Hydraphiles: design, synthesis and analysis of a family of synthetic, cation-conducting channels

George W. Gokel*

Bioorganic Chemistry Program and Department of Molecular Biology and Pharmacology, Washington University School of Medicine, 660 S. Euclid Ave., Campus Box 8103, St. Louis, MO 63110, USA.
E-mail: ggokel@molecool.wustl.edu

Received (in Cambridge, UK) 12th May 1999, Accepted 17th August 1999

The concept of channels has been with us more than a century. For half a century, biologists have studied the remarkable workings of protein and peptide channels that permit various cations and small molecules to pass through the phospholipid bilayer membrane. During the past decade, attempts have been made by chemists and biochemists to examine the action of channel compounds from the chemical point of view and to model their function using synthetic structures. What follows is a description of our own efforts to design, synthesize, and characterize a cation transporter that functions in a phospholipid bilayer.

Introduction

During the second half of the 20th century, there have been three important trends in organic chemistry. By the 1950s, the study of physical organic chemistry had moved to the forefront of the science. The study of steric and electronic effects and their influence on mechanism was at center stage. The refinement of physical organic principles provided the critical underlayment for the systematic development of synthetic methodology and strategy. Synthetic chemistry was built on the dual foundations of imagination and physical organic chemistry and reached ascendancy during the 1970s and 1980s. The importance of these two areas continues to be profound. Our understanding of mechanism and our ability to synthesize essentially whatever we can envision has spurred the organic chemist's imagination into supramolecular chemistry, particularly into the realms of bioorganic chemistry and materials development. Both of these areas face a similar challenge. In short, it is to design a compound that has a desired property or function without knowing precisely how such function is controlled. We have referred to the effort to design compounds having specific functions rather than specific structures as 'property-directed synthesis'.[1] This article is about our efforts to design compounds that perform as transmembrane channels[2] in phospholipid bilayers.

George Gokel was born in New York City but moved as a child to Florida where he grew up. He studied chemistry at Tulane University in New Orleans and earned a doctorate in chemistry at the University of Southern California in Los Angeles. After post-doctoral work with Donald Cram at UCLA and a short stint at the DuPont Chemical Co., Dr Gokel began his academic career. He has held positions in chemistry departments at the Pennsylvania State University, the University of Maryland, and the University of Miami. He is currently Professor in the Department of Molecular Biology and Pharmacology and Director of the Bioorganic Chemistry Program at the Washington University School of Medicine in St. Louis.

At the beginning of our effort to design functional synthetic channel compounds, we confronted a difficulty faced by everyone who attempts to mimic nature. The problem is to design a chemical compound that will function as the natural material does even though Nature's mechanism or mode of action may be imperfectly understood. This problem was compounded in the case of channel models because many in the biological community viewed proteins as the only authentic channels. Even peptides that exhibited channel-like function were regarded by some as intriguing but marginally useful.

Design strategy

The basic issue that must be considered in the design of a cation-conducting channel is how to get the cation from one side of a bilayer membrane to the other. Organic chemists have dealt with the issue of transporting cations across various membranes by designing, preparing, and using a variety of carrier molecules. These carriers function by complexing a cation at one surface of a membrane, carrying it 'ferry-boat style' across the non-polar or insulator regime of the membrane, and then releasing it at the opposite membrane surface. Crown ethers have proved to be particularly successful in transporting cations across bulk membranes. In this context, many combinations of macrocycles, salts, and solvents have been studied.[3]

Our early work with macrocycles led us to confront an interesting problem. The cation complexation constant is given by K_S (usually as the decadic logarithm, *i.e.* log K_S). The equilibrium constant is determined by the rates at which complexation and decomplexation occur, *i.e.* $K_S = k_1/k_{-1} = k_c/k_d = k_{complex}/k_{decomplex}$. Simple crown ethers[4] such as 18-crown-6 show fast binding and release kinetics as required

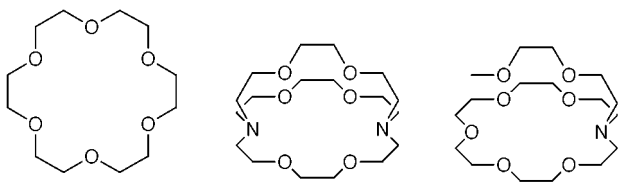

for successful carrier transport but cation binding selectivity is relatively poor. The cryptands are strong binders that show excellent cation selectivity but their binding and release kinetics are poor. We thus developed the family of compounds we named 'lariat ethers'[5] that could achieve the three-dimensional binding arrangement characteristic of cryptands and that also would exhibit good binding dynamics.[6]

The use of compounds that combine structural features thought to be important with flexibility (and therefore adaptability) was a cornerstone of our channel design philosophy. What

were the critical structural features? The first consideration was whether or not the channel would span the bilayer. This is a particularly intriguing question because in 1989, when the original design work was underway, the thickness of a bilayer was at least subject to interpretation if not unclear. Actually, there are three identifiable regions within the bilayer as shown in Fig. 1. These are the insulating regime or 'hydrocarbon slab', the polar headgroups, and the midpolar regime. The overall thickness of the membrane will depend upon the identities of the headgroups and the fatty acids.[7]

Chemists generally consider the 'membrane thickness' to be the entire width of the bilayer. This is known from X-ray structures of liposomes to be about 40 Å or more.[8] Biologists often regard the thickness of a membrane to be 30–35 Å since this is the value obtained from electrophysiological measurements that corresponds to the insulator regime.[9] The two values are different but both are correct in their context. The question of what, exactly, requires to be spanned by a channel model compound clearly remains. Should the channel's length be 30 or 50 Å?[10] Is the 'correct' length somewhere in between?

This issue illustrates a fundamental problem in modeling biological function. We may choose a span of either 30 or 40 Å to incorporate into our design. Assume we choose 40 Å, complete the design and synthesis, and then assess transport activity. If no cation transport is observed, does that mean that the length is wrong or that some other design feature is inappropriate? The length may be changed to 35 Å. If no cation transport occurs, should lengths of 30, 45 Å, *etc.* be tried? No variation in length will make the molecule function if some critical feature different from span is ill-designed. Combinatorial approaches could lead to optimization of this length but only after a functional design is in hand.

Several variables can immediately be recognized as bearing on channel function. These include the presence of donor groups, the 'relays', headgroups, and the conceptual models for the channel. Each of these variables has aspects that must be considered in the design of a synthetic channel. The consideration must, in the channel case, be done without having an adequate picture of how the wonderful and complex proteins actually work.

Donor groups

It seems reasonable that donor groups such as O, N or S must be present in a channel compound or how would the channel interact with a cation? In the design of the channel, one must consider which donor groups to incorporate. Do we wish only a few donors to be present or should they be numerous? Perhaps the decision about numbers will be influenced by whether the donors are strong or weak. The strength or weakness of a donor group depends on the cation with which it interacts. For example, sulfur (thioether) is a good donor for Zn^{2+} but less effective for K^+.

Ether oxygens, like water, are good donor groups for alkali metals. In that case, what sort of scaffolding should be used to organize the donor groups? Should the donor groups be incorporated into a macrocycle? 18-Crown-6 is selective for K^+ but will a channel incorporating 18-crown-6 also be selective for this cation? Indeed, can we think about cation selectivity in channels in the same way we conceive of complexation?[11] Let us consider 18-crown-6 and its ability to complex Na^+ and K^+. In aqueous solution, where binding constants are low, 18-crown-6 is selective for K^+ over Na^+. The respective binding constants are: K_S (Na^+) = 6.5; K_S (K^+) = 118.[12] This translates to an 18-fold selectivity for K^+ over Na^+. As noted above, $K_S = k_{complex}/k_{release} = k_1/k_{-1}$. The binding rates are known for these two cases and they differ by 2-fold: k_1 (Na^+) = 2.2×10^8 M^{-1}; k_1 (K^+) = 4.4×10^8 M^{-1}. The selectivity therefore lies principally in the ~10-fold difference in cation release rates: k_{-1} (Na^+) = 3.4×10^7 s^{-1}; k_{-1} (K^+) = 3.7×10^6 s^{-1}.

The reaction rates are important because a channel is a dynamic structure. The selectivity of a crown ether or cryptand is determined by what cation is bound relative to another. Which cations are transported rather than retained must define the selectivity of a channel. Thus, the *binding selectivity* of 18-crown-6 for K^+ over Na^+ may mean that a channel incorporating this macrocycle would pass Na^+ and thus show *transport selectivity* for it rather than for K^+. When we observed above that 'sulfur (thioether) is a good donor for Zn^{2+} but less effective for K^+', the context was binding rather than 'permitting' the cation to pass by. Thioether might be a 'good' channel donor group for an alkali metal or alkaline earth metal ion in the sense that it permits K^+ or Ca^{2+} but restricts Zn^{2+}.

Headgroups

An amphiphile is a compound having two different affinities or 'philicities'. The amphiphile sodium dodecyl sulfate has a polar sulfonic acid that constitutes the 'head' and a 12-carbon span that comprises the 'tail'. It seems reasonable that a channel would be an amphiphile since it must insert into a bilayer membrane that is constituted of phospholipid amphiphiles. If a single molecule spans the channel, it must be a twin-headed amphiphile.

In a channel molecule, the headgroup is required to play a second role: it must serve as, or lead to, a cation entry portal. One point of a membrane is, after all, to prevent salts from getting into or out of a cell. If the channel is to function, it must facilitate the entry and exit of cations (anions, small molecules

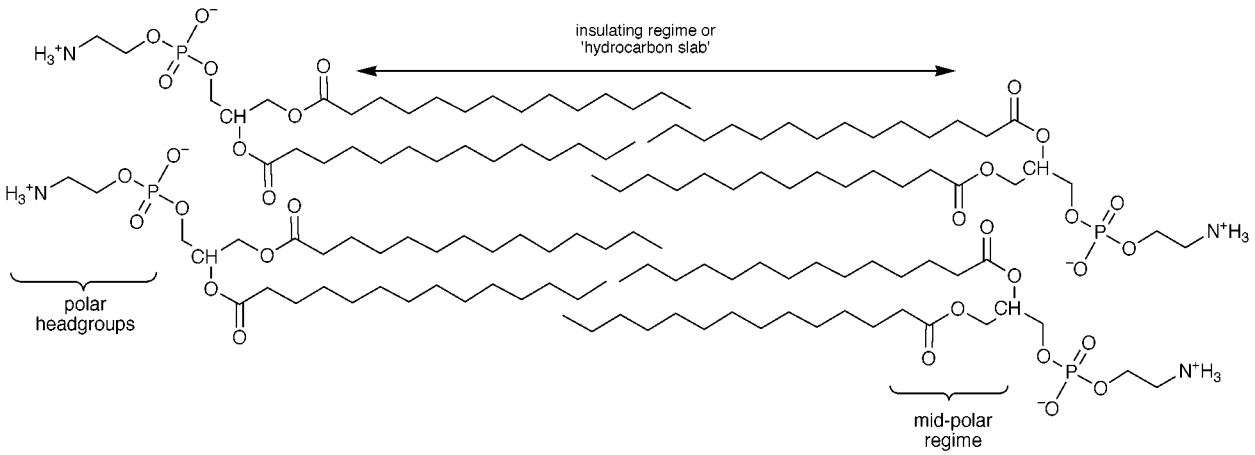

Fig. 1

etc.) without disrupting the membrane structure. It must create a controlled orifice in both the intra- and extra-vesicular surfaces of the bilayer.

There are two obvious challenges in the design of headgroups for a synthetic channel. First, where should the headgroup be placed relative to membrane elements? One possibility is at the membrane surface but an alternative is in the midpolar regime, which is the gateway to the hydrocarbon slab. Second, how polar should the headgroup be? If it is fully charged, should the field be positive or negative? It seems reasonable that a negatively charged headgroup would attract a cation and a cationic headgroup would favor an anion but this is more intuition than knowledge. Information about headgroup preferences might be gleaned from the specifics of protein channel structures. Although the amino acid sequences of many protein channels are known, the three dimensional structures of few have been established.

For most proteins, transmembrane segments are identified by subjecting the amino acid sequence to hydropathy analysis.[13] Typically, a computer program examines the entire length of the protein searching for sequences of amino acids that are hydrophobic. A transmembrane segment is about 20 amino acids if it is α-helical and it is about 10 amino acids if it is a β-sheet. Assuming an α-helical transmembrane segment (the common situation), the program looks for a sequence that is expected to partition into a low polarity medium. It is interesting to note that in an α-helix, each amino acid spans about 1.5 Å. Thus, a 20 amino acid sequence translates to a 30 Å span—the estimated thickness of the insulating regime. From this discussion, the problem is apparent. If one doesn't know the exact structure of the protein, it is hard to guess whether the polar residues, if any, are on the membrane surface or in the midpolar regime. In a synthetic channel, should there possibly be 'headgroups' in both positions? If one is unsure of the headgroup position(s), then guessing whether the environment is positively or negatively charged is obviously a challenge.

Water[14] is a ubiquitous element in biology and certainly present in bilayer membranes as well as in many proteins. What role will water play in transport? It seems reasonable to think that cations will be only partly desolvated as they pass through the membrane. Complete desolvation is a high-energy process and it is hard to see why all of the water would be stripped from a cation on the periplasmic side of the membrane when it must be rehydrated on the cytoplasmic surface. If water is attached to a cation, how does this affect transport? Must we consider the larger size of the fully hydrated cation rather than its crystallographic diameter? Will discrete molecules of water remain attached to individual ions or will there be exchange with the environment? How does the presence of water affect the choice of donor groups? Amidst all of these variables, one thing that seems clear is that it will be difficult for any positively charged species to traverse a 30 Å, nonpolar span without some interim stabilization.

Our original design for a cation-conducting channel is shown in Fig. 2. The questions posed above were dealt with as follows. Diaza-18-crown-6 polyethers were selected to serve as both headgroups and entry portals. It was known[15] that the crowns could bind both Na^+ ($\log K_S = 2.99$)[16] and K^+ ($\log K_S = 3.80$). It was also known from the early work of Kuwamura[17] and of Okahara[18] that alkyl-substituted crown ethers formed micellar aggregates when sonicated in aqueous suspension. We demonstrated that twin-tailed diazacrowns could form stable liposomes, suggesting that the crown would be effective as a head group.[19]

The two distal macrocycles were expected to serve both as headgroups and as entry portals. A K^+ cation (ionic diameter ~2.7 Å) can pass through the center of the macrocycle as can Na^+ (~2 Å). The central macrocycle was also expected to serve as a portal. Its role was predicted to be as a 'relay station' for the transient cation. The polar interaction of the crown with the transient cation at the least polar locale within the bilayer (the midplane) was expected to provide transient stabilization so the transmembrane journey could be completed. It was unknown at the time of the design how this might be accomplished within a protein channel.[20]

Dodecyl groups were chosen to be the hydrocarbon spacer chains and sidearms. The notion was that the two covalently attached chains would define the channel's overall length while the flexible sidearms organized along the lipid axis to provide the other 'wall' of the channel. A C–C bond is about 1 Å in the linear sense. The dodecyl chain is therefore just under 14 Å. This provides a span of ~28 Å plus the thickness of the macrocycle. Such a span was expected to cover the insulator regime of the bilayer. The arbitrary decision was made to locate the channel's headgroup in the bilayer's midpolar regime rather than on the membrane surface.

Diaza-18-crown-6 groups were chosen as the macrocycles because invertable nitrogen imparts flexibility to the system and obviates the problem of stereoisomerism. The protonation state of the nitrogen atoms within the bilayer is unknown at the time of this writing. It is worth noting that the schematic of the channel and four phospholipid monomers shows the latter with headgroups proportional to the lipid chain lengths.

Alternative designs

The development of synthetic channel models has been considered in a number of groups.[21] In some cases, compounds were designed *de novo* and in others the structures of the products of certain reactions suggested that they might possess channel activity. On occasion, the transport of Na^+, K^+ or Ca^{2+} was not studied but the assessment of transport efficacy was

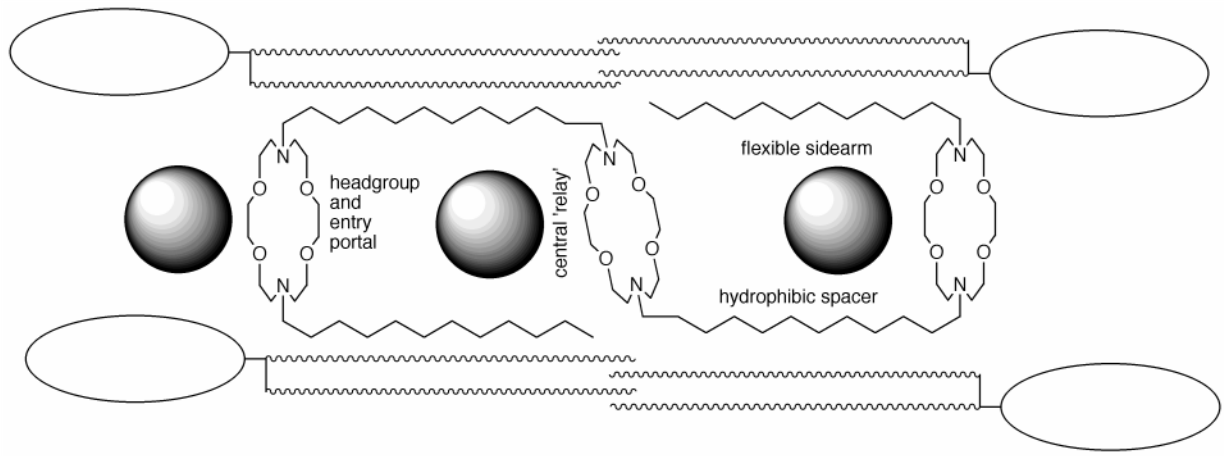

Fig. 2

limited to H^+ or Co^{2+}. Thus, the references cited represent a great range of approaches, designs, structural types and success.

Synthesis of channel 1

The first channel in the tris(macrocycle) family, designated C_{12}<N18N>C_{12}<N18N>C_{12}<N18N>C_{12} in a shorthand we developed some years ago,[22] presented the interesting problem of being nearly, but not quite, symmetrical. Of course, there is two-fold symmetry through the central macrocycle. The distal crowns, however, are attached to dodecyl chains on either side but are not symmetrical. Our best current synthetic approach[23] is accomplished as follows.

In the first step, diaza-18-crown-6 is monoalkylated by 1-bromododecane to give C_{12}<N18N> (Scheme 1). This, in turn, is treated with 1,12-dibromododecane to give C_{12}<N18N>C_{12}Br. Use of the latter to dialkylate diaza-18-crown-6 affords channel 1 (**1**). This approach was the model for the more than 30 members of this novel structural family now in hand.

Assessment of ionophoretic activity

Three methods were used to assess the efficacy of the synthetic cation transporters: fluorescence, ^{23}Na NMR and planar bilayer conductance. The fluorescence technique[24] was used for determining proton flux in a few compounds and only at an early stage of the study. Planar bilayer methods are discussed below. The bulk of the quantitative measurements were accomplished by using a dynamic NMR method. In short, phospholipid liposomes (vesicles) are created in the presence of NaCl. ^{23}Na NMR shows a single line for Na^+(inside) and Na^+ (outside). When Dy^{3+}, a shift reagent, is added to the external solution, the chemical shift of the external Na^+ changes. When an ionophore is added to the bilayer, internal and external Na^+ may equilibrate and the exchange rate constant may be determined from the concentration dependence of the linewidth change: $K = 1/\tau = \pi(\Delta\nu_1 - \Delta\nu_0)$.[25]

Multiple experiments at concentration ranges from 0–20 μM are required to determine the rate constant for a single transporter. The experiments were therefore done in tandem with a standard of known activity. In the early work, this standard was the naturally occurring, channel-forming peptide gramicidin.[26] Gramicidin is an excellent pore-former that sometimes functions even when experimental conditions are not properly maintained. Thus, the failure of a synthetic channel-former to transport Na^+ might occur due to poor experimental conditions rather than lack of efficacy and gramicidin might function despite the experimental problems. We have thus adopted Dn<N18N>C_{12}<N18N>C_{12}<N18N>Dn (Dn = dimethylaminonaphthylsulfonyl or dansyl) as our experimental standard. The 'dansyl channel' transports cations very reproducibly but fails when experimental conditions are not properly maintained. We have also modified the [Na^+] from 100 to 250 mM which gives better entrapment and more reproducible experimental results.

Using the ^{23}Na NMR method, we found channel **1** transported Na^+ across a phospholipid bilayer at a rate about 27% of that observed for gramicidin. The exchange rate observed for gramicidin is ~175 s^{-1} so channel **1** is transporting cations on the millisecond time scale. We were also able to correlate the transport rate with a number of structural variations although the details are beyond the scope of this review. It was interesting to note, however, that when terminal macrocycles were altered from C_{12}<N18N>~ to <18N>~ (aza-18-crown-6), Na^+ transport activity was lost. Replacement of the sidearm by benzyl, substituted benzyl, naphthyl, dansyl and others led to differences in transport rates but most sidearm changes afforded functional channels.

Naming the family of compounds

Many of the early channels were tris(macrocycle)s and we referred to these compounds as such. As structural variations led to the removal of one or more macrocycles, the name was no longer appropriate. We considered the name 'hydraphile' as a possibility because of its association with the two-headed monster slain by Hercules. The dictionary[27] provided additional inspiration in two other definitions. A hydra is 'any of several small freshwater polyps of the genus *Hydra* and related genera, having a naked cylindrical body and an oral opening surrounded by tentacles'. Clearly the shape and tentacles were highly suggestive. An additional definition added to the appropriateness of the name: 'A persistent or multifaceted problem that cannot be eradicated by a single effort'.

Control experiments

The fact that sodium flux was observed in the presence of **1** was very encouraging but not conclusive. It could mean that all of

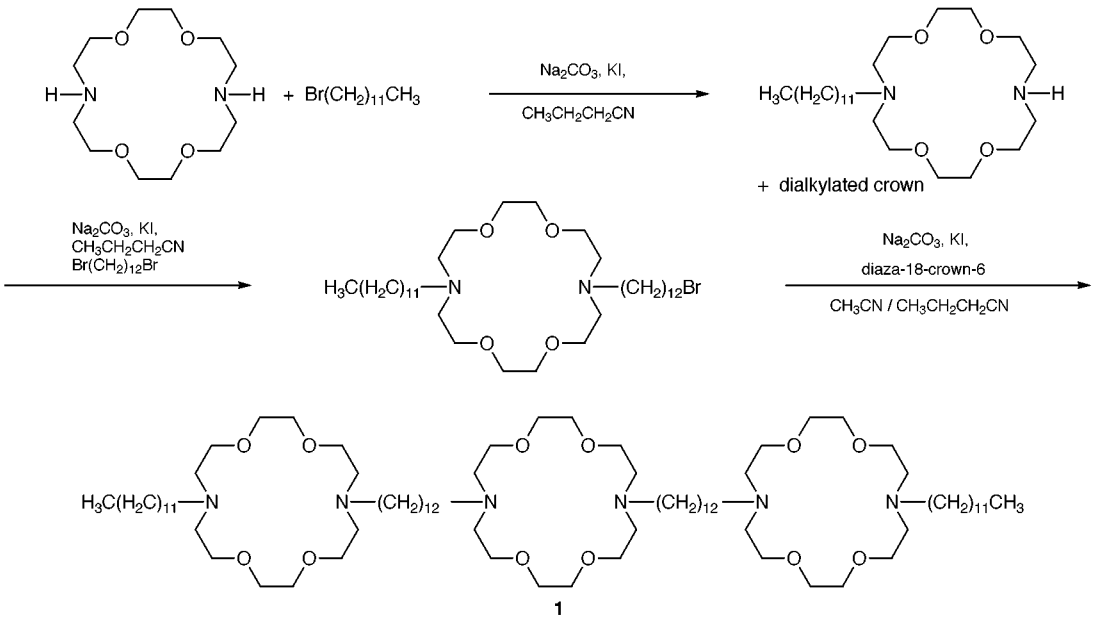

1

Scheme 1

the design concepts were as originally conceived. It is always nice to have one's ideas proven successful. Still, the fact of sodium transport was permissive rather than conclusive. It was possible, for example, that the tris(macrocycle) functioned simply by detergent action. To assess this possibility, the tris(macrocycle) ionophore was replaced by either Triton X-100, a neutral detergent, or sodium dodecyl sulfate, an anionic detergent. The concentration range in the ^{23}Na NMR experiment was expanded from the typical 0–20 μM by ten-fold to 0–200 μM but no cation flux (line broadening) could be detected in either case.[21]

It was possible that the tris(macrocycle)s were unusually active carrier molecules rather than pore-formers. A conventional concentric tube apparatus was used to assess carrier transport through a bulk $CHCl_3$ membrane in a group of 10 compounds.[28] In this experiment, a beaker is charged with $CHCl_3$ and water. A glass tube is then suspended in the beaker through the upper water layer and into the $CHCl_3$. The outer, upper aqueous ring is thus separated from the inner core of water. A NaX salt can be carried through the $CHCl_3$ bulk membrane from inner core to outer ring. On the atomic scale, a distance of $\sim 10^7$ Å must be traversed so the channel mechanism is precluded. The transport rates observed in this experiment (relative to valinomycin) were compared to those obtained for the same compounds in the ^{23}Na NMR/bilayer experiment (relative to gramicidin). In short, the data showed no discernible correlation. This does not prove the channel mechanism but clearly discounts carrier transport within the bilayer.[29] These findings comport with the observation that fragments of the channel such as $C_{12} < N18N > C_{12} < N18N > C_{12}$ or $< 18N > C_{12} < N18N > C_{12} < N18 >$ and known carriers such as $PhCH_2 < N18N > CH_2Ph$ were not sufficiently active to show transport when assessed by the NMR method.

It is interesting to note that addition of the tris(macrocycle)s to the $CHCl_3$ concentric tube system led to a dramatic increase in hydration of that solvent.[27] No further work was undertaken to resolve this issue because it was tangential to the main thrust of the effort.

It was possible that the rate differences observed for structurally related channels might be due only to variations in the extent of membrane penetration. Octanol–water partition coefficients[30] were determined for several substituted crown ethers and the experimentally determined values were compared to data calculated by the Hint module of Sybyl.[27] Agreement between experiment and calculation was good. The data showed that the tris(macrocycle)s favored octanol (*i.e.* the membrane) by $> 10^{10}$ up to as much as 10^{30}. Although the rate differential was not due to differences in partitioning, a minor kinetic effect was observed. When the ionophore was added to the preformed suspension of liposomes and then analyzed immediately, the plots of $1/\tau$ *vs.* [ionophore] showed curvature. If NMR analysis was delayed for an hour, the lines were essentially straight. Likewise, if the vesicles were formed in the presence of the ionophore (direct incorporation) linear data were obtained. Care was thus taken to permit equilibration of the sample system.

The channel's conformation

Changing the size of the central macrocycle diminished the transport rate but did not preclude it. Substituting the central macrocycle by an $O(CH_2CH_2O)_3$ chain again impeded but did not prohibit sodium transport. We concluded that the central macrocycle in $R < N18N > C_{12} < N18N > C_{12} < N18N > R$ was parallel to the lipid axis rather than parallel to the other two macrorings. Thus, we inferred that the cation passed by but not through the central macrocycle. This conformation is illustrated in Fig. 3.

Assessment of optimal distances

The tris(macrocyclic) channels were designed to function in a phospholipid bilayer but membrane dimensions and the placement of a channel within it are elusive. An attempt was therefore made to experimentally determine the optimal length of the channel. This was done by varying the length of the covalent, hydrophobic spacers in $PhCH_2 < N18N > C_{12} < N18N > C_{12} < N18N > CH_2Ph$. It was assumed that the overall conformation would remain similar as the chain length was varied by 2 methylenes on either side of the central macrocycle. The starting point for this exercise is indicated on the graph (Fig. 4) by an arrow. It was anticipated that incremental lengthening of a flexible assembly would lead to some reduction in efficacy as less favorable conformations were adopted. As chain length diminished, it was expected that a point would be reached at which the structure was simply too small to span the bilayer. Note that each change of 2 methylene units in the spacer is an overall change of 4 methylenes or ~ 4 Å in span. Shortening the chain by 4 Å or lengthening by 8 Å drops the transport rate to about half. Shortening by 8 Å leads to an inactive ionophore. Note that by 'inactive' we mean that no transport activity can be detected by the ^{23}Na NMR method.

Assessment of the conformation and location of the channel within the bilayer

The synthetic tris(macrocycle) channel compounds can readily be modified to incorporate various structural probes. In

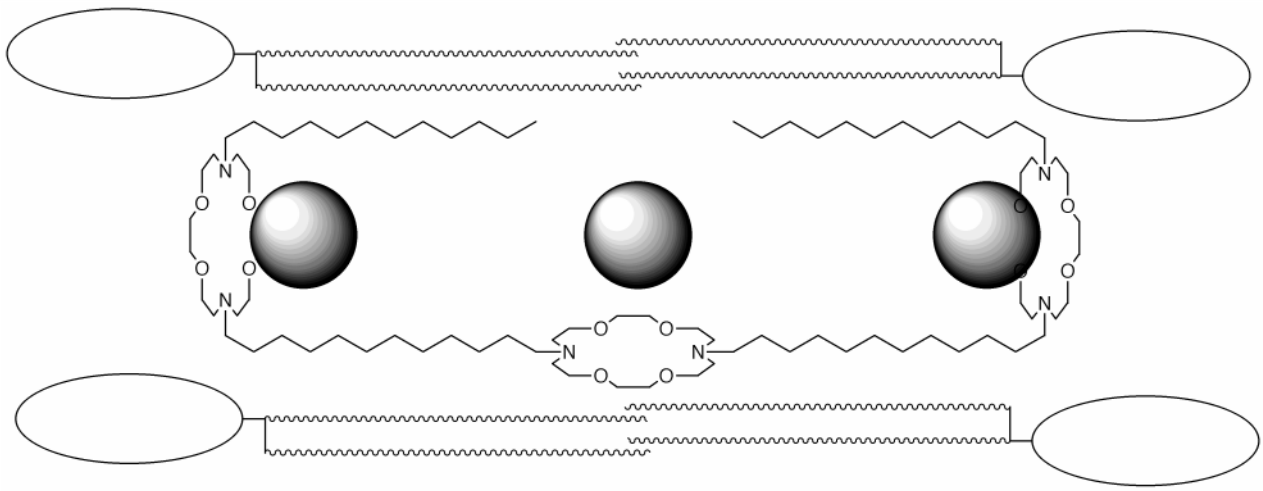

Fig. 3

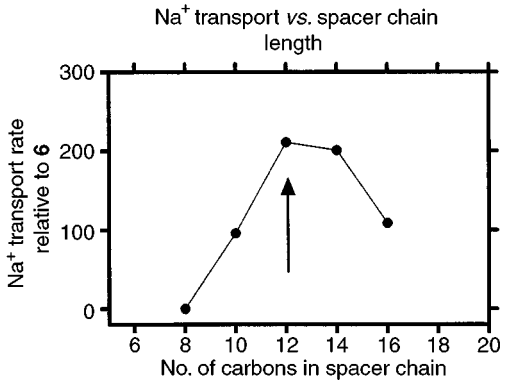

Fig. 4

particular, fluorescent headgroups can be included as an integral part of the structure. In biochemical studies, for example, the indolyl residue of tryptophan is often used as a fluorescent probe. Fluorescent dansyl residues were incorporated into the channel as headgroups: Dn < N18N > C_{12} < N18N > C_{12} < N18N > Dn, **2**. The fluorescence spectrum was determined in a variety of solvents from nonpolar to polar as well as in a phospholipid bilayer. Note that lipids were carefully screened to be sure that any fluorescent impurities were absent. The fluorescence maxima (λ_{max}) are shown in Fig. 5, plotted as a function of solvent polarity (the

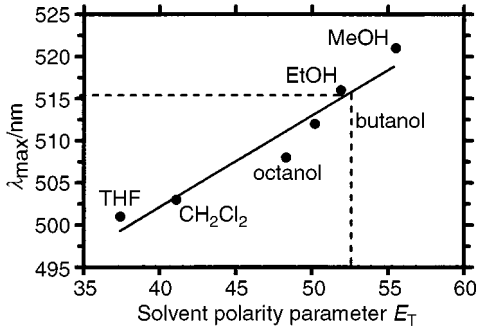

Fig. 5

Reichardt parameter, E_T).[31] A dashed line indicates the fluorescence maximum determined for the dansyl channel. The polarity experienced by the dansyl group is between that of ethanol and methanol—about what would be expected for the glyceryl ester regime of a phospholipid. In any event, the dansyl environment of the channel is significantly more polar than would be expected were it embedded in the membrane's 'hydrocarbon slab.

Fluorescence depth quenching

The heterocyclic 'doxyl' group quenches fluorescence by virtue of its unpaired electron spin. By using doxyl-substituted phospholipids, it is possible to estimate how far from the bilayer's midplane is the dansyl 'headgroup'. 7-Doxyl- and 12-doxyl-palmitoyl-substituted phosphatidylcholines were

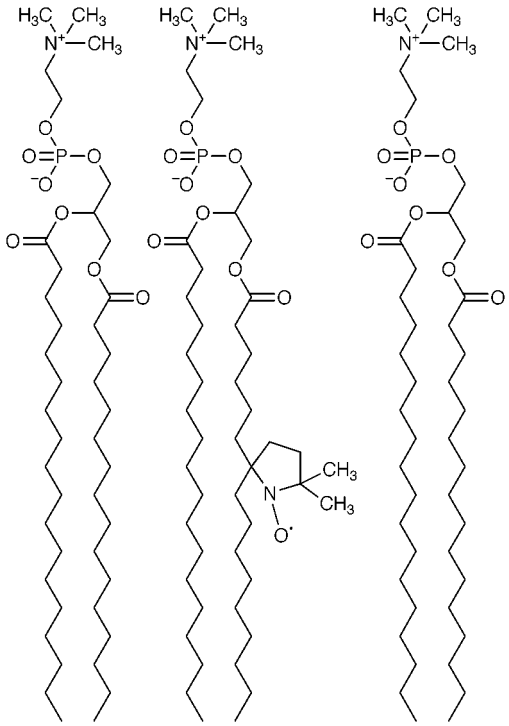

used along with the dansyl channel to estimate headgroup separation.[32] Application of the appropriate equations[33] gives a value for the headgroup separation of 28 Å (*i.e.* the distance of the headgroup from the bilayer's midplane is 14 Å). If the hydrocarbon slab is approximately 30 Å thick and the dansyl groups are ~6 Å, whether measured laterally or transversely, one concludes that the channel's termini are in or near the midpolar region created by the glyceryl ester residues. This comports with the position estimated from dansyl fluorescence.

Experiments designed to address headgroup issues

It was assumed that the conformation illustrated in Fig. 1 required the distal macrocycles to function both as headgroups and entry portals. An effort was made to confirm experimentally the ability of diaza-macrocycles to serve as amphiphile headgroups. It was found that a range of 2-armed diaza-18-crown-6 derivatives could form stable liposomes when sonicated in aqueous suspension.[34] In a molecule such as C_{18} < N18N > C_{18}, the octadecyl chains can function only as hydrophobic tails so the macrocycles must comprise the headgroups. Successful formation of stable liposomes from R < N18N > R clearly implies the efficacy of the crown as a headgroup. Evidence on the interaction of the headgroup with cations is discussed below.

The frequent observation of the rare amino acid tryptophan at the boundary margins of putative transmembrane segments of proteins suggested that it might play some important role in channel formation. In separate work, we demonstrated that indole, the sidechain of tryptophan, could function as a

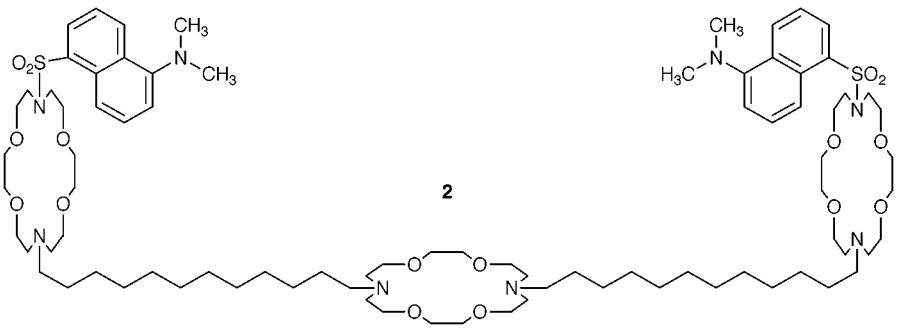

2

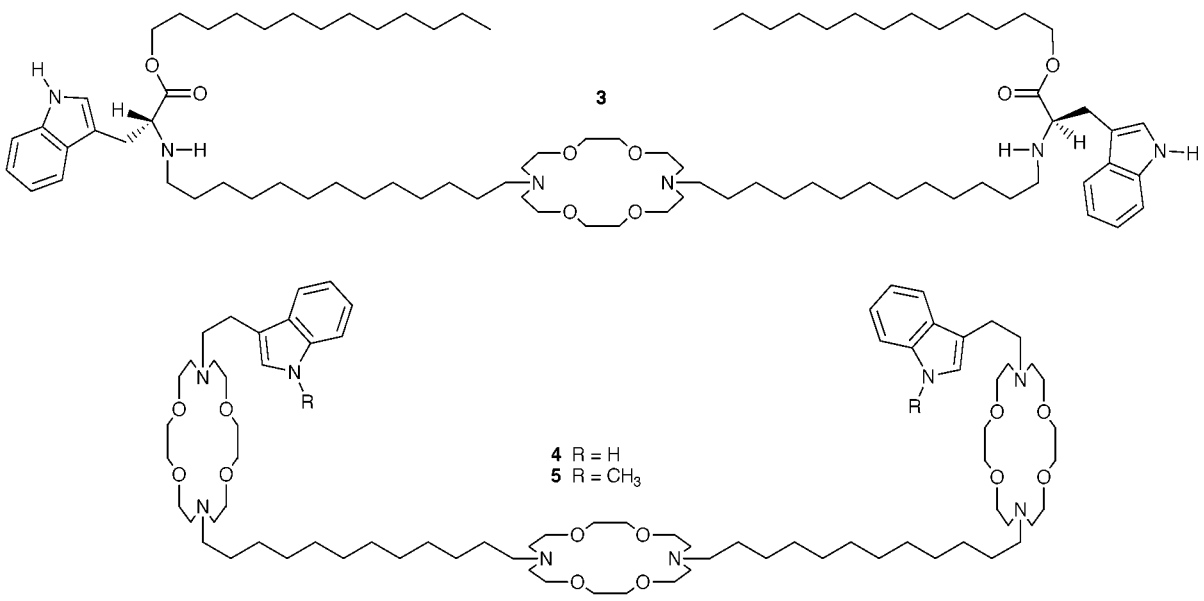

headgroup for the formation of stable liposomes.[35] Clearly, tryptophan cannot function as an entry portal for cations in the same sense that crowns do. We prepared **3**, which incorporated the essential channel elements shown in Fig. 1, but lacked the cation entry portal. Compound **3** showed no cation transport ability as judged by any of the analytical methods attempted.

H-bond-induced blockage of the headgroup

Because of our[35] and others'[33,36] speculation that tryptophan and/or its indole residue could play an anchoring role in phospholipid bilayer membranes, we prepared a tris(macrocycle) terminated in the indolylmethyl residue, *i.e.* $InCH_2CH_2 < N18N > C_{12} < N18N > C_{12} < N18N > CH_2CH_2In$**4**. Although structurally similar to the highly active benzyl channel ($PhCH_2 < N18N > C_{12} < N18N > C_{12} < N18N > CH_2Ph$), the indolyl channel showed no ability to transport Na^+.[37] Both CPK models and Monte Carlo simulations showed that a hydrogen bond between the indole NH and a macroring oxygen atom could form. An infrared band, attributable to H-bond formation, did not alter its position during 100-fold dilution. This suggests that the H-bond is intramolecular.

This result, although inferential, is clearly important. It implies that weak H-bond interactions can block the channel. This, in turn, implies that the conformation in Fig. 2 is correct or why would occlusion of the entry portal block the channel? Replacement of the indolyl residue by a methylindolyl, *i.e.* replacement of the NH group by NCH_3, gave a compound, **5**, that was fully active as a channel.

Application of the Hammett equation

If a cation enters the channel by going through or passing by the distal macrocycle(s), it should experience the stereoelectronics of that group. We prepared three channel compounds of the type $PhCH_2 < N18N > C_{12} < N18N > C_{12} < N18N > CH_2Ph$ in which the aromatic ring of the benzyl group was *para*-substituted. The substituents were H (shown), 4-methoxy and 4-nitro. A straight-line relationship was observed.[38] Admittedly, the graph (Fig. 6) involves only three points but the difficulty of synthesis and analysis will be apparent.

The critical results are as follows. First, r^2 for the three-point line is 0.95—a respectable value. Second, the slope of the line is negative as expected for the interaction of a cation with a neutral host. The slope is shallower than observed for complexation of cations by dibenzyldiaza-18-crown-6 derivatives.[39] This is expected for a transient interaction. A third point, not apparent from the graph, is that when relative transport rates obtained in the concentric tube experiment (see above) were plotted *vs.* Hammett σ^0, the straight-line 'correlation' had a zero slope and $r^2 = 0.4$.

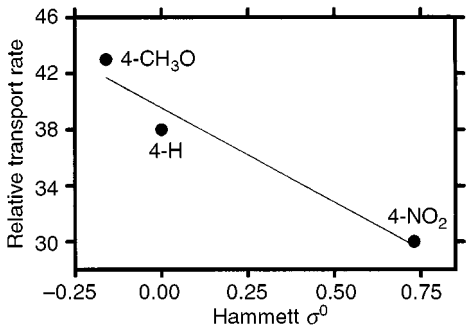

Fig. 6

Changes in headgroup size

Only limited work has thus far been completed to assess the influence of headgroup size. Two channels were prepared for this study. In both cases, the terminal residue ('flexible sidearm' in Fig. 1) was fluorobenzyl. The distal macrocycles were either 15- or 18-membered. When cation transport was assessed by using the NMR method, transport of Na^+ by the 15-membered ring channel was found to be about 60% of that determined for the compound having 18-membered distal macrocycles.[40]

The aggregation state of the channel

The availability of both the dansyl (**2**) and *N*-methylindolyl (**5**) channels provided an opportunity to assess the aggregation state of the channel. We found that the *N*-methylindolyl-sidearmed channel absorbed light at 283 nm and fluoresced at 343 nm—the wavelength at which the dansyl-terminated channel absorbs. An experiment was undertaken in which the amount of channel was held constant and the mole fractions of **2** and **5** were varied from 0→1 and 1→0, respectively. A logarithmic plot of the fluorescence ratio as a function of mole fraction gave a line with a slope of 1.12. The slope of this line has been interpreted to be the aggregation state. Thus, at least for these two compounds,

the channel operates, within experimental error, as a monomer.[41]

^{23}Na NMR transport results

The ^{23}Na NMR experiment as it is used to assess transport in a bilayer membrane was described above. A number of structural variations have been incorporated into channel **1** and the relative transport abilities of these compounds have been measured. Selected results are shown in Table 1 using the shorthand described above in which <N18N> represents 4,13-diaza-18-crown-6.

Table 1 Sodium ion transport by hydraphiles

Sidearm	Headgroup	Spacer	Center	k_{rel}
Dodecyl ($C_{12}H_{25}$)	<N18N>	$C_{12}H_{24}$	<N18N>	27
Benzyl ($CH_2C_6H_5$)	<N18N>	$C_{12}H_{24}$	O–2,6–$C_{10}H_6$–O	<2
Benzyl	<N18N>	$C_{12}H_{24}$	<N18N>	39
Dansyl	<N18N>	$C_{12}H_{24}$	<N18N>	24
Dansyl	<N18N>	$C_{12}H_{24}$	<N15N>	19
4-Fluorobenzyl	<N18N>	$C_{12}H_{24}$	<N18N>	26
2-(3-Indolyl)ethyl	<N18N>	$C_{12}H_{24}$	<N18N>	<2
2-(*N*-Methyl-3-indolyl)-ethyl	<N18N>	$C_{12}H_{24}$	<N18N>	23
None	<18N>	$C_{12}H_{24}$	<N18N>	<2

Patch clamping results

The ability of various synthetic and peptidic compounds to function as cation-conducting channels may be demonstrated by a technique called 'planar bilayer conductance', or PBC. In this technique, a phospholipid bilayer is formed in a pinhole separating two salt phases. When the membrane is formed over the pinhole, it turns dark and the system is sometimes referred to as a black lipid membrane. Using electrodes and a patch clamp amplifier, the electrical response of a bilayer membrane imbued with a transporter may be observed. A membrane is normally insulating so increases in the electrical response are interpreted as the passage of ions through it.

We conducted a number of experiments that confirmed ion transport. Our most recent PBC results are for a calixarene-based channel.[42] The patch clamp or PBC technique is wonderfully sensitive but it is a difficult method to master and to reproduce. In some cases, supposedly identical samples show high and no channel activity. In other cases, the membrane itself collapses and terminates the study before sufficient data have been acquired. We have thus preferred the NMR method; it is cumbersome but, so far at least, it has proved to be reliable.

Conclusions

Clearly many channel models are possible. Our basic design is effective and its modular design is proving useful to assess individual structural issues. In work that is yet to be published, we have explored covalent attachment of the sidearms and variations in the central relay unit. Cation/anion selectivity, ion selectivity in general, and rectification all remain important challenges in this emerging area.

Acknowledgment

I warmly thank the many co-workers whose names are on the cited references who have been intimately involved in this project. I appreciate their hard work, their clever ideas, and their keen insight and criticism. Support of this work by grants from NIH (GM 36262), NATO and NSF (CHE-9805840) is gratefully acknowledged.

Notes and references

1 G. W. Gokel, J. C. Medina and C. Li, *Synlett*, 1991, 677.
2 W. D. Stein, *Channels, Carriers, and Pumps*, Academic Press, New York, 1990; B. Hille, *Ionic Channels of Excitable Membranes*, 2nd edn., Sinauer Press, Sunderland, MA, 1992; D. J. Aidley and P. R. Stanfield, *Ion Channels: Molecules in Action*, Cambridge University Press, Cambridge, 1996.
3 B. A. Moyer, *Complexation and Transport*, in *Molecular Recognition: Receptors for Cationic Guests*, vol. 1, *Comprehensive Supramolecular Chemistry*, ed. G. W. Gokel, Elsevier, Oxford, 1996, pp. 377–416; T. Araki and H. Tsukube, *Liquid Membranes: Chemical Applications*, CRC Press, Boca Raton, 1990.
4 G. W. Gokel, *Crown Ethers and Cryptands*, in *Monographs in Supramolecular Chemistry*, ed. J. F. Stoddart, The Royal Society of Chemistry, London, England, vol. 3, 1991, p. 190.
5 The name lariat ether was suggested by the CPK models that resembled a looped rope. Moreover, the mode of complexation was envisioned as a 'rope and tie' combination of macroring and sidearm. When the first manuscript was submitted to this august Journal, it was accepted but an editor deleted the name lariat because he or she felt that the name was not officially sanctioned nomenclature. We felt the name was an important element in conceptualizing these compounds. We therefore withdrew the paper with the intention of submitting it elsewhere. The editor relented and the report appeared in due course: G. W. Gokel, D. M. Dishong and C. J. Diamond, *J. Chem. Soc., Chem. Commun.*, 1980, 1053.
6 G. W. Gokel and J. E. Trafton, *Cation Binding by Lariat Ethers*, in *Cation Binding by Macrocycles*, ed. G. W. Gokel and Y. Inoue, Marcel Dekker, New York, 1990, pp. 253-310; G. W. Gokel, *Lariat Ethers*, in *Inclusion Phenomena*, ed. J. L. Atwood, E. Davies and D. D. MacNicol, Oxford University Press, 1991, vol. 4, pp. 287–328; G. W. Gokel, *Chem. Soc. Rev.*, 1992, **21**, 39; G. W. Gokel and O. F. Schall, *Lariat Ethers*, in *Comprehensive Supramolecular Chemistry*, ed. G. W. Gokel, Elsevier, Oxford, 1996, pp. 97–152.
7 M. C. Wiener and S. H. White, *Biophys. J.*, 1992, **61**, 434.
8 Small unilamellar vesicles (SUV) formed by sonicating egg phosphatidylcholine lipids show internal and external radii of 65 and 105 Å respectively, suggesting a membrane thickness of 40 Å [P. Yeagle, *The Membranes of Cells*, Academic Press, New York, 1987, p. 47]. For a review of lipid packing in the solid state, see H. Hauser and G. Poupart, *Lipid Structure*, in ref. 9.
9 *The Structure of Biological Membranes*, ed. P. Yeagle, CRC Press, Boca Raton, 1992.
10 R. P. Rand and V. A. Parsegian, *The Forces between Interacting Bilayer Membranes and the Hydration of Phospholipid Assemblies*, in *The Structure of Biological Membranes*, ed. P. Yeagle, CRC Press, Boca Raton, 1992, pp. 251–306.
11 J. S. Bradshaw, R. M. Izatt, A. V. Bordunov, C. Y. Zhu and J. K. Hathaway, *Crown Ethers*, in *Molecular Recognition: Receptors for Cationic Guests*, ed. G. W. Gokel, Elsevier, Oxford, 1996, vol. 1, pp. 35–95.
12 G. W. Liesegang, A. Vasquez, N. Purdie and E. M. Eyring, *J. Am. Chem. Soc.*, 1977, 3240.
13 T. E. Creighton, *Proteins: Structures and Molecular Properties*, 2nd edn., Freeman, New York, 1993, p. 154.
14 F. Franks, *Water*, Royal Society of Chemistry, Cambridge, 1984, p. 69.
15 K. A. Arnold, J. C. Hernandez, C. Li, J. V. Mallen, A. Nakano, O. F. Schall, J. E. Trafton, M. Tsesarskaja, B. D. White and G. W. Gokel, *Supramol. Chem.*, 1995, **5**, 45.
16 Values are for *N,N′*-bis(*n*-dodecyl)-4,13-diaza-18-crown-6 in anhydrous CH_3OH at 25 °C.
17 T. Kuwamura and T. Kawachi, *Yukagaku*, 1979, **28**, 195 *(Chem. Abstr.*, 1979, **90**, 206248); T. Kuwamura, M. Akimaru, H. L. Takahashi and M. Arai, *Kenkyu Hokoku-Asahi Garasu Kogyo Gijutsu Shoreikai*, 1979, **35**, 45 *(Chem. Abstr.*, 1981, **95**, 61394q); T. Kuwamura and S. Yoshida, *Nippon Kagaku Kaishi*, 1980, 427 *(Chem. Abstr.*, 1980, **93**, 28168e).
18 M. Okahara, P. L. Kuo, S. Yamamura and I. Ikeda, *J. Chem. Soc., Chem. Commun.*, 1980, 586; I. Ikeda, K. Iwaisako, Y. Nakatsuji and M. Okahara, *Yukagaku*, 1986, **35**, 1001 *(Chem. Abstr.*, 1987, **106**, 86714).
19 L. E. Echegoyen, J. C. Hernandez, A. Kaifer, G. W. Gokel and L. Echegoyen, *J. Chem. Soc., Chem. Commun.*, 1988, 836; S. L. De Wall, K. Wang, D. L. Berger, S. Watanabe, J. C. Hernandez and G. W. Gokel, *J. Org. Chem.*, 1997, **62**, 6784.
20 B. Roux and R. MacKinnon, *Science*, 1999, **285**, 100.

21 I. Tabushi, Y. Kuroda and K. Yokota, *Tetrahedron Lett.*, 1982, **23**, 4601; F. M. Menger, D. S. Davis, R. A. Persichetti and J. J. Lee, *J. Am. Chem. Soc.*, 1990, **112**, 2451; Y. Kobuke, K. Ueda and M. Sokabe, *J. Am. Chem. Soc*., 1992, **114**, 7618; J. G. Neevel and R. Nolte, *Tetrahedron Lett.*, 1984, **25**, 2263; R. J. M. Nolte, A. J. M. Beijnen, J. G. Neevel, J. W. Zwikker, A. J. Verkley and W. Drenth, *Isr. J. Chem.*, 1984, **24**, 297; U. F. Kragten, M. F. M. Roks and R. J. M. Nolte, *J. Chem. Soc., Chem. Commun.*, 1985, 1275; L. Jullien and J. M. Lehn, *Tetrahedron Lett.*, 1988, **29**, 3803; L. Jullien and J. M. Lehn, *J. Inclusion Phenom.*, 1992, **12**, 55; J. Canceill, L. Jullien, L. Lacombe and J. M. Lehn, *Helv. Chim. Acta*, 1992, **75**, 791; M. Pregel, L. Jullien and J. M. Lehn, *Angew. Chem., Int. Ed. Engl.*, 1992, **31**, 1637; M. Pregel, L. Jullien, J. Canceill, L. Lacombe and J. M. Lehn, *J. Chem. Soc., Perkin Trans. 2*, 1995, 417; V. E. Carmichael, P. Dutton, T. Fyles, T. James, J. Swan and M. Zojaji, *J. Am. Chem. Soc.*, 1989, **111**, 767; T. Fyles, T. James and K. Kaye, *Can. J. Chem.*, 1990, **68**, 976; T. Fyles, K. Kaye, T. James and D. Smiley, *Tetrahedron Lett.*, 1990, 1233; K. Kaye and T. Fyles, *J. Am. Chem. Soc.*, 1993, **115**, 12 315; T. Fyles, T. James, A. Pryhitka and M. Zojaji, *J. Org. Chem.*, 1993, **58**, 7456; M. R. Ghadiri, J. R. Granja and L. K. Buehler, *Nature*, 1994, **369**, 301; N. Khazanovich, J. R. Granja, D. E. McRee, R. A. Milligan and M. R. Ghadiri, *J. Am. Chem. Soc.*, 1994, **116**, 6011; E. Stadler, P. Dedek, K. Yamashita and S. Regen, *J. Am. Chem. Soc.*, 1994, **116**, 6677; N. Voyer and M. Robitaille, *J. Am. Chem. Soc.*, 1995, **117**, 6599; Y. Tanaka, Y. Kobuke and M. Sokabe, *Angew. Chem., Int. Ed. Engl.*, 1995, **34**, 693; G. Deng, M. Merritt, K. Yamashita, V. Janout, A. Sadownik and S. L. Regen, *J. Am. Chem. Soc.*, 1996, **118**, 3308; A. Matsubara, K. Asami, A. Akagi and N. Nishino, *Chem. Commun.*, 1996, 2069; D. Seebach, A. Brunner, H. M. Buerger, R. N. Reusch and L. L. Bramble, *Helv. Chim. Acta*, 1996, **79**, 507; H. Wagner, K. Harms, U. Koert, S. Meder and G. Boheim, *Angew. Chem., Int. Ed. Engl.*, 1996, **35**, 2643; S. Matile, *J. Am. Chem. Soc.*, 1997, **119**, 8726; L. A. Weiss, N. Sakai, B. Ghebremariam, C. Ni and S. Matile, *J. Am. Chem. Soc.*, 1997, **119**, 12 142; J.-C. Meillon and N. Voyer, *Angew. Chem., Int Ed. Engl.*, 1997, **36**, 967; A. D. Pechulis, R. J. Thompson, J. P. Fojtik, H. M. Schwartz, C. A. Lisek and L. L. Frye, *Bioorg. Med. Chem.*, 1997, **5**, 1893; L. Chen, N. Sakai, S. T. Moshiri and S. Matile, *Tetrahedron Lett.*, 1998, **39**, 3627; T. D. Clark, L. K. Buehler and M. R. Ghadiri, *J. Am. Chem. Soc*., 1998, **120**, 651; C. Ni and S. Matile, *Chem. Commun*., 1998, 755; R. N. Reusch and H. L. Sadoff, *Proc. Natl. Acad. Sci. USA*, 1988, **85**, 4176.

22 J. C. Hernandez, J. E. Trafton and G. W. Gokel, *Tetrahedron Lett.*, 1991, 269.

23 O. Murillo, S. Watanabe, A. Nakano and G. W. Gokel, *J. Am. Chem. Soc*., 1995, **117**, 7665.

24 K. Kano and J. H. Fendler, *Biochim. Biophys. Acta*, 1978, **509**, 289.

25 F. G. Riddell and M. K. Hayer, *Biochem. Biophys. Acta*, 1985, **817**, 313; F. G. Riddell and S. J. Tompsett, *Biochim. Biophys. Acta*, 1990, **1990**, 193.

26 D. A. Doyle and B. A. Wallace, *Biomembranes*, 1996, **6**, 327; B. A. Wallace, *J. Struct. Biol.*, 1998, **121**, 123.

27 *American Heritage Dictionary*, 3rd edn., Houghton-Mifflin, 1992.

28 The apparatus is described in detail in ref. 20.

29 O. Murillo, I. Suzuki, E. Abel, C. L. Murray, E. S. Meadows, T. Jin and G. W. Gokel, *J. Am. Chem. Soc.*, 1997, **119**, 5540.

30 *Lipophilicity in Drug Action and Toxicology*, ed. V. Pliska, B. Testa and H. v. d. Waterbeemd, in *Methods and Principles in Medicinal Chemistry*, ed. R. Mannhold, H. Kubinyi and H. Timmerman, VCH, Weinheim, 1996, vol. 4.

31 C. Reichardt, *Chem. Rev.*, 1994, **94**, 2319.

32 E. Abel, G. E. M. Maguire, E. S. Meadows, O. Murillo, T. Jin and G. W. Gokel, *J. Am. Chem. Soc.*, 1997, **119**, 9061.

33 K. Kachel, E. Ascuncion-Punzalan and E. London, *Biochemistry*, 1995, **34**, 15 475.

34 S. L. De Wall, K. Wang, D. L. Berger, S. Watanabe, J. C. Hernandez and G. W. Gokel, *J. Org. Chem.*, 1997, **62**, 6784.

35 E. Abel, M. F. Fedders and G. W. Gokel, *J. Am. Chem. Soc*., 1995, **117**, 1265.

36 M. Schiffer, C.–H. Chang and F. J. Stevens, *Protein Eng.*, 1992, **5**, 213.

37 O. Murillo, E. Abel, G. E. M. Maguire and G. W. Gokel, *Chem. Commun.*, 1996, 2147.

38 O. Murillo, I. Suzuki, E. Abel and G. W. Gokel, *J. Am. Chem. Soc.*, 1996, **118**, 7628.

39 D. A. Gustowski, V. J. Gatto, J. Mallen, L. Echegoyen and G. W. Gokel, *J. Org. Chem.*, 1987, **52**, 5172.

40 C. L. Murray, E. S. Meadows, O. Murillo and G. W. Gokel, *J. Am. Chem. Soc.*, 1997, **119**, 7887.

41 E. Abel, G. E. M. Maguire, O. Murillo, I. Suzuki and G. W. Gokel, *J. Am. Chem. Soc*., 1999, **121**, 9043.

42 J. de Mendoza, F. Cuevas, P. Prados, E. S. Meadows and G. W. Gokel, *Angew. Chem., Int. Ed.*, 1998, **37**, 1534.

Paper a903825f

ChemComm

A rigid 1,3,5-phenylene-based metallodendrimer containing a ruthenium(II) bis(terpyridyl) complex

Mutsumi Kimura,* Tetsuo Shiba, Tsuyoshi Muto, Kenji Hanabusa and Hirofusa Shirai

Department of Functional Polymer Science, Faculty of Textile Science and Technology, Shinshu University, Ueda, Nagano 386-8567, Japan. E-mail: mkimura@giptc.shinshu-u.ac.jp

Received (in Cambridge, UK) 26th October 1999, Accepted Accepted 18th November 1999

A new 1,3,5-phenylene-based metallodendrimer containing a ruthenium bis(terpyridyl) complex was prepared and characterized; the rigid dendritic branches are found to affect the electrochemical properties of the redox-active core.

Dendrimers are well defined, highly branched macromolecules constructed from an interior core with a regular array of branch units.[1] To investigate the influence of dendritic structures on electrochemical, photochemical and catalytic properties, dendrimers containing functional units have been designed and synthesized.[2] The dendritic structures influence the microenvironment around the cores and modify their properties.[3] Polypyridyl ruthenium(II) complexes ($[Ru(bpy)_3]^{2+}$ and $[Ru(tpy)_2]^{2+}$) are widely used for the construction of dendrimers because of their unique electrochemical and photochemical properties.[4] However, these dendrimers have been prepared by attaching flexible dendron units around metal complexes. Rigid dendrimers have been prepared using phenylene, phenylacetylene and phenylenevinylene units as repeating units in the dendritic structures.[5] The construction of a well defined rigid dendritic structure around a redox-active metal complex unit may result in interesting electrochemical and optical changes.

Herein, we report the first rigid metallodendrimer containing $[Ru(tpy)_2]^{2+}$ in the interior core. The synthesis of the new 1,3,5-phenylene-based dendritic ligand **3** was performed using the methodology developed by Miller *et al.* (Scheme 1).[6] The terpyridyl core **1** was obtained from 3,5-dibromobenzaldehyde and 1-(2-pyridylcarbonylmethyl)pyridinium iodide according to the literature.[7] The dendron **2** was prepared in a stepwise manner through a Suzuki coupling reaction between an arylboronic acid and 3,5-dibromo-1-(trimethylsilyl)benzene.[8] Finally, the coupling of **2** to **1** using $Pd(PPh_3)_4$ as a catalyst proceeded smoothly to give the dendritic ligand **3** in 70% yield. This new dendritic ligand was characterized by ^{1}H NMR and matrix-assisted laser desorption ionization time of flight (MALDI-TOF) mass spectrometric techniques. MALDI-TOF mass spectra of **3** gave the correct molecular peak ($[M + H^+]$ *m/z* = 1823). Fig. 1 shows the ^{1}H NMR spectrum of **3** in $CDCl_3$ which provides structural information. The ^{1}H NMR spectrum in the aromatic region of **3** is very simple and readily assignable and indicates the successive generation of a highly symmetric layered structure.

Treatment of **3** with $RuCl_3 \cdot 3H_2O$ generated the desired metallodendrimer $[Ru(\mathbf{3})_2]^{2+}$ (Scheme 2) which was purified by column chromatography after anion exchange with hexafluorophosphate ion. The presence of *tert*-butyl groups at the exterior positions of the dendrimer completely encapsulates the $Ru(tpy)_2$ core and enhances the hydrophobicity with metallodendrimer $[Ru(\mathbf{3})_2]^{2+}$ being highly soluble in a variety of organic solvents such as alkanes, but not in polar solvents such as acetonitrile and alcohols. By contrast, the low molecular weight complex bis(4′-(*p*-tolyl)-2,2′:6′,2″-terpyridyl)ruthenium(II) complex ($[Ru(tpy\text{-}phMe)_2]^{2+}$) only showed solubility in polar solvents. The Homogeneity of $[Ru(\mathbf{3})_2]^{2+}$ was demonstrated by GPC analyses and MALDI-TOF mass spectrometry. Examination by GPC analysis showed that $[Ru(\mathbf{3})_2]^{2+}$ has a sharp and symmetrical elution peak with a polydispersity (M_w/M_n) of < 1.01. The MALDI-TOF mass spectrum of $[Ru(\mathbf{3})_2]^{2+}$ gave the correct mass at *m/z* 3891 for the $[M - PF_6]$ peak. Fig. 2 shows the absorption spectra of **3** and $[Ru(\mathbf{3})_2]^{2+}$, with absorption maxima (λ_{max}) and molar absorption coefficients (ε) collected in Table 1. The spectrum of $[Ru(\mathbf{3})_2]^{2+}$ in the visible region showed a characteristic MLCT transition at 490 nm, indicating the formation of a $[Ru(tpy)_2]^{2+}$ core.[10] The molecular coefficient for the MLCT band of $[Ru(\mathbf{3})_2]^{2+}$ was almost the same as that of $[Ru(tpy\text{-}phMe)_2]^{2+}$. Moreover, the absorbance at 260 nm of $[Ru(\mathbf{3})_2]^{2+}$ was approximately double that of the dendritic ligand **3**. As revealed by a computer generated ball-and-stick model, the dendritic ligand **3** is a hemispherical structure with a radius of *ca.* 1.5 nm (Scheme 2). The metallodendrimer $[Ru(\mathbf{3})_2]^{2+}$ is thus formed by metal-mediated

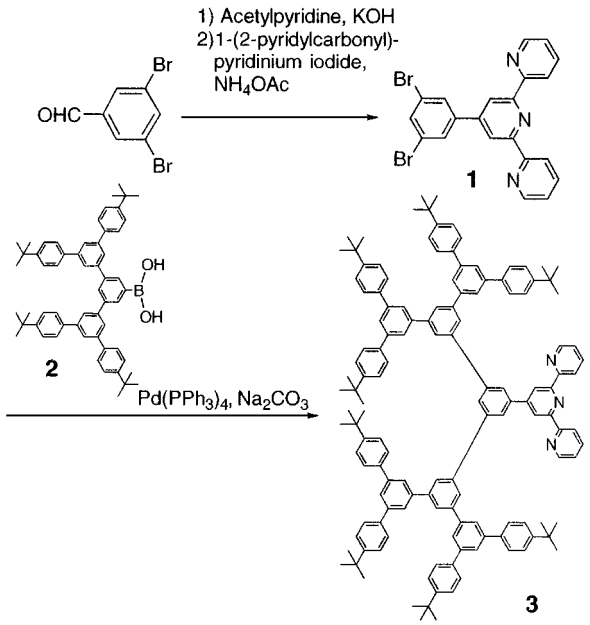

Scheme 1

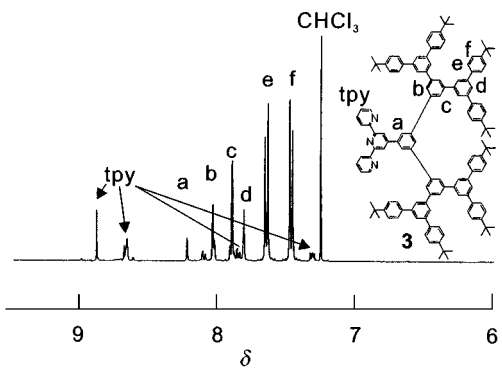

Fig. 1 ^{1}H NMR spectrum of **3** in $CDCl_3$.

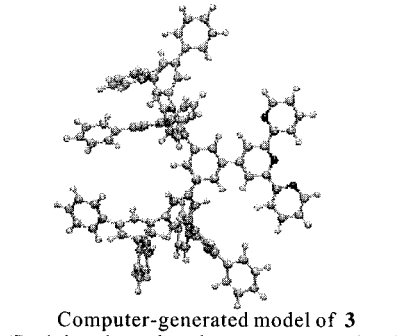

Computer-generated model of **3**
(Peripheral *tert*-butyl groups were omitted)

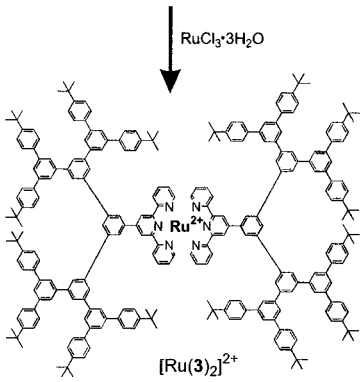

Scheme 2

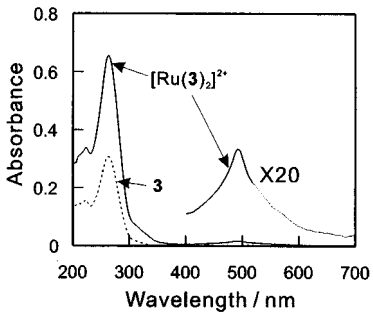

Fig. 2 UV–VIS absorption spectra of **3** and $[Ru(\mathbf{3})_2]^{2+}$ in CH_2Cl_2. ([**3**], $[Ru(\mathbf{3})_2]^{2+}$ = 1.0 μM).

assembly through the formation of a metal complex between two ligands possessing well defined hemispherical dendritic structures and one Ru^{2+} ion.

The influence of the rigid dendritic branches on the redox properties of the redox-active $[Ru(tpy)_2]^{2+}$ core was studied by cyclic voltammetry in CH_2Cl_2 using Bu_4NPF_6 (0.1 M) as supporting electrolyte (Table 1). The metallodendrimer $[Ru(\mathbf{3})_2]^{2+}$ exhibited one oxidation ($E_{1/2}$ = +1.25 V *vs.* SCE) and two reduction processes ($E_{1/2}$ = −1.28 and −1.43 V *vs.* SCE). The average peak potentials ($E_{1/2}$) for these processes were almost the same as those of the non-dendiritic $[Ru(tpy\text{-}phMe)_2]^{2+}$ complex.[4a,9] However, $[Ru(\mathbf{3})_2]^{2+}$ showed a large voltage difference between the current maxima of the reduction and return oxidation wave (ΔE), indicative of slower electron transfer than for the non-dendritic complex. This observation was similar to the electrochemical results of a flexible metallodendrimer containing redox-active core subunits.[3,4] The rigid dendritic branches around the $[Ru(tpy)_2]^{2+}$ core lead to a distance of 1.5 nm between the core and the electrode surface. The remoteness of the redox-active core from the electrode surface was found to hinder the electron transfer processes.

Table 1 Structural, spectroscopic and electrochemical data for $[Ru(\mathbf{3})_2]^{2+}$

	m/z[a]	Absorption[b] λ_{max}/nm (ε/M^{-1} cm^{-1})	$E_{1/2}$[c]/V *vs.* SCE	ΔE[c]/ mV
$[Ru(\mathbf{3})_2]^{2+}$	3891	490 (25000)	+1.25	180
	[M − PF_6^-]	260 (653000)	−1.28	120
			−1.43	125
$[Ru(tpy\text{-}phMe)_2]^{2+}$		490 (28900)	+1.20	76
			−1.24	71
			−1.46	83

[a] *m/z* Value determined by MALDI-TOF experiments. [b] CH_2Cl_2 solution. [c] From cyclic voltammetry in CH_2Cl_2 solution, 100 mV s^{-1} scan rate, Bu_4NPF_6 supporting electrolyte, Pt electrode, Ag/AgCl reference. $E_{1/2}$ is defined as the average of the two voltages at the current maximum/minimum of the redox waves. ΔE is defined as the difference of the peak voltages for the reduction and return oxidation waves.

In summary, we have reported the construction of a new rigid metallodendrimer, in which the metal complex is encapsulated in a precise position within the rigid dendritic macromolecule. Further photochemical investigations of the rigid metallodendrimer are currently in progress.

This research was supported in part by a Grant-in-Aid for COE Research 'Advanced Fiber/Textile Science and Technology' (#10CE2003) and Scientific Research (#11450366) from the Ministry of Education, Science, Sports and Culture of Japan.

Notes and references

1 D. A. Tomalia and H. Dupont Durst, *Top. Corr. Chem.*, 1993, **165**, 193; G. R. Newkome and C. N. Moorefield, *Comprehensive Supramolecular Chemistry*, Pergamon, 1996, vol. 10 pp. 777–832; J. M. J. Fréchet, *Science*, 1994, **263**, 1710; F. Zeng and S. C. Zimmerman, *Chem. Rev.*, 1997, **97**, 1681.

2 C. Gorman, *Adv. Mater.*, 1998, **10**, 295 and references therein; M. Fischer and F. Vögtle, *Angew. Chem., Int. Ed.*, 1999, **38**, 884 and references therein.

3 P. J. Dandliker, F. Diederich, M. Gross, C. B. Knobler, A. Louati and E. M. Sandford, *Angew. Chem., Int. Ed. Engl.*, 1994, **33**, 1739; P. J. Dandliker, F. Diederich, J.-P. Gisselbrecht, A. Louati and M. Gross, *Angew. Chem., Int. Ed. Engl.*, 1995, **34**, 2725; H.-F. Chow, I. Y.-K. Chan, D. T. W. Chan and R. W. M. Kwok, *Chem. Eur. J.*, 1996, **9**, 1085; C. B. Gorman, B. L. Parkhurst, W. Y. Su and K.-Y. Chen, *J. Am. Chem. Soc.*, 1997, **119**, 1141; C. M. Cardona and A. E. Kaifer, *J. Am. Chem. Soc.*, 1998, **120**, 4023.

4 (*a*) G. R. Newkome, R. Güther, C. N. Moorefield, F. Cardullo, L. Echegoyen, E. Pérez-Cordero and H. Luftmenn, *Angew. Chem., Int. Ed. Engl.*, 1995, **34**, 2023; (*b*) J. Issberner, F. Vögtle, L. De Cola and V. Balzani, *Chem. Eur. J.*, 1997, **3**, 706; (*c*) F. Vögtle, M. Plevoets, M. Nieger, G. C. Azzellini, A. Credi, L. De Cola, V. De Marchis, M. Venturi and V. Balzani, *J. Am. Chem. Soc.*, 1999, **121**, 6290; (*d*) V. Balzani, S. Campagna, G. Denti, A. Juris, S. Serroni and M. Venturi, *Acc. Chem. Res.*, 1998, **31**, 26 and references therein.

5 T. M. Miller and T. X. Neenan, *Chem. Mater.*, 1990, **23**, 34; Z. Xu, M. Kahr, K. L. Walker, C. L. Wilkins and J. S. Moore, *J. Am. Chem. Soc.*, 1994, **116**, 4537; C. Devadoss, P. Bharathi and J. S. Moore, *J. Am. Chem. Soc.*, 1996, **118**, 9635; D. J. Pesak, J. S. Moore and T. E. Wheat, *Macromolecules*, 1997, **30**, 6467; C. Devadoss, P. Bharathi and J. S. Moore, *Macromolecules*, 1998, **31**, 8091; H. Meier and M. Lehmann, *Angew. Chem., Int. Ed.*, 1998, **37**, 643; F. Morgenroth, A. J. Berresheim, M. Wagner and K. Müllen, *Chem. Commun.*, 1998, 1139.

6 T. M. Miller, T. X. Neenan, R. Zayas and H. E. Bair, *J. Am. Chem. Soc.*, 1992, **114**, 1018.

7 F. Kröhnke and K. F. Gross, *Chem. Ber.*, 1959, **92**, 22; J. P. Collin, S. Guillerez and J. P. Sauvage, *J. Chem. Soc., Chem. Commun.*, 1989, 776; K. Hanabusa, A. Nakamura, T. Koyama and H. Shirai, *Macromol. Chem.*, 1992, **193**, 1309.

8 N. Miyata, T. Yanagai and A. Suzuki, *Synth. Commun.*, 1981, **11**, 513.

9 E. C. Constable and M. D. Ward, *J. Chem. Soc., Dalton Trans.*, 1990, 14; J.-P. Collin, S. Guillerez, J.-P. Sauvage, F. Barigelletti, L. De Cola, L. Flamigni and V. Balzani, *Inorg. Chem.*, 1991, **30**, 4230; J. C. Chambron, C. Coudret and J.-P. Sauvage, *New J. Chem.*, 1992, **16**, 361; F. Barigelletti, L. Flamigni, V. Balzani, J.-P. Collin, A. Sour, E. C. Constable and A. M. W. Cargill Thompson, *J. Chem. Soc., Chem. Commun.*, 1993, 942; F. Barigelletti, L. Flamigni, V. Balzani, J.-P. Collin, J.-P. Sauvage, A. Sour, E. C. Constable and A. M. W. Cargill Thompson, *J. Am. Chem. Soc.*, 1994, **116**, 7692.

Communication a908500i

ChemComm

The first ester complexes of bismuth(III) using thiolate anchored bifunctional ligands

Glen G. Briand, Neil Burford* and T. Stanley Cameron*

Department of Chemistry, Dalhousie University, Halifax, Nova Scotia B3H 4J3, Canada. E-mail: burford@is.da.ca

Received (in Bloomington, IN, USA) 1st September 1999, Accepted 11th November 1999

The isolation and characterization of bismuth complexes involving ester functionalities on bifunctional ligands demonstrates the use of thiolates as anchors for weaker donors and in the context of the medicinal relevance of bismuth compounds, offers the opportunity to study the interaction of all biorelevant functional groups with bismuth.

The developing coordination chemistry of bismuth is hindered by the facile hydrolysis of most bismuth–element bonds to give the bismuthyl unit (BiO^+), which involves essentially quantitative precipitation.[1] Consequently, complexes of weakly donating functionalities can only be isolated in the absence of moisture and many conventional types of ligand have not yet been observed on bismuth. The high thermal and hydrolytic stability of the sulfur–bismuth bond[2] has enabled synthetic control using bifunctional ligands involving a thiolate anchor,[3] which offer the additional advantage of satisfying the high coordinative capacity of the bismuth center and thereby inhibit intermolecular interactions and coordination polymerisation. As a result, the complexes exhibit relatively high solubility allowing for crystallization and structural and spectroscopic characterization. We have exploited these realizations to prepare the first examples of ester complexes of bismuth, despite the relatively low basicity of the ester (carbonyl) (pK_b 21.5; *cf.* OH pK_b 16.5, NR_2 pK_b 9.2, CO_2^- pK_b 9.2) functionality. The significance of these new complexes lies in their relationship to the extensive and medicinally relevant carboxylate chemistry of bismuth. In this context, one of the new ester complexes adopts a pendant donor intermolecular arrangement that is reminiscent of the ubiquitous dimer structure **1** observed for the most extensively studied colloidal bismuth subcitrate (CBS).[1,4–7]

Reactions of potassium (methylester)methanethiolate with bismuth(III) chloride in 95% ethanol at the appropriate stoichiometry give bis[(methylester)methanethiolato]bismuth(III) chloride **2** (2:1) and tris[(methylester)methanethiolato]bismuth(III) **3** (3:1), respectively.†‡ Reaction of (methylester)methanethiol with bismuth(III) chloride also give **2**, which was identified by its distinctive Raman spectrum as the dominant product, independent of reaction stoichiometry (4:1, 3:1, 2:1).

Compound **2** adopts a one-dimensional polymeric array in the solid state (Fig. 1), with hepta-coordination for bismuth imposed by four equatorially disposed sulfur centers, two oxygen centers (carbonyl) and one chlorine center. The long and essentially equivalent Bi–S distances result from the strong

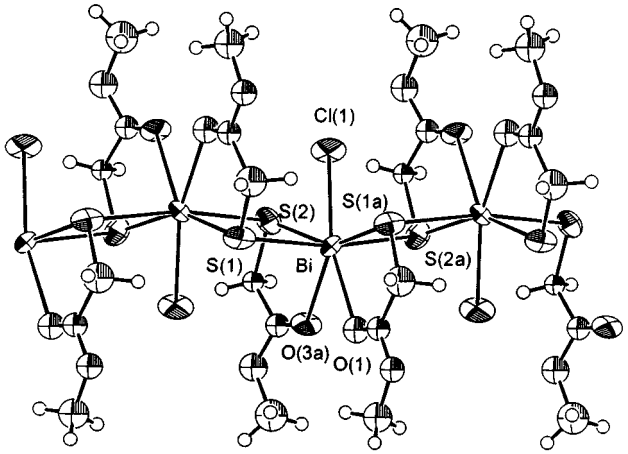

Fig. 1 Crystallographic view of polymeric arrangement of [Bi($SCH_2CO_2Me)_2Cl$] **2**. Thermal ellipsoids are drawn to 50% probability.

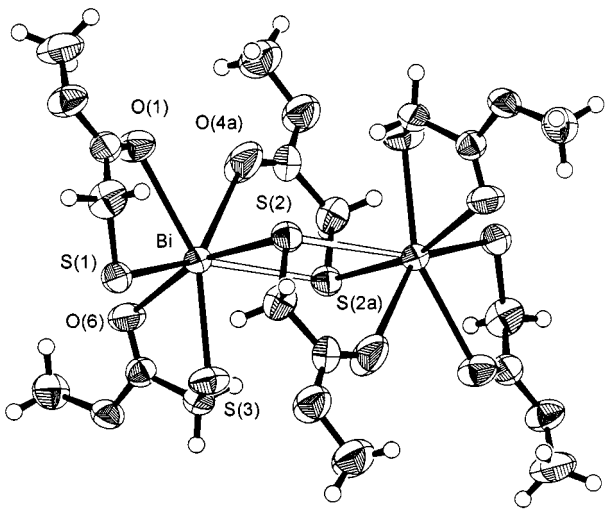

Fig. 2 Crystallographic view of the dimeric arrangement of [Bi($SCH_2CO_2Me)_3$] **3**. Thermal ellipsoids are drawn to 50% probability.

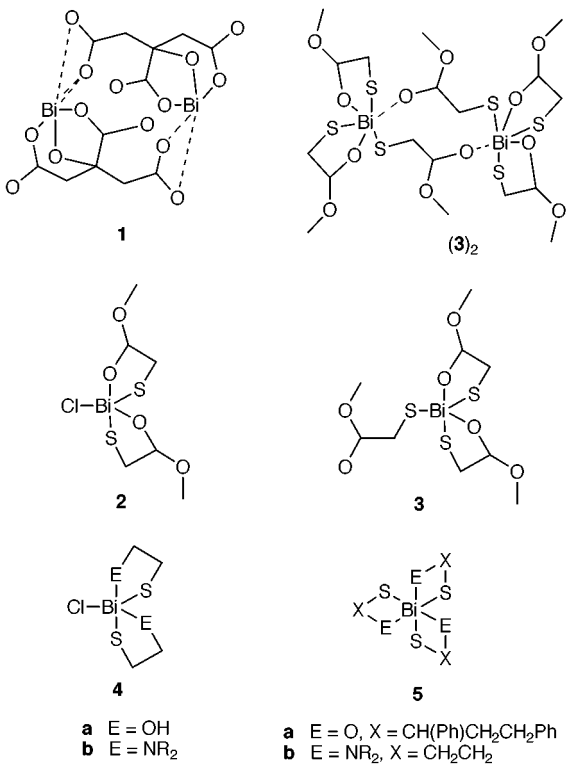

Table 1 Comparison of selected bond lengths (Å) in bismuth complexes with esters, hydroxy moieties, ketones and citrate

2		**3**		**4a**[9]		**5a**[11]		CBS[12,16–19]	
Bi–O(1)	2.68(2)	Bi–O(1)	2.807(5)	Bi–O	2.80(1)	Bi–O[a]	2.575(11)		
Bi–O(3a)	2.77(2)	Bi–O(6)	2.861(5)		2.86(1)		2.614		
							2.537(10)		
		Bi···O(4a)	3.071(7)					Bi···O	2.4–2.6
Bi–S(1)	2.849(7)	Bi–S(1)	2.568(2)	Bi–S	2.595(3)	Bi–S[a]	2.724(3)		
Bi–S(2)	2.884(6)	Bi–S(2)	2.608(2)		2.558(4)		2.581(4)		
Bi–S(1a)	2.963(7)	Bi–S(3)	2.574(2)			2.659(5)			
Bi–S(2a)	2.861(9)								
		Bi···S(2a)	3.331(2)	Bi···S	3.124(4)	Bi···S	3.494(5)		
Bi–Cl(1)	2.535(6)			Bi–Cl	2.589(3)		3.551(5)		
				Bi···Cl	3.488(4)				

[a] Average bond distances for two unique molecules.

trans influence[8] induced by intermolecular Bi–S contacts [S(1)-Bi–S(2a) 154.5(2) and S(2)–Bi–S(1a) 170.3(1)°]. Although a molecular unit represented by drawing **2** is indistinguishable in the polymeric solid state structure, the analogy with the more molecular hydroxy/thio **4a**[9] and amino/thio **4b**[3,9,10] derivatives is important. We attribute the more polymeric structure of **2** to the restrictions imposed by the backbone sp^2 hybridized carbonyl carbon center and the consequential chelate ring strain.

The structure of the tris(esterthiolato)bismuth complex (Fig. 2) may, at first glance, be viewed as two tris-chelated bismuth centers **3**, as observed for the keto/thiolate **5a**[11] and aminothiolate complexes **5b**.[3] However, closer inspection of the Bi–S bond distances [*i.e.* Bi···S(2a), 3.331(2) is substantially longer than Bi–S(2), 2.608(2), Table 1] reveals that one of the ligands clearly functions as an internuclear (Bi···Bi) bridge, rather than a chelating ligand, imposing a distinct dimer structure $(\mathbf{3})_2$. In comparison with the polymeric structure of **2**, substitution of the chloride for a third thiolate is manifested in the dislocation of the $\cdots S_2BiS_2Bi\cdots$ chain with consequential enhancement (shortening) of the three facial thiolate interactions (Table 1).

The dimeric structure $(\mathbf{3})_2$ imposed by the pendant ester is analogous to that observed for CBS **1**.[12] In contrast, the methyl groups preclude the interdimer interactions observed in the carboxylate complexes, resulting in a relatively simple molecular structure and highlighting the ester functionality as an important stepping stone to understanding the carboxylate chemistry of bismuth.

The identification and isolation of the first ester complexes of bismuth is demonstrative of the synthetic value of the thiolate as an anchor for weaker donors at the other terminus of bifunctional ligands. In the compelling quest to understand the bioactivity of bismuth compounds,[13–15] we now have the opportunity to study the interaction of all biorelevant functional groups with bismuth. For example, we are currently developing synthetic procedures towards bifunctional thiolate/amide [$C(O)NR_2$] ligand complexes, which represent an alternative derivatization of the carboxylate functionality and for which we anticipate an intermediate number of intermolecular interactions between those of the carboxylate and ester complexes.

Notes and references

† [$Bi(SCH_2CO_2Me)_2Cl$] **2**: $BiCl_3$ (1.67 g, 5.28 mmol) added to methylthioglycolate (1.12 g, 10.6 mmol) in 95% ethanol (150 mL) was allowed to stir overnight. The product was removed by suction filtration and recrystallized from DMF under vacuum (yellow needles). Yield 1.10 g (46%); mp 128 °C; Anal. Calc.: C, 15.85; H, 2.22%. Found: C, 16.08; H, 2.26%; IR(cm^{-1}): 555w, 681w, 770w, 874s, 886w, 986m, 994m, 1161m, 1206m, 1296m, 1318m, 1676s, 1707s; Raman (cm^{-1}): 95vs, 117s(sh), 147s, 187s, 227vs, 260vs, 350m, 399w, 561w, 686w, 768w, 888m, 984w, 1181w, 1204w, 1325w, 1376w, 1392w, 1428w, 1673w, 2903s, 2940m, 2959m, 3044w; ^{1}H NMR (dmso−d_6): δ 3.62, 4.69; ^{13}C NMR (dmso-d_6): δ 29.6, 52.3, 176.3; APCI−MS (rel. % intensity): 313(2), 349(100), 419(32).

[$Bi(SCH_2CO_2Me)_3$] **3**: $BiCl_3$ (1.65 g, 5.23 mmol) added to methylthioglycolate (1.67 g, 15.7 mmol) and KOH (0.88 g, 16 mmol) in 95% ethanol (150 mL) under N_2 was allowed to stir overnight. The solution was filtered and concentrated by rotary evaporation. Yellow needles of **1** appeared after 2 h at 4 °C, collected after 1 day. Yield 0.71 g (26%); mp 65 °C; Anal. Calc.: C, 20.61; H, 2.88%. Found: C, 20.71; H, 2.84%; IR(cm^{-1}): 569m, 583m, 681w, 711m, 772w, 864m, 880w, 889m, 899w, 909w, 992s, 1021w, 1141m, 1204s, 1287s, 1308s, 1397m, 1434s, 1558w, 1579w, 1605w, 1623w, 1691m, 1735m; Raman (cm^{-1}): 95vs, 146m, 195m, 221m, 266vs, 292vs, 334m, 402w, 580w, 714w, 769w, 885w, 908w, 990w, 1151w, 1181w, 1296w, 1397w, 1435w, 1696w, 2886s, 2956m, 2976m, 2988m, 3034w; ^{1}H NMR (dmso-d_6): δ 3.63, 4.46; ^{13}C NMR (dmso-d_6): δ 29.4, 52.3, 175.8; APCI-MS (rel. intensity): 313(4), 419(100).

‡ *Crystal data.* for **2**: $C_6H_{10}BiClO_4S_2$, M = 454.70, monoclinic, space group *Pa* (no. 7), light yellow needles, a = 8.092(2), b = 9.13(1), c = 8.128(3) Å, β = 102.90(2)°, V = 585.5(6) Å^3, D_c = 2.556 g cm^{-3}, Z = 2, T = 23.0 °C, R = 0.036, R_w = 0.027, GOF 1.57. For **3**: $C_9H_{15}BiO_6S_3$, M 524.36, triclinic, space group $P\bar{1}$ (no. 2), yellow needles, a = 9.340(1), b = 11.553(3), c = 8.168(1) Å, α = 109.18(2), β = 92.98(2), γ = 103.38(2)°, V = 798.4(3) Å^3, D_c = 1.993 g cm^{-3}, Z = 2, T = 23.0 °C, R = 0.0297, R_w = 0.0293, GOF 1.60.

All measurements were made on a Rigaku AFC5R diffractometer with graphite monochromated Mo-Kα radiation (λ = 0.71069 Å) and a 12 kW rotating anode generator. The structures were solved by direct methods (SHELXL97) and refined by full-matrix least least squares on F using 608 (**2**) and 3230 (**3**) reflections with $I > 3.00\sigma(I)$. A final difference-Fourier map yielded ρ(max.) = 0.72 e Å^{-3} and ρ(min.) = −0.69 e Å^{-3} for **2** and ρ(max.) = 1.26 e Å^{-3} and ρ(min.) = −0.80 e Å^{-3} for **3**. CCDC 182/1488.

1 G. G. Briand and N. Burford, *Adv. Inorg. Chem.*, 1999 in press.
2 L. Agocs, N. Burford, T. S. Cameron, J. M. Curtis, J. F. Richardson, K. N. Robertson and G. B. Yhard, *J. Am. Chem. Soc.*, 1996, **118**, 3225.
3 G. G. Briand, N. Burford, T. S. Cameron and W. Kwiatkowski, *J. Am. Chem. Soc.*, 1998, **120**, 11 374.
4 G. G. Briand and N. Burford, *Chem. Rev.*, 1999, **99**, 2601.
5 G. F. Baxter, *Pharm. J.*, 1989, **243**, 805.
6 G. F. Baxter, *Chem. Br.*, 1992, 445.
7 H. Sun, H. Li and P. J. Sadler, *Chem. Ber./Recueil*, 1997, **130**, 669; *Coord. Chem. Rev.*, 1999, **185–186**, 689.
8 F. J. Carmalt and N. C. Norman, in *Chemistry of Arsenic, Antimony and Bismuth*, ed. N. C. Norman, Blackie Academic and Professional, London, 1998, pp. 1–38.
9 L. Agocs, G. G. Briand, N. Burford, T. S. Cameron, W. Kwiatkowski and K. N. Robertson, *Inorg. Chem.*, 1997, **36**, 2855.
10 W. A. Herrmann, P. Kiprof, W. Scherer and L. Pajdla, *Chem. Ber.*, 1992, **125**, 2657.
11 A. K. Mishra, V. D. Gupta, G. Linti and H. Nöth, *Polyhedron*, 1992, **11**, 1219.
12 E. Asato, K. Katsura, M. Mikuriya, T. Fujii and J. Reedijk, *Inorg. Chem.*, 1993, **32**, 5322.
13 W. A. Herrmann, E. Herdtweck and L. Pajdla, *Chem. Ber.*, 1993, **126**, 895.
14 U. Dittes, E. Vogel and B. K. Keppler, *Coord. Chem. Rev.*, 1997, **163**, 345.
15 S. P. Summers, K. A. Abboud, S. R. Farrah and G. J. Palenik, *Inorg. Chem.*, 1994, **33**, 88.
16 E. Asato, K. Katsura, M. Mikuriya, U. Turpeinen, I. Mutikainen and J. Reedijk, *Inorg. Chem.*, 1995, **34**, 2447.
17 W. A. Herrmann, E. Herdtweck and L. Pajdla, *Inorg. Chem.*, 1991, **30**, 2579.
18 W. A. Herrmann, E. Herdtweck and L. Pajdla, *Z. Kristallogr.*, 1992, **198**, 257.
19 P. J. Barrie, M. I. Djuran, M. A. Mazid, M. McPartlin and P. J. Sadler, *J. Chem. Soc., Dalton Trans.*, 1996, 2417.

Communication a907094j

First triphenylene based non-symmetric donor–acceptor triple mesogen possessing disc-like and rod-like characteristics

Swen Mahlstedt,[a] Dietmar Janietz,*[a] Andreas Stracke[b] and Joachim H. Wendorff[b]

[a] *Universität Potsdam, Fachbereich Chemie und Institut für Dünnschichttechnologie, Kantstr. 55, D-14513 Teltow, Germany. E-mail: janietz@rz.uni-potsdam.de*

[b] *Universität Marburg, Institut für Physikalische Chemie und Wissenschaftliches Zentrum für Materialwissenschaften, Hans-Meerweinstr., D-35032, Marburg, Germany*

Received (in Cambridge) 27th September 1999, Accepted 16th November 1999

The synthesis and thermal properties of a novel donor–acceptor mesogen which is composed of a disc-like triphenyl ene donor group linked to a flat trinitrofluorenone acceptor *via* a rod-shaped azobenzene moiety are presented.

Thermotropic liquid crystals may be composed of molecules possessing rod-shaped as well as disc-like anisometric geometry. The molecular shape is known to determine the type of mesophase that is formed. Rod-like mesogens predominantly form smectic phases whereas molecules possessing on average a flat rigid core surrounded by a certain number of long flexible side chains preferably organize into columnar mesophases. A disadvantage for certain applications is that disc-like and rod-like mesogens are not miscible and that phase separation occurs on a macroscopic scale. Even the chemical linkage of molecular sub-units with different anisometric shapes *via* flexible spacers[1–3] does not necessarily lead to mesomorphic properties.

On the other hand, self-organization with formation of liquid crystalline structures can arise from attractive intermolecular interactions such as hydrogen bonding or charge-transfer complex formation between complementary molecules. For example, CT interactions between flat aromatic electron donors such as triphenylene ethers or radial multialkynylbenzene compounds with acceptor molecules may cause the stabilization as well as the induction of columnar mesophases.[4–6]

The combination of the two principles, molecular geometry and CT interactions, has led to the design of charge-transfer twin molecules with a flat electron donor group separated from an intramolecular acceptor function by a flexible alkyl spacer.[7–9] It could be shown that the chemical linkage of the donor with an acceptor molecular sub-unit gives rise to liquid crystalline structures that cannot be achieved by simple mixing of the components.

The concept is that the covalent linking of a disc-like donor to a calamitic moiety, with structure formation tendencies promoted by an additional intramolecular acceptor function, will avoid destruction of mesomorphic order. New aspects for the control of supramolecular structures may arise from this combination of three structural elements, differing in shape and functionality, within one molecule. Recently we reported the first compounds aimed to realize this concept. These are charge-transfer molecules with a calamitic group placed between an enlarged pentaalkynylbenzene donor and a flat acceptor moiety. The novel compounds were found to display a nematic-columnar like phase with the individual columns separated by rod-like groups.[10]

We present here the non-symmetric trimer **4** which is the first disc-rod triple mesogen composed of a disc-like alkoxy-substituted triphenylene donor group and a nitrofluorenone based acceptor unit, the two complementary parts being linked chemically *via* alkyl spacers to the termini of a rigid rod-shaped azobenzene moiety.

As shown in Scheme 1, the reaction sequence leading towards the donor–acceptor triple molecule **4** starts out from the alkoxytriphenylene **1** carrying one terminal bromine substituent. Compound **1** was converted into the non-symmetric dimer **3**, which combines a disc-like triphenylene donor and a rod-like sub-unit *via* an ether bridge, by reaction with the azobenzene derivative **2**.† Subsequent esterification of the remaining free aliphatic hydroxy group in the intermediate **3** with 3-(2,4,7-trinitrofluoren-9-ylideneaminooxy)propionic acid[7] in the presence of *N,N′*-dicyclohexylcarbodiimide and catalytic amounts of 4-dimethylaminopyridine yielded the triphenylene based trimer **4**.‡

Differential scanning calorimetry (DSC) gives evidence that the triphenylene donor–acceptor molecule **4** exhibits a glass transition at 19.4 °C followed by a phase transition into the isotropic phase at 56.3 °C (ΔH_i = 1.5 kJ mol^{-1}). Enantiotropic mesomorphic behaviour is confirmed by polarizing microscopy. The optical textures, however, are small-sized and non-specific. Considering the fact that there is no indication of liquid crystalline phase formation for the disc-rod dimer **3** it follows that, as found for charge-transfer triple mesogens based on a flat pentaalkynylbenzene donor moiety,[10] the mesophase of the triphenylene CT-triple **4** predominantly originates from donor–acceptor interactions due to the additional chemical linkage of the acceptor sub-unit. Further work is in progress to characterize charge-transfer complex formation of compound **4** spectroscopically.

The wide angle X-ray diffractogram of the triphenylene trimer **4** is presented in Fig. 1. It displays a distinct reflection in the small angle region corresponding to a distance of 1.56 nm. The value agrees approximately with the diameter of the triphenylene donor group. The amorphous halo which appears at larger scattering angles points to the liquid-like ordering of the flexible alkoxy chains. The halo is superimposed on an

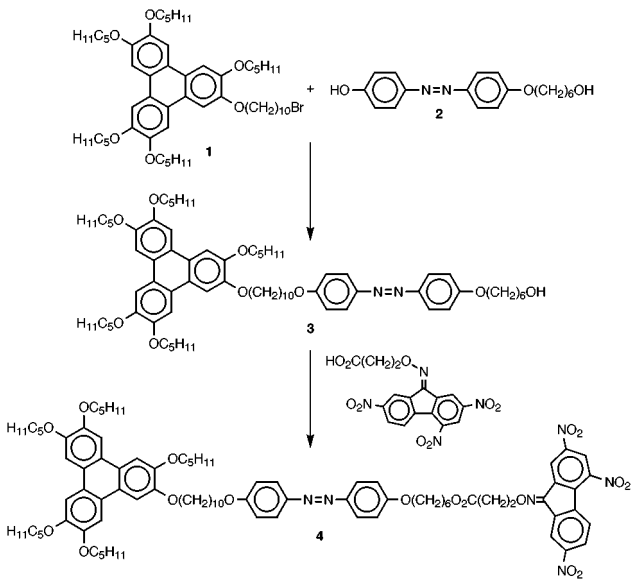

Scheme 1

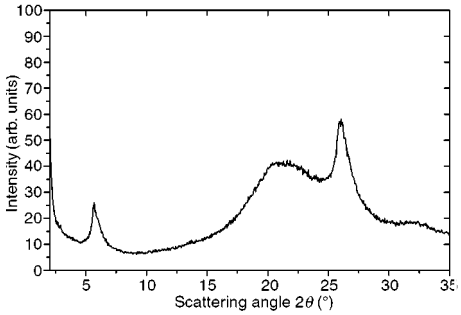

Fig. 1 Wide angle X-ray diffractogram of the triphenylene disc-rod triple mesogen **4**.

intense reflection which is characteristic for a periodical packing of flat anisometric cores in a column. The intracolumnar distances amount to 0.34 nm. This value is typical for columnar mesophases of hexaalkoxytriphenylenes doped with electron acceptors such as 2,4,7-trinitrofluoren-9-one (TNF).[4]

Certainly, the individual columns are formed through an intercalated stacking of the flat donor and acceptor groups of different molecules **4**. Furthermore, it is reasonable to suggest that the alkyl spacers connecting the three rigid molecular subunits preferably adopt more or less stretched conformations. This gives an arrangement of the calamitic moieties with their long axis predominantly oriented orthogonal rather than parallel to the column axis. The distance of 1.56 nm, corresponding to the small angle reflection, would be quite reasonable for the mean distance between adjacent columns perpendicular to the main axis of the molecules. We further have to take into account the unusually high viscosity that is observed by polarizing microscopy within the mesophase range of the triphenylene triple molecule **4**, which is typical for liquid crystalline polymers rather than for low molar mass mesogens. Therefore, we assume that as a result of the covalent linkage a one-dimensional quasi-chain incorporating the rod-shaped azobenzene units is realized which connects the alternating stacks of the donor and acceptor fragments of the molecules. A two-dimensional structure model arising from these considerations is presented schematically in Fig. 2.

The absence of mixed reflections in the small angle region indicates that the columns are not arranged on a two-dimensional lattice, rather that a layer structure exists along one direction. Further investigations are in progress to clarify this point.

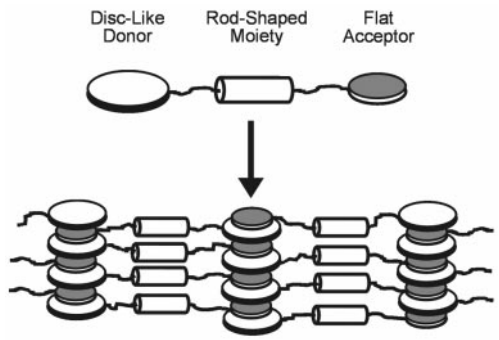

Fig. 2 Two-dimensional structure model for the novel mesophase of the donor–acceptor molecule **4** combining features of calamitic liquid crystalline phases with those of columnar mesomorphic structures. For sake of clarity the peripheral alkoxy substituents of the triphenylene donor are not shown. The appearance of only one small angle reflection along with the relatively small clearing transitional enthalpy seem to indicate a strongly distorted structure. Therefore, the model has to be considered as an 'ideal' structure at a local molecular level.

In summary, the CT-triple compound **4** is the first representative of a novel family of non-conventional thermotropic liquid crystals arising from the chemical linkage of a disc-like triphenylene donor, a rod-shaped moiety and an acceptor subunit. The concept of combining the three different structural elements in a defined manner within one molecule along with charge-transfer interactions introduced by the intramolecular acceptor function provides a powerful tool towards novel thermotropic mesophases, bridging the gap between smectic layer structures and columnar liquid crystalline phases.[12] Interesting properties such as optical biaxiality may be expected for such intermediate phases. Further work is currently in progress to modify molecular parameters such as the number of methylene groups in the spacer segments separating the three rigid moieties of the triphenylene based donor-acceptor triple mesogens.

The financial support of the Deutsche Forschungsgemeinschaft and of the Land Brandenburg is gratefully acknowledged.

Notes and references

† The 2-(6-bromodecyloxy)-3,6,7,10,11-pentapentyloxytriphenylene **1** used as the starting material was available *via* ferric chloride mediated regioselective coupling of 3,3′,4,4′-tetrapentyloxybiphenyl with 2-(6-bromodecyloxy)-1-pentyloxybenzene (ref. 11). The azobenzene compound **2** was prepared by alkylation of 4-acetylaminophenol with 6-chlorohexan-1-ol followed by acidic *N*-acetate cleavage, diazotisation of the resulting aniline and coupling with phenol.

‡ All new compounds **1**–**4** had spectroscopic data (IR, ^{1}H NMR, ^{13}C NMR) consistent with the assigned structure. *Selected data* for **4**: δ_H(300 MHz, $CDCl_3$) 8.90 (s, 1H, TNF), 8.56 (m, 2H, TNF), 8.25 (d, 1H, TNF, *J* 8.75) 8.03 (d, 1H, TNF, *J* 8.76), 7.70 (d, 4H, phenyl, *J* 8.71), 7.62 (s, 6H, phenyl), 6.89 (m, 4H, phenyl), 4.80 (t, 2H, CH_2-O-N, *J* 6.16), 4.15–4.24 (m, 12H, CH_2-O-phenyl and 2H, CH_2-O-CO), 3.95–4.02 (m, 4H, CH_2-O-phenyl), 2.95 (t, 2H, CH_2-COO, *J* 6.15), 1.25–2.05 (m, 54H, CH_2), 0.99 (t, 15H, CH_3, *J* 7.05); δ_C(300 MHz, $CDCl_3$): 170.50 (1C, COO), 161.10 (2C, phenyl C-O), 160.89 (1C, TNF C=N), 148.65 (6C, phenyl C-O), 148.42 (1C, TNF C-NO_2), 146.64 (1C, TNF C-NO_2), 146.56 (2C, phenyl C-N), 143.65 (1C, TNF C-NO_2), 138.85 (1C, TNF), 133.67 (1C, TNF), 131.25 (1C, TNF), 128.34 (1C, TNF CH), 128.78 (1C, TNF CH), 125.79 (1C, TNF), 124.13 (4C, phenyl CH), 122.72 (6C, phenyl and 1C, TNF CH), 120.52 (1C, TNF CH), 119.48 (1C, TNF CH), 114.48 (2C, phenyl CH), 114.43 (2C, phenyl CH), 106.26 (6C, phenyl CH), 72.75 (1C, CH_2-O–N), 69.29 (6C, CH_2-O-phenyl), 68.20 (1C, CH_2-O-phenyl), 67.88 (1C, CH_2-O-phenyl), 64.94 (1C, CH_2-O-CO), 34.26 (1C, CH_2-CO-O), 29.52–22.57 (27C, CH_2), 14.10 (5C, CH_3); ν(KBr)/cm^{-1} 1760 (COO), 1530 (NO_2), 1340 (NO_2).

1 W. Kreuder, H. Ringsdorf, O. Hermann-Schönherr and J. H. Wendorff, *Angew. Chem.*, 1987, **99**, 1300.
2 O. Karthaus, H. Ringsdorf, M. Ebert and J. H. Wendorff, *Makromol. Chem.*, 1992, **193**, 507.
3 I. D. Fletcher and G. R. Luckhurst, *Liq. Cryst.*, 1995, **18**, 175.
4 H. Bengs, M. Ebert, O. Karthaus, B. Kohne, K. Praefcke, H. Ringsdorf, J. H. Wendorff and R. Wüstefeld, *Adv. Mater.*, 1990, **2**, 141.
5 M. Ebert, G. Frick, C. Baehr, J. H. Wendorff, R. Wüstefeld and H. Ringsdorf, *Liq. Cryst.*, 1992, **11**, 293.
6 K. Praefcke and J. D. Holbrey, *J. Inclusion Phenom. Mol. Recognit. Chem.*, 1996, **24**, 19.
7 M. Möller, V. Tsukruk, J. H. Wendorff, H. Bengs and H. Ringsdorf, *Liq. Cryst.*, 1992, **12**, 17.
8 D. Janietz, *Chem. Commun.*, 1996, 713.
9 D. Goldmann, S. Mahlstedt, D. Janietz, P. Busch, C. Schmidt, A. Stracke and J. H. Wendorff, *Liq. Cryst.*, 1998, **24**, 881.
10 S. Mahlstedt, D. Janietz, C. Schmidt, A. Stracke and J. H. Wendorff, *Liq. Cryst.*, 1999, **26**, 1359.
11 N. Boden, R. J. Bushby and Z. B. Lu, *Liq. Cryst.*, 1998, **25**, 47 and references cited therein.
12 With respect to lamellar columnar phases, see: K. Ohta, H. Muroki, A. Takagi, K. Hatada, H. Ema, I. Yamamoto and K. Matsuzaki, *Mol. Cryst. Liq. Cryst.*, 1986, **140**, 131; H. Sakashita, A. Nishitani, Y. Sumiya, H. Terauchi, K. Ohta and I. Yamamoto, *Mol. Cryst. Liq. Cryst.*, 1988, **163**, 211.

Communication a907770g

$Hf_{27}Si_6P_{10}$, a novel metal-rich compound with P_2 groups

Chang-Cang Huang, Jörg Neuhausen and Wolfgang Tremel*

Institut für Anorganische Chemie und Analytische Chemie, Universität Mainz, Duesbergweg 10-14, D-55099 Mainz, Germany. E-mail: tremel@indigotrem1.chemie.uni-mainz.de

Received (in Cambridge, UK) 24th August 1999, Accepted 9th September 1999

The new ternary metal rich compound $Hf_{27}Si_6P_{10}$ has been synthesized by reduction of HfP with Hf and Si; $Hf_{27}Si_6P_{10}$ crystallizes in a new structure type, a characteristic and unexpected feature of which is the presence of P_2 groups; the structural results are interpreted with the aid of high-level band structure calculations.

The large family of metal-rich binary compounds that are formed between a transition metal (M) and a variety of main-group non-metals, metalloids and adjacent metals (Q) exhibit a remarkable range of compositions, structures and properties. It is surprising that these compounds challenge our basic assumptions about the chemistry of the transition elements and our chemical understanding in general. The existence and structure of none of these compounds can be predicted *a priori* and a rationalization of their structures *a posteriori* does not give chemically conclusive hints why seemingly simply binary compounds of the early transition metals (*e.g.* with composition M_2Q) display as many differences as they do.[1–5] Furthermore, the possibility of metal segregation in mixed-metal systems allows the formation of pseudo-binaries (M–M′)–Q which have no counterparts in the binary systems.[6]

Nonetheless, this group of compounds also shows some common characteristics regarding their structures as well as their electronic and bonding features. (i) In all known representatives the non-metal atoms are situated in capped trigonal-prismatic voids of the metal sublattice, and there are no filled voids adjacent to each other, *i.e.* from a topological point of view, there is no possibility for Q–Q bonding. (ii) Owing to appreciable differences in the electronegativities and valence energies of the component atoms, pnictides may be viewed as polar intermetallics; the more electronegative main-group element in these compounds contributes mostly to the low-lying valence band, especially for compounds of the early transition metals, whereas the conduction band has large contributions from the metal atoms. The stability is mostly based on strong heteroatom M–Q bonding; in addition, metal-rich phases also exhibit strong M–M but no Q–Q bonding.[7]

In the quest for new metal-rich quasi-binary early transition metal pnictides we have investigated reactions in the system M–Q–Q′ (M = Zr, Hf; Q = P, As, S, Se; Q′ = Si), the rationale behind this synthetic approach being to mimic the electron count in known binary compounds by the use of three components. $Hf_{27}Si_6P_{10}$ was prepared in a two step synthesis. To avoid a loss of P during the arc melting, HfP[8] was synthesised in a silica tube at 800 °C from the elements in a 1 : 1 ratio. In the second step, stoichiometric mixtures of HfP, Hf and Si were pressed into pellets with a hydraulic press. The pellets were melted under argon on a water-cooled copper hearth. Reactions with the approximate starting compositions 'Hf_6SiP_2' led to homogeneous products. EDX investigations on selected crystals indicated a phase width of ±10% within the limits of accuracy. According to the results of the X-ray structure determination[9] $Hf_{27}Si_6P_{10}$ crystallizes in a new structure type which contains fragments of a *bcc* packing. The crystal structure is depicted in a projection along the short *a* axis in Fig. 1. All atoms are located at $x = 0$ or 0.5 along the crystallographic *a* axis, *i.e.* each layer in Fig. 1 is fused to identical layers above and below the projection plane. The unit cell contains 54 metal atoms (nine crystallographically independent metal atoms per asymmetric unit) and 32 Si and P atoms (which cannot be distinguished by X-ray diffraction). The P and Si atoms are located in mono-, bi- and tri-capped trigonal Hf prisms with Hf–P/Si bond lengths ranging between 2.572(6) and 3.083(7) Å, where the larger Si atoms are assumed to be located in the nine-coordinate sites (Si and P mixing on the non-metal positions, however, cannot be ruled out). Based on this assumption the composition $Hf_{27}Si_6P_{10}$, in agreement with the analytical results, has been assigned. In an alternative description the $Hf_{27}Q_{16}$ structure may be viewed as being built up from M_6Q_8 clusters and cluster fragments.[10] The $Hf_{27}Q_{16}$ structure contains two variants of fused M_6Q_8 clusters that are condensed *via* common corners along [100]: Hf_5 fragments of the Hf_6Q_8 cluster where a Hf atom from the equatorial plane of the complete Hf_6X_8 unit is missing, and two types of Hf_6Q_8 clusters which are linked *via* common corners with Hf_5 and Hf_6 units. The first type of Hf_6Q_8 cluster (dark grey in Fig. 1) is linked to four Hf_5 units (medium grey) in the projection plane to give an entity with a 'bow-tie' shape. The second type of Hf_6Q_8 cluster (shown in light grey) is connected to two Hf_5 and two Hf_6 units in such a way that four type-2 Hf_6Q_8 clusters form a tetrameric entity. The entity in turn is linked by sharing common corners with four Hf_5 units. These condensed cluster units form a ribbon-like pattern along [001] which is highlighted in Fig. 1. Each of these ribbons is fused with two adjacent ribbons by Hf–Hf bonds and by sharing common P/Si atoms. Thus, all Hf atoms belong either to Hf_5 or Hf_6 units.

The shortest Hf–Hf bonds occur between the apical and basal atoms of the cluster units [distances ranging from 3.035(1) to 3.215(1) Å], whereas the equatorial Hf–Hf distances are significantly longer [3.544(2)–3.825(2) Å]. As is apparent from the length of the *b* axis, the octahedra are tetragonally compressed; as a result, the distances between the apical Hf atoms are 3.573(1) Å.

The most important and unexpected feature of the $Hf_{27}Q_{16}$ structure are two short P–P separations of 2.58(2) and 2.69(13) Å which are clearly in the bonding range. In addition, the Hf–Hf contacts across the P–P units are, at 3.270(2) and 3.225(1) Å,

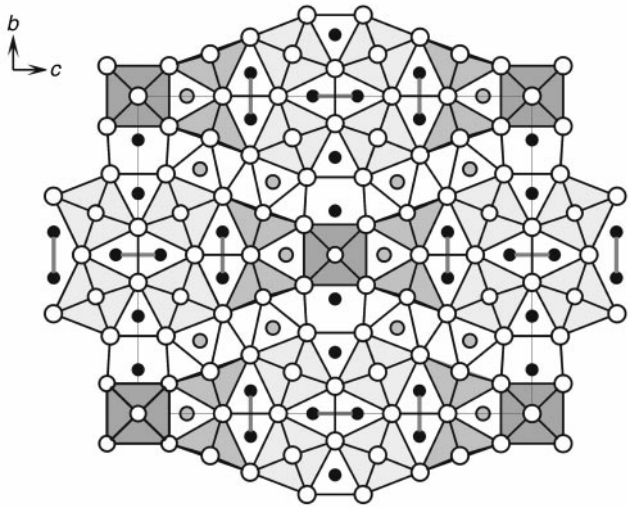

Fig. 1 View of the $Hf_{27}Si_6P_{10}$ structure along *a*. White circles, Hf atoms; grey circles, Si atoms; black circles, P atoms.

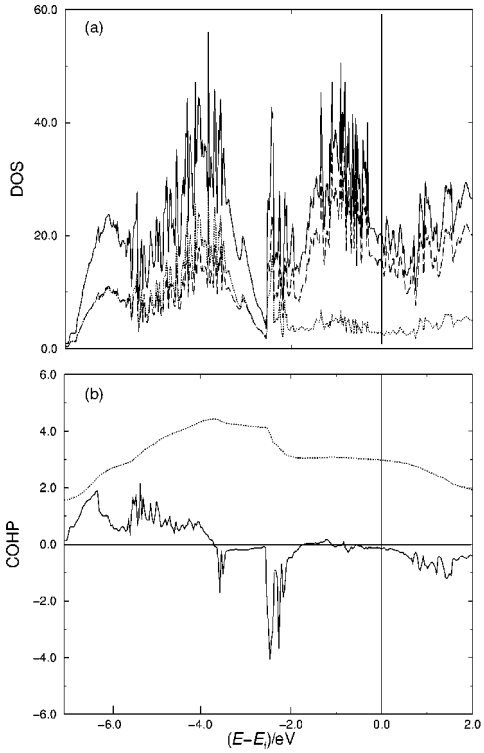

Fig. 2 (a) LMTO density of states for '$Hf_{27}P_{16}$'; solid line: total DOS; dashed line: Hf contribution; dotted line: Si/P contribution. The Fermi level is indicated by the vertical bar. (b) Crystal orbital Hamiltonian populations (COHP) for the P–P interactions. Upper part of the diagram is bonding, the lower part antibonding. The dotted line represents the integrated P–P overlap population.

very short. Based on Pauling's formula[11] $d_n = d_1 - 0.6 \log n$, the bond orders for the P–P contacts are 0.23 and 0.15 *i.e.* P–P bonding is present to a significant extent. These empirical results are also supported by the results of first-principles *ab initio* band structure calculations (*vide infra*) that have been performed on hypothetical $Hf_{27}P_{16}$ (the binary electron-rich end member of the ternary system $Hf_{27}Si_xP_{16-x}$ where the weakest P–P interactions might be expected). The presence of non-metal–non-metal bonding interactions in metal-rich compounds of an early transition metal is remarkable for at least two reasons: (i) since the non-metal atoms are the more electronegative partners in these compounds, the non-metal states should be occupied whereas the high-lying metal states are about to be filled. As a result, bonding interactions between non-metal atoms are unlikely. (ii) The non-metal atoms are situated in the voids of the metal sublattice and the probability of having filled voids adjacent to each other decreases with increasing M:Q ratio.

The $Hf_{27}Q_{16}$ structure contains two adjacent bicapped trigonal-prismatic sites. One of them is embranced by four Hf_6 clusters of the tetrameric unit, while the second is located at the intersection of the tetrameric unit and the 'bow-tie' shaped fragment. In order to clarify if this topological arrangement is only accidental, or if P–P interactions are significant for the structure stability, we have analysed the electronic structure of the title compound.

Considering the short P–P contacts as P–P bonds the electronic structure of $Hf_{27}Q_{16}$ may be formally described as $(Hf^{1.78+})_{27}(Si^{4-})_6(P_2{}^{4-})_3(P^{3-})_4$, *i.e.* approximately two electrons are available for each Hf atom for metal–metal bonding. According to the results of TB–LMTO–ASA calculations[12] the 3p block of the Si and P atoms is located well below the Fermi level. Fig. 2 shows the computed total density of states for hypothetical '$Hf_{27}P_{16}$' with the metal and non-metal contribution [Fig. 2(a)] as well as the results of the P–P bonding analysis in form of the COHP plot [Fig. 2(b)]. The P–P bonding states are separated by a small gap from the antibonding states that appear to be very localised just below −2 eV. The strong localisation indicates that a fraction of the P 3p orbitals is preferentially engaged in P–P bonding. A significant density of states is found at the Fermi level. Considering the M–M bonds along all directions in the structure of $Hf_{27}Q_{16}$, metallic properties can be safely assumed. The different site preferences for Si and P can be understood based on the differences in M–Q bonding. The bonding analysis of '$Hf_{27}P_{16}$' shows that higher bond orders are associated with the higher coordinated sites, and this situation should be increased for Si because of the greater expansion of the 3p orbitals and the lower electronegativity of Si relative to P.

In summary, $Hf_{27}Q_{16}$ is a metal-rich compound of an early transition metal whose structure is stabilized to a significant extent by bonding between the non-metal atoms. This is associated with a partial electron transfer from the anionic to the cationic components, which has also been observed for metal tellurides;[13,14] a comparable feature has been reported for two compounds of the heavy group homologues, Hf_6TiSb_4[15] and $(Zr, V)_{13}Sb_{10}$,[16] but is unprecedented for the lighter congeners.

This work was supported by the Fonds der Chemischen Industrie. We are indebted to Heraeus Quarzschmelze Hanau (Dr Höfer) for a generous gift of silica tubes.

Notes and references

1 Ti_2P: P. O. Snell, *Acta Chem. Scand.*, 1968, **22**, 1942; Zr_2P: P. J. Ahlsen, *Z. Kristallogr.*, 1989, **189**, 117; Hf_2P: T. Lundström, *Acta Chem. Scand.*, 1968, **22**, 1801; Zr_2As: S. Rundqvist, *Acta Chem. Scand.*, 1968, **22**, 2395; Hf_2As: J. O. Willerström, *Acta Chem. Scand., Ser. A*, 1984, **38**, 91.

2 Ti_2S: J. P. Owens and H. F. Franzen, *Acta Crystallogr.*, 1967, **23**, 77; Zr_2S: B. R. Conard, *High Temp. Sci.*, 1971, **3**, 491; Hf_2S: H. F. Franzen, *Z. Kristallogr.*, 1966, **123**, 1331; Zr_2Se: H. F. Franzen, *Acta Crystallogr., Sect. B*, 1968, **24**, 801; Ti_2Se, Hf_2Se: H. F. Franzen, J. Smeggil and B. R. Conard, *Mater. Res. Bull.*, 1967, **2**, 1087; Zr_2Te: G. Örlygsson and B. Harbrecht, *Inorg. Chem.*, 1999, **38**, 3377; Hf_2Te: B. Harbrecht, M. Conrad, T. Degen and R. Herbertz, *J. Alloys Compd.*, 1997, **255**, 178.

3 Nb_2P: Y. B. Kuzma, *Dop. Akad. Nauk Ukr. RSR, Ser. B*, 1988, **121**, 47; Ta_2P: A. Nylund, *Acta Chem. Scand.*, 1966, **20**, 2393; Ta_2As: S. Rundqvist, *Acta Chem. Scand.*, 1969, **23**, 2188.

4 Ta_2S: H. F. Franzen and J. Smeggil, *Acta Crystallogr., Sect. B*, 1969, **25**, 1736; Ta_2Se: B. Harbrecht, *Angew. Chem., Int. Ed. Engl.*, 1989, **28**, 1660.

5 Sc_2Te: P. A. Maggard and J. D. Corbett, *Angew. Chem., Int. Ed. Engl.*, 1997, **36**, 1974.

6 $Nb_{1.72}Ta_{3.28}S_2$: X. Yao and H. F. Franzen, *J. Am. Chem. Soc.*, 1991, **113**, 1426; $Zr_{6.45}Nb_{4.55}P_4$: *Chem. Mater.*, 1993, **5**, 678; $Hf_{5.08}Mo_{0.92}P_3$: J. Cheng and H. F. Franzen, *J. Solid State Chem.*, 1996, **121**, 362.

7 E. Garcia and J. D. Corbett, *Inorg. Chem.*, 1988, **27**, 2353.

8 W. Jeitschko and H. Nowotny, *Monatsh. Chem.*, 1962, **93**, 1284.

9 *Crystal data* (Bruker, CCD, T = 298 K) for $Hf_{27}Si_6P_{10}$: M = 1317, orthorhombic, space group *Immm*; a = 3.5739(7), b = 18.623(4), c = 23.081(5) Å, Z = 2, λ = 0.71073 Å, D_c = 11.443 g cm^{-3}, μ(Mo-Kα) = 91.46 mm^{-1}, 1029 independent reflections, unique data with $I > 2\sigma(I)$, 809, $R(F)$ = 0.035, $R_w(F^2)$ = 0.098, number of variables, 75. Structure solved and refined using the SHELXTL-Plus program system. Crystal needle-like, dimensions 0.005 × 0.005 × 0.1 mm. An empirical absorption correction was applied to the data (min. max. transmission, 0.080, 0.531). CCDC 182/1426. See http://www.rsc.org/suppdata/cc/a9/a906873b/ for crystallographic files in .cif format.

10 A. Simon, *Angew. Chem., Int. Ed. Engl.*, 1981, **20**, 1.

11 L. Pauling, *The Nature of the Chemical Bond*, Cornell University Press, Ithaca, New York3rd edn., 1948.

12 U. van Barth and L. Hedin, *J. Phys. C*, 1971, **4**, 2064; O. K. Andersen, *Phys. Rev. B: Condens. Mather*, 1975, **12**, 3060; H. L. Skriver, *The LMTO Method*, Springer, Berlin, 1984; O. Jepsen and O. K. Andersen, *Solid State Commun.*, 1971, 9.

13 J. Rouxel, *Chem. Eur. J.*, 1996, **2**, 1053.

14 Nb_2Te_3: H. Kleinke and W. Tremel, *Chem. Commun.*, 1999, 1175; Ta_4BTe_8: H.Kleinke, E. W. Finckh and W. Tremel, *Angew. Chem., Int. Ed.*, 1999, **38**, 2054.

15 H. Kleinke, *Inorg. Chem.*, 1999, **38**, 2931.

16 H. Kleinke, *Chem. Commun.*, 1998, 2219.

Communication a906873b

Bucky-bowls. A general approach to benzocorannulenes: synthesis of mono-, di- and tri-benzocorannulenes

Goverdhan Mehta* and P. V. V. Srirama Sarma

Department of Organic Chemistry, Indian Institute of Science, Bangalore, 560 012 India.
E-mail: diroff@admin.iisc.ernet.in

Received (in Cambridge, UK) 8th November 1999, Accepted 16th November 1999

We outline a conceptually simple and general route to bowl-shaped benzocorannulenes based on readily assembled PAHs which on flash vacuum pyrolysis result in the sequential formation of a five- and six-membered ring; following this approach, syntheses of mono-, di- and tri-benzocorannulenes have been achieved.

As a part of our continuing interest in the synthesis of C_{60} fullerene (bucky-ball) and its fragments (bucky-bowls),[1,2] we became interested in developing a synthetic approach to pentabenzocorannulene **1** *en route* (see transannular bridging indicated in **1**) to the 'deep-bowl' **2**, $C_{40}H_{10}$.[3] Bowl-shaped **1** and **2** represent 2/3 of the carbon content of C_{60} with eleven and sixteen rings, respectively, constituting a dominant cross-section on the fullerene surface. Both **1** and **2** evoke considerable synthetic interest and are formidable objectives. As a prelude to efforts towards **1** and **2**, we have developed a new and

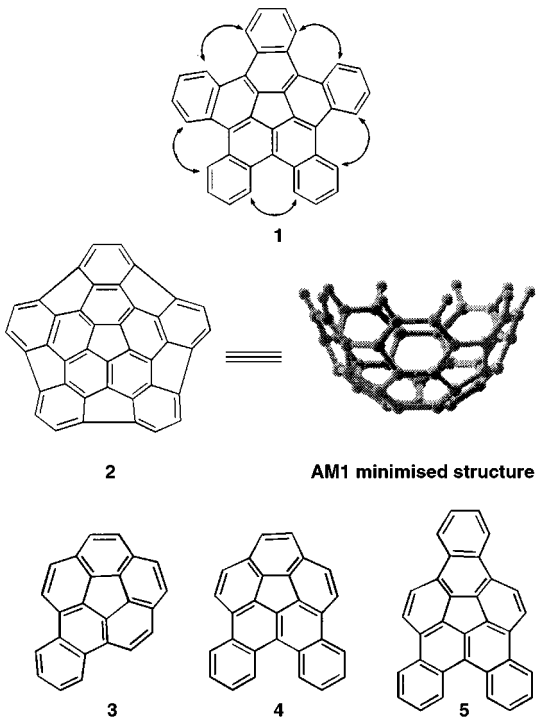

general synthetic route to benzoannulated corannulenes in which an appropriately constructed aromatic array upon flash vacuum pyrolysis (FVP) undergoes two-fold C–C bond formation involving cyclodehydrogenation to generate a five-membered ring, followed by insertion of vinylidene carbene or equivalent species to form a six-membered ring. Herein, we report the synthesis of mono-, di- and tri-benzocorannulenes **3**–**5**.

Our approach to benzocorannulene **3** emanated from 13-methylbenzo[*g*]chrysene **7**, readily available from 9-methylphenanthrene **6** through a tactical modification of the reported

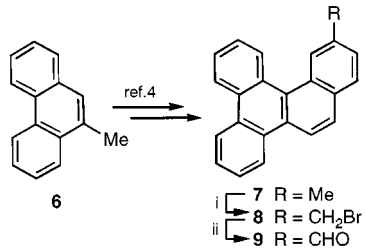

Scheme 1 *Reagents and conditions*: i, NBS, AIBN, CCl_4, 73%; ii, $(Bu_4N)_2Cr_2O_7$, $CHCl_3$, 76%.

procedure.[4] The methyl group in **7** was oxidised to the required aldehyde **9** in two steps *via* the intermediate bromide **8** (Scheme 1). The aldehyde functionality in **9** was then elaborated to **10**–**12** having active functionalities, which on thermal activation under FVP conditions were expected to result in the projected two-fold cyclization. Indeed, FVP of **10**–**12** furnished **3**, albeit in low yields characteristic of such reactions (Scheme 2).[2] Benzocorannulene **3** was readily identified through its spectral characteristics (UV, 2D NMR, mass).[5,6]

Our approach to dibenzocorannulene **4** originated from 5-methylbenzo[*c*]phenanthrene **13**, in turn readily accessible from commercial 2-methylnaphthalene.[7] Naphthoannulation on **13** through the intermediacy of the Wittig salt **14** and photocyclization of the resulting stilbene derivative **15** led to 13-methyldibenzo[*c*,*p*]chrysene **16** (Scheme 3). The methyl

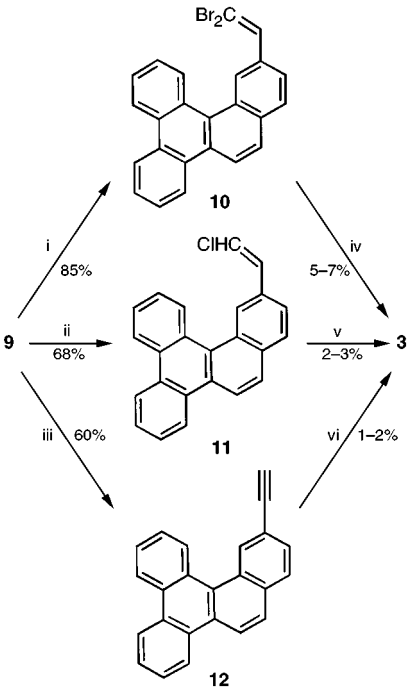

Scheme 2 *Reagents and conditions*: i, CBr_4, PPh_3, Zn, CH_2Cl_2, 85%; ii, $ClCH_2PPh_3Cl$, Bu^tOK, 0.5 h, 68%; iii, $ClCH_2PPh_3Cl$, Bu^tOK, 2 h, 60%; iv, FVP, 1150 °C, 5–7%; v, FVP, 1150 °C, 2–3%; vi, FVP, 1150 °C, 1–2%.

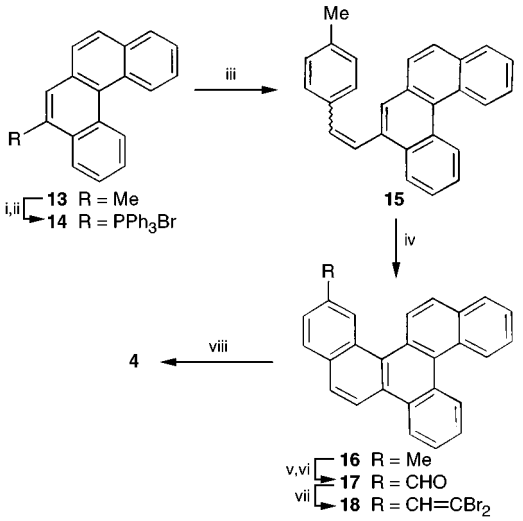

Scheme 3 *Reagents and conditions*: i, NBS 99%; ii, PPh_3, C_6H_6, 79%; iii, *p*-MeC_6H_4CHO, Cs_2CO_3, Pr^iOH, 80%; iv, *hv*, I_2, C_6H_6, propylene oxide, 65%; v, NBS, CCl_4, 44%; vi, $(Bu_4N)_2Cr_2O_7$, $CHCl_3$, 77%; vii, CBr_4, PPh_3, Zn, CH_2Cl_2, 85%; viii, FVP, 1150 °C, 5–7%.

group in **16** was oxidised to the aldehyde **17** and in the light of the relatively more efficient conversion **10**→**3** was further transformed to the hexacyclic *gem*-dibromoalkene **18**, the desired FVP precursor. On thermal activation **18** underwent the expected double cyclization to furnish the new dibenzocorannulene **4** and was fully characterised on the basis of incisive spectral analyses[5] (Scheme 3).

Interestingly, 5-methylbenzo[*c*]phenanthrene **13** and the Wittig salt **14** derived from it also served as the precursor for the synthesis of tribenzocorannulene **5**. Wittig coupling between **14** and 4-methylnaphthaldehyde gave **19** which on photocyclization led to the naphtho[1,2-*f*]picene derivative **20** (Scheme 4). The methyl group in **20** was again elaborated to the aldehyde **21** and further to the FVP precursor **22**. As planned, FVP on **22**

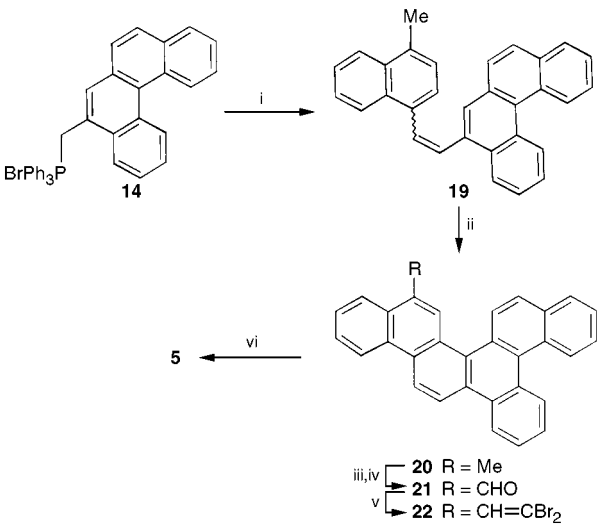

Scheme 4 *Reagents and conditions*: i, 4-methylnaphthaldehyde, Cs_2CO_3, Pr^iOH; ii, *hv*, I_2, C_6H_6, propylene oxide, 50% (2 steps); iii, NBS, CCl_4, 45%; iv, $(Bu_4N)_2Cr_2O_7$, $CHCl_3$, 70%; v, CBr_4, PPh_3, Zn, CH_2Cl_2, 55%; vi, FVP, 1150 °C, 1–2%.

furnished the desired tribenzocorannulene **5**, which was spectroscopically characterised (Scheme 4).[5,6]

In short, we have accomplished the syntheses of bowl-shaped benzocorannulenes **3**–**5** from appropriate polycyclic aromatics employing FVP as the key step, in which a five- and a six-membered rings are sequentially formed. The precursor polycyclic platforms were assembled from simple aromatic starting materials through an iterative sequence involving Wittig olefination and photocyclization steps. Notwithstanding the low yields in the final FVP step, which is not uncommon for such cyclizations,[1,2] this work demonstrates the generality of our approach and sets the stage for the synthesis of **1** and **2**.

We thank JNCASR for financial support and the SIF facility at I.I.Sc for high field NMR data. One of us (P. V. V. S. S.) thanks CSIR for a research fellowship. We thank Professor L. T. Scott for generously providing copies of spectra for comparison purposes.

Notes and references

1 Reviews: (*a*) R. Faust, *Angew. Chem., Int. Ed. Engl.*, 1995, **34**, 1429; (*b*) L. T. Scott, *Pure Appl. Chem.*, 1996, **68**, 291; (*c*) G. Mehta and H. S. P. Rao, in *Advances in Strain in Organic Chemistry*, ed. B. Halton, JAI, London, 1997, vol. 6; (*d*) G. Mehta and H. S. P. Rao, *Tetrahedron*, 1998, **53**, 13 325; (*e*) L. T. Scott, *Pure Appl. Chem.*, 1999, **71**, 209.

2 G. Mehta, S. R. Shah and K. Ravikumar, *J. Chem. Soc., Chem. Commun.*, 1993, 1006; G. Mehta and K. Venkateswara Rao, *Synlett*, 1995, 319; G. Mehta, K. Venkateswara Rao and K. Ravikumar, *J. Chem. Soc., Perkin Trans. 1*, 1995, 1787; G. Mehta, G. V. R. Sharma, M. A. Krishna Kumar, T. V. Vedavyasa and E. D. Jemmis, *J. Chem. Soc., Perkin Trans. 1*, 1995, 2529; G. Mehta, G. Panda, R. D. Yadav and K. Ravikumar, *Indian J. Chem., Sect. B*, 1997, **36**, 301; G. Mehta and G. Panda, *Tetrahedron Lett.*, 1997, **38**, 2145; G. Mehta and G. Panda, *Chem. Commun.*, 1997, 2081; G. Mehta, G. Panda, S. R. Shah and A. C. Kunwar, *J. Chem. Soc., Perkin Trans. 1*, 1997, 2269; G. Mehta, G. Panda and P. V. V. S. Sarma, *Tetrahedron Lett.*, 1998, **39**, 5835.

3 G. N. Sastry, E. D. Jemmis, G. Mehta and S. R. Shah, *J. Chem. Soc., Perkin Trans. 2*, 1993, 1867.

4 W. H. Laarhoven, Th. J. H. M. Cuppen and R. J. F. Nivard, *Tetrahedron*, 1970, **26**, 4865.

5 All new compounds reported here were fully characterised on the basis of their spectral (UV, IR, 2D ^1H and ^{13}C NMR, MS) and analytical data. *Selected data* for **3**: mp 253 °C; λ_{max}(MeOH)/nm 305, 275, 260 and 240; δ_H(300 MHz; $CDCl_3$), 8.68 (2H, dd, *J* 6 and 3.3), 8.26 (2H, d, *J* 8.7), 7.95 (2H, d, *J* 8.7), 7.84 (4H, ABq, *J* 8.7), 7.76 (2H, dd, *J* 5.7 and 3.3); δ_C(75 MHz; $CDCl_3$) 137.6 (qC), 135.4 (qC), 134.6 (qC), 133.1 (qC), 130.8 (qC), 130.5 (qC), 128.9 (qC), 127.5 (CH), 127.3 (CH), 127.1 (CH), 126.9 (CH), 125.1 (CH) and 124.3 (CH); *m/z* 300 (M^+). For **4**: mp >250 °C (decomp.); λ_{max}(MeOH)/nm 319, 272, 257 (sh), 242 (sh); δ_H(300 MHz; $CDCl_3$) 9.41 (2H, d, *J* 8.4), 8.83 (2H, d, *J* 7.5), 8.35 (2H, d *J* 8.7), 8.01 (2H, d, *J* 8.4), 7.91 (2H, s), 7.88–7.77 (4H, m); δ_C(75 MHz; $CDCl_3$) 136.7 (qC), 134.2 (qC), 134.0 (qC), 133.9 (qC), 133.7 (qC), 130.2 (qC), 128.5 (qC), 127.8 (CH), 127.5 (CH), 127.1 (CH), 127.0 (CH), 126.5 (CH), 125.5 (CH), 124.5 (qC), 123.9 (CH); *m/z* 350 (M^+). For **5**: λ_{max}(MeOH)/nm 347, 334, 279, 252; δ_H(400 MHz; $CDCl_3$) 9.41 (2H, d, *J* 8), 8.86 (2H, d, *J* 7.2) 8.73 (2H, dd, *J* 6.4 and 3.6), 8.45 (4H, ABq, *J* 8.4), 7.87 (2H, d, *J* 8), 7.83 (2H, d, *J* 9.2), 7.79 (2H, dd, *J* 6 and 3.2); *m/z* 400 (M^+).

6 Mono- **3** and tri-benzocorannulene **5** reported here have been prepared previously by Scott *et al.* [ref. 1(*b*), (*e*)] following entirely different routes. See also: B. McMahon, B.S. Thesis, Boston College, 1997; C. C. McComas, B.S. Thesis, Boston College, 1996. Since the details of this work are not published, we have provided here the spectral data and also compared the spectra of our synthetic compounds with theirs. Dibenzocorannulene **4** has been prepared for the first time.

7 D. L. Nagel, R. Kupper, K. Antonson and L. Wallcave, *J. Org. Chem.*, 1977, **42**, 1977.

Communication a908852k

ChemComm

Steric constraint generating large through-space ^{1}H–$^{203,205}Tl$ coupling in a dithallium(I) cryptate

Oliver W. Howarth,[a] Jane Nelson[bc] and Vickie McKee[c]

[a] *Chemistry Department, University of Warwick, Coventry, UK CV4 7AL*
[b] *Open University, Milton Keynes, UK MK7 6AA*
[c] *School of Chemistry, Queens University, Belfast, UK BT9 5AG. E-mail: jane.nelson@qub.ac.uk*

Received (in Basel, Switzerland) 21st October 1999, Accepted 12th November 1999

An aminocryptand host enforces approach of encapsulated Tl(I) ions to just within 4.4 Å; despite this relatively large separation, strong Tl(I)···Tl(I) interaction is observed and the aromatic proton of the bridging link exhibits a large through-space coupling to the pair of equivalent Tl nuclei.

In recent years we have become interested in the consequences of enforced proximity between cations encapsulated within azacryptand hosts.[1] In the transition series, this steric enforcement generates a previously uncharacterised bonding situation: a one-electron bond between copper ions in an average-valence +1.5 redox state.[2–6] Steric enforcement of close approach for transition ions implies use of relatively small hosts such as (imBT)† and amBT(= imBT + 12H), while larger hosts such as $(N[(CH_2)_2N{=}CH(C_6H_4\text{-}m)CH{=}N(CH_2)_2]_3N$ (L^1) and its amino form L^2 (= L^1 + 12H) have suitable cavity size to accommodate

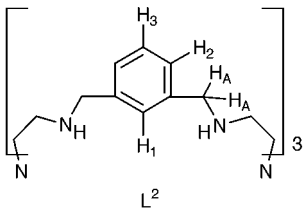

L^2

pairs of larger main group cations such as Tl^+. Our earlier studies with cryptates of L^2[7,8] and the analogous iminocryptand ligand, L^1, demonstrate[9,10] that these hosts offer internuclear distances of between 3 and 6 Å according to the preference of the guest cation, as the cryptands can make use of a triple helical twist mechanism[11,12] which allows them to adapt to the preferred coordination site separation of the cationic guests.

There is interest[13] among bonding theorists in interactions between the formally closed shell low-valent p-block cations. In a number of dimeric and oligomeric structures[13,14] with Tl···Tl distances (some supported by bridging donors) ranging from 3.5 to 4.0 Å, there is evidence for varying degrees of $s^2\cdots s^2$ interaction. Another point of interest is the possible existence of weakly attractive arene···heavy metal interactions,[15], which could assist the close approach of Tl(I) ions.

The dithallium(I) cryptates of L^2 are synthesised‡ by direct reaction of preformed ligand with the appropriate thallium(I) salt. ^1H NMR studies on the triflate salt, $Tl_2L^2(CF_3SO_3)_2$ **1,** in the solid state and in solution, suggest a simple and symmetric structure where each Tl(I) cation occupies the site defined by the N4 cap. There is evidence of a low-activation dynamic process in solution in that both methylene-cap signals of **1** present as broad temperature-independent singlet resonances with no discernible fine structure due to geminal or vicinal [^1H,^1H] methylene coupling. Sharp signals for the H_2 and H_3 resonances show well defined ortho coupling; however the expected singlet H_1 resonance (Ar_1), which in analogous L^1 disilver(I) and dicopper(I) iminocryptates[16] is strongly affected by guest encapsulation both in respect of breadth and position, appears here as a severely broadened triplet (apparent ^1J ($^{205,203}Tl$,^1H) ≈ 17 Hz) at δ *ca.* 6.8. The triplet structure is just discernible at 400 MHz; broadening is a function of the magnetic field, approximating to 16:9:6 for 400, 300 and 250 MHz spectra, in proportion to the square of the magnetic field used [Fig 1(a)]. The signal from the methylene H_A hydrogens adjacent to the aromatic ring is a similarly broadened triplet [Fig 1(b)] and decoupling experiments fail to relate the coupling of the broad triplets to any proton resonance. Also the resonances are not narrowed significantly at high temperature, thus ruling out broadening *via* an exchange process. These observations implicate through-space coupling to thallium, the latter relaxing by a chemical shift anisotropy mechanism.[17] The splitting of the α-methylene signal confirms that the two $^{205,203}Tl$ nuclei couple to each other with J(Tl,Tl) > > 17 Hz, an example of the strong coupling case.[17b] The size of the coupling to the lone Ar_1 hydrogen is unexpected because no formal bond to thallium exists. Nor can it be explained on a through-bond basis as, despite an identical bond pathway, the H_3 resonance shows no thallium coupling. It appears that this coupling has to be explained on the basis of interaction between the lone aromatic hydrogen Ar_1 and the pair of Tl(I) ions which, although unbonded, are constrained by geometry to lie in close proximity.

The low solubility of **1** in CD_3CN allows only a weak ^{13}C solution spectrum where the noise level hinders the unambiguous attribution of $^{205,203}Tl$, ^{13}C couplings. There are indications of such coupling in the unique Ar_1 carbon resonance which appears at δ *ca.*129.9 as a broadened ≈ 80 Hz triplet. The methylene carbons give rise to two sharp resonances at δ 57.5 and 49.3 with a broader, possibly Tl-coupled, feature at δ 54.1 representing the methylene carbon adjacent to the aromatic ring. In the CP MAS ^{13}C spectrum signal breadth is generally sufficient to conceal any $^{205,203}Tl$,^{13}C coupling although splitting of a weak resonance in the region δ 120–130 may derive from such a cause. The weak ^{15}N CP MAS spectrum obtained for **1** likewise fails to show any coupling to thallium; just one relatively broad signal (half-width 150 Hz) centered at

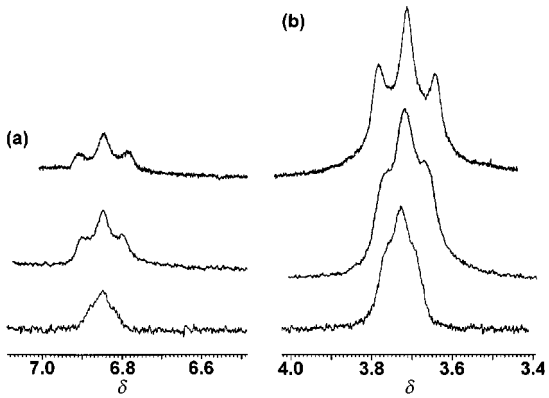

Fig. 1 The Tl-coupled Ar_1 (a) and CH_2(A) (b) resonances in different magnetic fields: bottom trace, 400; middle trace, 300; top trace, 250 MHz. (Spectra run in CD_3CN, 295 K, chemical shift in ppm from $SiMe_4$).

δ −307 (*vs.* NH_4NO_3 standard) appears, representing overlapped cryptand N(H) and N_{br} resonances.

In order to confirm the hypothesis of close approach of Tl nuclei, crystallographic evidence was sought,§ using the synchrotron source at Station 9.8 at CLRC Daresbury. The structure is illustrated in Fig. 2. The $[Tl_2L^2]^{2+}$ cation has $\bar{6}$ point symmetry and the anion lies on a threefold axis, so the asymmetric unit contains one sixth of the cation and one third of the anion. The Tl atom is coordinated to the bridgehead nitrogen (N1) and to three secondary amine groups (N11, N11A and N11B); it is displaced from the plane of the secondary amines by 1.087(3) Å towards the centre of the cavity and the Tl···TlA distance is 4.3755(4) Å. The Tl(I) cations are thus farther from the N_{br} apices than in other dinuclear cryptates we have studied.[1] The Tl–N distances are around 2.7–2.8 Å, at the long end of the range for Tl(I)–N distances,[14,18,19] suggesting a predominantly ionic character for bonding in this complex. The ligand host is fully extended to accommodate the pair of large spherical cations, and there is no helicity of cryptand strands. The structure is thus of unusually high symmetry for a cryptate. The distance between Tl(I) cations and the Ar_1 hydrogen is 3.816 Å. The shortest arene carbon···metal contact is 4.207 Å , almost 0.5 Å longer than the van der Waals sum. Edge to face intermolecular H···π contacts of *ca.* 2.49 Å involve all the arene rings.

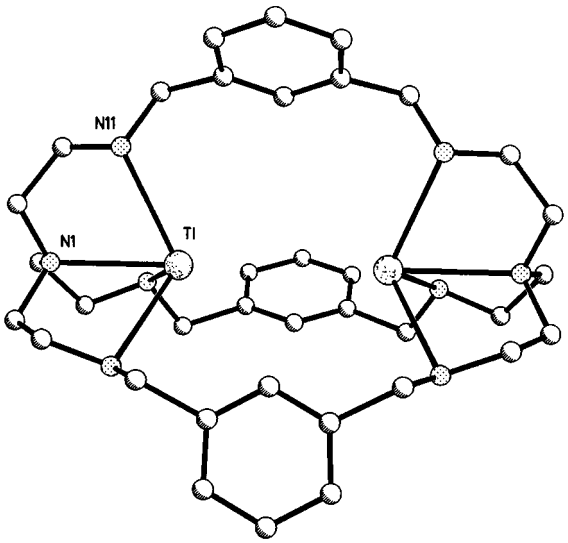

Fig. 2 Structure of $Tl_2L^2(CF_3SO_3)_2$. Selected distances (Å): Tl–N(I) 2.728(5), Tl–N(11) 2.796(3), Tl···Tl 4.3755(4), Tl··H(9) 3.816.

The structural data make it clear that the sizeable coupling between the Ar_1 proton and ^{205,203}Tl is formally through space, although the average separation of these nuclei in the dynamic solution environment may not be identical with that in the crystal where intermolecular H···π packing effects operate. The thallium–thallium coupling of >> 17 Hz must also be classified as a through space effect given the relatively large separation of Tl(I) cations, almost 1 Å greater than the internuclear distance (3.4 Å) in the element. We believe that this represents the largest recorded through-space coupling.

In most dimeric or quasi-dimeric structures,[13,14,19] Tl···Tl distances, in the range 3.6–3.9 Å are significantly shorter than noted here and the closest Tl···arene carbon distance of 3.816 Å in this structure exceeds that typical of weakly interacting arene–heavy metal systems.[19] Nonetheless, we have clear evidence of coupling between both the pair of Tl(I) cations and between this $Tl(I)_2$ pair and the unique aromatic proton Ar_1, despite the ionic character which explains the absence of ^{203,205}Tl, ^{1}H couplings elsewhere in the cryptate spectrum. It is intriguing that the only ^{203,205}Tl, ^{1}H couplings observed in this cryptate are mediated *via* a non-bonded pathway, *e.g.* that involving steric compression of the $Tl^+\cdots[H]\cdots Tl^+$ moiety. The implication is that coupling information can be efficiently transmitted in large soft cations like Tl(I) by non-directional overlap of electron density.

We thank EPSRC for access to the Solid State NMR service at Durham and to SRS station 9.8 at Daresbury. We are indebted to Dr M. Arthurs of Coventry University for the 250 MHz 1 H NMR spectrum.

Notes and references

† imBT = $N[(CH_2)_2N{=}CHCH{=}N(CH_2)_2]_3N$.

‡ Tl_2 $L^2(CF_3SO_3)_2 2H_2O{\cdot}MeOH$, **1**: To 0.5 mmol L^2 dissolved in 10 cm^3 MeOH was added 1 mmol Tl(OAc) dissolved in 2 ml water followed by 1 mmol of $LiCF_3SO_3$ as solid. A colourless precipitate was obtained in *ca.* 70% yield on concentrating the pale yellow solution. The final crop of this preparation yielded the small single crystals used for crystallography. Anal. Found (calc.): C, 33.8(34.2); H, 3.9(4.4); N 8.1(8.2)%.

§ *Crystal data*: $[Tl_2L^2](CF_3SO_3)_2$, $C_{38}H_{54}F_6N_8O_6S_2Tl_2$, colourless needle, 0.16 × 0.06 × 0.04 mm, hexagonal, a = 9.5074(2), c = 29.7005(4) Å, U = 2324.97(8) $Å^3$, space group $P6_3/m$, Z = 2, μ = 7.088 mm^{-1}, $F(000)$ = 1268. Data were collected at 150(2) K using a SMART CCD with synchrotron radiation (λ = 0.6885 Å, SRS station 9.8 at Daresbury). A hemisphere of data (16580 reflections, θ_{max} = 29.33°) was collected. The structure was solved by direct methods and refined on F^2, using all 2277 independent reflections (R_{int} = 0.0346). Non-hydrogen atoms were refined anisotropically and hydrogen atoms were inserted at calculated positions except for the amine proton, which was located and refined with a fixed ADP. The refinement, on 100 parameters, converged with $wR2$ = 0.0835, GOF = 1.060 (all data) and conventional $R1$ = 0.0357 (2σ data). The only significant residual peaks were close to the Tl atom. All programs used in the structure refinement are contained in the SHELX-97 package.[20] CCDC 182/1483. See http://www.rsc.org/suppdata/cc/a9/a908476b/ for crystallographic files in .cif format.

1 J. Nelson, V. McKee and G. Morgan, *Prog. Inorg. Chem.*, 1998, **47**, 167.
2 C. Harding, V. McKee and J. Nelson, *J. Am. Chem. Soc.*, 1991, **113**, 9684.
3 C. J. Harding, J. Nelson, M. C. R. Symons and J. Wyatt, *J. Chem. Soc., Dalton Trans.*, 1994, 2499.
4 J. A. Farrar, V. McKee, A. H. R. al Obaidi, J. J. McGarvey, J. Nelson and A. J. Thomson, *Inorg. Chem.*, 1995, **34**, 1302.
5 J. A. Farrar, R. Grinter, F. Neese, J. Nelson and A. J. Thomson, *J. Chem. Soc., Dalton Trans.*, 1997, 4083.
6 A. H. R. al-Obaidi, G. Baranovich, J. L. Coyle, C. Coates, J. J. McGarvey, V. McKee and J. Nelson, *Inorg. Chem.*, 1998, **37**, 3597.
7 C. J. Harding, F. Mabbs, E. MacInnes, V. McKee and J. Nelson, *J. Chem. Soc., Dalton Trans.*, 1996, 3227.
8 A. Escuer, C. J. Harding, Y. Dussart, J. Nelson, V. McKee and R. Vicente, *J. Chem. Soc., Dalton Trans.*, 1999, 223.
9 C. J. Harding, Q. Lu, J. F. Malone, D. J. Marrs, N. Martin, V. McKee and J. Nelson, *J. Chem. Soc., Dalton Trans.*, 1995, 1739.
10 R. Abidi, M. G. B. Drew, F. Arnaud-Neu, S. Lahely, M. J. Schwing-Weil, D. J. Marrs and J. Nelson, *J. Chem. Soc., Perkin Trans., 2*, 1996, 2747.
11 O. W. Howarth, G. G. Morgan, V. McKee and J. Nelson, *J. Chem. Soc., Dalton Trans.*, 1999 2097.
12 M. G. B. Drew, D. Farrell, G. G. Morgan, V. McKee and J. Nelson, to be published.
13 P. Pyykko, *Chem. Rev.*, 1997, **97**, 597.
14 H. Schuman, C. Janiak, J. Pickardt and U. Nborner, *Angew. Chem., Int. Ed. Engl.*, 1987, **26**, 789; P. Jutzi, J. Schnittger and M. B. Hursthouse, *Chem. Ber.*, 1991, **124**, 1693, and references therein.
15 C. Janiak, *Coord. Chem. Rev.*, 1997, **163**, 107; H. Schuman, C. Janiak, M. A. Khan and J. J. Zuckermann, *J. Organomet. Chem.*, 1988, **354**, 7.
16 Q. Lu, J.-M. Latour, C. J. Harding, N. Martin, D. J. Marrs, V. McKee and J. Nelson, *J. Chem. Soc., Dalton Trans.*, 1994, 1471.
17 (*a*) P. Ghosh, P. J. Desrosiers and G. Parkin, *J. Am. Chem. Soc.*, 1998, **120**, 10416; (*b*) R. Freeman, *Spin Choreography*, Spektrum, Oxford, 1997, ch. 1, p. 29.
18 A. J. Amoroso, J. C. Jeffrey, P. L. Jones, J. A. McCleverty, E. Psillakis and M. D. Ward, *J. Chem. Soc., Chem. Commun.*, 1995, 1175; K. Hellmann, L. H. Gade, R. Fleischer and T. Kottke, *Chem. Eur. J.*, 1997, **3**, 1801, and references therein.
19 C. H. Galka and L. H. Gade, *Inorg. Chem.*, 1999, **38**, 1038.
20 G. M. Sheldrick, SHELX-97, University of Göttingen, 1997.

Communication a908476b

ChemComm

Electrostatic interactions between positively charged porphyrins and nucleotides or amides: buffer-dependent dramatic changes of binding affinities and modes†

Mallena Sirish and Hans-Jörg Schneider*

FR 11.2 Organische Chemie der Universität des Saarlandes, D-66041 Saarbrücken, Germany. E-mail: ch12hs@rz.uni-sb.de

Received (in Cambridge, UK) 20th September 1999, Accepted 5th November 1999

The association strength of positively charged porphyrins with anionic species can be orders of magnitude higher than reported in the literature, depending on the chosen buffer; the buffer also determines the dominating interaction mechanism, leading to stronger stacking contributions at higher salt concentrations; even electroneutral amides show a hitherto not recognized interaction between the negatively charged carbonyl oxygen and the positively charged π-surface of the porphyrin system.

Porphyrins with pyridinium substituents (**R**) have been used for some time as partners in supramolecular complexes, in particular with nucleotides,[1] as well as ligands for DNA.[2] As major binding contributions, electrostatic and stacking interactions have been identified.[1,3] In the context of recent studies with a new porphyrin-based peptide receptor[4] we have measured associations with the underlying tetrapyridinium framework **R** under different conditions and have found large affinity changes to anionic species such as nucleotides. The results indicate at the same time strong changes in the binding modes, supported by the observed complexation-induced NMR shifts.

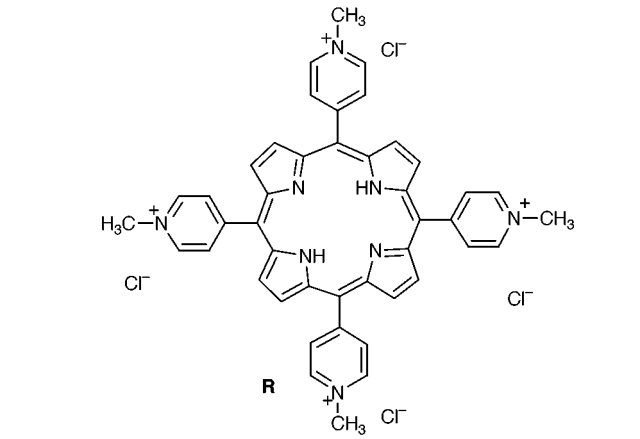

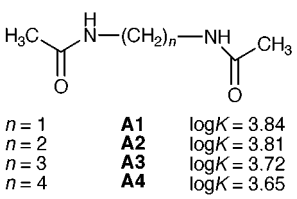

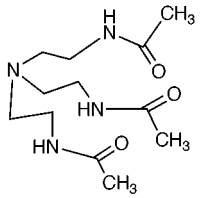

The binding constants were determined as reported earlier;[4] the titrations showed isosbestic points, in line with the fitting to a 1:1 equilibrium. It was secured that there was no pH change during titration; the very small change of the anyway very low ionic strength has a negligible influence on the association equilibria.[5] Measurements with amides like **A1**–**A5** showed changes of ΔA in the Soret band absorption similar to those observed earlier with a related receptor and peptides.[4] Association constants around 5000 M^{-1} with diamides **A1**–**A4** and over 10000 M^{-1} with the triamide **A5** reveal that even eletroneutral molecules can strongly interact with the positive charges in the extended aromatic receptor moiety. Experiments with corresponding diesters **E** (n = 1–3) and also α,ω-alkane diols with **R** showed in contrast to the other ligands no appreciable ΔA in the UV spectra, indicating that hydrophobic or lipophilic interactions cannot be a major binding force. These observations are only in line with additive interactions between the cationic porphyrin skeleton and the carbonyl oxygen atoms, which are known to bear a substantial negative charge in amides, in contrast to *e.g.* in esters where we cannot detect binding.

If such interactions with amide oxygens already lead to such high affinities, larger numbers should be expected with fully charged anions. In consequence, the association constants are expected to be substantially lowered by anions present in concentrations below the molarity of the amide type ligands. We therefore decided to re-eaxamine the affinity of the often used tetrapyridinium porphyrin **R** towards different anions, with and without the commonly used buffers.[1] Indeed we find that the binding constants are larger by one to two orders of magnitude than those reported in the literature (Table 1), if one measures them not in the presence of added buffer anions; this is illustrated with the selected isotherms in Fig. 1. Even with simple halides we find rather large log K values (Table 1).

Association of nucleotides with tetrapyridinium porphyrin is thus much stronger than known before; it increases as expected with the charges in the range AMP < ADP < ATP, and falls off steeply with higher buffer concentrations (Table 1). Noticeably, the distinct base selectivity observed, in the older work between purine and pyrimidine bases with **R**,[1] is almost absent at low salt concentrations, and appears again with higher buffer concentrations. Obviously, in the absence of competing buffer anions the electrostatic interactions between the nucleotide phosphate and the cationic receptor dominate so strongly that stacking interactions play a minor role. On the other hand, with decreased ion pairing at higher buffer concentrations the lipophilic interactions gain in energetic importance, as the salt

† Supramolecular Chemistry, Part 93; Part 92: V. A. Palyulin, S. V. Emets, V. A. Chertkov, C. Kasper and H.-J. Schneider, *Eur. J. Org. Chem.*, 1999, in the press.

Table 1 Logarithm of association constants for **R** and nucleotides[a]

	No buffer			0.1 M buffer			0.3 M buffer		
Ligands	log*K*	$\Delta\lambda$/nm	ΔA	log*K*	$\Delta\lambda$/nm	ΔA	log*K*	$\Delta\lambda$/nm	ΔA
Adenosine	4.54	3	0.11	2.64	5	0.39	2.79	6	0.35
AMP^{2-}	4.52	9	0.38	3.40	5	0.20	2.87	5	0.31
ADP^{3-}	4.95	10	0.38	3.40	7	0.10	3.14	7	0.33
ATP^{4-}	5.45	13	0.37	3.34	8	0.27	3.55	7	0.23
$dGMP^{2-}$	4.42	7	0.42	2.88	4	0.18	2.54	5	0.29
Thymidine	4.80	3	0.18	2.40	3	0.27	2.27	5	0.28
TMP^{2-}	4.42	6	0.27	2.56	3	0.21	2.33	3	0.25
$dUMP^{2-}$	4.09	6	0.32	3.98	2	0.07	2.44	2	0.30
$dCMP^{2-}$	4.02	5	0.29	4.03	1	0.06	2.38	3	0.24
$H_3PO_4^{2-}$	4.73	2	0.27	3.31	1	0.05	[b]	0	< 0.02
NH_4Cl	4.55	2	0.05						

[a] Measured by UV–visible titration of **R** with nucleotides in water in the absence and in the presence of 0.1 and 0.3 M phosphate buffer (pH 7.9 ± 0.2) at 25 °C. Titrations were carried out by adding concentrated stock solutions of nucleotides ([nucleotide] = 10 mM) containing *ca.* 2 μM of porphyrin to an equally concentrated solutions of porphyrin in a 10 mm cuvet. Error limits: log*K* ± 5%. [b] *K* value can not be determined accurately as the ΔA value is negligible.

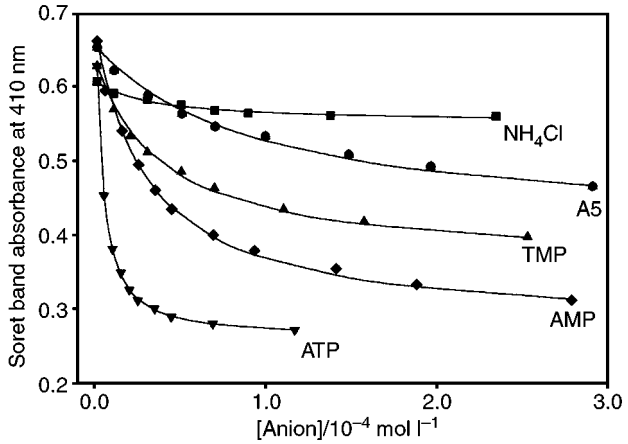

Fig. 1 Non-linear least square fit of UV–visible titration curves for receptor **R** with selected anions. Conditions: AMP, ATP and TMP without buffer (see Table 1); **A5** in water at pH 6.9 ± 0.2; NH_4Cl in water without buffer at pH 7.9 ± 0.2.

bridges do not 'draw away' as strongly the nucleobase from contacts to the porphyrin surface. That the nucleotide indeed stacks to the porphyrin moiety is established, by the significant shielding observed both at the nucleobase *and* the ribose protons.

In conclusion, the results show that the buffers used in host–guest complexation studies can significantly alter the dominating non-covalent interaction mechanisms, and thereby both the affinity and the selectivity seen in such systems. Moreover, permanent charges in a large receptor surface such as the tetrapyridinium porphyrin can even in water also lead to significant binding with the partial negative charges of electroneutral species such as amides.

Our work is supported by the Deutsche Forschungsgemeinschaft, Bonn, and the Fonds der Chemischen Industrie, Frankfurt. M. S. thanks the A. v. Humboldt foundation for a stipend.

Notes and references

1 R. F. Pasternack, E. J. Gibbs, A. Gaudemer, A. Antebi, S. Bassner, L. De Poy, D. H. Turner, A. Williams, F. Laplace, M. H. Lansard, C. Merienne and M. Perree-Fauvet, *J. Am. Chem. Soc.*, 1985, **107**, 8179; Y. Kuroda, H. Hatakeyama, N. Inakoshi and H. Ogoshi, *Tetrahedron Lett.*, 1993, **51**, 8285; B. L. Iverson, K. Shreder, V. Kral, P. Sansom, V. Lynch and J. L. Sessler, *J. Am. Chem. Soc.*, 1996, **118**, 1608; J. L. Sessler and A. Andrievsky, *Chem. Eur. J.*, 1998, **4**, 159.

2 B. Meunier, *Chem. Rev.*, 1992, **92**, 1411 and references cited therein; H. J. Schneider and M. Wang, *J. Org. Chem.*, 1994, **59**, 7473; P. Bigey, G. Pratviel and B. Meunier, *J. Chem. Soc., Chem. Commun.*, 1995, 181; N. E. Mukundan, G. Petho, D. W. Dixon and L. G. Marzilli, *Inorg. Chem.*, 1995, **34**, 3677; G. Pratviel, J. Bernadou and B. Meunier, *Angew. Chem.*, 1995, **107**, 819; *Angew Chem., Int. Ed. Engl.*, 1995, **34**, 746; D. W. Dixon and V. Steullet, *J. Inorg. Biochem.*, 1998, **69**, 25.

3 H.-J. Schneider, *Chem. Soc. Rev.*, 1994, **22**, 227 and references cited therein; H.-J. Schneider and M. Wang, *J. Org. Chem.*, 1994, **59**, 7464.

4 M. Sirish and H.-J. Schneider, *Chem. Commun.*, 1999, 907; M. Sirish, F. Eblinger and H.-J. Schneider, *Advances in Supramolecular Chemistry*, ed. G. W. Gokel, JAI, Stamford, 1999, vol. 6, in the press.

5 See Md. Alamgir Hossain and H.-J. Schneider, *Chem. Eur. J.*, 1999, **5**, 1284.

Communication a907620d

Selective nitration of aromatic compounds by solid acid catalysts

B. M. Choudary,* M. Sateesh, M. Lakshmi Kantam, K. Koteswara Rao, K. V. Ram Prasad, K. V. Raghavan and J. A. R. P. Sarma

Indian Institute of Chemical Technology, Hyderabad-500 007, India. E-mail: Choudary@iict.ap.nic.in

Received (in Cambridge, UK) 5th October 1999, Accepted 22nd November 1999

High activity and *para*-selectivity in the nitration of aromatic compounds is achieved by a high density of acidic sites and ready formation of the *para*-isomer in the pores of zeolite beta with low Si/Al ratio as revealed by molecular modeling studies.

Nitration of aromatic compounds is a ubiquitous reaction to realise organic intermediates required in large tonnages for the fine chemical industry. The conventional nitration process,[1] employing a nitrating mixture of nitric and sulfuric acid, for the last 150 years has remained unchallenged in the commercial arena owing to uneconomical alternative options. Selective synthesis of the desired isomer in the nitration of substituted aromatic compounds is of topical interest to reduce pollution caused by unwanted isomers and specifically to respond to market demand. Earlier we reported selective nitrations by employing a solid acid, Fe^{3+} montmorillonite in the presence of acetic anhydride–nitric acid.[2] Later, various novel options, meeting international environmental laws, and also avoiding the recovery of the spent acid in the conventional mixed acid process have been explored that include Laszlo's[3] claycop (copper nitrate impregnated on K10 montmorillonite) acetic anhydride and recently claycop–nitric acid–acetic anhydride, Smith's[4a] mordenite–benzoyl nitrate, Kwok's[5] ZSM-5-propyl nitrate and Olah's[6] Nafion-H–*n*-butyl nitrate. However these options fall short of expectations to commercial realisation in view of low space time yields, high dilution, and use of expensive mixtures in the form of acetic anhydride–nitric acid or expensive acyl or alkyl nitrate whereas Sato's[7] and Prins's[8] vapour phase nitrations of benzene conducted employing clays and mordenite zeolite provided low space time yields. The zeolite beta-acetic anhydride-nitric acid system developed later by Smith *et al.*,[4b,c] afforded good space time yields but required great care in large scale operations. Barrett and coworkers[4d] employed La(III) triflates as recyclable catalysts for aromatic nitrations but such systems required longer reaction times to obtain good yields without any explicit selectivity towards *o*-/*p*-isomer.

Herein, we present a unique methodology for the nitration of aromatic compounds that offers high space time yields, near zero emission of effluents, especially high *p*-selectivity for monosubstituted products, essential for commercial processes, employing nitric acid at a concentration of 60–90%, with reuse of the solid acid catalysts being possible by azeotropic removal of water formed in the reaction and present in nitric acid.†

We executed a two-fold approach employing modified clays and zeolites to realise a high space time yield as well as high selectivity of the desired *p*-isomer as indicated in Table 1. In an earlier investigation,[9] a series of different metal-exchanged and pillared clay catalysts were prepared[10] and employed in the nitration reactions of aromatic compounds under identical conditions. Fe^{3+} montmorillonite catalyst was found to be the most active owing to its high metal content and highly acidic sites. This catalyst (entry 1) is far superior in terms of space time yield, when compared even with gas phase reactions conducted with various metal-exchanged montmorillonites[7] and mordenite.[8] In the nitration of benzene, mononitrobenzene is obtained selectively without formation of any di- or poly-nitrobenzenes and the *p*-selectivities in the nitration of monosubstituted benzenes are improved.

Our main emphasis is to achieve higher *p*-selectivity to meet market demand. Accordingly, various zeolites which have well

Table 1 Selective nitration of aromatic compounds

Entry	Arene	Catalyst	HNO_3 (%)	Product yield[a] (%)	STY[b]	Product distribution[c]		
						o-	*m*-	*p*
1	C_6H_6	Fe^{3+} mont.	90	88	22.8	—	—	—
2	C_6H_6	Al^{3+} mont.[d]	60	48,[e] 95[f]	0.6	—	—	—
3	C_6H_5Me	Mixed Acid	90	—	—	58	4	38
4	C_6H_5Me	Fe^{3+} mont.	90	89	26.0	53	3	44
5	C_6H_5Me	K10 mont.	60	53	9.1	45	3	52
6	C_6H_5Me	Zeolite beta-I[g]	60	68, 96[f]	10.6	30	3	67
		5th recycle	60	67, 95[f]	10.3	33	3	64
7	C_6H_5Me	Zeolite beta-II[g]	60	40, 95[f]	6.8	41	4	55
8	C_6H_5Me	ZSM-5	60	32	5.6	49	7	44
9	C_6H_5Me	Mordenite	60	35	6.0	56	6	38
10	C_6H_5Me	HY	60	32	5.4	54	7	39
11	C_6H_5Me	TS-1	60	30	5.0	56	6	38
12	C_6H_5Cl	Fe^{3+} mont.	90	77	26.0	36	—	64
13	C_6H_5Cl	Zeolite beta-I	60	51, 98[h]	12.0	10	—	90
14	C_6H_5Br[i]	Zeolite beta-I	70	51, 96[h]	15.8	18	—	82
15	C_6H_5I[i]	Zeolite beta-I	70	52	19.8	28	—	72
16	C_6H_5Pr[i]	Zeolite beta-I	70	51	12.8	19	—	81
17	C_6H_5OMe	Zeolite beta-I	70	49, 96[h]	11.4	25	—	75

[a] Product yield based on total amount of HNO_3 used. [b] Space time yield: kg product/kg catalyst/h. [c] By GC. [d] Results from ref. 7. [e] Yields based on benzene. [f] Yields calculated based on HNO_3 actually consumed, *i.e.* subtracting the amount of nitric acid azeotropically distilled out from the reaction vessel and collected in the Dean–Stark trap from the total amount of nitric acid used. The nitric acid collected is reused after adjusting to the desired concentration. [g] Zeolite beta-I, II: SiO_2/Al_2O_3 molar ratio = 22, 27. [h] Yields based on aromatics with aromatic compound and HNO_3 in 1:2 ratio. [i] Dichloroethane used as solvent.

defined pore structures and channels that are derived from the networking of SiO_2 and Al_2O_3 making them attractive candidates for shape selective catalysis[11] were employed[12] to achieve higher shape selectivity in the nitration of substituted aromatics. Zeolite beta-I[13] (entry 6) is found to the best catalyst for the nitration of aromatic hydrocarbons to nitroaromatics with high *p*-selectivity. When compared with the selectivities obtained using classical mixed acid, zeolite beta-I catalyst displayed a major shift towards *p*-selectivity as is evident, for example; for toluene: from 38 to 67%, for cumene: 58 to 81%, for chlorobenzene: 64 to 90%, for anisole: 40 to 75% (Table 1). The production of the *p*-isomer in higher ratio for toluene and cumene meets the timely demand of the market and at the same time avoids the burning of undesired *o*-isomers occasionally resorted to by the manufacturers which causes environmental pollution. Increased formation of the *p*-isomer in the nitration of chlorobenzene eases the isomeric separation to a considerable extent and helps to save energy. Whereas the change from methyl (toluene) to the larger isopropyl (cumene) substituent increases the *para* selectivity, the reverse applies for halogens, for which the best *para* selectivity is obtained with the smaller substituent, namely chlorine owing to electronic factors.

We carried out nitration of toluene with various zeolite catalysts and zeolite beta of different Si/Al ratios (Table 1). Zeolite beta proved to be the best catalyst among the zeolites used in terms of space time yield and *p*-selectivity. On decreasing the Si/Al ratio in zeolite beta, an increase in *p*-selectivity as well as overall activity is observed (entry 6 and 7). An increased number of Bronsted acid sites reduces the available space in the pore and this result substantiates our inference that the formation of *o*-isomer, which requires more space, is unfavourable. These observations are in accord with the results observed by Bellussi *et al*. in alkylation reactions.[14] It is also found that with an increase of catalyst concentration the *p*-selectivity of toluene nitration increased further to 73%. Zeolite beta catalyst showed consistent activity and selectivity even after five cycles (entry 6). Careful analysis of the regenerated catalyst after recycling it five times showed no change in the Si/Al composition indicating that no dealumination of catalyst has taken place.

Sorption studies of the reactant and isomers of the product and their intermediates (transition states) undertaken using the sorption module of Cerius[2] which implements rapid Monte Carlo statistical mechanical calculations[15] clearly predicted high *p*-selectivity possible with ease of formation of the intermediate of the *p*-isomer in the pores. The result of shape selectivity observed employing zeolite beta derives further support from the results obtained with metal exchanged clays, wherein mesopores of montmorillonite formed due to acid treatment also induced some shift in *p*-selectivity (entries 4 and 5). The higher shape selectivity for the zeolite is ascribed to the induction of larger steric effects by the 3D structure of zeolite beta in comparison to the 2D structure of clay catalysts.

Nitration involves electrophilic attack on the aromatic ring by the nitronium ion, NO_2^+. Bronsted acidic sites are responsible for the generation of NO_2^+ ion from nitric acid. Reaction conducted with fuming nitric acid without azeotropic removal of water is totally inhibited after some time owing to a poisoning effect of water formed in the reaction. It is necessary to scavenge the water out of the reaction zone formed during the reaction to facilitate regeneration of active acid sites on the catalyst. The rate of addition of nitric acid to the reactor containing powder catalyst and substrate is matched with the rate of removal of water present in nitric acid and the reaction zone through extractive distillation with a Dean–Stark apparatus using the substrate as the solvent or chlorohydrocarbon solvent for high boiling aromatic compounds to afford optimum selectivity, activity and protection of the catalyst from degradation. This protocol envisages the instant reaction of added nitric acid and establishes that the solid acid catalysts used here act as bifunctional catalysts generating the electrophile, nitronium ion, as well as acting as an instant adsorbent for water formed during the reaction.

On the other hand ZSM-5 under such conditions affords low space time yield and selectivity (entry 8) in the nitration of toluene when compared to the high *p*-selectivity obtained by Kwok *et al*.[5] employing acyl nitrate as nitrating agent. This is attributed to low diffusion of aqueous HNO_3 in the hydrophobic pores of ZSM-5 and the resulting density of acidic sites is too low to promote the generation of nitronium ions from nitric acid. Therefore the reaction on ZSM-5 mainly takes place on the surface of the zeolite.

In conclusion, a simple methodology for nitration employing solid acids dispensing with the use of acetic anhydride or acyl nitrate described here leading to high space time yields and high *p*-selectivities, appears to be a promising alternative to the conventional acid mixture of nitric and sulfuric acid. Enhanced *p*-isomer formation to meet market demands, dispensing the use of sulfuric acid, achieving near zero emission of effluents, non-corrosivity and low water requirement are other attractions.

Notes and references

† *General procedure for the nitration of monosubstituted aromatics*: A mixture of toluene (161 ml; 1.5 mol) and zeolite beta-I catalyst (10 g) were added to in a 1 litre-reactor flask equipped with stirring rod and Dean–Stark apparatus. 60% nitric acid (120 ml, 1.5 mol) was added in a controlled manner with an infusion pump over a period of 80 min to the above mixture, which was preheated to the refluxing temperature. The liberated water collected into the Dean–Stark apparatus was continuously removed. After completion of the reaction, the catalyst was filtered off and the reaction mixture was concentrated to obtain the mixture of nitrotoluenes. Nitration of other aromatic hydrocarbons was similarly carried out on a 76 mmol scale.

1 G. A. Olah, R. Malhotra and S. C. Narang, *Nitration Methods and Mechanism*, VCH, New York, 1989, pp. 5–15; K. Schofield, *Aromatic Nitration*, Cambridge University Press, Cambridge, 1980.

2 B. M. Choudary, M. R. Sarma and K. V. Kumar, *J. Mol. Catal.*, 1994, **87**, 33.

3 L. Delaude, P. Laszlo and K. Smith, *Acc. Chem. Res.*, 1993, **26**, 607; B. Gigante, A. O. Prazeres, M. J. Marcelo-Curto, A. Cornelis and P. Laszlo, *J. Org. Chem.*, 1995, **60**, 3445; A. Cornelis, L. Delaude, A. Gerstmans and P. Laszlo, *Tetrahedron Lett.*, 1988, **29**, 5657.

4 (*a*) K. Smith, K. Fry, M. Butters and B. Nay, *Tetrahedron Lett.*, 1989, **30**, 5333; (*b*) K. Smith, A. Musson and G. A. DeBoos, *Chem. Commun.*, 1996, 469; (*c*) K. Smith, A. Musson and G. A. DeBoos, *J. Org. Chem.*, 1998, **63**, 8448; (*d*) F. J. Waller, A. G. M. Barrett, D. C. Braddock and D. Ramprasad, *Chem. Commun.*, 1997, 613.

5 T. J. Kwok, K. Jayasuriya, D. Reddy and B. W. Brodman, *J. Org. Chem.*, 1994, **59**, 4939.

6 G. A. Olah, R. Malhotra and S. C. Narang, *J. Org. Chem.*, 1978, **43**, 4628.

7 H. Sato, K. Hirose, K. Nagai, H. Yoshioka and Y. Nagaoka, *Appl. Catal. A*, 1998, **175**, 201.

8 L. Bertea, H. W. Kouwenhoven and R. Prins, *Appl. Catal. A* , 1995, **129**, 229.

9 B. M. Choudary, M. L. Kantam, M. Sateesh, K. K. Rao and K. V. Raghavan, EP 0949240 A, 1999.

10 P. Laszlo and A. Mathy, *Helv. Chim. Acta.*, 1987, **70**, 577; E. G. Rightor, M. Tzou and T. J. Pinnavaia, *J. Catal.*, 1991, **130**, 29.

11 S. M. Cseri, *Zeolites*, 1984, **4**, 202; W. Holderich and H. van Bekkum, *Stud. Surf. Sci. Catal.*, 1991, **58**, 631.

12 B. M. Choudary, M. Sateesh, M. L. Kantam, K. K. Rao, K. V. R. Prasad and K. V. Raghavan, *US Pat.*, Appl. No. 09/188589, 1998.

13 J. Perez-Pariente, J. A. Martens and P. A. Jacobs, *Zeolites*, 1991, **8**, 46.

14 G. Bellussi, G. Pazzuconi, C. Perego, G. Girotti and G. Terzoni, *J. Catal.*, 1995, **157**, 227.

15 Sorption module in Cerius[2] implements a rapid Monte Carlo statistical mechanics method: N. Metropolis, A. W. Rosenbluth, M. N. Rosenbluth, A. H. Teller and E. Teller, *J. Chem. Phys.*, 1953, **21**, 1087; M. P. Allen and D. J. Tildesley, *Computer Simulation of Liquids*, Clarendon Press, Oxford, 1987.

Communication a908011b

Reusable photographic films based on iron-containing clay minerals

Yea Wenn Liou and Chong Mou Wang*

Department of Chemistry, National Taiwan Normal University, Taipei 11718, Taiwan, Republic of China.
E-mail: checmw@scc.ntnu.edu.tw

Received (in Cambridge, UK) 25th October 1999, Accepted 15th November 1999

A non-silver-based photographic film has been developed from 9-methylacridinium-intercalated clay particles (denoted clay|AcH$^+$) and this inexpensive clay film showed potential reusability.

Substantial efforts have recently been directed towards the development of artificial photosynthetic systems,[1–5] which, in turn, unite the understanding of the structure of natural photosynthetic systems, the advances in instrumentation, and the development of novel materials for optical and chemical detection.[6–8] For the latter aspects, we recently carried out a series of investigations on clay modified electrodes, and found that iron-containing clay minerals proved useful in many applications, such as biosensing and optical recognition.[9–12] The iron containing species are likely to be key in mediating the electron reactions on the clay surface.[13,14] Besides, we also found that this inexpensive solid, if properly tailored, may be useful for lithography or image-recording.

Photography can be dated back to 1727 as Johann Heinrich Schulze reported that solid AgCl darkens when exposed to light. Thereafter, most color and black-and-white photography was developed on the basis of the photochemistry of AgBr. A representative example [eqn. (1)] is the following coupling reaction between α-naphthanol and *N*,*N*-diethyl-2-methyl-1,4-phenylenediamine (DEPD) sensitized by AgBr:[15,16]

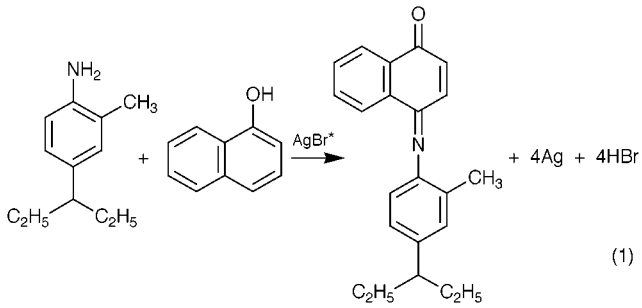

(1)

Meanwhile, many other dyes have showed excellent sensitivity to colored objects or to images only visible under IR or UV light. However, for most cases, silver bromide is sacrificed and the film is not recoverable. Here we describe that a potentially reusable photographic film can be developed from inexpensive iron-containing clay minerals.

When the clay|AcH$^+$ modified electrode is simultaneously biased at +0.4 V *vs*. SCE and illuminated with light of $\lambda > 350$ nm (100 W Hg lamp, 1 min), Fig. 1 shows that indophenol blue ($\lambda_{abs} \approx 625$ nm) is immediately formed on the surface of the clay film from a solution containing DEPD ($\lambda_{abs,max} = 257$ nm, pH 10) and α-naphthanol ($\lambda_{abs} = 250$, 337 nm, pH 10). Here, the clay|AcH$^+$ particles were prepared by reacting clay (Aldrich, montmorillonite K10, 0.5 g) with $AcHPF_6$ (10 mM, 50 mL in CH_3CN)[13] for two days followed by extensive washing with CH_3CN; the loading of AcH$^+$ in clay was estimated to be *ca*. 10^{-5} mol g^{-1}. The clay-modified electrode was fabricated on conductive ITO glass (indium-doped, 0.7 mm thick, 20 Ω cm^{-2}; Delta Technol.). Typically, a portion of the clay|AcH$^+$ slurry (30 μL cm^{-2}, 100 mg/100 mL water) was spin-coated onto glass sheets and dried at room temperature. Then, the clay

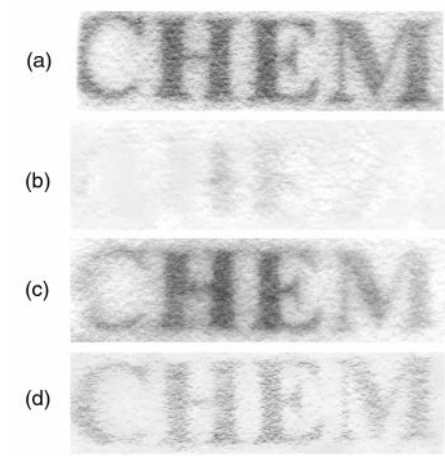

Fig. 1 (a) Photoimage formed on the clay|AcH$^+$ modified electrode in a solution containing 2 mM of DEPD and 3 mM of α-naphthanol (pH 4) under illumination ($\lambda > 350$ nm) and at $E = 0.4$ V *vs*. SCE for 1 min; (b) image erasing, after the image obtained in (a) was dipped in a dilute sulfuric acid for 1 s; (c) image recovering, the electrode in (b) was re-exposed to light in solution (a); (d) the image obtained after 20 consecutive exposure and erase cycles.

film was reinforced with polystyrene [PS, M_w 13000, Aldrich, 30 μL cm^{-2}, 10 mg mL^{-1} in ethyl acetate–toluene (1 : 1, v/v)]. The mechanism of formation of indophenol blue on the clay surface is proposed in Scheme 1 and control experiments support the proposed mechanism. As is evident in Fig. 2, insignificant photocurrent is detected for electrodes made from the bare clay particles in a pH 4 solution containing 1 mM of DEPD, whereas a greater photocurrent is obtained when the electrode is incorporated with AcH$^+$ ($\lambda_{abs,max} = 357$ nm; $\lambda_{em} = 500$ nm). Laser flash photolysis experiments (Fig. 3) show that the lifetime of $AcH^{+*}_{(aq)}$ (dotted lines) is 36 ns whereas the decay for $AcH^{+*}_{(clay)}$ (solid lines) occurs in the same time scale as the instrumental response ($\ll$10 ns), indicating that the excited acridinium, $AcH^{+*}_{(clay)}$, can be quickly quenched by iron species, presumably Fe^{2+}, in the clay particle, at Fe^{II} sites.[13] The fast decay of AcH^{+*} suggests a reductive quenching mechanism [eqn. (2)].

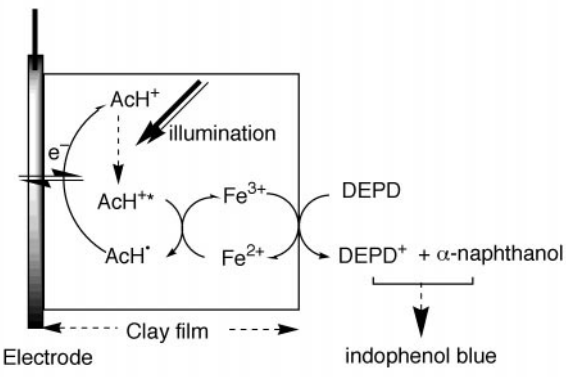

Scheme 1 Proposed mechanisms for the formation of indophenol blue on the illuminated clay|AcH$^+$ modified electrode.

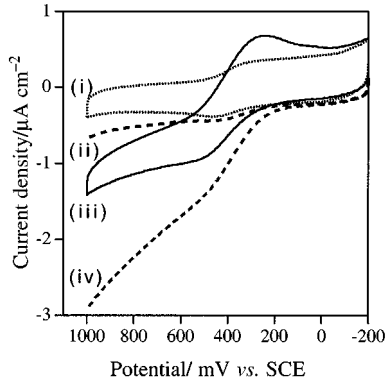

Fig. 2 *J*–*V* curves for DEPD (1 mM, pH 4): (i) with the electrode prepared with the bare clay particles, in the dark; (ii) with the clay|AcH$^+$ electrode, in the dark; (iii) with the electrode as in (a), under illumination; (iv) with the clay|AcH$^+$ electrode as in (b), under illumination. Scan rate: 50 mV s^{-1}.

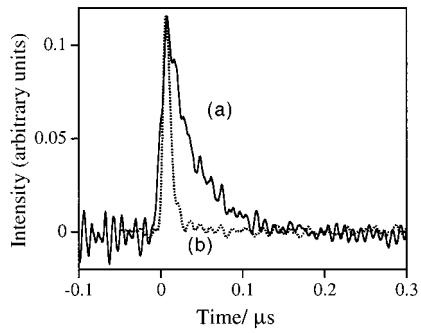

Fig. 3 Time-resolved laser spectroscopy (pH 4, acetic acid–acetate buffer, $I \approx 0.1$ M, $\lambda_{em} = 500$ nm) for free AcH$^+$ (a) and clay|AcH$^+$ (b).

$$AcH^{+*}{}_{(clay)} + Fe^{2+}{}_{(clay)} \longrightarrow AcH^{\cdot}{}_{(clay)} + Fe^{3+}{}_{(clay)} \quad (2)$$

The lack of an electron transfer product from AcH^{+*} in the clay is believed to be a consequence of the fast reaction of AcH$^{\cdot}$ with Fe^{3+} species in the Fe^{III} sites in the clay. To prevent the back reaction of eqn. (2) from occurring, an anodic regeneration for AcH$^+$ (at $E° \approx -0.4$ V *vs.* SCE, pH 4)[13] from AcH$^{\cdot}$ appears to be necessary.

The photoquality in terms of the contrast between the blue regions and the background is a function of the electrode potential, pH and the concentration ratio of the reactants. For instance, a high pH environment greatly favored the formation of indophenol blue. However, for a solution pH of >6, the formation of indophenol blue became too rapid to be controlled. As a consequence, a lower pH environment (pH 4), although less favorable for the formation of indophenol blue on the clay electrode, was, in turn, less interfering. The electrode potential is another key factor determining the image quality. Control experiments showed that the formation of indophenol blue tended to a limiting rate as the electrode potential approached 0.4 V *vs.* SCE (*i.e.* the formal potential of $Fe^{III/II}{}_{(clay)}$)[10] according to the absorbance monitored at 625 nm (the peak absorption of indophenol blue). This effect is attributed to the regeneration of $Fe^{III}{}_{(clay)}$ from $Fe^{II}{}_{(clay)}$ [eqn. (3)]

$$Fe^{II}{}_{(clay)} \longrightarrow Fe^{III}{}_{(clay)} + e^- \quad (3)$$

after the photooxidation of DEPD by $Fe^{III}{}_{(clay)}$ [eqn. (4)]

$$Fe^{III}{}_{(clay)} + DEPD \longrightarrow Fe^{II}{}_{(clay)} + DEPD^+ \quad (4)$$

The concentration ratio of DEPD to α-naphthanol is also an important factor for the performance of the clay film. Experiments showed that as [DEPD]/[α-naphthanol] approaches 3 : 2, a better contrast between the illuminated regions and the background could be obtained.

This filmed electrode appeared to be reusable since the image could be erased after dipping in dilute (1 mM) sulfuric acid [Fig. 1(b)] and once the electrode was reexposed a clear image could be restored [Fig. 1 (c)]. Long-term tests [Fig. 1 (d)], in addition, showed that although the clay|AcH$^+$ electrode gradually loses its sensitivity (tentatively ascribed to leaching of AcH$^+$), it could be reused more than twenty times. In summary, such very cheap iron-containing clay minerals after proper tailoring, may be useful materials for image-recording.

We thank the National Science Council, Republic of China and Chinese Petroleum Company for financial support (grant number: NSC 88-2113-M-003-016; NSC 88-CPC-M-003-002).

Notes and references

1 G. L. Closs and J. R. Miller, *Science*, 1988, **240**, 440.
2 M. R. Wasielewski, D. G. Johnson, W. A. Svec, K. M. Kersey, D. C. Cragg and D. W. Minsek, in *Photochemical Energy Conversion*, ed., J. R. Norris, Jr. and D. Mieisel, Elsevier, New York, 1989, pp. 1135–1147.
3 D. Gust and T. A. Moore, *Science*, 1989, **244**, 35.
4 M. R. Wasielewski, M. P. Niemczyk, W. A. Svec and E. B. Pewitt, *J. Am. Chem. Soc.*, 1985, **107**, 5562.
5 E. Danielson, C. M. Elliot, J. W. Merkert and T. J. Meyer, *J. Am. Chem. Soc.*, 1987, **109**, 2519.
6 M. A. Fox, *Adv. Photochem.*, 1986, **13**, 237.
7 *Chemical Sensors*, ed., T. E. Edmonds, Chapman & Hall, New York, 1988.
8 U. Schaller, E. Bakker, U. E. Spichiger and E. Pretsch, *Anal. Chem.*, 1994, **66**, 391.
9 S.-C. Shyu and C. M. Wang, *J. Electrochem. Soc.*, 1997, **144**, 3419.
10 S.-C. Shyu and C. M. Wang, *J. Electroanal. Chem.*, 1997, **440**, 27.
11 S.-C. Shyu and C. M. Wang, *J. Electrochem. Soc.*, 1998, **145**, 154.
12 C. F. Cheng and C. M. Wang, *J. Electroanal. Chem.*, 1999, **466**, 82.
13 Y. W. Teng, I.-J. Chang and C. M. Wang, *J. Phys. Chem. B*, 1997, **101**, 10386.
14 C. S. Ouyang and C. M. Wang, *J. Electrochem. Soc.*, 1998, **145**, 2654.
15 R. D. Theys and G. Sosnovsky, *Chem. Rev.*, 1997, **97**, 83.
16 *Braving the Elements*, ed., H. B. Gray, J. D. Simon and W. C. Trogler, University Science Books, Sausalito, 1995, pp. 300–314.

Communication a908503c

ChemComm

Porous gold structures through templating by echinoid skeletal plates

Fiona C. Meldrum[a] and Ram Seshadri[b]

[a] *Department of Chemistry, Queen Mary and Westfield College, London University, Mile End Road, London, UK E1 4NS. E-mail: F.C.Meldrum@qmw.ac.uk*

[b] *Solid State and Structural Chemistry Unit, Indian Institute of Science, Bangalore 560 012 India. E-mail: seshadri@sscu.iisc.ernet.in*

Received (in Oxford, UK) 27th August 1999, Accepted 18th November 1999

Porous gold structures with nearly regular 15 μm channels have been prepared by a novel route in which the calcium carbonate skeletal plates of echinoids (sea urchins) are used as templates.

Biological materials are characterised by unique structures and morphologies that cannot typically be replicated through laboratory synthesis. Nature uses materials not traditionally recognised for their engineering properties, such as calcium carbonate, to produce structures with superior mechanical properties. This is possible owing to control over morphology, composition and spatial organisation. Profiting from existing materials with unusual forms, we describe experiments using a structured calcium carbonate biomineral to template the production of porous inorganic solids (gold in this case) with pore diameters in the order of 15 μm. Few synthetic methods exist to produce materials that are spatially patterned on this length scale.

There is much interest in the preparation of materials with well defined pore sizes. Microporous solids, characterised by pore sizes of the order of 10 Å, include the zeolites. Mesoporous solids exhibit pore sizes in the range 10–1000 Å and represent a relatively new class of materials. A number of methods have been used to synthesise mesoporous materials based on surfactant templating.[1–5] These have been applied to a wide range of inorganic materials, including metals, silicates and metal oxides.[1–5] Reports on the synthesis of porous solids with pores in the micrometer size range are considerably more limited. Lamellar aluminophosphates with surface patterns on the sub-micrometer to millimeter size range have been produced using vesicle templates.[6] Bicontinuous microemulsions have been used to prepare porous shells of crystalline calcium carbonate with pore sizes ranging from 35 to 225 nm,[7] and calcium phosphate materials with microstructures comprising pore diameters of up to several micrometers.[8] The method of emulsion templating[9] is perhaps most general and has been used to produce macroporous titania, silica and zirconia with pore sizes from 50 nm to several microns.

Here we describe the use of the skeletal plates of echinoids (sea urchins) to template porous structures with pore sizes of the order of 15 μm.† The example material chosen here is gold, but the method is quite general. A continuous coating of gold is deposited over the entire surface area of the skeletal plates. Subsequent dissolution of the plate leaves the gold coating in the form of the original structure. Sea urchin plates were selected owing to their unique morphology. The skeletal plates and the spines of echinoids[10] are a low/high magnesium calcite (depending on genetic and geographical control) and each behave as single crystals when examined by diffraction or polarised light. The microstructure, however, is quite remarkable and complex, exhibiting a unique fenestrated structure of interconnected trabeculae and pores that are approximately 15 μm in diameter [Fig. 1(a)]. The porous network and inorganic fractions of the shell occupy approximately equal volumes, and display non-crystallographic curved surfaces. Indeed, the pore diameters and pore size distributions are highly controlled, and some species of urchin are characterised by highly uniform distributions of pores in very regular structures.[11]

A typical SEM image in cross section through a skeletal plate is presented in Fig. 1(a), showing the bicontinuous, sponge-like structure of the mineral with a length scale in the order of 15 μm. The mineral surface is very smooth even when viewed at higher magnification (not shown). Fig. 1(b) shows a similar skeletal plate after gold coating and annealing. The coating of gold particles on the surface of the mineral is clearly seen as a very marked roughening. Dissolution of the calcium carbonate component of a gold-coated echinoid plate produced the gold structures shown in Fig. 2(a) and (b). These images demonstrate that the echinoid plate acts as a template to produce porous gold with a structure mirroring that of the original plate. The gold particles produce a coating on the calcite, rather than filling the

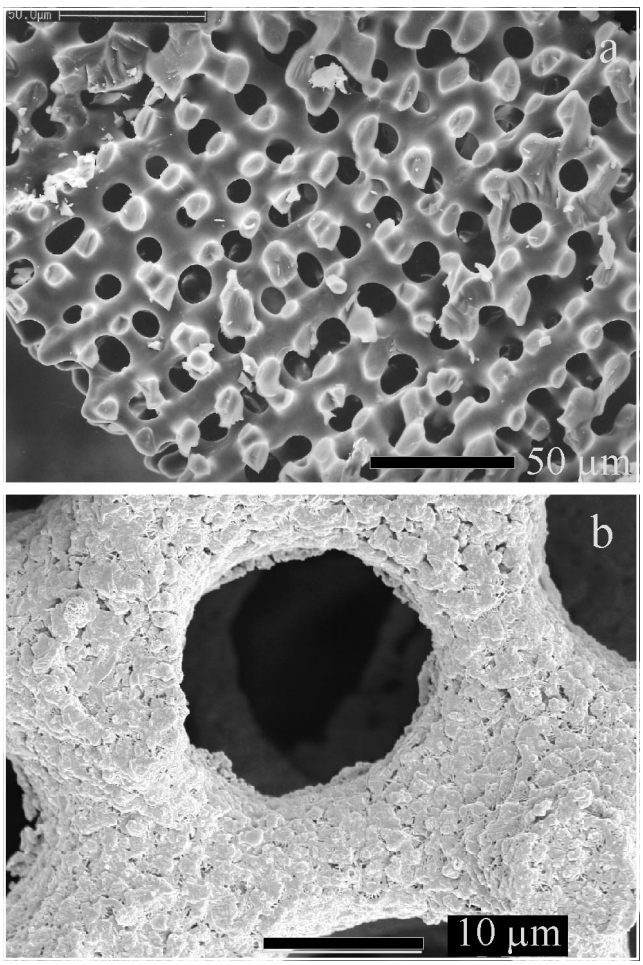

Fig. 1 Scanning electron micrographs of (a) a cleaned echinoid skeletal shell and (b) shell coated with gold and annealed. The bars correspond to (a) 50 μm and (b) 10 μm.

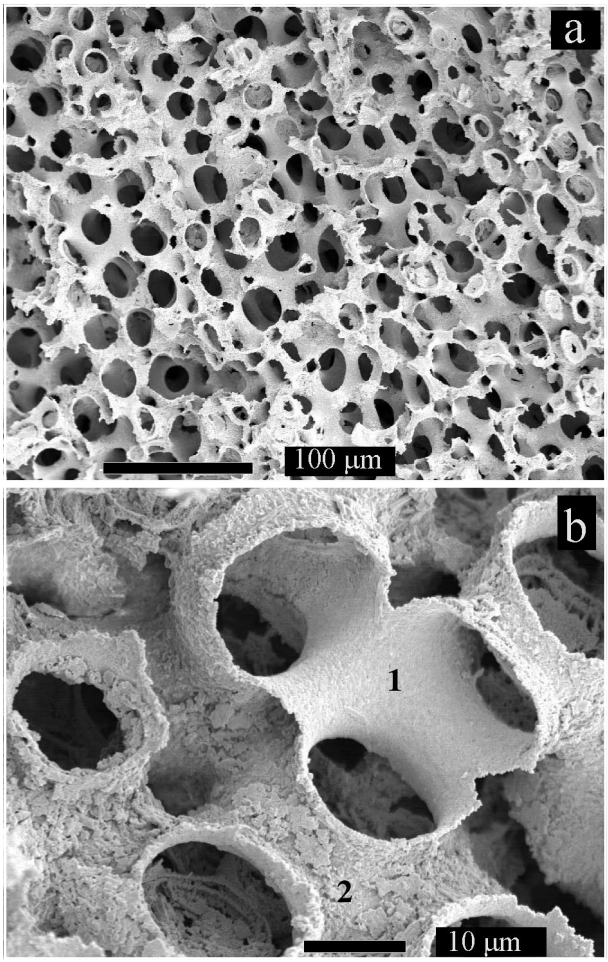

Fig. 2 SE micrographs of gold-coated echinoid skeletal shell after *in situ* dissolution of the calcium carbonate shell. 1 and 2 in (b) mark the smooth inner and rough outer surfaces of the templated gold structure. The bars correspond to (a) 100 μm and (b) 10 μm.

entire pore structure, so a double-sided surface is produced. This is clearly shown in Fig. 2(b), where the gold surface originally in contact with the calcite is smooth (area 1) while the surface directed into the original pore is rough (area 2).

Dissolution of the gold-coated plates in acid solution produced a solid of the same dimensions as the original plate. The solid produced was rather fragile and thus difficult to transfer to sample stubs without some damage to the structure. The best images of the porous gold were thus obtained from samples dissolved *in situ* on the sample stub. Further work will be directed to producing thicker metal coatings and even filling the entire pore structure to produce a replica of the original bicontinuous structure. This should produce a stronger material.

It is demonstrated that the skeletal plates of echinoids can be used to template the synthesis of porous materials (gold being chosen as an example) with unique structures. The technique is very general and it is envisaged that it can be applied to a wide range of inorganic solids. Indeed, preliminary experiments to produce macroporous TiO_2 structures *via* a sol–gel method suggest that the method is feasible, depending upon refinement of the kinetics of the reaction and control of shrinkage during annealing. Further experiments to deposit a wider range of solids and to control the thickness of the templated material are underway.

The class of new materials presented here may find application as light-weight structural ceramics. Ordered macroporous materials with pore dimensions comparable to optical wavelengths could display unique optical properties. Applications as catalyst supports are also possible, particularly in situations where the traditional materials with smaller pore sizes result in unacceptable pressure drops in the catalysis process.

R. S. thanks the RSC for a Journals Grant. We thank the Department of Materials, QMW College, for allowing access to electron microscope facilities.

Notes and references

† Specimens of the echinoid *Ircinia oros* were collected at Depot Beach, NSW, Australia, and were cleaned of organic material with hypochlorite solution using standard procedures.[12] Experiments were carried out with clean skeletal plates that had been abraded to a thickness of *ca.* 1 mm, sonicated in water to remove attached particles and subsequently dried. One end of a dry plate was then placed in gold paint (Johnson Matthey, Brilliant Gold, PM 002), and the paint was absorbed into the plate *via* capillary action, as evidenced from a colour change in the plate from white to dark brown–purple. The plate was then removed from the paint and was heated using a hot air gun to burn off the protective organic matter in the paint. The plate was allowed to cool slightly before repetition of the dipping/heating cycle. The cycle was repeated ten times and was then annealed in a furnace at 400 °C for 36 h.

The samples were examined using a JEOL 6300F scanning electron microscope (SEM), fitted with a field emission source and operating at 5 kV. Samples were prepared for (SEM) by mounting on aluminium stubs using adhesive carbon tape, either with the original outer surface of the plate exposed or in cross-section after fracture, and all were sputter-coated with a thin layer of gold prior to viewing to enhance conductivity. Pieces of echinoid plates were examined after cleaning [Fig. 1(a)] and subsequent to annealing of the absorbed gold [Fig. 1(b)]. Samples were also studied after dissolution of the calcium carbonate with acid. The annealed gold plates were immersed in solutions of 2% acetic acid or 2 M HCl until all of the original calcite plate has been dissolved, and the remaining gold material was mounted on SEM stubs. Plates were also mounted on SEM stubs and were dissolved *in stiu* with 2 M HCl [Fig. 2(a) and (b)].

1 Q. Huo, D. I. Margolese, U. Ciesla, P. Feng, T. E. Gier, P. Sieger, R. Leon, P. M. Petroff, F. Schüth and G. D. Stucky, *Nature*, 1994, **368**, 317.
2 K. M. McGrath, D. M. Dabbs, N. Yao, I. A. Aksay and S. M. Gruner, *Science*, 1997, **277**, 552.
3 N. K. Raman, M. T. Anderson and C. J. Brinker, *Chem. Mater.*, 1996, **8**, 1682.
4 Q. Huo, D. I. Margolese and G. D. Stucky, *Chem. Mater.*, 1996, **8**, 1147.
5 G. S. Attard, M. Edgar and C. G. Göltner, *Acta Mater.*, 1998, **46**, 751.
6 S. Oliver, A. Kuperman, N. Coombs, A. Lough and G. A. Ozin, *Nature*, 1995, **378**, 47.
7 D. Walsh and S. Mann, *Nature*, 1995, **377**, 320.
8 D. Walsh, J. D. Hopwood and S. Mann, *Science*, 1994, **264**, 1576.
9 A. Imhof and D. J. Pine, *Nature*, 1997, **389**, 948.
10 P. Dubois and C.-P. Chen, in *Echinoderm Studies*, ed. M. Jangoux and J. M. Lawrence, A. A. Balkema, Rotterdam, 1989, vol. 3, p. 109.
11 G. Donnay and D. L. Pawson, *Science*, 1969, **166**, 1147.
12 D. M. Swift, S. Sikes and A. P. Wheeler, *J. Exp. Zool.*, 1986, **240**, 65.

Communication a907074e

New chiral heterogeneous catalysts based on mesoporous silica: asymmetric diethylzinc addition to benzaldehyde

Sung Jin Bae,[a] Sang-Wook Kim,[b] Taeghwan Hyeon*[b] and B. Moon Kim*[a]

[a] *Department of Chemistry and Center for Molecular Catalysis, Seoul National University, Seoul 151-742, Korea. E-mail: kimbm@plaza.snu.ac.kr*

[b] *School of Chemical Engineering, Seoul National University, Seoul 151-742, Korea. E-mail: thyeon@plaza.snu.ac.kr*

Received (in Cambridge, UK) 11th November 1999, Accepted 18th November 1999

New heterogeneous catalyst systems have been developed employing a proline-derived ligand immobilized on mesoporous silicas; asymmetric diethylzinc addition to benzaldehyde was carried out using the catalyst systems; the reaction enantioselectivity was found to be largely dependent upon the pore size of the mesoporous silicas, capping of free silanol moieties with trimethylsilyl group and employment of Bu^{n}Li.

Optically active secondary alcohols are important intermediates for the construction of optically active natural products and biologically active compounds. Among various methods for the construction of optically active secondary alcohols, addition of diorganozinc reagents to aldehydes in the presence of a catalytic amount of a chiral β-aminoalcohol has been extensively studied.[1] Extremely high enantioselectivity has been reported in the reactions employing a variety of aminoalcohol ligands. However, in order for these reactions to be successfully exploited in large-scale applications, the chiral ligand has to be readily available or easily recycled. Toward this goal, immobilization of chiral ligands onto heterogeneous supports has been investigated and a number of support materials such as inorganic solids and polymers have been developed.[2] Recently, various mesoporous silicas with pore sizes ranging from 2 to 10 nm have been synthesized using self-assemblies of surfactants and block copolymers as templates.[3] These mesoporous silicas have been successfully employed as supports for various chiral catalysts.[4] Herein, we report on new heterogeneous catalyst systems that utilize proline derivatives anchored on the mesoporous silicas such as MCM-41 and SBA-15.

Although the reactions of diethylzinc with benzaldehyde using ephedrine immobilized onto amorphous silica gel[5] and mesoporous silica[6] have been investigated, the degree of enantioselection under these heterogeneous catalytic conditions has been less than satisfactory. In connection with the low enantioselectivty, several issues need to be addressed: (1) employment of a more selective ligand, (2) suppressing undesired catalytic activity on the silica surface, (3) changing silica pore sizes, and (4) addition of extra metal reagent. In terms of a more selective ligand system, a prolinol-based ligand developed by Soai *et al.*[7] was selected in our study. Since the free SiOH moieties of the silica surface could catalyze the reaction,[6] thus lowering the reaction enantioselectivity, mesoporous silicas containing the chiral ligand having its surface capped with trimethylsilyl groups[8] have been prepared. To investigate the effect of the pore size on the enantioselectivity, we have used two different mesoporous silicas, MCM-41 and SBA-15, which have similar hexagonal pore arrays but with different pore dimensions. We have also investigated reaction enantioselectivity when the catalyst system was treated with Bu^{n}Li before addition of the aldehyde.

The synthetic procedure including preparation of the ligand, immobilization onto silicas and capping with trimethylsilyl moieties is shown in Scheme 1. The new chiral aminoalcohol **3** was synthesized as follows. The amine group of 4-hydroxyproline (Aldrich Chemicals™) was protected using ethyl chloroformate and the acid was converted to a methyl ester to give the carbamate ester **2**. Treatment of compound **2** using phenylmagnesium chloride furnished a tertiary alcohol, and the carbamate group was converted to the corresponding methylamine through treatment with lithium aluminium hydride (LAH) yielding compound **3** in an overall yield of 72% from **1**. MCM-41 and SBA-15 were synthesized according to the previously reported procedures.[3] Chloropropyl linkers were grafted on the walls of mesoporous silicas by treating with $(CH_3CH_2O)_3Si–CH_2CH_2CH_2Cl$ in refluxing toluene. Reaction of the resulting chloropropyl-derivatized mesoporous silicas (**5b** and **5c**) with the chiral pyrrolidinemethanol **3** yielded silicas **6b** and **6c**, respectively. In order to cap remaining free SiOH groups on the walls of mesoporous silicas, **5b** and **5c** were treated in refluxing hexamethyldisiloxane (HMDS) for 12 h. To the best of our knowledge, this is the first anchoring of SBA-15 silica with a chiral ligand and the X-ray diffraction (XRD) patterns of SBA-15 derivatized samples have been taken during various stages of the preparation. The XRD results clearly demonstrated that the mesoporous structure of SBA-15 was preserved during the preparation of the catalyst. Table 1 lists the surface areas, the mean pore dimensions, and the amounts of grafted organic groups for the mesoporous silica based catalysts. The surface area decreased substantially during the chloropropyl-grafting step, especially for SBA-15. Nonetheless, the pore dimensions of the SBA-15 based systems did not change significantly during these synthetic steps. For comparison, the chiral ligand **3** was attached to amorphous silica to provide both non-TMS capped catalyst (**6a**) and TMS-capped catalyst (**8a**) using the same reaction conditions applied to the mesoporous silicas.

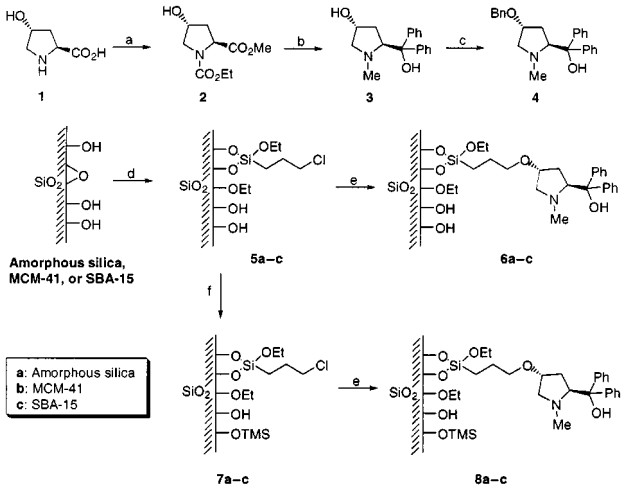

Scheme 1 The synthetic routes used in the preparation of various catalysts. *Reagents and conditions*: a: (i) ethyl chloroformate, $NaHCO_3$, H_2O, room temp., 16 h; (ii) $SOCl_2$, MeOH, room temp., 12 h; b: (i) PhMgCl, THF, 0 °C, 5 h; (ii) $LiAlH_4$, THF, reflux, 3 h; c: NaH, BnBr, THF, room temp., 16 h; d: Chloropropyltriethoxysilane, toluene, reflux, 12 h; e: **3**, xylene, reflux, 12 h; f: HMDS, reflux, 12 h

Table 1 Characterization of mesoporous silicas during various stages of catalyst preparation[a]

MCM-41 based catalysts				SBA-15 based catalysts			
Catalyst	Surface area/ $m^2\ g^{-1}$	Mean pore diameter/nm	Grafted amount/ mmol g^{-1}	Catalyst	Surface area/ $m^2\ g^{-1}$	Mean pore diameter/nm	Grafted amount/ mmol g^{-1}
Silica	919	3.1		Silica	800	8.9	
5b	750	3.0	0.55	**5c**	472	8.5	1.38
6b	655	2.4	0.40	**6c**	320	8.4	0.36
8b	648	2.3	0.59	**8c**	312	8.4	0.37

[a] N_2 adsorption and desorption isotherms were collected at STP on a Micrometrics ASAP2010 gas adsorption analyzer after the materials were degassed at 250 °C at 30 μTorr for 5 h. The surface areas were calculated by the BET method and the pore size distributions were calculated from the adsorption branch of the nitrogen isotherm by the BJH method.

We have investigated asymmetric addition of diethylzinc to benzaldehyde using these silica-based catalysts and the results are outlined in Table 2. For each silica catalyst, two different sets of reactions were run with 6 mol% of catalyst and either 3 equiv. of diethylzinc to benzaldehyde (method A) or 7.2 mol% of Bu^{n}Li followed by 3 equiv. of diethylzinc (method B). To evaluate our catalyst systems against the parent homogeneous catalyst, compound **4** was prepared from **3** through etherification of C(4)–OH with benzyl bromide. Reactions employing the homogeneous catalyst **4** provided products with 90 and 93% ee, respectively, *via* methods A and B (entries 1 and 2, Table 2). However, when the chiral catalysts anchored on amorphous silica were tested using method A, **6a** and **8a** gave only 16 and 37% ee, respectively (Table 2 entries 4 and 5). When the reactions were carried out using method B, slight improvements in the enantioselectivities were observed (entries 6 and 7). A noticeably higher enantioselectivity was observed in the reactions employing MCM-41-based catalyst (entries 8–11) and the best results were obtained with the catalysts based upon SBA-15 (entries 12–15). It is of particular note that catalysts based upon SBA-15 consistently gave higher enantioselectivity than that of MCM-41. In both MCM-41 and SBA-15 systems, TMS-capping as well as the employment of Bu^{n}Li improved the enantioselectivity significantly. Product of the highest ee (75%) was obtained for TMS-capped SBA-15 based catalyst utilized after treatment with Bu^{n}Li (entry 15). To test the catalytic activity of the silica without a chiral ligand, TMS-capped SBA-15 (**7c**) was used under otherwise the same reaction conditions, and a 15% yield of the product was observed. It appears that, even with TMS-capping, there remains some residual activity of the silica, resulting in a reduction of the enantioselectivity.

Table 2 Asymmetric diethylzinc addition to benzaldehyde using various catalysts

In summary, new mesoporous silica-based catalysts incorporating a chiral pyrrolidinemethanol derivative have been prepared and the asymmetric diethylzinc addition to benzaldehyde examined. Among various catalytic systems, the best result (75% ee) was obtained with the TMS-capped SBA-15 based catalyst treated with Bu^{n}Li.

T. H. would like to thank KISTEP (Critical Technology 21) and Korea Institute of Science and Technology (KIST) for the financial support and BASF-Korea for supplying P123 triblock copolymer. B. M. K. acknowledges generous financial support from the Korea Science and Engineering Foundation (97-0501-0201-3) and the KOSEF through the Center for Molecular Catalysis at Seoul National University.

Notes and references

1 R. Noyori and M. Kitamura, *Angew. Chem., Int. Ed. Engl.*, 1991, **30**, 49; K. Soai and S. Niwa, *Chem. Rev.*, 1992, **92**, 833.
2 *Heterogeneous Catalysis and Fine Chemicals IV*, ed. H. Blaser, A. Baiker and R. Prins, Elsevier, Amsterdam, 1997; J. H. Clark and D. J. Macquarrie, *Chem. Commun.*, 1998, 853; *Handbook of Heterogeneous Catalysis*, ed. G. Ertl, H. Knözinger and J. Weitkamp, Wiley-VCH, Weinheim, 1997, vol. 1.
3 C. T. Kresge, M. E. Leonowicz, W. J. Roth, J. C. Vartuli and J. S. Beck, *Nature*, 1992, **359**, 710; D. Zhao, J. Feng, Q. Huo, N. Melosh, G. H. Fredrickson, B. F. Chmelka and G. D. Stucky, *Science*, 1998, **279**, 548; J. Y. Ying, C. P. Mehnert and M. S. Wong, *Angew. Chem., Int. Ed.*, 1999, **38**, 57.
4 X. G. Zhou, X. Q. Yu, J. S. Huang, S. G. Li, L. S. Li and C. M. Che, *Chem. Commun.*., 1999, 1789; B. F. G. Johnson, S. A. Raynor, D. S. Shephard, T. Mashmeyer, J. M. Thomas, G. Sankar, S. Bromley, R. Oldroyd, L. Gladden and M. D. Mantle, *Chem. Commun.*, 1999, 1167; G.-J. Kim and J.-H. Shin, *Tetrahedron Lett.*, 1999, **40**, 6827.
5 K. Soai, M. Watanabe and A. Yamamoto, *J. Org. Chem.*, 1990, **55**, 4832.
6 M. Laspéras, N. Bellocq, D. Brunel and P. Moreau, *Tetrahedron: Asymmetry*, 1998, **9**, 3053.
7 K. Soai, A. Ookawa, T. Kaba and K. Ogawa, *J. Am. Chem. Soc.*, 1987, **109**, 7111.
8 T. Tatsumi, K. A. Koyano, Y. Tanaka and S. Nakata, *J. Phys. Chem. B.*, 1997, **101**, 9436.

Communication a908967e

Table 2 Asymmetric diethylzinc addition to benzaldehyde using various catalysts

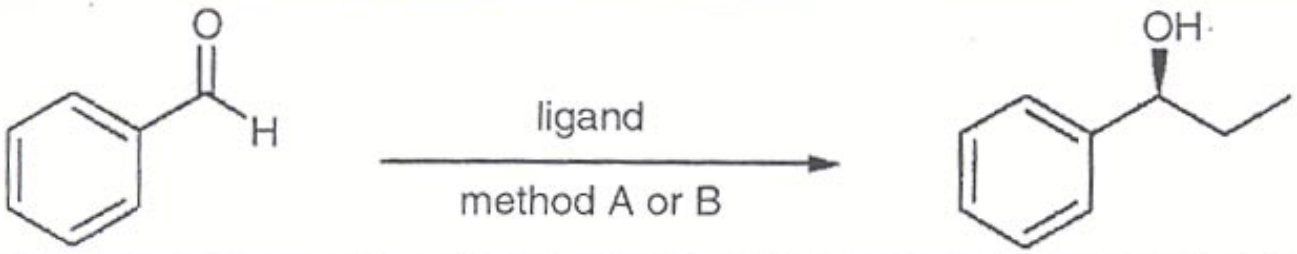

Entry	Catalyst	Method[a]	Ee(%)[b]	Yield(%)[c]
1	**4**	A	90	97
2	**4**	B	93	87
3	**7c**	B	0	15
4	**6a**	A	16	89
5	**8a**	A	37	78
6	**6a**	B	41	69
7	**8a**	B	43	74
8	**6b**	A	24	79
9	**8b**	A	36	77
10	**6b**	B	26	84
11	**8b**	B	64	96
12	**6c**	A	29	95
13	**8c**	A	45	96
14	**6c**	B	52	97
15	**8c**	B	75	98

[a] All reactions were carried out with 6 mol% catalyst at 0 °C for 4 h (entries 1 and 2) or 48 h (entries 3–15). Method A: Et_2Zn (3 equiv. to benzaldehyde), Method B: Bu^nLi (1.2 equiv. to catalyst) –Et_2Zn (3 equiv. to benzaldehyde). [b] Enantioselectivity was determined through chiral HPLC analysis using a Chiralcel OD column. [c] Yields were determined by GC analysis.

ChemComm

Easy and efficient processes for catalyst recycling and product recovery in organic biphase systems tested in the hydrogenation of hex-1-ene

Ricardo G. da Rosa,[a] Laura Martinelli,[a] Luís H. M. da Silva[b] and Watson Loh*[b]

[a] *Instituto de Química, Universidade Federal do Rio Grande do Sul, Caixa Postal 15003, Porto Alegre, RS, 91501-970, Brazil*

[b] *Instituto de Química, Universidade Estadual de Campinas, Caixa Postal 6154, 13083-970, Campinas, SP, Brazil. E-mail: wloh@iqm.unicamp.br*

Received (in Cambridge, UK) 17th November 1999, Accepted 26th November 1999

Two organic liquid biphase systems containg poly(ethylene oxide), heptane and either CH_2Cl_2 or methanol have been tested in the catalytic hydrogenation of hex-1-ene using, respectively, Wilkinson's catalyst and a cationic rhodium complex, both leading to high yields and selectivity, with the latter showing a better performance and enabling easy and efficient product separation and catalyst recycling.

Liquid biphase systems have been the focus of great attention in catalysis recently as media for alternative less polluting and more efficient catalytic processes, providing an easier separation between products and catalyst. Among the strategies studied so far, examples include the use of aqueous/organic biphase systems with water soluble catalysts,[1] fluorous biphase systems, where the use of fluorinated ligands leads to catalyst solubility in the perfluorinated phase,[2] functionalised thermosensitive polymers as supports for traditional organometallic homogeneous catalysts [3] and the application of molten salts as ionic liquids.[4] All these procedures present some advantages and disadvantages. Among the latter, is the need for specially prepared catalysts, occurrence of catalyst leaching, or the somewhat difficult handling of the biphase system.

We have recently described[5] an organic biphase system containing poly(ethylene oxide) (PEO), CH_2Cl_2 and heptane which shows a strong segregation between the polar polymer and the hydrocarbon solvent, the polymer being concentrated in the bottom phase. Further studies[6] revealed that this phenomenon is also observed in mixtures containing other polar solvents such as methanol, chloroform and acetonitrile. Because of its characteristics, this ternary mixture may be interchanged between homogeneous and biphasic regions by either composition or temperature changes. These features suggest a variety of applications in different separation processes where the absence of water is desirable including catalysis.

This communication describes studies on the application of these biphase systems in the hydrogenation of hex-1-ene catalysed by Wilkinson's complex, $RhCl(PPh_3)_3$, and by the cationic complex $[Rh(cod)(dppe)]PF_6$, cod = cycloocta-1,5-diene, dppe = 1,2-bis(diphenylphosphine)ethane].† Hydrogenation was chosen as a test reaction because of its technological importance and hex-1-ene was used as substrate owing to its easy product characterisation. The rhodium complexes used were selected considering their well established hydrogenation catalytic behaviour and poor solubility in apolar solvents. Therefore, ideally, this reaction may be conducted in a homogenous system and, after induced phase separation, the catalyst may be selectively separated from the products, allowing for their removal and recycling. In a similar procedure Bianchini *et al.*[7] performed two catalytic reactions in a mixture of methanol and hydrocarbons that was homogeneous at high temperatures and formed a biphase system at room temperature, using a rhodium complex with a chosen ligand that ensured the complex solubility only in the alcohol-rich phase.

The phase diagram for the ternary system PEO 3350–CH_2Cl_2–heptane has been previously reported[5] and that for the ternary system PEO 3350–MeOH–heptane (not shown) is similar, though with a larger biphase area. Additional experiments have shown that in both systems there are only small changes when the polymer molecular weight is varied from 200 to 10 000, provided the polymer content is expressed on a monomer basis. There are, however, some important changes of the phase boundaries with temperature, with the biphase region increasing as the temperature decreases.[6]

Of relevance to this investigation, there are some compositions at which the system may be moved from a biphasic to a homogeneous region by temperature increase, for instance, with 19.5% of PEO 3350, 51.6% of CH_2Cl_2 and 28.9% heptane [compositions expressed on the basis of mol% (for PEO this refers to mol of monomer units)], this transition occurs at 9 °C. However, a significant rhodium loss was spectrophotometrically detected to the upper phase (*ca.* 15%) for this and other compositions which presented temperature-driven phase separation, causing poor recycling properties.

For this reason, we developed another procedure to improve the selectivity of catalyst partitioning. As temperature decreases, these polymer solutions show phase separation of UCST (upper critical solution temperature) type. For PEO solutions in CH_2Cl_2, these phase separation temperatures range from −80 to −40 °C, for PEO 3350 concentrations between 1 and 60% (w/w). As the polymer phase separates, we have verified that most of the catalyst is also removed from the solution phase. Therefore, by cooling the reaction system with liquid N_2, it is possible to selectively separate the catalyst and the reaction products. The striking feature is that, probably owing to large density differences, this biphase system is kinetically stable for a long time (even hours) even at temperatures close to room temperature, allowing easy separation of the liquid phases. Although this system is not in thermodynamic equilibrium, this procedure has provided an easy way of catalyst recycling.

This procedure was employed using Wilkinson's catalyst in the hydrogenation of hex-1-ene,‡ allowing product recovery with no apparent catalyst leaching to the apolar phase (verified spectrophotometrically) and efficient and selective substrate conversion. However, a marked decrease in the catalytic activity was observed after the third recycle. This could be related to the recycling process, which may induce a continuous loss of the triphenylphosphine free ligand in equilibrium with the rhodium complex, as revealed by ^{31}P NMR spectra, generating inactive species.

In order to overcome this problem, a cationic rhodium complex containing a chelating phosphine, $[Rh(cod)(dppe)]PF_6$, was tested as a catalytic precursor. This complex showed poor catalytic activity using the ternary mixture containing CH_2Cl_2. On the other hand, as suggested by other catalytic hydrogenation studies,[8] its performance using methanol as the polar component of the ternary mixture was clearly enhanced. With this second ternary system, the procedure of inducing phase separation by cooling was not effective since the volume of the upper phase was too small thus impeding the

product separation. This reaction was then conducted in a homogenous system containing 14 mL of MeOH, 3.6 g of PEO, 0.0335 mmol of Rh complex and 8.01 mmol of hex-1-ene, at room temperature and under H_2 flow. This system requires an activation period of *ca.* 2.5 h to reach its maximum activity. The reaction products were analysed by GC§ 30 min after this period and during eight cycles, producing a 54 ± 5% conversion associated with 90 ± 10% selectivity to hydrogenation. Under these conditions, the estimated turnover frequency was 4 min^{-1}. Maintaining the reaction for 1 h, the substrate was completely and selectively converted to *n*-hexane, suggesting that the isomerisation reaction is faster than hydrogenation and that the isomers produced are reactive towards the catalyst being slowly, but continuously, converted to *n*-hexane. The product was then extracted by heptane addition, with three extractions with 4 mL heptane aliquots yielding 75% of product recovery. In the biphase system then formed, the extent of rhodium leaching was determined by ICP-atomic emission analyses of the upper phase,¶ revealing losses of only 0.083% of metal. Such a low rhodium loss qualifies this procedure as an efficient catalyst recycling.

This reaction is efficient even when performed under biphase conditions as, for instance, using a system composed of MeOH (14 mL), PEO (3.6 g) and *n*-heptane (14 mL), the same rhodium and olefin content as above, with 10 bar of H_2. Under these conditions five runs were made with complete conversion of the substrate to the hydrogenation product and no loss of catalytic activity or selectivity was noted. A kinetic study of this system allowed the determination of an activation time of 50 min. After this time, GC analysis revealed a complete conversion of hex-1-ene to *n*-hexane in 15 min, allowing determination of a turnover frequency of *ca.* 16 min^{-1}. This system can be recycled, at least eight times, with no changes in activity or selectivity.

In conclusion, this set of results, comprising experiments performed with two catalysts under different conditions, have proved the great potential for use of these organic biphase systems as reaction media that enable an easy product separation and efficient catalyst recycling. Furthermore, this procedure allows the use of common catalysts in homogeneous catalysis, requiring, therefore, no special reagents. These biphase systems also display advantages over binary solvent mixtures in that, owing to the presence of the polar polymer, the phase compositions are more different, increasing the partitioning selectivity, without the need of special ligands for the catalyst. The only requirement for their application is the selective partitioning of catalyst and of the desired product, however, this procedure is flexible enough to allow modifications (changing solvents, composition or temperature) that may suit a wide range of catalytic reactions and products.

R. G. da Rosa and L. Martinelli thank FAPERGS for financial support, L. H. M. da S. thanks CAPES-PICDT for a doctoral scholarship, and Universidade Federal de Viçosa for a leave of absence. The authors are grateful to R. F. de Souza and the Laboratório de Reatividade e Catálise - UFRGS for access to their facilities, and to M. Spitzer for providing phase equilibria data for some of the systems used.

Notes and references

† Wilkinson's catalyst was prepared according to the procedure described: J. A. Osborn and G. Wilkinson, *Inorg. Synth.*, 1967, **10**, 68 while $[Rh(cod)(dppe)]PF_6$ was prepared and characterised following R. R. Schrock and J. A. Osborn, *J. Am. Chem. Soc.*, 1971, **93**, 2397.

‡ In all the catalytic tests, the reactor, a 100 mL stainless steel autoclave, was previously purged by vacuum–argon cycles, then pressurised with hydrogen (99.999%). CH_2Cl_2, methanol and *n*-heptane were distilled prior to use, under argon from P_2O_5, activated molecular sieves (3 Å) and Na/benzophenone respectively. Hex-1-ene (Alpha, 99.9%) was stored over activated molecular sieves (3 Å) under argon. PEO 3350 (Sigma), was dried over P_2O_5. All reactions were conducted at room temperature under magnetic stirring.

§ The chromatographic analyses were performed using a Varian Star 3400 CX Chromatograph, equipped with a 30 m × 0.25 mm LM-1 capillary column, at 50 °C and 1 mL min^{-1} (10 psi) of H_2 as carrier gas.

¶ Rhodium analyses were performed by ICP-atomic emission spectrometry with a segmented-array charge coupled device detector (Optima 3000, Perkin Elmer, Newark, CT). Operating conditions: auxiliary argon flow 0.5 L min^{-1}, plasma argon flow 15 L min^{-1}, nebulizer argon flow 0.8 L min^{-1}, variable incident power (0.75–1.5 kW), cross-flow nebulizer and axial observation. Duplicate aliquots of the upper phase were digested with *aqua regia* for 12 h and then adjusted to produce concentrations close to 0.1 ppm. The final rhodium loss was determined as (0.083 ± 0.001)%.

1 O. Wachsen, K. Himmler and B. Cornils, *Catal. Today*, 1998, **42**, 373.
2 I. T. Horvath, *Acc. Chem. Res.*, 1998, **31**, 641.
3 D. E. Bergbreiter, *Catal. Today*, 1998, **42**, 389.
4 P. A. Z. Suarez, J. E. L. Dullius, S. Einloft, R. F. de Souza and J. Dupont, *Inorg. Chim. Acta*, 1997, **255**, 207; A. L. Monteiro, F. K. Zinn, R. F. de Souza and J. Dupont, *Tetrahedron: Asymmetry*, 1997, **8**, 177.
5 L. H. M. da Silva and W. Loh, *Chem. Commun.*, 1998, 787.
6 M. Spitzer, L. H. M. da Silva and W. Loh, unpublished work.
7 C. Bianchini, P. Frediani and V. Sernau, *Organometallics*, 1995, **14**, 5458.
8 B. D. Vineyard, W. S. Knowles, M. J. Sabacky, G. L. Bachman and D. J. Weinkauff, *J. Am. Chem. Soc.*, 1977, **99**, 5946.

Communication a909101g

A polymeric, layered bimetallic Mn(II)Fe(III) imidazolate network; crystal structure and magnetic properties

François Lambert,*[a] Jean-Philippe Renault,[a] Clotilde Policar,[a] Irène Morgenstern-Badarau[a] and Michèle Cesario[b]

[a] *Laboratoire de Chimie Bioorganique et Bioinorganique, Institut de Chimie Moléculaire d'Orsay, Université Paris-Sud, F-91405 Orsay, France. E-mail: flambert @icmo.u-psud.fr*
[b] *Institut de Chimie des Substances Naturelles, CNRS, F-91198 Gif-s/-Yvette, France.*

Received (in Oxford, UK) 27th August 1999, Accepted 22nd November 1999

The use of a C_3 complex bearing three imidazolate groups as a 'building block' allowed us to synthesize an infinite corrugated two-dimensional (2D) low-spin Fe(III)–high-spin Mn(II) polymer exhibiting weak ferromagnetic intralayer interaction through imidazolate bridge.

Imidazolate is a highly studied bridge in dimetallic compounds,[1a] as models of (Cu–Zn)SOD[1b,c] and cytochrome c oxidase.[1d] Imidazolate has been previously used in building two- or three-dimensional homo or poly-metallic polymers[2a,b] and is known to induce moderate magnetic coupling.[3]

In order to construct bidimensional structures, we used a pseudo-octahedral iron complex from a N-tripodal ligand (LH_3 = tris{[2-(2-imidazol-2-yl)methyl]iminoethyl}amine) bearing an imidazolate group at the end of each chain as a building block. A dimer based on an analogous iron complex with imidazole substituted in the 4-position has been previously prepared.[2c] We chose a 2-substituted imidazole group to design a more planar M1–imidazolate-M0–imidazolate–M1 geometry.† The iron monomer used is a stable neutral triimidazolate Fe(III) low-spin complex.[4]

Here, we report the X-ray structure of $[Mn(hfac)_2]_3[Fe(L)]_2$ (hfac = 1,1,1,5,5,5-hexafluoroacetylacetonate), an infinite 2D polymer and a preliminary magnetic study of this compound.

Small dark-blue crystals suitable for X-ray diffraction‡ were obtained readily by slow evaporation of a mixture of methanolic solutions of the iron and manganese complexes [Fe(L)] and $[Mn(hfac)_2]$.§ X-Ray crystallography shows an infinite honeycomb-like layered structure in the product. Each Fe(III)(L) entity is linked by imidazolate bridges with three Mn(II), whereas each $Mn(hfac)_2$ is bound in *cis* position to two Fe(III) complexes. The

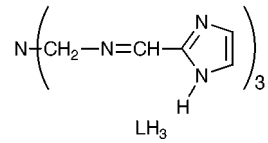

iron atoms are alternately capped above and below by the tripodal ligand L [Fig. 1(a)]. Within each layer the iron complexes display the same helicity, however, the crystal is non-chiral as revealed by the space group. The iron atoms of a given layer are located at the vertices of a chair-like structure (see Fig. 2) leading to a corrugated 2D-network similar to the Cr–Ni cyanide-bridged compound described by Ferlay *et al.*[5a] A remarkable feature is the *cis* substitution of imidazolate bridges around the manganese. This probably favours overall compactness and therefore the formation of a very stable hexagonal structure.[5a,b] Also, the small imidazolate–Mn–imidazolate angles) compensate for the large Mn–imidazolate–Fe–imidazolate–Mn distance.

The magnetic properties of $[Mn(hfac)_2]_3[Fe(L)]_2$ (Fig. 3) were recorded using a SQUID magnetometer with an applied field H = 1 kOe in the temperature range 50–300 K and with an

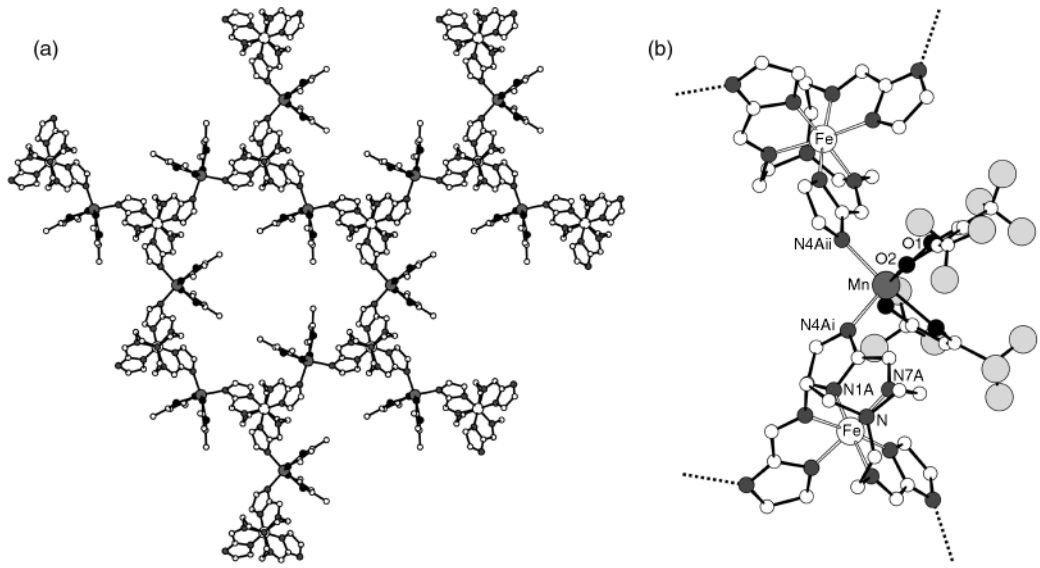

Fig. 1 (a) View of a sheet down the *c* axis. H atoms and F atoms have been omitted for clarity. Shortest Fe···Mn, Fe···Fe and Mn···Mn separations are 5.889(3), 11.26(1) and 9.62(1) Å, respectively. The Mn–Fe–Mn angle is 109.5°; (b) Molecular structure of two iron units bonded to one manganese unit. H atoms have been omitted for clarity. Each F atom has two partially occupied positions with those shown being in the major sites. Selected bond lengths (Å): Fe–N 3.130(10), Fe–N(1A) 1.924(5), Fe–N(7A) 1.983(5), Mn–N(4A) 2.176(5), Mn–O(1) 2.209(6), Mn–O(2) 2.164(5). Symmetry operations: i = x, y, z; ii = $x - y + 1/3, -y + 2/3, -z + 1/6$).

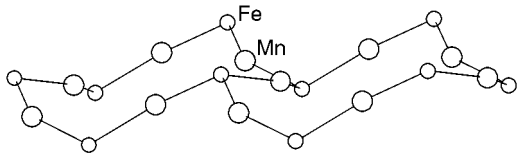

Fig. 2 View of the iron–manganese network showing the corrugated structure of a layer. Only two adjacent chair-like arrangements are represented.

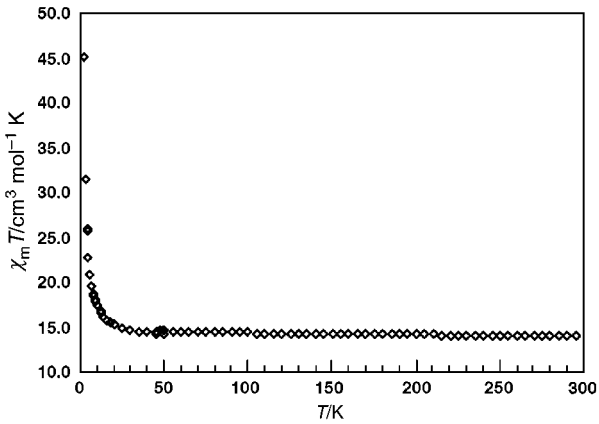

Fig. 3 Experimental temperature dependence of $\chi_M T$ (χ_M susceptibility). From 300 to 50 K, the magnetization was recorded with an applied field of 10 kOe, and from 50 to 2 K with an applied field of 100 Oe. The diamagnetic contribution of the ligands has been subtracted as usual.

applied field H = 100 Oe in the temperature range 2–50 K to avoid saturation.¶ At 300 K $\chi_M T$ = 14.1 cm^3 K mol^{-1}, in good agreement with the expected value for two non-coupled low-spin iron(III) (g = 2.28) and three high-spin manganese(II) (g = 2) ions.‖ Upon cooling, $\chi_M T$ increases and reaches a value of 45 cm^3 K mol^{-1} at 2 K. This behavior indicates the occurrence of a short range ferromagnetic exchange coupling between low-spin Fe(III) and high-spin Mn(II) through the imidazolato bridge. The variation of magnetization as a function of field has also been measured at 2 K. At saturation, expected values would be 17 μ_B (S = 17/2) and 13 μ_B (S = 13/2) for ferromagnetic and antiferromagnetic coupling, respectively (assuming an average g-value of 2). The observed magnetization reaches a value of 16.27 μ_B per Fe_2Mn_3 unit at 5.5 kOe which clearly indicates a ferromagnetic coupling. The overall shape of the M = f(H) curve and the low value (45 cm^3 K mol^{-1}) observed at 2 K for $\chi_M T$ shows only weak magnetic correlation within a layer,** restricted approximately to one Fe_2Mn_3 unit. Moreover, no interaction between the layers is observed down to 2 K. The compound can be considered at most as two dimensional from the magnetic point of view.

This compound is a good example of the ability for C_3 complexes, derived from a tripodal ligand bearing three bridging groups, to be a building block for 2D polymers. As far as we know, it is the first example of a 2D-bimetallic compound containing imidazolate bridges.[6]

We thank Dr E. Rivière for his contribution to magnetic measurements and Professor T. Mallah for useful discussions.

Notes and references

† The Mn–Fe–Mn angle for the present compound is 109°. For a 4-imidazolate iron complex this angle is estimated to be 80°.

‡ *Crystal data*: $[C_{66}N_{20}O_{12}H_{48}F_{36}Mn_3Fe_2]_n$, M = 2273.76, trigonal, space group $R\bar{3}c$, a = b = 18.328(9), c = 48.80(2) Å, γ = 120°, V = 14196(11) Å^3, Z = 6, D_c = 1.596 g cm^{-3}. The asymmetric unit is 1/6 of the molecular entity as defined above with Fe, the tripodal N atom and Mn, located in special positions (symmetry 3, 3 and 2). A blue dark prism single crystal (0.2 × 0.3 × 0.5 mm) was mounted on an Enraf-Nonius CAD4 diffractometer with graphite monochromated Mo-Kα radiation (λ = 0.7107 Å). The unit cell dimensions were refined from setting angles of 25 reflections ($6 < \theta < 9°$). The data collection was *via* the θ–2θ scan technique mode (range 2–25.8°). Three standard reflections were measured every hour and showed no significant decay. A total of 7674 reflections was collected ($-22 \leqslant h \leqslant 19$, $0 \leqslant k \leqslant 22$, $0 \leqslant l \leqslant 54$). From 2294 independent reflections, 1279 were considered with [$I > 2\sigma(I)$]. Lorentz-polarisation and absorption corrections were applied. The structure was solved by direct methods (program SHELXS86) and refined on F^2 for all reflections by the least-squares method using SHELXL-93. Hydrogen atoms were included in the refinement at their ideal positions with an isotropic thermal parameter 1.2 times that of the bonded atoms. The crystal structure is affected by disorder. Two different sites of each CF_3 group were found from difference Fourier syntheses. Best convergence was obtained with occupancy factors of 60 and 40%. Refinement was performed with constraints. The final conventional residuals are $R1$ = 0.054 and $wR2$ = 0.14 for [$I > 2\sigma(I)$] and $R1$ = 0.11 and $wR2$ = 0.19 (all data). CCDC 182/1490. See http://www.rsc.org/suppdata/cc/a9/a907068k/ for crystallographic files in .cif format.

§ Sample elemental analysis is in agreement with the proposed formula while the IR spectrum of the polymer is the superimposition of the spectra of iron and manganese building blocks. This is consistent with the geometric similarity of the Fe unit in the monomer and in the polymer (X-ray structure).

¶ Magnetic properties have been recorded for ground crystals from the same batch used for X-ray diffraction and elemental analysis.

‖ At 300 K, $\chi_M T$ = {[0.125$g_{Fe}^2 S(S+1)$] × 2} + {[0.125$g_{Mn}^2 S(S+1)$] × 3}. A g_{Fe}-value of 2.28 is consistent with the g_{Fe} value obtained for the iron monomer (2.35).[4]

** This is entirely consistent with imidazolate bridges which are known to induce only very weak magnetic interactions.[1]

1 (*a*) H. M. Hu, H. S. Sun, Q. Zhao, Z. Yu, X.Y. Huang and X. Z. You, *J. Coord. Chem.*, 1998, **43**, 361; (*b*) G. Tabbi, W. L. Driessen, J. Reedijk, R. P. Bonomo, N. Veldman and A. Spek, *Inorg. Chem.*,1997, **36**, 1168; (*c*) J. L. Pierre, P. Chautemps, S. Refaif, C. Begin, A. El Marzouki, G. Serratrice, E. Saint-aman and P. Rey, *J. Am. Chem. Soc.*, 1995, **117**, 1965; (*d*) J. T. Landrum, C. A. Reed, K. Hatano and W. R. Scheidt, *J. Am. Chem. Soc.*, 1978, **37**, 3232.

2 (*a*) E. Colacio, J. M. Dominguez-vera, M. Ghazi, R. Kivekäs, M. Klinga and J. M. Moreno, *Inorg. Chem.*, 1998, **37**, 3040; (*b*) S. J. Retting, A. Storr, D. A. Summers, R. C. Thompson and J. Troter, *J. Am. Chem. Soc.*, 1997, **119**, 8675; (*c*) C. T. Brewer, G. Brewer, M. Shang, W. R. Scheidt and I. Muller, *Inorg. Chim. Acta*, 1998, **278**, 197.

3 G. Kolks, S. J. Lippard, J. V. Waszczak and H. R. Lilienthal, *J. Am. Chem. Soc.*, 1982, **104**, 717.

4 F. Lambert, J. P. Renault, C. Policar, I. Morgenstern-Badarau, M. Cesario, J. Guilhem, B. Keita and L. Nadjo, manuscript in preparation.

5 (*a*) S. Ferlay, T. Mallah, J. Vaissermann, F. Bartolomé, P. Veillet and M. Verdaguer, *Chem. Commun.*, 1996, 2481; (*b*) S. Decurtins, H. W. Schmalle, H. R. Oswald, A. Linden, J. Ensling, P. Gütlich and A. Hauser, *Inorg. Chim. Acta*, 1994, **216**, 65.

6 We thank one of the referees for having suggested this.

Communication a907068k

High-resolution ^{1}H MAS NMR spectra of 2:1 phyllosilicates

María D. Alba,* Ana I. Becerro, Miguel A. Castro and Ana C. Perdigón

Departamento de Química Inorgánica, Instituto de Ciencia de Materiales, Universidad de Sevilla, Consejo Superior de Investigaciones Científicas, Avda. Américo Vespucio s/n. 41092-Sevilla, Spain. E-mail: alba@cica.es

Received (in Oxford, UK) 9th August 1999, Accepted 22nd November 1999

Solid-state ^{1}H MAS NMR at high magnetic fields and high spinning speeds provides a powerful means of identifying the different proton sites in smectites and affects information on the octahedral nature, the octahedral layer charge deficit and the charges on the cations residing in the interlayer space of the silicate.

Solid-state magic angle spinning nuclear magnetic resonance, MAS NMR, spectroscopy has long been recognised as a powerful tool for the study of the structural and physicochemical properties of inorganic silicates, aluminosilicates and zeolites, as well as for the study of the structure of adsorbed molecules and the sorbate–sorbent interactions between molecules and such solids. In consequence, MAS NMR is an experimental technique widely used in solid state chemistry research, both from basic and applied points of view.[1]

In particular, solid-state proton NMR offers an extremely useful tool in the characterization of both the proton-containing parts of the solids, *i.e.* structural hydroxyls and water, and the adsorbed molecules in these materials.[2] Moreover, it provides several advantages over other experimental techniques, such as X-ray diffraction and IR spectroscopy: (i) it is an intrinsically quantitative measurement, the area of the spectrum being directly proportional to the amount of hydrogen present;[3] (ii) the chemical shifts are characteristic of the hydrogen environment, different bands being associated with different structural sites;[4] (iii) both the inter-hydrogen distances, $d_{H–H}$,[5] and the hydrogen bonding distances[6] can be determined; and (iv) the strength and concentration of Brönsted acid sites can be quantitatively studied.[7]

However, conventional proton MAS NMR spectra in the solid state are usually very broad due to homo- and heteronuclear dipolar interactions and, to a lesser extent, chemical shift anisotropy. The main problem generally encountered in ^{1}H MAS NMR is the strength of the homogeneous dipolar interactions among protons, which produce significant linebroadening. Experimental techniques that make use of combined rotation and multiple-pulse spectroscopy, such as CRAMPS and WAHUHA, improve the quality of these spectra but imply the acquisition of more complicated experimental systems.[8] Partial deuteration of the samples reduces the spectral broadening but, again, a more complicated manipulation of the samples and a much more expensive preparation is involved.[9]

In contrast with these disadvantages, the advent of higher field magnets and the technical possibility of achieving very high spinning speeds has allowed the acquisition of high-resolution proton spectra through conventional single-pulse MAS NMR experiments on solids samples, provided that either the hydrogen density in the sample is less than about 15 atoms nm^{-3} or the motions of the molecules containing protons are fast enough, which is in accordance with classical works on the subject.[10] This technique has been successfully used to characterise many hydrous species in minerals, including pyrophyllite and talc, the two end-members of the smectite family.[11] However, the application of the solid-state ^{1}H MAS NMR technique to the study of clay minerals and their reactions has been largely unexplored, even when the information which could be obtained might be extremely useful for those numerous researchers who employ these samples in various areas of the chemistry.

This report details the study of proton spectra of samples representative of the smectite group and analyses the relationship between the spectra and the mineralogical composition of the samples. Likewise, useful applications for such measurements are proposed.

Samples of representative species among smectites with mineralogical compositions close to ideal were selected and homoionised in sodium. The set of samples was supplied by the Source Clay Minerals Repository of Missouri University (Columbia), and includes members of the dioctahedral and trioctahedral series as well as others with different tetrahedral Si/Al ratios. Additionally, the samples were also homoionised with different interlayer cations. The structural formulae of the samples studied in this report are included in Table 1 and characterised in more detail elsewhere.[12]

High-resolution ^{1}H MAS NMR spectra were recorded at room temperature for the smectites equilibrated in air (hydrated samples) and after heating at 150 °C, to ensure the complete removal of interlayer water (dehydrated samples), in order to separate both contributions. A more detailed description of the experimental procedure is given elsewhere.[12] Spectra were acquired in a magnetic field of 9.39 T and rotors were spun at 12 kHz. Pulse spaces of 5 s were used and the radiofrequency field for protons was 60 kHz.

^{1}H MAS NMR spectra of the different sodium-saturated smectites described in Table 1, after dehydration at 150 °C, are given in Fig. 1 (dotted lines in the right-hand column). The spectra of talc and pyrophyllite have also been included. All of the spectra show a single component, assigned to structural hydroxyl groups, which have been fitted with a Lorentzian curve (solid lines in the right-hand column of Fig. 1). The chemical shift (δ) and the full-width at half-height (fwhh) values are displayed in the upper-right-hand graph of Fig. 1.

Table 1 Structural formulae of the selected smectites

Short name	$^{[4]}Si^{4+}$	$^{[4]}Al^{3+}$	$^{[6]}Al^{3+}$	$^{[6]}Fe^{3+}$	$^{[6]}Mg^{3+}$	$^{[6]}Li^{+}$	$^{[6]}Ti^{4+}$	M^{+}
Talc	8.00	—	—	—	6.00	—	—	—
SHCa-1[a]	7.96	0.04	0.04	—	5.30	0.66	—	0.66
SapCa-1[b]	7.20	0.80	—	0.14	5.79	—	—	0.80
Pyrophyllite	8.00	—	4.00	—	—	—	—	—
Trancos[c]	7.64	0.36	3.09	0.28	0.69	—	—	0.87
SAz-1[c]	7.97	0.03	2.71	0.14	1.13	—	0.02	1.14

[a] Hectorite. [b] Saponite. [c] Montmorillonite.

The hydroxyl NMR bands show a value of *ca*. 0.5 ppm for the trioctahedral samples and of *ca*. 2.0 ppm for the dioctahedral ones. The difference in chemical shift between these samples is a consequence of differences in the composition of the octahedral sheet and is in agreement with the ^{29}Si MAS NMR data reported for these materials.[13] In trioctahedral minerals, OH bond axes are perpendicular to the layers and point toward the hexagonal cavities, while they are almost parallel to the layers in dioctahedral minerals.[14] In consequence, the proton position in the dioctahedral smectites allows an interaction between these OH groups and the apical oxygen atoms of the tetrahedral sheets, a hydrogen bond, which causes a deshielding of the protons and, hence, a displacement of their resonances to lower fields.

Within each series, the chemical shift value is related to the octahedral layer charge: the higher the octahedral layer charge, the higher the field. This fact is explained on the basis of the localisation of charge deficits created by isomorphous substitutions in the smectites.[15] If the deficit originates in the octahedral sheet, the excess negative charge tends to be delocalised around the whole sheet and the proton shielding of the structural hydroxyls increases as the octahedral charge is elevated. However, if the deficit occurs in the tetrahedral sheet, the excess negative charge tends to be localised on single oxygen atoms and the effect on the hydroxyl proton shielding is negligible.

As regards the band widths, these are influenced by both structural and compositional parameters. Firstly, trioctahedral structures provide a more symmetrical environment for the hydroxyl protons than dioctahedral minerals. In the latter structures, the hydroxyls are tilted and pointing toward one of the tetrahedra of the hexagonal array, a librational motion being allowed. In consequence, the trioctahedral minerals show a unique hydroxyl chemical environment and narrower ^{1}H NMR signals, whilst dioctahedral minerals show an average of different hydroxyl orientations and wider bands.

Secondly, the mineralogical composition affects the band width in a two-fold manner: those samples without isomorphic substitutions show the narrowest bands in each series and the incorporation of paramagnetic impurities and NMR-active nuclei causes a broadening of the signals.

In order to evaluate the influence of the interlayer cation, ^{1}H MAS NMR spectra of saponite exchanged with different cations are included in the left-hand column of Fig. 1, similar results being obtained for the other smectites. Dehydrated and exchanged saponites display similar ^{1}H NMR hydroxyl signals regardless of the identity of the interlayer cations, indicating that these species have no influence on the OH protons.

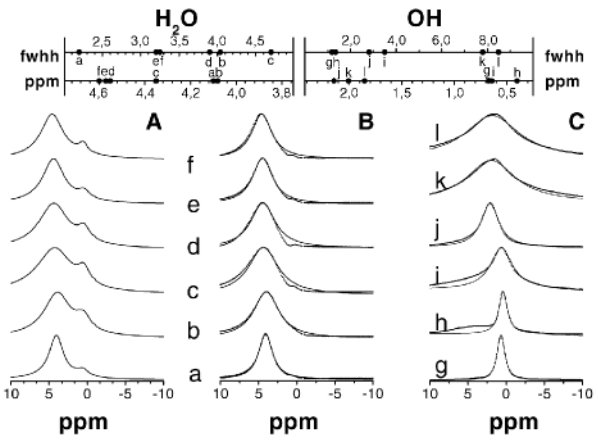

Fig. 1 A: ^{1}H MAS NMR spectra of saponite saturated with Na^{+} (a), Li^{+} (b), Mg^{2+} (c), Al^{3+} (d), La^{3+} (e), and Lu^{3+} (f) ions. **B**: Subtraction from ^{1}H MAS NMR spectra shown in the left column of the ^{1}H MAS NMR spectra obtained from the samples after dehydrating at 150 °C (dotted lines) and Lorentzian fitting curves (solid lines). Chemical shifts and full-widths at half-height are shown in the upper-left diagram for each fitting curve. **C**: ^{1}H MAS NMR spectra of (g) talc, (h) Na-hectorite, (i) Na-saponite, (j) pyrophyllite, (k) Na-Trancos montmorillonite, and (l) Na-SAz-1 montmorillonite after dehydrating at 150 °C (dotted lines). Lorentzian fitting curves have been included for each experimental curve (solid lines). Chemical shfts and full-widths at half-height are shown in the upper-right diagram for each fitting curve.

As regards the ^{1}H NMR water signal, the centre column of Fig. 1 exhibits, as dotted lines, the experimental spectra shown in the left-hand column, after subtraction of the corresponding spectra of the dehydrated samples. These spectra are composed of a single component, associated with the interlayer water of these materials. A clear relationship between the chemical shift value and the interlayer cation charge is observed. As the charge of the cation increases, the proton acidity increases and the band is shifted to lower fields: chemical shifts for the water protons of samples exchanged with trivalent cations are found to lie within the narrow range 4.60–4.55 ppm; those of samples exchanged with divalent cations lie close to 4.36 ppm; and those of samples exchanged with monovalent cations lie around 4.10 ppm. Identical chemical shifts were found for the other smectites exchanged with the same cations. Therefore, the position of the water band is uniquely affected by the charge of the interlayer cation.[16,17]

However, the fwhh is less influenced by both the charge and the size of the cation, the response being much more complicated. The variations in the linewidths of proton spectra in similar systems are affected by the mobility of water and, in consequence, complicated diffusion processes are involved, more sophisticated models being necessary for a discussion of these effects.

In summary, this report shows that the combined use of high magnetic fields and spinning speeds affords single-pulse ^{1}H MAS NMR spectra of smectites of similar quality to those currently obtained by using multiple-pulse sequences. Moreover, these spectra require only very short acquisition times and a simple instrumental set up. The spectra directly provide information on the octahedral nature, the octahedral layer charge, and the charge of the interlayer cation of the mineral, structural aspects of elevated importance in the study of these materials. In particular, they can be used as initial characterization measurements and can be valuable for monitoring structural changes in the course of many treatments in which smectites can change their layer charge, suffer leaching processes, or modify their interlayer compositions. Finally, such spectra afford the opportunity to develop two-dimensional cross-polarisation experiments with other nuclei, such as ^{27}Si, ^{29}Al and ^{7}Li, which would improve the information currently obtained from MAS NMR spectroscopy.

We thank DGICYT for financial support (Project No. PB97-0176).

Notes and references

1 J. M. Trillo, M. D. Alba, R. Alvero and M. A. Castro, *J. Chem. Soc., Chem. Commun.*, 1993, 1809.
2 J. Klinowski, *Chem. Rev.*, 1991, **91**, 1459.
3 S. C. Kohn, *Am. Mineral.*, 1996, **81**, 1523.
4 A. J. Vega and Z. Luz, *J. Phys. Chem.*, 1987, **91**, 365.
5 B. L. Phillips, P. C. Burnley, K. Worminghaus and A. Navrotsky, *Phys. Chem. Miner.*, 1997, **24**, 179.
6 D. Freude and J. Klinowski, *J. Chem. Soc., Chem. Commun.*, 1988, 1411.
7 H. Pfeifer, *Colloids Surf.*, 1990, **45**, 1.
8 D. R. Kinney, I. Chuang and G. E. Maciel, *J. Am. Chem. Soc.*, 1993, **115**, 6786.
9 A. Thursfield and M. W. Anderson, *J. Phys. Chem.*, 1996, **100**, 6698.
10 S. F. Dec, R. A. Wind and G. E. Maciel, *Macromolecules*, 1987, **20**, 2754.
11 J. P. Yesinowski, H. Eckert and G. R. Rossman, *J. .Am. Chem. Soc.*, 1988, **110**, 1367.
12 A. I. Becerro, Ph.D. Thesis, University of Seville, 1997.
13 J. Sanz and J. M. Serratosa, *J. Am. Chem. Soc*, 1984, **106**, 4790.
14 J. M. Serratosa and W. F. Bradley, *J. Phys. Chem.*, 1958, **62**, 1164.
15 G. Sposito and R. Prost, *Chem. Rev.*, 1982, **82**, 553.
16 P. H. Kasai and P. M. Jones, *J. Mol. Catal.*, 1984, **27**, 81.
17 J. N. Shoolery and B. Alder, *J. Chem. Phys.*, 1955, **23**, 805.

Communication a906577f

A novel hybrid layer compound containing silver sheets and an organic spacer

C. N. R. Rao,* Anupama Ranganathan, V. R. Pedireddi and A. R. Raju

Chemistry & Physics of Materials Unit and CSIR Centre for Excellence in Chemistry, Jawaharlal Nehru Centre for Advanced Scientific Research, Jakkur P.O., Bangalore 560 064, India. E-mail: cnrrao@jncasr.ac.in

Received (in Cambridge, UK) 12th October 1999, Accepted 23rd November 1999

A novel compound of the formula Ag_2·CA (CA = cyanuric acid) possessing Ag sheets and hydrogen-bonded CA chains, exhibits anisotropic conductivity and acts as an infinite parallel plate capacitor with a high dielectric constant.

Design of infinite two- and three-dimensional arrays of metal–ligand networks has attracted considerable attention in the last few years not only because of the structural and topological novelty of such engineered solids but also due to the potentially interesting electrical, magnetic and other properties.[1,2] Recently, interesting structures containing polymeric Ag(I) species and heterocyclic as well as aromatic compounds have been described.[2–4] For instance, Ag(I)–benzenesulfonate has a layered structure containing a planar hexagonal array of Ag(I) ions incorporating the anion.[4] A coordination network of dicyanodiphenylacetylene comprising Ag(I) sheets with an Ag···Ag separation of 3.39 Å has also been reported.[5] Equally interesting are the supramolecular Ag(I) complexes constructed with several aromatic compounds involving novel stacking of the aromatics such as the herringbone packing pattern.[6,7] Many of these compounds have Ag···Ag separation significantly shorter than the van der Waals contact distance, with Ag(I) having linear, trigonal, tetrahedral or hexagonal coordination,[8] however, the materials are generally either insulators or semiconductors with no unusual properties.

During the course of our investigations of supramolecular assemblies of cyanuric acid, $C_3H_3N_3O_3$ (CA), involving both hydrogen bonding and metal-ion coordination, we have isolated a novel silver compound possessing two-dimensional Ag sheets with the CA molecules in the interlayer space, forming linear hydrogen-bonded chains. This compound of composition Ag_2·CA, is a unique organic–inorganic hybrid with novel electrical properties, and is entirely different from the supramolecular assemblies described above, and from other Ag complexes and salts with short Ag···Ag distances.[9] Here, we describe the fascinating structure and properties of this Ag(I) compound.

Reaction of $AgNO_3$ with CA under hydrothermal conditions† gave single crystals of composition Ag_2·CA suitable for X-ray diffraction studies. The structure was determined‡ using the SHELXTL package,[10] with the intensity data collected on a Siemens smart diffractometer equipped with CCD area detector. The asymmetric unit of the compound is shown in Fig. 1. The structure viewed down the *b*-axis (Fig. 2) reveals the presence of two-dimensional sheets of Ag atoms separated by CA molecules, the inter-sheet separation being *ca*. 6 Å. The average Ag···Ag distance in the sheets is 2.95 Å, slightly longer than the Ag–Ag distance in metallic silver (2.89 Å). The dative Ag–O and Ag–N bond distances are in the range 2.22–2.76 and 2.09–2.12 Å, respectively, and the CA molecules are linked by relatively short N–H···O hydrogen bonds (H···O 1.90 Å, N···O, 2.75 Å), giving rise to a linear chain (Fig. 2). The arrangement of the CA molecules in the layers perpendicular to the Ag sheets is illustrated in Fig. 3. Another noteable feature of Ag_2·CA is that the organic spacer itself is the anion. Ag_2·CA can also be compared with Ag_3O with an *anti*-BiI_3 structure with the O atoms occupying 2/3 of the octahedral holes.[11] The Ag···Ag and Ag–O distances in Ag_2·CA are slightly longer than in Ag_3O, except for one Ag–O bond of 2.22 Å.

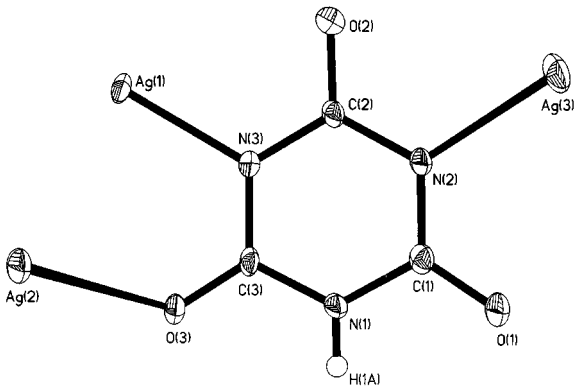

Fig. 1 ORTEP drawing showing the asymmetric unit of Ag_2·CA.

The presence of multipoint recognition patterns between CA and Ag in Ag_2·CA is of interest. For instance, the hydrogen bonding motif (a) in Scheme 1, found in the structure of CA,[12] is replaced by the motif (b) in Ag_2·CA by the substitution of Ag for H. Motif (b) is similar to that present in Ag carboxylates, except that two of the O atoms are replaced by N atoms. In addition, there are three-point recognition patterns (c) and (d) in Ag_2·CA, comparable to the hydrogen bonding pattern (e) found in the adduct of CA with melamine.[13]

Ag_2·CA crystals are mica-like and are readily cleaved because of the layer structure and the presence of weakly bound Ag sheets. The presence of two-dimensional Ag sheets is expected to give rise to anisotropic conductivity. Accordingly, the values of the dc conductivity parallel and perpendicular to the Ag sheets (*bc* plane) are *ca*. 5×10^{-3} and *ca*. 2×10^{-5} S cm^{-1}, respectively, at 300 K. The conductivity along the sheets is temperature-independent down to 15 K. Ag_2·CA, in which the conducting Ag sheets are separated by the organic spacer molecules, can be considered as an infinite parallel plate capacitor. In accord with this, the crystals possess a high static dielectric constant of *ca*. 22 000 at 300 K, a phenomenally high value which promises potential applications. This value of the

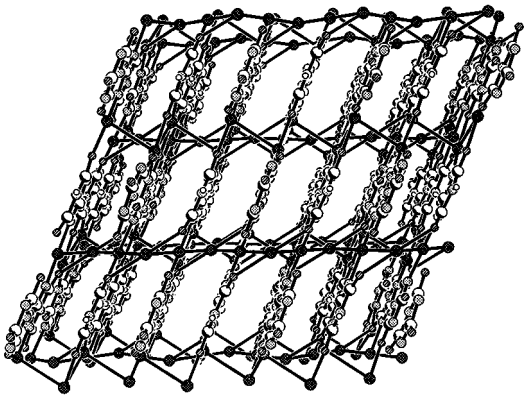

Fig. 2 Structure of Ag_2·CA showing Ag sheets and linear CA chains.

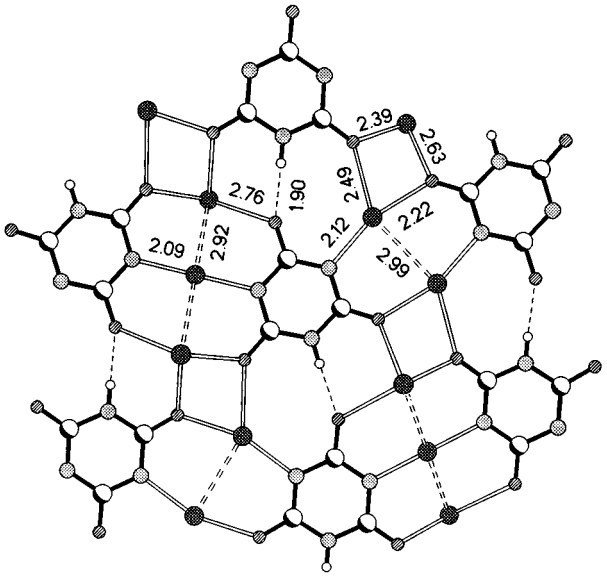

Fig. 3 Structure of a layer (*ab* plane) perpendicular to the Ag sheets: Solid lines, covalent bonds; double lines, dative bonds; dashed lines, hydrogen bonds; double dashed lines, Ag–Ag bonds.

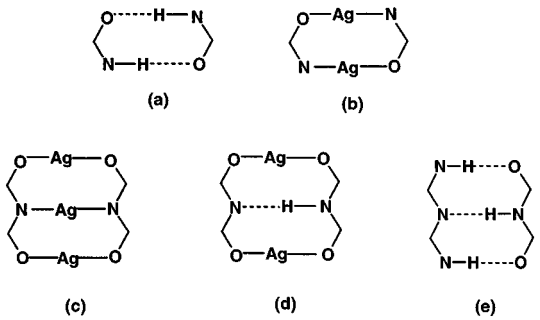

Scheme 1

dielectric constant is comparable with that of barium titanate (*ca*. 12000 at 300 K).

Notes and references

† A solution (10 mL) consisting of a mixture of $AgNO_3$ (0.170 g) and CA (0.129 g) in water in a Teflon flask was placed in a steel bomb. The bomb was placed in an oven maintained at 180 °C for 24 h and then cooled to room temperature (25 °C) over a period of 3 h. Good quality off-white plate-like single crystals, were obtained and the composition of the product was established as Ag_2·CA, consistent with that derived from X-ray crystallography. There were no other products in the reaction.

‡ *Crystal data* for Ag_2·CA($Ag_2C_3N_3HO_3$): crystal dimensions, 0.35 × 0.25 × 0.20 mm, monoclinic, space group, *C*2/*c*, a = 12.726(1), b = 13.064(1), c = 6.623(1) Å, β = 97.35(1)°, V = 1092.0(2) Å^3, Z = 8, D_c = 4.170 Mg m^{-3}, μ(Mo-Kα) = 7.11 mm^{-1}, F(000) = 1264, λ = 0.71073 Å, ω–2θ scan, 2 < θ < 24° (−13 ⩽ h ⩽ 14, −11 ⩽ k ⩽ 14, −6 ⩽ l ⩽ 7), 2266 total reflections, 785 independent reflections which were used in the refinement. The structure was solved to $R1$ = 0.035 and $wR2$ = 0.083. Hydrogen atoms were placed in calculated positions.

CCDC 182/1491. See http://www.rsc.org/suppdata/cc/a9/a908171b/ for crystallographic files in .cif format.

1 R. Robson, B. F. Abrahams, S. R. Batten, R. W. Gable, B. F. Hoskins and J. Liu, *Supramolecular Architecutre*, ACS Symp. Ser., Washington, D.C., 1992, vol. 449, 1992, ch. 19.
2 L. Carlucci, G. Ciani, D. M. Proserpio and A. Sironi, *Angew. Chem., Int. Ed. Engl.*, 1995, **34**, 1895 and references therein.
3 G. K. H. Shimizu, G. D. Enright, C. I. Ratcliffe, J. A. Ripmeester and D. D. M. Wayner, *Angew. Chem., Int. Ed.*, 1998, **37**, 1407.
4 G. K. H. Shimizu, G. D. Enright, C. I. Ratcliffe, K. F. Preston, J. L. Reid and J. A. Ripmeester, *Chem. Commun.*, 1999, 1485.
5 K. A. Hirsch, S. R. Wilson and J. S. Moore, *Inorg. Chem.*, 1997, **36**, 2960.
6 M. Munakata, L. P. Wu, T. Kuroda-Sowa, M. Maekawa, Y. Suenaga, G. L. Ning and T. Kojima, *J. Am. Chem. Soc.*, 1998, **120**, 8610.
7 G. L. Ning, L. P. Wu, K. Sugimoto, M. Munakata, T. Kuroda-Sowa and M. Maekawa, *J. Chem. Soc., Dalton Trans.*, 1999, 2529.
8 D. Venkataraman, Y. Du, S. R. Wilson, P. Zhang, K. Hirsch and J. S. Moore, *J. Chem. Educ.*, 1997, **74**, 915.
9 A. F. Wells, *Structural Inorganic Chemistry*, Oxford University Press, Oxford, 5th edn., 1995, p. 1099.
10 G. M. Sheldrick, SHELXTL, Users Manual, Siemens Analytical X-ray Instruments Inc., Madison, WI, 1993.
11 W. Beesk, P. G. Jones, H. Rumpel, E. Schwarzmann and G. M. Sheldrick, *J. Chem. Soc., Chem. Commun.*, 1981, 664.
12 P. Coppens and A. Vos, *Acta Crystallogr., Sect. B*, 1971, **27**, 146.
13 A. Ranganathan, V. R. Pedireddi and C. N. R. Rao, *J. Am. Chem. Soc.*, 1999, **121**, 1752.

Communication a908171b

Molecular capsule constructed by multiple hydrogen bonds: self-assembly of cavitand tetracarboxylic acid with 2-aminopyrimidine

Kenji Kobayashi,*[a] Toshiaki Shirasaka,[a] Kentaro Yamaguchi,[b] Shigeru Sakamoto,[b] Ernst Horn[ac] and Naomichi Furukawa[a]

[a] *Department of Chemistry and Tsukuba Advanced Research Alliance Center, University of Tsukuba, Tsukuba, Ibaraki 305-8571, Japan. E-mail: kenjinor@staff.chem.tsukuba.ac.jp*
[b] *Chemical Analysis Center, Chiba University, Inage-ku, Chiba 263-8522, Japan*
[c] *Department of Chemistry, Rikkyo University, Nishi-Ikebukuro, Toshima-ku, Tokyo 171-8501, Japan*

Received (in Cambridge, UK) 18th October 1999, Accepted 17th November 1999

Two molecules of cavitand tetracarboxylic acid and four molecules of 2-aminopyrimidine assemble into a capsule *via* 16 hydrogen bonds, as shown by ^{1}H NMR titration and X-ray crystallographic analysis; in the solid state, two molecules of nitrobenzene are encapsulated in the capsule.

Error correction through thermodynamic equilibration, minimization of synthetic effort by use of modular subunits and control of assembly processes through subunit design are characteristic of supramolecular approaches to self-assembly.[1,2] Carcerands, in which two calix[4]resorcinarene cavitands are held together by four covalent linkages, have been synthesized and well-characterized by Cram and others, and have attracted considerable attention from the viewpoint of stabilization of reactive intermediates and microvesicles for drug delivery by confinement of guest molecules inside the capsules away from bulk phases.[3] Recently, the field of molecular capsules has advanced to a stage where self-assembly through noncovalent interactions such as hydrogen bonds and metal coordination has proved to be a reliable tool.[4,5] Based on hydrogen bonds, homodimers of functionalized cavitands in solution[6,7] and multicomponent assemblies of calix[4]resorcinarenes with solvent water or alcohol molecules as linkers in the solid state[8,9] have been reported. Metal-bridged assemblies of functionalized cavitands have also proved to be a viable alternative.[10] We have chosen the cavitand tetracarboxylic acid **1** as a concave subunit[11] and 2-aminopyrimidine (2-AP) as a hydrogen-bonded linker subunit. Our strategy for capsule formation is based on the combination of carboxylic acids with 2-AP to form a 2:1 hydrogen-bonded complex in the solid state.[12] Herein we report the construction of capsule **2** from six components *via* 16 hydrogen bonds: two molecules of **1** are indirectly held together in a rim-to-rim fashion by hydrogen bonding bridges involving four molecules of 2-AP (Scheme 1).

The cavitand **1** alone has a low solubility in $CHCl_3$ at room temperature { < 5 mM for **1a** [R = $(CH_2)_6CH_3$] and < 1 mM for **1b** [R = $(CH_2)_2Ph$]}. On the other hand, in the presence of 2 equiv. of 2-AP, **1** becomes very soluble in $CHCl_3$ (> 100 mM). The titration of a suspension of **1a** in $CDCl_3$ at 25 °C with aliquots of 2-AP was monitored by ^{1}H NMR spectroscopy. Fig. 1 shows the chemical shift changes for the NH_2 protons of 2-AP and the inward and outward methylene protons at the rim of **1a** as a function of 2-AP/**1a**.† Below the 2:1 ratio of 2-AP/**1a**, the NH_2 protons of 2-AP apparently give a saturated downfield shift ($\Delta\delta_{obs}$ = 2.95 ppm), independent of 2-AP/**1a**, while the methylene protons of **1a** are increasingly shifted downfield upon addition of 2-AP. At the 2:1 stoichiometry of 2-AP/**1a**, the mixture becomes completely homogeneous.† Beyond the 2:1 ratio, the former chemical shift changes decrease due to the average of signals between the free and complex 2-AP, whereas the latter ones remain unchanged. The fact that both titration curves have an inflection point at the 2:1 stoichiometry of 2-AP/**1a** indicates that an *n*:2*n* complex of **1a** with 2-AP is formed *via* hydrogen bonds and that this formation may be a cooperative process. The cavitand **1a** and 2-AP possess four and two hydrogen bonding sites, respectively. In principle, 1:2 and/or 1:4 complexes of **1a** with 2-AP may be conceivable. In such complexes, however, half of the hydrogen bonding sites still remain intact. The titration data obtained here suggests the formation of a capsule **2a** in solution from two molecules of **1a** and four molecules of 2-AP (Scheme 1).‡ The capsule **2a** in $CDCl_3$ was disrupted upon addition of DMSO-d_6 as a cosolvent.

The stability of **2a** was evaluated by the dilution method in $CDCl_3$ at 25 °C using ^{1}H NMR, where the ratio of 2-AP/**1a** is maintained at 2:1. The chemical shift changes for the NH_2 protons of 2-AP decreased at less than 10 mM of 2-AP. The association constant for the formation of **2a** calculated from a nonlinear curve fitting was estimated to be $K_a = 3.7 \times 10^{19}$ M^{-5} in $CDCl_3$ at 25 °C with $\Delta\delta_{sat}$ = 2.96 ppm and a correlation

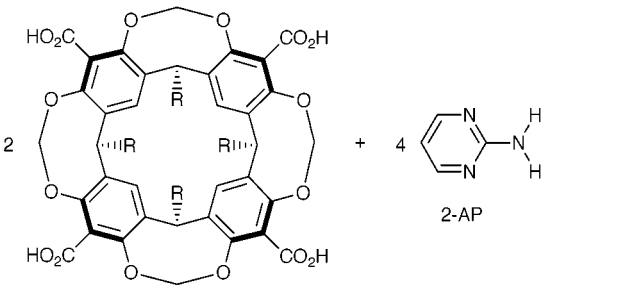

1a R = $(CH_2)_6CH_3$
1b R = $(CH_2)_2Ph$

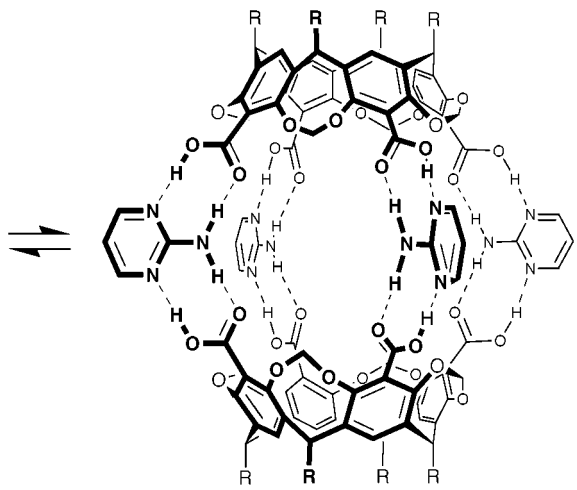

2a R = $(CH_2)_6CH_3$
2b R = $(CH_2)_2Ph$

Scheme 1

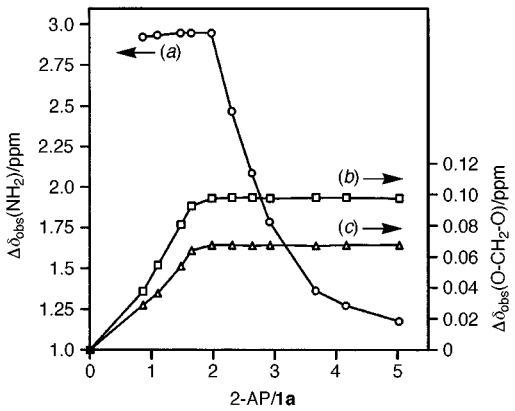

Fig. 1 Chemical shift changes for (*a*) the NH_2 protons of 2-AP and (*b*) the inward and (*c*) outward methylene protons at the rim of **1a** as a function of 2-AP/**1a** in $CDCl_3$ at 25 °C.

coefficient r = 0.99.§ This corresponds to an average $\Delta G°$ = −1.6 kcal mol^{-1} per hydrogen bond.[13]

Recrystallization of a mixture of **1** and 2-AP from various solvents such as *p*-xylene, anisole–$CHCl_3$ and nitrobenzene–$CHCl_3$ gave co-crystals composed of **1**:2-AP = 1:2 without exception. The IR spectra showed a shift (10 cm^{-1}) to lower wavenumbers of the $\nu_{C=O}$ for **1** upon adduct formation. The O–H stretching bands appeared at 2500 and 1900 cm^{-1}, which are characteristic of a carboxylic acid hydrogen bonded to an aromatic ring nitrogen.[12] When pyridine was used in place of 2-AP, co-crystals of **1**:pyridine = 1:4 were obtained. These results support the formation of **2** from **1** and 2-AP in the solid state.

Single crystals suitable for X-ray diffraction analysis were grown by allowing a hot solution of **1b** and 2-AP in nitrobenzene to slowly cool to room temperature.¶ As shown in Fig. 2, the molecular structure after symmetry operations unambiguously reveals the capsule **2b** in which two molecules of the hemispherical cavitand **1b** associate indirectly in a rim-to-rim fashion by hydrogen bonding bridges involving four molecules of 2-AP located on an equatorial position. The NH_2 protons and aromatic ring nitrogens of 2-AP form hydrogen bonds with the acid carbonyl oxygens and OH protons of **1b**, respectively. The hydrogen bonding distances of N(H)···O are 2.866(7), 2.841(7), 2.897(7) and 2.872(7) Å, and those of N···(H)O are 2.770(7), 2.604(7), 2.711(6) and 2.718(6) Å. Thus, the capsule **2b** is constructed *via* 16 hydrogen bonds between two molecules of **1b** and four molecules of 2-AP. The

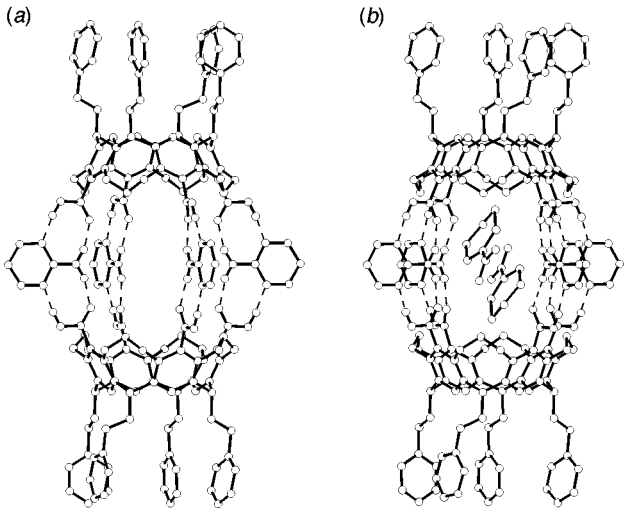

Fig. 2 Molecular structure of capsule **2b** (*a*) without and (*b*) with encapsulated nitrobenzenes. Nitrobenzenes which are not located inside the cavity and hydrogen atoms except for NH_2 protons of 2-AP and acid protons of **1b** are omitted for clarity. Dashed lines represent intermolecular hydrogen bonds.

dihedral angles between the carboxylic acid groups and the resorcinol rings of **1b** are almost perpendicular (83.5, 85.7, 105.9 and 80.2°), probably due to the electronic repulsion between the oxygen atoms of their moieties. This orientation plays an important role in the formation of the capsule. The capsule **2b** features dimensions of *ca.* 9 × 15 Å. Two molecules of nitrobenzene are encapsulated in the cavity of **2b** in an antiparallel fashion with an inter-ring distance of *ca.* 3.3 Å. They are oriented with the nitro groups towards the equatorial windows of **2b**.

In summary, we have demonstrated the capsule **2**, composed of two molecules of the cavitand tetracarboxylic acid **1** and four molecules of 2-aminopyrimidine, as a hydrogen-bonded linker. Exploration of linkers such as bipyridine derivatives and transition metals in order to control the cavity size of the capsules is currently underway in our laboratory.

Notes and references

† The concentration of **1a** is 20 mM if completely soluble in $CDCl_3$. The equilibrium is reached immediately. At the 2:1 stoichiometry of 2-AP/**1a**, the signal of the acid protons of **1a** was observed at δ 16.00 at −30 °C. Irradiation of the C(4,6) hydrogens of 2-AP showed a 3% NOE at the acid protons of **1a** at −30 °C.

‡ No evidence for the encapsulation of guests into **2a** in $CDCl_3$ is available, probably due to favorable accommodation of $CDCl_3$ as a bulk phase in **2a**.

§ A constant ratio [2-AP]:[**1a**] = 2:1, and the assumption that free **1a**, free 2-AP and capsule **2a** are the only components present, give eqn. (1),

$$[\text{2-AP}] = \{(\Delta\delta_{obs}/\Delta\delta_{sat})/[K_a(1 - (\Delta\delta_{obs}/\Delta\delta_{sat}))^6]\}^{0.2} \quad (1)$$

where $\Delta\delta_{obs} = \delta_{obs} - \delta_{free}$ and $\Delta\delta_{sat} = \delta_{sat} - \delta_{free}$ are the observed and saturated chemical shift changes of the NH_2 protons of 2-AP, respectively.

¶ *Crystal data* for **1b**·2(2-AP)·6($PhNO_2$): $C_{112}H_{96}N_{12}O_{28}$, M = 2058.05, crystal size 0.52 × 0.45 × 0.40 mm, triclinic, space group $P\bar{1}$, a = 17.79(2), b = 19.78(1), c = 15.047(5) Å, α = 107.32(4), β = 96.18(3), γ = 79.05(5)°, U = 4955(6) Å^3, Z = 2, D_c = 1.379 g cm^{-3}, μ(Mo-Kα) = 1.00 cm^{-1}, $2\theta_{max}$ = 50.2°. Intensity data (11593) were measured on a Rigaku RAXIS-II diffractometer at 120 K. The final least-squares refinement based on F for 8815 unique reflections [with $I > 3.0\sigma(I)$] and 1396 parameters converged with R = 0.110 and R_w = 0.124. CCDC 182/1489. See http://www.rsc.org/suppdata/cc/a9/a908315d/ for crystallographic data in .cif format.

1 J.-M. Lehn, *Supramolecular Chemistry: Concepts and Perspectives*, VCH, Weinheim, 1995.
2 G. M. Whitesides, E. E. Simanek, J. P. Mathias, C. T. Seto, D. N. Chin, M. Mammen and D. M. Gordon, *Acc. Chem. Res.*, 1995, **28**, 37; D. S. Lawrence, T. Jiang and M. Levett, *Chem. Rev.*, 1995, **95**, 2229.
3 D. J. Cram and J. M. Cram, *Container Molecules and Their Guests*, Royal Society of Chemistry, Cambridge, 1994; A. Jasat and J. C. Sherman, *Chem. Rev.*, 1999, **99**, 931.
4 For molecular capsules *via* hydrogen bonds, see: M. M. Conn and J. Rebek Jr., *Chem. Rev.*, 1997, **97**, 1647; J. de Mendoza, *Chem. Eur. J.*, 1998, **4**, 1373; J. Rebek Jr., *Acc. Chem. Res.*, 1999, **32**, 278.
5 For molecular capsules *via* metal coordination, see: M. Fujita, D. Oguro, M. Miyazawa, H. Oka, K. Yamaguchi and K. Ogura, *Nature*, 1995, **378**, 469; B. Olenyuk, A. Fechtenkötter and P. J. Stang, *J. Chem. Soc., Dalton Trans.*, 1998, 1707.
6 R. G. Chapman and J. C. Sherman, *J. Am. Chem. Soc.*, 1995, **117**, 9081; R. G. Chapman, G. Olovsson, J. Trotter and J. C. Sherman, *J. Am. Chem. Soc.*, 1998, **120**, 6252.
7 T. Heinz, D. M. Rudkevich and J. Rebek Jr., *Nature*, 1998, **394**, 764.
8 L. R. MacGillivray and J. L. Atwood, *Nature*, 1997, **389**, 469.
9 K. N. Rose, L. J. Barbour, G. W. Orr and J. L. Atwood, *Chem. Commun.*, 1998, 407; K. Murayama and K. Aoki, *Chem. Commun.*, 1998, 607.
10 P. Jacopozzi and E. Dalcanale, *Angew. Chem., Int. Ed. Engl.*, 1997, **36**, 613; O. D. Fox, N. K. Dalley and R. G. Harrison, *J. Am. Chem. Soc.*, 1998, **120**, 7111.
11 H.-J. Choi, D. Bühring, M. L. C. Quan, C. B. Knobler and D. J. Cram, *J. Chem. Soc., Chem. Commun.*, 1992, 1733.
12 M. C. Etter and D. A. Adsmond, *J. Chem. Soc., Chem. Commun.*, 1990, 589.
13 C. T. Seto and G. M. Whitesides, *J. Am. Chem. Soc.*, 1993, **115**, 1330.

Communication a908315d

Kinetic resolution of amines by acylation using 3-diacylaminoquinazolin-4(3*H*)-ones

Abdullah G. Al-Sehemi, Robert S. Atkinson, John Fawcett and David R. Russell

Department of Chemistry, Leicester University, Leicester, UK LE1 7RH. E-mail: vow@le.ac.uk

Received (in Cambridge) 4th October 1999, Accepted 16th November 1999

Four diastereoisomeric 3-diacylaminoquinazolinones 8a–d have been separated and identified by X-ray structure determinations on three of them: their stoichiometric reactions with α-phenylethylamine and with 2-methylpiperidine (2 equiv. of amine) gave the corresponding *N*-(2-acetoxypropanoyl)amine and unreacted amine in high diastereomeric/enantiomeric excess.

3-Diacylaminoquinazolinones (DAQs), *e.g.* **1**, are highly selective acylating agents for primary amines in the presence of secondary amines and for the less hindered of two secondary amines.[1] Recently the *N*,*N*-diacetamide **2** has been claimed to be even more chemoselective than DAQ **1** as an acetylating agent: a 1:1 mixture of pyrrolidine and piperidine (ΔpK_a = 0.01) reacts with **2** to give a 15:1 ratio of the corresponding *N*-acetylated amines.[2]

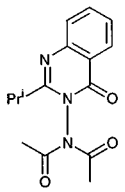

1

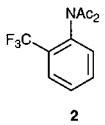

2

The DAQs **3**, **4** and **5** were available to us by acetylation of the corresponding 3-aminoquinazolinones[3] and, when reacted with a mixture of pyrrolidine and piperidine (1 equiv. each) at 0 °C in CH_2Cl_2 gave the ratios of the corresponding amides shown in Scheme 1. Unexpectedly, the chemoselectivity increases as the substituent R on the chiral centre decreases in size from Bu^t → Me with a 20:1 ratio for methyl.†

Since DAQs **3**, **4** and **5** are enantiopure we were particularly interested in a greater potential advantage which their use offered over that of *e.g.* **2**, namely as enantioselective acetylating agents.[4] However, reaction of DAQ **3** (1 equiv.) with racemic 2-methylpiperidine (2 equiv.) gave a sample of recovered amine having zero optical rotation and hence there is no kinetic resolution in this acetylation.

For 3-aminoquinazolinones *N*,*N*-disubstituted with different acyl groups, we have previously shown that the *N*–*N* bond is a chiral axis: in DAQ **6** the presence of two chiral elements gives rise to diastereoisomers with a barrier $\Delta G^{\#}$ = 121 kJ mol^{-1} for their interconversion by rotation around the *N*–*N* bond.[4]

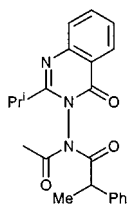

6

Successive acylation of enantiopure 3-aminoquinazolinone **7**[3] with (*S*)-2-acetoxypropanoyl chloride and isobutanoyl chloride (Scheme 2) gave four DAQ diastereoisomers **8a**–**d** in order of their elution on chromatography (see below). The major diastereoisomer **8b** was separated by crystallisation (35%) after flash chromatography to remove unreacted mono-acylquinazolinone (MAQ) and pure samples of the other three, **8a** (5%), **8c** (7%) and **8d** (26%), were obtained by separation using a chromatotron.

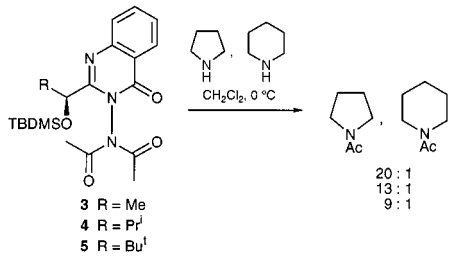

Scheme 1

X-Ray crystal structure determinations of DAQs **8b** and **8c** (Fig. 1) showed them to have the expected (*S*)-configuration at their α-acetoxypropanoyl chiral centres but different configurations at their *N*–*N* chiral axes.‡ Heating ($CDCl_3$, 60 °C, 42 h) interconverted **8b** and **8c** and gave a 5:4 ratio respectively at equilibrium, presumably as a result of rotation around the *N*–*N* bond: no interconversion with **8a** or **8d** occurred.

Diastereoisomers **8a** and **8d** arise from epimerisation at the α-acetoxypropanoyl centre as shown by the (*R*)-configuration in the X-ray crystal structure of **8d** (Fig. 1).‡ Interconversion of **8a** and **8d** by heating ($CDCl_3$, 60 °C, 13 h) gave a 6:1 ratio at equilibrium, respectively: no interconversion with **8b** and **8c** occurred in this equilibrium.

Although in their crystal structures DAQ **8b**–**d** all have the usual[4] *exo*/*endo* conformation for their imides, **8b** and **8c** have their α-acetoxypropanoyl groups *endo* and the isobutanoyl group *exo* whereas **8d** has the positions of these two groups reversed.

We find that these DAQs **8a**–**d** are enantioselective acylating agents for racemic amines. Thus DAQ **8c** (1 equiv.) reacts with α-phenylethylamine (2 equiv.) in CH_2Cl_2 at 5 °C to give (2*R*,2′*S*)-*N*-(-2-acetoxypropanoyl)-α-phenylethylamine [77% based on (*R*)-α-phenylethylamine, 88% de] by NMR comparison with authentic samples of both diastereoisomers: the recovered *S* enantiomer of the amine [90% based on (*S*)-α-phenylethylamine] was of 91% ee from its specific rotation (Scheme 3).

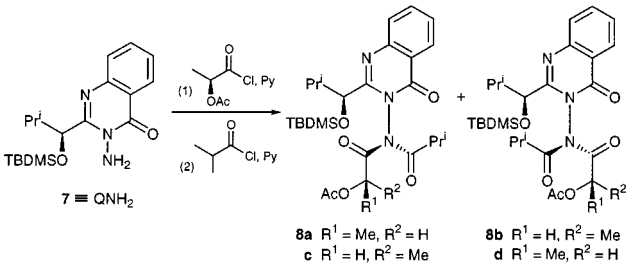

Scheme 2

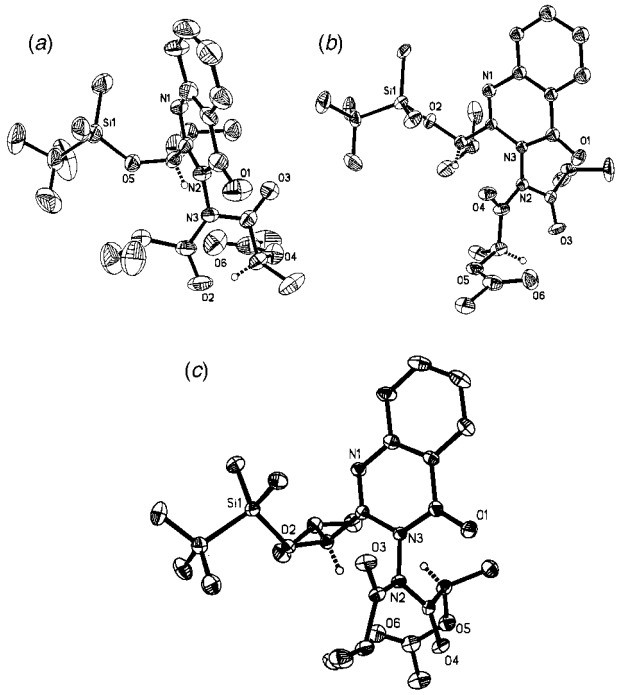

Fig. 1 Molecular structures of (*a*) **8b**, (*b*) **8c** and (*c*) **8d** showing atom labelling schemes and 30% probability displacement parameters. H atoms at chiral centres are shown with dashed bonds, all other H atoms are omitted for clarity.

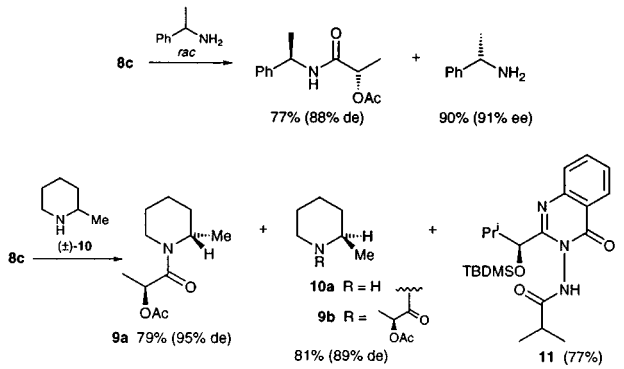

Scheme 3

Reaction of DAQ **8c** (1 equiv.) with racemic 2-methylpiperidine **10** (2 equiv.) in CH_2Cl_2 at 5 °C for 24 h gave, after chromatography, monoacylquinazolinone (MAQ) **11** (77%) and (2*S*,2′*S*)-1-(2′-acetoxypropanoyl)-2-methylpiperidine **9a** (79%) (Scheme 3) whose diastereopurity (de) as measured by NMR spectroscopy was 95%. The unreacted 2-methylpiperidine enantiomer was recovered from the crude reaction mixture by extraction with HCl (2 M) and derivatised by reaction with (*S*)-2-acetoxypropanoyl chloride to give **9b** (81%) of 89% de: at 400 MHz and 50 °C the OCOC*H*$_3$ signals of diastereoisomers **9a** and **9b** are well separated.§

Since DAQ **8b** was recovered unchanged when re-subjected to the conditions of the second acylation in Scheme 2, it appears that epimerisation at the 2-acetoxypropanoyl chiral centre occurs in the second acylation step.¶ An alternative, more stereoselective route to these DAQs was to carry out the second acylation using the lithium salt of the MAQ. Thus reaction of the lithium salt of MAQ **11** with (*S*)-2-acetoxypropanoyl chloride gave DAQ **8c** (71%) and **8a** (8%) (based on recovered starting material), *i.e.* with less epimerisation than previously.

Kinetic resolution is usually carried out in the presence of excess of the substrate to maximise enantiopurity in its derivatised enantiomer. Even under the most testing conditions of stoichiometry as in Scheme 3, DAQ **8c** delivers both derivatised and unreacted enantiomers of the substrate with high enantioselectivity.

We thank the Ministry of Education, Saudi Arabia for funding (to A. G. Al-S).

Notes and references

† This increase may be related to the preference for a defined conformation around the C–OSi bond in the (Q) 2-substituent in **3** but not in **4** or **5** (see R. S. Atkinson, M. P. Coogan and I. S. T. Lochrie, *Tetrahedron Lett.*, 1996, **37**, 5179.

‡ *Crystal data* for **8b**: $C_{27}H_{41}N_3O_6Si$, M = 531.72, orthorhombic, space group $P2_12_12_1$, a = 10.146(1), b = 13.296(2), c = 22.618(3) Å, V = 3051.4(7) Å^3, Z = 4, μ(Mo-Ka) = 0.118 mm^{-1}, 3845 reflections measured, 3639 unique (R_{int} = 0.013) which were all used in calculations. Final R_1 = 0.052 and wR_2 = 0.114 (all data). For **8c**: $C_{27}H_{41}N_3O_6Si$, M = 531.72, orthorhombic, space group $P2_12_12_1$, a = 9.391(2), b = 13.554(6), c = 23.908(13) Å, V = 3043(2) Å^3, Z = 4, μ(Mo-Ka) = 0.118 mm^{-1}, 3756 reflections measured, 3592 unique (R_{int} = 0.035) which were all used in calculations. Final R_1 = 0.102 and wR_2 = 0.309 (all data). For **8d**: $C_{27}H_{41}N_3O_6Si$, M = 531.72, orthorhombic, space group $P2_12_12_1$, a = 12.152(9), b = 13.170(7), c = 18.293(9) Å, V = 2928(3) Å^3, Z = 4, μ(Mo-Ka) = 0.118 mm^{-1}, 3666 reflections measured, 3455 unique (R_{int} = 0.155) which were all used in calculations. Final R_1 = 0.044 and wR_2 = 0.099 (all data). Data were measured on a Siemens P4 diffractometer at 190 K using graphite monochromated Mo-Ka radiation (λ = 0.7107 Å) using an ω-scan technique. Three standard reflections monitored every 100 scans showed no significant variation in intensity, the reflections were corrected for Lorentz and polarisation effects. The structures were solved by direct methods and refined by full-matrix least-squares on F^2. The absolute configurations of the compounds were established by the known configuration at the silyloxy substituted carbon atom. All examined crystals of **8c** diffracted weakly; to preserve an observed data to variable ratio of 6:1 the 13 most closely isotropic atoms were constrained to be isotropic. All hydrogen atoms were included in calculated positions (C–H = 0.96 Å) using a riding model. CCDC 182/1486. See http://www.rsc.org/suppdata/cc/a9/a907970j/ for crystallographic data in .cif format.

§ A mixture of amide diastereoisomers **9a** and **9b** was prepared by reaction of (*S*)-2-acetoxypropanoyl chloride with racemic 2-methylpiperidine. An authentic sample of amide **9b** was prepared from (*R*)-2-methylpiperidine, $[\alpha]_D$ (HCl salt) 8.9 (*c* 2, EtOH), itself prepared from the racemic amine by resolution using (*R*)-mandelic acid.

¶ Significantly, the MAQ recovered from the reaction in Scheme 2 was also found to be a mixture of two diastereoisomers, epimeric at the 2-acetoxypropanoyl chiral centre.

1 R. S. Atkinson, E. Barker and M. J. Sutcliffe, *Chem. Commun.*, 1996, 105.
2 Y. Murakami, K. Kendo, K. Miki, Y. Akiyama, T. Watanabe and Y. Yokoyama, *Tetrahedron Lett.*, 1997, **38**, 3751.
3 R. S. Atkinson, A. P. Ayscough, W. T. Gattrell and T. M. Raynham, *J. Chem. Soc., Perkin Trans. 1*, 1998, 2783.
4 R. S. Atkinson, E. Barker, P. J. Edwards and G. A. Thomson, *J. Chem. Soc., Perkin Trans. 1*, 1996, 1047.

Communication a907970j

Nucleobase molecular recognition in supercritical carbon dioxide by using a highly sensitive 27 MHz quartz-crystal microbalance

Toshiaki Mori, Masanobu Naito, Yoshinobu Irimoto and Yoshio Okahata*

Department of Biomolecular Engineering, Tokyo Institute of Technology, 4259 Nagatsuda, Midori-ku, Yokohama 226-8501, Japan. E-mail: yokahata@bio.titech.ac.jp

Received (in Columbia, MO, USA) 14th September 1999, Accepted 8th November 1999

Nucleobase molecular recognition on a self-assembled monolayer was studied in supercritical carbon dioxide and obtained kinetics were compared with those in air and liquid phases.

Molecular recognition is an essential phenomenon in living systems, as observed in complementary hydrogen bond formation in DNA. In recent years, a number of artificial receptors containing base pairing models of DNA have been reported.[1] They confirm selective binding of small guest molecules *via* complementary hydrogen bonds in hydrophobic organic solvents and at the air-water interface, although it hardly occurs in bulk water.[2] Molecular recognition in the gas phase has also been investigated, as it would form a most simple system avoiding any solvation effects on both host and guest molecules.[3] Supercritical fluid is attractive as a third medium, in addition to the liquid and gas phases, because its physical properties (*e.g.* solvation, density, diffusiveness and viscosity) are intermediate between those of a gas and a liquid, and can be manipulated by small changes in pressure or temperature.[4] Several spectral studies of hydrogen bonding interactions[5a–c] and inclusion phenomena[5a,e] have been carried out in supercritical fluid. It is useful to study and compare molecular recognition in these three different states of matter. A quartz-crystal microbalance (QCM) is a useful instrument for detecting directly guest molecular binding processes by measuring mass changes at a host monolayer, as it is independent of media and can be used in an air phase,[3a–c] in aqueous solution,[6] and even in supercritical fluid.

Here we report the binding behavior and kinetics of small guest molecules in supercritical carbon dioxide ($scCO_2$) at a self-assembled monolayer of decanethiol having thymine at the terminus on a highly sensitive 27 MHz QCM (see Fig. 1); these data are then compared with those obtained in the gas phase[3a–c] and in aqueous solution.[6]

A 27 MHz, AT-cut QCM was connected to a handmade oscillator.[6,7] Frequency changes were followed by a universal counter (Hewlett Packard Co., Ltd., model 53131A) attached to a microcomputer system. Calibration of the 27 MHz QCM showed that 0.62 ng cm^{-2} of substrate binding corresponds to 1 Hz of frequency decrease, which was consistent with the Sauerbrey equation[8] and our previous papers.[6,7] The thymine monolayer was immobilized on Au electrodes on both sides (4.9 $mm^2 \times 2$) of the QCM according to the previous papers.[3a–c] The frequency decreased by 500–600 Hz (mass increase, Δm = 310–370 ng cm^{-2}) due to the monolayer immobilization. The theoretical mass of the monolayer on the two gold electrodes was calculated to be 350 ng cm^{-2}, if the surface roughness was assumed to be about 2. These values indicate that the Au electrode was covered with a monolayer of the thymine derivative.

Liquid CO_2 was pumped into a reservoir vessel containing guest molecules at 10–15 MPa using a LC pump (Jasco PU-980 HPLC pump) connected to a CO_2 cylinder. The vessel was warmed up to 40 °C to create the supercritical state. A mixture of guest saturated $scCO_2$ and pure $scCO_2$ was passed at a rate of 3–5 ml min^{-1} into a reaction vessel at 40 °C and 10 MPa, in which the monolayer immobilized QCM was set with a magnetic stirrer. Guest concentrations were controlled by changing the mixture ratio of the two fluids.

Fig. 2 shows typical time courses of frequency changes of the 27 MHz QCM immobilized with the thymine monolayer responding to exposure to the same concentration (1.0×10^{-4} M) of various guest molecules in $scCO_2$ at 40 °C and 10 MPa. Both 9-ethyladenine and 2-aminopyridine (an adenine analogue) were bound reasonably well onto the thymine monolayer, probably due to complementary two-point hydrogen bonding with the host thymine membrane. In spite of having a two-point hydrogen bonding ability with thymine, 1-cyclohexyluracyl and 2-pyrrolidone (a uracil analogue) were hardly adsorbed onto the thymine monolayer. Similar selective binding of adenine derivatives to the thymine monolayer was observed when the binding experiments were carried out in the air phase[3a–c] and on the thymine monolayer at the air-water interface.[6]

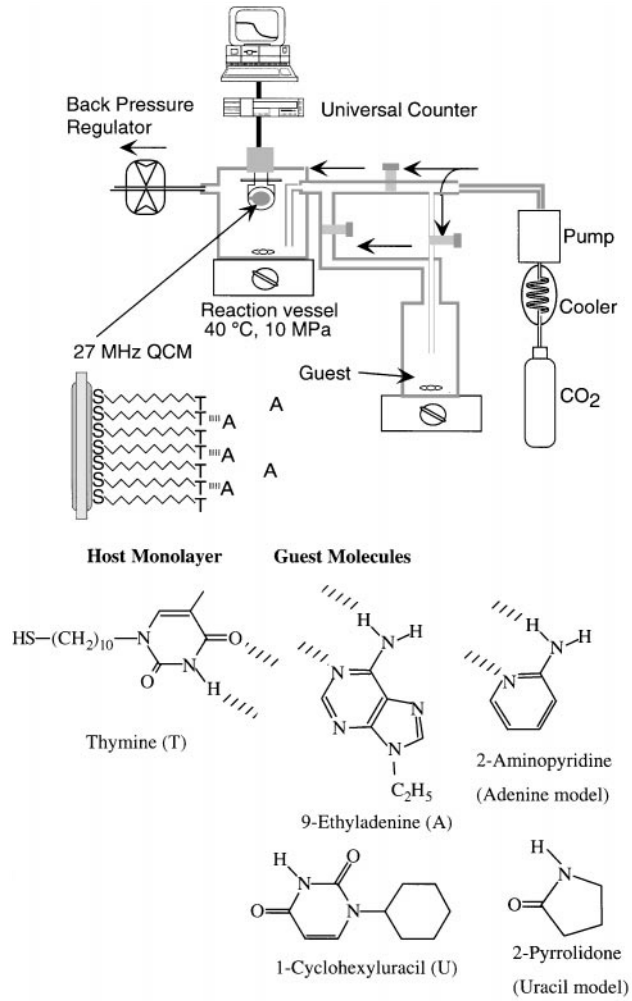

Fig. 1 Schematic illustration of nucleobase binding to a thymine monolayer on a 27 MHz QCM in a supercritical CO_2 flow system.

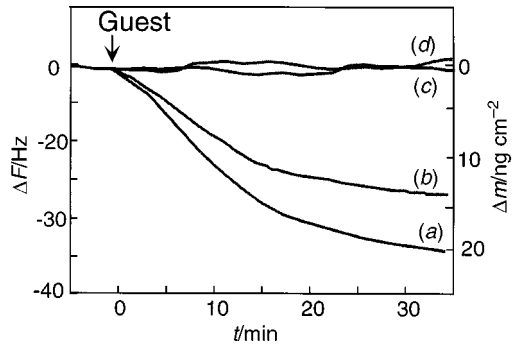

Fig. 2 Time courses of frequency decreases (mass increases) of the 27 MHz QCM immobilized with the thymine monolayer, responding to exposure of guest molecules (1.0×10^{-4} M) in supercritical CO_2 (40 °C and 10 MPa); (*a*) 9-ethyladenine, (*b*) 2-aminopyridine (an adenine model), (*c*) 1-cyclohexyluracil and (*d*) 2-pyrrolidone.

Table 1 Association constants (K_a) and initial binding rate constants (k_1) for guest bindings to the thymine monolayer in various media

Media	Guests	$K_a/10^3$ M^{-1}	k_1/M^{-1} s^{-1}
$scCO_2$[a]	9-ethyladenine	1.2	2.0
	2-aminopyridine (an adenine model)	2.6	8.0
	1-cyclohexyuracil	0.02	0.1
	2-pyrrolidone (a uracil model)	0.02	0.2
Air[b]	2-aminopyridine (an adenine model)	73 000	190 000
	2-pyrrolidone (a uracil model)	780	21 000
Water[c]	adenosine	0.23	0.5
	uridine	< 0.01	< 0.01

[a] 40 °C, 10 MPa. [b] 25 °C, see refs. 3(*a*) and 9. [c] 25 °C, pH 7.5, 0.01 M phosphate buffer, see refs. 6 and 10.

When the concentration of guest molecules increased (2×10^{-5} to 5×10^{-4} M), the typical saturation binding curves were obtained. From the reciprocal plots, association constants (K_a) could be obtained from linear correlations. From the initial slopes of the frequency decreases (mass increases) of Fig. 2, the apparent binding rate constants (k_1) were calculated. These data are summarized in Table 1, as are those values obtained using the same QCM system in the air[3a,9] or on the monolayer at the air-water interface.[6,10]

Complementary binding between the thymine monolayer and 9-ethyladenine or 2-aminopyridine (an adenine model) showed $K_a = (1.2–2.6) \times 10^3$ M^{-1}, which is about 100 times larger than K_a = 10–20 M^{-1} for noncomplementary binding of 1-cyclohecyluracil or 2-pyrrolidone. Similar selectivity was observed between the thymine monolayer and 2-aminopyridine (an adenine model) or 2-pyrrolidone (a uracil model) in the air phase at 25 °C, and between the thymine monolayer and adenosine or uridine in the aqueous solution (25 °C, pH 7.5, 0.01 M phosphate buffer). In the air phase, 2-aminopyridine and 2-pyrrolidone were employed as adenine and thymine models, respectively, since nucleobases are difficult to vaporize under the usual conditions. In aqueous solution, adenosine and uridine were employed due to their high solubility to aqueous solution.

Complementary hydrogen bonding between nucleobases has been confirmed by FT-IR spectral measurements in $CDCl_3$ solution.[11] We measured FT-IR spectra in the bulk $scCO_2$ using a pressure-resistant stainless steel vessel with ZnSe windows.[12] The $\delta_{N–H}$ at 1604 cm^{-1} for 2-aminopyridine (an adenine model) was shifted to 1616 cm^{-1} in the presence of an equal amount of 2-pyrrolidone (a uracil model) in $scCO_2$ (40 °C, 10 MPa), indicating that both molecules interact through hydrogen bonding as efficiently as in $CDCl_3$ solution.[11]

The selectivity (about 100 times) of the thymine monolayer for complementary guest molecules was similar among the three phases (air, water and super critical fluid). However, association constants (K_a) and initial binding rate constants (k_1) largely depended on the medium. K_a and k_1 values obtained in the air phase were very large due to the lack of solvent effects in the gas state, and those values in supercritical fluid were closer to, but still 10 times larger than, those in the aqueous phase. In supercritical fluid, the medium itself is thought to form fluid clusters, by which substrates are weakly solvated like a monolayer.[4a] This means that the very thin, weak solvation of the host and/or guest molecules in the supercritical fluid significantly reduced the interaction compared with the bare interaction in gas phase, and became close to the fully solvated interaction in the solution. Although the reaction conditions and guest molecules are slightly different for the three media, the K_a and k_1 values reflect the physical properties such as solvation and diffusiveness in each medium.

In conclusion, we could observe selective interactions between nucleobases in a supercritical fluid, and the QCM system is useful to monitor this binding behavior even in supercritical fluid, as well as in the liquid and air phases. One of advantages of supercritical fluid as a medium is that its physical properties, such as density, diffusion rate and solvation, can be reversibly changed by varying the temperature or pressure of the $scCO_2$ state.[13] We are currently studying the effect of solvation on molecular recognition by changing the physical state of the supercritical fluid.

Notes and references

1 J. Rebek Jr., *Angew. Chem., Int. Ed. Engl.*, 1990, **29**, 245; A. D. Hamilton, *J. Chem. Educ.*, 1990, **67**, 821.

2 K. Kurihara, K. Ohta, Y. Honda and T. Kunitake, *J. Am. Chem. Soc.*, 1991, **113**, 5077; R. Ahuja, P.-L. Caruso, D. Möbius, W. Paulus, H. Ringsdorf and G. Wildburg, *Angew. Chem., Int. Ed. Engl.*, 1993, **32**, 1033.

3 (*a*) K. Matsuura, Y. Ebara and Y. Okahata, *Langmuir*, 1997, **13**, 814; (*b*) Y. Okahata, K. Matsuura and Y. Ebara, *Supramol. Sci.*, 1996, **3**, 165; (*c*) K. Matsuura and Y. Okahata, *Chem. Lett.*, 1996, 119; (*d*) I.-H. Chu, D. V. Dearden, J. S. Bradshaw, P. Huszthy and R. M. Izatt, *J. Am. Chem. Soc.*, 1993, **115**, 4318.

4 (*a*) A. A. Clifford, in *Supercritical Fluids, vol. 273*, ed. E. Kiran and J. M. H. L. Segers, Kluwer, Netherlands, 1994, pp. 449–479; (*b*) O. Kajimoto, *Chem. Rev.*, 1999, **99**, 353; (*c*) P. G. Jessop, T. Ikariya and R. Noyori, *Science*, 1995, **269**, 1065; (*d*) T. Mori and Y. Okahata, *Chem. Commun.*, 1998, 2215; (*e*) T. Mori, A. Kobayashi and Y. Okahata, *Chem. Lett.*, 1998, 921.

5 (*a*) R. B. Gupta, J. R. Combes and K. P. Johnston, *J. Phys. Chem.*, 1993, **97**, 707; (*b*) S. G. Kazarian, R. B. Gupta, M. J. Clarke, K. P. Johnston and M. Poliakoff, *J. Am. Chem. Soc.*, 1993, **115**, 11 099; (*c*) H. Ochel and G. M. Schneider, *Ber. Bunsenges. Phys. Chem.*, 1994, **98**, 610; (*d*) J. D. Glenmon, S. Hutchinson, S. J. Harris, A. Walker, M. A. McKerrey and C. C. McSweeney, *Anal. Chem.*, 1997, **69**, 2207; (*e*) J. Ke, S. Jin, B. Ham, H. Yan and D. Shen, *J. Supercrit. Fluids*, 1997, **11**, 53.

6 Y. Ebara, K. Itakura and Y. Okahata, *Langmuir*, 1996, **12**, 5165.

7 Y. Okahata, Y. Matsunobu, K. Ijiro, M. Mukai, A. Murakami and K. Makino, *J. Am. Chem. Soc.*, 1992, **114**, 8299; Y. Okahata, M. Kawase, K. Niikura, F. Ohtake, H. Furusawa and Y. Ebara, *Anal. Chem.*, 1998, **70**, 1288; Y. Okahata, K. Niikura, Y. Sugiura, M. Sawada and T. Morii, *Biochemistry*, 1998, **37**, 5666; K. Niikura, H. Matsuno and Y. Okahata, *J. Am. Chem. Soc.*, 1998, **120**, 8537; K. Niikura, H. Matsuno and Y. Okahata, *Chem. Eur. J.*, 1999, **5**, 1609.

8 G. Z. Sauerbrey, *Z. Phys.*, 1959, **155**, 206.

9 In the air phase, the thymine monolayer-immobilized QCM was set in the atmospheric flow of dry N_2 gas and guest molecules were added into the flow using a system similar to that shown in Fig. 1.

10 In the aqueous phase experiments, the monolayer of the amphiphile having thymine as a hydrophilic head group was spread on the water phase, the bare QCM plate was attached horizontally from the air phase on the amphiphile monolayer, and then guest molecules were injected into the water phase (ref. 6).

11 Y. Kyogoku, R. C. Lord and A. Rich, *Science*, 1966, **154**, 518.

12 Although we attempted direct detection of the hydrogen bond formation on the monolayer using an RAS-IR at the interface, we could not obtain clear results due to a lack of the sensitivity.

13 For example, density and relative permittivity can be changed over the ranges 0.1–0.8 and 0.1–0.5, respectively, by changing the pressure from 7 to 20 MPa at 40 °C.

Communication a907478c

The insertion of sulfur dioxide into palladium–methyl bonds: the synthesis and X-ray crystal structure of an unusual $[(dppp)PdOS(Me)O]_2[BAr'_4]_2$ dimer

Derek P. Gates, Peter S. White and Maurice Brookhart*

Department of Chemistry, University of North Carolina at Chapel Hill, Chapel Hill, NC 27599-3290, USA. E-mail: brook@net.chem.unc.edu

Received (in Bloomington, IN, USA) 26th July 1999, Accepted 22nd October 1999

The migratory insertion of sulfur dioxide into the palladium(II)–methyl bond of [(dppp)Pd(Me)(OEt_2)]BAr'_4 [Ar′ = $C_6H_3(CF_3)_2$-3,5] to yield a unique dimeric eight-membered palladacycle was followed by NMR spectroscopy, and the product characterised by X-ray crystallography.

Palladium(II) complexes possessing bidentate ligands are known to efficiently catalyse the copolymerisation of olefins with carbon monoxide to form polyketones.[1] Sulfur dioxide is an attractive monomer for catalytic copolymerisations with olefins since SO_2, like CO, is known to undergo facile insertion reactions into a variety of transition metal–alkyl bonds.[2,3] Indeed, Drent recently patented alternating copolymerisation of ethylene with SO_2 using various palladium(II) complexes.[4] In 1998, Sen and coworkers also reported that [(dppp)PdMe(NCMe)]BF_4 was an effective catalyst for the copolymerisation of SO_2 with ethylene, propylene and cyclopentene.[5] Here, we report our preliminary investigations of the insertion reactions of SO_2 into Pd(II)–methyl bonds and the attempted spectroscopic detection of the copolymerisation of ethylene and SO_2.

The cationic 1,3-bis(diphenylphosphino)propane (dppp) palladium(II) complex **1** can be prepared by the low temperature

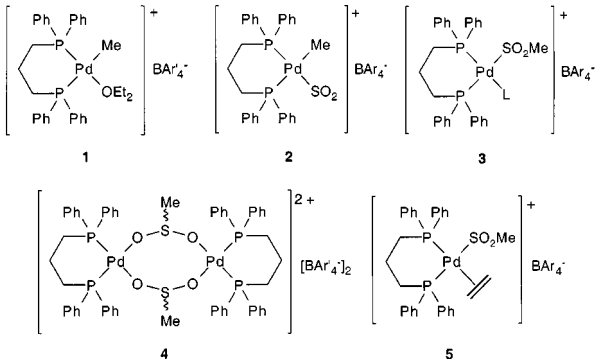

1 **2** **3** **4** **5**

reaction of $(dppp)PdMe_2$ **6** with $H(OEt_2)_2[BAr'_4]$ [Ar′ = $C_6H_3(CF_3)_2$-3,5].[6] We have previously studied the reactions of carbon monoxide with **1** at −70 °C, and have found that insertion proceeds *via* initial displacement of diethyl ether with CO followed by migratory insertion into the Pd–Me bond.[7] Immediately after treating a solution of **1** in CD_2Cl_2 with an excess of SO_2 (*ca.* 25 equiv.) at 193 K, the ^{1}H NMR spectrum shows the presence of free diethyl ether. Analysis of the reaction mixture by ^{31}P NMR spectroscopy (193 K) shows the formation of a major product (*ca.* 80%) which exhibits a singlet at δ 15.7 indicating equivalence of the phosphorus nuclei. In addition, two minor products (*ca.* 20%) with singlet resonances at δ 15.4 and 14.5 are also observed. The expected products, **2** and **3**, both of which would possess inequivalent phosphorus atoms, are not observed under these conditions. In addition, the ^{1}H NMR spectrum exhibits three new singlets[5] at δ 0.52 (78%), 0.42 (8%) and 0.25 (14%) which are assigned to $-CH_3$ groups, no signals were observed downfield at *ca.* 2–3 where resonances for an $-S(O)_2CH_3$ group would be expected.[8] A preparative scale reaction† was carried out in an attempt to isolate single crystals. Indeed, pale yellow crystals suitable for X-ray diffraction were isolated after recrystallisation of the crude product from dichloromethane–hexanes at −30 °C.‡

The molecular structure of the isolated product **4** is shown in Fig. 1, and confirms that insertion of SO_2 into the Pd–Me bond had taken place, however dimerisation resulted in the formation of an eight-membered cyclic compound in which the phosphorus atoms are equivalent, consistent with the ^{31}P NMR observations. In particular, the eight-membered ring consists of a plane of palladium and oxygen atoms, with the sulfur atoms located above and below the plane. The six-membered rings formed by the dppp ligand are in the chair conformation.

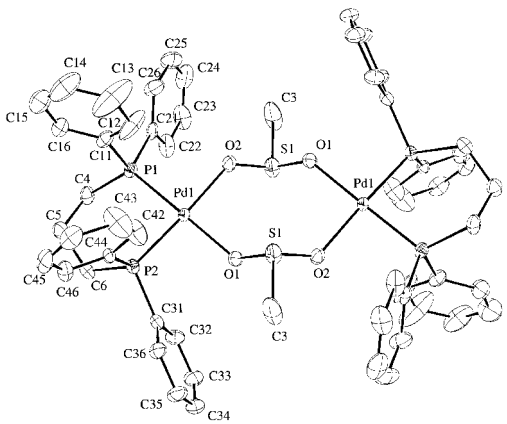

Fig. 1 Molecular structure of **4** (BAr'_4 anion omitted for clarity) with thermal ellipsoids shown at the 50% probability level. Selected bond lengths (Å) and angles (°): Pd(1)–P(1) 2.2354(20), Pd(1)–P(2) 2.2393(19), Pd(1)–O(1) 2.078(5), Pd(1)–O(2) 2.088(5), O(1)–S(1) 1.494(5), O(2)–S(1) 1.507(5), S(1)–C(3) 1.786(10); P(1)–Pd(1)–P(2) 90.12(7), P(1)–Pd(1)–O(2) 89.00(15), P(2)–Pd(1)–O(1) 90.47(15), O(1)–Pd(1)–O(2) 90.92(19), O(1)–S(1)–O(2) 109.5(3), O(1)–S(1)–C(3) 98.4(5), Pd(1)–O(1)–S(1) 128.0(3).

A variable temperature NMR experiment was carried out on **4** in CD_2Cl_2 solution. As the temperature is raised from 193 K the three singlet ^{31}P resonances (δ 15.7, 15.4, 14.5) begin to broaden at *ca.* 260 K and coalesce to a singlet above *ca.* 300 K. This process is reversible. Similarly, the three methyl signals also coalesce to a singlet but at a somewhat lower temperature (*ca.* 280 K) owing to the smaller spread in resonance frequencies. Since the inversion barrier at tetrahedral sulfur in **4** is expected to be high, the most likely source of the isomerism observed here[9] comes from ring inversion of the chair conformation of the dppp ligand.

We have also studied the behaviour of **1** towards mixtures of ethylene and SO_2 in an attempt to spectroscopically observe the insertion of SO_2 and ethylene in an alternating fashion. Thus, treatment of a solution of **1** in CD_2Cl_2 with a mixture of ethylene (10 equiv.) and SO_2 (10 equiv.) results in quantitative displacement of ether with ethylene at 193 K forming [(dppp)Pd(Me)(η^2-C_2H_4)]BAr'_4[10] which was characterised by ^{31}P [δ = 17.5 (d, *J* 56 Hz), −1.5 (d, *J* 56 Hz)] and ^{1}H NMR spectroscopy [δ 5.18 (bound C_2H_4), 0.34 (dd, Pd–CH_3, *J* 7, 4 Hz)]. Upon warming the reaction mixture to 223 K for *ca.* 30

min complex **4** was formed in nearly quantitative yield. No evidence for insertion of ethylene into the Pd–Me bond was detected, nor was any direct insertion of SO_2 into the Pd–Me bond of the methyl ethylene complex observed to form **5**. This suggests that formation of **4** from [(dppp)Pd(Me)(η^2-C_2H_4)]BAr′$_4$ (or **1**) involves displacement of ethylene (or diethyl ether for **1**) to yield **2** which then undergoes a rapid migratory insertion reaction to form **3** which then dimerises yielding **4**. This is in contrast to observations by Jones for analogous L_2PtMe_2 complexes which readily insert SO_2 *via* a five coordinate intermediate.[8] We have also carried out the analogous reaction of Pd complex **6** with SO_2 to form **7** presumably also *via* a five coordinate intermediate [eqn. (1)].†

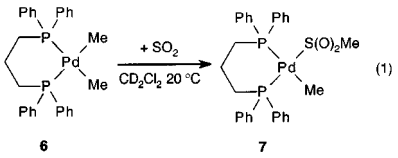

6 **7** (1)

In an attempt to obtain conclusive evidence for a migratory insertion mechanism, a low-temperature NMR experiment was carried out using $CDCl_2F$ as solvent. Thus, SO_2 (10 equiv.) was added to a solution of ether complex **1** in $CDCl_2F$ at 153 K. Upon warming to 173 K several new products could be detected in addition to **1**. The ^{31}P NMR spectrum exhibited resonances assigned to **4**, and also two sets of doublets at δ 22.0 and −5.5 (J_{PP} 50 Hz) and δ 18.8 and 17.4 (J_{PP} 20 Hz). In the ^{1}H NMR spectrum, in addition to **4**, two new products were observed which exhibited a methyl singlet at δ 1.6 and a methyl doublet of doublets at δ 0.0 (J_{HP} 7, 4 Hz). The signal at δ 0.0 is clearly due to a Pd–CH_3 group of a (dppp)Pd$(CH_3)^+$ moiety and, since this species is not observed in the absence of SO_2, we assign this resonance to complex **2**, [(dppp)Pd$(CH_3)(SO_2)]^+$. The ^{31}P resonances at δ 22.1 (d, *J* 50 Hz) and δ −5.6 (d, *J* 50 Hz) can be assigned to **2**. The low field methyl resonance at δ 1.6 [^{31}P resonances δ 18.8 (d, *J* 20 Hz), δ 17.4 (d, *J* 20 Hz)] is assigned to monomer **3**, a precursor to dimer **4**, formed *via* a migratory insertion reaction of **2**. The ligand (L) occupying the fourth coordination site in **3** is likely to be either SO_2 or Et_2O. As the reaction mixture was warmed in 5 °C increments, the signals for **2**, **3** and **4** increased in intensity and those for **1** decreased. At 213 K, only isomers of **4** could be detected. We speculate that in **3** the SO_2Me is bound through oxygen, rather than sulfur, based on the molecular structure of the final product **4**.

A copolymerisation was attempted using hex-1-ene (10% v/v) in CH_2Cl_2 purged with SO_2 in the presence of a catalytic quantity of **1** (14 mg).[11]† After *ca.* 14 h, the reaction was quenched with methanol. Solvent removal *in vacuo*, yielded a small amount of a polymeric material (23 mg). The polymer was precipitated with methanol and was characterised by gel permeation chromatography (M_n = 61 000: PDI = 5.8), and the ^{1}H and ^{13}C NMR data are identical with those reported for the hex-1-ene/SO_2 alternating copolymer prepared using a free-radical initiator.[12] Comparing the amount of **1** used as initiator (9×10^{-6} mol), the amount of hex-1-ene consumed (1.6×10^{-4} mol) and the estimated M_n of the polymer produced (61000) suggests that if chain growth occurred at Pd only a very small fraction of the Pd centers were active (< 5%). Results from repeated polymerisations proved quite erratic with varying amounts of polymer produced both in the presence and absence of **1**. Reactions conducted in the presence of the radical scavenger galvinoxyl failed to produce polymer.[13] These results, coupled with the failure to spectroscopically observe ethylene insertion in these systems and the ready formation of the stable dimer **4**, suggest that the copolymerisation of hex-1-ene and SO_2 under conditions reported above does not occur by a coordination–insertion process initiated by **1**. A radical chain growth mechanism appears very likely, although we cannot rule out copolymerization in the presence of **1** which is initiated by traces of a palladium complex of unknown structure present in **1** and which can be deactivated by galvinoxyl. The copolymerizations reported by Sen and coworkers[5] were carried out at higher pressures (600 psi), so it is uncertain how these results relate to those experiments.

We thank NSF for support of this work. D. P. G gratefully acknowledges NSERC of Canada for a Postdoctoral Fellowship. Thanks to S. Svejda for providing a sample of $CDCl_2F$ and to S. Shultz for useful discussions.

Notes and references

† *Preparation* of **4**: under an atmosphere of argon, SO_2(g) (150 mL, 6 mmol) was slowly purged through a cloudy white stirred suspension of **1** (102 mg, 0.07 mmol) in CH_2Cl_2 (7 mL) at −78 °C. After stirring for 10 min a clear yellow solution was observed and the solvent was removed *in vacuo* yielding a yellow solid. The crude product was recrystallized by dissolution in 3 mL of CH_2Cl_2 at −78 °C and layering pentanes (1.5 mL) over the solution. Overnight at −30 °C light yellow crystals formed. Yield 28 mg (30%). ^{1}H NMR (CD_2Cl_2, 193 K); major isomer (78%): δ 7.72 (s, 8H, BAr′$_4$: *o*-H), 7.53 (s, 4H, BAr′$_4$: *p*-H), 7.5–7.2 (m, 20H, C_6H_5), 2.49 (br, 2H, PCH_2), 2.34 (br, 2H, PCH_2), 2.07 (m, 2H, CH_2), 0.52 (s, CH_3), minor isomers: δ 0.42 (s, CH_3) (8%), 0.25 (s, CH_3) (14%); ^{31}P (CD_2Cl_2, 193 K) δ 15.7 (major isomer, *ca.* 80%), 15.4, 14.5 (minor isomers, *ca.* 20%). Anal. Calc.: C, 49.32; H, 2.83. Found: C, 49.37; H, 2.81%.

(dppp)Pd(Me)S(O)$_2$Me **7**: ^{1}H NMR (CD_2Cl_2, 293 K) δ 7.6–7.2 (m, 20H, C_6H_5), 2.4 (m, 4H, PCH_2), 2.21 (s, 3H, SO_2CH_3), 2.1 (m, 2H, CH_2), 0.52 (pseudo t, J_{PH} 6 Hz, 3H, CH_3); ^{31}P NMR (CD_2Cl_2, 293 K); δ 18.9 (J_{PP} 48 Hz), 3.1 (J_{PP} 48 Hz).

Polymerisation studies: a 10% solution of freshly distilled hex-1-ene (5 mL) in CH_2Cl_2 (45 mL) was purged with SO_2 for 7 min at room temperature. A solution of **1** (14 mg, 9 μmol) was added at −78 °C, and the reaction was stirred at room temperature for 14 h. Methanol (*ca.* 10 mL) was added to quench the reaction, the solution concentrated *in vacuo*, and methanol added to precipitate the polymer. Yield 23 mg. ^{1}H NMR ($CDCl_3$) δ 4.1–3.6 [br, 2H, SO_2CH_2], 3.3 [br, 1H, C*H*(Bu)SO_2], 2.5–1.7 (br, α-CH_2), 1.7–1.3 (br, 4H, CH_2CH_2), 0.9 (t, 3H, CH_3); GPC (THF, *vs.* PS standards): M_n = 61000, PDI 5.8. Identical conditions were applied for the reactions in the absence of **1** or in the presence of galvinoxyl (10 mg).

‡ *Crystal data* for $C_{65}H_{44}BCl_4F_{24}O_2P_2PdS$ **4**: M = 1666.04, triclinic, space group $P\bar{1}$, a = 13.0395(6), b = 17.1606(8), c = 17.9784(8) Å, α = 72.309(1), β = 78.658(1), γ = 68.341(1)°, V = 3545.8(3) Å^3, T = 173 K, Z = 2, μ(Mo-Kα) = 0.59 mm^{-1}, $2\theta \leqslant 56°$, 42774 reflections measured, 17105 unique (R_{int} = 0.031), 10812 observed [$I_{net} > 2.5\sigma(I_{net})$]. R_f = 0.079 (observed data), R_w = 0.104 (unique data). The data were collected using a Bruker SMART diffractometer using the ω scan mode, and solved using direct methods and refined by full matrix least squares on F_o. CCDC 129/236.

1 See, for example: A. Sen, *Adv. Polym. Sci.*, 1986, **73/74**, 125; E. Drent, J. A. M. van Broekhoven and M. J. Doyle, *J. Organomet. Chem.*, 1991, **417**, 235; M. Brookhart, F. C. Rix, J. M. DeSimone, J. C. Barborak, *J. Am. Chem. Soc.*, 1992, **114**, 5894; F. C. Rix, M. Brookhart and P. S. White, *J. Am. Chem. Soc.*, 1996, **118**, 4746.
2 For general reviews, see: G. J. Kubas, *Acc. Chem. Res.*, 1994, **27**, 183; A. Wojcicki, *Adv. Organomet. Chem.*, 1974, **12**, 31; W. Kitching and C. W. Fong, *Organomet. Chem. Rev. A*, 1970, **5**, 281.
3 The reaction of SO_2 with ethylene in the presence of catalytic amounts of $PdCl_2$ has been reported to produce $EtS(O)_2CH_2CH{=}CHCH_3$. See: H. S. Klein, *Chem. Commun.*, 1968, 377.
4 E. Drent, *US Pat.* 4 808 697, 1989.
5 L. M. Wojcinski, M. T. Boyer and A. Sen, *Inorg. Chim. Acta*, 1998, **270**, 8.
6 M. Brookhart, B. Grant and A. F. Volpe, *Organometallics*, 1992, **11**, 3920.
7 J. Ledford, C. S. Shultz and M. Brookhart, unpublished work.
8 M. S. Morton, R. J. Lachicotte, D. A. Vicic and W. D. Jones, *Organometallics*, 1999, **18**, 227.
9 Quantitative analysis of the spectra were not performed but the barrier to isomer interconversions must lie in the range 14–15 kcal mol^{-1} based on ^{31}P NMR linewidths at 263 K.
10 J. Ledford and M. Brookhart, unpublished work.
11 Hex-1-ene was chosen as comonomer because the ethylene/SO_2 copolymers are poorly soluble and difficult to characterise.
12 K. J. Ivin, M. Navratil and N. A. Walker, *J. Polym. Sci. Part A-1*, 1972, **10**, 701.
13 Polysulfones are generally prepared by radical initiated copolymerisation of SO_2 with olefins. Temperatures as low as −100 °C can be used. C. P. Tsonis, in *Polymeric Materials Encyclopedia*, ed. J. C. Salamone, CRC Press, New York, 1996, vol. 9, p. 6866.

Communication a905993h

Vanadium [dicyanoperfluorostilbene]$_2$·*y*THF: a molecule-based magnet with $T_c \approx 205$ K†

Jeffrey P. Fitzgerald,[a] Bharat B. Kaul[b] and Gordon T. Yee*[b]

[a] *Department of Chemistry, United States Naval Academy, Annapolis, MD 21402, USA*
[b] *Department of Chemistry and Biochemistry, University of Colorado, Boulder, CO 80309, USA. E-mail: yeeg@colorado.edu*

Received (in Bloomington, IN, USA) 16th September 1999, Accepted 17th November 1999

A new radical anionic bridging ligand, derived from the *in situ* reduction of α,α′-dicyanoperfluorostilbene, is reported to support ferrimagnetic ordering below 205 K in a three-dimensional vanadium-based coordination polymer.

In 1991, Miller and coworkers reported that the reaction of $V(C_6H_6)_2$ and tetracyanoethylene (TCNE), in dichloromethane yields an air-sensitive solid that is magnetically ordered at room temperature.[1] This compound, formulated as $V(TCNE)_2 \cdot 0.5CH_2Cl_2$ based on elemental analysis, represented the first example of ferrimagnetism above room temperature in a molecule-based system. The structure is presumed to be a three-dimensional coordination polymer consisting of solvent-ligated V^{2+} cations bridged by $TCNE \cdot^{1-}$ anions, though only limited structural information has been obtained.[2] One factor perhaps contributing to the amorphous nature of the solid is that, in principle, TCNE may bridge up to four metal centers, resulting in a degree of structural randomness.[3] Miller and coworkers have subsequently studied the effects of coordinating solvent[2] and improved on the synthesis, replacing $V(C_6H_6)_2$ with the more readily available precursor, $V(CO)_6$.[4] In recent work, they have shown that $MI_2 \cdot x$MeCN salts, (M = Mn, Fe, Co or Ni), are viable sources of building blocks for analogous $M(TCNE)_2$ magnets in which T_c ranges from 44 to 121 K.[5]

Despite this progress, no organic acceptor has been reported to substitute for TCNE in reactions with $V(CO)_6$ or $V(C_6H_6)_2$ to give a magnetically ordering compound.[2] Although many candidates possess the requisite electrochemical properties, those that have been examined, including 7,7,8,8-tetracyanoquinodimethane (TCNQ), 2,3-dichloro-5,6-dicyano-1,4-benzoquinone (DDQ) and tetrachloro-1,4-benzoquinone, react to yield paramagnetic solids, none of which show any signs of magnetic order.[2] These results have left it unclear what special properties of TCNE, such as molecular size, shape, redox properties or the ability to coordinate more than two metal centers, are critical to achieving a magnetically ordered solid. The *absence* of another efficacious acceptor has hampered efforts to elucidate the detailed mechanism of magnetic coupling in $V(TCNE)_2$ and to further develop this intriguing family of ferrimagnetic three-dimensional coordination polymers.

Here we report the discovery of a second magnetically ordering compound in the V(acceptor)$_2$·*y*(solvent) family. Pursuing a strategy involving the design and synthesis of ethylenic acceptors related to TCNE,[6] has led to the discovery that α,α′-dicyanoperfluorostilbene, (DCPFS), reacts with $V(CO)_6$ in THF to give an air-sensitive, charge-transfer coordination polymer, $V(DCPFS)_2 \cdot y$THF, a compound that orders, apparently ferrimagnetically, with $T_c \approx 205 \pm 5$ K. Because many of the characteristics of DCPFS are so unlike those of TCNE, its examination helps to delineate the properties that are unimportant in the design of potential new radical anionic bridging ligands. The construction of coordination polymer magnets with radical anionic bridging ligands is an attractive approach because the versatility of organic chemistry can be exploited and because the compounds produced are inherently three-dimensional, which favors higher T_c values.

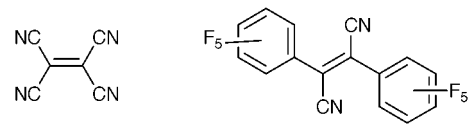

TCNE DCPFS

DCPFS was prepared by the oxidative dimerization of pentafluorophenylacetonitrile utilizing a modification of the method described by Cook and Linstead.[7,8] Both *cis* and *trans* products are fully characterized, air-stable, crystalline, white solids. Using cyclic voltammetry, it was found that *trans*-DCPFS exhibits a quasi-reversible one-electron reduction at *ca.* −1.0 V *vs.* ferrocene.[8] This value is 0.7 V more negative than the first reduction of TCNE, revealing that DCPFS is only a modest electron acceptor. It does not, for instance, oxidize decamethylmanganocene in CH_2Cl_2.

In spite of its relatively negative reduction potential, DCPFS reacts readily with $V(CO)_6$. In a typical preparation, $V(CO)_6$ in THF is treated with 2.2 equiv. of *trans*-DCPFS at room temp. in an inert atmosphere glove box.[8] The color immediately changes from yellowish green to reddish purple, but in sharp contrast to reactions between $V(CO)_6$ and TCNE, this reaction appears to remain homogeneous for at least several minutes after mixing of the two reactants. Over the course of 1 h, however, a small amount of dark precipitate deposits on the sides of the flask. This initial precipitate exhibits magnetic order, but at a relatively low T_c, perhaps because the degree of polymerization is still low. To obtain the higher T_c material, the solvent is removed under vacuum and the residue is triturated in Et_2O for 15 min. The black solid is collected on a fritted glass filter and washed with Et_2O until the filtrates run clear. Once precipitated, the solid cannot be redissolved in the original solvent.

Unfortunately, despite the greater solubility of incipient $V(DCPFS)_2 \cdot y$THF in organic solvents, we have not yet been able to crystallize it. Powder X-ray diffraction shows that the isolated compound is amorphous. IR spectrometry reveals little about the coordination environment except that there is no CO present. Elemental analysis of the product is variable, as was previously observed for the TCNE analog.[4] However, the results on five independently prepared samples are roughly consistent with the formulation, $V(DCPFS)_2 \cdot y$THF, ($y \approx 2$). The analyses were usually high in vanadium, a fact not too surprising given the method of isolation.

To support this proposed formulation, additional experiments have been performed in which the reactant ratios were varied. As expected, preparing the compound beginning with a 1:1 ratio of acceptor to donor, resulted in a product with a much lower critical temperature, and in much lower yield. In contrast, the product obtained from the 4:1 reactant ratio was magnet-

† Electronic supplementary information (ESI) available: preparation and spectral data for α,α′-dicyanoperfluorostilbene. See http://www.rsc.org/suppdata/cc/a9/a907535f/

ically equivalent to that obtained from the 2:1 procedure and the quantity of isolated product was essentially the same.

A sample [henceforth abbreviated $V(DCPFS)_2$] for magnetic studies was sealed under vacuum in a glass holder as previously described.[9] The plot of gram magnetization, *M*, *vs.* temperature, *T*, measured in 2 G applied field is shown in Fig. 1. It clearly shows the onset of magnetic order below *ca.* 205 K. The continuous decrease in magnetization with increasing temperature is reminiscent of the behavior observed for the TCNE analog. The feature at *ca.* 120 K might be the result of a second magnetic phase transition or indicate the presence of a second magnetic phase. The plot of ac susceptibility for $V(DCPFS)_2$ is also quite similar to that observed for $V(TCNE)_2$.[10] The data appear as a broad, featureless, frequency-independent maximum in χ' with a small non-zero χ'' component.[8]

Like $V(TCNE)_2$, $V(DCPFS)_2$ is a soft ferromagnet. Fig. 2 shows the plot of gram-magnetization, *M*, *vs.* applied field, *H*, at 5 K. At this temperature, the amount of hysteresis is very small; the coercive field is < 20 G. Gram-magnetization was plotted because of the uncertainty in the formula unit. However, assuming the stoichiometry $V(DCPFS)_2 \cdot 2THF$, one calculates the saturation magnetization to be *ca.* 7000 emu-G mol^{-1}, roughly consistent with ferrimagnetic coupling of two spin 1/2 anions and one spin 3/2 cation per formula unit.

It is important to note that the observed magnetic properties are not due to an impurity phase: by cooling a sample to 77 K in a sealed round bottom flask, one can easily attract and move the entire sample with a Sm–Co permanent magnet. Further, while one might suspect the presence of a vanadium-based Prussian blue-type ferrimagnet *via* the reductive decomposition of DCPFS, that seems very unlikely given no such rationally designed phase has been reported that contains only vanadium and no other metal.[12–14] Also, if such a compound did exist, it would have to possess ordered CN ligands around ordered mixed-valent V cations (no low-spin electron configurations exist for octahedral V in oxidation states two or higher) and these would have to arise from our one-pot synthesis.

Several modifications of the above standard procedure for preparing $V(DCPFS)_2$ were found to result in samples with inferior magnetic properties. For instance, carrying out the reaction in CH_2Cl_2 instead of THF gives a material with $T_c \approx 100$ K. This result is in sharp contrast with the corresponding reaction of $V(CO)_6$ with TCNE for which CH_2Cl_2 is the solvent of choice and coordinating solvents such as THF give rise to products with lower T_c values.[14] In THF, using $V(C_6H_6)_2$ in place of $V(CO)_6$ as a source of V^0 results in an ordering phase,

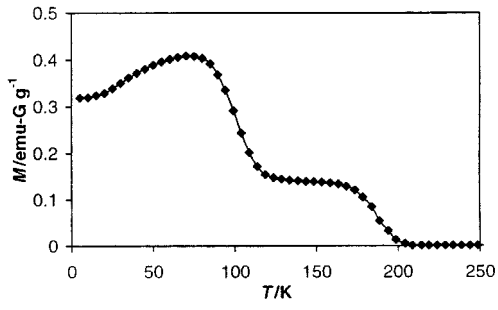

Fig. 1 Plot of magnetization, *M*, *vs.* temperature, *T*, measured at 2 G.

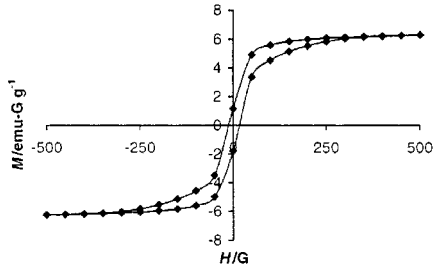

Fig. 2 Plot of magnetization, *M*, *vs.* applied field, *H*, measured at 5 K.

although the T_c is considerably lower (*ca.* 80 K). On the other hand, we have found that *cis*-DCPFS reacts with $V(CO)_6$ to give a magnetically identical product to that obtained from *trans*-DCPFS. This result, coupled with the observation that the Et_2O washes contain mixtures of *cis*- and *trans*-DCPFS, suggests that isomerization about the double bond occurs upon formation of the radical anion.

In conclusion, we have discovered $V(DCPFS)_2 \cdot y$THF to be a molecule-based magnet possessing a T_c of 205 K. Its magnetic behavior is quite reminiscent of the room temperature magnet, $V(TCNE)_2$. It is unclear what sets TCNE and DCPFS apart from other organic acceptors in reactions with $V(CO)_6$ and $V(C_6H_6)_2$. At this point, we can comment more meaningfully on the differences between DCPFS and TCNE and their impact on the choice of future synthetic targets:

1 Redox properties; TCNE is a relatively good acceptor, but DCPFS is a poor acceptor. This means that many more weak acceptor bridging ligands need to be investigated for their ability to mediate exchange.
2 Number of N donor sites; TCNE has four, but DCPFS has only two. Thus, despite the fact that each DCPFS ligand can act as a bridge between only two V cations, a ratio of two acceptors per donor is sufficient to form a three-dimensionally ordered magnetic solid.
3 Molecular size and shape; planar TCNE is the smallest acceptor and DCPFS is one of the largest and probably not flat. This result can be interpreted to mean that steric repulsion does not play a significant role, provided the fumaronitrile unit is left intact. Thus, larger, more complex ligands can be envisioned and should be investigated.

We thank the National Science Foundation for support of this work and the National Institute of Standards and Technology for use of the SQUID magnetometers. We also acknowledge Mr Christopher M. Holloway for synthetic help and Mr Roger Sommer for electrochemistry experiments.

Notes and references

1 J. M. Manriquez, G. T. Yee, R. S. McLean, A. J. Epstein and J. S. Miller, *Science*, 1991, **252**, 1415.
2 J. S. Miller and A. J. Epstein, *Chem. Commun.*, 1998, 1319.
3 W. Kaim and M. Moscherosch, *Coord. Chem. Rev.*, 1994, **129**, 157 and references therein.
4 J. Zhang, J. S. Miller, C. Vazquez, P. Zhou, W. B. Brinckerhoff and A. J. Epstein, in *Molecule-Based Magnetic Materials, Theory, Techniques, and Applications*, ed. M. M. Turnbull, T. Sugimoto and L. K. Thompson, *ACS Symp. Ser.*, Washington DC, 1996, vol. 6444, pp. 311–318.
5 J. Zhang, J. Ensling, V. Ksenofontov, P. Gütlich, A. J. Epstein and J. S. Miller, *Angew. Chem., Int. Ed.*, 1998, **37**, 657.
6 B. B. Kaul, W. S. Durfee and G. T. Yee, *J. Am. Chem. Soc.*, 1999, **121**, 6862.
7 A. H. Cook and R. P. Linstead, *J. Chem. Soc.*, 1937, 929.
8 See Electronic Supplementary Information (ESI) for complete experimental procedures and the plot of ac susceptibility [http://www.rsc.org/suppdata/cc/a9/a907535f/].
9 S. P. Sellers, B. J. Korte, J. P. Fitzgerald, W. M. Reiff and G. T. Yee, *J. Am. Chem. Soc.*, 1998, **120**, 4662.
10 B. G. Morin, P. Zhou, C. Hahm, A. J. Epstein and J. S. Miller, *J. Appl. Phys.*, 1993, **73**, 5648.
11 W. R. Entley, C. R. Treadway and G. S. Girolami, *Mol. Cryst. Liq. Cryst.*, 1995, **273**, 153.
12 S. M. Holmes and G. S. Girolami, *J. Am. Chem. Soc.*, 1999, **121**, 5593 and references therein.
13 O. Hatlevik, W. E. Buschmann, J. Zhang, J. L. Manson and J. S. Miller, *Adv. Mater.*, 1999, **11**, 914.
14 P. Zhou, S. M. Long, J. S. Miller and A. J. Epstein, *Phys. Lett. A*, 1993, **181**, 71.

ChemComm

Metal catalysed addition of B–H and N–H bonds to aminopropyl vinyl ethers

Christopher M. Vogels, Paul G. Hayes, Michael P. Shaver and Stephen A. Westcott*

Department of Chemistry, Mount Allison University, Sackville, NB E4L 1G8, Canada. E-mail: swestcott@mta.ca

Received (in Bloomington, IN, USA) 12th October 1999, Accepted 18th November 1999

The rhodium catalysed addition of pinacolborane to aminopropyl vinyl ethers gave selective formation of the corresponding alkenylboronate esters while palladium or platinum complexes catalysed the hydroamination of aminopropyl vinyl ether to give tetrahydro-2-methyl-1,3-oxazine.

The catalytic addition of B–H bonds to unsaturated carbon–carbon bonds using 1,3,2-benzodioxaborole (catecholborane) is of significant importance in organic synthesis.[1] Indeed, the use of a metal catalyst can give organoboronate ester products with stereo-, chemo- and regio-selectivities complementary or opposite to those obtained from the corresponding uncatalysed variants. As part of our ongoing study of generating novel aminoboron compounds,[2] we have examined the catalysed addition of B–H bonds to aminopropyl vinyl ethers ($R_2NCH_2CH_2CH_2OCH{=}CH_2$) and report our initial findings herein.

We have found that addition of catecholborane to commercially available aminopropyl vinyl ether **1a** and dialkylated derivatives **1b**–**e**† using 5 mol% of $RhCl(PPh_3)_3$ gave a number of products derived from an initial dehydrogenative borylation pathway. Formation of products derived from such pathways are well precedented[2a,3–5] and presumably occur *via* initial oxidative addition of the catecholborane B–H bond to the rhodium centre. This step is followed by insertion of the alkene into the Rh–B bond with subsequent ß–H abstraction to give dihydrogen and alkenylboronate esters.[2a] Further reaction of alkenylboronate esters formed in this study with catecholborane or dihydrogen occurs rapidly, as evidenced by the disappearance of the alkenyl peaks in the ^{1}H NMR spectra, to give a number of borated products. Product distributions were further complicated by the formation of Lewis acid–base adducts between the amine moiety and either unreacted catecholborane or the borated products. Although a number of rhodium complexes‡ were investigated as possible catalysts for this reaction, all gave several boron-containing products.

Pinacolborane (HBpin, pin = 1,2-$O_2C_2Me_4$), a less reactive hydroborating agent than catecholborane, was used in an attempt to improve selectivities for this reaction. Interestingly, reactions using HBpin and 5 mol% of $RhCl(PPh_3)_3$[6] at 65 °C gave the corresponding alkenylboronate esters **2a**–**e** (Scheme 1) as the *only* new boron-containing species.§ Similar reactivities were observed using other rhodium catalysts.‡ Although metal catalysed alkenylboronate ester formation using catecholborane is well established,[3–5] analogous products derived from such a pathway using pinacolborane are much less common and only occur in low yields.[6]

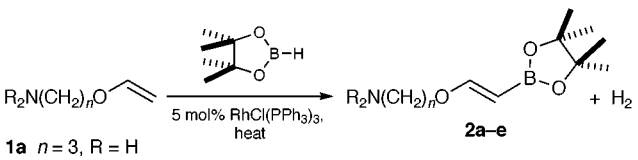

1a $n = 3$, R = H
1b $n = 3$, R = Me
1c $n = 3$, R = Et
1d $n = 2$, R = Et
1e $n = 3$, R = $SiMe_3$

Scheme 1

Unlike hydroborations of aminoalkenes using 9-BBN (9-borabicyclo[3.3.1]nonane),[7] protection of the amine hydrogens is not necessary when R = H, as HBpin reacts rapidly with **1a** to form the intermediate $(pinB)NHCH_2CH_2CH_2OCH{=}CH_2$ with loss of dihydrogen. The weak Lewis-acidic nature of HBpin also precludes the formation of adducts, which are observed in reactions with catecholborane.

The formation of alkenylboronate esters in these reactions is intriguing as previous studies on the addition of B–H bonds to vinyl ethers using BH_3 have shown exclusive formation of *anti*-Markovnikov hydroboration products.[8] We have also found that addition of HBpin to ethyl vinyl ether under similar catalytic conditions gave the corresponding borated product $CH_3CH_2OCH{=}CHBpin$, suggesting that the amine group is not responsible for the formation of alkenylboronate products in reactions with aminopropyl vinyl ethers.[9] The directive effects exerted by heteroatoms on the hydroboration of substituted vinyl derivatives has been reported elsewhere.[8,10–12]

The methodology described above provides a rapid and efficient means of generating novel air-stable alkenylboronate esters, which have remarkable synthetic utility in Suzuki–Miyaura cross-coupling reactions.[13] Vinyl ether derivatives are also versatile synthetic intermediates in polymer chemistry.[14] Further work is currently being conducted on the role the catalyst and the effect the heteroatom α to the vinyl group plays on selectivities in these reactions.

Interestingly, while some palladium and platinum complexes are known to be efficient hydroboration catalysts,[1] we have found that 'hydroboration reactions' using **1a** and catalytic amounts of palladium and platinum compounds gave products derived from addition of the corresponding borane to tetrahydro-2-methyl-1,3-oxazine **3**. Formation of cyclic **3**[15] presumably proceeds *via* an intramolecular hydroamination of the starting aminopropyl vinyl ether (Scheme 2). In fact, in the absence of a hydroborating agent, a number of platinum and palladium complexes effectively catalyse (using 5 mol% of metal) this reaction with high turnover numbers (Table 1).¶ The

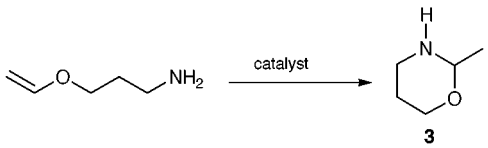

3

Scheme 2

Table 1 Metal catalysed hydroamination of aminopropyl vinyl ether **1a**

Entry	Catalyst[a]	TON[b]
1	PdI_2	1500
2	PdI_2L_2; (L = **3**)	1500
3	$PtMe_2(cod)$	300
4	$[MCl_2(coe)]_2$ (M = Pd, Pt)	250
5	$PtI_2(cod)$	100
6	$Pt(dba)_2$[c]	25
7	$PdCl_2$	2
8	$RhCl(PPh_3)_3$	0

[a] All reactions were carried out in toluene (10 mL) at room temperature. [b] Turnover number. [c] dba = dibenzylideneacetone.

palladium catalysed intramolecular hydroamination reaction is generally believed to occur *via* initial coordination of the alkene to the metal centre, which acts to polarize the alkene moiety and thereby making it more susceptible to nucleophilic attack by the amine.[16] In this study, subsequent addition of the N–H bond to the alkene moiety results in selective formation of the six-membered ring product.

While palladium iodide (Table 1, entry 1) is an active catalyst precursor for this hydroamination reaction, reduced activities (entry 7) were observed in reactions utilizing the corresponding chloride salt. Higher turnover numbers were achieved, however, using the cyclooctene metal chloride dimers (entry 4), presumably owing to their increased solubility in common organic solvents.[2b] Reactions using preformed bis-amine complexes (for instance PdI_2L_2, where L = **3**, entry 2) also gave oxazoline formation in high turnover numbers suggesting that these complexes may be resting states in the catalytic cycle. Attempts to affect the intermolecular hydroamination of ethyl vinyl ether and propylamine using these catalysts proved unsuccessful. Likewise, no reaction was observed when 2-(1-cyclohex-enyl)ethylamine was treated with these metal complexes, suggesting that the ether group in aminopropyl vinyl ether may also facilitate in activating the alkene towards nucleophilic attack. Studies of an asymmetric variant of the hydroamination chemistry, as well as expanding the scope of this reaction, are currently under investigation.

Thanks are gratefully extended to Drs Terri Bright, Giuliano Muccin and Sabine Weiguny (BASF) for the generous gift of aminopropyl vinyl ether and diethylaminoethyl vinyl ether, Dr R. Tom Baker (LANL) for helpful discussions, the Natural Sciences and Engineering Research Council of Canada, Mount Allison University, and Johnson Matthey Ltd. for the palladium and platinum salts.

Notes and references

† Dialkylated aminopropyl vinyl ethers were prepared by addition of 2.2 equivalents of Bu^nLi to **1a** at −78 °C in THF under an atmosphere of dinitrogen. After 2 h, 2 equivalents of the corresponding alkyl halide were added dropwise at 0 °C. Removal of solvent and extraction with hexane, followed by distillation, gave the desired products. *Spectroscopic NMR data* ($CDCl_3$): **1b** (15% yield): ^{1}H δ 6.37 (q, *J* 5 Hz, 1H), 4.08 (d, *J* 16 Hz, 1H), 3.87 (d, *J* 5 Hz, 1H), 3.62 (t, *J* 5 Hz, 2H), 2.29 (t, *J* 5 Hz, 2H), 2.10 (s, 6H), 1.74 (m, 2H); ^{13}C{^{1}H} δ 151.8, 86.4, 66.3, 56.4, 45.5, 27.3. **1c** (10% yield): ^{1}H δ 6.41 (q, *J* 5 Hz, 1H), 4.11 (d, *J* 16 Hz, 1H), 3.89 (d, *J* 5 Hz, 1H), 3.65 (t, *J* 5 Hz, 2H), 2.47 (overlapping m, 6H), 1.76 (m, 2H), 0.95 (t, *J* 5 Hz, 6H); ^{13}C{^{1}H} δ 152.0, 86.3, 66.6, 49.5, 47.1, 26.9, 11.9. **1e** (27% yield): ^{1}H δ 6.50 (q, *J* 5 Hz, 1H), 4.18 (d, *J* 16 Hz, 1H), 3.99 (d, *J* 5 Hz, 1H), 3.65 (t, *J* 5 Hz, 2H), 2.92 (t, *J* 8 Hz, 2H), 1.76 (m, 2H), 0.07 (s, 18H); ^{13}C{^{1}H} δ 152.1, 86.2, 65.9, 42.6, 34.8, 2.24.

‡ Other complexes examined include $[RhCl(cod)]_2$ (cod = cycloocta-1,5-diene), $RhH(PPh_3)_4$, $RhH(CO)(PPh_3)_3$, $[RhCl(coe)_2]_2$ (coe = *cis*-cyclooctene) and $[RhCl(coe)_2]_2/2PPh_3$.

§ The following procedure was used for the dehydrogenative borylation of aminopropyl vinyl ethers. Pinacolborane (190 mg, 1.5 mmol) was added to a solution of aminopropyl vinyl ether (1 mmol) and catalyst (5 mol%) in 10 mL of THF. The mixture was heated to reflux for 3 h under an atmosphere of dinitrogen whereupon solvent was removed and the reaction mixture analyzed by multinuclear NMR spectroscopy. *Selected NMR data* ($CDCl_3$): **2a**: ^{1}H δ 7.07 (d, *J* 16 Hz, 1H), 4.43 (d, *J* 16 Hz, 1H), 3.80 (m, 2H), 3.47 (m, 2H), 1.81 (m, 2H), 1.22 (s, 12H); ^{11}B{^{1}H} δ 34.0; ^{13}C{^{1}H} δ 162.2, 88.0 (br, C–B), 82.2, 68.0, 40.5, 32.2, 23.9. **2b**: ^{1}H δ 6.99 (d, *J* 16 Hz, 1H), 4.41 (d, *J* 16 Hz, 1H), 3.81 (t, *J* 5 Hz, 2H), 2.99 (m, 2H), 2.64 (s, 6H), 2.08 (br m, 2H), 1.24 (s, 12H); ^{11}B{^{1}H} δ 31.0; ^{13}C{^{1}H} δ 162.5, 87.7 (br, C-B), 82.7, 67.9, 51.6, 46.3, 26.2, 24.7. **2c**: ^{1}H δ 7.04 (d, *J* 16 Hz, 1H), 4.43 (d, *J* 16 Hz, 1H), 3.81 (t, *J* 5 Hz, 2H), 3.42 (t, *J* 5 Hz, 2H), 2.51 (overlapping m, 6H), 1.24 (s, 12H), 1.03 (t, *J* 5 Hz, 6H); ^{11}B{^{1}H}, δ 31.4; ^{13}C{^{1}H} δ 163.0, 87.3 (br, C–B), 82.6, 67.0, 48.9, 46.5, 26.2, 24.5, 11.0. **2d**: ^{1}H δ 7.09 (d, *J*16 Hz, 1H), 4.46 (d, *J* 16H z, 1H), 3.87 (t, *J* 8 Hz, 2H), 2.76 (t, *J* 5 Hz, 2H), 2.61 (q, *J* 8 Hz, 4H), 1.25 (s, 12H), 1.05 (t, *J* 8 Hz, 6H); ^{11}B{^{1}H} δ 31.5; ^{13}C{^{1}H} δ 162.6, 87.3 (br, C–B), 82.9, 66.0, 51.0, 47.5, 24.8, 10.6. **2e**: ^{1}H δ 7.06 (d, *J* 16 Hz, 1H), 4.41 (d, *J* 16 Hz, 1H), 3.68 (t, *J* 8 Hz, 2H), 2.87 (m, 2H), 1.69 (m, 2H), 1.23 (s, 12H), 0.07 (s, 18H); ^{11}B{^{1}H} δ 32.0; ^{13}C{^{1}H} δ 163.4, 87.3 (br, C–B), 82.8, 66.6, 42.4, 34.7, 24.9, 2.2.

¶ In a typical reaction, a known amount of aminopropyl vinyl ether was added to a stirred solution or suspension of catalyst (5 mol%) in 10 mL of toluene. The reaction mixture was allowed to stir for an additional 6 h upon which solvent was removed and the reaction analyzed by ^{1}H NMR spectroscopy.[15]

1 For an excellent review on hydroborations catalysed by transition metal complexes, see: I. Beletskaya and A. Pelter, *Tetrahedron*, 1997, **53**, 4957.
2 (*a*) T. M. Cameron, R. T. Baker and S. A. Westcott, *Chem. Commun.*, 1998, 2395; (*b*) C. M. Vogels, H. L. Wellwood, K. Biradha, M. J. Zaworotko and S. A. Westcott, *Can. J. Chem.*, 1999, **77**, 1196.
3 K. Burgess, W. A. van der Donk, S. A. Westcott, T. B. Marder, R. T. Baker and J. C. Calabrese, *J. Am. Chem. Soc.*, 1992, **114**, 9350.
4 S. A. Westcott, T. B. Marder and R. T. Baker, *Organometallics*, 1993, **12**, 975.
5 J. M. Brown and G. C. Lloyd-Jones, *J. Am. Chem. Soc.*, 1994, **116**, 866.
6 S. Pereira and M. Srebnik, *Tetrahedron Lett.*, 1996, **37**, 3283.
7 G. W. Kabalka, N.-S. Li and R. D. Pace, *Synth. Commun.*, 1995, **25**, 2135.
8 H. C. Brown and R. L. Sharp, *J. Am. Chem. Soc.*, 1968, **90**, 2915.
9 R. T. Baker, R. D. Broene, C. M. Vogels and S. A. Westcott, unpublished data.
10 D. J. Pasto and J. Hickman, *J. Am. Chem. Soc.*, 1967, **89**, 5608.
11 For other directive effects in hydroborations, see: B. Singaram, C. T. Goralski and G. B. Fisher, *J. Org. Chem.*, 1991, **56**, 5691.
12 A. H. Hoveyda, D. A. Evans and G. C. Fu, *Chem. Rev.*, 1993, **93**, 1307.
13 N. Miyaura and A. Suzuki, *Chem. Rev.*, 1995, **95**, 2457.
14 P. Kohli, A. B. Scranton and G. J. Blanchard, *Macromolecules*, 1998, **31**, 5681.
15 H. Booth and R. U. Lemieux, *Can. J. Chem.*, 1971, **49**, 777.
16 T. E. Muller and M. Beller, *Chem. Rev.*, 1998, **98**, 675; Y. Li and T. J. Marks, *J. Am. Chem. Soc.*, 1998, **120**, 1757; P. J. Walsh, A. M. Baranger and R. G. Bergman, *J. Am. Chem. Soc.*, 1992, **114**, 1708; M. R. Gagné, C. L. Stern and T. J. Marks, *J. Am. Chem. Soc.*, 1992, **114**, 275; L. S. Hegedus, *Angew. Chem., Int. Ed. Engl.*, 1988, **27**, 1113; M. S. Driver and J. F. Hartwig, *Organometallics*, 1997, **16**, 5706.

Communication a908206i

ChemComm

Synthesis, photoluminescent and electroluminescent behaviour of four-coordinate tetrahedral gold(I) complexes. X-Ray crystal structure of $[Au(dppn)_2]Cl$†

Vivian Wing-Wah Yam,* Chui-Ling Chan, Sam Wing-Kin Choi, Keith Man-Chung Wong, Eddie Chung-Chin Cheng, Sze-Chit Yu, Po-King Ng, Wai-Kin Chan and Kung-Kai Cheung

Department of Chemistry, The University of Hong Kong, Pokfulam Road, Hong Kong SAR, P.R. China. E-mail: wwyam@hku.hk

Received (in Cambridge, UK) 26th October 1999, Accepted 18th November 1999

Two tetrahedral four-coordinate Au(I) complexes, $[Au(4\text{-}R\text{-}dppn)_2]PF_6$ (R = H or Me), have been synthesized and the crystal structure of $[Au(dppn)_2]Cl$ has been determined by X-ray crystallography; the complexes have been found to exhibit both photoluminescent and electroluminescent behaviour.

Unlike d^{10} Cu(I) and Ag(I) species in which complexes with coordination number greater than two are commonly observed, most Au(I) complexes adopt a two-coordinate linear geometry.[1] Studies on four-coordinate Au(I) systems[2,3] have mainly been confined to those of structural characterization, with a few examples on cytotoxic[4a] and antitumor activities.[4b] Despite the recent growing interest in the study of luminescent two-[5] and three-coordinate[6] Au(I) systems, there have been no reports on the luminescence behaviour of four-coordinate Au(I) complexes. Besides, with the growing interest in the design and construction of light-emitting diodes (LEDs)[7] and the employment of metal complexes[8] as the emissive layer in electroluminescence (EL) devices, the use of Au(I) complexes in such studies is rare[8f,g] despite the rich luminescence behaviour associated with a number of Au(I) systems.[5,6,9]

Here, we report the synthesis of two four-coordinate Au(I) complexes, $[Au(4\text{-}R\text{-}dppn)_2]X$ [dppn = 1,8-bis(diphenylphosphino)naphthalene; R = H, X = PF_6 **1a**, Cl **1b**; R = Me, X = PF_6 **2**], and the X-ray crystal structure of **1b**. The first report on the photoluminescent and electroluminescent properties of this tetrahedral four-coordinate Au(I) system is also described.

To the freshly reduced solution of Au(I), prepared *in situ* by treatment of $K[AuCl_4]$ (0.1 mmol) with an excess of 2,2′-thiodiethanol in methanol (20 ml), was added the diphosphine ligand, 4-R-dppn (0.2 mmol). The chloride salt of the product was isolated by slow evaporation of the solvent. Diffraction quality crystals of **1b** were obtained by recrystallization from acetonitrile. Orange solids of **1a** and **2** were collected after the metathesis reaction with NH_4PF_6 in methanol. Recrystallization from dichloromethane–diethyl ether afforded **1a** and **2** as orange crystals. The identities of both have been confirmed by ^{1}H NMR spectroscopy, IR, positive FAB-MS, and elemental analyses.† The X-ray crystal structure of **1b** has also been determined.‡

Fig. 1 depicts the perspective view of the complex cation of **1b**. The structure shows a Au(I) centre in a highly distorted tetrahedral coordination geometry, as required by the steric demand of the dppn ligand. The P–Au–P angle of 86.9(2)–133.3(2)° are comparable to other four-coordinate Au(I) diphosphine complexes such as $[Au(dppe)_2]^+$ [P–Au–P 85.4(1)–129.6(1)°][3c] and $[Au(pdma)_2]^+$ [pdma = *o*-phenylenebis(dimethylarsine), P–Au–P 86.7–121.8°].[3a] The Au–P bonds of 2.379(6)–2.388(6) Å are slightly shorter than those of $[Au(dppe)_2]^+$ [2.389(3)–2.416(3) Å],[3c] but are longer than those of two-coordinate Au(I) phosphine complexes.[5e,f,9]

The electronic absorption spectra of **1a** and **2** are very similar, and are dominated by an intense high energy absorption band at *ca.* 300 nm with a weak low energy band at *ca.* 400 nm with tails extending to *ca.* 500 nm. The photophysical data of **1a** and **2** are collected in Table 1. With reference to previous spectroscopic work,[9,10] the intense absorption at *ca.* 300 nm which closely resembles that found in the free ligand, is assigned as an intraligand $\pi\rightarrow\pi^*$(naphthalene) transition while the lowest energy absorption band is a $\sigma\rightarrow\pi^*$(naphthalene) transition. An assignment of these low-energy absorption bands as d→p transitions, similar to those suggested for three-coordinate d^{10} complexes of Au(I)[6b,c] and Pt(0)[5a,11] is unlikely, given the approximately tetrahedral AuP_4 structure in which the valence p orbitals are strongly σ antibonding. Such d→p transitions are expected to occur at fairly high energy, for example, at 240 nm for $[Au(dcpe)_2]^+$ [dcpe = 1,2-bis(dicyclohexylphosphino)ethane].[6b] Excitation of solid samples of **1a** and **2** gave intense orange emission both at room temperature and 77 K. Room temperature luminescence in degassed dichloromethane solution has also been observed. The observation of the emission lifetime in the microsecond range is suggestive of an emission origin associated with a spin-forbidden transition. No such emission was observed in the related $[Au(dcpe)_2]^+$ complex, which was reported to be non-emissive both in the solid state and in solution.[6b] However, similar emission bands were observed in a related two-coordinate $[Au_2(dppn)(C{\equiv}CR)_2]$,[9d] in which an assignment of the emission origin as derived from states of $\sigma\rightarrow\pi^*$(naphthalene) transition is suggested. It is likely that the photoluminescent properties of **1a** and **2** are characteristic of the dppn unit. The observation that the emission of **2** in

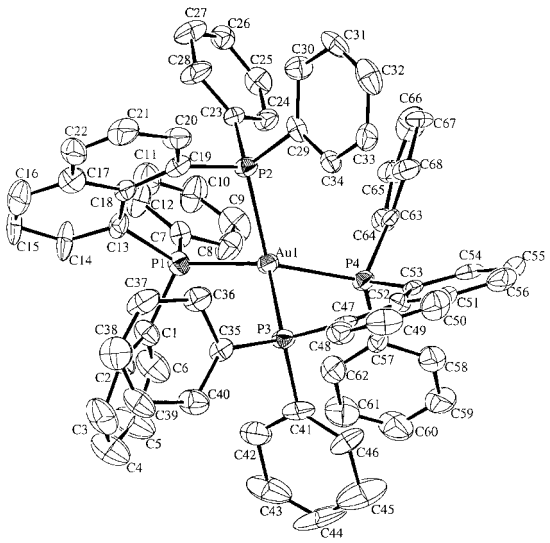

Fig. 1 Perspective drawing of the complex cation of **1b**.

† Electronic supplementary information (ESI) available: characterisation data and crystal structure refinement and data for **1b**, experimental details for EL measurements. See http://www.rsc.org./suppdata/cc/a9/a908521a/

Table 1 Photophysical data for **1a** and **2**.

Complex	Medium (T/K)	λ_{abs}/nm (ε/dm^3 mol^{-1} cm^{-1})	λ_{em}/nm (τ_o/μs)
$[Au(dppn)_2]PF_6$ **1a**	Solid (298)		640 (3.2)
	Solid (77)		653
	CH_2Cl_2 (298)	294 (35 870), 398(sh) (5000)	693 (0.7)
$[Au(4\text{-Me-dppn})_2]PF_6$ **2**	Solid (298)		642 (1.3)
	Solid (77)		647
	CH_2Cl_2 (298)	300 (33 720), 400(sh) (5330)	666 (1.5)

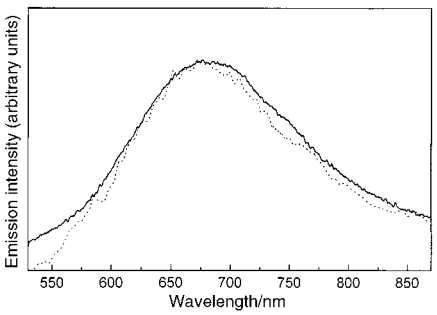

Fig. 2 EL (———) and PL (·····) spectra of **2** in thin films.

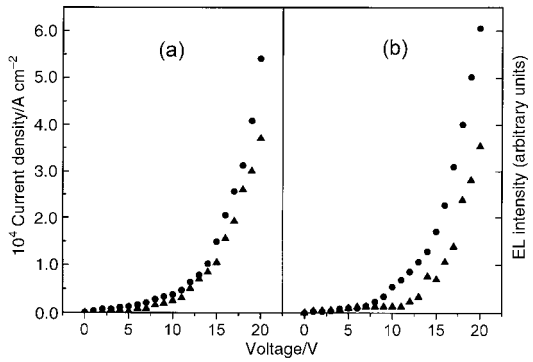

Fig. 3 Current density–voltage (●) and EL intensity–voltage (▲) curves for EL devices of ITO|**1a**–PC|Al (a) and ITO|**2**–PC|Al (b).

dichloromethane is at higher energy than **1a** is in agreement with an assignment of emissive states derived from the σ→π*(naphthalene) transition, since introduction of the methyl group would enhance the hyperconjugation effect, leading to an increase in the σ→π*(naphthalene) transition energy.

Besides exhibiting photoluminescence (PL) behaviour, both **1a** and **2** are also found to show electroluminescence (EL) when doped in polycarbonate (PC) as the emissive layer in a single-layered EL device (ITO|Au–PC|Al).† Upon being forward biased with the ITO electrode at positive polarity, the EL devices exhibit intense orange emission. The EL and PL spectra of **2** in thin films are shown in Fig. 2. The close resemblance of the EL and PL spectra suggests that the EL of these four-coordinate Au(I) complexes probably involves the same excited state as PL, *i.e.* triplet state of σ→π*(naphthalene) transition. The current density–voltage and EL intensity–voltage characteristics of the two single-layered EL devices, (ITO|**1a**–PC|Al) and (ITO|**2**–PC|Al), are shown in Fig. 3. The EL intensity exhibits an approximately linear relationship with current density and has a turn-on voltage of *ca.* 7 V. The EL intensities of the devices of **1a** and **2** at 13 V were 82 and 73 cd m^{-2} with an estimated external quantum efficiency of 0.02 and 0.01% respectively.

V. W.-W. Y. acknowledges financial support from the Research Grants Council and The University of Hong Kong, C.-L. C. the receipt of Croucher Foundation Studentship and Scholarship, K. M.-C. W. the receipt of a research associateship supported by the Vice-Chancellor's Development Fund of The University of Hong Kong, and E. C.-C. C., S. W.-K. C., S.-C. Y. and P.-K. N. the receipt of a postgraduate studentship from The University of Hong Kong.

Notes and references

‡ *Crystal data* for $[Au(dppn)_2]Cl$: M = 1225.47, monoclinic, space group $P2_1/n$ (no. 14), a = 16.981(4), b = 13.527(4), c = 26.399(4) Å, β = 98.75(2)°, V = 5993(2) Å^3, Z = 4, D_c = 1.358 g cm^{-3}, μ(Mo-Kα) = 26.53 cm^{-1}, F(000) = 2464, T = 298 K. Convergence for 666 variable parameters by least-squares refinement of F with $w = 4F_o^2/\sigma^2(F_o^2)$, where $\sigma^2(F_o^2) = [\sigma^2(I) + (0.036F_o^2)^2]$ for 4753 reflections with $I > 3\sigma(I)$ was reached at R = 0.060 and wR = 0.088 with a goodness-of-fit of 2.79. CCDC 182/1487. See http://www/rsc.org/suppdata/cc/a9/a908521a/ for crystallographic files in .cif format.

1 M. C. Gimeno and A. Laguna, *Chem. Rev.*, 1997, **97**, 511; *Gold: Progress in Chemistry, Biochemistry and Technology*, ed. H. Schmidbaur, John Wiley & Sons, Chichester, 1999 and references therein.

2 P. G. Jones, *J. Chem. Soc., Chem. Commun.*, 1980, 1031; R. C. Elder, E. H. K. Zeiher, M. Onady and R. R. Whittle, *J. Chem. Soc., Chem.Commun.*, 1981, 900; P. G. Jones, G. M. Sheldrich, J. A. Muir, M. M. Muir and L. B. Pulgar, *J. Chem. Soc., Dalton Trans.*, 1982, 2123; P. G. Jones, *Acta Crystallogr. Sect. C*, 1992, **48**, 1487; J. M. Forward, Z. Assefa, R. J. Staples and J. P. Fackler Jr., *Inorg. Chem.*, 1996, **35**,16.

3 (*a*) R. Usón, A. Laguna, J. Vicente, J. Garcia, P. G. Jones and G. M. Sheldrich, *J. Chem. Soc., Dalton Trans.*, 1981, 655; (*b*) P. A. Bates and J. M. Waters, *Inorg. Chim. Acta*, 1984, **81**, 151; (*c*) S. J. B. Price, M. A. Mazid and P. J. Sadler, *J. Chem. Soc., Dalton Trans.*, 1984, 969; (*d*) A. L. Balch, M. M. Olmstead, P. E. Reedy Jr. and S. P. Rowley, *Inorg. Chem.*, 1988, **27**, 4289.

4 (*a*) O. M. N. Dhubhghaill, P. J. Sadler and R. Kuroda, *J. Chem. Soc., Dalton Trans.*, 1990, 2913; (*b*) S. J. B. Price, P. S. Jarrett and P. J. Sadler, *Inorg. Chem.*, 1987, **26**, 3074.

5 (*a*) R. F. Ziolo, S. Lipton and Z. Dori, *J. Chem. Soc., Chem. Commun.*, 1970, 1124; (*b*) C. King, J.-C. Wang, M. N. I. Khan and J. P. Fackler Jr., *Inorg. Chem.*, 1989, **28**, 2145; (*c*) A. Vogler and H. Kunkeley, *Chem. Phys. Lett.*, 1988, **150**, 135; (*d*) V. W.-W. Yam, T.-F. Lai and C.-M. Che, *J. Chem. Soc., Dalton Trans.*, 1990, 3747; (*e*) Z. Asefa, B. G. McBurnett, R. J. Staples and J. P. Fackler Jr., B. Assmann, K. Angermaier and H. Schmidbaur, *Inorg. Chem.*, 1995, **34**, 75; (*f*) M. A. Mansour, W. B. Connick, R. J. Lachicotte, H. J. Gysling and R. Eisenberg, *J. Am. Chem. Soc.*, 1998, **120**, 1329; (*g*) W.-F. Fu, K.-C. Chan, V. M. Miskowski and C.-M. Che, *Angew. Chem., Int. Ed.*, 1999, **38**, 2783; (*h*) L. H. Gade, *Angew. Chem., Int. Ed. Engl.*, 1997, **36**, 1171; (*i*) V. W.-W. Yam and K. K.-W. Lo, *Chem. Soc. Rev.*, 1999, **28**, 323 and references therein.

6 (*a*) C.-M. Che, H.-K. Yip, V. W.-W. Yam, P.-Y Cheung, T.-F. Lai, S.-J. Shieh and S.-M. Peng, *J. Chem. Soc., Dalton Trans.*, 1992, 427; (*b*) T. M. McCleskey and H. B. Gray, *Inorg. Chem.*, 1992, **31**, 1733; (*c*) C. King, M. N. I. Khan, R. J. Staples and J. P. Fackler Jr., *Inorg. Chem.*, 1992, **31**, 3236; (*d*) S.-J. Shieh , S.-M. Peng and C.-M. Che, *J. Chem. Soc., Dalton Trans.*, 1993, 195; (*e*) M. N. I. Khan, R. J. Staples, C. King, J. P. Fackler Jr. and R. E. P. Winpenny, *Inorg. Chem.*, 1993, **32**, 5800; (*f*) V. W.-W. Yam and W.-K. Lee, *J. Chem. Soc., Dalton Trans.*, 1993, 2097; (*g*) J. M. Forward, Z. Assefa and J. P. Fackler Jr., *J. Am. Chem. Soc.*, 1995, **117**, 9103.

7 J. H. Burroughes, D. D. C. Bradley, A. R. Brown, R. N. Marks, K. Mackay, R. H. Friend, P. L. Burn and A. B. Holmes, *Nature*, 1990, **347**, 539; A. Kraft, A. C. Grimsdale and A. B. Holmes, *Angew. Chem., Int. Ed.*, 1998, **37**, 402 and references therein.

8 (*a*) C. W. Tang and S. A. VanSlyke, *Appl. Phys. Lett.*, 1987, **51**, 913; (*b*) C. Adachi, S. Tokito, T. Tsutsui and S. Saito, *Jpn. J. Appl. Phys.*, 1988, **28**, L269; (*c*) J.-K. Lee, D. S. Yoo, E. S. Handy and M. F. Rubner, *Appl. Phys. Lett.*, 1996, **69**, 1686; (*d*)M. A. Baldo, D. F. O'Brien, Y. You, A. Shoustikov, S. Sibley, M. E. Thompson and S. R. Forrest, *Nature*, 1998, **395**, 151; (*e*) X. Gong, P.-K. Ng and W.-K. Chan, *Adv. Mater.*, 1998, **10**, 1337; (*f*) Y. Ma, X. Zhou, J. Shen, H.-Y. Chao and C.-M. Che, *Appl. Phys. Lett.*, 1999, **74**, 1361; (*g*) Y. Ma, C. M. Che, H.-Y. Chao, X. Zhou, W.-H. Chan and J. Shen, *Adv. Mater.*, 1999, **11**, 852.

9 (*a*) T. E. Müller, S. W.-K., Choi, D. M. P. Mingos, D. Murphy, D. J. Williams and V. W.-W. Yam, *J. Organomet. Chem.*, 1994, **484**, 209; (*b*)V. W.-W. Yam, S. W.-K. Choi and K. K. Cheung, *J. Chem. Soc., Dalton Trans.*, 1996, 3411; (*c*) V. W.-W. Yam, S. W.-K. Choi and K. K. Cheung, *Organometallics*, 1996, **15**, 1734; (*d*) V. W.-W. Yam and S. W.-K. Choi, *J. Chem. Soc., Dalton Trans.*, 1996, 4227.

10 V. W.-W. Yam, S. W.-K. Choi and K. K. Cheung, *Chem. Commun.*, 1996, 1173.

11 P. D. Harvey and H. B. Gray, *J. Am. Chem. Soc.*, 1988, **110**, 2145.

Communication a908521a

^{29}Si and ^{27}Al MAS NMR spectra are affected by alkali metal cluster formation in zeolite LTA

Kelly L. Moran,[a] Peter D. Barker,[b] Jennifer E. Readman,[b] Peter P. Edwards,[b] Ray Dupree*[a] and Paul A. Anderson*[b]

[a] *Department of Physics, University of Warwick, Coventry, UK CV4 7AL*
[b] *School of Chemistry, The University of Birmingham, Edgbaston, Birmingham, UK B15 2TT. E-mail: p.a.anderson@bham.ac.uk*

Received (in Oxford, UK) 5th October 1999, Accepted 18th November 1999

We report the application of ^{27}Al and ^{29}Si MAS NMR to provide a direct probe of alkali metal cluster formation and distribution in the α-cages of zeolite A (LTA).

The reaction of alkali metals with framework aluminosilicates produces a rich variety of inclusion compounds comprising metal clusters and filamentary structures, confined and ordered, within the intracrystalline channels and cavities.[1] With zeolite pore dimensions typically *ca.* 1 nm or less, these may be regarded as the ultimate nanostructured materials, and as such have justifiably attracted considerable experimental and theoretical attention on account of a range of remarkable electronic, magnetic, optical and catalytic properties.[2–6] Although the presence in such compounds of low-nuclearity (n = 6) paramagnetic clusters is well documented,[7–12] these are present as minority species in all but a few cases.[1,2] Pioneering ^{23}Na MAS studies by Nakayama *et al.*[13] have suggested the possible formation of Na_5^{3+} and Na^-, in zeolites X, Y and A, but in general there is a dearth of information about the diamagnetic species present, in particular higher nuclearity clusters (n > 10) presumed to occupy the larger zeolite cages. Here, we report the first application of ^{27}Al and ^{29}Si MAS NMR to provide a direct probe of cluster formation and distribution in the α-cages of zeolite A.

We prepared a number of deeply coloured compounds M'_x/M-A (where A denotes the LTA framework)[14] by exposing alkali metal (M) ion-exchanged and dehydrated zeolite samples to a measured amount of alkali metal (M′) vapour in sealed, evacuated quartz tubes.[15,16] The products, which were virtually black, were subsequently handled under dry Ar. Unusual MAS NMR[17] spectral shifts (Table 1) were observed for several compositions, and for the first time in zeolite A, a number of compounds exhibited two distinct signals (Figs. 1 and 2) for each T_d nucleus (T_d = ^{27}Al and ^{29}Si), even though the materials were crystallographically single phase.[18] When exposed to air the colour centres were gradually quenched, yielding white powders, whose MAS NMR spectra closely resembled those of the 'empty' dehydrated hosts, with only one T_d signal. Dehydrated zeolite K-A exhibited a single sharp resonance in both the ^{27}Al and ^{29}Si MAS NMR spectra, at the usual shifts for zeolite A (δ *ca.* 58 and −89, respectively). In metal-loaded 'black' K_5/K-A, however, sharp T_d resonances shifted to lower frequency, δ 52.5 and −100.2, respectively, were observed. The magnitudes of the shifts suggest a structural and/or electronic perturbation of the framework.

Topologically, LTA is a cubic array of sodalite cages mutually separated by double 4-ring (D4R) windows to form a large α-cage. Each T_d atom in the structure belongs to one sodalite cage, two α-cages and one double 4-ring. In dehydrated K-A, all the α-cages contain eight K^+ cations that are coordinated to oxygen atoms in the 6-rings and partly balance the negative charge of the framework. The structure has a pseudo unit cell size (assuming no Si, Al ordering) of *ca.* 12.3 Å in space group $Pm\bar{3}m$. In K_5/K-A, alternate α-cages contain either eight K^+ cations coordinated to 6-rings as in the dehydrated host, or a K_{12}^{4+} cluster whose partly reduced potassium cations occupy 4-ring sites. This results in a doubling of the unit cell to 24.6324 Å in space group $Fm\bar{3}m$.[16,19] Owing to the strict alternation of the cage contents, the structure retains a single unique crystallographic T_d site.[16] We suggest that the observed low frequency T_d shifts in K_5/K-A may be due to an increase in the average T_d–O–T_d bond angles[20] in the cluster-containing material relative to those in the empty host, which is consistent with an observed increase in lattice parameter.[16,19] It is interesting that there is no paramagnetic T_d shift or broadening of lines observed in this compound, suggesting that the T_d atoms do not interact appreciably with the paramagnetic clusters known to be present.[16,19]

Similar low frequency NMR shifts were observed for Cs_5/K-A, but in this case, the deeply coloured material exhibited two sharp resonances for both T_d nuclei (Fig. 1). The first one, labelled line 1, is only slightly shifted relative to the dehydrated host and is assigned to T_d atoms at the vertices of α-cages that contain only 6-ring cations. Line 2 resembles the T_d resonance in K_5/K-A, both in shift and signal breadth, and therefore is assigned to T_d atoms which are part of one α-cage that contains 6-ring cations and one that contains a 'reduced' cluster. As caesium cations are both less likely to occupy the 4-ring site in preference to potassium, and less likely to be found partly reduced, we speculate that K_{12}^{4+} clusters may again be present. Structural studies are under way to confirm this hypothesis.[18] The relative intensities of the two lines are consistent with the

Table 1 Summary of 156.4 MHz ^{27}Al and 71.5 MHz ^{29}Si MAS NMR shifts (ppm), linewidths [$\Delta\nu_{1/2}$ (Hz)] and intensity ratios of the framework T_d resonances

Material	^{27}Al (line 1)	^{27}Al (line 2)	^{29}Si (line 1)	^{29}Si (line 2)	Ratio 1:2
Cs_5/K-A	59.3	52.2 (2150, total)	−89.7 (540)	−101.9 (420)	3:2
Exposed Cs_5/K-A	59.9 (1160)	—	−89.5 (320)	—	—
K_5/K-A	—	52.5[a]	—	−100.2 (400)	—
K-A host (dehydrated)	57.7 (890)	—	−89.3 (490)	—	—
Rb_7/Rb-A	83.8	67.9 (4320, total)	−64.1 (910)	−86.1 (840)	3:1
Exposed Rb_7/Rb-A	61.0 (940)	—	−86.1 (570)	—	—
Rb-A host (dehydrated)	57.8 (700)	—	−89.1 (490)	—	—

[a] ^{27}Al shift measured at 93.8 MHz. For comparison, the 93.8 MHz ^{27}Al shifts of Cs_5/K-A are at δ 57.5 and 51.0

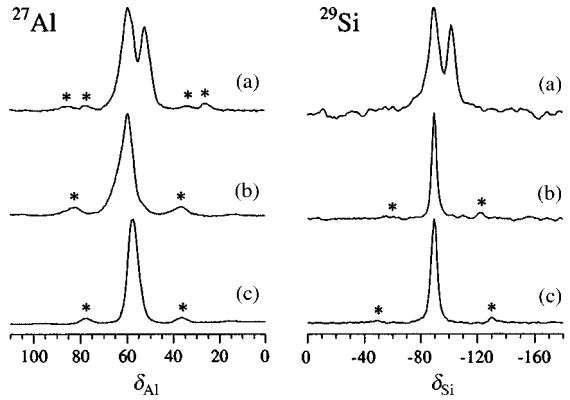

Fig. 1 ^{27}Al and ^{29}Si MAS NMR spectra of (a) 'black' Cs_5/K-A, and (b) air-exposed 'white' Cs_5/K-A and (c) dehydrated 'empty' K-A. Asterisks denote positions of spinning sidebands.

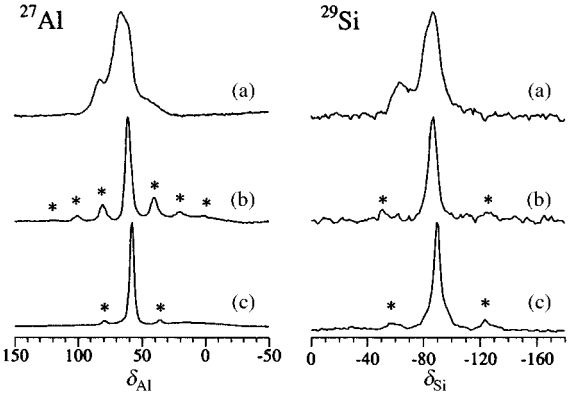

Fig. 2 ^{27}Al and ^{29}Si MAS NMR spectra of (a) 'black' Rb_7/Rb-A, (b) air-exposed 'white' Rb_7/Rb-A and (c) dehydrated 'empty' Rb-A. Asterisks denote spinning sidebands.

presence of a cluster in about one fifth of the α-cages. Exposure of 'black' Cs_5/K-A to air resulted in complete loss of colour and a single T_d resonance in both the ^{27}Al and ^{29}Si MAS NMR spectra (Fig. 1).

Two distinct T_d resonances were also observed in 'black' Rb_7/Rb-A and these collapsed to a single signal when the samples were exposed to air (Fig. 2). In this case the lines are significantly broader than in the dehydrated host, which may indicate some site distribution (static disorder) or broadening from nearby paramagnetic clusters. Additionally, both lines are shifted to higher frequency relative to the host. The framework in this fully loaded zeolite is also expanded relative to the empty host,[18] therefore there is no straightforward structural explanation for the observed shifts. One plausible explanation is that the framework in this case is directly affected by paramagnetic clusters of guest atoms, similar to the shift trends observed in 'black' sodalite.[12]

We thank the EPSRC for financial support. PAA is a Royal Society University Research Fellow.

Notes and references

1 P. P. Edwards, P. A. Anderson and J. M. Thomas, *Acc. Chem. Res.*, 1996, **29**, 23 and references therein; see also refs. 2–13, 15, 16 and 19.
2 P. P. Edwards, L. J. Woodall, P. A. Anderson, A. R. Armstrong and M. Slaski, *Chem. Soc. Rev.*, 1993, **22**, 305.
3 T. Kodaira, Y. Nozue, S. Ohwashi, T. Goto and O. Terasaki, *Phys. Rev. B*, 1993, **48**, 12245.
4 Y. Nozue, T. Kodaira, S. Ohwashi, T. Goto and O. Terasaki, *Phys. Rev. B*, 1993, **48**, 12253.
5 V. I. Srdanov, K. Haug, H. Metiu and G. D. Stucky, *J. Phys. Chem.*, 1992, **96**, 9309.
6 L. R. M. Martens, P. J. Grobet and P. A. Jacobs, *Nature*, 1985, **315**, 568.
7 J. A. Rabo, C. L. Angell, P. H. Kasai and V. Schomaker, *Discuss. Faraday Soc.*, 1966, **41**, 328.
8 P. A. Anderson, R. J. Singer and P. P. Edwards, *J. Chem. Soc., Chem. Commun.*, 1991, 914.
9 P. A. Anderson and P. P. Edwards, *J. Chem. Soc., Chem. Commun.*, 1991, 915.
10 P. A. Anderson, D. Barr and P. P. Edwards, *Angew. Chem., Int. Ed. Engl.*, 1991, **30**, 1501.
11 B. Xu and L. Kevan, *J. Chem. Soc., Faraday Trans.*, 1991, **87**, 2843.
12 G. Engelhardt, M. Feuerstein, P. Sieger, D. Markgraber, G. Stucky and V. Srdanov, *Chem. Commun.*, 1996, 729.
13 H. Nakayama, D. D. Klug, C. I. Ratcliffe and J. A. Ripmeester, *J. Am. Chem. Soc.*, 1994, **116**, 9777.
14 The parent zeolite Na-A has a pseudo unit cell composition of $Na_{12}Al_{12}Si_{12}O_{48}$.
15 P. A. Anderson and P. P. Edwards, *J. Am. Chem. Soc.*, 1992, **114**, 10 608.
16 A. R. Armstrong, P. A. Anderson and P. P. Edwards, *J. Solid State Chem.*, 1994, **111**, 178.
17 NMR experiments were performed on samples sealed inside quartz MAS rotor inserts (Fluorochem/Wilmad) with epoxy. ^{29}Si MAS spectra were measured at 71.5 MHz, at spinning speeds of up to 4 kHz, using a Chemagnetics 6 mm MAS probe in a Bruker MSL-360 spectrometer. Chemical shifts were measured relative to TMS. Field-dependent ^{27}Al MAS spectra were collected at 93.8 MHz as above, and at 156.4 MHz using a 9.5 mm Chemagnetics probe in a Varian/Chemagnetics Infinity 600 spectrometer. ^{27}Al shifts were measured relative to aqueous $AlCl_3$.
18 Rietveld refinement of powder neutron diffraction data from these samples is in progress.
19 L. J. Woodall, P. A. Anderson, A. R. Armstrong and P. P. Edwards, *J. Chem. Soc., Dalton Trans.*, 1996, 719.
20 R. Dupree, S. C. Kohn, C. M. B. Henderson and A. M. T. Bell, in *NATO ASI Ser., Ser. C*, 1993, **386**, 421.

Communicaton a908027i

A novel calamitic liquid crystalline oligomer composed of three non-identical mesogenic entities: synthesis and characterization

C. V. Yelamaggad,* U. S. Hiremath, D. S. Shankar Rao S. Krishna Prasad

Centre for Liquid Crystal Research P.B. No. 1329, Jalahalli, Bangalore-560013, India.
E-mail: uclcr@giasbg01.vsnl.net.in

Received (in Cambridge, UK) 4th October 1999, Accepted 23rd November 1999

The synthesis and evaluation of the mesomorphic properties of the first trimesogen consisting of three non-identical calamitic mesogenic entities have been described.

Liquid crystalline dimers[1] (dimesogens) consisting of two identical (symmetrical) or non-identical (non-symmetrical) mesogenic units have gained attention as these are regarded as model compounds for main chain[2] and side chain liquid crystalline polymers.[3] The non-symmetrical dimers are markedly different from those of symmetrical ones as they exhibit interesting polymorphic sequence[4] and stabilize wide range chiral nematic (N*)[5a] and smectic A (SmA) mesophases.[5b] The addition of one more mesogenic moiety to a dimer *via* a flexible spacer results in the next higher oligomer, which has been called a trimesogen, trimer or triplet liquid crystal.[6] We shall adopt the term 'trimesogen' in this article. Based on the molecular structure of the individual calamitic entities there can be three possible combinations: (i) all of them are structurally identical, (ii) two of them are identical while the third entity is different, and (iii) all three are different. These trimesogens are of interest because of the recent demonstration that a flexible backbone based virtual trimer model successfully accounts for the transitional properties of side chain liquid crystalline polymers.[3b] Trimesogens of type (i) and (ii) were reported for the first time in 1986[7] and since then a few other examples of these types have been reported.[6] To the best of our knowledge trimesogens of type (iii) have not been reported to date. In continuation of our work on oligomeric liquid crystals, here we present the synthesis of the first type (iii) trimesogen composed of three different calamitic mesogenic entities, namely, cholesteryl ester, diphenylacetylene (tolan) and azobezene moieties.

In our recent investigations we had demonstrated that the combination of a cholesteryl ester unit and a tolan unit through an *n*-pentyl (odd) spacer stabilizes a wide-range N* phase.[5a] Owing to a change in the helical pitch the N* phase shows a temperature dependent wavelength of selective reflectivity (thermochromism). Another field of materials research that has been of considerable current interest is the phenomenon of photochromism, which holds lot of promise for applications such as optical information storage technology.[8] Therefore we aimed to synthesize a trimesogen which is multifunctional, satisfying two criteria: (i) it exhibits thermochromism over a wide range of temperature, and (ii) it is photochromic at the same time. A major advantage of single component multifunctional liquid crystal is that the problem of phase separation, which occurs in mixtures of mesogenic monomers and functional monomers, is avoided.[9] Here we report the synthesis of such a multifunctional liquid crystal and a preliminary investigation of the mesomorphic properties of this novel trimesogen.

The synthetic approach employed for the trimesogen, cholesteryl 6-{4-[4-[(4-butylphenylazophenoxy)butoxy]phenylethynyl]phenoxy}hexanoate (**CII-105**), is shown in Scheme 1. It was conceived that **CII-105** could be prepared by combining two key fragments, the non-symmetrical dimeric phenol **CII-76** and butylbromo azobenzene **7**. Accordingly, both the fragments were synthesized and coupled under mild basic conditions to give **CII-105** as a yellow crystalline compound.†

The liquid crystalline properties of **CII-105** were studied using an optical polarizing microscope (Leitz DMRXP) and a differential scanning calorimeter (Perkin Elmer DSC7). For polarizing microscopic observations, glass plates coated with a polyimide solution and unidirectionally rubbed were used. On cooling from the isotropic phase (I) at 247.7 °C the N* phase with a characteristic planar texture is seen in which the nematic director lies in the plane of the substrates. This ensures that the helical axis is perpendicular to the glass plates, *i.e.* along the viewing direction. At a second transition below 215 °C, the texture changes to a square grid pattern, which persists down to 119 °C, when it transforms into a third mesophase. If the sample is observed in a wedge type cell with similar surface treatment to the parallel cell, Grandjean Cano dislocation lines are observed in both the cholesteric and second mesophases demonstrating that there is a helical twist normal to the plates in both cases. Thus the low temperature phase shows the Cano lines superposed on the square grid pattern (see Fig. 1). If the plates are treated to give a homeotropic alignment, a filament texture is observed with an undulatory structure whose

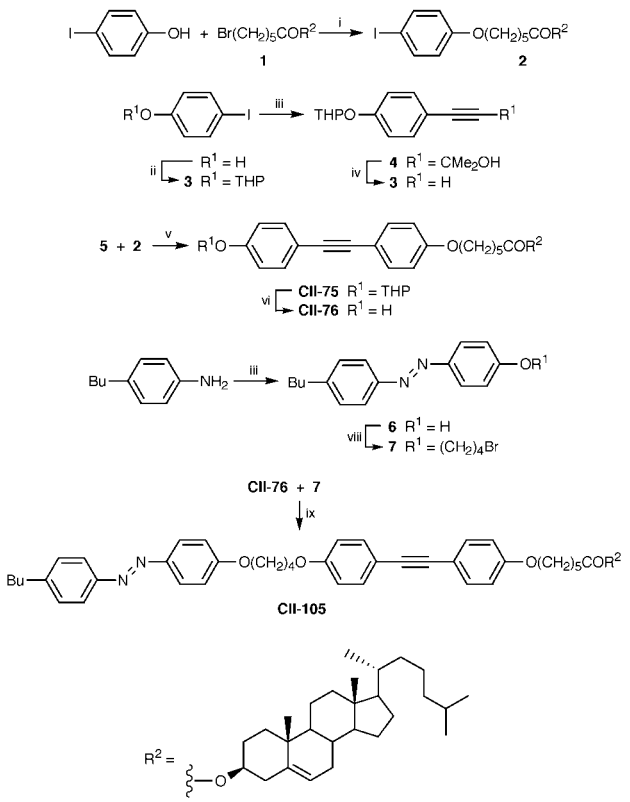

Scheme 1 *Reagents and conditions*: i, anhydrous K_2CO_3, cat. KI, butan-2-one, 70 °C, 24 h, 84%; ii, dihydropyran, PPTS, CH_2Cl_2, room temp., 12 h, quant.; iii, 2-methylbut-3-yn-2-ol, $(PPh_3)_2PdCl_2$, CuI, PPh_3, Et_3N, 65 °C, 16 h, 80%; iv, KOH, toluene, 110 °C, 2 h, 64%; v, $(PPh_3)_2PdCl_2$, CuI, PPh_3, Et_3N, 75 °C, 16 h, 75%; vi, TsOH, MeOH–THF, room temp., 30 min, 68%; vii, $NaNO_2$, HCl, phenol, 0–5 °C, 2 h, 78%; viii, 1,4-dibromobutane, anhydrous K_2CO_3, acetone, 60 °C, 90%; ix, anhydrous K_2CO_3, DMF, 80 °C, 24 h, 52%.

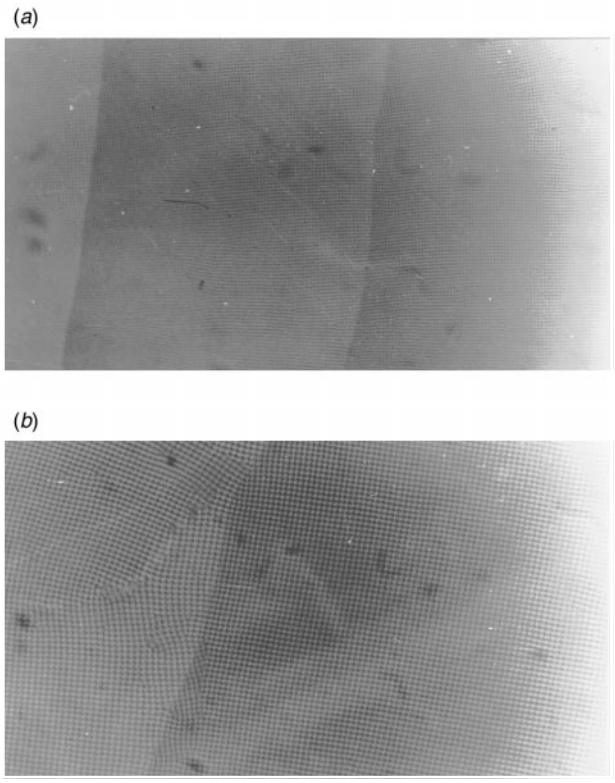

Fig. 1 Optical microscopic texture observed (magnification 400×) for the $UTGB_{C*}$ phase at 212.3 °C while cooling from the N* phase. (*a*) The Grandjean Cano lines (the two striations running from the top to the bottom of the picture) indicate the presence of a helix whose axis is normal to the photograph.The square grid patterns [shown on an enlarged scale in (*b*)] arise from a two-dimensional modulation perpendicular to the helix. The simultaneous existence of both these features is supposed to be proof of the existence of the $UTGC_{C*}$ phase.

periodicity is approximately the same as that of the spacing in the square grid pattern mentioned above. Again, the filament texture remains unchanged down to 119 °C. The features described here for the low temperature mesophase are identical to the textural observations for the very recently reported[10] undulated twist grain boundary ($UTGB_{C*}$) phase in a binary system as well as in a single compound. While in the binary mixture the $UTGB_{C*}$ phase is reported to occur over a narrow range of temperature (~4 °C),[10a] the range is not mentioned in the case of the single compound.[10c] In view of these observations it is remarkable that the second mesophase in **CII-105**, which shows the essential features of the $UTGB_{C*}$ phase, *viz.* simultaneous existence of a square grid texture and a helical structure perpendicular to it, exists over a large temperature range of 90 °C. According to the proposed model,[10a] the $UTGB_{C*}$ phase is a highly frustrated phase characterized by modulations in all the three dimensions, with the two-dimensional undulation of the smectic C*-like blocks being orthogonal to the helix of the TGB structure. Hence, it is all the more interesting to see that a phase with such a highly-frustrated structure exists over a wide temperature range. The mesophase below 119 °C seems to be a highly ordered one, and its detailed characterisation is underway.

The transition temperatures obtained from the cooling mode DSC scan along with the enthalpies are given in Scheme 2 (the transition from the cholesteric to the second mesophase was too weak for any reliable calculation of the enthalpy). It is worth mentioning here that the trimesogen **CII-105** is thermally stable during repeated heating and cooling cycles through the mesophases–isotropic transition, as confirmed by a ^{1}H NMR scan of the same sample which had been subjected to the DSC experiments. The profile obtained was identical, within experimental error, to that for the pristine sample.

In conclusion we have achieved the synthesis of the first trimesogen containing three non-identical calamitic mesogenic

Scheme 2 The number in parenthesis indicates the transition enthalpy; X is a highly ordered mesophase and yet to be fully characterized; K = crystal.

entities connected by flexible spacers. The compound is multifunctional, containing themochromic and photochromic mesogenic units. Such substances have potential as materials for information storage technology and replace mixtures of mesogenic compound in different applications, thereby solving phase separation problems associated with such mixtures. These may perhaps also serve as model compounds (which are yet to be realized) for co-polymeric liquid crystals. Interestingly, this oligomer stabilizes a recently discovered $UTGC_{C*}$ phase—supposed to be a highly frustrated phase—over a wide temperature range of 90 °C and thus invites systematic investigations so as to understand this behavior.

We are grateful to Professor S. Chandrasekhar for many useful discussions and thankfully acknowledge Dr Geeta G.Nair for her help in the experiments.

Notes and references

† The trimesogen **CII-105** and other intermediates exhibited spectral data consistent with their molecular structure. *Selected data* for **CII-105**: ν_{max}(KBr)/cm^{-1} 2950, 2863, 1729, 1607 and 1578; δ_H(500 MHz, $CDCl_3$) 7.89 (d, *J* 8.9, 2H, Ar), 7.8 (d, *J* 8.15, 2H, Ar), 7.44 (d, *J* 5.9, 2H, Ar), 7.42 (d, *J* 5.8, 2H, Ar), 7.3 (d, *J* 8.15, 2H, Ar), 7.0 (d, *J* 8.95, 2H, Ar), 6.87 (d, *J* 8.75, 2H, Ar), 6.84 (d, *J* 8.85, 2H, Ar), 5.36 (br d, *J* 4.85, 1H, olefinic), 4.6 (m, 1H, C*H*OCO), 4.12 (br t, 2H, OCH_2), 4.06 (br t, 2H, OCH_2), 3.96 (t, *J* 6.4, 2H, OCH_2), 2.68 (t, *J* 7.65, 2H, ArCH_2), 2.31 (m, 4H, 2 × C=CH_2), 2.01–0.9 (m, 40H, 17 × CH_2, 6 × C*H*), 1.02 (s, 3H, CH_3), 0.94 (t, *J* 7.25, 3H, CH_3), 0.91 (d, *J* 6.5, 3H, CH_3), 0.87 (d, *J* 2.1, 3H, CH_3), 0.86 (d, *J* 2.1, 3H, CH_3) and 0.67 (s, 3H, CH_3); δ_C(100 MHz, $CDCl_3$) 172.93, 161.22, 158.87, 158.75, 151.05, 147.1, 145.73, 139.67, 132.83, 128.99, 124.54, 122.59, 122.51, 115.8, 115.61, 114.67, 114.5, 88.04, 87.91, 73.82, 67.77, 67.69, 67.48, 56.69, 56.16. 50.05, 42.31, 39.74, 39.51, 38.16, 36.99, 36.59, 36.19, 35.77, 35.52, 34.54, 33.41, 31.88, 28.87, 28.2, 27.82, 25.95, 25.57, 24.76, 24.26, 23.83, 22.77, 22.53, 22.3, 21.03, 19.28, 18.71, 13.88 and 11.835; *m/z* (FAB) 1001 $[MH]^+$ (calc. for $C_{67}H_{88}N_2O_5$).

1 For a brief but recent review on dimers and oligomers see: C. T. Imrie and G. R. Luckhurst, *HandBook of Liquid Crystals*, ed. D. Demus, J. Goodby, G. W. Gray, H.-W. Spiess and V. Vill, Wiley-VCH, Weinheim, 1998, vol. 2B, p. 801.
2 A. C. Griffin and T. R. Britt, *J. Am. Chem. Soc.*, 1981, **103**, 4957; J. C. W. Chien, R. Zhou and C. P. Lillya, *Macromolecules*, 1987, **20**, 2340.
3 (*a*) C. T. Imrie, F. E. Karasz and G. S. Attard, *Macromolecules*, 1993, **26**, 545; (*b*) C. T. Imrie, F. E. Karasz and G. S. Attard, *Macromolecules*, 1993, **26**, 3803.
4 J.-I. Jin, H.-S. Kim, J.-W. Shin, B. Y. Chung and B.-W. Jo, *Bull. Korean Chem. Soc.*, 1990, **11**, 209; F. Hardouin, M. F. Achard, J.-I. Jin, J.-W. Shin and Y.-K. Yun, *J. Phys. II*, 1994, **4**, 627; C. V. Yelamaggad, A. Srikrishna, D. S. Shankar Rao and S. Krishna Prasad, *Liq. Cryst.*, 1999, **26**, 1545.
5 (*a*) C. V. Yelamaggad, *Mol. Cryst. Liq. Cryst.*, 1998, **326**, 149; (*b*) C. V. Yelamaggad, D. S. Shankar Rao and S. Krishna Prasad, unpublished work.
6 G. S. Attard and C. T. Imrie, *Liq. Cryst.*, 1989, **6**, 387; R. Centore, A. Roviello and A. Sirigu, *Mol. Cryst. Liq. Cryst.*, 1990, **182B**, 233; T. Ikeda, T. Miyamoto, S. Kurihara, M. Tsukada and S. Tazuke, *Mol. Cryst. Liq. Cryst.*, 1990, **182B**, 357; A. T. M. Marcelis, A. Koudijs and E. J. R. Sudholter, *Liq. Cryst.*, 1995, **18**, 851; A. T. M. Marcelis, A. Koudijs and E. J. R. Sudholter, *Liq. Cryst.*, 1996, **21**, 87; J. Andersch, S. Diele, D. Lose and C. Tschierske, *Liq. Cryst.*, 1996, **21**, 103.
7 H. Furuya, K. Asahi and A. Abe, *Polym. J.*, 1986, **18**, 779.
8 S. H. Chen, D. Katsis, A. W. Schmid, J. C. Mastrangelo, T. Tsutsui and T. N. Blanton, *Nature*, 1999, **397**, 506; D. J. Broer, J. Lub and G. N. Mol, *Nature*, 1995, **378**, 467; E. Sackmann, *J. Am. Chem. Soc.*, 1971, **93**, 7088.
9 G. Attard and G. Williams, *Nature*, 1987, **326**, 544.
10 (*a*) P. A. Pramod, R. Pratibha and N. V. Madhusudhana, *Curr. Sci.*, 1997, **73**, 761; (*b*) G. G. Nair, *Curr. Sci.*, 1998, **74**, 98; (*c*) B. K. Sadashiva, *Pramana*, 1999, **53**, 213.

Communication a907974b

ChemComm

Multi-functionalization of oligodeoxynucleotide: a facile post-synthetic modification technique for the preparation of oligodeoxynucleotides with two different functional molecules

Kazuo Shinozuka, SatoruKohgo, Hiroaki Ozaki and Hiroaki Sawai*

Department of Chemistry, Faculty of Engineering, Gunma University, 1-5-1 Tenjin-cho, Kiryu City 376-8515, Japan. E-mail: sinozuka@chem.gunma-u.ac.jp

Received (in Cambridge, UK) 30th September 1999, Accepted 23rd November 1999

Treatment of the support-bound novel multi-functionalizable oligodeoxyribonucleotides bearing both 5-cyanomethoxycarbonylmethyl- and 5-methoxycarbonylmethyl-uridine with tyramine followed by tris(2-aminoethyl)amine facilitated multi-functionalization of oligodeoxyribonucleotides having different amine molecules.

Modification of oligodeoxyribonucleotides (ODNs) through incorporation of an appropriate molecule such as an intercalating agent, metal chelating agent, fluorescent dye, *etc*. has been widely studied to produce functionalized ODNs which can be used for biological and biophysical studies.[1] Recently, a new and convenient post-synthetic modification method for the functionalization of ODNs has been reported. In this method, ODNs containing a specially designed convertible unit is assembled first by an automated solid-phase synthesizer, then a functional molecule is introduced to the ODNs.[2] Previously, we have reported that the nucleoside analogs 5-methoxycarbonylmethyl- and 5-cyanomethoxycarbonylmethyl-uridine can be utilized as the convertible unit in the post-synthetic modification technique.[3] Thus, the treatment of ODNs substituting the normal thymidine residue with the convertible nucleoside unit with mono-, di- or poly-amine molecules resulted in the corresponding oligomers carrying the amine derivatives at the 5-position of the uridine derivatives *via* nucleophilic displacement reaction. The method is very attractive since one can site-specifically introduce the desired functional molecules into ODNs after the assembly of the oligomer and, therefore, avoid the tedious preparation of each nucleoside precursor and the corresponding phosphoramidite prior to the assembly of the oligomers.

Meanwhile, further investigation of the nucleoside analogs revealed that reactivity towards the amine-involved nucleophilic displacement reaction is significantly different between the analogs. So far, a report dealing with the site-specific modification of ODNs with several different functional molecules *via* a post-synthetic modification technique has not been known. This background prompted us to develop a versatile method which allows the site-specific introduction of several different functional molecules into ODNs by a facile one-pot reaction. Here, we report preliminary results of our study to produce multi-functionalized oligonucleotides *via* a post-synthetic modification technique.

Phosphoramidite derivatives of 5′-*O*-dimethoxytrityl-5-methoxycarbonylmethyl- and 5-cyanomethoxycarbonylmethyl-uridine were prepared according to the previously reported procedure.[3,4] Preparation of CPG-bound ODNs containing 5-methoxycarbonylmethyl- and 5-cyanomethoxycarbonylmethyl-uridine residues was performed by a DNA synthesizer (ABI 381-A) using the corresponding phosphoramidites on a 1 μmol scale. Two different ODNs, namely, ODN-1 (T**X²**TT**X¹**T) and ODN-2 (**X²**TCC**X¹**GCCA**X¹**AG), were prepared (Scheme 1). In the ODNs, **X¹** and **X²** denote the 5-methoxycarbonylmethyl- and 5-cyanomethoxycarbonylmethyl-uridine residues, respectively. An extended coupling period of 360 s for **X¹** and **X²** phosphoramidites was required to obtain reasonable coupling yields (*ca.* 95%) in the synthesis of the ODNs. *N*⁴-Acetyldeoxycytidine (dC^{ac})phosphoramidite[5] was utilized in the synthesis instead of the usual dC^{bz} phosphoramidite to avoid possible transamination[6] during the amine treatment of the oligomers. The normal synthetic protocol was followed otherwise. It should be noted that the sequence of ODN-2 is complementary to the *rev* region of HIV-1 mRNA.[7]

To check the feasibility of the current multi-functionalization concept, we first studied ODN-1. Thus, the CPG support attached to the oligomer (CPG-ODN-1) was removed from the column and placed into a vial with a Teflon-coated screw cap. The support was first treated with a saturated DMA solution of tyramine in the presence of 1,2,4-triazole for 3 days at room temperature.[3b] The support was then washed thoroughly with

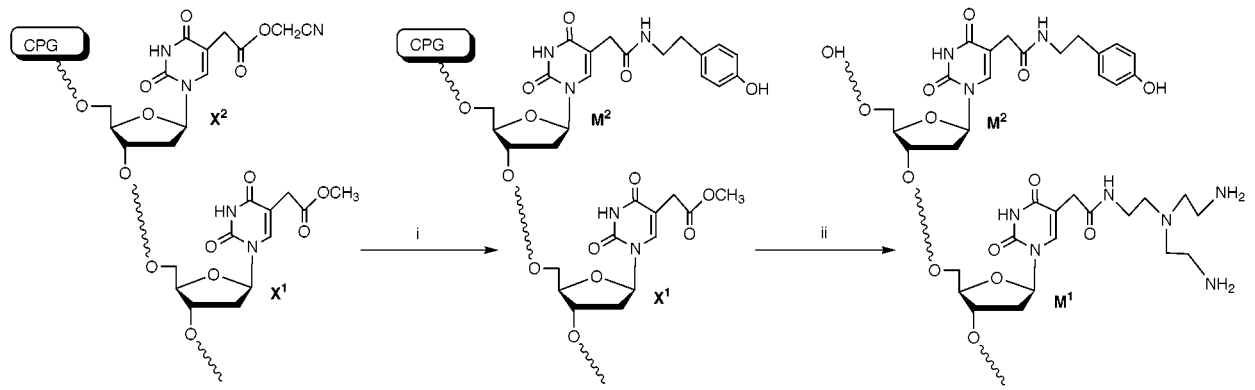

CPG-ODN-1 $^{5'}$T**X²**T T**X¹**T $^{3'}$- CPG
CPG-ODN-2 $^{5'}$**X²**TC C**X¹**G CCA **X¹**AG $^{3'}$- CPG

M-ODN-1 $^{5'}$T**M²**T T**M¹**T $^{3'}$
M-ODN-2 $^{5'}$**M²**TC C**M¹**G CCA **M¹**AG $^{3'}$

Scheme 1 *Reagents and conditions*: i, tyramin, 1,2,4-triazole, DMA; ii, 50% tris(2-aminoethyl)amine in dry EtOH.

Table 1 The sequence, yields and nucleoside compositions of the multi-functionalized ODNs (M-ODNs)

Oligodeoxynucleotide sequence	Isolated yield (OD units)	Nucleoside composition A : G : C : T : M_1 : M_2
TM²TTM¹T	13.2	4.0 : 0.9 : 1.1
M²TCOM¹GCCAM¹AG	22.7	1.7 : 1.8 : 4.3 : 1.2 : 1.7 : 1.2

DMA, followed by MeCN.After drying by Savant Speed Vac concentrator, the support was treated with 50% tris(2-aminoethyl)amine in dry ethanol (1 ml) for 48 h.[3a] After collection and concentration with an N_2 evaporator to remove volatile material, the obtained solution was diluted with 1 M tetraethylammonium acetate buffer (pH 7.0) to adjust the volume to approximately 1 ml and applied to gel filtration using a Sephadex G-25 column. The appropriate fractions were collected and purified by reversed-phase (C-18) HPLC. The obtained oligomer was treated with 20% acetic acid to remove the 5′-*O*-DMTr group, followed by EtOH precipitation and gel filtration (Sephadex G-25). The isolated oligomer (M-ODN-1) was subjected to enzymatic digestion to confirm its structure using snake venom phosphodiesterase, alkaline phosphatase and nuclease P1. In reversed-phase HPLC (C-18) analysis, the digested M-ODN-1 gave three peaks corresponding to thymidine and the modified 2′-deoxyuridine residues (**M¹** and **M²**, Scheme 1). The structures of the modified nucleosides were identified by the co-injection of independently prepared authentic samples. As listed in Table 1, the nucleoside composition calculated from the HPLC analysis agrees well with the expected ratio of dT : **M¹** : **M²** (4 : 1 : 1, respectively) for M-ODN-1.

We further examined the applicability of the current method to the ODN consisting of four natural nucleoside units. Thus, CPG-ODN-2 was treated with tyramine and tris(2-aminoethyl)-amine as mentioned above except that the treatment of the CPG-bound oligomer with tris(2-aminoethyl)amine–EtOH mixture was extended to 3 days. After the work up as above, the obtained oligomer (M-ODN-2) was subjected to enzymatic digestion. As shown in Table 1, HPLC analysis of enzyme digested oligomer indicates that the multi-functionalized oligomer was generated *via* the sequential treatment of the amine derivatives (expected ratio of dA : dG : dC : dT : **M¹** : **M²** = 2 : 2 : 4 : 1 : 2 : 1 for M-ODN-2).† Although in Table 1, **M**² residue was slightly over represented in both oligomers, we could not detect any measurable amount of side products which would result from the reaction of the tyramine with the 5-methoxycarbonylmethyl residue. Thus, the introduction of two different functional molecules to DNA having all four natural nucleoside units was also successful. It should be noted that tyramine in M-ODNs can be used as the substrate for ^{125}I labeling *via* the chloramine-T method,[8] and tris(2-aminoethyl)-amine in M-ODNs is effective to enhance the stability of the duplex formed by the ODN and its complement.[9] The T_m study suggested, indeed, that the M-ODN-2 containing duplex has a slightly enhanced stability (higher T_m value) compared to the corresponding duplex having the unmodified oligomer (N-ODN-2).‡ The yields of the multi-functionalized oligomers obtained by the current method were short of excellent but still within the acceptable range (Table 1).

In conclusion, we were able to successfully demonstrate the feasibility of a facile one-pot modification method to produce multi-functionalized oligonucleotides in a post-synthetic manner. The current method would provide an easy access to ODNs which have a combination of a variety of functional molecules useful for chemical and biological studies.

References and notes

† In electron mass spectrometry, *m/z* 4104.2 ($M - 2H^+$, 4104.0 calc. for $C_{139}H_{192}N_{49}O_{76}P_{11}$ in which two tertiary amine functions in the polyamine moieties are presumably protonated) was obtained.

‡ The following T_m values were obtained with complementary DNA (11-mer); M-ODN-2, 44.7 °C, unmodified N-ODN-2, 43.5 °C. Conditions; 2 μM concentration of the each strand, 100 mM NaCl, 50 mM sodium phosphate buffer (pH 7.2).

1 J. Goodchild, *Bioconjugate Chem.*, 1990, **1**, 165; E. Uhlmann and A. Peyman, *Chem. Rev.*, 1990, **90**, 543; S. L. Beaucage and R. P. Iyer, *Tetrahedron*, 1993, **49**, 1925; S. L. Beaucage and R. P. Iyer, *Tetrahedron*, 1993, **49**, 6123; S. Verma and F. Eckstein, *Ann. Rev. Biochem.*, 1998, **67**, 99.

2 A. Ono, N. Haginoya, M. Kiyokawa, M. Minakawa and A. Matsuda, *Bioorg. Med. Chem.*, 1994, **4**, 361; Y. Nomura, N. Haginoya, Y. Ueno and A. Matsuda, *Bioorg. Med. Chem.*, 1996, **6**, 2811; S. I. Khan and M. W. Grinstaff, *J. Am. Chem. Soc.*, 1999, **121**, 4704.

3 (*a*) K. Shinozuka, A. Umeda, T. Aoki and H. Sawai, *Nucleosides Nucleotides*, 1998, **17**, 291; (*b*) S. Kohgo, K. Shinozuka, H. Ozaki and H. Sawai, *Tetrahedron Lett.*, 1998, **39**, 4067.

4 H. Sawai, A. Nakamura, S. Sekiguchi, K. Yumoto, M. Endo and H. Ozaki, *J. Chem. Soc., Chem. Commun.*, 1994, 1997; H. Ozaki, A. Nakamura, M. Arai, M. Endo and H. Sawai, *Bull. Chem. Soc. Jpn.*, 1995, **68**, 1981.

5 M. P. Reddy, F. Farooqui and N. B. Hanna, *Tetrahedron Lett.*,1996, **37**, 8691.

6 P. S. Miller, M. P. Reddy, A. Murakami, K. P. Blake, S. B. Lin and C. H. Agris, *Biochemistry*, 1986, **25**, 5092.

7 L. Ratner, W. Haseltine, R. Patarca, K. J. Livak, B. Starcich, S. F. Josephs, E. R. Doran, J. A. Rafalski, E. A. Whitehorn, K. Baumeister, L. Ivanoff, S. R. Pettway Jr, M. L. Pearson, J. A. Lautenberger, T. S. Papas, J. Ghrayeb, N. T. Chang, R. C. Gallo and F. Wong-Staal, *Nature*, 1985, **313**, 277.

8 W. M. Hunter and F. C. Greenwood, *Nature*, 1962, **194**, 481.

9 K. Shinozuka, M. Matsukura, T. Okamoto and H. Sawai, *Nucleosides Nucleotides*, 1998, **17**, 2081.

Communication a907867c

Total spontaneous resolution of a cyanoguanidine showing only conformational chirality

Ian D. Cunningham,*[a] Simon J. Coles[b] and Michael B. Hursthouse[b]

[a] *Department of Chemistry, School of Physics and Chemistry, University of Surrey, Guildford, UK GU2 5XH. E-mail: i.cunningham@surrey.ac.uk*

[b] *Department of Chemistry, University of Southampton, Highfield, Southampton, UK SO17 1BJ*

Received (in Cambridge, UK) 16th September 1999, Accepted 23rd November 1999

The total spontaneous resolution of *N*-(4-chlorophenyl)-*N′*-cyano-*N*,*N″*,*N″*-trimethylguanidine, a compound which shows only conformational chirality, is described; variable temperature NMR experiments show that rotation of the dimethylamino group is rapid in solution at room temperature as is conformer interconversion by rotation of the arylmethylamino group.

Total spontaneous resolution is a relatively rare phenomenon whereby a racemic mixture crystallises as a single enantiomer.[1] It may be seen where a potentially chiral molecule is configurationally labile in solution, but stable in the solid state. These criteria are most commonly met when chirality is due *solely* to a chiral conformation and to the maintenance of this conformation by topology in the solid state. Despite its relative rarity, examples of total spontaneous resolution are known and the phenomenon is best illustrated by *rac*-1,1′-binaphthyl which has been known to crystallise in up to 95% ee.[2]

What raises the phenomenon of total spontaneous resolution above a mere curiosity is its importance in crystal engineering,[3] its potential for asymmetric synthesis starting from achiral reagents,[4] and its relevance to the origin of enantiomeric homogeneity in nature.[5]

Of course many organic compounds, while lacking a 'traditional' asymmetric carbon, adopt a chiral conformation in the solid state. However, as with more configurationally stable chiral compounds, crystallisation as a racemic compound is most common, or in certain cases as a conglomerate.[6] Examples of the latter are not uncommon, and the synthetic use of homochiral crystals has been reviewed.[7] However, in many cases the so-called 'absolute asymmetric synthesis' is based on selection of a 'single crystal' from what may well be a conglomerate, *or* on use of homochiral crystals obtained by seeding.[8] What is of more fundamental interest is where such a chiral conformer can not only be isolated in the crystalline state, but can be shown to be an example of total spontaneous resolution. Total spontaneous resolution is usually described for examples such as 1,1′-binaphthyl where racemization following dissolution is slow enough to be detected (k_{rac} *ca.* 10^{-2} s^{-1}). However, such examples are very rare and if studies can be extended to include solid state conformational isomers where the racemization in solution is fast (k_{rac} *ca.* 10^{4} s^{-1}), the scope of these studies can be greatly increased. We herein report such a material.

The compound *N*-(4-chlorophenyl)-*N′*-cyanoguanidine **1**, prepared from 4-chloroaniline and dicyanamide,[9] is weakly acidic.[10] Treatment of **1** with BuLi and excess MeI yielded *N*-(4-chlorophenyl)-*N′*-cyano-*N*,*N″*,N″-trimethylguanidine **2** (Scheme 1) as a mass of small microcrystals (56 mg, 17% yield).[11] Preliminary X-ray crystallographic analysis of *one* of these crystals indicated a chiral space group $P2_12_12_1$. Since no chirality was present in the starting material or in any of the reagents used to prepare **2**, this suggested a chiral conformation in the solid state. At this stage it was not possible to distinguish whether this material existed as a conglomerate or was an example of total spontaneous resolution. Therefore, a sample

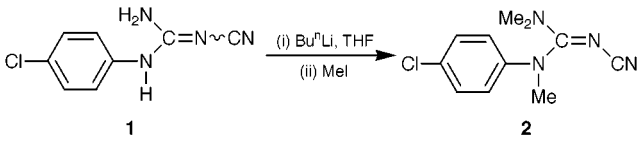

Scheme 1

comprising 18.2 mg was selected at random from the fine mass, dissolved in CH_2Cl_2 and allowed to recrystallise by slow evaporation of solvent to yield a single crystal of weight 16.2 mg (89% recovery).

X-Ray crystallographic analysis of a carefully cut piece of this single crystal again showed the $P2_12_12_1$ space group and the chiral conformation shown in Fig. 1 and schematically in Fig. 2;[12] the absolute configuration was a*S*.[13]

The chirality arises due to the twisting of the ArMeN portion relative to the rest of the molecule by *ca.* 47° (C4–N1–C8–N2). The twisting of the ArMeN group is all the more remarkable in that it results in loss of conjugation between the ArMeN lone pair and the C=N system. This is reflected in the increased length of 1.385(2) Å for the ArMeN–C bond compared to the Me_2N–C and C=N bonds at 1.340(2) and 1.325(2) Å, respectively.[14] The lack of planarity can be attributed to 'steric crowding', and the fact that the ArMeN nitrogen lone pair can delocalise 'towards' the Ar, as an alternative to the C=N–CN, probably explains why this group, rather than the Me_2N, is rotated.

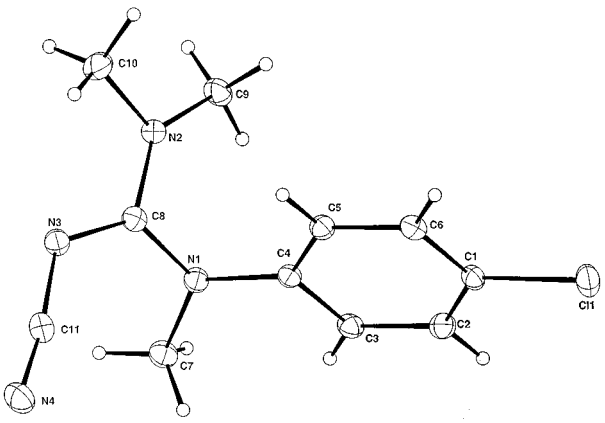

Fig. 1 ORTEP diagram of compound **2**; The numbering is arbitrary.

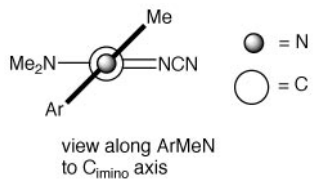

Fig. 2 Schematic representation of the conformation of **2**.

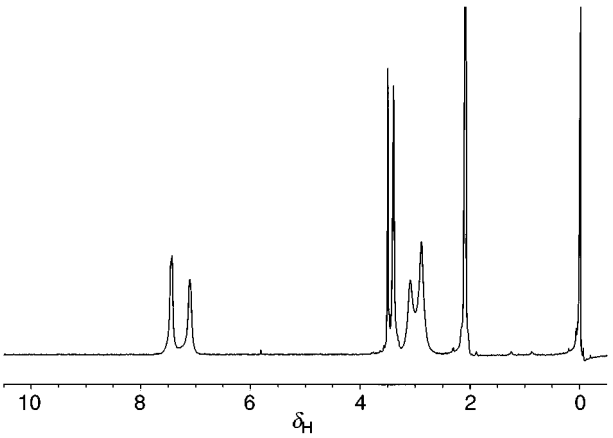

Fig. 3 Spectrum of **2** in acetone-d_6 at 223 K. Peaks at *ca.* δ 2.0, 3.4 and 3.5 are due to residual acetone, the Ar*Me*N and water, respectively.

The following facts prove that this is an example of total spontaneous resolution of a chiral conformer. Firstly, the X-ray crystallographic analysis shows that the *whole* crystal consists of only one chiral conformer [Flack *x* parameter = 0.02(6)[15]]. Secondly, this single crystal constitutes an almost quantitative yield of precipitate from homogeneous solution. Thirdly, the homogeneous solution was obtained using a relatively large randomly selected sample of the original material.[16]

Interestingly, in acetone-d_6 solution the formally non-equivalent dimethyl groups (of Me_2N) separated into two peaks at low temperature and variable temperature NMR experiments gave a coalescence temperature of 231 K. A value for $\Delta G^{\ddagger}_{rot}$ of 46 ± 1 kJ mol^{-1} is obtained from eqn. (1) where R, h and k_b are gas, Planck and Boltzman constants, respectively, and T_c is the coalescence temperature).[17]

$$\Delta G^{\ddagger}_{rot} = -RT_c\ln[\pi h(\Delta\nu)/1.4142k_bT_c] \quad (1)$$

As the Me_2N rotates 'out of plane' so the 'twisted' ArMeN would be expected to rotate 'into plane' and beyond.[18] Therefore, the $\Delta G^{\ddagger}_{rot}$ barrier of 46 ± 1 kJ mol^{-1} measured for the former sets an upper limit for rotation of the latter and also therefore for interconvertion of the chiral conformers in solution (see Fig. 2 where rotation of the ArMeN group yields the mirror image conformer). This translates to an interconversion, rate constant of $> 10^4$ s^{-1} in solution at 25 °C. Given this relatively high interconversion rate (compared to binaphthyl at *ca.* 10^{-2} s^{-1}) it is clear that the chirality is maintained (as opposed to effected) by the topology within the crystal.

Experimental support for possible 'coupled' rotation of the Me_2N and ArMeN groups comes from the NMR. On warming from *below* T_C, one of the methyl peaks (that at higher δ) becomes noticeably broader than the other one (see Fig. 3: NMR spectrum at 223 K, Me_2N signals at δ 3.10 and 2.85) before a broad but symmetrical peak is obtained on coalescence. We attribute this to restricted rotation of the methyl closer to the ArMeN group because of mutual steric interaction as the Me_2N fragment begins to rotate 'past' the ArMeN; some evidence of broadening of the aryl *ortho* hydrogens is also evident in the NMR spectrum at 223 K.

We are grateful to Dr D. C. Povey and Mr G. W. Smith of the University of Surrey for some preliminary X-ray crystallographic studies.

Notes and references

1 E. L. Eliel and S. H. Wilen, *Stereochemistry of Organic Compounds*, Wiley, New York, 1994, ch. 7.
2 K. R. Wilson and R. E. Pincock, *J. Am. Chem. Soc.*, 1975, **97**, 1474; R. Kuroda and S. F. Mason, *J. Chem., Soc., Perkin Trans. 2*, 1981, 167.
3 G. R. Desiraju, *Angew. Chem., Int. Ed. Engl.*, 1995, **34**, 2311; G. R. Desiraju, *Crystal Engineering. The Design of Organic Solids*, Materials Science Mongraphs 54, Elsevier, Amsterdam, 1989.
4 Defined as *absolute asymmetric synthesis*, see M. Sakamoto, *Chem. Eur. J.*, 1997, **3**, 684 and references therein.
5 L. Addadi and M. Lahav, *Origins of Optical Activity in Nature*, ed. D. C. Walker, Elsevier, Amsterdam, 1979, ch. 14; E. L. Eliel and S. H. Wilen, *Stereochemistry of Organic Compounds*, Wiley, New York, 1994, ch. 6.
6 A *racemic compound* is where a particular chiral molecule is partnered *within* the crystal by its enantiomer. A *conglomerate* is a mixture of crystals, *each* of one or the other chiral form; J. Jacques, A. Collet and S. H. Wilen, *Enantiomers, Racemates and Resolutions*, Wiley, New York, 1981.
7 See ref 4.With a conglomerate where the molecules owe their chirality only to conformational differences, selection of a single homochiral crystal followed by a suitable transformation can yield a configurationally stable chiral product and qualify as an *absolute asymmetric synthesis*. However, a pedant might point to the requirement of a chiral human auxilliary!
8 See for example, T. Suzuki, T. Fukushima, Y. Yamashita and T. Miyashi, *J. Am. Chem. Soc.*, 1994, **116**, 2793; A. Sekine, K. Hori, Y. Ohashi, M. Yagi, M. Toda and F. Toda, *J. Am. Chem. Soc.*, 1989, **111**, 697; M. Sakamoto, M. Takahashi, T. Fujita, S. Watanabe, I. Iida, T. Nishio and N. H. Aoyama, *J. Org. Chem.*, 1993, **58**, 3476.
9 I. D. Cunningham, B. G. Cox and N. C. Wan, *J. Chem. Soc., Perkin Trans. 2*, 1994, 1849.
10 I. D. Cunningham, B. G. Cox and N. C. Wan, *J. Chem. Soc., Perkin Trans. 2*, 1999, 693.
11 The remaining 'yield' was made up of a monomethylated product, a dimethylated product, recovered starting material and a cyanamide product (See ref. 10).
12 *Crystal data* for **2**: $C_{11}H_{13}ClN_4$, M = 236.7, colourless, 0.35 × 0.15 × 0.15 mm, orthorhombic, $P2_12_12_1$, a = 6.0730(10), b = 13.401(3), c = 14.091(3) Å, V = 1146.8(4) Å^3, T = 150(2) K, Z = 4, μ = 0.311 mm^{-1}, 7762 reflections collected, 2630 independent reflections, R = 0.0351, Rw = 0.0885. The structure solution was by direct methods with refinement by full-matrix least squares on F^2. CCDC 182/1491.
13 See E. L. Eliel and S. H. Wilen, *Stereochemistry of Organic Compounds*, Wiley, New York, 1994, ch. 14, p. 1120 for rules for specifying configuration due to axial chirality.
14 The less substituted and more planar *N*-cyano-*N*-(4-methoxyphenyl)guanidine has bond lengths of 1.328, 1.317 and 1.342 Å for the analogous bonds (see I. D. Cunningham, N. C. Wan, D. C. Povey, G. W. Smith and B. G. Cox, *Acta Crystallogr.*, 1997, **C53**, 984). See also 'mean geometry' for guanidines from CCDC data, T. Krigowski and K. Wozniak, in *Chemistry of Amidines and Imidates, Vol. 2*, ed. S. Patai and Z. Rappoport, Wiley, Chichester, 1991, p116.
15 H. D. Flack, *Acta Crystallogr.*, 1983, **A39**, 876; G. Bernardinelli and H. D. Flack, *Acta Crystallogr.*, 1985, **A41**, 500.
16 It is quite possible that the original sample had already undergone total spontaneous resolution, but with a material which is conformationally labile in solution and which consists of a large number of microcrystals proving this is almost impossible.
17 Experimental and calculated values for guanidinium range 20–81 kJ mol^{-1}, C. L. Perrin, in *Chemistry of Amidines and Imidates, Vol. 2*, ed. S. Patai and Z. Rappoport, Wiley, Chichester, 1991, p. 201; Y. Yamamoto and S. Kojima, in *Chemistry of Amidines and Imidates, Vol. 2*, ed. S. Patai and Z. Rappoport, Wiley, Chichester, 1991, p. 509.
18 A concerted rotation has been observed for a tertiary aromatic amide where, as here, planarity is lost due to 'steric crowding', J. Clayden and J. H. Pink, *Angew. Chem., Int. Ed.*, 1998, **37**, 1937.

Communication a907518f

N-(2-Methoxycarbonyl-2-yloethyl)phenylaminyl: EPR observation of a triplet nonconjugated 1,3-diradical with two different kinds of radical centers

Hideyuki Tukada

Graduate School of Integrated Science, Yokohama City University, Kanazawa-ku, Yokohama 236-0027, Japan. E-mail: htht@yokohama-cu.ac.jp

Received (in Cambridge, UK) 6th October 1999, Accepted 24th November 1999

EPR observation of *N*-(2-methoxycarbonyl-2-yloethyl)phenylaminyl at cryogenic temperature shows that the diradical has a triplet ground state, and is thermally labile for ring-closure reaction with low and distributive activation energies centered around 3.2 kJ mol^{-1}.

Diradicals,[1] reactive intermediates frequently appearing in both thermal and photochemical reactions, are unique in that they show dichotomous reactivities depending on their spin states. Recently numerous conjugated diradicals have been explored in efforts to develop building blocks for organic magnetic substances.[2] On the other hand, localized diradicals linked with σ-bonds have not yet received sufficient attention as magnetic molecules. Among the localized diradicals, 1,3-diradicals, such as trimethylene,[3] are the simplest and representative.[1] Here we report *N*-(2-methoxycarbonyl-2-yloethyl)phenylaminyl **1**, a diradical with two different kinds of formal radical centers,[4] localized and conjugated, on N and C atoms. To the best of our knowledge this is the first example of EPR observation of an open-chain nonconjugated 1,3-diradical. It is of interest how the energy gap between the singlet and the triplet in **1** is affected by heteroatom substitution on one side of the radical site in trimethylene, and how the lone pair on the nitrogen atom affects the kinetic stability of **1**.

Photolysis (330 ± 20 nm) of methyl 1-phenyl-4,5-dihydro-1*H*-1,2,3-triazole-4-carboxylate **2**[5] in a 1:1 mixture of C_2D_5OD–CD_3OD (50 mmol dm^{-3}) was performed in an EPR cavity (X-band) with a 500 W super-high-pressure mercury lamp and glass filters at 5 K. The EPR spectrum after irradiation for 5 min persisted for at least 1 h at this temperature, and showed a set of signals characteristic of a triplet biradical (half-field signal; 0.1569 mT) with zero-field-splitting (ZFS) parameters of $|D| = 3|E|$[6] (Fig. 1).

The signals at 2516 and 3953 mT were assigned to overlapping signals due to transition of Z and Y with the ZFS parameters $|D/hc| = 0.06716$ cm^{-1} and $|E/hc| = 0.02239$ cm^{-1}. The *D* value is close to those of cyclobutane-1,3-diyls[7] ($|D/hc| = 0.050$–0.11 cm^{-1}) and cyclopentane-1,3-diyls[8] ($|D/hc| = 0.041$–0.084 cm^{-1}), and is fully consistent with a localized 1,3-diradical structure with an average distance of 0.34 nm between two unpaired electrons.[8]

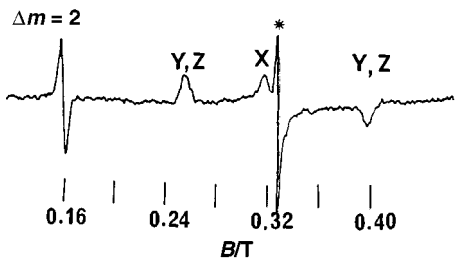

Fig. 1 X-Band EPR spectrum of **1** obtained after UV irradiation (330 ± 20 nm) to methyl 1-phenyl-4,5-dihydro-1*H*-1,2,3-triazo-4-carboxylate **2** in a 1:1 mixture of C_2D_5OD–CD_3OD matrix for 5 min at 5 K ($\nu = 9.0067$ GHz, power = 0.2 mW, modulation = 1 mT). Asterisk denotes doublet impurities.

EPR measurements were then performed on warming from 5 to 50 K in the dark. At each temperature (T_i) the signal intensity (I) stabilized within 3 min. Re-cooling from T_i to 5 K did not regenerate the initial intensity, which indicates that the biradical was irreversibly diminished by the reactions. However, no further decrease in signal intensity was observed between T_i and 5 K. The temperature dependence of the signal intensity for the annealed sample obeyed the Curie law (IT = constant) between 5 and T_i.

Consequently, the *IT vs. T* plot for the warming process did not become flat [line (i) in Fig. 2], whereas the plot for the post-annealed process showed a constant value [line (ii) in the Fig. 2]. The latter indicates that the triplet is the ground state of biradical **1**.

It seems reasonable that the initial decrease in signal intensity of the triplet can be attributed to decay through a ring-closure reaction to give methyl 1-phenylaziridine-2-carboxylate, which is the main photo-product at room temperature in solution (Scheme 1).[5] Decay by hydrogen abstraction from the matrix can probably be excluded because no new signals and no increase in the doublet species (indicated as * in Fig. 1) were observed up to 50 K. At 35 K, the triplet EPR signals originating from the biradical dissappeared immediately and simultaneously.

The same thermal behaviour of **1** was observed using 2-methyltetrahydrofuran as the matrix, indicating that the hardness of the surroundings of the diradical had little influence on ring-closure.

The former behavior [line (i)] can be interpreted as decay through transition states with distributive activation energies due to matrix site effects and conformers of **1**, rather than classical or tunneling processes having a single activation

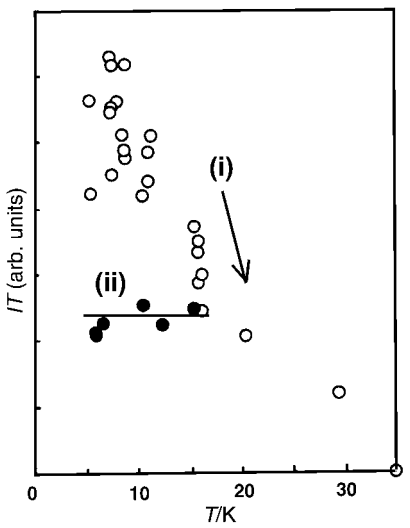

Fig. 2 *IT vs. T* plots, where I is the EPR signal intensity of the $|\Delta M_s| = 2$ transition of **1** in a 1:1 mixture of C_2D_5OD–CD_3OD, and T is the absolute temperature. (i) Open circles indicate a heating process from 5 to 35 K, and closed circles show the temperature dependence of the signal intensity between 5 and 18 K after annealing at 18 K.

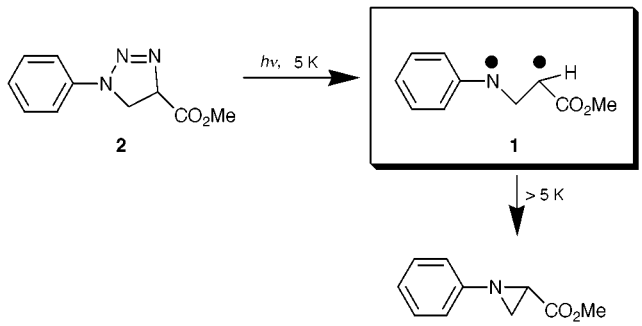

Scheme 1

energy. Such a mechanism with distributive activation energies was successively analyzed by a 'distribution slicing method' in the case of cyclobutane-1,3-diyls by Dougherty's group.[7] Applying this method to our case (50% of **1** decayed at 16 K) gave an average activation energy, E_a = 3.2 kJ mol^{-1}, under the assumption that $A = 10^8$ and t = 180 s, where A is a frequency factor in the Arrhenius equation and t is the slicing time. The activation energy, which possibly corresponds to that required for spin inversion (ISC), is slightly smaller than that in the case of cyclobutane-1,3-diyls (E_a = 4.0–9.7 kJ mol^{-1}) or cyclopentane-1,3-diyls (E_a = 8–> 20 kJ mol^{-1}).

The low activation energy in the case of **1** is attributable primarily to the flexible open chain structure and secondly to the interaction between a lone-pair on the aminyl radical and the p-orbital of the counterpart carbon radical.

According to density functional theory calculations (U-B3LYP/6-13G*)[9] for the biradical **1**, the triplet has a (0,0) conformation (following the notation for trimethylene)[3] and lies below the singlet by 1.3 kJ mol^{-1} (vertically; the singlet biradical has no minimum on the energy surface, and the optimization of the structure gives methyl 1-phenylaziridine-2-carboxylate). The computed energy gap $\Delta E_{S\text{-}T}$ is consistent with the result of the EPR experiment. Most of the spin populations of triplet **1** are distributed on both the formal radical centers (spin/charge = 0.63/−0.47 on the N atom, and 0.90/−0.16 on the C2′ atom), and agree with the average distance between unpaired electrons as estimated from the experimental D parameter.

In conclusion, we have been able to detect triplet diradical **1**, a heteroatom analogue of trimethylenemethane, and found that the diradical is thermally labile above 5 K with low and distributive activation energies.

The present work was financially supported by the Nagase Science and Technology Foundation, and by a Grant-in-Aid for Scientific Research on Priority Areas 'Creation of Delocalized Electronic Systems' (10146244) from the Ministry of Education, Science, Sports, and Culture, Japan.

Notes and references

1 *Diradicals*, ed. W. T. Borden, Wiley, New York, 1982; C. Wentrup, *Organic Reactive Intermediates*, Wiley, New York, 1984, ch. 3.
2 H. Iwamura, *Adv. Phys. Org. Chem.*, 1990, **26**, 179; J. A. Berson, *Acc. Chem. Res.*, 1997, **30**, 238; A. Rajca, *Chem. Rev.*, 1994, **94**, 871; W. M. Nau, *Angew. Chem., Int. Ed. Engl.*, 1997, **36**, 2445.
3 A. Skancke, D. A. Hrovat and W. T. Borden, *J. Am. Chem. Soc.*, 1998, **120**, 7079; S. J. Getty, E. R. Davidson and W. T. Borden, *J. Am. Chem. Soc.*, 1992, **114**, 2085; J. E. Baldwin, Y. Yamaguchi and H. F. Schaefer III, *J. Phys. Chem.*, 1994, **98**, 7513.
4 Heterospin molecules: for examples, see M. Rule, A. R. Matrinand, D. A. Doughtery, E. Hilinski and J. A. Berson, *J. Am. Chem. Soc.*, 1979, **101**, 5098.; H. Tukada, K. Mutai and H. Iwamura, *J. Chem. Soc., Chem. Commun.*, 1987, 1159; H. Tukada, *J. Chem. Soc., Chem. Commun.*, 1993, 302; K. Matsuda and H. Iwamura, *Chem. Commun.*, 1996, 1131; P. M. Lahti, B. Esat and R. Walton, *J. Am. Chem. Soc.*, 1998, **120**, 5122; D. A. Shultz and G. T. Farmer, *J. Org. Chem.*, 1998, **63**, 6254.
5 R. Huisgen, G. Szeimies and L. Mobius, *Chem. Ber.*, 1966, **99**, 475.
6 Diradicals having ZFS parameters of $D = 3E$, for example: T. Hirano, T. Kumagai, T. Miyashi, K. Akiyama and Y. Ikegami, *J. Org. Chem.*, 1992, **57**, 876.
7 M. B. Sponsler, R. Jain, F. D. Coms and D. A. Dougherty, *J. Am. Chem. Soc.*, 1989, **111**, 2240; 1988, **110**, 1356.
8 W. Adams, O. Emmert and T. Heidenfelder, *J. Org. Chem.*, 1999, **64**, 3417; S. L. Buchwalter and G. L. Closs, *J. Am. Chem. Soc.*, 1975, **97**, 3857; 1979, **101**, 4688.
9 The DFT calculations were performed using a Gaussian98 program package (Revision A7, Gaussian, Inc., USA).

Communication a908039b

A spirooxazine showing crystalline state photochromism

Sophie Bénard and Pei Yu*

Laboratoire de Chimie Inorganique, Bat. 420, UMR 8613, Université Paris Sud, F-91405, Orsay, France.
E-mail: yupei@icmo.u-psud.fr

Received (in Oxford, UK) 18th September 1999, Accepted 24th November 1999

A cationic spiroquinoxazine (SO2) is found to be photochromic both in solution and in the crystalline state.

Among the large number of investigated so far photochromic molecules,[1,2] few have been found to be photochromic in the crystalline state.[3–8] Photochromic organic crystals are interesting not only for the design of new materials for optical data processing and storage,[4,6] but also because the photoinduced molecular transformations might be used to gain control over other physical properties in the solid state. For instance, the photoswitching of NLO properties has been recently achieved in a photochromic organic crystal.[9] Spirooxazines (SO) are known to offer remarkable stability towards photo-fatigue in solution and in various matrices,[10–14] but to the best of our knowledge none of them has been reported to be photochromic in the crystalline state. We report herein the first spirooxazine to exhibit photochromism both in solution and in the pure crystalline state.

N-Methylation of spiroquinoxazine[10,12c] (SO1) with MeI in THF yielded the yellow microcrystalline cationic SO[15a] (SO2, see Scheme 1).

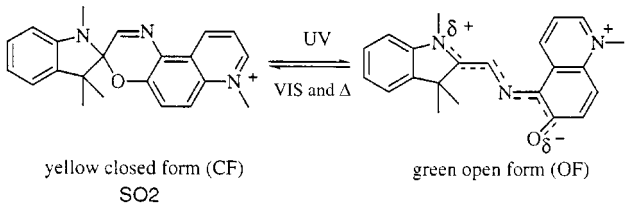

Scheme 1

Photochromism of spirooxazines is based on photocleavage of the C(spiro)–O bond, giving rise to an equilibrium between a colorless or weakly colored closed form and a strongly colored open form. The usually less stable open form reverts back to the closed form both photochemically and thermally. In the present case such an equilibrium is shown in Scheme 1.

Electronic absorption spectral changes of SO2 upon UV irradiation (365 nm)[15b] in $CHCl_3$ are depicted in Fig. 1. The main characteristics of the closed and open forms as well as the thermal color fading rate (k) of the latter are reported in Table 1.

Table 1 Spectral and kinetic properties of SO2 in different solvents

Compound	Solvent	Form	λ/nm (ε/dm^3 mol^{-1} cm^{-1})	k/s^{-1}
SO1[a]	EtOH	Open	564,[b] 599	0.23
	Toluene	Open	561,[b] 590	0.34
SO2	EtOH	Closed	375 (5700)	9.3×10^{-5}
		Open	592, 563[b]	
	$CHCl_3$	Closed	387 (4700)	8.2×10^{-6}
		Open	611, 575,[b] 469	
	Toluene	Closed	370 (4400)	2.5×10^{-4}
		Open	615, 580[b]	

[a] Ref. 12(*a*). [b] Shoulder.

The photochromic properties of SO2 are markedly different from those of SO1. First, at room temperature the thermal color decay of the open form of SO2, which follows a single exponential equation in the same manner as SO1, is very slow. Depending on the solvent, the constant k of this decay is about 10^3 to 10^4 times smaller than that of SO1. In other words, the *N*-methylation of the quinoline on the oxazine moiety stabilizes in a dramatic way the open form. Second, in contrast to the parent SO1 and other SO molecules, which are known to show positive solvatochromism,[10,12a] the open form of SO2 is characterized by a negative solvatochromism (Table 1), indicating that its ground state is more polar than the exited one. These two observations suggest a predominantly zwitterionic structure for the open form of SO2 rather than the less polar quinoidal one.

Irradiation of a microcrystalline sample of SO2 was carried out using an ultra-thin pressed pellet. The UV–VIS absorption spectra after different irradiation times are shown in Fig. 2. Upon UV irradiation (365 nm) a broad absorption band appeared between 550 and 650 nm and continuously increased while the initial yellow pellet turned green. When the sample

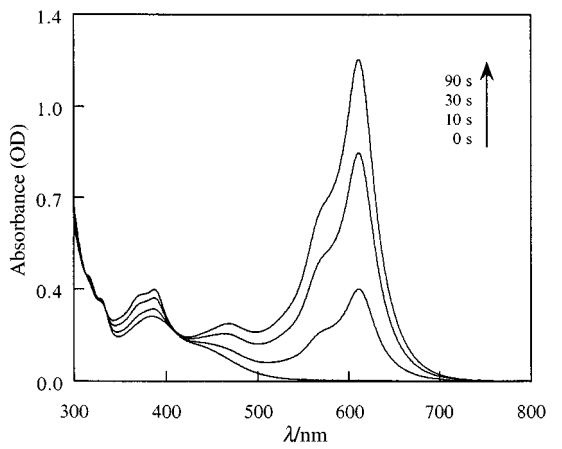

Fig. 1 UV–VIS spectral changes of SO2 in $CHCl_3$ solution (5×10^{-5}M, room temperature) upon UV irradiation.

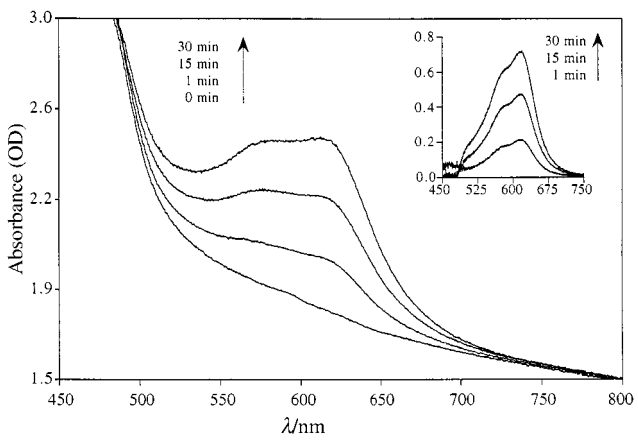

Fig. 2 Crystalline state UV–VIS spectral changes of SO2 upon UV irradiation. Insert shows the differential optical density between the spectra before and after UV irradiation.

was left in the dark at room temperature after irradiation, the green color faded slowly and the yellow colour returned very slowly. In contrast, visible light (550 nm) irradiation considerably accelerated the color decay. This behavior is similar to that observed in solution and indicates clearly that SO2 is photochromic in the crystalline state.

By monitoring the decay of the absorption band in the visible region at room temperature, the thermal decoloration rate of the thin pellet was found to deviate significantly from first order kinetics, but can be fairly well fitted to a biexponential equation with $k_1 = 1.6 \times 10^{-4}$ s^{-1} and $k_2 = 5.8 \times 10^{-6}$ s^{-1}. This behavior can be tentatively interpreted as the result of two different environments surrounding the open form of SO2 in the bulk sample. The open form molecules located near the surface of the solid are surrounded mostly by similar open form molecules. On the contrary an open form molecule lying deeper inside the bulk would have mainly closed form molecules as neighbors.

Finally, it is worth pointing out that the color change was not accompanied by any significant structure modifications, as the X-ray powder pattern of the irradiated sample did not show any detectable changes as compared to that of the initial one, while the large differences in geometry between the closed and open forms would lead one to expect rather large structure changes. A possible explanation would be that under current experimental conditions the photochemical process is mainly limited to the surface of the bulk sample, so the amount of the photoinduced open form is too small to give any significant changes in the X-ray powder pattern.

The reasons why SO2 shows crystalline state photochromism are not yet clearly understood. Nevertheless, the large stabilization of a predominantly zwitterionic open form brought about by the *N*-methylation of the quinoline ring seems to be an important factor in permitting solid state photochromism. On the other hand, the presence of iodide ions could result in more space or free volume in the crystal structure of SO2 as compared to the parent SO1. In other words, the anion, although not directly involved in the photochemical process, may have a kind of dilution or matrix-like effect on the cationic photoactive spirooxazine. These remarks are supported by the following observation: two derivatives of SO2, prepared by replacing the iodide anion in SO2 by nitrate or toluene-*p*-sulfonate, were also found to show similar behavior. This rather anion-independent behavior strongly suggests that crystalline state photochromism in this class of compounds depends mainly on the cationic nature of the photoactive species, and the role of the anion is probably minor. This particular feature would be of interest in the perspective of associating solid state photochromism with other properties that could be introduced through the anion.

We are grateful to Dr Keitaro Nakatani and Professor René Clément for many helpful discussions.

Notes and references

1 *Photochromism. Molecules and Systems*, ed. H. Durr and H. Bouas-Laurent, Elsevier, Amsterdam, 1990.
2 B. L. Feringa, W. F. Jager and B. de Lange, *Tetrahedron*, 1993, **49**, 8267.
3 E. Hadjoudis, in ref. 1, ch. 17.
4 M. Irie and K. Uchida, *Bull. Chem. Soc. Jpn.*, 1998, **71**, 985.
5 S. Kobatake, T. Yamada, K. Uchida, N. Kato and M. Irie, *J. Am. Chem. Soc.*, 1999, **121**, 2380 and references cited therein.
6 Y. Eichen, J. M. Lehn, M. Scherl, D. Haarer, J. Fischer, A. DeCian, A. Corval and H. P. Trommsdorff, *Angew. Chem., Int. Ed. Engl.*, 1995, **34**, 2530.
7 Y. H. Zhou, W. E. Baker, P. M. Kazmaier and E. Buncel, *Can. J. Chem.*, 1998, **76**, 884.
8 K. Okada, K. Imamura, M. Oda, M. Kozaki, Y. Morimoto, K. Ishino and K. Tashiro, *Chem. Lett.*, 1998, 891.
9 K. Nakatani and J. A. Delaire, *Chem. Mater.*, 1997, **9**, 2682.
10 N. Y. C. Chu, in ref. 1, ch. 10.
11 S. Kawauchi, H. Yoshida, N. Yamashina, M. Ohira, S. Saeda and M. Irie, *Bull. Chem. Soc. Jpn.*, 1990, **63**, 267.
12 *(a)* E. Pottier, R. Dubest, R. Guglielmetti, P. Tardieu, A. Kellmann, F. Tfibel, P. Levoir and J. Aubard, *Helv. Chim. Acta*, 1990, **73**, 303; *(b)* R. Gautron, D. Eloy, P. Escaffre, R. Guglielmetti, E. Pottier and P. Tardieu, *Bull. Soc. Chim. Belg.*, 1991, **100**, 315; *(c)* E. Pottier, M. Sergent, R. Phan Tan Luu and R. Guglielmetti, *Bull. Soc. Chim. Belg.*, 1992, **101**, 719; *(d)* G. Baillet, G. Giusti and R. Guglielmetti, *Bull. Chem. Soc. Jpn.*, 1995, **68**, 1220.
13 J. Biteau, F. Chaput and J. P. Boilot, *J. Phys. Chem.*, 1996, **100**, 9024.
14 B. Schaudel, C. Guermeur, C. Sanchez, K. Nakatani and J. Delaire, *J. Mater. Chem.*, 1997, **7**, 61.
15 (*a*) *Selected data* for SO2: (calc. for $C_{22}H_{22}IN_3O$: C, 56.06; H, 4.70; N, 8.91; O, 3.39. Found: C, 55.92; H, 4.77; N, 8.98; O, 3.34%); $\delta_H(CDCl_3)$ 1.34 (s, 3 H), 1.38 (s, 3 H), 2.75 (s, 3 H), 4.90 (s, 3 H), 6.61 (d, 1 H), 6.97 (t, 1 H), 7.10 (d, 1 H), 7.22 (t, 1 H), 7.68 (d, 1 H), 7.90 (s, 1 H), 8.10 (dd, 1 H), 8.19 (d, 1H), 9.60 (d, 1H), 10.18 (d, 1H). (*b*) An UV lamp for chromatography (365 nm with stained glass filter, 6 W) was used as a UV source.

Communication a907675a

Photo-induced tautomerisation of methyltrioxorhenium(VII): the intermediate in olefin metathesis?

Leigh J. Morris,[a] Anthony J. Downs,[a] Tim M. Greene,[a] G. Sean McGrady,[b] Wolfgang A. Herrmann,[c] Peter Sirsch,[c] Odd Gropen[d] and Wolfgang Scherer[d]

[a] *Inorganic Chemistry Laboratory, University of Oxford, South Parks Road, Oxford, UK OX1 3QR. E-mail: tony.downs@chem.ox.ac.uk*
[b] *Department of Chemistry, King's College London, Strand, London, UK WC2R 2LS*
[c] *Anorganisch-chemisches Institut, Technische Universität München, Lichtenbergstrasse 4, D-85747 Garching bei München, Germany*
[d] *Institute of Mathematical and Physical Sciences, University of Tromsø, N-9037 Tromsø, Norway*

Received (in Basel, Switzerland) 28th September 1999, Accepted 1st December 1999

Matrix-isolated $[CH_3ReO_3]$ tautomerises to $[H_2C{=}Re(O)_2OH]$ under the influence of UV light; the carbene has been characterised in its normal and ^2H- and ^{13}C-enriched isotopic forms by its IR spectrum with results well replicated by quantum chemical calculations.

Since methyltrioxorhenium(VII), $[CH_3ReO_3]$ **1**, was first described, its rôle in promoting and catalysing numerous organic reactions has been explored in detail.[1,2] In fact, **1** is probably the most widely active organometallic catalyst reported to date. This activity encompasses two general areas: (i) oxidation reactions (including olefin epoxidation, Baeyer–Villiger and aromatic oxidation);[2–5] and (ii) olefin isomerisation and metathesis.[6] The peroxo derivatives of **1** active in many reactions of type (i) have been isolated and characterised both structurally and spectroscopically.[7] By contrast, the species responsible for catalytic activity of type (ii) have eluded direct detection, although a tautomer of the form $[H_2C{=}Re(O)_2OH]$ **2**, has long been presumed to be the active form of **1**.[2,8] There are numerous reports of rhenium–carbon multiple bonds in the literature generally, but not exclusively, involving rhenium in formal oxidation states $< +7$.[8,9]

Photolysis of **1** in solution appears to result in homolysis of the Re–C bond.[10] Our studies reveal, however, that the matrix-isolated molecule exhibits altogether different behaviour, initially tautomerising to the previously unknown carbene derivative **2** under the influence of UV light at wavelengths near 254 nm (Scheme 1). Tautomer **2** is also photolabile, broad-band UV–VIS irradiation (λ = 200–800 nm) causing it to decay to a product containing an Re–CO fragment, **3**, possibly $[H_2Re(O)(OH)CO]$.

Exposure of **1** isolated in an Ar matrix at 14 K to UV radiation with λ = *ca.* 254 nm for several minutes results in the decay of the IR absorptions due to **1** and the simultaneous appearance and growth of new absorptions apparently due to a single product **2** (Fig. 1). Irradiation of the matrix with broad-band UV–VIS light (λ = 200–800 nm) was observed to cause the evolution from **2** of at least one further product **3** which could not be conclusively identified by its IR spectrum. The IR bands identified on the evidence of their growth-decay patterns enable **2** to be characterised as $[H_2C{=}Re(O)_2OH]$, the conclusions being underpinned (i) by the observed effects of ^2H- and ^{13}C-enrichment of the products derived from the species $[CD_3ReO_3]$ **1**-d_3, and $[^{13}CH_3ReO_3]$ **1**-^{13}c, (ii) by parallels with the spectra of related carbene and Re=O derivatives, *e.g.* $CoCH_2$[11] and ReO_2F_3,[12] and (iii) by comparisons with the results of Density Functional Theory (DFT) calculations. (Calculations were carried out in Gaussian 98[13] with geometries optimised at the BPW91/LANL2DZ level of theory; standard 6-31G(d,p) basis sets were used for C, O and H, whilst the Re basis set was augmented with an additional f-type polarisation function.) Prominent among its IR absorptions were those at 3650.0, 992.2, 963.3 and 668.4 cm^{-1} which are identifiable by their frequencies, intensities and responses to ^2H- and ^{13}C-enrichment with the modes ν(O–H), ν_s(Re=O), ν_{as}(Re=O) and ν(Re–OH), respectively. The presence of the $Re{=}CH_2$ unit is signalled by bands at 3079.6, 2985.8, 1320.9, 778.8, 756.4 and 627.9 cm^{-1} which we associate with the modes detailed in Table 1; each assignment is attested by analogy with the corresponding mode of $CoCH_2$[11] and by the ^2H and ^{13}C isotopic shifts, although the description of the motion is sometimes less than exact. The spectrum is well simulated by a scaled force field computed for **2** on the basis of DFT calculations (Table 1), the 36 frequencies measured for **2**, **2**-d_3 and **2**-^{13}c being matched with an r.m.s. deviation of only 1.66%. It is also evident that mixing of the ν(Re=C), $\rho(CH_2)$ and δ(OH) motions complicates the interpretation of the spectrum in the region 600–800 cm^{-1}, preventing the identification of any one feature with the ν(Re=C) mode. The relative intensities of the bands due to the well defined modes ν_{as}(Re=O) and ν_s(Re=O) imply an O=Re=O angle in the order of 116°, in good agreement with the optimum geometry computed for **2**.

Similar experiments with $[CH_2DReO_3]$ **1**-d_1 give rise not only to $[H_2C{=}Re(O)_2OD]$, but also to the isotopomer

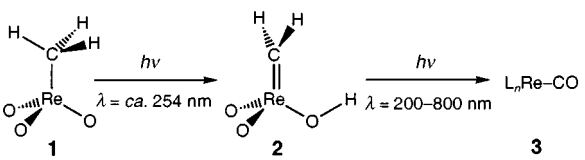

Scheme 1

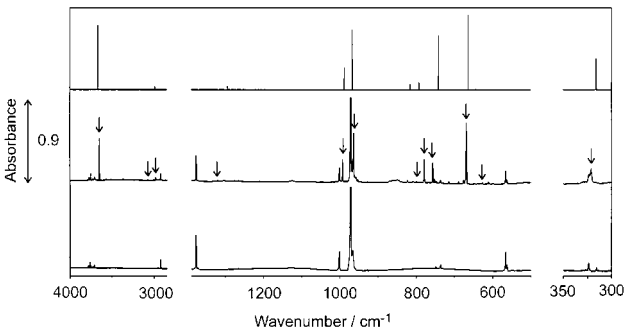

Fig. 1 (a) IR spectrum of $[CH_3ReO_3]$ **1** isolated in an argon matrix at 14 K; (b) IR spectrum showing the effect of irradiation at λ = 254 nm for 15 min ($\downarrow$ indicates a feature associated with $[H_2C{=}Re(O)_2OH]$ **2**); and (c) the spectrum of **2** based on the results of DFT calculations.

Table 1 Observed and calculated fundamental vibrational frequencies for **2**, **2**-^{13}c, and **2**-d_3 under C_s symmetry. Observed and calculated intensities are in parentheses[a]

$H_2{}^{12}CReO_2(OH)$		$H_2{}^{13}CReO_2(OH)$		$D_2{}^{12}CReO_2(OD)$		
Obs.	Calc.[b]	Obs.	Calc.[b]	Obs.	Calc.[b]	Description of mode
3650.0 (100)	3669.6 (87)	3650.4 (100)	3669.6 (87)	2694.2 (73)	2672.3 (63)	ν(O–H)
2985.8 (3)	2994.4 (5)	2980.2 (4)	2989.0 (5)	2195.1 (5)	2171.4 (6)	$\nu_s(CH_2)$
1320.9 (2)	1295.0 (5)	1311.8 (2)	1286.7 (5)	1009.9 (2)	1018.8 (6)	$\delta(CH_2)$
992.2 (25)	988.4 (30)	991.9 (26)	988.3 (30)	992.2 (31)	987.1 (42)	$\nu_s(ReO_2)$
799.2 (2)	815.4 (8)	798.7 (3)	812.4 (9)	622.6 (3)	631.0 (3)	
778.8 (34)	792.0 (10)	768.3 (53)	770.4 (14)	578.9 (43)	556.8 (81)	δ(O–H) + $\rho(CH_2)$
756.4 (30)	741.9 (73)	739.6 (19)	736.5 (67)	685.9 (10)	698.2 (6)	+ ν(Re=C) + ν(Re–OH)
668.4 (83)	664.2 (100)	668.8 (87)	664.2 (100)	660.0 (69)	664.7 (75)	
[c]	286.4 (2)	[c]	286.4 (2)	[c]	286.0 (2)	ReO_2 wag
[c]	255.6 (1)	[c]	255.6 (1)	[c]	252.7 (2)	ReO_2 scissor
[c]	239.8 (3)	[c]	239.8 (3)	[c]	217.6 (3)	δ(CReOH)
3079.6 (3)	3091.9 (0.6)	3068.4 (1)	3079.5 (0.6)	2315.2 (1)	2299.0 (0.3)	$\nu_{as}(CH_2)$
963.3 (64)	967.2 (81)	963.4 (80)	967.1 (81)	961.8 (100)	965.0 (100)	$\nu_{as}(ReO_2)$
627.9 (3)	644.2 (1)	625.7 (5)	639.3 (2)	500.2 (2)	504.1 (0.3)	CH_2 scissor
[c]	526.4 (0.2)	[c]	525.8 (0.2)	[c]	386.1 (0.01)	CH_2 wag
321.2 (33)	315.9 (42)	320.7 (38)	315.2 (43)	239.3 (19)	253.4 (6)	δ(O–H)
[c]	266.8 (15)	[c]	266.8 (15)	[c]	237.3 (15)	$\delta(CReO_2)$
[c]	233.2 (0.03)	[c]	233.2 (0.03)	[c]	208.5 (16)	$d(CReO_2)$

[a] Frequencies in cm^{-1}; all intensities normalised to that of the most intense band set equal to 100 (in parentheses). [b] Calculated frequency scaled by a factor of 0.9740. The r.m.s. deviation between observed and scaled calculated frequencies is 1.66%. [c] Indicates a feature too weak to be observed.

[H(D)C=Re(O)$_2$OH] **2**-d_1. Here the ν(C–H) fundamental is isolated from all other modes in the molecule and so gives access, in principle, to relatively precise estimates of the dimensions of the CH_2 unit.[14] The measured value of ν^{is}(C–H) (3035.4 cm^{-1}), taken together with ν(^{12}C–H), ν(^{13}C–H) and ν(^{12}C–D) data for the other isotopomers, affords values that tally with the results of the DFT optimisations given in parentheses: r_0 = 1.088 Å (r_e = 1.099 Å), ∠HCH = 119 ± 4° (∠$_e$HCH = 115.8°).

Although **2** was formed almost exclusively when matrix-isolated **1** was photolysed at wavelengths near 254 nm, exposure to broad-band UV–VIS light gave rise to a secondary change. The sole detectable product **3** formed from **2** under these conditions, but always in the presence of an abundance of **1** and **2**, could be identified by a single IR band at 2051.4 cm^{-1}. Assignment to the ν(C–O) mode of an Re–CO moiety is strongly urged by a minimal change of frequency when **3** is formed from **1**-d_3 or **1**-d_1 but by a shift to 2003.8 cm^{-1} when it is formed from **1**-^{13}c. The circumstances preclude positive identification, but a possible candidate for **3** is the novel rhenium(v) compound [H_2Re(CO)(O)OH] formed by photo-isomerisation of [H_2C=Re(O)$_2$OH] in a change that would parallel the conversion of [H_2COSi] to [H_2Si:CO].[15] DFT calculations provide some support for [H_2Re(CO)(O)OH], finding a potential energy minimum 126 kJ mol^{-1} above that of [H_2C=Re(O)$_2$OH] with a structure approximating to a square-based pyramid having the unique oxide ligand at the apex, and a calculated ν(C–O) frequency of 2040 cm^{-1} (^{12}C/^{13}C shift = 44.5 cm^{-1}).

[CH_3ReO_3] is active in olefin metathesis only when activated by a co-catalyst (S_4N_4/$AlCl_3$), or when supported on silica or alumina.[8] DFT calculations indicate that **2** lies *ca.* 89 kJ mol^{-1} higher in energy than **1**, and hence is inaccessible under normal thermal conditions. Model calculations on [CH_3ReO_2{(η^2-$OSiH_2$)$_2$O}] **4**, the product formed by condensation of [CH_3ReO_3] with disilanol ([H_2Si(OH)]$_2$O), show the tautomeric H-atom transfer to occur preferentially to an Re–O–Si bridging oxygen atom rather than to an Re=O unit. The resulting carbene species [H_2C=ReO_2{(η^2-$OSiH_2$)(O)(SiH_2OH)}] **5** is effectively stabilised by *ca.* 48 kJ mol^{-1} relative to complex **4**. This alternative H-atom transfer to the Re–O–Si bridge would seem to be a more realistic mechanism for carbene formation on supported [CH_3ReO_3].

Notes and references

1 W. A. Herrmann, *J. Organomet. Chem.*, 1995, **500**, 149.
2 C. C. Romão, F. E. Kühn and W. A. Herrmann, *Chem. Rev.*, 1997, **97**, 3197.
3 W. A. Herrmann, R. W. Fischer and D. W. Marz, *Angew. Chem., Int. Ed. Engl.*, 1991, **30**, 1638.
4 W. A. Herrmann, R. W. Fischer and J. D. G. Correira, *J. Mol. Catal.*, 1994, **94**, 213.
5 R. A. Sheldon, *Top. Curr. Chem.*, 1993, **164**, 21.
6 W. A. Herrmann, W. Wagner, U. N. Flessner, U. Volkhardt and H. Komber, *Angew. Chem., Int. Ed. Engl.*, 1991, **30**, 1636.
7 A. M. Al-Ajlouni and J. H. Espenson, *J. Org. Chem.*, 1996, **61**, 3969; M. M. Abu-Omar and J. H. Espenson, *Organometallics*, 1996, **15**, 3543.
8 D. M. Hoffman, in *Comprehensive Organometallic Chemistry II*, ed. C. P. Casey, Pergamon, Oxford, 1995, vol. 6, p. 231.
9 J. M. O'Connor, in *Comprehensive Organometallic Chemistry II*, ed. C. P. Casey, Pergamon, Oxford, 1995, vol. 6, p. 200.
10 H. Kunkely, T. Türk, C. Teixeira, C. de Meric de Bellefon, W. A. Herrmann and A. Vogler, *Organometallics*, 1991, **10**, 2090.
11 W. E. Billups, S.-C. Chang, R. H. Hauge and J. L. Margrave, *J. Am. Chem. Soc.*, 1995, **117**, 1387.
12 I. R. Beattie, R. A. Crocombe and J. S. Ogden, *J. Chem. Soc., Dalton Trans.*, 1977, 1481; W. J. Casteel Jr., D. A. Dixon, H. P. A. Mercier and G. J. Schrobilgen, *Inorg. Chem.*, 1996, **35**, 4310.
13 M. J. Frisch, G. W. Trucks, H. B. Schlegel, G. E. Scuseria, M. A. Robb, J. R. Cheeseman, V. G. Zakrewski, J. A. Montgomery, R. E. Stratmann, J. C. Burant, S. Dapprich, J. M. Millam, A. D. Daniels, K. N. Kudin, M. C. Strain, O. Farkas, J. Tomasi, V. Barone, M. Cossi, R. Cammi, B. Mennucci, C. Pomelli, C. Adamo, S. Clifford, J. Ochterski, G. A. Petersson, P. Y. Ayala, Q. Cui, K. Morokuma, D. K. Malick, A. D. Rabuck, K. Raghavachari, J. B. Foresman, J. Cioslowski, J. V. Ortiz, B. B. Stefanov, G. Lui, A. Liashenko, P. Piskorz, I. Komaromi, R. Gomperts, R. L. Martin, D. J. Fox, T. Keith, M. A. Al-Laham, C. Y. Peng, A. Nanayakkara, C. Gonzalez, M. Challacombe, P. M. W. Gill, B. G. Johnson, W. Chen, M. W. Wong, J. L. Andres, M. Head-Gordon, E. S. Replogle and J. A. Pople, Gaussian 98, Revision A.3, Gaussian Inc., Pittsburgh PA, 1998.
14 D. C. McKean, *Chem. Soc. Rev.*, 1978, **7**, 399; *Croat. Chem. Acta*, 1988, **61**, 447.
15 G. Maier, H. P. Reisenauer and H. Egenolf, *Organometallics*, 1999, **18**, 2155.

Communication a907908d

Photoactivated DNA cleavage *via* charge transfer promoted N_2 release from tris[3-hydroxy-1,2,3-benzotriazine-4(3*H*)-one]iron(III)

Tucker D. Maurer,[a] Brian J. Kraft,[a] Susan M. Lato,[a] Andrew D. Ellington[b] and Jeffrey M. Zaleski[a]*

[a] *Department of Chemistry and Biochemistry, Indiana University, Bloomington, IN 47405, USA. E-mail: zaleski@indiana.edu*

[b] *Department of Molecular Biology, University of Texas, Austin, TX 78712, USA*

Received (in Bloomington, IN, USA) 5th October 1999, Accepted 18th November 1999

Visible wavelength ligand-to-metal (LMCT) activated N_2 release from tris(3-hydroxy-1,2,3-benzotriazine-4(3*H*)-one]iron(III) produces localized ligand radical intermediates capable of cleaving DNA and represents a new chemical approach to photonuclease design for biological applications.

The antibiotic 6-diazo-5-oxo-L-norleucine utilizes a terminal diazo unit to generate unimolecular diradical intermediates following thermal incubation and loss of N_2.[1] The kinamycin antibiotics also possess the reactive terminal diazo unit,[2] and UV photolysis of kinamycin analogs is thought to generate diradical intermediates that effect DNA cleavage.[3] Bioorganic chemists have incorporated this strategy into the design of synthetic photonucleases by preparing diazene and benzotriazole agents that produce diradical intermediates capable of cleaving DNA upon UV excitation.[4,5] Although effective, the ability to promote diradical formation using visible region excitation would have significant advantages for *in vivo* photodynamic therapy applications owing to the increased optical penetration depth by longer wavelengths.[6] To this end, we have recently initiated efforts toward developing novel transition metal diazo compounds that use the metal center to activate ligands for N_2 release upon optical excitation into metal–ligand charge transfer transitions typically occurring in the visible spectral region. Application of the resulting radical intermediates to DNA cleavage provides approach toward the development of self-contained unimolecular photonucleases for biological applications.

Photochemical activation of diazo compounds occurs *via* UV irradiation of the $^1(n–\pi^*)$ transition which leads to extrusion of N_2 and formation of radical intermediates.[7] However, diazo compounds are also unstable to chemical and electrochemical oxidation and rapidly release N_2 as a reaction product.[8–10] We have chosen to exploit this property by preparing Fe(III) complexes with ligands that posses the reactive –N=N– subunit. Fe(III) is a powerful excited state oxidant[11] and is thermodynamically potent to activate these ligands for N_2 release.

The compound 3-hydroxy-1,2,3-benzotriazine-4(3*H*)-one **1** (Aldrich) contains the target N_2 subunit, and in its deprotonated form, the 3-hydroxy-4-one functionalities strongly chelate Fe(III).[12] Reaction of **1** with 3 equiv. of $Fe(NO_3)_3{\cdot}9H_2O$ in THF–Et_3N yields the tris-(chelate **2** as a red powder in nearly quantitative yield.[13] The electronic absorption spectrum of **1** in acetonitrile exhibits pronounced $\pi–\pi^*$ transitions in the 300 nm region and a shoulder at 325 nm corresponding to the forbidden $n–\pi^*$ transition of the diazo unit.[7] Photolysis of **1** at $\lambda \geq 345$ nm yields a triplet radical EPR signal (5 K, EtOH) with the signature half-field transition at 1700 G, as well as copious N_2 evolution as detected by GC–MS, reflecting the propensity for diradical formation *via* N_2 loss from this organic framework. The absorption spectrum of **2** in the same solvent (Fig. 1) reveals three distinct bands corresponding to a ligand-centered transition (λ_{max} = 300 nm), and two moderately intense O→Fe ligand-to-metal charge transfer (LMCT) bands (λ_{max} = 340, 425 nm) similar to those of Fe(III) tris-catecholates.[14]

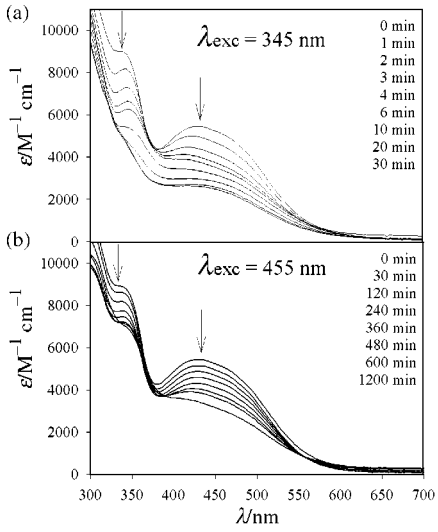

Fig. 1 Electronic absorption profiles for anaerobic photolyses of 0.1 mM acetonitrile solutions of **2** at (a) $\lambda \geq 345$ nm and (b) $\lambda \geq 455$ nm.

Anaerobic photolyses of **2** were performed in acetonitrile (0.1 mM) at $\lambda \geq 345$ and 455 nm and monitored with UV–VIS spectrophotometry (Fig. 1). In both cases, rapid photobleaching of the optical spectra are observed upon LMCT excitation of the complex, with partial recovery upon exposure to O_2, consistent with formation of Fe(II) in solution. This is confirmed by the disappearance of the rhombic Fe(III) EPR signal at g = 4.3 (Fig. 2) following variable time photolyses at 20 °C. Both reactions exhibit first-order kinetics at early photolysis times, with the reaction at $\lambda \geq 345$ nm ($k_{obs} = 9.3 \times 10^{-2}$ min^{-1}) proceeding considerably more efficiently than photolysis at $\lambda \geq 455$ nm ($k_{obs} = 4.0 \times 10^{-3}$ min^{-1}) under identical experimental conditions. In addition to excitation of both LMCT bands with $\lambda \geq 345$ nm, the disparate reactivity can be attributed to the greater quantum yield for decay of the starting compound upon excitation into the higher energy transition ($\phi_{365} = 2.1 \times 10^{-4}$ *cf.* $\phi_{436} = 3.6 \times 10^{-5}$). This results in simultaneous excitation of both the LMCT and ligand centered $n–\pi^*$ transitions of the Fe(III) compound. To verify LMCT activation of the triazine ligand, photolysis of **1** was conducted in acetonitrile with $\lambda \geq$ 455 nm and yielded no reactivity over a 12 h period indicating that photoactivation of **2** at lower energies derives solely from

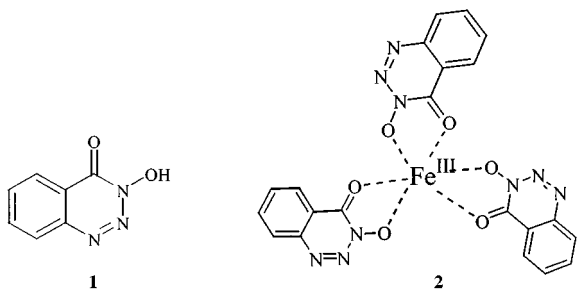

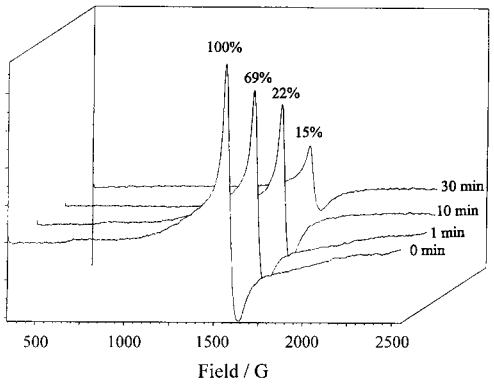

Fig. 2 Disappearance of the high spin Fe(III) EPR signal of **2** at $g = 4.3$ as a function of photolysis ($\lambda \geq 345$ nm) time. Relative spin quantitations are denoted above each trace.

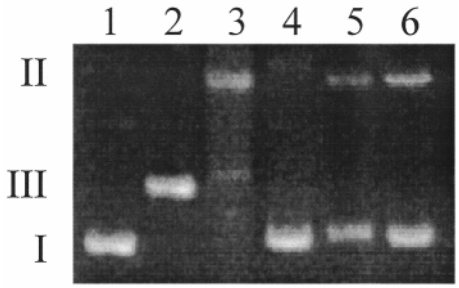

Fig. 3 Photoinduced DNA-cleavage of 30 μM/bp pUC 118 by 300 μM **2** following 400 nm photolysis for 12 h at 20 °C (2% agarose gel). Form I: supercoiled plasmid. Form II: nicked plasmid. Form III: linear plasmid. Lane 1: supercoiled DNA; lane 2: linear DNA from EcoRI digest; lane 3: DNA + **2** + *hν*; lane 4: DNA + **2**, no *hν*; lane 5: DNA + *hν*; lane 6: 900 μM **1** + DNA + *hν*.

LMCT excitation. Furthermore, reactivity of **2** has been demonstrated at wavelengths up to 500 nm, effectively ruling out the requirement for participation by higher energy excited states in the photoactivation of the triazine ligand.

To correlate the observed reactivity with N_2 extrusion, wavelength dependent photolyses ($\lambda \geq 345$ and 455 nm) were performed on 800 μL solutions of 15 mM **2** under argon in degassed benzonitrile. From headspace GC–MS analysis, N_2 production was gauged by comparison of the N_2/O_2 ratios above the photolyzed solutions relative to unphotolyzed controls. The average of four trials at each wavelength produced an increased N_2 content of 112% at $\lambda \geq 345$ nm and 9.7% at $\lambda \geq 455$ nm).[15] Together, these results demonstrate that the overall strategy to induce radical formation from charge transfer excited states is indeed operative.

Electronic structure studies of Fe(catecholate)$_3^{3-}$ have shown that the LMCT excited state is best described as a charge-separated Fe^{2+}–ligand radical. The energy required to photochemically produce a Fe^{2+}–$L^{\cdot+}$ state can be estimated by the sum of the redox potentials for the free ligand and the metal center, where $\Delta E = -E_{ox}(\mathbf{1}) + E_{red}(\mathbf{2})$. The cyclic voltammogram (CV) of **1** demonstrates an irreversible oxidation wave at a peak potential of +1.7 V *vs.* Ag/AgCl [E_{ox}(**1**)], derived from rapid denitrogenation.[8–10] The CV of **2** exhibits a reversible Fe(III)/(II) redox couple with a half potential of −0.3 V *vs.* Ag/AgCl [E_{red}(**2**)]. Therefore, the minimum energy required to produce the charge-separated excited state, ΔE, is *ca.* −2.48 eV, or 500 nm from the ground state. However, the energy of this state is exergonic with respect to LMCT excitation at $\lambda \geq 455$ nm and is therefore consistent with charge transfer induced activation and denitrogenation of the triazine ligand at these wavelengths.

The ligand radical intermediate produced upon LMCT excitation of **2** is an effective DNA photocleaving agent. Cleaving ability (%) was determined by quantitating the effectiveness in converting circular supercoiled plasmid DNA (form I) to nicked (form II) and linear DNA (form III) following subtraction of background cleavage due to photolysis of DNA alone (35%). Fig. 3 illustrates the agarose gel electrophoresis of photolysis products of 300 μM **2** in the presence of pUC 118 plasmid DNA (30 μM/bp where bp represents a base pair). Solutions were irradiated anaerobically for 12 h in 1:9 DMSO–Tris buffer (20 mM, pH 7.55) at $\lambda \geq 400$ nm.[16] Photolysis produced a mixture of linear (38%) and nicked (27%) forms (lane 3), while thermal incubation effected no DNA cleavage (lane 4). As Fig. 3 shows, the relative amount of cleavage by **2** is significant as photolysis of both plasmid alone (lane 5) and 900 μM free ligand (lane 6) yield identical amounts of nicked DNA (35%), indicating only background levels of DNA photodegradation. Our results demonstrate that although **2** did not generate exclusively linear DNA, it is the only species in Fig. 3 to produce the linear form and consume 100% of the supercoiled form. Additionally, the absence of O_2 from the reaction and the presence of the hydroxy radical scavenger DMSO in the buffer effectively rule out participation by O_2-derived radicals in the cleavage reaction and implicate a ligand-centered radical as the key intermediate.

In conclusion, the above studies describe the preparation and photoreactivity of a novel transition metal triazine compound. The overall strategy of metal complex activation *via* LMCT excitation in the visible spectral region is operative. Irradiation of the Fe(III) complex in the presence of plasmid DNA affords both single- and double-strand cleavage, with significantly greater efficiency than photolysis of free ligand in threefold higher concentration. From a mechanistic perspective, detection of Fe(II) as a reaction product raises important questions concerning the mode of activation of the kinamycins and 6-diazo-5-oxo-L-norleucine. Are these antibiotics redox activated, and if so, are diradicals or radical ions responsible for the DNA-cleaving reactivity of these agents? Further studies designed to probe the specific nature of the intermediates as well as modulate the reactivity of this system are ongoing.

The generous support of the American Cancer Society (RPG-99-156-01-C) and the Donors of the Petroleum Research Fund (PRF#33340-G4), administered by the American Chemical Society, are gratefully acknowledged.

Notes and references

1 K. Hiramoto, T. Fujino and K. Kikugawa, *Mutat. Res.*, 1996, **360**, 95.
2 S. J. Gould, N. Tamayo, C. R. Melville and M. C. Cone, *J. Am. Chem. Soc.*, 1994, **116**, 2207.
3 B. G. Maiya, C. V. Ramana, S. Arounaguiri and M. Nagarajan, *Bioorg. Med. Chem. Lett.*, 1997, **7**, 2141.
4 T. M. Bregant, J. Groppe and R. D. Little, *J. Am. Chem. Soc.*, 1994, **116**, 3635.
5 S. M. Touami, C. C. Poon and P. A. Wender, *J. Am. Chem. Soc.*, 1997, **119**, 7611.
6 T. J. Dougherty, C. J. Gomer, B. W. Henderson, G. Jori, D. Kessel, M. Korbelik, J. Moan and Q. Peng, *J. Natl. Cancer Inst.*, 1998, **90**, 889.
7 N. J. Turro, *Modern Molecular Photochemistry*, The Benjamin/Cummings Publishing Company, Inc., Menlo Park, 1978.
8 J. Adamson, D. L. Forster, T. L. Gilchrist and C. W. Rees, *Chem. Commun.*, 1969, 221.
9 R. J. Kobylecki and A. McKillop, *1,2,3 Triazines* in *Advances in Heterocyclic Chemistry*, vol. 19, ed. A. R. Katritzky and J. Boulton, Academic Press, Inc., New York, 1976.
10 V. D. Parker and D. Bethell, *J. Am. Chem. Soc.*, 1987, **109**, 5066.
11 O. Horvath and K. L. Stevenson, *Iron, Ruthenium, Osmium*, in *Charge Transfer Photochemistry of Coordination Compounds*, VCH, New York, 1993, pp. 207–266.
12 R. J. Motekaitis and A. E. Martell, *Inorg. Chim. Acta*, 1991, **183**, 71.
13 Compound afforded satisfactory analysis. Calc. for $FeC_{21}H_{12}N_9O_6 \cdot 0.5\ H_2O$; Fe 10.13; C 45.75; H 2.37; N 22.87. Found: Fe 10.16; C 46.01; H 2.36; N 22.95%. Positive ion ESI-MS match of *m/z* 543.2.
14 T. B. Karpishin, M. S. Gebhard, E. I. Solomon and K. N. Raymond, *J. Am. Chem. Soc.*, 1991, **113**, 2977.
15 Photolyses were performed for 12 h at $\lambda \geq 345$ nm and 72 h at $\lambda \geq 455$ nm.
16 Photolyses were performed at $\lambda \geq 400$ nm owing to the solvatochromatic blue shift of the LMCT transitions of **2** in water/buffer.

Communication a908005h

Study of the accessibility of phosphorus centres incorporated within ordered mesoporous organic–inorganic hybrid materials

Robert J. P. Corriu,* Christian Hoarau, Ahmad Mehdi and Catherine Reyé

Laboratoire de Chimie Moleculaire et Organisation du Solide, UMR 5637 CNRS, Université de Montpellier II, Sciences et Techniques du Languedoc, Place E. Bataillon, F-34095 Montpellier Cedex 5, France.
E-mail: reye@crit.univ-montp2.fr

Received (in Oxford, UK) 22nd September 1999, Accepted 18th November 1999

Phosphorus centres incorporated within surfactant-directed mesoporous hybrid materials are shown to be more easily accessible than those incorporated within the corresponding materials prepared in the absence of surfactant.

The one step preparation of organically functionalised ordered mesoporous silica by using non-ionic[1,3] and ionic surfactants[4–9] as structure-directing agents constitutes a new and very promising route to hybrid materials with organised functionalities. Our contribution in this field was the preparation of surfactant-directed mesoporous hybrid materials incorporating phosphino groups.[3] We showed that such materials are easily accessible and undergo further chemical reactions at phosphorus (sulfuration and quaternization) without disrupting the ordered structure and without changing notably the textural characteristics, thus suggesting the location of the P centres within the mesopore channels.[5] The potential applications of these materials containing P centres for catalysis[10] and separation which are strongly connected with the chemical accessibility of the functionalities have led us to further studies. Here, we show that, in surfactant-directed mesoporous hybrid materials, phosphorus centres are more easily accessible than in the corresponding materials prepared in the absence of surfactants.

The hybrid materials $\mathbf{X}_n$ and $\mathbf{X'}_n$ were obtained by co-hydrolysis and polycondensation of mixtures $Ph_2P(CH_2)_3Si(OMe)_3/nSi(OEt)_4$ (n = 6, 9 and 19) in the presence of *n*-hexadecylamine as template for $\mathbf{X}_n$ and in the absence of template but in the presence of 1% TBAF as catalyst for $\mathbf{X'}_n$ (Scheme 1). The molar composition of each mixture was: $1 - x$ $Si(OEt)_4$:$xPh_2P(CH_2)_3Si(OMe)_3$: 0.27 *n*-hexadecylamine : 24.2 H_2O : 9.1 EtOH. The xerogels were prepared according to previously published procedures[3] and some relevant physical properties are given in Table 1. The BET surface areas were determined by N_2 adsorption–desorption isotherm measurements. $\mathbf{X}_n$ (n = 6, 9, 19) exhibit type IV isotherms,[11] characteristic for mesoporous materials. In contrast, the isotherms of $\mathbf{X'}_n$ are indicative of macroporosity.[11] XRD patterns for $\mathbf{X}_n$ exhibit a single diffraction peak corresponding to d_{100} spacing while no peak was observed for $\mathbf{X'}_n$. Organic incorporation was calculated by thermogravimetric analysis. It is worth noting that the calculated values are slightly closer to theoretical values for the mesoporous xerogels than for the others and this, in particular for high 'dilutions' of the organic moiety in silica. Another interesting observation in relation to the effect of dilution was made from the ^{31}P NMR data of the materials. As shown in Fig. 1, the ^{31}P NMR spectra for $\mathbf{X'}_n$ displayed signals which are always broader than those for $\mathbf{X}_n$. This is an indication of a greater mobility for the P centres in $\mathbf{X}_n$ than in $\mathbf{X'}_n$. Furthermore, on going from the 'dilution' n = 9 to the higher 'dilution' n = 19, the $Dn_{1/2}$ values remain stable for the ordered hybrid materials while for the others $\mathbf{X'}_n$, they regularly decrease as the 'dilution' increases. Thus it can be concluded that from n = 9 all the P centres within $\mathbf{X}_n$ have the same surroundings, the organic pendants being regularly dispersed at the surface of the mesopores while for the solids $\mathbf{X'}_n$ the distribution of the organic groups is random.

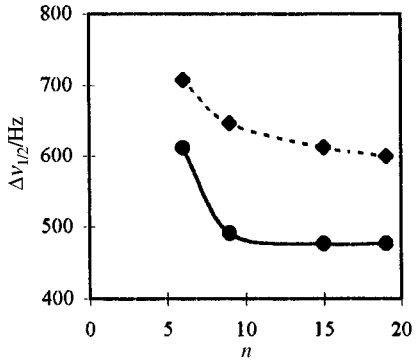

Fig. 1 Half linewidth ($\Delta\nu_{1/2}$) of the solid state ^{31}P NMR signals for $\mathbf{X}_n$ (———) and $\mathbf{X'}_n$ (-----) as a function of the 'dilution' n.

The accessibility of the P centres in these materials was investigated by using the reactions of quaternization and complexation of phosphorus centres. All the reactions at phosphorus were monitored by solid state ^{31}P NMR spectroscopy which is a reliable and sensitive probe for immobilized phosphorus groups.[12]

The solids $\mathbf{X}_n$ (n = 6, 9, 19) were treated with 1 equiv. of benzyl bromide **1** or 0.5 equiv. of α,α′-dibromoparaxylene **2** per P centre in CH_2Cl_2 at 20 °C. It is to be noted that after treatment, the ^{31}P NMR spectra of materials exhibited no signal corre-

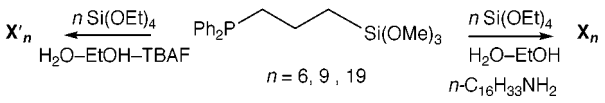

Scheme 1

Table 1 Physical characteristics for $\mathbf{X}_n$ ($\mathbf{X'}_n$)

Xerogel	d_{100} Lattice spacing/Å	BET surface area/m^2 g^{-1}	Total pore volume/cm^3 g^{-1}	Pore diameter[a]/Å	^{31}P CP MAS NMR (δ)	Organic incorporation[b] (%)	
$\mathbf{X_6}$ ($\mathbf{X'_6}$)	41.86 (—)	385 (149)	0.30 (—)	27 (≈300)	−15.84	14.2[c]	11 (10)
$\mathbf{X_9}$ ($\mathbf{X'_9}$)	34.41 (—)	1100 (350)	0.53 (—)	35 (≈300)	−15.71 (−15.61)	10[c]	9.4 (8.8)
$\mathbf{X_{19}}$ ($\mathbf{X'_{19}}$)	38.91 (—)	1380 (640)	0.61 (—)	34 (≈300)	−15.13 (−15.0)	5[c]	5 (4.7)

[a] Measured using the Horvath–Kawazoe pore size distribution model. [b] Percentage of Si atoms present as organosilane with respect to total Si content calculated by thermogravimetric analysis. [c] Theoretical values.

Table 2 Percentage of quaternization of P centres within $\mathbf{X}_n$ treated with **1** or (**2**) as reagent

Reaction time/h	$\mathbf{X_6}$	$\mathbf{X_9}$	$\mathbf{X_{19}}$
2	48 (35)	56 (58)	78 (74)
16	63 (68)	72 (82)	95 (90)
72	83 (83)	100 (93)	100 (100)

Table 3 Percentage of quaternization of P centres within $\mathbf{X}_n$ and $\mathbf{X'}_n$ after treatment for 24 h at 20 °C with **1** or (**2**) as reagent

n	6	9	19
$\mathbf{X}_n$	71 (73)	87 (92)	94 (95)
$\mathbf{X'}_n$	60 (72)	64 (82)	79 (70)

sponding to the oxidation of the P centres. The results given in Table 2 show that the percentage of quaternization of P centres increase with the dilution of the organic moieties in silica with both reagents. The reaction is quantitative with **1** after 72 h from $\mathbf{X_9}$ and $\mathbf{X_{19}}$. It is also quantitative with the bifunctional compound **2** from $\mathbf{X_{19}}$ after 72 h and almost quantitative from $\mathbf{X_9}$ which is noteworthy as in that case all the P centres are bridged. The same reactions were carried out on $\mathbf{X'}_n$ and the percentage of quaternization was calculated after 24 h of reaction. These results are compared to those obtained from $\mathbf{X}_n$ after the same reaction time in Table 3. It appears that the percentage of reaction with **1** is always lower from $\mathbf{X'}_n$ than from $\mathbf{X}_n$, whatever the dilution. Thus the P centres are more easily accessible within ordered mesoporous materials $\mathbf{X}_n$ than within the amorphous $\mathbf{X'}_n$. Interestingly, with the bifunctional reagent **2**, the gap between the percentage of quaternization of P centres obtained from $\mathbf{X}_n$ and $\mathbf{X'}_n$ increases with the dilution in favour of the ordered materials $\mathbf{X}_n$. This result is due to the regular distribution of organic moieties in $\mathbf{X}_n$. Indeed, while the substitution of the second bromide of **2** is promoted by the dilution within $\mathbf{X}_n$, it is rendered difficult within $\mathbf{X'}_n$ because of the random distribution of the organic groups in silica. The distribution of the organic moieties within the solids was further studied by treating the materials with 0.5 equiv. *cis*-$(PPh_3)_2PdCl_2$ per P centre. We observed that the solid state ^{31}P NMR spectra of the materials after 24 h of reaction at 20 °C in CH_2Cl_2 displayed a resonance at δ −16 corresponding to the remaining starting phosphine and a resonance at δ +16 which was assigned to the *trans* anchored phosphine Pd^{II} complex.[12] A further resonance at δ +36 was attributed to starting phosphine oxidation, which never exceeded 15%. Treatment of the materials with a large excess of the nucleophile PBu^n_3 allowed the complete elimination of the palladium liberating the starting phosphine (δ −16). The presence of the unchanged signal at δ +36 after this treatment confirmed the oxidation of the starting phosphine. The extent of the anchored phosphine Pd^{II} complex obtained from $\mathbf{X}_n$ and $\mathbf{X'}_n$ determined by ^{31}P NMR spectroscopy is shown in Fig. 2. The difference between the reactivity of materials $\mathbf{X}_n$ and $\mathbf{X'}_n$ (n = 9, 19) is important. Thus the diffusion of a bulky molecule like $(PPh_3)_2PdCl_2$ through

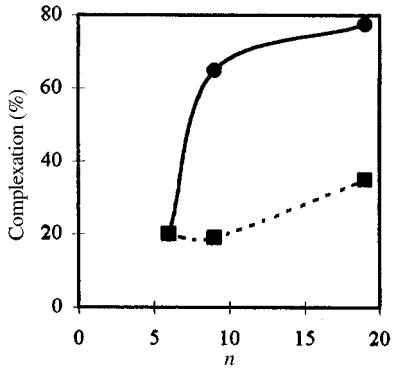

Fig. 2 Percentage of anchored phosphine Pd^{II} complex within $\mathbf{X}_n$ (———) and $\mathbf{X'}_n$ (-----).

materials $\mathbf{X'}_n$ is much more difficult than through the ordered mesoporous materials $\mathbf{X}_n$. The very low extent of reaction for $\mathbf{X_6}$ compared to $\mathbf{X_9}$ and $\mathbf{X_{19}}$ should be due to steric hindrance, which implies also that P centres are mostly located within the mesopores of $\mathbf{X}_n$.

In conclusion, we have shown that in surfactant-directed mesoporous hybrid materials, phosphorus centres are more easily accessible than in the corresponding materials prepared in the absence of surfactants. Furthermore the accessibility of phosphorus centres within ordered mesoporous hybrid materials depends on the 'dilution' of the organic part in silica. The higher the 'dilution', the greater the accessibility of the organic part in particular towards bulky reagents for which a minimum 'dilution' (n > 6) seems to be required. The study of hybrid materials with very low concentration of organo groups is in progress.

Notes and references

1 D. J. Macquarrie, *Chem. Commun.*, 1996, 1961.
2 D. J. Macquarrie, D. B. Jackson, J. E. G. Mdoe and J. H. Clark, *New J. Chem.*, 1999, **23**, 539.
3 R. J. P. Corriu, A. Mehdi and C. Reyé, *C.R. Acad. Sci. Paris, Sér. IIc*, 1999, 35.
4 S. L. Burkett, S. D. Sims and S. Mann, *Chem. Commun.*, 1996, 1367.
5 M. H. Lim, C. F. Blanford and A. Stein, *J. Am. Chem. Soc.*, 1997, **119**, 4090.
6 C. E. Fowler, S. L. Burkett and S. Mann, *Chem. Commun.*, 1997, 1769.
7 M. H. Lim, C. F. Blanford and A. Stein, *Chem. Mater.*, 1998, **10**, 467.
8 F. Babonneau, L. Leite and S. Fontlupt, *J. Mater. Chem.*, 1999, **9**, 175.
9 S. R. Hall, C. E. Fowler, B. Lebeau and S. Mann, *Chem. Commun.*, 1999, 201.
10 B. F. G. Johnson, S. A. Raynor, D. S. Shephard, T. Mashmeyer, J. Meurig Thomas, G. Sankar, S. Bromley, R. Oldroyd, L. Gladden and M. D. Mantle, *Chem. Commun.*, 1999, 1167.
11 S. J. Gregg and K. S. W. Sing, *Adsorption, Surface Area and Porosity*, Academic Press, New York, 2nd edn., 1982.
12 R. A. Komoroski, A. J. Magistro and P. P. Nicholas, *Inorg. Chem.*, 1986, **25**, 3917.

Communication a907700f

ChemComm

Cationic palladium(II) complex-catalyzed [2 + 2] cycloaddition and tandem cycloaddition–allylic rearrangement of ketene with aldehydes: an improved synthesis of sorbic acid

Tetsutaro Hattori,* Yutaka Suzuki, Osamu Uesugi, Shuichi Oi and Sotaro Miyano*

Department of Biomolecular Engineering, Graduate School of Engineering, Tohoku University, Aramaki-Aoba 07, Aoba-ku, Sendai 980-8579, Japan. E-mail: hattori@orgsynth.che.tohoku.ac.jp

Received (in Cambridge, UK) 2nd November 1999, Accepted 24th November 1999

Cationic palladium(II) complexes $[PdL_2(PhCN)_2](BF_4)_2$ efficiently catalyze the [2 + 2] cycloaddition of ketene with aldehydes to give the corresponding oxetan-2-ones, among which 4-vinyl-substituted ones are further isomerized under the conditions to give 3,6-dihydro-2*H*-pyran-2-ones in good yields.

There has been much current interest in the preparation of oxetan-2-ones (β-lactones) because they are not only structural units in biologically active natural products but also versatile synthetic intermediates.[1] Among various synthetic routes to this class of compounds, the most efficient and concise is the Lewis acid-catalyzed [2 + 2] cycloaddition of ketenes with aldehydes.[1] Recently, we have reported the first asymmetric version of the cycloaddition mediated by a catalytic amount of Corey's aluminium-based bissulfonamides.[2] However, the reaction requires the use of at least 10 mol% of the catalyst to obtain the lactones in practical yields, as has been revealed in the related reactions catalyzed by typical metal-based Lewis acids. This may be ascribed to the highly oxophilic nature of the acid, which causes competitive ligation between the reactants and the product to the catalyst to reduce the catalytic efficiency. Deactivation of the catalyst by a trace amount of incidental water in the reaction system is another plausible problem.

On the other hand, it has been recognized in the last decade that certain transition metal complexes have considerable Lewis acid character and can displace conventional Lewis acids in a variety of the so-called Lewis acid-catalyzed reactions.[3] Furthermore, some of the transition metal-based Lewis acids are reported to be effective even in the presence of water.[4] These facts prompted us to examine whether this class of Lewis acids can effect the cycloaddition reaction. Herein, we report a highly efficient [2 + 2] cycloaddition of ketene with aldehydes **1** using cationic palladium(II) complexes $[PdL_2(PhCN)_2](BF_4)_2$ **2**[5] as the catalyst (Scheme 1).

The general procedure for the [2 + 2] cycloaddition is as follows (Method A): to a solution of complex **2** (50.0 μmol) in dry CH_2Cl_2 (20 cm^3) was added aldehyde **1** (1.00 mmol) under nitrogen at an appropriate temperature. Gaseous ketene (*ca.* 2.5 mmol) was bubbled into the mixture over a period of 5 min and the resulting mixture was stirred at this temperature for 1 h.

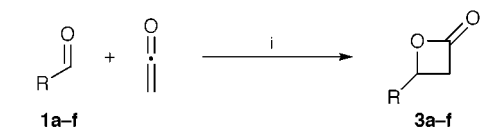

1,3a R = Cy
b R = Et
c R = hexyl
d R = Pr^i
e R = Bu^t
f R = Ph

$[PdL_2(PhCN)_2](BF_4)_2$
2a $L_2 = (PPh_3)_2$
b L_2 = dppe
c L_2 = dppp
d L_2 = dppb
e L_2 = dppf

Scheme 1 *Reagents and conditions*: i, **2**, CH_2Cl_2. dppp = 1,3-bis(diphenylphosphino)propane, dppf = 1,1′-bis(diphenylphosphino)ferrocene.

After usual work-up, the crude product was subjected to GC analysis to determine the yield of lactone **3**.

The results are listed in Table 1. The reaction of cyclohexanecarbaldehyde **1a** with ketene in the presence of 5 mol% of a palladium complex **2a**–**e** proceeded even at −78 °C to give the lactone **3a** (entries 1–5). The catalytic activity of the palladium complexes **2a**–**e** varied depending on the coordinating phosphine ligands, among which dppb (**2d**) was the most effective. Addition of powdered molecular sieves (3 Å) did not improve the yield of lactone **3a** (entry 6). An irregular temperature dependence of the product yield was found in the reaction conducted at −40 °C (entry 7, as compared with entries 4, 8 and 9). This may be ascribed to the balance between an increase in the rate constant with the rise in the reaction temperature and a significant decrease in the concentration of ketene around its boiling point (−41 °C). Lactone **3a** was obtained in quantitative yield at room temperature, even if the quantity of the catalyst was reduced to 1 mol% (entry 10). Judging from the high catalytic activity and the lack of apparent effect of the dehydrating agent (entry 6), the catalyst seems to be compatible with the trace amounts of water in the system. The reaction of several other aldehydes **1b**–**f** with ketene afforded the corresponding lactones **3b**–**f** in good to excellent yields (entries 11–15).

Next, our interest was directed toward the possibility of using the palladium complex **2d** as the catalyst for the cycloaddition of ketene with α,β-unsaturated aldehydes **1g**–**k** (Scheme 2). The reaction of ketene with crotonaldehyde **1g** under the standard conditions (Method A, *vide supra*) afforded not the β-lactone **3g** but a δ-lactone, 3,6-dihydro-6-methyl-2*H*-pyran-2-one (isoparasorbic acid) **4g**,[6] though only in poor yield, along with an unidentifiable polymer (*vide infra*) (Table 2, entry 1).[7] Low-

Table 1 Cycloaddition of ketene with aldehydes **1a**–**f** catalyzed by palladium complexes **2a**–**e**

Entry	**1**	**2**	*T*/°C	**3**	Yield (%)[a]
1	**1a**	**2a**	−78	**3a**	33
2	**1a**	**2b**	−78	**3a**	46
3	**1a**	**2c**	−78	**3a**	55
4	**1a**	**2d**	−78	**3a**	66
5	**1a**	**2e**	−78	**3a**	56
6	**1a**	**2d**	−78	**3a**	63[b]
7	**1a**	**2d**	−40	**3a**	52
8	**1a**	**2d**	0	**3a**	97
9	**1a**	**2d**	room temp.	**3a**	98
10	**1a**	**2d**[c]	room temp.	**3a**	99
11	**1b**	**2d**	room temp.	**3b**	99
12	**1c**	**2d**	room temp.	**3c**	97
13	**1d**	**2d**	room temp.	**3d**	99
14	**1e**	**2d**	room temp.	**3e**	63
15	**1f**	**2d**	room temp.	**3f**	61[d]

[a] Determined by GC analysis on ASTEC Chiraldex G-TA column (0.25 mm i.d. × 20 m) by the internal standard method. [b] Powdered molecular sieves (3 Å) (100 mg) were added. [c] 1.0 mol%. [d] Isolated yield of the 1,3-diol derived from compound **3f**.

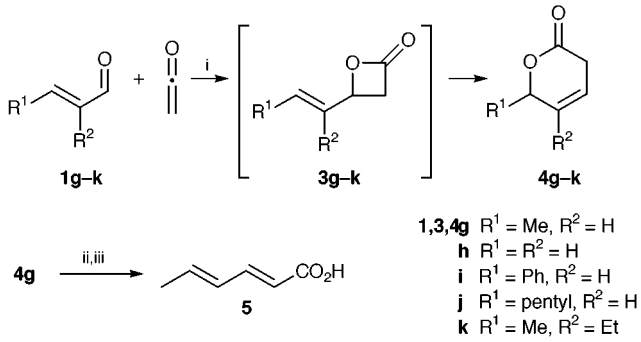

Scheme 2 *Reagents and conditions*: i, **2d**, CH_2Cl_2; ii, EtOH, conc. HCl, reflux; iii, KOH, aqueous EtOH, reflux.

Table 2 Tandem cycloaddition–allylic rearrangement of ketene with α,β-unsaturated aldehydes **1g–k** catalyzed by palladium complex **2d**

Entry	1	Method[a]	CH_2Cl_2/cm^3	4	Yield (%)[b]
1	**1g**	A	20	**4g**	13
2	**1g**	A	200	**4g**	55
3	**1g**	B	200	**4g**	70
4	**1g**	B	200	**4g**	50[c]
5	**1g**	B	500	**4g**	81
6	**1g**[d]	B	200	**4g**	65
7	**1h**	B	200	**4h**	0[e]
8	**1i**	B	200	**4i**	77[c]
9	**1j**	B	200	**4j**	58[c]
10	**1k**	B	200	**4k**	66[c]

[a] See text. [b] Determined by GC analysis on Quadrex MPS-10 column (0.32 mm i.d. × 25 m) by the internal standard method. [c] Isolated yield after column chromatography on silica gel with hexane–EtOAc (1:1) as the eluent. [d] 2.00 mmol. [e] Lactone **3h** was obtained in 96% yield.

ering the reaction temperature and changing the molar ratios of ketene and catalyst **2d** to aldehyde **1g** did not improve the product yield, while dilution of the reaction solution was found to be highly effective (entry 2). Eventually, lactone **4g** could be obtained in good yields by adding aldehyde **1g** and ketene portionwise to a dilute solution of catalyst **2d** (Method B†) (entries 3 and 5). Under these conditions, 2.5 mol% of the catalyst **2d** was sufficient to complete the reaction (compare entry 6 with entry 3). Similar δ-lactones **4i–k** were also obtained in the reaction of α,β-unsaturated aldehydes **1i–k**, while acrolein **1h** afforded β-lactone **3h** under the same conditions (entries 7–10).

The formation of lactone **4** can be rationalized by the initial [2 + 2] cycloaddition of aldehyde **1** with ketene to give the allyl ester **3**, followed by its allylic rearrangement to form lactone **4**. It is known that this type of 1,3-rearrangement of allylic esters is promoted by Pd^0 and Pd^{II} complexes.[8] It should be noted, however, that the palladium(II)-catalyzed reaction is reportedly a [3,3]-sigmatropic rearrangement of allyl esters, which is impossible for the said lactones **3g–k** due to steric reasons. On the other hand, the palladium(0)-catalyzed rearrangement is believed to involve a π-allylpalladium(II) intermediate. It is also reported that palladium(II) salts promote the ring opening of 4-vinyl- (**3h**), and 4-isopropenyl-oxetan-2-one to afford the corresponding penta-2,4-dienoic acids.[9] A metallacyclic σ-allylpalladium intermediate generated by oxidative addition of the C(4)–O bond of the oxetan-2-ones to a palladium(0) species is proposed for the reaction. Thus, an allylpalladium species may be a possible intermediate for the present reaction. We found, however, that $BF_3{\cdot}OEt_2$ also catalyzed the rearrangement to give lactone **4g**, though only in 13% yield, when aldehyde **1g** was treated with ketene (method B) in Et_2O (200 cm^3) at room temperature in the presence of 1.5 equiv. of the acid.[10] This observation, along with the result that lactone **3h** did not isomerize to lactone **4h**, may suggest another possibility, that coordination of the carbonyl oxygen of 4-vinyl lactones **3g**, **i–k** to Lewis acid **2d** promoted the heterolytic cleavage of the C(4)–O bond of the lactones to form a zwitterion, recombination of which at the other allylic terminus afforded lactones **4**.

Further treatment of lactone **4g** with EtOH in the presence of HCl followed by saponification of the resulting ethyl sorbate, gave hexa-2,4-dienoic acid (sorbic acid) **5** in 90% yield (Scheme 2). Therefore, the present method provides an easy access to the acid **5**. It should be noted that sorbic acid **5** is important as a mould and yeast inhibitor, the first step of an industrial synthesis of which relies on the cycloaddition of ketene with crotonaldehyde **1g** catalyzed by a zinc carboxylate.[11] However, the product obtained from the reaction is not the β-lactone **3g** but its ring-opening polymer, poly(3-hydroxyhex-4-enoic acid), the viscosity of which causes a great deal of trouble during the subsequent destructive distillation of the polyester to the acid **5**. Further studies on the scope and limitations of the allylic rearrangement, as well as the [2 + 2] cycloaddition, are in progress.

This work was supported in part by grants from the Center of Interdisciplinary Research (Tohoku University), the Takasago International Corporation and the Chisso Corporation.

Notes and references

† Method B: To a solution of complex **2d** (50.0 μmol) in CH_2Cl_2 (200 or 500 cm^3) was added aldehyde **1** (200 μmol). Ketene (*ca.* 250 μmol) was bubbled into the mixture over a period of 1 min and the mixture was stirred for 5 min. This series of operations was repeated until added aldehyde **1** reached the total amount of 1.00 mmol. To the mixture was added an additional amount of ketene (*ca.* 1.0 mmol) and the resulting mixture was stirred for 1 h before work-up.

1 Review: A. Pommier and J.-M. Pons, *Synthesis*, 1993, 441.
2 Y. Tamai, H. Yoshiwara, M. Someya, J. Fukumoto and S. Miyano, *J. Chem. Soc., Chem. Commun.*, 1994, 2281.
3 Review: B. Bosnich, *Aldrichim. Acta*, 1998, **31**, 76.
4 W. Odenkirk, A. L. Rheingold and B. Bosnich, *J. Am. Chem. Soc.*, 1992, **114**, 6392; S. Kanemasa, Y. Oderaotoshi, S. Sakaguchi, H. Yamamoto, J. Tanaka, E. Wada and D. P. Curran, *J. Am. Chem. Soc.*, 1998, **120**, 3074.
5 J. A. Davies, F. R. Hartley and S. G. Murray, *J. Chem. Soc., Dalton Trans.*, 1980, 2246; S. Oi, K. Kashiwagi, E. Terada, K. Ohuchi and Y. Inoue, *Tetrahedron Lett.*, 1996, **37**, 6351.
6 R. Stevenson and J. V. Weber, *J. Nat. Prod.*, 1988, **51**, 1215.
7 Only one report was found in literature, which described a formation of similar δ-lactones in the cycloaddition of ketene with ketones: F. G. Young, *J. Am. Chem. Soc.*, 1949, **71**, 1346.
8 Reviews: R. P. Lutz, *Chem. Rev.*, 1984, **84**, 205; L. E. Overman, *Angew. Chem., Int. Ed. Engl.*, 1984, **23**, 579.
9 A. F. Noels, J. J. Herman and P. Teyssié, *J. Org. Chem.*, 1976, **41**, 2527.
10 Hagemeyer reported that the boron trifluoride-catalyzed reaction of ketene with crotonaldehyde **1g** gave lactone **3g**: H. J. Hagemeyer, Jr., US 2,478,388/1949 (*Chem. Abstr.*, 1950, **44**, 1132). See also: J. H. McCain and E. Marcus, *J. Org. Chem.*, 1970, **35**, 2414.
11 H. J. Hagemeyer Jr., *Ind. Eng. Chem.*, 1949, **41**, 765.

Communication a908709e

ChemComm

Oligoacetylenic sulfides

Albert W. M. Lee,* Anissa B. W. Yeung, Mabel S. M. Yuen, H. Zhang, X. Zhao and W. Y. Wong

Department of Chemistry, Hong Kong Baptist University, Kowloon Tong, Kowloon, Hong Kong. E-mail: alee@hkbu.edu.hk

Received (in Cambridge, UK) 13th October 1999, Accepted 26th November 1999

Linear acetylenic and diacetylenic sulfides consisting of up to eight triple-bond units with alternating sulfur atoms and acetylene units were synthesized.

The synthesis of conjugated or homoconjugated cyclic or linear oligoacetylene systems is a rapidly developing research frontier and has attracted considerable attention from both fundamental and applied viewpoints.[1] These all-carbon or carbon-rich acetylene-based scaffolds are expected to exhibit a variety of unusual structural, electronic, electrical and optical properties.[2–4] Linear rigid oligoacetylenic molecular rods of defined length in nanometer-sized structures could also serve as molecular wires in molecular electronic application.[5–7]

For the conjugated oligoacetylenic systems, a representative example is a compound with six conjugated diacetylene units synthesized by Diederich's group through end-capping polymerization.[8] Molecular wires end-capped with redox-active metal groups have also been reported.[9,10] The longest molecule of this group has up to ten conjugated acetylene units. Novel heterocycles comprising alternating phosphorus atoms and acetylene units reported by Scott's group are also known.[11] Dendrimers with acetylenic units[12] and alkynyl sulfides[13] have also been prepared. However, to the best of our knowledge, there is no report on linear oligoacetylenic compounds containing heteroatom bridging between all or some of the acetylene units. Based on our experience in the preparation and uses of acetylenic sulfoxides and related compounds in organic synthesis,[14] a systematic approach to the syntheses of oligomeric acetylenic sulfides with up to eight acetylene units is reported here.

Two key reactions, namely sulfurization and oxidative coupling *via* Hay and Glaser-type related methods,[15] were used in building up the oligomeric acetylenic sulfides. Chain length is doubled in each cycle of the reaction.

The crucial starting material, a mono-protected bis-acetylene sulfide **7**, was first prepared. When an equal molar ratio of trimethylsilylacetylene **1** and triisopropylsilylacetylene **2** was treated with 1 equiv. of BuLi followed by 0.5 equiv. of SCl_2 at −78 °C, a mixture of silylated bis-acetylene sulfides (**3**–**5**) were formed (Scheme 1). The reaction mixture was placed under mild desilylation conditions (K_2CO_3/MeOH). The TMS group was hydrolyzed while the TIPS group remained intact. The volatile bis-acetylene sulfide **6** resulting from the hydrolysis of **3** was lost during work up and solvent evaporation. The remaining mono- and di-TIPS bis-acetylene sulfides **7** and **4** could be easily separated by column chromatography, with the mono-silylated compound **7** being the more polar component. The overall isolated yield of the desirable mono-protected compound **7** was 40%. The recovered di-TIPS acetylene sulfide **4** could also serve as the precursor of **7** through careful monodesilylation with KF in MeOH under close monitoring with TLC.

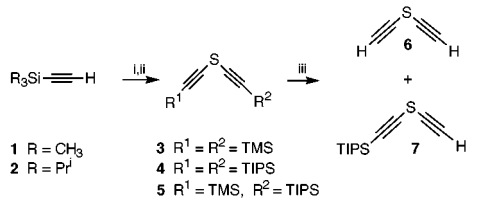

Scheme 1 *Reagents and conditions*: i, BuLi; ii, SCl_2, −78 °C; iii, K_2CO_3, MeOH.

Oxidative coupling and sulfurization reactions were then used in the chain elongation of the acetylenic sulfide. Several sets of oxidative coupling conditions for acetylene compounds were studied. Eventually, we found that the original Hay conditions[16] using CuCl and TMEDA afforded satisfactory results. For sulfurization, freshly distilled SCl_2 was used. Alternatively, a stable solid sulfurization agent, bis(benzenesulfonyl) sulfide **8**,[17] used extensively by Scott could also be used. As shown in Scheme 2, oxidative coupling of **7** afforded diacetylene compound **9** in 94% yield. Sulfurization of **7** with SCl_2 afforded sulfide **10** in 72% yield. Mono-deprotection of **10** to **12** was achieved by a carefully controlled desilylation procedure using KF in THF–H_2O in the presence of a catalytic amount of Bu_4NBr. The reaction was monitored closely *via* TLC and was stopped when **11** started to appear. Mono-deprotected **12** could be isolated in 35% yield after column chromatography with the recovery of about 16% of the starting material. If the desilylation reaction was allowed to run for a longer time at room temperature, the unprotected terminal acetylene compound **11** could also be isolated. The unprotected

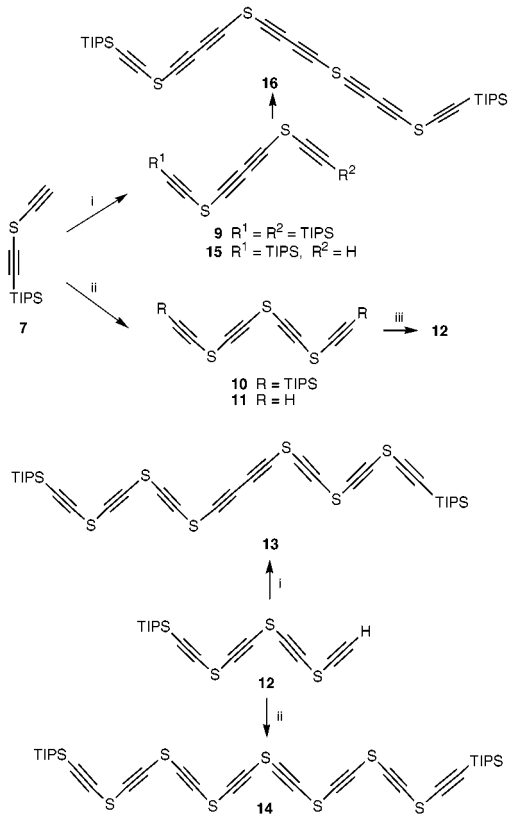

Scheme 2 *Reagents and conditions*: i, CuCl, TMEDA, air, $CHCl_3$; ii, BuLi or LIHMDS, then SCl_2 or **8** ($PhSO_2SSO_2Ph$); iii, KF, THF–H_2O, Bu_4NBr (cat.).

Table 1 Spectral data of acetylenic sulfides

Compound	δ_C sp^3 (Pr^i)	δ_C sp	δ_H	ν_{max}/cm^{-1}	λ_{max}[a]/nm (ε/dm^3 mol^{-1} cm^{-1})
4	11.23, 18.49	87.75, 100.49	1.05(s)	2098	231 (20600)
7	11.23, 18.49	67.82, 84.22,[b] 86.18, 101.29	1.06(s), 2.97(s)	3303, 2103	
9	11.23, 18.51	68.50, 82.09, 84.48, 102.84	1.11(s)	2104	
10	11.22, 18.51	81.56, 83.06, 85.97, 101.37	1.07(s)	2102	231 (41500)
11		66.38, 81.94, 82.16, 84.66[b]	2.99(s)	3289, 2098	
12	11.20, 18.51	66.51, 81.21, 81.65, 82.53, 83.58, 84.58[b], 85.77, 101.47	1.07(s), 2.99(s)	3297, 2103	
13	11.23, 18.53	67.45, 79.87, 80.66, 81.69,83.85, 83.92, 85.68, 101.65	1.12(s)	2101	260 (97400)
14	11.22, 18.53	80.85, 81.26, 81.74, 82.01,82.55, 83.67, 85.72, 101.58	1.07(s)	2100	237 (63900)

[a] In cyclohexane. [b] C≡*C*H.

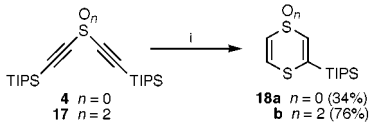

Scheme 3 *Reagents and conditions*: i, Na_2S, Al_2O_1, DMF–MeOH.

and mono-protected acetylenic sulfides **11** and **12** are very unstable, especially when concentrated.

Freshly prepared **12** was subjected to the coupling and sulfurization cycles to extend the chain to eight acetylene units. Coupling afforded diacetylene compound **13** in 55% yield. For the sulfurization process, we found that BuLi reacted with the triple bonds of **12** to give complicated products. Therefore, LIHMDS was used instead and **14** was prepared in 25% yield using **8** as the sulfurization agent. Monodesilylation of **9** to **15** could also be achieved under carefully controlled conditions. However, the coupling product **16**, which could be detected by FAB MS, was extremely unstable and could not be isolated in pure form.

All these new acetylenic sulfides were characterized by NMR, IR and MS. Some of the spectral data are summarized in Table 1. The typical IR frequency of the triple bond is around 2100 cm^{-1}, and the terminal acetylene C–H signal appears around 3300 cm^{-1}. UV spectra of oligoacetylene sulfides **4**, **10**, **13** and **14** were also recorded. There is no observable bathochromic shift (λ_{max} = 231–237 nm) for compounds **4**, **10** and **14** as the chain length increased. This indicated that the degree of conjugation between the acetylene units is weak. Compound **13**, being a diacetylene compound, showed a slight bathochromic shift (λ_{max} = 260 nm) relative to compounds **4**, **10**, **14** and had a large molar absorptivity.

We also explored the chemistry of double conjugate addition of nucleophiles to the terminal positions of the bis-acetylene sulfides and the corresponding sulfones.[18] Reactions with Na_2S impregnated on neutral alumina[19] took place readily in DMF–MeOH mixture at 0 °C and room temperature respectively for **4** and **17** (Scheme 3). However, to our surprise the mono-desilylated compounds **18a**,**b** were the only isolated products. The structure of cyclic sulfone **18b** was confirmed by X-ray analysis (Fig. 1).†

In summary, the first syntheses of a series of oligoacetylenic sulfides with alternating sulfur atoms and acetylene or diacetylene units were accomplished using the monoprotected bis-acetylene sulfide **7** as the starting material. Studies on the synthesis of some cyclic and metal end-capped analogs[20] are in progress.

Financial support from the Research Grants Council (RGC/97-98/48, HKBU 2048/97P) is gratefully acknowledged.

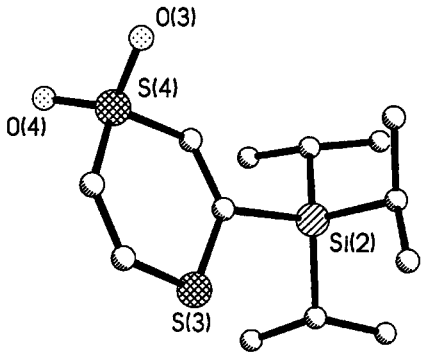

Fig. 1 X-Ray structure of **18b**.

Notes and references

† *Crystal data* for **18b**: $C_{13}H_{24}O_2S_2Si$, M = 304.53, triclinic, $P\bar{1}$ (no. 2), a = 7.9504(5), b = 15.857(1), c = 16.001(1) Å, α = 118.632(1), β = 98.449(1), γ = 97.355(1)°, V = 1705.0(2) Å^3, Z = 4, T = 293 K, μ(Mo-Kα) = 3.76 cm^{-1}, 10061 reflections measured, 7271 unique, R(int) = 0.0128, final R_1 = 0.039, wR_2 = 0.1061 (based on F^2) for 7271 [$I > 2\sigma(I)$] observed reflections. CCDC 182/1493. See http://www.rsc.org/suppdata/cc/a9/a908220d/ for crystallographic data in .cif format.

1 P. J. Stang and F. Diederich, *Modern Acetylene Chemistry*, VCH, Weihheim, 1995.
2 R. Gleiter, *Angew. Chem., Int. Ed. Engl.*, 1992, **31**, 27.
3 D. Bloor, *Chem. Br.*, 1995, 385.
4 F. Diederich, *Nature*, 1994, **369**, 199.
5 J. M. Tour, *Chem. Rev.*, 1996, **96**, 537.
6 J.-M. Lehn, *Angew. Chem., Int. Ed. Engl.*, 1988, **27**, 89.
7 M. D. Ward, *Chem. Br.*, 1996, 568.
8 J. Anthony, C. Boudon, F. Diederich, J.-P. Gisselbrecht, V. Gramlich, M. Gross, M. Hobi and P. Seiler, *Angew. Chem., Int. Ed. Engl.*, 1994, **33**, 763.
9 W. Weng, T. Bartik, M. Brady, B. Bartik, J. A. Ramsden, A. M. Arif and J. A. Gladysz, *J. Am. Chem. Soc.*, 1995, **117**, 11 922.
10 N. L. Narvor, L. Toupet and C. Lapinte, *J. Am. Chem. Soc.*, 1995, **117**, 7129.
11 L. T. Scott and M. Unno, *J. Am. Chem. Soc.*, 1990, **112**, 7823.
12 Z. Xu and J. J. Moore, *Angew. Chem., Int. Ed. Engl.*, 1993, **32**, 246; 1993, **32**, 1354.
13 G. Lábbée, B. Haelterman and W. Dehaen, *J. Chem. Soc., Perkin Trans. 1*, 1994, 2203.
14 A. W. M. Lee and W. H. Chan, *Top. Curr. Chem.*, 1997, **190**, 103.
15 G. Eglinton and W. McCrae, in *Advances in Organic Chemistry: Methods and Results*, ed. R. A. Raphael, E. C. Taylor and H. Wynberg, Interscience, New York, 1963.
16 A. S. Hay, *J. Org. Chem.*, 1962, **27**, 3320.
17 F. DeJong and M. J. Janssen, *J. Org. Chem.*, 1971, **36**, 1645.
18 J. Meijer, P. Vermeer, H. D. Verkruijsse and L. Brandsma, *Recl. Trav. Chim. Pays-Bas.*, 1973, **92**, 1326.
19 B. Czech, S. Quici and S. L. Regen, *Synthesis*, 1980, 113.
20 S. L. James, M. Younus, P. R. Raithby and J. Lewis, *J. Organomet. Chem.*, 1997, **543**, 233.

Communication a908220d

Synthesis and characterization of cross-conjugated polyenynes

Yuming Zhao, Robert McDonald and Rik R. Tykwinski*

Department of Chemistry, University of Alberta, Edmonton, Alberta, Canada T6G 2G2. E-mail: rik.tykwinski@ualberta.ca

Received (in Corvallis, OR, USA) 24th August 1999, Accepted 9th November 1999

Extended, cross-conjugated polyenynes are reported as well as a description of their electronic (UV–VIS) characteristics and an X-ray crystallographic analysis of hexayne 9 that shows solid-state molecular alignment suitable for topochemical polymerization.

The sequential combination of sp and/or sp^2 hybridized carbons affords a series of wire-like π-conjugated carbon chains typified by the structures of polyacetylene (**1**),[1] polydiacetylene (PDA, **2**)[2,3] and polytriacetylene (PTA, **3**)[4] in a progression that ultimately concludes with the one-dimensional carbon allotrope, carbyne (**4**).[5–7]

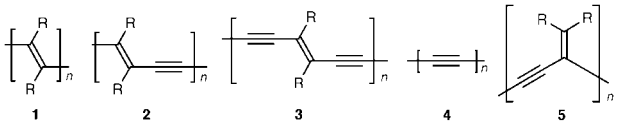

1 **2** **3** **4** **5**

The most recent addition to this mélange of enyne oligomers is *iso*-polydiacetylene (*iso*-PDA, **5**),[8] the cross-conjugated isomer of **2**.[9] Studies of *iso*-PDAs have shown that π-electron communication is present along the cross-conjugated framework, albeit to a much lesser extent than for PDAs. To provide a better understanding of the physical and electronic characteristics of cross-conjugated enynes, we have extended the skeleton of **5** by inserting additional alkyne groups. Herein, we report the first synthesis of these cross-conjugated polyenynes and a preliminary description of their electronic, X-ray crystallographic and solid-state chemical characteristics.

The enyne oligomers were synthesized as outlined in Scheme 1. Vinyl triflate **6**[10] was coupled with triisopropylsilylacetylene in THF at ambient temperature. Work-up and flash column chromatography, gave the triyne **7** in 93% yield.† Protodesilylation of **7** gave terminal alkyne **8**, which was then oxidatively homocoupled[11] to hexayne **9** in 96% yield as a stable, light yellow solid.

Triyne **8** was also elaborated to pentayne **10** in 71% yield *via* reaction with vinyl triflate **6**, as described for the formation of **7**. Desilylation of **10** gave the terminal alkyne **11**, which afforded a good yield of decayne **12**. Notably, the ^{13}C NMR of **12** shows individual resonances for all 10 acetylenic carbons, as well as four unique signals for the alkylidene methyl carbons.‡

Yellow single crystals of hexayne **9** were grown by diffusion of MeOH into a CH_2Cl_2 solution at –20 °C, and the structure was determined by X-ray crystallographic analysis (Fig. 1).§ The π-framework of **9** is virtually planar, with a maximum deviation of 0.130(17) Å from the least-squares plane for the 16-carbon conjugated skeleton.¶ All six triple bonds are essentially the same length, suggesting little bond length alteration as a result of π-conjugation and contrasting results for PDA oligomers of similar size.[12] The eight tetrayne carbons are virtually linear, showing only a gradual curvature with bond angles deviating less than 3° from 180°.

Analysis of the crystal packing of **9** down the *b*-axis shows the molecules are aligned in a parallel fashion (Fig. 1). The intermolecular proximity of the tetraynes in the crystal suggests the potential for topochemical polymerization as is well established for suitably aligned butadiynes and hexatriynes.[2,13,14a] The solid-state polymerization of octatetraynes has also been previously described, albeit in much less detail.[14]

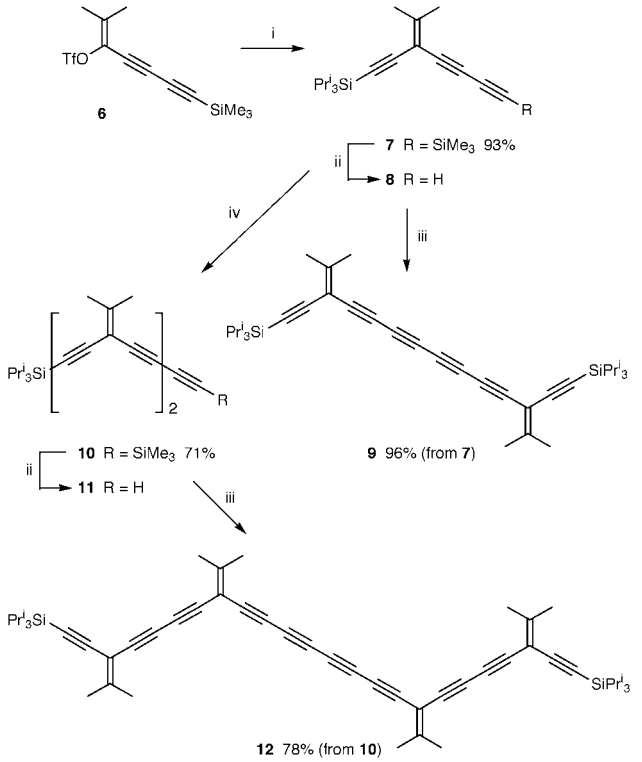

Scheme 1 *Reagents and conditions*: i, triisopropylsilylacetylene, $PdCl_2(PPh_3)_2$, CuI, Pr^i_2NH, THF, room temp; ii, K_2CO_3, wet MeOH–THF (1:1), room temp; iii, CuI, TMEDA, O_2, CH_2Cl_2 room temp; iv, **6**, $PdCl_2(PPh_3)_2$, CuI, Pr^i_2NH, THF, room temp.

The parameters describing the intermolecular relationship of molecules **9** are depicted in Fig.1(*c*).[2,13a,14a] Polymerization of **9** *via* 1,2- or 1,4-addition, as described for tetrayne systems,[14] is unlikely considering that $R_{1,2}$ (6.7 Å) and $R_{1,4}$ (4.7 Å) are both considerably more than the ideal distance of 4 Å between reacting carbon atoms. The angle ϕ between the tetrayne rod and the stacking axis at *ca*. 28° is significantly less than the optimum value of 45° determined for 1,4-addition in di-, tri- and tetraynes.[2,13a,14a] Thus, two alternative addition patterns might occur for **9**, namely 1,6-addition ($R_{1,6}$ = 3.6 Å) and 1,8-addition ($R_{1,8}$ = 4.2 Å). The stacking angle ϕ is nearly identical to the value of 27° that denotes highest 1,6-reactivity in triacetylenes, and the stacking distance between monomer units at 7.7 Å is quite near the desired value of 7.5 Å.[13a] In view of these values, 1,6-addition is the expected mode of reaction for **9**.

Differential scanning calorimetry showed that crystals of **9** have a well-defined melting point at 103–104 °C that is followed by decomposition at 145 °C. Attempts to thermally effect polymerization of single crystalline **9** were conducted at 90 °C. Over the course of 8 h, the crystals darken slightly to yield an opaque solid. A loss of crystal integrity for the resultant material was confirmed by the absence of any X-ray diffraction pattern. To date, the product(s) of this thermal reaction has not been identified.

Photochemical polymerization of a single crystal of **9** was attempted by monochromatic irradiation at 280 nm.[15,16] After

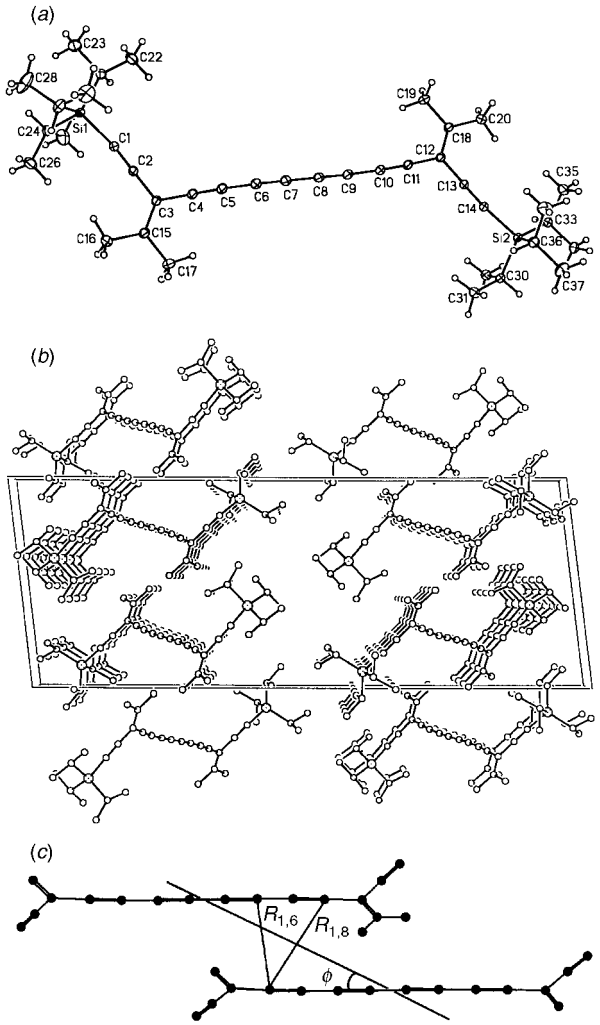

Fig. 1 (*a*) ORTEP drawing (20% probability level) of **9**, (*b*) crystal packing of **9** as viewed along the *b*-axis, and (*c*) crystal packing parameters for **9**.

approximately 2 h, a darkening of the crystal to yellow–orange was observed. Irradiation was continued for another 4 h with little additional darkening. X-Ray analysis of the crystal afforded a diffraction pattern and cell parameters identical to that of pure **9**, indicating little change in the solid beyond that which may have occurred at the outer surface of the crystal.

The electronic absorption spectra of **9**, **12** and 1,8-bis(4-*tert*-butylphenyl)-octa-1,3,5,7-tetrayne **13**, are shown in Fig. 2. The lower energy region is dominated by the absorption pattern of the tetrayne moiety and is remarkably similar to that of **13**.[17] Each compound displays three absorptions at *ca*. 405, 374 and 348 nm. Whereas the UV spectra of elongated *iso*-PDAs show evidence of π-electron communication *via* cross-conjugation,[8] this effect is absent in **9** and **12**, as the three lowest energy absorptions of **12** are each red-shifted by only 1 nm *versus* those of **9**.

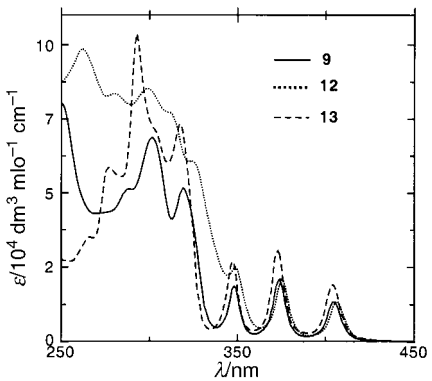

Fig. 2 UV–VIS spectra in $CHCl_3$ comparing polyynes **9**, **12** and **13**.

In conclusion, cross-conjugated polyenynes **7**–**12** can be synthesized in high yields as relatively stable solids. The UV–VIS spectra of **9** and **12** show a minimal contribution from cross conjugation. The solid state organization of **9** is suitable for topochemical polymerization, although initial attempts to effect thermal and photochemical polymerization have been unsuccessful. Further studies on **9** and **12** are currently underway.

This work was supported by a Gen-Science Endowment from the University of Alberta and by NSERC. We thank Professor M. M. Haley for providing a sample of **13**.

Notes and references

† The purity and structure of all new compounds were confirmed by ^1H and ^{13}C NMR, IR, UV, MS and either EA or HRMS.

‡ *Selected data* for **9**: yellow solid, mp 103–104 °C; δ_H(300 MHz, $CDCl_3$) 2.07 (s, 6H), 2.05 (s, 6H), 1.07 (s, 42H); δ_C(75 MHz, $CDCl_3$) 162.3, 101.2, 100.9, 94.9, 76.3, 75.0, 67.8, 64.1, 23.4, 23.2, 18.7, 11.3. For **12**: yellow solid, decomposition begins at *ca*. 80 °C; δ_H(300 MHz, CD_2Cl_2) 2.11 (s, 12H), 2.09 (s, 6H), 2.06 (s, 6H), 1.10 (s, 42H); δ_C(125 MHz, CD_2Cl_2) 166.6, 160.8, 102.3, 101.2, 99.7, 94.3, 80.2, 77.5, 77.0, 76.9, 75.4, 74.4, 68.1, 64.2, 23.7, 23.6, 23.3, 23.1, 18.8, 11.7.

§ *Crystal data* for **9**: $C_{38}H_{54}Si_2$, M = 566.99, monoclinic space group $P2_1/c$ (No. 14), Dc = 1.018 g cm^{-3}, Z = 4, a = 13.5571(8), b = 7.7132(5), c = 35.616(2) Å, β = 96.5990(10)°, V = 3699.7(4) Å^3, μ = 0.118 mm^{-1} Final $R(F)$ = 0.0472, $wR_2(F^2)$ = 0.1366 for 365 variables and 7039 data with $F_o^2 \geqslant -3\sigma(F_o^2)$ (4842 observations [$F_o^2 \geqslant 2\sigma(F_o^2)$]). CCDC 182/1485.

¶ The known X-ray structures of tetraynes and a pentayne have been summarized in refs. 7(*b*) and 7(*c*).

1 *Conjugated Polymers and Related Materials: The Interconnection of Chemical and Electronic Structure*, ed. W. R. Salaneck, I. Lundström and B. Rånby, OUP, Oxford, 1993.
2 V. Enkelmann, *Adv. Polym. Sci.*, 1984, **63**, 91.
3 G. Wegner, *Makromol. Chem., Suppl.*, 1984, **6**, 347.
4 R. E. Martin, T. Mäder and F. Diederich, *Angew. Chem., Int. Ed.*, 1999, **38**, 817.
5 P. P. K. Smith and P. R. Buseck, *Science*, 1982, **216**, 984; R. Hoffmann, *Tetrahedron*, 1966, **22**, 521.
6 R. J. Lagow, J. J. Kampa, H.-C. Wei, S. L. Battle, J. W. Gegne, D. A. Laude, C. J. Harper, R. Bau, R. C. Stevens, J. F. Haw and E. Munson, *Science*, 1995, **267**, 362; R. Eastmond, T. R. Johnson and D. R. M. Walton, *Tetrahedron*, 1972, **28**, 4601.
7 For metal endcapped polyynes, see: (*a*) T. B. Peters, J. C. Bohling, A. M. Arif and J. A. Gladyz, *Organometallics*, 1999, **18**, 3261; (*b*) R. Dembinski, T. Lis, S. Szafert, C. L. Mayne, T. Bartik and J. A. Gladysz, *J. Organomet. Chem.*, 1999, **578**, 229; (*c*) B. Bartik, R. Dembinski, T. Bartik, A. M. Arif and J. A. Gladysz, *New J. Chem.*, 1997, **21**, 739; (*d*) J. T. Lin, J. J. Wu, C.-S. Li, Y. S. Wen and K.-J. Lin, *Organometallics*, 1996, **15**, 5028; (*e*) M. Altmann, V. Enkelmann and U. H. F. Bunz, *Chem. Ber.*, 1996, **129**, 269.
8 Y. Zhao and R. R. Tykwinski, *J. Am. Chem. Soc.*, 1999, **121**, 458.
9 For cross-conjugated PTAs, see: A. M. Boldi, J. Anthony, V. Gramlich, C. B. Knobler, C. Boudon, J.-P. Gisselbrecht, M. Gross and F. Diederich, *Helv. Chim. Acta*, 1995, **78**, 779.
10 P. J. Stang and M. Ladika, *Synthesis*, 1981, 29.
11 A. S. Hay, *J. Org. Chem.*, 1962, **27**, 3320.
12 R. Giesa and R. C. Schulz, *Polym. Int.*, 1994, **33**, 43.
13 For polymerization of triynes, see: (*a*) V. Enkelmann, *Chem. Mater.*, 1994, **6**, 1337; (*b*) J. Kiji, J. Kaiser, G. Wegner and R. C. Schulz, *Polymer*, 1973, **14**, 433; (*c*) S. Okada, H. Matsuda, H. Nakanishi, M. Kato and M. Otsuka, *Thin Solid Films*, 1989, **179**, 423.
14 (*a*) R. H. Baughman and K. C. Yee, *J. Polym. Sci., Macromol. Rev.*, 1978, **13**, 219; (*b*) S. Okada, H. Matsuda, A. Masaki, H. Nakanishi and K. Hayamizu, *Proc. SPIE-Int. Soc. Opt. Eng.*, 1991, **1560**, 25; (*c*) K. Hayamizu, S. Okada, S. Tsuzuki, H. Matsuda, A. Masaki and H. Nakanishi, *Bull. Chem. Soc. Jpn.*, 1994, **67**, 342; (*d*) A. Sarkar, S. Okada, K. Komatsu, H. Nakanishi and H. Matsuda, *Macromolecules*, 1998, **31**, 5624.
15 A. E. Keating and M. A. Garcia-Garibay, in *Organic and Inorganic Photochemistry*, ed. V. Ramamurthy and K. S. Schanze, Marcel Dekker, New York, 1998.
16 H. Bässler, *Adv. Polym. Sci.*, 1984, **63**, 1.
17 M. M. Haley, M. L. Bell, S. C. Brand, D. B. Kimball, J. J. Pak and W. B. Wan, *Tetrahedron Lett.*, 1997, **38**, 7483.

Communication a906900c

Thermotropic and lyotropic behavior of novel amphiphilic liquid crystals having hydrophilic poly(ethyleneimine) units

Seiji Ujiie* and Yumi Yano

Department of Material Science, Interdisciplinary Faculty of Science and Engineering, Shimane University, Matsue 690-8504, Japan

Received (in Cambridge, UK) 27th September 1999, Accepted 25th November 1999

Novel ionic amphotropic liquid crystals, in which a hydrophilic poly(ethyleneimine) chain with hydroxy side-groups was attached to an azobenzene mesogenic core through an alkylene chain, showed a thermotropic smectic A mesophase and lyotropic smectic A and C mesophases.

Amphiphilic compounds such as ionic and nonionic surfactants always consist of hydrophilic and lipophilic groups. They can form thermotropic liquid crystalline phases in themselves and lyotropic liquid crystalline phases upon the addition of a solvent such as water.[1] The thermotropic liquid crystalline systems of the amphiphiles build up layered structures with distinct arrangements of the molecules within their layers. In the lyotropic liquid crystalline systems, the hydrophilic group conveys water solubility, while the hydrophobic group drives the formation of self-assembled aggregates. Lyotropic liquid crystalline systems can form liquid crystalline phases such as lamellar mesophases, which resemble thermotropic smectic A phases, columnar and cubic mesophases. Surfactants with an aromatic mesogenic group can show liquid crystal formation due to the anisotropy formed by aggregation of the polar head groups and interactions between the aromatic mesogenic groups.[2–4] They can show both thermotropic and lyotropic liquid crystalline behavior. It is of high importance in the field of supramolecular chemistry that new thermotropic and lyotropic liquid crystal forming amphiphilic compounds are sought. This makes it possible to develop novel types of functional liquid crystalline materials. During our study of new ionic liquid crystals,[5–8] we synthesized novel types of ionic liquid crystalline amphiphiles in which a hydrophilic poly(ethyleneimine) unit with hydroxy side-groups is attached to an aromatic mesogenic core. They showed amphotropic behavior. Here we describe the phase transitions and orientational behavior in the thermotropic and lyotropic liquid crystalline systems containing these novel amphiphilic compounds.

The ionic amphiphilic compounds prepared by us were obtained by ring-opening polymerization of aziridine-1-ethanol (AE) using 6-bromo-1-[4-(4-nitrophenylazo)phenoxy]hexane (Br6N) [or 12-bromo-1-[4-(4-nitrophenylazo)phenoxy)dodecane (Br12N)] as the polymerization initiator. AE (0.05 or 0.07 mol) and Br6N (0.01 mol) were dissolved in $CHCl_3$, and the mixture was stirred for 300 h at room temperature. After the reaction, the solution was concentrated and diluted in THF. The target material precipitated from the solution and was filtered off. The degree of polymerization (n) of the poly(ethyleneimine) unit was estimated by ^{1}H NMR. The ratio of the numbers of protons involved in methylene groups directly attached to the hydroxy group (3.7 ppm) and the phenyl ring (7.05 ppm) was examined. The existence of a terminal ionic group was shown by the peak at 3.5 ppm in the ^{1}H NMR spectra. The phase transitions of the samples were examined by DSC (Mettler DSC-20 and Shimadzu DSC-50Q) and polarizing microscopy (Nikon polarizing microscope equipped with a Mettler hot stage FP82). The X-ray diffraction measurements were performed using a Rigaku Rint 2100 X-ray diffractometer with Ni-filtered Cu-Kα radiation at various temperatures; the samples were inserted into a Linkam hot stage HFS91.

Table 1 Phase transitions of thermotropic liquid crystalline systems

Sample	Phase transition temperatures[a]/°C					
4E-6N	T_g = −2.78	K	31.1	SmA	109.6	Iso
6E-6N		G	−28.2	SmA	101.0	Iso
3E-12N		K	115.2	SmA	185.4	Iso

[a] T_g = glass transition point; K: solid phase; G: glass phase; SmA: smectic A phase; Iso: isotropic phase.

The phase transition temperatures of the thermotropic liquid crystalline systems are summarized in Table 1. The amphiphilic liquid crystals (6E-6N, 4E-6N) having a hexamethylene linkage

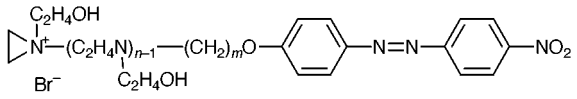

Sample	n	m
4E-6N	4	6
6E-6N	6	6
3E-12N	3	12

chain showed a thermotropic smectic A phase upon heating and cooling. Both 6E-6N and 4E-6N formed focal conics and a perpendicular alignment in the smectic A phase. The amphiphilic liquid crystal (3E-12N) with a dodecamethylene spacer unit also exhibited a thermotropic smectic A phase with focal conic fan and oily streak textures. The smectic A liquid crystal formation in 6E-6N, 4E-6N and 3E-12N is due to the aggregation of the hydrophilic poly(ethyleneimine) units and an overlapping arrangement of the aromatic mesogenic groups due to the strong interaction of the nitro terminal groups.

In this study, the lyotropic systems of 3E-12N were prepared, and their lyotropic liquid crystalline properties were estimated. 3E-12N was water-miscible and easily dissolved in water. The lyotropic systems (L1) consisting of 3E-12N and water formed a lyotropic smectic C phase, as well as the lyotropic smectic A phase (Fig. 1). In L1, focal conics and a perpendicular alignment were formed upon cooling from the isotropic phase to the

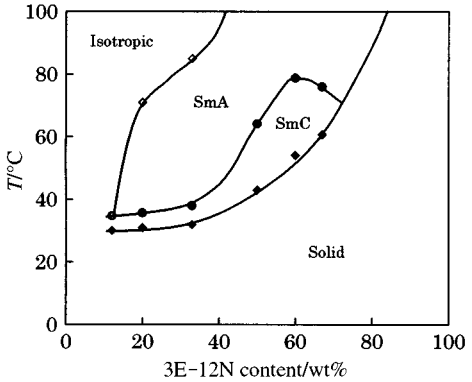

Fig. 1 Phase diagram of lyotropic system (L1) of 3E-12N.

lyotropic smectic A phase, and in the lyotropic smectic C phase, broken fan and schlielen textures clearly appeared (Fig. 2).

The lyotropic smectic C phase is induced by the addition of water to the amphiphilic 3E-12N because anhydrous 3E-12N cannot form the smectic C phase by itself. It is common that lyotropic liquid crystals form nematic, smectic A-like lamellar, columnar and cubic mesophases. However, a tilted smectic type of lyotropic mesophase, such as a smectic C phase, is seldom formed, and only a few reports have described the observation of the lyotropic smectic C phase for nonionic amphiphile/water mixtures.[9] The formation of the lyotropic smectic C phase in L1 is a rare case and is probably related to the balance of the hydrophilic and hydrophobic units in the 3E-12N molecule.

The X-ray diffraction pattern of thermotropic 3E-12N consists of sharp reflections at small angles and a broad reflection in the wide-angle region. The layer spacing of thermotropic 3E-12N was 44 Å. In the thermotropic smectic A

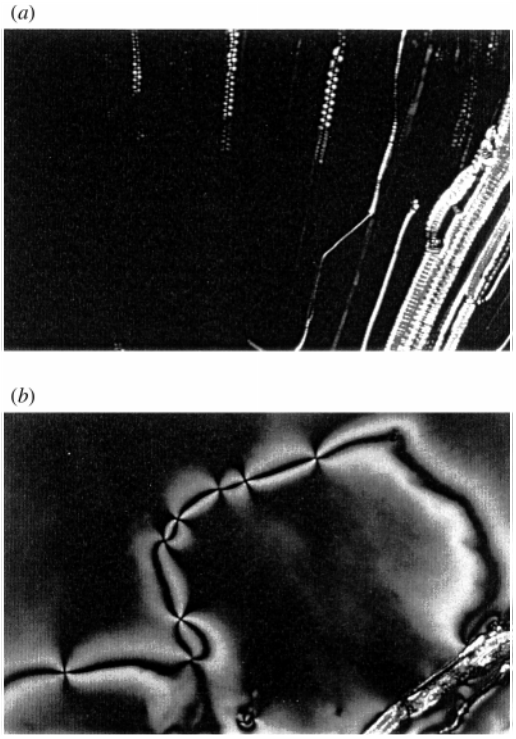

Fig. 2 Optical textures of L1 (50wt%): (*a*) lyotropic smectic A phase (70 °C); (*b*) lyotropic smectic C phase (50 °C).

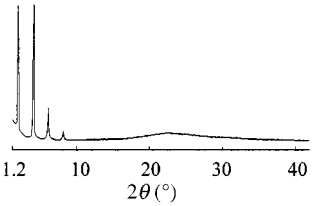

Fig. 3 X-Ray diffraction pattern for lyotropic smectic C phase of L1 (50 wt%) at 45 °C.

structure with hydrophobic and hydrophilic sublayers, the nitroazobenzene groups form the interdigitated structure, and poly(ethyleneimine) groups aggregate through hydrogen bondings and ionic interactions.

In the lyotropic mesophase, L1 showed X-ray diffraction patterns consisting of sharp reflections at small angles and a broad reflection in the wide-angle region (Fig. 3).

In L1 (50 wt%), the smectic A and C layer spacings were 50 (65 °C) and 45 Å (45 °C), respectively. In the lyotropic smectic phases, the nitroazobenzene mesogenic units overlap each other, and the poly(ethyleneimine) units and water aggregate through hydrogen bonding. It is expected that the layer structure of the lyotropic smectic A phase resembles that of the thermotropic smectic A phase. In the lyotropic smectic C phase, the hydrophobic sublayers, in which the mesogenic units were tilted with respect to the layer normal, are separated by the hydrophilic units and water.

Notes and references

1 *Handbook of Liquid Crystals*, ed. D. Demus, J. Goodby, G. W. Gray, H.-W. Spiess and V. Vill, Wiley-VCH, Weinheim, 1998, vol. 3, ch. VI and VII.
2 H. Ringsdorf, B. Schlarb and J. Venzmer, *Angew. Chem., Int. Ed. Engl.*, 1988, **27**, 115.
3 D. W. Bruce, D. A. Dunmur, E. Lalinde, P. M. Maitlis and P. Styring, *Nature*, 1986, **323**, 791; D. W. Bruce and S. A. Hudson, *J. Mater. Chem.*, 1994, **4**, 479.
4 E. Bravo-Grimaldo, D. Navarro-Rodriguez, A. Skoulios and D. Guillon, *Liq. Cryst.*, 1996, **20**, 393.
5 S. Ujiie, S. Takagi and M. Sato, *High Perform. Polym.*, 1998, **10**, 347.
6 Y. Haramoto, S. Ujiie and M. Nanasawa, *Liq. Cryst.*, 1996, **21**, 923.
7 S. Ujiie and K. Iimura, *Macromolecules*, 1992, **25**, 3174.
8 S. Ujiie and K. Iimura, *Polym. J.*, 1993, **25**, 347.
9 M. A. Schafheutle and H. Finkelmann, *Liq. Cryst.*, 1988, **3**, 1369; N. Pictschmann, A. Lunow, G. Brezesinski, C. Tschierske, F. Kuschel and H. Zaschke, *Colloid Polym. Sci.*, 1991, **269**, 636.

Communication a907765k

End-group modification of regioregular poly(3-alkylthiophene)s

Bea M. W. Langeveld-Voss, René A. J. Janssen,* A. J. H. Spiering, Joost L. J. van Dongen, Erik C. Vonk and Henk A. Claessens

Laboratory of Macromolecular and Organic Chemistry and Laboratory of Instrumental Analysis, Eindhoven University of Technology, PO Box 513, 5600 MB Eindhoven, The Netherlands. E-mail: r.a.j.janssen@tue.nl

Received (in Cambridge, UK) 8th November 1999, Accepted 22nd November 1999

An efficient and simple procedure for end-group modification of poly(3-alkylthiophene)s is presented which can be incorporated into the last step of the polymerisation reaction or employed as a post-polymerisation modification.

Poly(3-alkylthiophene)s (P3ATs) constitute an important class of conjugated polymers.[1] Being chemically and thermally stable materials, soluble P3ATs are attractive for exploring their electronic and optical properties. The side chains not only ensure solubility, but are a key parameter for the mesoscopic structure in thin films and, hence, as a property determining element. Perfection of the primary structure of the polymer, including molecular weight and polydispersity, is a prerequisite to obtain well-defined materials in a reproducible manner. Recently, regioregular P3ATs have been incorporated as the active material in transistors in which a preferential supramolecular ordering of the polymer chains induces a high field-effect mobility of up to 0.1 $cm^2\ V^{-1}\ s^{-1}$,[2,3] approaching that of single crystal oligothiophenes.[4] End-group functionalisation of these polymers would open the possibility to graft P3ATs onto surfaces, prepare block copolymers, or attach specific electroactive end groups and thereby extend the range of applications of these materials. Here we describe a simple and convenient procedure to introduce new end groups on the P3ATs.

Various synthetic routes to obtain regioregular P3ATs have been advanced over the last decade.[5-8] The McCullough route is most frequently employed to prepare regioregular P3ATs (Scheme 1). Typically a 3-alkyl-2-bromothiophene is converted to the (4-alkyl-5-bromo-2-thienyl)magnesium bromide Grignard reagent, which is polymerised *in situ* using $Ni(dppp)Cl_2$ as catalyst.[5] The work-up procedure involves extensive Soxhlet extractions with MeOH, hexanes, CH_2Cl_2 and $CHCl_3$,[9] and provides fractionated polymers with a polydispersity (PD) = 1.3–1.5 and molecular weight (M_w) increasing from 4–5 kg mol^{-1} for the hexanes fraction to ~30 kg mol^{-1} for the $CHCl_3$ fraction as determined by SEC analysis in $CHCl_3$ against polystyrene standards. Although regioregularities exceeding 99% have been claimed previously for P3ATs synthesised in this way, it has become clear that these polymers are less perfect than presumed initially.[10,11] Elemental analysis has revealed that synthesised P3ATs (where the alkyl group is *n*-butyl, *n*-hexyl, *n*-octyl or *n*-decyl) may contain a considerable amount of bromine (typically 1–2 wt%).[10,11]†

By investigating the hexane Soxhlet fraction of poly(3-hexylthiophene) (P3HT) with HPLC and preparative SEC in combination with MALDI-TOF mass spectrometry, it became clear that polymer chains terminated with 0, 1 and 2 bromines are present (Fig. 1).[10,11]‡ HPLC analysis of the hexane fraction confirms the presence of at least two series of P3HTs with alternating signal intensities [Fig. 2(*a*)]. The main progression in the HPLC trace [Fig. 2(*a*)] is identified as regioregular P3HT

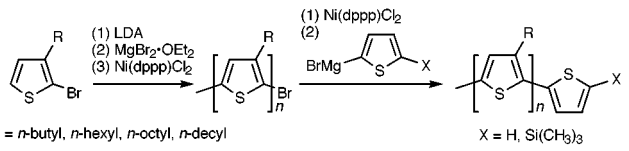

Scheme 1

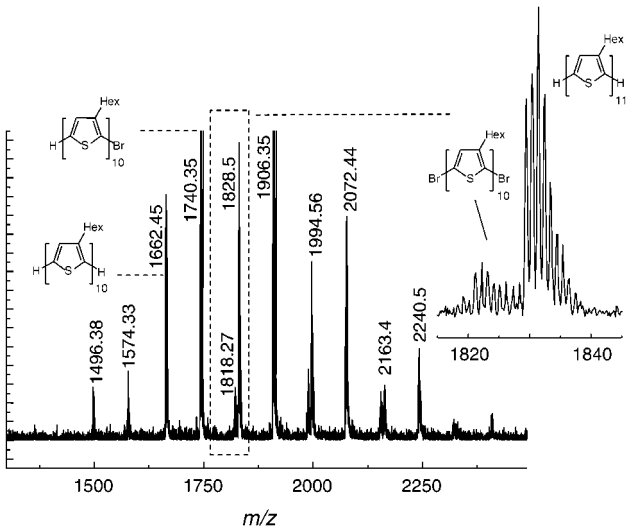

Fig. 1 MALDI-TOF of a narrow molecular weight fraction (M_w = 2.96 kg mol^{-1}, PD = 1.05) of P3HT obtained by preparative SEC showing the signals of chains with no, one and two bromine end groups. Note that SEC calibrated against polystyrene standards overestimates the molecular weight by a factor of 1.6.

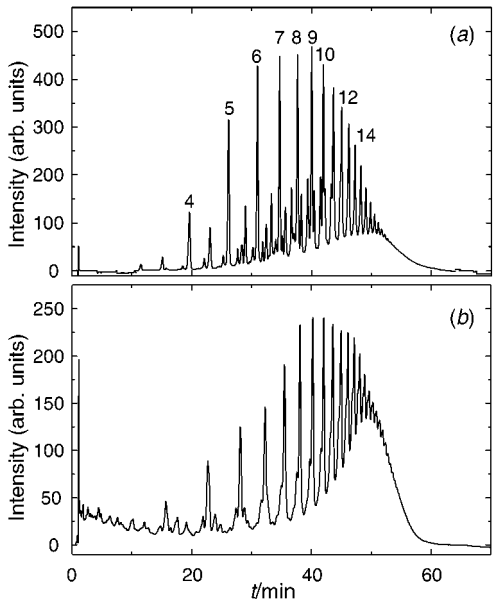

Fig. 2 HPLC of P3HT hexanes fraction before (*a*) and after (*b*) introduction of thiophene end groups. The numbers in the top graph indicate the number of thiophene rings of P3HT oligomers carrying one bromine end group.

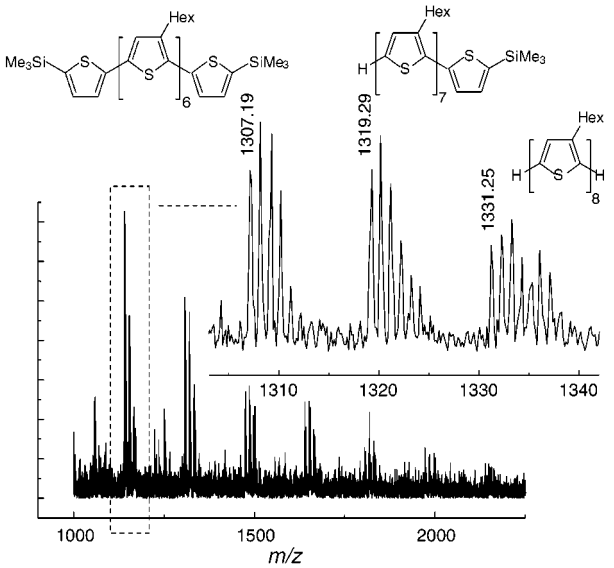

Fig. 3 MALDI-TOF of P3HT after end-capping with 5-trimethylsilyl-2-thienyl groups.

containing one bromine end group. This result is corroborated by the ^{1}H NMR spectrum of the $CHCl_3$ fraction of these polymers, which typically exhibits peaks for the benzylic resonances at δ 2.80 and 2.60 in a 20 : 1 ratio. While the δ 2.80 signal is due to benzylic protons in a regioregular head-to-tail dyad, the signal at δ 2.60 can be assigned to regioirregular head-to-head dyads and bromine terminated thiophene end groups.[9,12] The ratio of the benzylic ^{1}H NMR signals is a more sensitive gauge[6] to determine the regularity of the polymer than the aromatic protons and provides values on the order of 95% for the best materials.

Although the terminal bromines constitute a structural and chemical imperfection, they can be utilised to modify the polymers by introducing new end groups. We found that a post-polymerisation reaction of the polymer with a thiophene Grignard reagent under addition of fresh catalyst works rather well.§ Analysis with HPLC of a sample treated in this way showed essentially a single progression of P3HT chains [Fig. 2(*b*)]. To get a greater insight into the efficiency of the end-group modification reaction, a sample of P3HT was treated with 5-trimethylsilyl-2-thienylmagnesium bromide to introduce 5-trimethylsilyl-2-thienyl end groups under addition of fresh catalyst. MALDI-TOF analysis of short chains gives unambiguous evidence of the incorporation of the (5-trimethylsilyl-2-thienyl) end groups, with no signals for bromine-terminated chains (Fig. 3). The MALDI-TOF spectrum shows that both α and α,ω substitution occurs. The introduction of trimethylsilyl groups is also supported by the ^{1}H NMR spectrum, which shows a signal at δ 0.33.

In addition to adding a Grignard reagent at the end of the polymerisation reaction together with a fresh amount of catalyst to introduce specific end groups, the same reaction can also be performed on previously synthesised and isolated material.¶ This post-polymerisation reaction leaves the polymer intact, as inferred from a comparison of the molecular weights before and after performing the end-capping reaction.

In conclusion we have shown that *via* the Ni(dppp)Cl_2 mediated Grignard coupling it is possible to modify the bromine end groups that result from a McCullough type polymerization reaction of P3ATs, either as the last step in the polymerization or in a post-synthesis procedure on already isolated material. The procedure can be used to introduce end groups that are reactive to surfaces or to other functional groups. This opens the way to use P3ATs in adhesion, block-copolymerisation, electrooptical end groups and energy harvesting.

Financial support from the European Commission (Esprit 24793) is gratefully acknowledged.

Notes and references

† The bromine content was determined by Schöniger combustion.

‡ The molecular mass of the polymers was measured using a Perseptive DE PRO Voyager MALDI-TOF spectrometer utilising a α-cyano-4-hydroxy-cinnamic acid matrix. A solution of 1 mg ml^{-1} P3AT in THF was mixed with the matrix material at a molar ratio of *ca.* 1 : 10^{-3} (matrix : P3AT) and crystallised on the target immediately before measurement. HPLC column specifications: Waters, Nova-Pak C18, 60 Å, 4 μm, dimensions 3.9 × 150 mm. The HPLC runs (detected at 400 nm) were performed with an MeCN–THF gradient of 90 : 10 to 20 : 80, 1% min^{-1}, with Supra Gradient solvents from Biosolve.

§ In a typical procedure distilled Pr^i_2NH (2.8 ml, 20 mmol) was dissolved in 70 ml of dry THF. At room temperature BuLi (10.6 ml, 1.6 M in hexane, 17 mmol) was added. After stirring for 1.5 h, the solution was cooled to −60 °C and 2-bromo-3-hexylthiophene (4.0 g, 16 mmol) was added. The mixture was stirred for 1 h at –60 °C, and for 1 h at −40 °C. At −65 °C $MgBr_2{\cdot}OEt_2$ (4.4 g, 17 mmol) was added. The mixture was allowed to warm to 0 °C slowly. When all $MgBr_2{\cdot}OEt_2$ was dissolved, 0.09 g (0.18 mmol) Ni(dppp)Cl_2 was added and the mixture was stirred at room temperature for 20 hs. Then 20 mmol of freshly prepared 2-thienylmagnesium bromide (X = H) or 5-trimethylsilyl-2-thienylmagnesium bromide [X = $Si(CH_3)_3$] in Et_2O were added together with another portion of 0.18 mmol of Ni(dppp)Cl_2 and stirring was continued for 20 h. The reaction mixture was precipitated in MeOH, and further purified *via* Soxhlet extractions using MeOH, hexane and CH_2Cl_2. Isolation *via* Soxhlet extraction with $CHCl_3$ gave M_w = 25.6 kg mol^{-1} (PD = 1.42) for X = H and M_w = 14.6 kg mol^{-1} (PD = 1.48) for X = $Si(CH_3)_3$.

¶ To a mixture of P3HT (0.50 g, M_w = 11.0 kg mol^{-1}, PD = 1.4) in 15 ml THF and Ni(dppp)Cl_2 (0.4 g, 0.7 mmol) was added freshly prepared 2-thienyl magnesium bromide (5.9 g, 36 mmol 2-bromothiophene and 0.9 g, 37 mmol Mg) in 15 ml THF. The mixture was refluxed for 3 h. After removal of THF the P3HT was fractionated by Soxhlet extractions with MeOH, CH_2Cl_2 (0.32 g, M_w = 10.8 kg mol, PD = 1.51) and $CHCl_3$ (0.15 g, M_w = 19.4 kg mol^{-1}, PD = 1.23), respectively. The same work-up procedure on the original P3HT sample afforded M_w = 12.0 kg mol^{-1} (PD = 1.27) and M_w = 19.9 kg mol^{-1} (PD = 1.23).

1 J. Roncali, *Chem. Rev.*, 1992, **92**, 711; *Handbook of Organic Conductive Molecules and Polymers*, ed. H. S. Nalwa, Wiley, New York, 1997, vol. 1–4; *Polythiophenes: Electrically Conductive Polymers*, ed. G. Schopf and G. Koβmehl, Springer, Berlin, 1997; *Handbook of Conducting Polymers*, 2nd edn., ed. T. A. Skotheim, R. L. Elsenbaumer and J. R. Reynolds, Marcel Dekker, New York, 1998.
2 H. Sirringhaus, P. J. Brown, R. H. Friend, M. M. Nielsen, K. Bechgaard, B. M. W. Langeveld-Voss, A. J. H. Spiering, R. A. J. Janssen, E. W. Meijer, P. Herwig and D. M. de Leeuw, *Nature*, 1999, **401**, 685.
3 Z. Bao, A. Dodabalapur and A. Lovinger, *Appl. Phys. Lett.*, 1996, **69**, 4108.
4 G. Horowitz, F. Garnier, A. Yassar, R. Hajlaoui and F. Kouki, *Adv. Mater.*, 1996, **8**, 52; J. H. Schön, C. Kloc, R. A. Laudise and B. Batlogg, *Phys. Rev. B*, 1998, **58**, 12 952.
5 R. D. McCullough and R. D. Lowe, *J. Chem. Soc., Chem. Commun.*, 1992, 70; R. D. McCullough, R. D. Lowe, M. Jayaraman and D. L. Anderson, *J. Org. Chem.*, 1993, **59**, 904.
6 T.-A. Chen, X. Wu and R. D. Rieke, *J. Am. Chem. Soc.*, 1995, **117**, 233.
7 S. Guillerez and G. Bidan, *Synth. Met.*, 1998, **93**, 123.
8 A. Bolognesi, W. Porzio, G. Bajo, G. Zannoni and L. Fannig, *Acta Polym.*, 1999, **50**, 151; R. S. Loewe, S. M. Khersonsky and R. D. McCullough, *Adv. Mater.*, 1999, **11**, 251.
9 M. Trznadel, A. Pron, M. Zagorska, R. Chrzaszcz and J. Pielichowski, *Macromolecules*, 1998, **31**, 5051.
10 B. M. W. Langeveld-Voss, Thesis, Eindhoven University of Technology, ISBN 90-386-0668-0, 1998.
11 J. Liu, R. S. Loewe and R. D. McCullough, *Macromolecules*, 1999, **32**, 5777.
12 G. Bidan, A. De Nicola, V. Enée and S. Guillerez, *Chem. Mater.*, 1998, **10**, 1052.

Communication a908848b

ChemComm

First Dewar benzene approach to acetylenic oligophenylene macrocycles: synthesis and structure of a molecular rectangle bearing two spindles

Masakazu Ohkita, Kohta Ando, Ken-ichi Yamamoto, Takanori Suzuki and Takashi Tsuji*

Division of Chemistry, Graduate School of Science, Hokkaido University, Sapporo 060-0810, Japan. E-mail: tsuji@sci.hokudai.ac.jp

Received (in Cambridge, UK) 2nd November 1999, Accepted 29th November 1999

A novel Dewar benzene approach to the construction of oligophenylene macrocycles has been developed by introducing Dewar benzene 1 as a building block and applied to the synthesis of a molecular rectangle 8, whose structure was characterized crystallographically.

During the course of our study on small cyclophanes generated from the corresponding Dewar derivatives,[1] we were interested in exploiting a Dewar benzene for the construction of macrocyclic structures, especially for the synthesis of *p*-phenylene-based rigid, and thus strained, macrocycles. Since the bent shape of Dewar benzene is expected to provide a unique template effect on the cyclization, novel macrocyclic systems which are difficult to access from planar benzene derivatives may well become available based on the Dewar benzene approach. Here we report the rational and efficient synthesis of a novel rectangular macrocycle **8** using acetal-bridged Dewar benzene **1** as a building block, together with its crystallographic characterization. Phenylene acetylene macrocycles have attracted considerable recent attention in supramolecular chemistry and materials science.[2]

Dewar benzene **1** was readily prepared in four steps and on a gram scale from DMAD and 1,2-dichloroethylene.[3] Palladium-catalyzed coupling of **1** with **2**† afforded diethynylation product **3** (55% yield), which was then deprotected to **4** in 80% yield (Scheme 1). Copper-mediated oxidative coupling of **4** with $CuCl/Cu(OAc)_2$[4] in pyridine under pseudo-high-dilution conditions produced cyclic dimer **5**‡ in 70% yield. Acid hydrolysis of **5** followed by the silylation of resulting tetraol **6** afforded **7**§ in 73% yield. Photochemical isomerization of **7** proceeded smoothly and cleanly by irradiation with a high-pressure mercury lamp through Pyrex at 12 °C to afford **8**§ in quantitative yield. The less symmetrical product resulting from the rearrangement of only one of the Dewar benzene units was not detected by ^{1}H NMR monitoring of the reaction.

It is interesting to note that, in the ^{1}H NMR spectra, the benzylic protons of **7** appear as a pair of AB doublets (δ 4.10 and 4.12, J = 11 Hz) while those of **8** appear as a singlet (δ 4.95), indicating that these protons are diastereotopic in **7** and operationally enantiotopic in **8**. These observations would be most reasonably explained by postulating fast interconversion between the rotamers **8a** and **8b**, namely, fast rotation of the *p*-phenylene unit(s) in **8** on the NMR timescale despite the strained nature of the macrocycle.[5]

Crystals of **8** suitable for X-ray structure determination (Fig. 1) were obtained by slow diffusion of EtOH into a solution of **8** in $CHCl_3$ at room temperature.¶ The molecule adopts a nearly planar conformation in the crystal and the dimension of framework is 7.32 × 11.54 Å, as defined by the four inner *m*-phenylene carbon atoms. Interestingly, the framework appears to be distorted to a parallelogram to accommodate two $SiMe_2OCH_2$ moieties inside the cavity. The twist angles of the benzene rings from the least-square plane formed by the acetylenic carbon atoms are 3.7 and 0.4° in the *m*-phenylene units and 3.4° in the *p*-phenylene units. The benzene rings are essentially planar (deviation < 0.01 Å) while the acetylene units show small deviation from linearity with the C≡C–C angles of 168.7(3)–179.9(3)°.

In conclusion, we have successfully synthesized and characterized a novel rectangular macrocycle **8** by introducing **1** as a building block. The high efficiency of the macrocyclization of **4** into **5** demonstrates the synthetic utility of a Dewar structure as a 'masked' *p*-phenylene unit. Further elaboration and application of the present Dewar benzene strategy are now in progress.

We thank Professor Tamotsu Inabe, Hokkaido University, for the use of X-ray analytical facilities. This work was supported in part by a Grant-in-Aid for Scientific Research (No. 09640620) from the Ministry of Education, Science, Sports and Culture of Japan.

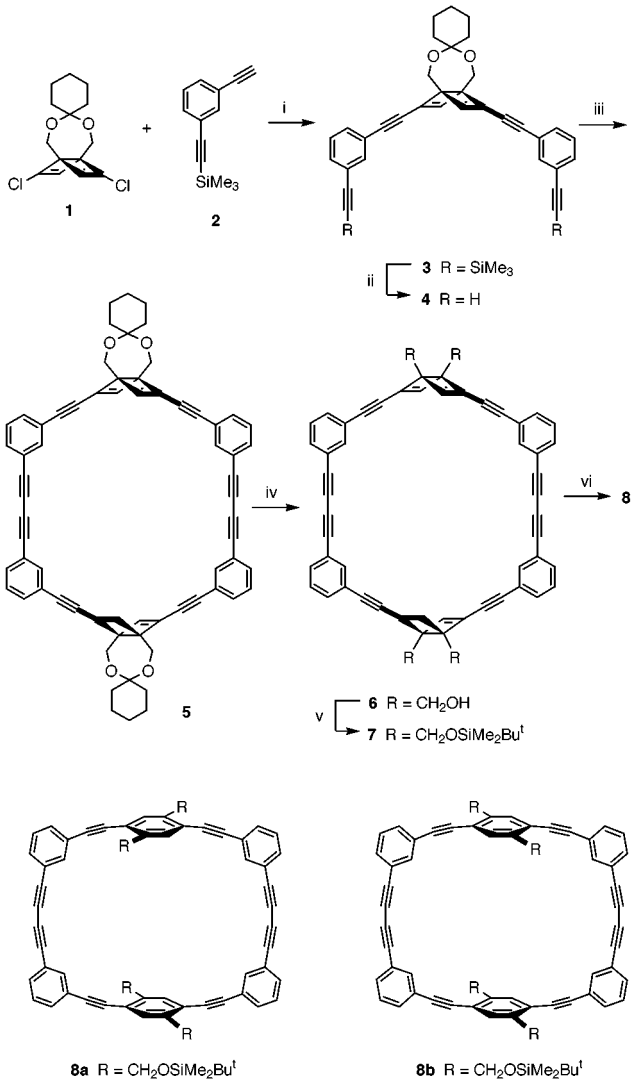

Scheme 1 *Reagents and conditions*: i, $Pd(PPh_3)_4$, CuI, Et_3N, 45 °C, 55%; ii, Bu_4NF, THF, 0 °C, 80%; iii, CuCl, $Cu(OAc)_2$, Py, syringe-pump addition over 2 h, 60 °C, 70%; iv, aq. HCl, THF, room temp., 98%; v, Bu^tMe_2SiOTf, Et_3N, CH_2Cl_2, room temp., 75%; vi, *hν*, CH_2Cl_2, 12 °C, 100%.

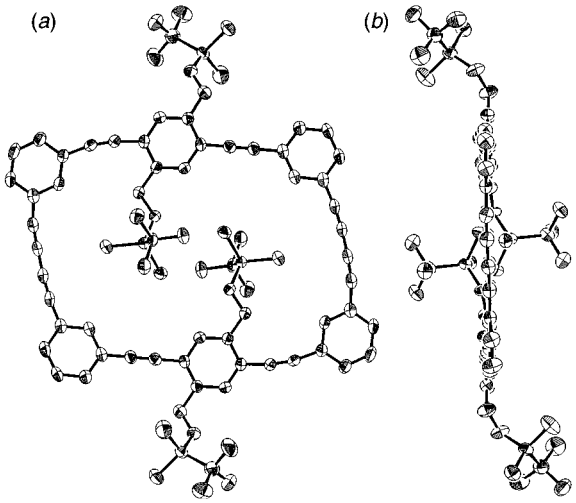

Fig. 1 Molecular structure of **8**: (*a*) top view, (*b*) side view. Hydrogen atoms are omitted for clarity.

Notes and references

† Compound **2** was prepared by partial desilylation of 1,3-bis[(trimethylsilyl)ethynyl]benzene (ref. 6) with aqueous KOH/MeOH in 60% yield.

‡ The isolated **5** was spectroscopically homogeneous although two stereoisomers arising from relative orientation of the Dewar units are possible. Only one of the possible isomers is depicted in Scheme 1. Compounds **6** and **7** were also spectroscopically homogeneous.

§ *Selected data* for **7**: δ_H(400 MHz, CD_2Cl_2) 0.08 (s, 24H), 0.92 (s, 36H), 4.10 (d, *J* 11.0, 4H), 4.12 (d, *J* 11.0, 4H), 6.83 (s, 4H), 7.29 (t, *J* 7.8, 4H), 7.38 (dt, *J* 7.8, 1.5, 4H), 7.52 (dt, *J* 7.8, 1.5, 2H), 7.70 (t, *J* 1.5, 2H); δ_C(100 MHz, CD_2Cl_2) −5.36, −5.23, 18.61, 26.05, 60.93, 66.42, 74.62, 81.31, 85.05, 94.77, 122.42, 124.11, 129.12, 131.75, 131.85, 136.18, 137.14, 146.02. For **8**: δ_H(400 MHz, CD_2Cl_2) 0.15 (s, 24H), 0.96 (s, 36H), 4.95 (s, 8H), 7.36 (t, *J* 7.8, 4H), 7.41 (dt, *J* 7.8, 1.5, 4H), 7.49 (dt, *J* 7.8, 1.5, 2H), 7.66 (s, 4H), 7.88 (t, *J* 1.5, 2H); δ_C(100 MHz, CD_2Cl_2) −5.07, 18.82, 26.24, 63.56, 75.37, 82.73, 89.08, 95.11, 120.79, 122.62, 124.36, 129.32, 130.13, 130.34, 130.92, 139.73, 142.36.

¶ *Crystal data* for **8**: $C_{80}H_{88}O_4Si_4$, M = 1224.6, colorless plate (0.60 × 0.30 × 0.05 mm), triclinic, $P\bar{1}$, a = 12.926(1), b = 17.570(2), c = 8.074(1) Å, α = 93.356(4), β = 97.690(3), γ = 79.755(4)°, V = 1787.1(3) Å^3, D_c = 1.14 g cm^{-3}, Z = 1, Mo-Kα radiation (λ = 0.71073 Å), T = 203 K, μ = 1.3 cm^{-1}, F(000) = 656. A total of 7513 unique reflections ($2\theta_{max}$ = 55°) were collected, of which 5339 observed reflections [$I > 3\sigma(I)$] were used in the structure solution (direct methods) and refinement (full-matrix least-squares with 398 parameters) to give final R = 0.063 and wR = 0.069. Residual electron density is 0.45 e Å^{-3}. CCDC 182/1496.

1 T. Tsuji, *Advances in Strained and Interesting Organic Molecules*, ed. B. Halton, JAI Press, Greenwich, 1999, vol. 7, p. 103 and references cited therein.
2 Reviews: U. H. F. Bunz, Y. Rubin and Y. Tobe, *Chem. Soc. Rev.*, 1999, **28**, 107; R. Faust, *Angew. Chem., Int. Ed.*, 1998, **37**, 2825.
3 T. Tsuji, H. Watanabe, J. Tanaka, M. Inada and S. Nishida, *Chem. Lett.*, 1990, 1193.
4 A. de Meijere, S. Kozhushkov, T. Haumann, R. Boese, C. Puls, M. J. Cooney and L. T. Scott, *Chem. Eur. J.*, 1995, **1**, 124.
5 Similar rotaion of spindles in strain-free phenylacetylene macrocycles, see: T. C. Bedard and J. S. Moore, *J. Am. Chem. Soc.*, 1995, **117**, 10 662; S. Höger, A.-D. Meckenstock and S. Muller, *Chem. Eur. J.*, 1998, **4**, 2423.
6 T. X. Neenan and G. M. Whitesides, *J. Org. Chem.*, 1988, **53**, 2489.

Communication a908711g

ChemComm

Novel liquid-crystalline PPE-naphthalene copolymers displaying blue solid-state fluorescence

Neil G. Pschirer, Mary E. Vaughn, Y. B. Dong, Hans-Conrad zur Loye and Uwe H. F. Bunz*

Department of Chemistry and Biochemistry, The University of South Carolina, Columbia, South Carolina 29208, USA. E-mail: bunz@psc.sc.edu

Received (in Columbia, MO, USA) 14th September 1999, Accepted 5th October 1999

Synthesis of poly(*p*-phenyleneethynylene)s (PPEs) containing 1,5-diethynyl-3,7-di-*tert*-butylnaphthalene leads to novel phenylene-naphthylene-ethynylene copolymers which show strong blue luminescence in the solid state.

Conjugated polymers are organic semiconductors and find *inter alia* applications in electroluminescent devices[1,2] and 'plastic lasers'.[3] We have recently reported an efficient synthesis of high molecular weight poly(*p*-phenyleneethynylene)s (PPEs) by alkyne metathesis utilizing simple 'instant catalysts'.[4] PPEs are promising materials, because they show quantum yields of 1.0 and blue emission in dilute solution. However, in the solid state, the emission spectra of PPEs are much weaker and considerably red-shifted as a consequence of aggregation and concomitant excimer formation in the solid state.[5,6] Likewise poly(3,7-di-*tert*-butylnaphthyleneethynylene), which we recently synthesized, is effectively non-fluorescent as film or powder.[7]

Herein we repot the synthesis and characterization of the unsaturated copolymers **3** which are efficient blue emitters in the solid state (Fig. 1). The polymers **3** are obtained by adding defined amounts of 3,7-di-*tert*-butyl-1,5-dipropynylnaphthalene **2**[7] to 1,4-dipropynyl-2,5-dialkylbenzenes **1** (Scheme 1) in our alkyne metathesis protocol utilizing an instant catalyst formed of $Mo(CO)_6$ and 4-chlorophenol.[8]† The catalyst and a varying ratio of monomers **1** and **2** were stirred in 1,2-dichlorobenzene at 140 °C for 11–25 h under a flow of N_2. This protocol results in a series of high molecular weight copolymers **3**. Longer polymerization times give rise to higher degrees of polymerization, as examined in the PPE system in detail.[8]

The UV–VIS spectra of **3a**–**d** in dilute solution show a λ_{max} of 388–395 nm, very similar to that of dialkyl-PPEs (388 nm). To our surprise, thin film absorption spectra of **3a**–**d** are identical to those in solution, which is in stark contrast to the PPE case where a dramatic red-shift is observed. The unusual optical behavior prompted us to investigate fluorescence of **3a**–**d**. In solution an intense blue emission is observed (**3a**, 425 nm; **3d**, 419 nm), again similar to dialkyl-PPEs (425 nm). In the solid state, however, the situation is different, and in thin films

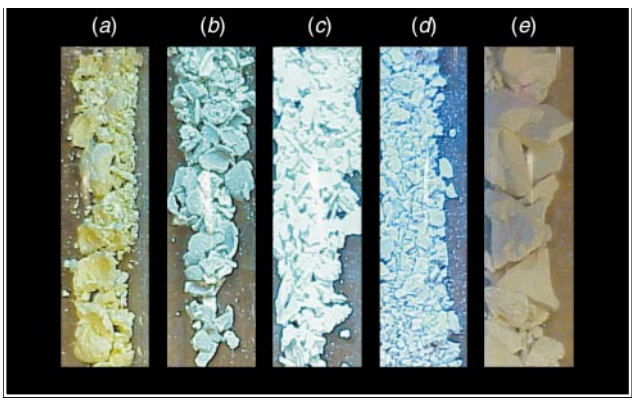

Fig. 1 Solid-state emission (hand held fluorescence lamp, λ_{max} = 366 nm) of PPE and PPE-napthalene copolymers **3**: (*a*) didodecyl-PPE; (*b*) polymer **3a**; (*c*) polymer **3c**; (*d*) polymer **3d**; (*e*) poly(3,7-di-*tert*-butylnaphtyleneethynylene).

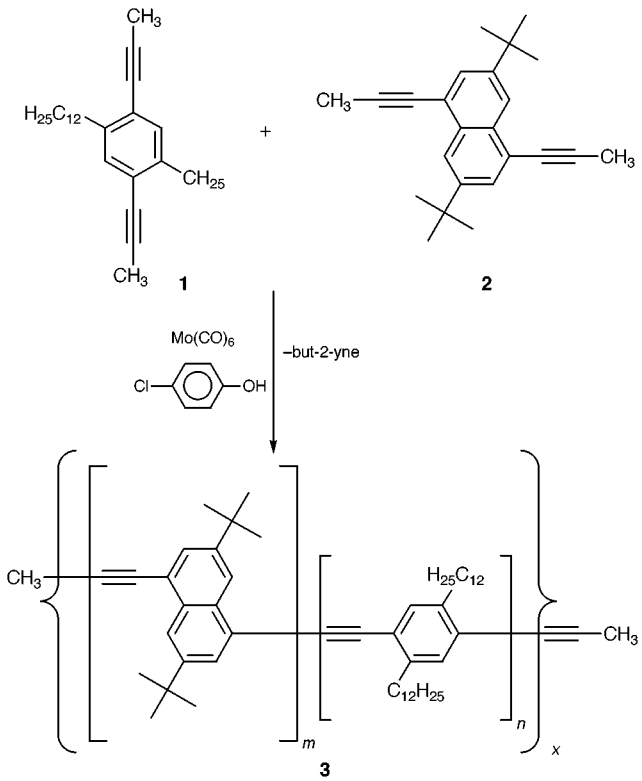

Scheme 1

Table 1 Characterization of **3a**–**d**

Entry	Ratio **1**:**2**	*t*/h	Yield (%)	GPC D_p[a]	GPC P_n[a]	Absorbance/nm $CHCl_3$	Absorbance/nm Thin film	Emission/nm $CHCl_3$	Emission/nm Thin film
3a	5:1	25.5	86	96	2.9	395	395, 420	425, 446	446
3b	2:1	11	64	49	2.9	390	390, 420	422, 443	442
3c	1:1	17	79	56	4.7	391	391	421, 444	433
3d	1:2	12.5	77	42	2.3	388	388	419, 440	422

[a] Gel permeation chromatography results based on polystyrene standard.

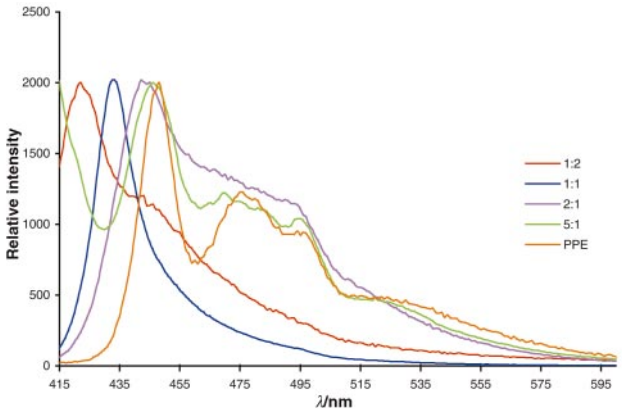

Fig. 2 Solid-state emission spectra of thin films of **3a**–**d** and PPE.

of **3a**–**d** we find emission maxima ranging from 446 (5 : 1, **3a**) to 422 nm (1 : 2, **3d**), (Fig. 2), thus allowing the manipulation of solid-state emission maximum from yellow–green to blue *via* the amount of added monomer **2**. The less PPE character the copolymer **3** has, the further its emission is blue-shifted towards that observed in dilute solution. We conclude that in the copolymers **3** aggregation and supramolecular ordering are efficiently suppressed by the presence of the bulky *tert*-butylnaphthyl groups.[9] This scenario must lead to a disordered solid state in **3**. To test this hypothesis we performed powder diffraction on polymers **3** (Fig. 3). The polymers **3a**–**c** display a broad diffraction peak of large intensity according to d = 4.2 Å. This diffraction peak can be attributed to the interchain distance of the polymers. A second, weak diffraction peak is observed at d = 8.8–11.7 Å, but is very weak in **3a**–**c**. In the naphthalene-rich polymer **3d** the small-angle diffraction at 11.7 Å is most prevalent. Molecular modeling indicates that this represents the distance between the two 3,7-*tert*-butyl groups on individual naphthalene units.[10]

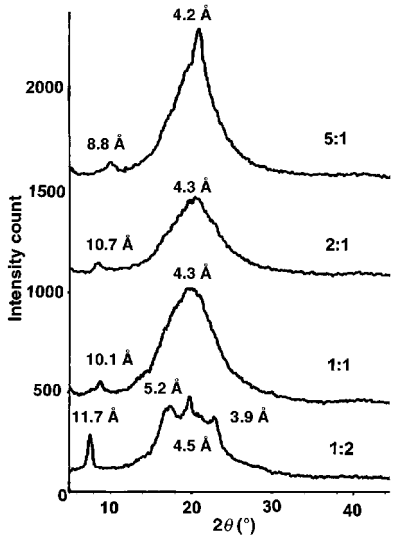

Fig. 3 Diffraction data of polymers **3a**–**d**.

For device purposes, liquid crystalline behavior offers the entry to polarized emission. DSC and polarizing microscopy performed upon **3a**–**c** shows that **3a**,**b** are thermotropic nematic (**3a**: isotropic → nematic 160 °C DSC; nematic → isotropic 170 °C → nematic 149 °C, evidenced by polarizing microscopy, cooling. **3b**: 194 °C polarizing microscopy, cooling isotropic → nematic), both displaying Schlieren textures. Copolymer **3c** displays a broad halo at 4.3 Å, and a weak small angle feature, suggesting either small domain sizes or a disordered structure. No identifiable textures develop upon thermal treatment. Only in the case of **3a** is the isotropic → nematic transition observed in the DSC and it is exothermic, with 0.27 kcal mol^{-1} per repeating unit, a small but not unexpected value.[11] Polymer **3d** is crystalline and does not show any phase transition up to 300 °C.

In conclusion we have presented the synthesis and characterization of a new series of liquid-crystalline PPE copolymers **3** which exhibit blue solid state fluorescence. The blue shift increases with the amount of naphthalene. Particularly attractive is the intensity of luminescence of **3** in the solid state. The increased solid-state fluorescence is attributed to the absence of aggregates and excimers, which normally reduce PPE's quantum efficiencies of emission in the solid state. Application of **3** in LEDs and sensory materials[12] is currently being explored.

We acknowledge Professor C. J. Murphy and L. Gearhart for help with the fluorescence spectra. This work was generously supported by the NSF (CHE 9814118, PI Bunz) and the Research Corporation.

Notes and references

† Sample coploymerization: **1** (0.35 g, 0.71 mmol), **2** (0.24 g, 0.71 mmol), $Mo(CO)_6$ (0.034 g, 0.07 mmol), 4-chlorophenol (0.091 g, 0.71 mmol) and 1,2-dichlorobenzene (20 mL) were held at 140 °C under a steady stream of N_2 for 17 h. Addition of chloroform acid and base washes and precipitation into methanol furnish **3c** in 80% yield. *Selected data* for **3c**: δ_H 8.58–8.54 (m), 8.07 (br s), 7.94 (br s), 7.60–7.42 (m), 3.02–2.89 (m), 2.13 (br s), 2.12 (br s), 1.79–1.68 (m), 1.51–1.22 (m), 0.88–0.87 (br s); δ_C 148.4, 141.9, 132.5, 131.3, 123.0, 122.8, 121.1, 93.5, 92.7, 35.1, 34.4, 32.0, 31.4, 31.3, 30.8, 29.8, 29.5, 29.4, 22.8, 14.2; ν_{max}(KBr)/cm^{-1} 3444, 2957, 2923, 2853, 2350, 1651, 1463, 1384, 1025, 886, 771.

1 D. Neher, *Adv. Mater.*, 1995, **7**, 691; A. Kraft, A. C. Grimsdale and A. B. Holmes, *Angew. Chem.*, 1998, **37**, 402; J. H. Burroughes, D. D. C. Bradley, A. R. Brown, R. N. Marks, K. Mackay, R. H. Friend, P. L. Burns and A. B. Holmes, *Nature*, 1990, **347**, 539.
2 S. A. Jenekhe and J. A. Osaheni, *Science*, 1994, **265**, 765; J. A. Osaheni and S. A. Jenekhe, *Macromolecules*, 1994, **27**, 739; X. Zhang, A. S. Shetty and S. A. Jenekhe, *Acta Polym.*, 1998, **49**, 52; E. Conwell, *Trends Polym. Sci.*, 1997, **5**, 218.
3 F. Hide, M. A. Diaz-Garcia, B. J. Schwartz and A. J. Heeger, *Acc. Chem. Res.*, 1997, **30**, 430.
4 L. Kloppenburg, D. Song and U. H. F. Bunz, *J. Am. Chem. Soc.*, 1998, **120**, 7973.
5 C. E. Halkyard, M. E. Rampey, L. Kloppenburg, S. L. Studer-Martinez and U. H. F. Bunz, *Macromolecules*, 1998, **31**, 8655; R. Fiesel, C. E. Halkyard, M. E. Rampey, L. Kloppenburg, S. L. Studer-Martinez, U. Scherf and U. H. F. Bunz, *Macromol. Rapid Commun.*, 1999, **20**, 107.
6 D. Ofer, T. M. Swager and M. S. Wrighton, *Chem. Mater.*, 1995, **7**, 418; Q. Zhou and T. M. Swager, *J. Am. Chem. Soc.*, 1995, **117**, 12 593; C. Weder and M. S. Wrighton, *Macromolecules*, 1996, **29**, 5157.
7 N. G. Pschirer, A. Marshall, C. Stanley, H. W. Beckham and U. H. F. Bunz, *Macromol. Rapid Commun.*, 2000, **21**, in the press.
8 L. Kloppenburg, D. Jones and U. H. F. Bunz, *Macromolecules*, 1999, **32**, 4194.
9 B. R. Hsieh, W. C. Wan, Y. Yu, Y. L. Gao, T. E. Goodwin, S. A. Gonzalez and W. A. Feld, *Macromolecules*, 1998, **31**, 631; W. J. Oldham, R. J. Lachicotte and G. C. Bazan, *J. Am. Chem. Soc.*, 1998, **120**, 2987; G. C. Bazan, Y. J. Miao, M. L. Renak and B. J. Sun, *J. Am. Chem. Soc.*, 1996, **118**, 2618; Z. H. Peng, J. H. Zhang and B. B. Xu, *Macromolecules*, 1999, **32**, 5152.
10 U. H. F. Bunz, V. Enkelmann, L. Kloppenburg, D. Jones, K. D. Shimizu, J. B. Claridge, H.-C. zur Loye and G. Lieser, *Chem. Mater.*, 1999, **11**, 1416; L. Kloppenburg, D. Jones, J. B. Claridge, H. C. zur Loye and U. H. F. Bunz, *Macromolecules*, 1999, **32**, 4460.
11 M. Altmann and U. H. F. Bunz, *Angew. Chem.*, 1995, **35**, 569.
12 J. S. Yang and T. M. Swager, *J. Am. Chem. Soc.*, 1998, **120**, 11 864.

Communication a907479a

Ring-closing alkyne metathesis with simple catalyst systems: an access to molecular triangles and rhomboids

Neil G. Pschirer, Wei Fu, Richard D. Adams* and Uwe H. F. Bunz*

Department of Chemistry and Biochemistry, The University of South Carolina, Columbia, South Carolina 29208 USA. E-mail: bunz@psc.sc.edu

Received (in Columbia, MO, USA) 26th October 1999, Accepted 30th November 1999

Treatment of the siloxane monomer 2 with a mixture of molybdenum hexacarbonyl and 4-chlorophenol at 140 °C furnished the corresponding cyclotrimer 3 and the cyclotetramer 4.

Ring-closing alkene metathesis utilizing well-defined organometallic catalysts[1–4] has developed into a powerful synthetic tool. A variety of rings have been prepared by this method. Cyclic polyynes are also of great interest,[5] but their synthesis *via* ring-closing alkyne metathesis is much less explored.[6] Fürstner[7] has reported the preparation of large-ring alkynes by ring-closure of suitable dipropynylated precursors utilizing Schrock's tungsten carbyne.[8]

We have recently developed an efficient and simple protocol for alkyne metathesis[9,10] and we now report the first examples of ring-closing metathesis using our 'instant' catalyst. This powerful catalyst is formed *in situ* from $Mo(CO)_6$ and 4-chlorophenol using off-the-shelf quality solvents.

The synthesis of shape-persistent macrocycles, potentially useful as molecular boxes, presents a new and interesting challenge.[11,12] We have chosen diyne **2** to be a convenient precursor to the novel molecular siloxane triangles/boxes **3** and **4**. Compound **2** was prepared in two steps from **1**, which was, itself, obtained from 4-iodophenol by treatment with $Pr^i_2SiCl_2$ in Et_3N (Scheme 1). A palladium-catalyzed coupling of **1** with propyne affords the monomer **2** in 61% yield.[13] Alkyne metathesis of **2** with $Mo(CO)_6$ and 4-chlorophenol at 140 °C in 1,2-dichlorobenzene under a steady stream of N_2 (Scheme 1) furnished the novel cycles **3** and **4**.† Sufficient dilution is an important factor for obtaining cyclic rather than polymeric products, although minor changes in concentration did not result in decreased yields of the macrocycles. Separation was difficult due to the similar retention times of **3** and **4**, and their corresponding open congeners. However, we were able to isolate **3** (14% yield) and **4** (18% yield). GC-MS confirmed that the isolated fractions of **3** and **4** were uncontaminated by other cycloisomers. The molecular structures of **3** and **4** were established by single crystal X-ray diffraction analyses.‡

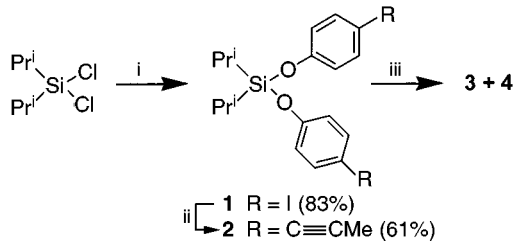

Scheme 1 *Reagents and conditions*: i, 4-IC_6H_4OH, Et_3N, THF; ii, propyne, $Pd(PPh_3)_2Cl_2$, CuI, piperidine; iii, $Mo(CO)_6$, 4-ClC_6H_4OH.

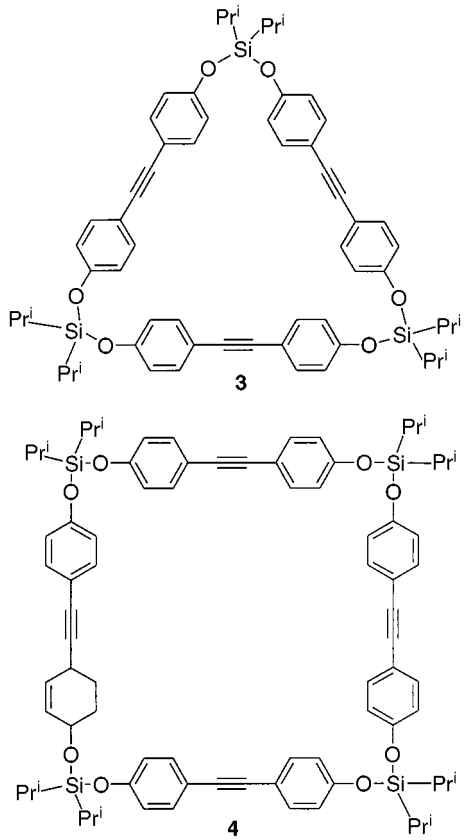

The crystal of **3** contains three symmetry-independent molecules. All three display similar conformations and the molecular structure of one of these is shown in Fig. 1. The cyclotetramer **4** is crystallographically centrosymmetric. It exhibits a rhomboidal structure with a large interior cavity that contains two molecules of hexane as solvate, from which it was crystallized (Fig. 2). This feature indicates the potential of these box-shaped molecules to engage in important host–guest chemistry.

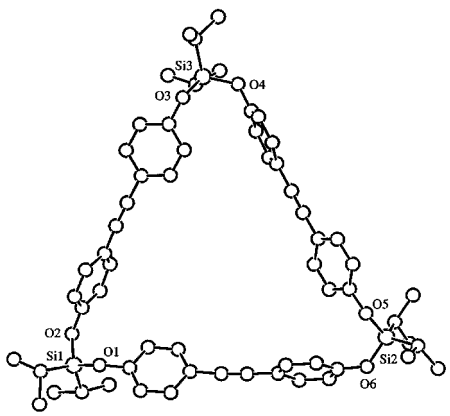

Fig. 1 A structural diagram of the cyclic triyne **3**. Selected bond distances (Å) and angles (°) are C≡C = 1.22(2), 1.20(2) and 1.16(2), Si(1)–O(1) = 1.616(9), Si(1)–O(2) = 1.624(9), Si(2)–O(5) = 1.67(1), Si(2)–O(6) = 1.63(1), Si(3)–O(3) = 1.63(1), Si(3)–O(4) = 1.66(1); O(1)–Si(1)–O(2) = 109.8(5), O(5)–Si(2)–O(6) = 106.9(5), O(3)–Si(3)–O(4) = 108.1(6).

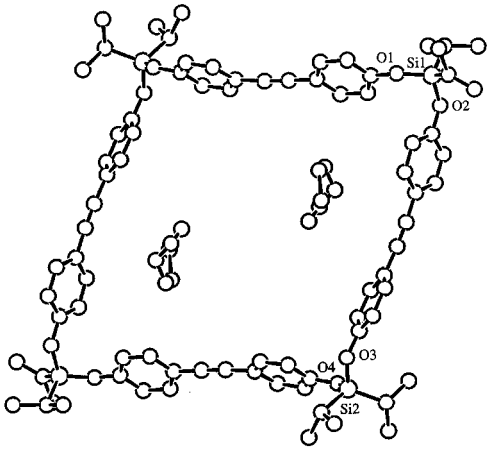

Fig. 2 A structural diagram of the cyclic tetrayne **4** showing two molecules of occluded hexane in the interior of the ring. Selected bond distances (Å) and angles (°) are C≡C = 1.179(9) and 1.213(9), Si(1)–O(1) = 1.635(4), Si(1)–O(2) = 1.646(4), Si(2)–O(3) = 1.654(4), Si(2)–O(4) = 1.652(4); O(1)–Si(1)–O(2) = 110.6(2), O(3)–Si(2)–O(4) = 109.9(2).

We have now demonstrated that ring-closing alkyne metathesis with our 'instant' catalyst system provides a convenient route to novel alkyne-containing macrocycles. Functionalized rings should also be accessible *via* this methodology as we have already shown that the mixtures of $Mo(CO)_6$ and 4-chlorophenol are metathesis-active in the presence of a variety of different functional groups.[8,9]

This work was generously supported by the NSF (CHE 9814118, PI Bunz) and the Research Corporation (PI Bunz).

Notes and references

† Sample cyclization: **2** (1.00 g, 2.66 mmol), $Mo(CO)_6$ (0.66 g, 0.27 mmol), 4-chlorophenol (0.206 g, 1.60 mmol) and 1,2-dichlorobenzene (100 ml) were held at 140 °C under a steady stream of N_2 for 17 h. The solution was allowed to cool, then dissolved in hexanes and washed with dilute acid and base. Separation of the resulting products was achieved by chromatography over silica gel (Merck silica gel 60, 40–63 μm particle size; eluent 3:1 hexanes–CH_2Cl_2–). *Selected data* for **3**: δ_H(400 MHz, $CDCl_3$) 7.31 (d, *J* 8.6, 12H), 6.71 (d, *J* 8.6, 12H), 1.30 (m, *J* 7.1, 6H), 1.16 (d, *J* 7.1, 36H); δ_C(400 MHz, $CDCl_3$) 154.1, 132.7, 119.9, 116.8, 88.2, 17.2, 12.7. For **4**: δ_H(400 MHz, $CDCl_3$) 7.35 (d, *J* 8.8, 16H), 6.88 (d, *J* 8.8, 16H), 1.40 (m, 8H), 1.09 (d, *J* 7.3, 48H); δ_H(400 MHz, $CDCl_3$) 154.4, 132.9, 119.7, 116.8, 88.1, 17.2, 12.7.

‡ *Crystal data*: for **3**: $Si_3O_6C_{60}H_{68}$, triclinic, M = 936.12 g cm^{-3}, space group = $P\bar{1}$ (No. 2). T = 293 K, Mo-Kα, a = 23.76(2), b = 24.07(3), c = 18.7192(5) Å, α = 92.0(1), β = 96.25(7), γ = 93.70(9)°, Z = 6, D = 1.083 g cm^{-3}, μ = 0.13 cm^{-1}, 15889 measured reflections, 7703 independent reflections, R (R_w) = 0.091 (0.126), hydrogen atoms calculated, not refined. For **4**: $Si_4O_8C_{80}H_{176}\cdot 2(C_6H_{14})$, triclinic, M = 1378.60, Space group = $P\bar{1}$ (No. 2), T = 293 K, Mo-Kα, a = 13.977(8), b = 14.25(1), c = 12.144(7) Å, α = 106.29(5), β = 108.21(5), γ = 69.68(5)°, Z = 1, D = 1.083 g cm^{-3}, μ = 0.12 cm^{-1}, 4534 measured reflections, 2740 independent reflections, R (R_w) = 0.0599 (0.0814). Hydrogen atoms calculated, not refined. CCDC 182/1494. See http://www.rsc.org/suppdata/cc/a9/a908638b/ for crystallographic data in .cif format.

1 R. R. Schrock, *Polyhedron*, 1995, **14**, 3177.
2 R. H. Grubbs and S. Chang, *Tetrahedron*, 1998, **54**, 4413 and references therein.
3 R. H. Grubbs, S. J. Miller and G. C. Fu, *Acc. Chem. Res.*, 1995, **28**, 446.
4 M. Schuster and S. Blechert, *Angew. Chem., Int. Ed. Engl.*, 1997, **36**, 2036; A. Fürstner, *Top. Catal.*, 1997, **4**, 285.
5 R. Gleiter and R. Merger, in *Modern Acetylene Chemistry*, ed. P. J. Stang and F. Diederich, VCH, Weinheim, 1995, ch. 8; L. T. Scott and M. J. Cooney, in *Modern Acetylene Chemistry*, ed. P. J. Stang and F. Diederich, VCH, Weinheim, 1995, ch. 9.
6 U. H. F. Bunz and L. Kloppenburg, *Angew. Chem., Int. Ed.*, 1999, **38**, 478.
7 A. Fürstner and G. Seidel, *Angew. Chem., Int. Ed.*, 1998, **37**, 1734.
8 R. R. Schrock, D. N. Clark, J. Sancho, J. H. Wengrovius and S. F. Pedersen, *Organometallics*, 1982, **1**, 1645; X.-I. Zhang and G. C. Bazan, *Macromolecules*, 1994, **27**, 4627.
9 L. Kloppenburg, D. Song and U. H. F. Bunz, *J. Am. Chem. Soc.*, 1998, **120**, 7973; L. Kloppenburg, D. Jones and U. H. F. Bunz, *Macromolecules*, 1999, **32**, 4194.
10 N. G. Pschirer and U. H. F. Bunz, *Tetrahedron Lett.*, 1999, **40**, 2481.
11 P. J. Stang and B. Olenyuk, *Acc. Chem. Res.*, 1997, **30**, 502; P. J. Stang, *Chem. Eur. J.*, 1998, **4**, 19; B. Olenyuk, A. Fechenkötter and P. J. Stang, *J. Chem. Soc., Dalton Trans.*, 1998, 1707; B. Olenyuk, A. J. A. Whiteford, A. Fechenkötter and P. J. Stang, *Nature*, 1999, **398**, 796.
12 For similar, conjugated silicon containing macrocycles, see F. Q. Liu, G. Harder and T. D. Tilley, *J. Am. Chem. Soc.*, 1998, **120**, 3271; S. S. H. Mao, F. Q. Liu and T. D. Tilley, *J. Am. Chem. Soc.*, 1998, **120**, 1193.
13 M. Altmann and U. H. F. Bunz, *Angew. Chem., Int. Ed. Engl.*, 1995, **34**, 569.

Communication a908638b

ChemComm

Formation of a benzenetrienoid resonance structure in a cyclophane containing a trinitrotriaminobenzene unit

J. Jens Wolff,* Uwe Seibold and Thomas Oeser

Organisch-Chemisches Institut der Ruprecht-Karls-Universität Heidelberg, Im Neuenheimer Feld 270, D-69120 Heidelberg, Germany. E-mail: wolff@donar.oci.uni-heidelberg.de

Received (in Liverpool, UK) 8th October 1999, Accepted 26th November 1999

The [6_3](1,5,9)triphenyleno(1,3,5)cyclophane 1 shows a trienoid Kekulé-type structure for the planar donor–acceptor substituted benzene part.

The deviation of small aromatic molecules like benzene and naphthalene from the usual equal bond lengths to bond length alternations has been the object of synthetic and theoretical investigations.[1,2] The known X-ray structures with considerable bond length alternations reminiscent of the extremum of a Kekulé structure require a threefold incorporation into strained rings which shorten the incorporated bonds. This leads to almost single-bond character for the bonds not incorporated. At first glance, steric strain may not be the only way to ease the formation of such structures with a Kekulé bond length alternation: the complete symmetrical substitution with three electron donating and three accepting groups might also lead to it. In an extreme situation, the interaction between donors and acceptors could equally result in Kekulé-type structures with three groups of separated double bonds that bear one donor and one acceptor, each interacting only with each other. Thus, this type of bond length alternation might also occur within such a ring without great strain.

A closer look, however, shows disappointing results. For example, while all 1,3,5-trinitro-2,4,6-triamino-substituted benzene derivatives known[3–5] do show bond length alternations, they are far from the threefold symmetry required for a Kekulé structure: the six-membered ring has a clear maximum of C_{2v} or C_2 symmetry. Almost all of the central rings of the molecules analyzed by X-ray adopt either a strongly nonplanar boat or a twist form. The same holds true for substitution with other donors like the hydroxy group or its anion. For these highly nonplanar molecules, the shown quinoid and bis-trimethine cyanoid resonance forms are the only geometric structures observed (Scheme 1). Planar ones correspond to usual benzene derivatives with some substituent-dependent bond length alternation.

We were therefore surprised when an X-ray structure† (Scheme 2) was obtained of an intermediate **3** in the construction of bis-hexaaminobenzene derivatives[6] used by us for the study of intramolecular electron transfer.[7] Both aromatic rings are close to planar.[8] While this would not be very surprising for most benzene derivatives, it has never been observed before for trinitrotriaminobenzenes, which are only close to planar in the hydrogen-bonded solid state structure of trinitrotriaminobenzene itself; even with only two amino groups and one alkylamino group, some folding of the ring is observed.[4] In addition, the donor–acceptor substituted ring shows C_3 symmetry and the bond lengths within the ring are 1.399(4) and 1.416(4) Å. Thus, the clear formation of a benzene ring with a Kekulé structure can be observed which lacks significant steric strain but has symmetrical donor–acceptor substitution. The higher C–C bond length occurs between the nitro and the amino groups that are linked by a weak intramolecular hydrogen bond (2.29 Å). Some interaction is also visible to the other direction, between the other oxygen of the nitro group and a proton of the methylene group next to the nitrogen (2.27 Å).[9] The oxygen of the nitro group which is engaged in intramolecular hydrogen bonding with the amino group also shows intermolecular contact to the NH of the hexaazatriphenylene (2.34 Å). Both possible enantiomeric forms are present in the crystal, related to each other by inversion symmetry.

A closer inspection provides a reason for the unexpected planarity. Since the bridges between the two rings need to keep approximately the same distance between them, they have to adopt comparable conformations. The hexaaminobenzene derivative part of **3** is expected to exist with a stable planar conformation for its central benzene ring.[7,10,11] Then, the second, donor–acceptor substituted ring can adopt neither boat nor twist forms, because the distance of the chains to the first ring would become quite different (Scheme 3). These conformations are thus unlikely to be observed. While equality of the distances would be possible in a chair conformation, it is not truly compatible with the electronic requirements of the push–pull interaction between the substituents and is thus rarely found even for non-polar benzene derivatives with strong steric interactions.[12] The only possible conformation for the usually

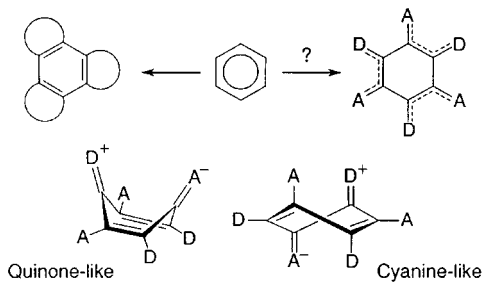

Scheme 1

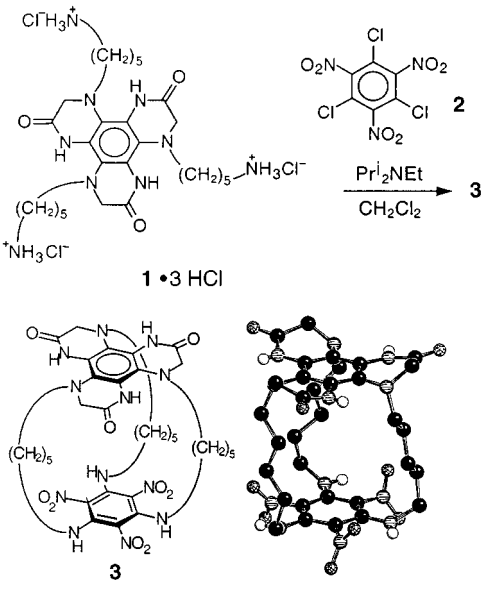

Scheme 2

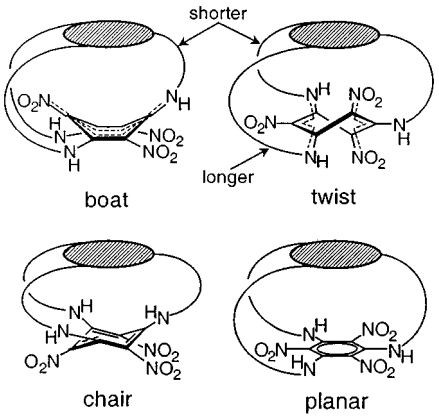

Scheme 3

highly distorted six-membered ring is therefore a planar one. While in this conformation the donor–acceptor interactions are quite reduced in comparison with known structures, they are nevertheless still present. Therefore a moderate, but definitely existent Kekulé distortion can be detected.

Support by the German Research Council ('DFG', Wo495/3-1 and Heisenberg fellowship for J. J. W.) is acknowledged. We would like to thank Mrs U. Wiesinger for assistance in the structural determination and also one of the reviewers for valuable comments.

Notes and references

† *Crystal data* for **3**: Orange hexagonal plates, $C_{33}H_{42}N_{12}O_9 \cdot 3H_2O \cdot 0.5\ CH_2Cl_2$ (750.3 + 96.5), T = 298 K, numerical absorption correction (μ = 0.16 mm^{-1}). Trigonal space group $P\bar{3}$ with $a = b$ = 15.267(3), c = 10.921(6) Å, Z = 2; solution by direct methods with SHELXS-97, refinement with SHELXL-97. 3941 reflections, 3549 unique, 1715 observed [$I > 2\sigma(I)$]. N–H refined isotropically, remaining H calculated. R = 0.067, R_w = 0.187, GOF = 0.98. CCDC 182/1497. See http://www.rsc.org/suppdata/cc/a9/a908200j/ for crystallographic data in .cif format.

1 F. Cozzi, F. Ponzini, R. Annunziata, M. Cinquini and J. S. Siegel, *Angew. Chem.*, 1995, **107**, 1092; *Angew. Chem., Int. Ed. Engl.*, 1995, **34**, 1019.

2 K. P. C. Vollhardt and D. L. Mohler, *The Phenylenes: Synthesis, Properties, and Reactivity*, in *Advances in Strain in Organic Chemistry, Vol. 5*, ed. B. Halton, JAI, Greenwich, 1996.

3 J. J. Wolff, *Structures of Benzene Derivatives with Symmetrical Substitution by Three Donor and Three Acceptor Groups*, in *Advances in Strained and Interesting Organic Molecules, Vol. 7*, ed. B. Halton, JAI, Stamford, 1999.

4 J. J. Wolff, F. Gredel, D. Hillenbrand and H. Irngartinger, *Liebigs Ann. Chem.*, 1996, 1175.

5 K. K. Baldridge and J. S. Siegel, *J. Am. Chem. Soc.*, 1993, **115**, 10782.

6 *Synthesis* of **3**: The synthesis of starting material will be described elsewhere. To a suspension of **1**·3 HCl (235 mg, 0.360 mmol) in dry CH_2Cl_2, a mixture of Hünig's base (282 mg, 2.18 mmol) and 1,3,5-trichloro-2,4,6-trinitrobenzene **2** (ref. 13) (114 mg, 0.360 mmol) in CH_2Cl_2 (100 ml) was added within 3 h. The mixture was stirred overnight and then, after addition of four drops of AcOH, filtered over silica gel (CH_2Cl_2–MeOH = 25/1). The solvents were removed and the chromatography was repeated. The cyclophane **3** was obtained as a yellow powder (18 mg, 0.024 mmol, 7%), decomp. > 230 °C. Crystals for X-ray analysis were obtained from diffusion of pentane into a solution in CH_2Cl_2. δ_H(300 MHz, DMSO-d_6) 1.08 (m, 6H), 1.26 (m, 6 H), 1.42 (m, 6H), 2.76 (m, 6H), 3.12 (m, 3H), 3.19 (m, 3H), 3.41 (d, J 17.1, 3H), 3.50 (d, J 16.9, 3H), 9.09 and 9.12 (br s, together 6H); δ_C(75.5 MHz, DMSO-d_6) 23.30, 24.82, 27.38, 45.67, 53.53, 56.21, 114.82, 115.07, 126.57, 147.40, 168.97 [FAB-MS: calc. for $C_{33}H_{42}N_{12}O_9$: 750.32, found 750.48 (15, M^+); $C_{33}H_{42}N_{12}O_9 + Na^+$: 773.31, found: 773.48 (3, $M + Na^+$)].

7 J. J. Wolff, A. Zietsch, H. Irngartinger, and T. Oeser, *Angew. Chem.*, 1997, **108**, 637; *Angew. Chem., Int. Ed. Engl.*, 1997, **36**, 621.

8 The sum of absolute torsional angles within the donor-substituted six-membered ring is 19°, and 15° in the donor–acceptor substituted one.

9 C–H···O interaction (see, *e.g.*: G. R. Desiraju, *Acc. Chem. Res.*, 1996, **29**, 441) could influence which type of bond is lengthened, and which one shortened. While the distance between NO and the second methylene group is fairly large (2.55 Å for C–H···O, 3.45 for C···O), it is smaller for the contact between the non-hydrogen-bonded oxygen and the first methylene group (2.27 and 2.99 Å). Since the nitrogen of the amino group will draw electron density from this carbon atom, it will also give a slightly more electron-deficient hydrogen more engaged in the dipolar interaction. AM1 or PM3 calculations indeed give a bond length alternation (0.026 *vs.* 0.017 Å) for a tris(diethylamino)trinitrobenzene with torsional angles derived from the structure of **3**, which decreases for the corresponding trimethyl derivative (0.014 Å), and vanishes for the corresponding triamino derivative.

10 J. Thomaides, P. Maslak and R. Breslow, *J. Am. Chem. Soc.*, 1988, **110**, 3970.

11 J. M. Chance, B. Kahr, A. B. Buda, J. P. Toscano and K. Mislow, *J. Org. Chem.*, 1988, **53**, 3226.

12 *E.g.*: H. Sakurai, K. Ebata, C. Kabuto and A. Sekiguchi, *J. Am. Chem. Soc.*, 1990, **112**, 1799.

13 P. Engelbertz (Inv.), Chemische Fabrik Griesheim, D.R.P. 767510, 1936, *Chem. Abstr.*, 1955, **49**, 14803d; M. E. Hill and F. Taylor Jr., *J. Org. Chem.*, 1960, **25**, 1037.

Communication a908200j

ChemComm

Delamination of layered double hydroxides by use of surfactants

Mariko Adachi-Pagano, Claude Forano* and Jean-Pierre Besse

Laboratoire des Matériaux Inorganiques, CNRS ESA 6002, Université Blaise Pascal, 63177 Aubière Cedex, France. E-mail: forano@chimtp.univ-bpclermont.fr

Received (in Oxford, UK) 29th November 1999, Accepted 29th November 1999

Delamination of the layered double hydroxide structure $[Zn_2Al(OH)_6][C_{12}H_{25}SO_4{\cdot}nH_2O]$ was realized by dispersion in butanol; translucent colloidal solutions are stable for at least 8 months with oriented LDH materials with extended crystallite size being obtained; the results presented here suggest that total delamination occurs in the colloidal solution.

Delamination of low dimensional solids is of tremendous practical importance in applications ranging from polymer reenforcement,[1] self assembling monolayers (SAM) and Langmuir–Blodgett film preparation[2] or emulsion stabilizations.[3] Dispersions of clay minerals have been studied more extensively owing to their extended swelling properties and a great ability to undergo surface modification with organophilic cations.[4] Exfoliation of other layered structures such as MoS_2, layered phosphates and metal oxides have also been achieved by manipulation of the interlayer interactions.[5]

Layered double hydroxides (LDHs) are layered materials constituted by a stacking of positive hydroxylated layers $[M^{2+}_{1-x}M^{3+}_{x}(OH)_2]^{x+}$ separated by interlayered anionic species and water molecules $[X^{q-}_{x/q}{\cdot}nH_2O]$. They are known for their unique anion exchange properties and their rich chemistry which make them good catalysts or catalyst precursors.[6] However, the high charge density of the LDHs layers and the high content of anionic species and water molecules result in strong interlayer electrostatic interactions between the sheets and significantly hydrophilic properties. Such dense interlamellar hydrogen bonding networks lead to a tight stacking of the lamellae. The rigid spheroidal 'sand rose' morphology of intergrown platelets prevents both accessibility to the major part of the surface or exfoliation of the sheets in water or in any other non-aqueous solvents. However, exchange of inorganic anions by organophilic anions, such as fatty acid salts or anionic surfactants proceeds readily.[10] This leads to a substantial modification of the surface properties, from hydrophobic to hydrophilic. Moreover, the van der Waals interlayer interactions introduced by the introduction of such species weakens the stacking of the layers and favours interactions with non-aqueous solvents.

The purpose of this study was to develop a method of delamination of LDHs which will lead to a novel generation of LDH based materials in which the total surface of the layered compound will be rendered accessible for chemical reactivity or for the preparation of new porous or oriented materials. The delaminated structure of the $Zn_2Al(OH)_6Cl{\cdot}2H_2O$ LDH phase ([Zn–Al]) would reach a theoretical specific surface aera of 800 $m^2\ g^{-1}$, while the experimental BET measured surface areas reach only 10–50 $m^2\ g^{-1}$.

We have already reported the influence of organic solvents (ethanol, methanol, acetone, ethylene glycol, glycerol) on the modification of the surface and porosity properties of LDHs.[7] However, complete delamination of LDHs has, as yet not been reported. Now successful LDH delamination has been achieved using various anionic surfactants and we report, for the first time, stable colloidal solutions of LDHs. In this study, we demonstrate total delamination of the [Zn–Al] LDH using dodecyl sulfate (DS) as an anionic surfactant and butanol as the dispersant.

The $Zn_2Al(OH)_6Cl{\cdot}2H_2O$ LDH precursor ([Zn_2Al–Cl]) was prepared by the coprecipitation method previously described by Bonnet *et al*.[9] The preparation of the surfactant modified LDH ([Zn_2Al–DS]) was realized by the anion exchange reaction in deionised water of 1.00 g of [Zn_2Al–Cl] with a 1.54 molar excess (1.34 g) of sodium dodecyl sulfate (Across). Intercalation of the surfactant was monitored by X-ray diffraction (Siemens D501 X-ray powder diffractometer, Cu-Kα radiation) and FTIR spectroscopy (Perkin-Elmer-FTIR16PC). The chemical formulae of the various compounds were calculated from elemental analysis. In all cases, the Zn/Al ratio was 2.2 and for the DS exchanged LDH, S/Al was equal to 0.98 in accord with total exchange of the Cl anions.

Intercalation of dodecyl sulfate in $Zn_2Al(OH)_6Cl{\cdot}2H_2O$ leads to the expanded phase $Zn_2Al(OH)_6(C_{12}H_{25}SO_4){\cdot}nH_2O$ ([Zn_2Al-DS]) with an increase of the basal spacing from 0.77 to 2.52 nm (Fig. 1) as reported in the literature.[12] The particle widths for both precursor and modified LDHs were measured by SEM (Cambridge Stereoscan 360, 20 kV, at Techinauv S.A). The measured thickness of [Zn_2Al–Cl] platelets was 0.05 μm, corresponding to a stacking of *ca.* 60 layers, while expansion of the basal spacing for [Zn_2Al-DS] leads to lamellae thickness of 0.15 μm. The number of stacked layers is retained after anion exchange confirming that the anion exchange proceeds by a topotactic mechanism.

Dispersion of [Zn_2Al–DS] in water, methanol, ethanol, propanol or hexane under reflux conditions leads to unstable suspensions which settle after a few hours and only a minor part of the material was dispersed. Dispersion in methanol appears to be kinetically controlled by the slow replacement of water molecules by methanol. After one week stirring, *ca.* 50% of the LDH can be exfoliated. By contrast, reflux in butanol at 120 °C for 16 h leads to a translucent colloidal solution, which remains stable for at least 8 months. Up to 1.5 g of [Zn_2Al–DS] per liter of butanol can be dispersed. Similar results have been obtained with higher alcohols such as pentanol and hexanol.

The size of the LDH colloids was measured by dynamic light scattering (Zetasizer–Malvern instrument). The mean equiva-

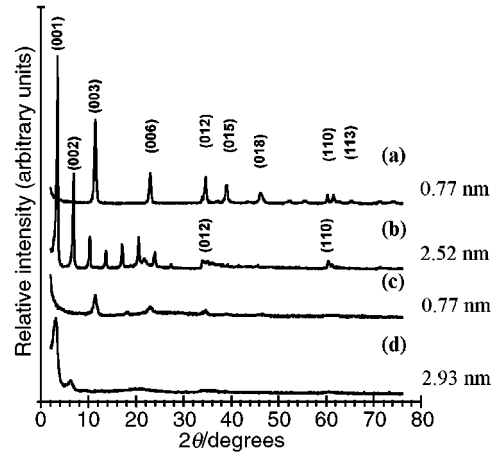

Fig. 1 Diffraction patterns of (a) [Zn_2Al–Cl], (b) [Zn_2Al–DS], (c) [Zn_2Al–Cl]$_{recov}$, (d) [Zn_2Al–DS]$_{recov}$.

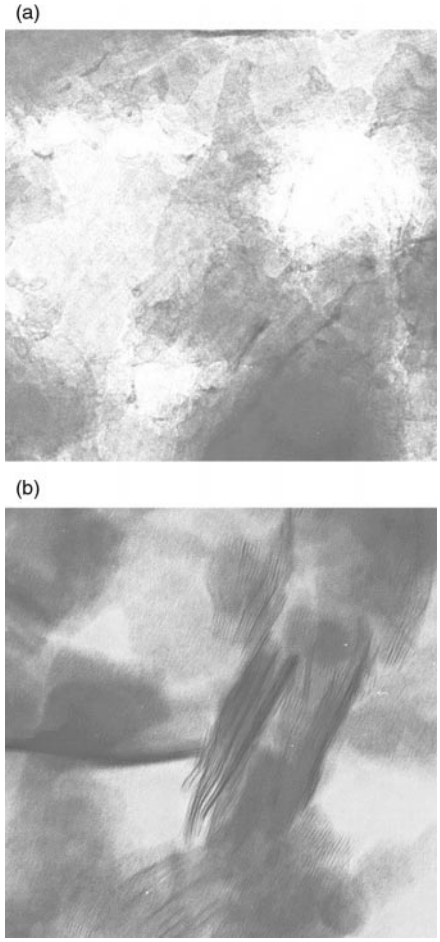

Fig. 2 TEM micrographs of [Zn_2Al–DS] dispersed in (a) butanol and (b) ethanol.

lent spherical diameter (d_s) is *ca.* 140 nm, smaller than the width of the hexagonal sheets measured by SEM (200 nm). Transmission electron micrographs of [ZnAl–DS] particles recovered from the colloidal solution [Fig. 2(a)] show assemblies of dispersed platelets all oriented parallel to the grid surface and confirm that delamination has occurred at the layer level while aggregates of stacked sheets are observed for the same materials dispersed in ethanol [Fig. 2(b)]. This argues in favour of a total delamination in butanol.

We note that the hydration state of the modified LDH is a critical parameter. Delamination was only observed when the organo-LDH compounds were previously dried under vacuum at room temperature for 1 day but not when a freshly wet prepared LDH was used or if the [Zn_2Al–DS] was thoroughly dried under vacuum at 80 °C for 4 h. Such intense drying leads to a new DS containing LDH phase with a smaller basal spacing of 1.68 nm corresponding to a tilted intertwined DS single layer. This LDH displays a densely packed structure which is resistent to exfoliation. It appears that the use of butanol with a boiling point higher than that of water and reflux conditions allows for a rapid replacement of all the intercalated water molecules by the solvent molecules. This seems to be the key process to completely exfoliate of the solid material.

When butanol is removed from the colloidal solution by evaporation (120 °C) or by lyophilization, a new LDH phase ([Zn_2Al–DS]$_{recov}$) is obtained with larger size and well oriented platelets as shown by an SEM micrograph [Fig. 3(a)]. This extended bidimensional orientated material displays a basal spacing of 2.93 nm in accord with incorporation of butanol in the interlamellar spaces. The typical 'sand rose' morphology of the LDH precursor is then lost and a thin film of LDH is obtained.

Comparison between FTIR spectra of the oriented LDH and [Zn_2Al–DS], particularly in the 400–1800 cm^{-1} wavenumber

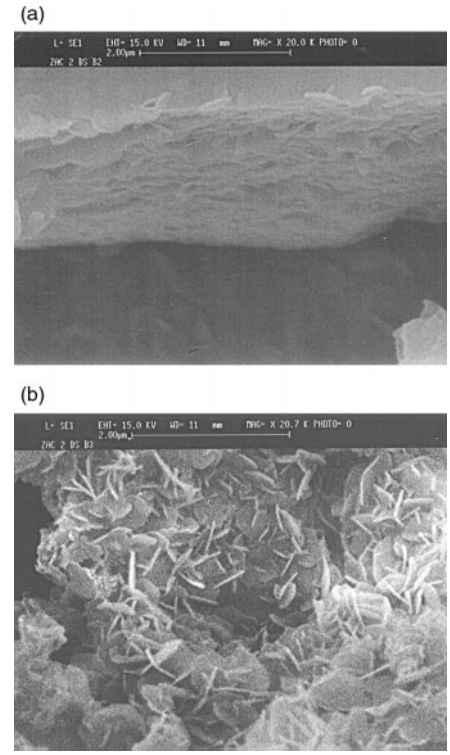

Fig. 3 SEM micrographs of (a) [Zn_2Al–DS]$_{recov}$ and (b) [Zn_2Al–CO_3]$_{recov}$.

range in with unchanged lattice vibrations are superimposed on surfactant vibrations, confirms that the LDH structure is retained after delamination. When NaCl or Na_2CO_3 are added to the colloidal solution, flocculation of particles occurs and reversible back anion exchanges to give [Zn_2Al–Cl]$_{recov}$ and [Zn_2Al–CO_3]$_{recov}$ results (Figs. 1, 3(b)). The recovering of LDH structures under solvent extraction or precipitation confirms the presence of delaminated LDH in the colloidal solution.

The preparation of colloidal solutions of LDHs appears to be of substantial importance for the development of novel chemistry of the LDHs. It is now possible to develop the chemistry of LDHs in non-aqueous media, *e.g.* for electrochemistry applications. Ultrathin films based on LDHs can now easily be prepared by a soft chemistry route. Preparations of novel based-LDH materials with improved chemical or porosity properties are now envisaged through interstratified LDH/LDH, LDH/clay, LDH/polymer or nanoporous LDH/SiO_2 materials.

Notes and references

1 A. Usuki, Y. Kojima, M. Kawasumi, A. Okada, Y. Fukushima, T. Kurauchi and O. Kamigaito, *J. Mater. Res.*, 1993, **8**, 1179.
2 T. E. Mallouk, H. N. Kim, P. J. Ollivier and S. W. Keller, *Supramolecular Comprehensive Chemistry*, Pergamon, Oxford, 1996, p. 189.
3 I. Dekany, F. Berger, K. Imrik and G. Lagaly, *Colloid Polym. Sci.*, 1997, 681.
4 T. Permien and G. Lagaly, *Clays Clay Miner.*, 1995, **2**, 229.
5 A. J. Jacobson, *Comprehensive Supramolecular Chemistry: Colloidal dispersion of compounds with layer and chain structures*, ed. G. Alberti and T. Bein, Elsevier, Oxford, 1996, vol. 7, p. 315.
6 F. Cavani, F. Trifiro and A. Vaccari, *Catal. Today*, 1991, **11**, 173.
7 F. Malherbe, C. Forano and J. P. Besse, *Microporous Mater.*, 1997, **10**, 67.
8 A. De Roy, C. Forano, K. El Malki and J. P. Besse, *Synthesis of Microporous Materials*, ed. L. Occelli and H. Robson, Van Nostrand, Reinhold, 1992, vol. 2, p. 108.
9 S. Bonnet, C. Forano, A. De Roy, J. P. Besse, P. Maillard and M. Momenteau, *Chem. Mater.*, 1996, **8**, 1962.
10 M. Meyn, K. Beneke and G. Lagaly, *Inorg. Chem.*, 1990, **29**, 5201.
11 S. Sundell, *Acta. Chem. Scand., Ser. A*, 1971, **31**, 799.
12 A. Clearfield, M. Kieke, J. Kwan, J. L. Colon and R. C. Wang, *J. Inclusion Phenom. Mol. Recognit. Chem.*, 1991, **11**, 361.

Communication a908251d

ChemComm

Luminescent molecular logic gates: the two-input inhibit (INH) function

Thorfinnur Gunnlaugsson,*[a] Dónall A. Mac Dónail[a] and David Parker[b]

[a] *Department of Chemistry, University of Dublin, Trinity College Dublin, Dublin 2, Ireland. E-mail: gunnlaut@tcd.ie*
[b] *Department of Chemistry, University of Durham, South Road, Durham, UK DH1 3LE*

Received (in Cambridge, UK) 10th November 1999, Accepted 3rd December 1999

The Tb(III) complex 3, is the first example of a molecular logic gate corresponding to a two-input INHIBIT function, A ∧ B′ where the 'output', a sharp, line-like, terbium emission, is only observed with two chemical inputs (i) the presence of protons and (ii) the absence of molecular oxygen.

Developments in supramolecular chemistry and nanotechnology have stimulated interest in the construction of simple electronic or photonic driven systems and networks that function as molecular-level devices.[1] Examples include simple host–guest complexes as well as more advanced switches,[2] wires,[3] grids,[4] shuttles[5] and molecular machines.[6] Mimicking the functions of semiconductor logic gates used in modern computing is of particular interest,[7] where the relationship between input and the output may be described by truth tables, where 1 represents an active input/output and 0 an inactive one.[8] For a two input system there are 16 different logic gate functions.[8b]† Some of these functions have recently been demonstrated where ions and molecules are used as inputs,[7] including the ID (or YES), AND, OR and NOT logic functions designed by de Silva *et. al.*[9] and the XOR function designed by Balzani *et al.*[10] Among the remaining logic gates is the inhibit (INH) function which can be interpreted as a particular integration of an AND and a NOT logic functions, where the output signal is inhibited by one of the active inputs.‡ Recently the more complex three-input integrated INH logic gate was demonstrated.[11] However, the fundamental two-input INH gate has not been reported.

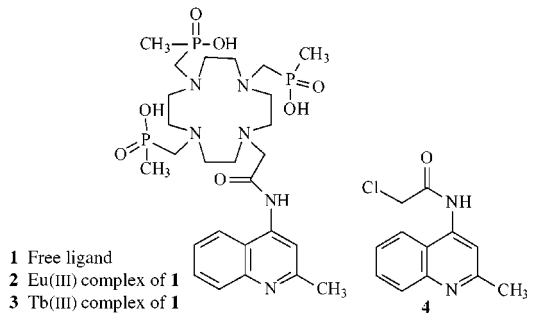

Here, we demonstrate that in water the Tb(III) based quinolyl derived macrocyclic 1,4,7,10-tetraazacyclododecane (cyclen) conjugate, **3**, yields such an INH logic gate. The two inputs are H^+ (the nitrogen moiety of the quinoline acting as a proton acceptor) and O_2 (or rather the absence of O_2, since this input is not asserted when O_2 is present). The output signal is a delayed line like Tb luminescence (owing to the deactivation of the Tb $^5D_4$ excited state to the ^7F_J, J = 6, 5, 4 and 3), occurring at long wavelengths. These are important features since sharp, long wavelength emissions give minimal signal interference, critical for high performance signalling systems. Tb was chosen because, unlike Eu(III), pyridine based Tb and related complexes are known to be spectroscopically sensitive to O_2,[12] opening the possibility of a gate with O_2 as a second input. Moreover, lanthanide based cyclen derivatives have been shown to be kinetically stable in water.[13]

The syntheses of the α-chloroamide **4**, the free ligand in **1** and the Eu complex **2**, have previously been described; **2** was designed as a delayed Eu luminescence pH sensor.[14] **3**, the Tb complex of **1**, was synthesised in a similar manner to **2**, and obtained in 55% yield after treating **1** with $Tb(CF_3SO_3)_3$ in refluxing acetonitrile, followed by a purification on alumina. Complexation was established by electrospray (ES^+) mass spectrometry and ^{31}P NMR.§

The absorption spectrum of **3** showed a similar pH dependence to **2** and **4**, with λ_{max} at 314 nm (log ε = 4.18) and a band at 261 nm under acid conditions with λ_{max} shifting to 295 nm (log ε = 4.0) in the presence of base (isosbestic points at 299 and 271 nm). The Eu luminescence (occurring from $^5D_0$, E = 17200 cm^{-1})[15] of **2** (1×10^{-5} mol dm^{-3}) in H_2O under ambient conditions ([O_2] *ca.* 0.23 mmol dm^{-3}) was highly pH dependent when excited at 330 nm, with a 250 fold luminescence enhancement (LE) observed upon addition of acid ([CF_3CO_2H] = 3 mmol dm^{-3}/pH = 2.5). This pH dependence signals the protonation of the remote quinoline nitrogen moiety (pK_a = 5.8) and the 'tuning' of the so-called antenna effect, the energy transfer mechanism from the singlet excited state (S_1) of the chromophore (*via* the triplet, T_1) to the lanthanide excited state.[12,13]¶

The Tb luminescence of **3** (appearing at 491.5, 547.5, 588.0 and 623.0 nm, J = 6, 5, 4 and 3 respectively) was somewhat different. The excited state emission from $^5D_4$ (E = 20500 cm^{-1}) was only weakly observed in alkaline solution under ambient conditions, with only a 1.7 fold enhancement upon acidification as seen in Fig. 1(a) ([CF_3CO_2H] = 1.26 mmol dm^{-3}/pH = 2.9) when excited at 330 nm. The corresponding fluorescence changes were more apparent; both a hypsochromic shift from 373 to 357 nm (isoemissive point at 387 nm) and intensity changes were observed upon acidification (two shoulders at 371 and 345 nm).

The measurements were repeated in degassed solution ('freeze–pump–thaw', [O_2] < 10^{-6} mol dm^{-3}). In alkaline solution the Tb emission spectrum and lifetime (τ_{Tb} = 0.39 ms) were unaffected (owing to the inefficient population of the lanthanide excited state¶). However, in acid solution degassing yielded a *ca.*50 fold increase in the Tb luminescence intensity at 547.5 nm [Fig. 1(b)], and an almost threefold increase in the lifetime (τ_{Tb} = 0.98 ms); these conditions 'switch on' the Tb emission [note the different scales in Fig. 1(a) and 1(b)]. The fluorescence spectra were however only marginally affected by the removal of O_2.

The small Tb emission in aerated acidic solution arises from the fact that the T_1 state of the quinoline (T_1 E = 21978 cm^{-1}, as measured for the protonated form of **4**) is partly quenched by an ambient level of O_2. The Tb $^5D_4$ state can also participate in a back-energy transfer mechanism to the T_1 state (the energy difference being 1478 cm^{-1}); these combined processes lead to efficient quenching of the $^5D_4$ state (*i.e.* the Tb emission is switched off). Upon removal of O_2 this quenching process is largely suppressed leading to more efficient population of the Tb $^5D_4$ state (the antenna effect is more efficient) and switching on of the Tb emission.[12]

From the perspective of logic functions, the Eu emission (**2**) is determined only by the presence of single ionic input (H^+), back energy transfer from $^5D_0$ is inefficient and the complex is

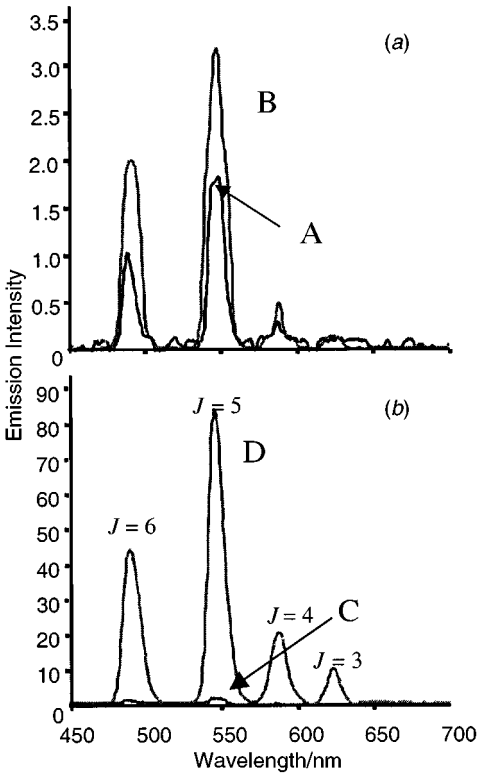

Fig. 1 Tb(III) emission of **3** (1×10^{-5} mol dm^{-3}) in water at 293 K, 10.0 mmol dm^{-3} NMe_4ClO_4 (to maintain constant ionic strength): (a) in *aerated* solution at: (A) pH = 11, (B) pH = 2.9; (*b*) in *degassed* solution at: (C) pH = 11, (D) pH = 2.9. Note the difference in the intensity scales.

thus insensitive to O_2,[7] and can as such be regarded as a pass logic function (YES[9] or ID[8b] logic gate). The emission of the Tb complex (**3**) is more interesting and is switched on *only* in the presence of H^+ and absence of O_2. Under other circumstances, the absence of H^+, the presence of O_2, or both, no significant Tb emission is observed (based on discrimination in LE factors; *ca.* 50 when O_2 *absent cf.* 1.7 with O_2 *present*, at 547.5 nm, Fig. 1). This behaviour may be conveniently described using logic notation,[7,9] written A ∧ B′, where A and B represent the H^+ and O_2 inputs respectively. The corresponding truth table is shown in Fig. 2(a), where an active output (X = 1, corresponding to emission) is obtained only when A = 1 and B = 0.[8] This logic gate is the inhibit (INH) function, Fig. 2(b).

(a)

A	B	X
0	0	0
0	1	0
1	0	1
1	1	0

(b)

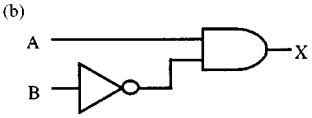

Fig. 2 (a) A truth table for the INH logic gate; inputs A and B correspond to the H^+ and O_2 respectively; X [Tb(III) emission], is the output signal. (b) The INH gate represented using a conventional gate notation; an active output signal (Tb emission) is obtained when A = 1 and B = 0.

Even though more advanced practical integration of such molecular level logic gates into circuits is somewhat beyond the horizon, progress depends of the generation of all fundamental logic operations. Our goal was to generate a two-input INH logic gate, and the Tb emission based gate reported herein is the first example of such a two-input molecular gate. Importantly, unlike many previous molecular logic gates where the output is a broad emission,[7,9,11] the output signal for **3**, is a set of line-like Tb emission bands occurring at long wavelengths (Stokes shifts of 160–300 nm for *J* = 6–3, respectively) with narrow bandwidth (*ca.* 10 nm) giving rise to a high signal quality. Complex **3**, is thus an important contribution to the development of molecular logic devices, not least since the current silicon based computer chips are expected to reach their physical limits in the near future.[16]

We are grateful to the BBSRC and Kinerton Ltd. for financial support, Professor John M. Kelly, Dr J. C. Penedo Esteiro and Dr Hazel M. Moncrieff for valuable discussions.

Notes and references

† The ONE and ZERO functions are trivial, the output being a 1 or 0 respectively, regardless of the input. Four functions depend on a single input, namely both ID and both INV (or NOT) functions. The remaining ten are functions of two inputs, and of these AND, OR, XOR, NAND, NOR and EQU (or XNOR) satisfy commutation. The last four functions corresponding to INH and IMP gates do not satisfy commutation.

‡ The INH function, A ∧ B′, should not be confused with the NAND function, (A ∧ B)′.

§ ES^+: *m/z* 802.94 (15, $M^+ + 1$), 826.30 (13, M + Na^+). ^{31}P NMR (101 MHz, CH_3CN): δ 441.71 (br s) and 427.76 (br s) *cf.* δ 42.95 and 33.54 for **1**.

¶ Population of the quinoline S_1 (λ_{ex} = 330 nm) and subsequent population of the lanthanide excited state (the antenna effect) is inefficient in alkaline solution since the chromophore is only weakly absorbing at this wavelength. On acidification the S_1 population is greatly enhanced since absorption is shifted to longer wavelengths.

1 *Molecular Electronics and Molecular Electronic Devices*, ed. K. Sienicki, CRC Press, USA, vol. 1, 1993; J.-M. Lehn, *Supramolecular Chemistry, Concepts and Prespectives*, VCH, Weinheim, 1995; V. Balzani and F. Scandola, *Supramolecular Photochemistry*, Ellis Horwood, Chichester, 1991.

2 P. R. Ashton, V. Balzani, J. Becher, A. Credi, M. C. T. Fyfe, G. Mattersteig, S. Menzer, M. B. Nielsen, F. M. Raymo, J. F. Stoddart, M. Venturi and D. J. Williams, *J. Am. Chem. Soc.*, 1999, **121**, 3951; A. P. de Silva, H. Q. N. Gunaratne, T. Gunnlaugsson, A. J. M. Huxley, C. P. McCoy, J. T. Rademacher and T. E. Rice, *Chem. Rev.*, 1997, **97**, 1515.

3 R. Ziessel and A. Harriman, *Coord. Chem. Rev.*, 1998, **171**, 331; A. Harriman and R. Ziessel, *Chem. Commun.*, 1996, 1707.

4 A. M. Garcia, D. M. Bassani, J.-M. Lehn, G. Baum and D. Fenske, *Chem. Eur. J.*, 1999, **5**, 1234; L. DeCola, *Chimia*, 1996, **50**, 214.

5 D. J. Cardenas, D. J. Collin, P. Gavina, J. P. Sauvage, A. De Cian, J. Fischer, N. Armaroli, L. Flamigini, V. Vicinelli and V. Balzani, *J. Am. Chem. Soc.*, 1999, **121**, 5481; R. A. Bissel, E. Cordova, A. E. Kaifer and J. F. Stoddart, *Nature*, 1994, **369**, 133.

6 N. Koumura, R. W. J. Zijlstra, R. A. van Delden, N. Harada and B. L. Feringa, *Nature*, 1999, **401**, 152; C. D. Mao, W. Q. Sun, Z. Y. Shen and N. C. Seeman, *Nature*, 1999, **397**, 144; V. Balzani, M. GomezLopez and J. F. Stoddart, *Acc. Chem. Res.*, 1998, **31**, 405.

7 A. P. de Silva, H. Q. N. Gunaratne and C. P. McCoy, *Nature*, 1993, **364**, 42; C. P. Collier, E. W. Wong, M. Belohradsky, F. M. Raymo, J. F. Stoddart, P. J. Kuekes, R. S. Williams and J. R. Heath, *Science*, 1999, **285**, 391; M. Asakawa, P. R. Ashton, V. Balzani, A. Credi, G. Mattersteig, O. A. Matthews, M. Montalti, N. Spencer, J. F. Stoddart and M. Venturi, *Chem. Eur. J.*, 1997, **7**, 1992; C. R. Copper and T. D. James, *Chem. Commun.*, 1997, 1419; P. Ghosh, P. K. Bharadwaj, S. Mandal and S. Ghosh, *J. Am. Chem. Soc.*, 1996, **118**, 1553; S. Iwata and K. Tanaka, *J. Chem. Soc., Chem. Commun.*, 1995, 1491.

8 (*a*) R. H. Katz, *Contemporary Logic Design*, Benjamin Cummings, CA 1994; (*b*) P. Burger, *Digital Design: A Practical Course*, Wiley, New York, 1988.

9 A. P. de Silva, H. Q. N. Gunaratne and C. P. McCoy, *J. Am. Chem. Soc.*, 1997, **119**, 7891; A. P. de Silva, H. Q. N. Gunaratne, T. Gunnlaugsson, C. P. McCoy, P. R. S. Maxwell, J. T. Rademacher and T. E. Rice, *Pure Appl. Chem.*, 1996, **68**, 1443; A. P. de Silva, H. Q. N. Gunaratne and G. E. Maguire, *J. Chem. Soc., Chem. Commun.*, 1994, 1213.

10 V. Balzani, A. Credi and M. Venturi, *Coord. Chem. Rev.*, 1998, **171**, 3; A. Credi, V. Balzani, S. J. Langford and J. F. Stoddart, *J. Am. Chem. Soc.*, 1997, **119**, 2679.

11 A. P. de Silva, I. M. Dixon, H. Q. N. Gunaratne, T. Gunnlaugsson, P. R. S. Maxwell and T. E. Rice, *J. Am. Chem. Soc.*, 1999, **121**, 1393.

12 N. Sabbatini, M. Guardigli and J.-M. Lehn, *Coord. Chem. Rev.*, 1993, **123**, 201; D. Parker and J. A. G. Williams, *Chem. Commun.*, 1998, 245; A. P. de Silva, H. Q. N. Gunaratne, T. E. Rice and S. Stewards, *Chem. Commun.*, 1997, 1891; J.-C. G. Bunzli, in *Lanthanide Probes in Life, Chemical and Earth Sciences, Theory and Practice*, ed. J.-C. G. Bunzli and G. R. Choppin, Elsevier, New York, 1989, p. 219.

13 D. Parker and J. A. G. Williams, *J. Chem. Soc., Dalton Trans.*, 1996, 3613; D. Parker and J. A. G. Williams, *J. Chem. Soc. Perkin Trans., 2*, 1996, 1581.

14 T. Gunnlaugsson and D. Parker, *Chem. Commun.*, 1998, 511.

15 G. Stein and E. Würzberg, *J. Chem, Phys.*, 1975, **62**, 208.

16 D. A. Muller, T. Sorsch, S. Moccio, F. H. Baumann, K. Evans-Lutterodt and G. Timp, *Nature*, 1999, **399**, 759.

Communication a908951i

Liquid phase methanol carbonylation catalysed over rhodium supported on hydrotalcite

M. P. Kapoor and Yasuyuki Matsumura*†

Osaka National Research Institute, 1-8-31 Midorigaoka, Ikeda, Osaka 563-8577, Japan

Received (in Cambridge, UK) 19th October 1999, Accepted 29th November 1999

A solid catalyst, Mg–Al hydrotalcite containing nanometer size rhodium particles, is active for liquid phase methanol carbonylation to methyl acetate at 473 K in the presence of methyl iodide.

Acetic acid and methyl acetate are industrially synthesised by carbonylation of methanol with a homogeneous rhodium catalyst promoted by methyl iodide.[1,2] Attempts have been made to use heterogeneous catalysts for methanol carbonylation,[3,4] because such a system would be advantageous in separation and recovery of the products and recycling of the catalyst, providing greater economic advantages and minimizing the environmental impact of the process. A number of supported rhodium systems such as zeolites,[5,6] polymers,[7] activated carbon[8] and inorganic oxides[9] are reported to be active under vapour phase conditions. In the liquid phase, polymer supported Rh(I) catalysts have been reported,[10] however, this system is unstable due to loss of rhodium.

Hydrotalcite, $[Mg_{1-x}Al_x(OH)_2(CO_3)_{x/2}{\cdot}yH_2O]$, consists of positively charged brucite-like layers with charge–balancing anions and water molecules.[11] The material shows strong basicity and is often employed as a precursor for catalysts or catalyst supports owing to its structure.[12] In the present work, we have demonstrated that nanometer size rhodium particles can be stabilized on hydrotalcite and the solid effectively catalyses the liquid phase carbonylation of methanol in the presence of methyl iodide. This may provide a realistic solution to problems such as separation, recovery, *etc.* associated with homogeneous catalytic systems.

An Mg–Al hydrotalcite (Mg/Al = 2/1) was synthesised using the procedure reported by Reichle.[13] Rhodium was loaded on the Mg–Al hydrotalcite by a deposition–precipitation method. In a typical procedure, Mg–Al hydrotalcite was placed in an aqueous solution of $Rh(NO_3)_3$ (Kanto Chemical) at 343 K and an aqueous solution of Na_2CO_3 (1 M) was added dropwise. The pH of the solution was kept at 10 for 1 h. The resulting solid was filtered off and washed thoroughly with distilled water, dried and then calcined in air at 673 K for 4 h. A rhodium catalyst was also prepared by the impregnation technique. After evaporation of a mixture of the solution of $Rh(NO_3)_3$ and hydrotalcite, the wet solid was dried and calcined in air at 673 K for 4 h. The Rh contents in the samples was analysed by ICP emission spectrometry.

Adsorption experiments were performed with a vacuum system equipped with Baratron vacuum gauges after the samples were reduced with hydrogen at 673 K for 2 h. The BET surface areas of the samples were determined from nitrogen physisorption isotherms.

Powder X-ray diffraction (XRD) patterns of the samples were recorded with a Rigaku Rotaflex 20 diffractometer using nickel-filtered Cu-Kα (40 kV, 150 mA) radiation.

Catalytic tests were performed in an autoclave (0.2 dm^3). Prior to the reaction, the catalyst (0.20 g) was activated under evacuation followed by reduction with hydrogen at 673 K for 2 h and sealed in a glass capsule. The capsule was placed in the reactor along with a mixture of methanol (780 mmol) and methyl iodide (35 mmol), and CO was introduced at 0.5 MPa (42 mmol) after displacing air inside the reactor with argon. The capsule was broken during pressurization and the reactor was heated to 473 K. The products were analysed with an Ohkura-802 gas chromatograph (TCD) with PEG 1500 (2 m) and Porapak T (2 m) columns.

The powder XRD pattern of the parent hydrotalcite confirmed that the sample was well crystallised, but broadening of the peaks was observed for the hydrotalcite containing rhodium (Fig. 1). A change in the BET surface area after modification with rhodium was also observed. The surface area decreased with an increase in the rhodium content for the hydrotalcite with an original surface area of 232 $m^2\ g^{-1}$ (Table 1). The surface area of the sample prepared by the impregnation method was very small in comparison with the samples prepared by deposition–precipitation.

Carbon monoxide was adsorbed on the samples containing rhodium reduced at 673 K. The amount of carbon monoxide adsorbed was saturated at *ca.* 1 kPa. On the basis of the amounts saturated, the surface areas of rhodium in the samples were tentatively calculated, assuming atomic adsorption of CO on a

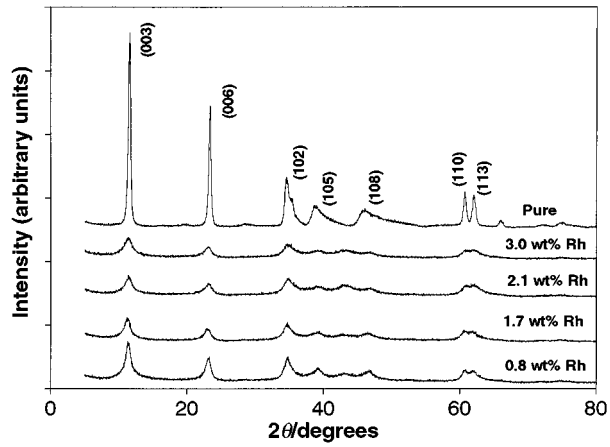

Fig. 1 XRD patterns of hydrotalcite modified with rhodium by deposition-precipitation.

Table 1 Some surface properties of Rh/Mg–Al hydrotalcite catalysts prepared by the deposition–precipitation method

Rhodium content (wt%)	BET surface area/ $m^2\ g^{-1}$	CO uptake/ (μmol g^{-1}	Rhodium surface area/ $m^2\ g^{-1}$
0.8	159	n.d.[a]	n.d.
1.7	116	44	1.5
2.1	104	50	1.7
3.0	86	39	1.3
1.5[b]	80	18	0.6

[a] Not determined. [b] Prepared by impregnation.

† Present address: Research Institute of Innovative Technology for the Earth, Kizu-cho, Soraku-gun, Kyoto 619-0292, Japan. E-mail: yasuyuki@rite.or.jp

Table 2 Methanol carbonylation over Rh/Mg–Al hydrotalcite catalysts at 473 K for 4 h

Rhodium content (wt %)	MeOH conversion (%)	Products/mmol		
		MeCHO	MeOAc	DME
0.8	12.7	0.1	21	29
1.7	16.3	0.2	30	33
1.7[a]	5.8	0.1	2	20
2.1	16.2	0.5	32	31
3.0	15.0	0.3	23	35
1.5[b]	7.7	0.2	9	21

[a] Reaction time = 1 h. [b] Prepared by impregnation.

rhodium site and a site density of 0.058 nm^2 (Table 1). The mean particle sizes of rhodium were calculated from the data in Table 1 assuming that all the rhodium particles are spherical and on the surface, and gave values of 5, 6 and 11 nm, respectively, for deposition–precipitation samples containing 1.7, 2.1 and 3.0 wt% of rhodium. The Rh particle size for the sample prepared by the impregnation method (1.5 wt% of Rh) was calculated as 12 nm. Particles of > 10 nm are expected to be large enough to enable detection by XRD. However, no peaks attributed to rhodium metal were evident in the patterns of any of the samples after reduction, with the XRD patterns being similar to those of Fig. 1. Since the stoichiometry of the adsorption varies with the chemisorption mode of CO (for bridge-type adsorption a CO molecule occupies two rhodium sites), the rhodium surface areas in Table 1 may be underestimates and would result in larger particle sizes. Hence, the actual particle sizes of rhodium may well be smaller than the values estimated by adsorption of carbon monoxide. The reduction of the BET surface area after modification of rhodium suggests that some of the rhodium particles are incorporated in the bulk phase of the hydrotalcite and so will be another reason for the apparent contradiction of the adsorption and XRD results.

Mg–Al hydrotalcites containing rhodium were found to be active for methanol carbonylation at 473 K. The main products were methyl acetate (MeOAc) and dimethyl ether (DME) with a small amount of acetaldehyde (Table 2). Neither acetic acid, nor other decomposition products such as hydrogen were detected. Loss of methyl iodide was not observed and no trace of rhodium was detected in the liquid phase after the reaction. The XRD patterns of the catalyst recovered after the reaction were very similar to those prior to the reactions, showing that the catalysts retain the hydrotalcite structure during reaction. No reaction products were obtained with rhodium-free Mg–Al hydrotalcite. An increase in rhodium content to 2.1 wt% enhanced formation of MeOAc while a further increase of rhodium to 3.0 wt% resulted in a lower yield of MeOAc. The catalyst prepared by the impregnation method with a rhodium content of 1.5 wt% was the least active. The activity towards MeOAc mainly depends on the estimated surface area of rhodium (*cf.* Tables 1 and 2).

No methanol carbonylation occurred in the absence of methyl iodide for the catalyst containing 1.7 wt% of rhodium except for formation of a small amount of DME. Hence, methanol cannot be directly carbonylated over the catalyst, and the presence of methyl iodide is essential in the carbonylation. This suggests that carbonylation of methyl iodide to acetyl iodide is a key step of the carbonylation as also found for homogeneous carbonylation with rhodium complexes.[14] Formation of MeOAc was low after reaction for 1 h with the catalyst containing 1.7 wt% of Rh while DME formation was considerable (Table 2). This result indicates an induction period for the formation of MeOAc. Formation of homogeneous rhodium species during the induction period might be possible. However, no acetic acid, which is one of the major products in homogeneous carbonylation,[2] was detected in the reaction with the heterogeneous catalyst. In the mechanism for homogeneous carbonylation, methyl acetate is formed as a product of a subsequent esterification of acetic acid and methanol.[2] The product distribution with the heterogeneous catalys is similar to that found for the vapour phase carbonylation of methanol in the presence of methyl iodide over rhodium supported on activated carbon[8] while methyl acetate appears to be directly produced in the reactions. The similarity suggests that the carbonylation with rhodium containing hydrotalcite takes place on the surface of rhodium particles. Carbonylation of DME to MeOAc has been proposed in the vapour phase reaction, and can account the selective formation of MeOAc and the induction period.[15]

In summary, nanometer sized rhodium particles can be stabilised on hydrotalcite, and methyl acetate is directly formed in the liquid-phase methanol carbonylation with supported rhodium catalysts. A detailed kinetic study is in progress, which should provide stimulating results for practical modifications of the methanol carbonylation process.

Notes and references

1 F. E. Paulik, A. Hershman, W. R. Knox and J. F. Roth, *U.S. Pat.*, 3 769 329, 1973.
2 F. E. Paulik and J. F. Roth, *Chem. Commun.*, 1968, 1578.
3 M. J. Howard, M. D. Jones, M. S. Roberts and S. A. Taylor, *Catal. Today*, 1993, **18**, 325.
4 B. K. Nefedov, N. S. Segeeva and Ya. T. Eidus, *Izv. Akad. Nauk, SSSR, Ser. Khim.*, 1976, 2271.
5 T. Yashima, Y. Orikasa, N. Takahashi and N. Hara, *J. Catal.*, 1979, **59**, 53.
6 N. Takahashi, Y. Orikasa and T. Yashima, *J. Catal.*, 1979, **59**, 61.
7 N. De Blasio, E. Tempesti, A. Kaddouri, C. Mazzocchia and D. J. Cole-Hamilton, *J. Catal.*, 1998, **176**, 253.
8 A. S. Merenov and M. A. Abraham, *Catal. Today*, 1998, **40**, 397.
9 A. Krywicki and M. Marczewski, *J. Mol. Catal.*, 1979, **6**, 431.
10 R. S. Drago, E. D. Nyberg, A. El A'mma and A. Zombeck, *Inorg. Chem.*, 1981, **20**, 641.
11 R. Allmann, *Acta Crystallogr., Sect B*, 1968, **24**, 972.
12 F. Canavi, F. Trifiro and A. Vaccari, *Catal. Today*, 1991, **11**, 173.
13 W. T. Reichle, *J. Catal.*, 1985, **94**, 547.
14 J. B. Cooper, *Eur Pat.*, 87070, 1982 (BP Chemicals).
15 T. Shikada, K. Fujimoto, M. Miyauchi and H. Tominaga, *Appl. Catal.*, 1983, **7**, 361.

Communication a908350b

Induction and reversal of chirality of heterohelicene by charge transfer interaction in aqueous SDS micelles

Koh-ichi Yamada,* Yuuki Kobori and Hiroko Nakagawa

Faculty of Pharmaceutical Sciences, Josai University, Sakado, Saitama 350-0295, Japan. E-mail: kyama@josai.ac.jp

Received (in Cambridge, UK) 1st November 1999, Accepted 30th November 1999

2-Hydroxymethylthieno[3,2-*e*:4,5-*e*′]di[1]benzothiophene and 2-(2,4,5,7-tetranitrofluoren-9-ylideneaminooxy)propionic acid in SDS micelles initially formed a 1:2 complex with a negative Cotton effect around 360 nm, which with time or sonication gradually changed to a 1:1 complex giving a reversed Cotton effect.

Chiral recognition occurs in artificial chiral environments such as membranes[1] and micelles[2] despite their intrinsically high fluidity. This is of interest because it mimics chiral recognition in biological receptors. Differences in diastereomeric interactions between each enantiomer of an incorporated racemic guest and the chiral host molecules have effected such recognition and have been sustained, so far, mainly by hydrogen bonding. Since charge-transfer (CT) interaction is one of the fundamental forces in molecular recognition by biological macromolecules,[3] we investigated whether CT bonding exerts effective chiral discrimination between enantiomers in aqueous sodium dodecyl sulfate (SDS) micelles. We used 2-hydroxymethylthieno[3,2-*e*:4,5-*e*′]di[1]benzothiophene (5HM) as a

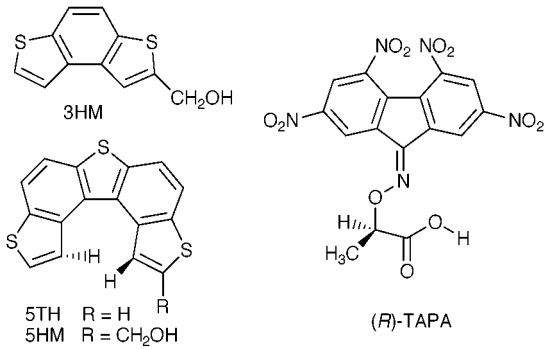

donor and 2-(2,4,5,7-tetranitrofluoren-9-ylideneaminooxy)propionic acid (TAPA) as a chiral acceptor. Although the helical shape of 5HM arises from steric repulsion between the terminal hydrogen atoms in the molecule,[4] inversion of the helix readily occurs in solution, causing a rapid racemization at room temperature.[5] However, the racemic 5HM is totally converted into the (*P*) enantiomer[6] on uptake by the serum albumin of several species,[7] and exhibits a slight (*M*) enantiomeric excess on incorporation into alkyl β-D-pyranoside micelles.[8] Furthermore, X-ray crystallographic analysis determined that racemic 5TH was entirely converted into the (*P*) enantiomer upon crystallization to give the deep-red 1:1 CT complex with (*S*)-TAPA.[9]

Both 5HM and TAPA are practically insoluble in water. A dioxane solution of (*R*)-TAPA (120 μl, 1.0×10^{-2} mol dm^{-3}) was added to an aqueous SDS solution (2 ml, 2×10^{-2} mol dm^{-3}), which resulted in a pale yellow transparent solution. Then, a dioxane solution of 5HM (27 μl, 1.0×10^{-2} mol dm^{-3}) was dissolved in this, and a pale red colour developed due to the CT interaction between the two components. The total volume of the solution was adjusted to 3 ml by adding SDS solution, which yielded concentrations of (*R*)-TAPA (4.0×10^{-4} mol dm^{-3}) and 5HM (9.0×10^{-5} mol dm^{-3}) in the SDS micellar solution (2×10^{-2} mol dm^{-3}) containing *ca.* 5% dioxane. CD measurements of this micellar solution at 20 °C gave intense absorptions in the range of 250–400 nm [Fig. 1(*b*), state (*b*)]. The wavelengths of these CD absorptions almost corresponded to those of the UV absorptions[8] of 5HM in $CHCl_3$ and in SDS micelles. A $CHCl_3$ solution of a mixture of (*R*)-TAPA and 5HM with the same concentrations as above, despite the development of a reddish colour, demonstrated small CD absorptions which were quite similar to those of (*R*)-TAPA alone in the micelles [Fig. 1(*a*)]. Moreover, a lower planar homologue of 5HM, 2-hydroxymethylbenzo[1,2-*b*:4,3-*b*′]dithiophene (3HM), showed no special CD absorptions in the presence of (*R*)-TAPA in the micelles, though the colour did change to yellow. These facts lead to the following reasoning: (1) the appearance of the CD absorptions [Fig.1(*b*)] is attributable to chiral 5HM being fixed to one enantiomer by the CT bonding of 5HM with chiral TAPA, and (2) the configuration of that enantiomer is determined as (*M*) by comparing the negative Cotton effect around 360 nm with the Cotton effects of 5HM incorporated in several albumins[7] or in chiral micelles,[8] and the CD spectrum of the 5TH-(*S*)–TAPA complex crystals in a KBr disk.[9]

On standing the micellar solution of 5HM and (*R*)–TAPA, the CD absorptions changed slowly with time. The intensity of Fig. 1(*b*) decreased to one fifth after 15 h at 20 °C. The decrease became faster with a rise in temperature. After *ca.* 10 h at 30 °C, the absorptions almost disappeared; instead, new absorptions began to appear in the opposite direction. Subsequently, the intensity increased very slowly over time, and finally the micellar solution became turbid after *ca.* 3 days, presumably because of the slow formation of the precipitate of the CT complex. This spontaneous alteration in the CD absorptions was accelerated by ultrasonic irradiation [Fig. 1(*b*)–(*f*)].[10] Only 1 min of sonication converted the sign of the Cotton effect around 360 nm to the opposite sign [Fig. 1(*c*)]. By subsequent sonication, the absorption intensities were gradually enhanced so as to reach the maximum in *ca.* 15 min [Fig. 1(*f*), state (*f*)]. These changes with time imply the reversal of handedness of 5HM in the micelles, that is, an (*M*) enantiomer to a (*P*). It is noteworthy that the shape of curve (*f*) is not strictly symmetrical

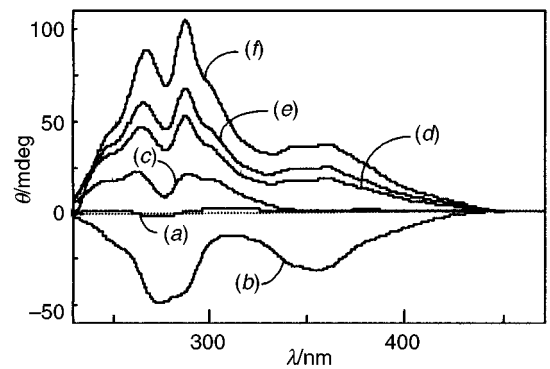

Fig. 1 Alterations in CD absorptions of 5HM–(*R*)-TAPA complex in SDS micelles: (*a*) (*R*)-TAPA alone, (*b*) immediately after the sample preparation, (*c*) sonication for 1, (*d*) 2, (*e*) 5 and (*f*) 15 min. [5HM] = 9.0×10^{-5} mol dm^{-3}, [(*R*)-TAPA] = 4.0×10^{-4} mol dm^{-3}, [SDS] = 2.0×10^{-2} mol dm^{-3}.

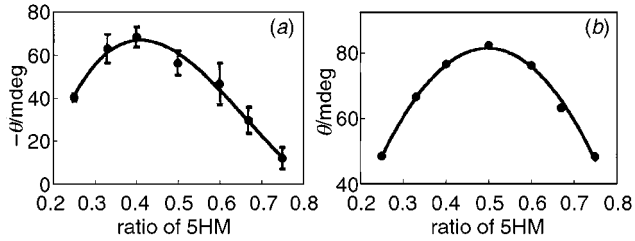

Fig. 2 Continuous variations experiments on the CD intensities at 359.2 nm: (*a*) for state (*b*) in Fig.1, (*b*) for state (*f*) in Fig.1, (the standard deviations are within the circles). [5HM] + [(*R*)-TAPA] = 5.0×10^{-4} mol dm^{-3}, [SDS] = 2.0×10^{-2} mol dm^{-3}.

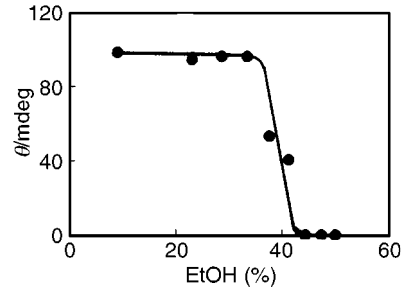

Fig. 3 Effect of an increase of EtOH content on the CD intensities at 287.0 nm for state (*f*) in Fig.1.

with that of the initial curve (*b*), though they are similar to each other.

In order to account for this phenomenon, binding stoichiometries between 5HM and TAPA were determined for both states (*b*) and (*f*) by the methods of continuous variations[11] and HPLC. Fig. 2 illustrates how the CD intensities at the trough [state (*b*)] or the peak [state (*f*)] around 360 nm vary with the mole ratio of 5HM to TAPA. For state (*b*), the plots reveal a maximum in the vicinity of the ratio = 0.35, indicating the presence of a 1:2 complex. On the other hand, a 1:1 complex can be estimated for state (*f*) because the maximum is observed in the vicinity of the ratio = 0.5. These stoichiometries were substantiated by HPLC experiments. On preparing a micellar solution containing (*R*)-TAPA (9×10^{-4} mol dm^{-3}) and 5HM (9×10^{-5} mol dm^{-3}), the precipitation occurred immediately. The precipitate collected was extracted with $CHCl_3$, the $CHCl_3$ solution being washed with water. The content of 5HM and TAPA in the $CHCl_3$ solution was determined by HPLC (silica gel column, $CHCl_3$–hexane–EtOH = 15:4:1), revealing a ratio of 5HM/TAPA = 0.47. Furthermore, the micellar solution containing (*R*)-TAPA (6×10^{-4} mol dm^{-3}) and 5HM (9×10^{-5} mol dm^{-3}) was sonicated for *ca.* 15 min, giving CD absorptions similar to Fig. 1(*f*). After the solution was left for 3 days, the resulting precipitate was collected and treated in the same way as above. The 5HM/TAPA ratio was estimated by HPLC to be 1.02. The results provided by the HPLC experiments were in excellent agreement with those of the continuous variations method.

TAPA is a carboxylic acid that has a tendency to dimer formation. Therefore, TAPA incorporated by way of a dimeric form in the micelles can be expected to encounter 5HM and produce the 1:2 CT complex. The 1:2 complex thus formed would be gradually converted into a more stable 1:1 complex as observed in the 1:1 complex crystals of (*S*)-TAPA and 5TH. Accompanying such change in the composition of the complex, configurational alteration is evoked in the 5HM molecules, causing the reversal of chirality of 5HM. These phenomena can be said to result from micellar effects. With an increase of ethanol content in the solution of state (*f*), the CD absorptions were rapidly decreased and completely missing (Fig. 3) owing to destruction of the micellar structure. When the same experiments concerning the alternative combination, 5HM and (*S*)-TAPA, were carried out, the same results were obtained except for the difference in the handedness of the 5HM molecules. In summary, the CT interactions have been proved to achieve effective recognition of chirality of heterohelicene in the SDS micelles. In particular, it is of interest that the initially fixed handedness of heterohelicene came to be spontaneously reversed with the composition change of the complex, although the structure of the 1:2 complex remains uncertain.

Notes and references

1 D. Dieudonne, A. Gericke, C. R. Flash, X. Jiang, R. S. Farid and R. Mendelsohn, *J. Am. Chem. Soc.*, 1998, **120**, 792; J. Partyka and K. Hiltrop, *Liq. Cryst.*, 1996, **20**, 611; N. Usol'tseva, K. Praefcke, D. Singer and B. Gundogan, *Liq. Cryst.*, 1994, **16**, 617; Y. Matsumoto and R. Ueoka, *Bull. Chem. Soc. Jpn.*, 1983, **56**, 3370.

2 P. Walde, E. Blochigner and K. Morigaki, *Langmuir*, 1999, **15**, 2346; S. Borocci, M. Erba, G. Mancini and A. Scipioni, *Langmuir*, 1998, **14**, 1960; D. Tickle, A. George, K. Jennings, P. Camilleri and A. J. Kirby, *J. Chem. Soc., Perkin Trans. 2*, 1998, 467; M. Lecouvey, C. Frochot, L. Miclo, P. Orlewski, M. Marraud, J. L. Gaillard, M. T. Cung and R. Vanderesse, *Lett. Pept. Sci.*, 1997, **4**, 359; K. Kano and T. Ishimura, *J. Chem. Soc., Perkin Trans. 2*, 1995, 1655; B. S. Jursic, *Tetrahedron Lett.*, 1993, **34**, 963.

3 H. Dugas, *Bioorganic Chemistry: A Chemical Approach to Enzyme Action*, 3rd edn., Springer-Verlag, New York, 1996.

4 H. Nakagawa, K. Yamada, H. Kawazura and H. Miyamae, *Acta Crystallogr.*, 1984, **C40**, 1039.

5 K. Yamada, H. Nakagawa and H. Kawazura, *Bull. Chem. Soc. Jpn.*, 1986, **59**, 2429.

6 The symbols (*P*) and (*M*) represent 'right-handed' and 'left-handed', respectively.

7 K. Yamada, R. Ishii, H. Nakagawa and H. Kawazura, *Tetrahedron: Asymmetry*, 1996, **7**, 737; K. Yamada, R. Ishii, H. Nakagawa and H. Kawazura, *Chem. Pharm. Bull.*, 1997, **45**, 936.

8 H. Nakagawa, K. Gomi and K. Yamada, *Enantiomer*, 1998, **3**, 175.

9 H. Nakagawa, K. Yamada and H. Kawazura, *J. Chem. Soc., Chem. Commun.*, 1989, 1378.

10 A titanium probe (Dr Hielscher GmbH, UP 50H, diameter 3 mm) sonication was carried out on samples in an ice bath at 270 W cm^{-2}.

11 In the continuous variations, individual components are mixed in variable ratios, but with constant total concentration. P. Job, *Ann. Chim.*, 1928, **9**, 113; J. O. Smith, D. A. Olson and A. Armitage, *J. Am. Chem. Soc.*, 1999, **121**, 2686.

Communication a908681a

ChemComm

The detection of intermediates in the ruthenium(II) catalysed asymmetric hydrogenation of ketones using electrospray ionisation mass spectrometry

Jennifer A. Kenny,[a] Kees Versluis,[b] Albert J. R. Heck,[b] Tim Walsgrove[c] and Martin Wills*[a]

[a] *Department of Chemistry, University of Warwick, Coventry, UK CV4 7AL. E-mail: m.wills@warwick.ac.uk.*
[b] *Department of Biomolecular Mass Spectrometry,Bijvoet Center for Biomolecular Research and Utrecht Institute for Pharmaceutical Sciences, Utrecht University, Sorbonnelaan 16, 3584 CA Utrecht, The Netherlands*
[c] *SmithKline Beecham Pharmaceuticals, Old Powder Mills, Nr Leigh, Tonbridge, Kent, UK TN11 9AN*

Received (in Liverpool, UK) 7th October 1999, Accepted 26th November 1999

The use of electrospray ionisation mass spectrometry for the detection of the intermediate species involved in the ruthenium(II)/amino alcohol reduction of ketones to alcohols is described.

The use of transfer hydrogenation for the asymmetric reduction of ketones to enantiomerically enriched secondary alcohols has recently been the subject of intense international research work.[1] Of the many methods reported for this process, complexes of η6-arene/ruthenium(II) species with β-amino alcohols[2] or monotosylated 1,2-diamines[3] give some of the very best results in terms of activity and enantioselectivity. In the case of monotosylated diamines the resulting complexes may be employed in conjunction with either Pr^{i}OH–KOH or formic acid–Et_3N as hydrogen source.[3] In contrast we have found that the corresponding amino alcohol complexes appear to be compatible only with the Pr^{i}OH system. In order to gain an insight into the mechanism of the reduction using ruthenium(II)

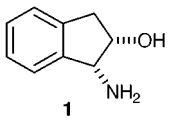

1

complexes of aminoindanol **1**, on which we have recently published, we wished to identify the key intermediates likely to be involved in the process.

Our initial speculation, taking as a starting point the results obtained by Noyori on the analogous monotosylated diamine system, was that the 'pre-catalyst' formed by the combination of **1** with ruthenium(II) dimer $[RuCl(\eta6\text{-cymene})]_2$ was likely to be the 18-electron species **2**. Treatment of **2** with base would, we predicted, lead to elimination of HCl to give the 16-electron intermediate **3** which would subsequently be reduced to the 18-electron ruthenium hydride complex **4** by hydrogen transfer from the solvent. In the case of monotosylated diamines Noyori was able to isolate, and characterise through the use of X-ray crystallography, all three intermediates **5**–**7** analogous to **2**–**4**.[4] Despite a number of efforts on our part, we have as yet been unable to obtain crystalline derivatives of any of our speculated intermediates, possibly due to lack of stability relative to the monotosylated diamine variants.

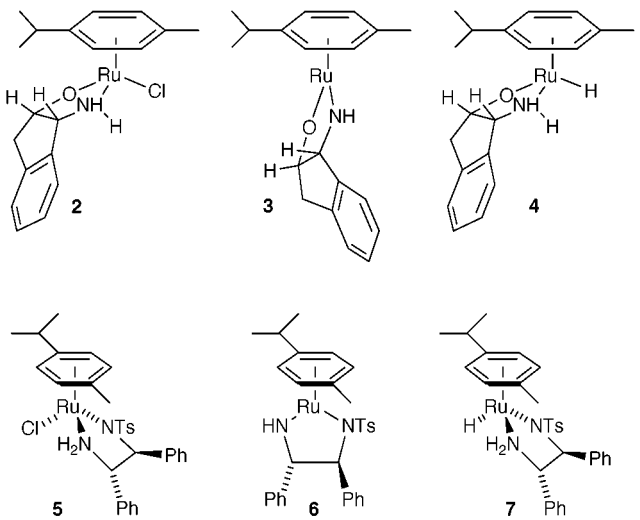

2 **3** **4** **5** **6** **7**

An alternative approach to this problem was, we considered, through the use of electrospray ionisation mass spectrometry (ESI-MS). This technique has been employed recently for the determination of intermediates in a number of catalytic processes, including the oxidative coupling of arylboronic acids[5] and a study of the aggregation states of organocopper complexes in solution.[6] In the event, this proved to be a highly valuable approach, as described below.

In our first experiment, we prepared a 0.1 M solution of our speculated 'pre-catalyst' **2** by combining a slight excess of *cis*-aminoindanol **1** with ruthenium(II) dimer $[RuCl(\eta6\text{-cymene})]_2$ in Pr^{i}OH solution.[7] ESI-MS [8] of the resulting solution diluted to 25 mM concentration gave a clean spectrum showing an isotope cluster centred around m/z = 420 (Fig. 1). The masses observed for this cluster and the intensity ratio of the different isotope peaks are in excellent agreement with the calculated pattern for the protonated expected molecule $C_{19}H_{25}NORuCl$.

In the next step of our investigation we added *ca*. 2 equiv. of an Pr^{i}OH solution of KOH to the initial solution of **2**. After a short period of time (5–10 min) at room temperature, this solution was again examined by ESI-MS by direct injection into the instrument. The resulting spectrum (Fig. 2) showed clearly, in addition to the isotope cluster of compound **2**, a new isotope cluster with the isotope at m/z 386 as the highest signal, but starting at m/z 378. The shape of this isotope cluster revealed that both expected molecules **3** and **4** were present. Fig. 3 shows a comparison between the experimentally observed intensities in this cluster and the calculated intensities when it is assumed that the protonated forms of the products **3** and **4** were present at a ratio of 1 to 3. This indicates that the reduction of compound **3** to **4** is likely to be faster than the production of **3** from **2**. The

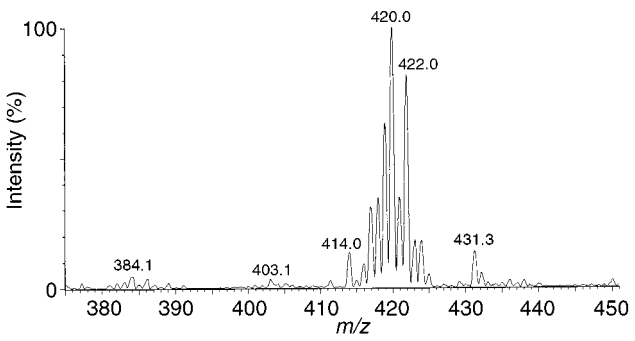

Fig. 1 ESI-MS of complex **2** in Pr^{i}OH.

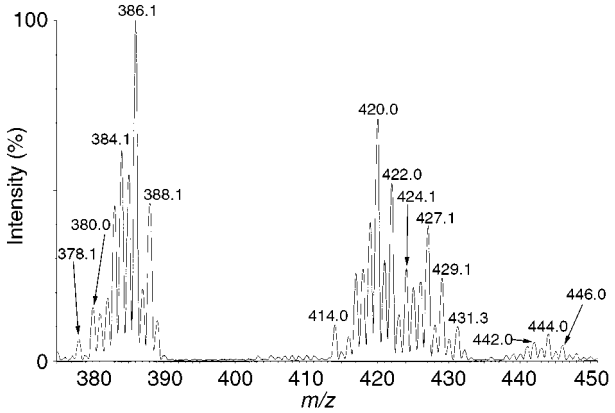

Fig. 2 ESI-MS of complex **2** in Pr^{i}OH, following addition of KOH.

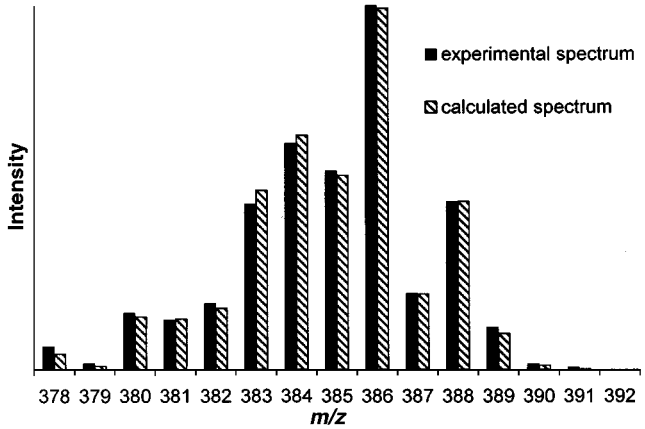

Fig. 3 Comparison of calculated *vs.* experimental ESI-MS spectra for a mixture of **3** and **4**.

less abundent isotope clusters observed around *m/z* 427 and 444 may be explained by assuming that Pr^{i}OH can also react with compound **3** (*m/z* 444) followed by loss of ammonia (*m/z* 427).

In an attempt to obtain evidence for the reduction of **3** by Pr^{i}OH we repeated the above reaction but with the use of CH_2Cl_2 as solvent. An ESI-MS spectrum was recorded shortly after the addition of base (Fig. 4) in which a strong set of peaks centred at *m/z* 384 was observed. The masses and the measured isotope signal intensities correspond to the mass predicted for the compound **3**. In the CH_2Cl_2 solution no suitable hydride source exists for reduction of **3**, therefore its lifetime is longer in this solvent.

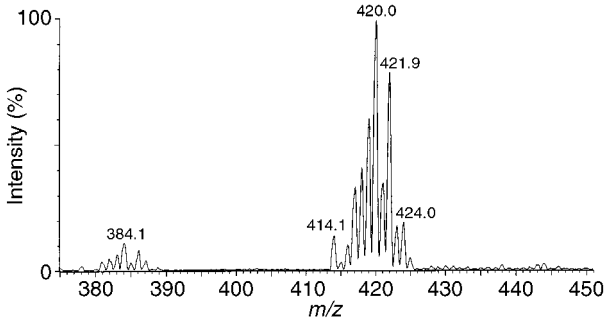

Fig. 4 ESI-MS of complex **2** in CH_2Cl_2 following addition of KOH.

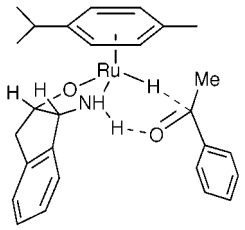

Fig. 5 Mechanism of hydrogen transfer.

In a final revealing set of studies, samples were taken of a solution of **4** in Pr^{i}OH (formed by addition of base) over a period of 90 min following addition of a quantity of acetophenone, which was reduced during this time. Remarkably, species **3** was observed to persist in solution, together with a quantity of unreacted **2**, but **4** was not observed. This observation is somewhat at odds with the result illustrated in Figs. 2 and 3, which suggested that **3** was shorter lived than **4**. Clearly the presence of ketone (and alcohol reduction product) has an effect of the equilibrium of the reaction.

In view of the results described above, and the lack of evidence for any complex of reduction product (1-phenethanol) with ruthenium, we believe that the hydrogen transfer mechanism probably proceeds *via* a 6-centre transition state proposed by Noyori for the corresponding reactions of monotosylated diamine complexes of ruthenium(II) (Fig. 5).[5] Whilst caution should be exercised in the interpretation of any transition state through inferences from observed intermediates, particularly since the method provides no information on the relative configurations of chiral centres in the complexes, we would consider that our evidence thus presented represents a solid foundation on which to build further studies of the synthetically important process of asymmetric transfer hydrogenation.

We thank the EPSRC and SmithKline Beecham Pharmaceuticals for support of a CASE studentship (to J. A. K.) and the British Council for a UK–Dutch Joint Scientific Research Programme Travel Grant.

Notes and references

1 M. J. Palmer and M. Wills, *Tetrahedron: Asymmetry*, 1999, **10**, 2045; R. Noyori and S. Hashiguchi, *Acc. Chem. Res.*, 1997, **30**, 97.

2 (*a*) J. Takehara, S. Hashiguchi, A. Fujii, S. Inoue, T. Ikariya and R. Noyori, *Chem. Commun.*, 1996, 233; (*b*) M. Palmer, T. Walsgrove and M. Wills, *J. Org. Chem.*, 1997, **62**, 5226; (*c*) D. A. Alonso, D. Guijarro, P. Pinho, O. Temme and P. G. Andersson, *J. Org. Chem.*, 1998, **63**, 2749; (*d*) J. A. Kenny, M. J. Palmer, A. R. C. Smith, T. Walsgrove and M. Wills, *Synlett*, 1999, 1615.

3 A. Fujii, S. Hashiguchi, N. Uematsu, T. Ikariya and R. Noyori, *J. Am. Chem. Soc.*, 1996, **118**, 2521; S. Hashiguchi, A. Fujii, J. Takehara, T. Ikariya and R. Noyori, *J. Am. Chem. Soc.*, 1995, **117**, 7562; K. Matsumura, S. Hashiguchi, T. Ikariya and R. Noyori, *J. Am. Chem. Soc.*, 1997, **119**, 8738; K. Püntener, L. Schwink and P. Knochel, *Tetrahedron Lett.*, 1996, **37**, 8165.

4 K.-J. Haack, S. Hashiguchi, A. Fujii, T. Ikariya and R. Noyori, *Angew. Chem., Int. Ed. Engl.*, 1997, **36**, 285.

5 M. A. Aramadia, F. Lafont, M. Morena-Manas, R. Pleixats and A. Roglans, *J. Org. Chem.*, 1999, **64**, 3592.

6 B. H. Lipshutz, J. Keith and D. J. Buzard, *Organometallics*, 1999, **18**, 1571.

7 The catalyst solutions, with the exception of the CH_2Cl_2 solutions, were prepared in an analogous manner to those used in the transfer hydrogenation reactions described in ref. 2(*b*).

8 Mass spectra were acquired on a Micromass Platform single quadrupole instrument. Samples were introduced by loop injection at concentrations of 25 mM.

Communication a908098h

Self assembly of a novel water soluble iron(II) macrocyclic phosphine complex from tetrakis(hydroxymethyl)phosphonium sulfate and iron(II) ammonium sulfate: single crystal X-ray structure of the complex $[Fe(H_2O)_2\{RP(CH_2N(CH_2PR_2)CH_2)_2PR\}]SO_4\cdot 4H_2O$ (R = CH_2OH)

John C. Jeffery,*[a] Barbara Odell,*[b] Nicola Stevens*[c] and Robert E. Talbot*[c]

[a] *School of Chemistry, University of Bristol, Cantocks Close, Bristol, UK BS8 1TS. E-mail: john.jeffery@bristol.ac.uk*
[b] *Dyson Perrins Laboratory, University of Oxford, South Parks Road, Oxford, UK OX1 3QY. E-mail: barbara.odell@chemistry.oxford.ac.uk*
[c] *Albright and Wilson UK Ltd., PO Box 80, Trinity Street, Oldbury, West Midlands, UK B69 4LN. E-mail: bob_e_talbot@albriw.com*

Received (in Cambridge, UK) 18th October 1999, Accepted 6th December 1999

The water soluble Fe(II) macrocyclic phosphine complex $[Fe(H_2O)_2\{RP(CH_2N(CH_2PR_2)CH_2)_2PR\}]SO_4\cdot 4H_2O$ (R = CH_2OH) has been characterised by single crystal X-ray diffraction and is formed by a remarkable self-assembly reaction between iron(II) ammonium sulfate and tetrakis(hydroxymethyl)phosphonium sulfate (THPS).

There is increasing interest in catalytic transformations carried out in aqueous media employing water soluble phosphine metal complexes.[1–4] In the latter context, phosphine ligands such as $P(CH_2OH)_3$ have been shown to be useful precursors for the synthesis of water soluble transition metal complexes.[4] Albright and Wilson have an interest in the related phosphonium salt $[P(CH_2OH)_4]_2SO_4$[5] because of its effectiveness as a biocide in oil wells. Recently, it was noted that $[P(CH_2OH)_4]_2SO_4$ also aids the dissolution of iron sulfide deposits and particulates. Iron sulfide arises both from anaerobic microbial activity in oil wells and as a result of indigenous H_2S; deposits cause flow restrictions in vessels and pipework and particulates can upset oil/water separation and lead to damage. In oil well situations, the dissolution of FeS by $[P(CH_2OH)_4]_2SO_4$ is accompanied by a red coloration of produced water from the well. The aim of this study was to explain how $[P(CH_2OH)_4]_2SO_4$ aids the dissolution of FeS and to identify the origin of the resulting red coloration which it was believed might be due to a water soluble iron complex.

The reactions of $[P(CH_2OH)_4]_2SO_4$ and the related phosphine $P(CH_2OH)_3$ with various Fe(II) and Fe(III) salts, *e.g.* FeS, $[Fe(NH_4)_2(SO_4)_2]$, $FeCl_3$, $FeCl_2$ and $FeSO_4$, were investigated to find an iron containing laboratory reagent that would model the red complex formed in the oil wells. Only $[Fe(NH_4)_2(SO_4)_2]$ produced a red colour with $[P(CH_2OH)_4]_2SO_4$ or $P(CH_2OH)_3$ and it was shown that other alkyl phosphonium salts do not give red complexes. Thus it appears that the formation of red water soluble complexes requires an Fe(II) salt, $[P(CH_2OH)_4]_2SO_4$ or $P(CH_2OH)_3$ and, crucially, the presence of ammonium ions. Following optimisation of the reaction conditions it was found that addition of 2 equiv. of $[P(CH_2OH)_4]_2SO_4$ to iron(II) ammonium sulfate in water at room temperature, followed by the slow addition of base (NaOH), so that the pH was maintained between 4.5 and 5.0, immediately produced a deep red solution which gave deep red crystals of $[Fe(H_2O)_2\{RP(CH_2N(CH_2PR_2)CH_2)_2PR\}]SO_4\cdot 4H_2O$ (R = CH_2OH) **1** on standing at 5 °C for two weeks.

The X-ray crystal structure† of **1** (Fig. 1) reveals a cationic octahedral Fe(II) complex with a remarkable tetradentate phosphine ligand in which alternating phosphorus and nitrogen atoms are linked by CH_2 spacers to form an eight-membered macrocyclic ring which functions as a *cis* bidentate phosphine donor to iron. The two nitrogen atoms carry pendant CH_2PR_2 groups which occupy *trans* diaxial sites in the metal coordination sphere. Two molecules of H_2O occupy the remaining *cis* coordination sites at iron. The complex is highly symmetric and has crystallographically imposed twofold symmetry leading to chemically equivalent pairs of axial and equatorial phosphorus sites. The $^{31}P\{^1H\}$ and ^1H NMR spectra‡ of the low spin d^6 complex **1** are consistent with the solid state structure being maintained in solution. Thus the $^{31}P\{^1H\}$ NMR spectrum shows two triplets at δ 20.1 [t, ^2J(PP) 53 Hz] and −1.5 [t, ^2J(PP) 53 Hz] as expected for the two pairs of chemically inequivalent phosphine sites in the complex.

The precise mechanism by which complex **1** is formed is uncertain but it seems likely that the reaction involves a Mannich-like condensation of $[P(CH_2OH)_4]_2SO_4$ with two ammonium ions, with the iron(II) ion acting as a template which controls the formation of the macrocycle and its pendant phosphine arms. When the reaction of $[P(CH_2OH)_4]_2SO_4$ and iron(II) ammonium sulfate with more prolonged base addition was monitored by $31P\{^1H\}$ it was observed that the triplets associated with **1** gradually diminished with concomitant

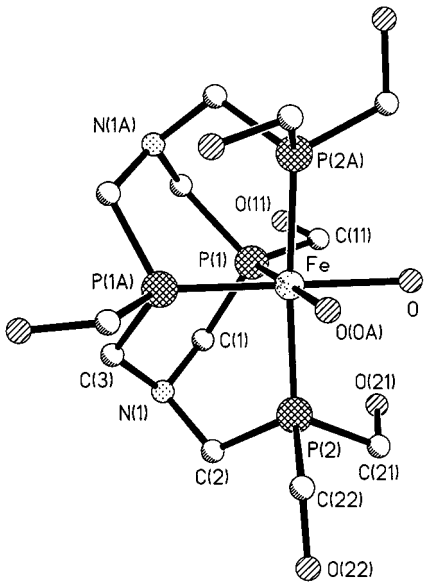

Fig. 1 Molecular structure of the cation of **1** with hydrogen atoms omitted for clarity. Selected bond lengths (Å) and angles (°): Fe–O 2.071(2), Fe–P(1) 2.1797(8), Fe–P(2) 2.2408(8), P(1)–C(11) 1.849(2), P(1)–C(1) 1.865(2), N(1)–C(3) 1.458(2), N(1)–C(1) 1.467(2), N(1)–C(2) 1.475(2), P(2)–C(21) 1.836(2), P(2)–C(22) 1.842(2), P(2)–C(2) 1.845(2); P(1)–Fe–P(1A) 80.63(4), P(1)–Fe–P(2) 92.41(2), O–Fe–P(2) 88.66(5), O–Fe–P(1) 98.25(5), O–Fe–O(OA) 82.87(9), P(2A)–Fe–P(2) 174.89(3), O(OA)–Fe–P(1) 178.87(4), C(3)–N(1)–C(1) 113.7(2), C(3)–N(1)–C(2) 113.0(2), C(1)–N(1)–C(2) 113.0(2).

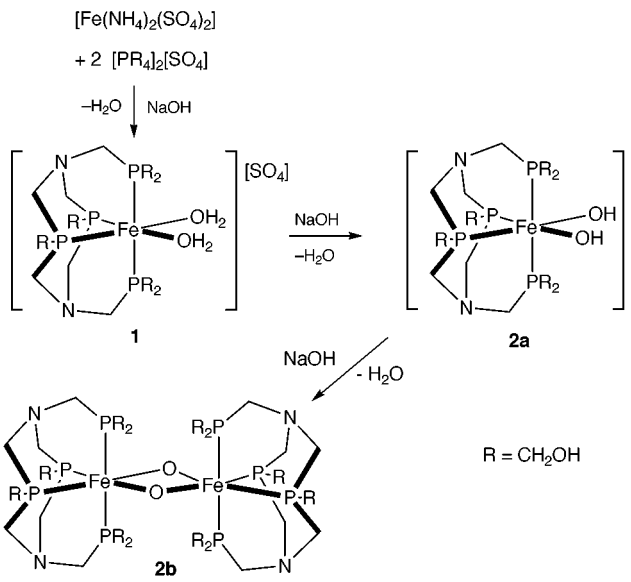

Scheme 1 Proposed mechanism for formation of **1** and **2**.

formation of a new complex **2** characterised by two new triplet resonances at δ −12.0 [t, ^2J(PP) = 76 Hz] and −22.8 [t, ^2J(PP) 76 Hz]. The latter pattern is very similar to that observed for the complex **1** suggesting a related structure, and although complex **2** has not yet been isolated and fully characterised, we tentatively suggest that it might be a neutral hydroxy **2a** or oxy-bridged complex **2b** of the type shown (Scheme 1) arising from base induced deprotonation of the coordinated H_2O molecules in **1**.

This investigation was stimulated by the need to explain how $[P(CH_2OH)_4]_2SO_4$ aids the dissolution of FeS in oil fields leading to a red coloration of the treated water. The speciation of the Fe/S system in natural environments such as oil wells is necessarily complex but our model reactions allow us to tentatively propose that $[P(CH_2OH)_4]_2SO_4$ and NH_4^+ ions self-assemble iron complexes similar to **1** from FeS that has formed in oil wells owing to sulfate reducing bacteria or indigenous H_2S. The key ammonium ions required for the condensation reaction are usually naturally present in oil field waters where $[P(CH_2OH)_4]_2SO_4$ is used. Also, ammonium bisulfite is often added as an oxygen scavenger to oil field injection water used to pressurise oil-bearing formations, thus providing an additional source. The observation that $[P(CH_2OH)_4]_2SO_4$ and FeS do not appear to react in the absence of NH_4^+ ions, but immediately give red solutions on addition of NH_4^+, adds further support for the proposed mechanism.

Whilst it was not the original intention of this study to prepare new water soluble catalysts, the novel tetradentate macrocyclic phosphine ligand which has been prepared has obvious potential in this context because it imposes facial octahedral coordination whilst leaving two *cis* sites free for potential catalytic transformations. Moreover, the ability of self assembled phosphine ligands of this type to strongly bind transition metals suggests that such systems might have a role to play in waste clean-up procedures. The chemistry involved in the self-assembly of the new Fe complex **1** is novel and a patent has been raised to protect its potential applications.[1]

The authors would like to thank Gary Woodward (Albright & Wilson UK Ltd) and Martin Murray (School of Chemistry, University of Bristol) for their help in spectral interpretation.

Notes and references

† *Crystal data for* **1**: $C_{12}H_{42}Fe\,N_2O_{16}P_4S$, M = 682.3, monoclinic, space group $C2/c$, a = 12.106(4), b = 14.103(6), c = 15.032(4) Å, β = 90.68(2)°, U = 2566(2) Å^3, Z = 4, D_c = 1.766 g cm^{-3}, F(000) = 1432, μ(Mo-Kα) = 0.995 mm^{-1}, $R1$ = 0.030 [$I \geq 2\sigma(I)$], $wR2$ = 0.081 for 2912 unique data, 7820 reflections collected ($2\theta \leq 55°$, 173 K). A full sphere of low temperature data was collected using a Siemens SMART three-circle area detector diffractometer (Mo-Kα X-radiation, graphite monochromator, λ = 0.71069 Å). The structure was solved by direct methods and refined by full matrix least squares on all F^2 data using the SHELXTL 5.03 package on a Silicon Graphics Indy computer.[6] An empirical absorption correction was applied using SADABS.[7] The asymmetric unit contains one half of a molecule of the Fe cation and one half of a disordered SO_4^{2-} anion both lying astride a twofold axis. There are also two molecules of water of crystallisation. CCDC 182/1498. See http://www.rsc.org/cc/a9/a908309j/ for crystallographic files in .cif format.

‡ *Selected spectroscopic data* for **1**: ^{1}H NMR (D_2O, 500 MHz) δ 4.63, 4.56 [AB, 8H, diastereotopic P(CH_2OH)$_2$, ^2J(HH) 13 Hz], 4.37 [s, 4H, P(CH_2OH)], 3.67 (s, 4H, CH_2N), 3.17, 3.10 [AB, 8H, diastereotopic CH_2N, ^2J(HH) 15 Hz]. ^{31}P{^{1}H} NMR: δ 20.1 [t, ^{2}P, ^2J(PP) 53 Hz] and −1.5 [t, 2P, ^2J(PP) 53 Hz]. UV–VIS(H_2O) λ_{max} 475 nm, (ε = 1496.0 × 10^{-2} m^2 mol^{-1}). Combined yields of **1** and **2** of *ca*. 88% were estimated by monitoring the conversion of $[P(CH_2OH)_4]_2SO_4$ to products by ^{31}P NMR. Analysis for $C_{12}H_{42}FeN_2O_{16}P_4S$: calc.(obs.) C 21.1 (21.3), H 6.2 (6.5), N 4.1 (4.0%).

1 *UK Pat.*, HB1103, September 8, 1998.
2 L. Higham, A. Powell, M. Whittlesley, S. Wocadlo and P. Wood, *Chem. Commun.*, 1998, 1107.
3 D. J. Darensbourg, F. Joo, M. Kannisto, A. Katho, J. H. Reibenspies and D. J. Daigle, *Inorg. Chem.*, 1994, **33**, 200.
4 J. W. Ellis, K. N. Harrison, P. A. Hoye, A. G. Orpen, P. G. Pringle and M. Smith, *Inorg. Chem.*, 1992, **31**, 3026.
5 Albright & Wilson Ltd, *UK Pat.*, 2,145,708B, 1983.
6 SHELXTL 5.03 program system, Siemens Analytical X-ray Instruments, Madison, WI, 1995.
7 SADABS, A program for absorption correction with the Siemens SMART system, G. M. Sheldrick, University of Göttingen, 1996.

Communication a908309j

Expression and assay of an *N*-methyltransferase involved in the biosynthesis of a vancomycin group antibiotic

Dominic P. O'Brien,[a] Peter N. Kirkpatrick,[a] Simon W. O'Brien,[a] Thomas Staroske,[a] Timothy I. Richardson,[b] David A. Evans,[b] Andrew Hopkinson,[c] Jonathan B. Spencer[a] and Dudley H. Williams*[a]

[a] *Cambridge Centre for Molecular Recognition, University Chemical Laboratory, Lensfield Road, Cambridge, UK CB2 1EW. E-mail: dhw1@cam.ac.uk*
[b] *Department of Chemistry and Chemical Biology, Harvard University, 12 Oxford Street, Cambridge, MA 02138, USA. E-mail: evans@chemistry.harvard.edu*
[c] *DP 4–4A, Unilever Research Port Sunlight Laboratory, Quarry Road East, Bebington, Wirral, UK L63 3JW. E-mail: Andrew.Hopkinson@unilever.com*

Received (in Cambridge, UK) 4th October 1999, Accepted 15th November 1999

An *N*-methyltransferase responsible for methylating the *N*-terminal leucine of a vancomycin group antibiotic has been expressed, and its activity assayed against a series of putative vancomycin precursors.

Vancomycin (**1**) and teicoplanin are the drugs of choice against methicillin-resistant *Staphylococcus aureus* (MRSA).[1] The

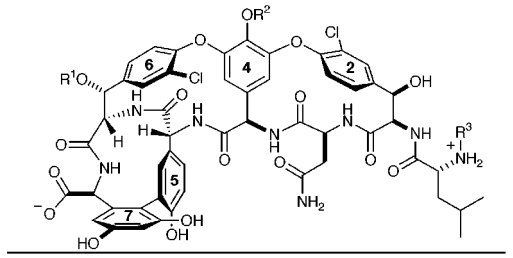

Compound	R^1	R^2	R^3
1	H	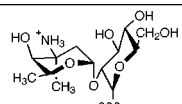	CH_3
2	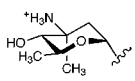	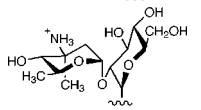	CH_3
3	H	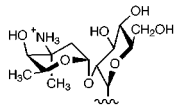	H
4	H	H	H

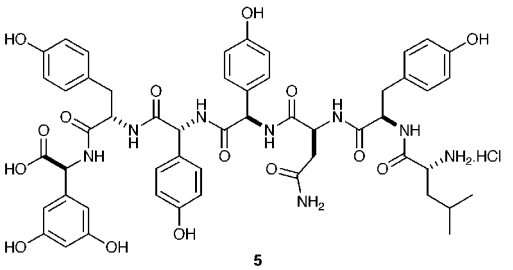

5

emergence of vancomycin-resistant enterococci (VRE) has highlighted the need for the development of new antibiotics.[2–4] We have sequenced the DNA containing a gene cluster assumed to encode enzymes for the biosynthesis of chloroeremomycin (**2**).[5,6] This assumption is strongly supported by the expression of a glycosyl transferase within the cluster, which was able to add glucose to an aglycone form of chloroeremomycin.[7] Recently, gene disruption in another glycopeptide producing strain has indicated the oxidative genes involved in cross-linking the aromatic groups along the peptide backbone, and led to the isolation of a linear heptapeptide precursor of a vancomycin group antibiotic.[8]

We now report the successful expression and assay of an *N*-methyltransferase from this cluster (MtfA, previously referred to as ORF 16) responsible for *N*-methylating the *N*-terminal leucine of chloroeremomycin. MtfA has significant sequence homology to the *N*-methyltransferase EryCVI which is involved in the synthesis of the desosamine moiety of erythromycin D.[9] The MtfA gene was amplified from cosmid pCZA361 using primers which introduced suitable restriction sites for cloning into the expression vector pET28a(+) (Novagen). The protein was then expressed in *E. coli* BL21 (DE3) under the control of the T7*lac* promoter as a His_6-tagged fusion protein which allowed one-step purification using Novagen His-Bind Quick 900 Cartridges. The relative molecular mass of the purified protein (which gave rise to a single band following SDS-PAGE) was found to be 32.52 kDa (using ESI-MS) which was in excellent agreement with that calculated (32.519 kDa) from the protein sequence.

We assayed MtfA against four different substrates. Each substrate represents a putative precursor corresponding to a different stage of the pathway. The first substrate was *N*-demethylvancomycin (**3**) which is identical in structure to *N*-demethylchloroeremomycin with the exception that the latter has an additional residue 6 amino-sugar (4-*epi*-vancosamine) and the residue 4 sugar is *epi*-vancosamine rather than vancosamine. The second substrate was the aglycone of **3** (**4**). These substrates allow assays for putative late stage methylation in the biosynthetic pathway. The third substrate was the linear heptapeptide D-Leu-D-Tyr-L-Asn-D-Phpg-D-Phpg-L-Tyr-L-Dhpg-OH (**5**).[10] This has the same linear peptide sequence as vancomycin but has no cross-linking between the aromatic side chains, no chlorine atoms or benzylic hydroxy groups and lacks the residue 4 sugars. This substrate allows an assay for a methylation step near to the middle of the biosynthetic pathway. The final substrates were the *R*- and *S*-enantiomers of leucine. These substrates allow assays for methylation at the start of the biosynthetic pathway. Although the *N*-terminal leucine of chloroeremomycin is the *R*-isomer, the possibility of post-methylation epimerisation cannot be ruled out.

Assays were performed in 50 mM Tris–HCl buffer, pH 7.5 at 25 °C. The concentrations of substrate (100 μM), (*S*)-adenosyl-L-methionine (200 μM) and enzyme (1 mg) were identical in each assay, as was the incubation time (24 h). Reaction mixtures were then subjected to analytical reverse phase HPLC and fractions analysed by FT-ICR mass spectrometry. The extent of methylation was determined by comparing the ratios of the intensities of the peaks corresponding to the singly charged parent ions of the substrates and their methylated products (Table 1). Appropriate controls were carried out.[11,12] Where

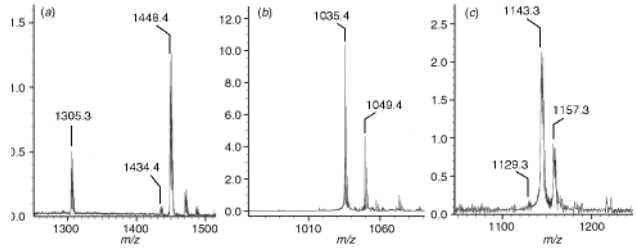

Fig. 1 FT-ICR spectra showing the MH^+ peaks due to substrate and methylated product(s) following MtfA assays for (*a*) **3**, (*b*) **5** and (*c*) **4**.

Table 1 Extent of methylation of various substrates by MtfA determined by FT-ICR spectrometry and HPLC analysis (parentheses). Each assay was performed under identical conditions of 100 μM substrate, 200 μM (*S*)-adenosylmethionine and 1 mg of enzyme for 24 h

Substrate	Substrate monomethylation (%)	Substrate dimethylation (%)
3	95 (> 95)	0 (0)
4	68	30
5	30	0
(*R*)-Leucine	0	0
(*S*)-Leucine	0	0

HPLC retention times of products and substrates did not overlap significantly, peak integration was also used to determine the extent of methylation (Table 1). Leucine and *N*-methylleucine have very weak UV absorption properties and mass spectrometry was used for their detection.[13]

Approximately 95% of **3** was monomethylated by MtfA to vancomycin [Table 1 and Fig. 1(*a*), *cf.* peaks at *m/z* 1434 and 1448]. In Fig. 1(*a*) the fragmentation peak at *m/z* 1305 corresponds to the loss of the residue 4 vancosamine from the methylated product, indicating that *N*-methylation occurs at the *N*-terminal leucine and not the amino group of vancosamine. Species **4** also proved a good substrate for MtfA with over 95% methylation. Interestingly, 30% underwent a second methylation to form a dimethylated product [Table 1 and Fig. 1(*c*), *cf.* peaks at *m/z* 1129, 1143 and 1157]. In contrast, only 30% of **5** was monomethylated [Fig. 1(*b*), *cf.* peaks at *m/z* 1049 and 1035] and no methylation of (*R*)- or (*S*)-leucine was detected. Each substrate was additionally assayed in the absence of MtfA and no methylation was observed.

We also carried out competition experiments in which an equimolar concentration of two substrates (100 μM each) was incubated with enzyme (2 mg) and (*S*)-adenosyl-L-methionine (200 μM) (Table 2).[14] In the competition experiment between substrates **3** and **5**, approximately 95% of **3** was monomethylated whereas no methylation of **5** was detected, confirming that **3** is a much better substrate than **5**. In the competition experiment between substrates **3** and **4,** 90% of **4** was monomethylated whereas only 30–35% of **3** was monomethylated. No dimethylated products were detected. The lack of a second methylation of **4** in this competition experiment implies that the *N*-methylated aglycone is a poorer substrate for the enzyme than is **3**. Most importantly, this result also implies that **4** is a better substrate than **3** and hence the best substrate of those tested.

Table 2 Extent of methylation of substrates after competition experiments in which mixtures of two substrates (100 μM each) and MtfA (1 mg) are subjected to a limiting concentration of *S*-adenosyl-L-methionine (200 μM). % values determined by FT-ICR spectrometry and HPLC analysis (parentheses)

	Substrate methylation[a] (%)		
Substrates	**3**	**4**	**5**
3,4	35 (30)	90	—
3,5	95 (> 95)	—	0

[a] All values refer to monomethylation only, since no dimethylation was observed in either experiment.

These results indicate that the order of specificity of the substrates tested for MtfA is **4** > **3** > **5** > (*R*)- and (*S*)-leucine. This order suggests that *N*-methylation is a late step in the biosynthetic pathway of chloroeremomycin, taking place after the oxidative crosslinking of the heptapeptide backbone but before the addition of the ring 4 disaccharide. However, the importance of the chlorine atoms on substrate specificity is yet to be determined.

We thank Dr Yan Husheng of Nankai University, People's Republic of China, for providing *N*-demethylvancomycin, Dr Jochen Görlitzer for synthesising the aglycone of demethylvancomycin, and the Royal Society (University Research Fellowship to J. B. S), Eli Lilly (S. O'B.), the EPSRC (T. S, D. O'B. and P. N. K), the BBSRC and Unilever for funding.

Notes and references

1 M. Foldes, R. Munro, T. C. Sorrell, S. Shankar and M. Toohey, *J. Antimicrob. Chemother.*, 1983, **11**, 21.
2 P. Courvalin, *Antimicrob. Agents Chemother.*, 1990, **34**, 2291.
3 H. C. Neu, *Science*, 1992, **257**, 1064.
4 C. T. Walsh, S. L. Fisher, I.-S. Park, M. Prahalad and Z. Wu, *Chem. Biol.*, 1996, **3**, 21.
5 A. M. A. v. Wageningen, P. N. Kirkpatrick, D. H. Williams, B. R. Harris, J. K. Kershaw, N. J. Lennard, M. Jones, S. J. M. Jones and P. J. Solenberg, *Chem. Biol.*, 1998, **5**, 155.
6 D. H. Williams and B. Bardsley, *Angew. Chem., Int. Ed.*, 1999, **38**, 1172.
7 P. J. Solenberg, P. Matsushima, D. R. Stack, S. C. Wilkie, R. C. Thompson and R. H. Baltz, *Chem. Biol.*, 1997, **4**, 195.
8 R. D. Süssmuth, S. Pelzer, G. Nicholson, T. Walk, W. Wohlleben and G. Jung, *Angew. Chem., Int. Ed.*, 1999, **38**, 1976.
9 R. G. Summers, S. Donadio, M. J. Staver, E. Wendt-Pienkowski, C. R. Hutchinson and L. Katz, *Microbiology*, 1997, **143**, 3251.
10 This peptide was synthesised using a combination of solution phase and solid phase methodology. Phpg and Dhpg refer to 4-hydroxyphenylglycine and 3,5-dihydroxyphenylglycine, respectively.
11 Equimolar mixtures of (*R*)-*N*-methylleucine and (*R*) leucine, vancomycin and *N*-demethylvancomycin and vancomycin aglycone and *N*-demethyvancomycin aglycone were subjected to FT-ICR mass spectrometry. For a given solution, the intensities of the singly and doubly charged parent ion peaks of each component were the same to within 10%.
12 Fragmentation peaks corresponding to *N*-demethylvancomycin, *N*-demethylvancomycin aglycone and (*R*)-leucine were not observed in the FT-ICR spectra of vancomycin, vancomycin aglycone and (*R*)-*N*-methylleucine, respectively.
13 Solutions of leucine and *N*-methylleucine were subjected to reverse phase HPLC and fractions were collected at intervals of 30 s. Each fraction was then subjected to FT-ICR mass spectrometry to test for the presence of the corresponding compound. By progressively narrowing the time interval between collections the retention time of the compounds was determined to within five seconds. For each reaction assay, samples corresponding to these retention times were collected and subjected to FT-ICR mass spectrometry.
14 60% of 100 μM substrate **3** is methylated in the presence of 100 μM (*S*)-adenosyl-L-methionine and MtfA, whereas 95% is methylated under the same conditions with 200 μM (*S*)-adenosyl-L-methionine. Hence, a 1:1 mixture of (*S*)-adenosyl-L-methionine and substrate provides a cofactor concentration which limits the extent of conversion.

Communication a907953j

Typeset and printed by Black Bear Press Limited, Cambridge, England

Microelectrochemical enzyme transistors

Philip N. Bartlett and Yann Astier

Department of Chemistry, University of Southampton, Highfield, Southampton, UK SO17 1BJ.
E-mail: p.n.bartlett@soton.ac.uk

Received (in Cambridge, UK) 12th April 1999, Accepted 13th July 1999

Conducting polymers, such as poly(aniline) or poly(3-methylthiophene), change their conductivity by many orders of magnitude upon oxidation or reduction. This modulation of the conductivity of the polymer by redox reactions can be utilised to fabricate microelectrochemical transistors—electrochemical devices that behave in many ways as analogues of solid state junction field effect transistors. When combined with suitable redox enzymes these devices can be developed as miniature biosensors which offer a number of interesting advantages, particularly for use with small sample volumes or at low analyte concentrations.

Introduction

Electrochemical biosensors have been extremely successful as disposable devices for the measurement of blood glucose for use by diabetics world-wide. This success is based on ease of manufacture at low cost but with high control of quality and reproducibility combined with ease of use. The clinical range for glucose in blood lies between 1 and 20 mM. In this concentration range direct amperometric measurement at millimetre sized electrodes yields readily measured currents in the microamp range. Future applications will require much smaller devices so that more assays can be carried out in a single drop of blood and assays for analytes such as hormones, drugs or enzymes present at much lower concentrations (typically nano- and micro-molar). Taken individually and together these requirements will be difficult to meet with present types of amperometric biosensor because as the size of the electrode and/or the concentration of the analyte decreases the current measured also decreases. It is therefore appropriate to look for other types of electrochemical biosensor which, while retaining the simplicity of use and low cost of the amperometric devices, also provide the potential for greater sensitivity and small size.

The majority of electrochemical biosensors are based on either potentiometric or amperometric detection (Fig. 1). In the case of a potentiometric enzyme electrode the electrode senses the steady state concentration of some species, usually a product of the enzyme catalysed reaction (such as H^+, NH_4^+ *etc.*), at the electrode surface. This steady state concentration is determined by the kinetics of the enzyme catalysed reaction and by the mass transport of reactants to, and products away from, the electrode. Under suitable circumstances this steady state concentration is directly related to the concentration of the analyte in the solution. The operation of potentiometric enzyme electrodes suffers from a number of problems which limit their sensitivity for many applications.[1] In addition an accurate and stable reference electrode is essential and this is not easy to fabricate as a disposable structure. Consequently amperometric approaches have generally been favoured, although this is not always possible (for example in measurement of urea or penicillin). In an amperometric enzyme electrode the current is a direct measure of the rate of the enzyme catalysed reaction and therefore, under suitable circumstances, is directly related to the concentration of analyte. The great majority of redox enzymes or coenzymes such as NADH and NADPH do not undergo rapid, direct electrochemical reaction at electrode surfaces and

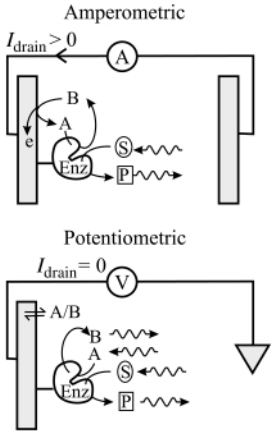

Fig. 1 Schematic representations of an amperometric enzyme electrode and a potentiometric enzyme electrode. In the amperometric enzyme electrode the conversion of substrate, S, to product, P, by the enzyme is linked to the electrode through the mediator couple A/B. The current for the conversion of B to A is then related to the rate of the enzyme catalysed reaction and thus to the substrate concentration. In the potentiometric enzyme electrode the electrode senses the concentrations of A and B at the electrode surface. These concentrations depend on the rate of the enzyme catalysed reactions and the rates of mass transport of the A/B couple and the substrate in solution.

Philip Bartlett did his first degree in Oxford and his PhD at Imperial College, London, under the supervision of Professor John Albery FRS. In 1984 he was appointed as a lecturer in Physical Chemistry at the University of Warwick, in 1991 he became Professor of Physical Chemistry at the University of Bath and in 1993 Professor of Electrochemistry at the University of Southampton. His research interests focus on the design, modification and characterisation of electrode surfaces and the application of electrochemically deposited thin films as chemical sensors. He has worked extensively in the areas of redox enzyme and coenzyme electrochemistry studying the mechanism and kinetics of modified electrodes and immobilised enzymes. He is currently chair of the organising committee for Faraday Discussion 116 on Bioelectrochemistry to be held in Southampton in July 2000.

Yann Astier was born in Rennes, France, in 1973. He received his degree in molecular chemistry from Rennes 1 University in 1997 and is now doing his PhD in electrochemistry at the University of Southampton with Professor P. N. Bartlett on electrochemical immunoassays.

consequently it is necessary to provide some means to couple the enzyme catalysed reaction to oxidation or reduction at the electrode surface. In the first amperometric enzyme electrodes, such as the Clark glucose electrode,[2] this was done by oxidising or reducing one of the co-reactants or products of the enzyme catalysed reaction at a metal electrode. The enzyme glucose oxidase (E.C. 1.1.3.4) catalyses the reaction of β-D-glucose with oxygen to give D-glucono-δ-lactone and hydrogen peroxide. This reaction occurs in two stages. In the first step [eqn. (1)] the oxidised flavin prosthetic group, FAD, bound in the enzyme active site is reduced by reaction with glucose to give the bound reduced flavin, $FADH_2$, and the product gluconolactone, which undergoes hydrolysis to give gluconic acid [eqn. (2)]. In a subsequent step the reduced flavin is reoxidised by reaction with molecular oxygen [eqn. (3)].

$$GOx(FAD) + \beta\text{-D-glucose} \rightarrow GOx(FADH_2) + \text{D-glucono-}\delta\text{-lactone} \quad (1)$$

$$\text{D-glucono-}\delta\text{-lactone} + H_2O \rightarrow \text{D-gluconate} + H_3O^+ \quad (2)$$

$$GOx(FADH_2) + O_2 \rightarrow GOx(FAD) + H_2O_2 \quad (3)$$

These reactions can be followed electrochemically by either measuring the rate of consumption of molecular oxygen or by measuring the rate of production of hydrogen peroxide. Although both approaches have been adopted they suffer from a number of problems. At high glucose concentrations, or in situations where the supply of oxygen is restricted, the response can be limited by the oxygen supply rather than by the concentration of glucose. In addition both oxygen and hydrogen peroxide are difficult species to measure electrochemically because of their poor electrode kinetics. Consequently measurements in whole blood, serum or other biological media are often difficult because of interference from other, readily oxidised compounds such as uric acid or ascorbate present in the sample. For these reasons it is preferable to avoid the use of oxygen and replace the second reaction by one in which a redox mediator is used to reoxidise the enzyme [eqn. (4)].

$$GOx(FADH_2) + 2M^+ + 2H_2O \rightarrow GOx(FAD) + 2M + 2H_3O^+ \quad (4)$$

Using this approach the mediator can be chosen so that it has both a fast reaction with the reduced enzyme, good stability and fast electrode kinetics at a potential where the interferences from other species present in the sample are minimal. The most successful example of this approach has been the use of ferrocene derivatives to mediate oxidation of glucose oxidase first suggested by Cass *et al.*[3] and subsequently the basis of a very successful commercial disposable glucose sensor.

For glucose oxidase, direct electrochemical oxidation of the enzyme is slow because the active site is buried deep within the enzyme core.[4] Homogeneous solution mediators, such as the ferrocene derivatives, are presumably able to diffuse into and out of the enzyme's active site and thus to act as a shuttle carrying electrons from the active site to the electrode. Although the use of homogeneous, freely diffusing mediators has proved a very successful and flexible approach to the problem it is not ideal for all applications because the mediator can diffuse away from the electrode surface and be lost. For this reason other approaches have been investigated including the co-immobilisation of the enzyme and mediator in carbon paste electrodes and sol-gel electrode structures, the covalent modification of the enzyme by attachment of the redox mediator to amino acid residues of the protein,[5,6] and the immobilisation of the enzyme in redox polymer films containing the covalently attached mediator. This last approach, pioneered by Heller,[7] has been very successful in linking the re-oxidation of several flavoproteins, including glucose oxidase, to electrodes for use in amperometric biosensors.

Despite these successes in designing amperometric enzyme electrodes there are important limitations to their performance if we wish to go towards either smaller sensors or analytes at lower concentrations. In an amperometric enzyme electrode the current is directly related to the rate of turnover of the enzyme. For example for glucose oxidase the maximum rate of turnover of the enzyme is 800 s^{-1}. For a monolayer coverage of the enzyme (1.6×10^{-12} mol cm^{-2})[8,9] on a 1 cm^2 electrode this corresponds to a maximum current of 240 μA. As the size of the electrode is decreased the current will also decrease because the number of enzyme molecules decreases. For a 70 micron diameter electrode (the diameter of a human hair, 3.85×10^{-5} cm^2) the maximum current for a monolayer coverage of glucose oxidase will be 9.2 nA; for a 1 micron diameter electrode (7.85×10^{-9} cm^2, a realistic size using present fabrication techniques) the current will be reduced to 1.9 pA. Clearly, in principle, this current can be increased if the enzyme coverage is increased from a monolayer to multilayer. However the increase in current will be less than linear with increasing enzyme coverage because of the restriction on diffusion of the substrate through the enzyme layer at the electrode surface. Thus, realistically we can probably only expect an increase of one or two orders of magnitude in the current if we use multilayer enzyme coverage on the electrode.

These currents are for high concentrations of the analyte (> 20 mM) and for an enzyme with fast kinetics. At lower concentrations, or for many other enzymes, the currents would be less. This also becomes a problem when we try to develop amperometric biosensors for analytes such as hormones or drugs which are biologically active at much lower concentrations.

To address these problems it is appropriate that we investigate other electrochemical sensing strategies which maintain the advantages of electrochemical biosensors in terms of low cost and ease of use and manufacture, but which offer other mechanisms to allow enhanced sensitivity at low analyte concentrations for devices of small size. One such approach is provided by the microelectrochemical transistor or switch devices first described by Wrighton and colleagues.[10] These devices make use of the ability to switch the conductivity of thin conducting polymer films by five or more orders of magnitude on oxidation or reduction. This large change in conductivity of the polymer leads to amplification of the signal and can be used as the basis of a chemical sensor or biosensor which acts as a electrochemical transistor analogous to a junction field effect transistor in its operation and characteristics. In addition these devices can be made very small so that they may be suitable for use in small sample volumes.

Conducting polymers

The microelectrochemical transistors and diodes described by Wrighton make use of the very large changes in the conductivity of electronically conducting polymers which accompany oxidation or reduction of the polymer backbone. Conducting polymers, such as poly(pyrrole) or poly(3-methylthiophene) are formed by oxidative coupling of the respective monomers. This coupling can be carried out chemically or electrochemically. The latter approach has the advantage that the polymerisation process is localised at the electrode surface and that the amount of polymer deposited can be controlled through the total amount of charge passed. On cycling the potential of the conducting polymer film in a solution of background electrolyte the polymer can be repeatedly oxidised and reduced (Fig. 2). The amount of charge passed in this process depends on the amount of polymer present. For polymers such as poly(pyrrole) and poly(3-methylthiophene) the oxidised form is conducting and the reduced form is insulating. Conduction in the oxidised form of the polymer is through the mobile bipolarons[11] (Fig. 2).

The oxidation and reduction of the conducting polymer is also accompanied by the ingress and egress of anions, cations and solvent and by polymer chain relaxation processes. Thus the dynamics of the redox transformation of these films is a complex process and one which we are only now beginning to

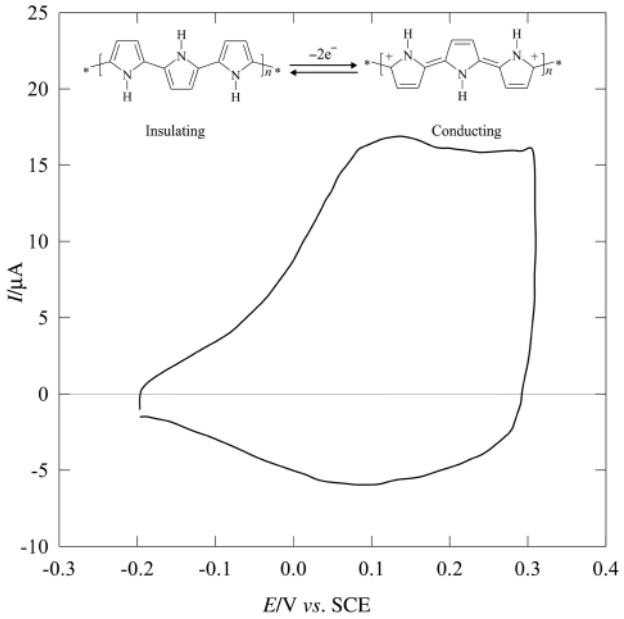

Fig. 2 A cyclic voltammogram of a poly(pyrrole) film recorded at 200 mV s^{-1} in 2 mol dm^{-3} H_2SO_4. The film was grown on a 0.5 mm diameter platinum electrode at 0.65 V *vs.* SCE from a solution of 0.5 mol dm^{-3} pyrrole in 1 mol dm^{-3} KCl. The inset shows the schematic structures for the insulating and conducting forms of the polymer. Note that in the fully oxidised polymer there is typically one charge for every four monomer units.

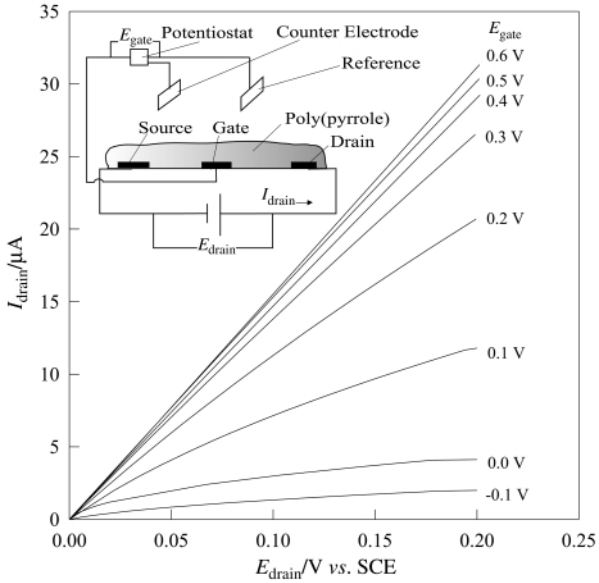

Fig. 3 Plots of the drain current, I_{drain}, as a function of the drain voltage, E_{drain}, for a poly(pyrrole) based microelectrochemical transistor operated in MeCN containing 0.1 mol dm^{-3} Bu_4NClO_4. Each curve corresponds to a different value of the gate voltage, E_{gate}. As the gate voltage increases from –0.1 V *vs.* SCE to 0.6 V the resistance of the poly(pyrrole) film decreases. The inset shows the arrangement used to make the measurements. (Adapted with permission from White *et al.*[10] Copyright 1984 American Chemical Society.)

fully comprehend through the use of a variety of *in situ* techniques.[12,13] This movement of ions is essential to maintain the electroneutrality of the polymer film. This requirement for the motion of ions to accompany the oxidation and reduction of the polymer constrains the maximum rate at which these films can switch between conducting and insulating states.

Microelectrochemical transistors and diodes

The first microelectrochemical transistor, described by Wrighton and colleagues in 1984,[10,14] comprised a poly(pyrrole) film deposited across the gaps between three independent gold microband electrodes 1.4 μm apart on a oxidised silicon substrate (Fig. 3). By analogy with a junction field effect transistor the three gold electrodes are referred to as the source, gate and drain. By using the central gate electrode Wrighton and colleagues were able to alter the redox state of the poly(pyrrole) film. With the gate at potentials, E_{gate}, negative of −0.2 V *vs.* SCE the polymer is insulating and no current flows through the polymer film between the outer source and drain electrodes when a voltage, E_{drain}, is applied between them—the device is in the 'off' state. When the gate potential, E_{gate}, is changed to more positive values the poly(pyrrole) film becomes oxidised and changes to its conducting state. Now when a voltage is applied between source and drain a significant drain current, I_{drain}, flows between the source and drain electrodes through the poly(pyrrole) film—the device is in the 'on' state. Fig. 3 shows the current–voltage characteristics of the device at different gate voltages. In this device a small signal applied to the gate electrode leads to a large change in the drain current flowing through the polymer; thus the device amplifies the signal in the same way that a solid state transistor can be use to amplify a signal.

A significant difference between the type of microelectrochemical transistor described here and conventional solid-state devices lies in their response times. In a solid-state semiconductor device the switching is achieved by movement of electrons or holes within the semiconductor. In the microelectrochemical enzyme transistor the switching is accompanied by the movement of ions and solvent within the film (see above). Consequently the process is much slower; switching for Wrighton's first poly(pyrrole) device took on the order of 10 s.[10] In subsequent studies Wrighton and colleagues demonstrated that other conducting polymer such as poly(3-methylthiophene) and poly(aniline) could be used to make microelectrochemical transistors[15,16] and that these devices could be made to operate faster by careful choice of the polymer film and by reducing the size of the inter-electrode gap. In this way they were able to demonstrate power amplification up to frequencies of 10 kHz.[17] Nevertheless this is still considerably slower than for solid-state devices.

However although switching in microelectrochemical transistors is slow they have other properties which solid state devices do not possess, notably that the devices can be switched by chemical reactions and therefore can, in principle, be used as chemical sensors. Thus, instead of using a potentiostat and external circuit the redox state of the polymer film can be changed by oxidation or reduction by a species in solution and this change can again be sensed by a change in the drain current flowing through the device—the chemical reaction switches the device between 'on' and 'off' states. The first examples of this used simple outer sphere redox couples such as $[Fe(CN)_6]^{3-/4-}$ or $[Ru(NH_3)_6]^{3+/2+}$ to turn devices based on poly(aniline) films 'on' and 'off' respectively.[16] The amount of redox reagent which can be detected with this type of device is very small. For example for a poly(3-methylthiophene) based transistor Wrighton *et al.* were able to detect the injection of 1×10^{-9} mol of $[IrCl_6]^{2-}$ corresponding to the reaction of 8×10^{-16} mol of the reagent at the polymer surface.[18] Subsequently responses to molecular hydrogen and oxygen were demonstrated for microelectrochemical transistors based on poly(3-methylthiophene) films modified with platinum particles to catalyse the reactions of hydrogen and oxygen[19] (Fig. 4). Despite the use of the platinum particles to catalyse the reduction of oxygen the response of the devices was still rather slow, taking around 2 min to respond to 1 atm of dissolved molecular oxygen. In these devices the microelectrochemical transistor acts as a sensor for the redox potential of the solution without any particular chemical selectivity for the species present.

Whilst these initial studies by Wrighton and colleagues demonstrated the concept of using a microelectrochemical

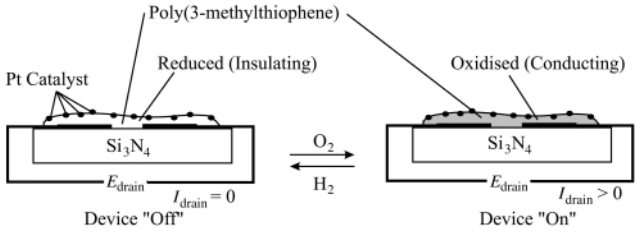

Fig. 4 A two terminal poly(3-methylthiophene) based microelectrochemical enzyme transistor. The device can be turned 'off' by reduction with hydrogen or 'on' by oxidation with oxygen. The platinum particles are necessary to catalyse the reactions of the gases at the surface of the polymer. (Adapted with permission from Thackeray *et al.*[19] Copyright 1986 American Chemical Society.)

transistor as a chemical sensor they did not go on to demonstrate selective devices or to look at the possible use of other types of catalyst to provide selectivity in the device response.

Microelectrochemical enzyme transistors

An obvious way to impart chemical selectivity to a microelectrochemical transistor is to use an immobilised enzyme as the catalyst.[20] However this has proved to be difficult because of the problems of coupling the enzyme electrochemistry to the conducting polymer film and finding the right conducting polymer with the correct properties for the application. The obvious starting point is to use poly(pyrrole) or one of its derivatives since these polymers can be deposited from neutral aqueous solutions and can be used to entrap enzymes such as glucose oxidase during deposition of the polymer.[21–23] This was the approach adopted by Matsue to make the first microelectrochemical enzyme transistor, an NADH responsive device based on diaphorase.[24] They used an interdigitated platinum electrode structure fabricated on glass with 10 μm wide bands separated by 10 μm wide gaps. These were coated with a thin electropolymerised film of co-polymerised pyrrole and *N*-methylpyrrole containing diaphorase (E.C. 1.6.99.- purified from *Bacillus stearothermophilus*). In order to couple the enzyme catalysed reaction to the reduction of the polymer 1 mM anthraquinone-2-sulfonate was added to the solution as a mediator. On addition of NADH the oxidation of NADH, catalysed by the diaphorase, led to reduction of the pyrrole–*N*-methylpyrrole copolymer film causing the device to switch from 'on' to 'off'. This change in the conductivity of the polymer was observed by recording the change in the drain current, I_{drain}, flowing through the device as a function of time after exposure to NADH (Fig. 5). After exposure to NADH the device is in its 'off' state and must be reset by reoxidising the polymer before it can be used to make another measurement of NADH. This was achieved by electrochemical oxidation of the polymer film.

Despite proving to be a useful way of immobilising enzymes at electrode surfaces for amperometric enzyme electrodes,[21–23] poly(pyrrole) and its derivatives are not the most suitable polymers for the fabrication of microelectrochemical enzyme transistors because the stability of the polymer in solution at neutral pH is not good, it is hard to reproducibly deposit the films from neutral aqueous solutions, and the electrical conductivity of the polymer is irreversibly destroyed by reaction with hydrogen peroxide.[25,26] This is a particularly serious problem if one wants to use flavoproteins, such as glucose oxidase, which inevitably generate some peroxide even when a redox mediator is incorporated into the film with the enzyme.[27]

These problems can be overcome by using poly(aniline) which is stable, does not react with hydrogen peroxide and which can be deposited very reproducibly by electrochemical methods. The electrochemistry of poly(aniline) is more complex that that of poly(pyrrole) because there are three accessible oxidation states: the leucoemeraldine, emeraldine, and pernigraniline forms[28,29] (Fig. 6). Of these three forms only the protonated emeraldine form is electronically conducting. The emeraldine base (Fig. 6) is an insulator. Thus poly(aniline) generally only exists in its conducting form in acidic solution and the polymer is normally electrochemically deposited from

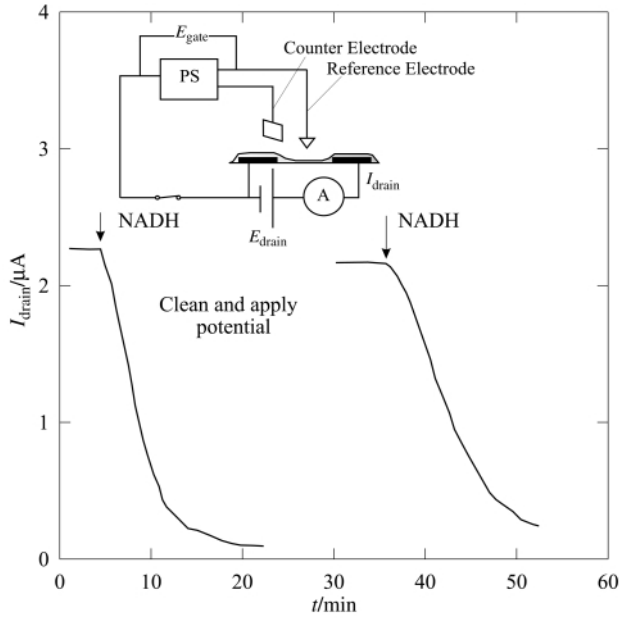

Fig. 5 Response of the drain current, I_{drain}, to the addition of 1 mmol dm^{-3} NADH for a microelectrochemical enzyme transistor based on a copolymer of pyrrole and *N*-methylpyrrole and incorporating diaphorase and anthraquinone-2-sulfonate. The device was operated at a drain voltage of 20 mV in 0.1 mol dm^{-3} KNO_3 in 20 mmol dm^{-3} phosphate buffer at pH 6.8. The inset shows the experimental arrangement for the measurement. (Adapted from Matsue *et al.*[24])

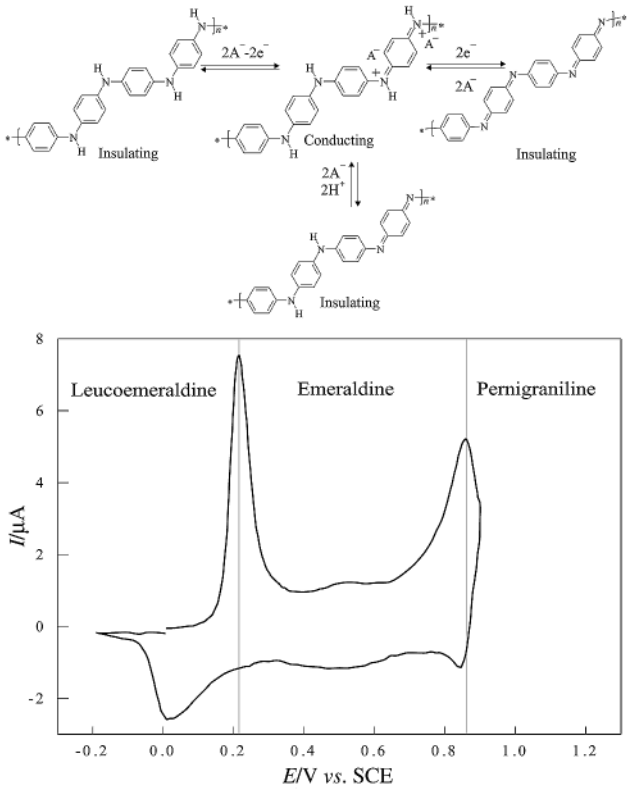

Fig. 6 Cyclic voltammogram for a poly(aniline) film recorded at 20 mV s^{-1} in 2 mol dm^{-3} H_2SO_4. The film was grown on a 0.5 mm diameter platinum electrode at 0.9 V *vs.* SCE from a solution of 0.4 mol dm^{-3} aniline in 2 mol dm^{-3} H_2SO_4. The three different forms of the material are indicated. Of the three only the protonated emeraldine form is electronically conducting. The diagram also shows schematic representations of the structures of the different forms.

acidic solutions (such as 1 M H_2SO_4). Poly(aniline) films can be cycled between the three redox states electrochemically in acidic solutions (Fig. 6) but at low pH the pernigraniline form is unstable and undergoes hydrolysis leading to degradation of the film.

In order to use poly(aniline) films with flavoproteins it is essential to work in neutral, or at best weakly acidic, solutions to avoid the destruction of the enzyme. The workable pH range for poly(aniline) films grown from sulfuric acid solution is determined by the pK_a of the emeraldine form of the polymer. This is around 5.5, so that these films can be operated in buffered solutions at pH 5. Microelectrochemical enzyme transistors responsive to glucose were fabricated by electrochemically depositing a thin film of poly(aniline) from sulfuric acid solution across a 20–25 μm gap between two screen printed carbon microbands.[30,31] Glucose oxidase was then immobilised on to the surface of the poly(aniline) in a second step carried out in buffered solution at pH 5. The glucose oxidase was immobilised on the poly(aniline) surface in an electropolymerised film of 1,2-diaminobenzene. 1,2-Diaminobenzene forms a thin insulating film under these conditions which is permselective and can be used to give selectivity against interferents in solution.[32] Thus the film serves the dual purpose of immobilising the enzyme onto the surface of the poly(aniline) and providing some selectivity against interference from solution species. The fact that the film is deposited electrochemically also means that it coats the surface of the device evenly. The construction of the device is shown in Fig. 7. To

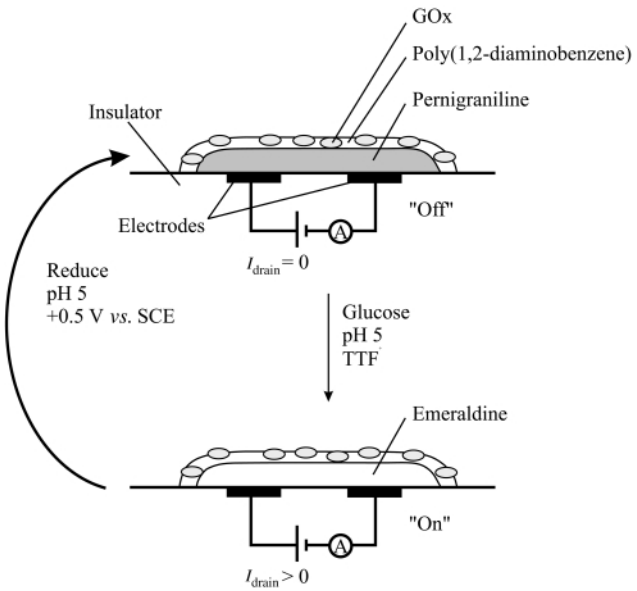

Fig. 7 The construction and operation of a microelectrochemical enzyme transistor responsive to glucose. The device is based on a poly(aniline) film deposited across the gap between two electrodes. On top of the film the enzyme glucose oxidase (GOx) is immobilised in a electropolymerised film of poly(1,2-diaminobenzene). The device is switched from 'off' to 'on' on exposure to glucose. The device can be reset by electrochemical oxidation of the poly(aniline) film at +0.5 V *vs.* SCE at pH 5.0 to the insulating pernigraniline state.

couple the enzyme catalysed oxidation of glucose to the reduction of the poly(aniline) film tetrathiafulvalene (TTF) was used as a mediator. The overall reaction scheme is then given by eqns. (5)–(8),

$$\text{GOx(FAD)} + \beta\text{-D-glucose} \rightarrow \text{GOx(FADH}_2\text{)} + \text{D-glucono-}\delta\text{-lactone} \quad (5)$$

$$\text{D-glucono-}\delta\text{-lactone} + H_2O \rightarrow \text{D-gluconate} + H_3O^+ \quad (6)$$

$$\text{GOx(FADH}_2\text{)} + 2\text{TTF}^+ + 2H_2O \rightarrow \text{GOx(FAD}^+\text{)} + 2\text{TTF} + 2H_3O^+ \quad (7)$$

$$\text{TTF} + \text{PANI(ox)} \rightarrow \text{TTF}^+ + \text{PANI(red)} \quad (8)$$

where PANI(ox) represents the fully oxidised, insulating, pernigraniline form of poly(aniline) and PANI(red) the partially oxidised, conducting, emeraldine form. Thus the enzyme catalysed reaction turns the device from 'off' to 'on' (Fig. 7). Following exposure to glucose the device can be reset by electrochemical oxidation of the poly(aniline) to the pernigraniline form at 0.5 V *vs.* SCE.

For a device of this type the rate at which the drain current increases upon exposure to the analyte and the time taken for it to switch between states depend on the concentration of analyte. Fig. 8 shows a set of response curves for a single device exposed

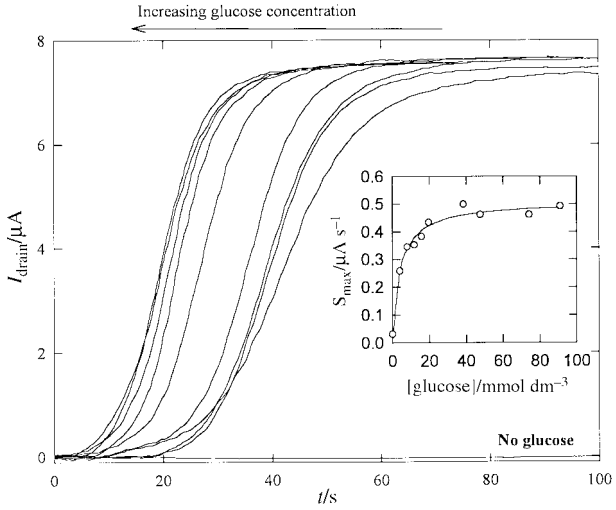

Fig. 8 A set of response curves for a glucose oxidase based microelectrochemical enzyme transistor. The structure of the transistor is shown in Fig. 7. Between each measurement the device was reset electrochemically to its insulating state at 0.5 V vs. SCE. Measurements were made with a drain voltage, E_{drain}, of 20 mV in pH 5 phosphate/citrate buffer containing 0.5 mol dm^{-2} Na_2SO_4 and 0.5 vol % Triton X100 saturated with tetrathiafulvalene. In each case aliquots of sample solution were added at time zero. In the absence of glucose the drain current, I_{drain}, flowing through the device does not change. When an aliquot of glucose is added the drain current increases with time following the addition until it eventually reaches a plateau when the device is in the 'on' state. The time taken for the device to switch on and the maximum switching rate, S_{max} (defined as the maximum slope of the plot of drain current against time), depends on the concentration of glucose. The inset shows the calibration curve for this device. (Reprinted from Bartlett and Birkin.[30] Copyright 1993 American Chemical Society.)

to different concentrations of glucose. First it is clear that the device can be reused at least nine times with no apparent loss in function, in fact many more than nine consecutive operations are possible for this device under these conditions. It is also clear that the response of the device depends on the concentration of glucose added to the solution. Without added glucose there is no change in the drain current over the course of the experiment. When glucose is added there is initially no change in the drain current flowing through the poly(aniline) film but then, as the enzyme catalysed reaction begins to reduce the polymer it is converted to its conducting, emeraldine state and the drain current increases, eventually reaching a plateau when the polymer is highly conducting and the drain current is limited by the base resistance of the carbon microband structure (in this case about 3 kΩ). Note that on switching from 'off' to 'on' the resistance of this device changes by around 3 orders of magnitude. We can show that the device does indeed operate through changes in the oxidation state of the poly(aniline) film by following the potential of the film during switching [Fig. 9(*a*)]. Before addition of glucose the potential of the polymer is around +0.28 V vs. SCE, where the poly(aniline) film is insulating. On addition of glucose the potential immediately begins to shift cathodic as the poly(aniline) is reduced and then the drain current increases as the polymer becomes more conducting. Fig. 9(*b*) shows the variation of the polymer resistance with potential.

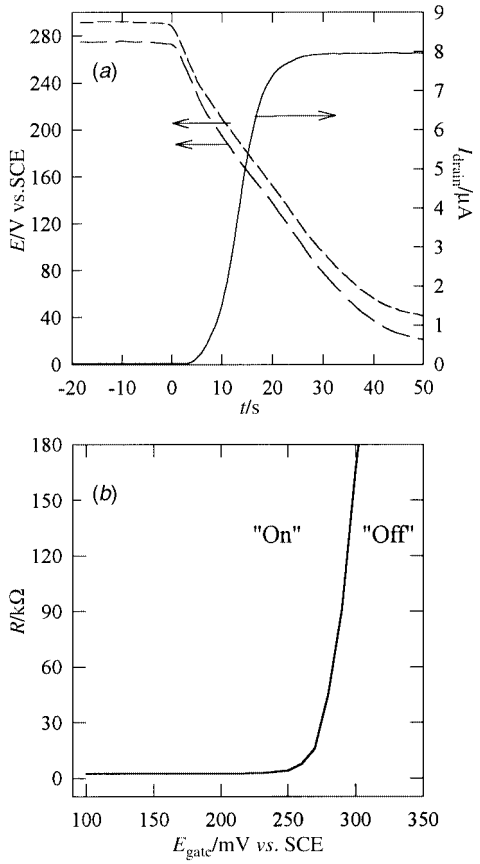

Fig. 9 (*a*) Simultaneous measurement of the drain current, I_{drain}, and the potentials of the two microband electrodes as a function of time after addition of glucose. (*b*) resistance of a poly(aniline) film as a function of the redox potential at pH 5. (Reprinted from Bartlett and Birkin.[31] Copyright 1994 American Chemical Society.)

Studies of the effect of varying the amount of polymer deposited onto the device and the enzyme loading allow us to optimise the speed of response of these devices to glucose and support our model of the operation of these devices.[31] By optimising the amount of poly(aniline) deposited across the 20 μm gap a switching time of less than 10 s can be achieved. This is significantly faster than the best switching times reported by Matsue *et al.* for their NADH responsive device.[24] The selectivity of this type of device for glucose over other sugars is largely determined by the selectivity of the enzyme itself, with D-(+)-glucose giving much faster switching rates than D-(+)-mannose or D-(+)-galactose (Table 1).

Table 1 Comparison of the relative homogeneous rates, amperometric response, and switching rate recorded for a single device in the presence of 0.15 mol dm^{-3} substrate and 1.4 mmol dm^{-3} TTF^+ (from ref. 31)

Substrate	Relative homogeneous rate[a]	Amperometric response/μA	Switching rate/s^{-1}
D-(+)-Glucose	100	63	0.209
2-Deoxy-D-glucose	25	42.5	0.218
D-(+)-Mannose	0.98	8.8	0.081
D-(+)-Galactose	0.14	3.3	0.034

[a] Ref. 53.

Advantages of microelectrochemical enzyme transistors

Microelectrochemical enzyme transistors have a number of potential advantages as biosensor devices which could be beneficial in some applications. First, the devices do not require a potentiostat or a reference electrode to operate. Measurement of the drain current can be achieved with very simple instrumentation and, at least for devices operating in the 'off' to 'on' direction (see below), the instrumentation required to re-set the device after each measurement can be very simple. Second, the devices can be made very small without loss of sensitivity. As the gap between the electrodes is decreased and the polymer film is made thinner the speed of response will increase and the magnitude of the drain current will increase. Third, these devices can be thought of as counting the number of molecules which have reacted with the enzyme. Thus it will take a certain number of glucose molecules to switch the device from its 'off' state to its 'on' state. This number of molecules depends on the amount of poly(aniline) in the device—for a device 50 μm by 50 μm we estimate that 60 fmol of glucose is required to reach the halfway point where I_{drain} is one half its maximum value. As the size of the device decreases the number of moles of glucose will also decrease. Fourth, the device integrates the analytical signal. Thus if the device is removed from the solution containing glucose the drain current does not fall back to zero but stays at the value reached. If the device is returned to the glucose solution the drain current increases once more. This is because the enzyme catalysed reaction causes the reduction of the polymer so that each molecule of glucose which reacts injects one charge carrier into the polymer and these charge carriers accumulate there leading to the increase in conductivity. This is in direct contrast of the operation of superficially similar devices also based on conducting polymer films and enzymes which operate by sensing a local change in pH caused by the enzyme catalysed reaction.[33–35] In these devices the response returns to the baseline value when the analyte is removed and in their operation they resemble potentiometric enzyme electrodes and suffer from the same problems as these devices in terms of sensitivity and effect of solution buffer concentration.[1]

We have made use of this ability of the microelectrochemical enzyme transistor to integrate the analyte signal in the measurement of low glucose concentrations using a device of the type described above.[36] In this work we were able to show that by the choice of suitable deposition and fabrication conditions we can make microelectrochemical enzyme transistors responsive to glucose with good reproducibility and that they can be used with good repeatability to make measurements of glucose concentration down to 2 μM in air-saturated buffer at pH 5. This was 40 times better than the performance of the corresponding amperometric device.

Despite the success in fabricating working devices responsive to glucose some problems and disadvantages remain. First it is important to realise that devices of this type will suffer from similar problems of interference, enzyme kinetics and selectivity as amperometric enzyme electrodes. Indeed if a device works as a microelectrochemical enzyme transistor then it will generally also function as an amperometric sensor simply by holding it at the appropriate potential and measuring the current. The advantages of the microelectrochemical enzyme transistor over the amperometric enzyme electrode lie in its sensitivity and simplicity of measurement. Second, for the devices described above freely diffusing mediator species have been necessary to couple the enzyme reaction to the reduction or oxidation of the polymer. Third, the use of poly(aniline) with bisulfate counterion is restricted to pH 5 and below and this is not compatible with all enzymes or enzyme assays. In the next section we address some of these challenges.

Further developments

Not all enzymes require the use of redox mediators to achieve oxidation or reduction at electrode surfaces. For glucose oxidase the flavin redox active site is buried deep within the core of the protein, making direct oxidation at an electrode very difficult, but this is not the case for all enzymes. For horseradish

peroxidase (E.C. 1.11.1.7) the haem redox site is located at the periphery of the enzyme and is solvent accessible. In this case direct reduction of the haem at electrode surfaces is possible.[37–39] Horseradish peroxidase can also be directly reduced at poly(aniline) coated electrodes[40] and so it is possible to make microelectrochemical enzyme transistors responsive to hydrogen peroxide using horseradish peroxidase as the catalyst.[41] In this case the reactions are those in eqns. (9) and (10).

$$H_2O_2 + HRP(red) \rightarrow HRP(compound\ I) + H_2O \quad (9)$$

$$HRP\ (compound\ I) + PANi(red) \rightarrow HRP(red) + PANi(ox) \quad (10)$$

In this case the poly(aniline) is converted from its reduced, conducting, emeraldine form to its oxidised, insulating, pernigraniline form so that the device operates in the 'on' to 'off' direction [see Fig. 9(*b*)], rather that the other way around, as was the case for the glucose responsive device. This has an important consequence. Because the device starts in the conducting state the time taken to switch the device in any given concentration of analyte is much more sensitive to the choice of setting potential for the poly(aniline) film (the initial value of E_{gate}). This is because the more cathodic the initial gate potential the greater the amount of charge that must be removed from the polymer before its conductivity will change significantly, switching the device 'off'. In contrast, for the glucose responsive device the poly(aniline) starts in the insulating state where the capacitance of the polymer is orders of magnitude lower. As a result small differences in the initial gate voltage make no difference in the switching time for the device and for the same reason the switching times are significantly faster.[41] The clear conclusion from this comparison is that, if possible, it is better to configure devices so that they operate in the 'off' to 'on' direction than *vice versa*.

The work described above for both glucose and hydrogen peroxide responsive devices was all carried out using poly(aniline) at pH 5. It is obviously desirable to remove this constraint and to be able to work at neutral pH. For poly(aniline) the problem is that the emeraldine form of the polymer deprotonates above about pH 5 (see Fig. 6 above) and that the deprotonated form is not an electronic conductor. For a poly(aniline) film the deprotonation of the emeraldine form is associated with the egress from the film of both the protons and the associated counter anions, [Fig. 10(*a*)]. This is only possible if the counter anions are small and mobile, for example chloride or bisulfate anions. If these mobile counter anions are replaced by long chain polymeric counter anions these become trapped within the poly(aniline) film and the overall process changes [Fig. 10(*b*)]. Now if the protons leave the film they must be replaced by cations from the solution in order to maintain electroneutrality. As a consequence of this change the conductivity of the poly(aniline) can be maintained to much higher pH[42] [in effect there is a Donnan type potential established across the poly(aniline) solution interface which alters the electrochemical potential of the protons within the film]. We have made use of this effect to deposit films of poly(aniline) with polymer counterions such as poly(vinylsulfonate) or poly(styrenesulfonate) which remain electrochemically active and conducting at neutral pH. These composite films can be used to make microelectrochemical enzyme transistors responsive to glucose[43] and to make devices responsive to NADH operating at pH 7.[44] In the latter case no enzyme is required because poly(aniline) is an excellent catalytic surface for the oxidation of NADH to NAD^+.[45]

Thus for glucose we have shown that we can make microelectrochemical enzyme transistors which respond rapidly and reproducibly,[25,30,31] that such devices show sensitivity to low glucose concentrations,[36] and that we can make them operate at pH 7.[43] However in all cases it has been necessary to use a freely diffusing redox mediator to couple the oxidation of the reduced flavin to the reduction of the poly(aniline). There

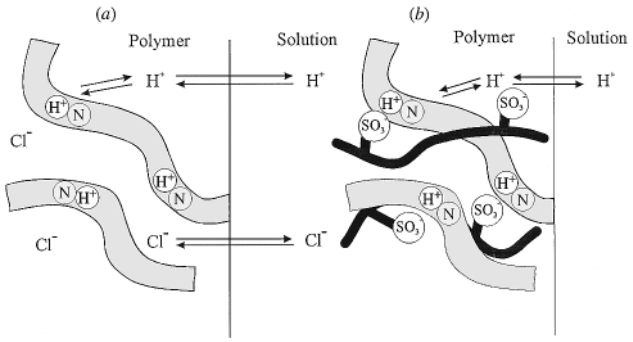

Fig. 10 Protonation equilibria for poly(aniline) films. For poly(aniline) grown with a mobile anion (*a*), such as chloride, the emeraldine state of the polymer can deprotonate on contact with neutral solutions by simultaneous expulsion of protons and chloride ions to leave the insulating emeraldine base. In contrast, for poly(aniline) films grown with long chain polymeric anions (*b*), such as poly(styrenesulfonate), the polymer can only deprotonate if it exchanges protons for cations from the solution. As a result the emeraldine form of the polymer remains protonated even when placed in contact with neural solution.

are two potential strategies to overcome this problem. The first, following the work of Heller on redox hydrogels,[7] is to use a redox polymer deposited on top of the poly(aniline) to establish electrochemical communication between the enzyme and the conducting polymer. Another alternative is to covalently attach the redox mediator to the enzyme.[5,6,46] Both approaches have been demonstrated in amperometric measurements and should work with microelectrochemical enzyme transistors if the redox potentials and rate constants for mediation are suitable.

Conclusions

Microelectrochemical enzyme transistors are good examples of integrated chemical systems as described by Wrighton[47] and Bard.[48] They are constructed by combining together, in a spatially organised manner, a number of distinct chemical components. These components (conducting polymer, insulating polymer, redox enzyme, redox mediator *etc*.) are each individually selected to perform a particular role in the final device and each possess different specific properties. By combining these discrete components in the proper way we are able to make functioning molecular devices. An important aspect of this approach is in the methods used to construct the final devices. These methods need to allow spatial control over the localisation of the different components. In constructing our microelectrochemical enzyme transistors we have used electrochemical polymerisation and adsorption to localise and immobilise the different components onto structures made using screen printing or photolithographic methods.

We believe that the prospects for the exploitation of microelectrochemical enzyme transistors and related devices are good. Their construction and operation is compatible with the current developments of disposable microsensor structures, sensor arrays[49–51] and conducting polymer based electronic circuits.[52] Microelectrochemical enzyme transistors offer significant advantages for the detection of analytes at low concentrations as a result of the inherent integration of the analyte signal and amplification that they provide. These features could be of significant benefit in developing small, disposable devices for immunoassay and DNA assay applications. Finally we note that the output of a microelectrochemical enzyme transistor can be treated digitally, that is it is possible to use such devices to make digital, as opposed to the conventional analogue, chemical sensors. In such devices the concentration of the analyte is encoded as a frequency of switching rather than as an analogue voltage or current. This is an as yet unexplored area. In addition, by combining arrays of microelectrochemical

enzyme transistors responsive to different analytes it is, in principle, possible to make devices which perform simple logical operations, again opening up a new and potentially useful field of study.

Notes and references

1 M. J. Eddowes, D. G. Pedley and B. Webb, *Sens. Actuators*, 1985, **7**, 233.
2 L. C. Clark, *Biosens. Bioelectron.*, 1993, **8**, iv.
3 A. E. G. Cass, G. Davis, G. D. Francis, H. A. O. Hill, W. J. Aston, I. J. Higgins, E. V. Plotkin, L. D. L. Scott and A. P. F. Turner, *Anal. Chem.*, 1984, **56**, 667.
4 H. J. Hecht, H. M. Kalisz, J. Hendle, R. D. Schmid and D. Schomburg, *J. Mol. Biol.*, 1993, **229**.
5 P. N. Bartlett, R. G. Whitaker, M. J. Green and J. Frew, *J. Chem. Soc., Chem. Commun.*, 1987, 1603.
6 Y. Degani and A. Heller, *J. Phys. Chem.*, 1987, **91**, 1285.
7 A. Heller, *J. Phys. Chem.*, 1992, **96**, 3579.
8 C. Sun, P.-H. Ho-Si and D. J. Harrison, *Langmuir*, 1991, **7**, 727.
9 A. Szucs, G. D. Hitchens and J. O. M. Bockris, *J. Electrochem. Soc.*, 1989, **136**, 3748.
10 H. S. White, G. P. Kittlesen and M. S. Wrighton, *J. Am. Chem. Soc.*, 1984, **106**, 5375.
11 J. Heinze, *Top. Curr. Chem.*, 1990, **152**, 3.
12 E. J. Calvo, R. Etchenique, P. N. Bartlett, K. Singhal and C. Santamaria, *J. Chem. Soc., Faraday Discuss.*, 1997, **107**, 141.
13 A. R. Hillman, D. C. Loveday, M. J. Swann, S. Bruckenstein and C. P. Wilde, *J. Chem. Soc., Faraday Trans.*, 1991, **87**, 2047.
14 G. P. Kittlesen, H. S. White and M. S. Wrighton, *J. Am. Chem. Soc.*, 1984, **106**, 7389.
15 E. P. Lofton, J. W. Thackeray and M. S. Wrighton, *J. Phys. Chem.*, 1986, **90**, 6080.
16 E. W. Paul, A. J. Ricco and M. S. Wrighton, *J. Phys. Chem.*, 1985, **89**, 1441.
17 T. E. Turner Jones, O. M. Chyan and M. S. Wrighton, *J. Am. Chem. Soc.*, 1987, **109**, 5526.
18 J. W. Thackeray, H. S. White and M. S. Wrighton, *J. Phys. Chem.*, 1985, **89**, 5133.
19 J. W. Thackeray and M. S. Wrighton, *J. Phys. Chem.*, 1986, **90**, 6674.
20 M. S. Wrighton, J. W. Thackeray, M. J. Natan, D. K. Smith, G. A. Lane and D. Belanger, *Phil. Trans. R. Soc. Lond. B*, 1987, **316**, 13.
21 M. Umãna and J. Waller, *Anal. Chem.*, 1986, **58**, 2979.
22 N. C. Foulds and C. R. Lowe, *J. Chem. Soc., Faraday Trans. 1*, 1986, **82**, 1259.
23 P. N. Bartlett and J. Cooper, *J. Electroanal. Chem.*, 1993, **362**, 1.
24 T. Matsue, M. Nishizawa, T. Sawaguchi and I. Uchida, *J. Chem. Soc., Chem. Commun.*, 1991, 1029.
25 P. N. Bartlett and P. R. Birkin, *Synth. Met.*, 1993, **61**, 15.
26 D. Belanger, J. Nadreau and G. J. Fortier, *J. Electroanal. Chem.*, 1989, **274**, 143.
27 P. N. Bartlett, Z. Ali and V. Eastwick-Field, *J. Chem. Soc., Faraday Trans.*, 1992, **88**, 2677.
28 G. Inzelt and G. Horanyi, *Electrochim. Acta*, 1990, **35**, 27.
29 W. S. Huang, B. D. Humphrey and A. G. MacDiarmid, *J. Chem. Soc., Faraday Trans. 1*, 1986, **82**, 2385.
30 P. N. Bartlett and P. R. Birkin, *Anal. Chem.*, 1993, **65**, 1118.
31 P. N. Bartlett and P. R. Birkin, *Anal. Chem.*, 1994, **66**, 1552.
32 C. Malitesta, F. Palmisano, L. Torsi and P. G. Zambonin, *Anal. Chem.*, 1990, **62**, 2735.
33 M. Nishizawa, T. Matsue and I. Uchida, *Anal. Chem.*, 1992, **64**, 2641.
34 M. Nishizawa, T. Matsue and I. Uchida, *Sens. Actuators, B*, 1993, **13-14**, 53.
35 D. T. Hoa, T. N. Suresh Kumar, N. S. Punekar, R. S. Srinivasa and R. Lal, *Anal. Chem.*, 1992, **64**, 2645.
36 P. N. Bartlett, J. H. Wang and W. James, *Analyst*, 1998, **123**, 387.
37 L. Gorton, G. Jonsson-Peterson, E. Csoregi, K. Johansson, E. Dominguez and G. Marko-Varga, *Analyst*, 1992, **117**, 1235.
38 U. Wollenberger, J. Wang, M. Ozsos, E. Gonzalez-Romero and F. Scheller, *Bioelectrochem. Bioenerg.*, 1991, **26**, 287.
39 G. Jonsson and L. Gorton, *Electroanalysis*, 1989, **1**, 465.
40 P. N. Bartlett, P. R. Birkin, F. Palmisano and G. De Benedetto, *J. Chem. Soc., Faraday Trans.*, 1996, **92**, 3123.
41 P. N. Bartlett, P. R. Birkin, J. H. Wang, F. Palmisano and G. De Benedetto, *Anal. Chem.*, 1998, **70**, 3685.
42 G. E. Asturias, G. W. Jang, A. G. MacDiarmid, Z. Doblhofer and C. Zhong, *Ber. Bunsenges. Phys. Chem.*, 1991, **95**, 1381.
43 P. N. Bartlett and J. H. Wang, *J. Chem. Soc., Faraday Trans.*, 1996, **92**, 4137.
44 P. N. Bartlett, J. H. Wang and E. N. K. Wallace, *Chem. Commun.*, 1996, 359.
45 P. N. Bartlett, P. R. Birkin and E. N. K. Wallace, *J. Chem. Soc., Faraday Trans.*, 1997, **91**, 1951.
46 P. N. Bartlett, S. Booth, D. J. Caruana, J. D. Kilburn and C. Santamaria, *Anal. Chem.*, 1997, **69**, 734.
47 M. S. Wrighton, *Comments Inorg. Chem.*, 1985, **4**, 269.
48 A. J. Bard, *Integrated Chemical Systems. A Chemical Approach to Nanotechnology*, Wiley, New York, 1994.
49 M. B. Madaras, I. C. Popescu, S. Ufer and R. P. Buck, *Anal. Chim. Acta*, 1996, **319**, 335.
50 M. B. Madaras and R. P. Buck, *Anal. Chem.*, 1996, **68**, 3832.
51 G. Nagy, X. X. Clarke and R. P. Buck, *Anal. Chem.*, 1998, **70**, 2156.
52 C. J. Drury, C. M. J. Mutsaers, C. M. Hart, M. Matters and D. M. de Leeuw, *Appl. Phys. Lett.*, 1998, **73**, 108.
53 M. Dixon and E. C. Webb, *Enzymes*, Longman, London, 1979.

Paper a902905b

Stabilisation of charge-separated states *via* gain of aromaticity and planarity of the donor moiety in C_{60}-based dyads

Nazario Martín,*[a] Luis Sánchez[a] and Dirk M. Guldi*[b]

[a] *Departamento de Química Orgánica I, Facultad de Química, Universidad Complutense, E-28040 Madrid, Spain*
[b] *Radiation Laboratory, University of Notre Dame, Indiana, USA. E-mail: nazmar@eucmax.sim.ucm.es*

Received (in Liverpool, UK) 2nd November 1999, Accepted 26th November 1999

The gain of aromaticity and planarity, associated with the oxidation of a π-extended TTF electron donor, is the key feature for obtaining strong stabilisation of photolytically generated radical pairs in novel C_{60}-based dyads.

The remarkable electron-acceptor properties of fullerenes[1] evoked the implementation of fullerenes as an electron acceptor unit in the design of novel artificial light harvesting superstructures.[2] One viable approach to photosynthesis modelling has been the covalent linkage of various redox active chromophores. In this context, light-induced intramolecular charge-separation (CS) has been reported for several C_{60}-based donor–acceptor systems endowed with various electron donors. CS evolves, in most of these systems, from the singlet excited state of the fullerene unit through a series of small distance intramolecular electron transfer events yielding a charge-separated state.[3,4]

The ultimate goal is to design a system that converts sunlight into a usable form of energy with a near unit quantum efficiency. The key to accomplish this is to optimise the stability of the charge-separated state. This requirement led researchers to pursue two important concepts: (i) the increase of the donor–acceptor separation, and (ii) the use of multicomponent systems (donor–acceptor triads, tetrads, *etc.*) either in conjunction or separately.[5]

We reported recently a strategy probing organic donor molecules [*e.g.* tetrathiafulvalenes (TTFs)], linked to the fullerene core, that gain rather than lose aromaticity on CS. In particular, the one-electron oxidised form of TTF forms the 1,3-dithiolium cation, which, in contrast to the ground state, displays an extended aromatic character.[6] In fact, the lifetime of the charge-separated state was increased by a factor of *ca.* 4 relative to comparable systems that do not contain TTF.[6]

Here we present the synthesis of novel fulleroids and methanofullerenes endowed with highly conjugated TTFs having a *p*-quinodimethane structure. Cyclic voltammetry is combined with optical absorption and emission spectroscopy to study the electronic properties and excited-state interactions in dyads **3a**,**b** and **4a**,**b**.

The motivation for the current work stems from the possibility of obtaining a higher degree of stabilisation of the oxidised donor *via* adding aromatic arenes to the heteroaromatic rings of TTF. Addition of the latter is expected to enhance the aromatic stabilisation energy. In the oxidised form, the π-conjugation is extended over the entire anthracene backbone and as a net result, the dicationic species is completely aromatic.[7]

The syntheses of dyads **3a**,**b** and **4a**,**b** were carried out by a cycloaddition reaction of diazo compounds with C_{60}.[8] In the present case, diazo compounds are generated *in situ* from the extended TTF containing *p*-tosylhydrazones (**2a**,**b**) by treatment with base. Compounds **2a**,**b** are in turn prepared in good yields from the respective aldehydes (**1a**,**b**)[9] and toluene-*p*-sulfonohydrazide (Scheme 1).

The reaction of *p*-tosylhydrazones (**2a**,**b**) with C_{60} under basic conditions in toluene at 70 °C afforded the kinetic product **3a**,**b** in 27–31% yield as a mixture of the two possible [5,6] isomers.[10] [6,6]Methanofullerenes (**4a**,**b**) were prepared either under basic conditions from *p*-tosylhydrazones (**2a**,**b**) with C_{60} in refluxing toluene or from the respective [5,6]fulleroid (**3a**,**b**) by refluxing for 30 h in toluene in quantitative yield.

The ^{1}H NMR spectra of fulleroids **3a**,**b** confirm the presence of both [5,6] isomers, showing the combination of two singlets at δ 6.9 ppm (*i.e.* the isomer with the methylene hydrogen atom above a five-membered ring) and 4.1 (*i.e.* the isomer with the methylene hydrogen atom above a six-membered ring).[11] In contrast, [6,6]methanofullerenes (**4a**,**b**) give rise to a typical ^{1}H NMR singlet at δ ~5.2 corresponding to the cyclopropane proton.†

All compounds studied show the presence of four one-electron reduction steps of the fullerene core, similar to those found for the parent C_{60}, though the underlying reduction potentials are shifted to more negative values. This shift evolves from the partial loss of conjugation of the C_{60} sphere, which raises the LUMO energy of the resulting modified fullerenes.[12] Although the [5,6]fulleroids do not undergo the loss of conjugation and retain the 60π electron configuration of C_{60}, essentially no difference in the reduction potentials were found between the two isomers (*i.e.* [5-6] *vs.* [6-6], see Table 1).[13] In the anodic region, a single two-electron oxidation wave, to form the dication of the TTF moiety, was noticed for all dyads (**3a**,**b** and **4a**,**b**).[7]

Pico- and nano-second-resolved transient absorption measurements with C_{60}–(π-extended)TTF donor–acceptor dyads (**3a**,**b** and **4a**,**b**) in toluene, CH_2Cl_2 and PhCN reveal the instantaneous formation of the fullerene singlet excited state.

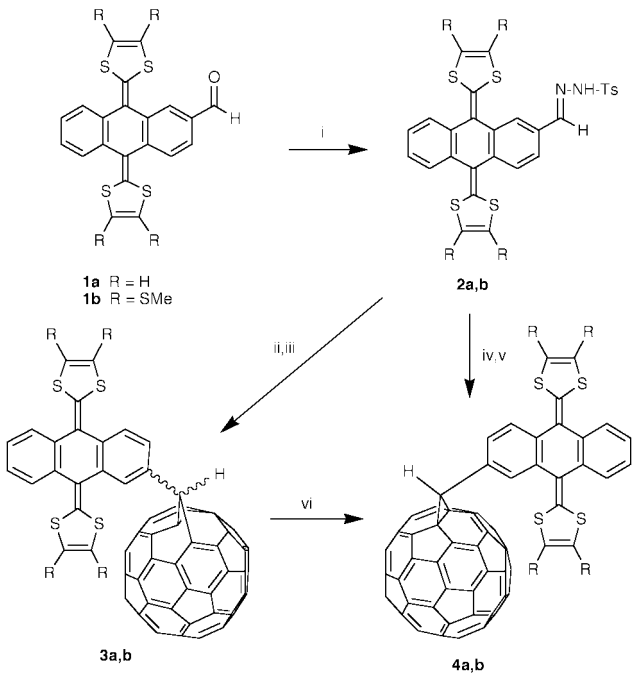

Scheme 1 *Reagents and conditions*: i, $TsNHNH_2$, $CHCl_3$; ii, MeONa, Py; iii, C_{60}, PhMe, 70 °C; iv, MeONa, Py; v, C_{60}, PhMe, reflux; vi, PhMe, reflux.

Table 1 Data for **3a**,**b** and **4a**,**b**

Compound	Solvent	$\Theta/10^{-4}$	τ/ns			E_{red}/V[a]	E_{ox}/V[a]
		Fluorescence	Fluorescence	Singlet	Charge separation		
3a	PhMe	0.42	0.191	0.124	not measured		
3a	CH_2Cl_2	0.18	0.135	0.104	150	−0.68, −1.12, −1.62, −2.00	0.48
3a	PhCN	0.06	< 0.1	0.051	202		
3b	PhMe	1.86	0.410	0.329	not measured		
3b	CH_2Cl_2	1.04	0.250	0.176	107	−0.65, −1.07, −1.59, −1.95	0.59
3b	PhCN	0.41	< 0.1	0.104	211		
4a	PhMe	0.48	0.230	0.176	not measured		
4a	CH_2Cl_2	0.18	0.190	0.113	110	−0.67, −0.99, −1.59, −1.95	0.45
4a	PhCN	0.06	< 0.1	0.099	220		
4b	PhMe	2.1	0.379	0.400	not measured		
4b	CH_2Cl_2	1.34	0.343	0.316	95	−0.64, −0.98, −1.61, −1.95	0.55
4b	PhCN	0.54	< 0.1	0.140	180		
C_{60}						−0.60, −1.07, −1.64, −1.93	
5[b]							0.45

[a] In V *vs.* SCE; GCE; $Bu_4N^+ClO_4^-$ (0.1 M); PhMe–MeCN (4:1); 200 mV s^{-1}; **5**: 9,10-bis(1,3-dithiol-2-ylidene)-9,10-dihydroanthracene; in CH_2Cl_2.

Due to the presence of the electron donor [*i.e.* (π-extended)TTF] the singlet excited state absorption (λ_{max} ~ 880 nm) transforms rapidly into a broadly absorbing product. It should be noted that the decay kinetics of the singlet excited state absorption correlates with the grow-in kinetics of the new species.

Spectroscopic evidence suggests that this newly formed transient can be ascribed to the charge-separated radical pair, namely, $C_{60}^{\bullet-}$–(π-extended)$TTF^{\bullet+}$. In particular, maxima at 660 and 680 nm are in excellent agreement with the pulse radiolytically generated (π-extended)TTF π-radical cations at 660 (R = H) and 675 nm (R = SMe), respectively.[14] On the other hand, the two isomeric fullerenes give rise to different π-radical anion absorptions at 1040 ([6-6]-closed)[15] and 1070 nm ([6-5]-open).[16]

Generally, the intramolecular ET rates (see Table 1) depend on (i) the donor strength of the π-extended tetrathiafulvalene derivative (*e.g.* R = H *vs.* R = SMe), (ii) the excited state energy of the fullerene derivative (*e.g.* [6-6]-closed *vs.* [6-5]-open isomer) and (iii) the solvent polarity (*e.g.* toluene *vs.* PhCN).

Independent confirmation for the rapid and, more importantly, solvent-dependent deactivation of the fullerene singlet excited state in dyads **3a**,**b** and **4a**,**b** evolves from complementary fluorescence measurements. The fluorescence quantum yields (Θ) and also the fluorescence lifetimes (τ) showed, beside a marked solvent dependence, a correlation with the donor strength of the TTF moiety. Specifically, Θ and τ values in photoexcited **3a** and **4a** are lower relative to **3b** and **4b**, respectively.

The lifetimes of the charge-separated states in all these C_{60}–(π-extended)TTF dyads (**3a**,**b** and **4a**,**b**) are remarkable. For example, they are in the range of several hundred nanoseconds in deoxygenated PhCN and slightly lower in the less polar CH_2Cl_2. In contrast, the parent TTF dyads (*e.g.* a donor moiety that undergoes simply a gain of aromaticity upon oxidation) or zinc tetraphenylpoprhyrin dyads (*e.g.* an electron donor which lacks both the gain in planarity and in aromaticity upon oxidation) yielded radical pairs with lifetimes of about 2[6] and 0.5 ns,[4] respectively. Therefore, we rationalise the increased stability of the $C_{60}^{\bullet-}$-(π-extended)$TTF^{\bullet+}$ pair with the stabilisation of the donor. The gain of aromaticity and planarity, associated with this oxidation, yields a state of lower energy. Consequently, reduction of the oxidised (π-extended)TTF donor, in a sense of charge recombination, requires a higher activation energy to proceed than the corresponding processes in C_{60}–TTF and C_{60}–ZnTPP dyads.

We are indebted to DGICYT (Project PB98-0818) for financial support. Part of this work was supported by the Office of Basic Energy Sciences of the U.S. Department of Energy (contribution No. NDRL-4188 from the Notre Dame Radiation Laboratory).

Notes and references

† *Selected data* for **4b**: 34% yield (100% from **3b**); ν_{max}(KBr)/cm^{-1} 1545, 1450, 1276, 800, 754, 644, 526 cm; δ_H($CDCl_3$–CS_2, 2:1, 300 MHz) 8.08 (1H, s), 7.87 (1H, m), 7.69 (1H, m), 7.53 (2H, m), 7.31 (2H, m), 5.41 (1H, s), 2.43 (12H, m); δ_C($CDCl_3$–CS_2, 2:1, 75 MHz) 151.6, 149.4, 145.5, 145.0, 144.9, 144.5, 144.4, 144.2, 143.9, 143.5, 142.8, 140.7, 136.4, 136.3, 135.1, 134.5, 134.3, 134.2, 134.1, 130.8, 130.5, 128.9, 128.6, 127.8, 126.4, 126.3, 125.5, 125.4, 125.3, 125.2, 122.9, 109.8, 107.5, 77.2, 75.1, 43.1, 29.8, 29.7, 29.6, 29.4; λ_{max}(CH_2Cl_2)/nm (log ε) 264 (4.49), 326 (4.18), 364 (4.18), 420 (4.00), 434 (4.03); *m/z* (FAB^+) 1296 (M^+, 21%).

1 L. Echegoyen and L. Echegoyen, *Acc. Chem. Res.*, 1998, **31**, 593.
2 H. Kurreck and M. Hüber, *Angew. Chem., Int. Ed. Engl.*, 1995, **34**, 849.
3 N. Martín, L. Sánchez, B. Illescas and I. Pérez, *Chem. Rev.*, 1998, **98**, 2527.
4 H. Imahori and Y. Sakata, *Adv. Mater.*, 1997, **9**, 537; H. Imahori and Y. Sakata, *Eur. J. Org. Chem.*, 1999, 2445.
5 K. A. Jolliffe, S. J. Langford, M. G. Ranasinghe, M. J. Shephard and M. N. Paddon-Row, *J. Org. Chem.*, 1999, **64**, 1238.
6 N. Martín, L. Sánchez, M. A. Herranz and D. M. Guldi, submitted for publication.
7 N. Martín, L. Sánchez, C. Seoane, E. Ortí, P. M. Viruela and R. Viruela, *J. Org. Chem.*, 1998, **63**, 1268; M. R. Bryce, A. J. Moore, M. Hasan, G. J. Ashwell, A. T. Fraser, W. Clegg, M. B. Hursthouse and A. I. Karaulov, *Angew. Chem., Int. Ed. Engl.*, 1990, **29**, 1450.
8 T. Suzuki, Q. Li, K. C. Khemani, F. Wudl and Ö. Almarsson, *Science*, 1991, **254**, 1186.
9 N. Martín, I. Pérez, L. Sánchez and C. Seoane, *J. Org. Chem.*, 1997, **62**, 5690.
10 For the first preparation of fulleroids from *p*-tosylhydrazones, see: J. C. Hummelen, B.W. Knight, F. LePeq and F. Wudl, *J. Org. Chem.*, 1995, **60**, 532.
11 M. Prato, V. Luccini, M. Maggini, E. Stimpfl, G. Scorrano, G. Eirmann, T. Suzuki and F. Wudl, *J. Am. Chem. Soc.*, 1993, **115**, 8479.
12 M. Maggini, A. Karlsson, G. Scorrano, G. Sandona, G. Farnia and M. Prato, *J. Chem. Soc., Chem. Commun.*, 1994, 589.
13 M. Eiermann, F. Wudl, M. Prato and M. Maggini, *J. Am. Chem. Soc.*, 1994, **116**, 8364.
14 D. M. Guldi, N. Martín and L. Sánchez, unpublished results.
15 D. M. Guldi, H. Hungerbühler and K.-D. Asmus, *J. Phys. Chem.*, 1995, **99**, 9380.
16 Since this is the first report on the π-radical anion absorption band of a [6-5]-open fulleroid, we conducted complementary pulse radiolytic experiments to reduce the fullerene under experimental conditions described in ref. 15. The recorded spectrum with λ_{max} at 1070 nm is identical to the photolytically generated spectrum and, thus, serves as additional confirmation for the spectral assignment.

Communication a908770b

Conjugate addition of diethylzinc to α,β-unsaturated lactones catalyzed by copper–phosphite complexes

Ming Yan, Zhong-Yuan Zhou and Albert S. C. Chan*

Open Laboratory of Chirotechnology and Department of Applied Biology and Chemical Technology, The Hong Kong Polytechnic University, Hong Kong, China. E-mail: bcachan@polyu.edu.hk

Received (in Cambridge, UK) 25th October 1999, Accepted 23rd November 1999

Highly enantioselective conjugate addition of diethylzinc to α,β-unsaturated lactones was achieved by using chiral diphosphite–copper catalysts; the structure of a chiral diphosphite–copper(I) catalyst was determined by single crystal X-ray diffraction.

The enantioselective conjugate addition of organometallic reagents to α,β-unsaturated ketones and esters provides an efficient method for asymmetric carbon–carbon bond formation in organic synthesis.[1] In recent years copper complexes of various chiral phosphorus ligands have been used as efficient catalysts for the conjugate addition of organozinc reagents to enones,[2] but there are no reports concerning the asymmetric conjugate addition of organozinc reagents to α,β-unsaturated lactones. Tomioka reported the enantioselective conjugate addition of Grignard reagents to 5,6-dihydro-2*H*-pyran-2-one catalyzed by a chiral phosphine–copper iodide catalyst with good enantioselectivity. However, a high loading of chiral ligand (32 mol%) was necessary to achieve high enantioselectivity.[3] Recently we found chiral aryl diphosphites to be efficient ligands for the copper-catalyzed conjugate addition of diethylzinc to cyclic enones.[4,5] Here we report the enantioselective conjugate addition of diethylzinc to α,β-unsaturated lactones with chiral diphosphite–copper catalysts. A cationic chiral diphosphite–copper(I) catalyst was isolated and its structure was determined by single crystal X-ray diffraction.

Table 1 Conjugate addition of diethylzinc to α,β-unsaturated lactones catalyzed by copper–phosphorus complexes[a]

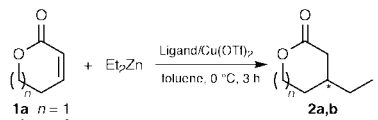

1a $n = 1$
b $n = 0$

2a,b

Entry	Ligand	Substrate	Conversion (%)[b]	Ee (%)[b]
1	—	**1a**	—	—
2	PPh_3	**1a**	14.3	—
3	$P(OPh)_3$	**1a**	10	—
4	$P(OEt)_3$	**1a**	17	—
5	$\mathbf{L_a}$	**1a**	68.4	10
6	$\mathbf{L_b}$	**1a**	66.9	16.8
7	$\mathbf{L_c}$	**1a**	100	73
8	$\mathbf{L_c}$	**1b**	85.2	38.5
9	$\mathbf{L_d}$	**1a**	100	92
10[c]	$\mathbf{L_d}$	**1a**	100	91.1
11[d]	$\mathbf{L_d}$	**1a**	100	86.7
12[e]	$\mathbf{L_d}$	**1a**	93	88.3
13	$\mathbf{L_d}$	**1b**	77	56.0
14	$\mathbf{L_e}$	**1a**	94.6	89.5
15	$\mathbf{L_e}$	**1b**	100	38.6

[a] The reactions were carried out in toluene at 0 °C for 3 h (copper : ligand : substrate : Et_2Zn = 0.01 : 0.02 : 1 : 1.5). [b] The data on conversion and the ee values of **2a** and **2b** were determined by GC with a Chiraldex A-TA column (30 m × 0.25 mm). [c] $[Cu(OTf)]_2$·benzene was used as the source of copper ($\mathbf{L_d}$/Cu = 2). [d] $[Cu(OTf)]_2$·benzene was used as the source of copper ($\mathbf{L_d}$/Cu = 1). [e] Isolated $[Cu\mathbf{L_d}(MeCN)_2]^+$ $CF_3SO_3^-$ was used as the catalyst.

The conjugate addition of diethylzinc to 5,6-dihydro-2*H*-pyran-2-one **1a** was selected as a model reaction. Typically the reaction was carried out in toluene at 0 °C for 3 h, using 1 mol% $Cu(OTf)_2$ and phosphorus ligands (4 mol% monodentate phosphorus ligands or 2 mol% bidentate phosphorus ligands) as the catalysts, and the results are summarized in Table 1.

$Cu(OTf)_2$ did not show catalytic activity activity in the absence of phosphorus ligands (entry 1). The $Cu(OTf)_2$ complexes of PPh_3, $P(OPh)_3$ and $P(OEt)_3$ showed low catalytic activity (entries 2–4).[6] Chiral phosphite $\mathbf{L_a}$ and phosphorus amidite $\mathbf{L_b}$ provided higher acceleration effects, but the enantioselectivities were rather poor (entries 5 and 6).[7,8] When aryl diphosphite $\mathbf{L_c}$ and $\mathbf{L_d}$ were examined in the reaction, high catalytic activity was achieved (entries 7 and 9). In addition excellent enantioselectivity was obtained when $Cu(OTf)_2$–$\mathbf{L_d}$

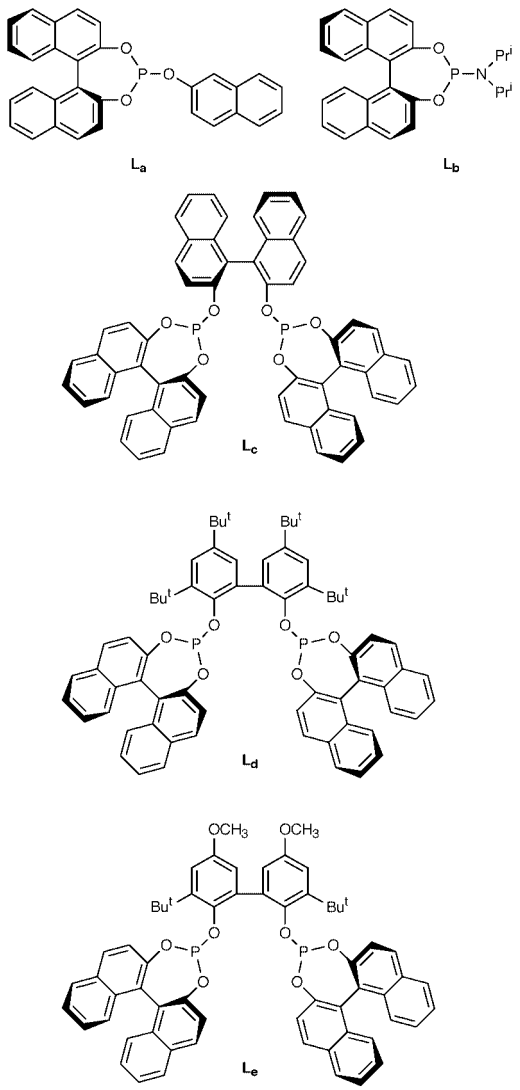

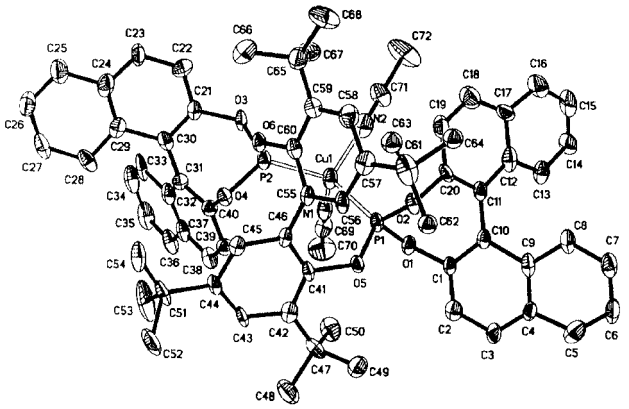

Fig. 1 ORTEP drawing of the molecular structure of [Cu$\mathbf{L_d}$(MeCN)$_2$]$^+$OTf$^-$. The triflate and hydrogen atoms have been omitted for clarity. The *tert*-butyl group (C47–C50) is disordered and only one of the disordered sets of atoms is shown. The P1–Cu–P2 angle is 119.1°. The bond lengths of P1–Cu and P2–Cu are 2.242 and 2.214 Å, respectively. The dihedral angles of the two binaphthyl units are 57.4 and 55.7°. The bridging 3,3′,5,5′-tetra-*tert*-butylbiphenol unit has a dihedral angle 61.5°.

complex was used as the catalyst (entry 9). To the best of our knowledge, this is the first example of the highly enantioselective conjugate addition of an organozinc reagent to an α,β-unsaturated lactone. The reaction was found to be highly regioselective and no 1,2-addition product was observed by GC analysis. When [Cu(OTf)]$_2$·benzene–$\mathbf{L_d}$ was tested as the catalyst in the conjugate addition of diethylzinc to **1a**, similar enantioselectivity was observed as that from using Cu(OTf)$_2$–$\mathbf{L_d}$ complex (entry 10 *vs.* entry 9). The $\mathbf{L_c}$–Cu(OTf)$_2$ and $\mathbf{L_d}$–Cu(OTf)$_2$ complexes were also tested in the addition of diethylzinc to 5*H*-furan-2-one **1b** and 38.5 and 56.0% ee were obtained respectively (entries 8 and 13).

A catalytic cycle for copper-catalyzed conjugate addition of diethylzinc to cyclic enones had been proposed by Fergina.[2a] A copper(I) species was proposed to be the catalyst in the reaction and direct evidence to support this hypothesis is desirable. To this end we carefully chose crystallization conditions and obtained colorless crystals from an MeCN solution of $\mathbf{L_d}$ and [Cu(OTf)]$_2$·benzene. A single crystal X-ray diffraction study of this species revealed a Cu$^{\text{I}}$ complex with the molecular formula [Cu$\mathbf{L_d}$(MeCN)$_2$]$^+$ OTf$^-$ which took a twist tetrahedron geometry (Fig. 1).† The *tert*-butyl group (C47–C50) is disordered.

As expected the isolated [Cu$\mathbf{L_d}$(MeCN)$_2$]$^+$OTf$^-$ crystals were also found to be an efficient catalyst in the conjugate addition of diethylzinc to **1a** (entry 12) and the enantioselectivity was similar to that obtained using the [Cu(OTf)]$_2$·benzene–$\mathbf{L_d}$ catalyst prepared *in situ* ($\mathbf{L_d}$/Cu = 1. entry 11). The X-ray crystallography of the [Cu$\mathbf{L_d}$(MeCN)$_2$]$^+$OTf$^-$ complex showed that the two terminal binaphthyl units form a good chiral pocket around the copper atom. In addition the four *tert*-butyl groups in the bridging biphenyl unit effectively fix the conformation of the complex and shield the space above the copper atom. In order to assess the importance of the *tert*-butyl groups at the 5,5′-positions of the bridging biphenyl unit, ligand $\mathbf{L_e}$ was prepared and tested for the reaction. The Cu(OTf)$_2$–$\mathbf{L_e}$ complex also gave good enantioselectivity in the conjugate addition of diethylzinc to **1a** (entry 14).

We thank The Hong Kong Polytechnic University and The Hong Kong Research Grant Council (Project number PolyU34/96P) for financial support of this study.

Notes and references

† *Crystal data* for [CuL$_\mathbf{d}$(MeCN)$_2$]OTf: $C_{72}H_{70}N_2O_6P_2Cu{\cdot}CF_3SO_3$, M = 1333.85, orthorhombic, a = 17.518(4), b = 17.524(4), c = 27.033(5) A, T = 293(2) K, space group $P2_12_12_1$, Z = 8299(3) Å^3, μ = 0.381 mm^{-1}, 18368 (R_{int} = 0.1071) independent reflections, refinement converged at a final R = 0.0623, wR = 0.1684. CCDC 182/1492. See http://www.rsc.org/suppdata/cc/a9/a908467c/ for crystallographic data in .cif format.

1 Reviews: B. E. Rossiter and H. M. Swingle, *Chem. Rev.*, 1992, **92**, 771; R. Noyori, *Asymmetric Catalysis in Organic Synthesis*, VCH, New York, 1993.
2 (*a*) B. L. Feringa, M. Pineschi, L. A. Arnold, R. Imbos and A. H. M. de Vries, *Angew. Chem., Int. Ed. Engl.*, 1997, **36**, 2620; (*b*) A. K. H. Knobel, I. H. Escher and A. Pfaltz, *Synlett*, 1997, 1429; (*c*) A. Alexakis, J. Vastra, J. Burton, C. Benhaim and P. Mangency, *Tetrahedron Lett.*, 1998, **39**, 7869.
3 M. Kanai and K. Tomioka, *Tetrahedron Lett.*, 1995, **36**, 4275.
4 M. Yan, L. W. Yang, K. Y. Wong and A. S. C. Chan, *Chem. Commun.*, 1999, 11.
5 M. Yan and A. S. C. Chan, *Tetrahedron Lett.*, 1999, **40**, 6645.
6 A. Alexakis, J. Vastra and P. Mangeney, *Tetrahedron Lett.*, 1997, **38**, 7745.
7 A. Alexakis, J. Vastra, J. Burton and P. Mangeney, *Tetrahedron: Asymmetry*, 1997, **8**, 3193.
8 A. H. M. De Vries, A. Meetsma and B. L. Feringa, *Angew. Chem., Int. Ed. Engl.*, 1996, **35**, 2374.

Communication a908467c

Pd^0-catalyzed cyclization reaction of aryl or alk-1-enyl halides with 1,2-dienyl ketones: a general and efficient synthesis of polysubstituted furans

Shengming Ma* and Junliang Zhang

Laboratory of Organometallic Chemistry, Shanghai Institute of Organic Chemistry, Chinese Academy of Sciences, 354 Fenglin Lu, Shanghai 200032, P. R. China. E-mail: masm@pub.sioc.ac.cn

Received (in Cambridge, UK) 29th October 1999, Accepted 30th November 1999

Under catalysis by Pd^0 and Ag_2CO_3, the reaction of 1,2-allenyl ketones and organic halides in PhMe using Et_3N as the base provides a new general access to polysubstituted furans with good to excellent yields.

Furans, one of the most prominent classes of heterocyclic compounds, can be found in many naturally occurring products,[1] commercially important pharmaceuticals, and flavor and fragrance compounds.[2] They are also considered as important synthetic intermediates for the preparation of numerous cyclic and acyclic compounds.[3] Usually, 3-, 2,3-, 2,4-, 3,4-, 2,3,4- and 2,3,5-substituted furans[4] can be synthesized *via* acyclic precursors or derivatization of simple furans.[5] Owing to its potential and diversity, much attention has been paid to the synthesis of furans from acyclic precursors. Some of the most important and interesting methodologies are as follows: (i) cyclization of alk-4-yn-1-ols;[6] (ii) cyclization of alk-3-yn-1-ols;[7] (iii) $AlCl_3$-catalyzed cyclization of acyl chlorides with 1,2-allenyl silanes;[8] (iv) epoxidation and subsequent HgO-catalyzed cyclization of alk-1-enyl alk-1′-ynyl methanols;[9] and (v) Pd-catalyzed cyclization of (*Z*)-2-iodoalk-2-enyl ketones.[10]

Recently, Marshall *et al.*[11] reported the Rh^+- or Ag^+-catalyzed direct one-component cyclization of 1,2-dienyl ketones to afford substituted furans with obvious limitations (mainly R^3 = H, Scheme 1). Since the introduction of substituents at the 3- and/or 4-position of the corresponding unsubstituted furans is difficult, efficient and general methodologies for furans with substituents at some or all of the four positions are still of current interest. During the course of our study of functionalized allenes,[12,13] we envisioned that a Pd^0-catalyzed cyclization of an organic halide with a 1,2-dienyl ketone would provide an efficient and general route to polysubstituted furans with the unique assembly of substituents at the different positions, depending on the substitution of both reactants (Scheme 1).[14]

1,2-Dienyl ketones with different substitution patterns are easily available.[12c,14b,15] As a starting point, we studied the Pd^0-

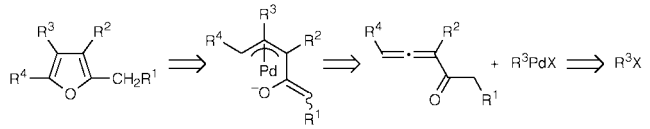

Scheme 1

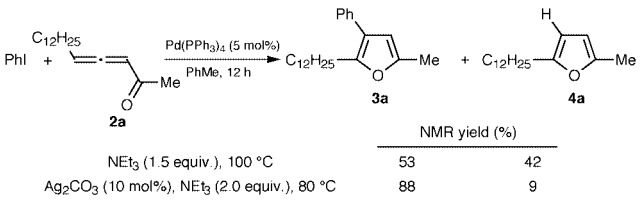

Scheme 2

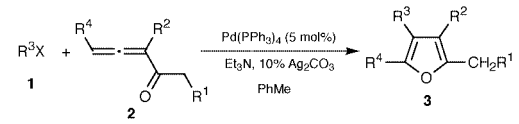

R^3X = PhI (**1a**)
p-Nitrophenyl iodide (**1b**)
p-Methoxycarbonylphenyl iodide (**1c**)
5-Bromopyrimidine (**1d**)
Methyl (*Z*)-3-iodopropenoate (**1e**)
p-Methoxyphenyl iodide (**1f**)

Scheme 3

Table 1 Efficient synthesis of polysubstituted furans[a]

Entry	R^3X[b]	Ketone **2**	R^1	R^2	R^4	*T*/°C	*t*/h	Product (% yield)[c]
1	**1a** (2.0)	**2a**	H	H	$C_{12}H_{25}$	80	12	**3a** (75)
2	**1b** (2.0)	**2a**	H	H	$C_{12}H_{15}$	80	13	**3b** (90)
3	**1c**	**2a**	H	H	$C_{12}H_{15}$	80	14	**3c** (94)
4	**1a**	**2b**	H	H	Bu	80	12	**3d** (73)
5	**1b**	**2b**	H	H	Bu	80	9	**3e** (92)
6	**1c**	**2b**	H	H	Bu	80	9	**3f** (85)
7	**1d**	**2b**	H	H	Bu	80	11	**3g** (71)
8	**1e**	**2b**	H	H	Bu	80	11	**3h**[d] (61)
9	**1c**	**2c**	H	Me	H	100	14	**3i** (68)
10	**1b**	**2c**	H	Me	H	100	11	**3j** (79)
11	**1d**	**2d**	H	Bu	H	100	17	**3k** (97)
12	**1b**	**2e**	H	H	Ph	80	10	**3l** (51)
13	**1c**	**2e**	H	H	Ph	80	10	**3m** (51)
14	**1b**	**2f**	Et	H	Ph	80	12	**3n** (77)
15	**1c**	**2f**	Et	H	Ph	80	12	**3o** (73)
16	**1f**	**2b**	H	H	Bu	80	11	**3p** (66)
17	**1f**	**2g**	H	H	C_7H_{15}	80	11	**3q** (63)

[a] Generally, the reaction was carried out using 1,2-allenyl ketone (1.5 equiv.), R^3X (1.0 equiv.), and 5 mol% of $Pd(PPh_3)_4$ in PhMe, unless otherwise stated. [b] The numbers in the parenthesis are the equiv. of R^3X used. [c] Isolated yield. [d] The configuration of the C=C bond in R^3 is *trans*.

catalyzed cyclization reaction of heptadeca-3,4-dien-2-one **2a** with PhI under various reaction conditions. After some screening, we found that the $Pd(PPh_3)_4$-catalyzed cyclization reaction of PhI with **2a** afforded the expected product **3a** in 88% yield together with the formation of **4a** in only 9% yield by using 5 mol% ($Pd(PPh_3)_4$ as the catalyst, toluene as the solvent, and Et_3N (2.0 equiv.)–Ag_2CO_3 (10 mol%) as the base. Similar to the cyclization reaction of 1,2-allenic carboxylic acids, we observed that a catalytic amount of Ag_2CO_3 is crucial to this reaction (Scheme 2).

Using these standard conditions, we studied this new and efficient synthetic methodology for the synthesis of polysubstituted furans with differently substituted 1,2-dienyl ketones as well as different kinds of organic halides (Scheme 3). The results are summarized in Table 1.

The results in Table 1 show that (i) the yields for this reaction range from moderate to excellent, with the highest being 97% (entry 11, Table 1); (ii) both electron-rich and electron-deficient aryl halides afforded the corresponding furans; (iii) substituents at different positions of furans could be introduced, depending on the structure of allenyl ketones and organic halides; and (iv) the reaction of methyl (*Z*)-3-iodopropenoate[16] yielded the product **3h**, providing an opportunity for further elaboration of the substitutions at the 4-position (entry 8, Table 1).

In conclusion, we have developed an efficient method for the synthesis of substituted furans with different substitution patterns. The study of new methodologies for differently substituted 1,2-allenyl ketones and the scope of this cyclization reaction, as well as its application in the synthesis of target molecules with potential activities, are currently being carried out in our laboratory.

We are grateful to the National Natural Science Foundation of China, the Chinese Academy of Sciences and the Shanghai Municipal Committee of Science and Technology for financial support. S.M. thanks the Hong Kong Qiu Shi Foundation of Science and Technology for the 1999 Qiu Shi Award for Young Scientific Workers (1999–2003).

Notes and references

1 F. M. Dean, in *Comprehensive Heterocyclic Chemistry*, ed. A. R. Katrizky and C. W. Rees, Pergamon, New York, 1984, vol. 4, p. 313; M. U. Sargent, p. 599; D. M. X. Donnelly, p. 651; R. Benassi, in *Comprehensive Heterocyclic Chemistry*, ed. A. R. Katrizky, C. W. Rees and E. F. U. Scriven, Pergamon, New York, 1996, vol. 2, p. 259; H. Heaney, p. 297; B. A. Keay, p. 395; K. Nakanishi, *Natural Products Chemistry*, Kodamsha, Tokyo, 1974; M. Shipman, *Contemp. Org. Synth.*, 1995, **2**, 1.

2 *Common Fragrance and Flavor Materials*, ed. K. Bauer and D. Garbe, VCH, Weinheim, 1985.

3 B. H. Lipshutz, *Chem. Rev.*, 1986, **86**, 795.

4 For most recent reviews, see: X. Hou, H. Y. Cheung, T. Y. Hon, P. L. Kwan, T. H. Lo, S. Y. Tong and H. N. C. Wong, *Tetrahedron*, 1998, **54**, 1955; B. A. Keay, *Chem. Soc. Rev.*, 1999, **28**, 209.

5 E. Bures, J. A. Nieman, S. Yu, P. G. Spinazzé, J. J. Bontront, I. R. Hunt, A. Rauk and B. A. Keay, *J. Org. Chem.*, 1997, **62**, 8750; E. Bures, P. G. Spinazz, G. Beese, I. R. Hunt, C. Rogers and B. A. Keay, *J. Org. Chem.*, 1997, **62**, 8741; T. Bach and L. Krüger, *Tetrahedron Lett.*, 1998, **39**, 1729.

6 I. Heilbron, E. R. H. Jones and F. Sondheimer, *J. Chem. Soc.*, 1947, 1586; T. L. Jacobs, D. Dankner and A. R. Dankner, *J. Am. Chem. Soc.*, 1958, **80**, 864; S. R. Landor and E. S. Pepper, *J. Chem. Soc. (C)*, 1966, 2283; G. Büchi and H. Wüest, *J. Org. Chem.*, 1969, **34**, 857; B. Gabriele, G. Salerno, F. De Pascali, G. T. Sciano, M. Costa and G. P. Chiusoli, *Tetrahedron Lett.*, 1997, **38**, 6877; S. Cacchi, G. Fabrizi and L. Moro, *J. Org. Chem.*, 1997, **62**, 5327; A. Arcadi and E. Rossi, *Tetrahedron*, 1998, **54**, 15253; D. I. MaGee, J. D. Leach and S. Setiadji, *Tetrahedron*, 1999, **55**, 2847.

7 I. M. Heilbron, E. R. H. Jones, P. Smith and B. C. L. Weedon, *J. Chem. Soc.*, 1946, 54; D. Miller, *J. Chem. Soc. (C)*, 1969, 12; Y. Wakabayashi, Y. Fukuda, H. Shiragami, K. Utimoto and H. Nozaki, *Tetrahedron*, 1985, **41**, 3655; Y. Fukuda, H. Shiragami, K. Utimoto and H. Nozaki, *J. Org. Chem.*, 1991, **56**, 5816.

8 R. L. Danheiser, E. J. Stoner, H. Koyama, D. S. Yamashita and C. A. Klade, *J. Am. Chem. Soc.*, 1989, **111**, 4407.

9 C. M. Marson and S. Harper, *J. Org. Chem.*, 1998, **63**, 9223.

10 F.-T. Lou, A. C. Bajji and A. Jeevanandam, *J. Org. Chem.*, 1999, **64**, 1738; F.-T. Lou, A. Jeevanandam and A. C. Bajji, *Tetrahedron Lett.*, 1999, **40**, 121.

11 J. A. Marshall and E. D. Robinson, *J. Org. Chem.*, 1990, **55**, 3450; J. A. Marshall and X. Wang, *J. Org. Chem.*, 1991, **56**, 960; J. A. Marshall and E. M. Wallace, *J. Org. Chem.*, 1995, **60**, 796.

12 For the hydrohalogenation reaction of electron-deficient allenes, see: (*a*) S. Ma, Z. Shi and L. Li, *J. Org. Chem.*, 1998, **63**, 4522; (*b*) S. Ma and Q. Wei, *J. Org. Chem.*, 1999, **64**, 1028; (*c*) S. Ma and L. Li, H. Xie, *J. Org. Chem.*, 1999, **64**, 5325.

13 For the Pd^0/Ag^+-cocatalyzed cyclization of organic halides with 1,2-allenyl carboxylic acids to afford β-butenolides, see: S. Ma and Z. Shi, *J. Org. Chem.*, 1998, **63**, 6387; For the corresponding reaction with 2,3-dienols with organic halides to afford oxiranes, see: S. Ma and S. Zhao, *J. Am. Chem. Soc.*, 1999, **121**, 7943.

14 For the Pd^{II}-catalyzed direct cyclization and dimerization of terminal allenyl ketones to afford a mixture of 2-monosubstituted furans and 2,4-disubstituted furans, see: (*a*) A. S. K. Hashmi, *Angew. Chem.*, 1995, **107**, 1749; *Angew. Chem., Int. Ed. Engl.*, 1995, **34**, 1581; (*b*) A. S. K. Hashmi, T. L. Ruppert, T. Knofel and J. W. Bats, *J. Org. Chem.*, 1997, **62**, 7295. In most cases, the dimerization products are predominant.

15 N. A. Petasis and K. A. Teets, *J. Am. Chem. Soc.*, 1992, **114**, 10328.

16 S. Ma, X. Lu and Z. Li, *J. Org. Chem.*, 1992, **57**, 709. For a review, see: X. Lu and S. Ma, *Chin. J. Chem.*, 1998, **16**, 388.

Communication a908627g

ChemComm

A new benchmark for the non-enzymatic enantioselective acylation of amines: use of a planar-chiral derivative of 4-pyrrolidinopyridine as the acylating agent

Yutaka Ie and Gregory C. Fu*

Department of Chemistry, Massachusetts Institute of Technology, Cambridge, Massachusetts 02139 USA. E-mail: gcf@mit.edu

Received (in Corvallis, OR, USA) 27th October 1999, Accepted 23rd November 1999

_N_-Acetylated Ph-PPY*, a new planar-chiral derivative of PPY, serves as an effective reagent for the enantioselective acylation of racemic amines, providing amides with very good stereoselectivity.

In recent years substantial progress has been made in the development of non-enzymatic catalysts for the enantioselective acylation of alcohols.[1,2] In contrast, to the best of our knowledge there have been no reports of effective non-enzymatic catalysts for the enantioselective acylation of amines.[3,4] Indeed, there has been only limited success even with stoichiometric chiral acylating reagents.[5]

We have recently described applications of planar-chiral

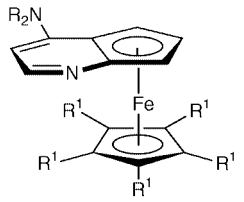

R^1 = Me, NR_2 = dimethylamino (–)-**1** (DMAP*)
R^1 = Me, NR_2 = pyrrolidino (–)-**2** (PPY*)
R^1 = Ph, NR_2 = dimethylamino (–)-**3** (Ph-DMAP*)
R^1 = Ph, NR_2 = pyrrolidino (–)-**4** (Ph-PPY*)

heterocycles (*e.g.* **1**–**3**) as nucleophilic catalysts for a variety of processes, including the enantioselective acylation of secondary alcohols.[6,7] Unfortunately, our attempts to extend this catalytic process to amines were frustrated by the facility with which amines react directly with acylating agents such as acetic anhydride, thereby providing a competitive, non-enantioselective pathway.

We therefore defined our immediate objective to be the development of a highly enantioselective stoichiometric reagent for the acylation of amines. Since progress toward this goal has been quite modest,[5] we felt that this in itself would be a worthwhile achievement.[8] Building on our recent discovery that planar-chiral Ph-DMAP* (**3**) undergoes *N*-acylation when treated with 1 equiv. of acetyl chloride,[2d] we examined the use of the acylated derivatives of iron complexes **1**–**4** as chiral reagents for the stereoselective acylation of (±)-1-phenylethylamine.

Our initial studies revealed that 4-pyrrolidino complexes provide higher ee than do 4-dimethylamino complexes and that complexes that bear the more bulky C_5Ph_5 group furnish better enantioselectivity than do those that bear the C_5Me_5 group. These cumulative substituent effects lead to the acylated form of a new planar-chiral PPY derivative (**4**; Ph-PPY*) being the most enantioselective acylating agent among complexes **1**–**4** [eqn. (1)].[9–11]

An optimization study established that the enantioselectivity with which acylated Ph-PPY* reacts with (±)-1-phenylethylamine varies with solvent. Although at room temperature several solvents furnish greater enantiomeric excess than does CH_2Cl_2 (Table 1), the stereoselection in CH_2Cl_2 is significantly

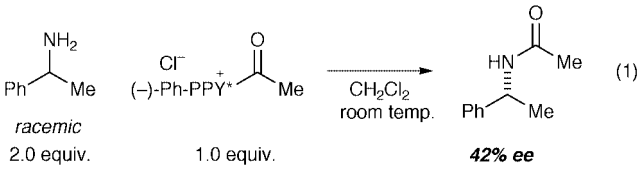

racemic 2.0 equiv. 1.0 equiv. 42% ee (1)

temperature-dependent, and acylation in CH_2Cl_2 at −78 °C affords the highest ee of the conditions that we have examined (78% ee; entry 3). Interestingly, the relationship between ee and solvent that we observe for the acylation of (±)-1-phenylethylamine differs from what we have observed for the catalytic asymmetric acylation of (±)-1-phenylethanol.[2b]

For enantioselective acylations of this sort, the ee of the amide product should increase when the ratio of amine to acylating agent is increased.[12] Consistent with this expectation, under otherwise identical conditions we obtain amide with 87% ee when we employ 8.0 equiv. of amine (Table 2, entry 1), compared with 78% ee when we use 2.0 equiv. of amine (Table 1, entry 3).

Under these reaction conditions, we can achieve the stereoselective acylation of a family of racemic amines with very good enantioselection (Table 2).[13] With respect to substituent effects, we observe somewhat lower ee as the steric demand of the alkyl substituent increases (entry 1 *vs.* entry 2). The stereoselectivity appears to be modestly dependent on the electronic nature of the aryl substituent, with acylations of (±)-1-phenylethylamine proceeding with higher enantioselection than either more electron-rich or more electron-poor derivatives (entry 1 *vs.* entries 3 and 4, respectively). As illustrated in Table 2, *N*-acylated Ph-PPY* efficiently differentiates the enantiomers of amines that bear a range of aromatic substituents (*e.g.* see entries 5 and 6).

Table 1 Effect of solvent and temperature on enantioselectivity

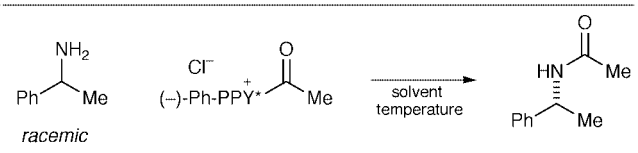

racemic 2.0 equiv. 1.0 equiv.

		Ee of amide (%)	
Entry	Solvent	room temp.	−78 °C
1	Et_2O	17	30
2	THF	41	48
3	CH_2Cl_2	42	78
4	EtOH	44	45
5	Toluene	52	56
6	Pr^iOH	54	69
7	Acetone	58	66
8	*tert*-Amyl alcohol	66	——

Table 2 Enantioselective acylation of amines

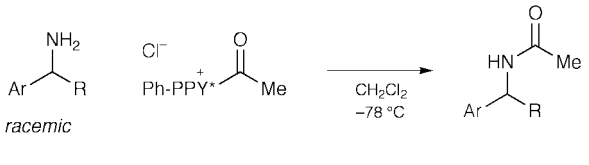

Entry	Amine		Ee of amide (%)[a]
	Ar	R	
1	Ph	Me	87
2	Ph	Et	66
3	4-$MeOC_6H_4$	Me	81
4	4-$CF_3C_6H_4$	Me	85
5	1-Naphthyl	Me	90
6	2-MeC_6H_4	Me	91

[a] Average of two runs.

In summary, we have established that *N*-acylated Ph-PPY*, a new planar-chiral derivative of PPY, can serve as an effective reagent for the enantioselective acylation of racemic amines. Compared with other reagents that have been reported for this process, the level of stereoselectivity furnished by *N*-acyl Ph-PPY* represents a significant advance in the state of the art. This work thus marks an important first step toward the development of an efficient non-enzymatic catalyst for the asymmetric acylation of amines. Ongoing investigations are focused on the discovery of acylating agents that will permit this challenging goal to be achieved.

Support has been provided by Bristol-Myers Squibb, Merck, the National Institutes of Health (National Institute of General Medical Sciences, R01-GM57034), Pfizer, Pharmacia & Upjohn, and Procter & Gamble. We thank J. Craig Ruble and Beata Tao for preliminary studies.

Notes and references

1 E. Vedejs, O. Daugulis and S. T. Diver, *J. Org. Chem.*, 1996, **61**, 430; E. Vedejs and O. Daugulis, *J. Am. Chem. Soc.*, 1999, **121**, 5813; T. Oriyama, Y. Hori, K. Imai and R. Sasaki, *Tetrahedron Lett.*, 1996, **37**, 8543; T. Sano, K. Imai, K. Ohashi and T. Oriyama, *Chem. Lett.*, 1999, 265; T. Kawabata, M. Nagato, K. Takasu and K. Fuji, *J. Am. Chem. Soc.*, 1997, **119**, 3169; S. J. Miller, G. T. Copeland, N. Papaioannou, T. E. Horstmann and E. M. Ruel, *J. Am. Chem. Soc.*, 1998, **110**, 1629; G. T. Copeland, E. R. Jarvo and S. J. Miller, *J. Org. Chem.*, 1998, **63**, 6784.

2 (*a*) J. C. Ruble, H. A. Latham and G. C. Fu, *J. Am. Chem. Soc.*, 1997, **119**, 1492; (*b*) J. C. Ruble, J. Tweddell and G. C. Fu, *J. Org. Chem.*, 1998, **63**, 2794; (*c*) C. E. Garrett, M. M.-C. Lo and G. C. Fu, *J. Am. Chem. Soc.*, 1998, **120**, 7479; (*d*) B. Tao, J. C. Ruble, D. A. Hoic and G. C. Fu, *J. Am. Chem. Soc.*, 1999, **121**, 5091.

3 Even enzymatic acylation of amines can be problematic. For a discussion and leading references, see: S. Takayama, S. T. Lee, S.-C. Hung and C. H. Wong, *Chem. Commun.*, 1999, 127.

4 For a review of methods for the asymmetric synthesis of amines, see: A. Johansson, *Contemp. Org. Synth.*, 1995, **2**, 393; For leading references to applications of enantiopure amines, see: M. J. Burk, Y. M. Wang and J. R. Lee, *J. Am. Chem. Soc.*, 1996, **118**, 5142.

5 See: K. Kondo, T. Kurosaki and Y. Murakami, *Synlett*, 1998, 725 and references cited therein.

6 For the enantioselective acylation of secondary alcohols, see ref. 2.

7 For other processes, see: J. C. Ruble and G. C. Fu, *J. Org. Chem.*, 1996, **61**, 7230; J. Liang, J. C. Ruble and G. C. Fu, *J. Org. Chem.*, 1998, **63**, 3154; J. C. Ruble and G. C. Fu, *J. Am. Chem. Soc.*, 1998, **120**, 11 532; B. L. Hodous, J. C. Ruble and G. C. Fu, *J. Am. Chem. Soc.*, 1999, **121**, 2637.

8 For example, with respect to the development of non-enzymatic methods for the kinetic resolution of alcohols, the discovery of effective stoichiometric reagents (D. A. Evans, J. C. Anderson and M. K. Taylor, *Tetrahedron Lett.*, 1993, **34**, 5563; E. Vedejs and X. Chen, *J. Am. Chem. Soc.*, 1996, **118**, 1809) preceded the discovery of effective catalysts (refs. 1 and 2).

9 The stereochemical preference of the complex appears to be the 'same', regardless of whether the substrate is an amine or an alcohol: acylated (−)-Ph-PPY* preferentially acylates (*R*)-1-phenylethylamine, and (−)-Ph-PPY*/Ac_2O preferentially acylates (*R*)-1-phenylethanol.

10 A preliminary study indicated that other *N*-acyl groups (*e.g.* pivaloyl) furnish lower enantioselectivity.

11 In contrast to our earlier papers on kinetic resolutions, in which we assessed stereoselection by focusing on the selectivity factor, in this work we have chosen to focus instead on the enantiomeric excess of the product. This is due to the fact that, because amine hydrochloride is the other product of these acylation reactions, calculation of a selectivity factor is not completely straightforward (the amine substrate is being 'consumed' both by acylation and by protonation).

12 H. B. Kagan and J. C. Fiaud, *Top. Stereochem.*, 1988, **18**, 249.

13 We have established that at the end of a reaction we can recover Ph-PPY* in 95% yield.

Communication a908625k

ChemComm

Unprecedented pentadenticity of the HB(3-Phpz)$_3$ (= Tp^{Ph}) ligand†

Christian Slugovc,*[a] Kurt Mereiter,[b] Swiatoslaw Trofimenko[c] and Ernesto Carmona*[a]

[a] *IIQ-Departamento de Química Inorgánica, CSIC - Universidad de Sevilla, Avda. Américo Vespucio s/n - Isla de la Cartuja, 41092 Sevilla, Spain. E-mail: guzman@cica.es (for E.C.); slugi@mail.zserv.tuwien.ac.at (for C.S.)*

[b] *Institute of Mineralogy, Crystallography and Structural Chemistry, Vienna University of Technology, Getreidemarkt 9, A-1060 Vienna, Austria*

[c] *Department of Chemistry and Biochemistry, University of Delaware, Newark, Delaware 19716-2522, USA*

Received (in Basel, Switzerland) 21st October 1999, Accepted 6th December 1999

Previously unobserved pentadentate coordination of a tris(pyrazolyl)borate ligand has been ascertained in the compound Ir[κ^5(*N*,*N*′,*N*″,*C*^{Ph},*C*$^{Ph'}$)-Tp^{Ph}](η^2-C$_2$H$_4$) (Tp^{Ph} = hydridotris(3-phenylpyrazolyl)borate] that forms by thermal activation of a mixture of [IrCl(coe)$_2$]$_2$ (coe = cyclooctene) with TlTp^{Ph} and ethene, through the intermediacy of Ir[κ^4(*N*,*N*′,*N*″,*C*^{Ph})-Tp^{Ph}](Et)(η^2-C$_2$H$_4$).

Denticity beyond κ^4 has never been encountered for Tp^R where R contains no heteroatoms. We are reporting herewith the synthesis of the first examples of a Tp^{Ph} ligand acting in an unprecedented pentadentate, as well as tetradentate, fashion in Ir(III) complexes, and the structural characterization of representative compounds.

Homoscorpionate ligands, Tp^R, where R is a 3-substituent on the pyrazolyl ring, have overwhelmingly exhibited a κ^3 coordination mode, usually κ^3-*N*, *N*′,*N*″,[1] and sometimes also κ^3-*N*, *N*′,*H*,[2,3] although lower denticity, such as κ^2-*N*,*N*′, κ^2-*N*,*H*, κ^1-*N*, and even κ^0 (where the Tp^R ligand serves only as an uncoordinated counter ion) has also been encountered.[4] By contrast, expansion of Tp^R denticity beyond κ^3 is rare. On the one hand this can occur by way of the 3-R substituent containing donor atoms, as in the demonstrably hexadentate Tp^{py},[5] or in the potentially hexadentate ligands Tp^{oAn},[6] or Tp$^{2,4(OMe)2Ph}$.[7] On the other hand, tetradenticity has been reported in Tp^R ligands where R contained no donor atoms, either by way of agostic bonding,[8] or through cyclometalation taking place at one of the aliphatic R groups per ligand,[9] or when an oxidative functionalization of one R group per ligand took place, leading to a C–O–M bond.[10,11] An example of reversible oxidative addition of the *ortho*-C–H of the phenyl group in the RhTp^{Ph}(CO)$_2$ complex, thus making the Tp^{Ph} ligand κ^4, has been reported in a dissertation.[12]

The reaction of [IrCl(coe)$_2$]$_2$ (coe = cyclooctene) with ethene and TlTp^{Ph} in CH$_2$Cl$_2$ produced the cyclometalated compound Ir[κ^4(*N*,*N*′,*N*″,*C*^{Ph})-Tp^{Ph}](Et)(η^2-C$_2$H$_4$) **1** (Scheme 1).† This was in sharp contrast to the related reactions of [IrCl(coe)$_2$]$_2$ with ethene and KTp or KTp^{Me2}, which under identical conditions produced the Ir(I) complexes IrTp^{Me2}(η^2-C$_2$H$_4$)$_2$. The propensity of the Ir(I)Tp^R fragments to induce C–H bond activation, enhanced in the present case by the increased steric bulk of the Tp^{Ph} ligand, and coupled with the close proximity of the phenyl rings to the metal, can be used to rationalize the facile activation of one of the phenyl rings, and one of the ethene ligands. The X-ray structure of **1** (see ESI) showed Ir in a distorted octahedral environment,‡ as indicated by the bite angles of the Tp^{Ph} ligand: N(3)–Ir–N(5) 83.3(1)°, N(1)–Ir–N(3) 92.8(2)°, N(1)–Ir–N(5) 76.1(1)°. The difference between the latter two (16.7°) is substantially larger than usual values (< 10°). The metalated phenylpyrazolyl unit showed a strong distortion by which the boron atom and the phenyl ring are considerably displaced from the plane of the pz ring: B by 0.73 Å, Ir by 0.37 Å and C(4) by 0.28 Å. At this stage, it appears appropriate to draw attention on the similarity of the cyclometalation of the phenylpyrazolyl unit of the Tp^{Ph} ligand that leeds to complex **1**, with related transformations that involve donors such as 2-phenylpyridine, 1-phenylpyrazole or bipyridine.[13,14] The metalation of the benzene ring of these compounds attached to the functional group that possesses the donor atom, requires, in general, more forcing conditions[14] than those needed for the generation of **1** but yields related organometallic complexes that incorporate the heterocyclic donor atom.[14]

Refluxing complex **1** in benzene for 17 h produced the bismetalated species Ir[κ^5(*N*,*N*′,*N*″,*C*^{Ph},*C*$^{Ph'}$)-Tp^{Ph}](η^2-C$_2$H$_4$) **2**, as the only product (NMR monitoring).§ The proposed κ^5 coordination mode was suggested by the presence of four carbon signals in the range δ 123.2–122.5 (this is also the case in compound **3**, *vide infra*). Refluxing **1** in toluene, converted it completely to **2** in 4.5 h. It can be concluded, therefore, that **2** is thermodynamically favored over the *a priori* expected compound Ir[κ^3(*N*,*N*′,*N*″)-Tp^{Ph}](Ph)$_2$(L), where L could be either ethene or dinitrogen, as was in the case with IrTp*(η^2-C$_2$H$_4$)$_2$.[15]

A related compound, which also contained a κ^5-Tp^{Ph} ligand, Ir[κ^5(*N*,*N*′,*N*″,*C*^{Ph},*C*$^{Ph'}$)-Tp^{Ph}](κ^1(*N*^{1})-3-phenylpyrazole) **3**, was formed upon treatment of [IrCl(coe)$_2$]$_2$ with 2,3-dimethylbutadiene and TlTp^{Ph}, the 3-phenylpyrazole resulting from partial ligand degradation. Surprisingly, a direct reaction of **2** with the free pyrazole, Hpz^{Ph}, proceeded only slowly, and yielded other products, in addition to **3**. Spectroscopic data for **3** were in agreement with the proposed structure. While ^{11}B NMR and ν(B–H) data for **3** (as for **1** and **2**) did not indicate the coordination mode of the Tp^{Ph} ligand,[16] the ^{13}C NMR spectrum showed characteristic signals for carbon atoms of the metalated rings at δ 122.9, 122.5, 122.4, and 121.5. By comparison, **1** had only two signals in this region, at δ 122.2 and 121.9. It is

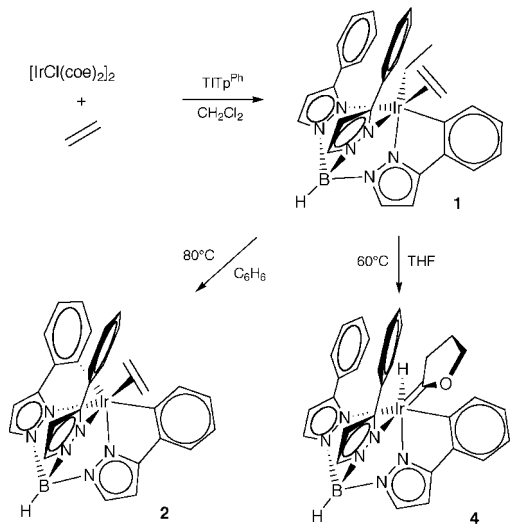

Scheme 1

† Electronic supplementary information (ESI) available: preparation and characterization data for compounds **1**–**4** and ORTEP plot of **1**. See http://www/rsc/org/suppdata/cc/a9/a908478i/

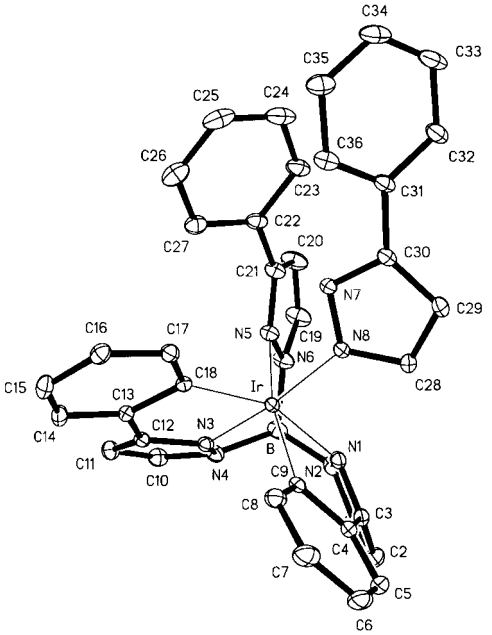

Fig. 1 ORTEP plot of **3** (hydrogen atoms omitted for clarity; thermal ellipsoids are at the 20% probability level). Selected bond lengths (Å) and angles (°): Ir–N(1) 2.114(2), Ir–N(3) 1.989(2), Ir–N(5) 2.219(2), Ir–C(9) 2.053(2), Ir–C(18) 2.051(2), Ir–N(8) 2.059(2), N(3)–Ir–N(1) 84.1(1), N(3)–Ir–N(5) 79.2(1), N(1)–Ir–N(5) 88.7(1), N(3)–Ir–N(8) 172.7(1), N(3)–Ir–C(9) 103.6(1), N(3)–Ir–C(18) 79.3(1), C(9)–Ir–N(1) 77.7(1), C(18)–Ir–C(9) 91.4(1).

noteworthy, that both **2** and **3** contained inequivalent pyrazolyl and phenyl rings. Thus, the diastereoselective cyclometalation of the 3-phenyl group of the pz^{Ph} ring *trans* to the monodentate ligand (in the case of **3**, 3-phenylpyrazole), gave rise to asymmetry of the molecule.

The ORTEP diagram of **3**, along with important bond lengths and angles is shown in Fig. 1.‡ The two Ir–C bond lengths are identical within experimental error [2.053(2) Å] and are also identical to the two Ir–C_6H_5 bonds of the somewhat related compound $[IrTp^*(Ph)_2]_2(\mu\text{-}N_2)$ [2.06(2) Å],[15] while Ir–C(9) of **1** is slightly shorter [2.030(4) Å]. Considerable distortion of the pentadentate Tp^{Ph} ligand is evident from Fig. 1. Whereas the d^6 Ir(III), and the bonding implicit in the coordination to the three N atoms of a Tp^R ligand strongly favour octahedral coordination,[17] an unstrained metalation of the two phenyl rings would lead to trigonal prismatic geometry. Reconciling these two desiderata, the dimetalated Tp^{Ph} ligand becomes highly distorted. The degree of distortion of the two Ir–C^{Ph} bonded entities is manifested by the values of the bond angles around iridium [77.7–103.6(1)°, *cisoid*; 157.4–172.7(1)°, *transoid*], and also by the out-of-plane bending of B, Ir and the C atoms C(4) and C(13) of the phenyl substituents with respect to the pz planes. These deviations are 0.763(4), 0.889(4) and 1.101(4) Å for B, Ir and C(4), respectively, referred to the N(1)N(2)C(1)C(2)C(3) ring, and 0.619(4), 0.860(3) and 0.294(3) for B, Ir and C(13), respectively, with respect to the ring containing N(3) and N(4).

In conclusion, we have demonstrated the first instance of κ^5 coordination of a Tp^R ligand. This work also shows that the tendency of Tp^R ligands to strongly favor octahedral geometry at the coordinated metal centers is so pronounced that even severe ligand distortions can be accommodated. The thermodynamic stability of the metalated compounds in refluxing benzene is surprising, in view of the results observed in related systems, and may be due to the chelate effect. The presently reported compounds and related Ir(I) complexes seem to be suitable for various C–H activation reactions. As represented in Scheme 1, compound **1** reacts in THF at 60 °C to yield the Fischer carbene complex **4** as the sole product. Moreover, the phenyl groups could be used as internal probes for C–H activation, as was demonstrated by the incorporation of 1.6 deuterium atoms into only one of the phenyl rings during the reaction of **1** with THF-d_8, producing the appropriate analog of **4**. These, and related, C–H activation reactions are currently being studied.

This work was supported by the 'Fonds zur Förderung der wissenschaftlichen Forschung' with a Schrödinger Stipendium for C. S. (J1756-CHE), the Spanish Ministry of Education, and the DGES (Project PB97-0733).

Notes and references

‡ *Crystal data*: $C_{31}H_{30}BIrN_6$ **1**: M = 689.62, monoclinic, space group $P2_1/n$ (no. 14), a = 16.399(5), b = 8.691(3), c = 19.809(5) Å, β = 91.77(2)°, U = 2821.9(15) Å^3, T = 295(2) K, Z = 4, μ(Mo-Kα) = 4.763 mm^{-1}, F(000) = 1360, 32 315 reflections measured, 6013 unique (R_{int} = 0.029), R_1 = 0.032 [$I \geq 2\sigma(I)$], R_1 = 0.036 (all data), wR_2 = 0.064 (all data). The structure was solved using direct methods and refined by full-matrix least squares on F^2.

For $C_{36}H_{28}BIrN_8$ **3**: M = 775.67, triclinic, space group $P\bar{1}$ (no. 2), a = 9.543(2), b = 12.043(4), c = 13.941(4) Å, α = 85.35(2), β = 77.78(2),γ = 78.63(2)°, U = 1533.9(7) Å^3, T = 223(2) K, Z = 2, μ(Mo-Kα) = 4.393 cm^{-1}, F(000) = 764, 21 402 reflections measured, 8675 unique (R_{int} = 0.022), R_1 = 0.018 [$I \geq 2\sigma(I)$], R_1 = 0.021 (all data), wR_2 = 0.042 (all data). The structure was solved using direct methods and refined by full-matrix least squares on F^2. CCDC 182/1500. See http://www.rsc.org.suppdata/cc/a9/a908478i/ for crystallographic files in .cif format.

§ Following an NMR-tube reaction (benzene-d_6, 60 °C) an intermediate could be observed, which was not characterized, but was thought to be Ir[κ^4(*N*,*N*′,*N*″,*C*^{Ph})-Tp^{Ph}](Ph)(η^2-C_2H_4). Cyclohexane and hexafluorobenzene as the solvents gave **2**, but a related intermediate was not observed. Using C_6D_6 as the solvent results in perdeuteration of **2** but not of the ethene-ligand.

1 For a comprehensive review of Tp^R complexes see: S. Trofimenko, *Scorpionates; The Coordination Chemistry of Polypyrazolylborate Ligands*, Imperial College Press, London, 1999; earlier reviews: S. Trofimenko, *Chem. Rev.*, 1993, **93**, 943; G. Parkin, *Adv. Inorg. Chem.*, 1995, **42**, 291.

2 J. C. Calabrese, P. J. Domaille, J. S. Thompson and S. Trofimenko, *Inorg. Chem.*, 1990, **29**, 4429.

3 A. Kremer-Aach, W. Kläui, R. Bell, A. Strerath, H. Wunderlich and D. Mootz, *Inorg. Chem.*, 1997, **36**, 1552.

4 U. E. Bucher, A. Currao, R. Nesper, H. Rüegger, L. M. Venanzi and E. Younger, *Inorg. Chem.*, 1995, **34**, 66; H: F. Malbosc, P. Kalck, J.-C. Daran and M. Etienne, *J. Chem. Soc., Dalton Trans.*, 1999, 271; E. Gutiérrez-Puebla, A. Monge, M. Paneque, S. Sirol, M. Trujillo and E. Carmona, *Angew. Chem.*, in press.

5 A. J. Amoroso, J. C. Jeffery, P. L. Jones, J. A. McCleverty, E. Psillakis and M. D. Ward, *Chem. Commun.*, 1994, 2751; A. J. Amoroso, J. C. Jeffery, P. L. Jones, J. A. McCleverty, L. Rees, A. L. Rheingold, Y. Sun, J. Takats, S. Trofimenko, M. D. Ward and G. P. A. Yap, *Chem. Commun.*, 1995, 1881.

6 P. L. Jones, K. L. V. Mann, J. C. Jeffery, J. A. McCleverty and M. D. Ward, *Polyhedron*, 1997, **16**, 2435.

7 A. L. Rheingold, B. S. Haggerty, L. M. Liable-Sands and S. Trofimenko, *Inorg. Chem.*, in press.

8 M. C. Keyes, V. G. Young Jr. and W. B. Tolman, *Organometallics*, 1996, **15**, 4133.

9 Y. Takahashi, S. Hikichi, M. Akita and Y. Moro-oka, *Organometallics*, 1999, **18**, 2571.

10 N. Kitajima, M. Osawa, M. Tanaka and Y. Moro-oka, *J. Am. Chem. Soc.*, 1991, **113**, 8952.

11 Y. Takahashi, S. Hikichi, M. Akita and Y. Moro-oka, *Chem. Commun.*, 1999, 1491.

12 R. Krentz, Ph.D. Dissertation, University of Alberta, Edmonton, 1989.

13 E. C. Constable, *Polyhedron*, 1984, **3**, 1037.

14 P. J. Steel, *J. Organomet. Chem.*, 1991, **408**, 395; S. Spouse, K. A. King, P. J. Spellane and R. J. Watts, *J. Am. Chem. Soc.*, 1984, **106**, 6647; W. A. Wickramasinghe, P. H. Bird and N. Serpone, *J. Chem. Soc., Chem. Commun.*, 1981, 1284.

15 E. Gutiérrez-Puebla, A. Monge, M. C. Nicasio, P. J. Pérez, M. L. Poveda and E. Carmona, *Chem. Eur. J.*, 1998, **4**, 2225.

16 M. Akita, K. Ohta, Y. Takahashi, S. Mikichi and Y. Moro-oka, *Organometallics*, 1997, **16**, 4121; T. Nurthcutt, R. J. Lachicotte and W. D. Jones, *Organometallics*, 1998, **17**, 5148.

17 M. D. Curtis, K. B. Shiu and W. M. Butler, *J. Am. Chem. Soc.*, 1986, **108**, 1550; M. D. Curtis, K. B. Shiu, W. M. Butler and J. C. Huffman, *J. Am. Chem. Soc.*, 1986, **108**, 3335.

Communication a908478i

Clusters containing metal–metal bonds linking high- and low-valent metal centres: synthesis and structure of $Ru_3(CO)_{12}\{Mo(NAr)_2\}$

Shahbano Ali,[a] Arthur J. Carty,*[b] Antony J. Deeming,[a] Gary D. Enright[b] and Graeme Hogarth*[ab]

[a] *Chemistry Department, University College London, 20 Gordon Street, London, UK, WC1H 0AJ. E-mail: g.hogarth@ucl.ac.uk*

[b] *The Steacie Institute for Molecular Sciences, National Research Council of Canada, 100 Sussex Drive, Ottawa, Ontario, Canada, K1A 0R6. E-mail: Arthur.Carty@NRC.CA*

Received (in Basel, Switzerland) 8th November 1999, Accepted 7th December 1999

Room temperature reaction of $K_2[Ru_3(CO)_{11}]$ with the molybdenum(VI) bis(imido) complexes $Mo(NAr)_2Cl_2(dme)$ (Ar = $C_6H_3X_2$-2,6; X = Me, Pr^i, Cl; dme = 1,2-dimethoxyethane) affords new high-low valent clusters $Ru_3(CO)_{12}\{Mo(NAr)_2\}$ which adopt a butterfly arrangement of metal centres with $[Ru_3(CO)_{12}]^{2-}$ acting as a ligand at a molybdenum(VI) centre.

Molecular transition metal complexes can broadly be divided into those containing the metal centre in either a high and or low oxidation state. While in most respects the chemistry displayed in these two areas is quite different, metal–metal bonding is prevalent in both. Moreover, there is an increasing number of examples in which metal–metal bonds are formed between high- and low-valent metal centres. These include the classic W(V)–W(I) complex $Cp^*W(CO)_3$–WO_2Cp^* prepared by Alt *et al.*,[1] while Sundermeyer has recently reported a range of related bi- and tri-nuclear imido-containing complexes.[2] In these, metal–metal bonds are found between the high- and low-valent centres but, even when more than one of the former is present, there are no metal–metal bonds between the low-valent centres. That is, clusters of this type are of the linear variety. Chi and coworkers[3,4] have synthesised a number of group 6/8 mixed-metal clusters containing imido ligands, however, here it is noted that the π-donor ligands are rarely bound in a monodentate fashion,[4] but rather bridge two or more metal centres.[3] As such, all metal centres in such clusters can be considered to be of similar valency. In contrast, Puddephatt and coworkers[5] have prepared the tetrahedral cluster cation $[Pt_3(ReO_3)(\mu\text{-dppm})_3]^+$ where the formal metal oxidation states may be considered as Re(VII) and Pt(0), yet it is characterised by three strong Pt–Re interactions.

Over the past thirty years, low-valent carbonyl clusters have been the focus of intensive research and a wide range of cluster geometries have been found.[6] Cluster frameworks are generally soft and deformable, with the geometries adopted dependent upon the number of electrons. Further, many are easily oxidised and/or reduced and as such have the ability to act as efficient electron sinks. Both of these properties, if controllable, would make the cluster useful as a ligand. Herein we describe the use of the low-valent cluster $[Ru_3(CO)_{12}]^{2-}$ as a ligand to a high-valent, bis(imido) stabilised molybdenum centre.

Room temperature addition of thf solutions of $K_2[Ru_3(CO)_{11}]$[7] and $Mo(NAr)_2Cl_2(dme)$[8] resulted in the formation of very dark solutions which were left to stir overnight. Work-up in an aerobic atmosphere resulted after chromatography in the isolation of $Ru_3(CO)_{12}$ and the new clusters $Ru_3(CO)_{12}\{Mo(NAr)_2\}$ **1a**–**c** in yields of 20–30% Clusters **1a**–**c** show good solubility in hexane and are air-stable in this solvent. Characterisation was made on the basis of IR, NMR and mass spectra.† Crystals of **1a** suitable for X-ray analysis were easily grown upon cooling a saturated hexane solution to −20 °C, the results of which are summarised in Fig. 1.‡

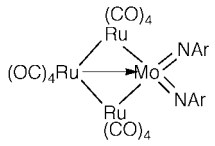

1

Ar = $C_6H_3R_2$-2,6: **a** R = Me, **b** R = Pr^i, **c** R = Cl

The molecule consists of a butterfly arrangement of one molybdenum and three ruthenium atoms, with a fold angle of 25.4° about the hinge vector, Mo(1)–Ru(1). The molybdenum centre retains its two imido ligands while each ruthenium centre is ligated by four CO ligands. Of the three ruthenium–molybdenum interactions, two are extremely short [Mo(1)–Ru(2) 2.7165(5), Mo(1)–Ru(3) 2.7025(4) Å] while the third, the hinge vector, is much longer [Mo(1)–Ru(1) 3.1094(8) Å]. Indeed, as far as we are aware, these bonds within **1a** span the range of all known molybdenum–ruthenium bonds in mixed-metal clusters.[9] The very short Mo–Ru interactions are probably a result of the smaller radii of high- *vs.* low-valent metal centres and high polarity of the heterometallic interaction $M^{\delta+}$–$M^{\delta-}$ as noted previously by Sundermeyer *et al.*[2] The longer hinge vector is dative in origin, the electron-rich ruthenium tetracarbonyl unit acting as a donor to the high-valent molybdenum centre. One way of looking at **1a** is as a molybdenum(VI) bis(imido) centre bound to a chelating $[Ru_3(CO)_{12}]^{2-}$ ligand. In the free state this dianion would lose CO to afford

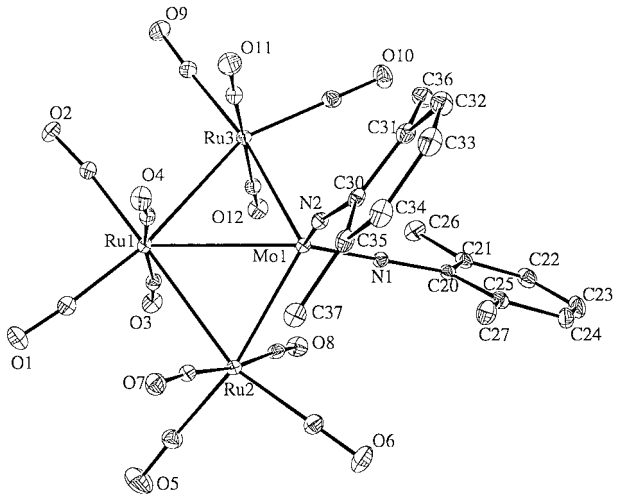

Fig. 1 Molecular structure of **1a** with selected bond lengths (Å) and angles (°): Mo(1)–Ru(1) 3.1094(8), Mo(1)–Ru(2) 2.7165(5), Mo(1)–Ru(3) 2.7025(4), Ru(1)–Ru(2) 2.9315(5), Ru(1)–Ru(3) 2.9556(5), Mo(1)–N(1) 1.766(2), Mo(1)–N(2) 1.761(2), Ru(2)–Mo(1)–Ru(3) 115.88(2), Mo(1)–Ru(3)–Ru(1) 66.50(2), Ru(3)–Ru(1)–Ru(2) 102.54(2), Ru(1)–Ru(2)–Mo(1) 66.68(2), N(1)–Mo(1)–N(2) 112.39(7), Mo(1)–N(1)–C(20) 163.60(13), Mo(1)–N(2)–C(30) 162.26(13).

$[Ru_3(CO)_{11}]^{2-}$, however, on the basis of a localised bonding model it would be expected to contain one long and two short ruthenium–ruthenium vectors. Ruthenium–ruthenium distances [Ru(1)–Ru(2) 2.9315(5), Ru(1)–Ru(3) 2.9556(5) Å] are *ca.* 0.1 Å longer than the average of 2.854 Å found in $Ru_3(CO)_{12}$,[10] however, this is expected as the outer ruthenium atoms carry a negative charge, while the Ru(2)–Ru(3) distance of 4.593 Å is clearly non-bonding. Thus, the triruthenium unit has the attributes expected of $[Ru_3(CO)_{12}]^{2-}$. Ignoring the dative Ru–Mo interaction, the molybdenum centre is approximately tetrahedral and related tetrahedral bis(imido) units are common for Mo(VI)[11] and known for Mo(IV).[12] Metal–nitrogen bond lengths in imido complexes are known to vary only slightly over a wide-range of complexe,[13] with no clear distinction between Mo(VI) and Mo(IV). Molybdenum–nitrogen distances in **1a** [Mo(1)–N(1) 1.766(2), Mo(1)–N(2) 1.761(2) Å] and the N(1)–Mo(1)–N(2) angle of 112.39(7)° are within the ranges found for both Mo(VI) and Mo(IV) complexes.[11–13]

Butterfly clusters are usually associated with an effective atomic number (EAN) of 62 electrons. As the imido ligands are linear [Mo(1)–N(1)–C(20) 163.60(13), Mo(1)–N(2)–C(30) 162.26(13)°] then both might be expected to be able to act as four-electron donors and such a scenario would give the expected 62-electron count. However, there are only three d orbitals of π-symmetry on any one metal centre, and thus the total donor capacity of the two imido ligands is six.[13] This suggests that cluster **1** has only 60 electrons and is formally electron deficient at molybdenum.

The mode of formation of **1** is not yet fully understood. Clearly CO scavenging must occur and this would be a reasonable explanation for the moderate yields obtained. The major byproduct of all reactions is $Ru_3(CO)_{12}$. This probably results from electron-transfer being competitive with nucleophilic substitution. We have also, however, noted that while **1a**–**c** are all indefinitely stable in hexane, thf solutions decompose over a period of hours under anaerobic conditions giving $Ru_3(CO)_{12}$ and an as yet unidentified molybdenum product. The differing stabilities of **1** in coordinating and non-coordinating solvents may reflect the strong polarisation of the Mo–Ru bonds and the electron deficiency at molybdenum.

Attempts to extend this type of cluster to aryl imido ligands without *ortho* substituents has so far been fruitless. For example, addition of $K_2[Ru_3(CO)_{11}]$ to $Mo(NPh)_2Cl_2(dme)$ yielded $Ru_3(CO)_{12}$ and $H_2Ru_4(CO)_{13}$ as the only tractable products. The reason for this is unclear but given the instability of **1a**–**c** in thf (the reaction solvent), it may be that $Ru_3(CO)_{12}$-$\{Mo(NPh)_2\}$ decomposes as rapidly as it is generated. We are currently exploring different solvents for these reactions, and plan to extend the metathesis methodology to other group 8 cluster anions and high-valent metal complexes, and explore the reactivity of this new class of high-low valent cluster complexes.

We are grateful to the National Research Council of Canada and the Natural Sciences and Engineering Research Council for financial support of this work. S. A. thanks University College London for financial support and the award of a Thomas Witherton Batt scholarship (1997–8).

Notes and references

† *Spectroscopic data:* for **1a**: IR (C_6H_{14}) ν(CO) 2106m, 2070s, 2055m, 2038w, 2030s, 2026(sh), 2006m, 2003w cm^{-1}; ^1H NMR ($CDCl_3$): δ 6.98 (s, 6H, Ar), 2.17 (s, 12H, Me): MS(FAB$^+$) *m/z* 945 (M − CO); Anal. Calc. for $MoRu_3C_{28}H_{18}N_2O_{12}$, C, 34.53, H, 1.85, N, 2.87. Found: C, 34.77, H, 1.83, N, 2.95%.

‡ *Crystal data*: X-ray intensity data were collected on a Siemens CCD diffractometer using Mo-Kα radiation and the ω-scan mode; T = 293 K, $MoRu_3C_{28}H_{18}N_2O_{12}$, M_r = 973.59, monoclinic, space group $P2_1/c$, a = 19.409(4), b = 9.887(2), c = 17.947(4) Å, β = 109.98(3)°, F(000) = 1880, D_c = 1.998 g cm^{-3}, Z = 4, μ = 1.81 mm^{-1}, 2θ(max) = 58.4°, R(R_w) = 0.0192 (0.0441) for 8668 reflections [$I > 2\sigma(I)$] and 487 parameters. CCDC 182/1499. See http://www.rsc.org/suppdata/cc/a9/a908982i/ for crystallographic files in .cif format

1 H. G. Alt, H. I. Hayen and R. D. Rodgers, *J. Chem. Soc., Chem. Commun.*, 1987, 1795.
2 J. Sundermeyer, D. Runge and J. S. Field, *Angew. Chem., Int. Ed. Engl.*, 1995, **33**, 678; J. Sundermeyer and D. Runge, *Angew. Chem., Int. Ed. Engl.*, 1995, **33**, 1255.
3 C.-J. Su, P.-C. Su, Y. Chi, S.-M. Peng and G.-H. Lee, *J. Am. Chem. Soc.*, 1996, **118**, 3289; Y. Chi, H.-F. Hsu, L.-K. Liu, S.-M. Peng and G.-H. Lee, *Organometallics*, 1992, **11**, 1763; R.-C. Lin, Y. Chi, S.-M. Peng and G.-H. Lee, *J. Chem. Soc., Dalton Trans.*, 1993, 227.
4 R.-C. Lin, Y. Chi, S.-M. Peng and G.-H. Lee, *J. Chem. Soc., Chem. Commun.*, 1992, 1705.
5 J. Xiao, R. J. Puddephatt, L. Manojlovic-Muir, K. W. Muir and A. A. Torabi, *J. Am. Chem. Soc.*, 1994, **116**, 1129; J. Xiao, R. J. Puddephatt, L. Manojlovic-Muir and K. W. Muir, *J. Am. Chem. Soc*., 1995, **117**, 6316.
6 D. M. P. Mingos, in *The Chemistry of Metal Cluster Complexes*, ed. D. F. Shriver, H. D. Kaesz and R. D. Adams, VCH, NY, 1990.
7 A. A. Bhattacharyya, C. C. Nagel and S. G. Shore, *Organometallics*, 1983, **2**, 1187.
8 R. R. Schrock, J. S. Murdzek, G. C. Bazan, J. Robbins, M. DiMare and M. O'Regan, *J. Am. Chem. Soc*., 1990, **112**, 3875; H. H. Fox, K. B. Yap, J. Robbins, S. Cai and R. R. Schrock, *Inorg. Chem.*, 1992, **31**, 2287.
9 R. D. Adams, J. E. Babin and M. Tasi, *Polyhedron*, 1988, **7**, 2263 and references cited therein.
10 M. R. Churchill, F. J. Hollander and J. P. Hutchinson, *Inorg. Chem.*, 1977, **16**, 2655.
11 A. C. Sullivan, G. Wilkinson, M. Motevalli and M. B. Hursthouse, *J. Chem. Soc., Dalton Trans.*, 1988, 53; N. Bryson, M.-T. Youinou and J. A. Osborn, *Organometallics*, 1991, **10**, 3389; W. Clegg, M. R. Elsegood, P. W. Dyer, V. C. Gibson and E. L. Marshall, *Acta. Cryst., Sect. C.*, 1999, **55**, 916.
12 P. W. Dyer, V. C. Gibson, J. A. K. Howard, B. Whittle and C. Wilson, *J. Chem. Soc., Chem. Commun.*, 1992, 1666; P. W. Dyer, V. C. Gibson, J. A. K.Howard and C. Wilson, *J. Organomet. Chem.*, 1993, **462**, C15; P. W. Dyer, V. C. Gibson and W. Clegg, *J. Chem. Soc., Dalton Trans.*, 1995, 3313.
13 D. E. Wigley, *Prog. Inorg. Chem.*, 1994, **42**, 239.

Communication a908982i

ChemComm

A new route to the metastable FCC molybdenum carbide α-MoC_{1-x}

Christophe Bouchy, Sharifah Bee Derouane-Abd Hamid* and Eric G. Derouane

Leverhulme Centre for Innovative Catalysis, Department of Chemistry, The University of Liverpool, Liverpool, UK L69 3BX. E-mail: sharifhd@liverpool.ac.uk

Received (in Cambridge, UK) 16th September 1999, Accepted 6th December 1999

The carburisation of a prereduced MoO_3 provides a new method for the synthesis of the metastable α-MoC_{1-x}.

Because of their potential as catalysts substituting noble metals, transition metal interstitial compounds,[1] especially carbides and nitrides of group VI (Mo, V, W),[2–5] have received considerable interest. Several routes have been proposed for their preparation and their catalytic properties have been evaluated for a variety of reactions.

The direct temperature programmed reduction (TPR) and carburisation of MoO_3 using methane allows the preparation of the thermodynamically stable β-phase of molybdenum carbide, β-Mo_2C, whose structure is hexagonal close packed (HCP), with specific surface areas in the range 50–100 $m^2\ g^{-1}$.[6] The metastable α-phase of molybdenum carbide, α-MoC_{1-x}, whose structure is face-centred cubic (FCC), possesses catalytic properties which differ from those of the β-phase as observed, for example, in the hydrogenolysis of ethane.[7] Two procedures have been proposed for its synthesis. The first one involves the initial reduction and nitridation of MoO_3 by ammonia followed by the carburisation of the γ-Mo_2N nitride.[8] The second consists in the direct reduction and carburisation of MoO_3 containing a small amount of platinum.[9] The first method is rather tedious whereas the second leads to α-MoC_{1-x} contaminated by platinum, which may affect its catalytic behaviour. We now report a new and direct route for the synthesis of α-MoC_{1-x} using pure MoO_3 as precursor.

The MoO_3 used was analytical grade and obtained from Aldrich. The structural transformations occuring during its reduction and carburisation were followed *in situ* using powder X-ray diffraction (XRD). A Paar XRD *in situ* cell, capable of operation up to *ca*. 900 °C and 10 bar, was mounted in a Siemens D5001 powder X-ray diffractometer (θ–2θ mode) equipped with a position sensitive detector enabling the fast (< 6 min) acquisition of detailed X-ray diffraction patterns.

The new synthesis route to α-MoC_{1-x} can be described as follows. MoO_3 is first reduced at 350 °C under pure dihydrogen flow for 24 h. *In situ* XRD characterisation showed (Fig. 1) that MoO_3 is converted by this reduction treatment into a mixture of the sub-oxide MoO_2 and of another phase previously identified as the oxyhydride MoO_xH_y.[10] The oxyhydride has an FCC structure with a_{cub} = 0.410 nm and is formed by reduction and hydrogen insertion in the MoO_3 lattice, the overall process being topotactic.[11]

Dihydrogen was then replaced by methane and the sample (mixture of MoO_2 and MoO_xH_y) heated progressively to 710 °C (3 °C min^{-1}). *In situ* fast scan XRD analyses were performed at regular 30 °C temperature intervals to follow the carburisation of the sample. As shown in Fig. 2, carburisation started at 620 °C and yielded eventually (680–710 °C) the nearly pure metastable carbide α-MoC_{1-x} with only traces of the stable carbide β-Mo_2C. The unit cell parameter (a_{cub}) of the FCC structure was found to be 0.428 nm, confirming that a pure carbide, and not an oxycarbide (lower a_{cub} values),[11,12] was synthesised. The particle size (coherent domain size) of α-MoC_{1-x}, calculated from the broadening of the XRD pattern, is *ca*. 3.4 nm, corresponding to an estimated surface area of 187 $m^2\ g^{-1}$. However, the specific surface area of the sample measured by the BET method was found to be much smaller (S_{BET} = 90 $m^2\ g^{-1}$), possibly because of the plugging of mesoporosity owing to carbon deposition on the sample during synthesis. The presence of carbon deposits was confirmed using the method of Lee *et al*.[6] and a $C/Mo_{surface}$ atomic ratio of 7 was found. The C_{bulk}/Mo_{bulk} atomic ratio of the sample was then estimated by *in situ* TPO of sample whose surface was coke-free, as a result of the former treatment. This ratio was found to be equal to 0.7 ± 0.1. The value of this ratio and of a_{cub} support the deduction that the carbide synthesised is similar to the FCC carbide previously reported in the literature.[13] An FCC carbide without coke contamination, *i.e.* directly usable for catalytic application, was synthesised by replacing the pure CH_4 gaseous flow by a H_2–CH_4 (9:1) mixture. In this case, S_{BET} was 179 $m^2\ g^{-1}$, with a pore size distribution centred around 3 nm. The formation of β-Mo_2C, in very small amount, is attributed to the

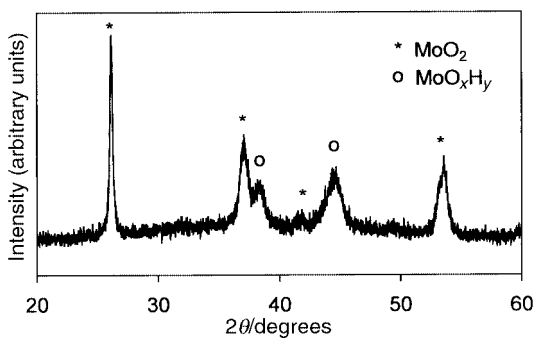

Fig. 1 *In situ* XRD pattern of the material obtained following reduction of MoO_3 by dihydrogen at 350 °C for 24 h.

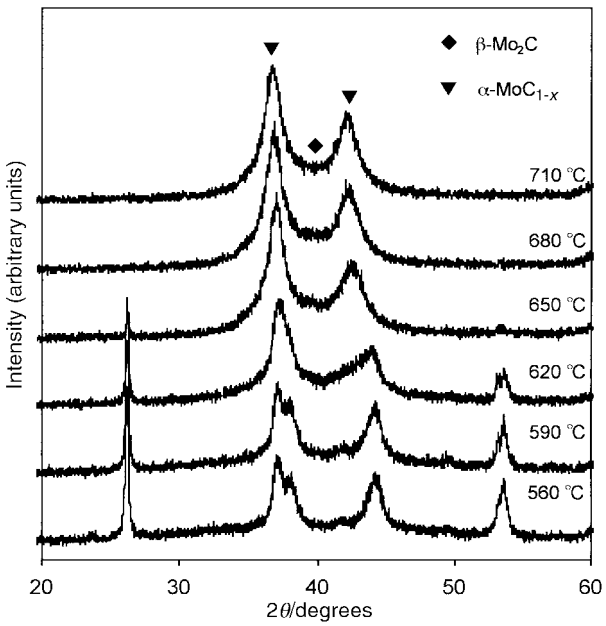

Fig. 2 *In situ* XRD characterisation of the MoO_2–MoO_xH_y mixture during methane carburisation.

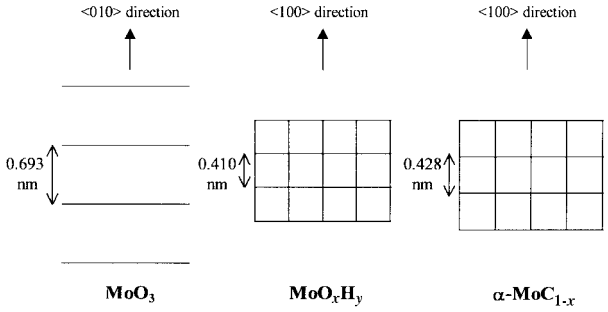

Fig. 3 Topotactic synthesis of FCC MoC_{1-x}: the < 010 > direction of the starting material is conserved during the synthesis.

carburisation of the MoO_2 sub-oxide as reported in the literature[14] whereas the carburisation of the oxyhydride MoO_xH_y yields α-MoC_{1-x}, both compounds having a FCC structure.

The synthesis of the FCC α-MoC_{1-x} carbide is enabled by the topotactic formation at low temperature of the FCC MoO_xH_y oxyhydride whose subsequent carburisation, occurring *via* a topotactic process,[11] leads to the FCC carbide. It appears that, as in the case of the topotactic synthesis of γ-Mo_2N from MoO_3,[15] the < 100 > direction of the FCC carbide is parallel to the < 010 > direction of the starting oxide (Fig. 3). The first step, *i.e.* the oxyhydride synthesis, is a further illustration of Figlarz's concepts about the usefulness of "soft chemistry"[16] when applied to the synthesis of new compounds in the MoO_3-WoO_3 system.

When compared to the two methods previously reported for the synthesis of α-MoC_{1-x}, the new route described above has two advantages. The first is its simplicity as no initial nitridation of MoO_3 with ammonia is required. The second is that the FCC carbide is obtained directly from pure MoO_3 and is thus not contaminated by traces of platinum.

These facts are certainly relevant if the α-MoC_{1-x} carbide is to be used as a catalyst, in order to avoid secondary reactions resulting from contamination by either γ-Mo_2N nitride (and its further reaction products) or platinum.

For example, it is known that bifunctional Mo-containing H-MFI zeolites, using $(NH_4)_6Mo_7O_{24}{\cdot}4H_2O$ or MoO_3 as molybdenum sources, are efficient catalysts for the direct aromatisation of methane and that the active Mo-species in such systems is molybdenum carbide.[17,18] The new procedure proposed here for the preparation of α-MoC_{1-x} has enabled the quantitative evaluation and comparison of the performance of acidic zeolites modified by both the α- and β-phases of molybdenum carbide[19] without secondary effects owing to the presence of platinum impurities or to possible structural modifications of the zeolite or microporous solid following its prolonged exposure to ammonia at high temperature.[20]

In addition, as the carburisation of MoO_2 and MoO_xH_y leads to two different Mo-carbides, the treatment described above may be used to evidence the formation of the MoO_xH_y oxyhydride phase after a low temperature reductive treatment of MoO_3.[21,22]

In conclusion, a new simple and direct route has been found for the synthesis of the pure α-MoC_{1-x} carbide. This should enable a better quantification of its surface properties and reactivity and may impact on its use as catalyst for a variety of reactions.

R. Anderson, I. Schmidt and Dr A. Green are gratefully acknowledged for having performed some of the experiments.

Notes and references

1 S. T. Oyama, *The Chemistry of Transition Metal Carbides and Nitrides*, Blackie Academic and Professional, London, 1996.
2 S. T. Oyama and G. L. Haller, *Surface and Defect Properties of Solids*, Specialist Periodical Reports, the Chemical Society, London, 1982, vol. 5, p. 332.
3 L. Leclerq, *Surface Properties and Catalysis by Non-metals*, ed. J. P. Bonnelle, D. Delmon and E. G. Derouane, Nato ASI Series, Washington DC, 1983, vol. 433.
4 M. J. Ledoux, C. Pham-Huu, J. Guille and H. Dunlop, *J. Catal.*, 1992, **134**, 383.
5 P. W. Lednor, *Catal. Today*, 1992, **15**, 243.
6 J. S. Lee, S. T. Oyama and M. Boudart, *J. Catal.*, 1987, **106**, 125.
7 G. S. Ranhotra, A. T. Bell and J. A. Reimer, *J. Catal.*, 1987, **108**, 40.
8 L. Volpe and M. Boudart, *J. Solid State Chem.*, 1985, **59**, 348.
9 J. S. Lee, L. Volpe, F. H. Ribeiro and M. Boudart, *J. Catal.*, 1988, **112**, 44.
10 P. Delporte, F. Meunier, C. Pham-Huu , P. Vennégues, M. J. Ledoux and J. Guille, *Catal. Today*, 1995, **23**, 251.
11 C. Bouchy, *PhD Thesis*, University Louis Pasteur, Strasbourg, 1998.
12 I. F. Ferguson, J. B. Ainscough, D. Morse and A. W. Miller, *Nature*, 1964, **202**, 1327.
13 E. Rudy, S. Windisch, A. J. Stosick and J. R. Hoffman, *Trans. TMS-AIME*, 1967, **239**, 1247.
14 S. T. Oyama, *Catal. Today*, 1992, **15**, 179.
15 L. Volpe, *PhD Thesis*, University of Stanford, 1985.
16 M. Figlarz, *Prog. Solid State Chem.*, 1989, **19**, 1.
17 F. Solymosi, A. Szoke and J. Cserenyi, *Catal. Lett.*, 1996, **39**, 157.
18 D. Wang, J. H. Lunsford and P. Rosynek, *J. Catal.*, 1997, **169**, 347.
19 S. B. Derouane-Abd Hamid, R. Anderson, I. Schmidt, C. Bouchy, K. Jacobsen and E. G. Derouane, oral presentation accepted at *APCAT 2000*, January, Australia *Catal. Today*, submitted.
20 E. Segal, I. Ivanova and E. G. Derouane, *Rev. Roum. Chim.*, 1993, **38**, 1127.
21 A. Katrib, V. Logie., P. Wehrer, L. Hilaire and G. Maire, *J. Chim. Phys.*, 1997, **94**, 1923.
22 T. Matsuda, H. Shiro, H. Sakagami and N. Takahashi, *Catal. Lett.*, 1997, **47**, 99.

Communication a907534h

Facile synthesis and crystal structure of a $Ga_{22}R_8$ cluster†

Gerald Linti* and Alexander Rodig

Institut für Anorganische Chemie der Universität, Engesserstr. Geb. 30.45, 76128 Karlsruhe, Germany. E-mail: linti@achpc9.chemie.uni-karlsruhe.de

Received (in Basel, Switzerland) 31st August 1999, Accepted 30th November 1999

A new metalloid cluster $Ga_{22}R_8$ with a central gallium atom exhibiting an unusual coordination number of 13 and the gallatetrahedrane Ga_4R_4 are obtained by reaction of 'GaI' with the lithium tris(trimethylsilyl)germanide $Li(thf)_3R$.

In the past decade, the chemistry of low valent gallium compounds has garnered widespread interest.[1] An appropriate and easily accessible starting material for gallium cluster compounds is 'GaI', prepared by treating gallium and iodine in toluene with ultrasound.[2] 'GaI', the structure of which is still unknown, has been used to synthesize a gallium(I) pyrazolyborate derivative[3] and the trigallane Ga_3I_5•$3PEt_3$.[4] The reaction of 'GaI' with lithium tris(trimethylsilyl)silanide as its thf solvate $Li(thf)_3R'$ (Scheme 1) afforded the gallatetrahedrane **1**, the electron-precise tetragallane **2** and the nonagallane **3** together with the disproportionation products **4** and **5**[5] as well as a silagallane cluster.[6] The structure of **3**, a cluster anion of composition $[Ga_9R'_6]^-$, is, in conformity with Wade–Williams cluster rules, a Ga_7 *closo* cluster with four R′ and two GaR′ ligands. Obviously, three Ga atoms are attached to other Ga atoms only. Such ligand free cluster atoms are rare in main group chemistry but are also found in $\{Al_{77}[N(SiMe_3)_2]_{20}\}^{2-}$ [7] and $In_{12}(SiBu^t_3)_8$.[8] In **1** and **3** the ligands shield the gallium core entirely. Thus, the question arises whether other ligands allow the preparation of cluster compounds with different gallium cores. Here, we report on the use of the tris(trimethylsilyl)germanyl group (R) in gallium cluster chemistry and the easy, high yield synthesis of a Ga_{22}-cluster.

When sonochemically prepared 'GaI' is reacted with $Li(thf)_3R$ in toluene (Scheme 2), a dark red–violet solution is obtained from which colourless gallium(III) products of the type R_2GaI_2•$Li(thf)_n$ **6** precipitate.‡ Obviously, a disproportionation reaction has occurred, but the formation of elemental gallium was not observed, implying that gallium species with oxidation states of $\leqslant 1$ had formed. Consequently, the gallatetrahedrane **7** was isolated in considerable yields while the main product of the reaction was $Ga_{22}[Ge(SiMe_3)_3]_8$ **8**. The tris(trimethylsilyl)silyl analogue of **8**, $Ga_{22}[Si(SiMe_3)_3]_8$,[9] was not accessible *via* 'GaI' but was synthesised *via* metastable GaBr solutions, the preparation of which is very complicated.

Compound **7** (Fig. 1)§ exhibits a nearly ideal tetrahedral Ga_4 core with average Ga-Ga distances of 258.7 pm. Thus, **7** is very similar to **1** ($d_{Ga–Ga}$ = 258.8 pm)[10] and $Ga_4(SiBu^t_3)_4$ ($d_{Ga–Ga}$ = 257.9 pm),[11] but has shorter Ga–Ga contacts than $Ga_4[C(SiMe_3)_3]_4$ ($d_{Ga–Ga}$ = 268.8 pm).[12]

X-Ray structure analysis of **8** (Fig. 2)§ shows a cluster consisting of 22 Ga atoms with eight R substituents and can be viewed as a Ga_{14} core with eight attached GaR units. The Ga_{14} core can be regarded as metalloid, yet this framework has no equivalent in any known modification of elemental gallium. The Ga_{14} core consists of a central gallium atom Ga(1), which is surrounded by 13 other gallium atoms with long Ga–Ga distances ranging from 285.5 to 312.4 pm (av. 295.1). The coordination sphere around the central gallium atom is an unusual Ga_{13} polyhedron of the type M_3–M_6–M_4 with eight four-membered and four three-membered ring facets. This is similar to the M_{12} cuboctahedron (M_3–M_6–M_3) in closest packing spheres of metals. The Ga–Ga distances within the Ga_{13} shell average 282.9 pm, longer than the Ga–Ga distances in elemental gallium (240–280 pm)[13] or in the Ga_{12} icosahedra in $Na_xMg_{5-x}Ga_9$ ($d_{Ga–Ga}$ = 269–273 pm).[14] All four-membered ring facets of this Ga_{13} shell are capped by GaR units in μ_4 and μ_3-modes [$d_{Ga–Ga}$ = 256.6 pm (av.)]. The gallium atoms

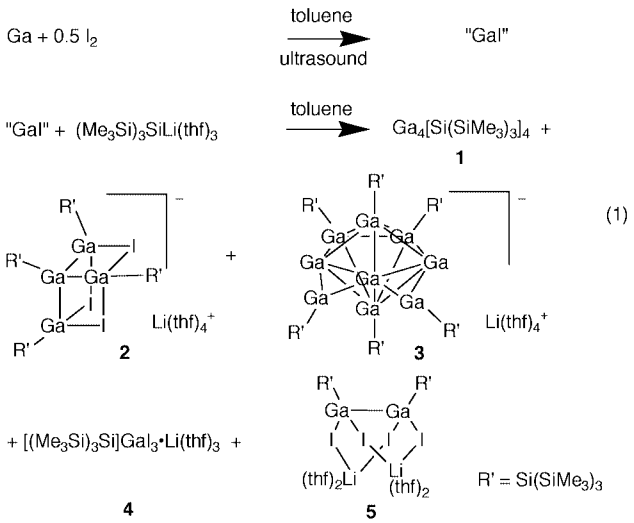

Scheme 1

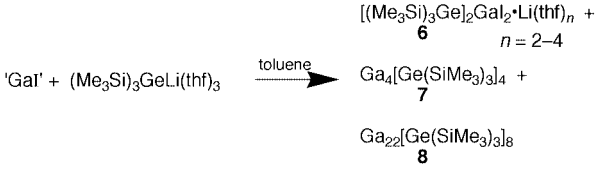

Scheme 2

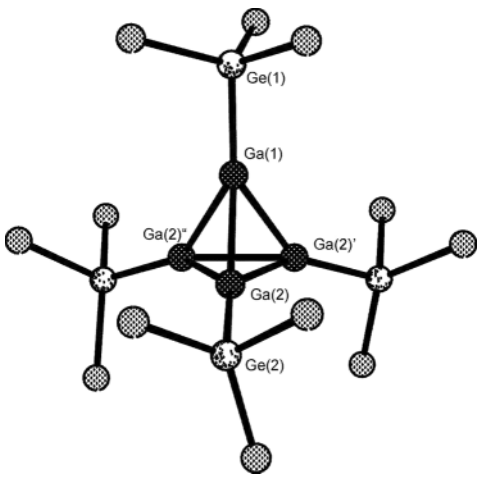

Fig. 1 View of a molecule of **7**. Methyl groups are omitted for clarity. Selected bond lengths (pm): Ga(1)–Ga(2) 258.2(5), Ga(2)–Ga(2)′ 259.1 (5), Ga(1)–Ge(1) 246.8(6), Ga(2)–Ge(2) 245.5(4), Ge–Si 235(2)–238(2).

† Dedicated to Prof. Nils Wiberg on the occasion of his 65th birthday.

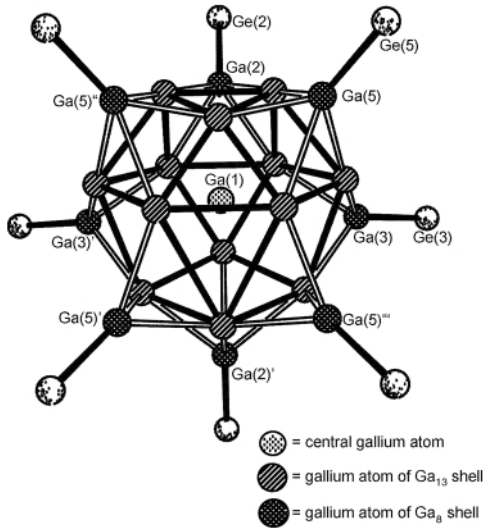

Fig. 2 View of a molecule of **8**. Trimethylsilyl groups are omitted for clarity. Selected bond lengths (pm): Ga(1)–Ga_{Ga13} 285.5(5)–312.4(5), Ga(2)–Ga_{Ga13} 244.7(5), 244.7(5), 245.8(4), 245.8(4), Ga(3)–Ga_{Ga13} 258.9(7), 246.0(5), 246.9(5), Ga(5)–Ga_{Ga13} 236.5(7), 240.3(7), 268.4(6), 269.3(5), Ga(2)′–Ga_{Ga13} 269.0(6), 274.6(8), 274.6(8), 300.5(8), Ga(2)–Ge(2) 243.0(2), Ga(3)–Ge(3) 242.8(2), Ga(5)–Ge(5) 242.9(3), Ge–Si 236.1(4)–238.4(5).

[Ga(2), Ga(3), Ga(5) and symmetry equivalents] of these eight GaR units form a quadratic antiprism ($d_{Ga–Ga}$ = 481–505 pm). Again, the bulky tris(trimethylsilyl)germyl ligands completely shield the gallium core.

Compound **8** is certainly not a typical Wade type cluster and should be viewed as a metalloidal cluster, in accordance with the jellium model.[9] However, when taking into consideration the long Ga–Ga distances involving Ga(1) and within the Ga_{13}-shell, as well as the short distances between the RGa units and the atoms of the Ga_{13} shell, the RGa groups may be viewed as electron pair donating ligands, attached to the Ga_{13} shell by two-electron multicenter bonds. Assuming a central Ga^+ ion, 15 cluster binding electron pairs are counted; thus the Ga_{13} shell may be regarded as a *nido* polyhedron. This 13-atom polyhedron resembles the M_3–M_6–M_4 arrangement recently reported for $(AlMe)_8C(CH_2Ph)_5H$.[15]

The results presented show the great synthetic potential of 'GaI' for the preparation of gallium cluster compounds. Examples include compounds **3** and **8**, which are intermediates in the disproportionation of low valent gallium species into metal and higher oxidized gallium compounds. Our current efforts are directed towards the synthesis of other silyl and germyl ligands with modified steric and electronic properties in order to influence the size of the gallium cluster.

This work was supported by the Deutsche Forschungsgemeinschaft and the Fonds der Chemischen Industrie. We thank Prof. Dr D. Fenske for diffractometer time.

Notes and references

‡ *Experimental*: $Li(thf)_3Ge(SiMe_3)_3$[16] (1.9 g, 3.7 mmol) dissolved in 25 mL of toluene at −78 °C was slowly added to a suspension of 'GaI' (0.7 g, 3.7 mmol) (prepared by the procedure given in ref. 2) in toluene (30 ml) at the same temperature. The mixture was stirred for 5 h at –78 °C and then allowed to warm to room temp. All volatiles were removed *in vacuo*, and the residue was extracted with methylcyclohexane (30 ml). The resulting dark red solution was filtered. Crystals of **6**, **7** and **8**, suitable for X-ray crystallography, were obtained from the concentrated filtrate at 0 and –30 °C, respectively.

Spectral data: for **7**•$0.5Ge_2Si_8C_{24}H_{72}O$•$0.5C_7H_8$ (*M* = 1867.1): yield: 259 mg (15%); ^{1}H NMR (C_6D_6): δ 0.46 [s, $OGe_2(SiMe_3)_6$], 0.39 [s, $GaGe(SiMe_3)_3$]; ^{13}C NMR (C_6D_6): δ 4.83 [$GaGe(SiMe_3)_3$], 4.65 [$OGe_2(SiMe_3)_6$]; MS (70 eV, EI): *m/z* (%) 1438 (2.7) $[M]^{\cdot+}$, 1365 (0.3) $[M - SiMe_3)]^+$, 1145 (5.0) $[M - Ge(SiMe_3)_3]^+$, 854 (1.3) $[M - 2\,Ge(SiMe_3)_3]^{\cdot+}$, 594 (2.6) $[OGe_2(SiMe_3)_6]^{\cdot+}$, 358 (34.5) $[GaGe(SiMe_3)_3]^{\cdot+}$, 293 (100.0) $[Ge(SiMe_3)_3]^+$.

For **8**•$0.25GeSi_4C_{12}H_{36}$ (*M* = 3962.9): yield: 127 mg (19%); MS (70 eV, EI): *m/z* (%) 362 (6.4) $[Ge(SiMe_3)_4]^{\cdot+}$, 293 (100.0) $[Ge(SiMe_3)_3]^+$.

§ *Crystal data*: STOE IPDS, Mo-Kα radiation, direct methods, full-matrix least squares against F^2, hydrogen atoms as riding model with Bruker AXS SHELXTL 5.1 (PC).

$Ga_4Ge_4Si_{12}C_{36}H_{108}$•$0.5Ge_2Si_8C_{24}H_{72}O$•$0.5C_7H_8$ **7**: crystal size: 0.20 × 0.20 × 0.10 mm, cubic, space group $Pa\bar{3}$ (no. 205), a = 2697.5(3) pm, V = 19.628(4) nm^3, Z = 8, D_c = 1.214 g cm^3, μ = 2.796 mm^{-1}, F(000) = 7424, 14038 measured reflections for 2θ = 2.5 − 42°, 3337 [1193 with $F > 4\sigma(F)$] independent reflections, 228 parameters. R_1 = 0.108, wR_2 = 0.289, max. residual electron density 1.56 e Å^{-3}. Several crystals tested were all very weakly diffracting, so this structure should be regarded as a preliminary one. Only Ga, Ge and Si atoms were refined anisotropically, C and O atoms isotropically. The nearly spherical molecules of **7** (residing on a threefold axis) pack in a primitive cubic lattice, providing large holes in the structure, which are occupied by disordered toluene and $[(Me_3Si)_3Ge]_2O$ molecules. The high residual electron density is due to partial oxidation resulting in a RGa_4O_4-heterocubane. Only *ca.* 10% of the oxygen positions are occupied, the R-values being unaffected, whether these are included in the refinement or not.

$Ga_{22}Ge_8Si_{24}C_{72}H_{216}$•$0.25GeSi_4C_{12}H_{36}$ **8**: crystal size: 0.20 × 0.10 × 0.02 mm, orthorhombic, space group *Pmmn* (no. 59), a = 2401.2(3), b = 2461.5(2), c = 1605.9(1) pm, V = 9.492(1) nm^3, Z = 2, D_c = 1.361 g cm^{-3}, μ = 4.520 mm^{-1}, F(000) = 3860, 16797 measured reflections for 2θ = 4 − 42°, 4661 [2160 with $F > 4\sigma(F)$] independent reflections, 366 parameters. R_1 = 0.088, wR_2 = 0.244 (all data), max. residual electron density 1.23 e Å^{-3}. The $GaGa_{14}$ core is disordered, so that two orientations of the Ga_{13} core overlie each other, interchanging the M_3 and M_4 facets. Thus the disordered molecule has crystallographic *mm* symmetry, while **8** has only mirror symmetry. Although the data were inspected thoroughly, no hint of a larger cell or superstructure was found. The almost spherical clusters are packed in a primitive cubic lattice, the cubic holes of which are occupied in part (*ca.* 25%) by disordered $Ge(SiMe_3)_4$ and pentane. Only the central Ge atoms were included in the refinement. Owing to the intensive disorder and the thinness of the crystal plates virtually no peaks with 2θ > 42° could be observed. Therefore, only gallium, germanium and silicon atoms were refined anisotropically.

CCDC 182/1495. See http://www.rsc.org/suppdata/cc/a9/a907039g/ for crystallographic files in .cif format.

1 W. Uhl, *Angew. Chem.*, 1993, **105**, 1449; *Angew. Chem., Int. Ed. Engl.*, 1993, **32**, 1386; C. Dohmeier, D. Loos and H. Schnöckel, *ibid.*, 1996, **108**, 141; 1996, **35**, 129.
2 M. L. H. Green, P. Mountford, G. J. Smout and S. R. Speel, *Polyhedron*, 1990, **9**, 2763.
3 M. C. Kuchta, J. B. Bonnano and G. Parkin, *J. Am. Chem. Soc.*, 1996, **118**, 10 914.
4 A. Schnepf, C. Doriat, E. Möllhausen and H. Schnöckel, *Chem. Commun.*, 1997, 2111.
5 G. Linti and W. Köstler, *Angew. Chem.*, 1997, **109**, 2758; *Angew. Chem., Int. Ed. Engl.*, 1997, **36**, 2644
6 G. Linti, W. Köstler, H. Piotrowski and A. Rodig, *Angew. Chem.*, 1998, **110**, 2331; *Angew. Chem., Int. Ed.*, 1998, **37**, 2209. This is the preceeeding paper in the series 'On the chemistry of gallium'. The present paper is regarded as part 16.
7 A. Ecker, E. Weckert and H. Schnöckel, *Nature*, 1997, **387**, 379.
8 N. Wiberg, T. Blank, H. Nöth and W. Ponikwar, *Angew. Chem.*, 1999, **111**, 887; *Angew. Chem., Int. Ed.*, 1999, **38**, 839.
9 A. Schnepf, E. Weckert, G. Linti and H. Schnöckel, *Angew. Chem.*, 1999, **111**, 3578; *Angew. Chem., Int. Ed.*, 1999, **38**, 3381.
10 G. Linti, *J. Organomet. Chem.*, 1996, **520**, 107.
11 N. Wiberg, *Coord. Chem. Rev.*, 1997, **163**, 217.
12 W. Uhl, W. Hiller, M. Layh and W. Schwarz, *Angew. Chem.*, 1992, **104**, 1378; *Angew. Chem., Int. Ed. Engl.*, 1992, **31**, 1364.
13 A. F. Wells, *Structural Inorganic Chemistry*, Clarendon Press, Oxford 5th edn., 1984.
14 R. Nesper, *Angew. Chem.*, 1989, **101**, 99; *Angew. Chem., Int. Ed. Engl.*, 1989, **28**, 58.
15 W. Uhl and F. Breher, *Angew. Chem.*, 1999, **111**, 1578; *Angew. Chem. Int. Ed.*, 1999, **38**, 1477.
16 A. G. Brook, F. Abdesaken and H. Söllradl, *J. Organomet. Chem.*, 1986, **299**, 9.

Communication a907039g

Cycloruthenated tertiary amines and ethylene: further insight to the Ru-mediated olefin–aryl coupling reaction

Vincent Ritleng, Jean Pascal Sutter,† Michel Pfeffer* and Claude Sirlin

Laboratoire de Synthèses Métallo-Induites, UMR CNRS 7513 Université Louis Pasteur, 4 rue Blaise Pascal, 67070 Strasbourg, France. E-mail: pfeffer@chimie.u-strasbg.fr

Received (in Basel, Switzerland) 29th October 1999, Accepted 6th December 1999

The reaction between cycloruthenated *N*,*N*-dimethylbenzylamine and ethylene under very mild conditions afforded 2-vinyl-*N*,*N*-dimethylbenzylamine and an organometallic Ru derivative resulting from the overall insertion of one carbon atom in the Ru–C bond of the starting material.

The insertion of an olefin in a transition metal–carbon σ-bond is a classical reaction in organometallic chemistry. With palladium, this process is followed by β-hydrogen elimination and is widely known as the Heck reaction.[1] Recently, functionalisation reactions of aryl C–H bonds with terminal olefins catalysed by ruthenium hydride complexes were reported.[2,3] In these reactions the products are alkyl substituted compounds resulting from the 'formal' insertion of the olefinic double bond into a C–H bond. We now report that air stable cycloruthenated *N*,*N*-dimethylbenzylamine derivatives react at low pressure (1.5 atm) and room temperature (RT) with ethylene to afford vinylbenzylamines, as in the Heck reaction, and an organometallic compound resulting from the insertion of ethylene into the Ru–C bond.

In a typical experiment, an orange suspension of (η^6-C_6H_6)Ru($C_6H_4CH_2NMe_2$)Cl **1a** in methanol was stirred at room temperature under 1.5 bar of ethylene over 1.5 h [eqn. (1)]. 2-Vinyl-*N*,*N*-dimethylbenzylamine **2a**‡ and the new organoruthenium compound **3a**‡ were isolated. The ^{1}H and ^{13}C NMR spectra and combustion analyses of **3a** are consistent with the structure depicted in eqn. (1).

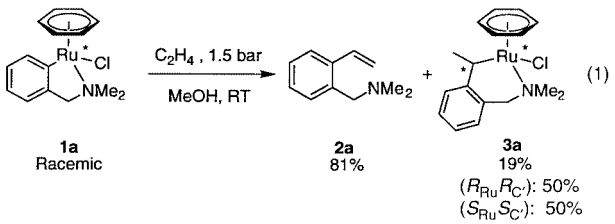

We found that it was possible to influence the ratio of **2a** to **3a** by removing the chloride ligand of the starting material. Thus, the yellow cationic derivative **1a′**[4c] led to a much higher yield of the red organometallic species **3a′** when it was treated with ethylene [eqn. (2)].

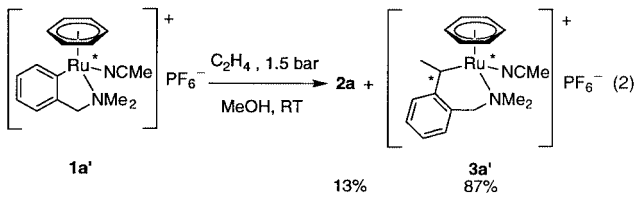

These reactions led to the formation of a chiral C atom σ-bonded to Ru, the Ru atom being itself a stereogenic center.[4] Interestingly, only one enantiomeric pair was observed by ^{1}H NMR in both cases, indicating that these reactions occur with a high level of diastereoselectivity. The stereochemistry of **3a** has been investigated by a ^{1}H NOE experiment. The η^6-benzene ring was found to interact strongly with one of the *N*-methyl and with the *C*-methyl which also interacts with the proton of the aryl ligand. The proton on the carbon α to Ru (C′) interacts neither with the latter nor with the η^6-benzene ring. Consequently, **3a** displays a boat conformation, with the C-methyl and the η^6-benzene ring in the equatorial and the axial positions respectively. The absolute configuration of the enantiomers are thus ($R_{Ru}R_{C'}$) and ($S_{Ru}S_{C'}$).

In order to confirm the chiral control of the reaction, the optically active complex (η^6-C_6H_6)Ru(C_6H_4-2-(*R*)-CH(Me)N-Me_2)Cl **1b** (de = 90%)[4] was treated with ethylene under the same conditions. Surprisingly in addition to **2b** and **3b**,‡ the respective analogues of **2a** and **3a**, a third product **4b**‡ was observed in trace amounts [eqn. (3)]. Its structure is that of a new cyclometallated benzylamine derivative displaying an ethyl substituent in position 3.

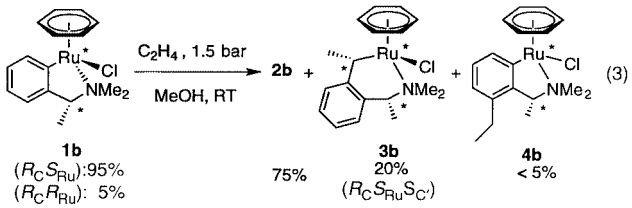

For complexes **3b** and **4b**, one diastereoisomer only was observed by ^{1}H NMR indicating that these compounds are the result of highly diastereoselective processes. Unfortunately owing to its instability, **3b** could not be isolated as a pure solid. Nevertheless its stereochemistry was investigated through a ^{1}H ROESY experiment of the crude reaction mixture. The methyl substituent of the carbon atom σ-bonded to Ru (C′) interacts with the proton of the aryl ligand and with the η^6-C_6H_6 ring whereas the corresponding proton interacts with none of these. These results indicate an equatorial position for the methyl group and axial position for the η^6-benzene ring as in **3a**. The methyl group α to N interacts equally with both *N*-methyls and with the proton of the aryl ligand but not with the η^6-benzene indicating an equatorial position as well. Moreover, the absence of any interaction between the η^6-benzene ring and the benzylic proton attached to N, together with the deshielding of the latter signal, indicate that this proton should be close to the chlorine atom as in the starting material **1b**. Consequently, **3b** should display a boat conformation with the protons α to Ru and N on bridgehead positions and its absolute configuration should therefore be ($R_CS_{Ru}S_{C'}$).

When **3b** was left in solution it isomerised slowly into **4b** together with decomposition but no conversion into **2b** was detected. Thus **2b** and **3b** are independent products which, however, are likely to come from the same intermediate (see below). The important instability of **3b** as compared to that of **3a** might be due to steric congestion around the Ru atom. The

† *Present address*: Institut de Chimie de la Matière Condensée de Bordeaux - UPR CNRS 9048-Avenue du Dr. Schweitzer 33608 Pessac, France.

rearrangement process **3b** → **4b** remains unclear yet. Running the reaction in CD_3OD did not result in deuterium incorporation in the new ethyl group. Moreover, when a sample of the crude reaction mixture was left in an aprotic solvent such as $CDCl_3$ this demetallation–remetallation process also occured. These observations tend to indicate that **4b** may be formed through an intramolecular rearrangement as demonstrated by Steenwinkel *et al.* for a related ruthenocyclic molecule.[5]

To the best of our knowledge the only precedent of a Ru-mediated functionalization of a C–H bond to afford a vinyl derivative such as **2a**,**b** was reported by Murai and coworkers[6] when reacting aromatic imines or imidates with mono-substituted olefins in the presence of catalytic amounts of $Ru_3(CO)_{12}$. It is generally assumed that this type of product is formed by β-H elimination from a carbometallation intermediate. Consequently the formation of **2a**,**b** and **3a**,**b** can be rationalised according to the reaction path depicted in Scheme 1. The first step involves the insertion of ethylene into the C–Ru bond followed by a β-H elimination leading to an olefin–hydride complex.[7] This leads on one hand to the metal free substituted olefin **2a**,**b** as in the Heck reaction and on the other hand to the one carbon-atom insertion complex **3a**,**b** by anti-Markovnikov hydrometallation of the olefinic unit (Scheme 1).

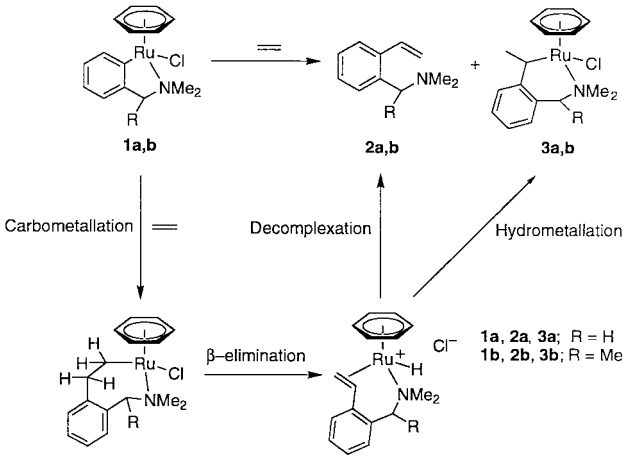

Scheme 1

Studies are currently under way to determine the conditions that would allow us to direct the reaction toward the exclusive formation of one of these products.

We thank INTAS (INTAS-97-166) for financial support of this work.

Notes and references

‡ *Selected data* (*J*/Hz): **2a**: δ_H(200 MHz, $CDCl_3$) 7.55 (m, 1H, C_6H_4), 7.26 (m, 3H, C_6H_4), 7.17 (dd, 1H, C*H*=CH_2, ^3J 17.5, ^3J 11.0), 5.68 (dd, 1H, CH=CH_EH_Z, ^3J 17.5, ^2J 1.4), 5.30 (dd, 1H, CH=CH_EH_Z, ^3J 11.0, ^2J 1.4), 3.44 (s, 2H, CH_2N), 2.24 (s, 6H, NMe_2). **2b**: δ_H(200 MHz, $CDCl_3$) 7.44 (m, 2H, C_6H_4), 7.24 (m, 2H, C_6H_4), 7.23 (dd, 1H, C*H*=CH_2, ^3J 17.4, ^3J 11.0), 5.57 (dd, 1H, CH=CH_EH_Z, ^3J 17.4, ^2J 1.6), 5.29 (dd, 1H, CH=CH_EH_Z, ^3J 11.0, ^2J 1.6), 3.53 (q, 1H, C*H*CH_3, ^3J 6.6), 2.21 (s, 6H, NMe_2), 1.31 (d, 3H, CHCH_3). **3a**: Anal. Calc. (found) for $C_{17}H_{22}NClRu{\cdot}0.25CH_2Cl_2$: C, 52.04 (52.27); H, 5.70 (5.72); N, 3.52 (3.66)%. δ_H(300 MHz, $CDCl_3$) 7.58 (d, 1H, C_6H_4, ^3J 7.7), 7.33 (m, 2H, C_6H_4), 6.88 (d, 1H, C_6H_4, ^3J 4.0), 4.90 (s, 6H, C_6H_6), 3.53 (q, 1H, C*H*CH_3, ^3J 7.1), 3.39 and 2.29 (AB, 2H, CH_2N, ^2J 11.4), 3.24 and 2.28 (2s, 6H, NMe_2), 2.14 (d, 3H, CHCH_3). δ_C(75 MHz, $CDCl_3$) 153.8, 133.3, 129.4, 129.0, 121.6 and 120.4 (C_6H_4), 83.0 (C_6H_6), 64.7 (CH_2N), 56.5 and 56.3 (NMe), 36.8 (CHRu), 24.5 (CH*C*H_3). **3a′**: δ_H(200 MHz, CD_3CN) 7.62 (d, 1H, C_6H_4, ^3J 7.4), 7.34 (m, 2H, C_6H_4), 6.99 (d, 1H, C_6H_4, ^3J 6.6), 5.14 (s, 6H, C_6H_6), 3.24 and 2.63 (AB, 2H, CH_2N, ^2J 11.8), 3.09 (q, 1H, C*H*CH_3, ^3J 7.4), 3.01 and 2.38 (2s, 6H, NMe_2), 2.14 (s, 3H, CH_3CN), 2.08 (d, 3H, CHCH_3). **3b**: δ_H(500 MHz, CD_2Cl_2) 7.57 (d, 1H, C_6H_4, ^3J 7.7), 7.29 (t, 1H, C_6H_4), 7.02 (d, 1H, C_6H_4). 6.90 (t, 1H, C_6H_4), 4.88 (s, 6H, C_6H_6), 3.57 (2q, 2H, C*H*CH_3Ru and C*H*CH_3N), 3.32 and 2.07 (2s, 6H, NMe_2), 2.11 (d, 3H, CHCH_3Ru, ^3J 7.1), 1.29 (d, 3H, CHCH_3N, ^3J 6.9). **4b**: δ_H(500 MHz, CD_2Cl_2) 7.51 (d, 1H, C_6H_3, ^3J 7.4), 6.94 (t, 1H, C_6H_3). 6.68 (d, 1H, C_6H_3), 5.32 (s, 6H, C_6H_6), 3.45 (q, 1H, C*H*CH_3, ^3J 6.6), 3.10 and 2.33 (2s, 6H, NMe_2), 2.44 (q, 2H, C$H_2$$CH_3$, ^3J 7.6), 1.16 (d, 3H, CHCH_3), 1.14 (t, 3H, CH_2CH_3).

1 R. F. Heck, *Org. React. (New York)*, 1982, **27**, 345.
2 S. Murai, F. Kakiuchi, S. Sekine, Y. Tanaka, A. Kamatani, M. Sonoda and N. Chatani, *Nature*, 1993, **366**, 529; F. Kakiuchi, S. Sekine, Y. Tanaka, A. Kamatani, M. Sonoda, N. Chatani and S. Murai, *Bull. Chem. Soc. Jpn.*, 1995, **68**, 62.
3 Y. Guari, S. Sabo-Etienne and B. Chaudret, *J. Am. Chem. Soc.*, 1998, **120**, 4228.
4 (*a*) H. C. L. Abbenhuis, M. Pfeffer, J. P. Sutter, A. de Cian, J. Fischer, H. Li Ji and J. H. Nelson, *Organometallics*, 1993, **12**, 4464; (*b*) S. Attar, J. H. Nelson, J. Fischer, A. de Cian, J. P. Sutter and M. Pfeffer, *Organometallics*, 1995, **14**, 4559; (*c*) S. Fernandez, M. Pfeffer, V. Ritleng and C. Sirlin, *Organometallics*, 1999, **18**, 2390.
5 P. Steenwinkel, S. L. James, R. A. Gossage, D. M. Grove, H. Kooijman, W. J. J. Smeets, A. L. Spek and G. van Koten, *Organometallics*, 1998, **17**, 4680.
6 F. Kakiuchi, M. Yamauchi, N. Chatani and S. Murai, *Chem. Lett.*, 1996, 111; F. Kakiuchi, T. Sato, M. Yamauchi, N. Chatani and S. Murai, *Chem. Lett.*, 1999, 19.
7 For a leading reference concerning olefin–hydride complexes, see: J. W. Faller and K. J. Chase, *Organometallics*, 1995, **14**, 1592.

Communication a908703f

Synthesis and characterization of a chiral nonplanar porphyrin

Cinzia M. Muzzi,[a] Craig J. Medforth,*[a] Kevin M. Smith,*[a] Song-Ling Jia[b] and John A. Shelnutt*[b]

[a] *Department of Chemistry, University of California, Davis, CA 95616 USA. E-mail: medforth@indigo.ucdavis.edu*
[b] *Nanomolecular Materials and Interfaces Department, Sandia National Laboratories, Albuquerque, New Mexico 87185-1349, USA*

Received (in Corvallis, OR, USA) 14th October 1999, Accepted 29th November 1999

The chiral nonplanar porphyrin zinc(II) 3,7,8,12,13,17,18-heptabromo-2-(2-methoxyphenyl)-5,10,15,20-tetraphenylporphyrin has been synthesized and its properties investigated.

The porphyrin macrocycle provides a versatile platform upon which to build elaborate superstructures, and this feature coupled with a rich and well-developed synthetic chemistry has led to the synthesis of many models of heme protein active sites[1] and numerous porphyrin-based receptor molecules.[2] One characteristic which is not normally considered in the design of porphyrin-based receptors is nonplanarity of the porphyrin macrocycle,[3] although the nonplanar systems that have been investigated (*e.g.* a pyridine sensitive Venus Flytrap[4] and a chirality-memory molecule[5]) have displayed quite unusual properties. Herein, we describe the synthesis and characterization of a new porphyrin-based chiral receptor molecule (**1**)

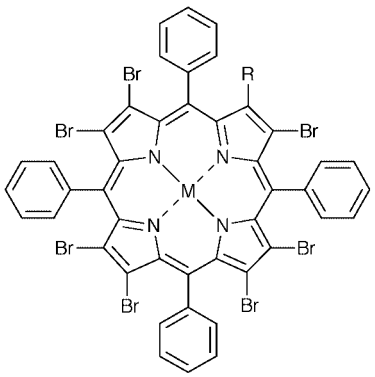

1 R = 2-MeOC$_6$H$_4$, M = Zn
3 R = 2-MeOC$_6$H$_4$, M = 2H
4 R = Br, M = 2H

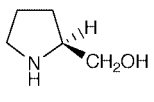

2

which exploits some structural features unique to nonplanar porphyrins.

Fig. 1 shows the four structures expected for porphyrin **1**. Structures **A** and **B** (or **C** and **D**) are enantiomers, structures **A** and **C** (or **B** and **D**) are related by rotation of the 2-methoxyphenyl group, and structures **A** and **D** (or **B** and **C**) are related by inversion of the nonplanar porphyrin macrocycle. Porphyrin **1** was calculated[6] to have a very high barrier for rotation of the 2-methoxyphenyl group (>146 kJ mol^{-1}), a low barrier for inversion of the porphyrin macrocycle[7] (*ca.* 40 kJ mol^{-1}), and a strong preference (ΔE = 8 kJ mol^{-1}) for structures **A** and **B** *vs.* structures **C** and **D**. Hence, it should be resolvable into two optically active components consisting primarily of structures **A** or **B**. Porphyrin **1** was designed with the aim of using a cavity formed by the nonplanar macrocycle to orient an axial ligand,[8] such that a hydrogen bond acceptor site (the methoxy group) could interact stereospecifically with hydrogen bond donor sites on the axial ligand. Fig. 2 shows the lowest energy structure calculated for a complex of **1** with (*S*)-2-pyrrolidinemethanol (**2**) which illustrates this ligand orientation effect and the formation of stereospecific hydrogen bonds with one enantiomer of the porphyrin (structure **B**). Note that the nonplanar deformation of the macrocycle serves a dual function as it also moves the methoxy substituent closer to the ligand than would be possible if the porphyrin were planar.

To prepare porphyrin **1**, porphyrin **3** was first synthesized using a Suzuki coupling reaction.[9] In this reaction, porphyrin **4** (1 equiv.), 2-methoxyphenylboronic acid (5 equiv.), Pd[(PPh$_3$)]$_4$ (0.15 equiv.) and K_2CO_3 (20 equiv.) in toluene under argon were heated at 90–100 °C for two days. MALDI mass spectrometry of the crude product revealed the presence of unreacted **4**, porphyrin **3**, and porphyrins with two or more 2-methoxyphenyl groups. Porphyrin **3** was isolated from this mixture using column chromatography (silica gel eluted with 3 : 2 $CHCl_3$–hexane) and obtained in 12% yield. The structure of **3** was confirmed by MALDI mass spectrometry and ^{1}H NMR spectroscopy. Zinc was then inserted using the metal acetate method to give **1**.

When porphyrin **1** was subjected to HPLC using a Chiralcel OD column eluted with 89 : 10 : 1 hexanes–$CHCl_3$–Pr^{i}OH, two fractions (elution times 12 and 28 min) were obtained. These fractions had identical optical spectra but their CD spectra were mirror images of each other. Leaving each fraction in the eluent and reinjecting it through the HPLC column 24 h after

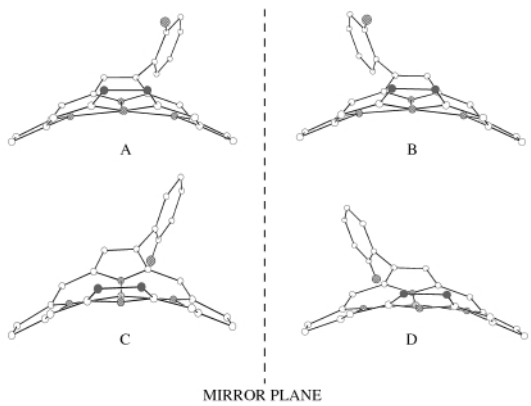

Fig. 1 Representations of the four structures expected for porphyrin **1**.

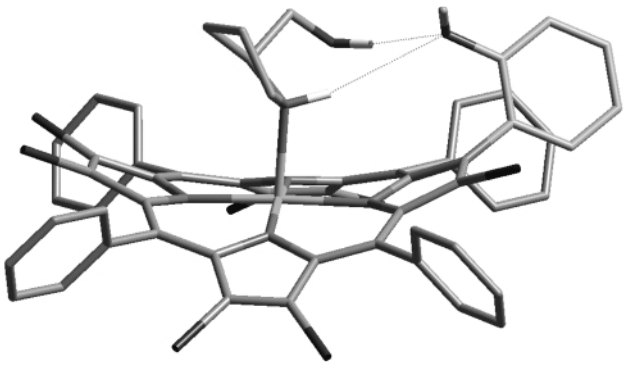

Fig. 2 Minimum energy structure calculated (ref. 6) for the complex of porphyrin **1** with ligand **2**. Porphyrin–ligand hydrogen bonds are indicated by broken lines.

separation revealed only a trace of racemization, in agreement with the high rotational barrier calculated for the 2-methoxyphenyl group. The isolation of only two HPLC fractions together with ^{1}H NMR studies of **1** confirmed that structures **A** and **D** (or **B** and **C**) were being interconverted by inversion of the porphyrin macrocycle.[7] The ^{1}H NMR spectrum of **1** showed a single broad methoxy signal at 295 K (δ 2.77) which split into two signals at 193 K (δ 2.30, integration 11.5 and δ 3.61, integration 1). As the methoxy signals at δ 2.30 and 3.61 could be assigned to **A** and **B** or **C** and **D** based on the expected ring current shifts of the methoxy protons in these structures, it was clear that the interconversion of **A** and **D** (or **B** and **C**) was rapid at room temperature and that **A** and **B** were significantly favored over **C** and **D**. Both the conformational energy difference (4 kJ mol^{-1} at 193 K) and the activation energy for macrocylic inversion (51 kJ mol^{-1} at the coalescence temperature of 273 K) were in reasonable agreement with the energies obtained from the modelling studies.

Despite repeated attempts we were unable to determine the X-ray structures of the porphyrins in the two HPLC fractions. However, modelling studies suggested that it should be possible to differentiate enantiomers **A** and **B** by their interactions with ligand **2**. In the case of structure **B**, ligand **2** should bind in essentially a single orientation because there is an energy difference of at least 5 kJ mol^{-1} between the minimum energy structure (Fig. 2) and other low energy structures (where the ligand is rotated approximately 180° in the cavity or is bound in either orientation in the cavity on the other face of the porphyrin). For structure **A**, the energy difference between these ligand binding geometries is calculated to be smaller, suggesting that the ligand should bind in multiple orientations. The hydrogen bonding seen in the lowest energy calculated structure of **B** (Fig. 2) is also expected to produce a downfield shift of the ligand NH and OH proton signals that should be absent or less pronounced for structure **A**. NMR spectra of the HPLC fractions dissolved in toluene-d_8 containing approximately 1 equiv. of **2** are shown in Fig. 3. The spectra were measured at 193 K where ligand exchange, ligand rotation, inversion of the porphyrin macrocycle, and rotation of the 2-methoxyphenyl group can all be demonstrated to be slow on the NMR timescale. The ligand proton region of the HPLC fraction with a retention time of 28 min shows only a single downfield-shifted pyrrolidine NH signal (definitively assigned by deuteration with D_2O) and agrees with the spectrum expected for structure **B**. In contrast, the HPLC fraction with a retention time of 12 min displays four NH signals (none of which are shifted downfield) consistent with the spectrum expected for structure **A**. Ligand signals were not seen for **C** and **D** in agreement with the higher energies calculated for these structures.

The results reported here provide further confirmation that nonplanar deformations of the porphyrin macrocycle can be exploited to produce unusual porphyrin-based receptor molecules. The present work also demonstrates the usefulness of molecular modelling techniques in the design and characterization of new porphyrin-based materials.

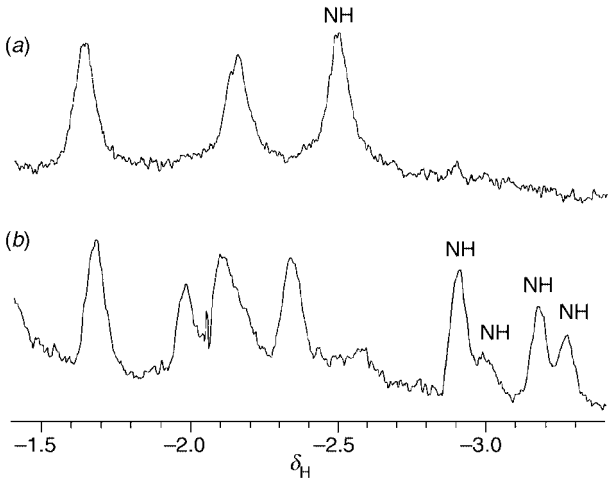

Fig. 3 Part of the ligand proton region from the 300 MHz ^{1}H NMR spectra of the complexes of **1** with ligand **2**: (*a*) fraction of **1** with 28 min HPLC retention time, and (*b*) fraction of **1** with 12 min HPLC retention time.

This work was supported by grants from the National Institutes of Health (HL 22252) and the National Science Foundation (CHE-99-04076). Sandia is a multiprogram laboratory operated by Sandia Corporation, a Lockheed-Martin company, for the United States Department of Energy under Contract DE-ACO4-94AL85000.

Notes and references

1 J. P. Collman, *Inorg. Chem.*, 1997, **36**, 5145.
2 H. Ogoshi, T. Mizutani, T. Hayashi and Y. Kuroda, in *The Porphyrin Handbook*, ed. K. M. Kadish, K. M. Smith and R. Guilard, Academic Press, Burlington, MA, 1999, vol. 6, ch. 46.
3 J. A. Shelnutt, X.-Z. Song, J.-G. Ma, S.-L. Jia, W. Jentzen and C. J. Medforth, *Chem. Soc. Rev.*, 1998, **27**, 31.
4 M. Mazzanti, J.-C. Marchon, M. Shang, W. R. Scheidt, S. Jia and J. A. Shelnutt, *J. Am. Chem. Soc.*, 1997, **119**, 12400.
5 Y. Furusho, T. Kimura, Y. Mizuno and T. Aida, *J. Am. Chem. Soc.*, 1997, **119**, 5267.
6 For details of the force field used in the calculations see: X.-Z. Song, L. Jaquinod, W. Jentzen, D. J. Nurco, S.-L. Jia, R. Khoury, J.-G. Ma, C. J. Medforth, K. M. Smith and J. A. Shelnutt, *Inorg. Chem.*, 1998, **37**, 2009.
7 C. J. Medforth, in *The Porphyrin Handbook*, ed. K. M. Kadish, K. M. Smith and R. Guilard, Academic Press, Burlington, MA, 1999, vol. 5, ch. 35, pp. 70–73.
8 C. J. Medforth, C. M. Muzzi, K. M. Smith, R. J. Abraham, J. D. Hobbs and J. A. Shelnutt, *J. Chem. Soc., Chem. Commun.*, 1994, 1843.
9 K. S. Chan, X. Zhou, B.-S. Luo and T. C. W. Mak, *J. Chem. Soc., Chem. Commun.*, 1994, 271.

Communication a908269g

Synthesis of novel (bis)(diarylamino)thiophenes *via* palladium-catalysed reaction of (di)bromothiophenes with diarylamines

Makoto Watanabe,* Toshihide Yamamoto and Masakazu Nishiyama

Yokkaichi Research Laboratory, Tosoh Corporation, 1–8 Kasumi, Yokkaichi, Mie 510-8540, Japan.
E-mail: m_wata@tosoh.co.jp

Received (in Cambridge, UK) 12th October 1999, Accepted 2nd December 1999

Synthesis of novel (bis)(diarylamino)thiophenes including 2,5-bis(diarylamino)thiophenes was attained by PBu^t_3-ligated palladium-catalysed coupling of (di)bromothiophenes with diarylamines.

Thiophene-containing compounds are widely known as an important class of materials which show intrinsic electronic properties such as luminescence,[1,2] redox activity,[3] nonlinear optical chromism[4] and electron-transport.[5] While triarylamines generally bear a role of hole-transport for organic electroluminescent (EL) display devices,[6] thienylphenylene-containing triarylamines showed different properties.[1,4] Thus, incorporation of a thiophene moiety into the triarylamine system is of current interest due to the product's potential applications. Nevertheless, synthesis of triarylamines bearing thienylamino group(s) is quite rare. 1,3,5-Tris(*N*-phenylthienylamino)benzenes have been synthesized by Ullmann coupling of tris(phenylamino)benzene and 2- and 3-iodothiophenes,[7] but there have been no reports of the synthesis of other (diarylamino)thiophenes.

Palladium-catalysed amination technology is widely known as a useful synthetic method for making arylamines from aryl halides with amines, and has been intensively examined for the synthesis of a wide range of arylamines since Buchwald and Hartwig reported the reaction.[8] However, halothiophenes have not been employed as substrates for the amination reaction. On the other hand, we recently reported that PBu^t_3 served as an excellent ligand for palladium-catalysed amination of aryl halides.[9] The catalytic system consisting of a palladium compound and PBu^t_3 also showed exceedingly high catalytic activity in the synthesis of triarylamines.[10] Herein we report the first palladium-catalysed synthesis of novel (diarylamino)thiophenes and 2,5-bis(diarylamino)thiophenes from (di)bromothiophenes and diarylamines [eqn. (1)].

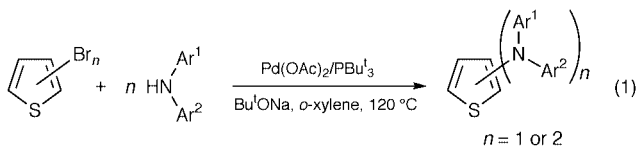

(1)

The coupling of (di)bromothiophenes with diarylamines is most suitable for synthesizing (bis)(diarylamino)thiophenes because (di)bromothiophenes are commercially available and inexpensive. The coupling reaction was examined using Bu^tONa in *o*-xylene at 120 °C (Table 1).† Reaction of 3-bromothiophene with Ph_2NH smoothly proceeded in the presence of 0.25 mol% of $Pd(OAc)_2$ to afford 69% yield of 3-(diphenylamino)thiophene **1a** (entry 1). On the other hand, although 0.75 mol% palladium catalyst was required to give complete conversion of 2-bromothiophene (entry 2), the reaction with Ph_2NH gave the desired product using a small amount of the catalyst. 2-Bromo-3-methylthiophene was similarly coupled without any significant steric effect due to the methyl group (entry 3). Double amination of dibromothiophene with diarylamines gives larger molecules of bis(diarylamino)thiophenes with higher molecular weight, which can be expected to be morphologically more stable than mono(diarylamino)thiophenes for organic EL devices. The palladium catalyst was so active that 2,5-dibromothiophene in the reaction with Ph_2NH could be converted to 2,5-bis(diphenylamino)thiophene **1d** in 57% yield in the presence of 2 mol% of palladium catalyst per dibromothiophene (entry 4). When 2 mol% of $Pd(dba)_2$/BINAP was used as catalyst in the same reaction, the catalytic activity was low, and after 24 h at 120 °C, 2-bromo-5-(diphenylamino)thiophene and 2,5-bis(diphenylamino)thiophene were obtained in 34 and 6% GC yield, respectively. These results indicate that PBu^t_3, which is a bulky and electron-rich phosphine, facilitates the amination of highly electron-rich aryl halides. Reaction of 3,4-dibromothiophene with Ph_2NH was also attempted and gave only a 12% yield of 3-bromo-4-(diphenylamino)thiophene, which is the monoamination product (entry 5). Using the same catalyst, reaction of *o*-dibromobenzene with Ph_2NH gave no product.[10] Although amination of 3,4-dibromothiophene afforded a low yield of monoaminated product, the difference in the reactivity between 3,4-dibromothiophene and *o*-dibromobenzene may be ascribed to the difference of the angle of C–C–Pd bond of the resulting arylpalladium complex after oxidative addition, in which the intramolecular coordination of a vicinal bromine to the palladium complex obtained from *o*-dibromobenzene is more likely to prevent Ph_2NH from ligating to the Pd complex. The coupling of 2,5-dibromothiophene with other diarylamines such as 3-methyldiphenylamine and *N*-phenyl-1-naphthylamine was performed to give 2,5-bis(diarylamino)thiophenes (**1e** and **1f**) (entries 6 and 7). 2,5-Bis(*N*-phenyl-2-fluorenylamino)thiophene **1g** could be prepared by Pd-catalysed reaction of 2-bromofluorene with aniline followed by addition of 2,5-dibromothiophene to the resulting reaction mixture (entry 8). Therefore, this synthetic method can be applied to the synthesis of a variety of elaborate diarylaminothiophenes with aromatic fused ring systems *via* secondary arylamines.

We have demonstrated that the catalytic system consisting of a palladium compound and PBu^t_3 catalysed coupling of bromothiophenes and diarylamines to afford novel (bis)(diarylamino)thiophenes in good yields. Although 2(,5)-(di)bromothiophenes were presumed not to undergo the amination reaction due to their strong coordination to the palladium catalyst, this catalytic system allows the amination with diarylamines to occur in the presence of a small amount of catalyst. The employment of PBu^t_3, which is a bulky and electron-rich ligand, realised the Pd-catalysed formation of (bis)(diarylamino)thiophenes.

Notes and references

† *General procedure*: $Pd(OAc)_2$ (44.9 mg, 0.2 mmol), PBu^t_3 (2.4 ml, 50 mg ml^{-1} in *o*-xylene, 121.4 mg, 0.6 mmol), 2,5-dibromothiophene (2.42 g, 10 mmol), diarylamine (20 mmol), sodium *tert*-butoxide (2.11 g, 22 mmol) and *o*-xylene (40 ml) were mixed at room temperature and heated at 120 °C for 3 h under N_2. After addition of water and extractive work-up with Et_2O, *o*-xylene was stripped off *in vacuo*. The residue was purified by reprecipitation by adding MeOH (30 ml) for **1a** (1.73 g, 6.9 mmol), **1b** (0.90 g, 3.6 mmol), **1d** (2.39 g, 5.7 mmol), **1f** (2.90 g, 5.6 mmol) or column chromatography on Al_2O_3 (eluent; hexane–EtOAc = 100 : 0–1 : 1) for **1c**

Table 1 Palladium-catalysed synthesis of (bis)(diarylamino)thiophenes[a]

Entry	Substrate	Diarylamine	Product
1		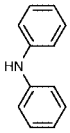	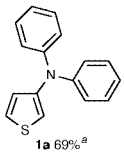 **1a** 69%[e] mp 91–92 °C
2		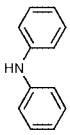	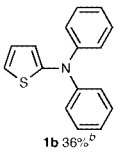 **1b** 36%[b] mp 77–79 °C
3		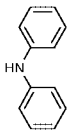	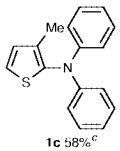 **1c** 58%[c] mp 66–67 °C
4	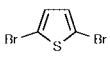	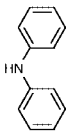	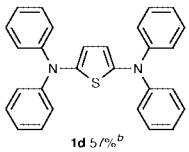 **1d** 57%[b] mp 144–145 °C
5		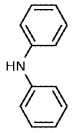	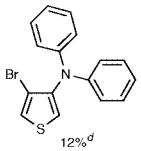 12%[d]
6	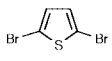	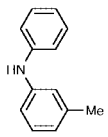	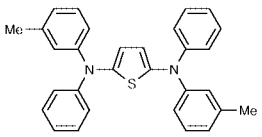 **1e** 81%[c] oil
7	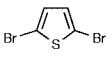	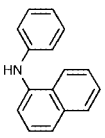	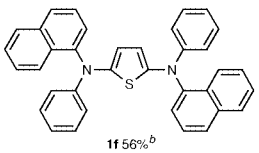 **1f** 56%[b] mp 120–125 °C
8[e]	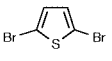	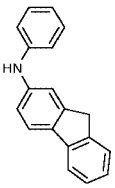	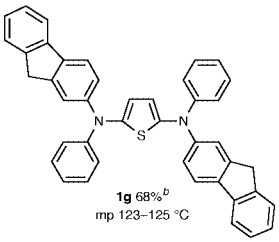 **1g** 68%[b] mp 123–125 °C

[a] All reactions were performed in *o*-xylene with 0.25–2.0 mol% $Pd(OAc)_2$, 0.75–6 mol% PBu^t_3 and 1.1–2.2 equiv. of Bu^tONa at 120 °C for 3 h unless otherwise stated. Satisfactory spectral (^1H and ^{13}C NMR and mass) analyses data were obtained for each isolated compound. [b] Isolated yield by reprecipitation with MeOH, which is not optimised, [c] Isolated yield by column chromatography on Al_2O_3 (hexane–EtOAc = 100:0–1:1). [d] Determined by GC analysis. [e] The reaction was conducted at 120 °C for 24 h *in situ* after preparation of *N*-phenylfluoren-2-ylamine by Pd-catalysed reaction of aniline with 2-bromofluorene at 120 °C for 3 h.

(1.54 g, 5.8 mmol), **1e** (3.62 g, 8.1 mmol) and **1g** (4.04 g, 6.8 mmol). *Selected data* for **1a**: $\delta_H(CDCl_3)$ 6.62 (s, 1H), 6.86 (d, *J* 6.1, 1H). 6.98 (t, *J* 7.8, 2H), 7.08 (d, *J* 7.8, 4H), 7.14–7.24 (m, 5H); $\delta_C(CDCl_3)$ 113.00, 122.21, 123.52, 125.04, 129.02, 146.30, 148.01; *m/z* 251 (M^+). For **1b**: $\delta_H(CDCl_3)$ 6.71 (s, 1H), 6.85 (d, *J* 6.1, 1H), 6.92–7.04 (m, 3H), 7.13 (d, *J* 7.8, 4H), 7.24 (t, *J* 7.8, 4H); $\delta_C(CDCl_3)$ 121.05, 121.70, 122.40, 123.02, 126.02, 129.03, 148.32, 151.20; *m/z* 251 (M^+). For **1c**: $\delta_H(CDCl_3)$ 1.94 (s, 3H), 6.78 (d, *J* 6.1, 1H), 6.96 (d, *J* 7.7, 2H), 7.01–7.10 (m, 5H), 7.22 (t, *J* 7.7, 4H); $\delta_C(CDCl_3)$ 13.12, 121.22, 122.05, 122.10, 128.86, 129.02, 132.64, 143.62, 147.13; *m/z* 265 (M^+). For **1d**: $\delta_H(CDCl_3)$ 6.46 (s, 2H), 7.01 (t, *J* 7.7, 4H), 7.14 (d, *J* 7.7, 8H), 7.24 (t, *J* 7.7, 8H); $\delta_C(CDCl_3)$ 120.10, 122.65, 123.00, 129.52, 145.45, 147.80; *m/z* 418 (M^+). For **1e**: $\delta_H(CDCl_3)$ 2.26 (s, 6H), 6.64 (s, 2H), 6.82 (d, *J* 7.4, 2H), 6.90–6.99 (m, 6H), 7.10–7.16 (m, 6H), 7.23 (t, *J* 7.4, 4H); $\delta_C(CDCl_3)$ 21.56, 119.91, 122.27, 122.65, 123.34, 123.98, 129.11, 139.04, 145.60, 148.02; *m/z* 446 (M^+). For **1f**: $\delta_H(CDCl_3)$ 6.43 (s, 2H), 6.83 (t, *J* 7.8, 2H), 6.89 (d, *J* 7.8, 4H), 7.10 (t, *J* 7.8, 4H), 7.30–7.52 (m, 8H), 7.75 (d, *J* 7.7, 2H), 7.84 (d, *J* 7.7, 2H), 7.98 (d, *J* 7.7, 2H); $\delta_C(CDCl_3)$ 117.93, 118.78, 118.97, 120.59, 123.99, 126.28, 126.34, 126.57, 127.11, 128.45, 128.95, 130.81, 135.19, 143.08, 145.42, 149.33; *m/z* 518 (M^+). For **1g**: $\delta_H(CDCl_3)$ 3.79 (s, 4H), 6.49 (s, 2H), 6.98 (t, *J* 7.4, 2H), 7.10–7.38 (m, 16H), 7.45 (d, *J* 7.4, 2H), 7.63 (d, *J* 8.1, 2H), 7.66 (d, *J* 7.4, 2H); $\delta_C(CDCl_3)$ 36.95, 119.43, 119.83, 120.43, 122.06, 122.15, 122.62, 124.93, 126.10, 126.80, 129.18, 137.24, 141.41, 143.13, 144.58, 145.63, 146.84, 148.21; *m/z* 594 (M^+).

1 T. Noda, H. Ogawa, N. Noma and Y. Shirota, *Appl. Phys. Lett.*, 1997, **70**, 699; T. Noda, I. Imae, N. Noma and Y. Shirota, *Adv. Mater.*, 1997, **9**, 239.

2 E. C. Constable, C. E. Housecroft, E. R. Schofield, S. Encinas, N. Armaroli, F. Barigelletti, L. Flamigni, E. Figgemeier and J. G. Vos, *Chem. Commun.*, 1999, 869.

3 H. Kurata, M. Inase and M. Oda, *Chem. Lett.*, 1999, 519.

4 S. Thayumanavan, J. Mendez and S. R. Marder, *J. Org. Chem.*, 1999, **64**, 4289.

5 Y. Cui, X. Zhang and S. A. Jenekhe, *Macromolecules*, 1999, **32**, 3824.

6 C. W. Tang and S. A. VanSlyke, *Appl. Phys. Lett.*, 1987, **51**, 913; C. W. Tang, S. A. VanSlyke and C. H. Chen, *J. Appl. Phys.*, 1989, **65**, 3610; S. A. VanSlyke, C. H. Chen and C. W. Tang, *Appl. Phys. Lett.*, 1996, **69**, 2160; Y. Shirota, Y. Kuwabara, H. Inada, T. Wakimoto, H. Nakada, Y. Yonemoto, S. Kawami and K. Imai, *Appl. Phys. Lett.*, 1994, **65**, 807; Y. Kuwabara, H. Ogawa, H. Inada, N. Noma and Y. Shirota, *Adv. Mater.*, 1994, **6**, 677; S. Tokito, H. Tanaka, A. Okada and Y. Taga, *Appl. Phys. Lett.*, 1996, **69**, 878; H. Inada, Y. Yonemoto, T. Wakimoto, K. Imai and Y. Shirota, *Mol. Cryst. Liq. Cryst.*, 1996, **280**, 331.

7 E. Ueta, H. Nakano and Y. Shirota, *Chem. Lett.*, 1994, 2397.

8 A. S. Guram, R. A. Rennels and S. L. Buchwald, *Angew. Chem., Int. Ed. Engl.*, 1995, **34**, 1348; J. Louie and J. F. Hartwig, *Tetrahedron Lett.*, 1995, **36**, 3609; Reviews: J. F. Hartwig, *Synlett*, 1997, 329; J. F. Hartwig, *Angew. Chem., Int. Ed.*, 1998, **37**, 2046; B. H. Yang and S. L. Buchwald, *J. Organomet. Chem.*, 1999, **576**, 125.

9 M. Nishiyama, T. Yamamoto and Y. Koie, *Tetrahedron Lett.*, 1998, **39**, 617.

10 T. Yamamoto, M. Nishiyama and Y. Koie, *Tetrahedron Lett.*, 1998, **39**, 2367.

Communication a908195j

The first mixed-valence $Mn^{II,III}$ gallium phosphate: synthesis and structural characterization of $(C_4H_{12}N_2)_2Mn_2Ga_5(H_2O)(PO_4)_8$†

Kuei-Fang Hsu and Sue-Lein Wang*

Department of Chemistry, National Tsing Hua University, Hsinchu 300, Taiwan. E-mail: slwang@mx.nthu.edu.tw

Received (in Cambridge, UK) 18th October 1999, Accepted 5th December 1999

The synthesis and characterization of a novel mixed-valence MnGaPO phase is described; the 3D open-framework consists of discrete bioctahedra of $Ga_2O_{10}(H_2O)$ and GaO_5 trigonal bipyramids, connected *via* $Mn^{II}O_4$, $Mn^{II}O_4$ and PO_4 tetrahedra to generate intersecting tunnels within which piperazinium cations reside.

Substitution of first-row transition metal (TM) ions for Al^{3+} in the frameworks of aluminium phosphates is of particular interest for the enhancement of catalytic activity and the design of novel catalysts,[1,2] exemplified by MnAlPO-31 for the isomerization of but-1-ene,[3] and MnAlPO-5 which demonstrates reversible oxidation and reduction cycles.[4] The location and environment of the TM ion site is of considerable importance for understanding the catalytic and adsorptive properties of molecular sieves. As few single-crystal data are available for MAlPO-*n* samples,[5] evidence for incorporation of TM ions into the tetrahedral frameworks is difficult to establish.[1] Owing to the similarity in framework topology and the presence of even wider pores, in *e.g.* cloverite,[6] the search for gallium phosphates adopting microporous structures has attracted much attention. In contrast to MAlPOs, only a limited number of MGaPO compounds (M = V^{3+}, Mn^{2+}, Fe^{2+}, Co^{2+}, Zn^{2+})[7–12] have been synthesized. Up to now, only three Mn-substituted gallium phosphates have been reported.[10–12] None of these MAlPOs and MGaPOs contain the same TM ions in mixed oxidation states, which would offer more possibility in understanding and designing redox-catalytic or magnetic molecular sieves.[13] By employing hydrothermal crystallization, we have synthesized the first mixed-valence manganese gallium phosphate phase, $(pipz)_2Mn_2Ga_5(H_2O)(PO_4)_8$ (pipz = $C_4H_{12}N_2^{2+}$), denoted MnGaPO-4. A reaction mixture of piperazine (0.258 g, 3 mmol), $Ga(NO_3)_3{\cdot}xH_2O$ (0.307 g, 1.2 mmol), $MnCl_2{\cdot}2H_2O$ (0.065 g, 0.4 mmol), H_3PO_4(aq) (85%, 6 mmol), ethylene glycol (5.8 mL) and H_2O (5.8 mL), was placed in a Teflon-lined digestion bomb (internal volume = 23 mL) and heated at 180 °C under autogenous pressure for 72 h. The final product contained a lot of light-brown tabular crystals mixed with a small amount of uncharacterized powder. A single-crystal structure analysis‡ indicated the tabular crystals to be $(pipz)_2Mn_2Ga_5(H_2O)(PO_4)_8$. The Mn:Ga:P ratios determined from single-crystal data (2:5:8) were corroborated by EMPA data (2.09:5.18:8.00). Elemental analysis also confirmed the organic content (Observed: C, 6.71; N, 4.19; H, 2.42%. Calc: C, 6.80; N, 3.97; H, 1.84%). Thermogravimetric analysis (N_2 atmosphere, heating rate 10 °C min^{-1}) on selected crystats showed a two-stage weight loss from *ca*. 200 to 1100 °C, with a total loss of 19.7%, corresponding to the removal of three water, two piperazine molecules and 1/5 P_4O_{10}.[9] It is also noted that another new Mn^{II}GaPO phase[14] results when piperazine is replaced by the bulkier 4,4′-trimethylenedipiperidine in the reaction mixture.

The three-dimensional anionic framework of MnGaPO-4 consists of GaO_6 octahedra and GaO_5 trigonal bipyramids, connected *via* MnO_4 and PO_4 tetrahedra (Fig. 1) to form intersecting tunnels along all three axial directions (Fig. 2). The pipz cations are located at the tunnel intersections, and four unique types of cages with different Mn content are found (Fig. 3). The open-framework nature of the structure is emphasized by a PLATON analysis[15] of the accessible solvent volume not occupied by the framework Ga, Mn, P and O atoms. The result showed that 457.5 Å^3 (*ca*. 28% of a unit cell volume) is 'solvent accessible'.

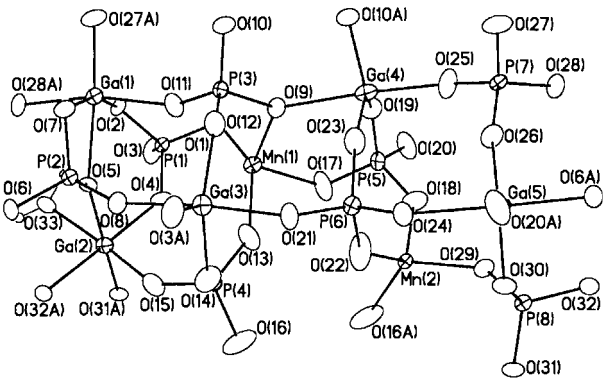

Fig. 1 ORTEP drawing of the building unit in MnGaPO-4. Average bond lengths (Å): Mn(1)–O 2.044(6), Mn(2)–O 1.888(6), Ga(1)–O 1.988(5), Ga(2)–O 1.974(5), Ga(3)–O 1.911(5), Ga(4)–O 1.909(5), Ga(5)–O 1.895(5), P–O 1.526(5) Å.

One remarkable feature of the structure is that the two distinct sites of the Mn ions adopt different charges, *i.e.* 2+ for Mn(1) and 3+ for Mn(2) based on bond-valence sum calculations.[16] The mixed-valence character is also evidenced by the color of the crystals of MnGaPO-4. According to a literature search, only three mixed-valence manganese phosphates have been previously structurally characterized *i.e.* $Cs_3Mn_4(P_6O_{18})_2$,

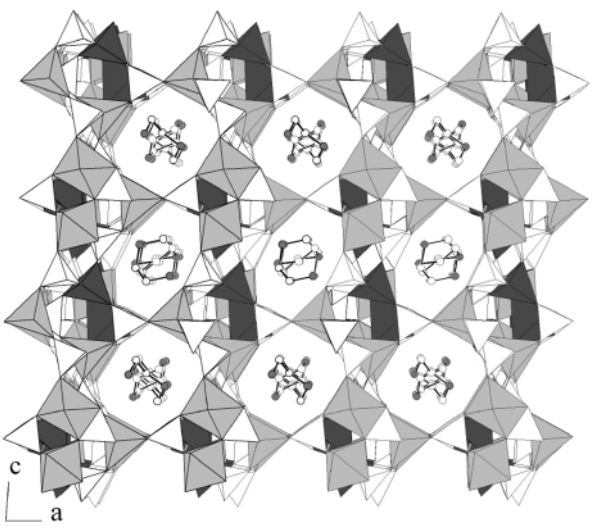

Fig. 2 View of the frameowork along [010], showing tunnels enclosed by eight-membered rings of diameter *ca*. 8 Å. The darker polyhedra are MnO_4, the lighter ones are GaO_5 and GaO_6, and the open tetrahedra are PO_4.

† Electronic supplementary information (ESI) available: thermal analysis and magnetic susceptibility data for $(C_4H_{12}N_2)Mn_2Ga_5(H_2O)(PO_4)_8$. See http://www.rsc.org/suppdata/cc/a9/a908334k/

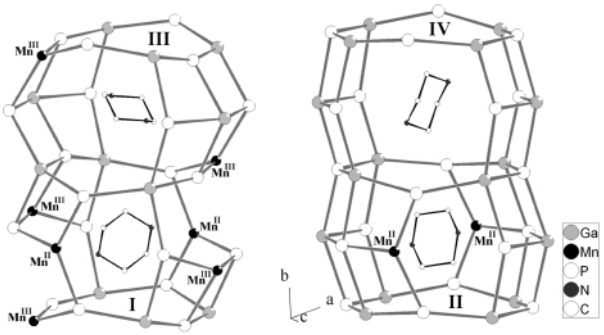

Fig. 3 Cages located at the interactions of three-dimensional tunnels. The pipz cations are located on inversion centers. Cages I show 8-ring windows and II, III and IV 4-ring windows when viewed along the *a*-axis direction.

$CsMn_2(P_6O_{18})$[17] and $Mn(H_2O)_4[Mn_2(OH)_2(PO_4)_2]$.[18] Unlike these, both Mn^{2+} and Mn^{3+} ions are tetrahedrally coordinated in our compound, having a distance to the fifth contact O atom at 2.61 and 3.06 Å, respectively. The four-coordinate Mn^{3+} ion in MnGaPO-4 is unprecedented for manganese phosphates where all of the Mn^{3+} ions are six-coordinate, typical of d^4 high-spin transition-metal ions. Furthermore, the charge distribution of the Mn centers varies in the enclosing structure of the cages; cage I has both Mn^{2+} and Mn^{3+} centers whilst cage II has Mn^{2+}, and cage III Mn^{3+} centers only (Fig. 3). This feature offers considerable possibilities in selective redox-catalytic applications. From the structural point of view, it may be anticipated that the Mn atoms have substituted for Ga rather than P atoms since the parent structure is an orthophosphate instead of a polyphosphate framework. The magnetic susceptibility data in the temperature range 50–300 K can be fitted to a Curie–Weiss law with $\theta = -17.2$ K and $C = 4.8$ emu, which corresponds to an effective magnetic moment per manganese ion of 6.2 μ_B, as expected, lower than that observed for pure Mn^{2+} ions in MnGaPO-2.[11]

Another interesting feature of the compound is in that an isolated $Ga_2O_{10}(H_2O)$ unit, built of corner-shared $Ga(1)O_6$ and $Ga(2)O_5(H_2O)$ octahedra, exists in the framework. Relative to gallium oxides, discrete gallium–oxygen cluster-containing phosphates are rare. The only example, $GaPO_4$-21,[19] was found to contain a dimer of corner-shared GaO_5 trigonal bipyramids. In the dimeric $Ga_2O_{10}(H_2O)$ cluster, a significant repulsion between the two Ga centers may arise since the distance between atoms Ga(1) and Ga(2) at 3.699 Å, is longer than that for two corresponding octahedral centers, 3.473 Å. As compared with $Ga(2)O_5(H_2O)$, the octahedron $Ga(1)O_6$ is much more distorted since it also shares a common edge with the $P(2)O_4$ tetrahedron. Atom O(5) bridges the Ga(1), Ga(2) and P(2) centers with the Ga(1)–O(5)–P(2) angle of 92.8°, deviating significantly from 120°, characteristic of trigonal planar geometry typical of a μ_3-O atom. In addition, the bridging Mn–O–P angles between corner-shared MnO_4 and PO_4 tetrahedra, ranging from 123.1 to 147.6°, span a rather wider range than those found in MnGaPOs and MnAlPOs.

We thank the National Science Council and Chinese Petroleum Corp. of Taiwan for support of this work (NSC 87–CPC–M–007–001 and NSC 89–2113–M–007–025).

Notes and references

‡ *Crystal data* for $(C_4H_{12}N_2)_2Mn_2Ga_5(H_2O)(PO_4)_8$: triclinic, space group $P\bar{1}$; $a = 9.1314(2)$, $b = 12.7496(1)$, $c = 14.7479(3)$ Å, $\alpha = 89.480(1)$, $\beta = 86.249(1)$, $\gamma = 72.419(1)°$, $U = 1633.17(5)$ Å^3, $Z = 2$, $M_r = 1412.57$, $D_c = 2.872$ g cm^{-3}, μ(Mo-Kα) = 53.37 cm^{-1}, $\lambda = 0.71073$ Å. A crystal of dimensions 0.30 × 0.13 × 0.03 mm was selected for indexing and intensity data collection at 296 K. Total number of measured and observed independent reflections ($I_{obs} > 2\sigma_I$) are 7814 and 5536 and $R_{int} = 0.0516$. Least-squares refinements were based on F^2 and converged at $R1 = 0.0567$ and $wR2 = 0.1386$. CCDC 182/1502. See http://www.rsc.org/suppdata/cc/a9/a908334k/ for crystallographic files in .cif format.

1 M. Hartmann and L. Kevan, *Chem. Rev.*, 1999, **99**, 635 and references therein.
2 A. K. Cheetham, G. Ferey and T. Loiseau, *Angew. Chem., Int. Ed.*, 1999, **38**, 3268 and references therein.
3 H. L. Zubowa, M. Richter, U. Roost, B. Parlitz and R. Fricke, *Catal. Lett.*, 1993, **19**, 67.
4 A. Katzmarzyk, S. Ernst, J. Weitkamp and H. Knoezinger, *Catal. Lett.*, 1991, **9**, 85.
5 N. Zabukovec, L. Golic, P. Fajdiga and V. Kaucic, *Zeolites*, 1995, **15**, 104.
6 M. Estermann, L. B. McCusker, C. Baerlocher, A. Merrouche and H. Kessler, *Nature*, 1991, **352**, 320.
7 A. M. Chippindale, K. J. Peacock and A. R. Cowley, *J. Solid State Chem.*, 1999, **145**, 379.
8 A. R. Cowley and A. M. Chippindale, *Microporous Mesoporous Mater.*, 1999, **28**, 163.
9 A. R. Cowley and A. M. Chippindale, *Chem. Commun.*, 1996, 673.
10 A. D. Bond, A. M. Chippindale, A. R. Cowley, J. E. Readman and A. V. Powell, *Zeolites*, 1997, **19**, 326.
11 A. M. Chippindale, A. D. Bond, A. R. Cowley and A. V. Powell, *Chem. Mater.*, 1997, **9**, 2830.
12 A. M. Chippindale, A. R. Cowley and A. D. Bond, *Acta Crystallogr., Sect. C*, 1998, **54**, 1; A. R. Overweg, J. W. de Haan, P. C. M. M. Magusin, R. A. van Santen, G. Sankar and J. M. Thomas, *Chem. Mater.*, 1999, **11**, 1680.
13 Q. Gao, N. Guillou, M. Nogues, A. K. Cheetham and G. Ferey, *Chem. Mater.*, 1999, **11**, 2937.
14 A new monoclinic phase with $a = 8.9468(4)$, $b = 10.1481(5)$, $c = 13.5540(7)$ Å, $\beta = 108.249(1)°$, $V = 1168.71(10)$ Å^3 and $Z = 2$; *Inorg. Chem.*, submitted.
15 L. Spek, *Acta Crystallogr., Sect. A*, 1990, **46**, C34.
16 I. D. Brown and D. Altermatt, *Acta Crystallogr., Sect. B*, 1985, **41**, 244.
17 E. V. Murashova and N. N. Chudinova, *Kristallografiya*, 1996, **41**, 248.
18 R. K. Anthony and B. M. Paul, *Am. Mineral.*, 1976, **61**, 1241.
19 Z. Levi, Z. D. Goldfarb and J. Batista, *J. Am. Chem. Soc.*, 1993, **115**, 1106.

Communication a908334k

ChemComm

Ti-ferrierite and TiITQ-6: synthesis and catalytic activity for the epoxidation of olefins with H_2O_2

A. Corma,* U. Diaz, M. E. Domine and V. Fornés

Instituto de Tecnología Química, UPV-CSIC, Universidad Politécnica de Valencia, Avda. de los Naranjos, s/n, Valencia, 46022 Spain. E-mail: acorma@itq.upv.es

Received (in Cambridge, UK) 3rd November 1999, Accepted 8th December 1999

A new zeolitic material TiITQ-6 has been obtained by the direct synthesis of a layered titanosilicate precursor, followed by delamination; titanium is tetrahedrally coordinated in framework positions and, while the zeolite derived from the precursor has little activity owing to geometrical constraints, the delaminated TiITQ-6 material is active and selective for the epoxidation of hex-1-ene with H_2O_2.

A new generation of oxidation catalysts started when TS-1[1] was synthesized and showed excellent catalytic activity in aqueous media using H_2O_2 as oxidant. Since then other Ti containing molecular sieves have been synthesized but only a few of them, of which TS-2[2] and Ti-beta[3] are outstanding, have shown to be active and selective for the epoxidation of linear olefins with H_2O_2. Recently[4] it has been proposed that the presence of Ti^{4+} ions tends to impede or to decrease the nucleation rates in the organothermal Ti-ferrierite (TiFER) system but by seeding with Si-ferrierite it was possible to prepare a Ti containing ferrierite. Unfortunately no catalytic activity for the sample was detected.[4] It was also demonstrated that it was possible to synthesize a laminar aluminosilicate precursor of ferrierite (PREFER)[5] that upon calcination could produce the ferrierite structure. In our case, we have succeeded in synthesizing directly, without seeding, the titanium containing laminar analogue TiPREFER. This was prepared in the following manner: 10 g silica (Aerosil 200, Degussa), 0.759 g of titanium(IV) ethoxide (Alfa 98%), 28.186 g H_2O (MiliQ), 26.008 g of 4-amino-2,2,6,6-tetramethylpiperidine (Fluka 98%), 9.246 g NH_4F (Aldrich 98%) and 3.462 g HF (Aldrich, 48.1 wt%) were mixed in an autoclave at 408 K for 10 days. The resulting product TiPREFER was filtered off, washed three times, and dried at 333 K. The X-ray diffraction (XRD) pattern of the product is shown in Fig. 1(a). The UV spectrum of the sample shows a single absorption band at *ca.* 210 nm corresponding to isolated framework Ti in tetrahedral coordination [Fig. 2(a)] and this band was maintained after calcination at 923 K for 12 h [Fig. 2(b)] to produce

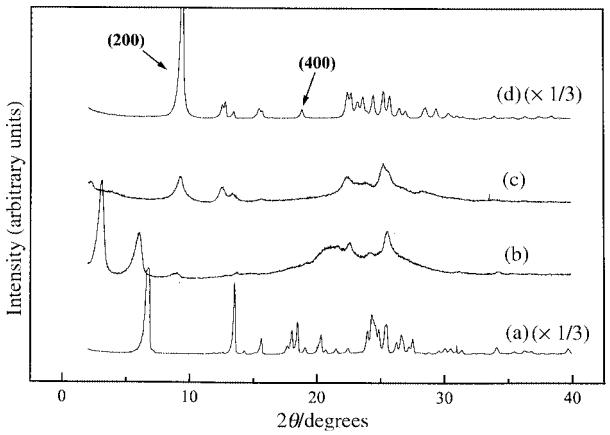

Fig. 1 X-Ray diffraction patterns of (a) TiPREFER, the laminar precursor of Ti-ferrierite, (b) TiPREITQ-6, the expanded material, (c) TiITQ-6, the delaminated zeolite and (d) TiFER, a Ti-ferrierite zeolite obtained after calcination of TiPREFER.

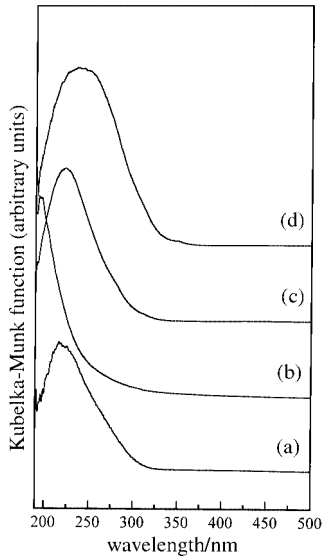

Fig. 2 Diffuse UV–VIS reflectance spectra of TiITQ-6: (a) as synthesised (TiPREFER), (b) Ti-Ferrierite, (c) TiITQ-6 and (d) TiITQ-6 after two reaction–calcination cycles.

the well crystallised Ti containing ferrierite TiFER [Fig. 1(d)]. The catalytic activity of this material for the epoxidation of hex-1-ene with H_2O_2 was tested in a batch reactor in the following way: 16.5 mmol olefin, 11.8 acetonitrile and 300 mg TiFER (1.3 wt% TiO_2) were introduced in a three necked glass flask which was heated to 323 K in a temperature controlled silicon bath. 4.5 mmol H_2O_2 (30% vol) was then added dropwise and the catalytic results obtained are given in Table 1. Very little conversion of hex-1-ene was observed for TiFER owing to diffusion limitation in the pores of this structure, in a similar manner found to that for another unidirectional 10-member ring pore zeolite Ti-ZSM-48.[6]

Table 1 Catalytic activity of Ti zeolites for hex-1-ene epoxidation[a]

Sample	$X_{\text{hex-1-ene}}$ (% of maximum)	Selectivity to epoxide (%)	Selectivity to H_2O_2 (%)	TON
TiFER	3.2	85.2	23	6
Ti-beta	18.0	97.2	77	20
TiITQ-6	19.7	95.5	73	23
TiITQ-6[b]	17.7	93.2	56	21

[a] *Reaction conditions*: 16.5 mmol olefin; 11.8 g acetonitrile; 4.5 mmol H_2O_2; 300 mg catalyst; 323 K, 5 h. [b] After two regeneration cycles.

Recently,[7] a new approach has been undertaken for expanding the use of zeolites to catalyze reactions when the accessibility of the reactants to the active sites is hindered. This involves the preparation of lamellar precursors of zeolites whose structure is subsequently delaminated making potentially catalytically active sites accessible through the external surface. Up to now the only delaminated material reported has been ITQ-2 which shows outstanding adsorption and catalytic

properties as an acid catalyst for large reactant molecules.[8] Unfortunately, the titanosilicate counterpart of ITQ-2 was not synthesized, and oxidation catalysts based on this material could only be prepared *via* secondary synthesis by anchoring Ti on external silanol groups.[9] The resultant materials were active and selective for epoxidation of olefins with organic peroxides, but they were not active when using the more desirable H_2O_2 as oxidating agent.

Here, we have succeeded in delaminating the Ti laminar precursor of TiFER in the following way: TiPREFER was suspended in a aqueous solution of cetyltrimethylammonium bromide ($CTMA^+Br^-$,29 wt%) and tetrapropylammonium hydroxide (TPA^+OH, 40 wt%) and refluxed for 16 h at 368 K. The XRD pattern of the expanded material is shown in Fig. 1(b). Delamination was performed by placing the slurry in an ultrasound bath (50 W, 40 kHz) at 323 K for 1 h, and maintaining the pH at 12.5. Finally the solid phase was washed thoroughly with water, dried at 333 K and calcined at 853 K for 7 h yielding TiITQ-6 with the XRD pattern shown in Fig. 1(c). The Ti in TiITQ-6 remained in tetrahedral coordination as shown by its UV spectrum [Fig. 2(c)]. Some removal of Ti has occurred during the delamination process (*ca.* 25%), nevertheless, when a sample of TiITQ-6 with a similar amount of Ti (1 wt% TiO_2) as in TiFER was prepared it showed a much higher activity and better selectivity for epoxidation of hex-1-ene than TiFER itself (Table 1). The increase in activity of TiITQ-6 is due to the higher accessibility of Ti-sites as a consequence of delamination of the TiPREFER structure. The external surface area of TiITQ-6 is 610 $m^2\ g^{-1}$ while that of the TiFER is only 60 $m^2\ g^{-1}$. In addition, the micropore volume of TiFER is 0.1304 cm g^{-1}, *cf.* 0.0016 cm g^{-1} for TiITQ-6. From these results it is clear that practically full delamination of the TiPREFER structure has occurred.

In order to have a reference for the catalytic activity of TiITQ-6, we carried out the same under the same conditions using Ti-beta with a similar Ti content (1.3 wt% Ti). The results in Table 1 show that the activity of TiITQ-6 is similar to that of Ti-beta. Moreover, the stability of TiITQ-6 under the reaction conditions is high since its activity remains close to that of the fresh catalyst after being subject to two reaction-regeneration cycles (calcination at 853 K for 7 h) (Table 1).

In conclusion, TiFER and a new zeolitic titanosilicate material (TiITQ-6) have been synthesized and, while the former presents a low catalytic activity for epoxidation of hex-1-ene with H_2O_2 owing to diffusional limitations of the reactants and products through the unidirectional 10MR channel of the zeolite, TiITQ-6 shows activities and selectivities similar to those of Ti-beta, owing to the good accesibility of the reactants to the active sites achieved by delamination of the TiPREFER laminar precursor.

Financial support by the Spanish CICYT (Project MAT97-0723 and Project MAT97-1207-C03-01) is gratefully acknowledged. U.D. and M.E.D. thank the M.E.C. and M.E.A. respectively, for their doctoral fellowships.

Notes and references

1 M. Taramaso, G. Perego and B. Notari, *US Pat.*, 4 410 501, 1983.
2 J. S. Reddy, K. Kumar and O. Ratnasamy, *Appl. Catal.*, 1990, **58**, L1.
3 A. Corma, P. Esteve and A. Martínez, *J. Catal.*, 1996, **161**, 11.
4 R. K. Ahedi and A. N. Kotasthane, *J. Mater. Chem.*, 1998, **8**, 1685.
5 L. Schreyeck, P. H. Caullet, J. Ch. Mongenel, J. L. Guth and B. Marler, *Chem. Commun.*, 1995, 2187; *Microporous Mater.*, 1996, **6**, 259.
6 D. P. Serrano, H. X. Li and M. E. Davis, *J. Chem. Soc., Chem. Commun.*, 1992, 745.
7 A. Corma, V. Fornés, S. B. Pergher, Th. L. M. Maesen and J. G. Buglass, *Nature*, 1998, **396**, 353.
8 A. Corma, V. Fornés, J. Martinez-Triguero and S. B. Pergher, *J. Catal.*, 1999, **186**, 57.
9 A. Corma, U. Diaz, V. Fornés, J. L. Jordá, M. Domine and F. Rey, *Chem. Commun.*, 1999, 779.

Communication a908748f

ChemComm

A highly *dl*-stereoselective pinacolization of aromatic aldehydes mediated by $TiCl_4$–Zn

Tingyou Li, Wei Cui, Jigang Liu, Jianzhang Zhao and Zongmu Wang*

College of Life Science, Jilin University, Changchun, 130023, P.R. China. E-mail: liwei@mail.jlu.edu.cn

Received (in Cambridge, UK) 15th November 1999, Accepted 2nd December 1999

Reduction of $TiCl_4(THF)_4$ with Zn in CH_2Cl_2 gave a green solution, which was found to promote the reductive coupling of aromatic aldehydes to yield 1,2-diols with high *threo* selectivity.

The pinacol coupling reaction, which allows the generation of 1,2-diols in one step, is a powerful synthetic reaction, and therefore has been recognized as one of the most significant C–C bond forming processes in synthetic organic chemistry.[1,2] In addition, *threo*-1,2-diols have, after resolution, frequently been utilized as auxiliaries in asymmetric synthesis.[3] Although a number of methods have been developed for the reductive coupling of carbonyl compounds,[4–6] selective pinacolization to *threo*-diols has only been found with stannylene precursors,[7] 'active titanium(III) reagents' prepared from $TiCl_4$/BuLi in Et_2O at −78 °C,[8] $TiCl_4$/$Bu^i{}_2Te$ in DME,[9] $TiCl_3$/CH_2Cl_2 solution[10] or $(Cp_2TiCl)_2$.[11,12] $(Cp_2TiCl)_2$, a binuclear complex, can be easily prepared from Cp_2TiCl_2 and used in stiochiometric or catalytic amounts in the pinacol coupling reaction. Many of these reagents are expensive and/or air sensitive.

Here we report the $TiCl_4$–Zn promoted reductive coupling of aromatic aldehydes in anhydrous solvent at room temperature. By the choice of an appropriate mole ratio of $TiCl_4$ and Zn and an appropriate coordinating additive such as TMEDA, TiCl-Zn and $TiCl_4$–Zn–TMEDA reduce benzaldehyde and other actived aromatic aldehydes to the corresponding pinacols in good yields and, what is more important, the coupling is highly *dl* selective.

It is noteworthy that the reagents used are readily available, inexpensive and stable to air oxidation, and the method is easier and more convenient compared with those so far reported. Thus, we produced 'actived titanium' and reduced aldehydes in one pot in only a short time.

In 1973, Mukaiyama[13] reported that $TiCl_4$–Zn reduced aromatic aldehydes or ketones to produce the corresponding 1,2-diols in high yield, but the stereoselectivity was not reported. At the outset of the study, we used THF as solvent, with an aldehyde to $TiCl_4$ to Zn ratio of 1 : 1.5 : 3, and obtained the hydrobenzoin with a *dl* : *meso* ratio of 3 : 1. When CH_2Cl_2 was selected as the solvent, with THF as a ligand and a mole ratio of $TiCl_4$ to Zn of 2 : 1, better results were obtained.

A typical procedure is as follows: THF (11.7 mmol) was added dropwise to a solution of $TiCl_4$ (3.65 mmol) in 10 ml of CH_2Cl_2 under an atmosphere of argon at room temperature. To this solution Zn (1.82 mmol) was added in one portion. The color of the solution changed to green immediately. After stirring for 3 min benzaldehyde (3.65 mmol) in 3 ml of CH_2Cl_2 was added in one portion. After 30 min of stirring, the reaction was quenched with 15 ml of 10% K_2CO_3 and extracted with EtOAc followed by chromatography to give 0.22 g of hydrobenzoin (57%, 94 : 1 *dl* : *meso*).

When the reduction time was less than 20 min, acceptable yields and high *dl* selectivities were obtained. However, when the reduction time was greater than 1 h, the color of solution changes from green to black, and no product was obtained. According to the reports of Piotr Sobota[14] and Kirrsten Foling,[15] we assume that the $TiCl_4(THF)_2$ was first reduced to $[Ti_2(\mu\text{-}Cl)_2Cl_4(THF)_4]$ by Zn in CH_2Cl_2; $ZnCl_2$ can then abstract chlorine from $[Ti_2(\mu\text{-}Cl)_2Cl_4(THF)_4]$ and form ionized $[TiCl_2(THF)_4{}^+ \cdot ZnCl_3(THF)^-]$. We think the binuclear complex $[Ti_2(\mu\text{-}Cl)_2Cl_4(THF)_4]$ is the active compound which reduces the benzaldehyde to pinacol with high *dl*-selectivity, exactly as $(Cp_2TiCl)_2$ has high *dl*-selectivity. The ionized $[TiCl_2(THF)_4{}^+ \cdot ZnCl_3(THF)^-]$ has no activity to benzaldehyde. In order to lower the Lewis activity of the $ZnCl_2$ and suppress ionization of the $[Ti_2(\mu\text{-}Cl)_2Cl_4(THF)_4]$, a coordinating additive, especially Lewis bases such as Py and TMEDA, is added. When the reduction was carried out in the presence of 1.5 equiv. of TMEDA as an additive the yield improved to 76% and only the *dl*-isomer was obtained.

Under the optimised conditions, a variety of symmetrical 1,2-diols were synthesized in good yields and excellent selectivity, and could be obtained diastereomerically pure after

Table 1 Coupling of benzaldehyde mediated by $TiCl_4$–Zn

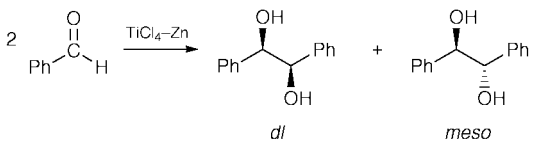

Entry	Additive (mmol)	Yield (%)[a]	*dl* : *meso*[b]
1[c]		57	94 : 1
2[d]		55	108 : 1
3[e]		0	—
4[c]	Py[f] (10.95)	42	5.2 : 1
5[c]	DME[f] (5.48)	58	129 : 1
6[c]	TMEDA[f] (5.48)	77	*dl* only

[a] Pinacol isolated yield. [b] Determined by ^{1}H NMR (400 MHz). [c] $TiCl_4$ reduction 3 min. [d] $TiCl_4$ reduction 18 min. [e] $TiCl_4$ reduction 1 h. [f] Added and stirred for 2 min prior to addition of benzaldehyde.

Table 2 Reductive coupling of aldehyes under optimised conditions

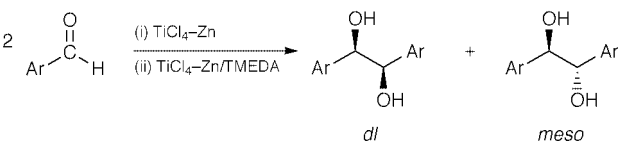

Entry	Ar	Yield (%)[a]	*dl* : *meso*[b]
1[c]	Ph	57	94 : 1
2[d]	Ph	77	*dl* only
3[c]	*p*-FC_6H_4	80	25 : 1
4[d]	*p*-FC_6H_4	88	*dl* only
5[c]	*p*-ClC_6H_4	86	52 : 1
6[d]	*p*-ClC_6H_4	86	*dl* only
7[c]	*p*-BrC_6H_4	90	51 : 1
8[d]	*p*-BrC_6H_4	92	*dl* only
9[c]	*m*-BrC_6H_4	92	54 : 1
10[d]	*m*-BrC_6H_4	94	346 : 1
11[c]	*p*-CNC_6H_4	92	*dl* only
12[d]	*p*-CNC_6H_4	96	*dl* only

[a] Pinacol isolated yield. [b] Ratio determined by ^{1}H NMR (400 MHz). [c] Conditions (i). [d] Conditions (ii).

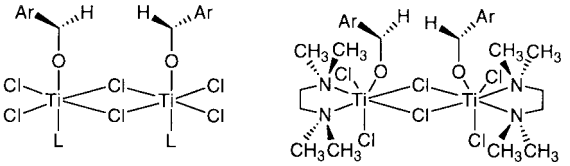

Fig. 1

a single recrystallization. Functional groups, such as halide and cyano groups, are tolerated. Aromatic aldehydes bearing an electron-donating group showed lower reactivity, for example, *p*-anisaldehyde afforded no significant conversion *via* TLC observation.

Mechanistically it seems reasonable to assume that the active species is a binuclear titanium complex binding both ketyl radicals, in which the Ar groups are arranged *anti* to each other to minimized steric interaction. When the binuclear titanium complex is coordinated with TMEDA, the sterically crowded environment drastically improved the pinacol diastereoselectivities (Fig. 1).

Notes and references

1 G. M. Robertson, in *Comprehensive Organic Synthesis*, ed. B. M. Trost, I. Fleming and G. Pattenden, Pergamon, Oxford, 1991, vol. 3, p. 563.
2 J. E. McMurry, *Chem. Rev.*, 1989, **89**, 1513.
3 B. Schmidt and D. Seebach, *Angew. Chem., Int. Ed. Engl.*, 1991, **30**, 99.
4 J. M. Khurana, A. Sehgal and A. Gogia, *J. Chem. Soc., Perkin Trans. 1*, 1996, 2213.
5 T. Honda and M. Katoh, *Chem. Commun.*, 1997, **4**, 370.
6 E. J. Corey, R. L. Danheiser and S. Chandrasekaran, *J. Org. Chem.*, 1976, **42**, 260.
7 C. Grugel, W. P. Neumann and J. Seifert, *Tetrahedron Lett.*, 1978, 2847.
8 H. G. Raubenheimer and D. Seebach, *Chimia*, 1986, **40**, 12.
9 H. Suzuki, H. Manabe and R. Enokiya, *Chem. Lett.*, 1986, **13**, 9.
10 A. Clerici, L. Clerici and O. Porta, *Tetrahedron Lett.*, 1996, **37**, 3035.
11 M. C. Barden and J. Schwartz, *J. Am. Chem. Soc.*, 1996, **118**, 5484.
12 A. Gansauer and D. Bauer, *J. Org. Chem.*, 1998, **63**, 2070.
13 T. Mukaiyama, T. Santo and J. Hanna, *Chem. Lett.*, 1974, 1041.
14 P. Sobota, J. Ejfler and S. Szafert, *J. Chem. Soc., Dalton Trans.*, 1993, 2353.
15 K. Folting, J. C. Huffman and R. L. Bansemer, *Inorg. Chem.*, 1984, **23**, 3289.

Communication a909032k

Self-assembled monolayers of bis-thioctic ester derivatives of oligoethyleneglycols: remarkable selectivity for K^+/Na^+ recognition†

Krisanu Bandyopadhyay, Haiying Liu, Sheng-Gao Liu and Luis Echegoyen*

Department of Chemistry, University of Miami, Coral Gables, Florida 33124, USA.
E-mail: lechegoyen@umiami.ir.miami.edu

Received (in Columbia, MO, USA) 15th July 1999, Accepted 23rd November 1999

Bis-thioctic ester terminated derivatives of oligoethylene glycols form extremely stable self-assembled monlayers (SAMs) on gold electrodes and these can recognize K^+ selectively over Na^+, as measured by cyclic voltammetry and impedance spectroscopy.

The incorporation of crown-ether groups into self-assembled monolayers (SAMs) and their potential as metal ion sensors was reported very recently and almost simultaneously by Moore *et al.*[1] and by Flink *et al.*[2] In one case they prepared simple 12-crown-4 and 15-crown-5 derivatives with appended single chains terminated in thiol groups, and impedance spectroscopy was used to monitor ion binding events on the surface.[2] The other reported crown-annelated TTF derivatives which also contained single alkyl chains terminated in thiol groups.[1] The latter work exploited the direct response of the electroactive surface-confined crown-TTF groups to measure the effect of ion complexation, similar to previously reported work in homogeneous solution by Hansen *et al.*[3] These SAMs were apparently not very stable under several sets of conditions and the electrochemical responses observed were very weak and poorly resolved.[1] We have recently prepared and studied bis-thioctic ester derivatives of crown ether annelated TTFs, and these form remarkably stable SAMs, some of which are able to detect alkali metal ion binding electrochemically.[4] Here we report the easy synthesis, remarkable stability, and electrochemical (cyclic voltammetric and impedance) responses of SAMs of bis-thioctic ester derivatives of oligoethylene glycols (podands). The general idea was to use the glycols to form ion binding domains on the surface (similar to crown ethers) *via* self-assembly. The SAMs prepared showed amazing stabilities and selectivities for K^+ over Na^+ binding, making them potentially useful monolayer sensors.

Compounds **1**–**3** were easily synthesized in high yield by reacting the corresponding bis-alcohols [$HO(CH_2CH_2O)_4CH_2CH_2OH$ or $HO(CH_2)_{12}OH$] with thioctic acid in CH_2Cl_2 in the presence of DCC and 4-pyrrolidinopyridine or DMAP.[5] Compounds **1** and **3** were obtained from the same reaction as two separate products.

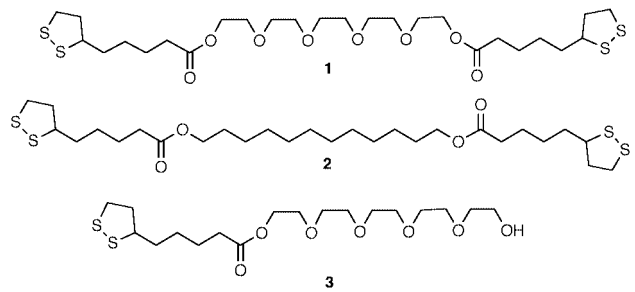

Glass-sealed, ultra-clean spherical gold bead electrodes prepared from ϕ 250 μm gold wire (99.9999%) were dipped into 5 mM EtOH solutions of the corresponding bis- or mono-thioctic ester compounds **1**–**3** for 24 h to form the corresponding SAMs.[6] After washing these with absolute EtOH and drying them in an Ar flow, these SAM modified electrodes were placed into 0.1 M aqueous Et_4NCl and the cyclic voltammograms (CVs) for 1 mM $Ru(NH_3)_6^{3+/2+}$ were recorded, using a platinum coil as counter and a Ag/AgCl as reference electrodes. The impedance response was also measured at the $E_{1/2}^0$ (−0.25 V) for the $Ru(NH_3)_6^{3+/2+}$ redox couple, between 1 kHz and 0.1 Hz.[7]

The CV response for the $Ru(NH_3)_6^{3+/2+}$ couple at a modified gold electrode of **1** is shown in Fig. 1(*a*) (dotted line).[8] It is clear that the insulating effect of the monolayer is poor, since the redox couple relatively easily undergoes electron transfer at the interface. This probably reflects poor surface coverage or good electron permeability through the monolayer. Interestingly, addition of 30 mM KCl to the solution results in a drastically reduced cathodic current and in the disappearance of the

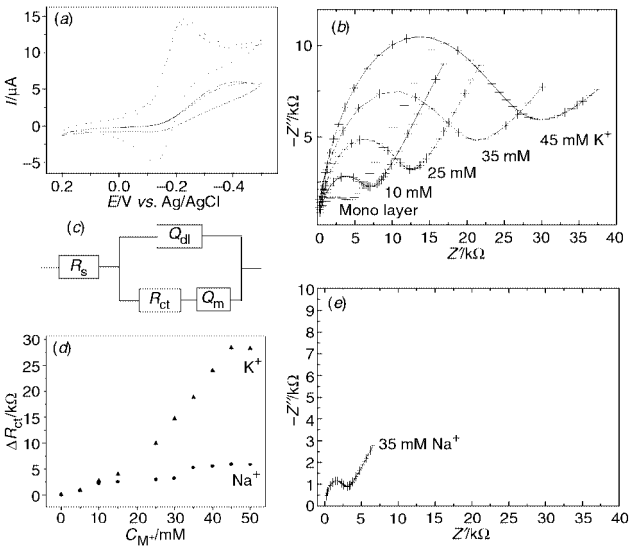

Fig. 1 (*a*) Cyclic voltammogram of $Ru(NH_3)_6^{3+/2+}$ in 0.1 M Et_4NCl using a monolayer-modified gold electrode (area = 0.02 cm^2) prepared from **1** before (dotted line) and after (solid line) addition of 30 mM of K^+ to the solution at a scan rate of 100 mV s^{-1}. (*b*) Impedance response of the same modified gold electrode in the absence and in the presence of varying amounts of [K^+]. The solid lines represent the fits of the experimental points to the equivalent circuit shown in (*c*). (*c*) Equivalent circuit used to fit the experimental data: R_S represents the solution resistance. The monolayer is described by a constant phase element Q_{dl} (used here as a generalized capacitance) in parallel with a resistance R_{CT} (the charge transfer resistance) and another constant phase element (Q_m) (related to diffusion controlled processes) in series. In admittance representation, a constant phase element is defined as $Y(\omega) = Y_0(j\omega)^n$ where Y_0 and n are adjustable parameters, n = 0, 1 and 0.5 correspond to an ideal resistor, a capacitor and a Warburg element, respectively, and ω is the angular frequency. The R_{CT} values can also directly be obtained from the diameter of the high frequency 'semicircle'. (*d*) Plot of the relative change of R_{CT} with [K^+] and with [Na^+]. (*e*) Impedance response of the same modified gold electrode in the presence of 35 mM NaCl. The response is essentially identical to that of the initial monolayer, see Fig. 1(*b*).

† Dedicated to Professor Jean-Marie Lehn on the occasion of his 60th birthday.

corresponding anodic process, indicating that electron transfer at the interface is dramatically inhibited, see Fig. 1(*a*) (solid line). On the other hand, addition of Na^+ has essentially no effect on the voltammetric response of this redox couple. These observations are consistent with complexation of K^+ (but not Na^+) with the monolayer, resulting in partial repulsion of the positively charged $Ru(NH_3)_6^{3+/2+}$ redox pair when K^+ is present. Note that the blocking effect due to K^+ addition is not perfect and some current is still observed.

Since none of the structural components of the SAM are electroactive, impedance spectroscopy was used to further probe ion recognition at the interface.[2] The impedance response for the same monolayer for which the CV is shown in Fig. 1(*a*) was measured in the absence and in the presence of increasing [K^+], and the data are presented in Fig. 1(*b*), as a Nyquist plot. Note that a very small R_{CT} (charge transfer resistance, determined as the diameter of the high frequency semicircle) is observed for the monolayer alone in the absence of K^+, 4.8 kΩ, and a significant diffusion component is observed as the linear portion at lower frequencies, indicating inefficient blocking to charge transfer. The fractional surface coverage (θ) was calculated to be 0.96 following well-established procedures.[9] These observations are consistent with the CV data already described, which showed that the SAM is either loosely packed or allows close approach of the redox probe to the modified electrode surface. Addition of K^+ to the solution resulted in dramatic and *reversible* increases in the R_{CT} values, from 7 kΩ at 5 mM to a limiting value of 31 kΩ at 45 mM, indicative of K^+ complexation at the interface and repulsion of the positively charged redox probe, in perfect agreement with the CV observations.[2] These values were obtained by a non-linear least-square fit of the experimental data to the equivalent circuit shown in Fig. 1(*c*), using the program EQUIVALENT CIRCUIT.[2] A plot of ΔR_{CT} *vs.* [K^+] shows two linear regions at different concentration ranges, and these intersect around 17 mM [K^+]. This complex ion response is in agreement with the non-linear fits, which yield different slopes for the CPE [Fig. 1(*b*)] and thus different '*n*' parameter values. At 45 mM KCl the surface binding sites must be saturated and no R_{CT} changes are observed with further salt additions. These SAMs are very stable and the results can be reproduced repeatedly over the course of days. With a useful range of 17–45 mM [K^+], this is not a practical sensor, but the novel principles established here should lead to improved designs in the future.

The same SAM electrode used to probe [K^+] was placed in solutions with increasing NaCl concentrations. The impedance results are presented in Fig. 1(*e*). In agreement with the results obtained by cyclic voltammetry, Na^+ showed almost no effect on the R_{CT} value of the monolayer [Fig. 1(*d*)], indicating that it is not binding significantly with the surface and thus not increasing its blocking effect. Simply based on the observations presented in Fig. 1(*b*) and (*e*) it is fair to say that a monolayer of **1** can act as a reversible and highly selective sensor for K^+ over Na^+. The selectivity for K^+ over Na^+ suggests the formation of a surface-confined *pseudo*-18-crown-6 structure, but further characterization is needed. Sensitivity, on the other hand, is not high, partly due to the inherent limitations of impedance response under the present conditions.

Control experiments with compounds **2** and **3** confirm the stated hypothesis. Compound **2** forms an initial monolayer which is a better insulator than **1** for charge transfer, as indicated by a high R_{CT}, 25 kΩ, but it exhibits no R_{CT} changes upon exposure to either K^+ or Na^+. That the initial monolayer is a good insulator is not surprising in view of its high hydrocarbon content. The mono-ester compound **3** has almost no charge transfer blocking ability in the absence or presence of alkali metal ions, and behaves essentially as a bare gold electrode.

In summary, we have prepared remarkably stable monolayers containing oligoethylene glycols on gold beads, and these exhibit impedance changes in the presence of K^+ but not with Na^+. While far from being useful sensors, the present SAMs are conceptually novel structures with unique cation binding properties exhibiting high selectivity.

This work was supported by the National Science Foundation (grants CHE-9816503 and DMR-9803088).

Notes and references

1 A. J. Moore, L. Goldenberg, M. R. Bryce, M. C. Petty, A. P. Monkman and S. N. Port, *Adv. Mater.*, 1998, **10**, 395.

2 S. Flink, B. A. Boukamp, A. Van den Berg, F. C. J. M. van Veggel and D. N. Reinhoudt, *J. Am. Chem. Soc.*, 1998, **120**, 4652; S. Flink, F. C. J. M. van Veggel and D. N. Reinhoudt, *J. Phys. Chem. B*, 1999, **103**, 6515.

3 T. K. Hansen, T. Jorgensen, P. C. Stein and J. Becher, *J. Org. Chem.*, 1992, **57**, 6403.

4 H. Liu, S. Liu and L. Echegoyen, *Chem. Commun.*, 1999, 1493.

5 All new compounds were fully characterized by spectroscopic techniques. *Selected data* for **1**: yellow liquid, yield 72%; δ_H ($CDCl_3$) 4.23 (4H, t, *J* 6.0), 3.65–3.70 (16H, m), 3.53–3.62 (2H, m), 3.07–3.20 (4H, m), 2.42–2.51 (2H, m), 2.35 (4H, t, *J* 7.2), 1.86–1.96 (2H, m), 1.61–1.69 (8H, m), 1.41–1.50 (4H, m); δ_C($CDCl_3$) 173.61, 70.99, 70.95, 70.93, 69.52, 63.76, 56.66, 40.55, 38.82, 34.91, 34.29, 29.00, 24.98; *m/z* (FAB^+) 614 (M^+, 60%) [HRMS (FAB^+): found 614.2074, calc. for $C_{26}H_{46}O_8S_4$: 614.2074]; ν_{max}(neat)/cm^{-1} 2918, 2851, 1733, 1457, 1380, 1247, 1128, 947, 857, 733. For **2**: yellow liquid, yield 71%; δ_H($CDCl_3$) 4.06 (4H, t, *J* 6.6), 3.52–3.61 (2H, m), 3.09–3.22 (4H, m), 2.43–2.49 (2H, m), 2.31 (4H, t, *J* 7.2), 1.87–1.96 (6H, m), 1.59–1.76 (16H, m), 1.43–1.51 (4H, m), 1.24–1.32 (8H, m); δ_C($CDCl_3$) 173.85, 140.08, 64.82, 40.55, 38.81, 38.78, 36.94, 35.25, 34.44, 34.39, 33.56, 29.86, 28.99, 26.71, 25.08, 25.01, 23.38; *m/z* (FAB^+) 578 (M^+, 100%). For **3**: yellow solid, yield 45%; δ_H($CDCl_3$) 4.22–4.25 (2H, m), 3.66–3.73 (18H, m), 3.59–3.62 (1H, m), 3.13–3.19 (2H, m), 2.41–2.52 (1H, m), 2.33—2.38 (2H, m), 2.13 (1H, s), 1.90–1.94 (1H, m), 1.59–1.75 (4H, m), 1.23–1.34 (2H, m); *m/z* (FAB^+) 426 (M^+, 100%).

6 F. Arias, L. A. Godínez, A. E. Kaifer and L. Echegoyen, *J. Am. Chem. Soc.*, 1996, **118**, 6086.

7 Impedance measurements were performed using a three electrode cell configuration with a monolayer-coated gold bead, a coiled platinum wire and Ag/AgCl as working, counter and reference electrode, respectively. The potential was held at the formal potential of the redox couple, and readings were taken at ten discrete frequencies per decade with an ac amplitude of 5 mV. The formal redox potential [$E_{\frac{1}{2}} = (E_p^c + E_p^a)/2$], where [$Ru(NH_3)_6^{3+}$] = [$Ru(NH_3)_6^{2+}$] was determined from cyclic voltammetry. Impedance analysis was carried out using the commercially available program EQUIVALENT CIRCUIT written by B. A. Boukamp (University of Twente), which determines the parameters of the assumed equivalent circuit by a non-linear least-square fit.

8 All electrochemical experiments were performed using a BAS-100W system. Electrolyte solutions were prepared from recrystallized materials using spectroscopic grade solvents and purged with argon prior to use. A three-electrode configuration was used with a Ag/AgCl reference electrode and a platinum wire as the counter electrode.

9 H. O. Finklea, D. A. Snider, J. Fedyk, E. Sabatani, Y. Gafni and I. Rubinstein, *Langmuir*, 1993, **9**, 3660; R. P. Janek, W. R. Fawcett and A. Ulman, *Langmuir*, 1998, **14**, 3011.

Communication a905839g

ChemComm

Synthesis and single crystal X-ray structure of the first cationic Pd(II) complex of a tellurium-containing polyaza macrocycle: contrasting reactions of Pd(II) and Pt(II) with a 22-membered macrocyclic Schiff base

Saija C. Menon,[a] Arunashree Panda,[a] Harkesh B. Singh*[a] and Ray J. Butcher[b]

[a] *Department of Chemistry, Indian Institute of Technology, Powai, Bombay 4000 076 India. E-mail: chhbsia@chem.iitb.ernet.in*

[b] *Department of Chemistry, Howard University, Washington, DC 20059, USA*

Received (in Cambridge, UK) 1st November 1999, Accepted 7th December 1999

The reaction of the tellurium containing macrocyclic Schiff base 1 with $Pd(PhCN)_2Cl_2$ and NH_4PF_6 gives the expected cationic complex $[Pd^{II}\mathbf{1}][PF_6]_2$; by contrast the reaction of 1 with $Pt(cod)Cl_2$ proceeds *via* novel transmetallation to yield an organoplatinum complex.

The chemistry of macrocycles bearing nitrogen or sulfur atoms has been very well developed.[1] The considerable effort which has been directed towards studying the coordination chemistry of polythio crowns in recent years has established that these macrocyclic ligands exhibit very different coordinating properties from their acyclic counterparts. This is principally due to the greater σ-donor effects caused by their cyclic nature which has facilitated stabilization of a wide range of metal ions in relatively unusual oxidation states. Polyselenoether macrocycles have an equally good potential to serve as ligands, however, the number of known polyselenoether macrocycles is very small.[2]

Recent studies by Levason *et al.* and others have established that the acyclic telluroether ligands are significantly better σ-donors compared to the lighter group 16 congeners.[3] Despite this, extension of this type of chemistry to the corresponding tellurium macrocycles is virtually unknown. A few notable examples include, 21-telluraporphyrins[4a] and 1,1,5,5,9,9-hexachloro-1,5,9-tritelluracyclododecane.[4b] Recently we have reported an easy, high yield template free synthesis, structure and preliminary coordination behaviour of the novel tellurium azamacrocycle **1**.[4c] The high yield and template free synthesis of **1** arises from intramolecular Te···N interactions in the macrocyclic ring.[4c] In continuation of this work, we report here, the synthesis and structure of the first cationic Pd(II) complex of the tellurium containing macrocyclic Schiff base **1**[4c] and the contrasting reaction of $Pt(cod)Cl_2$ with **1**. Both complexes **2** and **3** have been characterized by ^1H, ^{13}C, ^{125}Te NMR, mass and X-ray crystallography.

The reaction of **1** with 1 equivalent of $Pd(PhCN)_2Cl_2$ in $CHCl_3$ afforded a reddish yellow powder which was dissolved in methanol and treated with an excess of NH_4PF_6 to give the yellow complex **2** (Scheme 1). Slow diffusion of diethyl ether into an acetonitrile solution of this complex afforded yellow needles of **2**. This complex is fairly soluble in MeCN, $MeNO_2$, acetone, DMF and DMSO but insoluble in common chlorinated solvents. The IR spectrum of the complex confirmed the presence of PF_6^- [ν(P–F) 836, δ(F–P–F) 556 cm^{-1}] and showed a peak at 1639.8 cm^{-1} corresponding to the azomethine stretching frequency. The ^1H NMR spectrum of complex **2** exhibited two peaks in equal intensity at 8.99 and 8.82 ppm for the azomethine protons. The ^{13}C NMR spectrum showed two signals for the azomethine carbons at 170.81 and 163.76 ppm and for the methylene carbons at 58.11 and 63.75 ppm, suggesting coordination through only two imine nitrogens. However, the ^{125}Te NMR spectrum showed a single deshielded signal at 739.96 ppm *cf.* 607.1 ppm for the free ligand **1**[4c] thus indicating the coordination of Te to Pd and the presence of an identical environment around both the tellurium atoms. Elemental analysis data for complex **2** suggested the formation of a 1:1 product. The FAB mass spectrum of **2** showed a highest mass peak at *m/z* 977 corresponding to $\mathbf{2}^+ - PF_6^-$. Hence a formulation of $[Pd^{II}\mathbf{1}][PF_6]_2$ for the complex is suggested. The structure was further confirmed by single crystal X-ray diffraction studies‡.

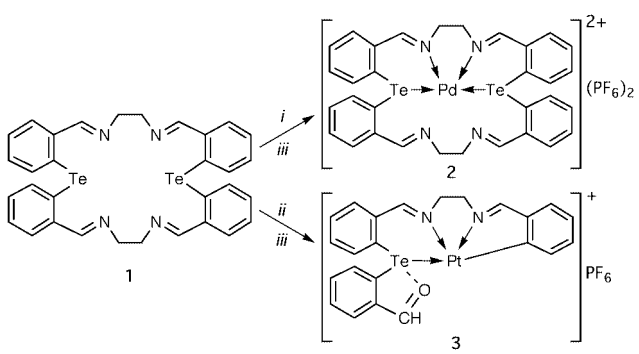

Scheme 1 *Reagents and conditions*: i, $Pd(PhCN)_2Cl_2$, $CHCl_3$, 2 h; ii, $Pt(cod)Cl_2$, CH_2Cl_2, 16 h; iii, MeOH, NH_4PF_6, room temp.

Interestingly, a similar reaction of **1** with $Pt(cod)Cl_2$ in dichloromethane yielded a reddish brown precipitate of the complex **3**† (Scheme 1) which could be recrystallized by slow evaporation from acetonitrile. The IR spectrum of **3** showed peaks consistent with the presence of ν(C=O) and ν(C=N) stretching frequencies at 1697 and 1647 cm^{-1}, respectively. The peak at 10.24 ppm in the ^1H NMR spectrum of **3** was assigned to an aldehydic proton. In addition, two peaks at 9.17 and 8.73 ppm were observed for the azomethine protons. The ^{125}Te NMR spectrum showed a high intensity peak at 708.39 ppm and a low intensity peak at 684.12 ppm. Similar behaviour has been observed for $[Pt([16]aneSe_4)][PF_6]_2$ by Reid and coworkers who observed two resonances for ^{77}Se at 187 and 147 ppm in MeCN at 300 K.[5] These authors suggested the presence of at least two invertomers in solution. The FAB mass spectrum showed a highest peak at *m/z* 665 corresponding to $\mathbf{3}^+ - PF_6^-$. Elemental analysis also suggested the formation of complex **3** the structure of which was confirmed from X-ray crystallographic studies.‡ The novel organoplatinum complex **3** results from facile C–Te bond cleavage and transmetallation. McWhinnie *et al.*, we and others have observed a similar transfer of organic groups from tellurium to another metal in the reactions of $HgCl_2$,[4c,6] copper salts,[7] Pd(II)[8,9] and Pt(II)[3d,9] with telluroethers. The facile cleavage of the C–Te bond is due to strong N → Te intramolecular interactions which activate the *trans* C–Te bond.

A view of the cation of the Pd(II) complex **2** is shown in Fig. 1. The cation adopts a four coordinate geometry, with coordination by two nitrogen and two tellurium atoms. The N–Pd–N, Te–Pd–Te and N–Pd–Te angles are close to 90 and 180°. The Pd–Te(1A) and Pd–Te(1B) bond distances of 2.5443(7) and 2.5483(7) Å are comparable to the Pd(1)–Te(1) and Pd(2)–Te(3) distances of 2.540(2) and 2.549(20 Å,

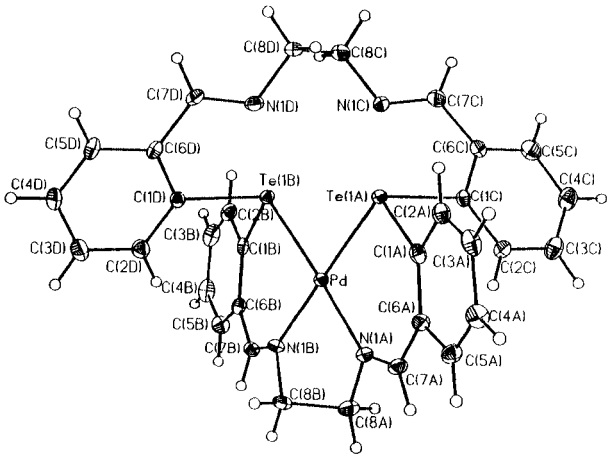

Fig. 1 An ORTEP diagram of Pd complex **2**. Selected bond lengths (Å) and angles (°): Te(1A)–Pd 2.5443(7), Te(1B)–Pd 2.5483(7), Pd–N(1A) 2.097(6), Pd–N(1B) 2.099(6), Te(1A)–N(1C) 2.739, Te(1B)–N(1D) 2.737, Te(1A)···Te(1B) 3.591, N(1B)–Pd–Te(1A) 176.9(2), N(1A)–Pd–Te(1B) 175.9(2), Te(1A)–Pd–Te(1B) 89.68(2), N(1A)–Pd–Te(1A) 94.4(2), N(1B)–Pd–Te(1B) 93.1(2).N(1A)–Pd–N(1B) 82.8(2).

respectively, in [{Pd(C_6H_4(TeMe)Te-*o*)I}$_4$].[8] The Te···N distances of 2.739 and 2.737 Å are well within the van der Waals distance (3.7 Å following Pauling[10]) and the Te–C–C–C–N moieties are planar. The tellurium is acting simultaneously as a Lewis acid and Lewis base. The Te···Te transannular bond distance of 3.591 Å is significantly shorter than the sum of the van der Waals radii (4.4 Å). This distance is also shorter than the transannular Te···Te bond distance (4.979 Å)[4c] in free ligand **1**.

The cation of complex **3** is shown in Fig. 2. The structure shows square planar geometry around the Pt(II) ion with coordination of carbon, tellurium and two nitrogen atoms. The angles around the Pt(II) ion lie in the range 80–100° and 162–177°, indicating the distorted square planar geometry. The Pt–Te bond distance of 2.5180(6) Å is comparable with the Pt–Te distance of 2.512(1) Å in [Pt{(NC_5H_4-2-$(CH_2)_2$-Te-C_6H_4-4-OMe}Cl_2].[11] The intramolecular Te···O distance of 3.004 Å implies a weak coordination of oxygen to tellurium as it is significantly shorter than the sum of the van der Waals radii (3.6 Å) of Te and O. However, this bond distance is longer than the mean tellurium–oxygen distance of 2.76 Å observed in bis(*o*-formylphenyl)ditelluride.[12] In addition, the cations are linked into weak dimers by weak intermolecular Te···Pt contacts (3.483 Å). Complex **3** is the first example of a structurally characterized organoplatinum complex having both intramolecular Te→Pt and intermolecular Pt···Te interactions.

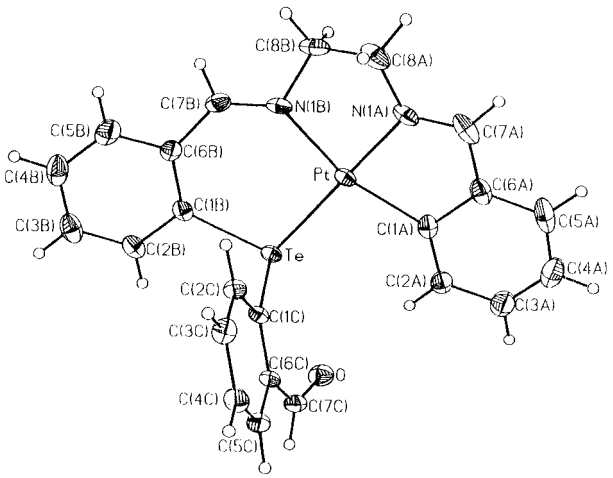

Fig. 2 An ORTEP diagram of Pt complex **3**. Selected bond lengths (Å) and angles (°): Pt–N(1A) 1.994(7), Pt–N(1B), 2.087(7), Pt–C(1A) 2.028(8), Pt–Te 2.5180(6), Te···O 3.004, Te···Pt 3.483; N(1A)–Pt–N(1B) 82.4(3), C(1A)–Pt–N(1B) 162.4(3), N(1A)–Pt–Te 177.0(2), N(1A)–Pt–C(1A) 80.3(4), N(1B)–Pt–Te 96.8(2), Te–Pt–C(1A) 100.7(2).

We are grateful to the Department of Science and Technology (DST), New Delhi for funding this work. We thank Prof. C. P. Morley for providing the mass and NMR facilities. R. J. B. acknowledges the DOD-ONR programme for funds to upgrade the diffractometer.

Notes and references

† *Analytical data*: **2** yield, 0.13 g (87%), mp 202–204 °C (decomp.); Anal. ($C_{32}H_{28}N_4Te_2PdP_2F_{12}$, 1120.16). Calc.: C, 34.29; H, 2.52; N, 5.00. Found: C, 34.42; H, 2.45; N, 5.13%. **3** Yield 0.060 g (46%), mp 260–262 °C (decomp.); Anal. ($C_{23}H_{19}N_2TePtOPF_6$, 807.07). Calc.: C, 34.23; H, 2.37; N, 3.47. Found: C, 34.24; H, 2.43; N, 3.45%.

‡ *Crystal data*: for **2**: $C_{32}H_{28}N_4Te_2PdP_2F_{12}$, M = 1120.12; monoclinic, space group $P2_1/n$, a = 8.2250(10), b = 21.280(4), c = 21.150(4) Å, V = 3691.9(11) Å^3, Z = 4, 8490 reflections collected, 8467 independent reflections (R_{int} = 0.0155), D_c = 2.015 Mg m^{-3}, $R(R_w)$ = 0.0512(0.1162).

For **3**: $C_{23}H_{19}F_6N_2OPPtTe$, M = 807.06; monoclinic, $P2_1/n$, a = 12.3253(14), b = 14.6557(14), c = 13.4054(11) Å, V = 2403.4(4) Å^3, Z = 4, 5352 reflections collected, 5108 independent reflections (R_{int} = 0.0225), D_c = 2.230 Mg m^{-3}, $R(R_w)$ = 0.0422(0.1071). CCDC 182/1501.

1 P. Comba, A. Kühner and A. Peters, *J. Chem. Soc., Dalton Trans.*, 1999, 509; J. Nelson, V. McKee and G. Morgan, *Prog. Inorg. Chem.*, 1998, **47**, 167; J. P. Danks, N. R. Champness and M. Schröder, *Coord. Chem. Rev.*, 1998, **174**, 417 and references therein; H. Furutachi, A. Ishida, H. Miyasaka, N. Fukita, M. Ohaba, H. Okawa and M. Koikawa, *J. Chem. Soc., Dalton Trans.*, 1999, 367; G. Musie, J. H. Reibenspies and M. Y. Darensbourg, *Inorg. Chem.*, 1998, **37**, 302; S. Mohanta, K. K. Nanda, L. K. Thompson, U. Flörke and K. Nag, *Inorg. Chem.*, 1998, **37**, 1465; F. Avecilla, A. de Blas, R. Bastida, D. E. Fenton, J. Mahía, A. Macías, C. Platas, A. Rodríguez and T. Rodríguez-Blas, *Chem. Commun.*, 1999, 125; S. Brooker, P. D. Croucher, T. C. Davidson, G. S. Dunbar, A. J. McQuillan and G. B. Jameson, *Chem. Commun.*, 1998, 2131.

2 R. J. Batchelor, F. W. B. Einstein, I. D. Gay, J. Gu, B. D. Johnston and B. M. Pinto, *J. Am. Chem. Soc.*, 1989, **111**, 6582; R. J. Batchelor, F. W. B. Einstein, I. D. Gay, J. Gu, B. M. Pinto and X. Zhou, *Inorg. Chem.*, 1996, **35**, 3667 and references therein; R. D. Adams and K. T. McBride, *Chem. Commun.*, 1997, 525; S. Tomoda and M. Iwaoka, *J. Chem. Soc., Chem. Commun.*, 1990, 231; R. Bhula, A. P. Arnold, G. J. Gainsford and W. G. Jackson, *Chem. Commun.*, 1996, 143; M. K. Davies, M. C. Durrant, W. Levason, G. Reid and R. L. Richards, *J. Chem. Soc., Dalton Trans.*, 1999, 1077 and references therein; C. Bornet, R. Amardeil, P. Meunier and J. C. Daran, *J. Chem. Soc., Dalton Trans.*, 1999, 1039 and references therein.

3 W. Levason, S. D. Orchard and G. Reid, *Chem. Commun.*, 1999, 1071 and references therein; W. Levason, S. D. Orchard, G. Reid and V. Tolhurst, *J. Chem. Soc., Dalton Trans.*, 1999, 2071; N. Al-Salim, T. A. Hamor and W. R. McWhinnie, *J. Chem. Soc., Chem. Commun.*, 1986, 453; N. I. Al-Salim and W. R. McWhinnie, *Polyhedron*, 1989, **8**, 2769; A. Khanna, A. Bala and B. L. Khandelwal, *J. Organomet. Chem.*, 1995, **494**, 199; R. Batheja, S. K. Dhingra and A. K. Singh, *J. Organomet. Chem.*, 1995, **487**, 173 and references therein.

4 (*a*) L. Latos-Grazynski, E. Pacholska, P. J. Chmielewski, M. M. Olmstead and A. L. Balch, *Angew. Chem., Int. Ed. Engl.*, 1995, **34**, 2252; (*b*) Y. Takaguchi, E. Horn and N. Furukawa, *Organometallics*, 1996, **15**, 5112 and references therein; (*c*) S. C. Menon, H. B. Singh, R. P. Patel and S. K. Kulshreshtha, *J. Chem. Soc., Dalton Trans.*, 1996, 1203.

5 N. R. Champness, P. F. Kelly, W. Levason, G. Reid, A. M. Z. Slawin and D. J. Williams, *Inorg. Chem.*, 1995, **34**, 651.

6 S. A. Mbogo, W. R. McWhinnie and T. S. Lobana, *J. Organomet. Chem.*, 1990, **384**, 115.

7 S. A. Mbogo, W. R. McWhinnie and T. S. Lobana, *Inorg. Chim. Acta*, 1990, **172**, 221.

8 T. Kemmitt, W. Levason, M. D. Spicer and M. Webster, *Organometallics*, 1990, **9**, 1181.

9 S. A. Mbogo, W. R. McWhinnie and T. S. Lobana, *Inorg. Chim. Acta*, 1992, **193**, 5.

10 L. Pauling, *The Nature of the Chemical Bond*, 3rd edition, Cornell University Press, Ithaca, New York, 1960.

11 A. Khalid, B. L. Khandelwal, A. K. Singh, T. P. Singh and B. Padmanabhan, *J. Coord. Chem.*, 1994, **31**, 19.

12 S. C. Menon, H. B. Singh, R. P. Patel, K. Das and R. J. Butcher, *Organometallics*, 1997, **16**, 563.

Communication a908683h

Hetero-dinuclear sodium–lanthanide(III) complexes with an asymmetric compartmental macrocycle

Umberto Casellato,[a] Sergio Tamburini,[a] Patrizia Tomasin,[a] Pietro A. Vigato,*[a] Silvio Aime,*[b] Alessandro Barge[b] and Mauro Botta[c]

[a] *Istituto di Chimica e Tecnologie Inorganiche e dei Materiali Avanzati, CNR, Corso Stati Uniti 4, 35127 Padova, Italy*
[b] *Dipartimento di Chimica I.F.M., University of Torino, Via P. Giuria 7, 10125 Torino, Italy. E-mail: aime@silver.ch.unito.it*
[c] *Dipartimento di Science e Tecnologie Avanzate, Università del Piemonte Orientale, 'Amedeo Avogadro', Corso Borsalino 54, 10131 Alessandria, Italy*

Received (in Basel, Switzerland) 26th November 1999, Accepted 10th December 1999

A heterodinuclear macrocyclic complex containing both Yb^{3+} and Na^+ ions has been synthesized and characterized by X-ray crystallography and ^1H and ^{23}Na solution NMR; at room temperature the coordinated Na^+ ion is in slow chemical exchange with free Na^+ ions and its NMR resonance is strongly shifted.

In recent years asymmetric compartmental ligands have been under intense scrutiny because it is expected that well defined bimetallic systems may find interesting applications in several areas of chemical research.[1–4] The synthesis of compartmental macrocycles is commonly pursued by a step-by-step condensation of 2,6-diformyl-4-substituted phenols with polyamines which may also contain other donor atoms. Heterodinuclear (M,M′) complexes may be conveniently prepared by reacting the intermediate [2 + 1] acyclic complex, obtained by template synthesis in the presence of M^{m+} ions, with a suitable polyamine in the presence of M'^{n+} ions.[5]

A marked difference in the set of donor atoms of the two adjacent chambers favours the formation of heterodinuclear complexes (with respect to homodinuclear complexes) thus limitating the possibility of positional heterodinuclear isomers.[6,7]

Here, we investigate the synthesis and characterisation of a Yb–Na dinuclear complex which represents the first example of macrocyclic compartmental complex containing a lanthanide and an alkali metal ions.

On the basis of the above considerations, it was thought that a suitable ligand should contain a Schiff base chamber for the lanthanide coordination and a crown-ether moiety for the coordination of the alkali metal ion. As diformyl precursor we used 3,3′-(3-oxapentane-1,5-diyldioxy)-bis(2-hydroxybenzaldehyde) which, upon reaction with 1,5-diamino-3-aza-methylpentane (Scheme 1) yields the asymmetric compartmental macrocycle shown in Fig. 1.[8,9]

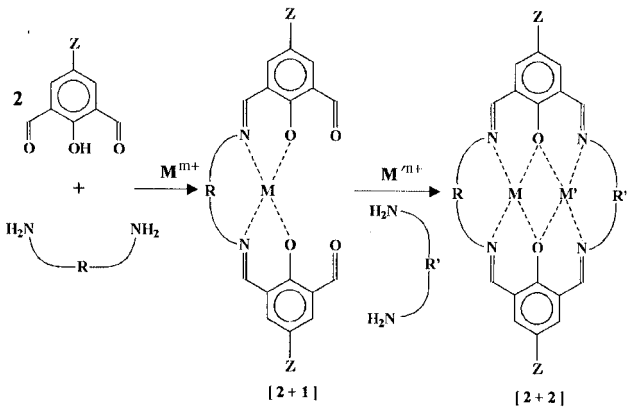

Scheme 1

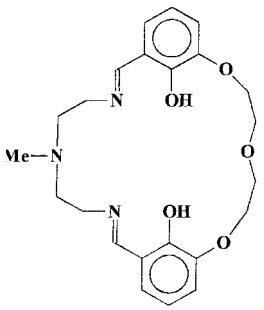

Fig. 1 Schematic representation of the compartmental macrocycle (L) designed for coordinating a lanthanide(III) ion into the Schiff base (N_3O_2) chamber and an alkali metal ion into the crown-ether moiety.

Rather surprisingly it was found that this macrocyclic ligand coordinates lanthanide(III) ions into the crown-ether chamber rather than into the N_3O_2 Schiff base.[9,10] On the other hand the same crown-ether chamber is involved in the coordination of alkali ions in the case of homonuclear alkaline metal containing species.[11] Thus, although both ions prefer coordination at the O_2O_3 chamber, we surmise that the use of the Na^+ containing complex may force the coordination of the lanthanide(III) ion into the Schiff-base chamber.

This synthetic strategy was successful as shown by the spectroscopic properties and X-ray structure of the obtained $YbNa(L)Cl_2$ derivative (Fig. 2).†

The ytterbium ion is coordinated by two chlorine atoms in *trans* positions and by three nitrogen and two negatively charged phenyl oxygen atoms of the ligand, reaching hepta-coordination with a pentagonal bipyramidal geometry. The sodium ion is coordinated by the three etheric oxygen atoms and the same two phenyl oxygens that act as a bridge. A methanol molecule is also coordinated in the apical position of the resulting pentagonal pyramidal polyhedron. The oxygen atom of the methanol is disordered and two positions have been found. The Yb···Na contact distance is 3.555(2) Å.

The high temperature ^1H NMR spectrum (65 °C, CD_3OD) of $YbNa(L)Cl_2$ (Fig. 3) is consistent with the occurrence of a motion in the macrocyclic ring which reduces to half (twelve) the number of the observed resonances. Although the spectrum covers a range of *ca.* 70 ppm, the resonances associated with the two N_3O_2 and O_2O_3 chambers can be unambiguously assigned. In fact, the paramagnetic Yb(III) ion causes a large spread of the five protons (and of the methyl group) associated with the Schiff base compartment (−15 to −57 ppm) whereas the proton associated with the crown ether and aromatic moieties fall in the region +7 to −8 ppm *i.e.* they 'feel' only in part the paramagnetism of the lanthanide ion.

The ^{23}Na NMR spectrum at ambient temperature consists of the broad absorption of the bound ion (Na^b) at *ca.* 40 ppm

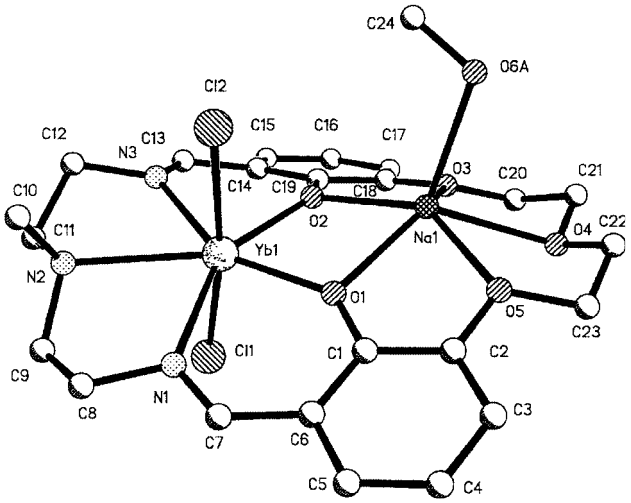

Fig. 2 ORTEP drawing of $[YbNa(L)Cl_2]\cdot MeOH$ with ellipsoids at the 50% probability level. Selected bond lengths (Å) and angles (°): Yb–O(1) 2.204(3), Yb–O(2) 2.226(3), Yb–N(1) 2.459(4), Yb–N(2) 2.593(4), Yb–N(3) 2.474(4), Yb–Cl(1) 2.582(1), Yb–Cl(2) 2.638(1), Na–O(1) 2.343(4), Na–O(2) 2.296(4), Na–O(3) 2.370(5), Na–O(4) 2.444(5), Na–O(5) 2.316(4), Na–O(6)(methanol) 2.35(mean); Cl(1)–Yb–Cl(2) 172.14(4), Yb–O(1)–Na 102.2(1), Yb–O(2)–Na 103.0(1).

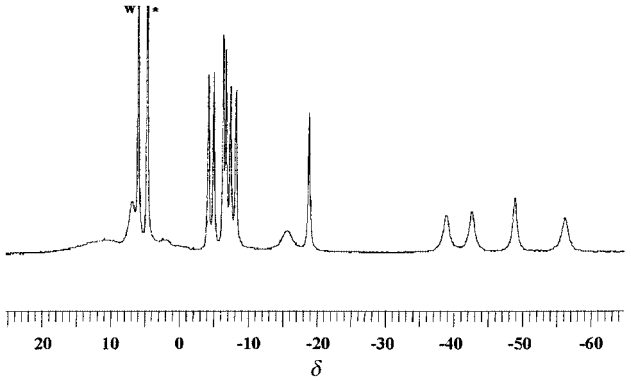

Fig. 3 400 MHz ^{1}H NMR spectrum of $YbNa(L)Cl_2$ at 65 °C in CD_3OD. The water and methanol resonances have been labelled with the symbols w and *, respectively.

upfield from that of the free ion (Na^f) [Fig. 4]. Upon increasing the temperature the exchange between Na^f and Na^b becomes fast on the NMR timescale [Fig. 4] and, at 65 °C, a relatively narrow absorption at *ca.* −16 ppm is observed. It seems reasonable to suggest that the release of Na^+ ion from the crown-ether chamber induces an overall flexibility of the macrocycle as the ^{1}H NMR spectrum recorded at ambient temperature is more complex than that obtained at 65 °C.

The high and negative paramagnetic ^{23}Na NMR shift observed for Na^b strongly suggests that the principal axis of the magnetic susceptibility tensor associated with the Yb(III) ion lies along the Yb–Na direction rather than along an axis perpendicular to the macrocyclic plane. This finding may be highly relevant to development of a novel class of ^{23}Na-shift

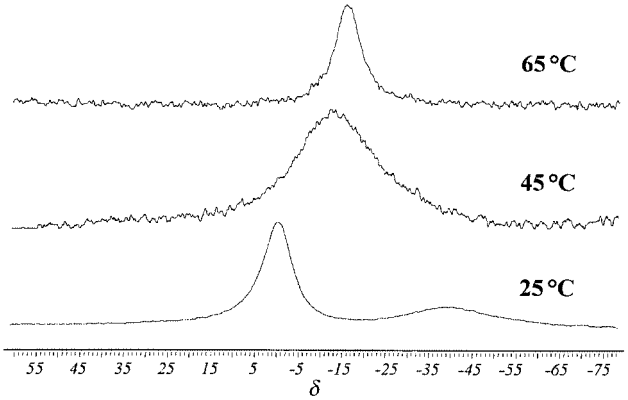

Fig. 4 Variable temperature ^{23}Na NMR spectra of $YbNa(L)Cl_2$ (25 mM) at 9.4 T in the presence of NaCl (30 mM) in CD_3OD.

reagents which could be very useful in separating the ^{23}Na NMR resonances for intra- and extra-cellular components.[12]

Notes and references

† *Crystal data* for $YbNa(L)Cl_2\cdot MeOH$: $C_{24}H_{30}Cl_2N_3NaO_6Yb$, yellow crystal, 0.30 × 0.35 × 0.25 mm, M = 723.44, monoclinic, space group $P2_1/n$, a = 12.586(3), b = 13.127(3), c = 16.690(3) Å, β = 101.08(3)°, U = 2706(1) Å^3, Z = 4, D_c = 1.776 g cm^{-3}, μ(Mo-Kα) = 3.713 mm^{-1}, T = 293(2) K, 7338 reflections measured, 6903 reflections with $I > 4\sigma(I)$ used in all calculations, $R(F^2)$ = 0.0411, $wR(F^2)$ = 0.112. The structure was solved using direct methods and refined by full-matrix least squares on F^2. CCDC 182/1503.

1 P. Guerriero, S. Tamburini and P. A. Vigato, *Coord. Chem. Rev.*, 1995, **139**, 17.
2 D. M. Rudkevich, J. D. Mercer-Chalmers, W. Verboom, R. Ungaro, F. de Jong and D. N. Reinhoudt, *J. Am. Chem. Soc.*, 1995, **117**, 6124.
3 D. G. McCollum, I. Hall, C. White, R. Ostrander, A. I. Rheingold, J. Whelan and B. Bosnich, *Inorg. Chem.*, 1994, **33**, 924 and references therein.
4 M. Yonemura, Y. Matsumura, H. Furutacki, M. Okawa and D. E. Fenton, *Inorg. Chem.*, 1997, **36**, 2711.
5 H. Okawa, H. Furutacki and D. E. Fenton, *Coord. Chem. Rev.*, 1998, **174**, 51.
6 J. Lisowki and P. Starynowicz, *Inorg. Chem.*, 1999, **38**, 1351.
7 M. Mikuriya, M. Nakamura, H. Okawa and S. Kida, *Chem. Lett.*, 1982, 839 and references therein.
8 C. J. Van Staveren, J. Van Eerden, F. C. J. M. Van Veggel, S. Harkema and D. N. Reinhoudt, *J. Am. Chem. Soc.*, 1988, **110**, 4994.
9 U. Casellato, S. Tamburini, P. Tomasin and P. A. Vigato, *Inorg. Chim. Acta*, 1998, **262**, 117.
10 U. Casellato, S. Tamburini, P. Tomasin, P. A. Vigato, S. Aime and M. Botta, *Inorg. Chem.*, 1999, **38**, 2906; N. Brianese, U. Casellato, S. Tamburini, P. Tomasin and P. A. Vigato, *Inorg. Chem. Commun.*, 1999, **2**, 149.
11 P. Zanello, S. Tamburini, P. A. Vigato and G. A. Mazzocchin, *Coord. Chem. Rev.*, 1987, **77**, 165; P. A. Vigato, S. Tamburini and D. E. Fenton, *Coord. Chem. Rev.*, 1990, **106**, 25; D. E. Fenton and P. A. Vigato, *Chem. Soc. Rev.*, 1988, **17**, 89; T. M. Sorrel, *Tetrahedron*, 1989, **45**, 3.
12 D. Sherry and C. F. G. C. Geraldes, *Lanthanide Probes in Life, Chemical and Earth Sciences*, ed. J. C. G. Bünzli and G. R. Choppin, 1989, Elsevier, Amsterdam, ch. 4.

Communication a909367b

ChemComm

Solid-phase oligosaccharide synthesis with tris(alkoxy)benzyl amine (BAL) safety-catch anchoring

Jakob F. Tolborg and Knud J. Jensen*

Department of Organic Chemistry, Building 201, Kemitorvet, Technical University of Denmark, DK-2800 Lyngby, Denmark. E-mail: okkj@pop.dtu.dk

Received (in Liverpool, UK) 20th October 1999, Accepted 29th November 1999

A tris(alkoxy)benzylamine (BAL) handle strategy was developed for safety-catch anchoring of D-glucosamine derivatives in solid-phase synthesis of oligosaccharides; the linkage between the BAL handle and the amine proved stable to conc. TFA and Lewis acids, but after *N*-acylation the amide could be released by treatment with TFA–H_2O (19 : 1).

Cell-surface oligosaccharides are involved in many biological recognition processes.[1] Also, free oligosaccharides can have biological effects such as in rhizobial lipochitin oligosaccharides which function as nodulation factors.[2] Amino sugars are found in many biologically important poly- and oligo-saccharides, *e.g.* in glycans of *O*- and *N*-glycoproteins and -peptides, lipochitin nodulation factors, and amino glycoside antibiotics such as streptomycin.

Solid-phase synthesis of oligosaccharides, when performed combinatorially, offers the prospect of easy access to very large numbers of well-defined oligosaccharides as tools for glycobiology. Despite Frechet and Schuerch's early pioneering work[3] and recent significant progress,[4] considerable developments are required before solid-phase oligosaccharide synthesis can be put to general use. Crucial to any solid-phase synthesis plan is the efficient and reliable anchoring of the first building block, the stability of the anchoring linkage to the synthesis conditions, and upon completion of the synthesis the efficient release under conditions compatible with the structural integrity of the final product. The most common cleavage reagent in solid-phase peptide synthesis is conc. TFA. Previously reported handles for anchoring of carbohydrates to solid supports have included esters,[4a] silyl ethers,[4b] sulfonyl esters,[4c] acetals[4d] and thioalkyls[4e] and ethers.[4f,g]

For the solid-phase synthesis of amino sugar containing oligosaccharides, we decided upon a strategy relying on release of final products by treatment with conc. TFA, with semi-permanent protecting groups to be removed in solution after purification and characterization.[5] The recently developed Backbone Amide Linker (BAL) handle strategy relies on anchoring of a peptide not through a carboxy group but through a backbone amide nitrogen leaving the *C*-terminus available for modifications.[6] Applied to anchoring of amino sugars, a BAL strategy would allow anchoring through an acetamido functionality leaving all hydroxy groups, including the anomeric, available for modification.

To investigate the anchoring concept, *o*-PALdehyde **1** was coupled to high-loading aminomethylated polystyrene **2** and unprotected D-glucosamine **3a** anchored through a BAL linkage by reductive amination in DMF–AcOH (99 : 1) in the presence of $NaBH_3CN$ (Scheme 1).† Perbenzoylation with BzCl followed by treatment with TFA–H_2O (19 : 1) yielded after column chromatography the α-pentabenzoate **4a** in 41% for a four step synthesis sequence. The presence of five benzoyl groups in the final product confirmed that anchoring had occurred through the amine rather than the putative *O*,*O*- or *O*,*N*-acetals.

For fast and efficient quantification of resin-bound carbohydrates we used two techniques. In the first, UV-active amino sugar derivatives were released into solution with TFA–H_2O (19 : 1) followed by quantification with HPLC–UV from standard curves.

In the second technique, the resin-bound monosaccharide was treated with 4,4′-dimethoxytrityl chloride (DMTCl) to attach a DMT moiety at the primary 6-OH group. For quantification, the resin was exposed to TFA–MeCN (1 : 49) and released DMT estimated by UV. Quantification using DMT was performed on resin bound monosaccharides in order to determine the efficiency of the coupling of *o*-PALdehyde to the resin as well as the coupling of the amino sugar to the linker. The methyl and benzyl glycosides of D-glucosamine **3b** and **3c** were coupled with an efficiency of at least 95% (four steps from **2**, including DMT coupling and cleaving) independently of the resin loading. The solid-phase bound benzyl α-D-glucosaminide **3c** was then per-acylated with Ac_2O or BzCl. This yielded the fully acetylated and benzoylated products **4b** and **4c** in 91–96 and 82% yield, respectively, measured by HPLC standard curves.

Several solution-phase glycosylation methods have been adapted for solid-phase; they all require Lewis acids for activation.[4] While studying the use of trichloroacetimidates in

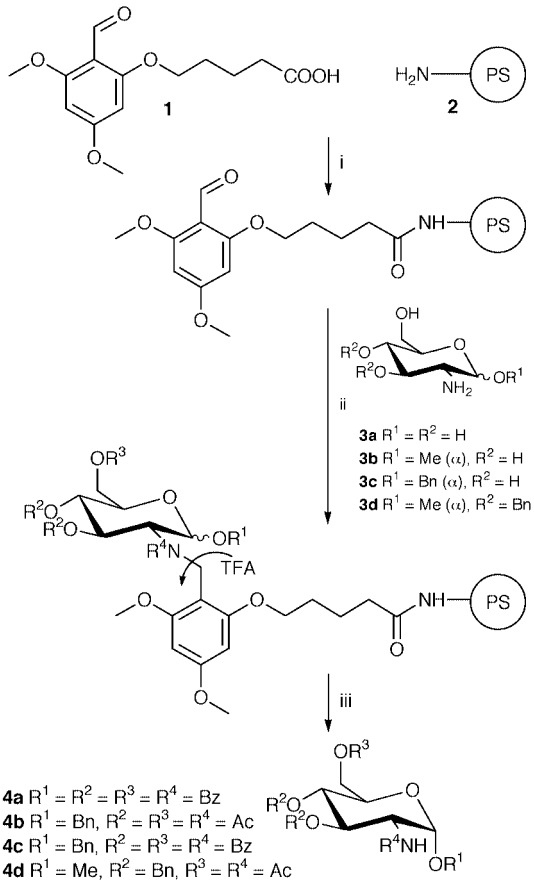

Scheme 1 *Reagents and conditions*: i, aminomethylated polystyrene **2**, **1** (2.0 equiv.), HBTU (1.9 equiv.), HOBt (2.0 equiv.), Pr^i_2NEt (3.9 equiv.), DMF, 10 h; ii, amino sugar (2.0 equiv.), $NaBH_3CN$ (10 equiv.), DMF–AcOH (99 : 1), 16 h, then protecting group chemistry including *N*-acylation; iii, TFA–H_2O (19 : 1), 30 min.

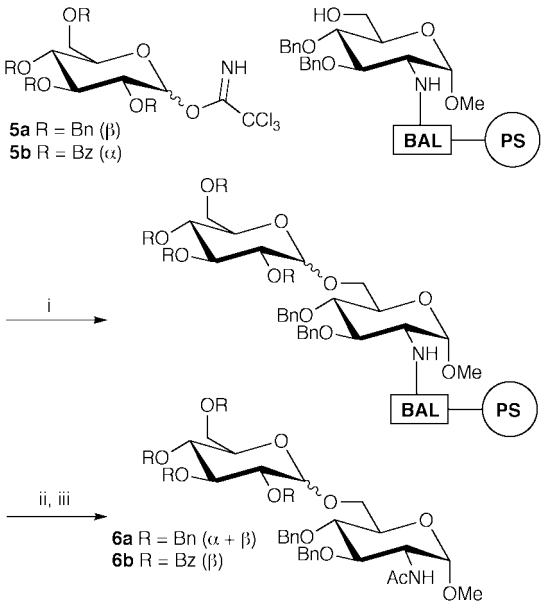

Scheme 2 *Reagents and conditions*: i, TMSOTf, CH_2Cl_2, 3 Å (Table 1); ii, Ac_2O–Py (2:1), 16 h; iii, TFA–H_2O (19:1), 30 min.

the presence of Lewis acid promoters for the glycosylation of BAL anchored D-glucosaminides, we realized that BAL anchoring could be operated in a safety-catch mode. The amine–BAL linkage proved stable to treatment with conc. TFA and more than stoichiometric amounts of Lewis acids such as $BF_3{\cdot}OEt_2$ and TMSOTf. After acylation to form the amide, the linkage became acid-labile and the carbohydrate could be released with conc. TFA.

For solid-phase glycosylations, we first synthesized the partially protected D-glucosamine derivative **3d**. Anchoring through a BAL handle to a polystyrene support was achieved as above, leaving the 6-OH free. In initial studies we used 2,3,4,6-tetra-*O*-benzyl-β-D-glucopyranosyl trichloroacetimidate **5a**[7] in the presence of $BF_3{\cdot}OEt_2$ or TMSOTf as promoters (Scheme 2). Solid-phase reactions are most conveniently carried out at room temperature, but this gave only low yields of the disaccharide. However, when performing the glycosylation at −50 °C the disaccharide **6a** was obtained in 35% yield as an α/β mixture (five steps from **2**).

When using the *less reactive* benzoyl protected glycosyl donor 2,3,4,6-tetra-*O*-benzoyl-α-D-glucopyranosyl trichloroacetimidate **5b** in the presence of TMSOTf, yields of up to 82% of the disaccharide **6b**[8] were obtained (five steps from **2**), leaving as little as 2% of the unglycosylated monosaccharide (Table1). The disaccharide was obtained with an α:β ratio of < 1:10, the high β-selectivity being due to the neighboring group participation of the benzoyl group. Stoichiometric and sub-stoichiometric amounts of Lewis acids were used, relative to the donor. We found that TMSOTf was superior to $BF_3{\cdot}OEt_2$ as promoter, and MAS NMR revealed that the secondary amine did *not* carry a TMS group after exposure to TMSOTf in glycosylations. The high yield of 82% for the five step synthesis of **6b** also indicated that release of the final product with TFA–H_2O was near quantitative.

Table 1 Reaction conditions for synthesis of **6b**

T/°C	**5b**/equiv.	TMSOTf/ equiv.	Yield of **6b** (%) (β/α)
Room temp.	5.0	1.0	0
Room temp.	5.0	2.0	76 (14)
Room temp.	5.0	5.0	74 (20)
Room temp.	5.0	10.0	64 (17)
Room temp.	10.0	2.0	82 (11)
Room temp.	10.0	5.0	82 (16)
Room temp.	10.0	10.0	67 (17)

The initial resin loading of the aminomethylated polystyrene **2** was 0.40 mmol g^{-1}, which dropped to 0.36 mmol g^{-1} after coupling of *o*-PALdehyde **1** to the resin, and 0.32 mmol g^{-1} after attaching the partly protected monosaccharide **3d**. With high-loading resin (1.20 mmol g^{-1}) glycosylation became much less efficient..

In conclusion, we have developed a new and efficient strategy for anchoring amino sugars through a BAL handle to a solid support in which the amino sugar is attached by an efficient reductive amination. BAL anchoring was operated in a safety-catch mode as BAL linked amines were stable to Lewis acids and conc. TFA, whereas the corresponding amides were released from the support with conc. TFA. This allowed the use of Lewis acids in excess in solid-phase glycosylations. Using this strategy, we synthesized 1-6 linked disaccharides in high yields. The safety-catch protocol for BAL anchoring should also be useful for other applications.

We thank Flemming Jensen and Annette Lind Nordestgaard, Phytera, for MS, Drs Charlotte Godfredsen and Henrik Pedersen for MAS NMR, and the Lundbeck Foundation (K. J.) and the Danish Technical Research Council ('Talent Project' grant to K. J.) for financial support.

Notes and references

† All solid-phase reactions were carried out in plastic syringes at room temperature, except for glycosylations at −50 °C, which were carried out in glass flasks. Syringes were fitted with a polypropylene filter, a Teflon valve in the bottom, and closed in the top with the syringe plunger. For glycosylations, the syringe was instead closed with a septum, after the solid reactants were placed in the syringe. It was then dried in a desiccator *in vacuo* with the Teflon valve open. The desiccator was opened under argon, the Teflon valve closed, and the solvent and Lewis acid added through the septum. After 18 h the resins were washed and dried; final products were released from the support with TFA–H_2O (19:1). Glycosylations were typically performed on a 5 μmol scale. Quantifications were done by HPLC–UV integration of peak areas and use of standard curves established from benzyl and benzoyl containing compounds. Benzyl groups were monitored at λ = 215 nm, and benzoyl groups at λ = 265 nm. At the 5 μmol scale and without purification, the structure of **6b** was established by MS, ^{1}H NMR and gCOSY spectroscopy (ref. 8).

1 A. Varki, *Glycobiology*, 1993, **3**, 97; K. J. Yarema and C. R. Bertozzi, *Curr. Opin. Chem. Biol.*, 1998, 49.
2 P. Lerouge, *Glycobiology*, 1994, **4**, 127.
3 J. M. Frechet and C. Schuerch, *J. Am. Chem. Soc.*, 1971, **93**, 492.
4 (*a*) M. Adinolfi, G. Barone, L. D. Napoli, A. Iadonisi and G. Piccialli, *Tetrahedron Lett.*, 1998, **39**, 1953; (*b*) C. Zheng, P. H. Seeberger and S. J. Danishefsky, *J. Org. Chem.*, 1998, **63**, 1126; (*c*) J. A. Hunt and W. R. Roush, *J. Am. Chem. Soc.*, 1996, **118**, 9998; (*d*) Y. Ito and T. Ogawa, *J. Am. Chem. Soc.*, 1997, **119**, 5562; (*e*) J. Rademann and R. R. Schmidt, *J. Org. Chem.*, 1997, **62**, 3650; (*f*) G. Hodosi and J. J. Krepinsky, *Synlett*, 1996, 159; (*g*) S. P. Douglas, D. M. Whitfield and J. J. Krepinsky, *J. Am. Chem. Soc.*, 1995, **117**, 2116.
5 Conc. TFA has been used extensively for release of final products in solid-phase synthesis of glycopeptides. Glycosidic bonds appear in general to be fully stable to these conditions, especially while retaining ester protecting groups. For a review see M. Meldal, in *Neoglycoconjugates: Preparation and Applications*, ed. Y. C. Lee and R. T. Lee, Academic Press, San Diego, 1994, p. 145.
6 K. J. Jensen, J. Alsina, M. F. Songster, J. Vágner, F. Albericio and G. Barany, *J. Am. Chem. Soc.*, 1998, **120**, 5441.
7 R. R. Schmidt, J. Michel and M. Roos, *Liebigs Ann. Chem.*, 1984, 1343.
8 *Selected data* for **6b**: δ_H($CDCl_3$, 500 MHz) 8.01 (dd, *J* 1.3, 8.5, 2H), 7.90 (dd, *J* 1.3, 8.5, 4H), 7.82 (dd, *J* 1.7, 8.5, 2H), 7.54–7.48 (m, 2H), 7.44–7.41 (m, 2H), 7.38–7.22 (m, 16H), 7.14 (dd, *J* 1.7, 7.7, 2H), 5.91 (dd, *J* 9.8, 9.4, 1H), 5.69 (dd, *J* 9.8, 9.4, 1H), 5.59 (dd, *J* 9.8, 8.1, 1H), 5.21 (d, *J* 9.4, 1H), 4.91 (d, *J* 7.7, 1H), 4.71 (d, *J* 11.5, 1H), 4.63 (dd, *J* 12.0, 3.4, 1H), 4.57–4.53 (m, 2H), 4.52 (d, *J* 11.5, 1H), 4.48 (d, *J* 3.4, 1H), 4.39 (d, *J* 11.1, Hz, 1H), 4.19–4.13 (m, 3H), 3.75 –3.68 (m, 2H), 3.57 (dd, *J* 10.7, 9.0, 1H), 3.42 (dd, *J* 9.4, 9.0, 1H), 3.07 (s, 3H), 1.81 (s, 3H); LC-MS ($C_{57}H_{55}NO_{15}$) calc. [M+H$^+$], 994.4, [M − MeO$^-$], 962.4; found 994.9, 962.8.

Communication a908446k

Enhanced cell binding using liposomes containing an artificial carbohydrate-binding receptor

Yvonne R. Vandenburg,[a] Zhi-Yi Zhang,[a] Douglas J. Fishkind[b] and Bradley D. Smith*[a]

[a] *Department of Chemistry and Biochemistry, University of Notre Dame, Notre Dame, IN 46556-5670, USA. E-mail: smith.115@nd.edu*

[b] *Department of Biological Sciences, University of Notre Dame, Notre Dame, IN 46556-5670, USA*

Received (in Columbia, MO, USA) 7th October 1999, Accepted 1st December 1999

Liposomes containing phospholipids bearing a sugar-binding boronic acid group exhibit enhanced binding to erythrocyte cells.

There is a need to develop liposomes that selectively self-assemble,[1] or interact with specific cell-types,[2] as this will likely lead to improved delivery systems and imaging agents.[3,4] The standard approach is to embed in the liposome membrane high molecular weight, biotic receptors (*e.g.* lectins) that have a selective affinity for cell-surface ligands, or conversely, to coat the liposome exterior with small ligands (*e.g.* folate) that bind selectively to receptor-containing cells.[5] If there is no natural binding partner for a desired cell-surface target then the only alternative is to construct an immunoliposome,[6] or perhaps a liposome coated with a rationally-designed synthetic receptor.†

Here we evaluate the cell-binding ability of a liposome system that contains phospholipids bearing a boronic acid. Over the last ten years a large number of boronic acid host compounds have been prepared and evaluated as synthetic saccharide-binding receptors.[13,14] In general, simple arylboronic acids have modest affinities ($K_a \sim 10$–10^4 M^{-1}) for saccharides containing a vicinal *cis*-diol. Since virtually all cell membranes include glycoproteins and/or glycolipids,[15,16] it is reasonable to expect that compounds containing boronic acid groups will bind to cell surfaces.[17] We find that liposomes containing the phospholipid–boronic acid conjugate DOPEBA have enhanced affinity for erythrocyte ghosts (red blood cells) as compared to related control liposomes that contain DOPEB, a structurally similar phospholipid that lacks a boronic acid residue.‡

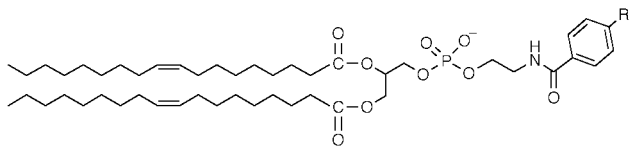

DOPEBA (R = B(OH)$_2$)
DOPEB (R = H)

Erythrocytes are the simplest and best characterized human cells.[16] They are good models for binding and fusion studies since they cannot undergo endocytosis. Liposome-cell binding and membrane fusion were monitored using fluorescently labelled liposomes containing 0.3% of the phospholipid probe NBD-PE [*N*-(7-nitro-2,1,3-benzoxadiazol-4-yl)phosphatidylethanolamine] and its resonance energy transfer quencher Rh-PE [*N*-(lissamine rhodamine B sulfonyl)phosphatidylethanolamine].[19] Two measurements are listed in Table 1, the percentage of liposomes bound to the erythrocyte ghosts, and the percentage of the bound liposomes that appear to undergo lipid mixing with the erythrocyte membranes. These values were determined using a centrifugation method to separate the cell-bound liposomes from unbound liposomes.[20] NBD-PE/Rh-PE labeled liposomes (100 nmol) and erythrocyte ghosts (5×10^8 cells) were incubated for 40 min at 37 °C in 150 μl of EDTA containing MOPS buffered saline, pH 7.4, then the mixture was centrifuged at 6000 rpm. The pellet was suspended in buffer solution and liposome binding was determined from the Rh-PE fluorescence intensity in the presence of 0.2% $C_{12}E_8$ (octaethylene glycol monododecyl ether). The fluorescence of ghosts alone in the presence of 0.2% $C_{12}E_8$ was used as 0% binding while the fluorescence of a freshly prepared liposome–ghost mixture (no incubation and spin) in the presence of $C_{12}E_8$ was taken as 100% binding. The percent of cell-bound liposomes that subsequently underwent lipid mixing with the unlabelled erythrocyte ghosts was determined from the increase in NBD-PE fluorescence which was initially attributed to dilution of the NBD-PE/Rh-PE probes. The NBD-PE fluorescence for a freshly prepared liposome–ghost mixture (without incubation and spin) was measured in the presence and absence of 0.2% $C_{12}E_8$ to determine the 100 and 0% lipid mixing, respectively. The values listed in Table 1 were calculated using the formula described by Shangguan.[20]

The erythrocyte binding and subsequent lipid mixing of 4:1 DOPEBA/POPC (1-palmitoyl-2-oleoyl-*sn*-glycero-3-phosphocholine) liposomes was compared to 4:1 DOPEB/POPC liposomes, in the presence and absence of competing sodium D-glucarate or 4-carboxyphenylboronic acid.§ As described in Table 1, only 3% of the DOPEB/POPC (4:1) liposomes were bound to the erythrocytes at neutral pH, which is in agreement with another study on related liposome systems.[20] In the case of DOPEBA/POPC (4:1) liposomes, about 33% were erythrocyte-bound. Addition of 10 mM glucarate decreased this number by half, whereas addition of 10 mM 4-carboxyphenylboronic acid had no measurable effect. It appears that binding of dianionic glucarate to the surface of DOPEBA/POPC (4:1) liposomes makes them more negatively charged and decreases their affinity for the negatively charged surfaces of glycosylated erythrocyte cells. The inability of 4-carboxyphenylboronic acid to affect liposome-erythrocyte binding is likely an example of

Table 1 Binding and apparent lipid mixing of labelled liposomes with unlabelled erythrocytes

Liposomes	Additive	Liposomes bound to cells[a] (%)	Apparent lipid mixing[ab] (%)
DOPEBA/ POPC (4:1)	none	33	18
	sodium D-glucarate	17	19
	4-carboxyphenyl boronic acid	34	15
DOPEB/ POPC (4:1)	none	3	26
	sodium D-glucarate	3	25
	4-carboxyphenyl boronic acid	3	22

[a] Each value is the average of six runs, uncertainty ± 3%. [b] Percentage of cell-bound liposomes that appear to undergo lipid mixing.

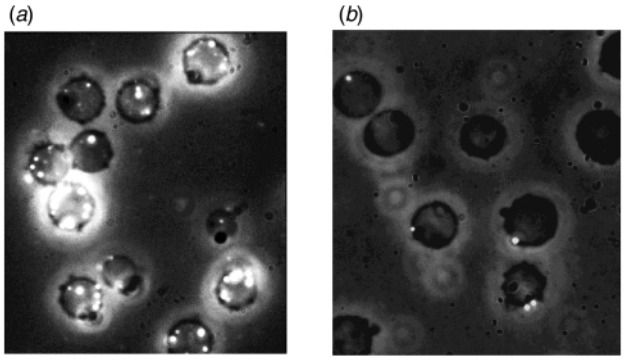

Fig. 1 Fluorescence and phase microscopy co-illumination images of Rh-PE containing liposomes bound to erythrocyte ghosts after a 10 min incubation followed by four wash cycles. The large dark circles are erythrocyte ghosts and the bright fluorescent dots are labelled liposomes. (*a*) DOPEBA/POPC (4:1) liposomes; (*b*) DOPEB/POPC (4:1) liposomes.

multivalency, where the binding constant for a monovalent boronic acid compound to the erythrocyte surface is quite weak, but the binding of a liposome that presents a partially organized array of boronic acid groups is much stronger. As expected, addition of glucarate or 4-carboxyphenylboronic acid had no effect on the binding of control DOPEB/POPC (4:1) liposomes (Table 1).

About 18% of the erythrocyte-bound DOPEBA/POPC (4:1) liposomes and 24% of the bound DOPEB/POPC (4:1) liposomes appeared to undergo lipid mixing (Table 1). Since the NBD-PE/Rh-PE lipid mixing assay is known to be susceptible to artefacts,[23,24] we decided to confirm binding and lipid mixing using a more direct method, namely, fluorescence microscopy.[20,25] In agreement with the binding data listed in Table 1, significantly more DOPEBA/POPC (4:1) liposomes were bound to the erythrocyte cells than control DOPEB/POPC (4:1) liposomes (Fig. 1). However, the fluorescence imaging showed no evidence for any lipid mixing (*i.e.* no evidence for the transfer of NBD-PE or Rh-PE probes from the liposomes to the erythrocytes),[20] which contrasts with the bulk solution data (Table 1). It appears that the increase in NBD-PE fluorescence seen in the bulk solution assay is not due to lipid mixing but is an artefact most likely due to liposome binding to the glycosylated structures on the cell surface. This result demonstrates the importance of using an alternative method to confirm the conclusions derived from lipid mixing assays.[23,24] Finally, we note that fluorescence imaging studies using liposomes filled with the water soluble dye, sulforhodamine B, produced no detectable evidence for enhanced delivery of liposomal contents.

Overall, the data is rationalized in terms of the following binding model. Unlike the DOPEB-containing liposomes, the DOPEBA-containing liposomes are able to bind strongly to the glycocalyx that projects from the erythrocyte cellular membrane. However, the DOPEBA-containing liposomes are still a significant distance from the erythrocyte membrane surface and there is no decrease in the energetic barrier to liposome–erythrocyte membrane adhesion and subsequent fusion.

The development of surface functionalized liposomes that bind to specific target cells appears to be feasible using current supramolecular technology.[2,7–12] A more difficult undertaking is the invention of structures that induce membrane fusion and thus facilitate drug delivery. Our initial efforts to address this problem will be published shortly.[26] This work was supported by the National Institutes of Health and the University of Notre Dame (Molecular Biosciences fellowship to Y. R. V.).

Notes and references

† There appears to be no previous report of enhanced cell-binding using a liposome coated with a rationally designed synthetic receptor. However, there are examples of artificial receptors enhancing small molecule recognition (ref. 7), liposome aggregation (ref. 8), and the binding and fusion of two different liposome populations (ref. 9). Also, the molecular recognition of monolayer surfaces using abiotic receptors and abiotic ligands is an active research area (refs. 10–12).

‡ The synthesis of DOPEBA has been reported before (ref. 18). DOPEB was prepared by treating dioleoylphosphatidylethanolamine with benzoyl cyanide. *Selected data* for DOPEB: δ ($CDCl_3$) 8.05 (s, 1H, N*H*), 7.86 (d, 2H, Ar*H*, *J* 7.2), 7.29–7.38 (m, 3H, Ar*H*), 5.27–5.39 (m, 4H, 2C*H*=C*H*), 5.13 (m, 1H, $POCH_2CH$), 4.27 (d, 1H, $POCH_2$), 3.83–4.04 (m, 5H, CH_2O-$POCH_2CHCH_2$), 3.60 (m, 2H, $NHCH_2$), 2.18 (t, 4H, $2COCH_2$, *J* 7.5), 2.00 (m, 8H, $2CH_2CH{=}CHCH_2$), 1.49 (m, 4H, $2COCH_2CH_2$), 1.26 [s br, 40H, $2COCH_2CH_2(CH_2)_4$ and $2(CH_2)_6CH_3$], 0.87 (t, 6H, $2CH_3$, *J* 6.6); HRMS (FAB) calc. for $C_{48}H_{81}O_9PNNa_2$ 892.5444, found 892.5475.

§ The liposomes were prepared by extrusion through polycarbonate filters as previously described (ref. 18). In each case, unilamellar vesicles (~100 nm diameter) were formed as determined by dynamic light scattering, encapsulation of aqueous contents, and lamellarity assays (ref. 21). Control experiments with liposomes containing NBD-PE/Rh-PE showed that the liposomes do not undergo significant morphology changes in the presence of sodium D-glucarate or 4-carboxyphenylboronic acid. This is in contrast to results obtained with non-liposomal aggregates of neutral and cationic amphiphiles with appended boronic acids (ref. 22).

1 S. A. Walker, M. Kennedy and J. Zasadzinski, *Nature*, 1997, **387**, 61.
2 N. Yagi, Y. Ogawa, M. Kofaka, T. Okada, T. Tomhiro, T. Konakahara and H. Okuno, *Chem. Commun.*, 1999, 1687.
3 D. D. Lasic, *Liposomes in Gene Delivery*, CRC, Boca Raton, 1997.
4 D. D. Lasic, *Liposomes: from Physics to Applications*, Elsevier, Amsterdam, 1993, ch. 18.
5 F. Schuber, A. Kichler, C. Boekler and B. Frisch, *Pure Appl. Chem.*, 1998, **70**, 89.
6 T. M. Allen, C. B. Hansen and S. Zalipsky, in *Stealth Liposomes*, ed. D. Lasic and F. Martin, CRC Press, Boca Raton, 1995, ch. 20.
7 Y. Murakami and O. Hayashida, *Proc. Natl. Acad. Sci. U.S.A.*, 1993, **90**, 1140.
8 E. C. Constable, W. Meier, C. Nardin and S. Mundwiler, *Chem. Commun.*, 1999, 1483.
9 V. Marchi-Artzner, L. Jullien, T. Gulik-Kryzwicki and J.-M. Lehn, *Chem. Commun.*, 1997, 117.
10 K. Ariga and T. Kunitake, *Acc. Chem. Res.*, 1998, **31**, 371.
11 D. Berti, L. Franchi, P. Baglioni and P. L. Luisi, *Langmuir*, 1997, **13**, 3438.
12 M. Weck, R. Fink and H. Ringsdorf, *Langmuir*, 1997, **13**, 3515.
13 B. D. Smith, *Supramol. Chem.*, 1996, **7**, 55.
14 T. D. James, K. R. A. S. Sandanayake and S. Shinkai, *Angew. Chem., Int. Ed. Engl.*, 1996, **35**, 1910.
15 H. R. Petty, *Molecular Biology of Membranes*, Plenum, New York, 1993.
16 E. A. Repasky and C. C. Gregorio, in *The Structure of Biological Membranes*, ed. P. Yeagle, CRC Press, Boca Raton, 1991, ch. 10.
17 T. J. Burnett, H. C. Peebles and J. H. Hageman, *Biochem. Biophys. Res. Commun.*, 1980, **96**, 157.
18 Z. Zhang and B. D. Smith, *J. Am. Chem. Soc.*, 1998, **129**, 7141.
19 A. L. Bailey and P. R. Cullis, *Biochemistry*, 1997, **36**, 1628.
20 T. Shangguan, C. C Pak, S. Ali, A. S. Janoff and P. Meers, *Biochim. Biophys. Acta*, 1998, **1368**, 171.
21 H. J. Gruber and H. Schindler, *Biochim. Biophys. Acta*, 1994, **1189**, 212.
22 T. Kimura, M. Takeuchi and S. Shinkai, *Bull. Chem. Soc. Jpn.*, 1998, **71**, 2197.
23 N. Düzgünes, T. M. Allen, J. Fedor and D. Papahadjopoulos, *Biochemistry*, 1987, **26**, 8435.
24 D. Hoekstra and N. Düzgünes, *Methods Enzymol.*, 1993, **220**, 15.
25 D. J. Fishkind, L. Romenskaia, Y. Bao, and C. M. Manubay, in *The Cytoskeleton and Signaling: A Practical Approach*, ed. K. L. and C. A. Carraway, Oxford University Press, Oxford, 1999, ch. 6.
26 Z. Zhang and B. D. Smith, unpublished work.

Communication a908142i

ChemComm

Catalytic production of urethanes from amines and alkyl halides in supercritical carbon dioxide

Masaaki Yoshida,* Namiko Hara and Sanae Okuyama

Applied Chemistry, Faculty of Engineering, Utsunomiya University, Utsunomiya 321-8585, Japan.
E-mail: yoshidam@cc.utsunomiya-u.ac.jp

Received (in Cambridge, UK) 5th November 1999, Accepted 7th December 1999

Some common onium salts catalysed selective urethane production from amines and alkyl halides in supercritical carbon dioxide, which acted not only as an alternative to organic solvents but also as a phosgene replacement; the reaction efficiency was 50–100 times higher than that attained in heptane.

The most widely utilized method for the synthesis of urethanes uses highly toxic phosgene as a reagent in organic solvents, which are also toxic and flammable. Therefore the conventional method involves environmental and safety problems.

Owing to the above mentions, much effort has been directed toward alternative routes for preparation of urethanes using carbon dioxide as a phosgene replacement.[1–8] Carbon dioxide is well known to react rapidly with amines to form carbamic acid ammonium salts.[9] However, as the nucleophilicity of the carbamate anion is lower than that of the amine formed in the equilibrium of the salt formation reaction, the reaction of the carbamate salts with alkyl halides does not selectively afford urethanes.[2] So, the activation of the carbamate anion was attempted by addition of crown ethers[5] and strong bases.[4] Monsanto's chemists have achieved a highly selective urethane synthesis process using very strong bases (*e.g.* CyTMG: *N*-cyclohexyl-*N′*,*N′*,*N″*,*N″*-tetramethylguanidine).[7] However, because a stoichiometric amount of CyTMG was necessary in the reaction, the Monsanto process could not replace the conventional method.

We have successfully synthesized urethanes in high yields from amines, alkyl halides, potassium carbonate and a catalytic amount of an onium salt in supercritical carbon dioxide ($scCO_2$) [eqn. (1)]. Supercritical carbon dioxide is an attractive

$$R^1R^2NH + R^3X + K_2CO_3 \xrightarrow[scCO_2]{\text{onium salt}} R^1R^2NCOOR^3 \quad (1)$$

alternative to organic solvents as it is environmentally benign, essentially nontoxic, inexpensive, nonflammable and has relatively low critical conditions (P_c = 73 atm, T_c = 31 °C).†

The results of the one-pot urethane production are summarized in Table 1. Not only aliphatic primary and secondary amines but also aromatic amines reacted well. As these are catalytic reactions, the low yields should be improved by increasing the amount of catalyst or extending the reaction time.

The effect of catalyst on the conversion of a pyrrolidine, butyl chloride and potassium carbonate system in $scCO_2$ is given in Table 2. The reaction could be catalysed by amonium salts and a phosphonium salt. Among these, the catalysts that afforded the best results were tetrabutylammonium bromide and trioctylammonium chloride, which are commonly used in industry.

Sanchez and co-workers also reported a phosgene-replaced urethane synthesis in heptane using amines, alkyl halides, potassium carbonate and tetrabutylammonium hydrogensulfate, as a solid/liquid phase-transfer reagent, without any additional carbon dioxide.[3] In their system, the carbonyl source was potassium carbonate. In order to determine the carbonyl source in our system, we tried a reaction in $scCO_2$ with pyrrolidine, butyl chloride and potassium phosphate in place of potassium carbonate. From the resulting 98% yield of urethane, it was confirmed that $scCO_2$ acts not only as a solvent but also as a direct starting material for the urethane in our reaction system.[10]

Consequently, the mechanism of the reaction could be explained as follows (Scheme 1). First, the amine readily forms the carbamic acid ammonium salt upon the introduction of liquid carbon dioxide. The salt starts to dissolve in $scCO_2$ as the temperature increases. At the reaction temperature (100 °C), the ion exchange reaction takes place between the carbamate salt and tetrabutylammonium bromide. As a result, the carbamate anion is activated by the tetrabutylammonium ion and readily reacts with alkyl halide to form urethane and potassium halide in the presence of potassium carbonate. At the same time, tetrabutylammonium bromide is regenerated to complete the catalytic reaction cycle. If tetrabutylammonium bromide is absent, the amine formed by the reverse reaction of the equilibrium of the carbamate salt formation attacks alkyl halide

Table 1 Bu_4NBr catalysed urethane production from R^1R^2NH, R^3X and K_2CO_3 in $scCO_2$[a]

R^1	R^2	R^3X	Bu_4NBr/mol%	*t*/h	Yield (%)[b]
	$-(CH_2)_4-$	BuCl	5	2	quant. (85)
	$-(CH_2)_4-$	$CH_3(CH_2)_7Cl$	5	2	76
	$-(CH_2)_4-$	Bu^sBr	5	2	73
	$-(CH_2)_5-$	BuCl	5	2	quant. (85)
	$-(CH_2)_2O(CH_2)_2-$	BuCl	15	2	72 (62)
Me	Me	BuCl	5	2	86 (81)
Et	Et	BuCl	5	2	90 (82)
Bu	Bu	BuCl	5	2	74
C_6H_{11}	C_6H_{11}	BuCl	5	2	72
Ph	Me	BuCl	5	2	quant. (94)
Bu	H	BuBr	5	1	quant. (90)
CH_2=$CHCH_2$	H	BuBr	5	1	quant. (90)
Bn	H	BuBr	5	1	91 (85)
Ph	H	BuCl	20	4	75

[a] Reaction was conducted at 100 °C, 80 atm in a 50 ml stainless steal autoclave containing amine (5 mmol), alkyl halide (8 mmol) and K_2CO_3 (10 mmol). [b] Estimated by ^{1}H NMR, isolated yield in parentheses.

Table 2 Effect of catalyst on conversion of pyrrolidine, butyl chloride and K_2CO_3 in $scCO_2$[a]

Catalyst	Yield (%)[b]
Bu_4NHSO_4	69
Bu_4NBr	74
Bu_4NI	51
Bu_4PBr	48
$[CH_3(CH_2)_{15}NMe_2Et]Br$	66
$[CH_3(CH_2)_7]_3MeNCl$	73

[a] Reaction was conducted at 100 °C, 80 atm in a 50 ml stainless steal autoclave containing pyrrolidine (5 mmol), butyl chloride (6 mmol), K_2CO_3 (10 mmol) and catalyst (0.5 mmol) without stirring for 2 h. [b] Estimated by ^{1}H NMR.

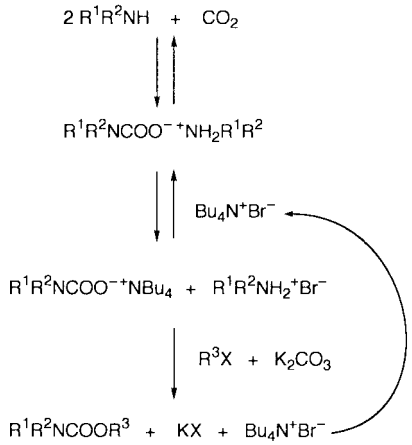

Scheme 1

to form highly alkylated amines, and as a result the selectivity of the urethane formation decreases.

Our reaction system is the first example of catalytic urethane production. Also we found that the efficiency of the reaction in $scCO_2$ is 50–100 times higher than that attained in heptane. Indeed, the urethane yield was less than 2% with pyrrolidine and butyl chloride, and less than 1% with butylamine and butyl bromide, in heptane.

In conclusion, we have achieved catalytic one-pot urethane synthesis from amines and alkyl halides in supercritical carbon dioxide and also achieved a phosgene replacement and organic solvent replacement by using common onium salts as catalysts. Our process is environmentally benign and also has benefits economically.

Notes and references

† *Typical experimental procedure*: For carrying out the reactions in $scCO_2$, a 50 ml stainless steel autoclave (Taiatsu Techno portable reactor TVS-N2) was used. Potassium carbonate (10 mmol), tetrabutylammonium bromide (0.25 mmol), pyrrolidine (5 mmol) and butyl chloride (8 mmol) were successively placed in the reaction vessel. The vessel was sealed and then liquid carbon dioxide (*ca.* 12.3 g) was introduced from a cylinder at room temperature. The reaction system was heated with a boiling water bath (*ca.* 100 °C). The pressure of the mixture reached *ca.* 80 atm and the mixture was stirred magnetically for 2 h. In completion, the reaction vessel was cooled with an ice bath and the pressure was released slowly to atmospheric pressure. The residual mixture was extracted with chloroform and the yields of urethane were estimated by ^{1}H NMR.

1 T. Tsuda, H. Washita, K. Watanabe, M. Miwa and T. Saegusa, *J. Chem. Soc., Chem. Commun.*, 1978, 815; T. Tsuda, K. Watanabe, K. Miyata, H. Yamamoto and T. Saegusa, *Inorg. Chem.*, 1981, **20**, 2728.
2 Y. Yoshida, S. Ishii and T. Yamashita, *Chem. Lett.*, 1984, 1571; Y. Yoshida, S. Ishii, M. Watanabe and T. Yamashita, *Bull. Chem. Soc. Jpn.*, 1989, **62**, 1534.
3 V. G. Parra, F. Sanchez and T. Torres, *Synthesis*, 1985, 282.
4 Y. Hori, Y. Nagano, J. Nakao, T. Fukuhara and H. Taguchi, *Chem. Express*, 1986, **1**, 224.
5 M. Aresta and E. Quaranta, *J. Org. Chem.*, 1988, **53**, 4153; M. Aresta and E. Quaranta, *J. Chem. Soc., Dalton Trans.*, 1992, 1893; M. Aresta and E. Quaranta, *Tetrahedron*, 1992, **48**, 1515.
6 K. J. Butcher, *Synthesis*, 1994, 825.
7 W. D. McGhee, B. L. Parnas, D. P. Riley and J. J. Talley, U.S. Patent No. 5,223,638, June 29, 1993; W. McGhee, Y. Pan and D. P. Riley, *J. Chem. Soc., Chem. Commun.*, 1994, 699; W. McGhee, D. P. Riley, K. Christ, Y. Pan and B. Parnas, *J. Org. Chem.*, 1995, **60**, 2820.
8 A. Inesi, V. Mucciante and L. Rossi, *J. Org. Chem.*, 1998, **63**, 1337.
9 J. T. Edsall, *Biophysical Chemistry*, Academic Press, New York, 1958, vol. 1, 571.
10 We also tried the reaction without potassium carbonate in $scCO_2$, and the urethane was obtained in a yield of 8%.

Communication a908819i

Keggin unit supported transition metal complexes: hydrothermal synthesis and characterization of $[Ni(2,2'\text{-bipy})_3]_{1.5}[PW_{12}O_{40}Ni(2,2'\text{-bipy})_2(H_2O)]\cdot 0.5H_2O$ and $[Co(1,10'\text{-phen})_3]_{1.5}[PMo_{12}O_{40}Co(1,10'\text{-phen})_2(H_2O)]\cdot 0.5H_2O$

Yan Xu,[a,b] Ji-Qing Xu,*[b] Kou-Lin Zhang,[a] Yong Zhang[a] and Xiao-Zeng You*[a]

[a] *Coordination Chemistry Institute, State Key Laboratory of Coordination Chemistry, Nanjing University, Nanjing, 210093, P.R. China. E-mail: SKLC@nju.edu.cn*

[b] *Department of Chemistry, Jilin University, Changchun, 130023, P.R. China*

Received (in Cambridge, UK) 26th October 1999, Accepted 9th December 1999

Two new Keggin unit supported transition metal complexes, $[Ni(2,2'\text{-bipy})_3]_{1.5}[PW_{12}O_{40}Ni(2,2'\text{-bipy})_2(H_2O)]\cdot 0.5H_2O$ 1 and $[Co(1,10'\text{-phen})_3]_{1.5}[PMo_{12}O_{40}Co(1,10',\text{-phen})_2(H_2O)]\cdot 0.5H_2O$ 2, are synthesized by a hydrothermal method; complex 1 is characterized by X-ray crystallography, showing that the $[Ni(2,2'\text{-bipy})_2(H_2O)]^{2+}$ units are covalently bonded to the α-Keggin cluster $[PW^{V}_2W^{VI}_{10}O_{40}]^{5-}$.

There is considerable current interest in metal–oxo cluster compounds reflecting their diverse properties, with applications to sorption clathration, catalysis, electrical conductivity, magnetism and photochemistry.[1–11] Recently an important advance in transition metal oxide cluster chemistry has been study of polyanions substituted by transition-metal and polyoxoanion-supported inorganic or organometallic complexes.[12–20] Structures determined included $[\{Cu(4,4'\text{-bipy}\}_4(Mo_8O_{26})]$[16] and $[\{Cu(en\}_2(Mo_8O_{26})]$,[17] which possess infinite extended structures, $[La(Mo_8O_{26})_2]^{5-}$,[18] a molecular cluster and the organometallic compounds $[(CO)_3Mn(cis\text{-}Nb_2W_4O_{19})]$[19] and $[\{(C_5Me_5)Rh\}_2(Mo_{13}O_{40})]^{2+}$,[20] which have discrete cluster structures.

Here, we reported the hydrothermal synthesis and characterization of a α-Keggin heteropoly anion-supported nickel–bipyridyl and cobalt–phenanthroline complexes, $[Ni(2,2'\text{-phen})_3]_{1.5}[PW_{12}O_{40}Ni(2,2'\text{-bipy})_2(H_2O)]\cdot 0.5H_2O$ **1** and $[Co(1,10'\text{-phen})_3]_{1.5}[PMo_{12}O_{40}Co(1,10'\text{-phen})_2(H_2O)]\cdot 0.5H_2O$ **2**. No previous structural examples of transition metal complexes coordinated to Keggin anions have been reported. The structure determination of $[PW_{12}O_{40}Ni(2,2'\text{-bipy})_2(H_2O)]^{3-}$ in **1** indicates a novel α-Keggin heteropolyanion coordinated to a transition metal complex.

Compound **1** was synthesized as black blocks in 34% yield based on W (0.37 g) by a hydrothermal method. A mixture of $Ni(OAc)_2$ (0.4 g), Na_2WO_4 (1.0 g), 2,2′-bipyridine (0.4 g), and water (10 ml) was neutralized to pH = 4.0 with 50% H_3PO_3 and sealed in a 15 cm^{-1} Teflon-lined reactor, which was heated to 160 °C for seven days. After cooling to room temperature, black block crystals were isolated. The IR spectrum of **1** exhibited an intense band at 950 cm^{-1}, attributed to ν(W=O), and features at 1595, 1475, 1432 and 1309 cm^{-1} characteristic of 2,2′-bipyridine, bands at 1060 and 1090 cm^{-1}, can be attributed ν(P–O). Black prism crystals of **2** (0.30 g, yield 30% based on Mo) were obtained under the same reaction conditions using $CoCl_2$ (0.4 g), Na_2MoO_4 (0.8 g) and 1,10′-phenanthroline (0.4 g). Compound **2** was characterized by elemental analyses† and IR spectroscopy, while compound **1** was characterized by elemental analyses IR spectroscopy and single-crystal analyses.‡ Compounds **1** and **2** were soluble in DMF but not in water.

Crystals of **1** contain $[PW^{VI}_{10}W^{V}_2O_{40}Ni(2,2'\text{-bipy})_2(H_2O)]^{3-}$ heteropoly anions and $[Ni(2,2'\text{-biby})_3]^{2+}$ cations. As shown in Fig. 1, the novel anion $[PW_{12}O_{40}Ni(2,2'\text{-bipy})_2(H_2O)]^{3-}$ consists of a reduced Keggin heteropolyanion $[PW^{VI}_{10}W^{V}_2O_{40}]^{5-}$ and the cation $[Ni(2,2'\text{-bipy})_2(H_2O)]^{2+}$. As in other Keggin structures,[1] the reduced polyanion is formed from twelve WO_6 octohedra and one PO_4 tetrahedron. For PO_4, the P–O distances are 1.509(5)–1.565(5) Å while the O–P–O angles vary from 108.8(3) to 111.1(3)°. The W–O distances can be grouped into three sets: W–O_t 1.677(5)–1.727(5), W–O_b 1.780(4)–1.957(5), W–O_a, 2.378(5)–2.467(5), while bond angles at the W atoms range from 70.8(2) to 103.2(3)°. In comparison with other Keggin polyanions,[1] the unusual feature here is that the Keggin structural unit $[PW^{VI}_{10}W^{V}_2O_{40}]^{5-}$ acts as a ligand towards Ni^{2+}, to give a novel transition metal anion. A μ-oxygen, O(29) links the Keggin unit and Ni(3), the [W(12) –O(29) 1.780(4) Å, O(29)–Ni(3) 2.010(4) Å, Ni(3)–O(29)–W(12) 160.6(3], the W(12)–O(29) distance is longer than the other W–O_t bond lengths but shorter than W–O_b. In the polyanion, the Ni atom is coordinated by two 2,2′-bipy, one water molecule and one Keggin unit, with Ni–OW(1) 2.140(6) Å and Ni–N 2.072(7)–2.106(6) Å. The coordinated water

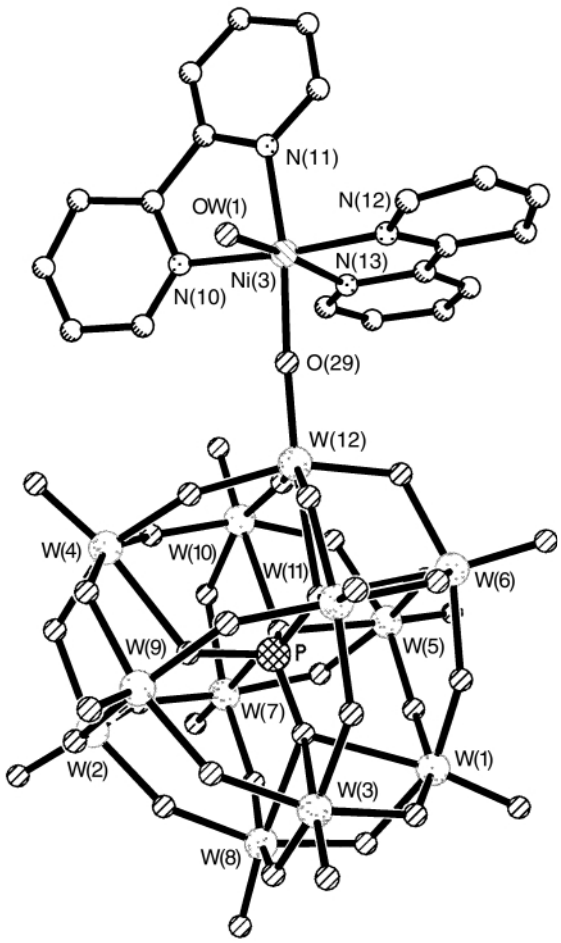

Fig. 1 The structure of the Keggin unit supported transition complex anion $[PW^{VI}_{10}W^{V}_2O_{40}Ni(2,2'\text{-bipy})_2(H_2O)]^{3-}$ in **1**.

molecule [OW(2) and its symmetry-related partner] link different polyanions by hydrogen bonding, to form a supramolecular assembly [Ow(2)··O(17a)(−*x*,1−*y*,1−*z*) 2.768(12) Å]. In each unit of **1**, the water molecules and heteropolyanion are involved in hydrogen bonding interactions, with OW(2)··OW(1) and OW(1)··O(29) 2.810(11) and 2.934(12) Å, respectively. In the cation $[Ni(2,2'\text{-bipy})_3]^{2+}$ of **1**, Ni is coordinated by three 2,2′-bipy molecules, with Ni–N 1.966(7)–2.102(6) Å. There are two W^V centres in the Keggin unit of **1**, and the assignment of the oxidation state for the W atoms is consistent with the electric charge and confirmed by bond valence sum calculations. Using an empirical bond valence calculation,[21] $S = \exp[-(R - 1.898)/0.315]$ (S = bond valence, R = bond length), leads to S values for W(1), W(2), W(3), W(4), W(5), W(6), W(7), W(8), W(9), W(10), W(11) and W(12) of 5.788, 5.950, 5.750, 6.081, 6.04, 5.786, 5.751, 6.060, 5.590, 5.946, 6.070 and 5.577, respectively. The average value for the calculated oxidation state of W is 5.866 (expected value 5.833 for $W^{VI}_{10}W^{V}_{2}$), consistent with the formula of **1**. Absorption of 600–2000 nm in the reflectance UV–VIS spectrum can be ascribed to d–d transitions and electron transitions between W^V and W^{VI} centres. Only a Ni^{2+} signal was observed (g = 2.013) in the room temperature EPR spectrum of **1**, the lack of signals for W^V indicate that the two unpaired electrons of the Keggin unit are delocalised.[1]

This work was supported by the National Science Foundation of China(29733090) and State Key Project of Fundanental and the National Nature Science Foundation of China.

Notes and references

† Anal. Calc. for $W_{12}Ni_{2.5}PO_{41.5}N_{13}C_{65}H_{55}$ **1**: W, 54.01; Ni, 3.61; P, 0.76; C, 19.18; N, 4.48; H, 1.35. Found : W, 53.74; Ni, 3.42; P, 0.84; C, 19.39; N, 4.52; H, 1.31%. Calc. for $Mo_{12}Co_{2.5}PO_{41.5}N_{13}C_{78}H_{55}$ **2**: Mo, 36.36; Co, 4.65; P, 0.98; C, 29.55; N, 5.75; H, 1.74. Found : Mo, 36.06; Co, 4.56; P, 1.03; C, 29.50; N, 5.69; H, 1.79%.

‡ *Crystal data*: diffraction data for **1** were collected on a crystal with dimensions 0.38 × 0.21 × 0.21 mm using a Siemens P4 diffractometer and Mo-Kα radiation, at 193 K. Monoclinic, space group $C2/c$, a = 46.768(9), b = 14.340(3), c = 25.945(5) Å, β = 90.21(3)°, Z = 8, D_c = 3.114 g cm^{-3}. Of 14314 data collected ($2\theta_{max}$ = 23.02°). 12113 were independent (R_{int} = 3.11%) and 7841 were observed [$2\sigma(I)$]. An empirical absorption correction from ψ-scans was applied (μ = 16.434 mm^{-1}). All metal, P, O and N atoms atoms were refined anisotropically, while all C atoms were refined isotropically, R_1 = 0.0732, R_w = 0.1827 for 891 parameters. CCDC 182/1504. See http://www.rsc.org/suppdata/cc/a9/a908527k/ for crystallographic files in .cif format.

1 M. T. Pope, *Herteropoly and Isopoly Oxometalates*, Springer-Verlag, Berlin, 1983.
2 V. W. Day and W. G. Klemperer, *Science*, 1985, **228**, 533.
3 M. T. Pope and A. Müller, *Angew. Chem., Int. Ed. Engl.*, 1991, **30**, 34.
4 M. T. Pope and A. Muller, *Polyoxometalates: From Platonic Solids to Anti-Retroviral Activity*, Kluwer Academic Publishers, Dordrecht, The Netherlands, 1994.
5 C. L. Hill, *Chem. Rev.*, 1998, **98**, 1.
6 L. C. W. Baker and D. C. Glick, *Chem. Rev.*, 1998, **98**, 3.
7 Y. P. Jeannin, *Chem. Rev.*, 1998, **98**, 51.
8 P. Gouzerh and A. Proust, *Chem. Rev.*, 1998, **98**, 77.
9 N. Mizuno and M. Misono, *Chem. Rev.*, 1998, **98**, 199.
10 A. Müller, F. Peters, M. T. Pope and D. Gatteschi, *Chem. Rev.*, 1998, **98**, 239.
11 E. Coronado and C. J. Gómez-García, *Chem. Rev.*, 1998, **98**, 273.
12 T. J. R. Weakley, *J. Crystallogr. Spectrosc. Res.*, 1987, **17**, 383.
13 H. T. Evans, Jr. C. Tourme, G. Tourme and T. J. R. Weakley, *J. Chem. Soc., Dalton Trans*, 1986, 2699.
14 J. M. Clemente-Juan, E. Coronado, J. R. Galàn-Mascarós and C. J. Gómez-García, *Inorg. Chem.*, 1999, **38**, 55.
15 J. Q. Xu, R. Z. Wang and G. Y. Yang, *Chem. Commun.*, 1999, 815.
16 D. Hagraman, C. Zubieta, D. J. Rose, J. Zubieta and R. C. Haushalter, *Angew Chem., Int. Ed. Engl.*, 1997, **36**, 873.
17 J. R. D. Debord, R. C. Haushalter, L. M. Meyer, D. J. Rose, P. J. Zapf and J. Zubieta, *Inorg. Chim. Acta*, 1997, **256**, 165.
18 Y. Zhang, P. J. Zapf, L. M. Meyer, R. C. Haushalter, D. J. Rose and J. Zubieta, *Inorg. Chem.*, 1997, **36**, 2159.
19 A. Kitamuura, T. Ozeki and A. Yagasaki, *Inorg. Chem.*, 1997, **36**, 4285.
20 C. J. Besecher, V. W. Day, W. G. Klemperer and T. A. Eberspacher, *Inorg. Chem.*, 1992, **31**, 3187.
21 I. D. Brown and D. Altermatt, *Acta Crystallogr., Sect. B*, 1985, **41**, 244.

Communication a908527k

Synthesis of Chiraphos *via* asymmetric hydrogenation of 2,3-bis(diphenylphosphinoyl)-buta-1,3-diene

Valentina Beghetto, Ugo Matteoli* and Alberto Scrivanti

Dipartimento di Chimica, Università di Venezia, Calle Larga S. Marta, 2137, 30123 Venezia, Italy.
E-mail: matteol@unive.it

Received (in Liverpool, UK) 20th October 1999, Accepted 1st December 1999

(*S*,*S*)-2,3-Bis(diphenylphosphinoyl)butane, an immediate precursor of (*S*,*S*)-CHIRAPHOS, can be obtained with 70% de and 71% op *via* double asymmetric hydrogenation of 2,3-bis(diphenylphosphinoyl)buta-1,3-diene in the presence of Ru–(*S*)-BINAP catalysts.

Recently, we have described a new strategy for the synthesis of Chiraphos,[1]† a well-known bidentate chiral ligand for asymmetric catalysis. The key step of the synthesis is the diastereoselective hydrogenation of 2,3-bis(diphenylphosphinoyl)-buta-1,3-diene **1** which affords a pair of enantiomers (*R*,*R*)- and (*S*,*S*)-**2** and the *meso* species (*R*,*S*)-**2**. This latter isomer is useless, therefore its formation must be avoided in order to remove the need for a difficult purification step. In the previously reported synthesis,[1] a racemic mixture of (*R*,*R*)- and (*S*,*S*)-**2** was obtained in *ca*. 70% yield by reacting **1** with $NaBH_4$. Using this reducing agent, *ca*. 30% of *meso*-**2** was also produced, but was promptly separated and discarded since it forms an insoluble adduct with one molecule of NaOH and one molecule of $NaBH_4$.[1]

The recent improvements achieved in asymmetric hydrogenation[2] by means of homogeneous chiral transition metal catalysts prompted us to investigate the direct synthesis of enantiopure (*R*,*R*)-**2** or (*S*,*S*)-**2** by hydrogenation of **1** in the presence of an asymmetric catalyst (Scheme 1).

Interest in this subject goes beyond the synthetic application envisaged here since, although a large number of reports concerned with asymmetric reduction of monoenes have been published, only a few examples of asymmetric reduction of dienes have appeared so far.[3] Further interest is added by the peculiar nature of **1**.

Two different Ru-BINAP complexes, *i.e.* [RuCl(*p*-cymene){(*S*)-BINAP}]Cl[4] and $[Ru(OAc)_2\{(S)\text{-BINAP}\}]$,[5] were tested as catalysts. The relevant data, together with the reaction conditions, are reported in Table 1.

The reactions were carried out in a magnetically stirred stainless steel autoclave. The product's composition was determined by NMR spectroscopy, since in previous studies we found that all the species which may form during the reaction (see Scheme 1) give well-separate signals in the ^{31}P NMR spectrum.[1]

When only the stereoisomers of **2** were present into the crude reaction mixture, the enantioselectivity of the reaction was determined by polarimetry on samples recrystallized from benzene/n–hexane to remove the catalyst.[6] In the case of runs 1 and 4, owing to the presence of the chiral intermediate **3**, a catalyst-free sample of the crude reaction mixture was treated with (1*S*)-(+)-camphorsulfonic acid to form *inter alia* the corresponding (*S*,*S*)-**2**–(1*S*)-(+)-camphorsulfonic and (*R*,*R*)-**2**–(1*S*)-(+)-camphorsulfonic adducts. The enantioselectivity of the reaction was then calculated by integration of their relevant resonances in the ^{31}P NMR spectrum.[7]

Both catalysts require rather severe reaction conditions to carry out the hydrogenation. With [RuCl(*p*-cymene){(*S*)-BINAP}]Cl the hydrogenation of **1** proceeds with complete

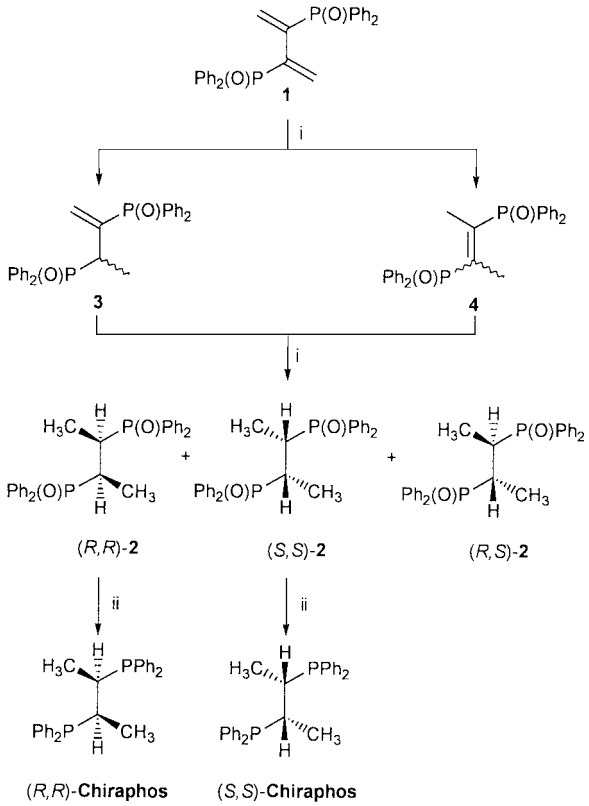

Scheme 1 *Reagents and conditions*: i, H_2, catalyst; ii, $HSiCl_3$, NEt_3.

Table 1 Hydrogenation of 2,3-bis(diphenylphosphinoyl)buta-1,3-diene **1** with Ru–BINAP catalysts[a]

				Yield (%)			
Run	Catalyst	*T*/°C	*t*/h	**3**	(*R*,*S*)-**2**	(*S*,*S*)-**2** + (*R*,*R*)-**2**	Op **2** (%)[b]
1	[RuCl(*p*-cymene){(*S*)-BINAP}]Cl[c]	50	216	53	0	47	0
2	[RuCl(*p*-cymene){(*S*)-BINAP}]Cl[c]	100	120	0	0	100	8
3	$[Ru(OAc)_2\{(S)\text{-BINAP}\}]$[d]	100	67	45	10	45	ND[e]
4	$[Ru(OAc)_2\{(S)\text{-BINAP}\}]$[d]	100	163	18	13	69	68
5	$[Ru(OAc)_2\{(S)\text{-BINAP}\}]$[d]	100	310	—	15	85	71

[a] MeOH (15 ml), substrate (2.0 mmol), $P(H_2)$ = 100 atm. [b] In all cases the prevailing configuration is (*S*,*S*)-**2**. [c] Substrate/Ru = 120. [d] Substrate/Ru = 10. [e] Not determined.

diastereoselectivity since no *meso*-**2** is formed. Surprisingly, operating at 50 °C in the presence of this catalyst, a racemic mixture of **2** is obtained, while working at 100 °C a modest induction is observed (run 2). This rather unusual enhancement of the enantioselectivity on increasing the reaction temperature suggests that different catalytic species are actually at work; an example of such behaviour has been previously reported in the literature.[8]

With [Ru(OCOCH$_3$)$_2$\{(*S*)-BINAP\}] lower reaction rates are obtained. Thus, even at 100 °C and using a substrate/catalyst ratio of 10, long reaction times are necessary to achieve complete hydrogenation of diene **1** (run 5). Most significant is that the reaction proceeds with good diastereo- (de = 70%) and enantio-selectivity [the op of the prevailing (*S*,*S*)-**2** isomer is 71%]. Presumably the P=O bond is acting as a co-ordinating group in the reaction, rather as an amide does in the hydrogenation of acylamino acrylates.[9,10]

Concerning the reaction mechanism, there are two possible pathways for the hydrogenation of the diene **1** (Scheme 1): (i) two consecutive 1,2-hydrogen additions; (ii) an initial 1,4-hydrogen addition to give (*cis* or *trans*) **4** followed by hydrogenation of the remaining double bond.

At shorter reaction times (runs 3 and 4) only **2** and **3** are detected in the reaction mixture, suggesting that the reaction proceeds *via* two consecutive 1,2-hydrogen additions; moreover it appears that the first double bond hydrogenation is faster than the second one. On the other hand, an independent experiment showed that a pure sample of **4**[11] is not hydrogenated in the presence of [Ru(OCOCH$_3$)$_2$\{(*S*)-BINAP\}] under the conditions in Table 1.

In conclusion, even if the process is not yet ready for practical application owing to the incomplete stereoselectivity this work demonstrates the possibility of employing the asymmetric catalysis in the synthesis of a chiral diphosphine. According to this strategy a chiral ligand could be synthesised using another chiral phosphine ligand, thus giving a new example of chiral amplification.

Notes and references

† Chiraphos: 2,3-bis(diphenylphosphino)butane.

1 U. Matteoli, V. Beghetto, C. Schiavon, A. Scrivanti and G. Menchi, *Tetrahedron: Asymmetry*, 1997, **8**, 1403.

2 *Catalytic Asymmetric Synthesis*, ed. I. Ojima, VCH, New York, 1993.

3 H. Muramatstu, H. Kawano, Y. Ishii, M. Saburi and Y. Uchida, *J. Chem. Soc., Chem. Commun.*, 1989, 769.

4 K. Mashima, K. Kusano, T. Ohta, R. Noyori and H. Takaya, *J. Chem. Soc., Chem. Commun.*, 1989, 1208.

5 M. Kitamura, M. Tokunaga and R. Noyori, *J. Org. Chem.*, 1992, **57**, 4053.

6 Polarimetry measurements on different recrystallised samples of **2** have shown that there is no variation in the op due to recrystallisation from benzene–*n*-hexane.

7 The adducts between **2** and (1*S*)-(+)-camphorsulfonic acid were prepared as follows: an 80:20 mixture of **2**:**3** (~500 mg recovered by recrystallisation of a sample of run 4) was dissolved in 10 ml of $CHCl_3$ and the mixture was heated to reflux temperature (mixture A). Separately, 220 mg (0.88 mmol) of (1*S*)-(+)-camphorsulfonic acid were dissolved in 15 ml of EtOAc (mixture B). The hot mixture B was added to mixture A and the system was further heated for 2 min. The crude solid recovered after evaporation of the solvents was characterised by ^{31}P NMR ($CDCl_3$): δ 40.7 (s), 40.4 (s). Signals due to the adducts between **3** and (1*S*)-(+)-camphorsulfonic acid were also present: δ 38.23 (d, $J_{P,P}$ 20.0), 38.21 (d, $J_{P,P}$ 21.0), 35.06 (d, $J_{P,P}$ 21.0), 35.00 (d, $J_{P,P}$ = 20.0). Pure samples of (*S*,*S*)-(−)-**2**–(1*S*)-(+)-camphorsulfonict and (*R*,*R*)-(+)-**2**–(1*S*)-(+)-camphorsulfonic adducts were synthesised as described above starting from pure samples of (*S*,*S*)-(−)-**2** or (*R*,*R*)-(+)-**2** and (1*S*)-(+)-camphorsulfonic acid to identify the two species present in the ^{31}P NMR spectrum. *Selected data* for (*S*,*S*)-(−)-**2**–(1*S*)-(+)-camphorsulfonic adduct: δ_P($CDCl_3$, 85% H_3PO_4) 40.7 (s); δ_H($CDCl_3$) 0.83 (3H, s, C*H*$_3$C), 1.07 (3H, s, C*H*$_3$C), 1.25 (6H, m, C*H*$_3$) 1.50–2.70 (7H, m, C*H*$_2$C*H*$_2$C*H*C*H*$_2$), 3.00 (2H, m, C*H*$_3$CH), 3.00 (1H, d, C*H*$_2$SO$_3$H, $J_{H,H}$ 15.0), 3.50 (1H, d, C*H*$_2$SO$_3$H, $J_{H,H}$ 15.0), 7.30–-7.80 (20H, m, arom), 8.20 (1H, s, CH$_2$SO$_3$*H*); ν_{max}(KBr)/cm^{-1} 3400 (OH, br), 3000–2900 (aliphatic and aromatic C–H, w), 1700 (C=O, s); $[\alpha]_D^{23}$ −14.0 (*c* 2.0 in CH_2Cl_2). For (*R*,*R*)-(+)-**2**–(1*S*)-(+)-camphorsulfonic adduct: δ_P ($CDCl_3$, 85% H_3PO_4) 40.4 (s); δ_H($CDCl_3$) 0.91 (3H, s, C*H*$_3$C), 1.08 (3H, s, C*H*$_3$C), 1.30 (6H, m, C*H*$_3$) 1.54–2.60 (7H, m, C*H*$_2$C*H*$_2$C*H*C*H*$_2$), 2.95 (2H, m, C*H*$_3$CH), 3.05 (1H, d, C*H*$_2$SO$_3$H, $J_{H,H}$ 15.2), 3.54 (1H, d, C*H*$_2$SO$_3$H, $J_{H,H}$ 15.2), 7.30–7.80 (20H, m, arom), 8.20 (1H, s, CH$_2$SO$_3$*H*); ν_{max}(KBr)/cm^{-1} 3400 (OH, br), 3000–2900 (aliphatic and aromatic C–H, w), 1700 (C=O, s); $[\alpha]_D^{23}$+25.0 (*c* 2.0 in CH_2Cl_2). Slight differences in the ^{31}P NMR ($CDCl_3$) chemical shifts of the mixture containing the two diastereoisomers may be observed due to variations in sample concentration.

8 M. Kitamura, M. Tokunaga, T. Ohkuma and R. Noyori, *Tetrahedron Lett.*, 1991, **32**, 4163.

9 A. S. Chan, J. J. Pluth and J. Halpern, *J. Am. Chem. Soc.*, 1980, **102**, 5952; H. Kawano, T. Ikariya, Y. Ishii, S. Yoshikawa, Y. Uchida and H. Kumobayashi, *J. Chem. Soc., Perkin Trans. 1*, 1989, 1571.

10 We are indebted to a referee for this suggestion.

11 A sample of pure monoene **4** was obtained by hydrogenation of **1** in the presence of Pd on carbon (10% Pd) at 80 °C and $P(H_2)$ = 100 bar followed by recrystallisation from benzene. δ_P ($CDCl_3$, 85% H_3PO_4) 31.88 (s); δ_H($CDCl_3$) 1.99 (6 H, m, C*H*$_3$), 7.4–7.8 (20H, m, arom); δ_C($CDCl_3$) 22.2 [*C*H$_3$, appt t, X part of an AA′X (A and A′ are the P atoms) spin system], 128.6 (*C*, arom, appt t), 131.4 (*C*, arom, appt t), 131.9 (*C*, s, arom.), 133.3 (*C*, s, arom.), 145.3 (C=, quin, AA′X spin system). Owing to the high symmetry of the molecule, the NMR data do not allow determination of the stereochemistry of the molecule.

Communication a908447i

ChemComm

Symmetrical and unsymmetrical 2,6-dialkyl-1,1′-biaryls by combined catalysis of aromatic alkylation *via* palladacycles and Suzuki-type coupling

Marta Catellani,* Elena Motti and Monica Minari

Dipartimento di Chimica Organica e Industriale dell'Università Parco Area delle Scienze 17A, I-43100 Parma, Italy. E-mail: catell@unipr.it

Received (in Cambridge, UK) 17th November 1999, Accepted 6th December 1999

The title compounds are made readily accessible by a catalytic procedure, occurring under mild conditions, based on palladium-mediated *ortho* alkylation of aromatic iodides with alkyl bromides followed by reaction with arylboronic acids.

Biaryls are ubiquitous compounds, their unit being present in a variety of natural products and bioactive molecules as well as in many functional advanced materials, and there is wide interest in the development of new synthetic methodologies in spite of the many methods already available.[1] We recently described a new methodology for aromatic *ortho* alkylation based on the formation of palladium(II) and palladium(IV) metallacycles (Scheme 1).[2]

Combining this new alkylation procedure with the Heck reaction enabled us to achieve the catalytic synthesis of vinylarenes selectively substituted in both *ortho* positions with equal or different alkyl groups in a one-pot procedure.[3]

We have now found that a Suzuki-type coupling reaction[1k,l] can be caused to occur directly in the reaction mixture with selective formation of *ortho* substituted biaryls.

To this end we added an arylboronic acid to a reaction mixture containing an iodoarene, norbornene, an alkyl bromide (in two-fold excess), palladium acetate as catalyst and potassium carbonate in DMF. In spite of the possibility that the Suzuki coupling could occur with the initially formed arylpalladium iodide[1k,l] and with other intermediates involved in the aromatic alkylation, as described in the literature,[4] the desired 2,6-dialkylated 1,1′-biaryls were obtained in satisfactory to excellent yields at room temperature.

The overall reaction leading to the synthesis of symmetrically *ortho*-dialkylated biaryls is shown in Scheme 2 for iodobenzene. Thus the reaction of iodobenzene (82 mg, 0.4 mmol), 1-bromopropane (220 mg, 1.6 mmol), 2-norbornene (38 mg, 0.4 mmol) and phenylboronic acid (59 mg, 0.48 mmol) with $Pd(OAc)_2$ (9.0 mg, 0.04 mmol) as the catalyst and K_2CO_3 (332 mg, 2.4 mmol) as the base, in DMF (5 mL) at room temperature for 72 h afforded 2,6-di-*n*-propyl-1,1′-biphenyl in 95% yield.† Higher substrate-to-catalyst ratios can be used but so far no optimisation work has been carried out. The course of the reaction can be concisely represented as shown in Scheme 3.

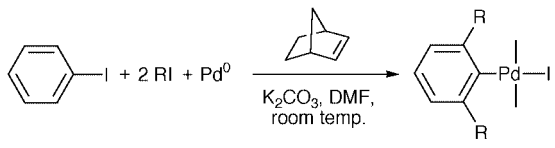

Scheme 1

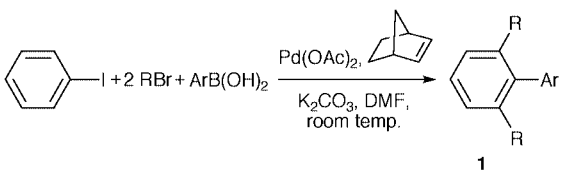

Scheme 2

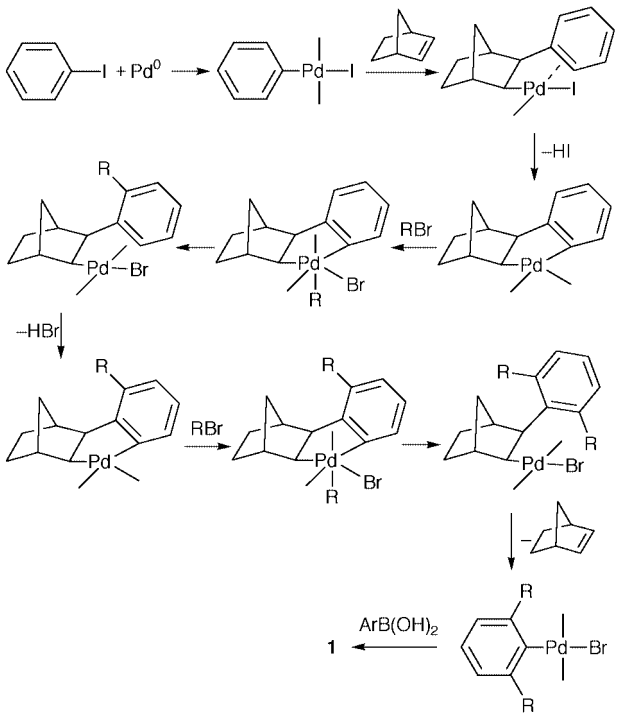

Scheme 3

The reaction was also extended to *ortho*-substituted aromatic iodides. This offers the possibility of obtaining biaryls **2** with two different *ortho* alkyl groups, as shown in Scheme 4.

The scope of the reaction is currently being studied. As shown in Table 1, however, the procedure appears to be tolerant of substituents both in the iodoarene and in the phenylboronic acid, and it can be carried out with different alkyl bromides. Thus it offers a simple and direct tool to gain access to 2,6-dialkyl substituted 1,1′-biaryls. *ortho*-Substituted arylboronic acid gave very poor results both in terms of yield and selectivity, and are not reported.

The reaction is sensitive to the bulkiness of the reagents. Although the reaction becomes slow and longer reaction times are required, selectivity remains high (runs 9–11).

Small amounts (1–4%) of by-products are also obtained, corresponding to *o*,*o*′-disubstituted biaryls, formed as a consequence of aryl exchange between arylpalladium bromide and arylboronic acid,[5] or to *o*,*o*′-disubstituted norbornylbenzenes which result from hydrogenolysis of the palladium complex

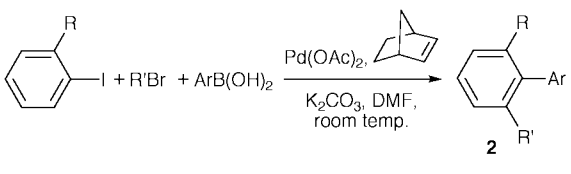

Scheme 4

Table 1 Reaction of aryl iodides, alkyl bromides and arylboronic acids in the presence of norbornene, $Pd(OAc)_2$ and K_2CO_3[a]

Run	Aryl iodide	Alkyl bromide R or R′	Boronic acid Ar	Biaryl yield (%)[b]	Aryl iodide conversion (%)[b]
1	PhI	Pr	Ph	95 (90)	98
2	PhI	Bu	Ph	83 (81)	86
3	4-$MeO_2CC_6H_4I$	Bu	Ph	89	97
4	4-MeC_6H_4I	Bu	Ph	74 (63)	93
5	4-MeC_6H_4I	Bu	4-MeC_6H_4	86 (84)	98
6	PhI	Bu	4-MeC_6H_4	71 (66)	77
7	PhI	Bu	4-FC_6H_4	62 (59)	72
8	2-MeC_6H_4I	Bu	Ph	89	96
9	2-BuC_6H_4I	Pr	Ph	70[c]	91[c]
10	2-$Pr^iC_6H_4I$	Bu	Ph	82[c]	84[c]
11	2-$Pr^iC_6H_4I$	Pr^i	Ph	71[c]	74[c]

[a] Molar ratio of the reagents 1 : 4 : 1.2 : 1 : 0.1 : 6; room temperature, 72 h, DMF as solvent, under nitrogen. [b] GC yield on the charged amount of the aryl iodide; isolated yields in brackets. [c] 144 h.

before norbornene deinsertion (Scheme 3), while biaryls resulting from homocoupling[6] of the arylboronic acids are not formed.

In conclusion the present reaction allows the selective preparation of symmetrical and unsymmetrical *o*,*o*′-dialkylated biaryls, an important class of not easily accessible compounds, in a one-pot procedure under mild conditions.

We thank Ministero Università e Ricerca Scientifica and National Research Council for financial support. Access to facilities of Centro Interfacoltà di Misure of the University of Parma is acknowledged.

Notes and references

† All isolated products gave satisfactory elemental analyses. *Selected data* for 2,6-di-*n*-propyl-1,1′-biphenyl: δ_H(300.13 MHz, $CDCl_3$, TMS, 20 °C) 7.40 (2H, m, H3′, H5′), 7.33 (1H, m, H4'), 7.23, 7.11 (3H, AB_2 system, *J* 7.3, H4, H3, H5), 7.15 (2H, m, H2′, H6′), 2.27 (4H, m, 2CH_2Ar), 1.41 (4H, m, 2C$H_2$$CH_3$), 0.75 (6H, t, *J* 7.3 Hz, 2CH_3); δ_C(75.4 MHz, $CDCl_3$, TMS, 20 °C) 141.1, 140.7, 140.4 (q), 129.6 (C2′, C6′), 127.9 (C3′, C5′), 127.0 (C4), 126.5 (C4′), 126.3 (C3, C5), 35.8 (*C*H_2Ar), 24.4 (*C*$H_2$$CH_3$), 14.1 ($CH_3$); *m*/*z* (EI, 70 eV) 238 (M^+, 25%) 209 (20), 178 (23), 167 (100), 165 (50).

1 (*a*) H. Weissman and D. Milstein, *Chem. Commun.*, 1999, 1901; (*b*) J. P. Wolfe and S. L. Buchwald, *Angew. Chem., Int. Ed.*, 1999, **38**, 2413; (*c*) D. S. McGuinness, K. J. Cavell, B. W. Skelton and A. H. White, *Organometallics*, 1999, **18**, 1596; (*d*) W. A. Herrmann, C.-P. Reisinger and M. Spiegler, *J. Organomet. Chem.*, 1998, **557**, 93; (*e*) A. F. Indolese, *Tetrahedron Lett.*, 1997, **38**, 3513; (*f*) S. Darses, T. Jeffery, J.-P. Genet, J.-L. Brayer and J.-P. Demoute, *Tetrahedron Lett.*, 1996, **37**, 3857; (*g*) M. Beller, H. Fischer, W. A. Herrmann, K. Öfele and C. Brossmer, *Angew. Chem., Int. Ed. Engl.*, 1995, **34**, 1848; (*h*) J. Clayden and M. Julia, *J. Chem. Soc., Chem. Commun.*, 1993, 1682; (*i*) S. P. Stanforth, *Tetrahedron*, 1998, **54**, 263; (*j*) I. P. Beletskaya, *Pure Appl. Chem.*, 1997, **69**, 471; (*k*) N. Miyaura and A. Suzuki, *Chem. Rev.*, 1995, **95**, 2457; (*l*) A. Suzuki, *Pure Appl. Chem.*, 1994, **66**, 213.

2 M. Catellani and M. C. Fagnola, *Angew. Chem., Int. Ed. Engl.*, 1994, **33**, 2421; for a recent review on metallacycles: G. Dyker, *Chem. Ber.*, 1997, **130**, 1567.

3 M. Catellani, F. Frignani and A. Rangoni, *Angew. Chem., Int. Ed. Engl.*, 1997, **36**, 119; M. Catellani and F. Cugini, *Tetrahedron*, 1999, **55**, 6595.

4 M. Catellani, G.P. Chiusoli and S. Concari, *Tetrahedron*, 1989, **45**, 5263.

5 M. Moreno-Mañas, M. Pérez and R. Pleixats, *J. Org. Chem.*, 1996, **61**, 2346.

6 K.-C. Kong and C.-H. Cheng, *J. Am. Chem. Soc.*, 1991, **113**, 6313; R. van Asselt and C. J. Elsevier, *Organometallics*, 1994, **13**, 1972.

Communication a909099a

Rapid synthesis of colossal magnetoresistance manganites by microwave dielectric heating

Kay E. Gibbons,[a] Martin O. Jones,[a] Stephen J. Blundell,[b] Amalia I. Mihut,[b] Ian Gameson,[a] Peter P. Edwards,*[a] Yuzuru Miyazaki,[a] Neil C. Hyatt[a] and Adrian Porch[c]

[a] *School of Chemistry, The University of Birmingham, Edgbaston, Birmingham, UK B15 2TT. E-mail: p.p.edwards@bham.ac.uk*
[b] *Clarendon Laboratory, University of Oxford, Parks Road, Oxford, UK OX1 3PU*
[c] *School of Electrical Engineering, The University of Birmingham, Edgbaston, Birmingham, UK B15 2TT*

Received (in Oxford, UK) 18th September 1999, Accepted 8th December 1999

Colossal magnetoresistance manganites have been synthesised by the microwave dielectric heating of metal nitrates, which act both as effective microwave susceptors, and a ready source of oxidizing NO_2 to induce mixed valency.

The perovskite mixed-valent manganites of generic formula $La_{1-x}A_xMnO_3$ (A = Ca, Sr, Ba; $0 \leqslant x \leqslant 1$), are currently the subject of intense enquiry in relation to the so-called 'colossal magnetoresistance' (CMR) effect.[1,2] The traditional ceramic (solid-state) synthesis of these CMR materials invariably requires conductive heating for extended periods at elevated temperatures; in some reported cases,[3] heating for 7 days at temperatures up to 1500 °C. Here, we illustrate the application of microwave dielectric heating to synthesise, in a period of minutes, a range of lanthanum alkaline-earth manganites exhibiting CMR. Importantly, we take advantage of the high intrinsic microwave susceptibility of component metal nitrate compounds [*e.g.* $Mn(NO_3)_2$] as compared to their moderately absorbing oxide counterparts (*e.g.* MnO_2, Mn_2O_3, *etc.*) in the synthesis of CMR materials. These findings are a clear illustration of the potential of microwave reaction selectivity—in this case *via* anion selectivity—in solid state chemical synthesis.

The microwave dielectric heating effect originates from the natural ability of certain substances to efficiently absorb, and then to transform electromagnetic (radiation) energy into heat. If sufficient heat can be generated at a local level, then chemical reactions may be initiated at a very rapid rate. More than a decade ago Mingos and co-workers carried out pioneering studies[4–6] of the use of microwave dielectric heating for the synthesis of advanced ceramic materials, most notably the high-temperature superconducting cuprates, $YBa_2Cu_3O_7$ and $La_{2-x}Sr_xCuO_4$. The strong microwave absorbing properties of one of the reactant (constituent) oxides, CuO, leads to a rapid and highly effective synthetic pathway. In fact, CuO reaches a temperature of *ca.* 700 °C after only 30 s of irradiation in a commercially available microwave oven. By contrast, the binary oxide constituents of the ternary CMR perovskites, *e.g.* La_2O_3, MnO_2, *etc.* attain temperatures of only 107 and 321 °C, respectively, after 1800 s (30 min) in a similarly configured microwave oven, while $SrCO_3$ does not absorb microwaves to any significant degree.[6]

The addition of fine-grained, graphitic carbon (known to be an efficient microwave absorber), homogeneously distributed through the starting materials, achieves the desired effect of significantly increasing the temperature of the reaction mixture and results in compound formation. However, the presence of this reactive carbon at elevated temperatures results in highly reducing synthetic conditions and this adversely affects the formation of mixed-valent manganese (Mn^{3+}/Mn^{4+}), known to be essential for the CMR phenomenon in the perovskite manganite materials.[1,2]

We have directly measured the room temperature microwave reflection of a variety of constituent starting materials over the frequency range 1–6 GHz using a HP8722A network analyser in conjunction with a specially designed open-ended coaxial probe; a selection of the data are shown in Fig. 1.

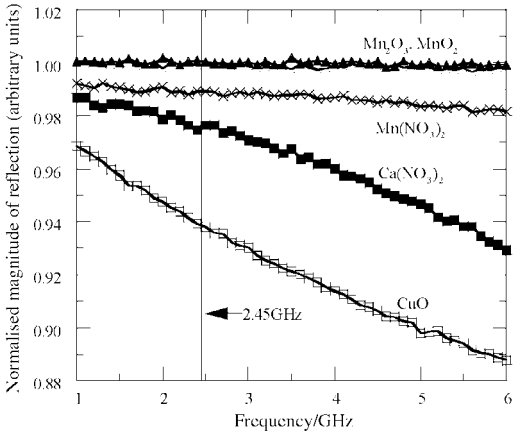

Fig. 1 Normalised magnitude of microwave reflection *vs.* frequency for various metal oxides and nitrates. The vertical line indicates the operating frequency of the microwave oven.

Whilst MnO_2 is frequently reported to be a good microwave susceptor,[5,7,8] we find that MnO_2 (and Mn_2O_3) are not as effective susceptors as compared with nitrate starting materials, *e.g.* $Ca(NO_3)_2$ and $Mn(NO_3)_3$. Moreover, there is another advantage in the use of nitrates; they decompose to yield highly oxidising NO_2 which facilitates the formation of the mixed Mn^{3+}/Mn^{4+} couple.

The manganites $La_{0.7}Sr_{0.3}MnO_{3+\delta}$, $La_{0.97}MnO_3$ and $La_{0.5}Ca_{0.5}MnO_{3+\delta}$ were formed by first dissolving stoichiometric amounts of the constituent metal nitrates in distilled water. The resulting solution was then transferred to an open quartz tube, supported in a firebrick. A small piece of aluminium foil was placed over the end of the tube to prevent the mixture boiling over, whilst allowing NO_2 to escape. This assembly was then placed in the centre of the turntable of a domestic 950 W microwave oven, operating at 2.45 GHz, and irradiated for 5 min at the full power setting. Following the loss of H_2O and NO_2, the sample glowed bright orange and continued to do so until the microwave power was switched off. The sample was then left to cool at a natural rate in the microwave oven. The resulting black, well sintered fine powder was ground using a pestle and mortar before being subjected to a further 5 min of microwave irradiation.

X-Ray powder diffraction patterns (Fig. 2) were collected using a Siemens D5000 system (Cu-Kα_1 radiation) and these clearly show the presence of the desired phases, but the diffraction peaks are consistently broader than those generally

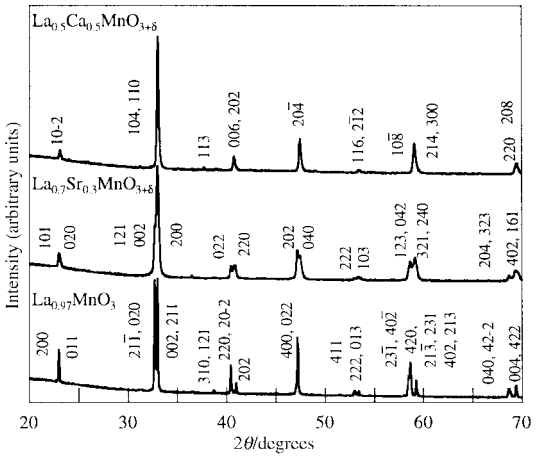

Fig. 2 X-Ray powder diffraction patterns for three manganites prepared using microwave dielectric heating.

produced by conventional solid state techniques.[9] This difference probably arises because microwave synthesis is somewhat akin to combustion synthesis in producing samples with small particle size.[10] The Rietveld method was applied to the refinement of crystal structures using the GSAS suite of programs.[11] The material $La_{0.7}Sr_{0.3}MnO_{3+\delta}$ is orthorhombic, a = 5.4640(4), b = 7.7277(6), c = 5.5285(4) Å, space group *Pnma*; $La_{0.97}MnO_3$ is monoclinic, a = 7.7970(4), b = 5.5271(3), c = 5.4842(3) Å, β = 90.8(2)°, space group *I2/a*; $La_{0.5}Ca_{0.5}MnO_{3+\delta}$ is rhombohedral, a = 5.4763(5), c = 13.379(1) Å, space group $R\bar{3}c$. These Rietveld refinements, combined with thermogravimetric analyses, indicated that these materials were fully oxygenated, with δ *ca*. zero.

The CMR properties of sintered pellets of the above materials were examined using a four-point resistivity probe in magnetic fields of 0 and 12 T. All three samples were found to exhibit CMR and the data are shown in Fig. 3. Whilst these samples show a very clear CMR effect, $La_{0.7}Sr_{0.3}MnO_{3+\delta}$ shows rather different CMR behaviour to materials produced by the conventional ceramic route.[12] This may be due to the orthorhombic symmetry of this sample resulting in reduced transfer of e_g electrons when compared with rhombohedral or pseudocubic phases.[13] The structural and CMR properties of the $La_{1-\delta}MnO_3$ system are extremely sensitive to synthesis conditions. For instance, the orthorhombic form shows no CMR properties at all.[14] Our sample of $La_{1-\delta}MnO_3$ adopts the less common monoclinic form and exhibits good CMR behaviour.[14] $La_{0.5}Ca_{0.5}MnO_{3+\delta}$ shows CMR comparable with previous literature reports.[12] Thermogravimetric analyses of these materials indicated no oxygen stoichiometry. Recently we have extended the microwave synthesis procedure to include the spinel manganates such as the battery material $LiMn_2O_4$ *etc*.

In summary, we have illustrated that dielectric heating represents a rapid and effective route to the synthesis of CMR manganites. Moreover, the direct measurement of microwave-reflecting properties (Fig. 1) greatly aids the choice of constituent starting materials.

We thank Merck Ltd. and the EPSRC for financial support, and Rod Riddle (Merck) for support and encouragement.

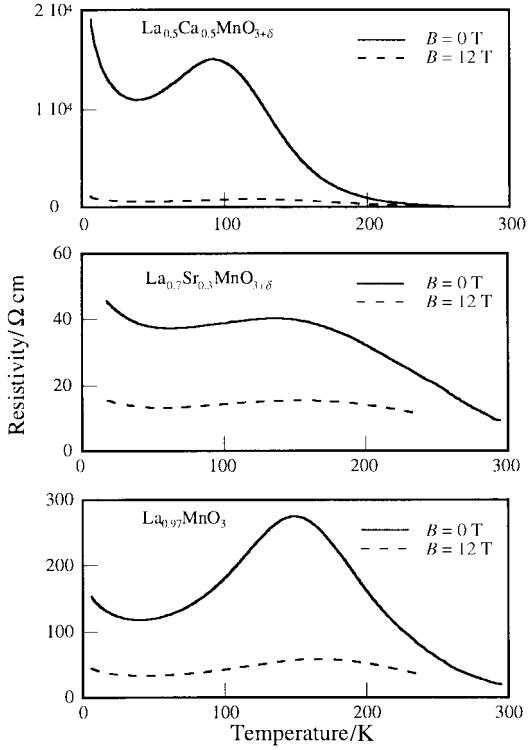

Fig. 3 Temperature variation of the electrical resistivity in magnetic fields (B) of 0 and 12 T for manganites produced using microwave dielectric heating.

Notes and references

1 S. Jin, T. H. Tiefel, M. McCormack, R. A. Fastnacht, R. Ramesh and L. H. Chen, *Science*, 1994, **264**, 413.
2 R. Mahesh, R. Mahendiran, A. K. Raychaudhuri and C. N. R. Rao, *J. Solid State Chem.*, 1995, **114**, 297.
3 G. Q. Gong, C. L. Canedy, G. Xiao, J. Z. Sun, A. Gupta and W. J. Gallagher, *J. Appl. Phys.*, 1996, **79**, 4538.
4 D. R. Baghurst, A. M. Chippindale and D. M. P. Mingos, *Nature*, 1988, **332**, 311.
5 D. R. Baghurst and D. M. P. Mingos, *J. Chem. Soc., Chem. Commun.*, 1988, 829.
6 D. M. P. Mingos and D. R. Baghurst, *Chem. Soc. Rev.*, 1991, **20**, 1.
7 W. H. Sutton, *Ceram. Bull.*, 1989, **68**, 376.
8 B. Vaidhyanathan and K. J. Rao, *J. Solid State Chem.*, 1997, **132**, 349.
9 A. Hammouche, E. Siebert and A. Hammou, *Mater. Res. Bull.*, 1989, **24**, 367.
10 S. S. Manoharan and K. C. Patil, *J. Solid State Chem.*, 1993, **102**, 267.
11 A. C. Larson and R. B. Von Dreele, General Structure Analysis System, University of California, 1994.
12 R. Mahendiran, S. K. Tiwary, A. K. Raychaudhuri, T. V. Ramakrishnan, R. Mahesh, N. Rangavittal and C. N. R. Rao, *Phys. Rev. B*, 1996, **53**, 3348.
13 C. N. R. Rao, A. K. Cheetham and R. Mahesh, *Chem. Mater.*, 1996, **8**, 2421.
14 A. Maignan, C. Michel, M. Hervieu and B. Raveau, *Solid State Commun.*, 1997, **101**, 277.

Communication a907677h

ChemComm

The first example of a substrate spanning the calix[4]arene bilayer: the solid state complex of *p*-sulfonatocalix[4]arene with L-lysine†

Mohamed Selkti,[a] Anthony W. Coleman,*[b] Ioannis Nicolis,[c] Nathalie Douteau-Guével,[b] Françoise Villain,[c] Alain Tomas[a] and Colette de Rango*[c]

[a] *CNRS EP2075, Faculté de Pharmacie, Université Paris V, 75270 Paris Cedex 06, France*
[b] *IBCP, CNRS UPR412, 7, Passage du Vercors, 69367 Lyon Cedex 07, France*
[c] *Laboratoire de Physique, Centre Pharmaceutique, Université Paris-Sud, 92296 Châtenay-Malabry Cedex, France. E-mail: colette.rango@cep.u-psud.fr*

Received (in Columbia, MO, USA) 6th August 1999, Accepted 23rd November 1999

The complex of *p*-sulfonatocalix[4]arene with L-lysine shows a new type of intercalation behaviour with regard to the achiral hydrophobic bilayer assembly of the calixarenes, and represents the first structural example of a cationic organic substrate spanning such a bilayer.

It has recently been shown that the *p*-sulfonatocalix[*n*]arenes can act as heparin mimics,[1] and their interactions with the positively charged amino acids, lysine and arginine, has been investigated.[2] In the case of *p*-sulfonatocalix[4]arene, 1:1 complexes with lysine and arginine are observed, with binding constants derived from ^{1}H NMR spectroscopy at pH 5 of 600 and 1700. Undoubtedly such electrostatic interactions are also important in the activity of the sulfonatocalixarenes as chloride ion blockers.[3] In recent years, *p*-sulfonatocalix[4]arene salts have been extensively studied; these complexes crystallize with a large variety of cations in bilayer-type structures.[4] The basic molecular motif is achiral and formed by two calixarenes related by crystallographic symmetry. They are arranged in the up-down fashion with the sulfonate groups covering the surfaces of the bilayers which are separated by a hydrophilic layer containing the majority of the water molecules and cationic counterions. The structures of complexes of *p*-sulfonatocalix[4]arene with transition metal compounds[5] have demonstrated that an aromatic organic substrate can be intercalated into the bilayer. However, no example of substrates traversing the bilayer have been observed. We report here on a new type of intercalation within the calixarene bilayer system showing that a chiral cationic organic molecule possessing a flexible aliphatic side chain, in this case L-lysine, can span the bilayer. The crystalline title compound also exhibits a chiral hydrophilic layer, containing three other L-lysine molecules, which separates the bilayers.

The crystal structure belongs to the triclinic *P*1 space group,‡ and consists of two [calix[4]arenesulfonate]$^{4-}$ anions (**A** and **B**), four L-lysine counterions and 17.5 water molecules distributed over 20 sites. The calix[4]arene pattern is strongly pseudo-centrosymmetrical and similar to those already described in other complexes.[4,5] The four L-lysine molecules and the sulfonate groups interact largely with water molecules. No water sites have been detected within the calixarene cavities.

For all the L-lysine molecules, the α- and ε-amino groups show contacts indicative of N–H···O hydrogen bonds with oxygen atoms on the sulphonate groups of the calixarenes, but they display different types of interactions. One L-lysine molecule (**L1**) is seen to traverse the hydrophobic bilayer with the main chain directed towards the sulfonate groups of the 'up', (**A**), calixarenes. As its side chain is in the fully extended conformation [χ_1 = −68(1)°, χ_2, χ_3, χ_4 values close to 180°], the ε-amino group points towards the opposite edge of the bilayer, nearly at the level of the S atoms of the 'down' (**B**), calixarenes (Fig. 1). While the α-amino group is in short contact with one sulfonate group of an **A** calixarene [N···O separation of 2.75(1) Å], the ε-amino group is connected to three **B** calixarenes, related by crystallographic translations along the *a*- and *b*-axes [N···O separations ranging from 2.853(6) to 3.013(6) Å]. This L-lysine molecule is thus the first example of a ligand which truly spans the hydrophobic calixarene bilayer.

Of further interest in the structure is the chiral hydrophilic layer separating the bilayers which contains the other three L-lysine molecules. One L-lysine molecule (**L2**) is placed in the core of this layer§ and aligned parallel to the *a*-axis. As with **L1**, the side chain adopts the fully extended conformation [χ_1 = −66(1)°, χ_2, χ_3, χ_4 values close to 180°], which is that most usually observed.[6] The other two L-lysine molecules (**L3** and **L4**) lie just above the calixarene macrocycles (**A** and **B** for **L3** and **L4**, respectively). Their arrangement is illustrated in Fig. 2. For both, the α-amino and α-carboxylate groups are directed into the chiral layer and the side chain is nearly at the level of the S atoms of their respective calixarene, with the ε-amino group pointed towards the exterior of the cavity. A common structural characteristic of **L3** and **L4** is that their side chains exhibit a folded conformation (χ_1 = 65.7(6) and 54.2(7)°, χ_4 = −46.2(7) and −63.5(7)°, χ_2, χ_3 values close to 180°]. This unusual conformation[6] allows N–H···O contacts between one sulfonate group of the parent calixarene and the two amino groups of the same L-lysine molecule (Table 1). This conformation has been previously observed in the structure of the L-lysine

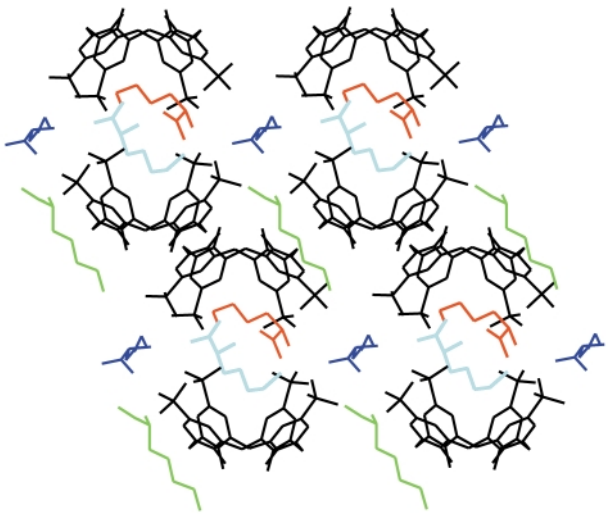

Fig. 1 Packing view along the *a*-axis of the structure demonstrating the spanning of one L-lysine molecule (**L1**, green) within the bilayer formed with the **A** (up) and **B** (down) *p*-sulfonatocalix[4]arenes. The other three L-lysine molecules are shown within the chiral layer which separates the bilayers (**L2**, dark blue; **L3**, light blue; **L4**, red).

† A figure showing the arrangement of the three L-lysine molecules within the chiral layer is available from the RSC web site, see http://www.rsc.org/suppdata/cc/a9/a906546f/

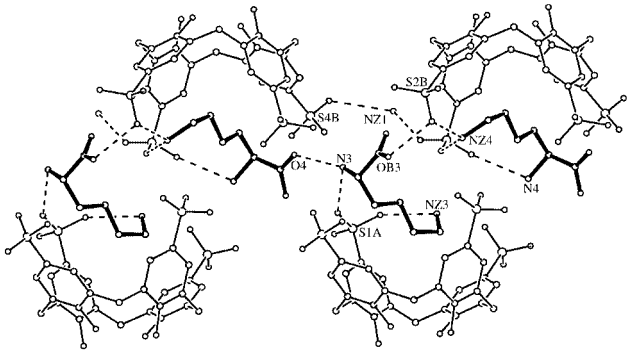

Fig. 2 A view of a section of the structure illustrating the arrangement of **L3** and **L4** within the chiral layer and representing the N(amino)··O(sulfonate) contacts (dashed lines) referred to in the text. The position of the ε-amino group of **L1** (NZ1) is also shown, the contacts between NZ1 and the sulfonate groups of two **B** calixarenes are indicated in dashed lines.

Table 1 Selected contacts (Å) between sulphonate oxygen atoms and the L-lysine molecules **L3** and **L4**

L3		**L4**	
N3···O41A	2.988(8)	N4···O43B	2.939(6)
NZ3···O21A	2.864(8)	NZ4···O33B	3.071(8)
OB3···O42B[a]	2.672(6)	NZ4···O42B	2.899(8)
N3···O31B	2.890(7)	OB4···O41A	2.635(7)
NZ3···O33B[a]	2.961(6)	NZ4···O23A[b]	2.806(10)

Symmetry codes: [a] $x + 1, y, z$. [b] $x - 1, y, z$. The minor components of the ε-amino groups are not considered.

sulfate,[7] with similar specific interactions between the L-lysine molecule and the sulfate anion. **L3** and **L4** are connected by an N–H··O contact between the α-amino group of **L3** and the carbonyl oxygen of **L4** [N··O separation 2.928(7) Å]. These dimers are only interconnected indirectly through one sulfonate oxygen atom (O42B) of the **B** calixarene, which is simultaneously in contact with the ε-amino group of **L4** and the hydroxy group of **L3**. The dimers are stacked along the *a*-axis. Thus, the L-lysine network within the chiral layer is composed of alternating rows of dimers and monomers. The bilayers are cross-linked through the chiral layer as **L3** and **L4** are also in contact with sulfonate groups of two calixarenes (**B** and **A**) lying in an adjacent bilayer (Table 1).

Thus, in contrast to the situation in solution, where a 1:1 complexation is observed, in the solid state a lysine–calixarene complex of 2:1 stoichiometry may be obtained. Actually, the system may be considered as two similar 1:1 complexes, each involving a folded L-lysine molecule (**L3** and **L4**), which would correspond to the situation observed in solution.[2] The other two L-lysine molecules, both with the side chain in the fully extended conformation, would be implicated in the solid state structure. Of the four independent L-lysine molecules, three are found within the hydrophobic layer separating the typical sulfonatocalix[4]arene bilayer, while the remaining molecule (**L1**) spans this bilayer in a manner resembling biomolecules traversing a lipid bilayer.¶ Further studies are underway to investigate the structural behaviour of the sulfonatocalix[*n*]arenes with peptides containing lysine and arginine.

Notes and references

‡ *Crystal data* for $2(C_{28}H_{20}O_{16}S_4)\cdot4(C_6H_{16}O_2N_2)\cdot17.5H_2O$: M_r = 2389.5; suitable crystals for X-ray diffraction were grown in sealed tubes from two to one lysine–calix[4]arene aqueous solution, at room temperature during six months; triclinic *P*1, a = 13.599(4), b = 14.369(2), c = 15.169(3) Å, α = 111.02(1), β = 100.02(2), γ = 99.02(2)°, V = 2646(1) Å^3, Z = 1, ρ_{calc} = 1.50 g cm^{-3}, $2\theta_{max}$ = 46°, μ(Mo-Kα) = 0.28 mm^{-1}, T = 293 K; 7673 independent reflections, 6530 with $I > 2\sigma(I)$; R_1 = 0.0863, wR_2 = 0.2553. The structure was solved by direct methods (SHELXS-86) and refined using the program SHELX-97. 17.5 water molecules were located, distributed over 20 sites. For three sulfonate groups, two O atoms are positionally disordered (two partially occupied sites for each). The ε-amino groups of **L3** and **L4** are disordered over two sites (0.75 and 0.25 occupancy factors). The parameters of the **A** and **B** calixarenes were refined in separate blocks. CCDC 182/1505. See http://www.rsc.org/suppdata/cc/a9/a906546f/ for crystallographic data in .cif format.

§ The **L2** molecule is situated in a large intermolecular space and all the atoms show high isotropic displacement parameters. Nevertheless, the amino groups of **L2** show contacts having relatively large separation distances with sulfonate oxygen atoms of two **B** calixarenes related by the *a*-translation [N··O separations of 3.02(1) and 3.07(1) Å]. A contact with a somewhat long N··O separation distance [3.09(1) Å] is also seen between the ε-amino group of **L3** and the carbonyl oxygen of **L2**.

¶ It is of interest to note that there was debate concerning whether the original sulfonatocalix[4]arene structures resembled those of bilipid membranes or clay minerals.

1 E. Aubert-Foucher, A. W. Coleman and D. J. S. Hulmes, French Patent, pending; K. M. Hwang, Y. M. Qi, S.-Y. Liu, T. C. Lee, W. Choy and J. Chen 1995, U.S. Patent No 5,409,959.

2 N. Douteau-Guével, A. W. Coleman, J.-P. Morel and N. Morel-Desrosiers, *J. Phys. Org. Chem.*, 1998, **11**, 693; N. Douteau-Guével, A. W. Coleman, J.-P. Morel and N. Morel-Desrosiers, *J. Chem. Soc., Perkin Trans. 2*, 1999, 629.

3 A. K. Singh, R. K. Juneja, J. L. Atwood and R. J. Bridges, *Biophys. J.*, 1993, **64**, 17; A. K. Singh, R. K. Juneja, R. Wang, J. L. Atwood and R. J. Bridges, *Ped. Pulm.*, 1993, **9**, 227; J. L. Atwood, R. J. Bridges, R. K. Juneja and A. K. Singh, 1996, U.S. Patent No 5,489,612.

4 J. L. Atwood, F. Hamada, K. D. Robinson, G. W. Orr and R. L. Vincent, *Nature*, 1991, **349**, 683; A. W. Coleman, S. G. Bott, S. D. Morley, C. M. Means, K. D. Robinson, H. Zhang and J. L. Atwood, *Angew. Chem., Int. Ed. Engl.*, 1988, **27**, 1361; S. G. Bott, A. W. Coleman and J. L. Atwood, *J. Am. Chem. Soc.*, 1988, **110**, 610; J. L. Atwood, A. W. Coleman, H. Zhang and S. G. Bott, *J. Inclusion Phenom.*, 1989, **7**, 203; S. Sinkai, K. Araki, T. Matsuda, N. Nishiyama, H. Ikeda, I. Takasu and M. Iwamoto, *J. Am. Chem. Soc.*, 1990, **112**, 9053; J.-M. Lehn, R. Meric, J.-P. Vigneron, M. Cesario, J. Guilhem, C. Pascard, Z. Asfari and J. Vicens, *Supramol. Chem.*, 1995, **5**, 97; J. L. Atwood, L. J. Barbour, E. S. Dawson, P. C. Junk and J. Kienzle, *Supramol. Chem.*, 1996, **7**, 271.

5 J. L. Atwood, G. W. Orr, F. Hamada, R. L. Vincent, S. G. Bott and K. D. Robinson, *J. Am. Chem. Soc.*, 1991, **113**, 2760; J. L. Atwood, G.W. Orr, F. Hamada, S. G. Bott and K. D. Robinson, *Supramol. Chem.*, 1992, **1**, 15; J. L. Atwood, G. W. Orr, K. D. Robinson and F. Hamada, *Supramol. Chem.*, 1993, **2**, 309.

6 G. S. Prasad and M.Vijayan, *Acta Crystallogr.*, 1991, **B47**, 927.

7 S. Capasso, C. A. Mattia, L. Mazzarella and A. Zagari, *Acta Crystallogr.*, 1983, **C39**, 281.

Communication a906546f

Epoxidation of alkenes using alkyl hydroperoxides generated *in situ* by catalytic autoxidation of hydrocarbons with dioxygen

Takahiro Iwahama, Gou Hatta, Satoshi Sakaguchi and Yasutaka Ishii*

Department of Applied Chemistry, Faculty of Engineering & High Technology Research Center, Kansai University, Suita, Osaka 564-8680, Japan. E-mail: ishii@ipcku.kansai-u.ac.jp

Received (in Cambridge, UK) 2nd November 1999, Accepted 10th December 1999

Olefins were smoothly epoxidized under O_2 (1 atm) in the presence of a hydrocarbon such as ethylbenzene or tetralin, using *N*-hydroxyphthalimide (NHPI) and $Mo(CO)_6$ as catalyst; the present reaction involves autoxidation of the hydrocarbon assisted by NHPI and epoxidation of alkenes with the resulting hydroperoxide catalyzed by $Mo(CO)_6$; *cis*-alkene was epoxidized in a stereospecific manner to form the corresponding *cis*-epoxide in high yield.

The epoxidation of alkenes using molecular oxygen *via* a catalytic process is a challenging subject in the field of oxidation chemistry.[1] Since the direct epoxidation of alkenes with molecular oxygen, which lies in triplet ground state, is inhibited, epoxidation using O_2 is carried out in the presence of a compound like an aldehyde which serves as an active oxygen carrier.[2] Although there have been many reports on the metal-catalyzed epoxidation of alkenes by O_2 in the presence of aldehydes, only a limited number of methods using O_2 as terminal oxidant have been developed.[3] There has been long-standing interest in the epoxidation of alkenes with alkyl hydroperoxides, as an active oxygen carrier, generated *in situ* from hydrocarbons and O_2. To the best of our knowledge, however, only one report has appeared on the epoxidation of alkenes by the use of cumene and O_2 with heteropolyoxometalates as catalyst.[4] A major difficulty in the epoxidation is attributed to the following: (i) autoxidation of aldehydes takes place very fast, at least two orders of magnitude faster than that of hydrocarbons; (ii) as a result, the epoxidation using hydrocarbons must be carried out under severe reaction conditions; and (iii) the epoxidizing ability of alkyl hydroperoxides is considerably lower than that of peracids or acylperoxy radicals derived from aldehydes and O_2.[5] Therefore, stepwise procedures are commonly utilized in epoxidations using alkyl hydroperoxides. For example, the Halcon process consists of the aerobic oxidation of ethylbenzene to α-hydroperoxyethylbenzene, and the Mo-catalyzed epoxidation of propylene with the α-hydroperoxyethylbenzene.[6] Consequently, development of an epoxidation system using a hydroperoxide generated *in situ* from ethylbenzene and molecular oxygen is very attractive from the synthetic and industrial points of view.

Recently, we have shown that hydrocarbons are efficiently oxidized with O_2 by *N*-hydroxyphthalimide (NHPI), which serves as a radical catalyst under mild conditions.[7] In this oxidation, hydrocarbons are converted into oxygen-containing compounds such as alcohols or ketones through *alkyl hydroperoxides (**B**)* as transient intermediates. If the alkyl hydroperoxides formed can be utilized as oxidants, it is possible to epoxidize alkenes using hydrocarbons and molecular oxygen. Here we report the Mo-catalyzed epoxidation of alkenes with hydroperoxides generated *in situ* by the NHPI-catalyzed aerobic oxidation of hydrocarbons such as ethylbenzene (Scheme 1).

Table 1 shows representative results for the epoxidation of oct-2-ene (**1**) with O_2 using hydrocarbons as a hydroperoxide source.† The epoxidation of **1** using ethylbenzene (**2a**) in the presence of NHPI (10 mol%), $Co(OAc)_2$ (0.1 mol%) and $Mo(CO)_6$ (5 mol%) at 60 °C under O_2 (1 atm) gave epoxide **3** in 61% selectivity at 67% conversion (run 1). An improvement of the present epoxidation by the addition of molecular sieves 4A (MS-4A) was observed, and thus the conversion of **1** and selectivity of epoxide **3** reached 81% and 70%, respectively (run 2). Using tetralin (**2b**) instead of **2a**, it was found that the selectivity of epoxide **3** was considerably improved (run 3). However, when toluene (**2c**) was employed as a hydrocarbon source, the selectivity of **3** was lowered to 44% (run 4). This is believed to be due to the occurrence of allylic hydrogen atom abstraction from **1** in competition with the benzylic hydrogen atom abstraction of **2c** by PINO.[8] Although AIBN was used as a radical source instead of NHPI, **1** was difficult to epoxidize to **3** (run 5). It is very interesting to note that the present epoxidation was induced even at room temperature to afford epoxide **3** in high selectivity (97%) at 31% conversion (run 7).[9] On the other hand, metal complexes such as $MoO_2(acac)_2$, $VO(acac)_2$ and $TiO(acac)_2$ were found to be inadequate for the present reaction (runs 8–10). Although molybdenum(VI) complexes have high catalytic activity for the epoxidation of alkenes with *tert*-butyl hydroperoxide,[10] $MoO_2(acac)_2$ was found to depress the formation of the hydroperoxide from **2b** under these conditions (run 8).

On the basis of these results, the epoxidation of various alkenes with O_2 using **2a** or **2b** was examined in the presence of catalytic amounts of NHPI, $Co(OAc)_2$ and $Mo(CO)_6$ under selected reaction conditions (Table 2).

trans-Oct-2-ene (*trans*-**1**) was epoxidized with excellent stereoselectivity to give *trans*-2,3-epoxyoctane (*trans*-**3**) (*trans* : *cis* = > 99 : 1) with 88% selectivity together with a small amount of octane-2,3-diol (4%) in 78% conversion. Similarly, the epoxidation of *cis*-**1** gave *cis*-2,3-epoxyoctane (*cis*-**3**) (*cis* : *trans* = 99 : 1) in good selectivity. It is noteworthy that the present epoxidation of *cis*-olefin proceeds with nearly complete stereoselectivity to give *cis*-epoxide, although the metal-catalyzed epoxidation of *cis*-olefins using an aldehyde and O_2 leads to a mixture of *cis*- and *trans*-epoxides.[11] This is because the resulting alkylperoxyl radical can abstract the hydrogen

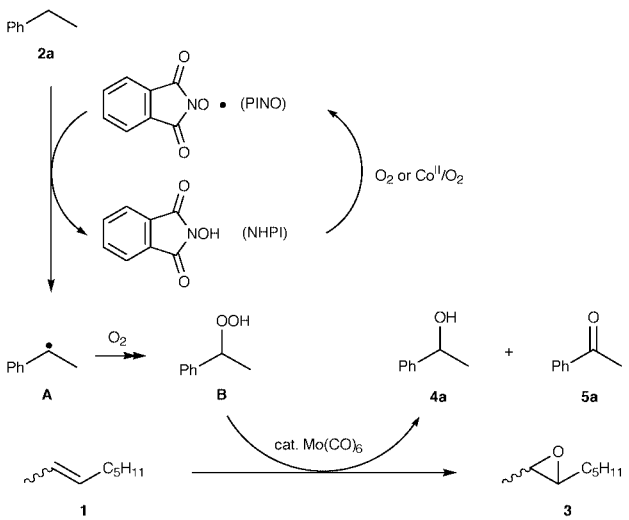

Scheme 1

Table 1 Epoxidation of oct-2-ene (**1**) to 2,3-epoxyoctane (**3**) with O_2 in the presence of hydrocarbons using NHPI, $Co(OAc)_2$ and various transition metals as catalysts[a]

Run	Hydrocarbon	Transition metal	*T*/°C	Conversion (%)		Selectivity (%)		
				1	**2a**,**b**	**3**	**4a**,**b**	**5a**,**b**
1	Ethylbenzene **2a**	$Mo(CO)_6$	60	67	10	61	65	25
2[b]	**2a**	$Mo(CO)_6$	60	81	12	70	71	19
3	Tetralin **2b**	$Mo(CO)_6$	50	67	25	86	62	30
4[c]	Toluene **2c**	$Mo(CO)_6$	60	59	—	44	—	—
5[d,e]	**2b**	$Mo(CO)_6$	80	12	7	67	88	11
6[f]	**2b**	$Mo(CO)_6$	50	58	18	91	79	17
7	**2b**	$Mo(CO)_6$	25	31	11	97	72	21
8	**2b**	$MoO_2(acac)_2$	50	8	< 5	95	> 90	< 8
9	**2b**	$VO(acac)_2$	50	12	15	79	31	64
10	**2b**	$TiO(acac)_2$	50	15	21	80	47	40

[a] Oct-2-ene (**1**) (4 mmol) was allowed to react with O_2 (1 atm) in the presence of NHPI (10 mol%), $Co(OAc)_2$ (0.1 mol%), transition metal (5 mol%) and hydrocarbon (**2a**,**b**) in PhCN (2 mL) for 12 h. **2a** (40 mmol) and **2b** (20 mmol) were used, respectively. [b] MS-4A (200 mg) was added. [c] 6 h. [d] AIBN (5 mol%) was used instead of NHPI. [e] 8 h. [f] NHPI (5 mol%) was used.

Table 2 Epoxidation of various alkenes with molecular oxygen in the presence of tetralin (**2b**) or ethylbenzene (**2a**) catalyzed by NHPI, $Co(OAc)_2$ and $Mo(CO)_6$[a]

Run	Alkene	*T*/°C	Conversion (%)[b]	Selectivity (%)[b]
1	*trans*-Oct-2-ene	60 (60)	78 (71)	88 (79)[c]
2	*cis*-Oct-2-ene	50 (60)	83 (75)	87 (71)[d]
3	2,4,4-Trimethylpent-2-ene	70 (70)	90 (76)	84 (80)
4	Oct-1-ene	60 (70)	38 (37)	80 (81)
5[e]	Cyclohexene	60	80	74
6[e]	Cyclooctene	60	89	83
7	*trans*-Hex-2-ene-1-ol **6**	60	79	65
8[f,g]	**6**	60	97	92

[a] Alkenes (4 mmol) and **2a** (40 mmol) or **2b** (20 mmol) were allowed to react with O_2 (1 atm) in the presence of NHPI (10 mol%), $Co(OAc)_2$ (0.1 mol%), $Mo(CO)_6$ (5 mol%) and MS-4A (200 mg) in PhCN (2 ml) for 14 h. [b] The results using **2a** are in parentheses. [c] *trans*:*cis* = > 99:1. [d] *cis*:*trans* = 99:1 for **2b**, 94:6 for **2a**. [e] **2b** (40 mmol) was used. [f] $VO(acac)_2$ (0.5 mol%) was used instead of $Co(OAc)_2$ and $Mo(CO)_6$. [g] 6 h.

atom from NHPI or **2** to give hydroperoxide **B**, which serves as the oxidant of the molybdenum-catalyzed epoxidation of alkenes.‡ Therefore, the present epoxidation of *cis*-olefin proceeds in a stereospecific manner, in contrast to the epoxidation of *cis*-alkene using aldehyde and O_2, which leads to a mixture of *cis*- and *trans*-epoxides.

Trisubstituted olefins afforded the corresponding epoxides in good selectivity. A terminal olefin, oct-1-ene, was a reluctant substrate for epoxidation using the present catalytic system, forming 1,2-epoxyoctane in moderate conversion. Cyclohexene was also epoxidized to 1,2-epoxycyclohexene in satisfactory yield.

On the other hand, the epoxidation of allylic alcohol, *trans*-hex-2-en-1-ol, to epoxy alcohol was achieved in high yield when $VO(acac)_2$ was employed instead of $Mo(CO)_6$. The epoxidation of allylic alcohols with *tert*-butyl hydroperoxide is known to result in epoxides with higher rates and better yields using vanadium(V) complexes rather than molybdenum(VI) catalysts.[10] It is interesting to note that the present epoxidation of allylic alcohols was promoted smoothly even with a very small amount of $VO(acac)_2$ (0.5 mol%) in the absence of $Co(OAc)_2$. It is thought that $VO(acac)_2$ induces not only the generation of PINO from NHPI under O_2 but also acts as the epoxidation catalyst of alkenes.

In conclusion, we have developed a selective one-pot epoxidation of alkenes with molecular oxygen using hydrocarbons such as ethylbenzene and tetralin as the hydroperoxide source under mild conditions.

This work was partly supported by the Japan Society for the Promotion of Science under the Research for the Future program JSPS.

Notes and References

† *Typical procedure for the epoxidation of* **1**: A PhCN (2 ml) solution of **1** (4 mmol), NHPI (10 mol%), $Co(OAc)_2$ (0.1 mol%), $Mo(CO)_6$ (5 mol%) and **2a** (40 mmol) was placed in a two-necked flask equipped with a balloon filled with O_2. The mixture was stirred at 60 °C for 12 h, and then analyzed by GLC with an internal standard.

‡ In general, the reaction of acylperoxy radicals derived from an aldehyde with olefins has been reported to be *ca.* 10^5 times faster than that of alkylperoxyl radicals derived from hydrocarbons such as **2**: see Y. Sawaki and Y. Ogata, *J. Org. Chem.*, 1984, **49**, 3344.

1 R. Neumann and M. Dahan, *Nature*, 1997, **388**, 24.
2 T. Mukaiyama, T. Takai, T. Yamada and O. Rhode, *Chem. Lett.*, 1990, 1.
3 T. Punniyamurthy, B. Bhatia and J. Iqbal, *Tetrahedron Lett.*, 1993, **34**, 4657; K. Yorozu, T. Takai, T. Yamada and T. Mukaiyama, *Bull. Chem. Soc. Jpn.*, 1994, **67**, 2195; T. Mukaiyama and T. Yamada, *Bull. Chem. Soc. Jpn.*, 1995, **68**, 17 and references cited therein. Recently, we have reported the epoxidation of alkenes with O_2 in the presence of alcohols; T. Iwahama, S. Sakaguchi and Y. Ishii, *Chem. Commun.*, 1999, 727.
4 R. Neumann and M. Dahan, *J. Chem. Soc., Chem. Commun.*, 1995, 171.
5 R. A. Sheldon and J. K. Kochi, *Metal Catalyzed Oxidations of Organic Compounds*, Academic Press, New York, 1981.
6 R. Landau, G. A. Sullivan and D. Brown, *CHEMTECH*, 1979, 602.
7 Y. Yoshino, Y. Hayashi, T. Iwahama, S. Sakaguchi and Y. Ishii, *J. Org. Chem.*, 1997, **62**, 6810; T. Iwahama, K. Syojyo, S. Sakaguchi and Y. Ishii, *Org. Proc. Res. Dev.*, 1998, **2**, 255 and references cited therein.
8 C. Ueda, M. Nayama, H. Ohmori and M. Masui, *Chem. Pharm. Bull.*, 1987, **35**, 1372.
9 We have reported the aerobic oxidation of alkylbenzenes such as toluene at room temperature catalyzed by NHPI combined with $Co(OAc)_2$ (see ref. 7).
10 K. A. Jorgensen, *Chem. Rev.*, 1989, **89**, 431.
11 T. Yamada, T. Takai, O. Rhode and M. Mukaiyama, *Bull. Chem. Soc. Jpn.*, 1991, **64**, 2513.

Communication a908731a

Experimental test of the validity of the use of the *n*-alkanes as model compounds for polyethylene

Stewart F. Parker,*[a] John Tomkinson,[a] Dale A. Braden[b] and Bruce S. Hudson[c]

[a] *ISIS Facility, Rutherford Appleton Laboratory, Chilton, Didcot, Oxon, UK OX11 0QX. E-mail: S.F.Parker@RL.AC.UK*
[b] *Department of Chemistry, University of Oregon, Eugene, OR 97403-1253, USA*
[c] *Department of Chemistry, Syracuse University, Syracuse, NY 13244-4100, USA*

Received (in Cambridge, UK) 15th October 1999, Accepted 10th December 1999

_n_-Alkanes are widely used as model compounds for the dynamics of the crystalline region of polyethylene; this use relies on the assumption of the transferability of the forcefield of the _n_-alkanes, a stringent test of this assumption is a comparison of the dispersion curves of the _n_-alkanes with those of polyethylene; the only direct measurements of the dispersion curves of polyethylene are for the ν_5 acoustic branch, the longitudinal acoustic mode (LAM), an in-plane skeletal mode of perdeuterated polyethylene; in the present work we have observed (by inelastic neutron scattering spectroscopy) and assigned (by the use of density functional theory calculations) the LAM modes of perdeuterated _n_-hexadecane in order to provide the first experimental test of the validity of the assumption.

Polyethylene is a major commodity polymer that is still the subject of active development.[1] Vibrational spectroscopy has played a key role in the characterisation of the material[2] and fundamental to the understanding of the dynamics of the polymer is a knowledge of the dispersion curves for the vibrational modes. The only direct method for the experimental determination of dispersion curves is by coherent inelastic neutron scattering (INS) spectroscopy. For hydrogenous polyethylene, this method fails because the background caused by the incoherent scattering from hydrogen completely swamps the coherent signal. This problem has been circumvented in two ways; the incoherent INS spectrum is related to the vibrational density-of-states which is in turn related to the dispersion curves. Comparison of the experimental spectrum[3] with dispersion curves and the density-of-states derived theoretically allows the quality of the calculations to be assessed. The second method is the use of the *n*-alkanes as model compounds for polyethylene.[4,5] This method relies on the assumption that the *n*-alkanes forcefield is directly transferable to polyethylene and that the end-effects caused by the finite length of the alkane chain can be neglected.

For perdeuterated polyethylene, the larger coherent and smaller incoherent cross-sections of deuterium[6] (H: incoherent 79.7 barns, coherent 1.758, deuterium: incoherent 2.0 barns, coherent 5.597 barns, 1 barn $= 1 \times 10^{-28}$ m^2) has allowed the ν_5 acoustic branch, the longitudinal acoustic mode (LAM), an in-plane skeletal mode, to be mapped by coherent INS.[7–10] These results are the only *direct* experimental measurement of any of the dispersion curves of polyethylene. Thus any test of the validity of the assumption that the *n*-alkanes are good models for polyethylene requires the determination of the LAM modes of a perdeuterated *n*-alkane. Unfortunately, while the LAM modes are formally IR and Raman active, their intensities are usually so small as to be unobservable for any but the first few modes (Raman) and the highest energy ones (IR).

We have recently shown that it is possible to both observe[11] and assign[12,13] the LAM modes of the *n*-alkanes (n = 5–25) by a combination of incoherent INS spectroscopy and *ab initio* calculations. In the present report we have extended the method to perdeutero-*n*-hexadecane in order to compare the experimental data for perdeuterated polyethylene with the measured LAM frequencies of $C_{16}D_{34}$.

It is only with the development of pulsed neutron sources with their high flux of epithermal neutrons that it has been possible to record incoherent INS spectra of perdeuterated compounds. With the increase in detected flux resulting from the recent installation of TOSCA[14] at ISIS (Rutherford Appleton Laboratory, Chilton, UK) it is now possible to routinely record spectra from such samples. Fig. 1 shows the incoherent INS spectrum of $C_{16}D_{34}$ in the region[15] below 500 cm^{-1}. All of the modes between 200 and 400 cm^{-1} are LAM modes, a further five modes occur below 200 cm^{-1} where the out-of-plane transverse acoustic modes and the external

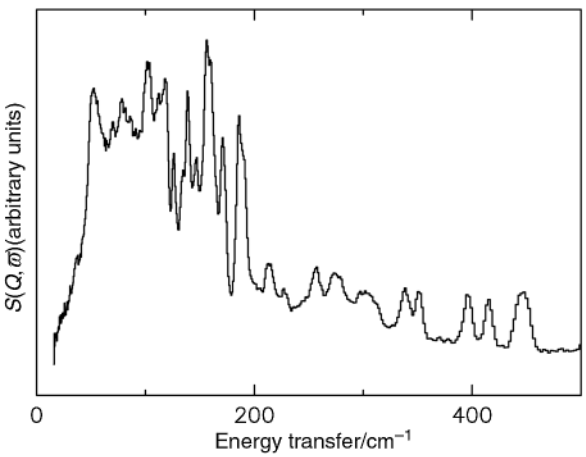

Fig. 1 Inelastic neutron scattering spectrum of $C_{16}D_{34}$ in the region 0–500 cm^{-1} showing the longitudinal acoustic modes, transverse acoustic modes and the external modes.

Table 1 Observed and calculated (DFT) frequencies (cm^{-1}) for the longitudinal acoustic modes of $C_{16}D_{34}$

	κ													
	0.067	0.133	0.200	0.267	0.333	0.400	0.467	0.533	0.600	0.667	0.734	0.800	0.867	0.934
Obs.	(159)	257	353	416	449	449	399	339	277	213	(127)	(102)	(54)	(25)
DFT	152	253	350	416	454	447	398	339	275	211	131	98	54	24
Symmetry	A_g	B_u	A_g	B_u	A_g	B_u	A_g	B_u	A_g	B_u	A_g	B_u	A_g	B_u

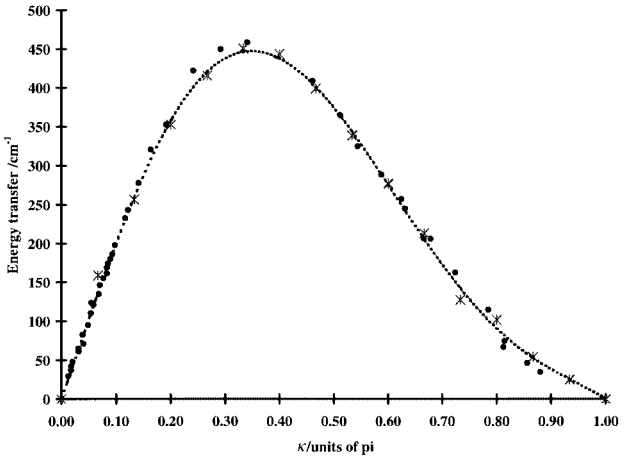

Fig. 2 Comparison of experimental data for the ν_5 mode of deuterated polyethylene (●) and the experimental LAM frequencies of $C_{16}D_{34}$ (*). The dashed line is a quintic least squares fit to the DFT data for perdeutero-*n*-hexadecane.

modes also occur. The density functional theory (DFT) calculations were performed using the GAUSSIAN-94[16] program in the B3LYP density functional approximation. The basis set used was 6-31-G**. The DFT results allow the modes to be assigned to a specific phase angle, κ. The results are shown in Table 1. The experimental frequencies below 200 cm^{-1} are given in parentheses since the DFT calculations show that out-of-plane modes lie close-by, thus there is some uncertainty (a few wavenumbers) in the exact value of the frequency.

Fig. 2 shows a comparison of experimental data for the ν_5 mode of perdeuterated polyethylene, the experimental frequencies and the frequencies calculated by DFT. The solid line is a quintic least squares fit to the DFT results for perdeuterated *n*-hexadecane as a guide to the eye. It can be seen that there is excellent agreement between all three sets of data. This provides the *first* experimental validation of the assumption that the forcefields derived from the *n*-alkanes are transferable to polyethylene.

This work is noteworthy for two other reasons: first that it is now possible to routinely obtain high quality incoherent inelastic neutron scattering spectra of perdeuterated samples and second the demonstration of the success of DFT calculations for the analysis of inelastic neutron scattering spectra provides a benchmark against which other methods can be tested.

This work was partially supported by the US National Science Foundation under grant CHE 9803058 and utilised the computer systems Exemplar and SGI PCarray at the National Centre for Supercomputing Applications, University of Illinois at Urbana-Champaign. The Rutherford Appleton Laboratory is thanked for access to neutron beam facilities.

Notes and references

1 C. Jenny and P. Maddox, *Curr. Opin. Solid State Mater. Sci.*, 1998, **3**, 94.
2 D. I. Bower and W. F. Maddams, in *The Vibrational Spectroscopy of Polymers*, Cambridge University Press, Cambridge, 1989, ch. 5.
3 S. F. Parker, *J. Chem. Soc., Faraday Trans.*, 1996, **92**, 1941.
4 P. C. Painter, M. L. Coleman and J. L. Koenig, *The Theory of Vibrational Spectroscopy and its Application to Polymeric Materials*, Wiley-Interscience, New York, 1982, ch. 13.
5 J. H. Schachtschneider and R. G. Snyder, *Spectrochim. Acta*, 1963, **19**, 85, 117.
6 V. F. Sears, *Neutron News*, 1992, **3**, 26.
7 L. A. Feldkamp, G. Vankataraman and J. S. King, *Neutron Inelastic Scattering*, International Atomic Energy Authority, Vienna, 1968, vol. 2, p. 159.
8 J. F. Twistleton and J. W. White, *Neutron Inelastic Scattering*, International Atomic Energy Authority, Vienna, 1972, p. 301.
9 G. Pepy and H. Grimm, *Neutron Inelastic Scattering*, International Atomic Energy Authority, Vienna, 1968, vol. 1, p. 607.
10 J. F. Twistleton, J. W. White and P. A. Reynolds, *Polymer*, 1982, **23**, 578.
11 S. F. Parker, *Macromol. Symp.*, 1997, **119**, 227.
12 S. F. Parker, D. A. Braden, J. Tomkinson and B. S. Hudson, *J. Phys. Chem. B*, 1998, **102**, 5955.
13 D. A. Braden, S. F. Parker, J. Tomkinson and B. S. Hudson, *J. Chem. Phys.*, 1999, **111**, 429.
14 S. F. Parker, C. J. Carlile, T. Pike, J. Tomkinson, R. J. Newport, C. Andreani, F. P. Ricci, F. Sachetti and M. Zoppi, *Physica B*, 1998, **241–243**, 154.
15 The complete spectrum 16–4000 cm^{-1} is available at http://www.isis.rl.ac.uk/insdatabase.
16 M. J. Frisch, G. W. Trucks, H. B. Schlegel, P. M. W. Gill, B. G. Johnson, M. A. Robb, J. R. Cheeseman, T. Keith, G. A. Petersson, J. A. Montgomery, K. Raghavachari, M. A. Al-Laham, V. G. Zakrzewski, J. V. Ortiz, J. B. Foresman, J. Cioslowski, B. B. Stefanov, A. Nanayakkara, M. Challacombe, C. Y. Peng, P. Y. Ayala, W. Chen, M. W. Wong, J. L. Andres, E. S. Replogle, R. Gomperts, R. L. Martin, D. J. Fox, J. S. Binkley, D. J. Defrees, J. Baker, J. P. Stewart, M. Head-Gordon, C. Gonzalez and J. A. Pople, Gaussian 94, Revision D.4, Gaussian, Inc., Pittsburgh, PA, 1995.

Communication a908263h

ChemComm

Metal ion effects on the asymmetric dimerization of 1-phenyl-3,4-dimethylphosphole

Guosen He, Ying Qin, K. F. Mok and Pak-Hing Leung*

Department of Chemistry, National University of Singapore, Kent Ridge 119260, Singapore.
E-mail: chmlph@nus.edu.sg

Received (in Cambridge, UK) 29th September 1999, Accepted 10th December 1999

An optically pure P-chiral diphosphine has been prepared efficiently from the asymmetric dimerization of 3,4-dimethyl-1-phenylphosphole in the presence of an organoplatinum(II) complex derived from (*R*)-*N*,*N*-dimethyl-1-(1-naphthyl)ethylamine.

Recently we have reported a series of asymmetric Diels–Alder reactions between the cyclic diene 3,4-dimethyl-1-phenylphosphole (DMPP) and various dienophiles in the presence of an organopalladium complex containing the enantiomerically pure forms of *N*,*N*-dimethyl-1-(1-naphthyl)ethylamine.[1] This organopalladium complex has been employed frequently because it is perhaps the most efficient reaction promoter and stereochemical controller for the activation of DMPP in these asymmetric syntheses. In cases where vinylphosphines were used as dienophiles, optically pure P-chiral diphosphines were obtained in high yields.[2] In theory, the [4 + 2] *exo*-cycloaddition reaction between two DMPP molecules will produce a rigid chiral diphosphine containing two phosphorus and four carbon stereogenic centres. Interestingly, this asymmetric dimerization process could not be achieved with the chiral organopalladium complex despite the fact that it has activated DMPP effectively as a cyclic diene in many cycloaddition reactions. Apparently, the organopalladium complex is not an efficent promoter for the activation of the dienophilicity of DMPP. Here we report the application of an analogous organoplatinum complex for the high yield synthesis of the desired optically active DMPP dimer.

As illustrated in Scheme 1, the reaction between the chiral platinum (−)-**1**[3] and 2 mol of DMPP in $CHCl_3$ at 30 °C for 60 d gave a 3:1 mixture of the regioisomers (−)-**2** and (−)-**3** in quantitative yield. The cationic complexes, which could not be separated by fractional crystallization, were separated efficiently by silica gel chromatography. The 202 MHz ^{31}P NMR spectrum of each regioisomer in $CDCl_3$ exhibited a pair of doublets. For the major isomer (−)-**2**, the doublet resonances occurred at δ 37.7 (J_{PtP} 3285 Hz, J_{PP} 7 Hz) and 133.7 (J_{PtP} 1548 Hz, J_{PP} 7 Hz). For the minor regioisomer (−)-**3**, the doublets were observed at δ 52.3 (J_{PtP} 1476 Hz, J_{PP} 7 Hz) and 104.8 (J_{PtP} 3216 Hz, J_{PP} 7 Hz). The low field doublets in these isomeric complexes are typical for bridgehead phosphorus adopting the *exo-syn* stereochemistry.[4] It is noteworthy that the Pt–P(bridgehead) coupling of (−)-**2** is significantly smaller than that of (−)-**3** as the former P(bridgehead) donor is located *trans* to a strong π-accepting aromatic carbon atom.[5] Treatment of both isomeric complex mixtures with conc. HCl removed the naphthylamine auxiliary chemoselectively to give the same dichloro complexes (+)-**4** as pale yellow prisms (70%), mp 200–202 °C (decomp.), $[\alpha]_D$ +58.4 (*c* 0.7, CH_2Cl_2). The ^{31}P NMR spectrum of (+)-**4** in $CDCl_3$ exhibited a pair of doublets at δ 39.6 (J_{PtP} 3193 Hz, J_{PP} 16.8 Hz) and 107.0 (J_{PtP} 3265 Hz, J_{PP} 16.8 Hz). The molecular structure and the absolute stereochemistry of (+)-**4** were determined by X-ray structural analyses (Fig. 1).† The studies reveal that the absolute configurations at P(1), P(2), C(1), C(4), C(5) and C(6) in the complex are *S*, *R*, *R*, *S*, *R*, and *R*, respectively. It should be noted that the dimerization process could be completed in 8 d by heating the reaction mixture at 100 °C in a sealed tube. Under these more vigorous conditions, however, product formation becomes less regioselective and a 1.5:1 mixture of (−)-**2** and (−)-**3** was obtained in somewhat lower yields.

Treatment of a CH_2Cl_2 solution of (+)-**4** with aqueous cyanide liberated the optically pure diphosphine (+)-**5** quantitatively as an air-sensitive oil with $[\alpha]_D$ +145 (*c* 0.5, CH_2Cl_2). The ^{31}P NMR spectrum of the free diphosphine in $CDCl_3$ exhibited a pair of doublets at δ 4.9 and 104.2 (J_{PP} 43.9 Hz). The low field ^{31}P resonance indicates that the *exo-syn* stereochemistry is retained. It is noteworthy that the apparent inversion of configuration that takes place at both phosphorus stereogenic centres during the liberation reaction is merely a consequence of the Cahn–Ingold–Prelog (CIP) rules.[6] The optical purity of (+)-**5** was confirmed by the quantitative repreparation of (−)-**2** and (−)-**3** from the liberated ligand and (−)-**1**; the 202 MHz ^{31}P NMR spectrum of the crude product exhibited signals due to the two regioisomers only. Unlike those obtained directly from the coupling reaction, the simple complexation process between (+)-**5** and (−)-**1** regenerated (−)-**2** and (−)-**3** as a 1:3 diastereomeric mixture. In a further test of optical purity, (+)-**5** was coordinated to the equally accessible (S_c)-(+)-**1**. The ^{31}P NMR spectrum of the crude product in $CDCl_3$ exhibited two new doublet resonances at δ 56.7 (J_{PtP} 1506 Hz, J_{PP} 10 Hz) and

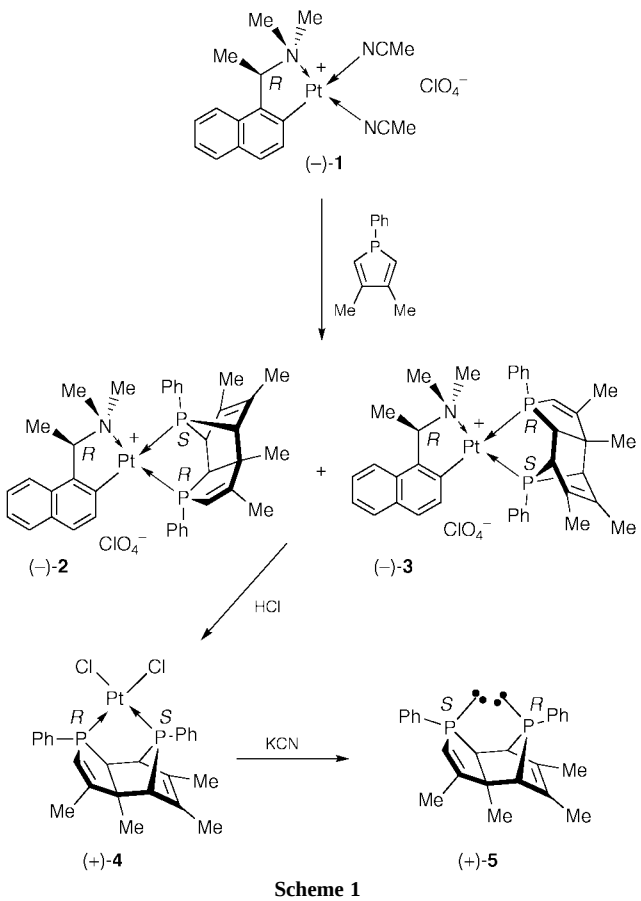

Scheme 1

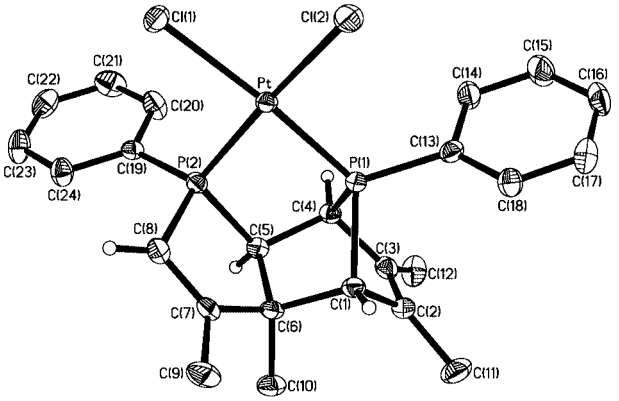

Fig. 1 Molecular structure and absolute stereochemistry of (+)-**4**. Selected bond lengths (Å) and angles (°): Pt–P(1) 2.214(1), Pt–P(2) 2.222(1), Pt–Cl(1) 2.381(1), Pt–Cl(2) 2.369(1), P(1)–C(1) 1.887(4), P(1)–C(4) 1.850(4), P(1)–C(13) 1.799(4), P(2)–C(5) 1.854(4), P(2)–C(8) 1.791(4), P(2)–C(19) 1.802(4), C(5)–C(6) 1.578(5), C(6)–C(7) 1.526(5), C(7)–C(8) 1.332(5), P(1)–Pt–P(2) 82.4(1), P(1)–Pt–Cl(1) 172.0(1), P(1)–Pt–Cl(2) 96.2(1), P(2)–Pt–Cl(1) 90.4(1), P(2)–Pd–Cl(2) 172.9(1), Cl(1)–Pt–Cl(2) 91.4(1), C(1)–P(1)–C(4) 80.2(2).

107.7 (J_{PtP} 3131 Hz, J_{PP} 10 Hz). According to the Pt–P coupling constants, these new signals are due to the S_c diastereomer of complex **3**. Interestingly, the S_c diastereomer of complex **2** was not formed *via* this coordination pathway, presumably due to steric reasons. More importantly, no resonance signals were detected at δ 37.7, 52.3, 104.8 and 133.7. It is noteworthy that the enantiomeric diphosphine (−)-**5** can be prepared similarly from the dimerization of DMPP using (+)-**1** as the chiral reaction promoter. However, diphosphine **5** was not obtained when the palladium analogue of **1** was used as the reaction promoter.

Finally, it is interesting to note that under different reaction conditions, complex **1** is able to activate DMPP both as a cyclic diene and as a dienophile toward the chemically reactive cyclopentadiene. Thus, when a $CHCl_3$ solution of (−)-**1**, DMPP, excess cyclopentadiene and a small quantity of NH_4Cl was heated at 60 °C for 24 h,[1] the ^{31}P NMR spectrum of the crude reaction mixture in $CDCl_3$ exhibited only two low field singlets of similar intensities at δ 98.3 and 98.1. The two singlets are of the same Pt–P coupling (3781 Hz). These low field NMR signals confirmed that two diasteromeric cycloadducts were formed and DMPP reacted as the cyclic diene under these conditions. On the other hand, when the reaction was carried out at room temperature for 24 h in the absence of the chloride anion,[1] only one isomer was produced. The ^{31}P NMR spectrum of the crude product exhibited a sole singlet at δ 14.5 (J_{PtP} 3703 Hz). This relatively high field ^{31}P NMR signal indicated that DMPP had reacted as the dienophile rather than the cyclic diene in this cycloaddition reaction. Investigations on the absolute stereochemistry of these cyclic adducts and the dienophilicity of DMPP toward other dienes are currently in progress.

We are grateful to the National University of Singapore for support of this research (Grant No. RP960675) and research scholarships to GSH.

Notes and references

† *Crystal data* for (+)-**4**: $[C_{24}H_{26}Cl_2P_2Pt]$, M = 642.38, orthorombic, space group $P2_12_12_1$, a = 11.288(1), b = 13.478(1), c = 15.818(1) Å, V = 2406.6(1) Å^3, Z = 4, D_c = 1.773 g cm^{-3}, μ(Mo-Kα) = 17.73 cm^{-1}, F(000) = 1248. A pale yellow prism with dimensions 0.20 × 0.14 × 0.10 mm was used for diffraction studies. A total of 5275 independent reflections were measured on a Siemens SMART CCD diffractometer with Mo-Kα radiation (graphite monochromator) using ω-scans. All the non-hydrogen atoms were refined anisotropically. In the full-matrix least-squares based on F^2 with absorption corrected data to give R_1 = 0.0199, wR_2 = 0.0434. The absolute stereochemistry was determined unambiguously by refining the Flack parameter [x = 0.01(1)]. CCDC 182/1507. See http://www.rsc.org/suppdata/cc/a9/a907846k/ for crystallographic data in .cif format.

1 G. S. He, S. K. Loh, J. J. Vittal, K. F. Mok and P. H. Leung, *Organometallics*, 1998, **17**, 3931 and references cited therein.
2 Y. C. Song, K. F. Mok, P. H. Leung and S. H. Chan, *Inorg. Chem.*, 1998, **37**, 6399.
3 S. Y. M. Chooi, J. D. Ranford, P. H. Leung and K. F. Mok, *Tetrahedron: Asymmetry*, 1994, **5**, 1805.
4 L. D. Quin and A. N. Hughes, in *The Chemistry of Organophosphorus Compounds*, ed. F. R. Hartley, John Wiley, New York, 1990, vol. I, ch. 10.
5 R. J. Cross, I. G. Dalgleish, G. J. Smith and R. Wardle, *J. Chem. Soc., Dalton Trans.*, 1996, 4443.
6 R. S. Cahn, C. K. Ingold and V. Prelog, *Angew Chem., Int. Ed. Engl.*, 1966, **5**, 385.

Communication a907846k

Highly enantioselective propargylic monofluorination established by carbon-13 and fluorine-19 NMR in chiral liquid crystals

Valérie Madiot,[a] Philippe Lesot,*[b] Danielle Grée,[a] Jacques Courtieu[b] and René Gree*[a]

[a] *Laboratoire de Synthèses et Activations de Biomolécules CNRS ESA 6052, ENSCR, Avenue du Général Leclerc, 35700 Rennes Beaulieu, France. E-mail: gree@ensc-rennes.fr*

[b] *Laboratoire de Chimie Structurale Organique, CNRS ESA 8074, ICMO, Bât 410, Université de Paris-Sud, 91405 Orsay, France. E-mail: philesot@icmo.u-psud.fr*

Received (in Liverpool, UK) 12th November 1999, Accepted 6th December 1999

Carbon-13 and fluorine-19 NMR experiments in a chiral polypeptide liquid crystalline solvent (PBLG) are used to establish enantioselective propargylic monofluorination.

Fluorine strongly modifies the physical, chemical and biological properties of organic molecules, giving access to new drugs or pharmacological tools and useful agrochemicals.[1] Monofluorination remains a challenging problem in terms of regio- and stereo-control,[2] especially in positions vicinal to unsaturated systems, even if some transition metal complexes can control the dehydroxyfluorination.[3] An alternative is to prepare small, chiral, fluorinated building blocks which can be elaborated into the target molecules.[4] Since acetylenic derivatives have high potentialities for stereoselective synthesis,[5] propargylic fluorides should be versatile intermediates.[6] In this strategy, control of the absolute configuration at the stereogenic center is important, therefore the preparation of optically active propargylic fluorides becomes a central question.[7,8]

Here we report the first study of enantioselectivity in dehydroxyfluorination using alcohols **1a** and **1b** as models. Furthermore, we demonstrate NMR in chiral liquid crystals as a powerful method for the analysis of the enantiomeric purity of these propargylic fluorides.

The reaction of (±)-**1a** with diethylaminosulfur trifluoride (DAST) at −50 °C is regiocontrolled,[9] giving exclusively (55% yield) the propargylic fluoride (±)-**2a** (Scheme 1).[10] Such chiral propargylic fluorides appear rather difficult to discriminate, and until now, none of the usual tools in the field of enantiomeric analysis (chiral GC or HPLC, chiral shift reagents *etc.* have allowed the differentiation of the enantiomers of (±)-**2a** for instance. It was therefore of interest to explore other analytical approaches such as NMR in chiral liquid crystalline solvents.[11–13] Indeed, it has been demonstrated that ^{2}H, ^{13}C or ^{19}F NMR in organic solutions of poly(γ-benzyl L-glutamate) (PBLG) can provide a competitive alternative when normal methods fail. In proton-decoupled natural abundance ^{13}C NMR (^{13}C{^{1}H}), enantiomeric discrimination is observed through a difference in the ^{13}C chemical shift anisotropies (CSA), leading to two separated peaks for each discriminated carbon of the molecule. This allows the measurement of ees with an accuracy of about ±5%.[12] As the parameters governing the strength of the ^{13}C CSA mainly increases with the electronegativity of the substituents and the hybridization state of the carbons [$\Delta\sigma$ (sp) > $\Delta\sigma$ (sp^2) > $\Delta\sigma$ (sp^3)], we could expect to obtain a measurable chiral discrimination on the acetylenic carbons of the fluorinated propargylic compounds.[12]

Fig. 1(*a*) presents the 100.62 MHz ^{13}C{^{1}H} spectrum associated with the ethynyl carbons of (±)-**2a** recorded in the PBLG/$CHCl_3$ phase.†‡ Analysis of the spectrum shows two doublets centred at different chemical shifts for the C-1 and the C-2 carbons. The splittings, noted T_{CF}, arise from the ^{13}C–^{19}F scalar (J_{CF}) and dipolar (D_{CF}) couplings, the latter being also order sensitive ($T_{CF} = J_{CF} + 2D_{CF}$).[12] However, as indicated in Fig. 1(*a*), it appears that the two enantiomers are mainly discriminated through a difference of CSA. The chemical shift differences ($\delta_R - \delta_S$) for C-1 and C-2 are of 0.07 and 0.06 ppm, respectively. Note also that a small chiral discrimination was also observed on the sp^3 chiral carbon of (±)-**2a**.

With this tool in hand, it now becomes possible to study the enantioselectivity of the dehydroxyfluorination reaction on (+)-**1a** and (−)-**1a** at various temperatures. The synthesis of (+)-**1a** or (−)-**1a** (ee ⩾ 95%) is straightforward, starting from commercially available (*R*)- or (*S*)-but-3-yn-2-ol (Scheme 2). Fig. 1(*b*) presents the ^{13}C{^{1}H} NMR signals associated with the C-1 and C-2 carbons of (−)-**2a** prepared at −55 °C from (−)-**1a**. When comparing these data with that of (±)-**2a**, we clearly observe a difference in peak intensity for both sp carbons. The measurement of the ee for the spectrum in Fig. 1(*b*) is, therefore, possible using both the signal of C-1 and C-2, which enhances the confidence interval in the determination of the ee. Thus, at −55 °C, the ee calculated using either peak integration or deconvolution tools is 45 ± 5%, whereas the ee increases to 75 ± 5% when the reaction temperature is lowered to −95 °C. Note that the (*S*)-enantiomer exhibits the most shielded signal for both carbons and all these experimental values were confirmed when (−)-**1a** was replaced by (+)-**1a**.

Thus, the dehydroxyfluorination reaction of (+)-**1a** or (−)-**1a** has a good enantioselectivity (⩾75%) at low temperature. This

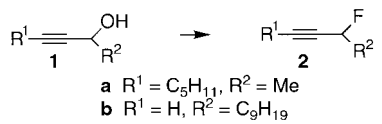

Scheme 1

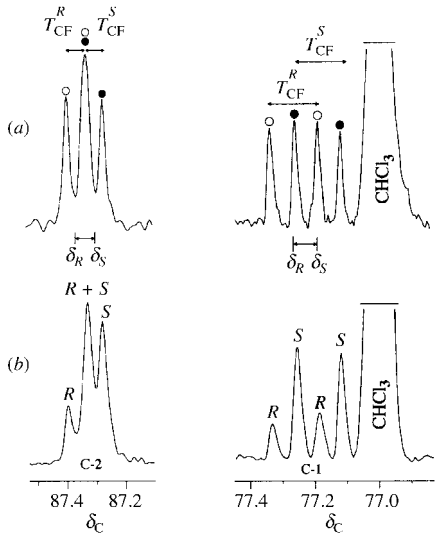

Fig. 1 ^{13}C{^{1}H} spectrum associated with the ethynyl carbons of (*a*) (±)-**2a** and (*b*) (−)-**2a** recorded at 298 K. Gaussian filtering was applied to enhance the spectral appearance. For (±)-**2a**, we measure T^R_{CF} = ± 14.9 Hz, T^S_{CF} = ± 14.4 Hz for the C-1 carbon, and T^R_{CF} = ± 6.9 Hz, for the C-2 carbon.

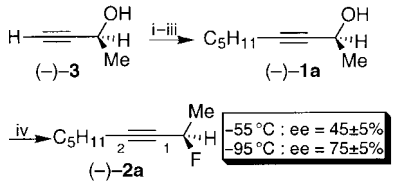

Scheme 2 *Reagents and conditions*: i, TBDMSCl, imidazole, DMAP, THF (84%); ii, BuLi, $C_5H_{11}Br$, THF–HMPA (3:1), −30 °C (85%); iii, Bu_4NF, THF (93%); iv, DAST, CH_2Cl_2 (55%).

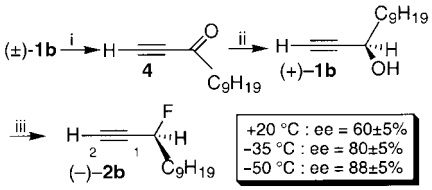

Scheme 3 *Reagents and conditions*: i, PCC, AcONa, CH_2Cl_2 (56%); ii, *R*-Alpine-Borane (89%); iii, DAST, CH_2Cl_2 (51%).

reaction exhibits a strong temperature dependence since the ee is only 45% at *ca.* −55 °C. In agreement with the mechanism generally accepted for DAST fluorination,[14] inversion of configuration is assumed.

A similar sequence was followed by the case of **2b**. Starting from (±) = **1b**[6] the racemic derivative (±)-**2b** is obtained, together with a small amount of the corresponding enyne separated by chromatography. The optically active alcohol (+)-**1b** (ee = 90%) is obtained by asymmetric reduction of **4** (Scheme 3).[15] Once again, ^{13}C NMR in PBLG allowed the study of the enantioselectivity of the fluorination.

In this example, the results were also confirmed through 376.49 MHz $^{19}F\{^1H\}$ NMR. Fig. 2(*a*) presents the $^{19}F\{^1H\}$ spectrum and $^{13}C\{^1H\}$ NMR signal associated with the C-2 carbon of (±)-**2b**. As before, the analysis of the ^{13}C signal shows two doublets centred at two different chemical shifts ($\delta_S - \delta_R$ = 0.14 ppm). Note that the C-1 carbon was also significantly discriminated through a chemical shift difference ($\delta_S - \delta_R$ = 0.20 ppm). Unlike the compound (±)-**2a**, which showed no chiral discrimination *via* $^{19}F\{^1H\}$ NMR, the derivative (±)-**2b** exhibits specific ^{19}F CSAs for each enantiomer ($\delta_S - \delta_R$ = 0.03 ppm). This example is the first case of chiral discrimination through $^{19}F\{^1H\}$ NMR on a monofluorinated compound using a chiral liquid crystal.

Fig. 2(*b*) reports the $^{19}F\{^1H\}$ and $^{13}C\{^1H\}$ NMR signal of (−)-**2b** synthesised at −35 °C starting from (+)-**1b**. We can observe unambiguously the strong difference in intensity of the doublets of each enantiomer compared with (±)-**2b**, thus showing the high enantioselectivity of this reaction. For this example, the ee calculated through peak integration or deconvolution processes is 80 ± 5% at −35 °C. It is noteworthy that the synthesis of (+)-**2b** at −50 °C enable us to further enhance the ee to 88 ± 5%. Therefore, the dehydroxyfluorination of (+)-**1b** has a very high stereoselectivity (≥97%) at −50 °C. As for **1a**, the reaction shows a temperature dependence, since the ee is 80% at −35 °C and only 60% at room temperature. Note here that the (*R*)-enantiomer exhibits the most shielded signals for C-1 and C-2. These results were confirmed using (−)-**1b** as starting material.

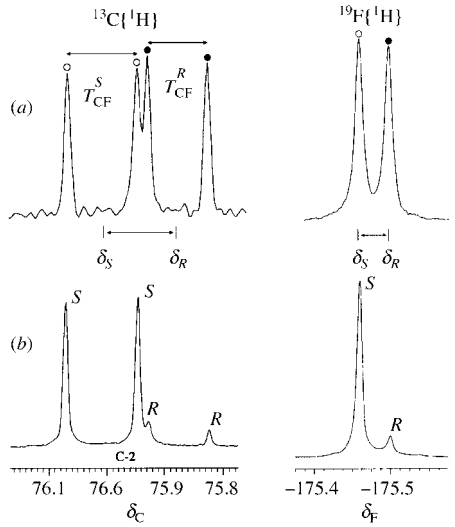

Fig. 2 $^{19}F\{^1H\}$ spectrum and $^{13}C\{^1H\}$ NMR signal associated to the C-2 carbon of (*a*) (±)-**2b** and (*b*) (−)-**2b** recorded at 294 K by adding 64 and 1500 scans, respectively. Gaussian filtering was applied to enhance the spectral appearance. For (±)-**2b**, we measure T_{CF}^S = ± 12.8 Hz, T_{CF}^R = ±11.1 Hz for the C-2 carbon.

These data appear to indicate a competition between S_N2 and S_N1 type processes. In the case of **1a**, the pentyl group can provide better stabilization for the carbocationic intermediate, leading to lower selectivities and a stronger temperature dependence compared to the hydrogen in **1b**. In addition, this study highlights the noteworthy potential of NMR in PBLG as an analytical method. Finally, these results, especially in the case of **2b**,[6] are of interest with regard to the preparation of fluorinated analogues of natural products.

We thank the region Bretagne for a fellowship to V. M.

Notes and references

† *Sample composition*: The liquid crystalline NMR samples were made from 100 mg of PBLG (DP = 534), 100 mg of a chiral material and 350 mg of $CHCl_3$. Sample preparation, see refs. 11–13.

‡ *NMR experiments*: NMR experiments were performed on Bruker DRX-400 (5 mm BBI probe) and ARX-400 (5 mm QNP probe) spectrometers. Broad-band proton decoupling was applied using the WALTZ-16 sequence. The interferograms were acquired using a pulse angle of ~60°, a recycle delay of ~1.5 s and 8 or 16 K of data points. Zero filling to 16 or 32 K was applied to increase the digital resolution.

1 See for instance: J. T. Welch, *Tetrahedron*, 1987, **43**, 3123; *Selective Fluorination in Organic and Bioorganic Chemistry*, ed. J. T. Welch, ACS symposium series 456, Washington DC, 1991; *Biomedical Frontiers of Fluorine Chemistry*, ed. I. Ojima, J. R. McCarthy and J. T. Welch, ACS symposium series 639, Washington DC, 1996.

2 R. L. Gree and J. P. Lellouche, *Enantiocontrolled Synthesis of Fluoro-Organic Compounds*, ed. V. A. Soloshonok, Wiley, Chichester, 1999.

3 D. M. Gree, C. J. M. Kermarrec, J. T. Martelli, R. L. Gree, J. P. Lellouche and L. J. Toupet, *J. Org. Chem.*, 1996, **61**, 1918; C. Kermarrec, V. Madiot, D. Gree, A. Meyer and R. Gree, *Tetrahedron Lett.*, 1996, **37**, 5691; S. Legoupy, C. Crevisy, J. C. Guillemin and R. Gree, *J. Fluorine Chem.*, 1999, **93**, 171.

4 F. A. Davis and P. V. N. Kasu, *Tetrahedron Lett.*, 1998, **39**, 6135.

5 F. Diederich and P. J. Stang, *Metal-catalysed Cross-coupling Reactions*, Wiley, Weinheim, 1998

6 For a synthesis of stereodefined systems with allylic fluorides (V. Madiot, D. Gree and R. Gree, *Tetrahedron Lett.*, 1999, **40**, 6403).

7 Few propargylic monofluorides have been described, see: (*a*) C. D. Poulter, P. L. Wiggins and T. L. Plummer, *J. Org. Chem.*, 1981, **46**, 1532; (*b*) F. Benayoud, D. J. de Mendonca, C. A. Digits, G. A. Moniz, T. C. Sanders and G. B. Hammond, *J. Org. Chem.*, 1996, **61**, 5159; (*c*) T. Munyemana, PhD Thesis, Louvain la Neuve, Belgium, 1991.

8 Only two optically active compounds have been previously reported, see: Y. Matsumura, T. Shimada, T. Nakayama, M. Urushirara, T. Asai, Y. Morizawa and A. Yasuda, *Tetrahedron*, 1995, **51**, 8771.

9 For exceptions, see: R. E. A. Dear and E. E. Gilbert, *J. Org. Chem.*, 1968, **33**, 819. See also ref. 7(*b*).

10 The isolated yields are rather low due to the volatility of this type of derivative.

11 I. Canet, J. Courtieu, A. Loewenstein, A. Meddour and J. M. Péchiné, *J. Am. Chem. Soc.*, 1995, **117**, 6520.

12 A. Meddour, P.Berdagué, A. Hedli, J. Courtieu and P. Lesot, *J. Am. Chem. Soc.*, 1997, **119**, 4502.

13 M. Jakubcova, A. Meddour, J. M. Péchiné, A. Baklouti and J. Courtieu, *J. Fluorine Chem.*, 1997, **86**, 149.

14 M. Hudlicky, *Org. React.*, 1988, **35**, 516.

15 For the *n*-octyl derivative, see: F. Baludri, V. Fiandanese, O. Hassan, A. Punzi and F. Naso, *Tetrahedron*, 1998, **54**, 4327.

Communication a909012f

A direct conversion of α,β-unsaturated ketones to vinylcyclopropanes: new zirconium-mediated reaction†

Philippe Bertus, Vincent Gandon and Jan Szymoniak*

Réactions Sélectives et Applications (UMR 6519), Université de Reims, 51687 Reims Cedex 2, France.
E-mail: jan.szymoniak@univ-reims.fr

Received (in Liverpool, UK) 5th November 1999, Accepted 6th December 1999

Various vinylcyclopropanes are synthesized from α,β-unsaturated ketones *via* a zirconium-mediated [1,2]-addition–deoxygenative cyclopropanation sequence; the latter step surprisingly proceeds under specific protic conditions.

Vinylcyclopropane derivatives are useful intermediates for a wide variety of transformations including rearrangements and stereoselective ring expansions, nucleophilic and electrophilic ring opening, and transition metal catalyzed reactions.[1] On the other hand, many natural or synthetic biologically active molecules contain a vinylcyclopropane moiety. The latter can be constructed using procedures that involve direct formation of the cyclopropane ring.[1,2] The limitation of these methods lies in the necessary use of the carbon–carbon double bond entity as a precursor. Thus, it appears worthwhile to search for new synthetic procedures aimed at relating the vinylcyclopropane moiety to other frequently encountered structural subunits.

Here we present a new approach to vinylcyclopropane derivatives.[3] The described procedure makes it possible to obtain them directly from α,β-enones, by zirconium-assisted deoxygenative addition of an ethylene dianion equivalent (in a formal sense). In practice, zirconocene (ethylene) complex, formed from Cp_2ZrEt_2, was used as a reagent.[4] In the first experiment, Cp_2ZrEt_2 was formed from Cp_2ZrCl_2 and EtMgBr (2 equiv.) in THF at −78 °C, and Cp_2Zr (ethylene) generated by allowing the reaction mixture to warm to 0 °C. Afterwards, benzylideneacetone (**1**) was added, and the reaction carried out at room temperature for 2 h.[5] The hydrolysis of the reaction mixture with 3 M HCl afforded alcohol **2** and an unexpected minor vinylcyclopropane derivative **3** (**3**:**2** = 22:78) (Scheme 1).[6]

Deuterolysis of the reaction mixture with DCl in D_2O (3 M) gave [^{2}H]-**2**, namely 5-deuterio-3-methyl-1-phenylpent-1-en-3-ol, with > 98% D incorporation. This result suggested that the reaction had involved an intermediate oxazirconacyclopentane (**A**), similar to those postulated for the reactions employing saturated ketones.[6]

Using 3 M H_2SO_4 instead of 3 M HCl for hydrolysis, the course of the final reaction changed. Thus, quenching of the reaction with 3 M H_2SO_4 resulted in predominant formation of vinylcyclopropane derivative **3** (**3**:**2** = 92:8) which was isolated in 45% yield (Scheme 1). We next ascertained that the cyclization process had not occurred before protonolysis, under the reaction conditions. In fact, no trace of **3** was detected in THF at 0 °C or at room temperature even after prolonged reaction time (36 h). This observation confirmed the crucial role of H_2SO_4 for cyclization. Thus, the title reaction markedly differs from the somewhat similar Kulinkovich hydroxy-cyclopropanation, which allows the preparation of cyclopropanols or cyclopropylamines from esters (carbonates) or amides and a Grignard reagent, in the presence of $Ti(OPr^i)_4$.[7] Whereas the latter involves the spontaneous rearrangement of the intermediate oxatitanacycle, specific protic conditions proved to be necessary for our cyclization to occur. Finally, we noticed that no cyclization reaction occurred with H_2SO_4 starting from the saturated ketones, and only the corresponding alcohols were isolated in all cases.

To further explore the scope of the title reaction other α,β-unsaturated ketones were tested. As shown in Table 1, the reaction can be applied to the synthesis of various vinylcyclopropane derivatives. Particularly, the spiro cyclopropane derivatives **11**–**15** (entries 3–7) could be prepared in moderate to excellent yields starting from the cyclic substrates. Thus, isophorone (**5**) and cholestenone (**6**) were transformed into the corresponding vinylcyclopropane derivatives **11** and **12**, respectively, in 75 and 91% yield (entries 3 and 4). The easily prepared **12** should be considered as a new potentially useful steroidal intermediate.[8] The carbonyl-conjugated C=C double bond may be in an exocyclic as well as endocyclic position, and even an additional isolated C=C double bond may be present in the substrate (entries 5 and 6). The reactions have also been accomplished starting from the relatively crowded tetramethylcyclopentenone (**9**) (entry 7). The absence of the corresponding alcohols using the cyclic substrates **5**–**9** is noteworthy. The less reactive acyclic enones **1** and **4** gave lower yields on average (entries 1 and 2). We thought that this might be due to the relative thermal instability of the Cp_2Zr(ethylene) complex,[4] performed *in situ* in the absence of the substrate. To overcome this limitation we tried to stabilize the complex by adding 1 equiv. of trimethylphosphine prior to increasing the temperature from −78 to 0 °C.[6] As a result, only slightly higher yields were observed (53 and 42% for **3** and **10**). Nevertheless, the phosphine-based procedure could also be applied to the preparation of substituted vinylcyclopropane derivatives, as exemplified by the synthesis of **16** (Scheme 2). This reaction did not proceed with a significant yield without PMe_3, possibly

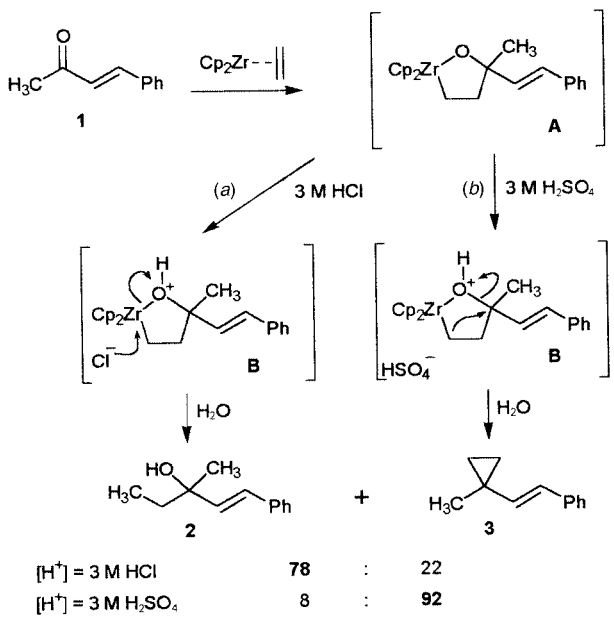

Scheme 1

† Dedicated to Professor Pierre Sinaÿ on the occasion of his 62nd birthday.

Table 1 Reaction of α,β-enones with Cp_2Zr/(ethylene), followed by hydrolysis with H_2SO_4

Entry	α,β-Enone	Product	Yield (%)[a,b]
1	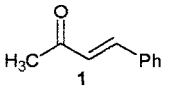 1	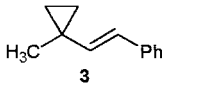 3	45 (53)
2	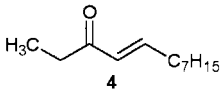 4	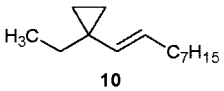 10	31 (42)
3	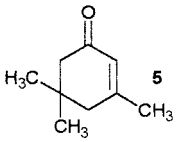 5	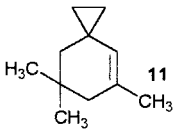 11	75
4	6 (4-cholesten-3-one)	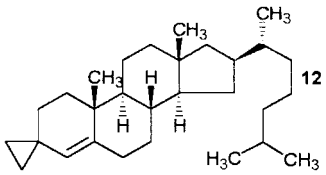 12	91
5	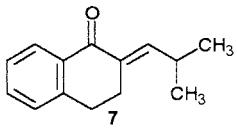 7	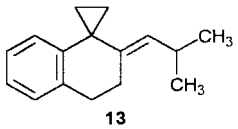 13	47
6	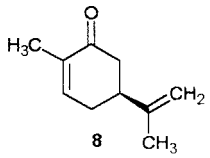 8	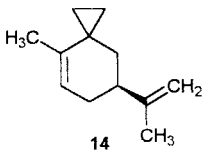 14	40 (59)
7	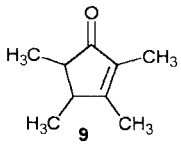 9	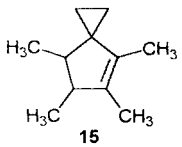 15	55

[a] Yields of isolated products after column chromatography. [b] Yields for the reaction employing PMe_3 (1 equiv.) are given in parentheses.

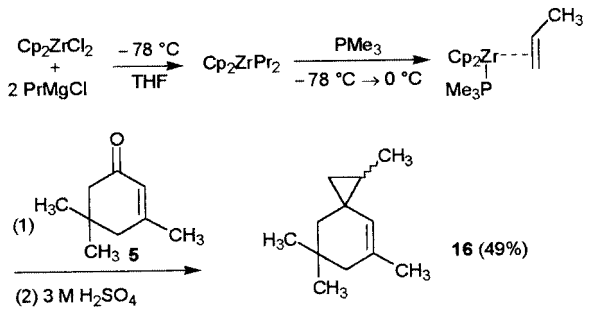

Scheme 2

because of the generally more difficult incorporation of higher alkenes.[4]

Two aspects of the title reaction are remarkable: (i) the cyclopropanation (C–C bond formation) step occurs under protic conditions, and (ii) this selective reaction requires 3 M H_2SO_4, whereas the use of 3 M HCl leads to the predominant formation of the alcohol. Further studies are necessary to clarify the specific role of H_2SO_4 in the cyclization process. However, based on the dichotomous behavior of the two strong protic acids, 3 M HCl and 3 M H_2SO_4, a hypothetical rationale for the two different reaction modes can be proposed (Scheme 1). In the first step, oxazirconacyclopentane **A** must invariably be protonated under the strongly acidic conditions to give the oxonium intermediate **B**. Depending on whether HCl or H_2SO_4 is employed, strikingly different mechanistic pathways [(*a*) or (*b*)] can follow. The reasonably nucleophilic Cl^- apparently attacks at the Cp_2Zr residue with cleavage of the Zr–O bond, which is favourably accompanied by the formation of the relatively strong Zr–Cl bond. In contrast, the attack of the weakly nucleophilic HSO_4^- on Cp_2Zr is slower than the competing ring contraction, leading to a cyclopropane derivative. In this concerted process,[9] the partial positive charge developing on the allylic carbon atom is efficiently stabilized by the neighbouring double bond. Studies are underway to fully elucidate the cyclization step and to extend the synthetic scope of the reaction, and the results will be published in due course.

Notes and references

1 L. A. Paquette, *Comprehensive Organic Synthesis*, ed. B. M. Trost and I. Fleming, Pergamon, Oxford, 1991, vol. 5, p. 899; P. J. Murphy, *Comprehensive Organic Functional Group Transformations*, ed. A. R. Katritzky, O. Meth-Cohn and C. W. Rees, Pergamon, Oxford, 1995, vol. 1, p. 801.

2 T. Hudlicky, F. Rulin, T. C. Lovelace and J. W. Reed, *Studies in Natural Product Chemistry, Stereoselective Synthesis*, ed. Atta-ur-Rahman, Elsevier, Amsterdam, 1989, Part B, vol. 3, p. 3; T. Tsuji and S. Nishida, *The Chemistry of the Cyclopropyl Group*, ed. Z. Rappoport, Wiley, New York, 1987, p. 307.

3 A similar reaction involving allylindium reagents was reported; this reaction is restricted, however, to the synthesis of homoallyl-substituted vinylcyclopropanes, see H. A. Höppe, G. C. Lloyd-Jones, M. Murray, T. M. Peakman and K. E. Walsh, *Angew. Chem., Int. Ed.*, 1998, **37**, 1545.

4 E. Negishi and T. Takahashi, *Bull. Chem. Soc. Jpn.*, 1998, **71**, 755 and references therein; E. Negishi and T. Takahashi, *Acc. Chem. Res.*, 1994, **27**, 124.

5 Usually, zirconocene (alkene) complexes are generated in the presence of a substrate. However, in our case, a complex mixture of products was formed using this procedure.

6 Cp_2Zr (ethylene) adds to saturated aldehydes and ketones to afford the corresponding alcohols, see T. Takahashi, N. Suzuki, M. Hasegawa, Y. Nitto, K. Aoyagi and M. Saburi, *Chem. Lett.*, 1992, 331; N. Suzuki, C. J. Rousset, K. Aoyagi, M. Kotora and T. Takahashi, *J. Organomet. Chem.*, 1994, **473**, 117.

7 O. L. Epstein, A. I. Savchenko and O. G. Kulinkovich, *Tetrahedron Lett.*, 1999, **40**, 5935 and references therein.

8 *Selected data* for **12**: δ_H(500 MHz, $CDCl_3$, TMS) 0.30–0.52 (m, 4 H), 0.70 (s, 3 H), 0.80–2.05 (m, 39 H), 2.15–2.25 (m, 1 H), 4.67 (s, 1 H); δ_C(125 MHz, $CDCl_3$) 12.0, 13.7, 15.1, 18.7, 19.1, 21.7, 22.6, 22.9, 23.9, 24.3, 28.0, 28.3, 30.0, 32.3, 33.2, 35.8, 36.0, 36.2, 37.0, 37.3, 39.5, 40.1, 42.5, 126.4, 144.1; *m/z* (70 eV) 397 (100%) [M^+], 382 (17) (calc. for $C_{29}H_{48}$: C, 87.80; H, 12.20; found: C, 87.56; H, 12.51%).

9 A concerted process for this ring contraction is in accordance with the fact that the double bond configuration in the acyclic products **3** and **10** is retained.

Communication a908897k

Typeset and printed by Black Bear Press Limited, Cambridge, England

ChemComm
FEATURE ARTICLE

Taming early transition metals: the use of polydentate amido-donor ligands to create well defined reactive sites in reagents and catalysts

Lutz H. Gade

Laboratoire de Chimie Organométallique et de Catalyse, UMR 7513, Institut Le Bel, Université Louis Pasteur, 4, rue Blaise Pascal, 67000 Strasbourg, France. E-mail: gade@chimie.u-strasbg.fr

Received (in Cambridge, UK) 15th October 1999, Accepted 7th December 1999

Ligand design in early transition metal chemistry has focussed recently on amide chemistry. The availability of two substituent positions at the amido N-donor atom allows its integration into ligand systems of both podand and macrocyclic topology. Amido functions may be combined with other donor functionalities which possess a different formal charge and chemical hardness and, more generally, a different thermodynamic and kinetic stability of their interaction with the metal centre. Early transition metal complexes containing polydentate amido-donor ligands not only display unprecedented patterns of reactivity but are the focus of recent developments in olefin polymerization catalysis.

Introduction

Amido–transition metal chemistry, a field which developed with limited momentum after the pioneering work of the 1960s and early 1970s,[1,2] has grown dramatically during the past decade. These recent advances are not due to the received wisdom of the structural chemistry and reactive behaviour gained in the early studies having undergone dramatic changes. It is the realization that the amido donor function R_2N^- may be placed into a great variety of structural environments which has ultimately led to the dramatic expansion of the area. It may be readily incorporated into complex polydentate ligand structures and combined with other donor functionalities. Amido units are thus suitable tools in ligand design for early transition metal complexes.

The stabilization, *i.e.* protection, of part of the coordination sphere of a high valent, Lewis acidic early transition metal may be achieved by considering several important aspects. First, the ligands chosen for the non-reactive metal ligand interactions (frequently referred to as *spectator* or *ancillary* ligands) should adequately match the electronic demands of the metal centre.[3] In the case at hand this requires strong σ- and π-donor capabilities and, given the hard nature of the Lewis acid, matching chemically hard donor atoms. Secondly, the ancillary ligands must obviously have significantly different bonding and reactive properties in comparison to the *reactive* ligands, *i.e.* those which undergo transformations in the stoichiometric or catalytic processes of interest. Third, the distribution of donor functions over the protected sector of the coordination sphere should be well balanced. This latter situation is demonstrated particularly well by the early transition metal metallocenes and their derivatives which are at the centre of a vast area of modern organometallic chemistry.[4] During the past decade the dominating position of the cyclopentadienide complexes in the coordination chemistry of the d-electron poor metals has been challenged by the rapid development of amido complex chemistry.

The availability of two substituent positions at the amido N-donor atom allows its integration into ligand systems of both podand and macrocyclic topology (Fig. 1).[5] This not only leads to a well defined relative orientation of the ligating atoms but opens up manifold possibilities of steric control. Moreover, amido functions may be combined with other donor functionalities which possess a different formal charge and chemical hardness and, more generally, a different thermodynamic and kinetic stability of their interaction with the metal centre. In the latter case the strong metal–amide bonds form the anchoring elements of the polyfunctional ligands while the remaining donor functions may either influence the electronic properties of the central atom or mask potentially reactive coordination sites by virtue of their hemilabile nature. In catalytic applications of amido complexes, the availablity of additional weakly coordinating donor functions may crucially determine the lifetimes of certain intermediates in the catalytic cycle and thus the nature of the reaction products. It is the aim of this article to provide an overview of the present state of the area of amido complex chemistry in which the amido functions in the ligand are combined with other *neutral donors* and in which all these considerations have played a role.

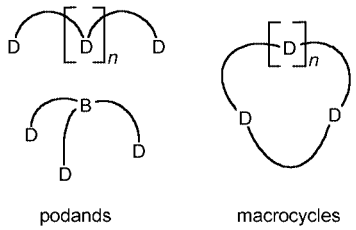

Fig. 1 Topologies of polydentate ligands (D = donor function, B = bridgehead function).

Combining anionic and neutral donor functions: amidoamine and amidopyridine ligands

The addition of a neutral tertiary amino function to a polydentate amido ligand may lead to a variety of conse-

Lutz H. Gade is Professor of Chemistry at the Université Louis Pasteur, Strasbourg. His research interests are in the fields of coordination chemistry, organometallic chemistry and catalysis. After completing his undergraduate studies at the University of Bonn and the Technical University of Munich, he went to Cambridge to work for his Ph.D. with Jack Lewis. Having returned to Germany after completing his thesis in 1991, he joined the Chemistry Department at the University of Würzburg where he finished his habilitation in 1996 and where he subsequently worked as a lecturer. In 1998 he moved to Strasbourg to take up his present position. His scientific work has found recognition through the award of the ADUC prize for 1994, the Heinz–Maier–Leibnitz Preis of the DFG and the Federal Ministry of Research and Education (1997), the Gerhard–Hess-Research Award of the DFG (1998) as well as the Award in Chemistry of the Academy of Sciences at Göttingen (1999).

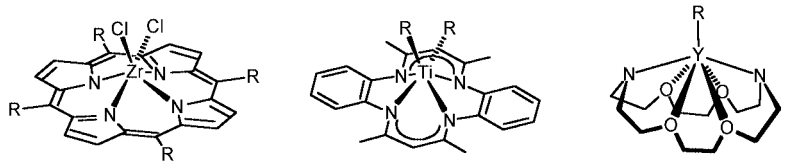

Fig. 2 N-donor macrocycles of different flexibility which have been employed in early transition metal chemistry.

quences. Incorporated within more or less rigid *macrocylic* structures they mostly remain coordinated to an early transition metal centre during transformations at the remaining coordination site(s) and thus serve the 'passive' purpose of maintaining a particular ligand environment with a given overall ligand charge thoughout the transformations. The extremes of macrocyclic rigidity and flexibility are represented by early transition metal porphyrins on the one hand[6] and metallated azacrown ethers on the other[7] as exemplified in Fig. 2. In both cases, the macrocycle–metal complex fragment does not seem to undergo significant changes in chemical reactions involving the reactive ligands. Other macrocyclic systems of intermediate flexibility include tetraazaanulenes the coordination chemistry of which has been recently reviewed.[8]

On the other hand, neutral amino groups (as well as ether or organosulfido groups, *vide infra*) are more readily displaced from early transition metal centres than anionic amido units and therefore may play a flexible role in organometallic transformations. The latter is of particular importance in the development of new early transition metal polymerization catalysts which will be discussed in detail below.

In contrast to the macrocyclic structures discussed so far, neutral donors in *bridgehead* positions of *podands* with amido 'arms' may remain essentially passive within the cage structure of the metal complexes containing these ligands. The paradigm for the use of such ligand systems are the triamidoamine ligands found in the azametallatranes **1** studied by Verkade, Schrock and others.[9,10] These are essentially tripodal ligands in which the apical bridgehead atom participates in the coordination to the metal centre generating a particularly stable cage structure. The arrangement of the triamidoamine creates a reactive site at the metal centre, occupied by the remaining ligand, which may be varied in size and geometry by choice of the appropriate peripheral substituents at the amido nitrogen donor atoms. A set of frontier orbitals comprising one σ and two π orbitals is in principle available for ligand binding at the remaining coordination site (Fig. 3).[10]

This situation is thought to provide the appropriate frontier orbital set at the metal for the extremely rich metal–ligand multiple bond chemistry found for these systems to date.[11] Whereas the tertiary amino function at the apex influences the orbital energies of the frontier orbitals, it apparently adopts a 'passive' role in most of the compounds studied to date. Only in rare cases has it been posssible to establish the involvement or association/dissociation of the amino function in reactions of

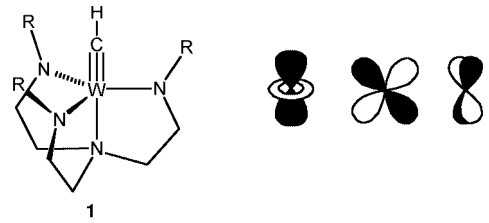

Fig. 3 Molecular structure of an azametallatrane, **1**, along with a depiction of the metal centred frontier orbitals which may be involved in ligand binding.

azametallatranes.[12] The chemistry of this class of complexes has developed rapidly during this decade and has been reviewed in detail.[9,10] It will therefore not be discussed in this overview of the field.

Greater flexibility in the coordination geometry and more open structures are found in a number of early transition metal complexes containing new types of diamidoamine ligands (Fig. 4). In these the amino donor function is less strongly bound and its *active* participation in chemical transformations, *i.e.* the coordination and dissociation, is possible. Whereas the tridentate diamidoamine ligand **A**, first reported by Cloke *et al.* adopts a facial coordination mode in **2**,[13] a meridional arrangement was observed in the crystal structure of the analogous complex **3** studied in Schrock's group.[14] Both compounds are precursors of cationic olefin polymerization catalysts the reactivity of which is strongly influenced by the availability of a neutral (dissociable) donor function (*vide infra*).

In contrast to these catalytically active dialkyldiamido zirconium complexes, complex **3a** bearing a tridentate ligand in which the aminofunction is not positioned between the anionic amido units has been found to be inactive in attempted polymerizations.[15]

The combination of a pyridyl unit with two amido functions leads to tridentate ligands which, depending upon their topology, may adopt meridional or facial coordination modes. Meridional coordination is achieved using ligands of type **D** (Fig. 5)[16] which have found application in the development of novel olefin polymerization catalysts of high activity (**4**, *vide infra*).[17] We first developed and studied the coordination chemistry of type **E** diamido pyridine ligands[18] which were found to adopt facial arrangents in early transition metal complexes such as **5**.[19]

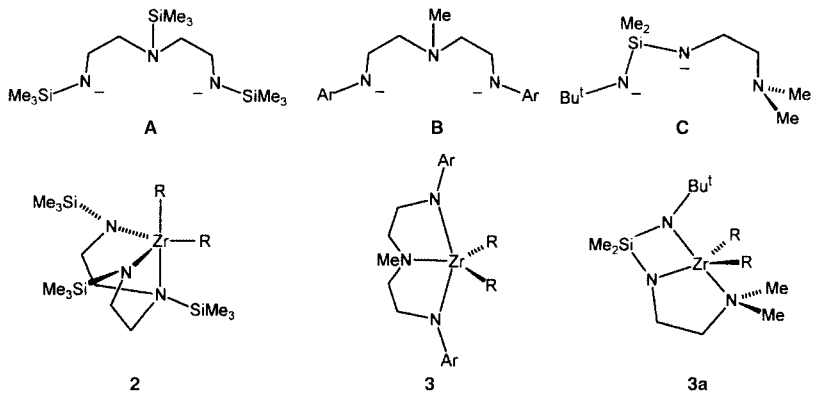

Fig. 4 Zirconium complexes containing the diamidoamine ligands **A**, **B** and **C**.

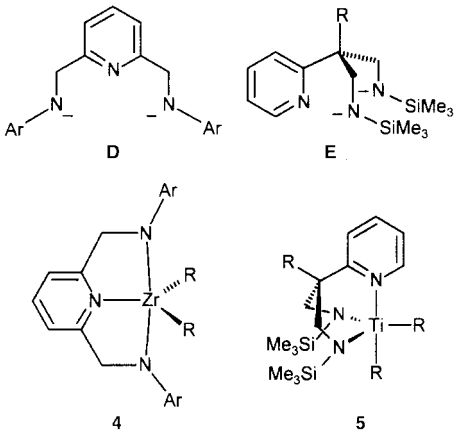

Fig. 5 The diamidopyridine ligands **D** and **E** adopting meridional and facial coordination modes, respectively.

Formally, the dianionic tripods may be derived from the threefold symmetrical tripodal ligands through the replacement of one of the anionic amido 'claws' by the neutral pyridyl function. This class of ligands has been employed in the synthesis of tetravalent titanium and pentavalent vanadium group metal complexes. For the complexes of the Ti triad the ancillary ligand system has allowed the coordination of either two additional anionic (*e.g.* alkyl) ligands or,[19] alternatively, a formally dianionic unit as achieved in the synthesis of a series of stable imido complexes (Scheme 1).[20,21]

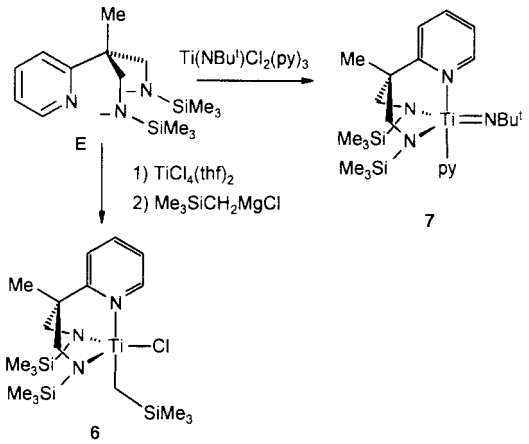

Scheme 1 Synthesis of pentacoordinate titanium complexes containing the diamidopyridine ligand **E**.

The coordination of the pyridyl unit to the metal centre and thus the formation of a pentacoordinate complex **7** (Fig. 6) of distorted trigonal bipyramidal coordination geometry depends upon the steric requirements of the additional ligands in axial and equatorial position. Decoordination of the pyridyl function has been observed in solution for a dialkyltitanium complex **8** bearing bulky neopentyl groups for which the fourfold coordination mode with a dangling py-unit has been established by NMR spectroscopy, or in the solid state, as demonstrated by the

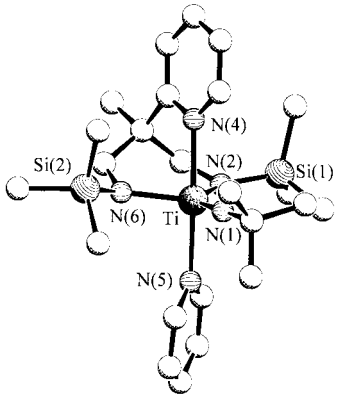

Fig. 6 Molecular structure of complex **7**.[20]

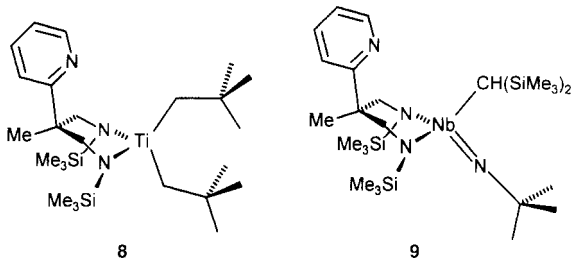

X-ray crystal structure analysis of [Nb{MeC(C$_5$H$_4$N-2)-(CH$_2$NSiMe$_3$)$_2$}(NBu^t){CH(SiMe$_3$)$_2$}] **9**.[19,21]

The imidotitanium complexes such as [Ti{MeC(C$_5$H$_4$N-2)-(CH$_2$NSiMe$_3$)$_2$}(NBu^t)(py)] **7** were found to have considerable thermal stability which allows their facile isolation and manipulation. However, they possess labile pyridine and pyridyl ligands that, under appropriate reaction conditions, may dissociate to yield unsaturated and highly reactive imido complexes of the type investigated by Wolczanski and coworkers *via* irreversible thermolysis of the respective precursor molecules (Fig. 7).[22] In fact, sublimation of **7** in high vacuum has yielded the four-coordinate complex **7a** which has been structurally characterized by X-ray crystallography.[21] In contrast, there has been no evidence, as yet, for the postulated highly unsaturated, three-coordinate species **7b**.

It is this flexibility of the tridentate ligand which is thought to be responsible for the remarkable reactivity of **7** towards a variety of organic substrates and represents an example of the 'taming' of a reactive structural element as implied in the title of this article. In reactions with methyl acetylenes we have found slow but selective cyclization yielding the metalla-azetidines **10**.[23]

This conversion is thought to occur *via* a C–H bond activation step of the methyl group to the Ti=N unit, as has been established for transiently generated imido compounds by Wolczanski and others,[22] and subsequent cyclization. The observation that the same products were obtained from the analogous substituted allenes may imply that an allenetitanium intermediate is involved in this conversion.

A cascade of C–-N and C–C coupling reactions is the result of exposing **7** to alkyl isocyanides to give metal bound

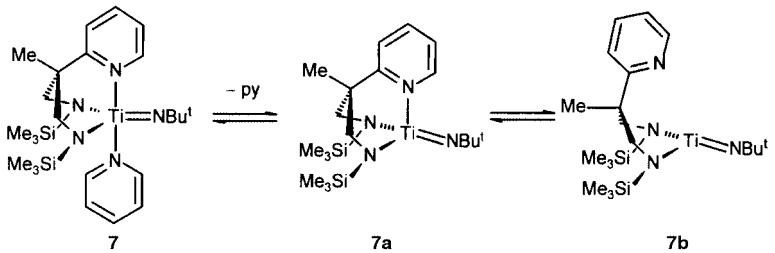

Fig. 7 Stabilization and "masking" of low-coordinate imidotitanium complexes.

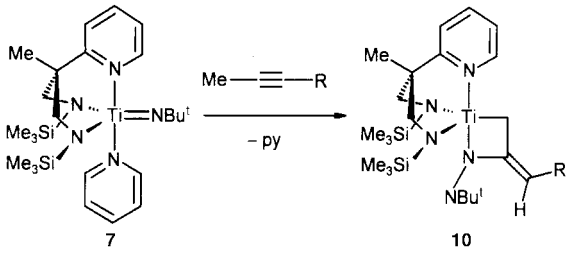

7 10

5,6-diamino-2,3-dihydropyrimidines **11**.[20] The reaction sequence is thought to occur along the pathway shown in Scheme 2.[24] Remarkably, no reaction intermediate could be detected for most of the isocyanide derivatives we studied. However, it has been possible to isolate and structurally characterize a derivative of **ii** which could be converted to **iii** upon addition of another molar equivalent of an isocyanide.

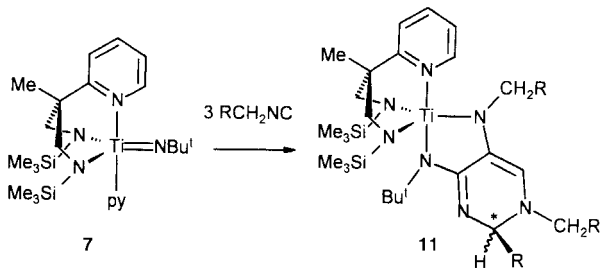

7 11

Several potentially tetra- and hexa-dentate amidopyridine ligands have been reported which contain deprotonated 2-aminopyridine units. Two of these have been connected *via* a bridging siloxane unit **F** and have been employed in the synthesis of heterodinuclear complexes in which they link neodymium and late transition metal fragments (for example **12**).[25] The combination of three aminopyridine fragments has been achieved in a trisilylmethane and trisilylsilane derived tripodal ligands for which titanium, zirconium and niobium complexes have been reported.[26,27] Although the pyridine donors in these systems are all coordinated to the respective metal centres in the crystal structures, their bonding situation in solution is not clear.

Stabilizing cationic early transition metal amido complexes: a new generation of non-metallocene polymerization catalysts

Few developments have fueled the interest in the organometallic chemistry of the early transition metals in the same way as the discovery of well defined olefin polymerization catalysts. To date, the majority of the systems, mainly based on titanium or zirconium, which have been investigated contain one or two cyclopentadienyl rings or their derivatives.[4] However, in recent years the focus has shifted to non-metallocene catalysts of which those containing chelating diamido ligands have received particular attention.[28] An ever increasing number of such complexes are currently being studied with regard to their activity as catalyst precursors for the polymerization of ethylene or longer chain α-olefins. The three complexes displayed in Fig. 8 were found to be procatalysts for highly active catalytic systems.[29]

In particular, the titanium complex **13** studied by McConville and coworkers,[29a,b] was found to behave as a living polymerization catalyst for hex-1-ene. The active species in these systems is thought to be a cationic monoalkyl complex which would be a solvated three coordinate species. In order to stabilize this

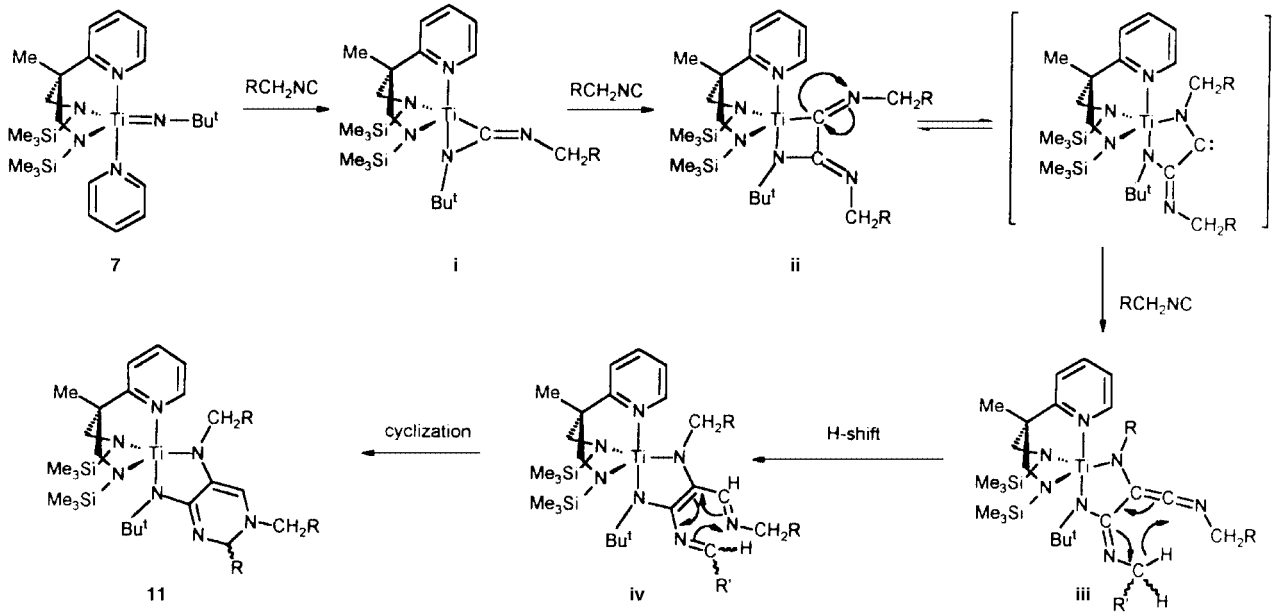

7 i ii iii iv 11

Scheme 2 Proposed mechanism of the icocyanide coupling with **7** to give Ti-bound 5,6-diamino-2,3-dihydropyrimidenes.

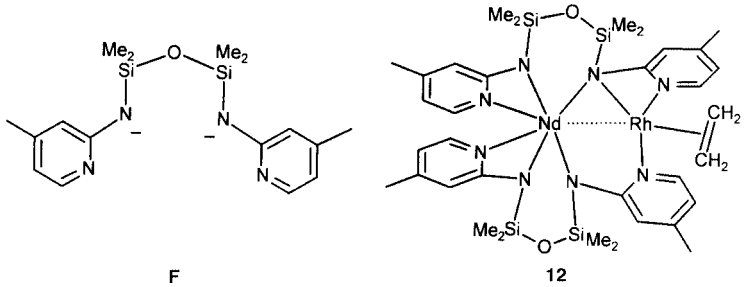

F 12

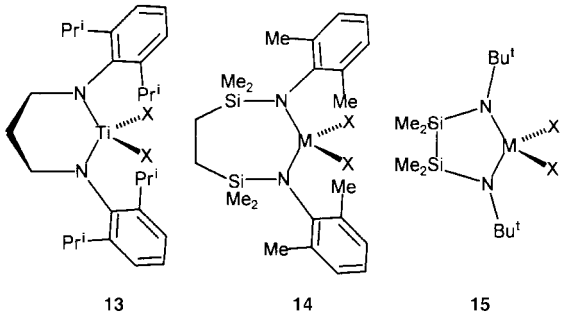

Fig. 8 Group 4 metal complexes containing chelating diamido ligands which are active catalysts for olefin polymerization.

cationic intermediate, ligand design has very recently been extended to include chelating diamido ligands which contain a third neutral donor function. As noted above, activity in olefin polymerization has mainly been observed for those systems in which the neutral donor is placed between the two anionic amido groups. In the five coordinate procatalysts shown in Fig. 9 the tridentate ligand may adopt either meridional or facial arrangements.[13,14,17,30–33]

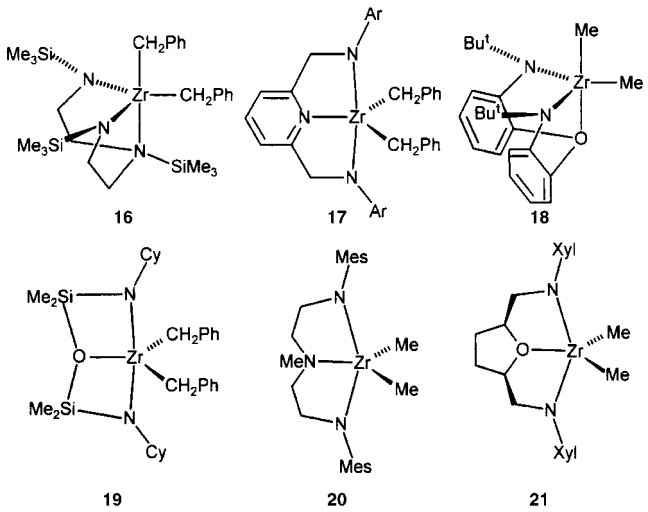

Fig. 9 Dialkylzirconium complexes, containing diamido-donor ligands, which are active olefin polymerization catalysts.

Compounds **16** and **17** have been studied by Cloke, Horton and McConville and represent the two possible arrangements of the donor functions.[13,17,30] While complex **16** was found to be moderately active in ethylene polymerization, the procatalyst **17** displays high activity. Very detailed studies into the mechanism of the polymerization and the role of the neutral donor functions have been carried out in Schrock's group. Compounds **18**, **20** and **21** are active catalysts for the polymerization of hexene.[14,31,33] An important feature in these complexes is the absence of N-bonded silyl groups which are not only easily hydrolyzed but may undergo cyclometallations. The chemically robust nature of **18**,[31] in particular, not only allows the living polymerization of hexene but has rendered the cationic intermediate suffiently stable to be characterized in solution.[34] The isolation and X-ray crystallographic characterization of the ionic adduct [{($Bu^tNC_6H_4$)$_2$O}ZrMe][MeB(C_6F_5)$_3$] **18a** upon reaction of **18** with the cocatalyst B(C_6F_5)$_3$, in which the boranate ion occupies the apical position, supports the notion that it is the apical alkyl group which is removed by the Lewis acid.[31]

Using $^{13}CH_3$-labeled **18**, it has been possible to detect the cationic solvent-stabilized catalyst by ^{13}C NMR spectroscopy in solution and to demonstrate that the 'insertion' of hex-1-ene into the Zr–CH_3 bond occurs in a 1,2 manner.[34]

Based on these studies, Schrock and Baumann have proposed the mechanism initiating the chain growth which is shown in

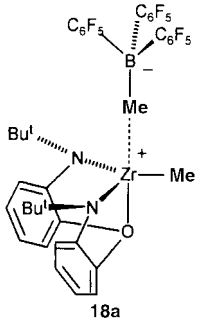

Scheme 3.[34] In the first step, the dissociation of the base in the apical position in **18b** generates the four-coordinate cationic complex **18c** to which the olefin monomer may coordinate generating a five coordinate cation **18d**. The monomer occupies the apical coordination site in this intermediate. In contrast to the mechanism proposed for the cationic metallocene catalysts, which adopt a pseudo-trigonal structure and in which the olefin may approach the metal–alkyl unit from two faces,[4] the pseudo-tetrahedral nature of **18c** restricts access to the metal centre to one face.

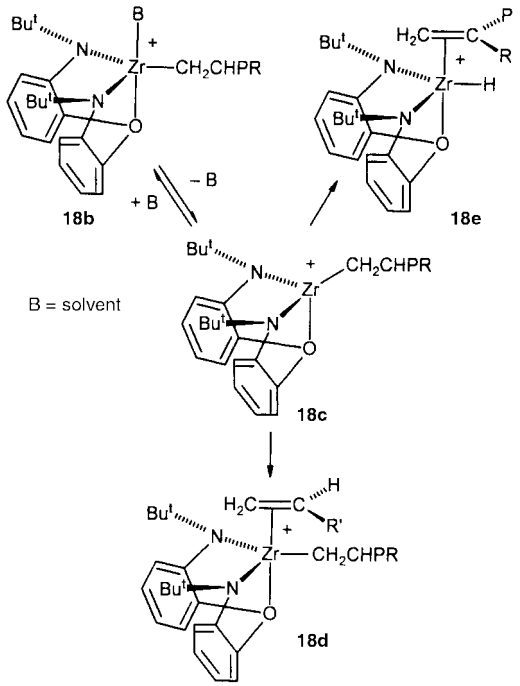

Scheme 3 Mechanism for the chain growth catalyzed by **18**.

That β-elimination which would terminate the living polymerization is a slow process is attributed to the steric congestion of the ligand sphere induced by the bulky N-bound *tert*-butyl groups. This renders the conversion of **18c** to **18c** kinetically unfavourable.

The studies discussed in this section impressively demonstrate the role played by the ancillary ligand in the control of the reactivity of a catalytic system. It is the combination of the electronic properties of the donor functions, the conformational degrees of freedom of the ligand backbone as well as the steric demand of both ligand backbone and peripheral substituents which influences their performance. This point is particularly apparent in the results of a comparative study of the catalytic properties of **21** and the simple dialkyl ether analogue [{O(CH_2CH_2NXyl)$_2$ZrMe$_2$] **22**.[33,35] Catalyst **21**, which contains a conformationally more rigid and sterically more demanding tetrahydrofuran-derived diamido-donor ligand, produced polyhexene of almost twice the molecular weight as compound **22**.

Amido ligands containing weakly coordinating donor functions: the *ortho*-fluorophenyl periphery

The neutral ligating units in the polyfunctional ligands discussed in the previous sections bind fairly strongly to the metal centres and are therefore thought to remain coordinated throughout most of the chemical conversions at the 'reactive' coordination site(s). However, the integration of very labile coordinating units into amido ligands enables the 'masking' of low coordination numbers and thus of potentially highly reactive species. The size of the reactive site in these systems is readily adjustable through coordination and decoordination of the hemilabile donors. We introduced such an *active ligand periphery* in several tripodal amido ligands in the form of *ortho*-fluorophenyl groups (Fig. 10).[36]

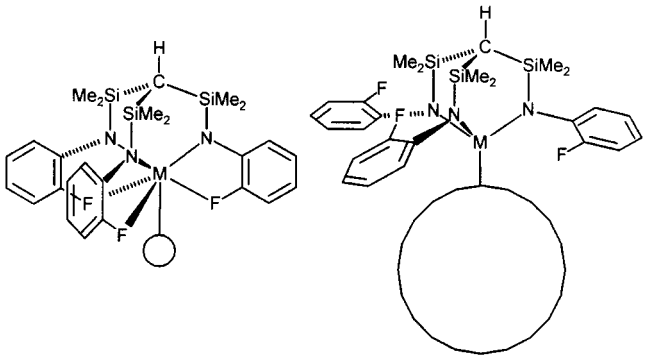

Fig. 10 Participation and non-participation of an active *ortho*-fluorophenyl ligand periphery in tripodal amido complexes.

The stabilization of Lewis acidic metal centres by weak C–F···M coordination has also been used in complexes containing appropriately functionalized monodentate amido ligands as well as in several metallocene derivatives.[37] The use of partially fluorinated aryl groups reduces the basicity at the amido N-atoms and thus increases their stability towards protolytic cleavage. Depending on the ionic radius of the metal centre and steric demand of the remaining anionic ligand(s), the coordination of one or more of the fluorine atoms both sterically shields and partially saturates the Lewis acidic metal centre. We have extended this approach to include N-bonded 2,3,4-trifluorophenyl groups which were found to stabilize complexes of the titanium triad even more efficiently.[36*b*]

The involvement of one, two or three *ortho*-F atoms in the coordination to the metal has been established by a systematic structural study. Coordination of all three C–F units has been observed for the yttrium complex **23** which together with an additional diethyl ether ligand leads to a sevenfold coordination geometry (Fig. 11).[36] This system was studied at the beginning of our work in view of its NMR-active metal nucleus ^{83}Y and indeed, ^{19}F NMR studies of the complex established the metal–fluorine interaction in solution by observation of ^{83}Y–^{19}F coupling.

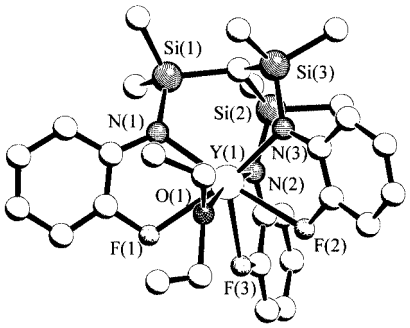

Fig. 11 Molecular structure of the yttrium complex [Y{HC[SiMe$_2$N(2-FC$_6$H$_4$)]$_3$}(OEt$_2$)] (**23**).

The structures of compounds **24**–**26** nicely demonstrate the relationship between the size of the anionic monodentate ligand(s) and the number of coordinated C–F groups.[37–39] While the coordination of the ligand periphery in **24** and **25** leads to sixfold coordination in the zirconium complexes, the large metal complex fragment {FeCp(CO)$_2$} which essentially acts as an anionic ligand in **26** enforces the dissociation of the hemilabile units (Fig. 12).

The role which the fluorine atoms adopt in the structures discussed above may be rationalized by assuming that the highly Lewis-acidic metal centre accepts as many additional donors as may be accommodated in their coordination sphere. The question of their importance in the chemical reactions of such species is more difficult to answer since intermediates are generally not detectable. However, we have carried out a comparative study of the kinetics of insertion reactions of unsaturated polar organic substrates into the polar metal–metal bonds in compounds such as **26**. These were related to the results obtained for complexes in which the fluorophenyl substituents were replaced by 'innocent' *para*-tolyl groups. In this study we found that the second order reaction rates of the fluorinated species are greater by a factor of *ca*. 10–50.[36*b*,39–41]

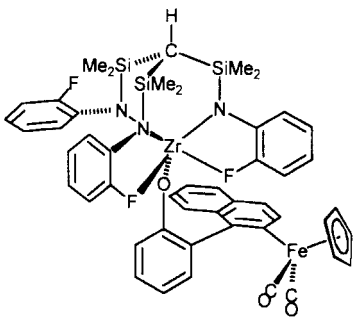

24

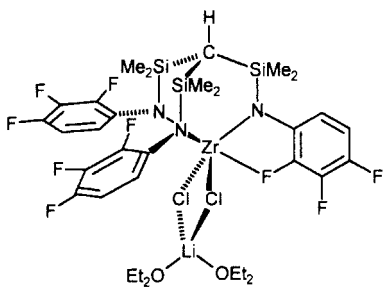

25

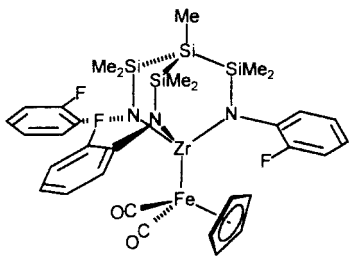

26

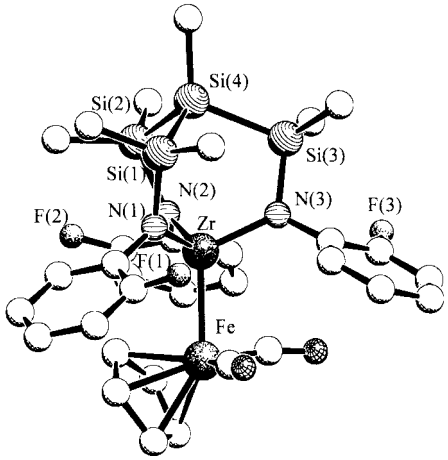

Fig. 12 Molecular structure of the Zr–Fe complex **26** showing the 'dangling' *ortho*-fluorophenyl groups.

The active periphery thus enhances the reactivity of the early–late heterobimetallics, an observation which may be understood in both possible mechanistic scenarios: an early or a late involvement of the F-donors in the process of metal–metal bond cleavage. Experimental evidence suggests that the attack of a Lewis-base at the early transition metal centre is the first step in the insertion reactions of polar substrates. The re-adjustment of electron density in the metal–metal bond destabilizes it and induces its subsequent scission. This process may be aided by the coordination of the CF groups before the cleavage of the Zr–M bond. On the other hand, the coordination of the fluorine atoms also stabilizes the fragments obtained after metal–metal bond breaking has occurred, a situation which will be reflected in the kinetics in the case of a late transition state. It has not been possible to differentiate between these two possibilities and it is quite likely that both play a role.

Labile coordination of *ortho*-fluorine atoms in N-bonded fluorinated aryl substituents has recently been observed in several other polydentate amides. X-Ray crystallographic studies carried out for [{$(C_6F_5NCH_2CH_2)_3$N}V] (V–F 2.65 Å)[42] and [{$(C_6F_5NCH_2CH_2)_2$N}$TaMe_2$] (Ta–F *ca.* 2.4 Å)[43] have also established metal–fluorine distances which are significantly longer than those found in binary fluorides or related compounds. This fact is to be seen in connection with the fluxionality of the orthofluorophenylamido complexes in solution which suggests that the strength of the interaction between the metal centres and the labile donor functions amounts to less than *ca.* 10 kcal mol^{-1}.

Combining hard and soft donor functions: chelating and macrocyclic amidophosphines

The stability of the metal–nitrogen bonds in amido complexes of the early transition metals enables their use as 'anchors' for polydentate ligands which also contain donor functions with less well matched electronic properties. This was part of the rationale behind the ligand design discussed in the previous sections. However, a particularly interesting variant of this concept has been developed and very successfully employed by Fryzuk *et al.* by combining the hard amido ligand with soft phosphine units in polydentate ligand systems.[3,44,45] The open chain PNP and NPN ligands **G** and **H** as well as the macrocyclic P_2N_2 ligand **I** displayed in Fig. 13 have been applied in the synthesis of organometallic complexes of the group 3–5 metals. Early work using **G**, which has been reviewed elsewhere, revealed that these systems may in fact be employed in the synthesis of stable late transition metal complexes with reversed roles of the two donor functions.[3,44] In d-electron rich complexes the soft phosphine ligands with their π-acceptor properties are to be viewed as the anchoring units which ensure the stabiliy of the molecules.

A series of early transition metal complexes containing the macrocyclic ligand **I** has been reported recently.[46,47] Particularly noteworthy is the coupling of two aryl rings in an yttrium(III) complex (Scheme 4).[47] This dinuclear species was

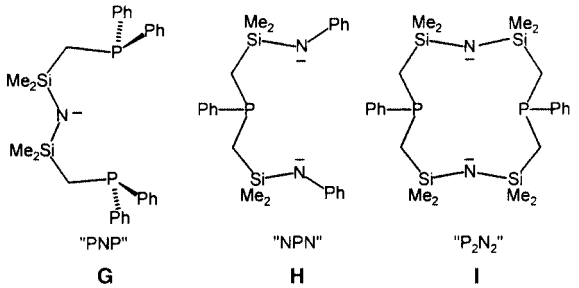

Fig. 13 Three polydentate amido-phosphine ligands introduced by Fryzuk and coworkers.

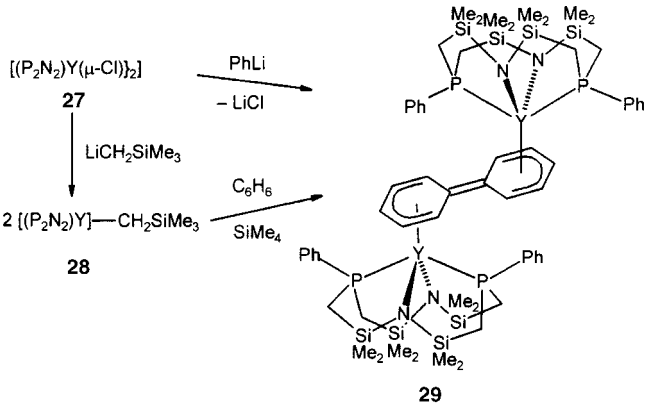

Scheme 4 Phenyl coupling induced by an yttrium complex stabilized by the macrocyclic P_2N_2 ligand **I**.

first discovered as the thermal decomposition product of the Me_3SiCH_2 complex **28** in benzene which yielded $SiMe_4$ and the dinuclear species **29** in which the bridging diphenyl ligand may be understood as being formally dianionic and thus leaving the oxidation state of the yttrium unchanged. The mechanism of this conversion which involved C–H bond activation is not yet fully understood. However, the same product was obtained upon reaction of the chloroyttrium(III) complex **27** with phenyllithium. This reaction of an aryllithium compound with a transition metal halide to give a product with a π-bonded arene unit is reminiscent of the chromium species which were first investigated in 1919 by Hein and coworkers but were only structurally understood after Fischer's synthesis of bis(benzene)chromium in 1955.[48]

It is remarkable that this coupling reaction may be extended to other aryl fragments as was shown in the generation of the ditolyl ligand on reaction of **27** with *para*-tolyllithium.[47] The structure of complex **30** which contains this bridging ditolyl

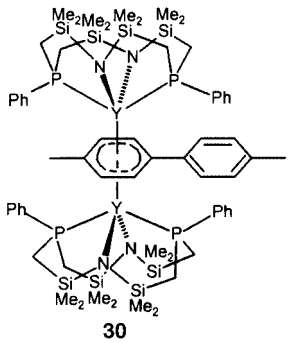

dianion shows that the arrangement of the two metal complex fragments coordinated to the organic unit appears to depend upon the substitution pattern of the latter. NMR studies carried out at variable temperature suggest a rapid migration of the complex fragments between the two ring positions in solution at room temperature.

The macrocyclic diamidodiphosphine ligand **I** has been used in the synthesis of the trimethyltantalum complex **31** in which

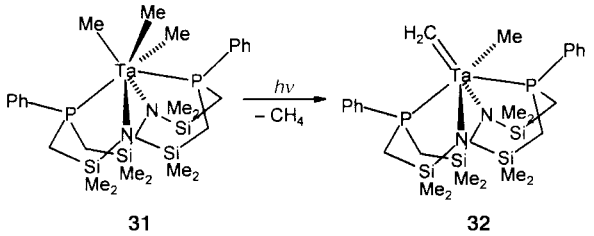

31 **32**

all ligand donor atoms are bonded to the metal centre and which consequently adopts a sevenfold coordination geometry best described as capped trigonal prismatic.[49] This compound undergoes a photochemically induced methane abstraction to give the methylmethylidene complex **32**. The latter displays an interesting dynamic behaviour in solution which amounts to a libration and/or rotation of the Ta(=CH_2)Me unit relative to the macrocycle–Ta fragment.

The most spectacular application of the amidophosphine ligands **G** – **I** has been in the synthesis of the dinitrogen-zirconium and -tantalum complexes **33–37** (Fig. 14) which not

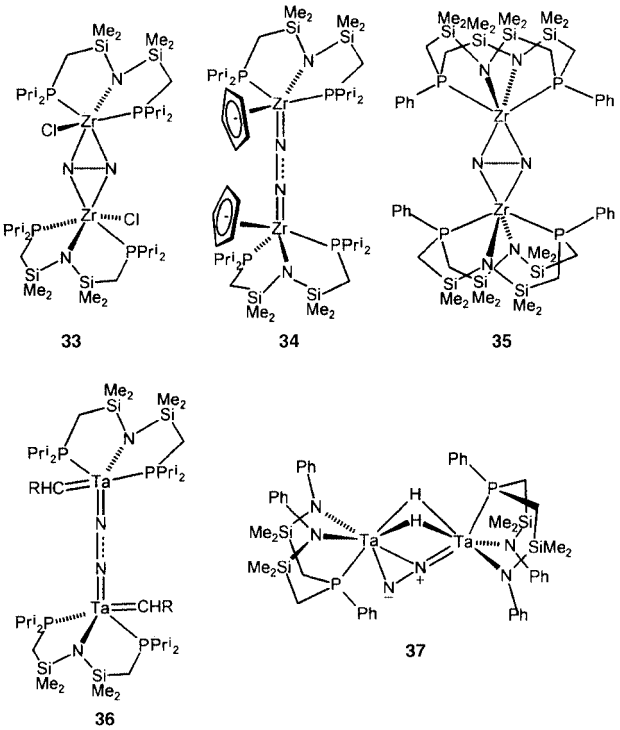

33 **34** **35**

36 **37**

Fig. 14 Different structural types in dinuclear zirconium and tantalum complexes containing bridging N_2 ligands.

only display different N_2 bonding modes but remarkable chemical reactivity.[50–53] The different coordination modes in the zirconium complexes have been explained by the way the monodentate ancillary ligands, Cl^- or Cp^-, influence the set of frontier orbitals available for N_2 binding at the metal centre. In the chloro complex **33** the unavailability of one of the d-orbitals at the zirconium which would normally be involved in an end-on coordination mode favours the side-on coordination observed in the molecular structure of the compound.

The coordination mode of the dinitrogen ligand in the tantalum complex **37** is unprecedented in transition metal chemistry.[53] The compound was obtained by displacement of dihydrogen from the dinuclear tetrahydridotantalum complex [{(PhNSi$Me_2CH_2)_2$PPh}Ta(μ-H)$_2$]$_2$ which is the first time that N_2-binding is observed by substitution of hydrido ligands. This observation may be relevant to a potential catalytic cycle for the reduction of N_2 to NH_3. The second step would then entail N–H formation and addition of further H_2 to regenerate the hydride.

That N–H coupling is indeed feasible in such hydrido N_2-complexes has been shown for compound **35**.[52] Stirring of the dinitrogen complex in hexane under an H_2 atmosphere slowly produced the remarkable dinuclear μ-η^2-N_2H complex **38** (Scheme 5).

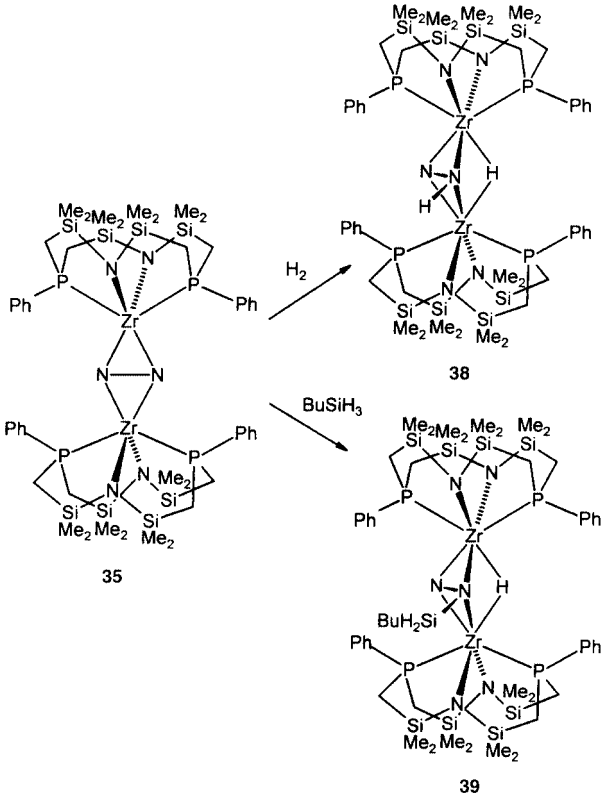

35 **38** **39**

Scheme 5 Hydrogenation of the (μ-N_2)Zr_2 complex **35** giving the (HN_2)Zr complex **38** and addition of Bu^nSiH_3 to **35** to give the {(BuH_2Si)N_2}Zr complex **39**.

The molecular structure of **38** was established by NMR spectroscopy in solution and by a single crystal neutron diffraction study for the solid state. An X-ray diffraction study of a closely related complex **39** has been carried out which was obtained by reaction of **35** with Bu_3SiH. This result confirms the previously noted close analogy between H–H and H–Si bonds in metal induced bond activation reactions.[54]

Conclusions and outlook

The amido function offers many possibilities of inclusion within a complex polydentate ligand system and the combination with other types of donor functionalities. This combination of hard, anionic amido functions with a range of neutral donor functions within the same ligand systems has led to the stabilization and isolation of new types of early transition metal complexes. Moreover, this concept has found its way into the systematic design of new olefin polymerization catalysts. Stabilization of the reactive site by additional ligating functions within a polydentate amide may play a role both in the isolated complexes themselves and in reactive intermediates in catalytic cycles.

The development of this area is still at an early stage, and the potential of creating novel types of reactive sites in the complexes of early transition metals is largely untapped. In particular, the combination of hard and soft donor functions appears to lead the way to novel patterns of structure and reactivity. The use of weakly coordination units, such as the CF fragments discussed above may offer an alternative strategy not only to stabilize otherwise highly reactive compounds but also to control the catalytic activity of molecular catalysts. More-

over, it is the combination of both the renewed academic interest in amide chemistry and the prospect of the commercial application of its results which provides the driving force for current and future progress.

Acknowledgements

I thank my coworkers who contributed to this area, in particular, Stefan Friedrich, Harald Memmler, Martin Schubart, Andreas Schneider and Dominique Trösch, for their enthusiasm and dedication. I also would like to acknowledge the fruitful collaborations with the research groups of Mary McPartlin (London), Philip Mountford (Oxford) and Joe Lauher (Stony Brook). Our own work has been supported by the Deutsche Forschungsgemeinschaft and the Fonds der Chemischen Industrie.

Notes and references

1 M. H. Chisholm and I. P. Rothwell, in *Comprehensive Coordination Chemistry*, ed. G. Wilkinson, R. D. Gillard and J. A. McCleverty, Pergamon, Oxford, 1987, vol 2, p. 161.
2 M. F. Lappert,, P. P. Power, A. R. Sanger and R. C. Srivastava, *Metal and Metalloid Amides*, Ellis Horwood-Wiley, Chichester, 1980.
3 See, for example: M. D. Fryzuk, T. S. Haddad, D. J. Berg and S. J. Rettig, *Pure Appl. Chem.*, 1991, **63**, 845.
4 H. H. Brintzinger, D. Fischer, R. Mühlhaupt, B. Rieger and R. M. Waymouth, *Angew. Chem., Int. Ed. Engl.*, 1995, **34**, 1143; W. Kaminski and M. Arndt, *Adv. Polym. Sci.*, 1997, **127**, 144; M. Bochmann, *J. Chem. Soc., Dalton Trans.*, 1996, 255.
5 L. H. Gade, *Koordinationschemie*, Wiley-VCH, Weinheim, 1998, p. 51.
6 H. Brand and J. Arnold, *Coord. Chem. Rev.*, 1995, **140**, 137; C. Floriani, *Chem. Commun.*, 1996, 1257; C. Floriani, *Pure Appl. Chem.*, 1996, **68**, 1.
7 L. Lee, D. J. Berg and G. W. Bushnell, *Organometallics*, 1995, **14**, 8; L. Lee, D. J. Berg and G. W. Bushnell, *Organometallics*, 1995, **14**, 5021.
8 P. Mountford, *Chem. Soc. Rev.*, 1998, **27**, 105.
9 J. G. Verkade, *Acc. Chem. Res.*, 1993, **26**, 483.
10 R. R. Schrock, *Acc. Chem. Res.*, 1997, **30**, 9.
11 See, for example: K.-Y. Shi, K. Totland, S. W. Seidel and R. R. Schrock, *J. Am. Chem. Soc.*, 1994, **116**, 12 103; N. C. Zanetti, R. R. Schrock and W. M. Davis, *Angew. Chem., Int. Ed. Engl.*, 1995, **34**, 2044; R. R. Schrock, S. W. Seidel, N. C. Mösch-Zanetti, K.-Y. Shih, M. B. O'Donoghue, W. M. Davis and W. M. Reiff, *J. Am. Chem. Soc.*, 1997, **119**, 11 876; S. W. Seidel, R. R. Schrock and W. M. Davis, *Organometallics*, 1998, **17**, 1058.
12 J. S. Freundlich, R. R. Schrock, C. C. Cummins and W. M. Davis, *J. Am. Chem. Soc.*, 1994, **116**, 6476.
13 F. G. N. Cloke, P. B. Hitchcock and J. B. Love, *J. Chem. Soc, Dalton Trans.*, 1995, 25; H. C. S. Clark, F. G. N. Cloke, P. B. Hitchcock, J. B. Love and A. P. Wainright, *J. Organomet. Chem.*, 1995, **503**, 333; J. B. Love, H. C. Clark, F. G. N. Cloke, J. C. Green and P. B. Hitchcock, *J. Am. Chem. Soc.*, 1999, **121**, 6843.
14 L.-C. Liang, R. R. Schrock, W. M. Davis and D. H. McConville, *J. Am. Chem. Soc.*, 1999, **121**, 5797.
15 F. J. Schattenmann, R. R. Schrock and W. M. Davis, *Organometallics*, 1998, **17**, 989.
16 S. Cai and R. R. Schrock, *Inorg. Chem.*, 1991, **30**, 4105.
17 F. Guérin, D. H. McConville and J. J. Vittal, *Organometallics*, 1996, **15**, 5596.
18 S. Friedrich, L. H. Gade, A. J. Edwards and M. McPartlin, *J. Chem. Soc., Dalton Trans.*, 1993, 2861.
19 S. Friedrich, M. Schubart, L. H. Gade, I. J. Scowen, A. J. Edwards and M. McPartlin, *Chem. Ber./Recueil*, 1997, **130**, 1751.
20 A. J. Blake, P. E. Collier, L. H. Gade, M. McPartlin, P. Mountford, M. Schubart and I. J. Scowen, *Chem. Commun.*, 1997, 1555.
21 P. E. Collier, L. H. Gade, P. Mountford, S. E. Pugh and D. J. M. Trösch, unpublished work.
22 J. L. Bennet and P. T. Wolczanski, *J. Am. Chem. Soc.*, 1997, **119**, 10696 and references therein.
23 A. Bashall, P. E. Collier, L. H. Gade, M. McPartlin, P. Mountford and D. J. M. Trösch, *Chem. Commun.*, 1998, 2555.
24 A. Bashall, P. E. Collier, L. H. Gade, M. McPartlin, P. Mountford, S. E. Pugh, S. Radojevic, M. Schubart, I. J. Scowen and D. J. M. Trösch, in preparation.
25 A. Spannenberg, M. Oberthür, H. Noss, A. Tillack, P. Arndt and R. Kempe, *Angew. Chem., Int. Ed.*, 1998, **37**, 2079.
26 B. Findeis, M. Schubart, L. H. Gade, F. Möller, I. J. Scowen and M. McPartlin, *J. Chem. Soc., Dalton Trans.*, 1996, 125.
27 G. Hillebrand, A. Spannenberg, P. Arndt and R. Kempe, *Organometallics*, 1997, **16**, 5585.
28 G. J. P. Britovsek, V. C. Gibson and D. F. Wass, *Angew. Chem., Int. Ed.*, 1999, **38**, 428.
29 (*a*) J. D. Scollard and D. H. McConville, *J. Am. Chem. Soc.*, 1996, **118**, 10008; (*b*) J. D. Scollard, D. H. McConville, N. J. Payne and J. J. Vittal, *Macromolecules*, 1996, **29**, 5241.
30 A. D. Horton, J. de With, A. J. van der Linden and H. van de Weg, *Organometallics*, 1996, **15**, 2672.
31 R. Baumann, W. M. Davis and R. R. Schrock, *J. Am. Chem. Soc.*, 1997, **119**, 3830.
32 N. A. H. Male, M. Thornton-Pett and M. Bochmann, *J. Chem. Soc., Dalton Trans.*, 1997, 2487.
33 M. A. Flores, M. R. Manzoni, R. Baumann, W. M. Davis and R. R. Schrock, *Organometallics*, 1999, **18**, 3220.
34 R. Baumann and R. R. Schrock, *J. Organomet. Chem.*, 1998, **557**, 69.
35 R. R. Schrock, F. Schattenmann, M. Aizenberg and W. M. Davis, *Chem. Commun.*, 1998, 199.
36 (*a*) H. Memmler, K. Walsh, L. H. Gade and J. W. Lauher, *Inorg. Chem.*, 1995, **34**, 4062; (*b*) L. H. Gade, H. Memmler, U. Kauper, A. Schneider, S. Fabre, I. Bezougli, M. Lutz, C. Galka, I. J. Scowen and M. McPartlin, *Chem. Eur. J.*, 2000, **6**, 692.
37 S. L. Stokes, W. M. Davis, A. L. Odom and C. C. Cummins, *Organometallics*, 1996, **15**, 4521. Examples for C-F···M stabilization in zirconocenes: A. R. Siedle, R. A. Newmark, W. M. Lamanna and J. C. Huffman, *Organometallics*, 1993, **12**, 1491; J. Karl, G. Erker and R. Fröhlich, *J. Am. Chem. Soc.*, 1997, **119**, 11 165.
38 A. Schneider, L. H. Gade, M. Breuning, G. Bringmann, I. J. Scowen and M. McPartlin, *Organometallics*, 1998, **17**, 1643.
39 L. H. Gade, M. Schubart, B. Findeis, S. Fabre, I. Bezougli, M. Lutz, I. J. Scowen and M. McPartlin, *Inorg. Chem.*, 1999, **38**, 5282.
40 H. Memmler, U. Kauper, L. H. Gade, I. J. Scowen and M. McPartlin, *Chem. Commun.*, 1996, 1751.
41 H. Memmler and L. H. Gade, unpublished work.
42 C. Rosenberger, R. R. Schrock and W. M. Davis, *Inorg. Chem.*, 1997, **36**, 123.
43 R. R. Schrock, J. Lee, L.-C. Liang and W. M. Davis, *Inorg. Chim. Acta*, 1998, **270**, 353.
44 M. D. Fryzuk, *Can. J. Chem.*, 1992, **70**, 2839.
45 M. D. Fryzuk, J. B. Love and S. J. Rettig, *Chem. Commun.*, 1996, 2783.
46 M. D. Fryzuk, J. B. Love and S. J. Rettig, *Organometallics*, 1998, **17**, 846.
47 M. D. Fryzuk, J. B. Love and S. J. Rettig, *J. Am. Chem. Soc.*, 1997, **119**, 9071.
48 C. Elschenbroich and A. Salzer, *Organometallics, A Concise Introduction*, VCH, Weinheim, 1992.
49 M. D. Fryzuk, S. A. Johnson and S. J. Rettig, *Organometallics*, 1999, **18**, 2.
50 M. D. Fryzuk, T. S. Haddad, M. Mylvaganam, D. H. McConville and S. J. Rettig, *J. Am. Chem. Soc.*, 1993, **115**, 2782.
51 J. D. Cohen, M. Mylvaganam, M. D. Fryzuk and T. M. Loehr, *J. Am. Chem. Soc.*, 1994, **116**, 9529.
52 (*a*) M. D. Fryzuk, J. B. Love, S. J. Rettig and V. G. Young, *Science*, 1997, **275**, 1445; (*b*) H. Basch, D. G. Musaev, K. Morokuma, M. D. Fryzuk, J. B. Love, W. W. Seidel, A. Albinati, T. F. Koetzle, W. T. Klooster, S. A. Mason and J. Eckert, *J. Am. Chem. Soc.*, 1999, **121**, 523.
53 M. D. Fryzuk, S. A. Johnson and S. J. Rettig, *J. Am. Chem. Soc.*, 1998, **120**, 11024.
54 X.-L. Luo, G. L. Kubas, J. C. Bryan, C. J. Burns and C. J. Unkefer, *J. Am. Chem. Soc.*, 1994, **116**, 10312; X.-L. Luo, G. J. Kubas, C. J. Burns, J. C. Bryan and C. J. Unkefer, *J. Am. Chem. Soc.*, 1995, **117**, 1159; J. J. Schneider, *Angew. Chem., Int. Ed. Engl.*, 1996, **35**, 1068.

Paper a908273e

ChemComm

A simple one phase preparation of organically capped gold nanocrystals

Mark Green† and Paul O'Brien*‡

Department of Chemistry, Imperial College of Science, Technology and Medicine, London, UK SW7 2AY. E-mail: paul.obrien@man.ac.uk

Received (in Oxford, UK) 14th September 1999, Accepted 9th December 1999

A simple reproducible one-phase preparation of highly monodispersed organically passivated gold nanoparticles is described. The effect of the capping ligand on the particle size is discussed along with the manipulation of the nanoparticles into colloidal crystals and 2D arrays.

Recently, Brust *et al.* reported a simple two phase method for the preparation of high quality thiol passivated gold nanoparticles which were soluble in many organic solvents.[1,2] These nanoparticles have subsequently been used in the preparation of superlattices and electroactive materials.[3,4] Other applications of nanoparticles of gold include biomarkers in TEM experiments,[5] and more recently in single-electron transistors.[6]

One popular method for the preparation of (II/VI) or III/V) semiconductor quantum dots is the use of tri-*n*-octylphosphine oxide (TOPO) as both a reaction medium and passivating ligand.[7,8] Recent developments include the preparation of other compound semiconductors,[9] the use of single-molecular precursors such as dithio- or diseleno-carbamates, and the incorporation of nanoparticles into devices.[10–12] Sun and Murray have recently reported the preparation of cobalt nanoparticles using a similar methodology.[13]

We now report that the reduction of gold(IV) chloride by sodium borohydride in hot TOPO or a mixture of polar Lewis base solvents results in gold nanoparticles.§ The reduction of gold chloride (added as a solution in 4-*tert*-butylpyridine) in TOPO at *ca.* 190 °C resulted in relatively uncontrolled growth to particles with a wide range of shapes and sizes. Fig. 1(a) shows a typical TEM image in which square, triangular and spherical particles ranging in size from 10 to 100 nm in diameter can be seen. The isolated re-suspended nanoparticles were stable in toluene for only a matter of hours. In contrast, growth in a mixture of TOPO and octadecylamine (1 : 0.57 molar ratio) at 190 °C resulted in the controlled growth of spherical nanoparticulate gold particles (8.59 ± 1.09 nm), which have proved stable in toluene for months [Fig. 1(b)].

The morphology of the gold nanoparticle is controlled by various properties of the capping ligands. The Lewis basicity must be sufficient for significant interaction to occur and the bond formed has to be sufficiently labile to allow controlled growth. The length of the alkyl group on the capping ligand further affects the tuning of the size. Longer chain ligands tend to favour slower growth and hence the formation of, relatively, smaller nanoparticles. Hence, a balance must be achieved between the growth rate and ligand stability to facilitate growth of nanoparticle of a uniform size. A similar discussion of the role of organic capping agents in controlling particle size has been presented by Murray *et al.*, in describing processes in the growth of organically passivated cadmium chalcogenides[7] or cobalt nanoparticles.[13] The effect of capping group on particle size is being investigated further.

Evidence for the presence of the capping groups was obtained using IR spectroscopy, mass spectrometry and NMR. IR spectroscopy of the gold nanoparticles capped with octadecylamine and TOPO showed the bands associated with both ligands. There is a weak, broad feature not seen in the free amine spectrum at *ca.* 500 cm^{-1}, possibly a ν(Au–N) stretch.[14] TOPO also binds to the surface gold sites and a feature at *ca.* 1130 cm^{-1} is consistent with the shifted ν(P=O) bond deformation observed in other TOPO capped nanoparticles.[15] It is assumed that both TOPO and octadecylamine bind through the electron rich O or N atoms respectively.

The ^{1}H NMR spectrum of gold nanoparticles passivated with TOPO/octadecylamine displayed resonances associated with

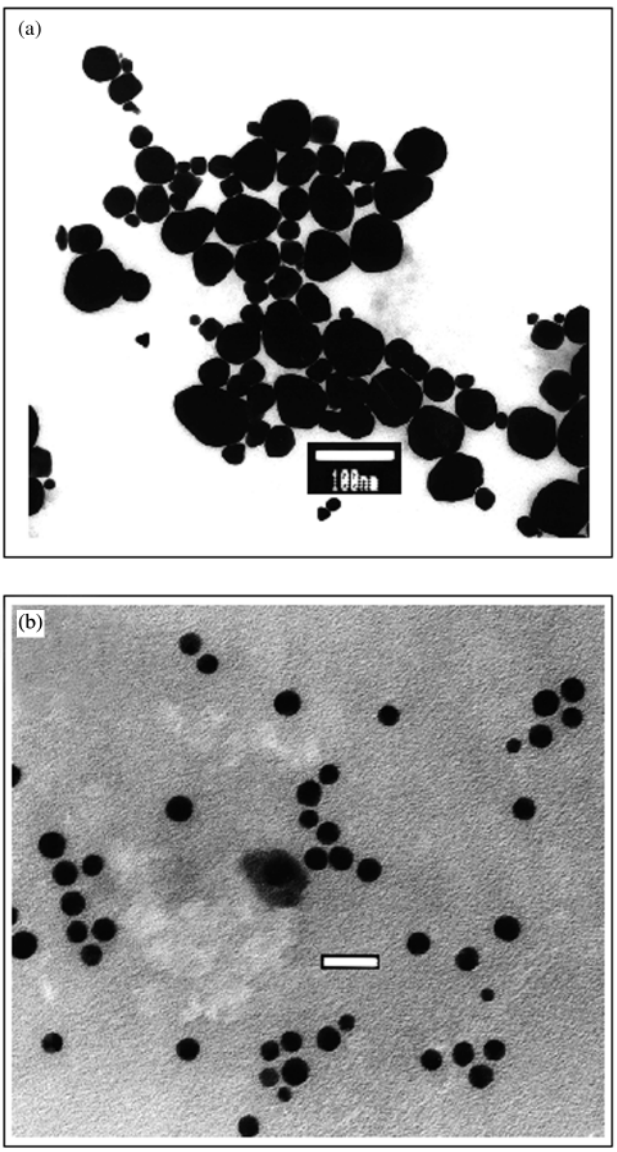

Fig. 1 (a) TEM of TOPO capped Q–Au (190 °C, 30 min), bar = 100 nm; (b) TEM of TOPO/octadecylamine capped Q–Au (190 °C, 30 min), bar = 20 nm.

† Present address: Department of Inorganic Chemistry, University of Oxford, South Parks Road, Oxford, UK OX1 3QR.

‡ Present address: The Manchester Materials Science Centre and The Chemistry Department, The University of Manchester, Oxford Road, Manchester, UK M13 9PL. E-mail: paul.obrien@man.ac.uk

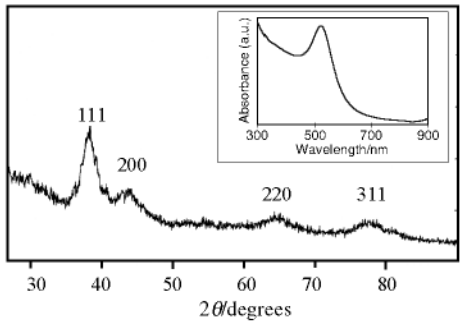

Fig. 2 XRD pattern of TOPO/octadecylamine capped Q–Au (190 °C, 30 min). Inset, electronic spectrum of TOPO/octadecylamine capped Q–Au (190 °C, 30 min).

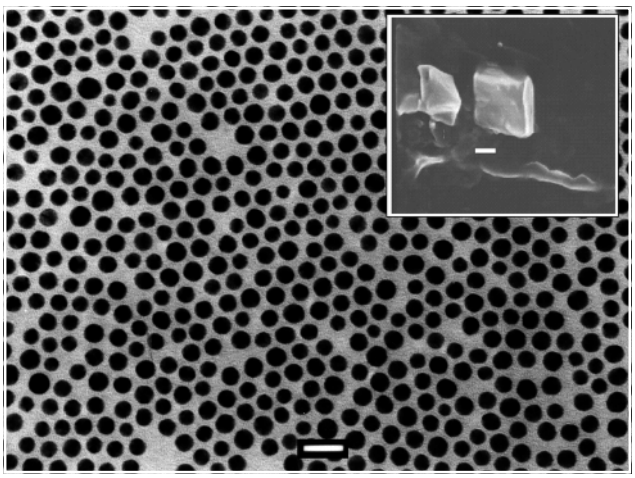

Fig. 3 2D lattice of octadecylamine/TOPO capped gold, bar = 20 nm. Inset; SEM of cubic colloidal crystal prepared from octadecylamine/TOPO capped gold nanoparticles (190 °C), bar = 80 μm.

organic ligands anchored to the nanoparticulate surface. Broad singlets at δ 0.9 and between δ 1.2 and 1.5 cannot be assigned as either TOPO or octadecylamine; broadening effects render resonances indistinguishable. The broadening of ^{1}H resonances of nanoparticle capping agents has previously been observed and attributed to either a reduction in rotational freedom at the surface site, or the inhomogeneous distribution of magnetic environments found on the nanocrystalline surface.[16,17] The ^{31}P NMR of capped gold nanoparticles show a single resonance at δ *ca.* 45; free TOPO displays a single resonance at δ 50. The upfield shift of 5 ppm is consistent with the surface metal shielding the phosphorus nuclei. This evidence again infers that the TOPO ligand bonds through the lone pair on the oxygen atom. FAB mass spectrometry of dots prepared in the mixed solvent system revealed the presence of not only TOPO (*m/z* 387) and octadecylamine (*m/z* 270), but also 4-*tert*-butylpyridine (*m/z* 136). It is assumed that only small amounts of 4-*tert*-butylpyridine are attached to the nanoparticle as no evidence for the ligand is found in either the ^{1}H NMR or the IR spectra. Powder X-ray diffraction data for the TOPO/octadecylamine capped dots showed broad peaks for the 111, 220, 200 and 311 planes of fcc gold (Fig. 2). Electronic spectroscopy of TOPO/octadecylamine gold dots showed the well documented plasmon resonance associated with colloidal gold at *ca.* 540 nm (2.29 eV).[18]

Murray *et al.* previously reported the controlled evaporation of solutions of TOPO capped CdSe and organically passivated Co, resulting in the preparation of superlattices and films.[13,19] Samples of as prepared octadecylamine/TOPO capped gold nanoparticles were washed with methanol removing all excess capping ligands and redispersed in the minimum amount of toluene. Aliquots of the toluene solutions were then placed either in a glass flask or on a glass slide and left to dry slowly (over *ca.* 3 days). Optical and electron microscopy revealed the presence of small cubic colloidal crystals with dimensions of the order of micrometers (Fig. 3, inset). XRD experiments on these colloidal crystals are currently in progress.

The as prepared octadecylamine/TOPO capped gold dots were found to spontaneously self assemble when deposited on a copper grid, forming ordered hexagonal close packed two-dimensional lattices (Fig. 3). Spontaneous self assembly has been observed before for highly monodispersed TOPO capped semiconductor nanoparticles.[20] We are at present developing this novel approach in the preparation of nanometric particles of different metals.

We acknowledge Keith Pell (QMW College) for electron microscopy and Jin-Ho Park (IC) for XRD. P. O. B. was Sumitomo/STS Professor of Material Chemistry during the duration of this work.

Notes and references

§ Nanoparticles were prepared using two different solvent systems. (1) In a typical synthesis, 0.07 g (23 mmol) $AuCl_4$ was dissolved in 7 ml 4-*tert*-butylpyridine. The solution was injected into a reaction flask containing 15 g TOPO and 0.0325 g $NaBH_4$ stabilised at 190 °C, left for 30 min, then removed from the heat source. The nanoparticles were isolated by solvent–non-solvent interactions at 60 °C, 30 ml of dry methanol was added leading to a precipitate which was isolated by centrifugation. The precipitate was stable in toluene for *ca.* 10 h.

(2) As above, injecting gold chloride dissolved in 4-*tert*-butylpyridine into a mixture of 10 g octadecylamine, 25 g TOPO and 0.0325 g $NaBH_4$ at 190 °C, with a growth time of 30 min. Upon injection, the reactants turned deep red. The nanoparticles were isolated using methanol as described above, and were found to be indefinitely stable in toluene. Once isolated as a powder, the nanoparticles were washed several times with methanol to remove excess capping agent before analysis.

1 M. Brust, J. Fink, D. Bethell, D. J. Schiffrin and C. Kiely, *J. Chem. Soc., Chem. Commun.*, 1995, 1655.
2 M. Brust, M. Walker, D. Bethell, D. J. Schiffrin and R. Whyman, *J. Chem. Soc., Chem. Commun.*, 1994, 801.
3 J. Fink, C. J. Kiely, D. Bethell and D. J. Schiffrin, *Chem. Mater.*, 1998, **10**, 922.
4 D. Gittens, D. J. Schiffrin, R. Nichols and D. Bethell, *Adv. Mater.*, 1999, **11**, 737.
5 J. W. Slot and H. J. Geuze, *J. Cell. Biol.*, 1981, **90**, 533.
6 T. Sato, H. Ahmed, D. Brown and B. F. G. Johnson, *J. Appl. Phys.*, 1997, **82**, 696.
7 C. B. Murray, D. J. Norris and M. G. Bawendi, *J. Am. Chem. Soc.*, 1993, **115**, 8706.
8 O. I. Micic and A. J. Nozik, *J. Lumin*, 1996, **70**, 95.
9 T. Trindade, O. C. Monteiro, P. O'Brien and M. Motevalli, *Polyhedron*, 1999, **18**, 1171.
10 T. Trindade, P. O'Brien and X. Zhang, *Chem. Mater.*, 1997, **9**, 523.
11 V. L. Colvin, M. C. Schlamp and A. P. Alivisatos, *Nature*, 1994, **370**, 354.
12 D. L. Klein, R. Roth, A. K. L. Lim, A. P. Alivisatos and P. L. McEuen, *Nature*, 1997, **389**, 699.
13 S. Sun and C. B. Murray, *J. Appl. Phys.*, 1999, **85**, 4325.
14 D. M. P. Mingos, J. Yau, S. Menzer and D. J. Williams, *J. Chem. Soc, Chem. Commun.*, 1995, 319.
15 J. E. Bowen-Katari, V. L. Colvin and A. P. Alivisatos, *J. Phys. Chem.*, 1994, **98**, 4109.
16 M. Kuno, J. K. Lee, B. O. Dabbousi, F. V. Mikulec and M. G. Bawendi, *J. Chem. Phys.*, 1997, **106**, 9869.
17 J. R. Sackleben, E. W. Wooten, L. Emsley, A. Pines, V. L. Colvin and A. P. Alivisatos, *Chem. Phys. Lett.*, 1992, **198**, 431.
18 M. M. Alvarez, J. T. Khoury, T. Gregory Scaaff, M. N. Shafigullin, I. Vezmar and R. L. Whetten, *J. Phys. Chem. B*, 1997, **101**, 3706.
19 C. B. Murray, C. R. Kagan and M. G. Bawendi, *Science*, 1995, **270**, 1335.
20 U. Banin, J. C. Lee, A. A. Guzelian, A. V. Kadavanich and A. P. Alivisatos, *Superlattices Microstruct.*, 1997, **22**, 559.

Communication a907532a

ChemComm

Controlling oxygen states at a Cu(110) surface: the role of coadsorbed sulfur and temperature

Albert F. Carley, Philip R. Davies, Rhys V. Jones, K. R. Harikumar and M. Wyn Roberts

Department of Chemistry, Cardiff University, P.O. Box 912, Cardiff, UK CF10 3TB. E-mail: robertsmw@cf.ac.uk

Received 23rd August 1999, Accepted 9th December 1999

Chemisorbed oxygen induces a disorder–order phase change in adsorbed sulfur at Cu(110) to give a c(2 × 2) adlayer at 295 K with oxygen present as isolated (2 × 1)-O strings, while warming a disordered oxygen state present at 80 K to 295 K generates a biphasic oxygen adlayer exhibiting both c(6 × 2) and (2 × 1) structures.

It is well established that at 295 K the chemisorbed oxygen adlayer at a Cu(110) surface consists of copper–oxygen chains oriented perpendicular to the copper substrate rows.[1a]

With increasing surface coverage the chains increase in length and coalese to form well ordered close packed islands with a (2 × 1)-O structure. At low oxygen coverages the oxygen chains are short, isolated, mobile and highly reactive to ammonia to form well ordered imide species through an oxydehydrogenation reaction accompanied by desorption of water.[2] By comparison, the oxygen islands are less reactive, with only those oxygen adatoms present at the island peripheries showing comparable dehydrogenation activity.

Here, we establish that a coadsorbate, chemisorbed sulfur, can influence the structure of chemisorbed oxygen states at a Cu(110) surface and how these oxygen states can simultaneously activate a disorder–order transition in the sulfur adlayer. The coadsorbates therefore exhibit cooperative effects which promote within the mixed-adlayer specific structural arrangements of each separate component. We also show that disordered oxygen adatoms present at 80 K are thermally ordered on warming to 295 K to generate a two phase system composed of (2 × 1)-O strings and c(2 × 6)-O structure.

An ultra-high vacuum spectrometer combining facilities for both scanning tunnelling microscopy (STM) and X-ray photoelectron spectroscopy (XPS) was supplied by Omicron Vacuum Physik. The Cu(110) crystal was cleaned by argon ion sputtering (0.6 keV beam energy; *ca.* 10 μA ion current) followed by annealing at 750 K for 30 min. The surface was shown to be clean by XPS and the purity of gases checked mass spectrometrically.

A Cu(110) surface was exposed to hydrogen sulfide at 295 K and the intensity of the S 2p binding energy region monitored by XPS. The signal was centred at 162 eV, indicative of chemisorbed sulfur,[3] and corresponded to a concentration of 2.4 × 10^{14} S adatoms cm^{-2}. The STM image [Fig. 1(a)] showed no evidence for chemisorbed sulfur although the copper atoms of the Cu(110) surface are resolved. This is consistent with a high surface mobility for the sulfur adatoms, most likely occurring along the $\langle 1\bar{1}0 \rangle$ directed troughs where the activation energy for surface diffusion is least.

However, when the disordered sulfur adlayer corresponding to a surface coverage $\theta \cong 0.28$ (σ_s = 3.0 × 10^{14} cm^{-2}) was exposed to oxygen at 295 K, ordered structures were immediately observed in the STM images [Fig. 1(b) and (c)]. A disorder–order phase transition with increasing sulfur coverage

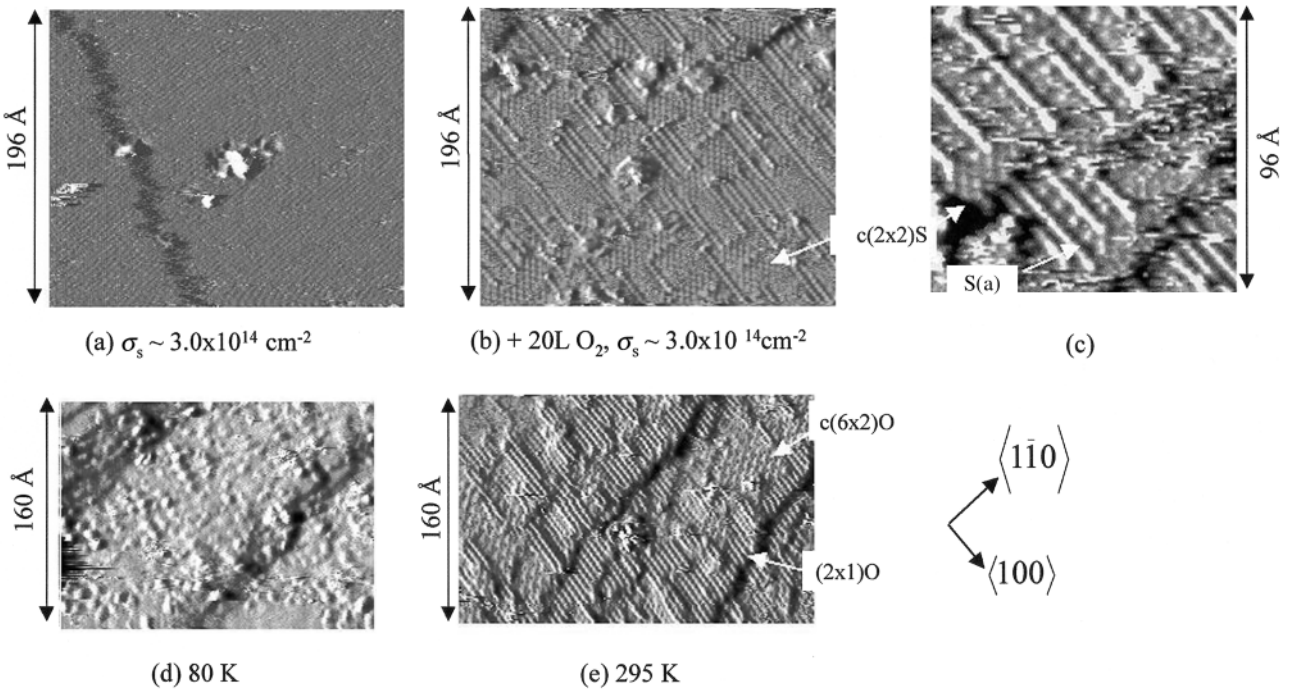

Fig. 1 STM images of (a) disordered chemisorbed mobile sulfur adatoms (σ_s = 3 × 10^{14} cm^{-2}; θ = 0.28) at a Cu(110) surface at 295 K, note the resolved copper atoms in the $\langle 1\bar{1}0 \rangle$ direction; (b) and (c) ordered structures of (2 × 1)-O and c(2 × 2)-S formed by an exposure of (a) to 20 L oxygen at 295 K [1 L (Langmuir) ≡ 10^{-6} Torr s]; chemisorbed sulfur adatoms separating (2 × 1)-O strings are visible in image (c); (d) disordered oxygen states present at a Cu(110) surface at 80 K; (e) ordered (2 × 1)-O and (6 × 2)-O states present after warming (d) to 295 K. The tunnelling conditions were typically [image (b)]: sample bias −0.38 V, feedback current 2.5 nA; loop gain 0.19%.

has been observed[1b] previously for Re(0001) but the role of a second adsorbate, in the present case oxygen, has not been reported. There are two distinct structures present at the Cu(110) surface, c(2 × 2) structures due to chemisorbed sulfur and (2 × 1) string or chain structures characteristic of chemisorbed oxygen. The presence of chemisorbed oxygen has clearly induced a disorder–order phase transition in the previously mobile disordered sulfur adlayer but with the simultaneous formation of oxygen strings well separated from each other (10 Å or more). The latter are distinctly different from the close packed oxygen island structures characteristic of the chemisorbed oxygen adlayer and more akin to the isolated oxygen chains present at Cu(110) at low oxygen coverage. In view of having established[2] that isolated oxygen chains were highly reactive in oxydehydrogenation reactions at Cu(110), we exposed this mixed sulfur–oxygen adlayer to ammonia at 295 K and confirmed the formation of imide species.

We, therefore, have an unusual phenomenon where during coadsorption two physiochemical processes occur: first chemisorbed oxygen inducing a phase change in the disordered S-adlayer to generate an ordered c(2 × 2)-S structure and second the presence of chemisorbed sulfur adatoms acting as a structural promoter of the isolated (2 × 1)-O strings. In some cases we have shown that the oxygen strings are separated from each other by just a single row of chemisorbed sulfur adatoms [Fig. 1(c)], in other cases the strings are well separated and present on terraces occupied predominantly by c(2 × 2) S-structures [Fig. 1(b)].

Although oxygen interaction at 295 K results in a well ordered (2 × 1)-O structure, if the Cu(110) is first exposed to oxygen at 80 K and the adlayer warmed to 295 K, the STM image indicates the presence of a biphasic oxygen adlayer [Fig. 1(d) and (e)]. In addition to the (2 × 1) structure there is also a (6 × 2)-O structure.

A c(6 × 2)-O structure has previously been reported by Wintterlin and Behm[1a] to exist at a Cu(110) surface when a (2 × 1)-O structure is exposed to 'much higher amounts of oxygen at $T \geqslant 300$ K'. Our STM results indicate that the same structure can develop through warming the chemisorbed adlayer at 80 K to room temperature, which offers a possible explanation for work function studies reported[4] some 30 years ago where the surface potential (change in work function) of chemisorbed oxygen on copper and nickel surfaces at 295 K differed by as much as 1 eV depending on whether or not the oxygen was chemisorbed first at 80 K. An earlier low energy electron diffraction study[5] also drew attention to the role of temperature in controlling the formation of the c(6 × 2) structure; Fig. 1(e) however provides atom-resolved evidence for the co-existence of the two phases at 295 K and the disorder–order transition that occurs between 80 and 295 K.

Since it is now well established that the chemical reactivity of oxygen at a Cu(110) surface is dependent on its structural state (isolated oxygen adatoms, isolated oxygen strings or close packed island structures), the ability to control the structural nature of the chemisorbed oxygen state through coadsorbed sulfur offers a novel approach to controlling selectivity in oxygenation catalysis. Sulfur, although more usually considered to be a surface 'poison', can also be a catalytic promoter with lateral interactions controlling surface structural states of oxygen.

We are grateful to the EPSRC for their support.

Notes and references

1 (*a*) J. Wintterlin and R. J. Behm, in *Scanning Tunelling Microscopy I*, ed. H.-J. Güntherodt and R. Wiesendanger, Springer-Verlag, Berlin, 1994; A. F. Carley, P. R. Davies and M. W. Roberts, *Catal. Lett.*, 1999, **58**, 93 and references therein; X.-C. Guo and R. J. Madix, *Faraday Discuss., Chem. Soc.*, 1996, **105**, 139; (*b*) M. Salmeron and J. Dunphy, *Faraday Discuss., Chem. Soc.*, 1996, **105**, 151.
2 A. F. Carley, P. R. Davies and M. W. Roberts, *Chem. Commun.*, 1998, 1793.
3 L. Moroney, S. Rassias and M. W. Roberts, *Surf. Sci.*, 1981, **105**, L249.
4 C. M. Quinn and M. W. Roberts, *Trans. Faraday Soc.*, 1964, **60**, 899.
5 G. R. Gruzalski, D. M. Zehner and J. F. Wendelken, *Surf. Sci.*, 1984, **147**, L623.

Communication a906827i

Novel dual-host approach in ion pair extraction: a simple tripodal nitrate host facilitates $CsNO_3$ transfer to 1,2-dichloroethane by a large crown ether

Konstantinos Kavallieratos,[a] Richard A. Sachleben,[a] Gary J. Van Berkel[b] and Bruce A. Moyer*[a]

[a] *Chemical Separations Group, Chemical and Analytical Sciences Division, Oak Ridge National Laboratory, PO Box 2008, Oak Ridge, TN 37831-6119, USA. E-mail: moyerba@ornl.gov*

[b] *Organic and Biological Mass Spectrometry Group, Chemical and Analytical Sciences Division, Oak Ridge National Laboratory, PO Box 2008, Oak Ridge, TN 37831-6365, USA*

Received (in Columbia, MO) 27th October 1999, Accepted 29th November 1999

The readily available benzene-1,3,5-tricarboxamide 1 enhances $CsNO_3$ extraction by tetrabenzo-24-crown-8 *via* hydrogen bonding to the nitrate anion, as demonstrated by NMR and electrospray ionization mass spectrometry.

Considerable effort has been expended toward developing host molecules for recognition of cations[1] and, more recently, anions.[2] Surprisingly little attention, though, has been given to recognition of targeted ion pairs,[3] despite potential applications.[4] Historically, ion-pair extraction of alkali and alkaline earth metal salts[5] has tended to be weak, owing to unfavorable dehydration–resolvation energetics for co-extraction of the common inorganic anions.[6,7] This effect simply reflects the normal electrostatic 'bias'[7b] disfavoring small, charge-dense anions (Hofmeister series).[8] Although various successful approaches have been developed to circumvent this 'anion problem',[5a,9] it was our thought that the combination of an anion host with a cation host would represent a singular advance by making anion transfer to the organic phase both more favorable and selective.[10] The idea was shown to work under some conditions in supported liquid membranes,[11] whereas we sought simpler and more synthetically accessible anion receptors as the key to widespread application. Nitrate represents an ion of particular significance in separation chemistry,[4] and certain of its salts, especially $CsNO_3$, are important components of nuclear waste.[4a] However, few designed nitrate receptors have been reported,[12] and neutral lipophilic nitrate hosts are rare.[12a,b] We now report that crown ether extraction of $CsNO_3$ is increased by a simple tripodal host that directly binds nitrate ion through amide N–H hydrogen bonds.

The anion host **1** and controls **2** and **3** were synthesized by standard methods from the corresponding anilines and acid

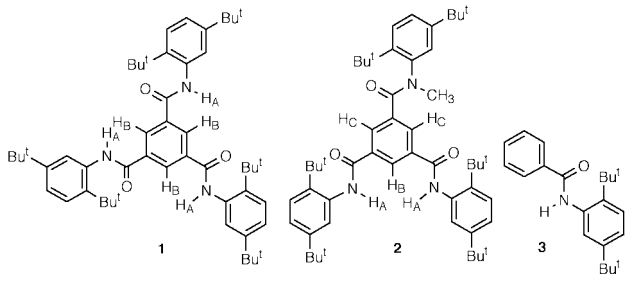

chlorides.[13] The chosen benzene-1,3,5-tricarboxamide skeleton combines the desired C_3 symmetry environment for recognition of the nitrate anion with synthetic ease and flexibility. Amides and ureas have been employed in anion host–guest chemistry.[2,14–17] Moreover, the potential for variation of the aniline moiety allows 'tuning' of the electronic and steric contributions to the binding, as well as solubility and hydrophobicity. Tetrabenzo-24-crown-8[18] was used as the cation host because it effectively complexes the caesium cation[19] in 1,2-dichloroethane, while keeping the encapsulated Cs^+ cation and the NO_3^- anion fully dissociated.[20]

The distribution results[21] (Fig. 1) show that amides **1** and **2** (but not monoamide **3**) enhance the extraction of $CsNO_3$ by tetrabenzo-24-crown-8. At 10 mM, tripodal amide **1** enhances the extraction by a factor of 1.9 ($D_{Cs} = 6.3 \times 10^{-3}$ for **1** *vs.* 3.3×10^{-3} for the crown-only experiment), whereas the same concentration of bipodal amide **2** enhances Cs extraction by a factor of 1.3 ($D_{Cs} = 4.2 \times 10^{-3}$). The enhancement is dependent on the amide concentration, as expected (Fig. 1). No extraction was detected with the amides alone ($D_{Cs} < 2 \times 10^{-5}$).

The nitrate binding affinities of **1** and **2** were determined by ^{1}H NMR titrations with $(Bu_4N)NO_3$ in 1,2-dichloroethane-d_4. Non-linear regression analysis[22] of the binding isotherms[23] obtained from the downfield chemical shift changes for the N–H amide (H_A) resonances ($\Delta\delta$ N–H), as well as for the *ortho* C–H aromatic (H_B) resonances ($\Delta\delta$ C–H), gave 1:1 association constants (K_a) of 250 M^{-1} for the formation of **1**·NO_3^- *vs.* 23 M^{-1} for **2**·NO_3^- (Table 1). For the diamide **2**, both H_A and H_B gave significant downfield shift changes, while the H_C chemical shift remained virtually constant. This is indicative of nitrate complexation by two hydrogen bonds.[16] In contrast, **1**·NO_3^- exhibited a single downfield-shifted resonance for H_B, suggest-

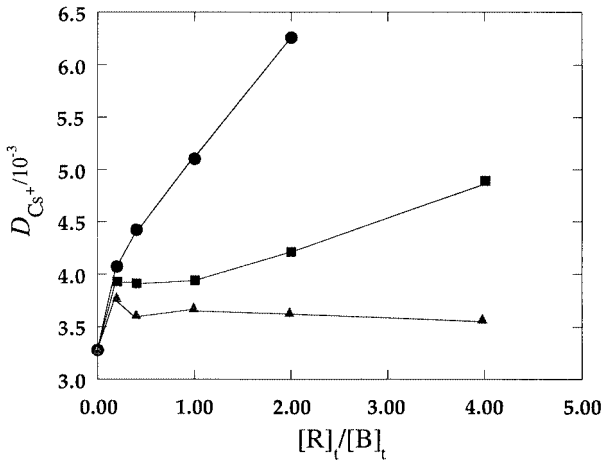

Fig. 1 Plot of D_{Cs} *vs.* $[R]_t/[B]_t$ at 25 °C, where $[R]_t$ is the total amide (R = **1**–**3**) concentration and $[B]_t$ is the total crown concentration (5 mM): (●) **1**, (■) **2** and (▲) **3**. Errors are estimated to be < 5%.

Table 1 Chemical shift changes, association constants, and ΔG^o values at 18.1 °C for **1**·NO_3^- and **2**·NO_3^- formation

Compound	δ_H(N–H)	δ_H(2-C–H)	K_a/M^{-1}	ΔG^o/kJ mol^{-1}
1	8.01	8.61		
1·[NO_3^-]	9.32	8.78	250[a]	−13.4
2	7.58	8.22		
2·[NO_3^-]	9.54	8.75	23[a]	−7.5

[a] Errors are estimated to be < 5%.

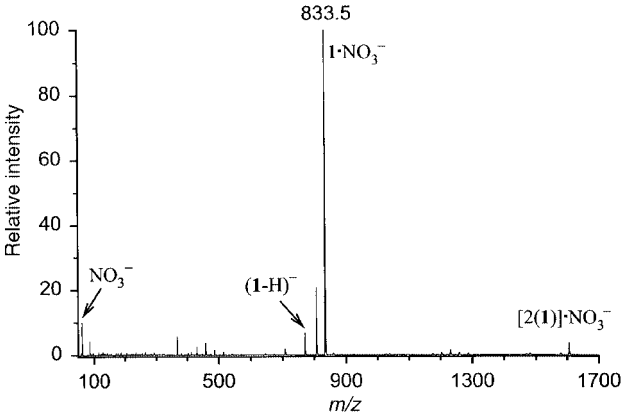

Fig. 2 Negative ion electrospray ionization mass spectrum for **1**·NO_3^- in extraction solvent. The peak at *m/z* 806.5 corresponds to **1**·Cl^- (ref. 25). The results were reproduced in solutions of **1** and $(Bu_4N)NO_3$.

ing participation of all three N–H groups, whether by pairs in fast equilibrium or in concert.

Negative ion mode electrospray ionization mass spectrometry[24] confirms the ^{1}H NMR conclusion of a 1:1 **1**·NO_3^- complexation stoichiometry (*m/z* = 833.5; Fig. 2). Receptor **2** also gave a peak corresponding to **2**·NO_3^-, but with a lower intensity. No evidence for **3**·NO_3^- was observed.

Based on these observations, and taking into consideration the ten-fold higher K_a for **1**·NO_3^- *vs.* **2**·NO_3^-, which cannot be attributed solely to the statistical factor (3), we suggest that a contribution of the third amide group in **1**·NO_3^- is primarily responsible for the higher extraction enhancement for **1** *vs.* **2**. The ^{1}H NMR association constants would ideally imply extraction enhancements of 3.5 and 1.2, respectively, which are consistent with the actual values of 1.9 and 1.3.[26]

In conclusion, the present results demonstrate the viability of employing two simple host molecules for transporting a selected salt *vs.* targeting only a single ion. The extraction enhancement obtained sets the ground for further research into using different hosts and target guest systems, as well as in elucidating aspects of speciation, selectivity, and structure of the supramolecular complexes involved.

We thank Peter V. Bonnesen, Tamara J. Haverlock, Jeffrey C. Bryan and Professor Robert H. Crabtree (Yale) for experimental assistance, information and useful suggestions. This research was sponsored by the Division of Chemical Sciences, Office of Basic Energy Sciences, U.S. Department of Energy, under contract number DE-AC05-96OR22464 with Oak Ridge National Laboratory, managed by Lockheed Martin Energy Research Corp. ES-MS instrumentation was provided through a cooperative research and development agreement with Perkin-Elmer Sciex Instruments (CRADA No. ORNL 96-0458). The participation of K. K. was made possible through an appointment to the ORNL Postgraduate Program, administered by ORAU.

Notes and references

1 B. Dietrich, P. Viout and J.-M. Lehn, *Macrocyclic Compounds Chemistry, Aspects of Organic and Inorganic Supramolecular Chemistry*, VCH, Weinheim, 1992.
2 *The Supramolecular Chemistry of Anions*, ed. A. Bianchi, K. Bowman-James and E. García-España, Wiley-VCH, New York, 1997; J. L. Atwood, K. T. Holman and J. W. Steed, *Chem. Commun.*, 1996, 1401; F. P. Schmidtchen and M. Berger, *Chem. Rev.*, 1997, **97**, 1609.
3 M. T. Reetz, in *Comprehensive Supramolecular Chemistry*, ed. F. Vögtle, Pergamon, Oxford, 1996, vol. 2, pp. 553–562.
4 (*a*) *Science and Technology for Disposal of Radioactive Tank Wastes*, ed. W. W. Schultz and N. J. Lombardo, Plenum, New York, 1998; (*b*) C. F. Mason, *Biology of Freshwater Pollution*, 2nd edn., Longman, New York, 1991.
5 (*a*) W. J. McDowell, *Sep. Sci. Technol.*, 1988, **23**, 1251. For calixarene complexants see: (*b*) C. D. Gutsche, *Calixarenes Revisited*, The Royal Society of Chemistry, Cambridge, 1998, ch. 7, pp. 185–208.
6 Y. Marcus, M. J. Kamlet and R. W. Taft, *J. Phys. Chem.*, 1988, **92**, 3613.
7 (*a*) B. A. Moyer, in *Comprehensive Supramolecular Chemistry*, ed. G. W. Gokel, Pergamon, Oxford, 1996, vol. 1, pp. 401–405; (*b*) B. A. Moyer and P. V. Bonnesen, in *The Supramolecular Chemistry of Anions*, ed. A. Bianchi, K. Bowman-James and E. García-España, Wiley-VCH, New York, 1997, pp. 31–33.
8 F. Hofmeister, *Arch. Exp. Pathol. Pharmakol.*, 1888, **24**, 247.
9 Y. Marcus, *Solvent Extr. Ion Exch.*, 1989, **7**, 567; E. P. Horwitz, M. L. Dietz and D. E. Fisher, *Solvent Extr. Ion Exch.*, 1990, **8**, 199; 1991, **9**, 1; B. K. Tait and D. P. Shillington, *Solvent Extr. Ion Exch.*, 1993, **11**, 877; P, V. Bonnesen, T. J. Haverlock, N. L. Engle, R. A. Sachleben and B. A. Moyer, in *Calixarene Molecules for Separations*, The American Chemical Society, Washington, DC, in press.
10 Related work in a collaboration led by K. Bowman-James at the University of Kansas uses receptors derived from *N*,*N*,*N*-tris(aminoethyl)amine; K. Kavallieratos, R. A. Sachleben, J. C. Bryan, B. A. Moyer, A. M. Danby and K. Bowman-James, 217th National Meeting of the American Chemical Society, Anaheim, CA, March 1999; K. Kavallieratos, A. M. Danby, G. J. Van Berkel, M. A. Kelly, R. A. Sachleben, B. A. Moyer and K. Bowman-James, manuscript in preparation.
11 F. de Jong and H. C. Visser, in *Comprehensive Supramolecular Chemistry*, ed. D. N. Reinhoudt, Pergamon, Oxford, 1996, vol. 10, pp. 13–51; L. A. J. Chrisstoffels, PhD Thesis, University of Twente, 1998.
12 (*a*) P. Bisson, V. Lynch, M. K. C. Monahan and E. V. Anslyn, *Angew. Chem., Int. Ed. Engl.*, 1997, **36**, 2340; (*b*) R. Jagessar and D. H. Burns, *Chem. Commun.*, 1997, 1685; (*c*) M. Staffilani, K. S. B. Hancock, J. W. Steed, K. T. Holman, J. L. Atwood, R. K. Juneja and R. S. Burkhalter, *J. Am. Chem. Soc.*, 1997, **119**, 6324; (*d*) R. D. Schnebeck, E. Freisinger and B. Lippert, *Angew. Chem., Int. Ed.*, 1999, **38**, 168; (*e*) P. D. Beer, M. G. B. Drew, D. Hesek and R. Jagessar, *J. Chem. Soc., Chem. Commun.*, 1995, 1187; (*f*) S. Mason, T. Clifford, L. Seib, K. Kuczera and K. Bowman-James, *J. Am. Chem. Soc.*, 1998, **120**, 8899; (*g*) G. Y. S. Chan, M. G. B. Drew, M. J. Hudson, N. S. Isaacs, P. Byers and C. Madic, *Polyhedron*, 1996, **15**, 3385; (*h*) R. J. Motekaitis, A. E. Martell, J.-M. Lehn and E.-I. Watanabe, *Inorg. Chem.*, 1982, **21**, 4253.
13 Purity was confirmed by TLC and ^{1}H NMR prior to extraction.
14 Y. Morzherin, D. M. Rudkevich, W. Verboom and D. N. Reinhoudt, *J. Org. Chem.*, 1993, **58**, 7602; C. Seel and F. Vögtle, *Angew. Chem., Int. Ed. Engl.*, 1992, **104**, 542.
15 A. P. Davis, J. J. Perry and R. P. Williams, *J. Am. Chem. Soc.*, 1997, **119**, 1793.
16 (*a*) K. Kavallieratos, S. R. de Gala, D. J. Austin and R. H. Crabtree, *J. Am. Chem. Soc.*, 1997, **119**, 2325; (*b*) K. Kavallieratos, C. M. Bertao and R. H. Crabtree, *J. Org. Chem.*, 1999, **64**, 1675.
17 E. Fan, S. A. van Arman, S. Kincaid and A. D. Hamilton, *J. Am. Chem. Soc.*, 1993, **115**, 369.
18 C. J. Pedersen, *J. Am. Chem. Soc.*, 1967, **89**, 7017.
19 R. A. Sachleben, Y. Deng, D. R. Bailey and B. A. Moyer, *Solvent. Extr. Ion Exch.*, 1996, **14**, 995; R. A. Sachleben, Y. Deng and B. A. Moyer, *Sep. Sci. Technol.*, 1997, **32**, 275.
20 Y. Deng, R. A. Sachleben and B. A. Moyer, *J. Chem. Soc., Faraday Trans.*, 1995, 4215; T. G. Levitskaia, J. C. Bryan, R. A. Sachleben, J. D. Lamb and B. A. Moyer, *J. Am. Chem. Soc.*, in press.
21 The aqueous phase was 10 mM $CsNO_3$, spiked with 10^{-7} M $^{137}CsNO_3$ tracer, and made acidic with 0.1 mM HNO_3. The distribution of Cs^+ was determined by gamma scintillation.
22 KaleidaGraph, Version 3.0.2. Synergy Software (PCS Inc.), Reading, PA 19606. Developed by Abelbeck Software Inc.
23 K. A. Connors, *Binding Constants*, Wiley, New York, 1987.
24 J. S. Brodbelt and D. V. Dearden, in *Comprehensive Supramolecular Chemistry*, ed. J. E. D. Davies and J. A. Ripmeester, Pergamon, Oxford, 1996, vol. 8, ch. 14, pp. 567–589 and references therein.
25 The strong affinity for the impurity Cl^- ion is under investigation.
26 The enhancement factors are approximated as $1 + K_a[R]_t$ assuming formation of 1:1 **R**·NO_3^- complexes. Probable aggregation of **R** or formation of **R**·crown complexes would be expected to reduce the enhancement and to be stronger for **1** than for **2**.

Communication a908562i

Can α-sultone exist as a chemical species? First experimental implication for intermediacy of α-sultone

Yoshiki Morimoto,* Hajime Kurihara and Takamasa Kinoshita

Department of Chemistry, Graduate School of Science, Osaka City University, Sumiyoshiku, Osaka 558-8585, Japan. E-mail: morimoto@sci.osaka-cu.ac.jp

Received (in Cambridge, UK) 17th November 1999, Accepted 15th December 1999

The treatment of 2,4,6-trimethylpyridine *N*-oxide 8 with $BnSO_2Cl$ and Et_3N in the presence of various olefins afforded unexpected γ-sultones 10 along with 2,4,6-trimethylpyridine 9, *via* the possible generation and/or intermediacy of an α-sultone 2 as a new reactive intermediate.

Sultones **1** are the internal esters of hydroxy sulfonic acids and

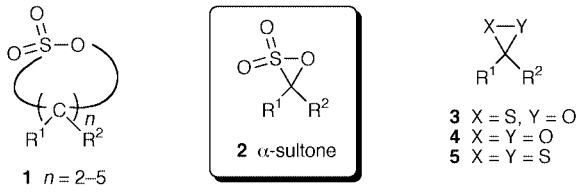

are the sulfur analogs of lactones. Since the term 'sultone' was first introduced into the literature by Erdmann in 1888,[1] there have been many new developments in sultone chemistry,[2] including industrial applications, biological properties and the current mechanistic research into the role of β-sultones in olefin sulfonation.[3,4] However, most of the sultones mentioned above have been restricted to four- to seven-membered rings. Can the α-sultone **2** exist as a chemical species? To the best of our knowledge, the description of an α-sultone has never been reported in the literature. On the other hand, S- and/or O-containing three-membered ring compounds such as **3–5** have attracted recent interest as labile reactive intermediates in organic chemistry.[5] From the viewpoints of labile reactive intermediates, the chemistry of small rings containing two heteroatoms and organosulfur chemistry as well as sultone chemistry, the question of whether α-sultone **2** can exist as a chemical species or not is a very stimulating and interesting subject in organic chemistry. Here we suggest the possibility of the generation and/or intermediacy of α-sultones as new reactive intermediates for the first time.

The reason why we suspected that the α-sultone might be generated as a reactive intermediate originated from an unexpected phenomenon. In the course of our recent synthetic studies on macrocyclic marine alkaloids, halicalmines A and B,[6] it was determined that an excess of MsCl resulted in the deoxygenation of pyridine *N*-oxides **6** under standard mesylation conditions (MsCl, Et_3N, CH_2Cl_2) without chlorination of the pyridine nucleus [eqn. (1)].[7] The problem is the reaction

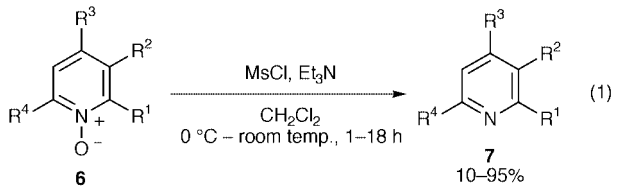

mechanism of these unusual deoxygenations. After many unsuccessful experiments, products, which are very significant for deducing the reaction mechanism, have been trapped. The treatment of 2,4,6-trimethylpyridine *N*-oxide **8** with 7 equiv. of $BnSO_2Cl$ and 9 equiv. of Et_3N in the presence of 30 equiv. of 2,3-dimethylbut-2-ene afforded γ-sultone **10** ($R^1 = R^2 = R^3 = R^4 = Me$) in 21% yield as an isolable and identifiable product along with deoxygenated 2,4,6-trimethylpyridine **9** (entry 1 in Table 1).† How can the production of γ-sultone **10** be explained?

Possible reaction pathways leading to the γ-sultone **10** are depicted in Scheme 1. The generation of sulfenes by treating

Table 1 Production of γ-sultones **10** in the presence of several olefins

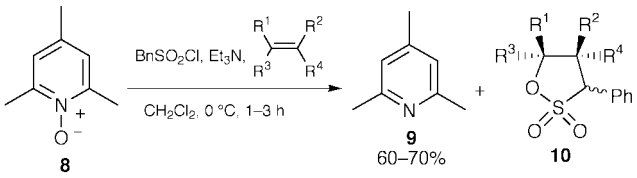

Entry	Olefin	Yield of **10**[a] (%)	α-Ph:β-Ph
1	$R^1 = R^2 = R^3 = R^4 = Me$	21	—
2	$R^1 = R^2 = R^3 = Me$, $R^4 = H$	26	60:40[b]
3	$R^1 = R^2 = Me$, $R^3 = R^4 = H$	36	35:65[b]
4	$R^1 = R^2 = (CH_2)_6$, $R^3 = R^4 = H$	40	45:55[c]

[a] Isolated yield. [b] Ratios were determined by ^1H NMR integration of the mixture. [c] Ratio was based on the isolated yields.

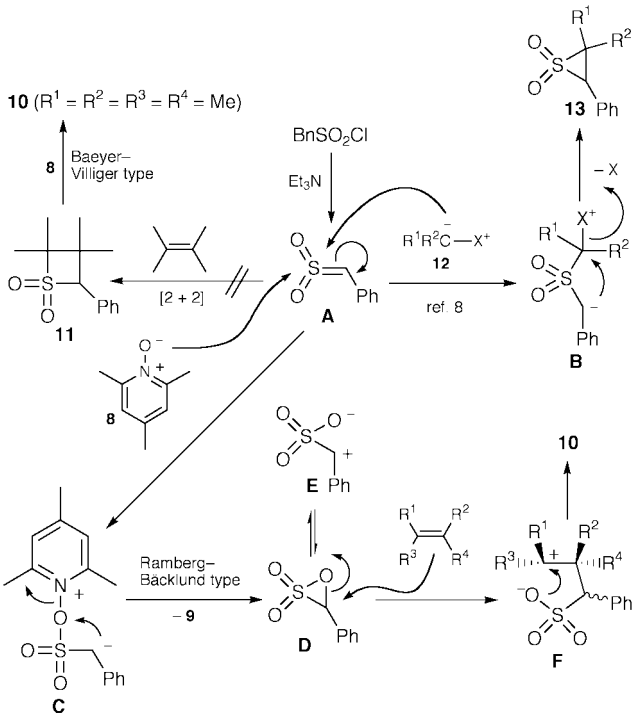

Scheme 1

alkanesulfonyl chloride derivatives possessing an α-hydrogen with triethylamine is a well-established process in sulfene chemistry.[8] The formation of thietane 1,1-dioxide **11**[9] by [2 + 2] cycloaddition between the sulfene intermediate **A** and 2,3-dimethylbut-2-ene and the subsequent Baeyer–Villiger type oxidation of **11** with *N*-oxide **8** may be considered as one possibility. This reaction pathway, however, appears to be ruled out, because the thietane 1,1-dioxide **11** could not be produced in the reaction of $BnSO_2Cl$ and Et_3N with 2,3-dimethylbut-2-ene in the absence of the *N*-oxide **8**. Furthermore, treatment of thietane 1,1-dioxide **14**‡ with *N*-oxide **8** in the presence of Et_3N in CH_2Cl_2 did not give γ-sultone **15**, but resulted in quantitative recoveries of **8** and **14** [eqn. (2)].

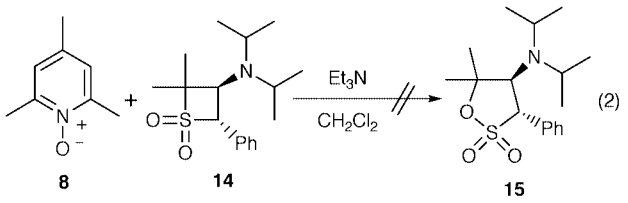

8 **14** **15** (2)

On the other hand, it is also well known that the reaction of sulfenes with diazoalkanes (X = N_2) and phosphonium (X = PPh_3), sulfonium (X = SR^3R^4) and sulfoxonium (X = SOR^3R^4) ylides **12** provides episulfones **13** *via* elimination of the neutral leaving group X from the intermediary adduct **B**.[8] Therefore, another possible reaction pathway closely related to this episulfone route may be more plausible to explain the production of γ-sultone **10**. The similar attack of the *N*-oxide **8** on the sulfur atom in the sulfene intermediate **A** may generate α-sultone **D** through the ring-closing reaction[10] such as the Ramberg–Bäcklund type[11] in the adduct **C** together with liberation of 2,4,6-trimethylpyridine **9**. The α-sultone **D** is postulated to be highly labile for the following reasons: (i) an intrinsic ring strain in the three-membered rings; (ii) a large polarization of the C–O bond which is characteristic of sulfonates and makes them good leaving groups; and (iii) the presence of carbon geminally disubstituted by two kinds of heteroatoms (oxygen and sulfur). Therefore, the alternative zwitterionic structure **E**, which is produced by spontaneous cleavage of the highly strained and polarized C–O bond, may then predominate over the α-sultone structure **D**. Finally, the interaction of α-sultone **D** or zwitterion **E** with 2,3-dimethylbut-2-ene could lead to the γ-sultone **10** ($R^1 = R^2 = R^3 = R^4$ = Me) by way of the cationic intermediate **F**.

The γ-sultones **10** were also obtained as stereoisomeric mixtures§ in the presence of olefins other than 2,3-dimethylbut-2-ene (entries 2–4). In the case of 2-methylbut-2-ene, the observation of only one regioisomeric γ-sultone **10** ($R^1 = R^2 = R^3$ = Me, R^4 = H) supports the intervention of the cationic intermediate **F** (tertiary *vs.* secondary). In entry 3, the fact that the stereochemistry of *cis*-but-2-ene was retained in the γ-sultone **10** ($R^1 = R^2$ = Me, $R^3 = R^4$ = H) may imply that in the carbocation **F** the ring-closure is much faster than the C–C single bond rotation. It is also of interest to note that yields of γ-sultones **10** reflect the reactivities (strain and steric hindrance) of the olefins examined.

In conclusion, we have proposed the possible generation and/or intermediacy of α-sultone **2** as a new chemical species for the first time in organic chemistry. Clarification of the detailed reaction mechanism for the production of γ-sultones **10** and determination of direct evidence for the α-sultone are in progress.

H. K. thanks the Suntory Institute for Bioorganic Research for a SUNBOR Scholarship. This work was partially supported by the Saneyoshi Scholarship Foundation and a Grant-in Aid for Encouragement of Young Scientists from the Japan Society for the Promotion of Science.

Notes and references

† All new compounds were satisfactorily characterized using ^1H and ^{13}C NMR, IR, MS and HRMS spectra and also by elemental analyses whenever possible. *Selected data* for **10** ($R^1 = R^2 = R^3 = R^4$ = Me): mp 190.5–191.5 °C; δ_H (400 MHz, $CDCl_3$) 7.56–7.48 (2H, m), 7.46–7.36 (3H, m), 4.52 (1H, s), 1.68 (3H, s), 1.49 (3H, s), 1.17 (3H, s), 0.97 (3H, s); δ_C (100 MHz, $CDCl_3$) 131.3, 129.2, 128.4, 127.9, 92.9, 70.6, 48.3, 24.2, 23.4, 22.1, 19.1; $\nu_{max}(CHCl_3)/cm^{-1}$ 2995, 1450, 1338, 1172, 1152, 1130, 1109, 940, 894, 835; *m/z* (EI-MS) 254 (M^+, 10%), 132 (100), 117 (67), 91 (41), 84 (54) (EI-HRMS: calc. for $C_{13}H_{18}O_3S$ (M^+), 254.0976; found, 254.0973) (Calc. for $C_{13}H_{18}O_3S$: C, 61.39; H, 7.13. Found: C, 61.46; H, 7.07%).

‡ Thietane 1,1-dioxide **14**, prepared according to the procedure of ref. 9(*b*), was subjected to the control experiment instead of the inaccessible **11**.

§ The relative stereochemistries in γ-sultones **10** were unambiguously assigned by the diagnostic coupling constants and NOE experiments in their ^1H NMR spectra.

1 H. Erdmann, *Liebigs Ann. Chem.*, 1888, **247**, 306.
2 For reviews, see: A. Mustafa, *Chem. Rev.*, 1954, **55**, 195; D. W. Roberts and D. L. Williams, *Tetrahedron*, 1987, **43**, 1027.
3 J. L. Boyer, B. Gilot and J.-P. Canselier, *Phosphorus Sulfur*, 1984, **20**, 259; W. A. Thaler and C. duBreuil, *J. Polym. Sci.*, 1984, **22**, 3905; H. Cerfontain, J. B. Kramer, R. M. Schonk and B. H. Bakker, *Recl. Trav. Chim. Pays-Bas*, 1995, **114**, 410 and references cited therein.
4 D. W. Roberts, D. L. Williams and D. Bethell, *J. Chem. Soc., Perkin Trans. 2*, 1985, 389; D. W. Roberts, P. S. Jackson, C. D. Saul and C. J. Clemett, *Tetrahedron Lett.*, 1987, **28**, 3383; J. Haller, B. R. Beno and K. N. Houk, *J. Am. Chem. Soc.*, 1998, **120**, 6468; J. O. Morley, D. W. Roberts and S. P. Watson, *J. Chem. Soc., Perkin Trans. 2*, 1999, 1819.
5 R. W. Murray and M. Singh, in *Comprehensive Heterocyclic Chemistry II*, ed. A. R. Katritzky, C. W. Rees and E. F. V. Scriven, Pergamon, Oxford, 1996, vol. 1A, p. 429; W. Adam and S. Weinkötz, *Chem. Commun.*, 1996, 177; R. Huisgen, G. Mloston, K. Polborn and F. Palacios-Gambra, *Liebigs Ann./Rec.*, 1997, 187; A. Kirschfeld, S. Muthusamy and W. Sander, *Angew. Chem., Int. Ed. Engl.*, 1994, **33**, 2212; A. Ishii, T. Akazawa, T. Maruta, J. Nakayama, M. Hoshino and M. Shiro, *Angew. Chem., Int. Ed. Engl.*, 1994, **33**, 777.
6 Y. Morimoto and C. Yokoe, *Tetrahedron Lett.*, 1997, **38**, 8981; Y. Morimoto, C. Yokoe, H. Kurihara and T. Kinoshita, *Tetrahedron*, 1998, **54**, 12 197.
7 Y. Morimoto, H. Kurihara, C. Yokoe and T. Kinoshita, *Chem. Lett.*, 1998, 829.
8 For reviews, see: G. Opitz, *Angew. Chem., Int. Ed. Engl.*, 1967, **6**, 107; N. H. Fischer, *Synthesis*, 1970, 393; J. F. King, *Acc. Chem. Res.*, 1975, **8**, 10.
9 For the formation of the thietane 1,1-dioxides from sulfenes and nucleophilic olefins such as enamines and enol ethers, see: (*a*) W. E. Truce and J. R. Norell, *J. Am. Chem. Soc.*, 1963, **85**, 3231; (*b*) W. E. Truce and J. F. Rach, *J. Org. Chem.*, 1974, **39**, 1109.
10 The readiness for intramolecular cyclization of carbanions to three-membered rings has been theoretically suggested as a proximity effect. See: S. Gronert, K. Azizian and M. A. Friedman, *J. Am. Chem. Soc.*, 1998, **120**, 3220. During the deoxygenations of tertiary amine oxides with carbon disulfide, the formation of three-membered ring intermediates from the analogous adduct such as **C** has been invoked. See: T. Yoshimura, K. Asada and S. Oae, *Bull. Chem. Soc. Jpn.*, 1982, **55**, 3000.
11 L. A. Paquette, in *Mechanism of Molecular Migrations*, ed. B. S. Thyagarajan, Interscience, New York, 1968, vol. I, p. 121; L. A. Paquette, *Acc. Chem. Res.*, 1968, **1**, 209.

Communication a909094k

Resolution of racemic Sb-chiral stibindoles using an optically active *ortho*-palladated benzylamine derivative, *via* their diastereomeric complexes

Jyoji Kurita,*[a] Fujiko Usuda,[a] Shuji Yasuike,[a] Takashi Tsuchiya,[a] Yoshisuke Tsuda,[b] Fumiyuki Kiuchi[b] and Shinzo Hosoi[b]

[a] *Faculty of Pharmaceutical Sciences, Hokuriku University, Kanazawa 920-1181, Japan. E-mail: j-kurita@hokuriku-u.ac.jp*
[b] *Faculty of Pharmaceutical Sciences, Kanazawa University, Kanazawa 920-1155, Japan*

Received (in Cambridge, UK) 22nd November 1999, Accepted 17th December 1999

Resolution of racemic Sb-chiral (±)-1-phenyl-2-trimethylsilylstibindole 1 has been achieved by the separation of a mixture of the diastereomeric palladium(II) complexes 3A and 3B derived from the reaction of (±)-1 with di-μ-chlorobis{(*S*)-2-[1-(dimethylamino)ethyl]phenyl-*C*,*N*}dipalladium(II) 2, and optically pure 1-phenylstibindoles (-)-4 and (+)-4 have also been obtained from resolved (−)-1 and (+)-1, respectively.

The asymmetric synthesis and resolution of optically active trivalent phosphines and arsines have been extensively studied because of their use as chiral auxiliaries for a wide range of enantioselective transition-metal-catalyzed processes, such as hydrogenation of olefins, ketones and imines,[1,2] hydrosilylation of ketones, coupling reactions of olefins, and allylic alkylations.[2,3] For the preparation of optically active P-chiral phosphines and As-chiral arsines, a variety of chiral organometallic reagents, *e.g. ortho*-palladated α-arylalkylamines,[4–7] π-pinenyl nickel halides,[8] bisphosphine platinum complexes[9] and iron cationic complexes,[10] have been used as efficient resolving reagents. However, as far as optically active antimony(III) compounds are concerned, only a few limited examples of Sb-chiral stibafluorenes and triarylstibines bearing a hydroxycarbonyl or an amino group have been reported;[11] these functional groups are essential for resolution. Here, we report on an efficient and stereoselective resolution of the racemic Sb-chiral (±)-1-phenyl-2-trimethylsilylstibindole **1**,[12] *via* the separation of the diastereomeric stibindole–palladium complexes **3A** and **3B**, formed by the reaction of (±)-**1** with an optically active *ortho*-palladated benzylamine derivative **2**, and on the molecular structures of the complexes **3A** and **3B**. Optically pure Sb-chiral 1-phenylstibindole (−)-**4** and (+)-**4** are also obtained from resolved (−)-**1** and (+)-**1**, respectively. The present results are the first examples of resolution of neutral Sb-chiral compounds.

Treatment of racemic **1** with 0.5 equiv. of di-μ-chlorobis{(*S*)-2-[1-(dimethylamino)ethyl]phenyl-*C*,*N*}dipalladium(II) **2** (Scheme 1) resulted in coordination of the antimony atom to the palladium atom to give a 1 : 1 mixture of the diastereomeric Pd-complexes **3A** and **3B** quantitatively, which could be separated by silica gel column chromatography; **3A**: mp 158−159 °C, $[\alpha]_D^{23}$ −16.2 (*c* 0.6, acetone) and **3B**: mp 161–162 °C, $[\alpha]_D^{23}$ −79.7 (*c* 0.6, acetone).† Treatment of **3A** and **3B** with triphenylphosphine resulted in decomplexation to afford optically pure (−)-**1** and (+)-**1** {mp 73–75 °C; $[\alpha]_D^{23}$ ±415 (*c* 0.6 MeOH)}, respectively, in quantitative yields. The optically active (−)-**1** and (+)-**1** revert back to **3A** and **3B** on treatment with (*S*)-**2**. The trimethylsilyl group in (−)-**1** and (+)-**1** can be readily removed by treatment with TBAF in water-containing THF to give the corresponding optically pure 1-phenylstibindoles (−)-**4** and (+)-**4** {mp 49–50 °C; $[\alpha]_D^{23}$ ±726 (*c* 0.5 MeOH)}, without any loss of optical purity.‡ The racemic stibindole **4**[12] having no trimethylsilyl group also reacts with (*S*)-**2**, however, the resulting complexes are relatively unstable and attempts at separation were unsuccessful. Unlike stibafluorenes which have been reported to racemize in solution,[11a,b] the optically active stibindoles **1** and **4** possess high optical stability and did not undergo racemization even when heated at 80 °C for 8 h in benzene, although they gradually decomposed at that temperature. Furthermore, the rotations of optically active **1** and **4** were unchanged in either an acidic (10% AcOH–MeOH) or a basic (10% Et_3N–MeOH) solution over 48 h at room temperature.

When the dimeric palladium reagent (*S*)-**2** was treated with 8 equiv. of (±)-**1** and the resulting residue was recrystallized from benzene–hexane, the pure complex **3B** was obtained in 95% yield (calculated from (*S*)-**2**) without chromatographic separation. However, the reaction of (*S*)-**2** with 4 mol equiv. of (±)-**1** gave a 1 : 2.4 mixture of **3A** and **3B** in 94% yield. These results indicate preferential stereoselective formation of **3B** over **3A**. The use of a naphthalene-substituted palladium complex, di-μ-chlorobis{(*R*)-dimethyl-[1-(1-naphthyl)ethyl]-aminato-*C*^{2},*N*}dipalladium(II)[5,7] which has been reported to be a superior

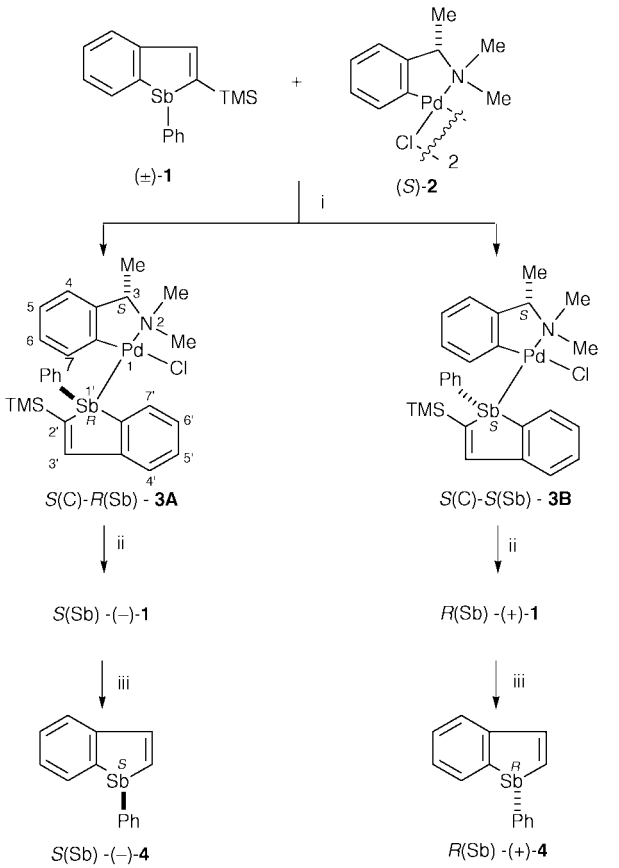

Scheme 1 *Reagents and conditions*: i, dichloromethane, room temp., 5 min, quantitative; ii, PPh_3 (1.05 equiv.), dichloromethane, room temp., 30 min, quantitative; iii, TBAF/5% H_2O–THF, 60–65 °C, 3 h, 92–94%.

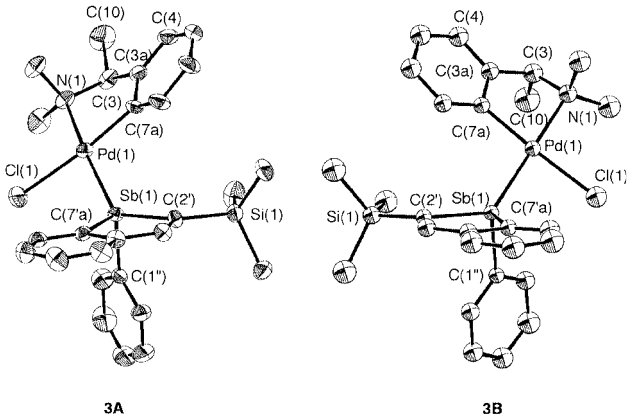

Fig. 1 Molecular structures of **3A** and **3B**. All hydrogen atoms are omitted for clarity. Selected bond lengths (Å) and angles (°). For **3A**: Pd(1)–Sb(1) 2.4926(8), Pd(1)–C(7a) 1.984(8), Pd(1)–N(1) 2.144(7), Pd(1)–Cl(1) 2.407(3), Sb(1)–Pd(1)–N(1) 170.2(2), Cl(1)–Pd(1)–C(7a) 171.0(3), C(10)–C(3)–C(3a)–C(4) 17(1), plane N(1)–Pd(1)–C(7a)–plane Sb(1)–Pd(1)–Cl(1) 14.12. For **3B**: Pd(1)–Sb(1) 2.4942(6), Pd(1)–C(7a) 2.003(6), Pd(1)–N(1) 2.161(6), Pd(1)–Cl(1) 2.408(2), Sb(1)–Pd(1)–N(1) 178.1(2), Cl(1)–Pd(1)–C(7a) 176.2(2), C(10)–C(3)–C(3a)–C(4) 91(1), plane N(1)–Pd(1)–C(7a)–plane Sb(1)–Pd(1)–Cl(1) 4.099.

chiral reagent relative to **2** for the resolution of trivalent phosphines and arsines, was found to give inferior results for the resolution of (±)-**1**.

The solid-state molecular structures of **3A** and **3B**, including absolute configuration were determined by single crystal X-ray analyses (Fig. 1),§ which reveals that in **3A** and **3B**, the coordinated antimony ligand is situated *trans* to the dimethylamine moiety as in the related phosphine[4,5] and arsine[6] complexes. Also apparent is that the antimony atom in **3A** and **3B** has *S*- and *R*-configuration, respectively, and no noticeable difference in the Pd–Sb distance is seen between **3A** (2.493 Å) and **3B** (2.494 Å). One of the most conspicuous differences in molecular structure between **3A** and **3B** is the geometry of their benzylic methyl groups. The methyl groups are located in a pseudo-equatorial orientation for **3A** and are pseudo-axial for **3B**. It is known that both equatorial and axial conformations of the benzylic methyl group are accessible in phosphine–palladium complexes of phenyl ethylamino derivatives.[7b]

Despite a detailed inspection of the X-ray structures of **3A** and **3B**, no significant intracomplex H···H or H···C interactions between the stibindole and the palladacycle moiety were observed. It has recently been suggested that square planarity around the palladium atom is important when considering the conformational stability of bidentate phosphine–palladium complexes, since deviation from square planarity around palladium will occur to prevent hard atomic contacts between the ligands and palladacycles.[7b] In both diastereomers **3A** and **3B**, the four substituents around the palladium atom lead to a distorted square planar geometry and significant differences in the bond angles Sb(1)–Pd(1)–N(1) and Cl(1)–Pd(1)–C(7a) between **3A** (170–171°) and **3B** (176–178°) are observed. These differences give rise to a difference in the dihedral angles between the planes N(1)–Pd(1)–C(7a) and Sb(1)–Pd(1)–Cl(1), *i.e.* 14.1° for **3A** and 4.1° for **3B**. These results indicate that **3A** is more distorted than **3B**. Consequently, the more sterically stable **3B** forms preferentially to the less stable **3A** in the present reaction.

Notes and references

† For a typical procedure; a mixture of (±)-**1** and (*S*)-**2** in dichloromethane was stirred for 5 min at room temperature. After removal of the solvent *in vacuo*, the resulting residue was separated by chromatography on silica gel [dichloromethane–hexane–diethyl ether (10 : 10 : 1)], followed by recrystallization from benzene–hexane (1 : 8) to give **3A** and **3B**. *Selected* ^{1}*H NMR data* (400 MHz, $CDCl_3$, *J*/Hz): **3A**, δ 0.13 (9H, s, TMS), 1.66 (3H, d, *J* 6.6, CHCH_3), 2.75 and 2.99 (3H, s, NCH_3), 4.03 (1H, q, *J* 6.6, C*H*CH$_3$), 6.61 (1H, m, 5-H), 6.85 (1H, br d, *J* 7.3, 7-H), 6.9–7.0 (2H, m, 4- and 6-H), 7.25–7.7 (8H, 4′-, 5′-, 6′- and Ph-H), 7.82 (1H, br d, *J* 7.3, 7′-H), 8.00 (1H, s, 3′-H). **3B**, δ 0.08 (9H, s, TMS), 1.76 (3H, d, *J* 6.6, CHCH_3), 2.84 and 2.89 (3H, s, NCH_3), 3.81 (1H, q, *J* 6.6, C*H*CH$_3$), 6.63 (1H, m, 5-H), 6.86 (1H, br d, *J* 7.3, 7-H), 6.9–7.0 (2H, m, 4- and 6-H), 7.2–7.7 (8H, 4′-, 5′-, 6′- and Ph-H), 7.81 (1H, br d, *J* 7.3, 7′-H), 8.00 (1H, s, 3′-H).

‡ The optical purities of (−)-**4** and (+)-**4** could be determined by comparison of the ^{1}H NMR signals due to the 3′- and 7′-protons of their Pd complexes with those of (*S*)-**2**. *Selected* ^{1}*H NMR data* (400 MHz, $CDCl_3$, *J*/Hz): (−)-**4**+(*S*)-**2**, δ 1.67 (3H, d, *J* 6.6, CHCH_3), 2.79 and 2.98 (3H, s, NCH_3), 3.94 (1H, q, *J* 6.6, C*H*CH$_3$), 6.80 (1H, m, 5-H), 6.95–7.05 (2H, m, 4- and 6-H), 7.16 (1H, br d, *J* 7.7, 7-H), 7.25–7.75 (9H, 2′-, 4′-, 5′-, 6′- and Ph-H), 7.79 (1H, d, *J* 8.8, 3′-H), 8.01 (1H, br d, *J* 7.3, 7′-H). (+)-**4**+(*S*)-**2**, δ 1.72 (3H, d, *J* 6.6, CHCH_3), 2.82 and 3.93 (each 3H, each s, NCH_3), 3.90 (1H, q, *J* 6.6, C*H*CH$_3$), 6.81 (1H, m, 5-H), 6.95–7.05 (2H, m, 4- and 6-H), 7.18 (1H, br d, *J* 7.7, 7-H), 7.25–7.7 (9H, 2′-, 4′-, 5′-, 6′- and Ph-H), 7.82 (1H, d, *J* 8.8, 3′-H), 7.97 (1H, br d, *J* 7.3, 7′-H).

§ *Crystal data* for **3A**{**3B** where different}: $C_{27}H_{33}ClNPdSbSi$, *M* = 663.25, *a* = 11.679(2) {11.738(3)}, *b* = 20.597(3) {20.626(2)}, *c* = 11.631(1) {11.494(2)} Å, *V* = 2797.8(7) {2782.6(7)} Å^3, *T* = 296 {298} K, space group $P2_12_12_1$ (no. 19), *Z* = 4, μ(Mo-Kα) = 17.59 {17.70} cm^{-1}, 3641 {3608} reflections measured (Rigaku AFC5R diffractometer), 3365 {3151} reflections [$I > 3\sigma(I)$] were used in all calculations, *R* = 0.049 {0.028}, R_w = 0.060 {0.046}. The structures of **3A** and **3B** were solved by direct methods and all of the non-hydrogen atoms were refined anisotropically using full-matrix least squares based on F^2. The absolute configurations of the antimony atoms in **3A** and **3B** were determined by comparison with the known configuration (*S*) of the benzylic methine moiety of the palladium reagent (*S*)-**2**, used as a resolving agent. CCDC 182/1510.

1 For reviews, see: W. S. Knowles, *Acc. Chem. Res.*, 1983, **16**, 106; W. A. Nugent, T. V. RajanBabu and M. J. Burk, *Science*, 1993, **259**, 479; K. Inoguti, S. Sakuraba and K. Achiwa, *Synlett.*, 1992, **3**, 169; R. Noyori, *Science*, 1990, **248**, 1194; M. Sawamura and Y. Ito, *Chem. Rev.*, 1992, **92**, 857; R. Noyori, *Asymmetric Catalysis in Organic Synthesis*, Wiley, New York, 1994.

2 S. B. Wild, in *The Chemistry of Organic Arsenic, Antimony and Bismuth Compounds*, ed. S. Patai, Wiley, Chichester, 1994, ch. 3; A. Kojima, C. D. J. Boden and M. Shibasaki, *Tetrahedron Lett.*, 1997, **38**, 3459; S. Y. Cho and M. Shibasaki, *Tetrahedron Lett.*, 1998, **39**, 1773.

3 P. R. Auburn, P. B. Mackenzie and B. Bosnich, *J. Am. Chem. Soc.*, 1985, **107**, 2033; B. M. Trost and D. L. V. Vranken, *Chem. Rev.*, 1996, **96**, 395.

4 K. Tani, L. D. Brown, J. Ahmed, J. A. Ibers, M. Yokota, A. Nakamura and S. Otsuka, *J. Am. Chem. Soc.*, 1977, **99**, 7876; M. K. Pietrusiewicz and M. Zablocka, *Chem. Rev.*, 1994, **94**, 1375; C. E. Barclay, G. Deeble, R. J. Doyle, S. A. Elix, G. Salem, T. L. Jones, S. B. Wild and A. C. Willis, *J. Chem. Soc., Dalton Trans.*, 1995, 57.

5 V. V. Dunina, E. B. Golovan, N. S. Gulyukina and A. V. Buyevich, *Tetrahedron: Asymmetry*, 1995, **6**, 2731.

6 J. W. L. Martin, F. S. Stephens, K. D. W. Weerasuria and S. B. Wild, *J. Am. Chem. Soc.*, 1988, **110**, 4346; S. B. Wild, *Coord. Chem. Rev.*, 1997, **166**, 291.

7 (*a*) N. W. Alcock, J. M. Brown and D. I. Hulmes, *Tetrahedron: Asymmetry*, 1993, **4**, 743; (*b*) N. W. Alkock, D. I. Hulmes and J. M. Brown, *J. Chem. Soc., Chem. Commun.*, 1995, 395; (*c*) H. Doucet and J. M. Brown, *Tetrahedron: Asymmetry*, 1997, **8**, 3775.

8 B. Henc, H. Pauling, G. Wilke, C. Krüger, G. Schroth and E. G. Hoffmann, *Liebigs Ann. Chem.*, 1974, 1820.

9 A. Bader, G. Salem, A. C. Willis and S. B. Wild, *Tetrahedron: Asymmetry*, 1992, **3**, 1227.

10 G. Salem and S. B. Wild, *J. Organomet. Chem.*, 1989, **370**, 33; A. A. Watson, A. C. Willis and S. B. Wild, *J. Organomet. Chem.*, 1993, **445**, 71.

11 (*a*) I. G. M. Campbell, *J. Chem. Soc.*, 1952, 4448; (*b*) I. G. M. Campbell and D. J. Morrill, *J. Chem. Soc.*, 1955, 1662; (*c*) I. G. M. Campbell, *J. Chem. Soc.*, 1955, 3116; (*d*) I. G. M. Campbell and A. W. White, *J. Chem. Soc.*, 1958, 1184.

12 J. Kurita, M. Ishii, S. Yasuike and T. Tsuchiya, *J. Chem. Soc., Chem, Commun.*, 1993, 1817; J. Kurita, M. Ishii, S. Yasuike and T. Tsuchiya, *Chem. Pharm. Bull.*, 1994, **42**, 1437.

Communication a909200e

ChemComm

Selective oxygen capture to give a unique mixed-anion lithium aluminate: the synthesis and solid-state structure of {[PhC(O)N(Me)Al(Me)(Bu^t)OMe]Li·[PhC(O)N(Me)Al(Me)(OBu^t)OMe]Li}$_2$

Robert P. Davies, David J. Linton, Ronald Snaith† and Andrew E. H. Wheatley*

Department of Chemistry, University of Cambridge, Lensfield Road, Cambridge, UK CB2 1EW. E-mail: aehw2@cam.ac.uk

Received (in Cambridge, UK) 18th November 1999, Accepted 17th December 1999

While reaction of a solution of the amidoalane PhC(O)N(Me)AlMe$_2$ 3 with 1 equiv. of Bu^{t}Li affords the lithium aluminate PhC(O)N(Me)Al(Me)$_2$(Bu^t)Li 4, deliberate treatment of the reaction mixture with oxygen affords the unique mixed-anion species {[PhC(O)N(Me)Al(Me)(Bu^t)OMe]Li·[PhC(O)N(Me)Al(Me)(OBu^t)OMe]Li}$_2$ 5; in the solid state 5 has a (LiO)$_4$ ladder structure containing terminal mono-oxygenated aluminate ligands and tripodal bis-oxygenated aluminate ligands spanning end and central Li$^+$ cations.

There is much current interest in the syntheses, structures and reactivities of lithium-containing heterobimetallic species.[1–3] Recently, we have synthesised lithium aluminate monomers Me$_2$Al(μ$_2$-OAr)$_2$Li (Ar = aryl) by treating bis(aryloxy)methylalanes of type MeAl(OAr)$_2$ with RLi reagents (R = Me, Bu^t) and demonstrated the role of such species in 1,4-conjugate additions to α,β-unsaturated ketones.[1] We have also shown that BuLi reagents react with the (amido)methylalane Me$_2$AlN(2-C$_5$H$_4$N)Ph, **1**, to afford remarkable hydride-containing compounds,[2] *e.g.* Bu^{t}Li reacts with **1** to give [Li(Me$_2$AlBu$^t_2$)$_2$]$^-$·{Li$_8$(H)[N(2-C$_5$H$_4$N)Ph]$_6$}$^+$ **2**. With a view to investigating the effect that the choice of organic residue has on the formation of species such as **2** we have recently carried out reactions of Bu^{t}Li with a variety of molecules containing a Me$_2$AlN(C=X)C– unit (X = N, O *etc.*) akin to that found in **1**. We report here, on the reaction of the *N*-methylbenzamidoalane[4] **3** with Bu^{t}Li to afford the lithium aluminate, **4**, and on the isolation of the unique heterobimetallic mixed-anion ladder, **5**, which results when oxygen is subsequently and deliberately introduced to the reaction mixture (Scheme 1).

Reaction of a prepared solution of **3** with 1 equiv. of Bu^{t}Li affords a solution from which **4** can be obtained as the only isolable product.‡ ^{1}H NMR spectroscopy shows that, rather than being a hydride-containing compound, **4** is, in fact, a simple lithium aluminate. However, the controlled treatment of a solution of **4** with air followed by storage at −30 °C affords crystals of the unique mixed-metal/mixed-anion species [PhC(O)N(Me)Al(Me)(Bu^t)OMe]Li·[PhC(O)N(Me)Al(Me)(OBu^t)OMe]Li **5**.§ X-Ray crystallography¶ shows that in the solid state **5** is a dimer of this formulation (Fig. 1) with one molecule of toluene in the lattice. At the core of the solid-state structure is a (LiO)$_4$ ladder composed of three precisely planar edge-fused (LiO)$_2$ rings which incorporate the original carbonyl O-centres of **4**. Supplementary to this core, the two types of oxygenated aluminate anions, which have been afforded by treatment of **4** with air, operate in distinct ways. The two mono-oxygenated anions are terminal, using their generated OMe groups to complete the six-membered OCNAlO(Me)Li chelate rings [Li1–O4 1.900(6) Å] which stabilise the Li$^+$ centres at the ends of the ladder. In contrast, the two bis-oxygenated anions span ladder end- and central-Li$^+$ cations (Li1 and Li2A, respectively), coordinating to these metal centres through interactions involving their OBu^t [Li1–O3 1.935(6) Å] and OMe [Li2A–O5 1.896(5) Å] units, respectively. The observation that these Li–OR (R = Me, Bu^t) bonds differ significantly presumably derives from the shortness of the Li1–O4 bond in the mono-oxygenated monomer. Overall, these bis-oxygenated anions act as tripodal ligands forming, with the involved Li$^+$ centres of the ladder (Li1, Li2A), fused tricyclic arrangements. It is probably the contiguous nature of these three rings which accounts for the relatively long Li1–O2 and Li2A–O2 distances (mean 2.054 Å). While two of the ring systems incorporate one Li$^+$ centre each [OCNAlO(Bu^t)Li and OCNAlO(Me)Li stabilise Li1 and Li2 respectively], the third six-membered ring, involving two Li$^+$ centres, is based on a fairly symmetrical MO(M′O)$_2$ (M = Al, M′ = Li) heterocycle.

Aside from the method used for its synthesis, the solid-state stucture of **5** shows a series of particularly noteworthy features. While several structurally characterised lithium aluminates incorporate intramolecular Li–O interactions, these have generally been based either on simple heterobimetallic motifs [Al(μ$_2$-O)Li[5,6] or Al(μ$_2$-O)$_2$Li[1,5,7]] or on (AlO)$_n$ rings (*n* = 2,

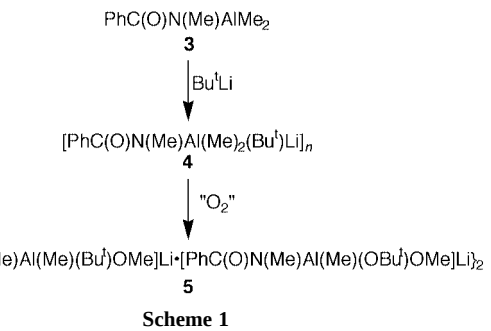

Scheme 1

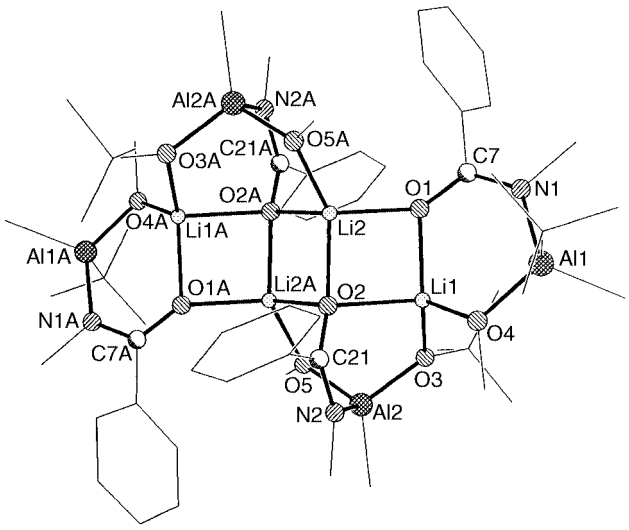

Fig. 1 Molecular structure of **5**; hydrogen atoms and lattice toluene molecule omitted for clarity.

† Deceased.

3).[6] Here, however, **5** is constructed around a $(LiO)_4$ ladder. Only a very limited number of such homometallic ladders are known,[8] the vast majority of Li–O-containing metallo-organic species (*e.g.* alkoxides, enolates) being pseudo-cubane tetramers,[5] hexamers[5,9] or even higher[10] aggregates in the solid state. It is salient, therefore, that the adoption of an $(LiO)_4$ intercepted-ladder motif by **5** represents the first crystallographic evidence that ladder structures, known for a range of lithiated organic compounds (particularly lithium amides),[5,11] can also pertain for Li–Al heterobimetallic ones. Furthermore, whereas the $(LiO)_4$ core of **5** utilises the original carbonyl *O*-centres, it is clear that the coordinative requirements of the *different* types of Li^+ centre (Li1 and Li2) in the assembled ladder are satisfied by the *variability* of ligand oxygenation.

The final interesting aspects of **5** concern how and why it is formed in the first place. The complex can be obtained repeatedly, albeit so far in moderate yields, from exposure of a pre-formed solution of **4** to either normal (*i.e.* moist) or (P_2O_5) dry air. However, the use of normal air affords samples of **5** which ^{1}H NMR spectroscopy shows to be significantly contaminated with (expected) aluminoxane[12] hydrolysis products. These observations point to oxygen rather than moisture being responsible for the observed multiple oxo-insertion process. In this context, it is known that air-sensitive R_3Al species afford *tris*-oxygenated compounds, $(RO)_3Al$, upon exposure to oxygen.[13] The surprise in the synthesis of **5** is the *controlled* nature and dual s*pecificity* of oxo-insertion. Preliminary ^{1}H NMR spectroscopic evidence suggests that the treatment of **3** alone [having two Al–C(Me) bonds] with pre-dried air fails to afford any detectable reaction and it is only when **3**, Bu^{t}Li and O_2 are combined, *in that order*, that **5** results. Complete *tris*-oxygenation of the Al–C bonds has not occurred in **5**, but rather two of the aluminate anions have each undergone single oxo-insertion and two have each inserted oxygen atoms into two Al–C bonds. In this way, the two types of ligands produced are perfect for provision of additional coordination (terminal and spanning respectively) to the Li^+ centres of the $(LiO)_4$ core of **5**, raising each such centre to a coordination number of four. While the precise mechanism by which **5** is formed is not yet understood, the observations noted above suggest that oxo-insertion is either directly templated [*i.e.* that lithium aluminate **4** is, itself, a $(LiO)_4$ ladder] or else that the conversion of **4** to **5** requires that the processes of ladder formation *and* oxo-insertion occur concurrently.

Attempts to learn the *precise* structural nature of **4**, and to thus better understand the reasons for the dual specificity of oxo-insertion, are ongoing. Further work will also seek to investigate the effects of employing pure oxygen in place of dry air and will attempt to follow the reaction by low-temperature multinuclear NMR spectroscopy. More generally, it is planned to look at related systems of general type R_2AlL and R′Li (R, R′ = alkyl, aryl; L = *N*- or *O*-centred ligands) and to deliberately treat these with oxygen. In this way, it is hoped to judge how widespread and how useful the oxo-insertion process, and the concomitant ligand amendments, might be. It is clear already, from this and other work,[3] that deliberate aeration of selected main group organometallic species (usually handled under strictly inert-atmosphere conditions) can produce much interesting new chemistry.

We thank the UK EPSRC (D. J. L.) for a Studentship and St. Catharine's (R. P. D.) and Gonville & Caius (A. E. H. W) Colleges for Research Fellowships. This work is dedicated to the memory of Ron Snaith.

Notes and references

‡ Toluene (1 ml) was added to *N*-methylbenzamide (0.14 g, 1 mmol) at −78 °C under nitrogen and the resultant suspension treated with $AlMe_3$ (0.5 ml, 1 mmol, 2 M in hexane). The reaction mixture was warmed to room temperature and stirred for 30 min whereupon it was returned to −78 °C and Bu^{t}Li (0.59 ml, 1 mmol, 1.7 M in pentane) was added. The resultant solution was warmed to room temperature whereupon removal of the solvent afforded crude **4** as a white powder. Yield 65%, mp 86–88 °C. Satisfactory C,H,N. ^{1}H NMR spectroscopy (400 MHz, CD_3CN), δ 7.72–6.99 (m, 5H, Ph), 2.87–2.76 (m, 3H, NMe), 0.87–0.66 (m, 9H, Bu^t), −1.21, −1.36, −1.53 (m, 6H, AlMe).

§ As for **4** but upon returning to room temperature the resultant pale yellow solution was treated with dry air (P_2O_5) for 1 min and with hexane (0.5 ml) before being stored at −30 °C for 3 days whereupon colourless microcrystals of **5** were deposited. Yield 15% (based on Bu^{t}Li consumed), mp 128–130 °C. Satisfactory C,H,N. ^{1}H NMR spectroscopy (500 MHz, [$^2H_8$]THF), δ 8.05–7.20 (m, 10H, Ph), 7.19–6.98 (m, 2.5H, C_6H_5Me), 3.51–3.44 (m, 6H, OMe), 3.04–2.66 (m, 6H, NMe), 2.32 (s, 1.5H, C_6H_5*Me*), 1.20–1.15, 0.86 (m, 18H, Bu^t), −1.02, −1.07 (m, 6H, AlMe).

¶ *Crystal data* for **5**: $C_{31.5}H_{50}Al_2Li_2N_2O_5$; M = 604, triclinic, space group $P\bar{1}$, a = 12.333(3), b = 13.439(3), c = 14.021(4) Å, α = 109.87(1), β = 91.58(2), γ = 114.21(1)°, U = 1955.2(9) Å^3, Z = 2, D_c = 1.105 g cm^{-3}, Cu-Kα (λ = 1.54178 Å), μ = 0.972 mm^{-1}, T = 180(2) K. 8243 reflections (4837 unique, θ < 54.98°, R_{int} = 0.0301), data were collected on a Stoe Siemens four-circle diffractometer. Refinement on F^2 values of all data gave $wR2$ = 0.1766, conventional R = 0.0640 on F values of 4242 reflections with $F^2 > 2\sigma(F^2)$, 428 parameters. Residual electron density extrema are 0.69 and −0.24 Å^{-3}. CCDC 182/1509. See http://www.rsc.org/suppdata/cc/a9/a909135a/ for crystallographic files in .cif format.

1 W. Clegg, E. Lamb, S. T. Liddle, R. Snaith and A. E. H. Wheatley, *J. Organomet. Chem.*, 1999, **573**, 305.
2 W. Clegg, R. P. Davies, S. T. Liddle, D. J. Linton, P. R. Raithby, R. Snaith and A. E. H. Wheatley, *Angew. Chem., Int. Ed.*, 1999, **38**, 3367.
3 A. R. Kennedy, R. E. Mulvey and R. B. Rowlings, *Angew. Chem., Int. Ed.*, 1998, **37**, 3180; A. R. Kennedy, R. E. Mulvey and R. B. Rowlings, *J. Am. Chem. Soc.*, 1998, **120**, 7816; A. R. Kennedy, R. E. Mulvey, C. L. Raston, B. A. Roberts and R. B. Rowlings, *Chem. Commun.*, 1999, 353.
4 For the analogous *N*-phenylbenzamidoalane, see: Y. Kai, N. Yasuoka, N. Kasai and M. Kakudo, *J. Organomet. Chem.*, 1971, **32**, 165.
5 *Lithium Chemistry: A Theoretical and Experimental Overview*, ed. A. M. Sapse and P. von R. Schleyer, John Wiley and Sons, New York, 1995.
6 See, for example: W. Uhl, I. Hahn, M. Kock and M. Layh, *Inorg. Chim. Acta*, 1996, **249**, 33; T. Arai, H. Sasai, K. Aoe, K. Okamura, T. Date and M. Shibasaki, *Angew. Chem., Int. Ed. Engl.*, 1996, **35**, 104; J. Storre, C. Schnitter, H. W. Roesky, H.-G. Schmidt, M. Noltemeyer, R. Fleischer and D. Stalke, *J. Am. Chem. Soc.*, 1997, **119**, 7505.
7 See, for example: T. J. Barbarich, S. T. Handy, S. M. Miller, O. P. Anderson, P. A. Grieco and S. H. Strauss, *Organometallics*, 1996, **15**, 3776; A. G. Avent, W.-Y. Chen, C. Eaborn, I. B. Gorrell, P. B. Hitchcock and J. D. Smith, *Organometallics*, 1996, **15**, 4343; H. Nöth, A. Schlegel, J. Knizek and H. Schwenk, *Angew. Chem., Int. Ed. Engl.*, 1997, **36**, 2640.
8 See, for example: C. Lambert, F. Hampel, P. von R. Schleyer, M. G. Davidson and R. Snaith, *J. Organomet. Chem.*, 1995, **487**, 139; M. Montevalli, D. Shah and A. C. Sullivan, *J. Organomet. Chem.*, 1996, **513**, 239; N. A. Khanjin and F. M. Menger, *J. Org. Chem.*, 1997, **62**, 8923.
9 See, for example: T. Maetzke, C. P. Hidber and D. Seebach, *J. Am. Chem. Soc.*, 1990, **112**, 8248.
10 See, for example: T. Maetzke and D. Seebach, *Organometallics*, 1990, **9**, 3032.
11 K. Gregory, P. von R. Schleyer and R. Snaith, *Adv. Inorg. Chem.*, 1991, **37**, 47; W. Clegg, L. Horsburgh, F. M. Mackenzie and R. E. Mulvey, *J. Chem. Soc., Chem. Commun.*, 1995, 2011; R. E. Mulvey, *Chem. Soc. Rev.*, 1991, **20**, 167; R. E. Mulvey, *Chem. Soc. Rev.*, 1998, **27**, 339; W. Clegg, S. T. Liddle, R. E. Mulvey and A. Robertson, *Chem. Commun.*, 1999, 511.
12 J. J. Eisch, *Comprehensive Organometallic Chemistry*, ed. E. W. Abel, F. G. A. Stone and G. Wilkinson, Pergamon, Oxford, 1995, vol. 1, p. 462.
13 J. P. Oliver, R. Kamur and M. Taghiof, *Coordination Chemistry of Aluminium*, ed. G. H. Robinson, Wiley-VCH, New York, 1993, p. 171.

Communication a909135a

Reactive polymer membranes containing cuprous complexes in olefin/paraffin separation

Young Hee Kim,[a] Jae Hee Ryu,[b] Jin Yong Bae,[b] Yong Soo Kang[b] and Hoon Sik Kim*[a]

[a] *CFC Alternatives Research Center, Korea Institute of Science and Technology, PO Box 131, Cheongryangri, Seoul, 130-650 Korea. E-mail: khs@kist.re.kr*

[b] *Center for Facilitated Transport Membranes, Korea Institute of Science and Technology, PO Box 131, Cheongryangri, Seoul, 130-650 Korea*

Received (in Cambridge, UK) 20th October 1999, Accepted 17th December 1999

The reduction of $Cu(BF_4)_2{\cdot}xH_2O$ in 1 wt% poly(vinyl pyrrolidone)–methanol solution with trimethyl phosphite produced a solution containing cuprous complexes; the membrane prepared from this solution showed a maximum selectivity of 10 for propylene over propane at room temperature.

Separation of olefin/paraffin mixtures is one of the most important processes in the petrochemical industry.[1] Currently, the separation is often carried out by highly energy-intensive low temperature distillation. Among a number of alternative separation processes, separation by a facilitated transport membrane with Cu^+ or Ag^+ has attracted much interest because of its low energy consumption, compact unit and simple operation.[2] The basis for the separation is the reversible formation of a π-bonded complex between metal ions, like Cu^+ or Ag^+, and the olefin.[3,4] Many studies have been reported on the facilitated transport of olefins by using supported liquid membranes,[5] ion-exchange membranes[6] or dense polymer membranes[7] containing silver ions as carriers. Cuprous ions have also been applied as carriers for facilitated transportation in liquid membranes, but only for transportation of carbon monoxide and not for olefins.[8] Recently, Lin *et al*. reported the use of CuCl coated γ-alumina membranes in the separation of ethylene/ethane mixtures, but obtained a maximum selectivity of only 1.4 for ethylene over ethane.[9] To the best of our knowledge, reactive solid polymer membranes containing cuprous ions have never been reported, probably due to the low solubility and the instability of cuprous complexes in water or organic solvents.[10]

We report here, for the first time, the direct synthesis of reactive solid polymer membranes containing cuprous complexes and the application of such membranes to the separation of olefin/paraffin mixtures. The addition of trimethyl phosphite to a methanol solution of a cupric salt and an appropriate polymer produced a solution containing cuprous species, which was subsequently coated onto a porous asymmetric membrane. Trimethyl phosphite is known to reduce Cu(II) to Cu(I) as in eqn. (1).[11] The copper ions were found to exist only in the Cu(I) state, as identified by iodometry.[12]

$$Cu(BF_4)_2 + H_2O + P(OMe)_3 + PVP \rightarrow CuBF_4/PVP + 2HBF_4 + OP(OMe)_3$$

PVP: poly(vinyl pyrrolidone) (1)

The membranes were prepared as follows: $Cu(BF_4)_2{\cdot}xH_2O$ (3 mmol, 1 g) and $P(OMe)_3$ (6 mmol, 1.5 mL) were added to 1 wt% poly(vinyl pyrrolidone) (0.5 mmol, 0.05 g) solution in methanol. The resulting solution was applied to a 5 cm × 5 cm asymmetric porous polysulfone membrane. The membrane was dried for 12 h in air and then vacuum-dried for 12 h at room temperature. Membranes consisted of a thin nanoporous cuprous-poly(vinyl pyrrolidone) top layer and an asymmetric coarse-pore polysulfone support. The thickness of the active layer was 2–3 μm, determined by scanning electron microscopy (not shown).

Separation measurements were performed with the coated membrane placed in a stainless steel separation module with the olefin/paraffin (50/50) gas mixture as described elsewhere.[13] The flow rates of the mixed gas and the sweep gas (helium) were controlled using mass flow controllers. The total feed pressure of mixed gas was set at 20 psig by back pressure regulators. Average fluxes of ethylene/ethane and of propylene/propane through the membranes were 2×10^{-5} and 1×10^{-5} $cm^3\ cm^{-2}\ s^{-1}\ cmHg^{-1}$, respectively at room temperature. The permeated gas was analyzed by gas chromatography.[14]

Fig. 1 and 2 show the effects of molar ratios of $P(OMe)_3$/Cu(II) and Cu(II)/PVP on the separation of olefin/paraffin mixtures. The selectivity for olefin over paraffin increased with increasing molar ratio of $P(OMe)_3$/Cu(II) up to 2 and then

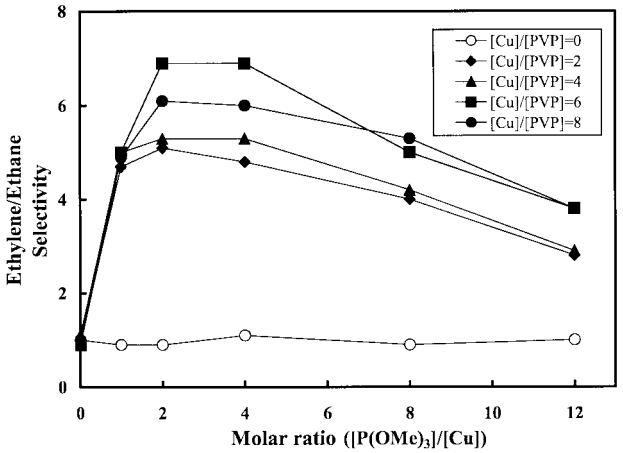

Fig. 1 Effects of molar ratios of $[P(OMe)_3]/[Cu]$ and [Cu]/[PVP] on the permeation selectivity of ethylene over ethane at 25 °C.

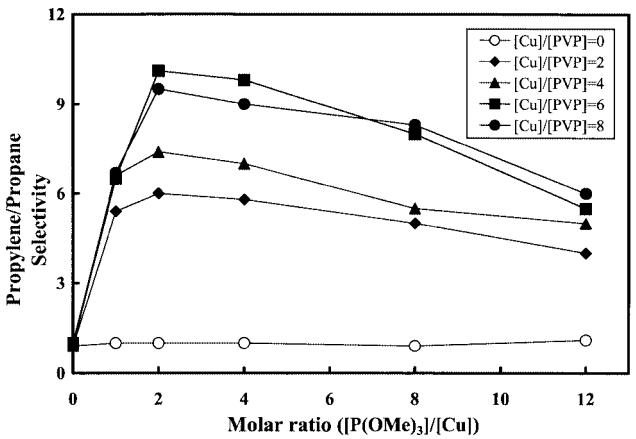

Fig. 2 Effects of molar ratios of $[P(OMe)_3]/[Cu]$ and [Cu]/[PVP] on the permeation selectivity of propylene over propane at 25 °C.

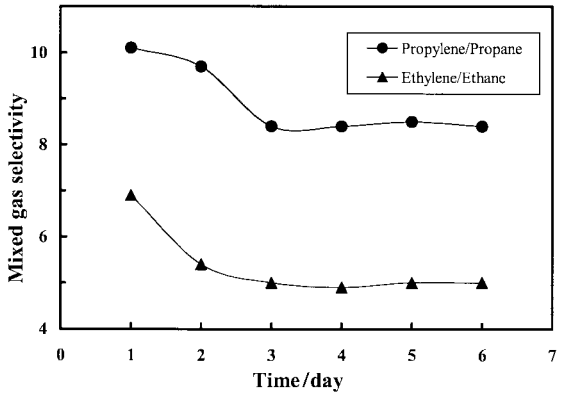

Fig. 3 Change of mixed gas selectivities with time.

gradually decreased with further increase in the molar ratio. It is likely that coordination of trimethyl phosphite is taking place to a certain extent, which could reduce the complexation ability of cuprous ion towards olefin. As expected, the membranes did not show any selectivity for olefin over paraffin at $P(OMe)_3/Cu(II) = 0$, confirming that only Cu(I) is responsible for the selectivity. The copper ions present in the membrane prepared in the absence of $P(OMe)_3$ exist only as Cu(II), for which complexation with olefin is impossible. The higher permeability ratio of propylene/propane in comparison with that of ethylene/ethane can be ascribed to the difference in diffusion rates of the mixed gases. The molar ratio of Cu(II)/PVP was also varied in the range from 0 to 8. As shown in Fig. 1 and 2, the selectivity increased with increasing molar ratio of Cu(II)/PVP up to 6. No appreciable selectivity at Cu(II)/PVP = 0 demonstrates that the PVP-only membrane is not effective for the olefin/paraffin separation and the separation is not taking place by simple diffusion and desorption across the PVP only membrane. Membranes with the molar composition of $P(OMe)_3$:Cu(II):PVP = 2:1:6 were subjected to a seven day permeation test as shown in Fig. 3. The selectivity decreased from 8 to 5 for ethylene/ethane and from 10 to 7 for propylene/propane during the first two days of the experiments and remained constant thereafter, demonstrating that the membranes were stable for at least a week. It is assumed that trimethyl phosphite present in the membranes may play a role in preventing Cu(I) from being oxidized to Cu(II) by trace amounts of oxygen or water in the feed gas.

Other cuprous membranes were also prepared using $Cu(ClO_4)_2$ and $Cu(SO_3CF_3)_2$, and tested for the separation of olefin/paraffin mixtures. The selectivities were lower by a factor of approximately 2 than the selectivities from the $Cu(BF_4)_2$ membranes. This can be attributed to the fact that ClO_4^- and $CF_3SO_3^-$ are more strongly binding anions than BF_4^- and consequently the reversible complexation of olefins is somewhat inhibited. In fact, the membranes containing CuCl showed much lower ethylene/ethane permeation selectivity, possibly due to the competitive complexation of ethylene and Cl^-.[9]

In a separate experiment, a polymer membrane containing $Cu(CO)PF_6$ was prepared according to eqn. (2).

$$1/2Cu_2O + HPF_6 + CO + PEOx \rightarrow Cu(CO)PF_6/PEOx + 1/2H_2O$$

PEOx: poly(2-ethyl-2-oxazoline) (2)

The membrane thus obtained was very unstable and showed no selectivity for the separation of propylene/propane mixtures. However, interestingly, when small amounts of trimethyl phosphite were added to the polymer solution of eqn. (2), the resulting membrane showed a maximum separation factor of 5 for the propylene/propane mixture. This result implies that trimethyl phosphite is functioning as a stabilizer for cuprous ion.

Investigations on the interactions between polymers and copper salts are in progress to improve the properties of cuprous ion-containing membranes.

We gratefully acknowledge financial support from the Ministry of Science and Technology of Korea through the Creative Research Initiatives.

Notes and references

1 S. U. Rege, J. Padiu and R. T. Yang, *AIChE J.*, 1998, **44**, 799.
2 R. B. Eldridge, *Ind. Eng. Chem. Res.*, 1993, **32**, 2208.
3 H. W. Quinn, *Progress in Separation and Purification*, Wiley-Interscience, New York, 1971, vol. 4, p. 133.
4 M. Bochmann, *Organometallics 2*, Oxford Science, New York, 1994, ch. 2.
5 R. D. Noble, C. A. Koval and J. J. Pellegrino, *Chem., Eng. Prog.*, 1989, **85**, 58.
6 O. H. Leblanc, W. J. Ward, S. L Matson and S. G. Kimura, *J. Membr. Sci.*, 1980, **6**, 339.
7 M. Teramoto, H. Matsuyama, T. Yamashiro and Y. Katayama, *J. Chem. Eng. Jpn.*, 1986, **19**, 115.
8 D. R. Smith and J. A. Quinn, *AIChE J.*, 1980, **26**, 229.
9 Y. S. Lin, W. Ji and R. J. Higgins, *Ind. Eng. Chem. Res.*, 1999, **38**, 2292.
10 R. B. Long, *Recent Developments in Separation Science*, CRC Press, Cleveland, Ohio, 1973, vol. 1, p. 35.
11 J. I. G. Cadogan, *Quart. Rev. (London)*, 1962, **16**, 208; B. W. Cook, R. G. J. Miller and P. F. Todd, *J. Organomet. Chem.*, 1969, **19**, 421.
12 I. M. Kolthoff, E. B. Sandell, E. J. Meehan and S. Bruckenstein, *Quantitative Chemical Analysis*, Macmillan, London, 1971, ch. 44.
13 S. Bai, A. Sridhar and A. A. Khan, *J. Membr. Sci.*, 1998, **147**, 131.
14 Gow-Mac gas chromatograph equipped with a thermal conductivity detector with unibead 2S 60/80 packed column.

Communication a908395b

Poly(zinc(II)-5,15-porphyrinylene) from silver(I)-promoted oxidation of zinc(II)-5,15-diarylporphyrins

Naoya Yoshida, Naoki Aratani and Atsuhiro Osuka*

Department of Chemistry, Graduate School of Science, Kyoto University, Sakyo-ku, Kyoto 606-8502, Japan. E-mail: osuka@kuchem.kyoto-u.ac.jp

Received (in Cambridge, UK) 30th November 1999, Accepted 23rd December 1999

Zinc(II)-5,15-diarylporphyrins have been effectively polymerized to give poly(Zn(II)-porphyrinylene) in high yields in the reaction with 1.5 equiv. $AgPF_6$ in $CHCl_3$ either in the presence of 0.5% *N*,*N*-dimethylacetamide or upon heating.

Linearly π-conjugated polymers and oligomers have attracted considerable attention in light of their potential applications in the fields of electronics, optical devices, sensors and solar energy conversion.[1] Among these, poly(arene)s represented by poly(*para*-phenylene)s (PPP), poly(pyrrole)s, and poly(thiophene)s have attracted considerable attention owing to their increasing conductivities upon doping.[2] Porphyrins are an appealing building block for the modular construction of such linear π-conjugated systems, since they offer a variety of desirable features such as rigidity, high stability, intense electronic absorption, a small band gap, strong fluorescence emission, and the possibility to tailor optical and redox properties by appropriate metallation.[3] However, to the best of our knowledge, directly linked poly(porphyrinylene) has not been reported so far. Recently we found that a *meso–meso* coupling reaction of 5,15-diaryl zinc(II)-porphyrins can be effected by treatment with an Ag(I) salt[4a] or by anodic electrochemical oxidation.[4b] Interestingly the *meso–meso* coupling regioselectivity is quite high, allowing the formation of straight and directly linked porphyrin arrays up to the octamer by the latter method.

Now we report that the Ag(I)-promoted *meso–meso* coupling reaction can be extended to the preparation of long poly(porphyrinylene)s simply by the addition of *N*,*N*-dimethylacetamide (DMA) or slight heating [reaction (1)]. Formally, the

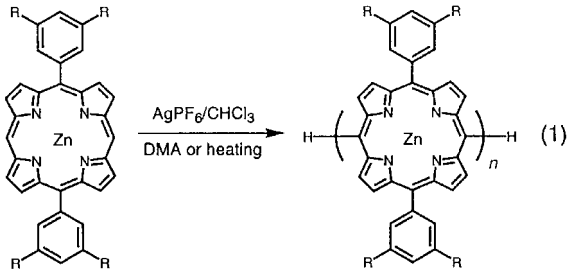

(1)

1a; R = Bu^t
1b; R = OC_8H_{17}

formation of one *meso–meso* bond is accompanied by the loss of two hydrogens and thus seems to need two equivalents of oxidant. This is nicely illustrated by the reaction of **1a** with 1.5 equiv. $AgPF_6$ in $CHCl_3$ at 20 °C for 4 h which gave, besides the recovery of unreacted **1a** (40–50%), **2a** (25–30%), **3a** (5–7%), and **4a** (1–2%) together with small amounts of higher oligomers (Fig. 1a).[4] In marked contrast, reaction under similar conditions but with the presence of a small amount of DMA (0.5% to $CHCl_3$) gave rise to enhanced oligomerization in only 0.5 h (Fig. 1b). The reaction mixture was examined by MALDI-TOF MS and a combined GPC–HPLC and UV-vis absorption method (Fig. 2). The former registered detectable peaks from 688 to 16500 Da (corresponding to 1- to 22-mers) with a repeat unit of *ca.* 750 Da, indicating the formation of diverse

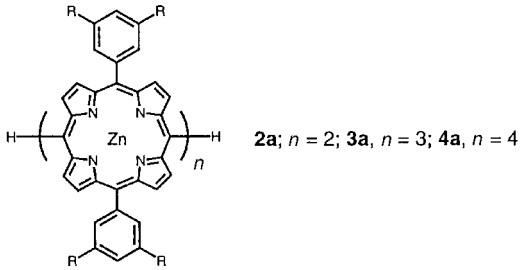

2a; *n* = 2; **3a**, *n* = 3; **4a**, *n* = 4

oligomeric porphyrin arrays up to the 22-mer.[5] The spectra in Fig. 2b that were taken for the GPC–HPLC fractions as their free bases[6] display progressive red-shifts and broadening of the split Soret bands and Q-bands and are consistent with the highly regioselective *meso–meso* coupling even for larger porphyrin arrays. On the basis of the relationship of the molecular weights of discrete oligo(porphyrinylene)s *versus* the retention time of

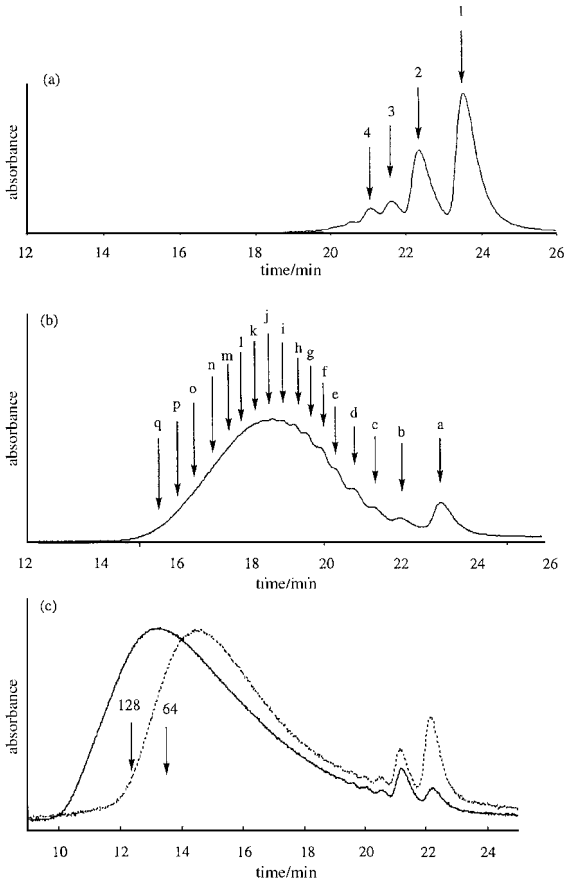

Fig. 1 GPC–HPLC charts of the reaction of **1a** and **1b** with 1.5 equiv. $AgPF_6$ in $CHCl_3$ detected at 413 nm: (a) **1a**, room temperature, 4 h, no DMA, arrows 1–4 indicate bands corresponding to **1a**, **2a**, **3a**, and **4a**, respectively; (b) **1a**, room temperature, 4 h, 0.5% DMA; (c) **1b**, 45 °C, 0.5% DMA, 11 h (dotted line); **1b**, 45°C, 0.5% DMA, 82 h (solid line), the retention times of the discrete 64-mer and 128-mer are indicated by arrows. The absorption spectra of fractions indicated by arrows a–q are shown in Fig. 2b.

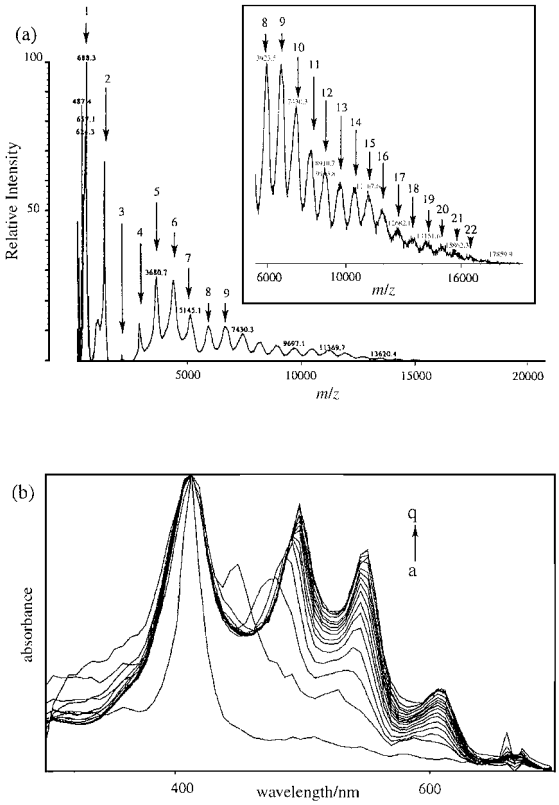

Fig. 2 Product mixture in the reaction of **1a** with 1.5 equiv. $AgPF_6$ in $CHCl_3$ containing 0.5% DMA: (a) MALDI-TOF MS spectrum; (b) absorption spectra of GPC–HPLC fractions after addition of TFA.

GPC–HPLC, we estimated M_w = 12 000 Da with a polydispersity of 1.46; the major oligomers eluting at *ca*. 19 min correspond to 8,9-mers and the detectable largest oligomers eluting at *ca*. 14.5 min correspond to *ca*. 50-mers. The polymerization depends on the amount of DMA, and is most effective upon addition of 0.5–3% DMA. The acceleration effect is only modest with less than 0.5% DMA and decreases with increasing amounts of DMA over 3%, and is completely suppressed upon addition of 20% DMA. Similar enhanced polymerization was also observed in the presence of DMF, HMPA, and DMSO with the enhancement order of DMA > DMF ≈ HMPA > DMSO. On the other hand, nitrogen bases such as pyridine, lutidine, triethylamine, and *N*,*N*-dimethylaniline were found to completely suppress the *meso–meso* coupling. It is also notable that even heating at 45 °C led to polymerization (M_w = 13 000 Da with a polydispersity of 1.37) after 24 h. In this thermally accelerated polymerization, however, the conversion of the monomer **1a** reached a maximum of *ca*. 70% after only 1–2 h but the increase of chain length proceeded rather slowly.

In the reaction of **1a**, there is a possibility that further polymerization may be interrupted owing to the poor solubility of the formed long porphyrin arrays. In order to circumvent this problem, we employed the much more soluble substrate **1b** as the starting monomer. **1b** turned out to be less reactive than **1a** probably due to its bulky dioctyloxy substituents; only 5% of **1b** was consumed even after 24 h in the reaction with 1.5 equiv. $AgPF_6$ in $CHCl_3$ at 20 °C [reaction (1)]. However, the addition of 0.5% DMA indeed accelerated the coupling to give poly(porphyrinylene) with M_w = 45 000 Da and a polydispersity of 1.7 after 24 h. As for **1a**, heating at 45 °C also led to the polymerization of **1b** (M_w = 21 500 Da with a polydispersity of 1.59), although a substantial induction period (10 h) was necessary to start the polymerization. When the reaction of **1b** with 1.5 equiv. $AgPF_6$ was conducted in the presence of 0.5% DMA at 45 °C, the polymerization proceeded extensively, giving poly(porphyrinylene)s with M_w = 75 000 Da and a polydispersity of 1.60 after 11 h, and M_w = 250 000 Da and a polydispersity of 2.78 after 82 h (Fig. 1c). Note that these large poly(porphyrinylene)s exhibit absorption and emission spectra similar to those of oligo(porphyrinylene) 64- and 128-mers of discrete size, which were separately prepared from **1b**.[7] Another merit of these polymers lies in their easy transformation to Ni(II) and Cu(II) complexes.[8]

The mechanism of this polymerization is not fully understood but can be considered to be initiated by one-electron oxidation of zinc(II)-porphyrin with silver(I) and the chain elongation process may be similar to those proposed for oxidative formation of PPP,[2a] involving a poly(5,15-dihydroporphyrinylene) intermediate which will be oxidized to poly(5,15-porphyrinylene)s. The superior acceleration effects of DMA over DMF suggest that it may play a reducing role to convert the cation radical intermediate to a biradical intermediate which may be more active for elongation of the chain.

In summary, sterically uncongested metalloporphyrins, **1a** and **1b**, can be polymerized in a regioselective manner to poly(zinc(II)-5,15-porphyrinylene)s in the reaction with silver(I) salt either in the presence of 0.5–3% of DMA or upon heating. Not fully optimized yet, it is evident that zinc(II)-5,15-diarylporphyrin can be polymerized under much milder conditions compared to the polymerization conditions of smaller aromatic and heteroaromatic molecules. Exploring synthetic conditions that allow the preparation of poly(porphyrinylene) with less polydispersity would be an interesting next target and is actively in progress in our laboratory.

This work was supported by Grants-in-Aid for Scientific Research from the Ministry of Education, Science, Sports and Culture of Japan and by CREST (Core Research for Evolutional Science and Technology) of Japan Science and Technology Corporation (JST). N. Y. is grateful for a JSPS Research Fellowship for Young Scientists.

Notes and references

1 R. E. Martin and F. Diederich, *Angew. Chem., Int. Ed.*, 1999, **38**, 1350; J. M. Tour, *Chem. Rev.*, 1996, **96**, 537; M. R. Wasielewski, *Chem. Rev.*, 1992, **92**, 435.

2 P. Kovacic and M. B. Jones, *Chem. Rev.*, 1987, **87**, 357; G. Wegner, *Angew. Chem., Int. Ed. Engl.*, 1981, **20**, 361; J. G. Speight, P. Kovacic and F. W. Koch, *J. Macromol. Sci. Rev. Macromol. Chem.*, 1971, **C5(2)**, 295; T. Yamamoto, *Bull. Chem. Soc. Jpn.*, 1999, **72**, 621.

3 M. J. Crossley and P. L. Burn, *J. Chem. Soc., Chem. Commun.*, 1991, 1569; D. P. Arnold, G. A. Heath and D. A. James, *J. Porphyrins. Phthalocyanines*, 1999, **3**, 5; L. Jaquinod, O. Siri, R. G. Khoury and K. M. Smith, *Chem. Commun.*, 1998, 1261; V. S.-Y. Lin, S. G. DiMagno and M. J. Therien, *Science*, 1994, **264**, 1105; R. W. Wagner and J. S. Lindsey, *J. Am. Chem. Soc.*, 1994, **116**, 9759; P. N. Taylor, J. Huuskonen, G. Rumbles, R. T. Aplin, E. Williams and H. L. Anderson, *Chem. Commun.*, 1998, 909; O. Mongin and A. Gossauer, *Tetrahedron*, 1997, **53**, 6835; D. A. Shultz, H. Lee and K. P. Gwaltney, *J. Org. Chem.*, 1998, **63**, 7584; J. L. Sessler, V. L. Capuano and A. Harriman, *J. Am. Chem. Soc.*, 1993, **115**, 4618.

4 A. Osuka and H. Shimidzu, *Angew. Chem., Int. Ed. Engl.*, 1997, **36**, 135; T. Ogawa, Y. Nishimoto, N. Yoshida, N. Ono and A. Osuka, *Chem. Commun.*, 1998, 337; *Meso–meso* coupled porphyrin dimers were prepared independently by others: K. Susumu, T. Shimidzu, K. Tanaka and H. Segawa, *Tetrahedron Lett.*, 1996, **37**, 8399; R. G. Khoury, L. Jaquinod and K. M. Smith, *Chem. Commun.*, 1997, 1057; M. O. Senge and X. Feng, *Tetrahedron Lett.*, 1999, **40**, 4165.

5 MALDI-TOF MS was measured for the reaction mixture of **1a**. The peak at 688 corresponds to a parent peak of the demetallated free base form of **1a** and the envelopes in the higher molecular weight region contain many species with variable numbers of incorporated Zn(II) ions.

6 Owing to the poor solubilities of zinc(II)-porphyrin arrays formed from **1a**, GPC–HPLC analysis was performed on the reaction mixtures of free base porphyrin arrays by addition of a small amount of TFA. The observed absorption spectra were quite similar to those of discrete long free base porphyrin arrays. The reaction mixtures of **1b** were directly analyzed as Zn(II) complexes.

7 N. Aratani, A. Osuka, Y. H. Kim, D. H. Jeong and D. Kim, submitted for publication.

8 Polymers with M_w = 6–7 × 10^4 are quite soluble in common organic solvents and are quantitatively converted to completely metallated polymers.

Communication a909444j

Rhodium-catalyzed silylative carbocyclization on C_{60}

Takako Muraoka, Hirotaka Asaji, Yoshihiko Yamamoto, Isamu Matsuda and Kenji Itoh*

Department of Applied Chemistry and Department of Molecular Design and Engineering, Graduate School of Engineering, Nagoya University, Chikusa, Nagoya 464-8603, Japan. E-mail: itohk@apchem.nagoya-u.ac.jp

Received (in Cambridge, UK) 16th November 1999, Accepted 17th December 1999

Rhodium-catalyzed three component coupling of hepta-1,6-diyne, hydrosilane and C_{60} proceeded smoothly to give a fullerene derivative in good yield.

Studies on the functionalization of C_{60} fullerene have attracted considerable attention,[1] because fullerene derivatives are expected to be effective precursors for advanced composite materials,[1c] photoconductive thin films,[2] electron transfer dyad,[3] efficient photosensitizers,[4] *etc*. Fullerene derivatives are also anticipated to form materials with stimulating biological properties,[1b,d] such as inhibition of HIV-1 protease,[5] promotion of DNA cleavage,[6] and enzymatic inhibition.[6e,7] In order to prepare a wide range of designed C_{60} derivatives, cycloadditions have proved the most useful method because well-defined mono-adducts can be easily obtained in most cases.[8] The obtained C_{60}-fused carbo- and heterocycles are interesting key molecular components for the construction of the aforementioned functionalized materials, which are often composed of organized molecular aggregates. In particular, the Diels–Alder reaction, employing C_{60} as a dienophile, is a reliable tool to obtain the cyclohexene-fused C_{60} derivatives.[8a] In addition, cycloaddition protocols include the reaction of C_{60} with appropriate addenda, such as carbenes, nitrenes, conjugated dienes, 1,3-dipoles, *etc*.[8b] No example of *a catalytic multicomponent coupling strategy* involving C_{60}, however, has been reported so far, although domino-type multi-component couplings catalyzed by a wide variety of transition metal complexes are now becoming a major focus in organic synthesis.[9] We herein report the first example of three-component coupling involving C_{60} catalyzed by a rhodium complex. Transition-metal promoted coupling reactions on fullerene are quite rare. This is ascribed to the finding that fullerenes preferentially form stable complexes with a wide range of transition metals. They are frequently too stable to show catalytic activity toward carbon–carbon bond formation with fullerene itself.[10] Only recently, the stoichiometric Ni-promoted cycloaddition of hepta-1,6-diynes and C_{60} was reported by Cheng *et al*.[11] Catalytic methods, however, are desirable as they are metal-economical and environmentally friendly processes. With these ideas in mind, we developed the Rh^{I}-catalyzed three-component domino coupling of C_{60}, hepta-1,6-diyne and hydrosilane *via* the silylative cyclization of the diyne followed by the Diels–Alder cycloaddition of the resultant diene and C_{60}.

We recently reported the rhodium-catalyzed silylative cyclization of hepta-1,6-diynes **1** with trialkylsilanes **2** leading to *cisoid* dienylsilane derivatives **3** (Scheme 1).[12] The obtained **3** has an exocyclic 1,3-diene moiety and can be utilized as a diene counterpart in the Diels–Alder cycloaddition toward fullerene. In fact, the thermal reaction between C_{60} and 1.5 equiv. of **3** [X = $C(CO_2Me)_2$, R_3Si = $PhMe_2Si$] in refluxing toluene for 1 h gave the desired cycloadduct **4a** in 58% isolated yield (88% yield based on consumed C_{60}). The structure of **4a** was determined on the basis of its ^{1}H and ^{13}C NMR, IR, and MS analyses.[13] First, its IR spectrum revealed that **4a** is the adduct of C_{60} and **3**, *i.e.* the typical absorption of the C_{60} core was observed at 527 cm^{-1} as well as the absorptions corresponding to the ester carbonyl groups and the silyl group at 1735 and 1249 cm^{-1}, respectively. In the ^{1}H NMR spectrum, cyclohexene ring protons [δ 3.13 (d, 1H, *J* 16.8 Hz), 3.38 (s, 1H), and 3.48 (m, 1H)] and cyclopentene ring protons [δ 3.64-3.77 (m, 2H) and 3.97–4.07 (m, 2H)] were observed along with the peaks assigned to the methyl and phenyl proton signals of the organic silyl group, and the methyl ester protons.[13] The molecular ion peak at *m/z* 1064 in the FAB-MS spectrum clearly indicated that **4a** is the expected 1:1 adduct. Furthermore, the ^{13}C NMR spectrum shows that the cycloaddition took place on the junction of two six-membered rings; among the ten peaks in the aliphatic region, the lowest-field signal at δ 66.62 is reasonably attributed to the fullerene sp^3 carbons of the 6,6-ring junction. The four sp^2 signal observed at δ 155.76, 156.39, 159.61 and 161.21 are also assigned to the C_{60} carbons next to the sp^3 carbon of the 6,6-junction.

The dienylsilane **3** is definitely an effective diene component in the Diels–Alder cycloaddition with C_{60}. Next, we investigated the three-component coupling from **1a**, **2** and C_{60}. Such three-component coupling is an attractive and more straightforward protocol for transition-metal-catalyzed carbocyclization on the fullerene framework in a single operation. The reaction of C_{60} (0.05 mmol) with **1a** (0.5 mmol) and **2** (0.5 mmol) under N_2 in refluxing toluene for 35 min in the presence of 3 mol% $RhCl(PPh_3)_3$ gave the expected **4a** in 36% isolated yield (55% yield based on consumed C_{60}; entry 1, Table 1). The spectral features of the product are identical to those from the Diels–Alder adduct of **3** with C_{60}. A decrease in the amounts of the diyne and the silane gave better results although longer reaction times are required (entries 2 and 3). The best yield (71%) was realized when 7 equiv. of **1a** and **2** were employed in refluxing toluene for 1 h (entry 2).

The significant feature of the present three-component domino coupling is that C_{60}, in spite of its strong tendency to form complexes with various transition metals,[10] never suppressed the catalytic silylative cyclization step. In sharp contrast, the three-component couplings of **1a**, **2** and *N*-phenylmaleimide (**5**) or maleic anhydride (**6**) failed although the Diels–Alder reaction of the isolated **3** gave the corresponding adducts with **5** or **6** in high yield.[14] These results suggest that

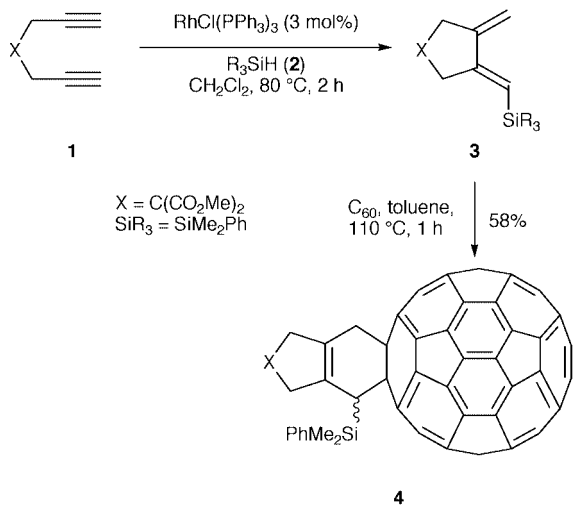

Scheme 1

Table 1 Rhodium-catalyzed three-component coupling of C_{60} with diynes **1a–c** and silane **2**

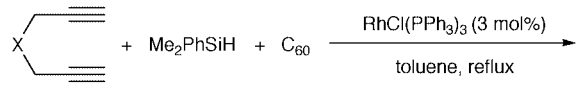

1a–c **2**

a X = $C(CO_2Me)_2$
b X = O
c X = NTs

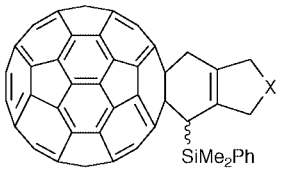

4a–c

Entry	1	Amount of 1 and 2/ equiv.	Product	t/min	Yield (%)[a]
1	**1a**	10	**4a**	40	53 (36)
2	**1a**	7	**4a**	60	71 (58)
3	**1a**	5	**4a**	110	63 (34)
4	**1b**	15	**4b**	200	41 (34)
5	**1c**	10	**4c**	45	32 (28)

[a] The yield was based on comsumed C_{60} and isolated yield was shown in parenthesis.

these strong dienophiles inhibited the catalytic cycle *via* complex formation with a Rh^I species.

The other important feature is that dipropargyl ether **1b** and *N*,*N*-dipropargyl tosylamide **1c** were successfully adapted to the domino coupling, whereas they hardly gave silylative cyclization products in the absence of C_{60}.[14] As a result, interesting C_{60}-bound heterocycles **4a** and **4b** were successfully isolated in 41 and 32% conversion yields, respectively (entries 4 and 5). It seems reasonable to assume that unstable exocyclic diene intermediates **3b** and **3c** were immediately coupled with C_{60} before decomposition under the reaction conditions.

In conclusion, we have developed the Rh^I-catalyzed three-component domino coupling of C_{60}, hepta-1,6-diynes and a hydrosilane. Dienophile C_{60} did not interfere with the catalytic silylative cyclization and efficiently trapped the exocyclic 1,3-diene intermediates to furnish the corresponding C_{60}-linked carbo- and heterocycles in fair to good yields. The present method is the first example of transition-metal catalyzed domino coupling on the fullerene conducted in a single operation.

We gratefully acknowledge financial support (09305059, 10132222, and 11119223) from the Ministry of Education, Science, Sports, and Culture, Japanese Government. We also thank to Mr Kazumoto Kondo for mass measurements.

Notes and references

1 (*a*) F. Diederich and R. Kessinger, *Acc. Chem. Res.*, 1999, **32**, 537; (*b*) T. D. Ros and M. Prato, *Chem. Commun.*, 1999, 663; (*c*) M. Prato, *J. Mater. Chem.*, 1997, **7**, 1097; (*d*) A. W. Jensen, S. R. Wilson and D. I. Schuster, *Bioorg. Med. Chem.*, 1996, **4**, 767.

2 For a recent example, see: W. Zhang, L. Gan and C. Huang, *J. Mater. Chem.*, 1998, **8**, 1731; J.-F. Nierengarten, C. Schall, J.-F. Nicoud, B. Heinrich and D. Guillon, *Tetrahedron Lett.*, 1998, **39**, 5747; T. Nakanishi, H. Murakami and N. Nakashima, *Chem. Lett.*, 1998, 1219; A. L. Balch, D. A. Costa and K. Winkler, *J. Am. Chem. Soc.*, 1998, **120**, 9614.

3 For a recent example, see: P. Cheng, S. R. Wilson and D. I. Schuster, *Chem. Commun.*, 1999, 89; T. D. Ros, M. Prato, D. Guldi, E. Alessio, M. Ruzzi and L. Pasimeni, *Chem. Commun.*, 1999, 635; A. Polese, S. Mondini, A. Bianco, C. Toniolo, G. Scorrano, D. M. Guldi and M. Maggini, *J. Am. Chem. Soc.*, 1999, **121**, 3446; M. Diekers, A. Hirsch, S. Pyo, J. Rivera and L. Echegoyen, *Eur. J. Org. Chem.*, 1998, 1111 and references cited therein; J.-P. Bourgeois, F. Diederich, L. Echegoyen and J.-F. Nierengarten, *Helv. Chim. Acta*, 1998, **81**, 1835; E. Dietel, A. Hirsch, E. Eichhorn, A. Rieker, S. Hackbarth and B. Röder, *Chem. Commun.*, 1998, 1981.

4 H. Nagashima, K. Hosoda, T. Abe, S. Iwamatsu and T. Sonoda, *Chem. Lett.*, 1999, 469; T. Hamano, K. Okuda, T. Mashino, M. Hirobe, K. Arakane, A. Ryu, S. Mashiko and T. Nagano, *Chem. Commun.*, 1997, 21; J. L. Anderson, Y.-Z. An, Y. Rubin and C. S. Foote, *J. Am. Chem. Soc.*, 1994, **116**, 9763; H. Tokuyama and E. Nakamura, *J. Org. Chem.*, 1994, **59**, 1135.

5 S. H. Friedman, D. L. DeCamp, R. P. Sijbesma, G. Srdanov, F. Wudl and G. L. Kenyon, *J. Am. Chem. Soc.*, 1993, **115**, 6506; R. Sijbesma, G. Srdanov, F. Wudl, J. A. Castoro, C. Wilkins, S. H. Friedman, D. L. DeCamp and G. L. Kenyon, *J. Am. Chem. Soc.*, 1993, **115**, 6510.

6 N. Higashi, T. Inoue and M. Niwa, *Chem. Commun.*, 1997, 1507; N. Yamakoshi, T. Yagami, S. Sueyoshi and N. Miyata, *J. Org. Chem.*, 1996, **61**, 7236; Y.-Z. An, C.-H. B. Chen, J. L. Anderson, D. S. Sigman, C. S. Foote and Y. Rubin, *Tetrahedron Lett.*, 1996, **52**, 5179; A. Boutorine, H. Tokuyama, M. Takasugi, H. Isobe, E. Nakamura and C. Hélène, *Angew. Chem., Int. Ed. Engl.*, 1994, **33**, 2462; H. Tokuyama, S. Yamago, E. Nakamura, T. Shiraki and Y. Sugiura, *J. Am. Chem. Soc.*, 1993, **115**, 7918.

7 E. Nakamura, H. Tokuyama, S. Yamago, T. Shiraki and Y. Sugiura, *Bull. Chem. Soc. Jpn.*, 1996, **69**, 2143.

8 (*a*) W. Sliwa, *Fullerene Sci. Technol.*, 1997, **5**, 1133; (*b*) A. Hirsch, *Synthesis*, 1995, 895.

9 H.-W. Frühauf, *Chem. Rev.*, 1997, **97**, 523; M. Lautens, W. Klute and W. Tam, *Chem. Rev.*, 1996, **96**, 49; L. F. Tietze, *Chem. Rev.*, 1996, **96**, 115; I. Ojima, M. Tzamarioudaki, Z. Li and R. J. Donovan, *Chem. Rev.*, 1996, **96**, 635.

10 Reviews: A. L. Balch and M. M. Olmstead, *Chem. Rev.*, 1998, **98**, 2123; A. Stephens and M. L. H. Green, *Adv. Inorg. Chem.*,1997, **44**, 1; J. R. Bowser, *Adv. Organomet. Chem.*, 1994, **36**, 57; P. J. Fagan, J. C. Calabrese and B. Malone, *Acc. Chem. Res.*,1992, **25**, 134.

11 T.-Y. Hsiao, K. C. Santhosh, K.-F. Liou and C.-H. Cheng, *J. Am. Chem. Soc.*, 1998, **120**, 12232.

12 T. Muraoka, I. Matsuda and K. Itoh, *Tetrahedron Lett.*, 1998, **39**, 7325.

13 *Selected data* for **4a**: ν_{max}(KBr)/cm^{-1} 1735 (s), 1428 (m), 1249 (m), 1159 (w), 1112 (m), 820 (w), 699 (w), 527 (m); δ_H(300 MHz, $CDCl_3$) 0.79 (s, 3H), 0.88 (s, 3H), 3.13 (d, 1H, *J* 16.8), 3.38 (s, 1H), 3.48 (m, 1H), 3.64–3.77 (m, 2H), 3.80 (s, 3H), 3.87 (S, 3H), 3.97–4.07 (m, 2H), 7.34–7.39 (m, 3H), 7.70–7.74 (m, 2H); δ_C(75 MHz, $CDCl_3$) −0.71, −0.53, 40.58, 44.37, 45.47, 45.83, 52.95, 52.98, 58.92, 66.62, 128.08, 129.50, 133.09, 133.57, 134.32, 135.26, 135.32, 135.60, 137.75, 138.85, 139.70, 139.97, 140.07, 140.36, 141.35, 141.51, 141.61, 141.73, 141.80, 141.92, 142.05, 142.09, 142.18, 142.56, 142.59, 142.63, 142.64, 142.68, 143.12, 143.18, 144.07, 144.58, 144.63, 144.73, 144.80, 144.86, 144.92, 145.28, 145.34, 145.37, 145.44, 145.46, 145.61, 145.73, 145.84, 145.85, 146.10, 146.16, 146.23, 146.28, 146.43, 146.52, 147.62, 147.68, 155.76, 156.39, 159.61, 161.21, 172.30, 172.52 (*cf.* because of signal coincidence, only 52 peaks of the expected 58 peaks of the C_{60} core were observed); *m/z* (FAB-MS) 1064 (M^+, 11%), 720 (100).

14 T. Muraoka, I. Matsuda and K. Itoh, unpublished results.

Communication a909050i

Photoswitchable trinuclear transition-metal complexes. Intramolecular triplet–triplet energy transfer from *fac*-(diimine)$Re^{I}(CO)_3$ chromophores to a stilbene-like bridging ligand†

Shih-Sheng Sun,[a] Elizabeth Robson,[a] Nicholas Dunwoody,[a] Alexsandra S. Silva,[a,b] Ira M. Brinn[b] and Alistair J. Lees*[a]

[a] *Department of Chemistry, State University of New York at Binghamton, Binghamton, New York 13902-6016, USA. E-mail: alees@binghamton.edu*

[b] *DQI, Instituto de Química, Universidade Federal do Rio de Janeiro, 21949-900, Rio de Janeiro, RJ, Brasil*

Received (in Bloomington, IN, USA) 7th October 1999, Accepted 23rd December 1999

A series of novel trinuclear metal complexes containing *fac*-(diimine)$Re^{I}(CO)_3$ chromophores and a stilbene-like bridging ligand have been synthesized and in CH_3CN exhibit photoswitchable luminescence arising from photoinduced intramolecular energy transfer from the *fac*-(diimine)-$Re(CO)_3$ chromophores to the bridging ligand.

Recently, molecular systems containing multiple electron or energy transfer donor–acceptors have been widely studied for potential applications as optical switches or gates in which the emission from these molecular systems can be switched on or off by external stimuli or environmental changes such as light or pH.[1] Polynuclear transition-metal complexes containing *fac*-(diimine)$Re^{I}(CO)_3$ chromophores have been used for extensive studies of photoinduced intramolecular energy transfer and electron transfer.[2] Earlier studies on ligand-bridged dimeric systems have illustrated that the bridging ligand π*-electron system has a profound effect on the spectroscopic, photochemical, and redox behavior of these complexes.[2,3]

The light-driven *cis–trans* isomerization processes of stilbenes and compounds containing stilbene units have undergone active investigation both through fundamental studies and practical applications.[4] The *cis*- or *trans*-stilbenes and their analogues are good triplet energy acceptors for exploring photosensitization and energy transfer processes.[5,6] We herein report the photophysics and photochemistry of trinuclear metal complexes containing *fac*-(diimine)$Re^{I}(CO)_3$ chromophores bridged by a stilbene-like tridentate ligand. The results show that following excitation into the Re (dπ) → diimine (π*) MLCT manifold, efficient triplet–triplet energy transfer from the ^{3}MLCT state to the bridging ligand occurs and this results in *trans–cis* isomerization of the bridging ligand. The structures of the bridging ligands and complexes studied here are shown in Scheme 1.

Complexes $[(NN)Re(CO)_3]_3(\mu\text{-TEEPB})(PF_6)_3$, where NN = bpy, 4,4′-$Me_2$bpy or 4-$NO_2$bpy, and TEEPB = 1,3,5-tris(2-ethenyl-4-pyridyl)benzene, were synthesized by refluxing a 3 : 1 molar ratio of $[(NN)Re(CO)_3(CH_3CN)]PF_6$ and TEEPB in THF solution and then standard workup procedures.[2c,7] All new complexes have been characterized by infrared spectra, ^{1}H, ^{13}C NMR and elemental analysis.‡

Photophysical parameters obtained from compounds **1**–**7** are summarized in Table 1. The absorption spectra of all these compounds feature a series of ligand localized π → π* and metal (dπ) to ligand (π*) charge transfer (MLCT) bands. Unlike most metal complexes containing the *fac*-(diimine)$Re^{I}(CO)_3$ unit, which are typically highly luminescent in solution,[2,3,6] compounds **1** and **3** show only weak luminescence (Φ_{em} < 0.0015) in room temperature CH_3CN solution. The quenching appears to occur *via* intramolecular sensitization of the π → π* transition localized on the olefin link of the bridging ligand accompanied by a *trans–cis* isomerization process.

$$[(NN)Re^{I}(CO)_3]_3(\mu\text{-}t\text{-TEEPB}) \xrightarrow{h\nu} [^3(NN^{\bullet-})Re^{II}(CO)_3]_3{}^*(\mu\text{-}t\text{-TEEPB}) \underset{k_{-ENT}}{\overset{k_{ENT}}{\rightleftharpoons}}$$

$$[(NN)Re^{I}(CO)_3]_3{}^3(\mu\text{-}t\text{-TEEPB})^* \xrightarrow[\text{isomerization}]{trans\text{–}cis} [(NN)Re^{I}(CO)_3]_3(\mu\text{-}c\text{-TEEPB})$$

This is supported by steady-state photolysis experiments. Fig. 1 shows the difference absorption spectrum of compound **1** in CH_3CN solution as a function of photolysis time. Photolysis into the MLCT band at 366 nm bleaches the ππ* absorption of the bridging ligand at *ca.* 280–370 nm and induces small increases at *ca.* 200–270 nm. A similar bleaching effect at *ca.* 280–330 nm was also observed for free TEEPB photolyzed at 313 nm. Furthermore, changes observed in the emission are very substantial and the emission quantum yield is 18 times greater for **1** (see inset in Fig. 1) and 21 times greater for **3** after 7 h of photolysis at 366 nm compared to the original spectra. The UV–VIS spectral changes and large increase in the luminescence intensity for **1** and **3** are consistent with the *trans–cis* isomerization of the bridging ligand, TEEPB,§[6a,b,8] and highly efficient energy transfer (*vide infra*). The energy transfer from the ^{3}MLCT state to the higher energy triplet excited state

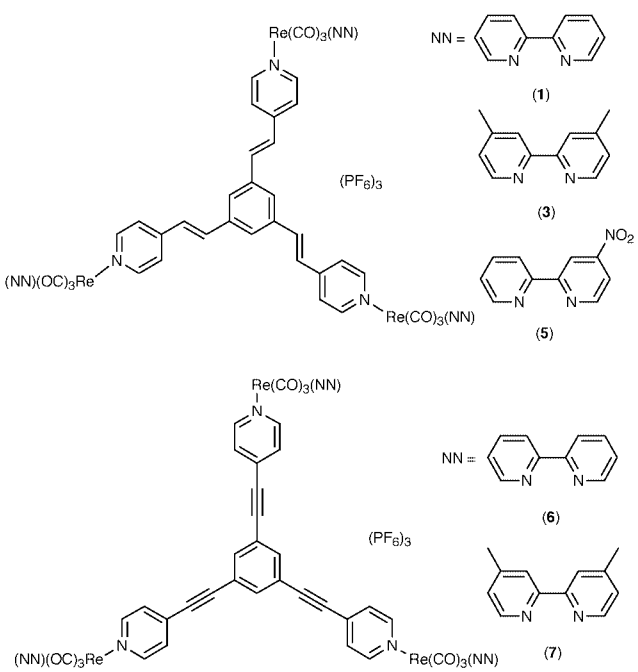

Scheme 1

† Spectral and analytical data for **1**, **3**, **5**, **6** and **7** are available from the RSC web site, see http://www.rsc.org/suppdata/cc/a9/a908074k/

Table 1 Photophysical properties of TEEPB and compounds **1**–**7**[a]

Compound	Absorption spectra λ_{max}/nm (10^{-3} ε/M^{-1} cm^{-1})	Emission						
		λ_{max}/nm	$10^2\Phi_{em}$[b]	τ/ns	k_r/s^{-1}	k_{nr}/s^{-1}	k_{ENT}/s^{-1}[c]	Φ_{ENT}[d]
1 [(bpy)Re(CO)$_3$]$_3$(μ-*t*-TEEPB)(PF$_6$)$_3$	341 (85), 320 (88), 280 (48), 239 (49)	574	0.14	15.1	9.3×10^4	3.1×10^6	6.3×10^7	0.94
2 [(bpy)Re(CO)$_3$]$_3$(μ-*c*-TEEPB)(PF$_6$)$_3$[e]		568	2.57	166	1.5×10^5	5.9×10^6		
3 [(4,4′-Me$_2$bpy)Re(CO)$_3$]$_3$(μ-*t*-TEEPB)(PF$_6$)$_3$	341 (94), 318 (86), 280 (50), 240 (55)	562	0.099	10.2	9.9×10^4	1.9×10^6	9.8×10^7	0.98
4 [(4,4′-Me$_2$bpy)Re(CO)$_3$]$_3$(μ-*c*-TEEPB)(PF$_6$)$_3$[e]		556	2.13	187	1.1×10^5	5.2×10^6		
5 [(4-NO$_2$bpy)Re(CO)$_3$]$_3$(μ-*t*-TEEPB)(PF$_6$)$_3$	402 (sh, 21), 336 (90), 285 (sh, 57), 238 (60)	[f]						
6 [(bpy)Re(CO)$_3$]$_3$(μ-TEPB)(PF$_6$)$_3$	342 (sh, 47), 319 (88), 301 (94), 283 (84), 251 (66)	576	3.03	246	1.2×10^5	3.9×10^6		
7 [(4,4′-Me$_2$bpy)Re(CO)$_3$]$_3$(μ-TEPB)(PF$_6$)$_3$	326 (sh, 75), 316 (95), 304 (94), 288 (79), 251 (71)	566	6.11	507	1.2×10^5	1.9×10^6		

[a] The excitation wavelengths are 380 nm. [b] The emission quantum yields were determined using [(bpy)Re(CO)$_3$(4-Etpy)](PF$_6$) ($\Phi_{em}^{CH_3CN}$ = 0.027) as reference.[2d] [c] Triplet–triplet energy transfer rate constant: see text for detail. [d] Quantum yield for generating ^{3}TEEPB excited state: see text for detail. [e] Generated by photolysis at 366 nm for 36 h. The k_r and k_{nr} values are calculated based on 100% *cis*-TEEPB presence in solution. [f] No emission detected.

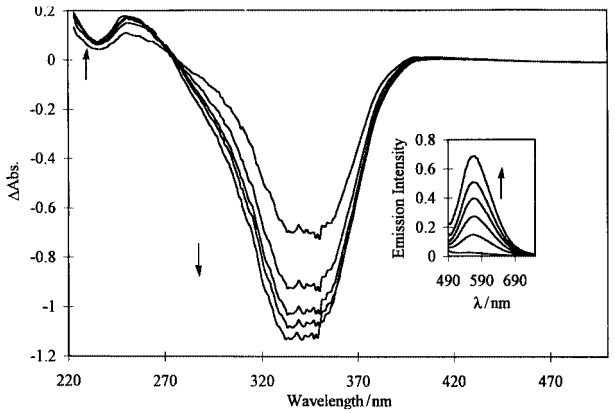

Fig. 1 UV–visible difference absorption spectra ($\Delta_{Abs} = A_t - A_{t=0}$) of [(bpy)Re(CO)$_3$]$_3$(μ-TEEPB)(PF$_6$)$_3$ in CH_3CN at 293 K as a function of photolysis time (λ = 366 nm; 0, 1, 2, 3, 4, 6 h). The inset shows the emission spectra before and after the photolysis.

localized on the *cis*-configuration bridging ligand is blocked or, at least, more unfavorable than direct deactivation from the ^{3}MLCT excited state to the ground state.

On the other hand, there is no emission detected from **5**, even after prolonged irradiation at 366 nm for 48 h. The lack of emission from **5** is attributed to the energy gap law, that is, the lower energy ^{3}MLCT excited state results in better vibrational overlap between the ground and excited states and the nonradiative decay increases as vibrational overlap increases.[9] The low energy ^{3}MLCT excited state in **5** also makes the energy transfer process energetically unfavorable.

Assuming that the MLCT intersystem crossing efficiency is unity, radiative (k_r) and nonradiative (k_{nr}) decay to the ground state and energy transfer (k_{ENT}) to TEEPB are the only deactivation processes for the ^{3}MLCT excited state, and that the decay from the ^{3}TEEPB excited state is much faster than energy transfer, then Φ_{em} and τ for [(NN)Re(CO)$_3$]$_3$(μ-TEEPB)(PF$_6$)$_3$ can be expressed as : $\Phi_{em} = k_r/(k_r + k_{nr} + k_{ENT})$ and $\tau = (k_r + k_{nr} + k_{ENT})^{-1}$. Calculated photophysical parameters are shown in Table 1. As expected, all the k_r values are very similar, *ca.* 1×10^5 s^{-1}, for the series of *fac*-(diimine)Re^{I}(CO)$_3$L complexes and in agreement with related Re(I) chromophores.[10] The energy transfer rate constant, k_{ENT}, and the efficiency for generating the ^{3}TEEPB excited state, Φ_{ENT}, at 293 K can be determined based on: $k_{ENT} = \tau^{-1} - \tau_{model}^{-1}$ and $\Phi_{ENT} = k_{ENT}/(k_r + k_{nr} + k_{ENT})$ with **6** and **7** as model compounds and their values are listed in Table 1.

It is not surprising that both the k_{ENT} and Φ_{ENT} values for **3** are larger than the corresponding values for **1**. The higher ^{3}MLCT excited energy in **3** results in a larger energy gap between the triplet donor and acceptor and, thus, a larger driving force that enhances the efficiency of energy transfer process.

We are grateful to the U.S. Department of Energy (Grant DE-FG02-89ER14039) for support of this research and CAPES for a scholarship to A. S. S.

Notes and references

‡ Two structurally similar compounds, [(NN)Re(CO)$_3$]$_3$(μ-TEPB)(PF$_6$)$_3$ [NN = bpy (**6**) or 4,4′-Me$_2$bpy (**7**) and TEPB = 1,3,5-tris(2-ethynyl-4-pyridyl)benzene] were prepared as model complexes (Scheme 1). Compounds **6** and **7** contain an sp-hybridized carbon link and, thus, avoid photoisomerization deactivation from the ^{3}MLCT excited state.

§ In a control experiment, the photolysis was performed in CD_3CN solution. The ^{1}H NMR spectra of both **1** and **3** showed the appearance of ethylene proton signals with coupling constants, J_{H-H} = 12 Hz (J_{H-H} = 16 Hz before photolysis), which unambiguously confirmed the formation of the *cis*-configuration bridging ligand. On the basis of the integrated areas in the ^{1}H NMR spectra, it was determined that all-*trans*-TEEPB in both **1** and **3** was less than 5% after 36 h of photolysis. The photolysis products are mixtures of *trans*-*trans*-*cis*-TEEPB, *trans*-*cis*-*cis*-TEEPB, and all-*cis*-TEEPB.

1 A. P. de Silva, H. Q. N. Gunaratne, T. Gunnlaugsson, A. J. M. Huxley, C. P. McCoy, J. T. Rademacher and T. E. Rice, *Chem. Rev.*, 1997, **97**, 1515 and references therein.
2 (*a*) R. Ziessel, A. Juris and M. Venturi, *Inorg. Chem.*, 1998, **37**, 5061; (*b*) K. M. Omberg, J. R. Schoonover and T. J. Meyer, *J. Phys. Chem. A*, 1997, **101**, 9531; (*c*) R. Lin, Y. Fu, C. P. Brock and T. F. Guarr, *Inorg. Chem.*, 1992, **31**, 4346; (*d*) G. Tapolsky, R. Duesing and T. J. Meyer, *Inorg. Chem.*, 1990, **29**, 2285.
3 A. J. Lees, *Chem. Rev.*, 1987, **87**, 711.
4 H. Meier, *Angew Chem., Int. Ed. Engl.*, 1992, **31**, 1399.
5 A. A. Gorman, I. Hamblett, F. A. P. Rushton and D. J. Unett, *J. Chem. Soc., Chem. Commun.*, 1993, 983; K. Sandros, M. Sundahl, O. Wennerstrom and U. Norinder, *J. Am. Chem. Soc.*, 1990, **112**, 3082; J. Saltiel, G. R. Marchand, E. Kirkor-Kaminska, W. K. Smothers, J. L. Charlton and W. B. Mueller, *J. Am. Chem. Soc.*, 1984, **106**, 3144.
6 (*a*) K. S. Schanze, L. A. Lucia, M. Cooper, K. A. Walters, H.-F. Ji and O. Sabina, *J. Phys. Chem. A*, 1998, **102**, 5577; (*b*) V. W.-W. Yam, V. C.-Y. Lau and L.-X. Wu, *J. Chem. Soc. Dalton Trans.*, 1998, 1461; (*c*) J. R. Shaw and R. H. Schmehl, *J. Am. Chem. Soc.*, 1990, **113**, 389; (*d*) M. S. Wrighton and D. L. Morse, *J. Am. Chem. Soc.*, 1974, **96**, 998; (*e*) P. P. Zarnegar, C. R. Bock and D. G. Whitten, *J. Am. Chem. Soc.*, 1973, **95**, 4367.
7 J. T. Lin, S.-S. Sun, J. R. Wu, Y. C. Liaw and K.-J. Lin, *J. Organomet. Chem.*, 1996, **517**, 27.
8 H. Gorner and H. J. Kuhn, *Adv. Photochem.*, 1995, **19**, 1.
9 L. A. Worl, R. Duesing, P. Chen, L. D. Ciana and T. J. Meyer, *J. Chem. Soc., Dalton Trans.*, 1991, 849; J. V. Caspar and T. J. Meyer, *J. Phys. Chem.*, 1983, **87**, 952.
10 A. I. Baba, J. R. Shaw, J. A. Simon, R. P. Thummel and R. H. Schmehl, *Coord. Chem. Rev.*, 1998, **171**, 43.

Communication a908074k

ChemComm

The room-temperature crystallisation of a one-dimensional gallium fluorophosphate, $Ga(HPO_4)_2F{\cdot}H_3N(CH_2)_3NH_3{\cdot}2H_2O$, a precursor to three-dimensional microporous gallium fluorophosphates

Richard I. Walton,[a] Franck Millange,[a] Armel Le Bail,[b] Thierry Loiseau,[c] Christian Serre,[c] Dermot O'Hare[a]* and Gérard Férey[c]

[a] *Inorganic Chemistry Laboratory, University of Oxford, South Parks Road, Oxford, UK OX1 3QR. E-mail: dermot.ohare@chem.ox.ac.uk*

[b] *Université du Maine, Laboratoire des Fluorures, CNRS ESA 6010, Avenue O. Messiaen, 72085 Le Mans Cedex 9, France*

[c] *Institut Lavoisier, UMR CNRS 8637, Université de Versailles Saint Quentin-en-Yvelines, 45, Avenue des Etats-Unis, 78035 Versailles Cedex, France*

Received (in Cambridge, UK) 1st November 1999, Accepted 5th January 2000

The one-dimensional gallium fluorophosphate $Ga(HPO_4)_2F{\cdot}H_3N(CH_2)_3NH_3{\cdot}2H_2O$ 1 crystallises at room temperature from an aqueous mixture of Ga_2O_3, H_3PO_4, 1,3-diaminopropane, and HF; compound 1 converts to the three-dimensional microporous fluorophosphate ULM-3 on heating to 160 °C under hydrothermal conditions.

The determination of the crystallisation mechanisms of microporous solids is currently a great challenge in solid-state chemistry, because of the huge importance of these materials in many industrial applications (for example the use of aluminosilicate zeolites in catalysis, ion-exchange and gas absorption).[1] It is hoped that a detailed understanding of how microporous solids are formed will enable the rational design of new materials with properties required for a particular use.[2,3] We have studied the hydrothermal crystallisation of fluorophosphates of aluminium and gallium *in situ*, using both time-resolved energy-dispersive X-ray diffraction (EDXRD)[4–6] and NMR spectroscopy.[7] In our EDXRD study of open-framework gallium fluorophosphates of the ULM-*n* family[8] we have observed novel crystalline intermediate phases when the source of phosphorus was changed from H_3PO_4 to P_2O_5.[4–6] The compounds are only stable under hydrothermal conditions, and so structural characterisation has proved extremely difficult. In order to gain a greater understanding of these new transient phases we have investigated the crystallisation of metastable frameworks structures from reaction gels at low temperature.

We now report the crystallisation of a one-dimensional fluorophosphate, $Ga(HPO_4)_2F{\cdot}H_3N(CH_2)_3NH_3{\cdot}2H_2O$ **1**, at room temperature. Compound **1** was prepared by standing at room temperature the reaction mixture usually heated in a hydrothermal bomb to prepare ULM-3 $[Ga_3(PO_4)_3F_2{\cdot}H_3N(CH_2)_3NH_3{\cdot}H_2O]$.[9] 1 g of Ga_2O_3 was used, the mixture placed in a Teflon tube covered with film and stood for 1 week. A laboratory powder X-ray diffraction pattern of the solid product after recovering and washing with water showed that a novel crystalline phase had been produced, although contaminated with unreacted GaOOH and poorly crystalline β-Ga_2O_3, present in the Ga_2O_3 starting material. Examination of the solid product using a JEOL 2000FX transmission electron microscope, equipped with a Link 'Pentafet' EDX detector, revealed it to consist of well-formed thin sheets of maximum dimension ≈ 3 μm, mixed with a small quantity of shapeless material. X-Ray microanalysis using a $GaPO_4$ calibrant showed the plate-like crystallites to contain Ga and P in the ratio 1:2, and emissions characteristic of O, F, C and N were observed. The contaminant material contained only Ga and O, presumably the unreacted gallium oxides. A sample of the phosphorus-rich gallium fluorophosphate was subsequently prepared in a virtually pure form, by changing the reagent ratios; the Ga:P ratio in the initial gel was changed to be 1:2, the amount of HF doubled, and the pH adjusted to the same value as in the first reaction mixture (≈ 5.5) by addition of the appropriate amount of 1,3-diaminopropane. This sample exhibits only the strongest Bragg reflection of GaOOH, and the impurity is present in a very small amount (less than 0.5% on the basis of the diffraction results, *vide infra*). It has not been possible to prepare crystals of suitable size for single-crystal diffraction studies; for example if the reaction mixture is stood for longer periods (up to four months) no change in the sample nature is observed and seeding the mixture with pre-made sample afforded no larger crystals. If HF is omitted from the reaction mixture, then the only crystalline material produced is 1,3-propanediammonium phosphate hydrate.[10]

Powder X-ray diffraction data were collected from the new gallium fluorophosphate at room temperature on Station 2.3 of the Daresbury SRS in a 0.5 mm diameter glass capillary. An X-ray wavelength of 1.30041 Å was used, selected using a Si(110) double-crystal monochromator. The data were successfully indexed by the autoindexing program TREOR[11] on a triclinic unit cell (a = 7.0736 Å, b = 8.5062 Å, c = 11.6205 Å, α = 107.48°, β = 102.10°, γ = 90.28°) with good figures of merit [$M(25)$ = 24, $F(25)$ = 90.6]. An *ab initio* approach was taken to the structure solution† and the final Rietveld plot is shown in Fig. 1.

The X-ray structure determination reveals that **1** is constructed from only $\{GaO_4F_2\}$ octahedra and $\{PO_3OH\}$ tetrahedra. All bond distances [Ga–O_{av} = 1.99(2) Å, Ga–F_{av} = 1.869(2) Å, P–O_{av} = 1.54(1) Å, P=O_{av} = 1.51(2) Å] agree very well with those previously reported for gallium fluorophos-

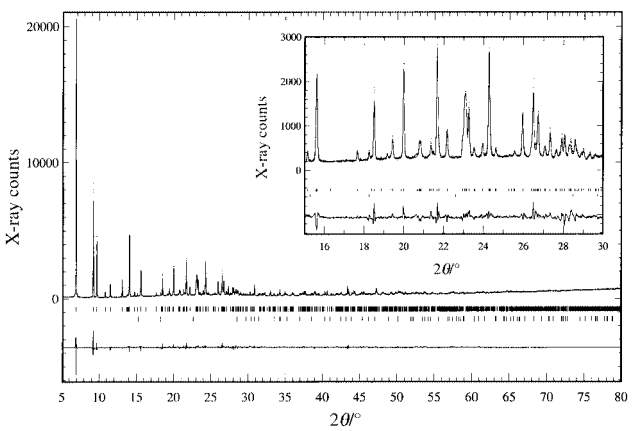

Fig. 1 Final Rietveld fit for $Ga(HPO_4)_2F{\cdot}H_3N(CH_2)_3NH_3{\cdot}2H_2O$. Inset is an expanded region of a small part of the data illustrating the small amount of the impurity GaOOH. Points are the experimental data, the line is the Rietveld fit, upper tick marks are for $Ga(HPO_4)_2F{\cdot}H_3N(CH_2)_3NH_3{\cdot}2H_2O$, and lower tick marks for GaOOH. The lower line is the difference curve.

phates.[8] The Ga polyhedra share the axial fluorines to produce an almost linear chain and all the (equatorial) oxygens are shared with the $\{PO_4\}$ tetrahedra. These phosphorus polyhedra bridge pairs of gallium octahedra along the chain on both sides (Fig. 2). Two of the phosphorus oxygens are terminal; these are assigned as one P–OH and one P=O per tetrahedron on the basis of charge-balancing considerations. Infra-red spectroscopy gave further evidence for the presence of this bonding; bands at 1380 cm^{-1} and 1005 cm^{-1} are assigned to the vibrations of phosphorus–oxygen bonds of P=O and P–OH respectively[12] and these are absent in ULM-3 in which all $\{PO_4\}$ oxygens are shared with Ga.[9] The chains of composition $Ga(HPO_4)_2F^{2-}$ are separated by charge-balancing $H_3N(CH_2)_3NH_3^{2+}$ cations and occluded water molecules. Thermogravimetric analysis is in agreement with the formulation of $Ga(HPO_4)_2F{\cdot}H_3N(CH_2)_3NH_3{\cdot}2H_2O$: a mass loss between 50 °C and 90 °C corresponds to the loss of the occluded water (observed 8.7%, expected 9.1%), and a mass loss between 300 °C and 700 °C corresponds to loss of the amine (observed 22.3%, expected 21.3%), presumably accompanied by collapse of the structure. The structure type has not previously been observed for an anionic gallium phosphate with organic counterions, although the arrangement of octahedra and tetrahedra is well known in the mineral chemistry of metal silicates, sulfates and phosphates,[13] Two one-dimensional anionic gallium phosphates, $Ga(PO_4)(HPO_4)^{2-}$, with charge-compensating alkylammonium cations are known and both of these were made using solvothermal methods.[14,15] In these compounds gallium is found only in tetrahedral sites. It is noteworthy that the previously reported one-dimensional gallophosphates have a Ga:P ratio of 1:2, and our new compound follows this pattern.

The use of ambient conditions to crystallise metal phosphates has previously received some attention, but the reagents used differ considerably from those usually used in solvothermal crystallisations.[16] It is interesting that the use of mild reaction conditions favours the formation of phosphates with low-dimensional structures, and thus it would appear that solvothermal conditions are necessary to synthesise three-dimensional (microporous) phosphates. The importance of the current work is that we have prepared a novel 1D phase at room temperature from *exactly* the same reaction mixture which yields a 3D phase if treated hydrothermally. The fact that the new chain phase contains only 6-coordinate gallium, whereas the hydrothermally-prepared ULM-3 contains both 5- and 6-coordinate gallium, is entirely consistent with recent *in situ* NMR spectroscopy results for related systems. For the aluminium fluorophosphate AlPO-CJ2 it was determined that there is a modification of Al coordination in solution from 6 to 5 on going from room temperature to hydrothermal conditions.[7]

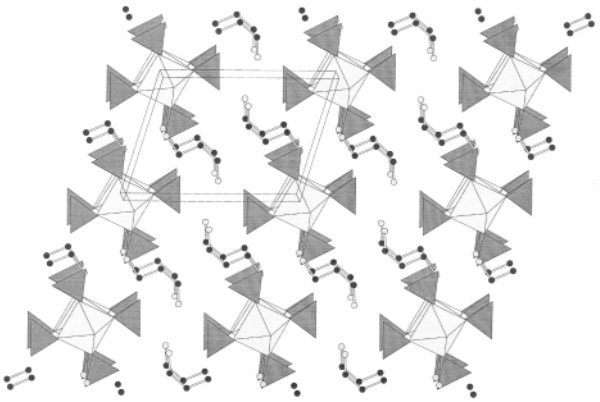

Fig. 2 A polyhedral view of the structure of $Ga(HPO_4)_2F{\cdot}H_3N(CH_2)_3NH_3{\cdot}2H_2O$ along *a*. Dark grey polyhedra are $\{PO_3OH\}$ tetrahedra and light grey polyhedra $\{GaO_4F_2\}$ octahedra. Black circles are carbon, and grey circles nitrogen. Occluded water molecules are not shown for clarity. The unit cell is shown by the faint line.

Such an observation will be of utmost importance in describing a reaction mechanism for the crystallisation and our structural data give some independent confirmation of this result. Heating **1** at 160 °C under hydrothermal conditions results in complete dissolution after ≈40 min followed by the almost immediate appearance of the 3D framework solid ULM-3.[17] Compound **1** may be thought of as a solid precursor to ULM-3 and we are investigating its possible transformation to other related gallium fluorophosphates, by the addition of other reagents. We have also recently shown that if H_3PO_4 is replaced by P_2O_5 in the room temperature reaction, a different gallium fluorophosphate is produced with a Ga:P ratio of 1:2. The structure of this second phase, which closely resembles material recovered by quenching from the hydrothermal synthesis of ULM-3 using P_2O_5,[6] we will report elsewhere.

We are grateful to the EPRSC, the Leverhulme Trust, the British Council (Alliance project) and the Novartis Trust Fund for financial support. We thank Dr C. C. Tang of Daresbury Laboratory for his assistance with measuring the powder diffraction data and Dr Lei Lixu for recording the infra-red spectra.

Notes and references

† The data were first analysed with a 'whole pattern fitting' algorithm to determine accurately the profile shape function, background and cell parameters. This preliminary study provided good estimates of R_{wp} and χ^2 that could be reached during structure refinement (16.9% and 2.0 respectively). The structure was solved in the space-group $P\bar{1}$. The gallium positions were located using the program EXPO.[18] The Reverse Monte Carlo program ESPOIR[19] was used to locate phosphorus and oxygen atoms of the inorganic framework, with gallium atoms fixed at the positions found by direct methods. The positions of the nitrogen and carbon atoms of the 1,3-diaminopropane and oxygen atoms of occluded water were found using Fourier difference maps with the previously found atoms constrained. In the final refinement cycle, atomic constraints on the inorganic macroanion (Ga–O, P–O and O–O distance constraints) were removed. A two-phase refinement was performed to account for the presence of the crystalline impurity GaOOH and the refinement converged with agreement factors R_p = 20.0%, R_{wp} = 18.4%, R_B = 9.6% χ^2 = 2.8.

1 M. T. Weller and S. E. Dann, *Curr. Opin. Solid State Mater. Sci.*, 1998, **3**, 137; A. K. Cheetham, G. Férey and T. Loiseau, *Angew. Chem., Int. Ed.*, 1999, **38**, 3268.
2 A. K. Cheetham and C. F. Mellot, *Chem. Mater.*, 1997, **9**, 2269.
3 R. J. Francis and D. O'Hare, *J. Chem. Soc., Dalton Trans.*, 1998, 3133.
4 R. J. Francis, S. J. Price, S. O'Brien, A. M. Fogg, D. O'Hare, T. Loiseau and G. Férey, *Chem. Commun.*, 1997, 521.
5 R. J. Francis, S. O'Brien, A. M. Fogg, P. S. Halasyamani, D. O'Hare, T. Loiseau and G. Férey, *J. Am. Chem. Soc.*, 1999, **121**, 1002.
6 R. I. Walton, T. Loiseau, D. O'Hare and G. Férey, *Chem. Mater.*, 1999, 3201.
7 M. Haouas, C. Gerardin, F. Taulelle, C. Estournes, T. Loiseau and G. Férey, *J. Chim. Phys.*, 1997, **95**, 302.
8 G. Férey, *J. Fluorine Chem.*, 1995, **72**, 187.
9 T. Loiseau, R. Retoux, P. Lacorre and G. Férey, *J. Solid State Chem.*, 1994, **111**, 427.
10 S. Kamoun, A. Jouini and A. Dauod, *Acta Crystallogr., Sect. C*, 1991, **47**, 117.
11 TROER, P. E. Warner, University of Stockholm, Sweden, 1990.
12 K. Nakamoto, *Infrared and Raman Spectra of Inorganic and Coordination Compounds Part B*, 5th edn., John Wiley, New York, 1997, p. 266.
13 F. C. Hawthorne, *Am. Mineral.*, 1985, **70**, 455.
14 T. Loiseau, F. Serpaggi and G. Férey, *Chem. Commun.*, 1997, 1093.
15 A. M. Chippindale, A. D. Bond, A. D. Law and A. R. Cowley, *J. Solid State Chem.*, 1998, **136**, 227.
16 M. A. Leech, A. R. Cowley, K. Prout and A. M. Chippindale, *Chem. Mater.*, 1998, **10**, 451.
17 R. I. Walton and D. O'Hare, unpublished results, 1999.
18 A. Altomare, M. C. Burla, M. Camalli, G. Cascarano, C. Giacovazzo, A. Guagliadi and G. Polidori, *J. Appl. Crystallogr.*, 1994, **27**, 435.
19 ESPOIR, A. Le Bail, Université du Maine, Le Mans, France, 1999.

Communication a908662e

Characterisation of a triply thiolate-bridged Ni–Fe amine–thiolate complex: insights into the electronic structure of the active site of [NiFe] hydrogenase†‡

Gunther Steinfeld and Berthold Kersting*

Institut für Anorganische und Analytische Chemie, Universität Freiburg, Albertstr. 21, D-79104 Freiburg, Germany. E-mail: kerstber@sun2.ruf.uni-freiburg.de

Received (in Basel, Switzerland) 7th October 1999, Accepted 5th January 2000

The synthesis and structural characterisation of a new Ni–Fe amine–thiolate complex are described; its chemical properties are related to the active site of [NiFe] hydrogenase.

The active site of the [NiFe] hydrogenase from *D. gigas* consists of a $(cys\text{-}S)_2Ni(\mu\text{-}cys\text{-}S)_2XFe(CO)(CN)_2$ bimetallic complex[1–3] that can exist in various redox states. Spectroscopic studies[4] and recent X-ray crystal structures of biological [NiFe] hydrogenases in their reduced, active forms[5] are indicative of changes in the electron density of both active site metal ions. The differences in the electron density could be due to the absence of a third bridging ligand X (which is a putative O^{2-} or OH^- ion in the oxidized, inactive form) or by the electron count of the Ni–Fe cluster. Despite the discovery of these active site features, the mechanism of biological hydrogen activation is still not well understood.[6] Model compounds are therefore being studied to understand the function of the more complex enzymes.[7] They also hold promise for cheap hydrogen catalysts, for example, in solar energy conversion.[3] Current studies focus on mono- and binuclear Fe thiolate complexes with Fe(CO) and Fe(CN) fragments[8] and Ni thiolate complexes.[9] However, only a few relevant NiFe complexes have been described.[10] We here describe the syntheses, X-ray structure and properties of a new heterobinuclear NiFe amine–thiolate complex which differs from previous examples by its reversible redox reactions.

The new complex $[Ni^{II}Fe^{II}(L)]^+$ (**1a**, Scheme 1) was obtained by reaction of $[Ni^{II}(L)]^-$ (prepared *in situ* from the nonadentate N_6S_3 ligand $H_3L{\cdot}6HCl$,[11] $NiCl_2{\cdot}6H_2O$, and NEt_3) with one equivalent of anhydrous $FeCl_2$ in methanol. It was isolated as the one-electron-oxidized form $[Ni^{II}Fe^{III}(L)]^{2+}$ in $\{[Ni^{II}Fe^{III}(L)]_2Cl\}[BPh_4]_3$ (**1b**) by exposing the reaction mixture to air and adding excess $NaBPh_4$.§

Crystallographic characterization of complex **1b**¶ confirmed the crystal structure to consist of a face-sharing bioctahedral NiFe complex, $[Ni^{II}Fe^{III}(L)]^{2+}$. The different metal–ligand bond lengths reflect the heterobinuclear nature of the C_3-symmetric complex (Fig. 1). It is assigned a $N'_3Ni^{II}(\mu\text{-}SR)_3Fe^{III}N_3$ core

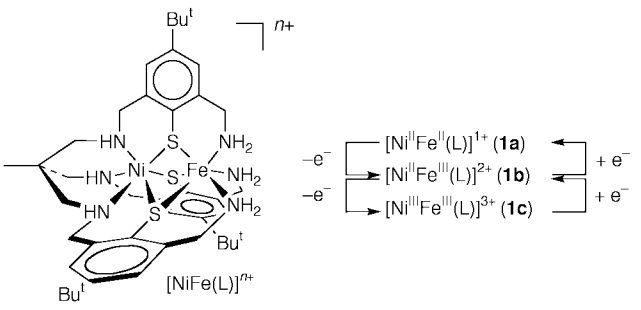

Scheme 1

† Electronic Supplementary Information (ESI) available: CV; Electronic absorption, EPR and ^{57}Fe Mössbauer spectra. See http://www.rsc.org/suppdata/cc/a9/a908201h/

‡ Dedicated to Professor Dr H. Vahrenkamp on the occasion of his 60th birthday.

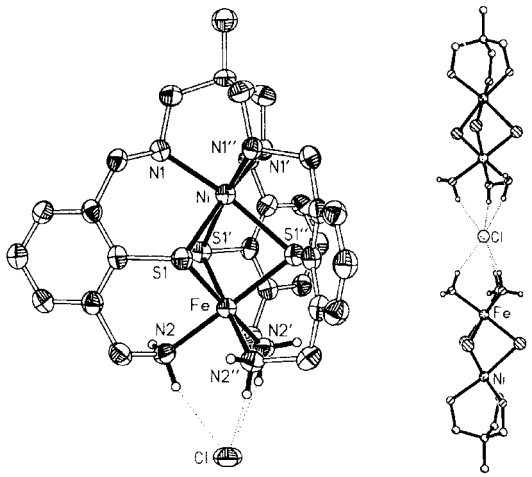

Fig. 1 Thermal ellipsoid plot of the $[Ni^{II}Fe^{III}(L)]^{2+}$ cation (left) and schematic representation of intermolecular hydrogen bonding interactions (right) in **1b**·12MeCN·H_2O. *tert*-Butyl groups and hydrogen atoms are omitted for clarity. Selected distances (Å) and angles (°): Ni–N(1) 2.083(4), Ni–S(1) 2.430(1), Fe–N(2) 2.047(4), Fe–S(1) 2.291(1); Fe–S(1)–Ni 79.79(5). Symmetry codes used to generate equivalent atoms: $1-x, x-y, z$ (′) and $1-x+y, 1-x, z$ (″).

structure‖ as the average M–N and M–S bond lengths of the N'_3NiS_3 site at 2.083(4) and 2.430(1) Å, respectively, match more closely with those of related $Ni^{II}N_3S_3$ complexes.[11] The short average M–N and M–S bond lengths of the other N_3MS_3 site at 2.047(4) and 2.291(1) Å confirm this assignment. These distances are too short for an octahedral $Ni^{II}N_3S_3$ complex, but are in excellent accord with those of low-spin Fe^{III} complexes in an octahedral N_3S_3 environment.[12–14] Preliminary results of ^{57}Fe Mössbauer spectroscopic investigations also support this oxidation state distribution (Fig. 2). At $T = 298$ K, **1b** gives rise to a single quadrupole doublet with $\delta = 0.26$ mm s^{-1} and $|\Delta E_Q| = 1.47$ mm s^{-1}, while at $T = 77$ K, $\delta = 0.32$ mm s^{-1} and $|\Delta E_Q| = 1.83$ mm s^{-1}. The temperature dependence of the quadrupole

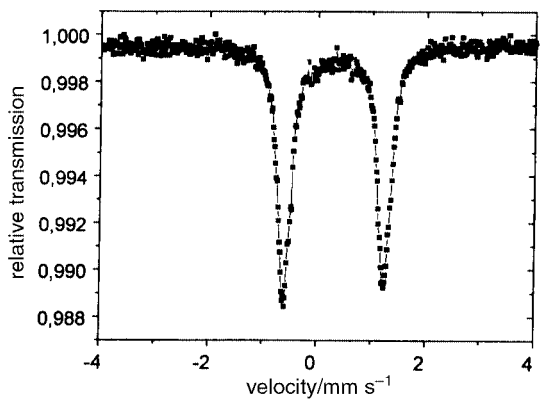

Fig. 2 ^{57}Fe Mössbauer spectrum of **1b**·12MeCN·H_2O at 77 K (relative to α-Fe).

splitting is consistent with the presence of a low-spin Fe^{III} ion.

It should be noted that the Ni···Fe distance at 3.030(1) Å is slightly longer than the Ni···Fe separation of 2.90 Å reported for the as isolated, inactive form of [NiFe] hydrogenase. The wide M–S–M angles [79.79(5)°], however, imply little, if any, attraction between the metal atoms.[14] The intermolecular hydrogen bonding interactions found for **1b** in the solid state are also worth mentioning: a chloride ion links two $[NiFe(L)]^{2+}$ dications *via* six equivalent N–H···Cl hydrogen bonding interactions (N···Cl 3.208 Å). In the resulting LNiFe···Cl···FeNiL subunit the intermolecular Fe···Fe and Ni···Ni distances are at 7.910(1) Å and 13.971(1) Å, respectively. It is unclear at present whether this assembly is retained in solution.

The 77K EPR powder spectrum of **1b** displayed a complex multiplet centered at $g \approx 2$ as the main component, a weaker resonance was observed at $g \approx 4$ (see ESI). Room temperature magnetic susceptibility measurements revealed the complex to be a paramagnetic species with $\mu_{eff} = 2.3\ \mu_B$. The results are indicative of an $S = \frac{1}{2}$ spin ground state which is most likely attained by an intramolecular antiferromagnetic exchange interaction between the Ni^{II} ($S_1 = 1$) and low-spin Fe^{III} ($S_2 = \frac{1}{2}$) ions. A cyclic voltammogram of **1b** in DMF solution displays two electrochemically reversible one-electron steps at $E^1_{1/2} = +0.45$ V [$\equiv E_{1/2}(Ni^{III}Fe^{III}/Ni^{II}Fe^{III})$] and at $E^2_{1/2} = -0.43$ V [$\equiv E_{1/2}(Ni^{II}Fe^{III}/Ni^{II}Fe^{II})$] *vs*. SCE. The CV is significantly different from those of homobinuclear complexes, $[Ni_2(L)]^{n+}$ and $[Fe_2(L)]^{n+}$,[11] and unambiguously confirms the heterobinuclear nature of **1b**.

There is a clearly discernible mutual influence of the constituent Fe^{III} and Ni^{II} ions on the respective $M^{III/II}$ potentials. Comparison with the electrochemical properties of homodinuclear complexes $[Ni_2(L)]^{n+}$ and $[Fe_2(L)]^{n+}$ reveals that the ferric ion raises the $Ni^{III/II}$ couple by *ca*. +400 mV to more anodic potentials, whereas the divalent Ni ion shifts the $Fe^{III/II}$ potential to more cathodic potentials. It is therefore plausible to assume that the reverse effects would occur in a complex in which $E_{1/2}(Fe^{III/II}) > E_{1/2}(Ni^{III/II})$, as for instance in the hydrogenase active site. Since the strong field ligands CO and CN^- keep the iron atom formally at the $+II$ oxidation level, a relatively low $Ni^{III/II}$ redox potential would result (at least for the oxidised, inactive form of the enzyme).

Compound **1b** is not a particularly close structural model of the active site of [NiFe] hydrogenase (lack of Fe-bound CO and CN^- ligands), however, it is an initial example for a thiolate-bridged NiFe complex which can exist in several different oxidation states. The effects of partial replacement of N or S donors of H_3L on the $M^{III/II}$ potentials of heterobinuclear NiFe complexes will be investigated in the future.

Financial support from the Deutsche Forschungsgemeinschaft is gratefully acknowledged. The authors thank Professor Dr C. Janiak for providing facilities for Mössbauer spectroscopic measurements.

Notes and references

§ An argon-purged solution of $H_3L{\cdot}6HCl$ (96 mg, 0.10 mmol) and $NiCl_2{\cdot}6H_2O$ (24 mg, 0.10 mmol) in methanol (10 mL) was treated with NEt_3 (90 mg, 0.90 mmol) to give a pale green solution. $FeCl_2$ (12.6 mg, 0.10 mmol) was then added. The mixture was stirred for 1 h under argon and then for 2 h with exposure to air. The resulting green-black solution was filtered. To the filtrate was added a solution of $NaBPh_4$ (0.17 g, 0.50 mmol) in methanol (1 mL). The green-black precipitate was isolated by filtration, washed with methanol and air-dried. Recrystallisation from acetonitrile afforded large single crystals of **1b**·12MeCN·H_2O (78 mg, 58%). CHN analyses for $\{[NiFe(L)]_2Cl\}[BPh_4]_3$ **1b**: found: C 68.23, H 6.57, N 5.97; calc. for $C_{154}H_{186}N_{12}S_6Ni_2Fe_2ClB_3$: C 68.65, H 6.96, N 6.24%.

¶ Crystal data for **1b**·12MeCN·H_2O: $C_{178}H_{224}N_{24}B_3ClFe_2Ni_2S_6O$, M_r = 3205.21, hexagonal, space group $R\bar{3}c$ (no. 167), T = 180(2) K, μ(Mo-Kα) = 0.51 mm^{-1}, a = 19.849(3) Å, c = 79.08(2) Å, V = 26982(8) $Å^3$, Z = 6; 54984 measured reflections, 7430 were unique [R(int) = 0.1943], structure determined by direct methods in SHELXS 86,[15] refinement with SHELXL-93,[15] R_1, wR_2 = 0.0687, 0.1675 [$I > 2\sigma(I)$]. CCDC 182/1512. See http://www.rsc.org/suppdata/cc/a9/a908201h/for crystallographic files in .cif format.

‖ N and N′ denote primary and secondary amine nitrogen atoms, respectively.

1 R. Cammack, *Nature*, 1995, **373**, 556.
2 A. Volbeda, M.-H. Charon, C. Piras, E. C. Hatchikian, M. Frey and J. C. Fontecilla-Camps, *Nature*, 1995, **373**, 580.
3 R. P. Happe, W. Roseboom, A. J. Pierik, S. P. J. Albracht and K. A. Bagley, *Nature*, 1997, **385**, 126.
4 L. M. Roberts and P. A. Lindahl, *J. Am. Chem. Soc.*, 1995, **117**, 2565; A. L. deLacey, E. C. Hatchikian, A. Volbeda, M. Frey, J. C. Fontecilla-Camps and V. M. Fernandez, *J. Am. Chem. Soc.*, 1997, **119**, 7181; Z. Gu, J. Dong, C. B. Allan, S. B. Choudhoury, R. Franco, J. J. G. Moura, I. Moura, J. LeGall, A. E. Przybyla, W. Roseboom, S. P. J. Albracht, M. J. Axley, R. A. Scott and M. J. Maroney, *J. Am. Chem. Soc.*, 1996, **118**, 11 155; J. E. Huett, M. Carepo, A. Pamplona, R. Franco, I. Moura, J. J. G. Moura and B. M. Hoffman, *J. Am. Chem. Soc.*, 1997, **119**, 9291.
5 E. Garcin, X. Vernede, E. C. Hatchikian, A. Volbeda, M. Frey and J. C. Fontecilla-Camps, *Structure*, 1999, **7**, 557; Y. Higuchi, H. Ogata, K. Miki, N. Yasuoka and T. Yagi, *Structure*, 1999, **7**, 549.
6 M. Pavlov, P. E. M. Siegbahn, M. R. A. Blomberg and R. H. Crabtree, *J. Am. Chem. Soc.*, 1998, **120**, 548.
7 R. T. Hembre and J. S. McQueen, *J. Am. Chem. Soc.*, 1996, **118**, 798.
8 C.-H. Lai, W.-Z. Lee, M. L. Miller, J. H. Reibenspies, D. J. Darensbourg and M. Y. Darensbourg, *J. Am. Chem. Soc.*, 1998, **120**, 10 103; D. Sellmann, T. Becker and F. Knoch, *Chem. Eur. J.*, 1996, **2**, 1092; H.-F. Hsu, S. A. Koch, C. V. Popescu and E. Münck, *J. Am. Chem. Soc.*, 1997, **119**, 8371; V. E. Kaasjager, R. K. Henderson, E. Bouwman, M. Lutz, A. L. Spek and J. Reedijk, *Angew. Chem., Int. Ed.*, 1998, **37**, 1668.
9 M. A. Halcrow and G. Cristou, *Chem. Rev.*, 1994, **94**, 2421; A. J. Atkins, D. Black, A. J. Blake, A. Marin-Becerra, S. Parsons, L. Ruiz-Ramirez and M. Schröder, *Chem. Commun.*, 1996, 457; S. Brooker and P. D. Croucher, *Chem. Commun.*, 1997, 459; S. Brooker, P. D. Croucher, T. C. Davidson, G. S. Dunbar, A. J. McQuillan and G. B. Jameson, *Chem. Commun.*, 1998, 2131.
10 D. K. Mills, Y. M. Hsiao, P. J. Farmer, E. V. Atnip, J. H. Reibenspies and M. Y. Darensbourg, *J. Am. Chem. Soc.*, 1991, **113**, 1421; C.-H. Lai, J. H. Reibenspies and M. Y. Darensbourg, *Angew. Chem., Int. Ed. Engl.*, 1996, **35**, 2390; F. Osterloh, W. Saak, D. Haase and S. Pohl, *Chem. Commun.*, 1997, 979; W.-F. Liaw, C.-M. Lee, L. Horng, G.-H. Lee and S.-M. Peng, *Organometallics*, 1999, **18**, 782; E. Bouwman, R. K. Henderson, A. L. Spek and J. Reedijk, *Eur. J. Inorg. Chem.*, 1999, 217; S. C. Davies, D. J. Evans, D. L. Hughes, S. Longhurst and J. R. Sanders, *Chem. Commun.*, 1999, 1935.
11 B. Kersting, D. Siebert, D. Volkmer, M. J. Kolm and C. Janiak, *Inorg. Chem.*, 1999, **38**, 3871; B. Kersting and D. Siebert, *Inorg. Chem.*, 1998, **37**, 3820.
12 T. Glaser, F. Kesting, T. Beissel, E. Bill, T. Weyhermüller, W. Meyer-Klaucke and K. Wieghardt, *Inorg. Chem.*, 1999, **38**, 722.
13 A. C. Moreland and T. B. Rauchfuss, *J. Am. Chem. Soc.*, 1998, **120**, 9376.
14 T. Glaser, T. Beissel, E. Bill, T. Weyhermüller, V. Schünemann, W. Meyer-Klaucke, A. X. Trautwein and K. Wieghardt, *J. Am. Chem. Soc.*, 1999, **121**, 2193.
15 G. M. Sheldrick, *Acta Crystallogr., Sect. A*, 1990, **46**, 467; G. M. Sheldrick, SHELXL-93, Program for the Refinement of Crystal Structures, University of Göttingen, 1993.

Communication a908201h

ChemComm

Syntheses of a dinuclear Ir complex containing bridging tetraselenide ligands $[(C_5Me_5)Ir(\mu\text{-}Se_4)_2Ir(C_5Me_5)]$ and its conversion into $Ir_2Pd_2Se_3$ and $Ir_2Pd_3Se_5$ clusters

Shoken Nagao,[a] Hidetake Seino,[a] Yasushi Mizobe*[ab] and Masanobu Hidai*[c]

[a] *Institute of Industrial Science, The University of Tokyo, Roppongi, Minato-ku, Tokyo 106-8558, Japan. E-mail: ymizobe@cc.iis.u-tokyo.ac.jp*

[b] *Institute for Molecular Science, Myodaiji, Okazaki 444-8585, Japan*

[c] *Department of Chemistry and Biotechnology, Graduate School of Engineering, The University of Tokyo, Hongo, Bunkyo-ku, Tokyo 113-8656, Japan*

Received (in Cambridge, UK) 29th November 1999, Accepted 17th December 1999

Treatment of $Cp^*IrCl(\mu\text{-}Cl)_2IrCp^*Cl$ ($Cp^* = \eta^5\text{-}C_5Me_5$) with Li_2Se_4 gave a tetraselenide-bridged diiridium complex $Cp^*Ir(\mu\text{-}Se_4)_2IrCp^*$, which reacted further with two equiv. of $Pd(PPh_3)_4$ to afford a mixture of bimetallic tetra- and penta-nuclear selenido clusters $(Cp^*Ir)_2\{Pd(PPh_3)\}_2(\mu_3\text{-}Se)_2(\mu_2\text{-}Se)$ and $(Cp^*Ir)_2\{Pd(PPh_3)\}_3(\mu_3\text{-}Se)_3(\mu_3\text{-}Se_2)$.

The chemistry of metal polysulfides has been progressing rapidly owing to their potential as synthetic reagents or catalysts as well as new materials. Stable polysulfide ligands are now known to be isolable with a variety of ring sizes and coordination modes,[1] which include a novel bridging nona-sulfide chain in $Cp^*Ir(\mu\text{-}SPr^i)_2(\mu\text{-}S_9)IrCp^*$ ($Cp^* = \eta^5\text{-}C_5Me_5$) prepared in this laboratory.[2] Recently, the coordination chemistry of inorganic selenium and tellurium ligands has also been attracting considerable attention.[1b,3] Hence, our studies on dinuclear noble metal–sulfur complexes consisting of half-sandwich Cp*M units[4] have been extended to related noble metal–selenium compounds.[5] Now we have found that reaction of $Cp^*IrCl(\mu\text{-}Cl)_2IrCp^*Cl$ **1** with Li_2Se_4 gives a complex containing a unique diiridium core bridged by two Se_4 ligands, $Cp^*Ir(\mu\text{-}Se_4)_2IrCp^*$ **2**.†

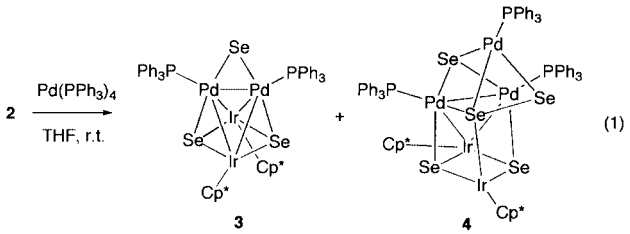

The structure of **2** has been determined in detail by X-ray analysis (Fig. 1).‡ In **2**, each of the Ir atoms has a chelating Se_4 ligand and is further bonded to either an α- or β-Se atom in the other Se_4 ligand. The distance between the two 18-electron Ir(III) centres is 4.179(3) Å. The Ir–Se bond lengths, varying from 2.42 to 2.50 Å, are comparable to those in $Cp^*Ir(PMe_3)(Se_4)$ [2.468(2) and 2.472(2) Å][6] and slightly shorter than that in $[Ir(Me_2PCH_2CH_2PMe_2)_2(Se_4)]Cl$ [2.542(3) Å],[7] while the Se–Se bond distances (2.28–2.41 Å) are unexceptional when compared with those in chelating tri- to penta-selenide ligands previously reported.[3b,c] The two $IrSe_4$ planes are folded and have envelope geometries. Thus, in the ring consisting of Ir(1) and Se(1)–Se(4), the Ir(1), Se(1), Se(3) and Se(4) atoms are almost coplanar within 0.003(4) Å while the distance of Se(2) from this least-square plane is 1.31 Å. For the other ring, the Se(6) atom is displaced 1.36 Å from the least-square plane defined by the Ir(2), Se(5), Se(7) and Se(8) atoms which show deviations of $< 0.10(2)$ Å. The $M(\mu\text{-}Se_4)_2M$ core observed in **2** is unprecedented, although the sulfur analogue has been demonstrated *via* the Rh complex $Cp^*Rh(\mu_2\text{-}S_4)_2RhCp^*$ obtained from the reaction of $Cp^*_2Rh_2(CO)_2$ with S_8.[8] More recently, the Ir complex $Cp^*Ir(\mu_2\text{-}S_4)_2IrCp^*$, produced from the reaction of $Cp^*Ir(2,5\text{-}Me_2C_4H_2S)$ with S_8 has been shown unequivocally to have a similar $M(\mu\text{-}S_4)_2M$ core,[9] while the complex generated by photolysis or thermolysis of $Cp^*Ir(S_4)(CO)$ was also formulated as $Cp^*Ir(\mu_2\text{-}S_4)_2IrCp^*$ based on spectroscopic data.[10]§

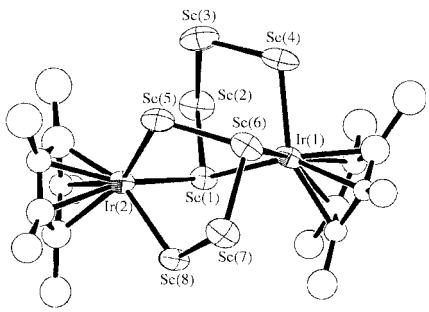

Fig. 1 Molecular structure of **2**. Hydrogen atoms are omitted for clarity. Selected bond distances (Å): Ir(1)–Se(1) 2.456(5), Ir(1)–Se(4) 2.468(5), Ir(1)–Se(6) 2.423(4), Ir(2)–Se(1) 2.454(5), Ir(2)–Se(5) 2.423(5), Ir(2)–Se(8) 2.496(5), Se(1)–Se(2) 2.405(7), Se(2)–Se(3) 2.285(7), Se(3)–Se(4) 2.309(8), Se(5)–Se(6) 2.312(7), Se(6)–Se(7) 2.391(7), Se(7)–Se(8) 2.325(7).

Although structures and reactivities of mixed-metal chalcogenido clusters are of particular interest, syntheses of mixed-metal selenido or tellurido clusters are still poorly explored in contrast to those of the corresponding sulfur compounds which have progressed rapidly. Employment of polychalcogenido complexes as precursors for synthesizing such clusters is essentially unexplored except for the reactions of certain dichalcogenido complexes with other low valent metal species giving chalcogenido clusters through E–E bond scission (E = S, Se or Te).[11] Transformation of **2** into mixed-metal clusters was therefore attempted, which led to the finding that when **2** was allowed to react with 2 equiv. of $Pd(PPh_3)_4$ in THF at room temperature, two readily characterizable Ir–Pd–Se clusters, $(Cp^*Ir)_2\{Pd(PPh_3)\}_2(\mu_3\text{-}Se)_2(\mu_2\text{-}Se)$ **3** and $(Cp^*Ir)_2\{Pd(PPh_3)\}_3(\mu_3\text{-}Se)_3(\mu_3\text{-}Se_2)$ **4**, were obtained in 11 and 12% yields, respectively.‡¶ In contrast, analogous treatment of **2** with $Pt(PPh_3)_4$ did not afford any tractable products.

Cluster **3** (Fig. 2) has a tetrahedral Ir_2Pd_2 framework having two capping selenido ligands on the Ir_2Pd faces and one bridging selenido ligand on the Pd–Pd bond. Among the six edges of the Ir_2Pd_2 tetrahedron, only the Ir–Ir separation of 3.4733(5) Å corresponds to a non-bonding interaction. The Ir–Se and Pd–Se bond lengths for the face-bridged Se(1) and Se(2) atoms, which are in the range 2.445(1)–2.455(1) Å, are slightly longer than the Pd(1)–Se and Pd(2)–Se distances for the edge-bridged Se(3) centre at 2.389(1) and 2.373(1) Å, respectively, and are not exceptional. In the ^1H and $^{31}P\{^1H\}$ NMR spectra, the protons of the two Cp* groups and the two P atoms appear

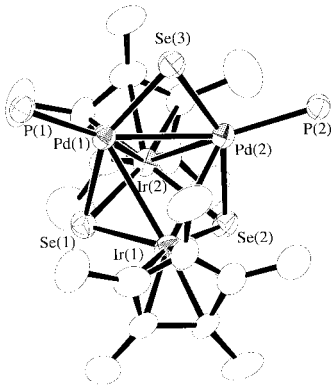

Fig. 2 Molecular structure of **3**. Hydrogen atoms are omitted for clarity. Selected interatomic distances (Å): Ir(1)–Pd(1) 2.9399(8), Ir(1)–Pd(2) 2.9530(8), Ir(2)–Pd(1) 2.9079(8), Ir(2)–Pd(2) 2.8584(8), Pd(1)–Pd(2) 2.773(1), Ir(1)–Ir(2) 3.4733(5).

as singlets, indicating a symmetrical structure with two mirror planes for **3** in solution.

Fig. 3 shows the structure of **4**,‡ whose core is composed of the $Ir_2Pd_2Se_3$ cluster framework of **3** as well as a triangular Pd(3)–Se(4)–Se(5) unit bound to it at the Pd(3) and Se(4) centres. The Se(4) atom is bound to Ir(2) and Pd(3) [2.472(1) and 2.526(1) Å], and weakly to Pd(2) [2.8510(9) Å], but not to Pd(1) [3.650(1) Å]. Owing to this unsymmetrical binding of the Se_2 ligand, no mirror plane exists for the cluster core and ^{1}H and ^{31}P NMR data are diagnostic of this structural feature. Metal–metal single-bonds are observed only for each of the three edges of the Ir(1)–Pd(1)–Pd(2) plane, although some bonding interaction may also be present between the Pd(1) and Pd(3) centres. Ignoring these metal–metal interactions, the geometries around Pd(1) and Pd(3) are distorted trigonal and square planar, respectively, while the Pd(2) atom has a trigonal pyramidal configuration with Se(4) at an apical position.

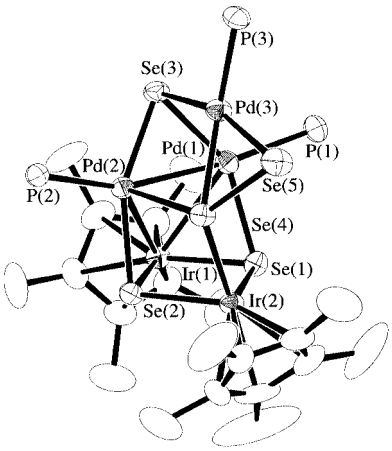

Fig. 3 Molecular structure of **4**. Hydrogen atoms are omitted for clarity. Selected interatomic distances (Å): Ir(1)–Pd(1) 2.8832(7), Ir(1)–Pd(2) 2.9175(8), Pd(1)–Pd(2) 2.7779(9), Ir(1)–Ir(2) 3.7640(4), Ir(2)–Pd(1) 3.9343(6), Ir(2)–Pd(2) 3.7644(7), Pd(1)–Pd(3) 3.079(9), Pd(2)–Pd(3) 3.2184(9).

In summary, a diiridium complex **2** containing two bridging Se_4 ligands has been prepared and characterized. A study on the reaction of **2** with $Pd(PPh_3)_4$ has verified that it serves as a versatile precursor for preparing mixed-metal Ir–Pd–Se clusters. It is of note that the sulfur analogue of **2**, $Cp^*Ir(\mu\text{-}S_4)_2IrCp^*$, did not give any characterizable products upon analogous treatment with $Pd(PPh_3)_4$. The reactivity of **2** towards other metal species as well as organic molecules is now under investigation.

Financial support by the Ministry of Education, Science, Sports, and Culture of Japan and The Iwatani Naoji Foundation's Research Grant (to Y. M.) is appreciated.

Notes and references

† Grey Se (1.74 g, 22.0 mmol) was suspended in THF (200 mL) and treated with 1.0 M $Li[BHEt_3]$ in THF (11 mL, 11 mmol) for 1 h at room temp. The resultant dark brown solution was warmed to 50 °C and **1** (1.99 g, 2.50 mmol) added. After stirring for 1 h at 50 °C, the mixture was dried *in vacuo* and the residue extracted with benzene. Addition of methanol to the concentrated extract afforded dark brown crystals of **2**·C_6H_6 (1.36 g, 40%). ^{1}H NMR ($CDCl_3$): δ 1.97, 1.71 (s, 15H, Cp*), 7.36 (s, 6H, C_6H_6). Anal. Calc. for $C_{26}H_{36}Se_8Ir_2$: C, 22.88; H, 2.66. Found: C, 22.71; H, 2.64%.

‡ *Crystal data*: **2**·C_7H_8 (obtained after recrystallization from toluene–MeOH): $C_{27}H_{38}Ir_2Se_8$, M = 1378.72, triclinic, space group $P\bar{1}$ (no. 2), a = 8.519(4), b = 14.081(3), c = 14.262(6) Å, α = 95.60(2), β = 94.51(5), γ = 91.88(3)°, U = 1695(1) Å^3, room temp., Z = 2, μ(Mo-Kα) = 164.64 cm^{-1}, R = 0.057 and R_w = 0.059 for 1658 reflections with $I > 3.00\sigma(I)$ and 178 variables.

3: $C_{56}H_{60}P_2Se_3Ir_2Pd_2$, M = 1629.16, monoclinic, space group $P2_1/c$ (no. 14), a = 18.844(4), b = 11.066(1), c = 26.778(2) Å, β = 104.843(8)°, U = 5409(1) Å^3, room temp., Z = 4, μ(Mo-Kα) = 76.87 cm^{-1}, R = 0.043 and R_w = 0.042 for 8181 reflections with $I > 3.00\sigma(I)$ and 587 variables.

4·C_6H_6: $C_{80}H_{81}P_3Se_5Ir_2Pd_3$, M = 2233.88, triclinic, space group $P\bar{1}$ (no. 2), a = 14.789(3), b = 16.151(3), c = 17.590(2) Å, α = 94.48(1), β = 99.85(1), γ = 108.86(1)°, U = 3877(1) Å^3, Z = 2, μ(Mo-Kα) = 65.63 cm^{-1}, R = 0.050 and R_w = 0.074 for 10195 reflections with $I > 3.00\sigma(I)$ and 587 variables. CCDC 182/1508. See http://www.rsc.org/suppdata/cc/a9/a909403b/ for crystallographic files in .cif format.

§ Reaction of **1** with Li_2S_4 gave fully characterizable $Cp^*Ir(\mu_2\text{-}S_4)_2IrCp^*$ in satisfactory yield, which will be reported in a subsequent paper.

¶ A THF solution (30 ml) of **2**·C_6H_6 (273 mg, 0.200 mmol) was treated with $Pd(PPh_3)_4$ (462 mg, 0.400 mmol) at room temperature for 1 day. The evaporated reaction mixture residue was extracted with benzene and subjected to column chromatography (Al_2O_3–benzene), affording first a dark brown band and then a green fraction. Recrystallization from benzene–hexane of the products from the latter and the former afforded green **3** (36 mg, 11% yield) and dark brown **4**·C_6H_6 (52 mg, 12% yield), respectively. **3**: ^{1}H NMR ($CDCl_3$): δ 1.38 (s, 30H, Cp*), 7.27–7.41 (m, 18H, Ph), 7.90–7.96 (m, 12H, Ph). $^{31}P\{^1H\}$ NMR ($CDCl_3$): δ 24.2 (s). Anal. Calc. for $C_{56}H_{60}P_2Se_3Ir_2Pd_2$: C, 41.29; H, 3.71. Found: C, 41.46; H, 3.74%.

4·C_6H_6: ^{1}H NMR ($CDCl_3$): δ 1.45 and 1.54 (s, 15H, Cp*), 6.87–7.16 (m, 27H, Ph), 7.63–7.68 (m, 18H, Ph), 7.36 (s, 6H, C_6H_6). $^{31}P\{^1H\}$ NMR ($CDCl_3$): δ 2.2 (dd, J 6 and 15 Hz, 1P), 10.0 (dd, J 15 and 179 Hz, 1P), 14.9 (dd, J 6 and 179 Hz, 1P). Anal. Calc. for $C_{80}H_{81}P_3Se_5Ir_2Pd_3$: C, 43.01; H, 3.65. Found: C, 42.93; H, 3.78%.

1 (*a*) M. Draganyac and T. B. Rauchfuss, *Angew. Chem., Int. Ed. Engl.*, 1985, **24**, 742; (*b*) J. W. Kolis, *Coord. Chem. Rev.*, 1990, **105**, 195.
2 M. Nishio, H. Matsuzaka, Y. Mizobe and M. Hidai, *Angew. Chem., Int. Ed. Engl.*, 1996, **35**, 872.
3 (*a*) L. C. Roof and J. W. Kolis, *Chem. Rev.*, 1993, **93**, 1037; (*b*) M. A. Ansari and J. A. Ibers, *Coord. Chem. Rev.*, 1990, **100**, 223; (*c*) M. G. Kanatzidis and S.-P. Huang, *Coord. Chem. Rev.*, 1994, **130**, 509.
4 See, for example: M. Hidai and Y. Mizobe, in *Transition Metal Sulfur Chemistry: Biological and Industrial Significance*, ed. E. I. Stiefel and K. Matsumoto, American Chemical Society, Washington, D.C., 1996, p. 310; M. Hidai, Y. Mizobe and H. Matsuzaka, *J. Organomet. Chem.*, 1994, **473**, 1; M. Hidai, S. Kuwata and Y. Mizobe, *Acc. Chem. Res.*, in press.
5 H. Matsuzaka, J.-P. Qü, T. Ogino, M. Nishio, Y. Nishibayashi, Y. Ishii, S. Uemura and M. Hidai, *J. Chem. Soc., Dalton Trans.*, 1996, 4307; H. Matsuzaka, T. Ogino, M. Nishio, M. Hidai, Y. Nishibayashi and S. Uemura, *J. Chem. Soc., Chem. Commun.*, 1994, 223.
6 M. Herberhold, G.-X. Jin and A. L. Rheingold, *Chem. Ber.*, 1991, **124**, 2245.
7 A. P. Ginsberg, W. E. Lindsell, C. R. Sprinkle, K. W. West and R. L. Cohen, *Inorg. Chem.*, 1983, **22**, 1781.
8 H. Brunner, N. Janiets, W. Meier, B. Nuber, J. Wachter and M. L. Ziegler, *Angew. Chem., Int. Ed. Engl.*, 1988, **27**, 708.
9 J. Chen and R. J. Angelici, *Inorg. Chim. Acta*, 1995, **235**, 61.
10 M. Herberhold, G.-X. Jin and W. Milius, *Chem. Ber.*, 1995, **128**, 557.
11 S. Kuwata, Y. Mizobe and M. Hidai, *J. Am. Chem. Soc.*, 1993, **115**, 8499; V. W. Day, D. A. Lesch and T. B. Rauchfuss, *J. Am. Chem. Soc.*, 1982, **104**, 1290; D. Seyferth, R. S. Henderson and M. K. Gallagher, *J. Organomet. Chem.*, 1980, **193**, 75.

Communication a909403b

ChemComm

Peptide-encapsulated CdS nanoclusters from a combinatorial ligand library†

Glen Spreitzer, Jacqueline M. Whitling, Jeffry D. Madura and David W. Wright*

Department of Chemistry and Biochemistry, Duquesne University, Pittsburgh, PA 15282-1530, USA. E-mail: wrightd@duq.edu

Received (in Bloomington, IN, USA) 9th September 1999, Accepted 23rd December 1999

A spatially addressable combinatorial library of peptides, based on cysteine containing phytochelatins, has been shown to stabilize a variety of discrete CdS nanoclusters ranging in size from 19 to 26 Å in diameter.

Quantum confined structures have elicited a great deal of recent interest.[1] An important class of these compounds is the II–VI semiconductor nanoclusters exemplified by CdS. Although there are a variety of excellent techniques for the synthesis of these clusters, the use of thiolate ligands to cap the growing CdS cluster *in situ* yields nanoclusters more resistant to aggregation and more readily processable.[1e] Interestingly, a variety of yeast, plants and bacteria use a class of cysteine containing peptides known as phytochelatins to trap nearly monodisperse CdS nanoclusters, thereby efficiently sequestering a large number of cadmium ions per peptide.[2] The sequence of the phytochelatins is generally $(\gamma\text{-GluCys})_n\text{Gly}$, where *n* is the number of dipeptide repeats.[3] Comparisons between the $(\gamma\text{-GluCys})_2\text{Gly}$ peptide and the more common α-peptide linkage show that $(\alpha\text{-GluCys})_2\text{Gly}$ stabilizes smaller nanoclusters with higher band gap transitions than those with γ-linkages.[4] To investigate the influence of thiolate separation in multidentate capping peptides on the stabilization of various populations of CdS nanoclusters, a spatially addressable combinatorial library in which the spacer amino acids have been systematically varied for the n_3 phytochelatin, X-Cys-Y-Cys-Z-Cys-Gly, has been synthesized. We report, herein, the analysis of those peptides that lie along the library's diagonal in which X, Y, and Z are equivalent amino acids.

Based on the n_3 phytochelatin sequence X-Cys-Y-Cys-Z-Cys-Gly, the cysteine residues are kept constant, while the spacer residues are varied over all combinations of the spacer amino acids, resulting in an initial library of 125 peptide ligands. The five selected spacer residues include α-Glu, γ-Glu, γ-aminobutyric acid (GABA), SerGly and ε-aminohexanoic acid (ε-Ahx). The spacer residues include natural and non-natural amino acids having between 3 to 7 atoms in the backbone and spanning an idealized extended C_α–C_α distance between the cysteines ranging from 3.75 Å to 8.7 Å, respectively.[5] Additionally, the spacer residues provide a wide range of hydrophilicity. The library was synthesized using Chiron Technologies PepSets system.[6] Peptide synthesis yielded approximately 1 mmol of each target ligand. Control peptides were greater than 97% pure by HPLC and mass spectrometry (see Electronic Supplementary Information).

The peptides were reacted anaerobically with Cd^{2+} and S^{2-} in aqueous Tris buffer (100 mM, pH 8.6) in a 1.25 : 1 : 1 ratio, respectively, for 4 h.‡ Since all of the ligands in the library are likely to stabilize CdS cluster formation, it is important that multiple screens be applied to the reaction mixtures in order to develop meaningful selection criteria for a specific nanocluster characteristic. The resulting reaction mixtures were subjected to an array of screens to assess size, monodispersity, photooptical properties, photocatalytic potential and stability. The selected screens encompass many of the most commonly cited critical parameters for this class of compounds.[1] It should be emphasized that the employed screens are designed to maximize the information about any given peptide–cluster aggregation reaction, not to definitively characterize the reaction product. The results from the analysis of the library's diagonal are given in Table 1.

Table 1 Results of combinatorial library screens

Peptide[a]	$\lambda_{abs,\ max/nm}$	R_{est}[d]/Å	$\lambda_{em,\ max/nm}$	MV^{2+} assay	PNP oxidation
ECG[b]	365	13.02	548	+	+
ECECECG	306	10.43	400	+	—
eCeCeCG	320	10.97	408	+	—
gGCgCgCG	308	10.51	419	+	—
SGCSGCSGCG	302	10.29	422	+	—
hChChCG[c]	284	9.65	423	+	—
	318	10.89	426		

[a] e, γ-Glu; E, α-Glu; g, GABA; h, ε-Ahx; S, Ser; G, Gly. [b] These results are consistent with those reported in refs. 2, 7 and 8. [c] After 24 h reaction time λ_{max} was 338 nm. R_{est} was 11.7 Å. All other reactions were unchanged after 24 h. [d] Ref 11.

The UV-visible absorption spectra of the resulting nanoclusters are shown in Fig. 1. The results indicate that each of the examined peptides is capable of stabilizing discrete populations of nanoclusters. The observed λ_{max} for the absorption spectra of the encapsulated $(\alpha\text{-GluCys})_3\text{Gly/CdS}$ (**1**) and $(\gamma\text{-GluCys})_3\text{Gly/CdS}$ (**2**) clusters at 306 and 320 nm, respectively, correspond well with previous reports for the *in vitro* synthesis of CdS nanoclusters using these peptides obtained from solid-phase peptide synthesis techniques or isolated from biological sources.[3] The absorption spectra for $(\text{GABACys})_3\text{Gly/CdS}$ (**3**) and $(\text{SerGlyCys})_3\text{Gly/CdS}$ (**4**) reveal similar distributions of clusters with λ_{max} near 313 nm. The absorption spectrum of the CdS clusters encapsulated by $(\varepsilon\text{-AhxCys})_3\text{Gly}$ (**5**) show two distinct populations of clusters centered with λ_{max} of 284 and 318 nm. Examination of **5** after 24 h shows a marked decrease in the cluster populations with λ_{max} centered near 282 and a new major population with λ_{max} centered at 338 nm. These results suggest that the cluster populations observed for the capping ligand $(\varepsilon\text{-AhxCys})_3\text{Gly}$ at 4 h represent intermediate metastable clusters which over time aggregate into the final cluster.

The photophysical properties of synthetic semiconductor nanoclusters are dictated by surface-mediated phenomena.[1a,b] Ultraviolet irradiation of the individual reaction mixtures at the respective absorption maxima resulted in luminescence in the visible spectral region with emission maxima ranging from 410 to 460 nm (Electronic Supplementary Information). The fluorescence behavior of clusters **1** and **2** is in good agreement with previously reported values.[3] Anaerobic excitation of all of the peptide encapsulated CdS nanoclusters in the presence of methyl viologen resulted in the reduction of the dye as monitored by characteristic absorbances near 380 and 600 nm. A significant back-reaction attributable to reoxidation of the dye by trapped holes (h+) on the particle's surface was also observed (Electronic Supplementary Information). In contrast to reports of glutathione (γ-GluCysGly) stabilized CdS nano-

† Electronic supplementary information (ESI): Schematic representation of the spatially addressable combinatorial library, HPLC, mass and fluorescence spectra, MV^{2+} assay, chromatograms, M_w calibration curve, model of CdS–peptide cluster. See http://www.rsc.org/suppdata/cc/a9/a907178d/

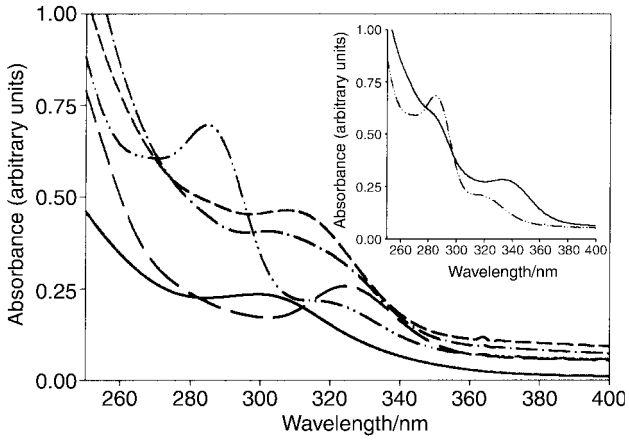

Fig. 1 UV-vis absorption spectra of the peptide–CdS cluster reaction after 4 hours. ——— **1**, — — — **2**, –·–· **3**, – – – – **4**, –···– **5**. Insert shows –···– **5** after 4 hours and ——— **5** after 24 hours.

clusters,[7,8] none of the examined nanoclusters were competent photocatalysts for the oxidative degradation of *p*-nitrophenol (PNP).

Each reaction mixture was examined for dispersity by size exclusion chromatography (Electronic Supplementary Information).[9] Chromatographic analysis of **1** and **2** revealed one major nanocluster containing fraction each, with an absorption maxima and full width at half maximum (FWHM) of the absorption peak essentially unchanged from that of the reaction mixture. Chromatograms of **3** and **4** had one major nanocluster fraction each, with a significant red shift in both the absorption maxima by 4 and 13 nm, respectively, and a 10–17% change in the absorption peak's FWHM. The resulting red shift is indicative of the separation of some fraction of smaller CdS clusters. The chromatogram of **5** resolved two major nanocluster fractions, the first containing only clusters with λ_{max} of 284 nm, while the second peak was a mixture of clusters with λ_{max} at 284 and 318 nm. The ratio of the two cluster populations is significantly altered from the crude reaction mixture demonstrating that two clusters are in fact being resolved. The chromatographic analysis clearly reveals that increasing the degree of rotational freedom within the spacer residue of the trapping ligand decreases the monodispersity of the resulting nanoclusters at the arbitrarily fixed end-point of the assay.

To verify the size of the resulting peptide-encapsulated CdS nanoclusters, a simplified compositional model of **1** and **2** was constructed using the methods of Dameron and Dance.[10] The model for the CdS core assumes an approximately equidimensional fragment of the cubic (sphalerite) lattice.§ The sizes of the CdS cores were estimated from the UV-vis spectra using Brus' effective mass model.[11] With a limiting cluster size, the number of peptides coating the particle was extrapolated from an analysis of S atom coordination. Based upon these models, the combined molecular weight of the peptide coat and CdS core was determined to be approximately 28 000 Da for nanoclusters **1** and **2**. The observed molecular weights from size-exclusion chromatographic analysis for **1** (30 137 + 5% Da) and **2** (28 438 + 5% Da) are in excellent agreement with this simplified compositional model. Similar modeling of clusters **3**–**5** is currently underway.

Through the use of a spatially addressable combinatorial library of peptide ligands inspired by the known phytochelatin sequence, peptide-coated CdS quantum-confined clusters have been synthesized. Analysis of the library's diagonal shows that the cluster size increases with the number of spacer bonds between the cysteine residues from 19.2 Å diameter for the peptide chelate $(\alpha\text{-GluCys})_3$Gly to 23.4 Å diameter for $(\varepsilon\text{-AhxCys})_3$Gly, resulting in a series of robust, photo-reductive clusters. The mechanism of size stabilizing selectivity is probably mediated by those peptides and/or peptide–$(Cd^{2+})_n$ complexes that trap growing nanoclusters when the surface of the aggregate presents sites which match the conformational spacing of the peptide or peptide complex. Such a mechanism, analogous to those proposed for the *in vivo* response of CdS sequestering organisms,[2] has important ramifications in the ability to control aggregation. From the perspective of the trapping moiety, it predicts that those peptides with greater degrees of rotational freedom in the peptide backbone may trap a variety of intermediate cluster sizes that are metastable due to steric crowding of the surface peptide coat and non-optimal surface coordination. From the perspective of the growing cluster, a trapping mechanism leads to stabilization of intermediate clusters with coordinatively unsaturated Cd^{2+} or S^{2-} ions that are shielded by the packing of the surface peptide coat. Such intermediate clusters eventually aggregate to more optimal sizes and surface coordination. This trapping termination of the growing aggregate is consistent with the intermediate clusters observed in the formation of **5**, as well as the increase in dispersity for those clusters encapsulated by peptides with greater degrees of rotational freedom. The complete analysis of the entire library is expected to produce important conceptual information about chelate features and lattice matching critical for the stabilization of CdS nanoclusters of specific size.

Notes and references

‡ The peptide (1 mmol) was disolved in 100 μL DMSO + 900 μL 0.1% TFA solution. In a 4 mL septum sealed vial, 250 μL peptide (1 mM) solution, 100 μL $CdCl_2$ (2 mM, 0.01 M HCl) solution and 1550 μL Tris (0.1 M, pH 8.5) were combined. With stirring, 100 μL aqueous Na_2S solution (2 mM) was added dropwise to the reaction mixture. After 4 h, the reaction solution was filtered through a 0.2 μm PVDF syringe filter for analysis.

§ The CdS lattice was constructed using the crystal builder feature of MOE (Chemical Computing Group, Inc., http://www.chemcomp.com). The lattice parameters used were space group $F\bar{4}3m$ with $a = b = c = 5.832$ Å and $\alpha = \beta = \gamma = 90°$. The unique Cd position was (0,0,0) and the unique S position was (0.25, 0.25, 0.25). The sphere was cut from a $6 \times 6 \times 6$ supercell using the proximity feature of MOE.

1 (*a*) M. Gratzel, *Acc. Chem. Res.*, 1981, **14**, 376; (*b*) H. Weller, *Angew. Chem., Int. Ed. Engl,*, 1993, **32**, 41; (*c*) G. Stucky and J. MacDougall, *Science*, 1990, **247**, 664; (*d*) C. B. Murray, D. J. Norris and M. G. Bawendi, *J. Am. Chem. Soc.*, 1993, **115**, 8706; (*e*) C. J. Murphy, *J. Cluster Sci.*, 1996, **7**, 341.

2 (*a*) R. N. Reese and D. R. Winge, *J. Biol. Chem.*, 1988, **263**, 12 832; (*b*) R. N. Reese, C. A. White and D. R. Winge, *Plant Physiol.*, 1992, **98**, 225; (*c*) C. T. Dameron, B. R. Smith and D. R. Winge, *J. Biol. Chem.*, 1989, **264**, 17 355; (*d*) C. T. Dameron and D. R. Winge, *Inorg. Chem.*, 1990, **29**, 1343; (*e*) D. R. Winge, C. T. Cameron and R. K. Mehra, in *Metallothioneins: Synthesis, Structure, and Properties of Metallothioneins, Phytochelatins, and Metal Complexes*, ed. M. J. Stilman, C. F. Shaw and K. T. Suzuki, VCH, New York, 1992, p. 257.

3 (*a*) E. Grill, E.-L. Winnacker and M. H. Zenk, *Science*, 1985, **230**, 674; (*b*) W. E. Rauser, *Annu. Rev. Biochem.*, 1990, **59**, 61. The number of dipeptide (γ-GluCys) repeats in phytochelatins typically ranges from 2 to 13. The number of dipeptide repeats commonly observed in the capping of CdS nanoclusters is 2 to 4.

4 (*a*) C. T. Dameron and D. R. Winge, *Trends Biotechnol.*, 1990, **8**, 3; (*b*) W. Bae and R. K. Mehra, *J. Inorg. Biochem.*, 1997, 201.

5 The C_α–C_α distance is based on an extended conformation.

6 The Chiron Mimetope and PepSets technology (Chiron Technologies, San Diego, CA) has recently been reviewed by M. C. Pirrung, *Chem. Rev.*, 1997, **9**, 473.

7 L. Nguyen, R. Kho, W. Bae and R. K. Mehra, *Chemosphere*, 1999, **38**, 155.

8 W. Bae and R. K. Mehra, *J. Inorg. Biochem.*, 1998, **69**, 33.

9 (*a*) C. H. Fisher, H. Weller, L. Katsikas and A. Henglein, *Langmuir*, 1989, **5**, 429; (*b*) H. Determann, *Gelchromatographie*, Springer, Berlin, 1967, p. 115.

10 C. T. Dameron and I. G. Dance, in *Biomimetic Materials Chemistry*, ed. S. Mann, VCH, New York, 1996, p. 69.

11 (*a*) L. E. Brus, *J. Chem. Phys.*, 1983, **79**, 5566; (*b*) L. E. Brus, *J. Chem. Phys.*, 1984, **80**, 4403; (*c*) R. Rossetti, J. L. Ellison, J. M. Gibson and L. E. Brus, *J. Chem. Phys.*, 1984, **80**, 4464.

Communication a907178d

New and efficient routes to $CpRe(CO)_3$ substituted steroids

Franck Le Bideau,[a] El Bachir Kaloum,[a] Pierre Haquette,[a] Ulrich Kernbach,[a] Jérôme Marrot,[b] Elie Stephan,[a] Siden Top,[a] Anne Vessières[a] and Gérard Jaouen*[a]

[a] *Ecole Nationale Supérieure de Chimie de Paris, 11 rue Pierre et Marie Curie, 75231 Paris Cedex 05, France. E-mail: jaouen@ext.jussieu.fr*

[b] *Université de Versailles Saint-Quentin-en-Yvelines, IREM, bâtiment Lavoisier, 45 av des Etats-Unis, 78035 Versailles Cedex, France*

Received (in Basel, Switzerland) 21st October 1999, Accepted 2nd January 2000

Two new methods for the formation of $CpRe(CO)_3$ substituted steroids are presented; both imply a one-pot procedure involving a transmetallation process.

The emergence of bioorganometallic chemistry[1] has benefited from the enormous amount of synthetic work that has been done to prepare all kinds of organometallic compounds over the last half-century. However, access to compounds for use in bioorganometallic chemistry is not always achieved merely by adopting synthetic methods used in classical organometallic chemistry. This is particulary true in the challenging area of low valent organometallic radiopharmaceuticals of ^{186}Re, ^{188}Re and ^{99m}Tc[2] which requires the devising of new reactions in order to introduce the radioactive element onto the bioligand in the last step of the process. The fixation of a small, compact, robust and non polar substituted cyclopentadienyltricarbonylrhenium unit [$CpRe(CO)_3$] appears to be a strategic objective with this respect. In this field, we previously reported the synthesis of a large number of substituted steroids. Among them, a non-radioactive $CpRe(CO)_3$ oestradiol derivative has been shown to have an excellent binding affinity for the oestrogen receptor (ER) when fixed at the 17α position.[3] We present here another route to attach this organometallic unit based on the introduction of fulvenes in other selected positions of steroids, which allows the introduction of the $CpRe(CO)_3$ fragment in the last step of the synthesis.

Fulvenes are easier to characterize and synthesize than the corresponding cyclopentadienes, which are often not stable and exist as mixtures of isomers.[4] As a source of rhenium we chose bromorhenium pentacarbonyl [$BrRe(CO)_5$] which can be used in a transmetallation process leading to substituted $CpRe(CO)_3$. Furthermore, we recently reported[5] a mild one pot access to this reagent starting from ammonium perrhenate, a Re^{VII} precursor which is easily accessible in radioactive forms.[6,7]

In a preliminary study, we began with cholest-4-en-3-one **1**. This compound was first submitted to the conditions reported by Little and Stone[8] for other substrates, to afford the corresponding fulvene **2** in less than 30% yield (Scheme 1). These results were attributed to the poor solubility of starting materials in MeOH. A thorough screening of solvents showed that the use of CH_2Cl_2 as cosolvent (MeOH–CH_2Cl_2 = 1:1) greatly enhanced yield (up to 70%) for the formation of **2**.

According to path (*a*) fulvene **2** was treated with MeLi in toluene at −78 °C and warmed to room temperature for 3 h. The resulting intermediate **3** was then submitted to transmetallation conditions[9]—$BrRe(CO)_5$ was added and the reaction mixture was heated to reflux for 15 h. Under these conditions, two diastereomers **5α/β** were produced in a 2:1 ratio in 39% yield which are distinguished by their relative configuration at the newly formed stereogenic center (steroid carbon center C-3). The major product was crystallized from CH_2Cl_2–hexane. An X-ray structural analysis shows that the newly introduced methyl substituent is attached to the α face of the steroid framework (Fig. 1).†

According to path (b), the fulvene **2**, KH and $BrRe(CO)_5$ were heated (110 °C) in a mixture of THF and toluene for only 1.6 h to give, after flash chromatography, the substituted $CpRe(CO)_3$ **6** in 67% yield.‡ No products resulting from the

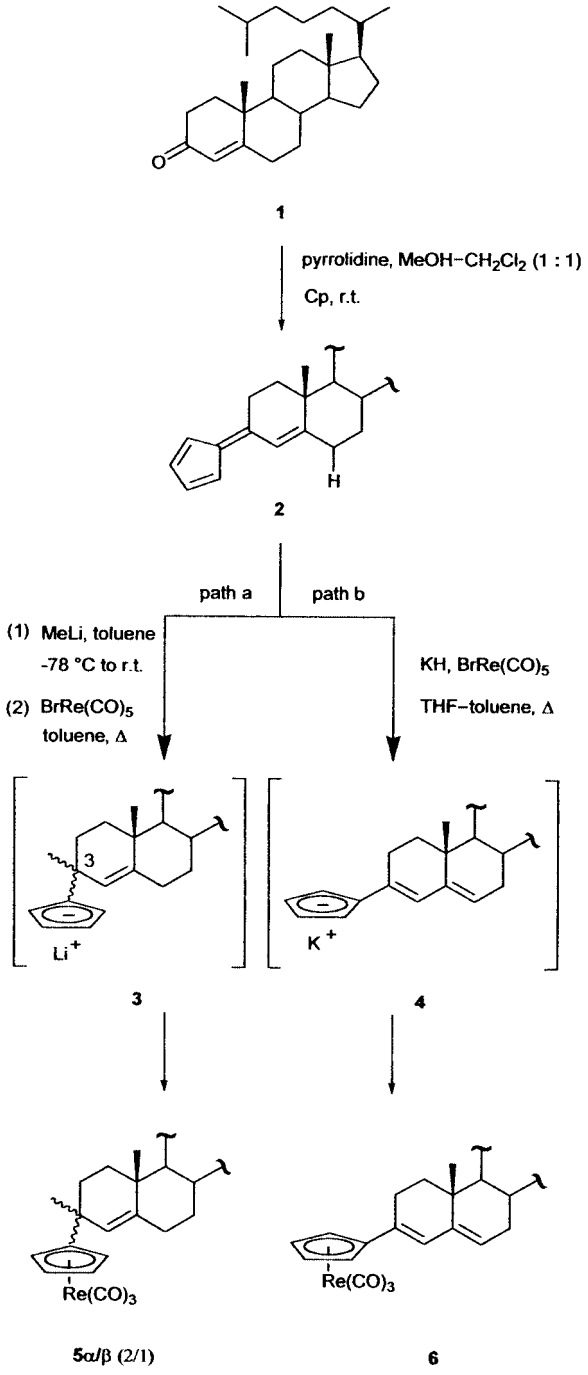

Scheme 1

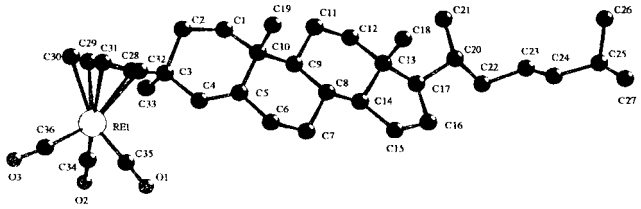

Fig. 1 X-Ray structure of **5α**.

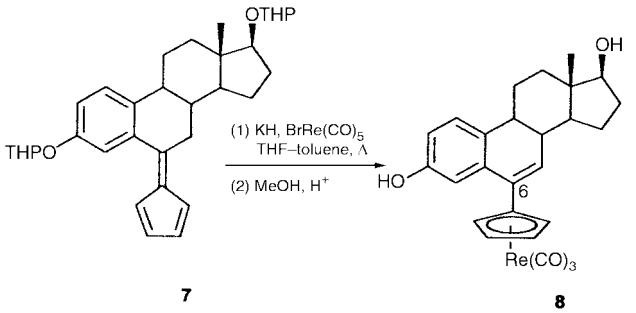

7 **8**

Scheme 2

deprotonation of the C-2 position were isolated using these conditions. In both cases, longer reaction times did not improve the yield, probably because of the degradation of the starting materials.

This second strategy was applied to the synthesis of an oestradiol derivative (Scheme 2). Thus, the fulvene **7**, obtained from the corresponding 6-oxoestradiol,[10] was submitted to the conditions of path (b). An acidic work up (MeOH, cat. TsOH) gives access to **8,** the first oestradiol derivative bearing an organometallic unit at the C-6 position. The relative binding affinity (RBA) of this complex for the ER was measured on lamb uterine cytosol according to a previously reported procedure.[11] Compound **8** is still recognized by the ER even if the RBA value is low (0.5%). This result confirms that a bulky substitution at C-6 induces a dramatic decrease in the affinity of the modified hormone for the ER.[12–14]

In conclusion, the results presented illustrate a new route to $CpRe(CO)_3$ substituted steroids. They show that (i) the introduction of the metal carbonyl unit on a steroid in the last step of the synthesis is possible [for this purpose, fulvenes are more interesting than the corresponding cyclopentadienes because of the great number of products accessible according to the conditions (basic versus nucleophilic) used] and (ii) $BrRe(CO)_5$ is a suitable precursor for the elaboration of $CpRe(CO)_3$ units in organic solvents.[15] We thus hope that this new strategy will greatly enhance progress in the area of organometallic radiopharmaceuticals.

F. L. B. thanks the Société de Secours des Amis des Sciences' for his fellowship

Notes and references

† *Crystal data* for **5α**: $C_{36}H_{51}O_3Re$, M = 717.97, monoclinic, a = 14.992, b = 7.18410(10), c = 15.4819(2) Å, U = 1665.98(3) Å^3, T = 296 K, space group $P2_1$, Z = 2, μ = 3.679 mm^{-1}, 11750 reflections measured, 8046 unique (R_{int} = 0.0457) which were used in all calculations. The final $wR(F^2)$ was 0.003 (all data). The molecular structure shows clearly that the organorhenium moiety is on the β face of the hormone. CCDC 182/1516. See http://www.rsc.org/suppdata/cc/a9/a908481i/ for crystallographic data in .cif format.

‡ *Procedure for the preparation* of **6**: The reaction was carried out in a flame-dried flask, under argon. Fulvene **2** (0.108 g, 0.25 mmol), KH (0.012 g, 0.3 mmol) washed twice with pentane and $BrRe(CO)_5$ (0.122 g, 0.3 mmol) in THF–toluene (2 ml/2 ml) were heated at reflux for 1.6 h. The reaction mixture was cooled to room temperature and diluted in CH_2Cl_2 (20 ml). The organic layer was washed with brine (2 × 20 ml), dried ($MgSO_4$), filtered and concentrated. Purification by flash chromatography (CH_2Cl_2–pentane = 95:5) afforded **6** (0.118 g, 67%) as a white solid. *Selected data* for **6**: δ_H (200 MHz, $CDCl_3$) 6.26 (1H, sl), 5.6–5.5 (3H, m), 5.2–5.3 (2H, m), 2.4–0.9 (29H, m), 0.95 (3H, s), 0.91 (3H, s), 0.87 (3H, s), 0.73 (3H, s); δ_C (50 MHz, $CDCl_3$) 194.4, 141.1, 126.7, 126.6, 124.8, 110.7, 84.4, 83.2, 79.8, 79.4, 56.8, 56.1, 48.1, 42.4, 39.7, 39.5, 36.2, 35.8, 34.9, 33.4, 32.0, 31.7, 28.2, 28.0, 24.6, 24.1, 23.8, 22.8, 22.5, 21.0, 19.0, 18.7, 12.0; ν_{max}(KBr)/cm^{-1} 2950–2850, 2020, 1900, 1466, 822; *m*/*z* 702, 614, 441 (Calc. for $C_{35}H_{47}O_3Re$: C, 59.89; H, 6.75. Found: C, 59.76; H, 6.89%).

1 G. Jaouen, A. Vessières and I. S. Butler, *Acc. Chem. Res.*, 1993, **26**, 361.
2 J. R. Dilworth and S. J. Parrott, *Chem. Soc. Rev.*, 1998, **27**, 43.
3 S. Top, H. El Hafa, A. Vessières, J. Quivy, J. Vaissermann, D. W. Hughes, M. J. McGlinchey, J.-P. Mornon, E. Thoreau and G. Jaouen, *J. Am. Chem. Soc.*, 1995, **117**, 8372. Katzenellenbogen *et al*. recently shifted from their N and S coordinated oxorhenium chelate complexes (R. K. Hom and J. A. Katzenellenbogen, *Nucl. Med. Biol.*, 1997, **24**, 485) to $CpRe(CO)_3$ substituted steroids (F. Minutolo and J. A. Katzenellenbogen, *J. Am. Chem. Soc.*, 1998, **120**, 13 264).
4 N. Neuenschwander, in *The Chemistry of Doubled-Bonded Functional Groups*, ed. S. Patai, Wiley, 1989, p. 1131.
5 S. Top, P. Morel, M. Pankowski and G. Jaouen, *J. Chem. Soc., Dalton Trans.*, 1996, 3611.
6 F. F. Knapp, A. L. Beets, S. Guhlke, P. O. Zamora, H. Bender, H. Palmedo and H.-J. Biersack, *Anticancer Res.*, 1997, **17**, 1783
7 P. P. Venkatesan, S. Shortkroff, M. R. Zalutsky and C. B. Sledge, *Nucl. Med. Biol.*, 1990, **17**, 357.
8 K. J. Stone and R. D. Little, *J. Org. Chem.*, 1984, **49**, 1849.
9 P. A. Deck, W. F. Jackson and F. R. Fronczek, *Organometallics*, 1996, **15**, 5287.
10 R. Tedesco, R. Fiaschi and E. Napolitano, *Synthesis*, 1995, 1493.
11 A. Vessières, S. Top, A. A. Ismail, I. S. Butler, M. Louer and G. Jaouen, *Biochemistry*, 1988, **27**, 6659.
12 E. R. Clark, A. M. E. Omar and G. Prestwich, *J. Med. Chem.*, 1977, **20**, 1096.
13 S. Top, A. Vessières, J.-P. Abjean and G. Jaouen, *J. Chem. Soc., Chem. Commun.*, 1984, 428.
14 G. Eisenbrand, J. Fischer, K. Mühlbauer, G. Schied, J. Schreiber, W. Tang and O. Zelezny, *Arch. Pharm.*, 1989, **322**, 863.
15 Alberto *et al*. recently reported the synthesis of a promising organometallic aqua ion $[^{99}Tc(OH_2)_3(CO)_3]^+$ and its ^{188}Re homologue. These species are very good precursors for potential radiopharmaceuticals in water as exemplified by the formation of $[Tc(PADA)(CO)_3]$; R. Alberto, R. Schibli, A. Egli and A. P. Schubiger, *J. Am. Chem. Soc.*, 1998, **120** , 7987.

Communication a908481i

Synthesis, characterization and application of a novel polymer solid photosensitizer

Masahiro Suzuki,[a] Yuko Ohta,[a] Hidetoshi Nagae,[a] Takashi Ichinohe,[a] Mutsumi Kimura,[a] Kenji Hanabusa,[a] Hirofusa Shirai*[a] and Dieter Wöhrle[b]

[a] *Department of Functional Polymer Science, Faculty of Textile Science and Technology, Shinshu University, Ueda, Nagano 386-8567, Japan. E-mail: smasa@giptc.shinshu-u.ac.jp*

[b] *Universität Bremen, Institut für Organische und Makromolekulare Chemie, Fachbereich 2, NW II, PO Box 330 440, Bremen 28334, Germany*

Received (in Cambridge, UK) 29th November 1999, Accepted 4th January 2000

A new water-insoluble polymer solid photosensitizer, prepared from an aluminium(III) tetracaboxyphthalocyanine and poly(styrene-*co*-chloromethylstyrene), has a photosensitizing ability for the photo-oxidation of phenol with singlet oxygen.

The photo-oxidation reactions of sulfides,[1,2] thiols,[3,4] phenols[5–7] and other organic compounds[8–11] have been reported using various low molecular weight photosensitizers such as Rose Bengal, Methylene Blue, porphyrins and phthalocyanines. Although these photosensitizers show high reaction activity, they are difficult to remove from the reaction cell because they are homogeneous. The use of polymer solid photosensitizers is expected to overcome this problem. Compared with low molecular weight photosensitizers, however, there are few reports on the application of polymer solid photosensitizers to photo-oxidation reactions.[12–14] Here, we describe the synthesis and characterization of a new water-insoluble polymer solid photosensitizer prepared from an aluminium(III) tetracaboxyphthalocyanine and poly[(styrene)-*co*-(4-chloromethylstyrene)] (polymer-AlPTC). Furthermore, the photo-oxidation of phenol is investigated in aqueous solution.

The poly[(styrene)-*co*-(4-chloromethylstyrene)] (St-*co*-CMSt) was prepared by free-radical copolymerization of styrene and 4-chloromethylstyrene with benzoyl peroxide as initiator in bulk. The degree of copolymerization was styrene:chloromethylstyrene = 0.8:0.2 (molar percentage), determined by elemental analysis and ^{1}H NMR. Gel permeation chromatography (GPC) measurements using polystyrene standards showed an average molecular weight of 8.0×10^4. The preparation of polymer-AlPTC was carried out as follows. St-*co*-CMSt (2.0 g) and aluminium(III) tetracarboxyphthalocyanine[3] (0.05 g) were heated at 90 °C for 24 h under a nitrogen atmosphere in a mixture of freshly distilled DMSO (20 ml) and acetone (10 ml). An excess of pyridine (20 ml) was added, and the heating was continued for 24 h. After the unreacted pyridine and acetone were completely removed by evaporation, the solution was slowly poured onto vigorous stirring Et_2O. The light green precipitate was filtered, washed with Et_2O, and then dried *in vacuo* for 12 h. The pure polymer-AlTPC, which is identified by elemental analysis, FTIR, and absorption spectrum measurements,[15] is shown below.

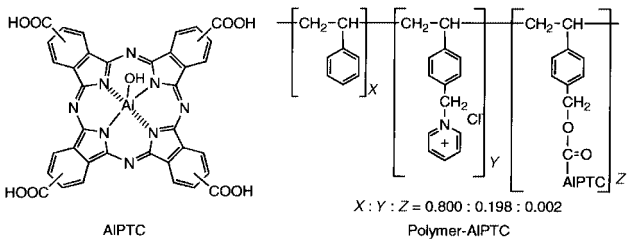

The absorption spectrum of the polymer-AlPTC in DMF showed an absorption maximum at 688 nm with a molecular absorption coefficient of *ca.* 40 000 in the visible region, which almost corresponded with that of AlPTC.[3] Although the copolymer of styrene and pyridiniomethylstyrene, corresponding to the parent copolymer of the polymer-AlPTC, is water-soluble, the polymer-AlPTC is water-insoluble. This is because the polymer-AlPTC has a structure which is partially bridged by AlPTC.

The photo-oxidation experiments were performed at 25 °C in an oxygen-saturated aqueous solution of pH 7, adjusted using a KH_2PO_4/Na_2HPO_4 buffer. A sample tube containing 2.0×10^{-6} mol dm^{-3} AlPTC or 0.84 mg polymer-AlPTC film (the same molarity as AlPTC) and 2.0×10^{-4} mol dm^{-3} phenol in aqueous solution (3 ml) was bubbled with oxygen for 10 min, and the capped sample solution was irradiated with a 300 W slide projector equipped with a UV cut-off filter ($\lambda > 440$ nm). The reaction was monitored by UV–VIS absorption spectrum measurements and also followed by GC and FTIR analyses.

Upon visible light irradiation of an oxygen-saturated aqueous solution of phenol and polymer photosensitizer, a new absorption band around 248 nm, characteristic for 1,4-benzoquinone (BQ),[14] increased. Fig. 1 shows the absorption spectral change in the heterogeneous reaction solution upon visible light irradiation at pH 7, and the initial formation rates of 1,4-benzoquinone are summarized in Table 1 In the presence of NaN_3 as

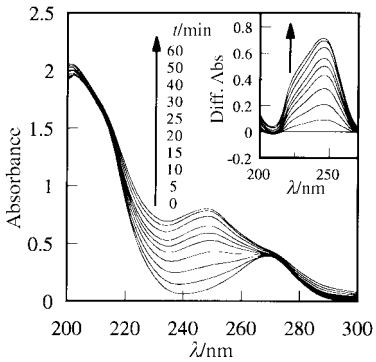

Fig. 1 Absorption spectral changes in an aqueous solution of polymer-AlPTC and phenol at pH 7 upon visible light irradiation. Inset: differential absorption spectral changes.

Table 1 Initial formation rates at pH 7 for polymer-AlPTC and AlPTC systems

	Initial rate[a]/mol dm^{-3} min^{-1}	[BQ][b]/mol dm^{-3}
Polymer-AlPTC[c]	1.05×10^{-6}	3.39×10^{-5}
NaN_3[cd]	1.71×10^{-9}	2.03×10^{-7}
Under Ar	—	—
AlPTC	—	—

[a] Experimental errors are within ±5%. [b] After irradiation for 120 min. [c] In oxygen-saturated aqueous solution. [d] $[NaN_3] = 2.0 \times 10^{-4}$ mol dm^{-3}.

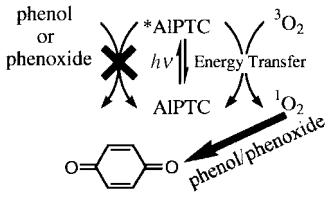

Scheme 1

a singlet oxygen quencher, the reaction rate and the amount of BQ formed are very small, and BQ does not form under Ar. Moreover, the absorption spectral change was not observed in the dark. These facts indicate that the present reaction is induced by excitation of the sensitizer itself and is the oxidation of phenol with singlet oxygen generated as shown in Scheme 1. Surprisingly, the photo-oxidation reaction using AlPTC photosensitizer, corresponding to the low molecular weight model complex, did not occur in a homogeneous aqueous solution at pH 7.[16] The polymer-AlPTC has hydrophobic segments (styrene residues) and positively charged segments (pyridinium residues) in the polymer backbone. These residues would concentrate phenol and/or phenoxide anion through hydrophobic and electrostatic attraction. Furthermore, the polymer-AlPTC can be readily separated by filtration from the reaction solution.

This work was supported by a Grant-in-Aid for COE Research (10CE2003) by the Ministry of Education, Science, Sports and Culture of Japan.

Notes and references

1 W. Spiller, D. Wöhrle, G. Schulz-Ekloff and J. Stark, *J. Photochem. Photobiol.*, 1996, **95**, 161.
2 D. Wöhrle, W. Spiller, G. Schneider, G. Schulz-Ekloff and J. Stark, *J. Inf. Rec. Mater.*, 1994, **21**, 1.
3 G. Schneider, D. Wöhrle, W. Spiller, J. Stark and G. Schulz-Ekloff, *Photochem. Photobiol.*, 1994, **60**, 333.
4 D. Wöhrle, G. Schneider, J. Stark and G. Schulz-Ekloff, *J. Mol. Catal.*, 1992, **75**, L39.
5 H. E. Gsponer, C. M. Previtali and N. A. Garcia, *Toxicol. Environ. Chem.*, 1987, **16**, 23.
6 M. C. Palumbo and N. A. Garcia, *Toxicol. Environ. Chem.*, 1988, **17**, 103.
7 R. Gerdes, D. Wöhrle, W. Spiller, G. Schneider, G. Schnurpfeil and G. Schulz-Ekloff, *J. Photochem. Photobiol. A: Chem.*, 1997, **111**, 65.
8 R. C. Straight and J. D. Spikes, in *Singlet Oxygen, Vol. IV*, ed. A. A. Frimer, CRC Press, Boca Raton, 1985, p. 91.
9 J.-L. Ravanat, M. Berger, F. Benard, R. Langlois, R. Ouellet, J. E. van Lier and J. Cadet, *Photochem. Photobiol.*, 1992, **55**, 809.
10 X.-F. Zhang and H.-J. Xu, *J. Photochem. Photobiol. B: Biol.*, 1994, **24**, 109.
11 J. D. Spikes, J. E. van Lier and J. C. Bommer, *J. Photochem. Photobiol. A: Chem.*, 1995, **91**, 193.
12 V. Iliev, A. Ileva and L. Bilyaska, *J. Mol. Catal. A: Chem.*, 1997, **126**, 99.
13 F. Amat-Guerri, M. Carrascoso, M. Luiz, A. T. Soltermann, A. Biasutti and N. A. Garcia, *J. Photochem. Photobiol. A: Chem.*, 1998, **113**, 221.
14 M. Nowakowska and M. Kepczynski, *J. Photochem. Photobiol. A: Chem.*, 1998, **116**, 251.
15 For AlPTC-polymer, elemental analysis: C: 79.55; H: 7.29; N: 2.07%, FTIR of polymer film: 1687 (COOH) and 1711 cm^{-1} (COO–CH_2–), and UV–VIS spectrum in DMF: λ_{max} = 688 nm and ε_{max} = 40500 mol^{-1} dm^3 cm^{-1}. Even when the polymer-AlPTC was immersed into water for 1 month, the polymer and unreacted AlPTC were not observed in water. Therefore, the polymer-AlPTC is completely water-insoluble and does not contain the unreacted AlPTC.
16 For AlPTC system, the photo-oxidation reaction was carried out in a homogeneous aqueous solution because of its water-solubility.

Communication a909406g

Tetrathiafulvalene–phenanthroline macrocycles as redox responsive sensors for metal ions

Kia Svane Bang, Mogens Brøndsted Nielsen, Roman Zubarev and Jan Becher*

Department of Chemistry, University of Southern Denmark (Odense University), Campusvej 55, DK-5230, Odense M, Denmark. E-mail: jbe@chem.sdu.dk

Received (in Cambridge, UK) 29th November 1999, Accepted 5th January 2000

Macrocycles containing a redox-active tetrathiafulvalene unit together with a phenanthroline ligand are able to recognise different metal ions (Cu^+, Ag^+ and Li^+) when part of a precatenate complex.

The redox responsive unit tetrathiafulvalene (TTF) has been incorporated into a number of oxygen, nitrogen and sulfur based crown ethers, resulting in sensors that are able to recognise alkali metal ions as well as silver and barium ions.[1] The strategy of using the templating abilities of Cu^+ to coordinate two phenanthroline ligands in a tetrahedral complex, originally developed by Sauvage and coworkers,[2] has been employed to prepare a TTF-containing Cu(I)-catenate.[3] Using this same strategy, we now report the use of TTF as a sensor unit for the metal ions Cu^+, Ag^+ and Li^+ in precatenate complexes (**5a**,**b**, **7**).

Synthesis of TTF–phenanthroline macrocycles **4a**,**b** were accomplished, using a modified procedure,[2] according to the route outlined in Scheme 1. First, *p*-anisyllithium was prepared by lithiation of *p*-bromoanisole using Bu^{t}Li and it was subsequently treated with 1,10-phenanthroline, affording a disubstituted tetrahydrophenanthroline derivative. Re-aromatisation upon treatment with MnO_2 afforded 2,9-di(*p*-methoxyphenol)-1,10-phenanthroline. Cleavage of the methylphenyl ether proceeded almost quantitatively in a reaction with anhydrous pyridinium hydrochloride, and after neutralisation with NaOH the diphenol **2** was isolated. *O*-alkylation of **2** with the TTF–diiodide **3**[4] under high-dilution conditions in the presence of Cs_2CO_3 gave the TTF–phenanthroline macrocycles **4a**,**b** in yields of 50–60%.

To a 1:1 mixture of the macrocycle and a metal salt, either $Cu(CH_3CN)_4BF_4$, $AgBF_4$, $NiSO_4{\cdot}7H_2O$ or $LiPF_6$, in CH_2Cl_2–CH_3CN (1:1) was added one equivalent of the molecular thread **2** dissolved in a very small amount of DMF (Scheme 2). In order to ensure the highest possible degree of complexation, the mixture was stirred overnight and then concentrated *in vacuo* to the solid complexes **5a**,**b**. The macrocycle **6** and its Cu^+ precatenate **7** were prepared in a similar manner.

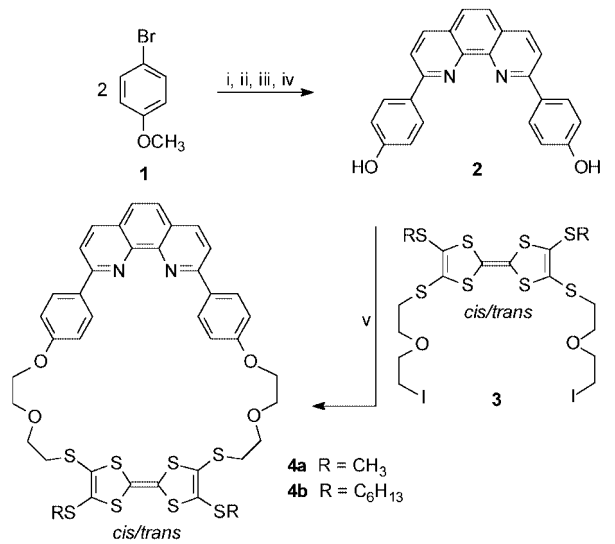

Scheme 1 *Reagents and conditions:* i, Bu^{t}Li (2.5 equiv.), Et_2O, −30 °C; ii, 1,10-phenanthroline (0.27 equiv.), toluene, room temp.; iii, MnO_2, CH_2Cl_2, room temp.; iv, C_5H_5N, conc. HCl, 210 °C; 39% (4 steps); v, Cs_2CO_3 (3 equiv.), DMF, 60 °C, 50–60%.

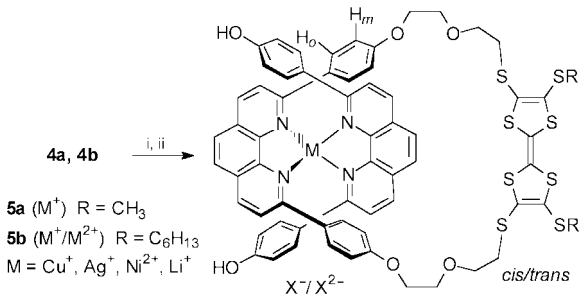

Scheme 2 *Reagents and conditions:* i, MX (1 equiv.) [$Cu(CH_3CN)_4BF_4$, $AgBF_4$, $NiSO_4{\cdot}7H_2O$ or $LiPF_6$], CH_2Cl_2–CH_3CN (1:1), room temp.; ii, 2,9-(*p*-hydroxyphenyl)-1,10-phenanthroline (1 equiv.)/DMF, room temp.

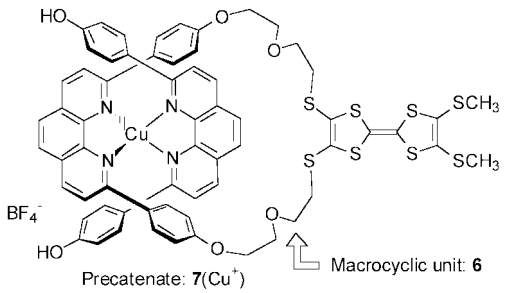

The isolated complexes were first studied by ^{1}H NMR spectroscopy.† Significant chemical shift changes relative to the free macrocycle were observed for the aromatic protons of **5a**,**b** when M^+ = Cu^+, Ag^+ or Li^+ and for **7**(Cu^+) (Table 1). In particular, a *ca.* 1 ppm upfield shift of the eight *ortho* and *meta* phenolic protons on the macrocyclic unit confirmed that the complexations had occurred nearly quantitatively for these three metal ions, however, integration of signals were compli-

Table 1 Selected ^{1}H NMR chemical shifts[a] in $CDCl_3$–CD_3CN (1:1)

Compound	δH_m	$-\Delta(\delta H_m)$/ppm	δH_o	$-\Delta(\delta H_o)$/ppm
4a	7.17	—	8.44	—
5a(Cu^+)	6.00	1.17	7.38	1.06
5b(Ag^+)	6.20 (br)	~0.97	7.50 (br)	~0.94
5b(Li^+)	6.13 (br)	~1.04	7.35 (br)	~1.09
5b(Ni^{2+})	7.16	0.01	8.47	−0.03
6	7.22	—	8.46	—
7(Cu^+)	5.97	1.25	7.26	1.20

[a] For **7**: values from the macrocyclic unit; for **5a**,**b**: average values from the macrocyclic and thread units.

cated by rather broad signals for both the Ag^+ and Li^+ precatenates. A purity of *ca*. 95% is estimated for the isolated complex **7**(Cu^+) from its relatively simple ^1H NMR spectrum (devoid of *cis/trans* isomerism). No significant changes in the proton resonances of the macrocyclic unit were observed for the isolated product containing Ni^{2+}, indicating that the Ni^{2+}-precatenate had not been formed at all. This zero-yield is probably a result of the reluctance of a Ni^{2+} complex to adopt the tetrahedral geometry enforced by the precatenate structure.

Both MALDI and ESI mass spectrometry are useful techniques for characterising precatenates of this type. Studies on the Cu^+ based precatenates show that an applicable amount of the complex is transferred to the gas phase without dethreading. Thus, the mass spectra of **5a**(Cu^+) and **7**(Cu^+) reveal a peak at *m/z* 1291 ($z = 1$) which can be assigned to the singly charged Cu^+ containing precatenate (without the BF_4^- counter ion). However, fragmentation peaks corresponding to the dethreaded macrocycle with and without Cu^+ are also seen.

The redox behaviour of the complexes was studied by cyclic voltammetry and differential pulse voltammetry.[5] The voltammograms of the precatenate **5a**(Cu^+) (Fig. 1(a),(b)) show large anodic shifts relative to the free macrocycle of both the first and second TTF redox potentials as a result of the electrostatic influence exerted by the metal ion (Table 2). In between the two TTF oxidations, Cu^+ is oxidised to Cu^{2+}. The generated Cu^{2+} is not expelled but maintained in the complex since the second TTF oxidation is also affected by the presence of a positively charged metal center. It is noteworthy that the cyclic voltammogram of **5a**(Cu^+) shows the three redox processes to be reversible.

For **5b**(Ag^+) the two TTF oxidations are also shifted to higher potentials, which indicates that the Ag^+ ion is also complexed after the first TTF oxidation. However, even though the ^1H NMR spectrum in $CDCl_3$–CD_3CN (1 : 1) showed clear evidence for the formation of the **5b**(Li^+) precatenate, the TTF redox potentials were almost unaltered according to differential pulse

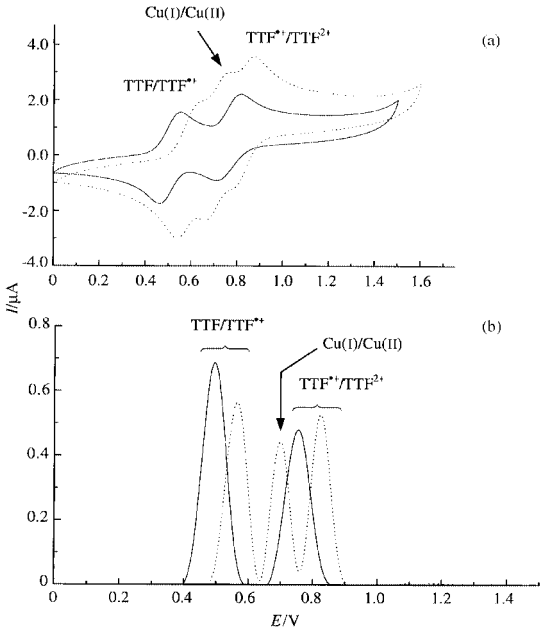

Fig. 1 (a) Cyclic voltammogram (scan rate 100 mV s^{-1}) and (b) differential pulse voltammogram of **4a** (—) and **5a**(Cu^+)BF_4^- (···) in CH_2Cl_2 containing 0.1 M NBu_4PF_6.

Table 2 Differential pulse data (*vs.* Ag/AgCl) in CH_2Cl_2 containing 0.1 M NBu_4PF_6

Compound	E_{ox}^1/V ($TTF^{\cdot+}/TTF^{+}$)	ΔE_{ox}^1/V	E_{ox}^2/V ($TTF^{\cdot+}/TTF^{2+}$)	ΔE_{ox}^2/V
4a	0.49	—	0.75	—
4b	0.53	—	0.78	—
5a(Cu^+)[a]	0.56	0.07	0.82	0.07
5b(Ag^+)	0.58	0.05	0.85	0.07
5b(Li^+)	0.54	0.01	0.79	0.01
6	0.44	—	0.80	—
7(Cu^+)[b]	0.54	0.10	0.83	0.03

[a] $E_{ox}(Cu^+/Cu^{2+}) = 0.70$ V. [b] $E_{ox}(Cu^+/Cu^{2+}) = 0.69$ V.

voltammetry. Thus, it seems that the precatenate is disrupted in the relatively polar solvent (0.1 M NBu_4PF_6 in CH_2Cl_2) used for the electrochemical studies. In agreement with this observation, Sauvage and coworkers found that the Li^+ complex was unstable in the polar solvent DMF.[6] For **7**(Cu^+) the first TTF oxidation is significantly shifted, whereas the second is less influenced.

In conclusion, we have investigated the ability of TTF–phenanthroline macrocycles to form precatenate complexes with different metal ions. The appearance of large shifts in the two TTF redox potentials for the Cu^+ and Ag^+ complexes demonstrates the advantage of employing such macrocycles as possible redox responsive sensors for transition metal ions.

Notes and references

† *Selected data* for **6**: δ_H(250 MHz, $CDCl_3$–CD_3CN 1 : 1): 8.46 (d, *J* 8.9 Hz, 4H, H_o), 8.35 (d, *J* 8.5 Hz, 2H, $H_{4/7}$), 8.14 (d, *J* 8.5 Hz, 2H, $H_{3/8}$), 7.82 (s, 2H, $H_{5/6}$), 7.22 (d, *J* 8.9 Hz, 4H, H_m), 4.34 (t, *J* 4.9 Hz, 4H, OCH_2), 3.85 (t, *J* 4.9 Hz, 4H, OCH_2), 3.79 (t, *J* 6.4 Hz, 4H, SCH_2), 3.08 (t, *J* 6.4 Hz, 4H, SCH_2), 2.24 (s, 6H, SCH_3); MS(PD): *m/z* 865 (M^+). Calc. for $C_{40}H_{36}N_2O_4S_8$: C, 55.53; H, 4.19; N, 3.24. Found: C, 55.33; H, 4.11; N, 3.16%. For **7**(Cu^+)BF_4^-: δ_H (250 MHz, $CDCl_3$–CD_3CN 1 : 1): δ8.63 (d, 2H, *J* 8.4 Hz, $H_{4'}/H_{7'}$), 8.53 (d, 2H, *J* 8.4 Hz, H_4/H_7), 8.24 (s, 2H, $H_{5'}/H_{6'}$), 8.05 (s, 2H, H_5/H_6), 7.88 (d, 2H, *J* 8.6 Hz, $H_{3'}/H_{8'}$), 7.85 (d, 2H, *J* 8.6 Hz, H_3/H_8), 7.41 (d, 4H, *J* 8.6 Hz, $H_{o'}$), 7.26 (d, 4H, *J* 8.6 Hz, H_o), 6.86 (s, 2H, OH), 5.98 (d, 4H, *J* 8.6 Hz, $H_{m'}$), 5.97 (d, 4H, *J* 8.6 Hz, H_m), 3.74 (t, 4H, *J* 6.2 Hz, OCH_2), 3.53 (2 × t, 8H, *J* 5.0 Hz, OCH_2), 3.26 (t, 4H, *J* 6.2 Hz, SCH_2), 2.41 (s, 6H, SCH_3); MS(ES): *m/z* 1291 $(M-BF_4)^+$.

1 T. Jørgensen, T. K. Hansen and J. Becher, *Chem. Soc. Rev.*, 1994, **23**, 41; M. B. Nielsen and J. Becher, *Liebigs Ann.*, 1997, 2177; R. Dieing, V. Morrison, A. J. Moore, L. M. Goldenberg, M. R. Bryce, J.-M. Raoul, M. C. Petty, J. Garín, M. Savirón, I. K. Lednev, R. E. Hester and J. N. Moore, *J. Chem. Soc., Perkin Trans. 2*, 1996, 1587; F. Le Derf, M. Sallé, N. Mercier, J. Becher, P. Richomme, A. Gorgues, J. Orduna and J. Garin, *Eur. J. Org. Chem.*, 1998, 1861; F. Le Derf, M. Mazari, N. Mercier, E. Levillain, P. Richomme, J. Becher, J. Garín, J. Orduna, A. Gorgues and M. Sallé, *Chem. Commun.*, 1999, 1417; H. Liu, S. Liu and L. Echegoyen, *Chem. Commun.*, 1999, 1493.

2 C. O. Dietrich-Buchecker, P.A. Marnot and J.-P. Sauvage, *Tetrahedron Lett.*, 1982, **23**, 5291; C. O. Dietrich-Buchecker and J.-P. Sauvage, *Chem. Rev.*, 1987, **87**, 795.

3 T. Jørgensen, J. Becher, J.-C. Chambron and J.-P. Sauvage, *Tetrahedron Lett.*, 1994, **35**, 4339.

4 Compound **3** was prepared according to a general procedure: M. B. Nielsen, Z.-T. Li and J. Becher, *J. Mater. Chem.*, 1997, **7**, 1175.

5 For comparison to polymetallorotaxanes based on a bipyridine thiophene backbone, see: S. S. Zhu and T. M. Swager, *J. Am. Chem. Soc.*, 1997, **119**, 12 568.

6 C. Dietrich-Buchecker, J.-P. Sauvage and J.-M. Kern, *J. Am. Chem. Soc.*, 1989, **111**, 7791.

Communication a909320f

Stereoselective catalytic hydrogenation of sorbic acid and sorbic alcohol with new Cp*Ru complexes†

Stephan Steines,[a] Ulli Englert[b] and Birgit Drießen-Hölscher*[a]

[a] *Institut f. Technische Chemie und Petrolchemie, RWTH Aachen, Templergraben 55, D-52056 Aachen, Germany. E-mail: drihoel@itc.rwth-aachen.de*

[b] *Institut f. Anorganische Chemie, RWTH Aachen, Templergraben 55, D-52056 Aachen, Germany*

Received (in Cambridge, UK) 26th November 1999, Accepted 6th January 2000

The new Cp*Ru complexes [Cp*Ru(η⁴-MeCH=CHCH=CHCO$_2$H)]$^+$X$^-$ (X$^-$ = $CF_3SO_3^-$ or [B{C$_6$H$_3$(CF$_3$)$_2$-3,5}$_4$]$^-$) are very effective catalysts for the hydrogenation of sorbic acid to *cis*-hex-3-enoic acid and of sorbic alcohol to *cis*-hex-3-en-1-ol (leaf alcohol) under mild conditions in liquid two-phase systems.

When sorbic acid **1**, a widely used preservative, or sorbic alcohol are hydrogenated, different products might occur. The mono-unsaturated products are of technical interest for the production of fragrances and vitamins.[1] This work focuses on the stereoselective preparation of *cis*-hex-3-enoic acid **2** [eqn. (1)] and of *cis*-hex-3-en-1-ol **3**, a fragrance commercialized as 'leaf alcohol'.

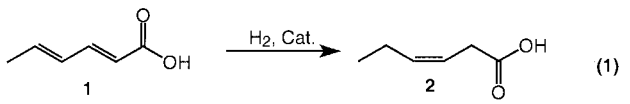

(1)

In early studies Frankel and coworkers showed that methylsorbate and sorbic alcohol can be catalytically hydrogenated by chromium(0) carbonyl compounds with high selectivities to methyl-*cis*-hex-3-enoate and to *cis*-hex-3-en-1-ol, respectively.[2a–d] Unfortunately the reaction only works with sorbic acid esters and sorbic alcohol but not with the cheaper sorbic acid **1**, and one must use toxic chromium catalysts and high catalyst/substrate ratios. Since the start of our studies on stereoselective hydrogenations of **1**[3,4] with complexes like [Cp*Ru(MeCN)$_3$]Tf **4**, we came to the conclusion that the [Cp*Ru]$^+$ fragment is essential for the stereoselectivity of the reaction. 'Naked' Cp*Ru complexes without inhibiting ligands should thus be more active and very selective.

We thus synthesized the model complexes [Cp*Ru(η⁴-MeCH=CHCH=CHCO$_2$H)]$^+$X$^-$ (X = Tf **5a**, X = tetrakis[3,5-bis(trifluoromethyl)phenyl]borate (BARF) **5b**), in which the [Cp*Ru]$^+$ fragment is stabilized by a η⁴-bonded sorbic acid molecule. We assumed, that these complexes should have a similar structure as [Cp*Ru (η⁴-H$_2$C=CHCH=CH$_2$)I],[5] but should bear weakly coordinating ligands instead of an iodide ligand. The new complexes **5a**,**b** have been synthesized from [(Cp*Ru(μ-OMe))$_2$] [6] which was cleaved by 2 equivalents of trifluoromethanesulfonic acid or tetrakis[3,5-bis(trifluoromethyl)phenyl]boric acid (HBARF) in the presence of a slight excess of sorbic acid [eqn. (2)].

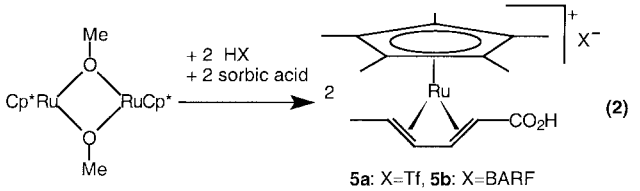

(2)

5a: X=Tf, **5b**: X=BARF

† Dedicated to Professor Wilhelm Keim on the occasion of his 65th birthday.

The complexes have been obtained as orange powders or crystals in 72% (**5a**) and 41% (**5b**) yield and have been characterized by ^{1}H NMR, ^{13}C NMR, secondary ion mass spectrometry and a crystal structure analysis.‡§ The η⁴-bonding mode of the sorbic acid in the complexes has been determined by a strong up-field shift of the olefinic proton signals in the ^{1}H NMR spectrum in comparison to free sorbic acid and by the crystal structure. In solution, the complexes may exist as monomers whereas Fig. 1 shows that complex **5b** is a dimer in the crystalline state which is bridged by the carbonyl oxygens of the acid. The hydroxy groups form hydrogen bridges to a THF molecule, the BARF anions do not interact with the cationic ruthenium complex. **5a**,**b** are the first sorbic acid–ruthenium complexes.

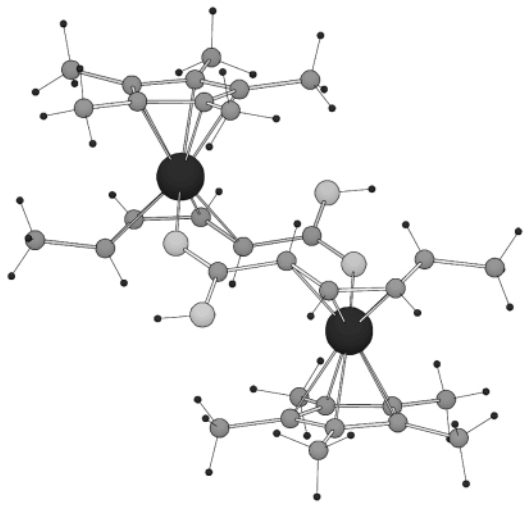

Fig. 1 Crystal structure of the cationic part of **5b**.

Complex **5a** is soluble in polar organic solvents such as alcohols, nitromethane or sulfolane, but it is insoluble in water and nonpolar organic solvents like ethers or alkanes. **5a** can thus be used as catalyst in liquid two-phase systems such as nitromethane–dibutyl ether, ethylene glycol–MTBE (methyl tertiary butyl ether) or sulfolane–MTBE, in which the complex remains in the polar phase. After the reaction the complex can be separated easily by decantation. Table 1 presents the results of the hydrogenation of sorbic acid in different solvents at 60 °C. At 60 °C the solvents in the systems nitromethane–dibutyl ether and sulfolane–MTBE become miscible, and at room temperature the two solvents form two phases.

The results obtained with the nitromethane systems (Table 1, entries 1 and 2) show that **5a** is about 30 times more active than [Cp*Ru(MeCN)$_3$]Tf **4**, which shows, that a naked [Cp*Ru]$^+$ fragment is more active. **5a**,**b** are active at room temperature whereas **4** is active only above 60 °C. Nitromethane is normally used as a weakly coordinating, aprotic solvent, therefore we expected good catalytic results. However, in this case the hydrogenation activities and the selectivities to *cis*-hex-3-enoic acid are lower in comparison to the stronger coordinating sulfolane and in comparison to the protic ethylene glycol.

Table 1 Stereoselective hydrogenation of **1** with **4** and **5a,b** as catalysts in various two-phase systems[a]

Entry	Solvent system	Catalyst	$p(H_2)$/bar	Conv. **1** (%)	Selectivity (S) *cis*-hex-3-enoic acid **2** (%)	Selectivity (S) *trans*-hex-3-enoic acid (%)	TOF/h^{-1}
1	$MeNO_2$–$Bu^n{}_2O$	**4**	60	45	93	6	3.1
2	$MeNO_2$–$Bu^n{}_2O$	**5a**	60	95	66	34	92
3[b]	Ethylene glycol–MTBE	**5a**	60	94	86	7	300
4[b]	Ethylene glycol–MTBE	**5a**	10	78	96	1	97
5	Sulfolane–MTBE	**5a**	60	68	71	29	580
6[c]	MTBE	**5b**	16	85	96	3	1057

[a] *Reagents and conditions*: 60 °C; 20 mmol sorbic acid; 0.06 mmol catalyst; catalyst phase: 30 ml solvent; nonpolar product phase: 44 ml solvent; Conv. = conversion; selectivity (S) = (*n*(product)/$\sum n$ (all products)) × 100; TOF = turnover frequency = ($\sum n$ (all products))/(*n*(catalyst) h).; [b] Some *trans*-hex-2-enoic acid is formed: (3) S = 7%, (4) 3%. [c] 40 mmol sorbic acid, 75 ml MTBE, 50 °C.

Table 2 Stereoselective hydrogenation of sorbic alcohol with **5a** as catalyst in ethylene glycol–MTBE[a]

Entry	*T*/°C	$p(H_2)$/bar	*n* (**5a**)/mmol	*t*/h	Conv. sorbic alcohol (%)	Selectivity to leaf alcohol **3** (%)	TOF/h^{-1}
1	21	20	0.0424	1.5	44	98.3	184
2	40	20	0.0426	0.42	70	98.9	1055
3	60	20	0.0219	0.40	88	98.6	2495
4	60	4	0.0428	0.77	86	97.8	714

[a] *Reagents and conditions*: 25–27 mmol sorbic alcohol; 25 ml ethylene glycol; 45 ml MTBE; in each experiment 1–2% *trans*-hex-3-en-1-ol is formed. Conv. = conversion; selectivity = (*n*(product) / $\sum n$ (all products)) × 100; TOF = turnover frequency = ($\sum n$ (all products))/(*n*(catalyst) h).

The highest selectivities (S) (S(*cis*-hex-3-enoic acid) = 96%) were obtained in ethylene glycol when the hydrogen pressure was reduced from 60 to 10 bar.

The highest activities with **5a** as catalyst (TOF = 580 h^{-1}) were obtained in sulfolane, but the selectivity was not as high as in ethylene glycol.

Since the BARF anion is much more lipophilic than the triflate anion, complex **5b** is more soluble in nonpolar solvents than **5a**. For this reason **5b** was used as catalyst in an MTBE solution instead of using it in a two-phase system. Experiments 5 and 6 in Table 1 can be compared because they both have been carried out in one-phase systems at the same reaction temperature. Evidently, **5b** is a more active catalyst than **5a** because the BARF anion has much weaker coordinating properties than the triflate anion.[7] Thus, the BARF anion does not compete with sorbic acid and hydrogen for free coordination sites at the ruthenium center in the catalytic steps of the reaction.

We also used hexa-2,4-diene-1-ol (sorbic alcohol) as substrate, which can be directly hydrogenated to *cis*-hex-3-ene-1-ol **3** (leaf alcohol). Preliminary results have shown that the catalytic hydrogenation is much faster with sorbic alcohol than with sorbic acid. It was thus possible to reduce the hydrogen pressure from 60 to 20 bar in the experiments shown in Table 2.

The best results were obtained with **5a**, which hydrogenates sorbic alcohol with a TOF of *ca*. 2500 h^{-1} at 60 °C in the two-phase system ethylene glycol–MTBE. Even at low hydrogen pressures of 4 bar, which allows working in glassware reactors, the reaction rate stays fairly high (TOF = 714 h^{-1}). The very high selectivity (98–99%) to leaf alcohol is virtually independent of the reaction temperature, while the hydrogenation activity raises as expected with increasing temperature. Other than in hydrogenations of sorbic acid the selecivity depends negligibly on the conversion. While the selectivity to *cis*-hex-3-enoic acid often decreases at conversion rates of > 90%, the selectivity to *cis*-hex-3-enoic alcohol remains constant even at 100% conversion.

We have thus shown that the concept of using 'naked' Cp*Ru complexes for stereoselective hydrogenations of functionalized dienes to *cis*-olefins is successful. In further work we will try to elucidate the mechanism and the kinetics of the reaction.

We thank the Bundesministerium für Bildung und Forschung and the Ministerium für Wissenschaft und Forschung des Landes NRW (Katalyseverbund NRW) for financial support.

Notes and references

‡ The complexes were synthesized in an argon atmosphere with dried solvents. Before the hydrogenation experiments the solutions of the complexes and the substrates were handled under argon.

General procedure for the synthesis of **5a**,**b**: 2.94 mmol [(Cp*Ru(μ-OMe))$_2$], which was prepared from 2.94 mmol [(Cp*$RuCl_2$)$_2$] according to the procedure described in the literature,[6b] were dissolved in 30 ml dichloromethane and 10 ml diethyl ether. A solution of 3.44 mmol sorbic acid and 3.15 mmol triflic acid (or HBARF) in 12 ml diethyl ether was added to the stirred solution of the complex at −78 °C. The reaction mixture changed immediately from deep red to brown. The reaction mixture was stirred for 10 min at −78 °C and was slowly brought to room temperature. After being stirred for a further 5 min at room temperature, the solvent was evaporated under reduced pressure. The residue was treated with 10 ml ethyl acetate to effect formation of an orange solid. For a better precipitation, 10 ml diethyl ether were added. The solid was filtered off washed twice with 10 ml diethyl ether and dried in high vacuum. 2.11 mmol **5a** were obtained (71.7% yield based on [(Cp*$RuCl_2$)$_2$]).

§ *Crystal data* for $C_{56}H_{51}BF_{24}O_4Ru$ **5b:** M_r 1355.87, triclinic, a = 12.648(6), b = 14.323(3), c = 16.711(6) Å, α = 78.23(2), β = 80.09(3), γ = 84.53(3)°, V = 2914(2) Å^3, T = 203 K, Z = 2, space group $P\bar{1}$ (no. 2), μ(Mo-Kα) = 3.80 cm^{-1}, 12258 independent reflections measured (R_{int} = 0.032). The final $wR(F^2)$ = 0.1497 (all data). The structure was solved using direct methods and refined by full matrix least squares on F^2. Single crystals of [Cp*Ru(μ-O-(η:*s*-*cis*-2,3,4,5-Me(CH)$_4$CO(OH)))]$_2$[B(C$_6$H$_3$-(CF$_3$)$_2$-3,5)$_4$]$_2$·4THF **5b** were crystallized from THF–dibutyl ether and washed with pentane.

CCDC 182/1513.

1 S. Arctander, *Perfume and Flavour Chemicals II*, Montclair, USA, 1969.
2 (*a*) M. Cais, E. N. Frankel and A. Rejoan, *Tetrahedron Lett.*, 1968, 1919; (*b*) E. N. Frankel, E. Selke and C. A. Glass, *J. Am. Chem. Soc.*, 1968, **90**, 2446; (*c*) A. Furuhata, K. Onishi, A. Fujita and K. Kogami, *Agric. Biol. Chem.*, 1982, **46**, 1757; (*d*) A. A. Vasil'ev and E. P. Serebryakov, *Mendeleev Commun.*, 1994, 4.
3 J. Heinen and B. Drießen-Hölscher, *J. Organomet. Chem.*, 1998, **570**, 141.
4 J. Heinen, Ph.D. Thesis, 1997, RWTH-Aachen.
5 P. J. Fagan, W. S. Mahoney, J. C. Calabrese and I. D. Williams, *Organometallics*, 1990, **9**, 1843.
6 (*a*) U. Kölle and J. Kossakowski, *J. Chem. Soc., Chem. Commun.*, 1988, 549; (*b*) U. Kölle and J. Kossakowski, *J. Organomet. Chem.*, 1989, **362**, 383.
7 G. M. DiRenzo, P. S. White and M. Brookhart, *J. Am. Chem. Soc.*, 1996, **118**, 6225.

Communication a909355i

Convergent synthesis of adenophostin A analogues *via* a base replacement strategy

Rachel D. Marwood, Satoshi Shuto, David J. Jenkins and Barry V. L. Potter*

Wolfson Laboratory of Medicinal Chemistry, Department of Pharmacy and Pharmacology, University of Bath, Claverton Down, Bath, UK BA2 7AY. E-mail: b.v.l.potter@bath.ac.uk

Received (in Cambridge, UK) 26th November 1999, Accepted 5th January 2000

The first totally synthetic base-modified analogues of the natural product and potent D-*myo*-inositol 1,4,5-trisphosphate receptor agonist adenophostin A were efficiently synthesised from D-xylose and D-glucose using methodology employing base and surrogate base addition to a common disaccharide intermediate.

D-*myo*-Inositol 1,4,5-trisphosphate [Ins(1,4,5)P_3, **1**] is a second messenger which mediates the release of intracellular Ca^{2+} on binding to its own ligand-gated receptor.[1] The synthesis of Ins(1,4,5)P_3 analogues has provided insights into the structural requirements for binding and Ca^{2+} release at the Ins(1,4,5)P_3 receptor,[2] although inositol-based mimics with a potency exceeding that of Ins(1,4,5)P_3 have yet to be synthesised.

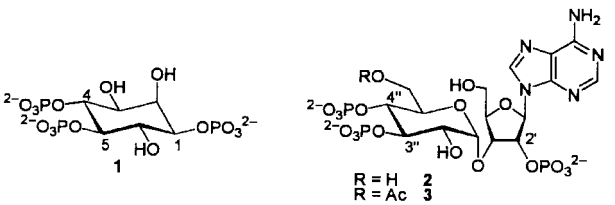

Adenophostins A and B (**2** and **3**)[3] were isolated from broths of *Penicillium brevicompactum*, and were found to be 10- to 100-fold more potent than Ins(1,4,5)P_3 in releasing Ca^{2+} and in receptor binding assays.[4,5] Design of chiral ligands based upon carbohydrates rather than cyclitols could provide novel synthetic signal transduction modulators. The biological activity of minimal structural analogues synthesised so far has not exceeded that of Ins(1,4,5)P_3[5–11] and it is likely that the adenine base is crucial for potency. Adenophostin A is finding widespread use as a tool to investigate cell signalling mechanisms[12] and there have been three syntheses of the molecule.[13–15] We required base-modified analogues of **2** and report here an efficient convergent route to five such compounds *via* a common disaccharide intermediate.

The disaccharide required for Vorbrüggen condensations, 1,2,3′,4′-tetra-*O*-acetyl-2′,5,6′-tri-*O*-benzyl-3-*O*-α-D-glucopyranosyl-D-ribofuranose (**4**), was prepared as follows. Species **5**[16] (Scheme 1) was selectively 5-*O*-benzylated by two different methods. Regioselective ring opening of a 3,5-*O*-dibutylstannylene derivative with BnBr yielded the 5-*O*-benzyl ether **6** (mp 45–47 °C; $[\alpha]_D$ +2.9) in one step. A 78% yield of benzylated products was isolated containing 90% of the desired regioisomer **6**. This method has since been reported by another group.[17] Alternatively, acid-catalysed treatment of **5** with benzaldehyde dimethyl acetal gave the crystalline benzylidene acetal **7** (mp 125 °C; $[\alpha]_D$ +3.8) as a single diastereoisomer in 89% yield; regiospecific cleavage of this acetal with $NaCNBH_3$–HCl also gave **6** in 68% yield. Inversion of the 3-hydroxy group to give the acceptor **8** (mp 83–85 °C; lit.[18] 81–83 °C) was achieved by oxidation with Ac_2O and DMSO and reduction of the corresponding 3-ulose with $NaBH_4$.[17] Acetylation of **9**, available in two steps from D-glucose,[6] gave diacetate **10** quantitatively and cleavage of the allyl glycoside was achieved using $PdCl_2$[19] to give **11** (mp 71–74 °C; $[\alpha]_D$ +83.0). Phosphitylation[15] gave the phosphite donor **12** as an oil in a 1:1 anomeric mixture as judged by ^1H and ^{31}P NMR spectroscopy.

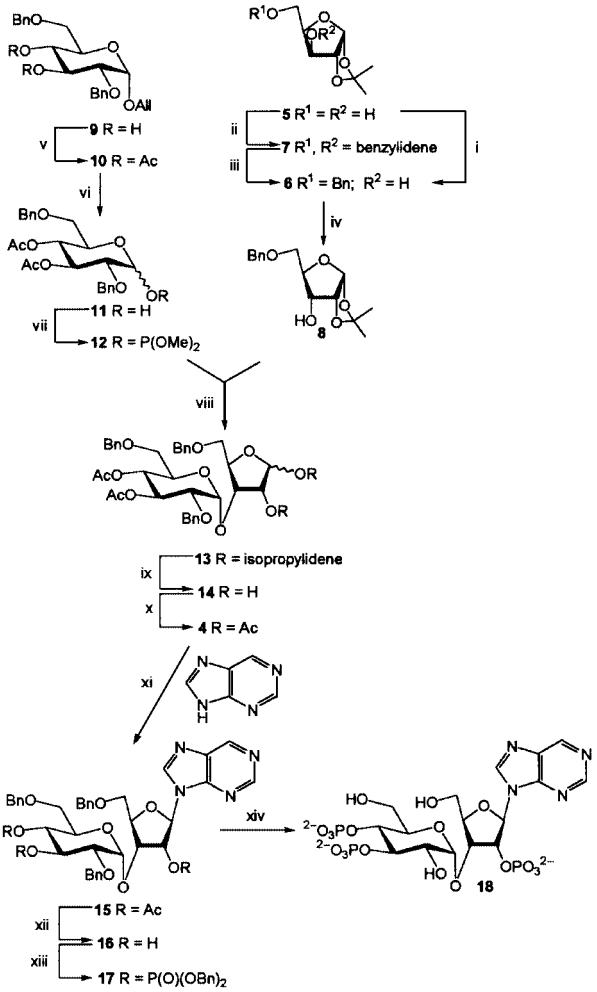

Scheme 1 *Reagents and conditions*: i, Bu_2SnO, BnBr, Bu_4NBr, MeCN, 4 Å sieves, Soxhlet, reflux, 24 h, 78%; ii, $PhCH(OMe)_2$, TsOH, DMF, 70 °C, –MeOH, 2 h, 89%; iii, $NaCNBH_3$–HCl, THF–Et_2O, 3 Å sieves, room temp., 5 min, 68%; iv, (*a*) Ac_2O–DMSO, 18 h, room temp., (*b*) $NaBH_4$, EtOH–H_2O (5:4), room temp., 1 h, 50% over two steps; v, Ac_2O, pyridine, room temp., 20 h, 100%; vi, $PdCl_2$, MeOH–CH_2Cl_2 (1:1), room temp., 3 h, 78%; vii, $(MeO)_2PNEt_2$, 1*H*-tetrazole, CH_2Cl_2, room temp., 30 min; viii, dioxane–toluene (3:1), 4 Å sieves, room temp., 2 h then $ZnCl_2$, $AgClO_4$, dark, room temp., 20 h, 81% (based on **8**); ix, AcOH–H_2O–$(CH_2OH)_2$ (14:6:3), reflux, 15 min, 75%; x, Ac_2O, pyridine, room temp., 20 h, 82%; xi, (*a*) purine, $(Me_3Si)_2NH$–Me_3SiCl (2:1), reflux, 20 h, (*b*) TMSOTf, $(CH_2Cl)_2$, reflux, 7 h, 61%; xii, conc. aq. NH_3–MeOH (1:5), sealed vessel, room temp., 20 h, 97%; xiii, $(BnO)_2PNPr^i_2$, 1*H*-tetrazole, CH_2Cl_2, room temp., 30 min, then MCPBA, −78 °C, 5 min, 80%; xiv, wet $Pd(OH)_2$/C, MeOH–cyclohexene–H_2O (11:5:1), reflux, 17 h, 56%.

Donor **12** and acceptor **8** were coupled together in a similar fashion to that described[11*b*] to give the desired disaccharide **13**

(mp 125–127 °C; $[\alpha]_D$ +101.6) in 81% yield; the reaction time had to be extended because of the deactivating effects[20] of the donor 3,4-di-*O*-acetate protecting groups. Note the high regiospecificity of this glycosylation, the α-coupled anomer being the sole isolated product in high yield. Cleavage of the isopropylidene acetal was accomplished by heating **13** at reflux in aqueous AcOH containing ethylene glycol[14] to give **14** (mp 126–128 °C; $[\alpha]_D$ +116.5) which was acetylated to give **4**.†

To exemplify our route the condensation of **4** with purine is described, using the method of Vorbrüggen *et al.*[21] with TMSOTf as catalyst. The major product was the 9-β-D-ribofuranosidopurine nucleoside (nebularine) derivative **15** ($[\alpha]_D$ +73.6) which exhibited a deshielded doublet at δ_H 6.44 (*J* 4.9 Hz) corresponding to H-1′ of a β-substituted product; purine signals in the ^{13}C NMR spectrum also corresponded closely to those of the known[22] 2′,3′,5′-tri-*O*-acetyl nebularine. Stirring **15** in a mixture of concentrated aqueous ammonia and methanol gave triol **16** ($[\alpha]_D$ +23.5) required for phosphorylation. Triol **16** was phosphitylated and the resulting trisphosphite was oxidised to trisphosphate **17** ($[\alpha]_D$ +17.9).[15] Deprotection of **17** to the purine analogue of **2** ('purinophostin', **18**) was achieved with catalytic transfer hydrogenation. The free acid was eluted from MP1 AG ion exchange resin with a gradient of aqueous TFA and converted into the sodium salt.

Other adenine-related base surrogates used were benzimidazole and imidazole, condensation being achieved similarly to above to give **19** and **20**. The imidazole analogue of adenophostin A ('imidophostin') **20**, in which the adenine six-membered

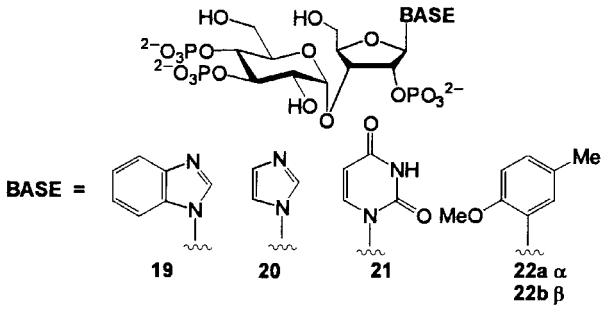

ring had been effectively deleted, was readily accessible by condensation of **4** with *N*-trimethylsilylimidazole.[23] A small amount of bis-glycosylated material was also formed. The desired product was deprotected, phosphorylated and deprotected as previously. We also synthesised an analogue ('uridophostin', **21**†) possessing the natural nucleic acid base, uracil. Condensation of **4** with 4-methylanisole gave both α- and β-substituted aryl C-glycosides in a *ca.* 1:1 ratio from ^1H NMR spectroscopy; these products were used to prepare the α- and β-4-methyl anisole analogues of adenophostin A, **22a** and **22b** respectively, by the coupling of 4-methylanisole and **4** in the presence of $AgCO_2CF_3$ and $SnCl_4$. This demonstrates the utility of our route also for the preparation of C-nucleoside analogues.

Convergent construction of **2** was described by van Straten *et al.*[14] This elegant approach was somewhat hampered, however, by a large number of protection/deprotection steps. Our present route allows efficient access to a central disaccharide **4**, whilst the choice of protecting groups requires minimal manipulation between Vorbrüggen condensation and target trisphosphates.

In summary, we report here an efficient route to the first synthetic base-modified analogues of adenophostin A.

We thank the Wellcome Trust for a Prize Studentship (R. D. M.) and Programme Grant Support (045491 to B. V. L. P.), the Ministry of Education, Science, Sports and Culture of Japan for support to S. S. and acknowledge discussions with Dr A. M. Riley and C. Mort for technical assistance.

Notes and references

† *Selected data* for **4**: mp 105–107 °C (EtOAc–hexane); R_f 0.29 (EtOAc–hexane 3:7); $[\alpha]_D^{20}$ +98.2 (*c* 0.2, $CHCl_3$) (Found: C, 64.00; H, 6.15. Calc. for $C_{40}H_{46}O_{14}$: C, 63.98; H, 6.18%); δ_H(400 MHz; $CDCl_3$) 1.86, 1.87, 1.93, 1.96 (12H, 4s, CH_3CO), 3.29, 3.36 (2H, ABX, $^2J_{AB}$ 10.7, $^3J_{AX}$ 3.9, $^3J_{BX}$ 2.4, H-6′$_A$, H-6′$_B$), 3.56 (1H, *J* 9.8, 3.4, H-2′), 3.63, 3.72 (2H, ABX, $^2J_{AB}$ 11.2, $^3J_{AX}$ 3.9, $^3J_{BX}$ 2.9, H-5$_A$, H-5$_B$), 3.88 (1H, ddd, *J* 10.3, 2.9, H-5′), 4.29 (1H, AB, J_{AB} 12.2, OCH*H*Ar), 4.37–4.40 (1H, m, H-4), 4.47–4.57 (4H, m, 2 × OC*H*$_2$Ar), 4.63–4.64 (2H, m, H-3, OCH*H*Ar), 5.03–5.08 (2H, m, H-1′, H-4′), 5.33 (1H, d, *J* 4.9, H-2), 5.38 (1H, dd, *J* 9.3, H-3′), 6.12 (1H, s, H-1), 7.23–7.34 (15H, m, ArCH); δ_C (100.4 MHz; $CDCl_3$) 20.45, 20.56, 20.63, 20.74, 20.83, 20.94, 21.05, 21.16 (8q, 4 × *C*H$_3$CO$_{\alpha \text{ and } \beta}$), 67.52 (t, C-6′), 68.85 (d, C-5′), 69.00, 69.28 (2t, C-5$_{\alpha \text{ and } \beta}$), 71.89, 72.02 (2d, C-3′$_{\alpha \text{ and } \beta}$), 73.02 (d, C-2), 73.17, 73.26, 73.35, 73.41, 73.48, 73.55 (4t and 2d, C-3$_{\alpha \text{ and } \beta}$, OCH$_2Ar_{\alpha \text{ and } \beta}$), 76.59, 76.76 (2d, C-2′$_{\alpha \text{ and } \beta}$), 81.27 (d, C-4), 96.28, 96.47 (2d, C-1′$_{\alpha \text{ and } \beta}$), 98.46, 98.50 (d, C-1$_{\alpha \text{ and } \beta}$), 127.32, 127.61, 127.74, 127.91, 128.02, 128.36, 128.46 (7d, ArCH), 137.51, 137.76, 138.11 (3s, 3 × C-1 of Bn rings), 169.35, 169.69, 170.17, 170.28 (4s, 4 × CH_3CO); α and β subscripts denote signals arising from α and β-anomers respectively; *m/z* (FAB$^+$) 750 (M^+, 1%), 91 (100). For uridophostin: δ_H (D_2O) 3.90–3.50 (7H, m, H-4′, H-5′, H-2″, H-5″, and H-6″), 4.17 (1H, m, H-4″), 4.32–4.28 (2H, m, H-3′ and H-3″), 4.74 (1H, m, H-2′), 5.15 (1H, br s, H-1″), 5.74 (1H, d, *J* 8.3, H-5), 5.95 (1H, d, *J* 4.4, H-1′), 7.65 (1H, d, *J* 8.3, H-6); δ_P(100 MHz, D_2O, ^1H-decoupled) 0.23, 1.09, 1.78; HRMS (triethylammonium salt, FAB) calc. for $C_{15}H_{24}N_2O_{20}P_3$ 645.0135, found 645.0130 (100%, M^-); $\lambda_{max}(H_2O)$/nm 260.

1 M. J. Berridge, *Nature (London)*, 1993, **361**, 315.
2 B. V. L. Potter and D. Lampe, *Angew. Chem., Int. Ed. Engl.*, 1995, **34**, 1933.
3 S. Takahashi, T. Kinoshita and M. Takahashi, *J. Antibiot.*, 1994, **47**, 95.
4 M. Takahashi, K. Tanzawa and S. Takahashi, *J. Biol. Chem.*, 1994, **269**, 369; J. Hirota, T. Michikawa, A. Miyawaki, M. Takahashi, K. Tanzawa, I. Okura, T. Furuichi and K. Mikoshiba, *FEBS Lett.*, 1995, **368**, 248.
5 J. S. Marchant, M. D. Beecroft, A. M. Riley, D. J. Jenkins, R. D. Marwood, C. W. Taylor and B. V. L. Potter, *Biochemistry*, 1997, **36**, 12 780 and references therein.
6 D. J. Jenkins and B. V. L. Potter, *Carbohydr. Res.*, 1996, **287**, 169.
7 R. A. Wilcox, C. Erneux, W. U. Primrose, R. Gigg and S. R. Nahorski, *Mol. Pharmacol.*, 1995, **47**, 1204.
8 N. Moitessier, F. Chrétien, Y. Chapleur and C. Humeau, *Tetrahedron Lett.*, 1995, **46**, 8023.
9 C. T. Murphy, A. M. Riley, C. J. Lindley, D. J. Jenkins, J. Westwick and B. V. L. Potter, *Mol. Pharmacol.*, 1997, **52**, 741.
10 D. J. Jenkins, R. D. Marwood and B. V. L. Potter, *Chem. Commun.*, 1997, 449; Corrigendum, 805.
11 (*a*) S. Shuto, K. Tatani, Y. Ueno and A. Matsuda, *J. Org. Chem.*, 1998, **63**, 8815; (*b*) R. D. Marwood, A. M. Riley, V. Correa, C. W. Taylor and B. V. L. Potter, *Bioorg. Med. Chem. Lett.*, 1999, **9**, 453.
12 Y. Huang, M. Takahashi, K. Tanzawa and J. W. Putney Jr., *J. Biol. Chem.*, 1998, **273**, 31 815; G. S. Bird, M. Takahashi, K. Tanzawa and J. W. Putney Jr., *J. Biol. Chem.*, 1999, **274**, 20 643; L. M. Broad, D. L. Armstrong and J. W. Putney Jr., *J. Biol. Chem.*, 1999, **274**, 32 881 and references therein.
13 H. Hotoda, M. Takahashi, K. Tanzawa, S. Takahashi and M. Kaneko, *Tetrahedron Lett.*, 1995, **36**, 5037.
14 N. C. R. van Straten, G. A. van der Marel and J. H. van Boom, *Tetrahedron*, 1997, **53**, 6509.
15 R. D. Marwood, V. Correa, C. W. Taylor and B. V. L. Potter, *Tetrahedron: Asymmetry*, 2000, in press.
16 J. Moravcova, J. Capkova and J. Stanek, *Carbohydr. Res.*, 1994, **263**, 61.
17 T. Q. Chen and M. M. Greenberg, *Tetrahedron Lett.*, 1998, **39**, 1103; P. B. Alper, M. Hendrix, P. Sears and C.-H. Wong, *J. Am. Chem. Soc.*, 1998, **120**, 1965.
18 T. Desai, J. Gigg and R. Gigg, *Carbohydr. Res.*, 1996, **280**, 209.
19 W. Liao and D. Lu, *Carbohydr. Res.*, 1996, **296**, 171.
20 N. L. Douglas, S. V. Ley, U. Lücking and S. L. Warriner, *J. Chem. Soc., Perkin Trans. 1*, 1998, 51.
21 H. Vorbrüggen, K. Krolikiewicz and B. Bennua, *Chem. Ber.*, 1981, **114**, 1234.
22 V. Nair and S. G. Richardson, *J. Org. Chem.*, 1980, **45**, 3969.
23 A. Al Mourabit, M. Beckmann, A. Poupat, A. Ahond and P. Potier, *Tetrahedron: Asymmetry*, 1996, **7**, 3455.

Communication a909347h

ChemComm

High internal phase emulsions (HIPEs) containing divinylbenzene and 4-vinylbenzyl chloride and the morphology of the resulting PolyHIPE materials

Andrea Barbetta, Neil R. Cameron* and Sharon J. Cooper

Department of Chemistry, University of Durham, South Road, Durham, UK DH1 3LE. E-mail: n.r.cameron@durham.ac.uk

Received (in Oxford, UK) 15th November 1999, Accepted 5th January 2000

The cell size of DVB–VBC PolyHIPEs decreases with increasing VBC content, which appears to be due to the adsorption of VBC at the emulsion interface leading to a lower interfacial tension and a smaller droplet size.

High internal phase emulsions (HIPEs) are defined as emulsions in which the droplet phase occupies greater than 74.05% of the emulsion volume, this figure representing the maximum volume occupiable by uniform spheres. Such systems have been known for many years, and features such as their preparation, stabilisation, structure and rheology have been investigated in detail.[1] Our interest[2] in HIPEs, and that of several other groups,[3] lies in their ability to be used as templates for the production of highly porous polymers. Such materials, known as PolyHIPEs using Unilever's nomenclature,[4] are prepared by polymerising the thin monomer films that surround the droplets of inert solvent-in-monomer solution HIPEs. Subsequent removal of the droplets produces a highly porous material (Fig. 1).

During the course of our work on developing novel PolyHIPE materials we undertook the preparation of species containing 4-vinylbenzyl chloride (VBC, **1**). This monomer is

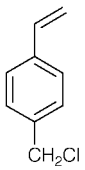

1

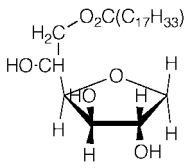

2

sufficiently hydrophobic to allow successful HIPE preparation, and results in materials possessing reactive chloromethyl functionalities that are amenable to functionalisation, potentially leading to a wide range of derivatised highly porous materials. VBC has been used previously to prepare HIPEs where it was present in either the droplet[5] or the continuous[6] phase, leading to the production of agglomerates of particles or foams, respectively. However, the influence of VBC on the emulsion and resulting polymer morphology was not described.

VBC-containing materials were easily prepared by addition of an aqueous solution of $CaCl_2.2H_2O$ and $K_2S_2O_8$ to a mixture of monomer(s) plus surfactant, using conditions optimised for the production of styrene–divinylbenzene (S–DVB) PolyHIPEs.[4,7] The ratio (wt%) of VBC to DVB[8] was varied, to give a range of foams, each with a pore volume of 90%. To our surprise, the resulting materials had smaller average cell sizes than those obtained from styrene and DVB (*e.g.* Fig. 1). SEM photographs (Fig. 2) clearly show that increasing the VBC content in the formulation causes a decrease in average cell size from 10 μm [Fig. 2(*a*)] to less than 5 μm [Fig. 2(*e*)]. Interestingly, the foam composed entirely of polyVBC [Fig. 2(*f*)] has no discernible cell structure. Previously, Williams[9] found that increasing the DVB concentration in styrene–DVB PolyHIPEs from 0 to 100% resulted in a decrease in average cell diameter by about 10 μm. He reasoned that DVB,

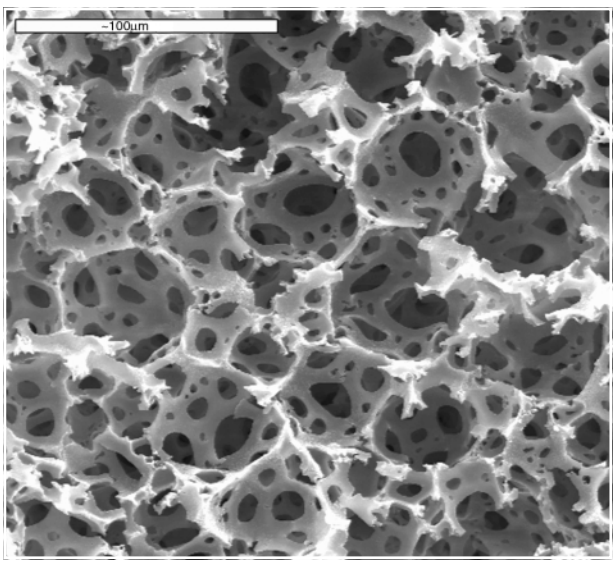

Fig. 1 SEM of a S–DVB PolyHIPE foam (pore volume *ca.* 90%, nominal crosslink density *ca.* 15%). Scale bar = 100 μm.

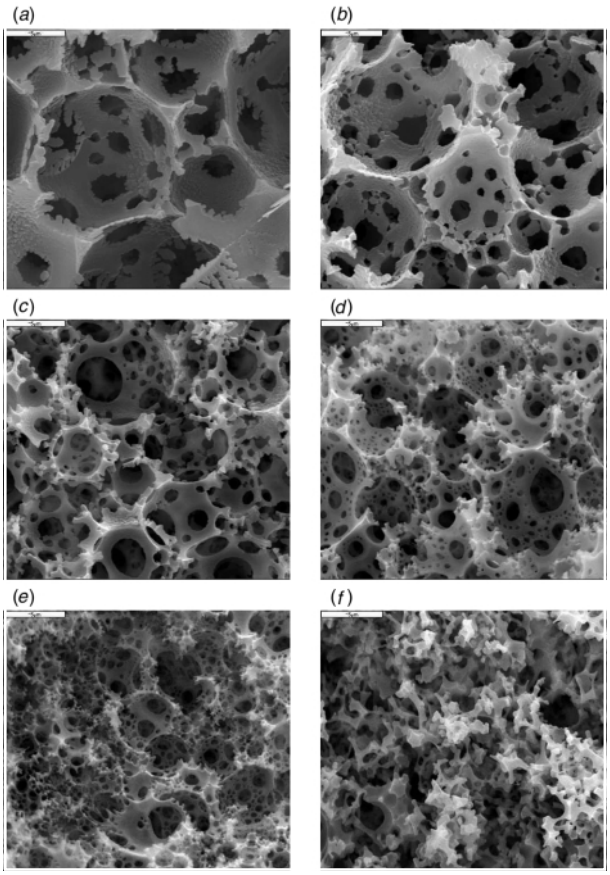

Fig. 2 SEMs of VBC–DVB PolyHIPE foams (ref. 16): (*a*) X80PV90; (*b*) V12.5X70PV90; (*c*) V37.5X50PV90; (*d*) V62.5X30PV90; (*e*) V87.5X10PV90; (*f*) V100X0PV90. Scale bar = 5 μm.

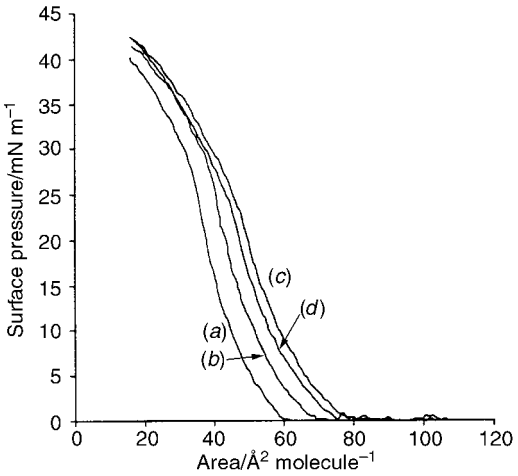

Fig. 3 π–*A* curves for films containing Span 80 alone (*a*) and Span 80 (17 mol% relative to total oil phase) plus DVB (*b*), VBC (*c*) and DVB–VBC (50 : 50 mol. mixture) (*d*).

being more hydrophobic, was leading to more stable emulsions. It is well known that droplet size decreases with increasing emulsion stability since the surface energy per unit area is lower. A decrease in emulsion droplet size leads to a decrease in PolyHIPE cell size since the foam is effectively a replica of the emulsion structure immediately prior to gel formation.

In our case, with VBC–DVB foams, increasing DVB concentration causes an increase in average cell size of the resulting foam. This implies that VBC leads to more stable emulsions than DVB. Emulsion stability is influenced by such factors as temperature, surfactant nature and concentration, phase composition and viscosity. Since the surfactant used was Span 80 (sorbitan monooleate, **2**) in each case, at constant concentration (20 wt% relative to monomer content), the polymerisation temperature was constant and emulsion preparation conditions were identical, the different behaviour must be due to differences in the physical chemistries of DVB and VBC. Both species being low molar mass entities, one would not anticipate tremendous differences in the viscosities of VBC and DVB.[10] We therefore concluded that the marked difference in their behaviour must be as a result of different interfacial properties. In particular, we wondered whether VBC could be concentrating at the interface and acting as a cosurfactant with Span 80.

It is well known that small molecules bearing polar and non-polar functionalities can adsorb at the interface of emulsions, the polar group locating in the aqueous phase and the non-polar group in the organic phase. Additionally, small molecule surface-active species can co-adsorb with surfactants possessing large head-groups, such as Span 80, leading to a better-packed interfacial film and consequently a more stable emulsion.[11] The presence of an aromatic moiety in the hydrophobic part of the cosurfactant may enhance its adsorption at the interface.[12]

Using a Langmuir trough, we measured the surface pressure against area (π–*A*) curves of films of Span 80 alone, and Span 80 with DVB, VBC and a 50 : 50 mixture of DVB and VBC.[13] The interfacial behaviour of the various components can be inferred from their π–*A* curves (Fig. 3). Span 80 [Fig. 3(*a*)] displays the behaviour of a typical surfactant; surface pressure is low and constant until critical film compression is reached, whereupon it increases drastically. The area corresponding to this compression represents the area of the condensed interfacial film where the surfactant molecules are densely packed. Adsorption of the other species (VBC, DVB) at the interface will cause greater crowding and lead to an increase in π at higher area (lower compression), which is indeed observed. From fig. 3 it can be inferred that DVB [Fig. 3(*b*)] is slightly adsorbed at the interface, but VBC [Fig. 3(*c*)] is adsorbed to a significantly greater extent. Therefore, VBC is co-adsorbed with Span 80 at the interface and leads to a more dense film. These results appear to confirm our hypothesis that VBC is acting as a cosurfactant. Williams[14] previously investigated the influence of 22 cosurfactants on the stability of S–DVB HIPEs and found that none enhanced stability.[15] However, all but three of those additives were alcohols and none possessed halide residues.

Further information on the interfacial behaviour of systems containing VBC can be deduced from closer inspection of Fig. 3. The curve of the film containing a 50 : 50 mixture of VBC and DVB [Fig. 3(*d*)] lies nearer to that of VBC [Fig. 3(*c*)] than to that of DVB [Fig. 3(*b*)], indicating that the greatest changes in interfacial properties occur on initial addition of VBC. This behaviour can also be inferred from the morphology of the PolyHIPE materials (Fig. 2); the decrease in cell size is more dramatic up to addition of 30% VBC [Fig. 2(*c*)], after which the cell size decreases only slightly. This implies that the interface is close to saturation at a VBC concentration in the HIPE of around 30%.

To conclude, we have prepared reactive PolyHIPE materials from VBC and DVB. These possess smaller average cell sizes than corresponding materials prepared from styrene and DVB. This phenomenon appears to be due to the adsorption of VBC at the interface, which lowers the interfacial tension, leads to a more stable emulsion with smaller droplets and therefore to the production of a foam with a smaller average cell diameter. The ability to control the morphology of these porous materials is crucial to their technological development.

Notes and references

1 See N. R. Cameron and D. C. Sherrington, *Adv. Polym. Sci.*, 1996, **126**, 163; E. Ruckenstein, *Adv. Polym. Sci.*, 1997, **127**, 163; and references therein.

2 N. R. Cameron and D. C. Sherrington, *Colloid Polym. Sci.*, 1996, **274**, 592; N. R. Cameron, D. C. Sherrington, I. Ando and H. Kurosu, *J. Mater. Chem.*, 1996, **6**, 719; N. R. Cameron and D. C. Sherrington, *Macromolecules*, 1997, **30**, 5860; N. R. Cameron and D. C. Sherrington, *J. Mater. Chem.*, 1997, **7**, 2209.

3 E. Ruckenstein and X. Wang, *Biotechnol. Bioeng.*, 1993, **42**, 821; J. R. Duke Jr., M. A. Hoisington, D. A. Langlois and B. C. Benicewicz, *Polymer*, 1998, **39**, 4369; R. J. Wakeman, Z. G. Bhumgara and G. Akay, *Chem. Eng. J.*, 1998, **70**, 133.

4 D. Barby and Z. Haq, *U.S. Pat. 4,522,953*, 1985.

5 L. Hong and E. Ruckenstein, *Polymer*, 1992, **33**, 1968; *React. Polym.*, 1991/1992, **16**, 181; E. Ruckenstein and L. Hong, *Chem. Mater.*, 1992, **4**, 1032.

6 K. Jones, B.R. Lothian, A. Martin, G. Taylor and Z. Haq, *U.S. Pat. 4,668,709*, 1987; H. F. M. Schoo, G. Challa, B. Rowatt and D. C. Sherrington, *React. Polym.*, 1991/1992, **16**, 125; B. C. Benicewicz, G. D. Jarvinen, D. J. Kathios and B. S. Jorgensen, *J. Radioanal. Nucl. Chem.*, 1998, **235**, 31; S. D. Alexandratos, R. Beauvais, J. R. Duke and B. S. Jorgensen, *J. Appl. Polym. Sci.*, 1998, **68**, 1911.

7 P. Hainey, I. M. Huxham, B. Rowatt and D. C. Sherrington, *Macromolecules*, 1991, **24**, 117.

8 Commercial grade DVB used in this study contains 80% actual DVB, the remainder being a mixture of ethylstyrene isomers.

9 J. M. Williams, A. J. Gray and M. H. Wilkerson, *Langmuir*, 1990, **6**, 437.

10 Viscosities of VBC and DVB (55%) at 25 °C are 1.830 and 1.007; from: *Kirk-Othmer Encyclopedia of Chemical Technology*, 4th edn., ed. J. I. Kroschwitz, Wiley, New York, 1991.

11 D. Myers, *Surfactant Science and Technology*, VCH, Weinheim, 1988, p. 228.

12 M. J. Rosen, *Surfactants and Interfacial Phenomena*, 2nd edn., Wiley, 1989, p. 6.

13 Film compositions were chosen to reflect as closely as possible the composition of the HIPE organic phase. In each case, 30 μl of a $CHCl_3$ solution ([Span 80] = 2.33×10^{-3} mol dm^{-3}, [additive] = 1.17×10^{-2} mol dm^{-3}) was spread on an aqueous solution of calcium chloride (0.075 mol dm^{-3}).

14 J. M. Williams, *Langmuir*, 1991, **7**, 1370.

15 One example, Brij 78, was found to produce a bimodal cell size distribution, the smaller of which were smaller than those commonly observed in S/DVB foams.

16 PolyHIPE coding system: V*a*X*b*PV*c*, *a* = wt. % of VBC relative to total monomer phase; *b* = nominal crosslink density (wt. % of actual DVB in monomer phase); *c* = pore volume (vol. % internal phase of HIPE).

Communication a909060f

ChemComm

Pentanuclear asymmetrical ladder structure of the 1,4-dimethylpiperazine solvate of lithium anilide and its implication for the unknown structure of amorphous lithium anilide

William Clegg,[a] Stephen T. Liddle,[a] Robert E. Mulvey*[b] and Alan Robertson[b]

[a] *Department of Chemistry, University of Newcastle, Newcastle upon Tyne, UK NE1 7RU*
[b] *Department of Pure and Applied Chemistry, University of Strathclyde, Glasgow, UK G1 1XL. E-mail: r.e.mulvey@strath.ac.uk*

Received (in Cambridge, UK) 13th December 1999, Accepted 7th January 2000

The weak solvating ligand 1,4-dimethylpiperazine appears to only partially disrupt the aggregation within lithium anilide, as evidenced by the structure of the title solvate: a three-dimensional polymer of solvent-linked irregularly shaped $(NLi)_5$ substructures, which can be interpreted as two interconnected ladders.

Long in the shadow of their better known secondary counterparts,[1] lithiated primary amines [{RN(H)Li}$_n$] are now emerging as valuable and versatile chemical intermediates themselves. Their ability to function as either amido [RN(H)$^-$][2] or imido (RN^{2-})[3] transfer agents, or sometimes as both simultaneously,[4] has proved particularly useful for the development of new heterometallic[5] and/or hetero-anionic[6] compositions. This paper focuses on one of the most important primary amides, lithium anilide. While its simple solvates with THF[7,8] or PMDETA[9] have been structurally elucidated, the pure solvent-free structure remains elusive. This situation is relatively common for lithium amides (whether primary or secondary) suspected of having polymeric constitutions (lithium anilide is thought to exist as a high oligomeric/polymeric ladder structure). Adding solvent ligands often produces smaller oligomers which can be crystallised and are therefore suitable for X-ray crystallographic study, unlike their solvent-free parent compounds which tend to be amorphous. Thus while lithium anilide is easy to prepare as a powder, so far it has not been possible to grow single crystals of it. However, keeping in mind that competition between aggregation and solvation can be delicately balanced, we have subjected it to the weak (weaker than THF or PMDETA) coordinating solvent 1,4-dimethylpiperazine (DMP) in the hope of crystallising a solvate with a structure more representative of the pure solvent-free compound, *i.e.* one in which the high (or infinite) aggregation has been only partially disrupted. As reported herein, the new solvate produced in this way, [{[{PhN(H)Li}$_5$·(DMP)$_2$]·(C$_6$H$_5$Me)$_2$·(DMP)$_{0.5}$}$_\infty$] **1**, possesses a remarkable structure. Besides fulfilling the aim of revealing a sizable ladder fragment (spanning five N–Li rungs), the structure also exhibits a new tetraanilido–lithium [{PhN(H)}$_4$Li] coordination mode, which facilitates the grafting of an additional N–Li bond onto a ladder edge. This unprecedented connectivity may provide an important clue as to the cause of the amorphous character of unsolvated lithium anilide.

The weak solvating power of DMP was reflected in the molar excess required (2.2 equivalents, 11 mmol) to dissolve a freshly prepared slurry of lithium anilide (5 mmol) in hexane–toluene solution. Cooling the resulting pale yellow solution to −30 °C for 2 days, afforded a crop of colourless crystalline **1**.† A standard inert-atmosphere protocol was used throughout this preparative and subsequent isolation procedure.

As determined by an X-ray crystallographic study,‡ the structure of **1** is made up of novel pentanuclear $(NLi)_5$ crossed ladder substructures (Fig. 1), linked together by bridging DMP ligands (Fig. 2) into a three-dimensional polymeric network. The crystal packing arrangement leaves spacious cavities in the

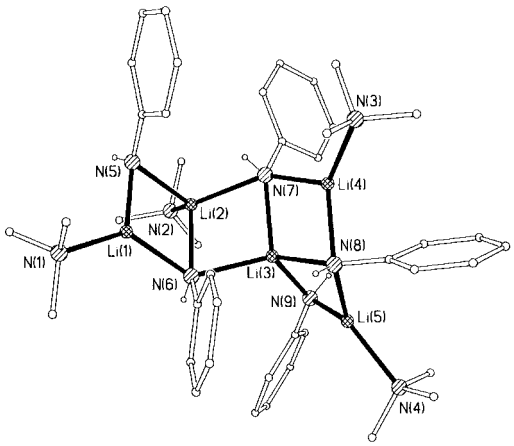

Fig. 1 Asymmetric unit of **1** showing atom labelling. Hydrogen atoms, except for N–H, are omitted for clarity, and solvent molecules are not shown.

structure which are filled by toluene solvent and free DMP molecules of crystallisation [2 and 0.5, respectively, per $(NLi)_5$ ladder]. Two essentially planar (anilidoN–Li)$_2$ rings, Li(1)N(6)Li(2)N(5) and Li(3)N(8)Li(4)N(7), joined together by Li(3)–N(6) and Li(2)–N(7) bonds, make up the main run of the ladder, the undulation of which is 'U-shaped' rather than 'stepped'. These rings can be classified as *cisoid*[10] (or *syn*), because their N–H substituents lie on the same side of the $(NLi)_2$ plane in each case. In contrast, at the junction of these two rings the conformation is *transoid* (*anti*) and the Li(2)N(7)Li(3)N(6) ring is butterfly shaped with an N···N hinge (folding angle, 138.4°) and Li wingtips. Located within the smaller cross-run of the ladder, the remaining Li(3)N(8)Li(5)N(9) ring is also *transoid* and butterfly shaped (folding angle, 151.7°). Those Li atoms positioned at ladder 'ends', Li(1), Li(4) and Li(5), have three-

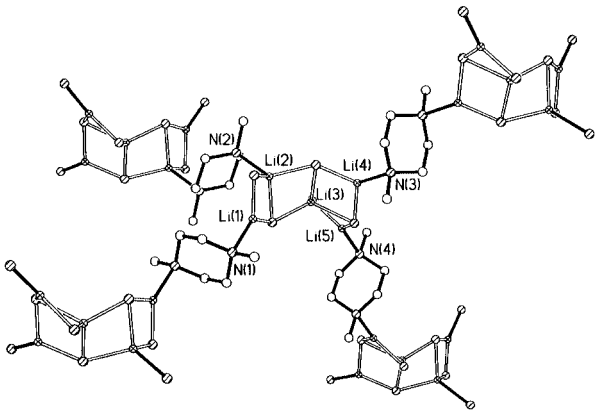

Fig. 2 View of **1** showing the bridging of four DMP ligands to neighbouring ladder substructures of which only Li and N atoms are shown.

coordinate, distorted trigonal planar geometries, though Li(4) is slightly pyramidalised (sum of bond angles, 353.2°). Occupying an inner rung, Li(2) displays a four-coordinate distorted tetrahedral geometry [bond angles, 99.8(3)–121.6(3)°]. Each of these Li atoms binds to one N atom from a chair-shaped DMP molecule which bridges through its second N atom to a Li atom of a neighbouring $(NLi)_5$ ladder. Connecting both runs of the ladder, Li(3) is unique as its distorted tetrahedral environment [bond angles, 96.7(3)–124.0(3)°] does not include a DMP molecule, but is made up exclusively of anilido N atoms. This coordination of Li by four monodentate anions is unprecedented for an anilide (and, to the best of our knowledge, for any amide). It is also rare generally in the wider context of organolithium chemistry, but not unknown, as a C_4Li coordination exists in the contact-ion pair structure of sodium tetraphenyllithate [{Na·(TMEDA)}$_3${$LiPh_4$}].[11] Three anilide anions in **1** [at N(6), N(7) and N(8)] engage in μ_3 bonding with Li atoms, while the other two situated in the end rungs [at N(5) and N(9)] are μ_2 bonded. These end rungs, N(5)–Li(1) and N(9)–Li(5), display the shortest lengths [1.934(8) and 1.954(7) Å, respectively] in the $(NLi)_5$ ladder framework reflecting the low coordination numbers (C.N.) involved (four for N; three for Li). Similarly, the longest such bond, N(8)–Li(3) [2.208(6) Å], reflects the high C.N. involved (five for N; four for Li). The remaining N–Li ladder lengths lie in the range 2.014(8)–2.178(7) Å. There is also a correlation between the dative (DMP)N–Li bond lengths and Li C.N. [where C.N. = 3, the mean length is 2.073 Å; where C.N. = 4, the length increases to 2.176(6) Å]. Turning to angular values, despite the ladder having an irregular shape and a variety of C.N., its endocyclic bond angles subtended at N cover a narrow range [73.1(3)–77.9(3)°]. The corresponding bond angles at Li cover a wider range [96.7(3)–107.8(3)°].

Pentanuclear aggregation is extremely rare in lithium structural chemistry. A previous example was reported for the anion of the lithium ketimidolithate complex [{Li·$(HMPA)_4$}$^+$-{$Li_5(N{=}CPh_2)_6$·(HMPA)}$^-$],[12] but in this case the (N_6Li_5) substructure is of a discrete cage anion, rather than a segment of a polymeric chain. The asymmetric unit of **1** represents the first pentanuclear Li_5 ladder conformation. Hitherto, homoaggregated lithium amide ladders generally have regular, symmetrical structures of laterally connected $(NLi)_2$ rings, the opposite facing N–Li bonds of which become either pairs of rungs or pairs of edges. Representative examples include the tetrameric 'concave' ladder of the piperidide [{$H_2C(CH_2)_4NLi{\cdot}HN(CH_2)_4CH_2$}$_4$],[13] the octameric cyclic ladder of [{$Bu^tN(H)Li$}$_8$],[14] and the polymeric sinusoidal wave-shaped ladder of [{$H_2NCH_2CH_2N(H)Li$}$_\infty$].[15] Aside from having an odd number of rungs, the ladder of **1** differs by virtue of the additional rung [N(9)–Li(5)] grafted onto the N(8)–Li(3) 'edge'. This is a new structural development§ since ladder edges usually stand alone, or in rare cases, are solvated at Li.[16] The presence of this special feature implies that removal of the DMP ligands from **1** would allow the laddering process to extend in several directions. Viewing the $(NLi)_5$ framework as two interconnected ladders, there are four end-rungs N(5)–Li(1), N(8)–Li(4), N(9)–Li(5) and N(7)–Li(4), from which further laddering might be possible, though the kinetics of growth at each site may be different. The amorphous nature of unsolvated lithium anilide may have its origin in the availability of such irregular branching. Hence this contrasts with the situation so far found in crystalline lithium amide polymeric ladders[15,16] where the laddering process is mono-directional.

We gratefully acknowledge the continued financial support of the EPSRC.

Notes and references

† Yield of first batch, 21%. Mp: decomp. from 290 °C. ^{1}H NMR (300 K, 400 MHz, d_5-pyridine) δ 2.20 (s, 3H, Me of DMP), 2.40 (s, 4H, CH_2 of DMP), 4.33 (s, 1H, NH), 6.49 (t, 1H, *p*-Ph), 6.89 (d, 2H, *o*-Ph) and 7.18 (t, 2H, *m*-Ph). Trace quantities of toluene are also present. ^{13}C NMR (300 K, 100.6 MHz, d_5-pyridine) δ 46.64 (Me of DMP), 55.94 (CH_2 of DMP), 110.58 (*p*-Ph), 116.72 (*o*-Ph), 130.03 (*m*-Ph) and 162.94 (*ipso*-Ph).

‡ *Crystal data* for **1**: $C_{59}H_{81}Li_5N_{10}$, M = 965.0, triclinic, space group $P\bar{1}$, a = 11.205(2), b = 16.726(3), c = 17.152(3) Å, α = 64.592(3), β = 80.095(4), γ = 85.225(4)°, U = 2860.1(8) Å^3, Z = 2, D_c = 1.121 g cm^{-3}, μ = 0.065 mm^{-1} (Mo-Kα, λ = 0.71073 Å), T = 160 K; R_w = 0.2625 on F^2 values of all 9732 unique data, conventional R = 0.0851 on F values of 5443 reflections with $F_o^2 > 2\sigma(F_o^2)$, 683 parameters; final difference map within ±0.65 e Å^{-3} except for one peak of 1.00 e Å^{-3} in a disordered toluene molecule. Restraints were applied for the toluene molecules. H atoms were constrained except for free refinement of positions for N–H. CCDC 182/159. See http://www.rsc.org/suppdata/cc/a9/a909754f/ for crystallographic files in .cif format.

§ The homoaggregated ladders described herein should not be confused with heteroanionic systems which have ladder shapes, for example, as in the amidinate–hydroxide [{(Li[(Bu^n)C(NBu^t)$_2$])$_2$·LiOH·THF}$_2$],[17] in which O–Li 'edges' interact with N–Li 'rungs'.

1 K. Gregory, P. v. R. Schleyer and R. Snaith, *Adv. Inorg. Chem.*, 1991, **37**, 47.
2 A. A. Danopoulos, D. M. Hankin, G. Wilkinson, S. M. Cafferkey, T. K. N. Sweet and M. B. Hursthouse, *Polyhedron*, 1997, **16**, 3879.
3 P. J. Brothers, R. J. Wehmschulte, M. M. Olmstead, K. Ruhlandt-Senge, S. R. Parkin and P. P. Power, *Organometallics*, 1994, **13**, 2792.
4 A. A. Danopoulos, G. Wilkinson, T. K. N. Sweet and M. B. Hursthouse, *J. Chem. Soc., Dalton Trans.*, 1996, 271.
5 R. E. Allan, M. A. Beswick, N. Feeder, M. Kranz, M. E. G. Mosquera, P. R. Raithby, A. E. H. Wheatley and D. S. Wright, *Inorg. Chem.*, 1998, **37**, 2602.
6 R. Holland, J. C. Jeffery and C. A. Russell, *J. Chem. Soc., Dalton Trans.*, 1999, 3331.
7 W. Clegg, L. Horsburgh, F. M. Mackenzie and R. E. Mulvey, *J. Chem. Soc., Chem. Commun.*, 1995, 2011.
8 R. v. Bülow, H. Gornitzka, T. Kottke and D. Stalke, *Chem. Commun.*, 1996, 1639.
9 D. Barr, W. Clegg, L. Cowton, L. Horsburgh, F. M. Mackenzie and R. E. Mulvey, *J. Chem. Soc., Chem. Commun.*, 1995, 891.
10 W. Clegg, K. W. Henderson, L. Horsburgh, F. M. Mackenzie and R. E. Mulvey, *Chem. Eur. J.*, 1998, **4**, 53.
11 U. Schümann and E. Weiss, *Angew. Chem.*, 1988, **100**, 573; *Angew. Chem., Int. Ed. Engl.*, 1988, **27**, 584.
12 D. Barr, W. Clegg, R. E. Mulvey and R. Snaith, *J. Chem. Soc., Chem. Commun.*, 1984, 226.
13 G. Boche, I. Langlotz, M. Marsch, K. Harms and N. E. S. Nudelman, *Angew. Chem.*, 1992, **104**, 1239; *Angew. Chem., Int. Ed. Engl.*, 1992, **31**, 1205.
14 N. D. R. Barnett, W. Clegg, L. Horsburgh, D. M. Lindsay, Q.-Y. Liu, F. M. Mackenzie, R. E. Mulvey and P. G. Williard, *Chem. Commun.*, 1996, 1639.
15 G. R. Kowach, C. J. Warren, R. C. Haushalter and R. J. DiSalvo, *Inorg. Chem.*, 1998, **37**, 156.
16 A. R. Kennedy, R. E. Mulvey and A. Robertson, *Chem. Commun.*, 1998, 89.
17 T. Chivers, A. Downard and M. Parvez, *Inorg. Chem.*, 1999, **38**, 4347.

Communication a909754f

Probing the catalytic oxidation of alcohols *via* an anionic dimolybdate centre using multistage mass spectrometry

Tom Waters, Richard A. J. O'Hair* and Anthony G. Wedd

School of Chemistry, University of Melbourne, Parkville, Victoria 3052, Australia.
E-mail: r.ohair@chemistry.unimelb.edu.au

Received (in Cambridge, UK) 26th November 1999, Accepted 6th January 2000

Multistage mass spectrometry experiments in a quadrupole ion trap combined with isotope labelling have revealed a novel gas phase catalytic cycle for the oxidation of alcohols *via* an anionic dimolybdate centre.

We report the catalytic oxidation of alcohols in the gas phase using a dimolybdate anion as the active species. The nature of each step in the catalytic cycle can be probed through (i) multistage mass spectrometry experiments using a modified quadrupole ion trap mass spectrometer[1] and (ii) isotope substitution experiments which involve labelling of neutral reagents and the dimolybdate centre.

Complex reactivity of alcohols in the gas phase has been observed for highly unsaturated transition metal ionic species,[2,3] including oxo–molybdenum cations.[2] In contrast, the present study demonstrates 'simple' modes of reactivity with an oxo–molybdenum anion which allow catalytic behaviour. The observation by multistage mass spectrometry of true gas phase oxidation catalysed by transition metal ions remains rare.[4] In addition, the present system may shed light on the industrial oxidation of methanol to formaldehyde as catalysed by amorphous solid state molybdate catalysts.[5] A detailed molecular understanding of the mechanisms of this process remains elusive.[6]

Quaternary ammonium salts of the dimolybdate anion in MeCN can be transferred to the gas phase *via* electrospray ionisation.[7] The main species observed are the dianion, $[Mo_2O_7]^{2-}$ **A** and the ion pair, $\{N(CH_2R)_4^+[Mo_2O_7]^{2-}\}^-$ **B**.[8] Both these species can act as precursors of $[Mo_2O_6(OCH_2R)]^-$ **C** which catalyses the oxygen atom transfer reaction (1) (Scheme 1; R = alkyl, R′ = aryl, alkyl):

$$RCH_2OH + R'NO_2 \rightarrow RCHO + H_2O + R'NO \qquad (1)$$

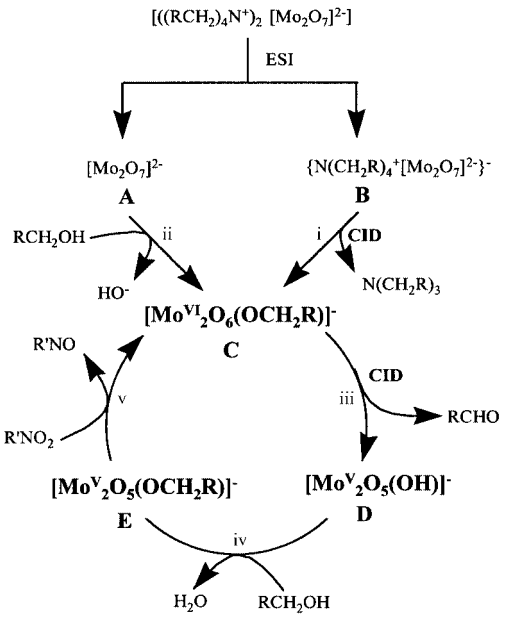

Scheme 1

Collision induced dissociation (CID) of **B** initiates an ion pair S_N2 reaction,[9] resulting in loss of trialkylamine and O-alkylation of **A** to form an alkylated dimolybdate species, **C** (Scheme 1(i)). Note that: (i) this is the first report of an ion pair S_N2 reaction involving an inorganic dianion and a tetraalkylammonium cation (*cf.* ref. 10) and (ii) thermolysis of trialkyloxonium salts of $[PMo_{12}O_{40}]^{3-}$ in the condensed phase also results in S_N2 O-alkylation.[11]

Gas phase ion–molecule reactions of **A**with various alcohols also yields **C**.[12] Labelling studies with $CH_3{}^{18}OH$ clearly reveal that this is not an S_N2 reaction (Fig. 1(a)). Rather, deprotonation of alcohol by a terminal oxo ligand[13] is followed by displacement of the resultant hydroxo ligand by the alkoxy anion (Scheme 1(ii), Table 1).

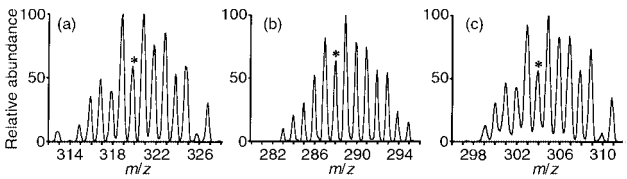

Fig. 1 Expansion of the isotope patterns for key product ions from gas phase reactions involving ^{18}O labelling experiments. The central peak of lower intensity in the isotope pattern is denoted by an asterisk, and is used to evaluate the outcome of the reaction. The numbering of the species and reactions is as according to Scheme 1. (a) shows that the product ion **C** from reaction (ii) is $[Mo_2O_6(^{18}OMe)]^-$; (b) shows that $[Mo_2O_6(^{18}OMe)]^-$ loses $CH_2{}^{18}O$ in reaction (iii), with concomitant formation of the product ion **D** $[Mo^V{}_2O_5(OH)]^-$; (c) shows that the product ion **E** from reaction (iv) is $[Mo^V{}_2O_5(^{18}OMe)]^-$.

CID of the alkylated dimolybdate species **C** results in reductive elimination of the alkoxo ligand as the aldehyde (Scheme 1(iii)). This corresponds to the formal redox half reaction: $RCH_2O^- \rightarrow RCHO + H^+ + 2e^-$. In the complementary half reaction, the dimolybdate(VI) centre is reduced by $2e^-$ and protonated to form $[Mo^V{}_2O_5(OH)]^-$ **D**. Labelling studies indicate that the oxygen from the alkoxo ligand is lost in this step (*i.e.* $CH_2{}^{18}O$ is lost; Fig. 1(b), Table 1).

The cycle is continued when **D** rapidly reacts with alcohol to form $[Mo^V{}_2O_5(OCH_2R)]^-$ **E** (Scheme 1(iv)). Once again the labelling studies reveal that this is not an S_N2 reaction (Fig. 1(c)), but rather a gas phase esterification reaction.

To complete the cycle, **E** is oxidised *via* an oxygen atom transfer to regenerate **C** (Scheme 1(v)). This reaction requires the presence of a second neutral reagent (along with alcohol) in the ion trap. To date we have used *m*-fluoronitrobenzene and nitromethane (*i.e.* $R'NO_2$ where R′ is Me or *m*-C_6H_4F) as oxygen atom donors.[14] Injection of $R'NO_2$ in the absence of alcohol indicates that oxygen atom transfer to **D** is also possible. This pathway does not compete with reaction (v) in Scheme 1 in the presence of alcohol owing to the fast rate of esterification.[15]

The present system raises questions about the mechanism(s) involved in the industrial oxidation of alcohols as catalysed by solid state molybdate catalysts.[5,6] In particular, can a related cycle (*cf.* reactions (iii)–(v) of Scheme 1) be applied to the layer compound $Mo_2O_5(OMe)_2$, proposed as a model heterogeneous

Table 1 Ionic products from reactions of $[Mo_2O_7]^{2-}$ **A** and $\{NBu_4^+[Mo_2O_7]^{2-}\}^-$ **B** under multistage mass spectrometry conditions

	m/z of ionic products from reaction sequence:[a,b]				
	A $\xrightarrow{MS^2}$	**C** $\xrightarrow{MS^3}$	**D** $\xrightarrow{MS^4}$	**E** $\xrightarrow{MS^5}$	**C**
Alcohol	reaction (ii)	reaction (iii)	reaction (iv)	reaction (v)	
CH_3OH	151.5	318	288	302	318
CH_3OD[c]	151.5	318	288	302	318
CD_3OD[d]	151.5	321	289	305	321
$CH_3{}^{18}OH$[e]	151.5	320	288	304	320
EtOH	151.5	332	288	316	332
Pr^nOH	151.5	346	288	330	346
	B $\xrightarrow{MS^2}$	**C** $\xrightarrow{MS^3}$	**D** $\xrightarrow{MS^4}$	**E** $\xrightarrow{MS^5}$	**C**
	reaction (i)	reaction (iii)	reaction (iv)	reaction (v)	
CH_3OH	546	360	288	302	318
CH_3OD	546	360	288	302	318
CD_3OD	546	360	288	305	321
$CH_3{}^{18}OH$	546	360	288	304	320
EtOH	546	360	288	316	332
Pr^nOH	546	360	288	330	346

[a] *m/z* refers to the central peak of lower intensity in the isotope pattern. [b] Refer to Scheme 1 for labelling of ionic species. [c] A sample from Cambridge Isotope Laboratories (99% D). [d] A sample from Cambridge Isotope Laboratories (99.9% D). [e] A sample from Isotec (95%^{18}O).

catalyst?[6] Given its layer structure features alternating *trans*-$Mo^{VI}O(OMe)$ centres separated by bridging oxo ligands, a simple mechanism can be devised for the oxidation of MeOH to H_2CO involving two Mo^{VI} sites on adjacent layers. This accommodates the fact that O_2 transfers two O atoms (eqn. (2)), rather than the single O atom from $R'NO_2$ (eqn. (1))

$$2\ MeOH + O_2 \rightarrow 2\ CH_2O + H_2O \qquad (2)$$

Further gas phase work is underway to examine (i) whether larger polyoxoanions also catalyse the oxidation of alcohols; (ii) the behaviour of other oxygen atom transfer reagents (*e.g.* O_2); (iii) models of oxo–molybdenum and –tungsten enzymes which catalyse oxygen atom transfer reactions.[16]

R. A. J. O. acknowledges support from the Australian Research Council, the University of Melbourne for funds to purchase the LCQ and the trustees of the Selby foundation for a Selby Research Award. A. G. W acknowledges support from the Australian Research Council.

Notes and references

1 *Practical Aspects of Ion Trap Mass Spectrometry*, ed. R. E. March and J. F. J. Todd, CRC Press, Boca Raton, FL, 1995: (*a*) vol. 1 *Fundamentals of Ion Trap Mass Spectrometry*; (*b*) vol. 2 *Ion Trap Instrumentation.* The operation of the modified instrument has been described previously: G. E. Reid, R. J. Simpson and R. A. J. O'Hair, *Int. J. Mass Spectrom.*, 1999, **190**/**191**, 209.

2 E. F. Fialko, A. V. Kikhtenko and V. B. Goncharov, *Organometallics*, 1998, **17**, 25.

3 I. K. Gregor and R. C. Gregor, *J. Organomet. Chem.*, 1995, **486**, 109 and references cited therein.

4 For FTICR studies on catalytic oxidation of (*a*) olefins, see: D. Stockigt and H. Schwarz, *Liebigs. Ann.*, 1995, 429; (*b*) CO, see: E. F. Fialko, A. V. Kikhtenko, V. B. Goncharov and K. I. Zamaraev, *Catal. Lett.*, 1996, **41**, 7.

5 H. R. Gerberich, A. L. Stautzenberger and W. C. Hopkins, *Formaldehyde*, in *Kirk-Othmer Encyclopedia of Chemical Technology*, ed. M. Grayson and D. Eckroth, Wiley, New York, 3rd edn., 1980, vol. 11, pp. 231–250.

6 E. M. McCarron, R. L. Harlow, Z. G. Li, C. Suto and Y. Yuen, *J. Solid State Chem.*, 1998, **136**, 247 and references therein.

7 Electrospray solutions were made to 0.1 g mL^{-1} in MeCN. Typical ESI conditions: Sheath gas flow rate 50 (arbitrary units), auxilliary gas flow rate 0 (arbitrary units), spray voltage 3 kV, capillary temp. 100 °C, capillary voltage –5 V, tube lens offset –5 V.

8 For previous studies on ESI/MS of polyoxoanions, see: T.-C. Lau, J. Wang, R. Guevremont and K. W. M. Siu, *J. Chem. Soc., Chem. Commun.*, 1995, 877.

9 We have also observed gas phase S_N2 reactions of **A** with neutral reagents such as MeI and Me_3SiCl.

10 S. Gronert and J. Azebu, *Org. Lett.*, 1999, **1**, 503.

11 W. H. Knoth and R. D. Farlee, *Inorg. Chem.*, 1984, **23**, 4765.

12 A range of molybdenum alkoxides $[Mo_2O_6(OCH_2R)]^-$ **C** where R = H, Me, Et or Pr^n can be 'synthesised' using reactions (i) and (ii) of Scheme 1. We have also discovered an alternative gas phase synthesis, involving a gas phase ion–molecule 'transesterification' reaction whereby one alkoxo ligand is replaced by another. Unfortunately the related *tert*-butoxide $[Mo_2O_6(OBu^t]^-$ is unavailable presently owing to the poor volatility of Bu^tOH.

13 We have also synthesised a dimolybdate centre in which the six terminal oxo ligands are labelled with ^{18}O (for related O isotope labelling studies of polyoxoanions, see: G. D. Hinch, D. E. Wycoff and R. K. Murmann, *Polyhedron*, 1986, **5**, 487). Upon reaction of labelled **A** with $CH_3{}^{16}OH$ a mass increase of 13 Da was observed (*cf.* 15 Da with unlabelled **A**) indicating loss of a terminal oxo ligand with $^{18}OH^-$.

14 For a review on related oxygen atom transfer reactions, see: R. H.Holm and J. P. Donahue, *Polyhedron*, 1993, **12**, 571.

15 Neutral reagents were injected at a flow rate of 3 μL min^{-1} at a split of 1:5000 in the ratio RCH_2OH: $R'NO_2$ = 4:1. At these conditions, reaction of $[Mo^V{}_2O_5(OH)]^-$ with EtOH and *m*-$FC_6H_4NO_2$ results in the formation of $[Mo^V{}_2O_5(OEt)]^-$ (*m/z* 316, from esterification) at the almost complete exclusion of $[Mo^{VI}{}_2O_6(OH)]^-$ (*m/z* 304, from oxidation). This confirms oxygen atom addition to $[Mo^V{}_2O_5(OH)]^-$ does not compete with esterification. All MS^n experiments were carried out using a *Q* value of 0.25. Ion-molecule reactions times were typically: reaction (ii) = 5 s; reaction (iv) = 20 ms; reaction (v) = 200 ms. Typical CID reactions were carried out for 30 ms using the following activation amplitudes: reaction (i) = 0.75 V; reaction (iii) = 0.65 V.

16 C. G. Young and A. G. Wedd, *Chem. Commun.*, 1997, 1251.

Communication a909353b

Asymmetric synthesis of *N*-acetylneuraminic acid

Sung Ho Kang,*[a] Hyeong-wook Choi,[a] Joon Seop Kim[a] and Joo-Hack Youn[b]

[a] *National Creative Research Institute Center for Asymmetric Reactions, Department of Chemistry, Korea Advanced Institute of Science and Technology, Taejon 305-701, Korea. E-mail: shkang@kaist.ac.kr*
[b] *Department of Chemical Engineering, Sun Moon University, Asan Si, Chung-Nam 336-840, Korea*

Received (in Cambridge, UK) 29th November 1999, Accepted 6th January 2000

A highly diastereoselective synthesis of *N*-acetylneuraminic acid 1 has been completed by stereoselective functionalization of *cis*-olefin 6 and *trans*-olefin 10 *via* intramolecular phenylselenoamidation and osmylation, respectively.

Sialic or neuraminic acids are a family of amino sugars comprising nine or more skeletal carbon atoms, and usually occur at the nonreducing terminal positions of oligosaccharides, glycoproteins and glycolipids.[1] They are involved in the modulation of a variety of important biological phenomena[2] such as cellular aggregation,[3] recognition,[4] lifetime[5] and viscosity of biofluids.[6] The family provides a potential therapeutic lead in developing inhibitors of sialidase[7] and sialyltransferase.[8] The most common member is the nine-carbon derivative 5-(acetylamino)-3,5-dideoxy-D-*glycero*-D-*galacto*-2-nonulosonic acid **1** (*N*-acetylneuraminic acid, Neu5Ac),[9] which is an essential constituent of sialoglycosphingolipids (ganglioside) and other glycoconjugates which mediate cellular interactions, differentiations and growth.[10]

While most of the known syntheses of Neu5Ac have been attained from carbohydrate sources,[11] only two syntheses have been established from noncarbohydrate precursors *via* hetero-Diels–Alder cycloaddition[12] and azido hydroxylation of *cis*-1,2-dihydrocatechol,[13] respectively. Its intriguing molecular structure and biological significance also led us to the enantioselective synthesis of *N*-acetylneuraminic acid **1** from diol **4**, which had been readily prepared from (*S*)-butane-1,2,4-triol.[14] The key steps of our synthetic route to **1** include the intramolecular phenylselenoamidation of *cis*-olefinic allylic trichloroacetimidate **3** and the stereoselective dihydroxylation of *trans*-olefin **2**, followed by introduction of the indispensable α-keto carboxylic acid functional group (Scheme 1).

Diol **4** was regioselectively protected by reacting with dibutyltin oxide in toluene using a Dean–Stark trap and subsequently with 2,4,6-trimethylbenzyl chloride in the presence of TBAB[15] to give a 7:1 mixture of the desired ether **5**, $[\alpha]_D^{20}$ + 19.9 (*c* 1.2, $CHCl_3$), and the isomeric secondary alkyl benzyl ether in 96% combined yield (Scheme 2). For the disposition of the required amino group and (*E*)-olefinic double bond, the allylic alcohol **5** was sequentially subjected to Cl_3CCN in the presence of DBU in MeCN and benzeneselenyl bromide in the presence of methyl trichloroacetimidate in a 4:1 mixture of MeCN and propylene oxide to provide *trans*-oxazoline **7**, $[\alpha]_D^{21}$ −18.4 (*c* 1.1, $CHCl_3$), in 67% yield. While the stereoisomeric *cis*-oxazoline could not be identified in the phenylselenocyclization, 9% of the enantiomerically pure tetrahydrofuran **8** was isolated as the major side product after hydrolysis. It is noted that methyl trichloroacetimidate and propylene oxide were expected to function as dehydrating agent and acid scavenger. The oxazoline ring of **7** was partially hydrolyzed in the presence of PPTS in aqueous acetone and the residual phenylselenyl group was oxidatively eliminated to afford *trans*-olefin **9**, $[\alpha]_D^{24}$ + 19.0 (*c* 1.2, $CHCl_3$), in 75% overall yield along with 5–6% of the corresponding *cis*-isomer.

The pendent amino and hydroxy groups of **9** were variously functionalized in order to induce the best stereoselectivity in the subsequent dihydroxylation of the olefinic double bond. In consequence, **9** was converted into dihydroxy oxazolidinone **10**, mp 110.3–111.0 °C, $[\alpha]_D^{25}$ + 23.9 (*c* 1.05, $CHCl_3$), in 91%

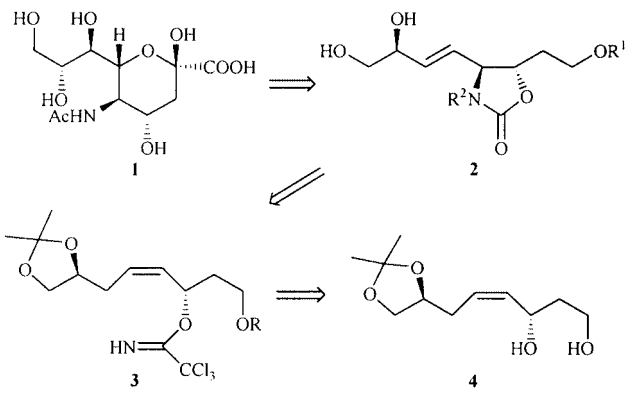

Scheme 1

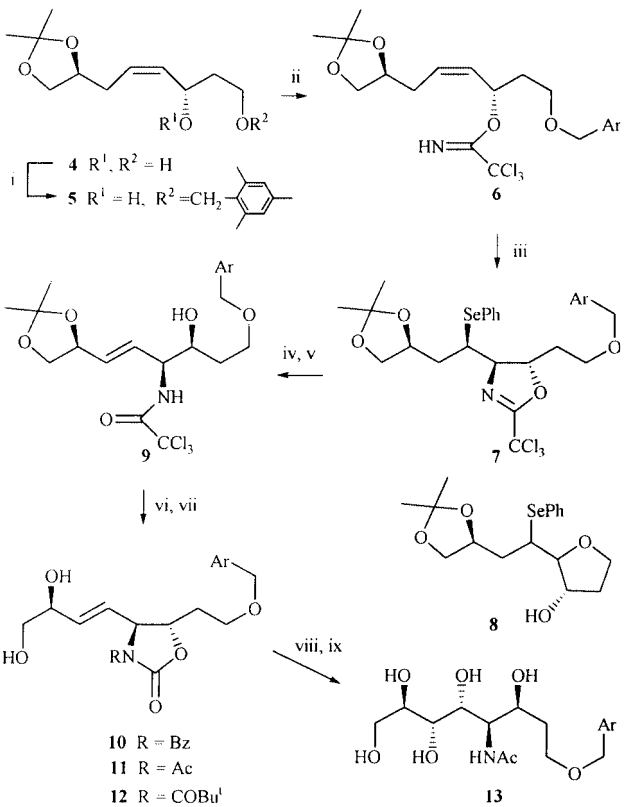

Scheme 2 *Reagents and conditions*: i, Bu_2SnO, PhMe, Dean–Stark trap, then 2,4,6-trimethylbenzyl chloride, Bu_4NBr, 80 °C; ii, Cl_3CCN, DBU, MeCN, −30 to −20 °C; iii, PhSeBr (3 equiv.), $MeOC(=NH)CCl_3$ (3 equiv.), propylene oxide–MeCN (1:4), −30 to 0 °C; iv, PPTS, H_2O–acetone (1:4), 20 °C; v, 30% H_2O_2, THF, 20 °C; vi, DBU, CH_2Cl_2, 20 °C, then BzCl, DMAP, Et_3N, 0 °C; vii, H_2O–AcOH (1:4), 20 °C; viii, OsO_4, NMO, H_2O–acetone (1:7), 0 °C; ix, $Ba(OH)_2$, H_2O–EtOH (1:2), 70 °C, then Ac_2O, 0 to 20 °C.

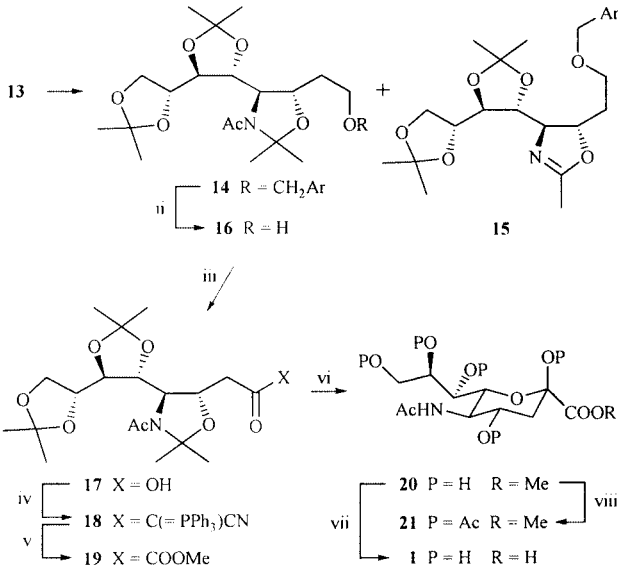

Scheme 3 *Reagents and conditions*: i, $C(OMe)_2Me_2$, PPTS, $CHCl_3$, 70 to 80 °C; ii, H_2, 20% $Pd(OH)_2/C$, $NaHCO_3$, EtOH, 20 °C; iii, $RuCl_3$ hydrate, $NaIO_4$, MeCN–CCl_4–H_2O (2:2:3), 20 °C; iv, $CH(=PPh_3)CN$, EDCl, DMAP, CH_2Cl_2, 20 °C; v, O_3, MeOH, −78 °C; vi, AcCl, MeOH, 20 °C; vii, K_2CO_3, H_2O, MeOH, 20 °C, then Dowex 50WX8-100 ion-exchange resin; viii, Ac_2O, DMAP, pyridine, 20 °C.

overall yield by a sequence of cyclization with DBU, *in situ* benzoylation with BzCl and deprotection in aqueous AcOH. The following dihydroxylation of **10** produced a mixture of several compounds, which seemed to be generated from migration of *N*-benzoyl group in the dihydroxylated products. The mixture was completely hydrolyzed with $Ba(OH)_2$ and the demasked amino group was acetylated in one pot to furnish an 18:1 mixture of the desired pentaol **13**, mp 190.4–191.0 °C, $[\alpha]_D^{22}$ −23.0 (*c* 0.3, MeOH) and the diastereomeric pentaol in 81% combined overall yield. Interestingly, dihydroxylation of acetyl carbamate **11** and pivaloyl carbamate **12** resulted in much lower stereoselectivities of 9:1 and 7:1, respectively.

Since **13** comprises all the requisite chiral functional groups of *N*-acetylneuraminic acid **1**, the remaining synthetic operation is to transform the benzyloxy group into an α-keto carboxylic acid functionality. Accordingly, **13** was protected as a triacetonide using 2,2-dimethoxypropane in the presence of PPTS in $CHCl_3$ to give the desired triacetonide **14** $[\alpha]_D^{22}$ −14.3 (*c* 1.2, $CHCl_3$), in 74% yield along with 12% of diacetonide oxazoline **15**, which was more significantly formed under a variety of other attempted reaction conditions (Scheme 3). After debenzylation of **14** in 94% yield by hydrogenolysis, Wasserman's protocol[16] was employed for the installation of α-keto carboxylate moiety to primary alcohol **16**, $[\alpha]_D^{24}$ −16.0 (*c* 0.9, $CHCl_3$). Alcohol **16** was oxidized with $NaIO_4$ in the presence of $RuCl_3$, followed by coupling with $CH(=PPh_3)CN$ in the presence of EDCI and DMAP. The resulting phosphorane **18** was exposed to O_3 in MeOH to provide α-keto ester **19**, $[\alpha]_D^{16}$ −11.9 (*c* 1.46, $CHCl_3$), in 71% overall yield from **16**. Triacetonide **19** was consecutively deprotected and cyclized with methanolic HCl, and then the generated methyl ester **20**[17,18] was hydrolyzed to *N*-acetylneuraminic acid **1**, $[\alpha]_D^{17}$ −32.0 (*c* 1.19, H_2O),[11b] in 84% overall yield. For further identification, **20** was peracetylated with Ac_2O to produce a 6:1 mixture of pentaacetate **21**, $[\alpha]_D^{18}$ −32.0 (*c* 0.54, $CHCl_3$),[11f,17c,18] and the corresponding anomeric acetate.[19]

This work was supported by Creative Research Initiatives of the Korean Ministry of Science and Technology.

Notes and references

1 *Sialic Acids: Chemistry, Metabolism and Function in Cell Biology Monographs*, ed. R. Schauer, Springer Verlag, Wien, New York, 1982, vol. 10.
2 M. von Itzstein and R. J. Thompson, *Top. Curr. Chem.*, 1997, **186**, 119.
3 R. B. Kemp, *J. Cell Sci.*, 1970, **6**, 751.
4 R. Schauer, *Pure Appl. Chem.*, 1984, **56**, 797; R. Schauer, *Trends Biochem. Sci.*, 1985, **10**, 357.
5 J. M. Jancik, R. Schauer and H. J. Z. Streicher, *Physiol. Chem.*, 1975, **356**, 1329.
6 F. Ahmad and P. McPhie, *Int. J. Biochem.*, 1980, **11**, 91.
7 E. Zbiral, E. Schreiner, R. Chiristian, R. G. Kleineidam and R. Schauer, *Liebigs Ann. Chem.*, 1989, 159.
8 M. Hartann, R. Chiristian and E. Zbiral, *Liebigs Ann. Chem.*, 1990, 83; E. Schreiner, R. Chiristian and E. Zbiral, *Liebigs Ann. Chem.*, 1990, 93.
9 A. Gottschalk, *Nature*, 1951, **167**, 845; M. Czarnicki and E. Thornton, *J. Am. Chem. Soc.*, 1977, **99**, 8279.
10 W. Spevak, J. O. Nagy, D. H. Charych, M. E. Schaefer, J. H. Gilbert and M. D. Bednarski, *J. Am. Chem. Soc.*, 1993, **115**, 1146; A. Giannis, *Angew. Chem., Int. Ed. Engl.*, 1994, **33**, 178.
11 For the references of earlier syntheses, see (*a*) M. P. DeNinno, *Synthesis*, 1991, 583; (*b*) T. Yamamoto, T. Teshima, K. Inami and T. Shiba, *Tetrahedron Lett.*, 1992, **32**, 325; (*c*) L.-H. Lin, T. Sugai, R. L. Halcomb, Y. Ichigawa and C.-H. Wong, *J. Am. Chem. Soc.*, 1992, **114**, 10 138; (*d*) D. M. Gordon and G. M. Whitesides, *J. Org. Chem.*, 1993, **58**, 7937; (*e*) T.-H. Chan and M.-C. Lee, *J. Org. Chem.*, 1995, **60**, 4228; (*f*) T. Takahashi, H. Tsukamoto, M. Kurosaki and H. Yamada, *Synlett*, 1997, 1065.
12 S. J. Danishefsky, M. P. DeNinno and S. Chen, *J. Am. Chem. Soc.*, 1988, **110**, 3929.
13 M. Banwell, C. D. Savi and K. Watson, *J. Chem. Soc., Perkin Trans. 1*, 1988, 2251.
14 S. H. Kang and J. S. Kim, *Chem. Commun.*, 1998, 1353.
15 S. David and S. Hanessian, *Tetrahedron*, 1985, **41**, 643.
16 H. H. Wasserman and W.-B. Ho, *J. Org. Chem.*, 1994, **59**, 4364.
17 (*a*) J. Haverkamp, H. Van Halbeek, L. Donald, J. F. G. Vliegenthart, R. Pfeil and R. Schauer, *Eur. J. Biochem.*, 1982, **122**, 305; (*b*) F. Baumberger and A. Vasella, *Helv. Chim. Acta*, 1986, **69**, 1205; (*c*) A. Marra and P. Sinay, *Carbohydr. Res.*, 1989, **190**, 317.
18 The spectroscopic data of the synthetic **20** and **21** are identical to those of **20** and **21** prepared from the commercially available Neu5Ac **1** (Aldrich).
19 All new compounds showed satisfactory spectral data.

Communication a909400h

ChemComm

A molecular colour sensor for monosaccharides†

Christopher J. Ward,[a] Prakash Patel,[b] Peter R. Ashton[a] and Tony D. James*[a]

[a] *The University of Birmingham, School of Chemistry, Edgbaston, Birmingham, UK B15 2TT. E-mail: tdjames@chemistry.bham.ac.uk*
[b] *AVECIA Limited, Hexagon House, PO Box 42, Blackley, Manchester, UK M9 8ZS*

Received (in Cambridge, UK) 22nd November 1999, Accepted 23rd December 1999

Boronic acid colour sensor 2 undergoes a large visible colour change, from purple to red in aqueous solution on the addition of monosaccharides.

Much recent attention has been paid to the development of synthetic molecular receptors with the ability to recognise neutral organic species, including saccharides. A large majority of these systems have utilised hydrogen bonding interactions for the purposes of recognition and binding of guest species. However, there is still no designed, monomeric receptor which can compete effectively with bulk water for low concentrations of monosaccharide substrates.[1]

Boronic acids readily and reversibly form cyclic esters with diols in aqueous basic media. Saccharides contain a linked array of hydroxy groups ideal for binding to boronic acids. The most common interaction is with 1,2- and 1,3-diols of saccharides to form five- or six-membered rings respectively *via* two covalent bonds. Lorand and Edwards determined the selectivity and first stability trends of various polyols and saccharides towards phenylboronic acid.[2]

The complex stability increases from ethylene glycol to D-fructose, *i.e.* from the simple acyclic diols to the rigid, vicinal *cis*-diols of saccharides. This observed selectivity order is common to all monoboronic acids, not just to phenylboronic acid.[3] The suitability of the boronic acid functionality as a receptor for saccharides has been established in both circular dichroism and fluorescence detection studies. Indeed, a number of fluorescent sensors have been reported in the literature.[4–6]

A fairly recent development has been the study of the effect of saccharides on the colour of dyes containing boronic acid functionality. Russell[7] synthesised a boronic acid azo dye from *m*-aminophenylboronic acid which was found to be sensitive to saccharides. Nagasaki, Shinmori and Shinkai observed that chromophores containing boronic acid moieties and which aggregate in water, changed colour and deaggregated upon addition of saccharides.[8] This year Strongin[9] reported a system based on resorcinarenes for the visual sensing of saccharides. However, for a colour change to be observed the saccharide must be heated (90 °C) in DMSO.

In 1994 Sandanayake and Shinkai reported 'the first known synthetic molecular colour sensor for saccharides'.[10] This designed molecular internal charge transfer (ICT) sensor, dye molecule **1**, was based on the intramolecular interaction between the tertiary amine and the boronic acid group.[11,12] The electron-rich amine creates a basic environment around the electron-deficient boron centre, which has the effect of inducing the boronic acid–saccharide interaction and reducing the working pH of the sensor.[13] Electronic changes associated with this decrease in the pK_a of the boronic acid moiety on saccharide complexation were shown to be transmitted to the neighbouring amine. This creates a spectral change in the connected ICT chromophore, which can be detected spectrophotometrically. The pK_a value associated with the boron–nitrogen interaction shifted on saccharide addition.

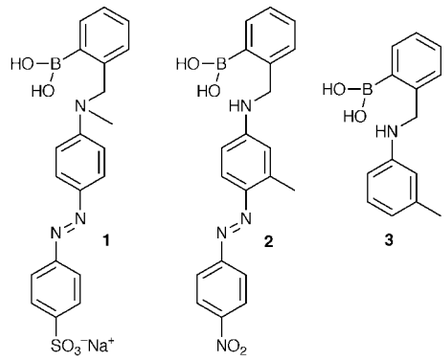

The main drawback of this system is the relatively small shifts in the absorption bands of the chromophore upon saccharide binding. The aim with this research was to develop a molecular ICT sensor, which produces a large visible colour change on saccharide binding. If a system with a large colour change can be developed it could be incorporated into a diagnostic test paper for D-glucose, similar to universal indicator paper for pH. Such a system would make it possible to measure D-glucose concentrations without the need of specialist instrumentation. This would be of particular benefit to diabetics in developing countries.

Dye molecule **2** was prepared in three steps in high yield.‡ The imine formed between comercial 2-formylphenylboronic acid and *m*-toluidine was reduced using $NaBH_4$ to give amine **3** in 75% yield. The final step is to couple **3** with the diazonium salt of 4-nitroaniline to give the boronic acid azo dye molecule **2** in 74% yield. The *m*-methyl group of **3** ensures that only the *p*-isomer is obtained.[14]

Absorption–pH titrations, from pH 2 to 12, of **2** in 0.05 mol dm^{-3} NaCl in MeOH–H_2O (1:2, w/w), were followed using a UV-VIS spectrometer. The experiments were then repeated with 0.05 mol dm^{-3} D-fructose also present. The NaCl present acts as an ionic buffer because small amounts of NaCl are formed on adjustment of the pH with NaOH and HCl. Because the titrations are carried out in a MeOH–H_2O mixture rather than simply water, the concept of pH is not strictly applicable to this situation. However, De Ligny and Rehbach have shown that for solutions in 50% MeOH the pH is only changed by 0.1 of a pH unit compared to a 100% water solution.[15]

The pK_a of compound **2** calculated from the absorption–pH titrations[16] was 10.2 and in the presence of 0.05 M fructose the value drops to 6.95. This shift on saccharide binding is in agreement with previous work[2,3,5,6,10] and can be explained by the decrease in oxygen–boron–oxygen bond angle upon saccharide binding, which increases the acidity of the boron centre.[3]

During these titrations it was noted that the UV–VIS absorption maxima of **2** does not move to as long a wavelength at high pH with D-fructose present. To investigate this phenomenon D-fructose, D-glucose and ethylene glycol titrations were performed at pH 11.32. The absorption spectra of the D-glucose titrations are shown in Fig 1.

† Details of the colour changes upon addition of D-glucose to **2** are available as supplementary data, see http://www.rsc.org/suppdata/cc/a9/a909204h/

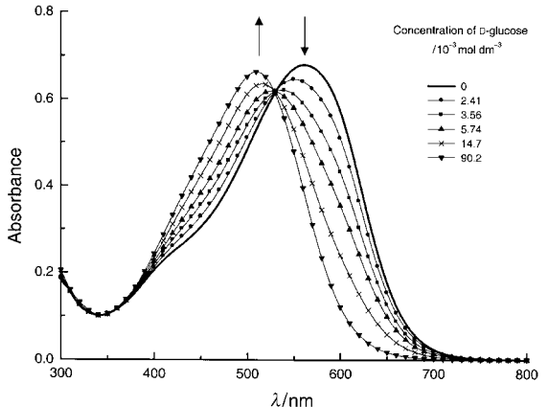

Fig. 1 Absorption spectral changes of dye molecule **2** (5.66×10^{-5} mol dm^{-3}) with increasing concentration of D-glucose at pH 11.32. pH 11.32 buffer: 0.01000 mol dm^{-3} KCl, 0.002771 mol dm^{-3} $NaHCO_3$, 0.002771 mol dm^{-3} Na_2CO_3 in 52.1% MeOH–47.9% H_2O (ref. 23).

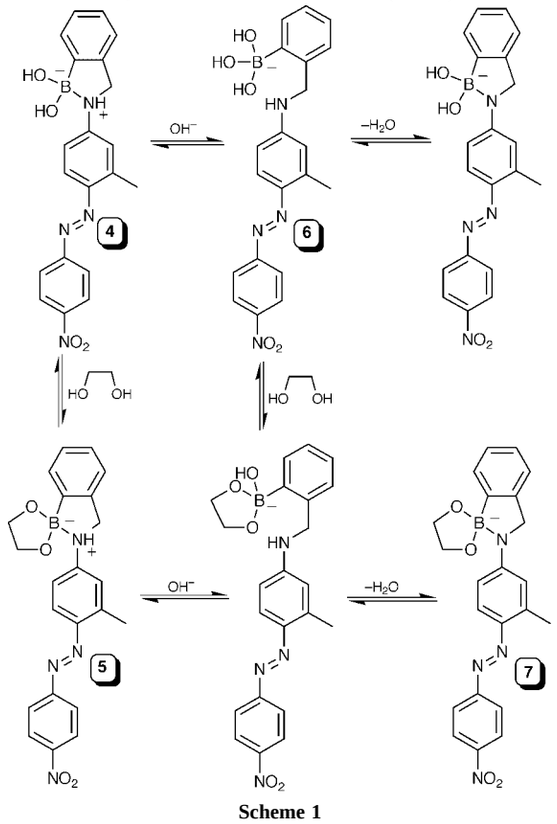

Scheme 1

The wavelength shifts by *ca.* 55 nm to shorter wavelength upon guest complexation. The concentration of the guest required to produce the change is different in each case, which is due to the different stability constants of the binding species, as mentioned earlier.[2] The wavelength shift obtained with **2** on addition of diols is the largest observed to date. The stability constants (log*K*) of the boronic acid dye–saccharide complexes were calculated from UV–VIS absorption–concentration profiles. The log*K* vales are D-fructose (3.75), D-glucose (1.85) and ethylene glycol (0.66) respectively.

Scheme 1 shows the species in equilibria responsible for the observed colour change, consistent with the experimental results. With dye molecule **1** Shinkai proposes that at intermediate pH a boron–nitrogen interaction is prevalent, whereas at high and low pH this bond is broken.[10] What makes the equilibria of dye molecule **2** more interesting is the presence of the *anilinic hydrogen*, which can give rise to different species at high pH. This apparently simple modification in the molecular structure is responsible for the enhanced response of these dyes relative to those previously reported.

In the absence of saccharide, at pH 11.32, the observed colour is purple and in the presence of saccharide the colour is red.† From previous work it is known that when saccharides form cyclic boronate esters with boronic acids, the Lewis acidity of the boronic acid is enhanced and therefore the Lewis acid–base interaction between the boronic acid and the amine is strengthened.[3,12] This stronger B–N interaction will favour the red species over the equivalent saccharide bound purple species. The reason for this can be understood by considering species **4** and **5** from Scheme 1. In the presence of saccharide the B–N interaction in species **5** is stronger than that in species **4**. The increased B–N interaction of species **5** will make the N–H proton of species **5** more acidic than the corresponding proton in species **4**. Therefore at higher pH, species **5** will deprotonate to form the red species **7**, whereas the weaker B–N bond in species **4** is broken by hydroxide ion to form the purple coloured species **6**.§

The colour change arises from the different electronic environment of the anilinic nitrogen. The anilinic nitrogen is conjugated to the azo chromophore. A change in the environment of this nitrogen leads to changes in the energy levels of the n and π^* orbitals of the azo chromophore and hence to a change in the absorption energy and wavelength. The proposal of these equilibrium species may also explain why dye molecule **1** did not give a visible spectral shift on saccharide binding. Because the anilinic nitrogen is tertiary in nature rather than secondary, there is no possibility of deprotonation, so the high pH boron–nitrogen bond cannot be formed. Hence there is no differentiation between the equilibrium species at high pH and consequently no spectral shift is observed.

T. D. J. wishes to acknowledge the Royal Society for support through the award of a University Fellowship. C. J. W. wishes to acknowledge the EPSRC and AVECIA Limited for support through the award of a Studentship.

Notes and references

‡ *Selected data* for **2**: mp 120–122 °C (decomp.) (HRMS: Found: $[M]^+$, 372.1381, $C_{20}H_{17}BN_4O_3$ requires 372.1394); ν_{max}(KBr)/cm^{-1} 1602s, 1518s and 1333s; δ_H(300 MHz; CD_3OD; Me_4Si) 2.63 (3 H, m), 4.45 (2 H, br s), 6.52–6.58 (1 H, m), 6.99–7.04 (1 H, m), 7.18–7.40 (5 H, m), 7.63–7.72 (1 H, m), 7.87–7.93 (1 H, m), 8.21–8.36 (2 H, m); δ_C(125 MHz; CD_3OD; Me_4Si) 18.1, 49.7, 113.2, 114.7, 118.3, 122.7, 123.6, 125.7, 127.6, 128.1, 129.8, 130.2, 132.8, 144.3; *m/z* (EI) 373 ($[MH - H_2O]^+$, 66%), 222 ($[M - H_2O–N_2C_6H_4NO_2]^+$, 100).

§ Negative ion electrospray ionisation (ESI) mass spectrometry using a Micromass LCT spectrometer confirmed the presence of the red species **7** (*m/z* 533).

1 A. P. Davis and R. S. Wareham, *Angew. Chem., Int. Ed.*, 1999, **38**, 2978.
2 J. P. Lorand and J. O. Edwards, *J. Org. Chem.*, 1959, **24**, 769.
3 T. D. James, K. Sandanayake and S. Shinkai, *Angew. Chem., Int. Ed. Engl.*, 1996, **35**, 1911.
4 C. R. Cooper and T. D. James, *Chem. Commun.*, 1997, 1419.
5 C. R. Cooper and T. D. James, *Chem. Lett.*, 1998, 883.
6 T. D. James, P. Linnane and S. Shinkai, *Chem. Commun.*, 1996, 281.
7 A. P. Russell, WO 91/04488, 1991.
8 N. Nagasaki, H. Shinmori and S. Shinkai, *Tetrahedron Lett.*, 1994, **35**, 2201.
9 C. J. Davis, P. T. Lewis, M. E. McCarroll, M. W. Read, R. Cueto and R. M. Strongin, *Org. Lett.*, 1999, **1**, 331.
10 K. Sandanayake and S. Shinkai, *J. Chem. Soc., Chem. Commun.*, 1994, 1083.
11 H. S. Snyder, M. S. Konecky and W. J. Lennarz, *J. Am. Chem. Soc.*, 1958, **80**, 3611.
12 R. T. Hawkins and H. R. Snyder, *J. Am. Chem. Soc.*, 1960, **82**, 3863.
13 G. Wulff, *Pure Appl. Chem.*, 1982, **54**, 2093.
14 P. Gordon and P. Gregory, *Organic Chemistry in Colour*, Springer-Verlag, Berlin, 1990.
15 C. S. De Ligny and M. Rehbach, *Recl. Trav. Chim. Pays-Bas*, 1960, **79**, 727.
16 B. Valeur, J. Pouget, J. Bourson, M. Kaschke and N. P. Ernsting, *J. Phys. Chem.*, 1992, **96**, 6545.
17 D. D. Perrin and B. Dempsey, *Buffers for pH and Metal Ion Control*, Chapman & Hall, London 1974.

Communication a909204h

ChemComm

Photodimerisation of a styrylpyrazine amphiphile suppresses the release of glucose entrapped in its mixed vesicle with DPPC

Jong-Mok Park, Shigeru Aoyama, Wanbin Zhang, Yohji Nakatsuji and Isao Ikeda*

Department of Applied Chemistry, Faculty of Engineering, Osaka University, Yamadaoka 2-1, Suita, Osaka 565-0871, Japan. E-mail: ikeda@ap.chem.eng.osaka-u.ac.jp

Received (in Cambridge, UK) 1st October 1999, Accepted 5th January 2000

Photolysis of a styrylpyrazine amphiphile in the bilayer of a vesicle made from its mixture with DPPC, with irradiation above 300 nm, effectively suppressed the release of glucose entrapped in the vesicle, while the stilbene analogue induced a sudden perturbation to release the glucose under the same conditions.

Vesicles of lipid bilayers have been extensively studied as an excellent model for a drug-delivery system (DDS) over 20 years.[1] The study of DDSs using vesicles can be generally classified into two main areas: the transport of vesicles targeting a specified site in a living body, and the release control of drugs entrapped in the interior space of vesicles. Concerning the latter case, much effort has been devoted to introducing photochromic molecules such as azobenzene, spiropyran and stilbene into the bilayer of vesicles as a device for changing the permeability of the bilayer membrane in response to light irradiation.[2,3] Most of these studies, however, have been focused on application of intramolecular photochromism, such as *cis–trans* isomerism and a conformational isomerism in the case of spiropyran, to the release control system of substances entrapped in vesicles by light. Although this intramolecular photochromism has been successfully used to regulate the release rate with irradiation at two independent wavelengths, it was impossible to stabilize the bilayer and suppress the release using this strategy.

In our previous paper,[4] we reported that styrylpyrazine amphiphile **1** showed very fast and topochemically-controlled photodimerisation and intermolecular photochromism between

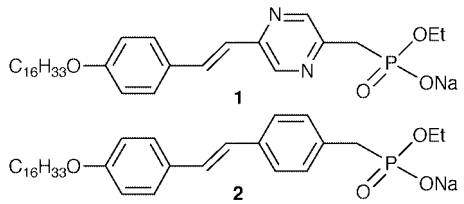

the monomer and its *syn* head-to-head cyclobutane dimer in aqueous dispersion. Our recent study has been directed toward application of this intermolecular photochromism to the photo-regulated release control of substances entrapped in vesicles. In the course of this study, we found that styrylpyrazine amphiphile **1** stabilizes the bilayer of the vesicle made from its mixture with L-α-dipalmitoyl phosphatidylcholine (DPPC) to suppress the release of glucose entrapped in the vesicle with irradiation above 300 nm, while the stilbene analogue **2** induces a sudden perturbation of the bilayer to release the glucose. Here we discuss these interesting observations from the point of view of the difference in molecular stacking modes of the two chromophores in the bilayer of the vesicles.

The mixed vesicles of **1** or **2** with DPPC were prepared by the conventional sonication method.† Permeability properties of the vesicles were studied by the measurement of glucose (%) released from vesicles in the course of storage time at 25 °C, as shown in Fig. 1. The release rate of glucose was decreased by incorporating **1** into the DPPC vesicle compared to that from the DPPC vesicle, whereas the release rate was greatly increased by incorporating **2** into the DPPC vesicle. Upon irradiation of the vesicle of **1** (**1**:DPPC = 1:4 molar ratio, hereafter referred to as vesicle **1**), which was stored for 13 h before irradiation, for 10 min under Ar atmosphere with a 500 W Xenon short-arc lamp through Pyrex glass, the release of glucose from the vesicle **1** was more suppressed than that from the untreated one. The mixtures of **1** with DPPC (**1**:DPPC = 1:3 and 1:2), however, were not able to form vesicles entrapping glucose under the same dispersion conditions. On the other hand, upon irradiation of the vesicle of **2** (**2**:DPPC = 1:6 molar ratio, hereafter referred to as vesicle **2**), which was stored for 17 h before irradiation, for 30 min under the same conditions, the release was initially accelerated and then suppressed. The vesicle of **2** (**2**:DPPC = 1:4 molar ratio) also indicated a similar acceleration effect of the release rate by the photolysis.

In order to explain these interesting results, we investigated the photochemical reactivities of **1** and **2** by irradiation above 300 nm in the bilayer matrix of DPPC vesicles by ^{1}H NMR spectroscopy. The aqueous dispersion of **1** (**1**:DPPC = 1:4) or **2** (**2**:DPPC = 1:6) obtained by the same procedure as referred to above was irradiated under Ar atmosphere with a 500 W Xenon short-arc lamp through Pyrex glass. ^{1}H NMR measurements were conducted in a mixed solvent (CD_3OD–$CDCl_3$ = 2:3) after removing the water *in vacuo*. It is obvious that the overall reaction process of **1** is very different from that of **2**, as shown in Fig. 2. In the case of **1**, the content (%) of the *trans*-monomer decreased rapidly with irradiation to give directly the corresponding *syn* head-to-head cyclobutane dimer, although a trace of the *cis*-isomer was detected. In the case of **2**, however, the content (%) of the *cis*-monomer increased rapidly to the

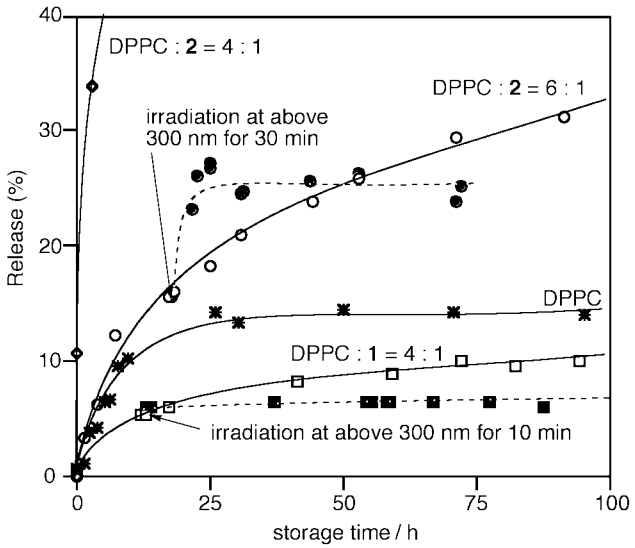

Fig. 1 Release (%) of glucose entrapped inside vesicles made from (※) DPPC, (□) a mixture of DPPC:**1** = 4:1, (■) DPPC:**1** = 4:1 after irradiation above 300 nm for 10 min at time = 13 h, (○) DPPC:**2** = 6:1, (●) DPPC:**2** = 6:1 after irradiation above 300 nm for 30 min at time = 17 h and (◇) DPPC:**2** = 4:1 as a function of storage time at 25 °C.

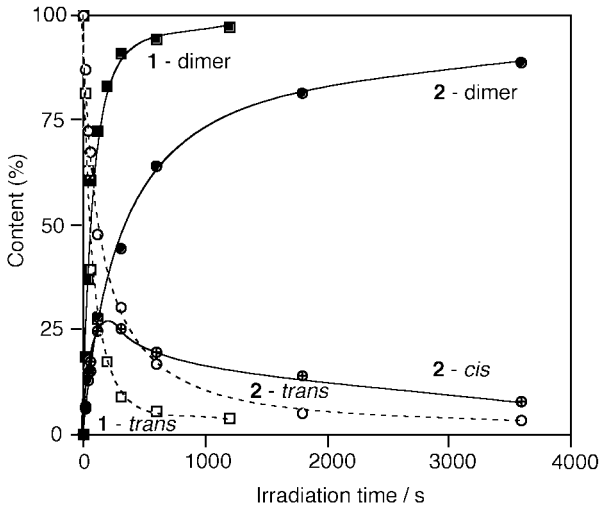

Fig. 2 Comparison of photoreactivities of **1** and **2** incorporated in the bilayer matrix of DPPC with irradiation at above 300 nm. Variation of content (%) of (□) **1**-*trans*, (■) **1**-*syn* head-to-head dimer, (○) **2**-*trans*, (⊕) **2**-*cis* and (●) **2**-*syn* head-to-head dimer as a function of the time of irradiation, where the suspension of **1** or **2** was prepared by dispersion of the mixture (**1**:DPPC = 4 μmol:16 μmol) or (**2**:DPPC = 2.8 μmol:17.2 μmol) in 2 ml of Milli-Q water, respectively.

level of 25% at the initial stage of irradiation with simultaneous formation of the corresponding *syn* head-to-head cyclobutane dimer, and then decreased progressively with the increase of the dimer formation. The reaction behavior of **1** in the bilayer matrix of DPPC was similar to that in the pure aqueous dispersion.[4] This observation suggests that **1** forms aggregates with a 'translation' structure having a strong face-to-face stacking through the multipole-multipole interaction even when **1** is diluted in the bilayer matrix of DPPC and, therefore, the photoisomerism is suppressed by the strong aggregation. On the other hand, the reaction behavior of **2** in the bilayer matrix of DPPC was considerably different from that in the aqueous dispersion.[4] The pure aqueous dispersion of **2** did not form the *cis*-monomer upon irradiation above 300 nm, while 5.5 mol% of 4-hexylstilbene-4′-butyric acid in a dihexadecyl phosphate vesicle gave a photostationary state containing 80% *cis*- and 20% *trans*-isomer upon irradiation at 315 nm.[3] These observations suggest that the intermolecular interaction of **2** is much weaker than that of **1** in the aggregate and, therefore, the fluidity of the bilayer membrane of the vesicle **2** is much higher than that of the vesicle **1**. This speculation is supported by the higher phase transition temperature (T_c) from the gel state to the liquid crystalline state of pure **1** (64 °C) than that of pure **2** (53 °C),[4] and the much lower permeability of the vesicle **1** (1:4) than that of the vesicle **2** (1:4). The weak intermolecular interaction of **2** may be due to the 'pinwheel' unit[5] aggregate having a face-to-edge stacking, as proposed by Whitten *et al.*

It is well known that the photoisomerisation of amphiphilic compounds containing *trans*-azobenzene and *trans*-stilbene to the *cis*-isomers in the bilayer membrane of vesicles increases the permeability of substances entrapped in their vesicles.[2] Therefore, the drastic acceleration of the release from the vesicle **2** at the initial stage of photolysis can be reasonably explained by considering the perturbation of the bilayer membrane induced by formation of the *cis*-isomer, and the suppression of the release from the vesicle **2** at the late stage and from the vesicle **1** may be ascribed to the formation of the corresponding *syn* head-to-head cyclobutane dimers. This was confirmed by investigating the release from the vesicle made from the pure *syn* head-to-head cyclobutane dimer of **1** and DPPC (1:8), the extent of which was smaller than that from the vesicle **1**.

Recently, a 'catastrophic' destruction of the vesicle made from a mixture of a styrylthiophene amphiphile with DPPC through the photodimerisation of the styrylthiophene,[6] inducing the release of substance entrapped within the vesicle, has been reported by Whitten *et al.* They proposed that the aggregation structure of the styrylthiophene amphiphile is a 'pinwheel' tetramer having face-to-edge stacking in the bilayer matrix of DPPC and, therefore, on the occasion of photodimerisation, some additional motion should be necessary to bring adjacent molecules close enough to dimerise. They pointed out the dimerisation, including a structural change, as the main reason for the vesicle disruption.

Considering the release property of the vesicle **2** and Whitten's result,[6] suppression of the release from the vesicle **1** without any perturbation during the dimerisation is unique. A simple topologically-controlled photodimerisation is expected to result in minimal disruption of the vesicle microstructure. Obviously, the vesicle **1** is just such a case. To the best of our knowledge, this is the first case for clean suppression of the release of substances from vesicles by [2 + 2] cycloaddition.

From the viewpoint of using the photochromism between a 1,2-diarylethylene monomer and the corresponding cyclobutane dimer as a new strategy for controlling the release of substances entrapped in vesicles, this clean suppression of the release is noteworthy. Naturally, since the reverse reaction, the cleavage of the cyclobutane dimer to the monomer,[4] is expected to increase the release rate, further study on the reversible release-control of vesicles by using **1** is now in progress in our laboratory.

Notes and references

† The thin layers of the mixtures **1** (**1**:DPPC = 4 μmole:16 μmole), or **2** (**2**:DPPC = 4 μmole:16 μmole, 2.8 μmole:17.2 μmole) with DPPC were prepared on the inside wall of a test tube by dissolving them in 2.5 ml of a MeOH–$CHCl_3$ (1:4, v/v) mixed solvent and evaporating the solvent *in vacuo*. After drying in a vacuum desiccator, 2 ml of an aqueous solution of glucose (300 mM) was added and sonicated for 5 min at 70 °C with a probe-type sonicator. Small unilamellar vesicles containing glucose were separated from the untrapped glucose by gel-filtration chromatography (Sephadex G-50, 1.5 × 18 cm, eluent: 150 mM NaCl aqueous solution). The formation of vesicles was confirmed by a well-established gel-filtration method (ref. 7). The determination of glucose was conducted by the measurement of absorbance at 505 nm of quinone dye produced by the Mutarotase GOD method described by Miwa *et al.* (ref. 8). The amount of glucose released (%) from the vesicles was calculated using eqn. (1),

$$\text{Glucose released (\%)} = A_t/A_{total} \times 100 \quad (1)$$

where A_t is the absorbance of the suspension after a definite period of storage, and A_{total} is the absorbance after addition of an aqueous solution of Triton X-100 (200 g l^{-1}) to the suspension.

1 A. D. Bangham, M. M. Standish and J. C. Watkins, *J. Mol. Biol.*, 1965, **13**, 238.
2 Y. Ohya, Y. Okuyama, A. Fukunaga and T. Ouchi, *Supramol. Sci.*, 1998, **5**, 21; C. G. Morgan, Y. P. Yianni, S. S. Sandhu and A. C. Mitchell, *Photochem. Photobiol.*, 1995, **62**, 24; C. G. Morgan, E. W. Thomas, S. S. Sandhu, Y. P. Yianni and A. C. Mitchell, *Biochim. Biophys. Acta*, 1987, **903**, 504.
3 Y. Lei and J. K. Hurst, *Langmuir*, 1999, **15**, 3424.
4 J. Park, W. Zhang, Y. Nakatsuji, T. Majima and I. Ikeda, *Chem. Lett.*, 1999, 1309.
5 X. Song, C. Geiger, U. Leinhos, J. Perlstein and D. G. Whitten, *J. Am. Chem. Soc.*, 1994, **116**, 10 340; H. Chen, M. S. Farahat, K. Law and D. G. Whitten, *J. Am. Chem. Soc.*, 1996, **118**, 2584; S. Vaday, H. C. Geiger, B. Cleary, J. Perlstein and D. G. Whitten, *J. Phys. Chem. B*, 1997, **101**, 321.
6 X. Song, J. Perlstein and D. G. Whitten, *J. Phys. Chem. A*, 1998, **102**, 5440.
7 M. Sugimoto, K. Shibahara, K. Kuroda, T. Hirao, H. Kurosawa and I. Ikeda, *Langmuir*, 1996, **12**, 2785.
8 I. Miwa, J. Okuda, K. Maeda and G. Okuda, *Clin. Chim. Acta*, 1972, **37**, 538.

Communication a907923h

Controlled/'living' radical polymerization of MMA *via in situ* ATRP process

Xiao-Ping Chen and Kun-Yuan Qiu*

Department of Polymer Science and Engineering, College of Chemistry and Molecular Engineering, Peking University, Beijing 100871, China. E-mail: kyqiu@chemms.chem.pku.edu.cn

Received (in Cambridge, UK) 19th November 1999, Accepted 23rd December 1999

Well-defined PMMA with very low polydispersity and α-Et_2NCS_2 and ω-Cl end groups was synthesized *via* a novel controlled/'living' radical polymerization (*in situ* ATRP process) using a tetraethylthiuram disulfide (TD)/$FeCl_3$/PPh_3 initiating system.

Recently, some effective controlled/'living' radical polymerization systems have been reported, such as stable free radical polymerization with 2,2,6,6-tetramethylpiperidinyl-1-oxyl (TEMPO),[1] atom transfer radical polymerization (ATRP) systems,[2,3] and reversible addition–fragmentation chain transfer (RAFT) systems.[4] Thus, the controlled/'living' radical polymerization has become a reality.

So far, there are two kinds of ATRP, *i.e.* conventional ATRP and reverse ATRP. In conventional ATRP, organic halides (RX) are used as initiators, transition-metal compounds in their lower oxidation state (M^n, where n is the oxidation state) are used as catalysts and electron-donating compounds are used as ligands (L). In this process, a dynamic equilibrium is established where the dormant polymer chains are reversibly activated *via* a halogen atom transfer reaction.

In reverse ATRP,[5–9] a radical initiator and a higher oxidation state transition-metal catalyst complex $M^{n+1}XL_m$ (where m is the number of ligands) are used. Reverse ATRP differs from conventional ATRP in the initiation step, where the initiating active species or the propagating active species can abstract a halogen atom from the oxidized transition-metal complex to form the dormant species and the reduced transition-metal species.

Here we report a novel ATRP (*in situ* ATRP), using TD/$FeCl_3$/PPh_3 as the initiating system. In the *in situ* ATRP process, the essential initiator [halide species (Et_2NCS_2Cl)], and the catalyst [transition-metal compound in its lower oxidation state ($FeCl_2$)] were both produced *in situ* from the reactions of TD and $FeCl_3$. The subsequent polymerization proceeded *via* a conventional ATRP process. The PMMAs synthesized using the TD/$FeCl_3$/PPh_3 system have very narrow polydispersities (1.04–1.07) and a very fast rate of polymerization.

The polymerization of MMA was carried out in bulk with the TD/$FeCl_3$/PPh_3 initiation system at 100 °C. Results for the system with the initial ratio of $[MMA]_0:[TD]_0:[FeCl_3]_0:[PPh_3]_0 \approx 200:1:10:30$ are shown in Fig. 1. It shows that the $M_{n\,(GPC)}$ (number-average molecular weight measured by GPC), increases linearly with conversion from 2200 to 7100, and the polydispersity index is very narrow (1.04–1.07) as the monomer conversion is increased from 21.5 to 85% in 8 min. The $M_{n\,(GPC)}$ is close to the $M_{n(th)}$, a theoretical number-average molecular weight computed from $M_{n(th)} = ([MMA]_0/2[TD]_0) \times MW_{MMA} \times$ conversion. The efficiencies of initiator f as calculated from $f = M_{n(th)}/M_{n(GPC)}$ are around 1.0. In a plot of $\ln([M]_0/[M])$ *vs.* time as shown in Fig. 2, a straight line is observed, indicating that the kinetics is first order in monomer. This means that the concentration of propagating radicals is constant during the polymerization.

When $[MMA]_0:[TD]_0:[FeCl_3]_0:[PPh_3]_0 \approx 200:1:10:30$, the results of solution polymerization of MMA in anisole are similar to those of bulk polymerization, while a lower rate of polymerization and slightly broader polydispersities (about 1.1) were obtained.

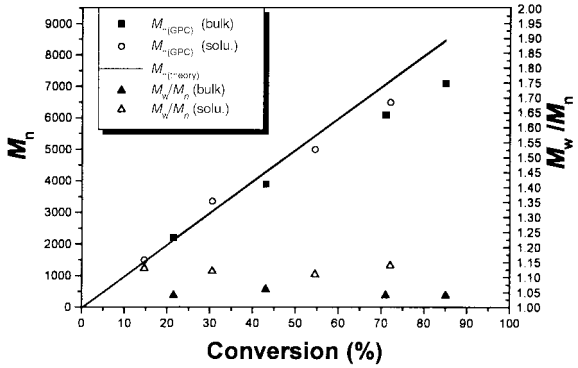

Fig. 1 Dependence of the PMMA molecular weight and polydispersity on the monomer conversion at 100 °C. Conditions: in bulk, $[MMA]_0 = 9.38$ mol l^{-1}, $[TD]_0 = 4.69 \times 10^{-2}$ mol l^{-1}, $[FeCl_3]_0 = 4.69 \times 10^{-1}$ mol l^{-1}, $[PPh_3]_0 = 1.41$ mol l^{-1}; in anisole, $[MMA]_0 = 4.69$ mol l^{-1}, $[TD]_0 = 2.35 \times 10^{-2}$ mol l^{-1}, $[FeCl_3]_0 = 2.35 \times 10^{-1}$ mol l^{-1}, $[PPh_3]_0 = 7.05 \times 10^{-1}$ mol l^{-1}. $M_{n(th)} = ([MMA]_0/2[TD]_0) \times MW_{MMA} \times$ conversion. Molecular weights and molecular weight distributions of polymer samples were measured using a Waters 515 GPC with polystyrene calibration standards.

From the results mentioned above, it can be observed that the MMA polymerization with the TD/$FeCl_3$/PPh_3 initiation system at 100 °C proceeds in a controlled/'living' manner.

From the FTIR, UV and NMR spectra, it can be seen that the Et_2NCS_2– group is one of the end groups of the polymer. The signals at 1267 and ~3450 cm^{-1} in the FTIR spectrum are characteristic absorption bands of the Et_2NCS_2– group. The UV spectrum of the PMMA powder identifies Et_2NCS_2– (~283 nm) is an end group. The number of Et_2NCS_2– groups was determined by UV spectroscopy in $CHCl_3$ to be *ca.* 1. In the ^1H NMR spectrum of the PMMA, the signal at δ_H 3.07 is that of the methylene of $Et_2NCS_2CH_2$–, and that at δ_H 3.70 is from the methylene of $(CH_3CH_2)_2NCS_2$–. The signal at δ_H 3.79 is that of the protons of the methoxy group, and that at δ_H 2.50 is from the methylene protons of the terminal MMA unit capped with an ω-chlorine, similar with that reported by Ando *et al.*[10] The $M_{n(NMR)}$ (6600) is close to $M_{n(GPC)}$ (6500), indicating that all the polymer chains have chlorine end groups. So, the polymers

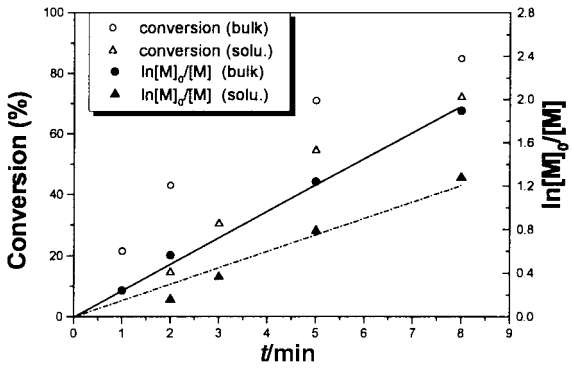

Fig. 2 Time dependence of $\ln[M]_0/[M]$ and conversion at 100 °C, where $[M]_0$ and $[M]$ are the MMA concentration at times 0 and t, respectively. Under the same conditions as in Fig. 1.

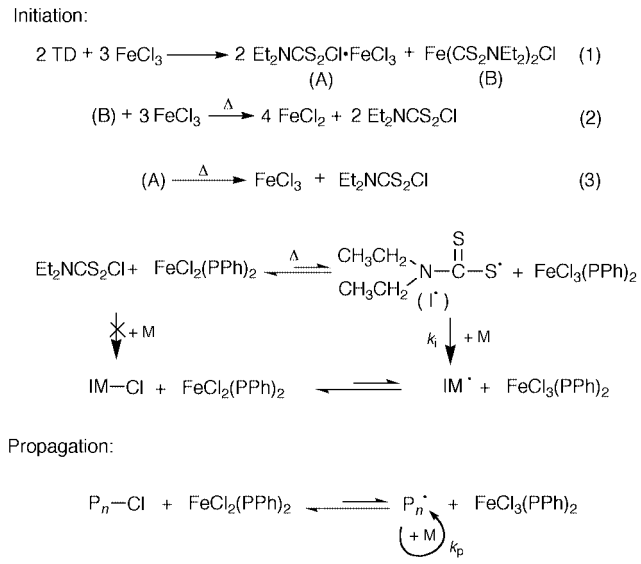

Scheme 1

produced using the initiation system are well-defined, not only with very narrow polydispersity but also with precise end groups, *i.e.* α-Et_2NCS_2– and ω-chlorine groups. The presence of an ω-chlorine end group in the obtained PMMA suggests the polymerization proceeds *via* an ATRP process.

In order to clarify the nature of the polymerization, we carried out some control experiments under fixed conditions: $[MMA]_0$ = 9.38 mol l^{-1}, $[TD]_0$ = 4.69 × 10^{-2} mol l^{-1}, $[FeCl_3]_0$ = 4.69 × 10^{-1} mol l^{-1}, $[PPh_3]_0$ = 1.41 mol l^{-1}, 100 °C. In this case, the conversion was 85% (8 min). However, the conversion decreased to 75% after 20 min in the presence of TEMPO ($[TEMPO]_0$ = 12.57 × 10^{-2} mol l^{-1}). This suggests that the activate species are possibly radicals. When H_2O was added ($[H_2O]_0$ = 281.4 × 10^{-2} mol l^{-1}), the polymerization still proceeded at a moderate rate with 49.3% conversion after 20 min. Generally speaking, MMA is an electron poor monomer and cannot be polymerized *via* a cationic process. It is impossible to perform an ionic polymerization in the presence of water ($[H_2O]_0/[TD]_0$ = ~60). Therefore, the polymerization with the TD/$FeCl_3$/PPh_3 system is a radical polymerization. When the polymerization was carried without the PPh_3 ligand, no polymer was obtained after 16 h but precipitated $FeCl_2$ was produced.

According to the results mentioned above, we propose a mechanism for the *in situ* ATRP as depicted in Scheme 1.

When TD was added to the mixture of $FeCl_3$, MMA and PPh_3 at room temperature, the color of the system instantly became dark green.[11] This indicated that TD rapidly reacted with $FeCl_3$ and two complex products of halide, $Et_2NCS_2Cl·FeCl_3$ (A) and $Fe(Et_2NCS_2)_2Cl$ (B) were produced,[12] as depicted in eqn. (1) in Scheme 1. At high temperature, such as 100 °C, (B) reacted with $FeCl_3$ to form Et_2NCS_2Cl and $FeCl_2$ [eqn. (2) in Scheme 1)]. (A) thermally decomposed into Et_2NCS_2Cl and $FeCl_3$ [eqn. (3) in Scheme 1]. Thus, the initiator (Et_2NCS_2Cl) and the transition-metal catalyst in its lower oxidation state ($FeCl_2$) for an ATRP system were *in situ* created. The primary radical $Et_2NCS_2^{\cdot}$, formed from the reaction of Et_2NCS_2Cl with $FeCl_2(PPh_3)_2$, can initiate MMA polymerization. The subsequent reactions proceeded following a conventional ATRP.

Due to the presence of an ω-chlorine end group on the polymer chain, chain extension polymerization of the PMMA can be carried out using a conventional ATRP initiation system. The results are as follows: in bulk at 100 °C, M_n of PMMA = 18 400, M_w/M_n = 1.11, $[PMMA]_0$ = 5.33 × 10^{-3} mol l^{-1}, $[MMA]_0$ = 8.23 mol l^{-1}, $[FeCl_2]_0$ = 5.33 × 10^{-3} mol l^{-1}, $[PPh_3]_0$ = 1.6 × 10^{-2} mol l^{-1}; a conversion of 70% was achieved after 36 h, M_n of the chain-extended PMMA = 157 700, M_w/M_n = 1.43.

Notes and references

1 M. K. Georges, R. P. N. Verergin, P. M. Kazmaier and G. K. Hamer, *Macromolecules*, 1993, **26**, 2987.
2 M. Kato, M. Kamigaito, M. Sawamoto and T. Higashimura, *Macromolecules*, 1995, **28**, 1721.
3 J. S. Wang and K. Matyjaszewski, *J. Am. Chem. Soc.*, 1995, **117**, 5614.
4 J. Chiefari, Y. K. (Bill) Chong, F. Ercole, J. Krstina, J. Jeffery, T. P. T. Le, R. T. A. Mayadunne, G. F. Meijs, C. L. Moad, G. Moad, E. Rizzardo and S. H. Thang, *Macromolecules*, 1998, **31**, 5559.
5 G. Moineau, Ph.Dubois, R. Jérôme, T. Senninger and Ph. Teyssié, *Macromolecules*, 1998, **31**, 545.
6 J. S. Wang and K. Matyjaszewski, *Macromolecules*, 1995, **28**, 7572.
7 J. Xia and K. Matyjaszewski, *Macromolecules*, 1997, **30**, 7692.
8 D. Q. Qin, S. H. Qin and K. Y. Qiu, *J. Polym. Sci., Part A: Polym. Chem.*, in press.
9 X. P. Chen and K. Y. Qiu, *Macromolecules*, in press.
10 T. Ando, M. Kamigaito and M. Sawamoto, *Macromolecules*, 1998, **31**, 6708.
11 In order to be sure that the polymerization was performed almost without TD at 100 °C, the reaction mixture of MMA, TD, $FeCl_3$, and PPh_3 contained in a tube sealed, with stirring, was placed overnight at room temperature; TD completely reacted with $FeCl_3$ according to eqn. (1) in Scheme 1.
12 V. Tamminen and E. Hjelt, *Suomen Kemistilehti*, 1950, **23B**, 39 (*Chem. Abstr.*, 1951, **45**, 2356b).

Communication a909162i

ChemComm

A palladium metallacalix[4]arene capped with a gadolinium atom

Jorge A. R. Navarro* and Juan M. Salas

Departamento de Química Inorgánica, Universidad de Granada, E-18071 Granada, Spain. E-mail: jarn@ugr.es

Received (in Basel, Switzerland) 15th November 1999, Accepted 7th January 2000

A molecular vase, analogous to a calix[4]arene, has been generated from (en)Pd^{II} and 4,6-dimethyl-2-hydroxypyrimidine, the X-ray crystallographic study showing that this compound is able to incorporate a gadolinium atom.

Calixarenes have been the subject of high interest owing to their wide range of applications.[1,2] Their cyclic frameworks associated with the presence of phenol oxygen atoms afford efficient complexing agents for metal ions,[3] while their hydrophobic cavities allow the inclusion of guest molecules. Formation of analogous inorganic macrocycles, metallacalixarenes, can be achieved by combining 120 and 90° bond angles provided respectively, by an appropriate ligand and a suitable metal entity.[4,5] Other angle combinations lead to molecular triangles,[6] squares,[7] and other structures of higher complexity.[8]

Reaction of $[(en)Pd(H_2O)_2]^{2+}$ with 4,6-dimethyl-2-hydroxypyrimidine (Hdmpymo) generates the cyclic species $[(en)Pd(dmpymo\text{-}N^1,N^3)]_4^{4+}$ **1**, (Scheme 1) by a self-assembly process. The presence of four exocyclic oxygen atoms of the pyrimidine moieties, suggested the possible coordination of additional metal atoms. Lanthanide metal ions were thought to be ideally suited in terms of both size and oxygen affinity. Addition of an excess of $Gd(NO_3)_3{\cdot}6H_2O$ to an aqueous solution of **1** affords $\{Gd(NO_3)_2(H_2O)[(en)Pd(dmpymo)]_4\}^{5+}$ **2** (Scheme 1),† which has been structurally characterised‡ and has been proved to be a metallacalix[4]arene of C_s symmetry (Fig. 1). The four Pd centres lie in a plane forming an almost perfect square with *ca.* 5.7 Å sides. The pyrimidine rings are not coplanar to the Pd_4 plane showing deviations of 35.2, 64.0 and 37.8°, respectively, for rings A, B and C, which results in the formation of a molecular vase. This is a consequence of Gd binding to the oxygen donor atoms of the dmpymo ligands which forces the four pyrimidine moieties to orient, from a high number of possibilities, in the same direction. The resulting conformation adopted by the metallacalixarene is that of a pinched cone. In classic organic calix[4]arenes stabilisation of the cone conformation, after binding of a single transition metal atom simultaneously to four phenol oxygens, is usual.[3] In metallacalix[4]arenes, however, the larger size of the oxo-surface, with O··O separations of *ca.* 4.4 Å, does not fit to transition metals, for which simultaneous binding to only two adjacent oxygen atoms has been observed.[9] The larger size of Gd^{3+} ideally suits the geometric requirements of the oxo-surface of **1** forming strong bonds to the four exocyclic dmpymo oxygens. The coordination sphere about Gd is completed by two bidentate nitrate anions placed over the calix lower rim and a water molecule completely encapsulated in the calix cavity. Calixarenes are well known for their ability to include guest molecules in their hydrophobic cavity.[1] Likewise, metallacalixarenes also possess a hydrophobic cavity which is also able to encapsulate organic residues.[9] In the present case, the opening of the cavity measured as the separation between C(5A)··C(5C) of 7.82(2) Å and C(5B)··C(5B#1) of 10.64(2) Å is big enough to permit inclusion of guest molecules. Additionally there is a water molecule coordinated to the Gd center which is completely included in the metallacalixarene cavity. This alters, the hydrophobic nature of the cavity[9] permitting the inclusion of an additional water molecule and a nitrate anion inside the cavity, which gives rise to strong H bonding interactions, namely O(1W)··O(5W) and O(1W)··O(91), with separations of 2.77(2) and 2.88(3) Å, respectively. This change in the hydrophobic nature of the cavity explains why it was not possible to find any host–guest chemistry of organic molecules for the $La[(en)Pt(uracilate)]_4(NO_3)_3$ species for which no X-ray structure was available.[9]

^{1}H NMR spectra of **1** are diagnostic of the N1, N3 bridging coordination mode of dmpymo, with retention of the original equivalence of its two methyl substituents. Replacement of the acidic protons at N1 and N3 in $H_2dmpymo^+$ by two metal entities is responsible for a significant downfield shift of the resonance of the aromatic proton H5 (−0.51 ppm) and upfield shift of the resonance of the methyl groups (δ +0.44 ppm) of dmpymo. The presence of only one set of dmpymo resonances in **1** is in agreement with its probable conformational flexibility.[5] We were also able to measure the ^{1}H NMR spectrum of **2** even thought it is paramagnetic. The spectrum is more complex than that of **1** with now two sets of signals for the

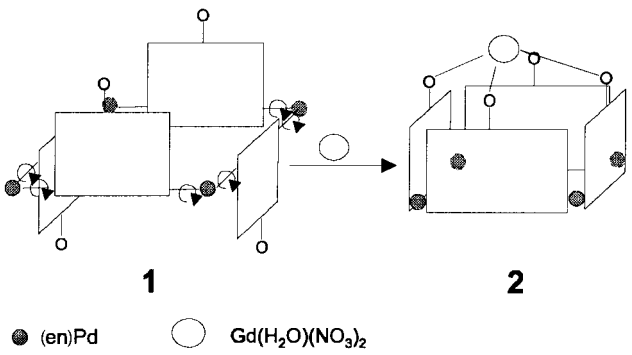

Scheme 1 Metallacalix[4]arene **1** presents conformational flexibility as a consequence of free rotation about the Pd–dmpymo bonds. In **2** Gd coordination to the oxo-surface of the metallacalix[4]arene is responsible for its fixed cone conformation.

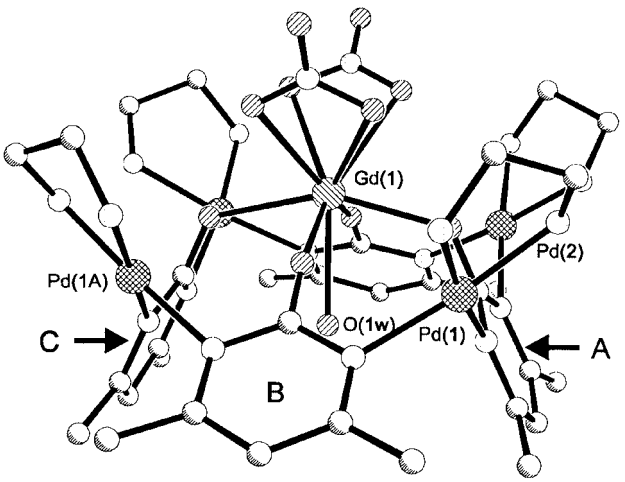

Fig. 1 Perspective view of the cation $\{Gd(NO_3)_2(H_2O)[(en)Pd(dmpymo)]_4\}^{5+}$ in the crystal structure of **2**. Pyrimidine rings A, B and C are labelled. Selected band lengths (Å): Gd(1)–O(2A) 2.309(8), Gd(1)–O(2C) 2.306(8), Gd(1)–O(2B) 2.323(6), Gd(1)–O(1W) 2.49(1), Gd(1)–O(41) 2.504(6), Gd(1)–O(31) 2.535(6), Pd(1)–N(1C) 2.071(7), Pd(1)–N(3B) 2.087(7), Pd(2)–N(3A) 2.072(7), Pd(2)–N(1B) 2.082(7).

dmpymo resonances of H5 (δ 6.31, 6.58) and methyl protons (δ 2.86, 3.04). We believe this can be attributed to the increased rigidity introduced to the metallacalixarene after Gd^{3+} coordination to **1**. Addition of La^{3+} has, however, no effect on the resonances of **1**. It is thought that the more polarising nature of Gd^{3+} with respect to La^{3+} leads to stronger bonds to the oxygen donor atoms of **1**.

This work was supported by the Spanish Ministry of Education and Culture (Project PB97-0786-CO1). J. A. R. N. thanks the University of Granada for a Research Contract and Johnson Matthey for a loan of K_2PdCl_4.

Notes and references

† $[(en)Pd(dmpymo)]_4(NO_3)_4$ **1** was obtained as follows: $(en)PdCl_2$ (3 mmol) was suspended in water (30 mL), $AgNO_3$ (6 mmol) added and the mixture stirred for 2 h at 60 °C. The mixture was cooled and AgCl removed by filtration. Hdmpymo (3 mmol) was added to the filtrate, at this point the pH was adjusted to 5.0 by means of 1 M NaOH, and the resulting pale yellow solution heated to 60 °C for 5 h. Subsequent concentration of the solution to 15 mL by rotary evaporation gives **1** in 32% yield, after 7 days at room temperature. Satisfactory elemental analysis for $C_{32}H_{68}N_{20}O_{20}Pd_4$: Anal. Calc. for **1**: C, 25.99; H, 4.64; N, 18.94. Found: C, 25.76; H, 4.99; N, 18.98%. δ_H(300 MHz, D_2O): 2.77 (CH_2, s, 4H), 3.02 (CH_3, s, 3H), 6.26 (H5, s, 1H). $\{Gd(NO_3)_2(H_2O)[(en)Pd(dmpymo)]_4\}(NO_3)_5{\cdot}8H_2O$ **2** was obtained after adding an excess of $Gd(NO_3)_3{\cdot}6H_2O$ (1 mmol) to an aqueous solution of **1** (0.125 mmol in 10 mL of H_2O). The resulting solution (pH 2.6) affords, after one week, yellow crystals of **2** in low yield (9%). Satisfactory elemental analysis for $C_{32}H_{76}N_{23}O_{33}Pd_4Gd$: Anal. Calc. for **2**: C, 20.29; H, 4.04; N, 17.01. Found: C, 20.13; H, = 3.98; N, 16.90. δ_H(400 MHz, D_2O): 2.77 (CH_2, s, 4H), 2.86, 3.04 (CH_3, s, 3H), 6.31, 6.58 (H5, s, 1H).

‡ *Crystal data* for **2**: M = 1876.0, orthorhombic, space group *Pnma*, a = 26.883(1), b = 13.2671(7), c = 17.961(1) Å, U = 6405.8(5) Å^3, Z = 4, D_c = 1.964 g cm^{-3}, μ = 2.228 mm^{-1}, λ(Mo-Kα) = 0.71069 Å, F(000) = 3764, T = 293(2) K. Stoe STADI4 diffractometer, crystal size 0.550 × 0.397 × 0.280 mm, 8075 reflections measured, 7668 unique, reflections observed 4269 $F_o^2 > 4\sigma(F_o^2)$, R_1 = 0.0590, wR_2 = 0.1489 (observed data), S = 1.029. The structure was solved by the Patterson method and refined using least-square methods.[10] The disorder found in one of the nitrate anions was modelled considering two positions with half occupancy. All non-hydrogen atoms were refined anisotropically with the exception of some of the nitrate anions and water molecules. CCDC 182/1515. See http://www.rsc.org/suppdata/cc/a9/a909150e/ for crystallographic files in .cif format.

1 C. D. Gutsche, *Calixarenes*, Royal Society of Chemistry, Cambridge, 1989; V. Böhmer, *Angew. Chem., Int. Ed. Engl.*, 1995, **34**, 713; A. Ikeda and S. Shinkai, *Chem. Rev.*, 1997, **97**, 1713.
2 See, for example: G. G. Talanova, H.-S. Hwang, V. S. Talanov and R. A. Bartsch, *Chem. Commun.*, 1998, 1329; B. Xu and T. M. Swager, *J. Am. Chem. Soc.*, 1993, **115**, 1159.
3 C. Wieser, C. B. Dieleman and D. Matt, *Coord. Chem. Rev.*, 1997, **165**, 93; V. C. Gibson, C. Redshaw, W. Clegg and M. R. J. Elsegood, *Chem. Commun.*, 1998, 1969; L. Charbonnière, C. Balsiger, K. J. Schenk and J.-C. G. Bünzli, *J. Chem. Soc., Dalton Trans.*, 1998, 505; L. Giannini, E. Solari, A. Zanottigerosa, C. Floriani, A. Chiesivilla and C. Rizolli, *Angew. Chem., Int. Ed. Engl.*, 1997, **36**, 753.
4 H. Rauter, E. C. Hillgeris, A. Erxleben and B. Lippert, *J. Am. Chem. Soc.*, 1994, **116**, 616; H. Rauter, I. Mutikainen, M. Blomberg, C. J. L. Lock, P. Amo-Ochoa, E. Freisinger, L. Randaccio, E. Zangrando, E. Chiarparin and B. Lippert, *Angew. Chem., Int. Ed. Engl.*, 1997, **36**, 1296.
5 J. A. R. Navarro, E. Freisinger and B. Lippert, *Inorg. Chem.*, submitted.
6 R.-D. Schnebeck, L. Randaccio, E. Zangrando and B. Lippert, *Angew. Chem., Int. Ed.*, 1998, **37**, 128; R.-D. Schnebeck, E. Freisinger and B. Lippert, *Chem. Commun.*, 1999, 675.
7 M. S. Lüth, E. Freisinger, F. Glahé and B. Lippert, *Inorg. Chem.*, 1998, **37**, 5044; M. Fujita, J. Yazaki and K. Ogura, *J. Am. Chem. Soc.*, 1990, **112**, 5645.
8 A. J. Stemmler, J. W. Kampf, M. L. Kirk, B. H. Atasi and V. L. Pecoraro, *Inorg. Chem.*, 1999, **38**, 2807; D. W. Johnson, J. Xu, R. W. Saalfrank and K. N. Raymond, *Angew. Chem., Int. Ed.*, 1999, **38**, 3058.
9 J. A. R. Navarro, M. Janik, E. Freisinger and B. Lippert, *Inorg. Chem.*, 1999, **38**, 426.
10 G. M. Sheldrick, SHELX-97, Program for structure solution and refinement, University of Göttingen, Germany, 1997.

Communication a909150e

Radical cyclization of *O*-trityl oximino esters: a ring closure that preserves the oxime function

Derrick L. J. Clive* and Rajendra Subedi

Chemistry Department, University of Alberta, Edmonton, Alberta, Canada T6G 2G2.
E-mail: derrick.clive@ualberta.ca

Received (in Corvallis, OR, USA) 4th November 1999, Accepted 16th December 1999

_O_-Trityl oximino esters 1 undergo stannane-induced radical cyclization to regenerate an oxime function, affording oximino lactones 4; these can be converted into enamides (*e.g.* 11b), and such a transformation was used to make the natural product 14c.

We report radical ring closures of the type summarized in Scheme 1 (X = homolyzable group).[1,2] The special feature of such reactions is that the sp^2 status of the acceptor carbon is preserved—a result that is different from the one seen in the classical cyclization of hexenyl radicals or the radical cyclization of *O*-alkyl oxime ethers.[3–5] Regeneration of the oxime function after the radical closure must involve[6] tautomerization of an intermediate nitroso compound, as shown in Scheme 1, **3** → **4**.†

The starting oximino esters (*cf.* **1**) are prepared using the crystalline reagent **5** (mp 165–166 °C), which is easily made (76%) by stirring equimolar amounts of *O*-trityl hydroxylamine and glyoxylic acid monohydrate in THF for 4 h. Evaporation of

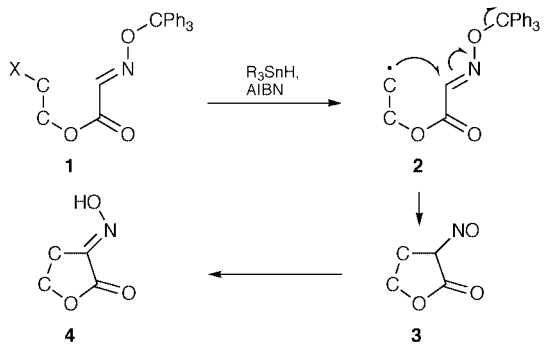

Scheme 1

Table 1 Esterification of various alcohols and subsequent radical cyclizations[a]

Entry	Ester	Lactone	Entry	Ester	Lactone
1	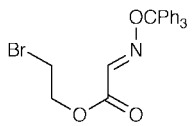 **6**, 99%	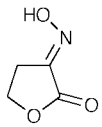 **6a**, 72%	5	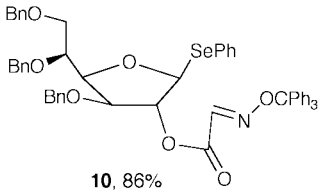 **10**, 86%	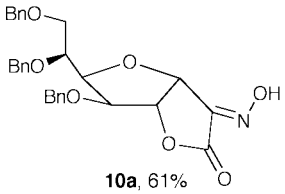 **10a**, 61%
2	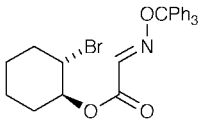 **7**, 80%	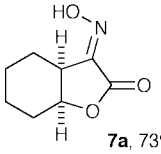 **7a**, 73%	6	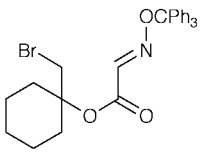 **11**, 68%	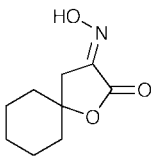 **11a**, 80%
3	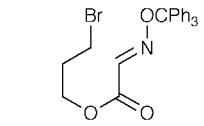 **8**, 83%	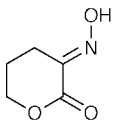 **8a**, 46%[b]	7	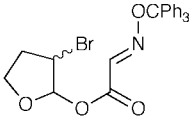 **12**, 86%[d]	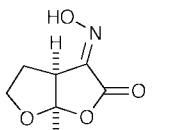 **12a**, 41%
4	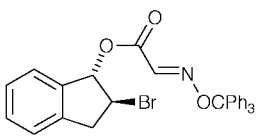 **9**, 79%	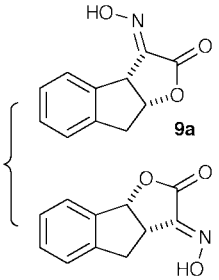 **9a** + **9b** 66%[c]	8	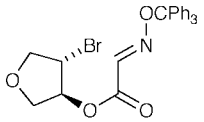 **13**, 83%	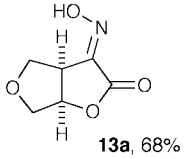 **13a**, 68%
			9	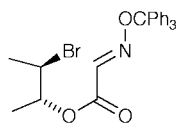 **14**, 84%	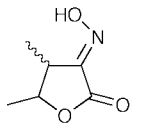 **14a**, 68%[e]

[a] Oxime geometries shown are arbitrary, except for **11** and **14a**. [b] A single product, which isomerizes on storage in MeOH. [c] Combined yield. Isomers **9a** and **9b** were obtained in a ratio of *ca.* 1:2. [d] Two isomers were isolated in yields of 61 and 25%. [e] A mixture (*ca.* 55:45) of two isomers was obtained.

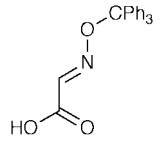

5

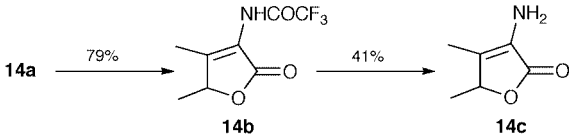

Scheme 2

the solvent and column chromatography over silica gel (3:7 hexane–EtOAc) gives pure **5**, whose geometry in the solid state was established by X-ray analysis. The reagent (1 mmol) reacts smoothly with alcohols (1.1 mmol) in CH_2Cl_2 in the presence of DCC (1.1 mmol) and DMAP (1.1 mmol) to give the corresponding esters, after 1–26 h. Yields in these esterifications are generally high (see Table 1, entries 1–6 and 8–9). The parent alcohol for **11** is a known compound,[8,9] but one tentative structural assignment given[8] in the literature [(1-bromocyclohexyl)methanol] is incorrect; our X-ray analysis of **11** establishes the actual structure. In one case (Table 1, entry 7) we prepared the required starting ester by reaction of **5** (1.1 mmol) with a THF solution of the alkene (1.0 mmol) in the presence of NBS (1.1 mmol), and again the yield was high.

The radical cyclizations were done by slow addition (*ca*. 10 h, syringe pump) of separate toluene solutions of Bu_3SnH (0.17 M, 1.5–2.5 mmol per mmol ester) and AIBN (0.012 M, 0.1–0.2 mmol per mmol ester) to a refluxing toluene solution of the ester (1.0–1.8 mmol, 0.016 M). Refluxing was continued for an arbitrary period of 2 h after the end of the addition. The products were isolated in the yields indicated in Table 1, by evaporation of the solvent and flash chromatography. While the oxime geometry for **5**, **11** and **14a** was determined by X-ray analysis, the geometries shown for the other oximes are arbitrary assignments. All the cyclization products were single isomers, except for **14a**. In that example, the material was obtained crystalline, and X-ray analysis showed the crystals to be composed of the *trans,E* and *cis,E* isomers in a ratio of *ca*. 55:45; the same composition was evident from the ^{1}H NMR spectrum. During cyclization of **9** a 1,2-acyloxy rearrangement[10] occurs, driven by formation of a benzylic radical.

We have examined briefly the partial reduction of several of our α-oximino lactones. For example, treatment of **7a** with iron

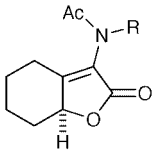

7b R = H, 54%
7c R = Ac, 30%

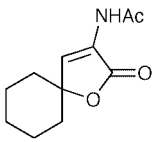

11b, 80%

powder in Ac_2O[11] (room temperature, 14 h) gave a mixture of enamide **7b** (54%) and the doubly acetylated analog **7c** (30%). Under the same conditions, **11a** gave **11b** (80%), and no bis-acetylated product was isolated.

Treatment of **14a** with iron powder in TFAA gave enamide **14b** (Scheme 2), the fluorinated anhydride being used because we expected this choice to facilitate subsequent amide hydrolysis. In the event, treatment of **14b** with aqueous K_2CO_3 afforded enamine **14c**, which is a naturally-occurring substance[12,13] that is present in the flowers of the tree *Quararibea funebris* (Llave). Extracts of the flowers have been used[14] by the Zapotec Indians of Oaxaca, Mexico, to treat a number of disorders, including some of a psychological nature, but it is not known whether **14c** itself is biologically active. It has been suggested that the compound may be the biosynthetic precursor of several pyrrole alkaloids present in the flower extract.[14]

All new compounds were characterized spectroscopically, including high resolution mass measurements, except for **9b**, which was isolated as a mixture with **9a**.

Acknowledgment is made to the Natural Sciences and Engineering Research Council of Canada and to Merck Frosst for financial support.

Notes and references

† No blue color was observed during the reaction. Tautomerization of a *C*-nitroso compound, as the terminating step of an intermolecular reaction, is known (see ref. 7)

1 Radical cyclizations of glyoxylic diphenylhydrazones and *O*-benzyloximes: D. L. J. Clive and J. Zhang, *Chem. Commun.*, 1997, 549.
2 For intermolecular radical addition to a glyoxylic oxime ether, see: H. Miyabe, C. Ushiro and T. Naito, *Chem. Commun.*, 1997, 1789.
3 Recent examples involving *O*-methyl oximes: T. Naito, K. Nakagawa, T. Nakamura, A. Kasei, I. Ninomiya and T. Kiguchi, *J. Org. Chem.*, 1999, **64**, 2003; G. E. Keck, S. F. McHardy and A. Murry, *J. Org. Chem.*, 1999, **64**, 4465.
4 Radical cyclizations involving oximes (and other nitrogen-containing species) have been reviewed: A. G. Fallis and I. M. Brinza, *Tetrahedron*, 1997, **53**, 17543.
5 Homolytic *C*-alkylation of aldoximes: A. Citterio and L. Filippini, *Synthesis*, 1986, 473.
6 For other radical sequences that result in C=N regeneration, see: G. Pattenden and D. J. Schultz, *Tetrahedron Lett.*, 1993, **34**, 6787; S. Kim and J. H. Cheong, *Chem. Commun.*, 1998, 1143; S. Kim, I. Y. Lee, J.-Y. Yoon and D. H. Oh, *J. Am. Chem. Soc.*, 1996, **118**, 5138; U. Iserloh and D. P. Curran, *J. Org. Chem.*, 1998, **63**, 4711.
7 M. Kizil and J. A. Murphy, *Tetrahedron*, 1997, **53**, 16 847.
8 See footnote 23 in J. G. Traynham and W. G. Hines, *J. Am. Chem. Soc.*, 1968, **90**, 5208.
9 M. Chini, P. Crotti, C. Gardelli and F. Macchia, *Tetrahedron*, 1992, **48**, 3805.
10 A. L. J. Beckwith, D. Crich, P. J. Duggan and Q. Yao, *Chem. Rev.*, 1997, **97**, 3273.
11 *Cf.* D. H. R. Barton and S. Z. Zard, *J. Chem. Soc., Perkin Trans. 1*, 1985, 2191; M. J. Burke, G. Casy and N. B. Johnson, *J. Org. Chem.*, 1998, **63**, 6084; G. Zhu, A. L. Casalnuovo and X. Zhang, *J. Org. Chem.*, 1998, **63**, 8100.
12 R. F. Raffauf, T. M. Zennie, K. D. Onan and P. W. Le Quesne, *J. Org. Chem.*, 1984, **49**, 2714.
13 For a structurally related natural product, see: A. J. Pallenberg and J. D. White, *Tetrahedron Lett.*, 1986, **27**, 5591.
14 T. M. Zennie and J. M. Cassady, *J. Nat. Prod.*, 1990, **53**, 1611.

Communication a908842c

ChemComm

Metallatubulane: synthesis and structural analysis of an infinite tubular coordination network formed by the self-assembly of a tetracyanocyclophane and silver cations

Cédric Kleina,[a] Ernest Graf,[a] Mir Wais Hosseini,*[a] André De Cian[b] and Jean Fischer[b]

[a] *Laboratoire de Chimie de Coordination Organique, Université Louis Pasteur, UMR CNRS, 7513, F-67000 Strasbourg, France. E-mail: hosseini@chimie.u-strasbg.fr*

[b] *Laboratoire de Cristallochimie et Chimie Structurale, Université Louis Pasteur, UMR CNRS, 7513, F-67000 Strasbourg, France*

Received (in Basel, Switzerland) 15th November 1999, Accepted 7th January 2000

Reaction of a tetracyano[1,1,1,1]metacyclophane blocked in the 1,3-alternate conformation and silver cations under self-assembly conditions leads to a tubular coordination network formed by double bridging of consecutive rings by linearly coordinated metal centres.

Tubular structures are interesting architectures, in particular with respect to their ability to transport ions and molecules. In principle, such structures may be obtained either using non reversible covalent bond formation processes or under self-assembly conditions using reversible interactions. It has been shown that tubular systems may be formed by 1-D chains adopting a helical structure, as observed for polypeptides in natural systems.[1,2] On the abiotic side, helical coordination polymers composed of synthetic organic ligands and metal centres,[3,4] which may be considered as tubular systems, have also been reported. Using self-assembly of silver ions and polydentate ligands, tubular systems formed by the interconnection of metallamacrocycles have been reported.[5,6] Other strategies based on the organisation of cyclic units into tubular arrangements using liquid crystalline phases[7] or polymeric backbones[8] have been shown to be successful as well. Finally, the formation of carbon nanotubes by rolling 2-D graphite sheets has also been demonstrated.[9]

Following the above-mentioned strategy based on the use of H-bonds between cyclic peptides, we reasoned that, by making the appropriate choice of ligands and metal centres, tubular coordination networks may be formed using the self-assembly strategy based on the formation of reversible coordination bonds. The formation of such a structure requires a complementary pair of ligand and metal cation that affords their reversible and mutual interconnection (Fig. 1).

Here, we report the synthesis of the exo-ligand **1** as well as the structural analysis of its tubular coordination network obtained in the presence of silver cations.

We believed that the exo-ligand **1** (Scheme 1) would be promising for the formation of infinite metallatubulanes. Ligand **1** is based on a [1,1,1,1]metacyclophane backbone that is blocked in the 1,3-alternate conformation and bears four nitrile groups as coordination sites, which are located below and above the main plane of the macrocycle in an alternate fashion and thus occupy the apexes of a pseudo-tetrahedron. The choice of **1** was based on the structural study of its hydroxy analogue **3**, which was demonstrated to be in the 1,3-alternate conformation,[10] the mercapto analogue **4**,[11] and on our previous observation dealing with the formation of 1-D coordination networks using ligand **6**.[12] Indeed, it was found that when using the calix **6**, owing to its inherent flexibility, two nitrile groups located on the same face of the ligand could act as a chelate for Ag^+ cations (Fig. 1). Thus, for the linear coordination network formed by bridging consecutive calix units by Ag^+ cations, the coordination geometry adopted by the latter was tetrahedral. In terms of topology, the above mentioned network is in principle of the tubular type; however, the presence of metal centres

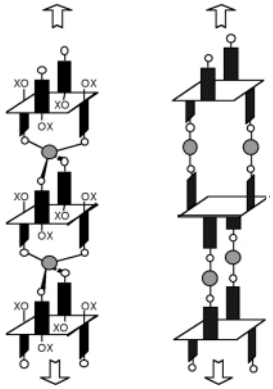

Fig. 1 Schematic representation of two types of tubular coordination networks which can be formed by the self-assembly of ligand **6** with Ag^+ cations adopting a tetrahedral coordination geometry (left) or ligand **1** and Ag^+ cations adopting a linear coordination geometry (right).

aligned along the tube axis obstructs the channel. In order to circumvent this, the ligand **1** was designed, which incorporates methyl groups that induce considerable rigidity and thus prevent the chelation process.

The synthesis of **1** (Scheme 1) was based on the strategy used for the preparation of **3**.[10] Starting with **4**, compound **5** was obtained in 84% yield upon treatment with $ClCH_2OMe$ in CH_2Cl_2 in the presence of $SnCl_4$ at −15 °C. Upon heating an equimolar mixture of **4** and **5** in $EtNO_2$ and in the presence of $SnCl_4$ for 6 h at 60 °C , the cyclic cyclophane **2** was obtained in 74% yield. The desired **1** was obtained in 54% yield upon treatment of **2** with CuCN in refluxing DMF for 15 h.[13] The 1,3-alternate conformation was established in the solid state by X-ray diffraction for both **1** and **2** (structures not reported here).

The metal cation used for the self-assembly of **1** into a tubular network was Ag(I), which forms kinetically labile complexes and can adopt a linear coordination geometry.[14] Furthermore, Ag^+ has been extensively used for the formation of coordination networks,[15] in particular using nitrile containing ligands.[16]

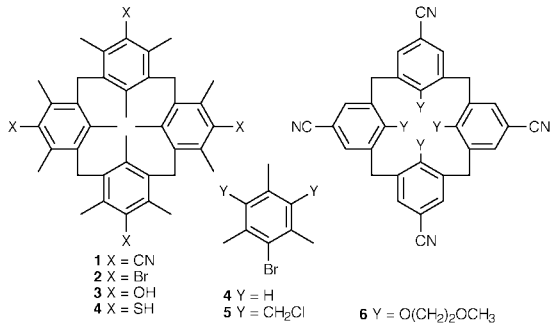

Scheme 1

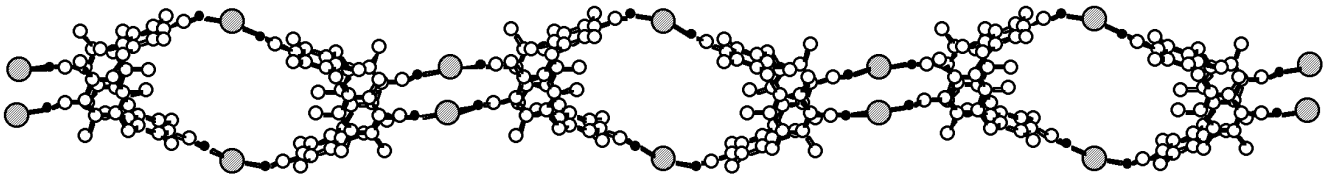

Fig. 2 A portion of the X-ray structure showing the formation of a cationic tubular coordination networks obtained by mutual bridging of Ag+ cations and ligands **1** (view perpendicular to the tube axis). For clarity, H atoms, solvent molecules and anions are not shown.

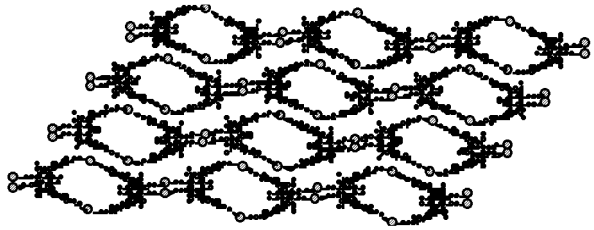

Fig. 3 A portion of the structure showing the packing of the cationic tubular coordination networks (projection normal to the tube axis). For clarity, H atoms and solvent molecules (CH_2Cl_2 and MeOH) are not shown.

Upon slow diffusion of a CH_2Cl_2 (0.75 ml) solution of the ligand **1** (2 mg, 3.18×10^{-6} mol) into a MeOH (1 ml) solution of $AgPF_6$ (8 mg, 3.18×10^{-5} mol) in large excess, colourless crystalline material was obtained. The analysis of single-crystals by X-ray crystallography† revealed the presence of disordered CH_2Cl_2 and MeOH solvent molecules in the lattice in addition to **1**, Ag^+ and PF_6^- anions. As predicted (Fig. 1), in addition to the anions and solvent molecules, the crystal was composed of cationic tubular coordination networks formed by the bridging of consecutive cyclic units by Ag^+ cations (Fig. 2). The ligand **1** adopts the imposed 1,3-alternate conformation. The nitrile groups are almost linear with an average C–C–N angle of *ca*. 177.5° and an average C–N distance of 1.142 Å. In the unit cell, two different Ag^+ cations are present. The coordination sphere around both crystallographically non-equivalent Ag^+ cations is composed of two nitrogen atoms (N–Ag–N 153.8 and 162.3°, C–N–Ag 171.5 and 150.3, 178.3°, N–Ag 2.155 and 2.126, 2.138 Å) and PF_6^- anions with Ag–F distances varying from 2.811 to 2.983 Å. Two Ag^+ cations located on the same face of the molecule are separated by 9.891 and 9.593 Å. The packing of the cationic component (Fig. 3) shows parallel disposition of tubular networks. Interestingly, the 1-D tubular networks are interconnected in a dihapto mode by strong metal–π interactions between Ag^+ cations and the aromatic moiety belonging to the next tubular strand (Ag^+–centroid distance of 3.087 Å). The same observation has been made with metallamacrocyles formed by connecting two cyclic *para*-dimethylaminopyridine derivatives with two Ag^+ cations.[14] Thus, taking into account the above interactions, the arrangement obtained may be described as a 2-D network with translations into two directions of space of two distinct assembling cores based on N–Ag^+–N and Ag^+–π interactions. Thus, the overall structure may be described as stacks of 2-D networks separated by PF_6^- anions. The tubular arrangement is not empty and occupied by solvent molecules. However, none of the solvent molecules (disordered CH_2Cl_2 and MeOH) present are included within the cavity of the cyclophanes but are rather located within cavities formed by interconnection of the cyclic units by silver cations.

In conclusion, employing the self-assembly strategy, the formation of a silver tubular coordination network using a [1,1,1,1]metacyclophane backbone that is blocked in the 1,3-alternate conformation and bears four nitrile groups was achieved and structurally characterised in the solid state by single-crystal X-ray analysis. The exchange of included solvent molecules, as well the enhancement of the size of the tubulane are currently under investigation.

Notes and references

† *Crystal data* for $C_{22}H_{22}N_2AgPF_6$•MeOH•0.75CH_2Cl_2: M = 663.01, monoclinic, space group $C2/m$, a = 24.2853(5), b = 19.1082(7), c = 11.9631(4) Å, β = 108.051(2)°, V = 5278.2(5) Å^3, Z = 8, D_c = 1.67 g cm^{-3}, μ(Mo-Kα) = 1.039 mm^{-1}. Data were collected on a Nonius KappaCCD diffractometer using Mo-Kα graphite monochromated radiation (λ = 0.71073 Å) at 173 K. A colourless crystal of dimensions 0.20 × 0.16 × 0.14 mm was used and a total of 28 326 reflections were collected, $2.5 < \theta < 27.5°$. 3937 unique reflections having $I > 3\sigma(I)$ were used for structure determination and refinement. Absorption corrections were partially integrated in the data reduction procedure. The structure was solved using direct methods and refined against $|F|$. Hydrogen atoms were introduced as fixed contributors when a residual electronic was observed near their expected positions. The MeOH and one of the CH_2Cl_2 molecules are disordered over two positions lying near symmetry elements of the space group. Site C28 was refined as containing a mixture of 50% of Cl and 50% of C and site C29 was refined as containing a mixture of 50% of C and 50% of O. Three solvent atoms were kept with isotropic temperature factors, all other atoms were refined with anisotropic temperature factors. Final results: $R(F)$ = 0.063, $Rw(F)$ = 0.083, GOF = 1.521, maximum residual electronic density = 0.98 e Å^{-3}. For all computations the Nonius OpenMoleN package17 was used. CCDC 182/1514. See http://www.rsc.org/suppdata/cc/a909029k/ for crystallographic data in .cif format.

1 D. H. Lee and M. R. Ghadiri, in *Comprehensive Supramolecular Chemistry*, ed. J. L. Atwood, J. E. D. Davies, D. D. Macnicol and F. Vögtle, Pergamon, vol. 9 (ed. J.-P. Sauvage and M. W. Hosseini), 1996, p. 451; J. D. Lear, Z. R. Wasserman and W. F. DeGrado, *Science*, 1988, **240**, 1177.

2 P. De Santis, S. Morosetti and R. Rizzo, *Macromolecules*,1974, **7**, 52; M. R. Ghadiri, J. R. Granja, R. A. Milligan, D. E. McRee and N. Khazanovich, *Nature*,1993, **366**, 324.

3 C. Kaes, M. W. Hosseini, C. E. F. Rickard, B. W. Skelton and A. White, *Angew. Chem. Int. Ed.*, 1998, **37**, 920.

4 O. J. Gelling, F. van Bolhuis and B. L. Feringa, *J. Chem. Soc., Chem. Commun.*, 1991, 917; Y. Dai, T. J. Katz and D. A. Nichols, *Angew. Chem., Int. Ed. Engl.*, 1996, **35**, 2109; B. Wu, W.-J. Zhang, S.-Y. Yu and X.-T. Wu, *Chem. Commun.*, 1997, 1795.

5 M. J. Hannon, C. L. Painting and W. Errington, *Chem. Commun.*, 1997, 1805.

6 M. Loï, M. W. Hosseini, A. Jouaiti, A. De Cian and J. Fischer, *Eur. J. Inorg. Chem.*, 1999, 1981.

7 J.-M. Lehn, J. Malthête and A.-M. Levelut, *J. Chem. Soc., Chem. Commun.*, 1985, 1794; V. Percec, G. Johansson, J. A. Heck, G. Ungar and S. V. Betty, *J. Chem. Soc., Perkin Trans. 1*, 1993, 1411; T. Komori and S. Shinkai, *Chem. Lett.*, 1993, 1455.

8 U. F. Kragten, M. F. M. Roks and R. J. M. Nolte, *J. Chem. Soc., Chem. Commun.*, 1985, 1275; C. Mertesdorf and H. Ringsdorf, *Mol. Cryst. Liq. Cryst.*, 1989, **5**, 1757.

9 S. Iijima, *Nature*, 1991, **354**, 56.

10 S. Pappalardo, G. Ferguson and J. F. Gallagher, *J. Org. Chem.*, 1992, **57**, 7102.

11 X. Delaigue and M. W. Hosseini, *Tetrahedron Lett.*, 1993, **34**, 8111.

12 G. Mislin, E. Graf, M. W. Hosseini, A. De Cian, N. Kyritsakas and J. Fischer, *Chem. Commun.*, 1998, 2545.

13 L. Friedman and H. Shechter, *J. Org. Chem.*, 1961, **26**, 2522.

14 R. Schneider, M. W. Hosseini, J.-M. Planeix, A. De Cian and J. Fischer, *Chem. Commun.*, 1998, 1625.

15 J. Blake, N. R. Champness, S. S. M. Chung, W-S. Li and M. Schröder, *Chem. Commun.*, 1997, 1675; M. A. Withersby, A. J. Blake, N. R. Champness, P. Hubberstey, W.-S. Li and M. Schröder, *Chem. Commun.*, 1997, 2327.

16 D. Perreault, M. Drouin, A. Michel and P. D. Harvey, *Inorg. Chem.*, 1992, **31**, 3688; K. A. Hirsch, S. R. Wilson and J. S. Moore, *Inorg. Chem.*, 1997, **36**, 2960; K. A. Hirsch, S. R. Wilson and J. S. Moore, *Chem. Eur. J.*, 1997, **3**, 765; G. B. Gardner, D. Venkataraman, J. S. Moore and S. Lee, *Nature*, 1995, **374**, 792; G. B. Gardner, Y.-H. Kiang, S. Lee, A. Asgaonkar and D. Venkataraman, *J. Am. Chem. Soc.*, 1996, **118**, 6946; B. F. Abrahams, S. J. Egan, B. F. Hoskins and R. Robson, *Chem. Commun.*, 1996, 1099; F.-Q. Liu and T. Don Tilley, *Inorg. Chem.*, 1997, **36**, 2090.

17 OpenMoleN, Interactive Structure Solution, Nonius B.V., Delft, The Netherlands, 1997.

Communication a909029k

ChemComm

Reactions of permethylmetallocene alkyne complexes of titanium and zirconium with tris(perfluorophenyl)borane

Vladimir V. Burlakov,[a] Paul-Michael Pellny,[b] Perdita Arndt,[b] Wolfgang Baumann,[b] Anke Spannenberg,[b] Vladimir B. Shur*[a] and Uwe Rosenthal*[b]

[a] *A. N. Nesmeyanov Institute of Organoelement Compounds, Russian Academy of Sciences, Vavilov St. 28, 117813, Moscow, Russia*

[b] *Institut für Organische Katalyseforschung an der Universität Rostock, Buchbinderstr. 5 - 6, D-18055 Rostock, Germany*

Received (in Cambridge, UK) 20th October 1999, Accepted 11th January 2000

Functionalization of the pentamethylcyclopentadienyl ligands by an electrophilic substitution of hydrogen atoms by $[B(C_6F_5)_3]$ is observed at the Cp* ligands of the alkyne complexes $[Cp^*_2M(\eta^2\text{-}PhC_2SiMe_3]$, connnected with (M = Ti, formation of 1) or without (M = Zr, formation of 2) loss of the alkyne and molecular hydrogen.

Recently we have published the reaction of the bis(trimethylsilyl)acetylene complex of titanocene $[Cp_2Ti(\eta^2\text{-}Me_3SiC_2\text{-}SiMe_3)]$[1] with $[HNMe_3][BPh_4]$ giving cationic complexes of the type $[Cp_2TiL_2][BPh_4]$ with L = THF and pyridine.[2] More recently we have found that in the interaction of $[Cp_2Ti(\eta^2\text{-}Me_3SiC_2SiMe_3)]$ with $[B(C_6F_5)_3]$ an electrophilic substitution of a hydrogen atom in one of the $\eta^5\text{-}C_5H_5$ rings takes place, and the paramagnetic zwitterionic titanium complex $[(\eta^5\text{-}C_5H_5)Ti\{\eta^5\text{-}C_5H_4B(C_6F_5)_3\}]$ is formed together with liberation of dihydrogen.[3] In this complex the *ortho*-fluorine atoms of two perfluorphenyl groups coordinate at the titanium centre.

Such an interaction but with only one perfluorphenyl group was described previously in the reaction product of the zirconacyclopentadiene $[Cp_2Zr(C_4Me_4)]$ with $[B(C_6F_5)_3]$ giving $[(\eta^5\text{-}C_5H_5)Zr\{\sigma\text{-}C(Me)=C(Me)\text{–}C(Me)=CHMe\}\{\eta^5\text{-}C_5H_4B(C_6F_5)_3\}]$.[4] Starting from the alkyne complex $[Cp_2Zr(PMe_3)(\eta^2\text{-}EtC_2Et)]$ and $[HB(C_6F_5)_2]$ the alkenyl complex $[(\eta^5\text{-}C_5H_5)Zr\{\sigma\text{-}C(Et)=CHEt\}\{\eta^5\text{-}C_5H_4BH(C_6F_5)_2\}]$ was obtained in which the hydrogen of the B–H groups coordinate at the Zr centre.[5]

Also, the so-called 'tuck in' permethylmetallocene complexes[5] were obtained with $[B(C_6F_5)_3]$ and $[HB(C_6F_5)_2]$. Some aspects of these compounds were reviewed by Piers in 1998.[5]

Here, we report the different reactions of the permethylmetallocene alkyne complexes $[Cp^*_2M(\eta^2\text{-}PhC_2SiMe_3)]$ (M = Ti[6] and Zr[7]) with $[B(C_6F_5)_3]$, leading to functionalization of the pentamethylcyclopentadienyl ligand.

The compound $[(\eta^5\text{-}C_5Me_5)Ti\{\eta^5\text{-}C_5Me_4CH_2B(C_6F_5)_3\}]$ **1** is formed by dissociation of the alkyne and an electrophilic substitution of a hydrogen atom in one methyl group of the Cp^* ligand together with liberation of dihydrogen (Scheme 1).†

The composition of the Ti(III) complex **1** was verified by elemental analysis‡ and crystallography.

The X-ray crystal structure analysis of **1**§ (Fig. 1) revealed a bent permethyltitanocene which consists of one unsubstituted and one substituted pentamethylcyclopentadienyl ligand. In this complex the *ortho*-fluorine atom of only one of the perfluorphenyl groups coordinates at the titanium centre [Ti–F152.406(3) Å]. This is longer than found in $[(\eta^5\text{-}C_5H_5)Ti\{\eta^5\text{-}C_5H_4B(C_6F_5)_3\}]$[3] (2.248, 2.223 Å).

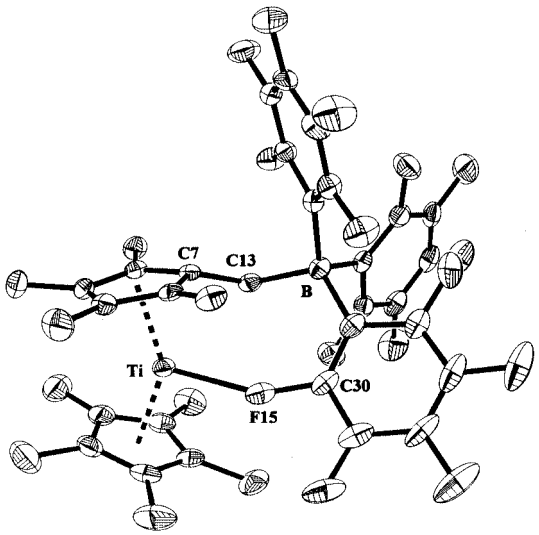

Fig. 1 Crystal structure of **1** at the 30% probability level for thermal ellipsoids. Hydrogen atoms are omitted for clarity. Selected bond lengths (Å) and angles (°): Ti–F15 2.406(3), C30–F15 1.391(5), C7–C13 1.514(5), C13–B 1.649(6); B–C13–C7 124.8(3).

The alkenyl compound $[(\eta^5\text{-}C_5Me_5)Zr\{C(Ph)=CH(SiMe_3)\}\{\eta^5\text{-}C_5Me_4CH_2B(C_6F_5)_3\}]$ **2** is formed also by an electrophilic substitution of a hydrogen atom in one methyl group of the Cp^* ligand but without dissociation of the alkyne and liberation of dihydrogen (Scheme 2).¶

The composition of the diamagnetic complex **2** was verified by elemental analysis and crystallography. For solubility reasons, NMR investigations had to be carried out in THF-d_8, but some undefined changes prevented a full analysis of the spectra.‖ However, the borane attack at one methyl group is evident from a strong line broadening of both the ^1H and ^{13}C methylene signals (diastereotopic protons at 2.65 and 2.81 ppm). The chemical shifts for the vinyl group, a strong deshielding for the α carbon atom (228.9 ppm) and an upfield

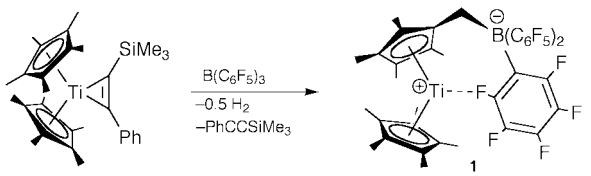

Scheme 1

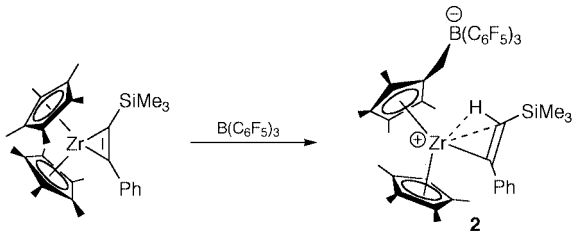

Scheme 2

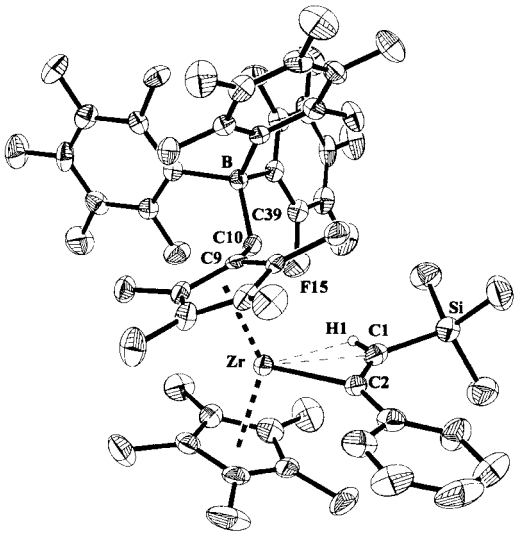

Fig. 2 Crystal structure of **2** at the 30% probability level for thermal ellipsoids. Hydrogen atoms except H1 are omitted for clarity. Selected bond lengths (Å) and angles (°): Zr–C1 2.518(6), Zr–C2 2.238(5), C9–C10 1.487(6), C10–B 1.694(6), Zr–H1 2.250, Zr–F15 4.744, C39–F15 1.369(5); C1–C2–Zr 86.5(4), B–C10–C9 121.6(4).

shift with a small coupling constant $^1J_{CH}$ (104.9 ppm, 111 Hz) for the β position, are characteristic for a 'β-CH agostic' structure[8] although the deshielding of the proton is not as pronounced for complex **2** as was found for other zirconium cyclopentadienyl compounds with this structural feature.[8,10*b*,12]

The X-ray crystal structure analysis of **2**§ (Fig. 2) revealed, similarly as found also for complex **1**, a bent permethylmetallocene which consists also of one unsubstituted and one substituted pentamethylcyclopentadienyl ligand, but no fluorine atom coordinates at the zirconium centre [shortest distance Zr–F15 4.744 Å]. Additionally an alkenyl group is σ-bonded with an agostic interaction[8] to the zirconium atom presenting the typical small angle Zr–C2–C1 of 86.5° for such a type of bonding. In complexes **1** and **2** an identically functionalized Cp* ligand [η^5-$C_5Me_4CH_2B(C_6F_5)_3$] is shown. Owing to the additional interaction in **1** the angle B–C13–C7 of 124.8(3)° is larger compared to the corresponding angle B–C10–C9 of 121.6(4)° in **2**.

The reactions of the corresponding complexes of bis-(trimethylsilyl) acetylene [$Cp^*_2M(\eta^2$-$Me_3SiC_2SiMe_3)$] (M = Ti[6] and Zr[9]) gave with [$B(C_6F_5)_3$] only oils or such solids which could not be purified by crystallisation.

The novelty of the reactions in this work is, in contrast to former observed *inter*molecular reactions for titanium[7*b*,10] and zirconium[7*b*,11] an *intra*molecular course *via* C–H activation for the formation of **1** and **2**. In the *inter*- and the *intra*molecular reactions the higher stability of the Ti(III) oxidation state as well as the larger zirconium atom can give an explanation for the different types of reaction: elimination or addition of the reacting substrate or group.

The work was supported by the Max-Planck-Gesellschaft, the Fonds der Chemischen Industrie and the Russian Foundation for Basic Research (Project code 99-03-33008).

Notes and references

† *General procedure* for the preparation of complex **1**: 0.507 g (0.990 mmol) of [$B(C_6F_5)_3$] was dissolved in 10 mL of toluene and added to 0.474 g (0.962 mmol) of [$Cp^*_2Ti(\eta^2$-$PhC_2SiMe_3)$].[6] The yellow–brown solution was filtered. After standing for 2 days at room temperature 0.123 g (15.4%) of yellow–brown crystals of **1** were formed which were separated from the mother-liquor, washed with cooled toluene and dried *in vacuo*; mp 141–143 °C (decomp.).

‡ *Data* for **1**: elemental analysis for $C_{38}H_{29}TiBF_{15}$ (*M* = 829.31). Calc.: C, 55.04; H, 3.52. Found: C, 55.02; H, 3.59%. NMR: As expected for Ti(III),[3] no NMR signals (^{1}H and ^{13}C) could be obtained from solutions of **1** in THF.

§ *X-Ray structure analysis* of **1** and **2**: STOE-IPDS diffractometer, graphite monochromated Mo-Kα radiation, solution of structures by direct methods (SHELXS-86: G. M. Sheldrick, *Acta. Crystallogr., Sect. A*, 1990, **46**, 467), refinement with full matrix least square techniques against F^2 (SHELXL-93: G. M. Sheldrick, University of Göttingen, Germany, 1993).

1: monoclinic, space group *C*2/*c*, a = 37.705(8), b = 10.990(2), c = 18.178(4) Å; β = 106.48(3)°; V = 7223(3) Å^3, Z = 8, D_c = 1.525 g cm^{-3}; 10465 reflections measured, 5758 were symmetry independent and 2868 were observed [$I > 2\sigma(I)$], R = 0.052, wR^2 (all data) = 0.116, 496 parameters.

2: monoclinic, space group $P2_1/c$; a = 12.827(3), b = 18.862(4), c = 19.499(4) Å, β = 94.26(3)°; V = 4704.6(18) Å^3, Z = 4, D_c = 1.480 g cm^{-3}; 13886 reflections measured, 7099 were symmetry independent and 3131 were observed [$I > 2\sigma(I)$], R = 0.045, wR^2 (all data) = 0.074, 608 parameters. CCDC 182/1520. See http://www.rsc.org/suppdata/cc/a9/a908591b/ for crystallographic files in .cif format.

¶ *General procedure* for the preparation of complex **2**: 0.368 g (0.719 mmol) of [$B(C_6F_5)_3$] was dissolved in 15 mL of toluene and added to 0.370 g (0.690 mmol) of [$Cp^*_2Zr(\eta^2$-$PhC_2SiMe_3)$].[7] The green solution was filtered. After standing for one day at room temperature red crystals deposited which were separated from the mother liquor, washed with cooled toluene and dried *in vacuo* to give 0.684 g (94.6%) of **2**;. mp 176–178 °C (decomp.).

‖ *Data* for **2**: elemental analysis for $C_{49}H_{44}SiBZrF_{15}$ (*M* = 1047.98). Calc.: C, 56.16; H, 4.23. Found : C, 55.99; H, 4.24%. ^{1}H NMR (THF-d_8, 297 K): δ 0.07 (s, 9H, $SiMe_3$); 1.30, 1.51, 1.64, 1.80 (4 s, 3H each, Cp-Me); 1.95 (s, 15H, Cp*); 2.65, 2.81 (br, 1H each, BCH_2); 4.49 (s, 1H, CH); 7.14 (2H, *o*-Ph); 7.19 (1H, *p*-Ph); 7.34 (2H, *m*-Ph). ^{13}C NMR (THF-d_8, 297 K, not all signals unambiguously identified): δ 1.2 ($SiMe_3$); 12.2, 12.4, 12.6, 12.7 (Cp-Me); 12.7 (Cp*); 22.9 (br, BCH_2); 104.9 (CH); 123.7 (Cp*); 126.6 (*o*-Ph); 126.8 (*p*-Ph); 128.7 (*m*-Ph); 228.9 (Zr–C).

1 (*a*) V. V. Burlakov, U. Rosenthal, P. V. Petrowsky, V. B. Shur and M. E. Vol'pin, *Metalloorg. Khim.*, 1988, **1**, 953; *Organomet. Chem. USSR*, 1988, **1**, 526; (*b*)V. V. Burlakov, A. V. Polyakov, A. I. Yanovsky, Yu. T. Struchkov, V. B. Shur, M. E. Vol'pin, U. Rosenthal and H. Görls, *J. Organomet. Chem.*, 1994, **476**, 197.

2 (*a*) A. Ohff, R. Kempe, W. Baumann and U. Rosenthal, *J. Organomet. Chem.*, 1996, **520**, 241; (*b*) W. Ahlers, B. Temme, G. Erker, R. Fröhlich and F. Zippel, *Organometallics*, 1997, **16**, 1440.

3 (*a*) V. V. Burlakov, S. I. Troyanov, A. V. Letov, E. I. Mysov, G. G. Furin and V. B. Shur, *Izv. Akad. Nauk, Ser. Khim.*, 1999, 1022; *Russ. Chem. Bull.*, 1999, **48**, 1012, (*Engl. Transl.*); (*b*) V. V. Burlakov, S. I. Troyanov, L. I. Strunkina, M. Kh. Minacheva, A. V. Letov, G. G. Furin, U. Rosenthal and V. B. Shur, *J. Organomet. Chem.*, 2000, in press.

4 J. Ruwwe, G. Erker and R. Fröhlich, *Angew. Chem.*, 1996, **108**, 108; *Angew. Chem., Int. Ed. Engl.*, 1996, **35**, 80.

5 W. E. Piers, *Chem. Eur. J.*, 1998, **4**, 13; and references therein.

6 (*a*) V. V. Burlakov, U. Rosenthal, R. Beckhaus, A. W. Polyakov, Yu. T. Struchkov, G. Oehme, V. B. Shur and M. E. Vol'pin, *Metalloorg. Khim.*, 1990, **3**, 476; *Organomet. Chem. USSR*, 1990, **3**, 237; (*b*) U. Rosenthal, H. Görls, V. V. Burlakov, V. B. Shur and M. E. Vol'pin, *J. Organomet. Chem.*, 1992, **426**, 53.

7 (*a*) A. K. List, K. Koo, A. L. Rheingold and G. L. Hillhouse, *Inorg. Chim Acta*, 1998, **270**, 399; (*b*) P.-M. Pellny, V. V. Burlakov, W. Baumann, A. Spannenberg and U. Rosenthal, *Z. Anorg. Allg. Chem.*, 1999, **625**, 910.

8 I. Hyla-Kryspin, R. Gleiter, C. Krüger, R. Zwettler and G. Erker, *Organometallics*, 1990, **9**, 517 and references therein.

9 J. Hiller, U. Thewalt, M. Polasek, L. Petrusova, V. Varga, P. Sedmera and K. Mach, *Organometallics*, 1996, **15**, 3752.

10 (*a*) C. Lefeber, A. Ohff, A. Tillack, W. Baumann, R. Kempe, V. V. Burlakov, U. Rosenthal and H. Görls, *J. Organomet. Chem.*, 1995, **501**, 179; (*b*) P. Arndt, C. Lefeber, R. Kempe, A. Tillack and U. Rosenthal, *Chem. Ber.*, 1996, **129**, 1281.

11 C. Lefeber, A. Ohff, A. Tillack, W. Baumann, R. Kempe, V. V. Burlakov and U. Rosenthal, *J. Organomet. Chem.*, 1995, **501**, 189.

12 (*a*) U. Rosenthal, A. Ohff, M. Michalik, H. Görls, V. V. Burlakov and V. B. Shur, *Angew. Chem.*, 1993, **105**, 1228; (*b*) D. Thomas, N. Peulecke, V. V. Burlakov, B. Heller, W. Baumann, A. Spannenberg, R. Kempe, U. Rosenthal and R. Beckhaus, *Z. Anorg. Allg. Chem.*, 1998, **624**, 919.

Communication a908591b

ChemComm

Preparation of silica aerogel using ionic liquids as solvents

Sheng Dai,*[a] Y. H. Ju,[ac] H. J. Gao,[b] J. S. Lin,[b] S. J. Pennycook[b] and C. E. Barnes[c]

[a] *Chemical Technology, Oak Ridge National Laboratory, PO Box 2008, Oak Ridge, TN 37831, USA. E-mail: i9d@ORNL.GOV*
[b] *Solid State Divisions, Oak Ridge National Laboratory, PO Box 2008, Oak Ridge, TN 37831, USA*
[c] *Department of Chemistry, University of Tennessee, Knoxville, TN 37996-1600, USA*

Received (in Bloomington, IN, USA) 3rd September 1999, Accepted 23rd December 1999

Ionic liquids have been used as effective solvents to synthesize aerogels; a long aging time can be used to produce stable aerogel structures without the need for supercritical drying processes.

Aerogels are a novel class of porous materials with wide-ranging applications. The unique properties include low density, high surface area, low thermal conductivity and low dielectric permittivity.[1–3] So far, the synthesis of silica-based aerogels has been accomplished mainly through the controlled condensation of small colloidal particles produced by sol–gel processing in alcoholic aqueous solutions, followed by a supercritical drying process. A highly desirable goal in aerogel synthesis is the elimination of the supercritical drying process, the most expensive and risky aspect of the process. For example, Guo and Guadalupe have succeeded in synthesizing a silica-based aerogel from a metastable lamellar composite through cooperative interaction between silica and surfactant species.[4] The surfactant molecules used to generate pores can be removed from the silica network through conventional solvent extraction. The porous structure is stable during this procedure, and no supercritical extraction is used. Here, we report a new aerogel synthesis methodology based on the use of ionic liquids as solvents. The structural features of the synthesized silica aerogel are characterized.

Ionic liquids are a unique class of solvents that have virtually no vapor pressure and possess versatile solvent properties.[5–7] Recently, they have been effectively demonstrated as a superior solvent for conducting many organic reactions. For example, Chauvin *et al.* have shown that oligomers of alkenes can be efficiently synthesized using ionic liquid solvents.[8,9] More recently, many new organic reactions in various ionic liquids have been carried out by Seddon's group.[10,11] Our interest is in exploring the ionic liquids as solvents to conduct inorganic polymeric reactions for synthesizing novel inorganic materials. Conventional sol–gel synthesis of aerogels involves hydrolysis and condensation of tetraalkylorthosilicates to form gels in alcoholic aqueous solutions. During the aging process, the solvents evaporate, causing gel shrinkage before formation of a stable sol–gel network. If the aging period is too long, the pore volume tends to be reduced to that of the corresponding xerogel. However, too short an aging time may cause instability of the gel network, which can result in its collapse after extraction of the solvent. Therefore, control of the aging time is critical to the success of the aerogel synthesis. Ionic liquids offer an attractive method for achieving longer aging times without shrinkage of the gel network. When used as the solvent for sol–gel processes, their negligible vapor pressure prevents solvent evaporation, and their high ionic strength increases the rate of aggregation. These and other effects allow hydrolysis and condensation to proceed to completion, accordingly producing a stable gel network before solvent extraction.[12] All the preceding assertions concerning the advantages of using ionic liquids as solvents for the aerogel synthesis, of course, rely on the solvation capability of ionic liquids to form homogeneous solutions with aerogel precursors.

Tetramethylorthosilicate (TMOS) is used as the sol–gel precursor. The room-temperature ionic liquid used in this work is 1-ethyl-3-methylimidazolium bis[(trifluoromethyl)sulfonyl] amide ($EtMeIm^+Tf_2N^-$). This melt was synthesized as described in the literature.[13–15] Acid-catalyzed sol–gel processing was conducted: in a typical run,[16] 1 mL of TMOS, 2 ml of formic acid (Aldrich Chemical Co., 99%) and 1 mL of $EtMeIm^+Tf_2N^-$ were mixed. The sol–gel reaction can be described by eqn. (1).[17] The final mixture gelled overnight

$$2\ HC(O)OH + (CH_3O)_4Si \rightarrow SiO_2 + 2\ CH_3OH + 2\ HC(O)OCH_3 \quad (1)$$

and was cured at ambient temperature for three weeks. A transparent monolith glass was obtained. The entrapped ionic liquid was extracted by refluxing the above monolith in acetonitrile (Baker Chemical Co., HPLC grade) overnight. The extraction procedure did not result in any visible shrinkage of the gel. This may be attributed to the long curing time used to stabilize the aerogel network before the extraction. The C–H stretching vibrational IR features of the ionic liquid around 2900 cm^{-1} disappeared after extraction and vacuum drying. This indicates that all ionic liquid molecules were removed through extraction. Immersion of the aerogel in solvents with a high dielectric constant (*e.g.* water) can result in cracking of the aerogel monolith. However, the aerogel monolith is very stable in air.

The N_2 adsorption isotherm (Fig. 1) of the monolith glass after removal of the ionic liquid is identical to those of aerogels prepared using different solvent and supercritical extraction.[2,3] The surface area and pore volume calculated from Fig. 1 are 720 $m^2\ g^{-1}$ and 1.4 $cm^3\ g^{-1}$, respectively.[18] Further supports for the aerogel structure come from investigation by small-angle X-ray scattering (SAXS). Fig. 2 shows a typical SAXS curve of the aerogel prepared using the ionic liquid. The analysis of the SAXS data indicates that the aerogel is mass fractal with a fractal dimension of 1.4. This small fractal dimension indicates a highly porous sol–gel network and is consistent with the mass fractal dimension for the aerogel materials.[12] The constituent particles have a size distribution and the value of R_g (radius of gyration) ranges from 80 to 14 Å, based on Guinier analysis.

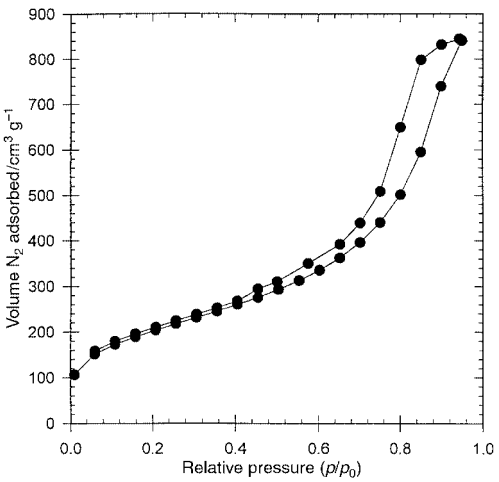

Fig. 1 Nitrogen adsorption–desorption isotherm.

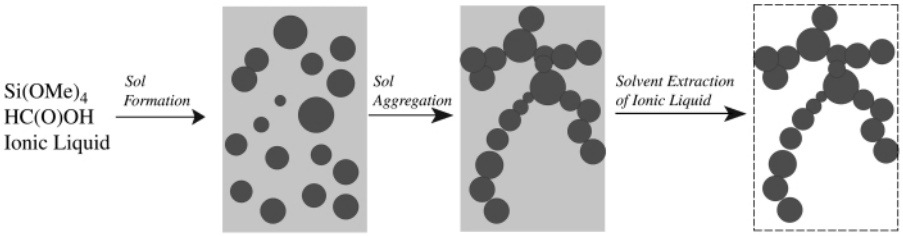

Scheme 1

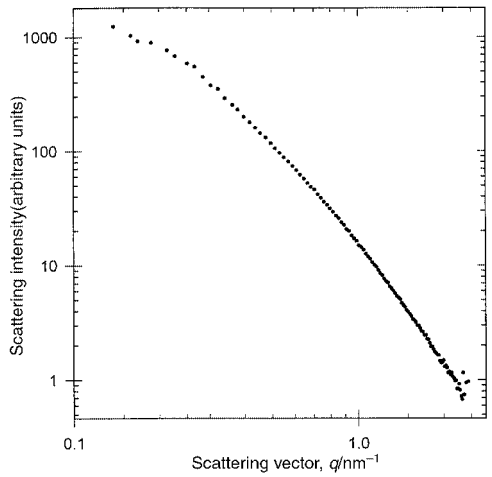

Fig. 2 Small-angle X-ray scattering curve for the aerogel.

Both the nitrogen adsorption and the SAXS data for our aerogel agree well with those obtained for the aerogels synthesized by conventional protocols.[1,3,13]

A possible mechanism for the aerogel formation in the ionic liquid is shown in Scheme 1. Formic acid initiates the formation of the sol particles, which effectively aggregate in the ionic liquid into a sol–gel network. Concurrently, the ionic liquid becomes entrapped in the growing covalent silica network, rather than being chemically bound to the inorganic matrix. A long aging time implemented before extraction of the non-volatile ionic liquid further enhances the stability of the aerogel network. No macroscopic phase separation between the gel and the ionic liquid solvent has been observed. The homogeneity is retained throughout the entire aging process. This indicates that the interaction between the sol particles and the ionic liquids is favored thermodynamically. The ionic liquid forms a homogeneous solution with sol–gel precursors. If other solvents (*e.g.* DMSO, water) are used in the sol–gel preparation, no appreciable pore volumes (< 0.1 cm^3 g^{-1}) are found. In fact, similar results have been reported in the literature concerning the doping of silica with organic liquids through sol–gel processes.[19]

In conclusion, the silica aerogel has been synthesized using an ionic liquid as a reaction solvent. This technique allows aerogel synthesis under mild chemical conditions and eliminates the risky supercritical drying process. We expect that this new methodology can find applications in synthesizing new aerogels and aerogel films for separation, catalysis, and insulation.

This work was supported by the Division of Chemical Sciences, Office of Basic Energy Sciences, U.S. Department of Energy, under contract No. DE-AC05-96OR22464 with Lockheed Martin Energy Research Corp. We also thank reviewers for their valuable comments.

Notes and references

1 N. Husing and U. Schubert, *Angew. Chem., Int. Ed.*, 1998, **37**, 22.
2 C. A. Morris, M. L. Anderson, R. M. Stroud, C. I. Merzbacher and D. R. Rolison, *Science*, 1999, **284**, 622.
3 M. L. Anderson, C. A. Morris, R. M. Stroud, C. I. Merzbacher and D. R. Rolison, *Langmuir*, 1999, **15**, 674.
4 Y. Guo and A. R. Guadalupe, *Chem. Commun.*, 1999, 315.
5 T. Welton, *Chem. Rev.*, 1999, **99**, 2071.
6 C. L. Hussey, *Pure Appl. Chem.*, 1988, **60**, 1763.
7 K. R. Seddon, *J. Chem. Tech. Biotechnol.*, 1997, **68**, 351.
8 Y. Chauvin and H. Olivier-Bourbigou, *CHEMTECH*, 1995, **25(9)**, 26.
9 Y. Chauvin, S. Einloft and H. Olivier, *Ind. Eng. Chem. Res.*, 1995, **34**, 1149.
10 M. J. Earle, P. B. McCormac and K. R. Seddon, *Chem. Commun.*, 1998, 2245.
11 C. J. Adams, M. J. Earle, G. Roberts and K. R. Seddon, *Chem. Commun.*, 1998, 2097.
12 C. J. Brinker and G. W. Scherer, *Sol–Gel Science: the Physics and Chemistry of Sol–Gel Processing*, Academic Press, Inc., New York, 1990.
13 J. S. Wilkes and M. J. Zaworotko, *J. Chem. Soc., Chem. Commun.*, 1992, 965.
14 P. Bonhote, A. P. Dias, N. Papageorgiou, K. Kalyanasundaram and M. Gratzel, *Inorg. Chem.*, 1996, **35**, 1168.
15 S. Dai, Y. H. Ju and C. E. Barnes, *J. Chem. Soc., Dalton Trans.*, 1999, 1201; S. Dai, Y. Shin, L. M. Toth and C. E. Barnes, *Inorg. Chem.*, 1997, **36**, 4900.
16 S. Dai, Y. Shin, C. E. Barnes and L. M. Toth, *Chem. Mater.*, 1997, **9**, 2521.
17 W. H. Green, K. P. Le, J. Grey, T. T. Au and M. J. Sailor, *Science*, 1997, **276**, 1826.
18 Nitrogen porsimetry often gives misleading pore volume data for aerogels, as noted in G. W. Scherer, D. M. Smith and D. Stein, *J. Non-Cryst. Solids*, 1995, **186**, 309.
19 H. Bottcher, K.-H. Kallies, H. Haufe and J. Seidel, *Adv. Mater.*, 1999, **11**, 138.

Communication a907147d

A convenient method of preparing optically active (*S*)-*N*-tritylaziridine-2-carboxylate esters from (*S*)-β-haloamino acids

Yasuo Kato*[ab] and Kenji Fukumoto[b]

[a] *Biotechnology Research Center, Toyama Prefectural University, Kosugi, Toyama 939-0398, Japan. E-mail: yasu@pu-toyama.ac.jp*

[b] *Life Science Research Center, Advanced Technology Research Laboratories, Nippon Steel Corporation, Nakahara-ku, Kawasaki 211-0035, Japan*

Received (in Cambridge, UK) 18th November 1999, Accepted 6th January 2000

A convenient method of preparing optically active (*S*)-*N*-tritylaziridine-2-carboxylate esters *via* intramolecular cyclization of (*S*)-*N*-trityl-β-haloamino acid esters is described.

The development of novel methods of synthesizing optically pure unnatural amino acids is an area of current interest.[1] (*S*)-*N*-Tritylaziridine-2-carboxylate [*N*-Tr-(*S*)-AZC] esters represent an interesting class of compounds since they can be considered a versatile synthetic equivalent of the 'β-alanyl cation' synthon suitable for elaboration into β-substituted (*S*)-amino acids,[2] enzyme substrates,[3] and irreversible inhibitors of proteases.[4] Despite their importance for synthetic use, only a few studies on the syntheses of *N*-Tr-(*S*)-AZC esters have been reported [5–9] and these methods involve multi-step procedures, require expensive starting materials, and produce a low yield or partial racemization of the intermediate in the synthetic scheme.

During the course of our studies on the application of enzymes in organic syntheses, we have discovered an efficient method for the production of halogen-containing α-amino acids *via* chemo-enzymatic reaction.[10] Using this process, optically pure (*S*)-β-haloamino acids, especially, (*S*)-β-chloroalanine (BCA) and *threo*-(2*R*,3*S*)-3-chloroaspartic acid, can be obtained in large quantities. We report herein a convenient method of synthesizing *N*-Tr-(*S*)-AZC esters *via* intramolecular cyclization of (*S*)-*N*-trityl-β-chloroalanine (*N*-Tr-BCA) esters,† which were derived from the enzymatically prepared BCA (Scheme 1).

In our first attempt at a base-catalyzed intramolecular cyclization reaction of *N*-Tr-BCA benzyl ester **1** to benzyl *N*-Tr-(*S*)-AZC **2** with 2 equiv. of strong base, such as NaH, Bu^{t}OK, DBU, DBN and Bu^{t}Li, in THF at room temperature, however, only the 1,2-elimination of hydrogen and chloride atoms occurred and *N*-trityldehydroalanine benzyl ester **3**‡ was obtained as the sole product (Table 1, entry 1). Reaction in another solvent, such as hexane, Et_2O, CH_2Cl_2, MeCN, DMF and DMSO, also gave **3**. It turned out that the expected aziridine **2**§ was formed when a weak inorganic base, KF, was used as the base in refluxing MeCN (entry 2) with some formation of **3**. Encouraged by this result, we further investigated the inorganic bases by changing their basicity and counter ions. Weaker bases and neutral salts such as LiF, NaF, LiCl, NaCl, KCl, NaBr, KBr, CsBr, RbBr, MgF_2 and SrF_2 were ineffective and afforded BCA benzyl ester **4** which was formed by deprotection of the trityl group of **1** (entry 4). However, the use of bisulfite salt, $KHSO_3$, could suppress both the 1,2-elimination and deprotection reaction to give the aziridine **2** as the sole product, although the reaction rate was decreased to one-third of that with KF (entry 5). Elongation of the reaction time could solve this problem and afforded **2** in almost quantitative yield (entry 6). The choice of the reaction solvent was quite important; alkyl nitriles *i.e.* MeCN, EtCN, PrCN, Pr^{i}CN, BuCN and Bu^{i}CN, were the only suitable solvents to form aziridine **2**. Other organic solvents such as THF, DMSO, DMF, 1,4-dioxane, CH_2Cl_2 and Et_2O were not useful; only the recovery of the starting material **1** was observed. The other weak acid salts of the potassium ion, $KHSO_3$, K_2SO_3, K_2HPO_4, K_2WO_4 and $K_2S_2O_5$, and weak organic amines, Et_3N and Pr^i_2NEt, were effective bases for the cyclization reaction and gave the cyclized aziridine **2** as the sole product. Interestingly, only a deprotected compound **4** was obtained using sulfate and persulfate salts, $KHSO_4$, K_2SO_4 and $K_2S_2O_7$. However, the use of stronger inorganic bases such as RbF and CsF deserves comment and produced only **3** (*e.g.* entry 7).

Under such suitable conditions,¶ the cyclization reactions of various esters of *N*-Tr-BCA were examined. Methyl, ethyl, *n*-propyl, *n*-butyl, *n*-pentyl, isopropyl and isobutyl esters of BCA were converted to the corresponding aziridines in yields of 90, 95, 94, 98, 92, 97 and 96%, respectively. These results suggest

Table 1 Base-catalyzed transformation of (*S*)-*N*-Tri-β-chloroalanine benzyl ester

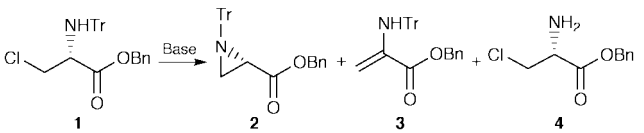

				Products (%)			
Entry	Base	Solvent	Conditions	**1**	**2**	**3**	**4**
1	NaH	THF	rt 4 h	0	0	95	0
2	KF	MeCN	reflux, 24 h	0	64	36	0
3	KF	DMF	90 °C, 4 h	0	0	98	0
4	NaF	MeCN	reflux, 24 h	0	5	2	90
5	$KHSO_3$	MeCN	reflux, 24 h	66	34	0	0
6	$KHSO_3$	MeCN	reflux, 48 h	0	98	0	0
7	CsF	MeCN	reflux, 4 h	0	0	97	0

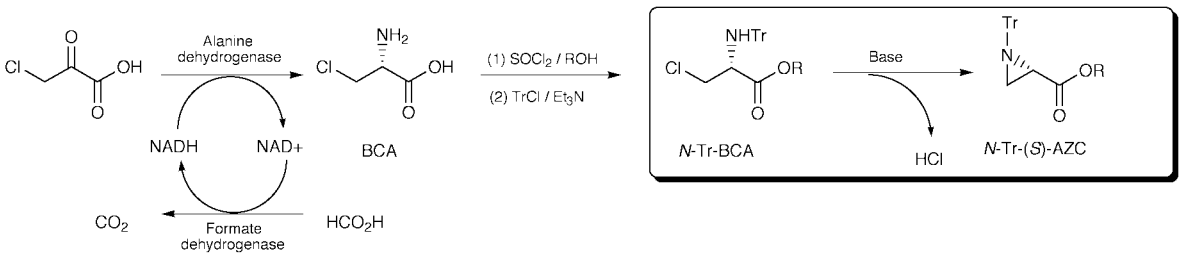

Scheme 1 Chemoenzymatic synthesis of (*S*)-*N*-tritylaziridine-2-carboxylate esters.

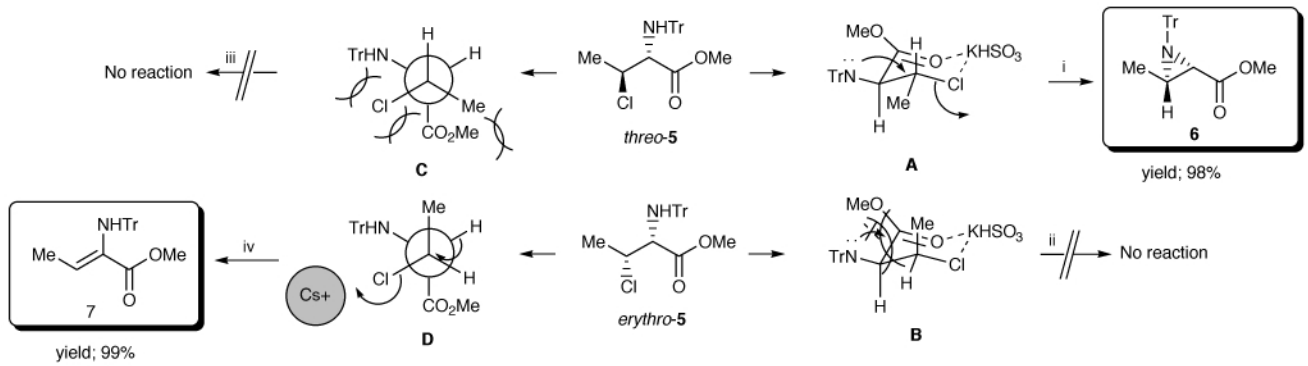

Scheme 2 *Reagents and conditions*: i, $KHSO_3$, MeCN, reflux, 63 h; ii, $KHSO_3$, MeCN, reflux, 120 h; iii, CsF, DMF, 100 °C, 60 h; iv, CsF, MeCN, reflux, 4 h.

that changing the ester moiety does not affect the yield or reaction rate of the formation of aziridine.

Based on these observations, we propose the following reaction mechanisms for the cyclization or 1,2-elimination reactions: (i) when the reagent is neutral or has Lewis acidity, only deprotection of the trityl group is seen; (ii) if the reagent exhibits basicity and dissociates into ions, the metal ions act as a base and catalyzed the 1,2-elimination reaction; (iii) if the reagent cannot dissociate into ions, it chelates both the chloride atom and carbonyl oxygen, allowing the cyclization reaction. This is supported by the fact that the KF-catalyzed cyclization reaction proceeds only in MeCN; the 1,2-elimination reaction preferentially occurred in polar solvents, such as DMF, DMSO, THF and 1,4-dioxane, in which the reagents dissociate more easily into the ion pairs (*e.g.* Table 1, entry 3).

We next examined the cyclization or 1,2-elimination reaction for each diastereomer of methyl (*S*)-*N*-trityl-3-chloro-2-amino-butyrate (*N*-Tr-BCAB), prepared from (*S*)-threonine or *allo*-(*S*)-threonine. As shown in Scheme 2, only the *threo* isomer of *N*-Tr-BCAB (*threo*-**5**) was cyclized to form (2*S*,3*R*)-3-methylaziridine-2-carboxylate **6**,‖ but *erythro*-**5** was not. If we assume a chair-like transition state, we can conceive a reaction mechanism. In the transition state, $KHSO_3$, which does not dissociate into K^+ and HSO_3^-, is chelated by both the chloride atom and the carbonyl oxygen; it allows an attack by a lone pair from nitrogen, giving cyclization and eliminating the chloride ion *via* an S_N2-like reaction (transition state A), resulting in the formation of aziridine **6**. In the case of *erythro*-**5**, steric repulsion by the axial methyl group stopped the attack of nitrogen (transition state B). In contrast, the 1,2-elimination reaction occurred only for *erythro*-**5** to give (*E*)-dehydroamino acid **7**‖ as the sole product. The results are explainable by Newman projections. The dissociated caesium ion acts as a base allowing the elimination of the chloride ion and *anti*periplanar proton, afforded 1,2-eliminated product **7** from *erythro*-**5** (transition state D), while *threo*-**5** cannot adopt a conformation able to 1,2-eliminate due to steric repulsion between the methyl, *N*-trityl and methoxycarbonyl groups, blocking reaction (transition state C).

In summary, we have shown here that (*S*)-*N*-tritylaziridine-2-carboxylate esters are quantitatively synthesized *via* the weak base-catalyzed cyclization of (*S*)-*N*-trityl-β-haloamino acid esters under mild conditions. By changing slightly the reaction conditions, 1,2-elimination takes place and affords *N*-trityl-dehydroalanine esters in good yield. Syntheses of (*S*)-amino acid derivatives by ring opening of the aziridine esters without racemization are currently underway.

This work was performed at the Life Science Research Center, Nippon Steel Corporation. We are grateful to Professor Katsuyuki Ogura, Chiba University, for helpful discussions.

Notes and references

† BCA was enzymatically synthesized in high chemical (> 90%) and optical (> 99.9% ee) yields from 3-chloropyruvate using alanine dehydrogenase from *Bacillus stearothermophilus* (Unitika, Kyoto, Japan) with regeneration of NADH by formate dehydrogenase (Boehringer Mannheim GmbH, Germany) as described previously (ref. 10). The BCA was converted to *N*-Tr-BCA esters by an esterification with $SOCl_2$ in an appropriate alcohol followed by *N*-tritylation with Tr-Cl–Et_3N in CH_2Cl_2.

‡ *Selected data* for **3**: δ_H(400 MHz, $CDCl_3$) 7.19–7.38 (m, 20H), 5.85 (br, 1H), 5.19 (s, 2H), 4.86 (dd, 1H, *J* 0.85, 1.7), 3.73 (d, 1H, *J* 0.85); δ_C(100 MHz, $CDCl_3$) 165.9, 144.5, 136.6, 135.6, 129.1, 128.5, 128.3, 128.0, 127.8, 126.8, 95.4, 71.2, 67.3; ν_{max}/cm^{-1} (NaCl) 3400, 3060, 3030, 1705, 1615, 1485, 1440, 1295, 1195, 1170, 745, 695; mp 164–166 °C.

§ *Selected data* for **2**: δ_H(400 MHz, $CDCl_3$) 7.47–7.49 (m, 6H), 7.31–7.39 (m, 6H), 7.18–7.25 (m, 8H), 5.21 (ABq, 2H, *J* 3.8, 18.6), 2.28 (dd, 1H, *J* 1.5, 2.5), 1.92 (dd, 1H, *J* 2.5, 6.2), 1.41 (dd, 1H, *J* 1.5, 6.2); δ_C(100 MHz, $CDCl_3$) 171.4, 143.6, 135.8, 129.3, 128.6, 128.4, 128.3, 127.7, 126.9, 74.4, 66.7, 31.8, 28.8; ν_{max}/cm^{-1} (NaCl) 3060, 3030, 1740, 1590, 1485, 1445, 1235, 1170, 1015, 745, 705, 695, 625; mp 115–116 °C; $[\alpha]_D^{20}$ −96.9 (*c* 1.0, $CHCl_3$); optical purity > 99.9% ee [determined by HPLC with Crownpak CR(-) (Daicel, Tokyo, Japan) after derivatization of **3** to (*S*)-alanine by hydrogenation with Pd/C].

¶ Typical reaction procedure: to a stirred suspension of $KHSO_3$ (2.5 mmol) in anhydrous MeCN (15 ml) was added *N*-Tr-BCA ester (0.5 mmol) and the mixture was refluxed for several hours. After cooling to room temperature, 5 ml of 5% $NaHCO_3$ was added to the mixture and the product was extracted with CH_2Cl_2 (15 ml × 2). The combined organic layer was dried over anhydrous $MgSO_4$ and concentrated *in vacuo*. The residue was purified by preparative TLC (silica gel) and afforded aziridines as crystals or an oil.

‖ The structure of aziridine **6** and dehydroamino acid **7** were confirmed by ^1H and ^{13}C NMR and IR in comparison with reported values (ref. 11).

1 R. M. Williams, *Synthesis of Optically Active α-Amino Acids*, Pergamon Press, Oxford, 1989
2 J. A. Deyrup, in *Small Ring Heterocycles*, Part 1, ed. A. Hassner, Wiley, New York, 1983, p.11; O. C. Dermer and G. E. Ham, *Ethylenimine and Other Aziridines*, Academic Press, New York, 1969; R. J. Cherney and L. Wang, *J. Org. Chem.*, 1996, **61**, 2544; J. Legters, J. G. H. Williams, L. Thijs and B. Zwanenburg, *Recl. Trav. Chim. Pays-Bas*, 1992, **111**, 1; D. Tanner, *Angew. Chem., Int. Ed. Engl.*, 1994, **33**, 599.
3 B. P. Murphy and R. F. Pratt, *Biochemistry*, 1991, **30**, 3640.
4 F. Gerhart, W. Higgins, C. Tardif and J.-B. Ducep, *J. Med. Chem.*, 1990, **33**, 2157; Z. Zhong, J. A. Bibbs, W. Yuan and C.-H. Wong, *J. Am. Chem. Soc.*, 1991, **113**, 2259; L. Moroder, H.-J. Musiol and R. Scharf, *FEBS Lett.*, 1992, **299**, 51.
5 K. Nakajima, F. Takai, T. Tanaka and K. Okawa, *Bull. Chem. Soc. Jpn.*, 1978, **51**, 1577; K. Nakajima, H. Sakai, M. Neya, M. Morishita, S. Sakai and K. Okawa, in *Peptide Chemistry*, ed. S. Sakakibara, Protein Research Foundation, Osaka, 1983, p. 19; P. Wipf and C. P. Miller, *Tetrahedron Lett.*, 1992, **33**, 6267; R. J. Cherney and L. Wang, *J. Org. Chem.*, 1996, **61**, 2544.
6 K. Harada and I. Nakamura, *Chem. Lett.*, 1978, 1171; I. Nakamura and K. Harada, *Chem. Lett.*, 1979, 313.
7 D. Tanner, C. Birgersson and H. K. Dhaliwal, *Tetrahedron Lett.*, 1990, **31**, 1903; K. Mori and H. Ishikawa, *Tetrahedron*, 1980, **36**, 87.
8 P. Garner, O. Dogan and S. Pillai, *Tetrahedron Lett.*, 1994, **35**, 1653.
9 A. Bongini, G. Cardillo, L. Gentilucci and C. Tomasini, *J. Org. Chem.*, 1997, **62**, 9148.
10 Y. Kato, K. Fukumoto and Y. Asano, *Appl. Microbiol. Biotechnol.*, 1993, **39**, 301; Y. Asano and Y. Kato, *Biosci. Biotechnol. Biochem.*, 1994, **58**, 223.
11 C. Dugave and A. Menez, *Tetrahedron: Asymmetry*, 1997, **8**, 1453; J. E. Baldwin, R. M. Adlington, N. Moss and N. G. Robinson, *J. Chem. Soc., Chem. Commun.*, 1987, 1664.

Communication a909140h

The oxidation of polychlorinated benzenes by genetically engineered cytochrome $P450_{cam}$: potential applications in bioremediation

Jonathan P. Jones, Ellen J. O'Hare and Luet-Lok Wong*

Department of Chemistry, Inorganic Chemistry Laboratory, University of Oxford, South Parks Road, Oxford, UK OX1 3QR. E-mail: luet.wong@chem.ox.ac.uk

Received (in Cambridge, UK) 2nd December 1999, Accepted 6th January 2000

Polychlorinated aromatic compounds are persistent environmental contaminants; we describe here the redesign and engineering of the haem monooxygenase cytochrome $P450_{cam}$ to oxidise these compounds efficiently to the chlorinated phenols which are readily degraded by many micro-organisms, thus providing a basis for novel systems for biological clean-up of these inert compounds.

Polychlorinated aromatic compounds are among the most problematic environmental pollutants because of their chemical inertness, lipid solubility and toxicity.[1] Naturally occurring micro-organisms have evolved to degrade and mineralise many, but by no means all, of these compounds. For example, the dioxins and heavily chlorinated biphenyls are degraded very slowly or not at all. Similarly, numerous micro-organisms have been isolated which together degrade most of the chlorinated benzenes,[2] but the most heavily chlorinated compounds pentachlorobenzene (PeCB) and hexachlorobenzene (HCB), as well as 1,2-dichlorobenzene (1,2-DCB) and 1,3,5-trichlorobenzene (1,3,5-TCB) are particularly inert to biodegradation.[3] We noted that chlorinated phenols are readily degraded by micro-organisms.[4] We reasoned that if a monooxygenase can be prepared that can efficiently oxidise polychlorinated benzenes to the phenol derivatives, then the monooxygenase system could be introduced into chlorophenol-degrading micro-organisms such as *Pseudomonas* bacteria to enable them to degrade polychlorinated benzenes. We report here the genetic engineering of the haem monooxygenase cytochrome $P450_{cam}$ from *Pseudomonas putida* to oxidise 1,2-DCB, 1,3,5-TCB and PeCB, creating a basis for novel bioremediation systems.

The criteria for successful redesign of the $P450_{cam}$ active site for the oxidation of polychlorinated benzenes are reasonable rates of substrate turnover and tight coupling of NADH consumed to substrate oxidation. Uncoupling wastes NADH and can produce harmful hydrogen peroxide,[5] both of which will put metabolic stress on the host organisms and thus reduce their viability. We have shown that the Y96A and Y96F mutations greatly improved the activity of $P450_{cam}$ for the oxidation of a wide range of organic compounds, including simple alkanes,[6] styrene[7] and naphthalene.[8] We proposed that these mutations at Y96 (Fig. 1) improve the turnover of such hydrophobic compounds by increasing the hydrophobicity of the enzyme active site. We also noted that the oxidation by the Y96F mutant of naphthalene, which is larger than the chlorinated benzenes considered here, had a coupling of 55% compared to 17% for the Y96A mutant. Since the Y96A mutant should have a larger active site, the Y96F mutation should be our starting point. The coupling could then be increased by improving the enzyme–substrate fit and by forcing the chlorinated benzenes to bind closer to the haem. Hence the active site volume was reduced by further substitutions with amino acids with bulkier side-chains at three other active site residues. Phenylalanines 87 and 98 are at approximately the same height as Y96 above the haem and near the top of the active site (Fig. 1), and valine-247 is just below these residues and closer to the haem.[9] The new mutants F87W–Y96F, F87W–Y96F–F98W and F87W–Y96F–V247L were prepared and their activities compared to the WT enzyme.

1,2-DCB was oxidised by all the $P450_{cam}$ enzymes to 2,3-dichlorophenol (2,3-DCP) and 3,4-dichlorophenol (3,4-DCP) in 9:1 ratio (Fig 2), and 2,4,6-trichlorophenol (2,4,6-TCP) was the only product from 1,3,5-TCB. The predominant product from PeCB oxidation was pentachloro-

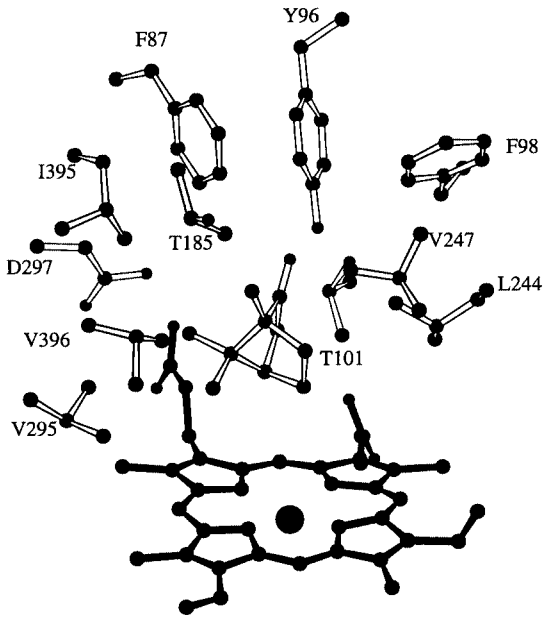

Fig. 1 The active site structure of wild-type $P450_{cam}$ with bound camphor.

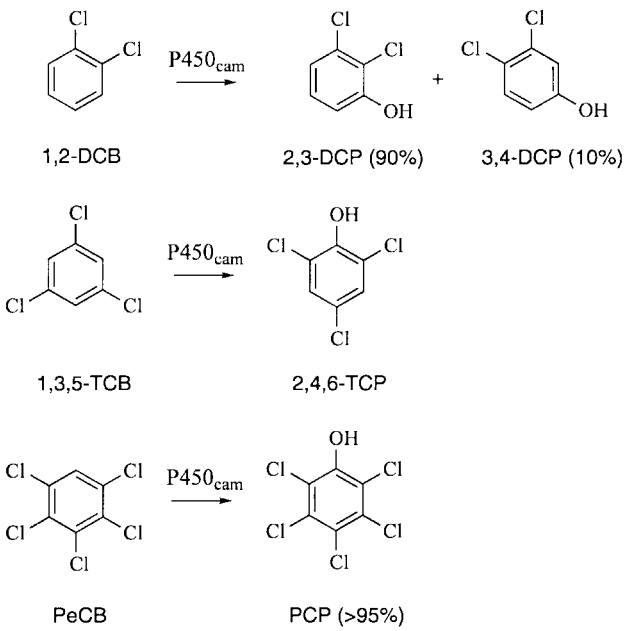

Fig. 2 The oxidation of chlorinated benzenes by wild-type $P450_{cam}$ and active site mutants.

Table 1 The activity of wild-type (WT) cytochrome $P450_{cam}$ and active site mutants for the oxidation of chlorinated benzenes. ND: no product observed by HPLC. The products of the reactions are shown in Fig. 2

	WT	F87W–Y96F	F87W–Y96F–V247L	F87W–Y96F–F98W
1,2-dichlorobenzene (1,2-DCB)				
Binding constant K_D/μM	3.0	2.0	0.9	1.2
NADH turnover rate[a]	20	408	391	158
Product formation rate (k_2)[b]	0.45	106	83	78
Coupling efficiency[c]	2.3%	26%	21%	49%
$(k_2/K_D)/M^{-1}\ s^{-1}$	2.50×10^3	8.83×10^5	1.54×10^6	1.08×10^6
1,3,5-trichlorobenzene (1,3,5-TCB)				
Binding constant K_D/μM	3.9	3.0	2.0	1.8
NADH turnover rate	6.5	224	308	121
Product formation rate (k_2)	0.07	115	175	119
Coupling efficiency	1.1%	51%	57%	97%
$(k_2/K_d)/M^{-1}\ s^{-1}$	3.00×10^2	6.39×10^5	1.46×10^6	1.10×10^6
Pentachlorobenzene (PeCB)				
NADH turnover rate	2.4	100	229	43
Product formation rate	ND	2.3	5.5	3
Coupling efficiency	—	2.3%	2.4%	7%

[a] Given as nanomoles of NADH consumed per nanomole of $P450_{cam}$ per minute and the average of at least 3 experiments with all the data within 10% of the means. Incubation mixtures (1.70 ml) contained 50 mM Tris.HCl, pH 7.4, 1 μM $P450_{cam}$, 10 μM putidaredoxin, 2 μM putidaredoxin reductase and 200 mM KCl. Both 1,2-DCB and 1,3,5-TCB (200 μM) were added as a 0.1 M stock in ethanol. The mixture was incubated at 30 °C for 2 min after the addition of NADH (100 μM) and the reaction initiated by the addition of substrate. NADH absorbance at 340 nm was monitored over the course of the reaction. [b] The total amount (in nanomoles) of chlorinated phenol products formed per nanomole of $P450_{cam}$ per minute. After the addition of 100 μl of an internal standard to a turnover incubation, organics were extracted by solid phase methods using Varian Bond-Elut columns and products were analysed by reverse phase HPLC. To obtain quantitative results, mixtures containing known concentrations of a product and all of the incubation components except NADH were extracted and analyzed as described above. Linear calibration plots that passed through the origin were obtained for all of the products. [c] The coupling efficiency is the ratio of the total amount of products formed to the amount of NADH consumed and is expressed as a percentage.

phenol (PCP), but two small peaks (*ca.* 2% each) were ascribed by co-elution experiments to 2,3,5,6- and 2,3,4,5-tetrachlorophenols formed by oxidative dehalogenation.

As shown in Table 1, the wild-type (WT) had low rates (< 0.5 min^{-1}) and couplings (1–2%) for the oxidation of the chlorinated benzenes compared to the totally coupled (100%) camphor oxidation rate of 1050 min^{-1} under identical conditions. The mutants all had 2–3 orders of magnitude faster chlorinated benzene oxidation rates than the WT. The NADH turnover rates were up to 400 min^{-1}, and the coupling efficiencies were also much higher. The 50% coupling for 1,2-DCB oxidation by the F87W–Y96F–F98W mutant is a dramatic improvement, and the near total coupling for 1,3,5-TCB oxidation is truly remarkable because the structure of this molecule is completely different from that of camphor. Very importantly, the results also showed that the low solubility of PeCB in water was not a problem, in that a very reasonable NADH turnover rate of 229 min^{-1} could be attained although the coupling was low. The data show that the rationale for active site redesign, whilst empirical and qualitative in nature, was very successful indeed.

The strength of binding and catalytic efficiency of the $P450_{cam}$ enzymes for 1,2-DCB and 1,3,5-TCB oxidation were investigated. The dissociation constants (K_D) in Table 1 show that, as expected, the binding of these compounds was strengthened by the mutations, but by no more than a factor of three. On the other hand, the substrate oxidation rates (k_2) showed 2–3 orders of magnitude increases. There was no direct correlation between the values of K_D and the NADH turnover rates or, notably, the coupling efficiency, which is a stringent measure of the enzyme–substrate fit. Nevertheless, it is instructive to compare the relative specificity (k_{cat}/K_M) of the mutants. It has been suggested that the k_2/K_D ratio is a fair approximation for the k_{cat}/K_M ratio for $P450_{cam}$.[10] The k_2/K_D ratios in Table 1 again highlight the very dramatic accelerating effects achieved by the mutations although they are well short of the near-optimal ratio for camphor oxidation by the WT enzyme ($K_D = 0.27$ μM, $k_2 = 1050$ min^{-1}, $k_2/K_D = 6.5 \times 10^7$ M^{-1} s^{-1}). However, we conclude that the F87W–Y96F–F98W mutant represents an excellent compromise between reasonable rate and tight coupling, especially for the *in vivo* oxidation of polychlorinated benzenes, where very fast turnover could lead to the build up of polychlorinated phenols to toxic levels.

All the chlorophenol products in Fig. 2 are known to be degraded by various micro-organisms,[4] and therefore the mutants can be the basis of novel bioremediation systems for polychlorinated benzenes by genetically introducing the genes encoding the three proteins of the $P450_{cam}$ system into chlorophenol-degrading micro-organisms such as *Pseudomonas* bacteria. The F87W–Y96F–F98W mutant can be used for the particularly inert 1,2-DCB and 1,3,5-TCB. The coupling for PeCB and HCB can be improved by further active site mutations, and then even these highly inert compounds can be efficiently degraded.

We thank HEFCE and BBSRC for support of this work. J. P. J. thanks the EPSRC for a Studentship.

Notes and references

1 S. Fetzner and F. Lingens, *Microbiol. Rev.*, 1995, **58**, 641.
2 S. Beil, B. Happe, K. N. Timmis and D. H. Pieper, *Eur. J. Biochem.*, 1997, **247**, 190; T. Potrawfke, K. N. Timmis and R. M. Wittich, *Appl. Environ. Microbiol.*, 1998, **64**, 3798; B. E. Haigler, C. A. Pettigrew and J. C. Spain, *Appl. Environ. Microbiol.*, 1992, **58**, 2237.
3 A. H. Neilson, *Int. Biodeterior. Biodegrad.*, 1996, 3; M. Haggblom, *FEMS Microbiol. Rev.*, 1992, **103**, 29.
4 I. P. Solyanikova and L. A. Golovleva, *Biochemistry (Engl. Transl.)*, 1999, **64**, 365.
5 P. J. Loida and S. G. Sligar, *Biochemistry*, 1993, **32**, 11 530.
6 J.-A. Stevenson, A. C. G. Westlake, C. Whittock, C. and L.-L. Wong, *J. Am. Chem. Soc.*, 1996, **118**, 12 836.
7 D. P. Nickerson, C. F. Harford-Cross, S. R. Fulcher and L.-L. Wong, *FEBS Lett.*, 1997, **405**, 153.
8 P. A. England, C. F. Harford-Cross, J.-A. Stevenson, D. A. Rouch and L.-L. Wong, *FEBS Lett.*, 1998, **424**, 271.
9 T. L. Poulos, B. C. Finzel and A. J. Howard, *J. Mol. Biol.*, 1987, **195**, 687.
10 W. M. Atkins and S. G. Sligar, *J. Biol. Chem.*, 1988, **269**, 18 842.

Communication a909536e

Typeset and printed by Black Bear Press Limited, Cambridge, England

Photochirogenesis: multidimensional control of asymmetric photochemistry†

Yoshihisa Inoue,*[ab] Takehiko Wada,[b] Sadayuki Asaoka,[b] Hirofumi Sato[b] and Jean-Pierre Pete[c]

[a] *Inoue Photochirogenesis Project, ERATO, JST, 4-6-3 Kamishinden, Toyonaka 565-0085, Japan*
[b] *Department of Molecular Chemistry, Faculty of Engineering, Osaka University, 2-1 Yamada-oka, Suita 565-0871, Japan. E-mail: inoue@chem.eng.osaka-u.ac.jp*
[c] *UMR CNRS et Université de Reims Champagne-Ardenne, BP 1039, 51687 Reims Cedex 2, France*

Received (in Cambridge, UK) 5th July 1999, Accepted 23rd August 1999

Photochirogensis, or photochemical induction of molecular chirality, is an attractive alternative to thermal or enzymatic asymmetric synthesis. Using the inherent advantage that the photochemical reaction is driven by light absorption, the effect of temperature on optical yield was investigated over a wide range. Unexpectedly, the stereochemistry of photoproduct was frequently inverted at a critical temperature (T_0), above which the optical yield increased with increasing temperature. The Eyring treatment of the relative rate constant for the production of each enantiomer revealed that the unusual temperature dependency originates from the non-zero differential entropy of activation for the enantiodifferentiating process. In this case, the enthalpy term dominates at lower temperatures, while the entropy term becomes more important above T_0, switching the product chirality. The absolute configuration of photoproduct obtained at temperatures lower than T_0 was correlated to that of the chiral sensitizer, except for those containing very bulky chiral auxiliaries, and the stereochemical outcomes are discussed on the basis of the molecular model examinations. Interestingly, similar switching behaviour was induced by varying the pressure from 0.1 to 400 MPa. The pressure effect was investigated at different temperatures to construct three-dimensional diagrams that correlate the optical yield with temperature and pressure as mutually independent factors. The combined use of temperature and pressure provides us with a convenient, powerful tool for controlling the product chirality and optical yield in asymmetric photochemistry.

† Dedicated to the memory of Professors Emeritus Yoshinobu Odaira and Setsuo Takamuka, who introduced me to photochemical research and who died on 21 March and 29 October 1999, respectively.

Introduction

Asymmetric synthesis is an area of vital importance in current chemistry, to which a considerable amount of effort has been devoted in recent years.[1–9] Thus, enantio- and diastereoselectivity are the principal objectives or prerequisites when developing a new asymmetric catalyst or synthetic methodology,[1–3] as well as in synthesizing chiral compounds such as naturally occurring compounds and pharmaceuticals.[4–9] The stereochemical outcome of these asymmetric reactions has been discussed in terms of empirical rules using the models of Cram,[10] Felkin-Anh[11,12] and others.[4,13] These models are based primarily on the relative steric bulk of the aligned substituents near the reaction centre, which are orientated by steric hindrance, dipole interactions or metal chelation. Obviously, the chiral discrimination mechanism based on these empirical rules can assess only the enthalpic contributions attributable to the steric/stereoelectronic

Yoshihisa Inoue was born in Nara (Japan). He received his PhD from Osaka University in 1977 (Professor H. Sakurai) before joining the Department of Applied Chemistry, Himeji Institute of Technology (Professor T. Hakushi). While on leave, he spent one year (1978–1979) at Columbia University (Professor N. J. Turro). In 1985, he moved to the Basic Research Laboratory as Associate Professor, and then to the Department of Material Science, Himeji Institute of Technology in 1990 (Professor A. Tai), where he was a PRESTO fellow of the JRDC from 1992 to 1994 (Professor K. Honda). In 1994, he returned to Osaka University to take a full professorship, and has also been engaged in the Inoue Photochirogenesis Project since 1996. His research interests include molecular recognition in the ground and excited states.

Takehiko Wada was born in Osaka (Japan) and received his PhD from Osaka University in 1989 (Professor K. Takemoto). He then joined the faculty of the Applied Fine Chemistry, Osaka University, where he worked with Professor K. Takemoto. In 1995, he moved to his current position as an Associate Professor, working with Professor Y. Inoue at the Department of Molecular Chemistry. His current research interests focus on asymmetric photochemistry and nucleic acids chemistry.

Sadayuki Asaoka was born in Osaka (Japan). He graduated from Kyoto University in 1992 and obtained his master's degree in 1994. After a short engagement (1994–1996) as a research chemist at Matsushita Battery Industrial Co., he resumed the study of photochemistry at the Department of Molecular Chemistry, Osaka University and is now finishing a PhD.

Hirofumi Sato was born in Osaka (Japan). He graduated from Osaka University in 1999 and is now a PhD student at the Department of Molecular Chemistry, Osaka University.

Jean-Pierre Pete is Professor of Chemistry in the Department of Chemistry of the University of Reims. After graduating as a Chemical Engineer from the University of Strasbourg (1961), he obtained his PhD in 1966 (Professor J. Levisalles). From 1961 to 1968 he was a research fellow at CNRS. He was a post-doctoral fellow (Professor P. de Mayo) at the University of Western Ontario (1966–1967), before joining the Faculty of Science at Reims in 1969. His research interests concern mainly organic photochemistry, photoinduced electron transfer processes asymmetric photoreactions and their applications to organic synthesis. He received the Grammaticakis–Neuman award from the Académie des Sciences in 1987 and is the co-author of more than 150 research publications.

interaction between the substituent and attacking reagent, while the entropic contribution arising from the conformational changes and re-positioning of the solvent molecules during the transition state has not been discussed explicitly for thermal and enzymatic asymmetric syntheses. Nevertheless, these empirical rules, which only take the enthalpy term into account, are generally successful and are frequently employed in interpreting and/or predicting the dominant stereoisomer formed, and also the trend in optical yield obtained in a variety of asymmetric induction and asymmetric catalysis processes. Consequently, the entropic contribution has not been discussed globally, or experimentally examined as a factor in the mechanism of most thermal asymmetric reactions until recently,[14] in spite of some early observations of small to moderate temperature effects on enantio- or diastereoselectivity, *e.g.* in the addition of alcohols or amines to ketenes in the presence of acetylquinine,[15] in the $LiAlH_4$ reduction of acetophenone in the presence of quinine,[16] and in the oxidation of sulfides with optically active peracids.[17] That entropy plays an important role does not seem unreasonable, since the temperature range available is rarely wide enough to thoroughly survey the effect of this variable, and the possible incorporation of different reaction mechanisms or a switch in intermediates resulting from a change in temperature is not rigorously ruled out in many thermal asymmetric reactions.

In contrast, photochemical reactions are driven by the absorption of high-energy photons and proceed through the excited state, which renders them inherently free from temperature restrictions, and they are, therefore, advantageous for investigating the effect of the entropy factor upon stereoselectivity over a wide temperature range without undergoing any essential changes in reaction mechanism or intermediates formed. However, the temperature effect has been rarely and only recently explored in the rather short history of asymmetric photochemistry.[18,19] Thus, in the diastereodifferentiating Paternò–Büchi photocycloaddition of optically active phenylglyoxylic esters with several alkenes,[20] Scharf *et al.* showed that the diastereoselectivity of the oxetane produced not only depends on the irradiation temperature, but also gives a bent Eyring plot as a consequence of the alteration of the rate limiting step that determines the diastereoselectivity. In the enantiodifferentiating *Z–E* photoisomerization of cyclooctene sensitized by optically active sensitizers,[21] we demonstrated that the antipodal (*E*)-cyclooctenes, *i.e.* (*S*)-(−)- and (*R*)-(+)-enantiomers, can be obtained simply by changing the irradiation temperature from −88 to +50 °C, and that the enantiomeric excess (ee) of the product increases with increasing temperature, an observation that conflicts with the belief that lowering the temperature will generally enhance the ee. This unprecedented temperature dependence and the switching of the major enantiomer produced was revealed to be exclusively entropic in origin through an analysis of the Eyring plot of the enantioselectivity of the reaction. A similar 'unusual' temperature dependence of stereoselectivity, which leads to the switching of product chirality and/or higher selectivity at higher temperature, has been observed in many enantio-[22–25] and diastereodifferentiating photoreactions[26–30] over the last decade. More recently, we have revealed that the product chirality can be controlled, and in some cases actually switched, by changing the pressure from atmospheric to 400 MPa in the photosensitized enantiodifferentiating isomerization of cyclooctene.[31]

Here we present a global view of recent advances in 'photochirogenesis', particularly in enantiodifferentiating photosensitization reactions. We will also demonstrate how the entropic and enthalpic factors share the role of manipulating the stereochemical outcome of these enantiodifferentiating photoreactions. Finally, we will show that the combined use of entropy-related factors, such as temperature, pressure and solvent, provides us with a new method for the control of asymmetric photochemistry. Indeed, the basic concepts revealed here by asymmetric photochemistry should also be applicable to thermal and biological asymmetric reactions.

Temperature effect

In the 'Photochirogenesis' project, which aims to devise methods for highly efficient photochemical generation, transfer and multiplication of molecular chirality, we have chosen the enantiodifferentiating geometrical photoisomerization of (*Z*)-cyclooctene (**1Z**) sensitized by optically active aromatic esters as one of the most promising processes for development (Scheme 1), simply because this photosensitization was known

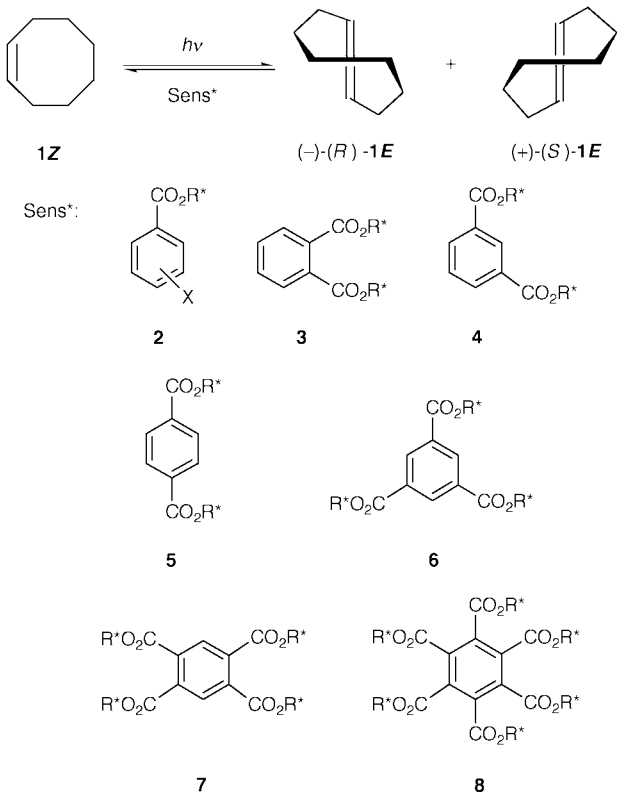

Scheme 1 Enantiodifferentiating *Z–E* photoisomerization of cyclooctene sensitized by chiral benzene(poly)carboxylates (Sens*).

to give chiral (*E*)-cyclooctene (**1E**) in high chemical and quantum yields and was also found to involve a singlet exciplex between the substrate and sensitizer.[32] The involvement of a structurally well-defined exciplex intermediate, which enables efficient transfer of chiral information in the excited state, is an essential condition for obtaining high optical yield in an enantiodifferentiating photosensitization.

Taking into account the simultaneous formation of the two enantiomers of **1E**, the original sensitization mechanism[32] was modified to include chirality, as shown in Scheme 2.[22a] The photosensitization is initiated by the formation of an encounter complex [**1Z**/**E**···^{1}**S***] between the excited sensitizer (^{1}**S***) and **1Z** or one of enantiomers of **1E**. Energy transfer within the exciplex intermediate and the subsequent rotation around the C=C bond of **1Z**/**1E** to a dihedral angle of *ca.* 90° afford a relaxed exciplex [^{1}***p***···**S***], which in turn releases the perpendicular singlet (^{1}***p***), regenerating the ground-state sensitizer (**S***). It should be noted that chirality is induced in ^{1}***p*** during the rotational relaxation step. The subsequent decay of ^{1}***p*** to **1Z** or **1E** concludes the photoisomerization cycle.

There are two steps in this mechanism that are potentially enantiodifferentiating: (i) the quenching of ^{1}**S*** by enantiomeric **1E**, and (ii) rotational relaxation within the exciplex [**1Z**···^{1}**S***]. Thus, the rate constants for quenching (k_{qS}, k_{qR}) and/or rotation (k_S, k_R) may be different from one another. Experimentally, no

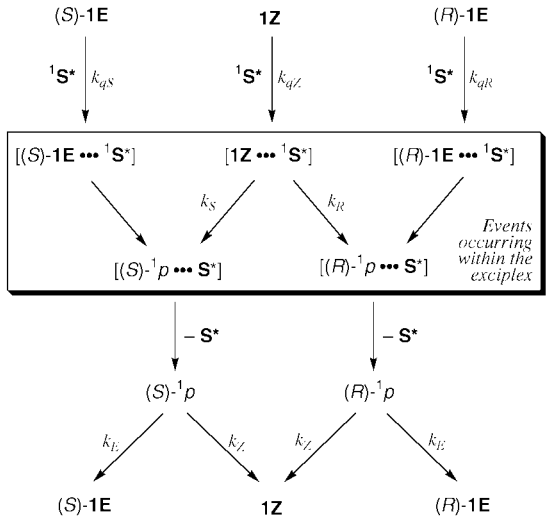

Scheme 2 Enantiodifferentiating mechanism for photosensitized isomerization of cyclooctene (**1**) *via* exciplex, where **S*** and ^{1}**S*** are the chiral sensitizer in the ground and excited singlet states, and ^{1}***p*** is the twisted, excited singlet of **1**.

appreciable optical rotation was detected in **1E** recovered during the initial stages of the enantiodifferentiating photosensitization of racemic **1E**, and the *ee* of product **1E** did not show any conversion dependency in the enantiodifferentiating photosensitization of **1Z**,[22b] both of which rule out the possibility of enantiodifferentiation in the quenching process, and thus $k_{qS} = k_{qR}$. Hence, the rotational relaxation of **1Z** to ^{1}***p*** within the exciplex intermediate can be the only enantiodifferentiating step in this asymmetric photosensitization, and the *ee* of **1E** is determined exclusively by the relative rate k_S/k_R. This seems quite reasonable, since intimate interaction, which leads to efficient chiral recognition, is more likely to occur in the long-lived exciplex intermediate that possesses a more defined structure than during the collisional quenching stage.

In order to discuss quantitatively the temperature dependence of the ees observed for this asymmetric photosensitization, the rate constants k_S and k_R were analyzed according to the Arrhenius, or Eyring equation. The relative rate constant, k_S/k_R, can then be expressed by eqns. (1a) and (1b), where $\Delta E_{S\text{-}R}$

$$\ln(k_S/k_R) = -\Delta E_{S\text{-}R}/RT + \ln(A_S/A_R) \quad (1a)$$

$$= -\Delta\Delta H^{\ddagger}_{S\text{-}R}/RT + \Delta\Delta S^{\ddagger}_{S\text{-}R}/R \quad (1b)$$

represents the differential energy of activation, A_S/A_R is the relative frequency factor, and $\Delta\Delta H^{\ddagger}_{S\text{-}R}$ and $\Delta\Delta S^{\ddagger}_{S\text{-}R}$ denote the differential enthalpy and entropy of activation, respectively.

The enantiodifferentiating photosensitizations of **1Z** were performed in several solvents at temperatures ranging from +50 to −90 °C, using a variety of optically pure (poly)alkyl benzene(poly)carboxylates as chiral sensitizers.[22] Interestingly, the product chirality switched at a specific, or equipodal, temperature T_0, upon sensitization with most *ortho*-substituted benzenepolycarboxylates, whereas no chirality inversion was observed for non-*ortho* sensitizers; typical examples are shown in Fig. 1. This is the first observation of an enantiodifferentiating reaction where the ee of the product is not only inverted by temperature, but also increased with increasing temperature above T_0. It is also important that both enantiomers can be prepared simply by changing the temperature without using the antipodal sensitizer.

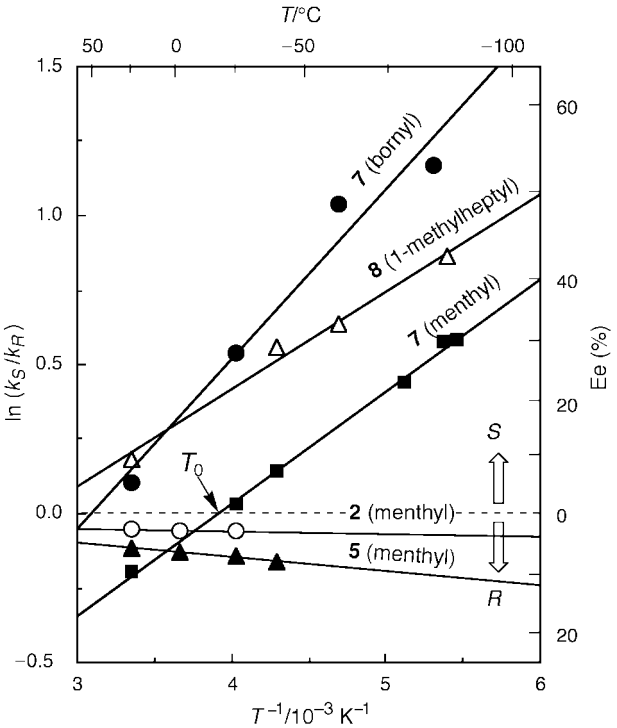

Fig. 1 Temperature dependence of the ee of the product in enantiodifferentiating photoisomerization of cyclooctene (**1Z**) sensitized by (−)-menthyl benzoate **2** (○) and terephthalate **5** (▲), (−)-menthyl and (−)-bornyl 1,2,4,5-benzenetetracarboxylate **7** (■ and △), and (−)-1-methylheptyl benzenehexacarboxylate **8** (●) in pentane. The chirality of product **1E** is switched at the equipodal temperature, T_0.

From eqns. (1a) and (1b) and the experimental plots exemplified in Fig. 1, the activation parameters were determined for these enantiodifferentiating photoisomerizations using various chiral benzenecarboxylate sensitizers; the relevant activation parameters and equipodal temperatures obtained for several sensitizers are listed in Table 1.

By examining eqn. (1), it is apparent that this temperature switching behavior of product chirality is attributable to the

Table 1 Activation parameters at 25 °C, determined from the temperature and pressure dependence of the *ee* of **1E** obtained in enantiodifferentiating photoisomerization of cyclooctene (**1Z**), sensitized by chiral benzenepolycarboxylates **2**–**5**, **7** and **8** in pentane

Sensitizer		$\Delta\Delta H^{\ddagger}_{S\text{-}R}$[a]/	$T\Delta\Delta S^{\ddagger}_{S\text{-}R}$[a]/			$\Delta\Delta V^{\ddagger}_{S\text{-}R}$[b]/
Compound	R*	kcal mol^{-1}	kcal mol^{-1}	A_S/A_R	T_0/°C	kcal mol^{-1}
2	(−)-Menthyl	+0.014	−0.039	0.99	[c]	−0.13
3	(−)-Menthyl	−0.19	−0.51	0.90	100	+0.83
	(−)-Bornyl	−0.50	−1.38	0.74	91	+1.48
4	(−)-Menthyl	+0.08	+0.15	1.16	530	+0.07
5	(−)-Menthyl	+0.09	+0.08	1.02	940	+0.36
7	(−)-Menthyl	−0.77	−3.00	0.52	−15	−3.71
	(−)-Bornyl	−0.61	−1.55	0.71	123	+0.29
	(−)-1-Methylheptyl	−0.54	−1.93	0.67	8	−1.44
8	(−)-Menthyl	−0.96	−3.85	0.43	−23	+3.50
	(−)-Bornyl	−0.86	−2.60	0.56	60	−5.56
	(−)-1-Methylheptyl	−1.13	−3.48	0.47	51	+0.56

[a] Ref. 22(*b*). [b] Ref. 31. [c] T_0 does not exist.

non-zero differential entropy of activation ($\Delta\Delta S^{\ddagger}_{S\text{-}R} \neq 0$) or the unequal frequency factor ($A_S \neq A_R$). Thus, the entropy factor is shown to play a decisive role in the enantiodifferentiation process. It should be emphasized that the *ortho*-substituted benzenepolycarboxylates, such as phthalate, benzenetetracarboxylate and benzenehexacarboxylate, afford very large deviations from unity for the ratio A_S/A_R, while benzoate and terephthalate show almost equal frequency factors for the (*R*)- and (*S*)-isomers, as can be seen in Table 1. This tendency is not incidental, but implies that the rotational motion of the double bond of **1** in the exciplex causes simultaneous global conformational changes of the closely situated *ortho*-alkoxycarbonyl groups of the sensitizer. Such dynamic changes during rotational relaxation in the exciplex inevitably produce large differences in the activation entropy of enantiodifferentiation.

Although we have hitherto concentrated on the enantiodifferentiating photoisomerization of **1**, similar chirality inversion phenomena have been observed in the enantiodifferentiating photosensitizations of 1-methylcyclooctene[22f] and cycloocta-1,3-diene,[24] as well as in the enantiodifferentiating anti-Markovnikov photoaddition of methanol to 1,1-diphenylpropene (**9**).[25b] Of these, the diphenylpropene case is particularly interesting, since this is the first bimolecular enantiodifferentiating photoreaction that affords the anti-Markovnikov adduct (**12**) upon sensitization with chiral 1,4-naphthalenedicarboxylates (**17**), with moderate ees of up to 33% observed (see Scheme 3 and Fig. 2). In this photosensitized polar addition, the

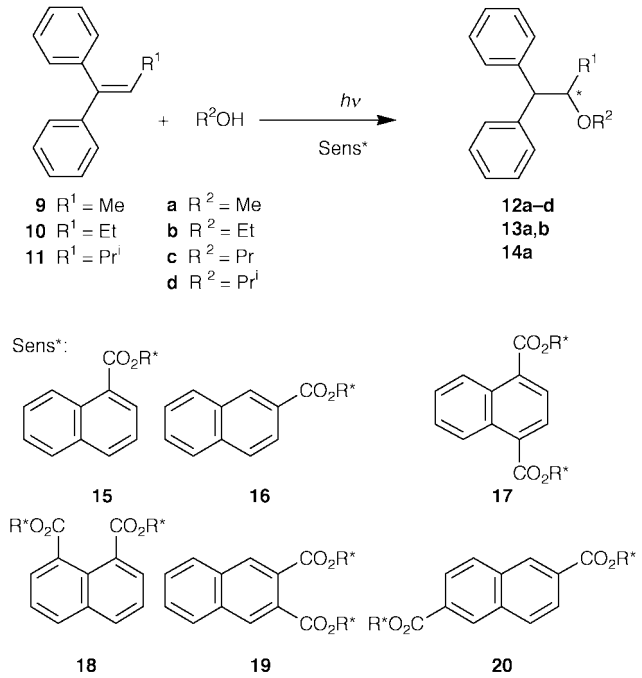

Scheme 3 Enantiodifferentiating photoaddition of alcohols to 1,1-diphenylalk-1-enes (**9**–**11**) sensitized by chiral naphthalene(di)carboxylates (**15**–**20**).

use of *ortho* aromatic esters is no longer required to cause the inversion of product chirality by altering the temperature, probably because the termolecular interaction of the attacking methanol with the initially formed sensitizer-substrate exciplex exaggerates the influence of the conformational differences on the enantiodifferentiating process.

The roles of entropy and enthalpy

The contributions of the enthalpy and entropy factors to the enantiodifferentiating process can be discussed in terms of eqn. (1b), or using the Gibbs–Helmholtz equation for the differential

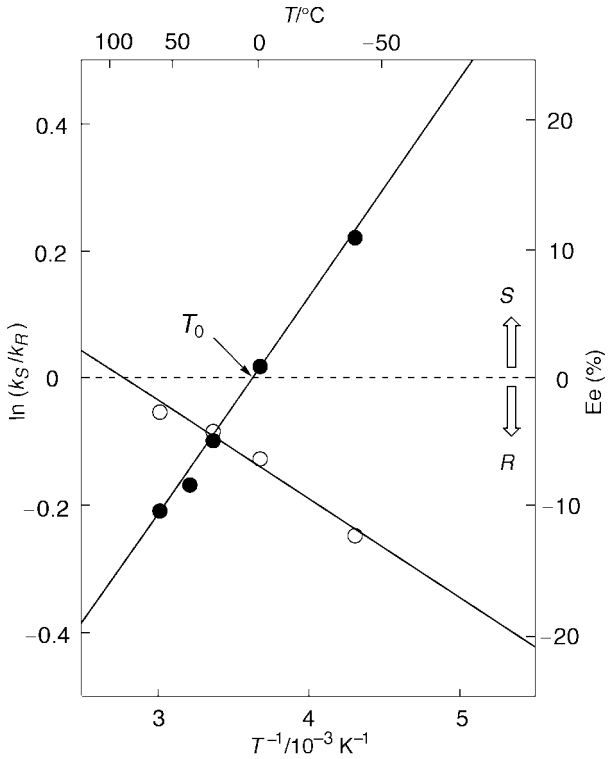

Fig. 2 Temperature dependence of the ee of the product in the enantiodifferentiating addition of methanol to **10**, sensitized by **17** with R* = (−)-menthyl (○) and 1,2:4,5-di-*O*-isopropylidene-β-D-fructopyranose (●) in methylcyclohexane.

activation free energy [eqn. (2)]. As can be seen from eqn. (2),

$$\Delta\Delta G^{\ddagger}_{S\text{-}R} = \Delta\Delta H^{\ddagger}_{S\text{-}R} - T\Delta\Delta S^{\ddagger}_{S\text{-}R} \qquad (2)$$

T_0 is the critical point at which the enthalpic and entropic contributions balance with each other ($\Delta\Delta H^{\ddagger}_{S\text{-}R} = T_0\Delta\Delta S^{\ddagger}_{S\text{-}R}$), affording no enantiodifferentiation. Below T_0, the enthalpy difference $\Delta\Delta H^{\ddagger}_{S\text{-}R}$ controls the enantiodifferentiating process, while the entropic term $T\Delta\Delta S^{\ddagger}_{S\text{-}R}$ is dominant at temperatures higher than T_0. If both $\Delta\Delta H^{\ddagger}_{S\text{-}R}$ and $\Delta\Delta S^{\ddagger}_{S\text{-}R}$ possess the same sign, switching of the dominant term in the enantiodifferentiation process leads to the inversion of product chirality, as exemplified above. In the enthalpy-controlled temperature region below T_0, the difference in the conformational freedom of the enantiodifferentiating transition states does not seriously affect the stereochemical consequence of the photoreaction, which is determined by the steric and stacking interactions in the exciplex intermediate. Since the π–π stacking interaction in the exciplex does not vary a great deal by changing the chiral auxiliary attached to the sensitizer, the majority of the enthalpy difference ($\Delta\Delta H^{\ddagger}_{S\text{-}R}$) may be attributed to different levels of steric interaction. In this context, it is reasonable to assume that the absolute configuration of the chiral sensitizer can be related directly and exclusively to that of the photoproduct. In the following section, we first examine the appropriateness of this simple theory and then explore its scope and limitations, using the enantiodifferentiating photoisomerization of cyclooctene as a representative system which can provide extensive information concerning the effects of temperature and chiral auxiliary on the ee of the product.

Stereochemical correlation

The chiral photosensitizers employed in the enantiodifferentiating photoisomerization of cyclooctene can be classified into two categories,[22] according to the temperature dependency of the ee of **1E** obtained. As shown in Fig. 1, non-*ortho* benzene(poly)carboxylate sensitizers give only small ee values and low gradient slopes in the Eyring plots, where the T_0 does not exist

at all, or appears only at an extreme temperature. In contrast, *ortho*-benzenepolycarboxylates, such as **3**, **7** and **8**, give much higher ees and steep slopes, and the product chirality is often switched at a readily accessible temperature. Since this contrasting behavior originates from the entropy term alone, it is probable that different enantiodifferentiation mechanism operates for the *ortho* and non-*ortho* sensitizers, from the conformational point of view.

In order to elucidate whether or not the absolute configuration of product **1E** can be correlated directly and globally to that of the stereogenic centre of the relevant chiral sensitizer, the data reported for the enantiodifferentiating photoisomerization of **1Z** sensitized by chiral benzene(poly)carboxylates in different solvents at ambient and low temperatures are summarized in Table 2.[22b,c] The sensitizers that carry phenyl group(s) in the chiral auxiliary are not included in Table 2, nor in the following

Table 2 Enantiodifferentiating photoisomerization of **1Z** sensitized by chiral (poly)alkyl benzene(poly)carboxylates in pentane at ambient and low temperatures

Sensitizer					**1E**	
Compound	R* (X)	Configuration[a]	Solvent	*T*/°C	Ee[b] (%)	Configuration[c]
2	(−)-Bornyl (H)	*R*	pentane	25	−1.0	*R*
	(−)-Cholesteryl (H)	*R*	pentane	25	−0.04	*R*
	(−)-1,3-Diphenylpropane-1,3-diyl[d] (H)	*S*	pentane	25	+1.2	*S*
	(+)-Isomenthyl (H)	*S*	pentane	25	+0.96	*S*
	(−)-Menthyl (H)	*R*	pentane	25	−2.7	*R*
				−25	−3.0	*R*
			cyclohexane	25	−2.7	*R*
	(−)-Menthyl (2-MeO)	*R*	pentane	25	−2.1	*R*
	(−)-Menthyl (4-MeO)	*R*	pentane	25	−4.3	*R*
	(−)-Menthyl (2-OH)	*R*	pentane	25	−7.0	*R*
				−60	−25.3	*R*
	(−)-Menthyl (2-Me)	*R*	pentane	25	−1.7	*R*
	(−)-Menthyl (3-Me)	*R*	pentane	25	−4.2	*R*
	(−)-Menthyl (4-Me)	*R*	pentane	25	−3.7	*R*
	(−)-Menthyl (4-Bu^t)	*R*	pentane	25	−3.5	*R*
	(−)-Menthyl (4-F)	*R*	pentane	25	−2.1	*R*
	(−)-Menthyl (2-CF_3)	*R*	pentane	25	−0.7	*R*
	(−)-Menthyl (3-CF_3)	*R*	pentane	25	−2.6	*R*
	(−)-Menthyl (4-CF_3)	*R*	pentane	25	−3.9	*R*
				−60	−4.4	*R*
	(−)-Menthyl (4-CN)	*R*	pentane	25	−3.3	*R*
	(−)-Menthyl [3,5-$(CF_3)_2$]	*R*	pentane	25	−2.4	*R*
	(+)-Neomenthyl (H)	*S*	pentane	25	+0.1	*S*
3	(−)-Bornyl	*R*	pentane	25	+7.6	*S*
				−60	+24.0	*S*
	(−)-Menthyl	*R*	pentane	25	+3.8	*S*
				−60	+10.3	*S*
	(−)-Menthyl, methyl[e]	*R*	pentane	25	+3.0	*S*
				−60	+10.8	*S*
4	(−)-Menthyl	*R*	pentane	25	−4.4	*R*
5	(−)-Menthyl	*R*	pentane	25	−6.0	*R*
				−40	−8.2	*R*
			cyclohexane	25	−5.9	*R*
			acetonitrile	25	−7.1	*R*
				−40	−8.5	*R*
			methanol	25	−5.8	*R*
	(−)-Menthyl, methyl[e]	*R*	pentane	25	−3.0	*R*
				−40	−4.0	*R*
6	(−)-Menthyl	*R*	pentane	25	−3.4	*R*
7	(−)-(1*S*,2*R*,3*S*)-*endo*-3-(Cyclohexylmethyl)-*endo*-2-bornyl	*R*	pentane	25	−19.5	*R*
				−40	−18.7	*R*
	(−)-(1*S*,2*R*,3*R*)-*exo*-3-(Cyclohexylmethyl)-*endo*-2-bornyl	*R*	pentane	25	+13.1	*S*
				−88	+53.3	*S*
	(−)-(1*S*,2*S*,3*R*)-*endo*-3-(Cyclohexylmethyl)-*exo*-2-bornyl	*S*	pentane	25	+6.9	*S*
				−88	−18.6	*R*
	(−)-(1*S*,2*S*,3*S*)-*exo*-3-(Cyclohexylmethyl)-*exo*-2-bornyl	*S*	pentane	25	+22.9	*S*
				−88	+51.4	*S*
	(−)-Bornyl	*R*	pentane	25	+11.5	*S*
				−88	+40.6	*S*
	(+)-Cedryl	*R*	pentane	−86	−22.5	*R*
	(+)-1-Cyclohexylethyl	*S*	pentane	25	+1.8	*S*
				−86	−11.4	*R*
	(−)-(1*R*,2*S*,5*R*)-8-Cyclohexylmenthyl	*R*	pentane	25	+49.2	*S*
				−89	+63.5	*S*
	(−)-(1*R*,2*S*,5*R*)-2-(Dicyclohexylmethyl)-5-methylcyclohexyl	*R*	pentane	−40	+3.3	*S*
				−86	−14.8	*R*
	(+)-1,2-Dimethylpropyl	*S*	pentane	25	+3.1	*S*
			pentane	−87	−16.1	*R*
	(−)-Fenchyl	*S*	pentane	25	−0.9	*R*
			pentane	−86	−8.0	*R*
	(+)-Isomenthyl	*S*	pentane	25	+6.0	*S*
			pentane	−88	−4.5	*R*
	(+)-Isopinocampheyl	*S*	pentane	25	+4.2	*S*
			pentane	−87	+4.4	*S*

Table 2 *Continued*

Sensitizer					1E	
Compound	R* (X)	Configuration[a]	Solvent	*T*/°C	Ee[b] (%)	Configuration[c]
	(−)-Menthyl	*R*	pentane	25	−9.6	*R*
				−90	+28.5	*S*
			heptane	25	−8.8	*R*
				−87	+30.7	*S*
			decane	25	−8.7	*R*
				−30	+7.1	*S*
			hexane	−85	+3.8	*S*
			isooctane	25	−14.2	*R*
				−87	+5.4	*S*
			isopentane	25	−13.1	*R*
				−87	+10.0	*S*
	(+)-1-(Methoxycarbonyl)ethyl	*S*	acetonitrile	25	−5.7	*R*
				−40	−13.2	*R*
	(+)-1-Methylheptyl	*S*	pentane	25	+1.5	*S*
				−85	−24.3	*R*
	(−)-1-Methylheptyl	*R*	pentane	25	−1.2	*R*
				−86	+24.0	*S*
			acetonitrile	25	−0.8	*R*
				−40	+5.6	*S*
			methanol	25	−0.03	*R*
				−86	+13.2	*S*
	(+)-1-Methylnonyl	*S*	pentane	25	+1.2	*S*
				−87	−27.0	*R*
	(+)-1-Methylpentyl	*S*	pentane	25	+1.8	*S*
				−90	−26.3	*R*
	(+)-1-Methylpropyl	*S*	pentane	25	−0.01	*R*
				−80	−13.4	*R*
	(+)-Neomenthyl	*S*	pentane	25	−8.4	*R*
				−88	−6.2	*R*
	(+)-1,2,2-Trimethylpropyl	*S*	pentane	25	+11.6	*S*
			pentane	−86	−15.6	*R*
8	(−)-Bornyl	*R*	pentane	25	+7.7	*S*
				−86	+47.0	*S*
	(−)-Menthyl	*R*	pentane	25	−16.8	*R*
				−86	+28.3	*S*
	(−)-1-Methylheptyl	*R*	pentane	25	+5.1	*S*
				−87	+52.7	*S*
	(−)-1-(Methoxycarbonyl)ethyl	*S*	acetonitrile	25	−4.9	*R*
				−40	−20.1	*R*

[a] Absolute configuration of the stereogenic center connected directly to the ester oxygen. [b] Enantiomeric excess of **1E**. Positive and negative signs for ee correspond to the formation of (*S*)-(+)- and (*R*)-(–)-isomers, respectively. [c] Absolute configuration of **1E**. [d] Dibenzoate. [e] Mixed ester.

discussion, since they are known to form an intramolecular exciplex, to which the substrate **1Z** approaches from the phenyl side.[22c]

Firstly, we will consider the stereochemical consequence observed upon sensitization with the non-*ortho* sensitizers (**2**, **4**, **5** and **7**). As demonstrated by several representative examples, these sensitizers do not exhibit chirality inversion behaviour caused by a change in temperature. It is reasonable, therefore, to discuss the relationship between the absolute configuration of **1E** obtained at any temperature with that of the stereogenic centre of the sensitizer. In examining this correlation, we will take into account only the stereogenic centre directly connected to the ester oxygen of the relevant sensitizer when the chiral auxiliary has many such centres. This approach may be justified, since the configuration around the stereogenic centre nearest to the benzenecarboxylate chromophore is expected, in general, to dominate the steric interactions in the exciplex intermediate. After examining the data for 23 different non-*ortho* sensitizers in a variety of solvents, we found a perfect stereochemical correlation between the stereogenic centres of the relevant sensitizer and product, in spite of the low ees obtained. Thus, non-*ortho* sensitizers with *R*-configuration at the nearest stereogenic centre afford (*R*)-(−)-**1E** without exception, and the opposite is true of *S*-configuration sensitizers.

Encouraged by the above result, we made further attempts to understand the seemingly complex stereochemical outcome observed for *ortho* sensitizers (*i.e.* **3**, **7** and **8**). *Ortho* sensitizers are known to cause the chirality inversion of product through a change in the reaction temperature as a consequence of the significant contribution of the entropy term. However, the entropic contribution is minimized or made negligible at temperatures below T_0. Under these conditions, the absolute configuration of the chiral sensitizer correlates to that of **1E**. Examining the results for the *ortho* sensitizers presented in Table 1, a highly consistent stereochemical correlation was observed again. Apart from those sensitizers that possess highly congested secondary and tertiary chiral auxiliaries, *e.g.* the *endo,endo*- and *exo,exo*-3-cyclohexylmethyl-2-bornyl, cedryl, 2-dicyclohexylmethyl-5-methylcyclohexyl and isopinocampheyl auxiliaries, the other 21 *ortho* sensitizers completely obey a rule which is opposite to that observed for the non-*ortho* sensitizers, *i.e. ortho* sensitizers with *R*-configuration afford (*S*)-(−)-**1E**.

These two mutually opposing stereochemical correlations, which are separately applicable to non-*ortho* and *ortho* sensitizers, urged us to derive plausible models which are compatible with them. A similar attempt to derive an exciplex model for a non-*ortho* sensitizer has already been carried out for (–)-menthyl benzoate, where an interaction of the ester carbonyl of excited benzoate with the C=C bond of **1Z** was proposed.[22b] This model is based on the fact that the ee values obtained upon sensitization with (−)-menthyl methyl terephthalate are exactly half of the values obtained with the (−)-dimenthyl analogue at

all temperatures examined, and that a semiempirical MNDO calculation for methyl benzoate indicates a good match between the MO lobes of the ester carbonyl and the C=C bond of **1Z**.[22b] In the present study, we carried out the MO recalculations on methyl benzoate and phthalate in the excited singlet state, using the PM3 program (MOPAC). The results are mostly consistent with the previous ones,[22b] except for the highly developed antibonding lobes on the carbonyl and the different pattern of the aromatic lobes in HSOMO. However, steric interactions in (−)-menthyl benzoate and phthalate are better evaluated by MM2 calculations to give the optimized conformations shown in Fig. 3. As can be seen from the front view [Fig. 3, bottom], the lower side of menthyl benzoate is covered by the menthyl isopropyl group preventing the approach of cyclooctene molecule to the ester carbonyl. If the top view is considered, it appears that the interaction of **1Z** with the C=O bond from the front side and the subsequent rotation of the C=C bond to the open side in the exciplex affords (*R*)-**1E**, in accord with the experimentally observed configuration. In the dimenthyl phthalate case (Fig. 3), the optimized conformation is substantially different from that of the benzoate due to steric hindrance between the adjacent menthoxycarbonyl groups. Thus, the two ester groups are non-equivalent, with one carbonyl orientated inside and the other outside. It is assumed that the less hindered C=O group, which is directed outwards, can interact with cyclooctene molecule from the open face, forming the exciplex (Fig. 3). The subsequent rotation in the exciplex towards the open side of the menthyl group results in the formation of (*S*)-**1E**, as observed experimentally at temperatures lower than T_0. In view of the low ees obtained, especially for non-*ortho* sensitizers, other rationales cannot be ruled out absolutely. However, we could not find any other model which was compatible with all of the experimental and MO calculation data.

Pressure effect

In the preceding sections, we have demonstrated that weak interactions in the exciplex intermediate can be controlled by temperature as a result of the contribution of the entropy term. In this context, it is interesting to study the way in which pressure can be used as an alternative tool for controlling the weak interactions that determine the stereochemical outcome in the excited state. Although pressure effects upon thermochemical and photochemical reactions have been studied in considerable detail,[33] very little effort has been extended to enantiodifferentiating photochemical reactions until recently, probably as a result of the low ees reported for such processes. However, we have recently discovered that the enantiodifferentiating photoisomerization of **1Z** (shown in Scheme 1) is significantly affected by pressure, resulting in inversion of product chirality.[31]

The pressure effect on the relative rate constant, k_S/k_R (Scheme 2), can be expressed as a linear function of pressure (P)

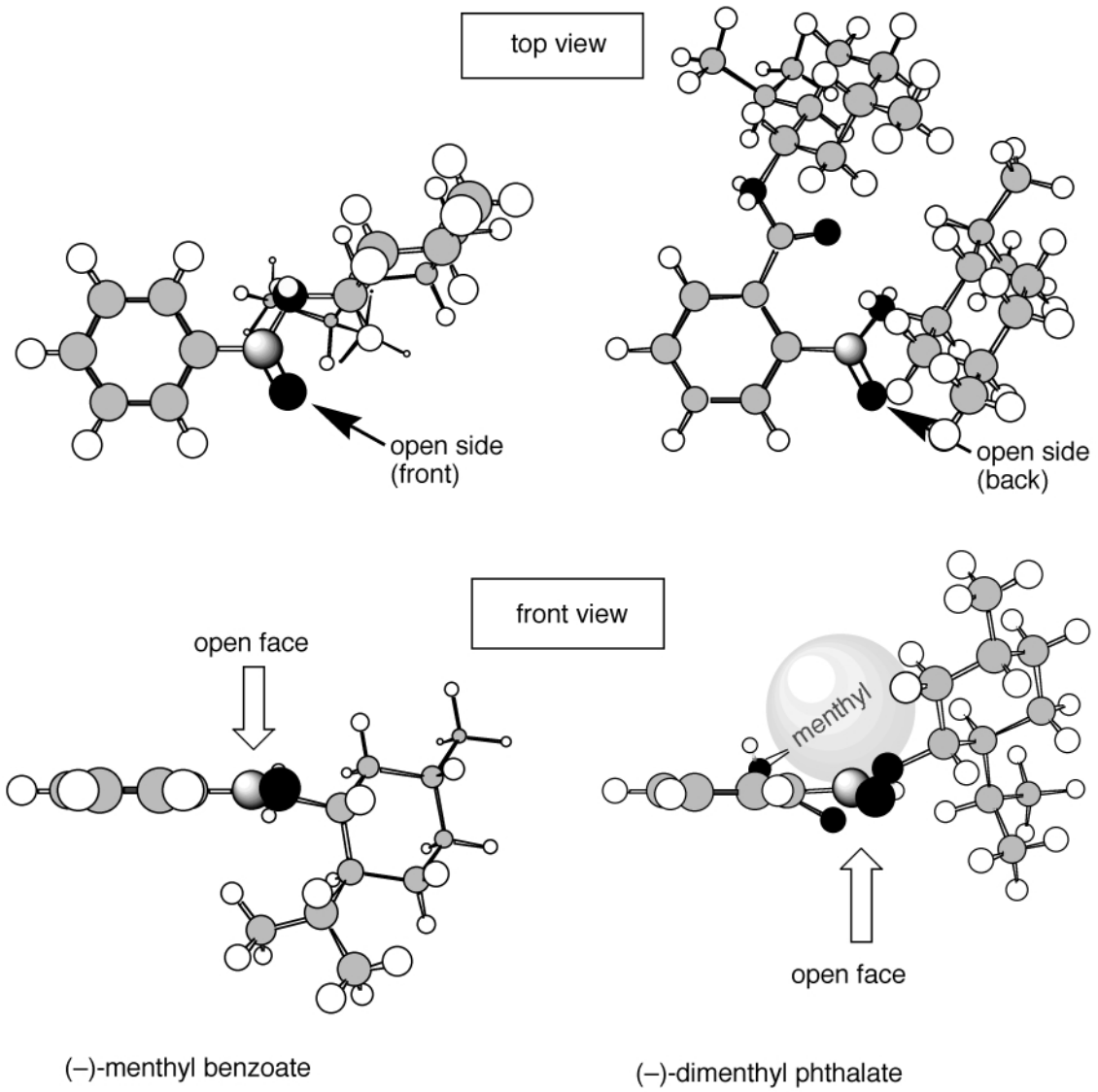

Fig. 3 Top and front views of MM2-optimized structures of (−)-menthyl benzoate **2** and phthalate **7**. In the latter structure, the shaded sphere represents the menthyl group located in the backside.

at a constant temperature [eqn. (3)][31] where $\Delta\Delta V^{\ddagger}_{S\text{-}R}$ represents

$$\ln (k_S/k_R) = -(\Delta\Delta V^{\ddagger}_{S\text{-}R}/RT)P + C \quad (3)$$

the difference in activation volume and C is equal to $\ln (k_S/k_R)$ at $P = 0$. The effect of hydrostatic pressures of up to 400 MPa was investigated in the enantiodifferentiating photoisomerization of **1Z** sensitized by chiral benzene(poly)carboxylates.[31] According to eqn. (3), the $\ln (k_S/k_R)$ values obtained were plotted against pressure.

As can be seen from Fig. 4, variations in the reaction pressure significantly affect the ee of **1E**, and often the product chirality is switched at the equipodal pressure (P_0) upon sensitization with *ortho* benzenepolycarboxylates (**3**, **7**, **8**). However, ees obtained for non-*ortho* sensitizers (**2**, **4**, **5**) were generally small and insensitive to pressure changes. This contrasting behaviour of the *ortho* and non-*ortho* sensitizers is similar to that observed for the temperature dependency of ee, again indicating a significant contribution of the entropy factor in the enantiodifferentiating process. However, the differential activation parameters obtained from the temperature- and pressure-dependence experiments,[22b,31] which are listed in Table 1, behave quite differently. Indeed, inconsistencies become evident particularly in the parameters obtained for *ortho* esters, as sensitizers that give large $\Delta\Delta H^{\ddagger}$ and $\Delta\Delta S^{\ddagger}$ values do not always show a strong pressure dependency, and no consistent relationship is found for the signs of $\Delta\Delta H^{\ddagger}$ or $\Delta\Delta S^{\ddagger}$ and $\Delta\Delta V^{\ddagger}$.

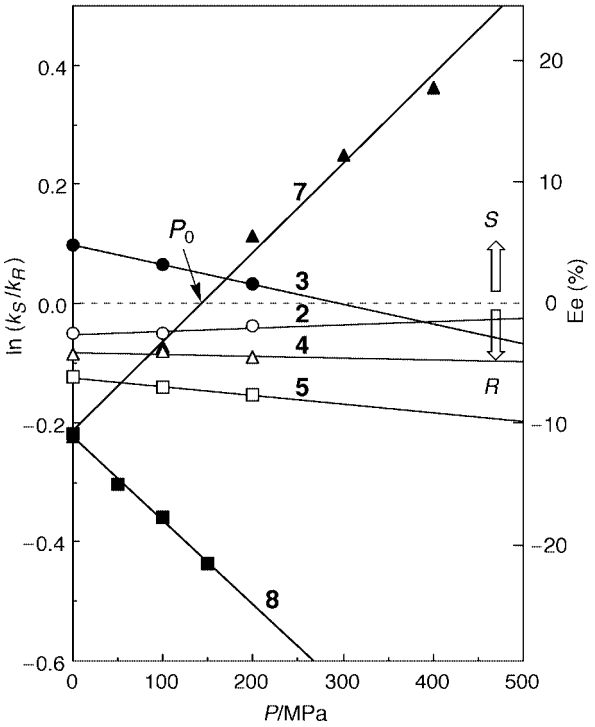

Fig. 4 Pressure dependence of the ee of the product in enantiodifferentiating photoisomerization of cyclooctene (**1Z**) sensitized by (−)-menthyl benzoate **2** (○), phthalate **3** (●), isophthalate **4** (△), terephthalate **5** (□), benzene-1,2,4,5-tetracarboxylate **7** (▲), and benzenehexacarboxylate **8** (■) in pentane at 25 °C; the chirality of product **1E** was switched at the equipodal pressure (P_0).

Multidimensional control of product chirality

The above discrepancy observed for temperature and pressure is not surprising, since both can be regarded as inherently independent variables. In order to verify this experimentally, and also to reveal the relationship between the ee of the product and these variables, we further investigated the effect of pressure on the enantiodifferentiating photoisomerization at several different temperatures, and found that the $\Delta\Delta V^{\ddagger}$ value depends critically on the reaction temperature.[31] From the data obtained, novel three-dimensional diagrams that correlate the ee with temperature and pressure were constructed for all possible cases. Two representative cases, which show inversion of the product chirality by temperature and/or pressure, are illustrated schematically in Fig. 5. In both cases, the enantiodifferentiating event occurs exclusively on one of the two intersecting planes that correspond to the antipodal sensitizers, and these two enantiodifferentiation planes are symmetrical to each other with respect to the T^{-1}–P plane. The temperature and pressure drive the product's ee in opposite directions in Fig. 5(*a*), where they act as independent factors, or in the same direction in Fig. 5(*b*). In spite of the limited number of sensitizers examined, a (−)-menthyl benzenetetracarboxylate sensitizer provides us with a fortuitous example, in which the ee of **1E** increases with decreasing temperature and increasing pressure, ultimately

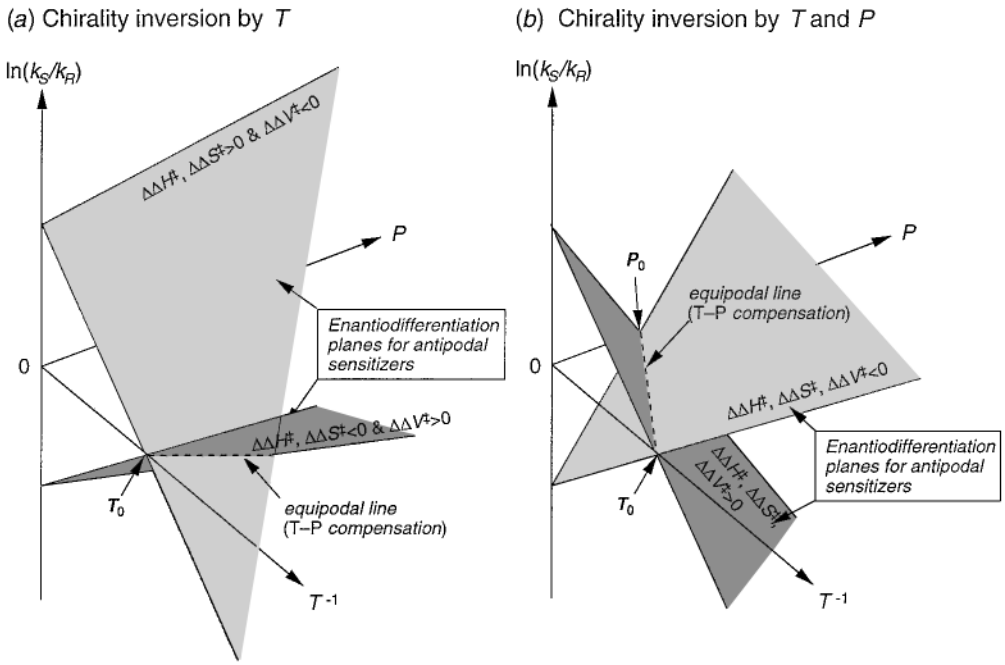

Fig. 5 Representative T^{-1}–P–$\ln(k_S/k_R)$ diagrams, correlating the ee of **1E** with temperature and pressure in the enantiodifferentiating photoisomerization of **1Z** sensitized by antipodal sensitizers; (*a*) the product chirality is inverted only by temperature as the signs of $\Delta\Delta H^{\ddagger}$ and $\Delta\Delta S^{\ddagger}$ are opposite to that of $\Delta\Delta V^{\ddagger}$; (*b*) the chirality is inverted by both temperature and pressure as the signs of $\Delta\Delta H^{\ddagger}$, $\Delta\Delta S^{\ddagger}$ and $\Delta\Delta V^{\ddagger}$ are all the same.

affording an extrapolated ee as high as 98.3% under conditions which are practically accessible, *i.e.* −9 °C and 1500 MPa.[31]

Conclusions

From the extensive experiments and comprehensive analyses of a variety of enantio- and diastereodifferentiating photochemical reactions,[20–31] it has been revealed that the entropy term plays an unexpectedly vital role in the stereodifferentiating processes where weak interactions determine rates and equilibria. However, it is important to emphasize that at temperatures below T_0, the stereoselectivity is dominated by the enthalpy difference arising mostly from steric and electrostatic interactions, while the dynamic behaviour of stereoselectivity over the whole temperature range, including the chirality switching phenomenon, is exclusively attributable to the entropy difference.

Experimental verification that temperature and pressure can function indeed as independent, yet cooperative, factors governing the product chirality in the enantiodifferentiating photosensitization gives us the new and versatile methodology of 'multidimensional control of asymmetric photochemistry'.[31] This strategy employs several entropy-related factors, such as temperature,[34] pressure, solvent,[35] concentration[36] and substituent flexibility, as tools for controlling the stereochemistry and stereoselectivity of photoproducts more conveniently and effectively through the manipulation of the steric and electronic weak interactions involved in the exciplex intermediates. Further, the concept of multidimensional control is not necessarily restricted to the asymmetric photochemical reactions described here, but may be applied in general to any thermal and biochemical reaction or equilibria where weak interactions are the principal driving force or determining factor, and therefore, where the entropy factor plays a major role.[37]

Acknowledgements

We would like to thank Dr Simon R. L. Everitt for corrections and improvements arising from a preliminary reading of this manuscript, and Ms Makiko Niki for her assistance in literature searching and manuscript preparation.

Notes and references

1 T. Hayashi, K. Tomioka and O. Yonemitsu, in *Asymmetric Synthesis: Graphical Abstracts and Experimental Methods*, Kodansha/Gordon and Breach, Tokyo/Amsterdam, 1998.
2 R. E. Gawley and J. Aubè, in *Principles of Asymmetric Synthesis*, ed. J. E. Baldwin, F. R. S. Magnus and P. D. Magnus, Pergamon, Oxford, 1996.
3 D. J. Ager and M. B. East, in *Asymmetric Synthetic Methodology*, CRC Press, Boca Raton, 1996.
4 J. Seyden-Penne, in *Chiral Auxiliaries and Ligands in Asymmetric Synthesis*, Wiley, New York, 1995.
5 M. Nógrádi, in *Stereoselective Synthesis*, 2nd edn., VCH, Weinheim, 1995.
6 R. Noyori, in *Asymmetric Catalysis in Organic Synthesis*, Wiley, New York, 1994.
7 C. H. Wong and G. M. Whitesides, in *Enzymes in Synthetic Organic Chemistry*, Pergamon, Oxford, 1994.
8 A. N. Collins, G. N. Sheldrake and J. Crosby, in *Chirality in Industry*, Wiley, Chichester, 1992, vol. 1; Wiley, Chichester, 1997, vol. 2.
9 R. A. Sheldon, in *Chirotechnology—Industrial Synthesis of Optically Active Compounds*, Marcel Dekker, New York, 1993.
10 D. J. Cram and D. R. Wilson, *J. Am. Chem. Soc.*, 1963, **85**, 1245; D. J. Cram and F. A. A. Elhafez, *J. Am. Chem. Soc.*, 1952, **72**, 5828; D. J. Cram and K. R. Kopecky, *J. Am. Chem. Soc.*, 1959, **81**, 2748.
11 N. T. Anh and O. Eisenstein, *Tetrahedron Lett.*, 1976, 1976; N. T. Anh and O. Eisenstein, *Nouv. J. Chim.*, 1977, **1**, 61; N. T. Anh, *Top. Curr. Chem.*, 1980, **88**, 145.
12 Y. D. Wu, K. N. Houk and B. M. Trost, *J. Am. Chem. Soc.*, 1987, **109**, 5560; Y. D. Wu, J. A. Tucker and K. N. Houk, *J. Am. Chem. Soc.*, 1991, **113**, 5018.
13 D. M. Huryn, in *Comprehensive Organic Synthesis*, ed. S. L. Schreiber, Pergamon, Oxford, 1991, vol. 1, p. 49.
14 For the temperature and solvent effects on diastereoselectivity in thermal asymmetric syntheses, see G. Cainelli, D. Ciacomini and P. Galletti, *Chem. Commun.*, 1999, 567 and the references cited therein.
15 H. Pracejus, *Justus Liebigs Ann. Chem.*, 1960, **634**, 9 and 23; H. Pracejus and A. Tille, *Chem. Ber.*, 1963, **96**, 854; S. Winter and H. Pracejus, *Chem. Ber.*, 1966, **99**, 151.
16 O. Cervinka, *Collect. Czech. Chem. Commun.*, 1965, **30**, 1685 and 2485; O. Cervinka and O. Belovsky, *Collect. Czech. Chem. Commun.*, 1967, **32**, 3897.
17 U. Folli, D. Iarossi, F. Montanari and G. Torre, *J. Chem. Soc. (C)*, 1968, 1317.
18 H. Rau, *Chem. Rev.*, 1983, **83**, 535.
19 Y. Inoue, *Chem. Rev.*, 1992, **92**, 741; S. R. L. Everitt and Y. Inoue, in *Organic Molecular Photochemistry*, ed. V. Ramamurthy and K. Schanze, Marcel Dekker, New York, 1999, p. 71.
20 H. Koch, J. Runsink, H.-D. Scharf and H. Leismann, *Chem. Ber.*, 1985, **118**, 1485; H. Buschmann, H. D. Scharf, N. Hoffmann, M. W. Plath and J. Runsink, *J. Am. Chem. Soc.*, 1989, **111**, 5367; for the first report on this diastereodifferentiating photocycloaddition, see H. Koch, J. Runsink and H.-D. Scharf, *Tetrahedron Lett.*, 1983, **24**, 3217.
21 Y. Inoue, T. Yokoyama, N. Yamasaki and A. Tai, *Nature*, 1989, **341**, 225; for the first report on this enantiodifferentiating photoisomerization, see Y. Inoue, Y. Kunitomi, S. Takamuku and H. Sakurai, *J. Chem. Soc., Chem. Commun.*, 1978, 1024.
22 (*a*) Y. Inoue, T. Yokoyama, N. Yamasaki and A. Tai, *J. Am. Chem. Soc.*, 1989, **111**, 6480; (*b*) Y. Inoue, N. Yamasaki, T. Yokoyama and A. Tai, *J. Org. Chem.*, 1992, **57**, 1332; (*c*) Y. Inoue, N. Yamasaki, T. Yokoyama and A. Tai, *J. Org. Chem.*, 1993, **58**, 1011; (*d*) Y. Inoue, F. Dong, K. Yamamoto, L.-H. Tong, H. Tsuneishi, T. Hakushi and A. Tai, *J. Am. Chem. Soc.*, 1995, **117**, 11 033; (*e*) H. Tsuneishi, T. Hakushi and Y. Inoue, *J. Chem. Soc., Perkin Trans. 2*, 1996, 1601; (*f*) H. Tsuneishi, T. Hakushi, A. Tai and Y. Inoue, *J. Chem. Soc., Perkin Trans. 2*, 1995, 2057; (*g*) M. Shi and Y. Inoue, *J. Chem. Soc., Perkin Trans. 2*, 1998, 1725.
23 Y. Inoue, N. Yamasaki, H. Shimoyama and A. Tai, *J. Org. Chem.*, 1993, **58**, 1785.
24 Y. Inoue, H. Tsuneishi, T. Hakushi and A. Tai, *J. Am. Chem. Soc.*, 1997, **119**, 472.
25 (*a*) Y. Inoue, T. Okano, N. Yamasaki and A. Tai, *J. Chem. Soc., Chem. Commun.*, 1993, 718; (*b*) S. Asaoka, T. Kitazawa, T. Wada and Y. Inoue, *J. Am. Chem. Soc.*, 1999, **121**, 8486.
26 R. Pelzer, H. D. Scharf, H. Buschmann and J. Runsink, *Chem. Ber.*, 1989, **122**, 1187; H. Buschmann, H.-D. Scharf, N. Hoffmann and P. Esser, *Angew. Chem., Int. Ed. Engl.*, 1991, **30**, 477.
27 D. Awandi, F. Henin, J. Muzart and J.-P. Pete, *Tetrahedron: Asymmetry*, 1991, **2**, 1101; J. Muzart, F. Hénin, J.-P. Pete and A. M'Boungou-M'Passi, *Tetrahedron: Asymmetry*, 1993, **4**, 2531.
28 N. Hoffmann, H. Buschmann, G. Raabe and H.-D. Scharf, *Tetrahedron*, 1994, **50**, 11 167.
29 T. Sugimura, H. Shimizu, S. Umemoto, H. Tsuneishi, T. Hakushi, Y. Inoue and A. Tai, *Chem. Lett.*, 1998, 233.
30 Y. Kubo, M. Yoshioka, S. Nakajima and I. Imamura, *Tetrahedron Lett.*, 1999, **40**, 2338.
31 Y. Inoue, E. Matsushima and T. Wada, *J. Am. Chem. Soc.*, 1998, **120**, 10 687.
32 Y. Inoue, S. Takamuku, Y. Kunitomi and H. Sakurai, *J. Chem. Soc., Perkin Trans. 2*, 1980, 1672.
33 T. Asano and W. J. le Noble, *Chem. Rev.*, 1978, **78**, 407; R. van Eldik, T. Asano and W. J. le Noble, *Chem. Rev.*, 1989, **89**, 549.
34 A paper on the effects of temperature and solvent upon enantiodifferentiating photoisomerization of (*Z*)-cycloheptene to the highly strained, optically active (*E*)-isomer has recently been published: R. Hoffmann and Y. Inoue, *J. Am. Chem. Soc.*, 1999, **121**, 10 702.
35 Switching of product chirality by changing solvent was observed in the enantiodifferentiating photoisomerization of **1Z**: Y. Inoue, H. Ikeda, M. Kaneda, T. Sumimura, S. R. L. Everitt and T. Wada, *J. Am. Chem. Soc.*, 2000, **122**, in the press.
36 Switching of product diastereoselectivity was also found to occur by changing the substrate concentration in the inter- and intramolecular photosensitized isomerization of 3-benzoyloxycyclooctene: T. Inoue, K. Matsuyama and Y. Inoue, *J. Am. Chem. Soc.*, 1999, **121**, 9877.
37 Y. Inoue and T. Wada, in *Advances in Supramolecular Chemistry*, ed. G. W. Gokel, JAI, Greenwich, 1997, vol. 4, p. 55.

Paper a905409j

ChemComm

$[Mo_{10}S_{10}O_{10}(OH)_{10}(H_2O)_5]$: a novel decameric molecular ring showing supramolecular properties

Emmanuel Cadot,* Bernadette Salignac, Jérôme Marrot, Anne Dolbecq and Francis Sécheresse

Institut Lavoisier. IREM, UMR 8637. Université de Versailles Saint Quentin, 45 Avenue des Etats-Unis, 78035 Versailles, France. E-mail: cadot@chimie.uvsq.fr

Received (in Basel, Switzerland) 15th November 1999, Accepted 10th January 2000

The new decameric $[Mo_{10}S_{10}O_{10}(OH)_{10}(H_2O)_5]$ oxo–thio ring was prepared by self-condensation of $[Mo_2S_2O_2]^{2+}$ upon addition of hydroxide ion; crystals were obtained in dimethylformamide in the presence of tetrabutylammonium iodide; X-Ray diffraction analysis reveals a 10-membered ring-shaped cluster; the cyclic architecture exhibits a supramolecular assembly resulting from hydrogen bonding between two iodide anions and inner water molecules of the open cavity of the Mo_{10}-ring.

The synthesis of large and discrete species resulting from transition metal and sulfur combinations is an exciting challenge for the inorganic chemist. Indeed, transition metal sulfides represent a prominent class of compounds involved in many areas of chemistry.[1] Especially, such systems are studied extensively for their implications in both biological and industrial catalytic processes. The nuclearity of the thiometalates is generally low with topologies often limited to a restricted number of archetypal architectures.[2] These features contrast with polyoxometalates which have now reached the nanometric scale with spectacular examples such as the 'big wheel' for molybdenum blues[3] and the 'giant butterfly' for heteropolytungstates.[4] We reported in a previous work the characterization of the first oxo–thio molecular ring with high nuclearity[5] and we have now indications that other derived compounds might be synthesized through the original and convenient route of synthesis we are developing. The $[Mo_2S_2O_2(H_2O)_6]^{2+}$ precursor (aqua ion) reacts rapidly with hydroxo ions to give cyclic polymeric oxo–thio molecules, the first compound (solid **1**) isolated at pH < 3 from concentrated potassium iodide solution, leading after crystallization in water to $[Mo_{12}S_{12}O_{12}(OH)_{12}(H_2O)_6]$ (denoted Mo_{12}) a cyclic iodide-free dodecameric neutral cluster **2**.[5]† The Mo_{12} ring-shaped molecule results from the cyclic linking of six $\{Mo_2S_2O_2\}$ fragments by face-shared connections. We have demonstrated that the six water molecules lining the inner ring are labile enough to be exchanged by small anions such as phosphate or arsenate ions.[6] These exchange properties arising from the cationic character of the central open cavity hold much promise for the elaboration of a new generation of 'multicomponent systems' based on host–guest chemistry. In the presence of anionic structuring agents, such as oxalate[7] or even metalates such as molybdate,[8] the self-condensation of $[Mo_2S_2O_2]^{2+}$ produces an octameric $\{Mo_8S_8O_8(OH)_8\}$ ring encapsulating the structuring anion. With more concentrated phosphate or arsenate solutions, the condensation leads exclusively to the hexameric $[(HXO_4)_4Mo_6S_6O_6(OH)_3]^{5-}$ anion (X = As, P)[9] in which three building units $\{Mo_2O_2S_2\}$ condense around a central phosphate group through hydroxo and peripheral phosphato bridges.

The structural characterization of the new $[Mo_{10}S_{10}O_{10}(OH)_{10}(H_2O)_5]$ ring-shaped cluster **3** (denoted Mo_{10}), obtained from **1** in a DMF solution containing tetrabutylammonium iodide represents a nice illustration of the self-condensation process. The synthesis is straightforward and consists of the dissolution of the reactants in dimethylformamide, leading to the crystallization of **3**‡ which has been fully characterized by X-ray diffraction, IR spectroscopy and elemental analysis.§

The results of the X-ray crystallographic investigation are shown in Figs. 1 and 2. The asymmetric unit contains one molecular Mo_{10}-ring, associated with two iodide anions and two tetrabutylammonium cations. The $[Mo_{10}S_{10}O_{10}(OH)_{10}(H_2O)_5]$ molecular ring consists of five $\{Mo_2S_2O_2\}$ units connected to each other by hydroxo double bridges to form a cyclic neutral decamer. Two types of Mo–Mo distances are observed: short Mo–Mo distances [2.835(2)–2.847(2) Å] within the $\{Mo_2S_2O_2\}$ building block and long Mo–Mo interblock distances (3.314–3.324 Å). A terminal oxygen atom and two bridging sulfur atoms, both belonging to the preformed building block, complete the coordination of the Mo^V centers. Five oxygen atoms located in the open cavity of the $\{Mo_{10}S_{10}O_{10}(OH)_{10}\}$ ring bridge two neighboring Mo atoms through long Mo–O distances (2.572–2.630 Å). This arrangement confers an overall zero charge to the cluster. The presence of two iodide anions symmetrically located on both sides of the mean plane defined by the ten Mo atoms is a remarkable feature of the molecular structure (Fig. 2). The distances between iodides and the five inner water molecules are short enough (3.570–3.622 Å) to suggest that the stability of the bis-halide complex is directly related to hydrogen bonds. The hydrogen atoms of the five inner water molecules are symmetrically distributed on each side of the ring cluster, in two planes parallel to those defined by the ten molybdenum atoms. The five

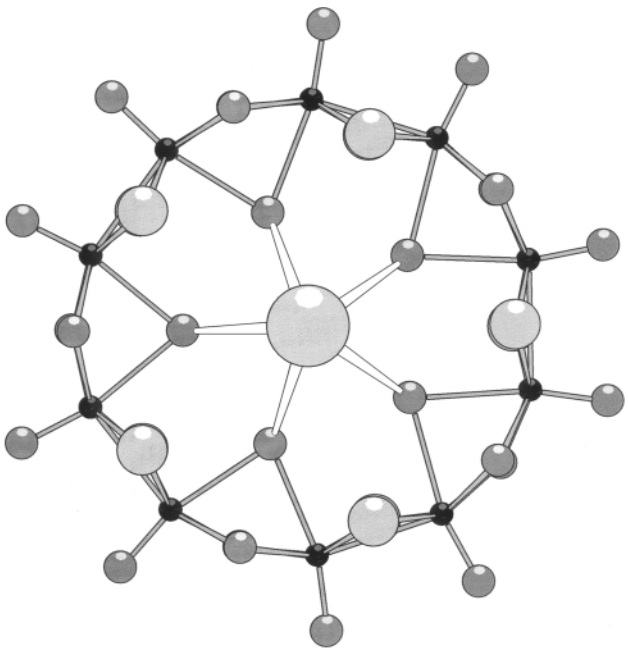

Fig. 1 Molecular structure of $[I_2Mo_{10}S_{10}O_{10}(OH)_{10}(H_2O)_5]^{2-}$: ball and stick model showing the 10 membered ring with the central iodide anions (black spheres: Mo, light grey spheres: S, dark grey spheres: O, light grey central sphere: I).

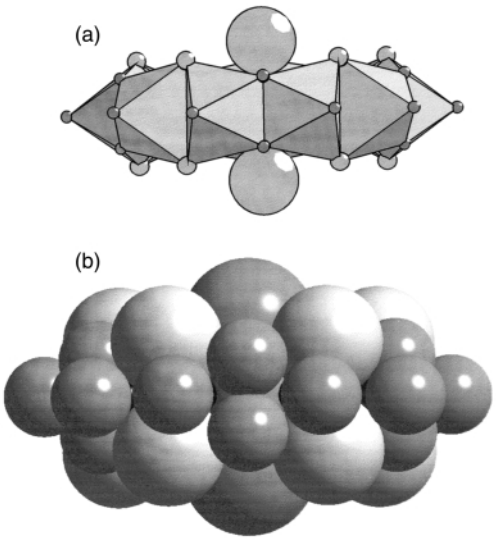

Fig. 2 Side view of $[I_2Mo_{10}S_{10}O_{10}(OH)_{10}(H_2O)_5]^{2-}$ showing the two symmetric iodide anions floating over the cavity of the Mo_{10} ring-shaped cluster through hydrogen interactions: (a) polyhedral representation; (b) space-filling sketch with ionic radii of the elements (O^{2-} = 1.32 Å, S^{2-} = 1.84 Å, I^- = 2.20 Å).

[I⁻···H–O–H···I⁻] interactions provoke a pronounced shortening of the I···I distances (4.783 Å), rather close to the sum of the ionic radii (4.40 Å). The electrostatic balance in the crystal is ensured by two tetrabutylammonium cations.

In conclusion, this work illustrates the flexibility and the versatility of the cyclic oxo–thio architecture: in water, **1** leads to the dodecamer $[Mo_{12}S_{12}O_{12}(OH)_{12}(H_2O)_6]$ **2** while in iodide containing DMF solution, **1** gives the cyclic decamer $[Mo_{10}S_{10}O_{10}(OH)_{10}(H_2O)_5]$ **3**. The solid state structure of **3** reveals a remarkable bis-halide complex resulting from the electrostatic interactions of two iodide ions with the inner cavity of the Mo_{10}-cluster. Such promising results demonstrate that supramolecular chemistry of anions can be considered in those inorganic systems.

Notes and references

† The crude product **1**, obtained by the synthetic procedure described in ref. 5 is a mixed K^+–NMe_4^+ salt of a neutral oxo–thio-cluster which incorporates iodide in the solid state. The elemental and thermogravimetric analysis for **1** led to the empirical molecular composition $\{K_{0.40}(NMe_4)_{0.1}I_{0.5}[Mo_2S_2O_2(OH)_2(H_2O)]\cdot 6.3H_2O\}_n$ with no direct evidence for the determination of the nuclearity *n*.

‡ *Synthesis of* $[NBu_4]_2I_2[Mo_{10}S_{10}O_{10}(OH)_{10}(H_2O)_5]\cdot H_2O\cdot 13DMF$ **3**. 1 g of **1** and tetrabutylammonium iodide (2.8 g, 7.6 mmol) were dissolved in 15 mL of DMF. After filtration, the solution was allowed to stand at room temperature for crystallization. After a week, well shaped orange crystals, suitable for X-ray diffraction were collected [yield: 41% (based on Mo)]. IR spectra (KBr pellet, ν/cm^{-1}) gave absorptions at *ca*. 1488w, 1434w, 1411w, 1388m, 1257m, 1150w, 1101m, 1063w, 968s, 876w, 666m, 533s, 413m, 378m. Crystals are strongly hygroscopic and not stable in air. Such a behavior explains the difference between the number of water molecules found in the solvate by X-ray diffraction (1.0 H_2O) and those determined by elemental analysis after hydration of the solid (18 H_2O). Anal. for $[NBu_4]_2I_2[Mo_{10}S_{10}O_{10}(OH)_{10}(H_2O)_5]\cdot 18H_2O\cdot 13DMF$. Calc.(Found): C, 23.40 (24.85); I, 6.86 (6.91); Mo, 25.96 (26.47); N, 5.67 (5.31); S, 8.65 (8.58)%.

§ *X-Ray crystal structure analysis* for $[NBu_4]_2I_2[Mo_{10}S_{10}O_{10}(OH)_{10}(H_2O)_5]\cdot H_2O\cdot 13DMF$ **3**. Intensity data collection was carried out on an orange crystal of 0.30 × 0.30 × 0.40 mm mounted in a glass tube, with a Siemens SMART three-circle diffractometer equipped with a CCD bidimensional detector, using monochromatized wavelength λ(Mo-Kα) = 0.71073 Å, at T = 293 K. An absorption correction was made in the data set using the SADABS program[10] based on the method of Blessing.[11] The asymmetric unit is composed of one Mo_{10}-ring, two iodide anions and two $[NBu_4]^+$ cations. Among the 13 DMF molecules per Mo_{10}-ring obtained by microanalysis, only 10 were located, the others being disordered in the lattice. *Crystal data* for $H_{185}C_{71}I_2Mo_{10}N_{15}O_{39}S_{10}$: a = 21.573(2), b = 21.075(2), c = 30.190(5) Å, β = 97.766(8)°, U = 13600(3) Å^3, Z = 4, M = 3405, D_c = 1.663 g cm^{-3}, monoclinic, space group $P2_1/c$, μ = 15.67 cm^{-1}, index ranges $-26 \leqslant h \leqslant 30$, $-15 \leqslant k \leqslant 23$, $-30 \leqslant l \leqslant 41$; total data 44152; unique data 29602 (R_{int} = 0.056), data with $I_0 > 2\sigma(I_o)$ 12749. The structure was solved by direct methods and refined by full matrix least squares, based on F^2, using the SHELX-TL software package.[12] All the non-hydrogen atoms were refined anisotropically except the water oxygen atoms, nitrogen, oxygen and carbon atoms of the DMF molecules and the three terminal carbon of the four alkyl chains in the two NBu_4^+ cations. No. of variables, 855; final $R(F)$ = 0.0782, $wR_2(F^2)$ = 0.1790; GOF 1.074; minimum and maximum peak in difference electron density map −1.761 and 1.415 e Å^{-3}. CCDC 182/1517. See http://www.rsc.org/suppdata/cc/a9/a909024j/ for crystallographic files in .cif format.

1 *Transition Metal Sulfur Chemistry: Biological and Industrial Significance*, ed. E. I. Stiefel and K Matsumoto, ACS Symp. Ser. 653, American Society, Washington, DC, 1996.
2 T. Shibahara, *Coord. Chem. Rev.*, 1993, **123**, 73.
3 A. Müller, S. Q. N. Shah, H. Bögge and M. Schmidtmann, *Nature*, 1999, **397**, 48.
4 K. Wassermann, M. H. Dickman and M. T. Pope, *Angew. Chem., Int. Ed. Engl.*, 1997, **36**, 1445.
5 E. Cadot, B. Salignac, S. Halut and F. Sécheresse, *Angew. Chem., Int. Ed.*, 1998, **37**, 611.
6 E. Cadot, B. Salignac, T. Loiseau, A. Dolbecq and F. Sécheresse, *Chem. Eur. J.*, 1999, 3390.
7 A. Dolbecq, B. Salignac, E. Cadot and F. Sécheresse, *Bull. Pol. Acad. Sci.*, 1998, **46**, 237.
8 A. Dolbecq, B. Salignac, E. Cadot and F. Sécheresse, *Chem. Commun.*, 1998, 2293.
9 E. Cadot, A. Dolbecq, B. Salignac and F. Sécheresse, *Chem. Eur. J.*, 1999, **5**, 2396.
10 G. M. Sheldrick, SADABS, Program for scaling and correction of area detector data, University of Göttingen, Germany, 1997.
11 R. Blessing, *Acta Crystallogr., Sect A*, 1990, **46**, 467; SHELX-TL version 5.03, Software Package for Crystal Structure Determination, Siemens Analytical X-Ray Instrument Division, Madison, WI, 1994.
12 G. M. Sheldrick, SHELX-TL version 5.03, Software package for crystal structure determination, Siemens Analytical X-ray Instruments Inc., Madison, WI, 1994.

Communication a909024j

Polymerisation of olefins catalysed by a palladium complex in supercritical carbon dioxide

Tjerk J. de Vries,*[ab] Robbert Duchateau,[bc] Marius A. G. Vorstman[a] and Jos T. F. Keurentjes[a]

[a] *Process Development Group, Department of Chemical Engineering and Chemistry, Eindhoven University of Technology, PO Box 513, 5600 MB Eindhoven, The Netherlands. E-mail: t.de.vries@tue.nl*
[b] *Dutch Polymer Institute, PO Box 902, 5600 AX Eindhoven, The Netherlands*
[c] *Schuit Institute of Catalysis, Eindhoven University of Technology, PO Box 513, 5600 MB Eindhoven, The Netherlands*

Received (in Cambridge, UK) 11th November 1999, Accepted 6th January 2000

A late transition metal catalyst has been used to polymerise hex-1-ene and ethene in supercritical carbon dioxide, yielding high molecular weight polymers; a comparison with polymerisations in CH_2Cl_2 reveal that polymers with identical molecular weight and polydispersity are formed.

Supercritical carbon dioxide ($scCO_2$) has recently emerged as an interesting substitute for organic solvents. CO_2 is environmental friendly compared to organic solvents and has a low critical temperature (31.1 °C) and pressure (73.8 bar). The physical properties of $scCO_2$ range from liquid-like to gas-like and can be manipulated by changing the pressure and the temperature. Physical properties like gas-like viscosities and diffusion rates, coupled with the liquid-like densities, can result in significant advantages in combined reaction, separation and purification processes. A drawback of $scCO_2$ is that only volatile or relatively non-polar compounds are soluble, as CO_2 is non-polar and has a low polarisability and relative permittivity.[1]

Polymerisation reactions using radical initiators and step growth mechanisms have been carried out in $scCO_2$.[2] More recently homogeneous catalysts have successfully been applied in $scCO_2$ for the preparation of small molecules[3] and polymers.[4–6] An interesting extension in the application of CO_2 is the use of CO_2 both as a reactant and as a solvent in a copolymerisation with cyclohexene oxide.[7] The goal of our research is to copolymerise α-olefins in $scCO_2$. Traditional catalysts for poly(olefin) production are based on early-transition-state metals, which are highly oxophilic and therefore not suitable for polymerisations in CO_2. As late-transition-state metal complexes are less oxophilic, they are more likely to be effective polymerisation catalysts in $scCO_2$. Here we describe the polymerisation of ethene and hex-1-ene catalysed by a homogeneous diimine palladium complex as catalyst,[8,9] also known as the Brookhart system, see Fig. 1.

In our polymerisation experiments we were primarily interested to see if high molecular weight polymers could be produced and whether the active catalyst would exhibit complexation behaviour with CO_2. The results of the polymerisations in CO_2 and in CH_2Cl_2 are listed in Table 1. The values of the turnover frequencies (TOFs) show that the activity of the catalyst is similar in both solvents, despite the large difference in phase behaviour of the reaction mixtures. Both the catalyst and the polymers are soluble in CH_2Cl_2. As expected, the polymer does not dissolve in $scCO_2$. Consequently, the polymerisations performed in CO_2 were all precipitation polymerisations as has been observed in the experiments. Although the differences in phase behaviour are rather large, the polymers produced are very similar, both in molecular weight and in molecular weight distribution. This behaviour indicates that there is no diffusion limitation, despite the precipitation in CO_2, suggesting strong swelling of the polymer, either by CO_2 or by the monomers used. More importantly, a similar molecular weight indicates that the active catalyst does not exhibit complexation behaviour with CO_2, since this would have resulted in a lower molecular weight.

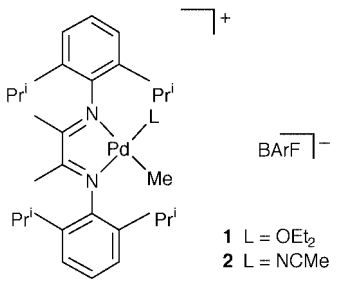

Fig. 1 Catalyst precursors used for polymerizations, BArF ≡ tetrakis[3,5-bis(trifluoromethyl)phenyl]borate.

Table 1 Polymerisation of ethene and hex-1-ene in CO_2 and CH_2Cl_2 for 2 h†

Experiment	Catalyst precursor	Catalyst/ 10^{-5} mol l^{-1}	Solvent	Pressure/bar	Monomer[a]/ mol l^{-1}	TOF[b]/h^{-1}	M_n[c]/kg mol^{-1}	M_w/M_n
1	**1**	42	CO_2	239	1.7	450	135	2.1
2	**2**	30	CH_2Cl_2	—	2.7	1010	93	1.5
3	**2**	30	CO_2	194	2.9	560	102	1.5
4	**2**	13	CH_2Cl_2	—	2.3	810	101	1.7
5	**2**	13	CO_2	193	2.1	990	103	2.0
6	**2**	2.6	CO_2	156	0.27	2250	88	2.0

† High pressure polymerisations were conducted in a 75 ml stainless steel high pressure reactor equipped with sapphire windows, a heating jacket and a magnetic stirring bar. The solid catalyst precursor **1** (air and temperature sensitive) was put in the reactor in a glass ampulla, which broke under pressure; catalyst precursor **2** (stable at room temperature in air) was placed directly in the reactor. The air was carefully flushed with CO_2 at low pressure and the reactor was heated. In the case of hex-1-ene as the monomer, the reactor was first filled with CO_2 and then the monomer was added. In the case of ethene, the reactor was flushed and filled with ethene after which CO_2 was added. [a] Experiments 1–5: hex-1-ene, reaction temperature 35 °C; experiment 6: ethene starting pressure 6.9 bar, reaction temperature 40 °C. [b] Turn Over Frequency: mol monomer converted per mol catalyst per hour. [c] GPC (against polystyrene standards).

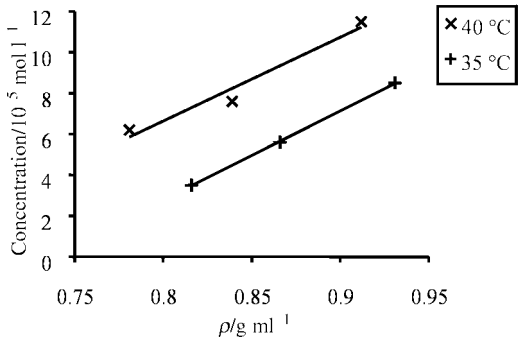

Fig. 2 Solubility of catalyst precursor **2** as a function of $scCO_2$ density.

To study the effect of catalyst concentration on the polymer yield two sets of experiments were conducted, one set with a relatively high catalyst concentration in CH_2Cl_2 and CO_2 (experiments 2 and 3, respectively) and one set with a low catalyst concentration (experiments 4 and 5, respectively). When the experiments were carried out with the high catalyst concentration, the TOF in CO_2 was lower than in the corresponding experiment in CH_2Cl_2. The experiments in the two solvents using the low catalyst concentration showed identical values for TOF, M_n and M_w/M_n, taking into account experimental error. In order to explain the effect of catalyst concentration to the TOF, the solubility of the catalyst precursor was measured in $scCO_2$ with a UV spectrophotometer‡ using a high-pressure view cell with sapphire windows. Although $scCO_2$ is a poor solvent for ionic compounds, the solubility at 35 and 40 °C was found to be in the order of 1×10^{-4} mol l^{-1}, see Fig. 2. However, the rate of solubilisation was low as it typically took 1 h to reach equilibrium. The relatively high solubility can be ascribed to the bulky anion (BArF). Generally, the solubility of an anion in hydrocarbon solvents is known to increase with increasing distribution of charge, *e.g.* the solubility increases in the order BF_4, PF_6, SbF_6, BArF and this is likely to apply for the apolar $scCO_2$ as well. All polymerisations of hex-1-ene in CO_2 were performed above the maximum solubility of the catalyst. Even in experiment 5 with the lowest catalyst concentration, only half of the added amount of catalyst is dissolved in the initial stage of the polymerisation, which follows from Fig. 2 and the density of the reaction mixture. During polymerisation, however, the solubility of the catalyst will be different from pure CO_2, since the catalyst is attached to a growing polymer chain. When the experiments with the low catalyst concentration are compared for the two solvents, no difference in TOF was observed. Obviously, the catalyst solubilisation was not limiting in experiment 5 using CO_2 as the activity was similar to experiment 4 using CH_2Cl_2. Comparing experiment 2 and 3 with the higher catalyst concentration, a difference in TOF was observed, which can be explained by the slow solubilisation and low solubility of the catalyst in CO_2. In experiment 6, ethene was polymerised in $scCO_2$ to high molecular weight polymer. It follows from this experiment that the catalyst is also active in $scCO_2$. In principle, this opens the possibility to copolymerise in $scCO_2$ with monomers such as ethene and propene.

From the foregoing it can be concluded that polymerisation of ethene and α-olefins can effectively be carried out in $scCO_2$. In the case of hex-1-ene, a comparison was made with polymerisation behaviour in an organic solvent, which yielded similar molecular weights and molecular weight distributions. In order to improve the solubility of the catalysts, we are currently modifying ligands to enhance the solubility in $scCO_2$.[10,11] Furthermore, a larger test set-up has been constructed to perform (co)polymerisations of propene, including the use of functional monomers as comonomers. Another extension to our work is the evaluation of other late-transition-state olefin polymerisation catalysts known from the literature.[12,13]

Notes and references

‡ Solubility experiments were conducted in a 1.4 ml high-pressure view cell equipped with sapphire windows and a heating jacket. The cell was filled with about 3 mg (2 μmol) solid catalyst. The air was carefully flushed with CO_2 at low pressure. The cell was then heated, filled with CO_2 at high pressure and placed in a UV spectrophotometer.

1 M. McHugh and V. Krukonis, *Supercritical Fluid Extraction*, 2nd edn., Butterworth-Heineman, Newton, 1994.
2 J. L. Kendall, D. A. Canelas, J. F. Young and J. M. DeSimone, *Chem. Rev.*, 1999, **99**, 543.
3 P. G. Jessop, T. Ikariya and R. Noyori, *Chem. Rev.*, 1999, **99**, 475.
4 C. D. Mistele, H. H. Thorp and J. M. DeSimone, *J. Macromol. Sci., Chem.*, 1996, **A33**, 953.
5 A. Fürstner, D. Koch, K. Langemann, W. Leitner and C. Six, *Angew. Chem., Int. Ed. Engl.*, 1997, **36**, 2466.
6 H. Hori, C. Six and W. Leitner, *Macromolecules*, 1999, **32**, 3178.
7 M. Super, E. Berluche, C. Costello and E. Beckman, *Macromolecules*, 1997, **30**, 368.
8 L. K. Johnson, C. M. Killian and M. Brookhart, *J. Am. Chem. Soc.*, 1995, **117**, 6414.
9 S. Mecking, L. K. Johnson, L. Wang and M. Brookhart, *J. Am. Chem. Soc.*, 1998, **120**, 888.
10 S. Kainz, D. Koch, W. Baumann and W. Leitner, *Angew. Chem., Int. Ed. Engl.*, 1997, **36**, 1628.
11 M. A. Carroll and A. B. Holmes, *Chem. Commun.*, 1998, 1395.
12 U. Klabunde and S. D. Ittel, *J. Mol. Catal.*, 1987, **41**, 123.
13 C. Wang, S. Friedrich, T. R. Younkin, R. T. Li, R. H. Grubbs, D. A. Bansleben and M. W. Day, *Organometallics*, 1998, **17**, 3149.

Communication a908966g

A novel magnetically coupled nonamanganese(II) 3 × 3 portcullis-like grid involving just oxygen bridges, generated by strict self assembly of the metal cation and a single heptadentate ligand

Liang Zhao,[a] Craig J. Matthews,[a] Laurence K. Thompson*[a] and Sarah L. Heath[b]†

[a] *Department of Chemistry, Memorial University of Newfoundland, St. John's, NFLD, A1B 3X7, Canada. E-mail: lthomp@morgan.ucs.mun.ca*

[b] *Department of Chemistry, The University, Sheffield, Brook Hill, UK S3 7HF*

Received (in Cambridge) 19th November 1999, Accepted 11th January 2000

The heptadentate ligand 2POAP combines two bridging alkoxide oxygen donors with diazine and pyridine terminal nitrogen donors in a linear array with the binding sites positioned critically to accommodate three metal centres, but on reaction with $Mn(ClO_4)_2·6H_2O$ a strict self assembly process occurs, producing a unique homoleptic nonamanganese 'square' grid complex, involving six ligands.

Self assembly strategies for the formation of clusters with predetermined topological architectures are limited, and succeed only when carefully programmed subunits are incorporated in the ligand(s). The use of a single ligand with a repeating array of coordination pockets arranged in a 'linear' fashion has the potential to create a grid-like arrangement of metal centers, and some success has been achieved with linear polytopic ligands of this sort based on pyridazine and pyrimidine as a bridging subunit. Essentially flat 2 × 2 homotetranuclear grids have been achieved with Cu(I)[1] and Co(II)[2] with pyridazine and pyrimidine based ligands respectively, and a flat 3 × 3 nonanuclear grid with Ag(I)[3] involving a pyridazine based ligand. The Co(II) centers were shown to be antiferromagnetically coupled within the cluster, despite long distances of separation between the metals (6.5 Å).[4] The *n*-topic nature of the ligand creates a grid-like cluster of n^2 metal centres.[3] The ordering of paramagnetic metal ions in these grid-like arrays presents the possibility of extended spin communication within a lattice of closely spaced metal ion centers, if appropriate bridge groups can be incorporated into the ligand backbone.

Previous studies on tetradentate ligands (*e.g.* POAP) built on a flexible diazine (N–N) backbone, with a strategically positioned alkoxide fragment, have been shown to organize

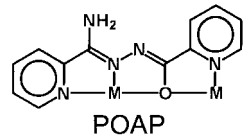

POAP

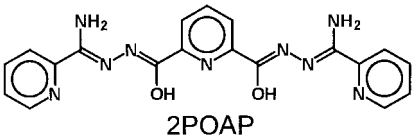

2POAP

Mn(II), Co(II), Ni(II) and Cu(II) centers into square homotetranuclear clusters with just alkoxide bridges between the metal centers.[5,6] These systems display dominant antiferromagnetic exchange, except in the copper case where ferromagnetic coupling prevails.[6] In addition a unique, spin coupled, homoleptic trigonal-bipyramidal alkoxo-bridged cluster has been produced with Mn(II).[7]

† Present address, Department of Chemistry, University of York, Heslington, York, UK YO10 5DD.

This report describes the synthesis‡ and study of a heptadentate ligand that is a systematic extension of POAP, in which repeating N_2O coordination pockets are built on a 2,6-disubstituted pyridine central fragment (2POAP). Reaction of 2POAP with $Mn(ClO_4)_2·6H_2O$ in MeCN–H_2O produced red crystals (72% yield)‡ suitable for structural analysis.§ The structure of $[Mn_9(2POAP–2H)_6](ClO_4)_6·3.57MeCN·11H_2O$ **1** is unique (Fig. 1) with a 3 × 3 grid of nine pseudo-octahedral, alkoxo-bridged Mn(II) centres coordinated by two groups of three roughly parallel dianionic ligands arranged above and below the metal pseudo-plane. The Mn centres comprise three different types; *trans*-MnN_2O_4 (central), *cis*-MnN_4O_2 (corners) and *mer*-MnN_3O_3 (sides). The Mn_9O_{12} core (Fig. 2) shows that within each Mn_4O_4 subunit a puckered boat-like bridging arrangement exists involving an alternation of oxygens above and below the Mn_4 pseudo-plane. This then translates symmetrically throughout the fused arrangement that comprises the whole grid.

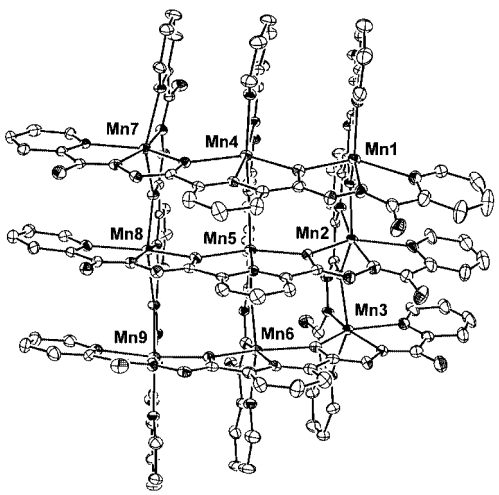

Fig. 1 Structural representation of the cation $[Mn_9(2POAP - 2H)_6]^{6+}$ (**1**) (40% probability thermal ellipsoids). Selected bond lengths (Å) and angles (°) Mn(1)–Mn(2) 3.953(3), Mn(1)–Mn(4) 3.956(4), Mn(2)–Mn(5) 3.918(4), Mn(4)–Mn(5) 3.928(3), Mn(2)–Mn(3) 3.909(3), Mn(3)–Mn(6) 3.956(4); Mn–O–Mn 126.6–130.0.

Variable temperature magnetic susceptibility measurements were carried out on a powdered sample of **1** in the temperature range 2–300 K.¶ Magnetic moments (per mol) drop smoothly from 16.9 μ_B at 300 K to 6.9 μ_B at 5 K, and then there is a very slight rise below this temperature. The room temperature value is consistent with the presence of nine high spin Mn(II) centers, and the drop to 6.9 μ_B at 5 K is associated with the presence of intramolecular antiferromagnetic exchange with the equivalent of one residual Mn(II) center in the spin coupled (S = 5/2) ground state. This situation is an exact parallel to that occurring in the pentamanganese(II) cluster of POAP.[7] The slight rise in μ_B at temperatures <5 K may be due to a very weak

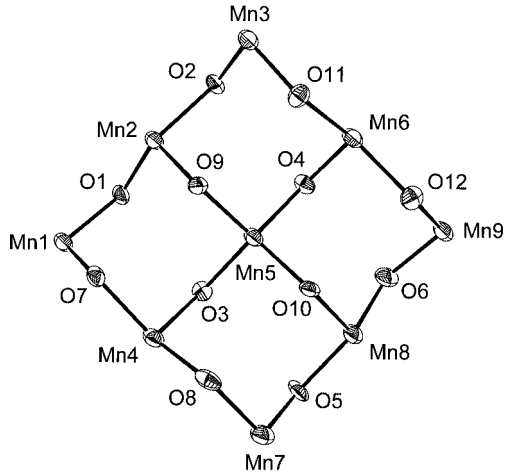

Fig. 2 Structural representation of the nonanuclear core in $[Mn_9(2POAP - 2H)_6]^{6+}$.

ferromagnetic component. An evaluation of the complex exchange coupling situation will be attempted and described elsewhere.

Electrochemical studies in acetonitrile revealed five sequential redox waves (cyclic voltammetry; $E^{1/2}$/(V)(ΔE_pmV) 0.61(220), 0.92(100), 1.13(140), 1.33(130), 1.53(110) at 100 mV s^{-1} (Fig. 3)). The $Zn(ClO_4)_2$ complex of 2POAP exhibits no significant waves in the range 0–1.6 V in acetonitrile. Coulometry (acetonitrile at 0.8 V) indicates that the first wave corresponds to a four-electron oxidation process, while the following four waves correspond to a further four-electron oxidation process in total (potential set at 1.65 V). Appropriate reduction sequences showed that eight electrons were required for complete reduction. The first wave reasonably corresponds to the oxidation of four equivalent Mn(II) centers to Mn(III), and is tentatively assigned to Mn(1), Mn(3), Mn(7) and Mn(9), which are equivalent and well separated. The sequence of four following waves is assigned to four other Mn(II) centers, which appear to be in communication, such that the oxidation potentials to Mn(III) become progressively more positive. These are assigned to Mn(2), Mn(6), Mn(4) and Mn(8), which are linked though Mn(5), and clearly all antiferromagnetically coupled to it. The visible spectrum of an oxidized acetonitrile solution of **1** shows the appearance of an intense band at 985 nm during the first four-electron oxidation process, followed by a further intensity increase after the full eight electron oxidation is complete. This band is reasonably assigned to an intervalence process.

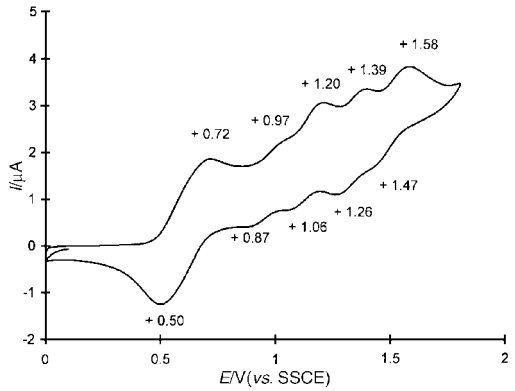

Fig. 3 Cyclic voltammetry for $[Mn_9(2POAP - 2H)_6](ClO_4)_6 \cdot 18H_2O$ **1** in acetonitrile (0.5 mM, 0.1 M NEt_4ClO_4; Pt working electrode, Pt counter electrode, SSCE reference electrode; BAS CV27 voltammograph; 100 mV s^{-1}).

The aggregation of nine octahedral manganese(II) centers (fifty four coordination positions) into an alkoxo-bridged, portcullis-like 3 × 3 grid by six heptadentate 2POAP ligands (fifty four donor positions) is a unique example of a self assembly process in which the coordination algorithm of the nine metal assembly is exactly matched by the aligned arrangement of the two sets of 'parallel' ligands arranged above and below the metal grid pseudo-plane. This strategy has general application, and $Cu(II)_9$ analogues have been prepared.[5] A simple extension of this type of ligand with additional five-membered chelate ring compartments can be envisaged to produce 4 × 4 and 5 × 5 grids, and even higher homologues. Efforts are currently underway to achieve this goal.

This research work was supported by NSERC (Natural Sciences and Engineering Research Council of Canada) and EPSRC.

Notes and references

‡ 2POAP was synthesized in 85% yield by the reaction of 2,6-pyridinedihydrazide with the methyl ester of iminopicolinic acid. 2POAP (0.403 g, 1.00 mmol) was added to a hot solution of $[Mn(H_2O)_6](ClO_4)_2$ (1.45 g, 4.00 mmol) in water (5 mL). MeCN (15 mL) was then added and the mixture left at room temperature. Red crystals (72% yield) formed after several days. Found (vacuum dried sample): C, 35.77; H, 2.63; N, 19.61. Calc. for $Mn_9(C_{19}H_{15}N_9O_2)_6\ (ClO_4)_6 \cdot 18H_2O$ **1**: C, 35.81; H, 3.29; N, 19.78%. IR (Nujol mull, cm^{-1}): νNH/H_2O 3450, 3339, 3247 ; νCO/CN 1689, 1654; νClO_4 1095. UV–VIS. (Nujol mull): 546 nm (sh); (MeCN) 1027 nm (ε 19.6 $dm^3\ mol^{-1}\ cm^{-1}$). μ_{RT} = 16.9 μ_B (mol^{-1}).

§ *Crystal data* for $[Mn_9(2POAP - 2H)_6](ClO_4)_6 \cdot 3.57MeCN \cdot 11H_2O$: $C_{121.14}H_{122.71}N_{57.57}O_{47}Cl_6Mn_9$ **1**; M = 3844.3, monoclinic, space group $C2/c$, a = 26.0641(16), b = 26.0910(16), c = 53.291(3) Å, β = 102.473(1)°, U = 35385(4) $Å^3$, Z = 8, D_c = 1.443 g cm^{-3}, T = 150(2) K, μ(Mo-Kα) = 0.800 mm^{-1}. 2075 parameters were refined with 17267 unique reflections ($I > 2.0\sigma(I)$) to give $R1$ = 0.1419, $wR2$ = 0.3936 (30409 independent reflections, R_{int} = 0.0668) (Bruker Smart three-circle diffractometer with a CCD area detector set at 6 cm, graphite-monochromatized Mo-Kα X-radiation). Only the non-hydrogen atoms of the cation and the chlorine atoms of the anions were refined anisotropically. Hydrogen atoms were fixed at idealized positions (U 1.2 × U (riding atom)), except for the amino groups, and the eleven identified waters of crystallization, where they were not included. The structure also contains three fully occupied acetonitrile molecules of crystallization and one partially occupied molecule refined to an occupancy of 0.57. The perchlorate anions are very disordered and the oxygen atoms were modeled isotropically, each with its own free variable, giving a total of 6.9 perchlorates in the final cycle of least-squares. Attempts to use a SUMP command to constrain the total perchlorate occupancy to six resulted in unstable refinements. The cation is however clearly defined, despite difficulties with the structural refinement and identification of all lattice fragments. A preliminary structure on $[Mn_9(2POAPZ - 2H)_6](NO_3)_6 \cdot xH_2O$ shows that it has the same structure (2POAPZ is the terminal pyrazine equivalent of 2POAP).[5]

CCDC 182/1521. See http://www.rsc.org/suppdata/cc/a9/a909180g/ for crystallographic files in .cif format.

¶ SQUID magnetometer (Quantum Design MPMS5S) with a field of 1000 Oe. Diamagnetic corrections for the sample holder and the sample were applied.

1 M.-T. Youinou, N. Rahmouni, J. Fischer and J. A. Osborn, *Angew. Chem., Int. Ed. Engl.*, 1992, **31**, 733.
2 G. S. Hannan, D. Volkmer, U. S. Schubert, J.-M. Lehn, G. Baum and D. Fenske, *Angew. Chem., Int. Ed. Engl.*, 1997, **36**, 1842.
3 P. N. W. Baxter, J.-M. Lehn, J. Fischer and M.-T. Youinou, *Angew. Chem., Int. Ed. Engl.*, 1994, **33**, 2284.
4 O. Waldmann, J. Hassmann, P. Müller, G. S. Hannan, D. Volkmer, U. S. Schubert and J.-M. Lehn, *Phys. Rev. Lett.*, 1997, **78**, 3390.
5 L. K. Thompson, C. J. Matthews, L. Zhao, D. O. Miller and S. R. Parsons, unpublished work.
6 C. J. Matthews, K. Avery, Z. Xu, L. K. Thompson, L. Zhao, D. O. Miller, K. Biradha, K. Poirier, M. J. Zaworotko, C. Wilson, A. E Goeta and J. A. K. Howard, *Inorg. Chem.*, 1999, **38**, 5266.
7 C. J. Matthews, Z. Xu, S. K. Mandal, L. K. Thompson, K. Biradha, K. Poirier and M. J. Zaworotko, *Chem. Commun.*, 1999, 347.

Communication a909180g

Molecular recognition on giant vesicles: coating of phytyl phosphate vesicles with a polysaccharide bearing phytyl chains†

Sangita Ghosh,[a] Stephen J. Lee,[a] Kensuke Ito,[b] Kazunari Akiyoshi,[b] Junzo Sunamoto,[b] Yoichi Nakatani*[a] and Guy Ourisson[a]

[a] *Centre de Neurochimie, Laboratoire de Chimie Organique des Substances Naturelles, associé au CNRS, Université Louis Pasteur, 5 rue Blaise Pascal, Strasbourg, France 67084. E-mail: nakatani@chimie.u-strasbg.fr*
[b] *Department of Synthetic Chemistry and Biological Chemistry, Graduate School of Engineering, Kyoto University, Yoshida-Hommachi, Sakyo-Ku, Kyoto, Japan 606-01*

Received (in Cambridge, UK) 5th November 1999, Accepted 6th January 2000

The molecular recognition between phytyl phosphate giant vesicles and a polysaccharide (pullulan) bearing phytyl or cholesteryl groups and a fluorescent tag was investigated; the pullulan bearing phytyl chains did coat the surface of the vesicles, in contrast with the pullulan bearing cholesteryl groups.

We have postulated that polyprenyl phosphates possibly formed the most primitive vesicles.[1] We have also suggested plausible processes for 'primitive' vesicles becoming more complex 'proto-cells'.[2,3] We have now studied whether giant vesicles (5 μm or more)[4] made from single-chain polyprenyl phosphates[5] could be coated by a polysaccharide (pullulan, MW ~55000 Da) bearing hydrophobic polyprenyl chains (Fig. 1). This would lead to an assembly somewhat reminiscent of the cell wall of microorganisms. To the polysaccharide was also covalently attached a fluorescent tag, to make it possible to clearly observe coated vesicles with optical fluorescence microscopy. We have recently reported that POPC (1-palmitoyl-2-oleoyl-*sn*-glycero-3-phosphocholine) vesicles can indeed be coated with pullulan, to which had been linked cholesteryl groups (FITC-CHP, 1.17

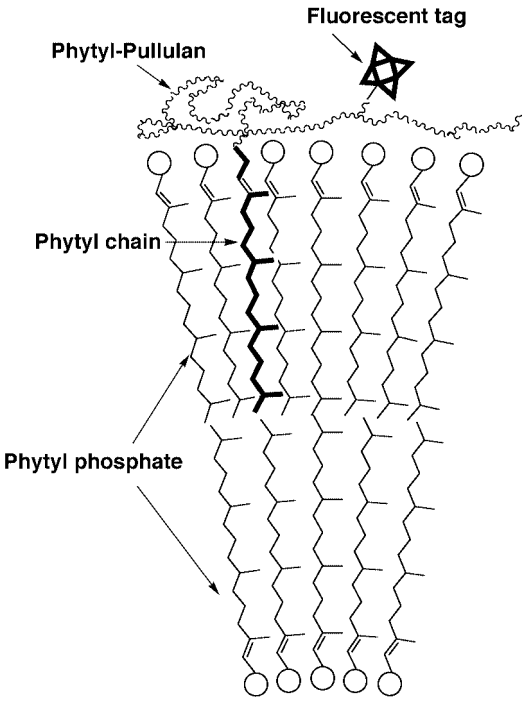

Fig. 1 Schematic representation of the coating of phytyl phosphate giant vesicles by phytyl-pullulan carrying fluorescent tags.

† Synthetic and spectroscopic data are available as supplementary data from the RSC web site, see http://www.rsc.org/suppdata/cc/a9/a908827j/

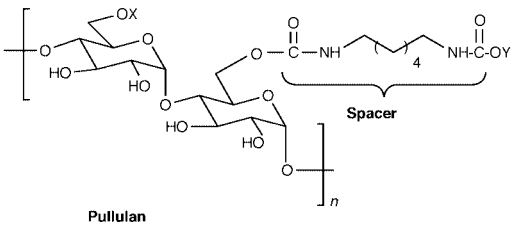

Pullulan

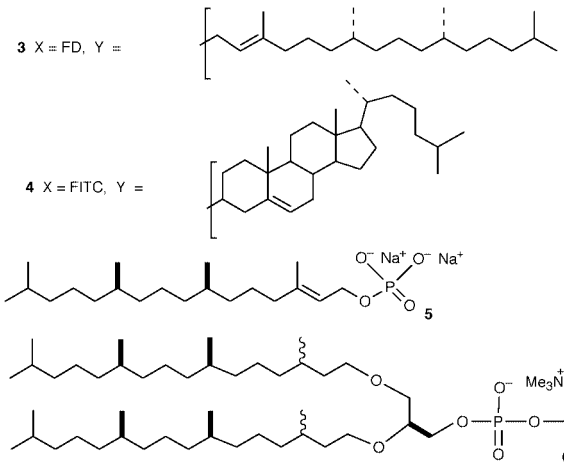

cholesteryl groups per 100 monosaccharide units) **4** (Scheme 1).[6] The cholesteryl groups of this 'cholesteryl-pullulan' insert themselves spontaneously into the membrane, in agreement with the fact that cholesterol itself is a widespread reinforcer of eucaryotic membranes, thereby spreading and anchoring the polysaccharide on the outer surface of the vesicles.

We first attempt to coat giant vesicles of phytyl phosphate **5** or of 2,3-diphytanyl-*sn*-glycero-1-phosphocholine (DPhPC) **6**, an archæal membrane constituent,[7] with 'cholesteryl-pullulan' **4**. This was unsuccessful, and cholesterol did *not* insert into either the monopolyprenyl phosphate or the dipolyprenyl phosphatidylcholine membranes. This was somewhat surprising, as cholesterol and phytol have similar amphiphilicity and overall shape. The non-incorporation of cholesteryl moiety does not depend on the nature of the head-group and must depend on the texture of the lipid part of the membrane. Indeed, Yamauchi *et al.*[8,9] have shown, by leakage studies, that diphytanyl phosphatidylcholine **6** membranes are relatively more rigid than those made of *n*-acyl lipids, which they explained by the lateral interdigitation of the phytanyl chains, which could also exclude the cholesteryl groups.

We then synthesized a novel pullulan derivative, replacing the cholesteryl moiety of (FITC-CHP) **4** by a phytyl chain (FD-

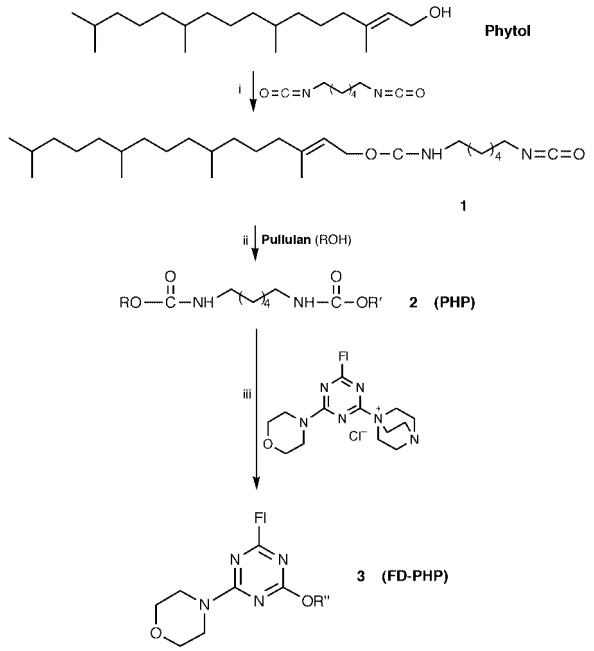

Scheme 1 *Reagents and conditions*: i, toluene–pyridine, 60 °C, 4 days, 100%; ii, DMSO–pyridine, 75 °C, 3 days, 55%; iii, rt, 24 h, 45%. ROH = pullulan, R′ = phytyl, R″ = hydrophobized pullulan (PHP), Fl = fluorescamine unit.

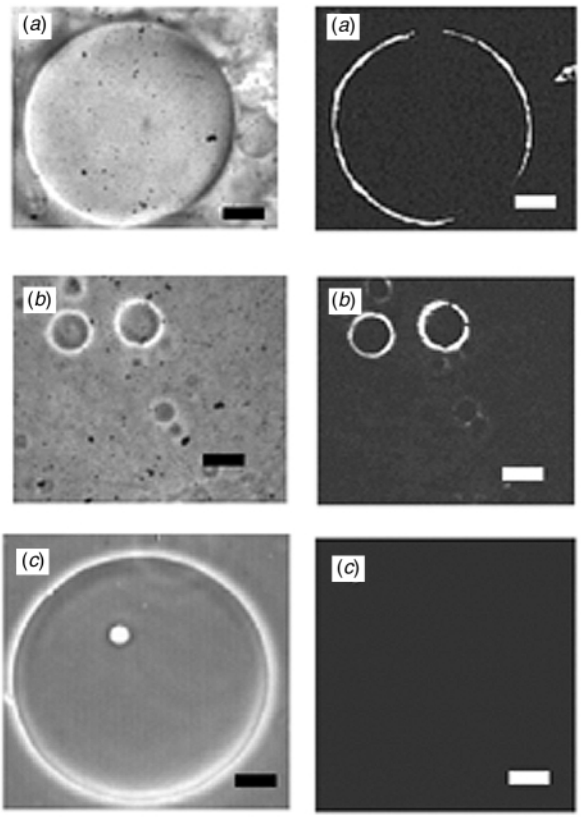

Fig. 2 Phase contrast image (left) and the corresponding fluorescent microscopic image (right) of coating (or not) of the surface of the preformed giant vesicles: (*a*) coating of phytyl phosphate vesicles by phytyl-pullulan (FD-PHP) **3**; (*b*) coating of diphytanyl phosphatidylcholine vesicles by phytyl-pullulan (FD-PHP) **3**; (*c*) absence of coating of phytyl phosphate vesicles by cholesteryl-pullulan (FITC-CHP) **4**. Bar: 10 μm.

PHP) **3**; this should of course be compatible with bilayers of phytyl phosphate **5** and permit the coating process. The synthetic route to obtain the fluorescent 'phytyl-pullulan' (FD-PHP) **3** is shown in Scheme 1. The phytyl moiety was linked to pullulan through an α,ω-dicarbamoylhexyl spacer, affording quantitatively a half-carbamate **1**, which was condensed with pullulan to produce the 'phytyl-pullulan' (PHP) **2** (55%). Finally, PHP was coupled to a morpholinyltriazine labelled with fluorescamine, followed by purification on a Sepharose gel, to yield a pure 'phytyl-pullulan' labelled with fluorescamine **3** FD-PHP (45%); content of phytyl groups: 2.9 per 100 glucose units; fluorescamine: 0.8 per 1 PHP molecule).‡

In contrast to the experiments with 'cholesteryl-pullulan', the entire outer surface of giant vesicles composed of phytyl phosphate **5** or DPhPC **6** could easily be coated with 'phytyl-pullulan' **3** (Fig. 2). Control experiments carried out with 'FITC-pullulan' (pullulan bearing the fluorescent tag but no hydrophobic moiety) confirmed that the coating of vesicles required the hydrophobic chains. Confocal microscopy showed that FD-PHP **3** spreads only on the surface of vesicles (not shown).

These results indicate that the criteria for efficient insertion of a lipophilic anchor into a bilayer are more stringent than we had initially expected; a near identical structure of the bilayer phospholipids and of the anchoring chains is required, or else the fit must be as closely adapted as is the case for cholesterol and *n*-acyl lipids.[10]

The recognition of a 'phytyl-pullulan' by a membrane of phytyl phosphate **5** or of diphytanyl phosphatidylcholine **6** is an interesting example of solubility guided by close structural similarity.

This work was supported in part by JST-ULP 'Supramolecules' Joint Research Project and by COST. We are grateful for support granted by the Ministry of National Education, France for a fellowship to S. J. Lee, CNRS to S. Ghosh. We express our gratitude to Dr S. Chasserot-Golaz, Strasbourg, for her help in obtaining the confocal microscopy images.

Notes and references

‡ Optical, fluorescence and confocal microscopies were carried out according to the procedures described in refs. 11–14. To coat the surface, it is sufficient to use oligosaccharide carrying 3% only of the stoichiometric amount of lipophilic chains.

1 G. Ourisson and Y. Nakatani, *Chem. Biol.*, 1994, **1**, 11.
2 G. Ourisson and Y. Nakatani, *C. R. Acad. Sci.*, 1996, **322**, 323.
3 G. Ourisson and Y. Nakatani, *Tetrahedron*, 1999, **55**, 3183.
4 P. L. Luisi, in *Giant Vesicles*, ed. P. L. Luisi and P. Walde, Wiley, Sussex, 1999, pp. 3–10.
5 G. Pozzi, V. Birault, B. Werner, O. Dannenmuller, Y. Nakatani, G. Ourisson and S. Terakawa, *Angew. Chem., Int. Ed. Engl.*, 1996, **35**, 177.
6 T. Ueda, S. J. Lee, Y. Nakatani, G. Ourisson and J. Sunamoto, *Chem. Lett.*, 1998, 417.
7 M. De Rosa and A. Gambacorta, *Prog. Lipid Res.*, 1998, **27**, 153.
8 K. Yamauchi, K. Doi, M. Kinoshita, F. Kii and H. Fukuda, *Biochim. Biophys. Acta.*, 1992, **1110**, 171.
9 K. Yamauchi, K. Doi, Y. Yoshida and M. Kinoshita, *Biochim. Biophys. Acta*, 1993, **1146**, 178.
10 K. Bloch, *C. R. C. Crit. Rev. Biochem.*, 1983, **14**, 47.
11 F. M. Menger and S. J. Lee, *Langmuir*, 1995, **11**, 3685.
12 S. Chasserot-Golaz, N. Vitale, I. Sagot, B. Delouche, S. Dirrig, L. A. Pradel, J. P. Henry, D. Aunis and M. F. Bader, *J. Cell Biol.*, 1996, **133**, 1217.
13 F. M. Menger, S. J. Lee and J. S. Keiper, *Langmuir*, 1996, **12**, 4479.
14 O. Dannenmuller, K. Arakawa, T. Eguchi, K. Kakinuma, S. Blanc, A.-M. Albrecht, M. Schmutz, Y. Nakatani and G. Ourisson, in *Giant Vesicles*, ed. P. L. Luisi and P. Walde, Wiley, Sussex, 1999, pp. 385–390.

Communication a908827j

ChemComm

Synthesis of new hybrid macromolecules with cyclo-dendritic architecture

Ivan Gitsov*[ab] and Pavlina T. Ivanova[a]

[a] *Department of Chemistry and Chemical Biology & Cornell Center for Materials Research, Cornell University, Ithaca, NY 14853, USA. E-mail: igivanov@mailbox.syr.edu*

[b] *Department of Chemistry, College of Environmental Science and Forestry, State University of New York, Syracuse, NY 13210, USA*

Received (in Corvallis, OR, USA) 28th September 1999, Accepted 22nd November 1999

Novel cyclo-dendritic hybrid macromolecules were synthesized using preformed blocks: hydroxymethyl crown ethers and poly(benzyl ether) monodendrons.

The highly symmetrical three-dimensional shape of dendrimers and their fractal construction make them excellent and unique biological models.[1] It is already known that the dendritic shell can provide specific and selective microenvironments greatly affecting host–guest interactions.[2,3] The combination of dendrimers and other macromolecular topologies as building blocks is an attractive and promising approach in the development of suitable biological replicas for the study of molecular recognition and other cell processes.[4,5]

Compounds containing both crown ethers and dendritic wedges might have interesting ligating properties.[6] The first example of this type was published by Percec and co-workers in 1993.[7] DCC-mediated transesterification was used to produce molecules containing a crown ether moiety and taper-shaped fragments that could also be regarded as first-generation monodendrons. In subsequent papers the same authors reported the intriguing self-assembling properties of these compounds that were able to form unique cylindrical supramolecular structures upon interaction with metal salts.[8] However, the investigation was limited only to a single type of crown ether (15-crown-5) and first-generation monodendrons with flat geometry. The influence of the size and shape of the reactive fragments and the reaction conditions on the formation of the cyclo-dendritic hybrids has not been explored.

Here we report the synthesis of a new series of hybrid compounds **1**–**9** (Scheme 1) containing crown ethers of different sizes and three generations of poly(benzyl ether) dendrimers with different geometry. These compounds can bind alkali and alkaline-earth metal ions *via* their crown ether cavities and complex other guest molecules through the voids and the peripheral shell in the dendritic part of the molecule. In distinction to previous reports, the Williamson reaction was used to create an ether bond between the dendrons and 2-hydroxymethyl crown ethers.

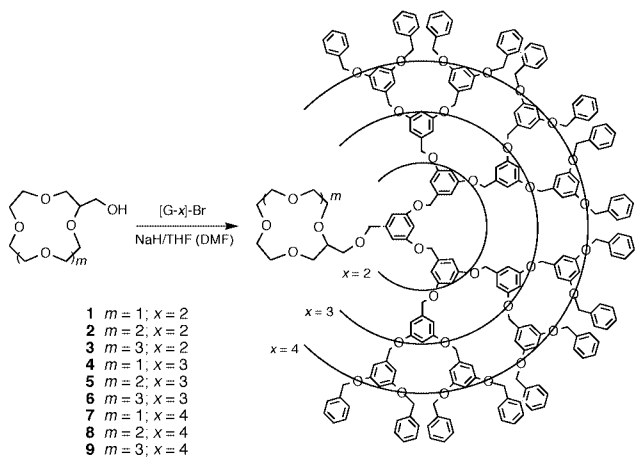

Scheme 1

The synthetic strategy for the formation of the dendritic crowns involves a reaction between two preformed fragments. Previously we have shown that this approach is a versatile tool for the generation of different types of dendrimer-containing hybrid macromolecules.[9] Because of the proven accessibility of the functional group at the 'focal' point of the dendrimer[10] it could be applied also in the present study. Earlier we found that linear aliphatic polyethers used as one of the building blocks in the formation of dendritic hybrids have a noticeable auto-acceleration effect on the Williamson reaction employed for their formation.[10] Therefore one of the additional goals in the present investigation is to trace the eventual influence of the size of the cyclic polyether on the speed and the efficiency of the synthetic procedure. The dendritic bromides were synthesized by a known method[11] and the 2-hydroxymethyl crown ethers (from Aldrich) were used without further purification.

Initially we explored the synthetic pathway based on typical phase-transfer reaction conditions that was successfully applied in the synthesis of the poly(benzyl ether) dendrimers.[10] The reaction, performed in refluxing acetone with K_2CO_3 and 18-crown-6 as catalyst, afforded a complex mixture, which did not contain the desired product. Stronger bases like dry THF/NaH or DMF/NaH systems proved to be more efficient. In a typical reaction procedure NaH (4 mmol) was added as a powder to a solution of 0.1 mmol of 2-hydroxymethyl-crown ether and 0.105 mmol of dendritic bromide in 10 ml dry THF. The reaction mixture was stirred under nitrogen at room temperature for 140 h. The progress of the reaction was monitored by TLC (CH_2Cl_2–Et_2O = 9:1). After no further change was observed the reaction was stopped and THF was evaporated under reduced pressure. The crude reaction product was purified by flash chromatography using gradient elution with a mixture of CH_2Cl_2–Et_2O for products containing the 12-crown-4 fragment (from 98:2 to 75:25 v/v) or CH_2Cl_2–acetone for larger cycles. When DMF was employed as the solvent at the end of the reaction the solution was precipitated into cold water and the crude filtered product was subsequently chromatographed.

The compounds composed of a second-generation dendritic bromide and all three 2-hydroxymethyl crown ethers are heavy oils; those of the higher generations are white foamy glassy solids. All reaction products were purified by flash chromatography and their purity was determined by TLC (single spot) on silica gel plates with fluorescent indicator and SEC at 40 °C in THF (single peak with double UV and RI detection). Their structure was confirmed by ^{1}H NMR spectroscopy.† All compounds yielded satisfactory elemental analyses and all exhibited very good correlation with the calculated molecular masses as evidenced by their MALDI-TOF spectra.

A summary of the reagents, reaction conditions and yields of the products is presented in Table 1. It can be seen that the Williamson synthesis performed in THF with NaH produced the desired products after long period of time in moderate yields. DMF (due to its higher polarity) facilitates the reaction and

Table 1 Influence of the reaction conditions and reagents' size on the yields of the cyclo-dendritic macromolecule[a]

Compound	Dendritic bromide	Crown ether	Yield (%) (purified)	*t*/h
1	[G-2]-Br	2-OH-12-crown-4	34.1	140
2	[G-2]-Br	2-OH-15-crown-5	29.2 (38.3)[b]	120 (24)[b]
3	[G-2]-Br	2-OH-18-crown-6	30.7 (37.1)[b]	96 (36)[b]
4	[G-3]-Br	2-OH-12-crown-4	20.2	140
5	[G-3]-Br	2-OH-15-crown-5	28.5 (45.4)[b]	120 (10)[b]
6	[G-3]-Br	2-OH-18-crown-6	24.1 (47.0)[b]	140 (24)[b]
7	[G-4]-Br	2-OH-12-crown-4	16.2 (17.0)[b]	140 (24)[b]
8	[G-4]-Br	2-OH-15-crown-5	21.5 (22.0)[b]	140 (24)[b]
9	[G-4]-Br	2-OH-18-crown-6	40.5 (39.8)[b]	140 (24)[b]

[a] Reaction conditions: dry THF, NaH, 5% excess of dendritic bromide. [b] Reactions performed in DMF at 70 °C.

improves the yields over reduced reaction times. An increase in reaction temperature to 70 °C and higher did not influence the reaction rate and the yields. To our surprise the ring size of the crown ethers did not effect substantially their nucleophilicity and all three of them have similar reactivity in the reaction with dendritic bromides. One would have expected 2-hydroxy-15-crown-5 to react faster and more effectively because of its additional complex binding towards Na^+, and this is partially true for the lower generations, but not with the fourth-generation dendritic bromide. The results from this study are not very conclusive in terms of dendritic activity. The change from a flat, two-dimensional geometry (second generation) to a globular shape (fourth generation) effects slightly the reactivity of the dendritic wedges. Despite the shielding effect of the large dendritic fragments, the focal point functionalities are still readily accessible for nucleophilic attack even in the fourth generation and this reconfirms our previous findings for the reactivity of dendrimers in Williamson reactions[10] and as macroinitiators for anionic ring-opening polymerization.[12]

The physical properties, self-assembling and binding capabilities of the new cyclo-dendritic hybrids are currently under investigation.

The authors would like to thank Rohm & Haas Co. and the Loctite Corporation for financial support. The analyses were performed in the Polymer Characterization Facility of the Cornell Center for Materials Research supported by the NSF (Award DMR-9632275).

Notes and references

† *Selected data* for **1**: $\delta_H(CDCl_3$, 200 MHz) 3.2–3.8 (7H, br), 4.45 (2H, s), 4.8–5.2 (12H, m), 6.5–6.8 (9H, d), 7.0–7.7 (20H, m); *m/z* (MALDI-TOF) 958.0 ($M^+ + Na^+$). For **2**: $\delta_H(CDCl_3$, 200 MHz) 3.3–3.9 (21H, br), 4.5 (2H, s), 4.8–5.2 (12H, m), 6.4–6.8 (9H, d), 7.0–7.7 (20H, m); *m/z* (MALDI-TOF) 1000.7 ($M^+ + Na^+$). For **3**: $\delta_H(CDCl_3$, 200 MHz) 3.4–3.8 (25H, br), 4.5 (2H, s), 4.8–5.2 (12H, m), 6.5–6.8 (9H, d), 7.0–7.7 (20H, br); *m/z* (MALDI-TOF) 1043.9 ($M^+ + Na^+$). For **4**: $\delta_H(CDCl_3$, 200 MHz) 3.4–3.8 (17H, br), 4.5 (2H, s), 4.8–5.2 (28H, m), 6.5–6.8 (21H, d), 7.0–7.7 (40H, m); *m/z* (MALDI-TOF) 1805.1 ($M^+ + Na^+$). For **5**: $\delta_H(CDCl_3$, 200 MHz) 3.4–3.8 (21H, br), 4.5 (2H, s), 4.8–5.2 (28H, m), 6.5–6.8 (21H, d), 7.0–7.7 (40H, m); *m/z* (MALDI-TOF) 1853.5 ($M^+ + Na^+$). For **6**: $\delta_H(CDCl_3$, 200 MHz) 3.4–3.8 (25H, br), 4.5 (2H, s), 4.8–5.2 (28H, br), 6.5–6.8 (21H, d), 7.0–7.7 (40H, m); *m/z* (MALDI-TOF) 1894.0 ($M^+ + Na^+$). For **7**: $\delta_H(CDCl_3$, 200 MHz) 3.4–3.9 (17H, br), 4.45 (2H, s), 4.7–5.2 (60H, m), 6.4–6.8 (45H, d), 7.0–7.6 (80H, m), *m/z* (MALDI-TOF) 3523.5 ($M^+ + 2Na^+$). For **8**: $\delta_H(CDCl_3$, 200 MHz) 3.4–3.8 (21H, br), 4.45 (2H, s), 4.6–5.2 (60H, m), 6.4–6.8 (45H, d), 7.0–7.7 (80H, m); *m/z* (MALDI-TOF) 3545.4 ($M^+ + Na^+$). For **9**: $\delta_H(CDCl_3$, 200 MHz) 3.4–3.8 (25H, br), 4.5 (2H, s), 4.6–5.2 (60H, m), 6.4–6.8 (45H, d), 7.0–7.6 (80H, m); *m/z* (MALDI-TOF) 3589.8 ($M^+ + Na^+$).

1 Several excellent reviews on dendrimers have been published recently: M. Fischer and F. Vögtle, *Angew. Chem., Int. Ed.*, 1999, **38**, 884; J. Roovers and B. Comanita, *Adv. Polym. Sci.*, 1999, **142**, 179; A. W. Bosman, H. M. Janssen and E. W. Meijer, *Chem. Rev.*, 1999, **99**, 1665; V. V. Narayanan and G. R. Newkome, *Top. Curr. Chem.*, 1998, **197**, 19; D. K. Smith and F. Diederich, *Chem. Eur. J.*, 1998, **4**, 1353; O. A. Mathews, A. N. Shipway and J. F. Stoddart, *Prog. Polym. Sci.*, 1998, **23**, 1.
2 C. J. Hawker, K. L. Wooley and J. M. J. Fréchet, *J. Am. Chem. Soc.*, 1993, **115**, 4375.
3 K. W. Pollak, E. M. Sanford and J. M. J. Fréchet, *J. Mater. Chem.*, 1998, **8**, 519; N. Tomioka, D. Takasu, T. Takahashi and T. Aida, *Angew. Chem., Int. Ed.*, 1998, **37**, 1531; H. Liu, A. Jiang, J. Guo and K. E. Uhrich, *J. Polym. Sci.: Part A: Polym. Chem.*, 1999, **37**, 703.
4 H. Frey, *Angew. Chem., Int. Ed.*, 1998, **37**, 2193.
5 M. Brewis, G. J. Clarkson, A. M. Holder and N. B. McKewon, *Chem. Commun.*, 1998, 969; J. P. Collman, L. Fu, A. Zingg and F. Diederich, *Chem. Commun.*, 1997, 193 and references therein.
6 T. Nagasaki, M. Ukon, S. Arimori and S. Shinkai, *Chem. Commun.*, 1992, 608.
7 V. Percec, G. Johansson, J. Heck, G. Ungar and S. V. Batty, *J. Chem. Soc., Perkin Trans. 1*, 1993, 1414.
8 V. Percec, G. Johansson, J. Heck, D Tomazos and G. Ungar, *Macromol. Symp.*, 1994, **77**, 235 and references therein; V. Percec, G. Johansson, G. Ungar and J. Zhou, *J. Am. Chem. Soc.*, 1996, **118**, 9855.
9 J. M. J. Fréchet and I. Gitsov, *Macromol. Symp.*, 1995, **98**, 441.
10 I. Gitsov, K. L. Wooley, C. J. Hawker, P. T. Ivanova and J. M. J. Fréchet, *Macromolecules*, 1993, **26**, 5621.
11 C. J. Hawker and J. M. J. Fréchet, *J. Am. Chem. Soc.*, 1990, **112**, 7638.
12 I. Gitsov, P. T. Ivanova and J. M. J. Fréchet, *Macromol. Rapid Commun.*, 1994, **15**, 387.

Communication a907914i

ChemComm

Polymer immobilised TEMPO (PIPO): an efficient catalyst for the chlorinated hydrocarbon solvent-free and bromide-free oxidation of alcohols with hypochlorite

Arné Dijksman, Isabel W. C. E. Arends and Roger A. Sheldon*

Laboratory for Organic Chemistry and Catalysis, Department of Biotechnology, Delft University of Technology, Julianalaan 136, 2628 BL Delft, The Netherlands. E-mail: secretariat-ock@stm.tudelft.nl

Received (in Cambridge, UK) 9th December 1999, Accepted 7th January 2000

PIPO, a readily prepared polymer immobilised TEMPO, can be employed as an efficient recyclable heterogeneous catalyst for the chlorinated hydrocarbon solvent-free and bromide-free bleach oxidation of a variety of alcohols and polyols.

The use of stable nitroxyl radicals, such as TEMPO, as catalysts for the oxidation of alcohols to aldehydes, ketones and carboxylic acids is well documented.[1] Typically, these transformations employ 1 mol% of the nitroxyl radical and a stoichiometric amount of a terminal oxidant, *e.g.* sodium hypochlorite,[2] MCPBA (*m*-chloroperbenzoicacid),[3] sodium bromite,[4] trichloroisocyanuric acid[5] and oxygen in combination with CuCl[6] or $RuCl_2(PPh_3)_3$.[7] In particular, the TEMPO-bleach protocol using bromide as co-catalyst introduced by Anelli *et al.*[2] is finding wide application in organic synthesis. Although only a small amount of catalyst is used, recyclability is an issue and several heterogeneous TEMPO systems have been reported.[8] For example, MCM-41[8g] and silica-supported TEMPO[8h,i] have been applied in oxidation reactions using hypochlorite as the oxidant. The preparation of these catalysts involves initial functionalisation of the support followed by covalent attachment of a 4-substituted TEMPO.

Here, we report the use of a readily prepared polymer immobilised TEMPO as a catalyst for alcohol oxidations. It was derived from a commercially available oligomeric, sterically hindered amine, poly[[6-[(1,1,3,3-tetramethylbutyl)amino]-1,3,5-triazine-2,4-diyl][2,2,6,6-tetramethyl-4-piperidinyl)-imino]-1,6-hexanediyl[(2,2,6,6-tetramethyl-4-piperidinyl-imino]], better known as Chimassorb 944 (MW ≈ 3000; see Scheme 1 for structure). This compound is used as an antioxidant and a light stabiliser for plastics. It contributes significantly to the long term heat stability of polyolefins and has broad approval for use in polyolefin food packaging.[9]

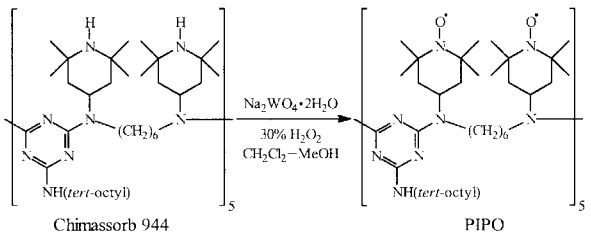

Scheme 1 Synthesis of PIPO.

Nitroxyl radicals are normally prepared by treating the analogous secondary amine with $Na_2WO_4 \cdot 2H_2O$ and hydrogen peroxide.[10] In the case of Chimassorb 944, the same procedure was applied resulting in the formation of an oligomeric TEMPO (Scheme 1). Probe-MS data revealed that the mass of each segment increased by 30 owing to transformation of two secondary amine moieties into the corresponding nitroxyl radicals. This new polymer immobilised TEMPO, further referred to as PIPO (polyamine immobilised piperidinyl oxyl), proved to be an effective catalyst for oxidations of alcohols with hypochlorite using the Anelli protocol.[2]†

Primary and secondary aliphatic and benzylic alcohols were smoothly converted to the corresponding aldehydes and ketones in CH_2Cl_2 (Table 1). Under these conditions the system was homogeneous as PIPO is soluble in dichloromethane. In contrast, in the absence of solvent (entry 3) PIPO was an active heterogeneous catalyst. The heterogeneous nature of the catalyst was confirmed in a filtration experiment, in which the reaction mixture was filtered after 10 min. The filtrate showed no activity at all during 1 h after filtration. The residue, however, could be reused at least twice as a catalyst. The minor loss of activity (< 5%) observed is probably due to mechanical losses occurring during filtration of the small amount of catalyst.

Table 1 PIPO-catalysed oxidation of alcohols with bromide/hypochlorite[a]

Entry	Substrate	Product	*t*/min	Conv.(%)[b]	Sel.(%)[b]
1	Octan-1-ol	Octanal	20	> 99	> 99
2	Octan-2-ol	Octan-2-one	20	> 99	> 99
3[c]			45	95	> 99
4	Benzyl alcohol	Benzaldehyde	20	> 99	> 99
5	1-Phenylethanol	Acetophenone	20	> 99	> 99

[a] 0.8 mmol substrate, 2.5 mg PIPO (1 mol% nitroxyl), 2 ml CH_2Cl_2, 0.16 ml 0.5 M KBr solution (10 mol%), 0.14 g $KHCO_3$, 2.86 ml 0.35 M hypochlorite solution (1.25 equiv.), 0 °C. [b] Conversion and selectivity determined by GC using *n*-hexadecane as internal standard. [c] No CH_2Cl_2 (solvent-free).

Further investigation revealed that the use of bromide was not necessary. Thus, in contrast to the conventional TEMPO-bleach oxidations, which use dichloromethane as solvent and bromide as a co-catalyst,[2] PIPO catalyses the oxidation of a variety of alcohols in the absence of organic solvent and using only a hypochlorite solution (0.35 M, pH 9.1) as the oxidant (Table 2). However, under these conditions primary aliphatic alcohols such as octan-1-ol, gave low selectivities to aldehydes owing to over-oxidation of octanal to octanoic acid (entry 1). This problem was circumvented by using MTBE as the organic solvent, in which PIPO is not soluble, affording an increase in selectivity to 94% (entry 2). Here again, filtration experiments confirmed that this system was heterogeneous, analogous to the solvent-free conditions.

In addition to primary and secondary aliphatic alcohols (entries 2–7), benzylic alcohols were also efficiently oxidised (entries 9 and 10), complete conversion being observed within 30 min. In competition experiments, the catalyst showed a marked preference for primary alcohols (entries 8 and 11). This is analogous to the already reported homogeneous[2] and heterogeneous[8h] TEMPO systems. Chirality on the α-position is not affected during oxidation as shown by the selective oxidation of (*S*)-2-methylbutan-1-ol to (*S*)-2-methylbutanal (entry 12).[11]

Table 2 PIPO-catalysed oxidation of alcohols with hypochlorite[a]

Entry	Substrate	Product	*t*/min	Conv. (%)[b]	Sel. (%)[b]
1	Octan-1-ol	Octanal	45	90	50[d]
2[c]	Octan-1-ol	Octanal	45	80	94
3[c]	Hexan-1-ol	Hexanal	45	89	95
4	Octan-2-ol	Octan-2-one	45	99	> 99
5	Hexan-2-ol	Hexan-2-one	45	99	> 99
6	Octan-3-ol	Octan-3-one	45	70	> 99
7	Cyclooctanol	Cyclooctanone	45	100	> 99
8[c]	Octan-1-ol/ octan-2-ol	Octanal/ octan-2-one	45	86/ < 1	96
9	Benzyl alcohol	Benzaldehyde	30	100	> 99
10	1-Phenylethanol	Acetophenone	30	100	> 99
11	Benzyl alcohol/ 1-Phenylethanol	Benzaldehyde/ acetophenone	30	95/4	> 99
12	(*S*)-2-Methyl-butan-1-ol	(*S*)-2-Methyl-butanal	45	90	> 99

[a] 0.8 mmol substrate, 2.5 mg PIPO (1 mol% nitroxyl), 0.14 g $KHCO_3$, 2.86 ml 0.35 M hypochlorite solution (1.25 equiv.), 0 °C. [b] Conversion and selectivity determined by GC using *n*-hexadecane as internal standard. [c] 2 ml MTBE as solvent. [d] Octanoic acid and octyl octanoate as side products.

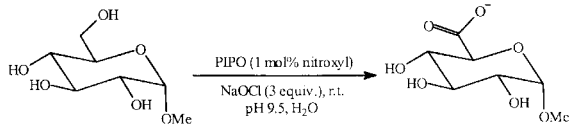

Scheme 2 Oxidation of methyl α-D-glucopyranoside using PIPO/NaOCl.

Carbohydrates are also oxidised by the PIPO/NaOCl system analogous to TEMPO/NaOCl.[12] For example, methyl α-D-glucopyranoside afforded methyl α-D-glucopyranosiduronate in 70% yield (Scheme 2).‡ As in the case of the oxidation of simple alcohols, filtration experiments confirmed that the catalyst is truly heterogeneous. Further investigation in the field of carbohydrate oxidations using PIPO/NaOCl is in progress and will be reported on in due course.

Besides hypochlorite, oxygen can also be used as oxidant.[6,7] Unfortunately, in contrast to homogeneous TEMPO the combination of PIPO and $RuCl_2(PPh_3)_3$ in chlorobenzene[7] is not able to catalyse the aerobic oxidation of octan-2-ol, probably owing to coordination of ruthenium to the polyamine. On the other hand, in combination with $CuCl/O_2$ in DMF,[6] it is capable of completely oxidising benzyl alcohol to benzaldehyde within 2 h. This system, however, is limited to benzylic and allylic alcohols as for homogeneous TEMPO.

In summary we have developed a recyclable heterogeneous catalyst for the bleach oxidation of alcohols and polyols. In contrast to previously reported systems, neither a chlorinated hydrocarbon solvent nor a bromide is necessary to achieve good activity. A further advantage of our system is that the catalyst is readily prepared from inexpensive and commercially available raw materials. We believe that it will find wide application in organic synthesis.

We gratefully acknowledge IOP (Innovation-Oriented Research Program) for financial support.

Notes and references

† *General procedure* for the oxidation of alcohols with PIPO as catalyst: in a glass reaction vessel was placed 2.5 mg of PIPO (8 μmol based on complete functionalisation; degree of functionalisation = 3.2 mmol g^{-1}). Then a CH_2Cl_2 solution (2 ml) of the alcohol (0.4 M) and *n*-hexadecane (0.12 M; as internal standard) was added followed by an aqueous solution (0.16 ml) of KBr (0.5 M). After the cooling of the reaction mixture to 0 °C, 2.86 ml of aqueous NaOCl (0.35 M and buffered by the addition of 0.14 g $KHCO_3$ to pH 9.1) was added. Then, the reaction mixture was vigorously shaken for 45 min. After destroying the excess of hypochlorite with Na_2SO_3, the reaction mixture was extracted with diethyl ether, dried over Na_2SO_4 and analysed on GC (Chrompack CP-WAX 52 CB column; 50 m × 0.53 mm).

‡ *Procedure* for the oxidation of methyl α-D-glucopyranoside with PIPO as catalyst: in a glass reaction vessel was placed 15.7 mg of PIPO (50 μmol based on complete functionalisation; degree of functionalisation = 3.2 mmol g^{-1}) and 200 mg methyl α-D-glucopyranoside (1.03 mmol). Then, 8 ml of aqueous NaOCl (0.56 M and brought to pH 9.5 with an aqueous 1 M hydrochloride solution) was added. During the reaction the pH was kept constant at 9.5 by automatic titration with a 0.1 M KOH solution. When the hydroxide consumption stopped (1.3 equiv. of hydroxide were consumed), Na_2SO_3 was added to destroy the excess of hypochlorite. The crude mixture was analysed using HPLC.

1 A. E. J. de Nooy, A. C. Besemer and H. van Bekkum, *Synthesis*, 1996, 1153 and references therein; J. M. Bobbitt and M. C. L. Flores, *Heterocycles*, 1988, **106**, 509.
2 P. L. Anelli, C. Biffi, F. Montanari and S. Quici, *J. Org. Chem.*, 1987, **52**, 2559.
3 J. A. Cella, J. A. Kelley and E. F. Kenehan, *J. Org. Chem.*, 1975, **40**, 1860; S. D. Rychovsky and R. Vaidyanathan, *J. Org. Chem.*, 1999, **64**, 310.
4 T. Inokuchi, S. Matsumoto, T. Nishiyama and S. Torii, *J. Org. Chem.*, 1990, **55**, 462.
5 C.-J. Jenny, B. Lohri and M. Schlageter, *Eur. Pat.*, 0775684A1, 1997.
6 M. F. Semmelhack, C. R. Schmid, D. A. Cortés and S. Chou, *J. Am. Chem. Soc.*, 1984, **106**, 3374.
7 A. Dijksman, I. W. C. E. Arends and R. A. Sheldon, *Chem. Commun.*, 1999, 1591.
8 (*a*) T. Osa, U. Akaba, I. Segawa and J. M. Bobbitt, *Chem. Lett.*, 1988, 1423; (*b*) Y. Kashiwagi, H. Ono and T. Osa, *Chem. Lett.*, 1993, 257; (*c*) T. Osa, Y. Kashiwagi and Y. Yanagisawa, *Chem. Lett.*, 1994, 367; (*d*) F. MacCorquodale, J. A. Crayston, J. C. Walton and J. Worsfold, *Tetrahedron Lett.*, 1990, **31**, 771; (*e*) T. Osa, Y. Kashiwagi, J. M. Bobbitt and Z. Ma, in *Electroorganic Synthesis*, Marcel Dekker Inc., New York, 1991, p. 343; (*f*) D. Brunel, P. Lentz, P. Sutra, B. Deroide, F. Fajula and J. B. Nagy, *Stud. Surf. Sci. Catal.*, 1999, **125**, 237; (*g*) M. J. Verhoef, J. A. Peters and H. van Bekkum, *Stud. Surf. Sci. Catal.*, 1999, **125**, 465; (*h*) A. Heeres, H. A. van Doren, K. F. Gotlieb and I. P. Bleeker, *Carbohydr. Res.*, 1997, **299**, 221; (*i*) C. Bolm and T. Fey, *Chem. Commun.*, 1999, 1795.
9 See: http://www.pidc.org.tw/enst/e-11.htm
10 E. G. Rozantsev and V. D. Sholle, *Synthesis*, 1971, 190.
11 For bleach oxidation of (*S*)-2-methylbutan-1-ol with homogeneous TEMPO, see: P. L. Anelli, F. Montanari and S. Quici, *Org. Synth.*, 1990, **69**, 212.
12 A. E. J. de Nooy, A. C. Besemer and H. van Bekkum, *Tetrahedron*, 1995, **51**, 8023; A. E. J. de Nooy, A. C. Besemer and H. van Bekkum, *Carbohydr. Res.*, 1995, **269**, 89; N. J. Davis and S. L. Flitsch, *Tetrahedron Lett.*, 1993, **34**, 1181.

Communication a909690f

A selective uranium extraction agent prepared by polymer imprinting†

Gregory D. Saunders,[a] Simon P. Foxon,[a] Paul H. Walton,*[a] Malcolm J. Joyce[b] and Simon N. Port[b]

[a] *Department of Chemistry, University of York, Heslington, York, UK YO10 5DD. E-mail: phw2@york.ac.uk*
[b] *BNFL Research and Technology, Salwick, Preston, Lancashire, UK PR4 0XJ*

Received (in Cambridge, UK) 24th September 1999, Accepted 7th January 2000

Using a modified method in the preparation of an imprinted polymer, we report here the synthesis of a uranyl-imprinted copolymer of chloroacrylic acid and ethylene glycol dimethacrylate, which—after removal of the template—selectively extracts uranium from dilute aqueous solution over a range of +2, +3 and +4 competitor metal ions.

The technique of polymer imprinting has shown considerable promise as a method for preparing materials which are capable of molecular recognition.[1] Of late, the technique has seen some impressive successes in the selective absorption of both organic molecules and metal ions.[2] One important goal is the preparation of absorbents specific for uranium, because of uranium's large environmental impact and importance as an energy resource. Recent progress has been made by Murray *et al*. who showed that a uranyl-imprinted polydivinylbenzene/styrene-based polymer absorbs uranium over a range of +1 and +2 metal ions and also La^{3+} (at pH > 3).[3] We report here the preparation and characterisation of a new selective uranium-binding polymer. Importantly the polymer shows excellent selectivity against a range of 'strong' competitor metal ions, including Th^{4+} and Fe^{3+} (at pH < 3).

In our studies we have used the uranyl complex of chloroacrylic acid (caaH) as a template [Scheme 1(a)]. ^{13}C NMR in CD_2Cl_2 studies of $UO_2(caa)_2(OH_2)_2$ suggest that this complex contains a uranyl ion coordinated by two bidentate chloroacrylate ligands and two water molecules.‡ We have been unable to crystallise this complex, but we have studied the analogous $UO_2(caa)_2(O{=}PPh_3)_2$ complex by single crystal X-ray diffraction (Fig. 1).§ The structure of this complex shows both bidentate and monodentate chloroacrylate ligands along with two triphenylphosphine oxide ligands coordinating to the uranyl ion.

Co-polymers of 2-chloroacrylic acid (caaH) and the cross-linking agent ethylene glycol dimethacrylate (egdma) can be prepared by free-radical solution polymerisation, thermally initiated with azoisobutyronitrile (aibn) in refluxing dichloromethane. Imprinting with uranyl is achieved by replacing caaH with the soluble template complex $UO_2(caa)_2(OH_2)_2$ [prepared *in situ* by reaction of caaH with NEt_3 and $UO_2(NO_3)_2{\cdot}6H_2O$ prior to polymerisation]. In the solution polymerisation reaction the ratio of reactants was 91/9 mol/mol% egdma/$UO_2(caa)_2(OH_2)_2$—typically a total of 3.5 g reactants in 100 cm^3 of CH_2Cl_2. The imprinted polymer was obtained as a pale yellow precipitate after 5 h [Scheme 1(a) and (b)]. The material was washed with CH_2Cl_2 and then dried *in vacuo* prior to grinding to a fine powder (particle diameter *ca.* 50 μm). As a comparison, a 'random polymer' was prepared in an analogous manner without the addition of NEt_3 and $UO_2(NO_3)_2{\cdot}6H_2O$. We denote this as a 'random polymer' since the orientations and relative positions of the α-chloropropionic acid (cpaH) groups in the polymer are presumed to be random.

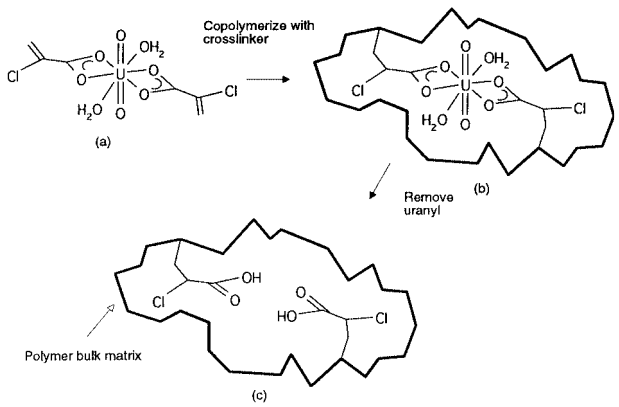

Scheme 1 Schematic reaction scheme for the preparation of uranyl-imprinted polymer.

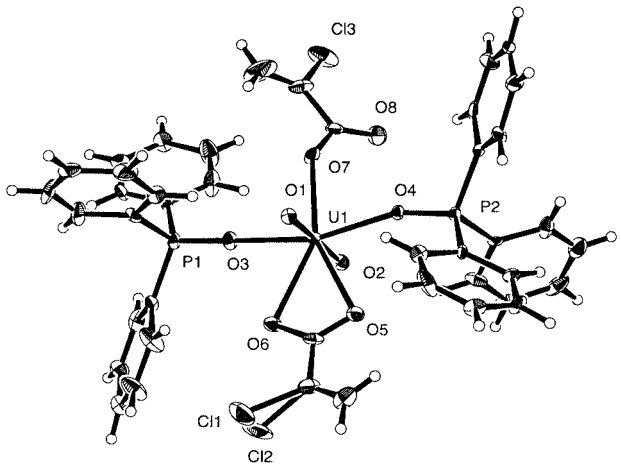

Fig. 1 ORTEP representation of the $[UO_2(caa)_2(O{=}PPh_3)_2]$ structure. Cl1 and Cl2 represent a single Cl atom disordered over two positions. Selected distances (Å): U1–O1 1.772(8), U1–O2 1.776(9), U1–O5 2.496(8), U1–O6 2.499(8), U1–O7 2.309(8), U1–O3 2.361(8), U1–O4 2.320(7).

Extraction of the uranyl from the imprinted polymer was achieved by treatment of the polymer with conc. HNO_3 under ultrasonication (30 kHz) for 15 min [Scheme 1(c)]. Following extraction, thorough washing of the polymer with deionised water and then drying *in vacuo* gave the imprinted polymer as a white powder. Elemental analysis of the polymer for uranium confirmed >95% extraction of the uranium from the polymer. Treatment of the random polymer with conc. HNO_3 in a 30 kHz sonic bath for 15 min did not change the percentage content of cpaH (determined by elemental analysis for chlorine), showing that the cpaH is tightly bound—probably *via* a covalent bond—to the polymer.

To investigate the effectiveness of the imprinting technique, rebinding of uranyl by the imprinted polymer was determined in the pH range 1–3. Approximately 2.60 g of polymer was stirred with a dilute aqueous solution of $UO_2(NO_3)_2{\cdot}6H_2O$ (50 cm^3, 0.5 mmol dm^{-3}) such that there was a fifty-fold mole excess of polymer-bound cpaH compared to uranyl. The pH was recorded after 4 min, after which the uranyl binding had equilibrated,¶ and the concentration of the uranyl ion in a small sample of the supernatant was determined by visible spectrophotometry using

† S. N. Port, M. J. Joyce, P. H. Walton and G. D. Saunders, *UK Pat. Appl.*, 979946.7, 1997; *Int. Pat.*, WO 99/15707, 1998.

the Arsenazo I method.[4] The pH was changed by the addition of small quantities of dilute HNO_3 or NaOH solutions and the extraction analysis procedure repeated.

The uranyl-binding behaviour of the imprinted and random polymers shows a reversible (*i.e.* the polymer can be reused) and smooth transition between low (*ca.* 10%) and high (> 98%) uranyl binding between pH 1.0 and 3.0. A plot of $\log_{10}[D_{ex}]$ *vs.* pH for the two polymers is shown in Fig. 2.‖ The near linearity of the data in the plots shows that the 'pH swing' binding model[5] is an accurate representation of this system. The gradient of the plots can be equated to *n*, the average stoichiometry of the $[UO_2(cpa)_n]$ complexes formed within the polymer, which, in turn, can be related to the fraction of imprinted binding sites (those containing two cpaH ligands) compared to non-imprinted binding sites (those with a single cpaH). In the random polymer *n* is approximately 1.1, showing that *ca.* 10% of the binding sites contain two cpaH ligands able to interact with a single uranyl ion. In contrast, for the imprinted polymer *n* increases to nearly 1.8 showing that *ca.* 80% of the uranyl binding sites contain two cpaH ligands. This increase can be attributed to the imprinting effect of the uranyl in the polymerisation process. The pH dependence of Th^{4+} binding to the polymer was also investigated, giving $n = 0.5$; a strong indication that most binding of Th^{4+} is associated with non-imprinted sites.

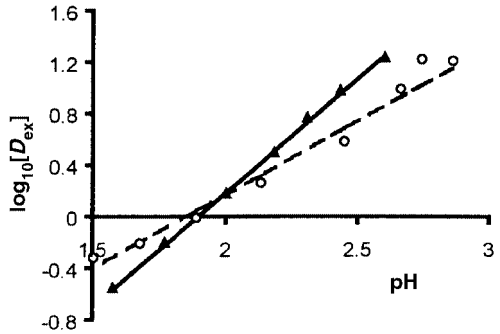

Fig. 2 $\text{Log}_{10}[D_{ex}]$ plots for the binding of uranyl by polymers as a function of pH. Black triangles, full line: imprinted polymer [gradient *n* - 1.77(3), R^2 = 1.00]. Circles, dashed line: random polymer [gradient $n = 1.14(7)$, R^2 = 0.97].

The selectivity of the imprinted polymer for uranyl was investigated by rebinding uranyl in the presence of various competitor metal ions. In a typical experiment 25 mg of polymer was mixed with a dilute aqueous solution of $UO_2(NO_3)_2$ (0.42 mmol dm^{-3}, 10 cm^3, 2.5 mmol dm^{-3} NO_3^- made up with KNO_3, constant pH 2.5) containing an equal concentration of one other competitor metal salt: hydrated salts of $Cu(NO_3)_2$, $VO(SO_4)$, $Al(NO_3)_3$, $Fe(NO_3)_3$ or $Th(NO_3)_4$. These competitor ions were chosen as the potentially strongest competitor ions for the uranyl binding sites. The resulting suspensions were shaken periodically over a period of 12 h before filtration. UO_2^{2+} and competitor metal concentrations in the supernatant were then determined by ICP-AES.

Table 1 lists the selectivity ratios ($S_{U/M}$) of uranyl *vs.* competitor metal binding to both random and imprinted polymers. It is clear that the random polymer exhibits no selectivity for the binding of the uranyl ion ($S < 1$), binding less uranyl than competitor ion in every case except Cu^{2+}. In contrast, the imprinted polymer displays a remarkable increase and even *reversal* of selectivity over the random polymer, increasing the relative polymer selectivity for uranium by over ten times in one case. The imprinted polymer exhibits a consistently higher binding of uranyl compared to each of the competitor ions, even against competitor ions such as Fe^{3+} and Th^{4+}, which would be expected to compete very strongly with UO_2^{2+} for the carboxylate binding sites. The results of the binding experiments show that the difference in metal binding between the random and imprinted polymers is due to the imprinting effect.

Table 1 Selectivity ratios for uranyl binding *vs.* competitor ion binding for random and imprinted polymers (23 °C, pH 2.5). U = uranyl, M = competitor ion. $S_{U/M} = S_U/S_M$. $S_M = V(C_i - C_f)/(C_f m)$ where C_i = concentration of solution before extraction, C_f = concentration of solution after extraction, $S' = (S_{U/M}$ imprinted$)/(S_{U/M}$ random), V = volume of solution, m = mass of polymer

	Selectivity ratios for U binding *vs.* competitor binding		
Competitor metal	Random polymer $S_{U/M}$ (random)	Imprinted polymer $S_{U/M}$ (imprinted)	Selectivity ratio increase S'
Cu^{2+}	6.5	8.1	1.2
V^{4+} (as VO^{2+})	0.32	3.8	11
Al^{3+}	0.29	2.5	8.6
Fe^{3+}	0.17	1.4	8.1
Th^{4+}	0.76	2.0	2.7

G. D. S. acknowledges BNFL and the University of York for funding. We thank Drs Rajiv Bhalla and David White for experimental assistance.

Notes and references

‡ $[UO_2(caa)_2(OH_2)_2]$ $^{13}C\{H\}$ NMR (270 MHz, CD_2Cl_2); δ 125.7 (s, CH_2), 136 [s, $C(Cl)=CH_2$], 176.4 (s, COO).

§ *Crystal data* for $C_{42}H_{34}O_8Cl_2P_2U_1$; monoclinic, space group $P2_1$ (no. 4), yellow block, a = 14.927(3), b = 8.8708(12), c = 15.795(3) Å, β = 97.735(15)°, V = 2072.4(6) $Å^3$, 150 K, Z = 2, $R1$ = 0.034, $wR2$ = 0.087, GOF = 1.007. CCDC 182/1518. See http://www.rsc.org/suppdata/cc/a9/a909691d/ for crystallographic files in .cif format.

¶ In separate experiments the maximum capacity of the polymer for uranyl was determined by measuring the extent of uranyl uptake by the imprinted polymer as a function of [uranyl]. (Contact time between polymer and solution was *ca.* 12 h.) The data were then fitted to a Langmuir isotherm, with excellent agreement. Further experiments showed that uranyl binding by the imprinted polymer was > 95% of maximum binding after 4 min, with no subsequent significant increase.

‖ D_{ex}, the distribution coefficient of extraction, defined for a given volume of solution, given nitrate concentration and given mass of polymer as: (mol of uranyl ion bound to the polymer)/(mol of uranyl ion left in solution) for eqn. (1).

$$m NO_3^- + UO_2^{2+} + \text{polymer}\cdot n H^+ = \text{polymer}\cdot UO_2^{2+}\cdot m NO_3^- + n H^+ \quad (1)$$

Separate experiments showed that 100% egdma polymers do not bind uranium to any significant extent; demonstrating that the amount of uranyl binding to non-carboxylic acid sites (*i.e.* $n = 0$) is low. It is also assumed that the number of sites where three carboxylic acids can interact with a single uranyl is statistically very low. Hence the average value of *n* obtained from our experiments is approximately the number weighted average of the $n = 1$ and $n = 2$ binding sites within the polymer. For non-integral values of *n* a slight curve is expected in the $\log[D_{ex}]$ *vs.* pH plots. However, this curve is very shallow over the pH range studied and the relationship can be considered as linear. For a treatment of D_{ex} and the calculation of complex stoichiometries and applications to solid phase absorbents, see ref. 5.

1 G. Wulff, *Angew. Chem., Int. Ed. Engl.*, 1995, **34**, 1812; M. Kempe and K. Mosbach, *J. Chromatogr. A*, 1995, **694**, 3; J. Steinke, D. C. Sherrington and I. R. Dunkin, *Adv. Polym. Sci.*, 1995, **123**, 81.

2 H. Chen, M. M. Olmstead, R. L. Albright, J. Devenyi and R. H. Fish, *Angew. Chem., Int. Ed. Engl.*, 1997, **36**, 642; Y. Kiode, H. Senba, H. Shosenji, M. Meada and M. Takagi, *Bull. Chem. Soc. Jpn.*, 1996, **69**, 125; K. Inoue, Y. Baba and K. Yoshizuka, *Bull. Chem. Soc. Jpn.*, 1993, **66**, 2915; M. Chanda and G. L. Rempel, *React. Polym.*, 1992, **16**, 149; W. Kuchen and J. Schram, *Angew. Chem., Int. Ed. Engl.*, 1988, **27**, 1695; R. Garcia, C. Pinel, C. Madic and M. Lemaire, *Tetrahedron Lett.*, 1998, **39**, 8651.

3 G. M. Murray and O. M. Uy, *Report to Environmental Management Science Program, Project ID Number 59977*, June 1998; Z. Xiangfei, A. Bzhelyansky, S. Y. Bae, A. L. Jenkins and G. M. Murray, *ACS Symp. Ser. 703*, Washington DC, p. 218.

4 J. S. Fritz and M. Johnson-Richard, *Anal. Chim. Acta*, 1959, **20**, 164.

5 H. Bernhard and F. Grass, *Monatsh. Chem.*, 1967, **98**, 1464; Y. Fujii, H. Maie, S. Kumagai and T. Sugai, *Chem. Lett.*, 1992, 995.

Communication a909691d

ChemComm

Hydrogen bonding networks and anion coordination in (η^6-arene)$Cr(CO)_3$ complexes: metal carbonyls as hydrogen bond acceptors

Salvatore Camiolo, Simon J. Coles, Philip A. Gale,* Michael B. Hursthouse, Thomas A. Mayer and Michael A. Paver*

Department of Chemistry, University of Southampton, Highfield, Southampton, UK SO17 1BJ. E-mail: philip.gale@soton.ac.uk or m.a.paver@soton.ac.uk

Received (in Cambridge, UK) 15th December 1999, Accepted 12th January 2000

A chloride selective amide cleft molecule 2 containing two $Cr(CO)_3$ moieties has been synthesised by condensation of (η^6-aniline)$Cr(CO)_3$ 3 with isophthaloyl dichloride; the X-ray crystal structure of 2 contains a network of Cr–CO···HN hydrogen bonds giving rise to an extended three-dimensional coordination array; the X-ray crystal structure of (η^6-aniline)$Cr(CO)_3$ 3 has been re-determined and found to contain bifurcated amine NH···OC–Cr hydrogen bonds.

The coordination chemistry of anionic[1–3] and neutral guest species[4] by hydrogen bond donating receptors is an area of supramolecular chemistry that continues to attract the attention of coordination chemists. One strategy that has been used to modulate the affinity or selectivity of a receptor for a particular guest is to alter the electronic environment of the guest-binding site. This may be achieved by synthesising a new receptor containing electron withdrawing or donating functional groups[5] or, alternatively, by coordinating transition metal fragments to a pre-existing receptor. This latter approach has been elegantly employed by Atwood *et al.* to transform calixarenes into anion-binding receptors.[6]

Receptors that contain hydrogen bond donating amide[7,8] or pyrrole[9] moieties have been shown to be effective and selective anion binding agents. Recently, Crabtree and coworkers have shown that simple amide cleft receptors based on compound **1**[10] are capable of binding halide anions.[11,12] As part of our programme of research in anion coordination,[13,14] we decided to synthesise an amide cleft receptor containing two electron withdrawing $Cr(CO)_3$ units that would serve to increase the acidity of the NH protons. However, we found that in addition to binding anions, hydrogen bonds were formed in the solid state between amide NH and chromium carbonyl moieties, leading to the formation of a three-dimensional coordination array.[15,16]

Compound **2** was synthesised by condensation of (η^6-aniline)$Cr(CO)_3$[17] **3** with isophthaloyl dichloride in dichloromethane in the presence of triethylamine and DMAP. The reaction mixture was purified by column chromatography on silica gel and crystallised from CH_2Cl_2–MeOH as yellow needles in 74% yield.

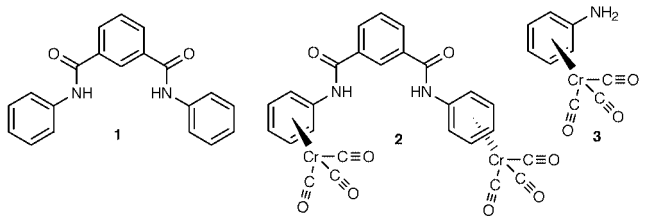

Crystals of **2** suitable for X-ray analysis† were obtained from CD_3CN solution. The crystal structure and atomic numbering scheme is shown in Fig. 1(a). The centrosymmetric nature of the space group causes the two (η^6-aniline)$Cr(CO)_3$ moieties to adopt orientations at 180° to each other on opposite sides of the molecule, fully enabling these groups to interact with other molecules. The presence of carbonyl and amide groups provide additional hydrogen bond donors and acceptors, facilitating the formation of a supramolecular assembly.[18] Each molecule of **2** donates six hydrogen bonds. These include an intramolecular interaction between H(5) and O(4) (2.22(3) Å), two intermolecular interactions between H(3) and O(4) and H(3′) and O(4′) (2.54(4) Å), and three intermolecular hydrogen bonds to metal carbonyl groups (H(1)··O(2) 2.47(2)Å and H(12) to two O(2) atoms in different adjacent molecules (2.50(3) Å)). This network of hydrogen bonds defines a continuous three-dimensional coordination array, a portion of which is shown in Fig. 1(b).

In light of the formation of this assembly, we decided to re-examine the solid state structure of (η^6-aniline)$Cr(CO)_3$ **3**. The

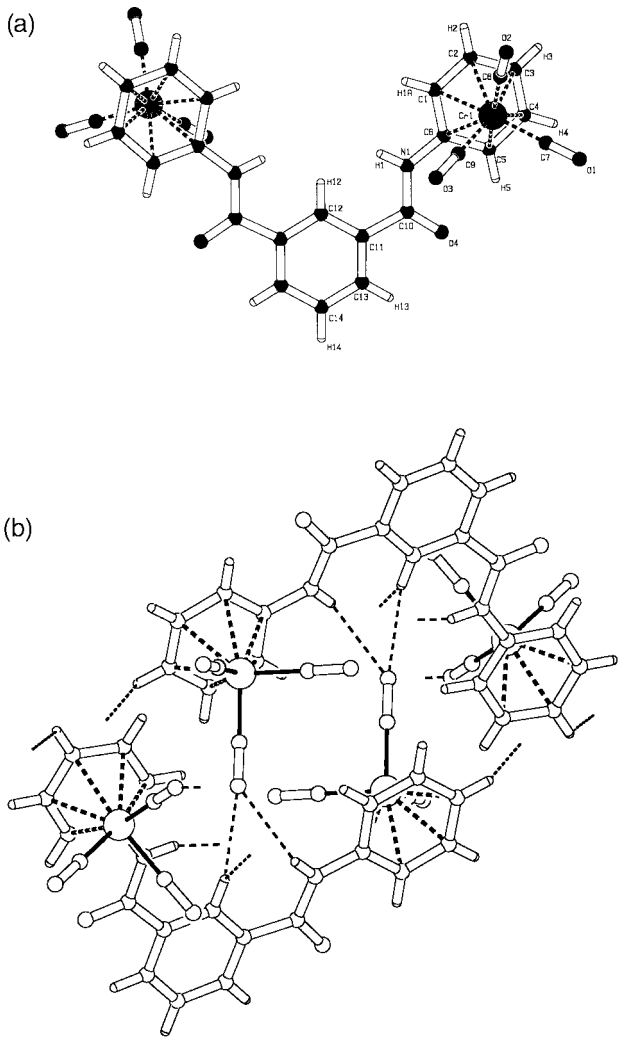

Fig. 1 (a) Crystal structure and atomic numbering scheme for **2** and (b) hydrogen bonding network.

structure of compound **3** was first solved in 1992 by Hunter, Zaworotko and co-workers.[19] In this case, compound **3** crystallised in a monoclinic lattice and contained no hydrogen bonding interactions. We found that if crystallisation occurs under different conditions (*i.e.* at room temperature from dichloromethane) from those used by Hunter *et al.*, a triclinic polymorph, with the same molecular geometry, reproducibly forms a hydrogen bonded network. These hydrogen bonds link molecules together into two-dimensional sheets (shown in Fig. 2). Two bifurcated hydrogen bonds are formed by one NH group to two OC–Cr moieties (H··O 2.55(6) and 2.32(7) Å) and a further hydrogen bond is formed from the other NH hydrogen to a OC–Cr moiety (H··O 2.50(6) Å) (Fig. 2). Each molecule therefore donates and accepts three hydrogen bonds.

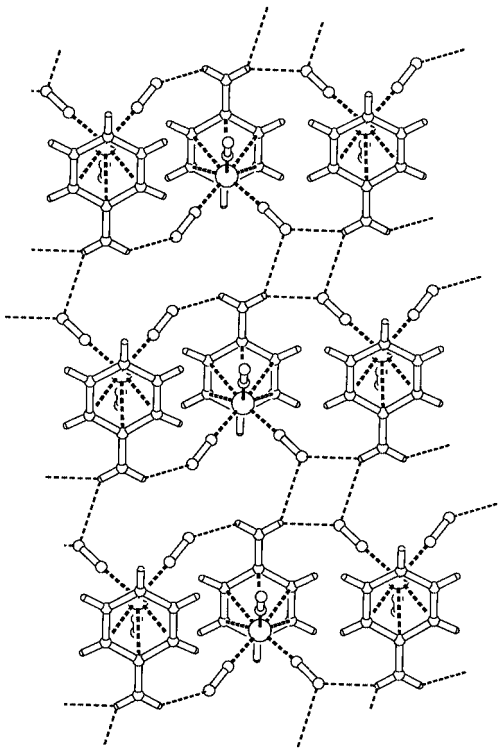

Fig. 2 Crystal structure of **3** emphasizing the hydrogen bonding network.

The anion coordination properties of **2** were studied using ^{1}H NMR titration techniques in CD_3CN by following the NH proton resonance. Stability constants were then calculated using the EQNMR computer program[20] and are presented in Table 1. Receptor **2** shows selectivity for chloride over the other putative anionic guests studied, with a stability constant that is higher than can be reliably measured by this technique (log K > 4). Interestingly the selectivity of **2** for chloride over dihydrogen phosphate is high. This may be due to the steric bulk of the $Cr(CO)_3$ moieties hindering the approach of the bulky dihydrogenphosphate anion to the amide cleft. A negative electrospray competititon experiment was run on an acetonitrile solution of **2** containing one equivalent of each of the anions shown in Table 1. Only peaks corresponding to the chloride complex were observed, confirming the chloride selectivity of **2**.

Table 1 Stability constants of compound **2** with a variety of anionic guests in CD_3CN at 298 K. Errors are estimated to be < 16%. All data fitted satisfactorily to a 1 : 1 receptor : anion binding model

Anion	Stability constant/ dm^3 mol^{-1}
F^{-a}	107
Cl^-	> 10^4
Br^-	2910
I^-	102
$H_2PO_4^{-a}$	119

[a] ArH proton used (broadening of the NH proton occurs during the titration).

The coordination of metal carbonyls by activated hydrogen bond donating ligands may lead to new strategies for the modification of the activity of carbonyl containing catalysts.[21] The presence of the hydrogen bonding networks in **2** and **3** leads us to suggest that the $Cr(CO)_3$ fragment in particular, may find future applications in the design of coordination polymers and extended networks in crystals as well as in the activation of NH groups for more effective or selective anion coordination.

P. A. G. thanks the Royal Society for a University Fellowship and the EPSRC for a project studentship (to S. C.).

Notes and references

† *Crystal data*: for $C_{26}H_{16}Cr_2N_2O_8$ **2**, M_r = 588.41, monoclinic space group $C2/c$, a = 17.283(3), b = 11.337(2), c = 14.586(3) Å, β = 125.16(3)°, U = 2333.6(8) Å^3, Z = 4, μ = 0.989 mm^{-1}, crystal size 0.15 × 0.025 × 0.025 mm, T = 150 K; refinement of 2621 unique reflections ($2\theta \leqslant 27.47°$, R_{int} = 0.0552) against 173 parameters gave R_1 = 0.0418 and wR_2 = 0.1100 [$I > 2\sigma(I)$] (R_1 = 0.0664 and wR_2 = 0.1265 for all data). For $C_9H_7CrNO_3$ **3**, M_r = 229.16, triclinic space group $P\bar{1}$, a = 7.0198(10), b = 7.3940(11), c = 9.4002(12) Å, α = 86.069(7), β = 86.591(8), γ = 69.457(7)°, U = 455.49(11) Å^3, Z = 2, μ = 1.232 mm^{-1}, crystal size 0.15 × 0.05 × 0.025 mm, T = 150 K; refinement of 1193 unique reflections ($2\theta \leqslant 22.48°$, R_{int} = 0.0912) against 127 parameters gave R_1 = 0.0774 and wR_2 = 0.1996 [$I > 2\sigma(I)$] (R_1 = 0.0934 and wR_2 = 0.2079 for all data).

Data were collected on a Nonius KappaCCD area detector diffractometer, at the window of a Nonius FR591 rotating anode (λ(Mo-Kα) = 0.71073 Å). Corrections were applied to account for absorption effects by means of comparing multiple and equivalent reflections. Solutions were obtained *via* direct methods and refined by full-matrix least squares on F_0^2, with hydrogens included in idealised positions and refined using the riding model. CCDC 182/1522. See http://www.rsc.org/suppdata/cc/a9/a909861e/ for crystallographic files in .cif format.

1 P. A. Gale, *Coord. Chem. Rev.*, 2000, in press.
2 M. M. G. Antonisse and D. N. Reinhoudt, *Chem. Commun.*, 1998, 443.
3 P. D. Beer, *Chem. Commun.*, 1996, 689.
4 W. E. Allen, P. A. Gale, C. T. Brown, V. M. Lynch and J. L. Sessler, *J. Am. Chem. Soc.*, 1996, **118**, 12 471.
5 P. A. Gale, J. L. Sessler, W. E. Allen, N. A. Tvermoes and V. Lynch, *Chem. Commun.*, 1997, 665.
6 J. L. Atwood, K. T. Holman and J. W. Steed, *Chem. Commun.*, 1996, 1401.
7 P. D. Beer, C. Hazlewood, D. Hesek, J. Hodacova and S. E. Stokes, *J. Chem. Soc., Dalton Trans.*, 1993, 1327; P. D. Beer, C. A. P. Dickson, N. Fletcher, A. J. Goulden, A. Grieve, J. Hodacova and T. Wear, *J. Chem. Soc., Chem. Commun.*, 1993, 828.
8 S. Valiyaveettil, J. F. J. Engbersen, W. Verboom and D. N. Reinhoudt, *Angew. Chem., Int. Ed. Engl.*, 1993, **32**, 900.
9 P. A. Gale, J. L. Sessler and V. Král, *Chem. Commun.*, 1998, 1.
10 Y. P. Khanna, E. M. Pearce, B. D. Forman and D. A. Bini, *J. Polym. Sci. Polym. Chem. Ed.*, 1981, **19**, 2799.
11 K. Kavallieratos, S. R. de Gala, D. J. Austin and R. H. Crabtree, *J. Am. Chem. Soc.*, 1997, **119**, 2325.
12 K. Kavallieratos, C. M. Bertao and R. H. Crabtree, *J. Org. Chem.*, 1998, **64**, 1675.
13 H. Miyaji, P. Anzenbacher Jr, J. L. Sessler, E. R. Bleasdale and P. A. Gale, *Chem. Commun.*, 1999, 1723.
14 P. A. Gale, L. J. Twyman, C. I. Handlin and J. L. Sessler, *Chem. Commun.*, 1999, 1851.
15 A. J. Blake, N. R. Brooks, N. R. Champness, M. Crew, L. R. Hanton, P. Hubberstey, P. C. Simon and M. Schroder, *J. Chem. Soc., Dalton Trans.*, 1999, 2813.
16 C. Kaes, M. W. Hossieni, C. E. F. Rickard, B. W. Skelton and A. H. White, *Angew. Chem., Int. Ed.*, 1998, **37**, 920.
17 B. Nicholls and M. C. Whiting, *J. Chem. Soc.*, 1959, 551.
18 Hydrogen bonds to metal carbonyl moieties have been observed previously. For examples, see: C. P. Casey, A. J. Shusterman, N. W. Vollendorf and K. J. Haller, *J. Am. Chem. Soc.*, 1982, **104**, 2417; S. E. Kabir and E. Rosenberg, *Organometallics*, 1995, **14**, 721.
19 A. D. Hunter, L. Shilliday, W. S. Furey and M. J. Zaworotko, *Organometallics*, 1992, **11**, 1550.
20 M. J. Hynes, *J. Chem. Soc., Dalton Trans.*, 1993, 311.
21 For an example of the modification of the activity of a chloride containing catalyst by a hydrogen bond donating ligand, see: J. Scheele, P. Timmerman and D. N. Reinhoudt, *Chem. Commun.*, 1998, 2613.

Communication a909861e

ChemComm

Hydrogen bonds C–H···Cl as a structure-determining factor in the gold(I) complex bis(3-bromopyridine)gold(I) dichloroaurate(I)†

Matthias Freytag and Peter G. Jones*

Institut für Anorganische und Analytische Chemie der Technischen Universität, Postfach 3329, D-38023 Braunschweig, Germany. E-mail: p.jones@tu-bs.de

Received (in Basel, Switzerland) 13th September 1999, Accepted 13th January 2000

The crystal structure of the title compound involves three types of secondary interaction; hydrogen bonds of the form C–H···Cl account for the mutually perpendicular arrangement of the cations and anions.

We are interested in gold(I) complexes with amine ligands and have recently reported the synthesis and structure of such complexes with aliphatic amines[1] and with pyridines.[2] Our other current studies involve the investigation of intermolecular contacts such as hydrogen bonds (including non-classical cases such as C–H···X), aurophilic interactions,[3] and halogen–halogen contacts.[4] These fields naturally overlap, and we have established the importance of classical hydrogen bonds in gold(I) amine complexes,[1] and of C–H···Cl contacts in some gold(I) dppm complexes.[5]

Here, we present the structure of bis(3-bromopyridine)gold(I) dichloroaurate(I) **1**.‡ The compound was obtained from 3-bromopyridine and tetrahydrothiophene(chloro)gold(I).§ As will be seen below, the primary structure is unexceptional but the secondary interactions extensive and varied.

The structure analysis shows that compound **1** crystallizes in the ionic form $(L_2Au)^+(AuCl_2)^-$ (L = pyridine ligand); in principle, such complexes can also display the alternative molecular form LAuCl. The balance between the two forms is very sensitive, as can be seen from the fact that the 2-picoline derivative is molecular but the 3-picoline derivative ionic.[2] The non-substituted bis(pyridine)gold(I) dichloroaurate(I) also displays the ionic form.[6]

The asymmetric unit of **1** consists of one cation and one anion, each without imposed crystallographic symmetry. In both ions the geometry at the gold centre is, as expected, linear, with normal dimensions Au1–N 2.009(10), 2.035(10) Å, N–Au1–N 173.8(4)°, Au2–Cl 2.259(3), 2.267(3) Å, Cl–Au(2)–Cl 177.61(12)°. The bromo substituents, like the methyl substituents of the 3-picoline analogue (which displays strict inversion symmetry)[2] are *trans* to each other.

The extended structure of **1** involves three distinct kinds of secondary interaction: *aurophilic interactions*,[3] C–H···Cl *hydrogen bonds* and Br···Cl *interhalogen contacts*. It is well known that gold(I) centres have a marked tendency to aggregation. In **1**, short aurophilic contacts are observed both within the asymmetric unit [Au1···Au2 3.2681(7) Å], and *via* the inversion operator $1 - x, 1 - y, 1 - z$ [Au1···Au1# 3.3113(10) Å]. The ions are thereby connected to form 'isolated' (see below!) dimeric units containing a zigzag chain of four gold atoms (Fig. 2), similar to the complex bis(pyridine)gold(I) dichloroaurate(I).[6] In the 3-picoline complex, Au···Au contacts lead to infinite zigzag chains with alternating cations and anions.[2] In all three structures, the L–Au–L axes of cation and anion are approximately perpendicular to each other; a typical torsion angle in **1** is N1′–Au1–Au2–Cl2 −90.1(3°).

A more detailed inspection shows that the extended structure of **1** is not solely characterised by aurophilic contacts. Within the dimeric unit (Fig. 1) there are eight (four independent) C–H···Cl contacts (Table 1, first four entries), formed *via* the H atoms *ortho* to nitrogen. These may reasonably be considered as C–H···Cl hydrogen bonds,[7] since they are essentially linear, with H···Cl distances appreciably less than the sum of the van der Waals radii (2.95 Å); they are *charge-assisted*[8] by the opposite charges of anion and cation.. The corresponding H···Cl–Au angles lie in the range 72–85°. Although steric factors must also play a role, the formation of such hydrogen bonds provides a good explanation for the mutually perpendicular orientation of anions and cations. As far as we are aware, this is the first time that C–H···Cl interactions have been explicitly cited as conformation-determining factors in metal complexes.[9] The presence of a 2-methyl group in the 2-picoline derivative blocks one of the potential hydrogen bonding sites, which may be one reason why a non-ionic structure is preferred.[2] Inspection of the bis(pyridine)gold(I) dichloroaurate(I) structure[6] shows an exactly analogous framework to that of **1**. The 3-picoline derivative[2] exhibits two C–H···Cl contacts within

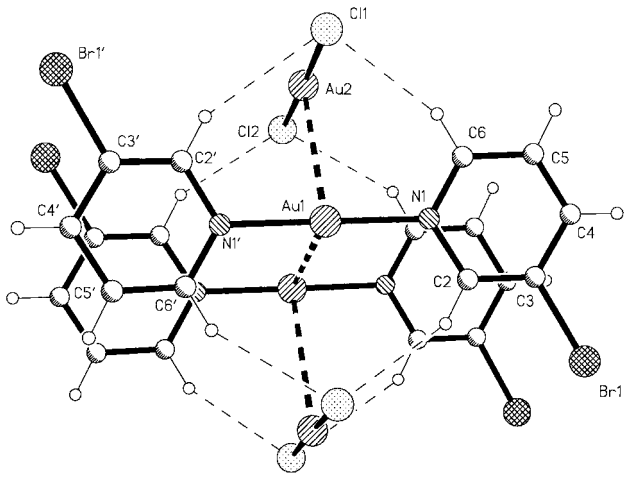

Fig. 1 Dimeric unit of **1** in the crystal. Radii are arbitrary. Only the asymmetric unit is numbered. Gold···gold contacts are represented by thick dashed lines, C–H···Cl contacts as thin dashed lines.

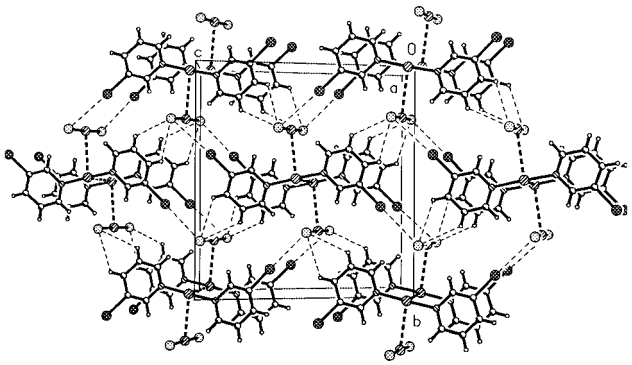

Fig. 2 Packing diagram of **1** parallel to the *x* axis. Gold···gold contacts are represented by thick dashed lines, C–H···Cl and Br···Cl contacts as thin dashed lines. C–H···Cl contacts within the dimeric units are omitted.

† Gold complexes with amine ligands, Part 5.[1]

Table 1 Geometrical data (Å, °) for the hydrogen bonds and interhalogen contacts in **1**[a]

System	*d*(H···Cl)[10]	∠(CH···Cl)	∠(H···Cl–Au2)
C2′–H2′···Cl1	2.69	151	72
C2–H2···Cl2#1	2.69	144	85
C6′–H6′···Cl2#1	2.62	144	80
C6–H6···Cl1	2.55	155	75
C4′–H4′···Cl2#2	2.92	120	92
C4–H4···Cl1#3	2.91	118	80
C5′–H5′···Cl2#2	2.87	123	75
C5–H5···Cl1#3	2.71	127	93
System	***d*(Br···Cl)**	**∠(CBr···Cl)**	
C3–Br1···Cl2#2	3.384(3)	169.6(4)	
C3′–Br1′···Cl1#4	3.441(4)	173.1(4)	

[a] Symmetry transformations: #1 1 − *x*,1 − *y*,1 − *z*; #2 1.5 − *x*,0.5 + *y*,1.5 − *z*; #3 −0.5 + *x*,0.5 − *y*, − 0.5 + *z*; #4 0.5 + *x*,0.5 − *y*,0.5 + *z*.

the chain and one between chains, with H···Cl 2.59, 2.84, 2.72 Å respectively;[10] regrettably, this did not attract our attention at the time.

An analysis of the packing of the dimeric units reveals further secondary interactions between the dimeric units. The packing diagram parallel to the *x* axis shows a layer structure (Fig. 2) with additional, slightly longer and less linear C–H···Cl contacts, leading to five-membered rings C4–H4···Cl···H5–C5 (Table 1, entries 5–8). Finally, there are Br···Cl contacts of 3.441(4) (Br1′···Cl1) and 3.384(3) Å (Br1···Cl2). These lie well below the sum of the van der Waals radii (3.6 Å), and the angles C3′–Br1′···Cl1 and C3-Br1···Cl2 [173.1(4) and 169.6(4)°] are essentially linear; thus these contacts may be classed as charge-assisted electrostatic interactions of the form $Br^{\delta+}\cdots Cl^{\delta-}$ (*cf.* analogous Cl···O [11] or Cl···Cl [4] contacts).

We conclude that non-conventional hydrogen bonds may play an important role in determining the structure of metal complexes. Furthermore, in view of the increasing interest in secondary interactions, great caution is needed in describing crystal packing in terms of *isolated* molecules or ions!

We thank the Fonds der Chemischen Industrie for financial support.

Notes and references

‡ *X-Ray structure analysis*: *Crystal data*: $C_{10}H_8Au_2Br_2Cl_2N_2$, monoclinic, space group $P2_1/n$, a = 7.5360(8), b = 14.4660(14), c = 14.0832(12) Å, β = 101.951(8)°, V = 1502.0(3) Å^3, Z = 4, μ(Mo-Kα) = 25.2 mm^{-1}, T = −100 °C. *Data collection*: colourless prism 0.45 × 0.10 × 0.06 mm, Siemens P4 diffractometer; absorption correction based on ψ-scans (transmissions 0.41–0.99). Measured reflections 3122 ($2\theta_{max}$ 50°), 2636 independent (R_{int} 0.053). *Structure solution and refinement*: heavy atom method, anisotropic refinement on F^2 (SHELXL-97, G. M. Sheldrick, University of Göttingen). Hydrogen atoms included using a riding model. Final *wR*2 0.087, with *R*1 0.037, for 163 parameters; *S* 0.91; max. $\Delta\rho$ 2.8 e Å^{-3}.

CCDC 182/1526. See http://www.rsc.org/suppdata/cc/a9/a907523b/ for crystallographic files in .cif format.

§ *Preparation* of **1**: To 2 ml (10 mmol) 3-bromopyridine were added 0.5 g (1.5 mmol) tetrahydrothiophene(chloro)gold(I). After 1 h stirring, the solution was transferred to small crystallisation tubes and left in the dark for 10 days. Small colourless crystals of **1** were formed in low yield, together with metallic gold. The quantity was insufficient for elemental analysis or spectroscopic studies. No product could be isolated from analogous reactions with other halogenated pyridines.

1 Part 4: B. Ahrens, P. G. Jones and A. K. Fischer, *Eur. J. Inorg. Chem.*, 1999, 1103 and references therein.
2 P. G. Jones and B. Ahrens, *Z. Naturforsch. Teil B*, 1998, **53**, 653.
3 H. Schmidbaur, *Gold Bull.*, 1990, **23**, 11; *Chem. Soc. Rev.*, 1995, 391.
4 M. Freytag, P. G. Jones, B. Ahrens and A. K. Fischer, *New J. Chem.*, 1999, **23**, 1137 and references therein.
5 P. G. Jones and B. Ahrens, *Chem. Commun.*, 1998, 2307.
6 H.-N. Adams, W. Hiller and J. Strähle, *Z. Anorg. Allg. Chem.*, 1982, **485**, 81.
7 C. B. Aakeröy, T. A. Evans, K. R. Seddon and I. Pálinkó, *New J. Chem.*, 1999, **23**, 145; O. Navon, J. Bernstein and V. Khodorkhovsky, *Angew. Chem.*, 1997, **109**, 640.
8 D. Braga and F. Grepioni, *New J. Chem.*, 1998, **22**, 1159.
9 The role of chlorine ligands as H bond acceptors with conventional donors is however documented: G. Aullón, D. Bellamy, L. Brammer, E. A. Bruton and A. G. Orpen, *Chem. Commun.*, 1998, 653.
10 Following T. Steiner (*Acta Crystallogr., Sect. B*, 1998, **54**, 456) and others, we have used normalised C–H distances of 1.08 Å to calculate the hydrogen bonding parameters.
11 J. P. M. Lommerse, A. J. Stone, R. Taylor and F. H. Allen, *J. Am. Chem. Soc.*, 1996, **118**, 3108.

Communication a907523b

ChemComm

Microwave effects on the selective reduction of NO by CH_4 over an In–Fe_2O_3/HZSM-5 catalyst

Xiaodong Wang, Tao Zhang,* Changhai Xu, Xiaoying Sun, Dongbai Liang and Liwu Lin

State Key Laboratory of Catalysis, Dalian Institute of Chemical Physics, Chinese Academy of Sciences, Dalian 116023, China. E-mail: taozhang@ms.dicp.ac.cn

Received (in Cambridge, UK) 30th November 1999, Accepted 7th January 2000

Microwave effects have been shown to promote the activation of NO_x molecules in the process of selective reduction of NO by CH_4 over an In–Fe_2O_3/HZSM-5 catalyst and to enhance the water tolerance of this catalyst for NO reduction.

Microwave radiation technology has been applied in heterogeneous catalysis research in the last ten years.[1] The use of microwave radiation to stimulate catalytic reactions has provided some remarkable results.[2,3] However, the effects of microwave radiation on heterogeneous catalysis have not been clearly elucidated yet. Recently the selective catalytic reduction (SCR) of nitrogen oxides by hydrocarbons has received much attention as this process has the advantage of using a gas mixture very similar to that found in automobile exhausts. Since methane exists in nearly all combustion exhausts, the CH_4-SCR has attracted increasing interest, and various types of catalysts have been reported for this reaction.[4] We studied the selective catalytic reduction of NO with CH_4 in a microwave field.[5] An In–Fe_2O_3/HZSM-5 catalyst has been found to show high activity at low reaction temperatures. Here, we report on the microwave effects on this process.

The In–Fe_2O_3/HZSM-5 catalyst was prepared by impregnating a mechanical mixture of commercial pure Fe_2O_3 and HZSM-5 powders (SiO_2/Al_2O_3 = 25, supplied by Nankai University, China) with a required amount of an aqueous solution of $In(NO_3)_3$ (Tianjin No. 3 Reagent Plant, China). The samples were dried at 120 °C for 6 h and subsequently calcined in air at 700 °C for 6 h. The catalysts were denoted by the weight ratios of indium, iron oxide and HZSM-5 zeolite, for example, In–Fe_2O_3/HZSM-5(1:8:20) indicates In:Fe_2O_3:HZSM-5 = 1:8:20 (weight ratio).

The SCR of NO by CH_4 was carried out in a quartz microcatalytic single-pass flow reactor. The feed gas contained 2500 ppm NO, 2000 ppm CH_4 and 4.0% O_2 (balance He); 3.3% H_2O was added to this feed gas when the water tolerance effect was investigated. Under standard reaction conditions, 60 ml min^{-1} of this mixture were fed over a catalyst loading of 500 mg, which results in a space velocity of 3600 h^{-1}. Product analyses were performed with a gas chromatograph and a NO_x analyzer. The catalytic activity was evaluated in terms of the conversion of NO_x to N_2.

The microwave reaction system consisted of a microwave generator, a rectangular waveguide, a circulator, a resonant cavity and a plunger. The microwave energy was supplied by a 200 W, 2.45 GHz microwave generator and the effective power for this experiment ranged from 10 to 50 W. The reactor was placed at the center of the single mode resonant cavity, which was parallel to the direction of the electric field. An IR thermometer and a thermocouple were employed to measure the reaction temperature of the catalyst bed in the microwave field, both of which have been proven to be relatively accurate methods.[3,6]

Fig. 1 shows the conversion of NO to N_2 as a function of temperature over In–Fe_2O_3/HZSM-5(1:8:20) and In/HZSM-5(1:20) catalysts in microwave and conventional reaction mode. Although In/HZSM-5 exhibited high activity for NO conversion, it was inactive when operated in the microwave mode (not shown in Fig. 1). Probably, this is associated with the fact that the In/HZSM-5 has poor microwave absorption ability. On the other hand, NO conversion was very high and even reached 100% over the In–Fe_2O_3/HZSM-5(1:8:20) catalyst. Obviously the Fe_2O_3 component in this catalyst was responsible for the good activity. This can be attributed to the fact that Fe_2O_3 is a good microwave medium, so that microwave energy can be effectively converted into the activation energy of the reacting molecules adsorbed on the catalyst.

It is worthwhile to note that although the In–Fe_2O_3/HZSM-5(1:8:20) catalyst also showed high NO reduction activity in the conventional reaction mode, the reaction temperature needed was much higher than that in the microwave reaction mode. The mechanism of microwave catalysis is, as yet, not clear. However, it can be rationalized that a direct interaction of microwaves with the catalyst bed would cause a strong coupling between the microwave and the absorbing materials in the catalyst. Since the molecules in the gas phase are transparent to microwaves, no interaction will take place between the microwaves and the gaseous molecules. Our TPD experiments on Fe_2O_3 also agree well with the report of Otto and Shelef[7] that Fe_2O_3 is a good material for NO_x adsorption. Thus, it is speculated that a coupling may also occur between microwaves and the adsorbed polar NO_x molecules *via* Fe_2O_3, which is not only a good NO_x adsorber but also a microwave absorber. It has been reported that NO_2 plays an important role in the SCR of NO by hydrocarbon,[8,9] so coupling between microwaves and NO_2 molecules may weaken the NO–O bond and promote their activation and, in turn, greatly facilitate the activation of CH_4 by NO_2. As a result, it is reasonable to speculate that the activation energy of NO reduction by CH_4 on the In–Fe_2O_3/HZSM-5(1:8:20) will be reduced, so that the microwave-radiated reactor can operate at a lower temperature than the conventional reactor. It should be noted that although the In–Fe_2O_3/HZSM-5 was inactive for the NO + CH_4 reaction in the conventional reaction mode (not shown in Fig. 1), the reaction took place over this catalyst in the microwave reaction mode and the highest NO

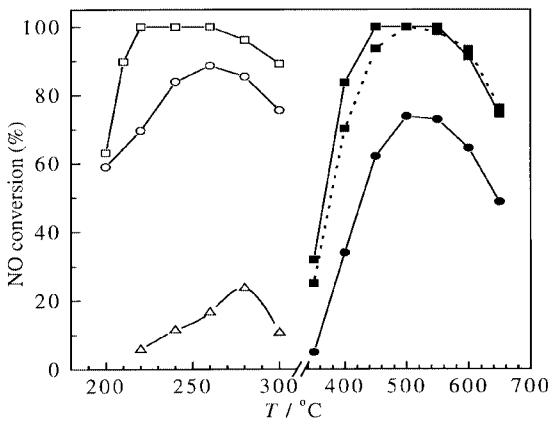

Fig. 1 NO conversions over In–Fe_2O_3/HZSM-5(1:8:20)(—) and In/HZSM-5(1:20)(----) in the microwave (open symbols) and conventional (filled symbols) reaction modes in the reaction systems NO + CH_4 + O_2 (squares), NO + CH_4 (triangles) and NO + CH_4 + O_2 + H_2O (circles).

conversion reached 23.6% (Fig. 1). This illustrates again that microwaves exhibit an effect on the activation of NO as the catalyst only chemisorbs NO_x.

The impact of H_2O on the NO conversion over the In–Fe_2O_3/HZSM-5(1:8:20) catalyst in both the conventional and the microwave reaction modes is also shown in Fig. 1. It is evident that the NO conversion suffered a more severe decrease in the conventional mode than in the microwave mode. As H_2O competes for the same adsorption sites as NO_x and inhibits the adsorption of the NO_x molecules, the catalyst will be deactivated in the presence of water vapor. However, H_2O is a strongly polar molecule and has a good microwave-absorbing ability, so that when H_2O molecules are adsorbed on the catalyst, they interact with the catalyst in the microwave field, leading to a strong coupling and resulting in the desorption of H_2O molecules from the adsorption sites, or in the weakening the adsorption of H_2O molecules on the catalytic surface. Therefore the microwave reaction mode provides the NO_x molecules with more adsorption sites than the conventional reaction mode when the feed contains water vapor. This suggests that microwave catalysis may lead to a new approach for the SCR of NO by hydrocarbons when dealing with feeds with high water content.

In conclusion, the In–Fe_2O_3/HZSM-5 catalyst shows some remarkable catalytic performances in the SCR of NO by CH_4 in a microwave field, indicating that microwaves have a beneficial effect on the activation of reacting molecules.

Notes and references

1 G. Bond, R. B. Moyes and D. A. Whan, *Catal. Today*, 1993, **17**, 427.

2 C. Y. Cha and Y. Kong, *Carbon*, 1995, **33**, 1141; C. Y. Cha and B. I. Kim, *Fuel Sci. Tech. Int.*, 1993, **11**, 1175; M. S. Ioffe, S. D. Pollington and J. K. S. Wan, *J. Catal.*, 1995, **151**, 349; L. Seyfried, F. Garin, G. Maire, J. M. Thiebaut and G. Roussy, *J. Catal.*, 1994, **148**, 281; S. Ringler, P. Girard, G. Maire, S. Hilaire, G. Roussy and F. Garin, *Appl. Catal. B*, 1999, **20**, 219.

3 Y. Chang, A. Sanjurjo, J. G. McCarty, G. Krishnan, B. Woods and E. Wachsman, *Catal. Lett.*, 1999, **57**, 187; C. Chen, P. Hong, S. Dai and J. Kan, *J. Chem. Soc., Faraday Trans.*, 1995, **91**, 1179.

4 Y. Li and J. N. Armor, *Appl. Catal. B*, 1992, **1**, L31; E. Kikuchi and K. Yogo, *Catal. Today*, 1994, **22**, 73; X. Zhou, T. Zhang, Z. Xu and L. Lin, *Catal. Lett.*, 1996, **40**, 35; C. J. Lougman and D. E. Resasco, *Appl. Catal. B*, 1995, **5**, 351; Z. Li and M. F. Stephanopoulos, *Appl. Catal. B*, 1999, **22**, 35.

5 X. Wang, T. Zhang, C. Xu, W. Guan, D. Liang and L. Lin, *Proceedings of the First International Conference on Microwave Chemistry, Prague*, 1998, p. P4.

6 W. L. Perry, J. D. Katz, D. Rees, M. T. Paffet and A. K. Datye, *J. Catal.*, 1997, **171**, 431.

7 K. Otto and M. Shelef, *J. Catal.*, 1970, **18**, 184.

8 H. Hamada, Y. Kintaichi, M. Sasaki, T. Ito and M. Tabata, *Appl. Catal.*, 1991, **70**, L15.

9 Y. Li and J. N. Armor, *J. Catal.*, 1994, **150**, 376; C. Yokoyama and M. Misono, *J. Catal.*, 1994, **150**, 9; M. Shelef, C. M. Montreuil and H. W. Jen, *Catal. Lett.*, 1994, **26**, 277; T. Beutel, B. J. Adelman, G.-D. Lei and W. M. H. Sachtler, *Catal. Lett.*, 1995, **32**, 83; K. A. Bethke, C. Li, M. C. Kung and H. H. Kung, *Catal. Lett.*, 1995, **31**, 287; D. B. Lukyanov, G. Still, J. L. d'Itri and W. K. Hall, *J. Catal.*, 1995, **153**, 265; E. Kikuchi, M. Ogura, N. Aratani, Y. Sugiura, S. Hiromoto and K. Yogo, *Catal. Lett.*, 1996, **27**, 35; M. Iwamoto, A. M. Hernandez and T. Zengyo, *Chem. Commun.*, 1997, 37.

Communication a909437g

ChemComm

Crystal engineering of 2-D hydrogen bonded molecular networks based on the self-assembly of anionic and cationic modules†

Olivier Félix, Mir Wais Hosseini,* André De Cian and Jean Fischer

Université Louis Pasteur, Institut Le Bel, F-67000 Strasbourg, France. E-mail: hosseini@chimie.u-strasbg.fr

Received (in Basel, Switzerland) 14th November 1999, Accepted 13th January 2000

Using a self-assembly strategy based on both H-bonding and ionic interactions, a molecular module composed of two cyclic amidinium units and that bears two additional OH groups, thus possessing a total of six H-bond donor sites, was used to engineer 2-D crystalline molecular networks in the presence of carboxylate anions.

Molecular networks, formed in the crystalline phase by the self-assembly[1] of structurally defined and energetically programmed molecular modules,[2] are molecular assemblies possessing translational symmetry of one or several assembling cores.[3] The latter may be regarded as a series of interaction patterns between complementary molecular building blocks comprising the solid. In principle, any type or combination of intermolecular interactions such as H-bond,[4] van der Waals interactions[1] or coordination-bonds[5] may be used to design the assembling core. In the present contribution, we focus on the formation of molecular networks based on H-bonds. The dimensionality of molecular networks (1-, 2- or 3-D) is defined by the number of translations (1, 2, or 3 respectively) of the assembling cores.[3] Although, one dimensional networks have become more commonplace,[4,6] the formation of 2-[7] and 3-D-networks[8] is still a matter of active research interest.

Here we report the formation of β-networks using the tecton **2**-2H$^+$ and mono- (**3**$^-$) and di-carboxylate (**4**$^{2-}$) anions.

Molecular networks may be generated through self-assembly processes using either a monocomponent system based on a single self complementary module or a polycomponent system composed of several complementary units. Although the former case is ideal in terms of atom economy, in practice, such a system often leads to amorphous powders and thus eludes structural investigations. On the other hand, using polycomponent systems, for which both thermodynamic and kinetic parameters may be monitored, the structure of the network may be investigated by X-ray crystallography in some cases.

Although the majority of reported molecular networks are mainly based on nonionic hydrogen bonding,[3] the simultaneous use of directional hydrogen bonds and strong but less directional ionic interactions has been also reported.[4e,6] It has been shown that bis-amidinium dications such as **1**-2H$^+$[6] (Scheme 1) are interesting building blocks for the crystal engineering of hydrogen bonded molecular networks. Indeed, the **1**-2H$^+$ dication, owing to the presence of four acidic NH protons oriented in a divergent fashion, acts as a tetra H-bond donor.[6] Furthermore, owing to the appropriate spacing of the two cyclic amidinium moieties by an ethylene spacer, compound **1**-2H$^+$ was shown to interact with two carboxylate units by a dihapto mode of recognition on each side of the module (Fig. 1). It has been shown that in the presence of the monoanion **3**$^-$ acting as stopper, **1**-2H$^+$ forms a discrete exobinuclear complex [Fig. 1(a)], and in the presence of dicarboxylates, such as iso- or terephthalate **4**$^{2-}$ acting as connectors, the same compound leads to 1-D networks [Fig. 1(b)].

The enhancement of the dimensionality of the above mentioned network from 1- to 2-D, requires interconnection of the 1-D networks. This may be achieved using different design strategies. The most obvious one would consist of increasing the number of components. This has indeed been achieved using a three-component system based on the dication **1**-2H$^+$, fumarate dianion and fumaric acid.[6d] On the other hand, while using a two-component system, another possibility would be to increase the number of interaction sites within the dianionic module. This may be achieved by using a sp^3 centre such as in pyrophosphate instead of sp^2 carboxylate units.[6c] Finally, one may introduce additional H-bond donor sites within the cationic partner [Fig 1(c)].

The design of the bisamidinium **2**-2H$^+$ is based on a combination of NH and OH groups as H-bond donors. The quadruple H-bond donor module **1**-2H$^+$ may be transformed into a sextuple H-bond donor **2**-2H$^+$ by introduction of two OH groups within its framework. Owing to the half-chair conformation adopted by both cyclic amidinium moieties, the OH group, by virtue of its axial positioning should be oriented below and above the main plane of the module and thus should allow the interconnection of consecutive 1-D networks through strong OH$\cdots$O$^-$ hydrogen bonds. The synthesis of **2** was achieved following the reported procedure for the bisamidine **1**.[9] 1,3-Diamino-2-hydroxypropane was first transformed into its

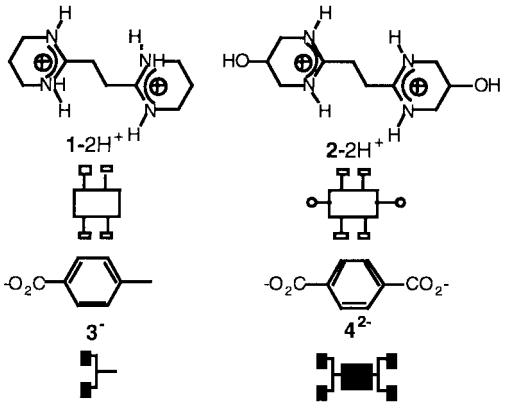

Scheme 1

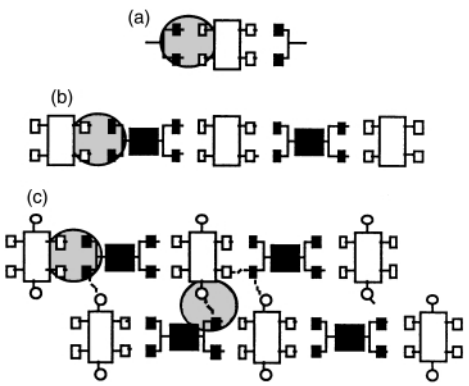

Fig. 1 Schematic representation of a discrete exo-binuclear complex (a), 1-D molecular network (b) based on the translation of a single assembling core (grey circle), and of a 2-D network based on the translation of two different assembling cores in two different spatial directions (c).

† Dedicated to the memory of Professor Olivier Kahn.

mono tosylate salt before it was treated with 0.5 equiv. of succinonitrile under argon for 1 h at 140 °C. Pure **2**-2TsOH was isolated as a white crystalline solid in 78% yield upon crystallisation from EtOH–H_2O.

Using the module **2**-2H$^+$, the formation of molecular networks in the crystalline phase was investigated using toluate **3**$^-$ (Fig. 2) as well as terephthalate dianions **4**$^{2-}$ (Fig. 3).

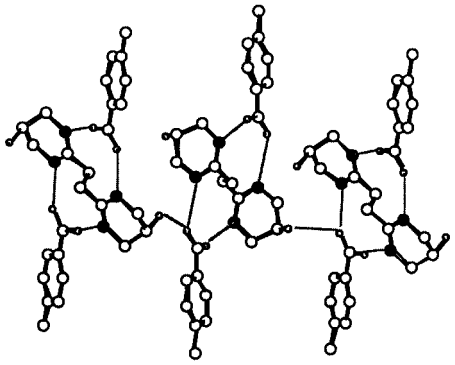

Fig. 2 A portion of the X-ray structure of (**2**-2H$^+$, 2**3**$^-$) co-crystals showing the formation of a 1-D network. In fact the co-crystal shows a 2-D network formed by H-bonds engaging the remaining OH groups.

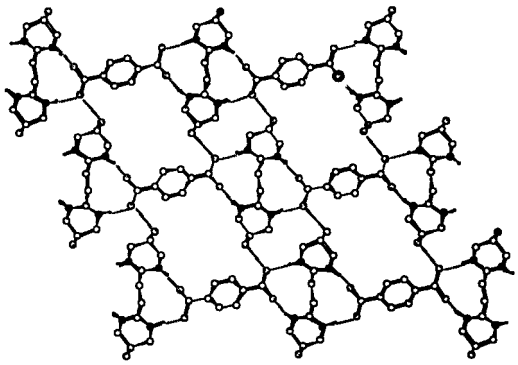

Fig. 3 A portion of the X-ray structure of (**2**-2H$^+$, **4**$^{2-}$) co-crystals showing the formation of a 2-D hydrogen bonded network that is formed by the interconnection of 1-D networks formed by the amidinium and carboxylate moieties, through strong OH··O$^-$ hydrogen bonds.

Upon mixing the free base **2** with 2 equiv. of toluic acid or 1 equiv. terephthalic acid in EtOH, colourless single crystals were obtained. The formation of molecular networks in the above mentioned co-crystals was investigated by X-ray crystallography which revealed the following common features for both structures (Fig. 2 and 3)‡: (i) for the centrosymmetric **2**-2H$^+$ unit, owing to the fully extended *trans* conformation of the ethylene chains, the two planes containing the amidinium groups are almost parallel but not coplanar; (ii) both six-member cycles adopt a half-chair conformation with the OH groups in axial positions, (iii) all four acidic protons are localised on **2** with an average N–H distance of *ca*. 1.01 Å; (iv) the N1··N3 and N2··N4 average distance is, as for **1**-2H$^+$,[6a], close to 5.0 Å, thus allowing the recognition of carboxylate groups through a dihapto mode of H-bonding (Fig. 2); (v) the recognition of two carboxylate moieties by the dication **2**-2H$^+$, as for **1**-2H$^+$,[6a] takes place in a symmetric mode on each side of the module through two strong H-bonds with an average N··O distance of *ca*. 2.72 Å an NH··O distance of *ca*. 1.72 Å and an average N–H–O angle value of *ca*. 172°.

Interestingly, whereas for (**1**-2H$^+$, 2**3**$^-$) co-crystals a 0-D solid composed of discrete units without any specific interactions between them was obtained[10] [Fig. 1(a)], for the (**2**-2H$^+$, 2**3**$^-$) salt, owing to the presence of the OH groups, the neutral complexes are interconnected into a β-network through strong H-bonds of the OH··O type (average d_{OHO} distance of *ca*. 2.64 Å) between the hydroxy moieties of **2** and carboxylate extremities of the anion **3**$^-$ (Fig. 3).

For the (**2**-2H$^+$, **4**$^{2-}$) co-crystals, as predicted and previously observed for the amidinum **1**-2H$^+$[6a] case, a 1-D network exclusively composed of **2**-2H$^+$ dication and **4**$^{2-}$ (Fig. 3) dianions interconnected through strong H-bonds was observed in the solid state. However, as for the (**2**-2H$^+$, 2**3**$^-$) salt, for (**2**-2H$^+$, **4**$^{2-}$) cocrystals, owing to the presence of the additional OH groups, the above mentioned 1-D networks were interconnected into a 2-D network through strong OH··O bonds with an average d_{OHO} distance of *ca*. 2.71 Å.

In conclusion, the dicationic molecular module **2**-2H$^+$ that bears both NH and OH groups and is capable of acting as a sextuple H-bond donor was designed and synthesised. The module **2**-2H$^+$, which is capable of specifically recognising two carboxylate units through strong H-bonds and ionic interactions, was assembled into 2-D networks using the additional hydrogen bond donor OH sites to interconnect 1-D networks formed between the amidinium dications and dicarboxylates in the crystalline phase. The extension of concepts discussed above for the design of 3-D networks is currently in progress.

Notes and references

‡ *Crystal data*: for (**2**-2H$^+$, 2**3**$^-$): data were collected on a MACH3 Nonius diffractometer at 294 K using colorless crystals (0.30 × 0.20 × 0.10 mm). $C_{10}H_{20}N_4O_2{\cdot}2C_8H_7O_2$, M = 498.58, triclinic, space group $P\bar{1}$, a = 6.0754(6), b = 14.989(1), c = 14.979(1) Å, α = 68.09(2), β = 89.34(2), γ = 87.19(2)°, U = 1264.0(2) Å, Z = 1, D_c = 1.16 g cm^{-3}, Mo-Kα graphite monochromated radiation, μ = 0.075 mm^{-1}, $R(F)$ = 0.071 using 1405 reflections with $I > 3\sigma(I)$.

For (**2**-2H$^+$, **4**$^{2-}$): data were collected on a Kappa CCD difractometer at 173 K using colorless crystals (0.26 × 0.10 × 0.10 mm). $C_{10}H_{20}N_4O_2{\cdot}C_8H_4O_4$, M = 392.42, triclinic, space group $P\bar{1}$, a = 5.0376(2), b = 9.5318(5), c = 10.5146(5) Å, α = 68.186(9), β = 81.393(9), γ = 75.452(9)°, U = 452.81(1) Å, Z = 1, D_c = 1.44 g cm^{-3}, Mo-Kα graphite monochromated radiation, μ = 0.102 mm^{-1}, $R(F)$ = 0.048 using 1615 reflections with $I > 3\sigma(I)$.

CCDC 182/1525.

1 M. W. Hosseini and A. De Cian, *Chem. Commun.*, 1998, 727.
2 J.-M. Lehn, *Supramolecular Chemistry, Concepts and Perspectives*, VCH, Weinheim, 1995; G. R. Desiraju, *Angew. Chem. Int. Ed. Engl.*, 1995, **34**, 2311; see also: *Crystallography of Supramolecular Compounds*, ed. G. Tsoucaris *et al.*, Kluwer, Dordrecht,1996; M. C. Etter, *Acc. Chem. Res.*, 1990, **23**, 120; G. M. Whitesides, J. P. Mathias and T. Seto, *Science*, 1991, **254**, 1312.
3 F. W. Fowler and J. W. Lauther, *J. Am. Chem. Soc.*, 1993, **115**, 5991.
4 (*a*) D. S. Lawrence, T. Jiang and M. Levett, *Chem. Rev.*, 1995, **95**, 2229; (*b*) J. F. Stoddart and D. Philip, *Angew. Chem., Int. Ed. Engl.*, 1996, **35**, 1155; (*c*) C. B. Aakeröy and K. R. Seddon, *Chem. Soc. Rev.*, 1993, **22**, 397; (*d*) S. Subramanian and M. J. Zaworotko, *Coord. Chem. Rev.*, 1994, **137**, 357; (*e*) V. A. Russell and M. D. Ward, *Chem. Mater.*, 1996, **8**, 1654; G. T. R. Palmore and J. C. MacDonald, in *Structure, Energetics, and Reactivity in Chemistry*, ed. A. Greenberg, C. M. Breneman and J. F. Liebman, Wiley, New York, 2000, p. 291.
5 S. R. Batten and R. Robson, *Angew. Chem., Int. Ed.*, 1998, **37**, 1461.
6 (*a*) M. W. Hosseini, R. Ruppert, P. Schaeffer, A. De Cian, N. Kyritsakas and J. Fischer, *J. Chem. Soc., Chem. Commun.*, 1994, 2135; (*b*) G. Brand, M. W. Hosseini, R. Ruppert, A. De Cian, J. Fischer and N. Kyritsakas, *New J. Chem.*, 1995, **19**, 9; (*c*) M. W. Hosseini, G. Brand, P. Schaeffer, R. Ruppert, A. De Cian and J. Fischer, *Tetrahedron Lett.*, 1996, **37**, 1405; (*d*) O. Félix, M. W. Hosseini, A. De Cian and J. Fischer, *Angew. Chem., Int. Ed. Engl.*, 1997, **36**, 102; (*e*) O. Félix, M. W. Hosseini, A. De Cian and J. Fischer, *New J. Chem.*, 1998, **22**, 1389.
7 M. D. Ward, P. J. Fagan, J. C. Calabrese and D. C. Johnson, *J. Am. Chem. Soc.*, 1989, **111**, 1719; E. Fan, J. Yang, S. J. Geib, T. C. Stoner, M. D. Hopkins and A. D. Hamilton, *J. Chem. Soc., Chem. Commun.*, 1995, 1251; K. E. Schiebert, D. N. Chin, J. C. MacDonald and G. M. Whitesides, *J. Am. Chem. Soc.*, 1996, **118**, 4018.
8 O. Ermer, *J. Am. Chem. Soc.*, 1988, **110**, 3747; M. Simard, D. Su and J. D. Wuest, *J. Am. Chem. Soc.*, 1991, **113**, 4696.
9 P. Oxley and W. F. Short, *J. Chem. Soc.*, 1947, 497.
10 O. Félix, M. W. Hosseini, A. De Cian and J. Fischer, *Tetrahedron Lett.*, 1997, **38**, 1755.

Communication a909093b

ChemComm

High-loading resin beads for solid phase synthesis using triple branching symmetrical dendrimers

Christophe Fromont and Mark Bradley*

Department of Chemistry, University of Southampton, Highfield, Southampton, UK SO17 1BJ

Received (in Liverpool, UK) 9th August 1999, Accepted 11th January 2000

Resin beads with a loading of 200 nmol per bead have been prepared using a Generation 2.0 tris-based dendrimer to amplify resin loading sites.

The process of split and mix by its very nature rapidly generates large libraries of compounds in such a manner that a single resin bead carries a single compound. It is one of the most efficient and cost effective chemical methods for the generation of large compound numbers,[1] with compound numbers increasing exponentially with only a linear increase in the number of synthetic steps. The single bead/single compound concept opens up the option of screening compounds released from single beads as a powerful tool for high throughput screening and thus several major pharmaceutical companies now use single bead screening in anger in the area of lead generation. The drawbacks to this process are the tiny amounts of compound found on single beads, usually in the order of a few hundred picomoles, and the identification of the compound on the bead. Compound quantity maybe sufficient for one or two biological assays but it is usually insufficient for IC_{50} determinations and chemical analysis/determination of the structure of the compound. These analysis issues have led to a number of elegant tagging solutions that encode the chemical sequence to which a bead has been exposed, although complicating the synthetic process.[2] However the need for encoding and resolution of the screening problems could be overcome if the loading of the solid support could be increased to a more practical level. We previously reported the synthesis of polyamine based Generation 3.0 PAMAM dendrimers on resins beads as a means of enhancing loading.[3]

Here we describe a practical approach to the synthesis of a tri-branching symmetrical dendrimer on the solid phase with an 18-fold amplification of resin loading per bead. Beads with a loading of 200 nmol per bead were prepared and used in a number of synthetic applications, with single beads containing more than sufficient compound for conventional analysis, including NMR!

The trifunctional dendrimer monomers[4] were prepared in bulk (> 50 g) by alkylation of tris **1** with acrylonitrile followed by nitrile hydrolysis in a saturated solution of HCl in dry MeOH to give the methyl ester **2**. Alternatively, the triacid could be obtained by direct hydrolysis. The hindered amine **2** was converted to the isocyanate **3** by treatment with Boc_2O and DMAP as described by Knölker[5] to give the stable symmetrical monomer **3**. Aminomethylpolystyrene resin (0.7 mmols g^{-1}, 250–300 μm, Polymer Laboratories) was directly derivatised with **3** as shown in Scheme 1. Displacement of the methyl ester by propane-1,3-diamine was followed by on-bead IR (ATR) and NMR analysis of cleaved material.† Repeating the process gave Generation 2.0 dendrimer beads with a loading of 85% of the theoretical maximum (36 nmol per bead). Swelling studies (Fig. 1) showed that the dendrimer beads swelled to a much greater degree in more polar solvents than the starting aminomethyl resin, as expected due to the nature of the dendrimer itself. It should however also be noted that swelling was measured in units of ml g^{-1}. Since the dendrimer beads have a density that is different to those of polystyrene (the mass of the generation 2.0 dendrimer is 2111 Da), trends rather than absolute swelling ratios in terms of bead sizes are being observed. The average diameters of the resin beads in DMF were: aminomethyl resin, 310 μm, PS-Gen 1.0, 400 μm and PS Gen. 2.0, 500 μm. These beads were extremely stable to solvation changes and extended manipulations and behaved in all respects as normal resin beads. They proved to be ideal for a broad range of chemistries. In addition, with *ca*. 27 000

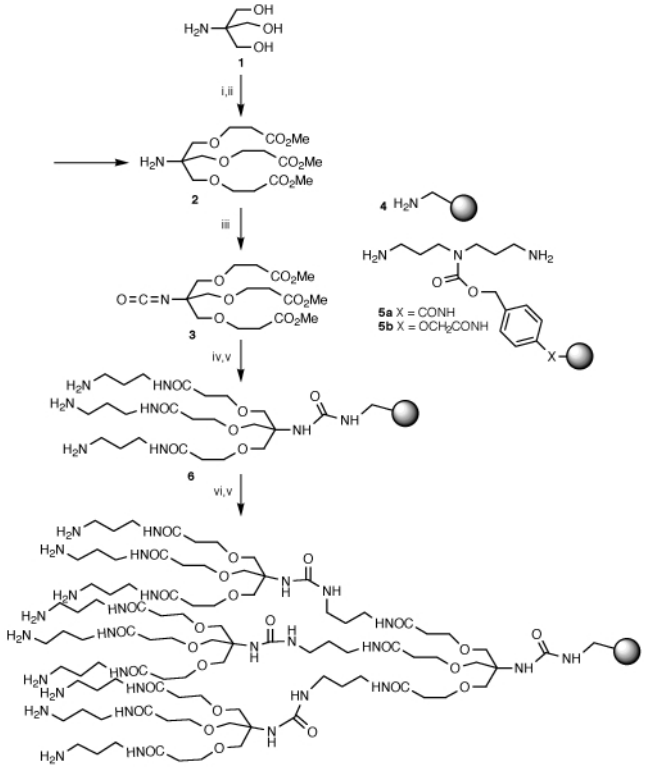

Scheme 1 *Reagents and conditions*: i, acrylonitrile, 1,4-dioxane, 40% KOH, room temperature, 3 days; ii, HCl, MeOH, 4–6 h, reflux; iii, Boc_2O, DMAP (cat), CH_2Cl_2, room temp., 30 min; iv, **4** or **5a**,**b**, DMAP (cat), Pr^i_2NEt (2 equiv.), CH_2Cl_2 or DMF, 12 h; v, propane-1,3-diamine, MeOH, 3 days or propane-1,3-diamine, DMSO, 3 days; vi, **3**, DMAP (cat), Pr^i_2NEt (2 equiv.), DMF, 12 h.

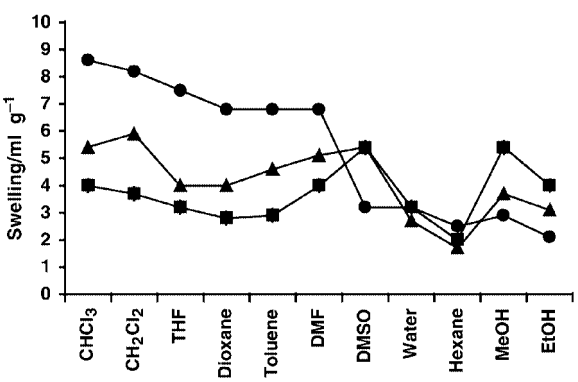

Fig. 1 Swelling studies: (●) aminomethyl resin; (▲) PS Gen 1.0; (■) PS Gen 2.0.

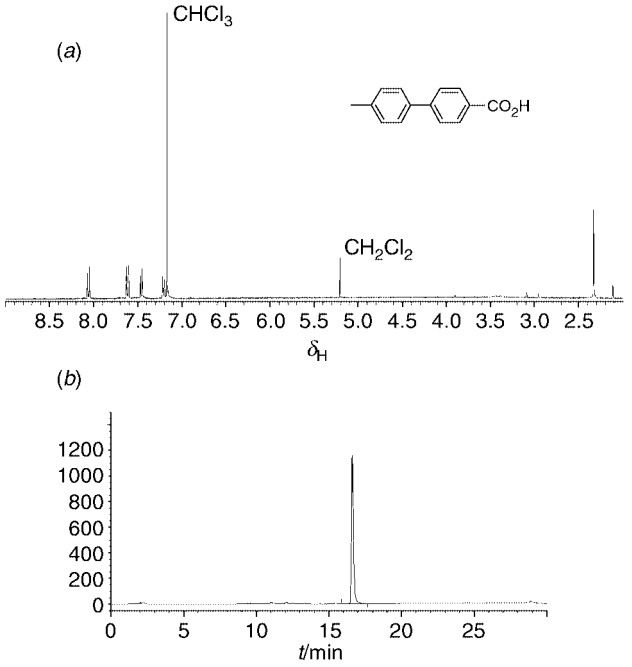

Fig. 2 (*a*) Crude ^{1}H NMR spectrum (5 mm NMR tube, 256 scans, 400 MHz) and (*b*) HPLC trace (10% of sample injected, 3.6 mm × 18 cm, C-18 column) for the Suzuki biaryl product cleaved from a single resin bead.

beads g^{-1} a split and mix synthesis on a gram of resin beads clearly provides the numbers of compounds and the amounts necessary for a serious single bead screening approach.

Dendrimer synthesis was also carried out on 400–500 μm aminomethyl polystyrene resin beads, loaded with the polyamine scaffolds **5a**,**b**,[3] as shown in Scheme 1. Generation 1.0 (8000 beads g^{-1}) had a loading of 116 nmol bead^{-1}, while Generation 2.0 (4300 beads g^{-1}) had a loading of 230 nmol bead^{-1}.‡ The dendrimer beads were used in a number of synthetic applications attaching a linker onto the free amino groups of the dendrimer to allow cleavage of the desired compound. This included peptide chemistry (synthesis of Fmoc-Val-Phe-Ala-OH) and a Suzuki coupling.[6] Thus 4-iodobenzoic acid was esterified onto the HMPB linker and 4-methylbenzene boronic acid coupled under standard conditions [K_2CO_3, $Pd(PPh_3)_4$, DMF, 110 °C, 16 h]. Cleavage of the biaryl compound from a single resin bead gave the HPLC and NMR data shown in Fig. 2. It should be noted that these very large beads were not as robust as the smaller beads used earlier, with solvent shock often causing the beads to shatter, necessitating a gradual change from one solvent to another and gentle handling, thereby limiting their utility.

We have thus devised a fast and efficient method of generating symmetrical tri-branched resin linked dendrimers in a very efficient manner. The smaller, robust Gen 2.0 beads with a loading of 36 nmol bead^{-1} (which has been extended to Gen 3.0, beads with a loading of 100 nmol bead^{-1}) are we believe ideally practical for single bead screening applications.

We acknowledge the Royal Society for a University Research Fellowship to M. B. and the BBSRC for generous support of this research (ROPA grant).

Notes and references

† Using cleavable linkers dendrimers were cleaved at the 0.5*n* and *n* generations and fully analysed, and clearly showed that dendrimer synthesis had proceeded cleanly and as anticipated.
‡ By Fmoc determination.

1 A. Furka, F. Sebestyen, M. Asgedom and G. Dibo, *Int. J. Pept. Protein Res.*, 1991, **37**, 487; R. A. Houghten, C. Pinilla, S. E. Blondelle, J. R. Appel, C. T. Dooley and J. H. Cuervo, *Nature*, 1991, **354**, 84; K. S. Lam, S. E. Salmon, E. M. Hersh, V. J. Hruby, W. M. Kazmierski and R. J. Knapp, *Nature*, 1991, **354**, 82.
2 H. P. Nestler, P. A. Bartlett and W. C. Still, *J. Org. Chem.*, 1994, **59**, 4723; J. J. Baldwin, J. J. Burbaum, I. Henderson and M. H. J. Ohlmeyer, *J. Am. Chem. Soc.*, 1995, **117**, 5588; J. J. Burbaum, M. H. J. Ohlmeyer, J. C. Reader, I. Henderson, L. W. Dillard, G. Li, T. L. Randle, N. H. Sigal, D. Chelsky and J. J. Baldwin, *Proc. Natl. Acad. Sci. U.S.A.*, 1995, **92**, 6027; M. H. J. Ohlmeyer, R. N. Swanson, L. W. Dillard, J. C. Reader, G. Asouline, R. Kobayashi, M. Wigler and W. C. Still, *Proc. Natl. Acad. Sci. U.S.A.*, 1993, **90**, 10 922.
3 N. J. Wells, M. Davies and M. Bradley, *J. Org. Chem.*, 1998, **63**, 6430; N. J. Wells, A. Basso and M. Bradley, *Biopolymers*, 1998, **47**, 381; V. Swali, N. J. Wells, G. J. Langley and M. Bradley, *J. Org. Chem.*, 1997, **62**, 4902; V. Swali and M. Bradley, *Anal. Commun.*, 1997, **34**, 15.
4 G. R. Newkome, C. N. Moorefield and G. R. Baker, *Aldrichim. Acta*, 1992, **25**, 31; G. R. Newkome, C. D. Weis and B. J. Childs, *Designed Monomers and Polymers*, 1998, **1**, 3.
5 H.-J. Knölker, T. Braxmeier and G. Schlechtingen, *Angew. Chem., Int. Ed. Engl.*, 1995, **34**, 2497.
6 B. Ruhland, A. Bombrun and M. A. Gallop, *J. Org. Chem.*, 1997, **62**, 7820.

Communication a906515f

On the role of planar chirality: a tunable enantioselectivity in palladium-catalyzed allylic alkylation with planar chiral 1,1′-P,N-ferrocene ligands

Wei-Ping Deng, Xue-Long Hou,* Li-Xin Dai, Yi-Hua Yu and Wei Xia

Laboratory of Organometallic Chemistry, Shanghai Institute of Organic Chemistry, Chinese Academy of Sciences, 354 Fenglin Lu, Shanghai 200032, China. E-mail: xlhou@pub.sioc.ac.cn

Received (in Cambridge, UK) 22nd November 1999, Accepted 7th January 2000

A series of planar chiral 1,1′-P,N-2′-substituted ferrocene ligands 9–12 and 16, prepared with diastereopurity > 99 : 1, have been used to examine the role of planar chirality, and significant effects on enantioselectivity as well as the control of absolute configuration in palladium-catalyzed allylic alkylation as a model reaction were observed.

Catalytic enantioselective reactions have attracted great interest among synthetic chemists in recent years, and many efforts in preparing efficient ligands have been made.[1,2] Most of the chiral ligands currently used consist of central chirality and/or axial chirality. Chiral ferrocene ligands with planar chirality began to be used in industrial processes only two or three years ago.[3] Ferrocene ligands have thus received more intensive attention.[4–7] Although these ferrocene ligands usually have planar chirality, the role of this chirality element is not clear. Some examples showed that the planar chirality had a significant effect on the enantioselectivity,[5] while in other examples the effect was not so apparent.[6] To date, there have been only a few attempts to ascertain the effect of planar chirality on stereochemical outcome in asymmetric synthesis.[5b,6a] Moreover, most works dealt with 1,2-disubstituted ferrocene ligands having two donor groups on the same Cp ring, such as compounds **1**,[7] **2**[5a] and **3**.[5b] Quite recently, Ikeda,[8a,b] Ahn[8c] and Knochel[9] reported new 1,1′-disubstituted ferrocenyl ligands

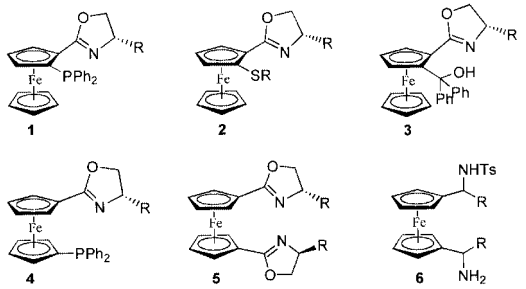

4–**6**, and good enantioselectivities have been obtained with these ligands. As a part of our program[5c,6] aimed at the design and application of chiral ligands to asymmetric synthesis, we studied the role of planar chirality in asymmetric induction. We envisage that, if planar chirality is introduced into this kind of 1,1′-disubstituted ferrocene ligand, it may provide a good model to investigate the role of planar chirality. Moreover, it is worthwhile to note that, after the planar chirality is introduced into such ligands, there are three elements of chirality—central, planar and axial chirality—upon their coordination with metal palladium. Herein we report the synthesis of planar chiral 1,1′-P,N-2′-disubstituted ferrocene ligands and the observation of significant effects on enantioselectivity as well as the control of absolute configuration in palladium-catalyzed allylic alkylation upon introducing a new element of chirality—planar chirality—into the 1,1′-P,N-ferrocene ligands.

As shown in Scheme 1, ferrocenyloxazoline derivative **7**, which was synthesized according to Bryce's method,[9] was treated with BuLi followed by trapping with Ph_2PCl to afford 1-diphenylphosphino-1′-oxazolinylferrocene **8** in 78% yield. Directed diastereoselective *ortho*-lithiation of **8** according to Richards' procedure[8e] and subsequent treatment with electrophiles gave 2′-substituted compounds **9**, **10** and **16**. Compound **9** was again lithiated followed by trapping with electrophiles to afford ferrocene derivatives **14** and **15**. Conversion of **14** and **15** to **11** and **13** respectively was accomplished by removing the TMS group with TBAF in THF at reflux. Then, a bromo–lithium exchange of **13** followed by quenching the resulting anion with TMSCl furnished **12**. The diastereopurities of all compounds containing planar chirality, determined by 300 MHz ^{1}H NMR, were > 99 : 1.

Chiral P,N-ligands have proved to be effective in several kinds of metal-catalyzed asymmetric reactions,[11] especially palladium-catalyzed allylic substitutions,[11a,b,12] and ligand **8** has also proved effective in palladium-catalyzed allylic substitutions with 91% ee.[8b–d] In our previous work, we studied the role of the planar chirality of 1,2-N,S-ferrocene ligands in palladium-catalyzed allylic alkylations.[6a] Therefore, in order to investigate the role of the planar chirality of this new kind of 1,1′-P,N-2′-disubstituted ferrocene ligand in metal-catalyzed asymmetric reaction, we also used allylic alkylation as the model reaction. The results are summarized in Table 1. Our attention was first focused on the role of planar chirality in this reaction. A dramatic change in the enantioselectivity of the reaction was observed with (S,S_p)-**9**; the enantioselectivity of the reaction product **22** changed from 91% with *S* configuration using ligand **8** to 69.7% with *R* configuration using ligand **9** (entries 1 and 3). In considering the change of absolute configuration, the effect of the newly introduced group is significant. This exciting result encouraged us to probe the effect of the newly introduced group with opposite planar

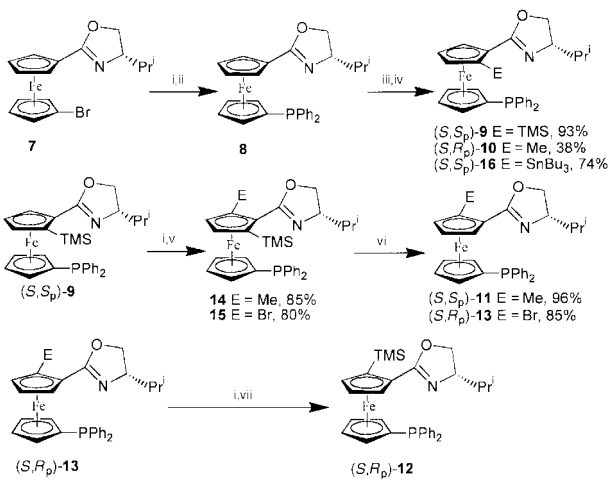

Scheme 1 *Reagents and conditions*: i, BuLi, THF, −78 °C; ii, Ph_2PCl, 78%; iii, BuLi, Et_2O, TMEDA, −78 °C; iv, E^+ (MeI, TMSCl or Bu_3SnCl); v, E^+ (MeI or $BrCF_2CF_2Br$); vi, TBAF, THF, reflux; vii, TMSCl, 73%.

Table 1 The effect of different ligands on enantioselectivity and configuration of product in palladium-catalyzed allylic alkylation[a]

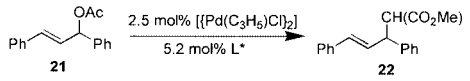

Entry	Ligand	Yield (%)[b]	Ee (%)[c]	Configuration[d]
1	**8**	99	91.0	*S*
2	**8**	98	92.8[e]	*S*
3	**9**	98	69.7	*R*
4	**9**	99	64.0[e]	*R*
5	**10**	98	34.2	*R*
6	**11**	99	98.5[e]	*S*
7	**11**	99	98.2	*S*
8	**11**	99	87.8[f]	*S*
9	**12**	99	98.6[e]	*S*
10	**12**	99	97.8	*S*
11	**16**	98	83.3	*R*
12	**16**	98	77.7[e]	*R*

[a] Molecular ratio: $[Pd(\eta^3\text{-}C_3H_5)Cl]_2$: ligand : **21** : dimethyl malonate : BSA : KOAc = 2.5 : 5.2 : 100 : 300 : 300 : 5. [b] Isolated yield. [c] The ee value for **22** was determined by HPLC analysis using a Chiralcel OD column. [d] Configurations were assigned by comparison of the sign of optical rotation. [e] No KOAc was used. [f] 10 equiv. KOAc was used *vs.* ligand.

chirality, which may increase the ee value in comparison with that of ligand **8**. Therefore, (S,S_p)-**11** was synthesized and subjected to the same reaction. Just as expected, a remarkable improvement in the ee value (98.5%, *S* configuration) was revealed. This result indicates that the effect of planar chirality on the stereochemical outcome is significant in this model reaction. In order to study the steric effect of the 2′-substituted group, (S,R_p)-**10** and (S,R_p)-**12** were synthesized and also used for this reaction. A reasonable result was obtained, that is, the steric bulkiness of the group was found to directly correlate with the enantioselectivity; the larger the group, the higher the ee value (compare ligand **9** *vs.* **10** and **11** *vs.* **12**). From this result, we envisaged that further increasing the steric bulkiness of the 2′-substituent of ligand **9** should also increase the enantioselectivity of the reaction. As expected, a higher ee value (83.3% ee, entry 11) was obtained when ligand **16** was used for this reaction. It was reported in the literature[12] that the addition of KOAc may sometimes increase the ee value. However, non-uniform results were obtained in our case (Table 1).

In order to explain the significant role of the planar chirality of this kind of ligand in this model reaction, the complexation behavior of **8**, **9** and **12** with $Pd(CH_3CN)_2Cl_2$ in CD_3CN was examined by ^{31}P NMR. The results showed that the ^{31}P NMR of the complex of **8** with $Pd(CH_3CN)_2Cl_2$ gave two peaks in a ratio of 7 : 3, which was consistent with the literature.[8b] However, for **9** the ratio dropped to 2 : 3, which might be assigned as diastereomers **17** and **18**, and for **12** the ratio became 22 : 1, which might be assigned as diastereomers **19** and **20** (Scheme 2). The ^{31}P NMR data showed that the addition of a third group

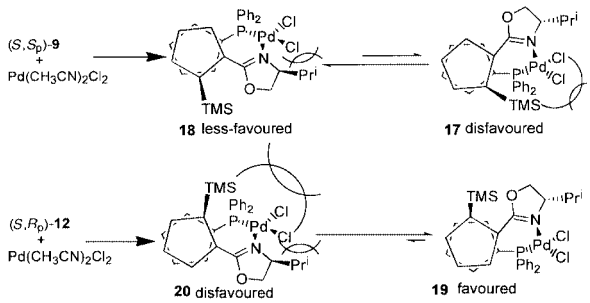

Scheme 2

in a proper disposition may favor the formation of one rotamer over the other, consistent with the ee values of the products. On the other hand, from Scheme 2, if the TMS group of compound **17** is replaced by the larger Bu_3Sn group, the balance should move towards the left. As a result, the entioselectivity of the reaction should also be increased by using ligand **16** in comparison with ligand **9**. In fact, the experimental results did agree with the above reasoning (entries 3 *vs.* 11).

In summary, we have synthesized a new kind of 1,1′-P,N-2′-disubstituted ferrocene ligand in which planar chirality was introduced. Comparison of the results for ligands **8**, **9** and **12** showed that the planar chirality is decisive in exerting control over both absolute configuration and enantiomeric excess. In addition, this kind of ligand is unique due to its multi-chirality (central, planar and axial chirality) upon coordination with Pd, and provides a new approach to the design of novel ligands. Further studies on the detailed transition-state structures, and the mechanism, and the exploration of the scope of asymmetric reactions with these promising ligands are in progress.

Financial support from The National Natural Science Foundation of China (projects 29790127 and 29872045), the Chinese Academy of Sciences, and the Shanghai Committee of Science and Technology are acknowledged. We thank Dr Yong Tang for helpful and inspiring discussions.

Notes and references

1 Reviews: I. Ojima, *Catalytic Asymmetric Synthesis*, VCH, New York, 1993; R. Noyori, *Asymmetric Catalysis in Organic Synthesis*, Wiley, New York, 1994.
2 Review: H. Brunner and W. Zettimeier, *Handbook of Enantioselective Catalysis with Transition Metal Compounds*, VCH, Weinheim, 1993.
3 A. Togni, *Angew. Chem., Int. Ed. Engl.*, 1996, **35**, 1475; H.-U. Blaser and F. Spindler, *Chimia*, 1997, **51**, 297; R. Imwinkelried, *Chimia*, 1997, **51**, 300.
4 For reviews, see: (*a*) *Ferrocenes*, ed. A. Togni and T. Hayashi, VCH, Weinheim, 1995 and references therein; (*b*) C. J. Richards and A. J. Locke, *Tetrahedron: Asymmetry*, 1998, **9**, 2377.
5 (*a*) T. Hayashi, M. Konishi, M. Fukushima, T. Mise, M. Kagotani, M. Tajika and M. Kumada, *J. Am. Chem. Soc.*, 1982, **104**, 180; (*b*) C. Bolm, K. M. Fernandez, A. Seger, G. Raabe and K. Gunther, *J. Org. Chem.*, 1998, **63**, 7860; (*c*) X.-T. Zhou, Y.-R. Lin and L.-X. Dai, *J. Org. Chem.*, 1999, **64**, 1331.
6 (*a*) S.-L. You, Y.-G. Zhou, X.-L. Hou and L.-X. Dai, *Chem. Commun.*, 1998, 2765; (*b*) X. D. Du, L.-X. Dai, X.-L. Hou, L. J. Xia and M. H. Tang, *Chin. J. Chem.*, 1998, **16**, 90.
7 T. Sammakia and H. A. Latham, *J. Org. Chem.*, 1995, **60**, 6002; C. J. Richards, T. Damalidis, D. E. Hibbs and M. B. Hursthouse, *Synlett*, 1995, 74; Y. Nishibayashi and S. Uemura, *Synlett*, 1995, 79; J. Park, S. Lee, K. H. Ahn and C.-W. Cho, *Tetrahedron Lett.*, 1995, **36**, 7263.
8 (*a*) W. Zhang, Y. Adachi, T. Hirao and I. Ikeda, *Tetrahedron: Asymmetry*, 1996, **7**, 451; (*b*) W. Zhang, Y. Yoneda, T. Kida, Y. Nakatsuji and I. Ikeda, *Tetrahedron: Asymmetry*, 1998, **9**, 3371; (*c*) J. Park, Z. Quan, S. Lee, K. H. Ahn and C.-W. Cho, *J. Organomet. Chem.*, 1999, **584**, 140; (*d*) The 91% ee value of compound **22** using ligand **8** was obtained in our laboratory, which is consistent with Ikeda's result [ref. 8(*b*)]. However, Ahn *et al.* reported that 99% ee was obtained using the same ligand [ref. 8(*c*)]; (*e*) L. Schwink, T. Ireland, K. Puntener and P. Knochel, *Tetrahedron: Asymmetry*, 1998, **9**, 1143.
9 A. Chesney, M. R. Bryce, R. W. J. Chubb, A. Batsanov and J. Howard, *Synthesis*, 1998, 413.
10 C. J. Richards and A. Mulvaney, *Tetrahedron: Asymmetry*, 1996, **7**, 1419.
11 Selected papers for P,N-chelating ligands: (*a*) P.-V. Matt and A. Pfaltz, *Angew. Chem., Int. Ed. Engl.*, 1993, **32**, 566; (*b*) A. Togni, U. Burckhardt, V. Gramlich, P. S. Pregosin and R. Salzmann, *J. Am. Chem. Soc.*, 1996, **118**, 1031; (*c*) I. Takei, Y. Nishibayashi, K. Segawa, Y. Arikawa, S. Uemura and M. Hidai, *Organometallics*, 1999, **18**, 2271; (*d*) O. Loiseleur, M. Hayashi, M. Keenan, N. Schmees and A. Pfaltz, *J. Organomet. Chem.*, 1999, **576**, 16.
12 B. M. Trost and D. Vranken, *Chem. Rev.*, 1996, **96**, 395.

Communication a909211k

ChemComm

Iron(II)-catalyzed intramolecular aminochlorination of alkenes

Thorsten Bach,* Björn Schlummer and Klaus Harms†

Fachbereich Chemie der Philipps-Universität Marburg, D-35032 Marburg, Germany.
E-mail: bach@chemie.uni-marburg.de

Received (in Liverpool, UK) 11th November 1999, Accepted 20th December 1999

2-Alkenyloxycarbonyl azides undergo an efficient intramolecular Fe^{II}-catalyzed aminochlorination with TMSCl in EtOH and furnish the corresponding 4-(chloromethyl)-oxazolidinones (60–84% yield), presumably *via* a stepwise single electron transfer pathway.

The catalytic aziridination of alkenes is a topic of current scientific interest.[1,2] In particular, transition metal catalysts which allow a nitrene transfer to alkenes and which can be modified by chiral ligands have attracted considerable attention.[3] Research in our group has been directed towards the transfer of *N*-alkoxycarbonyl substituted nitrene fragments to nucleophiles. We have shown that the reaction of *tert*-butoxycarbonyl azide ($BocN_3$) with sulfides and sulfoxides is catalyzed by $FeCl_2$ (10–25 mol%) and yields the corresponding sulfimides and sulfoximides in moderate to good yields.[4] We have now studied the Fe^{II}-catalyzed intramolecular nitrogen transfer to alkenes using the corresponding 2-alkenyloxycarbonyl azides.

Substrates of this type are known to undergo an intramolecular aziridination under thermal conditions.[5] The strained aziridines primarily formed are ring-opened readily by nucleophiles. Metal-catalyzed versions of this aziridination reaction have not been reported. Initial experiments in our laboratories were carried out with the azide **1a**[6] [eqn. (1)].

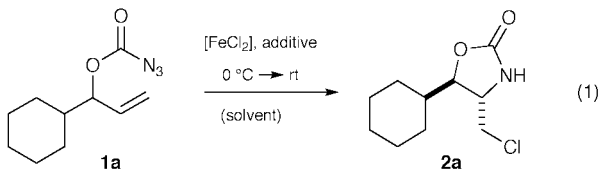

In all cases we studied, the *trans*-4-(chloromethyl)-oxazolidinone **2a** was obtained as the major nitrogen transfer product. An aziridine intermediate was not observed. In CH_2Cl_2 and THF the reaction proceeded sluggishly. MeCN proved to be a superior solvent for the desired transformation (Table 1, entry 1). Since a source of chloride ions was essential to guarantee an effective catalytic cycle we screened several candidates. TMSCl finally turned out to be the additive of choice (entry 2). It was, however, not possible to obtain acceptable yields using 0.1 equiv. of the catalyst in MeCN (entry 3). In search of another solvent which would allow a decreased catalyst loading we found EtOH to be ideally suited (entry 6). With 10 mol% of the catalyst a product yield of 72% was achieved (entry 7). In some instances, variation of the additive or the solvent led to complete inhibition of the reactions (entries 4, 5 and 8).

Table 1 Fe^{II}-catalyzed intramolecular aminochlorination of substrate **1a**

Entry	Solvent	$FeCl_2$/ equiv.	Additive	Yield (%)[a]	*trans*:*cis*[b]
1	MeCN	0.5	—	59	95:5
2	MeCN	0.5	TMSCl[c]	63	95:5
3	MeCN	0.1	TMSCl[c]	24	96:4
4	MeCN	0.5	$FeCl_3$[c]	< 5	—
5	MeCN	0.5	H_2O[d]	< 5	—
6	EtOH	0.5	TMSCl[c]	70	90:10
7	EtOH	0.1	TMSCl[c]	72	91:9
8	MeOH	0.5	TMSCl[c]	< 5	—

[a] Yield of isolated product after chromatographic purification. [b] Ratio of the two oxazolidinone diastereoisomers as determined by ^1H NMR spectroscopy. [c] 1.5 equiv. of the additive were employed.. [d] A 9:1 (v/v) solvent mixture of MeCN–H_2O was used.

† To whom inquiries about the X-ray analysis should be addressed.

Under optimized conditions (0.1 equiv. $FeCl_2$, 1.5 equiv. TMSCl, EtOH)[7] other substrates **1** reacted equally well [eqn. (2)]. In the case of the azides **1b** and **1c**, which bear a smaller

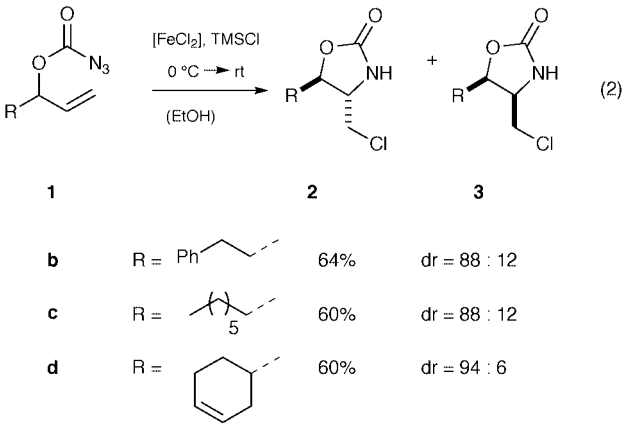

primary alkyl group at the stereogenic center, the facial diastereoselectivity was slightly lower than with the secondary alkyl substituted substrates **1a** and **1d**. The product **2d** obtained from the diastereomeric mixure of the 3-cyclohexenyl-substituted substrate **1d** was as a mixture of two 4,5-*trans*-isomers due to the additional stereogenic center at the cyclohexene ring.

Mechanistically, we initially assumed an aziridination–ring opening sequence to be responsible for the formation of the 4-(chloromethyl)oxazolidinones **2** and **3**. We started to cast doubt on this idea when we studied the Fe^{II}-catalyzed reaction of the achiral (2*E*)-alkenyloxycarbonyl azides **4** [eqn. (3)]. One

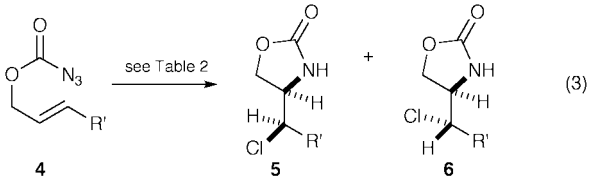

would expect the aziridination to occur stereospecifically to yield a *trans*-aziridine, which would upon ring opening form the *erythro*-product **6**. Contrary to this expectation, the azide **4a** gave only a mixture of diastereoisomers (Table 2, entry 1). We conducted the same reaction in boiling 1,1,2,2-tetrachloroethane (TCE) in the absence of Fe^{II} and obtained exclusively a single product, albeit in much lower yield (entry 2). In this case an aziridine is known to be the intermediate[5b] and the ring opening occurs most likely by HCl, which is formed from TCE upon heating.[5a] Based on analogy with the reactions of azide **4b**

Table 2 Yields and diastereoselectivities determined in the intramolecular aminochlorination of 2-alkenyloxycarbonyl azides **4**

Entry	Substrate	R′	Meth1od	Yield (%)[a]	**5**:**6**
1	**4a**	Pr	$FeCl_2$ (EtOH)	84	49:51
2	**4a**	Pr	Δ*T* (TCE)	62	<1:99
3	**4b**	Ph	$FeCl_2$ (EtOH)	76	>99:1
4	**4b**	Ph	Δ*T* (TCE)	42	<1:99

[a] Yield of isolated product after chromatographic purification.

under the same two different conditions (*vide infra*), structure **6a** was assigned to this product. A thermodynamic equilibration was ruled out because the *erythro*-product **6a** did not interconvert to the *threo*-product **5a** upon treatment with $FeCl_2$.

The difference between the two reaction variants was even more dramatic when we used azide **4b** as the starting material. The Fe^{II}-catalyzed reaction delivered exclusively the *threo*-product **5b** (entry 3), whereas the thermal reaction furnished the *erythro*-product **6b** (entry 4). In this case the relative configuration of one diastereoisomer (**5b**) could be unambiguously proven by single X-ray crystallography[8] (Fig. 1).

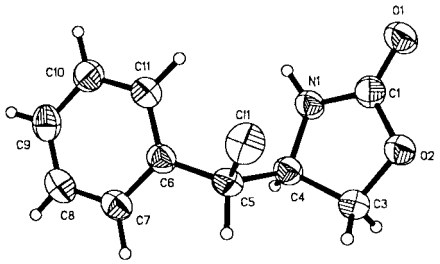

Fig. 1 A molecule of compound **5b** in the crystal.

These observations are in line with an Fe^{II}-catalyzed nitrogen transfer *via* radicals as intermediates. Apparently, the intermediate formed from $FeCl_2$ and the azide does not transfer the fragment to the alkene in a concerted fashion, but in a stepwise fashion. The reaction of **4a** is not stereospecific, as a free rotation can occur after N–C bond formation. A possible explanation for the high preference in favor of *threo*-product **5b** in the aminochlorination of substrate **4b** is shown below. The intermediate **7** formed from **4b** adopts the preferred conformation shown owing to 1,3-allylic strain; within this conformation intramolecular chloride transfer can occur diastereoselectively.

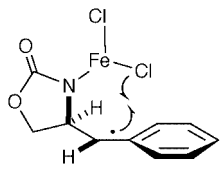

7

If this picture is correct there is an obvious analogy between the reaction we study and intermolecular radical-type aminochlorination reactions of *N*-chloro-*N*-alkenyl amines and *N*-chloroalkenamides.[9] Mechanistic evidence might consequently be deduced from comparing the stereochemical outcome of these reactions with the results obtained by the Fe^{II}-catalyzed reaction of similar substrates. A direct comparison is not yet possible as reactions of *N*-chloro-*O*-alkenyl carbamates related to **1** have to the best of our knowledge not been reported.

In further work which is currently underway we plan to undermine our mechanistic hypothesis based on the above-mentioned analogy and based on suitable radical clocks.

This work was generously supported by the *Deutsche Forschungsgemeinschaft* (SFB 260), and by the *Fonds der Chemischen Industrie* (Kekulé-fellowship to B. S.).

Notes and references

1 Review on the asymmetric synthesis of aziridines: H. M. I. Osborn and J. Sweeney, *Tetrahedron: Asymmetry*, 1997, **8**, 1693.

2 Some selected examples: D. A. Evans, M. M. Faul and M. T. Bilodeau, *J. Org. Chem.*, 1991, **56**, 6744; K. J. O'Connor, S.-J. Wey and C. J. Burrows, *Tetrahedron Lett.*, 1992, **33**, 1001; K. Noda, N. Hosoya, R. Irie, Y. Ito and T. Katsuki, *Synlett*, 1993, 469; D. A. Evans, M. M. Faul and M. T. Bilodeau, *J. Am. Chem. Soc.*, 1994, **116**, 2742; Z. Li, R. W. Quan and E. N. Jacobsen, *J. Am. Chem. Soc.*, 1995, **117**, 5889; P. Müller, C. Baud and Y. Jacquier, *Tetrahedron*, 1996, **52**, 1543; J. U. Jeong, B. Tao, I. Sagasser, H. Henniges and K. B. Sharpless, *J. Am. Chem. Soc.*, 1998, **120**, 6844.

3 Review: P. Müller, in *Advances in Catalytic Processes Vol. 2, Asymmetric Catalysis*, ed. M. P Doyle, JAI, , Greenwich, 1997, pp. 131–151.

4 T. Bach and C. Körber, *Tetrahedron Lett.*, 1998, **39**, 5015; T. Bach and C. Körber, *Eur. J. Org. Chem.*, 1999, 1033.

5 (*a*) S. C. Bergmeier and D. M. Stanchina, *Tetrahedron Lett.*, 1995, **36**, 4533; (*b*) S. C. Bergmeier and D. M. Stanchina, *J. Org. Chem.*, 1997, **62**, 4449.

6 The azides were prepared by successive treatment of the corresponding allylic alcohols with 1,1′-carbonyldiimidazole and NaN_3: P. Yuan, P. Plourde, M. R. Shoemaker, C. L. Moore and D. E. Hansen, *J. Org. Chem.*, 1995, **60**, 5360. **CAUTION**! Alkoxycarbonyl azides are potential explosives. Appropriate safety protection and utmost care are required while handling these compounds.

7 Representative procedure: A solution of **1a** (209 mg, 1.00 mmol) and TMSCl (163mg, 1.50 mmol) in dry ethanol (5 ml) was degassed with a stream of argon at 0 °C for 15 min. $FeCl_2$ (13 mg, 0.10 mmol) was added in one portion to the stirred solution. The formerly colorless reaction mixture turned yellow and nitrogen started to evolve. The solution was allowed to warm to room temperature and was stirred for another 20 h. It was then dissolved in EtOAc (20 ml) and washed with water (2 × 20 ml) and brine (20 ml). The organic layer was dried over $MgSO_4$ and the solvent was removed *in vacuo*. The brown residue was purified by chromatography on silica using pentane–*tert*-butyl methyl ether (2:8) as the eluent. A mixture of **2a** and **3a** was obtained as colorless crystals (156 mg, 72%, dr = 91:9). The analytical data were in agreement with the literature values (ref. 5).

8 *Crystal data* for **5b**: $C_{10}H_{10}ClNO_2$, *M* 211.64 g mol^{-1}, monoclinic, *a* = 789.0 (1), *b* = 583.8 (1), *c* = 2055.2 (1) pm, β = 94.175 (4)°; V = 944.1 (1) × 10^{-30} m^3, space group $P2_1/c$, *Z* = 4, λ = 3.358 mm^{-1}, reflections collected = 3750, independent reflections = 1922 [R_{int} = 0.0766], wR_2 = 0.1310, *R* = 0.0459 [$I > 2\sigma(I)$]. CCDC 182/1523.

9 Reviews: A. G. Fallis and I. M. Brinza, *Tetrahedron*, 1997, **53**, 17543; D. Savoia, in *Houben-Weyl Methoden der Organischen Chemie*, 4th edn., ed. G. Helmchen, R. W. Hoffmann, J. Mulzer and E. Schaumann, Thieme, Stuttgart, 1996, vol. E21, pp. 5265–5273.

Communication a909009f

ChemComm

New fluoroionophores from aniline dimer derivatives: a variation of cation signalling mechanism with the number of amino groups

Pascale Crochet, Jean-Pierre Malval and René Lapouyade*

Laboratoire d'Analyse Chimique par Reconnaissance Moléculaire (LACReM), Ecole Nationale Supérieure de Chimie et de Physique de Bordeaux (ENSCPB), Talence, France. E-mail: lapouyad@enscpb.u-bordeaux.fr

Received (in Liverpool, UK) 18th October 1999, Accepted 10th January 2000

New fluoroionophores, *N*-peralkylated dimers of aniline, are described.

The direct connection of an ionophore to a luminophore provides an optical ion sensor if these two components are in electronic interaction in the ground state or in the excited state.[1] Sensing is based on the modification of the two components interaction when the ion is recognized by the ionophore. According to the nature of the ionophore–fluorophore interaction, the fluorescence signal is modified in intensity or/and in energy. Fluoroionophores which undergo spectral shift on cation binding allow the measurement of the cation concentration from the ratio of the fluorescence intensity at two different wavelengths. To obtain this wavelength dependence of the fluorescence intensity, fluoroionophores with two emitting states, monomer–excimer (exciplex)[2] or ICT–TICT states,[3] the populations of which are ion-dependent, have been designed.[4] In particular, when the ionophore has a heteroatom which is a ligand of the ion and which also takes part in the first electronic transition of the fluorophore, the recognition of an ion stabilizes the heteroatom electronic pair and the fluorophore has the electronic configuration of the unsubstituted compound. The fluorescence spectrum of the ion-probe complex will be that of the probe or of the unsubstituted fluorophore (or a mixture of the two) depending on the relative rate constants of radiative emission and of the decoordination of the cation from the probe.[5] We have prepared and characterized the optical properties of *N*-peralkylated *meta*- and *para*-dimers of aniline with the monoaza-15-crown-5 ionophore replacing the dialkylamino group at one end of the molecules (**P1** and **P3**) and the

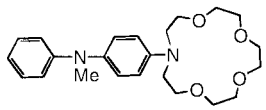

P1

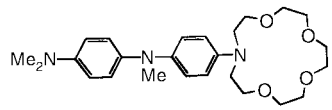

P2

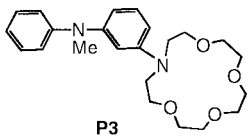

P3

para-dimethylamino derivative of **P1** with the amino group in the *para* position (**P2**). The comparison of **P1** and **P3** should provide an additional example of the '*meta* effect'.[6] The addition of the Me_2N group in **P2** should, upon cation binding, restore the photoinduced charge transfer encountered for **P1**, as we have recently observed with similar electronically symmetrical stilbenes.[7] We report here that the calcium complexes of the azacrown derivative of the peralkylated aniline dimer and its *p*-dimethylamino derivative (**P1** and **P2**) do not decoordinate in the excited state and consequently lead to new emission bands, upon cation recognition, blue-shifted for **P1** because of cation-inhibition of the CT process, and red-shifted for **P2** as a result of a cation-induced electron acceptor group which leads to a charge transfer band.

The three compounds[8] were synthesized from an Ullmann coupling of the aniline derivatives with iodonitrobenzene, followed by methylation of the secondary amine,[9] reduction of the nitro group and transformation of the resulting primary amine into the aza-15-crown-5.[10]

The absorption spectra of **P1**–**P3** extend to 340 nm and do not show significant shift with increasing solvent polarity, whereas the fluorescence, always unstructured, is red-shifted in polar solvents (Table 1). This behaviour could be attributed to rapid relaxation of the initially formed Franck–Condon excited state to a charge-transfer (CT) state. Let us assume that there is only one emitting state, whatever the polarity of the solvent; by applying the Lippert–Mataga equation[11] we can estimate dipole moments of 20.6, 8.8 and 12.2 D for **P1**, **P2** and **P3** respectively (Table 1). The monoexponential decay of **P1** implies one emitting state or several in fast equilibrium. Nevertheless the charge transfer (CT) character of the fluorescing state is large for the *p*-aniline dimer (**P1**) where we can calculate, from the Rhem–Weller equation[12] ($\Delta G = E_{ox} - E_{red} - E_{ex}$), neglecting the Coulomb part of the stabilization energy, an exergonic stabilisation energy $\Delta G = -0.36$ eV for charge separation from the *p*-phenylenediamine group in the excited state ($E_{ox} - E_{ex} = -3.78$ eV for *N*,*N*,*N*′,*N*′-tetramethyl-*p*-phenylenediamine) to the benzene substituent ($E_{red} = -3.42$ eV).[13] The excited state dipole moments of the *meta* isomer (**P3**) and of the symmetrical derivative (**P2**) are lower, relative to **P1**, because the electron donor group in **P3** has a higher oxidation potential and the potential electron acceptor substituent (dimethylaniline) in **P2** has a more negative reduction potential.

Addition of calcium perchlorate to solution of the probes in MeCN leads to the absorption spectra of the corresponding compounds without the azacrown substituent; for example, the absorption spectrum of the calcium–**P2** complex superposes with the absorption of **P1**. In fact the absorption spectra are not markedly shifted but the absorption intensity is altered enough to allow the measurement of the complexation constant K_s by a nonlinear least-squares analysis of the absorption intensity *versus* the concentration of the cation using the relation derived by Valeur[14] for probes with a sufficiently high K_s that the

Table 1 Fluorescence emission data for **P1**–**P3** and their calcium complexes

	λ_{max}/nm			ϕ_F[b]		τ_F/ns (preexp)
	Hexane	MeCN	μ_e/D[a]	Hexane	MeCN	MeCN
P1	391	489	20.6	0.05	0.03	4.20
P2	404	427	8.8			
P3	377	374	12.2			
P1–Ca		417				1.60 (66) 4.84 (34)
P2–Ca		536				

[a] Calculated according to $\nu_{flu} = -2\mu_e(\mu_c - \mu_g)/hca^3\{(\varepsilon - 1)/(2\varepsilon + 1) - (n^2 - 1)(4n^2 + 1)\}$ + constant, with $a = 4.55$ Å and $\mu_g = 1.67$ D from AM1 calculation for **P1**, $a = 4.81$ Å and $\mu_g = 0$ for **P2** and $a = 4.55$ Å and $\mu_g = 0$ for **P3**. [b] Diphenylanthracene ($\phi_F = 0.9$ in cyclohexane) as the actinometer for all compounds excited at 330 nm.

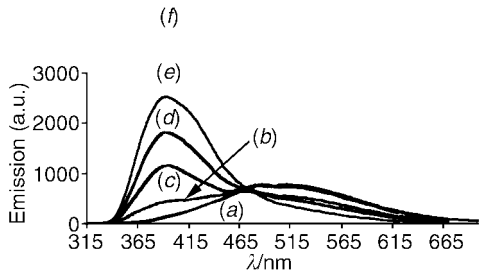

Fig. 1 Influence of Ca^{2+} on the fluorescence of a 1.86×10^{-5} M solution of **P1** in acetonitrile: $[Ca^{2+}] = 0$ M (*a*); 3.15×10^{-6} M (*b*); 6.3×10^{-6} M (*c*); 1.26×10^{-5} (*d*); 1.89×10^{-5} M (*e*); 5.67×10^{-4} M (*f*).

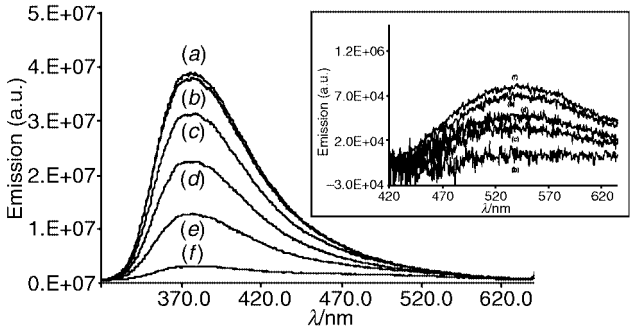

Fig. 2 Fluorescence spectra of **P2** (8.50×10^{-4} M) in acetonitrile with increasing amount of $Ca(ClO_4)_2$: $[Ca^{+2}] = 0$ M (*a*); 2.88×10^{-6} M (*b*); 8.64×10^{-6} M (*c*) 1.15×10^{-5} M (*d*); 1.73×10^{-5} M (*e*); 2.88×10^{-5} M (*f*).

concentration of the uncomplexed cation cannot be approximated to the concentration of the salt added. We obtained log K_s = 5.3 and 5.6 for **P1** and **P2**, respectively.[15] These values are higher than those found with fluoroionophores of the stilbene series built with the same ionophore but with the electron-accepting substituent in the *para* position (log $K_s \cong 4$) or even with a *p*-dimethylamino group (log $K_s \cong 4.9$).[7] The value of the complexation constants increases with the electron density on the nitrogen atom of the ionophore.

The effect of calcium on the fluorescence spectra of **P1** and **P2** is marked, while being peculiar for each compound (Fig. 1 and Fig. 2): the fluorescence of the probes is quenched, and a new emission appears of similar intensity and on the high energy side for **P1**, and with very low quantum yield ($< 10^{-4}$) and at longer wavelength for **P2**.

The complexation constants obtained from the fluorescence spectra have the same value as those from the absorption spectra. The fluorescence of the complex **P1**–Ca is in the same wavelength region as the fluorescence of Ph_2NMe and that of the complex **P2**–Ca corresponds to that of **P1**.

These characteristics indicate that there is no decoordination of the cation during the excited state lifetime of the probes. With **P1** the cation lowers the energy of the electron pair on the nitrogen atom of the azacrown, which accordingly is decoupled from the π aromatic system. In a first approximation we can estimate that the **P1**–Ca complex has the same electronic configuration as Ph_2NMe. With the same reasoning, we could consider that **P2**–Ca is identical to **P1**, but if the spectral position and the solvatochromism of the emission are comparable, the quantum yield of fluorescence of the **P2**–Ca complex is very low. The Ca–nitrogen atom interaction, which should be reinforced in the excited state, could open a new channel for non-radiative deactivation. In conclusion these *N*-peralkylated dimers of aniline provide interesting fluoroionophores with high complexation constants and distinct fluorescence shifts upon cation complexation. In conjugation with the phenyl-azacrown ionophore, the PhMeN substituent is an electron donor in the ground state of the probe, while the benzene group can be an electron acceptor with the probe in the excited state. As cation recognition by the azacrown should have the same electronic effect as protonation, the results reported here should be pertinent to the fluorescence modification of polyaniline when the protonic level of doping is increased. Longer and conformationaly constrained oligoanilines are under study to achieve oligomeric fluorescent cation probes[16*a*,*b*] and to better understand the electronic properties of polyaniline.

We thank Colette Belin and Jean-Pierre Desvergne for help with the fluorescence experiments and the Ecole Nationale Supérieure de Chimie et de Physique de Bordeaux for financial support.

Notes and references

1 *Chemosensors of Ion and Molecule Recognition*, ed. J.-P. Desvergne and A. W. Czarnik, Kluwer, Boston, 1997; W. Rettig and R. Lapouyade, *Topics in Fluorescence Spectroscopy*, ed. J. R. Lakowicz, Plenum, New York, 1994, vol. 4, pp. 109–149; B. Valeur and E. Bardez, *Chem. Br.*, 1995, **31**, 216.
2 H. Bouas-Laurent, A. Castellan, M. Daney, J.-P. Desvergne, G. Guinand, P. Marsau and M. Riffaud, *J. Am. Chem. Soc.*, 1986, **108**, 315.
3 J.-F. Letard, S. Delmond, R. Lapouyade, D. Braun, W. Rettig and M. Kreissler, *Recl. Trav. Chim. Pays-Bas*, 1995, **114**, 517.
4 For a review see: A. Prasanna de Silva, H. Q. Nimal Gunaratne, T. Gunnlaugsson, A. J. Huxley, C. P. McCoy, J. T. Rademacher and T. E. Rice, *Chem. Rev.*, 1997, **97**, 1515.
5 R. Mathevet, G. Jonusauskas, C. Rulliere, J.-F. Letard and R. Lapouyade, *J. Phys. Chem.*, 1995, **99**, 15 709.
6 F. D. Lewis and J.-S. Yang, *J. Am. Chem. Soc.*, 1997, **119**, 3834.
7 S. Delmond, J.-F. Letard, R. Lapouyade, R. Mathevet, G. Jonusauskas and C. Rulliere, *New. J. Chem.*, 1996, **20**, 861.
8 The structure of the compounds was confirmed by ^1H, ^{13}C NMR and MS.
9 A. Barco, S. Benetti, G. P. Pollini and P. G. Baraldi, *Synthesis*, 1976, 124.
10 H. Maeda, S. Furuyoshi, Y. Nakatsuji and M. Okahara, *Bull. Chem. Soc. Jpn.*, 1983, **56**, 212.
11 E. Z. Lippert, *Z. Naturforsch., Teil. A*, 1955, **10**, 541; N. Mataga, Y. Kaifu and M. Koizumi, *Bull. Chem. Soc. Jpn.*, 1956, **29**, 465.
12 D. Rehm and A. Weller, *Ber. Bunsenges. Phys. Chem.*, 1969, **73**, 834.
13 J. Mortensen and J. Heinze, *Angew. Chem., Int. Ed. Engl.*, 1984, **23**, 84.
14 J. Bourson, J. Pouget and B. Valeur, *J. Phys. Chem.*, 1993, **97**, 4552.
15 (*a*) When complexed with calcium the very efficient photoconversion of the *meta* isomer **P3** to carbazole derivatives precludes an accurate measurement of K_s. This photoreaction parallels the well-studied photocyclization of Ph_2NMe to *N*-methylcarbazole [ref. 15(*b*)]; (*b*) K. H. Grellmann, W. Kühnle, H. Weller and T. Wolff, *J. Am. Chem. Soc.*, 1981, **103**, 6889.
16 (*a*) B. Waug and M. R. Wasielewski, *J. Am. Chem. Soc.*, 1997, **119**, 12; (*b*) Q. Zhai and T. M. Swager, *J. Am. Chem. Soc.*, 1995, **117**, 12 593.

Communication a908393f

ChemComm

Efficient blue–green light emitting poly(1,4-phenylene vinylene) copolymers†

Rainer E. Martin,[a] Florence Geneste,[a] Robert Riehn,[b] Beng Sim Chuah,[a] Franco Cacialli,[b] Richard H. Friend[b] and Andrew B. Holmes*[a]

[a] *Melville Laboratory, Department of Chemistry, University of Cambridge, Pembroke Street, Cambridge, UK CB2 3RA. E-mail: abh1@cus.cam.ac.uk*

[b] *Cavendish Laboratory, Department of Physics, University of Cambridge, Madingley Road, Cambridge, UK CB2 0HE*

Received (in Cambridge, UK) 29th November 1999, Accepted 18th January 2000

2,3-Dialkoxy-substituted poly(1,4-phenylene vinylene) (PPV) homo- and co-polymers have been prepared by the Gilch dehydrohalogenation polycondensation of the corresponding bishalomethyl-substituted benzene monomers, and double layer light emitting devices fabricated with these materials exhibited high electroluminescence efficiencies with low turn-on voltages.

Semiconducting organic polymers exhibiting electroluminescence (EL) have recently attracted considerable interest owing to their high potential for application as the active layer in polymer light-emitting devices (PLEDs).[1–5] The 2,3-disubstituted derivatives of PPV are of interest owing to the potential distortion of the intra- and inter-molecular chain interactions as a result of steric effects.[6] Poly(2,3-dibutoxy-1,4-phenylene vinylene)[7] **1** exhibits a blue–green solid state photoluminescence (PL) with 40% efficiency which is considerably higher than the prototypical 2,5-dialkoxy-substituted analogue, MEH-PPV.[8] We have also reported a new class of 2-silylated and 2,5-disilylated PPV derivatives which essentially behave as organic solvent processible analogues of PPV itself, but which are much more luminescent (PL efficiency 60%). However, single layer (100 nm) devices fabricated from poly(2-dimethyloctylsilyl-1,4-phenylene vinylene) (DMOS-PPV)[9,10] **2** and poly[2,5-bis(dimethyloctylsilyl)-1,4-phenylene vinylene] (BDMOS-PPV)[11] **3** suffered from rather high turn-on voltages of *ca*. 15 V. It has recently been reported that high efficiencies may be realised in ternary statistical copolymers of PPV derivatives,[12] and that the degree of defects is determined in part by non-regioregular coupling of the putative quinomethide precursor in the Gilch polycondensation.[13]

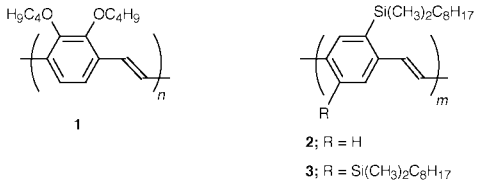

Here, we report an improved synthesis of 1,4-bis(bromomethyl)-2,3-dibutoxybenzene **8** and the exploitation of two important monomers to yield the statistical copolymers poly[(2-dimethyloctylsilyl-1,4-phenylene vinylene)-*co*-(2,3-dibutoxy-1,4-phenylene vinylene)] (DMOS-*co*-DB-PPV) **11** and poly-{bis[(2,5-dimethyloctylsilyl)-1,4-phenylene vinylene]-*co*-(2,3-dibutoxy-1,4-phenylene vinylene)} (BDMOS-*co*-DB-PPV) **12**, respectively, that combine the intrinsically high electroluminescence present in the three corresponding homopolymers **1**–**3** with the significantly reduced turn-on voltages of 2,3-dialkoxy-substituted PPVs.

The synthesis of the 2,3-dibutoxy monomer **8** is shown in Scheme 1. The key improvements were the use of the double Mannich reaction to introduce both carbon substituents and the conversion of the diol formed from saponification of the diacetate **7** with CBr_4 and PPh_3[14] into the crystalline 1,4-bis-bromomethyl compound **8**.‡ Statistical copolymersation under Gilch conditions of monomer **8** with **9**[9,10] and **10**,[11] using in both cases a feed ratio of 1:1, in the presence of excess KOBu^t in degassed THF at room temperature (Scheme 2) gave the copolymers **11** and **12**, respectively. The polymers were purified by precipitation from methanol and acetone or mixtures of methanol–water, respectively, and formed bright yellow fibres displaying high luminescence. ^{1}H NMR side-chain analysis of DMOS-*co*-DB-PPV **11** gave the ratio *n*:*m* of 3:4 and for BDMOS-*co*-DB-PPV **12** of 4:3.

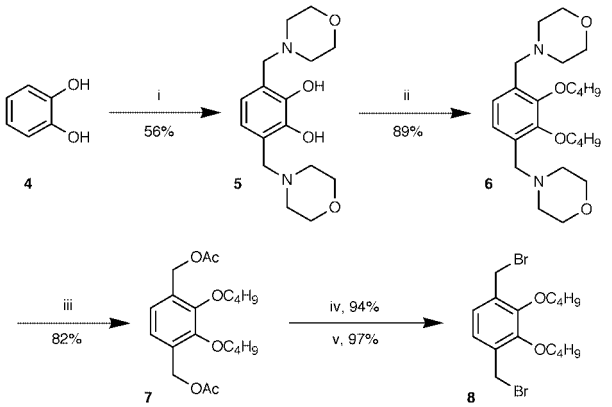

Scheme 1 *Reagents and conditions*: i, CH_2O, morpholine, Pr^{i}OH, reflux, 1 h. ii, C_4H_9Br, K_2CO_3, EtOH, reflux, 20 h. iii, Ac_2O, NaOAc, HOAc, reflux, 72 h. iv, K_2CO_3, MeOH–THF–H_2O (50:9:3), 48 h. v, CBr_4, PPh_3, THF, 4 h.

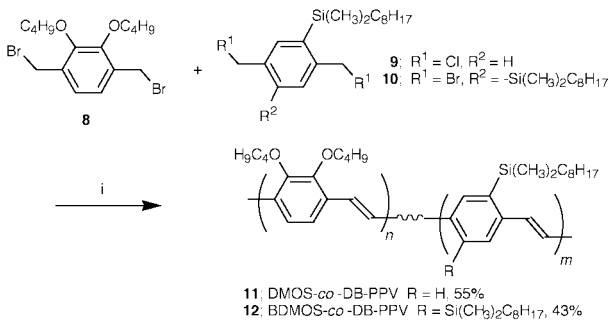

Scheme 2 *Reagents and conditions:* i,KOBu^t, THF, 18 h.

Molecular weight determination of the purified polymers using size-exclusion chromatography (SEC) calibrated with polystyrene standards and multiple angle light scattering revealed high molecular weights and polydispersities, typical of dehydrohalogenation polycondensations (DMOS-*co*-DB-PPV: M_n = 290 000, M_w/M_n = 7.1; BDMOS-*co*-DB-PPV: M_n = 180 000, M_w/M_n = 5.5). DMOS-*co*-DB-PPV **11** and BDMOS-

† Electronic supplementary information (ESI) available: normal optical absorption, PL and EL spectra (Fig. S1) and cyclic voltammograms (Fig. S2) for BDMOS-DB-PPV. See http://www.rsc.org/suppdata/cc/a9/a909382f/

co-DB-PPV **12** readily dissolved in aprotic solvents such as THF, chloroform or xylene and formed good uniform transparent films on ITO-coated glass substrates. The thermal properties of the polymers were investigated by thermal gravimetry (TG) and differential scanning calorimetry (DSC) under nitrogen. Analysis of the TG trace (heating rate 10 °C min^{-1}) for DMOS-*co*-DB-PPV and BDMOS-*co*-DB-PPV revealed a 5% weight loss at *ca*. 370 and 320 °C, respectively. BDMOS-*co*-DB-PPV showed an exothermic phase transition at *ca*. 170 °C.

Optical absorption measurements in $CHCl_3$ solutions for DMOS-*co*-DB-PPV and BDMOS-*co*-DB-PPV showed λ_{max} of 440 and 442 nm, respectively. Interestingly, DMOS-*co*-DB-PPV showed for the λ_{max} in the solid-state a bathochromic shift to 448 nm, whereas BDMOS-*co*-DB-PPV revealed a slightly hypsochromically shifted value of 440 nm (Fig. S1 in ESI). The longest wavelength absorption maxima reflected the statistical composition of the respective monomeric building blocks; DB-PPV **1**: λ_{max} = 454 nm; DMOS-PPV **2**: λ_{max} = 414 nm; BDMOS-PPV **3**: λ_{max} = 436 nm. Both polymers are bright yellow materials exhibiting high solid-state PL efficiencies of 35 and 28%, with the longest wavelength emission peaks at λ_{em} = 548 nm (2.26 eV) and λ_{em} = 544 nm (2.28 eV, (Fig. S1 in ESI)), respectively.

Cyclic voltammetry (CV) was perfomed on thin polymer films of BDMOS-*co*-DB-PPV **12** spin-coated onto Pt disk electrodes in MeCN using a Pt wire as counter electrode and Ag/AgCl as a reference. In the anodic scan the onset of oxidation occurred at *ca*. 1.2 V followed by three subsequent non-reversible oxidations at 1.38, 1.63 and 1.80 V, respectively (Fig. S2 in ESI). The cathodic sweep showed onset of reduction at *ca*. −1.6 V and a quasi-reversible reduction step at −1.83 V (Fig. S2 in ESI). The electrochemically measured band gap was 2.8 V, which compares well with the HOMO–LUMO energy gap of 2.82 eV as measured from UV–VIS spectroscopy. The HOMO and LUMO energy levels of BDMOS-*co*-DB-PPV were estimated from the oxidation and reduction onset potentials to be HOMO = 5.6 eV and LUMO = 2.8 eV, respectively.[15]

Double layer devices with the configuration ITO/PEDOT:PSS/polymer/cathode were fabricated, [PEDOT:PSS is poly(3,4-ethylenedioxythiophene):poly(styrene sulfonate)].§ Both polymers exhibited blue–green light emission. Interestingly, DMOS-*co*-DB-PPV LEDs only showed EL emission for Ca cathodes evaporated at pressures of *ca*. 10^{-3} mbar, but little or no EL for evaporation at pressures $\leqslant 3 \times 10^{-6}$ mbar. DMOS-*co*-DB-PPV **11** double layer LEDs with Al cathodes showed turn-on voltages of 2.0–2.4 V (threshold = 0.01 cd m^{-2}) with a power efficiency of 0.05 cd A^{-1} and a maximum luminance of 36 cd m^{-2} at 11 V. Substantially better performance (both efficiency and luminance) was noted for devices made with BDMOS-*co*-DB-PPV **12** and Ca cathodes compared with devices made with DMOS-*co*-DB-PPV **11**. The power efficiency was up to 0.72 cd A^{-1} with a maximum luminance of 1384 cd m^{-2} at 12 V and turn-on voltages of 4.0 V for a structure with an 80 nm active layer (Fig. 1). This compares well with a 6 V turn-on voltage for the BDMOS-PPV **3** based homopolymer device.[11] The EL emission peak was measured at λ_{em} = 533 nm (2.33 eV).

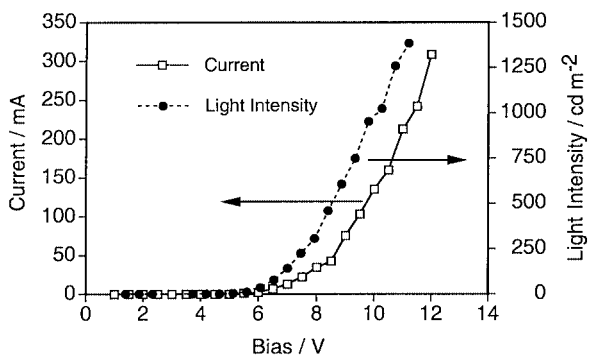

Fig. 1 Current–voltage–luminance (I–V–L) characteristics of an ITO/PEDOT (80 nm)/BDMOS-DB-PPV (80 nm)/Ca LED. The active area of the device is *ca*. 0.045 cm^2. EL emission turns on at 4.0 V and the maximum efficiency is 0.72 cd A^{-1}.

In summary, a new and versatile synthetic route for the preparation of 2,3-dialkoxy-1,4-bis(bromomethyl) monomers was developed. Improved EL performance of devices using statistical copolymers such as BDMOS-*co*-DB-PPV **12** as the active layer in comparison with the homopolymers was demonstrated, making this material a promising candidate for further optimisation.

We thank EPSRC for financial support and provision of the Swansea Mass Spectrometry Service, the Swiss National Science Foundation and Churchill College, Cambridge (Fellowships to R. E. M.), the Royal Society (University Research Fellowship to F. C.), the Commission of the European Union (Marie Curie Fellowship to F. G., TMR network 'SELOA' and Brite-Euram Contract BRPR-CT97-0469 'OSCA'), the Cambridge Commonwealth Trust and the CVCP (ORS studentship to B. S. C.) and Cambridge Display Technology (CDT) for generous support.

Notes and references

‡ All new monomers were characterised fully by their melting points, IR, ^1H and ^{13}C NMR spectroscopy, EI or CI MS spectrometry and elemental analysis.

§ Absorption and PL spectroscopy were carried out on thin films deposited onto spectrosil substrates by means of a Hewlett Packard B453 UV–VIS spectrophotometer (absorption) and of a CCD UV-enhanced spectrograph (PL). The PL efficiency was determined on films deposited on spectrosil substrates, using a nitrogen purged integrating sphere. Excitation was by means of the visible or multiline UV lines (*ca*. 351, 364 nm) of an Ar-ion laser. LEDs were prepared on commercial ITO substrates (Asahi), treated prior to use with a oxygen plasma for 10 min.[16] The PEDOT:PSS (Bayer) was coated from a water dispersion yielding a *ca*. 80 nm thick layer after drying (*ca*. 90 °C; 1 h).[17] Active layers were spin-coated from THF–*p*-xylene solutions on either the bare ITO or on ITO/PEDOT substrates to give film thickness of 80–100 nm. Cathodes (Al or Ca/Al) thermal evaporation (at *ca*. 5×10^{-6} mbar or less) completed the preparation of the diodes which were then tested in a 10^{-2} mbar vacuum.

1 A. Kraft, A. C. Grimsdale and A. B. Holmes, *Angew. Chem., Int. Ed.*, 1998, **37**, 402.
2 J. L. Segura, *Acta Polym.*, 1998, **49**, 319.
3 R. H. Friend, R. W. Gymer, A. B. Holmes, J. H. Burroughes, R. N. Marks, C. Taliani, D. D. C. Bradley, D. A. Dos Santos, J. L. Brédas, M. Lögdlund and W. R. Salaneck, *Nature*, 1999, **397**, 121.
4 J. R. Sheats, Y. L. Chang, D. B. Roitman and A. Stocking, *Acc. Chem. Res.*, 1999, **32**, 193.
5 F. Cacialli, *Curr. Opin. Coll. Int. Sci.*, 1999, **4**, 159.
6 B. R. Hsieh, Y. Yu, E. W. Forsythe, G. M. Schaaf and W. A. Feld, *J. Am. Chem. Soc.*, 1998, **120**, 231.
7 B. S. Chuah, F. Cacialli, D. A. dos Santos, N. Feeder, J. E. Davies, S. C. Moratti, A. B. Holmes, R. H. Friend and J. L. Brédas, *Synth. Met.*, 1999, **102**, 935.
8 N. C. Greenham, I. D. W. Samuel, G. R. Hayes, R. T. Philips, Y. A. R. R. Kessener, S. C. Moratti, A. B. Holmes and R. H. Friend, *Chem. Phys. Lett.*, 1995, **241**, 89.
9 D.-H. Hwang, S. T. Kim, H.-K. Shim, A. B. Holmes, S. C. Moratti and R. H. Friend, *Chem. Commun.*, 1996, 2241.
10 S. T. Kim, D.-H. Hwang, X. C. Li, J. Grüner, R. H. Friend, A. B. Holmes and H.-K. Shim, *Adv. Mater.*, 1996, **8**, 979.
11 H.-Y. Chu, D.-H. Hwang, L.-M. Do, J.-H. Jang, H.-K. Shim, A. B. Holmes and T. Zyung, *Synth. Met.*, 1999, **101**, 216.
12 H. Spreitzer, H. Becker, E. Kluge, W. Kreuder, H. Schenk, R. Demandt and H. Schoo, *Adv. Mater.*, 1998, **10**, 1340.
13 H. Becker, H. Spreitzer, E. Kluge, K. Ibrom and W. Kreuder, *Macromolecules*, 1999, **32**, 4925.
14 (*a*) C. J. Hawker and J. M. J. Fréchet, *J. Chem. Soc., Chem. Commun.*, 1990, 1010; (*b*) C. J. Hawker and J. M. J. Fréchet, *J. Am. Chem. Soc.*, 1990, **112**, 7638.
15 M. D. de Leeuw, M. M. J. Simenon, A. B. Brown and R. E. F. Einerhand, *Synth. Met.*, 1997, **87**, 53.
16 J. S. Kim, R. H. Friend and F. Cacialli, *J. Appl. Phys.*, 1999, **86**, 2774.
17 T. M. Brown, J. S. Kim, R. H. Friend, F. Cacialli, R. Daik and W. J. Feast, *Appl. Phys. Lett.*, 1999, **75**, 1679.

Communication a909382f

ChemComm

Radical pair recombination stereoselectivity as a probe of magnetic isotope and magnetic field effects

George Lem and Nicholas J. Turro*

Chemistry Department, Columbia University, New York, New York 10027, USA. E-mail: turro@chem.columbia.edu

Received (in Corvallis, OR, USA) 22nd November 1999, Accepted 7th January 2000

Photolysis of *meso*- or *dl*-2,4-diphenylpentan-3-one within NaY zeolites, coadsorbed with a chiral inductor, lead to enantioselective radical pair recombinations which are sensitive to ^{13}C isotope effects, but insensitive towards external magnetic field effects.

We report here rationally designed systems, based on well-established radical pair chemistry, which investigate the stereoselectivity of recombination of prochiral radical pairs for which significant magnetic field effects and magnetic isotope effects have been observed in micelles.[1,2] The concept of the systems is the following. A prochiral triplet radical pair that can be produced reversibly is generated in a chiral, supramolecular[3] environment that (i) allows the separation of the pair to distances allowing for the exchange interaction between the partners of the pair to decrease to values of the order smaller than those available from external or internal magnetic fields,[1] and (ii) encourages reencounters of the pair. Each recombination of the pair can produce either the (+) or (−)-enantiomer, but in the presence of a chiral inductor within the supramolecular environment, a certain enantiomeric selectivity can result.[4] For any given system in which some ee is observed, the efficiency of ee resulting from radical pair recombination is expected to depend on the radical pair lifetime, which has consequences in terms of the effective interactions between the pair and the chiral inductor. In this scenario, magnetic field and magnetic isotope effects on the enantioselectivity may result if the lifetime of the pair is extended or diminished. From a survey of published results, we selected the supercage of NaY faujasite zeolites[5] as the host supramolecular environment,[6] the photolyses of *meso*- and *dl*-2,4-diphenylpentan-3-one (*meso*-**1** and *dl*-**1**, respectively) to generate triplet radical pairs and a co-adsorbed chiral inductor such as diethyl L-tartrate and (+)- or (−)-ephedrine as chiral inductors.

As depicted in Scheme 1, photolysis of *meso*-**1** results in the formation of *dl*-**1** and *vice versa* (for simplicity only the photoprocesses of *meso*-**1** are shown).[7] According to the conventional paradigm of ketone photochemistry,[8] α-cleavage of triplet excited **1** leads to the formation of *sec*-phenethyl and *sec*-phenethylacyl triplet geminate radical pairs (GRP). If the space available in the supercage allows rapid diffusional separation of the primary geminate pair, then decarbonylation of the *sec*-phenethylacyl radical and subsequent formation of diastereomeric 2,3-diphenylbutanes **2** occurs.[7] If diffusion is restricted, but rotation of the triplet radical pairs relative to one another is permitted, intersystem crossing (ISC) of the radical pairs occurs to yield *meso*-**1** or *dl*-**1**. Additionally, if the environment is chiral, *dl*-**1** with some degree of enantiomeric enrichment can be produced. Of these processes, only the rate of ISC is sensitive towards magnetic effects.[1a,b] Thus, the ratios between decarbonylation products and recombination products,[2c] as well as the ee of photoproduced *dl*-**1** can serve as probes for magnetic effects on the radical pair recombination stereochemistry. While we expect the ratio of recombination products/decarbonylation products to increase as the rate of ISC increases, predictions on the direction of change of the ee of photoproduced *dl*-**1** cannot be made *a priori*.

Table 1 summarizes the ee values of recovered *dl*-**1** upon photolysis of *dl*-**1** in NaY co-loaded with diethyl L-tartrate as a function of both external magnetic field strength and isotope. It can be seen that there are no differences, within experimental error, in the ee (measured by chiral GC) of the photolyzed *dl*-**1** when the photoreaction is carried out at either 0 or 2 kG. However, upon photolysis at 0 kG of *dl*-**1** enriched in ^{13}C (98% enriched) at the carbonyl carbon, a significant increase in the ee of the recovered *dl*-**1** is observed when the ^{13}C labeled isomer is photolyzed relative to the unlabeled isotopomer (3.0 *vs.* 1.6%, respectively). Additionally, a slight increase in the amount of recombination product *vs.* decarbonylation products was observed in the photolysis of *dl*-**1**-^{13}CO relative to *dl*-**1**-^{12}CO.[9] However, no such trend has seen in the photolysis of *dl*-**1**-^{12}CO performed at 0 *vs.* 2 kG.

In order to assess the influence of initial stereochemistry of **1** on the enantioselectivity of *dl*-**1** as a function of external magnetic field and isotope effects, photolyses of *meso*-**1** were performed in NaY using ephedrine as the chiral inductor.[10] From Table 2, it can be seen that photolyses of *meso*-**1** in NaY in the presence of ephedrine, significantly higher ees for *dl*-**1** are obtained compared to utilizing *dl*-**1** as the starting material and diethyl L-tartrate as the inductor. However, similar to the results obtained with diethyl L-tartrate, only a ^{13}C isotope effect is observed while external field effects are absent. Thus, an

Table 1 Photolysis of *dl*-**1** in NaY co-loaded with diethyl tartrate[a]

Magnetic field/kG[b]	Ketone	Chiral inductor	Ee of *dl*-**1** (%)[cd]
2	*dl*-**1**-^{12}CO	diethyl L-tartrate	+2.0 ± 0.2
0	*dl*-**1**-^{12}CO	diethyl L-tartrate	+1.6 ± 0.3
0	*dl*-**1**-^{13}CO	diethyl L-tartrate	+3.0 ± 0.1

[a] The average occupancy of *dl*-**1** in NaY is ~0.05 molecules per cage and that of diethyl tartrate ~1 molecules per cage; *dl*-**1** was photolyzed to 35–45% conversion. [b] Ref. 12. [c] Errors correspond to standard deviations derived from three or more independent experiments. [d] After photolysis, *dl*-**1** is separated from *meso*-**1** *via* preparative TLC and analyzed by chiral GC.

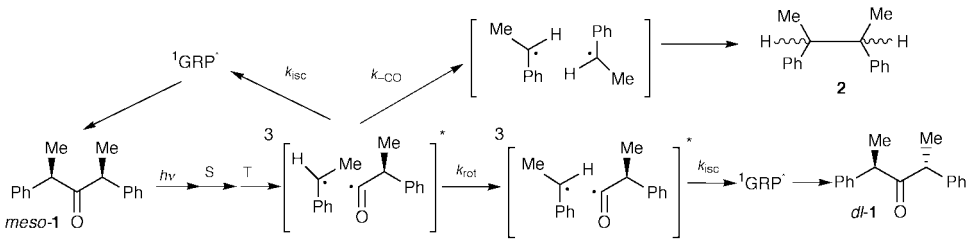

Scheme 1

Table 2 Photolysis of *meso*-**1** in NaY co-loaded with ephedrine[a]

Magnetic field/kG[b]	Ketone	Chiral inductor	Ee of *dl*-**1** (%)[cd]
2	*meso*-**1**-^{12}CO	(−)-ephedrine	+4.9 ± 1.9
0	*meso*-**1**-^{12}CO	(−)-ephedrine	+4.7 ± 1.9
0	*meso*-**1**-^{13}CO	(−)-ephedrine	+9.9 ± 1.3
2	*meso*-**1**-^{12}CO	(+)-ephedrine[e]	−4.3 ± 1.6
0	*meso*-**1**-^{12}CO	(+)-ephedrine[e]	−3.6 ± 0.6
0	*meso*-**1**-^{13}CO	(+)-ephedrine[e]	−7.1 ± 0.5

[a] The average occupancy of *meso*-**1** in NaY is ~0.05 molecules per cage and that of ephedrine ~1 molecules per cage; *meso*-**1** was photolyzed to 26–50% conversion. [b] Ref. 12. [c] Errors correspond to standard deviations derived from three independent experiments. [d] After the photolysis, *dl*-**1** is separated from *meso*-**1** *via* preparative TLC and analyzed by chiral GC. [e] The hemihydrate form was used.

approximate two-fold increase in the ee of *dl*-**1** is observed upon photolysis of *meso*-**1**-^{13}CO compared to that of *meso*-**1**-^{12}CO [+10% *vs.* +5%, with (−)-ephedrine] (Table 2). Additionally, more recombination product was observed for the photolysis of *meso*-**1**-^{13}CO compared to that of *meso*-**1**-^{12}CO.[11]

We can interpret the data in Tables 1 and 2 based on the mechanism of triplet–singlet ISC for triplet biradicals.[13,2c,f] It is recognized that if triplet radical pairs are separated by distances of several Å or more, the singlet–triplet energy gap is decreased and ISC is controlled by weak hyperfine couplings induced by nuclear-spin interactions which are magnetic field and isotope dependent. Thus, ^{13}C is expected to induce a faster ISC in the radical pair relative to ^{12}C, for which only protons provide a hyperfine mechanism for ISC. External magnetic fields can reduce the rate of ISC by increasing the S–T energy gap for two of the three triplet sublevels. Experimental results for such phenomena have been the subject of several reviews.[1,2]

In hydrocarbon solutions, *sec*-phenethylacyl radicals decarbonylate with a rate constant of $\sim 5 \times 10^7$ s^{-1}.[14] In polar solvents, the rate of CO loss can be reduced.[15] Since the internal cages of zeolite supercages are considered highly polar,[16] decarbonylation in the zeolite must be significantly slower than 5×10^7 s^{-1}. Recombination of structurally related benzoyl and cumyl radical pairs obtained from the photolysis of dimethyldeoxybenzoin, in SDS micellar solutions, has been measured to occur with a rate constant on the order of $\sim 1.2 \times 10^7$ s^{-1}.[17] This rate is expected to be increased by ^{13}C isotope effects, *via* changes in the rate of ISC. An increased rate of ISC can be manifested in the different ee values for recovered *dl*-**1** obtained upon irradiation of either *meso*- or *dl*-**1** containing different isotopic labels at the carbonyl carbon. Since there is a lack of information in the rotational dynamics between the prochiral GRPs and the chiral inductor, the trend of the ee of the photoreaction cannot be predicted *a priori*.

The experimental results show an increase in the ee of *dl*-**1**-^{13}CO relative to its ^{12}C isotopomer. Furthermore, photolysis of **1**-^{13}CO leads to a slight decrease in the amount of decarbonylated products relative to the ^{12}C labeled isotopomer.[9,11] Similar results have also been previously observed for the photolysis of dibenzylketone-^{13}CO in faujasites.[2c] Hence, an increase in the ee of the photoproduced *dl*-**1**-^{13}CO may be a function of its faster rate of ISC, leading to a greater number of recombinational processes from the primary GRP as compared to *dl*-**1**-^{12}CO which maintains a relatively lower rate of ISC from the triplet GRP and thus higher propensity to form decarbonylated products.[2a,b,4a,18]

According to the product ratios and the ee values expressed in Tables 1 and 2, there are no observable external field effects in the photolysis of either *meso*- or *dl*-**1**. At this time we lack a theoretical kinetic model to explain these experimental results. Although it has been widely demonstrated that magnetic field and magnetic isotope effects can influence the rate of ISC for triplet biradicals in opposite manners, there is a lack of information on the *magnitudes* of those rates. It can be argued that external field effects, as they pertain to **1** in faujasites, are very small and subtle as compared to magnetic isotope effects. Indeed, in similar product studies done with dibenzyl ketone (DBK) adsorbed in faujasites, external magnetic field effects were significantly smaller than those observed for ^{13}C isotope effects.[2c]

The results show that photochemical enantiomeric selectivity through geminate radical recombinations in zeolite cavities is feasible. The most important finding is that ee values are sensitive to magnetic isotope effects, and consequently can be used as a probe of radical pair dynamics in zeolites.

This work was supported in part by the NSF and the Department of Energy under Grant No. NSF CHE 9810367 to the Environmental Molecular Sciences Institute at Columbia University and National Science Foundation Grant No. CHE 98-12676. We are especially indebted to Dr Valery Tarasov of the Russian Academy of Sciences for helpful discussions and sharing unpublished data.

Notes and references

1 (*a*) U. E. Steiner and T. Ulrich, *Chem. Rev.*, 1989, **89**, 51; (*b*) K. M. Salikhov, Yu. N. Molin, R. Z. Sagdeev and A. L. Buchachenko, in *Spin Polarization and Magnetic Effects in Radical Reactions*, Elsevier, Amsterdam, 1984; (*c*) N. J. Turro, *Proc. Natl. Acad. Sci. U.S.A.*, 1983, **80**, 609; (*d*) N. J. Turro and B. Kraeutler, *Acc. Chem. Res.*, 1980, **13**, 369.

2 (*a*) E. N. Step, V. F. Tarasov, A. L. Buchachenko and N. J. Turro, *J. Phys. Chem.*, 1993, **97**, 363; (*b*) V. Tarasov, N. D. Ghatlia, A. L. Buchachenko and N. J. Turro, *J. Phys. Chem.*, 1991, **95**, 10 220; (*c*) N. J. Turro and Z. Zhang, *Tetrahedron Lett.*, 1989, **30**, 3761; (*d*) N. J. Turro, M. B. Zimmt and I. R. Gould, *J. Phys. Chem.*, 1988, **92**, 433; (*e*) M. B. Zimmt, C. Doubleday and N. J. Turro, *J. Am. Chem. Soc.*, 1985, **107**, 6727; (*f*) M. B. Zimmt, C. Doubleday and N. J. Turro, *J. Am. Chem.Soc.*, 1984, **106**, 3363; (*g*) N. J. Turro and G. C. Weed, *J. Am. Chem. Soc.*, 1983, **105**, 1861; (*h*) B. H. Baretz and N. J. Turro, *J. Am. Chem. Soc.*, 1983, **105**, 1309.

3 J.-M. Lehn, in *Supramolecular Chemistry*, VCH, Weinheim, 1995; V. Balzani and F. Scandola, in *Supramolecular Photochemistry*, Prentice-Hall, New York, 1991, ch. 3.

4 N. A. Kaprinidis, M. S. Landis and N. J. Turro, *Tetrahedron Lett.*, 1997, **38**, 2609; V. J. Rao, S. R. Uppili, D. R. Corbin, S. Schwarz, S. R. Lustig and V. Ramamurthy, *J. Am. Chem. Soc.*, 1998, **120**, 2480; A. Joy, R. J. Robbins, K. Pitchumani and V. Ramamurthy, *Tetrahedron Lett.*, 1997, **38**, 8825; G. Sundarababu, M. Leibovitch, D. R. Corbin, J. R. Scheffer and V. Ramamurthy, *Chem. Commun.*, 1996, 2159.

5 D. W. Breck, in *Zeolite Molecular Sieves: Structure, Chemistry and Use*, Wiley, New York, 1974.

6 V. Ramamurthy, in *Photochemistry in Organized and Constrained Media*, ed. V. Ramamurthy, VCH, New York, 1991.

7 N. D. Ghatlia and N. J. Turro, *J. Photochem. Photobiol. A: Chem.*, 1991, **57**, 7.

8 N. J. Turro, in *Modern Molecular Photochemistry*, Benjamin-Cummings, Menlo Park, CA, 1978, ch. 13.

9 Ratio of *meso*-**1**:**2** = 0.12 for the photolysis of *dl*-**1**-^{12}CO, ratio of *meso*-**1**:**2** = 0.19 for the photolysis of *dl*-**1**-^{13}CO.

10 No data is reported for the stereoselectivity of the photoreaction of *meso*-**1** in NaY–diethyl tartrate systems due to analytical difficulties in measuring the ee of *dl*-**1** recovered from such photolysis.

11 Ratio of *dl*-**1**:**2** = 0.64 for the photolysis of *meso*-**1**-^{12}CO, ratio of *dl*-**1**:**2** = 0.92 for the photolysis of *meso*-**1**-^{13}CO.

12 Irradiations at 2 kG were performed by photolyzing the sample between the poles of a permanent magnet.

13 N. J. Turro, in *Modern Molecular Photochemistry*, Benjamin-Cummings, Menlo Park, CA, 1978, ch. 6.

14 I. R. Gould, B. H. Baretz and N. J. Turro, *J. Phys. Chem.*, 1987, **91**, 925; N. J. Turro, I. R. Gould and B. H. Baretz, *J. Phys. Chem.*, 1983, **87**, 531.

15 Y. P. Tsentalovich and H. Fisher, *J. Chem. Soc., Perkin Trans. 2*, 1994, 729.

16 V. Ramamurthy, D. R. Sanderson and D. F. Eaton, *Photochem. Photobiol.*, 1992, **56**, 29; K. K. Iu and J. K. Thomas, *Langmuir*, 1990, **6**, 471.

17 I. R. Gould, M. B. Zimmt, N. J. Turro, B. H. Baretz and G. F. Lehr, *J. Am. Chem. Soc.*, 1985, **107**, 4605.

18 V. F. Tarasov, N. D. Ghatlia, A. L. Buchachenko and N. J. Turro, *J. Am. Chem. Soc.*, 1992, **14**, 9517; V. F. Tarasov, N. D. Ghatlia, N. I. Avdievich, I. A. Shkrob, A. L. Buchachenko and N. J. Turro, *J. Am. Chem. Soc.*, 1992, **116**, 2281; V. F. Tarasov, I. A. Shkrob and A. L. Buchachenko, *Chem. Phys. Lett.*, 1989, **135**, 391.

Communication a909256k

Crown-annelated 9,10-bis(1,3-dithiol-2-ylidene)-9,10-dihydroanthracene derivatives: a new efficient transducer in the electrochemical and spectroscopic monitoring of metal complexation

Martin R. Bryce,*[a] Andrei S. Batsanov,[a] Terry Finn,[a] Thomas K. Hansen,[a]† Judith A. K. Howard,[a] Marta Kamenjicki,[b] Igor K. Lednev[b] and Sanford A. Asher[b]

[a] *Department of Chemistry, University of Durham, Durham, UK DH1 3LE. E-mail: m.r.bryce@durham.ac.uk*
[b] *Department of Chemistry, University of Pittsburgh, Pittsburgh PA 15260, USA*

Received (in Liverpool, UK) 28th October 1999, Accepted 21st December 1999

S_2O_4-Crown annelated derivatives of 9,10-bis(1,3-dithiol-2-ylidene)-9,10-dihydroanthracene function as efficient ligands in the voltammetric and spectroscopic recognition of Na^+ and Ag^+.

Redox-active ligand systems are important in the field of electrochemically-controlled uptake and release of guest metal cations.[1] For large shifts of the redox potential to be observed upon metal binding the antennae [*e.g.* crown ether unit(s)] should be situated close to the redox-responsive centre (*i.e.* the transducer), thereby enhancing the intramolecular electrostatic (through-space) effect which modulates the redox signal. Typical molecular[2] redox species for this purpose are ferrocene,[3] metal coordinated dithiolate[4] and diimine,[5] and tetrathiafulvalene (TTF) derivatives,[6] *e.g.* **1**[6a,b] and **2**.[6d] For these systems cation binding induces a positive shift of the one-electron oxidation potential E_1^{ox}.

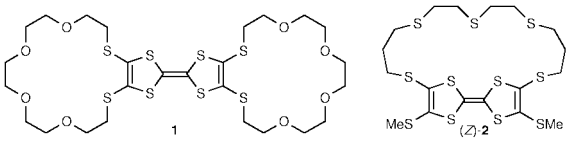

Derivatives of 9,10-bis(1,3-dithiol-2-ylidene)-9,10-dihydroanthracene are versatile building blocks in supramolecular and materials chemistry.[7] The special feature of this system is a *two-electron* oxidation wave [neutral → dication, E_1^{ox} *ca.* +0.35 V‡ (in MeCN, *vs.* Ag/AgCl) which is electrochemically quasi-reversible and chemically reversible].[8] Herein we report the first crown-annelated derivatives **5** and **8**.

Reaction of anthraquinone **3** with the new reagent **4**[9] under standard conditions[8,10] gave a mixture of the bis- and mono-crown annelated derivatives **5** and **6**, respectively (Scheme 1).§

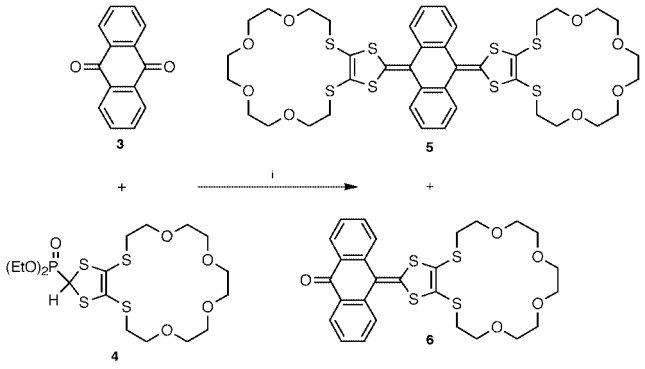

Scheme 1 i, **4**, LDA, THF, −78 °C, 3 h, then addition of **3**, then −78 to 20 °C.

† Present address: Medicinal Chemistry Research, Novo Nordisk A/S, Novo Nordisk Park, 2760 Maløv, Denmark.

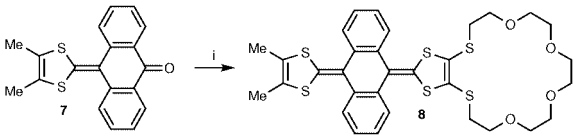

Scheme 2 i, **4**, LDA, THF, −78 °C, 3 h, then addition of **7**, then −78 to 20 °C.

The latter was characterised by X-ray diffraction.¶ Reaction of **4** with **7**[8a] gave the bis(1,3-dithiole) system **8** (Scheme 2).

An X-ray crystallographic study¶ of **8**·CH_2Cl_2 showed a motif of saddle-shaped molecules (Fig. 1) engulfing each other's dimethyldithiole ends. The anthracenediylidene moiety is folded along the C(9)···C(10) vector, the two benzene rings forming a dihedral angle of 39° (*cf.* 21° in **6**). The dithiole rings are folded along the S(1)···S(2) and S(3)···S(4) vectors by 15.5 and 8.7°, and the S(1)C(16)C(17)S(2) and S(3)C(19)C(20)S(4) planes form an acute dihedral angle of 81°.

The cation binding properties of **5** were assessed by ^{1}H NMR titration studies in $CDCl_3$ at 50 °C (at 20 °C a precipitate formed on addition of metal salts). In the presence of Na^+ and Ag^+ the resonances due to the $–SCH_2CH_2O–$ protons of the crown [(SCH_2) δ 3.05; (OCH_2) δ 3.66] shifted downfield by *ca.* 0.07 ppm in the presence of 10 equiv. of Na^+ and Ag^+, while the anthracenediylidene resonances were unaffected, confirming that cation binding occurs at the crown site. Li^+ and K^+ cations had essentially no effect on the ^{1}H NMR spectrum. UV–VIS absorption spectra for **5** in MeCN in the presence of both Na^+ and Ag^+ (as the perchlorate salts) resulted in a specific change in the spectra. No isosbestic points were observed, indicating that, most probably, both 1:1 and 1:2 complexes [*i.e.* **5**M^+ and **5**$(M^+)_2$] form simultaneously, and the absorption spectra of these species are different. Such behaviour is known for other bis(crown) chromoionophores.[11] Fig. 2 shows the changes in the spectrun of **5** upon complexation with Ag^+. The stability constants for the formation of **5**M^+ and **5**$(M^+)_2$ were estimated to be logK_1 *ca.* 3.4 and log K_2 *ca.* 5.5, respectively.

Cyclic voltammetry (CV) and square wave voltammetry (SQV) showed that **5** and **8** display a two-electron oxidation

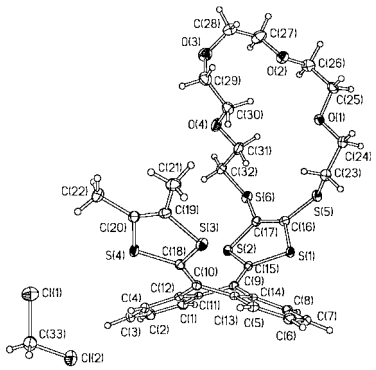

Fig. 1 Molecular structure of **8**·CH_2Cl_2 (50% displacement ellipsoids).

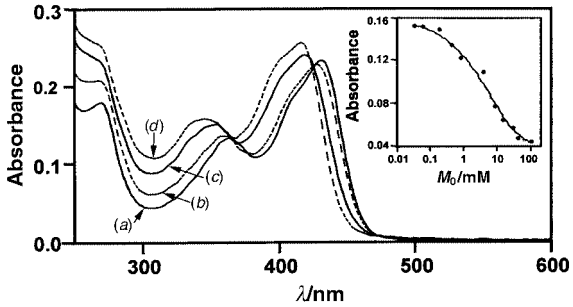

Fig. 2 Absorption spectra of **5** (2×10^{-5} M) in MeCN (1 cm cell) containing $AgClO_4$ at concentrations of (*a*) 0, (*b*) 0.5, (*c*) 8.0 and (*d*) 30 mM. Inset: absorption at 445 nm as a function of Ag salt concentration fitted with eqn. (1), where A_0, A_1 and A are the absorbances of the free ligand L and

$$A = A_0 + \frac{K_1M_0(A_1 - A_0)}{1 + K_1M_0 + K_2M_0^2} + \frac{K_2M_0^2(A_\infty - A_0)}{1 + K_1M_0 + K_2M_0^2} \quad (1)$$

complexes LM^+ and $L(M^+)_2$, respectively; K_1 and K_2 are equilibrium constants for complex formation.

wave: E_1^{ox} +0.405 V (**5**) and E_1^{ox} +0.345 V (**8**). A second reversible one-electron wave, ascribed to oxidation of the anthracene system[8b,c] (*i.e.* radical trication formation) was seen at E_2^{ox} 1.62 V for both compounds [CV data were recorded *vs.* Ag/AgCl, $Bu_4N^+ClO_4^-$ (0.1 M), MeCN, 20 °C, 100 mV s^{-1}]. The progressive addition of aliquots of metal triflate salts resulted in a positive shift of E_1^{ox} (and a similar positive shift of the coupled reductive peak on the cathodic scan), while E_2^{ox} remained unchanged, thereby acting as an internal reference. This is consistent with expulsion of the metal cation from the ionophore prior to the second oxidation wave. The maximum positive shifts (ΔE_1^{ox}) are as follows: Li^+ (15–20 mV), Na^+ (100 mV), K^+ (15–20 mV) and Ag^+ (115 mV). The values of ΔE_1^{ox} are essentially the same for the mono- and bis-crown systems **8** and **5**, respectively, whereas in the TTF series, *e.g.* **1**, a larger shift is observed for bis-crowns. This is likely to be a consequence of intramolecular steric interactions between the crown rings of **5**, and/or sandwich complexation between two crowns, favoured by the rigid saddle conformation. A comparison with related S_2O_4-crowned TTF systems[6] shows two important advantages of systems **5** and **8**: (i) the positive shifts for Na^+ and Ag^+ are significantly larger, and (ii) the system is significantly more sensitive, with saturation being achieved with < 10 equiv. of cation (Fig. 3) (*cf.* 200 equiv. for **1**[6a]).

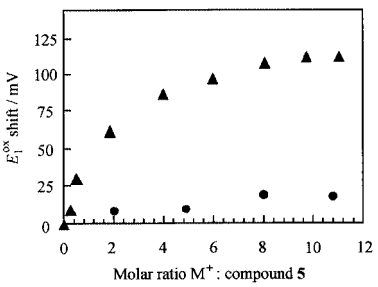

Fig. 3 Shift of E_1^{ox} in the CV of **5** with added equivalents of AgOTf (▲) and KOTf (●). Data were obtained in 0.2 M Bu_4NBF_4, MeCN, Pt disk electrode, 50 mV s^{-1}, Ag/AgCl reference electrode, referenced *vs.* decamethylferrocene.

We suggest that these results are a consequence of the unique combination of structural and redox properties of the 9,10-bis(1,3-dithiol-2-ylidene)-9,10-dihydroanthracene transducer unit: (i) the saddle-shape folding of the anthracenediylidene system places the crown ring(s) of **5** and **8** in close proximity to the redox-responsive moiety, and there is a marked conformational change upon oxidation,[7a] and (ii) the E_1^{ox} redox process which is monitored is a *two-electron* oxidation (*cf.* the one-electron wave of TTF, ferrocene *etc.*) thereby enhancing the electrostatic repulsion with the bound metal cation(s) leading to an increase in ΔE_1^{ox}.

In summary, using ligands **5** and **8** we have exploited for the first time the chromophoric and redox properties of the 9,10-bis(1,3-dithiol-2-ylidene)-9,10-dihydroanthracene system to provide efficient and controllable cation recognition within appended crown ether units. To enhance further these effects we suggest that redox species which undergo a *multi-electron* wave (*e.g.* certain dendrimers)[12] should be targets for future transducers in redox-controlled molecular recognition.

We acknowledge funding for this work from EPSRC, Office of Naval Research, Grant #: N00014-94-1-0592 (S. A. A.) and DOE Grant #: DE-FG07-98ER62708 (S. A. A.), and thank Dr A. J. Moore for helpful discussions.

Notes and references

‡ E_1^{ox} = anodic peak potential on the first wave of the oxidative scan.

§ Compounds **4**, **5**, **6** and **8** gave spectroscopic and analytical data consistent with their structures. *Selected data* for **5**: orange crystals, 67% yield, mp 216–218 °C (from CH_2Cl_2–cyclohexane); $\delta_H(CDCl_3)$ 3.05 (8H, m), 3.66 (32H, m), 7.33 (4H, m) and 7.56 (4H, m). For **8**: orange crystals, 53% yield; mp 223–225 °C (from CH_2Cl_2); $\delta_H(CDCl_3)$ 1.94 (6H, s), 3.00 (4H, m), 3.58 (16H, m), 7.29 (4H, m), 7.52 (2H, m) and 7.68 (12H, m).

¶ Diffraction data were measured on a SMART 1K CCD area detector (graphite-monochromated Mo-Kα radiation, λ = 0.71073 Å). Structures were solved by direct methods and refined against F^2 of all data, using SHELXL97 (G. M. Sheldrick, University of Göttingen, 1997). *Crystal data* for **6**: $C_{27}H_{28}O_5S_4$, M = 560.7, T = 150 K, orthorhombic, $P2_12_12_1$ (No. 19), a = 7.600(1), b = 18.395(1), c = 18.566(4) Å, U = 2596(1) Å^3, Z = 4, D_c = 1.435 g cm^{-3}, μ = 0.40 mm^{-1}, 10781 reflections (4219 unique, R_{int} = 0.037) with 2θ = 52.7°, 418 variables, R = 0.038 [3920 data, $I > 2\sigma(I)$], $wR(F^2)$ = 0.083, $\Delta\rho$ max./min. = 0.28, −0.21 e Å^{-3}. The absolute structure was determined from anomalous X-ray scattering: Flack parameter 0.07(8). For **8**: $C_{32}H_{34}O_4S_6{\cdot}CH_2Cl_2$, M = 759.9, T = 120 K, triclinic, $P\bar{1}$ (No. 2), a = 11.891(2), b = 12.546(1), c = 12.691(2) Å, α = 104.93(1), β = 97.02(1), γ = 106.60(1)°, U = 1713(1) Å^3, Z = 2, D_c = 1.473 g cm^{-3}, 9437 reflections (7080 unique, R_{int} = 0.025) with 2θ = 55°, 551 variables, R = 0.037 [6205 data, $I > 2\sigma(I)$], $wR(F^2)$ = 0.089, $\Delta\rho$ max./min. = 0.43, −0.29 e Å^{-3}. CCDC 182/1511. See http://www.rsc.org/suppdata/cc/a9/a908716h/ for crystallographic data in .cif format.

1 G. W. Gokel, *Chem. Soc. Rev.*, 1992, **21**, 39; P. L. Boulas, M. Gomez-Kaifer and L. Echegoyen, *Angew. Chem., Int. Ed.*, 1998, **37**, 216; A. E. Kaifer, *Acc. Chem. Res.*, 1999, **32**, 62.

2 Crown substituted conjugated polymers (*e.g.* polythiophenes) have also been widely studied in this context. Review: L. M. Goldenberg, M. R. Bryce and M. C. Petty, *J. Mater. Chem.*, 1999, **9**, 1957.

3 J. C. Medina, T. T. Goodnow, S. Bott, J. L. Atwood, A. E. Kaifer and G. W. Gokel, *J. Chem. Soc., Chem. Commun.*, 1991, 290; P. D. Beer, *Acc. Chem. Res.*, 1998, **31**, 71.

4 M. L. H. Green, W. B. Heuer and G. C. Saunders, *J. Chem. Soc., Dalton Trans.*, 1990, 3789.

5 F. Van Veggel, M. Bos, S. Harkema, H. van de Bovenkamp, H. Reedijk and D. Reinhoudt, *J. Org. Chem.*, 1991, **56**, 225.

6 (*a*) T. K. Hansen, T. Jørgensen, P. C. Stein and J. Becher, *J. Org. Chem.*, 1992, **57**, 6404; (*b*) R. Dieing, V. Morrison, A. J. Moore, L. M. Goldenberg, M. R. Bryce, J. M. Raoul, M. C. Petty, J. Garín, M. Saviron, I. K. Lednev, R. E. Hester and J. N. Moore, *J. Chem. Soc., Perkin Trans. 2*, 1996, 1587; (*c*) A. J. Moore, L. M. Goldenberg, M. R. Bryce, M. C. Petty, A. P. Monkman, C. Marenco, J. Yarwood, M. J. Joyce and S. N. Port, *Adv. Mater.*, 1998, **10**, 395; (*d*) F. Le Derf, M. Marari, N. Mercier, E. Levillain, P. Richomme, J. Becher, J. Garín, J. Orduna, A. Gorgues and M. Sallé, *Chem. Commun.*, 1999, 1417; (*e*) H. Liu, S. Liu and L. Echegoyen, *Chem. Commun.*, 1999, 1493.

7 (*a*) M. R. Bryce, A. J. Moore, M. Hasan, G. J. Ashwell, A. T. Fraser, W. Clegg, M. B. Hursthouse and A. I. Karaulov, *Angew. Chem., Int. Ed. Engl.*, 1990, **29**, 1450; (*b*) N. Martín, I. Pérez, L. Sánchez and C. Seoane, *J. Org. Chem.*, 1997, **62**, 5690; (*c*) Y. Yamashita and M. Tomura, *J. Mater. Chem.*, 1998, **8**, 1933; (*d*) C. Boulle, O. Desmars, N. Gautier, P. Hudhomme, M. Cariou and A. Gorgues, *Chem. Commun.*, 1998, 2197.

8 (*a*) A. J. Moore and M. R. Bryce, *J. Chem. Soc., Perkin Trans. 1*, 1991, 157; (*b*) M. R. Bryce, M. A. Coffin, M. B. Hursthouse, A. I. Karaulov, K. Müllen and H. Scheich, *Tetrahedron Lett.*, 1991, **32**, 6029; (*c*) N. Martín, L. Sánchez, C. Seoane, E. Ortí, P. M. Viruela and R. Viruela, *J. Org. Chem.*, 1998, **63**, 1268.

9 Reagent **4** was prepared from the corresponding 1,3-dithiole-2-thione derivative [ref. 6(*a*)] by the same route used for analogues [ref. 8(*a*)].

10 K. Akiba, K. Ishikawa and N. Inamoto, *Bull. Chem. Soc. Jpn.*, 1978, **51**, 2674.

11 R. M. Izatt, K. Pawlak and J. Bradshaw, *Chem. Rev.*, 1991, **91**, 1721.

12 W. Devonport, M. R. Bryce, G. J. Marshallsay, A. J. Moore and L. M. Goldenberg, *J. Mater. Chem.*, 1998, **8**, 1361 and references therein.

Communication a908716h

Encapsulation and biocatalytic activity of the enzyme pepsin in fatty lipid films by selective electrostatic interactions

Anand Gole,[a] Chandravanu Dash,[b] Mala Rao,*[b] and Murali Sastry*[a]

[a] *Materials Chemistry Division, National Chemical Laboratory, Pune-411 008, India. E-mail: sastry@ems.ncl.res.in*
[b] *Biochemical Sciences Division, National Chemical Laboratory, Pune-411 008, India. E-mail: malarao@dalton.ncl.res.in*

Received (in Cambridge, UK) 29th November 1999, Accepted 19th January 2000

The encapsulation of pepsin by electrostatically controlled diffusion from solution into thermally evaporated fatty amine films is described and the catalytic activity of the immobilized enzyme on hemoglobin is investigated.

The entrapment of proteins in different inert matrices with the aim of protecting the proteins against microbial degradation, hydrolysis, autoproteolysis, deamidation, *etc*.; retention of the native protein structure and accessibility of the encapsulated proteins to cofactors, substrates and redox agents is a problem of current interest especially where application in biosensors/ biocatalysis is sought. Proteins have been immobilized in phospholipid bilayers,[1] on self-assembled monolayers (SAMs),[2] in silicate sol–gels,[3] in polymer matrices,[4] in Langmuir–Blodgett films,[5] within the galleries of α-zirconium phosphates[6] as well as polymer microspheres.[7] Developing on our earlier work on the spontaneous self-organization of fatty acid salts[8] and electrostatic assembly of colloidal nanoparticles,[9,10] we show here, that the proteolytic enzyme pepsin (which occurs in the gastric juice of all mammals), can be encapsulated *via* electrostatic interaction in thermally evaporated fatty lipid matrices (octadecylamine, ODA) by simple immersion of the lipid film in the protein solution under extremely mild preparation conditions (Schematic 1, inset of Fig. 1). The encapsulated enzyme showed good biocatalytic activity using hemoglobin as the substrate. The biocatalytic activity was determined by estimating the amount of acid-soluble tyrosine and tryptophan residues released by reaction of the encapsulated pepsin on hemoglobin.

Pepsin (molecular weight = 37400; pI ≈ 1 where pI represents the isoelectric point)[11] was obtained from Sigma Chemicals and used as received. A 10^{-6} M solution of pepsin was prepared in glycine–HCl buffer (0.05 M, pH 3), close to the pH value at which pepsin exhibits maximum catalytic activity. 250 and 1000 Å thick ODA (Aldrich) films were deposited by thermal evaporation on gold coated AT cut quartz crystals (for quartz crystal microgravimetry (QCM) measurements) and Si(111) substrates (for FTIR and activity measurements) in an Edwards E306A chamber. Fig. 1 shows a plot of the QCM mass uptake recorded *ex situ* from a 250 Å thick ODA film as a function of time of immersion in the pepsin solution. Details of the QCM measurement procedure may be obtained from our earlier reports.[9,10] It can be seen that the diffusion of pepsin into the lipid matrix is extremely rapid with maximum protein uptake being accomplished within 10 min of immersion. The small time scale for encapsulation of the enzyme in the lipid matrix is a particularly attractive feature of this approach and considerably improves upon the days to weeks timeframe required in other techniques for synthesis of such bio-composites.[3,6] At pH 3, the ODA matrix is positively charged (pK_B of ODA = 10.5) while the pepsin molecules are negatively charged (pI of pepsin ≈ 1.0) thereby leading to attractive electrostatic interactions and a rapid diffusion of the proteins into the lipid matrix (see inset of Fig. 1). The maximum mass loading in the film (Fig. 1) is measured to be *ca*. 3900 ng cm^{-2} of the film yielding a pepsin concentration of 6.3×10^{13} molecules per cm^2 of the ODA–pepsin composite film.

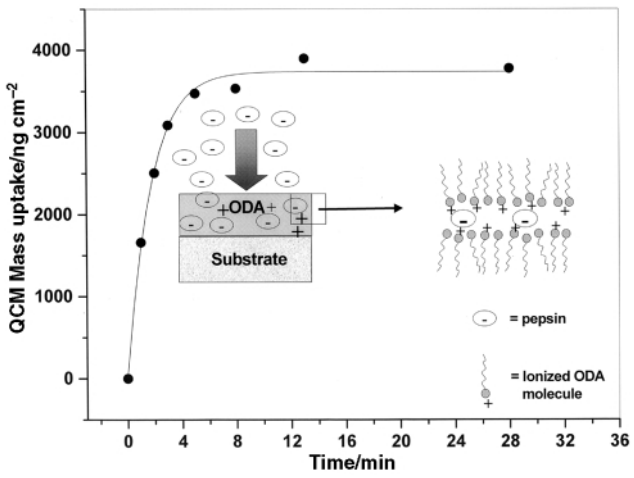

Fig. 1 QCM mass uptake curve measured *ex situ* as a function of time of immersion of 250 Å thick ODA films in 10^{-6} M pepsin solution at pH 3. The schematic in the figure illustrates the procedure adopted for synthesis of the pepsin–ODA composite and the probable microscopic structure of the film and enzyme encapsulation.

It is well known that proteins spontaneously concentrate at the phase boundaries[12] and simple surface adsorption of pepsin on the ODA film surface must be ruled out. Contact angle measurements of a sessile water drop (1 μl, Rame Hart 100 goniometer used) were carried out on a 250 Å thick ODA film on Si(111) substrates after immersion in 10^{-6} M pepsin solution at pH 3 for 60 min and careful washing of the film. The measurements carried out at different points on the film surface yielded a mean value of 90° which is very close to the contact angle of 100° recorded for the as-deposited ODA film. The contact angle recorded for the pepsin–ODA composite film is much higher than the values of 20 and 15° measured for the bare Si(111) substrate surface and a pepsin film formed on Si by evaporating a drop of the pepsin solution respectively, indicating clearly that the pepsin molecules are not adsorbed on the surface of ODA but within the lipid film.

Fig. 2 shows the FTIR spectra recorded from a 1000 Å thick as-deposited ODA film (curve 1), the ODA film after immersion in 10^{-6} M pepsin solution kept at pH 3 for 60 min (curve 2) and the pepsin–ODA nanocomposite film after testing the catalytic activity of the pepsin–ODA film by immersion in hemoglobin solution (curve 3, as discussed subsequently). A number of vibrational modes can be observed for the three films. The amide I band occurs at 1647 cm^{-1} for the pepsin–ODA nanocomposite film (feature A, curve 2, Fig. 2) and the film after reaction with hemoglobin (curve 3, Fig. 2). Whereas a small feature at this wavenumber does occur in the as-deposited ODA film, the intensity of this band increases in films 2 and 3 clearly showing that it originates in the pepsin molecules. The position of this band is close to that reported for native proteins in earlier reports[6,13] and indicates that the

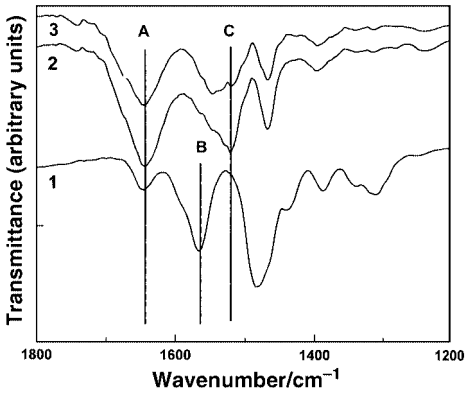

Fig. 2 FTIR spectrum recorded from a 1000 Å thick ODA film before (curve 1) and after immersion for 60 min in pepsin solution at pH 3 (curve 2). The spectrum measured from the pepsin–ODA film after assay with hemoglobin is also shown (curve 3). Features A–C are discussed in the text.

secondary structure of the enzyme in the ODA environment is unperturbed. The amide II band, which occurs at 1521 cm^{-1} (feature C, Fig. 2), can also clearly be seen for the pepsin–ODA composite film as well as the film after the activity test with hemoglobin (curves 2 and 3 respectively). This band also indicates that the secondary structure of the protein is maintained in the encapsulated form.[13] Small differences are observed in the amide II bands for the pepsin–ODA films before and after reaction with hemoglobin. This may be due to a contribution of hemoglobin molecules in the ODA matrix in the digested/undigested form and suggests a possible mechanism for the action of encapsulated pepsin on the heme-protein. However, further work is required before an unequivocal statement can be made on this observation. The origin of the band at 1564 cm^{-1} (feature B, Fig. 2) is as yet not fully understood but it clearly arises from the ODA matrix and its intensity is reduced on complexation of the ODA molecules with pepsin.

The biochemical activity of the enzyme encapsulated in the lipid matrix was determined by reaction with a solution of hemoglobin (5 mg ml^{-1}) prepared in glycine–HCl buffer (0.05 M, pH 3.0) and by incubating the reaction mixture at 37 °C for 30 min. Pepsin digests hemoglobin and yields acid soluble products which are readily detected by their strong UV signatures at 280 nm.[14] Quartz substrates of known dimensions coated with 250 Å thick ODA films were immersed in pepsin solution for 1 h until the pepsin density in the films reached equilibrium values (6.3×10^{13} pepsin molecules cm^{-2} of film, see QCM studies). These films were immersed in 1 ml of hemoglobin solution (5 mg ml^{-1}) and incubated at 37 °C for 60 min and then withdrawn. The reaction was quenched by addition of an equal volume of 1.7 M perchloric acid to the reaction mixture and the precipitate removed by centrifugation. The supernatant containing the acid soluble tyrosine and tryptophan residues was analysed using UV–VIS spectroscopy and the optical absorbance at 280 nm determined (Shimadzu-6201 PC spectrophotometer operated at a resolution of 1 nm). For comparison, the enzymatic activity of pepsin in solution was determined in a similar fashion. The values obtained from these activity measurements are given in Table 1. It is observed that the activity of pepsin in the ODA matrix is slightly less than that of the enzyme in solution. This may be a consequence of the orientation of the enzyme in the lipid matrix limiting the accessibility of the substrate hemoglobin to the active enzyme sites. Another possibility is that all the enzyme molecules do not participate in the biocatalysis in the first run. That this is so is indicated by the fact that one of the films showed enzymatic activity during three successive runs, albeit considerably reduced each time (Table 1).

Table 1 Comparison of enzymatic activity of pepsin in solution and ODA entrapped pepsin using hemoglobin as the substrate

System	Amount of pepsin/μg	Activity[a]/ units	Activity/ units μg^{-1}
Pepsin	2.0	7.5	3.75
Pepsin–ODA (film 1)	2.7	9	3.33
Pepsin–ODA (film 2, run 1)	3.6	10	2.77
Pepsin–ODA (film 2, run 2)	3.6	1.2	0.333
Pepsin–ODA (film 2, run 3)	3.6	0.5	0.136

[a] One unit of enzyme will produce a change in absorbance at 280 nm of 0.001 min^{-1} at pH 3.0 and 37 °C measured as PCA soluble products using hemoglobin as the substrate (ref. 14).

The different measurements on the pepsin–ODA composite films clearly establish the following. The electrostatically controlled diffusion of the enzyme molecules from the aqueous phase into the lipid matrix may be accomplished under conditions close to that where the enzyme shows maximum activity by suitable choice of the lipid (either cationic or anionic). The enzyme molecules are encapsulated within the ODA matrix without significant distortion to the native structure. The elasticity of the bilayers may be primarily responsible for this and enables the matrix to adopt the contours of the enzyme molecule (Schematic, inset of Fig. 1). The reasonably fast time-scales for the synthesis of the enzyme–lipid composites and the enzyme–friendly encapsulation conditions are a major improvement over other techniques currently being investigated.[1,3,4,6]

Two of us (A. G. and C. D.) thank the Council for Scientific and Industrial Research (CSIR), Government of India, for financial assistance.

Notes and references

1 I. Hamachi, A. Fujita and T. Kunitke, *J. Am. Chem. Soc.*, 1994, **116**, 8811.
2 J. Fang and C. M. Knobler, *Langmuir*, 1996, **12**, 1368.
3 I. Gill and A. Balleseros, *J. Am. Chem. Soc.*, 1998, **120**, 8587.
4 K. Yoshinaga, K. Kondo and A. Kondo, *Polym. J.*, 1995, **27**, 98.
5 A. Boussaad, L. Dziri, R. Arechabaleta, N. J. Tao and R. M. Leblanc, *Langmuir*, 1998, **14**, 6215.
6 C. V. Kumar and G. L. McLendon, *Chem. Mater.*, 1997, **9**, 863.
7 F. Karen, K. Griebenow, L. Hsieh, A. M. Klibanov and R. Langer, *J. Controlled Release*, 1999, **58**, 357.
8 P. Ganguly, S. Pal, M. Sastry and M. N. Shashikala, *Langmuir*, 1995, **11**, 1078.
9 M. Sastry, V. Patil and S. R. Sainkar, *J. Phys. Chem. B.*, 1998, **102**, 1404.
10 V. Patil, R. B. Malvankar and M. Sastry, *Langmuir*, 1999, **15**, 8197.
11 *The Enzymes: Vol. 4* ed. by P. D. Boyer, H. Lardy and K. Myrback, Academic Press, New York, 1960, ch. 4.
12 L. Razumovsky and S. Damodaran, *Langmuir*, 1999, **15**, 1392.
13 A. Dong, P. Huang and W. S. Caughey, *Biochemistry*, 1992, **31**, 182.
14 M. Anson, *J. Gen. Physiol.*, 22, **79**, 1938.

Communication a909385k

Synthesis of the chlorin macrocycle by the '3 + 1' approach

Dennis H. Burns,*[a] Dong Chuan Shi[a] and Timothy D. Lash[b]

[a] *Department of Chemistry, Wichita State University, Wichita, Kansas 67260, USA. E-mail: burns@wsuhub.uc.twsu.edu*

[b] *Department of Chemistry, Illinois State University, Normal, Illinois 61790, USA.*

Received (in Corvallis, OR, USA) 1st November 1999, Accepted 29th December 1999

The one-step regioselective synthesis of a chlorin macrocycle from a tripyrrane and bisformylpyrrole is described for the first time; the chlorin is furnished in 46% yield and is constructed from readily prepared pyrroles.

The magnesium chlorins (dihydroporphyrins) found in the photosynthetic proteins of green plants[1] are utilized in light harvesting arrays and electron transfer reaction centers. With similar photophysical characteristics to their chlorophyll counterparts, synthetic chlorins are potentially useful chromophores for use in molecular wires and antenna arrays, all of which make them interesting synthetic targets.[2] The preparation of chlorins regioselectively functionalized for supramolecular assembly is no small task, for in the preparation of an asymmetrically substituted macrocycle it is possible to produce a maximum of eight isomers: four pyrroline-ring regioisomers, each of which could exhibit *cis* or *trans* stereochemistry. We have recently reported the preparation of chlorins **1** from the rearrangement of metallated 5,15-porphodimethenes **2** (Scheme 1).[3] Advantages to this method are (i) the synthesis is highly regioselective, with only one out of four possible pyrroline ring isomers formed as shown, and (ii) the synthesis is short, as the porphodimethene is furnished directly from readily prepared open-chained pyrrolic intermediates *via* the '2 + 2' MacDonald condensation[4] of 1,9-diformyldipyrromethanes **3** and dipyrromethanes **4**. However, a general limitation to our approach is that one of the dipyrromethanes must be symmetrical or the '2 + 2' condensation will furnish two isomeric chlorin macrocycles.

The last few years have seen the active development of the '3 + 1' approach to the synthesis of porphyrins[5] and porphyrin analogs.[6] In this method the macrocyclic ring is furnished by the condensation of tripyrrane **5** with 2,5-diformylpyrrole **6** (Scheme 2). The tripyrrane is prepared in one step by the electrophilic substitution of pyrrole **7** with 2 equiv. of acetoxymethylpyrrole **8**. In theory, the method could allow the preparation of a porphyrin with four different pyrroles and the only symmetry constraint would be that the 2,5-diformylpyrrole must have identical β-substituents in order to form one isomeric porphyrin upon condensation with an asymmetrically substituted tripyrrane. The varied ring substituent pattern that this method allows makes the '3 + 1' approach to the construction of a chlorin macrocycle an attractive alternative to the more symmetry constrained '2 + 2' method. However, the intermediates of the condensation are not known. The 5,10-porphodimethene **9**, other dihydroporphyrins as well as porphyrinogens (5,10,15,20,22,24-hexahydroporphyrin) have all been postulated as intermediates.[5] The latter is not the correct oxidation state to rearrange to a chlorin, and it was not clear if all or just a portion of the dihydroporphyrin intermediates produced in the condensation could be easily metallated or then rearranged into a chlorin like the tautomer **2**. We now have determined the identity of the condensation intermediate and report the first synthesis of a chlorin that utilizes a '3 + 1' approach to prepare the macrocyclic ring.

The '3 + 1' synthesis of chlorin **10** is shown in Scheme 3. To demonstrate the utility of the '3 + 1' approach, chlorin **10** was chosen as a target because its substituent pattern was not efficiently accessible *via* the '2 + 2' approach. Pyrrole (**11**) was used because the absence of β-substituents on this ring was expected to control the regiochemistry by analogy to the earlier '2 + 2' chlorin syntheses and furnish only the one ring-reduced isomer as shown.[3] Its use also precluded the formation of pyrroline ring stereoisomers. The propanoate ester pyrroles were used because it was felt that the ensuing substituent pattern on the chlorin macrocycle could lend itself to the fabrication of supramolecular chlorin assemblies of interest. Our initial attempts to make the precursor tripyrrane **13** in the usual manner[5,6] by refluxing pyrrole with 2 equiv. of acetoxymethylpyrrole **12** in an EtOH–AcOH solution overnight did not furnish **13** as expected. This literature procedure works well when the 2,5-unsubstituted pyrrole is substituted in its 3,4-position with electron-donating alkyl substituents. However, the electrophilic substitution reaction of pyrrole with **12** was slow, allowing the solvolysis of **12** and the resultant production of the unreactive ether by-product. We therefore prepared the known dipyrromethane **14**[3] first and refluxed it in an EtOH–AcOH

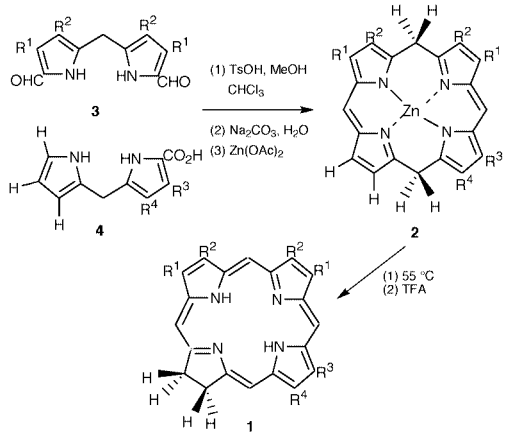

Scheme 1

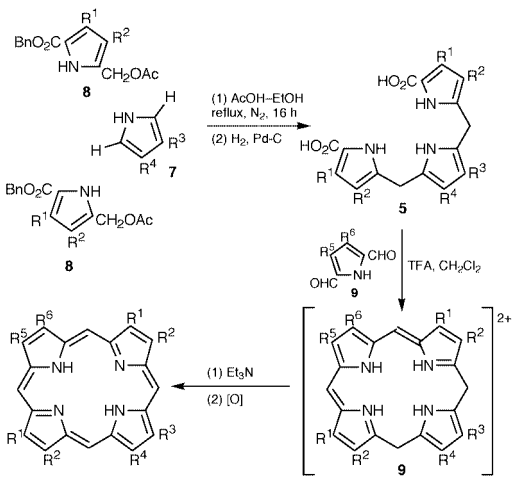

Scheme 2

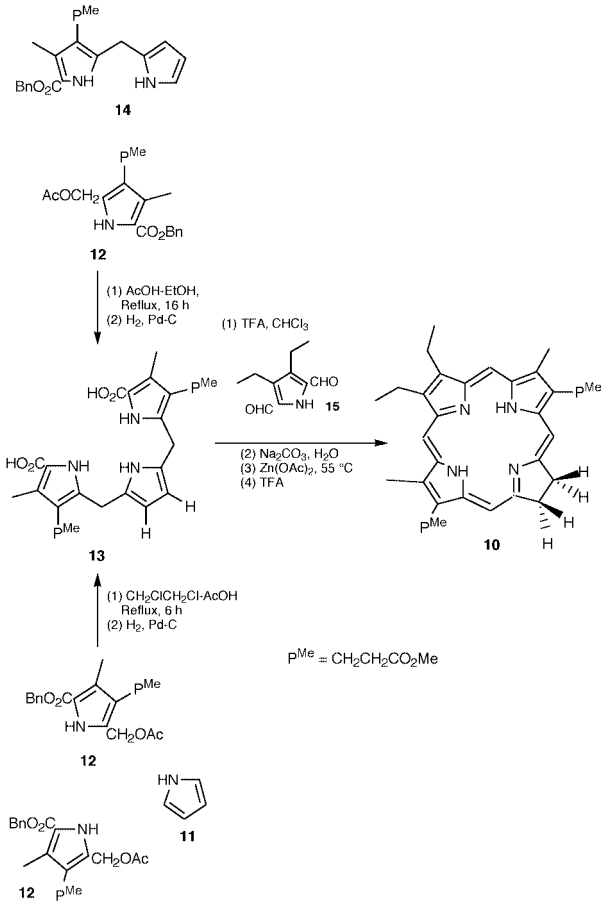

Scheme 3

solution overnight with the acetoxymethylpyrrole **12** to furnish tripyrrane **13** in 60% yield. This demonstrates for the first time that the mild reaction conditions which allow the formation of the acid-sensitive tripyrrane in one step from three pyrrole precursors also work well when using a dipyrromethane and acetoxymethylpyrrole. On the other hand, when pyrrole and 2 equiv. of acetoxymethylpyrrole **12** were refluxed in a 1,2-dichloroethane–AcOH solution for 6 h the tripyrrane **13** was furnished in 45% yield. Pyrrole **12** did not decompose to form an unreactive by-product in the modified reaction mixture.

The benzyl esters of tripyrrane **13** were hydrogenolysed over 10% palladium-on-charcoal and the resulting diacid tripyrrane condensed with 2,5-bisformylpyrrole **15**[5c] in the presence of 5% TFA in $CHCl_3$ under an inert atmosphere.[7] After 2 h the solution was neutralized with $NaHCO_3$, washed with water and dried over Na_2SO_4. The reaction mixture was filtered through an alumina plug, metallated with a saturated solution of $Zn(OAc)_2$ in MeOH, and heated to 55 °C for 2 h. The crude product was demetallated in TFA and chromatographed on alumina (Grade III, eluted with CH_2Cl_2–benzene 65 : 35) to furnish chlorin **10** in 46% yield along with 8% of the corresponding porphyrin.[8] UV–VIS spectroscopy of the reaction mixture after neutralization with $NaHCO_3$ and before metallation revealed that the main macrocyclic intermediate formed in the '3 + 1' condensation was a phlorin (432 nm, broad adsorption at 720 nm). This was a gratifying result, for we have previously shown that the reaction of $Zn(OAc)_2$ with a phlorin produced a metallated 5,15-porphodimethene that would rearrange to chlorin upon heating.[3a] If the 5,10-porphodimethene **9** was ever formed during the '3 + 1' condensation, it must have equilibrated rapidly to the thermodynamically more stable phlorin upon neutralization.

In conclusion, the '3 + 1' approach furnished chlorin in yields as high, if not higher, than with chlorins prepared *via* the '2 + 2' approach. The preparation of a tripyrrane from dipyrromethane and pyrrole precursors demonstrates the feasibility of synthesizing an asymmetrically substituted tripyrrane (*i.e.* one made from three different pyrroles), and corresponding asymmetrically substituted chlorin via the '3 + 1' approach. The relative brevity and simplicity of the synthetic route, utilizing readily prepared precursor pyrroles, makes this an attractive method for the regioselective synthesis of chlorins.

D. H. B. gratefully acknowledges the support of this work by the National Science Foundation (CHE - 9508653), and for the support of the NSF in the purchase of a departmental 400 MHz NMR (CHE - 9700421). TDL also acknowledges support from the NSF (CHE - 9732054).

Notes and references

1 H. Scheer, in *Chlorophylls*, ed. H. Scheer, CRC Press, Boca Raton, 1991, pp. 3–30; *Photosynthesis, A Comprehensive Treatise*, ed. A. S. Raghavendra, Cambridge University Press, Cambridge, 1998.
2 For reviews on chlorin assemblies, see M. R. Wasielewski, in *Chlorophylls*, ed. H. Scheer, CRC Press, Boca Raton, 1991, pp. 269–286; M. R. Wasielewski, *Chem. Rev.*, 1992, **92**, 435.
3 (*a*) D. H. Burns, T. L. Caldwell and M. W. Burden, *Tetrahedron Lett.*, 1993, **34**, 2883; (*b*) D. H. Burns, Y. H. Li, D. C. Shi and M. O. Delaney, *Chem. Commun.*, 1998, 1677.
4 G. Arsenault, E. Bullock and S. F. MacDonald, *J. Am. Chem. Soc.*, 1960, **82**, 4384.
5 For an overview, see (*a*) T. D. Lash, *Chem. Eur. J.*, 1996, **2**, 1197; (*b*) A. Boudif and M. Momenteau *J. Chem. Soc., Perkin Trans. 1*, 1996, 1235; (*c*) T. D. Lash, *J. Porphyrins Phthalocyanines*, 1997, **1**, 29.
6 (*a*) T. D. Lash, *Angew. Chem., Int. Ed. Engl.*, 1995, **34**, 2533; (*b*) T. D. Lash and S. T. Chaney, *Chem. Eur. J.*, 1996, **2**, 944.
7 The preparation and purification of the chlorin were performed in a Vacuum Atmosphere glove box under a nitrogen atmosphere.
8 All new compounds exhibited satisfactory spectral and elemental analysis.

Communication a908784b

Coordination polymerization of ethylene in water by Pd(II) and Ni(II) catalysts

Anke Held, Florian M. Bauers and Stefan Mecking*

Institut für Makromolekulare Chemie und Freiburger Materialforschungszentrum der Albert-Ludwigs-Universität Freiburg, Stefan-Meier-Str. 31, D-79104 Freiburg, Germany. E-mail: mecking@ruf.uni-freiburg.de

Received (in Cambridge, UK) 29th October 1999, Accepted 5th January 2000

Ethylene is polymerized in water as a reaction medium by Pd(II) and Ni(II) complexes to afford branched or linear homopolymer.

Water possesses unique properties as a reaction medium. It is highly polar and immiscible with most organic compounds, has a high heat capacity and also features a strong propensity for micelle formation. In addition, water is an ideal medium from an environmental and safety perspective. Thus, emulsion and suspension polymerization of olefinic monomers is employed on a vast scale, *e.g.* for the direct production of water-based lattices, used for coatings and paints. In contrast to these free radical polymerizations, transition metal catalyzed coordination polymerization reactions in water have received less attention, as the early transition metal catalysts[1] used predominately are extremely sensitive to moisture.

Late transition metal complexes are generally less sensitive to polar media due to their less oxophilic nature. Due to the propensity of late transition metal alkyl complexes for β-hydride elimination, dimers or oligomers are usually obtained in C–C linkage of ethylene.[2] Only a limited number of catalysts for polymerization to high molecular weight products are known. Most of them are based either on neutral Ni(II) complexes[3,14a] of formally monoanionic bidentate ligands or on cationic Fe, Co, Ni or Pd complexes[4] of neutral multidentate ligands with bulky substituted N donor atoms.[5] The aforementioned stability of late transition metal complexes is demonstrated by the tolerance of some of these polymerization catalysts towards polar functionalized comonomers[3d,4b,c] and polar organic solvents.[3c,d,4c,6]

In the context of possible side reactions in transition metal catalysis in aqueous media[7] (such as hydrolysis of metal alkyl species, attack of water on coordinated substrates or coordination of water to the metal center as a ligand), regarding polymerization reactions a conceivable effect of water on chain transfer[8] is of specific interest as small (absolute) changes in the overall chain transfer rate will strongly influence product molecular weight.

A very slow (*ca.* 1 turnover per day) coordination polymerization of ethylene in water catalyzed by a Rh complex has previously been investigated.[9] We now report on the homopolymerization of ethylene in water by neutral Ni(II) and cationic Pd(II) complexes.

Exposure of an aqueous suspension of Pd complex **1**[4c] to ethylene at elevated pressure results in formation of high molecular weight, highly branched polyethylene (Table 1). The reaction is effective under mild conditions (7 bar, room temperature), an increase of the ethylene pressure to 40 bar resulting in a doubling of productivity (entry 1 *vs.* 3). Comparison of 3 and 16 h experiments reveals no significant deactivation of the cationic catalyst in the presence of water (entry 2 *vs.* 3). In comparison to polymerization employing a homogeneous solution of **1** in CH_2Cl_2 as a non-aqueous solvent

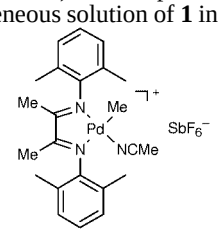

1

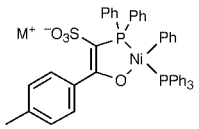

2a: $M^+ = Na^+$
2b: $M^+ = H_{33}C_{16}NMe_3^+$

(entry 3 *vs.* 4), activities are similar. However, branching is reduced in comparison to reaction in CH_2Cl_2 (69 to 83 branches per 1000 C atoms in runs 1 to 3 *vs.* 109 branches per 1000 C in run 4; determined by ^{1}H NMR). Also, GPC analysis reveals a much higher molecular weight of the polymers obtained in water (Table 1). These findings correspond to the physical appearance of the polymers: whereas the material obtained in CH_2Cl_2 is a highly viscous oil, the polymers obtained in the aqueous reaction medium are rubbery solids. In preliminary

Table 1 Polymerization results

	Reaction conditions					Results				
Entry No.	Catalyst	*n*(cat.)/ μmol	Ethylene pressure/bar	Reaction medium	Reaction time/h	Polymer yield/g	Productivity/ mol(ethylene) mol(cat.)$^{-1}$	Average activity/ mol(ethylene) mol(cat.)$^{-1}$ h^{-1}	M_w[a]/g mol^{-1}	M_n[a]/g mol^{-1} (M_w/M_n)
1	**1**	81	7	H_2O	23	7.4	3 260	140	160 000	70 600 (2.3)
2	**1**	61	40	H_2O	3	2.3	1 340	450	181 100	63 500 (2.8)
3	**1**	61	40	H_2O	16	10.9	6 380	400	179 400	77 700 (2.3)
4	**1**	61	50	CH_2Cl_2	14	14.4	8 430	600	32 300	14 500 (2.2)
5	**2a**[b]	130	50	acetone : H_2O 50 : 50	1.5	2.5	680	450	[c]	[c]
6	**2a**[b]	121	50	acetone : H_2O 50 : 50	3	3.2	940	310	[c]	[c]
7	**2a**[b]	108	50	acetone : H_2O 5 : 95	2	2.2	710	360	2 230	970 (2.3)
8	**2a**[b]	89	50	toluene : H_2O 5 : 95	2	5.9	2 360	1 180	3 030	960 (3.1)
9	**2b**[b]	116	50	toluene : H_2O 5 : 95	1.5	1.0	310	210	[c]	[c]
10	**2b**[b]	104	50	toluene : H_2O 5 : 95	3	1.6	550	180	[c]	[c]
11	**2a**[b]	12	50	toluene	2	9.0	26 680	13 340	580 000	13 900 (42)
12	**2a**[b]	26	50	acetone	2	22.2	30 440[d]	15 220[d]	94 000	3 770 (25)
13	**2b**[b]	9	50	toluene	1.75	5.2	20 600	11 780	28 800	5 440 (5.3)

Reaction temperature: room temp. (entries 1 to 4), 70 °C (entries 5 to 13). Total volume of water and/or organic solvent: 100 mL.

[a] Determined *vs.* polystyrene (entry 1 to 4) resp. linear polyethylene (entry 5 to 13) standards. [b] Phosphine scavenger [Rh(CH_2=CH_2)$_2$(acac)] (Ni : Rh 2 : 1). [c] Not determined. [d] Probably mass transfer limited.

experiments, the water ligand of the cationic complex [(ArN=C-(Me)C(Me)=NAr)PdMe(OH_2)]$^+SbF_6^-$ (Ar = 2,6-^{i}Pr$_2$C$_6$H$_3$)[10] was found to be displaced completely upon addition of ethylene in low temperature NMR experiments. This result implies that in catalysis in aqueous media with cationic complexes of this type no severe blocking of coordination sites by water should be expected, in accordance with the above polymerization experiments.

In ethylene polymerisation by a neutral Ni(II) complex with a P,O ligand, introduction of a sulfonate substituent has been reported to enhance formation of higher molecular weight products (toluene as reaction medium).[3c,d] At the same time, the sulfonate group affects water solubility. In order to produce higher molecular weight polymer the absence of strongly coordinating phosphine ligands is required.[3d,11] For this reason we have employed complex **2a**,[12,13] utilizing [Rh(H_2C=CH_2)$_2$(acac)] as a phosphine scavenger. For comparison to water-soluble **2a** with respect to aqueous polymerization in the presence of a water-immiscible solvent (*vide infra*) the novel complex **2b** was prepared by oxidative addition of 4-MeC_6H_4C(O)C($SO_3^-H_{33}C_{16}NMe_3^+$)=$PPh_3$ to [Ni(cod)$_2$] in the presence of PPh_3, or by addition to [Ni(PPh_3)$_4$].[13] Introduction of the large $H_{33}C_{16}NMe_3^+$ cation results in a strong increase in lipophilicity: whereas **2a** dissolves in the aqueous phase upon addition of water to a toluene solution of the complex, **2b** remains in the organic phase.

The stability of C–C linkage catalysts based on Ni complexes with anionic bidentate ligands towards protic media, including water, had been noted early on by the original inventors.[14] However, successful polymerization to afford higher molecular weight products in water has not been reported, to the best of our knowledge. The complex [{κ^2*P*,*O*-Ph_2PC(Ph)=C(OEt)O}NiPh-(PEt_3)] (removal of PEt_3 by phosphine scavengers) was reported to be completely inactive for ethylene polymerization in organic media in the presence of 1000 eq. water.[3d,15] For this reason, we were somewhat surprised to observe formation of linear polyethylenes employing catalysts **2a** and **2b** in an aqueous environment, utilizing only a small amount of water-miscible (acetone) or -immiscible (toluene) organic solvent to enable injection of the phosphine scavenger or the scavenger and **2b**, respectively (Table 1, entries 7 to 10). By comparison to polymerization in neat toluene or acetone[16] (entries 11 to 13), polymer molecular weight is significantly reduced and productivity is lowered in aqueous media. From the data presented, no dramatic effect of water on chain transfer reactions is evident, the lowering of polymer molecular weight also being attributable to a slower chain growth (as reflected by the lower productivity) caused by the lower solubility of ethylene in water. Considering catalyst stability, comparison of entries 5 *vs.* 6 and 9 *vs.* 10 shows that the catalysts are still active for polymerization after several hours in water. A preliminary comparison of the hydrophilic **2a** and the lipophilic **2b** in the multiphase system water/toluene/insoluble polymer (entries 8 and 9) reveals that phosphine abstraction from **2a** is not significantly hampered by the different solubilities of **2a** and [Rh(H_2C=CH_2)$_2$(acac)].

Interestingly, when performing the Ni(II)-catalyzed polymerization in the presence of ionic or non-ionic surfactants (SDS, Triton X-100), stable polyethylene emulsions are obtained. Typically, emulsions with particle sizes in the range of ϕ 80 to 300 nm are obtained at a catalyst productivity of, *e.g.* 1300 mol(ethylene) per mol(Ni) (conditions of run 7, surfactant added).

In conclusion, high molecular weight polymers can result from the coordination polymerizaton of ethylene in water at high catalyst activities. Branched or linear polymers are accessible in water as a reaction medium.

The authors thank R. Mülhaupt for his interest in our work. Financial support by BASF AG is gratefully acknowledged, and we thank B. Manders and M. O. Kristen for valuable discussions. A.H. thanks the Deutsche Forschungsgemeinschaft for a Graduiertenkolleg stipend. A generous loan of $PdCl_2$ was provided by Degussa-Huels AG. GPC analyses of linear polyethylenes were carried out by D. Lilge (BASF) and ^{31}P NMR analyses were provided by D. Hunkler (Freiburg).

Notes and references

1 *Ziegler Catalysts*, ed. G. Fink, R. Mülhaupt and H. H. Brintzinger, Springer, Berlin, 1995.

2 G. Wilke, *Angew. Chem., Int. Ed. Engl*, 1988, **27**, 185; *Angew. Chem.*, 1988, **100**, 189. M. Peuckert and W. Keim, *Organometallics*, 1983, **2**, 594.

3 (*a*) W. Keim, R. Appel, A. Storeck, C. Krueger and R. Goddard, *Angew. Chem., Int. Ed. Engl.*, 1981, **20**, 116; *Angew. Chem.*, 1981, **93**, 91. (*b*) W. Keim, F. H. Kowaldt, R. Goddard and C. Krueger, *Angew. Chem., Int. Ed. Engl.*, 1978, **17**, 466; *Angew. Chem.*, 1978, **90**, 493. (*c*) K. A. Ostoja-Starzewski and J. Witte, *Angew. Chem., Int. Ed. Engl.*, 1987, **26**, 63; *Angew. Chem.*, 1987, **99**, 76. (*d*) U. Klabunde and S. D. Ittel, *J. Mol. Catal.*, 1987, **41**, 123. (*e*) C. Wang, S. Friedrich, T. R. Younkin, R. T. Li, R. H. Grubbs, D. A. Bansleben and M. W. Day, *Organometallics*, 1998, **17**, 3149. (*f*) L. K. Johnson, A. M. A. Bennett, S. D. Ittel, L. Wang, A. Parthasarathy, E. Hauptman, R. D. Simpson, J. Feldman and E. B. Coughlin (DuPont), WO98/30609, 1998.

4 Ni, Pd: (*a*) L. K. Johnson,, C. M. Killian and M. Brookhart, *J. Am. Chem. Soc.*, 1995, **117**, 6414. (*b*) L. K. Johnson, S. Mecking and M. Brookhart, *J. Am. Chem. Soc.*, 1996, **118**, 267. (*c*) S. Mecking, L. K. Johnson, L. Wang and M. Brookhart, *J. Am. Chem. Soc.*, 1998, **120**, 888. (*d*) L. K. Johnson, C. M. Killian, S. D. Arthur, J. Feldman, E. McCord, S. J. McLain, K. A. Kreutzer, M. A. Bennett, E. B. Coughlin, S. D. Ittel, A. Parthasarathy, D. Tempel and M. Brookhart (UNC-Chapel Hill/DuPont) WO 96/23010, 1996. Co, Fe: (*e*) B. L. Small, M. Brookhart and A. M. A. Bennett, *J. Am. Chem. Soc.*, 1998, **120**, 4049. (*f*) G. J. P. Britovsek, V. Gibson, B. S. Kimberley, P. J. Maddox, S. J. McTavish, G. A. Solan, A. J. P. White and D. J. Williams, *Chem. Commun.*, 1998, 849.

5 A much larger variety of ligands is applicable for the particular case of palladium-catalyzed alternating olefin–carbon monoxide copolymerization as the involvement of CO can reduce the propensity for chain transfer: E. Drent and P. H. M. Budzelaar, *Chem. Rev.*, 1996, **96**, 663; A. Sen, *Acc. Chem. Res.*, 1993, **26**, 303. Alternating olefin–CO copolymerization in aqueous media: Z. Jiang and A. Sen, *Macromolecules*, 1994, **27**, 7215; G. Verspui, G. Papadogianakis and R. A. Sheldon, *Chem. Commun.*, 1998, 401; C. Bianchini, H. Man Lee, A. Meli, S. Moneti, V. Patinec, G. Petrucci and F. Vizza, *Macromolecules*, 1999, **32**, 3859.

6 Tolerance of the palladium diimine complexes towards moisture has previously been noted, ref. 4*b*,*c*.

7 *Aqueous-Phase Organometallic Chemistry*, ed. B. Cornils and W. A. Herrmann, Wiley-VCH, Weinheim, 1998.

8 *E.g.* the presence of additional ligands can promote chain transfer reactions in ethylene oligomerization: W. Keim and F. H. Kowaldt, *Erdoel, Erdgas, Kohle/Compend.-Dtsch. Ges. Mineraloelwiss. Kohlechem.*, 1978, **78–79**, 453.

9 L. Wang, R. S. Lu, R. Bau and T. C. Flood, *J. Am. Chem. Soc.*, 1993, **115**, 6999.

10 ^{1}H NMR (CD_2Cl_2, 300 MHz, −50 °C): 7.4–7.0 (m, 6H, H_{aryl}), 4.6 (s, 2H, OH_2), 2.90 and 2.86 (septet, *J* 7 Hz, 2 H, C*H*Me$_2$ and C′*H*Me$_2$), 2.18 [s, 6H, N=C(*Me*)C(*Me*)=N], 1.32, 1.26, 1.15 and 1.10 (d, *J* 7 Hz, 6H; CH*MeMe*′ and C′H*MeMe*′), 0.26 (s, 3H, PdMe).

11 For formation of polyethylene employing a PPh_3 complex in hexane suspension *cf.* ref. 3*b*.

12 D. L. Beach and J. J. Harrison (Gulf), *Eur. Pat.* A 52929, 1982.

13 Characteristic NMR data (^{13}C{^{1}H}, 75 MHz; ^{31}P{^{1}H}, 202 MHz), ligands 4-MeC_6H_4C(O)C($SO_3^-M^+$)=PPh_3. M^+ = $H_{33}C_{16}NMe_3^+$: NMR ($CDCl_3$), ^{13}C: δ 188.5 [d, ^2J(C,P) 6 Hz, C=O], 81.0 [d, ^1J(C,P) 104 Hz, C=P], 52.2 ($H_{33}C_{16}NMe_3^+$). ^{31}P: δ 16.8. M^+ = Na^+: NMR ($CDCl_3$), ^{13}C: δ 191.5 (C=O), 81.3 [d, ^1J(C,P) 113 Hz, C=P]. ^{31}P: δ 16.7. **2b** NMR ^{13}C (toluene-d_8): δ 187.1 [dd, ^2J(C,P) 23 Hz, ^3J(C,P) 8 Hz, C–O], 104.7 [d, ^1J(C,P) 44 Hz; =C(SO_3^-)P], 52.7 ($H_{33}C_{16}NMe_3^+$). ^{31}P (C_6D_6): δ 38.3 [d, ^2J(P,P) 272 Hz, =C(SO_3^-)P], 21.0 [d, ^2J(P,P) = 272 Hz, PPh_3]. **2a** NMR (C_6D_6), ^{13}C: δ 187.9 (br, C–O), 101.2 [d, ^1J(C,P) 42 Hz, =C(SO_3^-)P]. ^{31}P: δ 35.4 [d, ^2J(P,P) 276 Hz, =C(SO_3^-)P], 21.0 [d, ^2J(P,P) 276 Hz, PPh_3].

14 (*a*) R. Bauer, H. Chung, G. Cannell, W. Keim and H. van Zwet (Shell), *US Pat.* 3637636, 1972. (*b*) R. Bauer, H. Chung, K. W. Barnett, P. W. Glockner and W. Keim (Shell), *US Pat.* 3686159, 1972.

15 Polymerization in the presence of 'up to 100 eq.' of water/Ni for a neutral nickel complex with a chelating N,O-ligand has recently been claimed: D. A. Bansleben, S. Friedrich, T. R. Younkin, R. H. Grubbs, C. Wang and R. T. Li (W. R. Grace), WO 98/42664, 1998.

16 The broad molecular weight distributions observed in entries 11 and 12 are in agreement with previous studies: ref. 3*d*.

Communication a908633a

Reaction of tetracyanoethylene with SCl_2: new molecular rearrangements

Panayiotis A. Koutentis, Charles W. Rees, Andrew J. P. White and David J. Williams

Department of Chemistry, Imperial College of Science, Technology and Medicine, London, UK SW7 2AY. E-mail: c.rees@ic.ac.uk

Received (in Liverpool, UK) 23rd November 1999, Accepted 4th January 2000

The chloride ion catalysed addition of SCl_2 to TCNE gives the dicyanomethylene-1,2,6-thiadiazine 3 as major product together with two unexpected minor products, pyrimidine 4 and pyrroloimidazothiadiazine 5, whose X-ray crystal structures are described; the products are derived from interaction of SCl_2 with one cyano group with neighbouring group participation by two others.

1,2,6-Thiadiazines which are not oxidised on sulfur are rare.[1] One notable exception is 3,5-dichloro-4*H*-1,2,6-thiadiazin-4-one **1** which is readily prepared from dichlorodicyanomethane and SCl_2, followed by hydrolysis with formic acid; the chlorines in **1** can be successively displaced by a range of

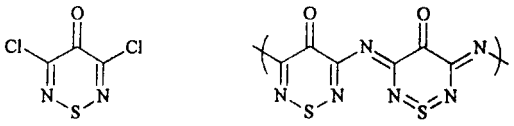

1 **2**

nucleophiles, the second requiring more vigorous conditions.[2] We needed a large scale synthesis of the 3,5-diamino derivative for incorporation into a conjugated polymer of type **2**. Since the displacement of the second chlorine of **1** by NH_3 required sealed tubes or pressure vessels, we decided to enhance the reactivity of the chlorines by replacing the 4-keto group in **1** by dicyanomethylene to give the monomer **3**.

The dicyanomethylene compound **3** was not formed by condensing the keto compound **1** with malononitrile, but it was formed slowly in up to 60% yield by the addition of SCl_2 to TCNE catalysed by $BnEt_3NCl$, in CH_2Cl_2 at room temperature (Scheme 1). However the formation of **3** was accompanied by the formation of two unexpected and puzzling minor products; 4,5,6-trichloropyrimidine-2-carbonitrile **4** (5%) and 4,8-dichloro-6,7-dicyanopyrrolo[1′,2′:1,2]imidazo[5,4-*c*][1,2,6]thiadiazine **5** (5%). The dicyanomethylene compound **3** was obtained as bright yellow flakes, mp 134–135 °C, the pyrimidine **4** as colourless, volatile needles, mp 64.5–65 °C, and the pyrroloimidazothiadiazine **5** as deep red needles or prisms, mp > 245 °C with sublimation.

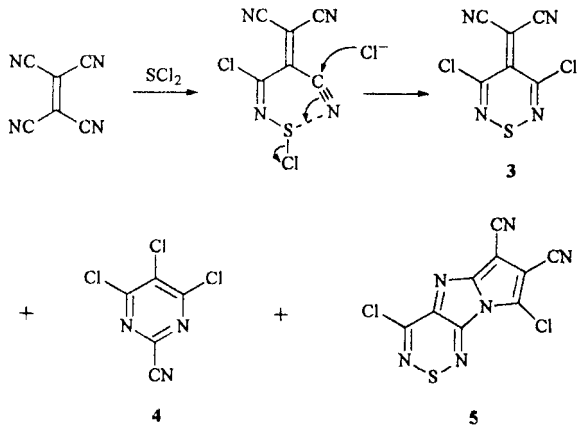

3 **4** **5**

Scheme 1

For the thiadiazinone **1**, which is almost planar,[3] Bird calculated his aromaticity index I_A to be 54,[4] indicating a modestly aromatic compound, *cf.* I_A = 53 for furan and 100 for benzene. The dicyanomethylene analogue **3**, however, has a distinctly non-planar, shallow boat conformation (Fig. 1).† In all four independent molecules in the crystal the N(2)–S(1)–N(6) and C(3)–C(4)–C(5) planes are inclined by *ca.* 25°, thereby distancing the cyano groups from the bulky chloro substituents. Whereas the two C=N bonds in the thiadiazine ring have pronounced double bond character, the C(4)–C(7) linkage is delocalised. Compound **3** has a slightly higher aromaticity index (I_A = 60) than **1**, in spite of being less planar, presumably because the more strongly electron withdrawing group in **3** allows greater contribution from dipolar resonance forms.

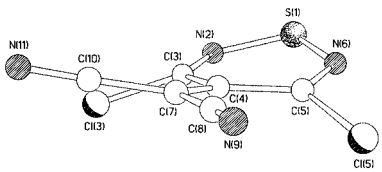

Fig. 1 The molecular structure of **3**. The average S–N, C=N and C(4)–C(7) distances over the four independent molecules are 1.616(7), 1.272(10) and 1.367(10) Å, respectively.

Compounds **4** (Fig. 2) and **5** (Fig. 3) are both planar and delocalised, the latter being the first example of this (14π aromatic) ring system. Crystals of **4** contain two independent molecules which are planar to within 0.031 and 0.071 Å, respectively. The molecules pack with the cyano group of one directed into the π system of the other (Fig. 2), the shortest N···ring centroid distance being 3.22 Å with a C≡N···π angle of 171°. Two polymorphs of **5** were identified; both are monoclinic but one crystallises in a centrosymmetric space group whereas the other is polar. The geometries of the two forms do not differ significantly, being planar to within 0.066 (form 1) and 0.117 Å (form 2), their tricyclic cores having maximum deviations from planarity of only 0.019 and 0.023 Å respectively (Fig. 3). There is distinct bond ordering in the thiadiazine ring and also to a lesser degree in the imidazole, whereas the terminal pyrrole exhibits delocalisation that

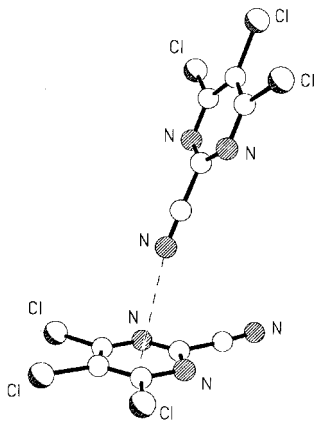

Fig. 2 The molecular structure of **4**.

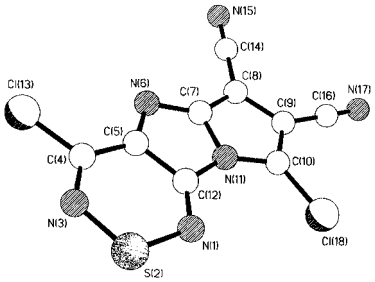

Fig. 3 The molecular structure of **5**.

extends from C(8) to C(9) *via* N(11). Despite the differences in packing, both polymorphs contain loosely linked tapes of molecules formed by electrostatic N···Cl interactions.

The formation of **3**, **4** and **5** from TCNE and SCl_2 at room temperature required the presence of chloride ions for a significant rate of reaction; all are presumably initiated by coordination of the electrophilic SCl_2 to a cyanide nitrogen, which activates nucleophilic addition of chloride. This process can be repeated by addition of chloride to a geminal cyano group (Scheme 1), and cyclisation to form the aromatic thiadiazine **3**, which was always the major product. The mechanism of formation of the minor, rearranged, products is much less obvious. However it is possible that a *cis*-vicinal cyano group could also participate in the SCl_2 reaction, with its nitrogen now attacking carbon to form a five-membered ring as shown in **6** (Scheme 2). Various examples of such neighbouring group participation in the reactions of dicyanides with electrophilic reagents have been reported.[5] The intermediate **7**, thus formed, is highly electrophilic and would be subject to successive, reversible attack by chloride ions, ultimately displacing the cyano groups, *via* **8** and **9**, to give the fully chlorinated derivative **10**. This could then undergo a Beckmann-type rearrangement with the developing carbocation being captured by cyanide, in the anhydrous medium, to give the observed pyrimidine **4**. A related, classical, Beckmann rearrangement has been observed in the conversion of analogous azacyclopentadienone oximes into pyrimidones,[6] and Beckmann carbocation intermediates have been efficiently intercepted by cyanide ions.[7]

Formation of **5** could arise by condensation of the major product **3** and the intermediate **7**. One of the chlorine atoms in **3** is very readily displaced by nucleophiles,[8] and it would be expected to react rapidly with the adducts of **7** and chloride ions, such as **8**. The amidine-like nitrogen of **8** would displace a chlorine from **3** (Scheme 3) to give **11**, which could collapse to **12** and finally aromatise to give **5**. It is not known how the dicyanomethylene and other substituents are lost from **12**, but one possibility is shown in Scheme 3. Other bis-nucleophiles react with **3**, displacing a chlorine and the dicyanomethylene to give related polycyclic systems.[8]

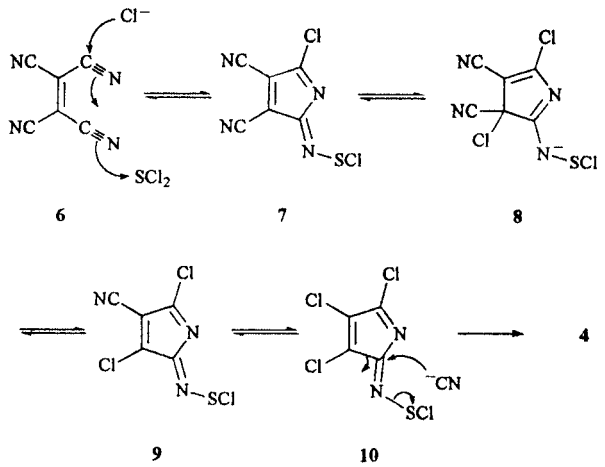

Scheme 2

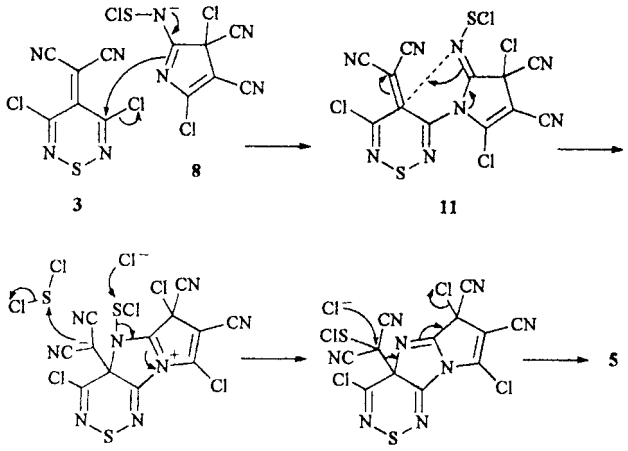

Scheme 3

Thus **3** has been prepared from TCNE and SCl_2, but this reaction is complicated by the involvement of geminal and vicinal cyano groups, after the initial interaction. These neighbouring group interactions lead to the formation of **3** (Scheme 1) or to new molecular rearrangements to give the minor products **4** and **5** (Scheme 2 and 3).

We thank the EPSRC for a Research Studentship (P. A. K.) and the Wolfson Foundation for establishing the Wolfson Centre for Organic Chemistry in Medical Science at Imperial College.

Notes and references

† *Crystal data* for **3**: $C_6N_4Cl_2S$, M = 231.1, orthorhombic, $Pc2_1b$ (no. 29), a = 10.474(6), b + 10.787(4), c = 31.348(10) Å, V = 3542(3) Å^3, Z = 16 (four independent molecules), D_c = 1.733 g cm^{-3}, μ(Mo-Kα) = 9.20 cm^{-1}, F(000) = 1824, T = 293 K; refined based on F, R = 0.045, Rw = 0.049, 2646 independent observed reflections [$|F_o| > 4\sigma(|F_o|)$, $2\theta \leqslant 50°$], 469 parameters. The polarity of the structure was determined by use of the η parameter, which refined to a value of −0.1(6). For **4**: $C_5N_3Cl_3$, M = 208.4, monoclinic, $P2_1/c$ (no. 14), a = 15.886(4), b = 6.994(2), c = 16.477(2) Å, β = 118.01(2)°, V = 1616.4(5) Å^3, Z = 8 (two independent molecules), D_c = 1.713 g cm^{-3}, μ(Cu-Kα) = 97.4 cm^{-1}, F(000) = 816, T = 293 K; refined based on F, R = 0.053, Rw = 0.055, 1318 independent observed absorption corrected reflections [$|F_o| > 4\sigma(|F_o|)$, $2\theta \leqslant 120°$], 200 parameters. For **5** (form 1): $C_9N_6Cl_2S$, M = 295.1, monoclinic, $P2_1/c$ (no. 14), a = 7.876(2), b = 20.334(10), c = 7.167(2) Å, β = 108.88(2)°, V = 1086.0(7) Å^3, Z = 4, D_c = 1.805 g cm^{-3}, μ(Mo-Kα) = 7.77 cm^{-1}, F(000) = 584, T = 293 K; refined based on F, R = 0.034, Rw = 0.037, 1470 independent observed reflections [$|F_o| > 4\sigma(F_o|)$, $2\theta \leqslant 50°$], 164 parameters. For **5** (form 2): $C_9N_6Cl_2S$, M = 295.1, monoclinic, $P2_1$ (no. 4), a = 6.303(7), b = 14.060(8), c = 6.466(5) Å, β = 105.08(2)°, V = 553.3(9) Å^3, Z = 2, D_c = 1.771 g cm^{-3}, μ(Mo-Kα) = 7.62 cm^{-1}, F(000) = 292, T = 293 K; refined based on F, R = 0.061, Rw = 0.058, 1249 independent observed reflections [$|F_o| > 4\sigma(|F_o|)$, $2\theta \leqslant 60°$], 164 parameters. The polarity could not be assigned. CCDC 182/1524.

1 C. J. Moody, in *Comprehensive Heterocyclic Chemistry*, ed. A. R. Katritzky and C. W. Rees, Pergamon, Oxford, 1984, vol. 3, p. 1039; R. K. Smalley, in *Comprehensive Heterocyclic Chemistry II*, ed. A. R. Katritzky, C. W. Rees and E. F. V. Scriven, Pergamon, Oxford, 1996, vol. 6, p. 695; R. E. Busby, *Adv. Heterocycl. Chem.*, 1990, **50**, 255.
2 J. Geevers and W. P. Trompen, *Recl. Trav. Chim. Pays-Bas*, 1974, **93**, 270.
3 S. Harkema, *Acta Crystallogr., Sect. B*, 1978, **34**, 2927.
4 C. W. Bird, *Tetrahedron*, 1986, **42**, 89; 1992, **48**, 335.
5 F. Johnson and R. Madroñero, *Adv. Heterocycl. Chem.*, 1966, **6**, 95; A. I. Meyers and J. C. Sircar, in *The Chemistry of the Cyano Group*, ed. Z. Rappoport, Interscience, London, 1970, p. 380.
6 T. Ajello, *Gazz. Chim. Ital.*, 1939, **69**, 460; 1940, **70**, 504; 1944, **72**, 325.
7 R. H. Poirier, R. D. Morin, R. W. Pfeil, A. E. Bearse, D. N. Kramer and F. M. Miller, *J. Org. Chem.*, 1962, **27**, 1547; K. Maruoka, T. Miyazaki, M. Ando, Y. Matsumura, S. Sakane, K. Hattori and H. Yamamoto, *J. Am. Chem. Soc.*, 1983, **105**, 2831.
8 P. A. Koutentis and C. W. Rees, unpublished observations.

Communication a909307i

ChemComm

Polymer-supported cobalt carbonyl complexes as novel solid-phase catalysts of the Pauson–Khand reaction

Alex C. Comely,*[a] Susan E. Gibson (née Thomas)[a] and Neil J. Hales[b]

[a] *Department of Chemistry, King's College London, Strand, London, UK WC2R 2LS. E-mail: alex.comely@kcl.ac.uk*
[b] *AstraZeneca UK Ltd., Mereside, Alderley Park, Macclesfield, UK SK10 4TG*

Received (in Liverpool, UK) 29th November 1999, Accepted 10th January 2000

Cobalt carbonyl complexes immobilised onto a 'polymer-bound triphenylphosphine' solid support are effective and practical catalysts of the Pauson–Khand reaction.

The synthesis of cyclopentenone derivatives *via* the cobalt carbonyl-mediated annulation of an alkyne, an alkene and carbon monoxide, the Pauson–Khand (P–K) reaction, was first described in 1971.[1] A synthetically very important process,[2] the P–K reaction is routinely applied using a stoichiometric amount of the transition metal complex. Although the catalytic process was reported as early as 1973,[1b] it was confined to the strained reactive alkenes norbornene and norbornadiene.

Ensuing years saw little development of the catalytic P–K reaction until a protocol developed by Rautenstrauch,[3] albeit one demanding extremely forcing conditions (310–360 bar ethene/CO, 150 °C) to realise only moderate yields, inspired several new approaches to catalysis. Promoters such as 1,2-dimethoxyethane or water have been investigated,[4] the addition of phosphites is shown to prevent inactive cluster formation[5] and the use of supercritical CO_2 as a reaction medium is described.[6] Alternative sources of zero valent cobalt [$Co(acac)_2/NaBH_4$[7] and (indenyl)Co(COD)[8]] and cobalt carbonyl clusters[9] have also been employed. Although yields and turnovers are excellent, these systems still suffer the requirement of high temperatures and pressures.

The current state-of-the-art can be attributed to Livinghouse who in 1996 reported a photochemically driven process requiring only mild temperatures (50–55 °C) and 1 atm CO.[10] A more recent report from the same group relates that careful control of temperature to within a narrow window (60–70 °C) dispenses with the need for photolytic promotion.[11] Rigorous purification of $Co_2(CO)_8$ in these systems can be obviated, reports Krafft, by prior base washing of the glassware.[12] Problems associated with the very labile $Co_2(CO)_8$, however, have also spurred the development of stable cobalt–alkyne catalyst precursors.[13]

Given our current interest in polymer-supported cobalt complexes[14] and increasing awareness of the environmental and handling advantages conferred by such solid-phase methodologies,[15] we decided to determine the viability of the catalytic P–K reaction using immobilised cobalt carbonyls.† Our preliminary investigations, which reveal for the first time that polymer-supported cobalt complexes do indeed catalyse the P–K reaction, are reported herein.

The cobalt carbonyl resins to be tested as catalyst precursors were prepared as follows.[14] Reaction of 'polymer-bound triphenylphosphine' **1**‡ with $Co_2(CO)_8$ in THF at room temperature generated a resin-bound mixture of phosphine-substituted cobalt carbonyl complexes **2** and **3** (*ca.* 1:1) (Scheme 1). The purple resin, which is significantly more air-stable than $Co_2(CO)_8$, was characterised on the basis of its IR and ^{31}P NMR spectra.[14] Heating this resin at 75 °C in 1,4-dioxane cleanly converted it into a second form, assigned the structure of the neutral bisphosphine **4** on the basis of its IR and ^{31}P NMR spectra.[14] Resin **4**, however, can be more conveniently prepared directly from **1** and $Co_2(CO)_8$§ without prior isolation of **2** + **3**.

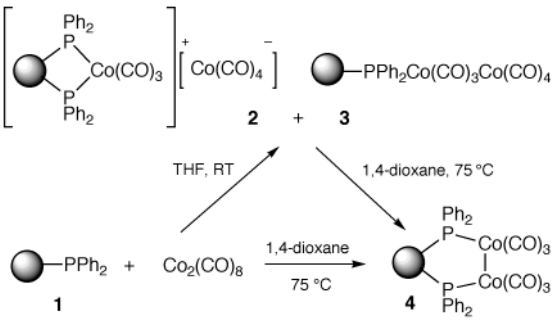

Scheme 1

In light of the mild and very attractive conditions reported by Livinghouse for the catalytic P–K reaction, and in particular the thermal window identified between 60 and 70 °C,[11] it was these conditions which were used as the basis for our initial experiments with the cobalt–carbonyl loaded resins.¶ At 65 °C we were very encouraged by the observation that 5 mol% of either precursor **2** + **3** or **4** effected a moderate conversion of enyne substrate **5**[17] to cyclopentenone **6**[10] after 24 h in THF

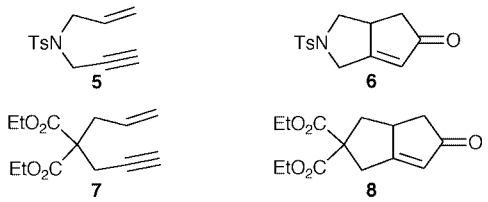

under a 50 mbar overpressure of CO (Table 1, entries 1 and 2). In preliminary steps to optimise the methodology, the first parameter investigated was temperature. An increase to 70 °C (Table 1, entries 3 and 4) resulted in a significant increase in conversion for both catalyst precursors, the bisphosphine-substituted complex **4** again proving to be the most effective

Table 1 Conversion of substrates **5** and **7** into **6** and **8** respectively *via* the catalytic Pauson–Khand reaction using cobalt resins **2** + **3** and **4**¶

Entry	Catalyst precursor (5 mol%)	*T*/°C	Substrate	Product	Yield (%)[a] (isolated)
1	**2** + **3**	65	**5**	**6**	22
2	**4**	65	**5**	**6**	48
3	**2** + **3**	70	**5**	**6**	37
4	**4**	70	**5**	**6**	66 (61)
5	**2** + **3**	75	**5**	**6**	21
6	**4**	75	**5**	**6**	28
7	**2** + **3**	70	**7**	**8**	28
8	**4**	70	**7**	**8**	57 (49)

[a] Describes percentage conversion measured by ^1H NMR spectroscopy. Isolated yields are those obtained after flash column chromatography. Products were characterised by comparison of their ^1H, ^{13}C and IR spectra with the literature values (ref. 10).

producing 66% conversion and 61% isolated yield of **6**. The consequence of a further 5 °C increase in temperature, however, was a precipitous drop in conversion for both forms of the catalyst alike (Table 1, entries 5 and 6).

A further substrate was subjected to our preliminarily optimised conditions. Hence, enyne **7**[10,18] was cyclised to cyclopentenone **6**[10] in a respectable 49% isolated yield, catalyst precursor **4** again resulting in the highest conversion (Table 1, entries 7 and 8).

In conclusion, we have shown for the first time that solid-phase cobalt carbonyl complexes have significant potential as catalysts of the P–K reaction. As with all supported catalysts, a very simple work-up procedure is required: filtration of the polymer-bound catalyst and concentration of the filtrate. A further advantage conferred by the increased air-stability of the immobilised cobalt complexes is ease of handling using readily available laboratory equipment. Our results, together with the environmental advantages of immobilising metal carbonyls on a solid support, suggest that this new approach to the P–K reaction is worthy of considerable further investigation.

The authors wish to thank AstraZeneca UK Ltd. for a studentship (A. C. C.).

Notes and references

† Polymer-bound P–K substrates have been cyclised in the presence of stoichiometric amounts of $Co_2(CO)_8$ (ref. 16).

‡ 'Polymer-bound triphenylphosphine' (commercially available from Fluka, ~1.6 mmol P g^{-1}) describes a diphenylphosphino polystyrene polymer crosslinked with 1% divinylbenzene.

§ The experimental procedure for the formation of **4** is as follows: commercial polymer-bound triphenylphosphine (1 g, ~1.6 mmol P) was suspended in oxygen-free anhydrous 1,4-dioxane (15 cm^3) and allowed to swell for 30 min under N_2 agitation. A solution of commercial $Co_2(CO)_8$ complex (383 mg, 1.12 mmol) in anhydrous, deoxygenated 1,4-dioxane (5 cm^3) was added under nitrogen agitation, the black mixture was left at room temperature for 30 min and subsequently heated to 75 °C for 16 h. After cooling, the resin beads were filtered, washed with alternate aliquots of THF and Et_2O until the filtrate became colourless, and dried *in vacuo* to afford deep purple beads of **4** {1.15 g, 50% P site complexation, 0.35 ± 0.05 mmol $[Co_2(CO)_6]$ g^{-1}}.

¶ A general experimental for the catalytic P–K reaction is as follows: resin **4** {63 mg, 0.025 mmol $[Co_2(CO)_6]$} and substrate **5** (125 mg, 0.5 mmol) were combined in a 10 cm^3 round-bottomed flask fitted with a condenser. The apparatus was thoroughly purged with CO and sealed under 1.05 bar CO. CO-saturated THF (5 cm^3) was added and the mixture was heated to 70 °C for 24 h. Filtration of the pale brown mixture, thorough washing of the polymer beads with alternate aliquots of THF and Et_2O, and concentration of the combined filtrates *in vacuo* afforded cyclopentenone **6** [66% conversion by ^1H NMR spectroscopy; 85 mg, 61% isolated by flash chromatography (SiO_2, EtOAc–light petroleum, 2:8 to 4:6 gradient elution), 0.31 mmol].

1 (*a*) I. U. Khand, G. R. Knox, P. L. Pauson and W. E. Watts, *J. Chem. Soc., Chem. Commun.*, 1971, 36; (*b*) I. U. Khand, G. R. Knox, P. L. Pauson, W. E. Watts and M. I. Foreman, *J. Chem. Soc., Perkin Trans. 1*, 1973, 977.
2 For recent reviews see: O. Geis and H.-G. Schmalz, *Angew. Chem., Int. Ed.*, 1998, **37**, 911; Y. K. Chung, *Coord. Chem. Rev.*, 1999, **188**, 297.
3 V. Rautenstrauch, P. Mégard, J. Conesa and W. Küster, *Angew. Chem., Int. Ed. Engl.*, 1990, **29**, 1413.
4 T. Sugihara and M. Yamaguchi, *Synlett*, 1998, 1384.
5 N. Jeong, S. H. Hwang, Y. Lee and Y. K. Chung, *J. Am. Chem. Soc.*, 1994, **116**, 3159.
6 N. Jeong, S. H. Hwang, Y. W. Lee and J. S. Lim, *J. Am. Chem. Soc.*, 1997, **119**, 10549.
7 N. Y. Lee and Y. K. Chung, *Tetrahedron Lett.*, 1996, **37**, 3145.
8 B. Y. Lee, Y. K. Chung, N. Jeong, Y. Lee and S. H. Hwang, *J. Am. Chem. Soc.*, 1994, **116**, 8793.
9 J. W. Kim and Y. K. Chung, *Synthesis*, 1998, 142; T. Sugihara and M. Yamaguchi, *J. Am. Chem. Soc.*, 1998, **120**, 10782.
10 B. L. Pagenkopf and T. Livinghouse, *J. Am. Chem. Soc.*, 1996, **118**, 2285.
11 D. B. Belanger, D. J. R. O'Mahony and T. Livinghouse, *Tetrahedron Lett.*, 1998, **39**, 7637.
12 M. E. Krafft, L. V. R. Bonaga and C. Hirosawa, *Tetrahedron Lett.*, 1999, **40**, 9171.
13 D. B. Belanger and T. Livinghouse, *Tetrahedron Lett.*, 1998, **39**, 7641; M. E. Krafft, C. Hirosawa and L. V. R. Bonaga, *Tetrahedron Lett.*, 1999, **40**, 9177.
14 A. C. Comely, S. E. Gibson and N. J. Hales, *Chem. Commun.*, 1999, 2075.
15 A. R. Brown, P. H. H. Hermkens, H. C. J. Ottenheijm and D. C. Rees, *Synlett*, 1998, 817; S. J. Shuttleworth, S. M. Allin and P. K. Sharma, *Synthesis*, 1997, 1217.
16 For reports of the P–K reaction on polymer-bound P–K substrates: N. E. Schore and S. D. Najdi, *J. Am. Chem. Soc.*, 1990, **112**, 441; J. L. Spitzer, M. J. Kurth, N. E. Schore and S. D. Najdi, *Tetrahedron*, 1997, **53**, 6791; G. L. Bolton, *Tetrahedron Lett.*, 1996, **37**, 3433; G. L. Bolton, J. C. Hodges and J. R. Rubin, *Tetrahedron*, 1997, **53**, 6611.
17 F. E. Scully Jr. and K. Bowdring, *J. Org. Chem.*, 1981, **46**, 5077; W. Oppolzer, A. Pimm, B. Stammen and W. E. Hume, *Helv. Chim. Acta*, 1997, **80**, 623.
18 S. C. Berk, R. B. Grossman and S. L. Buchwald, *J. Am. Chem. Soc.*, 1994, **116**, 8593.

Communication a909462h

Synthesis of the macrocyclic core of apoptolidin

K. C. Nicolaou,* Yiwei Li, Bernd Weyershausen and Heng-xu Wei

Department of Chemistry and The Skaggs Institute for Chemical Biology, The Scripps Research Institute, 10550 North Torrey Pines Road, La Jolla, California 92037, USA and Chemistry and Biochemistry, University of California San Diego, 9500 Gilman Drive, La Jolla, California 92093, USA. E-mail: kcn@scripps.edu

Received (in Cambridge, UK) 17th January 2000, Accepted 20th January 2000

The convergent synthesis of the apoptolidin macrocyclic core is described.

Apoptolidin (**1**) is a recently discovered natural product possessing impressive biological properties, including the

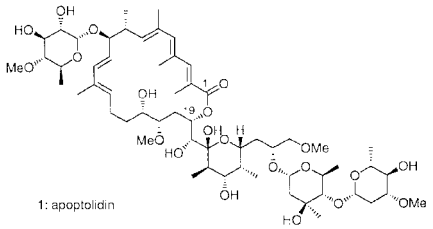

selective induction of apoptosis in rat glia cells transfected with adenovirus E1A oncogene[1] in the presence of normal cells.[2] Originally isolated from cultures of *Nocardiopsis* sp by Hayakawa and co-workers in 1997,[3] this compound possesses a novel molecular architecture whose central domain consists of a 20-membered macrocyclic lactone containing independent conjugated triene and diene systems. Because of its important biological activity and novel molecular features, apoptolidin (**1**) was deemed a prime target for total synthesis. Herein we report a convergent construction of the apoptolidin macrocyclic core (**2**) demonstrating a potential strategy for an eventual total synthesis of the natural product.

In developing a synthetic strategy to access **2** (Scheme 1), we envisaged union of key intermediates **3** and **4** *via* a Stille coupling reaction[4] followed by a Yamaguchi type macrolactonization[5] process as a means to construct the 20-membered macrocycle. Based on the expected conformational rigidity that would be conferred to the backbone of the seco, open-chain precursor of this macrocyclic system by the series of its double bonds, we hypothesize that C1–C19 lactonization would be highly preferred over C1–C16 or C1–C9 ring closures. To test this hypothesis, the synthetic strategy was tailored so that all three hydroxy groups (at C9, C16 and C19) would be free from protection prior to lactonization. The successful execution of this strategy is described below.

The construction of the C1–C11 fragment **3** began with **5** and proceeded as shown in Scheme 2. Thus, the known **5**[6] was treated with Brown's *cis*-crotylborane [(+)-Ipc$_2$B(*cis*-crotyl)][7] to furnish **6** (82% yield), which was readily protected as a TBS

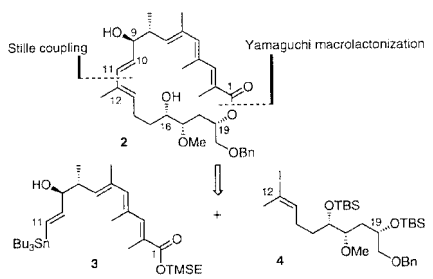

Scheme 1

ether (TBSOTf, 2,6-lutidine) to afford **7** (97% yield). Ozonolytic cleavage of the terminal olefin in **7** afforded **8**, which reacted with Ph$_3$P=C(CH$_3$)CO$_2$Et (toluene, 100 °C) to afford **9** in 90% yield after chromatography. Reduction of this intermediate using DIBAL-H (90% yield) followed by oxidation (NMO/TPAP) afforded **11** *via* **10**. Subsequent homologation employing a Horner–Wadsworth–Emmons reaction[8] [(EtO)$_2$P(=O)–CH(CH$_3$)CO$_2$Et, NaH] provided **12** in 90% overall yield from **10**. After reduction of the ester moiety in **12** (DIBAL-H, 89%) and TBAF-mediated removal of both silyl protecting groups (98% yield), it was found that upon exposure of the resulting diol **14** to MnO_2 in dilute CCl_4 solution, the primary hydroxy group was selectively oxidized to afford **15** in 97% yield. Use of a second Horner–Wadsworth–Emmons olefination [(EtO)$_2$P(=O)–CH(CH$_3$)CO$_2$TMSE, NaH, THF] provided the desired all-*trans* **16** in 65% yield. In the final transformation, Pd^0-catalyzed hydrostannation [Bu^{3}SnH, Pd(Ph$_3$P)$_2$Cl$_2$ cat., THF][9] provided a 4:1 mixture of β-(*E*) and α-regioisomers, which were separated chromatographically to afford the desired [β-(*E*)] vinylstannane **3** in 69% yield.

The synthesis of the C12–C19 fragment (**4**) commenced with PMB protection (PMBCl, NaH, 90%) of the commercially available (*S*)-glycidol (**17**) leading to **18** (Scheme 3). Addition

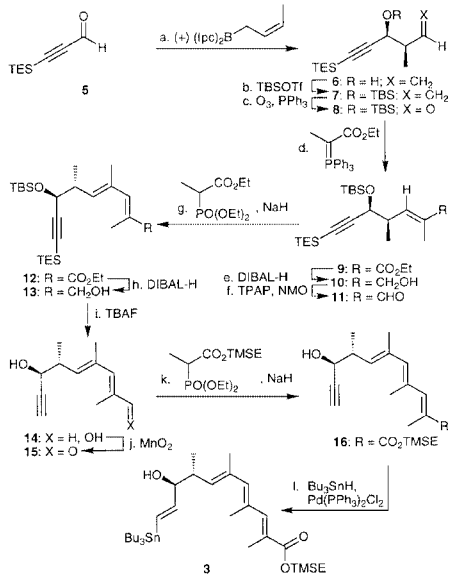

Scheme 2 *Reagents and conditions*: (a) (*Z*)-(+)-crotyldiisopinocampheylborane (2.5 equiv.), THF, −78 °C; then NaBO$_3$·4H$_2$O (15 equiv.), THF–H$_2$O (1:1), 25 °C, 12 h, 82%; (b) TBSOTf (1.5 equiv.), 2,6-lutidine (2.0 equiv.), CH_2Cl_2, 0 → 25 °C, 12 h, 97%; (c) O_3, Sudan red 7B (0.02 equiv.), CH_2Cl_2, −78 °C; then PPh_3 (1.5 equiv.), −78 → 25 °C, 12 h; (d) Ph$_3$P=C(CH$_3$)CO$_2$Et (10.0 equiv.), toluene, 100 °C, 12 h, 90% for 2 steps; (e) DIBAL-H (2.5 equiv.), −78 °C, 2 h, 90%; (f) TPAP (0.05 equiv.), NMO (6.0 equiv.), 4 Å MS, CH_2Cl_2, 25 °C, 30 min; (g) NaH (5.0 equiv.), (EtO)$_2$P(=O)CH(CH$_3$)CO$_2$Et (5.0 equiv.), THF, 0 → 25 °C, 1 h, 81% for 2 steps; (h) DIBAL-H (2.5 equiv.), −78 °C, 2 h, 89%; (i) TBAF (3.0 equiv.), THF, 0 → 25 °C, 1 h, 98%; (j) MnO_2 (20 equiv.), CCl_4, 25 °C, 3 h, 97%; (k) NaH (6.0 equiv.), (EtO)$_2$P(=O)CH(CH$_3$)CO$_2$TMSE (6.0 equiv.), THF, 0 → 25 °C, 5 h, 65%; (l) Bu$_3$SnH (4.0 equiv.). PdCl$_2$(PPh$_3$)$_2$ (0.05 equiv.), THF, 0 °C, 30 min, 69%. TPAP = Pr$_4$NRuO$_4$.

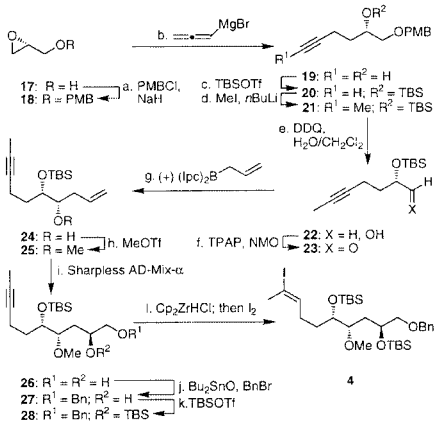

Scheme 3 *Reagents and conditions*: (a) PMBCl (2.0 equiv.), NaH (2.0 equiv.), $Bu_4N^+I^-$ (2.0 equiv.), DMF, 0 → 25 °C, 1 h, 90%; (b) Allenylmagnesium bromide (1.25 equiv.), Et_2O, −78 → 25 °C, 1 h, 90%; (c) TBSOTf (2.5 equiv.), 2,6-lutidine (4.0 equiv.), CH_2Cl_2, 0 → 25 °C, 97%; (d) BuLi (2.0 equiv.), MeI (5.0 equiv.), THF, −78 → 25 °C, 2 h, 95%; (e) DDQ (2.0 equiv.), CH_2Cl_2–H_2O (18:1), 0 → 25 °C, 97%; (f) TPAP (0.05 equiv.), NMO (6.0 equiv.), 4 Å MS, CH_2Cl_2, 0 → 25 °C, 2 h, 90%; (g) *B*-(+)-allyldiisopinocampheylborane (4.0 equiv.), Et_2O, −100 °C, 1 h; then $NaBO_3{\cdot}4H_2O$ (15 equiv.), THF–H_2O (1:1), 25 °C, 12 h, 85%, **24**: diastereoisomer *ca.* 10:1; h) MeOTf (3.0 equiv.), 2,6-di-*tert*-butyl-4-methylpyridine (5.0 equiv.), CH_2Cl_2, 40 °C, 24 h, 85%; (i) $K_3Fe(CN)_6$ (3.0 equiv.), K_2CO_3 (3.0 equiv.), $(DHQ)_2$-PYR (0.02 equiv.), OsO_4 (0.01 equiv. 2.5 wt% in Bu^tOH), Bu^tOH–H_2O (1:1), 0 °C, 12 h, 85%, **26**: diastereoisomer *ca.* 6:1; (j) Bu_2SnO (1.1 equiv.), toluene, 110 °C, 12 h; then BnBr (1.2 equiv.), $Bu_4N^+I^-$ (1.5 equiv.), toluene, 80 °C, 2 h, 85%; (k) TBSOTf (2.5 equiv.), 2,6-lutidine (4.0 equiv.), CH_2Cl_2, 0 → 25 °C, 97%; (l) Cp_2ZrHCl (2.0 equiv.), THF, 50 °C, 2 h; then I_2 (2.0 equiv.), THF, −15 → 25 °C, 0.5 h, 65%. $(DHQ)_2$-PYR = 2,5-diphenyl-4,6-bis(9-*O*-dihydroquinyl)pyrimidine.

of allenylmagnesium bromide[10] to **18** gave the desired hex-5-yne-1,2-diol (**19**) in 90% yield. Silylation of the free hydroxy group in **19** with TBSOTf–2,6-lutidine followed by methylation of the terminal alkyne (BuLi, McI) afforded **21** in 95% yield. Subsequent removal of the PMB group from **21** in the presence of DDQ in CH_2Cl_2–H_2O (18:1) (97% yield) followed by TPAP–NMO mediated oxidation of the resulting alcohol **22** readily provided **23** (90% yield). Exposure of **23** to β-(+)-allyldiisopinocampheylborane according to Brown *et al.*[11] furnished a mixture of diastereomeric alcohols (*ca.* 10:1 ratio, 85% combined yield) from which the major and desired isomer (**24**) was isolated chromatographically. Methylation of the hydroxy group (MeOTf, 2,6-di-*tert*-butyl-4-methylpyridine, 40 °C, 85% yield)[12] in **24** furnished **25** whose terminal olefin underwent stereoselective dihydroxylation in the presence of AD-mix-α[13] to provide **26** together with its (minor) diastereoisomer (*ca.* 6:1 ratio) in 85% combined yield. The two diastereoisomers could not be easily separated chromatographically at this stage, but after protection of the primary hydroxy group as a benzyl ether (Bu_2SnO, BnBr, toluene),[14] the desired diastereoisomer **27** was readily isolated by flash chromatography. Subsequent protection of the secondary hydroxy group of **27** as a TBS ether (TBSOTf, 2,6-lutidine, 97%) followed by hydrozirconation–iodonation (Cp_2ZHCl, THF, 50 °C; then I_2, −15 °C) generated the key intermediate **4** (65% overall yield) *via* **28**.

With both key intermediates **3** and **4** in hand, the stage was set for the crucial coupling and macrolactonization steps (see Scheme 4). Thus, upon treatment with catalytic amounts of $Pd(CH_3CN)_2Cl_2$ (0.05 equiv.) in DMF, **3** and **4** readily coupled to afford **29** in 60% yield. Subsequent exposure of **29** to TBAF resulted in concomitant removal of all three silyl protecting groups furnishing **30** in 80% yield. Finally, Yamaguchi macrolactonization of seco-acid **30** (2,4,6-trichlorobenzoyl chloride, DMAP, Et_3N) resulted in the ring-selective formation of macrocyclic core **2**† in 60% yield.

The described chemistry demonstrates the feasibility of the present strategy for the chemical synthesis of apoptolidin-like

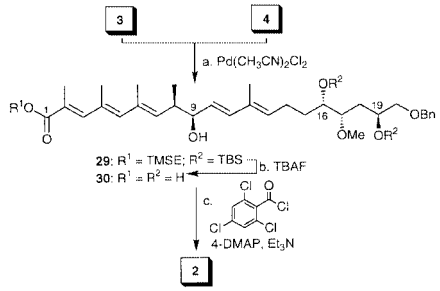

Scheme 4 *Reagents and conditions*: (a) $Pd(CH_3CN)_2Cl_2$ (0.05 equiv.), DMF, 25 °C, 48 h, 60%; (b) TBAF (6.0 equiv.), THF, 25 °C, 12 h, 80%; (c) Et_3N (6.0 equiv.), 2,4,6-trichlorobenzoyl chloride (1.5 equiv.), THF, 1.5 h, 0 °C; then 4-DMAP (5.0 equiv.), benzene, 25 °C, 1 h, 60%.

compounds for biological screening purposes and paves the way for an eventual total synthesis of apoptolidin itself. Alternative strategies towards this macrocycle, including a palladium(0)-catalysed coupling to form the C11–C12 single bond and an olefin metathesis approach to form the C10–C11 double bond of the construct are in progress.

We thank Drs G. Siuzdak and D. H. Huang for mass spectrometric and NMR assistance, respectively. This work was financially supported by The Skaggs Institute for Chemical Biology, the National Institutes of Health (USA), a Feodor Lynen Fellowship of the Alexander von Humboldt Stiftung (to B. W.) and grants from Abbott, Amgen, Boehringer-Ingelheim, Glaxo-Wellcome, Hoffmann-La Roche, Dupont, Merck, Novartis, Pfizer, Schering Plough, and Bristol-Myers Squibb.

Notes and references

† *Selected data* for **2**: R_f = 0.40 (silica gel, EtOAc–hexane 1:1); $[\alpha]_D^{20}$ −50.0 (MeOH, *c* 0.42); ν_{max}(film)/cm^{-1} 3419, 2925, 1696, 1453, 1381, 1243, 1104, 807, 712; δ_H(500 MHz, $CDCl_3$) 7.35–7.20 (m, 5H, C_6H_5), 7.18 (s, 1H, H-3), 6.08 (d, *J* 15.4, 1H, H-11), 6.08 (s, 1H, H-5), 5.56 (br t, *J* 8.0, 1H, H-13), 5.35 (dd, *J* 15.4, 8.1, 1H, H-10), 5.22–5.20 (m, 1H, H-19), 5.13 (br d, *J* 9.9, 1H, H-7), 4.58 (d, *J* 12.1, 1H, $OCH_2C_6H_5$), 4.51 (d, *J* 12.1, 1H, $OCH_2C_6H_5$), 3.90 (dd, *J* 8.4, 8.1, 1H, H-9), 3.60–3.46 (m, 3H), 3.42, (s, 3H, OCH_3), 3.44–3.40 (m, 1H), 2.90–2.87 (m, 1H), 2.55–2.43 (m, 2H), 2.30–2.24 (m, 1H), 2.13 (s, 3H), 2.07 (s, 3H), 1.97–1.89 (m, 1H), 1.87 (s, 3H), 1.85–1.78 (m, 1H), 1.68 (s, 3H), 1.65–1.52 (m, 2H), 1.13 (d, *J* 6.6, 3H, 8-CH_3); δ_C(150 MHz, $CDCl_3$) 168.7, 145.9, 145.1, 140.6, 138.0, 137.2, 136.5, 133.4, 132.5, 132.3, 131.7, 128.8 (2C), 127.6 (2C), 127.4, 123.2, 82.0, 79.7, 73.7, 73.2, 71.5, 71.0, 60.4, 39.5, 35.5, 34.6, 24.4, 17.5, 17.2, 16.2, 13.7, 12.0; HRMS (MALDI) calc. for $C_{33}H_{46}NaO_6$ (M + Na^+): 561.3192, found: 561.3216.

1 M. Debbas and E. White, *Genes Dev.*, 1993, **7**, 546.
2 J. W. Kim, H. Adachi, K. Shin-ya, Y. Hayakawa and H. Seto, *J. Antibiot.*, 1997, **50**, 628.
3 Y. Hayakawa, J. W. Kim, H. Adachi, K. Shin-ya, K. Fujita and H. Seto, *J. Am. Chem. Soc.*, 1998, **120**, 3524.
4 J. K. Stille, *Angew. Chem., Int. Ed. Engl.*, 1986, **25**, 508; J. Betzer, J. Lallemand and A. Pancrazi, *Synthesis*, 1998, 522.
5 J. Inanaga, K. Hirata, H. Saeki, T. Katsuki and M. Yamaguchi, *Bull. Chem. Soc. Jpn.*, 1979, **52**, 1989; K. C. Nicolaou, M. R. V. Finlay, S. Ninkovic and F. Sarabia, *Tetrahedron*, 1998, **54**, 7127.
6 R. L. Danheiser, D. J. Carini, D. M. Fink and A. Basak, *Tetrahedron*, 1983, **39**, 435.
7 H. C. Brown and K. S. Bhat, *J. Am. Chem. Soc.*, 1986, **108**, 293.
8 For reviews, see: W. S. Wadsworth Jr., *Org. React.*, 1977, **25**, 73; B. E. Maryanoff and A. B. Reitz, *Chem. Rev.*, 1989, **89**, 863.
9 H. X. Zhang, F. Guibe and G. Balavoine, *J. Org. Chem.*, 1990, **55**, 1857.
10 L. Brandsma and H. Verkruijisse, *Preparative Polar Organometallic Chemistry I*, Springer, Berlin, 1987, 63.
11 U. S. Racherla and H. C. Brown, *J. Org. Chem.*, 1991, **56**, 401.
12 D. M. Walba, W. N. Thurmes and R. C. Haltiwanger, *J. Org. Chem.*, 1988, **53**, 1046.
13 G. A. Crispino, K.-S. Jeong, H. C. Kolb, Z.-M. Wang, D. Xu and K. B. Sharpless, *J. Org. Chem.*, 1993, **58**, 3785.
14 T. B. Grindley, *Adv. Carbohydr. Chem. Biochem.*, 1998, **53**, 17.

Communication b000424n

Facile β-trimethylstannyl promoted 1,5-hydride shifts in cyclooctyl and cyclodecyl systems

Matthew P. Glenn, Kerry G. Penman and William Kitching*

Department of Chemistry, The University of Queensland, Brisbane, Queensland 4072, Australia.
E-mail: kitching@chemistry.uq.edu.au

Received (in Cambridge, UK) 30th November 1999, Accepted 19th January 2000

Deuterium labelling and ^{2}H NMR mapping demonstrate that cyclooctyl and cyclodecyl mesylates in aqueous EtOH exhibit greatly enhanced or exclusive levels of 1,5-hydride shift, provided a Me_3Sn group is β to the migrating hydrogen, and after tin group loss from the formal β-stannyl cation, results in regiospecific, transannular alkene formation.

Recently we have described how suitably located Group 14 centred substituents (*e.g.* Me_3Si, Me_3Sn) may regulate transformations of medium-ring epoxides and mesylates.[1] Although 1,5-H shift occurs to the extent of *ca.* 50% in solvolysis of cyclooctyl mesylate,[1,2] this phenomenon is essentially completely suppressed in *cis*- and *trans*-5-mesyloxycyclooctyltrimethylstannanes **1** and is attributable to the relatively unfavourable nature of the α-stannyl cation **2**.[1] Nor do 1,4-hydride shifts compete in these systems, despite the generation of a formal β-stannyl cation intermediate **3**. Other pathways intervene.[1] However, there would be justifiable anticipation that in the 4-mesyloxycyclooctyl- and 6-mesyloxycyclodecyltrimethylstannanes **4** and **5** transannular hydride migration would be especially facile if the 'β-stannyl effect'[3] can operate to stabilise intermediates resembling **3** and **6**, as stable ion data[4] require that cyclooctyl and cyclodecyl cations possess the 1,5-μ-hydrido bridged stuctures (Scheme 1). This proposition is now verified. *cis*-Cyclooctane-1,4-diol **7**[5] was processed as shown below (Scheme 2) to provide *trans*- and *cis*-4-hydroxycyclooctyltrimethylstannanes **8** and **9**, respectively, and the corresponding 4-$^2H_1$-isotopomers **8a** and **9a**.[6]

All stereochemically validated cases of stannyl anion displacement of sulfonate ester groups proceed with inversion of configuration at carbon,[1,7] and on this basis, *cis*-diol **7** provides *trans*-stannyl alcohol **8**. The similar patterns of ^{13}C chemical shifts, through-bond ^{119}Sn–^{13}C coupling constants (especially $^3J_{Sn-C}$)[8] and certain ^{1}H chemical shifts for **8** and **9** indicate that the *chair–chair* (**10**) and *boat–chair* (**11**) conformations are important for the *trans* (**8**) and *cis* stannanes (**9**), respectively.

The behaviour of the mesylates from **8**, **8a**, **9** and **9a** in 75% EtOH–H_2O, buffered with 2,6-lutidine, was examined and the product profiles and ^{2}H location were determined by a combination of ^{1}H, ^{2}H and ^{13}C NMR spectroscopy of (total) product solutions, combined GC-MS analyses and comparisons with the spectra of authentic compounds. This data is summarised in Scheme 3.

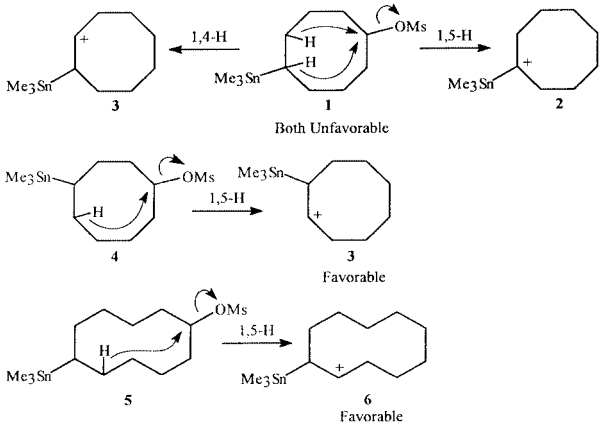

Scheme 1

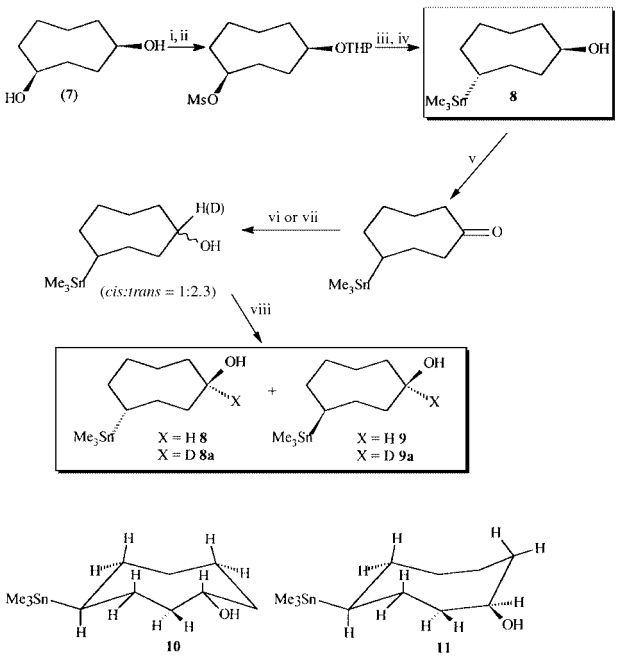

Scheme 2 *Reagents and conditions*: i, dihydropyran, TsOH, CH_2Cl_2, 52%; ii, MsCl, Et_3N, CH_2Cl_2, 93%; iii, Me_3SnLi, THF, 84%; iv, TsOH, MeOH, 89%; v, tetrapropylammonium perruthenate, NMO, CH_2Cl_2, 77%; vi, $LiAlH_4$, Et_2O, 91%; vii, $LiAlD_4$, Et_2O, 93%; viii, HPLC.

trans-Mesylates from **8** or **8a** afforded very predominantly (*E*)-cyclooctene **12**, whereas *cis*-mesylates provided almost exclusively (*Z*)-cyclooctene **13** and very little Me_3Sn-containing products **14**. The ^{2}H NMR spectra of the cyclooctenes **12** and **13** from the labelled mesylates (from **8a** and **9a**) each

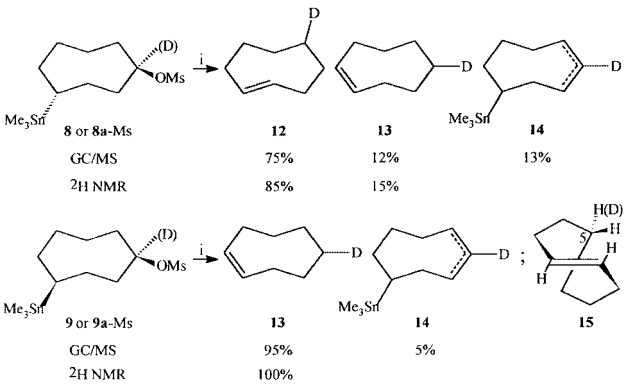

Scheme 3 *Reagents and conditions*: i, 75% EtOH–H_2O, 2,6-lutidine, 300 K.

consisted of a single, sharp high-field resonance at δ 1.42 for labelled (*Z*)-cyclooctene **13** and at δ 1.72 for (*E*)-cyclooctene **12**, confirming exclusive location of the label on a methylene carbon. Because we had already assigned the ^{13}C NMR spectra of a number of specifically ^{2}H-labelled (*Z*)- and (*E*)-cyclooctenes,[9] we were able to establish from the ^{13}C NMR spectra of the product that only 5-$^{2}H_1$-(*Z*)-cyclooctene **13** formed from **9a** and (as a minor product) from **8a** and only *one* diastereomer of **12** from labelled *trans*-mesylate **8a**.

Hence the H-shift was *complete* and *regiospecific* in a *1,5-sense*, and *diastereospecific* in the formation of **12**, which incorporates two stereogenic features. Furthermore, there is a substantial difference in the chemical shifts of the 'inside' and 'outside' protons on C-5 in the rigid (*E*)-cyclooctene systems[10] (see **15**) (δ 0.82 and 1.41;[11] δ 0.7 and 1.7[12]) that reflects the influence of the double bond. Deuterium is located only at an 'outside' position in **12** (δ 1.7) and this specificity appears to require that there is a nexus, perhaps weak, between ionisation and the 1,5-hydride shift. Consideration of the likely conformations **10** and **11** for the stannanes and likely distortions as ionisation proceeds, indicates a favourable pseudo-antiperiplanar disposition of the migrating C–H bond and β-Sn–C bond is accessible and meets the proximity and trajectory requirements of the migration.

β-Trimethylstannyl enhanced 1,5-H shifts have also been observed in similar reactions of the ^{2}H-labelled *trans*- and *cis*-6-mesyloxycyclodecyltrimethylstannanes **17** and **18**, which were acquired from *trans*-cyclodecane-1,6-diol[13,14] in the way summarised in Scheme 2 for the 1,4-cyclooctyl system.

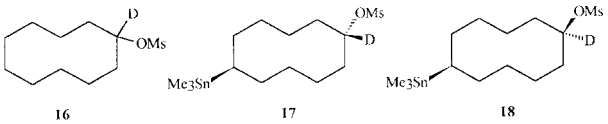

16 **17** **18**

For 1-$^{2}H_1$-cyclodecylmesylate **16** the major products (~90%) were the (*E*) and (*Z*) cyclodecenes with about 67% of the ^{2}H label on the double bond (δ 5.3–5.4) representing unrearranged products, with *ca.* 20% corresponding to rearranged transannular product (δ 1.26).[15,16] However, the *trans*-stannane **17** also provided largely cyclodecenes (~80%) but now the majority of the label (~75%) is located transannularly (δ 1.26), confirming considerably enhanced 1,5-H migration. [Small amounts of both *cis* and *trans* decalins also form (δ 1.55 and 0.76, corresponding to bridgehead absorption)]. The labelled *cis*-mesylate **18** also provides cyclodecenes that are substantially rearranged (δ 1.33, 65–70%), in addition to *cis*-decalin (~20%, δ 1.54) which may result from 'back-lobe' bond formation, as proposed for the exclusive formation of *cis*-bicyclo[3.3.0]octane from *cis*-5-mesyloxycyclooctyltrimethylstannane.[1]

For a variety of alkyl and stannyl substituted cyclooctyl sulfonate esters, and for the stannyl substituted cyclodecylmesylates, relative to the parent system,[17] there is a narrow rate spread within each system, despite substantial variations in the levels of associated transannular hydride shift.[1,18] This fact, along with values for α-secondary ^{2}H-isotope effects,[19] implies that hydride shift lags behind primary ionisation. The present results confirm that 1,5- and not 1,6-H shifts are generally operative in cyclooctyl and cyclodecyl systems and are strongly promoted by a β-Me_3Sn group. These results and those from cyclononyl systems will be discussed in full at a later date, but demonstrate that Me_3Sn-driven transannular functionalization is facile and regiospecific.

The authors are grateful to the Australian Research Council for financial support.

Notes and references

1 B. H. Riches and W. Kitching, *Chem. Commun.*, 1996, 1907; A. P. Wells, B. H. Riches and W. Kitching, *J. Chem. Soc., Chem. Commun.*, 1992, 1575.
2 R. Heck and V. Prelog, *Helv. Chim. Acta*, 1955, **38**, 1541; A. P. Wells and W. Kitching, *J. Org. Chem.*, 1992, **57**, 2517.
3 See for example, J. B. Lamberg, G.-T. Wang and D. H. Teramura, *J. Org. Chem.*, 1988, **53**, 5422.
4 R. P. Kirchen, T. S. Sorensen, K. Wagstaff and A. M. Walker, *Tetrahedron*, 1986, **42**, 1063 and references therein; M. Saunders and H. A. Jiménex-Vasquez, *Chem. Rev.*, 1991, **91**, 375; V. Galasso, *Int. J. Quantum Chem.*, 1998, **20**, 119.
5 A. C. Cope, J. M. Grisar and P. E. Petersen, *J. Am. Chem. Soc.*, 1959, **81**, 1640.
6 All new compounds exhibited concordant ^{1}H and ^{13}C NMR spectra and high resolution mass spectral (accurate mass) data.
7 W. Kitching, H. A. Olszowy and K. J. Harvey, *J. Org. Chem.*, 1982, **47**, 1893 and references therein. This is not the case for bromide or iodide systems, in which e-transfer and exchange processes compete.
8 D. Doddrell, I. Burfitt, W. Kitching, M. Bullpitt, C. Lee, R. J. Mynott, J. L. Considine, H. Kuivila and R. H. Sarma, *J. Am. Chem. Soc.*, 1974, **96**, 1640.
9 K. G. Penman, W. Kitching and A. P. Wells, *J. Chem. Soc., Perkin Trans. 1*, 1991, 721; G. Read and J. Shaw, *J. Chem. Soc., Perkin Trans. 1*, 1988, 2287; K. G. Penman and W. Kitching, unpublished results.
10 K. T. Burgoine, S. G. Davies, M. J. Peagram and G. H. Whitham, *J. Chem. Soc.*, 1974, 2629 and papers in this series.
11 I. Sauers, L. A. Grezzo, S. W. Staley and J. H. Moore, *J. Am. Chem. Soc.*, 1976, **98**, 4218; K. J. Shea and J.-S. Kim, *J. Am. Chem. Soc.*, 1992, **114**, 3044.
12 K. G. Penman and W. Kitching, unpublished results.
13 O. Ermer and J. D. Dunitz, *Isr. J. Chem.*, 1989, **29**, 137; O. Ermer, J. D. Dunitz and I. Bernal, *Acta Crystallogr.*, 1973, **1329**, 2278.
14 Large prisms of the *trans*-diol (we thank Dr P. Bernhardt for an X-ray structural analysis) were processed to a single stannane isomer (see Scheme 1) concluded to be the *cis* on the basis of argument presented in the text.
15 These figures agree well with the original data based on degradative studies of the ^{14}C and ^{2}H labelled cyclodecene products.
16 V. Prelog and J. G. Traynham, in *Molecular Rearrangements*, ed. P. de Mayo, Interscience, New York, 1963, vol. 1, p. 593; A. C. Cope, M. M. Martin and M. A. McKervey, *Quart. Rev. Chem. Soc.*, 1966, **20**, 119.
17 A. C. Cope and D. M. Gale, *J. Am. Chem. Soc.*, 1963, **85**, 3743; N. L. Allinger and W. Szknybal, *Tetrahedron*, 1968, **24**, 4699; A. C. Cope and R. B. Kinnel, *J. Am. Chem. Soc.*, 1966, **88**, 752; H.-J. Schneider and D. Heiske, *J. Am. Chem. Soc.*, 1981, **103**, 3501.
18 We are unaware of solvolytic data for any other stereochemically defined, substituted cyclodecylsulfonate esters.
19 W. Parker and C. I. F. Watt, *J. Chem. Soc., Perkin Trans. 1*, 1975, 1647; M. P. Glenn and W. Kitching, unpublished results.

Communication a909463f

ChemComm

Two different [1,3]-B shifts in phenalenyl(dipropyl)borane

Oleg L. Tok,* Ilya D. Gridnev,* Elena M. Korobach and Yuri N. Bubnov

A. N. Nesmeyanov Institute of Organoelement Compounds, Vavilova 28, 117813 Moscow, Russia.
E-mail: gridnev@scichem.c.chiba-u.ac.jp

Received (in Cambridge, UK) 6th December 1999, Accepted 24th January 2000

Both possible [1,3]-B sigmatropic shifts are observed in the title compound; benzylic rearrangement to position 9 is much faster than allylic migration to position 3.

Twenty years ago Butcher and Pagni argued that the phenalenyl ring system is an excellent choice for the exploration of fluxionality in its organometallic derivatives.[1] However, the trimethylsilyl and trimethylstannyl compounds prepared in their work were non-fluxional on the NMR time scale at temperatures up to 185 °C.[1] Due to orbital restrictions, both silicon[2] and tin[3–5] prefer to rearrange *via* [1,5]- or [1,9]-migration pathways (thermal [1,3]-Si shifts have very high activation barriers[6,7] and known [1,3]-Sn rearrangements are intermolecular).[3,4,8] However, there is only one possibility of intramolecular [1,5]-M migration in a molecule of monosubstituted phenalene, *i.e.* non-degenerate rearrangement to the central position. This is difficult to observe due to the obvious relative instability of the corresponding isomer.

On the other hand, introducing a [1,3]-migrating substituent into position 1 of phenalene provides the first example of a molecule where two different [1,3]-sigmatropic migrations may occur. Being interested in the regularities of the sigmatropic migrations of BR_2 groups,[9] which often migrate by the [1,3]-B shift mechanism,[10–14] we have synthesized a phenalenyl derivative of boron and studied its fluxional behaviour.

1-Phenalenyl(dipropyl)borane **1** was prepared by the reaction of phenalenyllithium **2**[1] with chloro(dipropyl)borane in pentane. Borane **1** is a light-yellow extremely air- and moisture-sensitive oil. It has only limited thermal stability that retards its purification. We failed to distil borane **1** and used samples of approximately 95% purity (main admixture is phenalene), obtained after evacuation of volatile products in vacuum, for the NMR studies.

Assignment of signals in the ^{1}H and ^{13}C NMR spectra of **1** was carried out by standard homo- and heteronuclear 2D chemical shift correlation techniques. The signal of H^9 in the ^{1}H NMR spectrum was distinguished from H^4 by its long-range coupling with H^1 [^4J(H^1–H^9) = 1.1 Hz, confirmed by double resonance].

The NMR spectra of **1** show reversible temperature dependence and are not affected by changes in concentration. Therefore, intramolecular rearrangements take place in **1**. The mechanism of these was elucidated by 2D ^{1}H–^{1}H EXSY (exchange spectroscopy) NMR experiments. Fig. 1 shows the chemical exchange NMR spectrum of **1** taken at 298 K. Four exchange cross-peaks observed in this spectrum unequivocally prove the mechanism of [1,3]-B sigmatropic migrations from position 1 to position 9 of the phenalene ring. The 2D EXSY experiments carried out at higher temperatures also show cross-peaks of lower intensity, corresponding to the second possible degenerate [1,3]-B migration from position 1 to position 3 (Fig. 2, Scheme 1). Thus, both [1,3]-B shifts are observed in **1**, but their rates differ significantly.

The kinetics of the [1,3][9]-sigmatropic migrations of the dipropylboryl group in **1** were measured from a series of 2D ^{1}H EXSY spectra recorded in the temperature interval 290–318 K. At this temperature, the second dynamic process does not manifest itself in the EXSY spectra at short mixing times (τ_m) and therefore, may be neglected. Rate constants were obtained from eqn. (1),[15] where I_{AA} and I_{BB} are the intensities of the diagonal peaks and I_{AB} and I_{BA} are the intensities of the cross-peaks. Rate constants and activation parameters so obtained, derived by Arrhenius and Eyring treatments of the kinetic data, are listed in Table 1.

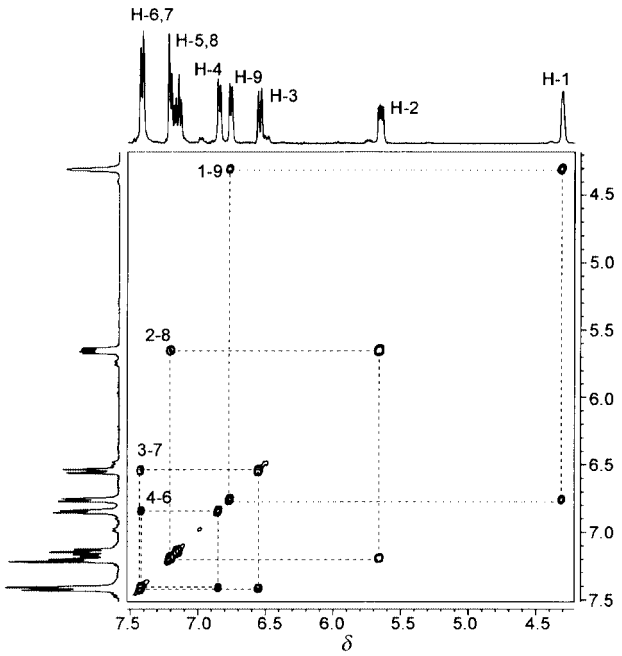

Fig. 1 2D ^{1}H–^{1}H EXSY spectrum (400 MHz, benzene-d_6) of dipropyl(phenalenyl)borane **1** at 298 K with a mixing time of 0.5 s.

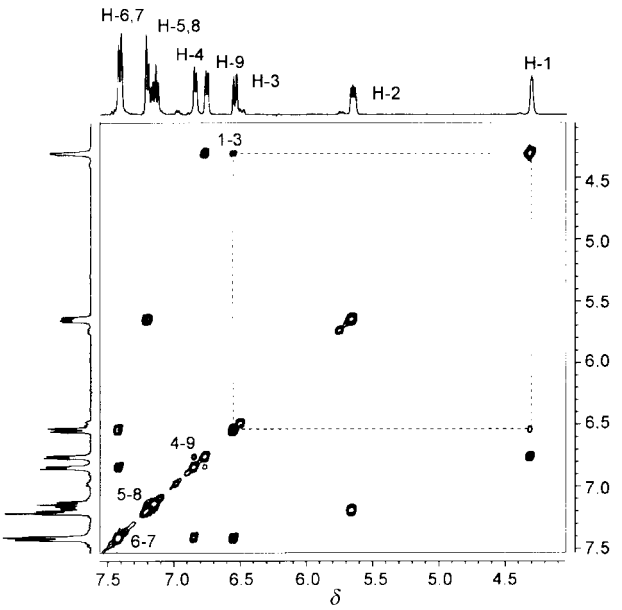

Fig. 2 2D ^{1}H–^{1}H EXSY spectrum (400 MHz, benzene-d_6) of dipropyl(phenalenyl)borane **1** at 313 K with a mixing time of 0.5 s.

$$k = \frac{1}{\tau_m} \ln \frac{r+1}{r-1}, \quad r = \frac{I_{AA} + I_{BB}}{I_{AB} + I_{BA}} \qquad (1)$$

The kinetic analysis of simultaneous dynamic processes is possible *via* matrix analysis.[15] However, in the present case this approach is complicated by a considerable difference in the rates of the two borotropic migrations and the overlap of some diagonal and cross-peaks. Approximate evaluation of the available data shows that the [1,3]^3-borotropic migration in **1** at 323 K is about 10 times slower the [1,3]^9-B shift.

Either of two [1,3]-B shifts in isolation is spatially fixed to one allylic or benzylic fragment of **1**. However, the *combination of both* results in the possibility for the dipropylboryl group to wander around the whole molecule. This is experimentally illustrated by difference SST (spin saturation transfer) ^{1}H NMR spectra (Fig. 3). Irradiation of the H^1 signal leads to a decrease in the intensities of all signals due to α-protons in **1** (Fig. 3a). Similarly, irradiation of H^2 shows that it is in exchange with both remaining β-protons, H^5 and H^8 (Fig. 3b).

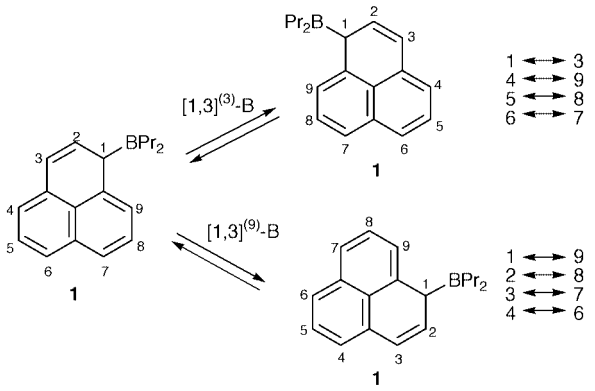

Scheme 1 Two possible borotropic migrations in **1**.

Table 1 Kinetic data and activation parameters for the [1,3]-B shift in borane **1**

T/K	k/s^{-1}	τ_m/s	
290	0.95	0.500	E_A = 19.1 ± 0.4 kcal mol^{-1}
295	1.41	0.300	ln A = 33.0 ± 0.7
298	1.97	0.200	$\Delta H^{\ddagger}_{298}$ = 16.6 ± 0.2 kcal mol^{-1}
303	3.33	0.050	$\Delta S^{\ddagger}_{298}$ = 5.0 ± 0.1 cal mol^{-1} K^{-1}
308	6.06	0.050	$\Delta G^{\ddagger}_{298}$ = 15.1 ± 0.2 kcal mol^{-1}
313	9.86	0.025	
318	14.80	0.010	

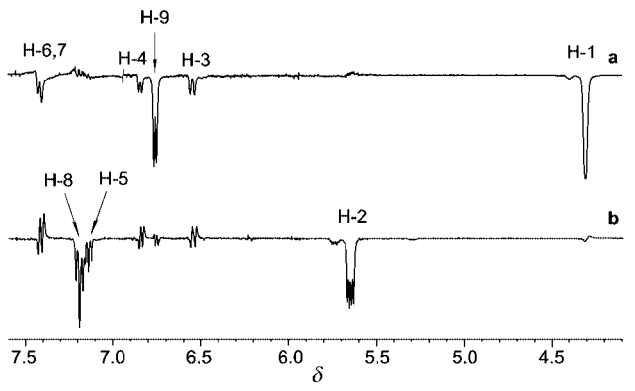

Fig. 3 Difference ^{1}H SST NMR spectra of borane **1** (400 MHz, benzene-d$_6$, 313 K): (a) irradiation of H^1; (b) irradiation of H^2.

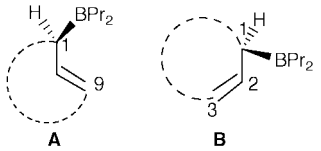

Scheme 2 Schematic representation of the geometries of allylic fragments for [1,3]^9-B (**A**) and [1,3]^3-B (**B**) shifts in **1**.

Since the configurations of the starting compounds and the product are equal for both observed rearrangements,[16] the difference in the activation barriers is exactly the difference in the energies of the corresponding transition states (TS). Therefore, one can conclude that the spatial arrangement of the allylic fragment **A** is much nearer in configuration to the TS than that of **B** (Scheme 2). This conclusion is in agreement with computational results for the [1,3]-B shift.[17]

Thus, we have observed for the first time two different [1,3]-B sigmatropic shifts in one molecule, *viz.* phenalenyl(dipropyl)borane. Further studies on the fluxional behaviour of organometallic derivatives of phenalene are underway in our laboratory.

Acknowledgements

The donation of research equipment by the Alexander von Humboldt Foundation is gratefully acknowledged. This work was supported by the Russian Foundation for Basic Research (grant no. 97-03-32714) and a Grant of the President of the Russian Federation (No. 00-15-97378).

Notes and references

1 J. A. Butcher and R. M. Pagni, *J. Am. Chem. Soc.*, 1979, **101**, 3997.
2 M. Stradiotto, S. S. Rigby, D. W. Hughes, M. A. Brook, A. D. Bain and M. J. McGlinchey, *Organometallics*, 1996, **15**, 5645.
3 M. J. Hails, B. E. Mann and C. M. Spencer, *J. Chem. Soc., Dalton Trans.*, 1983, 729.
4 Y. Naruta, Y. Nishigaichi and K. Maruyama, *J. Org. Chem.*, 1991, **56**, 2011.
5 I. D. Gridnev, P. R. Schreiner, O. L. Tok and Y. N. Bubnov, *Chem. Eur. J.*, 1999, **5**, 2042.
6 H. Kwart and T. Slutsky, *J. Am. Chem. Soc.*, 1972, **94**, 2515.
7 T. Yamabe, K. Nakamura, Y. Shiota, K. Yoshizawa, S. Kawauchi and M. Ishikawa, *J. Am. Chem. Soc.*, 1997, **119**, 807.
8 Y. Naruta, Y. Nishigaichi and K. Maruyama, *Tetrahedron*, 1985, **45**, 1067.
9 I. D. Gridnev, O. L. Tok, N. A. Gridneva, Y. N. Bubnov and P. R. Schreiner, *J. Am. Chem. Soc.*, 1998, **120**, 1034.
10 M. E. Gurskii, I. D. Gridnev, Y. V. Il'ichev, A. V. Ignatenko and Y. N. Bubnov, *Angew. Chem., Int. Ed. Engl.*, 1992, **31**, 781.
11 I. D. Gridnev, M. E. Gurskii, A. V. Ignatenko, Y. N. Bubnov and Y. V. Il'ichev, *Organometallics*, 1993, **12**, 2487.
12 I. D. Gridnev, M. E. Gurskii and Y. N. Bubnov, in *Current Topics in the Chemistry of Boron*, ed. G. W. Kakalka, Royal Society of Chemistry, Cambridge 1993, p. 56.
13 I. D. Gridnev, O. L. Tok, M. E. Gurskii and Y. N. Bubnov, *Chem. Eur. J.*, 1996, **2**, 1483.
14 I. D. Gridnev, P. R. Schreiner, M. E. Gurskii, Y. N. Bubnov, A. O. Krasavin and V. I. Mstislavski, *Chem. Commun.*, 1998, 2507.
15 C. L. Perrin and T. J. Dwyer, *Chem. Rev.*, 1990, **90**, 935.
16 More exactly, in each exchange **1** is transformed to its enantiomer.
17 M. Bühl, P. v. R. Schleyer, M. A. Ibrahim and T. Clark, *J. Am. Chem. Soc.*, 1991, **113**, 2466.

Communication a909574h

Hyperbranched porphyrins—a rapid synthetic approach to multiporphyrin macromolecules

Stefan Hecht, Todd Emrick and Jean M. J. Fréchet*

Department of Chemistry, University of California, Berkeley, California 94720-1460, USA.
E-mail: frechet@cchem.berkeley.edu

Received (in Corvallis, OR, USA) 22nd November 1999, Accepted 21st January 2000

A new class of porphyrin containing hyperbranched polymers has been prepared *via* proton-transfer polymerisation utilising an $A_2 + B_3$ approach, thus providing an accelerated entry into the construction of branched multiporphyrin architectures.

In recent years, significant effort has been made to prepare and study covalently linked multiporphyrin arrays[1] due to their promising role in artificial photosynthesis.[2] The incorporation of porphyrin units into the framework of a dendrimer[3] is of special interest since the dendritic architecture allows for maximum interactions between the chromophores, a necessary condition for efficient energy and electron transfer processes. However, access to such multiporphyrin compounds represents a difficult synthetic challenge, thus only low generation dendritic porphyrins have been prepared to date.[1,4]

We report on an alternative approach to the construction of branched multiporphyrin architectures that takes advantage of the rapid one pot synthesis used for generating hyperbranched polymers.[5] This approach is based on our recent work in proton transfer polymerisation[6] that used an $A_2 + B_3$ route for the preparation of hyperbranched aliphatic polyethers.[7] The system described herein is designed following similar principles. In this case, bisphenolic porphyrin **1** serves as the A_2 monomer and the aliphatic trisepoxide **2**[8] serves as the B_3 monomer (Scheme 1).

Initiation of the polymerisation is expected to proceed *via* deprotonation of the phenol by the base catalyst. This should be followed by ring opening of an epoxide substituent by the nucleophilic phenoxide. Regeneration of phenoxide should then occur by an efficient proton transfer from a different phenol to the formed secondary alkoxide.[7] This process leads to a highly branched polyether architecture incorporating multiple porphyrin units.[9] It was envisaged that the formed polymer chain in the *ortho*-position of the *meso*-phenyl substituents would lead to good solubility by decreasing the porphyrin–porphyrin stacking interactions. The metalated derivative, *e.g.* zinc complex, was chosen to prevent participation of the pyrrole hydrogens in the proton transfer event.

The asymmetric zinc porphyrin A_2 monomer **1**† is accessible in gram quantities *via* a three step procedure in 10% overall yield. The polymerisations employed equimolar ratios of the monomers as a 0.2 M solution in THF at 60 °C using a catalytic amount of base (25 mol% per phenolic group). The successful incorporation of both monomers into the polymer backbone was monitored by matrix assisted laser desorption ionisation time of flight (MALDI-TOF) mass spectrometry (Fig. 1). Unfortunately, ionisation of higher molecular weight material becomes increasingly difficult by the MALDI technique. Therefore, gel permeation chromatography (GPC)‡ was used as an additional complementary method for MW analysis (Fig. 2). The kinetic growth profile appeared as expected for a polycondensation reaction (Fig. 2, inset).[6,7] Upon reaching MW ~10 000,§ the reaction was stopped by removing the heating source, and the resulting polymer **3**¶ was purified by precipitation into methanol (THF–MeOH 1 : 50) giving rise to a fairly narrow polydispersity (PD) of less than 2 (Fig. 2). Control over MW can be achieved easily by variation of reaction time (typically a few days). We reason that slow polymerisation is due to the high dilution conditions made necessary by the relatively low

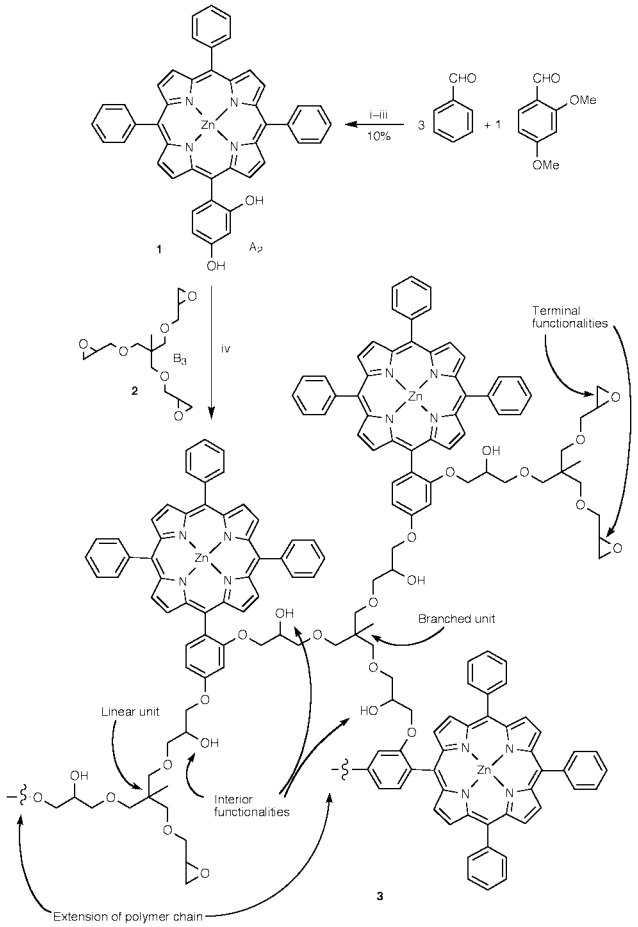

Scheme 1 *Reagents and conditions*: i, pyrrole, $EtCO_2H$, $PhNO_2$, 120 °C; ii, BBr_3, CH_2Cl_2, 0 °C to room temp.; iii, $Zn(OAc)_2$, $CHCl_3$–MeOH, reflux; iv, $KOBu^t$, THF, heat.

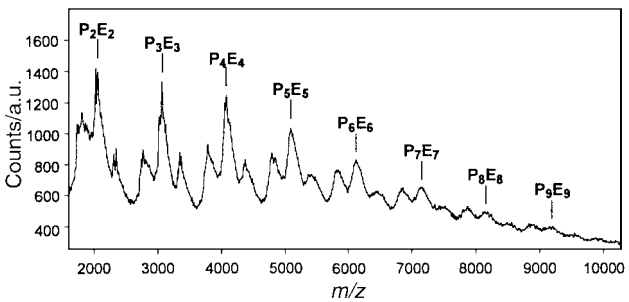

Fig. 1 MALDI-TOF mass spectrum of the polymerisation mixture showing the incorporation of the porphyrin (P) and epoxide (E) monomers. The peaks at lower (higher) mass of each major peak correspond to the loss (addition) of one epoxide unit.

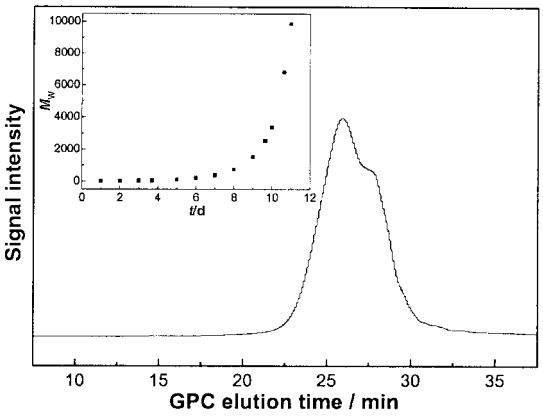

Fig. 2 GPC trace of polymer **3** after precipitation into MeOH (MW = 9900; PDI = 1.9). The inset shows polymer growth as a function of time for a polymerisation run at 60 °C.

solubility of **1**. Higher temperatures result in faster polymer growth, as well as increased PD of the polymers. The polymers were obtained as dark purple powders in 50–60% yields after precipitation, and showed good solubility in a variety of solvents such as $CHCl_3$, THF and DMSO.

Initial photophysical studies revealed only slight changes in the absorption behaviour of polymer **3** compared to monomer **1**, suggesting rather weak electronic coupling of the porphyrin units (Fig. 3).[10] However, a 30% decrease in fluorescence intensity of **3** compared to **1** was observed (Fig. 3, inset). This finding is attributed to an enhanced self-quenching of the chromophores within the macromolecule, presumably by cofacial interactions.

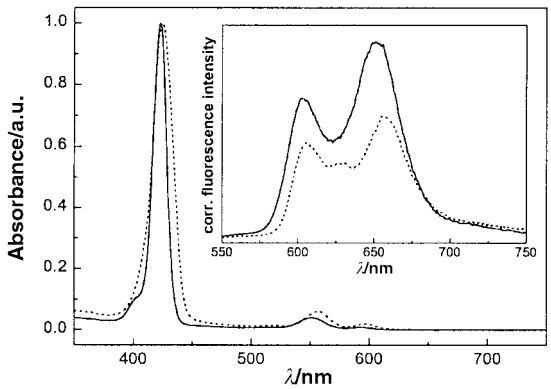

Fig. 3 UV–VIS absorption spectra of monomer **1** (—) and polymer **3** (···) in $CHCl_3$. The inset shows the corrected fluorescence spectra in $CHCl_3$ (λ_{exc} = 420 nm).

In summary, we have developed for the first time hyperbranched polymers incorporating porphyrin chromophores. The described methodology allows for the rapid synthesis of multiporphyrin architectures facilitated by the ease of purification, *e.g.* no chromatography, and it should be of general applicability. Such polymers could serve as interesting materials for a variety of photophysical and electrochemical studies as well as for the construction of optoelectronic devices.[11] Furthermore, structural modification of these polymers by transmetalation or derivatisation of residual functional groups should provide a diverse set of new materials.

Financial support from the AFOSR-MURI program and the National Science Foundation (NSF-DMR 9816166) is acknowledged with thanks.

Notes and references

† *Selected data* for **1**: δ_H(300 MHz, $CHCl_3$, 25 °C, TMS) 8.96 (d, ^3J(H,H) 5 Hz, 8H, β-H), 8.19–8.21 (m, 6H, Ph-*H*), 7.72–7.80 (m, 9 + 1H, Ph-*H* + 6′-*H*), 6.72–6.76 (s and d, ^3J(H,H) 8 Hz, 1 + 1H, 3′- and 5′-*H*), 5.12 (br s, 1H, O*H*), 5.04 (br s, 1H, O*H*); FAB-HRMS: *m/z* 708.1487 (M^+, $C_{44}H_{28}N_4O_2Zn$ requires 708.1504); λ_{max}($CHCl_3$)/nm (ε/dm^3 mol^{-1} cm^{-1}) 423 (517 000), 551 (19 600), 593 (3200); λ_{em}($CHCl_3$)/nm (λ_{exc} = 420 nm) 602, 651.

‡ The MW values of polymer **3** as given by GPC are merely estimates due to the differences in hydrodynamic volume between **3** and the polystyrene standards used for GPC calibration.

§ Polymers of much higher molecular weight (MW > 50 000) can be obtained; however, the polydispersity increases significantly above 10 kD.

¶ *Selected data* for **3**: GPC‡ (THF): M_w = 9900, M_n = 5100, PDI = 1.9; δ_H(300 MHz, DMSO-d_6, 25 °C) 8.72 (br s, β-*H*), 8.13 (br s, Ph-*H*), 7.72 (br s, Ph-*H* + 6′-*H*), 6.94 (br s, 3′- and 5′-*H*), 1.2–4.3 (very br, C*H*$_2$CHOH, CH$_2$C*H*OH and CH$_2$CHO*H*), 0.9 (br s, C*H*$_3$); λ_{max}($CHCl_3$)/nm (ε/dm^3 mol^{-1} cm^{-1}) 425, 557, 597; λ_{em}($CHCl_3$)/nm (λ_{exc} = 420 nm) 606, 655.

1 For larger branched covalent multiporphyrin arrays, see: D. L. Officer, A. K. Burrell and D. C. W. Reid, *Chem. Commun.*, 1996, 1657; C. C. Mak, N. Bampos and J. K. M. Sanders, *Angew. Chem., Int. Ed.*, 1998, **37**, 3020; C. C. Mak, D. Pomeranc, M. Montalti, L. Prodi and J. K. M. Sanders, *Chem. Commun.*, 1999, 1083; C. C. Mak, N. Bampos and J. K. M. Sanders, *Chem. Commun.*, 1999, 1085; A. Nakano, A. Osuka, I. Yamasaki, T. Yamasaki and Y. Nishimura, *Angew. Chem., Int. Ed.*, 1998, **37**, 3023; H. A. M. Biemans, A. E. Rowan, A. Verhoeven, P. Vanoppen, L. Latterini, J. Foekema, A. P. H. J. Schenning, E. W. Meijer, F. C. de Schryver and R. J. M. Nolte, *J. Am. Chem. Soc.*, 1998, **120**, 11 054; R. Dagani, *Chem. Eng. News*, 1999, (11/1), 9.

2 For a recent discussion, see: M. Freemantle, *Chem. Eng. News*, 1998, (10/26), 37; 1999, (11/1), 27.

3 For a comprehensive review on dendrimers, consult: G. R. Newkome, C. N. Moorefield and F. Vögtle, *Dendritic Molecules: Concepts, Synthesis, Perspectives*, VCH, Weinheim, 1996.

4 A first generation porphyrin dendrimer has recently been described: T. Norsten and N. Branda, *Chem. Commun.*, 1998, 1257.

5 Comprehensive reviews of hyperbranched polymers include: Y. H. Kim, *J. Polym. Sci., Part A: Polym. Chem.*, 1998, **36**, 1685; J. M. J. Fréchet and C. J. Hawker, in *Comprehensive Polymer Science, 2nd Suppl.*, ed. S. L. Aggarwal and S. Russo, Pergamon, 1996, pp. 71–132.

6 T. Emrick, H.-T. Chang and J. M. J. Fréchet, *Macromolecules*, 1999, **32**, 6380.

7 Hyperbranched aromatic epoxies prepared by proton-transfer polymerisation utilising an AB_2 monomer have been reported recently: H.-T. Chang and J. M. J. Fréchet, *J. Am. Chem. Soc.*, 1999, **121**, 2313.

8 T. Kita, M. Yokota, A. Masuyama, Y. Nakatsuji and M. Okahara, *Synthesis*, 1993, 487.

9 Related linear polyethers containing porphyrin units in the main chain have been reported by: E. Scamporrino and D. Vitalini, *Macromolecules*, 1992, **25**, 2625; 1992, **25**, 6605.

10 Strong electronic coupling has been observed for linear conjugated multiporphyrin arrays: V. S.-Y. Lin, S. G. Di Magno and M. J. Therien, *Science*, 1994, **264**, 1105; P. N. Taylor, J. Huuskonen, G. Rumbles, R. Aplin, E. Williams and H. L. Anderson, *Chem. Commun.*, 1998, 909.

11 A hyperbranched polymer containing carbazole units has been used in an electroluminescence application: X.-T. Tao, Y.-D. Zhang, T. Wada, H. Sasabe, H. Suzuki, T. Watanabe and S. Miyata, *Adv. Mater.*, 1998, **10**, 226.

Communication a909258g

ChemComm

Rhodium-catalyzed copolymerization of norbornadiene derivatives with carbon monoxide

Shi-Wei Zhang and Shigetoshi Takahashi*

The Institute of Scientific and Industrial Research, Osaka University, Mihogaoka, Ibaraki, Osaka 567-0047, Japan. E-mail: takahashi@sanken.osaka-u.ac.jp

Received (in Cambridge, UK) 24th November 1999, Accepted 19th January 2000

Alternate copolymerization of norbornadiene derivatives with carbon monoxide is catalyzed by a rhodium complex under water-gas shift reaction conditions selectively to give unsaturated polyketones in high yields.

Polyketones are of current interest in terms of functional materials exhibiting photo- and biodegradabilities as well as of starting materials for other classes of functionalized polymers.[1] As a useful method for the synthesis of polyketones, transition metal-catalyzed copolymerization between an olefin and carbon monoxide has been receiving much attention over the last few decades. Among transition metals, mono- and dicationic palladium complexes have predominantly been investigated and developed as excellent catalysts for the perfectly alternating copolymerization of olefins with carbon monoxide until recently.[2] The palladium catalytic system has also been extended to the copolymerization of several dienes with carbon monoxide, giving saturated poly(cyclic ketone)s.[3] Some reports described the copolymerization of norbornadiene with carbon monoxide in the presence of palladium complexes.[2a,4] but the resulting copolymers were characterized to be a mixture of structures A and B. Very recently, Novak and Safir have

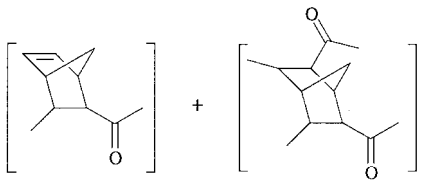

A **B**

described a palladium-catalyzed copolymerization of 2,3-substituted norbornadiene derivatives with carbon monoxide to give alternating copolymers.[5] Other than palladium complexes, few effective catalysts are known for the copolymerization of olefins with carbon monoxide,† although the copolymerization of ethylene[7] and arylallene[8] with carbon monoxide catalyzed by rhodium complexes has been reported. In the course of our studies on the rhodium-catalyzed carbonylations of alkynes under water-gas shift reaction conditions,[9] we have now found that norbornadiene and its derivatives can smoothly be copolymerized with carbon monoxide. Here we report the first rhodium-catalyzed copolymerization of norbornadiene and its derivatives with carbon monoxide, producing perfectly alternating polyketones in which one of the two carbon–carbon double bonds of norbornadiene remains intact [eqn. (1)]. The structure

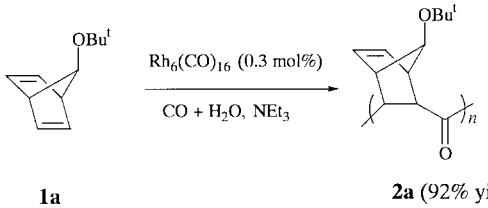

(1)

1a **2a** (92% yield)

has been characterized by chemical reactions as well as by spectral analyses.

Thus, a mixture of 7-*tert*-butoxynorborna-2,5-diene **1a** (5 mmol, 0.820 g), $Rh_6(CO)_{16}$ (0.015 mmol, 15 mg), triethylamine (2 ml) and water (1 ml) in benzene (15 ml) was stirred in an autoclave at 55 °C for 24 h under 100 atm of carbon monoxide. After venting the gases from the autoclave at room temperature, the reaction solution was poured into a large amount of methanol (*ca.* 200 ml). Precipitates formed were collected by filtration, washed several times with methanol, and dried *in vacuo* at 50 °C overnight to give product **2a** as a white powder (0.883 g, 92% yield). Product **2a** is soluble in a variety of organic solvents such as acetone, chloroform, benzene and THF, and the GPC analysis (polystyrene standards) indicated **2a** to be a polymer with a molecular weight of 24 500 and a narrow molecular weight distribution (M_w/M_n = 1.38). In its IR spectrum, polymer **2a** showed a characteristic absorption at 1715 cm^{-1} typical of the carbonyl groups of polyketones.[4b,5] The weak absorption band at 1630 cm^{-1} and the stronger band at 3059 cm^{-1} indicated the presence of a carbon–carbon double bond.[10] ^1H and ^{13}C NMR ($CDCl_3$) spectra of **2a** exhibited broad signals but a very simple pattern, suggesting that the copolymer may have a regular structure. The ^1H NMR spectrum showed broad signals in the range 2.55–3.95 ppm, indicating that **2a** contains a ring structure and may be a copolymer of **1a** with CO. Furthermore, the ^1H NMR spectrum revealed that the ratio of olefinic protons to the other protons present in the copolymer is consistent with that predicted on the basis of structure **2a**, suggesting that one of the two C=C bonds of norbornadiene remains intact. Indeed, the $^{13}C\{^1H\}$ NMR spectrum exhibited a signal at 132 ppm attributable to the C=C group and a carbonyl resonance at 208 ppm. When the $^{13}C\{^1H\}$ NMR experiment was performed using an NNE (Heterogated Decoupling without Nuclear Overhauser Effect) pulse sequence, the spectrum exhibited a ratio of sp^2 to sp^3 carbons for the norbornene units consistent with the proposed structure for **2a**, corresponding to an alternating 1:1 copolymer of **1a** with CO. Thermogravimetric analysis (TGA) revealed that **2a** appeared to degrade by a two-step process with a mass loss of 72% at the first degradation step. This mass loss rate corresponds to the theoretical value ($C_5H_5OBu^t/C_{12}H_{16}O_2$ = 0.719) calculated for the case where all of the *tert*-butoxycyclopentadiene moieties $(C_5H_5OBu^t)_n$ of **2a** are liberated by a retro-Diels–Alder reaction.

In order to characterize further and prove the structure of **2a**, we tried to convert it into functionalized polymers. Since **2a** has one C=O group and one C=C bond in the repeat unit, it may be easily modified chemically. Thus, as shown in eqn. (2), treatment of **2a** with an excess of bromine at room temperature gave dibromide **3a** in 84% yield. In the ^1H NMR spectrum of **3a**, the signal due to the olefinic protons of **2a** at 6.2 ppm disappeared completely and a new signal appeared at higher field around 4.5 ppm, while the IR spectrum showed that the absorption at 1715 cm^{-1} due to a carbonyl group remained, indicating that the polyketone structure was not affected.‡ In addition, the reaction of **2a** with $LiAlH_4$ in THF at 65 °C selectively gave polyol **4a** in 90% yield [eqn. (3)]. The IR spectrum of **4a** showed the disappearance of the C=O band at 1715 cm^{-1} of polyketone **2a** and the appearance of a new broad band at 3395 cm^{-1} attributable to a hydroxy group. The ^{13}C

NMR spectrum displayed the complete disappearance of the carbonyl carbon at 208 ppm, and the ^{1}H NMR spectrum is also consistent with the structure of **4a**.

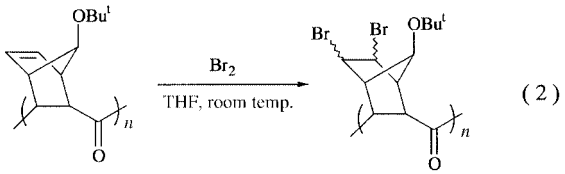

(2)

2a **3a** (84% yield)

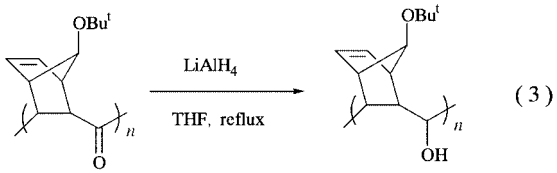

(3)

2a **4a** (90% yield)

Besides 7-*tert*-butoxynorborna-2,5-diene **1a**, norbornadiene and its derivatives smoothly reacted with carbon monoxide in the presence of $Rh_6(CO)_{16}$ under the same reaction conditions to give the corresponding copolymers in good yields. As shown in eqn. (4), the reaction of norbornadiene **1b** (R = H) gave

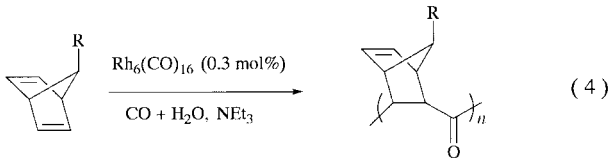

(4)

1b R = H **2b** (95% yield)

1c R = Ph **2c** (85% yield)

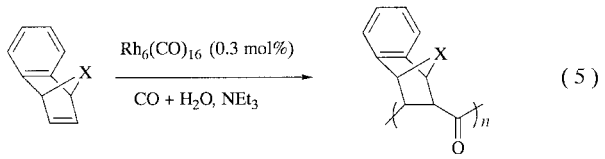

(5)

1d X = C=CMe$_2$ **2d** (90% yield)

1e X = O **2e** (81% yield)

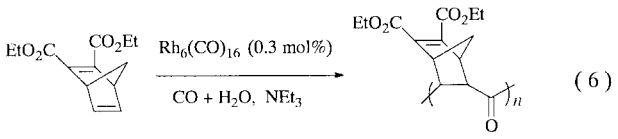

(6)

1f **2f** (81% yield)

copolymer **2b** which is almost insoluble in organic solvents. The high-resolution solid-state ^{13}C NMR (CPMAS) spectrum of **2b** suggested that **2b** has the same structure as **2a**. 7-Phenylnorbornadiene **1c** (R = Ph), which was prepared by treatment[11] of 7-*tert*-butoxynorbornadiene with PhMgBr, also reacted with carbon monoxide to give copolymer **2c** in good yield with a molecular weight of M_w = 9000 (M_w/M_n = 1.38). Interestingly, 1,4-dihydro-9-isopropylidene-1,4-methanonaphthalene **1d** having a norbornadiene skeleton was copolymerized with carbon monoxide to give copolymer **2d** with a high molecular weight (M_w = 25 500) in a high yield [eqn. (5)]. In contrast to **1d**, the reaction of **1e** gave the corresponding copolymer in good yield but with lower molecular weight (M_w = 2570, M_w/M_n = 1.24). Similarly, 2,3-substituted norbornadiene **1f** gave copolymer **2f** in 81% yield, but also with low molecular weight (M_w = 2530, M_w/M_n = 1.20), as shown in eqn. (6). Different electron densities on the C=C bonds of monomers **1d**, **1e** and **1f** could be considered to be a factor affecting the chain growth of the copolymers. In the present reaction system, the steric effect of the substituents on the norbornadiene skeleton might be another factor.

It should be noted that the copolymerization did not occur in the absence of water and amine, suggesting that the copolymerization could be catalyzed by an active rhodium species formed from the reaction of rhodium carbonyl species with water and amine.[7d,9] Detailed investigations are now in progress.

We thank Dr Kenji Wada, Kyoto University, for the measurement of solid-state ^{13}C NMR spectra, and are grateful to the Material Analysis Center of ISIR, Osaka University, for elemental analyses.

Notes and references

† The first transition metal-catalyzed copolymerization of ethylene with carbon monoxide was performed using nickel cyanide complexes in aqueous medium with carbon monoxide pressures as high as 200 atm and at a temperature up to 250 °C to form 'high molecular weight polyketones' (ref. 6). The subsequent advances made using a variety of nickel complexes were outlined in a review [ref. 2(*c*)].

‡ In fact the C, H and Br analyses of polymer **3a** gave a satisfactory result: calc. for $[C_{11}H_{16}OBr_2{\cdot}CO]_n$: C, 40.94; H, 4.58; Br, 45.39. Found: C, 40.81; H, 4.30; Br, 45.24%).

1 J. Guillet, *Polymer Photophysics and Photochemistry*, Cambridge University Press, Cambridge, 1985, p. 278; A. Sen, *Chemtech*, 1986, 48; A. Sen, *Acc. Chem. Res.*, 1993, **26**, 303; E. Drent and P. H. M. Budzelaar, *Chem. Rev.*, 1996, 663.

2 (*a*) A. Sen and T.-W. Lai, *J. Am. Chem. Soc.*, 1982, **104**, 3520; (*b*) T.-W. Lai and A. Sen, *Organometallics*, 1984, **3**, 6; (*c*) A. Sen, *Adv. Polym. Sci.*, 1986, **73/74**, 125; (*d*) A. Sen and Z. Jiang, *Macromolecules*, 1993, **26**, 911; (*e*) P. K. Wong, J. A. van Doorn, E. Drent, O. Sudmeijer and H. Stil, *Ind. Eng. Chem. Res.*, 1993, **32**, 986; (*f*) M. Brookhart and M. I. Wagner, *J. Am. Chem. Soc.*, 1992, **114**, 5894; (*g*) M. Brookhart and M. I. Wagner, *J. Am. Chem. Soc.*, 1994, **116**, 641; (*h*) S. Bronco, G. Consiglio, R. Hutterm, A. Batistini and U. W. Suter, *Macromolecules*, 1994, **27**, 4436; (*i*) Z. Jiang, S. E. Adams and A. Sen, *Macromolecules*, 1994, **27**, 2694; (*j*) Z. Jiang and A. Sen, *J. Am. Chem. Soc.*, 1995, **117**, 4455; (*k*) K. Nozaki, N. Sato and H. Takaya, *J. Am. Chem. Soc.*, 1995, **117**, 9911; (*l*) F. C. Rix, M. Brookhart and P. S. White, *J. Am. Chem. Soc.*, 1996, **118**, 4746; (*m*) M. Brookhart and M. I. Wagner, *J. Am. Chem. Soc.*, 1996, **118**, 7219; (*n*) P. Margel and T. Ziegler, *J. Am. Chem. Soc.*, 1996, **118**, 7337.

3 B. V. Maatschappij, *Neth. Appl.*, 8801168, 1988 (*Chem. Abstr.*, 1990, **113**, 24686f); E. Drent, *Eur. Pat. Appl.*, 504,985, 1992 (*Chem. Abstr.*, 1993, **118**, 103023); D. J. Liaw, *J. Polym. Sci., Part A: Polym. Chem.*, 1993, **31**, 309; S. L. Borkowsky and R. M. Waymouth, *Macromolecules*, 1996, **29**, 6377; K. Nozaki, N. Sato, K. Nakamoto and H. Takaya, *Bull. Chem. Soc. Jpn.*, 1997, **70**, 659.

4 (*a*) J. Tsuji and S. Hosaka, *Polym. Lett.*, 1965, **3**, 703; *JP Patent* 43020469, 1968; (*b*) D.-J. Liaw and J.-S. Tsai, *J. Polym. Sci., Part A: Polym. Chem.*, 1997, **35**, 1157.

5 A. L. Safir and B. M. Novak, *J. Am. Chem. Soc.*, 1998, **120**, 643.

6 Nickel cyanide complex as a catalyst for ethylene/CO copolymerization, also see: W. Reppe and A. Magin, *US Patent*, 2,577,208, 1950.

7 (*a*) Y. Iwashita and M. Sakuraba, *Tetrahedron Lett.*, 1971, 2490; (*b*) G. Consigilo, B. Studer, F. Oldani and P. Pino, *J. Mol. Catal.*, 1990, **58**, L9; (*c*) A. Sen and J. S. Brumbaugh, *J. Organomet. Chem.*, 1985, **279**, C5; (*d*) A. Sen, J. S. Brumbaugh and M. Lin, *J. Mol. Catal.*, 1992, **73**, 297.

8 K. Osakada, J.-c. Choi and T. Yamamoto, *J. Am. Chem. Soc.*, 1997, **119**, 12 390; J.-c. Choi, I. Yamaguchi, K. Osakada and T. Yamamoto, *Macromolecules*, 1998, **31**, 8731.

9 T. Joh, K. Doyama, K. Onitsuka, T. Shiohara and S. Takahashi, *Organometallics*, 1991, **10**, 2493; T. Sugioka, S.-W. Zhang, N. Morii, T. Joh and S. Takahashi, *Chem. Lett.*, 1996, 249; E. Yoneda, T. Kaneko, S.-W. Zhang and S. Takahashi, *Tetrahedron. Lett.*, 1998, **39**, 5061; S.-W. Zhang, T. Sugioka and S. Takahashi, *J. Mol. Catal.*, 1999, **143**, 211.

10 F. Hojabri, *J. Appl. Chem. Biotechnol.*, 1973, **23**, 601.

11 P. R. Story and S. R. Fahrenholtz, *J. Org. Chem.*, 1963, **28**, 1716.

Communication a909287k

ChemComm

Synthesis of (±)-kainic acid by dearomatising cyclisation of a lithiated *N*-benzyl *p*-anisamide

Jonathan Clayden* and Kirill Tchabanenko

Department of Chemistry, University of Manchester, Oxford Road, Manchester, UK M13 9PL. E-mail: j.p.clayden@man.ac.uk

Received (in Liverpool, UK) 24th November 1999, Accepted 12th January 2000

_N_-Benzyl _p_-anisamide 6, on lithiation with Bu^{t}Li in the presence of HMPA, undergoes a stereoselective anionic cyclisation with loss of aromaticity to give a bicyclic enone which may be converted in nine steps to (±)-kainic acid.

We recently described[1] the dearomatising cyclisation reaction of lithiated *N*-benzyl benzamides **1** to give bicyclic cyclohexadienes **2** and **3** (Scheme 1).[2] The reaction is stereoselective, creating three new stereogenic centres, and it is noticeable that the pyrrolidine ring of the major product **2** has the relative stereochemistry of kainic acid **4**. (−)-Kainic acid[3] **4** was first isolated in 1953 from the Japanese marine alga *Digenea simplex*.[4] It has diverse biological activity: as an anthelmintic, *D. simplex* is a traditional remedy in which kainic acid is the active component.[5] Kainic acid is an extremely potent neuroexcitor, binding specifically at the kainate receptor and leading to specific neuronal death.[6,7] Both the anthelmintic and neuroexcitatory properties of kainic acid are dependent on the *cis* C-3–C-4 relative stereochemistry: allokainic acid, the C-4 epimer, is inactive as an anthelmintic[8] and has lower neuroexcitatory activity than kainic acid.[9]

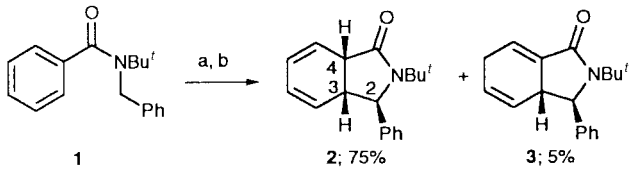

Scheme 1 *Reagents and conditions*: (a) Bu^{t}Li (1.3 equiv.), HMPA (6 equiv.), THF, −78 °C, 16 h; (b) NH_4Cl.

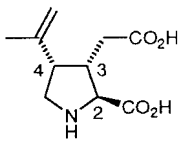

A number of syntheses of (−)-kainic acid[10] and (±)-kainic acid[11] have been reported, several of which[10g–k,p,s,11a] achieve control over the C-3–C-4 stereochemistry by forming these substituents from a cyclic precursor. Our approach to (±)-kainic acid, presented in Schemes 2 and 3, also uses this strategy, exploiting the relative stereochemistry of the dearomatising cyclisation reaction.

Acylation of cumylamine **5**[12] with *p*-anisoyl chloride, followed by alkylation of the secondary amide with benzyl bromide, gave the cyclisation substrate **6**. Tertiary *N*-substituents are necessary for good yields in the cyclisation step, and our early studies had all used *N*-Bu^t amides. However, we had considerable difficulty removing the *tert*-butyl group from the cyclised products: we turned to the cumyl group for ease of removal under acid conditions.[13] The *N*-cumyl-*N*-benzyl amide **6** was lithiated with Bu^{t}Li in the presence of HMPA, but the more bulky group slowed the reaction considerably and the cyclisation of **6** *via* **7** required 60 h at −40 °C to reach

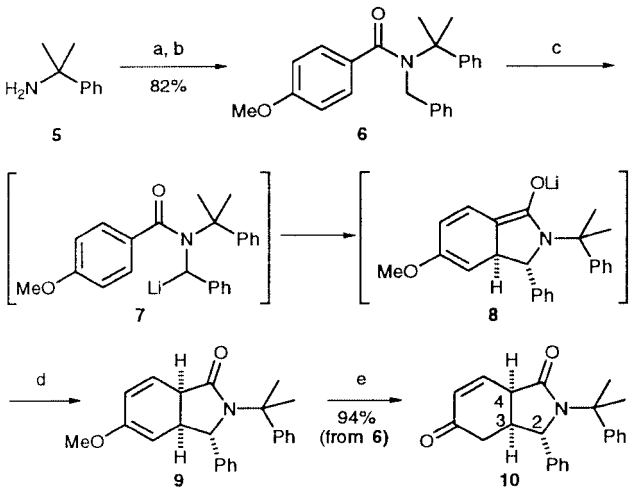

Scheme 2 *Reagents and conditions*: (a) *p*-anisoyl chloride, Et_3N, CH_2Cl_2; (b) NaH, DMF, BnBr, 18 h; (c) Bu^{t}Li (2 equiv.), HMPA (12 equiv.), THF, −40 °C, 60 h; (d) NH_4Cl; (e) THF, 1 M HCl (aq).

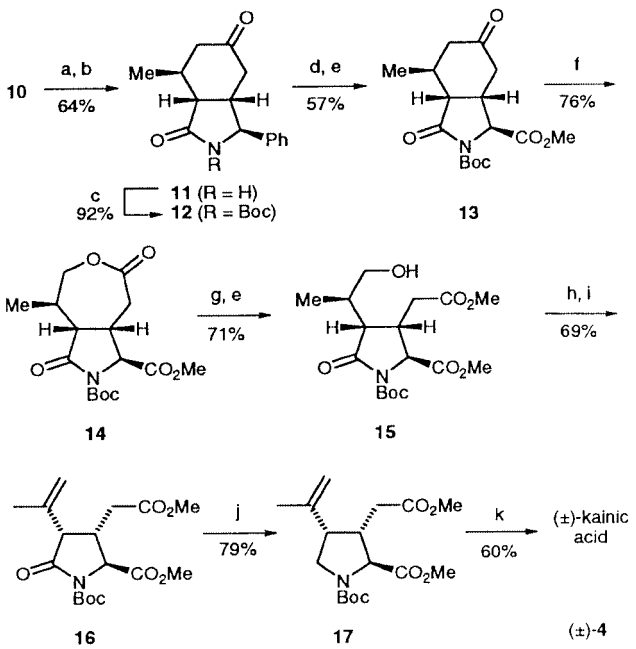

Scheme 3 *Reagents and conditions*: (a) Me_2CuLi, Me_3SiCl, THF, −78 °C, 1 h; (b) CF_3CO_2H, reflux, 6 h; (c) Boc_2O, Et_3N, DMAP, CH_2Cl_2, (d) $NaIO_4$, cat. $RuCl_2$, 1:1 acetone–H_2O; (e) Me_3SiCHN_2, PhH, MeOH; (f) MCPBA, CH_2Cl_2; (g) NaOH (2.2 equiv.), MeOH, reflux, 2 h; (h) *o*-$NO_2C_6H_4SeCN$, Bu_3P, THF, rt; (i) H_2O_2, Py, THF, −40 °C; (j) $NaBH(OMe)_3$ (2 equiv.), THF, reflux; (k) 10:1 CF_3CO_2H–H_2O, reflux, 4 h.

completion. The initial product of the cyclisation was the enolate **8**, which was protonated to give the dienyl ether **9** as a single regioisomer. This was hydrolysed *in situ* to the bicyclic

enone **10**, whose pyrrolidinone ring has the relative stereochemistry of kainic acid.

Lithium dimethyl cuprate, in the presence of trimethylsilyl chloride, attacked solely the *exo* face of the enone **10**: TFA catalysed both hydrolysis of the product silyl enol ether and removal of the cumyl group, and the lactam **11** was reprotected as its Boc derivative **12**.

The phenyl ring of **12** was oxidised with catalytic RuO_4, and we found that replacing the usual MeCN–CCl_4–H_2O system[14] with 1 : 1 acetone–water considerably improved the rate of the reaction. The carboxylic acid product was esterified with trimethylsilyldiazomethane[15] to give **13**.

We used Baeyer–Villiger oxidation to cleave the cyclohexanone ring of **13** into the two portions required in the target: remarkably, despite the fact that the ketone is almost identically substituted on both sides, the oxidation was fully regioselective and gave **14** with no trace of the other regioisomer. We tentatively propose that the regioselectivity is a consequence of the conformational preference of the intermediate peracid adduct in the Baeyer–Villiger reaction. Attack of the peracid on the *exo*-face of **13** gives **18**, whose pseudo-axial methyl group

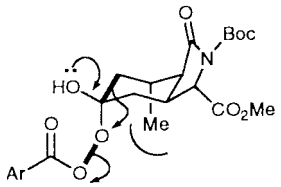

18

may favour a conformation with the breaking O–O bond antiperiplanar to the C–C bond shown in bold, rather than the C–C bond to the other side of the former ketone.

Seven-membered lactone **14** was converted to diester **15** by hydrolysis with methanolic NaOH (slow addition of base avoided cleavage of the Boc protecting group) and esterification with trimethylsilyldiazomethane.[15] The elimination of water to give the isopropenyl group of **16** was achieved in one step by direct formation of a selenide[16] which was oxidised and eliminated under mild conditions.

Sodium trimethoxyborohydride selectively reduced the lactam carbonyl group of **16** in the presence of the two esters,[17] and wet trifluoroacetic acid both deprotected the amino group and hydrolysed the esters of the product **17**. The racemic product (±)-**4** was recrystallised from methanol and had spectroscopic properties (^{1}H and ^{13}C NMR) identical with those of natural kainic acid.

We are grateful to the Leverhulme Trust for a grant.

Notes and references

1 A. Ahmed, J. Clayden and S. A. Yasin, *Chem. Commun.*, 1999, 231.

2 Dearomatising anionic cyclisations are also known in the naphthamide series: A. Ahmed, J. Clayden and M. Rowley, *Chem. Commun.*, 1998, 297; A. Ahmed, J. Clayden and M. Rowley, *Tetrahedron Lett.*, 1998, **39**, 6103; R. A. Bragg and J. Clayden, *Tetrahedron Lett.*, 1999, **40**, 8323; *Tetrahedron Lett.*, 1999, **40**, 8327. There are reports of similar reactions of aryl sulfones: J. K. Crandall and T. A. Ayers, *J. Org. Chem.*, 1992, **57**, 2993; A. Padwa, M. A. Filipkowski, D. N. Kline, S. S. Murphree and P. E. Yeske, *J. Org. Chem.*, 1993, **58**, 2061.

3 For recent reviews, see A. F. Parsons, *Tetrahedron*, 1996, **52**, 4149; M. G. Moloney, *Nat. Prod. Rep.*, 1998, **15**, 206; 1999, **16**, 485.

4 S. Murakami, T. Takemoto and Z. Shimizu, *J. Pharm. Soc. Jpn.*, 1953, **73**, 1026.

5 H. Watase, Y. Tomiie and I. Nitta, *Nature (London)*, 1958, **181**, 761.

6 E. G. McGeer, J. W. Olney and P. L. McGeer, *Kainic Acid as a Tool in Neurobiology*, Raven Press, New York, 1978.

7 H. Shinozaki, in *Excitatory Amino Acid Receptors. Design of Agonists and Antagonists*, ed. P. Krogsgaard-Larsen and J. J. Hansen, Ellis Horwood, New York, 1992, p. 261.

8 S. Husinec, A. E. A. Porter, J. S. Roberts and C. H. Strachan, *J. Chem. Soc., Perkin Trans. 1*, 1984, 2517.

9 J. J. Hansen and P. Krogsgaard-Larsen, *Med. Res. Rev.*, 1990, **10**, 55.

10 (*a*) W. Oppolzer and K. Thirring, *J. Am. Chem. Soc.*, 1982, **104**, 4978; (*b*) J. Cooper, D. W. Knight and P. T. Gallagher, *J. Chem. Soc., Chem. Commun.*, 1987, 1220; (*c*) J. Cooper, D. W. Knight and P. T. Gallagher, *J. Chem. Soc., Perkin Trans. 1*, 1992, 553; (*d*) J. E. Baldwin and C.-S. Li, *J. Chem. Soc., Chem. Commun.*, 1987, 166; (*e*) J. E. Baldwin, M. G. Moloney and A. F. Parsons, *Tetrahedron*, 1990, **46**, 7263; (*f*) S. Takano, Y. Iwabuchi and K. Ogasawara, *J. Chem. Soc., Chem. Commun.*, 1988, 1204; (*g*) S. Takano, T. Sugihara, S. Satoh and K. Ogasawara, *J. Am. Chem. Soc.*, 1988, **110**, 6467; (*h*) N. Jeong, S.-E. Yoo, S. J. Lee, S. H. Lee and Y. K. Chung, *Tetrahedron Lett.*, 1991, **32**, 2137; (*i*) S.-E. Yoo, S.-H. Lee, N. Jeong and I. Cho, *Tetrahedron Lett.*, 1993, **34**, 3435; (*j*) S.-E. Yoo and S.-H. Lee, *J. Org. Chem.*, 1994, **59**, 6968; (*k*) S. Takano, K. Inomata and K. Ogasawara, *J. Chem. Soc., Chem. Commun.*, 1992, 169; (*l*) A. Barco, S. Benetti, G. P. Pollini, G. Spalluto and V. Zanirato, *J. Chem. Soc., Chem. Commun.*, 1991, 390; (*m*) S. Hatakeyama, K. Sugawara and S. Takano, *J. Chem. Soc., Chem. Commun.*, 1993, 125; (*n*) S. Hanessian and S. Ninkovic, *J. Org. Chem.*, 1996, **61**, 5418; (*o*) Y. Nakada, T. Sugahara and K. Ogasawara, *Tetrahedron Lett.*, 1997, **38**, 857; (*p*) M. D. Bachi and A. Melman, *J. Org. Chem.*, 1997, **62**, 1896; (*q*) O. Miyata, Y. Ozawa, I. Ninomiya and T. Naito, *Synlett*, 1997, 275; (*r*) A. Rubio, J. Ezquerra, A. Escribano, M. J. Remuiñán and J. J. Vaquero, *Tetrahedron Lett.*, 1998, **39**, 2171; (*s*) J. Cossy, M. Cases and D. G. Pardo, *Tetrahedron*, 1999, **55**, 6153; (*t*) A. D. Campbell, T. M. Raynham and R. J. K. Taylor, *Chem. Commun.*, 1999, 245.

11 (*a*) J. A. Monn and M. J. Valli, *J. Org. Chem.*, 1994, **59**, 2773; (*b*) S.-E. Yoo, S.-H. Lee, K.-Y. Yo and N. Jeong, *Tetrahedron Lett.*, 1990, **31**, 6877.

12 D. Balderman and A. Kalir, *Synthesis*, 1978, 24.

13 The use of cumyl as an organolithium-resistant acid labile protecting group for nitrogen was recently independently reported by Snieckus and coworkers: C. Metallinos, S. Nerdinger and V. Snieckus, *Org. Lett.*, 1999, **1**, 1183.

14 Sharpless recommended the use of MeCN to keep Ru–carboxylate complexes in solution: P. H. Carlsen, T. Katsuki, V. S. Martín and K. B. Sharpless, *J. Org. Chem.*, 1981, **46**, 3936. See also M. T. Nuñez and V. S. Martín, *J. Org. Chem.*, 1990, **55**, 1928; T. Shioiri, F. Matsuura and Y. Hamada, *Pure Appl. Chem.*, 1994, **66**, 2151.

15 N. Hashimoto, T. Aoyama and T. Shioiri, *Chem. Pharm. Bull.*, 1981, **29**, 1475.

16 P. A. Grieco, S. Gilmann and H. Nishizawa, *J. Org. Chem.*, 1976, **41**, 1485.

17 We are not aware of other uses of this reagent to reduce lactams in the presence of esters. See, however, M. E. Kuehne and P. J. Shannon, *J. Org. Chem.*, 1977, **42**, 2082.

Communication a909325g

Typeset and printed by Black Bear Press Limited, Cambridge, England

ChemComm
FEATURE ARTICLE

Fullerenes: three dimensional electron acceptor materials

Dirk M. Guldi

University of Notre Dame, Radiation Laboratory, Notre Dame, IN 46556, USA. E-mail: guldi.1@nd.edu

Received (in Cambridge) 28th September 1999, Accepted 3rd November 1999

This feature article highlights the advantages of employing [60]fullerene as a viable electron accepting building block in novel donor acceptor systems. Different strategies that aim towards improving charge separation in fullerene containing systems are presented. This is accomplished, for example, *via* utilisation of additional stabilisation forces of the radical pair or, alternatively, diffusional splitting of the last mentioned. Fine-tuning the topology of the electron donor moiety has been shown to be a powerful means of influencing the relative energies of the two states involved (*e.g.* the charge-separated state *vs.* the singlet ground state). Remarkable effects concerning the lifetime of the charge-separated radical pair were observed, in particular, in systems that upon charge separation led to a gain of aromaticity and planarity of the oxidised fragment.

Introduction

In the photosynthetic reaction centre (PRC), a variety of short-range electron transfer (ET) and energy transfer (ENT) events occur between well-arranged organic pigments and other cofactors. Thereby, charges are separated with remarkable efficiency to yield a spatially and electronically well-isolated radical pair and thus eliminate the energy-wasting back electron transfer (BET). The arrangement of the donor–acceptor couples in the PRC is accomplished *via* non-covalent incorporation into a well-defined protein matrix.[1]

Owing to the importance and complexity of natural photosynthesis, the study thereof necessitates suitable simpler models. The ultimate goal is to design and assemble synthetic systems which can efficiently convert solar energy into useful chemical energy. An important approach to PRC modelling has been the covalent linking of a photoexcitable chromophore with an electron acceptor or an electron donor. It is important to note that in these artificial systems the organising property is the covalent linkage between the redox active moieties.[2]

A number of factors have been systematically altered over the past decades to overcome the difficulties encountered in the early artificial, covalently linked donor-acceptor dyads:[2] the energies of the donor and acceptor molecules have been adjusted to increase the rates of the forward ET and to slow down the BET. Also, the electronic coupling between donor and acceptor moieties has been tuned to alter ET rate constants in favourable directions. The most important strategy, however, focuses on the incorporation of secondary electron donor or acceptor moieties into multicomponent arrays (triads, tetrads, pentads *etc*.).

In the following contribution some noteworthy features are summarised concerning [60]fullerene as a new, three-dimensional electron acceptor unit in artificial reaction centres. Additionally, different strategies are presented which aim towards improving charge separation in fullerene containing supermolecular (*e.g.* covalently linked) and supramolecular (*e.g.* non-covalently linked) systems. It should be pointed out that the highlighted systems are restricted to composites that bear a single electron acceptor and a single electron donor block. The key feature in these dyads relies on additional stabilisation of the radical pair such as (i) a gain in aromaticity and planarity of the electron donor, or (ii) a dissociation of the charge-separated state. These effects are expected to result in diminishing of the BET.

Small reorganisation energies of fullerenes

One of the most fascinating phenomena in the field of fullerene chemistry is the small reorganisation energy associated with almost all their reactions, especially in photoinduced electron transfer (PET).[3] This is an important requisite for the directional control and also the efficiency of ET reactions, as illustrated by the well-organised special pair (*e.g.* bacterial chlorophyll and ubiquinone) in the photosynthetic reaction centre. The total reorganisation energy (λ) is the sum of a solvent-independent term λ_i and the solvent reorganisation energy λ_s.[4] The λ_i contribution stems from the nuclear configurations, associated with the transformation of the molecule, for instance, in a photochemical reaction from an initial to a final state. It is notable that the rigid structure of the fullerene core leads to small Raman shifts under reductive conditions, and small Stokes shifts in excitation experiments.[5] A reasonable interpretation for these observations is the structural similarity between [60]fullerene in the ground, reduced and also excited states. It is also believed that the solvent-dependent term (λ_s) is small, thus requiring little energy for the adjustment of a generated state (*e.g.* excited or reduced states) to the new solvent environment.

These effects have fundamental consequences upon the classical Marcus treatment of ET theory.[4] The latter predicts an increase in rate with increasing thermodynamic driving force in

Dirk M. Guldi graduated from the University of Cologne (Germany) in 1988, from where he received his PhD in 1990 (under the supervision of Professor Fritz Wasgestian). In 1992, after a postdoctoral appointment at the National Institute of Standards and Technology (with Dr Pedatsur Neta), he took a research position at the Hahn-Meitner-Institute Berlin in the group of Professor Klaus-Dieter Asmus. After a brief stay as a Feodor-Lynen Stipend at Syracuse University (within the framework of the Alexander von Humboldt Foundation) he joined in 1995 the faculty of the Notre Dame Radiation Laboratory where he was promoted to Associate Scientist in 1996. In 1999 he completed his Habilitation at the University of Leipzig (Germany). His primary research interests are in the areas of charge separation in super- and supramolecular systems with three-dimensional electron acceptors and mechanistic aspects of radiation and photosensitization. He is particularly interested in molecular recognition as a means to control the dynamics in intra- and intermolecular electron transfer events and the efficiency of charge separation in donor–acceptor assemblies.

DOI: 10.1039/a907807j

the 'normal' region up to a maximum value, where $-\Delta G°$ equals the reorganisation energy λ. As the standard free energy becomes more negative ($-\Delta G° > \lambda$) the ET rate decreases in the 'inverted' region. Based on the small λ value for fullerenes, the maximum of the Marcus curve should be reached at smaller $-\Delta G°$, relative to two-dimensional electron acceptors, which in general have less rigid structures and higher reorganisation energies than three-dimensional fullerenes. This shifts the more exothermic BET clearly into the Marcus 'inverted' region, far from the thermodynamic maximum ($-\Delta G° = \lambda$) and inhibits the undesired BET event. At the same time, the 'normal' region is steeper, which leads to a notable acceleration of ET.

In conclusion, the ability of these three-dimensional carbon allotropes to inhibit BET and still combine it with a fast forward ET renders them as unique probes for *inter*- and *intra*molecular ET studies. In addition, the low reduction potential of [60]fullerene ($E_{1/2} = -0.44$ V *vs.* SCE) appears profitable for their utilisation as novel electron acceptors or relays in multicomponent donor acceptor systems.[6]

To illustrate the benefits of incorporating a fullerene rather than a quinone acceptor, which has a similar reduction potential but higher reorganisation energy, a fullerene-based porphyrin dyad with a rigid spacer guaranteeing a fixed separation between the two redoxactive moieties was compared with a quinone-based porphyrin dyad. Remarkably, the fullerene-based dyad gives rise to an accelerated ET (~6 times) and decelerated BET process (~25 times) relative to the kinetics of the corresponding quinone dyad.[3a]

Fullerene containing donor–bridge–acceptor dyads

The covalent linkage of fullerenes to a number of interesting electro- or photoactive species offers new opportunities in the preparation of materials that may produce long-lived charge-separated states in high quantum yields. Most importantly, the covalent linkage eliminates diffusion as the rate determining ET step and helps to enhance the transfer dynamics in donor acceptor dyads. Consequently, the PET event is converted to a truly *intra*molecular reaction controlled only by the activation energy of the reaction. A fixed and short distance between the two electroactive components prevents the undesired loss of excitation energy *via* alternative radiation and radiationless decay channels.

In this context various fullerene-based donor acceptor dyads, encompassing the linkage of the fullerene core to different donor moieties, ranging from ferrocene and aniline derivatives to phenothiazine, have been reported in recent years.[7] In these systems the fullerene moiety operates as the photosensitizer, absorbing the visible light to generate an excited species. The electron donor is not initially affected and remains in its singlet ground state (see Fig. 1). In a follow-up step the sacrificial electron donor is oxidised *via* quenching of the photoexcited sensitizer.

The singlet excited state energies of monofunctionalized fullerene building blocks, such as methanofullerenes[8a] (1.796 eV) or pyrrolidinofullerenes[8b] (1.762 eV) are sufficiently high to activate an *intra*molecular ET from the appended donor moiety.[5b] This principally yields the $C_{60}^{\bullet -}$–$D^{\bullet +}$ charge-separated state, in which $D^{\bullet +}$ denotes the oxidised donor moiety. A diagnostic probe for the identification of the π-radical anion of the fullerene moiety (*e.g.* $C_{60}^{\bullet -}$) is the sharp band in the NIR around 1000 nm.[9] The spectral signature allows a precise analysis of *inter*- and *intra*molecular ET and BET dynamics in [60]fullerene containing donor acceptor systems.

The Coulombic term, which results from the destabilisation when charges are separated, governs the fate of the $C_{60}^{\bullet -}$-$D^{\bullet +}$ pair. Accordingly, BET is, in general, very fast and produces the singlet ground state. Increasing the distance between the donor and acceptor, by means of increasing the size of the spacer units,

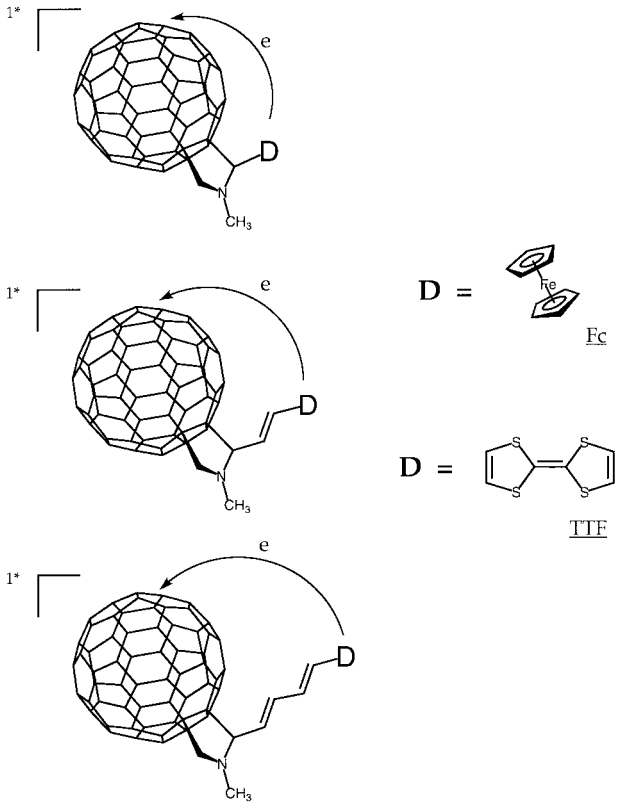

Fig. 1 Schematic illustration of photoinduced electron transfer processes from an electron donor [A = ferrocene (Fc) and tetrathiofulvalene (TTF)] to the singlet excited state of a fullerene moiety.

is one approach to reduce the Coulombic term and to slow down the BET kinetics. For example, substitution of a simple C–C linkage of the donor and acceptor moieties by various vinyl units or a norbornylogous bridge led to enhanced lifetimes of the charge-separated state.[10] At the same time, the spatial separation impacts the thermodynamic driving force ($-\Delta G°$) for an *intra*molecular ET event. Specifically, increasing the donor–acceptor separation lowers the free energy change. Thus, an ET that is exothermic in a closely spaced dyad may become endothermic or only weakly exothermic in a widely spaced dyad, and therefore cannot compete with other deactivation processes (*e.g.* radiation and radiationless decay channels).

One possible way to alter the free energy gap is to increase the chemical potential of the donor and/or acceptor moiety.[2,10] Alternatively, solvents with high relative permittivities may be used. Polar solvents impose two major effects on the ET dynamics: first, it assists in reactivating the ET even in widely separated dyads, and secondly, it helps stabilise the charge-separated radical pair by lowering the Coulombic term.

Employing the dielectric continuum model these solvents and separation effects can be quantified. This model handles the charge-separated radical pair as two spherical ions separated by a distance (R), submerged into a solvent of a static relative permittivity (ε).[11]

Gain of aromaticity

In addition to the Coulombic term, energetic considerations associated with the topology of the donor molecule also control the energies of the ground and oxidised states. Donor moieties, such as aniline and ferrocene, reveal aromatic structures in their ground states.[10,12] The delocalization that the aromatic core helps to stabilise the generated radical cation. For molecules whose ground state is aromatic, one-electron oxidation will result, however, in a partial loss of their aromatic resonance stabilisation (see case I in Fig. 2). This loss of aromaticity, consequently, yields a state of higher energy.

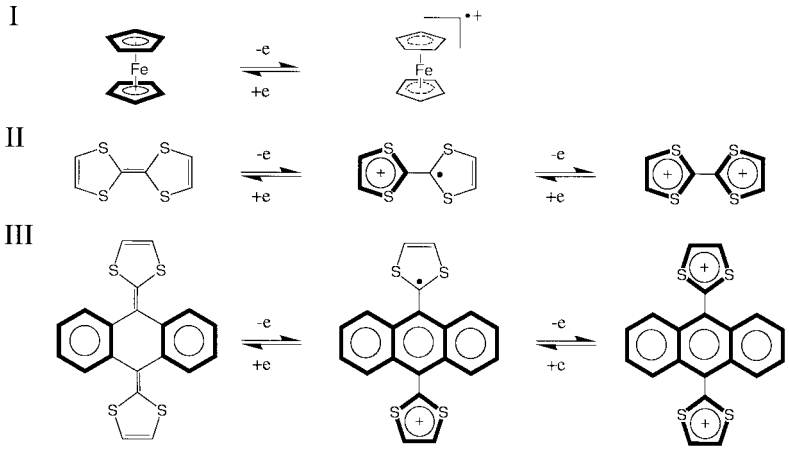

Fig. 2 Concept of gain of aromaticity and planarity. (I) Loss of aromaticity in one-electron oxidised ferrocene. (II) Gain of aromaticity in one- and two-electron oxidised TTF. (III) Gain of aromaticity and planarity in one- and two-electron oxidised (extended)TTF.

The gain in aromaticity associated with the reverse reaction (*e.g.* the BET reaction), on the other hand, provides a driving force for destabilisation of the oxidised species and acceleration of the BET in $C_{60}^{\bullet-}$-$D^{\bullet+}$ pairs. To circumvent this problem a strategy has been proposed for special donor–acceptor composites in which a series of novel organic donors were linked to the fullerene core that gain rather than lose aromaticity on charge separation (CS). This is an important difference to alternative approaches that imply stabilisation of the charge-separated state energy at the expense of subsequent, irreversible chemistry or decomposition of the oxidised donor. It is expected that the gain of aromaticity leads to noticeable effects by enhancing the lifetime of the charge-separated radical pair. This strategy was pursued using molecules, such as tetrathiafulvalenes (TTF), which contain donors whose electronic structure dictates that aromaticity is gained on CS. TTF molecules fulfil this important requisite by means of forming the 1,3-dithiolium cation, which, in contrast to the ground state, displays an aromatic character (see case II in Fig. 2).[13]

Steady-state and time-resolved photolysis studies reveal that the fullerene singlet excited states in C_{60}–TTF dyads[14] undergo rapid *intra*molecular ET events, yielding a charge-separated radical pair, namely, ($C_{60}^{\bullet-}$)-($TTF^{\bullet+}$). *Intra*molecular ET rate constants range between 1.2×10^{10} s^{-1} for closely spaced dyads (donor-acceptor separation of 4.8 Å) in benzonitrile and 1.5×10^{9} s^{-1} for widely spaced analogues (donor-acceptor separation of 10.5 Å) in toluene. The ET rate constants of these processes increase with increasing solvent polarity (*i.e.* larger $-\Delta G°$), which is consistent with the processes occurring in the 'normal' Marcus region. A radical pair lifetime of *ca.* 2 ns was observed for the closely spaced C_{60}–TTF dyads.[15] In comparison, lifetimes of 0.526, 0.05 and 0.294 ns are reported for similarly spaced carotene–C_{60}, ZnTPP–C_{60} and H_2TPP–C_{60} dyads, respectively.[16] This improvement is clearly an experimental demonstration of the 'gain of aromaticity' concept.

Gain of aromaticity and planarity

A further development with respect to increasing the degree of stabilisation is to add heteroaromatic rings to the aromatic arenes that posses larger aromatic stabilisation energies. This approach was successfully carried out by using conjugated TTF analogues with a *p*-quinodimethane structure (see case III in Fig. 2).[17] In addition to the aromatic 1,3-dithiolium cations, the π-conjugation in the oxidised form of the two isolated benzene rings is extended to the entire anthracene backbone. As a net result, the dicationic species is fully aromatic.

The geometrical features of *p*-quinodimethane analogues of tetrathiafulvalene further widens the scope of the stabilisation concept, from simply a gain of aromaticity to both a gain of aromaticity and of planarity.[18] In particular, the molecular geometries in π-extended tetrathiafulvalene derivatives with *p*-quinonoid structures reveal highly distorted orientations. They adopt a butterfly-shaped structure in the ground state to avoid the short contacts between the sulfur atoms and the hydrogen atoms. In contrast, optimisation of the two-electron oxidised state, *i.e.* the dication, with the aromatic anthracene as a basic constituent reveals a planar structure. The two aromatic 1,3-dithiolium cations align orthogonally with respect to the anthracene plane. It should be added that the oxidation process is fully reversible but necessitates, due to the loss of planarity and aromaticity, higher activation energies for the return process to occur.[18]

Pico- and nanosecond time-resolved transient absorption measurements with C_{60}–(extended)TTF dyads reveal that the initially formed singlet excited fullerene states transform rapidly into the charge-separated radical pairs. Generally, the *intra*molecular ET rates depend on (i) the spatial separation, (ii) the oxidation potential of the π-extended tetrathiafulvalene derivative, (iii) the reduction potential of the fullerene derivative, and (iv) the solvent polarity. They vary between 1.9×10^{10} s^{-1} (donor–acceptor separation of 4.4 Å) in benzonitrile and 1.3×10^{9} s^{-1} (donor–acceptor separation of 10.35 Å) in toluene. In all cases, the lifetimes of the charge-separated radical pair (*ca.* 100 ns) are promisingly increased relative to donor molecules which lack the gain in planarity or aromaticity upon oxidation (far less than 1 ns, see above).[19]

The above-summarised observations illustrate the key to controlling the structure *via* a combination of donor–acceptor potential and topology to fine-tune the relative energies of the two forms, namely, the singlet ground state and the charge-separated state.

Donor–acceptor complex association and dissociation

A major drawback, associated with *intra*molecular ET events, concerns the rapid BET, driven by the covalent linkage of the donor and acceptor moieties. The rate of BET determines the efficiency of a multicomponent system for practical applications.

In the following a supramolecular approach is summarised, which aims to retard the fast BET, commonly observed in supermolecular systems.[20] It entails the biomimetic assembly of two or more individual molecules, linked by weak *inter*molecular interactions such as van der Waals' forces, hydrogen bonding, salt bridges or ligand complexation. The reversible coordination of the acceptor moiety (ligand or substrate) to the donor (coordination centre or receptor) rather than their covalent linkage enables the diffusional splitting of the charge-separated radical pair after the initial ET takes place. Thus, complexation of the donor–acceptor couple appears a viable

alternative to supermolecular polyads (*e.g.* triads, tetrads, *etc*.) involving covalent links between the components. In the latter, a multistep electron relay along a vectorial redox gradient governs the lifetime of the radical pair: as the number of sequential steps involved in the electron relay increases, the lifetime lengthens. However, with each step the overall efficiency for transport of the charge from one end to the other decreases.

Ideally, light-induced intramolecular ET from the porphyrin chromophore to C_{60} proceeds very fast. Then, in a weakly coordinating solvent, complex dissociation should follow the ET event, which leads to diffusional separation of the charge-separated radical pair. As a consequence the BET is limited to a simple *inter*molecular process. In the case of the depicted fullerene complexes BET within the associated complex will compete with complex dissociation and, therefore, govern the quantum efficiencies of CS. Since the rate of complex dissociation depends on the strength of the coordination bond, optimisation of the CS is possible by using different coordination metals. For example, the strong π-back bonding in CO–RuTPP complexes *vs*. the weaker σ–bonding in ZnTPP composites leads to drastically different complexation strengths (see Fig. 3) with, for example, pyridine.[21] While the former complex is quite stable in solution, the latter exhibits a complexation equilibrium constant (K) of nearly 5900 $dm^3\ mol^{-1}$ (in toluene) and thus is only shifted towards the complexed form.

The assembly of a rigid but non-covalently connected dyad was obtained by coordinating a fullerene ligand to a zinc tetraphenylporphyrin (ZnTPP) *via* axial pyridine coordination to the metal. This ensemble gives rise to an edge-to-edge distance of 4.5 Å between the entities or a centre-to-centre distance of 9.5 Å. The complex association is conveniently followed by absorption spectroscopy (*e.g.* shift of the Q-band transitions) and also by steady state emission spectroscopy (*e.g.* fluorescence quenching). In particular, a concentration-dependent fluorescence quenching of the (^{1}*π–π)ZnTPP correlates with a very efficient CS upon irradiation.

It is pertinent to note that two different pathways for the ET processes exist (see Fig. 4). A fast *intra*molecular ET inside the associated fullerene-porphyrin complex follows the excitation of the porphyrin chromophore. Alternatively, the free porphyrin is excited and undergoes *inter*molecular ET as soon as the acceptor molecules approach closely enough during molecular diffusion. The former process, which occurs in all solvents, involves (^{1}*π–π)ZnTPP, while the *inter*molecular process is likely to dominate the quenching of the energetically lower lying (^{3}*π-π)ZnTPP. Complications arise from the fact that polar solvents, such as benzonitrile, interfere with the coordination of the zinc centre. It was shown that in coordinating media, the solvent displaces the fullerene ligand from the zinc, making the *inter*molecular route more effective.

Kinetic analysis of the fullerene π-radical anion transient absorption evolving from irradiation of the ZnTPP–C_{60} composite yields a remarkable lifetime of several hundred microseconds for the separated radical pair in deoxygenated benzonitrile. The quantum yield (Φ) for the truly separated radical pair, $C_{60}^{\bullet-}$ and $ZnTPP^{\bullet+}$ in deoxygenated dichloromethane is *ca.* 0.14.

The given example demonstrates the potential usefulness of these non-covalently linked systems in photovoltaic devices. But they also point to the fundamental challenge employment of a more polar environment, such as aqueous solutions, faces with respect to avoiding complexation of the zinc centre, while promoting the stabilisation of the radical pair. Future work will concentrate on water-soluble systems using additionally charged porphyrin macrocyclic ligands to slow down the BET step.

The coordination concept, namely, complexation of a fullerene–pyridine ligand by a macrocyclic π-system that bears

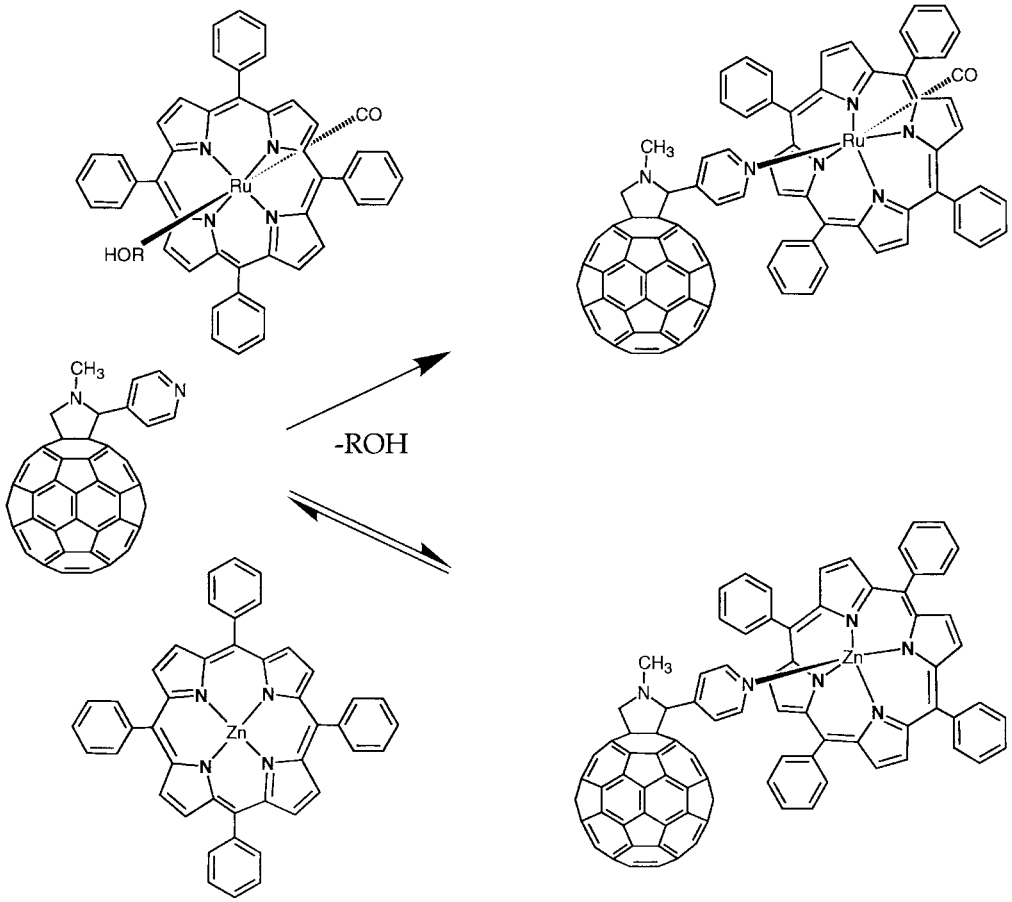

Fig. 3 Irreversible (upper case) and reversible complexation (lower case) of an electron acceptor (*e.g.* fullerene-pyridine derivative) to transition metal complexes (*e.g.* Zn^{II} and Ru^{II}) of tetraphenyl porphyrins.

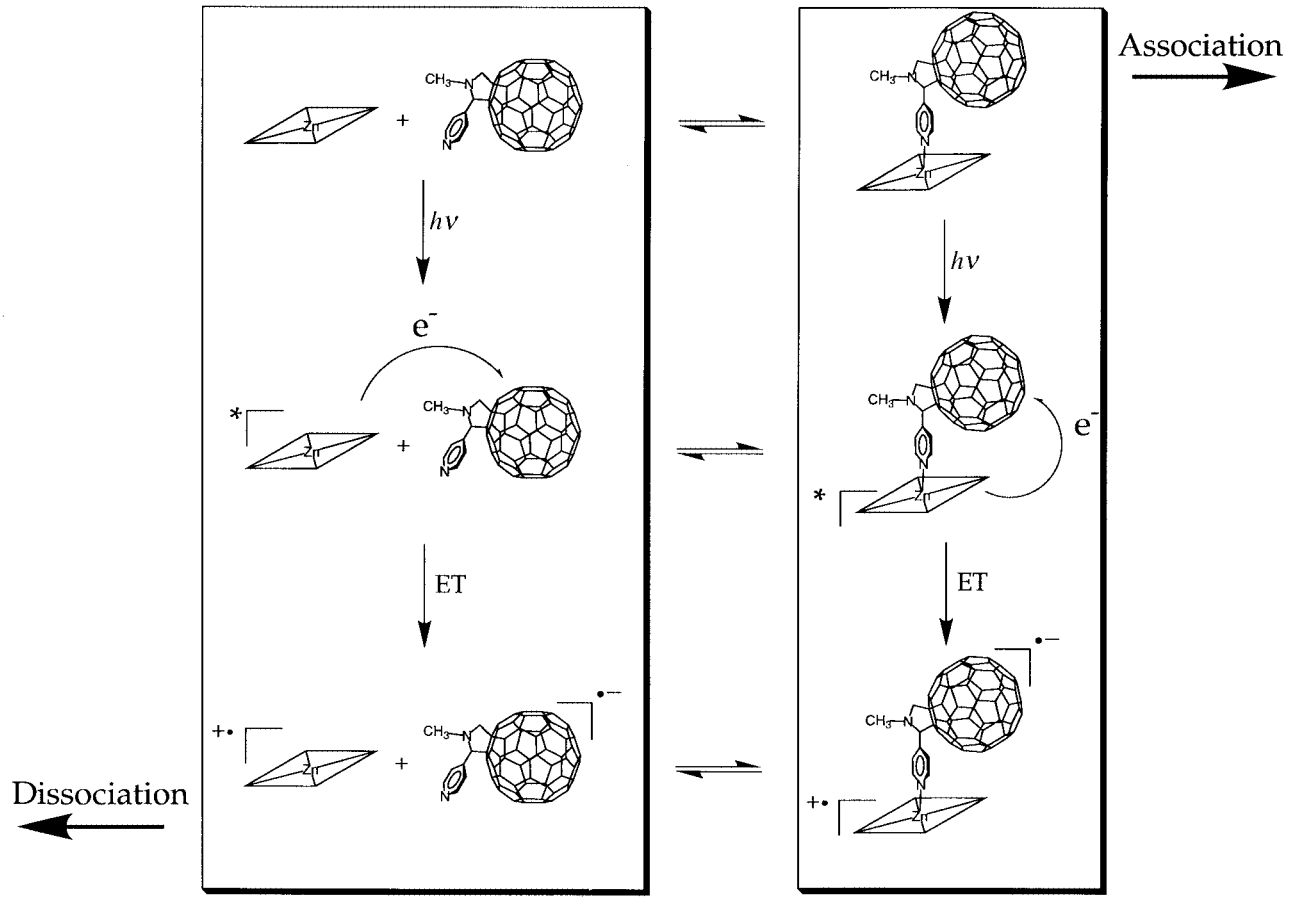

Fig. 4 Inter- and intramolecular electron transfer routes in an associated fullerene–porphyrin complex (right hand side) and in a free porphyrin fullerene mixture (left hand side), respectively.

a potential utilisation as a chromophore system, is very general and can be employed successfully for metallophthalocyanines and structural porphyrin isomers.[22]

Peptides as molecular rulers

Molecular systems that respond precisely to environmental changes occurring at a microscopic level and signal the response at a macroscopic level are of great interest in the field of chemical sensing and molecular electronics. Peptide-based interchromophore bridges are attractive probes since cooperative transitions between the secondary structure, *e.g.* between ordered and disordered states, can be conveniently monitored.[23] Hydrogen bonding is one means that was expected to influence donor–acceptor interactions in a peptide based donor–acceptor dyad. Also, the key role of hydrogen bonding should be noted, especially with respect to mediating ET processes in biological and artificial systems.[24]

Aib (α-aminoisobutyric acid) is a C^{α}-tetrasubstituted α-amino acid that strongly favours 3_{10}-helical structures more than any of the regular protein amino acids.[24] Tight helix–helix packing is a key feature of the α-helical bundle tertiary structures commonly found in biological proteins in which the photosynthetic reaction centre is embedded. In this context a hexapeptide (see Fig. 5) has been employed as a large molecular ruler to separate a pyrrolidinofullerene acceptor unit from a ruthenium(II) trisbipyridine (chromophore molecule) complex ($[Ru(bpy)_3]^{2+}$).[25]

The peptide-spaced ensemble, containing structurally constrained Aib, can be interrelated to rigid androstane- and flexible ethyleneglycol-spaced C_{60}–$[Ru(bpy)_3]^{2+}$ assemblies previously reported (see Fig. 5).[26] The role played by the spacer is not just structural since its chemical nature governs the electronic communication between the terminal units (*e.g.*

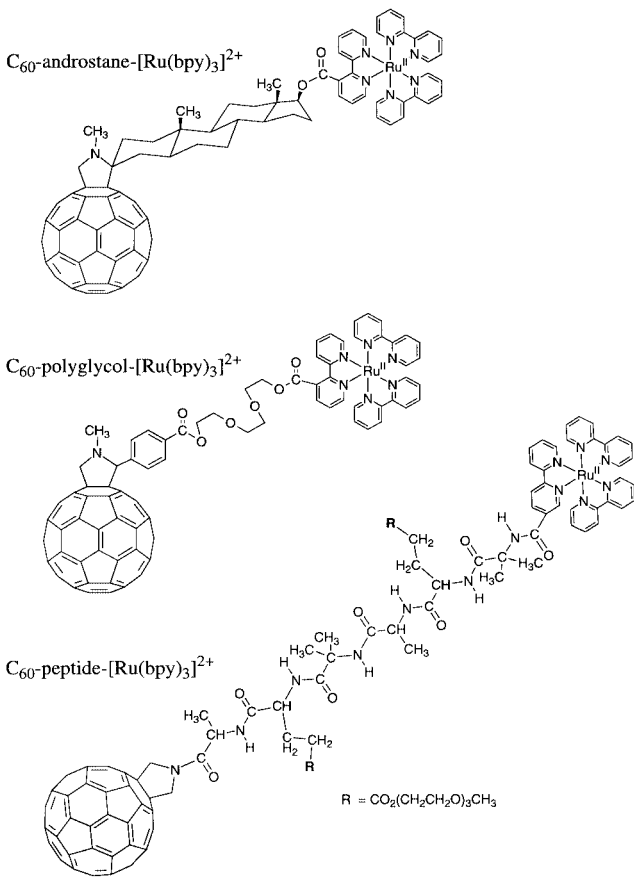

Fig. 5 Structures of C_{60}–androstane–$[Ru(bpy)_3]^{2+}$, C_{60}–polyglycol–$[Ru(bpy)_3]^{2+}$ and C_{60}–peptide–$[Ru(bpy)_3]^{2+}$ donor–bridge–acceptor dyads.

fullerene and $[Ru(bpy)_3]^{2+}$). Another important feature of the spacer is its modular composition, which allows alteration of the separation without affecting the electronic nature of the connection.

It may be pointed out that the geometry of the flexibly linked [*i.e.* $-(CH_2CH_2O)_n-$ chain] system is not well-defined, and the rapid deactivation of the ^{3}*(MLCT) $[Ru(bpy)_3]^{2+}$ state is ascribed to an '*intra*molecular exciplex' mechanism (case II in Fig. 6). Owing to the rigid structure of steroids, such as

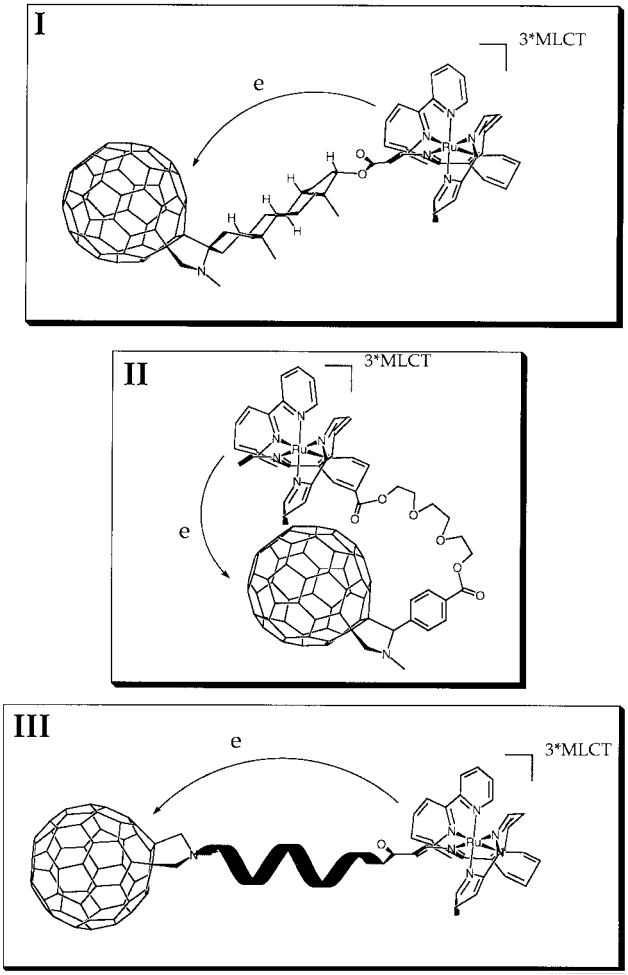

Fig. 6 Schematic illustration of photoinduced electron transfer processes from a ^{3}*(MLCT) state of a $[Ru(bpy)_3]^{2+}$ complex to an electron accepting fullerene moiety in (I) C_{60}–androstane–$[Ru(bpy)_3]^{2+}$, (II) C_{60}–polyglycol–$[Ru(bpy)_3]^{2+}$ and (III) C_{60}–peptide–$[Ru(bpy)_3]^{2+}$ dyads. Please note that the C_{60}–androstane–$[Ru(bpy)_3]^{2+}$ dyad is represented by one of the two possible diastereoisomers.

androstane, a 'through-bond' mediated ET(case I in Fig. 6) prevails in the C_{60}–androstane-$[Ru(bpy)_3]^{2+}$ dyad. The steroid acts as a wire allowing the electron to be passed from the donor to the acceptor through the intervening σ-bond framework. In both dyads (*e.g.* C_{60}–androstane–$[Ru(bpy)_3]^{2+}$ and C_{60}–polyglycol–$[Ru(bpy)_3]^{2+}$), quenching of the ^{3}*(MLCT) state of the $[Ru(bpy)_3]^{2+}$ complex by ET to the fullerene generates the $C_{60}^{\bullet-}$–$[Ru(bpy)_3]^{3+}$ radical pair. The different *intra*molecular ET mechanism in these dyads, leads, however, to quite different lifetimes for $C_{60}^{\bullet-}$–$[Ru(bpy)_3]^{3+}$. For example, in dichloromethane solutions the rigidly spaced C_{60}–androstane–$[Ru(bpy)_3]^{2+}$ dyad yields a lifetime of 304 ns, while no appreciable lifetime was noted for the flexibly spaced C_{60}–polyglycol–$[Ru(bpy)_3]^{2+}$ analogue.[26]

Structures, such as a 3_{10}-helix, are prone to conformational changes upon addition of protic solvents. In nonprotic solvents the helical secondary structure of the peptide spacer places the two redox active moieties into close proximity, which is favourable for their mutual electronic interaction. An edge-to-edge distance of *ca.* 12 Å provides the means for a rapid *intra*molecular ET from the ^{3}*(MLCT) $[Ru(bpy)_3]^{2+}$ state to the electron accepting fullerene (case III in Fig. 6). In fact, the initially formed ^{3}*(MLCT) $[Ru(bpy)_3]^{2+}$ state transforms readily (3.4×10^8 s^{-1}) into a long-lived charge-separated state (τ = 608 ns). Protic solvents, on the other hand, interfere with the *intra*molecular hydrogen bonding of the peptide backbone. Unfolding of the relatively compressed secondary structure of the ordered peptide results in a statistically unordered conformation. Consequently, the spatial separation between the two components, donor ($[Ru(bpy)_3]^{2+}$) and acceptor (C_{60}), located at the N- and C-termini of the peptide chain, respectively, tends to increase to a point that eventually disrupts their mutual electronic interactions. Despite the general flexibility of the peptide backbone, the experimental data fail to support either of the two possible ET mechanisms (*e.g.* a 'through bond' or an '*intra*molecular exciplex' route), instead the ^{3}*(MLCT)$[Ru(bpy)_3]^{2+}$ state decays with a lifetime of 535 ns (*e.g.* similar to a $[Ru(bpy)_3]^{2+}$ reference complex). This leads to the conclusion that the peptide backbone is relatively stiff in comparison to true flexibility found in a hydrocarbon chain.

An intriguing feature of the *intra*molecular hydrogen bonding within the peptide backbone is that the more randomised configuration can be reversibly transferred into the starting conformation (*e.g.* the 3_{10}-helical character). After careful removal of the protic component from a binary solvent mixture (protic and nonprotic; 1 : 1 *v/v*) the luminescence intensity of the $[Ru(bpy)_3]^{2+}$ chromophore becomes comparable again to that for the original non-protic solution prior to the addition of the protic solvent. The reversible activation–deactivation of the ET mechanism was successfully repeated many times (*e.g.* 10 times) and, thus, serves as a sensitive probe for the secondary structure of peptides.

The strong electrostatic fields (10^9 V m^{-1}) in helices have been used in rationalising the observation that only one of the two branches of the bacterial PRC is active.[27] An oriented dipole, which spans from the N- to the C-terminus of the helix, is responsible for this field. In the system presented a charge-separated radical pair is created which resembles the helices' own electrostatic field and, therefore, destabilises the charge-separated radical pair. The observed k_{ET}/k_{BET} ratio (209), as a meaningful measure of the usefulness of a PET system, is, nevertheless, promising. The k_{ET}/k_{BET} ratio may be further improved by exchanging the two building blocks. In such a system the ET will operate with the dipole moment of the helix and, thus, be accelerated, while simultaneously the BET is rendered more difficult.

Concluding remarks and outlook

The selected examples described in this article illustrate the continuing interest and potential of fullerenes as multifunctional electron storage moieties in well-ordered multicomponent composites. Noteworthy in this context is the recent introduction of elegant and versatile protocols concerning the chemical functionalization of the fullerene core.[8,28]

Remarkably, similar systems based on two-dimensional acceptors (*e.g.* quinone) failed to exhibit sufficient lifetimes of the charge-separated states formed because of the fast occurring BET. This is due, at least in part, to the slower ET and faster BET dynamics evolving from the larger reorganisation energies of two-dimensional electron acceptors. The unique delocalization, provided by the three-dimensional structure of the fullerene core, in combination with the small reorganisation energy, on the other hand, prevents a fast BET process in the contributed fullerene-containing systems.

The important idea presented by the current concepts (*e.g.* gain of aromaticity and planarity) is the stabilisation of the oxidised donor moiety and, in turn, of the resulting radical pair. In this line of thinking the diffusional splitting of the radical pair

in fullerene-metallocomplexes is the basis for the design of artificial photosynthetic systems with efficient and long-lived charge separation but fewer electron transfer steps and less energy loss.

In summary, the systematic investigation of fullerene chemistry has, already at a relatively early stage, played a significant role in the development of useful molecular composites. If the more technological problems can be solved, there is an almost unlimited field of application to be foreseen and eventually fullerenes may become important building blocks of future technologies, such as solar energy conversion, batteries and photovoltaics.

Acknowledgement

This work was supported by the Office of Basic Energy Sciences of the Department of Energy. This is document NDRL-4166 from the Notre Dame Radiation Laboratory. I am deeply indebted to Professors Nazario Martin, Michele Maggini and Maurizio Prato for their productive collaborations and numerous stimulating discussions. This paper is dedicated to my PhD supervisor, Professor Fritz Wasgestian, on the occasion of his retirement.

Notes and references

1 J. Deisenhofer, O. Epp, K. Miki, R. Huber and H. Michel, *J. Mol. Biol.*, 1984, **180**, 385; *The Photosynthetic Reaction Center*, ed. J. Deisenhofer and J. R. Norris, Academic Press, 1993; G. McDermott, S. M. Prince, A. A. Freer, A. M. Hawthornthwaite-Lawless, M. Z. Papiz, R. J. Cogdell and N. W. Isaacs, *Nature*, 1995, **374**, 517; W. Kuhlbrandt and D. N. Wang, *Nature*, 1991, **350**, 130.

2 Examples with leading references: D. Gust, T. A. Moore and A. L. Moore, *Acc. Chem. Res.*, 1993, **26**, 198; M. R. Wasielewski, *Chem. Rev.*, 1992, **92**, 435; M. N. Paddon-Row, *Acc. Chem. Res.*, 1994, **27**, 18; N. Sutin, *Acc. Chem. Res.*, 1983, **15**, 275; A. J. Bard and M. A. Fox, *Acc. Chem. Res.*, 1995, **28**, 141; T. J. Meyer, *Acc. Chem. Res.*, 1989, **22**, 163; A. C. Benniston, P. R. Macki and A. Harriman, *Angew. Chem., Int. Ed.*, 1998, **37**, 354; W. B. Davis, W. A. Svec, M. A. Ratner and M. R. Wasielewski, *Nature*, 1998, **396**, 60.

3 (*a*) H. Imahori, K. Hagiwara, T. Akiyama, M. Akoi, S. Taniguchi, T. Okada, M. Shirakawa and Y. Sakata, *Chem. Lett.*, 1996, **263**, 545; (*b*) D. M. Guldi and K.-D. Asmus, *J. Am. Chem. Soc.*, 1997, **119**, 5744.

4 R. A. Marcus, *J. Chem. Phys.*, 1956, **24**, 966; R. Marcus and N. Sutin, *Biophys. Acta*, 1985, **811**, 265.

5 (*a*) M. L. McGlashen, M. E. Blackwood and T. G. Spiro, *J. Am. Chem. Soc.*, 1993, **115**, 2074; (*b*) D. M. Guldi and K.-D. Asmus, *J. Phys. Chem. A*, 1997, **101**, 1472.

6 L. Echegoyen and L. E. Echegoyen, *Acc. Chem. Res.*, 1998, **31**, 593.

7 For recent reviews see H. Imahori and Y. Sakata, *Adv. Mater.*, 1997, **9**, 537; M. Prato, *J. Mater. Chem.*, 1997, **7**, 1097; N. Martin, L. Sanchez, B. Illescas and I. Perez, *Chem. Rev.*, 1998, **98**, 2527; A. L. Balch and M. M. Olmstead, *Chem. Rev.*, 1998, **98**, 2123; F. Diederich and M. GomezLopez, *Chem. Soc. Rev.*, 1999, **28**, 263; D. M. Guldi and P. V. Kamat, in *Fullerenes: Chemistry, Physics and Technology*, ed. K. M. Kadish and R. S. Ruoff, Wiley, New York, in press.

8 (*a*) F. Diederich, L. Isaacs and D. Philp, *Chem. Soc. Rev.*, 1994, **23**, 243; (*b*) M. Prato and M. Maggini, *Acc. Chem. Res.*, 1998, **31**, 519.

9 D. M. Guldi, H. Hungerbühler, E. Janata and K.-D. Asmus, *J. Chem. Soc., Chem. Commun.*, 1993, 84; T. Kato, T. Kodama, T. Shida, T. Nakagawa, Y. Matsui, S. Suzuki, H. Shiromaru, K. Yamauchi and Y. Achiba, *Chem. Phys. Lett.*, 1991, **180**, 446.

10 R. M. Williams, J. M. Zwier and J. W. Verhoeven, *J. Am. Chem. Soc.*, 1995, **117**, 4093; R. M. Williams, M. Koeberg, J. M. Lawson, Y.-Z. An, Y. Rubin, M. N. Paddon-Row and J. W. Verhoeven, *J. Org. Chem.*, 1996, **61**, 5055; D. M. Guldi, M. Maggini, G. Scorrano and M. Prato, *J. Am. Chem. Soc.*, 1997, **119**, 974; D. M. Guldi, M. Maggini, G. Scorrano, M. Prato, A. Bianco and C. Toniolo, *J. Inf. Rec. Mater.*, 1998, **24**, 33.

11 A. Weller, *Z. Physik. Chem.*, 1982, **132**, 93; G. L. I. Gaines, M. P. O'Neil, W. A. Svec, M. P. Niemczyk and M. R. Wasielewski, *J. Am. Chem. Soc.*, 1991, **113**, 719.

12 K. G. Thomas, V. Biju, M. V. George, D. M. Guldi and P. V. Kamat, *J. Phys. Chem. A*, 1998, **102**, 5341; K. G. Thomas, V. Biju, D. M. Guldi, P. V. Kamat and M. V. George, *J. Phys. Chem. A*, 1999, **103**, 10 755.

13 F. Wudl, G. M. Smith and E. J. Hufnagel, *J. Chem. Soc., Chem. Commun.*, 1970, 1453; S. Hünig, G. Klesslich, D. Schentzow, R. Zahradnik and P. Carsky, *Int. J. Sulfur Chem.*, 1971, **6**, 109.

14 N. Martin, L. Sanchez, C. Seoane, R. Andreu, J. Garin and J. Orduna, *Tetrahedron Lett.*, 1996, **37**, 5979.

15 N. Martin, L. Sanchez, M. A. Herranz and D. M. Guldi, submitted for publication.

16 D. Gust, T. A. Moore and A. L. Moore, *Res. Chem. Intermed.*, 1997, **23**, 621; D. Gust, T. A. Moore and A. L. Moore, *Pure Appl. Chem.*, 1998, **70**, 2189.

17 Y. Yamashita, Y. Kobayashi and T. Miyashi, *Angew. Chem., Int. Ed. Engl.*, 1989, **28**, 1052; M. R. Bryce, A. J. Moore, M. Hasan, G. J. Ashwell, A. I. Fraser, W. Clegg, M. B. Hursthouse and A. I. Karanlov, *Angew. Chem., Int. Ed. Engl.*, 1990, **29**, 1450.

18 N. Martin, L. Sanchez, C. Seoane, E. Orti and P. M. Viruela, *J. Org. Chem.*, 1998, **63**, 1268.

19 N. Martin, L. Sanchez and D. M. Guldi, *Chem. Commun.*, 2000, 113.

20 T. Da Ros, M. Prato, D. M. Guldi, E. Alessio, M. Ruzzi and L. Pasimeni, *Chem. Commun.*, 1999, 635; similar systems have been reported by: N. Armaroli. F. Diederich, L. Echegoyen, T. Habicher, L. Flamigni, G. Marconi and J. F. Nierengarten, *New J. Chem.*, 1999, **23**, 77; F. D'Souza, G. R. Deviprasad, M. S. Rahman and J.-P. Choi, *Inorg. Chem.*, 1999, **38**, 2157.

21 D. M. Guldi, T. Da Ros, M. Prato, L. Pasimeni and M. Ruzzi, submitted for publication.

22 M. Prato and D.M. Guldi, unpublished results.

23 C. Toniolo, G. M. Bonora, V. Barone, A. Bavoso, E. Benedetti, B. Di Blasio, P. Grimaldi, F. Lelj, V. Pavone and C. Pavone, *Marcomolecules*, 1985, **18**, 895; C. Toniolo and E. Benedetti, *Trends Biochem. Sci.*, 1991, **16**, 350; P. Hanson, G. Millhauser, F. Formaggio, M. Crisma and C. Toniolo, *J. Am. Chem. Soc.*, 1996, **118**, 7612.

24 P. J. F. de Rege, S. A. Williams and M. J. Therien, *Science*, 1995, **269**, 1409; J. A. Roberts, J. B. Kirby and D. G. Nocera, *J. Am. Chem. Soc.*, 1995, **117**, 8051; S. L. Springs, D. Gosztola, M. R. Wasielewski, V. Kral, A. Andievsky and J. L. Sessler, *J. Am. Chem. Soc.*, 1999, **121**, 2281.

25 A. Polese, S. Mondini, A. Bianco, C. Toniolo, G. Scorrano, D. M. Guldi and M. Maggini, *J. Am. Chem. Soc.*, 1999, **121**, 3456.

26 M. Maggini, D. M. Guldi, S. Mondini, G. Scorrano, F. Paolucci, P. Ceroni and S. Roffia, *Chem. Eur. J.*, 1998, **4**, 1992; M. Maggini, A. Dono', G. Scorrano and M. Prato, *J. Chem. Soc., Chem. Commun.*, 1995, 845; D. M. Guldi, M. Maggini, S. Mondini, F. Guerin and J. H. Fendler, *Langmuir*, in press; M. Maggini, D. M. Guldi, S. Mondini, G. Scorrano, F. Paolucci, P. Ceroni and S. Roffia, submitted for publication.

27 E. Galoppini and M. A. Fox, *J. Am. Chem. Soc.*, 1996, **118**, 2299; E. Galoppini and M. A. Fox, *J. Am. Chem. Soc.*, 1997, **119**, 5277.

28 A. Hirsch, *The Chemistry of the Fullerenes*, Thieme, Stuttgart, 1994; *Fullerenes and Related Structures*, ed. A. Hirsch, *Top. Curr. Chem.*, Springer, Berlin, vol. 199, 1999.

Paper a907807j

Catalytic effect of monovalent cations on the amine oxidation by cofactor TTQ of quinoprotein amine dehydrogenases

Shinobu Itoh,*[a] Masato Taniguchi[b] and Shunichi Fukuzumi*[b]

[a] *Department of Chemistry, Graduate School of Science, Osaka City University, 3-3-138 Sugimoto, Sumiyoshi-ku, Osaka 558-8585, Japan. E-mail: shinobu@sci.osaka-cu.ac.jp*

[b] *Department of Material and Life Science, Graduate School of Engineering, Osaka University; CREST, JAPAN Science and Technology Corporation, 2-1 Yamada-oka, Suikta, Osaka 565-0871, Japan*

Received (in Cambridge, UK) 9th November 1999, Accepted 19th January 2000

Oxidation of benzylamine by a model compound of cofactor TTQ (tryptophan tryptophylquinone) of quinoprotein amine dehydrogenases is made possible by coordination of a monovalent cation such as Li^+ in anhydrous MeCN.

Bacterial methylamine dehydrogenase (MADH) and aromatic amine dehydrogenase (AADH) comprise a new class of enzymes which contain a heterocyclic *o*-quinone cofactor, TTQ

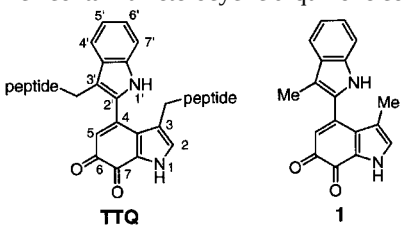

(tryptophan tryptophylquinone), at their active sites in the light subunits.[1–3]

Monovalent cations have recently been shown to influence not only the UV–VIS spectrum of the enzyme but also the redox reactivity of TTQ in the amine oxidation and the subsequent electron transfer to biological electron acceptor proteins such as amicyanin.[4–9] The enzymes have two different cation binding sites, one of which is located near the quinone carbonyl oxygen O(6) of the cofactor.[4] Thus, the cationic species incorporated into this binding pocket have been suggested to interact with the quinone moiety directly, affecting the electronic structure of the cofactor as well as the reactivity both in the amine oxidation reaction and the subsequent electron transfer process.[5–9] However, little is known about the binding model of the cationic species toward TTQ or how it affects the electronic structure as well as the reactivity of the TTQ cofactor. In this study, we have investigated the interaction of a TTQ model compound[10] with monovalent cations to demonstrate that an alkaline metal ion such as Li^+ binds to the quinone, leading to a significant enhancement of the amine oxidation reaction in anhydrous organic media.

Addition of a certain amount of $LiClO_4$ to an anhydrous MeCN solution containing TTQ model compound **1** (5.0×10^{-5} mol dm^{-3}) and benzylamine (1.0×10^{-2} mol dm^{-3}) caused a rapid spectral change in the UV–VIS region. Fig. 1 shows the spectral change of the titration of **1** with $LiClO_4$ (0–0.15 mol dm^{-3}) in the presence of benzylamine (1.0×10^{-2} mol dm^{-3}).[11] The characteristic absorption band at 408 nm due to the quinone itself decreases, accompanied by an increase in a new absorption band at 461 nm, with increasing the concentration of added $LiClO_4$. The binding constant K_{ML} for 1:1 complex formation between the quinone (Q) and the metal ion (M^+) can be expressed by eqn. (1), where A_0 and A_∞ are the initial and final absorptions of the titration, and $[M^+]_0$ and $[Q]_0$ denote the concentration of the added metal ion and the initial quinone concentration, respectively. The plot of $(A - A_0)/(A_\infty - A)$ *vs.* $([M^+]_0 - \alpha[Q]_0)$ [$\alpha = (A - A_0)/(A_\infty - A_0)$] gives a straight line passing through the origin, as shown in the inset in Fig. 1, from which a K_{ML} value of 15.6 dm^3 mol^{-1} was obtained from the slope. A similar spectral change was obtained in the titration of **1** with $NaClO_4$ although the binding constant was smaller (K_{ML} = 5.5 dm^3 mol^{-1}, λ_{max} = 454 nm).[12,13] It should be noted that the spectral change obtained in this system is fairly close to that observed in the titration of MADH with monovalent cations.[4,8] This result suggests that the monovalent cation binds to the quinone moiety of **1** at a similar position to that proposed in the enzymatic systems.[14]

$$\frac{A - A_0}{A_\infty - A} = K_{ML}([M^+]_0 - \frac{A - A_0}{A_\infty - A_0}[Q]_0) \quad (1)$$

Although *no* reaction takes place between benzylamine and quinone **1** in an aprotic solvent such as anhydrous MeCN, **1** was converted into the reduced form of TTQ in the presence of Li^+. Thus, the reaction of quinone **1** (5.0×10^{-5} mol dm^{-3}) and benzylamine (1.5×10^{-2} mol dm^{-3}) in the presence of $LiClO_4$ (0.15 mol dm^{-3}) in anhydrous MeCN at 25 °C under anaerobic conditions resulted in a drastic spectral change where the absorption band at 461 nm due to the Li^+ complex of the quinone decreases, accompanied by an increase in a new band at 323 nm due to the reduced TTQ in the aminophenol form (Fig. 2).[15] As reported in the previous model reactions between the TTQ model compound and benzylamine in MeOH,[16] the reaction consists of three distinct steps, where the first one [Fig. 2(*a*)] corresponds to addition of the amine to the quinone (k_1), the second one [Fig. 2(*b*)] is due to the spontaneous (k_2) and the amine-catalyzed (k_2') rearrangement from the substrate imine to the product imine intermediates, and the third one [Fig. 2(*c*)] is ascribed to the imine exchange reaction (k_3) to generate the aminophenol and *N*-benzylidenebenzylamine ($PhCH_2N{=}CHPh$), as summarized in Scheme 1.[15] Each process has its own isosbestic point, at 418, 383 and 372 nm, respectively, demonstrating the accuracy of the stepwise mechanism shown in Scheme 1. Since the difference in the rate

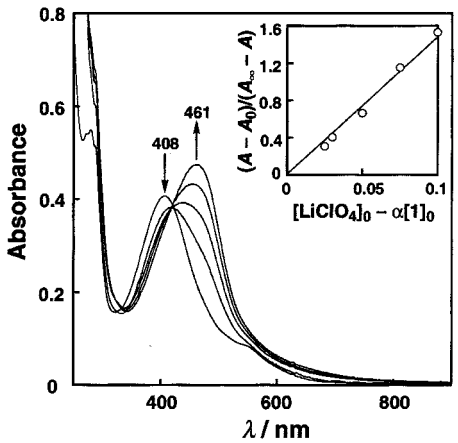

Fig. 1 Spectral change observed upon addition of $LiClO_4$ (0–0.15 mol dm^{-3}) to an MeCN solution of **1** (5.0×10^{-5} mol dm^{-3}) in the presence of benzylamine (1.0×10^{-2} mol dm^{-3}) at 25 °C. Inset: plot of $(A - A_0)/(A_\infty - A)$ *vs.* $[LiClO_4]_0 - \alpha[\mathbf{1}]_0$ $\{\alpha = (A - A_0)/(A_\infty - A_0)\}$.

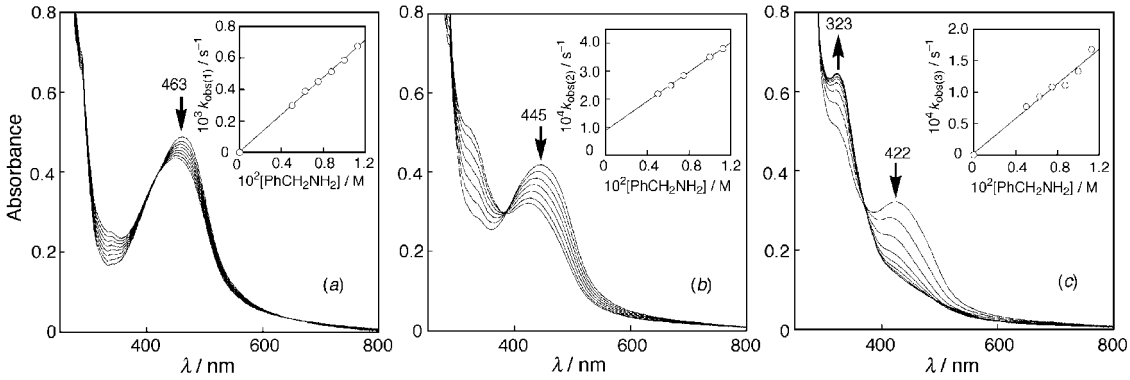

Fig. 2 Spectral change for the reaction of **1** (5.0×10^{-5} mol dm^{-3}) with benzylamine (1.5×10^{-2} mol dm^{-3}) in the presence of $LiClO_4$ (0.15 mol dm^{-3}) in anhydrous MeCN at 25 °C under anaerobic conditions. (*a*) The first stage (0–7200 s), 800 s interval. Inset: plot of $k_{obs(1)}$ *vs.* [$PhCH_2NH_2$]. (*b*) The second stage (9600–24000 s), 2400 s interval. Inset: plot of $k_{obs(2)}$ *vs.* [$PhCH_2NH_2$]. (*c*) The third stage (24000–49600 s), 3200 s interval. Inset: plot of $k_{obs(3)}$ *vs.* [$PhCH_2NH_2$].

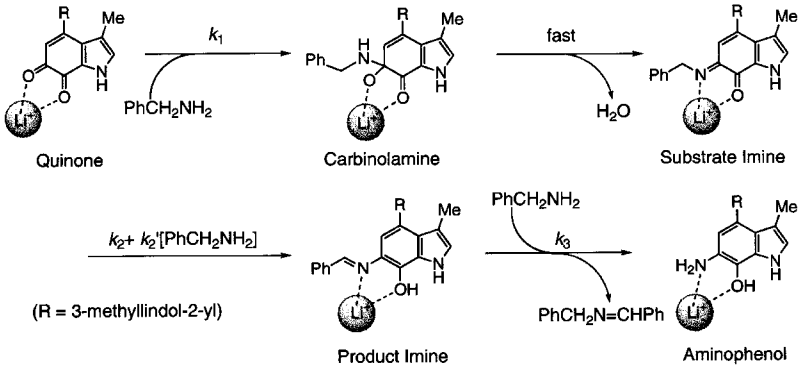

Scheme 1

of each step was not large enough to determine the rate independently, the pseudo-first order rate constants for the three steps ($k_{obs(1)}$, $k_{obs(2)}$ and $k_{obs(3)}$) were determined simultaneously by computer simulation of the time course of the absorption change using a non-linear curve-fitting program (Mac curve fit) as reported in the previous study.[16] From the dependence of k_{obs} in each step on the amine concentration the rate constants were determined as $k_1 = 5.9 \times 10^{-2}$ M^{-1} s^{-1}, $k_2 = 8.7 \times 10^{-5}$ s^{-1}, $k_2' = 2.6 \times 10^{-2}$ M^{-1} s^{-1}, and $k_3 = 1.4 \times 10^{-2}$ M^{-1} s^{-1}, as shown in the insets in Fig. 2. It should also be emphasized that the oxidation of benzylamine by the Li^+ complex of **1** proceeds catalytically, and molecular oxygen is used as an electron acceptor to regenerate the iminoquinone form from the reduced TTQ. Thus, benzylamine (0.10 mol dm^{-3}) was converted into *N*-benzylidenebenzylamine quantitatively when it was treated with a catalytic amount of **1** (1.0×10^{-3} mol dm^{-3}; 1 mol %) in the presence of $LiClO_4$ (1.0 mol dm^{-3}) under aerobic conditions for 24 h.

In summary, a monovalent cation such as Li^+ has been demonstrated for the first time to bind to TTQ at its quinone moiety and makes it possible for the catalytic amine oxidation to occur efficiently in anhydrous MeCN. The Li^+ binding may accelerate the addition step of the amine (k_1) and enhances the stability of the intermediates, leading to the efficient catalytic oxidation of benzylamine. These results gave us an important insight into the catalytic mechanism of the monovalent cations in MADH- and AADH-catalysed reactions.

The present study was financially supported in part by a Grant-in-Aid for Scientific Research from the Ministry of Education, Science, Culture, and Sports of Japan.

Notes and references

1 W. S. McIntire, D. E. Wemmer, A. Chistoserdov and M. E. Lidstrom, *Science*, 1991, **252**, 817.
2 L. Chen, F. S. Mathews, V. L. Davidson, E. G. Huizinga, F. M. D. Vellieux and W. G. J. Hol, *Proteins*, 1992, **14**, 288.
3 S. Govindaraj, E. Eisenstein, L. H. Jones, J. Sanders-Loehr, A. Y. Chistoserdov, V. L. Davidson and S. L. Edwards, *J. Bacteriol.*, 1994, **176**, 2922.
4 V. Kuusk and W. S. McIntire, *J. Biol. Chem.*, 1994, **269**, 26 136.
5 A. C. F. Gorren and J. A. Duine, *Biochemistry*, 1994, **33**, 12 202.
6 A. C. F. Gorren, S. de Vries and J. A. Duine, *Biochemistry*, 1995, **34**, 9748.
7 A. C. F. Gorren, P. Moenne-Loccoz, G. Backes, S. de Vries, J. Sanders-Loehr and J. A. Duine, *Biochemistry*, 1995, **34**, 12 926.
8 P. Moenne-Loccoz, N. Nakamura, S. Itoh, S. Fukuzumi, A. C. F. Gorren, J. A. Duine and J. Sanders-Loehr, *Biochemistry*, 1996, **35**, 4713.
9 G. R. Bishop and V. L. Davidson, *Biochemistry*, 1997, **36**, 13 586.
10 S. Itoh, M. Ogino, S. Haranou, T. Terasaka, T. Ando, M. Komatsu, Y. Ohshiro, S. Fukuzumi, K. Kano, K. Takagi and T. Ikeda, *J. Am. Chem. Soc.*, 1995, **117**, 1485.
11 Each spectrum in Fig. 1 was taken just after the addition of $LiClO_4$, since the redox reaction between **1** and benzylamine gradually proceeded over a prolonged reaction time.
12 Because of the low solubility of NH_4ClO_4, $KClO_4$, $CsClO_4$ and CsOTf in anhydrous MeCN, interaction between the quinone and those monovalent cations could not be examined accurately.
13 In the absence of benzylamine, the spectral changes (bathochromic shifts) and the K_{ML} values are much smaller than those measured in the presence of the amine: for Li^+, λ_{max} = 430 nm; K_{ML} = 3.6 dm^3 mol^{-1}; for Na^+, λ_{max} = 425 nm; K_{ML} = 2.3 dm^3 mol^{-1}. Benzylamine may abstract the pyrrole proton of **1** to enhance the Li^+ binding.
14 In spite of our great efforts, a single crystal of the Li^+ complex of **1** suitable for X-ray analysis has yet to be obtained. The ^{1}H NMR spectrum of **1** (1×10^{-3} mol dm^{-3}) in CD_3CN in the presence of $LiClO_4$ (1 mol dm^{-3}) showed downfield shifts for 1-H, 2-H and 5-H ($\Delta\delta$ = 0.39, 0.16 and 0.05 ppm, respectively), suggesting the coordination of Li^+ at the quinone moiety of **1**.
15 Although the reaction intermediates (substrate imine and product imine) and the aminophenol product of TTQ have been successfully isolated in the previous reaction in MeOH (ref. 16), isolation and detailed characterization of those species in the present system were hampered by Li^+ existing in large excess. The spectral change of the present reaction is, however, fairly close to that of the reaction of **1** and benzylamine in MeOH, (ref. 16), strongly supporting the idea that the intermediates and reduced product are the same in both systems.
16 S. Itoh, N. Takada, S. Haranou, T. Ando, M. Komatsu, Y. Ohshiro and S. Fukuzumi, *J. Org. Chem.*, 1996, **61**, 8967.

Communication a908914d

A novel hexakis(tetrathiafulvalene) derivative: synthesis, structure and electrochemical properties

Christian A. Christensen,[ab] Martin R. Bryce,*[a] Andrei S. Batsanov[a] and Jan Becher*[b]

[a] *Department of Chemistry, University of Durham, Durham, UK DH1 3LE. E-mail: m.r.bryce@durham.ac.uk*
[b] *Department of Chemistry, Odense University, Campusvej 55 DK 5230 Odense M, Denmark*

Received (in Cambridge, UK) 16th December 1999, Accepted 19th January 2000

The hexakis(TTF) derivative 3 has been synthesised in 89% yield by six-fold reaction of the thiolate anion of reagent 2 with hexakis(bromomethyl)benzene: the solution electrochemistry of 3 shows sequential formation of the hexa-(radical cation) and the dodecacation species, and spectroelectrochemistry shows interacting radical cations; the X-ray crystal structure of 3 is reported.

Oligo(tetrathiafulvalene) (TTF) derivatives,[1] including dendrimers[2] and main-chain and side-chain polymers,[3] have received considerable attention recently. The two-step electrochemical oxidation of TTF,[4] to form sequentially the radical cation and dication, offers the prospect of controlled generation of oligo(radical cation) and oligo(dication) species, which may engage in intramolecular or intermolecular interactions, act as multi-electron redox switches,[2e] or modulate redox processes of organic guests incorporated within the oligo(TTF) host framework.[5] To date, all the pure TTF oligomers ($n > 3$) which have been characterised have required multi-step syntheses. We now report the remarkably efficient synthesis of the novel hexakis(TTF) molecule **3** along with its X-ray crystal structure and solution electrochemistry.

Six-fold reaction of hexakis(bromomethyl)benzene **1**[6] with the thiolate anion of 4-(2-cyanoethyl)-4′,5,5′-tris(methylsulfanyl)TTF **2**, which was generated using $CsOH·H_2O$ as described previously,[7] proceeded remarkably cleanly to afford the TTF hexamer **3** in 89% yield (Scheme 1).†

The X-ray crystal structure of **3**‡ is shown in Fig. 1. As far as we are aware, no compound containing more than three TTF moieties has been structurally studied previously, and the structures of very few tris(TTF) compounds have been reported.[8–11] Molecule **3** has crystallographic C_i symmetry. The central benzene ring is planar, with CH_2–S bonds directed alternately above and below its plane. All three independent TTF moieties adopt a boat-like conformation: the inner dithiole rings are folded by 25.5, 29.6 and 13.2°, the outer ones by 18.4, 10.2 and 11.4°, with a small twist around the central C=C bond, by 6.3, 5.5 and 2.9°, respectively. Such flexibility and easy rotation around (exocyclic) C–S bonds may explain the fact that **3** forms a relatively dense crystal packing (21.6 Å^3 per non-H atom, *cf.* 22.8 and 22.1 Å^3 in monoclinic[12] and triclinic[13] polymorphs of MeS_4TTF, respectively) with no significant cavities, while its poly-aryl analogues crystallise as clathrates, *e.g.* $C_6(CH_2SPh)_6·2CCl_4$,[14a] $C_6(CH_2SO_2CHMePh)_6·4AcOH$,[14b] $C_6(CH_2SC_6H_4Bu^t)_6·1/2C_{30}H_{50}$[14c] and $C_6(CH_2SCH_2Ph)_6$·dioxane.[14d] Three of the six outer methyl groups in **3** are disordered between two positions each, indicating some residual looseness of the structure. There is no intramolecular S···S contact shorter than twice the van der Waals radius (3.60 Å)[15] of sulfur (excluding the contacts within the same TTF moiety) although each molecule participates in four significantly shorter intermolecular contacts.

Cyclic voltammetry (CV) of compound **3** (Fig. 2) showed two oxidation waves at $E_1^{1/2}$ 0.55 V and $E_2^{1/2}$ 0.88 V (*vs.* Ag/AgCl) typical of a tetra(alkylsulfanylTTF) system.[4b] The first wave is reversible; the second wave is quasi-reversible. (The criterion applied for reversibility was a ratio of 1.0 ± 0.05 for the intensities of the anodic and cathodic currents I_a/I_c, and no shift of the half wave potentials with varying scan rates between 50 and 500 mV s^{-1}.) There is no apparent interaction between the different TTF units. Thin layer CV was performed with the one-electron reduction peak of 2,3-dichloronaphthoquinone providing the internal reference, using procedures detailed previously.[2d] The number of electrons exchanged per oxidation

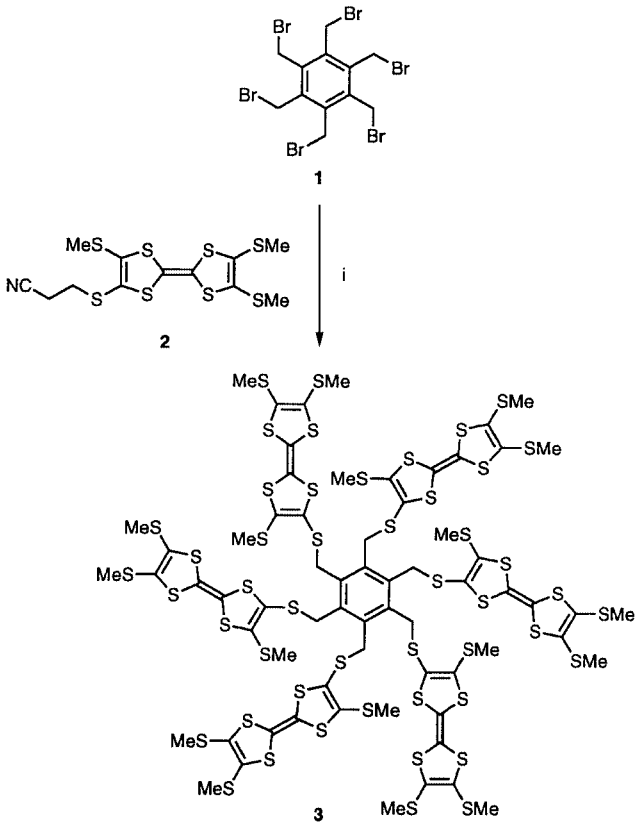

Scheme 1 *Reagents and conditions*: i, $CsOH·H_2O$, MeOH, DMF, 20 °C.

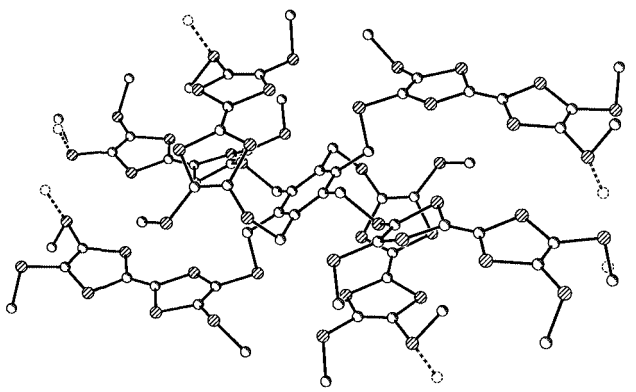

Fig. 1 Molecular structure of **3**, showing the disorder of the terminal methyl groups (H atoms are omitted).

DOI: 10.1039/a909882h

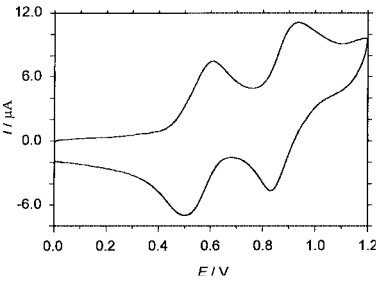

Fig. 2 Cyclic voltammogram of **3**.

wave was calculated to be 6.0 ± 0.5, which clearly suggests that complete oxidation occurs for all the TTF units. We note that in both CV and TLCV the reductive peak for the second redox couple (I_a/I_c = 0.8–0.9) is slightly smaller than for the first wave, as observed previously for some other multi(TTF) systems,[2d,16] indicating an associated chemical reaction, or a marked conformational change, at the highest oxidation level of the molecule.

The spectroelectrochemistry of compound **3** is shown in Fig. 3 [compound **3** (10^{-4} M), $BuNPF_6$ (10^{-1} M), $CHCl_3$]. The spectrum obtained at 0 V is consistent with neutral TTF units. On increasing the potential, as oxidation of the system proceeds, we see the concomitant emergence of the low energy absorption band of interacting TTF cation radicals (π–π dimers)[17] at λ_{max} 850 nm (Fig 3, spectrum at 0.65 V) along with a shoulder assigned to isolated (non-interacting) TTF cation radicals (λ_{max} 480 nm). On further increasing the potential to form the fully oxidised species precipitation of material was observed in the cell, so the spectra of the +12 species could not be obtained. It is apparent, therefore, that the dense packing of TTF moieties in **3** favours intramolecular interactions of their cation radicals. This contrasts with previous less densely packed TTF units for which isolated TTF cation radicals are clearly detected in the UV–VIS absorption spectra.[2c]

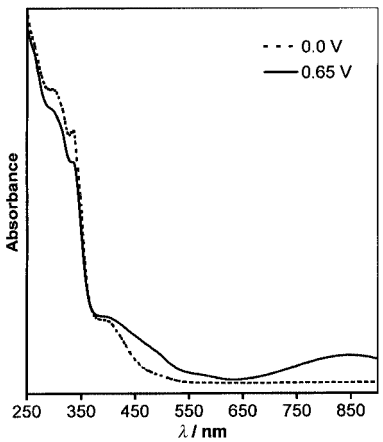

Fig. 3 Spectroelectrochemistry of **3**.

In summary, we report an extremely efficient one-pot synthesis of a hexakis(TTF) derivative **3**. This remarkably high-yielding six-fold reaction should make reagent **1** a suitable core unit for the convergent construction of higher TTF oligomers, including redox dendrimers, which are charged organic nanoparticles, relevant to miniaturisation in electronic materials.[18]

We thank the EPSRC and the Danish Research Academy for funding (C. A. C.), Dr L. M. Goldenberg for TLCV experiments and Dr P. Low for the design of the spectroelectrochemical cell.

Notes and references

† To a stirred solution of **2** (0.427 g, 1.00 mmol) in dry degassed DMF (60 cm^3) was added a solution of $CsOH·H_2O$ (0.185 g, 1.10 mmol) in dry MeOH (5 cm^3). The solution was stirred under nitrogen at 20 °C for 1 h. Compound **1** (0.095 g, 0.150 mmol) was added and the reaction mixture was stirred at 20 °C for 16 h to afford an orange suspension which was poured onto water (400 cm^3) and the orange pricipitate was filtered off, washed with MeOH (10 cm^3) and dried to afford analytically pure compound **3** (0.319 g, 89%), mp 214–215 °C. Recrystallisation from CS_2–hexane afforded red prisms. Elemental analysis: calc. for $C_{66}H_{66}S_{48}$: C, 33.05; H, 2.77. Found: C, 32.82; H, 2.62%; $\delta_H(CDCl_3)$ 4.45 (s, 12H), 2.46 (s, 18H), 2.45 (s, 18H), 2.42 (s, 18H); *m/z* (ES) 2397.6 [M^+], 1199.0 [M^{2+}], 799.3 [M^{3+}] (calc.: 2398.3, 1199.2, 799.4); CV $E_1^{1/2}$ 0.55 V; $E_2^{1/2}$ 0.88 V, CH_2Cl_2, Bu_4NPF_6, Pt electrode, *vs.* Ag/AgCl, scan rate 200 mV s^{-1}.

‡ *Crystal data* for **3**: $C_{66}H_{66}S_{48}$, M = 2398.1, T = 120 K, triclinic, space group $P\bar{1}$ (No. 2), a = 10.799(3), b = 15.117(1), c = 16.732(5) Å, α = 69.56(1), β = 76.88(1), γ = 77.89(1)°, U = 2467(1) $Å^3$, Z = 1, D_c = 1.614 g cm^{-3}, SMART 1K CCD area detector, λ = 0.71073 Å (Mo-Kα), 22999 reflections (8659 unique, R_{int} = 0.017) with 2θ = 50°, semi-empirical absorption correction (SADABS: G. M. Sheldrick, 1997; $T_{max,min}$ = 0.720, 0.591), least squares refinement against F^2 of all data (SHELXL97: G. M. Sheldrick, University of Göttingen, 1997), 541 variables, R = 0.028 [7731 data, $I > 2\sigma(I)$], $wR(F^2)$ = 0.076, Δρ max./min. = 0.70, −0.35 e $Å^{-3}$. CCDC 182/1528. See http://www.rsc.org/suppdata/cc/a9/a909882h/ for crystallographic files in .cif format.

1 Reviews: M. Adam and K. Müllen, *Adv. Mater.*, 1994, **6**, 439; T. Otsubo, Y. Aso and K. Takimiya, *Adv. Mater.*, 1996, **8**, 203; M. R. Bryce, W. Devonport, L. M. Goldenberg and C. Wang, *Chem. Commun.*, 1998, 945.
2 (*a*) M. R. Bryce, W. Devonport and A. J. Moore, *Angew. Chem., Int. Ed. Engl.*, 1994, **33**, 1761; (*b*) C. Wang, M. R. Bryce, A. S. Batsanov, L. M. Goldenberg and J. A. K. Howard, *J. Mater. Chem.*, 1997, **71**, 1189; (*c*) C. A. Christiansen, L. M. Goldenberg, M. R. Bryce and J. Becher, *Chem. Commun.*, 1998, 509; (*d*) W. Devonport, M. R. Bryce, G. J. Marshallsay, A. J. Moore and L. M. Goldenberg, *J. Mater. Chem.*, 1998, **8**, 1361; (*e*) M. R. Bryce, P. de Miguel and W. Devonport, *Chem. Commun.*, 1998, 2565.
3 S. Frenzel, S. Arndt, R. M. Gregorious and K. Müllen, *J. Mater. Chem.*, 1995, **5**, 1529; T. Yamamoto and T. Shimizu, *J. Mater. Chem.*, 1997, **7**, 1967; J. Roncali, *J. Mater. Chem.*, 1999, **9**, 1875.
4 (*a*) S. Hünig, G. Kiesslich, H. Quast and D. Scheutzow, *Liebigs Ann. Chem.*, 1973, 310; (*b*) D. L. Lichtenberger, R. L. Johnston, K. Hinkelmann, T. Suzuki and F. Wudl, *J. Am. Chem. Soc.*, 1990, **112**, 3302.
5 M. R. Bryce, W. Devonport and R. Kataky, unpublished results.
6 J. Závada, M. Pánková, P. Holý and M. Tichý, *Synthesis*, 1994, 1132.
7 J. Lau, O. Simonsen and J. Becher, *Synthesis*, 1995, 521.
8 M. Fourmigué and P. Batail, *J. Chem. Soc., Chem. Commun.*, 1991, 1370.
9 S. Yunoki, K. Takimiya, Y. Aso and T. Otsubo, *Tetrahedron Lett.*, 1997, **38**, 3017; M. Iyoda, M. Fukuda, S. Sasaki and M. Yoshida, *Synth. Met.*, 1995, **70**, 1171.
10 P. Blanchard, N. Svenstrup, J. Rault-Berthelot, A. Riou and J. Becher, *Eur. J. Org. Chem.*, 1998, 1743.
11 T. Akutagawa, Y. Abe, T. Hasegawa, T. Nakamura, T. Inabe, K. Sugiura, Y. Sakata, C. A. Christensen, J. Lau and J. Becher, *J. Mater. Chem.*, 1999, **9**, 2737.
12 C. Katayama, M. Honda, H. Kumagai, J. Tanaka, G. Saito and H. Inokuchi, *Bull. Chem. Soc. Jpn.*, 1985, **58**, 2272.
13 H. Endres, *Z. Naturforsch., Teil B*, 1986, **41**, 1351.
14 (*a*) A. D. U. Hardy, D. D. MacNicol and D. R. Wilson, *J. Chem. Soc., Perkin Trans. 2*, 1979, 1011; (*b*) A. Freer, C. J. Gilmore, D. D. MacNicol and S. Swanson, *Tetrahedron Lett.*, 1980, **21**, 205; (*c*) A. Freer, C. J. Gilmore, D. D. MacNicol and D. R. Wilson, *Tetrahedron Lett.*, 1980, **21**, 1159; (*d*) A. D. U. Hardy, D. D. MacNicol, S. Swanson and D. R. Wilson, *J. Chem. Soc., Perkin Trans. 2*, 1980, 999.
15 R. S. Rowland and R. Taylor, *J. Phys. Chem.*, 1996, **100**, 7384.
16 S. Booth, E. N. K. Wallace, K. Singhal, P. N. Bartlett and J. D. Kilburn, *J. Chem. Soc., Perkin Trans. 1*, 1998, 1467.
17 J. B. Torrance, B. A. Scott, B. Welber, F. B. Kaufman and P. E. Seiden, *Phys. Rev. B*, 1979, **19**, 730.
18 U. Simon, *Adv. Mater.*, 1998, **10**, 1487.

Communication a909882h

ChemComm

Novel arsine ligands for selective hydroformylation of alk-1-enes employing platinum/tin catalysts†

Lars A. van der Veen, Peter K. Keeven, Paul C. J. Kamer and Piet W. N. M. van Leeuwen*

Institute of Molecular Chemistry, University of Amsterdam, Nieuwe Achtergracht 166, 1018 WV Amsterdam, The Netherlands. E-mail: pwnm@anorg.chem.uva.nl

Received (in Basel, Switzerland) 25th August 1999, Accepted 20th January 2000

The synthesis and application of new wide bite angle arsine based ligands in the platinum/tin-catalysed hydroformylation of oct-1-ene is reported; an unprecedented high activity and selectivity is obtained employing a mixed phosphine/arsine ligand.

Hydroformylation of alkenes is one of the world's largest homogeneously catalysed reactions in industry (Scheme 1), producing more than six million tons of aldehydes and alcohols annually.[1] The commercial hydroformylation processes are run exclusively on cobalt or rhodium complexes as catalysts. Platinum complexes also give active hydroformylation catalysts, but are mainly of academic interest. Both terminal and internal alkenes can be hydroformylated selectively employing platinum–diphosphine complexes activated by tin chloride as the co-catalyst.[2] Tin-free catalyst systems have been reported as well.[3] Despite the very high linear over branched (l:b) aldehyde ratios induced by the platinum/tin–diphosphine catalysts, these systems have mainly been applied to asymmetric hydroformylation so far.[1,4] The major drawbacks of these catalysts are extensive isomerisation and hydrogenation of the substrate alkenes.

Both in the rhodium- and in the platinum/tin-catalysed hydroformylation of alk-1-enes, widening of the natural bite angle of the diphosphine ligands has proven to be favourable for the catalytic performance.[2a,5] Recently, it was also demonstrated that in the selective hydroformylation of internal alkenes toward linear aldehydes wide bite angle diphosphine ligands can be very efficient.[6] Based on these results we wondered whether wide natural bite angles could also improve the catalytic performance of ligands having donor atoms other than phosphorus. Since the xanthene backbone is an excellent scaffold for the construction of ligands with wide natural bite angles, we set out to synthesise the (mixed) group 15 derivatives of the xantphos ligand **1** (Fig. 1). Here, we report the synthesis of the arsine analogues of xantphos **1** and their excellent performance in the platinum/tin-catalysed hydroformylation reaction. To our knowledge, xantarsine and xantphosarsine ligands **2** and **3** constitute the first efficient arsine modified platinum/tin catalysts for selective hydroformylation of terminal alkenes.

The xantarsine and xantphosarsine ligands **2** and **3** were synthesised *via* procedures similar to the synthesis of xantphos **1** (Scheme 2).[6a] Dilithiation of 4,5-dibromo-2,7-di-*tert*-butyl-9,9-dimethylxanthene **5** with *n*-butyllithium in THF at −65 °C, followed by reaction with chlorodiphenylarsine gave xantarsine

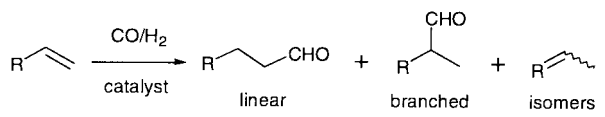

Scheme 1 The hydroformylation reaction.

† Electronic supplementary information (ESI) available: full characterisation data for the new compounds. See http://www.rsc.org/suppdata/cc/a9/a906903h/

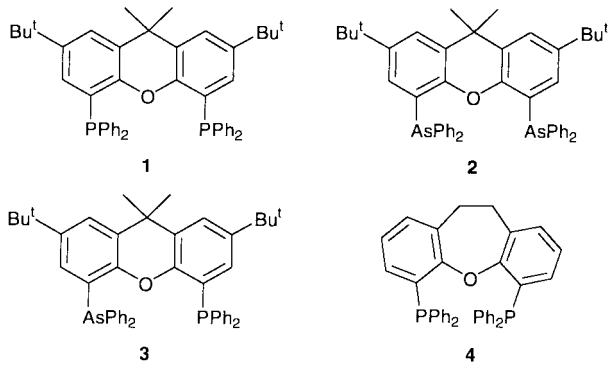

Fig. 1

2 in 83% yield. Xantphosarsine ligand **3** was obtained in 49% yield by monolithiation of bromoxantphos **6** and subsequent reaction with chlorodiphenylarsine. Bromoxantphos **6** was synthesised by monolithiation of compound **5**, followed by reaction with chorodiphenylphosphine. The calculated natural bite angles of ligands **1**, **2**, **3** and **4** are 110, 113, 111 and 102°, respectively.[7]

Ligands **1**–**4** were tested in the platinum/tin-catalysed hydroformylation of oct-1-ene (Table 1). In the hydro-

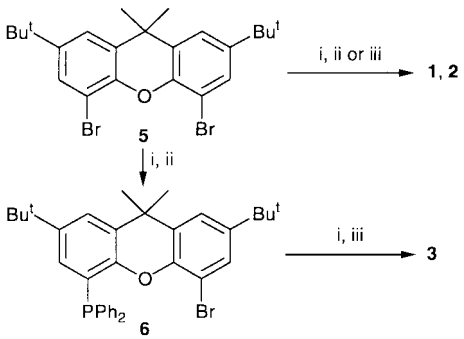

Scheme 2 Synthesis of ligands **1**–**3** and **6**: (i) Bu^{n}Li, THF, −65 °C; (ii) Ph_2PCl, THF, −65 to 25 °C, 81% (**1**), 48% (**6**); (iii) Ph_2AsCl, THF, −65 to 25 °C, 83% (**2**), 49% (**3**).

Table 1 Platinum/tin-catalysed hydroformylation of oct-1-ene at 60 °C[a]

Ligand	l:b Ratio[b]	% *n*-Nonanal[b]	% Isomerization[b]	TOF[bc]
1	230	95	4.5	18
2	> 250	92	8.0	210
3	200	96	3.1	350
4	> 250	88	12	720

[a] Reactions were carried out in a 180 mL stainless steel autoclave in dichloromethane at 60 °C under 40 bar of $CO–H_2$ (1:1), catalyst precursor $[Pt(cod)Cl_2]$, [Pt] = 2.5 mM, $Pt:SnCl_2:P$:1-octene = 1:2:4:255. [b] Determined by GC with decane as the internal standard. [c] Averaged turnover frequencies (TOF) were calculated as (mol of aldehyde) (mol Pt)$^{-1}$ h^{-1} at 20–30% conversion.

DOI: 10.1039/a906903h

formylation of oct-1-ene the arsine based ligands **2** and **3** proved to give more efficient catalysts than the parent xantphos ligand **1**. The xantarsine ligand **2** is only slightly less selective than xantphos **1**, but more than 10 times as active. The xantphosarsine ligand **3** is even 20 times as active as xantphos **1**, while displaying the same excellent selectivity for linear aldehyde formation. This is remarkable, since up to now, without exception, arsine ligands have performed worse than phosphine ligands in platinum/tin-catalysed hydroformylation.[2c,3a,8] To our knowledge the high activity and selectivity displayed by the mixed xantphosarsine ligand **3** under these mild conditions is unprecedented.

Comparison of the activities of the xantphos ligands **1** and **4** reveals a dramatic effect of the natural bite angle. Narrowing of the natural bite angle from 110 to 102°, results in a 40 fold higher hydroformylation rate. This is accompanied, however, by a considerable increase in isomerization activity. As a result, the selectivity for linear aldehyde obtained for xantphos **4** is lower than that for xantphos **1**. It is striking that the selectivities of the xantphos ligands **1** and **4** observed in the platinum/tin-catalysed hydroformylation are virtually identical to those obtained before for rhodium.[5c,6a]

The high selectivities of ligands **1**, **2** and **3** compared to xantphos **4** can be ascribed to the wider natural bite angles of the former ligands.‡ Widening of the bite angle of the ligand will increase the steric congestion around the platinum centre resulting in more selective formation of the sterically less hindered linear aldehydes. An explanation for the higher activities of ligands **2**, **3** and **4** compared to xantphos **1** is still lacking, but we speculate that it is caused by the coordination behaviour of the ligands in the platinum/tin complexes. Increasing the natural bite angle of bidentate ligands favours the formation of *trans* complexes. Compared to xantphos **1**, xantphos **4** and the arsine ligands **2** and **3** probably give more or easier formation of the *cis*-platinum complexes, a prerequisite for efficient hydroformylation.[10]

In conclusion, wide bite angle arsine based ligands can give very efficient catalysts for selective hydroformylation of terminal alkenes. The catalytic performances of the arsine modified platinum/tin systems can compete with the best results obtained using rhodium catalysts.[1,5c,11] Especially in applications where very high l:b ratios are a necessity these systems could be interesting alternatives for rhodium–diphosphine catalysts.

Financial support from the Technology Foundation (STW) of the Netherlands Organization for Scientific research (NWO) is gratefully acknowledged.

Notes and references

‡ When comparing the activities and selectivities of ligands **1**, **2**, and **3**, it should be noted that in general the σ-donor ability and the steric effects of substituents on the donor atom decrease in the order of P > As.[9]

1 M. Beller, B. Cornils, C. D. Frohning and C. W. Kohlpaintner, *J. Mol. Catal. A: Chem.*, 1995, **104**, 17; C. D. Frohning and C. W. Kohlpaintner, in *Applied Homogeneous Catalysis with Organometallic Compounds: a comprehensive handbook in two volumes*, ed. B. Cornils and W. A. Herrmann, VCH, Weinheim, 1996, vol. 1, pp. 27–104.
2 (*a*) Y. Kawabata, T. Hayashi and I. Ogata, *J. Chem. Soc., Chem. Commun.*, 1979, 462; (*b*) T. Hayashi, Y. Kawabata, T. Isoyama and I. Ogata, *Bull. Chem. Soc. Jpn.*, 1981, **54**, 3438; (*c*) I. Schwager and J. F. Knifton, *J. Catal.*, 1976, **45**, 256; (*d*) F. Ancillotti, M. Lami and M. Marchionna, *J. Mol. Catal.*, 1990, **63**, 15.
3 (*a*) S. C. Tang and L. Kim, *J. Mol. Catal.*, 1982, **14**, 231; (*b*) P. W. N. M. van Leeuwen, C. F. Roobeek, R. L. Wife and J. H. G. Frijns, *J. Chem. Soc.*, 1986, 31; (*c*) C. Botteghi, S. Paganelli, U. Matteoli, A. Scrivanti, R. Ciociaro and L. M. Venanzi, *Helv. Chim. Acta*, 1990, **73**, 284.
4 F. Agbossou, J.-F. Carpentier and A. Mortreux, *Chem. Rev.*, 1995, **95**, 2485.
5 (*a*) C. P. Casey, G. T. Whiteker, M. G. Melville, L. M. Petrovich, J. A. Gavney Jr. and D. R. Powell, *J. Am. Chem. Soc.*, 1992, **114**, 5535; (*b*) M. Kranenburg, Y. E. M. van der Burgt, P. C. J. Kamer and P. W. N. M. van Leeuwen, *Organometallics*, 1995, **14**, 3081; (*c*) L. A. van der Veen, P. H. Keeven, G. C. Schoemaker, J. N. Reek, P. C. J. Kamer, P. W. N. M. van Leeuwen, M. Lutz and A. L. Spek, *Organometallics*, 2000, **19**, in press.
6 (*a*) L. A. van der Veen, P. C. J. Kamer and P. W. N. M. van Leeuwen, *Angew. Chem., Int. Ed.*, 1999, **38**, 336; (*b*) P. Meessen, D. Vogt and W. Keim, *J. Organomet. Chem.*, 1998, **551**, 165.
7 C. P. Casey and G. T. Whiteker, *Isr. J. Chem.*, 1990, **30**, 299.
8 H. C. Clark and J. A. Davies, *J. Organomet. Chem.*, 1981, **213**, 503.
9 *Advanced Inorganic Chemistry: a comprehensive text*, ed. F. A. Cotton and G. Wilkinson, 5th edn., Wiley, New York, 1988, p. 432.
10 M. Gomez, G. Muller, D. Sainz, J. Sales and X. Solans, *Organometallics*, 1991, **10**, 4036; I. Toth, T. Kegi, C. J. Elsevier and L. Kollar, *Inorg. Chem.*, 1994, **33**, 5708.
11 E. Billig, A. G. Abatjoglou, D. R. Bryant, E. Billig, A. G. Abatjoglou, (to Union Carbide), EP 213639, 1987 (*Chem. Abstr.*, 1987 **107**, 7392r).

Communication a906903h

ChemComm

The chemical retro-Bingel reaction: selective removal of bis(alkoxycarbonyl)methano addends from C_{60} and C_{70} with amalgamated magnesium

Nicolle N. P. Moonen,[a] Carlo Thilgen,[a] Luis Echegoyen[b] and François Diederich*[a]

[a] *Laboratorium für Organische Chemie, ETH-Zentrum, Universitätstrasse 16, CH-8092 Zürich, Switzerland. E-mail: diederich@org.chem.ethz.ch*

[b] *Department of Chemistry, University of Miami, Coral Gables, FL 33124, USA*

Received (in Cambridge, UK) 9th December 1999, Accepted 25th January 2000

Bis(alkoxycarbonyl)methano addends are removed from C_{60} and C_{70} derivatives by reaction with amalgamated magnesium in dry THF; this facile and selective retro-Bingel reaction, which leaves pyrrolidine rings fused to C_{60} intact, opens up the possibility of using bis(alkoxycarbonyl)methano addends as protecting and reversible directing groups in the regioselective multiple functionalization of fullerenes.

Regioselective multiple functionalization of fullerenes is a subject of great interest. A major strategy used to accomplish this task is tether-directed remote functionalization.[1] Another protocol, often used in combination with tether-directed remote functionalization,[2] is the temporary introduction of an addend which protects specific positions and, at the same time, directs new incoming addends regioselectively to other bonds on the carbon sphere. Examples for such addends, which are readily introduced and removed, are the [9,10]anthraceno bridge[3] as well as fullerene-fused cyclohexene[2,4] and isoxazoline[5] rings.

One of the most common fullerene functionalization methods is the nucleophilic cyclopropanation with 2-halomalonates, the so-called Bingel reaction.[6] Although the resulting bis(alkoxycarbonyl)methanofullerenes are generally quite stable, there were early hints that the Bingel-type addends may be removed under certain circumstances.[7] Closer investigations led to the discovery of the electrochemical retro-Bingel reaction, consisting of the preparative removal of bis(alkoxycarbonyl)methano addends from fullerene adducts by exhaustive electrochemical reduction.[8] The first successful applications of the Bingel–electrochemical retro-Bingel reaction sequence were reported in the chemistry of the higher fullerenes, with the preparation of enantiomerically pure D_2-C_{76}[8] and D_2-C_{84},[9a] pure D_{2d}-C_{84}[9a] and a new C_{84} isomer,[9a] and C_{2v}-symmetric C_{78}.[9b] The potential of bis(alkoxycarbonyl)methano addends as general protecting and reversible directing groups in fullerene chemistry prompted us to investigate the possibility of carrying out the retro-Bingel reaction under chemical conditions. Such a method would have the advantages of not requiring electrochemical equipment, avoiding the use of supporting electrolyte, and allowing conversions on a larger scale.

Initial attempts to remove the Bingel-type addend from **1** by electron transfer from Na metal or sodium naphthalenide in THF failed, leading only to materials that were insoluble in THF or toluene. Another convenient reducing agent which is easy to handle is metallic magnesium. Heating **1** with Mg powder (25 equiv.) in dry refluxing THF under Ar led to the formation of a brownish precipitate after *ca.* 1 d, and after 3 d, varying yields of up to 81% of C_{60} could be isolated from the mixture. In analogy to Grignard reactions, starting the retro-Bingel reaction with pure Mg sometimes proved to be quite difficult. This situation could only be partially improved through activation of the metal by treatment with I_2 prior to the addition of the fullerene derivative. Use of the highly active Rieke magnesium[10] only led to products that were insoluble in THF or toluene. Also, treatment of the commercial magnesium with $CuCl_2$ did not lead to better or more reproducible yields. The best and most consistent results were obtained by amalgamation of the Mg powder with 10% $HgBr_2$ in THF, followed by a replacement of the solvent with fresh THF, addition of the

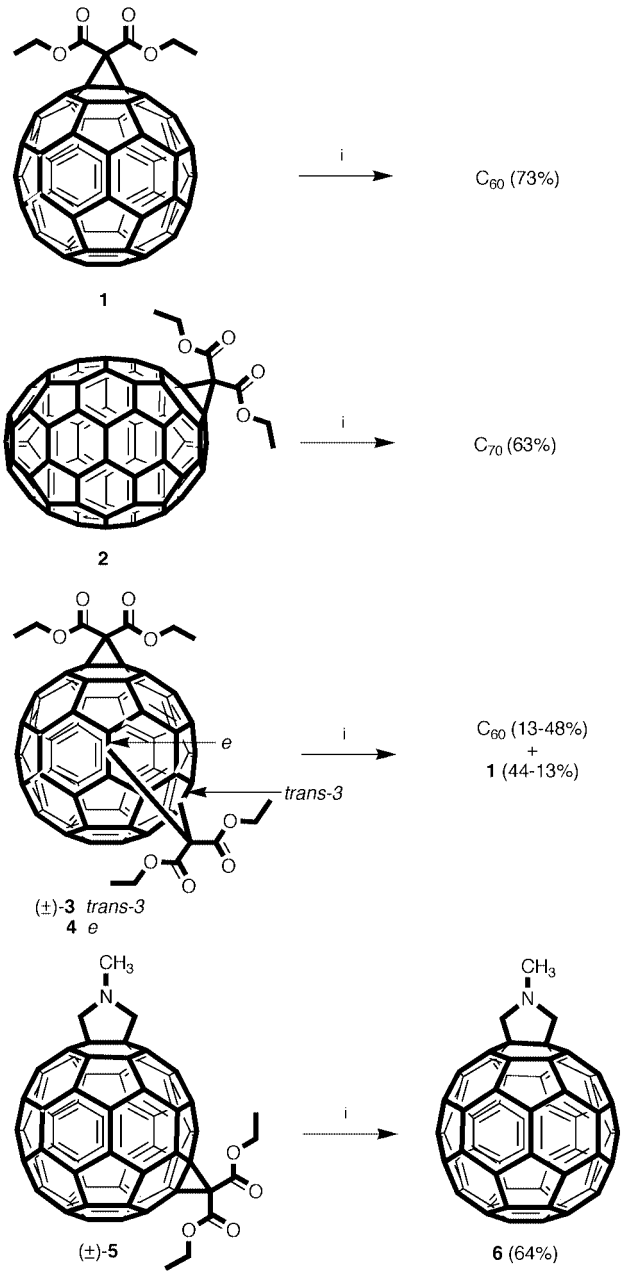

Scheme 1 *Reagents and conditions:* i, Mg/Hg, THF, Ar, 80 °C, 3 d.

DOI: 10.1039/a909704j

methanofullerene and heating to reflux for 3 d.† Under these conditions, **1** afforded C_{60} in 73% yield while unchanged starting material was recovered in 23% yield (Scheme 1). Similarly, the C_{70} mono-adduct **2** provided 63% of the parent fullerene. These yields are comparable to those obtained by the electrochemical retro-Bingel reaction.[8] Traces of as yet unidentified by-products, which may provide useful information with regard to the reaction mechanism, were detected during chromatographic purification of the products.

Zn dust and the Zn/Cu couple[11] are both active reducing agents in the retro-Bingel reaction of **1**, but the yields (Zn: 47% C_{60}, Zn/Cu: 29% C_{60}) are lower and, particularly with pure Zn, the amount of unidentified by-products is higher.

In the case of Bingel-type bis-adducts of C_{60}, the yields were variable (Scheme 1). In different experiments, the reduction of the pure *trans*-3 and *e* regioisomers (±)-**3** and **4**, or of a mixture of the seven known regioisomers,[12] with Mg (100 equiv.) amalgamated with 10% $HgBr_2$ afforded between 48% C_{60} (and 13% mono-adduct **1**) and 13% C_{60} (and 44% **1**). These fluctuations contrast the clean conversion (up to 75% yield) of the bis-adducts to C_{60} by the electrochemical retro-Bingel protocol,[8] but the reasons for these differences are not yet understood. Interestingly, whereas the product mixture recovered from the non-exhaustive electrochemical reduction of constitutionally pure bis-adducts contained regioisomers of the starting material resulting from an intramolecular 'walk-on-the-sphere' rearrangement,[13] such isomerization was not detected in the reduction of pure (±)-**3** or **4** with amalgamated Mg.

Fused pyrrolidines introduced by 1,3-dipolar cycloaddition are among the most versatile addends in fullerene chemistry. We therefore explored whether a bis(dialkoxycarbonyl)methano addend could be removed from bis-adducts such as (±)-**5**[14] while leaving the methaniminomethano bridge intact. When (±)-**5**[15] was reacted for 3 d with amalgamated Mg (50 equiv.), fulleropyrrolidine **6**[16] was isolated in 64% yield, showing that the heterocycle is stable under the conditions of the chemical retro-Bingel reaction. This result opens up the possibility of using Bingel-type addends as protecting and reversible directing groups in future syntheses of fullerene multi-adducts that are not otherwise accessible. Investigations along these lines are now under way.

Support from the Swiss National Science Foundation is gratefully acknowledged.

Notes and references

† In a typical experiment, a mixture of Mg powder (50–150 mesh, purity ≥99.8%; 14 mg, 576 mmol) and $HgBr_2$ (20 mg, 57 mmol) (both reagents from Fluka) was sonicated in dry THF (8 ml) for 30 min under Ar, after which the solvent was replaced by fresh dry THF (8 ml) and C_{60} monoadduct **1** (20 mg, 23 mmol) was added. The mixture was sonicated for another 30 min and then heated to reflux for 3 d. Column chromatography (SiO_2; toluene–hexane 1:1) provided 12 mg (73%) of C_{60}.

1 L. Isaacs, R. F. Haldimann and F. Diederich, *Angew. Chem., Int. Ed. Engl.*, 1994, **33**, 2339; F. Diederich and R. Kessinger, *Acc. Chem. Res.*, 1999, **32**, 537; F. Diederich and R. Kessinger, in *Templated Organic Synthesis*, ed. F. Diederich and P. J. Stang, Wiley-VCH, Weinheim, 1999, pp. 189–218.

2 F. Cardullo, L. Isaacs, F. Diederich, J.-P. Gisselbrecht, C. Boudon and M. Gross, *Chem. Commun.*, 1996, 797; W. Qian and Y. Rubin, *Angew. Chem., Int. Ed.*, 1999, **38**, 2356.

3 R. Schwenninger, T. Müller and B. Kräutler, *J. Am. Chem. Soc.*, 1997, **119**, 9317; I. Lamparth, C. Maichle-Mössmer and A. Hirsch, *Angew. Chem., Int. Ed. Engl.*, 1995, **34**, 1607.

4 Y.-Z. An, G. A. Ellis, A. L. Viado and Y. Rubin, *J. Org. Chem.*, 1995, **60**, 6353.

5 T. Da Ros, M. Prato, F. Novello, M. Maggini, M. De Amici and C. De Micheli, *Chem. Commun.*, 1997, 59.

6 C. Bingel, *Chem. Ber.*, 1993, **126**, 1957.

7 A. Hirsch, I. Lamparth, T. Grösser and H. R. Karfunkel, *J. Am. Chem. Soc.*, 1994, **116**, 9385; M. Keshavarz-K., B. Knight, R. C. Haddon and F. Wudl, *Tetrahedron*, 1996, **52**, 5149; F. Arias, Y. Yang, L. Echegoyen, Q. Lu and S. R. Wilson, in *Recent Advances in the Chemistry and Physics of Fullerenes and Related Materials*, ed. K. M. Kadish and R. S. Ruoff, The Electrochemical Society, Pennington, NJ, 1995, pp. 200–212; F. Cardullo, P. Seiler, L. Isaacs, J.-F. Nierengarten, R. F. Haldimann, F. Diederich, T. Mordasini-Denti, W. Thiel, C. Boudon, J.-P. Gisselbrecht and M. Gross, *Helv. Chim. Acta*, 1997, **80**, 343.

8 R. Kessinger, J. Crassous, A. Herrmann, M. Rüttimann, L. Echegoyen and F. Diederich, *Angew. Chem., Int. Ed.*, 1998, **110**, 1919.

9 (*a*) J. Crassous, J. Rivera, N. S. Fender, L. Shu, L. Echegoyen, C. Thilgen, A. Herrmann and F. Diederich, *Angew. Chem., Int. Ed.*, 1999, **38**, 1613; (*b*) C. Boudon, J.-P. Gisselbrecht, M. Gross, A. Herrmann, M. Rüttimann, J. Crassous, F. Cardullo, L. Echegoyen and F. Diederich, *J. Am. Chem. Soc.*, 1998, **120**, 7860.

10 R. D. Rieke and S. E. Bales, *J. Am. Chem. Soc.*, 1974, **96**, 1775; R. D. Rieke, *Acc. Chem. Res.*, 1977, **10**, 301.

11 The Zn/Cu couple was prepared according to: H. P. Spielmann, G.-W. Wang, M. S. Meier and B. R. Weedon, *J. Org. Chem.*, 1998, **63**, 9865.

12 A. Hirsch, I. Lamparth and H. R. Karfunkel, *Angew. Chem., Int. Ed. Engl.*, 1994, **33**, 437.

13 R. Kessinger, M. Gómez-Lopez, C. Boudon, J.-P. Gisselbrecht, M. Gross, L. Echegoyen and F. Diederich, *J. Am. Chem. Soc.*, 1998, **120**, 8545.

14 M. Prato and M. Maggini, *Acc. Chem. Res.*, 1998, **31**, 519.

15 R. Kessinger and F. Diederich, unpublished results.

16 M. Maggini, G. Scorrano and M. Prato, *J. Am. Chem. Soc.*, 1993, **115**, 9798.

Communication a909704j

ChemComm

Chemoselective oxidative debenzylation of tertiary *N*-benzyl amines

Steven D. Bull,[a] Stephen G. Davies,*[a] Garry Fenton,[b] Andrew W. Mulvaney,[a] R. Shyam Prasad[a] and Andrew D. Smith[a]

[a] *The Dyson Perrins Laboratory, University of Oxford, South Parks Road, Oxford, UK OX1 3QY. E-mail: steve.davies@chem.ox.ac.uk*

[b] *Rhône-Poulenc Rorer, Rainham Road South, Dagenham, Essex, UK RM10 7XS*

Received (in Liverpool, UK) 4th January 2000, Accepted 25th January 2000

Treatment of tertiary amines containing one or more *N*-benzyl protecting groups with aqueous ceric ammonium nitrate results in clean *N*-debenzylation to afford the corresponding secondary amine.

Differentially protected homochiral lithium amide additions to α,β-unsaturated esters have proved to be an extremely versatile route for the asymmetric synthesis of homochiral β-amino acids and β-lactams.[1–3] In the course of studies directed towards extending the versatility of this lithium amide methodology, the synthetic applications of a novel debenzylation reaction observed when *tert*-butyl 3-[benzyl(4-methoxybenzyl)amino]-3-phenylpropionate **1** was treated with aqueous ceric ammonium nitrate (CAN) are reported herein. Thus, while treatment of **1** with 2,3-dichloro-5,6-dicyano-1,4-benzoquinone (DDQ) resulted as expected in smooth cleavage of the 4-methoxybenzyl protecting group to afford *tert*-butyl 3-benzylamino-3-phenylpropionate **2**, treatment of **1** with 2.1 equiv. of CAN in CH_3CN–H_2O afforded a 50:50 mixture of the monodeprotected products **2** and *tert*-butyl 3-(4-methoxybenzylamino)-3-phenylpropionate **3** (Scheme 1). It is noteworthy that in both cases the isolated products were those resulting from cleavage of the primary benzylic amine; the secondary benzylic centre (β-centre) remained unaffected under these conditions. This lack of selectivity for deprotection of tertiary amine **1** is in direct contrast to the well-established use of CAN for the orthogonal deprotection of 4-methoxybenzyl ethers in the presence of *O*-benzyl ethers.[4]

This unexpected reaction implies oxidation at the tertiary nitrogen atom rather than at the arene ring since the outcome of the reaction is unaffected by arene substitution and therefore should be equally applicable to debenzylation of simple tertiary benzylamines. Thus, treatment of tribenzylamine **4** with CAN gave dibenzylamine **5** in 90% yield after chromatographic purification to remove benzaldehyde.[5] The chemoselectivity of this oxidative debenzylation protocol for tertiary amines was confirmed by treating dibenzylamine **5** with excess CAN (10 equiv.), which resulted in essentially quantitative recovery of starting material. Treatment of tertiary amine **6**, which contains two *N*-benzylic and one α-substituted *N*-benzylic groups, resulted in chemoselective monodebenzylation to afford exclusively secondary amine **7** in 79% isolated yield. Similarly, *N*-debenzylation of homochiral tertiary amine **8**, which contains one *N*-benzylic and two α-substituted *N*-benzylic protecting groups, occurred without epimerisation, to afford homochiral secondary amine **9** {$[\alpha]_D$ −15.8 (*c* 1.0, $CHCl_3$); lit.[2] −16.3 (*c* 1.5, $CHCl_3$)} in 86% isolated yield. Extension of this methodology to the deprotection of tertiary amines containing either two or one benzylic groups was also demonstrated *via* treatment of tertiary amines **10** and **12** to afford secondary amines **11** {$[\alpha]_D$ −46.4 (*c* 1.0, $CHCl_3$)} and **13** in 85 and 64% isolated yield respectively (Scheme 2). The lower isolated yield for amine **13** was a result of its inherent volatility, however, no other product was detected in the ^1H NMR spectrum obtained from the crude reaction mixture.

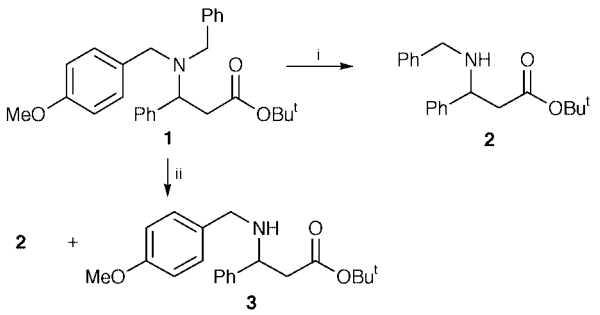

Scheme 1 *Reagents and conditions:* i, DDQ, CH_2Cl_2–H_2O (5:1); ii, CAN (2.1 equiv.), CH_3CN–H_2O (5:1).

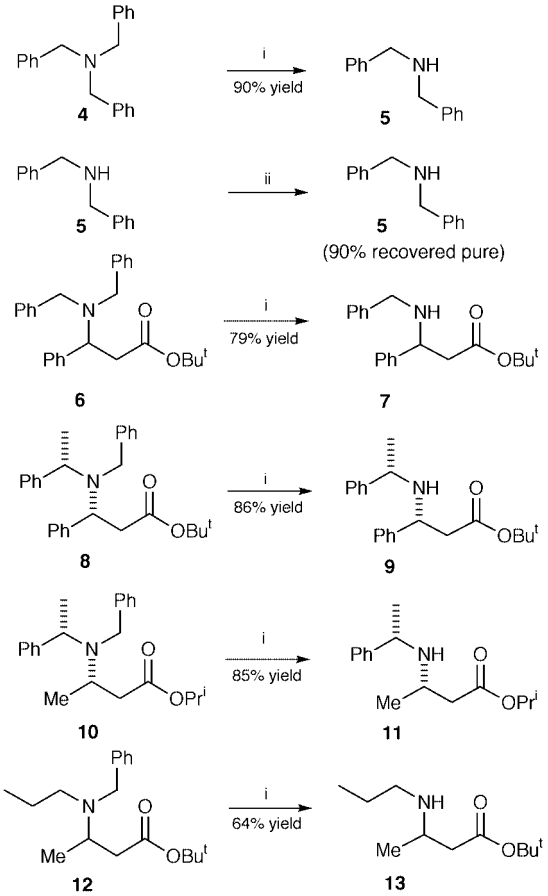

Scheme 2 *Reagents and conditions:* i, CAN (2.1 equiv.), CH_3CN–H_2O (5:1); ii, CAN (10.0 equiv.), CH_3CN–H_2O (5:1).

Since benzyl groups are commonly employed as protecting groups for other heteroatom functionality the chemoselectivity of this transformation was examined by carrying out the CAN-mediated tertiary amine debenzylation protocol on a range of perbenzylated *N*,*N*-dibenzylamines which also contained ben-

DOI: 10.1039/b000071j

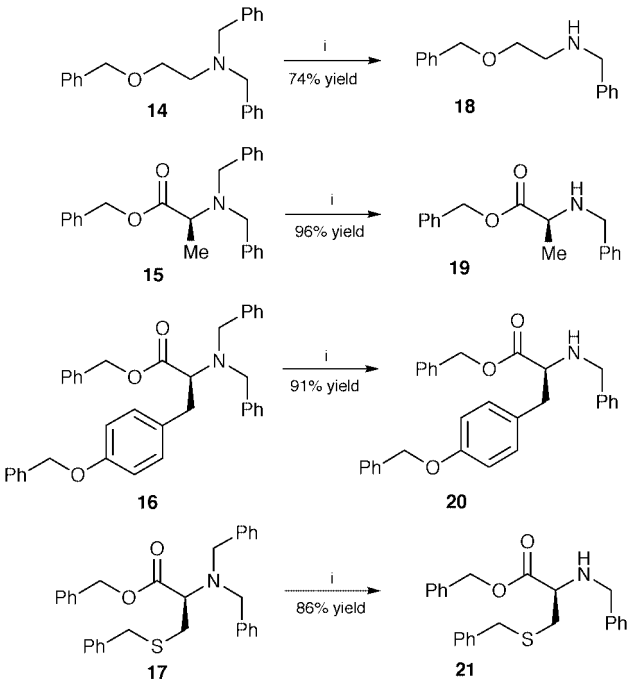

Scheme 3 *Reagents and conditions:* i, CAN (2.1 equiv.), CH_3CN–H_2O (5:1).

zyl ethers, benzyl esters, benzyl phenolates and benzyl thiolates. Thus, treatment of **14**–**17** resulted in clean *N*-deprotection to afford the mono-*N*-debenzylated secondary amines **18**, **19** {$[\alpha]_D$ −38.6 (*c* 1.0); lit.[6] $[\alpha]_D$ for *ent*-**19** 40.4 (*c* 1.0)}, **20** {$[\alpha]_D$ −8.3 (*c* 1.2} and **21** {$[\alpha]_D$ −21.9 (*c* 1.1)} in good to excellent isolated yields (Scheme 3).

With this chemoselective debenzylation of tertiary amines in hand, the application of this novel cleavage protocol for solid phase synthesis was apparent. Thus, consecutive reductive alkylation[7] of aminomethyl polystyrene resin **22** with hexanal afforded polymer supported tertiary amine **23**, which was treated with CAN to afford dihexylamine **24** in 72% overall yield over the five steps (Scheme 4). This cleavage protocol constitutes a novel oxidative traceless linker synthesis of secondary amines on a solid support[8] and is of potential further utility in that cleavage of the secondary amine liberates formyl polystyrene resin **25** (ν_{max} 1700 cm^{-1}; lit.[9] 1700 cm^{-1}), thus affording the possibility of resin recycling.

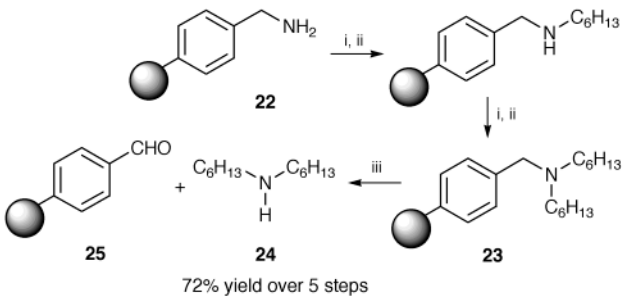

Scheme 4 *Reagents and conditions:* i, $CH_3(CH_2)_4CHO$ (5.0 equiv.), trimethyl orthoformate; ii, $NaBH_4$ (10.0 equiv.), DMF–EtOH (3:1); iii, CAN (5.0 equiv.), CH_3CN–H_2O (5:1), room temp.

In conclusion, treatment of *N*-benzyl tertiary amines with CAN results in smooth *N*-debenzylation to afford the corresponding secondary amines with complete chemoselectivity. While some *N*-debenzylations may be achieved under hydrogenolytic conditions in acid,[10] this novel debenzylation under oxidative conditions adds considerable versatility to *N*-benzylation protection–deprotection methodology and to regeneration of polymer supports in combinatorial chemistry. Investigations are currently underway to determine the reaction mechanism of this transformation.

The authors wish to acknowledge Rhône-Poulenc Rorer Ltd. (A. D. S) and Oxford Asymmetry International plc (R. S. P.) together with the EPSRC for CASE awards.

Notes and references

1 S. G. Davies and O. Ichihara, *Tetrahedron: Asymmetry*, 1991, **2**, 183; S. G. Davies, O. Ichihara and I. A. S. Walters, *Synlett*, 1993, 461; S. G. Davies, N. M. Garrido, O. Ichihara and I. A. S. Walters, *J. Chem. Soc., Chem. Commun.*, 1993, 1153; S. G. Davies, M. E. Bunnage and C. J. Goodwin, *J. Chem. Soc., Perkin Trans. 1*, 1993, 1375; S. G. Davies, M. E. Bunnage and C. J. Goodwin, *Synlett*, 1993, 731; S. G. Davies, O. Ichihara and I. A. S. Walters, *Synlett*, 1994, 117; S. G. Davies, M. E. Bunnage, A. J. Burke and C. J. Goodwin, *Tetrahedron: Asymmetry*, 1994, **5**, 203; S. G. Davies and I. A. S. Walters, *J. Chem. Soc., Perkin Trans. 1*, 1994, 1129; S. G. Davies, O. Ichihara and I. A. S. Walters, *J. Chem. Soc., Perkin Trans. 1*, 1994, 1141; S. G. Davies, M. E. Bunnage, C. J. Goodwin and O. Ichihara, *Tetrahedron*, 1994, **50**, 3975; S. G. Davies, O. Ichihara, I. Lenoir and I. A. S. Walters, *J. Chem. Soc., Perkin Trans. 1*, 1994, 1411; S. G. Davies, M. E. Bunnage, A. N. Chernega and C. J. Goodwin, *J. Chem. Soc., Perkin Trans. 1*, 1994, 2373; S. G. Davies, M. E. Bunnage and C. J. Goodwin, *J. Chem. Soc., Perkin Trans. 1*, 1994, 2385; S. G. Davies, J. F. Costello and O. Ichihara, *Tetrahedron: Asymmetry*, 1994, **5**, 1999; S. G. Davies, M. E. Bunnage, A. J. Burke and C. J. Goodwin, *Tetrahedron: Asymmetry*, 1995, **6**, 165; S. G. Davies, A. J. Edwards and I. A. S. Walters, *Recl. Trav. Chim. Pays-Bas*, 1995, **114**, 175; S. G. Davies and G. D. Smyth, *Tetrahedron: Asymmetry*, 1996, **7**, 1001; S. G. Davies and G. D. Smyth, *Tetrahedron: Asymmetry*, 1996, **7**, 1005; S. G. Davies and G. D. Smyth, *Tetrahedron: Asymmetry*, 1996, **7**, 1273; S. G. Davies and O. Ichihara, *Tetrahedron: Asymmetry*, 1996, **7**, 1919; S. G. Davies and D. J. Dixon, *Chem. Commun.*, 1996, 1797; S. G. Davies, A. J. Burke and C. J. R. Hedgecock, *Synlett.*, 1996, 621; S. G. Davies and G. D. Smyth, *J. Chem. Soc., Perkin Trans. 1*, 1996, 2467; S. G. Davies and O. Ichihara, *J. Synth. Org. Chem. Jpn.*, 1997, **55**, 26; S. G. Davies J. G. Urones, N. M. Garrido, D. Diez and S. H. Dominguez, *Tetrahedron: Asymmetry*, 1997, **8**, 2683; S. G. Davies, D. R. Fenwick and O. Ichihara, *Tetrahedron: Asymmetry*, 1997, **8**, 3387; S. G. Davies and D. J. Dixon, *J. Chem. Soc., Perkin Trans. 1*, 1998, 2629; S. G. Davies and D. J. Dixon, *J. Chem. Soc., Perkin Trans. 1*, 1998, 2635; S. G. Davies, I. Brackenridge, D. R. Fenwick, O. Ichihara and M. E. C. Polywka, *Tetrahedron*, 1999, **55**, 533; S. G. Davies, J. G. Urones, N. M. Garrido, D. Diez and S. H. Dominguez, *Tetrahedron: Asymmetry*, 1999, **10**, 1637; S. G. Davies, G. D. Smyth and A. M. Chippindale, *J. Chem. Soc., Perkin Trans. 1*, 1999, 3089; S. G. Davies, N. M. Garrido, P. A. McGee and J. P. Shilvock, *J. Chem. Soc., Perkin Trans. 1*, 1999, 3105; S. G. Davies and O. Ichihara, *Tetrahedron Lett.*, 1999, **40**, 9313.

2 S. G. Davies and D. R. Fenwick, *J. Chem. Soc., Chem. Commun.*, 1995, 1109; S. G. Davies and D. R. Fenwick, *Chem. Commun.*, 1997, 565; D. R. Fenwick, *D. Phil. Thesis*, University of Oxford, 1996.

3 S. G. Davies and O. Ichihara, *Tetrahedron Lett.*, 1998, **39**, 6045.

4 C. Murakata and T. Ogawa, *Carbohydr. Res.*, 1992, **234**, 75.

5 *Representative protocol*: To a solution of *N*-benzylated tertiary amine (1 mmol) in CH_3CN–H_2O (5:1), at room temperature, was added CAN (2.1 equiv.) and the reaction mixture stirred for 2 h. The reaction mixture was neutralised with $NaHCO_3$ (aq), extracted with Et_2O, dried ($MgSO_4$), and the solvent and benzaldehyde removed *in vacuo* to afford a crude oil which was purified by chromatography to afford the desired secondary amine.

6 H. Kubota, A. Kubo, M. Takahashi, R. Shimizu, T. Da-te, K. Okamura and K. Nunami, *J. Org. Chem.*, 1995, **60**, 6776.

7 S. Kobayashi and Y. Aoki, *J. Comb. Chem.*, 1999, **1**, 371.

8 For examples of traceless synthesis of amines on solid supports, see: S. Brandtner, S. Bräse, D. Enders, J. Köbberling, R. Lazny and M. Wang, *Tetrahedron. Lett.*, 1999, **11**, 2105; A. R. Brown, J. R. Morphy, Z. Rankovic and D. C. Rees, *J. Am. Chem. Soc.*, 1997, **119**, 3288; J. R. Morphy, Z. Rankovic and D. C. Rees, *Tetrahedron. Lett.*, 1996, **37**, 3209.

9 Y. Bing and L. Wenbao, *J. Org. Chem.*, 1997, **62**, 9347.

10 For example, see: J. P. Li, *J. Org. Chem.*, 1975, **40**, 3414.

Communication b000071j

ChemComm

Redox-active self-assembled monolayers as novel solid contacts for ion-selective electrodes†

Monia Fibbioli,[a] Krisanu Bandyopadhyay,[b] Sheng-Gao Liu,[b] Luis Echegoyen,*[b] Olivier Enger,[a] François Diederich,*[a] Philippe Bühlmann[c] and Ernö Pretsch*[a]

[a] *Laboratory of Organic Chemistry, Swiss Federal Institute of Technology (ETH), CH-8092 Zürich, Switzerland. E-mail: pretsch@org.chem.ethz.ch*

[b] *Department of Chemistry, University of Miami, Coral Gables, FL 33124, USA*

[c] *Department of Chemistry, School of Science, The University of Tokyo, Hongo 731, Bunkyo-ku, Tokyo 113-0033, Japan*

Received (in Cambridge, UK) 2nd December 1999, Accepted 25th January 2000

A new methodology to fabricate solid-contact ion-selective electrodes (SC-ISEs) using SAMs of a lipophilic redox-active compound to facilitate the charge transfer across the interface leads to improved potential stability and prevents redox or O_2 interference of valinomycin-based SC-ISEs.

In conventional solvent polymeric ion-selective electrodes (ISEs), the membrane is in electrical contact with the internal reference electrode through an inner solution. This arrangement provides stable potentials at the membrane/solution and solution/internal electrode interfaces.[1] For an ISE whose membrane is in direct contact with the inner electrode (coated wire electrodes),[2] however, the potential stability is generally not satisfactory owing to poorly defined redox reactions at the metal surface and formation of a thin aqueous layer between this metal and the membrane.[3a–c] ISFETs with an immobilized buffered hydrogel layer between the PVC membrane and the SiO_2 surface showed improved stability[3d] but since the need for an inner solution impedes true miniaturization of ISEs, several approaches to improve the EMF stability of solid-contact electrodes have been suggested.[3b,4,5]

Here, we introduce a novel approach to prepare SC-ISEs using redox-active self-assembled monolayers (SAMs). A lipophilic and redox-active compound (a fullerene **1** or tetrathiafulvalene, (TTF) **2** derivative, Fig. 1) is attached by self-assembly to the inner gold electrode (gold film or gold bead), and a conventional ion-selective membrane (with polyurethane matrix) is deposited on the modified solid substrate. The redox properties of the SAMs guarantee a stable potential, while their lipophilicities prevent the formation of an aqueous layer between the membrane and the metal electrode. Two new compounds were designed in view of their easy reduction (of fullerene in **1**) or oxidation (of TTF in **2**).

Compound **1** was synthesized by converting 8-chlorooctanol to the *S*-acetyl protected 8-mercaptooctanol[6] and then into the malonate derivative, which was added in a modified Bingel reaction to C_{60}.[7] Acidic deprotection of the monoadduct yielded **1**. The synthesis of **2** is described in the literature.[8–10] Detailed procedures, spectroscopic and voltammetric data are included in the electronic supplementary information.†

SAMs of **1** and **2** were formed by dipping freshly evaporated Au films (2000 Å, vacuum-deposited on glass slides with a buffer layer of 60 Å Cr) or glass-sealed ultra-clean spherical Au bead (diameter of exposed area *ca.*1 mm) electrodes into a 1 mM CH_2Cl_2 solution of the respective compound for 24 h, followed by rinsing with large amounts of CH_2Cl_2 and drying under Ar.[10] The resulting modified surfaces were characterized by contact-angle measurements, ellipsometry and IR spectroscopy (for Au films) or voltammetry (for Au films and beads).

† Electronic supplementary information (ESI) available: synthetic and spectroscopic data for **1** and **2** is available from the RSC web site: http://www.rsc.org/suppdata/a9/a909532b/

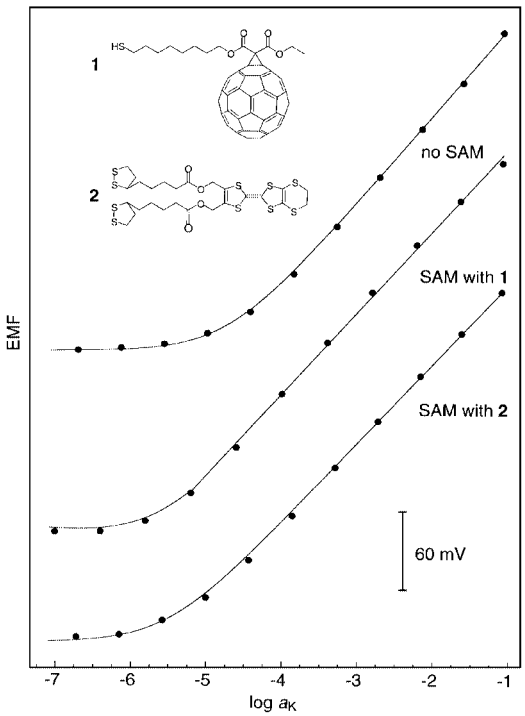

Fig. 1 K^+-Calibration curves of a valinomycin-based SC-ISE membrane with no SAM, and with a SAM of the fullerene derivative **1** or TTF derivative **2** (curves offset for clarity).

The cyclic voltammograms (CVs) recorded in a solution of 0.1 M NBu_4PF_6 in CH_2Cl_2 show a linear increase of the peak current related to the fullerene-based first reduction (for **1**) or TTF-based first oxidation (for **2**) with the scan rate, indicative of a surface-confined behavior (Fig. 2).[11] This was also confirmed by the small potential difference between the anodic and cathodic peaks: 22 mV for the fullerene reduction at $E_{1/2}$ = −680 mV and 35 mV for the TTF oxidation at $E_{1/2}$ = +575 mV (*vs.* an aqueous Ag/AgCl reference electrode at a scan rate of 1 V s^{-1}; Fig. 2). The SAMs derived from compounds **1** and **2** proved to be stable, exhibiting almost the same current responses after several scan cycles. The surface coverages[12] were found to be 3.9×10^{-10} and 1.9×10^{-10} mol cm^{-2} (estimated values for a monolayer: 1.9×10^{-10} and 3.6×10^{-10} mol cm^{-2})[13] for **1** and **2**, respectively.[8,14] The advancing contact angles of water revealed a higher lipophilicity (71 ± 2° for **1** and 70 ± 2° for **2**)[15] compared to that of the unmodified Au electrode, but a lower one than reported for highly hydrophobic surfaces (> 100°),[16] which apparently reflects the aromatic character of the terminal fullerene and TTF groups.

Both SAM-modified Au films and beads were used as internal electrodes for the potentiometric measurements[17] with

DOI: 10.1039/a909532b

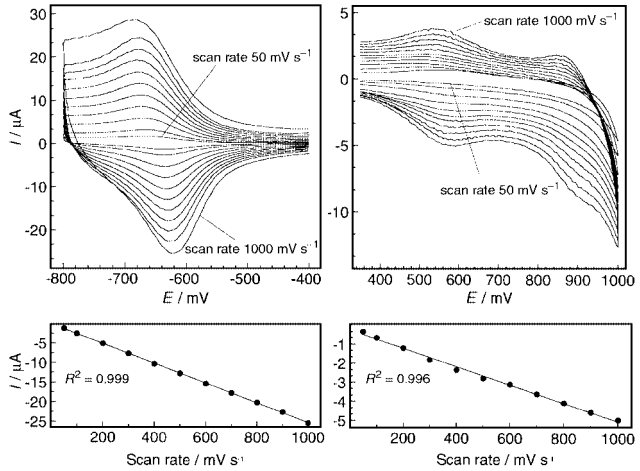

Fig. 2 Cyclic voltammograms of a SAM of **1** (left) or **2** (right) on a gold bead recorded in 0.1 M NBu_4PF_6 in CH_2Cl_2 with scan rates between 1000 (first scan) and 50 mV s^{-1} (last scan). All measurements were started at 0 mV.

K^+ selective polyurethane membranes.[18] Fig. 1 shows calibration curves for the SC-ISEs with different interfaces after conditioning in a 10^{-3} M KCl solution for 12 h. The SC-ISEs with SAMs exhibit linear responses down to 10^{-5} M K^+ with Nernstian slopes (the lower detection limit is due to H^+ interference[17]). Since the membrane composition for these SC-ISEs is the same as for conventional liquid-contact ISEs, the selectivity coefficients are also the same within experimental error. The EMF values of these SC-ISEs are more stable (long term drifts over 100 h 85 μV h^{-1} as compared to 220 μV h^{-1} without SAM) and not influenced by changes in the ratio of Fe(III)/Fe(II) in solutions of constant ionic strength (0.1 M KCl) and constant total amount of the redox couple (10^{-2} M $FeCl_3$/$FeCl_2$). In the absence of the redox-active SAM, the linear response range was reduced by about an order of magnitude (Fig. 1, the lower detection limit is no more due to H^+ inteference) and strongly drifting signals (> 5 mV min^{-1}) were observed when interfering ions were measured. Both of these effects can be explained by the presence of an aqueous layer between the polyurethane membrane and the gold surface. The composition of this layer changes upon contact of the SC-ISE with interfering sample ions and thereby affects both the phase boundary potential at the interface of the membrane and the aqueous layer as well as the interfacial potential at the metal surface, which is apparently determined by the reaction of O_2.[3b] The strong influence of O_2 on the EMF of coated wire electrodes[3b,5a] Fig. 3, top curve) is effectively reduced by the SAMs of **1**, **2** or *n*-$C_8H_{17}SH$ (Fig. 3), indicative of the absence of an aqueous layer. However, no Nernstian response could be obtained with the latter monolayer, corroborating the need for the redox active SAM.

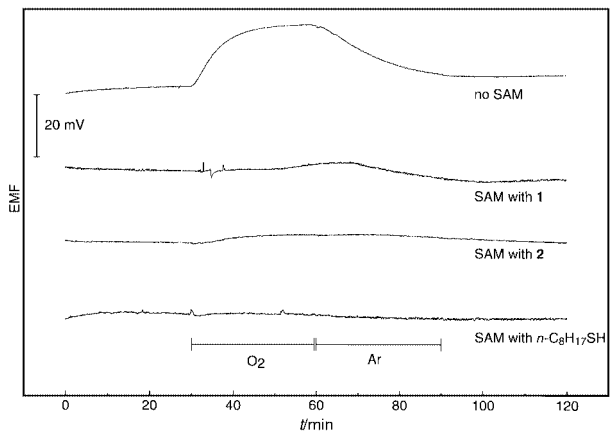

Fig. 3 EMF response of various SC-ISEs on introducing O_2 or Ar into a 10^{-3} M KCl solution (curves offset for clarity).

In summary, we have developed a new methodology to fabricate solid-contact ion-selective electrodes using SAMs of redox-active compounds. All the valinomycin-based SC-ISEs studied show Nernstian responses down to 10^{-5} M K^+, with improved stability, and no redox or O_2 interference.

The authors thank ETH Zurich for an internal research grant, Orion Research Inc. (Beverly, MA) for financial support, Dr M. Hirayama, H. Persson and Professor U. W. Sutter for their help in surface characterization, and Dr D. Wegmann for careful reading of the manuscript. L. E., S.-G. L., and K. B. wish to thank the US National Science Foundation (CHE-9816503 and DMR-9803088) and F. D. the Swiss National Science Foundation for financial support.

Notes and references

1 W. E. Morf, *The Principles of Ion-Selective Electrodes and of Membrane Transport*, Elsevier, 1981; B. P. Nikolskii and E. A. Materova, *Ion-Sel. Electrode Rev.*, 1985, **7**, 3; E. Bakker, P. Bühlmann and E. Pretsch, *Chem. Rev.*, 1997, **97**, 3083.
2 R. W. Cattrall and H. Freiser, *Anal. Chem.*, 1971, **43**, 1905.
3 (*a*) R. W. Cattrall, D. W. Drew and I. C. Hamilton, *Anal. Chim. Acta*, 1975, **76**, 269; (*b*) P. C. Hauser, D. W. L. Chiang and G. A. Wright, *Anal. Chim. Acta*, 1995, **302**, 241; (*c*) D. Liu, R. K. Meruva, R. B. Brown and M. E. Meyerhoff, *Anal. Chim. Acta*, 1996, **321**, 173; (*d*) E. J. R. Sudhölter, P. D. van der Wal, M. Skowronska-Ptasinska, A. van den Berg, P. Bergveld and D. N. Reinhoudt, *Anal. Chim. Acta*, 1990, **230**, 59.
4 G. S. Cha, D. Liu, M. E. Meyerhoff, H. C. Cantor, A. R. Midgley, H. D. Goldberg and R. B. Brown, *Anal. Chem.*, 1991, **63**, 1666.
5 (*a*) A. Cadogan, Z. Gao, A. Lewenstam, A. Ivaska and D. Diamond, *Anal. Chem.*, 1992, **64**, 2496; (*b*) J. Bobacka, M. McCarrick, A. Lewenstam and A. Ivaska, *Analyst*, 1994, **119**, 185; (*c*) J. Bobacka, T. Lindfors, M. McCarrick, A. Ivaska and A. Lewenstam, *Anal. Chem.*, 1995, **67**, 3819.
6 P. Ferraboschi, A. Fiecchi, P. Grisenti, E. Santiello and S. Trave, *Synth. Commun.*, 1987, **17**, 1569.
7 J.-F. Nierengarten, V. Gramlich, F. Cardullo and F. Diederich, *Angew. Chem.*, 1996, **108**, 2242; J.-F. Nierengarten, T. Habicher, R. Kessinger, F. Cardullo, F. Diederich, V. Gramlich, J.-P. Gisselbrecht, C. Boudon and M. Gross, *Helv. Chim. Acta*, 1997, **80**, 2238; C. Bingel, *Chem. Ber.*, 1993, **126**, 1957.
8 H.-Y. Liu, S.-G. Liu and L. Echegoyen, *Chem. Commun.*, 1999, 1493.
9 S.-G. Liu, M. Cariou and A. Gorgues, *Tetrahedron Lett.*, 1998, **39**, 8663; P. Blanchard, M. Sallé, G. Duguay, M. Jubault and A. Gorgues, *Tetrahedron Lett.*, 1997, **33**, 2685.
10 K. Bandyopadhyay, H. Liu, S.-G. Liu and L. Echegoyen, *Chem. Commun.*, 2000, 141.
11 A. J. Bard and L. R. Faulkner, *Electrochemical Methods*, Wiley, New York, 1980.
12 The geometric area of the electrode was obtained from the slope of a linear plot of the cathodic current *vs.* (scan rate)$^{1/2}$ for the reversible reduction of $[Ru(NH_3)_6]^{3+/2+}$ taking 7.5×10^{-6} cm^2 s^{-1} as the diffusion coefficient in 0.1 M aqueous NaCl.
13 K. Chen, W. B. Cadwell and C. A. Mirkin, *J. Am. Chem. Soc.*, 1993, **115**, 1193; C. M. Yip and M. D. Ward, *Langmuir*, 1994, **10**, 549.
14 H. Imahori, T. Azuma, S. Ozawa, H. Yamada, K. Ushida, A. Ajavakom, H. Norieda and Y. Sakata, *Chem. Commun.*, 1999, 557.
15 Mean and standard deviations of 36 measurements (6 different positions of 3 samples from both sides).
16 W. B. Caldwell, K. Chen, C. A. Mirkin and S. J. Babinec, *Langmuir*, 1993, **9**, 1945; Y. S. Shon, K. F. Kelly, N. J. Halas and T. R. Lee, *Langmuir*, 1999, **15**, 5329; C. D. Bain, E. B. Troughton, Y. T. Tao, J. Evall, G. M. Whitesides and R. G. Nuzzo, *J. Am. Chem. Soc.*, 1989, **111**, 321.
17 Composition of the ISE membrane: valinomycin (10 mg), potassium tetrakis[3,5-bis(trifluoromethyl)phenyl]borate (4.1 mg), tetradodecylammonium tetrakis(4-chlorophenyl)borate (11.5 mg), bis(2-ethylhexyl) sebacate (330.2 mg), Tecoflex® (661.7 mg). A membrane of 60 μm thickness was obtained by casting 2.5 mg of these components dissolved in 50 μL tetrahydrofuran. A Ag/AgCl reference electrode was used with a 1 M LiOAc bridge electrolyte.
18 E. Lindner, V. V. Cosofret, S. Ufer, R. P. Buck, W. J. Kao, M. R. Neuman and J. M. Anderson, *J. Biomed. Mater. Res.*, 1994, **28**, 591.

Communication a909532b

cis-Trihydrogen cyclotriphosphazenates—acidic anions in strongly basic media

Gavin T. Lawson, Frederic Rivals, Mathieu Tascher, Chacko Jacob, Jamie F. Bickley and Alexander Steiner*

Department of Chemistry, University of Liverpool, Crown Street, Liverpool, UK L69 7ZD.
E-mail: A.Steiner@liv.ac.uk

Received (in Cambridge) 10th November 1999, Accepted 26th January 2000

Exclusively *cis*-protonation occurs at axial N-atoms of chair shaped P_3N_9 ring cores in the protolysis of the lithium salt of hexaanionic cyclotriphosphazenate $[(CyN)_6P_3N_3]^{6-}$ with three equivalents of butan-1-ol and *cis*-deprotonation takes place at the hexaprotic cyclotriphosphazene $(PhNH)_6P_3N_3$ with three equivalents of Bu^nLi, respectively, yielding both times lithium salts of *cis*-trihydrogen cyclotriphosphazenates $[(RNH)_3(RN)_3P_3N_3]^{3-}$.

The formal replacement of oxy and hydroxy units (=O, –OH) by isoelectronic imino and amino groups (=NR, –NHR), respectively, has led to novel compounds with unusual properties, due to both the increased electron donating capability of the nitrogen centre and the steric demand of the lipophilic organic substituent.[1] Imino analogues of the classic oxy-anions $[SO_3]^{2-}$,[2] $[SO_4]^{2-}$,[3] $[PO_4]^{3-}$ [4] and the kinetically unstable $[PO_3]^-$ [5] exist as molecular aggregates and are highly soluble in aprotic organic solvents. However, little is known about multistep protonation pathways between corresponding acid–base pairs. Recently, we have discovered that cyclophosphazenes carrying RNH groups act as multiprotic acids in the presence of strong bases yielding multianionic phosphazenates, a novel class of highly charged ligand systems.[6] The hexaprotic cyclotriphosphazene $(CyNH)_6P_3N_3$ **1a** is fully deprotonated by Bu^nLi generating the lithium salt of the hexaanionic cyclotriphosphazenate $[(CyN)_6P_3N_3]^{6-}$ **3a** which is highly soluble in non-polar aprotic solvents.[6a] Its central P_3N_9 core is electronically related to the cyclotrisilicate ion $[Si_3O_9]^{6-}$. We have now revealed protonation and deprotonation pathways between hexaprotic phosphazenes and hexaanionic phosphazenates by monitoring reactions using ^{31}P NMR spectroscopy and determining crystal structures of trianionic intermediates.

Stepwise addition of Bu^nLi to a solution of **1a** (14.9 ppm) in thf leads to a complex signal pattern in the ^{31}P NMR spectrum (Fig. 1) which finally gives a single peak at 25.3 ppm due to the formation of fully deprotonated **3a**. However, stepwise protolysis of **3a** with Bu^nOH gives a single peak at 16.2 ppm after addition of three equivalents of Bu^nOH indicating the existence of the trianionic intermediate $[(CyNH)_3(CyN)_3P_3N_3]^{3-}$ **2a**. In contrast, the hexaanilino derivative $(PhNH)_6P_3N_3$ **1b** (3.2 ppm) gives directly $[(PhNH)_3(PhN)_3P_3N_3]^{3-}$ **2b** upon addition of three equivalents of Bu^nLi as indicated by the appearance of a single peak at 5.0 ppm. Addition of six equivalents to **1b** results in one signal at 16.2 ppm which can be attributed to hexaanionic $[(PhN)_6P_3N_3]^{6-}$ **3b**. In both cases tri- and hexa-anionic species are levelled by excess of Bu^nOH yielding **1** and exist only in aprotic non-acidic media or very weakly protic solvents such as cyclohexylamine.

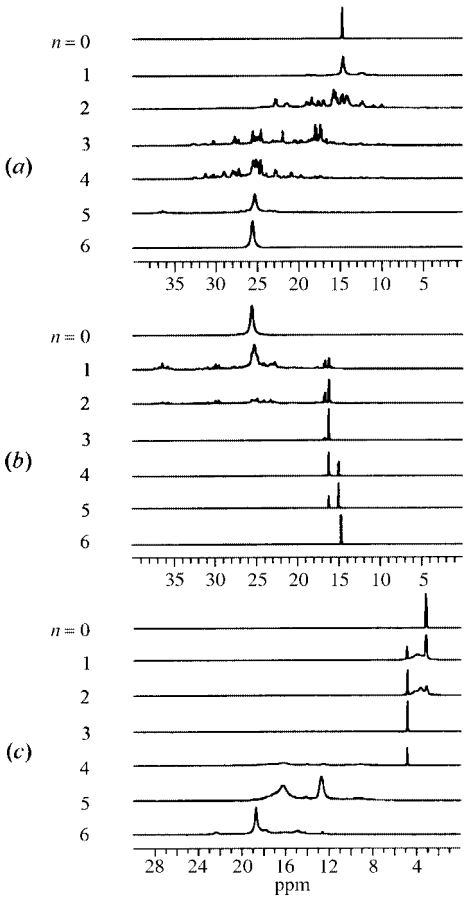

Fig. 1 ^{31}P NMR spectra (ppm) (161 MHz, thf, 25 °C) of stepwise reactions (a) **1a** + *n* Bu^nLi, (b) **3a** + *n* Bu^nOH and (c) **1b** + *n* Bu^nLi.

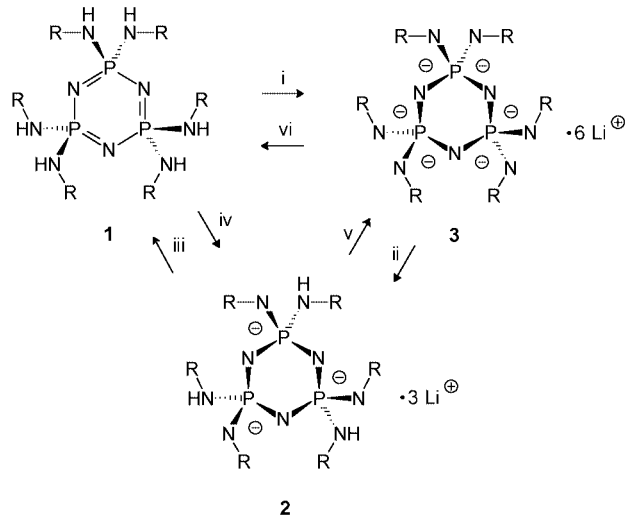

Scheme 1 *Reagents and conditions*: for **a** (R = Cy): i, Bu^nLi (6 equiv.), thf; ii, Bu^nOH (3 equiv.); iii, Bu^nOH (3 equiv.); for **b** (R = Ph): iv, Bu^nLi (3 equiv.), thf; v, Bu^nLi (3 equiv.), thf.

The X-ray structure† of **2a** reveals that exclusively axial N-atoms at the chair shaped P_3N_3 ring have been protonated (Fig. 2). The dimeric complex of **2a** is closely related to that of hexaanionic **3a** containing a centrally arranged polyhedral cage comprising six lithium cations which are encapsulated by two trianions. Each lithium cation is chelated by a bidentate N(eq)–P–N(ring) site of one of the anions and additionally coordinated by an equatorial N-atom of the other anion. The geometry of the central P_3N_9 core in **2a** is midway between those observed in **1a**

DOI: 10.1039/a908954c

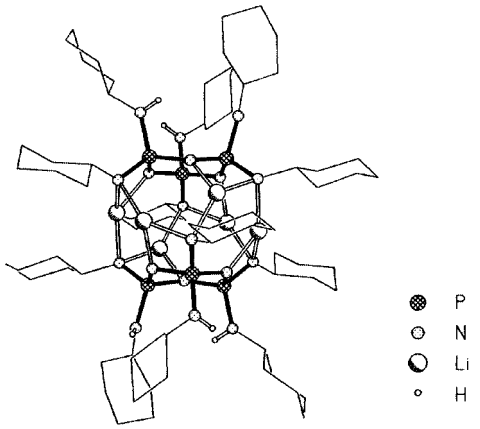

Fig. 2 Crystal structure of **2a**. Average bond lengths (Å) and angles (°): P–N(ring) 1.635, P–N(eq) 1.614, P–N(ax) 1.665, Li–N(ring) 1.99, Li–N(eq) 2.04, Li–N(eq) of the other trianion 2.03, N(ring)–P–N(ring) 112.3, N(eq)–P–N(ax) 111.3, P–N(ring)–P 121.9, av. P_3N_3 ring torsion = 33.2°.

and **3a**: torsion angles within the P_3N_3 ring show that the degree of ring puckering increases in the order **1a** (av. 3.6° ~planar), **2a** (av. 33.2°) and **3a** (av. 43.7°). The P–N ring stretching frequency in the IR-spectra undergoes a considerable red shift from **1a** (1194 cm^{-1}), **2a** (1095 cm^{-1}) to **3a** (1031 cm^{-1}) suggesting a decrease in bond order, also shown by the increase in P–N(ring) bond lengths from 1.598 (**1a**), 1.635 (**2a**) to 1.660 Å (**3a**) and decrease in N–P–N(ring) angles [116.3° (**1a**), 112.3° (**2a**), 109.7° (**3a**)] causing puckering of the central six-membered ring. The difference in exocyclic P–N bond lengths in **2a** [P–N(eq) 1.614, P–NH(ax) 1.665 Å] indicates that multiple bond character is partly transferred from ring onto equatorial P–N bonds.

2b exists as the monomeric C_3-symmetric complex $[(thf)_6Li_3$ *cis*-$(PhNH)_3(PhN)_3P_3N_3]$ in the solid state. Each lithium cation is chelated by an N(eq)–P–N(ring) site of the ligand and in addition coordinated by two thf molecules. Structural parameters of the P_3N_9 core in **2b** resemble those in **2a** (Fig. 3) and

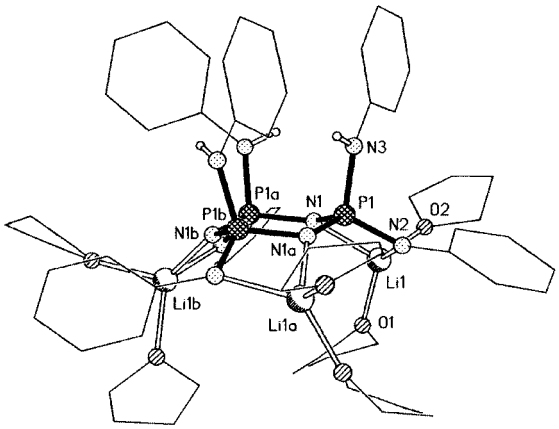

Fig. 3 Crystal structure of **2b**. Selected bond lengths (Å) and angles (°): P1–N1 1.621(3), P1–N1a 1.614(3), P1–N2 1.592(3), P1–N3 1.708(4), N1–Li1 2.054(8), N2–Li1 2.038(8); N1–P1–N1a 114.7(2), N2–P1–N3 112.3(2), P1–N1–P1a 119.8(2); P_3N_3 ring torsion = 32.3(4)°. Non-coordinated thf molecules have been omitted for clarity.

deprotonation also occurred in *cis* fashion at equatorial N-atoms. The difference in P–N bond lengths (P–N(ring) 1.617 (av.), P–N(eq) 1.592(3), P–NH(ax) = 1.708(4) Å) shows the same tendency as **2a**. The *cis*-arrangement in both structures can be rationalised as follows: charge repulsion within the P_3N_9 core forces the six-membered ring into a chair conformation, due to distribution of charge over ring and equatorial N atoms. This leaves axial sites protonated and provides three N(ring)–P–N(eq) chelates complexing the lithium cations on the opposite side of the trianion.

The successive protonation pattern of the above described $\{(RNH)_6P_3N_3/[(RNH)_3(RN)_3P_3N_3]^{3-}/[(RN)_6P_3N_3]^{6-}\}$ systems resembles that of mononuclear polyprotic oxy acids. It is, however, shifted towards the far basic region of the acidity scale and ion pairing seems to play a significant role. In contrast, condensed oxy acids lack corresponding acid–base reactions due to backbone cleavage in the presence of strong bases and related acidic oxy-anions such as $[H_3Si_3O_9]^{3-}$ are unknown. Another interesting feature of **2** is the site selective protonation pattern which is to our knowledge the first selective *cis*-trifunctionalisation of a cyclotriphosphazene.[7] This could lead to novel ligand systems equipped with a hexadentate coordination surface on one side and a non-polar surface on the other side of the molecule similar to calixarenes.

This work was supported by the EPSRC, the Royal Society and the Nuffield Foundation.

Notes and references

† Crystal data were collected on a Stoe-IPDS at 200 K using Mo-Kα radiation (λ = 0.71073 Å). Full-matrix least square refinements on F^2 using all data (SHELX97). *Crystal data*: **1a**: $C_{36}H_{72}N_9P_3$, M = 723.94, triclinic, space group $P\bar{1}$, a = 11.039(4), b = 12.001(4), c = 16.651(6) Å, α = 95.81(4), β = 91.38(4), γ = 108.77(3)°, V = 2074(1) Å^3, Z = 2, μ(Mo-Kα) = 0.180 mm^{-1}, $R1[I > 2\sigma(I)]$ = 0.061, $wR2$ (all 5408 data) = 0.145. **2a**: $C_{72}H_{138}Li_6N_{18}P_6{\cdot}C_7H_8$, M = 1575.60, monoclinic, space group $C2/c$, a = 25.993(5), b = 17.647(4), c = 20.639(4) Å, β = 109.81(3)°, V = 8920(3) Å^3, Z = 4, μ(Mo-Kα) = 0.172 mm^{-1}, $R1[I > 2\sigma(I)]$ = 0.068, $wR2$ (all 5676 data) = 0.210. **2b**: $C_{60}H_{81}Li_3N_9O_6P_3{\cdot}4C_4H_8O$, M = 1426.48, rhombohedral, space group $R\bar{3}c$, a = 21.620(3), c = 61.490(12) Å, V = 24891(7) Å^3, Z = 12, μ(Mo-Kα) = 0.129 mm^{-1}, $R1[I > 2\sigma(I)]$ = 0.059, $wR2$ (all 3619 data) = 0.166. Both coordinated and non-coordinated thf molecules in **2b** show disorder. CCDC 182/1530. See http//www.rsc.org/suppdata/cc/a9/a908954c/ for crystallographic files in .cif format.

1 D. E. Wigley, *Prog. Inorg. Chem.*, 1994, **42**, 239; C. C. Romão, F. E. Kühn and W. A. Herrmann, *Chem. Rev.*, 1997, **97**, 3197.
2 R. Fleischer, S. Freitag, F. Pauer and D. Stalke, *Angew. Chem., Int. Ed. Engl.*, 1996, **35**, 204; D. Ilge, D. S. Wright and D. Stalke, *Chem. Eur. J.*, 1998, **4**, 2275.
3 R. Fleischer, A. Rothenberger and D. Stalke, *Angew. Chem., Int. Ed. Engl.*, 1997, **36**, 1105; R. Fleischer, B. Walfort, A. Gbureck, P. Scholz, W. Kiefer and D. Stalke, *Chem. Eur. J.*, 1998, **4**, 2266.
4 P. R. Raithby, C. A. Russell, A. Steiner and D. S. Wright, *Angew. Chem., Int. Ed. Engl.*, 1997, **36**, 649.
5 E. Niecke, M. Frost, M. Nieger, V. von der Gönna, A. Ruban and W. W. Schoeller, *Angew. Chem., Int. Ed. Engl.*, 1994, **33**, 2111.
6 *(a)* A. Steiner and D. S. Wright, *Angew. Chem., Int. Ed. Engl.*, 1996, **35**, 636; *(b)* A. Steiner and D. S. Wright, *Chem. Commun.*, 1997, 283; *(c)* G. T. Lawson, C. Jacob and A. Steiner *Eur. J. Inorg. Chem.*, 1999, 1881.
7 C. W. Allen, *Chem. Rev.*, 1991, **91**, 119.

Communication a908954c

ChemComm

Synthesis and chloride binding properties of a Lewis acidic tetratin(IV) calixarene

Michael T. Blanda* and Michael A. Herren

Department of Chemistry, Southwest Texas State University, San Marcos, TX 78666, USA. E-mail: mb29@swt.edu

Received (in Columbia, MO, USA) 6th August 1999, Revised 9th December 1999, Accepted 9th December 1999

The Lewis acidic calix[4]arene with four covalently attached diphenylmonochlorotin(IV) centers was synthesized and its stannate complex with chloride was studied by ^{119}Sn NMR.

The supramolecular chemistry of anions including their detection, sequestration and transportation by calixarenes is an emerging area of research involving this versatile class of receptor molecules.[1] Compared to their positively charged counterparts, anions are inherently more difficult to bind due to their relatively larger ionic radii, higher solvation energies and diverse topologies.[2] Even with these formidable obstacles, calixarenes with incorporated hydrogen bond donors (*e.g.* ureas, amides and alcohols)[3] or electron-deficient metal centers (*e.g.* metallocenes and metal complexes)[4] have been synthesized which selectively bind different types of anions. Recently, there has been an increased interest in designing heteroditopic ligands for the simultaneous complexation of anions and cations suitable for extraction or transportation of metal salts. Since calixarenes can be functionalized on both their upper and lower rims, they are attractive molecular scaffolds for constructing heteroditopic hosts. Common design features of previously reported bifunctional calixarenes are hydrogen bond donors for anion complexation and crown ether or ester groups for cation recognition.[5] In this context, we report the synthesis and chloride-binding properties of a neutral, heteroditopic calixarene containing covalently attached Lewis acidic tin atoms for anion binding and ether oxygens for cation binding.

Incorporation of main group metals, particularly tin, represents a relatively unexplored area of calixarene chemistry. Two of the reported three examples are actually complexes containing mono- and ditin(II) centers wherein the calixarenes served as oxoligands.[6a,b] The lone example of a covalently attached tin(IV)-containing calixarene utilizes the tin atoms as the bridge between adjacent aromatic rings.[6c] The relatively longer C–Sn bonds allowed this compound to adopt a nearly planar geometry, thereby destroying the chalice-like structure.

The neutral Lewis acidic tetrastannacalix[4]arene host **4** was synthesized as outlined in Scheme 1.†‡ The principal starting material for the synthesis was the de-*tert*-butylated calix[4]arene **1**, which was readily obtained in multigram batches from literature procedures.[7] The dealkylated calixarene was used so that the Lewis acidic tin atoms could be appended to the upper rim. Alkylation of the lower rim of **1** with allyl bromide yielded the tetraallyl ether (85%), which when heated to 215 °C underwent a Claisen rearrangement that transferred the allyl groups to the upper rim (71%).[7]

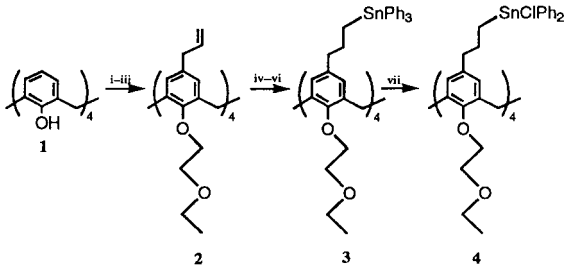

Scheme 1 *Reagents and conditions*: i, NaH, allyl bromide; ii, *N*,*N*-diethylaniline, heat; iii, NaH, 2-bromoethylethyl ether; iv, 9-BBN, H_2O_2, NaOH; v, Ph_3P, CCl_4; vi, $Ph_3SnSnPh_3$, Li; vii, HCl, CH_2Cl_2.

The cone conformation in the calix[4]arene framework of **2** was then fixed by appending ethoxyethyl groups on to the lower rim of the rearranged tetraallyltetrahydroxycalixarene (58%).[8] These ether groups were used to create a prototypical cation binding site for three reasons: (i) they were inert to the conditions of the subsequent reactions, (ii) their cation-binding properties were already known[9] and (iii) their conformational influence on the calixarene was predictable. Hydroboration of the double bonds in **2** with 9-BBN produced the tetraol (28%) which was converted to the corresponding tetrachloride by treatment with Ph_3P/CCl_4 (82%). The tetratin compound **3** was obtained by reacting the tetrachloride with Ph_3SnLi (40%).[10] The ^{119}Sn NMR spectrum of **3** contained only one signal at δ −101.27, which indicated that the four tins were equivalent in solution. Without the inductive effects of an electron withdrawing group, the tin atoms are not acidic enough to complex chloride ions, thus host **4** was obtained after careful treatment of **3** with anhydrous HCl at −78 °C (90%). The ^{119}Sn NMR spectrum of **4** also contained just a single signal at δ +14.75 which is within the range of typical Ph_2RSnCl species.[11a] What ultimately motivated us to employ the 3-carbon spacer group on the upper rim was the fact that the order of reactivity in this reaction is Ph > Bn > R.[11b] This meant that at least a 2-carbon spacer had to separate the tin atoms from the aromatic rings on which they were attached so that regiochemical control could be achieved in the chlorination reaction.

The chloride complexing properties of **4** were investigated in $CDCl_3$ by using ^{119}Sn NMR to observe the change from the tetravalent uncomplexed, stannane species to the pentavalent geometry of the stannate complex.[11b,12] Initial binding studies were restricted to chloride binding in order to eliminate complications introduced by ligand exchange at the tin atoms. The stoichiometry of the complex was determined by the method of continuous variation (Job plot).[13] This method is particularly useful for systems under rapid exchange conditions and can be adapted easily to ^{119}Sn NMR data.[12] The experiment required analysis of several solutions of **4** and Bu_4NCl prepared such that the mole fractions changed, but the concentration was constant. A plot of $(\Delta\delta X_H)$ *vs.* X_H, where $\Delta\delta = (\delta_{obs} - \delta_H)$, produced a parabolic curve that maximized at $X_H = 0.25$, indicating that each tin atom acted independently in the formation of a 4:1 (Cl:**4**) stannate complex. This result is not surprising, since the tin atoms are not structurally preorganized in a well-defined binding site that would facilitate cooperative binding.

Chloride association constants for **4** were determined by the Benesi–Hildebrand method as adapted to ^{119}Sn NMR data as shown in eqn. (1).[12]

$$(\delta_{obs} - \delta_H)^{-1} = (\delta_C - \delta_H)^{-1} + (K_{eq}(\delta_C - \delta_H))^{-1}[Cl^-] \quad (1)$$

The rate of exchange between the free host and complex was rapid on the NMR time scale, over the temperature range of −20 to +50 °C, as evidenced by a single weighted-average signal that was observed to shift from its initial value for the free host (δ +14.35) to higher field strengths upon the addition of

DOI: 10.1039/b000522n

chloride. For example, the signal for Cl^-/host = 4 was observed at δ −171.93 and continued to shift slightly further upfield with the addition of 8, 12, 16 and 20 equiv. of Cl^-. The total displacement ($\delta_{obs} - \delta_{host}$) was 207 ppm, with 90% displacement occurring at the addition 4 equiv. of Cl^-. This behavior is characteristic of weak binding, which was confirmed by the small K_{eq} values that ranged from a high of 52 M^{-1} at 253 K to a low of 13 M^{-1} at 328 K, with intermediate values of 25 and 33 M^{-1} at 295 and 273 K, respectively. Not only are these values similar to acyclic ditin model compounds,[14] they were anticipated since the tin atoms in **4** lack any preorganization and cooperative binding.

We are currently investigating the simultaneous ion pair complexing properties of **4** with NaCl as the metal salt. These studies are based on previous results that demonstrated that the ethoxyethyl ether groups were selective for sodium ions even though the percent extraction is relatively low.[9]

M. T. B. would like to thank the Robert A. Welch Foundation for financial support and Dr Norman Dean for assistance in acquisition of the ^{119}Sn NMR data.

Notes and references

† All new compounds were characterized by ^{1}H (400 MHz), ^{13}C (100 MHz) and ^{119}Sn (149 MHz) NMR spectroscopy and elemental analysis. Internal standards for NMR spectra were tetramethylsilane (^{1}H and ^{13}C) and tetramethyltin (^{119}Sn).

^{119}Sn Job plot experiments: Aliquots from 0.1 M stock $CDCl_3$ solutions of **4** and Bu_4NCl were mixed so that the mole fractions of each changed, but the total concentration of all species in solution remained constant. Spectra were acquired at 295 K (149 MHz) on samples containing mole fractions of **4** ranging from 0.1 to 0.8.

Binding constants: Equilibrium constants were determined by the Benesi–Hildebrand method, wherein a large excess of guest species was present relative to the amount of host. In these experiments, aliquots of a 1.72 M solution of Bu_4NCl were added to 0.780 ml (0.071 mmol) of a 0.091 M solution of **4** in 1 ml volumetric flasks. The solutions were mixed thoroughly and transferred to an NMR tube. Binding constants were determined at 328, 295, 273 and 253 K.

‡ *Selected data* for **2**: $\delta_C(CDCl_3)$ 15.29, 30.72, 39.36, 66.32, 69.63, 73.10, 114.82, 128.30, 133.11, 134.63, 138.22, 154.47. For tetraol: $\delta_C(CDCl_3)$ 15.25, 30.51, 31.22, 33.89, 61.86, 66.28, 69.61, 73.14, 127.87, 134.52, 135.11, 153.99. $\delta_C(CDCl_3)$ 15.28, 30.70, 31.91, 34.07, 44.17, 66.31, 69.65, 73.14, 128.12, 133.95, 134.68, 154.41. For **3**: $\delta_C(CDCl_3)$ 10.53, 15.31, 28.62, 30.83, 39.47, 66.29, 69.64, 72.93, 128.09, 128.43, 128.77, 134.34, 135.12, 137.04, 139.08, 154.32; δ_{Sn} −101.24. For **4**: $\delta_C(CDCl_3)$ 15.21, 16.89, 27.42, 30.69, 37.88, 38.79, 64.71, 68.64, 72.03, 127.69, 128.33, 128.77, 133.92, 134.86, 136.77, 138.59, 154.03. $\delta_{Sn}(CDCl_3)$ +14.75.

1 C. D. Gutsche, *Calixarenes, Monographs in Supramolecular Chemistry*, ed. J. F. Stoddart, Royal Society of Chemistry, Cambridge, 1989; C. D. Gutsche, *Calixarenes Revisited*, ed. J. F. Stoddart, Royal Society of Chemistry, Cambridge, 1998.
2 J. L. Atwood, K. T. Holmann and J. W. Steed, *Chem. Commun.*, 1996, 1401.
3 N. Pelizzi, A. Casnati and R. Ungaro, *Chem. Commun.*, 1998, 2607; B. R. Cameron and S. J. Loeb, *Chem. Commun.*, 1997, 573; J. Scheerder, M. Fochi, J. F. J. Engbersen and D. N. Reinhoudt, *J. Org. Chem.*, 1994, **59**, 7815.
4 P. A. Cale, Z. Chen, M. G. B. Drew, J. A. Heath and P. D. Beer, *Polyhedron*, 1998, **17**, 405; M. Staffilani, K. S. B. Hancock, J. W. Steed, K. T. Holman, J. L. Atwood, R. K. Juneja and R. S. Burkhalter, *J. Am. Chem. Soc.*, 1997, **119**, 6324.
5 P. Nicola, A. Casnati, A. Friggeri and R. Ungaro, *J. Chem. Soc., Perkin Trans. 2*, 1998, **6**, 1307; P. D. Beer and J. B. Cooper, *Chem. Commun.*, 1998, 129; D. M. Rudkevich, J. D. Mercer-Chalmers, W. Jerboom, R. Ungaro, F. de Jong and D. N. Reinhoudt, *J. Am. Chem. Soc.*, 1995, **117**, 6124.
6 (*a*) A. H. Cowley and B. G. McBurnett, *Chem. Commun.*, 1999, 17; (*b*) T. Hascall, A. L. Rheingold, I. Guzei and G. Parkin, *Chem. Commun.*, 1998, 101; (*c*) J. Hockeymeyer, B. Valentin, A. Castel, P. Riverie, J. Satge, C. J. Cardin and S. Teixeira, *Main Group Met. Chem.*, 1997, **20**, 775.
7 C. D. Claisen Gutsche, J. A. Levine and P. K. Sujeeth, *J. Org. Chem.*, 1985, **50**, 5802.
8 The cone conformations of calix[4]arenes **2**–**4** were characterized by an AB quartet for the $ArCH_2Ar$ protons in ^{1}H NMR spectra at δ 4.50–2.80 and a signal at δ 30–32 in the ^{13}C spectra (ref. 1).
9 A. Ikeda and S. Shinkai, *J. Am. Chem. Soc.*, 1994, **116**, 3102.
10 C. Tanborski, F. E. Ford and E. J. Soloski, *J. Am. Chem. Soc.*, 1963, **28**, 181.
11 (*a*) B. Wrackmeyer, *Annu. Rep. NMR Spectrosc.*, 1985, **16**, 115; (*b*) A. G. Davies, *Organotin Chemistry*, VCH, New York, 1997, p. 55.
12 In the NMR adaptation of the Benesi–Hildebrand method, the variable δ_{obs} is the observed chemical shift, δ_H is the chemical shift of the free host, δ_C is the chemical shift of the complex, [Cl] is the concentration of the free halide, and K_{eq} is the formation constant for the complex. One may plot $(\delta_{obs} - \delta_H)^{-1}$ *versus* $[Cl]^{-1}$ to obtain $(\delta_C - \delta_H)^{-1}$ as the intercept and $(K_{eq}(\delta_C - \delta_H))^{-1}$ as the slope. From these values, both δ_C and K_{eq} can be calculated. M. T. Blanda, J. H. Horner and M. Newcomb, *J. Org. Chem.*, 1989, **54**, 4626.
13 K. A. Connors, *Binding Constants*, Wiley, New York, 1987, pp. 24–28.
14 M. Newcomb, A. M. Madonik, M. T. Blanda and J. K. Judice, *Organometallics*, 1987, **6**, 145.

Communication b000522n

ChemComm

Synthesis of a hydrophilic phosphonic acid monomer for dental materials

Liyuan Mou,[a] Gurdial Singh*[a] and John W. Nicholson[b]

[a] *Department of Chemistry, University of Sunderland, Sunderland, UK SR1 3SD. E-mail: gurdial.singh@sunderland.ac.uk*

[b] *Dental Biomaterials Department, GKT Dental Institute, Kings College, University of London, London, UK SE1 9RT*

Received (in Liverpool, UK) 16th December 1999, Accepted 25th January 2000

A novel phosphonic acid monomer for use in dental composites was prepared by the base-catalysed rearrangement of the corresponding diethyl arylphosphonate.

In general dentistry may be described as a profession that is engaged with the repair and treatment of the teeth in order to restore proper function and good aesthetics. One of the major problems encountered in the treatment of teeth is dental caries, which is a preventable condition but one that is widespread and is possibly the most common disease in the world.[1] The onset of dental caries is due to metabolic activity by the bacteria of the plaque leading to production of acids from sugar in the diet, resulting in a localised attack on the enamel and dentine of the tooth.[2] The infection caused by caries can lead to other more serious conditions and can be fatal in the case of endocarditis,[3] and as a consequence dental repair can be seen as important. Repair materials have been the subject of considerable research, with recent emphasis on aesthetic materials that are capable of bonding to the cleaned tooth surface.

In the present work, we have sought to prepare an acid-functional monomer for use in dental restorative materials. There are existing filling materials that contain acid-functional monomers, but they are aliphatic, and the resulting materials have relatively poor mechanical properties.[4] We anticipate that aromatic monomers, such as **1**, will yield materials with

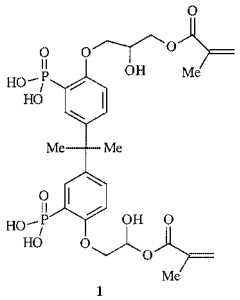

1

improved mechanical properties, because of the similarity with the aromatic dimethacrylate monomers currently used extensively in dentistry.

We also reasoned that the incorporation of a phosphonic function into monomer structures would result in increased biocompatability and adhesion to the tooth due to chelation with calcium ions in the tooth surface.

Here we report on the synthesis of the novel monomer **1** in which we have incorporated a phosphonic acid residue in both aromatic rings as well as incorporating a methylmethacrylate function that is capable of ionic or radical polymerisation.

At the outset we investigated the formation of the aryl phosphonate **6** employing Michaelis–Arbuzov reaction with the 2,2′-dibromobisphenol **2** and triethyl phosphite and with *O*-dimethoxy analogues under a wide range of conditions,[5] and all of these attempts proved to be unfruitful. As a result of these findings we explored the chemistry of the di-*O*-isopropylidene protected dibromoaryl ether **3** employing Michaelis–Arbuzov conditions and also the Hirao modification.[6] Once again these attempts at the introduction of the phosphonate group proved to

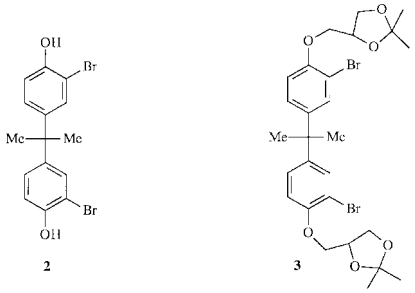

2 **3**

be unfruitful. The alternative strategy of lithio anion formation.[7] followed by subsequent trapping led to complex mixtures that contained a small amount of the desired product, as evidenced by NMR.

Our successful approach to the synthesis of **1** is detailed in reaction Scheme 1. Bisphenol **4** was treated with NaH and chlorodiethylphosphite and afforded the di-*O*-phosphate **5** in 50% yield.† An improved yield (75%) of **5** was obtained if the reaction was conducted using diethyl phosphite in the presence of CCl_4 and triethylamine.[8] With the diphosphate **5** in hand we examined its rearrangement to the C-phosphonate as similar processes had been reported by Melvin at Pfizer[9] for simpler systems.[10] Thus treatment of the diaryl phosphate **5** with a 2.5 fold excess of lithium diisopropylamide at −78 °C resulted in the clean rearrangement to the diarylphosphonate **6** in 86% isolated yield after recrystallisation. That the rearrangement had occurred to give **6** was strongly supported by its spectral properties, in particular the ^1H, ^{13}C and ^{31}P NMR were most

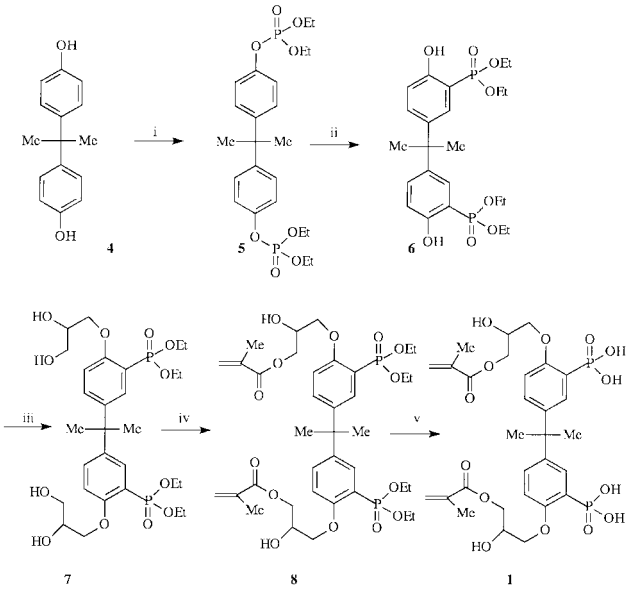

Scheme 1 *Reagents and conditions*: i, NEt_3 (2 equiv.), diethyl phosphite (2 equiv.), CCl_4, room temp., 30 h; ii, LDA (5 equiv.), THF, −78 °C, 1 h, then 3 h at room temp.; iii, glycidol (5 equiv.), cat. NEt_3, heat, 3 h; iv, Py, methacrylic anhydride (3.5 equiv.), cat. DMAP, room temp., 18 h; v, TMSBr (9 equiv.), room temp., 18 h, followed by aq. MeOH.

informative. In the ^{1}H NMR there was significant ^{1}H–^{31}P coupling to the *ortho* and *meta* protons (J_{P-H} 11.2 and 7.2 Hz) of the aromatic rings; this coupling was absent in **5**. In the ^{13}C NMR, coupling of ^{13}C–^{31}P was observed for the aromatic resonances (J_{C-P} 179.6, 13.5 Hz). The ^{31}P NMR also provided convincing support for the assignment, as the resonance due to the phosphonate was observed at δ −21.54 for **6** whilst in the phosphate **5** the resonance was found to be at δ −7.21.

This type of rearrangement reaction most likely proceeds *via ortho*-directed metallation of the aromatic ring followed by migration of the phosphorus to the cabanion centre, resulting in the formation of the phenolic phosphate. During the course of these studies we examined this rearrangement using ^{31}P NMR but we were unable to detect any intermediates during this process. We believe that this is the first example of this type of double phosphate rearrangement to provide the diphosphonate **6**.

Having the desired arylphosphonate **6** in hand alkylation of both the phenolic functions was accomplished with glycidol in the presence of triethylamine to afford **7** in 50% yield. Selective methacrylation of the primary hydroxy functions at both termini was accomplished with either methacroyl chloride in the presence of pyridine or with methacrylic anhydride in the presence of a catalytic amount of DMAP. The latter sequence was preferred as it gave rise to the desired product **8** in 50% yield as compared to 29% for the former reaction procedure. In both of these esterification reactions we observed the formation of doubly and singly esterifed products that were separated by column chromatography. The mono ester thus obtained could be converted to the diester on further treatment with either of the two acylating agents.

At this juncture it remained for us to selectively remove the ethyl ester protecting group of the phosphinates in **8**. We examined a range of procedures, including acid and base hydrolysis, and all of these methods proved to be unfruitful, with many resulting in C–O bond cleavage and removal of the methacroyl group. As a result of this we undertook model deprotection experiments with both the phosphonates **5** and **7** using trimethylsilyl bromide.[11] This treatment resulted in the formation of the respective phosphonic acids **9** and **10** as

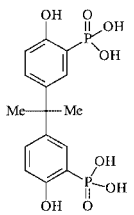

9

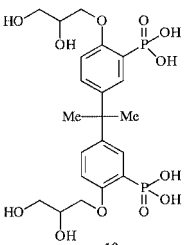

10

dicyclohexylammonium salts, after hydrolysis, in yields of 55 and 96%. As a result of these findings we used trimethylsilyl bromide followed by hydrolysis with aqueous methanol to undertake the removal of the phosphonate ester groups and gratifyingly this afforded the desired acid monomer **1** in 60%. Alternatively, it could be isolated as its dicyclohexylammonium salt.

In summary, we have successfully developed the synthesis of the phosphonic acids **1** employing a double phosphate rearrangement reaction in excellent overall yield.

Polymerisation studies of **1** will be reported elsewhere. To date preliminary biocompatability studies are showing promise and these are ongoing.

We thank the EPSRC for support of this work and for access to central facilities for high resolution mass spectrometric data at the University of Wales, Swansea.

Notes and references

† All new compounds gave satisfactory spectral, microanalytical and/or high resolution mass spectrometry. *Selected data* for **1**: δ_H(270 MHz, $CDCl_3$) 1.65 (s, 6H), 1.95 (s, 6H), 3.76–4.29 (m, 12H), 5.66 (m, 2H), 6.18 (s, 2H), 6.85 (br d, 2H, *J* 5.1), 7.28 (br d, 2H, *J* 8.5), 7.84 (br d, 2H, *J* 14.1); δ_P(109.25 MHz, $CDCl_3$) +18.48; δ_C(67.8 MHz, $CDCl_3$) 30.55, 41.83, 41.85, 64.62, 67.87, 70.92, 112.92 (J_{C-P} 10.9), 117.04 (J_{C-P} 189), 125.93, 131.62 (J_{C-P} 13.5), 132.35 (J_{C-P} 4.5), 135.84, 143.11 (J_{C-P} 21), 158.39 (J_{C-P} 3.6 Hz), 167.04; ν_{max}(thin film)/cm^{-1} 3324–2716, 1720, 1600, 1490, 1294, 1168, 941 (found: M^+ + H, 673.1840, $C_{29}H_{39}O_{14}P_2$ requires 673.1815; dicyclohexylammonium salt (FAB) found: M^+ + H, 1035, $C_{53}H_{85}N_2O_{14}P_2$ requires 1035). For **5**: δ_H(270 MHz, $CDCl_3$) 1.28 (t, 12H, *J* 7.2), 1.62 (s, 6H), 4.12 (q, 8H, *J* 7.2), 7.03–7.33 (m, 8H); δ_P(109.25 MHz, $CDCl_3$) −7.21; δ_C 15.98 (d, J_{C-P} 6.7), 30.81, 42.17, 64.43 (J_{C-P} 6.0), 119.31 (J_{C-P} 4.9), 127.96, 146.98 (J_{C-P} 1.3), 148.63 (J_{C-P} 7.1); ν_{max}(thin film)/cm^{-1} 3451, 3281, 1604, 1505, 1271, 1033, 967. For **6**: mp 93–94 °C; δ_H(270 MHz, $CDCl_3$) 1.28 (t, 12H, *J* 7.2), 1.62 (s, 6H), 4.10 (q, 8H, *J* 7.2), 6.86 (dd, 2H, *J* 9.5, 7.2), 7.20 (dd, 2H, *J* 11.2, 2.6), 7.23 (dd, 2H, *J* 9.5, 2.6); δ_P(109.25 MHz, $CDCl_3$) −21.54; δ_C(67.8 MHz, $CDCl_3$) 16.09 (d, J_{C-P} 6.2), 30.67, 41.65, 64.64 (J_{C-P} 4.7), 108.04 (J_{C-P} 179.6), 117.38 (J_{C-P} 13), 128.80 (J_{C-P} 7), 134.06 (J_{C-P} 2.1), 141.42 (J_{C-p} 12.7), 160.17 (J_{C-P} 7.2); ν_{max}(KBr)/cm^{-1} 3451, 3137, 1602, 1405, 1209, 1027, 979.

1 T. R. Pitt Ford, *The restoration of teeth*, Blackwell Scientific, Oxford, 1985.
2 J. W. Nicholson, *Educ. Chem.*, 1994, **31**, 12.
3 *A comprehensive guide to clinical dentistry*, ed. A. H. Rowel, Class, London, 1989, vol. 3.
4 K. Miyazaki, T. Horibe, J. M. Antoncucci, S. Takagi and L. C. Chow, *Dent. Mater.*, 1993, **9**, 41; J. W. Nicholson and M. Alsarhedd, *J. Oral Rehabil.*, 1998, **25**, 616.
5 P. Tavs and F. Korte, *Tetrahedron*, 1967, **23**, 4677; P. Tavs, *Chem. Ber.*, 1970, **103**, 2428.
6 T. Hirao and T. Masunaga, *Synthesis*, 1981, 56.
7 V. E. Baulin, V. Kh. Syundyukova and E. N. Tsvetkov, *Zh. Obsch. Khim.*, 1989, **59**, 62.
8 B. Dhawan and D. Redmore, *J. Org. Chem.*, 1984, **49**, 4018.
9 L. S. Melvin, *Tetrahedron Lett.*, 1981, **22**, 3375.
10 For the S-variant, see: S. Masson, J.-F. Saint-Clair and M. Saquet, *Synthesis*, 1993, 485.
11 G. A. Olah and S. C. Narang, *Tetrahedron*, 1982, **38**, 2225.

Communication a909877a

Enhanced regioselectivity of rhodium-catalysed alkene hydroboration in supercritical carbon dioxide

Charles A. G. Carter,[a] R. Thomas Baker,*[a] Steven P. Nolan[b] and William Tumas*[a]

[a] *Los Alamos Catalysis Initiative, Chemical Science and Technology Division, Los Alamos National Laboratory, MS J514, Los Alamos, NM 87545 USA. E-mail: weg@lanl.gov; tumas@lanl.gov*
[b] *Department of Chemistry, University of New Orleans, New Orleans, LA 70148 USA*

Received (in Cambridge, UK) 2nd December 1999, Accepted 26th January 2000

Catalysed alkene hydroboration proceeds in supercritical CO_2 with several rhodium(I) complexes using tunable fluorinated ligands and shows higher regioselectivity relative to tetrahydrofuran or perfluoromethylcyclohexane.

The power of homogeneous transition metal catalysis rests in chemists' ability to fine-tune the steric and electronic properties of the metal coordination environment and to optimize activity and selectivity by judicious choice of the reaction medium.[1] While a number of studies have employed fluorinated ligands [2–4] to conduct a variety of metal-catalysed reactions[5] in environmentally benign supercritical carbon dioxide ($scCO_2$), little work has been reported on catalyst tunability. Recently reported phosphines PR_2R_F[3,6,7] and phosphinites $PR_2(OR_F)$[6,7] (R_F = $CH_2CH_2C_6F_{13}$) are easily prepared and offer the ability not only to enhance catalyst solubility, but to control the stereoelectronic environment of catalysts in $scCO_2$. We chose to investigate Rh^I-catalysed alkene hydroboration[8,9] due to the importance of boronate ester products in synthetic organic chemistry, medicinal chemistry, materials science and molecular recognition. The catalyzed reaction exhibits higher rates and complementary regioselectivity compared to the uncatalysed reaction, and efficient chirality transfer has been demonstrated in the asymmetric variant.[9] We now report the first demonstration of catalysed alkene hydroboration in $scCO_2$, the ability to tune both regio- and chemo-selectivity, and the discovery of much higher selectivity in $scCO_2$ compared to perfluoromethylcyclohexane ($CF_3C_6F_{11}$).

Catalyzed hydroboration of styrene derivatives with catecholatoborane (HBcat) was carried out in $scCO_2$ at 40 °C and 2800 psi for 5 h with a rhodium catalyst precursor and added phosphorus ligands using magnetically-stirred, high-pressure reactors with sapphire view windows that have been described elsewhere.[10] Addition of HBcat to vinylanisole using only the hexafluoroacetylacetonate (hfacac) rhodium complex (hfacac)$Rh(coe)_2$ **1** (coe = cyclooctene) as catalyst precursor[2] led to a homogeneous solution and, after 5 h, high conversion to a mixture of alkylboronate esters **A** and **B**, alkenylboronate ester **C**, and 4-ethylanisole **D** (Scheme 1, Table 1). Products **C** and **D** result from a competing dehydrogenative borylation pathway which is favoured by phosphine-free rhodium catalysts.[11] Addition of triphenylphosphine to **1** gave turbid solutions due to poor ligand and/or catalyst solubility in $scCO_2$. The fluorinated ligands, including **5**–**8** led to homogeneous solutions demonstrating that a single fluorinated substituent is sufficient to impart high solubility in $scCO_2$. As shown in Table 1, added ligands dramatically influence the regioselectivity of hydroboration. Triphenylphosphine, its 3,5-bis(trifluoromethyl)phenyl analog, and $P(R_F)_3$ all greatly increased hydroboration regiochemistry, but chemoselectivity was improved only marginally. Alkylboronate ester **A** was formed exclusively with cyclohexyl-substituted phosphine **8** (L:Rh ratio = 2:1), demonstrating the ability to control regioselectivity and chemoselectivity by tuning the solubility and stereoelectronic properties of ligands and metal catalysts in $scCO_2$.

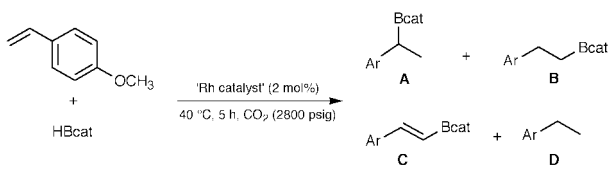

Scheme 1

Table 1 Ligand effects on catalysed hydroboration of vinylanisole in $scCO_2$[a]

Entry	L	Conversion (%)	Selectivity (%) A	B	C	D
1	No added ligand	89	14	14	31	41
2	PPh_3 (**2**)	92	71	13	13	3
3	$P[3,5\text{-}(CF_3)_2C_6H_3]_3$ (**3**)	94	75	—	19	6
4	$P(R_F)_3$ (**4**)[b]	94	82	—	17	1
5	Ph_2POR_F (**5**)[b]	81	88	—	12	—
6	Cy_2POR_F (**6**)[b,c]	89	90	—	—	—
7	Ph_2PR_F (**7**)[b]	88	89	—	11	—
8	Cy_2PR_F (**8**)[b]	100	100	—	—	—

[a] (hfacac)$Rh(coe)_2$ **1** (0.02 mmol), ligand L (0.04 mmol) and substrate (1.0 mmol). Conversion and product selectivity were determined by ^1H and ^{11}B NMR using hexamethyldisiloxane standard. [b] R_F = $CH_2CH_2C_6F_{13}$. [c] Some polymeric material was observed in this reaction.

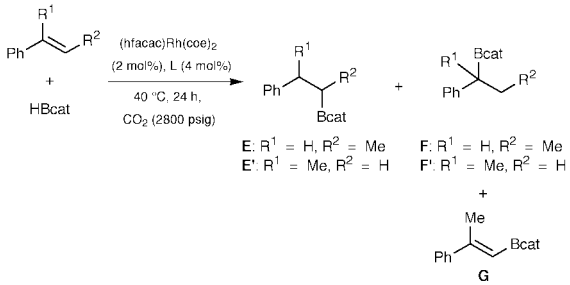

Scheme 2

In several studies of rhodium-catalyzed hydroboration of disubstituted alkenes, such as α- and β-methylstyrenes, monodentate ligands have been found to give poor selectivity to the desired Markovnikov addition product.[8] While conversions were low in some cases, the ability to control regiochemistry through tunable fluorinated ligands in $scCO_2$ is further illustrated in Scheme 2 and Table 2. For β-methylstyrene, the tris[3,5-bis(trifluoromethyl)phenyl]phosphine **3** and cyclohexyl-substituted ligands **6, 8** gave the highest activity, but with only fair regiocontrol. Ligands **4**, **5** and **7** gave alkylboronate ester **E** exclusively. The advantage of ligand tunability is also demonstrated for the reaction of α-methylstyrene and HBcat, as changing from cyclohexyl **6** to phenylphosphinite ligand **5** yields only the Markovnikov addition product **E′**.

Solvent effects play an important role in determining the selectivity of catalytic hydroboration reactions.[12] Gladysz and

DOI: 10.1039/a909636a

Table 2 Hydroboration of α- and β-methylstyrene[a] in $scCO_2$

Entry	L	Conversion (selectivity) (%) **E**:**F**:**G**	**E′**:**F′**
1	$P[3,5\text{-}(CF_3)_2C_6H_3]_3$ (**3**)	100 (0:24:76)	90 (78:22)
2	$P(R_F)_3$ (**4**)	56 (55:45:0)	13 (100:0)
3	Ph_2POR_F (**5**)	13 (100:0:0)	8 (100:0)
4	Cy_2POR_F (**6**)	3 (50:50:0)	71 (89:11)
5	Ph_2PR_F (**7**)	19 (96:4:0)	16 (100:0)
6	Cy_2PR_F (**8**)	38 (36:64:0)	77 (71:29)

[a] Conversion and selectivity were determined after 24 h.

Table 3 Effect of solvent on the regioselectivity of vinylanisole hydroboration[a]

Entry	L	Solvent	Conversion (%)	Selectivity (%) **A**	**B**	**C**	**D**
1	$P(R_F)_3$ (**4**)	THF	82	66	15	13	6
		$CF_3C_6F_{11}$	84	57	16	19	8
		$scCO_2$	94	82	—	17	1
2	Ph_2POR_F (**5**)	THF	100	52	21	16	11
		$CF_3C_6F_{11}$	98	37	23	23	17
		$scCO_2$	81	88	—	12	—
3	Cy_2POR_F (**6**)	THF	94	20	37	35	8
		$CF_3C_6F_{11}$	89	24	26	37	13
		$scCO_2$[b]	89	90	—	—	—
4	Ph_2PR_F (**7**)	THF	93	84	—	12	4
		$CF_3C_6F_{11}$	90	80	4	12	4
		$scCO_2$	88	89	—	11	—
5	Cy_2PR_F (**8**)	THF	100	32	34	17	17
		$CF_3C_6F_{11}$	91	25	41	17	17
		$scCO_2$	100	100	—	—	—

[a] Reactions in organic solvents were run in NMR tubes using 0.002 mmol **1**, 0.004 mmol ligand, and 0.1 mmol vinylanisole. Conversion and selectivity were determined by ^1H NMR. [b] Some polymeric material was observed in this reaction.

Horvath[13] reported an elegant study of alkene hydroboration in fluorous biphasic media using $RhCl[P(R_F)_3]_3$ derived from **4**; however, the regioselectivity for styrene derivatives was low. Comparing the reaction of vinylanisole and HBcat in $scCO_2$ to that in perfluoromethylcyclohexane led to some surprising results. Catalyst precursor **1** and ligand **4** showed significantly greater regiocontrol in $scCO_2$ (Table 3, entry 1). This trend held for ligands **5**–**8** and was particularly striking for Cy_2PR_F (entry 5) which afforded a single product in $scCO_2$. Remarkably, the selectivity in $scCO_2$ for **4**–**8** was also considerably higher than that observed in THF. Ligand **4** is not soluble in THF; however, partially fluorinated ligands **5**–**8** and their rhodium complexes are fully soluble under the reaction conditions. In THF, product selectivity using the nonfluorinated analog of ligand **8** (*i.e.* $Cy_2PC_8H_{17}$) was found to be similar to that observed for ligand **8**, confirming the insulating effect of the two methylene spacers in the R_F group.† There are several reports[4,5,14,15] of enhanced selectivity of catalysed reactions in $scCO_2$ compared to conventional organic solvents. Except for a few cases where density is controlled through pressure changes,[16] we are unaware of any examples presenting such a dramatic effect as that shown here. The origin of the higher selectivities for hydroborations is not clear. Since ligand-free rhodium complexes result in poor hydroboration selectivity,[11] stability and lability of the catalysts (*i.e.* keeping the ligand on the metal), which are likely solvent dependent, may play an important role. It is also possible that a Rh–η^3-benzyl intermediate[17] that would lead to **A** could be stabilized in $scCO_2$ relative to the η^1-regioisomer that would yield **B**.

In summary, we have demonstrated that catalysed alkene hydroboration can proceed in supercritical CO_2 without any difficulty from B–H reactivity with the solvent. Regiocontrol can be achieved using tunable ligands of the form R_2PR_F and R_2POR_F. Furthermore, significantly higher regioselectivities can be obtained for these ligands in $scCO_2$, relative to fluorocarbons and even THF. Given further advancements in catalyst separations and recovery in $scCO_2$,[18] catalysis in this medium can complement fluorous phase approaches. We are currently assessing the effects of pressure (solvent density) on selectivity, monitoring reactive species by *in situ* NMR spectroscopy, and studying stoichiometric reactions of isolable 16 electron rhodium–boryl complexes.[19]

This work was supported as part of the Los Alamos Catalysis Initiative by the Department of Energy through Laboratory Directed Research and Development (LDRD) funding and by the Department of Energy (DE-FG02-98ER45732) for work performed at UNO. We would like to thank Drs Chris Haar and Dale Smith (UNO) for providing ligands and Professor John Gladysz for a generous donation of $P(CH_2CH_2C_6F_{13})_3$.

Notes and references

† Triphenylphosphine and catalyst precursor **1** (3:1) or Wilkinson's catalyst (ref. 9) lead to high selectivity > 95% to **A** in THF; however, these catalysts are not effective for methylstyrenes (ref. 19).

1 B. Cornils and W. A. Herrmann, *Applied Homogeneous Catalysis with Organometallic Compounds*, VCH, Weinheim, 1996.
2 D. Koch and W. Leitner, *J. Am. Chem. Soc.*, 1998, **120**, 13 398.
3 M. A. Carroll and A. B. Holmes, *Chem. Commun.*, 1998, 1395.
4 D. K. Morita, D. R. Pesiri, S. A. David, W. H. Glaze and W. Tumas, *Chem. Commun.*, 1998, 1397.
5 P. G. Jessop, T. Ikariya and R. Noyori, *Chem. Rev.*, 1999, **99**, 475.
6 C. M. Haar, J. Huang and S. P. Nolan, *Organometallics*, 1998, **17**, 5018; D. C. Smith, Jr., E. D. Stevens and S. P. Nolan, *Inorg. Chem.*, 1999, **38**, 5277.
7 P. Bhattacharyya, D. Gudmunsen, E. G. Hope, R. D. W. Kemmitt, D. R. Paige and A. M. Stuart, *J. Chem. Soc., Perkin Trans.1*, 1997, 3609.
8 S. A. Westcott, H. P. Blom, T. B. Marder and R. T. Baker, *J. Am. Chem. Soc.*, 1992, **114**, 8863.
9 I. Beletskaya and A. Pelter, *Tetrahedron*, 1997, **53**, 4957.
10 S. Buelow, P. Dell'Orco, D. K. Morita, D. R. Pesiri, E. Birnbaum, S. L. Borkowsky, G. H. Brown, S. Feng, L. Luan, D. Morgenstern and W. Tumas, in *Frontiers in Benign Chemical Synthesis and Processing*, ed. P. Anastas and T. C. Williamson, Oxford University Press, 1998, p. 264.
11 J. M. Brown and G. C. Lloyd-Jones, *J. Chem. Soc., Chem. Commun.*, 1992, 710.
12 T. M. Cameron, R. T. Baker and S. A. Westcott, *Chem. Commun.*, 1998, 2395.
13 J. J. J. Juliette, D. Rutherford, I. T. Horváth and J. A. Gladysz, *J. Am. Chem. Soc.*, 1999, **121**, 2696.
14 G. Francio and W. Leitner, *Chem. Commun.*, 1999, 1663.
15 M. J. Burk, S. Feng, M. F. Gross and W. Tumas, *J. Am. Chem. Soc.*, 1995, **117**, 8277.
16 R. S. Oakes, T. J. Heppenstall, N. Shezad, A. A. Clifford and C. M. Rayner, *Chem. Commun.*, 1999, 1459; R. S. Oakes, A. A. Clifford, K. D. Bartle, M. T. Pett and C. M. Rayner, *Chem. Commun.*, 1999, 247.
17 T. Hayashi, Y. Matsumoto and Y. Ito, *Tetrahedron: Asymmetry*, 1991, **2**, 601.
18 S. Kainz, A. Brinkmann, W. Leitner and A. Pfaltz, *J. Am. Chem. Soc.*, 1999, **121**, 6421.
19 K. Burgess, W. A. van der Donk, S. A. Westcott, T. B. Marder, R. T. Baker and J. C. Calabrese, *J. Am. Chem. Soc.*, 1992, **114**, 9350.

Communication a909636a

Design of a nucleobase-conjugated peptide that recognizes HIV-1 RRE IIB RNA with high affinity and specificity

Tsuyoshi Takahashi,[a] Keita Hamasaki,[a] Ichiro Kumagai,[a] Akihiko Ueno[a] and Hisakazu Mihara*[ab]

[a] *Department of Bioengineering, Faculty of Bioscience and Biotechnology, Tokyo Institute of Technology, Nagatsuta, Yokohama 226-8501, Japan. E-mail: hmihara@bio.titech.ac.jp*

[b] *Form and Function, PRESTO, Japan Science and Technology Corporation, Tokyo Institute of Technology, Nagatsuta, Yokohama 226-8501, Japan*

Received (in Cambridge) 6th December 1999, Accepted 26th January 2000

A nucleobase-conjugated peptide, derived from HIV-1 Rev, was designed and synthesized, and the peptide which contained the cytosine moiety at the L-α-amino acid side chain bound RRE IIB RNA with high affinity and high specificity.

RNA–protein interactions play important roles in nature. Many cellular functions, including transcription, RNA splicing and translation, depend on the specific interaction of proteins and RNA. RNA-binding proteins seldom target fully double-stranded tracts for recognition, but interact with secondary structural domains such as hairpin loops, internal loops, and bulges of RNA.[1] In most cases, an RNA-binding domain of a protein forms a suitable conformation such as an α-helix or a β-strand to recognize a structured RNA, and amino acids orientated exactly in the protein structure make specific contacts to the RNA backbone and bases, resulting in high affinity and high specificity in the RNA binding. The study of the design and synthesis of novel molecules that recognize the structure of RNA might lead to drugs targeting RNA.

Peptide nucleic acid (PNA) is a DNA mimic with the nucleobases on a pseudopeptide backbone composed of *N*-(2-aminoethyl)glycine units.[2] A PNA molecule has the ability to efficiently and sequence-specifically bind both single-stranded DNA and RNA as well as double-stranded DNA. However, a simple PNA molecule itself may not recognize highly structured RNA with high specificity, because PNA alone would not have the ability to form the various conformations that proteins or peptides do. We have attempted to design peptides containing nucleobases that combine the advantages of peptides (formation of rigid structure such as α-helices) and nucleobases (specific recognition of a base in RNA). For this purpose, we have utilized an artificial L-α-amino acid, with a nucleobase at the side chain, in peptides for keeping the peptide conformation.

In order to demonstrate the applicability of a nucleobase amino acid (NBA) in peptides, we have chosen the regulatory protein of virion expression (Rev) of human immunodeficiency virus type-1 (HIV-1)[3–6] from among the enormous range of examples of proteins which bind RNA specifically. The Rev protein binds the corresponding response region of HIV-1 mRNA (RRE), and this protein–RNA interaction plays a key role in HIV-1 virus replication. The arginine-rich domain (34–50) of the Rev protein binds specifically the stem-loop IIB region of RRE RNA (Fig. 1) by forming an α-helix conformation.[7] The α-helix potential of the $Rev_{34–50}$ peptide affects the binding affinity and specificity of the peptide to RRE IIB RNA.[7,8] Moreover, it has been proposed that the Gln36 residue in the $Rev_{34–50}$ peptide is placed close to the guanine-48 base in the internal loop region of the RRE IIB RNA by NMR structural analyses.[9]

On the basis of these informations, we designed and synthesized the nucleobase-conjugated peptide, $Q36C_{NBA}$, in which L-α-amino γ-cytosine butanoic acid (cytosine nucleobase amino acid: C_{NBA}) was introduced instead of Gln36 in $Rev_{34–50}$ (Fig. 1), and examined the effect of the introduction of the C_{NBA} unit on the peptide conformation and the RNA-binding affinity. It was expected that the cytosine base in $Q36C_{NBA}$ could interact with the guanine-48 base in RRE IIB RNA and that the interaction may lead to an increase in affinity and specificity of the peptide for the RNA. Furthermore, the chiral C_{NBA} unit possibly gives a rigid conformation in the peptide. For the elucidation of the structural importance of $Q36C_{NBA}$, $Q36C_{PNA}$, in which Gln36 and Ala37 were replaced by Nielsen type cytosine PNA (C_{PNA}),[2] was also designed (Fig. 1). The two amino acids were replaced by C_{PNA}, because a PNA monomer has the length equivalent of two amino acids in the main chain. Q36A and Q36GG were used to evaluate the effect of introduction of the cytosine moiety in $Q36C_{NBA}$ and $Q36C_{PNA}$, respectively (Fig. 1). To increase the stability of the α-helix structure, the N-terminal amino and C-terminal carboxy groups of the peptides were succinylated and amidated, respectively.[7,8] To introduce the C_{NBA} unit in the peptide, (2*S*)-4-(*N*^{4}-benzyloxycarbonylcytosin-1-yl)-2-(fluoren-9-ylmethoxycarbonyl)aminobutanoic acid [Fmoc-C_{NBA}(Z)-OH] was synthesized according to the method in ref. 10 with some modifications. Peptides were synthesized by the solid phase method using an Fmoc-strategy[11] and purified by HPLC with high purity (> 98% on analytical HPLC). The peptides $Q36C_{NBA}$ and $Q36C_{PNA}$ gave a molecular ion peak at *m/z* 2602.3 [$(M + H)^+$] (calc. = 2603.9) and 2588.6 [$(M + H)^+$] (calc. = 2589.9), respectively, by matrix assisted laser desorption ionization time-of-flight mass spectrometry. RRE IIB RNA was prepared by *in vitro* transcription from a synthetic DNA template using T7 RNA polymerase and purified by polyacrylamide gel electrophoresis.[12]

Circular dichroism studies revealed that none of the peptides including $Rev_{34–50}$ had a rigid structure in aqueous buffer (pH

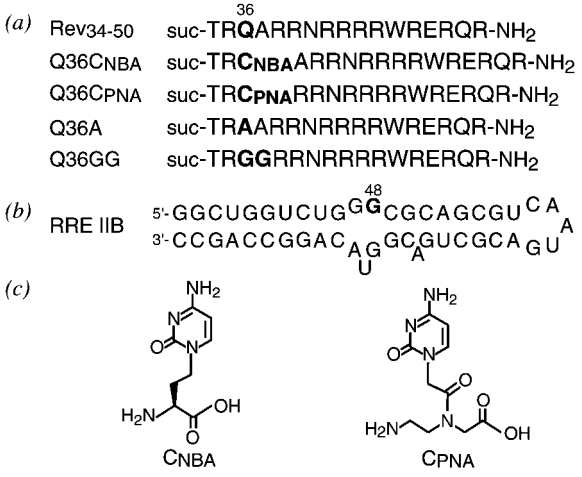

Fig. 1 (*a*) Amino acid sequences of $Rev_{34–50}$ and designed peptides; (*b*) the secondary structure of RRE IIB RNA; (*c*) structures of C_{NBA} and C_{PNA}.

DOI: 10.1039/a909579i

Table 1 α-Helix contents of the peptides in TFE solution, and dissociation constants (K_d) of the peptides with RRE IIB RNA

Peptide	α-Helicity (%)[a]	$K_d/10^{-9}$ mol dm^{-3}
$Rev_{34–50}$	59	3.4 ± 0.3
$Q36C_{NBA}$	60	1.7 ± 0.1
$Q36C_{PNA}$	41	10.9 ± 0.7
Q36A	76	3.4 ± 0.1
Q36GG	52	9.9 ± 1.1

[a] α-Helix contents were estimated from $[\theta]_{222}$ according to the method of ref 14.

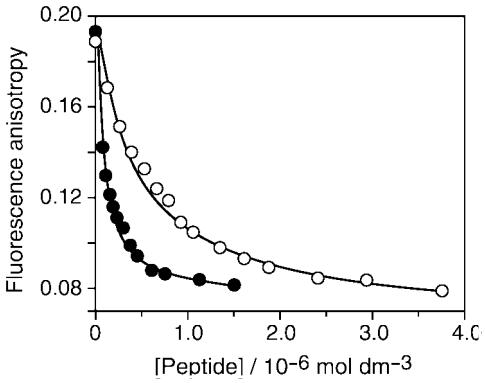

Fig. 2 Fluorescence anisotropy of Rhod-Rev containing RRE IIB RNA as a function of $Q36C_{NBA}$ (●) and $Q36C_{PNA}$ (○) concentration in 1.0×10^{-2} mol dm^{-3} Tris·HCl buffer (pH 7.5) containing 1.0×10^{-1} mol dm^{-3} KCl, 1.0×10^{-3} mol dm^{-3} $MgCl_2$, and 5.0×10^{-4} mol dm^{-3} EDTA at 25 °C. [Rhod-Rev] = 1.0×10^{-8} mol dm^{-3} and [RRE IIB] = 2.5×10^{-8} mol dm^{-3}.

7.5). On the contrary, in TFE, which is known to be an α-helix forming solvent,[13] the peptides showed an α-helix CD pattern. The α-helicity[14] (Table 1) of $Q36C_{NBA}$ was 60%, similar to that of $Rev_{34–50}$ (59%), suggesting that the C_{NBA} unit had a similar potential to the Gln36 residue in the Rev peptide for forming an α-helix structure. However, the α-helicity of $Q36C_{PNA}$ was decreased to 41% despite it being in TFE solution. These results indicate that the α-helix structure is disturbed by the flexible and achiral PNA unit, but not by the rigid and chiral C_{NBA}.

The binding properties of the peptides with RRE IIB RNA were evaluated by competition assay[15] using the Rev peptide modified with 5-carboxytetramethylrhodamine at the N-terminal (Rhod-Rev) as a fluorescence tracer. The dissociation constant (2.1×10^{-9} mol dm^{-3}) of Rhod-Rev with RRE IIB RNA was calculated from the anisotropy increase of the tracer upon the addition of the RNA using an equation with 1:1 stoichiometry.[15] In the mixture of Rhod-Rev (1.0×10^{-8} mol dm^{-3}) and RRE IIB RNA (2.5×10^{-8} mol dm^{-3}), fluorescence anisotropy values were decreased by the addition of the designed peptides as a competitor, affording the free Rhod-Rev (Fig. 2). This competition assay revealed that Rev_{34-50} bound RRE IIB RNA strongly with a dissociation constant (K_d) of 3.4 x 10^{-9} mol dm^{-3} (Table 1). Interestingly, $Q36C_{NBA}$ showed a K_d value of 1.7×10^{-9} mol dm^{-3}. Even though $Q36C_{NBA}$ has almost the same α-helix potential as $Rev_{34–50}$, it could bind RRE IIB RNA 2.0-fold stronger than $Rev_{34–50}$. These results suggest that the cytosine moiety of $Q36C_{NBA}$ contributes to the interaction of the peptide with the RNA by making a contact such as a hydrogen bond to a nucleobase of the RNA. Q36A showed the same affinity for the RNA ($K_d = 3.4 \times 10^{-9}$ mol dm^{-3}) as $Rev_{34–50}$. This result indicates that the higher α-helix content (76% in TFE) of Q36A enables it to maintain the same binding affinity as the $Rev_{34–50}$. On the other hand, the binding affinity of $Q36C_{PNA}$ for the RNA was significantly decreased ($K_d = 10.9 \times 10^{-9}$ mol dm^{-3}) to a level similar to Q36GG ($K_d = 9.9 \times 10^{-9}$ mol dm^{-3}), even if it has the same base in its sequence. These findings suggest that the introduction of the C_{PNA} residue at the Gln36 position does not improve the binding affinity with RNA. Furthermore, the decrease of the binding affinity is also attributed to the lower α-helix potential of $Q36C_{PNA}$ (41% in TFE).

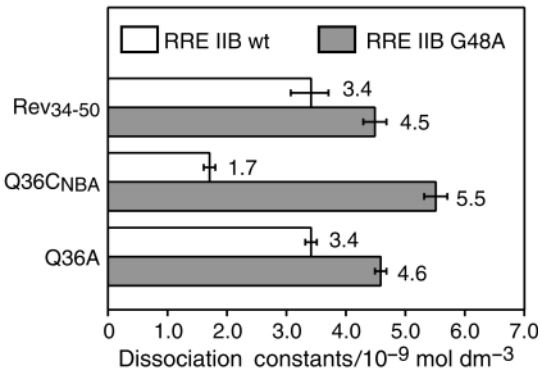

Fig. 3 Comparison of dissociation constants of the peptides with the wild-type and the mutant RNA.

In order to elucidate the selectivity of the designed peptide $Q36C_{NBA}$ for RRE IIB RNA, a mutant RNA (G48A), in which the guanine-48 base of RRE IIB RNA was replaced by adenine, was also prepared. $Rev_{34–50}$ bound G48A RNA with a dissociation constant of 4.5×10^{-9} mol dm^{-3}, comparable to that of the wild-type RRE IIB RNA (1.3-fold decrease) (Fig. 3). Q36A bound the mutant RNA with an affinity similar to $Rev_{34–50}$ ($K_d = 4.6 \times 10^{-9}$ mol dm^{-3}). $Q36C_{NBA}$ bound the mutant RNA with $K_d = 5.5 \times 10^{-9}$ mol dm^{-3}, 3.2-fold weaker than that of the wild-type RNA, that is, the affinity of $Q36C_{NBA}$ to the mutant RNA was lower than that of the $Rev_{34–50}$ and Q36A peptides. It seems that the cytosine base in $Q36C_{NBA}$ may interact with the guanine-48 moiety in RRE IIB RNA, and the interaction enhances the binding specificity to RRE IIB RNA more than Gln36 in $Rev_{34–50}$ does.

In conclusion, the nucleobase-conjugated peptide, $Q36C_{NBA}$, derived from HIV-1 Rev was successfully designed and synthesized. Introduction of the cytosine moiety as an artificial L-α-amino acid to the $Rev_{34–50}$ peptide increased the binding affinity and specificity to RRE IIB RNA, without changing the conformational properties of the peptide. This study should lead to a new strategy applicable to the construction of molecules that recognize a specific structure of an RNA molecule using various nucleobase amino acids.

Notes and references

1 I. W. Mattaj, *Cell*, 1993, **73**, 837.
2 P. E. Nielsen and G. Haaima, *Chem. Soc. Rev.*, 1997, **73**; H. Knudsen and P. E. Nielsen, *Nucleic Acids Res.*, 1996, **24**, 494.
3 C. Jain and J. G. Belasco, *Cell*, 1996, **87**, 115.
4 M. H. Malim, J. Hauber, S.-Y. Le, J. V. Maizel and B. R. Cullen, *Nature*, 1989, **338**, 254.
5 B. K. Felber, M. Hadzopoulou-Cladaras, C. Cladaras, T. Copeland and G. N. Pavlakis, *Proc. Natl. Acad. Sci. U.S.A.*, 1989, **86**, 1495.
6 M. Emerman, R. Vazeux and K. Peden, *Cell*, 1989, **57**, 1155.
7 R. Tan, L. Chen, J. A. Buettner, D. Hudson and A. D. Frankel, *Cell*, 1993, **73**, 1031.
8 R. Tan and A. D. Frankel, *Biochemistry*, 1994, **33**, 14579.
9 J. L. Battiste, H. Mao, N. S. Rao, R. Tan, D. R. Muhandiram, L. E. Kay, A. D. Frankel and J. R. Williamson, *Science*, 1996, **273**, 1547.
10 A. Lenzi, G. Reginato and M. Taddei, *Tetrahedron Lett.*, 1995, **10**, 1713.
11 E. Atherton and R. C. Sheppard, *Solid Phase Peptide Synthesis: A Practical Approach*,IRL Press, Oxford, 1989.
12 J. F. Milligan and O. C. Uhlenbeck, *Methods Enzymol.*, 1989, **180**, 51.
13 N. E. Zhou, B.-Y. Zhu, C. M. Kay and R. S. Hodges, *Biopolymers*, 1992, **32**, 419.
14 J. M. Scholtz, H. Qian, E. J. York, J. M. Stewart and R. L. Baldwin, *Biopolymers*, 1991, **31**, 1463.
15 K. Hamasaki, J. Killian, J. Cho and R. R. Rando, *Biochemistry*, 1998, **37**, 656.

Communication a909579i

ChemComm

Enhanced radical delivery from aldoxime esters for EPR and ring closure applications

Andrew J. McCarroll and John C. Walton*

University of St. Andrews, School of Chemistry, St. Andrews, Fife UK KY16 9ST. E-mail: jcw@st-and.ac.uk

Received (in Cambridge, UK) 24th December 1999, Accepted 26th January 2000

Arylmethaniminyl and alkyl radicals were generated from di- and tri-methoxyphenyl aldoxime esters, by photolysis in the presence of 4-methoxyacetophenone, and were detected by EPR spectroscopy: good yields of cyclised products were isolated from suitably unsaturated alkyl substituents.

Molecules suitable for direct photochemical or thermal generation of free radicals, other than peroxides and azo compounds, are quite limited, and therefore potential alternative types are of special interest. Oxime esters **2** are easily made from aldehyde (or ketone) oximes **1** and carboxylic acids (or acyl halides) (Scheme 1) and are much easier to handle and characterise than peroxides or azo compounds. These esters, which contain weak N–O bonds, appear to be a category of precursors for carbon-centred and iminyl radicals (**7**) with promise of considerable generality, but so far exploitation has been minimal. Thus, benzophenone oxime esters [$Ph_2C{=}NOC(O)R$] were shown to function as photolytic sources of alkyl and diphenylmethaniminyl radicals and used in preparations of alkyl aromatics,[1,2] alkyl chlorides,[2] and alkanes.[2] Radical induced homolysis of oxime benzoates by tributylstannane was found to be a useful method for generating iminyl radicals,[3,4] which were also produced, without the need for toxic organotin compounds, by use of Ni powder and acetic acid.[5,6]

Aldoxime esters **2** (Ar = Ph) displayed strong UV absorption bands at 208 and 254 nm. Inclusion of methoxy substituents in the aryl group (**3**, **4**) induced additional strong absorption bands at longer wavelengths (λ_{max} = 273, 312 nm) and this implied that photo-dissociation to radicals might be more efficient. We tested this prospect by monitoring solution phase photolyses of oxime esters containing a range of aromatic and alkyl substituents by means of 9 GHz EPR spectroscopy. No observable spectra were obtained from photolysis (500 W Hg arc, unfiltered) of degassed solutions of oxime esters **2** to **6** in *tert*-butylbenzene solution in the temperature range 200 to 320 K, except for a very weak spectrum of the allyl radical from **2e**. However, on addition of 4-methoxyacetophenone to the solutions as a photosensitiser (≥0.1 equiv.), good quality EPR spectra were obtained, especially from methoxy-substituted oxime esters of types **3** and **4**, but not from types **5** and **6** containing electron-withdrawing substituents. In the sensitised photolyses of **2d**, **3d** and **4d**, for example, the EPR spectra consisted of a superposition of two radicals [see Fig. 1(*a*), (*b*)]. The most prominent signals were due to the *tert*-butyl radical, with EPR parameters identical to those reported in the literature.[7] Two widely spaced groups of nitrogen triplets could also be discerned in the wings of the spectra [from **7** (Ar = Ph): a(H) = 80.5, a(N) = 10.0 G, g = 2.0034 at 250 K]. The exceptionally large a(H) values, as well as the other EPR parameters, are the signatures of rarely observed arylmethaniminyl radicals,[8] *i.e.* **7**. Fig. 1(*b*) shows the well-resolved second-order structure of the individual lines of the *tert*-butyl radical and the partly resolved long range splitting from ring hydrogens in iminyl radical **7** (Ar = Ph). The ratio of the concentrations of the alkyl and iminyl radicals depended on temperature and on the nature of R. For example, from **3e** (R = allyl) very intense spectra mainly of allyl were obtained, particularly for lower power and low modulation amplitude [Fig. 2(*a*), whereas for **4a** (R = Bu) the spectra were dominated by iminyl signals [Fig. 2(*b*)] and in general primary alkyls were difficult to detect. These differences in the concentrations of the two radicals were probably due to minor differences in the rates of their termination reactions. For highly reactive σ-radicals, *e.g.* cyclopropyl, generated from **4f** and trifluoromethyl generated from **4g**, the EPR spectra showed only the 2,4,6-trimethoxy-

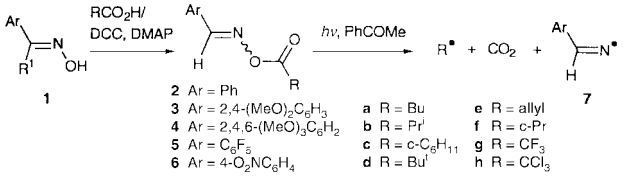

Scheme 1

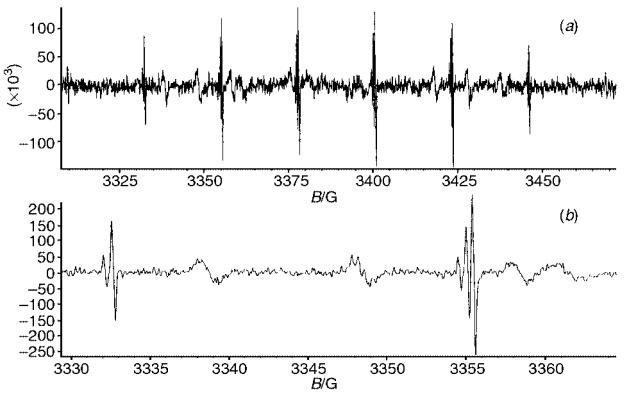

Fig. 1 (*a*) 9.4 GHz EPR spectrum obtained from photolysis of a solution of **2d** and MAP in *tert*-butylbenzene at 225 K showing the *tert*-butyl and iminyl radicals. (*b*) Scale expansion of a section of the above spectrum at 250 K showing the second order structure on the *tert*-butyl radical and partly resolved long range splittings on the iminyl radical **7** (Ar = Ph).

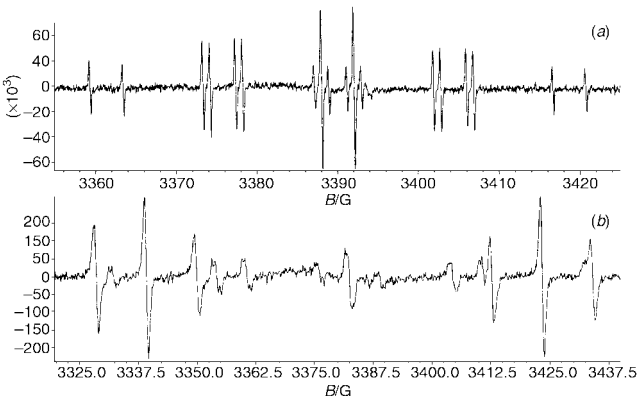

Fig. 2 (*a*) EPR spectrum of the allyl radical obtained on photolysis of a solution of **3e** and MAP in *tert*-butylbenzene at 200 K. Note the absence of iminyl **7** at low microwave power (0.2 mW) and low modulation amplitude (0.3 G_{pp}). (*b*) EPR spectrum of the iminyl radical **7** (Ar = TMP) and the butyl radical, from photolysis of a solution of oxime ester **4a** and MAP in *tert*-butylbenzene at 235 K.

DOI: 10.1039/a910346p

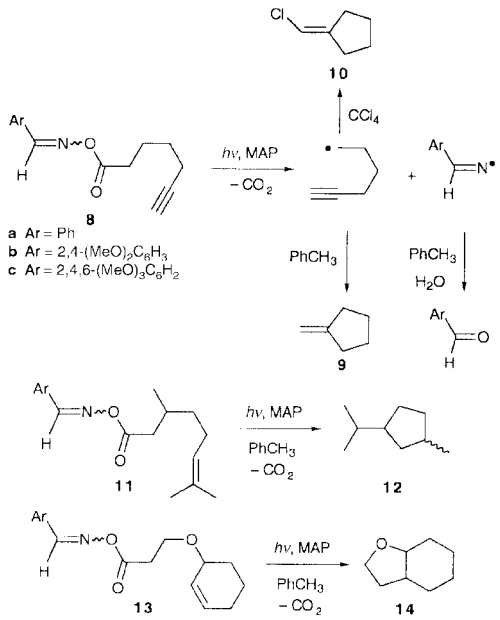

Scheme 2

Table 1 Results of irradiation of oxime esters

Oxime ester	Ar[a]	Solvent	MAP/equiv.	Product (%)[b]
8a	Ph	$PhCH_3$	—	**9** (6)
8a	Ph	$PhCH_3$	1	**9** (28)
8b	DMP	$PhCH_3$	—	**9** (39)
8b	DMP	$PhCH_3$	1	**9** (77)
8c	TMP	CCl_4	1	**10** (60)
11c	TMP	$PhCH_3$	1	**12** (34)
13c	TMP	CH_2Cl_2	1	**14** (72)

[a] DMP = 2,4-dimethoxyphenyl, TMP = 2,4,6-trimethoxyphenyl. [b] Yields determined by NMR.

phenylmethaniminyl radical [**7**, Ar = 2,4,5-$(MeO)_3C_6H_2$] except at low temperatures [< *ca.* 220 K], where cyclohexadienyl radicals from addition of cyclopropyl (or CF_3) to the *tert*-butylbenzene solvent were also visible.[9]

The large doublet H-hfs and comparatively few lines of the methaniminyl radicals provide a 'window' of *ca.* 60 G in the centre of the EPR spectrum which minimises overlap with the co-radical. Furthermore, the iminyl spectra act as useful standards with known *g*-factors so that spectral analysis of the co-radical is facilitated. Thus, these oxime esters constitute a convenient new class of radical precursors suitable for spectroscopic studies. Unlike the alternative diacyl peroxides, reagents **2** are innocuous and convenient to handle.

The EPR spectral results indicated that use of di- and trimethoxy oxime esters, in conjunction with a photosensitiser, could enhance their efficiency in preparative reactions. Accordingly, several ring closure reactions of oxime esters **8**, **11** and **13** were investigated. (Scheme 2).

Solutions of individual oxime esters (*ca.* 0.13 mol dm^{-3}) in a hydrogen donor solvent ($PhCH_3$, CH_2Cl_2) were photolysed with light from a 400 W medium pressure Hg lamp for *ca.* 3 h. Table 1 shows that for **8a** yields of the cyclised product, methylenecyclopentane (**9**), were low, but improved on inclusion of photosensitiser. Best yields of **9** were, however, obtained from the dimethoxy oxime ester **8b** when photosensitiser was included. Variation of the photosensitiser concentration showed that as little 0.1 equiv. could be used before serious loss of efficiency was experienced. The bicyclic ether **14** was obtained in good yield from photolysis of the trimethoxy oxime ester **13**, but the yield of 1-isopropyl-3-methylcyclopentane (**12**) from **11** was moderate, possibly because of poor hydrogen donation to the tertiary cyclised radical by the solvent.[10] No uncyclised products from direct reduction of the initial unsaturated alkyl radicals were detected. This is an advantage in that by-products are minimised, but indicates that, as expected, hydrogen donation is slow. An advantage of the method is that halogen-donor solvents can also be used for the preparation of functionalised rings. For example, photolysis of **8c** in CCl_4 afforded a good yield of chloromethylenecyclopentane (**10**). The main products derived from the iminyl radicals were the corresponding aldehydes, probably formed from intermediate imines, ArCH=NH, which are known to be highly susceptible to hydrolysis.

These results demonstrate that di- and tri-methoxy substitution of aryl oxime esters enhances their performance as photolytic sources of carbon-centred and iminyl radicals and that further improvement can be achieved by inclusion of a photosensitiser. These compounds are promising radical precursors of use in spectroscopic studies and as 'cleaner' tin-free reagents for preparative decarboxylative cyclisations of unsaturated carboxylic acids.

We thank the EPSRC (grant GR/L49185) for financial support.

Notes and references

1 M. Hasebe, K. Kogawa and T. Tsuchiya, *Tetrahedron Lett.*, 1984, 3887; M. Hasebe and T. Tsuchiya, *Tetrahedron Lett.*, 1986, 3239.
2 M. Hasebe and T. Tsuchiya, *Tetrahedron Lett.*, 1987, 6207; M. Hasebe and T. Tsuchiya, *Tetrahedron Lett.*, 1988, 6287.
3 J. Boivin, A.-M. Schiano and S. Z. Zard, *Tetrahedron Lett.*, 1994, **35**, 249.
4 J. Boivin, A.-C. Callier-Dublanchet, B. Quiclet-Sire, A.-M. Schiano and S. Z. Zard, *Tetrahedron*, 1995, **51**, 6517.
5 J. Boivin, A.-M. Schiano and S. Z. Zard, *Tetrahedron Lett.*, 1992, **33**, 7849.
6 S. Z. Zard, *Synlett*, 1996, 1148.
7 R. W. Fessenden and R. H. Schuler, *J. Chem. Phys.*, 1963, **39**, 2147.
8 A. R. Forrester, M. Gill, C. J. Meyer, J. S. Sadd and R. H. Thomson, *J. Chem. Soc., Perkin Trans. 2*, 1979, 606.
9 EPR experiments with **2g** were also carried out in liquid cyclopropane which enables lower temperatures to be accessed. However, due partly to poor solubility at low temperatures, only weak spectra of **7** (Ar = 2,4,6-$(MeO)_3C_6H_2$ were observed.
10 For example: oxime ester **13c** (0.25 g, 0.69 mmol) and MAP (0.12 g, 0.8 mmol) in CH_2Cl_2 (5 cm^3) were photolysed in a quartz tube for 3 h at 50 °C with light from a 400 W medium pressure Hg lamp. The solvent was evaporated and the solid remaining was extracted several times with Et_2O. Concentration and microdistillation at ambient temperature/0.01 Torr gave bicyclic ether **14** (ref. 11) (0.01 g, 12%) (ref. 12), δ_H(300 MHz, $CDCl_3$) 1.15–1.30 (2H, m), 1.39–1.68 (6H, m), 1.83–2.04 (3H, m), 3.77–3.87 (2H, m), 3.96 (1H, q, *J* 8).
11 P. A. Baguley and J. C. Walton, *J. Chem. Soc., Perkin Trans. 1*, 1998, 2073.
12 Low yield due to small scale reaction and volatile product: see final row Table 1 for a better measure of the true yield.

Communication a910346p

ChemComm

Amphiphilic polyenic push–pull chromophores for nonlinear optical applications

Valérie Alain,[a]† Mireille Blanchard-Desce,*[ab] Isabelle Ledoux-Rak[c] and Joseph Zyss[c]

[a] *Ecole Normale Supérieure, Département de Chimie (CNRS, UMR 8640), 24 rue Lhomond, 75231 Paris Cedex 05, France*

[b] *UMR 6510, Université Rennes 1, Campus de Beaulieu, Bât. 10A, 35042 Rennes cedex, France. E-mail: mireille.blanchard-desce@univ-rennes1.fr*

[c] *Laboratoire de Photonique Quantique et Moléculaire (UMR 8537), ENS Cachan, 61 avenue du Président Wilson, 94235 Cachan, France*

Received (in Liverpool, UK) 28th October 1999, Accepted 24th January 2000

Amphiphilic cationic polyenic push–pull chromophores which offer interesting supramolecular possibilities for second harmonic generation have been synthesised and their optical non-linearities studied for the first time by electric field induced second harmonic (EFISH) generation in solution.

Molecular nonlinear optics (NLO) has attracted increasing interest over the past ten years.[1] NLO materials are highly promising for applications in various fields including telecommunications, optical data storage and processing, optical power limitation *etc*. NLO phenomena also present interesting opportunities for probing and imaging purposes. For instance, second harmonic generation (SHG) has been successfully used for probing asymmetrical systems (such as interfaces)[2] or high resolution imaging of biological cells.[3]

Within this context, we have investigated a strategy based on the design of amphiphilic push–pull chromophores [*i.e.* molecules combining an electron-donating group (D) and an electron-withdrawing group (A) connected by a conjugated system] with enhanced quadratic molecular response (*i.e.* hyperpolarizability β) and prone to interact in an asymmetrical way with a lipid membrane. Such characteristics provide an interesting way to induce the asymmetry required for quadratic NLO phenomena both at the molecular and macroscopic levels, by taking advantage of specific interactions with hydrophilic–hydrophobic interfaces. Hereafter, we present the design and synthesis of amphiphilic cationic polyenic chromophores showing large nonlinearities. Their quadratic nonlinearities have been studied for the first time by electric field induced second harmonic (EFISH) generation in solution, a technique usually precluded for ionic species.

Stilbazolium dyes have been the topic of many studies in the field of NLO. They have led to highly SHG efficient crystals.[4] In addition, they are interesting candidates for designing NLO micro- and nanostructures. For examples, derivatives bearing an elongated alkyl chain have been deposited into Langmuir–Blodgett films showing SHG activity[5] and amphiphilic derivatives have been shown to be of interest for the design of optical probes for membrane potentials.[6] Our choice has been to investigate amphiphilic vinylogous derivatives of stilbazolium dyes (Fig. 1). The presence of two butyl hydrophobic tails grafted on the donor end group and of the positively-charged hydrophilic acceptor moiety confers an amphiphilic character to these push–pull chromophores and should facilitate their interaction with a lipidic membrane while avoiding deleterious detergent effects. Increasing the polyenic chain length is expected to lead to a marked increase of β as already known for other push–pull polyenic systems.[7–9] Similarly, by substituting the pyridinium acceptor end group by a quinolinium end group, larger nonlinearities are expected.

Stilbazolium dyes and analogous chromophores are usually prepared using Konevenagel condensation (Scheme 1).[6] However, this simple strategy proved ineffective in the case of polyenic analogues ($n > 1$) bearing long alkyl chains. It leads to both poor yields and purification problems due to the side formation of shorter homologues. To ensure satisfactory preparation yields, we have implemented an alternative synthetic scheme based on the Wittig–Horner condensation of a pyridine moiety[10] on a polyenal bearing the donating end group (Scheme 1). This allows for the preparation in medium to good yield of compounds of series **4** from polyenals of series **1** using solid–liquid phase transfer conditions. Polyenals of series **1** can be obtained in high yields from the generic molecule **1**[0] using a sequential vinylic homologation.[9] Molecules of series **4** were obtained as pure all-*E* isomers (as shown by NMR spectra and elemental analyses) after catalytic isomerisation and column chromatography ($n = 1$, 2) or recrystallisation ($n > 2$). Alkylation of molecules of series **4** in neat MeI readily afforded pure amphiphilic push–pull polyenic chromophores of series **2**.

The electric field induced second harmonic (EFISH) generation technique[11] is a useful method to derive the quadratic nonlinearity (and more precisely the projection of the dipolar part of the β tensor on the dipole moment μ) of dipolar chromophores. It is in principle precluded in the case of ionic species. Yet, we have been able to implement the EFISH technique for the determination of the $\mu\beta$ values of ionic amphiphilic chromophores **2** and **3** by operating in a solvent of low polarity thanks to the formation of close ion pairs. The EFISH experiments were carried out in chloroform ($\varepsilon_r = 4.7$) and at 1.907 μm in order to avoid absorption of the second harmonic. The $\mu\beta$ values and the wavelength of the maximum absorption (λ_{max}) are collected in Table 1. The static $\mu\beta(0)$ values extrapolated at zero frequency by using the two-level dispersion model for β[11] (valid in the case of 1-D intramolecular charge transfer only) are also included.

As clearly observed from Table 1, amphiphilic salts of series **2**[*n*] and **3**[1] show large $\mu\beta$ values. Lengthening the polyenic chain induces both a bathrochromic shift and a significant increase of the quadratic nonlinearity, although the effect seems to slow down for the longest derivatives. This leads to a $\mu\beta(0)$

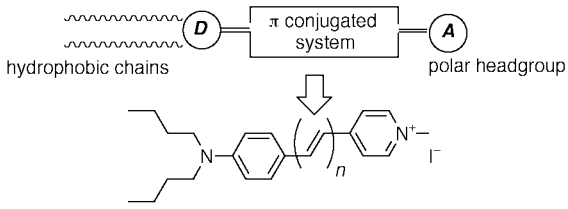

Fig. 1 Molecular engineering of amphiphilic push–pull chromophores.

† Present address: Laboratoire de Photophysique et de Photochimie Supramoléculaires et Macromoléculaires, ENS Cachan, 61 avenue du Président Wilson, 94235 Cachan, France.

DOI: 10.1039/a908717f

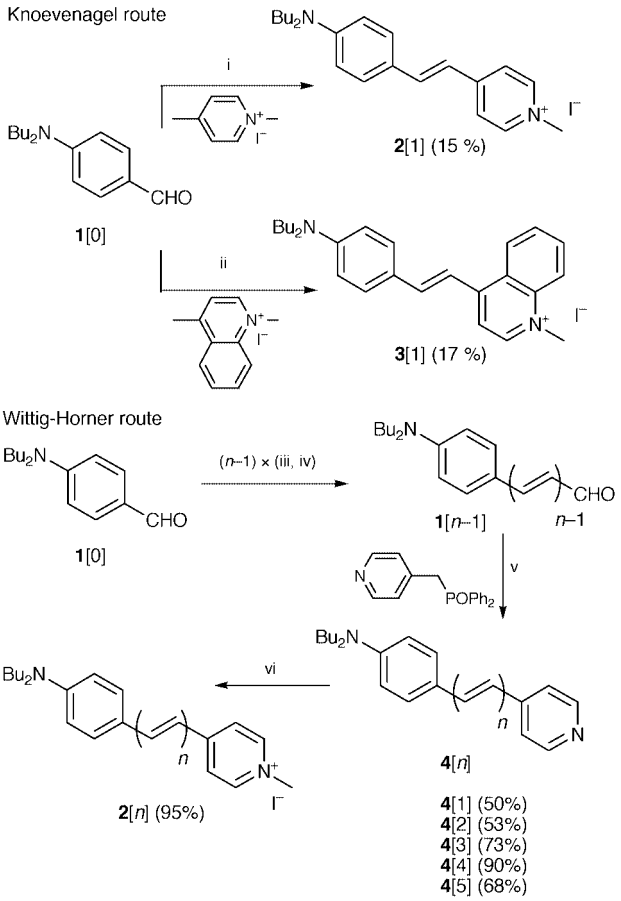

Scheme 1 *Reagents and conditions*: i, *N*-methyl-4-picolinium iodide (0.9 equiv.), cat. piperidine, EtOH, reflux, 16 h; ii, *N*-methyllepidinium iodide (0.9 equiv.), cat. piperidine, EtOH, reflux, 16 h; iii, (1,3-dioxolan-2-ylmethyl)tributylphosphonium bromide (1.1 equiv.), NaH (1.5 equiv.), cat. 18-C-6, THF, room temp., 20 h; iv, HCl (10%), THF, room temp., 1 h; v, diphenyl(4-pyridyl)methylphosphine oxide (1.1 equiv.), THF, NaH (1.5 equiv.), cat. 18-C-6, room temp. 15 h; vi, MeI, room temp., 1 h.

Table 1 Linear and nonlinear optical properties of amphiphilic push–pull chromophores **2**[1–5] and **3**[1] in chloroform; $\mu\beta$ values were derived from EFISH measurements at 1.907 μm

Compound	$\mu\beta(2\omega)^a/10^{-48}$ esu	λ_{max}/nm	$\mu\beta(0)/10^{-48}$ esu
2[1]	840	517	550
2[2]	2230	558	1340
2[3]	2700	581	1540
2[4]	3380	589	1890
2[5]	3690	598	2020
3[1]	1380	603	745

[a] The β values are defined using the X convention (ref. 15).

value as high as 2000×10^{-48} esu for the **2**[5] ion pair, which is more than four times larger than the corresponding experimental value (450×10^{-48} esu) determined in similar conditions for the benchmark *dipolar* chromophore Disperse Red 1. Compound **3**[1], which bears the stronger heterocyclic acceptor, shows a $\mu\beta(0)$ value about 50% larger than that of compound **2**[1], but at the expense of a much reduced transparency. Compound **2**[3] exhibits a $\mu\beta(0)$ value twice as large as that for compound **3**[1] for a similar molecular weight while remaining significantly blue-shifted. Elongation of the polyenic chain of derivatives of series **2** is thus preferable—in terms of nonlinearity–transparency trade-off—to turning to a stronger acceptor moiety.

Finally, cationic polyenic push–pull chromophores have been synthesised and their optical non-linearities studied for the first time by electric field induced second harmonic generation in solution, owing to the formation of ion pairs in a solvent of low relative permittivity. Their quadratic nonlinearities can be enhanced by increasing the polyenic chain length and/or adjusting the charged heterocyclic acceptor. Recent second harmonic generation and two-photon excited fluorescence experiments reported in ref. 12 provide evidence that chromophores of type **2** are incorporated in the outer leaflet of model bilayer lipid membranes and orientated perpendicular to the membrane surface. These amphiphilic chromophores hold promise as sensitive probes for SHG imaging of membrane potentials.[3,13] In addition, incorporation of the chromophores in the lipid bilayer is expected to significantly influence the molecular nonlinear responses, as shown recently for the inclusion of a stilbazolium dye in a supramolecular complex.[14]

The Délégation Générale pour l'Armement (DGA) is acknowledged for a fellowship to V.A. We thank Idrissa Njabira for his participation in EFISH measurements.

Notes and references

1 *Molecular Nonlinear Optics: Materials, Physics and Devices*, ed. J. Zyss, Academic Press, Boston, 1994; *Nonlinear Optics of Organic Molecules and Polymers*, ed. H. S. Nalwa and S. Miyata, CRC Press, 1994.
2 K. B. Eisenthal, *Chem. Rev.*, 1996, **96**, 1343.
3 A. Lewis, A. Khatchatouriants, M. Treinin, Z. Chen, G. Peleg, N. Friedman, O. Bouevitch, Z. Rothman, L. Loew and M. Sheres, *Chem. Phys.*, 1999, **245**, 133.
4 S. R. Marder, J. W. Perry and W. P. Schaefer, *Science*, 1989, **245**, 626.
5 I. R. Girling, N. A. Cade, P. V. Kolinsky, R. J. Jones, I. R. Peterson, M. M. Ahmad, D. B. Neal, M. C. Petty, G. G. Roberts and W. J. Feast, *J. Opt. Soc. Am. B*, 1987, **4**, 950.
6 A. Hassner, D. Birnbaum and L. M. Loewe, *J. Org. Chem.*, 1984, **49**, 2546.
7 M. Barzoukas, M. Blanchard-Desce, D. Josse, J.-M. Lehn and J. Zyss, *Chem. Phys.*, 1989, **133**, 323.
8 S. R. Marder, L.-T. Cheng, B. G. Tiemann, A. C. Friedli, M. Blanchard-Desce, J.W. Perry and J. Skindhøj, *Science*, 1994, **263**, 511.
9 M. Blanchard-Desce, V. Alain, P. V. Bedworth, S. R. Marder, A. Fort, C. Runser, M. Barzoukas, S. Lebus and R. Wortmann, *Chem. Eur. J.*, 1997, **3**, 1091.
10 M. Blanchard-Desce, T. S. Arrhenius and J.-M. Lehn, *Bull. Soc. Chim. Fr.*, 1993, **130**, 266.
11 J.-L. Oudar, *J. Chem. Phys.*, 1977, **67**, 446.
12 L. Moreaux, O. Sandre, M. Blanchard-Desce and J. Mertz, *Opt. Lett.*, 2000, **25**, 3220.
13 O. Bouevitch, A. Lewis, I. Pinevsky, J. P. Wuskell and L. Loew, *Biophy. J.*, 1993, **65**, 672.
14 K. Clays, G. Olbrechts, T. Munters, A. Persoons, O.-K. Kim and L.-S. Choi, *Chem. Phys. Lett.*, 1998, **293**, 337.
15 A. Willets, J. E. Rice, D. M. Burland and D. P. Shelton, *J. Chem. Phys.*, 1992, **97**, 7590.

Communication a908717f

ChemComm

Host–guest complexes with tuneable solid state structures

Simon J. Holder,*[ab] Johannes A. A. W. Elemans,[a] Joaquín Barberá,[c] Alan E. Rowan[a] and Roeland J. M. Nolte*[a]

[a] *Department of Organic Chemistry, NSR Center, University of Nijmegen, Toernooiveld, 6525 ED, Nijmegen, The Netherlands. E-mail: desiree@sci.kun.nl*
[b] *Centre for Materials Research, University of Kent, Canterbury, Kent, UK CT2 7NR*
[c] *Química Orgánica, Facultad de Ciencias-ICMA, Universidad de Zaragoza-CSIC, E-50009 Zaragoza, Spain*

Received (in Liverpool, UK) 23rd November 1999, Accepted 19th January 2000

Molecular clip receptors with long hydrocarbon tails self-assemble and form lamellar thin solid films, the architecture and properties of which can be fine-tuned by complexation of guest molecules

The generation of ordered thin films of organic materials is of fundamental importance to future molecular electronic applications.[1] A variety of methods have been utilized in the formation of these films, generally the sequential build-up of multilayers through procedures such as Langmuir–Blodgett film deposition,[2] the Sagiv method of thin film self-assembly,[3] alkanethiol binding to gold surfaces,[4] anionic–cationic polyelectrolyte alternation[5] and thermal evaporation *in vacuo*.[6] However the ideal route to the self-assembly of thin organic films would involve a system that spontaneously self-orders upon either being cast from solution or cooled from the melt—essentially a one-step process involving the minimum of experimental input. To date the only systems approaching this ideal are microphase separated block copolymers[7] and liquid-crystalline materials.[8]

Over the past years our group has studied a class of host compounds commonly referred to as 'molecular clips'.[9] These molecules of type **1** possess a rigid, U-shaped cavity in which

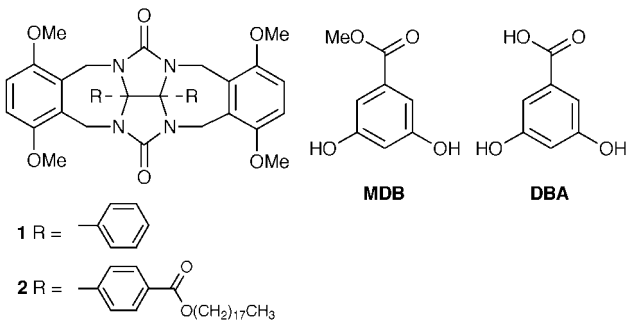

dihydroxybenzene guests can selectively be bound through hydrogen bonding, π–π stacking and cavity filling effects.[10] Recently it has been demonstrated that molecular clips also exhibit self-recognition and ultimately self-assembly properties: they can form dimers in organic solvents as well as in the solid state, in which the cavity of one molecule is filled by one of the side-walls of its dimeric partner and *vice versa*.[11] In aqueous solution clips with water-soluble functions can assemble to form well-defined nano-arrays.[12]

Here we describe a clip (**2**) which is derivatised at its convex side with two long aliphatic tails. This molecule was designed to generate liquid crystalline phases: upon dimerisation, it can adopt a structure analogous to that of a typical 'rod-like' mesogen [Fig. 1(*a*)]. It turned out, however, that it formed solid films, the structure of which can be tuned by adding guest molecules.

Clip **2** was prepared according to standard procedures.[13] The compound melted at 195.4 °C, and upon recrystallisation from the melt it displayed a birefringent platelet texture under the polarising optical microscope (PM), similar to that shown by classic smectic mesogens.[8] In addition, the material turned out to be highly malleable upon the application of pressure to the covering slide, again similar to that expected for a liquid crystalline substance. Below 84 °C, the texture was retained but the material was now completely solid. The enthalpy (ΔH = 21.3 kJ mol^{-1}) involved with the final isotropisation transition upon heating the sample, as measured by differential scanning calorimetry (DSC), was, however, far larger than would have been expected for a typical mesophase to isotropic liquid transition. X-Ray powder diffraction (XRPD) analysis suggested that the material was actually crystalline at all temperatures below 195.4 °C.† It showed a set of equally spaced peaks in the low-angle region of the diffraction pattern, corresponding to 1st, 2nd, 3rd *etc*. order reflections, indicating a layered structure. We attribute the origin of this lamellar structure to the dimerisation of the molecular clips *via* cavity filling in conjunction with π–π stacking interactions occurring between adjacent clip dimers, giving rise to 'bilayers' of molecular clips separated by aliphatic tails which display varying degrees of interdigitation depending on the temperature (Fig. 2). Evidence for this comes from the observed *d*-spacing of 28.4 Å at 20 °C, calculated from the low-angle reflections, which increases to 42 Å at 175 °C. These values correspond to the length of a tilted bilayer of dimerised clip molecules.‡ The solid state ^{13}C CPMAS NMR spectrum of **2** confirmed the decreased interdigitation of the aliphatic tails at higher temperatures, which followed from the downfield shifts of the resonances of the $CH_2CH_2CH_3$ termini of the hydrocarbon tails. In addition, the resonances of the main chain CH_2 protons significantly sharpened, indicative of increased mobility. A more detailed NMR study will be published elsewhere.[13]

We believe that strong π–π interactions between the dimeric units prevent the material from being truly liquid crystalline, and attribute its malleability at higher temperatures to a lessening of the interdigitation and an increased mobility of the aliphatic tails, so that the layers of clips can more readily slide over one another.

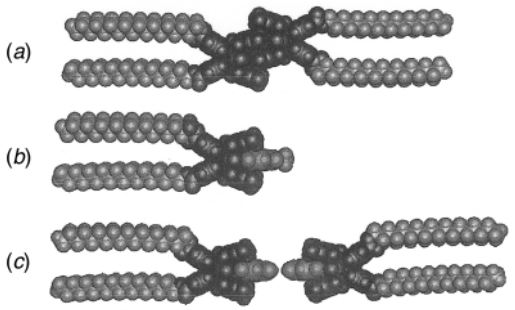

Fig. 1 Computer generated models of (*a*) a dimer of **2**, based on the X-ray structure of an analogue containing methyl instead of octadecyl ester groups, (*b*) the 1:1 complex of **2** and **MDB**, and (*c*) the 1:1 complex of **2** and **DBA**.

DOI: 10.1039/a909309e

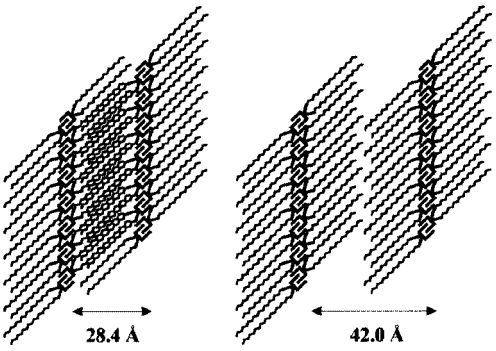

Fig. 2 Schematic representation of the proposed lamellar ordering of the molecules of **2** at 20 °C (left) and at 175 °C (right).

If, as postulated, the lamellar nature of **2** is a result of dimerisation *via* cavity filling, then addition of a guest molecule that can strongly bind in the cavity, such as methyl dihydroxybenzoate (**MDB**) [Fig. 1(*b*)], should result in the disruption of the bilayer structure and thus in the lamellar arrangement of the molecules.§ The 1 : 1 **2**:**MDB** complex was prepared by co-evaporation of an equimolar mixture of solutions of the two components in MeOH–$CHCl_3$ (1 : 4, v/v), followed by heating the mixture and recrystallisation of the complex from the isotropic melt. The complex recrystallised at 53 °C, displaying a white microcrystalline texture by polarised optical microscopy, typical of a crystalline organic material. Repeated heating and cooling runs were identical, and DSC analysis indicated the presence of only the 1:1 complex and no free clip or guest components.¶ The material showed no malleability under applied pressure, and XRPD revealed a unique diffraction pattern with no observable reflections corresponding to lamellar ordering.

Since complexation of **2** with **MDB** disrupts the lamellar arrangement of the molecules in the material, it was reasoned that complexation of **2** with 3,5-dihydroxybenzoic acid (**DBA**) might have the effect of 'stitching' together the bilayers of the clips, because the carboxylic acid groups of two guests can form a dimer without interfering with the bonding of the 3,5-dihydroxyaromatic parts to the clips. This then would result in the reimposition of the lamellar ordering. The 1 : 1 **2**:**DBA** complex was prepared in an identical manner to the 1 : 1 **2**:**MDB** complex. Upon cooling from the isotropic melt, the complex crystallised, displaying a clear 2D spherulitic morphology at 137 °C, indicative of a lamellar crystalline packing. As with free **2**, the complex proved to be malleable under applied pressure. XRPD measurements showed a set of equally spaced reflections yielding an interlayer spacing of 57.8 Å. This value is in line with an 'extended dimer' structure of the building blocks achieved through two independent molecular recognition processes, *viz.* host–guest binding and guest dimerisation [Fig. 1(*c*)]. Further evidence for this comes from infrared analysis, which confirmed that the C = O stretching vibration at 1690 cm^{-1}, due to benzoic acid dimerisation, was present in the material.

The ability of **2** to form highly ordered lamellar structures from the melt and the possibility to fine-tune this structure by adding guest molecules opens the way to design new functional materials that are easily melt-processed. Current research is focussed on the incorporation of functional guests, such as porphyrins and metal-coordination complexes, into these lamellar films.

Notes and references

† Compounds in the smectic mesophase in principle can still display Bragg lines in their XRPD patterns.

‡ When the clip dimers are tilted at an angle of *ca*. 40°, the width of the bilayer is *ca*. 42 Å. Strong evidence for such a tilting comes from the crystal structure of the methyl ester analogue of **2**, in which the clip dimers are packed with a similar tilt of 40° as a result of interdimer π–π stacking.

§ Binding of **MDB** by **2** in $CDCl_3$ solution was found to be several orders of magnitude stronger ($K_a > 10^4\ M^{-1}$) than dimerisation of **2** ($K_{dimer} = 18\ M^{-1}$).

¶ Complexation of the guest in the cavity of **2** was also supported by shifts in the C=O stretching vibration of the glycoluril urea functions of **2** and in the OH stretching vibration of **MDB** in the solid-state FTIR spectra.

1 R. H. Tredgold, *J. Mater. Chem.*, 1995, **5**, 1095; A. Ullman, *An Introduction to Ultrathin Organic Films*, Academic Press, Boston, 1991; R. H. Tredgold, *Order in Thin Organic Films*, Cambridge University Press, Cambridge, 1994.
2 G. G. Roberts, *Langmuir-Blodgett Films*, Plenum, New York, 1990.
3 L. Netzer and J. Sagiv, *J. Am. Chem. Soc.*, 1983, **105**, 674.
4 L. Strong and G. M. Whitesides, *Langmuir*, 1988, **4**, 316.
5 D. Decher, J. D. Hong and J. Schmitt, *Thin Solid Films*, 1992, **210/211**, 831.
6 M. Woolley, R. H. Tredgold and P. Hodge, *Langmuir*, 1995, **11**, 683.
7 T. Goldacker, V. Abetz, R. Stadler, I. Erukhimovich and L. Leibler, *Nature*, 1999, **398**, 137.
8 G. W. Gray and J. W. G. Goodby, *Smectic Liquid Crystals – Textures and Structures*, Leonard Hill, Glasgow, 1984.
9 For a review see: A. E. Rowan, J. A. A. W. Elemans and R. J. M. Nolte, *Acc. Chem. Res.*, 1999, **32**, 995.
10 J. N. H. Reek, A. H. Priem, H. Engelkamp, A. E. Rowan, J. A. A. W. Elemans and R. J. M. Nolte, *J. Am. Chem. Soc.*, 1997, **119**, 9956.
11 J. N. H. Reek, A. E. Rowan, R. de Gelder, P. T. Beurskens, M. J. Crossley, S. de Feyter, F. de Schryver and R. J. M. Nolte, *Angew. Chem., Int. Ed. Engl.*, 1997, **36**, 361.
12 J. N. H. Reek, A. Kros and R. J. M. Nolte, *Chem. Commun.*, 1996, 245; J. A. A. W. Elemans, R. de Gelder, A. E. Rowan and R. J. M. Nolte, *Chem. Commun.*, 1998, 1553.
13 S. J. Holder, J. A. A. W. Elemans, M. J. Boerakker, J. J. J. M. Donners, R. de Gelder, J. Barberá, A. E. Rowan and R. J. M. Nolte, manuscript in preparation.

Communication a909309e

ChemComm

Significant room temperature oxygen storage over 0.58% $Pt/Ce_{0.68}Zr_{0.32}O_2$ when H_2 is used as a reducing agent

N. Hickey,[a] P. Fornasiero,[a] J. Kašpar,*[a] M. Graziani,[a] G. Blanco[b] and S. Bernal[b]

[a] *Dipartimento di Scienze Chimiche, Università di Trieste, 34127 Trieste, Italy. E-mail: kaspar@univ.trieste.it*
[b] *Departamento de Ciencia de los Materials e Ingeniería Metalúrgica y Química Inorgánica, Universidad de Cádiz, Apartado 40, Puerto Real, 11510, Spain*

Received (in Oxford, UK) 13th December 1999, Accepted 27th January 2000

The investigation of the oxygen storage/release capacity (OSC) of 0.58 wt% $Pt/Ce_{0.68}Zr_{0.32}O_2$ catalyst by oscillating the feed-stream between reducing and oxidising conditions showed that a high OSC could be measured at room temperature, even for redox-aged sample, by using H_2 as the reducing agent.

The so-called oxygen storage/release capacity (OSC) of a three-way catalyst (TWC) is the ability to attenuate the negative effects of rich/lean oscillations of exhaust gas composition. By maintaining a stoichiometric composition at the catalyst, the highest conversion efficiency of the exhaust is attained. OSC, which in the modern TWCs is achieved by adding a CeO_2–ZrO_2 mixed oxide component, is usually discussed in terms of the ability to regulate the oxygen partial pressure in the exhaust through the Ce^{3+}/Ce^{4+} redox couple [eqn. (1)]:

$$CeO_2 \underset{H_2O-CO_2}{\overset{H_2-CO}{\rightleftharpoons}} CeO_{2-x} + x/2O_2 \quad (1)$$

Formation of vacancies is therefore either implied or assumed. Following the pioneering work of Yao and Yu-Yao,[1] dynamic-OSC measurement involves alternately pulsing the chosen reducing agent (usually CO but sometimes H_2) and O_2 over the material under investigation. More recently the oxygen buffering capacity (OBC) technique has been developed by Bernal *et. al.*[2] In this method O_2 is pulsed over the sample in a flow of inert gas, which effectively corresponds to oscillations between mildly reducing and oxidising conditions.

Here, we demonstrate that it is possible, using H_2 as reducing agent, to measure significant dynamic-OSC over $Pt/Ce_{0.68}Zr_{0.32}O_2$ under conditions where vacancy creation is unlikely (room temperature, r.t.). Such high r.t. OSC is not observed when either CO is used as reductant or when the OBC method is employed. The evidence suggests that this dynamic-OSC may be associated with the phenomenon of spillover. This opens the possibility that spilled-over H_2 can be a contributing factor to OSC measurements even at higher temperatures. The presence of H_2 in exhaust effluent in a ratio of *ca.* 1:3 with respect to CO[3] makes this finding a potentially important piece of information.

0.58 wt% $Pt/Ce_{0.68}Zr_{0.32}O_2$ and 0.53 wt% Pt/CeO_2 were prepared and supplied by RHODIA as part of the CEZIR-ENCAT network.[4] 0.5 wt% Pt/γ-Al_2O_3 (γ-Al_2O_3: Alfa products) was prepared using $Pt(NH_3)_2(NO_2)_2$ as precursor. An *in situ* oxidising cleaning procedure[5] (heating in flow of O_2 at 823 K for 1 h) was applied before all experiments, giving a sample designated as fresh. Redox-aged sample was prepared as follows: reduction up to 1273 K in 5 % H_2 in Ar (25 ml min^{-1}), holding at 1273 for 15 min, flushing in Ar at 1273 K; slow cooling to 700 K; re-oxidation at 700 K and cooling to 423 K in 5% O_2 in Ar; and, finally, cooling to r.t. in Ar (60 ml min^{-1}). Quantitative dynamic-OSC measurements were performed by increasing the temperature in a stepwise manner and, during the isothermal steps (60 min), alternately pulsing every 70 s H_2 (500 or 100 μl, H_2-OSC) or CO (100 μl, CO-OSC) and O_2 (250 or 100 μl) over the sample (20 mg, maintained in a flow of Ar of 25 ml min^{-1}). OSC was measured using a thermal conductivity detector as the uptake of O_2 from the O_2 pulse. Steady-state values are reported. When CO was used as the reducing agent, the evolved CO and CO_2 were separated on a Porapak Q column. TPR-MS profiles were obtained up to 1273 K as above reported for redox-ageing. OBC measurements were carried out as reported previously.[2] Hydrogen chemisorption measurements were conducted at 298 and 195 K.[6]

The redox behaviour was first investigated by means of the TPR-MS technique. The TPR profiles (not reported) of fresh and redox-aged $Pt/Ce_{0.68}Zr_{0.32}O_2$ showed single reduction features centred around 500 and 400 K, respectively. This behaviour is fairly consistent with a recent report[6] and is attributed to an initial reduction of supported PtO, which in turn results in support reduction through spillover of hydrogen species. The degree of reduction, *i.e.* the overall transferable oxygen, was measured by O_2 uptake at 700 K after the TPR experiment as previously reported.[6] An O_2 uptake of 20 ml g^{-1} was obtained for both fresh and redox-aged samples.

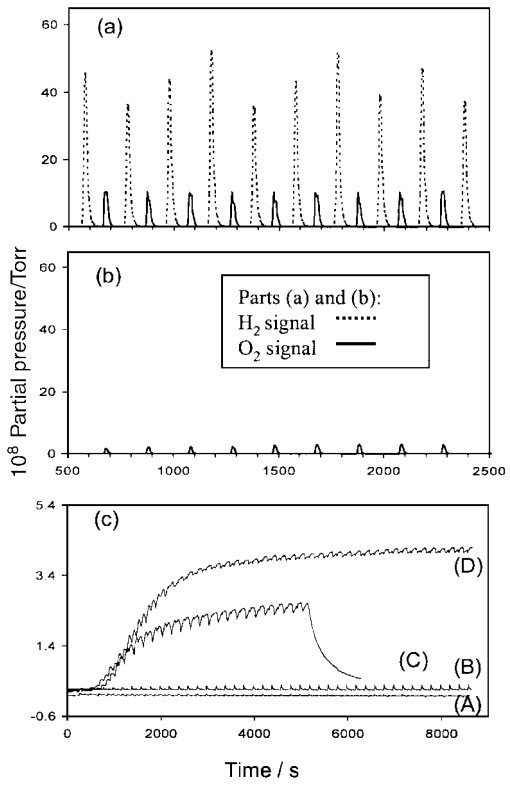

Fig. 1 H_2-OSC measured at r.t. H_2 (*m/z* = 2) and O_2 (*m/e* = 32) profiles over fresh/reduced at 500 K Pt/Al_2O_3 (for clarity this trace is displaced) (a) and $Pt/Ce_{0.68}Zr_{0.32}O_2$ (b), and water production (*m/e* = 18) (c) over: (A) fresh/reduced 500 K Pt/Al_2O_3, (B) fresh $Pt/Ce_{0.68}Zr_{0.32}O_2$; (C) redox-aged $Pt/Ce_{0.68}Zr_{0.32}O_2$, reaction stopped at 5000 s; (D) fresh/reduced 500 K $Pt/Ce_{0.68}Zr_{0.32}O_2$. MS was tuned to enhance the sensitivity to H_2 compared to O_2. 200 mg of sample and loop volumes of 1 ml were employed.

DOI: 10.1039/a909751a

Table 1 Oxygen storage and chemical/textural characterisation of the $Pt/Ce_{0.68}Zr_{0.32}O_2$ catalyst

	Oxygen storage capacity[a]/OBC[b]				H_2 chemisorption[c]			
					H_2 update/ml g^{-1}			N_2 physisorption
Sample	*T*/K	H_2-OSC[d]/ ml O_2 g^{-1}	CO-OSC/ ml O_2 g^{-1}	OBC (%)	*T*/K	0 Torr	20 Torr	Surface area/ m^2 g^{-1}
$Pt/Ce_{0.68}Zr_{0.32}O_2$ fresh/reduced	r.t.	6.3	0.0		298	6.78	7.09	100
	373	7.1	0.7		193	0.31	0.37	
	473	7.5	1.7					
	673	8.1	> 2.6	4				
	773	8.9	> 2.6	20				
$Pt/Ce_{0.68}Zr_{0.32}O_2$ redox-aged	r.t.	2.8	0.0		298	2.62	2.76	30
	373	4.1	0.0		193	0.09	0.09	
	473	9.1	0.1					
	673	9.8	> 2.6	8				
	773	11.6	> 2.6	21				
Pt/CeO_2 fresh/reduced	r.t.	4.2			298	3.88	4.02	88
					193	0.30	0.31	
Pt/CeO_2 redox-aged	r.t.	0.6			298	0.47	0.45	7
					193	0.04	0.04	
Pt/Al_2O_3 fresh/reduced	r.t.	0.3			298	0.28	0.30	99
					193	0.26	0.27	

[a] Quantitative analysis using TCD, standard deviation ± 0.4 ml O_2 g^{-1}. Steady state values measured as O_2 uptake (ml g^{-1}). For CO / O_2 experiments, an OSC of 2.6 ml O_2 g^{-1} corresponds to a maximum O_2 uptake using the experimental setup described in the text. [b] OBC (%): [100 $(A_{NA} - A_A)/A_{NA}$]; A_{NA}: area under non-attenuated pulse; A_A: area under the attenuated pulse. Pulse volume 0.25 ml of 5% O_2 in He. [c] Sample reduced at 500 K for 1 h, followed by evacuation at 673 K for 4 h. A range of H_2 pressure of 2 –20 Torr was employed. Adsorbed volumes were determined by extrapolation to zero pressure of the linear part of the adsorption isotherm (0 Torr). Cumulative H_2 adsorption at p = 20 torr is also given. [d] Using loop volumes of 100 μl for H_2 and O_2 a full O_2 uptake, *i.e.* 2.6 ml O_2 g^{-1}, was observed in all experiments.

Fig. 1 compares the H_2-OSC behaviour at r.t. of $Pt/Ce_{0.68}Zr_{0.32}O_2$ and Pt/Al_2O_3. Table 1 summarises quantitative OSC measurements and also some characterisation data. Fresh/reduced Pt/Al_2O_3 does not exhibit appreciable H_2-OSC at r.t. In contrast, a very high consumption of both H_2 and O_2 is observed over fresh/reduced $Pt/Ce_{0.68}Zr_{0.32}O_2$, indicating the crucial role of the $Ce_{0.68}Zr_{0.32}O_2$ in providing sites for the storage process. Water evolution is also observed in the latter case [Fig. 1(c), trace D], ruling out any kind of chromatographic effect. Negligible water production is observed over the fresh $Pt/Ce_{0.68}Zr_{0.32}O_2$, [Fig. 1(c), trace B], indicating that reduced Pt is necessary to promote hydrogen activation. In an attempt to establish the origin of this high r.t. H_2-OSC, H_2 chemisorption measurements were carried out on the $Pt/Ce_{0.68}Zr_{0.32}O_2$ at 193 and 298 K. Spilling of H_2 at 193 K is negligible allowing determination of H/Pt ratios.[7] 0.31 ml H_2 g^{-1} are adsorbed at 193 K which correspond to a dispersion of 94% upon assumption of H : Pt = 1 : 1 stoichiometry. The low H_2 uptake indicates that titration of hydrogen/oxygen adsorbed on the metal cannot be responsible for the observed H_2-OSC. Conversely, the amount of H_2 adsorbed/spilled over the support at 298 K is of the same order of magnitude of the values of H_2-OSC, suggesting a relevant role of the spillover phenomena in the oxygen storage. A higher relative pressure of H_2 during the H_2 pulse and presence of H_2O could account for the high values of O_2 uptake compared to the spilt H_2 detected in the chemisorption measurement. In fact, H_2 and O_2 consumption close to stoichoimetry is measured in the H_2-OSC experiment. Redox-ageing decreases both the surface area and the amount of adsorbed H_2 at 298 K by a factor of three. The H_2-OSC decreases by a factor of two. The important role of hydrogen spillover in giving high H_2-OSC at r.t. is supported by the data reported for Pt/Al_2O_3 and Pt/CeO_2. In particular, very small r.t. H_2-OSC is observed for the latter catalyst after redox-ageing, when spillover is negligible.

The comparison with CO as reducing agent and the OBC measurements is striking. Irrespectively of the pre-treatment, fresh/reduced or recycled, significant CO-OSC is observed only at and above 473 K, while OBC starts being significant at 673 K. In both these experiments, the reduction process may be envisaged as a measure of the oxygen diffusion towards the surface where it is removed either by interaction with CO or simple desorption, provided that surface processes are not rate limiting.[8] The very high H_2-OSC clearly points to a crucial role of H_2 in affecting the redox properties of these systems at low temperatures.

In conclusion, there is a dramatic dependence of the results obtained on the nature of the reducing environment with significantly high dynamic-OSC particularly apparent at low temperatures using H_2. At r.t. spillover phenomena seem to be a dominant factor. The implications of these findings need to be carefully considered when the results of such measurements are extended to the extremely complicated conditions encountered in three-way catalysis.

The present work has received financial support from the TMR Program of the European Commission (Contract FMRX-CT-96-0060). Financial support from University of Trieste, the Ministero dell'Ambiente (Roma), contract n. DG 164/SCOC/97, Regione Friuli Venezia-Giulia, 'Fondo regionale per la ricerca', the CICYT (Contract No.: MAT96-0931) and the Junta de Andalucía are also acknowledged.

Notes and references

1 H. C. Yao and Y. F. Yu Yao, *J. Catal.*, 1984, **86**, 254.
2 S. Bernal, G. Blanco, M. A. Cauqui, P. Corchado, J. M. Pintado and J. M. Rodriguez-Izquierdo, *Chem. Commun.*, 1997, 1545.
3 K. C. Taylor, *Catalysis-Science and Technology*, ed. J. R. Anderson M. Boudart, ch. 2, Springer-Verlag, Berlin, 1984.
4 The CEZIRENCAT project is a multi-laboratory project in the area of three-way catalysis funded by the European Union. Home page: http://www.dsch.univ.trieste.it/cezirencat/index.html.
5 M. Daturi, C. Binet, J. C. Lavalley, H. Vidal, J. Kašpar, M. Graziani and G. Blanchard, *J. Chim. Phys.*, 1998, **95**, 2048.
6 P. Fornasiero, J. Kašpar, V. Sergo and M. Graziani, *J. Catal.*, 1999, **182**, 56.
7 S. Bernal, F. J. Botana, J. J. Calvino, M. A. Cauqui, G. A. Cifredo, A. Jobacho, J. M. Pintado and J. M. Rodriguez-Izquierdo, *J. Phys. Chem.*, 1993, **97**, 4118.
8 A. Trovarelli, *Catal. Rev. -Sci. Eng.*, 1996, **38**, 439.

Communication a909751a

ChemComm

Encapsulation of two aromatics by a carcerand-like capsule of nanometre-scale dimensions†

Leonard R. MacGillivray,* Peter R. Diamente, Jennifer L. Reid and John A. Ripmeester

Steacie Institute for Molecular Sciences, National Research Council of Canada, Ottawa, Ontario, Canada K1A 0R6. E-mail: lmacgil@ned1.sims.nrc.ca

Received (in Columbia, MO, USA) 10th November 1999, Accepted 7th January 2000

Co-crystallization of *C*-methylcalix[4]resorcinarene 1 with 4,4′-bipyridine 2 in the presence of nitrobenzene 3 yields a six-component carcerand-like capsule, 2(1)·4(2), held together by 16 hydrogen bonds, in which two molecules of 3 are aligned within the interior of the complex in a head-to-head fashion.

Using a modular approach to molecular self-assembly, it has been shown that co-crystallization of *C*-methylcalix[4]resorcinarene **1** with 4,4′-bipyridine **2** typically yields a one-dimensional (1D) host–guest wave-like polymer, **1**·2(**2**), in which the cavity of **1** is deepened supramolecularly, interacting with two stacking pyridine units of **2** by way of four O–H···N hydrogen bonds.[1] The cavity created by the five molecules, which may be induced to form by way of guest template effects,[2] is remarkably flexible, being able to accommodate either single[3] or multiple guests,[4] many of which are too large to fit within the parent receptor **1**,[2] by way of a conformational change of the network.

During experiments aimed at attempts to isolate multiple guests within **1**·2(**2**), we have discovered the ability of the components of the wave-like framework to undergo a structural reorganization to form a discrete, six-component carcerand-like capsule,[5] 2(**1**)·4(**2**), held together by 16 hydrogen bonds (Fig. 1). The capsule, which is a supramolecular isomer[6] of the parent 1D material **1**·2(**2**), assembles in the solid state such that the cavity of the host, which is of nanometre-scale dimensions,[7] encapsulates two identical aromatic guests aligned within the complex in a head-to-head fashion. Whereas **1** has been shown to form multi-component capsules based upon protic solvent molecules (*e.g.* H_2O, PrOH, EtOH),[8–10] 2(**1**)·4(**2**) represents, to the best of our knowledge, the first example of a hydrogen-bonded capsule, based upon **1**, formed using an aromatic spacer as a 'bridging unit'. Our observations also confirm the ability of nano-sized capsules to accommodate more than one guest,[7] where understanding the spatial relationships displayed by the guests of such multi-guest host systems is of much current interest.[11]

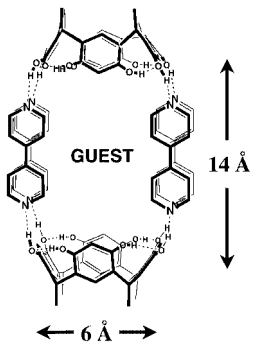

2(**1**)·4(**2**)

Fig. 1 Structure of 2(**1**)·4(**2**).

† Published as NRCC No. 43828.

Addition of **1** (0.021 g) to a boiling aliquot of THF (0.5 ml) and EtOH (1.0 ml) in the presence of **2** (0.012 g) and nitrobenzene **3** (3.0 ml) yielded, upon slow cooling, dark yellow crystals of **1**·2(**2**)·2(**3**) suitable for X-ray analysis. The formulation of **1**·2(**2**)·2(**3**) was confirmed by ^{1}H NMR spectroscopy and single-crystal X-ray diffraction.‡

An ORTEP perspective of 2(**1**)·4(**2**), along with a space-filling view, is shown in Fig. 2. As in the case of the wave-like framework **1**·2(**2**),[1–4] the components of 2(**1**)·4(**2**) have assembled in the solid state such that four pyridine units of **2**, in the form of two stacked dimers, interact with two opposite resorcinol units of **1** by way of four O–H···N hydrogen bonds [O···N separations (Å): O(1)···N(1) 2.75(1), O(2)···N(3) 2.71(1), O(5)···N(2) 2.74(1), O(6)···N(4) 2.68(1)]. The remaining hydroxy groups of **1** form four O–H···O hydrogen bonds [O···O separations (Å): O(3)···O(2) 2.76(1), O(4)···O(5) 2.79(1), O(7)···O(6) 2.79(1), O(8)···O(1) 2.71(1)] along the wider rim of **1** such that the macrocycle, as in **1**·2(**2**), adopts a bowl-like conformation with approximate C_{2v} symmetry. Unlike **1**·2(**2**), however, the four bipyridines of 2(**1**)·4(**2**), which act as bifunctional hydrogen bond acceptors, serve to bridge two, rather than three, molecules of **1**. This, in turn, gives rise to a discrete, six-component assembly held together by eight intermolecular O–H···N and eight intramolecular O–H···O hydrogen bonds, for a total of 16 structure-directing O–H···X (X = N, O) forces. In this arrangement, the cavities of **1**, which sit around a crystallographic center of inversion, are aligned in a head-to-head fashion such that the wider rims of the macrocycles, along with **2**, define a cylindrical cavity, of idealized D_{2h} symmetry, with dimensions ~6.0 × 14.2 Å. Indeed, the structure of 2(**1**)·4(**2**) is reminiscent of a carcerand[5] in which the eight covalent bonds that typically connect four spacer units to two molecules of **1** have been replaced by eight O–H···N forces.

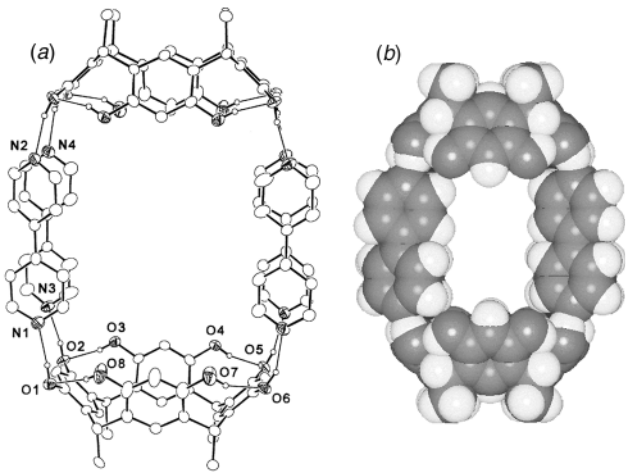

Fig. 2 (*a*) ORTEP perspective of the six-component capsule 2(**1**)·4(**2**), and (*b*) space-filling view. Selected interatomic distances (Å): O(1)···N(1) 2.75(1), O(2)···N(3) 2.71(1), O(5)···N(2) 2.74(1), O(6)···N(4) 2.68(1), O(3)···O(2) 2.76(1), O(4)···O(5) 2.79(1), O(7)···O(6) 2.79(1), O(8)···O(1) 2.71(1).

DOI: 10.1039/a909339g

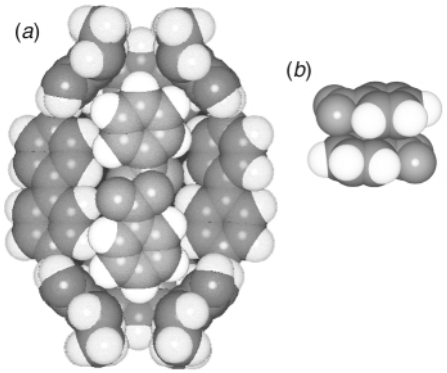

Fig. 3 Space-filling views of the guests of **1**·2(**2**)·2(**3**): (*a*) cut-away view of 2(**1**)·4(**2**)·2(**3**) displaying the two encapsulated aromatics (one occupied site is shown for clarity), and (*b*) the anti-parallel arrangement adopted by the guests exterior to 2(**1**)·4(**2**)·2(**3**).

A cut-away space-filling view depicting the guests of 2(**1**)·4(**2**) is shown in Fig. 3(*a*). Two molecules of **3**, which are disordered across two independent sites (75 : 25 occupancy), have assembled within the six-component complex in a head-to-head fashion such that the aromatic rings of the guests are directed into separate ends of the capsule,[7,11] each interacting with the interior of **1** by way of C–H···π interactions.[15] In these orientations, the phenyl groups of the guests of the major and minor occupied positions, in a way similar to **1**·2(**2**)·*p*-chlorotoluene,[2] lie approximately 20 and 27° off-axis to the principal rotation axis of the host and are rotated, in contrast to **1**·2(**2**)·*p*-chlorotoluene,[2] by approximately 78 and 21° along the symmetry axis of **1**, respectively.§ The nitro groups of the two encapsulated molecules are then observed to fill the center of the capsule, being separated by a distance of 3.6 Å. Interestingly, the organization displayed by the two molecules of **3** within 2(**1**)·4(**2**), in which two highly electron withdrawing substituents are oriented in close proximity,[11] contrasts that of pure **3** which self-assembles in the solid state, by way of C–H···O forces, to form antiparallel dimers.[16] Moreover, such observations confirm the ability of nano-sized capsules to encapsulate multiple guests where the cavities of such systems have been shown to impose spatial arrangements of guests not typically encountered in the free molecules.[7,11]¶

The capsule 2(**1**)·4(**2**) assembles in the solid state, in a tail-to-tail manner, to form 1D columnar arrays, which lie off-set and form a 2D layered architecture, in which two molecules of **3** are sandwiched between adjacent host–guest complexes. As shown in Fig. 3(*b*), in contrast to the two encapsulated guests, the aromatics located exterior to the host–guest complex assemble by way of face-to-face π–π interactions such that they form, in a way similar to pure **3**, antiparallel dimers (plane-to-plane separation: 3.35 Å).[16] Thus, **1**·2(**2**)·2(**3**) is an inclusion compound that possesses two different cavities, both of which accommodate two copies of the same guest in which the guests assemble in specific ways to meet the electronic and steric demands of each cavity.

In this report, we have revealed the ability of **1** to assemble with **2**, in the presence of a suitable guest, to form a six-component carcerand-like capsule, that is a supramolecular isomer of an extended 1D framework, held together by 16 hydrogen bonds.‖ The capsule, which is of nano-metre scale dimensions, features a cavity that hosts two identical aromatics as guests. With such observations realized, we are now investigating whether this system may be used to encapsulate additional guests where it may be possible to isolate two different molecules within the cavity of the assembly.[11] We are also investigating whether it is possible to lengthen 2(**1**)·4(**2**)[3] such that further analogies, in terms of structure and function, between discrete[8] and infinite[1–4] host–guest frameworks based upon **1** may be realized.

We are grateful for funding from the Natural Sciences and Engineering Research Council of Canada (graduate scholarship, J. L. R.; research grant, J. A. R.).

Notes and references

‡ *Crystal data* for **1**·2(**2**)·2(**3**): triclinic, space group $P\bar{1}$, a = 10.731(1), b = 15.075(1), c = 16.882(1) Å, α = 95.727(1), β = 94.860(1)°, γ = 93.915(2)°, U = 2699.4(3) Å^3, D_c = 1.36 g cm^{-3}, Mo-Kα radiation (λ = 0.71070 Å) for Z = 2. Least-squares refinement based on 3549 reflections with $I_{net} > 2.0\sigma(I_{net})$ (out of 6097 unique reflections) led to a final value of R = 0.071. Aromatic and hydroxy hydrogen atoms were placed by modelling the moieties as rigid groups with idealised geometry, maximising the sum of the electron density at the calculated hydrogen positions. Structure solution was accomplished using SHELXS-86 (ref. 12) and refinement was conducted using SHELXL93 (ref. 13) locally implemented on a pentium-based IBM compatible computer. Structure refinements and production of the figures were accomplished with the aide of RES2INS (ref. 14). CCDC 182/1533. See http://www.rsc.org/suppdata/cc/a9/a909339g/ for crystallographic data in .cif format.

§ For comparison, the aromatic guest of **1**·2(**2**)·*p*-chlorotoluene lies approximately 39° off-axis to the principle rotation axis of the host and is rotated by 0° along the axis of **1**.

¶ Such spatial constraints can, for example, give rise to reactivity (see ref. 11).

‖ Experiments are underway to determine if 2(**1**)·4(**2**) is maintained in solution.

1 L. R. MacGillivray and J. L. Atwood, *J. Am. Chem. Soc.*, 1997, **119**, 6931.
2 L. R. MacGillivray, J. L. Reid and J. A. Ripmeester, *CrystEngComm*, 1999, 1.
3 L. R. MacGillivray, K. T. Holman and J. L. Atwood, *Cryst. Eng.*, 1998, **1**, 87.
4 L. R. MacGillivray, K. T. Holman and J. L. Atwood, *Trans. Am. Crystallogr. Assoc.*, 1998, **33**, 129.
5 D. J. Cram and J. M. Cram, *Container Molecules and Their Guests*, ed. J. F. Stoddart, Royal Society of Chemistry, Cambridge, 1994.
6 T. L. Hennigar, D. C. MacQuarrie, P. Losier, R. D. Rogers and M. J. Zaworotko, *Angew. Chem., Int. Ed. Engl.*, 1997, **36**, 972.
7 T. Heinz, D. M. Rudkevich and J. Rebek, Jr., *Nature*, 1998, **394**, 764.
8 L. R. MacGillivray and J. L. Atwood, *Nature*, 1997, **389**, 469.
9 K. N. Rose, L. J. Barbour, G. W. Orr and J. L. Atwood, *Chem. Commun.*, 1998, 407.
10 K. Murayama and K. Aoki, *Chem. Commun.*, 1998, 607.
11 F. C. Tucci, D. M. Rudkevich and J. Rebek, Jr., *J. Am. Chem. Soc.*, 1999, **121**, 4928.
12 G. M. Sheldrick, *Acta. Crystallogr., Sect. A*, 1990, **46**, 467.
13 G. M. Sheldrick, SHELXL93, University of Göttingen, Germany, 1993.
14 L. J. Barbour, RES2INS, University of Missouri-Columbia, Missouri, USA, 1997.
15 G. R. Desiraju and T. Steiner, *The Weak Hydrogen Bond in Structural Chemistry and Biology*, OUP, Oxford, 1999.
16 R. Boese, D. Bläser, M. Nussbaumer and T. M. Krygowski, *Struct. Chem.*, 1992, **3**, 363.

Communication a909339g

ChemComm

Enhancement in helicity of an oligopeptide by its organization onto a dendrimer template

Nobuyuki Higashi,* Tomoyuki Koga, Norio Niwa and Masazo Niwa*

Department of Molecular Science & Technology, Faculty of Engineering, Doshisha University, Kyo-tanabe, Kyoto 610-0321, Japan. E-mail: nhigashi@mail.doshisha.ac.jp

Received (in Cambridge, UK) 6th December 1999, Accepted 27th January 2000

An oligopeptide comprised of γ-benzyl-L-glutamic acid has been successfully assembled on an amido amine dendrimer surface by graft polymerization and the resultant dendrimer has shown drastic enhancement in helicity of the peptide segment.

Here we describe the assembly of an oligopeptide onto the surface of an amine-terminated, poly(amido amine) (PAMAM) dendrimer and the enhancement in helicity of the oligopeptide.

Much effort has been dedicated to the molecular design and synthesis of model proteins to define interactions involved in protein folding[1,2] and to develop protein-based materials.[3] Protein tertiary structures can be looked upon as assemblies of secondary structural elements (α-helix, β-strand, reverse turn). This model has been the basis for the design of artificial proteins. A recent approach to protein design is to use a rigid template molecule.[4] Many artificial proteins have been prepared in aqueous solutions by attaching peptide blocks to templates that direct the component helices into a protein-like packing arrangement, *e.g.* a bundle structure of α-helices.[5] The amphiphilic properties of the helical blocks seem to be essential to stabilize such a bundle structure. We have devised a strategy in which purely synthetic polypeptides are aligned on two-dimensional media[6] such as on water and on Au surfaces. Poly(L-glutamic acid) has been chosen as a structural element because of its ease of synthesis and well-defined conformational characteristics in water. We now describe that complete surface modification of a three-dimensional dendrimer with an oligopeptide can be accomplished by graft polymerization of γ-benzyl-L-glutamate *N*-carboxy anhydride (BLG-NCA) and the resulting graft chains show interesting conformational properties.

Dendrimers are known to be hyperbranched macromolecules possessing a very high concentration of surface functional groups.[7] A variety of dendrimers have been developed by introducing functionalities into these terminal groups. For example, dendrimers terminated with an amino acid,[8] a sugar,[9] and a perfuluoroalky[10] or alkyl[11] chain show encapsulation functions for guest molecules. The other structural feature of dendrimers is the high degree of control over molecular weight and shape. The diameters of the spherical dendrimers range from 3 to 10 nm.[12] Taking account of these features in shape, the oligopeptide-attached dendrimer in this study may be a relevant candidate for model proteins.

The third-generation, amine-terminated PAMAM dentrimer (G3-NH_2) with branches and an ethylenediamine core was used as a template for assembly and an initiator for graft polymerization. As shown in Scheme 1, BLG-NCA (3.8 mmol) was polymerized with G3-NH_2 ([NH_2] = 0.30 mmol) in $CHCl_3$ at room temperature. A relatively short chain length of the peptide segment (degree of polymerization, n = 10–15) was employed because the number of amino acid units is appropriate for both characterization of the resultant dendrimer and elucidation of the effect of assembly. After stirring for 30 min, the reaction mixture was poured into a large excess of Et_2O and then purified and dried, giving a white powdery product (G3-PBLG) with a yield of 97%. The M_w/M_n value† determined by size exclusion chromatography was reasonably narrow (M_w/M_n = 1.06), indicating the absence of the polymerization catalyzed by the tertiary amine of the inner part of PAMAM dendrimer that produces a homopolymer of BLG-NCA with a broad molecular weight distribution.[9] ^{1}H and ^{13}C NMR spectroscopies (data not shown) supported the structure of G3-PBLG. In the ^{13}C NMR spectrum of G3-PBLG, no peaks assigned to the α- and β-carbons of the unreacted terminal amino groups of PAMAM dendrimer were observed, while those of G3-NH_2 appeared at δ_c 41 and 42, respectively. This means that the graft polymerization proceeded for all of the terminal amino groups located at the G3-NH_2 dendrimer surface. The n value of the grafted peptide segment was evaluated to be 12 on the basis of ^{1}H NMR analysis.‡

The secondary structure of G3-PBLG was investigated by means of circular dichroism (CD) and ^{1}H NMR spectroscopy. For comparison, Pr-PBLG, which possesses a propyl group at the C-terminus of the PBLG chain, was prepared by polymerization of BLG-NCA initiated with propylamine instead of G3-NH_2. The ^{1}H NMR analysis of Pr-PBLG showed that n for the PBLG segment was also 12. In the CD spectrum of this CH_2Cl_2 solution ([glutamate unit] = 1.0 mM), a trough appears at *ca.* 222 nm, indicating the exsitence of a right-handed α-helix

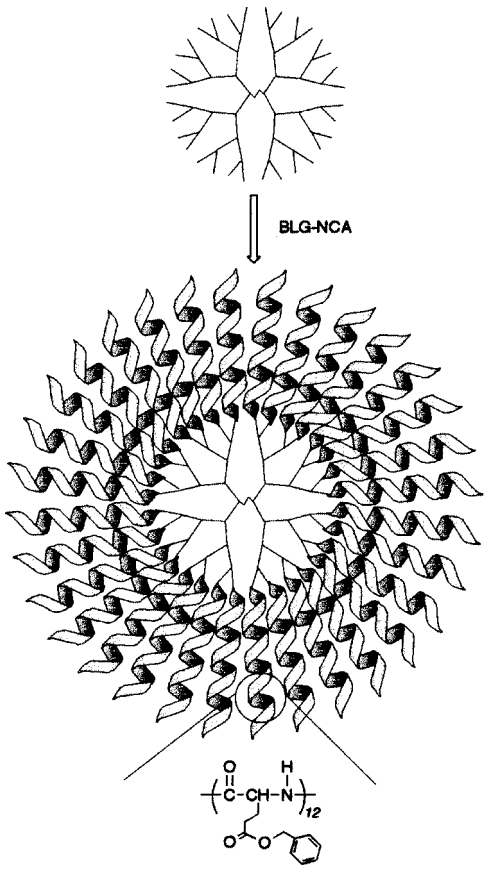

Scheme 1

DOI: 10.1039/a909586a

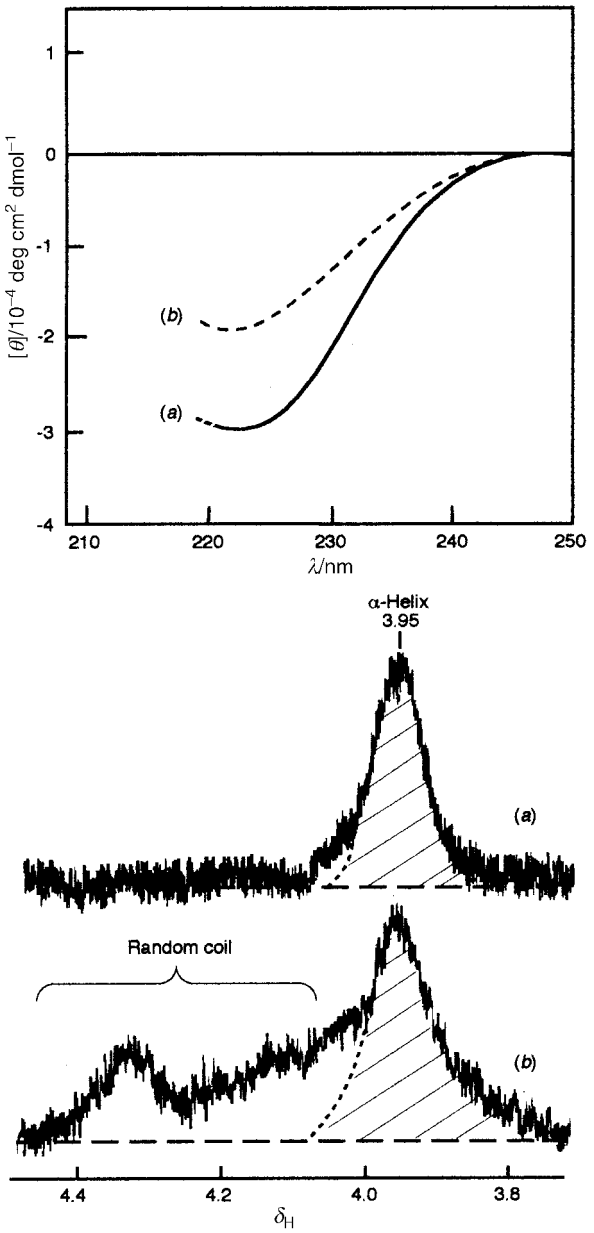

Fig. 1 CD and ^{1}H NMR spectra of G3-PBLG (*a*) and Pr-PBLG (*b*) in CH_2Cl_2 (for CD) or CD_2Cl_2 (for NMR) at 25 °C; [glutamate unit] = 1.0×10^{-3} M.

conformation (Fig. 1). The helix content of the Pr-PBLG solution is calculated to be 53% from the observed molar ellipticity $[\Theta]$ at 222 nm ($[\Theta] = 1.8 \times 10^{-4}$ deg cm^2 dmol^{-1}).§ This helix content is reasonable taking account of such a short segment length as $n = 12$.[13] On the other hand, the molar ellipticity of the G3-PBLG solution is found to be enhanced drastically, compared with that of the Pr-PBLG solution. Surprisingly, the helix content goes up to 92%. To obtain more quantitative information on the secondary structure, ^{1}H NMR spectra were measured in CD_2Cl_2 under the same conditions (Fig. 1). The α-C*H* resonance signal of the PBLG main chain was known to give a peak at δ_H 3.95 ascribed to the α-helix conformation, while giving an apparent lowfield shift on going from the helix to the random coil form.[14] From signal areas based on α-helix and random coil forms, the helix contents were evaluated to be 93 and 57% for G3-PBLG and Pr-PBLG, respectively. These values are consistent with those obtained by CD analysis. FTIR spectra (data not shown), in particular in amide II band region of the main chain, showed that β-sheet structures were absent for both PBLGs. It is clear from these spectral data that transfer and aggregation of the PBLG segment onto the dendrimer surface from bulk solution would cause such an enhancement in helicity since the PBLG segment lengths (*n*) of Pr-PBLG and G3-PBLG are the same. The enhancement of helicity due to aggregation of helices has sometimes been observed in aqueous solutions when a helix-bundle structure is formed by assembling with a template.[5] In those cases, it has been demonstrated that the hydrophobic effects among the side chain groups play an important role in stabilizing the helical conformation. Presumably, in our case, the driving force for causing such enhancement in helicity must also be the hydrophobic effect, resulting from the characteristic shape of the spherical dendrimer surface, at which the peptide segments are forced to assemble densely, which will require further exploration.

Notes and references

† M_w and M_n denote weight-average molecular weight and number-average molecular weight, respectively, determined by means of size exclusion chromatography, and the ratio of M_w/M_n is the polydispersity of the polypeptides prepared by polymerization of NCA. Size exclusion chromatography was performed in DMSO at 30 °C, with a Shimazu Model LC-5A high performance liquid-chromatograph apparatus (column, Shodex KD803 and 804).

‡ The *n* value was calculated by using the area ratio of the signal of CH_2 (benzyl) in the PBLG segment to that of CH_2 in the PAMAM dendrimer, observed in the ^{1}H NMR spectrum of G3-PBLG.

§ The helix content was calculated by using the following equation: helix content (%) = $([\Theta]_{222}/[\Theta]_h) \times 100$, where $[\Theta]_{222}$ and $[\Theta]_h$ are the molar ellipticity at 222 nm and −34 000 (deg cm^2 dmol^{-1} (ref. 15), respectively.

1 B. Gutte, M. Daumigngen and E. Wittschieber, *Nature*, 1979, **281**, 650.
2 M. H. Hecht, J. S. Richardson, D. C. Richardson and R. C. Ogden, *Science*, 1990, **249**, 884.
3 A. Nathan and J. Kohn, *Protein Engineering and Design*, ed. P. R. Carey, Academic Press, San Diego, 1996, p. 265.
4 M. Mutter and S. Vuilleumier, *Angew. Chem., Int. Ed. Engl.*, 1989, **28**, 535; P. Wallimann, R. J. Kennedy and D. S. Kemp, *Angew. Chem., Int. Ed.*, 1999, **38**, 1290.
5 T. Sasaki and E. T. Kaiser, *J. Am. Chem. Soc.*, 1989, **111**, 380; T. Hahn, W. A. Klis and J. M. Stewart, *Science*, 1990, **248**, 1544; R. M. Ghadiri, C. Soares and C. Choi, *J. Am. Chem. Soc.*, 1992, **114**, 825; P. E. Dawson and S. B. H. Kent, *J. Am. Chem. Soc.*, 1993, **115**, 7263.
6 For a recent review, see: N. Higashi and M. Niwa, *Colloids Surf. A*, 1997, **123/124**, 433 and references cited therein; M. Niwa, M.. Morikawa and N. Higashi, *Langmuir*, 1999, **15**, 5088.
7 For a recent review, see: F. W. Zeng and S. C. Zimmerman, *Chem. Rev.*, 1997, **97**, 1681 and references cited therein.
8 J. F. G. A. Jansen, E. M. M. de Brabander-van den Berg and E. W. Meijer, *Science*, 1994, **266**, 1226.
9 K. Aoi, K. Itoh and M. Okada, *Macromolecules*, 1995, **28**, 5391; K. Aoi, K. Tsutsumiuchi, A. Yamamoto and M. Okada, *Tetrahedron*, 1997, **53**, 15415.
10 A. I. Cooper, J. D. Londono, G. Wignall, J. B. McClain, E. T. Samulski, J. S. Lin, A.Dobrynin, M. Rubinstein, A. L. C. Burke, J. M. J. Fréchet and J. M. DeSimone, *Nature*, 1997, **389**, 368.
11 V. Chechik, M. Zhao and R. M. Crooks, *J. Am. Chem. Soc.*, 1999, **121**, 4910.
12 D. A. Tomalia and H. D. Durst, *Top. Curr. Chem.*, 1993, **165**, 193.
13 J. C. Mitchell, A. E. Woodward and P. Doty, *J. Am. Chem. Soc.*, 1957, **76**, 3955.
14 E. M. Bradbury, C. Crane-Robinson, H. Goldman and H. W. E. Rattle, *Nature*, 1968, **217**, 812.
15 K. T. O'Neil and W. F. DeGrado, *Science*, 1990, **250**, 646.

Communication a909586a

ChemComm

The self-assembly of benzyl alcohol derived deep-cavity cavitands: a new, highly efficient moiety for irreversible assemblies?†

Corinne L. D. Gibb, Edwin D. Stevens and Bruce C. Gibb*

Department of Chemistry, University of New Orleans, New Orleans, LA 70148, USA. E-mail: bgibb@uno.edu

Received (in Columbia, MO, USA) 7th October 1999, Accepted 29th November 1999

In the absence of an apparent (single) molecular template, the irreversible self-assembly of benzyl alcohol substituted, deep-cavity cavitands is shown to be a highly efficient process.

With aspirations to improve our understanding of self-assembly, chemists have begun to focus on systems where the convergence of the molecular subunits is not promoted by a single molecular template,[1–4] but rather where assembly occurs around multiple 'templates'.[5] When considering the nano-scale products which such manifold species 'templations' result in, two options are available. First, scientists have considered self-correcting systems as a means to product formation, an approach that utilizes thermodynamics to maximize the yield of the target.[6,7] Alternatively, using a (normally less efficient) irreversible process allows the potential isolation of intermediates, and hence a more detailed picture of the assembly process in question. In this latter paradigm, considerable work has been carried out in systems requiring a single template. Thus, extending the original work of Cram,[8–10] Sherman *et al.* have demonstrated how carceplex formation is governed by the topology of the molecular template so essential for their synthesis.[11] In contrast, probing irreversible self-assemblies that require manifold species 'templation' has been relatively unexplored, primarily because of a lack of suitable supramolecular motifs[12] that can effectively drive such assemblies. Thus in the formation of a number of large, cavity-containing molecules, it has been noted that when using phenol groups to form the supramolecular motif, yields have tended to decrease toward statistical or worse.[10,13,14] We report here on an irreversible assembly in which the subunit utilizes benzyl alcohol groups in its supramolecular motif. Although the assembly occurs in the absence of a single molecular template, and the eight new covalent bonds created in the process are formed in a non-correcting manner, each is formed with an efficiency greater than 97%. As a result therefore, the synthesis of the nanoscale host is highly efficient.

We recently demonstrated the stereoselective bridging of resorcinarenes with benzal bromide, a process which provided access to a new series of deep-cavity cavitands (DCCs) epitomized by structure **1**.[15] More recently, we have noted that this reaction can be applied to a range of benzal bromides to form a series of DCCs whose 'upper row' of aromatic rings may be substituted at the *o*, *m* or *p* position.[16] We chose one example of these, the *p*-Br derivative **2** as an entry point for the synthesis of DCCs **3** and **4** whose architecture should allow them to undergo an assembly process analogous to the carceplex reaction.[10,11] Our initial attempts to perform this 'dimerization' of DCCs centered around the tetrakis(4-hydroxyphenyl) derivative **3**. However, our studies showed that **3** was insufficiently stable in either acidic or basic conditions, a result we attribute to the ability of the electrons on the OH groups to conjugate through to the acetal bridges. Consequently, we synthesized DCC **4** whose essential nucleophilic centers possess slightly less preorganization, but are 'insulated' from the benzal bridging-carbon by the benzyl methylene group.

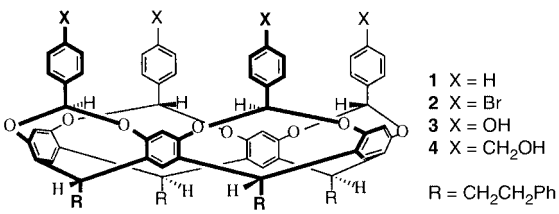

Our initial studies focused on the covalent joining of two molecules of **4** with the bis-electrophile CH_2BrCl (Scheme 1) in the absence of a large templating molecule. Our early results with a range of aprotic solvents[17] gave poor yields of **5**, the bulk of **4** being transformed into intractable polymeric material and trace quantities of DCC–solvent conjugates. DMSO on the other hand led to a considerable improvement, with a highly efficient[18] 80% yield of **5** being obtained under dilute conditions, a remarkable yield for an irreversible process.[19] Yields decreased at concentrations > *ca.* 2 mmolar, presumably because of the highly concentration-dependent formation of the superbase, methylsulfinyl carbanion.[20] However at these concentrations, yields could be increased by the addition of small quantities of water to generate the less basic hydroxide[21] and inhibit[20] the superbase formation.

Definitive formation of **5** came from an X-ray crystallographic determination (Fig. 1).[22] In the solid state, both hemispheres of **5** are rotated slightly with respect to each other, while the linker groups each display the anomeric effect with *gauche–gauche* conformations for the $CH_2OCH_2OCH_2$ units. A consideration of the salient inter-carbon atom distances indicates that the cavity of **5** is approximately 19 × 15 Å, while the portals are roughly 9.5 × 11.5 Å. Not surprisingly, disordered solvent molecules within the cavity precluded an accurate determination of its composition.

Although the assembly is highly efficient, DCC **4** is too large to fit within the cavity of the product. Thus, there is no suitable, single template to promote the formation of **5** over and above

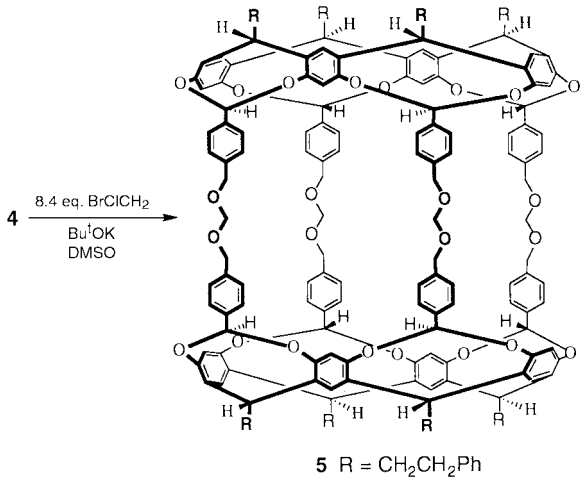

Scheme 1

† Synthetic and spectroscopic details for **3**–**6** and a full description of the term 'Assembly Number' are available from the RSC web site, see http://www.rsc.org/suppdata/cc/a9/a908144e/

DOI: 10.1039/a908144e

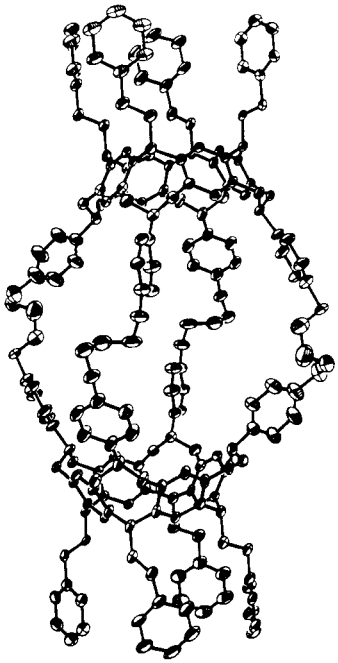

Fig. 1 ORTEP diagram of DCC dimer **5**. Hydrogen atoms have been omitted for clarity.

random polymer. As it seems entropically unlikely that several species in solution organize themselves into a multiple species template; we surmise that this efficient assembly process is occurring 'around' bulk solvent.

What lies behind this efficient assembly? In normal cavitands, the supramolecular motif that drives the reaction is constructed with the phenol group, a moiety that in the presence of base can form a charged hydrogen bond (CHB) with its conjugate base.[23] As yet, we have been unable to definitively ascertain if an analogous process is occurring in the assembly of **4**. However, variations in the base utilized for the reaction tentatively support this hypothesis.[24] Furthermore, work by Kolthoff[25]—who demonstrated that weakly acid phenols formed stronger CHBs with their conjugate bases than their more acidic counterparts—suggests that the poorly acidic benzyl alcohol group[21*a*] should form very strong CHBs.

In summary, we have demonstrated an efficient, irreversible self-assembly that occurs in the absence of a single, molecular template. Investigations into the use of the benzyl alcohol group in other molecular subunits are currently underway.

We are grateful to Richard B. Cole of the New Orleans Center for Mass Spectrometry Research for mass analysis of the deep-cavity cavitands. This work was partially supported by the Louisiana Board of Regents Support fund (1997-00)-RD-A-23, a Research Innovation Award from the Research Corporation, and the Donors of the Petroleum Research Fund, administered by the American Chemical Society.

Notes and references

1 R. G. Chapman and J. C. Sherman, *Tetrahedron*, 1997, **53**, 15 911.
2 J. S. Lindsey, *New J. Chem.*, 1991, **15**, 153.
3 D. H. Busch, *J. Inclusion Phenom. Mol. Recognit. Chem.*, 1992, **12**, 389.
4 S. Anderson, H. L. Anderson and J. K. M. Sanders, *Acc. Chem. Res.*, 1993, **26**, 469.
5 Although templation has been defined in a variety of publications (refs. 1–4), to the best of the authors' knowledge there has been no attempt in the supramolecular chemistry field to precisely delineate between the terms 'templation' and 'solvation'. The few examples (using two or more templating molecules) (refs. 6, 7, 10, 13, 14) that lie in the 'gray area' between these two terms have either not raised this semantic problem, or have referred to the process at hand as templation. Thus, we will refer to the described process as being 'templated' by bulk solvent, although 'solvated' may be an equally applicable term.
6 For systems using metal ion binding motifs see: N. Takeda, K. Umemoto, K. Yamaguchi and M. Fujita, *Nature*, 1999, **398**, 794 and references therein.
7 For assemblies using various hydrogen bonded motifs see: L. R. MacGillivray and J. L. Atwood, *Nature*, 1997, **389**, 469; Y. Tokunaga, D. M. Rudkevich, J. Santamaría, G. Hilmersson and J. Rebek Jr., *Chem. Eur. J.*, 1998, **4**, 1449; J. Kang, J. Santamaría, G. Hilmersson, J. Rebek Jr., *J. Am. Chem. Soc.*, 1998, **120**, 7389.
8 D. J. Cram, *Science*, 1983, **219**, 1177.
9 L. M. Tunstad, J. A. Tucker, E. Dalcanale, J. Weiser, J. A. Bryant, J. C. Sherman, R. C. Helgeson, C. B. Knobler and D. J. Cram, *J. Org. Chem.*, 1989, **54**, 1305.
10 D. J. Cram and J. M. Cram, *Container Molecules and Their Guests*, Royal Society of Chemistry, Cambridge, 1994.
11 A. Jasat and J. C. Sherman, *Chem. Rev.*, 1999, **99**, 932; R. G. Chapman, N. Chopra, E. D. Cochien and J. C. Sherman, *J. Am. Chem. Soc.*, 1994, **116**, 369; R. G. Chapman and J. C. Sherman, *J. Am. Chem. Soc.*, 1995, **117**, 9081; K. Nakamura, C. Sheu, A. E. Keating, K. N. Houk, J. C. Sherman, R. G. Chapman and W. L. Jorgensen, *J. Am. Chem. Soc.*, 1997, **119**, 4321.
12 We define here the term 'supramolecular motif' as the repeating pattern of functional groups that contribute significantly to the overall enthalpy (orentropy) change during assembly. We note that the term 'function groups' fails to differentiate between those moieties that drive the assembly process, and those that do not. The term 'functional groups' also invokes images of well-defined areas in a molecule that contain elements other than C and H, but ignores large tracts of hydrocarbon surface that are often important in the self-assembly of proteins.
13 J. A. Bryant, M. T. Blands, M. Vincenti and D. J. Cram, *J. Chem. Soc., Chem. Commun.*, 1990, 1403; T. A. Robbins, C. B. Knobler, D. R. Bellew and D. J. Cram, *J. Am. Chem. Soc.*, 1994, **116**, 111; R. C. Helgeson, K. Paek, C. B. Knobler, E. F. Maverick and D. J. Cram, *J. Am. Chem. Soc.*, 1996, **118**, 5590.
14 (*a*) N. Chopra and J. C. Sherman, *Angew. Chem., Int. Ed.*, 1999, **38**, 1955; (*b*) C. von dem Bussche-Hünnefeld, D. Bühring, C. B. Knobler and D. J. Cram, *J. Chem. Soc., Chem. Commun.*, 1995, 1085.
15 H. Xi, C. L. D. Gibb, E. D. Stevens and B. C. Gibb, *Chem. Commun.*, 1998, 1743.
16 H. Xi, G. L. D. Gibb and B. C. Gibb, *J. Org. Chem.*, 1999, 9286–9288.
17 Solvents were: DMF, DMA, tetramethyl urea and NMP.
18 As a measure of the efficiency of these assemblies, we define the term 'assembly number' (AN) as the ratio of the isolated yield of a compound over its theoretical yield (derived by assuming 100% efficiency for each of the possible reaction options available to the *isolated* self-assembly components which appear in the product). Such a derivation (see the supplementary data for a full description) provides a semi-quantitative guide to these (and other similar) assemblies: AN < 1 not an assembly process, AN > 1 (the higher the better), an assembly process. For **5**, AN = 4.04 for optimal carceplex formation (ref. 11), AN = 1.45; for extended hemicarcerands [ref. 14(*b*)], AN = 1.62.
19 Evidence of irreversibility will be published elsewhere.
20 J. I. Brauman, J. A. Bryson, D. C. Kahl and N. J. Nelson, *J. Am. Chem. Soc.*, 1970, **92**, 6679.
21 (*a*) F. G. Bordwell, *Acc. Chem. Res.*, 1988, **21**, 456; (*b*) W. N. Olmstead, Z. Margolin and F. G. Bordwell, *J. Org. Chem.*, 1980, **45**, 3295.
22 *Crystal data* for **5**: $C_{188}H_{160}O_{24}$ $(C_2H_6SO)_{10.5}$, monoclinic, space group $P2_1/c$, colorless prism, a = 20.068(2), b = 19.803(2), c = 25.310(3) Å, β = 92.747(2)°, V = 10047(2) Å^3, Z = 2, D_{calc} = 1.288 Mg m^{-3}, T = 130(2) K, μ = 0.195 mm^{-1}, 23737 reflections measured, 9842 unique reflections, R_{int} = 0.1046, $R(F)$ = 0.1081 for reflections with $I > 2\sigma(I)$. The molecule sits on an inversion center. DMSO solvent molecules are distributed over two fully occupied sites and eight partially occupied sites in each asymmetric unit. An additional 19 peaks corresponding to atoms of unresolved DMSO or $CHCl_3$ solvent are included as partially occupied oxygen atoms in the model. No peaks corresponding to solvent atoms are observed inside the cavity, indicating a high degree of disorder within the host. CCDC 182/1506. See http://www.rsc.org/suppdata/cc/a9/a908144e/ for crystallographic data in .cif format.
23 R. G. Chapman, G. Olovsson, J. Trotter and J. C. Sherman, *J. Am. Chem. Soc.*, 1998, **120**, 6252.
24 No reaction was observed when $KHCO_3$, K_2CO_3 or DBU were used as base. Stronger bases (the following pK_a values are noted in DMSO), KOMe (pK_a = 29.0) [ref. 21(*a*)], KOEt (pK_a = 29.8) [ref. 21(*b*)], KOH (pK_a = 31.2) [ref. 21(*a*)] gave poor results compared to Bu^{t}OK (pK_a = 32.2) [ref. 21(*a*)]. In these cases, the bulk of the product was polymeric. Using KOH and Bu^{t}OH did not give a high yield of **5**, a fact that, in conjunction with our observation that the reaction gave only polymer with < 8 equiv. of base, may be attributed to the slow dissolution of KOH.
25 I. M. Kolthoff, M. K. Chantooni and S. Bhowmik, *J. Am. Chem. Soc.*, 1968, **90**, 23.

Communication a908144e

Optical resolution of sulfoxides by inclusion in host dehydrocholic acid

Olga Bortolini, Giancarlo Fantin,* Marco Fogagnolo, Alessandro Medici and Paola Pedrini

Università di Ferrara, Dipartimento di Chimica, via Borsari 46, 44100 Ferrara, Italy. E-mail: fnn@dns.unife.it

Received (in Liverpool, UK) 12th November 1999, Accepted 18th January 2000

Dehydrocholic acid serves as an effective chiral host molecule for the optical resolution of aryl alkyl sulfoxides by inclusion.

The optical resolution of different classes of organic substrates by lattice inclusion compounds is receiving significant attention on account of its high efficiency and simplicity.[1] Bile acids have often been used as host molecules both in the direct resolution of a guest racemate[2,3] and in enantioselective transformation of an inclusion compound.[4] The resolution of aliphatic alcohols with cholanamide (3,7,12-trihydroxy-5-cholan-24-amide)[2] and that of lactones in the presence of cholic and deoxycholic acid[3] are examples of the former case.

Chiral sulfoxides are finding increasing use as auxiliaries in asymmetric synthesis[5] and as intermediates in the pharmaceutical industry.[6] Beside the classical resolution methods,[7] new strategies have been developed mainly based on the oxidation of prochiral sulfides by titanium peroxo species bearing chiral C_2 symmetric diols[8–10] (*e.g.* tartaric esters) or C_3 symmetric trialkanolamines.[11] However, the limited turnover numbers characterizing most of these oxidation procedures and the kinetic resolution *via* oxidation involving the sulfoxides so produced[12] prompted us to reconsider the resolution method to obtain enantiomerically pure sulfoxides.

Described here is the novel observation that dehydrocholic acid (3,7,12-triketo-5-cholan-24-oic acid) **1**, a bile acid derivative lacking steroidal hydroxy groups can serve as a host molecule to form inclusion compounds with different aryl alkyl sulfoxides **2**–**6**, leading to the effective optical resolution of this class of compounds.

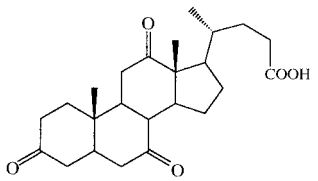

1

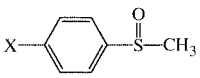

2 X = H,
3 X = CH_3
4 X = CH_3O
5 X = Cl
6 X = Br

The inclusion compounds of **1** with sulfoxides were obtained by two different methods based on direct absorption of the melted (method A) or solvent dissolved (method B) sulfoxide. The choice depends on the sulfoxide. In the former case the solid dehydrocholic acid is directly added to the melted sulfoxide in the absence of any solvent, whereas in the latter procedure **2**–**6** were dissolved in the minimum amount of Et_2O, and poured onto solid **1**. As shown in Table 1, both processes are equally effective, affording sulfoxides in good to high ees in the range 36–99%.

A view of the overall process is given in Scheme 1. On standing at room temperature for 48–72 h, dehydrocholic acid and the selected sulfoxide formed crystals[13] that were washed with Et_2O. The ethereal layer was separated from the solid phase and evaporated to give the crude sulfoxide in predominant (*S*) configuration. On the other hand, included sulfoxides were easily obtained in quantitative yields in (*R*) for **3**–**5** and (*S*) configuration for **2**, respectively, by dissolving the crystals with aqueous $NaHCO_3$ followed by extraction with Et_2O.[14] Furthermore, almost complete recovery of dehydrocholic acid can be obtained upon treatment of the aqueous basic layer with dilute mineral acid. No significant differences in optical and chemical yields were observed when recycled dehydrocholic acid was used.

The relative amount of the sulfoxide with respect to **1**, in the inclusion process, was expected to play an important role. Accordingly, a 3-fold excess of **2**–**6** over the bile acid favored high optical purities of the sulfoxides that are included in **1**, as shown from the data of Table 1, whereas a one-to-one stoichiometry increased the ees of the non-guest sulfoxides obtained from the Et_2O solution. As an example, when **6** is added in equimolar amounts to the bile acid, (*S*)-**6** is recovered from the solution and (*R*)-**6** is obtained from crystals in ees of about 70%. When a 3-fold excess of **6** is used the optical purity of (*R*)-**6** increased to 84% (Table 1).

Compared to **1** the efficiency of the well-known host cholic acid (3,7,12-trihydroxy-5-cholan-24-oic acid) is lower, affording sulfoxides with optical purities in the range 2–47%, depending on the sulfoxide. This is an example of the excellent ability of dehydrocholic acid, a non-naturally occurring steroid lacking hydroxy groups, to recognize sulfoxides according to

Table 1 Optical resolution of *p*-$XC_6H_4SCH_3$ sulfoxides **2**–**6** using dehydrocholic acid **1** as host

Sulfoxide	X	Method[a]	*t*/h	Ee[c] (%)	Predominant configuration[d]
2	H	A	72	74	*S*
		B	72	36	*S*
3	CH_3	A	72	86	*R*
		B	72	> 99	*R*
4	OCH_3	A	48	40	*R*
		B[b]	48	54	*R*
5	Cl	A	72	82	*R*
		B	72	77	*R*
6	Br	A	48	74	*R*
		B[b]	48	84	*R*

[a] Method A: 1 equiv. of **1** is added to 3 equiv. of melted sulfoxide. Method B: sulfoxide dissolved in Et_2O and added to **1**. [b] A few drops of EtOAc were added to Et_2O. [c] Determined by GC on Megadex DETTBS. [d] Absolute configurations of the material recovered from the crystals were determined by comparison of $[\alpha]_D$ with literature values, see refs. 8–11.

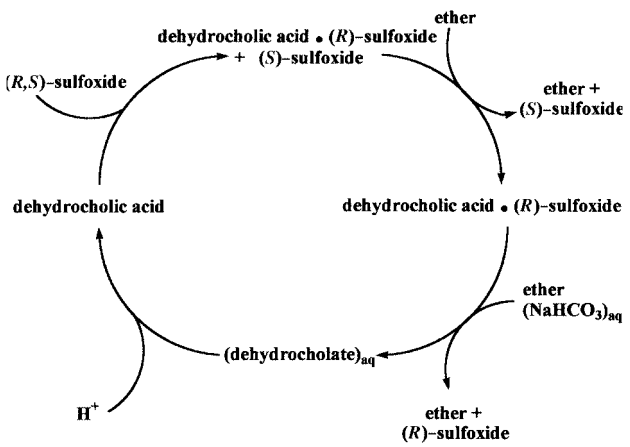

Scheme 1

DOI: 10.1039/a909013d

size, polarity and chirality. Work is in progress to extend this approach to other classes of organic chiral molecules.

This investigation was financially supported by Universita' di Ferrara.

Notes and references

1 F. Toda, *Top. Curr. Chem.*, 1987, **140**, 43.
2 K. Sada, T. Kondo and M. Miyata, *Tetrahedron: Asymmetry*, 1995, **6**, 2655.
3 M. Miyata, M. Shibakami and K. Takemoto, *J. Chem. Soc., Chem. Commun.*, 1988, 655.
4 F. Toda and K. Mori, *J. Chem. Soc., Chem. Commun.*, 1989, 1245.
5 M. C. Carreno, *Chem. Rev.*, 1995, **95**, 1717.
6 P. Pitchen, C. J. France, I. M. McFarlane, C. G. Newton and D. M. Thompson, *Tetrahedron Lett.*, 1994, **35**, 485.
7 C. Mioskowski and G. Solladiè, *Tetrahedron*, 1980, **36**, 227 and references therein.
8 J. M. Brunel, P. Diter, M. Duetsch and H. B. Kagan, *J. Org. Chem.*, 1995, **60**, 8086; F. Di Furia, G. Modena and R. Seraglia, *Synthesis*, 1984, 325 and references therein.
9 M. I. Donnoli, S. Supelchi and C. Rosini, *J. Org. Chem.*, 1998, **63**, 9392.
10 N. Komatsu, M. Hashizume, T. Sugita and S. Uemura, *J. Org. Chem.*, 1993, **58**, 4529.
11 F. Di Furia, G. Licini, G. Modena, R. Motterle and W. A. Nugent, *J. Org. Chem.*, 1996, **61**, 5175 and references therein.
12 A. Lattanzi, F. Bonadies, A. Senatore, A. Soriente and A. Scettri, *Tetrahedron: Asymmetry*, 1997, **8**, 2473.
13 The inclusion compounds have a host : guest ratio of 1 : 1 with **3**, **4** and **6** and 2 : 1 in the other cases. Work is in progress on this specific point.
14 For optical purity and absolute configuration, see footnotes of Table 1.

Communication a909013d

Covalent capture of dynamic hydrogen-bonded assemblies

F. Cardullo,[a] M. Crego Calama,[a] B. H. M. Snellink-Ruël,[a] J.-L. Weidmann,[a] A. Bielejewska,[a] R. Fokkens,[b] N. M. M. Nibbering,[b] P. Timmerman*[a] and D. N. Reinhoudt*[a]

[a] *Laboratory of Supramolecular Chemistry and Technology, MESA+ Research Institute, University of Twente, PO Box 217, 7500 AE Enschede, The Netherlands. E-mail: d.n.reinhoudt@ct.utwente.nl.*

[b] *Institute of Mass Spectrometry, University of Amsterdam, Nieuwe Achtergracht 129, 1018 WS Amsterdam, The Netherlands*

Received (in Liverpool, UK) 26th November 1999, Accepted 18th January 2000

Covalent linkage of the three calix[4]arene units in hydrogen-bonded assemblies $\mathbf{1}_3$•$(DEB)_6$ *via* a threefold ring closing metathesis (RCM) reaction quantitatively converts the dynamic assemblies into covalent systems (123-membered macrocycles) that can be easily characterized using MALDI-TOF MS and HPLC.

Dynamic combinatorial libraries have recently attracted a great deal of attention in the rapidly expanding field of combinatorial chemistry.[1] Such libraries have the potential to amplify the formation of the strongest binder as a result of a templating effect exerted by an added host or guest molecule.[2–7] Most literature examples involve dynamic systems based on the reversible formation of *covalent* bonds[2–5] or coordinative bonds.[6,7] Dynamic libraries based on the reversible formation of weak noncovalent interactions, like multiple hydrogen-bonding, have so far not received a great deal of attention, most likely because of severe characterization problems. Our group has reported the synthesis and characterization of a 4-membered dynamic library of hydrogen-bonded assemblies and recently we have shown that guest-templating effects are also applicable to these systems.[8,9] Increasing the structural diversity in these systems is easy and can be performed simply by mixing the appropriate number of individual components under thermodynamically controlled conditions. However, the serious lack of suitable characterization techniques currently limits the size of the libraries that can be made.

Here we describe the covalent capture of dynamic libraries of hydrogen-bonded assemblies $\mathbf{1}_3$•$(DEB)_6$, which converts these dynamic libraries into covalent analogues that can be readily characterized using conventional techniques like mass spectrometry and HPLC. We used the ring-closing metathesis (RCM) reaction,[10] because it is compatible with the hydrogen-bonded network in assembly $\mathbf{1}_3$•$(DEB)_6$. Moreover, it has been used previously for the cyclization of cyclic peptides,[11] catenane formation,[12,13] and post-modification of dendrimers.[14]

Reaction of assembly $\mathbf{1a}_3$•$(DEB)_6$ (R = H, n = 6),[15] carrying oct-7-enyl side chains, with Grubbs catalyst in CD_2Cl_2 resulted in the covalent linkage of the three calix[4]arene units **1a** (Fig. 1) *via* a threefold metathesis reaction giving the 123-membered macrocycle **2a** as the corresponding hydrogen-bonded assembly **2a**•$(DEB)_6$ in 96% yield (Fig. 2).† Monitoring the reaction by ^{1}H NMR spectroscopy (Fig. 3) clearly showed that the reaction occurs without destroying the assembly. The signals for the terminal vinylic protons at δ 5.8 and 4.9 gradually disappear during the reaction and a new signal at δ 5.47 for the internal vinylic protons in **2a**•$(DEB)_6$ is observed [Fig. 3(*b*)].‡ HPLC analysis of the reaction mixture (at different time intervals) showed that **1a** is rapidly consumed (> 95% after 36 min) upon addition of the Ru catalyst, initially giving intermediate products (linear dimer and trimer) that are slowly converted into the final product **2a**.§ The clean formation of assembly **2a**•$(DEB)_6$ (detected as **2a** after loss of DEB under the MS conditions) was confirmed by MALDI-TOF MS (observed m/z = 3100 for $[\mathbf{2a} + H]^+$ containing the most abundant natural isotopes; calc. for $C_{180}H_{240}N_{36}O_{12}$ = 3100; Fig. 4). Both HPLC and MALDI-TOF MS clearly showed that the cyclic monomer **3a** (calc. m/z for $C_{60}H_{80}N_{12}O_4$ = 1032) is not formed, which emphasizes the high degree of preorganization of the reactive double bonds within the assembly.

The clean formation of assembly **2a**•$(DEB)_6$ was only observed under conditions where assembly $\mathbf{1a}_3$•$(DEB)_6$ is present. Not a single trace of **2a** was formed when **1a** was reacted with the Ru catalyst either in the absence of DEB or in the presence of 4 equiv. of *N*-propyl-5,5-diethylbarbituric acid (PDB), a substitute for DEB that cannot form an assembly similar to $\mathbf{1a}_3$•$(DEB)_6$. Moreover, RCM reactions carried out at $[\mathbf{1a}_3$•$(DEB)_6]_{t=0}$ = 0.01 mM (250-fold dilution) gave the cyclic monomer **3a** as the major product due to extensive dissociation of the assembly at this concentration.

The presence of bromo or iodo substituents at position R in assembly $\mathbf{1}_3$•$(DEB)_6$ significantly decreases the yields of the corresponding cyclic trimers **2b** (21%) and **2c** (16%) (Fig. 2). When the covalent capture was carried out in CD_2Cl_2 significant amounts of the cyclic monomers **3b** (12%) and **3c** (28%) were formed.¶ In toluene-d_8 formation of the cyclic monomers **3b** and **3c** was not observed, but still the yields of the cyclic trimers **2b** (37%) and **2c** (10%) were low in comparison to that of **2a** under the same conditions (100%). These results clearly indicate that the bromo and iodo substituents at position R significantly reduce the thermodynamic stability of the

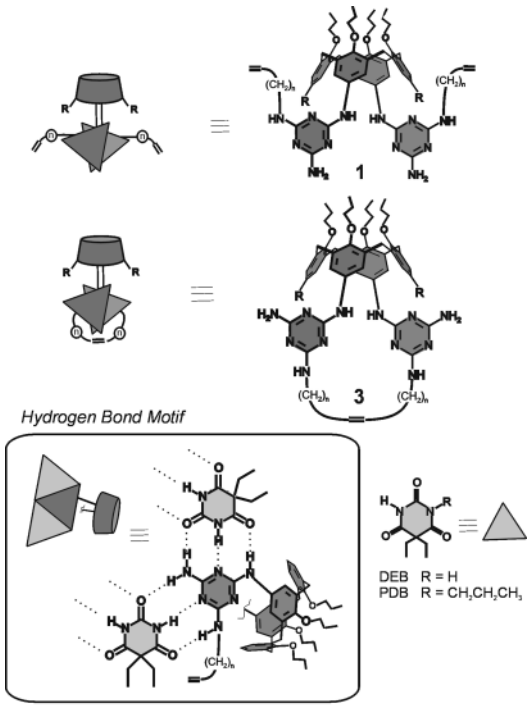

Fig. 1 Molecular structures and schematic representations of calix[4]arene dimelamine **1**, cyclic monomer **3** and barbituric acid derivatives DEB and PDB.

DOI: 10.1039/a909459h

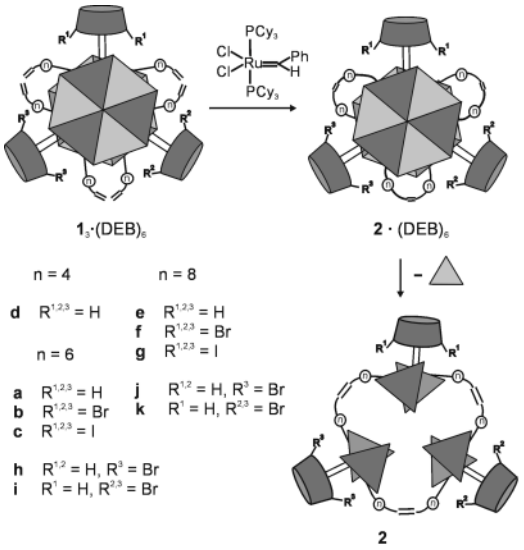

Fig. 2 Schematic representation of the covalent capture of hydrogen-bonded assemblies $\mathbf{1}_3$•$(DEB)_6$.

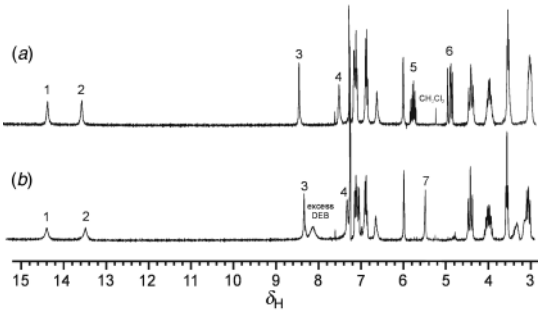

Fig. 3 ^{1}H NMR spectra of (*a*) assembly $\mathbf{1a}_3$•$(DEB)_6$ and (*b*) assembly **2a**•$(DEB)_6$ after reaction of assembly $\mathbf{1a}_3$•$(DEB)_6$ with Grubbs catalyst. Peak designations: NH_{barb} protons (1 and 2), NH_{Ar} protons (3), NH_{CH2} protons (4), terminal (5,6) and internal (7) vinylic protons. Spectra were recorded in $CDCl_3$ on a 300 MHz spectrometer.

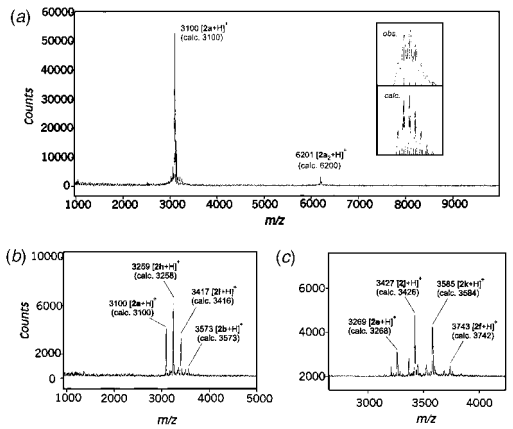

Fig. 4 MALDI-TOF mass spectra of the crude reaction mixtures of the covalent capture of (*a*) assembly $\mathbf{1a}_3$•$(DEB)_6$ (observed and calculated isotopic patterns for $[\mathbf{2a}+H]^+$ are given as inserts); (*b*) dynamic library $\mathbf{1a}_{3-x}\mathbf{1b}_x$•$(DEB)_6$ (x = 0–3, R = H, Br, n = 6); (*c*) dynamic library $\mathbf{1e}_{3-x}\mathbf{1f}_x$•$(DEB)_6$ (x = 0–3, R = H, Br, n = 8).

assemblies[15] and strongly hinder the reaction of the two alkene units, leading to competitive polymerization of the assemblies and/or intermediates.

Substitution of the oct-7-enyl chains in **1a** for hex-5-enyl chains, as in **1d**, completely inhibits the covalent capture of the corresponding assembly $\mathbf{1d}_3$•$(DEB)_6$ and formation of cyclic trimer **2d** does not occur to a significant extent either in CD_2Cl_2 or in toluene-d_8. The effect of an increase in the alkenyl chain length is much less pronounced. Covalent capture of assembly $\mathbf{1e}_3$•$(DEB)_6$, carrying dec-9-enyl side chains, in toluene-d_8 gave assembly **2e**•$(DEB)_6$ in 71% yield. The introduction of bromo substituents at positions R in these assemblies seems to decrease the yield of the corresponing assembly **2**•$(DEB)_6$ to a much smaller extent. For example, covalent capture of assembly $\mathbf{1f}_3$•$(DEB)_6$ (R = Br, n = 8) in toluene-d_8 gave assembly **2f**•$(DEB)_6$ in 61% yield.

Covalent capture of the 4-component dynamic libraries[8] $\mathbf{1a}_{3-x}\mathbf{1b}_x$•$(DEB)_6$ (x = 0–3, R = H, Br, n = 6), and $\mathbf{1e}_{3-x}\mathbf{1f}_x$•$(DEB)_6$ (x = 0–3, R = H, Br, n = 8) under standard RCM conditions in toluene-d_8 clearly showed the formation of all four possible trimers **2a**, **2b**, **2h** and **2i** (Fig. 4, relative ratio 20:43:30:7 determined by HPLC) and **2e**, **2f**, **2j** and **2k** (relative ratio 10:38:40:12 determined by HPLC), respectively. The product distribution for the library with oct-7-enyl side chains is slightly different from statistical (*i.e.* 12:38:38:12), due the lower stability of the Br-containing assemblies.

In conclusion we can state that the covalent capture of hydrogen-bonded assemblies $\mathbf{1}_3$•$(DEB)_6$ occurs with high efficiency and provides a new tool for the characterization of dynamic libraries using conventional techniques like HPLC and mass spectrometry.

We thank the EC for the Marie Curie Research Training Grant to Dr F. Cardullo (No. ERBFMBICT 972555) and Dr M. Crego Calama (No. ERBFMBICT 961445) as part of the TMR Programme.

Notes and refences

† Reaction conditions for RCM reactions: (*a*) CD_2Cl_2, room temp., 40 h; $[\mathbf{1}]_{t=0}$ = 9.0 mM; $[DEB]/[\mathbf{1}]_{t=0}$ = 2.5; $[Ru\ cat]_{t=0}$ = 20 mol%, additional 10 mol% at t = 18 h. (*b*) toluene-d_8, room temp., 48 h; $[\mathbf{1}]_{t=0}$ = 6.0 mM; $[DEB]/[\mathbf{2}]_{t=0}$ = 2.5; $[Ru\ cat]_{t=0}$ = 20 mol%, additional 10 mol% at t = 18 and 24 h. Reactions were quenched by extensive bubbling with oxygen.

‡ A mixture of *cis* (*c*) and *trans* (*t*) isomers is most probably formed (the HPLC analysis of assembly **3a**•$(DEB)_6$ shows two shoulders), but the different isomers (*ccc*, *cct*, *ctt*, *ttt*) were not resolved even in a 600 MHz ^{1}H NMR spectrum.

§ HPLC analysis was performed on crude reaction mixtures (no intermediate workup). Eluent: 95% CH_2Cl_2–4.75% MeOH–0.25% NH_3 (25% in H_2O); Column: Resolve Silica 90 Å 5 μm 3.9 × 150 mm. Yields were determined using DEB as an internal standard.

¶ In all reactions that show the formation of cyclic monomer **3** by MS and HPLC, precipitation of significant amounts of the monomer was observed, resulting in overall yields being much lower than 100%.

1 For recent overviews, see: A. Ganesan, *Angew. Chem., Int. Ed.*, 1998, **37**, 2828 and references therein; C. Gennari, H. P. Nestler, U. Piarulli and B. Salom, *Liebigs Ann. Recl.*, 1997, 637 and references therein; J.-M. Lehn, *Chem. Eur. J.*, 1999, **5**, 2455.
2 I. Huc and J.-M. Lehn, *Proc. Natl. Acad. Sci. U.S.A.*, 1997, **94**, 2106; S. Sakai, Y. Shigemassa and T. Sasaki, *Tetrahedron Lett.*, 1997, **38**, 8145; B. Klekota, M. H. Hammond and B. L. Miller, *Tetrahedron Lett.*, 1997, **38**, 8639.
3 A. V. Eliseev and M. I. Nelen, *Chem. Eur. J.*, 1998, **4**, 825.
4 P. A. Brady and J. K. M. Sanders, *J. Chem. Soc., Perkin Trans. 1*, 1997, 3237.
5 H. Hioki and W. C. Still, *J. Org. Chem.*, 1998, **63**, 904.
6 M. Albrecht, O. Bau and R. Fröhlich, *Chem. Eur. J.*, 1999, **5**, 48.
7 I. Huc, M. J. Krische, D. P. Funeriu and J.-M. Lehn, *Eur. J. Inorg. Chem.*, 1999, 1415.
8 M. Crego Calama, R. Hulst, R. Fokkens, N. M. M. Nibbering, P. Timmerman and D. N. Reinhoudt, *Chem. Commun.*, 1998, 1021.
9 M. Crego Calama, P. Timmerman and D. N. Reinhoudt, *Angew. Chem.*, in the press.
10 R. H. Grubbs and S. Chang, *Tetrahedron*, 1998, **54**, 4413.
11 T. D. Clark, K. Kobayashi and R. M. Ghadiri, *Chem. Eur. J.*, 1999, **5**, 782.
12 B. Mohr, M. Weck, J.-P. Sauvage and R. H. Grubbs, *Angew. Chem., Int. Ed. Engl.*, 1997, **36**, 1308; D. G. Hamilton and J. K. M. Sanders, *Chem. Commun.*, 1998, 1749.
13 T. J. Kidd, D. A. Leigh and A. J. Wilson, *J. Am. Chem. Soc.*, 1999, **121**, 1599.
14 M. S. Wendland and S. C. Zimmerman, *J. Am. Chem. Soc.*, 1999, **121**, 1389.
15 P. Timmerman, R. H. Vreekamp, R. Hulst, W. Verboom, D. N. Reinhoudt, K. Rissanen, K. A. Udachin and J. Ripmeester, *Chem. Eur. J.*, 1997, **3**, 1823.

Communication a909459h

ChemComm

Selectin ligands: 2,3,4-tri-*O*-acetyl-6-*O*-(2-naphthyl)methyl (NAP) α-D-galactopyranosyl imidate as a novel glycosyl donor for the efficient total synthesis of branched mucin core 2-structure containing the NeuAcα2,3(SO_3Na-6)Galβ1,3GalNAcα sequence

Wensheng Liao, Robert D. Locke and Khushi L. Matta*

Molecular & Cellular Biophysics, Roswell Park Cancer Institute, Elm & Carlton Streets, Buffalo, NY 14263, USA. E-mail: klmatta@yahoo.com

Received (in Corvallis, OR, USA) 21st October 1999, Accepted 10th January 2000

The stereo- and regioselective total synthesis of branched mucin core 2-structure 2, which contains the NeuAcα-2,3(SO_3Na-6)Galβ1,3GalNAcα sequence, is accomplished through the use of the key glycosyl donor 19.

Our recent study has shown that a core 2-branched sequence can enhance L- and P-selectin binding, *e.g.* our synthetic compound GalNAcβ1,4(Fucα1,3)GlcNAcβ1,6(NeuAcα2,3Galβ1,3)GalNAcαOMe **1** was found to be 5- to 6-fold better at inhibiting L- and P-selectins than sialyl Lewis^x-OMe.[1] It is now well established that natural selectin ligands, such as CD34, MadCAM-1, PSGL-1 and GlyCAM-1, are mucin type glycoproteins.[1] Both PSGL-1 and GlyCAM-1 contain the NeuAc2,3Galβ1,3GalNAcα sequence. In GlyCAM-1 it has been demonstrated that, in addition to sialylation and fucosylation, sulfation of the saccharide chains is important for high affinity binding to L-selectin.[2] Based upon this, we became interested in the synthesis of sulfated analogs of our previously reported **1** as

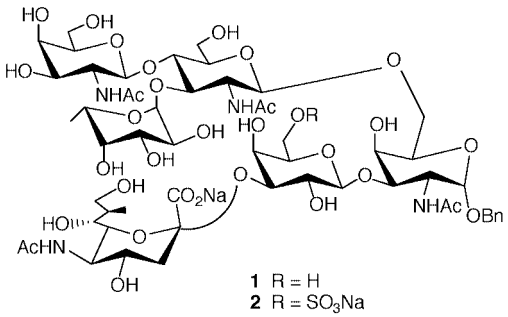

1 R = H
2 R = SO_3Na

potential ligands. Moreover, the sequences (SO_3Na-6)Galβ-1,3GalNAcα and especially NeuAcα2,3(SO_3Na-6)Galβ1,3GalNAcα have been found to be part of *O*-linked glycoproteins.[3] Thus, we turned our attention to the synthesis of our target molecule **2**, which contains the NeuAcα2,3(SO_3Na-6)Galβ-1,3GalNAcα sequence, as a potential ligand.

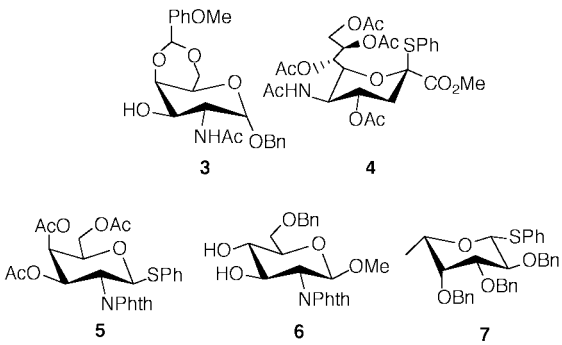

3 **4** **5** **6** **7**

Our present approach is based upon the use of imidate **19** bearing a 6-*O*-(2-naphthyl)methyl (NAP) group as a valuable glycosyl donor. Recently Spencer *et al.*[4] reported selective cleavage of the NAP group by hydrogenolysis (10% Pd/C, ethanol) even in the presence of benzyl groups. However, when we applied this method to the synthesis of oligosaccharides, our pilot experiments showed that the hydrogenation reactions went very slowly and the benzyl groups were also partially cleaved (Scheme 1). Meanwhile, in our lab we have found that DDQ can smoothly remove the NAP group and other usual protecting groups (such as Ac, pivaloyl, TBS, phthalimido, Bn and benzylidene) can still survive.[5] The donor **19** was prepared as shown in Scheme 2. On alkylation with 2-(bromomethyl)naphthalene, the readily accessible **14** provided **15** in quantitative yield. Deacetonation followed by acetylation furnished compound **17** (α:β 2:3). Selective removal of the anomeric *O*-acetyl group from **17** gave, in 87% yield, **18** which on treatment with CCl_3CN–DBU (−10 °C) afforded a 90% yield of trichloroacetimidate **19** as the pure α-anomer.

Glycosidation of alcohol **3** with imidate **19** was performed under Schmidt's 'inverse procedure'.[6] The β-linked disaccharide **20** was obtained in 74% yield, which was then *O*-deacetylated to furnish triol **21**. The sialylation of **21** with the sialic acid donor **4** under NIS–TfOH catalysis at −30 °C gave the trisaccharide **22** in 78% yield. Compound **22** was then acetylated to give **23**. The ^{1}H NMR spectrum of **23** displayed characteristic signals at δ 5.07 (dd, 1H, $J_{1',2'}$ 8.0, $J_{2',3'}$ 10.4 Hz, H-2′), 4.96 (d, 1H, $J_{3',4'}$ 2.8 Hz, H-4′), 5.27 (dd, 1H, $J_{6'',7''}$ 2.8, $J_{7'',8''}$ 9.6 Hz, H-7″) and 2.59 (dd, 1H, J_{gem} 12.8, $J_{3''eq,4''}$ 4.9 Hz, H-3″e) which confirmed an α(2 → 3) glycosidic linkage. Removal of the 4,6-benzylidene group in **23** (50% HOAc, 55 °C) afforded the trisaccharide diol **24** (90%).

Although preparation of the key GalNAc Le^x glycosyl donor **29** has been reported,[1] a simplified procedure based on employing diol **6** as an acceptor was developed (Scheme 3). Thus, regioselective condensation of phenylthio donor **5** and diol **6** under NIS–TfOH conditions (−65 °C) afforded the β(1 → 4) linked disaccharide **25** in 73% yield. Selectfluor–BF_3·Et_2O promoted[7] α-L-fucosylation of **25** with donor **7** in CH_3CN (0 °C) gave trisaccharide **27** in 75% yield. Hydrogenolysis of **27**, followed by acetylation and then acetolysis

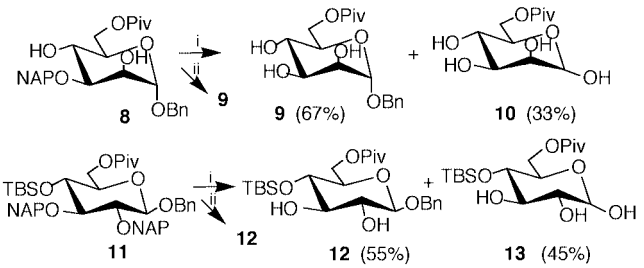

Scheme 1 *Reagents and conditions*: i, 10% Pd/C, HOAc–MeOH, 16 h; ii, DDQ (2.5 equiv. for **8**, 5 equiv. for **11**), CH_2Cl_2–H_2O (15:2), 3 h, quant.

DOI: 10.1039/a908511d

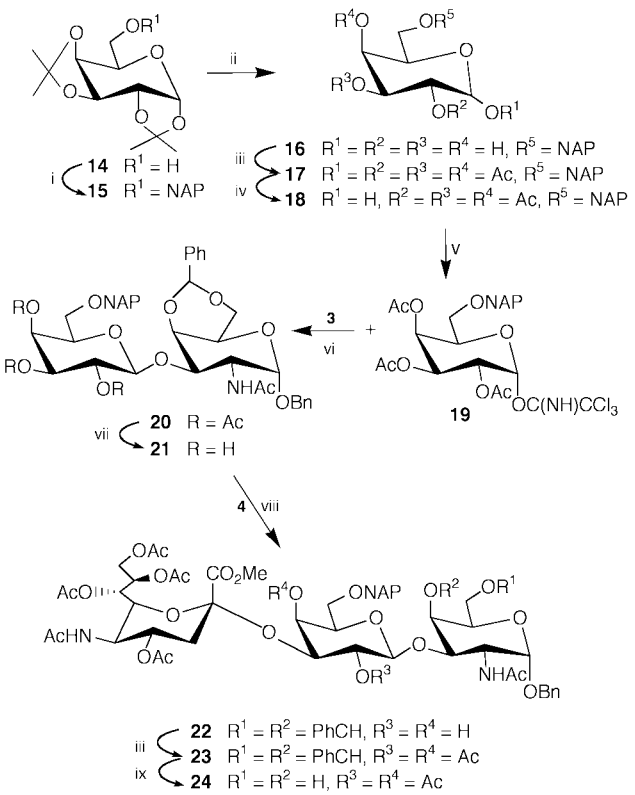

Scheme 2 *Reagents and conditions*: i, 2-(bromomethyl)naphthalene, KOH, 18-crown-6, THF, 2 h; ii, 80% AcOH, 75 °C, 95%; iii, pyridine–Ac_2O, DMAP; iv, hydrazine acetate, DMF, 2 h, 87%; v, CCl_3CN–DBU, CH_2Cl_2, −10 °C, 90%; vi, **19** (1.5 equiv.), TESOTf, 4 Å molecular sieves, CH_2Cl_2, room temp., 73%; vii, MeOH–Et_3N–H_2O, 4 °C; viii, **4** (2.0 equiv.), NIS–TfOH, 3 Å molecular sieves, CH_3CN–CH_2Cl_2, −30 °C, 3 h, 78%; ix, 50% AcOH, 55 °C, 4 h, 90%.

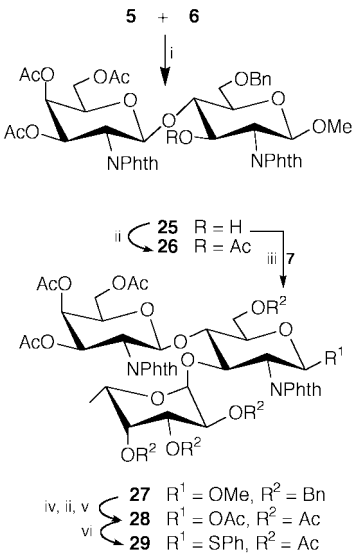

Scheme 3 *Reagents and conditions*: i, **5** (1.2 equiv.), NIS–TfOH, CH_2Cl_2, 4 Å molecular sieves, −65 °C; ii, pyridine–Ac_2O, DMAP; iii, **7** (3.0 equiv.), Selectfluor, $BF_3{\cdot}Et_2O$, 3 Å molecular sieves, CH_3CN, 0 °C, 75%; iv, 10% Pd/C, HOAc–MeOH; v, Ac_2O–HOAc–H_2SO_4, 70%; vi, PhSH, $BF_3{\cdot}Et_2O$, CH_2Cl_2, 73%.

with Ac_2O–HOAc–H_2SO_4 provided the fully acetylated trisaccharide **28**. Treatment of **28** with PhSH–$BF_3{\cdot}Et_2O$ furnished GalNAc Le^x glycosyl donor **29** in 73% yield.

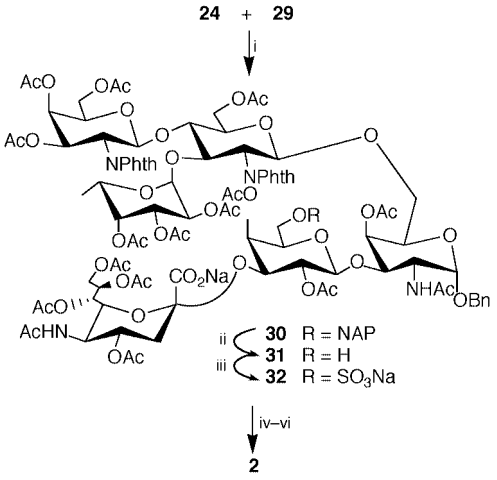

Scheme 4 *Reagents and conditions*: i, **29** (1.5 equiv.), NIS–TfOH, CH_2Cl_2, 4 Å molecular sieves, −60 °C, 2 h, 70%; ii, DDQ (2.5 equiv.), CH_2Cl_2–H_2O, 3 h, quant.; iii, SO_3·pyridine complex (5 equiv.), DMF, 0 °C, 3 h, 95%; iv, LiI (40 equiv.), pyridine, 110 °C, overnight, 90%; v, hydrazine hydrate–MeOH (1:4), 80 °C, 6 h; vi, MeOH–CH_2Cl_2 (1:1), Ac_2O, 0 °C, 1 h; Na^+ resin.

Glycosylation of **29** with diol **24** (NIS–TfOH, −60 °C) gave the expected hexasaccharide **30** in 70% yield (Scheme 4). Removal of the NAP group in the β-galactopyranosyl residue by DDQ in CH_2Cl_2–H_2O afforded **31**, which was further treated with 5 equiv. of sulfur trioxide–pyridine complex in DMF at 0 °C to give the sulfated compound **32**. Finally, **32** was converted to the target compound **2** in three successive steps: (i) LiI–pyridine at 110 °C (methyl ester to free acid); (ii) 4:1 MeOH–hydrazine hydrate at 80 °C (removal of the phthalimido and acetyl groups); (iii) 5:5:3 MeOH–CH_2Cl_2–Ac_2O (*N*-acetylation). The structure of **2** was confirmed by ^1H, ^{13}C NMR and FAB mass spectroscopy.†

We thank the National Cancer Institute for financial support (Grant No. CA 63218) of this work.

Notes and references

† *Selected data for* **2**: *m/z* (FAB) 1441.4 (M); $[\alpha]_D^{20}$ +3.1 (*c* 0.16, H_2O); δ_H(D_2O, 400 MHz) 5.12 (d, 1H, *J* 3.6, H-1‴), 4.99 (d, 1H, *J* 3.6, H-1), 4.56 (d, 1H, *J* 8.4, H-1″), 4.55 (d, 1H, *J* 8.4, H-1‴), 4.46 (d, 1H, *J* 8.0, H-1′), 4.09 (dd, 1H, *J* 3.3, 9.9, H-3′), 2.76 (dd, 1H, *J* 4.8, 12.2, H-3⁗e), 2.07, 2.04, 2.00 and 1.97 (each s, 12H, 4 × NHAc), 1.80 (t, *J* 12.0, H-3⁗a), 1.28 (d, 3H, *J* 7.2, CMe); δ_C(D_2O, 100.6 MHz) 105.21 (C-1″), 102.30 (C-1‴), 101.81 (C-1′), 101.00 (C-2⁗), 99.56 (C-1‴), 97.13 (C-1), 76.60 (C-3′), 71.47 (C-6), 70.36 (*C*H_2Ph), 68.73 (C-6′), 63.65 (C-6‴), 62.52 (C-6″), 61.15 (C-9⁗), 40.73 (C-3⁗), 23.46, 23.31, 23.15, 23.06 (4 × NHAc), 16.46 (C-6⁗).

1 R. K. Jain, C. F. Piskorz, B.-G. Huang, R. D. Locke, H.-L. Han, A. Koenig, A. Varki and K. L. Matta, *Glycobiology*, 1998, **8**, 707.
2 Y. Imai, L. A. Lasky and S. D. Rosen, *Nature*, 1993, **361**, 555.
3 C. Capon, C. L. Laboisse, J. M. Wieruszeski, J. J. Maoret, C. Augeron and B. Fournet, *J. Biol. Chem.*, 1992, **267**, 19 248; D. L. Chance and T. P. Mawhinney, *Carbohydr. Res.*, 1996, **295**, 157.
4 M. J. Gaunt, J. Yu and J. B. Spencer, *J. Org. Chem.*, 1998, **63**, 4172; M. J. Gaunt, C. E. Boschetti, J. Yu and J. B. Spencer, *Tetrahedron Lett.*, 1999, **40**, 1803.
5 J. Xia, S. A. Abbas, R. D. Locke, C. F. Piskorz, J. L. Alderfer and K. L. Matta, *Tetrahedron Lett.*, 2000, **41**, 169.
6 R. R. Schmidt and A. Toepfer, *Tetrahedron Lett.*, 1991, **32**, 3353.
7 M. D. Burkart, Z. Zhang, S.-C. Hung and C.-H. Wong, *J. Am. Chem. Soc.*, 1997, **119**, 11 743.

Communication a908511d

Enhancement effects of methanol on the reactivity for methane partial oxidation in the gas phase reaction of CH_4–O_2–NO_2

Yonghong Teng,*[a] Yoichi Yamaguchi,[b] Tetsuya Takemoto,[a] Lianxin Dai,[a] Kenji Tabata[a] and Eiji Suzuki[a]

[a] *Research Institute of Innovative Technology for the Earth (RITE), 9-2, Kizugawadai, Kizu-cho, Soraku-gun, Kyoto, 619-0292. Japan. E-mail: teng@rite.or.jp*

[b] *Kansai Research Institute (KRI), Kyoto Research Park, Science Center Bldg. 17, Chudoji-Minami-machi, Shimogyo-ku, Kyoyo, 600-8813 Japan*

Received (in Cambridge, UK) 6th December 1999, Accepted 31st January 2000

The partial oxidation of methane in the gas phase reaction of CH_4–O_2–NO_2 was enhanced with the addition of a small amount of methanol; the selectivity of methanol at the same level of CH_4 conversion was enhanced in the presence of methanol which showed this effect exclusively in the presence of NO_2.

Methanol is a desirable product in the partial oxidation of methane. Recently, we found high yield methanol formation at 808 K under atmospheric pressure in the gas phase reaction of CH_4–O_2 upon the addition of a small amount of NO_x (x = 1,2).[1,2] The transition barrier energy of hydrogen atom abstraction from CH_4 by NO_2 was lower than that by O_2.[3,4] This brought about the enhancement effect of NO_2 on the reactivity of methane in CH_4–O_2–NO_2. Since successive oxidation of the produced methanol has been reported at high temperatures for the CH_4–O_2 gas phase reaction,[5,6] the successive oxidation of methanol could also occur in the CH_4–O_2–NO_x gas phase reaction. The initial hydrogen atom abstraction is the first step of successive oxidation of methanol that probably initiates radical chain reactions to enhance methane partial oxidation, since Burch and co-workers[5] reported that the addition of C_2H_6 lowered the reaction temperature by *ca.* 50 K at the same conversion of CH_4 for the gas phase reaction of CH_4–O_2. On the other hand, it was found in our previous study that the selectivity of the produced methanol was scarcely affected by a change of space velocity at a given temperature.[1,2,4] This indicates that methanol could be a fairly stabilized product in the gas phase. In addition, gaseous additives have been examined under high pressure so far,[7–9] but an enhancement effect of methanol was not found. Therefore it is important to clarify the behavior of methanol in the gas phase reaction of CH_4–O_2–NO_2. In this study, a small amount of methanol was added to the CH_4–O_2–NO_2 system to investigate its effects on the partial oxidation of methanol in the gas phase.

The reaction was carried out with using a test gas (CH_4: 28%, O_2: 14%, NO_2: 0.5%, He: 57.3 or 57.5%, CH_3OH: 0 or 0.16%). A quartz tube (7 mm i.d.) was used as a reactor and the length of heated reaction zone was 200 mm. The temperature was measured with a thermocouple attached on the outside of the reactor. Products were analyzed with two gas chromatographs. The carbon balance before and after the reaction exceeded 98%. Each reaction was performed for 30 min under each of the conditions and then the products were analyzed. All experimental data shown here were shown to be reproducible. Conversion and selectivities were calculated as follows (unit is mol): CH_4 conversion = (initial CH_4 − final CH_4)/initial CH_4; selectivity of a product = product/reacted CH_4; selectivity of methanol = total methanol/reacted CH_4.

Fig. 1 shows CH_4 conversion in each different reaction gas mixture as a function of reaction temperature. The temperature at the level of 10% CH_4 conversion is lowered by *ca.* 30 K (827 K) with addition of methanol (0.16%) to CH_4–O_2–NO_2. CH_4 conversion was scarcely observed at 827 K for both CH_4–O_2 and CH_4–O_2–CH_3OH systems. These differences indicate that the decrease of reaction temperature is derived from the presence of both CH_3OH and NO_2 in the reaction mixture. The enhancement effects of CH_3OH are clearly seen on an ON–OFF experiment for the supply of methanol (Fig. 2). An increase of reaction temperature after the addition of methanol was observed but amounted to < 3 K in the center of the reactor.

On varying the methanol concentration, it was found that 0.016% CH_3OH was the lower limit for which CH_4 conversion was enhanced.

The selectivity of CH_3OH for the reaction in the presence of methanol is higher than that without methanol in the lower conversion region (Table 1). The selectivity of CH_2O in the system CH_4–O_2–NO_2–CH_3OH had somewhat smaller values in the same region. The selectivity of CH_3OH in the presence of methanol exceeded that in the absence of CH_3OH for the regions of CH_4 conversion shown in Table 1.

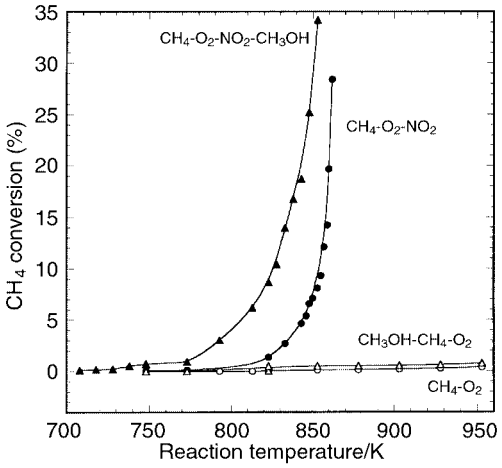

Fig. 1 CH_4 conversion *vs.* reaction temperature. Reaction gas: CH_4(28%)–O_2(14%)–NO_2(0.5%)–He(57.3%)–CH_3OH(0.16%) (▲), CH_4(28%)–O_2(14%)–NO_2(0.5%)–He(57.5%) (●), CH_4(28%)–O_2(14%)–He(57.8%)–CH_3OH(0.16%) (△), CH_4(28%)–O_2(14%)–He(58%) (○).

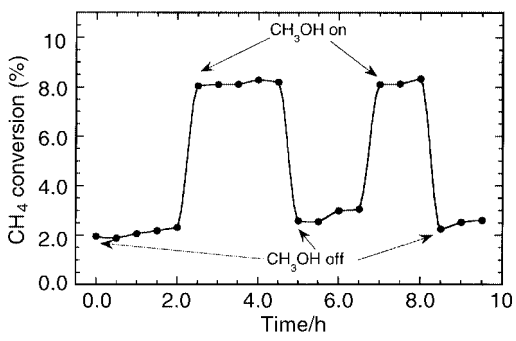

Fig. 2 The enhancement effect of CH_3OH on CH_4 conversion in CH_4–O_2–NO_2. 0.16% CH_3OH was fed into the reaction gas consisting of CH_4(28%)–O_2(14%)–NO_2(0.5%)–He(57.5%).

DOI: 10.1039/a909587j

Table 1 The effects of methanol addition on methane partial oxidation in the presence of NO_2[a]

			Selectivity (%)				
	T/K	CH_4 conversion (%)	HCHO	CH_3OH	CH_3NO_2	CO	CO_2
Without CH_3OH	831	2.3	38.0	11.7	10.8	33.5	6.0
	846	5.6	27.3	13.1	8.2	48.2	3.2
	851	8.1	19.8	13.1	8.0	55.9	3.1
	857	12.1	11.3	11.9	6.2	66.7	3.9
With CH_3OH	788	2.3 (0.3)[b]	29.1	18.8	11.7	35.1	5.3
	810	5.6 (0.7)[b]	25.0	17.1	11.9	42.3	3.7
	820	8.1 (2.3)[b]	19.6	15.7	11.1	50.4	3.2
	830	12.1 (5.6)[b]	14.0	14.0	7.4	60.7	3.9

[a] Reaction gas: CH_4(28.0%)–O_2(14.0%)–NO_2(0.5%)–He(57.3 ~ 57.5%), with or without 0.16% CH_3OH. [b] Values in parentheses are CH_4 conversion before CH_3OH addition.

It is of note that > 99% methanol was oxidized to CO and CO_2 in the CH_3OH–O_2–NO_2 system in the absence of methane below 750 K. Since all of the added methanol was completely oxidized up to 750 K, the obtained methanol in the CH_4–O_2–NO_2–CH_3OH system was assumed to be produced through the partial oxidation of methane. This indicates that the enhancement of reactivity of CH_4 in CH_4–O_2–NO_2–CH_3OH above 750 K was caused by reaction between NO_2 and CH_3OH.

In previous papers, we suggested reaction pathways to form C_1-oxygenates in the gas phase reaction of CH_4–O_2–NO_2.[1–4] The rate-determining step is hydrogen abstraction from methane with an activation energy of 37.6 kcal mol^{-1} at 800 K. The lowering of the initial reaction temperature upon CH_3OH addition indicated the presence of other lower barrier reaction pathways for the dissociation of methane. Furthermore, the enhancement of CH_4 conversion indicated the presence of radical chain reactions. We considered the most probable reaction between CH_3OH and NO_2 [eqn. (1)]:

$$CH_3OH + NO_2 \rightarrow CH_2OH + HNO_2 \quad (1)$$

Our theoretically obtained value for the activation energy of eqn. (1) was 28.4 kcal mol^{-1} at 800 K calculated using the Gaussian94 *ab initio* program package and was close to that reported by Bromly *et al.*[10] The produced CH_2OH was assumed to react easily with O_2 to produce formaldehyde [eqn. (2)]:

$$CH_2OH + O_2 \rightarrow CH_2O + HO_2 \quad (2)$$

This HO_2 could then react with CH_4 [eqn. (3)]:

$$CH_4 + HO_2 \rightarrow CH_3 + H_2O_2 \quad (3)$$

Since the reported[10] activation energy of eqn. (3) was 24.6 kcal mol^{-1} and is lower than 37.6 kcal mol^{-1} for the activation energy of hydrogen abstraction from methane, we considered that this difference lowered the commencement temperature of CH_4 conversion.

The higher selectivity of produced methanol is explained by assuming that the subsequent oxidation of methanol is retarded under the reaction conditions.

We acknowledge financial support of the New Energy and Industrial Technology Development Organization (NEDO). Y. T. was supported by a Fellowship from NEDO.

Notes and references

1 Y. Teng, F. Ouyang, L. Dai, T. Karasuda, H. Sakurai, K. Tabata and E. Suzuki, *Chem. Lett.*, 1999, 991.
2 Y. Teng, H. Sakurai, K. Tabata and E. Suzuki, *Appl. Catal. A*, 1999, **190**, 283.
3 Y. Yamaguchi, Y. Teng, S. Shimomura, K. Tabata and E. Suzuki, *J. Phys. Chem. A*, 1999, **103**, 8272.
4 K. Tabata, Y. Teng, Y. Yamaguchi, H. Sakurai and E. Suzuki, *J. Phys. Chem. A*, 2000, in press.
5 T. R. Baldwin, R. Burch, G. D. Squire and S. C. Tsang, *Appl. Catal. A*, 1991, **74**, 137.
6 R. Burch, G. D. Squire and S. C. Tsang, *J. Chem. Soc., Faraday Trans. 1*, 1989, **85**, 3561.
7 J.-W. Chun and R. G. Anthony, *Ind. Eng. Chem. Res.*, 1993, **32**, 788.
8 N. R. Hunter, H. D. Gesser, L. A. Morton and P. S. Yarlagadda, *Appl. Catal.*, 1990, **57**, 45.
9 A. S. Chellappa, S. Fuangfoo and D. S. Viswanath, *Ind. Eng. Chem. Res.*, 1997, **36**, 1401.
10 J. H. Bromly, F. J. Barnes, S. Muris, X. You and B. S. Haynes, *Combust. Sci. Technol.*, 1996, **115**, 259.

Communication a909587j

ChemComm

Charge-transfer in a π-stacked fullerene porphyrin dyad: evidence for back electron transfer in the 'Marcus-inverted' region

Dirk M. Guldi,*[a] Chuping Luo,[a] Maurizio Prato,*[b] Elke Dietel[c] and Andreas Hirsch*[c]

[a] *University of Notre Dame, Radiation Laboratory, Notre Dame, IN 46556, USA*
[b] *Dipartimento di Scienze Farmaceutiche, Università di Trieste, Piazzale Europa 1, 34127 Trieste, Italy*
[c] *Institut für Organische Chemie der Universität Erlangen-Nürnberg, Henkestrasse 42. D-91054 Erlangen, Germany. E-mail: hirsch@organik.uni-erlangen.de*

Received (in Cambridge, UK) 18th Decmeber 1999, Accepted 2nd February 2000

The 'Marcus-inverted' region for BET in a π–π stacked fullerene–porphyrin dyad was determined based on (i) the photoactivation of an intramolecular ET in a variety of solvents and (ii) the formation of a highly energetic charge-separated state

Photoinduced electron transfer (ET) to fullerenes is a subject of current interest.[1] Specifically, the moderate first reduction potentials of fullerenes[2] and their small reorganization energies in ET reactions[3] make them excellent building blocks for the design of novel donor–acceptor systems. According to the Marcus theory, electron transfer rates (k_{ET}) are expected to exhibit a parabolic dependence on the free energy gap of the electron transfer ($-\Delta G°_{ET}$).[4] In particular, k_{ET} decreases as the reaction becomes more exergonic, especially at large $-\Delta G°_{ET}$. The maximum of the theoretically expected bell-shaped energy gap dependence (*i.e.* $-\Delta G° \approx \lambda$, [$\lambda$ = reorganization energy (Marcus theory)]) is largely controlled by the nuclear reorganization energy including the solvent reorganization associated with the ET. Surprisingly, experimental support to ET kinetics clearly occurring in the inverted region, is limited to charge recombination processes in geminate radical pairs[5] and a few examples of non fullerene-containing donor–acceptor dyads.[6] In order to optimise the stability of a charge-separated state (*i.e.* retarding charge recombination) it is desirable to reach the thermodynamic maximum at small $-\Delta G°$ values and, thus, to push the exergonic back electron transfer (BET) into the 'Marcus-inverted' region. The small reorganization energy of the rigid C_{60} cage should be an ideal prerequisite to shift the maximum of the 'Marcus parabola' to smaller values and BET in fullerene-based donor–acceptor arrays is proposed to be decelerated compared with two-dimensional electron acceptors. Here, we present the first experimental evidence for an electron transfer within a C_{60} based compound in the 'Marcus-inverted' region.

The model compound that we used in this study is the π–π stacked C_{60}–ZnTPP dyad **1** involving a *trans*-2 addition pattern,[7] which we reported recently.[8] The fluorescence quantum yield of **1**, is strongly quenched ($\Phi = 1.26 \times 10^{-4}$) relative to a ZnTPP reference complex ($\Phi = 0.04$) even in a non-polar toluene solution. Similarly low fluorescence quantum yields were found in tetrahydrofuran ($\Phi = 1.16 \times 10^{-4}$), dichloroethane ($\Phi = 1.37 \times 10^{-4}$) and benzonitrile ($\Phi = 1.37 \times 10^{-4}$). This points to a very efficient electronic communication between the two moieties in the excited state. Significantly, the texture of the ZnTPP fluorescence is still preserved. Assuming that the lifetime of the ZnTPP singlet excited state is 2700 ps, the lifetime of the chromophore in dyad **1** can be estimated to be *ca.* 8.5 ps corresponding to an intramolecular rate constant of 1.18×10^{11} s^{-1}. The new emission band,[7] centered around 820 nm, was found exclusively in toluene solutions and is missing in the other solutions. To characterize this emission band, the phosphorescence of a ZnTPP reference compound was probed. The resemblance of the ZnTPP phosphorescence with the emission band of **1** in toluene suggests the spin-forbidden phosphorescence of the ZnTPP chromophore. The lifetime of the 820 nm emission band (τ = 2.84 ns)[7] matches nicely the proposed energy transfer rate measured by picosecond-resolved transient absorption spectroscopy (see below).

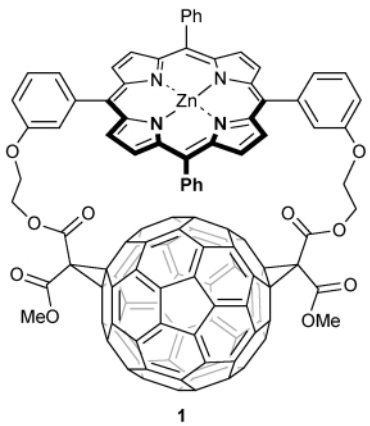

1

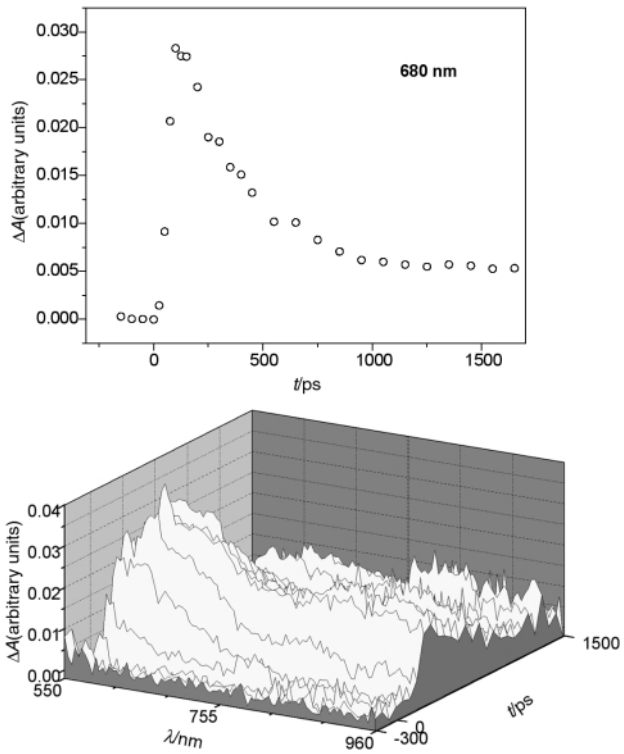

Fig. 1 (a) Differential absorption spectra obtained upon picosecond flash photolysis (532 nm) of *ca.* 10^{-5} M solutions of dyad **1** in nitrogen saturated toluene with time delays between −300 and 1500 ps. (b) Time-absorption profiles at 680 nm (*i.e.* maximum of the $ZnP^{\bullet+}$ absorption).

DOI: 10.1039/a909657d

Table 1 Photophysical properties of dyad **1** in various solvents

Solvent	ε^a	$10^4\ \Phi$ (fluorescence)	τ (radical pair)/ps	$\Delta G_{CR}°$/eV	$\Delta G_{ET}°$/eV	Product
Toluene	2.38	1.26	619	1.536	0.524	Triplet excited state
Tetrahydrofuran	7.6	1.16	385	1.452	0.608	Singlet ground state
Dichloromethane	9.08		121	1.445	0.615	Singlet ground state
Dichloroethane	10.19	1.37	66	1.441	0.619	Singlet ground state
Benzonitrile	24.8	1.37	38	1.424	0.636	Singlet ground state

[a] Dielectric constant.

In order to measure the absolute quenching rate constants and to unravel the underlying mechanism, **1** was studied in various solvents by means of picosecond-resolved transient absorption spectroscopy. In all solvents used, **1** gives rise to the rapid formation of the ZnTPP π-radical cation absorption between 670 and 680 nm (Fig. 1). However the rise time, representing the actual forward ET process, is masked by the instrument response time. Thus, we can only provide an upper limit of the ZnTPP lifetime, for example, in a toluene solution of ~35 ps. Despite this inaccuracy, the estimate is in reasonably good agreement with the steady-state emission study.

Taking into account the strong fluorescence quenching and the formation of $ZnTPP^{\bullet+}$, we can conclude that electron transfer prevails in the deactivation of the ZnTPP singlet excited state, to yield the $C_{60}^{\bullet-}$–$ZnTPP^{\bullet+}$ pair. In line with the spectral identification of the $C_{60}^{\bullet-}$–$ZnTPP^{\bullet+}$ pair is the assumption, which is based on the thermodynamic driving force ($-\Delta G_{ET}°$) for an intramolecular electron transfer from the photoexcited ZnTPP. The $\Delta G_{ET}°$ values are approximated by:

$$\Delta G_{ET}° = -[E^*_{0\text{–}0} + \Delta G_{CR}°] \quad (\text{with } \Delta G_{CR}° = -[\Delta E° + e^2/d\varepsilon_S]) \quad (1)$$

and summarized in Table 1.

The fact that ET rather than energy transfer events govern the fate of the photoexcited ZnTPP chromophore, can be rationalized by the close packing of the two moieties. This clearly reflects the higher efficiency of an electron exchange mechanism compared with a dipole–dipole energy transfer mechanism.

As determined by transient absorption spectroscopy the product of the charge-recombination is the singlet ground state in any solvent [eqn. 2(a)]. The only exception is toluene [eqn. 2(b)]: Nanosecond-resolved photolysis confirmed the

$$C_{60}^{\bullet-} - ZnTPP^{\bullet+} \xrightarrow{\text{BET}} C_{60} - ZnTPP \quad (2a)$$

$$C_{60}^{\bullet-} - ZnTPP^{\bullet+} \xrightarrow{\text{BET}} C_{60} - {}^3{*}ZnTPP \xrightarrow{\text{EnergyT}} {}^3{*}C_{60} - ZnTPP \quad (2b)$$

formation of the fullerene triplet excited state with an overall quantum efficiency of 0.196. To shed further light onto the exact formation mechanism, we reinvestigated the dynamics of **1** in toluene on the picosecond time scale. Here, the radical pair (1.54 eV) decays *via* a transient intermediate, before the fullerene triplet excited state evolves (τ = 3970 ps). Based on the close spectral reminiscence with the ZnTPP triplet excited state we propose the formation of the latter state as an intermediate step towards the fullerene triplet excited state. Its excited state energy (1.53 eV) is then a sufficient promoter to activate an intramolecular triplet–triplet energy transfer to the lower lying fullerene triplet (1.50 eV).

In more polar solvents the energy of the radical pair state is decreased (< 1.45 eV; see Table 1) and, as a consequence, charge recombination, yielding the porphyrin or fullerene triplet excited state is thermodynamically hindered. Instead, direct generation of the singlet ground state takes place [eqn. 2(a)].

The clean decay kinetics of the π-radical cation absorption allowed us to measure the lifetime of the radical pair as a function of solvent polarity. The lifetime is subject to an interesting trend: The lifetimes in tetrahydrofuran (τ = 385 ps) and dichloromethane (τ = 122 ps) are markedly increased relative to the more polar solvents dichloroethane (τ = 61 ps) and benzonitrile (τ = 38 ps) (Table 1). This dependency prompts to an important conclusion: The rates of the back electron transfer processes, from the $C_{60}^{\bullet-}$–$ZnTPP^{\bullet+}$ state to the ground state, are clearly in the 'Marcus-inverted' region [*e.g.* a region in which larger free energy changes ($-\Delta G°_{ET}$) lead to slower electron transfer rates (k_{ET})].

Since the correct choice of intermolecular separation is essential to the efficiency of light-driven electron transfer, especially in light of guaranteeing $-\Delta G° > \lambda$, a comparison of **1** with non-fullerene systems, that have similar van der Waals contacts, was deemed necessary. In these systems,[6e,g] the inverted BET reactions are activated only at values exceeding 1.9 eV, while in **1** the 'Marcus-inverted' region was established even at values smaller than 1.5 eV. This underlines the unique role of [60]fullerene, possessing a smaller reorganization energy than two-dimensional acceptor moieties, as a novel electron acceptor.

This work was supported by the Office of Basic Energy Sciences of the Department of Energy, the Stiftung Volkswagenwerk, by MURST (cofin. ex 40%, prot. n. 9803194198_005), by C.N.R. through the program 'Materiali Innovativi (legge 95/95)' and by the European Community (RTN program FUNCARS). This is document NDRL-4198 from the Notre Dame Radiation Laboratory.

Note added in proof: similar investigations on a different dyad were recently reported by D. Schuster *et. al.*[9]

Notes and references

1 H. Imahori and Y. Sakata, *Eur. J. Org. Chem.*, 1999, 2445; D. M. Guldi, *Chem. Commun.*, 2000, 321.
2 L. Echegoyen and L. E. Echegoyen, *Acc. Chem. Res.*, 1998, **31**, 593.
3 H. Imahori, K. Hagiwara, T. Akiyama, M. Akoi, S. Taniguchi, T. Okada, M. Shirakawa and Y. Sakata, *Chem. Lett.*, 1996, **263**, 545; D. M. Guldi and K.-D. Asmus, *J. Am. Chem. Soc.*, 1997, **119**, 5744.
4 R. A. Marcus, *J. Chem. Phys.*, 1956, **24**, 966; R. Marcus and N. Sutin, *Biophys. Acta*, 1985, **811**, 265.
5 Examples with leading references: T. Asahi and N. Mataga, *J. Phys. Chem.*, 1989, **93**, 6575; L. A. Kelly and M. A. J. Rodgers, *J. Phys. Chem.*, 1995, **99**, 13 132; I. R. Gould and S. Farid, *Acc. Chem. Res.*, 1996, **29**, 522; C. Turro, J. M. Zaleski, Y. M. Karabatsos and D. G. Nocera, *J. Am. Chem. Soc.*, 1996, **118**, 6060.
6 (*a*) M. R. Wasielewski, M. P. Niemczyk, W. A. Svec and E. B. Pewitt, *J. Am. Chem. Soc.*, 1985, **107**, 1080; (*b*) P. Chen, R. Duesing, D. K. Graff and T. J. Meyer, *J. Phys. Chem.*, 1991, **95**, 5850; (*c*) E. H. Yonemoto, R. L. Riley, Y. I. Kim, S. J. Atherton, R. H. Schmehl and T. E. Mallouk, *J. Am. Chem. Soc.*, 1992, **114**, 8081; (*d*) T. Asahi, M. Ohkohchi, R. Matsusaka, N. Mataga, R. P. Zhang, A. Osuka and K. Maruyama, *J. Am. Chem. Soc.*, 1993, **115**, 5665; (*e*) A. C. Benniston, A. Harriman, D. Philp and J. F. Stoddart, *J. Am. Chem. Soc.*, 1993, **115**, 5298; (*f*) E. H. Yonemoto, G. B. Saupe, R. H. Schmehl, S. M. Hubig, R. L. Riley, B. L. Iverson and T. E. Mallouk, *J. Am. Chem. Soc.*, 1994, **116**, 4786; (*g*) A. C. Benniston and A. Harriman, *J. Am. Chem. Soc.*, 1994, **116**, 11531.
7 E. Dietel, A. Hirsch, E. Eichhorn, A. Rieker, S. Hackbarth and B. Röder, *Chem. Commun.*, 1998, 1981.
8 For the synthesis of a similar dyad involving a *trans-1* addition pattern see: J.-P. Bourgois, F. Diederich, L. Echegoyen and J.-F. Nierengarten, *Helv. Chim. Acta*, 1998, **81**, 1835.
9 D. I. Schuster, P. Cheng, S. R. Wilson, V. Prokhorenko, M. Katterle, A. R. Holzwarth, S. E. Braslavsky, G. Klihm, R. M. Williams and C. Luo, *J. Am. Chem. Soc.*, 1999, **121**, 11 599.

Communication a909657d

ChemComm

Photoinduced electron transfer in multicomponent arrays of a π-stacked fullerene porphyrin dyad and diazabicyclooctane or a fulleropyrrolidine ligand

Dirk M. Guldi,*[a] Chuping Luo,[a] Tatiana Da Ros,[b] Maurizio Prato,*[b] Elke Dietel[c] and Andreas Hirsch*[c]

[a] *University of Notre Dame, Radiation Laboratory, Notre Dame, IN 46556, USA*
[b] *Dipartimento di Scienze Farmaceutiche, Università di Trieste, Piazzale Europa 1, 34127 Trieste, Italy*
[c] *Institut für Organische Chemie der Universität Erlangen-Nürnberg, Henkestrasse 42, D-91054 Erlangen, Germany. E-mail: hirsch@organik.uni-erlangen.de*

Received (in Cambridge, UK) 8th December 1999, Accepted 2nd February 2000

The kinetics of photoinduced electron transfer in new multicomponent arrays of a π-stacked fullerene porphyrin dyad and diazabicyclooctane or a fulleropyrrolidine ligand have been determined and depend on the molecular architecture

Owing to the importance of converting sunlight into electric current, suitable models are needed for the mimicry of the primary events in natural photosynthesis. A viable approach to artificial photosynthesis is to organize the donor–acceptor couple *via* covalent linkage and, thereby, controlling the separation and electronic coupling. To optimize the performance of such artificial systems, incorporation of secondary electron donor or acceptor moieties into multicomponent arrays (triads, tetrads, pentads *etc.*) has attracted considerable attention. Recently, different alternatives to address the critical issue of organizing the donor–acceptor couples has been forwarded, for example the assembly of individual molecules, linked by weak intermolecular interactions such as van der Waals' forces, hydrogen bonding, salt bridges or by complexation with metals.[1] In this contribution we present the formation and photophysical properties of new rigid electroactive arrays that evolve from complexation of a π–π stacked C_{60}-based ZnTPP dyad **1**[2] with diazabicyclooctane (DABCO) or a pyridine–fullerene ligand.[3]

The facile and selective formation of triad **2** or pentad **3** is based on the pronounced concentration dependence of ZnTTPs to form either square pyramidal 1:1- or 2:1 complexes with diazabicyclooctane (DABCO), respectively.[4] In analogy to related fullerene free TPPs[4] at low concentrations (*e.g.* 10^{-6} M) the exclusive formation of **2** was observed as shown, for example, with the titration experiment depicted in Fig. 1. Owing to the complexation the absorptions of the TPP moiety undergo a bathochromic shift of 9–10 nm which is very characteristic for a 1:1 complex.[4] The bathochromic shifts in 2:1 complexes are less pronounced (5–6 nm).[4] At higher concentrations the formation of the pentad **3** prevails. Titration of a 4.3×10^{-2} M solution of **1** in $CDCl_3$ with DABCO under ^{1}H NMR control showed the immediate appearance of one signal only for the 12 methylene protons of the axial ligand at δ −4.5 clearly demonstrating that exclusively **3** is formed. After the addition of 0.5 equiv. of DABCO only **3** can be detected in the NMR spectrum and all of free **1** is consumed. Upon formation of **3** the signals of the ZnTPP protons undergo an up-field shift of up to 0.5 ppm. Up-field shifts of up to 1 ppm for the ZnTPP C atoms and of 8.23 ppm for the C atoms of DABCO are observed in the ^{13}C NMR spectrum of **3**. Addition of more DABCO results in the formation of **2** being in an equilibrium with **3** as demonstrated by the appearance of a second signal for the DABCO ligand at δ −2.50 belonging to the three outer methylene groups of **2**. Similarly, triad **4** was prepared by mixing equimolar solutions of **1** and the corresponding fulleropyrrolidine.[3,5,6] The reversible formation of the complex was followed by visible and by ^{1}H NMR spectroscopies. In the former technique, a bathochromic shift of the porphyrin bands

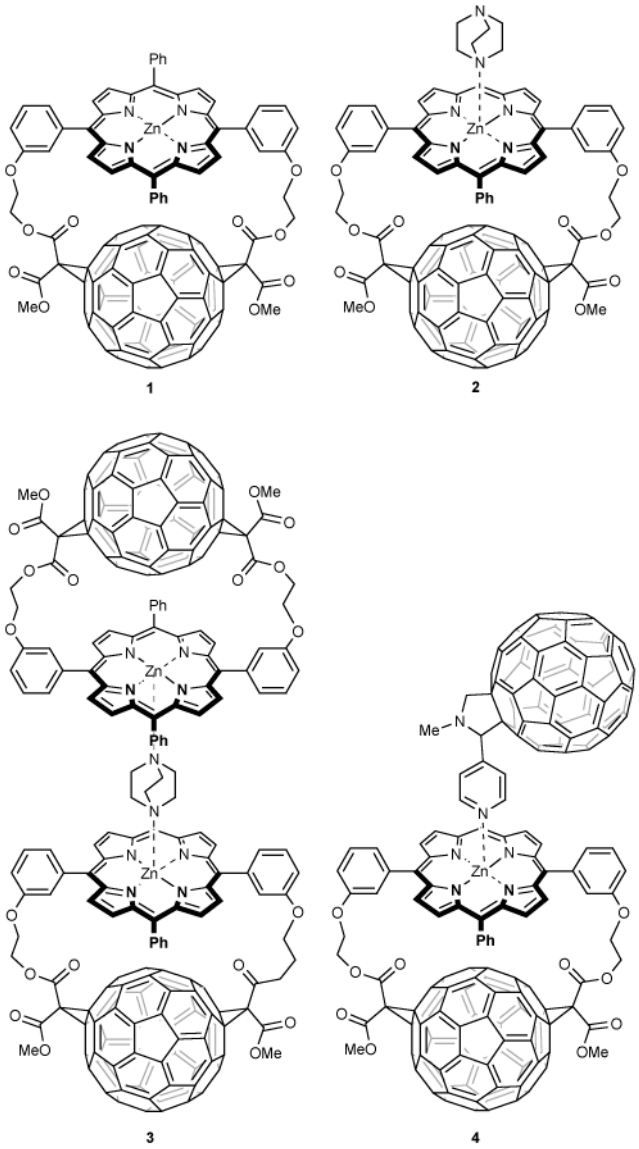

was observed, in analogy to **2**, whereas in the proton NMR a considerable upfield shift of the pyridine *2*-protons confirmed the presence of an equilibrium between **1** and the fulleropyrrolidine.[5]

Picosecond excitation of triad **2** resulted in the rapid transformation of the ZnTPP singlet excited state into a new transient, which displays a broad absorption maximum around 680 nm. Since the absorption spectrum is in close agreement with that of dyad **1**, we conclude that a rapid intramolecular electron transfer to yield a charge-separated radical pair follows the initial excitation event. The lifetime of the charge-separated

DOI: 10.1039/a909659k

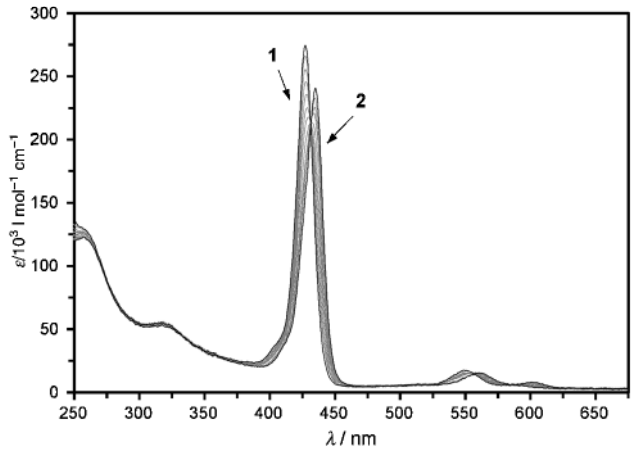

Fig. 1 Titration of **1** with DABCO in CH_2Cl_2: The appearance of **2** and disappearance of **1** is monitored by UV–VIS-spectroscopy.

state in triad **2** (1980 ± 30 ps) gives rise to a significant enhancement over dyad **1** (619 ps). Interestingly, the transient absorption spectra still revealed the characteristics of the ZnTPP π-radical cation. A reasonable rationalization for this observation implements the close energy of the $C_{60}^{\bullet-}$–$ZnTPP^{\bullet+}$–DABCO and $C_{60}^{\bullet-}$–ZnTPP–$DABCO^{\bullet+}$ states, as estimated by the oxidation potentials of the ZnTPP and DABCO electron donors. This leads to the assumption that the positively charge may be distributed over both moieties. In line with this assumption is the fact that the fullerene triplet quantum yield (*e.g.* the product of charge-recombination) did not change upon addition of the secondary electron donor (*i.e.* dyad **1** *cf.* triad **2**).

A qualitative similar picture was obtained with pentad **3**. Immediately after excitation of **3** in toluene the increase of absorbance between 600 and 800 nm is consistent with the formation of the radical pair, observed for dyad **1** and triad **2**. The kinetics of charge-recombination, as monitored around 660 nm, followed again first order kinetics, with a lifetime of 2280 ps.

As a viable alternative to DABCO (*e.g.* electron donor), addition of a fullerene derivative bearing a pyridine functionality (*e.g.* electron acceptor) to a toluene solution of dyad **1** was probed. In this context, the strong fluorescence quenching of **1** should be taken into account. Thus, addition of variable concentrations of the fullerene ligand ($0.5–5.0 \times 10^{-5}$ M) failed to show any meaningful effects on the fluorescence quantum yield of the resulting triad **4**. Photolysis (532 nm) of triad **4** in toluene or benzonitrile did not lead to any noticeable changes, relative to those described for dyad **1**. Owing to the rapid electron transfer occurring between the ZnTPP chromophore and the π–π stacked fullerene, the competing electron transfer route to the coordinated fullerene ligand is too slow that the latter reaction may contribute to the overall deactivation of the ZnTPP singlet excited state. Dramatic changes were, however, noted upon generating the fullerene singlet excited state (excitation at 337 nm). Now photoinduced electron transfer can be activated from both fullerene moieties, namely, the covalently linked one, which is still very fast (*e.g.* within the time-resolution of the apparatus) and the coordinatively one. Since benzonitrile is used as a solvent, its ability to coordinate to the zinc center and, therefore, interference with the fullerene–ligand complexation equilibrium between dyad **1** and triad **4** should be considered. This divides a reaction between the photoexcited fullerene and the ZnTPP into two processes. In particular, a fast intramolecular reaction (*ca.* 10^{10} s^{-1}) between the fullerene singlet excited state in the coordinated complex (triad **4**) is followed by a much slower intermolecular reaction (1.7×10^{10} $M^{-1}s^{-1}$) between the fullerene triplet excited state and the free dyad **1**. Spectroscopic evidence for this mechanism stems from the fact that the differential absorption changes reveal a two step formation of the $C_{60}^{\bullet-}/ZnTPP^{\bullet+}$ radical pair grow-in around 1010 and 680 nm, respectively.

In conclusion, we have shown that the reversible complexation of diazabicyclooctane or a fulleropyrrolidine ligand by a π–π stacked C_{60}–ZnTPP dyad **1** is a viable concept to construct novel supramolecular architectures. Rapid photoinduced electron transfer reactions in these multicomponent assemblies lead to charge-separated states, whose lifetimes are markedly improved relative to dyad **1**.

This work was supported by the Office of Basic Energy Sciences of the Department of Energy, the Stiftung Volkswagenwerk, by MURST (cofin. ex 40%, prot. n. 9803194198_005), by C.N.R. through the program 'Materiali Innovativi (legge 95/95)' and by the European Community (RTN program FUNCARS). This is document NDRL-4199 from the Notre Dame Radiation Laboratory.

Notes and references

1 For leading examples of noncovalent donor acceptor assemblies: P. Tecilla, R. P. Dixon, G. Slobodkin, D. S. Alavi, D. H. Waldeck and A. D. Hamilton, *J. Am. Chem. Soc.*, 1990, **112**, 9408; P. J. F. de Rege, S. A. Williams and M. J. Therien, *Science*, 1995, **269**, 1409; J. P. Kirby, J. A. Roberts and D. G. Nocera, *J. Am. Chem. Soc.*, 1997, **119**, 9230; S. L. Springs, D. Gosztola, M. R. Wasielewski, V. Kral, A. Andrievsky and J. L. Sessler, *J. Am. Chem. Soc.*, 1999, **121**, 2281; J. L. Sessler, B. Wang, S. L. Springs and C. T. Brown, in *Comprehensive Supramolecular Chemistry*, ed. Y. Murakami, Pergamon Press Ltd,, Oxford, UK, 1996, vol. 4, pp 311–335.

2 E. Dietel, A. Hirsch, E. Eichhorn, A. Rieker, S. Hackbarth and B. Röder, *Chem. Commun.*, 1998, 1981.

3 M. Prato, M. Maggini, C. Giacometti, G. Scorrano, G. Sandonà and G. Farnia, *Tetrahedron*, 1996, **52**, 5221.

4 A. Hunter, M. N. Meah and J. K. M. Sanders, *J. Am. Chem. Soc.*, 1990, **112**, 5773.

5 T. Da Ros, M. Prato, D. Guldi, E. Alessio, M. Ruzzi and L. Pasimeni, *Chem. Commun.*, 1999, 635.

6 For related approaches using bucky ligands see: N. Armaroli, F. Diederich, L. Echegoyen, T. Habicher, L. Flamigni, G. Marconi and J.-F. Nierengarten, *New J. Chem.*, 1999, 77; F. D'Souza, G. R. Deviprasad, M. S. Rahman and J.-P. Choi, *Inorg. Chem.*, 1999, **38**, 2157.

Communication a909659k

ChemComm

Synthesis, resolution and crystallographic characterization of a new C_2-symmetric planar-chiral bipyridine ligand: application to the catalytic enantioselective cyclopropanation of olefins

Ramon Rios, Jack Liang, Michael M.-C. Lo and Gregory C. Fu*

Department of Chemistry, Massachusetts Institute of Technology, Cambridge, Massachusetts 02139, USA. E-mail: gcf@mit.edu

Received (in Corvallis, OR, USA) 29th November 1999, Accepted 26th January 2000

The synthesis of a new C_2-symmetric planar-chiral bipyridine ligand is described, as well as its application to the enantioselective Cu^I-catalyzed cyclopropanation of olefins.

As Togni and Venanzi have recently documented, the use of transition metal catalysts that employ nitrogen-donor ligands is expanding rapidly.[1] With respect to neutral, bidentate, nitrogen donors, 2,2′-bipyridine is one of the most widely used.[2,3] As a consequence, the development of an effective chiral derivative of bipyridine is a challenge of considerable importance.[4,5] We have recently been exploring the application of planar-chiral heterocycles in asymmetric catalysis, both as enantioselective nucleophilic catalysts[6] and as chiral ligands for transition metals.[7] Here we describe our first investigation in the area of chiral bipyridine chemistry, specifically, the synthesis, resolution and crystallographic characterization of C_2-symmetric planar-chiral ferrocene derivative **1**. To benchmark this new

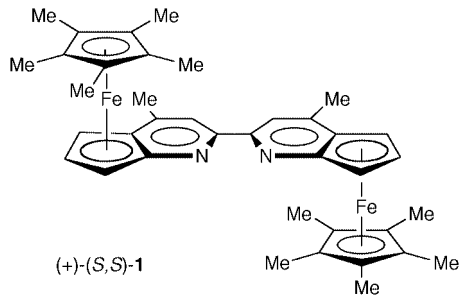

(+)-(*S*,*S*)-**1**

ligand, we have chosen to follow the lead of others by examining its utility in the Cu^I-catalyzed cyclopropanation of olefins [eqn. (1)].[8–10]

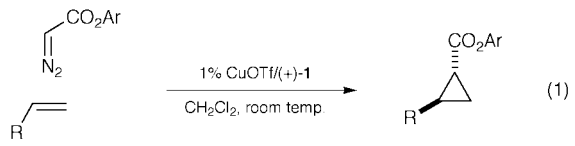

R = aryl, alkyl, silyl *up to 94% ee*

Our synthesis of ligand **1** begins with previously reported pyridine derivative **2**,[11] which is available in one step from commercially available materials (Scheme 1). Chlorination with $POCl_3$ affords compound **3** in 74% yield, and a standard sequence of oxidation, acetoxylation and elimination then furnishes pyrindine **6**.[6a] The five-membered ring of **6** is complexed to iron through reaction of its lithium salt with $(Cp^*FeCl)_n$ (59%),[6a] and the resulting ferrocene derivative is then reductively coupled with $NiBr_2(PPh_3)_2$/Zn/Et_4NI,[12] thereby providing racemic **1** as a single diastereomer in 58% yield. This route is amenable to the synthesis of multi-gram quantities of this new C_2-symmetric, planar-chiral bipyridine ligand.

The enantiomers of ligand **1** can be separated by chiral HPLC (Regis Whelk-O column). We have established the absolute configuration of (+)-**1** through X-ray crystallography.

In order to validate our ligand design, we chose to investigate the application of bipyridine **1** to the Cu^I-catalyzed cyclopropanation of olefins, a reaction that has previously been used to benchmark new chiral bipyridine designs.[8] We were pleased to observe that with the 2,6-di-*tert*-butyl-4-methylphenyl ester of diazoacetic acid as the carbene source, we can cyclopropanate an array of olefins with high stereoselectivity (Table 1). For example, treatment of styrene with 1% CuOTf, 1.2% (+)-**1**, and 2 equiv. of diazo ester in CH_2Cl_2 at room temperature furnishes the *trans*-cyclopropane in very good diastereomeric and enantiomeric excess (94% de, 87% ee; Table 1, entry 1). The stereoselection remains unchanged even at a very low catalyst loading (0.25%), although the yield drops somewhat (60%). It is worth noting that, in contrast to many previously reported Cu^I-catalyzed cyclopropanations wherein the diazo ester is the limiting reagent, our conditions employ the olefin as the limiting reagent. Among the copper sources and the solvents that we have examined, CuOTf and CH_2Cl_2 appear to be optimal.

In the presence of CuOTf/**1**, we can effect the catalytic enantioselective cyclopropanation of an array of olefins (Table

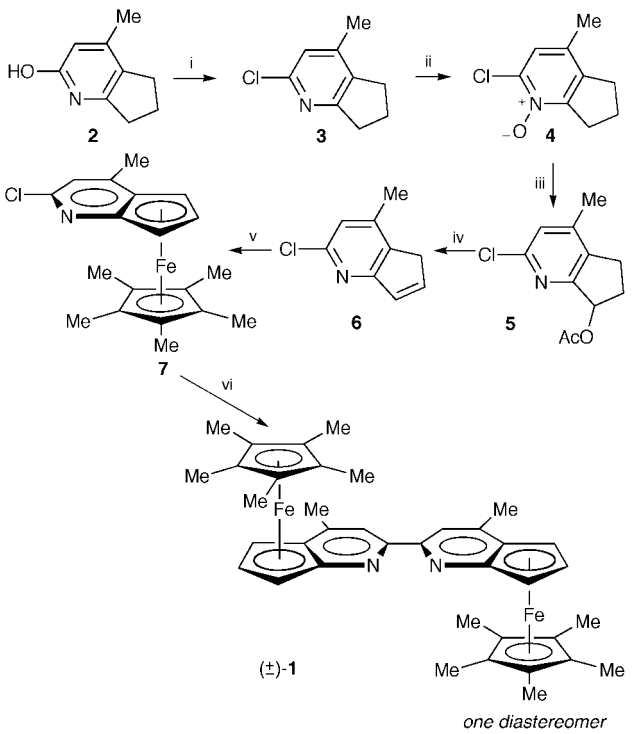

Scheme 1 *Reagents and conditions*: i, $POCl_3$, 74%; ii, H_2O_2, AcOH, 88%; iii, Ac_2O, 58%; iv, H_2SO_4, 79%; v, BuLi, then $(Cp^*FeCl)_n$, 58%; vi, 30% $NiBr_2(PPh_3)_2$, Zn, Et_4NI, 58%.

DOI: 10.1039/a909457a

Table 1 Scope of the Cu^{I}/**1**-catalyzed enantioselective cyclopropanation of olefins[a]

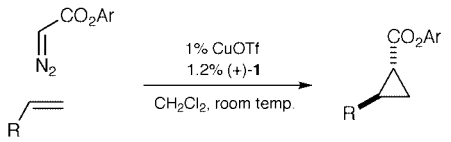

Entry	R	*trans*:*cis*	Ee (%) (*trans*)	Yield (%)
1	Ph	97:3	87	78
2	*p*-(MeO)C_6H_4	95:5	75	71
3	*p*-(F_3C)C_6H_4	94:6	94	83
4	*n*-Hexyl	94:6	78	78
5	Et_3Si	96:4	80	60

[a] All data represent the average of two runs.

1). For styrene derivatives, we have made the interesting observation that whereas the electronic nature of the aromatic ring has only a modest effect on *trans*:*cis* diastereoselectivity, it exerts a very significant impact on enantioselectivity (entries 1–3). Thus, reaction of electron-rich 4-methoxystyrene proceeds with relatively moderate ee (75%, entry 2), whereas reaction of electron-poor 4-trifluoromethylstyrene occurs with quite high ee (94%, entry 3). Alkyl-substituted olefins (entry 4) and vinylsilanes (entry 5) undergo cyclopropanation with excellent diastereoselectivity and good enantioselectivity.

An examination of the X-ray crystal structure of [Cu((−)-**1**)(styrene)]PF_6† clearly shows that bidentate complexation of ligand **1** to copper furnishes a well-defined C_2-symmetric binding pocket [Fig. 1(*a*)]. The styrene is bound to copper in an orientation that is predictable on the basis of minimizing steric interactions with ligand **1** [Fig. 1(*b*)].

In summary, we have described the synthesis, resolution and crystallographic characterization of a new class of C_2-symmetric planar-chiral bipyridine ligands, and we have demonstrated the effectiveness of our ligand design through a study of Cu^{I}-catalyzed cyclopropanations of olefins. The chiral environment afforded by this family of bidentate ligands should be readily tunable, both through a change in the metal fragment (*e.g.* FeCp* → FeC_5Ph_5[6b]) and through the incorporation of substituents in the 7 and 7′ positions. The large number of processes known to be catalyzed by bipyridine–metal complexes provides a wealth of opportunities for applications of these ligands in asymmetric catalysis.

Support has been provided by the Alfred P. Sloan Foundation, the American Cancer Society, Bristol-Myers Squibb, the Camille and Henry Dreyfus Foundation, Merck, the National Science Foundation, Novartis, Pfizer, Pharmacia & Upjohn, Procter & Gamble, the Spanish Ministry of Education, and Union Carbide.

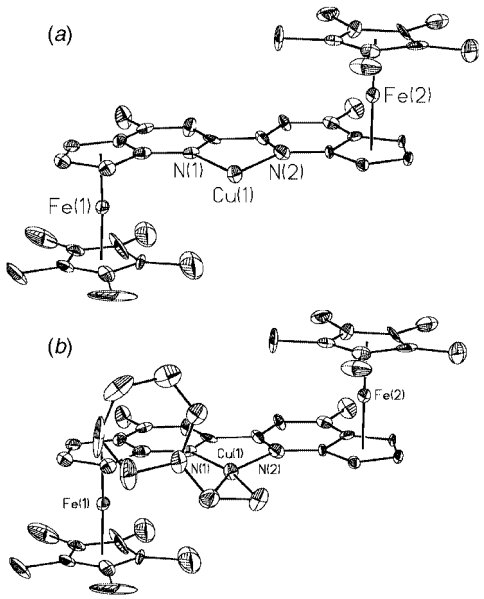

Fig. 1 X-Ray crystal structure of [Cu((−)-**1**)(styrene)]PF_6 (the non-coordinating PF_6 counter ion has been omitted for clarity): (*a*) without styrene; (*b*) with styrene.

Notes and references

† *Crystal data* for [Cu((*R*,*R*)-**1**)(PhCH=CH_2)]PF_6 (green): $C_{46}H_{52}CuF_6Fe_2N_2P$, M = 953.11, orthorhombic, space group $P2_12_12_1$, μ = 1.315 mm^{-1}, a = 7.8830(16), b = 20.670 (4), c = 25.167(5) Å, V = 4100.8(14) $Å^3$, Z = 4, T = 183(2) K, 16506 reflections collected, 5878 independent reflections (R_{int} = 0.1378), 518 variables, R = 0.0465, R_w = 0.0549 [$I > 2\sigma(I)$], Flack parameter = −0.02(2). CCDC 182/1534.

1 A. Togni and L. M. Venanzi, *Angew. Chem., Int. Ed. Engl.*, 1994, **33**, 497.
2 F. Blau, *Chem. Ber.*, 1888, **21**, 1077.
3 J. Reedijk, in *Comprehensive Coordination Chemistry*, ed. G. Wilkinson, Pergamon, New York, 1987; vol. 2, ch. 13.2.
4 For a review, see: G. Chelucci, *Gazz. Chim. Ital.*, 1992, **122**, 89. See also: C. Bolm, in *Organic Synthesis via Organometallics*, ed. K. H. Dötz and R. W. Hoffmann, Vieweg, Wiesbaden, 1990, pp. 223–240.
5 For examples of progress in achieving this goal (> 50% ee), see: rhodium-catalyzed hydrosilylation of ketones: C. Botteghi, A. Schionato, G. Chelucci, H. Brunner, A. Kürzinger and U. Obermann, *J. Organomet. Chem.*, 1989, **370**, 17; H. Nishiyama, S. Yamaguchi, S.-B. Park and K. Itoh, *Tetrahedron: Asymmetry*, 1993, **4**, 143; $ZnEt_2$ addition to benzaldehyde: C. Bolm, M. Zehnder and D. Bur, *Angew. Chem., Int. Ed. Engl.*, 1990, **29**, 205; P. Collomb and A. von Zelewsky, *Tetrahedron: Asymmetry*, 1998, **9**, 3911; nickel-catalyzed conjugate addition to enones: C. Bolm and M. Ewald, *Tetrahedron Lett.*, 1990, **31**, 5011; rhodium-catalyzed transfer hydrogenation of ketones: S. Gladiali, L. Pinna, G. Delogu, S. De Martin, G. Zassinovich and G. Mestroni, *Tetrahedron: Asymmetry*, 1990, **1**, 635; copper-catalyzed ring expansion of oxetanes to tetrahydrofurans: K. Ito and T. Katsuki, *Chem. Lett.*, 1994, 1857; palladium-catalyzed allylic alkylation: E. Pena-Cabrera, P.-O. Norrby, M. Sjögren, A. Vitagliano, V. De Felice, J. Oslob, S. Ishii, D. O'Neill, B. Akermark and P. Helquist, *J. Am. Chem. Soc.*, 1996, **118**, 4299; G. Chelucci, G. A. Pinna and A. Saba, *Tetrahedron: Asymmetry*, 1998, **9**, 531; zinc-catalyzed allylation of aldehydes: H.-L. Kwong, K.-M. Lau, W.-S. Lee and W.-T. Wong, *New J. Chem.*, 1999, **23**, 629.
6 (*a*) J. C. Ruble and G. C. Fu, *J. Org. Chem.*, 1996, **61**, 7230; (*b*) J. C. Ruble, H. A. Latham and G. C. Fu, *J. Am. Chem. Soc.*, 1997, **119**, 1492; (*c*) J. C. Ruble, J. Tweddell and G. C. Fu, *J. Org. Chem.*, 1998, **63**, 2794; (*d*) J. Liang, J. C. Ruble and G. C. Fu, *J. Org. Chem.*, 1998, **63**, 3154; (*e*) C. E. Garrett, M. M.-C. Lo and G. C. Fu, *J. Am. Chem. Soc.*, 1998, **120**, 7479; (*f*) J. C. Ruble and G. C. Fu, *J. Am. Chem. Soc.*, 1998, **120**, 11 532; (*g*) B. L. Hodous, J. C. Ruble and G. C. Fu, *J. Am. Chem. Soc.*, 1999, **121**, 2637; (*h*) B. Tao, J. C. Ruble, D. A. Hoic and G. C. Fu, *J. Am. Chem. Soc.*, 1999, **121**, 5091.
7 P. I. Dosa, J. C. Ruble and G. C. Fu, *J. Org. Chem.*, 1997, **62**, 444; M. M.-C. Lo and G. C. Fu, *J. Am. Chem. Soc.*, 1998, **120**, 10 270; S. Qiao and G. C. Fu, *J. Org. Chem.*, 1998, **63**, 4168.
8 (*a*) K. Ito, S. Tabuchi and T. Katsuki, *Synlett*, 1992, 575; (*b*) G. Chelucci, M. A. Cabras and A. Saba, *J. Mol. Catal. A.*, 1995, **95**, L7; (*c*) H.-L. Kwong, W.-S. Lee, H.-F. Ng, W.-H. Chiu and W.-T. Wong, *J. Chem. Soc., Dalton Trans.*, 1998, 1043; (*d*) U. Wörsdörfer, F. Vögtle, M. Nieger, M. Waletzke, S. Grimme, F. Glorius and A. Pfaltz, *Synthesis*, 1999, 597.
9 For the first study of transition metal-catalyzed asymmetric cyclopropanation, see: H. Nozaki, S. Moriuti, H. Takaya and R. Noyori, *Tetrahedron Lett.*, 1966, 5239; For an industrial application of copper-catalyzed olefin cyclopropanation with a diazo ester, see: T. Aratani, *Pure Appl. Chem.*, 1985, **57**, 1839.
10 For reviews of catalytic enantioselective cyclopropanation, see: M. P. Doyle and D. C. Forbes, *Chem. Rev.*, 1998, **98**, 911; M. P. Doyle, M. A. McKervey and T. Ye, *Modern Catalytic Methods for Organic Synthesis with Diazo Compounds*, Wiley, New York, 1998; H.-U. Reissig, in *Stereoselective Synthesis (Houben-Weyl)*, ed. G. Helmchen, R. W. Hoffmann, J. Mulzer and E. Schaumann, Thieme, New York, 1996, vol. E21c, ch. 1.6.1.5.
11 A. Sakurai and H. Midorikawa, *Bull. Chem. Soc. Jpn.*, 1968, **41**, 165.
12 M. Iyoda, H. Otsuka, K. Sato, N. Nisato and M. Oda, *Bull. Chem. Soc. Jpn.*, 1990, **63**, 80; M. Tiecco, L. Testaferri, M. Tingoli, D. Chianelli and M. Montanucci, *Synthesis*, 1984, 736.

Communication a909457a

Novel zirconium complexes of amine bis(phenolate) ligands. Remarkable reactivity in polymerization of hex-1-ene due to an extra donor arm†

Edit Y. Tshuva,[a] Israel Goldberg,[a] Moshe Kol,*[a] Hana Weitman[b] and Zeev Goldschmidt*[b]

[a] *School of Chemistry, Raymond and Beverly Sackler Faculty of Exact Sciences, Tel Aviv University, Tel Aviv 69978, Israel. E-mail: moshekol@post.tau.ac.il*

[b] *Department of Chemistry, Bar-Ilan University, Ramat-Gan 52900, Israel. E-mail: goldz@mail.biu.ac.il*

Received (in Cambridge, UK) 11th January 2000, Accepted 2nd February 2000

Zirconium complexes of two dianionic amine bis(phenolate) ligands have been synthesized, their X-ray structures solved, and their activity as hex-1-ene polymerization catalysts studied; upon treatment with $B(C_6F_5)_3$, an octahedral $[ONNO]Zr(CH_2Ph)_2$ complex, having an extra N-donor group on a side arm, shows exceptionally high polymerization activity and yields a high molecular weight poly(hex-1-ene), whereas a related pentacoordinate $[ONO]Zr(CH_2Ph)_2$ complex, having no extra donor group, shows only poor activity as a polymerization catalyst.

The increased interest in development of novel catalysts for polymerization of α-olefins has resulted in the introduction of a variety of non-metallocene group 4 metal complexes.[1] Most interest was drawn to pre-catalysts based on chelating di(amido) ligands,[2] while di(alkoxo) based pre-catalysts have attracted more limited attention.[3] Recently, we introduced the amine bis(phenolate) family of ligands to group 4 transition metal chemistry.[4] Here, we report on the synthesis, structure and hex-1-ene polymerization activity of two zirconium dibenzyl complexes of related amine bis(phenolate) ligands: a tetradentate $[ONNO]^{2-}$ ligand and a tridentate $[ONO]^{2-}$ ligand.

The ligand precursor $[ONNO]H_2$ **1** reacted cleanly with 1 mol equiv. of tetrabenzylzirconium at 65 °C yielding the dibenzyl complex $[ONNO]Zr(CH_2Ph)_2$ **2**, quantitatively, as a yellow crystalline solid (Scheme 1).† The spectral data of **2** indicate the formation of a rigid C_s symmetrical complex having symmetry related phenolate rings and two different benzyl groups.

The X-ray structure of **2** (Fig. 1)‡ features a complex having a slightly distorted octahedral geometry, in which the two oxygen atoms of the phenolate rings are in a *trans* configuration. Most importantly, the *cis* configuration of the two benzyl groups, expected from the arrangement of the donor atoms in this $[ONNO]^{2-}$ tetradentate ligand, is evident from the narrow C–Zr–C angle of 93.7°. A narrow angle between the active positions may facilitate the formation of a metallacyclobutane, in the rate determining step of the polymerization of α-olefins.[5]

The tridentate ligand precursor $[ONO]H_2$ **3**, having identical phenolate groups but lacking the extra donor group on the side arm, also reacted cleanly with 1 mol equiv. of tetrabenzylzirconium at 65 °C yielding the formally penta-coordinate dibenzyl complex $[ONO]Zr(CH_2Ph)_2$ **4**, quantitatively, as a yellow crystalline solid (Scheme 2).†

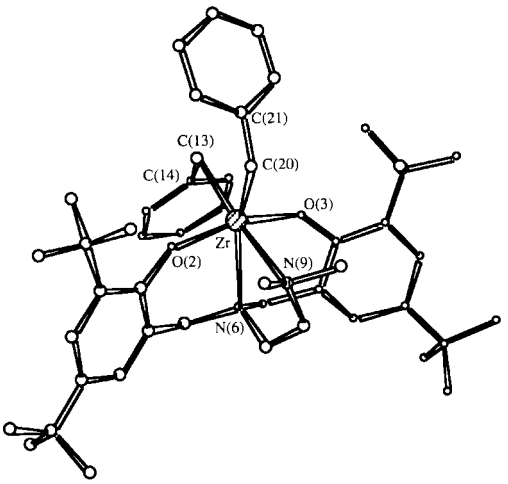

Fig. 1 Molecular structure of **2**. Selected bond lengths (Å) and angles (°): Zr–O(2) 1.995(5), Zr–O(3) 1.994(5), Zr–N(6) 2.446(6), Zr–N(9) 2.594(6), Zr–C(13) 2.305(7), Zr–C(20) 2.250(6); O(2)–Zr–O(3) 160.3 (2), N(6)–Zr–N(9) 69.7(2), C(13)–Zr–C(20) 93.7(2), Zr–C(13)–C(14) 104.9(5), Zr–C(20)–C(21) 115.8(5).

Interestingly, a homoleptic complex of the type $[ONO]_2Zr$, was not formed, apparently due to the steric effect of the *tert*-butyl groups in the *ortho* position of the phenolate rings.[4] In analogy to **2**, the spectral data of **4** also indicated the formation of a rigid C_s symmetrical complex having symmetry related phenolate rings and two different benzyl groups. However, the X-ray crystal structure of **4** indicated several differences between it and **2** (Fig. 2).‡

The structure features a complex having a pseudo-trigonal bipyramidal geometry, with axial O atoms and equatorial N, C, C atoms, as evident from an O–Zr–O angle of 157.3°, and sum of angles between the equatorial substituents around the zirconium of 360°. The angle between the two benzyl groups in **4** is much wider than in **2**, at 117.4°. An acute Zr–CH_2–C(Ar) angle of 89.4° as well as a short Zr–C(Ar) distance of 2.71 Å, for one of the benzyl groups, indicate that the π-system interacts with the metal, *i.e.* there is a non-classical η^2 binding of this group to the Zr atom.[6] The η^2 binding in **4** may reflect the

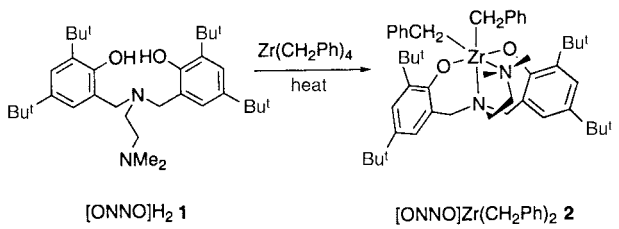

Scheme 1

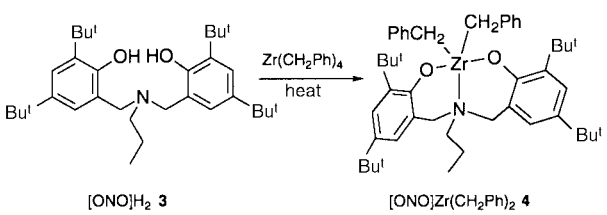

Scheme 2

† Electronic supplementary information (ESI) available: selected spectroscopic data. See http://www.rsc.org/suppdata/cc/b0/b000396o/

DOI: 10.1039/b000396o

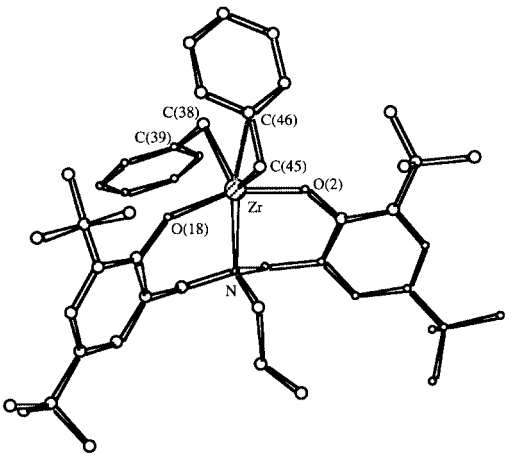

Fig. 2 Molecular structure of **4**. Selected bond lengths (Å) and angles (°): Zr–O(2) 2.002(2), Zr–O(18) 2.000(2), Zr–N 2.378(2), Zr–C(38) 2.272(2), Zr–C(45) 2.292(2), Zr–C(46) 2.714(2); O(2)–Zr–O(18) 157.33(6), C(45)–Zr–C(38) 117.39(9), Zr–C(45)–C(46) 89.4(1), Zr–C(38)–C(30) 108.7(2).

electron deficiency of this complex relative to **2**, or may simply result from the lower crowding around the metal, allowing the bending of one of the benzyl groups. It is noteworthy that the central nitrogen and the two phenolate rings bind very similarly in **2** and **4**, despite the additional donor in **2**, and difference in benzyl hapticities.

Which of these systems is expected to lead to a better catalyst for polymerization of α-olefins? Since additional donor groups have been reported to increase the reactivity in certain systems[7] and reduce the reactivity in other systems,[8] this prediction is not straightforward. **2** proved to be an extremely reactive catalyst in the presence of tris(pentafluorophenyl)borane: adding 0.01 mmol of **2** and 1 mol equiv. of $B(C_6F_5)_3$ to 10 mL of neat hex-1-ene at room temperature, initiated a fast polymerization reaction accompanied by heat release, causing boiling of the hex-1-ene.§ The monomer reacted almost completely within 2 min giving an activity of 15 500 g $mmol_{cat}^{-1}$ h^{-1}. To the best of our knowledge, this is the highest reactivity reported for polymerization of hex-1-ene under such mild conditions, namely a dibenzyl complex[9] activated by the mild Lewis acid tris(pentafluorophenyl)borane.[2a,10] In order to restrain the polymerization, the monomer was diluted in an inert solvent, and the quantity of catalyst was reduced. Thus, adding 0.005 mmol of **2** and 1 mol equiv. of $B(C_6F_5)_3$ to 3 mL of hex-1-ene in 7 mL of heptane resulted in a slower evolution of heat, and linear consumption of the monomer for 8 min, after which time 80% had reacted. The polymer obtained had a molecular weight of M_w = 170 000 and PDI M_w/M_n = 2.2, indicating that the catalytic system is homogeneous.

In contrast, **4** yielded a poor hex-1-ene polymerization catalyst: adding 0.01 mmol of **4** and 1 mol equiv. of $B(C_6F_5)_3$ to 2 mL of neat hex-1-ene at room temperature, yielded only oligo(hex-1-ene) chains (30 mg), giving a low activity of 23 g $mmol_{cat}^{-1}$ h^{-1}. Olefinic termination groups were observed in the ^1H NMR spectra, integration of which indicated an average of < 20 units of monomer per chain.

In summary, of the two amine bis(phenolate) zirconium complexes that were introduced, that having an extra donor arm was about three orders of magnitude more reactive than its counterpart. We therefore propose that the side arm nitrogen of the $[ONNO]^{2-}$ ligand remains attached to the metal in the reactive catalyst. Since the extra donor is supposed to *lower* the electrophilicity of the zirconium complex, it seems that, at least for these systems, electrophilicity does not play a major role in determining the polymerization activity.[11] The extreme reactivity of the catalyst derived from the $[ONNO]^{2-}$ ligand may result from steric effects, *e.g.* a narrow angle between the growing polymer chain and a coordinated olefin, as well as electronic effects induced by the N-donors being *trans* to the active positions. The synthesis of related systems and their application as polymerization catalysts is currently under way.

This research was supported in part by the Israel Science Foundation founded by the Israel Academy of Sciences and Humanities. We thank Sima Alfi (BIU) for technical assistance.

Notes and references

‡ *Crystal data*: for **2**: $C_{53}H_{80}N_2O_2Zr{\cdot}C_5H_{12}$, M = 868.41, orthorhombic, space group *Pbca*, a = 18.4520(10), b = 19.1310(19), c = 28.2390(10) Å, U = 9968.5(8) Å^3, Z = 8, D_c = 1.157 g cm^{-3}, μ(Mo-Kα) = 0.260 mm^{-1}, T = 117 K, Enraf-Nonius Kappa-CCD, 9375 reflections were measured (R_{int} = 0.000). The structure was solved by direct methods and refined by full-matrix least-squares on F^2. In the crystal, the dimethylamino(ethyl) arm was found to be disordered. The unit cell contains one molecule of disordered pentane, which could not be modelled precisely. When its contribution to the structure factors was substracted by the 'Bypass' procedure,[12] the final refinement converged at R_1 = 0.1028 and wR_2 = 0.2636 for observations with [$I > 2\sigma(I)$] and R_1 = 0.1480 and wR_2 = 0.2853 for all data. For **4**: $C_{54}H_{81}NO_2Zr{\cdot}C_7H_{16}$, M = 867.42, monoclinic, space group $P2_1/c$, a = 10.4840(1), b = 19.2970(4), c = 24.5940(5) Å, β = 91.048(1)°, U = 4974.77(15) Å^3, Z = 4, D_c = 1.158 g cm^{-3}, μ(Mo-Kα) = 0.259 mm^{-1}, T = 116 K, Enraf-Nonius Kappa-CCD, 12508 reflections were measured. The structure was solved by direct methods and refined by full-matrix least squares on F^2. In the crystal, one of the Bu^t groups was found to be disordered. The unit cell contains one molecule of disordered heptane. The final refinement converged at R_1 = 0.0493 and wR_2 = 0.1295 for observations with [$I > 2\sigma(I)$] and R_1 = 0.0624 and wR_2 = 0.1377 for all data. CCDC 182/1535. See http://www.rsc.org/suppdata/cc/b0/b000396o/for crystallographic files in .cif format.

§ The extreme reactivity of this catalytic system was even more pronounced in the polymerization of oct-1-ene: adding 0.01 mmol of **2** and 1 mol equiv. of $B(C_6F_5)_3$ to 2 mL of neat oct-1-ene at r.t. caused boiling of the oct-1-ene (bp = 123 °C), which was almost completely consumed within 2 min.

1 G. J. P. Britovsek, V. C. Gibson and D. F. Wass, *Angew. Chem., Int. Ed.*, 1999, **38**, 428.
2 (*a*) J. D. Scollard, D. H. McConville, N. C. Payne and J. J. Vittal, *Macromolecules*, 1996, **29**, 5241; (*b*) J. D. Scollard and D. H. McConville, *J. Am. Chem. Soc.*, 1996, **118**, 10 008; (*c*) R. Baumann, W. M. Davis and R. R. Schrock, *J. Am. Chem. Soc.*, 1997, **119**, 3830; (*d*) M. Aizenberg, L. Turculet, W. M. Davis, F. Schattenmann and R. R. Schrock, *Organometallics*, 1998, **17**, 4795; (*e*) L.-C. Liang, R. R. Schrock, W. M. Davis and D. H. McConville, *J. Am. Chem. Soc.*, 1999, **121**, 5797; (*f*) S. Tinkler, R. J. Deeth, D. J. Duncalf and A. McCamley, *Chem. Commun.*, 1996, 2623; (*g*) Y.-M. Jeon, S. J. Park, J. Heo and K. Kim, *Organometallics*, 1998, **17**, 3161; (*h*) V. C. Gibson, V. S. Kimberley, A. J. P. White, D. J. Williams and P. Howard, *Chem. Commun.*, 1998, 313.
3 A. van der Linden, C. J. Schaverien, N. Meijboom, C. Ganter and A. G. Orpen, *J. Am. Chem. Soc.*, 1995, **117**, 3008; E. B. Tjaden, D. C. Swenson, R. F. Jordan and J. L. Petersen, *Organometallics*, 1995, **14**, 371; S. Fokken, T. P. Spaniol, J. Okuda, F. G. Sernetz and R. Mülhaupt, *Organometallics*, 1997, **16**, 4240; L. Matilainen, M. Klinga and M. Leskalä, *J. Chem. Soc., Dalton Trans.*, 1996, 219.
4 E. Y. Tshuva, M. Versano, I. Goldberg, M. Kol, H. Weitman and Z. Goldschmidt, *Inorg. Chem. Commun.*, 1999, **2**, 371.
5 N. A. H. Male, M. Thornton-Pett and M. Bochmann, *J. Chem. Soc., Dalton Trans.*, 1997, 2487.
6 F. G. N. Cloke, T. J. Geldbach, P. B. Hitchcock and J. B. Love, *J. Organomet. Chem.*, 1996, **506**, 343.
7 L. Porri, A. Ripa, P. Colombo, E. Miano, S. Capelli and S. V. Meille, *J. Organomet. Chem.*, 1996, **514**, 213; F. G. Sernetz, R. Mülhaupt, S. Fokken and J. Okuda, *Macromolecules*, 1997, **30**, 1562.
8 F. J. Schattenmann, R. R. Schrock and W. M. Davis, *Organometallics*, 1998, **17**, 989.
9 A. D. Horton and J. de With, *Organometallics*, 1997, **16**, 5424.
10 Y.-X. Chen, P. F. Fu, C. L. Stern and T. J. Marks, *Organometallics*, 1997, **16**, 5958.
11 T. H. Warren, R. R. Schrock and W. M. Davis, *Organometallics*, 1998, **17**, 308.
12 P. Van der Sluis and A. L. Spek, *Acta Crystallogr., Sect. A*, 1990, **46**, 194.

Communication b000396o

ChemComm

High turnover number of γ-$SiW_{10}\{Mn^{III}(OH_2)\}_2O_{38}^{6-}$ for oxygenation of cyclohexane with 1 atm molecular oxygen†

Tetsuya Hayashi, Asako Kishida and Noritaka Mizuno*

Department of Applied Chemistry, Graduate School of Engineering, The University of Tokyo, Hongo, Bunkyo-ku, Tokyo 113-8656, Japan. E-mail: tmizuno@mail.ecc.u-tokyo.ac.jp

Received (in Cambridge, UK) 24th December 1999, Accepted 3rd February 2000

An all-inorganic oxo-bridged dimanganese-containing silicotungstate, γ-$SiW_{10}\{Mn^{III}(OH_2)\}_2O_{38}^{6-}$, showed the highest turnover number of 789 among various metal-substituted silicotungstates for the oxygenation of cyclohexane with 1 atm molecular oxygen; this is the highest level when compared with other catalysts reported so far.

Catalytic oxygenation of alkanes has attracted much attention. The utilization of molecular oxygen for catalytic oxygenation is a rewarding goal because among oxidants molecular oxygen has the highest content of active oxygen and forms no by-products.[1–7] Reducing reagents or radical initiators have been added for in an attempt to facilitate reaction lowering the reaction temperature and resulting in the suppression of overoxidation of oxygenated products.[8–13] However, there are only a few examples of ideal homogeneous oxygenation systems for alkanes with molecular oxygen in the absence of reducing reagents or radical initiators because of catalyst deactivation and difficulty of C–H bond/oxygen activation.[1–24] The oxidation of cyclohexane has been industrialized by using a cobalt catalyst with pressurized molecular oxygen above 423 K, low conversions, however, are a drawback in suppressing overoxidation of the products.[5,25,26] It is clearly desirable if oxygenation can be carried out with higher turnover numbers under milder conditions. Fe(DPA) (DPA = 2,6-dicarboxylatopyridine), $K[Ru^{III}(saloph)Cl_2]$ [saloph = *N*,*N*′-*o*-phenylenebis(salicylideneaminato)] $PW_9O_{37}\{Fe_{3-x}Ni_x(OAc)_3\}^{(9+x)-}$ (*x*) = predominantly 1) and γ-$SiW_{10}\{Fe^{III}(OH_2)\}_2O_{38}^{6-}$ are examples of catalysts for cyclohexane oxygenation with 1 atm molecular oxygen.[14–16,20]‡ Cobalt-containing aluminophosphate and $[Co(NCMe)_4](PF_6)_2$ have also been reported to be active for oxygenation of cyclohexane with pressurized molecular oxygen.[21–24] However, the turnover numbers are low at < 180.

Little is known of the structures of the active manganese centers for the oxygenation of cyclohexane with molecular oxygen. Here, we report that the oxo-bridged dimanganese-containing silicotungstate, γ-$SiW_{10}\{Mn^{III}(OH_2)\}_2O_{38}^{6-}$, can efficiently catalyze the oxygenation of cyclohexane with 1 atm molecular oxygen.

Cyclohexane was distilled and treated with activated alumina to remove impurities and cyclohexyl hydroperoxide. The other reagents were commercially obtained and used as received. The reaction was carried out in a glass vial containing a magnetic stir bar as described previously.[27] The reaction solution was periodically sampled and analyzed by gas chromatography on TC-WAX capillary columns. The oxidation of cyclohexane did not proceed without catalyst under the present conditions.

Cyclohexanol and cyclohexanone were mainly formed after an induction period for the catalytic oxygenation of cyclohexane with 1 atm molecular oxygen catalyzed by γ-$SiW_{10}\{Mn^{III}(OH_2)\}_2O_{38}^{6-}$ at 365 K. Only small amounts of dicyclohexyl and cyclohexyl hydroperoxide were observed and neither acids, oxoesters nor carbon oxides were observed. The selectivities changed little with time. The conversion was 6.4%, and the turnover number of γ-$SiW_{10}\{Mn^{III}(OH_2)\}_2O_{38}^{6-}$ reached 789 after 96 h, much higher than values reported for the oxygenation of cyclohexane catalyzed by Fe(DPA)/O_2(1 atm),[14] $K[Ru(saloph)Cl_2]/O_2$ (1 atm),[15] γ-$SiW_{10}\{Fe^{III}(OH_2)\}_2O_{38}^{6-}/O_2$ (1 atm),[20] $[Co(NCMe)_4](PF_6)_2/O_2$ (3 atm)[21] or cobalt-containing aluminophosphate/O_2 (15 atm).[23] In addition, the value was higher than those of 130, 90, 5 and 3 reported for $Mn(acac)_2$/NHPI (NHPI = *N*-hydroxyphthalimide),[11] $Co(acac)_2$/NHPI,[13] $[\{Fe(HBpz_3)(hfacac)\}_2O]$-/Zn ($HBpz_3$ = hydrotris(1-pyrazolyl)borate, hfacac = 1,1,1,5,5,5-hexafluoroacetylacetone)[28] and $[R_fMn(R_fTACN)]^{2+}$/TBHP (R_fTACN = tris-*N*-(4,4,5,5,6,6,7,7,8,8,9,9,10,10,11,11,11-heptadecafluoroundecyl)-1,4,7-triazacyclononane; R_f = C_8F_{17})[12] systems, respectively, which work in the presence of reducing reagents or radical initiators with 1 atm molecular oxygen.

The oxygenation of cyclohexane with 1 atm molecular oxygen proceeded catalytically even at 305 K,§ whilst no oxygenation was observed for γ-$SiW_{10}\{Fe^{III}(OH_2)\}_2O_{38}^{6-}$ at the same temperature. It has been reported that the commercial catalyst, $Co(oct)_2$ (oct = 2-ethylhexyl octanoate), was inactive at 348 K with 3 atm molecular oxygen.[21] All these results demonstrate that γ-$SiW_{10}\{Mn^{III}(OH_2)\}_2O_{38}^{6-}$ can catalyze the selective oxygenation of cyclohexane with high turnover number and under mild conditions.

Table 1 compares turnover numbers for cyclohexane oxygenation with molecular oxygen catalyzed by manganese-substituted silicotungstates. The turnover numbers for manganese-substituted silicotungstates decreased in the order γ-$SiW_{10}\{Mn^{III}(OH_2)\}_2O_{38}^{6-}$ > α-$SiW_{11}\{Mn^{III}(OH_2)\}O_{39}^{5-}$ > α-$SiW_9\{Mn^{III}(OH_2)\}_3O_{37}^{7-}$ ≈ α-$SiW_{12}O_{40}^{4-}$ ≈ 0. No oxygenation proceeded for γ-$SiW_{10}\{Mn^{II}(OH_2)\}_2O_{38}^{8-}$ in which the oxidation state of manganese is +2. In addition, among *mono*-transition metal-substituted silicotungstates, α-$SiW_{11}\{M^{n+}(OH_2)\}O_{39}^{(8-3n)-}$ (M = Mn^{3+}, Fe^{3+}, Cu^{2+}), the order of turnover numbers was Mn^{3+} > Fe^{3+} > Cu^{2+}. These facts show that manganese is an effective element for catalysis and that a dimanganese site with the oxidation state of +3 is the most effective for the oxygenation of cyclohexane with molecular oxygen.

Small amounts of dicyclohexyl, which is formed by the reaction of two cyclohexyl radicals, and cyclohexyl hydroperoxide were observed. The addition of an alkyl-radical scavenger, *p*-*tert*-butylcatechol, led to complete inhibition. These facts suggest that the reaction includes a radical-chain mechanism. Further mechanistic work is in progress.

We acknowledge Dr C. Nozaki for the preliminary experiments of this work. This work was supported in part by a Grant-in-Aid for Scientific Research from the Ministry of Education, Science, Sports and Culture of Japan.

† Electronic supplementary information (ESI) available: preparation and characterization of polyoxometalates. See http://www.rsc.org/suppdata/cc/a9/a910334l

Table 1 Oxidation of cyclohexane with molecular oxygen catalyzed by metal-substituted silicotungstates at 356 K[a]

Catalyst	Turnover number[b]	Conversion[c] (%)	Selectivity (%)			
			Cyclohexanol	Cyclohexanone	Cyclohexyl hydroperoxide	Dicyclohexyl
$[\alpha]$-$SiW_{12}O_{40}]^{4-}$	0	0.0	—	—	—	—
$[\alpha$-$SiW_{11}\{Mn^{III}(OH_2)\}O_{39}]^{5-}$	295	2.4	57	41	2	Trace
$[\gamma$-$SiW_{10}\{Mn^{III}(OH_2)\}_2O_{38}]^{6-}$	789	6.4	51	48	1	Trace
$[\gamma$-$SiW_{10}\{Mn^{II}(OH_2)\}_2O_{38}]^{8-}$	0	0.0	—	—	—	—
$[\alpha$-$SiW_9\{Mn^{III}(OH_2)\}_3O_{37}]^{7-}$	0	0.0	—	—	—	—
$[\gamma$-$SiW_{10}\{Fe^{III}(OH_2)\}_2O_{38}]^{6-}$ [d]	135	1.1	53	47	—	Trace
$[\gamma$-$SiW_{10}\{Cu^{II}(OH_2)\}_2O_{38}]^{8-}$	0	0.0	—	—	—	—

[a] *Reaction conditions*: catalyst, 1.5 μmol; solvent, 1,2-$C_2H_4Cl_2$ (1.5 mL–acetonitrile (0.1 mL); cyclohexane, 18.5 mmol; $P(O_2)$, 1 atm; reaction time, 96 h. [b] Mol of products/mol of catalysts used. [c] Mol of products/mol of cyclohexane used. [d] Cited from ref. 20.

Notes and references

‡ The turnover numbers for Fe(DPA), $K[Ru^{III}(saloph)Cl_2]$, $PW_9O_{37}\{Fe_{3-x}$-$Ni_x(OAc)_3\}^{(9+x)-}$ and γ-$SiW_{10}\{Fe^{III}(OH_2)\}_2O_{38}^{6-}$, cobalt-containing aluminophosphate and $[Co(NCMe)_4](PF_6)_2$ catalysts were 0.2 (reaction temperature, 295 K), 18 (298–318 K), 5 (356 K), 135 (356 K), 167 (403 K) and 180 (348 K), respectively.

§ The selectivity to cyclohexanone and turnover number for γ-SiW_{10}-$\{Mn^{III}(OH_2)\}_2O_{38}^{6-}$ catalyst were 100% and 3, respectively, after 96 h.

1 C. L. Hill, *Activation and Functionalization of Alkanes*, ed. C. L. Hill, Wiley, New York, 1989, p. 243.
2 A. Sobkowiak, H. Tung and D. T. Sawyer, *Prog. Inorg. Chem.*, 1992, **40**, 291.
3 C. L. Hill and C. M. Prosser-McCartha, *Coord. Chem. Rev.*, 1995, **143**, 407.
4 R. H. Crabtree, *Chem. Rev.*, 1995, **95**, 997.
5 A. E. Shilov and G. B. Shul'pin, *Chem. Rev.*, 1997, **97**, 2879.
6 N. Mizuno and M. Misono, *Chem. Rev.*, 1998, **98**, 199.
7 C. L. Hill, *Nature*, 1999, **401**, 436.
8 S. Murahashi, T. Naota and N. Komiya, *Tetrahedron Lett.*, 1995, **36**, 8059.
9 M. Kurioka, K. Nakata, T. Jintoku, Y. Taniguchi, K. Takaki and Y. Fujiwara, *Chem. Lett.*, 1995, 244.
10 I. Yamanaka, K. Nakagaki, T. Akimoto and K. Otsuka, *J. Chem. Soc., Perkin Trans. 2*, 1996, 2511.
11 Y. Ishii, T. Iwahama, S. Sakaguchi, K. Nakayama and Y. Nishiyama, *J. Org. Chem.*, 1996, **61**, 4520.
12 J.-M. Vincent, A. Rabion, V. K. Yachandra and R. H. Fish, *Angew. Chem., Int. Ed. Engl.*, 1997, **36**, 2346.
13 T. Iwahama, K. Syojyo, S. Sakaguchi and Y. Ishii, *Org. Proc. Res. Dev.*, 1998, **2**, 255.
14 C. Sheu, A. Sobkowiak, S. Jeon and D. T. Sawyer, *J. Am. Chem. Soc.*, 1990, **112**, 879.
15 M. M. Taqui Khan, D. Chatterjee, S. Kumar S, A. P. Rao and N. H. Khan, *J. Mol. Catal.*, 1992, **75**, L49.
16 N. Mizuno, M. Tateishi, T. Hirose and M. Iwamoto, *Chem. Lett.*, 1993, 2137.
17 M. W. Grinstaff, M. G. Hill, J. A. Labinger and H. B. Gray, *Science*, 1994, **264**, 1311.
18 J. E. Lyons, P. E. Ellis Jr. and H. K. Myers Jr., *J. Catal.*, 1995, **155**, 59 and references 25–37 therein.
19 R. Neumann and M. Dahan, *Nature*, 1997, **388**, 353.
20 C. Nozaki, M. Misono and N. Mizuno, *Chem. Lett.*, 1998, 1263.
21 A. S. Goldstein and R. S. Drago, *Inorg. Chem.*, 1991, **30**, 4056.
22 D. L. Vanoppen, P. E. De Vos, M. J. Genet, P. G. Rouxhet and P. A. Jacobs, *Angew. Chem., Int. Ed. Engl.*, 1995, **34**, 560.
23 G. Sanker, R. Raja and J. M. Thomas, *Catal. Lett.*, 1998, **55**, 15.
24 J. M. Thomas, R. Raja, G. Sanker and R. G. Bell, *Nature*, 1999, **398**, 227.
25 C. A. Tolman, J. D. Druliner, M. J. Nappa and N. Herron, *Activation and Functionalization of Alkanes*, ed. C. L. Hill, Wiley, New York, 1989, p. 303.
26 D. D. Davis and D. R. Kemp, *Kirk–Othmer Encyclopedia of Chemical Technology*, ed. J. I. Kroschwitz and M. Howe-Grant, Wiley, New York, 1991, vol. 1, p. 466.
27 N. Mizuno, C. Nozaki, I. Kiyoto and M. Misono, *J. Am. Chem. Soc.*, 1998, **120**, 9267; C. Nozaki, I. Kiyoto, Y. Minai, M. Misono and N. Mizuno, *Inorg. Chem.*, 1999, **38**, 5724.
28 N. Kitajima, M. Ito, H. Fukui and Y. Moro-oka, *Chem. Commun.*, 1991, 102.
29 T. Tézé, G. Hervé and M. T. Pope, *Inorg. Synth.*, 1990, **27**, 85.
30 M. Tourné, G. F. Tourné, S. A. Malik and T. J. R. Weakly, *J. Inorg. Nucl. Chem.*, 1970, **32**, 3875.
31 X. Zhang, C. J. O'Conner, G. B. Jameson and M. T. Pope, *Inorg. Chem.*, 1996, **35**, 30.
32 J. Liu, F. Ortéga, P. Sethuraman, D. E. Katsoulis, C. E. Costello and M. T. Pope, *J. Chem. Soc., Dalton Trans.*, 1992, 1901.
33 N. Mizuno, C. Nozaki, I. Kiyoto and M. Misono, *J. Catal.*, 1999, **182**, 285.

Communication a910334l

ChemComm

Mass spectrometric evidence for aggregation of a substituted sexithiophene

A. F. M. Kilbinger,[a] H. J. Cooper,[b] L. A. McDonnell,[b] W. J. Feast,*[a] P. J. Derrick,*[b] A. P. H. J. Schenning[c] and E. W. Meijer[c]

[a] *IRC in Polymer Science and Technology, University of Durham, Durham, UK DH1 3LE. E-mail: wj.feast@durham.ac.uk*
[b] *Institute of Mass Spectrometry and Department of Chemistry, University of Warwick, Coventry, UK CV4 7AL*
[c] *Laboratory of Macromolecular and Organic Chemistry, Eindhoven University of Technology, PO Box 513, 5600 MB Eindhoven, The Netherlands*

Received (in Cambridge) 9th December 1999, Accepted 7th February 2000

Nanospray FT-ICR mass spectroscopy provides unambiguous evidence for solvent-dependent aggregation of a substituted sexithiophene.

We report evidence for the solvent-dependent aggregation of an α,ω-disubstituted sexithiophene, obtained by nanospray Fourier-transform ion cyclotron resonance (FT-ICR) mass spectrometry[1–6] of solutions of varying polarity. Electrospray ionisation (ESI),[3] of which nanospray[4–6] is a variant, has been used for studying aggregation of proteins.[7,8] In this work, we used FT-ICR coupled with ESI (nanospray) to probe aggregation of an oligomer; high resolution was important in order to resolve overlapping signals due to differently sized aggregates.

Aggregation in solution is well known for α-oligothiophenes and poly(thiophenes).[9–11] Evidence for aggregation of such chromophores has been deduced from shifts in UV–VIS spectra, quenching of photoluminescence, broadening of linewidths in NMR or observation of a circular dichroism spectrum for aggregates of chiral chromophores.[12,13] Whereas these techniques give indirect evidence for aggregation, we have established direct evidence for solvent-dependent aggregation by FT-ICR mass spectrometry.

We have established a synthesis for 2,2′:5′,2″:5″,2‴:5‴,2⁗:5⁗,2⁗′:5⁗′-sexithiophene-5,5⁗′-dicarboxylic acid (2*S*)-2-methyl-3,6,9,12,15-pentaoxahexadecyl ester **1** (Fig. 1) and UV (absorption and emission) and CD spectroscopic evidence for its temperature dependent chiral aggregation in solution.[13] Compound **1** appears to aggregate in polar protic solvents such as THF–water mixtures and to be molecularly dissolved in organic solvents such as pure THF or $CHCl_3$. We have used nanospray FT-ICR mass spectrometry to investigate **1** in THF and THF–water mixtures. The nanospray technique provided the possibility of ionising the oligomer **1**, and its suspected aggregates, without fragmentation.

Experiments were performed using nanospray on a Bruker BioApex FT-ICR mass spectrometer equipped with a shielded 9.4 T magnet (Magnex Scientific Ltd., Abingdon, UK), a 6 cm diameter cylindrical infinity cell and electrospray ionisation source (Analytica of Branford, Branford, USA).[14,15] Low capillary and skimmer potentials were used to minimise any possibility of the non-covalent bonds of the aggregate being disrupted in the source. Solutions were made up using THF and a polar solvent mixture (PSM) containing equal volumes of ammonium acetate solution (10 mM, pH 6.0) and methanol, and 2% v/v concentrated acetic acid.

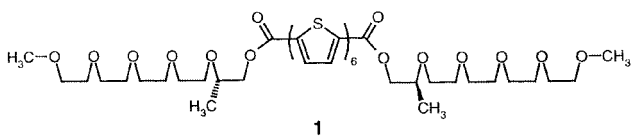

1

Fig. 1 2,2′:5′,2″:5″,2‴:5‴,2⁗:5⁗,2⁗′:5⁗′-sexithiophene-5,5⁗′-dicarboxylic acid (2*S*)-2-methyl-3,6,9,12,15-pentaoxahexadecyl ester **1**.

In agreement with our previous observations from UV–VIS and photoluminescence spectroscopy, the results from nanospray FT-ICR indicated that **1** did not aggregate in predominantly aprotic solution. Fig. 2 shows the mass spectrum obtained from a solution of **1** in 90% THF–10% PSM. The neutral oligomer is designated as 6T in the spectrum. Intense signals due to the ammonium and sodium ion adducts of the monomeric compound can be seen in Fig. 2. The experimental isotope patterns matched the theoretical, confirming that each cluster of peaks represented a single species. The measured mass-to-charge (*m*/*z*) ratios agreed with those calculated to within 1 ppm in all cases (all-^{12}C $[6T+NH_4]^+$, measured mass 1096.2811 *cf.* calc. 1096.2802; all-^{12}C $[6T+Na]^+$, measured mass 1101.2342 *cf*. calc. 1101.2356). There was no evidence for aggregation. Nanospray from a more polar solution of **1**, (75% THF–25% PSM), again gave mainly monomeric ammonium and sodium ion adducts but also a weak signal due to the dimeric diammonium ion adduct (Fig. 3). Peaks from the doubly charged dimer can lie underneath those from the singly charged monomer or appear between the singly charged monomer peaks. Thus, the all-^{12}C monomer peak and the all-^{12}C dimer peak both theoretically fall at *m*/*z* 1096.2802. The one-^{13}C monomer peak falls at *m*/*z* 1097.2836 but the one-^{13}C dimer peak falls between these two peaks at *m*/*z* 1096.7822 and is detected as a weak peak. The spectrum (Fig. 3) establishes that the bonding in the dimer between the constituent monomers is non-covalent, because the measured mass of the dimer is exactly twice that of the monomer. If the bonding had been covalent, loss of two hydrogen atoms might have been expected; there is no possibility of simple addition dimerisation of **1**. In the case of loss of two hydrogen atoms, there would have been a detectable peak at *m*/*z* 1095.2724 due to the doubly-charged all-^{12}C dimer, there was no peak at this *m*/*z*.

The diammonium ion adduct of the tetramer (Fig. 4), the diammonium ion adduct of the pentamer (Fig. 5) and the

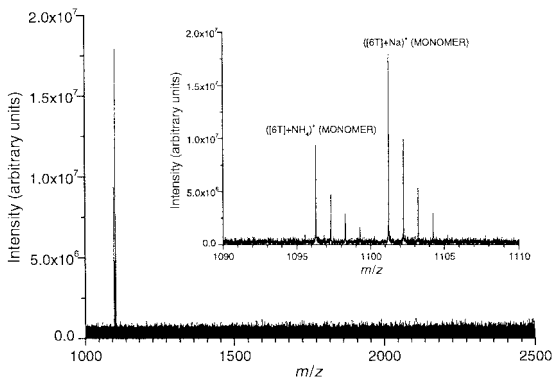

Fig. 2 Compound **1** (50 μM) in THF–PSM (90 : 10 v : v). Only monomeric species can be observed. The inset shows the isotope patterns of the ammonium adduct ion, $([6T]+NH_4)^+$ and of the sodium adduct ion, $([6T]+Na)^+$. 6T is a designation used for the neutral compound **1**.

DOI: 10.1039/a909686h

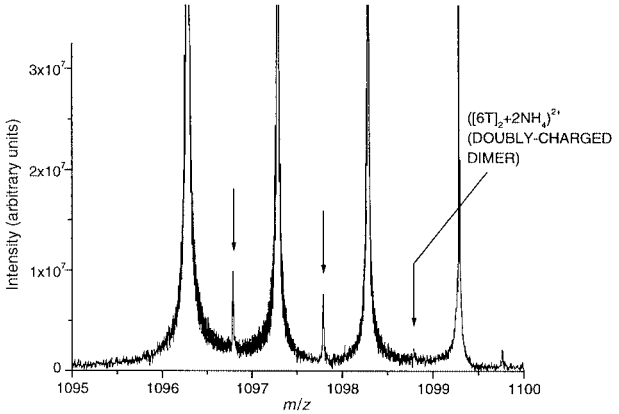

Fig. 3 Compound **1** (150 μM) in THF–PSM (75 : 25 v : v). The monomeric ammonium adduct ion (see also Fig. 2) and the dimeric diammonium adduct ion, $([6T]_2+2NH_4)^{2+}$ (see arrows) are observed.

triammonium ion adduct of the hexamer were observed when a solution of compound **1** in 50% THF–50% polar solvent mixture was investigated.

The diammonium adduct of the tetramer overlays the ammonium adduct of the dimer (Fig. 4). That the isotope distributions of the two ions were directly coincident indicates that the mass of the tetrameric species was exactly twice that of the dimer, *i.e.* bonding was non-covalent in the tetramer. The most intense peak in the isotope distribution of the diammonium pentamer adduct (Fig. 5) corresponds to the six-^{13}C species; the all-^{12}C isotopomer cannot be discerned in Fig. 5. The cluster of peaks shown in Fig. 6 represent isotopes of three species: the singly charged ammonium adduct of the dimer $([6T]_2+NH_4)^+$, the doubly-charged diammonium tetramer adduct

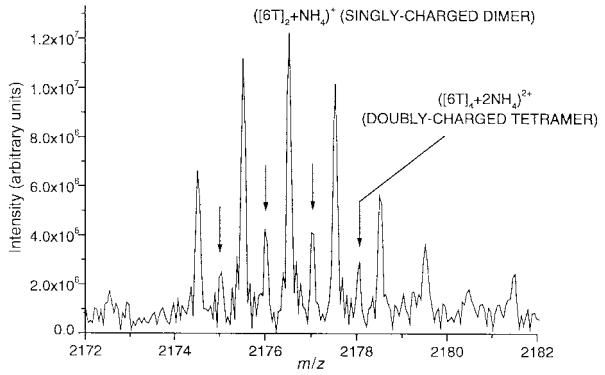

Fig. 4 Compound **1** (50 μM) in THF–PSM (50 : 50 v : v). Peaks due to the ammonium ion adduct of the dimer, $([6T]_2+NH_4)^+$, and the diammonium adduct ion of the tetramer, $([6T]_4+2NH_4)^{2+}$, are superimposed.

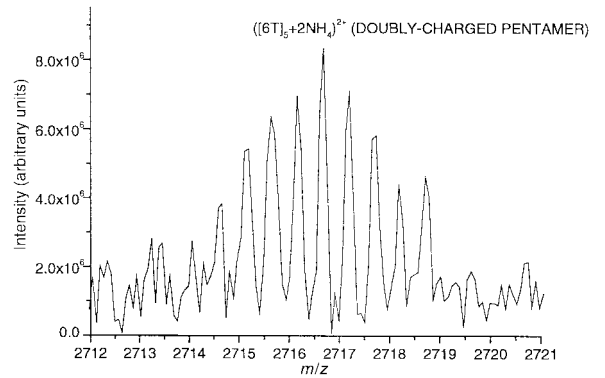

Fig. 5 Compound **1** (50 μM) in THF–PSM (50 : 50 v:v). Isotopic distribution of the diammonium adduct ion of the pentamer, $([6T]_5+2NH_4)^{2+}$.

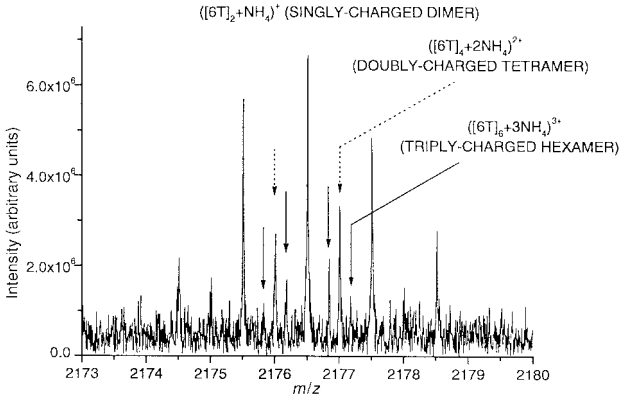

Fig. 6 Compound **1** (100 μM) in THF–PSM (50 : 50 v : v). Peaks due to the ammonium adduct ion of the dimer, $([6T]_2+NH_4)^+$, the diammonium adduct ion of the tetramer, $([6T]_4+2NH_4)^{2+}$ (dotted arrows) and the triammonium ion adduct of the hexamer, $([6T]_6+3NH_4)^{3+}$ (straight arrows) are overlaid.

$([6T]_4+2NH_4)^{2+}$ and the triply charged triammonium hexamer adduct $([6T]_6+3NH_4)^{3+}$.

The size of detectable aggregates is currently limited by the instrument configuration and the relationship between behaviour in solution and in the mass spectrometer source[16] is a matter for continuing study. However, we conclude that oligomeric aggregates of compound **1**, from the dimer to the hexamer have been observed by nanospray FT-ICR mass spectrometry when sprayed from polar solution, whereas the monomer alone was observed when sprayed from THF solution. Taken together these results constitute unambiguous evidence for the aggregation of **1** in solution, a process which intensifies with increasing solution polarity.

We thank Luc Brunsveld for the chiral penta(ethylene glycol), the European Commission Training and Mobility of Researchers Network SELOA (contract number ERBFMRX-CT960083) and the Royal Dutch Academy of Arts and Sciences. The FT-ICR laboratory at the University of Warwick is an EPSRC National Facility.

Notes and references

1 M. B. Comisarow and A. G. Marshall, *Chem. Phys. Lett.*, 1974, **25**, 282.
2 A. G. Marshall, M. B. Comisarow and G. Parisod, *J. Chem. Phys.*, 1979, **71**, 4434.
3 J. B. Fenn, M. Mann, C. K. Meng, S. F. Wong and C. M. Whitehouse, *Science*, 1989, **246**, 64.
4 M. S. Wilm and M. Mann, *Int. J. Mass Spectrom., Ion Proc.*, 1994, **136**, 167.
5 M. S. Wilm and M. Mann, *Anal. Chem.*, 1996, **68**, 1.
6 R. Korner, M. Wilm, K. Morand, M. Schubert and M. Mann, *J. Am. Soc. Mass Spectrom.*, 1996, **7**, 150.
7 D. Lafitte, A. J. R. Heck, T. J. Hill, K. Jumel, S. E. Harding and P. J Derrick, *Eur. J. Biochem.*, 1999, **261**, 337.
8 A. A. Rostom and C. V. Robinson, *J. Am. Chem. Soc.*, 1999, **121**, 4718.
9 E. Ramos Lermo, B. M. W. Langeveld, R. A. J. Janssen and E. W. Meijer, *Chem. Commun.*, 1999, 791.
10 B. M. W. LangeveldVoss, M. P. T. Christiaans, R. A. J. Janssen and E. W. Meijer, *Macromolecules*, 1998, **31**, 6702.
11 G. Bidan, S. Guillerez and V. Sorokin, *Adv. Mater.*, 1996, **8**, 157.
12 B. M. V. LangeveldVoss, D. Beljonne, Z. Shuai, R. A. J. Janssen, S. C. J. Meskers, E. W. Meijer and J. L. Bredas, *Adv. Mater.*, 1998, **10**, 1343.
13 A. F. M. Kilbinger, A. P. H. J. Schenning, F. Goldoni, W. J. Feast and E. W. Meijer, *J. Am. Chem. Soc.*, 2000, in press.
14 A. J. R Heck and P. J. Derrick, *Anal. Chem.*, 1997, **69**, 3603.
15 H. Lavanant, P. J. Derrick, A. J. R. Heck and F. A. Mellon, *Anal. Biochem.*, 1998, **255**, 74.
16 S. M. Hunt, M. M. Sheil, M. Belov and P. J. Derrick, *Anal. Chem.*, 1998, **70**, 1812.

Communication a909686h

Hydrolysis of an *N*-methylcarbamate by a catalytic antibody†

A. Nicole Dinaut,[a] Mei-Jin Chen,[a] Alex Marks,[b] Robert A. Batey[c] and Scott D. Taylor*[a]‡

[a] *Department of Chemistry, University of Toronto, 3359 Mississauga Rd. North, Mississauga, Ontario, Canada L5L 1C6*
[b] *Banting and Best Department of Medical Research, University of Toronto, 112 College Street, Toronto, Ontario, Canada M5G 1L6*
[c] *Department of Chemistry, University of Toronto, St. George Campus, 80 St. George Street, Toronto, Ontario, Canada M5S 1A1*

Received (in Corvallis, OR, USA) 23rd December 1999, Accepted 21st January 2000

The first example of antibody-catalyzed hydrolysis of an *N*-methylcarbamate, a highly challenging reaction for antibody catalysis, was achieved by raising a monoclonal antibody to a phosphoramidate transition state analogue.

The vast majority of antibody-catalyzed hydrolyses of carbonyl derivatives, such as esters, amides and carbamates, have been performed using substrates that are amenable to hydrolysis: half-lives for the spontaneous reactions usually range from hours to a few months under the assay conditions.[1] Antibody catalysis of more energetically demanding hydrolytic reactions of carbonyl derivatives in which the half-life for the spontaneous reaction is measured in years, rather than hours to months, is rare.[2a–f] As part of a project related to antibody-catalyzed 'remote' prodrug activation,[3] we became interested in examining the possibility of generating antibodies capable of catalyzing the hydrolysis of *N*-methylcarbamates. *N*-methylcarbamates are very resistant to hydrolysis[4] and there has yet to be a report describing an antibody capable of catalyzing this reaction. Several papers have appeared describing antibodies capable of catalyzing the hydrolysis of N–H carbamates.[2e,5] Of particular note is the work of Wentworth *et al.*[2e] These researchers obtained an antibody, DF8-D5, that catalyzes the hydrolysis of N–H carbamates of type **1** by raising antibodies to

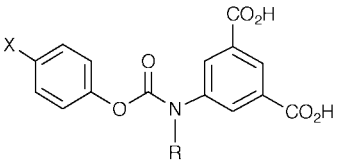

1 R = H, X = NO_2, Br, F, H, OMe
2 R = CH_3, X = NO_2

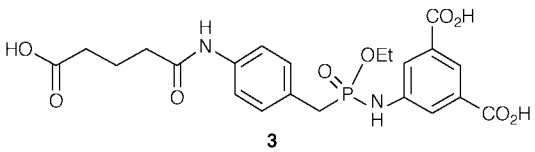

3

the phosphonamidate transition state analogue (TSA) **3**. Although this antibody did not hydrolyze *N*-alkylcarbamates such as **2**, the significantly smaller Hammett ρ value (ρ = + 0.53) obtained for the antibody-catalyzed reaction compared to that obtained for the uncatalyzed reaction (ρ = +2.68) suggested that the antibody reaction proceeded *via* the highly disfavoured $B_{Ac}2$ mechanism rather than the more favoured $E1_cB$ process found for the uncatalyzed reaction.[2e] These results suggest that antibodies raised to an appropriately designed TSA of the $B_{Ac}2$ process for *N*-methylcarbamate hydrolysis might be capable of catalyzing the hydrolysis of these stable compounds. Here we report the first example of antibody-catalyzed hydrolysis of an *N*-methylcarbamate, a highly challenging reaction for antibody catalysis.

Carbamate **4** was chosen as a model substrate for the antibody-catalyzed reaction (Scheme 1). Although this carbamate contains a *p*-nitrophenol leaving group, it is fairly resistant to hydrolysis, exhibiting a half life of approximately 5.7 years at pH 9.0.[4a,6] In the TSA used by Wentworth *et al.*,[2e] the phenolic oxygen of the substrate was replaced with a methylene unit. This was done to promote the $B_{Ac}2$ mechanism over the $E1_cB$ mechanism by minimizing recognition of the phenolate anion, an important feature of the $E1_cB$ transition state.[2e] However, during *N*-methylcarbamate hydrolysis, there is no competing $E1_cB$ mechanism. Consequently, we chose to employ a phosphoramidate TSA (hapten **5**), reasoning that a phosphoramidate should be a better mimic of the $B_{Ac}2$ transition state than a phosphonamidate.

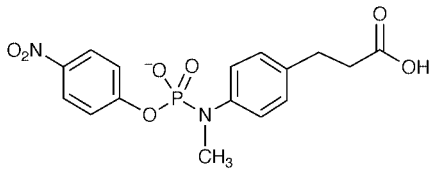

5

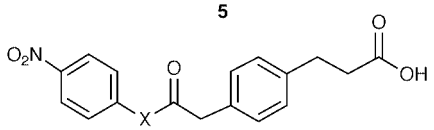

6 X = NH
7 X = O

Hapten **5** was constructed† and conjugated to Bovine Serum Albumin (BSA) and Keyhole Limpet Hemocyanin (KLH) *via* its *N*-hydroxysulfosuccinimide ester, which was prepared *in situ via* reaction of **5** with *N*-hydroxysulfosuccinimide in the presence of 1-(3-dimethylaminopropyl)-3-ethylcarbodiimide hydrochloride (EDC). The degree of conjugation to the carrier protein was determined using the trinitrobenzene sulfonic acid (TNBS) assay of Habeeb.[7] Balb/c mice were hyperimmunized with the KLH conjugate and monoclonal antibodies were obtained using hybridoma technology.[8]†

Thirty-two monoclonal antibodies were screened for catalytic activity by removing aliquots from a solution containing antibody (~ 4 μM) and substrate **4** (1 mM) in 50 mM bicine, 5% DMSO, pH 9.0, at various time intervals, and then examining the aliquots for *p*-nitrophenol using HPLC. Under these conditions, we were unable to detect any hydrolysis of **4** in the absence of antibody after 40 h. Several of the antibodies

† The synthesis and characterization of **4**, **5**, **6** and **7**, preparation of monoclonal antibodies and ST51 Fab, experimental details for kinetic studies and Lineweaver–Burk plots are provided as electronic supplementary information, see http://www.rsc.org/suppdata/cc/b0/b000468p/

‡ Current address: Department of Chemistry, University of Waterloo, 200 University Avenue West, Waterloo, Ontario, Canada N2L 3G1 E-mail: s5taylor@sciborg.uwaterloo.ca

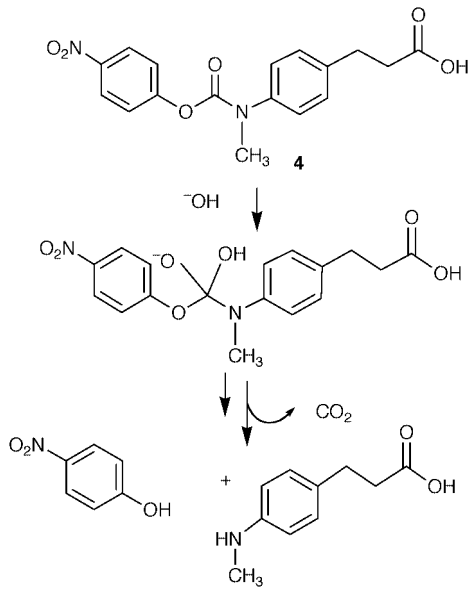

Scheme 1

exhibited catalytic activity. The most active antibody, ST51, was selected for a more detailed kinetic analysis. The ST51-catalyzed reaction obeys saturation kinetics and at pH 9.0 exhibited a $k_{cat} = 9.1 \times 10^{-2}$ h^{-1}, a $K_m = 2.6 \times 10^2$ μM, and $k_{cat}/K_m = 3.5 \times 10^{-4}$ μM^{-1} h^{-1}. The rate enhancement obtained for the reaction (k_{cat}/k_{uncat}) is 6.5×10^3, which is in the range of the average rate enhancement obtained for other antibody-catalyzed hydrolytic reactions of carbonyl derivatives such as esters, amides and carbamates.[1] The rate enhancement obtained with **4** and ST51 (6.5×10^3) is approximately 20 times greater than that obtained by Wentworth *et al.*[2e] for the hydrolysis of **1** when X = NO_2 with DF8-D5 (k_{cat}/k_{uncat} = 300). However, when DF8-D5 is assayed with other substrates (**1**, X = Br, F and OMe), it exhibits greater rate enhancements than that obtained with ST51 and substrate **4**.[2e]

That catalysis is indeed a result of the abzyme and not a contaminating protease or esterase is supported by the following results. First, the reaction is completely inhibited by stoichiometric quantities of the TSA. Second, pure ST51 Fab[10] exhibited the same catalytic activity as pure ST51 mAb. Finally, ST51 did not catalyze the hydrolysis of amide **6** *or even ester* **7**, two compounds that should be readily hydrolyzed by proteases or esterases and both of which undergo spontaneous hydrolysis under the assay conditions more readily than **4**.[11,12] The fact that ST51 does not hydrolyze **6** and **7** also indicates that ST51 is a remarkably selective abzyme compared to other abzymes that catalyze the hydrolysis of amides[2a] or carbamates.[5a]

Although ST51 is also active at pH 10.0 and exhibits a higher k_{cat} (2.5×10^{-1} h^{-1}) at pH 10.0 than at pH 9.0, it exhibits a considerably higher K_m (1.3 mM), and lower rate enhancement (1.8×10^3) at pH 10. ST51 is a robust abzyme, as evidenced by the fact that it can be stored at room temperature at pH 10.0 over several days without any loss of catalytic activity. In addition, ST51 is capable of multiple turnover, indicating that it is not subject to strong product inhibition as is often the case for hydrolase abzymes.[13] This may be due to the fact that carbamate hydrolysis yields CO_2, as opposed to a negatively charged carboxylic acid found with ester or amide hydrolysis, which should experience minimal charge interactions with positively-charged residues in the active site generated in response to the negatively-charged TSA.[13]

In summary, this work represents the first example of antibody-catalyzed hydrolysis of an *N*-methylcarbamate, a highly challenging reaction for antibody catalysis. This was achieved by raising antibodies to a phosphoramidate TSA. Studies concerning the application of this antibody to 'remote' prodrug activation[3] are in progress. In addition, X-ray crystallographic analyses to determine the structure of ST51 Fab are also in progress.[14] The results of the X-ray analysis and further kinetic studies will be used to elucidate the mechanism of this interesting abzyme.

We thank the Medical Research Council (MRC) of Canada and the Natural Sciences and Engineering Research Council (NSERC) of Canada (post-graduate scholarship for A. Nicole Dinaut) for financial support of this work. We would also like to thank Katherine Majewska for assistance in synthesizing compounds **6** and **7**, and Melanie Lea for assistence with hybridoma production.

Notes and references

1 Recent reviews: G. M. Blackburn, A. Datta, H. Denham and P. Wentworth, *Adv. Phys. Org. Chem.*, 1998, **31**, 249; N. R. Thomas, *Nat. Prod. Rep.*, 1996, **13**, 479.

2 (*a*) K. D. Janda, D. Schloeder, S. J. Benkovic and R. A. Lerner, *Science*, 1988, **241**, 1188; (*b*) M. T. Martin, T. S. Angeles, R. Sugusawara, N. I. Aman, A. D. Napper, M. J. Darsley, R. I. Sanchez, P. Booth and R. C. Titmas, *J. Am. Chem. Soc.*, 1994, **116**, 6508; (*c*) T. Li, S. Hilton and K. D. Janda, *J. Am. Chem. Soc.*, 1995, **117**, 2123; (*d*) C. Gao, B. J. Lavey, C-H. L. Lo, A. Datta, P. Wentworth and K. D. Janda, *J. Am. Chem. Soc.*, 1998, **120**, 2212; (*e*) P. Wentworth, A. Datta, S. Smith, A. Marshall, L. J. Partridge and G. M. Blackburn, *J. Am. Chem. Soc.*, 1997, **119**, 2315. (*f*) F. Benedetti, F. Berti, A. Colombatti, C. Ebert, P. Linda and F. Tonizzo, *Chem. Commun.*, 1996, 1417.

3 S. D. Taylor, M. J. Chen, A. N. Dinaut and R. A. Batey, *Tetrahedron*, 1998, **54**, 4223.

4 (*a*) A. F. Hegarty and L. N. Frost, *J. Chem. Soc., Perkin Trans. 1*, 1973, 1719; (*b*) I. Christenson, *Acta Chem. Scand.*, 1964, **18**, 904; (*c*) I. W. Dittert and T. Higuchi, *J. Pharm. Sci.*, 1963, **52**, 852.

5 (*a*) D. L. Van Vranken, D. Panomitros and P. G. Schultz, *Tetrahedron Lett.*, 1994, **35**, 3873; (*b*) P. Wentworth, A. Datta, D. Blakey, T. Boyle, L. J. Partidge and G. M. Blackburn, *Proc. Natl. Acad. Sci. U.S.A.*, 1996, **93**, 799.

6 The second order rate constant for the hydrolysis of **4** was determined by measuring its rate of hydrolysis in NaOH solutions (0.1–1.0 M) at 25 °C using spectrophotometry. This yielded a second order rate constant of 3.8×10^{-4} M^{-1} s^{-1}. This value is very close to that obtained (3.7×10^{-4} M^{-1} s^{-1}) by other workers [see ref. (4*a*)] for the hydrolysis of phenyl *N*-methyl-*N*-(*p*-nitrophenyl)carbamate in aq. NaOH solutions at 25 °C. Using a base concentration of 1×10^{-5} M , we obtained a half-life for **4** at pH 9.0 of 5.7 years.

7 A. F. S. A Habeeb, *Anal. Biochem.*, 1966, **14**, 328. The number of haptens per protein was approximately 13.

8 E. Harlow and D. Lane, *Antibodies: A Laboratory Manual*, Cold Spring Harbour, New York, 1988.

9 D. S. Tawfik, R. R. Zemel, R. Arad-Yellin, B. S. Green and Z. Eshhar, *Biochemistry*, 1990, **29**, 9916.

10 Generated by papain digestion of ST51 Mab. See: J. Rousseaux, R. Rousseaux-Prevost and H. Bazin, *J. Immunol. Methods*, 1983, **64**, 141.

11 Studies by other workers on similar systems have shown that esters of type **7** hydrolyze *via* an E1$_c$B mechanism. See: R. Chandrasekar and N. Venkatasubramanian, *J. Chem. Soc., Perkin Trans. 2*, 1982, 1625.

12 Kinetic studies with **4** and **6** in 1.0 M NaOH indicate that amide **6** hydrolyzes approximately twice as fast as carbamate **4**.

13 T. Nakatani, R. Umeshita, J. Hiratake, A. Shinzake, T. Suzuki, N. Nakajima and J. Oda, *Bioorg. Med. Chem.*, 1994, **2**, 457.

14 In the laboratory of Professor Emil Pai, University of Toronto.

Communication b000468p

Temperature programmed desorption of argon for evaluation of surface acidity of solid superacids

Hiromi Matsuhashi* and Kazushi Arata

Department of Science, Hokkaido University of Education, 1-2 Hachiman-cho, Hakodate 040-8567, Japan. E-mail: matsuhas@cc.hokkyodai.ac.jp

Received (in Cambridge, UK) 15th December 1999, Accepted 13th January 2000

The activation energy of Ar desorption from solid acids is determined by temperature programmed desorption (TPD) using Ar as 9.3, 7.6 and 6.0–6.7 kJ mol^{-1} for sulfated ZrO_2, $Cs_{2.5}H_{0.5}PW_{12}O_{40}$ and zeolites, respectively; the data indicate that Ar TPD is applicable to evaluation of the relative acid strengths of solid superacids.

Temperature programmed desorption (TPD) using ammonia is the most useful technique to evaluate relative acid strengths and the amount of acid sites on solid acids.[1–3] However, there are several problems when this technique is applied to solid acids with high acidity such as sulfated zirconia and zeolites. For instance, the ammonia desorption temperature is elevated owing to the strong interaction of ammonia with strong acid sites, and thus the acid sites may be decomposed by reaction with the adsorbents at such temperatures. Sikabwe *et al.* reported that Fe, Mn and Ni promoted sulfated zirconias were partially or completely decomposed in the temperature range 700–900 K when ammonia, pyridine or benzene were adsorbed.[4] An interaction of ammonia with both the acidic OH group and the basic oxygen site next to the acid site is another problem.[5] Therefore, accurate acid strengths of solid superacids can not be evaluated by TPD using probes such as ammonia or pyridine. To solve these problems, an inert molecule with lower basicity must be used as the probe molecule.

Argon is completely inert towards superacids, but shows an acid–base like interaction with acid sites at low temperature.[6] Argon has an induced dipole when it interacts with a strong dipole. The most polarized site on the solid acids must be the acid sites, and argon would be adsorbed on such sites in a polarized state. The strength of the interaction between Ar and acid sites would be expected to depend on the acid strength. Wakabayashi *et al.* reported that inert gases including Ar showed an interaction with acidic OH sites on zeolites giving 1 : 1 hydrogen-bonded complexes at low temperatures, and there was a linear correlation between the strength of the interaction and the proton affinities of the gases.[6,7] From their results, it is expected that the relative acid strength of solid superacids can be evaluated by TPD using Ar as a probe. Here, Ar TPD was applied to silica–alumina, several types of zeolites, sulfated zirconia and a Cs substituted heteropoly acid; the results clearly showed that Ar TPD was applicable for the evaluation of acid strength of solid superacids.

Silica–alumina and zeolites used in this study were supplied by the Catalysis Society of Japan as reference catalysis. Sulfated zirconia (SO_4^{2-}/ZrO_2) was prepared by the reported method,[8] and the heteropoly acid ($Cs_{2.5}H_{0.5}PW_{12}O_{40}$) was supplied by Professor T. Okuhara, Hokkaido University.[9] Both of these materials can convert *n*-butane into isobutane at room temperature. The solid acid (*ca.* 15–40 mg) was placed in a glass sample tube and pretreated in vacuum at 773 K (SiO_2–Al_2O_3 and zeolites) or 473 K (sulfated zirconia and heteropoly acid) for 2 h. After the pretreatment, the sample was exposed to 6.7 kPa of Ar at room temperature, then cooled to 113 K by N_2 gas which was bubbled out of liquid N_2. The sample cooling system is shown in Fig. 1. The adsorption of Ar was carried out at 113 K for 10 min. Then excess Ar was removed by evacuation at the same temperature. The final pressure of the system was $< 5.0 \times 10^{-3}$ Pa. Ar TPD was performed in the temperature range 113–223 K at a programmed rate of 2–5 K min^{-1}. The sample tube was heated by an electric heater regulated by a temperature controller. Argon desorbed from the surface of solid acid was detected by a mass spectrometer and an ionization gauge connected to the vacuum system.

Ar TPD profiles of solid acids are summarized in Fig. 2. The signal response (m/z = 40) was normalized by the weight of the samples. All the samples showed an Ar desorption peak at *ca.* 120–170 K, *i.e.* much higher than the boiling point of Ar (87.45 K). There was no relation between the BET surface area and the relative amounts of desorbed Ar. The profiles thus show evidence of interaction of Ar with the acid sites on the surface.

For zeolites, an acid site is constructed from Al^{3+} in the framework and the amount of Ar desorbed from the surface is expected to depend on the quantity of Al^{3+}. The amount of Ar desorbed from H-mordenite was much larger than that of H-ZSM-5 reflecting the higher content of Al^{3+} in H-mordenite (Table 1). However, the amount of Ar desorption from H-Y was much smaller than that expected from the Al^{3+} content. Only a small fraction of the acid sites on H-Y or SiO_2–Al_2O_3 appear to show an acid–base interaction with Ar.

An apparent activation energy of Ar desorption was calculated by applying eqn. (1).[10]

$$2\ln T_m - \ln\beta = E_d/RT_m + \text{const.} \quad (1)$$

Here, T_m is the peak temperature, β is the rate of temperature increase and E_d is the activation energy of desorption. E_d values are obtained from plots of $(2\ln T_m - \ln\beta)$ *vs.* $1/T_m$. For the

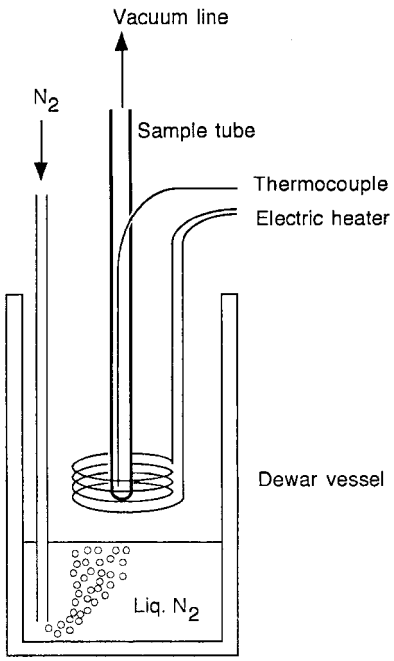

Fig. 1 An outline of the sample cooling system for Ar TPD.

DOI: 10.1039/a909844e

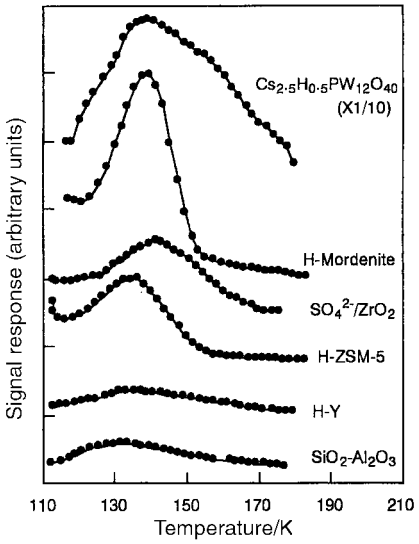

Fig. 2 Ar TPD profiles of solid acids; temperature programmed rate: 2 K min^{-1}.

Table 1 Solid acids and activation energies of Ar desorption

Solid acid	Surface area/ $m^2\ g^{-1}$	Al_2O_3 content (wt%)	Activation energy/ kJ mol^{-1}
SiO_2–Al_2O_3 (JRC-SAH-1)	511	28.61	5.5
H-Y (JRC-Z-HY-5.6)	650	22.0	6.0
H-ZSM-5 (JRC-Z5-70H)		1.99	6.6
H-Mordenite (JRC-Z-HM20)	399	7.76	6.7
SO_4^{2-}/ZrO_2	137		9.3
$Cs_{2.5}H_{0.5}PW_{12}O_{40}$	135		7.6

examples shown in Fig. 2, the estimated values of T_m were 131.5, 132.8, 136.0, 139.8, 139.5 and 138.9 K for SiO_2–Al_2O_3, H-Y, H-ZSM-5, SO_4^{2-}/ZrO_2, H-mordenite and $Cs_{2.5}H_{0.5}PW_{12}O_{40}$, respectively. The calculated activation energies of Ar desorption are summarized in Table 1. The order of the activation energies is as follows:

$$SO_4^{2-}/ZrO_2 \gg Cs_{2.5}H_{0.5}PW_{12}O_{40} \gg \text{H-mordenite} \geqslant \text{H-ZSM-5} > \text{H-Y} > SiO_2\text{–}Al_2O_3$$

The termination temperature of Ar desorption also followed this order, *viz.* 159.0, 158.7, 153.8, 153.9, 151.8 and 149.6 K for SO_4^{2-}/ZrO_2, $Cs_{2.5}H_{0.5}PW_{12}O_{40}$, H-mordenite, H-ZSM-5, H-Y and SiO_2–Al_2O_3, respectively. The polarization of the Ar molecule is induced by the polarized sites. The interaction between Ar and acid sites should be strong when Ar is adsorbed on strong acid sites because of higher polarization of Ar molecules on the more polarized acid sites. Therefore, the order of the activation energy reflects the acid strength of the solid acid sites. The strength order of zeolites evaluated in this study was consistent with previous reports.[11] From these results, it can be concluded that Ar TPD is applicable to the evaluation of relative acid strengths of solid acids of high acidity on the surface.

The energy of Ar desorption form the solid superacid of sulfated zirconia was 9.3 kJ mol^{-1} the highest among the tested catalysts. The highest acid strength of this sample ($H_0 \leqslant -16.04$) is reflected by the highest value of the desorption energy.[12] The Cs substituted heteropoly acid had a desorption energy (7.6 kJ mol^{-1}) which was higher than for the zeolites. Consequently, it can be stated that the heteropoly acid is a solid superacid.

In summary, the catalysis of solid superacids is characterized by activities for acid-catalyzed reactions at low temperatue and reactions are carried out below room temperature in many cases. The acidity of solid superacids should thus be evaluated at such lower temperatures. TPD using Ar can be performed in the temperature range 113–223 K, close to the reaction temperatures used. Destruction of acid sites can be avoided at these temperatures for themally sensitive sites as found, for example, in Cs-substituted heteropoly acids. In conclusion, TPD using Ar is a very useful technique to evaluate the acidity of solid superacids.

We thank Professor Toshio Okuhara, Hokkaido University, for his kindness in providing the Cs substituted-heteropoly acid.

Notes and references

1 M. Niwa, M. Iwamoto and K. Segawa, *Bull. Chem. Soc. Jpn.*, 1983, **59**, 3735.
2 H. G. Karge and V. Dondur, *J. Phys. Chem.*, 1990, **94**, 765.
3 T. Miyamoto, N. Katada, J.-H. Kim and M. Niwa, *J. Phys. Chem. B*, 1998, **102**, 6738.
4 E. C. Sikabwe, M. A. Coelho, D. E. Resasco and R. L. White, *Catal. Lett.*, 1995, **34**, 23.
5 E. H. Teunissen, A. P. J. Jansen and R. A. van Santen, *J. Phys. Chem.*, 1995, **99**, 1873.
6 F. Wakabayashi, J. N. Kondo, K. Domen and C. Hirose, *J. Phys. Chem.*, 1996, **100**, 4154.
7 F. Wakabayashi, J. N. Kondo, K. Domen and C. Hirose, *Microporous Mater.*, 1997, **8**, 29.
8 T. Tatsumi, H. Matsuhashi and K. Arata, *Bull. Chem. Soc. Jpn.*, 1996, **69**, 1191.
9 K. Na, T. Okuhara and M. Misono, *J. Chem. Soc., Faraday Trans.*, 1995, **91**, 367.
10 R. J. Cvetanovic and Y. Amenomiya, *Adv. Catal.*, 1967, **17**, 103.
11 H. Stach, J. Jänchen, H. Jerschkewitz, U. Lohse, B. Parlitz and M. Hunger, *J. Phys. Chem.*, 1992, **96**, 8480.
12 K. Arata, *Adv. Catal.*, 1990, **37**, 165.

Communication a909844e

Temperature-dependent helix–helix transition of an optically active poly(diarylsilylene)†

Julian R. Koe,[ab] Michiya Fujiki,*[ab] Masao Motonaga[b] and Hiroshi Nakashima[ab]

[a] *NTT Basic Research Laboratories, 3-1 Wakamiya, Morinosato, Atsugi, Kanagawa 243-0198, Japan. E-mail: jrkoe@with.brl.ntt.co.jp*

[b] *CREST-JST, 3-1 Wakamiya, Morinosato, Atsugi, Kanagawa 243-0198, Japan. E-mail: jrkoe@with.brl.ntt.co.jp*

Received (in Cambridge, UK) 26th November 1999, Accepted 28th January 2000

The poly(diarylsilylene) copolymer mainchain helix in $(Ar^*_2Si)_x(Ar_2Si)_{1-x}$ [Ar* = 3-(*S*)-2-methylbutylphenyl, Ar = 4-butylphenyl, x = 0.2] undergoes a thermally driven inversion of helical screw sense with a transition temperature of −10 °C.

Functional organic and polymeric materials with potential for application in devices in capacities such as switches, data storage, transmission and displays are attracting much attention owing to their relatively low cost, ease of fabrication of large area thin films, processability, and chemical tunability of optoelectronic properties through choice of substituents,[1] and particularly those with physical responses to stimuli, arising from higher order structural regularity.[2] Polymers adopting a preferential screw sense helical backbone conformation offer the possibility of a two state, switchable material if the opposite screw sense is energetically accessible and the helix–helix transition reversible.[3] Such helical inversions are rare and for discrete molecules in dilute solution responding to a change in temperature, have been reported only twice, first for a polypeptide, poly(β-propyl-L-aspartate)[4a] and very recently for a polyisocyanate, poly[3-{(*S*)-*sec*-butoxycarbonyl}phenylisocyanate].[4b] There is one example of a solid state helix inversion, for a polypeptide,[5] and change of sign of optical activity upon aggregation of other polyisocyanates,[6] polypeptides[7] and polythiophenes[3,8] is known.

Recently we showed using circular dichroism (CD) spectroscopy that poly(diarylsilylene)s (of significance owing to their electroluminescence (EL) properties)[9] with enantiopure chiral sidechains adopt preferential helical screw sense backbone conformations in solution.[10] Incorporation of the (*S*)-2-methylbutylphenyl group in polymers of the type $[(Ar')(Ar'')Si]_n$ (Ar′, Ar″ = 4-butylphenyl, 4-(*S*)-2-methylbutylphenyl or 3-(*S*)-2-methylbutylphenyl) afforded optically active materials with positive or negative Cotton effects in the CD spectra (solution state) for polymers with one or two chiral centres per silicon, respectively. We then set out to find poly(diarylsilylene)s which could exhibit either positive or negative Cotton effects, dependent upon the application of an external stimulus. Such materials could potentially find application in a polymer-based chiroptical photonic device (*e.g.* circularly polarised EL device or semiconducting small molecule chirality sensor). Now we report our preliminary findings that the copolymer, poly[{bis-3-(*S*)-2-methylbutylphenyl}$_{0.2}$-*co*-(bis-4-butylphenyl)$_{0.8}$silylene] **1** undergoes a reversible, thermally driven helix–helix transition in solution with a transition point at −10 °C.

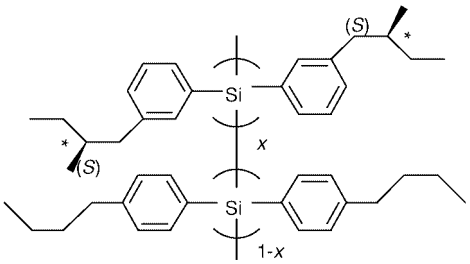

1: $x = 0.2$
2: $x = 0.5$
3: $x = 0.8$

Poly(diarylsilylene) copolymers **1**–**3** were obtained by the Wurtz coupling of the appropriate dichlorosilane monomer mixtures in toluene at 70 °C and the compositions, as verified by ^{13}C NMR spectroscopy, corresponded to the nominal addition ratios (for preparative and NMR details see ESI†). Polymerisation and spectroscopic data are given in Table 1.

The polymers show relatively narrow ($\Delta\nu_{1/2}$ *ca.* 16 nm) UV absorptions (peak maximum *ca.* 396 nm) due to the conjugated Si backbone σ–σ* transition, mirror image fluorescence emission spectra, small Stokes' shifts (*ca.* 13 nm) and fluorescence anisotropies in the range 0.20–0.38, indicating regular, semi-flexible polymer molecules with long segment lengths.[10] The CD and UV spectra of **1** are shown in Fig. 1. A negatively signed Cotton effect is evident in the CD spectrum at −70 °C, coincident with the absorption due to the Si σ–σ* transition, whereas at 50 °C, the effect is positive and at −10 °C the signal is approximately zero. This indicates a change in the

† Electronic supplementary information (ESI) available: polymer syntheses, fluorescence excitation and NMR data for **1**–**3**. See http://www.rsc.org/suppdata/cc/a9/a909368k/

Table 1 Polymerisation and spectroscopic data for **1**–**3**

		UV[b]	CD[b]						
	T[a]/°C	$\varepsilon/\lambda_{max}$/fwhm	$\Delta\varepsilon/\lambda_{max}$	$10^4\ g_{abs}$	FL λ_{max}	FL-A[c]	$10^{-3}\ M_w$[d]	PDI[e]	Yield[f] (%)
1	20	24 300/397/14.0	0.24/393	0.10	408.5	0.20–0.30	474	2.77	5.9
2	20	25 700/399/14.6	−0.61/400	−0.24	410.5	0.20–0.30	271	2.88	3.9
3	20	10 400/393/19.0	−1.06/392	−1.02	407.5	0.34–0.38	8	1.34	3.3

[a] UV and CD data in isooctane at 20 °C; fluorescence (FL) and fluorescence anisotropy (FL-A) data in toluene at room temperature (21 °C). [b] ε and $\Delta\varepsilon$ units: (Si repeat unit)$^{-1}$ dm^3 cm^{-1}; λ_{max} units: nm; fwhm = full width (nm) at half maximum of λ_{max}. [c] Fluorescence anisotropy measured over region of backbone σ–σ* transition. [d] Molecular weights determined by size exclusion chromatography (SEC) and relative to polystyrene standards; eluent: THF. [e] PDI = polydispersity index: M_w/M_n; given for isolated high M_w fractions. [f] Isolated yields of high M_w fraction.

DOI: 10.1039/a909368k

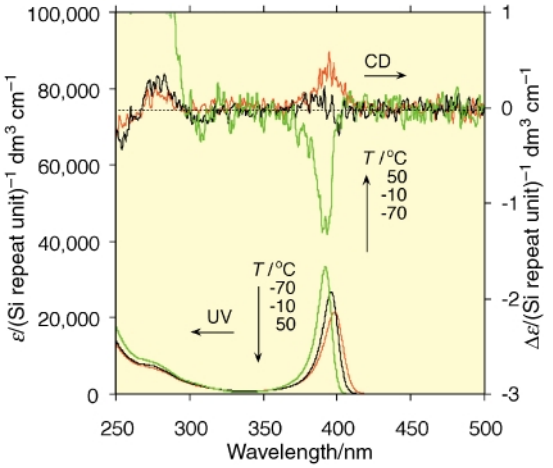

Fig. 1 CD and UV spectra of **1** at −70, −10 and 50 °C.

backbone from one prevailing helical screw sense to the other. The disymmetric ratio,[11] g_{abs}, defined as the ratio of CD and UV molar absorptivities, $\Delta\varepsilon/\varepsilon$ (and thus more appropriate as a gauge of helicity than simply $\Delta\varepsilon$), is small for **1** at the temperature listed in Table 1 (20 °C), since this is close to the transition temperature. However, at −70 °C, g_{abs} is −0.38, greater than that for **2** (−0.27), but less than that for **3** (−1.57). By comparison, g_{abs} for the related homopolymer, poly[bis{3-(*S*)-2-methylbutylphenyl}silylene],[10] at 20 °C is −2.00. The lower disymmetric ratios for **1**–**3**, therefore, are most probably the consequence of the coexistence of both helical screw senses in **1**–**3**, at all temperatures.

Consistent with the above suggestion, at −10 °C, the CD spectrum of **1** actually has a small negative component at *ca.* 401 nm in addition to the small positive peak at 390 nm. We ascribe these two bands to the two different screw senses, which should be characterised by different screw pitches.[12] It is not possible, however, in the present case to associate a particular screw sense with the sign of the Cotton effect.

The maximum magnitude of the positive Cotton effect for **1** occurs around 50 °C, but it is less than the maximum negative magnitude, as may be seen from the plot of CD intensity $\Delta\varepsilon$ *vs.* *T* in Fig. 2. Above 50 °C, the CD signal intensity decreases again, a feature in common with the poly(diarylpolysilylene) homopolymers in our earlier study,[10] which we attribute to thermal population of the higher energy screw sense state, but additionally, though to a much lesser degree, to thermal broadening of the bands as a result of slight bond length increase (the molar absorptivities for UV and CD spectra decrease with increasing temperature).

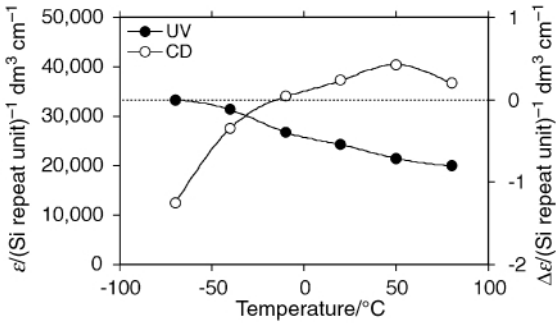

Fig. 2 Plots of CD ($\Delta\varepsilon$) and UV (ε) molar absorptivities per Si repeat unit *vs.* temperature for **1** (cubic spline fitting).

The corollary of this is an increase in $\Delta\varepsilon$ with decrease in temperature (in the absence of helical inversion), which has also been observed by other workers.[4b,13,14] Green *et al.* proposed that the optical activity of poly(alkyl isocyanate)s increases with decreasing temperature due to a diminishing number of helix reversals, allowing greater cooperation of backbone units.[14b]

A temperature cycling experiment comprising three cycles of −70/50 °C with CD and UV spectra recorded at each temperature for **1** indicated that the transition is reversible, negative and positive Cotton effects being observed, respectively. Excluding CD results, the data for polymer **2**, with a ratio of enantiopure chiral monomer to achiral monomer of 0.5 : 0.5, are similar to those of **1**. Polymer **3** (chiral : achiral = 0.8 : 0.2) with lower M_w (owing to lower solubility during synthesis) has slightly lower UV molar absorptivity but is otherwise also comparable to **1**, indicating similar polymer structures for **1**–**3**. The CD data, however, are markedly different: whereas **1** shows negative Cotton effects at low temperature and positive at high temperature indicating a transition from one helical screw sense to the other, **2**, **3** and the above mentioned related homopolymer, poly[bis{3-(*S*)-2-methylbutylphenyl}silylene],[10] show only negative Cotton effects at all temperatures and thus do not exhibit this phenomenon; *i.e.* this function is specific to **1**. It is apparent, therefore, that a subtle interplay of factors permits such a helix–helix transition, presumably as a result of the enthalpy and entropy terms in the Gibbs free energy equation being of the same sign, such that the free energy difference changes sign as a function of temperature, as was proposed in discussions of helix–helix transitions for certain polyisocyanates.[4b,15]

In conclusion, we have demonstrated a structure-specific, reversible, temperature-dependent helical screw sense inversion for a hybrid organic–inorganic chromophoric and fluorophoric polymer. Further investigation of poly(diarylsilylene) systems is in progress.

Notes and references

1 J. H. Burroughes, D. D. C. Bradley, A. R. Brown, R. N. Marks, K. Mackay, R. H. Friend, P. L. Burns and A. B. Holmes, *Nature (London)*, 1990, **347**, 539; M. Berggren, O. Inganas, G. Gustafsson, J. Rasmusson, M. R. Andersson, T. Hjertberg and O. Wennerstrom, *Nature (London)*, 1994, **372**, 444.

2 D. S. Schlitzer and B. M. Novak, *J. Am. Chem. Soc.*, 1998, **120**, 2196; B. Gallot, G. Galli, A. Ceccanti and E. Chiellini, *Polymer*, 1999, **40**, 2561 and references therein.

3 M. M. Bouman and E. W. Meijer, *Adv. Mater.*, 1995, **7**, 385.

4 (*a*) E. M. Bradbury, B. G. Carpenter and H. Goldman, *Biopolymers*, 1968, **6**, 837; (*b*) K. Maeda and Y. Okamoto, *Macromolecules*, 1998, **31**, 5164.

5 J. Watanabe, S. Okamoto, K. Satoh, K. Sakajiri, H. Furuya and A. Abe, *Macromolecules*, 1996, **29**, 7084.

6 M. M. Green, N. C. Peterson, T. Sato, A. Teramoto, R. Cook and S. Lifson, *Science*, 1995, **268**, 1860; M. M. Green, C. A. Khatri, M. P. Reidy and K. Levon, *Macromolecules*, 1993, **26**, 4723; J. Guenet, H. S. Jeon, C. Khatri, S. K. Jha, N. P. Palsara, M. M. Green, A. Brulet and A. Thierry, *Macromolecules*, 1997, **30**, 4590.

7 M. P. Reidy and M. M. Green, *Macromolecules*, 1990, **23**, 4225; S. Yue, G. C. Berry and M. M. Green, *Macromolecules*, 1996, **29**, 6175.

8 G. Bidan, S. Guillerez and V. Sorokin, *Adv. Mater.*, 1996, **8**, 157.

9 C.-H. Yuan, S. Hoshino, S. Toyoda, H. Suzuki, M. Fujiki and N. Matsumoto, *Appl. Phys. Lett.*, 1997, **71**, 3326; H. Suzuki, S. Hoshino, C.-H. Yuan, M. Fujiki, S. Toyoda and N. Matsumoto, *IEEE J. Sel. Top. Quant. Electron.*, 1998, **4**, 129; H. Suzuki, C.-H. Yuan, K. Furukawa and N. Matsumoto, *Polym. Prepr.*, 1998, **39**, 996.

10 J. R. Koe, M. Fujiki and H. Nakashima, *J. Am. Chem. Soc.*, 1999, **121**, 9734.

11 H. P. J. M. Dekkers, in *Circular Dichroism: Principles and Applications*, ed. K. Nakanishi, N. Berova and R. W. Woody, VCH, New York, 1994, ch. 6, p. 122.

12 M. Fujiki, S. Toyoda, C.-H. Yuan and H. Takigawa, *Chirality*, 1998, **10**, 667.

13 Y. Okamoto, M. Matsuda, T. Nakano and E. Yashima, *J. Polym. Sci. A, Polym. Chem.*, 1994, **32**, 309; K. Maeda, M. Matsuda, T. Nakano and Y. Okamoto, *Polym. J.*, 1995, **27**, 141.

14 (*a*) M. M. Green, C. Andreola, B. Munoz, M. P. Reidy and K. Zero, *J. Am. Chem. Soc.*, 1988, **110**, 4063; (*b*) M. M. Green, M. P. Reidy, R. J. Johnson, G. Darling, D. J. O'Leary and G. Willson, *J. Am. Chem. Soc.*, 1989, **111**, 6452.

15 H. Gu, Y. Nakamura, T. Sato, A. Teramoto, M. M. Green, C. Andreola, N. C. Peterson and S. Lifson, *Macromolecules*, 1995, **28**, 1016.

Communication a909368k

ChemComm

Cadmium- and zinc-directed assembly of nano-sized, resorcarene-based host architectures which strongly bind C_{60}†

O. Danny Fox,[a] Michael G. B. Drew,[b] Emma J. S. Wilkinson[a] and Paul D. Beer*[a]

[a] *Inorganic Chemistry Laboratory, University of Oxford, Oxford, UK OX1 3QR. E-mail: paul.beer@chem.ox.ac.uk*
[b] *Department of Chemistry, University of Reading, Whiteknights, Reading, UK RG6 6AD*

Received (in Cambridge) 17th January 2000, Accepted 3rd February 2000

Nano-sized molecular loops based on a trimer of resorcarene ligands assembled by six cadmium or zinc ions are shown to strongly bind the spherically shaped fullerene C_{60} in toluene and benzene solutions.

The chalice-shaped molecules, calixarenes, serve as excellent hosts for the binding of organic guest molecules through non-covalent interactions.[1] Pathways to multiple calixarene hosts employing self-assembly techniques that utilise numerous metal–ligand or hydrogen bonding interactions have been described recently.[2,3] The potential to exploit these and other nano-sized hosts as molecular receptors or containers in which large or multiple substrate molecules can be bound, stored, transported or even reacted upon has generated much recent interest in both their synthesis and properties.[4] Herein, we demonstrate the cadmium(II)- and zinc(II)-directed assembly of nano-sized host architectures based on a trimer of dithiocarbamate (dtc)-functionalised resorcarene ligands and show these loop-shaped hosts strongly bind buckminsterfullerene, C_{60}, in solution.

The C_4 symmetric resorcarenes are particularly suited for the generation of metal-assembled nano-hosts being easy to functionalise with a range of coordinating moieties. Reaction of tetra(bromomethyl)resorcarene with neat propylamine or butylamine yields tetrakis(alkylaminomethyl)resorcarenes **Am$_1$**, **Am$_2$**.† From these secondary amines, the dithiocarbamate cadmium(II) and zinc(II) resorcarene assemblies **1**–**4** were prepared in a one-pot synthesis from potassium hydroxide, carbon disulfide and metal(II) acetate and isolated as cream coloured powders. Recrystallisation from pyridine–water solutions afforded the pyridine adducts of the hexametallic hosts as pale yellow, prismatic crystals. All four compounds have been characterised by X-ray crystallography; three of the structures (**1**, **2** and **3**) are presented here (Fig. 1 and Table 1)‡ and **4** is described elsewhere.[2]

Metal complexes **1**–**4** are isomorphous and consist of three resorcarene cups linked by six divalent metal ions (all of which are crystallographically equivalent). The cup-shaped resorcarene ligands provide the corners of an equilateral molecular triangle whose sides are *ca*. 19–20 Å in length. In **1**, **2** and **3** the six metal(II) ions are five-coordinate with sulfur atoms of the bidentate dtc unit forming a square-plane [Cd–S 2.590(5)–2.635(5) **1**, 2.603(5)–2.641(5) **2**, Zn–S 2.444(4)–2.495(4) Å **3**]. Axial coordination *via* a pyridine molecule [Cd–N 2.35(2) **1**; 2.32(2) **2**, Zn–N 2.124(9) Å **3**] causes a pyramidal distortion which raises the metal ion slightly above the square plane [Cd 0.50 **1**, 0.49 **2**; Zn 0.53 Å **3**]. The trimeric loop-shaped assembly is formed by two parallel running sets of dtc–M(II)–dtc units on each side of the resorcarene bowl connecting to an adjacent resorcarene bowl.

Previously, calixarene and CTV macrocycles have been shown to bind fullerenes through favourable interactions between the π-electron system of the calixarene aromatics and the surface of the carbon sphere.[5–7].

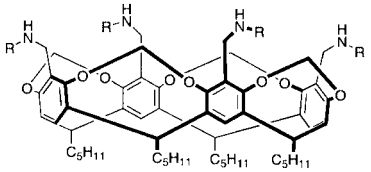

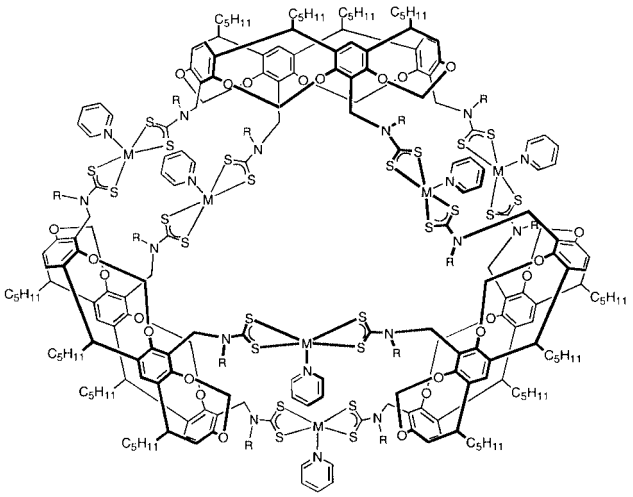

Purple solutions of C_{60} in toluene or benzene turn red–brown on addition of colourless hosts **1**–**4**. Such a colour change is

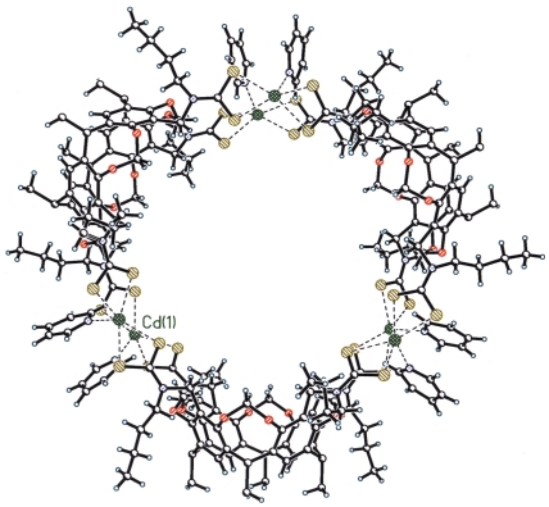

Fig. 1 View of the molecular structure of $Cd_6(L^1)_3$ **1**. For clarity, *n*-butyl chains at the bases of the resorcarenes have been removed.

† Electronic supplementary information (ESI) available: synthetic, spectroscopic and crystallographic date for **1**-**4**. See http://www.rsc.org/suppdata/cc/b0/b000481m/

DOI: 10.1039/b000481m

Table 1 Structural parameters for hosts **1**–**4**

Host	M(II)	R	Intramolecular distances (Å) M··M(adj)[a]	M··M(opp)[b]	Cavity dimensions (Å)[c]
1	Cd	Bu^n	6.74	14.65	19.58
2	Cd	Pr^n	6.73	14.72	19.59
3	Zn	Bu^n	6.65	14.59	19.18
4	Zn	Pr^n	6.61	14.69	19.13

[a] Adjacent metal ions. [b] Opposite metal ions, *i.e.* across the cavity. [c] Dimensions of the cavity defined by carbon atoms close to the base of the resorcarene.

Table 2 Association constants (log K_{ass}) for host structures **1**–**4** and guest C_{60} (T = 295 K)

Solvent	**1**	**2**	**3**	**4**
Benzene	4.7 ± 0.3	> 6[a]	4.41 ± 0.03	4.07 ± 0.03
Toluene	4.3 ± 0.2	5.1 ± 0.1	3.70 ± 0.05	3.47 ± 0.03

[a] Owing to the strength of binding a satisfactory convergence in the fitting program could not be reached.

indicative of a binding interaction between the host and the guest.[8] To determine the stoichiometry of this interaction, UV–VIS absorption spectra of mixtures of known concentrations of host and guest species in toluene were examined using a method of continuous variance, commonly known as Job's method.[9] Maxima in the curve of the Job's plot were observed at 1:1 concentration ratios of host and guest for all four compounds. The strength of binding was probed further by standard UV–VIS titration experiments of host and guest. Equivalents of host solutions **1**–**4** were added to a C_{60} solution (in benzene or toluene) and the absorbance in the UV–VIS spectrum monitored. From this data, binding constants for the host–C_{60} complexes in both toluene and benzene solutions were calculated using the computer programme Specfit. Table 2 shows all the host–guest stability constants are of substantial magnitudes and the binding is significantly stronger in benzene. It is noteworthy that the cadmium complexes **1** and **2** bind C_{60} much more strongly than the zinc complexes **3** and **4**, although the cavity dimensions are very similar. The association constants determined for cadmium hosts **1** and **2** exceed those reported by Fukazawa and coworkers who employed mono- and bis-calix[5]arene derivatives[7] and are comparable in magnitude with a bisporphyrin system reported most recently by Tashiro *et al.*[10]

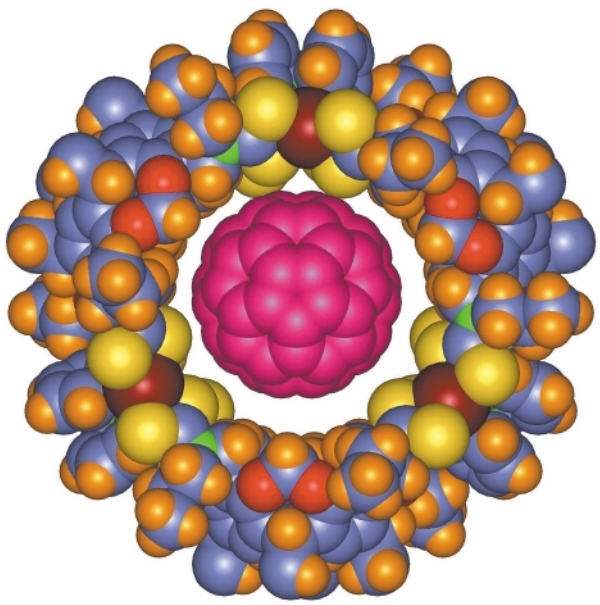

Fig. 2 Space filling model of host–C_{60} complex showing the proposed mode of fullerene binding by loop-shaped hosts **1**–**4**. For clarity, *n*-butyl chains at the base of the resorcarenes have been removed.

Space-filling CPK representations based on the crystal structures of **1**–**4** show that the cavity is circular with a diameter of *ca.* 16–17 Å and therefore suitable for the binding of spherically shaped molecules such as C_{60} (Fig. 2). The interatomic distances and molecular dimensions in **1**–**4** are all very similar (Table 1). Thus, it is unlikely that the modest differences in host size and shape can reasonably account for the large variation in binding constants observed. Molecular models of C_{60} inside hosts **1**–**4** indicate that a possible mode of receptor–guest binding is through the sulfur atoms of the dtc moieties;[11] the C_{60} resting in a cup-shaped cavity formed by sixteen sulfur atoms and the resorcarene bowl. It is the position and electronic nature of these donor atoms, which, affected by the choice of metal ion, may dictate the strength of binding to the electron-deficient fullerene guest species. Studies are in progress to elucidate further details of these binding interactions.

Financial support for this work was kindly provided by AWE Aldermaston. We thank the EPSRC and University of Reading for funds for the Image Plate System.

Notes and references

‡ *Crystal data* for complexes **1**–**3**: $Cd_6(L^1)_3(py)_6{\cdot}9H_2O{\cdot}15EtOH$ **1**, $C_{288}H_{450}Cd_6N_{18}O_{48}S_{24}$, M = 6376.5, rhombohedral, space group $R\bar{3}c$, Z = 6, a = 37.65(4), c = 55.36(6) Å, U = 67970 Å^3 D_c = 0.935 g cm^{-3}, 6903 unique data. $Cd_6(L^2)_3(py)_6{\cdot}27H_2O{\cdot}6EtOH$ **2**, $C_{258}H_{408}Cd_6N_{18}O_{57}S_{24}$, M = 6117.9, rhombohedral, space group $R\bar{3}c$, Z = 6, a = 37.52(4), c = 56.04(6) Å, U = 68312 Å^3, D_c = 0.892 g cm^{-3}, 7089 unique data. $Zn_6(L^1)_3(py)_6{\cdot}10.5H_2O{\cdot}9EtOH$ **3**, $C_{276}H_{417}Cd_6N_{18}O_{43.5}S_{24}$, M = 5844.9, rhombohedral, space group $R\bar{3}c$, Z = 6, a = 37.23(4), c = 55.63(6) Å, U = 66769 Å^3, D_c = 0.872 g cm^{-3}, 9055 unique data.

All the structures contained several molecules of disordered solvent and were refined on F^2 using SHELXL to R values for observed data of ($R1$, $wR2$) 0.141, 0.204 for Cd **1**, 0.112, 0.243 for Cd **2**, and 0.141, 0.212 for Zn **3**.

CCDC 182/1537. See http://www.rsc.org/suppdata/cc/b0/b000481m/ for crystallographic files in .cif format.

1 D. J. Cram and M. J. Cram, *Container Molecules and Their Guests, Monographs in Supramolecular Chemistry*, ed. J. F. Stoddart, The Royal Society of Chemistry, Cambridge, 1994 and references therein; A. Jasat and J. C. Sherman, *Chem. Rev.*, 1999, **99**, 931.

2 O. D. Fox, M. G. B. Drew and P. D. Beer, *Angew Chem., Int. Ed.*, 2000, **39**, 135.

3 O. D. Fox, N. K. Dalley and R. G. Harrison, *J. Am. Chem. Soc.*, 1998, **120**, 7111; O. D. Fox, N. K. Dalley and R. G. Harrison, *Inorg. Chem.*, 1999, **38**, 5860; E. Dalcanale and P. Jacopozzi, *Angew. Chem., Int. Ed. Engl.*, 1997, **36**, 613; M. M. Conn and J. Rebek, Jr., *Chem. Rev.*, 1997, **97**, 1647; L. R. MacGillivray and J. L. Atwood, *Nature*, 1997, **389**, 469.

4 M. Fujita, *Chem. Soc. Rev.*, 1998, **27**, 417; C. J. Jones, *Chem. Soc. Rev.*, 1998, **27**, 289; P. J. Stang, *Chem. Eur. J.*, 1998, **4**, 19.

5 F. Diederich and M. Gómez-López, *Chem. Soc. Rev.*, 1999, **28**, 263; S. Shinkai and A. Ikeda, *Pure Appl. Chem.*, 1999, **71**, 275; M. J. Hardie and C. L. Raston, *Chem. Commun.*, 1999, 1153.

6 J. L. Atwood, G. A. Koutsantonis and C. L. Raston, *Nature*, 1994, **368**, 229; A. Ikeda, M. Yoshimura, H. Udzu, C. Fukuhara and S. Shinkai, *J. Am. Chem. Soc.*, 1999, **121**, 4296.

7 T. Haino, M. Yanase and Y. Fukazawa, *Angew. Chem., Int. Ed.*, 1998, **37**, 997; T. Haino, M. Yanase and Y. Fukazawa, *Angew. Chem., Int. Ed. Engl.*, 1997, **36**, 259.

8 J. L. Atwood, M. J. Barnes, M. G. Gardiner and C. L. Raston, *Chem. Commun.*, 1996, 1449.

9 K. A. Connors, *Binding Constants*, Wiley, New York, 1987.

10 K. Tashiro, T. Aida, J-Y. Zheng, K. Kinbara, K. Saigo, S. Sakamoto and K. Yamaguchi, *J. Am. Chem. Soc.*, 1999, **121**, 9477.

11 The model shown in Fig. 2 was generated on an SG workstation using Cerius^2 with the Universal Force Field.†

Communication b000481m

Oxidative *N*-demethylation of *N*,*N*-dimethylanilines catalysed by lignin peroxidase: a mechanistic insight by a kinetic deuterium isotope effect study

Enrico Baciocchi,*[a] Maria Francesca Gerini,[b] Osvaldo Lanzalunga,[b] Andrea Lapi,[b] Simona Mancinelli[b] and Paolo Mencarelli[b]

[a] *Dipartimento di Chimica, Università 'La Sapienza', P.le A. Moro 5, 00185, Rome, Italy. E-mail: baciocchi@axcasp.caspur.it*

[b] *Dipartimento di Chimica and Centro CNR di Studio sui Meccanismi di Reazione, Università 'La Sapienza', P.le A. Moro 5, 00185, Rome, Italy*

Received (in Liverpool, UK) 18th October 1999, Accepted 13th January 2000

Lignin peroxidase can catalyse the *N*-demethylation of *N*,*N*-dimethylanilines by an electron transfer mechanism, where the deprotonation of the intermediate radical cation is also an enzymatic process.

Lignin peroxidase (LiP), a heme-containing glycoprotein isolated from the ligninolytic cultures of the white-rot fungus *Phanerochaete chrysosporium*, is a very important enzyme capable of performing the oxidative depolymerization of lignin with hydrogen peroxide.[1] For this reason, studies of this enzyme have been focused so far on the oxidation of non-phenolic electron rich aromatic lignin model compounds,[1c,d,2] while less information is available about the catalytic activity of LiP in the H_2O_2-promoted oxidation of other substrates.[3]

Here we report on the ability of LiP to catalyse the oxidative *N*-demethylation of *N*,*N*-dimethylanilines, a process of great biological importance. We also provide some information about the mechanism of this reaction *via* a kinetic deuterium isotope effect (KDIE) study.

4-X-Substituted *N*,*N*-dimethylanilines were reacted with an equimolar amount of hydrogen peroxide in the presence of LiP (purified from the *Phanerochaete chrysosporium* culture medium according to the literature method[4]) in an argon-degassed 50 mM sodium tartrate buffered solution at pH 4. A clean *N*-demethylation reaction was observed, but only when X is an electron withdrawing group (X = Br, CF_3, CN and NO_2). The yields are reported in Table 1. *N*,*N*-Dimethylaniline and anilines with electron donating substituents exhibited no reactivity, probably due to the fact that they were almost completely protonated at the low pH value necessary for the enzyme catalysis. In all cases, beside the demethylated products, formaldehyde was also formed, which was detected by GC-MS after conversion into the dimedone adduct.

The capacity of LiP to catalyse the oxidation of electron rich aromatics ($E° \leqslant 1.25$ V *vs.* SCE in water) by an electron transfer (ET) mechanism is well documented.[2c,3d] Therefore, it is reasonable to suggest that an ET mechanism also occurs in the *N*-demethylation reaction, as a value as low as 1.1 V *vs.* SCE[5] has been estimated for the redox potential of *N*,*N*-dimethyl-4-nitroaniline, the least oxidizable aniline in Table 1. This mechanism is also consistent with the absence of reactivity observed when the aniline is in the protonated form. Moreover, an ET mechanism has been proposed for the *N*-demethylation of *N*,*N*-dimethylaniline by other peroxidases.[7]

According to this mechanism (Scheme 1), an ET occurs between the substrate and the porphyrinato iron–oxo complex (Compound I), which is the active oxidant formed by reaction of the native form of LiP with H_2O_2. An anilinium radical cation and the reduced form of Compound I (Compound II) are obtained. The anilinium radical cation then undergoes deprotonation to give an α-amino carbon radical and it has been suggested by Guengerich and his associates that this process can either involve the enzyme or take place by a non-enzymatic pathway, depending on the nature of the peroxidase.[7b] In the former case [path (b) in Scheme 1], Compound II is suggested to be the proton abstracting base. The α-amino carbon radical then undergoes oxygen rebound to form a carbinolamine that is eventually converted to the *N*-demethylated product. In the second case, the deprotonation is promoted [path (a)] by the medium (H_2O). The α-amino carbon radical (a very easily oxidizable species) is oxidized to a carbocation which is then converted into a carbinolamine by reaction with H_2O.

Guengerich also suggested, on the basis of intramolecular KDIE values, that chloroperoxidase followed the enzymatic path, while horseradish peroxidase followed the non-enzymatic one, probably due to the difficult accessibility of the ferryl oxygen in the latter enzyme.[7b]

In the case of LiP, the size of the substrate-access channel to the heme is still smaller than in HRP so that the substrate should have access only to the heme edge, where the electron transfer

Table 1 Products and yields in the reaction of 4-substituted *N*,*N*-dimethylanilines with hydrogen peroxide catalyzed by LiP[a]

Substrate (4-substituent)	Product yield ArNHMe (%)	Material balance[b] (%)
Br	16	> 99
CF_3	28[c]	75
CN	62	86
NO_2	20	87

[a] Experimental procedures are as follows: the oxidant (10 μmol) was added, over a period of 1 h by an infusion pump, to a stirred degassed solution of the substrate (10 μmol), LiP (0.96 units, 1.16 nmol) and MeCN (50 μl) as the co-solvent, in 3 ml of Na–tartrate buffer (50 mM, pH 4) at 25 °C. Products analysis were performed by GC and GC-MS. [b] The sum of the moles of unreacted substrate and reaction product relative to the initial moles of substrate. [c] In this case 4-trifluoromethylaniline (5%) was also observed.

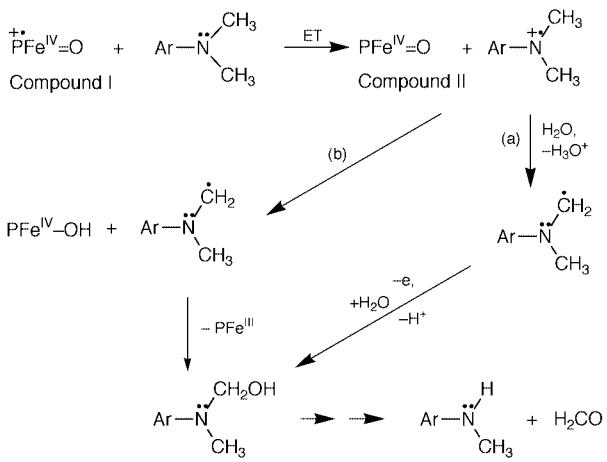

Scheme 1

DOI: 10.1039/a908394d

process can still take place, but not the deprotonation of the radical cation by the ferryl oxygen.[8] One would therefore predict a non-enzymatic pathway for the deprotonation of the radical cation in the LiP-catalysed *N*-demethylation reactions. However, strong evidence in favour of a deprotonation promoted by the enzyme has been provided by the complete masking [k_H/k_D = 1.04 (± 0.06)] of the intramolecular KDIE observed for the *N*-demethylation of *N*-methyl-*N*-trideuteromethyl-2,4,6-trichloroaniline **1** catalysed by LiP (25% yield).[9,10]

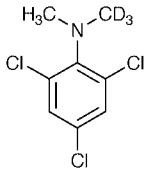

1

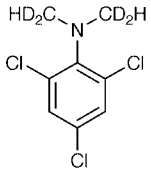

2

In this system, due to the steric effect of the two *ortho*-chlorine atoms, the two *N*-methyl groups are forced to stay one above and the other below the plane of aromatic ring as confirmed by theoretical calculations based on the Density Functional approach (DFT), carried out on the radical cation of *N*,*N*-dimethyl-2,6-dichloroaniline, a model compound for **1**.[11] These calculations moreover show that there is a quite large barrier (33.5 kJ mol^{-1}) to the rotation around the C(aromatic)–N bond.[12] Thus, the absence of a deuterium isotope effect for this substrate strongly suggests that deprotonation has to take place in the enzyme pocket, being significantly faster than rotation of CH_3 and CD_3 groups around the C(aromatic)–N bond.[13] Under these conditions, the loss of hydrogen or deuterium will only depend on which one of the two methyl groups in the radical cation is oriented towards the proton abstracting center and reasonably there is the same probability that this group is CH_3 or CD_3. Thus, the intramolecular KDIE with this substrate should be completely masked, as is actually observed. This interpretation is confirmed by the significant value of intramolecular KDIE (3.36 ± 0.07) found instead in the oxidation of *N*,*N*-bis(dideuteromethyl)-2,4,6-trichloroaniline **2** (27 % yield), where deuterium and hydrogen are bonded to the same carbon.[14] In **2**, the KDIE is no longer influenced by the hindered rotation mentioned before. Further support also comes from the high intramolecular KDIE value (7.0 ± 0.8) measured in the oxidation of *N*-methyl-*N*-trideuteromethyl-3,4,5-trichloroaniline, where the absence of *ortho*-substituents allows the two methyl groups to freely interchange within the enzyme pocket.

In conclusion, our data clearly show that LiP can catalyse the oxidative *N*-demethylation of aromatic tertiary amines with fairly good efficiency. Moreover, the intramolecular KDIEs measured with **1** and **2** indicate that the aminium radical cation is deprotonated by the enzyme. Concerning the basic center, Compound II seems unlikely, in the light of the already mentioned current views about the accessibility of the heme in this enzyme.[8] Another hypothesis is that the deprotonation of the radical cation is promoted by some specific amino acid residue located in or very close to the active site. Histidine 82 might be a suitable candidate in this respect. An additional possibility might be a medium induced deprotonation of an enzyme complexed radical cation.[15]

This work was carried out with the financial support of the Ministero dell'Università e della Ricerca Scientifica Tecnologica (MURST) and the Consiglio Nazionale delle Ricerche (CNR). We also thank Professor Pietro Tagliatesta, University of 'Tor Vergata', Rome, Italy, for cyclic voltammetry measurements.

Notes and references

1 (*a*) M. Tien and T. K. Kirk, *Science*, 1983, **221**, 661; (*b*) J. K. Glenn, M. A. Morgan, M. B. Mayfield, M. Kuwahara and M. H. Gold, *Biochem. Biophys. Res. Commun.*, 1983, **114**, 1077; (*c*) H. E. Schoemaker, *Recl. Trav. Chim. Pays-Bas*, 1990, **109**, 255; (*d*) G. Labat and B. Meunier, *Bull. Soc. Chim. Fr.*, 1990, **127**, 553.

2 (*a*) P. J. Kersten, M. Tien, B. Kalyanaraman and T. K. Kirk, *J. Biol. Chem.*, 1985, **260**, 2609; (*b*) K. E. Hammel, M. D. Mozuch, P. J. Kersten and K. A. Jensen, *Biochemistry*, 1994, **33**, 13 349 and references therein; (*c*) K. Joshi and M. H. Gold, *Eur. J. Biochem.*, 1996, **237**, 45.

3 (*a*) S. D. Haemmerli, M. S. A. Leisola, D. Sanglard and A. Fiechter, *J. Biol. Chem.*, 1986, **261**, 6900; (*b*) D. K. Joshi and M. H. Gold, *Biochemistry*, 1994, **33**, 10 969; (*c*) D. C. Goodwin, S. D. Aust and T. A. Grover, *Biochemistry*, 1995, **34**, 5060; (*d*) B. Kalyanaraman, *Xenobiotica*, 1995, **25**, 667; (*e*) A. Paszczynski, S. Goszczynski, R. L. Crawford and D. L. Crawford, *Microb. Processes Biorem.*, 1995, 187; (*f*) M. Chivukula, J. T. Spadaro and V. Renganathan, *Biochemistry*, 1995, **34**, 7765.

4 M. Tien and T. K. Kirk, *Methods Enzymol.*, 1988, **161**, 238.

5 (*a*) V. D. Parker and M. Tilset, *J. Am. Chem. Soc.*, 1991, **113**, 8778. (*b*) This value has been measured in MeCN, the value in water should be significanly lower (of *ca*. 0.4 V) (ref. 6).

6 M. Jonsson, D. D. M. Wayner and J. Lusztyk, *J. Phys. Chem.*, 1996, **100**, 17 539.

7 (*a*) *Peroxidases in Chemistry and Biology*, ed. J. Everse, K. E. Everse and M. B. Grisham, CRC Press, Boca Raton, 1991, vol. I and II; (*b*) O. Okazaki and F. P. Guengerich, *J. Biol. Chem.*, 1993, **268**, 1546 and references therein.

8 A. M. English and G. Tsaprailis, *Adv. Inorg. Chem.*, 1995, **43**, 79.

9 All the KDIE values reported in this work were determined by GC-MS analysis of the formaldehyde–dimedone adduct, and they are an average of at least three independent determinations.

10 Compound **1** was prepared by reacting 2,4,6-trichloroaniline with MeI and then with CD_3I.

11 (*a*) The calculations were carried out, with the GAUSSIAN 94 package [ref. 11(*b*)], by using the DFT approach at the B3LYP/6-311+G(d,p) level of theory. Spin contamination due to states of multiplicity higher than the doublet state was negligible, in that the $< S^2 >$ parameter was, in all cases, well within 10% of the expectation value for a doublet (0.75). (*b*) M. J. Frisch, G. W. Trucks, H. B. Schlegel, P. M. W. Gill, B. G. Johnson, M. A. Robb, J. R. Cheeseman, T. Keith, G. A. Petersson, J. A. Montgomery, K. Raghavachari, M. A. Al-Laham, V. G. Zakrzewski, J. V. Ortiz, J. B. Foresman, J. Cioslowski, B. B. Stefanov, A. Nanayakkara, M. Challacombe, C. Y. Peng, P. Y. Ayala, W. Chen, M. W. Wong, J. L. Andres, E. S. Replogle, R. Gomperts, R. L. Martin, D. J. Fox, J. S. Binkley, D. J. Defrees, J. Baker, J. P. Stewart, M. Head-Gordon, C. Gonzalez and J. A. Pople, GAUSSIAN 94, Revision D.2, Gaussian, Inc., Pittsburgh PA, 1995.

12 This can also be argued by the oxidation peak potential (E_p) measured for **1** (1.34 V *vs.* SCE) [ref. 5(*b*)] which is significantly higher than that measured for its isomer *N*,*N*-dimethyl-3,4,5-trichloroaniline (E_p = 1.16 V *vs.* SCE) [ref. 5(*b*)].

13 Even assuming that the barrier to rotation does not increase in the enzyme pocket, a deprotonation faster than rotation around the C(aromatic)–N bond is plausible, as an activation enthalpy less than 33.5 kJ mol^{-1} is possible for the former reaction [ref. 5(*a*)].

14 Compound **2** was prepared by reacting 2,4,6-trichloroaniline with CD_2O and $NaBH_4$ (S. B. Karki, J. P. Dinnocenzo, J. P. Jones and K. R. Korzekwa, *J. Am. Chem. Soc.*, 1995, **117**, 3657).

15 We thank one of the referees for this suggestion.

Communication a908394d

ChemComm

A convenient synthesis of porphodimethenes and their conversion to *trans*-porphyrins with two functionalized *meso*-naphthyl substituents

Michael Harmjanz and Michael J. Scott

Department of Chemistry, University of Florida, Gainesville, FL 32611-7200, USA. E-mail: mjscott@chem.ufl.edu

Received (in Bloomington, IN, USA) 4th October 1999, Accepted 20th January 2000

The Mac Donald-type 2 + 2 condensation of the readily available 5-mesityldipyrromethane with acenaphthenequinone leads to the *trans* (*syn* and *anti*) porphodimethenes, respectively, which, after treatment with KOH or NaOMe in THF and subsequent oxidation with air, yield the corresponding *trans*-8-carboxynaphthylporphyrins or their esters.

meso-Substituted porphyrins with rigid anthracene, biphenylene or naphthalene spacers have been widely used to determine the distance dependency of photo-induced electron transfer[1] as well as to prepare and examine cofacial diporphyrins[2] or other bridged porphyrins with well defined separations and varying relative arrangements of the porphyrin rings.[3] Porphyrins with a functionalized anthracene or naphthalene group have also found utility as building blocks for the synthesis of molecular receptors and for the design of dinuclear complexes.[4] Despite the numerous potential applications for these types of complexes, their development has been severely hampered by the inability to prepare large quantities of the porphyrin precursors. The syntheses, in general, require complex procedures for the preparation of the aromatic side arm and/or a multistep procedure for the porphyrin backbone. Chang *et al*.[5] and Therien and coworkers[6] have reported the preparation of porphyrins attached to the 1-position of an 8-functionalized naphthalene but to the best of our knowledge, a straightforward synthetic procedure for the synthesis of *trans* αα/αβ porphyrins bearing two 8-functionalized naphthalene derivatives has yet to be reported.

As part of our building block approach towards the preparation of new di- and tri-nuclear porphyrin based complexes, a general two-step synthesis, starting from 5-mesityldipyrromethane, has been developed to provide convenient amounts of the desired porphyrins. Reaction of commercially available acenaphthenequinone with 5-mesityldipyrromethane in the presence of catalytic amounts of $BF_3{\cdot}OEt_2$[7] gives, after oxidation with DDQ and subsequent filtration through neutral alumina, a mixture of the corresponding porphodimethene isomers in 26% yield. Separation by column chromatography yields the two isomers [**1** (*syn*), **2** (*anti*)] in an almost 1:2 ratio.†

The porphodimethenes **1** and **2** are air-stable, bright orange solids and they exhibit a characteristic absorption maxima in the visible region at λ_{max}/nm (log ε) 440(4.97) (**1**) and 438(4.93) (**2**), which when compared to previously described octaalkylporphodimethenes (414–426 nm) are bathochromically shifted.[8] The N–H and C=O stretch frequencies can be found, respectively, in the IR at 3345, 1732 cm^{-1} for **1** and 3279, 1720 cm^{-1} for **2**. The absolute configuration has been determined by ^{1}H NMR and by an X-ray structure analysis of the metallated (Zn^{2+}) porphodimethene **2b**. Although the X-ray structure analysis of **2** reveals a strong roof-like folded structure of the porphodimethene core,[9] only one type of acenaphtheneoyl can be identified in the ^{1}H NMR spectra of both **1** and **2**, suggesting a fast up and down motion of the acenaphtheneoyl groups together with a flexing of the two dipyrromethane units along a line joining the two saturated *meso* carbons. Even at 223 K, only minor changes were evident in the NMR spectra of **2**. Owing to the lack of aromaticity in the macrocycle, the signal of the N–H protons appears downfield at δ 13.92 (**1**) and 14.00 (**2**), respectively, characteristic of porphodimethenes.[8,10] Metal insertion has been demonstrated by reaction of **2** with $Zn(OAc)_2{\cdot}2H_2O$ in refluxing $CHCl_3$–MeOH. Complex formation can be easily monitored by UV–VIS-spectroscopy [Fig. 1, λ_{max} (log ε) 475 nm (5.17) (**2b**)]. As shown in Fig. 2, the Zn^{2+} in **2b** is complexed by a nearly planar, C_2 symmetric, tetrapyrrole macrocycle, although the metal is disordered over two positions in the solid-state structure. The

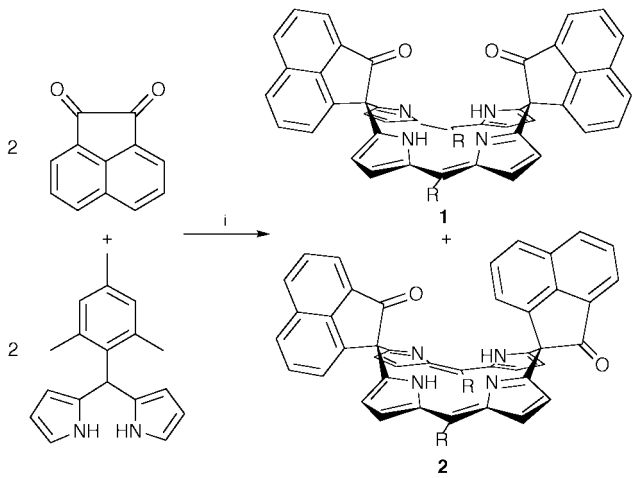

Scheme 1 *Reagents and conditions*: i, 1. $BF_3{\cdot}OEt_2$, CH_2Cl_2, room temp., 4 h, 2. DDQ, room temp., 1 h. R = mesityl.

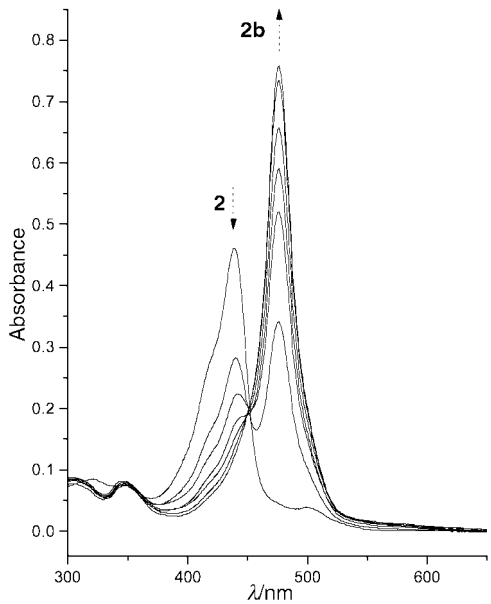

Fig. 1 UV-VIS spectra of **2** upon addition of $Zn(OAc)_2$ in boiling $CHCl_3$–MeOH. The arrows indicate the direction of change in peaks during metallation. Spectra were measured at 5 min intervals.

DOI: 10.1039/a907992k

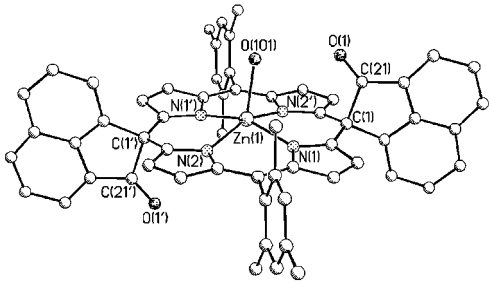

Fig. 2 Diagram of **2b**; the porphodimethene resides on inversion symmetry position, relating the prime and unprimed atoms. The zinc atom is disordered over two positions and the symmetry equivalent Zn(1′) and O(101′) atoms as well as all hydrogen atoms have been omitted for clarity. Selected bond lengths (Å) and angles (°): Zn(1)–N(1) 2.116(4), Zn(1)–N(2) 2.197(4), Zn(1)–N(1′) 2.038(4), Zn(1)–N(2′) 2.063(4), Zn(1)–O(101) 2.175(7), N(1)–Zn(1)–N(2) 85.2(1), N(1)–Zn(1)–N(2′) 88.6(1), N(1′)–Zn(1)–N(2) 87.0(1), N(1′)–Zn(1)–N(2′) 90.7(1), N(1)–Zn(1)–O(101) 97.9(2), N(2)–Zn(1)–O(101) 107.4(2), N(1′)–Zn(1)–O(101) 104.9(2), N(2′)–Zn(1)–O(101) 94.3(2).

largest out of plane displacements are observed for the saturated *meso* carbon atoms (0.11 Å) which are part of the five-membered rings of the two 1-acenaphthenone moieties aligned in an *anti* position. The Zn atom, coordinated by the four pyrrole nitrogens and an axial water molecule, resides 0.404 Å above the plane defined by the nitrogen donor set. The Zn–N bond lengths vary considerably from 2.038(4) to 2.197(4) Å, but the average distance of 2.10 Å is significantly larger than the corresponding linkage in tetra *meso*-aryl substituted porphyrins [mean: 2.036(6) Å; ZnTPP].[11]

Refluxing the porphodimethenes **1** and **2** in THF in the presence of 30% KOH results in ring opening and formation of the respective porphyrins without further oxidation by DDQ. Subsequent protonation with 6 M HCl gives the free acids (**3**, **4**) in high yields. While the αα isomer **3** is soluble in $CHCl_3$, the αβ atropisomer is virtually insoluble in most common organic solvents, possibly owing to strong intermolecular hydrogen-bonding interactions between the carboxylic acid groups. Accordingly, the αβ atropisomer has been fully characterized as the dipotassium salt.

Porphyrin formation has also been accomplished by reaction of **1** or **2** with NaOMe in THF–MeOH at room temp. After bubbling air through the reaction mixture, the corresponding esters (**5**, **6**) were isolated in moderate yields.‡ All of the porphyrins exhibit a characteristic Soret band between 425 and 432 nm in the UV–VIS spectra and they have been characterized by IR, NMR and MS. In addition, the αβ atropisomer **6** has been characterized by an X-ray structural analysis (Fig. 3), and although most of the structural parameters of the porphyrin core are indistinguishable from other *meso*-aryl substituted porphyrins, a few particular details are worth noting. The two mesityl residues are oriented nearly perpendicular to the porphyrin plane (85.3°) while the naphthalene moieties exhibit a twist of 61.8° relative to the macrocyclic ring. Owing to the electronic repulsion of the ester group and the electron rich porphyrin plane, the functionalized naphthalene groups are slightly inclined back away from the porphyrin, lifting the two oxygen atoms above the plane of the macrocycle by 2.667 Å [O(2)] and 3.087 Å [O(1)], respectively.

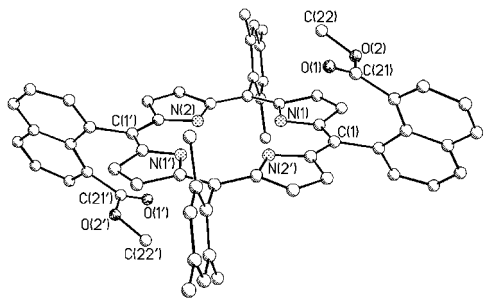

Fig. 3 Diagram of the structure of **6** outlining the atom numbering scheme. Primed and unprimed atoms are related by a center of inversion. The hydrogen atoms have been omitted for clarity.

In summary, we have demonstrated that acenaphthenone substituted porphodimethenes can be generated from 5-mesityldipyrromethane and acenaphthenequinone. Ring cleavage gives the desired porphyrins bearing two 8-functionalized naphthalene groups. Work is in progress to extend this reaction to other vicinale diketones. Other ring opening reactions are also under investigation.

We thank the Deutsche Forschungsgemeinschaft and the Research Corporation (Research Innovation Award) for providing financial support for this work. Support from the National Science Foundation (CAREER Award) is also gratefully acknowledged.

Notes and references

† 5-Mesityldipyrromethane was prepared as described before.[12] The formation of the porphodimethenes **1** and **2** and the porphyrins **5** and **6** were carried out under a nitrogen atmosphere in dried and degassed solvents. Satisfactory elemental analyses or HR-MS (MH^+) were obtained for new compounds. **1**: Yield: 8%. $\lambda_{max}(CH_2Cl_2)$/nm (log ε) 440 (4.97). IR (KBr): 3345 (ν_{N-H}), 1732 cm^{-1} (ν_{CO}). **2**: Yield: 18%. $\lambda_{max}(CH_2Cl_2)$/nm (log ε) 438(4.93). IR (KBr): 3279 (ν_{N-H}), 1720 cm^{-1} (ν_{CO}). **2b**: Yield: 91%. $\lambda_{max}(CH_2Cl_2)$/nm (log ε) 475(5.17). IR (KBr): 1720 cm^{-1} (ν_{CO}) **3**: Yield: 92%. λ_{max} ($CHCl_3$) 432 nm. IR (KBr): 3327 (ν_{N-H}), 1708 cm^{-1} (ν_{CO}). **4** (potassium salt after recrystallization): Yield: 65%. λ_{max} (MeOH) 431 nm. IR (KBr): 1563 cm^{-1} (ν_{CO}). **5**: Yield: 69%. λ_{max} ($CHCl_3$) 425 nm. IR (KBr): 3315 (ν_{N-H}), 1727 cm^{-1} (ν_{CO}). **6**: Yield: 59%. $\lambda_{max}(CHCl_3)$ 425 nm. IR (KBr): 3315 (ν_{N-H}), 1725 cm^{-1} (ν_{CO}).

‡ *Crystal data*: **2b**·$CHCl_3$: $C_{61}H_{45}N_4O_3Cl_3Zn$, tetragonal, space group, $I4_1/a$, a = 29.539(2), c = 12.104(1) Å, V = 10561(1) $Å^3$, T = 173 K, Z = 8, D_c = 1.325 g cm^{-3}, μ(Mo-Kα) = 0.667 mm^{-1}, 27 497 reflections collected, 4520 unique, of which 2954 with $I > 2\sigma(I)$ were used in the refinement. The structure was solved by direct methods and refined using full-matrix least squares refinement on F^2 and difference Fourier synthesis. Unless severely disordered, all non-hydrogen atoms were refined anisotropically; hydrogen atoms were included at calculated positions. At convergence, R_1 = 0.0704 [$I > 2\sigma(I)$], wR_2 = 0.2010, GOF = 1.029 for 381 parameters.

6·CH_2Cl_2: $C_{63}H_{52}N_4O_4Cl_2$, monoclinic, space group $C2/c$, a = 25.800(1), b = 12.7094(7), c = 17.6758(9) Å, β = 115.168(1)°, V = 5245.6(5) $Å^3$, T = 173 K, Z = 4, D_c = 1.266 g cm^{-3}, μ(Mo-Kα) = 0.177 mm^{-1}, data collection, refinement and solution as above, 11 105 reflections collected, 3433 unique, of which 3006 with $I > 2\sigma(I)$ were used in all calculations. R_1 = 0.0611 [$I > 2\sigma(I)$], wR_2 = 0.1766, GOF = 1.047 for 357 parameters.

CCDC 182/1536. See http://www.rsc.org/suppdata/cc/a9/a907992k/ for crystallographic files in .cif format.

1 H. A. Staab, B. Kratzer and S. Quazzotti, *Eur. J. Org. Chem.*, 1998, 2149.
2 R. Guilard, M. A. Lopez, A. Tabard, P. Richard, C. Lecomte, S. Brandes, J. E. Hutchison and J. P. Collman, *J. Am. Chem. Soc.*, 1992, **114**, 9877 and references therein.
3 Y. Naruta, M. Sasayama and K. Ichihara, *Russ. J. Org. Chem.*, 1996, **32**, 214.
4 Y. Liang and C. K. Chang, *Tetrahedron Lett.*, 1995, **36**, 3817; N. Bag, S.-S. Chern, S.-M. Peng and C. K. Chang, *Inorg. Chem.*, 1995, **34**, 753.
5 C. K. Chang and M. P. Kondylis, *J. Chem. Soc., Chem. Commun.*, 1986, 316.
6 A. G. Hyslop, M. A. Kellett, P. M. Iovine and M. J. Therien, *J. Am. Chem. Soc.*, 1998, **120**, 12676.
7 B. J. Littler, Y. Ciringh and J. S. Lindsey, *J. Org. Chem.*, 1999, **64**, 2864.
8 A. Botulinski, J. W. Buchler, K.-L. Lay and H. Stoppa, *Liebigs Ann. Chem.*, 1984, **7**, 1259.
9 M. Harmjanz and M. J. Scott, unpublished results.
10 M. Fontecave, J. P. Battioni and D. Mansuy, *J. Am. Chem. Soc.*, 1984, **106**, 5217.
11 W. R. Scheidt, M. E. Kastner and K. Hatano, *Inorg. Chem.*, 1978, **17**, 706.
12 C.-H. Lee and J. S. Lindsey, *Tetrahedron*, 1994, **50**, 11427.

Communication a907992k

ChemComm

TEMPO free radical derived β-aminoalkoxyketolactones: substrates for base-, acid- and radical-induced fragmentation reactions

Arthur G. Schultz† and Xuqing Zhang*

Department of Chemistry, Rensselaer Polytechnic Institute, Troy, NY 12180-3590, USA. E-mail: zhangx4@rpi.edu

Received (in Corvallis, OR, USA) 10th December 1999, Accepted 2nd February 2000

β-Aminoalkoxyketolactones 2 and 3 obtained from the TEMPO free radical substitution of iodolactones 1 undergo fragmentations under basic, acidic and free radical conditions.

Fragmentation reactions of iodoketolactones of general structure **1**, available as single enantiomers,[1] with LiOH under aqueous conditions afford butenolide carboxylic acids and 4-hydroxy-2-cyclohexenones by way of competing additions of hydroxide ion to the ketone and lactone carbonyl groups.[2] The bicyclo[3.2.1] ring system in **1** locks the conformation of the two carbonyl groups with respect to the iodo substituent. To examine the importance of stereoelectronic factors[3] in these fragmentation processes it was desirable to have access to not only the axial iodo substituent in **1** but also an equatorial leaving group. We have found that it is possible to carry out an exchange of iodide in **1** with 2,2,6,6-tetramethyl-1-piperidinyloxy free radical (TEMPO) to provide both the axial and equatorial substituted β-aminoalkoxyketolactones **2** and **3** (Scheme 1).[4] Herein we describe the fragmentation reactions of **2** and **3** under basic, acidic and free radical conditions.

Mixtures of β-aminoalkoxyketolactones **2** and **3** were produced from **1** and were separated by flash chromatography on silica gel. Treatment of **2a** with 2 equiv. of LiOH in a 5:1 mixture of THF and water gave butenolide carboxylic acid **4** in 78% isolated yield with no trace of the 4-hydroxycyclohexenone **5** (Scheme 2). Addition of aqueous LiOH to the isomer **3a** with an axial aminoalkoxy group gave mainly the 4-hydroxycyclohexenone **5** along with 18% of **4** (Scheme 2).

That **2a** undergoes fragmentation to give **4** rather than **5** is a result of the antiperiplanar relationship of the leaving group X and the cyclohexanone C–C bond in the tetrahedral intermediate generated by addition of hydroxide ion to the ketone carbonyl group. The formation of **5** is explained by addition of hydroxide ion to the lactone carbonyl group of **3a** followed by a relatively fast fragmentation of the lactone C–C bond along with elimination of the antiperiplanar aminoalkoxy group. A competing fragmentation of **3a** occurs by addition of hydroxide ion to the ketone carbonyl group followed by a relatively slow cleavage of the cyclohexanone C–C bond to give a lactone enolate; elimination of the poorly oriented aminoalkoxy group is probably not in concert with C–C bond cleavage, but must await a conformational adjustment in the enolate to bring orbitals into proper alignment.[3] It is noteworthy that iodolactone **1a** also gave a mixture of **4** and **5** on treatment with aqueous LiOH.[4]

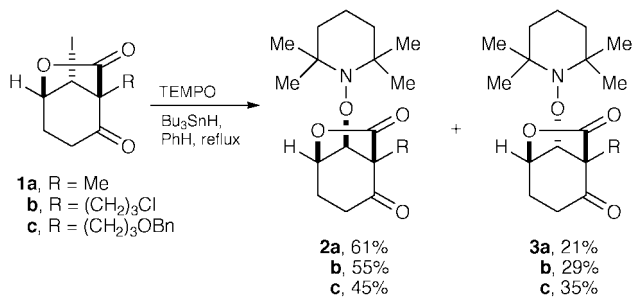

Scheme 1

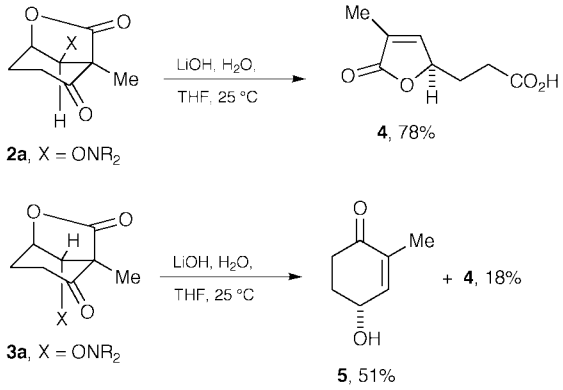

Scheme 2

We were interested in the development of fragmentation processes initiated by intramolecular carbonyl addition reactions. Hydrogenolysis of the benzyl ether **2c** in the presence of dilute hydrochloric or acetic acids provided the hemiketal **6**, and treatment of **6** with moderately concentrated HCl in ethanol at 25 °C resulted in fragmentation to give the medium ring lactone-butenolide **7** in 90% yield (Scheme 3).[5] Hemiketal **6** also was converted to **7** (88%) by fragmentation under basic reaction conditions (Et_3N in CH_2Cl_2, 25 °C). By contrast, hemiketal **8** obtained from hydrogenolysis of the isomeric benzyl ether **3c** did not undergo fragmentation to **7** under comparable acidic or basic reaction conditions (Scheme 3).

The utilization of aminoalkoxy substituents to initiate acid-catalyzed fragmentation reactions appears to be without precedent in the chemical literature. It is thought that fragmentation of **6** occurs from the *N*-protonated aminoalkoxy substituent to provide the oxide of a *sec*-amine as the leaving group; the amine oxide would be expected to rearrange to 1-hydroxy-

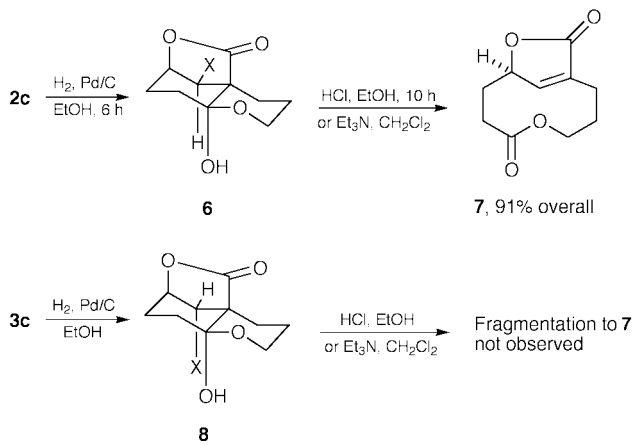

Scheme 3

† Deceased January 20th, 2000.

DOI: 10.1039/a909750c

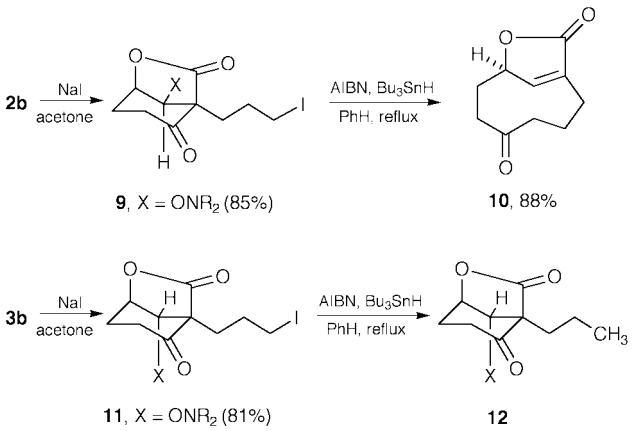

Scheme 4

2,2,6,6-tetramethylpiperidine.[6] Ionization of the protonated axial aminoalkoxy substituent in **8** does not occur because of the synclinal relationship of the C–ONR_2 bond and the cyclohexane C–C bond.[7] Fragmentation of **6** with Et_3N occurs by deprotonation of the hemiketal with concomitant elimination of R_2NO^-.

Perhaps the most interesting application of the aminoalkoxy substituent as a regulator of fragmentation reactions is in the area of free radical-mediated ring expansions.[8] Treatment of the alkyl iodide **9** with AIBN and Bu_3SnH (added over 6 h) in refluxing benzene gave the nine-membered-ring ketone **10** in 77% yield (88% based on recovered **9**) (Scheme 4).[9] However, the isomer **11** with an axial aminoalkoxy substituent gave the *n*-propyl derivative **12** with no trace of **10** (Scheme 4).

These data suggest that the primary alkyl radical generated from **9** undergoes addition to the ketone carbonyl group, followed by a relatively fast alkoxy radical-induced fragmentation to give **10** and the TEMPO free radical. The primary radical generated from **11** probably also undergoes addition to the ketone carbonyl group (reversible), but without proper alignment of the aminoalkoxy substituent this addition is nonproductive; reversion to the alkyl radical and eventual reduction with Bu_3SnH gives the *n*-propyl derivative **12**. It should be noted that alkyl radical addition to the lactone carbonyl group and fragmentation to a 2,4-lactone fused-2-cyclohexenone (structure not shown; *cf.* **3a** → **5**) is not competitive with reduction of the alkyl radical with Bu_3SnH.

In summary, the 2,2,6,6-tetramethyl-1-piperidinyloxy group has been found to be an effective leaving group in fragmentation reactions performed under basic, acidic and free radical conditions. It is important to note that elimination of 2,2,6,6-tetramethylpiperidine from **2** or **3** to give the corresponding β-diketone did not occur under any of these reaction conditions.[10] The availability of β-aminoalkoxyketolactones **2** and **3** as single enantiomers[1] suggests that these fragmentation reactions ought to have substantial utility in organic synthesis; the development of methods to selectively generate **2** and **3** and related substrates are under investigation.

We thank Dr P. R. Guzzo and Dr L. Pettus for early contributions to this project and the National Institutes of Health (GM 26568) for generous financial support.

Notes and references

1 A. G. Schultz, *Chem. Commun.*, 1999, 1263.
2 A. G. Schultz, M. Dai, S.-K. Khim, L. Pettus and K. Thakkar, *Tetrahedron Lett.*, 1998, **39**, 4203.
3 P. Deslongchamps, *Stereoelectronic Effects in Organic Chemistry*, Pergamon, Oxford, 1984; C. A. Grob, *Angew. Chem., Int. Ed. Engl.*, 1969, **8**, 535.
4 A. G. Schultz, M. Dai, F. S. Tham and X. Zhang, *Tetrahedron Lett.*, 1998, **39**, 6663; D. L. Boger and J. A. McKie, *J. Org. Chem.*, 1995, **60**, 1271.
5 Benzyl ether **2c** also was converted to **7** (91%) in one experimental operation by way of hydrogenolysis under more strongly acidic conditions (HCl in EtOH).
6 Ionization initiated by *O*-protonation or a bridging *N*,*O*-protonation should also be considered.
7 P. S. Wharton and G. A. Hiegel, *J. Org. Chem.*, 1965, **30**, 3254.
8 P. Dowd and W. Zhang, *Chem. Rev.*, 1993, **93**, 2091; G. H. Posner, K. S. Webb, E. Asirvatham, S. Jew and A. Degl'Innocenti, *J. Am. Chem. Soc.*, 1988, **110**, 4754.
9 For related free radical ring expansions that give cyclononenones, see: J. E. Baldwin, R. M. Adlington and J. Robertson, *J. Chem. Soc., Chem. Commun.*, 1988, 1404.
10 D. H. Hunter, D. H. R. Barton and W. J. Motherwell, *Tetrahedron Lett.*, 1984, **25**, 603 and references therein.

Communication a909750c

Development of a novel oxidatively removable and recyclable linker for combinatorial solid phase synthesis

Wen-Ren Li,* Nai-Mu Hsu, Hsueh-Hsuan Chou, Sung Tsai Lin and Yu-Sheng Lin

Department of Chemistry, National Central University, Chung-Li, Taiwan 32054, ROC.
E-mail: wenrenli@rs250.ncu.edu.tw

Received (in Cambridge, UK) 23rd November 1999, Accepted 28th January 2000

An appropriately derivatized phenanthridine is shown to behave as a novel, reusable linker which is based on a disubstituted amide anchorage and forms an acid group on oxidative cleavage, but tolerates exposure to acidic, basic and reductive reaction conditions.

Recently, a considerable amount of attention has been focused on the use of the combinatorial library approach for the discovery of new molecules with desired properties.[1] Up to now, syntheses of a variety of classes of chemical libraries have been constructed employing solid phase methods.[2,3] Many linkers have, therefore, been developed for anchoring and selectively removing the desired target molecule from polymer supports.[4–8] As far as we are aware, none of the available linkers used for carboxylic functions survive through a series of acidic, basic and reductive reactions and are also stable to *N*-alkylation conditions.[9–11] This void led us to devise a new type of recyclable phenanthridine linker for the synthesis of acids, which possesses greater stability under the above reaction processes and the capability to be removed by a mild oxidative reagent. In addition, it can be recycled.

The synthesis of an appropriately functionalized phenanthridine **1** is detailed in Scheme 1. The synthesis was initiated with protection of the acid group of 4-nitrophenylacetic acid as its methyl ester using $SOCl_2$ and MeOH. Reduction of the nitro group of the methyl ester was rapidly accomplished by catalytic transfer hydrogenation with NH_4HCO_2 as the hydrogen donor over a Pd/C catalyst.[12] Coupling of amine **3** with 2-iodobenzoic acid was followed by reduction using $NaBH_4$ and $BF_3{\cdot}OEt_2$ to form the secondary amine **4** in 73% yield for four steps from 4-nitrophenylacetic acid. Attempts to perform an internal biaryl cyclization of the aryl substituted amide, before $NaBH_4$ reduction, gave an undesired intermolecular coupling dimer. Acylation of the amino and hydroxy group of compound **4** with AcBr, followed by intramolecular Heck type cyclization[13] employing $Pd(OAc)_2$, PPh_3 and Ag_2CO_3 in MeCN led to the amide **5** in 70% yield. Oxidative cleavage of the resulting amide **5** with cerium ammonium nitrate (CAN) and subsequent hydrolysis of the acetate with LiOH afforded the amine-masked phenanthridine handle **1** as a crystalline compound. Of particular note is that the synthesis of all intermediates in Scheme 1 can be carried out on a preparative scale to afford ample quantities of the desired compound in roughly 40% overall yield.

The suitability for reductive processing and alkylation of the new linker and its applicability to peptide chemistry were demonstrated by the synthesis a trimethylated derivative of actarit,[14] an immunomodulating agent, and a *N*-acylated dipeptide on the Merrifield resin as shown in Schemes 2 and 3. The phenanthridine derivatized solid support **8** (Scheme 2) can readily be prepared by treating chloromethylpolystyrene with the sodium salt of phenanthridine in dry DMF at room temperature for 16 h. In this form the phenanthridine resin is stable and can be stored for long periods without loss of activity. Reduction of this functionalized resin furnished the resin-bound secondary amine, which was first derivatized with 4-nitrophenylacetic acid and then subjected to enolate alkylation by employing commonly used bases such as NaH or LDA.[15] Reduction of the nitro group of resin **6** with $SnCl_2$ in DMF afforded, after acetylation and *N*-alkylation, the trimethylated acid-bound resin. Treatment of the resulting resin with 2 equiv. of CAN in MeCN and water for 10 min resulted in complete cleavage of the desired acid from the solid support. After removal of the MeCN, the crude product was dissolved in EtOAc, washed successively with water and aqueous HCl and purified to give the trimethylated actarit derivative **7** in 57% overall yield for eight steps. The regenerated phenanthridine resin **8** could be reused for another synthetic sequence with only a slight loss in activity. The yields after one and two recycles are 90 and 84%, respectively. The resin-bound amides in Scheme 2 are stable under either basic or acidic hydrolytic conditions.

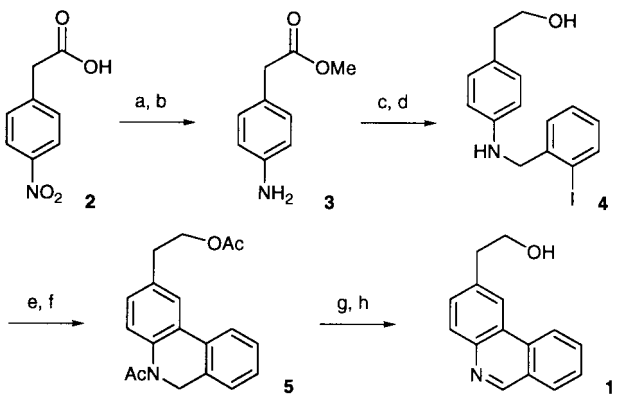

Scheme 1 *Reagents and conditions*: (a) $SOCl_2$, MeOH, 97%; (b) 10% Pd/C, HCO_2NH_4, MeOH, 97%; (c) 2-iodobenzoic acid, DIC, MeCN, 84%; (d) $NaBH_4/BF_3{\cdot}OEt_2$, THF, 93%; (e) AcBr, Et_3N, MeCN, 87%; (f) PPh_3, $Pd(OAc)_2$, Ag_2CO_3, MeCN, 70%; (g) CAN, MeCN, H_2O, 95%; (h) LiOH, THF, H_2O, 95%.†

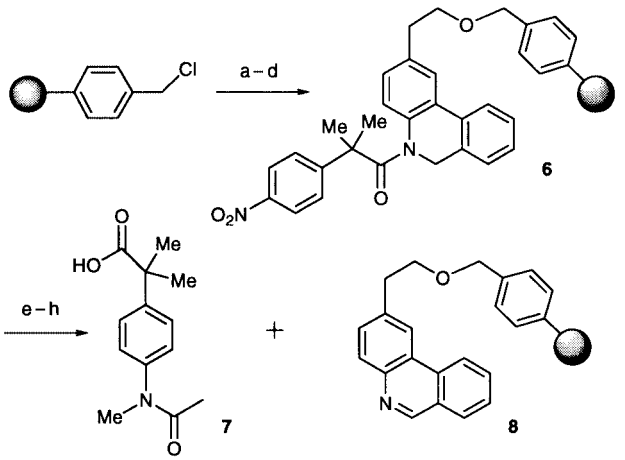

Scheme 2 *Reagents and conditions*: (a) NaH, DMF, linker **1**; (b) $NaBH_4$, $BH_3{\cdot}THF$, EtOH, 71%; (c) 4-nitrophenylacetic acid, DIC, CH_2Cl_2; (d) NaH, MeI, DMF or LDA, HMPA, THF, MeI; (e) $SnCl_2$, DMF, 88%; (f) Ac_2O, Et_3N, CH_2Cl_2; (g) NaH, MeI, DMF; (h) CAN, THF, H_2O, 92%.†

DOI: 10.1039/a909236f

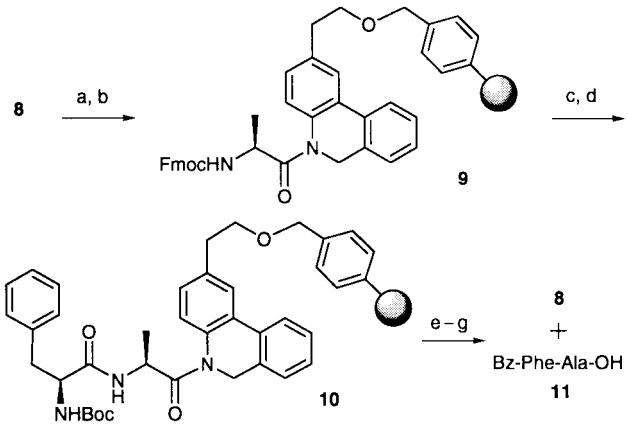

Scheme 3 *Reagents and conditions*: (a) $NaBH_4$, BH_3·THF, EtOH; (b) DIC, Fmoc-L-Ala-OH, CH_2Cl_2; (c) 20% piperidine, DMF, 89%; (d) HBTU, Pr^i_2NEt, Boc-L-Phe-OH, DMF; (e) TFA, CH_2Cl_2, 94%; (f) BzCl, Pr^i_2NEt, CH_2Cl_2; (g) CAN, THF, H_2O, 91%.

These amides were not hydrolyzed upon treatment with 1 M HCl or NaOH in THF–H_2O solution over 24 h. The further utility of this linker has been shown by synthesizing an *N*-acylated dipeptide **11** (Scheme 3). Similar results were achieved using a similar strategy to that employed for the previous syntheses. After *N*-Fmoc-L-alanine was coupled to the phenanthridine linker the resin was submitted to the peptide synthetic sequence to provide the desired dipeptide **11** in a nonoptimized yield of 76%, as shown in Scheme 3. At each step, the coupling efficiency was about 86–95% yield as monitored by photometric Fmoc determination and the ninhydrin method. Controls during these syntheses proved that the above reaction milieu did not cause either any premature cleavage or damage of the linker.

In conclusion, we have developed a new linker for solid phase organic synthesis of carboxylic acids and have successfully demonstrated its application. The advantages of this linker are: (i) it is orthogonal to the Fmoc/Boc and Boc/Bn protecting group strategies; (ii) it can be prepared in both large quantity and high purity; (iii) its attachment to the solid support is straightforward; (iv) it is anchored to the C-terminal residue by a disubstituted amide and not an ester bond, ensuring stability to *N*-alkylation and avoidance of diketopiperazine formation at the dipeptide stage; (v) the linker is rapidly cleaved under mild oxidative conditions and the reaction is very clean; (vi) the phenanthridine resin is sufficiently robust to be recovered and recycled through the reaction sequence. Therefore, the phenanthridine linker should find broad application in the field of solid phase combinatorial synthesis where orthogonal methods of release are required. Currently, we are investigating non-aqueous oxidative cleavage conditions which will afford the corresponding esters and are exploring the length and attachment position of the alkoxyacyl spacer that is needed to link the appropriate phenanthridine handle to aminated resins such as MBHA or BHA resin through an amide bond.

The authors are grateful to the National Science Council, ROC, for the financial support (NSC 86-2113-M-008-001) of this work.

Notes and references

† Abbreviations used: DIC = 1.3-diisopropylcarbodiimide, HBTU = 2-(1*H*-benzotriazol-l-yl)-1,1,3,3-tetramethyluronium hexafluorophosphate, MBHA = 4-methylbenzhydrylamine.

1 S. Booth, P. H. H. Hermkens, H. C. J. Ottenheijm and D. C. Rees, *Tetrahedron*, 1998, **54**, 15 385, and references therein.
2 K. S. Lam, M. Lebl and V. Krchnák, *Chem. Rev.*, 1997, **97**, 411.
3 N. K. Terrett, M. Gardner, D. W. Gordon, R. J. Kobylecki and J. Steele, *Tetrahedron*, 1995, **51**, 8135.
4 I. W. James, *Tetrahedron*, 1999, **55**, 4855.
5 J. S. Fruchtel and G. Jung, *Angew. Chem., Int. Ed. Engl.*, 1996, **35**, 17.
6 F. Stiber, U. Grether and H. Waldmann, *Angew. Chem., Int. Ed.*, 1999, **38**, 1073.
7 C. R. Millington, R. Quarrell and G. Lowe, *Tetrahedron Lett.*, 1998, **39**, 7201.
8 K. Fukase, Y. Nakai, K. Egusa, J. A. Poroco Jr. and S. Kusumoto, *Synlett*, 1999, 1074.
9 B. J. Backes, A. A. Virgilio and J. A. Ellman, *J. Am. Chem. Soc.*, 1996, **118**, 3055 and references therein.
10 A. N. Semenov and K. Gordeev, *Int. J. Peptide Protein Res.*, 1995, **45**, 303.
11 R. Sola, P. Saguer, M.-L. David and R. Pascal, *J. Chem. Soc., Chem. Commun.*, 1993, 1786.
12 S. Ram and R. E. Ehrenkaufer, *Tetrahedron Lett.*, 1984, **25**, 3415.
13 T. Harayama, T. Akiyama and K. Kawano, *Chem. Pharm. Bull.*, 1996, **44**, 1634.
14 T. Nishimura, H. Fujisawa, H. Suzuka, H. Yoshifusa, Y. Nakamura, K. Inoue, Y. Shibata, K. Kimura and M. Muramatsu, *Jpn. Pharmacol. Ther.*, 1993, **21**, 329; H. Munakata, M. Kobayashi, K. Wagatsuma, S. Sato, M. Tsurufuji, H. Enomoto, M. Sugiyama, Y. Shibata and I. Morita, *US Pat.*, 4720506; 880119.
15 F. Tanaka, M. Node, K. Tanaka, M. Mizuchi, S. Hosoi, M. Nakayama, T. Taga and K. Fuji, *J. Am. Chem. Soc.*, 1995, **117**, 12 159.

Communication a909236f

Preparation of synthetic steamcracker feed from cycloalkanes (or aromatics) on zeolite catalysts

Jens Weitkamp,*[a] Andreas Raichle,[a] Yvonne Traa,[a] Martin Rupp[b] and Franz Fuder[b]

[a] *Institute of Chemical Technology, University of Stuttgart, D-70550 Stuttgart, Germany. E-mail: jens.weitkamp@po.uni-stuttgart.de*
[b] *VEBA OEL AG, D-45876 Gelsenkirchen, Germany*

Received (in Cambridge, UK) 23rd December 1999, Accepted 4th February 2000

Methylcyclohexane is converted into a high-quality steamcracker feed over acidic zeolites with appropriate pore systems, thereby opening a new route for the utilisation of surplus aromatics.

Steamcrackers[1] are widely employed for the production of ethylene and propylene from naphtha,[2] ethane or similar light hydrocarbons. One of the by-products of steamcracking is pyrolysis gasoline which is rich in aromatics. Given the forecasted growth in the worldwide demand of ethylene[3] and propylene[4] from, respectively, 57×10^6 and 30×10^6 tonne yr^{-1} in 1990 to *ca.* 140×10^6 and 75×10^6 tonne yr^{-1} in 2010, the production of pyrolysis gasoline will necessarily increase as well. Up till now, pyrolysis gasoline has been used as an aromatics-rich and, hence, high-octane petrol component. With the so-called Auto Oil Programme of the European Community, the aromatics content of petrol has to be diminished from 45 to < 42 vol% until the year 2000, and to < 35 vol% until 2005.[5] Therefore, new outlets for surplus aromatics are urgently needed. We report here on a novel catalytic chemistry by which cycloalkanes (or aromatics, since these can easily be hydrogenated into cycloalkanes by state-of-the-art processes) are converted predominantly into light linear alkanes (ethane, propane, *n*-butane and *n*-pentane) the mixture of which is a premium steamcracker feedstock for high ethylene and propylene yields.[6]

Previous work on ring opening of cycloalkanes mostly relies on hydrogenolysis over noble metal catalysts designed predominantly to yield branched alkanes.[7–9] Such hydrocarbons are, however, less suitable as a steamcracker feed, since large amounts of undesired methane will be formed. Only few reports deal with cracking of cyclic hydrocarbons over acidic zeolites in an excess of hydrogen,[10–12] and yields of *n*-alkanes during the conversion of cycloalkanes or aromatics with seven or more carbon atoms are reported to be low.

On zeolite H-ZSM-5 at 400 °C, methylcyclohexane is converted[13] with a yield of 70.6% into ethane (9.4%), propane (47.7%), *n*-butane (12.4%) and *n*-pentane (1.1%), see Fig. 1 and Table 1, whereas on zeolite H-Y, much lower yields (42.8%) of these desirable products are obtained. On H-ZSM-5, the most important by-products are branched alkanes, *viz.* 17.6% isobutane, 6.2% isopentane and 0.6% isohexanes. Whereas on H-ZSM-5 virtually no aromatics are found, the total yield of aromatics on H-Y amounts to 15.9% (benzene 2.2%, toluene 6.4%, C_8-aromatics 5.6% and C_9-aromatics 1.7%). We tentatively attribute this difference to the lower activity of the larger-pore zeolite for cleavage of endocyclic carbon–carbon bonds.[14] The difference in selectivities becomes even more pronounced at lower conversions (Fig. 2) or at high times-on-stream (Table 1, entry 7). The deactivation observed on zeolite H-Y correlates qualitatively with the mass ratio of carbon in the coke formed on the catalyst[15] and in the methylcyclohexane fed (Table 1, entry 8).

The pronounced differences in the catalytic behaviour of both zeolites can be accounted for by introducing the so-called cracking mechanism ratio,[16] $\mathrm{CMR} \equiv (Y_{\mathrm{methane}} + Y_{\mathrm{C_2\ hydrocarbons}})/Y_{\mathrm{isobutane}}$ (Table 1, entry 9 and Fig. 3), which is considered as a quantitative measure for the relative contributions of monomolecular Haag–Dessau cracking[17] *versus* conventional bimolecular cracking. In the narrower pores of zeolite ZSM-5 and with increasing temperature, Haag–Dessau cracking, which produces large amounts of ethane and propane, is favoured over the spatially more demanding bimolecular mechanism which leads predominantly to isobutane. In line with this interpretation, much more hydrogen is incorporated into the cracked products on H-ZSM-5 than on H–Y (Table 1, entry 10): Clearly, H_2 can be activated on acidic zeolites, as demonstrated previously.[12,18,19]

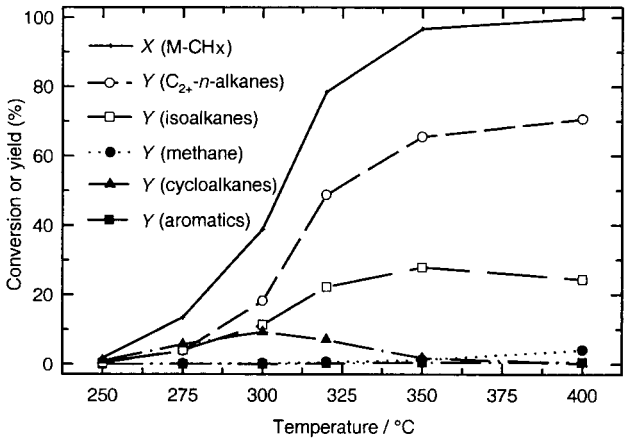

Fig. 1 Conversion of methylcyclohexane on H-ZSM-5 at various temperatures.

In conclusion, methylcyclohexane can be converted over acidic zeolites with suitable pore systems into a high-quality synthetic steamcracker feed consisting predominantly of eth-

Table 1 Conversion of methylcyclohexane at 400 °C and 30 min TOS[a]

Entry	Catalyst	H-ZSM-5	H-Y
1	$X_{\mathrm{M\text{-}CH}x}$ (%)	99.9	99.5
2	Y_{methane} (%)	4.0	0.6
3	$Y_{n\text{-alkanes}}$[b] (%)	70.6	42.8
4	$Y_{i\text{-alkanes}}$ (%)	24.4	39.3
5	$Y_{\mathrm{cycloalkanes}}$ (%)	0.2	0.8
6	$Y_{\mathrm{aromatics}}$ (%)	0.7	15.9
7	$Y_{n\text{-alk.}}$[b](440 min TOS)/$Y_{n\text{-alk.}}$ (30 min TOS)	1.00	0.84
8	$m_{\mathrm{C,\ coke}}/m_{\mathrm{C,M-CH}x}$[c] (%)	< 0.05	1.76
9	CMR[d]	0.76	0.15
10	H_2 incorporation[e]	2.3	1.2

[a] Time-on-stream. [b] Yield of *n*-alkanes = $Y_{\mathrm{ethane}} + Y_{\mathrm{propane}} + Y_{n\text{-butane}} + Y_{n\text{-pentane}}$, the individual yields being defined in the usual manner, *e.g.* $Y_{\mathrm{ethane}} = (2/7) \times (\dot{n}_{\mathrm{ethane,\ out}}/\dot{n}_{\mathrm{M-CH}x,\ \mathrm{in}})$. [c] Mass ratio of carbon in the coke formed on the catalyst after 500 min time-on-stream and in the methylcyclohexane cumulatively fed within the same time. [d] Cracking mechanism ratio, see text. [e] $\dot{n}_{\mathrm{H_2,\ consumed}}/\dot{n}_{\mathrm{M-CH}x,\ \mathrm{fed}}$.

DOI: 10.1039/a910284l

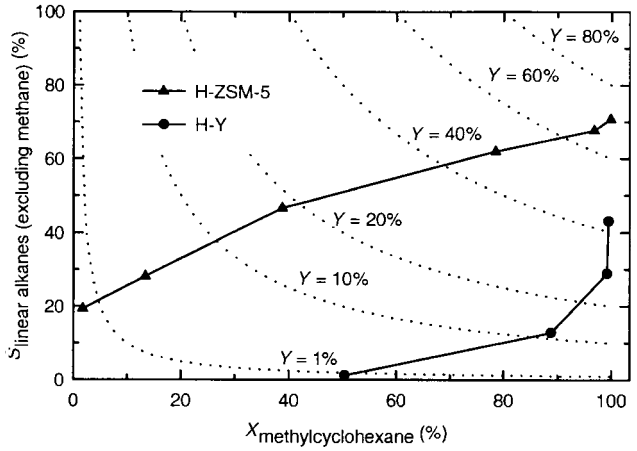

Fig. 2 Selectivity to linear alkanes (excluding methane) as a function of the methylcyclohexane conversion on zeolites H-ZSM-5 and H-Y after 30 min TOS.

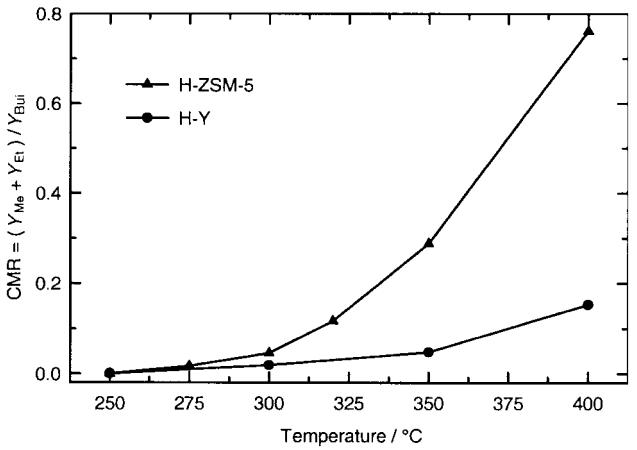

Fig. 3 Cracking mechanism ratio (CMR) after 30 min TOS as a function of temperature during the conversion of methylcyclohexane.

ane, propane and *n*-butane, thereby opening a new route for the utilisation of surplus aromatics. Instead of hydrogenating the aromatics to cycloalkanes and converting the latter into light *n*-alkanes separately, one can use a bifunctional form of the zeolite, such as Pd/H-ZSM-5 or Pt/H-ZSM-5, and produce light *n*-alkanes directly from aromatics in a single reactor. Such work is under way in our laboratories.

Notes and references

1 In steamcrackers, hydrocarbons are thermally cracked in the presence of steam as diluent.
2 Light petrol, especially hydrocarbons with five and six carbon atoms.
3 T. Chang, *Oil Gas J.*, 1999, **97**(13), 50.
4 J. Cosyns, J. Chodorge, D. Commereuc and B. Torck, *Hydrocarbon Process., Int. Ed.*, 1998, **77**(3), 61.
5 W. J. Petzny and C.-P. Hälsig, in *DGMK Tagungsbericht 9903, Proc. DGMK Conference: The Future Role of Aromatics in Refining and Petrochemistry, October 13–15, 1999, Erlangen, Germany*, ed. G. Emig, M. Rupp and J. Weitkamp, DGMK, Hamburg, 1999, p. 7.
6 C. Dembny, ref. 5, p. 115.
7 R. J. Schmidt, P. L. Bogdan, L. B. Galperin and J. S. Holmgren, *US Pat.*, 5 831 139, 1998.
8 G. B. McVicker, M. S. Touvelle, C. W. Hudson, D. E. W. Vaughan, M. Daage, S. Hantzer, D. P. Klein, E. S. Ellis, B. R. Cook, O. C. Feely and J. E. Baumgartner, *WO Appl.*, 97/09288, 1997.
9 K. J. Del Rossi, D. J. Dovedytis, D. J. Esteres, M. N. Harandi and A. Huss Jr., *US Pat.*, 5 334 792, 1994.
10 M. Chareonpanich, Z.-G. Zhang and A. Tomita, *Energy Fuels*, 1996, **10**, 927.
11 F. Hernandez, L. Moudafi, F. Fajula and F. Figueras, in *Proc. 8th Int. Congr. Catal., July 2–6, 1984, Berlin, Germany*, Verlag Chemie, Weinheim, 1984, vol. 2, p. 447.
12 T. Sano, K. Okabe, H. Hagiwara and H. Takaya, *J. Mol. Catal.*, 1987, **40**, 113.
13 The zeolites Y (n_{Si}/n_{Al} = 2.4, obtained from Union Carbide) and ZSM-5 (n_{Si}/n_{Al} = 20, hydrothermally synthesised after S. Ernst and J. Weitkamp, *Chem.-Ing.-Tech.*, 1991, **63**, 748) were ion-exchanged with aqueous solutions of NH_4NO_3 and pre-treated in a flow of nitrogen for 12 h at 400 °C to yield the Brønsted-acidic forms. The experiments were performed in a flow-type apparatus with a fixed-bed reactor. The mass of dry catalyst (particle size between 0.20 and 0.32 mm), the total pressure, the partial pressure of methylcyclohexane at the reactor inlet and the WHSV amounted to 500 mg, 6.0 MPa, 65 kPa and 0.68 h^{-1}, respectively. Product analysis was achieved by high-resolution capillary gas chromatography.
14 J. Weitkamp, P. A. Jacobs and S. Ernst, in *Structure and Reactivity of Modified Zeolites, Studies in Surface Science and Catalysis*, ed. P. A. Jacobs, N. I. Jaeger, P. Jírů, V. B. Kazansky and G. Schulz-Ekloff, Elsevier, Amsterdam, Oxford, New York, Tokyo, 1984, vol. 18, p. 279.
15 The carbon content of the used catalysts was determined by elemental analysis with an Elementar Vario EL instrument.
16 A. F. H. Wielers, M. Vaarkamp and M. F. M. Post, *J. Catal.*, 1991, **127**, 51.
17 W. O. Haag and R. M. Dessau, in *Proc. 8th Int. Congr. Catal., July 2–6, 1984, Berlin, Germany*, Verlag Chemie, Weinheim, 1984, vol. 2, p. 305.
18 K. Ebitani, J. Tsuji, H. Hattori and H. Kita, *J. Catal.*, 1992, **138**, 750.
19 J. Meusinger and A. Corma, *J. Catal.*, 1995, **152**, 189; 1996, **159**, 353.

Communication a910284l

ChemComm

The catalytic hydrolysis of CCl_4 to HCl and CO_2 over magnesium oxide

Ulrike Weiss, Michael P. Rosynek and Jack Lunsford*

Department of Chemistry, Texas A&M University, College Station, Texas 77843, USA.
E-mail: lundsford@mail.chem.tamu.edu

Received (in Cambridge, UK) 29th November 1999, Accepted 1st February 2000

At temperatures > 400 °C, CCl_4 reacts with H_2O over a MgO catalyst to yield HCl and CO_2.

The destruction of carbon tetrachloride found in ground water and in effluent streams is typically carried out by using incineration[1] or catalytic oxidation.[2] We describe here the catalytic reaction of CCl_4 with H_2O to form CO_2 and HCl, which has not been previously reported except for a brief comment in the patent literature.[3] The kinetics of the corresponding uncatalyzed reaction in water was studied by Fells and Moelwyn-Hughes,[4] who observed a rather small second order rate constant (with respect to CCl_4) of $k = 1.21 \times 10^{-3}$ L mol^{-1} s^{-1} at 373 K for an initial CCl_4 concentration of 0.903 mmol L^{-1}. The rate was unaffected by proton, hydroxide or chloride ion concentration.

The use of an alkaline earth oxide catalyst is based on a non-catalytic cycle in which CCl_4 was first reacted with BaO to form $BaCl_2$.[5] The $BaCl_2$ was subsequently reacted with aqueous CO_3^{2-} to produce $BaCO_3$ and aqueous HCl. The $BaCO_3$ could be converted to BaO at elevated temperatures (600 °C), and the process could then be repeated. However when CCl_4 and H_2O were passed over BaO at 500°C, the catalytic reaction [eqn. (1)]

$$CCl_4 + 2H_2O \rightarrow 4HCl + CO_2 \quad \Delta G^{o}_{500\,^{\circ}C} = -390\ \text{kJ mol}^{-1} \qquad (1)$$

did not occur. Magnesium oxide, however, is an effective catalyst for this reaction, in part because magnesium chloride is not extensively formed, and, more importantly, magnesium carbonate decomposes at temperatures near 400 °C.

The catalyst was prepared by the decomposition of $Mg(OH)_2$ obtained by stirring a slurry of MgO (Fisher, light) and water at 80 °C for 24 h. The $Mg(OH)_2$ (20–40 mesh size) was decomposed at 400 °C in flowing O_2 (100 mL min^{-1}). The reaction of CCl_4 with H_2O was carried out in a plug flow reactor at a total flow rate of 80 mL min^{-1} with He as the diluent. Gas chromatography was used to analyze for CCl_4, CO_2 and H_2O, while HCl was trapped in water and subsequently titrated with $AgNO_3$ (aq). X-Ray photoelectron spectra (XPS) were acquired using a Perkin-Elmer (PHI) model 5500 spectrometer.

The conversions of CCl_4 and H_2O are shown in Fig. 1 for the reaction carried out at 500 °C over 0.58 g MgO with $P(CCl_4)$ = 2 Torr and $P(H_2O)$ = 4 Torr. Under these conditions, the initial conversion of 88% decreased to *ca.* 74% during the first hour, but thereafter the conversion remained nearly constant. After 24 h on stream, the conversion was 68%. The surface area of the catalyst decreased from 90 to 38 m^2 g^{-1}, with most of the decrease occurring during the first hour. At the same partial pressures of CCl_4 and H_2O, but with 1.72 g MgO at 525 °C, the conversion was > 99% (no remaining CCl_4 was detected) for 72 h. Thus, nearly complete removal of CCl_4 can be achieved over a long period.

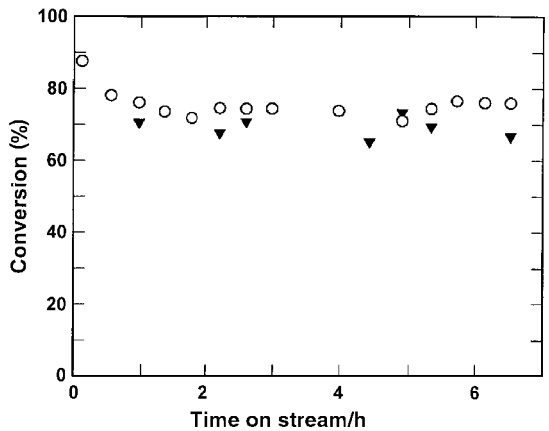

Fig. 1 Conversion of CCl_4 (○) and H_2O (▼) over 0.58 g MgO at 500 °C with $P(CCl_4)$ = 2 Torr and $P(H_2O)$ = 4 Torr.

Kinetic results were obtained under differential reaction conditions, which were achieved either by using a smaller amount of catalyst or by operating at lower temperatures. Over the temperature range 400–500 °C with 2 Torr CCl_4 and 4 Torr H_2O, the apparent activation energy was 85 kJ mol^{-1}. At the same initial pressures and at 450 °C, the specific activity was 0.167 μmol (g s)$^{-1}$ or 4.1 nmol (m^2 s)$^{-1}$ for a catalyst having a surface area of 38 m^2. The reaction orders with respect to CCl_4 and H_2O are given in Fig. 2. The reaction order with respect to H_2O at 400 °C was slightly dependent on the partial pressure of CCl_4 and increased to n = 0.16 at 6 Torr of CCl_4.

The amount of chloride in the sample after reaction was 4 wt%, which corresponds to a Cl/Mg ratio of 0.047. This value may be compared with a near-surface Cl/Mg ratio of 0.12 (as determined from XPS spectra), which was nearly the same for samples that had been on stream for 1 h at 500 °C or for 70 h at 525 °C. After steady state was attained, there was nearly a 100% chlorine balance between CCl_4 reacted and HCl formed.

The results are consistent with the mechanism described in Scheme 1, which is adapted from an earlier one that was proposed by Hooker and Klabunde[6] for the destructive adsorption of CCl_4. Although phosgene is a potential intermediate, none was detected in the gas phase by IR spectroscopy. The rate limiting step is believed to be the dissociative adsorption of CCl_4, although this is inhibited by the presence of chloride ions on the surface, which is consistent with the fact

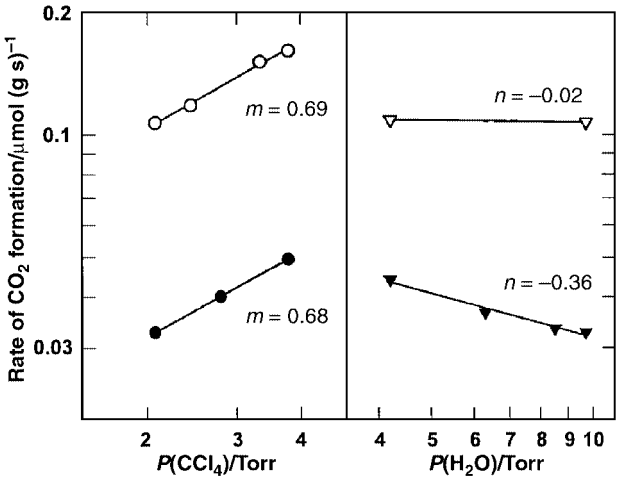

Fig. 2 Effect of CCl_4 and H_2O partial pressures on the rate of CO_2 formation over 0.40 g MgO: variation in CCl_4 pressure at 400 °C (●) and at 450 °C (○) with $P(H_2O)$ = 9.7 Torr; variation in H_2O pressure at 400 ° C (▼) and at 450 °C (▽) with $P(CCl_4)$ = 2.1 Torr.

DOI: 10.1039/a909552g

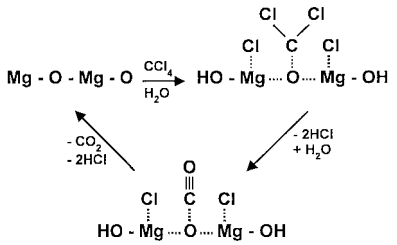

Scheme 1

that the reaction order with respect to CCl_4 is less than unity. The dissociative adsorption of H_2O to form hydroxide ions is very rapid at the reaction temperatures used. One might expect that the formation of carbonate ions, derived from CO_2, would inhibit the reaction, but this is not the case since the addition of CO_2 to the feed, in a 30-fold excess of that produced during the reaction, did not influence the reaction rate. The presence of chloride ions may decrease the basicity of the surface[7] and thereby minimize the formation of surface carbonates on MgO (see below).

The results described to this point were obtained using Fisher MgO (Ca < 1%, Fe < 0.05%); however, one experiment was carried out with Puratronic MgO (99.998%), and at comparable conditions the activity was the same, indicating that impurities such as iron do not play a role. By contrast, CaO and, as noted above, BaO were not active as catalysts. Both of these oxides are more effective than MgO for the activation of CCl_4 to form the metal chloride at 425 °C,[5] therefore, the first step in the reaction mechanism would readily occur. Moreover, the replacement of Cl^- ions by CO_3^{2-} ions on $BaO/BaCl_2$ can even take place at 25 °C, albeit slowly. It appears that the formation of stable carbonates on CaO and BaO inhibits the catalytic reaction over the temperature range employed in this study. At a pressure of 2 Torr CO_2, the decomposition temperatures of $MgCO_3$, $CaCO_3$ and $BaCO_3$ are 430, 600 and 970 °C, respectively.[8]

In summary, it has been found that MgO is a catalyst that promotes the reaction of CCl_4 with H_2O to yield CO_2 and HCl. For environmental purposes, the HCl could be easily removed from an effluent stream.

Notes and references

1 J. Josephson, *Environ. Sci. Technol.*, 1984, **18**, 222A; S. L. Huang and L. D. Pfefferle, *Environ. Sci. Technol.*, 1989, **23**, 1085.
2 J. J. Spivey, *Ind. Eng. Chem. Res.*, 1987, **26**, 2165; S. Chatterjee and H. L. Greene, *J. Catal.*, 1991, **130**, 76.
3 G. R. Lester, *US Pat.*, 5 176 897, 1993.
4 I. Fells and E. A. Moelwyn-Hughes, *J. Chem. Soc.*, 1959, 398.
5 B. M. Weckhuysen, G. Mestl, M. P. Rosynek, T. R. Krawietz, J. F. Haw and J. H. Lunsford, *J. Phys. Chem. B*, 1998, **102**, 3773.
6 P. D. Hooker and K. J. Klabunde, *Environ. Sci. Technol.*, 1994, **28**, 1243.
7 D. Wang, M. P. Rosynek and J. H. Lunsford, *J. Catal.*, 1995, **151**, 155.
8 *Treatise on Inorganic Chemistry*, ed. H. Remy, Elsevier, Amsterdam, 1956, vol. 1.

Communication a909552g

Unusually high cation-induced fluorescence enhancement of a structurally simple intrinsic fluoroionophore with a donor–acceptor–donor constitution†

Knut Rurack,*[ab] Wolfgang Rettig[b] and Ute Resch-Genger[a]

[a] *Federal Institute for Materials Research and Testing (BAM), Richard-Willstaetter Str. 11, D-12489 Berlin, Germany. E-mail: knut.rurack@bam.de*

[b] *Institute of Physical and Theoretical Chemistry, Humboldt-University Berlin, Bunsenstr. 1, D-10117 Berlin, Germany*

Received (in Liverpool, UK) 16th December 1999, Accepted 4th February 2000

Upon cation complexation, donor–acceptor–donor–substituted intrinsic fluoroionophore 3 shows red-shifted emission spectra accompanied by an extraordinarily high fluorescence enhancement.

Ionically controlling the fluorescence of molecular systems which contain an ion-sensitive receptor as an integral part of their signal generating fluorophore is of particular interest in fluorometric analysis.[1] These so-called intrinsic fluoroionophores usually combine an electron rich donor (D) as the ion-sensitive receptor and an electron acceptor unit (A) in a π-conjugated D–A arrangement.[2] Many such compounds are known including, *e.g.* styryl or stilbene dyes.[3] In highly polar solvents often encountered in sensing applications, the spectroscopic behaviour of such dyes is usually governed by an intramolecular charge transfer (ICT) process which leads to broad, structureless, and largely Stokes-shifted absorption and emission bands.[2,3] Upon cation binding to the receptor (= donor, R_D), strong hypsochromic shifts in absorption are found but the corresponding effects in emission are rather small.[2,3] The latter behaviour has been attributed to a decoordination reaction in the excited complex as a consequence of the ICT process, where a shift of negative charge from R_D to A leads to electrostatic repulsion between cation and formally positively charged donor.[4] Owing to complexation-induced fluorescence intensity changes as well as spectral shifts, these dyes are advantageous in terms of spectral discrimination as compared to PET (photoinduced electron transfer) systems[5] with electronically decoupled fluorophore and receptor. However, besides small shifts in emission the main disadvantage of intrinsic fluoroionophores is the relatively small change in fluorescence intensity (usually factors ≤5) upon ion binding.

In order to circumvent the problem of cation decoordination in the excited state and thus to achieve stronger shifts in emission, other design concepts were realized including D–D-substituted sensor molecules (*e.g.* **1**) as well as compounds with a D–A–D arrangement (*e.g.* **2**). Unfortunately, cation complexation to **1** resulted in fluorescence quenching[3c] unfavourable in terms of a high signal output and complex specific fluorescence lifetimes and **2** is already moderately fluorescent (ϕ_f = 0.33) in the uncomplexed state.[3a] As was shown in various mechanistical studies of such dyes,[6] the excited state reaction mechanism involves several emissive and non-emissive conformers, closely related to the theory of so-called twisted intramolecular charge transfer (TICT) and biradicaloid states.[7] Upon complexation, the change in fluorescence yield critically depends on the change of the relative energetic positions of the excited species involved and thus on the rate constants of the competing reactions from planar emissive locally excited E* to a highly polar single-bond-twisted species

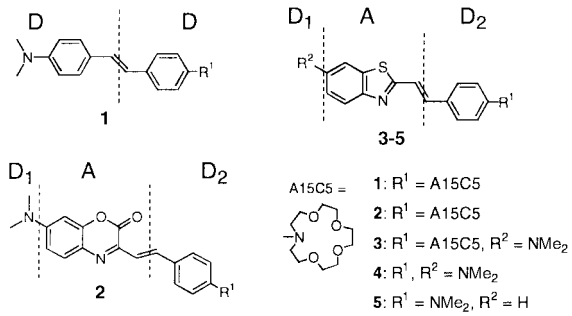

A* or to a non-emissive and weakly polar double-bond-twisted conformer P* of biradicaloid nature (three-state-model, Scheme 1).[6,7] Since for **2**, efficient formation of an emissive A* state is responsible for the moderate fluorescence in the uncomplexed dye in polar solvents,[3a,6a] reducing the acceptor strength promised to decrease the energy gap between emissive A* and quenching P* state and thus promised to lead to higher cation-induced fluorescence enhancement. With this in mind we designed the D–A–D fluoroionophore **3**.

Introduction of the electron donating dimethylamino group to the benzothiazole acceptor leads to slight shifts in both absorption (bathochromic) and emission (hypsochromic) accompanied by an increase in fluorescence quantum yield and lifetime (**4** *cf.* **5**, Table 1). A similar behaviour has been previously found for 4,4′-bis(dimethylamino)stilbene[6b] and corresponding 4-(dimethylamino)stilbene[6c] and quantum chemical calculations performed in analogy to those reported in ref. 6(*b*) support the validity of this model for **4** and **5**.[8] Based on the differences in bulkiness and donor strength of the two alkylated amino substituents, **3** and **4** show very similar spectroscopic properties and a slightly higher fluorescence yield in the case of **3** (Table 1).

Upon cation addition, the absorption band is slightly blue-shifted (Fig. 1) and the isosbestic points found in a titration indicate the formation of 1 : 1 complexes. This is supported by the fits of the titration data yielding complex stability constants in a range characteristic for neutral ICT fluoroionophores.[2,3] Concerning the cation-induced effects in fluorescence, **3** combines a red shift of the emission spectrum (Fig. 1) with extraordinarily high fluorescence enhancement factors (FEF),

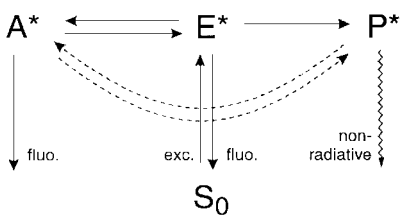

Scheme 1 Three-state-model involving multiple emissive states (A*, E*). E* is the planar conformer, A* corresponds to the different single-bond-twisted conformers and P* to the double-bond-twisted conformers.

† Electronic supplementary information (ESI) available: experimental details including synthesis of **3**–**5**, optical spectroscopy and the determination of complex stability constants. See http://www.rsc.org/suppdata/cc/a9/a909899b/

DOI: 10.1039/a909899b

Table 1 Spectroscopic data for **3** and its cation complexes **4** and **5** in acetonitrile at room temperature[a]

	λ_{abs}/nm	λ_{em}/nm	FEF[b]	τ_f/ns	log K_s[c]
3	409	502	1	0.19	—
3 ⊂ Li^I	399	517	4.4	1.12	2.96
3 ⊂ Na^I	396	522	9.6	1.98	2.43
3 ⊂ K^I	405	511	2.6	1.48	n.d.[d]
3 ⊂ Mg^{II}	395	541	26.7	2.87	2.98
3 ⊂ Ca^{II}	397	537	31.8	3.20	4.52
3 ⊂ Sr^{II}	397	534	26.7	3.12	3.67
3 ⊂ Ba^{II}	396	532	28.5	3.03	3.71
4	406	505	0.67	0.14	—
5	395	511	0.22	0.06	—

[a] *Experimental conditions*: see caption to Fig. 1, λ_{exc} = 425 nm for time-resolved fluorometry. [b] FEF relative to **3** (ϕ_f = 0.027). [c] K_s = Complex stability constant ($dm^3\ mol^{-1}$). [d] Not determined.

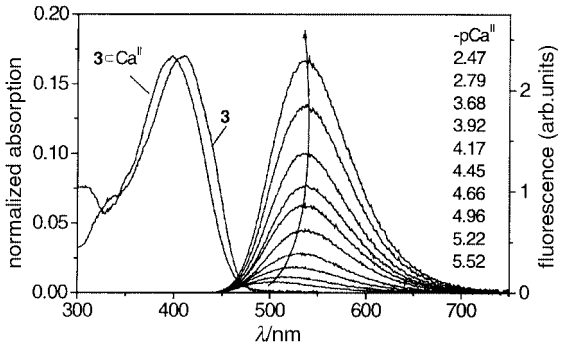

Fig. 1 Absorption spectra of **3** and **3** ⊂ Ca^{II} and fluorometric titration spectra of **3** and $Ca(ClO_4)_2$ in acetonitrile (c_{probe} = 1 × 10^{-6} M; λ_{exc} = 406 nm; $-pCa^{II}$ = $-\log c_{Ca}$ of the titration steps indicated in the plot).

normally only found for electronically decoupled PET systems,[5] and cation specific fluorescence lifetimes (Table 1).

These analytically favourable effects can be understood on the basis of the three-state-model introduced above. For **1**, the D–D substitution pattern is turned into a D–A pattern upon ion binding (Scheme 2), exemplified by a red shift in emission, and the decrease in fluorescence yield in the order of **1** > **1** ⊂ Ca^{II} > 4-dimethylamino-4′-cyanostilbene,[9] correlates with the increase in acceptor strength and should mainly be related to the relative energetic positions of E*, A* and P*.[6b,9] As follows from the blue-shifted emission band of **2** ⊂ Ca^{II}, complexation to **2** decreases the strength of D_2 (Scheme 2) slowing down the formation of (probably less) emissive A* and leads to enhanced emission owing to more efficient formation of an ICT state of planar conformation involving partial charge transfer from D_1 to A.[6a] This was also observed for highly fluorescent D–A(–A) benzoxazinone dyes with R^1 = H[6a] or CHO.[10] Accordingly, for **3** ⊂ $M^{I/II}$ the bathochromic shift in emission suggests the conversion of D_2 into an acceptor yielding a D_1–A–A_2 pattern (Scheme 2) and radiative deactivation of such a highly emissive

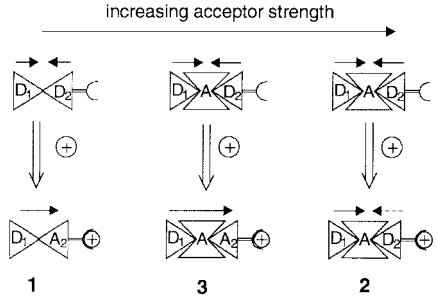

Scheme 2 Change of donor and acceptor strength upon complexation (arrows indicate CT interactions).

CT species successfully competes with any quenching channel (P*) restoring the fluorescence as a function of the charge density of the metal ion bound.

In summary, we have shown for the first time that efficient complexation-induced 'switching on' of the fluorescence can be achieved for simple intrinsic fluoroionophores by careful tuning of the donor–acceptor substitution pattern.

We gratefully acknowledge the financial support by the Deutsche Forschungsgemeinschaft.

Notes and references

1 A. W. Czarnik, *Chem. Biol.*, 1995, **2**, 423.
2 B. Valeur, *Probe design and chemical sensing*, ed. J. R. Lakowicz, 1994, Plenum, New York, p. 21.
3 (*a*) S. Fery-Forgues, M.-T. Le Bris, J.-P. Guetté and B. Valeur, *J. Phys. Chem.*, 1988, **92**, 6233; (*b*) J.-F. Létard, R. Lapouyade and W. Rettig, *Pure Appl. Chem.*, 1993, **65**, 1705; (*c*) S. Delmond, J.-F. Létard, R. Lapouyade, R. Mathevet, G. Jonusauskas and C. Rullière, *New J. Chem.*, 1996, **20**, 861; (*d*) I. K. Lednev, T.-Q. Ye, R. E. Hester and J. N. Moore, *J. Phys. Chem. A*, 1997, **101**, 4966; (*e*) S. I. Druzhinin, M. V. Rusalov, B. M. Uzhinov, S. P. Gromov, S. A. Sergeev and M. V. Alfimov, *J. Fluoresc.*, 1999, **9**, 33.
4 M. M. Martin, P. Plaza, Y. H. Meyer, F. Badaoui, J. Bourson, J.-P. Lefèvre and B. Valeur, *J. Phys. Chem.*, 1996, **100**, 6879; R. Mathevet, G. Jonusauskas, C. Rullière, J.-F. Létard and R. Lapouyade, *J. Phys. Chem.*, 1995, **99**, 15709.
5 R. A. Bissell, A. P. de Silva, H. Q. N. Gunaratne, P. L. M. Lynch, G. E. M. Maguire, C. P. McCoy and K. R. A. S. Sandanayake, *Top. Curr. Chem.*, 1993, **168**, 223.
6 (*a*) S. Fery-Forgues, M.-T. Le Bris, J.-C. Mialocq, J. Pouget, W. Rettig and B. Valeur, *J. Phys. Chem.*, 1992, **96**, 701; (*b*) J.-F. Létard, R. Lapouyade and W. Rettig, *Chem. Phys. Lett.*, 1994, **222**, 209; (*c*) J.-F. Létard, R. Lapouyade and W. Rettig, *J. Am. Chem. Soc.*, 1993, **115**, 2441.
7 W. Rettig, *Top. Curr. Chem.*, 1994, **169**, 253.
8 K. Rurack, J. L. Bricks, J. L. Slominskii, U. Resch-Genger and W. Rettig, to be submitted.
9 R. Lapouyade, K. Czeschka, W. Majenz, W. Rettig, E. Gilabert and C. Rullière, *J. Phys. Chem.*, 1992, **96**, 9643.
10 M.-T. Le Bris, J. Mugnier, J. Bourson and B. Valeur, *Chem. Phys. Lett.*, 1994, **106**, 124.

Communication a909899b

ChemComm

Synthesis of optically active *N*-hydroxylamines by asymmetric hydrogenation of nitrones with iridium catalysts

Shun-Ichi Murahashi,* Teturou Tsuji and Shuichi Ito

Department of Chemistry, Graduate School of Engineering Science, Osaka University, 1-3 Machikaneyama, Toyonaka, Osaka 560-8531, Japan. E-mail: mura@chem.es.osaka-u.ac.jp

Received (in Cambridge, UK) 21st December 1999, Accepted 2nd February 2000

Asymmetric hydrogenation of nitrones with the iridium catalyst system, prepared from $[IrCl(cod)]_2$, (*S*)-BINAP, and $NBu^n_4BH_4$, gives the corresponding *N*-hydroxylamines, which are important as biologically active compounds and precursors of amines, with high enantioselectivity (up to 86% ee).

Optically active *N*-hydroxylamines are of interest as biologically active compounds,[1] naturally occurring compounds,[2] and precursors of chiral amino compounds. A catalytic method for synthesis of these compounds is limited to the ruthenium-catalyzed asymmetric hydrosilylation of nitrones.[3] To explore more convenient and economical methods, we pursued the catalytic hydrogenation of nitrones which are obtained readily by catalytic oxidation of secondary amines with hydrogen peroxide.[4] We report herein asymmetric hydrogenation of nitrones with iridium catalysts to give optically active *N*-hydroxylamines. As shown in Scheme 1, catalytic oxidation of amines **1**, followed by catalytic asymmetric hydrogenation of nitrones **2** thus formed provides an efficient and useful route for synthesis of optically active *N*-hydroxylamines **3**. Furthermore, optically active secondary amines **4** can be prepared upon catalytic reduction of **3**.

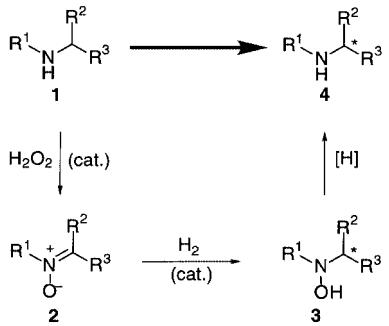

Scheme 1 Catalytic asymmetric synthesis of chiral amino compounds.

This method is particularly convenient and useful because of the configurational stability of nitrones, ease of handling, and readiness of preparation. Although asymmetric hydrogenation of imines with homogeneous catalysts has been studied extensively,[5] neither asymmetric nor simple hydrogenation of nitrones with homogeneous catalysts are, to our knowledge, known.

We examined the catalytic activity of metal complexes for the hydrogenation of configurationally pure (*E*)-*N*-[1-(4-chlorophenyl)ethylidene]methylamine *N*-oxide **5a**, whose stereochemistry was determined by NOE experiments [eqn. (1)]. When ruthenium complexes were used as catalysts, no hydrogenation occurred. This may be due to the strong affinity of nitrones for ruthernium complexes. Iridium and rhodium complexes, however, showed catalytic activity.

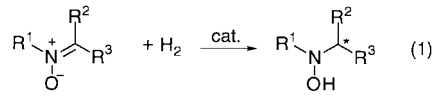

a; R^1=R^3=Me, R^2=4-ClC_6H_4
b; R^1=R^3=Me, R^2=Ph
c; R^1=R^3=Me, R^2=4-BrC_6H_4
d; R^1=R^3=Me, R^2=3-ClC_6H_4
e; R^1=R^3=Me, R^2=2-ClC_6H_4
f; R^1=R^3=Me, R^2=2-naphthyl
g; R^1=$PhCH_2$, R^2=Me, R^3=Ph

Metal complex catalysts bearing the BINAP [2,2′-bis(diphenylphosphino)-1,1′-binaphthyl] ligand[6] were examined for asymmetric hydrogenation and results are summarized in Table 1. Enantioselectivity was not observed with rhodium catalysts such as $[RhCl(cod)]_2$/(*S*)-BINAP or [Rh{(*S*)-BINAP}(cod)]-ClO_4 (entries 1 and 2). The cationic iridium catalyst, 2.0 mol% [Ir{*R*)-BINAP}(cod)]BF_4 is less reactive, and the enantioselectivity obtained was 27% ee (entry 3). The neutral iridium catalyst, 1.0 mol% $[IrCl(cod)]_2$/(*S*)-BINAP (1.0 : 2.2 mol/mol) gave *N*-hydroxylamine (*R*)-**6a** in 69% yield with 40% ee (entry 4).

These results indicate that iridium catalysts are promising and the ligand coordinated to the iridium plays an important role in the face discrimination of nitrones. A systematic study of neutral iridium catalysts revealed that catalyst systems obtained by treatment of the $[IrCl(cod)]_2$/(*S*)-BINAP complex with hydride sources such as $NBu^n_4BH_4$ or $NaBH_4$ gave higher reactivity and enantioselectivity. The highest enantioselectivity was obtained, when the iridium catalyst system, prepared from 1.0 mol% $[IrCl(cod)]_2$/(*S*)-BINAP/$NBu^n_4BH_4$ (1.0 : 2.2 : 2.0 mol/mol) *in situ*, was used at 0 °C (*R*)-**6a**, 82%, 83% ee, entry 5).† The absolute configuration of **6a** was determined to be *R* by comparison of the optical rotation of the secondary amine derived from **6a** with the reported data.[7] The opposite enantiomer (*S*)-**6a** was obtained, when (*R*)-BINAP was used as a ligand. In this reaction, hydrogen pressure did not affect the enantioselectivity in the range 1–80 kg cm^{-2}. The effect of the solvent on the enantioselectivity is dramatic with THF found to

Table 1 Asymmetric hydrogenation of nitrone **5a** with iridium and rhodium complex catalysts[a]

Entry	Catalyst	Yield[b] (%)	Ee[c] (%)	Configuration
1	$[RhCl(cod)]_2$/(*S*)-BINAP[d]	8[f]	2	—
2	[Rh{(*S*)-BINAP}(cod)]ClO_4[e]	33[f]	0	—
3	[Ir{(*R*)-BINAP}(cod)]BF_4[e]	36	27	(*S*)
4	$[IrCl(cod)]_2$/(*S*)-BINAP[d]	69	40	(*R*)
5	$[IrCl(cod)]_2$/(*S*)-BINAP/$NBu^n_4BH_4$[d]	85 82[g]	73 83[g]	(*R*) (*R*)

[a] Reactions were carried out in the presence of the metal catalyst at 22 °C in THF under hydrogen (80 kg cm^{-2}) for 18 h. [b] Isolated yield. [c] The optical yields were determined by HPLC analysis using a DAICEL CHIRALPAK AD column. [d] 1.0 mol%. [e] 2.0 mol%. [f] Solvent is benzene–methanol (1 : 1). [g] Reaction carried out at 0 °C.

DOI: 10.1039/a909927l

Table 2 Asymmetric hydrogenation of nitrones with $[IrCl(cod)]_2$/(*S*)-BINAP/$NBu^n_4BH_4$ catalyst system[a]

Entry	Nitrone[b]	Yield[c] (%)	Ee[d] (%)	Configuration[e]
1	**5a**	82	83	(*R*)
2	**5b**	45	69	(*R*)
3	**5c**	76	86	(+)
4	**5d**	68	81	(+)
5	**5e**	17	78	(−)
6	**5f**	64	80	(+)
7[f]	**5g**	78	75	(*R*)

[a] Reactions were carried out in THF at 0 °C under hydrogen (80 kg cm^{-2}) for 18 h in the presence of catalyst. The catalyst was prepared by mixing $[IrCl(cod)]_2$ (1.0 mol%), (*S*)-BINAP (2.2 mol%), and $NBu^n_4BH_4$ (2.0 mol%). [b] Nitrones were configurationally pure. The stereochemistry was determined by NOE experiments. [c] Isolated yield. [d] The optical yields were determined by HPLC analyses using chiral columns. **5a**, **c**–**f**: CHIRALPAK AD, **5b**: CHIRALCEL OD-H, **5g**: CHIRALCEL OJ. [e] See text. [f] Reaction carried out at 22 °C

be best.† Toluene led to moderate enantioselectivity while methanol and dichloromethane gave poor results.

Various nitrones can be hydrogenated enantioselectively with the $[IrCl(cod)]_2$/(*S*)-BINAP/$NBu^n_4BH_4$ catalyst system (Table 2). In the reaction of (*E*)-*N*-1-(arylethylidene)methylamine *N*-oxides, the reactivity and enantioselectivity are increased noticeably by introduction of an electron-withdrawing group on the aryl group. The hydrogenation of nitrones bearing *para*- and *meta*-halogens, **5c** and **5d**, proceeded smoothly to give the corresponding *N*-hydroxylamines with enantioselectivity of 86 and 81% ee, respectively (entries 3 and 4). However, the hydrogenation of *ortho*-chlorinated compound **5e** proceeded slowly (entry 5). The hydrogenation of nitrone **5f** bearing a naphthyl group at the α-position of nitrogen gave the corresponding *N*-hydroxylamine with 80% ee (entry 6). The *N*-benzyl substituted nitrone **5g** was hydrogenated with 75% ee (entry 7). The absolute configurations of **6b**[7] and **6g**[5j] were determined to be *R*.

We prepared $[IrH(\eta^1,\eta^3\text{-}C_8H_{12})\{(S)\text{-BINAP}\}]$ **7** in 59% yield from $[IrCl(cod)]_2$, (*S*)-BINAP and KOH in methanol–benzene (1 : 1). Under the conditions of hydrogenation, the C_8H_{12} group of **7** is reduced to cyclooctane, and complex **7** would be converted to $[IrH\{(S)\text{-BINAP}\}(THF)_n]$. Using complex **7** as a catalyst for the hydrogenation of **5a** led to *N*-hydroxylamine **6a** with 86% ee (*R*). This result is comparable to the 83% ee (*R*) obtained with the $[IrCl(cod)]_2$/(*S*)-BINAP/$NBu^n_4BH_4$ catalyst system above, indicating that iridium–hydride species appear to form from $[IrCl(cod)]_2$/(*S*)-BINAP/$NBu^n_4BH_4$ mixtures and lead to high enantioselectivity for asymmetric hydrogenation of nitrones.

This work was supported by Research for the Future program, the Japan Society for the Promotion of Science.

Notes and references

† *Typical experimental procedure*: a Schlenk flask was charged with $[Ir(cod)Cl]_2$ (3.4 mg, 0.0050 mmol), (*S*)-BINAP (6.8 mg, 0.011 mmol), $NBu^n_4BH_4$ (2.6 mg, 0.010 mmol) and degassed THF (2.5 mL) under argon atmosphere and the mixture stirred for 15 min at room temperature. The solution of the catalyst was transferred to an autoclave, and (*E*)-*N*-[1-(4-chlorophenyl)ethylidene]methylamine *N*-oxide **5a** (92.2 mg, 0.50 mmol) added under argon. The argon gas in the autoclave was replaced by hydrogen in three cycles (20 kg cm^{-2}) and finally pressurized with hydrogen to 80 kg cm^{-2}. The mixture was stirred at 0 °C for 18 h. After the autoclave was vented and opened, the reaction mixture was transferred to a flask. The solvent was evaporated under reduced pressure. The product was purified by SiO_2 column chromatography (**6a**; 76.1 mg, 0.41 mmol, 82% yield). The enantiomeric excess was determined to be 83% by HPLC using a DAICEL CHIRALPAK AD. Optically pure *N*-hydroxylamine **6a** was obtained by recrystallization from acetone {**6a**, mp 97.5–98 °C, $[\alpha]_D$ +50.0 (c = 1.00, EtOH)}. The corresponding optically pure secondary amine was obtained by treatment of optically pure **6a** with molecular hydrogen over a palladium catalyst or by treatment with zinc/HCl.

1 S. Pan, J. Wang and K. Zhao, *J. Org. Chem.*, 1999, **64**, 4; H. C. J. Ottenheijm and J. D. M. Herscheid, *Chem. Rev.*, 1986, **86**, 697.
2 J. Clardy, J. P. Springer, G. Büchi, K. Matsuo and R. Wightman, *J. Am. Chem. Soc.*, 1975, **97**, 663; G. Büchi, K. C. Luk, B. Kobbe and J. M. Townsend, *J. Org. Chem.*, 1977, **42**, 244.
3 S.-I. Murahashi, S. Watanabe and T. Shiota, *J. Chem. Soc., Chem. Commun.*, 1994, 725.
4 S.-I. Murahashi, H. Mitsui, T. Shiota, T. Tsuda and S. Watanabe, *J. Org. Chem.*, 1990, **55**, 1736; S.-I. Murahashi, T. Shiota and Y. Imada, *Org. Synth.*, 1992, **70**, 265; S.-I. Murahashi and T. Shiota, *Tetrahedron Lett.*, 1987, **28**, 2383; S.-I. Murahashi, T. Oda and Y. Masui, *J. Am. Chem. Soc.*, 1989, **111**, 5002.
5 Rh: (*a*) J. Bakos, I. Tóth, B. Heil and L. Markó, *J. Organomet. Chem.*, 1985, **279**, 23; (*b*) G. J. Kang, W. R. Cullen, M. D. Fryzuk, B. R. James and J. P. Kutney, *J. Chem. Soc., Chem. Commun.*, 1988, 1466; (*c*) A. G. Becalski, W. R. Cullen, M. D. Fryzuk, B. R. James, G. J. Kang and S. J. Rettig, *Inorg. Chem.*, 1991, **30**, 5002. Ir: (*d*) F. Spindler, B. Pugin and H. U. Blaser, *Angew. Chem., Int. Ed. Engl.*, 1990, **29**, 558; (*e*) Y. N. C. Chan and J. A. Osborn, *J. Am. Chem. Soc.*, 1990, **112**, 9400; (*f*) T. Morimoto and K. Achiwa, *Tetrahedron: Asymmetry*, 1995, **6**, 2661; (*g*) K. Tani, J. Onouchi, T. Yamagata and Y. Kataoka, *Chem. Lett.*, 1995, 955; (*h*) P. Schnider, G. Koch, R. Prétôt, G. Wang, F. M. Bohnen, C. Krüger and A. Pfaltz, *Chem. Eur. J.*, 1997, **3**, 887; (*i*) H.-U. Blaser and F. Spindler, *Comprehensive Asymmetric Catalysis*, ed. E. N. Jacobsen, A. Pfaltz and H. Yamamoto, Spingler, Berlin, 1999, vol. 3, p. 1427; Ti: (*j*) C. A. Willoughby and S. L. Buchwald, *J. Am. Chem. Soc.*, 1994, **116**, 8952.
6 R. Noyori and H. Takaya, *Acc. Chem. Res.*, 1990, **23**, 345.
7 S. Takenaka and M. Koden, *J. Chem. Soc., Chem. Commun.*, 1978, 830.

Communication a909927l

Model studies towards carbohydrate–base pair recognition. Relevance of hydrogen–bonding cooperativity

Manuela López de la Paz,[a] Carlos González[b] and Cristina Vicent*[a]

[a] *Departamento de Química Orgánica Biológica, Instituto de Química Orgánica, CSIC, Juan de la Cierva 3, E-28006 Madrid, Spain. E-mail: iqocv18@iqog.csic.es*

[b] *Instituto de Estructura de la Materia, CSIC, Serrano 119, 28006 Madrid, Spain*

Received (in Cambridge, UK) 16th December 1999, Accepted 3rd February 2000

The importance of intramolecular OH···OH hydrogen-bonds (H-bonds) in the effective molecular recognition of carbohydrates is highlighted; specifically, the 1,3-*cis*-diaxial H-bonded OH groups of 1 are shown to provide an efficient binding motif for bidentate coordination of the amino-carbonyl Hoogsteen site of the CG base-pair through the formation of two cooperative intermolecular H-bonds; this result suggests that intramolecularly H-bonded carbohydrate OH groups may be considered as multidentate units able to H-bond cooperatively.

Deoxygenated oligosaccharides which are present in natural products[1] and aminoglycoside antibiotics[2] are known to directly interact with a number of DNA and RNA sequences, respectively. However there is limited structural information on the molecular basis of such a saccharide–nucleic acid recognition in solution.[3]

The design of many low molecular weight nucleic acid ligands has been based on hydrogen-bonding (H-bonding) recognition of the Hoogsteen sites of the B-DNA grooves.[4] One of the most important characteristics of multiple H-bonded complexes is the non-additivity of the H-bonds therein; this property has given rise to the concept of cooperativity.[5] As part of a general project to study H-bonding cooperativity and its implications in the molecular recognition of carbohydrates, we present here our initial effort to use H-bonding cooperativity to efficiently bind sugars in the grooves of B-DNA.

Carbohydrate 1,2- and 1,3-diol motifs are present in many DNA and RNA binders.[1] We have previously demonstrated that the hydroxy groups of the 1,3-*cis*-diaxial diol **1** are intramolecularly H-bonded (OH-2→OH-4); the presence of this H-bond polarizes the σ O-H bonds and enhances the donor ability of OH-4 and acceptor ability of OH-2 [Fig. 1(a)].[6]

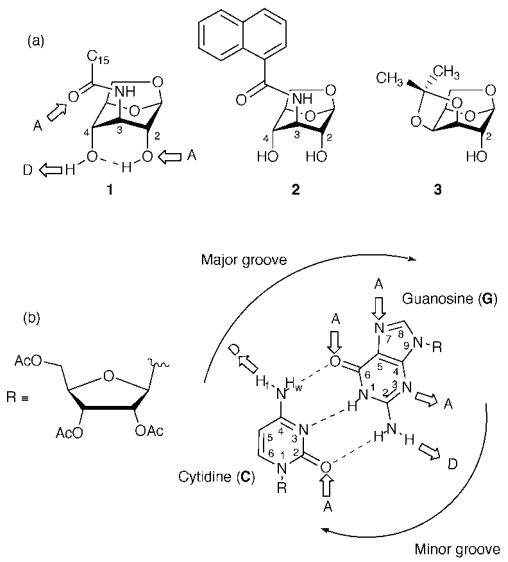

Fig. 1 Carbohydrate-derivatives and **CG** base-pair used in the binding studies.

Molecular modelling studies of the carbohydrate-derivative **1** and the cytidine–guanosine (**CG**) base-pair indicate that the hydroxy groups of **1** are suitably positioned to bridge both amino-carbonyl Hoogsteen binding sites of **CG** in a bidentate fashion [Fig. 1(b)]. A sugar–**CG** complex† could potentially be stabilized by two cooperative intermolecular H-bonds (Fig. 2); this would provide the first example of H-bonding cooperativity in carbohydrate-base pair recognition.

For the reasons outlined above, the binding of **1** to **CG** has been investigated.‡ Binding studies were performed by titrating **1** (0.08 mM) with an equimolar mixture of tri-*O*-acetylguanosine (**G**) and tri-*O*-acetylcytidine (**C**) (2 mM).[7]§ Under these experimental conditions only a 1 : 1 complex of the diol **1** and **CG** could be expected. The titration data were fitted to a 1 : 1 binding model, taking into account the dimerization of **CG** (Table 1).[8]¶ The measured association constant‖ for the **1–CG** complex was 1491 M^{-1}. The binding of the aromatic diol **2** to **CG** was also studied in the same way with the expectation of observing induced chemical shifts of the naphthyl proton resonances and thereby obtaining more data for model fitting. $\Delta G°$ values for the **1–CG** (-4.4 ± 0.1 kcal mol^{-1}) and **2–CG** (-4.2 ± 0.1 kcal mol^{-1}) complexes were greater than expected for a complex stabilized by a single H-bond, or two isolated H-bonds. This result implies the interplay of cooperative H-bonding in **1–CG** and **2–CG** recognition.

To quantify the effect of H-bonding cooperativity on the stabilization of the **1–CG** complex, it is necessary to know the number of intermolecular H-bonds formed between **1** and **CG**. ^{1}H NMR variable temperature experiments, NOESY, and deuterium exchange experiments were carried out with the aim of determining structural information.

The hydroxy proton resonances of **1** were deshielded upon complexation with **CG**, which indicates that the binding process is mediated by H-bonding of both OH groups of the carbohydrate (Table 2). In contrast, the amide proton (NH-3) of diol **1**

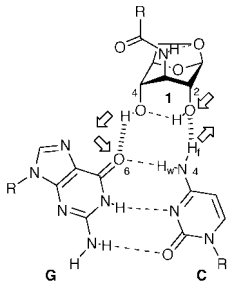

Fig. 2 Schematic representation of the complex formed by the carbohydrate **1** and the **CG** base-pair.

Table 1 Stability parameters of the interaction between the **CG** base-pair and the carbohydrate derivatives **1**–**3** (299 K, $CDCl_3$)

Compound	**1**	**2**	**3**
K_a/M^{-1}	1491	1091	6.7
$\Delta G°$/kcal mol^{-1}	-4.4 ± 0.1	-4.2 ± 0.1	-1.1 ± 0.1

Table 2 $\Delta\delta/\Delta T$ of the exchangeable resonances of **1** in the free and bound state to the **CG** base-pair[a]

Resonance of **1**	$\Delta\delta/\Delta T$ (**1**)[b]/ppb K^{-1}	$\Delta\delta/\Delta T$ (**1–CG**)[c]/ppb K^{-1}
OH-4	−5.2	−13.2
OH-2	−2.8	−6.8
NH-3	−2.9	−4.5

[a] Measured between 293–318 K. [b] [**1**] = 1.1 × 10^{-4} M. [c] [**1**] = 1.1 × 10^{-4} M; [**CG**] = 1.5 × 10^{-3} M (**1**:**CG** = 1:13).

showed minimal displacement on complexation. According to previous reports,[6a,9] comparison of $\Delta\delta/\Delta T$ of the OH resonances of the free ligand **1** and the **1–CG** complex also implies that both OH groups are involved in intermolecular H-bonds (Table 2).

NOESY spectra of mixed samples of **1** and **CG** in different ratios** revealed cross peaks between the OH proton resonances of **1** and the exchangeable protons of **CG**; these could not unambiguously be attributed to chemical exchange or intermolecular NOEs. However, the same experiments showed that the **C**(N^4–H)$_f$ proton resonates at lower field in the presence of a higher concentration of diol **1**, which further suggests its involvement in H-bonding with **1**.

Additional evidence for the preferred complexation site of **CG** was obtained by deuterium exchange experiments. An equal quantity of deuterated diol **1** (**1**–D) was added to separate samples of **CG** (experiment A: **CG** 2 mM) and **1**:**CG** in a 2:1 ratio (experiment B: **1**:**CG** 4 mM:2 mM), to facilitate the formation of the hypothetical 1:2 **CG**:**1** complex. In each case a control experiment was carried out (experiment A: **CG** 2 mM; experiment B: **1**:**CG** 4 mM:2 mM). ^{1}H-NMR spectra were acquired at t = 0 and 17 days. Both samples containing **1**–D showed complete H–D exchange of the **C** amino protons after 17 days, while the amino protons of **G** were only partially deuterated after the same period of time. In the control experiments a small and comparable decrease in the signal intensity of all the exchangeable **CG** protons was observed. From this result we infer that on average the **C**-amino group is in contact with the deuterated hydroxy groups of **1**–D for longer than the amino protons of **G**, and that a 1:1 **1–CG** complex is favoured over a 2:1 **1–CG** complex, which is in agreement with the Job plot determined stoichiometry.¶

Molecular modelling[11] of the **1–CG** complex supported the results of our ^{1}H-NMR experiments and confirmed that the carbonyl group **G**(C^6-O) is the H-bond acceptor best located to form a second H-bond to OH-4 of **1** .†† The calculated **1–CG** structure also showed that the non-exchangeable protons of the **1–CG** complex are very distant from each other, which could explain why only ambiguous intermolecular NOEs were detected.

To quantify the influence of the intramolecular OH-2→OH-4 H-bond on the formation of intermolecular H-bonds between **1** and **CG**, the complexation of monoalcohol **3** with **CG** was studied.‡‡ The K_a for the **3–CG** complex is 7 M^{-1} (Table 1); the formation of one H-bond between the monoalcohol **3** and the **CG** base-pair thus corresponds to a $\Delta G°$ value of −1.1 kcal mol^{-1}, while the $\Delta G°$ for two intermolecular H-bonds in the **1–CG** complex is more than four times greater than this value. This demonstrates that the formation of H-bonds between **1** and **CG** is non-additive (cooperative); furthermore the importance of intramolecular OH···OH H-bonds in the effective molecular recognition of carbohydrates is highlighted.

Our work has shown that in the future we may consider the intramolecularly H-bonded OH groups of carbohydrates as multidentate units capable of H-bonding cooperatively. Specifically, the 1,3-*cis*-diaxial relative configuration of carbohydrate OH groups serves in apolar medium as an efficient binding motif for bidentate coordination of the **C**(N^4–H)$_f$/**G**(C^6–O) site of **CG** through formation of two cooperative intermolecular H-bonds.

Financial support by DGES (Grant PB97–0832) and TMR (FMRX–CT98–0231) are acknowledged. M. L. P. is grateful to the Comunidad Autónoma de Madrid for a predoctoral fellowship. We thank Professor C. A. Hunter (University of Sheffield) for kindly providing the fitting program and Dr Joanne Hawley for critical reading of the manuscript.

Notes and references

† **C** (2',3',5'-tri-*O*-acetylcytidine) and **G** (2',3',5'-tri-*O*-acetylguanosine) were purchased (Sigma) and used without further purification. Carbohydrate-derivatives **1**, **2** and **3** were synthesized.[10] **1**–D was prepared by repeatedly dissolving **1** (1.4 mg, 3.5 mmol) in CD_3OD (5 × 0.5 mL) and evaporating to dryness. The deuterated residue (**1**–D) was dried under high vacuum and heated at 40 °C in the presence of P_2O_5 and dissolved in $CDCl_3$ (2 mL) to give a solution of concentration 1.8 mM.

‡ All binding studies were performed at 299 K using freshly prepared solutions in $CDCl_3$ which were always passed through basic alumina and collected over 4 Å molecular sieves prior to use; the alumina and molecular sieves employed were freshly activated by heating at 600 °C under high vacuum. Each experiment was carried out at least two times and $\Delta G°$ values were reproducible within ±0.1 kcal mol^{-1}.

§ The feasibility of this titration experiment relied on the high stability of the **CG** base-pair[7] in chloroform (K_a = 10^4–10^5 M^{-1}). The imino proton **G**(N^1–H) experienced minimal chemical shift displacement (upfield) upon complexation with **1** ($\Delta\delta$ < 0.1 ppm), which is consistent with the **CG** complex remaining intact during the titrations.[8a]

¶ The 1:1 stoichiometry of the complex **1**:**CG** was determined by a Job plot based on the chemical induced shifts of the hydroxy resonances. The **CG** base-pair dimerizes in chloroform.[8a] We have measured a dimerization constant of 55 M^{-1}.

‖ Reverse titration experiments (**CG** *vs.* **1**) were also performed. Fitting of the induced chemical shifts of the C(C^5–H) proton resonance to a 1:1 complexation model gave a value of K_a (1460 M^{-1}) which was in good agreement with the value determined experimentally from the **1** *vs.* **CG** titrations.

** NOESY spectra (500 ms, 278 K, 600 MHz) were recorded for two samples of different **1**:**CG** molar ratio: (i) **1**:**CG** 1:3, [**1**] = 6.7 × 10^{-4} M; [**CG**] = 2 × 10^{-3} M; (ii) **1**:**CG** 3:1, [**1**] = 6 × 10^{-3} M; [**CG**] = 2 × 10^{-3} M.

†† Molecular mechanics calculations were carried out using MM2[11a] (carbohydrates) and AMBER[11b] (nucleosides, CG base-pair and carbohydrate–CG complexes) with the GB/SA solvent model for chloroform.[11c] Molecular modelling of the complex involing the **C**(C=O) and **G**(N–N) of **CG** (minor groove of the base-pair) indicated that such a complex is not stable. This could be explained on the basis of steric hindrance of the acetylated ribose moieties.

‡‡ The use of **3** allowed us to evaluate the effect of a second OH in a 1,3-*cis*-diaxial relative configuration on the energetics of the recognition process between **1** and **CG**.

1 A. Kirschning, A. F. W. Bechthold and J. Rohr, *Bioorganic Chemistry Models and Applications*, ed. J. Rohr, Springer, Heidelberg, 1997, vol. 184, pp. 1–79.
2 U. von Ahsen and H. F. Noller, *Science*, 1993, **260**, 1501; M. L. Zapp, S. Stern and M. R. Green, *Cell*, 1993, **74**, 969; B. Clouet-d'Orval, T. K. Stage and O. C. Uhlenbeck, *Biochemistry*, 1995, **34**, 11 186.
3 K. C. Nicolaou, B. M. Smith, K. Ajito, H. Komatsu, L. Gómez-Paloma and Y. Tor, *J. Am. Chem. Soc.*, 1996, **118**, 2303; L. Jiang, A. K. Suri, R. Fiala and D. J. Patel, *Chem. Biol.*, 1997, **4**, 35.
4 P. E. Nielsen, *Chem. Eur. J.*, 1997, **3**, 505; S. White, J. W. Szewczyk, J. M. Turner, E. E. Baird and P. B. Dervan, *Nature*, 1998, **391**, 468.
5 H. S. Frank and W. Y. Wen, *Discuss. Faraday Soc.*, 1957, **24**, 133; G. A. Jefrey and W. Sainger, *Hydrogen Bonding in Biological Structures*, Springer-Verlag, Berlin, 1991, p. 569.
6 (*a*) M. López de la Paz, J. Jiménez–Barbero and C. Vicent, *Chem. Commun.*, 1998, 465; (*b*) F. J. Luque, J. M. López, M. López de la Paz, C. Vicent and M. Orozco, *J. Phys. Chem. A*, 1998, **102**, 6690.
7 Y. Kyogoku, R. C. Lord and A. Rich, *Biochim. Biophys. Acta*, 1969, **179**, 10.
8 (*a*) S. C. Zimmerman and P. Schmitt, *J. Am. Chem. Soc.*, 1995, **117**, 10 769; (*b*) N. Branda, G. Kurz and J.-M. Lehn, *Chem. Commun.*, 1996, 2443.
9 E. S. Stevens, N. Sugawara, G. M. Bonora and C. Toniolo, *J. Am. Chem. Soc.*, 1980, **102**, 7048.
10 M. López de la Paz, G. Ellis, S. Penadés and C. Vicent, *Tetrahedron Lett.*, 1997, **38**, 1659; C. W. Holzapfel, J. M. Koekemoer and C. F. Marais, *S. Afr. J. Chem.*, 1984, **37**, 19.
11 (*a*) N. L. Allinger, *J. Am. Chem. Soc.*, 1977, **99**, 8127; (*b*) S. J. Weiner, P. A. Kollman, D. T. Nguyen and D. A. Case, *J. Comput. Chem.*, 1986, **7**, 230; (*c*) W. C. Still, A. Tempczyk, R. C. Hawley and T. Hendrickson, *J. Am. Chem. Soc.*, 1990, **112**, 6127.

Communication a909878j

ChemComm

Chiral inclusion crystallization of tetra(*p*-bromophenyl)ethylene by exposure to the vapor of achiral guest molecules: a novel racemic-to-chiral transformation through gas–solid reaction

Koichi Tanaka,*[a] Daisuke Fujimoto,[a] Thomas Oeser,[b] Hermann Irngartinger[b] and Fumio Toda[c]

[a] *Department of Applied Chemistry, Faculty of Engineering, Ehime University, Matsuyama, Ehime 790-8577, Japan. E-mail: tanaka@en3.ehime-u.ac.jp*
[b] *Organisch-Chemisches Institut, Ruprecht-Kares-Universität, Heidelberg, Im Neuenheimer Feld 270, D-69120 Heidelberg, Germany*
[c] *Faculty of Science, Okayama University of Science, 1-1 Ridaicho, Okayama 700-0005, Japan*

Received (in Cambridge, UK) 14th December 1999, Accepted 7th February 2000

Racemic crystalline tetra(*p*-bromophenyl)ethylene was converted into chiral inclusion crystals in the solid state by contact with gaseous achiral guest compounds.

Chiral crystallization of achiral molecules in the absence of any external chiral source is of special interest not only for "so-called" absolute asymmetric synthesis[1] but also for its relationship to the prebiotic origin of chirality.[2] Such chiral crystals have been obtained previously during crystallization of achiral substrates from their solutions. We have now found that chiral inclusion crystals can be obtained by treatment of a racemic host compound with the vapor of achiral guest compounds. This is the first example of the formation of chiral inclusion crystals from achiral components through gas–solid inclusion complexation.

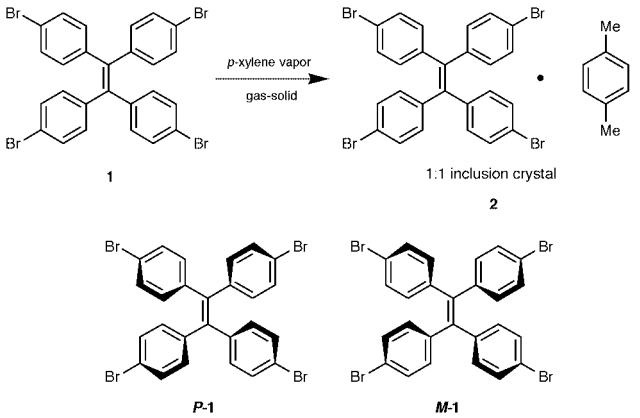

Recently, we have found that tetra(*p*-bromophenyl)ethylene **1**[3] forms chiral inclusion compounds with various kinds of achiral guest molecules. For example, recrystallization of **1** from *p*-xylene gave 1:1 inclusion crystals (**2**). The chiral arrangement of **1** molecules in **2** was easily detected by measurement of CD spectra of its Nujol mull. Hence, one single crystal of **2** showed a positive Cotton effect while another showed a negative Cotton effect (Fig. 1). The host compound **1** also formed chiral inclusion crystals with acetone (1:1), dioxane (1:1) and benzene (1:1), whereas it formed racemic inclusion crystals with cyclohexanone (1:1), THF (1:2), β-picoline (1:1) and toluene (1:1), by recrystallization (Table 1).

Very interestingly, however, when exposed to *p*-xylene vapor at room temperature for 24 h, a single crystal of pure **1** prepared by recrystallization from *m*-xylene was gradually changed into the chiral polycrystalline 1:1 inclusion complex (**2**) of **1** with *p*-xylene. The inclusion complex (**2**) thus obtained showed the same CD spectrum as that obtained by the recrystallization

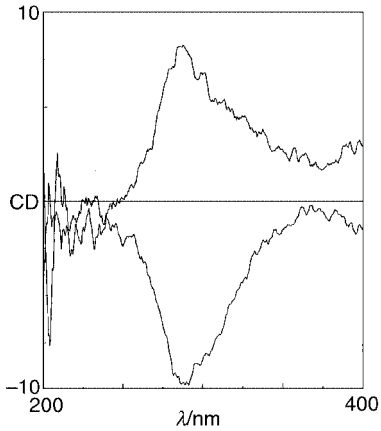

Fig. 1 CD spectra of the enantiomeric 1:1 inclusion crystals of **1** with *p*-xylene in Nujol mulls.

Table 1 Inclusion complexation of **1** with some guest compounds

	Inclusion complex				
	By recrystallization		By gas–solid reaction		
Guest	host:guest		host:guest		*t*/h
Acetone	chiral	1:2	—	—[a]	168
Cyclohexanone	*rac*	1:1	—	—[a]	168
THF	*rac*	1:2	chiral	1:2	2
1,4-Dioxane	chiral	1:1	chiral	1:1	24
Benzene	chiral	1:1	chiral	1:1	24
Toluene	*rac*	1:1	—	—[a]	168
p-Xylene	chiral	1:1	chiral	1:1	24
β-Picoline	*rac*	1:1	chiral	1:1	168

[a] No complexation occurred.

method, and its X-ray powder pattern was similar to that obtained by recrystallization (Fig. 2) Gas-solid reaction of **1** with THF, dioxane, benzene and β-picoline also produced their inclusion complexes with the same host–guest ratios as those obtained by recrystallization (Table 1). It is also remarkable that the inclusion crystals of **1** with THF and β-picoline obtained by gas–solid reaction were chiral, whereas those obtained by recrystallization were racemic. Gas–solid inclusion complexation did not occur, however, in the cases of acetone, cyclohexanone and toluene (Table 1). The chiral crystalline lattice formed by chiral arrangement of **1** molecules is very stable and still exists after removal of the guest molecules *via* heating compound **2** under reduced pressure. The chiral crystalline powder left after removal of the guest from **2** showed a very similar X-ray powder diffraction pattern to that of **2**. By

DOI: 10.1039/a909782a

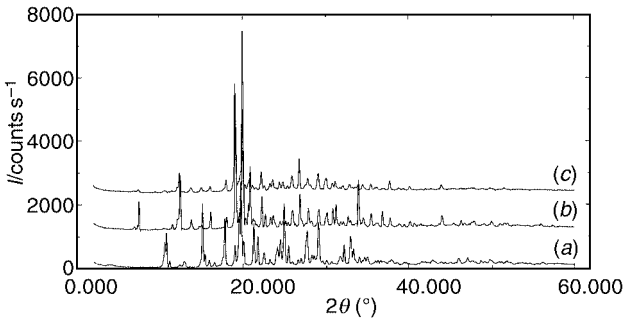

Fig. 2 The X-ray powder patterns of (*a*) *rac*-crystals of pure **1**, (*b*) chiral crystals of **2** prepared by recrystallization and (*c*) chiral crystals of **2** prepared by gas–solid reaction.

exposure to xylene vapor, this chiral crystalline powder was easily converted to the 1 : 1 inclusion crystals **2** with the same chirality.

X-Ray analysis of the *rac*-crystal of **1** showed that two halves of crystallographically independent molecules of *P*-**1** and *M*-**1** exist in the asymmetric unit (space group: *Pccn*). (Fig. 3)† Molecular layers of *P*-**1** and *M*-**1** are arranged perpendicular to the *a*-axis and within these layers the molecules are connected by Br··Br contacts along the *c*-direction. The *P*-**1** molecule has a right-handed and the *M*-**1** molecule has a left-handed propeller structure, respectively (Fig. 4).

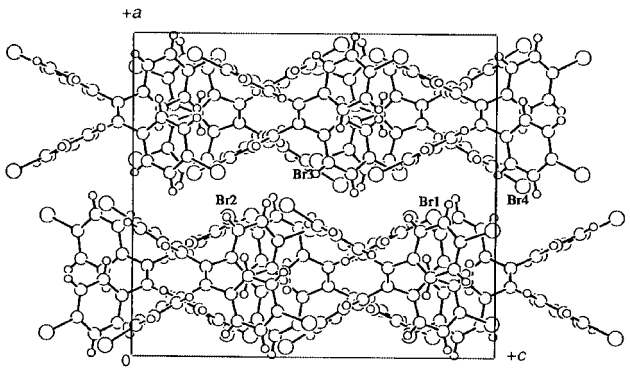

Fig. 3 Crystal structure of **1** viewed along the *b*-axis.

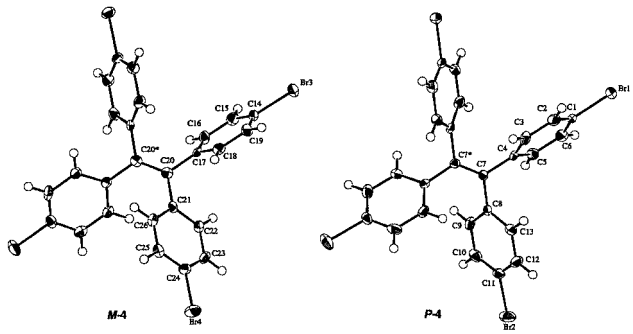

Fig. 4 Molecular structure of *P*-**1** (right molecule) and *M*-**1** (left molecule) in the crystal of **1**. Thermal ellipsoids are drawn at the 50% probability level.

The molecules in **2** occupied the chiral space group $P2_12_12_1$.‡ The *p*-xylene molecules are included in chiral cavities formed by the bromophenyl rings (Fig. 5) In **2**, molecular layers are arranged perpendicular to the *a*-axis, and within these layers the

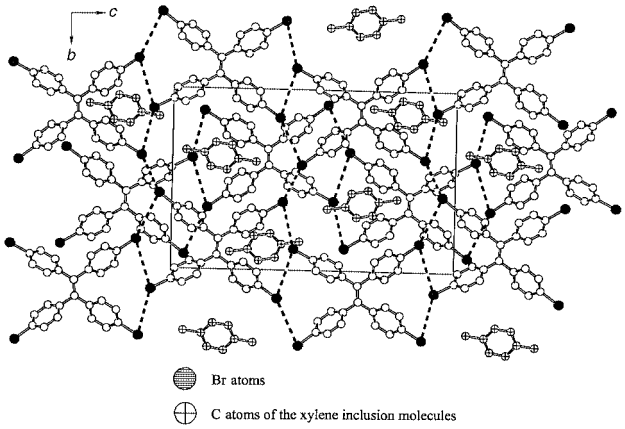

Fig. 5 Crystal structure of **2** viewed along the *a*-axis.

molecules are connected by Br··Br contacts along the *b* direction. It has been found that halogen··halogen contacts act as attractive interactions and the inclusion complex is stabilized by the Br··Br interactions between host molecules.[4] This is the first example of the construction of a chiral inclusion crystalline lattice by a Br··Br interaction network among achiral host molecules.

In conclusion, we have found a unique example of racemic-to-chiral transformation by exposing racemic crystalline material to the vapor of an achiral guest compound. This provides not only a new strategy for construction of chiral crystals but also a new model for studying the mechanism of generation of chirality in crystals.

The authors thank Dr M. Shiro of the Rigaku X-ray research laboratory for determining the X-ray structure of **1**.

Note and references

† *Crystal data* for **1**: $C_{26}H_{16}Br_4$, M = 648.03, colorless prisms 0.35 × 0.15 × 0.15 mm, orthorhombic, *Pccn*, a = 16.173(2), b = 16.512(1), c = 18.024(2) Å, V = 4813(1) Å^3, Z = 8, D_c = 1.788 g cm^{-3}, μ(Mo-Kα) = 67.19 cm^{-1}, F(000) = 2496, T = 133 K, final R = 0.033, Rw = 0.032 for 272 variables and 3159 reflections with $I > 2\sigma(I)$. The structures were solved by direct methods (SIR97) (ref. 5) and refined by full-matrix least-squares on F^2.

‡ *Crystal data* for **2**: $C_{26}H_{16}Br_4{\cdot}C_8H_{10}$, M = 754.2, colorless prisms 0.44 × 0.2 × 0.2 mm, orthorhombic, space group $P2_12_12_1$, a = 8.762(1), b = 14.942(2), c = 23.472(4) Å, V = 3073.0(8) Å^3, Z = 4, D_c = 1.63 g cm^{-3}, T = 218 K, μ(Mo-Kα) = 5.26 mm^{-1}, F(000) = 1480, final R = 0.047, Rw = 0.096 for 345 variables, 4119 reflections and 2148 observed reflections with $I > 2\sigma(I)$. The structures were solved by direct methods (SHELXS-97) (ref. 6) and refined by full-matrix least-squares on F^2. CCDC 182/1539. See http://www.rsc.org./suppdata/cc/a9/a909782a/ for crystallographic files in .cif format.

1 For reviews: M. Sakamoto, *Chem. Eur. J.*, 1997, **3**, 684; G. Kaupp and M. Haak, *Angew. Chem., Int. Ed. Engl.*, 1993, **32**, 694.
2 L. Addadi and M. Lahav, in *Origins of Optical Activity in Nature*, ed. D. C. Walker, Elsevier, New York, 1979, pp. 179–192.
3 R. E. Buckles, E. A. Hausman and N. G. Wheeler, *J. Am. Chem. Soc.*, 1950, **72**, 2494.
4 A. Farina, S. V. Meille, M. T. Messina, P. Metrangolo, G. Resnati and G. Vecchio, *Angew. Chem., Int. Ed.*, 1999, **38**, 2433.
5 A. Altomare, M. C. Burla, M. Camalli, G. L. Cascarano, C. Giacovazzo, A. Guagliardi, A. G. G. Moliterni, G. Polidori and R. Spagna, *J. Appl. Crystallogr.*, 1999, **32**, 115.
6 G. M. Sheldrick, SHELXS-97, Universität Gottingen, Germany, 1997.

Communication a909782a

A new redox-denitration reaction of aromatic nitro compounds

Charles W. Rees*[a] and Siu C. Tsoi[b]

[a] *Department of Chemistry, Imperial College of Science, Technology and Medicine, London, UK SW7 2AY. E-mail: c.rees@ic.ac.uk*

[b] *Kodak European Research and Development, Headstone Drive, Harrow, Middlesex, UK HA1 4TY*

Received (in Liverpool, UK) 23rd December 1999, Accepted 3rd February 2000

When 4,4-dimethyl-1-(2-nitrophenyl)pyrazolidin-3-one 9 is heated in pyridine containing pyridine hydrochloride it is transformed into 4,4-dimethyl-1-phenylpyrazolidin-3,5-dione 10 in which the methylene group has been oxidised and the nitro group has disappeared; two further examples of the same reaction, of pyrazolidinones 4 and 7, are reported together with a mechanistic rationalisation of this curious reaction.

New reactions of aromatic nitro groups are rare. We recently discovered one during an unsuccessful attempt to synthesise the 1-arylpyrazolidin-3-one **4** from 4,5-dimethoxy-2-nitrophenylhydrazine **1** and 3-chloropivaloyl chloride **2**. After an initial reaction in cold pyridine which gave **3**,† mp 163 °C (isolable in 90% yield), the reaction mixture was heated under reflux for 24 h. From this complex reaction we could not isolate any **4**, but only a rather low yield of the 1-arylpyrazolidin-3,5-dione **5**,† mp 189–191 °C (23%), in which the nitro group has been replaced by hydrogen and the pyrazolidinone methylene group oxidised to a carbonyl group (Scheme 1). Compound **5** was synthesised independently from 3,4-dimethoxyphenylhydrazine and dimethylmalonyl dichloride. We assume that **1** and **2** are converted *via* **3** into the desired pyrazolidinone **4**, but this has reacted further to give **5**. On heating preformed **3** in pyridine for 20 h, **5** was again formed as the major product. This unexpected conversion of **4** into **5** is a novel redox reaction in which the nitro group has presumably oxidised the adjacent methylene group and has undergone, most unusually, complete cleavage from the aromatic ring with overall loss of the elements of nitroxyl, HNO.

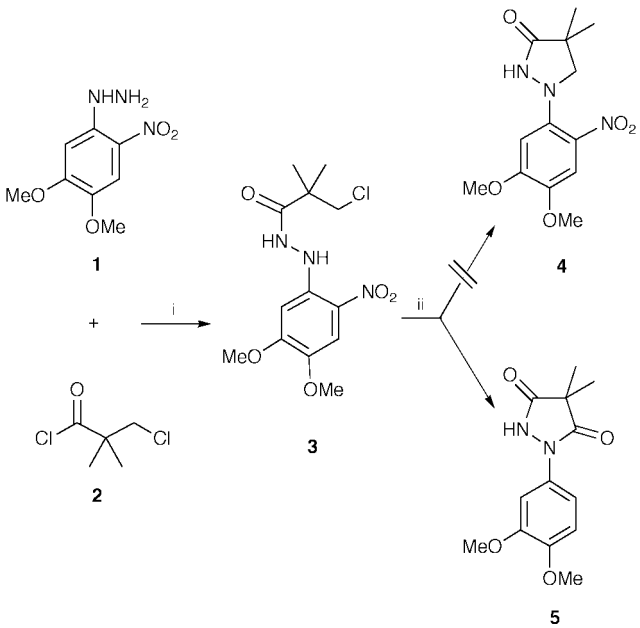

Scheme 1 *Reagents and conditions*: i, pyridine, 5 °C, N_2, 1 h; ii, pyridine, 115 °C, N_2, 24 h.

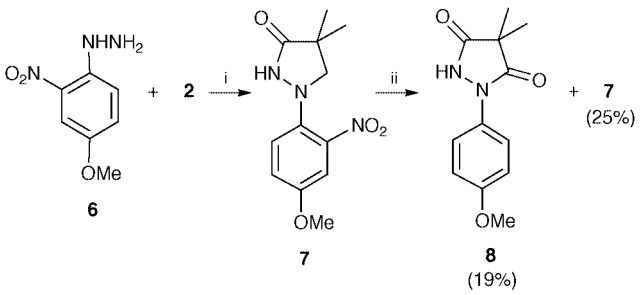

Scheme 2 *Reagents and conditions*: i, pyridine, 5 °C, N_2, 1 h, then room temp., 1 h, then 115 °C, 2 h, ii; pyridine 115 °C, N_2, 20 h.

We performed the same reaction (Scheme 2) with the monomethoxyphenylhydrazine **6** and acid chloride **2** in cold pyridine, to give the acylic hydrazide intermediate (TLC), followed by brief heating (2 h) to give the expected 1-arylpyrazolidin-3-one **7** as the major product. After extended heating (20 h) a mixture of **7** (25%) and the denitrated pyrazolidin-3,5-dione **8** (19%) was isolated. The formation of the monomethoxy product **8** is distinctly slower than for the dimethoxy product **5**.

Finally we treated 2-nitrophenylhydrazine with acid chloride **2** in cold pyridine and then at 90 °C for 11 h to give the nitrophenylpyrazolidin-3-one **9**,† mp 196–198 °C (43%) (Scheme 3). When pure compound **9** was heated in pyridine for up to 5 days there was very little reaction,‡ but when heated in pyridine containing pyridine hydrochloride (1 equiv.) to simulate the conditions of the reactions of **1** and **6**, the overall loss of HNO again occurred to give 1-phenylpyrazolidin-3,5-dione **10** (mp 180 °C, lit.[1] 180–182 °C) (23%) after 20 h. Product **10** was also synthesised from phenylhydrazine and dimethylmalonyl dichloride.

This new acid-catalysed redox-denitration reaction could thus be general for the conversion of 1-(2-nitroaryl)pyrazolidin-3-ones, like **4**, **7** and **9**, into 1-arylpyrazolidin-3,5-diones, like **5**, **8** and **10**. A possible mechanism is outlined in Scheme 4, for the simplest case. Aromatic nitro groups are well known to interact in thermal, photolytic and catalysed reactions with a range of *ortho* substituents,[2] often being reduced to nitroso, azo, azoxy or amino groups, but very rarely with concomitant cleavage of the aryl–nitrogen bond.[3] Since the methylene group would be activated towards oxidation by the adjacent pyrazolidinone

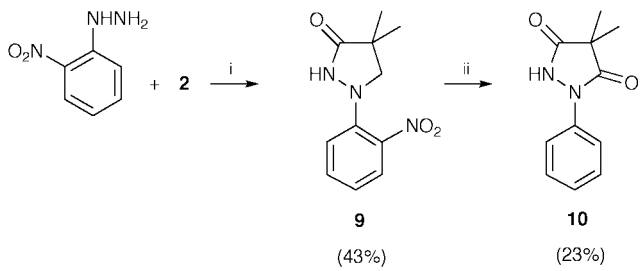

Scheme 3 *Reagents and conditions*: i, pyridine, 50 °C, N_2, 1 h, then 90 °C, 11 h; ii, pyridine, py·HCl (1 equiv.), 115 °C, N_2, 20 h.

DOI: 10.1039/a910290f

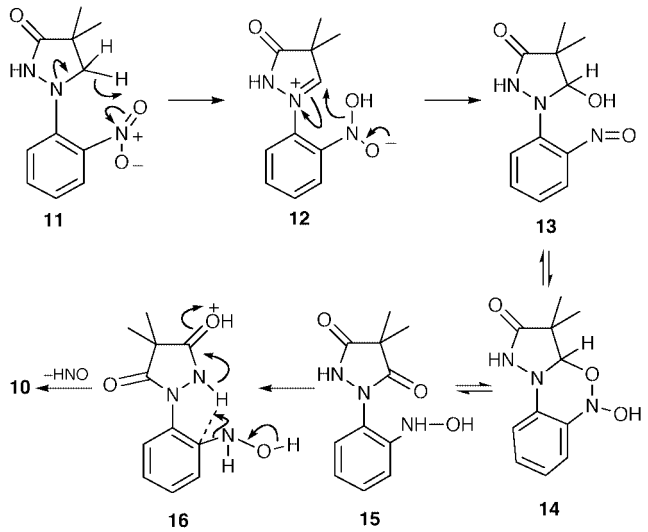

Scheme 4

nitrogen atom, it seems likely that the first step would be an intramolecular hydride transfer to the nitro group (arrows in **11**). This is exactly analogous to that proposed for tertiary amines, when the amine replaces our heterocyclic ring (the *tert*-amino effect).[4] This would give the iminium ion **12** which could collapse to the nitroso compound **13** or its tricyclic tautomer **14**; **13** and **14** would be in equilibrium with each other and with the hydroxylamine **15**.

The final and most unusual step would then be the loss of nitroxyl, HNO,[5] from **15** to give the isolated product **10**; this outcome may depend critically upon the particular structural features of the starting pyrazolidinones. Since protonation at the benzene 2-position must presumably be involved, the reaction should be acid-catalysed (as observed), inter- or intra-molecularly. It could occur, for example, in the conjugate acid **16** of **15** as shown (arrows in **16**). In this mechanism (Scheme 4) various steps would be facilitated by the electron releasing groups in the mono- and di-methoxy compounds, in accord with the observed relative rates of reaction. Further work is required to establish the scope and mechanism of this new reaction.

We are grateful to Kodak Ltd. for permission to publish this work and to Dr N. E. Milner for support and encouragement.

Notes and references

† The structures of all new compounds are based upon IR, MS, LCMS, HRMS and ^{1}H NMR spectroscopy.

‡ Some intractable material containing traces of **10** (mass spectrometry) was formed.

1 W. H. Pirkle and P. L. Gravel, *J. Org. Chem.*, 1978, **43**, 808.
2 P. N. Preston and G. Tennant, *Chem. Rev.*, 1972, **72**, 627.
3 R. Fielden, O. Meth-Cohn and H. Suschitzky, *Tetrahedron Lett.*, 1970, 1229 report such a reaction in the formation of a by-product in the thermolysis of 1-diethylamino-2-nitrobenzene but the loss of the nitro group is not accompanied by oxidation of an adjacent methylene group.
4 O. Meth-Cohn and H. Suschitzky, *Adv. Heterocycl. Chem.*, 1972, **14**, 211; O. Meth-Cohn, *Adv. Heterocycl. Chem.*, 1996, **65**, 1.
5 P. A. S. Smith and G. E. Hein, *J. Am. Chem. Soc.*, 1960, **82**, 5731; M. N. Hughes, *Q. Rev. Chem. Soc.*, 1968, **22**, 1

Communication a910290f

Ferrocenylsilylation of dendrons: a fast convergent route to redox-stable ferrocene dendrimers

Sylvain Nlate,[a] Jaime Ruiz,[a] Jean-Claude Blais[b] and Didier Astruc*[a]

[a] *Groupe de Chimie Supramoléculaire des Métaux de Transition, LCOO, UMR CNRS No 5802, Université Bordeaux I, 33405 Talence Cédex, France. E-mail: d.astruc@lcoo.u-bordeaux.fr*

[b] *Laboratoire de Chimie Structurale Organique et Biologique, EP CNRS No 103, Université Paris VI, 4 Place Jussieu, 75252 Paris, France*

Received (in Cambridge, UK) 4th November 1999, Accepted 4th February 2000

A 54-ferrocene dendrimer is synthesized by a convergent route and can be used to modify a Pt electrode in CH_2Cl_2; it can be reversibly oxidized in DMF in a single 54-electron wave (and with NO^+).

The redox activity of nanoscopic materials,[1,2] in particular that of dendrimers,[3] is of promise in considering applications as materials devices. Ferrocene dendrimers[4] illustrate the potential access to precise redox active nanoscopic molecules with original properties. We now report the ferrocenylsilylation of dendrons and a fast convergent route[5] to *redox stable* dendrimers using ferrocenyldimethylsilane **1**.[6] Hydrosilylation has already been used as an excellent synthetic route to dendrimers.[4e,7] and ferrocenylsilylation has been successfully carried out by Jutzi *et al*. with decaallylferrocene.[4e]

The ferrocenylsilylation of the phenoltriallyl dendron **2**[8] using **1** is achieved with Karstedt's catalyst[9] in the absence of air without protection of the phenol function (Scheme 1). After chromatographic separation, the triferrocenylsilane dendron **3**† is obtained in 90% yield. ^{1}H and ^{13}C NMR spectra indicate the absence of regioisomers, the analytical data are excellent, and the MALDI TOF mass spectrum shows the molecular peak at *m/z* 960.41 (calc. 960.91). A convergent route was developed for the synthesis of the nonaferrocene dendron. The protected dendron *p*-$EtO_2CC_6H_4C(CH_2CH_2I)_3$[8] reacts with **3** in DMF in the presence of K_2CO_3 to give **4**† in 60% yield after deprotection and chromatography. The MALDI TOF mass spectrum of **4** shows an excellent degree of purity, the molecular peak being largely dominant at *m/z* 3110.44 (calc. molecule 3111.09). Dendron **4** reacts with the core hexa(bromomethyl)benzene in EtOH in the presence of K_2CO_3 at 80 °C over two weeks to give the 54-ferrocene dendrimer **5**† in 20% yield after chromatographic separation (C analysis within 0.3%).

Cyclic voltammograms (CVs) of the ferrocenyl dendrons **3** and **4** and the ferrocenyl dendrimer **5** were recorded on a Pt anode in dichloromethane and dimethylformamide (DMF).[10] Dendrons **3** and **4** show a reversible oxidation wave in a diffusion process (no adsorption, as indicated by ΔE_p = 60 mV at 20 °C) in both solvents. The number of electrons involved in this ferrocene oxidation wave was determined using Bard's equation[11] and decamethylferrocene as the internal reference. The experimental number of electrons was found to be in full agreement within 5% with the actual number of dendritic branches. In DMF, the CV of **5** also gives a single reversible wave corresponding to the oxidation of the 54 ferrocene redox centers in a pure diffusion process as indicated by ΔE_p = 60 mV at 20 °C as for the decamethylferrocene reference. The number of redox centers determined experimentally as above is 54 ± 3. In dichloromethane, the CV of **5** shows a mixture of diffusion and adsorption as indicated by a value of ΔE_p = 30 mV at a scan rate of 0.1 V s^{-1}. Modified electrodes[12] with **5** could be prepared by cyclic scanning between the ferrocene and ferrocenium regions of potentials on a Pt electrode in dichloromethane solution, washing with dichloromethane and drying in air. Cycling about twenty times is necessary before observation of a constant curve. When such a derivatized electrode is used in a new dendrimer-free solution containing only the electrolyte, the cyclic voltammogram of the adsorbed dendrimers are obtained with ΔE_p = 0 and a linear relationship between the scan rate and the intensity, both features being characteristic of derivatized electrodes with ferrocene polymers[12] and dendrimers[4g] (Fig. 1). The orange–red dendrimer **5** can be instantaneously oxidized by $NOPF_6$ in dichloromethane, and the blue PF_6^- salt of the 54-ferrocenium dendrimer $\mathbf{5}^{54+}$ obtained as a precipitate can be reduced back to the 54-ferro-

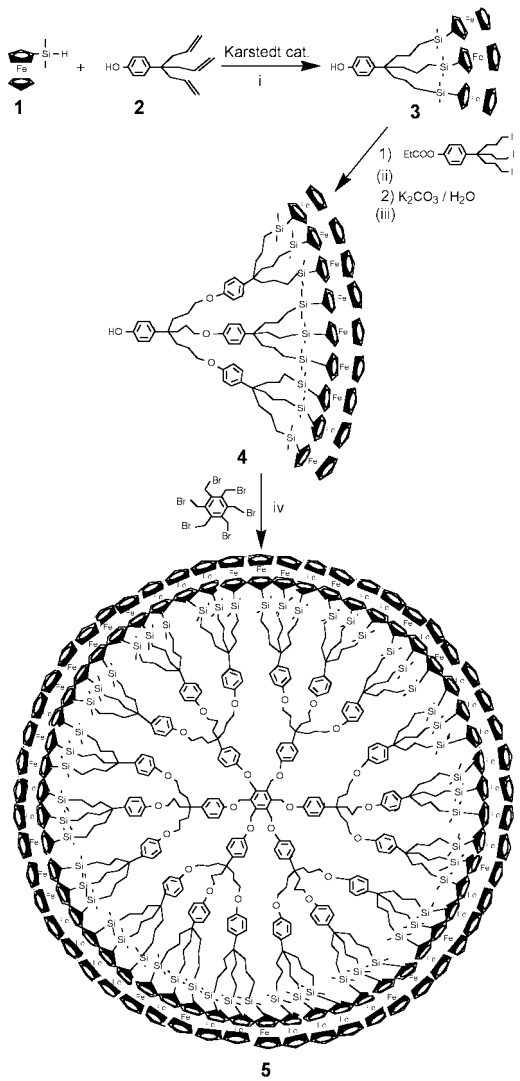

Scheme 1 *Reagents and conditions*: i, toluene, 40 °C, 1 d; ii, DMF, room temp., 2 d; iii, 40 °C, 2 d; iv, EtOH, K_2CO_3, reflux, 14 d.

DOI: 10.1039/a908791e

cene dendrimer **5** using the monoelectronic reducing agent decamethylferrocene. No decomposition of the dendrimer occurs during these redox processes as indicated by the indentity of the ^{1}H NMR spectra before and after the reactions.

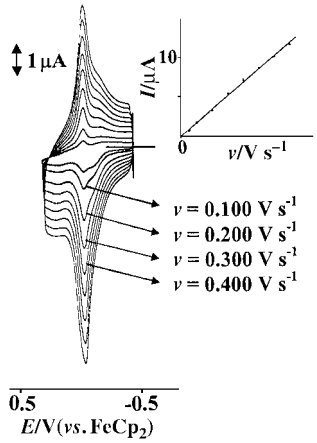

Fig. 1 Cyclic voltammogram of a Pt electrode modified with a film of the 54-ferrocene dendrimer **5**; CH_2Cl_2, 0.1 M $NBu^n_4PF_6$. Inset: plot of the peak intensity *vs.* sweep rate.

Whereas the mechanism of electron transfer in DNA is highly controversial,[13] that in multi-redox dendrimers is also of interest. The present study concerns a large dendrimer approaching a globular shape. The electrochemical reversibility observed for the oxidation of **5** indicates that the structural rearrangement between **5** and $\mathbf{5}^{54+}$ is small. Since the repulsion between the positively charged ferrocenium units in $\mathbf{5}^{54+}$ requires that they be at the periphery of the dendrimer with maximum space expansion, the shape of **5** is relatively closely related to that of $\mathbf{5}^{54+}$. The fact that a single reversible wave is observed is due to fast rotation of the dendrimer compared to the electrochemical timescale, so that all the redox centres come close to the electrode within this timescale.[14*b*] In addition, a kind of *relay*-mechanism from a ferrocene site to the next (hopping electron transfer or *via* π-stacking[14] of the ferrocene units or *via* the σ bonds between ferrocene units) may eventually occur. Otherwise, the heterogeneous electron transfer between the electrode and the most remote redox sites of the globular dendrimer would be slow, as it is when the redox site is isolated at the center of the dendrimer.[4*l*,*m*,15] This type of stable polyredox dendrimer in which the redox centers are all active and fully chemically and electrochemically reversible at about the same potential could find use in the future as molecular batteries and sensors.

Notes and references

† Satisfactory C and H elemental, and MALDI TOF mass spectral analyses were obtained for **3** and **4**. NMR: **3** δ_H($CDCl_3$, 250 MHz) 7.12 (d, 2H, C_6H_4), 6.75 (d, 2H, C_6H_4), 4.20 (t, 6H, C_5H_4), 4.09 (s, 15H, C_5H_5), 4.01 (t, 6H, C_5H_4), 1.59 (br s, 6H, CH_2Ar), 1.12 (br s, 6H, CH_2CH_2Ar), 0.61 (br s, 6H, CH_2Si), 0.17 (s, 18H, SiMe). δ_C($CDCl_3$, 62.9 MHz) 152.55 (C_q, ArOH), 139.88 (C_q, Ar), 127.66 (CH, Ar), 114.67 (CH, Ar), 72.95 (C_5H_4); 71.58 (C_q, C_5H_4), 70.52 (C_5H_4), 68.12 (C_5H_5), 43.12 (C_q-CH_2), 42.16 (CH_2), 18.08 (CH_2CH_2Si), 17.56 (CH_2Si), −1.93 (SiMe). **4**. δ_H($CDCl_3$, 250 MHz) 7.18 (m, 8H, C_6H_4), 7.04 (m, 8H, C_6H_4), 4.23 (br m, 18H, C_5H_4), 4.02 (s, 45H, C_5H_5), 3.94 (br m, 6H, C_5H_4), 3.89 (br s, 6H, CH_2O), 1.54 (br s, 24H, CH_2CH_2Ar); 1.18 (br s, 24H, CH_2CH_2Ar), 0.56 (br s, 18H, CH_2Si), 0.16 (s, 45H, SiMe); δ_C($CDCl_3$, 62.9 MHz) 156.11 (C_q, ArO), 152.39 (C_q, ArOH) 140.02 (C_q, Ar), 127.63 (CH, Ar), 127.60 (CH, Ar), 114.64 (CH, Ar), 113.69 (CH, Ar), 73.21 (C_5H_4), 71.83 (C_q, C_5H_4), 70.88 (C_5H_4), 68.38 (C_5H_5), 43.20 (C_q-CH_2), 42.16 (CH_2), 29.50 (CH_2CH_2Ar), 18.07 (CH_2CH_2Si), 17.56 (CH_2Si), −1.95 (SiMe). **5**, δ_H($CDCl_3$, 250 MHz) 7.12 (m, 60H, C_6H_4), 6.77 (m, 60H, C_6H_4), 5.21 (br s, 18H, PhCH_2O), 4.29 (br m, 108H, C_5H_4), 4.09 (s, 270H, C_5H_5), 4.01 (br m, 108H, C_5H_4), 3.86 (br s, 36H, CH_2O), 1.54 (br s, 108H, CH_2CH_2Ar), 1.12 (br s, 108H, CH_2CH_2Ar), 0.60 (br s, 108H, CH_2Si), 0.16 (s, 324H, SiMe). δ_C($CDCl_3$, 62.9 MHz) 156.11 (C_q, ArO), 139.56 (C_q, Ar), 127.60 (CH, Ar), 127.3 (CH, Ar), 114.68 (CH, Ar), 113.72 (CH, Ar), 72.92 (C_5H_4), 70.62 (C_q, C_5H_4); 70.58 (C_5H_4); 68.08 (C_5H_5); 66.00 (CH_2CH_2O) 43.99 (C_q-CH_2) 41.36 (CH_2), 29.73 (CH_2CH_2Ar), 18.08 (CH_2CH_2Si), 17.67 (CH_2Si), −1.87 (SiMe).

1 D. Astruc, *Electron Transfer and Radical Processes in Transition Metal Chemistry*, VCH, New York, 1995, ch. 4: *Molecular Electronics*.

2 J.-M. Lehn, *Supramolecular Chemistry: Concepts and Perspectives*, VCH, Weinheim, 1995, ch. 8: *Devices*; V. Balzani and F. Scandola, *Supramolecular Chemistry*, Ellis Horwood, New York, 1991.

3 D. A. Tomalia, A. N. Naylor and W. A. Goddard III, *Angew. Chem., Int. Ed. Engl.*, 1990, **29**, 138; N. Ardoin and D. Astruc, *Bull. Soc. Chim.*, 1995, **132**, 875; G. R. Newkome, C. N. Moorefield and F. Vögtle, *Dendritic Molecules: Concepts, Syntheses and Perspectives*, VCH, New York, 1996; M. R. Bryce and W. Devonport, in *Advances in Dendritic Macromolecules*, ed. G. R. Newkome, JAI Press Inc, CT, 1996, vol. 3, pp. 115–149; E. C. Constable, *Chem. Commun.*, 1997, 1073; V. Balzani, S. Campagna, G. Denti, A. Juris, S. Serroni and M. Venturi, *Acc. Chem. Res.*, 1998, **31**, 26; C. M. Casado, I. Cuadrado, M. Morán, B. Alonso, B. Garcia, B. Gonzalès and J. Losada, *Coord. Chem. Rev.*, 1999, **185**–**186**, 53; M. A. Hearshaw and J. R. Moss, *Chem. Commun.*, 1999, 1; G. R. Newkome, E. He and C. N. Moorefield, *Chem. Rev.*, 1999, **99**, 1689.

4 (*a*) J.-L. Fillaut and D. Astruc, *J. Chem. Soc., Chem. Commun.*, 1993, 1320; (*b*) B. Alonso, I. Cuadrado, M. Morán and J. Losada, *J. Chem. Soc., Chem. Commun.*, 1994, 2575; (*c*) B. Alonso, M. Morán, C. M. Casado, F. Lobete, J. Losada and I. Cuadrado, *Chem. Mater.*, 1995, **7**, 1440; (*d*) I. Cuadrado, M. Morán, C. M. Casado, B. Alonso, F. Lobete, R. Garcia, M. Ibisate and J. Losada, *Organometallics*, 1996, **15**, 5278; (*e*) P. Jutzi, C. Batz, B. Neumann and H. G. Stammler, *Angew. Chem., Int. Ed. Engl.*, 1996, **35**, 2118; (*f*) C. Valério, J.-L. Fillaut, J. Ruiz, J. Guittard, J.-C. Blais and D. Astruc, *J. Am. Chem. Soc.*, 1997, **119**, 2588; (*g*) J. Losada, I. Cuadrado, M. Morán, C. M. Casado, B. Alonso and M. Barranco, *Anal. Chim. Acta*, 1997, **338**, 191; (*h*) I. Cuadrado, C. M. Casado, B. Alonso, M. Morán, J. Losada and V. Belsky, *J. Am. Chem. Soc.*, 1997, **119**, 7613; (*i*) T. Takada, D. J. Diaz, H. D. Abruna, I. Cuadrado, C. Casado, B. Alonso, M. Morán and J. Losada, *J. Am. Chem. Soc.*, 1997, **119**, 10 763; (*j*) C. F. Shu and H. M. Shen, *J. Mater. Chem.*, 1997, **7**, 47; (*k*) C. Köllner, B. Pugin and A. Togni, *J. Am. Chem. Soc.*, 1998, **120**, 10 274; (*l*) C. M. Cardona and A. E. Kaifer, *J. Am. Chem. Soc.*, 1998, **120**, 4023; (*m*) G. E. Oosterom, R. J. van Haaren, J. N. H. Reek, P. C. J. Kamer and P. W. N. M. van Leeuwen, *Chem. Commun.*, 1999, 1119; (*n*) C. Valério, E. Alonso, J. Ruiz, J.-C. Blais and D. Astruc, *Angew. Chem., Int. Ed.*, 1999, **38**, 1747.

5 C. J. Hawker and J. M. J. Fréchet, *J. Am. Chem. Soc.*, 1990, **112**, 1010; T. M. Miller and T. X. Neenan, *Chem. Mater.*, 1990, **2**, 346.

6 K. H. Pannel and H. Sharma, *Organometallics*, 1991, **10**, 954.

7 D. Seyferth, D. Y. Son, A. L. Rheingold and R. L. Ostrander, *Organometallics*, 1994, **13**, 2682; S. W. Krska and D. Seyferth, *J. Am. Chem. Soc.*, 1998, **120**, 3604.

8 V. Sartor, L. Djakovitch, J.-L. Fillaut, F. Moulines, F. Neveu, V. Marvaud, J. Guittard, J.-C. Blais and D. Astruc, *J. Am. Chem. Soc.*, 1999, **121**, 2929.

9 B. Marciniec, in *Applied Homogeneous Catalysis with Organometallic Compounds*, ed. B. Cornils and W. A. Herrmann, VCH, Weinheim, 1996, vol. 1, ch. 2.6; L. N. Lewis, J. Stein and K. A. Smith, in *Progress in Organosilicon Chemistry*, ed. B. Marciniec and J. Chojnowski, Gordon and Breach, Langhorne, USA, 1995, p. 263.

10 For the redox chemistry of ferrocene derivatives, see for instance: N. G. Connelly and W. E. Geiger, *Adv. Organomet. Chem.*, 1984, **83**, 1; ref. 1, ch. 2: *Electrochemistry*.

11 J. B. Flanagan, S. Margel, A. J. Bard and F. C. Anson, *J. Am. Chem. Soc.*, 1978, **100**, 4268; for an example of the use of this formula, see: F. Moulines, L. Djakovitch, R. Boese, B. Gloaguen, W. Thiel, J.-L. Fillaut, M.-H. Delville and D. Astruc, *Angew. Chem., Int. Ed. Engl.*, 1993, **32**, 1075 (ref. 17 therein); ref. 10(*b*), p. 116.

12 R. Murray, in *Molecular Design of Electrode Surfaces*, ed. R. Murray, Wiley, New York, 1992, p. 1.

13 E. K. Wilson, *Chem. Eng. News*, Aug. 23, 1999, p. 43.

14 (*a*) C. A. Christensen, L. M. Goldenberg, M. R. Bryce and J. Becher, *Chem. Commun.*, 1998, 509; (*b*) S. J. Green, J. J. Pietron, J. J. Stokes, M. J. Hostleter, H. Wu, W. P. Wuelfing and R. W. Murray, *Langmuir*, 1998, **14**, 5612.

15 J. Issberner, F. Vögtle, L. De Cola and V. Balzani, *Chem. Eur. J.*, 1997, **3**, 706; C. B. Gorman, B. L. Parkhurst, W. Y. Su and K. Y. Chen, *J. Am. Chem. Soc.*, 1997, **119**, 1141.

Communication a908791e

Typeset and printed by Black Bear Press Limited, Cambridge, England

ChemComm
FEATURE ARTICLE

Panoscopic materials: synthesis over 'all' length scales

Geoffrey A. Ozin

Materials Chemistry Research Group, Chemistry Department, 80 St. George Street, University of Toronto, Toronto, Ontario, Canada M5S 3H6. E-mail: gozin@alchemy.chem.utoronto.ca

Received (in Cambridge, UK) 25th June 1999, Accepted 23rd August 1999

For the latter half of the 'Solid State 20th Century' materials science has been the engine that propelled technology. As we enter the 'Materials 21st Century' it is abundantly clear that the insatiable demand for new materials for emerging technologies is driving materials synthesis and change. Materials chemistry will play a central role in this endeavor through the creation of materials with structures and properties able to meet the demands required by up-and-coming technologies. In this paper a far-sighted and innovative materials chemistry strategy is proposed. It takes solid state chemistry beyond fifty years of thermodynamic phases and microscale structures, to a new era of self-assembly chemistry focused on metastable phases and mesoscale structures, with accessible surfaces and well defined interfaces that determine function and utility. It is an interdisciplinary approach that combines synthesis, solid state architecture and functional hierarchy to create an innovative strategy for materials chemistry in the new millennium. The attractive feature of the approach is the ability to assemble complex structures rationally from modular components and integrate them into self-assembling constructions for a range of perceived applications. By creating a series of purposeful design strategies it is believed that truly revolutionary advances in materials science and technology can result from this approach.

Room at the top and bottom

Not so long ago in materials chemistry it seemed that there was only 'room at the bottom'.[1] The trend was to synthesize and organize nanoscopic materials. As we enter the new millennium it is becoming abundantly clear that there is also 'room at the top'.[2] What has changed and why is this important? In this brief essay I will make the case that the paradigmatic shift comes from the realization that self-assembly, templating, patterning, capping, layering and molding methods have expanded the materials chemists tool box to include synthesis and organization of materials at 'all' length scales. Hierarchy has been introduced into materials chemistry and purely synthetic integrated chemical systems that are designed to achieve a particular function are becoming a reality. This augurs well for the development of materials, composites and systems with novel properties, new functions and perceived value in a range of applications in the biomedical, pharmaceutical, aerospace, automotive, construction, energy, electronics and photonics user sectors.

Self-assembling materials

This story is about interfaces between organics and inorganics and how they can be controlled synthetically at the molecular level to produce composite materials in which structure is prescribed from angstrom to centimeter length scales. The construction kit consists of complementary organics and inorganics that spontaneously assemble through lock-and-key intermolecular interactions. The driving forces for molecular organization are quite varied and as summarized in Scheme 1 can be based upon ionic, covalent, hydrogen, non-covalent, metal–ligand and colloidal bonding interactions, which may result in structures and properties not found in the individual components.

In this context, self-assembly may be viewed in terms of a map of bonding forces that operate between building blocks and over different length scales. In a self-organizing system, basic construction-units spontaneously associate to form a particular structure, the architecture of which is solely determined by the bonding properties and shapes of the individual components. The system proceeds towards a state of lower free energy and greater structural stability. Self-assembly is usually entropically driven in an aqueous system, where association of modules is accompanied by exclusion of ordered water molecules.

Hierarchy

A feature of self-assembly is hierarchy, where primary building blocks associate into more complex secondary structures that are integrated into the next size level in the hierarchy. This organizational scheme, which is illustrated in Scheme 2, continues until the highest level in the hierarchy is reached. These hierarchical constructions may exhibit unique properties that are not found in the individual components. Hierarchy is a characteristic of many self-assembling biological structures and is beginning to emerge as a hallmark of supramolecular materials. Self-assembly is considered to be distinct from template-directed assembly, which involves structure-directing additives, often organics or polymers, in addition to the constituent building-units, which may be inorganics. The

Geoffrey A. Ozin, born 23rd August 1943 in London, England, received his BSc degree in Chemistry from Kings College, University of London in 1965, and his DPhil degree in Inorganic Chemistry from Oriel College, Oxford University in 1967. He was an ICI Fellow at the University of Southampton from 1967–69 before joining the University of Toronto in 1969 where he is currently Professor of Chemistry. Recently he was a Canada Council Isaac Walton Killam Research Fellow and inducted into the Royal Society of Canada. He is a materials chemist and the current work of his group focuses on micro-, meso- and macro-structured materials and composites. The research exploits molecular recognition and self-assembly, to organize inorganic and organic building-units into materials with structural features that span angstrom to centimeter length scales. The methodology embraces concepts in supramolecular, host–guest inclusion, and biomimetic chemistry. Self-assembling mesostructures emerging from the research may find utility in areas such as electrically tunable membranes and chemical delivery systems, chemoselective sensors and solar cells, batteries and fuel cells, bone implants and photonics, nanocomposites and environmental clean-up of toxic waste.

DOI: 10.1039/a905090f

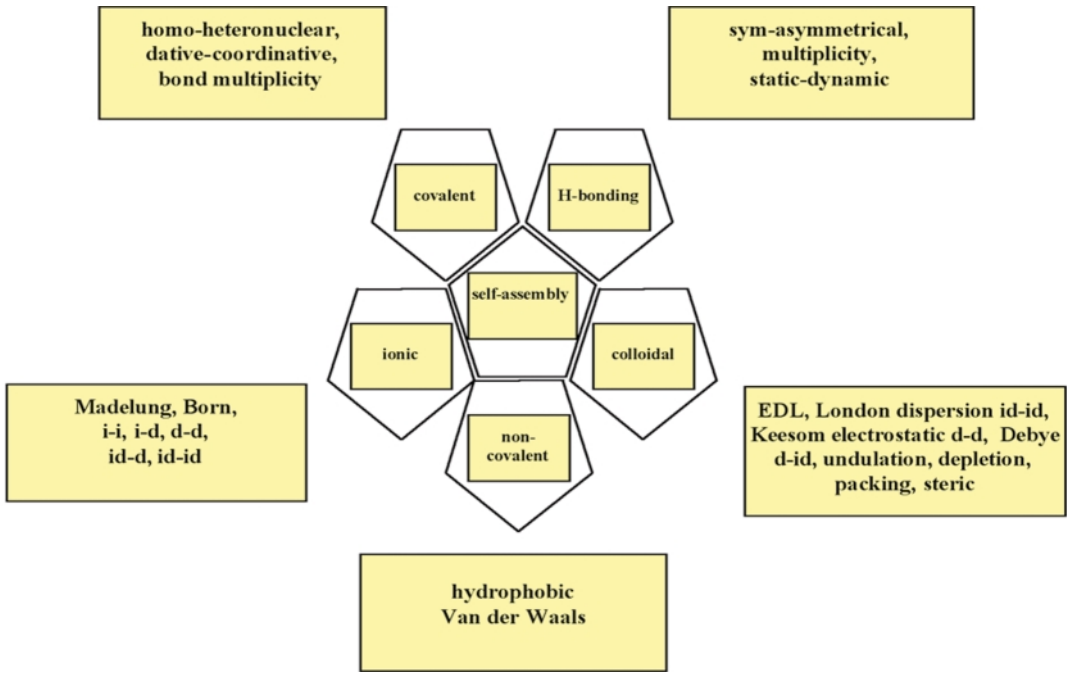

Scheme 1

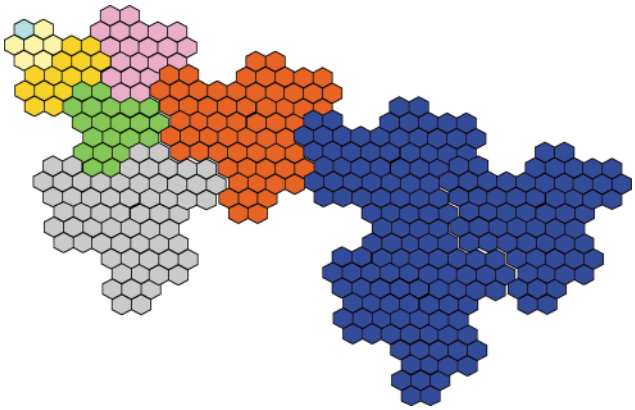

Scheme 2

template can serve to fill space, balance charge and direct the formation of a specific structure. In this definition, template assembly is synonymous with co-assembly and distinct from self-assembly.

Self-assembling materials over multiple length scales

Simple, elegant and robust attributes of self-assembly are now being combined with the powerful methods of inorganic and solid state chemistry to create supramolecular materials with unprecedented structures, compositions and morphologies. The paradigmatic shift of utilizing organics for templating,[3] capping,[4], layering,[5,6] wiring,[7] patterning[8] and molding[9] inorganics is having a revolutionary effect on the field of materials research. This is because it enables, for the first time, self-assembly of most elemental compositions of the periodic table but without the usual restriction of the dimension of structural components. This is facilitating purely synthetic approaches to hierarchical systems with the construction pieces integrated over micro-, meso- and macro-scopic length scales. This kind of 'panoscopic' synthesis, so to speak, has up until very recently been unparalleled in the field of solid state and materials chemistry. By combining the methodologies of self-assembly and microfabrication it has become feasible to assume the challenge of self-organizing and interconnecting functional organic, bio-organic, inorganic and polymeric chemical components into integrated electronic, photonic, mechanical, analytical and chemical systems for future 'panoscale' (panoscale: of any sizes, pano, L) devices.[10] Part of the motivation stems from the notion that the architecture of complex macrosystems in biology and engineering physics are generally based on hierarchical building principles, that is, smaller units are assembled into larger ones, which in turn are organized at a higher dimension. This construction process is continued until the highest level of structural complexity in the hierarchy has been attained.

The hallmark of an integrated chemical, physical or biological system is the assembly of components into a particular architecture that performs a certain function.[11] In the cell of a higher green plant the photosynthetic chloroplast and oxidative phosphorylation mitochondrion machines are perhaps two of the most impressive examples of functional integrated biological systems. Within the body of a computer the atoms are assembled into insulators, semiconductors and metals, dopants, junctions, metal leads and contacts. These are the building blocks that constitute the transistors, diodes and capacitors of the integrated circuits, which comprise circuit boards and subassemblies of an integrated microelectronic system. Familiar integrated chemical systems include heterogeneous catalysts, photoelectrochemical cells, solid state lithium batteries, hydrogen–oxygen fuel cells, instant color photographic film, sensors and chromatographic stationary phases.

The ability to self-assemble diverse kinds of materials over 'all' length scales and spatial dimensions has taken synthetic chemistry to a new level of structural complexity that begins to match those found in biology and engineering physics. It is now feasible to devise strategies for organizing, patterning and linking chemical components into functional architectures that were not previously accessible purely through synthesis. Representative examples taken from the recent literature include, layer-by-layer assembly of a thin film Zerner diode from conducting polymers and monodispersed capped semiconductor nanoclusters,[12] a metal–insulator–metal nanocluster–insulator–metal (MINIM) single electron transistor (SET),[13] a multicolor pixel voltage-controllable semiconductor cluster–luminescent polymer light emitting diode (LED)[14] an all-plastic field effect transistor driven light emitting diode (FET-LED),[15] and a high density rechargeable ultrathin graphite oxide

nanoplatelet–polyelectrolyte lithium ion battery.[16] These few examples serve to demonstrate the power and versatility of a self-assembly materials chemistry approach to 'panostructured' integrated chemical systems that perform a specific function.

'Panoscopic' synthesis can be viewed in terms of molecular level control of interfaces between organics and inorganics. As illustrated in Scheme 3, this allows one to embrace molecular,[17]

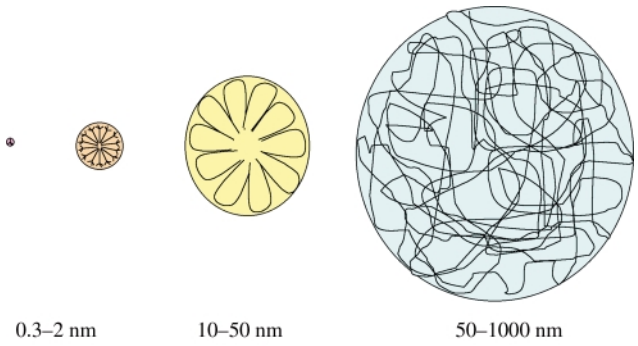

Scheme 3

supramolecular,[18] macromolecular,[19] and colloidal crystalline[20] assemblies under the umbrella of organic template-based assembly, facilitating the synthesis of inorganic materials over multiple length scales, with structural features that may span angstroms to microns.

Through a creative fusion of organic templating, inorganic chemistry, soft lithographic patterning and micromolding methodologies it is feasible to create functional hierarchical materials of the type sketched in Scheme 4. Entirely through

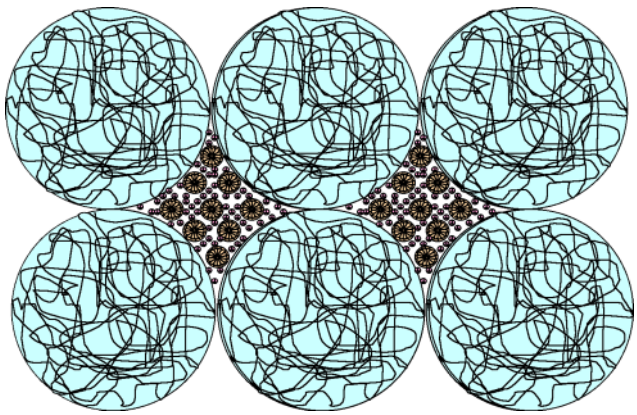

Scheme 4

chemistry one can plan how to synthesize, self-organize and interconnect different kinds of materials over 'all' length scales to create an integrated chemical system with single or multiple functions. In the following, I will briefly expand upon this theme by examining some case studies taken from our recent research to illustrate where 'panoscale' synthesis may find 'room at the bottom as well as the top' of the new materials world.

Faux diatoms and radiolaria

Interest in the synthesis of 'panascopic' materials may be traced to a report in 1995 of surfactant-templated mesolamellar aluminophosphates whose 'natural form' bore a striking resemblance to those of the lace-like siliceous microskeletons produced by the single cell marine organisms known as the diatoms and radiolarians.[21] When looking at scanning electron microscope (SEM) images of these purely synthetic forms it is sometimes difficult to distinguish them from the real thing, Fig. 1. This turned out to be the first synthesis that created a hybrid inorganic–organic material with a shape that mimicked an entire biomineralized skeleton found in the natural world.

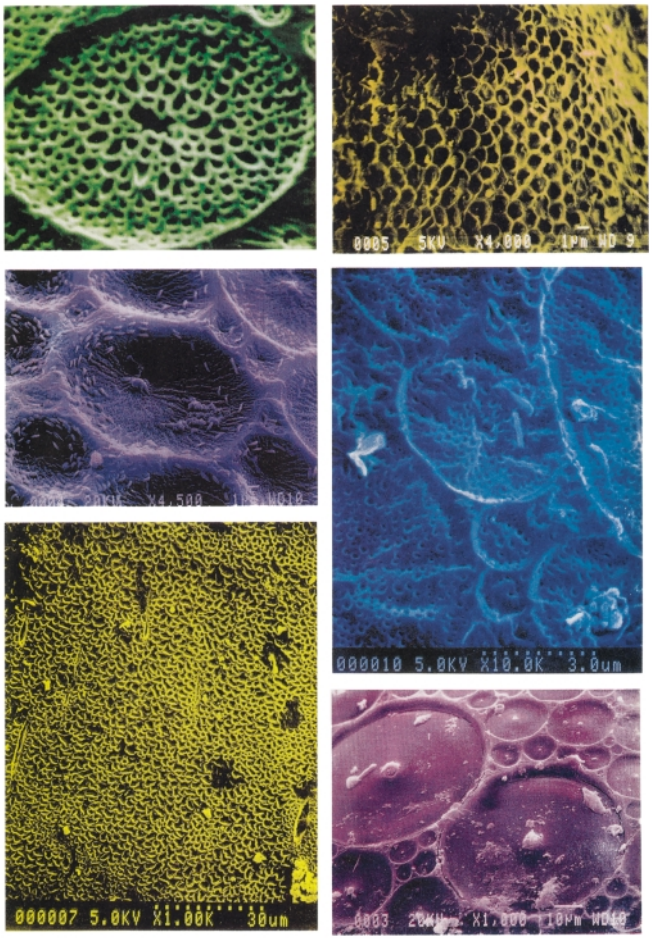

Fig. 1 Scanning electron micrograph images of synthetic examples of diatom and radiolarian microskeletons. Reprinted in part with permission from: *Adv. Mater.* (*London*) 1995, **7**, 943 (© 1995 Wiley-VCH) (top left, middle right); *Nature* (*London*) 1995, **378**, 47 (© 1995 Nature Publishing Group) (http://www.nature.com) (top right, middle left, bottom right); and *Acc. Chem. Res.* 1997, **30**, 22 (© 1997 American Chemical Society) (bottom left).

Fig. 2 Transmission electron microscopy image of the mesolamellar aluminophosphate material from which the synthetic diatoms and radiolaria mimics are built.

Multianalytical characterization of these synthetic natural forms revealed a hierarchical structure based upon a layered aluminophosphate.[21–25] The lamellae were well ordered at the mesoscale and glassy at the microscale, Fig. 2. Observed morphologies that emerged from a synthesis exhibited micron scale

patterns on millimeter sized solid and hollow spheres of a kind that are usually associated with the filigree microskeletons of diatoms and radiolaria. These aesthetically sculpted biological minerals continue to be admired in Ernst Haekel's *Art Forms in Nature*[26] and avidly read in D'Arcy Wentworth Thompson's *On Growth and Form*.[27]

How was such morphosynthesis possible in a laboratory setting? The template used to produce such shapes was dodecylamine, which in the presence of 85 wt% phosphoric acid formed dodecylammonium dihydrogen phosphate (DDP). Single crystal X-ray diffraction (SCXRD) established an interdigitated bilayer structure for DDP in which the ammonium head group was intricately hydrogen-bonded to the dihydrogen phosphate counter anion, Fig. 3. Powder X-ray diffraction (PXRD) and differential scanning calorimetry (DSC) showed that DDP transforms, under the reaction conditions that generate the patterned sphere shapes, to a thermotropic smectic liquid crystal phase. When observed between crossed-polarizers in a hot stage optical microscope (POM), as a film supported on a glass slide, the mesophase displayed the focal conic texture expected for a smectic liquid crystal,[22] Fig. 4. The optical birefringence pattern appeared even more pronounced when the DDP mesophase was formed in tetraethyleneglycol (TEG), which was the non-aqueous solvent used in the synthesis to create the patterned sphere shapes. The patterns seemed to be diagnostic of a microemulsion in which contiguous assemblies of phase separated water droplets were coated with a layer of the phosphate liquid crystal, Fig. 5. These observations suggested that the texture of the mesophase was 'fossilized' as a lamellar aluminophosphate by a POH + HOAl $\rightarrow$ P–O–Al + H_2O condensation–polymerization reaction of the dihydrogen phosphate anion with an aluminium(III) glycolate precursor located in the microphase separated domains of the DDP–TEG–H_2O liquid crystal microemulsion. This provided an appealing explanation for the origin of the micron-sized patterns observed on the surface of the mesolamellar aluminophosphate sphere shapes.

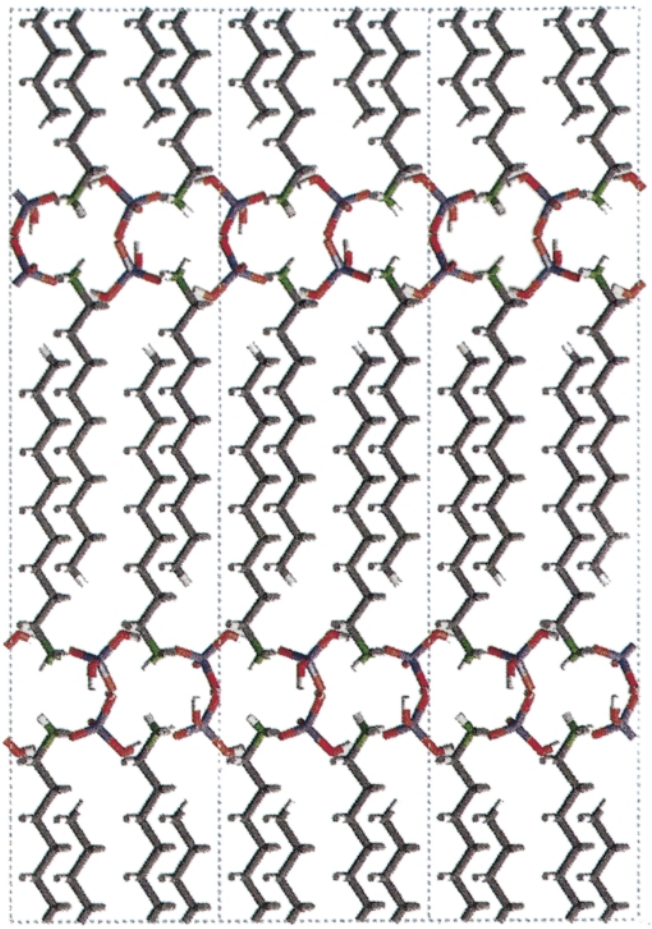

Fig. 3 Single crystal X-ray diffraction structure of dodecylammonium dihydrogen phosphate. Reprinted in part with permission from: *Acc. Chem. Res.* 1997, **30**, 24 (© 1997 American Chemical Society).

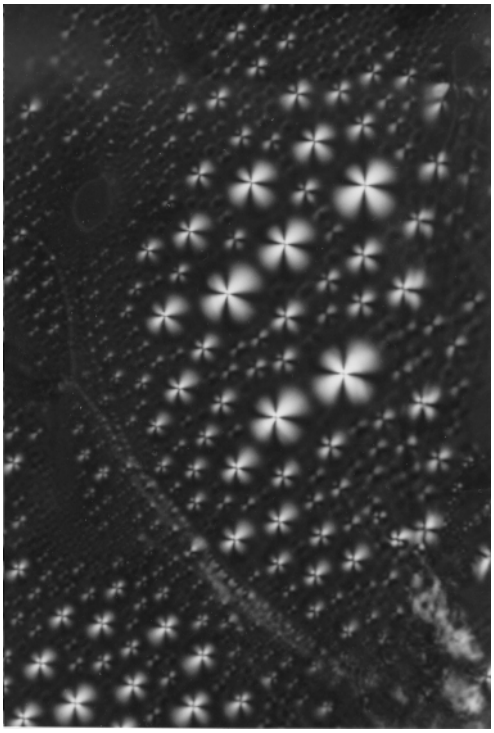

Fig. 4 Optical birefringence texture of smectic dodecylammonium dihydrogen phosphate mesophase.

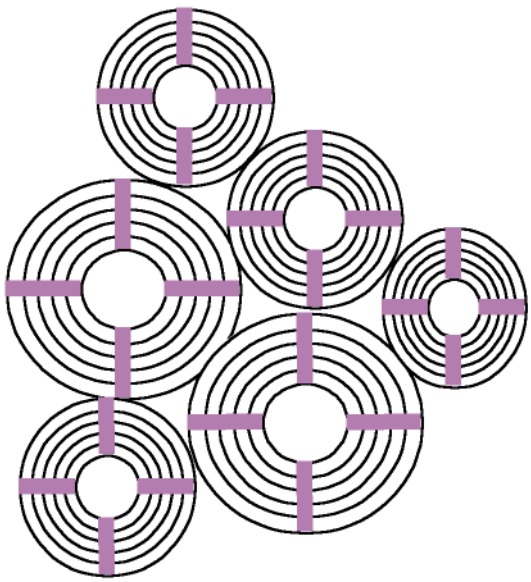

Fig. 5 Illustration of the smectic dodecylphosphate dihydrogen phosphate–tetraethyleneglycol–water liquid crystal microemulsion templating model for the morphogenesis of synthetic aluminophosphate diatom and radiolaria mimics.

It was the recognition that inorganic liquid crystals could be used to synthesize inorganic materials with complex form and structures spanning multiple length scales that raised the possibility of a purely synthetic approach to functional hierarchical materials such as bone mimics.

Synthetic bone implant materials

Synthetic analogues of bone are being actively pursued for biomedical applications in the field of bone replacement,

augmentation and repair.[28] Numerous stringent criteria have to be satisfied for a biomaterial to be acceptable as a bone implant, including the ability to integrate into bone and not cause any side effects. We recently described a biomimetic strategy to a new type of bone analogue material.[29,30] Bone consists of *ca.* 70% hydroxyapatite $Ca_{10}(PO_4)_6(OH)_2$, (OHAp), embedded in an organic matrix consisting mainly of the proteinaceous triple helix, collagen. Needle or plate-like morphologies of hydroxyapatite crystallize at regular intervals along the collagen fibers with the long *c*-axes oriented parallel to the fibrils. The presence of HPO_4^{2-} groups in bone apatites suggests that octacalcium phosphate $Ca_8(PO_4)_4(HPO_4)_2{\cdot}5H_2O$, (OCP), is a precursor to hydroxyapatite formation in bone. The OCP serves to establish the final morphology, composition, solubility and interfacial energy of apatitic materials, as well as controlling the nucleation and growth of OHAp. These result from the fact that OCP and OHAp have similar crystal structures and are able to epitaxially grow together.[31] A prime consideration in the preparation and performance of a bone implant material is the selection of a surface that is able to induce nucleation of OCP and growth of new bone.

With this background in mind we set out to synthesize an analogue of bone that comprised a porous hydroxyapatite–octacalcium phosphate–calcium dodecylphosphate (CDDP) composite film grown on a titania–titanium substrate. It has the hierarchical construction illustrated in Fig. 6. A macroporous

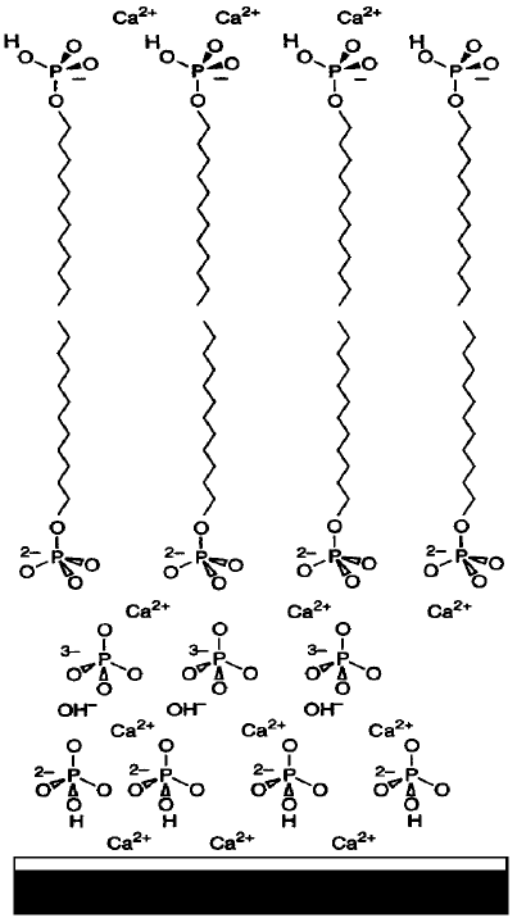

Fig. 6 Hierarchical construction of macroporous hydroxyapatite–octacalcium phosphate–calcium dodecylphosphate composite film grown on a titania–titanium substrate.

and oriented OHAp–OCP mineral phase was found to nucleate and grow, under physiological conditions, from TiOH Brønsted acid and base anchoring sites on the surface of a sputter-deposited titania film as seen in Fig. 7. The mesolamellar CaDDP phase was co-assembled with the OHAp phase in a 'mesoepitaxial' fashion as seen in Fig. 8. It is envisioned that if

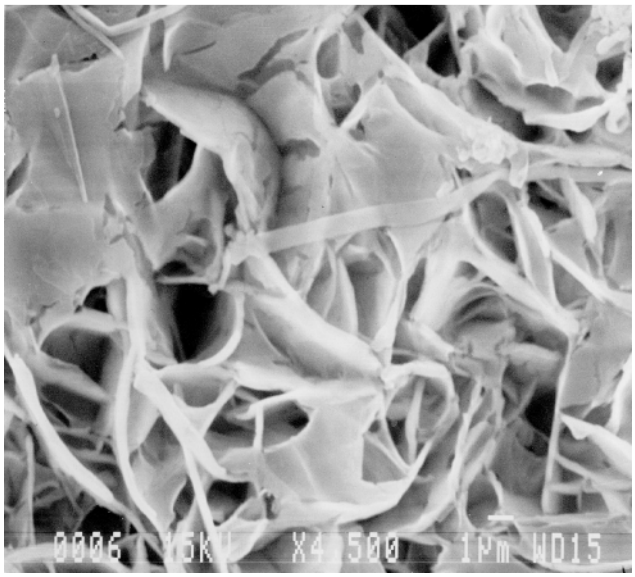

Fig. 7 Scanning electron microscopy image of macroporous hydroxyapatite–octacalcium phosphate–calcium dodecylphosphate composite film grown on a titania–titanium substrate.

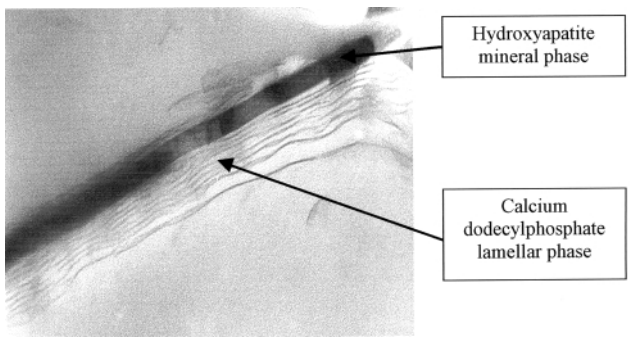

Fig. 8 Transmission electron microscopy image depicting the 'mesoepitaxial' relation between the calcium dodecylphosphate lamellar phase co-assembled with the hydroxyapatite mineral phase.

materials of this genre can integrate into bone they may be able to deliver bioeffectors and drugs, from the hydrophobic region of the CaDDP mesolamellar phase, to stimulate bone growth and combat disease. Notably, the macroporous structure of the material would facilitate the influx of cells and blood vessels to the site of the bone implant.

Tin sulfide mesh mesophase

The discovery of phosphate liquid crystals raised the possibility that other inorganic liquid crystals should exist and exhibit equally fascinating chemical and physical properties. Materials of this type are rare, they are anticipated to combine the fluidity of organic liquid crystals with for instance, the charge transport and optical properties of inorganic materials. This thinking led to the synthesis of a new class of tin sulfide liquid crystals with a novel structure based on a mesh mesophase.[32,33] The preparation involved the reaction of tin(IV) chloride with hexadecylamine and ammonium sulfide in aqueous ammonium hydroxide. The stoichiometry of the product, $HDA_{2{\cdot}67}SnS_{2{\cdot}05}$, suggested that the material had a structure with a very large void volume. In fact, it was found to have a structure based on regularly perforated layers of tin sulfide sandwiched between a bilayer of partially protonated and charge-balancing hexadecylamine. The room temperature phase was shown to be crystalline with well ordered inorganic and organic layers. The illustration depicts the structure of the as-synthesized crystalline tin(IV) sulfide mesoporous layers at room temperature (top), its semi-liquid crystalline form at 45 °C (middle) and its liquid

crystalline form at 85 °C (bottom), Fig. 9. Tapping mode atomic force microscopy (AFM) images of the material at room temperature revealed well ordered mesopores and mesola-

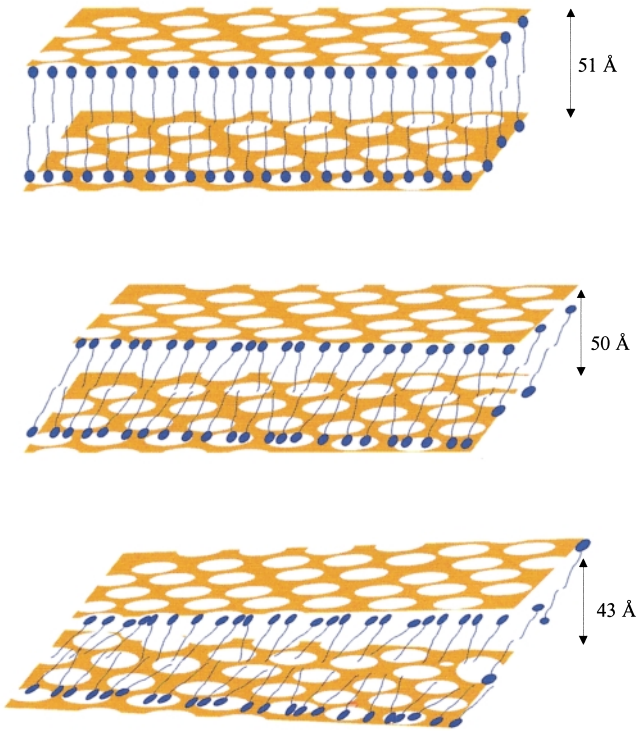

Fig. 9 Illustration of the structure of the tin sulfide mesh crystalline (top), semi-liquid crystalline (middle) and liquid crystalline (bottom) phase.

mellae, which was consistent with the results of powder X-ray diffraction (PXRD) and transmission electron microscopy (TEM), Fig. 10. The structure appeared to be best described as a tin sulfide replica of a mesh mesophase. A film of the room temperature crystalline phase had an electrical conductivity of 5.3×10^{-8} Ω^{-1} cm^{-1}. This increased by >1000 times on transforming to the liquid crystalline phase where it behaved as a semiconducting metallogen. Mesh type tin(IV) sulfide was found to be optically transparent and readily formed electrically conducting crystalline, semicrystalline or liquid crystalline thin films. Furthermore, it reversibly adsorbed molecules like H_2O and CO_2 with a concomitant and measurable electrical response. These observations bode well for the use of this new class of hybrid inorganic–organic semiconducting liquid crystals for display and chemical sensing applications.

Modular mesostructures

The work with tin sulfide liquid crystals suggested that metal sulfide cluster-based liquid crystals might be synthetically accessible and could provide a new and interesting way of assembling mesostructured metal sulfides from well defined building blocks. Earlier work involving the organic molecule templated assembly of adamantanoid $Ge_4S_{10}^{4-}$ clusters into crystalline microporous metal germanium sulfides showed that the integrity of the $Ge_4S_{10}^{4-}$ remained intact.[34] This suggested that cluster liquid crystals based on $Ge_4S_{10}^{4-}$ might be a good starting point to attempt the synthesis of mesostructured metal germanium sulfides. $TMA_4Ge_4S_{10}$ was readily accessible and could be ion exchanged for cationic surfactants like cetyltrimethylammonium chloride to form a lamellar germanium sulfide cluster mesophase $CTA_4Ge_4S_{10}$, Fig. 11. This appeared to be an attractive precursor for the assembly of mesostructured metal germanium sulfides, however the material was found to be insoluble in water, which prevented the formation of a lyotropic mesophase.

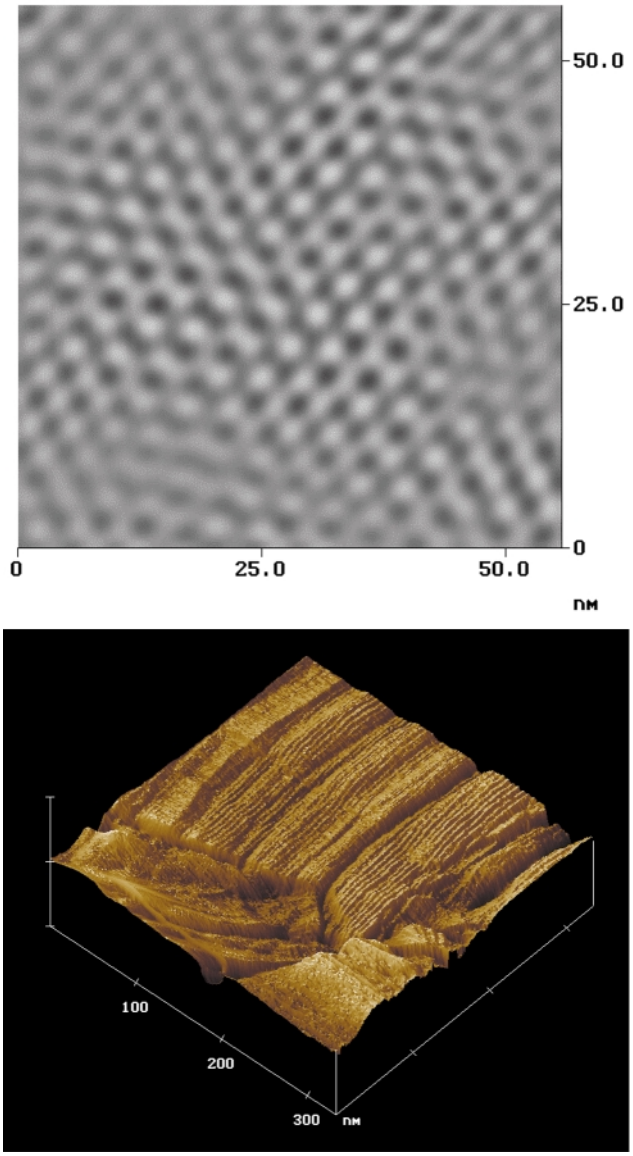

Fig. 10 Tapping mode atomic force microscopy images of the mesopores (top) and mesolamellae (bottom) in the crystalline tin sulfide mesh phase.

The solution to the problem, illustrated in Scheme 5, was found by using the interesting solvent formamide, $HCONH_2$, in which $CTA_4Ge_4S_{10}$ is soluble and self-assembles into a germanium cluster lyotropic liquid crystal.[35] Formamide is a strongly hydrogen-bonded solvent with a dielectric constant and boiling point higher than water. Moreover, the phase diagram of surfactants in formamide resembled that of surfactants in water. Using this knowledge it was discovered that adamantanoid $Ge_4S_{10}^{4-}$ clusters could be linked by divalent M^{2+} transition metal ions around a liquid crystal surfactant assembly in formamide to give exceptionally well ordered mesostructured metal germanium sulfide materials. Elemental analysis established the stoichiometry $CTA_2M_2Ge_4S_{10}$, which together with Raman spectroscopy of the precursor $CTA_4Ge_4S_{10}$ and microporous $TMA_2MGe_4S_{10}$ analogue proved that the cluster integrity remained intact, Fig. 12. These materials represented the first examples of 'coordination mesostructures', a new family of solids in which the $Ge_4S_{10}^{4-}$ cluster functions as a tetradentate ligand by coordinating through its four terminal sulfurs to transition metal ions like Co^{2+}, Ni^{2+}, Cu^{+}, Zn^{2+}.[35] By co-assembling the clusters and transition metal ions in this way, it proved possible to obtain a hexagonal mesostructure with metal linked adamantanoid clusters comprising the channel wall, Fig. 13. In the case of Cu^{+} compound the clusters were linked by Cu_2^{2+} dimers to create $CTA_2Cu_4Ge_4S_{10}$, an unusual example of a mesostructured material that contained a metal–

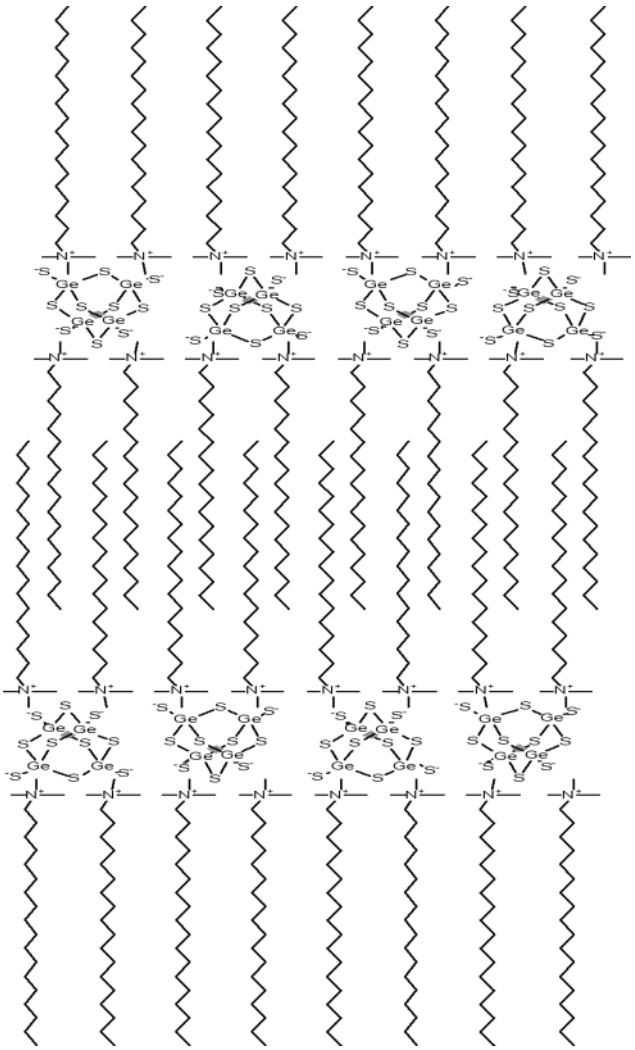

Fig. 11 Illustration of the lamellar adamantanoid germanium sulfide cluster crystalline phase.

metal bond like its microporous counterpart $TMA_2Cu_2Ge_4S_{10}$.[34,35] The supramolecular assembly of mesostructured materials from the linking of clusters was unprecedented. From consideration of the architecture and composition of mesostructured metal sulfide materials it is envisioned that they could prove effective in diverse applications, such as detoxification of heavy metals in polluted water streams, sensing of sulfurous vapors and semiconductor quantum anti-dot devices.

Sol–Gel mesophase

Continuing with the theme of inorganic liquid crystals that can mineralize into mesostructured inorganic replicas of the templating mesosphase, raised the possibility that a generalized non-aqueous synthesis of main group and transition metal oxide mesostructures could be developed based upon the hydrolytic condensation–polymerization of a sol–gel mesophase. This led to the discovery of glycosilicate and glycometallate surfactants that self-assemble into a hydrolyzable lamellar mesophase.[36,37] The surfactant was cationic and the glycometallate functioned as the charge compensating counter anion, Fig. 14. The main advantage of hydrolyzable glycometallate surfactants was found to be the control that could be exerted over the condensation–polymerization of source reagents like silicates, titanates, zirconates and niobates. This proved pivotal to the successful incorporation of two or more metals into the framework of binary or ternary mesoporous metal oxide materials. Glycometallate precursors may be considered as

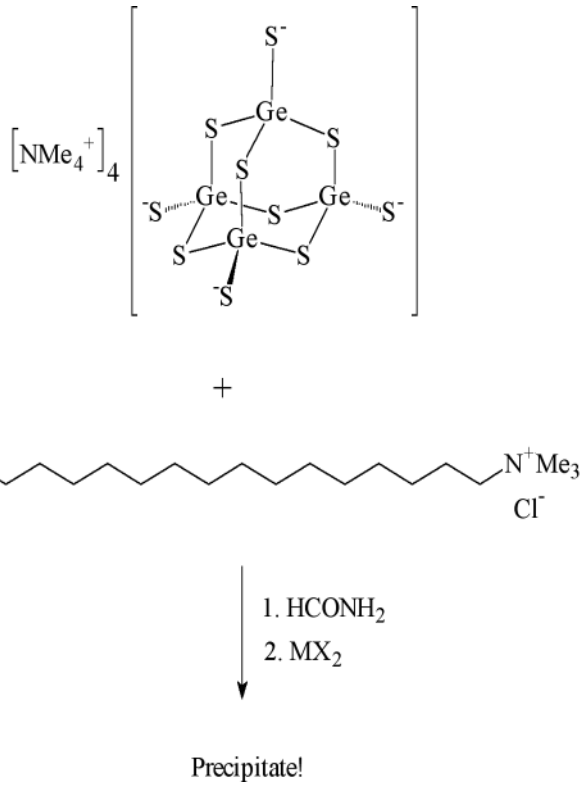

Scheme 5

bidentate metal alkoxides. They provide better command over differential rates of hydrolysis of binary combinations compared to traditional monodentate metal alkoxides or bulk metal oxide source materials.

Hydrolysis of Si(IV), Ti(IV), Zr(IV) and Nb(V) glycometallates was found to produce well-ordered mesoporous metal oxides, Fig. 15. Following treatment with metal alkoxides or disilane coupling reagents the surfactant template could be removed to create high surface area narrow pore size distribution mesoporous binary metal oxides. The glycosilicate mesophase showed a well defined lamellar to hexagonal structural transition, which appeared to originate from polymerization induced size and charge density changes in the headgroup region of surfactant. Binary silica–transition metal oxide, mesoporous materials that are rich in either the silica or metal component have been synthesized from a mesophase comprised of mixed glycometallates.

Glycometallate surfactants provide a facile synthetic entry to electroactive and photoactive mesoporous metal oxide materials. They are anticipated to function as electrodes, electrolytes and plasticisers in solid state batteries, fuel cells, solar energy conversion devices, and large molecule chemical sensors.

Mesostructured solid electrolytes

Inorganic liquid crystals again played a central role in the synthesis of a new class of solid electrolytes coined 'salted mesostructures'.[38] In a one-pot synthesis, a lithium triflate–silicate–oligo(ethylene oxide) surfactant mesophase was found to undergo an acid catalyzed polymerization to generate a lithium triflate–oligo(ethylene oxide) surfactant–mesoporous silica nanocomposite film. The optical birefringence fan texture observed for the film was that expected for a silicified version of the hexagonal symmetry mesophase, Fig. 16. $LiCF_3SO_3$ was found, by NMR and Raman spectroscopy, to be dissociated into free lithium (small solid black circle) and triflate (large hatched circle) ions, which were contained in the oligo(ethylene oxide) head group region of the surfactant assembly (thin black lines), all imbibed within the channels (thick black line) of the

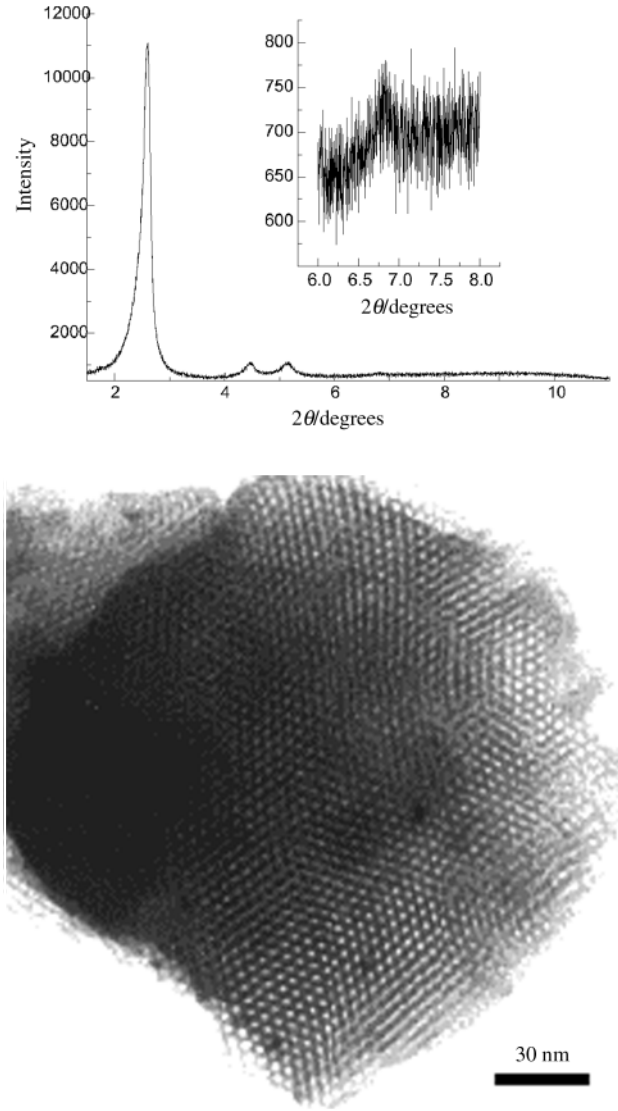

Fig. 12 Powder X-ray diffraction pattern (observed d_{hkl} = 100, 110, 200, 210) and transmission electron microscopy image of the hexagonal form of mesostructured nickel (top) and cobalt germanium sulfide (bottom).

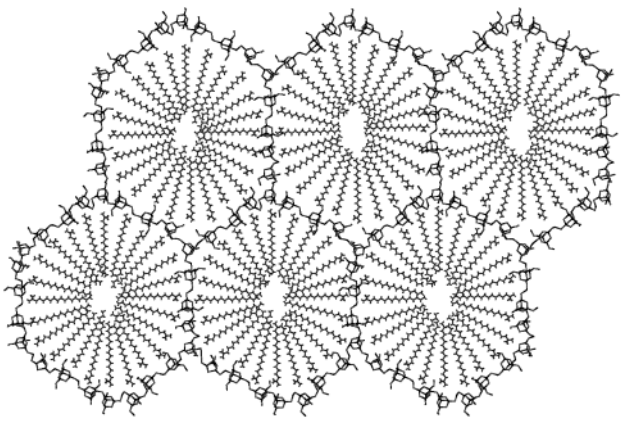

Fig. 13 Illustration of the structure of hexagonal symmetry mesostructured metal germanium sulfide assembled from metal linked adamantanoid germanium sulfide clusters around a surfactant mesophase.

mesoporous silica, Fig. 17. Nanocomposite materials of this genre have been found by ac impedance spectroscopy to behave as fast lithium ion conductors at room temperature, which bodes well for them finding utility in the important field of polymer electrolyte, plasticiser and battery technology.

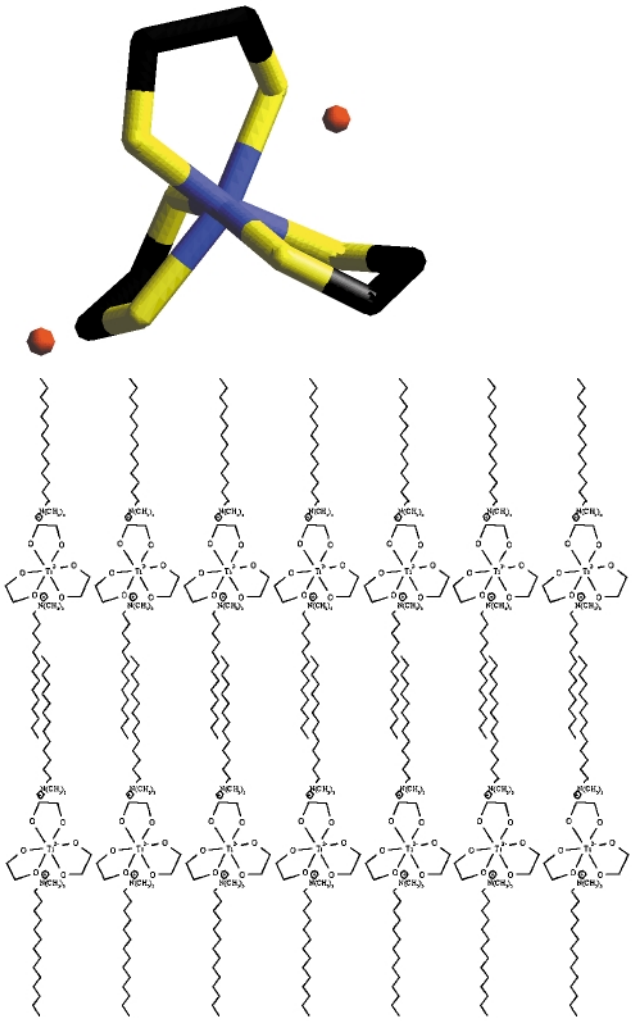

Fig. 14 Illustration of sodium glycotitanate(IV) (top) and lamellar cetyltrimethylammonium glycotitanate(IV) mesophase (bottom).

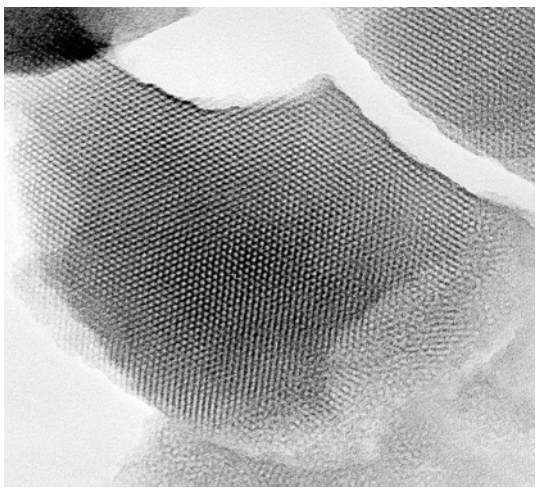

Fig. 15 Transmission electron microscopy image of mesosporous zirconia assembled from glycozirconate around a surfactant mesophase.

Polymer–mesoporous silica nanocomposites

The ability to control the morphology and mesostructure of surfactant-templated silica as fibers, films, spheres, gyroids, discoids, spirals and soft lithographically defined micron scale patterns depends on the integration of chemical and physical concepts in surfactant, sol–gel, liquid crystal, surface, colloid and crystal growth science.[39,40] This entailed command over topological defects, director fields, surface charge, nucleation

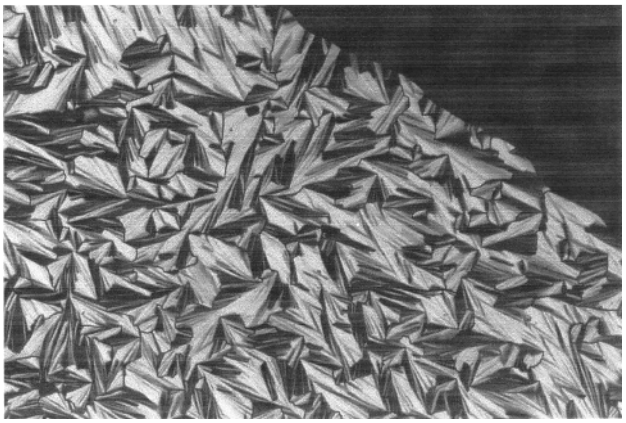

Fig. 16 Optical birefringence texture of lithium triflate–oligo(ethylene oxide) surfactant–mesoporous silica composite film.

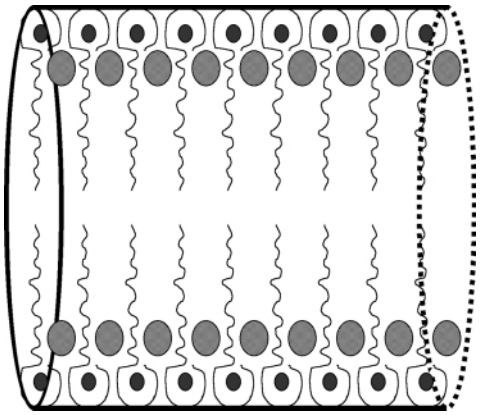

Fig. 17 Illustration of the channel architecture of lithium triflate–oligo(ethylene oxide) surfactant–mesoporous silica composite film.

and growth of polymerizable silicate micelles and liquid crystals. The availability of shaped forms of hexagonal mesoporous silica, like those illustrated in Scheme 6, raised the interesting possibility of using host–guest inclusion chemistry to synthesize a range of nanocomposites, nanowires and nanoclusters, which may possess unique electrical, optical and mechanical properties. Spatially self-limiting synthesis of this genre has enabled the production of polymer nanocomposites. Subsequent etching of the silica host was able to provide a route to polymer mesofibres with the same diameter as the channels of the host.

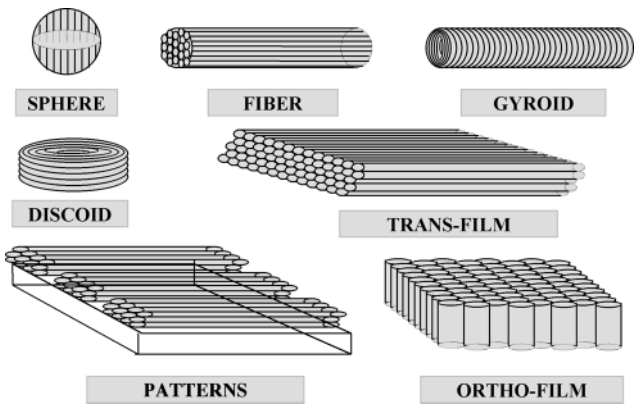

Scheme 6

To amplify, phenol and formaldehyde were introduced into the channels of hexagonal mesoporous silica. Exposure to gaseous hydrogen chloride induced a condensation polymerization of the monomer precursors in the channels to form a cross linked poly(phenolformaldehyde)–mesoporous silica nanocomposite material.[41] Proof for the formation of intrachannel poly(phenolformaldehyde) in mesoporous silica was obtained by TEM imaging of aqueous HF extracted fibers. They were found to have a diameter of *ca.* 20–30 Å and aspect ratios as high as 10^4, Fig. 18. Depending on the details of the HF extraction process the polymer could be formed as either individual strands or bundles of fibers.

Fig. 18 Transmission electron microscopy image of poly(phenolformaldehyde) mesofibers extracted from poly(phenolformaldehyde)–mesoporous silica composite. Scale bar = 10 nm.

Inorganic polymer–mesoporous silica nanocomposites

This paradigm has been effectively used to synthesize a poly(ferrocenylsilane)–mesoporous silica composite, Fig. 19, by the ring opening polymerization of a silaferrocenophane within the channels of hexagonal mesoporous silica.[42] Temperature controlled heating in the range 500–1000 °C caused the encapsulated polymer fibers to pyrolyze and form a well ordered, superparamagnetic ceramic–silica nanocomposite, Fig. 20. The composite materials were shown to contain monodisperse superparamagnetic iron nanoparticles embedded in a SiC/C matrix, housed within the channels of the mesoporous silica host.

Silicon–silica nanocomposite film

Work of a related kind concerns the synthesis of silicon nanoclusters in hexagonal mesoporous silica film that displays bright visible photoluminescence and nanosecond lifetimes.[43] This is notably distinct to the longer millisecond and microsecond emission lifetimes usually observed for nanocrystalline and bulk forms of silicon.[44–46] The process of creating the luminescent silicon–silica nanocomposite film is purely synthetic and works well under very mild conditions. It is simple to execute, low cost, may be integrated into existing silicon technology and could be suitable for mass production. The methodology may be useful for the fabrication of silicon-based light emitting diodes, optical interconnections, displays and chemical sensors.

To amplify, chemical vapor deposition (CVD) of disilane Si_2H_6 at 140 °C and 30 Torr in free standing, oriented hexagonal mesoporous silica film, yielded photoluminescent silicon nanoclusters. This mild CVD process necessitated the use of an incompletely polymerized mesoporous silica film that contained a high population of hydroxy SiOH wall sites as well as

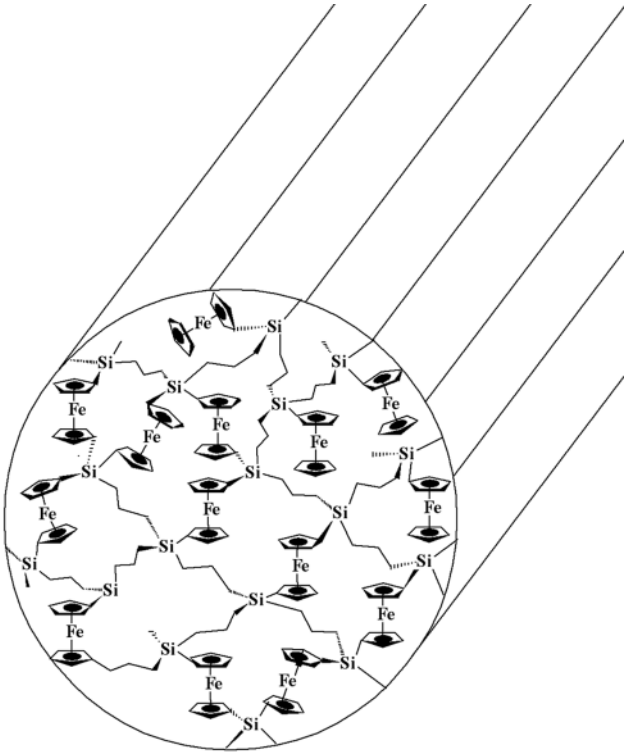

Fig. 19 Illustration of channel architecture of poly(ferrocenylsilane)–mesoporous silica composite.

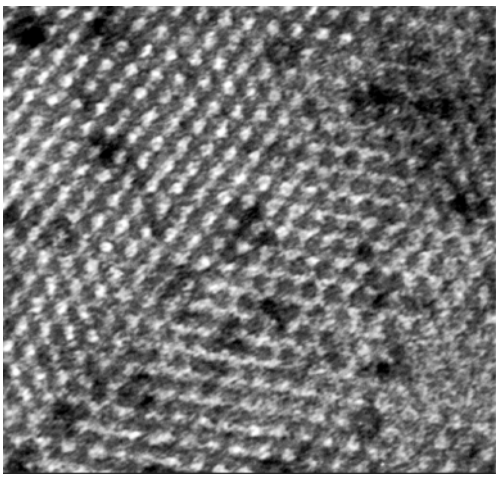

Fig. 20 Transmission electron microscopy image of superparamagnetic iron clusters in a silicon carbide–carbon matrix housed within the channels of a mesoporous silica host.

the surfactant template, required to make the film, within the channels. Exposure of the film to gaseous Si_2H_6 led to a silicon–silica nanocomposite film that displayed bright luminescence in the visible spectrum. Adsorption of Si_2H_6 into the film appeared to be facilitated by the surfactant imbibed within the channels. Anchoring of Si_2H_6 in the film occured at reactive SiOH sites located in the silica channel wall. Thermally induced hydrogen-elimination from anchored $Si_2H_6 \cdots SiOH$ and aggregation of silicon proceeded in the channel spaces of the film. This process restricted the growth of silicon clusters to the dimensions of the mesoscale channels. Raman, solid state NMR and luminescence spectroscopic techniques indicated that the size of the encapsulated silicon nanoclusters was *ca.* 1–2 nm and in this range they exhibited distinct structural and electronic properties compared to larger silicon nanocrystallites and bulk silicon, Fig. 21. This is believed to be the origin of the observed nanosecond lifetimes of the photoluminescence from the silicon–silica nanocomposite film.

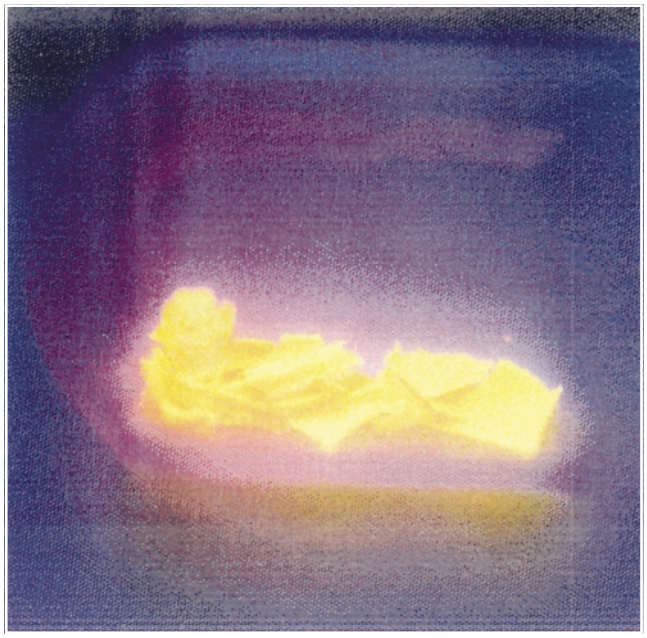

Fig. 21 Photoluminescence from 1–2 nm diameter silicon nanoclusters housed within the channels of hexagonal mesoporous silica film.

Buckling silicate liquid crystals

Morphosynthetic control of the nucleation, growth and polymerization of a lyotropic silicate liquid crystal has enabled sculpting of fiber, film and sphere shapes out of hexagonal mesoporous silica.[39,40] While topological defects (*e.g.* disclinations and dislocations) and colloidal interactions (*e.g.* electrical double layer, van der Waals) play a dominant role in the genesis of a particular form of mesoporous silica, more subtle elastic and compressive forces have been found to be responsible for the creation of radial patterns and twisted shapes like those shown in Fig. 22.

Patterning

Intriguing designs have been found on the surface of mesoporous silica shapes.[47] Radial patterns observed on discoid morphologies are particularly impressive, as judged by Fig. 23. While the relation between bulk and surface mesostructure, optical birefringence and morphology provided a useful insight into morphogenesis of curved mesoporous silica shapes, the origin of surface patterns remained an enigma and a challenge for materials chemistry. Analysis of the radial patterns of a large number of discoids showed the nodal frequency spans from zero to over a hundred with no obvious trend in the observed values. To gain an insight into the morphogenesis of radial patterns in mesoporous silica discoid shapes, the theory of elasticity for nematics with some modification was considered a logical starting point. The equilibrium shape of a hexagonal silicate mesophase confined to a regular discoid geometry (concentric co-axial director field, 2π line disclination) was obtained by integrating the free energy density over the volume of the liquid crystal, taking into account the surface tension term. It was found that the minimum energy of a regular discoid mesophase is attained by an elastic deformation to create a discoid with a radial pattern that was similar to those observed on mesoporous silica discoid shapes.

Although calculations predicted that radial patterns could appear on a planar discoid, it was found experimentally that radial patterns often occur on corrugated and/or sunken discoid shapes, Fig. 23. Clearly, some other distortion was operative in the silicate discoid mesophase besides just spontaneous elastic deformation and that had not been taken into account in the free energy calculations. The missing contribution to the growth process was believed to originate from longitudinal and radial

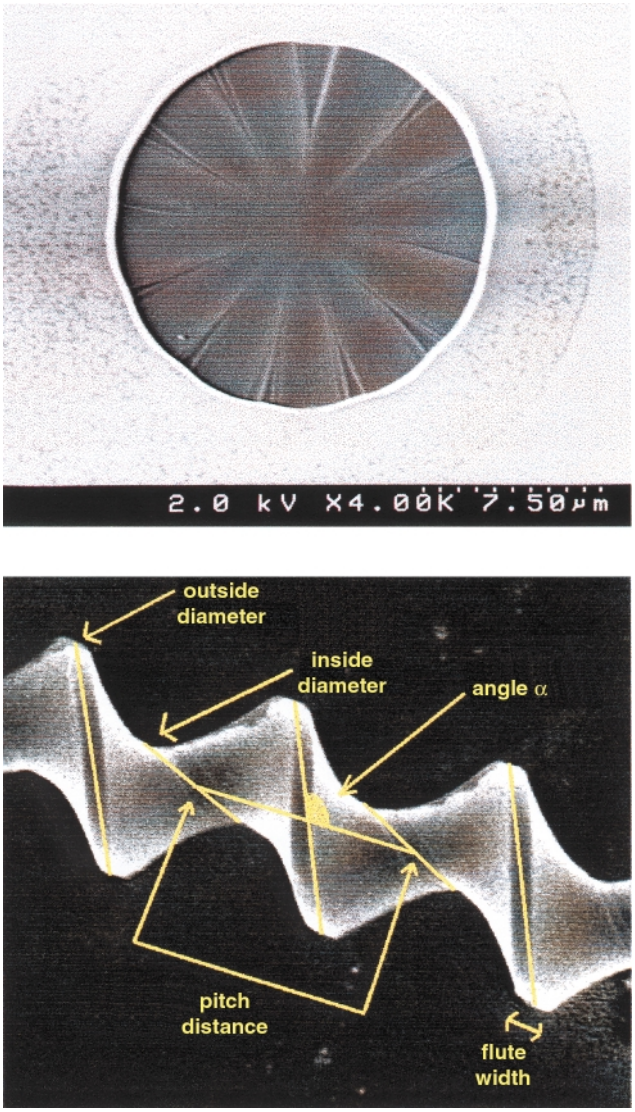

Fig. 22 Scanning electron microscope images of radially patterned discoid (top) and of hollow Archimedian screw (bottom) shapes both made of hexagonal mesoporous silica.

differential contraction of micelle rods that comprised the liquid crystal discoid and that was induced by polymerization of silicate to silica. Because growth of a discoid was imagined to occur from the center and radially outwards, the inner portion of the discoid was expected to be more polymerized than the outer region. The outcome of including polymerization induced differential contraction effects into the calculation of the shape of the radially patterned mesoporous silica discoid was to create sunken discoid shapes like those shown in Fig. 23.

Supramolecular origami

Similar kinds of polymerization induced differential contraction but now confined to a patch of hexagonal mesoporous silica film were found to be responsible for the morphogenesis of hollow helicoids of mesoporous silica.[48] It was found that a low acidity and high ionic strength medium favored a slow rate of silicification in a patch of mesoporous silica film. Hence polymerization-induced differential contraction of silicate micelle rods became influential in the formation of hollow helicoids rather than the formation of a mesoporous silica film. PXRD clearly defined the materials as hexagonal mesoporous silica and SEM images revealed shapes that resembled an Archimedian screw, Fig. 22. TEM images recorded for whole-mounted helicoids revealed that they were hollow with *ca.* 1 μm thick 'shell'. The shell was found to be composed of

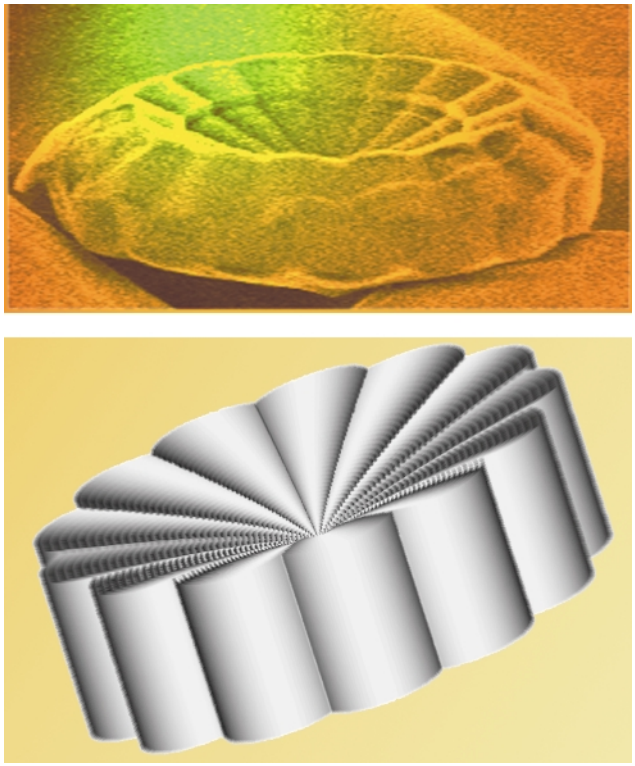

Fig. 23 Observed and calculated sunken and radially patterned hexagonal mesoporous silica discoid.

hexagonally close-packed *ca.* 5 nm diameter channels, which had a *ca.* 1 nm thick silica wall and appeared to spiral around the major axis of the helicoid. The dimensions of a significant collection of hollow helicoids were analyzed by measurements of SEM images. It was striking that diagnostic dimensions of the screw, namely pitch width and angle, flute width, and inside and outside diameter, were found to span a rather narrow range. Notably, the pitch angle α was centered at 70 and 110°, which, respectively, corresponded to left and right handed helices that occurred in essentially equal numbers within the same synthesis batch. From the collective evidence it was concluded that hollow helical cylinders originated from polymerization induced differential contraction of a hexagonal silicate liquid crystal 'patch', which contracted further into hollow helicoids made of hexagonal mesoporous silica, Fig. 24.

The folding mechanism illustrated in Fig. 24 is based upon both radial and longitudinal contractions across and parallel to the rods/channels, respectively, induced by polymerization of a hexagonal silicate mesophase to mesoporous silica. As the patch grows in area and thickness, older rods must undergo more polymerization and contraction than younger ones. Provided radial and longitudinal differential contractions in thickness are considered, they lead to diagonal bending of the patch because these two contractions act in mutually orthogonal directions. Within this diagonally folded patch, the volume of the micelle rods changes solely by contraction but not deformation. Therefore, the folded patch is stress-free, that is in an energetically favorable configuration.

Synthetic shape

The understanding that emerged from these studies has revealed new ways of controlling the growth and form of composite inorganic–organic mesostructured materials with novel topologies. Siliceous hollow helicoids with spiraling channels may find utility for separating viral or bacterial particles, in the synthesis of chiral macromolecules, and as micromolds for the fabrication of magnetically activated screws in microelectromechanical, microfluidic and microanalytical devices. The ability to intentionally synthesize micron-sized shaped objects

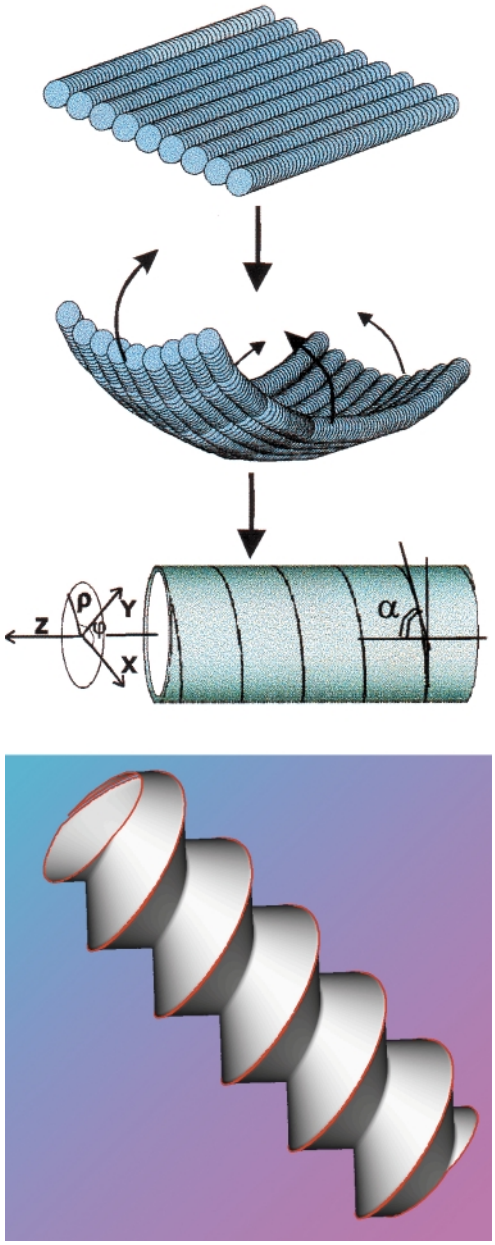

Fig. 24 Supramolecular origami: polymerization induced differential contraction and folding of a patch of hexagonal silicate liquid crystal film to give a mesoporous silica hollow cylinder (top) which further contracts to a hollow helicoid (bottom).

begins to point the way to self-assembling 'synthetic' micro-electro-mechanical machines (SMEMS), like the one imagined in Fig. 25. One might be able to employ this approach as an alternative or adjunct to currently employed MEMS techniques, which rely on the fabrication of components. This paradigm raises some intriguing possibilities for future 'panoscale' research aimed at the organization and integration of synthetically shaped materials for functional devices.

New nanocomposites: a fusion of synthetic organic and solid state materials chemistry

A brand new class of self-assembling nanocomposite materials called periodic mesoporous organosilica materials (PMOs) has recently been discovered.[49–53] What is so special about these nanocomposites is that for the first time organic functionality has been chemically integrated 'within' the framework of a solid state inorganic structure.

These organic–inorganic hybrids are prepared through the surfactant-templated hydrolytic polycondensation of bis(triethoxysilyl)organo precursors, $(EtO)_3SiRSi(OEt)_3$, in which

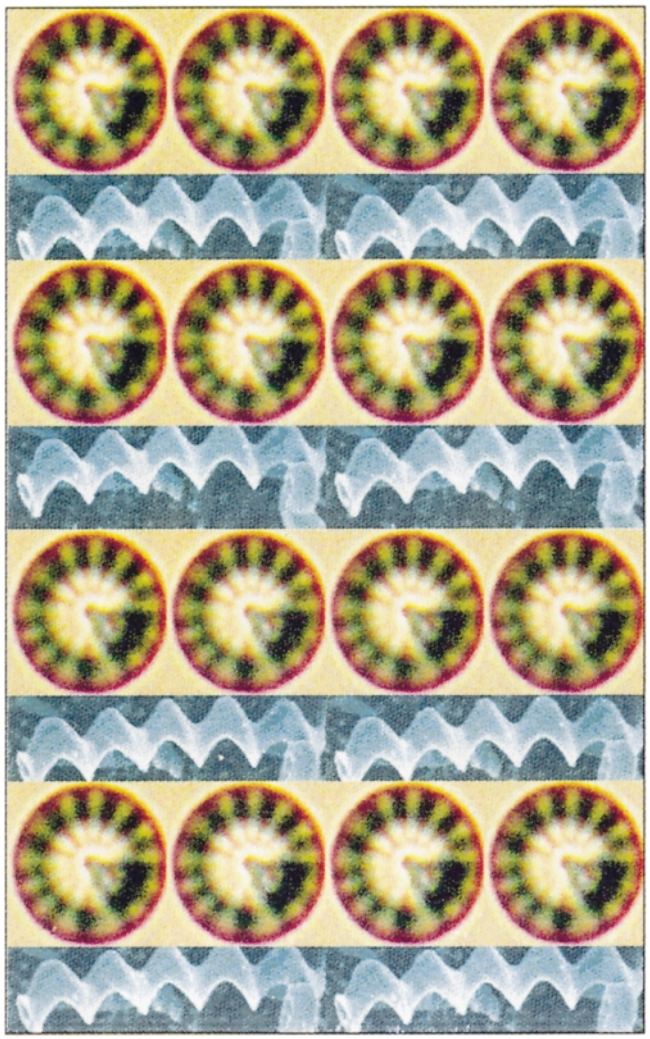

Fig. 25 Concept of futuristic synthetic microelectromechanical machines, SMEMS.

two sol–gel moieties are connected by an organic group R. Bridging organic groups that have been successfully integrated into the silica framework include ethane, ethene, methylene, benzene, thiophene, ferrocene and acetylene.[49–53] Significantly, the methodology also enables the synthesis of controlled morphology PMOs in the form of optically transparent monoliths and films (see Fig. 26).[54] This approach extends the realm of periodic mesoporous materials to 'chemistry of the channel walls' rather than limiting the 'chemistry to the channel space', which had been the situation until these reports.

The synthesis of PMOs fuses methodologies in organic synthesis, sol–gel chemistry and supramolecular assembly, to create a new class of nanocomposites in which the interface between the organic and inorganic components is under molecular scale control. What is so appealing about PMOs is the 'designed integration' of organic functionality 'inside' the actual framework of a solid state inorganic material, which exhibits crystalline mesoporosity. This is considered a breakthrough for several reasons. It allows the composition, hydrophobicity–hydrophilicity, and chemical properties of the mesoporous host to be tuned using chemistry. There is potential to chemically change the mesoporous material to modify the physical and mechanical properties of the mesoporous host—no other material designed thus far can claim this possibility. The functional groups do not hinder space inside the channels, as do terminally grafted organic groups. It permits a greater fraction (100% loading) of organic species to be placed in the framework of the material than other synthetic routes, which put organic groups inside the channel voids and are restricted to 25% loading before all order is lost. Also, it ensures a

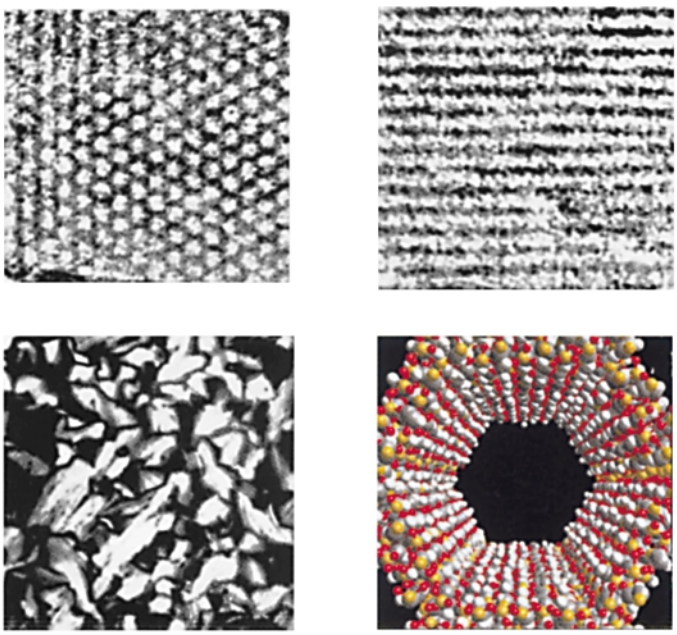

Fig. 26 Transmission electron micrograph (top left and right) and polarization optical microscope (bottom left) images and graphical representation of a single channel (bottom right) of optically transparent oriented hexagonal mesoporous ethenesilica film.[54]

homogeneous distribution of organic groups inside the walls of the materials.

Having reactive organic groups chemically integrated 'inside' the channel wall of periodic mesoporous silicas, rather than simply grafted to and hanging in the channel spaces, may prove to be advantageous for many applications. Moreover, there are additional advantages that may arise from the incorporation of organics into the 'backbone' of the material. Owing to the flexibility of organic spacers, PMO film and monolithic samples may be less prone to cracking, a problem that has always plagued research involving controlled morphology mesoporous silica materials. Moreover, the hardness and density of the bulk mesoporous organosilica may be tuned by changing the organic groups. This provides a new route to lightweight periodic mesoporous materials. Clearly, many opportunities abound for periodic mesoporous organosilicas with appropriately designed functional organics 'inside' the framework.

Value of panoscopic materials

Ultimately, the scientific and technological impact of any new class of materials depends on the ability to control the size, morphology and aggregate structure of primary particles. Self-assembling 'panoscopic' materials are no exception in this respect. They introduce hierarchy into materials chemistry and bode well for the development of materials and composites with novel properties, new functions and perceived utility in a range of applications in the biomedical, pharmaceutical, aerospace, automotive, construction, energy, electronics and photonics sectors. Possibilities for 'panostructured' materials include large molecule catalysis, membrane separation and sensing, battery electrolytes, low dielectric electronics packaging, chiral separation stationary phases, bone implants, chemical delivery vehicles, and toxic clean-up of water streams, The future looks very bright for self-assembling 'panoscopic' materials.

Acknowledgements

The research described in this personal account has profoundly influenced my way of thinking about materials chemistry. Chemical concepts in self-assembly, length scales, hierarchy, integration and topology have been introduced that hopefully will make a difference to the way materials research evolves in the new millennium. None of this would have been possible without the contributions of my talented coworkers whose names are listed in the references and who challenged me every day with important, insightful and creative ideas and suggestions. Dr Charles Kresge of Mobil, Dr Robert Bedard of UOP and Dr Juan Garces of Dow have championed the research in the U of T materials chemistry group for many years and were regular visitors in Toronto for many memorable brainstorming sessions, both in the laboratory and at great restaurants. During this exciting period of research, G. A. O. was awarded an Isaac Walton Killam Memorial Fellowship from the Canada Council. G. A. O. is also grateful to the Natural Sciences and Engineering Research Council (NSERC) of Canada for financial support of this work. Support and encouragement from the Chairman of the chemistry department, Dr Martin Moskovits, is appreciated. And last but not least I wish to express my gratitude to my best friend Linda Ozin who tries to make my writing more lucid.

References

1 R. Feynmann, *Sci. Eng.*, 1960, **23**, 22; G. A. Ozin, *Adv. Mater.*, 1992, **4**, 612.
2 G. A. Ozin, E. Chomski, D. Khushalani and M. MacLachlan, *Curr. Opin. Coll. Surf. Sci*, 1998, **3**, 181; S. Mann and G. A. Ozin, *Nature*, 1996, **382**, 313.
3 C. T. Kresge, M. Leonowicz, W. J. Roth, J. C. Vartuli and J. C. Beck, *Nature*, 1992, **359**, 710.
4 R. L. Whetten, M. N. Shafigullin, J. T. Khoury, T. G. Schaaff, I. Vezmar, M. M. Alvarez and A. Wilkinson, *Acc. Chem. Res.*, 1999, **32**, 397.
5 G. Decher, *Science*, 1997, **277**, 1232.
6 S. W. Keller, H. N. Kim and T. E. Mallouk, *J. Am. Chem. Soc.*, 1994, **116**, 8817.
7 R. C. Mucic, J. J. Storhoff, C. A. Mirkin and R. L. Letsinger, *J. Am. Chem. Soc.*, 1998, **120**, 12674.
8 Y. Xia and G. M. Whitesides, *Angew. Chem., Int. Ed.*, 1998, **37**, 550.
9 C. R. Martin, *Science*, 1994, **266**, 1961.
10 G. M. Whitesides, *Sci. Am.*, 1995, **273**, 146.
11 *Integrated Chemical Systems, A Chemical Approach to Nanotechnology*, ed. A. J. Bard, John Wiley and Sons, Inc., New York, 1994.
12 T. Cassagneau, T. E. Mallouk and J. H. Fendler, *J. Am. Chem. Soc.*, 1998, **120**, 7848.
13 D. L. Feldheim, K. C. Grabar, M. J. Natan and T. E. Mallouk, *J. Am. Chem. Soc.*, 1996, **118**, 7640.
14 J. E. Bowen Katari, V. L. Colvin and P. Alivasatos, in *Biomimetic Materials Chemistry*, ed. S. Mann, VCH, New York, 1996.
15 H. Sirringhaus, N. Tessler and R. H. Friend, *Science*, 1998, **280**, 1741.

16 T. Cassagneau and J. H. Fendler, *Adv. Mater.*, 1998, **10**, 877.
17 O. M. Yaghi, H. Li, C. Davis, D. Richardson and T. L. Groy, *Acc. Chem. Res.*, 1998, **31**, 474.
18 M. Antonietti and C. Göltner, *Angew. Chem., Int. Ed. Engl.*, 1997, **36**, 910.
19 M. Templin, A. Franck, D. Chense, H. Leist, Y. Zhang, R. Ulrich, V. Schädler and U. Wiesner, *Science*, 1997, **278**, 1795.
20 A. Van Blaaderen, *Science*, 1998, **282**, 887.
21 S. Oliver, A. Kuperman, N. Coombs, A. Lough and G. A. Ozin, *Nature*, 1995, **378**, 47.
22 S. R. J. Oliver and G. A. Ozin, *J. Mater. Chem.*, 1998, **8**, 1081.
23 S. Oliver, N. Coombs, A. Kuperman and G. A. Ozin, *Adv. Mater.*, 1995, **7**, 931.
24 G. A. Ozin, D. Khushalani, S. Oliver, N. Coombs, G. C. Shen, I. Sokolov and H. Yang, *J. Chem. Soc., Dalton Trans.*, 1997, 3941.
25 G. A. Ozin, *Acc. Chem. Res.*, 1997, **30**, 17.
26 *Art Forms in Nature*, ed. Ernst Haekel, Prestel, Munich, 1998.
27 *On Growth and Form, The Complete Revised Edition*, ed. D'Arcy W. Thompson, Dover, 1992.
28 *Structural Biomaterials*, ed. J. F. V. Vincent, Princeton University Press, Princeton, NJ, 1990.
29 I. Soten and G. A. Ozin, *J. Mater. Chem.*, 1999, **9**, 703.
30 N. Varaksa, N. Coombs, J. E. D. Davies, D. D. Perovic, M. Ziliox and G. A. Ozin, *J. Mater. Chem.*, 1997, **7**, 1601.
31 *Structure and Chemistry of the Apatites and Other Calcium Orthophosphates*, ed. J. C. Elliot, Elsevier, New York, 1994.
32 T. Jiang and G. A. Ozin, *J. Mater. Chem.*, 1997, **7**, 2213.
33 I. Sokolov, T. Jiang and G. A. Ozin, *Adv. Mater.*, 1998, **10**, 942.
34 R. W. J. Scott, M. J. MacLachlan and G. A. Ozin, *Curr. Op. in Solid State Mater. Sci.*, 1999, **4**, 113.
35 M. J. MacLachlan, N. Coombs and G. A. Ozin, *Nature*, 1999, **397**, 681; M. J. MacLachlan, N. Coombs, R. L. Bedard, S. White, L. Thompson and G. A. Ozin, *J. Am. Chem. Soc.*, 1999, **121**, 12005.
36 D. Khushalani, G. A. Ozin and A. Kuperman, *J. Mater. Chem.*, 1999, **9**, 1483.
37 D. Khushalani, Ö. Dag, G. A. Ozin and A. Kuperman, *J. Mater. Chem.*, 1999, **9**, 1491.
38 Ö. Dag, A. Verma, G. A. Ozin and C. T. Kresge, *J. Mater. Chem.*, 1999, **9**, 1475.
39 H. Yang, C. T. Kresge and G. A. Ozin, *Adv. Mater.*, 1998, **10**, 883.
40 G. A. Ozin, *Can. J. Chem.*, 1999, **77**, 2001.
41 S. A. Johnson, D. Khushalani, N. Coombs, T. E. Mallouk and G. A. Ozin, *J. Mater. Chem.*, 1998, **8**, 13.
42 M. J. MacLachlan, P. Aroca, N. Coombs, I. Manners and G. A. Ozin, *Adv. Mater.*, 1998, **10**, 144.
43 Ö. Dag, G. A. Ozin, H. Yang, C. Reber and G. Bussiere, *Adv. Mater.*, 1999, **11**, 474.
44 A. G. Cullis, L. T. Canham and P. D. J. Calcott, *J. Appl. Phys.*, 1997, **82**, 909.
45 G. A. Ozin, E. Chomski, Ö. Dag and A. Kuperman, *Adv. Mater. Chem. Vap. Deposit*, 1996, **2**, 8.
46 G. A. Ozin, Ö. Dag and A. Kuperman, *Adv. Mater.*, 1995, **7**, 72.
47 I. Sokolov, H. Yang, G. A. Ozin and C. T. Kresge, *Adv. Mater.*, 1999, **11**, 636.
48 S. M. Yang, I. Y. Sokolov, N. Coombs, C. T. Kresge and G. A. Ozin, *Adv. Mater.*, 1999, **11**, 1427.
49 S. Inagaki, S. Guan, Y. Fukushima, T. Ohsuna and O. Terasaki, *J. Am. Chem. Soc.*, 1999, **121**, 9611.
50 B. J. Melde, B. T. Holland, C. F. Blanford and A. Stein, *Chem. Mater.*, 1999, **11**, 3302.
51 T. Asefa, M. J. MacLachlan, N. Coombs and G. A. Ozin, *Nature*, 1999, **402**, 867.
52 T. Asefa, M. J. MacLachlan, N. Coombs and G. A. Ozin, *Angew. Chem.*, 1999, in press.
53 C. Ishii, T. Asefa, N. Coombs, M. J. MacLachlan and G. A. Ozin, *Chem. Commun.*, 1999, 2539.
54 O. Dag, C.-Y. Ishii, T. Asefa, M. J. MacLachlan, H. Grondey and G. A. Ozin, *Adv. Mater.*, 1999, submitted.

Paper a905090f

Aggregate formation from 3-alkylindoles: amphiphilic models for interfacial helix anchoring groups

Ernesto Abel, Stephen L. De Wall, W. Barry Edwards, S. Lalitha, Douglas F. Covey and George W. Gokel*

Bioorganic Chemistry Program and Department of Molecular Biology & Pharmacology, Washington University School of Medicine, 660 S. Euclid Ave., Campus Box 8103, St. Louis, MO 63110 USA. E-mail: ggokel@molecool.wustl.edu

Received (in Columbia, MO, USA) 30th November 1999, Accepted 9th December 1999, Published on the Web, 29th February 2000

Indole can function as an amphiphile headgroup, but the counter-intuitive observation that 3-substituted indoles form less stable aggregates than the *N*-substituted isomers has been addressed by use of a Langmuir–Blodgett trough.

Many proteins that control the passage of cations and small molecules across membrane boundaries are thought to involve multiple α-helical strands that organize into a pore.[1] In most cases, this notion is based on a combination of sequence analysis and hydrophobicity plots[2] but firm structural data has come to hand recently for the K*sc*A channel of *Streptomyces lividans*[3] and the mechanosensitive ion channel homologue from *Mycobacterium tuberculosis.*[4] In many cases, the α-helices are thought to be connected by 'loops' that do not enforce rigid structural arrangements on the transmembrane segments. It has been postulated, for example, that the tryptophan residues of gramicidin serve as anchors at the membrane boundary to stabilize the single-strand, head-to-head dimer structure.[5] The interesting recent controversy over the active channel structure of gramicidin[6] has been argued partly in terms of indole position within the phospholipid bilayer.[7] It has also been noted 'that Trp and Leu are equally hydrophobic in character and able to embed in a bilayer membrane'.[8]

If transmembrane proteins require alignment of multiple α-helical segments for effective function, tryptophan is a reasonable candidate to serve that purpose. Indeed, the known solvatochromism[9] of the indole sidechain and tryptophan-rich[10] and highly conserved periplasmic loops[11] suggest an anchoring function. In the first stage of the present work, the strategy was to determine if vesicles could be formed from single-strand alkanes[12] terminated with a headgroup corresponding to the tryptophan sidechain.

One measure of a group's 'anchoring potential'[13] could be obtained by evaluating amphiphiles in which indole served as headgroup.[14] We felt that the loss of the NH residue resulting from *N*-alkylation of indole constituted a stringent test of the potential for this group to function as an anchor. We thus prepared several *N*-alkylindoles and assessed their ability to form aggregates. When the alkyl chains were of sufficient length, *N*-alkylindoles formed stable aggregates that were characterized by laser light scattering, electron microscopy, and dye entrapment.[15] We report here that the isomeric 3-alkylindoles form aggregates as well but their behavior is quite different.

3-Methylindole **1** was obtained commercially. Compounds **2**–**6** were obtained by treatment of indole with LiH in THF followed by addition of the alkylating agent (Scheme 1). Yields were modest (20–40%); the major by-products were the *N*-substituted isomer and/or the disubstituted compound. The previously unknown materials **2**–**6** were obtained either as oils or low-melting solids.[16]

Aggregates were formed from aqueous suspensions of the amphiphiles reported here by using the lipid hydration[17] vesicle preparation method.[18] Aggregate size was assessed by using a standard laser light scattering instrument[19] and negative stain electron microscopy. Aggregates were not observed for **1** or **2**, which have 3-methyl and 3-hexyl sidechains, respectively.

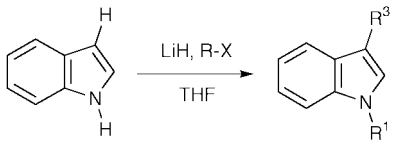

1 R^1 = H, R^3 = CH_3
2 R^1 = H, R^3 = $(CH_2)_5CH_3$
3 R^1 = H, R^3 = $(CH_2)_9CH_3$
4 R^1 = H, R^3 = $(CH_2)_{17}CH_3$
5 R^1 = $(CH_2)_{17}CH_3$, R^3 = H
6 R^1 = R^3 = $(CH_2)_{17}CH_3$

Scheme 1

Large aggregates (340 ± 93 nm) were observed for **3** (R′ = *n*-decyl) and when the 3-sidechain was *n*-octadecyl (**4**), the aggregate diameter was 142 ± 34 nm. The latter value compared with 138 nm (narrow size distribution) observed when the octadecyl chain was attached to indole at the 1-position. When both the 1- and 3-positions of indole were substituted by *n*-octadecyl groups, light scattering showed that the liposomes had an average diameter of 210 nm (size distribution was broad). Aggregates were further characterized by electron microscopy. Aggregates formed from **3** are shown in the accompanying photomicrograph (Fig. 1). These aggregates proved to be too fragile to stain with 0.2% uranyl acetate, converting into large, ill-defined structures. Previous studies with the corresponding *N*-alkylindoles suggested that the aggregates formed from those isomers were robust. Moreover, when an aqueous suspension of *N*-*n*-decylindole was maintained at ambient temperature in the dark for one week, the unimodal diameter increased from 272 ± 43 to 373 ± 130 nm. No other alteration in the system could be detected. In contrast, an aqueous suspension of the isomer **3** was monitored weekly

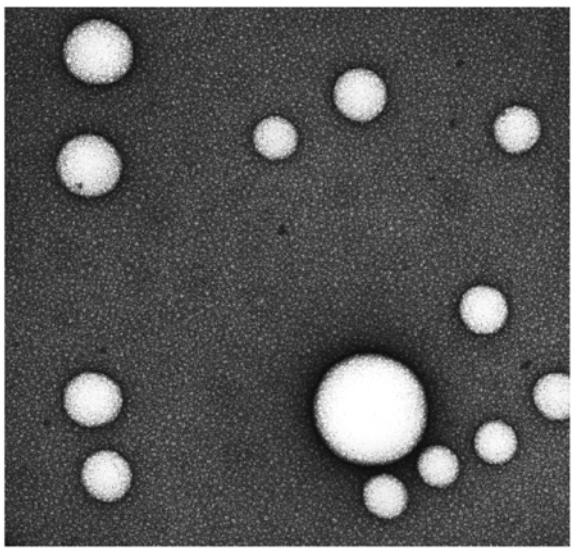

Fig. 1 Photomicrograph of **3** (field of view = 2000 × 2000 nm).

DOI: 10.1039/a909527f

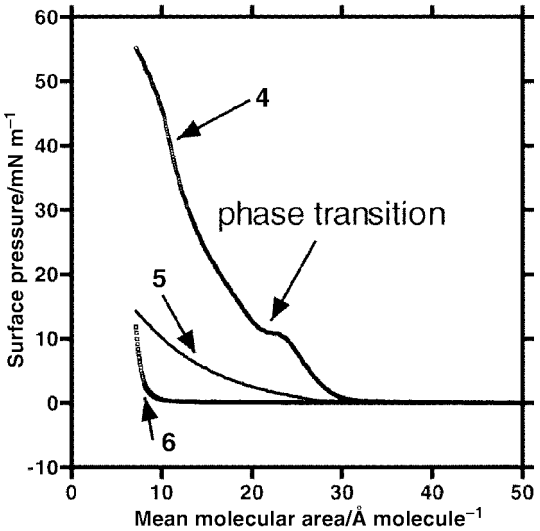

Fig. 2 Pressure–area isotherms for **4**–**6**.

during one month. The size observed for the aggregates, 340 ± 93 nm, remained constant. However, a foamy residue was observed to deposit on the walls of the vessel during this period and the amount of very large particles[20] detected by the laser light scattering instrument increased from 0% to 7%. It thus appears that some fusion[21] and precipitation have occurred.

A dye entrapment study conducted on vesicles formed from *N*-decylindole using the fluorescent dye carboxyfluorescein (1 and 100 mM) found inclusion to be 8%.[15] When such a study was undertaken with **3**, the observed aggregate size tripled from 340 to ~1000 nm. The inclusion was calculated to be 3.5% but the variation in aggregate size makes the meaning of the inclusion volume unclear. Alternative attempts to entrap other dyes, methylumbellyferyl-D-glucopyranose, or Na^{125}I also proved to be equivocal. The fragility of vesicles formed from 3-alkylindoles, which retain a free NH, compared to the stability of the *N*-substituted indoles, was remarkable. This seemed counter-intuitive as the free NH was expected to make the indole more capable of hydrogen bonding and thus interacting with water.

When the alkyl group is attached at indole's 3-position, the indolyl NH remains free and available to interact with proximate water. Hydrogen bonding could, in principle, compete with the organizational force[22] available from π-stacking.[23] When vesicles form, association of the lipid tails help to stabilize the overall structure. When there is no NH residue available for H-bonding, the hydrophobic forces are expected to dominate vesicular organization. The experimentally-determined pressure–area isotherm π–A curves (π = surface pressure, Langmuir–Blodgett trough) for compounds **4**–**6** at 20 °C are shown in Fig. 2. The *N*-alkylated indoles **5** and **6** gave no significant isotherm. 3-Octadecylindole **4** revealed a transition (20 °C) from expanded to condensed phase (surface pressure of the condensed phase, π_c, of ~12 mN m^{-1}) typical of many known amphiphiles when the monolayer is below its critical temperature.[24] The mean molecular area of the expanded phase at this pressure was 22.5 Å^2 molecule^{-1}. The area of the condensed phase was obtained by extrapolating the condensed isotherm **($\pi = \pi_c$).** The corresponding value is ~20.5 Å^2 molecule^{-1}. Unlike various other monolayer systems known in the literature,[25] the monolayers formed from **4**, which has an accessible NH functional group, did not collapse. Instead, the surface pressure rose until the trough barriers could not further compress the layer.

An important conclusion of the present work is that indole is capable of serving as a head group in the formation of stable aggregates, whether the alkyl chain is attached at the 1-(*N*) or 3-position. As expected for a typical amphiphile, aggregates are observed only when the alkyl chains are sufficiently long. These aggregates were characterized by standard methods. The difference in behavior for the isomeric indole amphiphiles may be understood in terms of hydrogen bonding. The Langmuir–Blodgett trough work suggests that lipid–lipid and headgroup stacking interactions control the formation of aggregates. When the NH residue is free (3-alkylindoles), the interaction with water becomes dominant, altering the stability of the aggregates. The multiple indolyl (Trp) headgroups in membrane-inserted gramicidin are focused to the aqueous boundary and stabilize the position of the structure. The present results demonstrate that indole may function generally as an organizing element in membrane-bound peptide[26] and protein structures.

We thank the NIH for grants (GM-36262 to G. W. G.) and (GM-47969 to D. F. C.) that supported this work.

Notes and references

1 G. Von Heijne, *Annu. Rev. Biophys. Biomol. Struct.*, 1994, **23**, 167.
2 T. E. Creighton, *Proteins: Structures and Molecular Properties*, 2nd edn., Freeman, New York, 1993.
3 D. A. Doyle, J. M. Cabral, R. A. Pfuetzner, A. Kuo, J. M. Gulbis, S. L. Cohen, B. T. Chait and R. MacKinnon, *Science*, 1998, **280**, 69.
4 G. Chang, R. H. Spencer, A. T. Lee, M. T. Barclay and D. C. Rees, *Science*, 1998, **282**, 2220.
5 W. Hu, K.-C. Lee and T. A. Cross, *Biochemistry*, 1993, **32**, 7035; R. R. Ketchem, W. Hu and T. A. Cross, *Science*, 1993, **26**, 1457.
6 B. M. Burkhart, N. Li, D. A. Langs, W. A. Pangborn and W. L. Duax, *Proc. Natl. Acad. Sci. USA*, 1998, **95**, 12 950; B. M. Burkhart, R. M. Gassman, D. A. Langs, W. A. Pangborn, W. L. Duax and V. Pletnev, *Biopolymers*, 1999, **51**, 129.
7 R. E. Koeppe II, F. J. Sigworth, G. Szabo, D. W. Urry and A. Woolley, *Nat. Struct. Biol.*, 1999, **6**, 609; T. A. Cross, A. Arseniev, B. A. Cornell, J. H. Davis, J. A. Killian, R. E. Koeppe II, L. K. Nicholson, F. Separovic and B. A. Wallace, *Nat. Struct. Biol.*, 1999, **6**, 610.
8 B. M. Burkhart and W. L. Duax, *Nat. Struct. Biol.*, 1999, **6**, 611; W.-M. Yau, W. C. Wimley, K. Gawrisch and S. H. White, *Biochemistry*, 1998, **37**, 14713.
9 T. B. Truong, *J. Phys. Chem.*, 1980, **84**, 964; S. R. Meech, D. Phillips and A. G. Lee, *Chem. Phys.*, 1983, **80**, 317; H. Lami and N. Glasser, *J. Chem. Phys.*, 1986, **96**, 4768.
10 M. Schiffer, C.-H. Chang and F. J. Stevens, *Protein Eng.*, 1992, **5**, 213.
11 R. E. Jacobs and S. H. White, *Biochemistry*, 1989, **28**, 3421.
12 T. Kunitake, Y. Okahata, M. Shimomura, S. Yasunami and K. Takarabe, *J. Am. Chem. Soc.*, 1981, **103**, 5401.
13 R. E. Jacobs and S. H. White, *Biochemistry*, 1986, **25**, 2605; 1989, **28**, 3421.
14 W. C. Wimley and S. H. White, *Biochemistry*, 1992, **31**, 12 813; A. S. Ladokhin and P. W. Holloway, *Biophys. J.*, 1995, **69**, 506.
15 E. Abel, M. F. Fedders and G. W. Gokel, *J. Am. Chem. Soc.*, 1995, **117**, 1265.
16 The spectral properties of all new compounds were as expected and combustion analytical data within ±0.4% for each element were obtained.
17 L. Saunders, J. Perrin and D. B. Gammock, *J. Pharm. Pharmacol.*, 1962, **14**, 567.
18 The *N*-alkylindole suspensions were sonicated using either a bath or tip sonicator (40 MHz) at ice-bath temperature and the 3-alkylindoles were irradiated at 40 °C. Sonication was maintained for 20–45 min, shorter times being required for the 3-alkylindoles.
19 The dynamic light scattering measurements were carried out by using a Coulter Model N4MD spectrophotometer equipped with a 4 mW helium–neon laser source, operated at 632.8 nm. The detection angle was fixed at 90°.
20 The light scattering instrument's internal calculation program reports large particles as 'dust'.
21 F. M. Menger and M. I. Angelova, *Acc. Chem. Res.*, 1998, **31**, 789.
22 E. E Tucker and S. D. Christian, *J. Phys. Chem.*, 1979, **83**, 426.
23 C. A. Hunter and J. K Sanders, *J. Am. Chem. Soc.*, 1990, **112**, 5525.
24 F. MacRitchie, *Chemistry at Interfaces*, Academic Press, New York, 1990; M. C. Phillips and D. Chapman, *Biochim. Biophys. Acta*, 1968, **163**, 301; M. W. Kim and D. S. Cannell, *Phys. Rev. A*, 1976, **13**, 411; O. Albrecht, H. Gruler and E. Sackmann, *J. Phys. Fr.*, 1978, **39**, 127; K. Motomura, T. Terazono, H. Matuo and R. Matuura, *J. Colloid. Interface. Sci.*, 1976, **57**, 52; D. A. Cadenhead, F. Muller-Landau and B. M. J. Kellner, *Ordering in Two Dimensions*, ed. S. K. Sinha, Elsevier, Amsterdam, 1980, p. 73.
25 J. P. Slorte, *Biochim. Biophys. Acta*, 1992, 326.
26 A. S. Ladokhin, M. E. Selsted and S. H. White, *Biophys. J.*, 1997, **72**,794.

Communication a909527f

Thin layer chromatography as a tool for reaction optimisation in microwave assisted synthesis

Lorenzo Williams

SINTEF Applied Chemistry, P.O. Box 124 Blindern, N-0314 Oslo, Norway.
E-mail: Lorenzo.Williams@chem.sintef.no

Received (in Liverpool, UK) 23rd November 1999, Accepted 18th January 2000,
Published on the Web, 1st March 2000

Reaction parameters for the microwave assisted synthesis of N′-substituted arylpiperazines were optimised *via* their rapid synthesis on thin layer chromatography (TLC) plates.

Piperazines form the backbone of many biologically interesting molecules.[1] Their incorporation into biologically active molecules has even been associated with an increase in potency.[2] Recent examples of piperazine-containing molecules include many fluoroquinolone antibiotics, the HIV protease inhibitor Crixivan™ and the PDE-5 inhibitor Viagra™, used for male erectile dysfunction. As part of a program dedicated to the development of new techniques for combinatorial chemistry,[3] we describe herein a simple procedure for reaction optimisation in microwave assisted synthesis.[4] This procedure is exemplified by the rapid derivatisation of a number of monoarylpiperazines.

Previously we synthesised several 2-iodobenzylamines as radical precursors for an investigation of the α-alkylation of amines *via* a 1,5-hydrogen shift.[5] During the synthesis of these precursors it was observed that, in some cases, amines would react partially with benzyl halides when co-spotted on a TLC plate.[6] After elution a new spot was sometimes seen that corresponded to that of the expected benzylated amine product. Product conversion was often poor since considerable amounts of unreacted starting materials were usually present. We were able to utilise this information in the design of methodology toward the rapid and efficient synthesis of the arylpiperazine derivatives shown in Table 1.†‡

Initial observations for the co-spotting of an arylpiperazine and an electrophile, either neat or as dilute solutions in CH_2Cl_2, onto a TLC plate confirmed the above in that reactions occurred sporadically if at all, and without complete consumption of the starting material. It was anticipated that the reactions could be accelerated by microwave irradiation of the reagents on a glass-backed TLC plate prior to elution, since the TLC plate would act as a support without the silica gel absorbing or restricting the transmission of microwaves. TLC plates (Merck silica gel 60 F254) with preadsorped reagents were irradiated in a domestic microwave oven with varying power outputs and at various time intervals. Method of application, loading and stoichiometry of the reagents were varied as an array on plates in order to discover the optimum conditions for the reaction. After cooling, the plates were eluted and viewed under UV light (254 nm) and by development with either I_2 or ninhydrin. The most convenient method involved the application of reagents in solution (at a concentration of *ca*. 1 mg in 1 ml CH_2Cl_2) in 5 μl aliquots onto a plate with a 0.2 mm layer of SiO_2. Complete consumption of one or other of the reagents occurred after irradiation for 5 min at an output of 585 watts. Reactions were complete under these conditions, regardless of the stoichiometry of the reagents. Only one product spot was seen, the R_f value of which was consistent with that of the expected product. Confirmation was later afforded through direct synthesis (*vide infra*). A rather serendipitous discovery was made in that excesses of sulfonyl chlorides appeared to degrade under these conditions to a product with a polar baseline spot, presumably the corresponding sulfonic acid. Fortunately the degradation appeared to occur rather more slowly than the desired transformation, and the reactions remained unaffected since the arylpiperazine component was completely consumed to yield the desired product.

Upon identification of the optimum reaction parameters, the reactions were scaled up to several hundred milligrams in size. Reagents were dissolved in a minimum amount of CH_2Cl_2 and adsorbed onto silica gel (230–400 mesh). After removal of solvent the mixture was irradiated for 5 min. The silica gel was allowed to cool and was then washed with CH_2Cl_2 and the washings filtered through a Celite pad. Evaporation of the solvent *in vacuo* yielded the desired product in high yield and purity. Although unnecessary, it was often advantageous to use a slight excess of the amine component to drive the reaction to completion and facilitate isolation of the final product in pure form, without the need to resort to chromatography. Reactions involving equimolar amounts of reagents worked equally as

Table 1 Arylpiperazine derivatives formed *via* microwave assisted synthesis

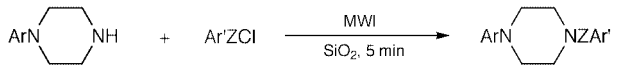

Entry	Ar	Ar′	Z	Isolated yield[a] (%)
1	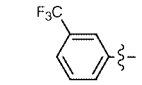		SO_2	91
2	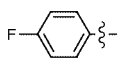	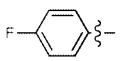	SO_2	77
3	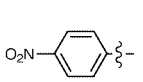	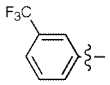	SO_2	96
4		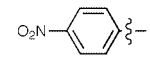	CH_2	99
5	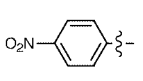	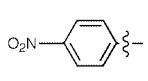	CH_2	99
6	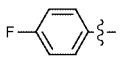		CH_2	75
7		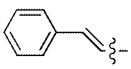	CO	93
8		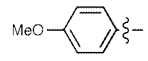	CO	97
9	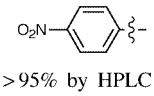	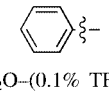	CO	72

[a] Purity >95% by HPLC [10% H_2O–(0.1% TFA)MeCN on a Hypersil column].

DOI: 10.1039/a909305b

well, though occasionally the purity of the final product was compromised due to the presence of small amounts of unreacted halides. Fortuitously, reactions involving an equimolar amount or excess of sulfonyl halides were unaffected since the unreacted material degraded under the reaction conditions (*vide supra*). Interestingly, all reactions were high yielding and afforded *N′*-substituted products in high purity. The presence of electron-withdrawing groups on the arylpiperazine, *e.g.* 1-(4-nitrophenyl)piperazine in entries 3, 5, and 9, didn't appear to impede reaction. It has been reported previously that the presence of electron-withdrawing groups in the aryl ring of arylpiperazines diminishes the nucleophilicity of the secondary amine.[7]

Reactions on silica gel were performed without incident and somewhat surprisingly without salt formation. It is thought that silica gel scavenges any HCl formed in the reaction, thereby negating salt formation. When reactions were performed in the absence of silica gel or by using finely ground glass as the support none of the desired products were isolated. TLC analysis of these reactions indicated the absence of product. However, the presence of a new and more polar baseline spot was seen, presumably the corresponding amine salt formed in the presence of HCl generated *in situ*.

In summary, reactions performed on a TLC plate are a powerful tool for rapid reaction optimisation. The method is suitable in particular for microwave assisted reactions since the plate can be used as an inert support. The technique is applicable to combinatorial chemistry where reactions often have to be optimised prior to library synthesis. Moreover it is possible to combine this technique with bioautographical screening and analytical methods.[8] Use of this technology for the synthesis and screening of combinatorial libraries will be described in due course.

Aud Bouzga and Ole Saastad are gratefully acknowledged for NMR and GCMS analysis.

Notes and references

† All compounds gave satisfactory spectral data.

‡ *Typical procedure*: 1-(α,α,α-trifluoro-*m*-tolyl)piperazine (0.25 g, 1.1 mmol) in CH_2Cl_2 (1 ml) and 2-nitrobenzenesulfonyl chloride (0.24 g, 1.1 mmol) in CH_2Cl_2 (1 ml) were mixed thoroughly with silica gel (Merck 230–400 mesh, 1 g) in a glass vial and the solvent removed under reduced pressure. The mixture was then irradiated in a domestic microwave oven (Electrolux NF4884) at an output of 585 watts for 5 min. Water (50 ml) was placed in another vessel and irradiated simultaneously. After cooling to room temperature the product was dissolved in CH_2Cl_2 (*ca.* 5 ml) and filtered through a Celite pad. The solvent was removed under reduced pressure to afford the corresponding sulfonamide as a yellow solid (0.41 g, 91%, > 98% pure by HPLC); R_f 0.55 (MeOH–CH_2Cl_2, 5%); δ_H($CHCl_3$, 300 MHz) 8.01 (1H, d, *J* 9.3), 7.72 (2H, m), 7.63 (1H, m), 7.37 (1H, t, *J* 7.7), 7.14 (3H, m), 3.51 (4H, m), 3.31 (4H, m).

1 See for example: M. Perez, C. Fourrier, I. Sigogneau, P. J. Pauwels, C. Palmier, G. W. John, J.-P. Valentin and S. Halazy, *J. Med. Chem.*, 1995, **38**, 3602.
2 M. E. Jung, E. C. Yang, B. T. Vu, M. Kiankarimi, E. Spyrou and J. Kaunitz, *J. Med. Chem.*, 1999, **42**, 3899 and references therein.
3 L. Williams, Proceedings of ECSOC-3, The Third International Electronic Conference on Synthetic Organic Chemistry, http://www.mdpi.org/ecsoc-3.htm, September 1–30, 1999, ed. E. Pombo-Villar, R. Neier and S.-K. Lin, CD-ROM edition ISBN 3-906980-04-9, to be published in 2000 by MDPI, Basel, Switzerland; L. Williams, 6th Annual Exploiting Molecular Diversity meeting, San Diego, 1999, 4th Annual High-Throughput Organic Synthesis meeting, San Diego, 1999.
4 For a comprehensive overview of microwave heating in synthesis, see *Microwave-Enhanced Chemistry. Fundamentals, Sample Preparation and Applications*, ed. H. M. Kingston and S. J. Haswell, ACS, Washington, DC, 1997.
5 K. Undheim and L. Williams, *J. Chem. Soc., Chem. Commun.*, 1994, 883; L. Williams, S. E. Booth and K. Undheim, *Tetrahedron*, 1994, **50**, 13 697.
6 L. Williams, unpublished results.
7 M. Hepperle, J. Eckert and D. Gala, *Tetrahedron Lett.*, 1999, **40**, 5655.
8 Patent pending.

Communication a909305b

Synthesis and ring enlargement of 2-ethoxycarbonyl-1-silacyclobutanes

Gerhard Maas* and Susanne Bender

Division of Organic Chemistry I, University of Ulm, Albert-Einstein-Allee 11, D-89081 Ulm, Germany. E-mail: gerhard.maas@chemie.uni-ulm.de

Received (in Liverpool, UK) 23rd November 1999, Accepted 4th February 2000, Published on the Web, 3rd March 2000

2-Ethoxycarbonyl-1-silacyclobutanes were synthesized by intramolecular C–H insertion of carbenes generated photochemically from α-(di-*tert*-butylsilyl)-α-diazoacetates; they undergo smooth thermal ring-expansion by a 1,3(C → O) silyl shift to form 6-ethoxy-1-oxa-2-silacyclohex-5-enes.

Silacyclobutanes are useful precursors for other organosilicon compounds (*e.g.* larger silaheterocycles by ring expansion,[1,2] silaethenes by cycloreversion,[3] organosilicon polymers by ring opening[4]) and can be employed in C–C bond forming processes, such as the aldol reaction,[5] allylation of carbonyl compounds,[1,6] and metal-catalyzed cross-coupling reactions.[7] Much of this chemistry has been carried out with silacyclobutanes functionalized only at the silicon atom, and the synthesis of these compounds begins typically with a Wurtz-type cylisation reaction of γ-halopropyl(chloro)silanes.[8] Silacyclobutanes bearing functional groups at the ring carbon atoms appear to be rare; some notable exceptions are 3-alkenylsilacyclobutanes[9] and 3-(alkoxycarbonyl)methyl-1-silacyclobutanes.[10]

During our investigations into the chemistry of silicon-substituted carbenes,[11] it occured to us that the intramolecular 1,4-C,H insertion of these reactive intermediates might offer a novel route to silacyclobutanes. While the 1,5-C,H insertion of silylcarbenes or silylcarbenoids under thermal,[12] photochemical,[13] and transition-metal catalyzed[14] conditions is well documented, the formation of a 1-oxa-2-silacyclobutane from trimethoxysilylcarbene in an argon matrix[15] represents so far the only reported 1,4-C,H insertion involving a silicon-attached substituent in a silylcarbene.

We report now that photolysis of α-(di-*tert*-butylsilyl)-α-diazoacetates **1** provides convenient access to 2-alkoxycarbonyl-1-silacyclobutanes **2**. When solutions of **1a**–**d**[16] in toluene were irradiated with 300 nm light, silacyclobutanes **2a**–**d** were formed (Scheme 1).† From the photolysis of **1a** and **1c**, silacyclobutanes **2a** and **2c**, respectively, were obtained as the only produts and in high yield. In both cases, only one diastereomer was detected by NMR. In the absence of spectroscopic evidence for its configuration (irradiation into the Bu^t resonance did not provide a NOE effect with the ring-CH proton), a *trans*-relationship between the Bu^t and ester groups is assumed for steric reasons. Photolysis of **1b**,**d** led to an unseparable mixture of the expected silacyclobutanes **2b**,**d**, formed again as single diastereomers, and the isomeric 1-oxa-2-silacyclohex-5-enes **3b**,**d**. We reasoned that the latter compounds are ring-expansion products of **2**, and in fact, conversion of **2** into **3** was achieved when these product mixtures as well as the isolated silacyclobutanes **2a**,**c** were heated at *ca*. 85 °C in toluene.‡ The constitution of the cyclic *O*-silylketene acetals **3** was indicated by some characteristic NMR signals [δ(=CH) 3.70–3.81; δ(C_{olefin}) 154.4 ± 0.3 and 72.0 ± 0.3] as well as by strong IR absorptions at 1650–1680 cm^{-1} which are assigned to the C=C stretching mode (Table 1).

The 4 → 6 ring expansion of silacyclobutanes **2** proceeds by a 1,3(C → O) silyl shift. Monitoring of the isomerisation **2c** → **3c** by ^{1}H NMR spectroscopy indicated a first-order reaction with k = 1.25 × 10^{-4} s^{-1} at 70 °C in [D_6]benzene, corresponding to a half-life time of 92.7 min. Compounds **3** constitute cyclic *O*-silyl ketene acetals, and it should be recalled that acyclic compounds of this type undergo reverse thermal isomerisation, *i.e.* they rearrange to form α-silylcarboxylates.[17] Certainly, the smooth ring-expansion of silacyclobutane-2-carboxylates is due largely to the relief of ring-strain[18] for this four-membered ring.

The cyclic ketene acetals **3** appear not to be storable for a long time, and signs of decomposition were detected by ^{1}H NMR after just a few days. Nevertheless, the different functional groups in these molecules should allow some useful transformations. As an example, we treated **3a**,**d** with an excess of $LiAlH_4$ and obtained 3-(hydroxybutyl)silane **4** in yields of 39 and 61% (Scheme 2).§ The IR absorptions at ν_{max} 2110, 922 and 848 cm^{-1} are in the ranges expected for dialkylsilanes.[19]

In summary, we have reported a novel synthesis of silacyclobutanes, namely by intramolecular 1,4-insertion of a carbene center into the C–H bond of a Si–Bu^t group. It appears that the presence of a $SiBu^t_2X$ group in (silyl)diazoacetates **1** is

Table 1 UV-irradiation of diazoacetates **1a**–**d** in toluene and conversion of silacyclobutanes **2** into 1-oxa-2-silacyclohex-5-enes **3**

Diazoacetate	X	Product(s) and relative Yields[a] (%)	Yield of **3**[b] (%)
1a	Cl	**2a** (100)	36
1b	N_3	**2b** (46), **3b** (54)	45
1c	N=C=O	**2c** (100)	39
1d	N=C=S	**2d** (26), **3d** (74)	67

[a] According to ^{1}H NMR spectra, product formation was nearly quantitative (90–95%). [b] The yield after thermal isomerization is given and is based on diazoacetate **1**.

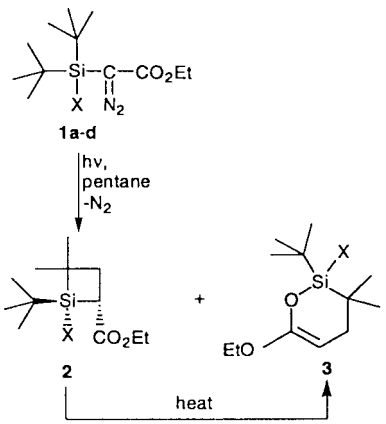

Scheme 1

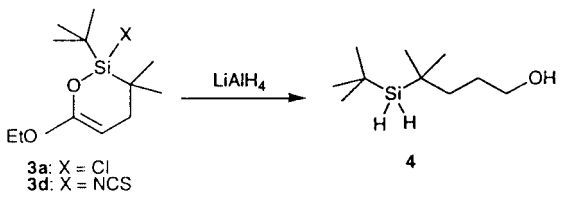

Scheme 2

DOI: 10.1039/a909306k

a favorable case for this type of C,H insertion which has not been reported so far for closely related α-silyl-α-diazoacetates with a β-C–H bond in the silyl group. For example, UV irradiation of the $SiEt_3$ and $SiPr^i_3$ substituted diazoacetates in benzene was unspecific while their copper- or rhodium-catalysed decomposition gave products derived from other carbene-type reactions.[20] α-Alkoxy(diisopropyl)silyl-α-diazoacetates, on the other hand, underwent a photochemical 1,5-C–H insertion of the carbene at the alkoxy chain but no 1,4-C,H insertion at the isopropyl substituents.[13] In spite of these apparent structural limitations, it is obvious that the transformation **1** → **2** represents an easy entry to silacyclobutanes with functionalities at both the silicon and the α-position of the ring which offer opportunities for further synthetic transformations.

This work was supported financially by the Deutsche Forschungsgemeinschaft.

Notes and references

† *General procedure* for the irradiation of diazoacetates **1**: a solution of **1a**–**d** (3–6 mmol) in dry pentane (80 ml) was irradiated with a high-pressure mercury lamp ($\lambda \geqslant 300$ nm) until evolution of nitrogen had ceased (2.5–4.5 h). The solvent was evaporated at 0.01 mbar to leave the crude product(s) (**2** or **2**/**3**) which, except for **2c**, could not be purified further. *Selected data* for ethyl 1-*tert*-butyl-1-chloro-4,4-dimethylcyclobutane-2-carboxylate **2a**: δ_H(500 MHz, $CDCl_3$) 1.13 (s, 9H, CMe_3), 1.22 (s + t, 6H, 4-Me and CH_2*Me*), 1.26 (s, 3H, 4-Me), 1.91 (dd, 1H, *J* 12.7, 9.5 Hz, 3-H^A), 2.41 (dd, 1H, *J* 12.7, 9.9 Hz, 3-H^B), 2.96 (pseudo-t, 1H, 2-H), 4.03–4.21 (m, 2H, OCH_2). δ_C(125.77 MHz, $CDCl_3$) 14.46 (CH_2*Me*), 23.03 (*C*Me_3), 25.44 and 25.51 (C*Me*$_2$), 25.67 (C*Me*$_3$), 32.36 (CH), 32.77 (*C*Me_2), 35.74 (CH_2-ring), 59.95 (OCH_2), 172.11 (C=O). For **2b**: δ_H(400 MHz, $CDCl_3$) 1.08 (s, 9H, CMe_3), 1.23 (s, 3H, 4-Me), 1.25 (t, 3H, CH_2*Me*), 1.26 (s, 3H, 4-Me), 1.98 (dd, 1H, *J* 12.9, 9.6 Hz, 3-H^A), 2.41 (dd, 1H, *J* 12.9, 9.6 Hz, 3-H^B), 2.86 (t, 1H, 2-H), 4.10 and 4.21 (2q, 2H, OCH_2). δ_C(100.61 MHz, $CDCl_3$) 14.3 (CH_2*Me*), 21.7 (*C*Me_3), 24.7 and 24.9 (C*Me*$_2$), 25.6 (C*Me*$_3$), 31.8 (CH), 32.9 (*C*Me_2), 36.4 (CH_2-ring), 60.1 (OCH_2), 172.7 (C=O). ν_{max}(film)/cm^{-1} 2148 (vs, N_3), 1720 (s, C=O). For **2c**: bp. 50 °C/0.01 mbar. δ_H(500 MHz, $CDCl_3$) 1.09 (s, 9H, CMe_3), 1.20 and 1.22 (2s, 6H, CMe_2), 1.24 (t, 3H, CH_2*Me*), 1.93 (dd, 1H, *J* 12.8, 9.5 Hz, 3-H^A), 2.36 (dd, 1H, *J* 12.8, 9.8 Hz, 3-H^B), 2.81 (pseudo-t, 1H, 2-H), 4.05–4.23 (m, 2H, OCH_2). δ_C(125.77 MHz, $CDCl_3$) 14.35 (CH_2*Me*), 21.07 (*C*Me_3), 24.94 and 25.15 (C*Me*$_2$), 25.42 (C*Me*$_3$), 30.95 (*C*Me_2), 31.10 (CH), 35.89 (CH_2-ring), 60.11 (OCH_2), 125.35 (NCO), 172.64 (C=O). ν_{max}(film)/cm^{-1} 2273 (vs, NCO), 1720 (C=O). For **2d**: δ_H(400 MHz, $CDCl_3$) 1.10 (s, 3H, 4-Me), 1.13 (s, 9H, CMe_3), 1.16 (s, 3H, 4-Me), 1.23 (t, 3H, CH_2*Me*), 1.96 (dd, 1H, *J* 12.7, 9.7 Hz, 3-H^A), 2.39 (dd, 1H, *J* 12.7, 9.7 Hz, 3-H^B), 2.82 (t, 1H, 2-H), 4.01–4.32 (m, 2H, OCH_2). ν_{max}(film)/cm^{-1} 2110–1940 (vs, br, NCS), 1725 (C=O).

‡ Diazoacetates **1a**–**d** were photolyzed as described above. The solvent was replaced by dry toluene (10 ml) and the solution was heated at 85 °C (**2c**: 82 °C, 2.5 h). The solvent was evaporated, and the residue was fractionated by bulb-to-bulb distillation. *Selected data* for **3a**: bp 70-80 °C (oven temp.)/0.01 mbar. δ_H(500 MHz, $CDCl_3$) 1.10 (s, 3H, 3-Me), 1.14 (s, 9H, CMe_3), 1.18 (s, 3H, 3-Me), 1.29 (t, 3H, CH_2*Me*), 1.63 (dd, *J* 16.2, 6.2 Hz, 1H, 4-H^A), 2.34 (dd, *J* 16.2, 2.6 Hz, 1H, 4-H^B), 3.74 (dd, 1H, 5-H), 3.79 (q, 2H, OCH_2). δ_C(125.77 MHz, $CDCl_3$) 14.47 (CH_2*Me*), 20.81 (*C*Me_2), 21.60 (*C*Me_3), 24.11 and 25.29 (C*Me*$_2$), 26.30 (C*Me*$_3$), 37.07 (CH_2-ring), 63.21 (OCH_2), 72.32 (=CH), 154.14 (C-6). ν_{max}(film)/cm^{-1} 1758, 1738, 1681, 1665, 1467, 1395, 1385, 1368, 1332, 1229. For **3b**: bp 90–100 °C/0.04 mbar. δ_H(500 MHz, $CDCl_3$) 1.10 (s, 3H, 3-Me), 1.11 (s, 9H, CMe_3), 1.12 (s, 3H, 3-Me), 1.31 (t, 3H, CH_2*Me*), 1.78 (dd, *J* 16.3, 6.0 Hz, 1H, 4-H^A), 2.23 (dd, *J* 16.3, 3.1 Hz, 1H, 4-H^B), 3.73 (dd, 1H, 5-H), 3.81 (q, 2H, OCH_2). δ_C(125.77 MHz, $CDCl_3$) 14.45 (CH_2*Me*), 20.00 (*C*Me_2), 20.48(*C*Me_3), 24.34 and 24.87 (C*Me*$_2$), 26.10 (C*Me*$_3$), 37.00 (CH_2-ring), 63.26 (OCH_2), 71.88 (=CH), 154.66 (C-6). ν_{max}(film)/cm^{-1} 2152 (N_3), 1678, 1662, 1466, 1368, 1330, 1229. For **3c**: bp 80–90 °C/0.02 mbar. δ_H(500 MHz, $CDCl_3$) 1.08 (s, 3H, 3-Me), 1.09 (s, 9H, CMe_3), 1.11 (s, 3H, 3-Me), 1.30 (t, 3H, CH_2*Me*), 1.75 (dd, *J* 16.3, 6.0 Hz, 1H, 4-H^A), 2.19 (dd, *J* 16.3, 3.1 Hz, 1H, 4-H^B), 3.70 (dd, 1H, 5-H), 3.78 (q, 2H, OCH_2). δ_C(125.77 MHz, $CDCl_3$) 14.46 (CH_2*Me*), 18.94 (*C*Me_2), 19.61 (*C*Me_3), 23.81 and 25.14 (C*Me*$_2$), 26.04 (C*Me*$_3$), 36.92 (CH_2-ring), 63.20 (OCH_2), 71.62 (=CH), 123.00 (NCO), 154.56 (C-6). ν_{max}(film)/cm^{-1} 2287 (NCO), 1679, 1664, 1469, 1368, 1337, 1230. For **3d**: bp 70–80 °C/0.01 mbar. δ_H(400 MHz, $CDCl_3$) 1.12 (s, 9H, CMe_3), 1.12 and 1.13 (2s, 6H, 3-Me), 1.30 (t, 3H, CH_2*Me*), 1.63 (dd, *J* 16.2, 6.2 Hz, 1H, 4-H^A), 2.34 (dd, *J* 16.2, 2.6 Hz, 1H, 4-H^B), 3.74 (dd, 1H, 5-H), 3.79 (q, 2H, OCH_2). δ_C(100.6 MHz, $CDCl_3$) 14.4 (CH_2*Me*), 19.2 (*C*Me_2), 19.9 (*C*Me_3), 24.9 and 25.7 (C*Me*$_2$), 25.9 (C*Me*$_3$), 36.8 (CH_2-ring), 63.3 (OCH_2), 71.9 (=CH), 144.3 (NCS), 154.4 (C-6). ν_{max}(film)/cm^{-1} 2115–1917 (vs, br, NCS), 1730, 1652, 1458, 1358, 1324, 1225, 1141, 1087, 1006.

§ Compound **2d** (547 mg, 1.91 mmol) in diethyl ether (10 ml) was added to a suspension of $LiAlH_4$ (593 mg, 15.6 mmol) in diethyl ether (30 ml) and the suspension was heated at reflux for 3 h. Work-up by addition of ice-water and extraction with diethyl ether yielded 220 mg (61%) of *tert*-butyl(1,1-dimethyl-4-hydroxybutyl)silane **4**. *Selected data*: δ_H(200 MHz, $CDCl_3$) 1.05 (s, 15H, CMe_3 and CMe_2), 1.33–1.72 (m, 4H, SiCH_2CH_2), 3.45 (s, 2H, SiH), 3.62 (t, 2H, OCH_2). δ_C(100.61 MHz, $CDCl_3$) 17.6 (*C*Me_2), 21.0 (*C*Me_3), 26.1 (C*Me*$_2$), 28.0 (CH_2), 28.9 (C*Me*$_3$), 37.7 (CH_2), 63.5 (OCH_2). ν_{max}(film)/cm^{-1} 3300 (br, OH), 2110 (Si–H), 922, 848. Anal. Calc. for $C_{10}H_{24}OSi$ (188.4): C, 63.76; H, 12.84. Found: C, 63.50; H, 12.10%.

1 Review on synthetic transformations of silacyclobutanes: K. Matsumoto, K. Oshima and K. Utimoto, *J. Synth. Org. Chem. Jpn.*, 1996, **54**, 289.

2 B. P. S. Chauhan, Y. Tanaka, H. Yamashita and M. Tanaka, *Chem. Commun.*, 1996, 1207; Y. Tanaka, H. Yamashita and M. Tanaka, *Organometallics*, 1996, **15**, 1524.

3 L. E. Gusel'nikov and N. S. Nametkin, *Chem. Rev.*, 1979, **79**, 529; G. Raabe and J. Michl, in *The Chemistry of Organic Silicon Compounds*, ed. S. Patai and Z. Rappoport, John Wiley & Sons, Chichester, 1989, ch. 17.

4 Recent examples: N. V. Ushakov, N. A. Pritula and A. I. Rebrov, *Russ. Chem. Bull.*, 1993, **42**, 1372; J. Lu and W. P. Weber, *Bull. Soc. Chim. Fr.*, 1995, **132**, 551; M. Birot, J.-P. Pillot and J. Dunoguès, *Chem. Rev.*, 1995, **95**, 1443; H. Yamashita, M. Tanaka and K. Honda, *J. Am. Chem. Soc.*, 1995, **117**, 8873.

5 A. G. Myers, S. E. Kephart and H. Chen, *J. Am. Chem. Soc.*, 1992, **114**, 7922; S. E. Denmark, B. D. Griedel and D. M. Coe, *J. Org. Chem.*, 1993, **58**, 988; S. E. Denmark and B. D. Griedel, *J. Org. Chem.*, 1994, **59**, 5136; S. E. Denmark, B. D. Griedel, D. M. Coe and M. E. Schnute, *J. Am. Chem. Soc.*, 1994, **116**, 7026.

6 K. Matsumoto, K. Oshima and K. Utimoto, *J. Org. Chem.*, 1994, **59**, 7152.

7 S. E. Denmark and Z. Wu, *Org. Lett.*, 1999, **1**, 1495; S. E. Denmark and J. Y. Choi, *J. Am. Chem. Soc.*, 1999, **121**, 5821.

8 L. H. Sommer and G. A. Baum, *J. Am. Chem. Soc.*, 1954, **76**, 5002; J. Lanne, *J. Am. Chem. Soc.*, 1967, **89**, 1144; N. Auner and J. Grobe, *J. Organomet. Chem.*, 1980, **188**, 25.

9 Reviews: N. Auner, *J. Prakt. Chem.*, 1995, **337**, 79; N. Auner, in *Organosilicon Chemistry: From Molecules to Materials*, ed. N. Auner and J. Weis, VCH, Weinheim, 1994, p. 103.

10 Y. Hatanaka, M. Watanabe, S. Onozawa, M. Tanaka and H. Sakurai, *J. Org. Chem.*, 1998, **63**, 422.

11 G. Maas, *Silicon-substituted carbenes*, in *The chemistry of organic silicon compounds*, ed. Z. Rappoport and Y. Apeloig, John Wiley & Sons, London, 1998, vol. 2, ch. 13.

12 J. W. Connolly, *J. Organomet. Chem.*, 1968, **11**, 429; J. W. Connolly and P. F. Fryer, *J. Organomet. Chem.*, 1971, **30**, 315.

13 G. Maas, F. Krebs, T. Werle, V. Gettwert and R. Striegler, *Eur. J. Org. Chem.*, 1999, 1939.

14 S. N. Kablean, S. P. Marsden and A. M. Craig, *Tetrahedron Lett.*, 1998, **39**, 5109.

15 M. Trommer and W. Sander, *Organometallics*, 1996, **15**, 736.

16 G. Maas and S. Bender, *Synthesis*, 1999, 1175.

17 S. Raucher and D. C. Schindele, *Synth. Commun.*, 1987, **17**, 637.

18 M. S. Gordon, J. A. Boatz and R. Walsh, *J. Phys. Chem.*, 1989, **93**, 1584; M. G. Voronkov, V. A. Klyuchnikov, E. V. Sokolova, T. F. Danilova, G. N. Shvets, A. N. Korchagina, L. E. Gussel'nikov and V. V. Volkova, *J. Organomet. Chem.*, 1991, **401**, 245.

19 D. Lin-Vien, N. B. Colthup, W. G. Fateley and J. G. Grasselli, *Infrared and Raman Characteristic Frequencies of Organic Molecules*, Academic Press, Boston, MA, 1991, pp. 252.

20 G. Maas, M. Gimmy and M. Alt, *Organometallics*, 1992, **11**, 3813.

Communication a909306k

ChemComm

Thiophene *S*-oxides: orbital energies and electrochemical properties

Alessandro Bongini,*[a] Giovanna Barbarella,[b] Massimo Zambianchi,[b] Catia Arbizzani[a] and Marina Mastragostino[c]

[a] *Dipartimento di Chimica, 'G.Ciamician', Università, Via Selmi 2, 40126 Bologna, Italy. E-mail: bongini@ciam.unibo.it*
[b] *CNR-I.Co.C.E.A., Area di Ricerca CNR, Via Gobetti 101, 40129 Bologna, Italy*
[c] *Dipartimento di Chimica Fisica, Università, Viale delle Scienze, 90128 Palermo, Italy*

Received (in Cambridge, UK) 29th November 1999, Accepted 3rd February 2000, Published on the Web, 29th February 2000

***Ab initio* calculations and experimental oxidation and reduction potentials show that the functionalization of thiophene to the corresponding *S*-oxide leads to only a minor change in ionization potential but to a dramatic increase in the electron affinity.**

Owing to their electrical and optical properties, α-conjugated oligo- and poly-thiophenes are currently the subject of intense research activity in the field of organic materials. There is great interest in finding functionalization capable of decreasing the energy of the LUMO orbital of these compounds. Indeed, easily reducible compounds are useful for application in a variety of electrochemical and electrooptical devices.[1]

Unsubstituted thiophene *S*-oxide has not yet been isolated; however, new oxidation methods have recently been developed that make it possible to obtain stable substituted thiophene *S*-oxides.[2] Thus, following our research line on thiophene *S,S*-dioxides,[3] we have commenced a study aimed at elucidating how the functionalization of the thienyl sulfur of thiophene-based materials to the corresponding *S*-oxide affects the orbital energies and the electrochemical properties of these compounds.

Here, we report *ab initio* theoretical calculations performed on the thiophene *S*-oxide and compare the results with related physical properties for 2,5- and 3,4-disubstituted counterparts. The results on thiophene and thiophene *S,S*-dioxide analogues are also reported for comparison.

MP2/6-31G* *ab initio* calculations[4] indicate a non-planar structure for thiophene *S*-oxide with the sulfur atom lying outside the plane formed by the other four atoms by 0.26 Å (Scheme 1).

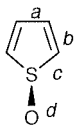

	I	II
a	1.455	1.404
b	1.356	1.397
c	1.768	1.676
d	1.512	1.500
>*ab*	113.0	113.9
>*bc*	110.6	106.9
>*cc'*	90.7	98.3
>*cd*	116.3	130.8
>*bab'*	0.0	0.0
>*abc*	9.8	0.0
>*bcd*	-132.9	180.0

Scheme 1 Selected bond lengths (Å) and angles (°) of the MP2/6-31G* ground state (**I**) and transition state (**II**) structures of thiophene *S*-oxide.

The results are in agreement with previous *ab initio* calculations at a lower level of theory[5] and with the X-ray structure reported for 2,5-diphenyl[2a] and 3,4-di-*tert*-butyl[2c] derivatives.

The non-planar geometry implies that thiophene *S*-oxide should be less aromatic than unmodified thiophene. Indeed, using this geometry, we calculated the aromaticity Bird index[6a] to be 37.4, which is much lower than that reported for thiophene (66)[6a] and similar to that of phosphole (35.5).[6b]

MP2/6-31G* calculations also show that inversion at the pyramidal sulfur proceeds through a fully planar transition state (Scheme 1) with a calculated energy barrier of 13.5 kcal mol^{-1}, in good agreement with the experimental value of 14.8 kcal mol^{-1} reported for 2,5-di-*tert*-octylthiophene *S*-oxide,[7] but much lower than the energy inversion barriers reported for sulfoxides (37–42 kcal mol^{-1}).[8] Clearly, in thiophene *S*-oxide the increased π-conjugation makes the planar transition state more aromatic than the ground state (the Bird index calculated for this planar geometry is 90.8) and furnishes extra stabilization that accounts for the lower value of the inversion barrier.

Table 1 reports the *ab initio* calculated frontier orbital energies of thiophene, thiophene *S*-oxide and thiophene *S,S*-dioxide (**1**–**3**) together with the oxidation and reduction potentials of the corresponding 2,5-disilylated derivatives (**4**–**6**) and of 3,4-di-*tert*-butylthiophene *S*-oxide **7**, measured by cyclic voltammetry (CV); UV maxima and optical edges for **4**–**7** are also reported.†

Table 1 MP2/6-31G* frontier orbital energies (E_{HOMO}, E_{LUMO}/eV) of thiophene **1**, thiophene *S*-oxide **2** and thiophene *S,S*-dioxide (**3**), along with oxidation and reduction potentials [I_p (A) I_p (C)/V *vs.* SCE], λ_{max} ($CHCl_3$/nm) and optical edge values (ΔE/eV) of the substituted derivatives **4**–**7**

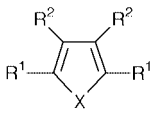

1 X = S, $R^1 = R^2 = H$
2 X = SO, $R^1 = R^2 = H$
3 X = SO_2, $R^1 = R^2 = H$
4 X = S, $R^1 = SiMe_3$, $R^2 = H$
5 X = SO, $R^1 = SiMe_3$, $R^2 = H$
6 X = SO_2, $R^1 = SiMe_3$, $R^2 = H$
7 X = SO, $R^1 = H$, $R^2 = Bu^t$

	E_{HOMO}	E_{LUMO}	I_p (A)[a]	I_p (C)[b]	λ_{max}	ΔE_{edge}
1	−8.71	3.57				
2	−9.58	1.84				
3	−10.09	1.27				
4			1.98	< −2.60	248	4.43
5			2.02	−1.70	256	2.95
					324	
6			2.74	−1.46	230	3.39
					314	
7			2.06	−1.90	227	3.14
					329	

[a] CV in MeCN–NEt_4BF_4 0.2 M at 100 mV s^{-1}. [b] CV in propylene carbonate–NEt_4BF_4 0.2 M at 100 mV s^{-1}.

The calculations show that the frontier orbitals of **1**–**3** are all π in character. The LUMO orbital of thiophene is spread over all five atoms of the ring, while the LUMO orbitals of **2** and **3** and the HOMO orbitals of **1**–**3** are essentially confined to the four carbon atoms. This indicates that it is the LUMO orbital that is most affected by the functionalization of thienyl sulfur to the *S*-oxide and that it is the first oxidation step that mostly affects the frontier orbitals. The trend of the electrochemical potentials of **4**–**7** is in agreement with the trend shown by the calculated frontier orbital energies. It appears that the functionalization of the thienyl sulfur to *S*-oxide affects the reduction potential to a greater extent than the oxidation potential strongly

DOI: 10.1039/a909390g

increasing the electroaffinity and bringing about much greater variation than the functionalization of the *S*-oxide to the corresponding *S*,*S*-dioxide. It is interesting that the potential values of sulfoxides **5** and **7** indicate that these compounds are both oxidizable and reducible at moderate potential values, in contrast to thiophene (which is easily oxidized and difficult to reduce) and thiophene *S*,*S*-dioxide (which is easily reduced but difficult to oxidize).

Examining the optical data, it is seen that the first functionalization to *S*-oxide leads to two distinct maxima, at 256 and 324 nm, the latter showing a strong bathochromic shift with respect to the parent thiophene **4**, and to a substantially smaller optical edge. Literature data for to 2,5-di-*tert*-butylthiophene and the corresponding *S*-oxide and *S*,*S*-dioxide show an analogous trend.[7] Similar λ_{max} and ΔE_{edge} values were found for compounds **5** and **7** which have different substituents and substitution pattern. Taking into account also the similarity of the oxidation and reduction potentials of **5** and **7**, it appears that it is the type of functionalization of the sulfur atom which is the main factor affecting the frontier orbitals energies.

A 4 × 4 singly excited CI ZINDO/S//PM3 analysis[9] performed on **1**–**3** shows that the low wavelength absorption in thiophene *S*-oxide and in thiophene *S*,*S*-dioxide is due to the mixing of transitions involving both S–O and π orbitals, while in all the compounds the highest wavelength absorption is due to the HOMO–LUMO π–π* transition. It is of note that in both **2** and **3** the lone pairs of the oxygen atoms are not involved in the HOMO–LUMO transition.

In conclusion, theoretical calculations and electrochemical data show that the functionalization of thiophene to the corresponding *S*-oxide produces a dramatic increase in the electron affinity, without requiring complete de-aromatization of the molecule as in the case of the *S*,*S*-dioxide. In addition, there is only a minor variation in the oxidation potential. Therefore, this type of functionalization of thiophene-based compounds could lead to a novel class of materials with new and interesting properties.

Thanks are due to MURST (Electrochemical and Electronic Devices with Polymer Components) for financial support.

Notes and references

† Compounds **4**,[2b] **5**,[2b] **6**[3a] and **7**[2c] were synthesized according to the literature

1 J. Roncali, *Chem. Rev.*, 1997, **97**, 173.
2 (*a*) P. Pouzet, I. Erdelmeier, D. Ginderow, J.-P. Mornon, P. Dansette and D. Mansuy, *J. Chem. Soc., Chem. Commun.*, 1995, 473; (*b*) N. Furukawa, S. Zang, S. Sato and M. Higaki, *Heterocycles*, 1997, **44**, 61; (*c*) J. Nakayama, T. Yu, Y. Sugihara and A. Ishii, *Chem. Lett.*, 1997, 499.
3 (*a*) G. Barbarella, O. Pudova, C. Arbizzani, M. Mastragostino and A. Bongini, *J. Org. Chem.*, 1998, **63**, 1742; (*b*) G. Barbarella, L. Favaretto, M. Zambianchi, O. Pudova, C. Arbizzani, A. Bongini and M. Mastragostino, *Adv. Mater.*, 1998, **10**, 551; (*c*) G. Barbarella, L. Favaretto, G. Sotgiu, M. Zambianchi, L. Antolini, O. Pudova and A. Bongini, *J. Org. Chem.*, 1998, **63**, 5497.
4 GAUSSIAN 94, Revision E.2, M. J. Frisch *et al.*, Gaussian Inc., Pittsburgh, PA, 1995.
5 I. Rozas, *J. Org. Phys. Chem.*, 1992, **5**, 74.
6 C. W. Bird, *Tetrahedron*, (*a*) 1985, **41**, 1409; (*b*) 1990, **46**, 5697.
7 W. L. Mock, *J. Am. Chem. Soc.*, 1970, **92**, 7610.
8 D. R. Rayner, A. J. Gordon and K. Mislow, *J. Am. Chem. Soc.*, 1968, **90**, 4854.
9 *HyperChem.*, release 4.5 from Hypercube, Inc. Waterloo, Ontario, Canada.

Communication a909390g

ChemComm

Unnatural natural triterpenes produced by altering isoleucine into alanine at position 261 in hopene synthase and the importance of having the appropriate bulk size at this position for directing the stereochemical destiny during the polycyclization cascade†

Tsutomu Hoshino,* Takamasa Abe and Masanori Kouda

Department of Applied Biological Chemistry, Faculty of Agriculture and Graduate School of Science and Technology, Niigata University, Ikarashi, Niigata 950-2181, Japan. E-mail: hoshitsu@agr.niigata-u.ac.jp

Received (in Cambridge, UK) 24th January 2000, Accepted 8th February 2000, Published on the Web, 29th February 2000

Incubation of squalene with the site-directed mutant of Ile261Ala of squalene-hopene cyclase from *Alicyclobacillus acidocaldarius* afforded multiple triterpenes consisting of tri-, tetra- and penta-cyclic skeletons, together with a final product of hopene, among which the previously unknown 6/6/6/6-fused tetracyclic skeletal compounds, denoted pro-hopene A and B, are included.

Squalene-hopene cyclase (SHC) catalyses the cyclization reaction of squalene **1** into pentacyclic triterpenes, hopene **2** and hopanol **3**, under a fine regio- and stereo-chemical specificity. The reaction has been believed to proceed through all *pre*-chair conformation,[1] but recent studies on the site-directed mutagenesis have indicated that the reaction proceeds *via* two expansion steps from the 5-membered C- and D-ring intermediates, which had been previously formed under Markovnikov closure, into the corresponding 6-membered rings (anti-Markovnikov adduct), as shown in Scheme 1.[2a,b] The ring-expansion processes have been further supported by trapping experiments of the 6/6/5-fused tricyclic intermediate **6** and the 6/6/6/5-fused tetracyclic intermediate **8** (Markovnikov adducts) using the substrate analogues having a highly nucleophilic hydroxyl group.[2a,b] The stereochemistry of 13H in **6** and 17H in **8** have been established to be of β-configuration; no enzymic products having the α-configurations have been obtained in the trapping experiments. Recently, we and Poralla's group have reported the isolation of the enzymatic products derived from the carbocation intermediates of mono- **4**,[3] bi- **5**,[4a,c] tri- **6**,[2b,4c] and tetra-cyclic **8**;[2a,b,4b,c] these discrete cationic intermediates were produced by a single amino acid replacement of D377N (D377C), F365A, Y420A, F601A, W169F, W169 H or W489F in *A. acidocaldarius* SHC (Scheme 1). The abortive cyclization products formed by each point mutation have revealed not only the catalytic function of given amino acids but also the cyclization mechanism for **1**; the cyclization is triggered by the DXDDTA motif;[3] D377 stabilises monocyclic cation **4** probably *via* the carboxylate anion; and both F365[4a] and F601[2b] stabilise the transient carbocations at each cyclization stage **5** → **8** possibly *via* a cation–π interaction. The aromatic residues of W169, W489 and Y420 are likely to play a significant role for folding the substrate **1**.[2a,4c] In a series of the site-directed mutagenesis experiments, we have focused on Ile261 as a next experiment, which is highly conserved among all the known SHCs and oxidosqualene cyclases. The mutated SHCs of I261A produced the unknown 6/6/6/6-fused tetracyclic **14** and **15** ('unnatural' natural products) together with the known **11**, **12**, **13** and **16**.[5] The stereochemistry at 13- and 17-positions of premature products **11** and **12** was of α-configuration and in contrast to those of true intermediates **6** and **8**. We report here, that the appropriate bulk size and shape at position 261 has a critical role in directing the steric control for constructing the hopane skeleton.

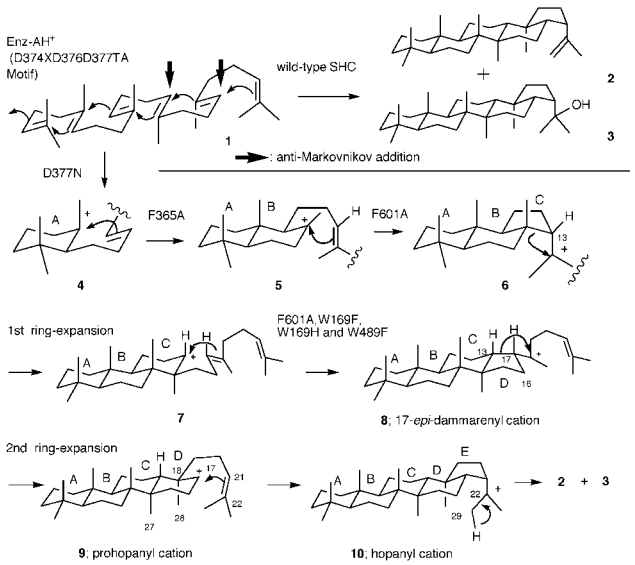

Scheme 1

† Electronic supplementary information (ESI) available: EIMS and NMR assignments. See http://www.rsc.org/suppdata/cc/b0/b000711k/

With the cell-free homogenates (150 ml), prepared from a 3 L culture of *E. coli* clone encoding I261A SHC, 100 mg of **1** was incubated for 15 h at optimum catalytic conditions (pH 6 and 55 °C). The GC analysis (30 m DB1, capillary column) showed six new enzymic products other than **2** in a hexane-extract of the reaction mixture.

Column chromatography over SiO_2 eluting with hexane afforded five fractions in the following order: **16**, **2** + **13**, **12** + **14** + **15**, **11** and the recovered **1**. The complete separation of each product was achieved by reverse-phase HPLC (C18) with THF–H_2O (6 : 4). The yields of each product, estimated by GC, were as follows: 4.0, 19.0, 4.1, 4.1, 3.7, 3.2, 48.6 and 3.1 mg for **11**, **12**, **13**, **14**, **15**, **16**, **2** and **3**, respectively, and 0.6 mg for the recovered **1**. No other products were observed in a detectable amount.

Structures of all the isolated compounds were determined as shown in Fig. 1 by EIMS and NMR spectra (H–H COSY 45, HOHAHA, NOESY, DEPT, HMQC and HMBC).† The EIMS, ^1H and ^{13}C NMR spectra of **11** were identical to those of the authentic (17*E*)-(13αH)-malabarica-14(27),17,21-triene,[2b] the stereochemistry of H13 being further confirmed to be of α-configuration by a strong NOE between H9 and H13. The epimer of **11**, (13βH)-malabaricatriene **11′**[2b] with a longer retention time (rt) on the GC than **11**, was never detected in the reaction mixture. The fragmentation pattern of **12** in the EIMS spectrum was superimposable to that of 17-*epi*-dammara-20(21),24-diene **12′**,[2a] but the rt of **12** on the GC is shorter than that of **12′**, and the NOE between 30-Me and H17 was found, thus proving the α-orientation of H17 in **12**. The double bond of **13** was $\Delta^{13,17}$ by HMBC correlation both from 30-Me to C13

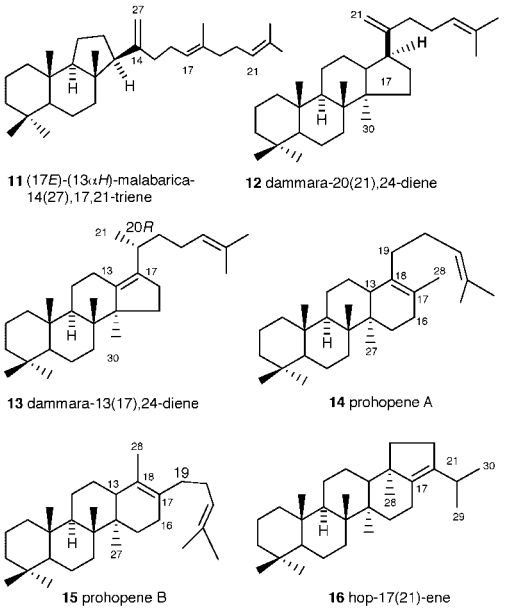

Fig. 1 Structures of the enzymatic products by the mutated I261A SHC.

and from 21-Me for C17. The proton chemical shift of 21-Me was 0.919 ppm (*J* 6.7 Hz) in $CDCl_3$, which allowed the assignment of 20*R*-stereochemistry.[6] The EIMS spectrum of **14** was essentially the same as that of **15**. The 6/6/6/6-fused tetracyclic skeletons of **14** and **15** were revealed by NMR analyses. An HMBC correlation between 28-Me and C13 was observed for **15**, but not for **14**. A strong NOE was observed between H16 and H19 for **15**, while no NOE was seen for **14**. Product **16** differed from **2** only in the double bond position, which was determined by the HMBC cross peaks of 28-Me/C17, 29-Me/C21 and 30-Me/C2l.

Tricyclic **11** could be produced *via* **6′** and two tetracyclics **12** and **13**, *via* **8′** (Scheme 2). Proton elimination from 21-Me of **8′** could give **12**, but a hydride shift to C18 of **8′** followed by deprotonation of the 13H could afford **13**. Formation of tri- and tetra-cyclic skeletons **11**–**13** may have occurred owing to the local change, especially near the site(s) responsible for the C/D-ring formation; the mutated SHC replaced by a smaller bulk size of Ala could not perfectly fit with **1**.[7] Compounds **11**–**13** were accumulated, while the corresponding epimers **11′** and **12′** from **6** and **8** were not detected. This suggests that **6′** and **8′** cannot undergo further cyclizations, whereas the intermediates **6** and **8**, which had been produced by this mutated SHC, could undergo

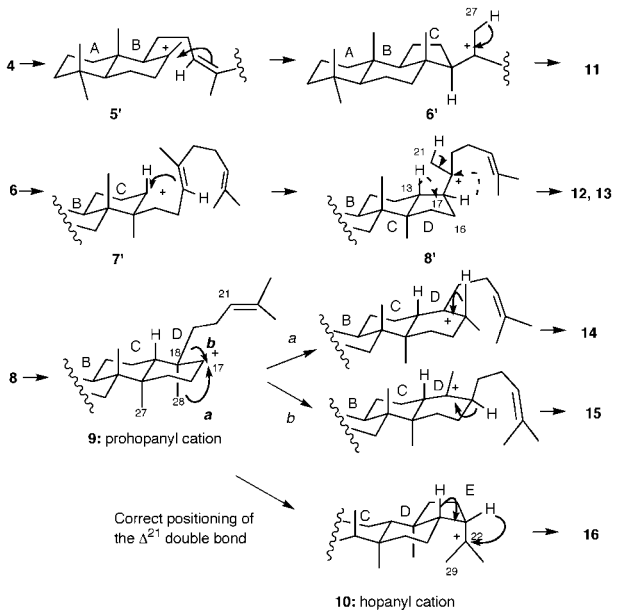

Scheme 2

subsequent cyclizations to yield **2**. Therefore, it is likely that the (13βH)- and (17βH)-configurations in 6/6/5- and 6/6/6/5-ring systems are required for the completion of two ring-expansion processes to give **9**. This hypothesis agrees well with the previous results[2a,b] that only **6** and **8** were trapped when the squalene analogues having a hydroxy group were incubated with the native SHC, but that **6′** and **8′** were not. The secondary cation **9** has been assumed as an intermediate in hopene biosynthesis, but no experimental evidence has been given. Formation of **14** and **15** gave definitive evidence for the involvement of intermediate **9**. The 1,2-shift of 28-Me to the C17 cation could give **14** (path *a* in Scheme 2), whereas rearrangement of the isoprenoid side chain to the cation could afford **15** (path *b*). Triterpenes **14** and **15** have never been reported before. We propose to denote the prohopane skeleton for **9**, prohopene A for **14** and prohopene B for **15**. It is noteworthy that **8′** is the biosynthetic intermediate of some plant triterpenes.[1] A looser binding near the C/D-ring could also perturb the correct positioning of the Δ^{21} double bond in **9**, thus leading to the accumulation of **14** and **15**; the appropriate arrangement of the double bond could allow a further cyclization to give **10** through the nucleophilic attack of the double bond toward cation **9**. Product **16** could be formed perhaps due to the erroneous positioning of the deprotonation site for introducing the $\Delta^{22,29}$ double bond of **2**, which may have also occurred concomitantly with the local change near the C/D-rings.

With respect to the mutated I261V SHC, no abortive cyclization product was found and the kinetic data were almost the same as that of the wild-type SHC,[7] but the mutant I261A gave a looser affinity and a slower velocity for hopene biosynthesis.[7] Site-directed mutagenesis not only helps to understand the fundamental issue of the reaction mechanism (molecular recognition and catalytic function), but also generates the previously unknown 'unnatural' natural products,[8a] as represented by **14** and **15**. The rational genetic engineering of the active and/or recognition sites is a promising tool for the creation of novel natural products.[4a,8b]

This work was supported by a Grant-in-Aid to T. H. (No. 11660104) from the Ministry of Education, Science, Sports and Culture, Japan.

Notes and references

1 I. Abe, M. Rohmer and G. D. Prestwich, *Chem. Rev.*, 1993, **93**, 2189.
2 (*a*) T. Sato, T. Abe and T. Hoshino, *Chem. Commun.*, 1998, 2617; (*b*) T. Hoshino, M. Kouda, T. Abe and S. Ohashi, *Biosci. Biotechnol. Biochem.*, 1999, **63**, 2038.
3 T. Sato and T. Hoshino, *Biosci. Biotechnol. Biochem.*, 1999, **63**, 2189.
4 (*a*) T. Hoshino and T. Sato, *Chem. Commun.*, 1999, 2205; (*b*) T. Merkofer, C. Pale-Grosdemange, M. Rohmer and K. Poralla, *Tetrahedron Lett.*, 1999, **40**, 2121; (*c*) C. Pale-Grosdemange, T. Merkofer, M. Rohmer and K. Poralla, *Tetrahedron Lett.*, 1999, **40**, 6009.
5 For **11**; K. Masuda, K. Shiojima and H. Ageta, *Chem. Pharm. Bull.*, 1989, **34**, 1140; for **12**; H. Yamashita, K. Masuda, T. Kobayashi, H. Ageta and K. Shiojima, *Phytochemistry*, 1998, **49**, 2461; for **13**; Y. Arai, K. Masuda and H. Ageta, *Chem. Pharm. Bull.*, 1982, **30**, 4219; for **16**, H. Ageta, K. Shiojima and Y. Arai, *Chem. Pharm. Bull.*, 1987, **35**, 2705.
6 I. Abe and M. Rohmer, *J. Chem. Soc., Perkin Trans 1*, 1994, 783.
7 Optimum catalysis was found at 55 °C for the mutants I261A, but at 60 °C for the wild-type and I261V. Kinetic values of K_m and V_{max} were determined at 55 °C and pH 6.0 from Lineweaver–Burk plots as follows; K_m: 25.8, 34.7 and 178 μM; V_{max}: 3.87, 3.57 and 0.43 nmol min^{-1} μg^{-1}, respectively, for the wild-type, I261V, and I261A. The I261G mutant, having the smallest size, also produced **11**–**13** in twice the quantity than I261A, despite the cyclase activity being significantly decreased (the amount of **2** was 17% of that of I261A), which further supports the importance of a bulk size at 261 position for the stereoselective cyclization reactions.
8 (*a*) Examples of 'unnatural' natural products by altering the active sites of sesquiterpenes or polyketide synthases. D. E. Cane and Q. Xue, *J. Am. Chem. Soc.*, 1996, **118**, 1563; R. McDaniel, A. Thamchaipenet, C. Gustafsson, H. Fu, M. Betlach, M. Betlach and G. Ashley, *Proc. Natl. Acad. Sci., USA*, 1999, **96**, 1846; (*b*) C. A. Roessner and A. I. Scott, *Chem. Biol.*, 1996, **3**, 325.

Communication b000711k

ChemComm

Dendrimers based on multiple 1,4,7-triazacyclononane derivatives

Paul D. Beer* and De Gao

Department of Chemistry, Inorganic Chemistry Laboratory, University of Oxford, South Parks Road, Oxford, UK OX1 3QR. E-mail: paul.beer@chem.ox.ac.uk

Received (in Cambridge, UK) 2nd December 1999, Accepted 9th February 2000, Published on the Web, 29th February 2000

New first and second generation dendritic poly-1,4,7-triazacyclononane molecules have been prepared and shown to coordinate multiple Cu(II) and Ni(II) metal cations.

The last decade has witnessed an enormous growth in the field of dendrimer chemistry with current interest being stimulated by the discovery of specific functions and novel properties that are a direct consequence of the dendritic architecture.[1] Metallodendrimers[2] in particular have been shown to exhibit novel electrochemical and photophysical properties. With a view to creating new efficient extraction and membrane transporting reagents for transition metals[3] and for the preparation of metal nanoclusters[4,7] we report here, the first examples of dendrimers containing the well established transition metal coordinating ligand, 1,4,7-triazacyclononane.[5]

The new key asymmetric functionalised triazacyclononane branching synthons **5** and **6** required for convergent and divergent syntheses of the target dendritic macrocyclic molecules were prepared as shown in Scheme 1. The reaction of **1**[5] with 2 equiv. of 3-nitrobenzyl chloride in the presence of K_2CO_3 in MeCN solution gave **2** in 90% yield. Detosylation of **2** using sulfuric acid produced **3** in 50% yield. Refluxing **3** with 1 equiv. of butyl bromoacetate in the presence of K_2CO_3 afforded **4** as a pale yellow solid in 82% yield. Hydrolysis of **4** with formic acid gave **5** in 80% yield and reduction of **4** using hydrogen and Raney Ni produced the diamine **6** quantitatively (Scheme 1).

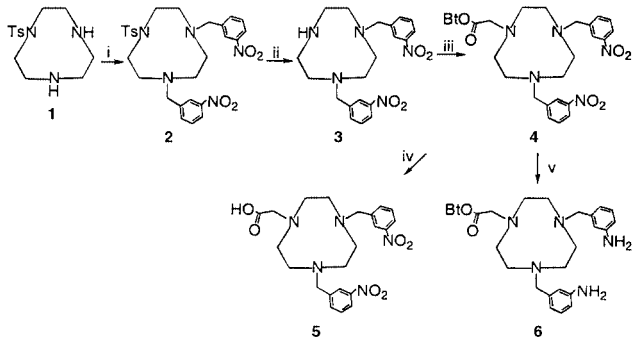

Scheme 1 *Reagents and conditions*: i, 2 equiv. 3-nitrobenzyl chloride, K_2CO_3, MeCN, reflux; ii, conc. H_2SO_4, 150 °C; iii, butyl bromoacetate, K_2CO_3, MeCN, reflux; iv, formic acid, reflux; v, H_2, Raney Ni, MeOH–THF, 55 °C.

The dendritic core triazacyclononane derivative **8** was synthesised *via* reaction of 1,4,7-triazacyclononane with 3 equiv. of 3-nitrobenzyl chloride to give **7** followed by reduction with Raney Ni and H_2 (Scheme 2).

Using a divergent synthetic procedure the first generation dendrimer compound **9** was synthesised *via* a condensation

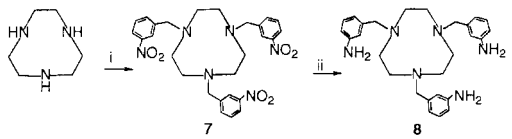

Scheme 2 *Reagents and conditions*: i, 3 equiv. 3-nitrobenzyl chloride, K_2CO_3, MeCN, reflux; ii, H_2, Raney Ni, MeOH–THF, 55 °C.

reaction of **8** with 3 equiv. of **5** in DMF in the presence of 1-(3-dimethylaminopropyl)-3-ethylcarbodiimide hydrochloride (EDC) and 1-hydroxybenzotriazole hydrate (HOBt) (Scheme 3). After column chromatography using alumina and CH_2Cl_2, **9** was isolated as a yellow solid in 90% yield. The convergent preparative approach is illustrated with the synthesis of **10** from **6** and 2 equiv. of **5** using a similar condensation reaction (Scheme 4).

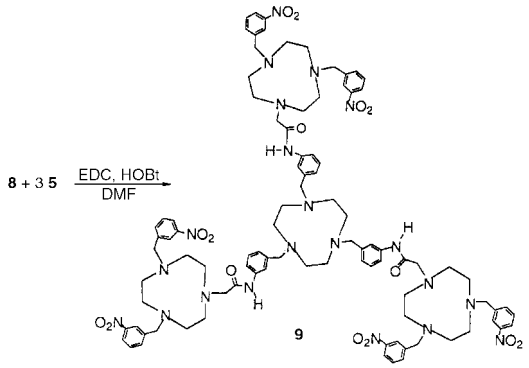

Scheme 3 *Reagents and conditions*: EDC, HOBt, DMF, room temp.

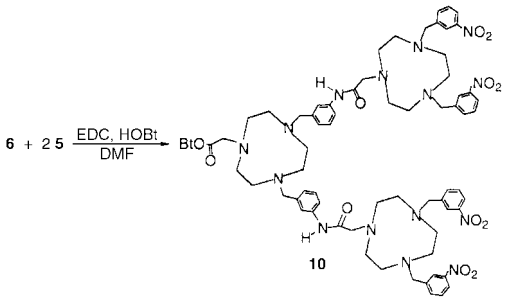

Scheme 4 *Reagents and conditions*: EDC, HOBt, DMF, room temp.

Raney Ni/H_2 reduction of **9** and reaction of the corresponding amine **11** with 6 equiv. of **5** in DMF gave the second generation dendrimer **12** in 60% yield (Scheme 5).†

Preliminary transition metal coordination investigations of dendrimers **9** and **12** with Cu(II) and Ni(II) metal cations have been undertaken using UV–VIS spectrophotometric titration experiments. In the absence of dendrimer, MeCN and DMF solutions of copper(II) acetate exhibit a broad d–d absorption at 710 nm. The addition of dendrimers **9** or **12** causes λ_{max} to undergo a blue shift to 646 nm which is characteristic of Cu(II) being bound by amine ligands.[5] The spectrophotometric titration curves (Fig. 1) suggest **9** binds four, and **12** ten Cu(II) metal cations, one Cu is coordinates to each triazacyclononane macrocyclic ligand of the respective dendrimer, suggesting the transition metal is complexed at the core, branches and surface dendritic recognition sites.‡ This result contrasts with PAMAM dendrimers which are thought to bind most Cu cations at the outermost tertiary amine donor sites of the dendrimer structure.[7] With Ni(II) preliminary spectrophotometric titration results with the first generation dendrimer **9** indicate as with Cu(II), each

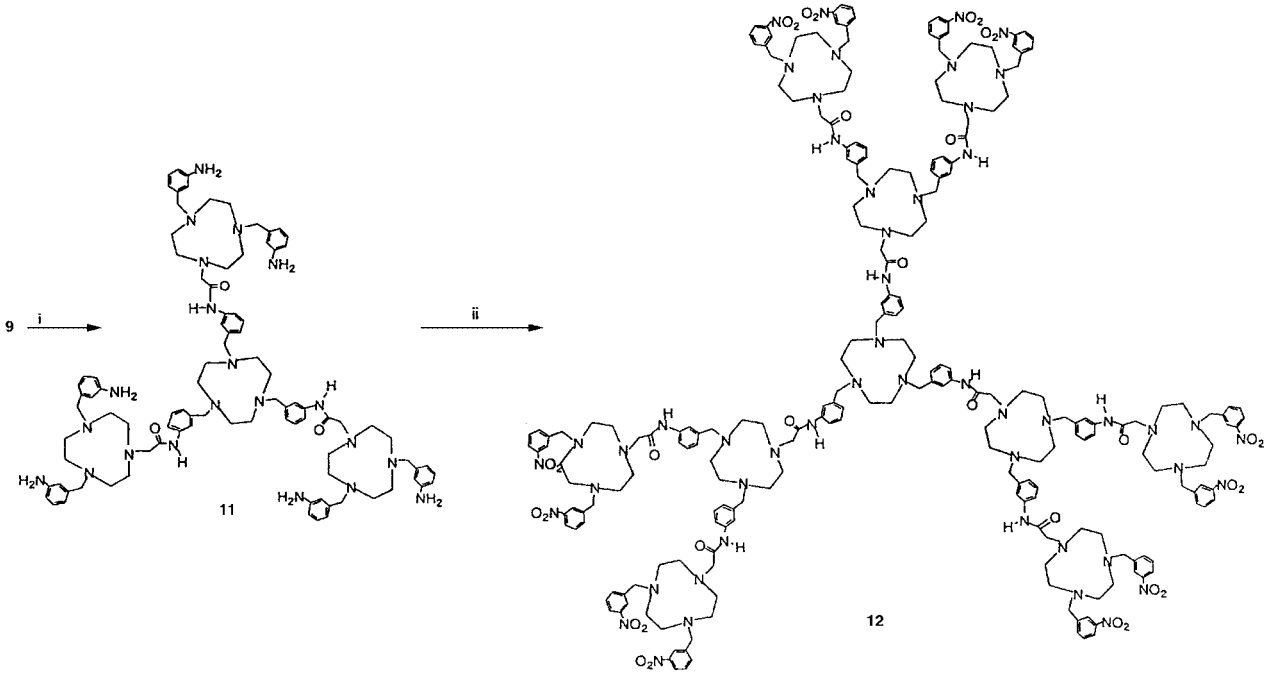

Scheme 5 *Reagents and conditions*: i, H_2, Raney Ni, MeOH–THF, 55 °C; ii, 6 equiv. **5**, EDC, HOBt, DMF, room temp.

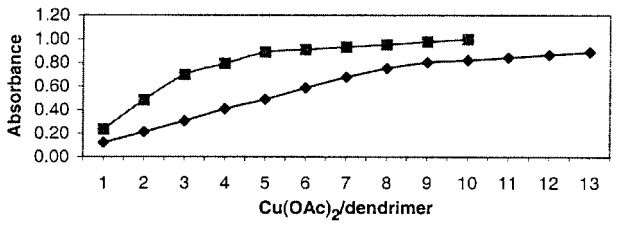

Fig. 1 Spectrophotometric titration of **8** (■) (3 mM) with $Cu(OAc)_2$ in acetonitrile, absorbance at 646 nm and of **12** (◆) (0.5 mM) with $Cu(OAc)_2$ in DMF, absorbance at 600 nm.

triazacyclononane ligand complexes one Ni(II) cation resulting in 4 Ni^{2+}: **9** solution stoichiometry.

Further transition metal coordination chemistry investigations with these novel dendritic poly-triazacyclononane-molecules are in progress.

We thank the Royal Society for a K. C. Wong Fellowship (D. G.) and the EPSRC mass spectrometry service at the University of Wales, Swansea.

Notes and references

† All new compounds were characterised by ^{1}H NMR, mass spectrometry and elemental analysis.

Selected data: **9**: ^{1}H NMR ($CDCl_3$) δ 2.76 (16H, s, CH_2CH_2, ring), 2.85 (32H, s, CH_2CH_2, ring), 3.27 (6H, s, CH_2), 3.54 (6H, s, CH_2), 3.78 (12H, s, CH_2), 7.06–8.18 (36H, m, aromatics), 9.96 (3H, s, amide). $C_{99}H_{111}N_{21}O_{15}$ requires C, 63.36; H, 6.35; N, 16.68. Found: C, 62.95; H, 6.41; N, 16.37%. FAB MS: *m/z* 1764 (M + H).

10: ^{1}H NMR ($CDCl_3$) δ 1.43 (9H, s, CH_3), 1.59–2.86 (36H, m, CH_2CH_2, ring), 3.27 (2H, s, CH_2), 3.52 (4H, s, CH_2), 3.60 (4H, s, CH_2), 3.78 (8H, s, CH_2), 6.46–8.20 (24H, m, aromatics), 9.96 (2H, s, amide). $C_{70}H_{89}N_{15}O_{12}$. FAB MS: *m/z* 1332 (M + H).

12: ^{1}H NMR ($CDCl_3$) δ 2.60–2.86 (120H, m, CH_2CH_2, ring), 3.20 (6H, s, CH_2), 3.32 (6H, s, CH_2), 3.50 (12H, s, CH_2), 3.64 (12H, s, CH_2), 3.76 (24H, s, CH_2), 6.95–8.20 (84H, m, aromatics), 9.96 (9H, s, amide). $C_{225}H_{273}N_{51}O_{33}$. ES MS: *m/z* $(2109.87)^{2+}$, $(1406.9)^{3+}$.

‡ This assumes the absorption coefficients are additive. Also the error in estimating the stoichiometry of metal uptake from the titration data is ±1 or 2.

1 G. R. Newkome, C. N. Moorefield and F. Vogtle, *Dendritic Molecules: Concepts, Syntheses, Perspectives*, VCH, Weinheim, Germany, 1996; A. Archut and F. Vogtle, *Chem. Soc. Rev.*, 1998, **27**, 233.
2 G. R. Newkome, E. He and C. N. Moorefield, *Chem. Rev.*, 1999, **99**, 1689.
3 A. M. Groth, L. F. Lindoy and G. V. Meehan, *J. Chem. Soc., Perkin Trans. 1*, 1996, 1553; D. J. White, N. Laing, H. Miller, S. Parsons, S. Coles and P. A. Tasker, *Chem. Commun.*, 1999, 2077.
4 L. N. Lewis, *Chem. Rev.*, 1993, **93**, 2693.
5 P. Chaudhuri and K. Wieghardt, *Prog. Inorg. Chem.*, 1987, **35**, 329.
6 J. L. Sessler, J. W. Sibert and V. Lynch, *Inorg. Chem.*, 1990, **29**, 4143.
7 M. Zhao, L. Sun and R. M. Crooks, *J. Am. Chem. Soc.*, 1998, **120**, 4877; L. Balogh and D. A. Tomalia, *J. Am. Chem. Soc.*, 1998, **120**, 7355.

Communication a909535g

Highly fluorescent and electroactive molecular squares containing perylene bisimide ligands

Frank Würthner* and Armin Sautter

Abteilung Organische Chemie II, Universität Ulm, Albert-Einstein-Allee 11, 89081 Ulm, Germany. E-mail: frank.wuerthner@chemie.uni-ulm.de

Received (in Cambridge, UK) 16th December 1999, Accepted 7th February 2000, Published on the Web, 29th February 2000

Large functional molecular squares have been assembled with ditopic perylene bisimide bridging ligands and Pt(II) and Pd(II) phosphine corner units and their optical, electrochemical and spectroelectrochemical properties have been studied.

Interest in functional supramolecular assemblies[1] has been triggered by examples from nature like the light harvesting system (LHS) in purple bacteria.[2] The supramolecular functionality of this natural assembly is realized by chlorophyll molecules organized in cyclic arrangements which control the electronic coupling of the dye molecules and allow accommodation of the reaction center of photosynthesis within the largest ring of LHS.[2] A straightforward access to cyclic structures in high yields was introduced by Fujita and Ogura[3] and Stang and Olenyuk[4] *via* the concept of molecular squares using ditopic bridging ligands and *cis*-coordinating square planar Pt(II) or Pd(II) corners. Some very interesting examples have been reported based on pyridyl-substituted porphyrin ligands,[5] where functionality is introduced by the ligand but porphyrin fluorescence is quenched upon metal complexation. Here, we report on a new ligand based on perylene tetracarboxylic acid bisimides[6,7] which exhibits fluorescence quantum yields Φ_F near 100%[6] as well as redox activity[8] and which conserves these properties in the metal-assembled state: a giant photo- and redox-active molecular square (metal–metal diagonal *ca*. 3.4 nm).

The perylene ligand **1** was synthesized in 66% yield by condensation of the corresponding perylene bisanhydride[7] with 4-aminopyridine in quinoline with catalytic amounts of zinc(II) acetate. The ligand exhibits an intense absorption band at λ_{max} = 585 nm and red fluorescence at λ_{max} = 618 nm with Φ_F = 0.94 for **1** in chloroform.[9]

Equimolar mixing of ditopic perylene ligand **1** with dpppM$(OTf)_2$ [M = Pt(II) or Pd(II), dppp = 1,3-bis(diphenylphosphino)propane; OTf = $CF_3SO_3^-$] in CH_2Cl_2 leads exclusively to the formation of molecular squares **2a**,**b** in 90 and 95% isolated yield, respectively (Scheme 1). The squares were characterized by elemental analysis, ^{1}H and ^{31}P{^{1}H} NMR spectroscopy and electrospray mass spectrometry (ESI–MS) (**2a**).† In the ^{31}P{^{1}H} NMR spectra of **2a**,**b** only one singlet is observed owing to the high symmetry of the squares, additionally there are Pt-satellites resulting from ^{195}Pt–^{31}P spin–spin coupling in the spectrum of **2a**. A typical change in chemical shifts of the phosphorus nuclei of *ca*. 10 ppm results upon complexation with **1**.[10] The ^{1}H NMR spectra show only a single set of signals for the ligand **1** and the dppp moiety with significant changes in the chemical shifts of the α- and β-pyridyl protons (*ca*. 0.3 ppm) owing to metal complexation.[10] In the ESI–MS of **2a** (acetone solution) we observed signals at *m/z* 2575.0 which we assign to the M−3OTf species with +3 charge state (separation of peaks by 1/3 mass unit) which corresponds to a molecular mass of 7725 for the square minus three triflate anions in excellent agreement with the calculated mass of 7724.89 ($C_{409}H_{360}N_{16}O_{47}F_{15}P_8S_5Pt_4$). Furthermore, we observed signals at *m/z* 1894, 1485 and 1213 which we assign to $(M-4OTf)^{4+}$, $(M-5OTf)^{5+}$ and $(M-6OTf)^{6+}$ species (THF–ethyl acetate solution). The less stable corresponding Pd-square

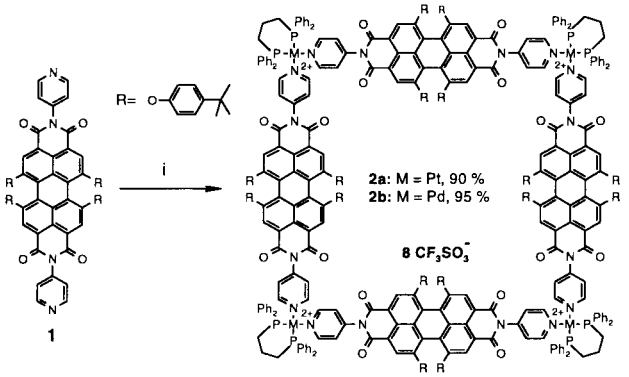

Scheme 1 *Reagents and conditions:* i, dpppM$(OTf)_2$, CH_2Cl_2, 24 h, 20 °C.

2b has not, as yet, been characterized by the ESI–MS technique.

The optical and electrochemical properties of the perylene ligand **1** remain almost unchanged upon formation of the complexes **2**. We ascribe this to the fact that in perylene tetracarboxylic acid bisimides, the imide substituents have only a small electronic coupling to the HOMO and LUMO of the perylene chromophore.[8,11] Therefore, the chromophoric perylene unit is largely decoupled of the binding site and only small bathochromic shifts of $\Delta\lambda$ = 5–7 nm in the absorption and emission spectra are observed upon complexation. The absorption maximum of **2a** is located at λ_{max} = 591 nm, the emission occurs at 625 nm. An even more important consequence is negligible quenching of the perylene fluorescence in these complexes with Φ_F (**2a**, $CHCl_3$) = 0.88.[9]

The ligand **1** and platinum complex **2a** exhibit reversible electrochemistry which was investigated by cyclic voltammetry in CH_2Cl_2. **1** displays two, reversible reductions at potentials of −1.08 and −1.23 V (*vs.* Fc/Fc$^+$), but oxidation is irreversible causing adsorption of **1** on the platinum electrode. The molecular square **2a** shows two reversible waves in the reductive cycle at similar potentials (−1.01, −1.14 V *vs.* Fc/Fc$^+$) but the oxidative cycle, in contrast to **1** shows a reversible wave at +0.93 V, probably as a consequence of the pyridyl nitrogen lone pairs which are now blocked by platinum-complexation (Fig. 1). The electrochemical studies of the palladium complex **2b** revealed a more complicated behavior displaying an irreversible reduction at $E < -1.15$ V which we attribute to electron transfer processes involving the Pd(II) corners.

A closer insight into the electrochemical processes was gained by spectroelectrochemical investigations of **2a** and **1**. By increasing the potential in a stepwise manner to the first reduction wave of **2a** (−1.01 V) the absorption bands of the perylene bisimide chromophores at 591 nm decrease while three bands in the UV–VIS–NIR appear with a maximum absorption at 791 nm [Fig. 2(a)]. Based on identical spectroscopic changes observed for the free perylene bisimide ligand **1**, we assign these optical transitions to perylene bisimide radical anionic species. After a further increase of the potential to the second reduction

DOI: 10.1039/a909892e

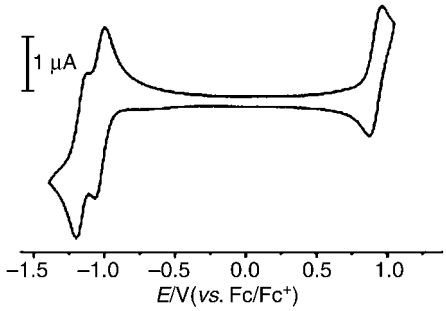

Fig. 1 Cyclic voltammogram of perylene–platinum square **2a** in CH_2Cl_2; scan rate 100 mV s^{-1}. Working electrode: Pt disc, auxiliary electrode: Pt wire, reference electrode: Ag/AgCl; concentration **2a** = 2.5×10^{-4} M; supporting electrolyte NBu_4PF_6 (0.1 M).

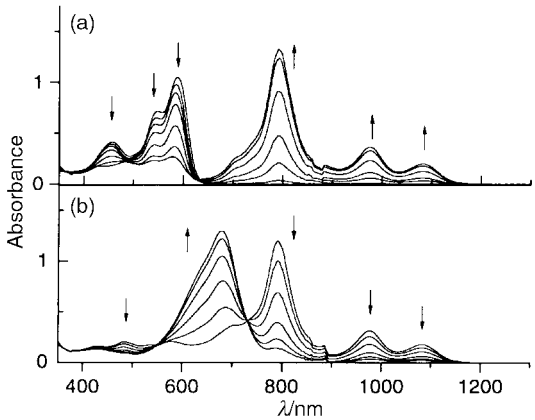

Fig. 2 Spectroelectrograms of perylene–platinum square **2a** in CH_2Cl_2 with NBu_4PF_6 (0.1 M) as supporting electrolyte. Working electrode: Pt disc; auxiliary electrode: Pt wire; reference electrode: Ag/AgCl; concentration **2a** = 1.4×10^{-4} M. Stepwise increase of the applied potential to radical anionic perylene species (a) and to dianionic perylene species (b).

wave of **2a** (−1.14 V) the perylene radical anion bands disappear completely whereas a broad and intense band appears, with a maximum absorption at 679 nm [Fig. 2(b)], corresponding to dianionic perylene bisimides. Oxidation to the radical cationic state results in less pronounced spectral changes in the visible but new broad bands appear in the NIR at 809, 908 and 1225 nm. The distinct isosbestic points in the absorption spectra for all redox couples confirm the reversibility of all oxidation and reduction processes. Therefore, we conclude that (i) the redox processes take place exclusively at the perylene ligands with the Pt(II) corner units being inert in the applied potential range and acting solely as structural building blocks, (ii) the perylene ligands assembled in the square do not interact with one another even in a charged state, and (iii) each perylene ligand in the square is reduced and oxidized at the same time at the given potentials.[12]

In summary, we report on a new functional ditopic perylene ligand **1** which has been used to construct nanosized molecular squares **2** with Pt(II) and Pd(II) phosphine corner units. The optical and electrical properties of the ligands are conserved in the metal-assembled state **2a** which shows a fluorescence quantum yield of almost unity and multiple, fully reversible redox couples. The giant inner volume of nanosquares **2** seems ideal to accommodate large functional guest molecules for studies on redox and photocatalytic processes.

We thank Dr Peter Weber (Scripps, La Jolla) for ESI mass spectrometry and helpful discussions. We gratefully acknowledge the Fonds der Chemischen Industrie, the BMBF, the DFG and the Ulmer Universitätsgesellschaft for financial support, the BASF AG and Degussa-Hüls AG for the donation of chemicals.

Notes and references

† *Selected data for* **2a**: mp > 330 °C. ^{1}H NMR ($CDCl_3$, 500 MHz), δ 9.13 (br s, 16H), 8.12 (s, 16H), 7.69 (br s, 32H), 7.40 (m, 32H), 7.32 (m, 16H), 7.20 (d, 32H, *J* 8.4 Hz), 7.09 (d, 16H, *J* 5.9 Hz), 6.77 (d, 32H, *J* 8.4 Hz), 3.29 (br s, 16H), 2.20 br s, 8H), 1.24 (s, 144H). ^{31}P{^{1}H} NMR ($CDCl_3$, 85% H_3PO_4, 202 MHz), δ −15.11 (s). UV–VIS(CH_2Cl_2), λ (ε) 591 (217000), 550 (135000), 459 nm (72000 dm^3 mol^{-1} cm^{-1}). $\lambda_{em,\,max}$(CH_2Cl_2) 625 nm. MS (ESI, acetone) Calc. $(M-3OTf)^{3+}$ *m/z* 2575.7. Found 2575.0. Found: C, 59.29; H, 4.59; N, 2.54; S, 3.03. $C_{412}H_{360}N_{16}O_{56}F_{24}P_8Pt_4S_8 \cdot 8H_2O$ requires C, 59.50; H, 4.56; N, 2.69; S, 3.08%.

1 J. M. Lehn, *Supramolecular Chemistry*, VCH, Weinheim, 1995; D. Philp and J. F. Stoddart, *Angew. Chem., Int. Ed. Engl.*, 1996, **35**, 1154; *Comprehensive Supramolecular Chemistry*, ed. J. M. Lehn, J. L. Atwood, J. E. D. Davies, D. D. MacNicol and F. Vögtle, Pergamon, Oxford, 1996, vol. 1–11.
2 G. McDermott, S. M. Prince, A. A. Freer, A. M. Hawthornthwaite-Lawless, M. Z. Papiz, R. J. Cogdell and N. W. Isaacs, *Nature*, 1995, **374**, 517; X. Hu and K. Schulten, *Phys. Today*, 1997, 28.
3 M. Fujita and K. Ogura, *Bull. Chem. Soc. Jpn.*, 1996, **69**, 1471.
4 P. J. Stang and B. Olenyuk, *Acc. Chem. Res.*, 1997, **30**, 502.
5 J. Fan, J. A. Whiteford, B. Olenyuk, M. D. Levin, P. J. Stang and E. B. Fleischer, *J. Am. Chem. Soc.*, 1999, **121**, 2741; C. M. Drain and J. M. Lehn, *J. Chem. Soc., Chem. Commun.*, 1994, 2313; R. V. Slone and J. T. Hupp, *Inorg. Chem.*, 1997, **36**, 5422; C. M. Drain, F. Nifiatis, A. Vasenko and J. D. Batteas, *Angew. Chem., Int. Ed.*, 1998, **37**, 2344.
6 G. Seybold and G. Wagenblast, *Dyes Pigments*, 1989, **11**, 303; R. Gvishi and B. Reisfeld, *Chem. Phys. Lett.*, 1993, **213**, 338.
7 D. Dotcheva, M. Klapper and K. Müllen, *Macromol. Chem. Phys.*, 1994, **195**, 1905; F. Würthner, C. Thalacker and A. Sautter, *Adv. Mater.*, 1999, **11**, 754.
8 S. K. Lee, Y. Zu, A. Herrmann, Y. Geerts, K. Müllen and A. J. Bard, *J. Am. Chem. Soc.*, 1999, **121**, 3513.
9 Fluorescence quantum yields were determined relative to 1,6,7,12-tetraphenoxy-*N*,*N*′-bis(2,6-diisopropylphenyl)perylene-3,4,9,10-tetracarboxylic acid bisimide (Φ_R = 0.96, $CHCl_3$)[6] by the optically dilute method ($A \leq 0.035$) in chloroform; J. N. Demas and G. A. Crosby, *J. Phys. Chem.*, 1971, **75**, 991.
10 P. J. Stang, D. H. Cao, S. Saito and A. M. Arif, *J. Am. Chem. Soc.*, 1995, **117**, 6273.
11 H. Langhals, S. Demmig and H. Huber, *Spectrochim. Acta, Part A*, 1988, **44**, 1189.
12 This conclusion is drawn from spectroelectrochemistry which shows complete disappearance of the bands of the neutral and the radical-anionic perylene species at the respective redox potentials.

Communication a909892e

ChemComm

Kinetic trapping of host–guest complexes in a polymeric matrix

Faysal Ilhan, Laura Diamondis, Leigh Gautreau and Vincent M. Rotello*

Department of Chemistry, University of Massachusetts, Amherst, MA 01003, USA. E-mail: rotello@chem.umass.edu

Received (in Columbia, MO, USA) 29th November 1999, Accepted 4th February 2000, Published on the Web, 29th February 2000

Diaminotriazine–flavin host–guest complexes are kinetically trapped in spin-cast polystyrene films.

Self-assembly is a powerful tool for the creation of nanoscale constructs. These non-covalently assembled host–guest complexes have been used to fabricate many molecular-scale components such as wires,[1] switches[2] and computers.[3] Central to the pragmatic utilization of these constructs, however, are the issues of immobilization and isolation. These attributes allow the utilization of molecular components to fabricate useful devices from the disorganized ensemble of components present in the solution phase.

Polymer matrix isolation is an effective technique for the isolation and immobilization of molecules.[4] Application of this methodology to the isolation of host–guest assemblies is hampered by issues of competition and aggregation. Matrix formation from polar polymers creates a competitive environment, disrupting the desired interactions such as hydrogen bonding. Conversely, creation of matrices using non-polar polymers can cause aggregation and concomitant phase separation of polar host–guest complexes. To overcome the issue of phase separation in non-polar polar matrices, we have explored methods of trapping host–guest complexes. We report here, the kinetic isolation of individual hosts and host–guest complexes in a highly non-polar polystyrene matrix through spin-casting of polymer solutions.

In preliminary investigations, we explored the fluorescence behavior of flavin **1** in different volumes of polystyrene films. The polymer-doped films were prepared by spin-casting[5] from solutions of 0.41, 0.87 and 1.75% w/w polystyrene ($M_n = 1{,}1 \times 10^5$, PDI = 2.3) and varying quantities of flavin **1**[6] in $CHCl_3$ on SiO_2 surfaces.[7] The optical transparency of these films[8] allowed direct observations of flavin **1** fluorescence behavior.[9] Addition of more equivalents of flavin **1** resulted in an increased quenching of fluorescence emission for the films prepared from solutions of 0.41 and 0.87% w/w polystyrene in $CHCl_3$ (Fig. 1).[10] This behavior is diagnostic of self-aggregation of flavin **1**. For films prepared from a solution of 1.75% w/w polystyrene in $CHCl_3$, increasing concentrations of flavin **1** resulted in a linear increase in fluorescence emission, demonstrating that self aggregation was effectively suppressed (Fig. 2). Heating of these films to temperatures higher than the T_g of the polystyrene (*ca.* 398 K) resulted in marked reduction in fluorescence and curvature of the fluorescence *vs.* concentration plot, both behaviors diagnostic of flavin aggregation.

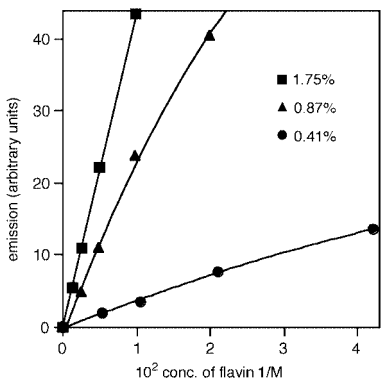

Fig. 1 Plot of fluorescence emission *vs.* concentration of flavin **1** in films prepared from solutions of 0.41, 0.87 and 1.75% w/w polystyrene in $CHCl_3$. Excitation: 445 nm, emission: 525 nm.

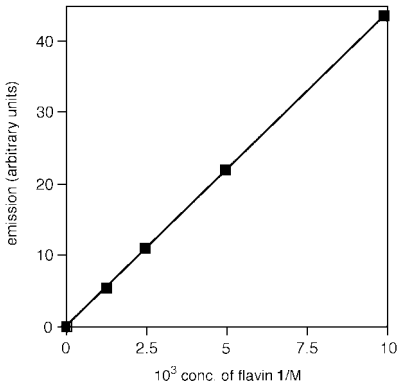

Fig. 2 Plot of fluorescence emission *vs.* concentration of flavin **1** in films prepared from a solution of 1.75% w/w polystyrene in $CHCl_3$. Excitation: 445 nm, emission: 525 nm.

To explore the complexation of flavin **1** *via* hydrogen bonding in the non-polar polystyrene matrix, films containing flavin **1** and complementary diaminotriazine-based[11] guest **2** were prepared. As shown in Fig. 3, increasing quantities of guest **2** resulted in only slightly decreased flavin **1** fluorescence emission for films prepared from solution of 0.41% w/w polystyrene in $CHCl_3$. This is consistent with non-specific aggregation between flavin **1** and triazine **2**. In contrast, titrations with 1.75% w/w polystyrene films showed marked decreases in fluorescence of flavin **1** with increasing concentrations of receptor **2**, reaching a limiting value. This is concordant with solution based investigations, where we established that hydrogen bonding between flavin **1** and guest **2** effectively quenches flavin fluorescence (Fig. 4).[12] Control experiments utilizing N(3)-methyl flavin **3** (Fig. 5), a molecule not capable

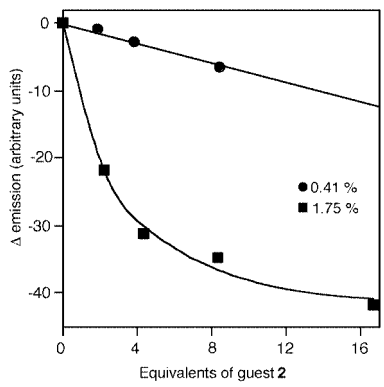

Fig. 3 Fluorescence emission changes of flavin **1** upon addition of triazine **2** in films prepared from solutions of 0.41 and 1.75% w/w polystyrene in $CHCl_3$. Excitation: 445 nm, emission: 525 nm. The curve for the titration performed with 1.75% w/w polystyrene films represents the best fit to the 1:1 binding isotherm. The line for the titration performed with 0.41% w/w polystyrene is a linear fit to the data points, and is intended only as a guide to the eye.

DOI: 10.1039/a909454g

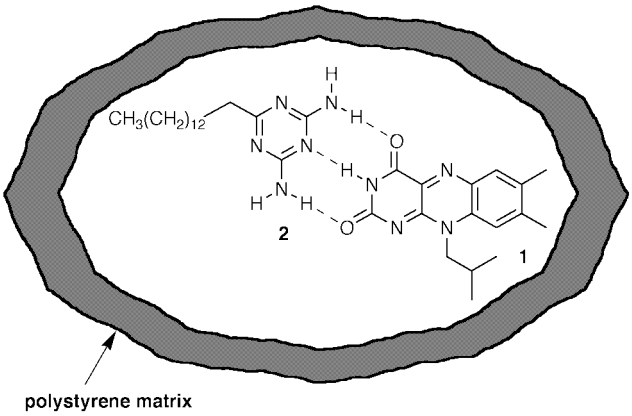

Fig. 4 Schematic illustration of isolated flavin **1**–triazine **2** host–guest complexes in a polystyrene matrix.

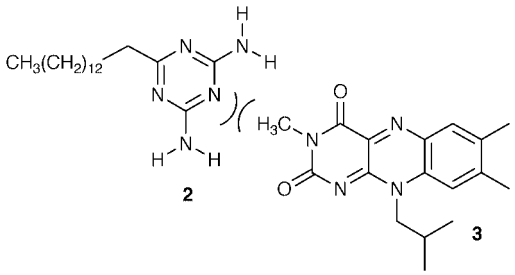

Fig. 5 N(3)-methyl flavin **3**–guest **2**.

of complementary binding through hydrogen bonding, in place of host **1** did not demonstrate any measurable complexation with guest **2**.

After calculating the volume of polymer matrices, the apparent association constants for flavin **1**–triazine **2** complexation were estimated by fitting the data to 1 : 1 binding isotherms for each different titration set of films. We did not observe any quantifiable recognition between flavin **1** and triazine **2** in films prepared from 0.41% w/w polystyrene solution, as a result of flavin **1** aggregation. For the films prepared from 1.75% w/w polystyrene solution, an estimated binding constant of 53 ± 12 M^{-1} was obtained.[13] This is considerably lower than the binding constant of 555 ± 8 M^{-1} which was obtained for the same host–guest complex formation in $CHCl_3$,[14] despite the non-competitive nature of the forming polystyrene matrix. This reduction in binding constant can be attributed to both the development of stress during polymer film formation[15] and the polymer entanglement during the deposition process, issues that we are currently exploring.

In summary, we have demonstrated the kinetic isolation of individual host flavin **1** and host flavin **1**–guest triazine **2** complexes in a highly non-polar polystyrene matrix through spin-casting of polymer solutions. Self-aggregation of polar flavin **1** in these non-polar polymer films was prevented by adjusting the ratio between polystyrene and flavin **1** in solution prior to spin casting. Fundamental and applied studies of this approach are underway and will be reported in due course.

This research was supported by the National Science Foundation (CHE 9905492 and 9703466 to V. M. R.), the National Institutes of Health (RO1 GM59249-01). V. M. R. acknowledges the Petroleum Research Fund of the ACS, the Alfred P. Sloan Foundation, Research Corporation, and the Camille and Henry Dreyfus Foundation

Notes and references

1 J. Lukkari, K. Kleemola, M. Meretoja and J. Kankare, *Chem. Commun.*, 1997, **12**, 1099; U. Simon, *Adv. Mater.*, 1998, **10**, 1487; G. Schmid and L. F. Chi, *Adv. Mater.*, 1998, **10**, 515.

2 A. P. Desilva, H. Q. N. Gunaratne, T. Gunnlaugsson, A. J. M. Huxley, C. P. Mccoy, J. T. Rademacher and T. E. Rice, *Chem. Rev.*, 1997, **97**, 1515; V. Balzani, M. Gomezlopez and J. F. Stoddart, *Acc. Chem. Res.*, 1998, **31**, 405; J. P. Launay and C. Coudret, *Anal. N. Y. Acad. Sci.*, 1998, **852**, 116.

3 J. M. Seminario and J. M. Tour, *Anal. N. Y. Acad. Sci.*, 1998, **852**, 68.

4 C. Higler and R. Stadler, *Macromolecules*, 1992, **25**, 6670; J. H. Golden, F. J. Disalvo, J. M. J. Frechet, J. Silcox, M. Thomas and J. Elman, *Science*, 1996, **273**, 782; N. Shinyashiki, S. Yagihara, I. Arita and S. Mashimo, *J. Phys. Chem. B*, 1998, **102**, 3249; P. Schuck, *Biophys. J.*, 1996, **70**, 1230; T. Werner, I. Klimant and O. S. Wolfbeis, *Analyst*, 1995, **120**, 1627.

5 For other studies utilizing spin-coating technique, see: C. J. Durning, B. O'Shaughnessy, U. Sawhney, D. Nguyen, J. Majewski and G. S. Smith, *Macromolecules*, 1999, **32**, 6772; R. J. Jackman, D. C. Duffy, O. Cherniavskaya and G. M. Whitesides, *Langmuir*, 1999, **15**, 2973; N. Tirelli, U. W. Suter, A Altomare, R. Solaro, F. Ciardelli, S. Follonier, Ch. Bosshard and P. Günter, *Macromolecules*, 1998, **31**, 2152.

6 A. Niemz, J. Imbriglio and V. Rotello, *J. Am. Chem. Soc.*, 1997, **119**, 892.

7 Films were spin-cast at 4500 rpm onto 22 mm square SiO_2 slides , using 200 μL of polymer/flavin solution in $CHCl_3$. Prior to coating, the slides were sonicated for 10 min sequentially in 1,1;2,2-tetrachloroethane, acetone and isopropyl alcohol. The slides were then dried for 2 h at 120 °C, and allowed to cool to ambient temperature in a $CaSO_4$ dessicator. After casting, films were dried *in vacuo* for 16 h prior to spectroscopic observations.

8 The polymer-doped films were highly transparent. For example, the film of 1.75% w/w polystyrene containing 1×10^{-2} M flavin **1** showed 96% transmittance at 445 nm.

9 Fluorescence measurements were performed using a machined slide holder. The slides were vertically set, with the polymer coated surface at an angle of 60° to the excitation beam.

10 The spin-coated films were homogeneous, indicating the lack of macroscopic phase separation.

11 For other examples of similar host–guest complexes, see: R. Deans and V. M. Rotello, *J. Org. Chem.*, 1997, **62**, 4528; E. Breinlinger, A. Niemz and V. M. Rotello, *J. Am. Chem. Soc.*, 1995, **117**, 5379; A. D. Hamilton and D. Van Engen, *J. Am. Chem. Soc.*, 1987, **109**, 5035; A. V. Muehldorf, D. Van Engen, J. C. Warner and A. D. Hamilton, *J. Am. Chem. Soc.*, 1988, **110**, 6561.

12 For binding experiments utilizing fluorescent probes, see: M. D. Greaves and V. M. Rotello, *J. Am. Chem. Soc.*, 1997, **119**, 10 569; D. C. Myles and K. Motesharei, *J. Am. Chem. Soc.*, 1994, **116**, 7413; K. Inoue, K. Kinoshita, H. Nakahara and T. Tanigaki, *Macromolecules*, 1990, **23**, 1227.

13 The uncertainty presented is the asymptotic standard error (A. S. E.). The value presented for K_a is for comparison purposes, as this system is obviously not in the standard state.

14 R. Deans, F. Ilhan and V. M. Rotello, *Macromolecules*, 1999, **32**, 4956.

15 For stress–strain effects on hydrogen bonding, see: M. J. Loboda and J. A. Seifferly, *J. Mater. Res.*, 1996, **11**, 391; M. Kawagoe and M. Morita, *J. Mater. Sci.*, 1994, **29**, 6041; R. E. Taylorsmith and R. A. Register, *Macromolecules*, 1993, **26**, 2802.

Communication a909454g

Electrosynthesis of cyclic carbamates from aziridines and carbon dioxide

Patricia Tascedda and Elisabet Duñach*

Laboratoire de Chimie Bioorganique, Associé au CNRS, Université de Nice-Sophia Antipolis, 06108 Nice Cedex 2, France. E-mail: dunach@unice.fr

Received (in Cambridge, UK) 23rd December 1999, Accepted 2nd February 2000, Published on the Web, 1st March 2000

A new and selective synthesis of five-membered ring cyclic carbamates involving nickel-catalyzed CO_2 incorporation into aziridines under mild electrochemical conditions was carried out in good yields.

Within our ongoing interest in carbon dioxide incorporation into small heterocyclic ring systems,[1,2] we present here our results on carbon dioxide incorporation into aziridines for the synthesis of 2-oxazolidones. 2-Oxazolidones are an important class of heterocyclic five-membered ring compounds.[3] These cyclic carbamates show good antibacterial properties[4,5] and are widely used in pharmaceutical chemistry.[6]

Their synthesis generally proceeds through the condensation of 1,2-aminoalcohols with toxic carbonyl derivatives such as phosgene[7] or cyanic acid (from urea decomposition).[8] The direct addition of CO_2 to β-amino alcohols at high pressure and temperature has been described in the patent literature.[9] Other methods of synthesis of 2-oxazolidones include the reaction of epoxides with cyanuric acid[10] or isocyanates[11] or the reaction of alkenes with *N*-bromosuccinimide and isocyanates.[12] 2-Oxazolidones can also be obtained from α-ketols and isocyanates or chloroformates.[13]

The direct functionalization of aziridines to cyclic carbamates has been reported *via* flash vacuum pyrolysis at 600 °C in the presence of ethyl chlorocarbonate[14] and by reaction with CO_2 at high pressure (50 atm, 60 °C) in the presence of tetraphenylantimony halides.[15]

We describe now a new and selective method of 2-oxazolidone synthesis using a simple electrochemical procedure, by which the cyclic carbamates **2** and **3** can be obtained in good yields from the direct reaction of substituted aziridines **1** with CO_2. Carbon dioxide insertion into the C–N bond of the aziridine ring takes place under very mild conditions, at room temperature and with atmospheric carbon dioxide pressure (Scheme 1). This new carboxylation reaction widens the field of utilization of CO_2 as a C-1 building block for organic chemicals.[16]

The reaction was catalyzed by a Ni(II) complex (10 mol%) and was carried out in a single-compartment cell fitted with a consumable magnesium anode and an inert cathode (*e.g.* stainless steel). Electrolyses were conducted at constant intensity in DMF as the solvent, and $[Ni(bipy)_3][BF_4]_2$ (bipy = 2,2′-bipyridine) was shown to be an efficient catalyst for this carboxylation. This same Ni(II)–bipy complex has already been used as a catalyst in other carbon dioxide incorporation reactions (*e.g.* into alkynes[17] or diynes[18]).

The electrochemical carboxylation of the *N*-Boc protected aziridine **1a**[19] led to the cyclic carbamates as a 60 : 40 mixture of two regioisomers **2a** and **3a** in 83% yield and 60% aziridine conversion (Table 1, entry 1). The major isomer corresponds to the incorporation of CO_2 at the less hindered side of the monosubstituted aziridine. No reaction occurred in the absence of current and in the absence of the nickel catalyst a very low yield of cyclic carbamates was obtained (< 10%).

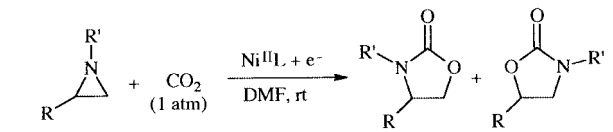

1a R = Et, R′ = Boc
b R = *n*-C_8H_{17}, R′ = Boc
c R = Ph, R′ = Boc
d R = *n*-$BuOCH_2$, R′ = Boc
e R = Ph, R′ = H

Scheme 1

From a mechanistic point of view, oxidation of the magnesium rod to Mg^{2+} ions in solution takes place at the anode. At the cathode, the reduction of the Ni(II) complex to Ni(0) occurs reversibly at −1.2 V *vs.* SCE. Cyclic voltammetry showed that upon addition of **1a** to the Ni(II)–bipy solution, the reduction peak of the Ni(II)/Ni(0) transition at −1.2 V became irreversible. This was taken to indicate that the electrogenerated Ni(0) reacted with **1a** by a possible insertion into the C–N bond of the aziridine ring. The oxidative addition of Ni(0) complexes to oxirane rings has already been reported.[20]

Table 1 Ni-catalyzed electrochemical CO_2 incorporation into aziridines[a]

Entry	Aziridine	Catalyst[b]	Conditions[c]	Conversion (%)	Carbamate yield[d] (%)	Ratio **2**:**3**
1	**1a**	Ni–bipy	Mg/st. steel KBr	60	83	60:40
2	**1a**	Ni–bipy	Mg/Ni KBr	20	100	75:25
3	**1a**	Ni–bpy	Mg/C KBr	45	88	50:50
4	**1a**	Ni–bipy	Al/st. steel KBr	30	50	66:34
5	**1a**	Ni–bipy	Mg/st. steel NBu_4BF_4	30	85	76:24
6	**1a**	Ni–bipy	Mg/st. steel KCl	45	75	73:27
7	**1a**	Ni–cyclam	Mg/st. steel KBr	85	94	75:25
8	**1b**	Ni–cyclam	Mg/st. steel KBr	65	93	67:33
9	**1c**	Ni–cyclam	Mg/st. steel KBr	99	94	78:22
10	**1d**	Ni–cyclam	Mg/st. steel KBr	99	100	86:14
11	**1e**	Ni–cyclam	Mg/st. steel KBr	63	100	84:16

[a] *General electrochemical conditions*: into a single-compartment cell[21] of *ca.* 50 mL capacity fitted with the corresponding couple of electrodes, 40 mL of freshly distilled DMF, the supporting electrolyte (2×10^{-2} M), the Ni(II) catalyst (0.3 mmol) and aziridine **1** (3 mmol) were introduced. The solution was stirred at room temperature and CO_2 was bubbled into it at atmospheric pressure. The electrodes were connected to a stabilized constant current supply (Sodilec, EDL 36.07) and electrolyzed at 60 mA (corresponding to a current density of *ca.* 0.3 A dm^{-2}) for 7 h, until the consumption of **1** was negligible. The reaction mixture was then stirred at 50 °C overnight, hydrolyzed with aqueous HCl and extracted with ethyl acetate. The crude product was analyzed by GC, NMR and mass spectrometry, purified by column chromatography on silica gel and the identity of the carbamate products compared to the known compounds. [b] Ni–bipy = $[Ni(bipy)_3][BF_4]_2$, Ni–cyclam = $[Ni(cyclam)]Br_2$; both are 10 mol% with respect to the aziridine **1**. [c] The experimental conditions relate to the anode/cathode couple of electrodes and the supporting electrolyte (2×10^{-2} M). [d] The carbamate yields of **2** + **3** are calculated on the basis of converted aziridine.

DOI: 10.1039/a910285j

On the other hand, electrogenerated Ni–bipy complexes are also known to catalytically react with CO_2 to form its radical anion,[17,22] which, under the reaction conditions, undergoes reductive dimerization to oxalate.

In the electrocarboxylation of aziridines (Scheme 1), there is a competition for the electrogenerated Ni(0) complexes between two processes: (i) Ni(0) insertion into the aziridine ring followed by further CO_2 uptake and ring closure to the carbamate and (ii) CO_2 reduction to oxalate. This competition, which was very dependent on the reaction conditions, accounts for the limited aziridine conversion rates in some cases.

The influence of several factors such as the nature of the electrodes, the supporting electrolyte and of the ligand(s) attached to nickel were examined in the electrocarboxylation of **1a**. As regards the electrode, a magnesium/stainless steel couple afforded the best results, as compared to the use of carbon fiber or nickel foam as cathodes (compare Table 1, entries 1–3). When an aluminium anode was used (with several cathode materials) low aziridine conversions and low carbamate yields (*e.g.* Table 1, entry 4) were observed, with CO_2 electroreduction being favored. Among supporting electrolytes, KBr, KCl and NBu_4BF_4 were tested with Mg/stainless steel electrodes. The use of NBu_4BF_4 (Table 1, entry 5) afforded a good yield of carbamate but a low conversion of **1a** while KCl led to a conversion of 45% (Table 1, entry 6); KBr afforded the best results (Table 1, entry 1).

In the related CO_2 incorporation into oxirane rings for the synthesis of cyclic carbonates,[2] we showed that both 2,2′-bipy and cyclam ligands on nickel (cyclam = 1,4,8,11-tetraazacyclotetradecane) were effective for the CO_2 insertion reaction. In the electrocarboxylation of **1a**, the use of [Ni(cyclam)]Br_2 as the catalyst afforded **2a** and **3a** in 94% yield with 85% aziridine conversion (Table 1, entry 7). With the Ni–cyclam catalytic system the electroreduction of carbon dioxide was almost completely inhibited, in favor of aziridine carboxylation. The observed regioselectivity **2a**:**3a** was 75:25.

The reaction was then extended to the carboxylation of several monosubstituted aziridines **1b**–**e** with [Ni(cyclam)]Br_2 as the catalyst. Thus, aliphatic, aromatic or ether substituted *N*-Boc aziridines (Table 1, entries 8–10) led regioselectively to the corresponding carbamates in good yields and excellent conversions (Table 1, entries 9, 10). The electrocarboxylation of the non-protected N–H aziridine **1e** was also efficient and led to a 84:16 regioisomeric ratio of **2e**:**3e** in quantitative yield and with a 63% conversion (Table 1, entry 11).

In conclusion, a novel catalytic system for incorporation of CO_2 into aziridines for the synthesis of cyclic carbamates was developed. Use of stable and readily available Ni(II) complexes of cyclam or bipyridine ligands and application of simple preparative electrochemical conditions, led to efficient catalytic insertion of the carbon dioxide into the C–N bond of aziridines with regioselectivities of 60–86%.

The electrochemical method described here employs very mild experimental conditions (CO_2 pressure of 1 atm, 20 °C), as compared to existing methods, which require harsh conditions or the use of toxic starting materials such as phosgene. It is also worth noting that this reported method utilizes carbon dioxide as the starting C-1 carbon source, and constitutes a new example in the field of green and catalytic chemistry.

Notes and references

1 P. Tascedda and E. Duñach, *J. Chem. Soc., Chem. Commun.*, 1995, 43.
2 P. Tascedda, M. Weidmann, E. Dinjus and E. Duñach, *Appl. Organomet. Chem.*, 2000, in press.
3 M. E. Dyen and D. Swern, *Chem. Rev.*, 1967, 197.
4 S. Sato, Y. Yoshida and S. Kuwahara, *Jpn. J. Microbiol.*, 1960, **4**, 419.
5 D. F. Kefauver and I. Drupa, *Antibiot. Chemother.*, 1960, **10**, 688.
6 G. Chakraborty, *Indian J. Pediat.*, 1964, **28**, 357; R. M. Stabler, *J. Parasitol.*, 1957, **43**, 280.
7 H. L. Crowther and H. McCombie, *J. Chem. Soc.*, 1913, **103**, 27; D. Ben-Ishai, *J. Am. Chem. Soc.*, 1956, **78**, 4962.
8 W. J. Close, *J. Am. Chem. Soc.*, 1951, **73**, 95.
9 J. W. Lynn, *US Pat.* 2 975 187, 1961; A. B. Steele, *US Pat.* 2 868 801, 1959.
10 R. W. Cummins, *J. Org. Chem.*, 1963, **28**, 85.
11 S. Knapp, P. J. Kukkola, S. Sharma, T. G. Murali Dhar and A. B. J. Naughton, *J. Org. Chem.*, 1990, **55**, 5700.
12 C. Heathcock and A. Hassner, *Angew. Chem.*, 1963, **75**, 344.
13 W. H. Pirkle and A. K. Simmons, *J. Org. Chem.*, 1983, **48**, 2520.
14 M. R. Banks, J. I. G. Cadogan, I. Gosney, K. G. Hodgson and D. E. Thomson, *J. Chem. Soc., Perkin Trans 1*, 1991, 961.
15 R. Nomura, T. Nakano, Y. Nishio, S. Ogawa, A. Ninagawa and H. Matsuda, *Chem. Ber.*, 1989, **122**, 2407.
16 A. Behr, *Carbon Dioxide Activation by Metal Complexes*, VCH, Weinheim, 1988; T. Inui, M. Anpo, K. Izui, S. Yanagida and T. Yamaguchi, *Advances in Chemical Conversions for Mitigating Carbon Dioxide, Studies in Surface Science and Catalysis*, Elsevier, Amsterdam, 1998.
17 S. Dérien, E. Duñach and J. Périchon, *J. Am. Chem. Soc.*, 1991, **113**, 8447.
18 S. Dérien, J. C. Clinet, E. Duñach and J. Périchon, *J. Org. Chem.*, 1993, **58**, 2578.
19 Aziridine **1a** was prepared according to: P. Wessig and J. Schwarz, *Synlett.*, 1997, 893.
20 R. J. De Pasquale, *J. Chem. Soc., Chem. Commun.*, 1973, 157; M. Weidmann, Doctoral Thesis, Universitat Jena, Germany, 1997.
21 J. Chaussard, J. C. Folest, J. Y. Nédélec, J. Périchon, S. Sibille and M. Troupel, *Synthesis*, 1990, **5**, 369.
22 L. Garnier, Y. Rollin and J. Périchon, *New J. Chem.*, 1989, **13**, 53; P. Daniele, G. Ugo, G. Bontempelli and M. Fioriani, *J. Electroanal. Chem., Interfacial Electrochem.*, 1987, **219**, 259.

Communication a910285j

Synthesis and structural characterization of a novel asymmetric distannene [{1-[N(Bu^t)C(SiMe$_3$)C(H)]-2-[N(Bu^t)(SiMe$_3$)CC(H)]C$_6$H$_4$}Sn→Sn{1,2-[N(Bu^t)(SiMe$_3$)CC(H)]$_2$C$_6$H$_4$}]†

Wing-Por Leung,* Hui Cheng, Rong-Bin Huang, Qing-Chuan Yang and Thomas C. W. Mak

Department of Chemistry, The Chinese University of Hong Kong, Shatin, New Territories, Hong Kong, China. E-mail: kevinleung@cuhk.edu.hk

Received (in Cambridge, UK) 4th January 2000, Accepted 9th February 2000, Published on the Web, 1st March 2000

The reaction of dilithium complex [{1,2-[N(Bu^t)C(SiMe$_3$)C(H)]$_2$C$_6$H$_4$}{Li$_2$(TMEDA)$_2$}] 1 with SnCl$_2$ yielded an unusual asymmetric distannene [{1-[N(Bu^t)C(SiMe$_3$)C(H)]-2-[N(Bu^t)(SiMe$_3$)CC(H)]C$_6$H$_4$}Sn→Sn{1,2-[N(Bu^t)(SiMe$_3$)CC(H)]$_2$C$_6$H$_4$}] 2 resulting from intramolecular self-rearrangements of the ligands; 2 has a tin–tin bond distance of 3.0087(3) Å.

Ethene analogues of tin containing homoleptic ligands such as [SnR$_2$]$_2$ have been an interesting topic of research. The first crystallographically characterized distannene [Sn{CH(SiMe$_3$)$_2$}$_2$]$_2$ [Sn–Sn 2.768(1) Å] was reported in 1976 by Lappert and coworkers.[1] Nearly two decades later, solid-state structures of three thermally stable compounds [Sn{Si(SiMe$_3$)$_3$}$_2$]$_2$,[2] [Sn{2,4,6-(CF$_3$)$_3$C$_6$H$_2$}$_2$]$_2$[3] and [Sn(4,5,6-Me$_3$-2-Bu^{t}C$_6$H)$_2$]$_2$[4] having tin–tin bonds [Sn–Sn 2.825(1), 3.64, 2.910(1) Å, respectively] were reported. These compounds were either partially or completely dissociated to the monomers SnR$_2$ in toluene or methylcyclohexane. There have been evidences for formation of an unstable dimer [Sn(2,4,6-Pr$^i_3$C$_6$H$_2$)$_2$]$_2$ from the photolysis of corresponding cyclotrimer [Sn(2,4,6-Pr$^i_3$C$_6$H$_2$)$_2$]$_3$ in methylcyclohexane at 205 K.[5] However, the dimer had not been structurally characterized owing to its complete reversion to the cyclotrimer at room temperature. To our knowledge, only two examples of structurally characterized bivalent tin complexes containing different ligands attached to each tin atom having a tin–tin bond have been reported. One of them reported by our group was a thermally labile compound [{8-(CHSiMe$_3$)C$_9$H$_6$N}$_2$Sn→SnCl$_2$] **I** with an Sn–Sn distance of 2.961(1) Å,[6] and the other compound [{2,6-(Me$_2$N)$_2$C$_6$H$_3$}$_2$Sn→Sn{1,8-(NCHBu^t)$_2$C$_{10}$H$_6$}] **II** [Sn–Sn 3.087(2) Å] reported recently by Lappert and coworkers.[7] These two complexes were obtained from the reactions of two tin(II) complexes, where each of the tin complexes either acts as a Lewis acid or a base. Here, we report a rare example of an asymmetric distannene having chelating ligands bonded in different modes to the tin metals resulted from intramolecular self-rearrangements within the binuclear tin(II) compound.

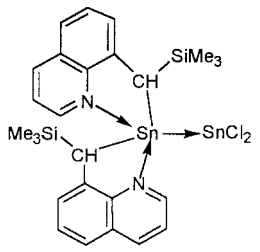

I

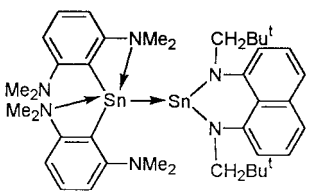

II

This novel distannene [{1-[N(Bu^t)C(SiMe$_3$)C(H)]-2-[N(Bu^t)(SiMe$_3$)CC(H)]C$_6$H$_4$}Sn→Sn{1,2-[N(Bu^t)(SiMe$_3$)CC(H)]$_2$C$_6$H$_4$}] **2** was prepared from the reaction of the bis(1-azaallyl) dilithium compound [{1,2-[N(Bu^t)C(SiMe$_3$)C(H)]$_2$-C$_6$H$_4$}{Li$_2$(TMEDA)$_2$}] **1** with SnCl$_2$ (Scheme 1). Dilithium compound **1** was prepared by the addition of isocyanide Bu^{t}NC to a diethyl ether solution of the dilithium dialkyl compound [{1,2-(CHSiMe$_3$)$_2$C$_6$H$_4$}{Li$_2$(TMEDA)$_2$}]. In this reaction, the isocyanide inserts into the Li–C bond followed by a 1,2-shift of the trimethylsilyl group along the carbon chains. Similar reaction with organonitrile Bu^{t}CN has been reported earlier.[8] Compound **1** has been characterized by ^{1}H and ^{13}C NMR spectroscopy, EI-MS spectrometry and elemental analysis.‡ The X-ray structure of **1** has been determined.

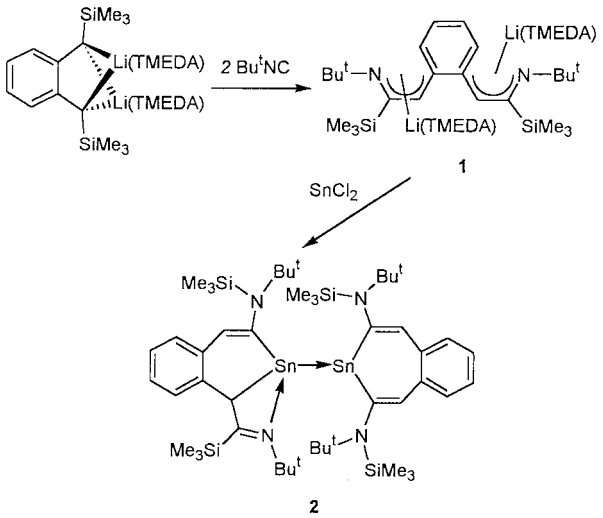

Scheme 1 Synthesis of complexes **1** and **2**.

Subsequent treatment of **1** with a slight excess of SnCl$_2$ led to the formation of **2** in 64.9% yield. By X-ray structure analysis of the product, it has found that the ligands bonded to the two tin(II) atoms undertake different rearrangements. One of the ligands undergoes two 1,2-shifts of the SiMe$_3$ group from C to N, and both of the 1-azaallyl arms are bonded to the tin(II) atom *via* the carbon atoms. The ligand attached to the other tin(II) core undergoes a 1,2-silyl migration. This rearrangement results in the two 1-azaallyl arms bonded to the tin atom in an η^1-C and η^2-C,N bonding mode, respectively. Compound **2** is soluble in toluene, Et$_2$O and THF, and slowly decomposes to tin metal in solution. It has been characterized by EI-MS spectrometry, ^{1}H, ^{13}C, ^{119}Sn NMR spectroscopy, elemental analysis‡ and X-ray structure analysis.§ The ^{1}H and ^{13}C NMR spectra of **2** in C$_6$D$_6$–C$_5$D$_4$N (4 : 1) showed only one set of signals corresponding to the ligand at ambient temperature. The ^{119}Sn NMR spectrum displayed a broad singlet at δ 333.04.

Compound **2** crystallized from a solvent mixture of THF and toluene (1 : 10) as a THF solvate (Fig. 1). It is comprised of two

† Electronic supplementary information (ESI) available: characterization data for compounds **1** and **2**. See http://www.rsc.org/suppdata/b0/b000268m/

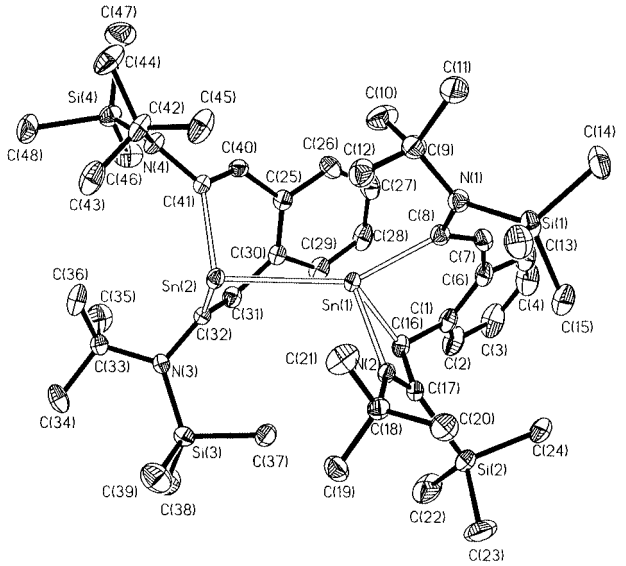

Fig. 1 Molecular structure of [{1-[N(Bu^t)C(SiMe$_3$)C(H)]-2-[N(Bu^t)(SiMe$_3$)CC(H)]C$_6$H$_4$}Sn→Sn{1,2-[N(Bu^t)(SiMe$_3$)CC(H)]$_2$C$_6$H$_4$}] **2**. Hydrogen atoms and solvent molecule have been omitted for clarity. Selected bond distances (Å) and angles (°): Sn(1)–Sn(2) 3.0087(3), Sn(1)–C(8) 2.208(2), Sn(1)–C(16) 2.219(2), Sn(1)–N(2) 2.266(1), Sn(2)–C(32) 2.209(2), Sn(2)–C(41) 2.255(2); C(8)–Sn(1)–C(16) 89.53(7), C(8)–Sn(1)–N(2) 91.32(6), C(16)–Sn(1)–N(2) 61.70(6), C(8)–Sn(1)–Sn(2) 144.21(4), C(16)–Sn(1)–Sn(2) 126.22(5), N(2)–Sn(1)–Sn(2) 106.25(4), C(32)–Sn(2)–C(41) 90.05(6), C(32)–Sn(2)–Sn(1) 93.42(4), C(41)–Sn(2)–Sn(1) 97.18(4).

independent stannylene moieties linked by a tin–tin bond at a distance of 3.0087(3) Å. The coordination geometries at the tin atoms are different. The Sn(1) centre adopts a distorted tetrahedron with the Sn(1)–Sn(2) vector residing on one of the vertices. The 1-azaallyl ligand attached to the Sn(1) atom undergoes a further 1,2-shift of the SiMe$_3$ group, resulting in a C(7)–C(8) double bond [1.352(2) Å] and C(8)–N(1) single bond [1.431(2) Å]. The other 1-azaallyl skeleton of the same ligand links to the Sn(1) atom in an η^2-C,N coordination mode, with an Sn(1)–C(16) bond distance of 2.219(2) Å and an Sn(1)–N(2) bond distance of 2.266(1) Å. The Sn(1)–N(2) bond distance is somewhat longer than the average Sn–N(amido) distances of 2.092 Å in [Sn{N(SiMe$_3$)$_2$}$_2$],[9] and 2.085 Å in **II**,[7] and comparable to the Sn–N distances of 2.153(4) and 2.288(4) Å in [Sn{C(SiMe$_3$)$_2$C(Ph)N(SiMe$_3$)}$_2$].[10] Unlike most 1-azaallyl complexes, no distinctive electron delocalization was found within the C(16)C(17)N(2) part. The C(16)–C(17) bond [1.539(3) Å] is a normal C–C single bond and the C(17)–N(2) bond distance [1.279(2) Å] coincides with the C–N double bond. The angle sum around N(2) is 359.97°, indicative of an sp^2 hybridization. Sn(2) adopts a trigonal pyramidal environment with an angle sum of 280.65° at Sn(2). This value is comparable to similar angles in **I** and **II**. In **I**, SnCl$_2$ acts as a Lewis acid, and the angle sum around Sn is 282.6°.[6] In **II**, the three-coordinate Sn core behaves as an acceptor with an angle sum of 279.4°.[7] The Sn(2) moiety in **2** can be viewed as an acceptor, and the Sn(1) fragment as a donor. Both of the 1-azaallyl ligands of Sn(2), undergo a 1,2-SiMe$_3$ migration, and are bonded to the Sn(2) atom in an η^1-C bonding mode. The Sn–C bond distances of 2.255(2) and 2.209(2) Å in **2** are shorter than those in [Sn{2-C(SiMe$_3$)$_2$C$_5$H$_3$N}$_2$] [2.334(6), 2.346(6), 2.377(7) Å],[11] and [Sn{2-C(SiMe$_3$)(Ph)C$_5$H$_3$N}$_2$] [2.329(4), 2.333(4) Å],[12] and comparable to the corresponding Sn–C distances in **I** [2.200(8), 2.203(8) Å],[6] and **II** [2.186(6), 2.196(7) Å].[7]

This work was supported by the Hong Kong Research Grants Council Earmarked Grant CUHK317/96P.

Notes and references

‡ *Selected spectroscopic data* for **1**: ^{1}H NMR [300 MHz, C$_6$D$_6$–C$_5$D$_4$N(2:1), 25 °C]: δ 0.52 (s, 18 H, SiMe$_3$), 1.57 (s, 18 H, CMe$_3$), 2.03 (s, 24 H, NMe$_2$), 2.12 (s, 8 H, CH$_2$N), 5.11 (s, 2 H, CH), 6.49 (br, 2 H, C$_6$H$_4$), 9.67 (br, 2 H, C$_6$H$_4$); ^{13}C{^{1}H} NMR [75.5 MHz, C$_6$D$_6$–C$_5$D$_4$N (2:1), 25 °C]: δ 4.95, 34.80, 46.03, 53.34, 57.73, 94.73, 119.22, 133.41, 137.45, 162.73; EI-MS (70 eV): *m/z* (%) 416 (21.9, M$^+$ − 2 Li − 2 TMEDA + 2). For **2**: ^{1}H NMR [300 MHz, C$_6$D$_6$–C$_5$D$_4$N(4:1), 25 °C]: δ 0.42 (s, 18 H, SiMe$_3$), 1.57 (s, 18 H, CMe$_3$), 6.69 (dd, 2 H, C$_6$H$_4$), 6.98 (dd, 2 H, C$_6$H$_4$), 7.51 (s, 2 H, CH); ^{13}C{^{1}H} NMR [75.5 MHz, C$_6$D$_6$–C$_5$D$_4$N (4:1), 25 °C]: δ 6.55, 32.93, 55.33, 123.51, 128.71, 132.71, 135.82, 182.27; ^{119}Sn NMR [149.2 MHz, C$_6$D$_6$–C$_5$D$_4$N (4:1), 25 °C]: δ 333.04 (br); EI-MS (70 eV): *m/z* 878 (2.6, M$^+$ − SiMe$_3$ − 2 Bu^t − 1).

§ *Crystal data* for **2**: C$_{52}$H$_{92}$N$_4$OSi$_4$Sn$_2$, M = 1139.04, crystal dimensions 0.36 × 0.20 × 0.14 mm, monoclinic, space group $P2_1/c$ (no. 14), a = 12.108(1), b = 36.869(3), c = 14.320(1) Å, β = 105.004(2)°, U = 6174.7(9) Å^3, Z = 4, μ = 0.922 mm^{-1}, T = 294(2) K, 42889 reflections collected for 1.57 < θ < 28.30°, 15255 independent reflections, $R1$ = 0.0540 for reflections with $I > 2\sigma(I)$, $wR2$ = 0.1435 (for all data). Data collection Bruker SMART CCD detector (0.3° ω scans), full-matrix least-squares refinement on F^2, SHELXTL-97. CCDC 182/1542. See http://www.rsc.org/suppdata/cc/b0/b000268m/ for crystallographic files in .cif format.

1 (*a*) D. E. Goldberg, P. B. Hitchcock, M. F. Lappert, K. M. Thomas, A. J. Thorne, T. Fjeldberg, A. Haaland and B. E. R. Schilling, *J. Chem. Soc., Dalton Trans.*, 1986, 2387; (*b*) D. E. Goldberg, D. H. Harris, M. F. Lappert and K. M. Thomas, *J. Chem. Soc., Chem. Commun.*, 1976, 261.

2 K. W. Klinkhammer and W. Schwarz, *Angew. Chem., Int. Ed. Engl.*, 1995, **34**, 1334.

3 U. Lay, H. Pritzkow and H. Grützmacher, *J. Chem. Soc., Chem. Commun.*, 1992, 260.

4 M. Weidenbruch, H. Kilian, K. Peters, H. G. von Schnering and H. Marsmann, *Chem. Ber.*, 1995, **128**, 983.

5 S. Masamune and L. R. Sita, *J. Am. Chem. Soc.*, 1985, **107**, 6390.

6 W.-P. Leung, W.-H. Kwok, F. Xue and T. C. W. Mak, *J. Am. Chem. Soc.*, 1997, **119**, 1145.

7 C. Drost, P. B. Hitchcock and M. F. Lappert, *Angew. Chem., Int. Ed.*, 1999, **38**, 1113.

8 M. F. Lappert and D.-S. Liu, *J. Organomet. Chem.*, 1995, **500**, 203.

9 T. Fjeldberg, H. Hope, M. F. Lappert, P. P. Power and A. J. Thorne, *J. Chem. Soc., Chem. Commun.*, 1983, 639.

10 P. B. Hitchcock, J. Hu, M. F. Lappert, M. Layh and J. Severn, *Chem. Commun.*,1997, 1189.

11 B. S. Jolly, M. F. Lappert, L. M. Engelhardt, A. H. White and C. L. Raston, *J. Chem. Soc., Dalton Trans.*, 1993, 2653.

12 W.-P. Leung, W.-H. Kwok, L.-H. Weng, L. T. C. Law, Z.-Y. Zhou and T. C. W. Mak, *J. Chem. Soc., Dalton Trans.*, 1997, 4301.

Communication b000268m

ChemComm

Synthesis and molecular structure of an unusual –Ga–Ga–Ga– linked organometallic

Xiao-Wang Li, Pingrong Wei, Brent C. Beck, Yaoming Xie, Henry F. Schaefer III, Jianrui Su and Gregory H. Robinson*

Department of Chemistry and the Center for Computational Quantum Chemistry, The University of Georgia, Athens, GA 30602-2556 USA. E-mail: robinson@sunchem.chem.uga.edu

Received (in Columbia, MO, USA) 24th November 1999, Accepted 5th February 2000, Published on the Web, 1st March 2000

Reaction of $[(2,4,6\text{-}Pr^i_3C_6H_2)_2C_6H_3]GaCl_2$ with $P(SiMe_3)_3$ affords the unusual organometallic compound $[(2,4,6\text{-}Pr^i_3C_6H_2)_2C_6H_3]Ga\{H_2PGa(H)PH_2\}Ga[C_6H_3(C_6H_2\text{-}Pr^i_3\text{-}2,4,6)_2]$ 1 characterized by multinuclear NMR, complete (C, H, Ga and P) elemental analyses, IR spectroscopy and single crystal X-ray diffraction; 1 is significant as it contains a rare Ga–Ga–Ga [2.5145(13) and 2.7778(14) Å] linkage even as its formation is facilitated by the unusual stripping of the sterically demanding *m*-terphenyl ligand from the central gallium atom.

One of the most extensively studied reactions in organo-group 13 chemistry of the past decade has been that of organometallic moieties with various phosphines.[1] The preference for tris-(trimethylsilyl)phosphine, $P(SiMe_3)_3$, as a phosphorus source may largely be traced to the considerable steric demands (*i.e.* large cone angle) of this compound coupled with the robust nature of the trimethylsilyl leaving groups.[2] Herein, we report the synthesis[3] and molecular structure[4] of $[(2,4,6\text{-}Pr^i_3C_6H_2)_2C_6H_3]Ga\{H_2PGa(H)PH_2\}Ga[C_6H_3(C_6H_2\text{-}Pr^i_3\text{-}2,4,6)_2]$ **1** isolated from reaction of $[(2,4,6\text{-}Pr^i_3C_6H_2)_2C_6H_3]GaCl_2$[5] with $P(SiMe_3)_3$. Compound **1**, characterized by

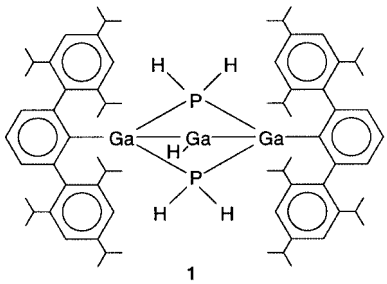

1

multinuclear NMR, complete elemental (C, H, Ga and P) analyses IR spectroscopy, and single crystal X-ray diffraction, is significant as it contains a rare –Ga–Ga–Ga– linkage even as its formation is facilitated by the unusual stripping of the sterically demanding *m*-terphenyl ligand from the central gallium atom.

The laboratory has had an interest in the organogallium chemistry of $P(SiMe_3)_3$ for some time having previously reported the synthesis and molecular structure of the phosphinogallane dimer $[Me_2Ga\text{–}P(SiMe_3)_2]_2$, isolated from reaction of $GaMe_3$ with $P(SiMe_3)_3$.[6] This compound contained a planar Ga_2P_2 four-membered ring with an independent Ga–P bond distance of 2.456(1) Å. Reaction of the Lewis acid–base adduct $Me_3Ga\text{–}PMe_3$ [Ga–P 2.455(4) Å] with $P(SiMe_3)_3$ was shown by this laboratory to afford $[(Me_3Si)_2P\{Me_2Ga\}_2PMe]_2$ – a novel bicyclic phosphinogallane consisting of two fused Ga_2P_3 five-membered rings sharing a common P–P base at a distance of 2.25(3) Å with a mean Ga–P bond distance of 2.44(4) Å.[7] Relative to sterically demanding ligands the *m*-terphenyl moiety $(2,4,6\text{-}Pr^i_3C_6H_2)_2C_6H_3$ has been most prominently utilized in the stabilization of $Na_2[\{(2,4,6\text{-}Pr^i_3C_6H_2)_2C_6H_3\}\text{–}Ga{\equiv}Ga\text{–}\{C_6H_3(C_6H_2Pr^i_3\text{-}2,4,6)_2\}]$, a novel gallyne possessing a short Ga–Ga bond distance of 2.319(3) Å.[8–10] Thus, as described herein, we endeavored to examine the organogallium chemistry of this ligand as a function of $P(SiMe_3)_3$.

The formation of **1** is at once both surprising and interesting. Although the stripping of a large organic moiety from a gallium center, as with the central gallium atom of **1**, is noteworthy, it is not unprecedented as a $Pr^i_3C_6H_2$ ligand has been shown to be stripped from a gallium atom.[11] While it may be reasonable to consider the five hydrogen atoms, two on each of the two phosphorus atoms and one on the central gallium atom, as having originated from the stripped *m*-terphenyl ligand, there are other possibilities. It is also possible, for example, that the ligand stripping may have initiated hydride abstraction from the solvent (or *vice versa*). It is noteworthy that the title compound has been repeatedly isolated in this laboratory under a number of conditions.[3] The phosphine hydrogen atoms and the gallium hydride are prominently manifest in IR and NMR spectroscopy. IR spectroscopic data for **1** indicate the presence of phosphine hydrogen atoms with bands at 2371 cm^{-1} [ν_{P-H} (m)] and 2337 cm^{-1} [ν_{P-H} (m)]. These values compare well to 2314 cm^{-1} [ν_{P-H} (m)] for $\{[Me_2Ga]_4[(\mu\text{-}PH)_2(C_6H_4)]_2\}$[12] and to 2343 cm^{-1} [ν_{P-H} (sym)] and 2335 cm^{-1} [ν_{P-H} (asym)] for the phosphinogallane trimer $[Bu^t_2Ga(\mu\text{-}PH_2)]_3$.[13] The gallium hydride IR bands at 1801 cm^{-1} [ν_{Ga-H} (vw)] and 1849 cm^{-1} [ν_{Ga-H} (vw)] of **1** are comparable to previously reported gallium hydride IR bands: $Me_2N\text{–}GaH_3$,[14] 1829 cm^{-1} [ν_{Ga-H} (vw)]; $[(PhCH_2(Me)_2NGaH_3]$,[15] 1835 cm^{-1} (ν_{Ga-H}) and $(Et_2O)_2Li[\mu\text{-}As(SiMe_3)_2]_2GaH_2$,[16] 1834 cm^{-1}. Similar to **1** which exhibits two Ga–H IR bands, the organometallic (mono)hydride $K[Ga(H)(CH_2SiMe_3)_3]$ also exhibits two Ga–H IR bands at 1915 cm^{-1} [ν_{Ga-H} (vw)] and 1840 cm^{-1} [ν_{Ga-H} (vw)].[17] It is important to note that our calculated IR spectrum agrees well with the experimental results of **1** reported herein.[18] A theoretical study of the model molecule $CH_3Ga\{H_2PGa(H)\text{-}PH_2\}GaCH_3$ at the DZP B3LYP level of theory in this laboratory reveals harmonic vibrational frequencies corresponding to P–H stretches of 2441, 2441, 2418 and 2415 cm^{-1}. Moreover, the calculated Ga–H IR band appears at 1882 cm^{-1}. In sum, these theoretical predictions are in good agreement (within 5%) with the experimentally observed IR spectrum. Although the Ga–H bond could not be unambiguously assigned in the ^1H NMR spectrum, P–H was clearly observed as a multiplet at δ 3.25; moreover the integration is indicative of two hydrogen atoms on each of the two phosphorus atoms. Consistent with its diamagnetic nature, the title compound did not prove to be EPR active.

A number of points are noteworthy relative to structure (Fig. 1) and bonding in the title compound. Compound **1** may be considered as a Ga_3P_2 trigonal bipyramidal core bridging the two *m*-terphenyl ligands. The Ga–C bonds in **1** of 1.969(6) and 1.982(6) Å are longer than the value reported for $[(2,4,6\text{-}Pr^i_3C_6H_2)_2C_6H_3]GaCl_2$ [1.949(8) Å] and yet are considerably shorter than that reported for the $Na_2[\{(2,4,6\text{-}Pr^i_3C_6H_2)_2C_6H_3\}\text{–}Ga{\equiv}Ga\text{–}\{C_6H_3(C_6H_2Pr^i_3\text{-}2,4,6)_2\}]$ gallyne (2.06 Å). The angles about the {–P–Ga–P–} core connecting the

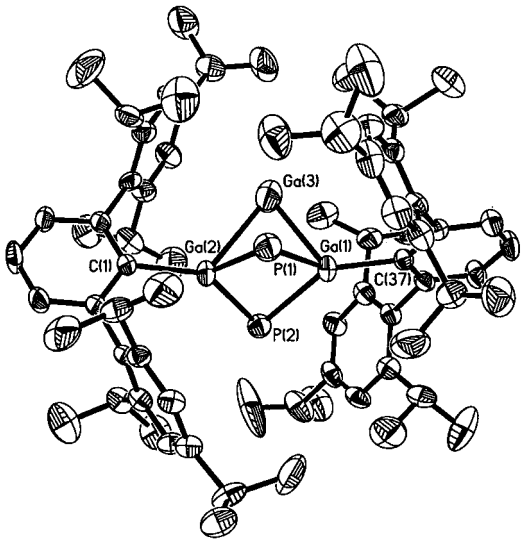

Fig. 1 Molecular structure of **1** (all hydrogen atoms, including that on Ga(3) and the two each on P(1) and P(2), have been omitted for clarity and only one position for each disordered phosphorus atoms is shown. Ellipsoids are shown at the 30% probability level): Bond distances (Å) and angles (°): Ga(1)–C(37) 1.969(6), Ga(2)–C(1) 1.982(6), Ga(1)–P(2) 2.564(5), Ga(1)–P(1) 2.660(6), Ga(1)–Ga(3) 2.5145(13), Ga(2)–P(1) 2.449(5), Ga(2)–P(2) 2.455(4), Ga(2)–Ga(3) 2.7778(14), Ga(1)···Ga(2) 3.031, Ga(3)···P(1) 3.327, Ga(3)···P(2) 3.314, P(1)···P(2) 3.930; C(37)–Ga(1)–P(2) 129.98(19), C(37)–Ga(1)–P(1) 130.3(2), P(2)–Ga(1)–P(1) 97.58(10), C(37)–Ga(1)–Ga(3) 115.97(18), P(2)–Ga(1)–Ga(3) 81.48(15), P(1)–Ga(1)–Ga(3) 79.96(18), C(1)–Ga(2)–P(1) 124.0(2), C(1)–Ga(2)–P(2) 128.1(2), P(1)–Ga(2)–P(2) 106.5(3), C(1)–Ga(2)–Ga(3) 119.69(18), P(1)–Ga(2)–Ga(3) 78.78(15), P(2)–Ga(2)–Ga(3) 78.33(13), Ga(1)–Ga(3)–Ga(2) 69.68(4), Ga(2)–P(1)–Ga(1) 72.65(17), Ga(2)–P(2)–Ga(1) 74.27(14).

two [(2,4,6-$Pr^i_3C_6H_2)_2C_6H_3$]Ga fragments are particularly acute at angles of 69.68(4), 72.65 and 74.27° for Ga(1)–Ga(3)–Ga(2), Ga(1)–P(1)–Ga(2) and Ga(1)–P(2)–Ga(2), respectively. The Ga(1)–Ga(3)–Ga(2) linkage is asymmetric at distances of 2.5145(13) and 2.7778(14) Å for Ga(1)–Ga(3) and Ga(2)–Ga(3), respectively. It should be noted, however, that compound **1** is not governed by a plane of symmetry or a twofold axis which would demand a symmetrical –Ga–Ga–Ga– linkage. Even though these Ga–Ga distances in **1** are rather long, they compare with a Ga–Ga range of 2.678–2.702 Å for the Ga_4-tetrahedral based [Ga{$C(SiMe_3)_3$}]$_4$.[19] Indeed, the Ga–Ga bond distances of **1** compare favorably with the Ga–Ga distances of 2.440(1) and 2.790(1) Å for the recently reported 'silicon-capped' Ga_4Si trigonal bipyramidal anion.[20]

The mean Ga–P distance in **1** is 2.461 Å. With Ga···P contacts of 3.327 and 3.314 Å for Ga(3)···P(1) and Ga(3)···P(2), respectively, the possibility of meaningful gallium–phosphorus interactions would appear to be remote. Likewise, the P(1)···P(2) approach of 3.930 Å is far beyond the realm of a phosphorus–phosphorus bond as typical P–P single bond distances are normally in the range 2.25(3)–2.35 Å.[21] Lastly, the Ga(1)···Ga(2) approach of 3.031 Å virtually rules out significant metal–metal interaction.

We are grateful to the National Science Foundation (H. F. S.: CHE-9815397; G. H. R.: CHE-9520162) and to the donors of The Petroleum Research Fund, administered by the American Chemical Society, for support of this work.

Notes and references

1 A. M. Arif, B. L. Benac, A. H. Cowley, R. Geerts, R. A. Jones, K. B. Kidd, J. M. Power and S. T. Schwab, *J. Chem. Soc., Chem. Commun.*, 1986, 1543.

2 R. L. Wells, S. R. Aubuchon, M. F. Self, J. P. Jasinski, R. C. Woudenberg and R. J. Butcher, *Organometallics*, 1992, **11**, 3370.

3 Compound **1** was prepared by a number of methods under a variety of conditions. All syntheses afforded **1** in comparable yields. *Method A*: inside a drybox (M Braun LabMaster 130), a Schlenk flask was charged with [(2,4,6-$Pr^i_3C_6H_2)_2C_6H_3$]$GaCl_2$ (1.30 g, 2.08 mmol), diethyl ether (40 mL) and a stirring bar. The resulting colorless solution was cooled to −78 °C. To this flask a solution of $P(SiMe_3)_3$ (0.52 g, 2.08 mmol) in diethyl ether (30 mL) was added *via* syringe over a period of 10 min. The solution was allowed to stir for 3 h at low temperature, after which it was allowed to slowly warm to room temperature and continued to stir for 72 h resulting in a slightly yellow solution. After filtration, the volume of the solution was reduced to *ca.* 20 mL *in vacuo*. Cooling the solution to −25 °C for one week gave colorless crystals of **1** (0.25 g, 0.20 mmol). Yield: 30%. mp: 191 °C (decomp.). Anal. Calc. (found) for $C_{72}H_{103}P_2Ga_3$ (E + R Microanalytical Laboratory, Corona, NY): C, 69.80 (70.30); H, 8.40 (8.19); Ga, 16.90 (16.88); P, 5.00 (4.86%). ^{1}H NMR (300 MHz, 298 K, C_6D_6): δ 0.87–1.31 [m, 72H, CH(CH_3)$_2$], 2.92 [m, 12H, –CH(CH_3)$_2$], 3.25 (m, 4H, PH_2), 7.10–7.21 [m, 14H, CH (aromatic)]. ^{13}C NMR (300 MHz, 298 K, THF-d_8): δ 23.5, 31.3, 35.4 (isopropyl); 120.0, 121.5, 128.8, 129.3, 140.6, 146.9, 148.0, 149.6 (aromatic carbon atoms). ^{31}P{^{1}H} NMR (300 MHz, 298 K, THF-d_8): δ −167.95 (s). Compound **1** was EPR inactive, thereby confirming its diamagnetic nature. IR (Perkin Elmer Paragon 1000PC FT-IR Spectrometer) (Nujol mull): 2371 [ν_{P-H} (m)], 2337 [ν_{P-H} (m)], 1801 [ν_{Ga-H} (vw)], 1849 cm^{-1} [ν_{Ga-H} (vw)].

4 A number of crystals of **1** were mounted and sealed in a glass capillaries under an atmosphere of nitrogen inside the drybox. The X-ray intensity data on an appropriate sample were collected at room temperature on a Bruker SMART TM CCD-based X-ray diffractometer system with graphite-monochromated Mo-Kα radiation (λ = 0.710 73 Å) using the ω-scan technique to a maximum 2θ value of 46.7°. *Crystallographic data*: $C_{72}H_{103}P_2Ga_3$: monoclinic, space group $P2_1/n$ (no. 14), a = 18.7040(16), b = 18.4955(16), c = 20.3393(17) Å, β = 92.588(2)°, V = 7029.0(10) Å^3, Z = 4, M = 1239.64, μ = 1.224 mm^{-1}, D_c = 1.171 g cm^{-3}. Of the 9812 independent reflections collected, 4427 were observed [$I > 2\sigma(I)$]. A routine absorption correction was applied by using SADABS and any decay correction was made with the SAINT program. The structure was solved by direct methods using the SHELXTL 5.1 Software Package. Each of the two bridging phosphorus atoms was found to be disordered over two adjacent positions with a refined occupancy factor of 0.50 for each position. The non-hydrogen atoms (except for the disordered phosphorus atoms) were refined anisotropically while hydrogen atoms were placed in ideal positions with their coordinates and thermal parameters riding on the attached carbon atoms (C–H 0.98 Å), the phosphorus atoms (P–H 1.50 Å) and the bridging gallium atom (Ga–H 1.50 Å). The final residual values based on 695 variable parameters and 4427 observed reflections [$I > 2\sigma(I)$] and $R1$ = 0.0637, $wR2$ = 0.1359 and those for all 9812 unique reflections are $R1$ = 0.1665, $wR2$ = 0.1711. CCDC 182/1538. See http://www.rsc.org/suppdata/cc/a9/a909451b/ for crystallographic files in .cif format.

5 J. Su, X.-W. Li and G. H. Robinson, *Chem. Commun.*, 1998, 2015.

6 M. D. B. Dillingham, J. A. Burns, W. T. Pennington and G. H. Robinson, *Inorg. Chim. Acta*, 1994, **216**, 267.

7 J. A. Burns, W. T. Pennington and G. H. Robinson, *Organometallics*, 1995, **14**, 1533.

8 J. Su, X.-W. Li, R. C. Crittendon and G. H. Robinson, *J. Am. Chem. Soc.*, 1997, **119**, 5471.

9 J. Xie, R. S. Grev, J. Gu, H. F. Schaefer III, P. v. R. Schleyer, J. Su, X.-W. Li and G. H. Robinson, *J. Am. Chem. Soc.*, 1998, **120**, 3773.

10 G. H. Robinson, *Acc. Chem. Res.*, 1999, **32**, 773.

11 K. M. Waggoner, S. Parkin, D. C. Pestana, H. Hope and P. P. Power, *J. Am. Chem. Soc.*, 1991, **113**, 3597.

12 R. L. Wells, H. Rahbarnoohi, P. B. Glaser, L. M. Liable-Sands and A. L. Rheingold, *Organometallics*, 1996, **15**, 3204.

13 A. H. Cowley, P. R. Harris, R. A. Jones and C. M. Nunn, *Oranometallics*, 1991, **10**, 652.

14 D. O'Hare, J. S. Ford, T. C. M. Page and T. J. Whitaker, *J. Chem. Soc., Chem. Commun.*, 1991, 1445.

15 P. C. Andrews, M. G. Gardiner, C. L. Raston and V.-A. Tolhurst, *Inorg. Chim. Acta*, 1997, **259**, 249.

16 J. F. Janik, R. L. Wells, V. G. Young Jr. and H. A. Halfen, *Organometallics*, 1997, **16**, 3022.

17 R. B. Hallock, O. T. Beachley Jr., Y.-J. Li, W. M. Sanders, M. R. Churchill, W. E. Hunter and J. L. Atwood, *Inorg. Chem.*, 1983, **22**, 3683.

18 H. F. Schaefer III and Y. Xie, unpublished results.

19 W. Uhl, W. Hiller, M. Layh and W. Schwarz, *Angew. Chem., Int. Ed. Engl.*, 1992, **31**, 1364.

20 G. Linti, W. Köstler, H. Piotrowski and A. Rodig, *Angew. Chem., Int. Ed.*, 1998, **37**, 2209.

21 *Compounds Containing Phosphorus–Phosphorus Bonds*, ed. A. H. Cowley, Dowden, Hutchinson and Ross, Inc., Stroudsburg, PA, 1973. A listing of typical P–P single bond values is found on p. 6 and references cited therein.

Communication a909451b

Microemulsion-promoted changes of reaction mechanisms: solvolysis of substituted benzoyl chlorides

L. García-Río* and J. R. Leis

Departamento de Química Física, Facultad de Química, Universidad de Santiago, 15706 Santiago, Spain. E-mail: qflgr3cn@usc.es

Received (in Cambridge, UK) 2nd December 1999, Accepted 14th February 2000, Published on the Web, 1st March 2000

When the hydrolysis of substituted benzoyl chlorides is carried out in a water/oil (w/o) microemulsion, the point in the substituent σ^+/lg *k* plot at which the mechanism changes from associative to dissociative depends on the water content of the microemulsion.

Water-in-oil (w/o) microemulsions[1] can be considered as consisting of three compartments in which small solutes may be located: the aqueous core of the droplets; the continuous non-polar phase; and the intervening micellar interface made up of surfactant molecules with their polar head groups facing the aqueous core.[2] They are extensively used for foods, cleaning products, drug delivery, tertiary oil recovery,[1] and as media for chemical reactions.[3] This latter application derives largely from their ability to catalyse reactions by bringing water-soluble reagents dissolved in the aqueous compartment into contact, at the micellar interface, with water-insoluble organic reagents dissolved in the non-polar compartment; microemulsion catalysis is an alternative to phase-transfer catalysis[4] and other techniques for favouring reaction between water-soluble and water-insoluble compounds. In addition, however, microemulsions can also bring about catalysis simply by concentrating water-soluble reagents in the aqueous droplet core and at the interface, the droplets thus acting as 'microreactors'.[5] Furthermore, reaction rates can be influenced by the altered properties of the water in droplets with very low water contents.[6,7]

In this work, we found that the altered properties of microemulsion water can affect not only reaction rates, but also the mechanism by which certain reactions take place. The specific class of reactions investigated was the hydrolysis of substituted benzoyl chlorides in water/AOT/isooctane microemulsions [AOT = sodium bis(2-ethylhexyl)sulfosuccinate] with water contents $W = [H_2O]/[AOT]$ ranging from 2 to 50.

The kinetics of the hydrolysis of benzoyl chlorides in microemulsions can be investigated using our extended pseudophase model of the latter.[8] Specifically, since the poor solubility of benzoyl chlorides in water makes it safe to assume that the amount of substrate dissolved in the aqueous compartment is negligible, we applied the model shown in Scheme 1, where K_S {$K_S = ([\text{Substrate}]_i Z)/[\text{Substrate}]_o$} governs the partition of substrate between the organic phase and the interface, the only region in which the reaction occurs. For the observed rate constant k_{obs}, this model affords eqn. (1), in which *k* is the

$$k_{obs} = \frac{kK_S}{K_S + Z} \quad (1)$$

pseudo first-order rate constant for the reaction in the interface and Z = [isooctane]/[AOT] is the ratio of the molar concentrations of the non-polar solvent and the surfactant.

As predicted by eqn. (1), plots of $1/k_{obs}$ *vs.* Z are linear in all cases studied (errors are always < 10–12% for the intercepts and *ca.* 1–2% for the slopes). Fig. 1 shows these results for some of the benzoyl chlorides used. For each value of *W*, the values of *k* (errors are always < 15%) so obtained were used to construct the corresponding Hammett plot. Fig. 2 shows the results for $W = 2$ and 50.

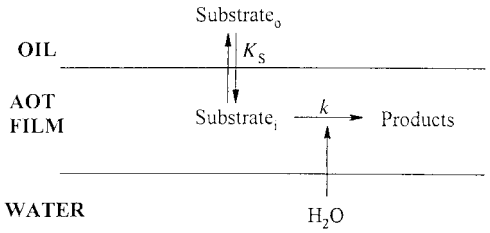

Scheme 1

Mechanistically, the solvolysis of benzoyl chlorides can proceed *via* either of two phenomenologically distinct kinds of mechanism: one in which the rate-limiting step includes a transition state with little or no cleavage of the bond binding the leaving group [an associative mechanism, Scheme 2(a)], and one in which it shows well advanced cleavage of the leaving group bond [a dissociative mechanism, Scheme 2(b)].[9,10] A positive ρ^+ value provides evidence for an associative transition state that involves bimolecular attack of water on the acyl chloride with little or no bond-breaking to the leaving group in the rate-limiting step. This corresponds to the initial step of an addition–elimination mechanism, but we do not know if there is an intermediate with a significant lifetime on the reaction path. An 'uncoupled concerted' reaction pathway may occur, in which there is no intermediate, but in which bond formation and bond cleavage are not balanced; *i.e.* bond-making and bond-breaking have not occurred to the same extent at the same time.[9]

The mechanism of a given reaction depends on the nature of the substituent and the solvent in which the reaction takes place.[9] The slope of a Hammett plot for solvolysis of benzoyl chlorides in water changes from negative (indicative of dissociative reactions, $\rho^+ = -3.0$[9]) to positive values (indicative of associative reactions) somewhere between the points corresponding to 3-(trifluoromethyl)benzoyl chloride and 4-ni-

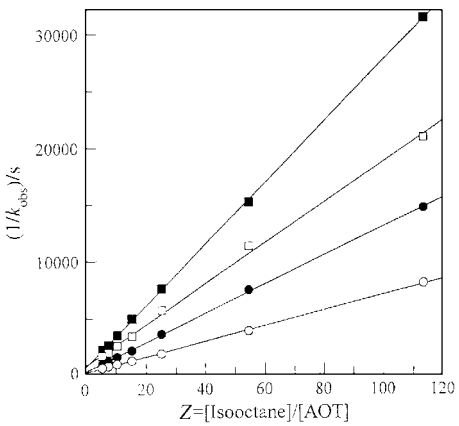

Fig. 1 Plots of $1/k_{obs}$ *vs.* Z = [isooctane]/[AOT] [see eqn. (1)] for the hydrolysis of substituted benzoyl chlorides at 25 °C in AOT/isooctane/water microemulsions with $W = 18$. (■) 4-Cl, (□) 4-H, (●) 4-Me, (○) 4-CF_3.

DOI: 10.1039/a909531d

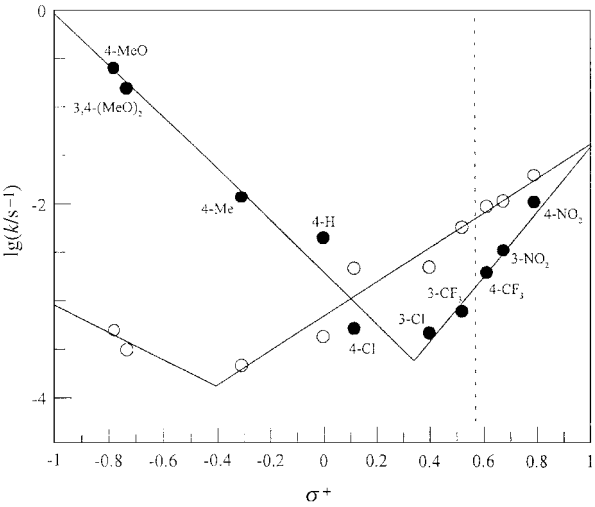

Fig. 2 Hammett plots for the hydrolysis of substituted benzoyl chlorides in AOT/isooctane/water microemulsions with different water contents: (●) W = 50 and (○) W = 2 at 25 °C. The dashed line indicates the point at which a similar plot for the reaction in water changes from negative to positive slope (ref. 9).

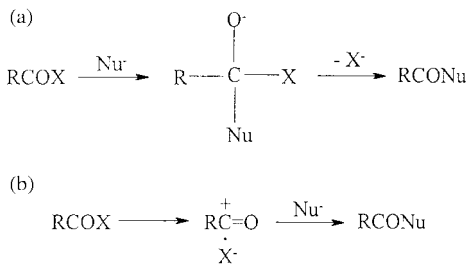

Scheme 2

trobenzoyl chloride, the latter of which reacts faster than the former.[9]

Fig. 2 shows that in microemulsions, as in water, there is indeed a switch from the dissociative to the associative mechanism. For the microemulsion with W = 50 this occurs at σ^+ *ca.* 0.3, between the points for 4-chlorobenzoyl chloride and 3-chlorobenzoyl chloride: for $\sigma^+ > 0.3$ there is very good Hammett correlation with a slope of $\rho^+ = 3.5 \pm 0.3$, whereas the least-squares line through the results for substituents with $\sigma^+ < 0.3$ has a slope of $\rho^+ = -2.7 \pm 0.3$, close to the value of −3.0 observed for reaction in pure water.[9] For the microemulsion with W = 2, the switch occurs at σ^+ *ca.* −0.4, just below the point for 4-methylbenzoyl chloride, with a Hammett slope of $\rho^+ = 1.8 \pm 0.2$ for $\sigma^+ > -0.4$ (the number of substrates with more negative σ^+ values was too few for accurate calculation of a Hammett slope for the dissociative branch).

As the water content of the medium falls, so too does the σ^+ value at which the mechanism switch occurs (see Fig. 2, in which the value at which the switch occurs in bulk water is shown by a dotted line). This can be attributed to the change in the properties of micelle-borne water.[11,12] The change from a dissociative to an associative reaction path with increasingly electron-withdrawing substituents occurs much later in water than in AOT/isooctane/water microemulsions with W = 50. The rate of the associative reaction is independent of the leaving group, while the dissociative reaction is strongly dependent on the nature of the leaving group and on its solvation.[9] For large values of W, water at the centre of the aqueous micelle core is similar in nature to that of bulk water, but water in or adjacent to the interface is devoted to solvating the surfactant head groups[12] and, hence, has a limited ability to assist the leaving group; in microemulsions with W = 2, all water is of this latter kind. Consequently, lowering W favours the associative pathway, with the result that the change in mechanism occurs at lower σ^+ values; in the microemulsion with W = 2, even 4-methylbenzoyl chloride, with its electron-donating substituent, is hydrolysed *via* the associative mechanism.

In conclusion, in this work we found that carrying out the hydrolysis of benzoyl chlorides in microemulsions allows not only the reaction rate but also the reaction mechanism to be controlled by modifying the quantitative composition of the microemulsion. The effect on the mechanism can be attributed to the dependence of the properties of micelle-borne water on the value of W = [H_2O]/[surfactant]. We envisage that this phenomenon may prove to be of use for investigation of other reaction mechanisms.

Financial support from the Dirección General de Investigación Científica y Técnica of Spain (project PB96-0954) is gratefully acknowledged.

Notes and references

1 *Reverse Micelles*, ed. P. L. Luisi and B. E. Straub, Plenum Press, New York, 1984.
2 *Structure and Reactivity in Reverse Micelles*, ed. M. P. Pileni, Elsevier, Amsterdam, 1989.
3 J. Yao and L. Romsted, *J. Am. Chem. Soc.*, 1994 **116**, 11 779; C. R. A. Bertoncini, M. F. S. Neves, F. Nome and C. A. Bunton, *Langmuir*, 1993, **9**, 1274; R. A. Mackay and C. Hermansky, *J. Phys. Chem.*, 1981, **85**, 739.
4 S. L. Regen, *Angew. Chem.*, 1979, **91**, 464; *Angew. Chem., Int. Ed. Engl.*, 1979, **18**, 421; D. A. Jaeger and M. R. Frey, *J. Org. Chem.*, 1982, **47**, 311.
5 M. J. Schwuger, K. Stickdorn and R. Schomäcker, *Chem. Rev.*, 1995, **95**, 849.
6 E. Keh and B. Valeur, *J. Colloid Interface Sci.*, 1981, **79**, 465; M. Wong, J. K. Thomas and T. Nowak, *J. Am. Chem. Soc.*, 1977, **99**, 4730; C. D. Borsarelli and S. E. Braslavsky, *J. Phys. Chem. B*, 1997, **101**, 6036.
7 P. E. Zinsli, *J. Phys. Chem.*, 1979, **83**, 3223; M. Wong, J. K. Thomas and M. Grätzel, *J. Am. Chem. Soc.*, 1976, **98**, 2391.
8 L.García-Río, J. R. Leis, M. E. Peña and E. Iglesias, *J. Phys. Chem.*, 1993, **97**, 3437; L. García-Río, J. R. Leis and E. Iglesias, *J. Phys. Chem.*, 1995, **99**, 12 318.
9 B. D. Song and W. P. Jencks, *J. Am. Chem. Soc.*, 1989, **111**, 8470.
10 T. W. Bentley and A. E. Freeman, *J. Chem. Soc., Perkin Trans. 2*, 1984, 1115; T. W. Bentley, G. E. Carter and H. C. Harris, *J. Chem. Soc., Perkin Trans. 2*, 1985, 983; T. W. Bentley and I. S. Koo, *J. Chem. Soc., Chem. Commun.*, 1988, 41; B. L. Knier and W. P. Jencks, *J. Am. Chem. Soc.*, 1980, **102**, 6789.
11 K. Tamura and N. Nii, *J. Phys. Chem.*, 1989, **93**, 4825.
12 T. K. De and A. Maitra, *Adv. Colloid Interface Sci.*, 1995, **59**, 95.

Communication a909531d

A novel self-assembled monolayer (SAM) coated microcantilever for low level caesium detection

Hai-Feng Ji,[a] Eric Finot,[b] Reza Dabestani,*[a] Thomas Thundat,[b] Gilbert M. Brown[a] and Phillip F. Britt[a]

[a] *Chemical and Analytical Science Division and* [b] *Life Science Division, Oak Ridge National Laboratory, PO Box 2008, MS-6100, Oak Ridge, TN 37831-6100, USA. E-mail: dabestanir@ornl.gov*

Received (in Columbia, MO, USA) 7th October 1999, Accepted 2nd February 2000, Published on the Web, 1st March 2000

We report a new sensor concept based on an ion-selective SAM modified microcantilever which can detect caesium ion concentrations *in situ* in the range 10^{-11}–10^{-7} M and shows potential for use in developing a new family of real time *in situ* metal ion sensors with high sensitivity/selectivity and low cost, for chemical and biological applications.

Research in the area of sensor development for metal ion detection in chemical and biological applications has received considerable attention in recent years.[1–3] In particular, the application of host–guest chemistry to sensor development has proved to be a very useful detection method.[4] Many different receptors (hosts) including crown ethers, cryptands and calixarenes have been synthesized as molecular recognition agents for the binding of various metal ions (guests).[5–7] Recent results from our laboratory on microcantilever based sensors have revealed that adsorption-induced stress on microcantilevers can be used to detect low concentrations (ppb) of chemical vapors.[8] This adsorption-induced stress can be detected by the change in bending[9] or resonance frequency[10] caused by changes in the cantilever surface. We have shown that microcantilevers can operate in both the gas and liquid phase for chemical sensing applications.[8,9] In liquid environments, the preferable mode of detection appears to be adsorbate induced cantilever bending. Chemical selectivity for inorganic ions can be obtained by coating an ion-selective polymer film or modified SAM containing ion selective binding sites.

Here we report the first example of a selective caesium ion sensor based on an ion-selective SAM coated microcantilever capable of detecting caesium ions in the presence of high concentrations of potassium of sodium ions. Our data shows that the sensitivity of this cantilever based sensor for *in situ* measurements is several orders of magnitude better than the currently available ion selective electrodes (ISE).

The caesium recognition agent used in this work was 1,3-alternate 25,27-bis(11-mercapto-1-undecanoxy)-26,28-calix[4]benzocrown-6 **1**, bound to a gold coated microcantilever. The crown cavity of the 1,3-alternate conformation of calix[4]benzocrown-6 has been shown to be very suitable for accommodating caesium ions with Cs/Na and Cs/K selectivity ratios in excess of 10^4 and 10^2, respectively, by a solvent extraction technique.[11] Binding constant values of 10, 2×10^4 and 2.5×10^6 have also been determined by a fluorescence technique for Na^+, K^+ and Cs^+ in MeOH–CH_2Cl_2 (1:1) solution.[12] Based on the high selectivity exhibited by these compounds, receptor molecule **1** was designed and anchored onto the gold surface of the microcantilever by standard techniques.[13] Decane-1-thiol was co-absorbed onto the gold surface in a 2:1 ratio to fill the gaps present between the two alkyl thiol arms of **1** and the adjacent molecules (Scheme 1) and to enhance the aqueous stability of the SAM.

The experiments were performed in a flow-through glass cell where the SAM coated V-shaped microcantilever was immersed in distilled water at a flow rate of 10 mL min^{-1}. Electrolyte solutions (Cs, K or Na nitrate) were introduced using a syringe pump by switching the syringe delivering pure water to the syringe containing the desired electrolyte solution. The volume of the glass cell was selected to be small enough (4 mL) to insure fast replacement of the liquid in contact with cantilever. The bending of the cantilever was measured by monitoring the position of a laser beam reflected off the top of the microcantilever onto a four-quadrant photodiode. The microcantilever was initially immersed into the cell exposed to a constant flow of distilled water and its deflection (bending) was measured as the background and set to 0 nm. Approximately 30 s later, the flow of distilled water was replaced with caesium ion solution. As the Cs^+ ions diffuse to the SAM coated microcantilever, the bending response of the cantilever changes reaching an equilibrium within 70–80 s (Fig. 1). Based on the large complexation constant calculated (*vida infra*) for caesium and 1,3-alternate calix[4]benzocrown-6, it is reasonable to assume that the initial rapid increase in bending response depends on the concentration of caesium in solution. Fig. 2 shows the observed change in bending response of the microcantilever as the concentration of caesium ions is varied. It is clear from the plot in Fig. 2 that the most dramatic response is exhibited when the concentration of caesium is in the range 10^{-7}–10^{-11} M. In contrast, the cantilever response to potassium ions (the most prevalent interfering ion) in the same concentration range is very small (*e.g.* 20 nm deflection for 1×10^{-8} M solution of K^+ compared to 330 nm deflection for caesium at the same concentration, Fig. 2). For Cs^+ ion concentrations $> 10^{-6}$ M, the bending response at equilibrium reaches its maximum value at *ca.* 330 nm (Fig. 2). A blank test performed on a gold coated silicon nitride cantilever without the SAM revealed that

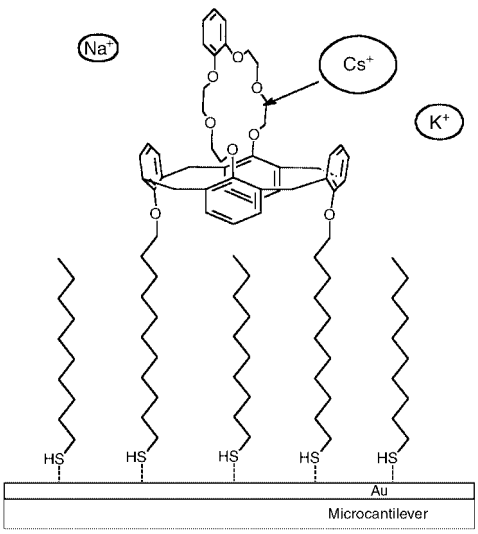

Scheme 1 Schematic representation of the molecular structure of receptor molecule 1,3-alternate 25,27-bis(11-mercapto-1-undecanoxy)-26,28-calix[4]benzocrown-6 (**1**) co-absorbed with decane-1-thiol on the gold surface of microcantilever by the SAM technique. The synthetic procedure for preparation of the thiol derivative of 1,3-alternate calix[4]arene **1** used in this work will be published elsewhere. The microcantilever is commercially available and has the following dimensions: 200 μm long, 40 μm base and 0.7 μm thick (Park Scientific Instruments, CA). The maximum number of molecules of **1** that can adsorb on the surface of cantilever is $\leqslant 2 \times 10^{10}$. The sensitivity of detection is 10.58 mV nm^{-1}

DOI: 10.1039/a908143g

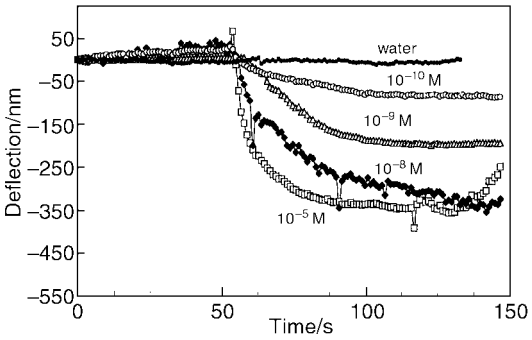

Fig. 1 Bending deflection response of the SAM coated microcantilever as a function of time, *t*, before and after exposure to different concentrations of Cs^+ ions in solution at room temperature. For the *y*-axis, the voltage has been converted to nm using the conversion factor 10.58 mV nm^{-1}.

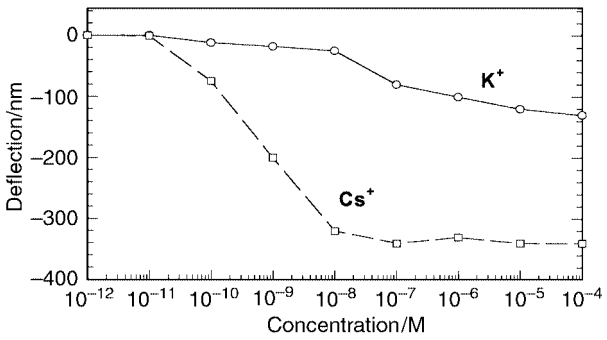

Fig. 2 Bending deflection response of the SAM coated microcantilever as a function of the change in concentration of Cs^+ and K^+ ions. For the *y*-axis, the voltage has been converted to nm using the conversion factor 10.58 mV nm^{-1}.

even at high Cs^+ ion concentration (*e.g.* 10^{-3} M) the bending response was unaffected (same as pure water). Such a finding clearly rules out any contribution to the cantilever bending response by the caesium ions in the absence of receptor molecule, and substantiates the role of molecular recognition agent (receptor) in inducing the observed change in bending response.

The relationship between the cantilever displacement, *z*, and the differential surface stress can be expressed by eqn. (1).

$$z = \left(\frac{3(1-\nu)L^2}{t^2E}\right)\delta s \quad (1)$$

where *L* is the length of the cantilever, *v* is Poisson's ratio, *E* is Young's modulus for the substrate, *t* is the thickness of the cantilever, and δs is the adsorption-induced differential surface stress. Since δs is directly proportional to ion absorption by the microcantilever, eqn. (1) can be re-arranged to eqn. (2) where *b* is a constant, *K* is the complexation constant between the ion receptor and the ions present in solution (1 : 1 stoichiometry), [M] is the concentration of ions in solution, and R_0 is the no of mol of ion receptor present on cantilever before complexation.

$$z = b\left(\frac{3(1-\nu)L^2}{t^2E}\right)\left(\frac{K[\mathrm{M}]R_0}{1+K[\mathrm{M}]}\right) \quad (2)$$

Since the change in concentration of ions present in solution after absorption by the receptor is essentially unchanged in a continuous flow system, the value of [M] will be the same as the initial concentration of ions. The complexation constants determined from the plot of 1/*z vs.* 1/[M] for caesium (K_{Cs}) and potassium (K_K) using eqn. (2) are 2×10^9 M^{-1} and 1.6×10^7 M^{-1}, respectively. These values are much higher (three orders of magnitude) than the corresponding values observed for the derivatives of similar compounds in MeOH–CH_2Cl_2 (1 : 1) solution[12] but the ratio of K_{Cs}/K_K is essentially the same. Similar enhancements in the association constant values for other SAM systems (relative to the free molecule) have also been reported.[14,15] The large value of association constant observed for Cs^+ ions indicates that binding is essentially irreversible. This notion is further supported by our experimental results that showed cycling pure water through the system (to rinse the SAM coated microcantilever containing Cs^+ ions) for several hours failed to regenerate the initial reading (water curve in Fig. 1).

The bending response of the SAM coated microcantilever upon Cs^+, K^+ and Na^+ complexation was also compared for the same concentration of each ion (10^{-5} M). The results indicated that SAM coated microcantilever was much more selective towards Cs^+ ions compared to K^+ and Na^+ ions (not shown). In fact, Na^+ ions have a minimal effect (if any) on the bending response while K^+ ions exhibit enough sensitivity to interfere (as a perturbing ion when present) in the detection of caesium ions.

In summary, our study has shown that the concept of ion-selective-SAM coated cantilever can be applied successfully to detect trace amounts (ppb) of caesium ions (*in situ*) in the presence of high concentrations of interfering potassium ions with remarkable sensitivity. This methodology can be applied to the detection of a wide variety of metal ions of chemical and biological importance. For example, we envision construction of a compact device capable of measuring low levels of metal ions in the blood stream *in situ* using this technique. This concept can be further expanded by constructing a multi-panel array device based on an SAM coated microcantilever for *in situ* detection of different metal ions present in solution or biological fluids. Along these lines, we are currently synthesizing molecular recognition agents containing different size cavities capable of complexing different metal ions.

This research was funded by the Environmental Management Science Program, Office of Environmental Management, US Department of Energy and in part by an appointment sponsored by the Oak Ridge National Laboratory Postdoctoral Research Associates Program administered jointly by the Oak Ridge Institute for Science and Education and Oak Ridge National Laboratory. Oak Ridge National Laboratory is operated by Lockheed Martin Energy Research Corporation for the US Department of Energy under contract number DE-AC05-96OR22464.

Notes and references

1 S. K. Menon, A. Sathyapalan and Y. K. Agrawal, *Rev. Anal. Chem.*, 1997, **16**, 333.
2 M. L. Davies, C. J. Hamilton, S. M. Murphy and B. J. Tighe, *Biomaterials*, 1992, **13**, 971.
3 K. Cammann, W. Kleibohmer, E. Mussenbrock, B. Ross and F. Zuther, *J. Anal. Chem.*, 1994, **349**, 338.
4 J. L. Atwood and J.-M. Lehn, *Comprehensive Supramolecular Chemistry*, Pergamon Press, Oxford, UK, 1996.
5 R. M. Izatt, K. Pawlak, J. S. Bradshaw and R. L. Bruening, *Chem. Rev.*, 1991, **97**, 1721.
6 A. Ikeda and S. Shinkai, *Chem. Rev.*, 1997, **97**, 1713.
7 A. P. deSilva, H. Q. N. Gunarante, T. Gunnlaugsson, A. J. M. Huxley, C. P. McCoy, J. T. Rademacher and T. E. Rice, *Chem. Rev.*, 1997, **97**, 1515.
8 T. Thandat, G. Y. Chen, R. J. Warmack, D. P. Allison and E. A. Wachter, *Anal. Chem.*, 1995, **67**, 519.
9 T. Thundat, R. J. Warmack, G. Y. Chen and D. P. Allison, *Appl. Phys. Lett.*, 1994, **64**, 2894.
10 J. P. Cleveland, S. Manne, D. Bocek and P. K. Hansma, *Rev. Sci. Instrum.*, 1993, **64**, 403.
11 T. J. Haverlock, P. V. Bonnesen, R. A. Sachleben and B. A. Moyer, *Radiochim. Acta*, 1997, **76**, 103.
12 H.-F. Ji, G. M. Brown and R. Dabestani, *Chem. Commun.*, 1999, 609.
13 C. D. Bain, E. B. Troughton, Y.-T. Tao, J. Evall, G. M. Whitesides and R. G. Nuzzo, *J. Am. Chem. Soc.*, 1989, **111**, 321.
14 A. Yoshizumi, N. Kanayama, Y. Maehara, M. Ide and H. Kitano, *Langmuir*, 1999, **15**, 482.
15 H. Yamamoto, Y. Maeda and H. Kitano, *J. Phys. Chem.*, 1997, **101**, 6855.

Communication a908143g

ChemComm

Synthesis of optically active amino sugar derivatives using catalytic enantioselective hetero-Diels–Alder reactions

Wei Zhuang, Jacob Thorhauge and Karl Anker Jørgensen*

Center for Metal Catalyzed Reactions, Department of Chemistry, Aarhus University, DK-8000 Aarhus C, Denmark. E-mail: kaj@kemi.aau.dk

Received (in Cambridge, UK) 17th November 1999, Accepted 5th February 2000, Published on the Web, 2nd March 2000

A new synthetic method for the formation of optically active amino sugars using catalytic enantioselective inverse-electron demand hetero-Diels–Alder reactions of γ-amino-protected β,γ-unsaturated α-keto esters with vinyl ethers is presented; the catalytic reactions proceed in good yield with high diastereo- and enantioselectivity and fully control of the stereochemistry at the amino-carbon center.

Sugars containing nitrogen atoms have a variety of different biological activities; they are, *e.g.* among the largest group of carbohydrate mimetics and belong to the strongest known inhibitors of glycosidases found.[1] Furthermore amino sugars are also applied as pharmaceuticals such as for treatment of diabetes[2] and promising drugs against influenza.[3]

The synthesis of optically active amino sugars normally takes its starting point from naturally occurring carbohydrates.[4] or amino acids.[5] A simple and convenient procedure for the formation of optically active amino sugars and their derivatives (**3**) could be the catalytic enantioselective inverse-electron demand hetero-Diels–Alder (HDA) reaction of γ-amino-protected β,γ-unsaturated α-keto esters **1** with vinyl ethers **2** [eqn. (1)]. This approach has previously been used in diastereoselective reactions.[6]

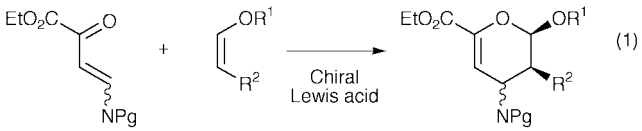

1 **2** **3**

Here, we present the first catalytic enantioselective synthesis of amino sugars **3** by inverse-electron demand HDA reactions using C_2-bisoxazoline-Lewis acid complexes as catalysts.[7,8]† The reaction has been developed for two different protected γ-amino β,γ-unsaturated α-keto esters **1a**, **b** which have the protected γ-amino substituent, *trans* or *cis*, respectively, as these by reaction, *e.g.* ethyl vinyl ether **2a**, will give the two different diastereomers of the optically active amino sugars **3a** and **4a**, respectively [eqn. (2)]. The (*S*)-Bu^t-BOX-Cu(OTf)$_2$ [(*S*)-**5a**] and (*R*)-Ph-BOX-Zn(OTf)$_2$ [(*R*)-**5b**] complexes are found to be good catalysts for the reaction among different C_2-bisoxazoline–Lewis acid complexes tested.

Table 1 Reaction of γ-amino-protected β,γ-unsaturated α-keto esters **1a**, **b** with ethyl vinyl ether **2a** in the presence of (*S*)-Bu^t-BOX-Cu(OTf)$_2$ [(*R*)-**5a**] and (*R*)-Ph-BOX-Zn(OTf)$_2$ [(*S*)-**5b**] at room temperature (r.t.)

Entry	Substrate	Cat./mol%	Yield[a] (%)	*endo*-de[b] (%)	Ee[c] (%)
1	**1a**	(*S*)-**5a**/10[e]	**3a**/98	88	98
2	**1a**	(*S*)-**5a**/5[e]	**3a**/67	95	> 99
3	**1a**	(*S*)-**5a**/10[e,f]	**3a**/94	90	> 99
4	**1a**	(*S*)-**5a**/10[g]	**3a**/82	29	99
5	**1b**	(*S*)-**5a**/10[g]	**4a**/96	74	94[d]
6	**1b**	(*R*)-**5b**/10[e]	**4a**/99	70	70[d]

[a] Isolated yield. [b] Diastereomeric excess measured by ^{1}H NMR. [c] Enantiomeric excess measured by chiral HPLC using a Daicel Chiralpak OJ column. [d] Enantiomeric excess measured by chiral GC using a Chrompack ChiralsilDex CB column. [e] Et_2O as solvent. [f] Reaction temperature 0 °C [g] THF as solvent.

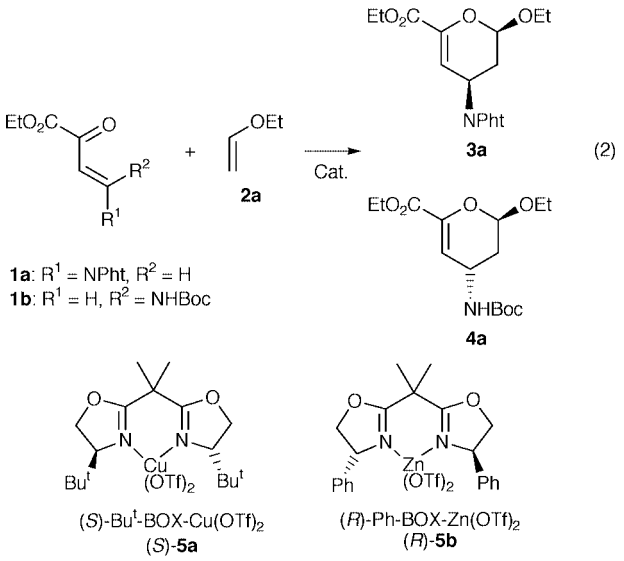

Table 1 presents some results obtained for the reaction of **1a**, **b** with **2a**. It appears that the γ-amino-protected β,γ-unsaturated α-keto esters **1a**, **b** react with ethyl vinyl ether **2a** in the presence of the (*S*)-**5a** catalyst giving the protected amino sugars **3a** and **4a**, respectively, in high yield, diastereo (de) and enantiomeric excess (ee) at room temperature. The reaction of **1a** with **2a** can proceed with 5 mol% of the catalyst with very high diastereoselectivity giving only one detectable enantiomer by chiral HPLC of **3a** (entry 2). The reaction can take place in several solvents and high yield, de and ee are obtained in, *e.g.* Et_2O and THF (entries 1, 4). However, it is notable that the de is reduced when THF is the solvent compared with Et_2O, and that the reaction performed in CH_2Cl_2 gives the *exo*-diastereomer as the major diastereomer (de_{exo} 43% and with 90% ee_{exo}). The reaction of **1b** leads to the other diastereomer of the protected amino sugar (**4a**) and this reaction proceeds also with high yield, de and ee using (*S*)-**5a** as the catalyst and **4a** is obtained in 96% yield, 74% de and 94% ee (entry 5). The yield of **4a** is slightly improved in the presence of (*R*)-**5b** as the catalyst, while the de is the same and the ee is reduced compared to (*S*)-**5a** as the catalyst (entry 6). The absolute configuration of a related series of compounds has been determined previously.[8e]

The application of this catalytic enantioselective approach for the preparation of various types of different amino sugar derivatives is shown in the following equations. In eqn. (3) the reaction of **1a** with *cis*-1-acetoxy-2-ethoxyethene **2b** in the presence of (*S*)-**5a** and (*R*)-**5b** as the catalysts is presented. The reaction proceeds in a highly regio-, diastereo- and enantioselective manner giving **3b** in 82% yield, 85% de and 99% ee when (*S*)-**5a** is the catalyst and an improvement in yield, and reduction in ee when (*R*)-**5b** is the catalyst. The reaction in eqn. (3) shows that it is possible to introduce two different

DOI: 10.1039/a909115g

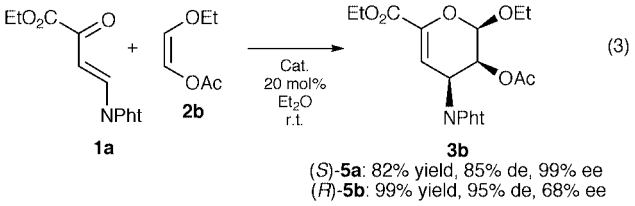

(3)

protected hydroxy functionalities in the amino sugar fragment by this reaction.

The results for the reaction of **1a** with 2,3-dihydrofuran **2c** is presented in eqn. (4). Both catalysts give good yield of the

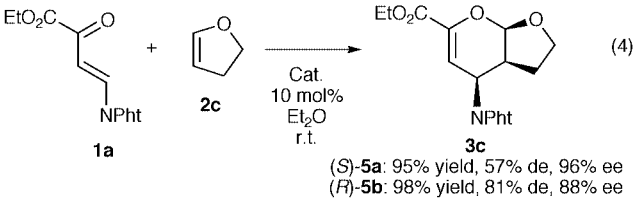

(4)

amino sugar **3c**; the (*S*)-**5a** catalyst gives the highest ee (96%) of the major diastereomer, formed with a de of 57%, while (*R*)-**5b** leads to the highest de (81%), and with only a slight reduction to 88% ee. It is notable that the same enantiomer of **3b** and **3c** in eqns. (3) and (4) are obtained using the (*S*)-**5a** and (*R*)-**5b** catalysts.

The catalytic enantioselective reaction of the activated cyclic alkene **2d** with **1a** gives **3d** in moderate yield (51%) and de (66%), and with high ee (92%) [eqn. (5)]. The highest yield of

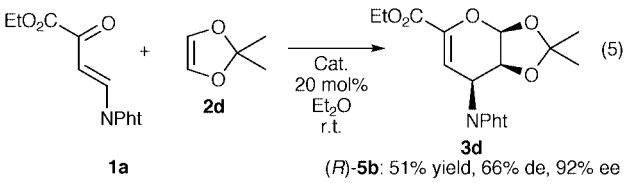

(5)

3d is obtained with the chiral zinc(II) catalyst (*R*)-**5b**, while catalyst (*S*)-**5a** only gives 12% isolated yield of **3d**, but formed in a highly enantioselective manner as 97% ee is obtained.

The catalytic enantioselective HDA reaction can also be used for the preparation of optically active spiro-amino sugars. The spiroacetal functionality is found in natural products such as pheromones, steroidal compounds, anti-parasitic agents and polyether antibiotics[9] and eqn. (6) shows how the reaction of

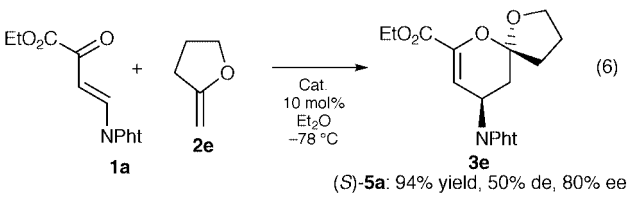

(6)

1a with the exo-cyclic vinyl ether **2e** catalyzed by (*S*)-**5a** leads to high yield, de and ee of the spiro-amino sugar **3e**.

The present work has shown a new development in catalytic enantioselective HDA reactions for the preparation of optically active amino sugars. It is demonstrated that the approach can be used for the synthesis of a series of different types of protected amino sugars in good yield with control of both the diastereo- and enantioselectivity. The new synthetic procedure introduces a new approach for the formation important amino sugars from simple substrates. Furthermore, can the products obtained also be considered as cyclic γ-amino acid esters. Further work is in progress in developing optically active highly functionalized molecules using this approach.

We are indebted to The Danish National Research Foundation for financial support.

Notes and references

† *Representative procedure* for the catalytic enantioselective HDA reaction: to a flame dried Schlenk tube was added $Cu(OTf)_2$ (18.1 mg, 0.05 mmol) and bisoxazoline (*S*)-**5a** (16.2 mg, 0.055 mmol). The mixture was dried under vacuum for 1–2 h and freshly distilled anhydrous solvent (2.0 mL) was added and the solution was stirred for 0.5–1 h. Subsequently, **1a** (137 mg, 0.5 mmol) and **2a** (70 μL, 1.5 eq.) were added. After stirring overnight at r.t., the reaction mixture was filtered through a pad of silica with EtOAc and pentane (1 : 1), concentrated *in vacuo*, and the product purified by flash chromatography (30% EtOAc in pentane) to afford compound **3a** in 98% yield, 88% de and 98% ee detected by HPLC using a Daicel Chiralpak OJ column hexane–Pr^iOH (95 : 5), $[\alpha]^{20}_D$ = +27.0° (*c* = 0.0074 g mL^{-1} in $CDCl_3$); ^1H NMR ($CDCl_3$): δ 7.79–7.76 (m, 2H, Ar), 7.69–7.67 (m, 2H, Ar), 5.94 (dd, 1H, *J* 3.0, 1.5 Hz, C=CH), 5.16–5.09 (m, 2H, OCHO and CHN), 4.19 (dq, 2H, *J* 5.4, 7.2 Hz, $CO_2CH_2CH_3$), 4.01 (dq, 1H, *J* 9.0, 7.2 Hz, $OCHHCH_3$), 3.61 (dq, 1H, *J* 9.0, 7.2 Hz, $OCHHCH_3$), 2.54 (ddd, 1H, *J* 12.8, 9.9, 8.7 Hz, CHH), 2.08 (ddt, 1H, *J* 12.8, 6.3, 1.5 Hz, CHH), 1.25 (t, 3H, *J* 7.2 Hz, $CO_2CH_2CH_3$), 1.18 (t, 3H, *J* 7.2 Hz, OCH_2CH_3)' ^{13}C NMR ($CDCl_3$): δ 167.4, 162.0, 143.7, 134.1, 131.7, 123.3, 109.4, 99.8, 64.9, 61.3, 42.9, 31.0, 15.0, 14.1.

Enone **1a** made according to ref. 6(*b*). **1b** was prepared as described in ref. 6(*f*) except for the last isomerization step which was performed by a simple destillation. Alkenes were obtained from commercial sources or synthesized using literature procedures.[10]

1 See, *e.g.*: A. E. Stütz, *Iminosugars as Glycosidases Inhibitors; Nojirimycin and beyond*, Wiley-VCH Verlag, Weinheim, 1999.
2 For some reviews, see *e.g.*: S. P. Clissold and C. Edwards, *Drugs*, 1988, **35**, 214; J. A. Balfour and D. McTavish, *Drugs*, 1993, **46**, 1025.
3 See, *e.g.*: M. von Itzstein, W.-Y. Wu, G. B. Kok, M. S. Pegg, J. C. Dyason, B. Jin, T. V. Phan, M. L. Smythe, H. F. White, S. W. Oliver, P. M. Colman, J. N. Varghese, D. M. Ryan, J. M. Woods, R. C. Bethell, V. J. Hotham, J. M. Cameron and C. R. Penn, *Nature*, 1993, **363**, 418; C. U. Kim, W. Lew, M. A. Williams, H. Liu, L. Zhang, S. Swaminathan, N. Bischofberger, M. S. Chen, D. B. Mendel, C. Y. Tai, W. G. Laver and R. C. Stevens, *J. Am. Chem. Soc.*, 1997, **119**, 681; D. P. Calfee and F. G. Hayden, *Drugs*, 1998, **58**, 537.
4 Amino sugars synthesized from natural occurring carbohydrates, see *e.g.*: P. Crotti, V. D. Bussolo, L. Favero, F. Macchia and M. Pineschi, *Tetrahedron: Asymmetry*, 1996, **7**, 779; B. Steiner, M. Koós, V. Langer, D. Gyepesová and L. Smcrok, *Carbohydrates Res.*, 1998, **311**, 1.
5 Amino sugars from amino acids, see *e.g.*: R. D. Groneberg, T. Miyazaki, N. A. Stylianides, T. J. Schulze, W. Stahl, E. P. Schreiner, T. Suzuki, Y. Iwabuchi, A. L. Smith and K. C. Nicolaou, *J. Am. Chem. Soc.*, 1993, **115**, 7593.
6 Amino sugars with diastereoselective HDA reactions with inverse-electron demand: (*a*) L. F. Tietze and E. Voß, *Tetrahedron Lett.*, 1986, **27**, 6181; (*b*) L. F. Tietze, A. Bergmann, G. Brill, K. Brüggemann, U. Hartfiel and E. Voß, *Chem. Ber.*, 1989, **122**, 83; (*c*) M. Buback, W. Tost, T. Hübsch, E. Voß and L. F. Tietze, *Chem. Ber.*, 1989, **122**, 1179; (*d*) L. F. Tietze and U. Hartfiel, *Tetrahedron Lett.*, 1990, **31**, 1697; (*e*) L. F. Tietze, U. Hartfiel, T. Hübsch, E. Voß and J. Wichmann, *Chem. Ber.*, 1991, **124**, 881; (*f*) P. D. Howes and P. W. Smith, *Tetrahedron Lett.*, 1996, **37**, 6595.
7 For reviews of C_2-bisoxazoline–Lewis acid complexes as catalysts for hetero-Diels–Alder reactions, see *e.g.*: A. K. Ghosh, P. Mathivanan and J. Cappiello, *Tetrahedron: Asymmetry*, 1998, **9**, 1; K. A. Jørgensen, M. Johannsen, S. Yao, H. Audrain and J. Thorhauge, *Acc. Chem. Res.*, 1999, **32**, 605.
8 Examples of catalytic enantioselective hetero-Diels–Alder reactions with inverse-electron demand: (*a*) E. Wada, H. Yasuoka and S. Kanemasa, *Chem. Lett.*, 1994, 1637; (*b*) E. Wada, W. Pei, H. Yasuoka, U. Chin and S. Kanemasa, *Tetrahedron*, 1996, **52**, 1205; (*c*) D. A. Evans and J. S. Johnson, *J. Am. Chem. Soc.*, 1998, **120**, 4895; (*d*) J. Thorhauge, M. Johannsen and K. A. Jørgensen, *Angew. Chem., Int. Ed.*, 1998, **37**, 2404; (*e*) D. A. Evans, E. J. Olhava, J. S. Johnson and J. M. Janey, *Angew. Chem., Int. Ed.*, 1998, **37**, 3372.
9 See, *e.g.*: F. Perron and K. F. Albizati, *Chem. Rev.*, 1989, **89**, 1617.
10 G. Wulff and P. Birnbrich, *Chem. Ber.*, 1992, **125**, 473; G. H. Posner and T. D. Nelson, *Tetrahedron*, 1990, **46**, 4573; R. E. Ireland and D. Häbich, *Chem. Ber.*, 1981, **114**, 1418.

Communication a909115g

ChemComm

Single-wall carbon nanotube colloids in polar solvents

Zujin Shi,[a] Yongfu Lian,[a] Xihuang Zhou,[a] Zhennan Gu,*[a] Yaogang Zhang,[b] Sumio Iijima,[b] Qihuang Gong,[c] Hongdong Li[c] and Shu-Lin Zhang[c]

[a] *Department of Chemistry, Peking University, Beijing 100871, P.R. China. Email: guzn@chemms.chem.pku.edu.cn*
[b] *Fundamental Research Laboratories, NEC Corporation, 34 Miyukigaoka Tsukuba, Ibaraki 305-8501, Japan*
[c] *Department of Physics, Peking University, Beijing 100871, P.R. China*

Received (in Oxford, UK) 22nd November 1999, Accepted 14th February 2000, Published on the Web, 2nd March 2000

Stable single-wall carbon nanotube (SWCNT) colloids in polar solvents, such as water, ethanol, acetone and DMF, have been prepared and the third-order optical nonlinearity of the SWCNTs measured using the femtosecond optical Kerr effect.

Owing to their novel structural, electronic and mechanical properties, single-wall carbon nanotubes (SWNTs) are likely to possess many potential applications.[1,2] However, it is difficult to study their chemical behavior and properties because of their insolubility in solvents. Chen *et al*.[3,4] obtained an SWCNT derivative which was soluble in organic solvents obtained from shortened SWCNTs[5] and studied the solution-phase EPR of such SWCNTs.[6] Liu *et al*.[7] successfully deposited individual short SWCNT segments on chemically functionalized nanolithographic templates from a 0.1 mg ml^{-1} carboxylated SWCNT suspension of DMF. Here, we report the preparation of stable SWCNT colloids by dispersing carboxylated SWCNTs in several polar solvents, which will facilitate the study of chemical properties and the engineering of electronic devices based upon SWCNTs. The third-order optical nonlinearity of colloidal SWCNTs in DMF was measured. The high third-order optical nonlinearity susceptibility obtained indicate potential applications of SWCNTs in optical information processes.

SWCNTs were produced by the dc arc-discharge method[8] and purified to > 90%.[9] The SWCNTs had a diameter of *ca*. 1.3 nm and existed as SWCNT bundles both in the raw-soot and purified samples. The SWCNT bundles had a diameter of 20–30 nm in the raw-soot and 50–60 nm in the purified sample with lengths of > 10 μm.[9] The preparation of aqueous colloids was carried out by dissolving 100 mg purified SWCNTs in 120 ml 98% H_2SO_4–70% HNO_3 (3 : 1) and subjecting to ultrasonication for 8 h. The obtained solution was diluted with deionized water to 500 ml and left to stand over night. After decanting the solution, 50 ml of deionized water was added to the residue which was allowed to stand for one day. After discarding the supernatant, 25 ml of deionized water was added to the residue to form a colloidal solution of SWCNTs in water. The pH value of the colloidal solution was *ca*. 3 for a concentration of 1.77 mg ml^{-1}. The colloid solution remained very stable for > 1 year.

In order to remove the residual acids, the colloid solution was passed through a PTFE membrane disc Filter (Gelman, 1 μm pore size) under vacuum followed by washing several times with deionized water. The SWCNTs on the membrane disc were readily dispersed in water, ethanol, acetone and DMF after ultrasonication for a few minutes to form black colloids in the absence of surfactants. The saturated concentration of SWCNTs in water, ethanol, acetone and DMF were 1.16, 0.5, 1.06 and 2.0 mg ml^{-1}, respectively, and the pH value of the colloid solution of SWCNTs in water was 5.5.

In our experiments, the saturated concentration of SWCNTs in water largely depended on the acidity of the solution. At pH < 1.5, SWCNTs in water precipitate in 1 or 2 h after standing while pH at 2.4, 1.97 mg SWCNTs can be dispersed in 1 ml of water to form a stable colloid. At a pH of 5.5 the saturated concentration of SWCNTs is reduced to 1.16 mg ml^{-1}. Thus, the pH range 2–3 is favorable for the formation and existence of stable colloids of SWCNTs in water.

The observation of stable colloids suggests the presence of carboxylic groups at open ends of the SWCNTs, which was verified by the characteristic stretching band ($\nu_{C=O}$) at 1710 cm^{-1} in the FTIR spectrum.[4] The structure of the SWCNTs was established by Raman spectroscopy. As shown in Fig. 1, no obvious change occurs in the Raman spectra of SWCNTs before or after treatment with mixed acids except for a decreasing peak ratio G : D, which implied that the SWCNTs were shortened after acid treatment. Compared to Liu's results for relatively longer nanotubes,[5] it can be anticipiated that SWCNTs should exist in a non-aggregated state in the various colloid solutions.

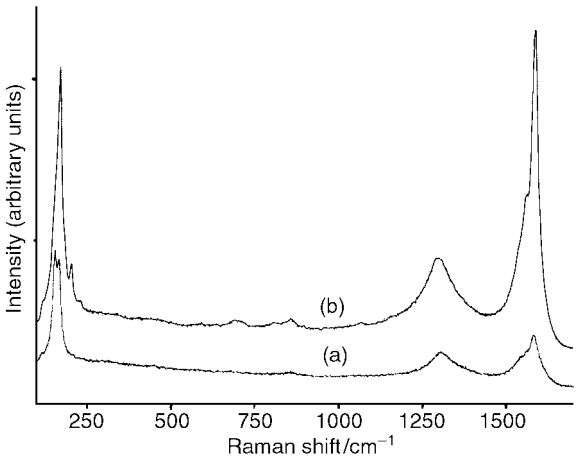

Fig. 1 Raman spectra of purified (b) and carboxylated (a) SWCNTs at 783 nm.

The tube length distribution of SWCNTs in solvents can be approximately estimated by the hydrodynamic radius *via* laser-scattering characterization. SWCNTs in water have a hydrodynamic radius in the range 23–300 nm with a mean of 81.1 nm (Fig. 2). In other words, the length of the SWCNTs ranges from 50 to 600 nm with a mean of *ca*. 160 nm. The length distribution is shorter than that reported by Liu *et al*.[5]

The successful preparation of the colloids made it possible to measure the third-order optical nonlinearity of the SWCNTs. Nonlinear optics (NLO) measurements were performed using the femtosecond optical Kerr technique[10] with a Ti:sapphire laser (Mira 900F, Coherent Co. Ltd., USA). The operating wavelength was centered at 820 nm, where the sample shows no absorption. In our experiments, three SWCNTs colloid solutions of 0.33, 0.22 or 0.13 mg ml^{-1}, in DMF were used and the sample cell thickness was 1 mm. The zero delay point was determined with a BBO crystal (0.3 mm thick) and the pulse duration was set at 120 fs.

The ultrafast NLO response of the SWCNT colloids is shown in Fig. 3 together with that for the reference sample of CS_2 under the same conditions. The instantaneous response proves that the NLO signal is attributed to conjugated π-electrons. The

DOI: 10.1039/a909240d

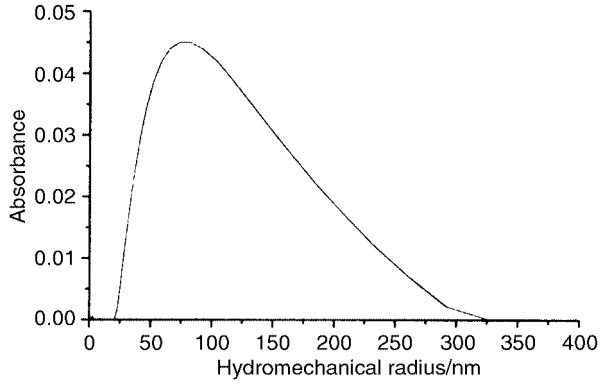

Fig. 2 Hydrodynamic radius distribution of an aqueous colloid of SWCNT measured using 514.5 nm laser-scattering.

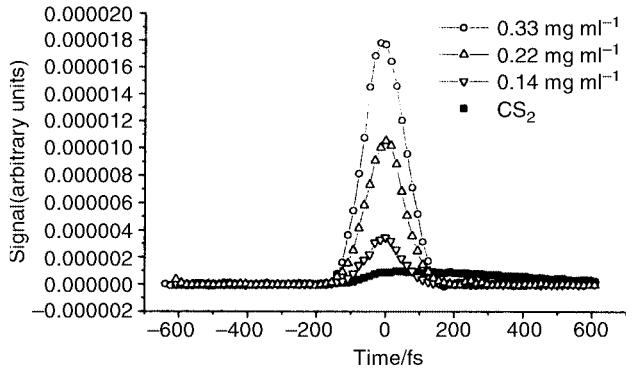

Fig. 3 Ultrafast OKE signals of SWCNT colloids in DMF together with a reference sample of CS_2.

signal caused by colloids at different concentrations indicates a square dependence of the signal on the concentration. The third-order optical nonlinearity susceptibility, $\chi^{(3)}$, of the colloid at a given concentration can be calculated[11] and a value of 4×10^{-13} esu was obtained for the 0.33 mg ml^{-1} SWCNT colloid in DMF. In this measurement, the contribution of DMF (*ca.* 1×10^{-14} esu) is reasonably neglected as the $\chi^{(3)}$ value for DMF is nearly ten times smaller than that of CS_2[12] (1×10^{-13} esu).[13] Furthermore, the magnitude of the second-order hyperpolarizabilities, γ_c, for each carbon atom can be calculated as 7.7×10^{-33} esu, which is much higher than those of C_{60} and multiwall carbon nanotubes,[14] and close to the value expected from theoretical calculation.[15] This is a remarkably large non-resonant and instantaneous NLO response for π-conjugated molecules, which indicates that SCWNTs may be useful as nonlinear optical materials.

In conclusion, stable SWCNTs colloid solutions in polar solvents, such as water, ethanol, acetone and DMF, have been prepared with purified SWCNTs and using a sulfuric acid–nitric acid mixture. This opens the possibility for template assembly or functionalization of SWCNTs in polar solvents. For colloids of SWCNTs in DMF, the third-order optical non-linearity of SWCNTs was measured and a large nonresonant and instantaneous NLO response was obtained, indicating the potential applications of SWCNTs in optical information process.

This work was supported by the National Natural Science Foundation of China, No. 29671030 & 29981001.

Notes and references

1 R. F. Service, *Science*, 1998, **281**, 940.
2 B. I. Yakobson and R. E. Smalley, *Am. Sci.*, 1997, **85**, 324.
3 J. Chen, M. A. Hamon, H. Hu, Y. S. Chen, A. M. Rao, P. C. Eklund and R. C. Haddon, *Science*, 1998, **282**, 95.
4 M. A. Hamon, J. Chen, H. Hu, Y. S. Chen, M. E. Itkis, A. M. Rao, P. C. Eklund and R. C. Haddan, *Adv. Mater*, 1999, **11**, 834.
5 J. Liu, A. G. Rinzler, H. Dai, J. H. Hafner, R. K. Bradley, P. J. Boul, A. Lu, T. Iverson, K. Shelimov, C. B. Huffman, F. Rodriguez-Macias, Y. S. Shon, T. R. Lee, D. T. Colbert and R. E. Smalley, *Science*, 1998, **280**, 1253.
6 Y. Chen, J. Chen, H. Hu, M. A. Hamon, M. E. Itkis and R. C. Haddon, *Chem. Phys. Lett.*, 1999, **299**, 532.
7 J. Liu, M. J. Casavant, M. Cox, D. A. Walters, P. Boul, W. Lu, A. J. Rimberg, K. A. Smith, D. T. Colbert and R. E. Smalley, *Chem. Phys. Lett.*, 1999, **303**, 125.
8 Z. J. Shi, Y. F. Lian, X. H. Zhou, Z. N. Gu, Y. G. Zhang, S. Iijima, L. X. Zhou, K. T. Yue and S. L. Zhang, *Carbon*, 1999, **37**, 1449.
9 Z. J. Shi, Y. F. Lian, F. H. Liao, X. H. Zhou, Z. N. Gu, Y. G. Zhang and S. Iijima, *Solid State Commun.*, 1999, **112**, 35.
10 T. Zhang, C. Chen, Q. Gong, W. Yan, S. Wang, H. Yang, H. Jian and G. Xu, *Chem. Phys. Lett.*, 1999, **301**, 243.
11 Q. Gong, Y. Sun, Z. Xia, Y. Zou, Z. N. Gu, X. H. Zhou and D. Qiang, *J. Appl. Phys.*, 1992, **71**, 3025.
12 Q. Gong, J. Li, T. Zhang and H. Yang, *Chin. Phys. Lett.*, 1998, **15**, 30.
13 R. Minoshima, M. Taija and T. Kobayashi, *Opt. Lett.*, 1991, **16**, 1683.
14 X. C. Liu, J. H. Si, B. H. Chang, G. Xu, Q. G. Yang, Z. W. Pan and S. S. Xie, *Appl. Phys. Lett.*, 1999, **74**, 164.
15 R. H. Xie and J. Jiang, *Chem. Phys. Lett.*, 1999, **280**, 66.

Communication a909240d

ChemComm

An extended network of twenty-membered $K_6Se_6P_4N_4$ rings: X-ray structure of $\{[(THF)K[Bu^tN(Se)P(\mu\text{-}NBu^t)_2P(Se)NBu^t]K(THF)_2]_2\}_\infty$

Tristram Chivers,* Mark Krahn and Masood Parvez

Department of Chemistry, University of Calgary, 2500 University Drive, N.W., Calgary, Alberta, Canada T2N 1N4. E-mail: chivers@ucalgary.ca

Received (in Cambridge, UK), 13th January 2000, Accepted 28th January 2000, Published on the Web, 2nd March 2000

The partially THF-solvated dipotassium salt of the novel bis-chelating dianion $[Bu^tN(Se)P(\mu\text{-}NBu^t)_2P(Se)NBu^t]^{2-}$ forms an infinite network of twenty-membered $K_6Se_6P_4N_4$ rings involving two types of K···Se interactions.

The coordination chemistry of monoanions of the type $[R_2P(E)NP(E)R_2]^-$ **1** is a very active area of investigation.[1] The interest in metal complexes of these acetylacetonate analogues includes their use in catalysis[2] or as lanthanide shift reagents,[3] as well as the stabilization of unusual geometries at main group metal centres.[4] The dianionic bis(amido) P(III) ligand **2** has also been studied recently for possible applications in catalysis[5] and as a ligand for main group metals.[6] Bischalcogenido derivatives of **2** are unknown. Such dianionic P(V) ligands **3** would be especially interesting in view of the possibility of (a) selective chelation of different metals *via* S,S′ or Se,Se′ (soft) and N,N′ (hard) centres or (b) generation of metal-containing polymers *via* bis-chelation. Here, we describe the synthesis and X-ray structures of the first alkali metal derivatives of **3a** and **3b**.

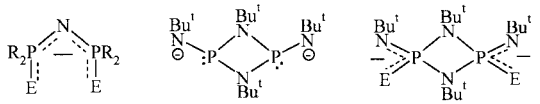

1 (E = O, S, Se) **2** **3a**, E = Se; **3b**, E = S

The dianions **3a** and **3b** are obtained as their dipotassium salts **6** and **7** in good yields *via* the deprotonation reaction depicted in Scheme 1.† The ^1H and ^{13}P $\{^1H\}$ NMR spectra of **6** and **7** are consistent with symmetrical bis-chelation of the dianions to two K^+ ions, but these spectroscopic data do not distinguish between two possible bonding modes: (a) bis-(N,E) chelation or (b) N,N′ and E,E′ chelation. The ^{31}P $\{^1H\}$ NMR spectrum of the diprotonated precursor **4** shows two pairs of ^{77}Se satellites attributable to the AA′X spin system of the isotopomer containing one ^{77}Se ($I = \frac{1}{2}$, 7.6%) atom.†[7] The value of $^1J(^{31}P–^{77}Se)$ is reduced from 880 to 684 Hz upon deprotonation consistent with a decrease in P–Se bond order (*cf.* 786 and 687 Hz for $Ph_2P(Se)NHP(Se)Ph_2$ and its K^+ salt).[7] The A–A′ $[^2J(^{31}P–^{31}P)]$ coupling is 25 Hz in **4**, but it is unresolved for **6**. A reliable estimate of the number of THF ligands per K^+ ion by integration of the ^1H NMR spectra of **6** and **7** could not be obtained owing to the facile loss of THF from the crystals.

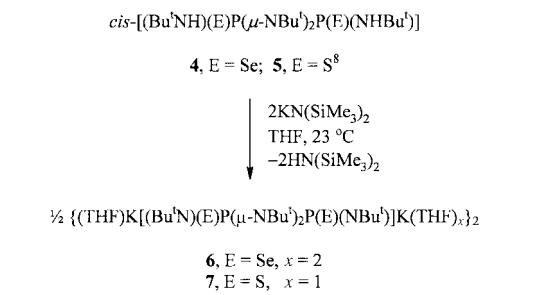

cis-$[(Bu^tNH)(E)P(\mu\text{-}NBu^t)_2P(E)(NHBu^t)]$

4, E = Se; **5**, E = S[8]

↓ $2KN(SiMe_3)_2$, THF, 23 °C, $-2HN(SiMe_3)_2$

½ $\{(THF)K[(Bu^tN)(E)P(\mu\text{-}NBu^t)_2P(E)(NBu^t)]K(THF)_x\}_2$

6, E = Se, $x = 2$
7, E = S, $x = 1$

Scheme 1

The X-ray structural analysis of **6** (Fig. 1)‡ reveals that bis-chelation occurs at the 'top' and 'bottom' of the dianion (Se,Se′ and N,N′) in preference to 'side-on' bis(N,Se) chelation. Presumably the formation of six-membered KNPNPN and KSePNPSe rings is preferred over the known four-membered KNPSe ring[9] for the relatively large K^+ ion. The mean K–Se distance in the monomeric unit is 3.312 Å, *cf.* 3.377 Å for $(K[Ph_2P(Se)NSiMe_3]\cdot THF)_2$.[9] Fig. 2 shows that dimerization occurs *via* two K···Se interactions (3.418(3) Å) to give a central K_2Se_2 ring as observed for $(K[Ph_2P(Se)NSiMe_3]\cdot THF)_2$.[9] For **6**, however, the K^+ ions involved in these four-membered rings are bis-solvated (five-coordinate). The X-ray crystal structure of the sulfur analogue **7** is similar to that of **6** except that both K^+ ions are monosolvated.[10] The dimeric units in **6** associate further *via* weak···Se interactions (3.644(3) Å) involving the monosolvated K^+ ions and the two-coordinate Se atoms to give an extended structure. Extended ladder structures involving K···E interactions have been reported previously for the unsolvated complexes $K[Ph_2P(E)NP(E)Ph_2]$ (E = S,[11a] Se[11b]). For **6** the

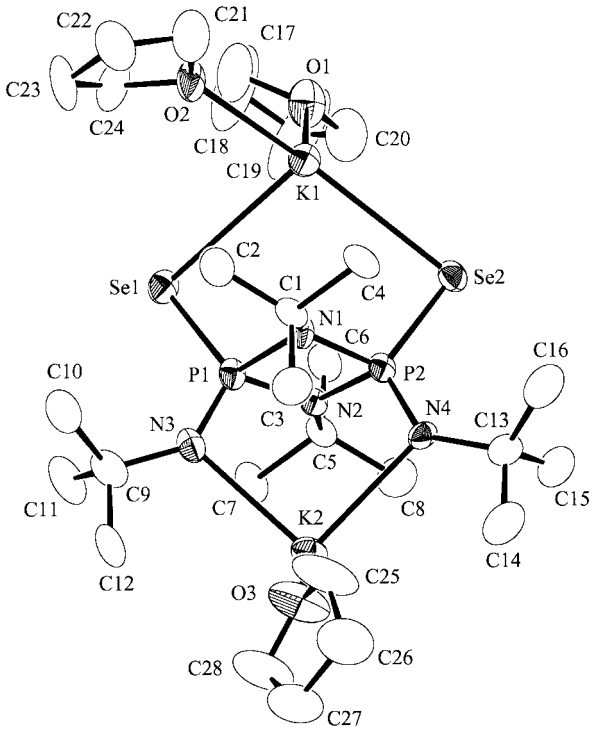

Fig. 1 The X-ray structure of the monomeric unit in **6** showing the numbering scheme. Selected bond lengths (Å) and angles (°): K(1)–Se(1) 3.354(3), K(1)–Se(2) 3.270(4), K(2)–N(3) 2.766(11), K(2)–N(4) 2.804(10), P(1)–Se(1) 2.171(4), P(2)–Se(2) 2.163(4), P(1)–N(3) 1.546(10), P(2)–N(4) 1.552(10), P(1)–N(1) 1.735(9), P(1)–N(2) 1.715(10), P(2)–N(1) 1.717(10), P(2)–N(2) 1.703(8); Se(1)–K(1)–Se(2) 97.14(8), N(3)–K(2)–N(4) 91.2(3), Se(1)–P(1)–N(3) 119.5(4), Se(2)–P(2)–N(4) 119.8(4), P(1)–Se(1)–K(1) 86.66 (11), P(2)–Se(2)–K(1) 87.64(12), P(1)–N(3)–K(2) 105.1(5), P(2)–N(4)–K(2) 104.0(5).

DOI: 10.1039/b000357n

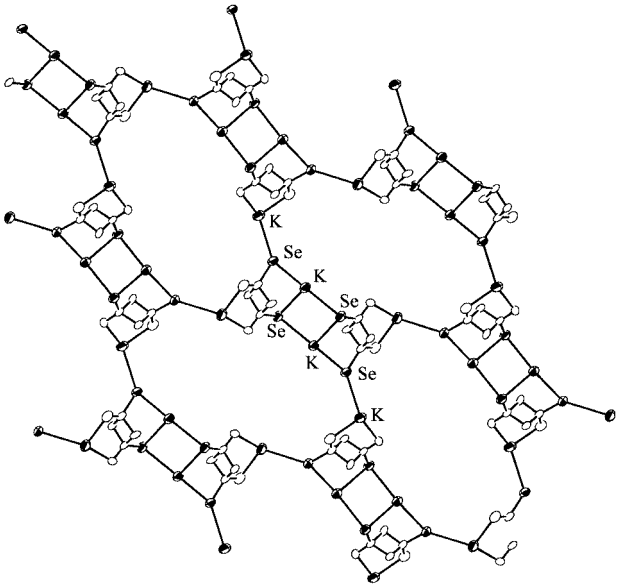

Fig. 2 The extended structure of **6** showing the two types of K···Se interactions. For clarity Bu^t groups and THF are omitted.

presence of two K^+ ions per monomeric building block allows the formation of an extended network of twenty-membered ($K_6Se_6P_4N_4$) rings (Fig. 2). The sulfur analogue **7** forms a similar extended structure.[10] By contrast, we note that the sodium salt of **3a**, $(THF)_2Na[Bu^tN(Se)P(\mu\text{-}NBu^t)_2P(Se)(NBu^t)]Na(THF)_2$ **8**, in which *both* Na^+ ions are bis-solvated, has a monomeric structure similar to that depicted in Fig. 1.[10] The ^{31}P {^1H} NMR parameters for **8** in d_8-THF are δ +3.9, $^1J(^{31}P–^{77}Se)$ = 678 Hz and $^2J(^{31}P–^{31}P)$ = 6.1 Hz.

Investigations of the formation of metal-containing coordination polymers involving the novel bis-chelating dianions **3a** and **3b** are in progress. Details of the structural characterization of **7** and **8** will be provided in the full account of this work.

We thank the NSERC (Canada) for financial support.

Notes and references

† *Synthesis* of **6**: *cis*-[(Bu^{t}NH)(Se)P(μ-NBu^t)$_2$P(Se)(NHBu^t)] **4** was obtained in *ca.* 80% yield from the reaction of [(Bu^{t}NH)P(μ-NBu^t)P(NHBu^t)] with elemental selenium in boiling toluene for 18 h. NMR (d_8-THF): ^1H, δ 4.56 (s, 2H, NH), 1.68 (s, 18H, Bu^t), 1.46 (s, 18H, Bu^t); ^{31}P {^1H}, δ 26.7 (s, $^1J(^{31}P–^{77}Se)$ 880, $^2J(^{31}P–^{31}P)$ 25 Hz; ^{77}Se, δ −128.4 (d, $J(^{31}P–^{77}Se)$ 877 Hz). IR (cm^{-1}): 3383 [ν(N–H)], 581 [ν(PSe)].

A solution of $KN(SiMe_3)_2$ (1.66 g, 7.90 mmol) in THF (10 mL) was added slowly to a stirred solution of **4** (2.00 g, 3.95 mmol) in THF at 23 °C. After 2 h solvent was removed under vacuum and the product was washed with hexane (2 × 10 mL) to give **6** (2.07 g, 2.59 mmol) as a yellow powder. X-Ray quality crystals were obtained from THF–hexane (1 : 1) solution at 23 °C. NMR (d_8-THF): ^1H, δ 3.58 (m, OCH_2CH_2), 1.74 (m, OCH_2CH_2), 1.66 (s, 18H, Bu^t), 1.33 (s, 18H, Bu^t); ^{31}P {^1H}, δ −0.03 (s, $^1J(^{31}P–^{77}Se)$ 686 Hz); ^{77}Se, δ 13.2 (d, $J(^{31}P–^{77}Se)$ 684 Hz). IR (cm^{-1}): 514 [ν(PSe)].

Synthesis of **7**: complex **7** was obtained in 81% yield as a yellow powder from $KN(SiMe_3)_2$ (5.00 mmol) and **5**[7] (2.50 mmol) in THF (20 mL) by a procedure similar to that described above for **6**. NMR (d_8-THF): ^1H, δ 3.58 (m, OCH_2CH_2), 1.75 (m, OCH_2CH_2), 1.60 (s, 18H, Bu^t), 1.31 (s, 18H, Bu^t); ^{31}P {^1H}, δ 26.6 (s), IR (cm^{-1}): 551 [ν(PS)].

‡ *Crystal data* for **6**: $C_{28}H_{60}N_4K_2O_3P_2Se_2$, M = 798.87, monoclinic, space group $P2_1/n$ (no. 14), a = 10.733(11), b = 14.085(10), c = 26.138(9) Å, β = 90.99(5)°, V = 3951(5) Å^3, Z = 4, D_c = 1.343 g cm^{-3}, μ(Mo-Kα) = 21.94 cm^{-1}. Crystal dimensions 0.50 × 0.30 × 0.20 mm. Data were measured on a Rigaku AFC6S diffractometer with graphite-monochromated Mo-Kα radiation using ω scans. The structure was solved by direct methods and refined anisotropically using data that were corrected for absorption. Three carbon atoms of a THF molecule (C18, C19 and C20) had large thermal displacement parameters. 2135 of the 6958 unique reflections has $I \geqslant 2.00\sigma(I)$. The final agreement factors were R = 0.0640, R_w = 0.1652.

CCDC 182/1532. See http://www.rsc.org/suppdata/cc/b0/b000357n/ for crystallographic files in .cif format.

1 For recent reviews, see: J. D. Woollins, *J. Chem. Soc., Dalton Trans.*, 1996, 2893; I. Haiduc, R. Cea-Olivares, S. Hernandez-Ortega and C. Silvestru, *Polyhedron*, 1995, **14**, 2041.
2 N. Platzer, H. Rudler, C. Alvarez, L. Barkaoui, B. Denise, N. Goasdoue, M. N. Rager, J. Vaissermann and J. C. Daran, *Bull. Chem. Soc. Fr.*, 1995, **132**, 95.
3 H. Rudler, B. Denise, J. R. Gregorio and J. Vaissermann, *Chem. Commun.*, 1997, 2299.
4 R. Cea-Olivares, J. Novosad, J. D. Woollins, A. M. Z. Slawin, V. Garcia-Montalvo, G. Espinosa-Pérez and P. Garcia y Garcia, *Chem. Commun.*, 1996, 519; V. Garcia-Montalvo, J. Novosad, P. Kilian, J. D. Woollins, A. M. Z. Slawin, P. Garcia y Garcia, M. Lopez-Cardoso, G. Espinosa-Pérez and R. Cea-Olivares, *J. Chem. Soc., Dalton Trans.*, 1997, 1029.
5 L. Grocholl, L. Stahl and R. J. Staples, *Chem. Commun.*, 1997, 1465.
6 L. Grocholl, I. Schranz, L. Stahl and R. J. Staples, *Inorg. Chem.*, 1998, **37**, 2496; I. Schranz, L. Stahl and R. J. Staples, *Inorg. Chem.*, 1998, **37**, 1493.
7 P. Bhattacharyya, J. Novosad, J. Phillips, A. M. Z. Slawin, D. J. Williams and J. D. Woollins, *J. Chem. Soc., Dalton Trans.*, 1995, 1607; P. Bhattacharyya, A. M. Z. Slawin, D. J. Williams and J. D. Woollins, *J. Chem. Soc., Dalton Trans.*, 1995, 2489.
8 T. G. Hill, R. C. Haltiwanger, M. L. Thompson, S. A. Katz and A. D. Norman, *Inorg. Chem.*, 1994, **33**, 1770.
9 T. Chivers, M. Parvez and M. A. Seay, *Inorg. Chem.*, 1994, **33**, 2147.
10 T. Chivers, M. Krahn and M. Parvez, unpublished results.
11 (*a*) A. M. Z. Slawin, J. Ward, D. J. Williams and J. D. Woollins, *J. Chem. Soc., Chem. Commun.*, 1994, 421; (*b*) J. D. Woollins, *J. Chem. Soc., Dalton Trans.*, 1996, 2893.

Communication b000357n

ChemComm

The synthesis of (+)-nemorensic acid

Timothy J. Donohoe,*[a] Jean-Baptiste Guillermin,[a] Christopher Frampton[b]† and Daryl S. Walter[b]

[a] *Department of Chemistry, The University of Manchester, Oxford Road, Manchester, UK M13 9PL. E-mail: t.j.donohoe@man.ac.uk*

[b] *Department of Chemistry, Roche Discovery Welwyn, Broadwater Road, Welwyn Garden City, Herts, UK AL7 3AY*

Received (in Liverpool, UK) 19th January 2000, Accepted 8th February 2000, Published on the Web, 2nd March 2000

The synthesis of (+)-nemorensic acid in nine steps is described; key steps in the route were the stereoselective Birch reduction of a substituted furan, and addition of allyltrimethylsilane to an oxonium ion at C-5; an X-ray crystal structure of (−)-nemorensic acid provided proof of the relative stereochemistry of the target.

We have recently initiated a research programme aimed at synthesising the pyrrolizidine alkaloids.[1] These alkaloids are a diverse series of compounds, isolated from the *Senecio* family of plants, which display a wide range of biological activities such as hepatotoxicity and carcinogenic activity; some of these alkaloids have the ability to cross-link DNA at specific points.[2] In particular we were drawn to pyrrolizidine alkaloids containing a macrocyclic bislactone. Hydrolysis of these bislactone alkaloids yields a diol (necine base) and a diacid (necic acid). While the synthesis of necine bases is well established, the necic acid moiety has received relatively little attention; indeed it is variation in this part of the molecule that is responsible for much of the diversity of these plant alkaloids. We now report our studies on the synthesis of nemorensic acid, which is obtained from hydrolysis of nemorensine (Scheme 1).[3] A survey of the literature reveals that nemorensic acid has been synthesised by the groups of Klein (±),[4] White (+),[5] Mascareñas (±)[6] and Honda (+).[7] Our retrosynthetic analysis of nemorensic acid identified the lactone **1** as a viable precursor for the target; we know from previous studies that **1** can be prepared from the commercially available 3-methyl-2-furoic acid *via* a Birch reduction on a chiral auxiliary (Xc) laden furan.[8]

Our synthesis began with **2**, which was coupled to (*R*,*R*)-(−)-bismethoxymethylpyrrolidine in excellent yield. We have already reported that the reductive methylation of **3** proceeds in high yield and with ⩾30:1 diastereoselectivity.[8] Subsequent Jones (allylic) oxidation gave **5** and hydrogenation with palladium provided **6** in good overall yield, and with high selectivity for the isomer shown (Scheme 2).[9]

The lactone **6** (structure proven by X-ray crystallography) was treated with 'Cp_2TiMe_2' which was freshly prepared from Cp_2TiCl_2 and MeLi, according to Petasis (Scheme 3).[10] The resulting enol ether **7** was rather sensitive to hydrolysis and was, therefore, converted immediately into the acetal **8** (1:1 mixture of epimers) with acidic methanol (72% overall yield). Introduction of carbon functionality at C-5 was accomplished by

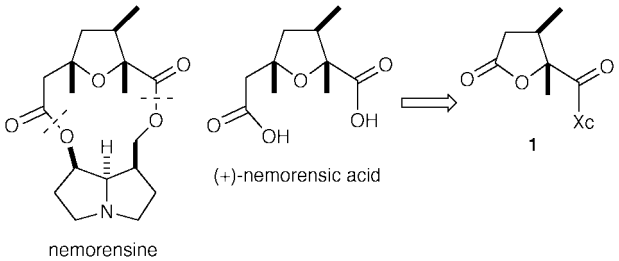

Scheme 1

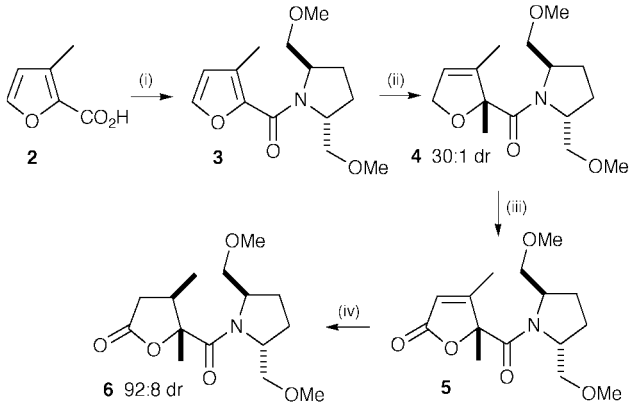

Scheme 2 *Reagents and conditions*: i, $SOCl_2$, then (*R*,*R*)-bismethoxymethylpyrrolidine, NaOH, 95%; ii, Na, NH_3, THF, −78 °C then MeI, 93%; iii, CrO_3, H_2SO_4, 89%; iv, H_2, Pd-C, EtOH, AcOH, 87% (pure *cis*).

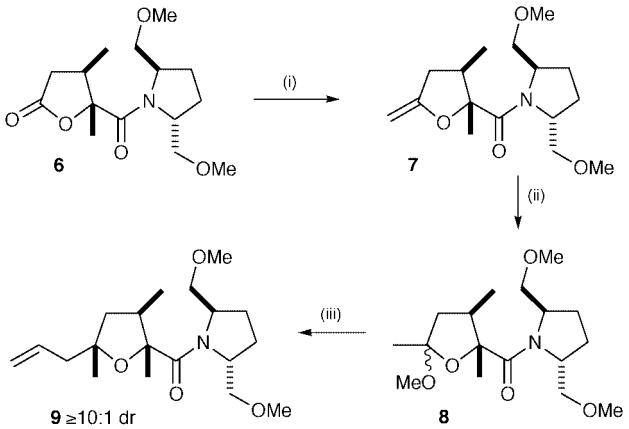

Scheme 3 *Reagents and conditions*: i, Cp_2TiCl_2, MeLi; ii, MeOH, HCl, 72% (two steps); iii, allyltrimethylsilane, $TiCl_4$, CH_2Cl_2, −78 °C, 79%.

reaction of the epimeric mixture of acetals with titanium tetrachloride and allyltrimethylsilane. The allylated compound **9** that resulted from this reaction was formed as a single diastereoisomer according to ^1H NMR analysis of the crude reaction mixture. We could assign the stereochemistry of the product with the aid of NOE experiments which showed a strong (and reciprocal) enhancement between the allylic methylene protons and the (*cis*) methine proton at C-3 (Fig. 1).

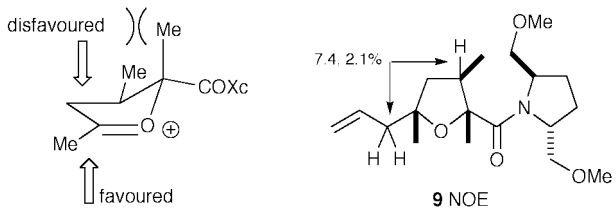

Fig. 1

† Author to whom correspondence on the X-ray crystal structure should be addressed.

DOI: 10.1039/b000565g

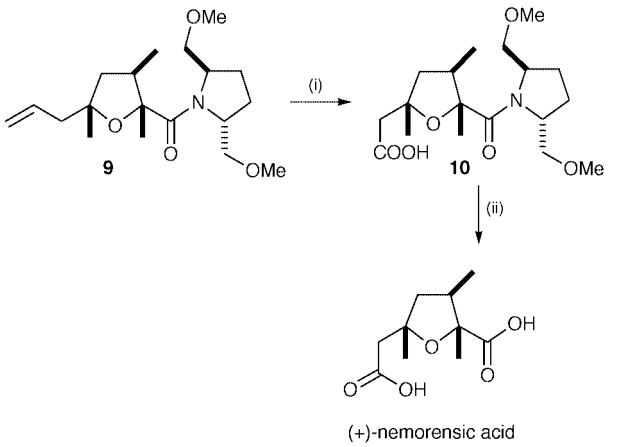

Scheme 4 *Reagents and conditions*: i, $RuCl_3$ (cat.) $NaIO_4$; ii, 6 M HCl, Δ, 65% (two steps).

The sense of diastereoselectivity displayed during the allylsilane addition to acetal **8** is interesting and is consistent with a recent observation by Woerpel *et al.* on related systems.[11] According to this model, geminal substitution at C-2 is crucial for high levels of selectivity, and the main reason for addition to the lower face of the oxonium ion derived from **8** is steric interaction with the pseudoaxial methyl group at C-2 (Fig. 1).

The synthesis was completed by oxidative cleavage of the alkene unit with catalytic ruthenium tetroxide; the acid **10** was immediately treated with aqueous acid to cleave the auxiliary and liberate nemorensic acid, (65% yield from **9**) (Scheme 4). The relative stereochemistry of the product was confirmed by X-ray crystallographic analysis (Fig. 2).‡

Nemorensic acid produced by this sequence had spectroscopic data (^1H, ^{13}C NMR) that were identical with those reported in the literature. Its melting point was 171–173 °C (lit.[3] 174–177 °C) and its optical rotation was $[\alpha]_D$ +84 (*c* 0.18, EtOH) (lit.[3] $[\alpha]_D$ +87 (*c* 0.84, EtOH)).

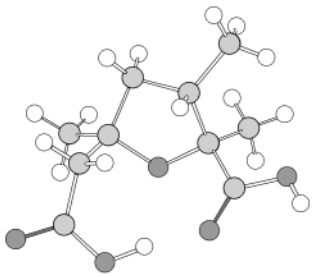

Fig. 2 Nemorensic acid.

To conclude, we have prepared (+)-nemorensic acid in nine steps and 25% overall yield using the Birch reduction of furan as the key step. This synthesis is particularly efficient and is amenable to the preparation of ample amounts of material.

We thank the EPSRC and Roche Pharmaceuticals for financial support. Clare Stevenson is thanked for some preliminary experiments.

Notes and references

‡ In the initial phase of our studies we prepared the unnatural (−) enantiomer of nemorensic acid and obtained X-ray crystallographic analysis on this material. *Crystal data* for (−)-nemorensic acid: $C_{10}H_{16}O_5$, M = 216.23, orthorhombic, a = 8.4556(2), b = 11.4227(2), c = 11.4637(2) Å, U = 1107.23(4) Å^3, T = 123(1) K, space group $P2_12_12_1$ (no. 19), Z = 4, D_c = 1.297 g cm^{-1}, μ(Mo-Kα) = 0.104 mm^{-1}. Data collected on a Bruker AXS SMART CCD diffractometer, 9403 reflections measured, data truncated to 0.80 Å (θ_{max} 26.37°, 99.8% complete), 2269 reflections unique (R_{int} = 0.0182). Final agreement factors for 161 parameters gave R_1 = 0.0274, wR^2 = 0.0773 and GOF = 1.001 based on all 2269 data, absolute structure not determined, final difference map +0.21 and −0.15 e Å^{-3}. Programs used: Bruker AXS SMART and SAINT control and integration software, SHELXTL Structure solution and refinement (G. M. Sheldrick, University of Göttingen, Germany). CCDC 182/1540. See http://www.rsc.org/suppdata/cc/b0/b000565g/ for crystallographic data in .cif format.

1 For a review see: D. J. Robins, *Nat. Prod. Rep.*, 1995, **12**, 413 and references therein..
2 See J. J. Tepe and R. M. Williams, *J. Am. Chem. Soc.*, 1999, **121**, 2951 and references therein..
3 A. Klásek, P. Sedmera, A. Boeva and F. Santavý, *Collect. Czech. Chem. Commun.*, 1973, **38**, 2504.
4 L. L. Klein, *J. Am. Chem. Soc.*, 1985, **107**, 257.
5 M. P. Dillon, N. C. Lee, F. Stappenbeck and J. D. White, *J. Chem. Soc., Chem. Commun.*, 1995, 1645.
6 J. R. Rodríguez, A. Rumbo, L. Castedo and J. L. Mascareñas, *J. Org. Chem.*, 1999, **64**, 4560.
7 T. Honda and F. Ishikawa, *J. Org. Chem.*, 1999, **64**, 5542.
8 T. J. Donohoe, M. Helliwell, C. A. Stevenson and T. Ladduwahetty, *Tetrahedron Lett.*, 1998, **39**, 3071.
9 T. J. Donohoe, C. A. Stevenson M. Helliwell, R. Irshad and T. Ladduwahetty, *Tetrahedron: Asymmetry*, 1999, **10**, 1315.
10 N. A. Petasis and E. I. Bzowej, *J. Am. Chem. Soc.*, 1990, **112**, 6392.
11 J. T. Shaw and K. A. Woerpel, *Tetrahedron*, 1999, **55**, 8747; see also C. Brückner, H. Lorey and H.-U. Reissig, *Angew. Chem., Int. Ed. Engl.*, 1986, **25**, 556.

Communication b000565g

High isolated yields in thermodynamically controlled peptide synthesis in toluene catalysed by thermolysin adsorbed on Celite R-640

Alessandra Basso, Luigi De Martin, Cynthia Ebert, Lucia Gardossi* and Paolo Linda

Dipartimento di Scienze Farmaceutiche, Università degli Studi, Piazzale Europa 1, 34127 Trieste, Italy. E-mail: gardossi@univ.trieste.it

Received (in Liverpool, UK) 27th January 2000, Accepted 14th February 2000, Published on the Web, 2nd March 2000

An innovative immobilisation method that allows peptide synthesis to be performed even at equimolar concentrations, by controlling water activity, is reported.

Enzymes have proved to be an attractive alternative to chemical methods in peptide synthesis since several proteases effect peptide bond formation under mild conditions, with minimum side-chain protection, and avoiding racemization. In spite of these benefits, enzymatic methods are not routinely employed, partly because they suffer from unfavourable thermodynamics in water.

There are two distinct mechanisms for protease-catalysed peptide synthesis: thermodynamically and kinetically controlled synthesis. In principle, replacing water with organic solvents as a reaction medium should be beneficial for both types of reaction. However, water is essential for proteases such as thermolysin and α-chymotrypsin, and various studies confirmed that these enzymes display no activity when insufficiently hydrated.[1] Unfortunately, water/solvent mixtures are not optimal media for peptidases since high percentages of co-solvents reduce the activity of the enzyme dramatically.

Owing to these two opposite roles of water in enzymatic peptide synthesis, various approaches have been developed in order to search for compromises. These include kinetically controlled syntheses in solvents containing low percentages of water [2] or methods to reverse the equilibrium towards synthesis, such as using an excess of the amino component and extracting/precipitating the product.[3]

Kitaguchi and Klibanov[1a] have given an alternative solution to the problem by demonstrating that water can be replaced partially by water mimics such as formamide, maintaining the activity of the enzyme in the organic solvent while minimising hydrolytic reactions. Finally, promising results have been obtained by Halling and coworkers by controlling the hydration of thermolysin in kinetically controlled peptide synthesis in hexane[4] and, more recently, by developing solid-to-solid peptide synthesis in the presence of minimum amounts of water.[1b]

Aiming to overcome the above drawbacks to a larger application of enzymes in peptide synthesis, the present work describes a novel approach for the non-covalent immobilisation of thermolysin in toluene and its application to thermodynamically controlled peptide synthesis at controlled water activity (a_w). The method exploits the ability of Celite R-640 rods (Fluka) to adsorb large amounts of water (> 90% of its weight) and to maintain the a_w constant in a reaction system within wide defined ranges of water concentrations.[5,6] Thermolysin was adsorbed on dry Celite R-640 according to an innovative and practical technique illustrated in Scheme 1. The enzymatic aqueous solution was added to the hydrophobic solvent containing the dry support. Owing to the presence of the hydrophobic solvent, a uniform coating of the aqueous phase formed around the Celite rods and the enzymatic solution was adsorbed on the Celite within 24 h.

The immobilised catalyst suspended in toluene gave, after equilibration, a_w values between 0.70 and 0.75. Enzymatic reactions can be carried out simply by adding the reactants to the toluene used for the adsorption and storage of the enzymes. The use of the hydrophobic organic solvent makes the leakage of the enzyme negligible so that the biocatalyst can be recycled. The hydrophobic solvent leads to further remarkable advantages in terms of stability, especially if compared to the detrimental effects of the water miscible solvents largely reported.[7] For instance, the hydrolases immobilised on Celite R-640 in toluene were stored in the same solvent at a controlled degree of hydration without any appreciable decrease of activity for at least 4 weeks. The same immobilisation technique can also be employed for the immobilisation of α-chymotrypsin and penicillin G amidase (PGA), which were shown to be effective in catalysing amino acid esterification and protection of amino groups, respectively. Table 1 reports some examples of syntheses catalysed by the three immobilised enzymes in toluene at controlled a_w. The water adsorbed by the porous support provides the enzymes with the hydration necessary to display their catalytic activity.[2–4] It should be noted that no reaction was observed when the three native enzymes were employed in dry toluene or acetonitrile in accordance with our observation that PGA is also active in organic solvents only when sufficiently hydrated (a_w > 0.4).[5]

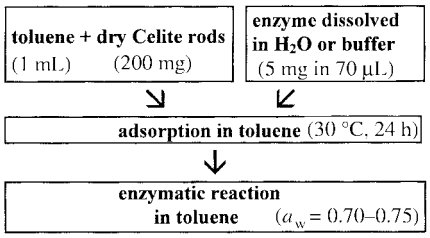

Scheme 1

Table 1 Enzymatic synthesis performed in toluene at a_w between 0.70 and 0.75 at 30 °C

Enzyme[a]	CO_2H donor[b]	Nucleophile[b]	Final conversion[c] (%)	*t*/h
Thermolysin/Celite	Z-L-Phe–CO_2H	L-Phe–OEt	98	48
Thermolysin/Celite	Z-L-Phe–CO_2H	L-Tyr–OEt	97	144
Thermolysin[d]/Celite	Z-L-Phe–CO_2H	L-Leu–NH_2[d]	95	96
PGA[e]/Celite	$PhCH_2CO_2Me$	L-Tyr–OEt	98	24
α-Chymotrypsin[e]/Celite	Z-L-Phe–CO_2H	MeOH	97	60

[a] Enzyme dissolved in buffer and adsorbed on 200 mg of Celite rods according to Scheme 1. [b] Equimolar concentrations of reactants (80 μmol) were employed in all reactions. An excess of MeOH (250 μmol) was used only in the esterification of Z-L-Phe-CO_2H. [c] Conversions calculated by means of RP-HPLC using an internal standard. Isolated yields of Z-L-Phe-L-Phe–OEt, Z-L-Phe-L-Tyr–OEt and Z-L-Phe-L-Leu–NH_2 were 93, 90 and 76%, respectively. Reactions catalysed by α-chymotrypsin and thermolysin were monitored also by titrating the Z-L-Phe–CO_2H with 0.1 M NaOH solution. [d] The enzyme was dissolved in 35 μL of buffer, adsorbed on the Celite rods and equilibrated for 24 h. Afterwards, a buffer solution (35 μL) containing L-Leu–NH_2 was added to the thermolysin/Celite system and equilibrated for 3 h. [e] The enzyme was dissolved in water before adsorption.

DOI: 10.1039/b000797h

The use of Celite R-640 as a support for thermolysin and α-chymotrypsin enables peptide bond synthesis and esterification to be performed using free carboxylic acids since the water produced during the reaction is adsorbed by the Celite rods. Therefore a_w was maintained sufficiently low and hydrolytic reactions were prevented so that nearly quantitative conversions were achieved even when employing equimolar concentrations of non-activated, and thus less expensive, substrates. It must be noted that when native thermolysin was employed in water–acetonitrile (13% v/v)† in the synthesis of Z-L-Phe-L-Tyr–OEt, a maximum of 22% of conversion was obtained in 6 h but during the reaction course a_w exceeded 0.90 so that hydrolytic reactions prevailed, causing a very low final conversion (11%).

Despite the fact that the poor solubility of peptides has often been viewed as a restriction for enzymatic reactions in organic solvents, results in Table 1 indicate that thermodynamically controlled peptide enzymatic synthesis in hydrophobic solvents can be carried out employing substrates having very low solubility and which are present in the reaction medium mainly as a suspension. This observation is in accord with previous studies concerning kinetically controlled peptide synthesis[4] and the solid-to-solid synthesis.[1b,c]

The dipeptide Z-L-Phe-L-Leu–NH_2 was synthesised following an alternative strategy since the poorly soluble L-Leu–NH_2 was previously dissolved in an aqueous buffer and then adsorbed on the Celite rods where thermolysin had been already immobilised. However, this second method led to lower isolated yields (76%) probably owing to some adsorption of the product on the Celite rods.

The time required to achieve complete conversion is mainly affected by the fact that equimolar concentrations of the reactants were used in all peptide synthesis, so that the reaction rate slows down dramatically at the end of the reaction when the concentrations of the two reactants become extremely low. Complete conversions are achievable in shorter times using a two fold excess of the amino component (> 98% yield of Z-L-Phe-L-Tyr–OEt in 48 h). Nevertheless, employing equimolar concentrations of reactants is advisable since this enables the recovery and isolation of the products very simply and, most importantly, avoiding any purification step.‡ As a consequence, remarkably high isolated yields (93 and 90%) are achievable. This is a factor of major importance in peptide synthesis, especially when various subsequent synthetic steps are required.

Reactions reported in Table 1 catalysed by α-chymotrypsin and PGA are also of practical use in peptide synthesis since they are potentially useful for the preparation and protection of activated amino acids suitable for kinetically controlled peptide synthesis. It is noteworthy that α-chymotrypsin catalysed the complete esterification of Z-L-Phe, despite it being previously reported that the enzyme accepts preferentially the *N*-acetyl amino acids,[1d] which, however, are deprotected with difficulty.

The novelty of our method lies not only in the synthetic results obtained but also in the immobilisation technique developed. The use of Celite R-640 allows control of the water activity, rather than water concentration, during the whole process, thus controlling effectively both the enzyme activity and the reaction equilibrium. No devices, such as hydrated salts,[8] equilibration with the atmosphere at known relative humidity,[9] or more complex methods[10] for adjusting the a_w of the system are required; also there is no need to remove the water produced during the process.[11] Furthermore, the immobilisation method fulfils the fundamental requirements for a larger application to biotransformations since the procedure is simple and inexpensive, it provides very high reproducibility in terms of enzyme and water content so leading to reproducible activity and quantitative adsorption yields. Detrimental effects caused by the removal of water under vacuum or with polar solvents[12–14] are avoided. Moreover, microbial contaminations are prevented, the support material is stable under the reaction conditions, and possesses no swelling capacity.

In conclusion, the present work describes the first example, to the best of our knowledge, of thermodynamically controlled enzymatic peptide synthesis performed in organic solvent leading to complete conversions and very high isolated yields even when equimolar concentrations of the reactants are employed.

Since it has been already demonstrated that peptidases catalyse the formation of the bond between oligopeptide fragments in organic solvents and that PGA is able to remove phenylacetic groups selectively from amino acids, we are currently investigating the application of this technique to a totally enzymatic approach for peptide synthesis competing with chemical routes.

We thank CNR and MURST (Roma) for financial support to P. Linda.

Notes and references

† 13% v/v of H_2O enables operation at $a_w \approx 0.73$[12d] in MeCN.

‡ The three synthesised dipeptides precipitated upon formation owing to their low solubility in toluene. The toluene was removed and the solid residue was washed with MeCN. The organic solutions were combined, filtered and taken to dryness obtaining products having > 98% purity by HPLC. Products of reactions catalysed by PGA and α-chymotrypsin are soluble in toluene and were isolated by removing the organic phase and evaporating the solvent.

1 (*a*) H. Kitaguchi and A. M. Klibanov, *J. Am. Chem. Soc.*, 1989, **111**, 9272; (*b*) M. Erbeldinger, X. Ni and P. J. Halling, *Biotechnol. Bioeng.*, 1998, **59**, 68; (*c*) P. Kuhl, U. Eichhorn and H.-D. Jakubke, *Biotechnol. Bioeng.*, 1995, **45**, 276; (*d*) P. Clapés and P. Adlercreutz, *Biochim. Biophys. Acta*, 1991, **1118**, 70.

2 K. Ohiama, S. Nishimura, Y. Nonaka, K.-I. Kihara and T. Hashimoto, *J. Org. Chem.*, 1981, **46**, 5242; P. Clapés, E. Pera and J. L. Torres, *Biotechnol. Lett.*, 1997, **19**, 1023; Y. Murakani, S. Hayashi, A. Takehara and A. Hirata, *Biotechnol. Tech.*, 1999, **13**, 165; R. A. Persichetti, N. L. St. Clair, J. P. Griffith, M. A. Nava and A. Margolin, *J. Am. Chem. Soc.*, 1995, **117**, 2732.

3 R. Didziapetris, B. Drabnig, V. Schellenberger, H.-D. Jakubke and V. Svedas, *FEBS Lett.*, 1991, **287**, 31; V. Kasche and B. Galusky, *Biotechnol. Bioeng.*, 1995, **45**, 261; M. Haensler, S. Thust, P. Klossek and G. Ullman, *J. Mol. Catal. B: Enzymatic*, 1999, **6**, 95; G. Lye and J. M. Woodley, *TIBTECH*, 1999, **17**, 395; M. Erbeldinger, X. Ni and P. J. Halling, *Biotechnol. Bioeng.*, 1999, **63**, 316.

4 P. Kuhl, P. J. Halling and H.-D. Jakubke, *Tetrahedron Lett.*, 1990, **31**, 5231.

5 L. De Martin, C. Ebert, G. Garau, L. Gardossi and P. Linda, *J. Mol. Catal. B: Enzymatic*, 1999, **6**, 437.

6 A. Basso, L. De Martin, C. Ebert, L. Gardossi and P. Linda, *J. Mol. Catal. B: Enzymatic*, 2000, **8**, 245.

7 J. Partridge, B. D. Moore and P. J. Halling, *J. Mol. Catal. B: Enzymatic*, 1999, **6**, 11.

8 P. J. Halling, *Enzyme Microb. Technol.*, 1994, **16**, 178.

9 E. Wehtje, H. de Wit and P. Adlercreutz, *Biotechnol. Tech.*, 1996, **10**, 947.

10 (*a*) E. Wehtje, I. Svensson, P. Adlercreutz and B. Mattiasson, *Biotechnol. Tech.*, 1993, **7**, 873; (*b*) S. J. Kwon, K. M. Song, W. H. Hong and J. S. Rhee, *Biotechnol. Bioeng.*, 1994, **46**, 393.

11 S. Bloomer, P. Adlecreutz and B. Mattiasson, *Enzyme Microb. Technol.*, 1992, **14**, 546; M. Otamiri, P. Adlercreutz and B. Mattiasson, *Biotechnol. Bioeng.*, 1994, **44**, 73; P. Mensah, J. L. Gainer and G. Carta, *Biotechnol. Bioeng.*, 1996, **20**, 434.

12 (*a*) J. Partridge, G. A. Hutcheon, B. D. Moore and P. J. Halling, *J. Am. Chem. Soc.*, 1996, **118**, 12873; (*b*) M. C. Parker, B. D. Moore and A. J. Blaker, *Biocatalysis*, 1994, **10**, 269; (*c*) T. Ke and A. M. Klibanov, *Biotechnol. Bioeng.*, 1998, **57**, 746; (*d*) J. Partridge, P. J. Halling and B. D. Moore, *Chem.Commun.*, 1998, 841.

13 K. Dabulis and A. M. Klibanov, *Biotechnol. Bioeng.*, 1993, **41**, 566.

14 P. Adlercreutz, *Eur. J. Biochem.*, 1991, **199**, 609; J. Kim and B. G. Kim, *Biotechnol. Bioeng.*, 1996, **50**, 687.

Communication b000797h

Preparation and characterization of homoleptic and ethoxy-bridged nitronato iron(III) complexes

Tibor Kovács,[a] Gábor Speier,*[ab] Marius Réglier,[c] Michel Giorgi,[c] Attila Vértes[d] and György Vankó[d]

[a] *Department of Organic Chemistry, University of Veszprém, 8201 Veszprém, Hungary. E-Mail: speier@almos.vein.hu*
[b] *Research Group for Petrochemistry of the Hungarian Academy of Sciences, 8201 Veszprém, Hungary*
[c] *Chimie, Biologie et Radicaux Libres, UMR CNRS 6517, Universites d'Aix-Marseille 1 et 3, Faculté des Sciences et Techniques de Saint Jerôme, case 432, avenue Escadrille Normandie-Niemen, 13397 Marseille Cedex 20, France*
[d] *Hungarian Academy of Sciences at Eötvös University, Research Group for Nuclear Methods in Stuctural Chemistry, 1518 Budapest, Hungary*

Received (in Basel, Switzerland) 1st January 2000, Accepted 10th February 2000, Published on the Web, 2nd March 2000

Iron(III) chloride reacts with potassium 2-propanenitronate to give the homoleptic tris(2-propanenitronato-*O*,*O*)iron(III) complex which in ethanol transfoms to an ethoxy-bridged diiron(III) 2-propanenitronate complex.

The conversion of nitro compounds to aldehydes and ketones is one of the most important functional group transformations.[1] It can be achieved conveniently by the Nef reaction, where conjugate bases of nitro compounds are treated with sulfuric acid leading to the hydrolysis of the C=N bond [eqn. (1)].[2]

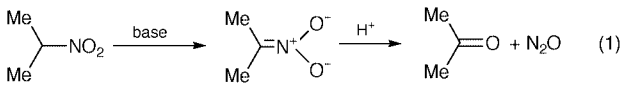

(1)

Alternative oxidative methods also exist for this reaction in the literature resulting in better yields and fewer side reactions.[3] Biological organisms can also transform aliphatic nitro compounds to the corresponding oxo species and nitrite ion [eqn. (2)]. Oxygenated flavoenzyme species,[4] glucose oxidase, D- and

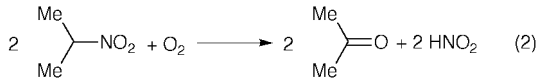

(2)

L-amino acid oxidase,[5] extracts of *Neurospora crassa*[6] pea seedlings and those from the hyphae of a nitrifying strain of *Aspergillus flavus*[7] and the intracellular enzyme 2-nitropropane dioxygenase of *Hansenula mraki*[8] oxidatively degrade nitroalkanes. The latter is believed to contain iron ions at its active center. Recently we demonstrated the facile copper-assisted oxygenation of nitroalkanes according to eqn. (2) and proposed a mechanism for the reaction.[3,9]

In order to understand the coordination of alkanenitronates to iron and their conversion to oxo compounds, we now describe the first fully characterised 2-propanenitronato-*O*,*O*–Fe(III) complexes and their oxygenation reaction.

Treatment of $FeCl_3$ with an equimolar amount of potassium 2-propanenitronate in benzene at room temperature for 4 h yielded the red–brown crystalline complex $[Fe(C_3H_6NO_2)_3]$ **1** in 24% yield.† If the reaction was carried out in a mixture of benzene and ethanol or **1** was recrystallised from ethanol the red crystalline complex $[Fe_2(C_3H_6NO_2)_4(C_2H_5O)_2]$ **2** was obtained in 27% yield.† In ethanol complex **1** undergoes ligand exchange, ethanolate displaces the nitronate ligand and bridges the two iron(III) ions to form **2** in an equilibrium [eqn. (3)].

The IR spectra of **1** and **2**, obtained as KBr pellets, reveal a particularly diagnostic absorption [ν(C=N)] at 1639 and 1644 cm^{-1}, respectively. The relative intensity of this absorption suggests a similar mode of coordination for both complexes and implies considerable carbon–nitrogen double bond character.[10] Magnetic measurements gave values of μ_B = 5.87 per Fe(III) for **1** and 7.29 per 2Fe(III) for **2** accord with high spin Fe(III) centers,

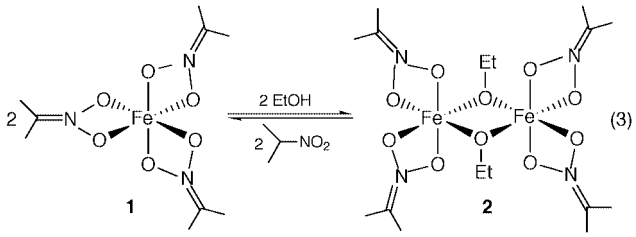

(3)

with a slight antiferromagnetic interaction in complex **2**. The Mössbauer spectra, recorded at 80 K, reflect the different coordination of Fe(III) in complexes **1** and **2**. Although the identical isomer shift values (δ_1 = 0.48 mm s^{-1} and δ_2 = 0.48 mm s^{-1}) reveal the same electron density on the iron in both compounds, the quadrupole splittings (Δ_1 = 0.90 mm s^{-1} and Δ_2 = 0.53 mm s^{-1}) differ significantly owing to different ligand contributions to the electric field gradient (EFG). The trigonal distortion of complex **1** makes the EFG rather large; however, this is considerably reduced upon dimerisation, when the local environment of the iron becomes closer to octahedral.

The crystal structure of **1**,‡ shown in Fig. 1 together with selected data, shows a distorted octahedral geometry around the

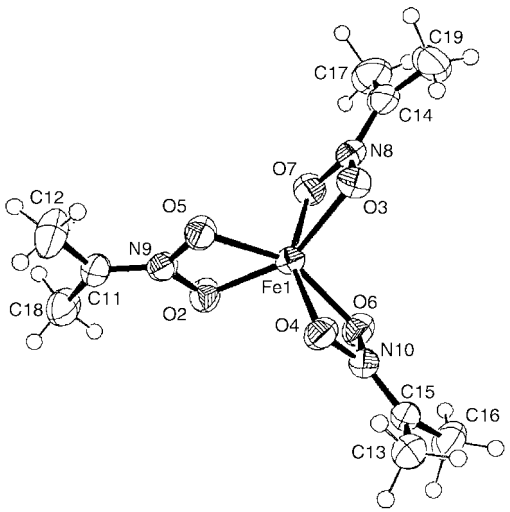

Fig. 1 Molecular structure of $[Fe(C_3H_6NO_2)_3]$ **1**. Selected distances (Å) and angles (°): Fe(1)–O(2) 2.021(3), Fe(1)–O(3) 2.026(3), Fe(1)–O(4) 2.016(3), Fe(1)–O(5) 2.016(2), Fe(1)–O(6) 2.019(3), Fe(1)–O(7) 2.013(3), O(2)–N(9) 1.342(4), O(3)–N(8) 1.342(4), O(4)–N(10) 1.338(4), O(5)–N(9) 1.346(4), O(6)–N(10) 1.344(4), O(7)–N(8) 1.339(4), N(8)–C(14) 1.293(5), N(9)–C(11) 1.283(4), N(10)–C(15) 1.288(5); O(2)–Fe(1)–O(5) 66.0(1), O(3)–Fe(1)–O(7) 66.0(1), O(4)–Fe(1)–O(6) 65.9(1), O(3)–N(8)–O(7) 110.3(3), O(2)–N(9)–O(5) 109.8(3), O(4)–N(10)–O(6) 109.9(3). Displacement ellipsoids are shown at 50% probability level.

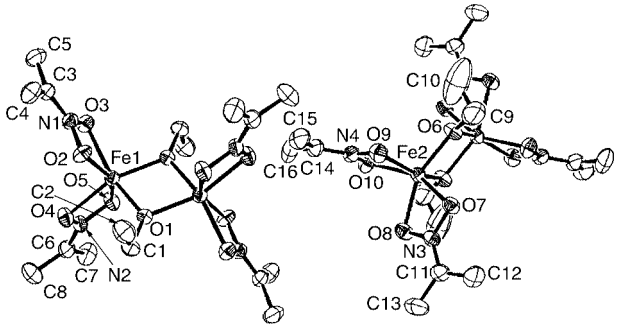

Fig. 2 Molecular structure of $[Fe_2(C_3H_6NO_2)_4(C_2H_5O)_2]$ **2**. Selected distances (Å) and angles (°): O(4)–N(2) 1.335(3), O(5)–N(2) 1.338(3), Fe(2)–O(6) 1.958(2), Fe(2)–O(6) 1.964(2), Fe(2)–O(7) 2.030(2), Fe(2)–O(10) 2.040(2), Fe(2)–O(8) 2.048(2), Fe(2)–O(9) 2.053(2), O(6)–Fe(2) 1.958(2), O(7)–N(3) 1.341(3), O(8)–N(3) 1.335(3), O(9)–N(4) 1.331(4), O(10)–N(4) 1.337(3), O(1)–Fe(1)–O(1) 77.65(8), O(2)–Fe(1)–O(3) 65.28(8), O(5)–Fe(1)–O(4) 65.13(8), Fe(1)–O(1)–Fe(1) 102.35(8), O(3)–N(1)–O(2) 110.6(2), O(4)–N(2)–O(5) 110.3(2), O(6)–Fe(2)–O(6) 77.43(10), O(7)–Fe(2)–O(8) 65.13(8), O(10)–Fe(2)–O(9) 4.85(9), Fe(2)–O(6)–Fe(2) 102.58(10), O(8)–N(3)–O(7) 110.2(20), O(9)–N(4)–O(10) 110.7(2). Displacement ellipsoids are shown at 50% probability level.

iron atom, with all coordination sites being occupied by the bidentate 2-nitropropanate ligands. The Fe–O bond distances are in the range 2.013(3)–2.026(3) Å and the bite-angles of the ligands lie in the range 109.8(3)–110.3(3)°. **1** exhibits a propeller-like structure with the iron atom being 0.007 Å out of the plane of the three N atoms of the three ligands. The crystal structure of **2**,‡ shown in Fig. 2 together with selected data, shows that there are two very similar ethoxy-bridged diiron molecules with slightly different bond distances and angles. The geometry around the iron atoms is aproximately octahedral, the six coordination sites being occupied by two ethoxy groups and two bidentate 2-propanenitronate ligands. The average Fe–O (bridging) bond distance is 1.966 Å with an Fe···Fe separation of 3.07 Å. The dimer lies on a crystallographic inversion center, the bridging Fe_2O_2 is perfectly planar with Fe–O–Fe and O–Fe–O angles of 102.35(8), 102.58(10) and 77.65(8), 77.43(10)°, respectively. The Fe–O bond lengths of the nitronato ligands are in the range 2.021(2)–2.053(2) Å while the N–O bond distances average 1.337 Å, only slightly shorter than the N–O single bond and larger than the N=O double bond (N–O 1.40 Å, N=O, 1.21 Å).[11] The carbon–nitrogen bonds in both complexes (1.283–1.291 Å) are essentially double bond in character (C–N 1.47 Å, C=N 1.27 Å).[11]

Complex **1** is very sensitive towards dioxygen and moisture while **2** is reasonably stable to both in the solid state. Preliminary oxygenation reactions of 2-nitropropane in the presence of **1** and **2** in pyridine at 90 °C resulted in the formation of acetone and HNO_2. Conversions of *ca.* 80% could be achieved at substrate : catalyst ratios of 20–40 : 1 during 20 h. The conversion–time profiles of the catalytic reactions were very similar for complexes **1** and **2** indicating that **2** transforms to **1** if an excess of 2-nitropropane is present. To our knowledge, these reactions represent the first examples of iron-catalysed oxygenation of 2-nitropropane resembling enzyme action, and indicating the possible role of iron ion as a cofactor. Further work is in progress for the elucidation of the mechanism of the reaction.

This work was supported by the Hungarian Research Fund (OTKA) grants # T-16285 and T-30400 and the French–Hungarian Joint Project (Balaton) # F-23/96.

Notes and references

† Satisfactory elemental analyses were obtained for compounds **1** and **2**.

‡ *Crystal data*: $C_9H_{18}FeO_6N_3$ **1**, M_r = 320.10, monoclinic, space group $P2_1/n$, a = 12.395(1), b = 9.226(1), c = 13.343(1) Å, β = 109.082(1)°, V = 1442.0(4) Å^3, Z = 4, T = 298 K, μ(Mo-Kα) 10.698 mm^{-1}, 4145 reflections measured, 3070 unique (R_{int} = 0.031) which were used in all calculations. The final $wR(F^2)$ was 0.33 (all data).

$C_{16}H_{34}Fe_2N_4O_{10}$ **2**, M_r = 554.16, triclinic, space group $P\bar{1}$, a = 10.1033(4), b = 10.3819(4), c = 13.8442(4) Å, α = 111.60(2), β = 95.66(2), γ = 99.77(1)°, V = 1309.7(2) Å^3, Z = 2, μ(Mo-Kα) 1.15 mm^{-1}, T = 297 K,: 4865 reflections measured, 4324 unique (R_{int} = 0.0318) which were used in all calculations. The final $wR(F^2)$ was 0.1038 (all data).

CCDC 182/1541. See http://www.rsc.org/suppdata/cc/b0/b000408l/ for crystallographic files in .cif format.

1 J. March, *Advanced Organic Chemistry, Reactions, Mechanisms and Structure*, Wiley, New York, 4th edn., 1992.
2 H. W. Pinnick, *Org. React.*, 1990, **38**, 655; A. H. Haines, *Methods for the Oxidation of Organic Compounds*, Academic Press, New York, 1988, pp. 220, 416.
3 É. Balogh-Hergovich, J. Kaizer and G. Speier, *Chem. Lett.*, 1996, 573 and references therein.
4 T. C. Bruice, in *Biomimetic Chemistry, Advances in Chemistry Series, 191*, ed. D. Dolphin, C. McKenna, Y. Murakami and I. Tabushi, ACS, Washington DC, 1980, p. 89.
5 D. J. T. Porter and H. J. Brigth, *J. Biol. Chem.*, 1977, **252**, 4361.
6 H. N. Little, *J. Biol. Chem.*, 1951, **193**, 347; H. N. Little, *J. Biol. Chem.*, 1957, **229**, 231.
7 J. A. E. Molina and M. Alexander, *J. Bacteriol.*, 1971, **105**, 489.
8 T. Kido, T. Yamamoto and K. Soda, *Arch. Microbiol.*, 1975, **106**, 165.
9 É. Balogh-Hergovich, G. Speier, G. Huttner and L. Zsolnai, *Inorg. Chem.*, 1998, **37**, 6535.
10 R. M. Silverstein, G. C. Bassler and T. C. Morril, *Spectrometric Identification of Organic Compounds*, Wiley, New York, 1981.
11 L. Pauling, *The Nature of the Chemical Bond*, Cornell University Press, Ithaca, New York, 3rd edn., 1960.

Communication b000408l

ChemComm

Total synthesis of new C-6 homologues of 1-deoxynojirimycin and 1-deoxy-L-idonojirimycin†

Peter Szolcsányi,[a] Tibor Gracza,*[a] Marian Koman,[b] Naïa Prónayová[c] and Tibor Liptaj[c]

[a] *Department of Organic Chemistry, Faculty of Chemical Technology, Slovak University of Technology, Radlinského 9, 812 37 Bratislava, Slovakia. E-mail: gracza@chelin.chtf.stuba.sk*

[b] *Department of Inorganic Chemistry, Faculty of Chemical Technology, Slovak University of Technology, Radlinského 9, 812 37 Bratislava, Slovakia*

[c] *Central NMR Laboratories, Faculty of Chemical Technology, Slovak University of Technology, Radlinského 9, 812 37 Bratislava, Slovakia*

Received (in Liverpool, UK) 21st October 1999, Accepted 25th January 2000, Published on the Web, 2nd March 2000

Novel piperidine lactones 1 and 2, which represent direct precursors to the new C-6 homologues of 1-deoxynojirimycin (3) and 1-deoxy-L-idonojirimycin 4, were prepared by key Pd^{II}-catalysed aminocarbonylation of protected aminoalkene 10.

The inhibitors of glycosidases, enzymes involved in many crucial biochemical pathways,[1] could be very valuable in the treatment of serious human diseases such as diabetes,[2] cancer[3] and viral infections including AIDS.[4] The prominent members of this class of compounds are polyhydroxylated piperidines (often referred to as 'azasugars'). There has been an enormous effort put toward their efficient syntheses as well as toward the preparation of their various derivatives over the last decade. However, only a few of the already published synthetic strategies deal with the preparation of C-6 homologues of azasugars.[5–8] Here we report on the synthesis of new homologues of 1-deoxynojirimycin (**3**) and 1-deoxy-L-idonojirimycin (**4**), (Fig. 1).

Our synthetic plan relies on the successful $PdCl_2$-catalysed aminocarbonylation of the benzyl protected aminoalkene **10** yielding the desired lactones **1** and **2**. Generally, aminocarbonylation of 3-hydroxypent-4-enylamines giving pyrrolidine lactones proceeds easily,[9,10] which is in contrast to 4-hydroxy-hex-5-enylamines producing the corresponding piperidine lactones (Scheme 1).

To the best of our knowledge, there are only a few papers in the literature which deal with such a transformation on similar but simpler substrates.[10,11] However, reported yields are fairly low and no further synthetic elaboration of the prepared piperidine lactones has been reported. The common feature of almost all published amino-/amido-carbonylations (either producing pyrrolidine or piperidine lactones) is the use of electron-withdrawing protecting groups (tosyl, CO_2Me, CO_2Bn, CONHMe, CONHPh, CONHBn) on the NH function of the aminoalkenes. However, properties of such protecting groups (introduction, deprotection, chemical inertness and stability) were not suitable for our proposed plan for the total synthesis. Therefore, we decided to explore the applicability of the benzyl protecting group in the aminocarbonylation producing the piperidine lactones. We report here the above-mentioned strategy in the total synthesis of new C-6 homologues of 1-deoxynojirimycin (**3**) and 1-deoxy-L-idonojirimycin (**4**).

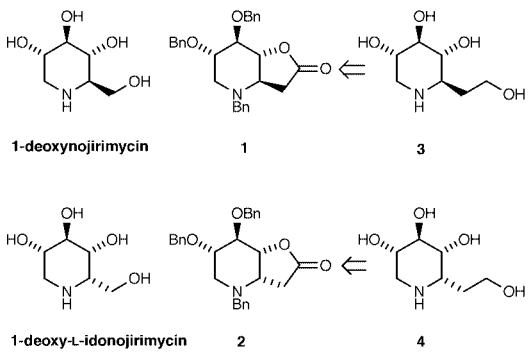

Fig. 1 Homologues of 1-deoxynojirimycin and 1-deoxy-L-idonojirimycin.

† Part of PhD Thesis of P. S. E-mail: szol@chelin.chtf.stuba.sk

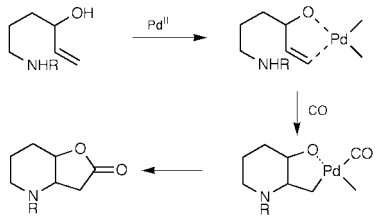

Scheme 1

Thus, the key substrate **10** was prepared by analogy with the known procedure according to the literature:[12] benzylidenation of the starting methyl-α-D-glucoside **5** afforded the diol **6**, which was subsequently benzylated to a fully-protected compound **7**. Acidic hydrolysis of **7** and nucleophilic displacement of the primary hydroxy function of **8** yielded bromide **9**, the latter being finally converted to the desired (2*S*,3*S*,4*R*)-*N*-benzyl-2,3-di-*O*-benzyl-2,3,4-trihydroxyhex-5-enylamine **10**.

First attempts to cyclise **10** under standard carbonylation conditions[11a] (1 atm CO, 0.1 equiv. $PdCl_2$, 3 equiv. $CuCl_2$, 3 equiv. AcONa, AcOH, conditions A) at room temperature failed and always the starting material was isolated. Gratifyingly, simply raising of temperature to 50 °C led to the complete consumption of aminoalkene **10** while the colour of the reaction mixture changed from dark green to ochre. However, aminocarbonylation of **10** yielded a complex mixture of compounds from which desired lactones **1** and **2** were isolated in the ratio 1 : 4.8 as main products. The major by-product of the reaction turned out to be *N*-benzyl-2,3-di-*O*-benzyl-6-chloro-1,6-dideoxy-L-idonojirimycin **11**‡ (Scheme 2).

We then searched for reaction conditions that would produce more of lactone **1** than **2** and suppress the formation of the side product **11**. We were pleased to find that a catalytic system consisting of 0.1 equiv. $PdCl_2$, 1 equiv. *p*-benzoquinone, 2 equiv. LiCl, 2 equiv. AcONa in THF under 1 atm CO at room temperature (conditions B) afforded a mixture of lactones **1** and **2** in the ratio 3.7 : 1 with no formation of **11**. Our suspicion that $CuCl_2$ (used in excess as reoxidant) might be responsible for the formation of undesired **11** was thus proved. The definitive confirmation came from the experiment in which aminoalkene **10** was subjected to conditions A but with exclusion of CO atmosphere. The only product we were able to isolate was the chloroderivate **11**§ (Scheme 3).

The separation and purification of **1** and **2** by FLC and subsequent reduction of both lactone rings gave the piperidine

DOI: 10.1039/a908449e

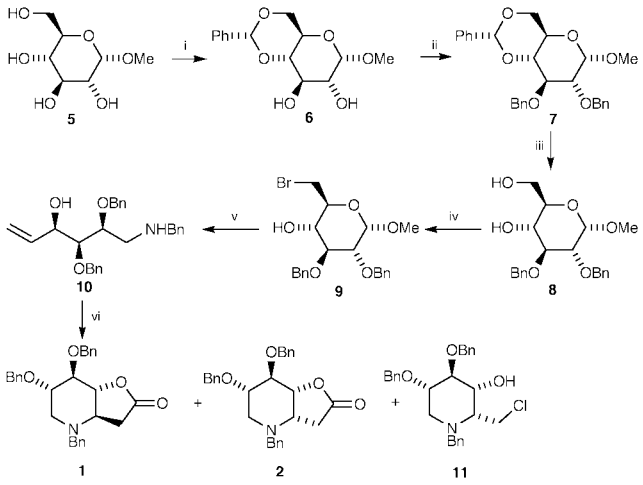

Scheme 2 *Reagents and conditions*: i, $PhCH(OEt)_2$, cat. CSA, $CHCl_3$, 81%; ii, BnBr, NaH, DMF, 75%; iii, H_2SO_4, MeOH, 97%; iv, Ph_3P, CBr_4, pyridine, 79%; v, Zn dust, $BnNH_2$, $NaBH_3CN$, PrOH–H_2O (19:1), 64%; vi, conditions A, 50 °C, 4–7 h, FLC, 46% of **1** + **2** (dr = 1:4.8), 9% of **11** or conditions B, room temp., 17 h, FLC, 66% of **1** + **2** (dr = 3.7:1).

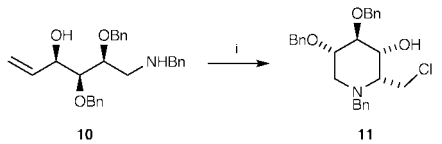

Scheme 3 *Reagents and conditions*: i, conditions A without CO, room temp., 48 h, FLC, 70%.

diols **12** [mp = 97–98 °C; $[\alpha]_D^{31}$ −19.4 (*c* 0.29, CH_2Cl_2); *m/z* 417 (M − $CH_2OH)^+$] and **13** [$[\alpha]_D^{31}$ −1.32 (*c* 0.34, CH_2Cl_2); *m/z* 447 (M − $1)^+$]. Final catalytic debenzylation of both tetraols afforded the desired (2*R*,3*R*,4*R*,5*S*)-2-(2-hydroxyethyl)-3,4,5-trihydroxypiperidine **3** [mp 177–179 °C; $[\alpha]_D^{26}$ +30 (*c* 0.55, MeOH); *m/z* 177 (M − $HCl)^+$] and (2*S*,3*R*,4*R*,5*S*)-2-(2-hydroxyethyl)-3,4,5-trihydroxypiperidine **4** (mp 202–203 °C; $[\alpha]_D^{32}$ +20.2 (*c* 0.42, MeOH); *m/z* 177 (M − $HCl)^+$] as hydrochlorides (Scheme 4).¶

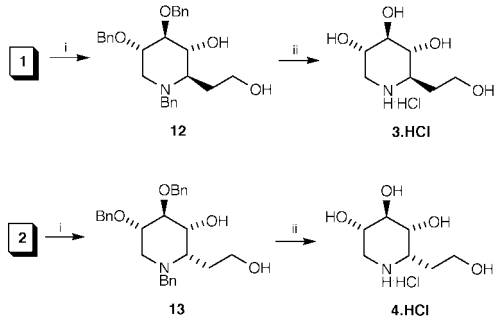

Scheme 4 *Reagents and conditions*: i, $LiBH_4$, THF, room temp., 64–65% ii, H_2, 10% Pd/C, MeOH, HCl, room temp., DOWEX (H^+), 82–90%.

In conclusion, we have performed the first successful Pd^{II}-catalysed aminocarbonylation of highly substituted 4-hydroxyhex-5-enylamine that contains a Bn-protected amine group.‖ In contrast to the literature precedents,[10,11] we observed the formation of both diastereoisomeric *cis*- and *trans*-fused piperidine lactones. Their ratio depended on the reaction conditions and these compounds represent direct precursors for the synthesis of new derivatives of polyhydroxylated piperidines. The applicability of this methodology has been demonstrated in the total synthesis of new C-6 homologues of 1-deoxynojirimycin (**3**) and 1-deoxy-L-idonojirimycin (**4**).

In addition, we have observed an interesting type of $PdCl_2$/$CuCl_2$ catalysed chloroaminocyclisation of substituted 4-hydroxyhex-5-enylamine producing the corresponding piperidine derivative **11** which could be useful in the synthesis of various piperidine and azepine alkaloids.[13] Investigation of the scope and limitations of the presented methodology is under progress and will be reported in due course.

We are grateful to Professor V. Jäger (Stuttgart) for very helpful ideas, discussions and unlimited support. This research was supported by VW Stiftung (Hannover) and The Slovak Grant Agency. We thank TauChem Ltd. (Bratislava) for providing us with carbon monoxide and to Dr Zálupsky for language corrections.

Notes and references

‡ The ratio of diastereoisomeric lactones **1** and **2** was determined by quantitative ^{13}C NMR spectroscopy with suppressed NOE effect. *Selected data* for **1**: $[\alpha]_D^{24}$ −64.9 (*c* 1.23, CH_2Cl_2); *m/z* 443 (M − $1)^+$. For **2**: $[\alpha]_D^{30}$ −6.05 (*c* 0.74, CH_2Cl_2); *m/z* 444 $(M)^+$. For **11**: $[\alpha]_D^{25}$ +35.1 (*c* 0.7, CH_2Cl_2); *m/z* 451 (M − $1)^+$. The relative configurations of **1**, **2** and **11** were established on the basis of NOESY and DIFNOE NMR experiments.

§ An analogous transformation using $PdCl_2(PhCN)_2$ and $CuCl_2$ in PrCN has been reported. However, neither the configuration of the product(s) nor the diastereoisomeric excess were given: M. Wada, H. Aiura and K. Akiba, *Heterocycles*, 1987, **26**, 929.

¶ All new compounds exhibit satisfactory elemental analyses and spectroscopic data. The absolute configuration of **3**·**HCl** was determined by single X-ray analysis (ref. 14).

‖ The benzylamino group was used in a similar type of process for the cyclisation of more reactive allenes that produced esters rather than lactones: T. Gallagher, I. W. Davies, S. W. Jones, D. Lathbury, M. F. Mahon, K. C. Molloy, R. W. Shaw and P. Vernon, *J. Chem. Soc., Perkin Trans 1*, 1992, 433.

1 B. Winchester and G. W. J. Fleet, *J. Glycobiol.*, 1992, **2**, 199; M. L. Sinnot, *Chem. Rev.*, 1990, **90**, 1171.
2 E. Truscheit, W. Frommer, B. Junge, L. Müller, D. D. Schmidt and W. Wingender, *Angew. Chem., Int. Ed. Engl.*, 1981, **20**, 744.
3 M. J. Humphries, K. Matsumoto and S. L. White, *Cancer Res.*, 1986, **46**, 5215.
4 A. Karpas, G. W. J. Fleet, R. A. Dwek, S. Petursson, S. K. Namgoong, N. G. Ramsden, G. S. Jacob and T. W. Rademacher, *Proc. Natl. Acad. Sci. U.S.A.*, 1988, **85**, 9229.
5 I. Lundt and R. Madsen, *Synthesis*, 1995, 787; C. Herdeis and T. Schiffer, *Tetrahedron*, 1996, **52**, 14 745.
6 G. Rassu, L. Pinna, N. Culeddu, G. Casiraghi, G. Gasparri Fava, M. Belicchi Ferrari and G. Pelosi, *Tetrahedron*, 1992, **48**, 727; J. P. Shilvock, K. Y. Hsia, R. J. Nash, J. D. Lloyd, A. L. Winters, N. Asano and G. W. J. Fleet, *Tetrahedron: Asymmetry*, 1998, **9**, 4157.
7 Y. Chen and P. Vogel, *J. Org. Chem.*, 1994, **59**, 2487; S. Picasso, Y. Chen and P. Vogel, *Carbohydr. Lett.*, 1994, **1**, 1; A. Baudat, S. Picasso and P. Vogel, *Carbohydr. Res.*, 1996, **281**, 277.
8 A. Kilonda, F. Compernolle, S. Toppet and G. J. Hoornaert, *Tetrahedron Lett.*, 1994, **35**, 9047; F. Compernolle, G. Joly, K. Peeters, S. Toppet, G. J. Hoornaert, A. Kilonda and B. Babady, *Tetrahedron*, 1997, **53**, 12 739.
9 Y. Tamaru, T. Kobayashi, S. Kawamura, H. Ochiai and Z. Yoshida, *Tetrahedron Lett.*, 1985, **26**, 4479; Y. Tamaru and Z. Yoshida, *J. Organomet. Chem.*, 1987, **334**, 213; W. Hümmer, E. Dubois, T. Gracza and V. Jäger, *Synthesis*, 1997, 634.
10 V. Jäger, T. Gracza, E. Dubois, T. Hasenöhrl, W. Hümmer, U. Kautz, B. Kirschbaum, A. Lieberknecht, L. Remen, D. Shaw, U. Stahl and O. Stephan, *Pd(II)-Catalyzed Carbonylation of Unsaturated Polyols and Aminopolyols*, in *Organic Synthesis via Organometallics OSM 5*, Vieweg, Germany, 1997, p. 331.
11 (*a*) Y. Tamaru, M. Hojo and Z. Yoshida, *J. Org. Chem.*, 1988, **53**, 5731; (*b*) Y. Tamaru and M. Kimura, *Synlett*, 1997, 749.
12 R. C. Bernotas, M. A. Pezzone and B. Ganem, *Carbohydr. Res.*, 1987, **167**, 305; R. C. Bernotas, *Tetrahedron Lett.*, 1990, **31**, 469.
13 T. Morie and S. Kato, *Heterocycles*, 1998, **48**, 427.
14 M. Koman, P. Szolcsányi and T. Gracza, submitted for publication.

Communication a908449e

ChemComm

Selective signalling of zinc ions by modulation of terbium luminescence†

Ofer Reany,[a] Thorfinnur Gunnlaugsson[ab] and David Parker*[a]

[a] *Department of Chemistry, University of Durham, South Road, Durham, UK DH1 3LE. E-mail: david.parker@durham.ac.uk*

[b] *Department of Chemistry, Trinity College Dublin, Dublin 2, Eire*

Received (in Cambridge, UK) 10th January 2000, Accepted 16th February 2000, Published on the Web, 2nd March 2000

Luminescence enhancement of terbium emission accompanies zinc ion binding at pH 7.4 with an apparent dissociation constant of 0.6 μM in a competitive ionic background.

Responsive luminescent lanthanide complexes have been defined recently in which the concentration variation of certain analytes has been signalled by changes in emission intensity,[1] lifetime[1,2] or polarisation.[3] For this purpose, kinetically robust complexes of Eu and Tb have been studied in particular and systems that respond to changes in pH,[4] pO_2[2,5] and pX[6] in water have been reported. We set out to prepare analogous complexes which respond sensitively and selectively to changes in metal ion concentration, in competitive aqueous media at physiological pH. The signalling of zinc ion concentration is of particular interest in this respect. Although total [Zn^{2+}] have long been established to be *ca.* 12 μM in serum,[7] there is considerable interest in defining the concentration of 'available' Zn^{2+}—both in the extracellular and intracellular environments. Different approaches have been adopted,[8,9] of which the most advanced involve the use of fluorescent 8-tosylamide-quinoline derivatives.[10,11] In seeking to prepare a suitable complex, the requirement for selectivity over Na^+, K^+ and more particularly Mg^{2+} (*ca.* 0.9 mM) and Ca^{2+} (1.2 mM extracellular; < 0.1 μM intracellular) was evident. Accordingly, we resolved to prepare the ligand L^{1a} and explore the complexation behaviour of the Eu and Tb complexes in the macrocyclic derivative L^2, as model systems for selective zinc binding.

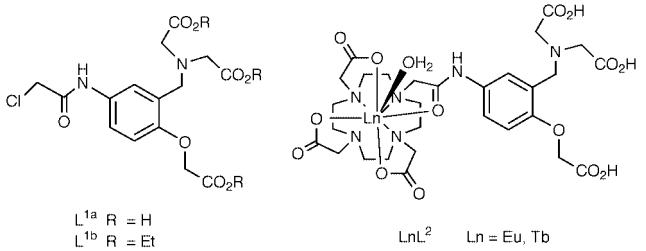

Stepwise alkylation of *o*-aminomethylphenol ($BrCH_2CO_2Et$, 5% KI, Na_2HPO_4; *O*-alkylation with $BrCH_2CO_2Et$, KI, K_2CO_3) followed by mild nitration (HNO_3–HOAc; −20 °C) yielded an intermediate nitro-ester which was reduced (H_2/Pd–C/MeOH) and acylated with chloroacetyl chloride (Et_3N, DEE) to yield the triethyl ester L^{1b}. Basic hydrolysis of L^{1b} (pH 12, 20 °C, aq. NaOH) afforded the amino acid L^{1a} which was purified by ion-exchange chromatography. Reaction of L^{1b} with 1,4,7-tris(*tert*-butoxycarbonylmethyl)-1,4,7,10-tetraazacyclododecane (MeCN, K_2CO_3) followed by treatment with CF_3CO_2H–CH_2Cl_2 and complexation with $Ln(NO_3)_3{\cdot}5H_2O$ (Ln = Eu, Tb; pH 5.5; 20 °C) gave the neutral lanthanide complexes; successive treatment with aqueous sodium hydroxide and then strong-acid cation exchange resin afforded the desired lanthanide complexes, [LnL^2].[12] Measurements of the rate constants for decay of the Eu or Tb excited state were made in H_2O and D_2O in the absence and presence of 10 mM $ZnCl_2$. Values for [EuL^2] (k_{H_2O} = 1.61, k_{D_2O} = 0.45 ms^{-1}; *q* (Ln hydration state) = 1.0[13]) were unchanged in the presence of zinc and data for [TbL^2] (k_{H_2O} = 0.55, k_{D_2O} = 0.29; *q* = 1.0) were similarly unaffected by addition of $ZnCl_2$ or $CaCl_2$.

Addition of $ZnCl_2$ to L^{1a} or [LnL^2] was monitored by changes in absorption, fluorescence and lanthanide emission at pH 7.4. The ligand L^{1a} absorbed at 248 nm and no change to the position and intensity of this band occurred on ion binding, suggesting that the aryl ether oxygen was not participating in ion binding. For [TbL^2], a small blue-shift was observed in absorption (λ_{max} 255 → 250 nm); in fluorescence emission two bands were observed at 440 nm and a second, half as intense at 365 nm, which may be ascribed to internal charge transfer and locally excited states, respectively. On binding zinc, the former band shifted (442 → 430 nm) and reduced in intensity, while the latter did not shift but increased in intensity. Zinc binding was also characterised by a small increase in absorbance ($\lambda_{max.}$ = 250 nm) and with a larger enhancement of lanthanide emission intensity, following excitation at the isosbestic wavelength (262 nm). Smaller changes in absorption and emission spectra were obtained following addition of $CaCl_2$ (*e.g.* < 3 nm shift in absorption $\lambda_{max.}$) and no significant variations in absorption wavelength were observed following $MgCl_2$ addition, consistent with reduced or insignificant aryl ether oxygen donation, in these cases. The enhancement of Tb (and Eu) emission intensity (26 and 42%, respectively) upon Zn^{2+} binding is likely to be related to suppression of a photo-induced electron transfer from the benzylic nitrogen to the intermediate aryl singlet excited state.[1,2] In addition for [EuL^2], the metal based emission and ligand based fluorescence intensity was *ca.* 20 times lower than for [TbL^2], owing to quenching of the intermediate singlet state by the Eu^{3+} ion.

Such spectral changes allowed titrations to be carried out, monitoring absorption and luminescence intensity variations as a function of added metal salt concentration. The data obtained reveal a consistent selectivity pattern (Table 1), with Zn^{2+} bound more strongly than Ca^{2+} or Mg^{2+} ions. Two other general features emerged from this analysis: metal ion complexation of the linking amide carbonyl enhanced the ion-binding affinity of the potentially pentadentate ligand and a slightly higher apparent affinity was also found in the excited state for the lanthanide complexes, *i.e.* when observing ligand or lanthanide emission intensity variations. The lanthanide ion may serve to promote intramolecular charge transfer involving conjugation of the ether oxygen lone pair in the ground and excited states, *via* a through-ring electron withdrawing effect. This may also lead to a better orientation of the oxygen lone pair, in those cases (*e.g.* Zn^{2+} binding) where chelation of the benzylic N and the aryl ether O occurs. Such behaviour allowed zinc concentrations to be monitored in the sub-micromolar range, even in a simulated extracellular environment, *i.e.* the presence of 0.9 mM $MgCl_2$, 1.26 mM $CaCl_2$, 140 mM NaCl and 4 mM KCl, with an apparent dissociation constant of 0.6 μmol (pH 7.4, 295 K). The observed zinc ion sensitivity and selectivity with [TbL^2] augur well for the development of practicable signalling

† Electronic supplementary information (ESI) available: representative examples of spectral changes and of data analysis. See http://www.rsc.org/suppdata/cc/b0/b000283f/

DOI: 10.1039/b000283f

Table 1 Affinity constants (log β_{ML}) for cation binding, based on modulation[c] of absorption (S_0) or lanthanide (Ln*) luminescence[d] (295 K, 10 mM HEPES, 20 mM NaCl, 115 mM KCl, pH 7.4[a])

Ligand/complex (parameter)	Zn^{2+}	Ca^{2+}	Mg^{2+}
$L^1(S_0)$	5.04	3.91	2.1
$[TbL^2](S_0)$	5.48	3.84	2.0
$[TbL^2]$(Tb*)	6.35[b]	4.03	2.5
$[EuL^2](S_0)$	5.38	3.90	2.1
$[EuL^2]$(Eu*)	5.99	4.06	1.9

[a] Potentiometric titration of L^1 (298 K, I = 0.1 M NMe_4NO_3) revealed a pK_a for N-protonation of 7.35, echoed by the pH variation of ligand absorption; for binding constant measurements, the pH was adjusted to 7.4 by addition of 'Tris' base and was also monitored at the end of the titration. [b] In a simulated extracellular environment (Na, K, Mg, Ca), the apparent binding affinity for $[TbL^2]$, based on Tb emission intensity changes, was 6.22. [c] Binding constants were obtained by iterative least-squares fitting to a 1:1 model and showed reasonably good agreement to Hill plot analysis. [d] Excitation of the Ln complexes was effected at the isosbestic wavelength (λ_{exc} = 262 nm), while absorption spectral changes were monitored at 240 or 250 nm (294 nm for L^1). Excitation was also performed in the tail at 320 nm and emission variation as a function of $[M^{2+}]$ gave slightly higher binding affinities, *e.g.* for Ca^{2+}; 4.37 with $[TbL^2]$ and 4.67 with $[EuL^2]$ with a luminescence enhancement of 20%.

systems, in which longer wavelength excitation is of course required and where changes in the form of the lanthanide emission are desirable.

We thank BBSRC for support.

Notes and references

1 A. P. de Silva, D. B. Fox, A. J. M. Huxley, N. D. McClenaghan and J. Roiron, *Coord. Chem. Rev.*, 1999, **185–186**, 297; for examples of Na/K perturbing Ln luminescence in methanol: A. P. de Silva, H. Q. N. Gunaratne, T. E. Rice and S. Stewart, *Chem. Commun.*, 1997, 1891.
2 D. Parker, K. Senanayake and J. A. G. Williams, *J. Chem. Soc., Perkin Trans. 2*, 1998, 2129.
3 R. S. Dickins, T. Gunnlaugsson, D. Parker and R. D. Peacock, *Chem. Commun.*, 1998, 1643.
4 T. Gunnlaugsson and D. Parker, *Chem. Commun.*, 1998, 511; T. Gunnlaugsson, D. Parker and D. A. McDonaill, *Chem. Commun.*, 2000, 93.
5 D. Parker and J. A. G. Williams, *Chem. Commun.*, 1998, 245.
6 D. Parker, K. Senanayake and J. A. G. Williams, *Chem. Commun.*, 1997, 1777.
7 M. M. Parker, F. L. Humaller and D. J. Mahler, *Clin. Chem.*, 1967, **13**, 40.
8 J. D. Stewart, V. A. Roberts, M. W. Crowder, E. D. Getzoff and S. J. Benkovic, *J. Am. Chem. Soc.*, 1994, **116**, 415; A. Godwin and J. M. Berg, *J. Am. Chem. Soc.*, 1996, **118**, 6514; P. S. Eis and J. R. Lakowicz, *Biochemistry*, 1993, **32**, 7981; B. Imperiali and G. K. Walkup, *J. Am. Chem. Soc.*, 1997, **119**, 3443.
9 F. Barigeletti, L. Flamigni, G. Calogero, L. Hammerström, J.-P. Sauvage and J.-P. Collin, *Chem. Commun.*, 1998, 2333.
10 P. D. Zalewski, I. J. Forbes and W. H. Betts, *Biochem. J.*, 1993, **296**, 403; P. Coyle, P. D. Zalewski, J. C. Philcox, I. J. Forbes, A. D. Ward, S. F. Lincoln, I. Mahadevan and A. M. Rofe, *Biochem. J.*, 1994, **303**, 781.
11 K. M. Hendrickson, T. Rodopoulos, P.-A. Pilfet, I. Mahadevan, S. F. Lincoln, A. D. Word, T. Kurucsev, P. A. Duckworth, I. J. Forbes, P. D. Zalewski and W. H. Betts, *J. Chem. Soc., Dalton Trans.*, 1997, 3879.
12 Complexes gave accurate masses (ESMS$^-$), ^{1}H NMR and micro-analytical data in accord with the proposed structures: *e.g.* $[EuL^2]$: *m/z* (ESMS$^-$) 847.1660, ($C_{29}H_{39}EuN_6O_{14}$ −H) requires 847.1659. L^{1a}: Found: C, 39.2, H, 6.34; N, 12.3. Calc.(as bisammonium salt dihydrate): C, 39.3; H, 5.93; N, 12.2%. $[TbL^2]$: *m/z* (ESMS$^-$) 853.1692; ($C_{29}H_{39}TbN_6O_{14}$ –H) requires 853.1699.
13 A. Beeby, I. M. Clarkson, R. S. Dickins, S. Faulkner, D. Parker, L. Royle, A. S. de Sousa, J. A. G. Williams and M. Woods, *J. Chem. Soc., Perkin Trans. 2.*, 1999, 493.

Communication b000283f

Intramolecular Diels–Alder reactions of masked *p*-benzoquinones: a novel methodology for the synthesis of highly functionalized *cis*-decalins

Yow-Fu Tsai, Rama Krishna Peddinti and Chun-Chen Liao*

Department of Chemistry, National Tsing Hua University, Hsinchu, Taiwan 300. E-mail: ccliao@mx.nthu.edu.tw

Received (in Cambridge, UK) 4th January 2000, Accepted 25th January 2000, Published on the Web, 2nd March 2000

Tethering of dienols to hydroquinones under Mitsunobu conditions followed by oxidation with diacetoxyiodobenzene in methanol resulted in the development of highly functionalized *cis*-decalins *via* intramolecular Diels–Alder reactions of *in situ* generated masked *p*-benzoquinones.

Because of their widespread occurrence in a large variety of natural products of biological importance, decalins remain a focus of attention for synthetic organic chemists.[1–3] Functionalized decalins with proper stereochemistry are possible intermediates for several terpenoids possessing biological activity. Not surprisingly, there has been a great deal of interest in developing methodologies for their synthesis, as evidenced by the growing number of reports in this area.[4–8] Most recently, we have shown that masked *o*-benzoquinones (MOBs), *i.e.*

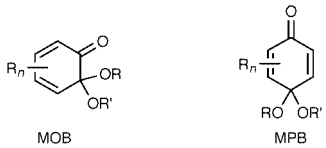

6,6-dialkoxycyclohexa-2,4-dienones, are efficient intermediates for the stereoselective synthesis of highly functionalized *cis*-decalins.[9] Herein, we report a novel method for the synthesis of highly functionalized decalins *via* the intramolecular Diels–Alder (IMDA) reactions of *in situ* generated masked *p*-benzoquinones (MPBs), a class of cross-conjugated cyclohexadienones. To the best of our knowledge this is the first detailed study of IMDA reactions of MPBs.[10]

Over the past ten years we have been investigating the inter- and intra-molecular Diels–Alder reactions of MOBs[11] and their synthetic potential has been exploited.[12] In contrast to the case of MOBs, the Diels–Alder chemistry of MPBs is less explored.[13] This may be due to the fact that the lesser reactivity of MPBs often requires harsh reaction conditions like high pressure[13*a*] or high temperature[13*c*,*d*] with prolonged reaction times. We envisioned that this problem could possibly be overcome by performing these reactions in an intramolecular fashion[14] *via* the *in situ* generation of MPBs by oxidizing *p*-methoxyphenols with diacetoxyiodobenzene (DAIB) in the presence of a dienol in a tandem oxidative acetalization process that would furnish stereoselective and highly functionalized *cis*-decalins.

As a prelude to this objective, we have carried out the reactions of *p*-methoxyphenols **1** and **2** with 10 equiv. of sorbic alcohol (**6**) in the presence of DAIB in different solvents, such as THF, CF_3CH_2OH and CH_2Cl_2. We have isolated the adducts **3** formed *via* IMDA reaction of *in situ* generated MPBs in rather poor yields (Scheme 1). Although the reasons for the lower reactivity of **1** and **2** with **6** are not known at this point, it is apparent that, unlike 2-methoxyphenols,[11*b*] 4-methoxyphenols cannot undergo facile tandem IMDA reactions. Consequently, we have switched our attention to tethering[15] the diene moiety to the hydroquinones *via* Mitsunobu reaction with dienols prior to oxidation by DAIB. For this purpose, we have performed the reactions of hydroquinone **4** and dienols **5**–**6** under Mitsunobu conditions to obtain the products in 38–55% yields (Scheme 2).

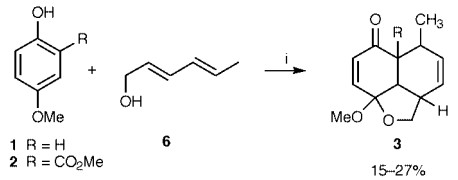

Scheme 1 *Reagents and conditions*: i, DAIB, solvent, room temp., 2 h.

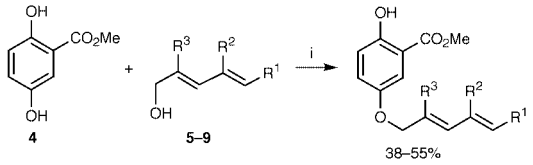

Scheme 2 *Reagents and conditions*: i, PPh_3, DEAD, THF.

Attempts to improve the yields by changing the reaction conditions were not successful. The use of DIAD in place of DEAD produced slightly better yields. However, we have conveniently produced the required phenols **13b**–**27b** by choosing selectively protected hydroquinones **10**–**12** as starting materials for Mitsunobu reaction followed by saponification in very good yields (Scheme 3, Table 1).

Masked *p*-benzoquinones **13c**–**27c** generated *via* oxidation of phenols **13b**–**27b** (0.5 mM) in MeOH (50 ml) using DAIB (0.75 mM) as oxidant underwent intramolecular cyclization at room temperature (Method A), or at reflux temperature in benzene (Method B) or in toluene (Method C) to afford the cycloadducts **13d**,**e**–**27d**,**e** in 78–90% yield (Scheme 3). Table 2 illustrates typical results of the IMDA reactions of MPBs.

The gross structures of all the IMDA adducts were determined by their IR, ^{1}H and ^{13}C NMR, DEPT, low- and high-resolution mass spectral analyses. The stereochemistries of

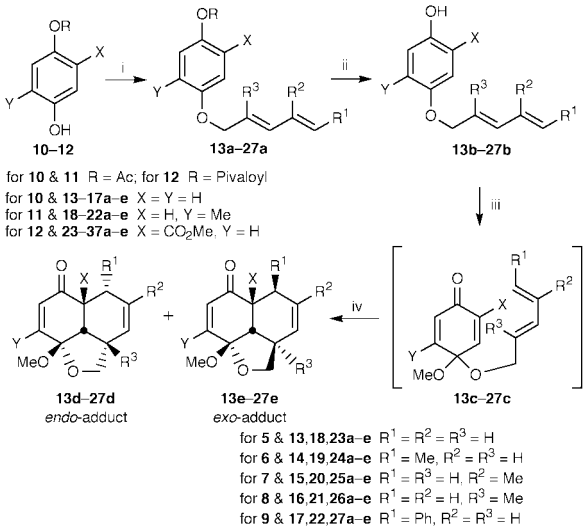

Scheme 3 *Reagents and conditions*: i, PPh_3, DIAD, THF, **5**–**9**; ii, K_2CO_3, MeOH, 0 °C; iii, DAIB, MeOH; iv, Methods A–C.

DOI: 10.1039/b000248h

Table 1 Synthesis of phenols **13b**–**27b**

Phenols **10**–**12**	Dienols **5**–**9**	Dienyl ethers **13a**–**27a** (% yield)	Phenols **13b**–**27b** (% yield)
10	**5**	**13a** (82)	**13b** (98)
	6	**14a** (86)	**14b** (98)
	7	**15a** (84)	**15b** (97)
	8	**16a** (87)	**16b** (99)
	9	**17a** (78)	**17b** (99)
11	**5**	**18a** (87)	**18b** (81)
	6	**19a** (85)	**19b** (85)
	7	**20a** (85)	**20b** (85)
	8	**21a** (83)	**21b** (88)
	9	**22a** (74)	**22b** (76)
12	**5**	**23a** (85)	**23b** (98)
	6	**24a** (83)	**24b** (96)
	7	**25a** (85)	**25b** (97)
	8	**26a** (83)	**26b** (97)
	9	**27a** (75)	**27b** (99)

Table 2 IMDA reactions of MPBs **13c**–**27c** generated from phenols **13b**–**27b**

Entry	Phenol	MPB	Method[a]	DA adduct	Yield (%)	*endo*:*exo*[b]
1	**13b**	**13c**	B	**13d** + **e**	88	1:1
2	**14b**	**14c**	A	**14d**	90	1:0
3	**15b**	**15c**	B	**15d** + **e**	85	3:1
4	**16b**	**16c**	C	**16d**	80	1:0
5	**17b**	**17c**	A	**17d**	78	1:0
6	**18b**	**18c**	B	**18d** + **e**	85	1:1
7	**19b**	**19c**	A	**19d**	84	1:0
8	**20b**	**20c**	B	**20d** + **e**	88	2.5:1
9	**21b**	**21c**	C	**21d**	79	1:0
10	**22b**	**22c**	A	**22d**	79	1:0
11	**23b**	**23c**	A	**23d** + **e**	83	1:1
12	**24b**	**24c**	A	**24d** + **e**	87	1.2:1
13	**25b**	**25c**	A	**25d** + **e**	88	2.5:1
14	**26b**	**26c**	C[c]	**26d**	83	1:0
15	**27b**	**27c**	A	**27d** + **e**	82	1:1

[a] All MPBs were generated at 0 °C and after usual workup, the crude residue was used as such for Methods B and C. Method A: room temp., 15 min; Method B: benzene, reflux, 4 h; Method C: toluene, reflux, 40 h. [b] Determined by ^{1}H NMR. [c] Reaction time: 18 h.

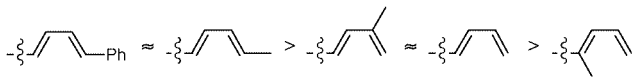

Fig. 1 Reactivity series for the diene moiety.

endo-adducts **14d**, **16d**, **17d**, **19d**, **21d**, **22d** and **26d** were established by NOE studies. The *endo*-adduct **25d** and the *exo*-adduct **25e** were separated from their mixture **25d** + **e** by recrystallizing from hexane–Et_2O to afford the former as an oil and the latter as crystals, and their stereochemistry was deduced from NOE studies. The stereochemistry of **25e** was further confirmed from its single crystal X-ray structure.[16] The *endo* and *exo* ratios of cycloadducts from entries 1, 3, 6, 8, 11–13 and 15 were determined from their ^{1}H NMR (400 MHz) spectra.

In the IMDA reactions of unsymmetrical MPBs **18c**–**22c** and **23c**–**27c**, the double bond with less electron density, *i.e.* the unsubstituted double bond in **18c**–**22c** and the CO_2Me-substituted double bond in **23c**–**27c**, behaved as a dienophile. The IMDA reactions of MPBs **23c**–**27c** bearing an additional electron-withdrawing group (CO_2Me) (entries 11–15) are faster than those of **13c**–**22c** (entries 1–10), where such a group is not present. The two sets of MPBs **13c**–**22c** and **23c**–**27c** show comparable reactivities. It appears that the reactivity pattern mainly depends on the tethered diene unit and could be explained on the basis of the position of the substituents attached to the diene moiety,[17] as shown in Fig. 1.

In most of the cases studied, the *endo*-adduct was obtained as either the sole product or the predominant product. The

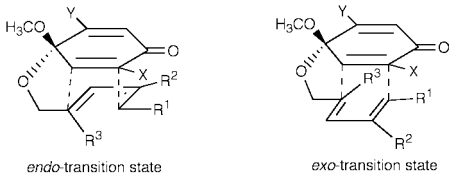

Fig. 2 Diels–Alder transition states.

transformation of transoid to cisoid conformation of the diene units in MPBs **16c**, **21c** and **26c** (R^1 = R^2 = H, R^3 = Me) required for Diels–Alder reaction needs more energy as reflected by the reaction conditions employed (entries 4, 9 and 14). Owing to the disfavored interactions in their *exo*-transition states (Fig. 2), *endo*-adducts **16d**, **21d** and **26d** were formed exclusively in these reactions.

In summary, we have shown for the first time that masked *p*-benzoquinones tethered to a diene moiety undergo efficient intramolecular cyclization to produce highly functionalized *cis*-decalins in very good yields. Our methodology provides an easy access to a series of stereoselective *cis*-decalins attached to five-membered oxygen heterocycles which may otherwise be difficult to synthesize. Further applications of MPBs in organic synthesis are under investigation in our laboratory.

We thank the National Science Council (NSC) of the Republic of China for financial support. R. K. P. thanks the NSC for a post-doctoral fellowship.

Notes and references

1 J. R. Hanson, *Nat. Prod. Rep.*, 1999, **16**, 209 and references therein.
2 S. V. Ley, A. A. Denholm and A. Wood, *Nat. Prod. Rep.*, 1993, **10**, 109.
3 A. T. Merritt and S. V. Ley, *Nat. Prod. Rep.*, 1992, **9**, 243.
4 R. B. Grossman, R. M. Rasne and B. O. Patrick, *J. Org. Chem.*, 1999, **64**, 7173.
5 K. Ohrai, K. Kondo, M. Sodeoka and M. Shibasaki, *J. Am. Chem. Soc.*, 1994, **116**, 11 737.
6 O. Z. Pereira and T. H. Chan, *J. Org. Chem.*, 1994, **59**, 6710.
7 H.-J. Liu and Y. Han, *Tetrahedron Lett.*, 1993, **34**, 423.
8 G. Müller and G. Jas, *Tetrahedron Lett.*, 1992, **33**, 4417.
9 P. D. Rao, C.-H. Chen and C.-C. Liao, *Chem. Commun.*, 1998, 155; P.-Y. Hsiu and C.-C. Liao, *Chem. Commun.*, 1997, 1085; T.-H. Lee, C.-C. Liao and W.-C. Liu, *Tetrahedron Lett.*, 1996, **37**, 5897.
10 A. E. Fleck, J. A. Hobart and G. W. Morrow, *Synth. Commun.*, 1992, **22**, 179.
11 (*a*) C.-C. Liao, C.-S. Chu, T.-H. Lee, P. D. Rao, S. Ko, L.-D. Song and H.-C. Shiao, *J. Org. Chem.*, 1999, **64**, 4102 and references therein; (*b*) C.-S. Chu, T.-H. Lee, P. D. Rao, L.-D. Song and C.-C. Liao, *J. Org. Chem.*, 1999, **64**, 4111; (*c*) M.-F. Hsieh, P. D. Rao and C.-C. Liao, *Chem. Commun.*, 1999, 1441; (*d*) C.-H. Chen, P. D. Rao and C.-C. Liao, *J. Am. Chem. Soc.*, 1998, **120**, 13 254.
12 W.-C. Liu and C.-C. Liao, *Chem. Commun.*, 1999, 117.
13 (*a*) E. R. Jarvo, S. R. Boothroyd and M. A. Kerr, *Synlett*, 1996, 897; (*b*) R. A. Russel, D. A. C. Evans and R. N. Warrener, *Aust. J. Chem.*, 1984, **37**, 1699; (*c*) M. C. Carreno, F. Farina, A. Galan and J. L. G. Ruano, *J. Chem. Res.*, 1981 (*S*) 370; (*M*) 4310; (*d*) M. C. Carreno, F. Farina, A. Galan and J. L. G. Ruano, *J. Chem. Res.*, 1979, (*S*) 296; (*M*) 3443.
14 W. R. Roush, *Combining C–C π-bonds*, in *Comprehensive Organic Synthesis*, ed. B. M. Trost, I. Fleming and L. A. Paquette, Pergamon, Oxford, 1991, vol. 5, ch. 4.1.
15 D. R. Gauthier Jr., K. S. Zandi and K. J. Shea, *Tetrahedron*, 1998, **54**, 2289; M. Bols and T. Skrydstrup, *Chem. Rev.*, 1995, **95**, 1253.
16 *Crystal data* for **25e**: $C_{15}H_{18}O_5$, M = 278.3. monoclinic, a = 9.1424(4), b = 11.5049(5), c = 13.4460(6) Å. β = 101.281(1)°, V = 1387.0(4) Å^3, T = 296 K, space group $P2_1/n$, Z = 4, μ(Mo-Kα) = 0.100 mm^{-1}. 8056 reflections measured, 3010 unique (R_{int} = 0.0325), final R indices [$I \geqslant 3\sigma(I)$] $R1$ = 0.0436, $wR2$ = 0.0492. CCDC 182/1531. See http://www.rsc.org/suppdata/cc/b0/b000248h/ for crystallographic files in .cif format.
17 R. Sustmann and R. Schubert, *Angew. Chem., Int. Ed. Engl.*, 1972, **11**, 840.

A facile preparation of transparent and monolithic mesoporous silica materials

Jie-Bin Pang,[a] Kun-Yuan Qiu,*[a] Yen Wei,*[b] Xiao-Jun Lei[c] and Zhong-Fan Liu[c]

[a] *Department of Polymer Science and Engineering, College of Chemistry and Molecular Engineering, Peking University, Beijing 100871, China. E-mail: kyqiu@chemms.chem.pku.edu.cn*
[b] *Department of Chemistry, Drexel University, Philadelphia, Pennsylvania 19104, USA. E-mail: weiyen@drexel.edu*
[c] *Center for Nanoscale Science and Technology, College of Chemistry and Molecular Engineering, Peking University, Beijing 100871, China*

Received (in Cambridge, UK) 2nd December 1999, Accepted 14th February 2000

Monolithic mesoporous silica samples of *ca.* 2 × 2 × 1 mm in dimension with large surface areas (> 900 m² g⁻¹) and pore volumes (> 0.80 cm³ g⁻¹) have been readily prepared *via* a sol–gel process in the presence of hydroxy-carboxylic acid compounds as non-surfactant templates, and their pore structure was observed directly by means of atomic force microscopy (AFM).

The synthesis and applications of mesoporous materials prepared using surfactants as templates have attracted great attention since the discovery of the M41S family of mesoporous molecular sieves by scientists at the Mobil Corporation.[1,2] So far, most synthetic methods typically yield products in the form of fine powders resulting from uncontrolled precipitation during the sol–gel synthesis or template removal. Such powder forms hamper their use in catalysis and separation technologies. For example, for potential use in membrane separation, it is important to be able to process mesoporous structures in the form of defect-free, oriented films. Mesostructured silica films with ordered or disordered mesopore channel arrangements have been prepared using surfactants as templates under very carefully controlled conditions.[3–6] Mesoporous silica materials with diverse and remarkable morphologies[7–9] have been prepared under some extreme synthetic conditions to prevent uncontrolled precipitation of the mesostructured silicates. However, the dimensions of the products which occur as hollow spheres, tubules or other shapes is still microscopic. Emulsion biphase chemistry has been demonstrated to yield hollow or hard mesoporous macroscale spheres.[10,11] Recently, Wei *et al.*[12,13] reported a non-surfactant templating route to mesoporous silica materials *via* a sol–gel process. Because of the mild conditions, this process facilitates the preparation of mesoporous silica bulk objects. Here, we present the synthesis of mesoporous silica samples of large size (*e.g.* 2 mm) *via* a non-surfactant sol–gel route with hydroxy-carboxylic acids as templates.

The synthetic procedure was similar to that in the literature.[12] The preparation of colourless, transparent disks (*ca.* 3 cm in diameter) of the template-containing silicas was achieved by HCl-catalyzed sol–gel reactions of tetraethyl orthosilicate (TEOS) in the presence of organic hydroxy-carboxylic acid compounds, *i.e.* citric acid (CA), lactic acid (LA), malic acid (MA) and tartaric acid (TA). In general, TEOS (Acros Organics, 98%) was prehydrolyzed with deionized water in ethanol using HCl as catalyst (at TEOS : HCl : H_2O : EtOH molar ratios of 1 : 0.01 : 4 : 3) at about 70 °C for 5–6 hours. Upon cooling to room temperature, the prehydrolyzed solution (*e.g.* 10.6 ml) was added to a designed volume of aqueous solution (*e.g.* 3 ml of 0.45 g ml⁻¹) of hydroxy-carboxylic acid compound under stirring. The transparent and monolithic template-containing silica disks were obtained after the gel formed and dried within about two months at room temperature. The template-containing silica disks were then broken into smaller pieces instead of being ground into fine powders as reported in the literature.[12] The transparent and monolithic mesoporous silica samples were readily obtained by removing the templates *via* Soxhlet

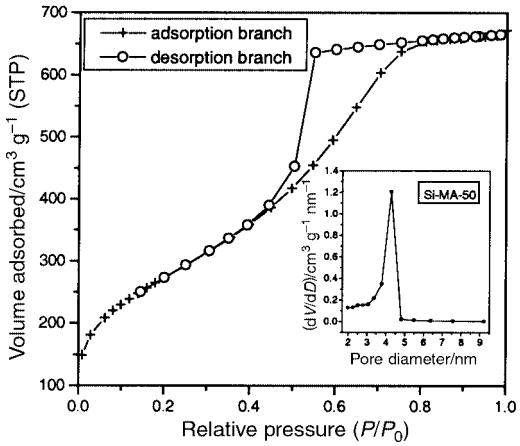

Fig. 1 Nitrogen adsorption–desorption isotherm for the sample Si-MA-50. Inset: BJH pore size distribution curve of the same sample.

Table 1 Physicochemical properties of the monolithic mesoporous silica materials

Sample code[a]	BET surface area/m² g⁻¹	Total pore volume/cm³ g⁻¹	Average pore diameter BET/nm	Average pore diameter BJH/nm	Micropore data[b] Surface area/ m² g⁻¹	Micropore data[b] Pore volume/ cm³ g⁻¹
Si-CA-50	959	0.888	3.7	3.6	42	0.0079
Si-LA-50	865	0.924	4.3	3.7	10	—
Si-MA-40	1053	0.863	3.3	3.4	24	—
Si-MA-50	991	1.028	4.1	3.8	30	0.0016
Si-MA-60	1030	1.474	5.7	4.8	22	—
Si-TA-50	911	0.977	4.3	3.9	42	0.0087

[a] The two letters in the middle of the sample codes are the abbreviations for the templates: CA = citric acid, LA = lactic acid, MA = malic acid, TA = tartaric acid. The numbers in the codes indicate the template concentrations (wt.%) in the template-containing silicas, as calculated from the feed composition under the assumption that TEOS is completely transformed into SiO_2. [b] The surface area and pore volume of micropores were obtained by t-plot analysis using the Harkins–Jura equation.

DOI: 10.1039/a909420b

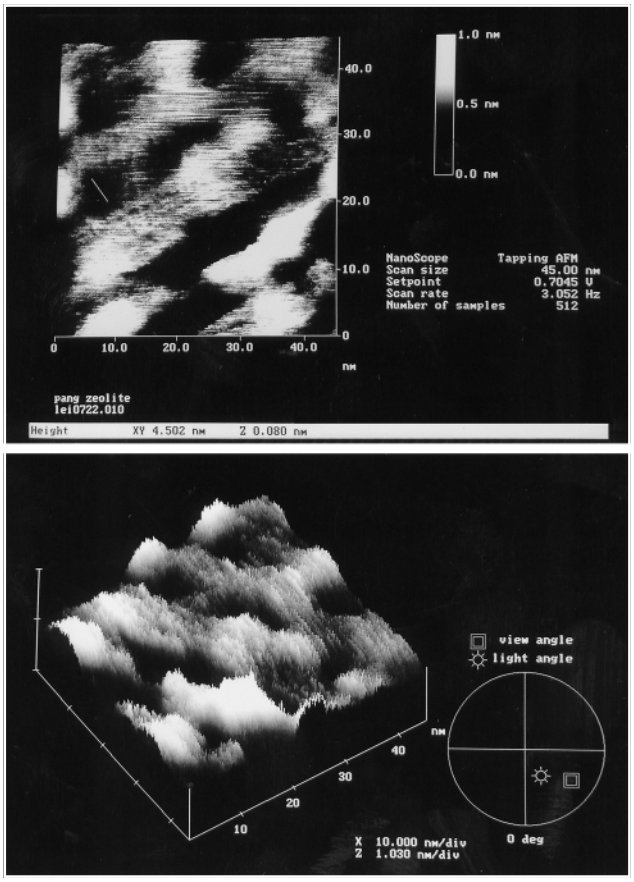

Fig. 2 AFM images of the surface of the sample Si-LA-50 (the scale bar in the top-view image is 4.50 nm).

extraction with ethanol for 3–4 days followed by drying. The samples before and after extraction were monitored by FTIR using a Bruker Vector22 FTIR spectrometer. Disappearance of the characteristic absorption band at *ca.* 1734 cm^{-1} for the carbonyl of the hydroxy-carboxylic acids indicated the completion of template removal. The Brunauer–Emmett–Teller (BET) surface area and pore parameters of the samples as small pieces after the removal of templates were determined by nitrogen adsorption–desorption isotherm measurements at 77 K on a Micromeritics ASAP2100 analyzer. Mesopore size distributions were calculated from the desorption branch of the isotherm by the Barrett–Joyner–Halenda (BJH) method using the Halsey equation. The AFM images were obtained on a Digital Instruments Nanoscope IIIa SPM by tapping mode AFM.

The BET surface area data and pore parameters of the silica samples after the removal of the templates are summarized in Table 1. Mesoporous materials with large surface areas (> 900 $m^2\ g^{-1}$) and pore volumes (> 0.80 $cm^3\ g^{-1}$) were obtained with CA, LA, MA or TA as template. As shown in the MA-templated synthesis, the pore diameter and volume tend to increase with the MA concentration. From the t-plot analysis with the Harkins–Jura equation, we conclude that the contributions from micropores to the measured surface areas and pore volumes are negligible.

The nitrogen adsorption–desorption isotherms of all the samples exhibit type IV-like isotherms with a sharp inflection at $P/P_0 \approx 0.5$ (type H2 hysteresis), as shown in Fig. 1. The pore size distributions are quite narrow in all the samples. As shown in the inset of Fig. 1, the pore size distribution has a peak pore diameter at *ca.* 4.3 nm with a peak width of *ca.* 0.6 nm at half-maximum. In contrast, the silica sample prepared in the absence of template under otherwise identical conditions shows a type I isotherm and a BET surface area of *ca.* 50 $m^2\ g^{-1}$.

Most reported mesoporous materials have been characterized with established techniques, such as transmission electron microscopy (TEM) or scanning electron microscopy (SEM).[1,2] Atomic force microscopy (AFM) enables resolution at the atomic level[14] and can be used to obtain nanoscale images of the surface of bulk materials and recently, AFM images of nanoporous ceramic films have appeared in a report.[15] The mesoporous silica samples obtained in this work are relatively easily characterized by AFM, as long as a smooth surface on freshly prepared samples could be identified. Fig. 2 shows AFM images (top-view and topographic view) of the sample Si-LA-50. From the images, we can readily identify the mesopores of *ca.* 4.5 nm diameter. Some channels are vertical to the observed surface and two are slanted to the surface, suggesting that the channel axes are largely disordered and three-dimensionally interconnected as reported in the literatures using TEM.[12] Although the images only reflect the surface pattern of the mesoporous materials, the inner mesostructures can be inferred from the large surface area, large pore volume and narrow pore size distribution as measured with the BET method.

This work was financially supported by the National Natural Science Foundation of China (Grant No. 29874002, to K-Y. Q.) and the Outstanding Young Scientist Award from NSFC (Grant No. 29825004, to Y. W.).

Notes and references

1 C. T. Kresge, M. E. Leonowicz, W. J. Roth, J. C. Vartuli and J. S. Beck, *Nature*, 1992, **359**, 710.
2 J. S. Beck, J. C. Vartuli, W. J. Roth, M. E. Leonowicz, C. T. Kresge, K. D. Schmitt, C. T. W. Chu, D. H. Olson, E. W. Sheppard, S. B. McCullen, J. B. Higgins and J. L. Schlenker, *J. Am. Chem. Soc.*, 1992, **114**, 10 834.
3 H. Yang, A. Kuperman, N. Coombs, S. Mamiche-Afara and G. A. Ozin, *Nature*, 1996, **379**, 703.
4 I. A. Aksay, M. Trau, S. Manne, I. Honma, N. Yao, L. Zhou, P. Fenter, P. M. Eisenberger and S. M. Gruner, *Science*, 1996, **273**, 892.
5 Y. Lu, R. Ganguli, C. A. Drewien, M. T. Anderson, C. J. Brinker, W. Gong, Y. Guo, H. Soyez, B. Dunn, M. H. Huang and J. I. Zink, *Nature*, 1997, **389**, 364.
6 S. H. Tolbert, T. E. Schaffer, J. Feng, P. K. Hansma and G. D. Stucky, *Chem. Mater.*, 1997, **9**, 1962.
7 H.-P. Lin and C.-Y. Mou, *Science*, 1996, **273**, 765.
8 H. Yang, N. Coombs and G. A. Ozin, *Nature*, 1997, **386**, 692.
9 P. S. Singh and K. Kosuge, *Chem. Lett.*, 1998, 101.
10 S. Schacht, Q. Huo, I. G. Voigt-Martin, G. D. Stucky and F. Schuth, *Science*, 1996, **273**, 768.
11 Q. Huo, J. Feng, F. Schuth and G. D. Stucky, *Chem. Mater.*, 1997, **9**, 14.
12 Y. Wei, D. Jin, T. Ding, W.-H. Shih, X. Liu and S. Z. D. Cheng, *Adv. Mater.*, 1998, **3**, 313.
13 Y. Wei, J. Xu, H. Dong, J.-H. Dong, K.-Y. Qiu and S. A. Jansen-Varnum, *Chem. Mater.*, 1999, **11**, 2023.
14 S. Manne, P. K. Hansma, J. Massie, V. B. Elings and A. A. Gewirth, *Science*, 1991, **251**, 183.
15 V. Z.-H. Chan, J. Hoffman, V. Y. Lee, H. Latrou, A. Avgeropoulos, N. Hadjichristidis, R. D. Miller and E. L. Thomas, *Science*, 1999, **286**, 1716.

Communication a909420b

ChemComm

Enantioselective deprotonation reactions using a novel homochiral magnesium amide base

Kenneth W. Henderson,* William J. Kerr* and Jennifer H. Moir

Department of Pure and Applied Chemistry, University of Strathclyde, 295 Cathedral Street, Glasgow, Scotland, UK G1 1XL. E-mail: cbas69@strath.ac.uk

Received (in Liverpool, UK) 11th January 2000, Accepted 7th February 2000

A novel homochiral magnesium bisamide base system has been prepared and reacted with a series of prochiral ketones in the presence of TMSCl to give efficient formation of the corresponding enol ethers in enantiomeric ratios of up to 95:5.

Optically pure lithium amide bases have proven to be versatile tools in modern asymmetric synthesis. Indeed, highly enantioselective deprotonation reactions have been accomplished for several sets of substrates, including conformationally locked ketones, epoxides, and tricarbonyl (η^6-arene)chromium complexes.[1] In turn, many of the more recent advances in this area have been accomplished by the development of new homochiral ligands and the tuning of reaction conditions to improve the selectivity of these lithium-mediated deprotonations.[2] In contrast to the Li-based strategies, magnesium reagents have received relatively little attention for use in asymmetric synthesis[3] and, in particular, as mediators of enantioselective deprotonation processes.

More recently, studies within our laboratories have shown how, in a racemic sense, magnesium amides can be employed as alternatives to their more widely used lithium counterparts in both enolisation and aldol addition reactions.[4] Indeed, advantages of the Mg-bases over the Li-analogues which have already been noted include their greater thermal stability (which, for example, allows aldol reactions between ketones to be promoted[4b]) and, in some instances, higher levels of more general reaction selectivity.[5] Consequently, with a view to developing asymmetric Mg-based protocols we considered that these observations, as well as the ability to formally bond two (chiral) ligands to the Mg centre, would allow good levels of stereoselectivity in organic transformations to be achieved. Herein, we report the first use of homochiral magnesium amide bases as reagents in the enantioselective deprotonation of conformationally locked ketones.

At the outset of this programme, and based on our recently reported structural study of the Li-amide (*R*)-**1**,[6] we chose to utilise readily available (*R*)-*N*-benzyl-α-methylbenzylamine, (*R*)-**2**. In due course, the Mg-amide base was readily prepared by the addition of dibutylmagnesium to 2 equiv. of the amine (*R*)-**2** in hexane solution, followed by heating to reflux for 90 min.† Analysis of the reaction mixture by ^{1}H NMR spectroscopy showed complete amination to the bisamide (*R*)-**3**.[7]

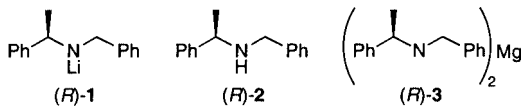

Subsequently, and based on extensive studies as reported in the chemical literature,[1] ketone **4a** was the substrate on which we chose to perform our initial deprotonation attempts. As shown in Table 1, a range of solvents, with and without HMPA as an additive,‡ were employed at −78 °C; from entries 1–5 it is clear that THF in the presence of 1 mol equiv. of HMPA provided good conversion to the silyl enol ether **5**.§ Furthermore and to our delight, even this simple Mg-amide base system displayed high levels of enantioselectivity for the (*S*)-silyl enol ether, (*S*)-**5a**.¶ Subsequent reaction optimisation (entries 5–8) showed that the use of only 0.5 mol equiv. of HMPA (entry 7) delivered a good reaction conversion and, at least as importantly, provided an enhanced level of enantioselection with a 91:9 enantiomeric ratio (82% ee) of (*S*)-**5a** over its optical isomer.‖ It should also be noted that reaction at −98 °C in THF, again with 0.5 mol equiv. of HMPA, gave a similar conversion (80%) and the same e.r. of 91:9, whereas reactions at more elevated temperatures with (*R*)-**3** led to a general reduction in enantioselectivity.

Table 1 Enantioselective deprotonations of **4a** and formation of silyl enol ether **5a**[a]

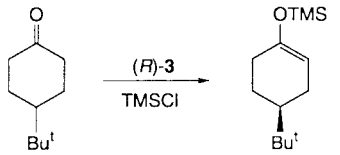

4a (*S*)-**5a**

Solvent	HMPA (mol equiv.)	Conversion (%)[b]	Enantiomeric ratio (e.r.)[b] (*S*):(*R*)
Et_2O	0	0	—
Et_2O	1	83	80:20
CH_2Cl_2	1	40	72:28
THF	0	33	90:10
THF	1	94	86:14
THF	2	26	84:16
THF	0.5	82	91:9
THF	0.1	53	91:9

[a] All reactions were performed at −78 °C for a period of 6 h. [b] Conversions and enantiomeric ratios were determined by separate GC analysis; see footnote ‖.

With these initial studies in hand and in order to investigate the wider applicability of this Mg-based strategy, a range of substituted cyclohexanones were subjected to our optimised reaction conditions. As can be seen from Table 2, using ketones **4a**–**e** the developed protocol with (*R*)-**3** was shown to consistently deliver the corresponding enol ethers **5a**–**e** with good efficiency and enantioselection, up to an excellent e.r. of 95:5 for **5d**.

To further extend our studies, as shown in Scheme 1, the less reactive 2,6-dimethyl ketone **4f** (82:18 *cis*:*trans* mixture; *trans*-ketone 50:50 e.r.) was also transformed with appreciable asymmetric induction (e.r. 90:10) to enol ether **5f** with the (*R*)-enantiomer in excess (55% conversion).** Notably, upon reaction completion the ratio of the returned ketone **4f** displayed a relatively unchanged 80:20 *cis*:*trans* ratio. However, the final enantiomeric ratio of the the *trans*-isomer of the starting ketone was 37:63. These latter observations and the elevated enantiomeric ratio for enol ether **5f** affirm that the Mg-amide base (*R*)-**3** had mediated a kinetic resolution process with the *trans*-ketone, as well as efficient asymmetric deprotonation with the *cis*-isomer.

DOI: 10.1039/b000425l

Table 2 Enantioselective deprotonations and silyl enol ether formation with Mg-amide (*R*)-**3**

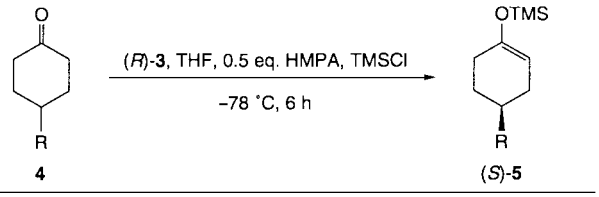

4 (*S*)-**5**

R	Product	Conversion[a] (%)	Enantiomeric ratio (e.r.) (*S*):(*R*)[b]
Bu^t (**4a**)	**5a**	82	91:9
Ph (**4b**)	**5b**	79	87:13
Me (**4c**)	**5c**	81	91:9
Pr^i (**4d**)	**5d**	77	95:5
Pr^n (**4e**)	**5e**	88	88:12

[a] Conversions were determined by GC analysis. [b] See footnote **.

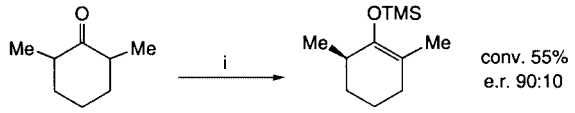

4f (*R*)-**5f**

Scheme 1 *Reagents and conditions*: i, (*R*)-**3**, HMPA (0.5 equiv.), TMSCl (4 equiv.), THF, −78 °C, 65 h.

Finally, in attempts to find a more practically acceptable additive to replace HMPA, equivalent quantities of DMPU were introduced to reactions of **4a** with (*R*)-**3**. In THF solvent at −78 °C, when 0.5 mol equiv. of DMPU were used, pleasingly an enantiomeric ratio of 90:10 in favour of (*S*)-**5a** was achieved in 89% conversion (Scheme 2); use of 1 mol equiv. of DMPU led to comparable conversion (93%) and e.r. (86:14).

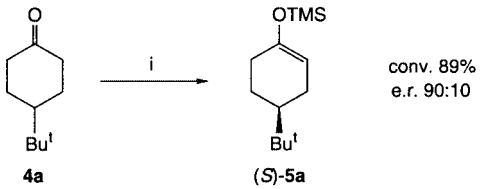

4a (*S*)-**5a**

Scheme 2 *Reagents and conditions*: i, (*R*)-**3**, DMPU (0.5 equiv.), TMSCl (4 equiv.), THF, −78 °C, 6 h.

In conclusion, having prepared a novel homochiral magnesium bisamide system, we have demonstrated, for the first time, that such bases can successfully mediate enantioselective deprotonation reactions. Indeed, significant levels of selection in these asymmetric processes have been realised, and to an extent that they are already approaching the optimum enantiomeric ratios achievable by more complex Li-base systems.[1] Furthermore, and more importantly for the widespread use of the Mg-based approach, this efficient enantioselection has been achieved using a reagent which is easily prepared from a simple, readily available, and inexpensive amine. The application of further Mg-bisamide systems and the development of related methodology is currently under investigation and will be reported in due course.

We gratefully acknowledge The Carnegie Trust for the Universities of Scotland for a postgraduate studentship (J. H. M.) and The Royal Society for a University Research Fellowship (K. W. H.). We also thank AstraZeneca Pharmaceuticals, Alderley Park for generous funding of our research endeavours *via* Strategic Research Funding, and the EPSRC Mass Spectrometry Service, University of Wales, Swansea for analyses.

Notes and references

† *Preparation* of Mg-amide base (*R*)-**3**: a Schlenk flask was charged with a solution of amine (*R*)-**2** (0.42 mL, 2 mmol) in dry hexane (8 mL) under N_2. To this stirred solution, dibutylmagnesium (0.85 mL of a 1.1 M solution in heptane, 1 mmol) was added dropwise and the mixture heated to reflux for 90 min. The reaction solution was then allowed to cool followed by removal of all solvent *in vacuo* and replacement by the solvent of choice for the subsequent deprotonation reaction. ^{1}H NMR spectroscopic analysis of the resultant yellow oil, after removal of the reaction solvent, is consistent with the formation of the bisamide (*R*)-**3**: (400 MHz, C_6D_6, 25 °C): δ 7.22–7.02 (m, 10H, Ph), 3.57–3.48 (m, 2H, 2 × CH), 3.40–3.35 (m, 1H, CH), 1.11 (d, *J* 6.6 Hz, 3H, CH_3).

‡ The beneficial use of HMPA as a co-solvent has been reported previously for various Li-mediated enantioselective reactions.[1a,c]

§ From the 94% conversion (by GC) shown as entry 5 in Table 1, following alumina column chromatography, an isolated yield of 64% was obtained for **5a** with a 90% recovery of the starting amine (*R*)-**2**.

¶ Formation of the (*S*)-silyl enol ether, (*S*)-**5a**, is consistent with the selectivity of the analogous Li-base (*R*)-**1**.[8] Additionally, GC analysis, by comparison with that of Knochel and co-workers[2b] allowed confirmation of the assignment of absolute stereochemistry for the enol ether **5a**.

‖ The typical procedure for the enantioselective deprotonation reactions is illustrated by a preparation of **5a**: a Schlenk flask containing base (*R*)-**3** (1 mmol) suspended in THF (10 mL) was cooled to −78 °C under N_2. The flask was then charged with TMSCl (0.5 mL, 4 mmol) and HMPA (0.09 mL, 0.5 mmol). After stirring for 20 min at −78 °C, 4-*tert*-butylcyclohexanone (123 mg, 1 mmol) was added as a solution in THF (2 mL) over 1 h using a syringe pump. The reaction was allowed to stir at −78 °C for a further 5 h and then quenched by the addition of saturated aqueous $NaHCO_3$ (5 mL). After warming to room temperature the reaction mixture was extracted with diethyl ether (50 mL) and washed with saturated aqueous $NaHCO_3$ (2 × 20 mL). The combined aqueous phase was extracted with diethyl ether (2 × 20 mL), the combined organic phase was then dried over Na_2SO_4, followed by removal of solvent *in vacuo*. The reaction conversion was determined as 82% by GC analysis [DB 179 fused silica capillary column, carrier gas H_2 (80 kPa), 60–190 °C; temperature gradient: 45 °C min^{-1}, t_r = 3.1 min (**4a**), t_R = 3.3 min (**5a**)]. The resultant yellow oil was then filtered through a silica plug and washed with a light petroleum–diethyl ether solution (9:1). This afforded **5a** as a colourless oil. The enantiomeric ratio was determined by GC analysis as 91:9 [Chirasil-DEX CB capillary column, carrier gas H_2 (30 kPa), 80 °C (1 min)–120 °C; temperature gradient: 1.5 °C min^{-1}, t_R = 32.2 min [(*S*)-**5a**], t_R = 32.8 min [(*R*)-**5a**)]].

** Enantiomeric ratios were determined by GC analysis. Additionally, the absolute configuration of the major and minor enantiomers for **5b**, **5c**, **5d** and **5f** were assigned by correlation of optical rotation measurements with those of Koga and coworkers;[9] for **5e** the major and minor isomer configurations were tentatively assigned by comparison with **5a–d**. Furthermore, all compounds exhibited satisfactory analytical and spectral data.

1 (*a*) P. O'Brien, *J. Chem. Soc., Perkin Trans. 1*, 1998, 1439; (*b*) N. S. Simpkins, *Pure Appl. Chem.*, 1996, **68**, 691; (*c*) K. Koga, *Pure Appl. Chem.*, 1994, **66**, 1487; (*d*) P. J. Cox and N. S. Simpkins, *Tetrahedron: Asymmetry*, 1991, **2**, 1.

2 For recent examples, see: (*a*) V. K. Aggarwal, P. S. Humphries and A. Fenwick, *J. Chem. Soc., Perkin Trans. 1*, 1999, 2883; (*b*) C.-D. Graf, C. Malan and P. Knochel, *Angew. Chem., Int. Ed.*, 1998, **37**, 3014.

3 For relevant examples of Mg-based reagents as used in different classes of organic transformations, see: D. A. Evans and S. G. Nelson, *J. Am. Chem. Soc.*, 1997, **119**, 6452; C. L. Elston, R. F. W. Jackson, S. J. F. MacDonald and P. J. Murray, *Angew. Chem., Int. Ed. Engl.*, 1997, **36**, 410; M. E. Bunnage, S. G. Davies, C. J. Goodwin and I. A. S. Walters, *Tetrahedron: Asymmetry*, 1994, **5**, 35.

4 (*a*) J. F. Allan, W. Clegg, K. W. Henderson, L. Horsburgh and A. R. Kennedy, *J. Organomet. Chem.*, 1998, **559**, 173; (*b*) J. F. Allan, K. W. Henderson and A. R. Kennedy, *Chem. Commun.*, 1999, 1325.

5 P. E. Eaton, C. H. Lee and Y. Xiong, *J. Am. Chem. Soc.*, 1989, **111**, 8016; G. Lessène, R. Tripoli, P. Cazeau, C. Biran and M. Bordeau, *Tetrahedron Lett.*, 1999, **40**, 4037.

6 D. Armstrong, K. W. Henderson, A. R. Kennedy, W. J. Kerr, F. S. Mair, J. H. Moir, P. H. Moran and R. Snaith, *J. Chem. Soc., Dalton Trans.*, 1999, 4063.

7 For previous studies into the formation of bis(amido)magnesium compounds, see: K. W. Henderson, J. F. Allan and A. R. Kennedy, *Chem. Commun.*, 1997, 1149; W. Clegg, F. J. Craig, K. W. Henderson, A. R. Kennedy, R. E. Mulvey, P. A. O'Neil and D. Reed, *Inorg. Chem.*, 1997, **36**, 6238.

8 R. P. C. Cousins and N. S. Simpkins, *Tetrahedron Lett.*, 1989, **30**, 7241.

9 K. Aoki, H. Noguchi, K. Tomioka and K. Koga, *Tetrahedron Lett.*, 1993, **34**, 5105; H. Kim, R. Shirai, H. Kawasaki, M. Nakajima and K. Koga, *Heterocycles*, 1990, **30**, 307.

Communication b000425l

The first hafnium methandiide complexes: the assembly of an entire triad of group 4 metal 'pincer' bis(phosphinimine) complexes possessing the M=C carbene–ylide structure

Ruppa P. Kamalesh Babu,[a] Robert McDonald[b] and Ronald G. Cavell*[a]

[a] *Department of Chemistry, University of Alberta, Edmonton, AB, Canada T6G 2G2. E-mail:Ron.Cavell@Ualberta.ca*
[b] *Structure Determination Laboratory, University of Alberta, Edmonton, AB, Canada T6G 2G2*

Received (in Cambridge, UK) 8th December 1999, Accepted 14th February 2000

Dichlorobis[bis(trimethylsilylamido)]hafnium(IV) reacts with $(R_2P{=}NSiMe_3)_2CH_2$ (R = Cy, Ph) cleaving the C–H bonds of the P–C–P backbone methylene group and eliminating 2 mol of hexamethyldisilazane to yield the hafnium methandiide (carbene) complexes 3 and 4, thus completing the triad of group 4 metal complexes containing the M=C moiety.

Although extensive systems of group 5, 6 and 7 carbene complexes are known,[1] similar group 4 carbene complexes are rare[2] being limited to a few titanium,[3] and zirconium alkylidene complexes[4] and some zirconium Fischer carbene complexes.[5] In particular, carbene complexes of hafnium have long eluded isolation. Whereas hafnium alkylidene species have been implicated as intermediates in stoichiometric reactions, attempted isolation gave orthometallated[6] or dimeric products.[7] We now report a novel, high yield synthesis of the first examples of hafnium bis(iminophosphorano)methandiide complexes which have a hafnium–carbon bond with multiple (hence carbene) character supported by phosphinimine substituents in a "pincer" structure. With these hafnium complexes we now complete the triad of group 4 metal complexes with similar structural features.[8]

The reaction of $[HfCl_2\{N(SiMe_3)_2\}_2]$[9] with $CH_2(R_2P{=}NSiMe_3)_2$ [R = Cy **1** (prepared by heating $(Cy_2P)_2CH_2$[10] with N_3SiMe_3), or Ph **2**[11]] in refluxing toluene (Scheme 1) gave the electron deficient methandiide complexes, $[HfCl_2\{C(R_2P{=}NSiMe_3)_2\text{-}\kappa^3C,N,N'\}]$ (R = Cy **3** or Ph **4**), as the result of a facile C–H bond cleavage process whereby the protons of the methylene group in the backbone of the ligand are removed;† 2 mol of hexamethyldisilazane were eliminated. This hafnium precursor reacts much more rapidly with the phenyl substituted bis(iminophosphorano)methane ligand, **2**, compared to the cyclohexyl analog, **1**, which we attribute to the higher acidity of the methylene protons in the former. Under similar conditions $[ZrCl_2\{N(SiMe_3)_2\}_2]$[9] reacts with **1** and **2** to yield the zirconium methandiide analogs, $[ZrCl_2\{C(R_2P{=}NSiMe_3)_2\text{-}\kappa^3C,N,N'\}$, prepared previously[8] by a different route. The hafnium methandiide complexes have a relatively high thermal stability, as do the Ti and Zr complexes,[8] which can be attributed to the steric protection of the carbene center by the formation of the tridentate chelate "pincer" structure.

The ^{31}P NMR spectra of complexes **3** and **4** consist of one sharp singlet showing that the two phosphorus nuclei are equivalent. The carbene resonances (δ 66.6 for **3**, 84.6 for **4**) appear as triplet signals because of coupling to two equivalent phosphorus atoms. The unusual upfield carbon chemical shift values for these carbene complexes relative to the general range exhibited by group 4 carbene complexes[2] may arise from the electronic influence of the phosphorus substituents, the presence of conjugated phosphinimine structures or because of the constrained geometry of the encapsulated carbene center.[12] We note that these shift values are similar to those of the previously reported carbodiphosphorane complexes of W[13] and Re[14] which show definitive M=C character. These latter complexes have neither the pincer nor the cyclic ring structure, thus the NMR properties probably devolve from the nature of the phosphorus–carbon interaction.

The molecular structure of $[HfCl_2\{C(Cy_2P{=}NSiMe_3)_2\text{-}\kappa^3C,N,N'\}]$ **3**,‡ shown in Fig. 1,[15] is similar to that of the zirconium analog.[8] The key structural feature of the complex is the relatively short Hf–C(1) bond length [2.162(6) Å] which is shorter than the Hf–C bonds in other hafnium hydrocarbyl complexes (mean Hf–CH_2C 2.300 Å, Hf–CHC_2 2.387 Å[16,17]). The two four-membered ring systems defined by the common Hf=C bond are nearly coplanar with a dihedral angle of 5.4(4)°. The C(1) atom lies above the least square plane defined by P(1), P(2), N(1), N(2) and Hf by 0.108(7) Å. The structure is consistent with a considerable degree of multiple bond character between the metal and the carbene center. A closer look at the bond lengths within the six-membered frame shows that the Hf–N bonds [mean 2.167(5) Å] are slightly shorter than values typical of neutral amine complexes but longer than values typical of amide complexes.[18] If we compare the P–C and P–N bond lengths in the complex to those of the free ligand,[19] we see that the endocyclic P–C bonds [mean 1.665(7) Å] of the P–C–P backbone are shorter and the P–N [mean 1.637(5) Å] bonds are

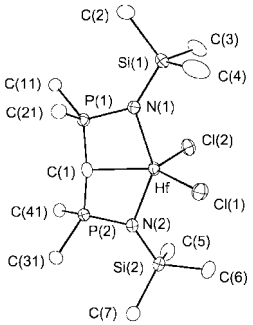

Fig. 1 An ORTEP[15] view of $[HfCl_2\{C(Cy_2P{=}NSiMe_3)_2\text{-}\kappa^3C,N,N'\}]$ **3** showing the atom labeling scheme. All cyclohexyl (except the *ipso*) carbon atoms and all hydrogen atoms have been removed for clarity. The remaining atoms are represented by Gaussian ellipsoids at the 20% probability level. Selected interatomic lengths (Å) and angles (°) Hf–Cl(1) 2.377(2), Hf–Cl(2) 2.389(2), Hf–C(1) 2.162(6), Hf–N(1) 2.164(5), Hf–N(2) 2.170(5), P(1)–N(1) 1.639(5), P(2)–N(2) 1.635(5), P(1)–C(1) 1.662(7), P(2)–C(1) 1.668(7), P(1)–C(11) 1.834(6), P(2)–C(31) 1.825(6), P(1)–C(1)–P(2) 169.9(4), Hf–C(1)–P(1) 93.5(3), Hf–C(1)–P(2) 93.6(3), N(1)–Hf–N(2) 143.3(2), N(1)–P(1)–C(1) 100.5(3), N(2)–P(2)–C(1) 100.3(3).

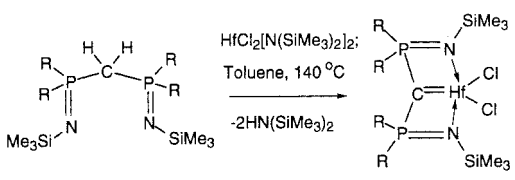

Scheme 1

DOI: 10.1039/a909771f

longer which implies delocalization of π-electron density in the four-membered planes which would arise from the conjugation of the P=N and the M=C bonds,[20] as delineated in Scheme 2. The central carbon NMR shifts in complexes **3** and **4** suggest that a tautomeric ylide–carbene formulation may be an appropriate description.

Scheme 2

Having assembled a complete triad of Ti, Zr and Hf complexes with the same chemical structures we are now in a position to conduct a comparison of the similarities and differences in reaction behaviour which derive from the metal alone. Such comparative reactivity studies are now in progress.

We thank the Natural Sciences and Engineering Research Council of Canada, NOVA Chemicals Corporation and the University of Alberta for financial support.

Notes and references

† *Preparation* of **3**: all experimental manipulations were performed under rigorously anaerobic conditions using Schlenk techniques or an argon-filled glovebox. The complex, $[HfCl_2\{N(SiMe_3)_2\}_2]$ (0.2 g, 0.35 mmol) was dissolved in 10 mL of toluene. Solid $CH_2(Cy_2P{=}NSiMe_3)_2$ **1** (0.204 g, 0.35 mmol) was added to this solution with stirring and the colorless solution was heated at 140 °C for seven days. The resultant pale yellow solution was concentrated and cooled to −15 °C for 24 h to obtain colorless crystals which were isolated by filtration (yield: 0.21 g, 72.1%). IR (Nujol mull): 1447s, 1404w, 1377w, 1356w, 1320s, 1297w, 1260s, 1246s, 1202w, 1192w, 1176w, 1168w, 1112m, 1024s br, 915w, 887m, 836s br, 783m, 771s, 754s, 747s, 707w, 679m, 654s, 635m, 615s, 552s, 542m, 495m, 485m, 464w. ^{1}H NMR (400.1 MHz, C_6D_6, 298 K): δ 2.1–1.1 (br m, 40 H, methylene-Cy and 4 H, methine-Cy), 0.47 (s, 18 H, $SiMe_3$). ^{13}C{^{1}H} NMR (100.6 MHz, C_6D_6, 298 K): δ 66.6 (t, $^1J_{PC}$ 158.0 Hz, 1 C, quaternary C-PCP), 40.7 (m, 4 C, methine-Cy), 26.8 (m, 8 C, *ortho* methylene-Cy), 26.6 (s, 4 C, *para* methylene-Cy), 26.4 (s, 4 C, *meta* methylene-Cy), 26.3 (s, 4 C, *meta* methylene-Cy), 3.5 (s, 6 C, $SiMe_3$). ^{31}P{^{1}H} NMR (161.9 MHz, C_6D_6, 298 K): δ 32.6 (2 P). Anal. Calc. for $C_{31}H_{62}Cl_2HfN_2P_2Si_2$: C, 44.84; H, 7.53; N, 3.37. Found: C, 45.04; H, 7.98; N, 3.29%.

Preparation of **4:** in a similar fashion, $[HfCl_2\{N(SiMe_3)_2\}_2]$ (0.104 g, 0.18 mmol) in toluene solution was treated with solid $CH_2(Ph_2P{=}NSiMe_3)_2$ **2** (0.102 g, 0.18 mmol) and heated at 140 °C for 3 d. The solution was reduced to a small volume and layered with hexane. After 2 days at ambient temperature, colorless crystals were deposited which were isolated by filtration (yield: 0.11 g, 74.8%). IR (Nujol mull): 1589w, 1574w, 1480w, 1463m, 1436s, 1378m, 1311s, 1251s, 1181w, 1156w, 1111s, 1070m, 1057s, 1037s, 999m, 843s, 787s, 772m, 754m, 738m, 716s, 696s, 654s, 631m, 622s, 615m, 576m, 524s. ^{1}H NMR (400.1 MHz, C_6D_6, 298 K): δ 7.63 (m, Ph), 6.97 (m, Ph), 6.91 (m, Ph), 0.22 (s, 18 H, $SiMe_3$). ^{13}C{^{1}H} NMR (100.6 MHz, C_6D_6, 298 K): δ 134.7 (m, 4 C, *ipso* Ph), 131.5 (t, $^2J_{PC}$ 6.0 Hz, 8 C, *ortho* Ph), 131.0 (s, 4 C, *para* Ph), 128.5 (t, $^3J_{PC}$ 5.6 Hz, 8 C, *meta* Ph), 84.6 (t, $^1J_{PC}$ 145.0 Hz, 1 C, quaternary C-PCP), 2.6 (s, 6 C, $SiMe_3$). ^{31}P{^{1}H} NMR (161.9 MHz, C_6D_6, 298 K): δ 12.2 (2 P). Anal. Calc. for $HfCl_2\{C(Ph_2P{=}NSiMe_3)_2$-$\kappa^3C,N,N'\}\cdot 0.5C_6H_5Me$, $C_{34.5}H_{42}Cl_2HfN_2P_2Si_2$: C, 48.62; H, 4.97; N, 3.29. Found: C, 48.24; H, 5.21; N, 3.34%.

‡ *Crystal data* for $[HfCl_2\{C(Cy_2P{=}NSiMe_3)_2$-$\kappa^3C,N,N'\}]$ **3**: monoclinic, space group, $P2_1/c$ (no. 14), a = 10.3572(7), b = 20.8156(10), c = 17.8865(10) Å, β = 93.226(5)°, V = 3850.1(4) Å^3, Z = 4, D_c = 1.433 g cm^{-3}, μ = 7.829 mm^{-1} (Cu-Kα, λ = 1.54178 Å), T = 213 K; the structure was solved by direct methods and refined by full matrix least squares procedures: R_1 = 0.0432 and 0.0495, (wR_2 = 0.1100 and 0.1148) for 4864 reflections with $F_o^2 > 2\sigma(F_o^2)$ and all data respectively.

CCDC 182/1543. See http://www.rsc.org/suppdata/cc/a9/a909771f/ for crystallographic files in .cif format.

1 For some recent review articles, see: K. H. Dötz and P. Tomuschat, *Chem. Soc. Rev.*, 1999, **28**, 187; M. P. Doyle and D. C. Forbes, *Chem. Rev.*, 1998, **98**, 911; R. R. Schrock, *Acc. Chem. Res.*, 1990, **23**, 158; D. M. Hoffman, ch 10, *High-valent Organorhenium Compounds*, in *Comprehensive Organometallic Chemistry II*, ed. E. W. Abel, F. G. A. Stone and G. Wilkinson, Pergamon, Oxford, 1995, vol. 6, pp. 231–255; W. D. Wulff, *Organometallics*, 1998, **17**, 3116.

2 R. Beckhaus, *Angew. Chem., Int. Ed. Engl.*, 1997, **36**, 686.

3 J. D. Meinhart, E. V. Anslyn and R. H. Grubbs, *Organometallics*, 1989, **8**, 583; P. Binger, P. Müller, P. Philipps, B. Gabor, R. Mynott, A. T. Herrmann, F. Langhauser and C. Krüger, *Chem. Ber.*, 1992, **125**, 2209; J. A. van Doorn, H. van der Heijden and A. G. Orpen, *Organometallics*, 1995, **14**, 1278; H. van der Heijden and B. Hessen, *J. Chem. Soc., Chem. Commun.*, 1995, 145; P. Sinnema, L. v. Veen, A. L. Spek, N. Veldman and J. H. Teuben, *Organometallics*, 1997, **16**, 4245; S. Kahlert, H. Görls and J. Scholz, *Angew. Chem., Int. Ed.*, 1998, **37**, 1857; R. Baumann, R. Stumpf, W. M. Davis, L.-C. Liang and R. R. Schrock, *J. Am. Chem. Soc.*, 1999, **121**, 7822.

4 M. S. Clift and J. Schwartz, *J. Am. Chem. Soc.*, 1984, **106**, 8300 and references therein; M. D. Fryzuk, P. B. Duval, S. S. S. H. Mao, M. J. Zaworotko and L. R. MacGillivray, *J. Am. Chem. Soc.*, 1999, **121**, 2478.

5 P. T. Barger, B. D. Santarsiero, J. Armantrout and J. E. Bercaw, *J. Am. Chem. Soc.*, 1984, **106**, 5178.

6 A. R. Bulls, W. P. Schaefer, M. Serfas and J. E. Bercaw, *Organometallics*, 1987, **6**, 1219.

7 B. Hessen, F. v. Bolhuis and J. H. Teuben, *Organometallics*, 1987, **6**, 1352; R. P. Planalp, R. A. Andersen and A. Zalkin, *Organometallics*, 1983, **2**, 16.

8 R. G. Cavell, R. P. Kamalesh Babu, A. Kasani and R. McDonald, *J. Am. Chem. Soc.*, 1999, **121**, 5805.

9 R. A. Andersen, *Inorg. Chem.*, 1979, **18**, 2928.

10 M. D. Fryzuk, D. H. McConville and S. J. Rettig, *J. Organomet. Chem.*, 1993, **445**, 245.

11 R. Appel and I. Ruppert, *Z. Anorg. Allg. Chem.*, 1974, **406**, 131.

12 R. H. Crabtree, *The Organometallic Chemistry of the Transition Metals*, John Wiley & Sons, Inc., New York, 1988, p. 260.

13 A. E. Bruce, A. S. Gamble, T. L. Tonker and J. L. Templeton, *Organometallics*, 1987, **6**, 1350.

14 J. Sundermeyer, K. Weber, K. Peters and H. G. v. Schnering, *Organometallics*, 1994, **13**, 2560.

15 C. K. Johnson, ORTEP, Report ORNL No. 5138, Oak Ridge Nat. Lab., Oak Ridge, TN, 1976.

16 F. H. Allen, J. E. Davies, J. J. Galloy, O. Johnson, O. Kennard, C. F. Macrae, E. M. Mitchell, G. F. Mitchell, J. M. Smith and D. G. Watson, *J. Chem. Inf. Comput. Sci.*, 1991, **31**, 187. The values were calculated from the data retrieved from the Cambridge Crystallographic Data Base.

17 R. D. Rogers, R. V. Bynum and J. L. Atwood, *J. Am. Chem. Soc.*, 1981, **103**, 692.

18 See, for example: $HfCl\{N(SiMe_3)_2\}_3$, Hf–$N(SiMe_3)_2$ 2.04(1) Å (C. Airoldi, D. C. Bradley, H. Chudzynska, M. B. Hursthouse, K. M. Abdul Malik and P. R. Raithby, *J. Chem. Soc., Dalton Trans.*, 1980, 2010); $Hf(NPh_2)_4$, Hf–NPh_2 2.047–2.085 Å (M. Polamo, I. Mutikainen and M. Leskelä, *Acta Crystallogr., Sect. C*, 1996, **52**, 1348); $Me_2NHf\{(Me_3SiNCH_2CH_2)_3N\}$, Hf–$NMe_2$ 2.048(6) Å (Z. Duan, A. A. Naiini, J.-H. Lee and J. G. Verkade, *Inorg. Chem.*, 1995, **34**, 5477); $(C_5Me_5)_2Hf(H)(NHMe)$; Hf–NHMe 2.027(8) Å (G. L. Hillhouse, A. R. Bulls, B. D. Santarsiero and J. E. Bercaw, *Organometallics*, 1988, **7**, 1309).

19 Unpublished results, R. P. Kamalesh Babu, R. McDonald and R. G. Cavell, The X-ray structure of $CH_2\{Cy_2P{=}NSiMe_3\}_2$, University of Alberta Structure Determination Laboratory, Report RGC 9802. The important bond parameters are: mean P–C (P–C–P frame) length, 1.819(2), P–C (Cy bonds) length, 1.837(2), P–N length, 1.547(2) Å and the P–C–P angle, 117.4(1)°.

20 R. P. Kamalesh Babu, R. McDonald, S. A. Decker, M. Klobukowski and R. G. Cavell, *Organometallics*, 1999, **18**, 4226.

Communication a909771f

ChemComm

$2C_{60}·3CS_2$: orientational ordering accompanies the reversible phase transition at 168 K

Marilyn M. Olmstead,* Feilong Jiang and Alan L. Balch

Department of Chemistry, University of California, Davis, CA 95616, USA. E-mail: olmstead@indigo.ucdavis.edu

Received (in Columbia, MO, USA) 7th October 1999, Accepted 2nd February 2000

At 168 K crystals of $2C_{60}·3CS_2$ undergo a reversible phase transition (from orthorhombic to monoclinic), which is accompanied by orientational ordering of both C_{60} molecules in the asymmetric unit.

Carbon disulfide and aromatic hydrocarbons are widely used as good solvents for C_{60} and for the higher fullerenes. Both carbon disulfide and benzene solutions of C_{60} form crystalline solvates when they are allowed to evaporate to dryness. The structure of $C_{60}·4C_6H_6$ has been reported[1–3] and shown to contain van der Waals interactions of the types: benzene–benzene, benzene–C_{60}, and C_{60}–C_{60}. In spite of numerous intermolecular interactions, the C_{60} molecule is disordered with two orientations of the molecules occupying a common site at 104 K. Solutions of C_{60} in carbon disulfide produce brown crystals of $2C_{60}·3CS_2$.[4–6] Crystallographic studies at room temperature have identified the space group as either orthorhombic,[5] *Pbnm*, a = 24.97(6), b = 25.52(3), c = 9.98(1) Å or as orthorhombic,[6] $Pn2_1a$, a = 25.588(2), b = 9.984(2), c = 24.997(2) Å. The latter study reported a complete structure determination and showed the gross packing of molecules. However the resulting R value was high (0.18), and each of the two independent C_{60} molecules was modeled with four different orientations of the C_{60} molecule at each of the two independent sites. Additionally, the carbon disulfide molecules were disordered with two orientations at each of the three sites, and the structure could only be refined using a set of bond constraints. In this report we examine the structure of $2C_{60}·3CS_2$ at low temperatures and show that a reversible phase transition occurs at 168 K.

The structure of $2C_{60}·3CS_2$, obtained by evaporation of a carbon disulfide solution, was determined at 90 K. At this temperature the crystals belong to the monoclinic space group $P2_1/n$, with a = 9.8722(12), b = 25.466(3), c = 24.671(3) Å, β = 90.047(3)°.† The crystal was treated as a pseudo-merohedral twin. Refinement proceeded satisfactorily with a model that included two fully ordered C_{60} molecules and three ordered carbon disulfide molecules in the asymmetric unit. The average values and average deviations for the low temperature form are: fullerene; C–C bond distance (5:6 ring junctions) = 1.382(11) Å; C–C (6:6 ring junctions) = 1.450(11) Å; carbon disulfide; C–S bond distance = 1.544(6) Å; S–C–S bond angle = 179.0(4)°. A stereoview of the monoclinic structure perpendicular to the shortest axis is given in Fig. 1. In this structure, the set of three CS_2 molecules approach one another end-on to form a triangle with non-bonded S··S contacts of 3.696, 3.697 and 3.808 Å (Fig. 2). The closest contact between any sulfur atom and C_{60} is 3.460 Å (between S6 and C59), and the next shortest (3.468 Å) involves S3 and C1. The twenty shortest contacts between sulfur atoms and fullerene carbon atoms have an average value of 3.602 Å. Interestingly, one of the sulfur atoms, S5, has no contacts in this group; its shortest contact to a fullerene carbon is 3.834 Å. The shortest contact between the central carbon of CS_2 and C_{60} is 3.278 Å.

In view of the similarities of the orthorhombic and monoclinic cell parameters, the structure at room temperature was reexamined, and we confirmed that at room temperature $2C_{60}·3CS_2$ has an orthorhombic cell with a = 24.988(9), b = 25.602(8), c = 9.984(3) Å. We also confirmed that the structure

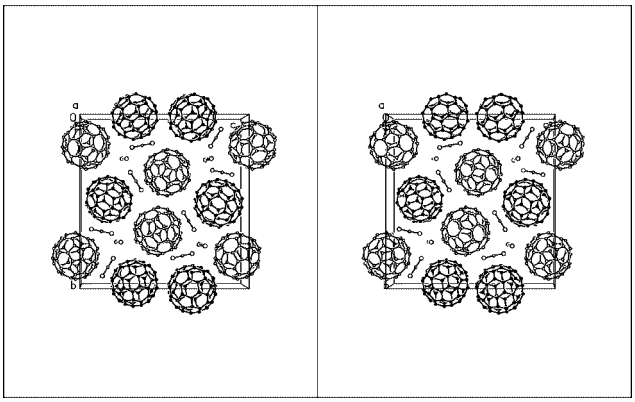

Fig. 1 A stereoview down the short (9.872 Å) axis of the monoclinic structure of $2C_{60}·3CS_2$. The two fullerene molecules are differentiated by using open circles for one and shaded circles for the other.

cannot be solved in the centrosymmetric space group, *Pbnm*. After two days of data collection a 25% reduction in the intensity of check reflections had occurred, presumably as a result of loss of CS_2.

In order to understand the relationship between the two crystallographically distinct forms of $2C_{60}·3CS_2$, variable temperature crystallographic studies were conducted. The orthorhombic setting for the high temperature form will match the monoclinic B setting of the low temperature form if it is described in the space group $P2_1nb$, the *cab* setting of $Pna2_1$, (no. 33). In this space group the symmetry elements differ from $P2_1/n$ by the addition of a b glide, and by a 2_1 screw axis that lies along the a-axis instead of the b-axis. Although the presence of

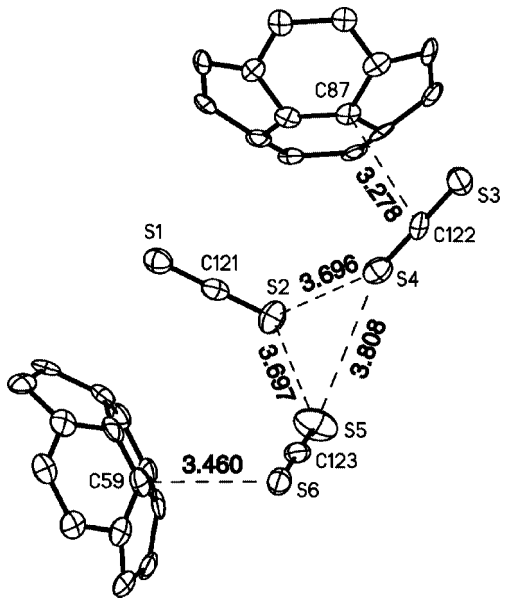

Fig. 2 A drawing showing selected intermolecular contacts associated with the CS_2 molecules in the monoclinic form.

DOI: 10.1039/a908147j

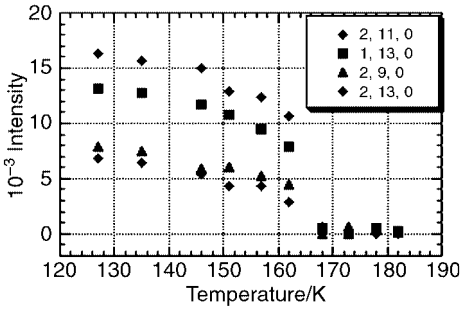

Fig. 3 A plot of the reflection intensity as a function of temperature for four selected *hk*0 reflections of $2C_{60}{\cdot}3CS_2$.

the screw axis does not confer any extra conditions; the presence of the *b* glide in the orthorhombic form leads to the condition, *hk*0, $k = 2n$, which is distinct from that of the monoclinic form, for which *hk*0 has no conditions.

A set of ten strong reflections in the set of *hk*0, $k = 2n + 1$ were identified in the low temperature form. A small data set was collected on these reflections at selected temperatures between 127 and 183 K. Without exception, extinction was observed at 168(2) K. This can be seen in the plot of the intensities of four of these reflections as a function of temperature shown in Fig. 3. The temperature was raised and lowered three times through the above range, and no loss in intensity of the benchmark reflections was observed.

Since the high temperature, orthorhombic, and low temperature, monoclinic, structures are interconvertible without loss of crystallinity, it is not surprising that they contain similar arrays of molecules. Each form has two distinct C_{60} sites and three CS_2 sites. The pattern of packing of these constituents is exactly the same, and the orientation of the CS_2 molecules matches. The orthorhombic space group has an additional glide plane, but the principal difference is that in the high temperature form there are four different orientations of the C_{60} molecules and two different orientations of the CS_2 molecules at sites which themselves contain no crystallographic symmetry. However, as a consequence of the higher orthorhombic symmetry, there would be higher order in the high temperature form if the disorder did not occur. Thus, the phase transition results in an increased disorder upon warming and is entropically driven.

Some compression of the structure at low temperature would be expected due to the reduction in temperature, and this is clearly seen by a comparison of the average center-to-center distances. For the orthorhombic form (298 K), the average value is 10.051 Å, while for the monoclinic form (90 K), the average value is 9.961 Å. An accurate comparison of the individual bond distances and angles cannot be made due to the disorder at room temperature. Likewise, comparison of temperature-dependent changes in the contact distances between C_{60} and CS_2 is flawed by the same inaccuracies due to the disorder, but, based upon the packing, no remarkable differences are expected.

Despite the ordering observed in this crystallographic study, the fullerene molecules in $2C_{60}{\cdot}3CS_2$ still undergo dynamic reorientation at low temperatures. Crystalline $2C_{60}{\cdot}3CS_2$ has been studied previously by solid state ^{13}C NMR spectroscopy.[7] Over the temperature range 125 to 263 K, the spectrum consists of a single narrow line which exhibits a minimum in the spin–lattice relaxation time, T_1 at 170 K. Those results were interpreted to indicate that an orientational ordering transition occurs and that the fullerene molecules jump between equivalent orientations with a correlation time of $< 10^{-5}$ s. The nature of the interactions between C_{60} and CS_2 has been examined by quantum mechanical calculations.[8]

Reversible phase transitions in molecular crystals are relatively rare occurrences. More commonly, molecular crystals undergo cooling without phase change or fragment upon cooling owing to irreversible phase changes which generally make determination of the structure of the low temperature phase inaccessible. Reversible phase changes in molecular crystals are likely to involve an aspect of increased molecular order at low temperature owing to a reorganization process such as the molecular ordering seen for $2C_{60}{\cdot}3CS_2$ or the side chain ordering and molecular reorientation observed in cholesterol.[9] Since orientational disorder is common in fullerenes, it is likely that other reversible phase changes will be seen in the large number of crystals in which a fullerene co-crystallizes with one or two other molecules. The present study emphasizes the value of examining fullerene structures at the lowest experimentally obtainable temperature.

Notes and references

† The crystal used was a dark brown lath of size $0.065 \times 0.13 \times 0.36$ mm. Data for the structure determination was collected on a Bruker SMART 1000 equipped with a CRYO Industries low-temperature apparatus. Selection of the monoclinic space group, $P2_1/n$, followed directly from the observation of systematic absences. The unit cell was based upon a least-squares fit of 5907 reflections with $2.3 < \theta < 24.3°$. Solution of the structure was achieved with some difficulty from direct methods and subsequent refinement and difference maps. Refinement of the structure stopped with an *R*1 of 0.28, yet there was no indication in the difference maps of another, rotationally disordered, C_{60} molecule. At this stage a twin law was introduced because there were two strong indicators of pseudo-merohedral twinning.[10] One was a mean $|E^2 - 1| = 0.749$, a value near to that expected for a non-centrosymmetric structure rather than a centrosymmetric one, and the other was the β angle very near 90°. A twin law [1 0 0 0 −1 0 0 0 −1] and twin component of 0.5 were introduced, which led to a 20% reduction in the value of *R*1. Another 2% reduction in the *R*1 value was achieved by the introduction of anisotropic thermal parameters for all atoms, leading to an *R*1 of 0.0579 computed for 8239 observed data [$> 2\sigma(I)$] and 1162 parameters. The twin component converged to 0.5032(10) and was subsequently set to 0.5000. The largest difference map peak had a value of 0.42 e Å^{-3}.

Crystal data for $2C_{60}{\cdot}3CS_2$, $M = 1669.59$, monoclinic, space group $P2_1/n$, $a = 9.8722(12)$, $b = 25.466(3)$, $c = 24.671(3)$ Å, $\beta = 90.047(3)°$, $U = 6202.5(7)$ Å^3, μ(Mo-Kα) = 0.297 mm^{-1}, $Z = 4$, $T = 90$ K, 60760 reflections collected, 14233 unique ($R_{int} = 0.115$), $wR(F^2)$ was 0.1224 (all data). CCDC 182/1546. See http://www.rsc.org/suppdata/cc/a9/a908147j/ for crystallographic files in .cif format.

A Siemens P4 diffractometer equipped with a rotating Cu anode and LT-2 low temperature apparatus was used for the study of the phase change. The temperature at the crystal and calibration of the readout were determined by a separate study of the phase transition (at 123 K) of potassium dihydrogen phosphate. The Bruker SMART diffractometer was funded in part by NSF grant CHE-9808259.

1 M. F. Meidine, P. B. Hitchcock, H. W. Kroto, R. Taylor and D. R. M. Walton, *J. Chem. Soc., Chem. Commun.*, 1992, 1534.
2 A. L. Balch, J. W. Lee, B. C. Noll and M. M. Olmstead, *J. Chem. Soc., Chem. Commun.*, 1993, 56.
3 H. B. Bürgi, R. Restori, D. Schwarzenbach, A. L. Balch, J. W. Lee, B. C. Noll and M. M. Olmstead, *Chem. Mater.*, 1994, **6**, 1325.
4 K. Kikuchi, S. Suzuki, K. Saito, H. Shiromaru, I. Ikemoto, Y. Achiba, A. Zakhidov, A. Ugawa, K. Imaeda, H. Inokuchi and K. Yakushi, *Physica C*, 1991, **185–189**, 415.
5 B. Morosin, P. P. Newcomer, R. J. Baughman, E. L. Venturini, D. Loy and J. E. Schirber, *Physica C*, 1991, **184**, 21.
6 J. C. A. Boeyens, M. Ramm, D. Zobel and P. Luger, *S. Afr. Tydskr. Chem.*, 1997, **50**, 28.
7 Y. Maniwa, K. Mizoguchi, K. Kume, K. Kikuchi, I. Ikemoto, S. Suzuki and Y. Achiba, *Solid State Commun.*, 1991, **80**, 609.
8 A. Tamulis, J. Tamuliene and A. Graja, *Fullerene Sci. Tech.*, 1998, **6**, 1097.
9 L.-Y. Hsu and C. E. Nordman, *Science*, 1983, **220**, 604.
10 R. Herbst-Irmer and G. M. Sheldrick, *Acta Crystallogr., Sect. B*, 1998, **54**, 443.

Communication a908147j

ChemComm

1,3-Dipolar cycloaddition of 2-azetidinone-tethered azomethine ylides. Application to the rapid, stereocontrolled synthesis of optically pure highly functionalised pyrrolizidine systems

Benito Alcaide,* Pedro Almendros, Jose M. Alonso and Moustafa F. Aly†

Departamento de Química Orgánica I, Facultad de Ciencias Químicas, Universidad Complutense, 28040-Madrid, Spain. E-mail: alcaideb@eucmax.sim.ucm.es

Received (in Liverpool, UK) 4th January 2000, Accepted 14th February 2000

A new straightforward methodology to prepare polyfunctionalised enantiopure pyrrolizidine systems, based on the 1,3-dipolar cycloaddition of 2-azetidinone-tethered azomethine ylides as the key reaction, is presented.

1,3-Dipolar cycloaddition employing azomethine ylides is an important process in organic synthesis, acquiring a prominent place of synthetic strategy for a variety of targets, including natural products such as azasugars and alkaloids.[1] Pyrrolizidine alkaloids occur in many natural products of potential use in medicine and agriculture.[2] In view of their potent and various biological activities, pyrrolizidine alkaloids as well as structurally related unnatural compounds are continuosly stimulating new synthetic approaches.[3] On the other hand, the importance of 2-azetidinones as synthetic intermediates has been widely recognized in organic synthesis. This usefulness is based on the impressive variety of transformations which can be derived from this system.[4] The application of β-lactams in stereoselective synthesis may be divided into two groups, namely, those processes based on transformation of the 2-azetidinone by external reagents and those based on rearrangements of the four-membered ring. The first type of reactivity is exemplified by the β-lactam synthon method.[5] The second group of reactions is based on the building of a conveniently functionalised 2-azetidinone to produce different types of, usually cyclic, compounds by selective bond breakage and rearrangement.[6] Despite the versatility of the 2-azetidinone ring, there is little information available on the use of β-lactams as chiral synthons for the synthesis of pyrrolizidine alkaloids, just the groups of Reuschling[7] and Palomo[8] have reported β-lactam routes to simple pyrrolizidines. Our interest in the use of 4-oxoazetidine-2-carbaldehydes as substrates for addition reactions and cyclization processes,[9] prompted us to evaluate the combination of the 1,3-dipolar cycloaddition of alanine (glycine) derived iminoester ylides with rearrangement reactions on the 2-azetidinone ring as a route to complex pyrrolizidine alkaloids (Scheme 1). We report here, a straightforward asymmetric synthesis of different kinds of highly fuctionalised bi- and tri-cyclic pyrrolizidine systems using β-lactams as chiral building blocks.

Cyclization precursors, 4-oxoazetidine-2-carbaldehydes **1**, were prepared both in the racemic form and in optically pure form using standard methodology.[9–12] Treatment of aldehydes **1** with various α-aminoesters in the presence of molecular sieves provided the corresponding aliphatic aldimines **2**. Imines **2** were obtained in quantitative yields and were used for next step without further purification

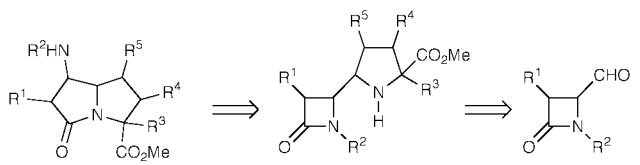

Scheme 1

We sought to explore the reactivity of 2-azetidinone-tethered azomethine ylides with cyclic and acyclic dienophiles such as *N*-phenyl maleimide and methyl acrylate.‡ The 1,3-dipolar cycloaddition was achieved *via* metal ion catalysis at room temperature. Treatment of aldimines **2** with the appropriate dienophile in the presence of $AgOAc–Et_3N$ in toluene at room temp. for 40 h gave with reasonable diastereoselectivity mixtures of cycloadducts **3** and **4** (Table 1) in moderate to excellent yields (45–90%).§ Fortunately, in all cases the diastereomeric cycloadducts were easily separated by flash chromatography. Furthermore, the reaction with an unsymmetric monoactivated alkene, methyl acrylate, proceeded with total regioselectivity. The steric properties of the C3 substituent on the 2-azetidinone ring influence the stereoselectivity of the cycloaddition, sterically less demanding groups increasing the diastereoisomeric ratio (Table 1). Next, our aim was to find an expedient transformation of the cycloadducts into pyrrolizidine systems. First we tested sodium methoxide as reagent for the conversion of adducts **3** or **4** into the framework of pyrrolizidine alkaloids. In the event, the pyrrolizidine skeleton was obtained. Sodium methoxide works well in maleimide derived cycloadducts, however epimerization was observed in adducts coming from methyl acrylate. This preliminary result encouraged us to find a more convenient reagent for this transformation. To our delight, when the reaction was conducted in a saturated solution of HCl(g) in isopropanol at room temperature for 36 h, optically pure pyrrolizidine systems **5** and **6** were obtained in moderate to good yields and without by-products (Scheme 2).¶ However, bicycle (−)-**6b** was more efficiently obtained in a saturated methanolic solution of HCl(g), with some isopropyl transesterification being observed when adduct (+)-**4d** was treated with HCl(g) in isopropanol. The reaction of (+)-**3d** in a saturated solution of HCl(g) in methanol for 36 h gave a quantitative yield of the monocyclic pyrrolidine (+)-**7**, which requires 2 h of heating in toluene under PTSA catalysis to give the expected tricyclic system (+)-**5b**.‖ The formation of pyrrolizidinones **5** and **6** involves a selective C–N bond cleavage of the four-membered ring, followed by a rearrangement under the reaction conditions. The relative *anti*-disposition of the ester and amine moieties in bicycles **6** must be responsible for the failure of the third cyclization to occur, preventing the formation of a highly strained tricyclic system. The polycyclic structures (by DEPT, HETCOR and COSY) and the stereochemistry (by vicinal proton couplings and NOE experiments) of compounds **5** and **6** were established by one- and two-dimensional NMR techniques.** Taking into account that separated diastereomeric cycloadducts **3** and **4** could be obtained and cyclized, the stereochemistry for compounds **3** and **4** was inmediately deduced by comparison with the NOE results of the polycyclic systems. Also, the *cis*-stereochemistry of the four-membered ring is set during the cyclization step to form the 2-azetidinone ring and it is transferred unaltered during the further synthetic steps.

† Permanent address: Department of Chemistry, Faculty of Science at Qena, South Valley University, Qena, Egypt.

DOI: 10.1039/b000249f

Table 1 1,3-Dipolar cycloaddition of 2-azetidinone-tethered azomethine ylides

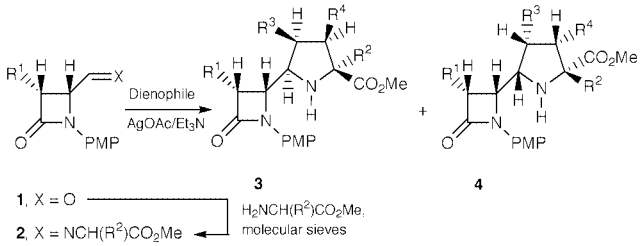

Entry	Aldehyde	R^1	R^2	R^3	R^4	Products	**3**:**4** ratio[a]	**3**:**4** yield[b]
1	**1a**	H	Me	CO_2Me	H	**3a**[c]	—[c]	48[d]
2	**1b**	Vinyl	H	CO_2Me	H	**3b**/**4b**	95:5	43/2
3	(+)-**1c**	MeO	Me	CO_2Me	H	(+)-**3c**/(+)-**4c**	65:35	39/21
4	(+)-**1c**	MeO	H	CO_2Me	H	(+)-**3d**/(+)-**4d**	70:30[e]	46/20

[a] The ratio was determined by integration of well resolved signals in the ^{1}H NMR spectra of the crude reaction mixtures before purification. PMP = 4-$MeOC_6H_4$. [b] Yield of pure, isolated product with correct analytical and spectral data. [c] The ^{1}H NMR spectrum of the crude mixture showed mainly **3a** togheter with unmeasurable traces of two other isomers. [d] Additional fractions containing the major cycloadduct together with traces of the minor isomers were isolated after column chromatography, accounting for an overall 80% yield. [e] Two additional diastereoisomeric cycloadducts were detected in the ^{1}H NMR spectra of the crude reaction mixture accounting, respectively, for 7 and 4% of the products formed.

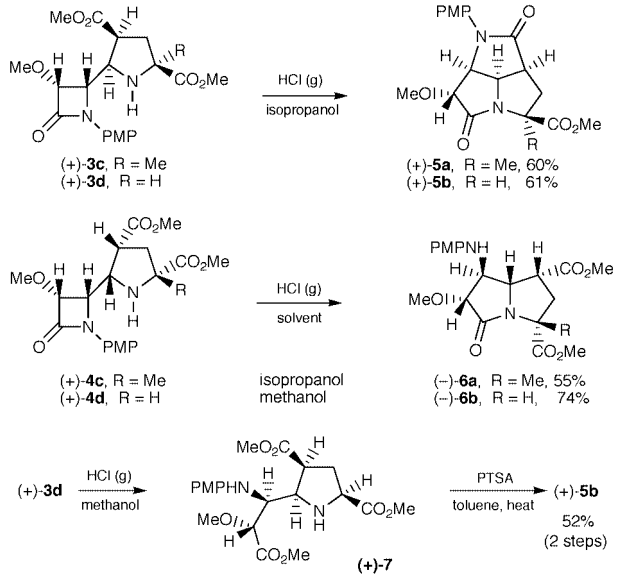

Scheme 2

In summary, we have demonstrated that the combination of 1,3-dipolar cycloaddition of 2-azetidinone-tethered azomethine ylides with rearrangement reactions on the 2-azetidinone ring is a powerful, hitherto unknown, strategy for the asymmetric synthesis of different types of highly functionalised pyrrolizidine systems. In addition, this methodology is very versatile offering the possibility of obtaining a variety of complex pyrrolizidine derivatives just by changing the substituents in readily available 4-oxoazetidine-2-carbaldehydes, α-amino-esters or dipholarophiles.

We thank the DGES (MEC-Spain, grant PB96-0565) for financial support. P. A. thanks the DGES (MEC, Spain) for a 'Contrato de Incorporación'. J. M. A. thanks the UCM for a predoctoral grant.

Notes and references

‡ During the evaluation of this manuscript a report appeared describing the 1,3-dipolar cycloaddition of closely related β-lactam azomethine ylides: R. Grigg, M. Thornton-Pett and L.-H. Xu, *Tetrahedron*, 1999, **55**, 13 841.

§ When DBU was used instead of Et_3N, complex mixtures of unidentified products were obtained, whereas pyridine gave erratic results. Perfoming the reaction in acetonitrile afforded poor yields of cycloadducts.

¶ *Representative experimental procedure* for the synthesis of pyrrolizidine systems: HCl(g) was bubbled, during 1 h, through an unstirred solution of the appropriate cycloadduct **3** or **4** (0.4 mmol) in isopropyl alcohol (6 ml) and the reaction solution left to stand in a sealed vessel for 36 h. The reaction mixture was concentrated under reduced pressure, diluted with dichloromethane (10 ml), washed with saturated aqueous sodium hydrogen carbonate and brine, dried ($MgSO_4$) and concentrated under reduced pressure. After purification by flash chromatography, pyrrolizidinones **5** and **6** were obtained in analytically pure form.

‖ Tricycle (+)-**5b** was alternatively obtained *via* heating overnight the adduct (+)-**3d** in methanol using 37% aqueous hydrochloric acid as a catalyst.

** All new compounds were fully characterised by spectroscopic methods and microanalysis and/or HRMS.

1 For reviews, see: G. Broggini and G. Zecchi, *Synthesis*, 1999, 905; K. V. Gothelf and K. A. Jorgensen, *Chem. Rev.*, 1998, **98**, 863.

2 For reviews, see: J. R. Liddell, *Nat. Prod. Rep.*, 1998, **15**, 363; J. P. Michael, *Nat. Prod. Rep.*, 1997, **14**, 619; H. Takahata and T. Momose, *The Alkaloids*, ed. G. A. Cordell, Academic Press, New York, 1993, vol. 26, p. 327; A. F. H. Rizk, *Naturally Ocurring Pyrrolizidine Alkaloids*, CRC Press, Boston, MA, 1991; A. R. Mattocks, *Chemistry and Toxicology of Pyrrolizidine Alkaloids*, Academic, New York, 1986.

3 A comprehensive investigation of the imine/azomethine ylide/cycloaddition cascade process for the synthesis of pyrrolizidine-type alkaloids has been carried out by Grigg. For recent references, see: R. Grigg, M. Thornton-Pett and G. Yoganathan, *Tetrahedron*, 1999, **55**, 8129; R. Grigg, S. Hargreves, J. Redpath, S. Turchi and G. Yoganathan, *Synthesis*, 1999, 441.

4 For reviews, see: I. Ojima, *The Organic Chemistry of β-Lactams*, ed. G. I. Georg, VCH Publishers, New York, 1993, p. 197; I. Ojima, *Adv. Asym. Synth.*, 1995, **1**, 95.

5 For a review, see: I. Ojima and F. Delaloge, *Chem. Soc. Rev.*, 1997, **26**, 377.

6 M. S. Manhas, D. R. Wagle, J. Chiang and A. K. Bose, *Heterocycles*, 1988, **27**, 1755; B. Alcaide, Y. Martín-Cantalejo, J. Pérez-Castells and M. A. Sierra, *J. Org. Chem.*, 1996, **61**, 9156 and references therein.

7 F. Cavagna, A. Linkies, H. Pietsch and D. Reuschling, *Angew. Chem., Int. Ed. Engl.*, 1980, **19**, 129.

8 C. Palomo, J. M. Aizpurua, C. Cuevas, P. Román, A. Luque and M. Martínez-Ripoll, *An. Quím. Int. Ed.*, 1996, **92**, 134.

9 B. Alcaide, P. Almendros and C. Aragoncillo, *Chem. Commun.*, 1999, 1913; B. Alcaide, I. M. Rodríguez-Campos, J. Rodríguez-López and A. Rodríguez-Vicente, *J. Org. Chem.*, 1999, **64**, 5377; B. Alcaide and P. Almendros, *Tetrahedron Lett.*, 1999, **40**, 1015.

10 B. Alcaide, Y. Martín-Cantalejo, J. Pérez-Castells, J. Rodríguez-López, M. A. Sierra, A. Monge and V. Pérez-García, *J. Org. Chem.*, 1992, **57**, 5921.

11 C. Palomo, F. P. Cossío, A. Arrieta, J. M. Odriozola, M. Oiarbide and J. M. Ontoria, *J. Org. Chem.*, 1989, **54**, 5736.

12 G. I. Georg and V. T. Ravikumar, in *The Organic Chemistry of β-Lactams*, ed. G. I. Georg, VCH, Weinheim, 1993, ch. 3, p. 295.

Communication b000249f

Aragonite $CaCO_3$ thin-film formation by cooperation of Mg^{2+} and organic polymer matrices

Ayae Sugawara and Takashi Kato*

Department of Chemistry and Biotechnology, Graduate School of Engineering, The University of Tokyo, Hongo, Bunkyo-ku, Tokyo 113-8656, Japan. E-mail: kato@chiral.t.u-tokyo.ac.jp

Received (in Cambridge, UK) 3rd December 1999, Accepted 15th February 2000

Aragonite thin films of calcium carbonate have been deposited on chitosan matrices by cooperation of chitosan, poly(aspartate) and $MgCl_2$ in $CaCO_3$ solution, and their double layered composite structures are obtained by the alternate operations of chitosan coating and thin-film crystallization.

Living organisms produce a great diversity of organic/inorganic composite materials by using interactions between biopolymers and inorganic substances. The nacre of mollusc shell, one of the most studied, has a laminated composite structure of $CaCO_3$ crystals in the aragonite polymorph and biological macromolecules such as chitin and silk-fibroin-like protein, which provides high mechanical strength and unusual optical properties.[1] Aragonite crystals are considered to enhance mechanical properties of the nacre owing to the absence of cleavage planes.[2] Polymorph control for aragonite crystals has been performed by the use of proteins extracted from shells,[3] synthetic polymers[4] and LB films.[5] A biofabrication method involving a biosystem, the mantle and shell of red abalone, led to the formation of flat aragonite films.[6] However, to our knowledge, no aragonite thin film has been formed by the use of simple polymers *in vitro*. Here, we report a synthetic approach to the fabrication of aragonite thin films which resemble a part of lamellar sheets in the nacre by using a cooperative effect of Mg^{2+} and organic polymers with simple repeating units.

For calcite and vaterite syntheses, thin films could be obtained on organic matrices such as polysaccharides[7,8] and aggregated amphiphilic molecules[9] in the presence of acid-rich macromolecules. In the present study, we selected poly(aspartate) (pAsp) as an organic additive. It was reported that aspartate-rich proteins are responsible for the controlled crystallization of $CaCO_3$ layers of shells.[1]

$CaCO_3$ was crystallized on chitosan matrices spin coated on glass substrates from supersaturated calcium hydrogen carbonate aqueous solution by slow evaporation of CO_2.† In the absence of additives, rhombohedral calcite crystals of size 10 μm were deposited, which suggests that the chitosan matrix does not solely exert any effects on the crystallization. In contrast, the addition of pAsp to the solution induced the deposition of thin film states of crystals with a homogeneous thickness, as shown in Fig. 1(a), for concentrations of pAsp between 4.4×10^{-4} and 1.0×10^{-2} wt%. The thickness of these films is *ca.* 1 μm. These thin films show circular symmetry around the center of nucleation. X-Ray diffraction patterns show that these crystals are mixtures of calcite, aragonite and vaterite [Fig. 2(a)]. The fraction of aragonite as well as vaterite increases with the concentration of pAsp.

To prepare thin films of high aragonite content, we added $MgCl_2$ ($Mg^{2+}/Ca^{2+} = 6$) to the solution in addition to pAsp as Mg^{2+} is known to induce aragonite formation.[10] Thin film crystals have also been deposited [Fig. 1(b)], although the appropriate concentration of pAsp is limited to *ca.* 4.4×10^{-4} wt%. The surface of the films is smoother than that without $MgCl_2$. X-Ray diffraction studies reveal that the fraction of aragonite in the films is 95 wt% or higher, and vaterite is absent [Fig. 2(b)]. By contrast, aragonite crystals with needle morphology were grown on chitosan matrices by the addition of $MgCl_2$

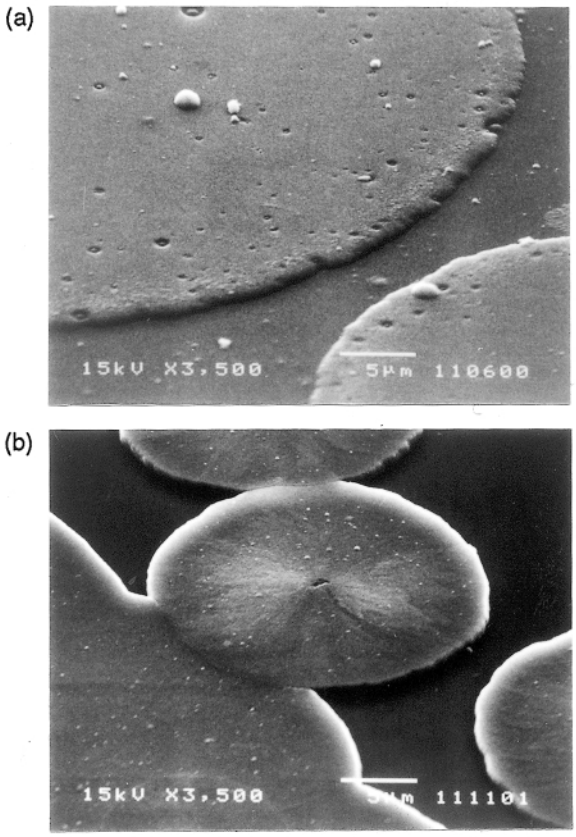

Fig. 1 Scanning electron micrographs of $CaCO_3$ thin films grown on chitosan matrices in the presence of pAsp (4.4×10^{-4} wt%): (a) in the absence of $MgCl_2$ and (b) in the presence of $MgCl_2$ ($Mg^{2+}/Ca^{2+} = 6$).

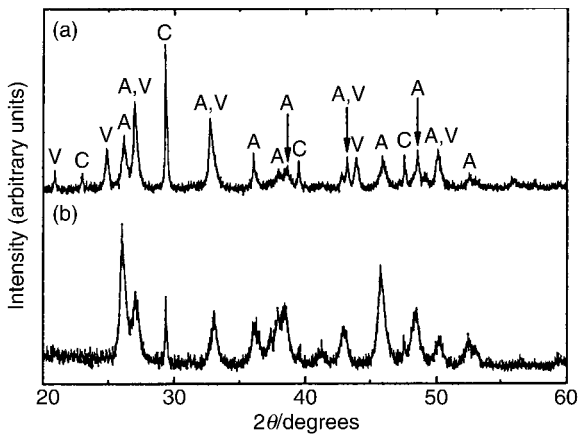

Fig. 2 X-Ray diffraction patterns of $CaCO_3$ thin films grown on chitosan matrices in the presence of pAsp (4.4×10^{-4} wt%): (a) in the absence of $MgCl_2$ and (b) in the presence of $MgCl_2$ ($Mg^{2+}/Ca^{2+} = 6$); aragonite (A), calcite (C) and vaterite (V).

DOI: 10.1039/a909566g

in the absence of pAsp. These results show that selective aragonite deposition by the addition of $MgCl_2$ and the formation of thin film crystals by chitosan and pAsp are compatible for aragonite thin-film formation. Furthermore, the stability of the film was so high that no flaking was observed upon microwave irradiation while needle-like aragonite crystals obtained with $MgCl_2$ in the absence of pAsp were observed to detach under such conditions.‡

By alternate operations of chitosan spin coating and aragonite crystallization,§ we could prepare double layered composite films of aragonite and chitosan. Fig. 3 shows an example of such a film; the upper aragonite layer has successfully grown on the underlying layer. It is expected that multi-layered composite materials resembling the nacreous structure can be prepared if adequate control is provided.

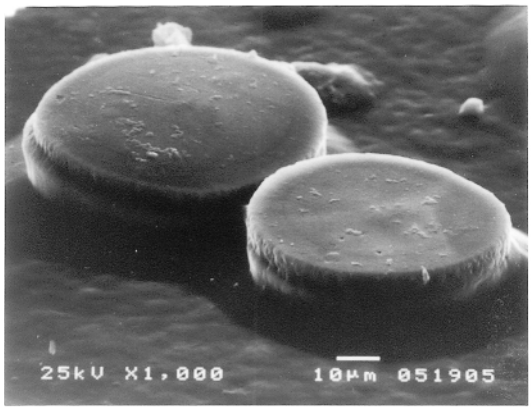

Fig. 3 Scanning electron micrograph of double layered aragonite thin films grown on a chitosan matrix in the presence of pAsp (4.4×10^{-4} wt%) and $MgCl_2$ ($Mg^{2+}/Ca^{2+} = 6$) by alternate spin coating and crystallization.

In summary, we have succeeded, for the first time, in the formation of aragonite thin films with a controlled homogeneous thickness. Double layer films have also been fabricated by the cooperative effect of $MgCl_2$ and functionalized organic polymers. These results offer potential for the design of high-performance organic/inorganic composite materials by simple synthetic procedures.

Partial financial support of a Grant-in-Aid for Scientific Research (No. 10875188) from the Ministry of Education, Science, Sports, and Culture is gratefully acknowledged.

Notes and references

† Crystals were grown from supersaturated calcium hydrogen carbonate solution in the presence of poly-L-(aspartic acid) sodium salt (DP = 360) (pAsp) and/or $MgCl_2$ at 30 °C. The detailed synthetic procedure has been described previously.[7] Polymorphs of $CaCO_3$ were studied by X-ray diffraction measurements. The fraction of aragonite in the crystals was calculated from the diffraction peak areas using a calibration curve obtained from crystal mixtures with known ratios of the polymorphs.

‡ The stability of the crystals formed on the matrix polymers was tested by microwave irradiation at 140 W for 30 min for the films placed in water.

§ After preparation of the aragonite thin films, chitosan was spin coated on them, and then $CaCO_3$ was subsequently crystallized.

1 S. Mann, in *Inorganic Materials*, ed. D. W. Bruce and D. O'Hare, Wiley, Chichester, 2nd edn., 1996, p. 255; L. Addadi and S. Weiner, *Proc. Natl. Acad. Sci. USA*, 1985, **82**, 4110; L. Addadi and S. Weiner, *Nature*, 1997, **389**, 912; N. Watabe, *J. Ultrastruct. Res.*, 1965, **12**, 351; I. A. Aksay, M. Trau, S. Manne, I. Honma, N. Yao, L. Zhou, P. Fenter, P. M. Eisenberger and S. M. Gruner, *Science*, 1996, **273**, 892.

2 S. Weiner and L. Addadi, *J. Mater. Chem.*, 1997, **7**, 689.

3 A. M. Belcher, X. H. Wu, R. J. Christensen, P. K. Hansma, G. D. Stucky and D. E. Morse, *Nature*, 1996, **381**, 56; G. Falini, S. Albeck, S. Weiner and L. Addadi, *Science*, 1996, **271**, 67.

4 Y. Levi, S. Albeck, A. Brack, S. Weiner and L. Addadi, *Chem. Eur. J.*, 1998, **4**, 389.

5 A. L. Litvin, S. Valiyaveettil, D. L. Kaplan and S. Mann, *Adv. Mater.*, 1997, **9**, 124.

6 M. Fritz, A. M. Belcher, M. Radmacher, D. A. Walters, P. K. Hansma, G. D. Stucky, D. E. Morse and S. Mann, *Nature*, 1994, **371**, 49.

7 T. Kato, T. Suzuki, T. Amamiya, T. Irie, M. Komiyama and H. Yui, *Supramol. Sci.*, 1998, **5**, 411; T. Kato and T. Amamiya, *Chem. Lett.*, 1999, 199.

8 S. Zhang and K. E. Gonsalves, *Langmuir*, 1998, **14**, 6761.

9 G. Xu, N. Yao, I. A. Aksay and J. T. Groves, *J. Am. Chem. Soc.*, 1998, **120**, 11977.

10 Y. Kitano, *Bull. Chem. Soc. Jpn.*, 1962, **35**, 1973; D. Walsh and S. Mann, *Nature*, 1995, **377**, 320; G. Falini, S. Fermani, M. Gazzano and A. Ripamonti, *Chem. Eur. J.*, 1997, **3**, 1807; G. Falini, M. Gazzano and A. Ripamonti, *J. Cryst. Growth*, 1994, **137**, 577; N. Wada, K. Yamashita and T. Umegaki, *J. Colloid Interface Sci.*, 1999, **212**, 357.

Communication a909566g

Unusual stability of the coordinated triethylborohydride anion in an alkaline-earth metal complex: crystallographic characterization of $[Ca(HBEt_3)\{1,2,4\text{-}C_5(SiMe_3)_3H_2\}(thf)_2]$

Melanie J. Harvey,[a] Timothy P. Hanusa*[a] and Maren Pink[b]

[a] *Department of Chemistry, Vanderbilt University, Nashville, TN 37235, USA. E-mail: t.hanusa@vanderbilt.edu*
[b] *Chemistry Department, University of Minnesota, Minneapolis, MN 55455, USA*

Received (in Bloomington, IN, USA) 1st November 1999, Accepted 11th February 2000

The triethylborohydride anion $[HBEt_3]^-$ transfers intact from $Na[HBEt_3]$ to a calcium center to form the monomeric organocalcium complex $[Ca(HBEt_3)\{1,2,4\text{-}C_5(SiMe_3)_3H_2\}(thf)_2]$, which is stable in solution and the solid state; the $[HBEt_3]^-$ anion is coordinated in a multidentate fashion to the metal, which likely contributes to the failure of attempts to abstract the triethylborane moiety from the compound.

Owing to its exceptional nucleophilicity and selectivity, the triethylborohydride anion ($[HBEt_3]^-$) has found extensive use in organic, organometallic, and materials chemistry as a reducing agent and hydride source.[1–5] Study of the structure and bonding of the $[HBEt_3]^-$ anion itself is complicated by its high reactivity; it is usually encountered only in the form of its Group 1 (Li–K) salts, and is rarely incorporated into complexes containing other metals.[6–8] When the latter is the case, the stability of the resulting compounds may not be high; the organolanthanide species $[Sm(C_5H_4Bu^t)_2(HBEt_3)(thf)_2]$[7] and $[Nd(C_5H_4Bu^t)_2(HBEt_3)]$,[8] for example, cannot be removed from solution without decomposing. We have been interested in the $[HBEt_3]^-$ anion as a synthon for molecular main-group element hydrides, and in the course of this work discovered the unusual stability and structural features of the triethylborohydride anion in a Group 2 complex.

Parallels between the structure and reactions of the heavier Group 2 and divalent lanthanide elements[9] suggest that an alkaline-earth mono(cyclopentadienyl) halide might serve as a precursor to an organometallic hydride by metathetical reaction with an appropriate hydride source.[10,11] To examine this possibility, the iodide-bridged dimer $\{Ca(\mu\text{-}I)[1,2,4\text{-}C_5(SiMe_3)_3H_2](thf)\}_2$[12] was allowed to react in toluene with $Na[HBEt_3]$; removal of the NaI precipitate and evaporation of the filtrate left an air- and moisture-sensitive white solid that could be recrystallized from thf and was characterized as the triethylborohydride complex $[Ca(HBEt_3)\{1,2,4\text{-}C_5(SiMe_3)_3H_2\}(thf)_2]$ **1**.†

Spectroscopic evidence indicates that the $[HBEt_3]^-$ anion in **1**, which has transferred intact from Na^+, is involved in a bridging $Ca\cdot\cdot H\cdot\cdot BEt_3$ interaction. A prominent B–H stretch occurs at 1935 cm^{-1} (KBr) in the IR spectrum, in the region associated with μ-BH bonds.[13] This vicinity is where ν(BH) appears in $M[HBEt_3]$ salts [1870, 1835 and 1950 cm^{-1} for M = Li (KBr), Na (cyclohexane) and K (toluene), respectively].[14] The ^{11}B NMR resonance (δ −13.3 in C_6D_6; J_{B-H} 50 Hz) of **1** is characteristic of a bridging BH contact (*cf.* 60–90 Hz for J_{B-H_b} in transition metal examples),[15] and is also similar to that of $Na[HBEt_3]$ (δ −12.5; J_{B-H} 50 Hz).[16]

An X-ray diffraction study of **1** provided the first details of the bonding of the triethylborohydride anion to an element other than a Group 1 metal.‡ The compound crystallizes from thf as a monomer, with the calcium center surrounded by a $[\eta^5\text{–}C_5(SiMe_3)_3H_2]^-$ ring, two thf molecules and the $[HBEt_3]^-$ ligand (Fig. 1). The average Ca–C(ring) and Ca–ring centroid distances of 2.707(9) and 2.42 Å in **1** are comparable to those in $\{Ca(C_5Pr^i_4H)[C{\equiv}CPh](thf)\}_2$ [2.713(15) and 2.43 Å, respectively],[17] which contains a formally seven-coordinate Ca^{2+} center.

In **1**, the calcium–carbon distances reflect the multidentate ligation of the triethylborohydride anion to the metal. The hydrogen atom on B(1) was located from difference maps and successfully refined, with B(1)–H(1) and Ca(1)–H(1) distances of 1.13(4) and 2.21(4) Å, respectively, and a Ca(1)–H(1)–B(1) angle of 110(2)°. These values are similar to those observed for the $[HBEt_3]^-$ anion in, for example, the dimeric complex $[Nb_2(hexahydropyrimido\{1,2\text{-}a\}pyrimidinate)_4\bullet NaHBEt_3]$ (B–H 1.24, Na···H(B) 2.17 Å; Na–H–B 108°).[18] In **1**, the niobium dimer, and in related compounds such as $[Pd_2(dippp)_2\text{-}H_2]\bullet[(Li,Na)(BEt_4)]$ [dippp = 1,3-bis(diisopropylphosphino)-propane][19] and $[TaH_5(dmpe)_2]\bullet[LiBEt_4]$,[20] there is a close contact between the metal center and a methylene hydrogen on one or more ethyl groups. In **1**, the methylene hydrogen positions are calculated from the carbon atom locations, so the Ca···H(α-C) distance is not as reliable as is the Ca···H(B) separation. Even so, the Ca···H(25a) contact in **1** (2.41 Å)

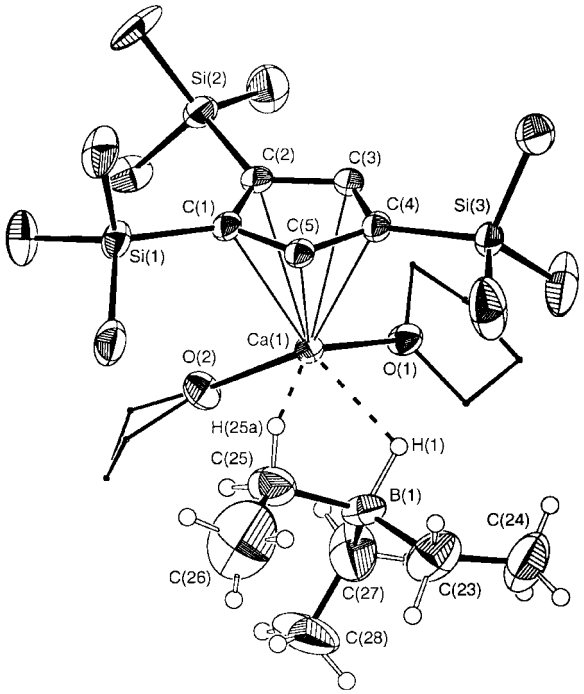

Fig. 1 ORTEP diagram of $[Ca(HBEt_3)\{1,2,4\text{-}C_5(SiMe_3)_3H_2\}(thf)_2]$ **1**. The trimethylsilyl groups on C(1) and C(2) were found to be disordered; for clarity, only one conformation for each is shown. Selected bond distances (Å) and angles (°): Ca(1)–C(1) 2.733(4), Ca(1)–C(2) 2.764(4), Ca(1)–C(3) 2.685(4), Ca(1)–C(4) 2.676(4), Ca(1)–C(5) 2.679(4), Ca(1)–C(19) 2.84(2), Ca(1)–O(1) 2.386(3), Ca(1)–O(2) 2.367(3), B(1)–C(23) 1.629(9), B(1)–C(25) 1.629(8), B(1)–C(27) 1.610(8), B(1)–H(1) 1.13(4); O(1)–Ca(1)–O(2) 86.3(1), Ca(1)–H(1)–B(1), 110(2).

DOI: 10.1039/a908674i

appears to be structurally significant, and the triethylborohydride group should be regarded as binding through both H(1) and H(25a).

The triethylborohydride anion in **1** proves to be remarkably robust, and several approaches to removing the BEt_3 moiety from **1** have been unsuccessful. For example, no reaction is observed with the competing base PMe_3 in toluene, and refluxing a solution of **1** in toluene leads to decomposition and the formation of the metallocene [Ca{η^5-1,2,4-C_5(SiMe_3)$_3H_2$}].[21] The bidentate bonding of the $[HBEt_3]^-$ anion to the calcium evidently strengthens the attachment of the BEt_3 fragment.

Several features of the complex are worth noting. (i) The similarity of the bonding arrangement of the triethylborohydride anion in **1** to complexes of the alkali metals may indicate that this is its typical ligation geometry to highly electropositive metals. The structure of **1** may thus serve as a model for the triethylborohydride complexes of the lanthanide elements, which have yet to be structurally characterized.[6–8]

(ii) The resistance of the BEt_3 moiety to removal from **1** may stem from several factors. Heavy organoalkaline-earth complexes containing the bulky 1,2,4-tris(trimethylsilyl)cyclopentadienyl ligand are kinetically stabilized against ligand redistribution,[12] and the presence of the thf ligands enables **1** to remain coordinately saturated without having to oligomerise. These structural features combined with the bidentate ligation of the $[HBEt_3]^-$ ion probably leave it without a facile pathway for decomposition. Knowledge of these bonding requirements may help in the use of the triethylborohydride anion with other metals.

Acknowledgment is made to the National Science Foundation for support of this research.

Notes and references

† To a flask with {Ca(μ-I)[1,2,4-C_5(SiMe_3)$_3H_2$](thf)}$_2$ (0.331 g, 0.64 mmol) dissolved in 50 mL of toluene was added a solution of Na[$HBEt_3$] (0.64 mL of a 1.0 M solution in toluene, 0.64 mmol) at room temperature. The reaction mixture was stirred for 30 min before filtration, and the filtrate evaporated to dryness. Recrystallisation of the crude product from thf led to [Ca($HBEt_3$){1,2,4-C_5(SiMe_3)$_3H_2$}(thf)$_2$] as air-sensitive, colorless crystals (0.285 g, 79%), mp 152 °C. Anal. Calc. for $C_{28}H_{61}BCaO_2Si_3$: C, 59.53; H, 10.88. Found: C, 58.18; H, 10.61%. The low value for carbon probably reflects the high air-sensitivity of the compound and/or partial loss of coordinated thf. Note for [Ca($HBEt_3$){1,2,4-C_5(SiMe_3)$_3H_2$}(thf)]: C, 58.49; H, 10.84%. ^{1}H NMR (300 MHz, thf-d_8, 20 °C): δ −0.03 (br, 6H, CH_2CH$_3$), 0.20 [s, 9H, Si(CH$_3$)$_3$], 0.27 [s, 18H, Si(CH$_3$)$_3$], 0.79 (t, ^3J 7.5 Hz, 9H, CH$_2$CH_3), 6.85 (s, 2H, ring-C*H*). ^{13}C NMR (75.5 MHz, thf-d_8, 20 °C): δ 1.0 [s, 1C, Si(CH$_3$)$_3$], 2.5 [s, 2C, Si(CH$_3$)$_3$], 12.7 (s, 3C, CH$_2$CH_3), 122.7 [s, 1C, ring-*C*Si(CH$_3$)$_3$], 127.8 [s, 2C, ring-*C*Si(CH$_3$)$_3$], 132.4 (s, 2C, ring-CH). No signal was observed from the carbon atoms on the boron. Principal IR bands (KBr, cm^{-1}): 2952 vs, br, 2898s, 1935m, br, 1456m, 1427m, 1407m, 1250vs (sh), 1089ms, 1062ms 1024ms, 979m, 831vs, br, 753s sh, 688m.

‡ *Crystal data* for $C_{28}H_{61}BCaO_2Si_3$ **1**: M = 564.93, orthorhombic, a = 22.306(2), b = 19.9944(9), c = 16.009(2) Å, U = 3568.9(6) Å^3, T = 173 ± 2 K, space group $Pna2_1$ (no. 33), Z = 4, μ(Mo-Kα) = 0.297 mm^{-1}, 24468 reflections measured, 6321 unique (R_{int} = 0.055) which were used in all calculations. The final $wR(F^2)$ was 0.1316 (all data) and 0.1175 [for 4440 reflections with $I > 2.0\sigma(I)$]. Single crystals of **1** were grown from toluene, attached to the tip of a 0.1 mm diameter glass capillary and transferred to the cold gas stream of a diffractometer at the University of Minnesota. The structure was solved using a combination of direct methods and Fourier difference maps, and refined by full-matrix least squares on F^2. CCDC 182/1544. See http://www.rsc.org/suppdata/cc/a9/a908674i/ for crystallographic files in .cif format.

1 J. A. Gladysz, *Aldrichim. Acta*, 1979, **12**, 13.
2 E. R. Burkhardt, *Chim. Oggi-Chem. Today*, 1998, **16**, 6.
3 T. D. Xiao, S. Torban, P. R. Strutt and B. H. Kear, *Nanostruct. Mater.*, 1996, **7**, 857.
4 C. K. Yee, R. Jordan, A. Ulman, H. White, A. King, M. Rafailovich and J. Sokolov, *Langmuir*, 1999, **15**, 3486.
5 H. Boennemann, W. Brijoux, R. Brinkmann, R. Fretzen, T. Joussen, R. Koeppler, B. Korall, P. Neiteler and J. Richter, *J. Mol. Catal.*, 1994, **86**, 129.
6 L. Hasinoff, J. Takats, X. W. Zhang, A. H. Bond and R. D. Rogers, *J. Am. Chem. Soc.*, 1994, **116**, 8833.
7 D. Baudry, A. Dormond, B. Lachot, M. Visseaux and G. Zucchi, *J. Organomet. Chem.*, 1997, **547**, 157.
8 M. Visseaux, D. Baudry, A. Dormond and C. Qian, *J. Organomet. Chem.*, 1999, **574**, 213.
9 T. P. Hanusa, *Chem. Rev.*, 1993, **93**, 1023.
10 T. Cuenca, M. Galakhov, E. Royo and P. Royo, *J. Organomet. Chem.*, 1996, **515**, 33.
11 R. B. Grossman, R. A. Doyle and S. L. Buchwald, *Organometallics*, 1991, **10**, 1501.
12 M. J. Harvey and T. P. Hanusa, *Organometallics*, in the press.
13 K. Nakamoto, *Infrared and Raman spectra of Inorganic and Coordination Compounds*, John Wiley, New York, 5th ed., 1997, vol. A. p. 356.
14 P. Binger, G. Benedikt, G. W. Rotermund and R. Koester, *Liebigs Ann. Chem.*, 1968, **717**, 21.
15 D. L. Reger, R. Mahtab, J. C. Baxter and L. Lebioda, *Inorg. Chem.*, 1986, **25**, 2046 and references therein.
16 J. L. Hubbard, *J. Chem. Soc., Chem. Commun.*, 1989, 1639.
17 D. J. Burkey and T. P. Hanusa, *Organometallics*, 1996, **15**, 4971.
18 F. A. Cotton, J. H. Matonic and C. A. Murillo, *J. Am. Chem. Soc.*, 1998, **120**, 6047.
19 M. D. Fryzuk, B. R. Lloyd, G. K. B. Clentsmith and S. J. Rettig, *J. Am. Chem. Soc.*, 1994, **116**, 3804.
20 D. M. Dawson, A. Meetsma, J. B. Roedelof and J. H. Teuben, *Inorg. Chim. Acta*, 1997, **259**, 237.
21 M. J. Harvey, T. P. Hanusa and V. G. Young, Jr., in preparation

Communication a908674i

ChemComm

Pyrrole as an NMR probe molecule to characterise zeolite basicity

Manuel Sánchez-Sánchez and Teresa Blasco*

Instituto de Tecnología Química (UPV-CSIC), Avenida de los Naranjos s/n 46022-Valencia, Spain. E-mail: tblasco@itq.upv.es

Received (in Cambridge, UK) 21st January 2000, Accepted 10th February 2000

The ^{1}H NMR chemical shift of the N–H group of pyrrole adsorbed on alkali metal ion exchanged FAU-type zeolites depends on the zeolite intrinsic basicity, while, as shown for zeolite LiY, the NMR of alkali metal nuclei reflects the interaction of the aromatic cycle with the cations at sites SII.

Zeolite molecular sieves have been extensively investigated mainly due to their application as acidic catalysts in the chemical and petrochemical industry. The large social and economical impact of such processes when compared with those using base catalysts can explain why much less attention has been paid to zeolite basicity. Only recently it has been realized that basic zeolites can also be successfully used as catalysts and have gained a growing interest in the last decade.[1,2]

Basic zeolites are, by definition, non-protonic, and the negative charge created by the presence of aluminium atoms into the network are compensated by extraframework usually monovalent metal cations. The zeolite oxygen atoms act as Lewis basic sites, while the compensating cations act as Lewis acid sites, forming an acid–base pair. The so-called intrinsic zeolite basicity increases with the negative charge on the oxygens, which is determined by their framework structure and chemical composition. The basic strength of zeolites is strongly enhanced by increasing the framework aluminium content, and for a given Si/Al molar ratio, when the electronegativity of the compensating cation decreases. These results can be understood in terms of the average charges over oxygen atoms calculated using the Sanderson principle of equalization of electronegativities based on the zeolite chemical composition.[3] whereas the effect of the crystalline structure was quantified by the more sophisticated electronegativity equalization method (EEM).[4]

The most used method to characterize zeolite basicity uses pyrrole as an IR probe molecule and is based on the shift to lower frequencies of the pyrrole N–H stretching band when the framework basicity increases.[1] Pyrrole is an amphoteric molecule which can interact with zeolite basic sites forming hydrogen bonds between the N–H group and framework oxygen atoms, and with cationic acid sites by donation of charge from its aromatic five-membered heterocycle. Hydrogen bonding is clearly shown by the shift of the IR N–H stretching frequency, while the pyrrole–cation interaction is only suggested from the IR CH out of plane deformation bands[5,6] and by theoretical calculation,[6,7] however, no direct experimental evidence has been reported so far. Here, we show that the ^{1}H NMR chemical shift of the N–H group of pyrrole adsorbed over basic zeolites is a very sensitive probe to measure the average intrinsic basicity, with the advantage that the NMR spectra of alkali metal nuclei provides direct information about the pyrrole–cation interaction, as illustrated for zeolite LiY.

The chemical composition of the zeolites X and Y used here were described previously.[8] Zeolites LiY, KY, CsY and LiX, KX also contains Na^+ as compensating cation owing to incomplete exchange. Samples were heated under dynamic vacuum at 673 K for 12 h up to a final pressure of $< 10^{-5}$ kPa, then contacted with the vapor pressure of pyrrole at room temperature for 5 min and subsequently evacuated at 338 K for 30 min to eliminate physisorbed pyrrole.

The ^{1}H NMR spectra of adsorbed pyrrole (Fig. 1), shows three peaks of relative intensity 1:2:2 corresponding to the three types of protons in the molecule. The less intense peak is due to the N–H group, whereas the other two are from the four C–H protons in the five-membered heterocycle; the two C–H groups in α and the two in β positions give rise to the intermediate and high field resonances, respectively. The N–H peak of liquid pyrrole appears at δ 7.1 and shifts to higher frequency when it is adsorbed on alkali zeolites X and Y, to an extent that depends on the sample. From the chemical composition and the characterization performed by other methods, the intrinsic basicity of the zeolites used here increases in the order LiY < NaY < KY < LiX < CsY < NaX < KX.[8] Therefore, the N–H proton resonance shifts to higher frequency when the framework basicity increases, giving differences of up to 3 ppm between LiY and KX (Fig. 1). This shift can be understood by the higher polarization of the N–H bond, which forms hydrogen bonds with the framework oxygen atoms, when the intrinsic zeolite basicity increases.

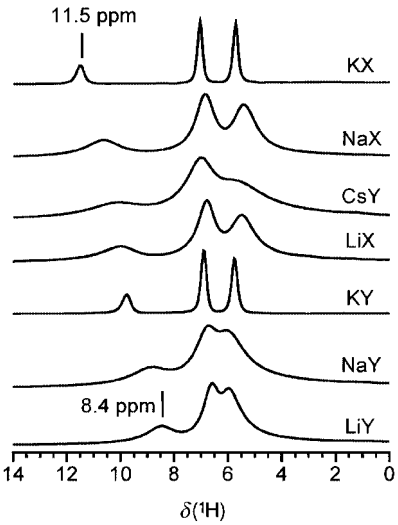

Fig. 1 ^{1}H magic angle spinning (MAS) NMR spectra of pyrrole adsorbed over the zeolites indicated. The samples were prepared by the method described in the text and transferred into the rotors in a glove box. The spectra were recorded at room temperature with a Varian VXR-S 400-WB spectrometer at 399.9 MHz, using a VT CP/MAS Varian probe with 5 mm silicon nitride rotors spinning at 13 kHz. $\pi/2$ rad pulses of 6 μs and a recycle delay of 5 s were used.

At the same time, solid state NMR of alkali metal cations reveals their interaction with the guest molecules as illustrated in Fig. 2 for zeolite LiY, where the degassing temperature after the pyrrole adsorption was varied. Very recently, an upfield shift of the ^{7}Li resonance has been reported to occur after the adsorption of benzene over Li-ZSM-5 as a result of 1:1 π-complexation between Li^+ and benzene, as confirmed by *ab initio* calculation of ^{7}Li chemical shifts.[9] Fig. 2(a) shows the ^{7}Li NMR spectrum of bare LiY, consisting of a peak formed by two

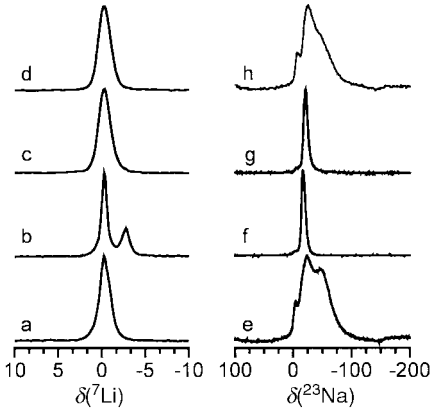

Fig. 2 ^{7}Li and ^{23}Na magic angle spinning (MAS) NMR spectra of: (a) and (e) bare zeolite LiY. Sample LiY after the adsorption of pyrrole at room temperature and evacuation at: (b) and (f) 338 K; (c) and (g) 423 K; (d) and (h) 473 K. The ^{7}Li and ^{23}Na spectra were recorded at room temperature with a Varian VXR-S 400-WB spectrometer at 155.4 and 105.8 MHz, respectively, using a VT CP/MAS Varian probe with 5 mm silicon nitride rotors spinning at 13 kHz. To record both ^{7}Li and ^{23}Na MAS NMR spectra, pulses of 1.5 μs to flip the magnetization π/8 rad and a recycle delay of 1 s were applied. ^{7}Li and ^{23}Na chemical shifts are referred to 0.1 M solutions of LiCl and NaCl, respectively.

overlapping signals at δ −0.2 and −1.0 which can be assigned to lithium atoms in front of six-ring windows at sites SI′ and SII in the sodalite and super-cages, respectively, of the faujasite structure, in agreement with published results for LiX.[10] From chemical analysis and NMR results the site occupancy per unit cell in zeolite LiY is 24 Li^+ at site SI′ and 10 at SII positions. As shown in Fig. 2(b), after pyrrole adsorption and subsequent evacuation at 338 K, the peak from ^{7}Li cations at sites SI′ remains at the same position, while the resonance from ^{7}Li atoms at sites SII shifts to δ −2.8 indicating the direct interaction of accessible Li cations with the π electrons of the pyrrole ring. As is apparent from Fig. 2(c), these pyrrole species are desorbed at 423 K and the original ^{7}Li spectrum is recovered. The corresponding ^{23}Na MAS NMR spectra are shown in Fig. 2(e)–(h). The ^{23}Na spectrum of bare LiY [Fig. 2(e)] shows a peak at δ −3 for cations within the hexagonal prism at site SI, and two broad bands from quadrupolar signals of sodium at sites SI′ and SII.[11] The site population per unit cell is *ca.* 0.8 Na^+ at SI and 20 Na^+ atoms at sites SII and SI′ (with a higher population of SII). After the adsorption of pyrrole, the signal from Na^+ at sites SI remains unchanged while the quadrupole coupling constant (QCC) of sodium atoms at sites SII and SI′ strongly decreases, as shown in Fig. 2(f). Consistent with the results for ^{7}Li, the modification of the ^{23}Na NMR signal of cations at sites SII must be attributed to direct interaction with the aromatic system of the pyrrole molecules. The changes observed for the ^{23}Na signal of Na^+ at site SI′, which are inaccessible to pyrrole molecules, could be attributed to the influence of pyrrole adsorption on nearby oxygen atoms, or interpreted in terms of cation migration to accessible positions.[12] The ^{23}Na spectrum of bare LiY zeolite is almost recovered and only some residual pyrrole is evident after evacuation at 473 K [Figs. 2(f)–(h)]. Simultaneously, the ^{1}H resonance of the pyrrole N–H group progressively shifts to higher frequency (up to 0.5 ppm) when the degassing temperature is increased to 473 K, indicating that pyrrole species at more basic sites remain.

The results reported here confirm the model proposed for the adsorption of pyrrole over alkali metal exchanged zeolites of FAU-type structure based on theoretical calculations.[6,7] Pyrrole adsorbs on zeolites Y at cations at sites SII by interaction of its aromatic ring, and the N–H group points towards framework basic oxygen sites forming hydrogen bonds.[6,7] For zeolite LiY, basic centres involving SII sites occupied by Na^+ are more basic than those occupied by Li^+, although the overall intrinsic zeolite basicity is also modified by the type of compensating cation. Heterogeneity of the basic sites is directly observed by the appearance of several components in the N–H stretching band of pyrrole adsorbed over basic zeolites,[1,13] which are not reflected in the ^{1}H MAS NMR spectra because of the different time scale of both spectroscopic techniques. However, the interpretation of the IR spectra is still controversial,[7,13] and the use of solid state NMR can shed some light in the knowledge of the host–guest interactions between the probe molecules and basic zeolites and the nature of the adsorbed species.

Financial support by the CICYT (Project MAT 97-1016-C02-01) is gratefully acknowledged.

Notes and references

1 D. Barthomeuf, *Catal. Rev.-Sci. Eng.*, 1996, **38**, 521.
2 A. Corma, *Mater. Res. Soc. Symp. Proc.*, 1991, **233**, 17.
3 W. J. Mortier, *J. Catal.*, 1978, **55**, 138.
4 K. A. Van Genechten and W. J. Mortier, *Zeolites*, 1988, **8**, 273; W. J. Mortier, *Stud. Surf. Sci. Catal.*, 1988, **37**, 253.
5 M. Huang and S. Kaliaguine, *J. Chem. Soc., Faraday Trans.*, 1992, **88**, 751.
6 H. Förster, H. Fuess, E. Geidel, B. Hunger, H. Jobic, C. Kirschhock, O. Klepel and K. Krause, *Phys. Chem. Chem. Phys.*, 1999, **1**, 593.
7 R. Heidler, G. O. A. Janssens, W. J. Mortier and R. A. Schoonheydt, *Microporous Mater.*, 1997, **12**, 1.
8 M. Sánchez-Sánchez. T. Blasco and F. Rey, *Phys. Chem. Chem. Phys.*, 1999, **1**, 4529.
9 D. H. Barich, T. Xu, J. Zhang and J. F. Haw, *Angew. Chem., Int. Ed.*, 1998, **37**, 2530.
10 M. Feuerstein, G. Engelhardt, P. L. McDaniel, J. E. McDougall and T. R. Gaffney, *Microporous Mesoporous Mater.*, 1998, **26**, 27.
11 M. Feuerstein, M. Hunger, G. Engelhardt and J. P. Amoureux, *Solid State Nucl. Magn. Reson.*, 1996, **7**, 95.
12 C. P. Grey, F. I. Poshni, A. F. Gualtieri, P. Norby, J. C. Hanson and D. R. Corbin, *J. Am. Chem. Soc.*, 1997, **119**, 1981.
13 D. Murphy, P. Massiani, R. Franck and D. Barthomeuf, *J. Phys. Chem.*, 1996, **100**, 6731.

Communication b000609m

ChemComm

Using a large calixarene as a polyalkoxide ligand: *tert*-butylcalix[12]arene and its complex with the uranyl cation

Pascal C. Leverd,*[a] Isabelle Dumazet-Bonnamour,[b] Roger Lamartine[b] and Martine Nierlich[a]

[a] *CEA-Saclay, Service de Chimie Moléculaire, Bât. 125, 91191 Gif sur Yvette, France. E-mail: leverd@drecam.cea.fr*
[b] *Laboratoire de Chimie Industrielle, CNRS-UMR 5078, Université Claude Bernard, 69622 Villeurbanne, France*

Received (in Basel, Switzerland) 31st January 2000, Accepted 16th February 2000

***tert*-Butylcalix[12]arene ($H_{12}L$) encompasses two uranyl bimetallic units inside its cavity to form $[HNEt_3]_2[\{(UO_2)_2(NO_3)(py)\}_2(H_4L)]$ 1, the first metal complex of a large calixarene; the comparison of the crystal structures of 1 and $H_{12}L$ shows a relatively limited influence of metal coordination on the conformation of the macrocycle.**

The coordination chemistry of the calixarenes exclusively concerns calix[4,5,6,7 and 8]arenes and their various derivatives.[1,2] Working with the large calix[$n > 8$]arenes is considered a challenge and very little organic and physical chemistry has been reported for this class of molecules.[3] The calixarene with the highest number of phenolic units for which structural information is currently available is calix[8]arene.[4] The major interest of the calix[$n > 8$]arenes in coordination chemistry is that these large and flexible polyalkoxide ligands have the potential to assemble several metallic units inside their cavity and could lead to new molecular architectures. In an attempt to widen the use of calixarenes in coordination chemistry, we set out to study *tert*-butylcalix[12]arene ($H_{12}L$)[3a,b] as a ligand for the uranyl cation. We report herein, the crystal structure of $H_{12}L\cdot10py$, the first of a large calixarene, and comparison with that of $[HNEt_3]_2[\{(UO_2)_2(NO_3)(py)\}_2(H_4L)]$ **1**, the first metal complex with a ligand of this class. To the best of our knowledge, **1** is a unique example of an organic macrocycle binding two bimetallic species inside its cavity.

Crystals of $H_{12}L$ suitable for X-ray crystallography were obtained from pyridine–acetonitrile (1:1) (0.050 g $H_{12}L$ in 10 ml) that was slowly evaporated at 290(1) K over 180 days.†‡ The structure was solved and revealed $H_{12}L\cdot10py$ a pyridine solvate of the fully protonated macrocycle (Fig. 1). In the solid state, $H_{12}L$ is located around a crystallographic centre of inversion. All its phenolic groups engage in strong H-bonding. Four successive intramolecular H-bonds are formed between O(4), O(3), O(2), O(1) and O(6) while O(5) and O(6) bind to pyridine molecules. The all-in conformation of the calixarene is at first reminiscent of that described for *tert*-butylcalix[8]arene.[5] However, a closer look at the dihedral angles between the adjacent phenolic faces indicates that the conformation cannot be described as a pleated loop or a cone.[6,7] In order to define the overall shape of the macrocycle, attention was paid to the relative positions of the phenolic rings [the centroid of the ring bearing O(n) is denoted X(n)]. X(2), X(5) and their two symmetry equivalents define a perfect plane above which are located X(3) and X(4) (+1.37 and +2.50 Å, respectively) and below which are positioned X(1) and X(6) (−4.70 and −3.90 Å, respectively). With this work, $H_{12}L$ becomes the first large calixarene to have its solid state conformation determined by X-ray crystallography.

When $UO_2(NO_3)_2\cdot6H_2O$ was treated with $H_{12}L$ in the presence of NEt_3 in pyridine, a red solution typical of a phenolate complex of uranyl was immediately obtained. The solution was allowed to stand and after a few days a red microcrystalline powder of **1** was obtained as the sole reaction product in 46% yield.†

The synthesis was repeated in a crystallisation vessel (10 mL) which was allowed to stand at 290(1) K. After 180 days, very small crystals suitable for X-ray crystallography were isolated from the same mixture of solvent as for $H_{12}L$.‡ The structure was solved and revealed a complex in which four uranyl cations are encompassed by the macrocyclic ligand (Fig. 2).

As for $H_{12}L$, **1** is located around a centre of symmetry in the solid state. The four uranyl dications form two symmetry related bimetallic units in which the two metal cations are bound by a tridentate nitrate ligand. Such a bis-chelating binding mode of $[NO_3]^-$ is not unusual for solid state polymers, however, it is more rarely found for discrete metal complexes.[8,9] The bimetallic units are bound to the macrocycle through five of its oxygen atoms, four of which are deprotonated [O(1), O(2), O(4) and O(5)]. The resulting short U–O distances (*ca.* 2.2 Å) are typical of uranyl phenolate complexes while the longer U(1)–O(3) distance [2.62(3) Å] corresponds to the dative bond

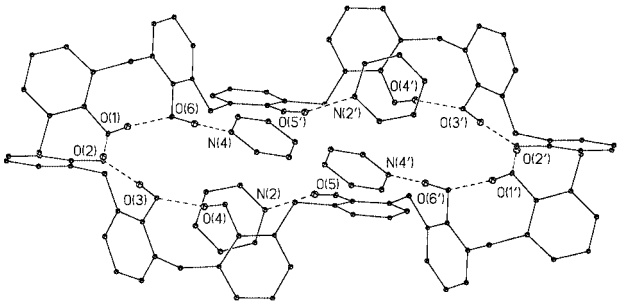

Fig. 1 Crystal structure of compound $H_{12}L$ (5% probability). All Bu^t groups and H atoms or solvent molecules not participating in H-bonding have been omitted for clarity. H-bond donor–acceptor distances (Å): O(1)–O(6) 2.57(3), O(2)–O(1) 2.63(3), O(3)–O(2) 2.61(3), O(4)–O(3) 2.66(3), O(5)–N(2) 2.82(4), O(6)–N(4) 2.56(4).

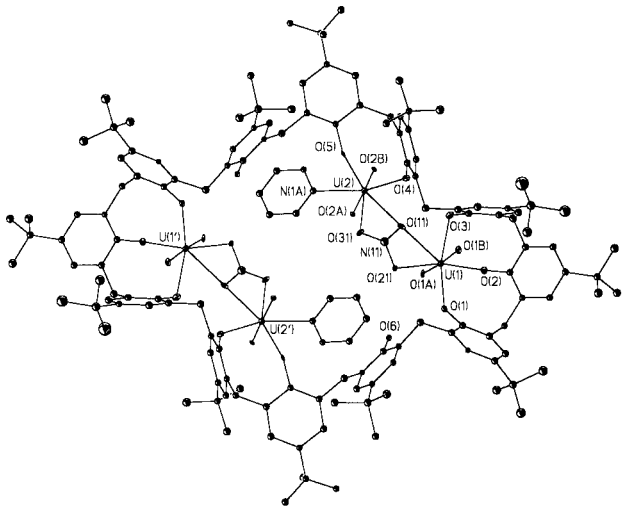

Fig. 2 Crystal structure of compound **1** (5% probability). All H atoms, $[HNEt_3]^+$ cations, as well as solvent molecules have been omitted for clarity. Selected bond lengths (Å): U(1)–O(1) 2.21(3), U(1)–O(2) 2.23(3), U(1)–O(3) 2.62(3), U(1)–O(11) 2.47(3), U(1)–O(21) 2.49(2), U(2)–O(4) 2.32(3), U(2)–O(5) 2.15(3), U(2)–O(11) 2.41(3), U(2)–O(31) 2.46(3), U(2)–N(1A) 2.58(2).

DOI: 10.1039/b000909l

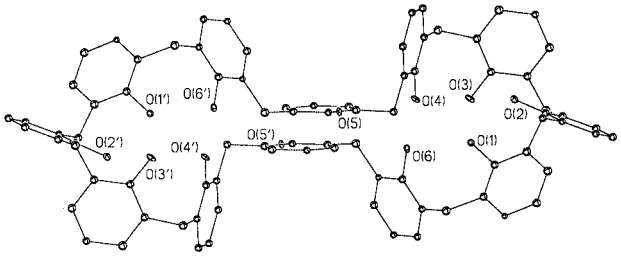

Fig. 3 Side view of the calixarene core in **1**.

formed by a phenolic group.[10] The geometry around the uranyl ion is five-coordinate pentagonal with one of the uranium atoms completing its coordination sphere with the nitrogen atom of a pyridine molecule.

Interestingly, the arrangement of the metallic species in **1** is reminiscent of that reported for the uranyl complex of an acyclic hexaphenol where the six oxygen atoms of the ligand are coordinated to the $[(UO_2)_2(NO_3)]^{3+}$ core.[9] The latter was presented as an open analogue of calix[6]arene but can also be viewed as the half of a calix[12]arene. The macrocyclic geometry of $H_{12}L$ does not enable such flexibility and is probably the cause of the unprecedented arrangement of the donor atoms observed for the metallic species of **1**, in which one of the cations is coordinated by five oxygen atoms and the other by only four, plus a nitrogen atom. To the best of our knowledge, **1** is the first example of an organic macrocycle carrying two bimetallic units inside its cavity. The isolation of **1** reinforces the notion that large polyalkoxide ligands such as calixarenes can be considered as potential 'cluster-keepers'.[3]

$H_{12}L$ acts as a double pentadentate ligand. As indicated by the stoichiometry and the U–O bond distances, only O(3) and O(6) have been able to retain their acidic proton. The calixarene is thus deprotonated eight times, with the negative charges evenly distributed around the macrocycle.[11] The conformation of the macrocycle is a regular succession of distorted pleated-loops and cones.[12] Although its structure appears different from that of $H_{12}L$, it essentially only differs by the positive sign of the fourth dihedral angle ϕ which is negative for the free macrocycle (−4.8°). Had the latter been positive, the conformation of $H_{12}L$ and **1** would have been similar.[13] This result follows Gutsche's postulate that flexible calixarenes seek conformations which possess as much cone and/or pleated loop character as their geometry permits.[1]

A good indication of the effect of metal coordination on the ligand is obtained by comparison of some intramolecular distances in $H_{12}L$ and **1**. The longest distance for the oxygen atoms of the phenolic groups in $H_{12}L$ is 17.815 Å between O(1) and O(1′) while the shortest is 4.66 Å between O(5) and O(5′). In **1**, these two distances are 15.68 Å between O(2) and O(2′) and 9.94 Å between O(5) and O(5′). Whereas the free ligand is a thin and elongated molecule, **1** is a shorter and wider compound. The macrocycle is stretched open by metal coordination inside its cavity, but retains its global geometry. The side view of the calixarene core (Fig. 3) emphasises best the shape of the macrocycle in **1** and its resemblance to that of the free ligand.

In conclusion, the encompassing of two metal dimers into one macrocycle has a surprisingly limited influence on the conformation of what was considered a very flexible molecule. The use of a large polyalkoxide ligand leads to a new combination of donor atoms around the uranyl cation and seems highly appropriate for the design of new metal complex architectures. Work is in progress to study other large calixarenes.

Notes and references

† *General*: $H_{12}L$ was prepared by the method described in ref. 3(*a*).

Synthesis of $[HNEt_3]_2[\{(UO_2)_2(NO_3)(py)\}_2(H_4L)]$ **1** : $UO_2(NO_3)_2{\cdot}6H_2O$ (0.052 g, 1.04×10^{-4} mol) was treated with $H_{12}L$ (0.050 g, 2.6×10^{-5} mol) and NEt_3 (0.021 g, 2.08×10^{-4} mol) in pyridine (2.5 mL) at 313 K for 2 h. After allowing the red solution to stand for 7 days at room temperature, a red microcrystalline powder of **1** was separated by decanting, washed twice with acetonitrile (2 mL) and dried for 2 h to afford $[HNEt_3]_2[\{(UO_2)_2(NO_3)(py)\}_2(H_4L)]{\cdot}py$ (0.045 g, 1.2 10^{-5} mol, 46%). $C_{159}H_{207}N_7O_{26}U_4$: Calc. C, 53.28; H, 5.78; N, 2.74. Found: C, 53.36; H, 5.35; N, 2.61%.

‡ *Crystal data*: for $H_{12}L{\cdot}10py$: $C_{182}H_{218}N_{10}O_{12}$, M = 2737.66, 0.12 × 0.03 × 0.03 mm, triclinic, $P\bar{1}$, Z = 1, a = 12.232(2), b = 16.072(3), c = 20.841(4) Å, α = 98.25(3), β = 103.53(3), γ = 91.77(3)°, V = 3933(2) Å^3, D_c = 1.156 g cm^{-3}, $F(000)$ = 1476, $2\theta_{max}$ = 49.34°, μ(Mo-Kα) = 0.072 cm^{-1}, T = 100 K. The structure was solved by direct methods[14] and refined on F^2.[15] Of the 23623 reflections measured, 12327 were found to be independent (R_{int} = 0.247), 3687 of which were considered as observed [$I > 2\sigma(I)$] and were used in the refinement of the 439 parameters, leading to a final R_1 of 0.1212 and a R_{all} of 0.3481. wR_{obs} and wR_2 were 0.2145 and 0.3373, respectively. All hydrogen atoms were introduced in the calculation as riding on calculated positions except those of the phenolic groups which were located on the Fourier map. The goodness-of-fit parameter S was 0.989 and the maximum residual density 0.308 e Å^{-3}.

For **1**·9py: $C_{199}H_{247}N_{15}O_{26}U_4$, M = 4217.22, 0.06 × 0.04 × 0.03 mm, triclinic, $P\bar{1}$, Z = 1, a = 10.099(2), b = 22.133(4), c = 25.109(5) Å, α = 114.39(3), β = 94.07(3), γ= 97.50(3)°, V = 5019(2) Å^3, D_c = 1.395 g cm^{-3}, $F(000)$ = 2120, $2\theta_{max}$ = 41.26°, μ(Mo-Kα) = 3.283 cm^{-1}, T = 100 K. The structure was solved and refined as above. Of the 16796 reflections measured, 9436 were found to be independent (R_{int} = 0.214), 3687 of which were considered as observed [$I > 2\sigma(I)$] and were used in the refinement of the 375 parameters, leading to a final R_1 of 0.1397 and a R_{all} of 0.3007. wR_{obs} and wR_2 were 0.2578 and 0.3604 respectively. Hydrogen atoms were introduced in the calculation as riding on calculated positions. The goodness-of-fit parameter S was 1.228 and the maximum residual density 0.988 e Å^{-3}. CCDC 182/1545. See http://www.rsc.org/suppdata/cc/b0/b000909l/ for crystallographic files in .cif format..

1 C. Wieser, C. B. Dieleman and D. Matt, *Coord. Chem. Rev.*, 1997, **165**, 93; J.-C. Bünzli and J. M. Harrowfield, in *Calixarenes, A Versatile Class of Macrocyclic Compounds*, ed. J. Vicens and V. Böhmer, Kluwer Academic Publishers, Dordrecht, 1991, p. 211.

2 J. M. Harrowfield, *Gazz. Chim. Ital.*, 1997, **127**, 663.

3 (*a*) I. Dumazet, J.-B. Regnouf-de-Vains and R. Lamartine, *Synth. Commun.*, 1997, **27**, 2547; (*b*) D. R. Stewart and C. D. Gutsche, *J. Am. Chem. Soc.*, 1999, **121**, 4136; (*c*) R. Mlika, I. Dumazet, M. Gamoudi, R. Lamartine, H. Ben Ouada, N. Jaffrezic-Renault and G. Guillaud, *Anal. Chim. Acta*, 1997, **354**, 283.

4 Mention of the existence of a uranyl complex of *tert*-butylcalix[9]arene can be found in ref. 2, but the experimental details have remained unpublished.

5 C. D. Gutsche, A. E. Gutsche and A. I. Karaulov, *J. Incl. Phenom.*, 1985, **3**, 447.

6 F. Ugozzoli and G. D. Andreetti, *J. Incl. Phenom.*, 1992, **13**, 337; C. D. Gutsche, in *Calixarenes Revisited*, ed. J. F. Stoddart, Monographs in Supramolecular Chemistry, Royal Society of Chemistry, Cambridge, 1998.

7 Pairs of torsion angles (°) in $H_{12}L$ between the rings bearing O(n) and O(n + 1) starting with n = 1: +86.3 −104.6, −97.6 +85.5, +90.5 −100.2, −4.8 −86.2, +69.6 −0.1, +89.6 −100.6. This succession designates the conformation as C_i [+ −, − +, + −, − −, + −, + −] away from the regular (+ −, − +) or (+ −, + −) sequences respectively expected for the pleated loop and cone conformation.

8 (*a*) T. J. R. Weakley, *Inorg. Chim. Acta*, 1982, **63**, 161; (*b*) C. L. Raston, B. W. Skelton, C. R. Whitaker and A. H. White, *Aust. J. Chem.*, 1989, **42**, 771.

9 P. Thuéry and M. Nierlich, *J. Chem. Soc., Dalton Trans.*, 1997, 1481.

10 P. C. Leverd, P. Berthault, M. Lance and M. Nierlich, *Eur. J. Inorg. Chem.*, 1998, 1859.

11 Succession of the oxygen atoms of the calixarene in **1** stressing the regular distribution of the negative charge: O(1)$^-$, O(2)$^-$, O(3)H, O(4)$^-$, O(5)$^-$, O(6)H, O(1′)$^-$, O(2′)$^-$, O(3′)H, O(4′)$^-$, O(5′)$^-$, O(6′)H.

12 Pairs of torsion angles (°) in **1** between the rings bearing O(n) and O(n + 1) starting with n = 1: +89.0 −79.5, −131.4 +76.6, +92.7 −95.0, −61.2 +103.4, −66.7 +8.1, −92 +70.4. The conformation is designated as C_i [+ −, − +, + −, − +, − +, − +]. The twelve pairs of dihedral angles are ordered into two (+ −, − +) alternate sequences, separated by two (− +, − +) regular sequences.

13 If the fourth dihedral angle ϕ (−4.8°) of the free macrocycle was to be positive,[7] the conformation would be designated as C_i [+ −, −+, + −, + −, + −, + −].

14 G. M. Sheldrick, *SHELXS 86, A Program for the Solution of Crystal Structures*, University of Göttingen, Germany, 1990.

15 G. M. Sheldrick, *SHELXS 90, A Program for the Solution of Crystal Structures*, University of Göttingen, Germany, 1993.

Communication b000909l

Enantiopure epoxidation of electrophilic alkenes

Otto Meth-Cohn,*[a] David J. Williams[b] and Yi Chen[a]

[a] *Chemistry Department, University of Sunderland, Sunderland, UK SR1 3SD. E-mail: otto.meth-cohn@sunderland.ac.uk*

[b] *Chemistry Department, Imperial College of Science, Technology and Medicine, London, UK SW7 2AY*

Received (in Liverpool, UK) 18th January 2000, Accepted 14th February 2000

Cinnamamides derived from prolinols (*e.g.* –CH_2OH and –CPh_2OH) and from proline amides (*e.g.* prolineanilide) are epoxidised with total retention of the alkene configuration, to give either epoxides or bicyclic derivatives thereof, essentially enantiopure, using *tert*-butyl hydroperoxide and butyllithium.

Recently we disclosed[1] that our general method for the stereocontrolled epoxidation of electrophilic alkenes using lithium *tert*-butylhydroperoxide[2] was capable of homochiral application using α,β-unsaturated amides derived from homochiral secondary amines (Scheme 1). However, the method produced two diastereomers, albeit easily separable, that could then be further converted into, for example, α,β-unsaturated ketones with organolithium derivatives. It would be much more elegant and extremely useful synthetically, if the epoxidation could be conducted to give solely one or other enantiopure diastereomer in a predictable manner. This would be especially worthwhile if the chiral auxiliary were cheap, easily available as both enantiomers and was recyclable. We herein present our recent endeavours to achieve these goals.

The first requirement in this search was to understand the basis of the diastereomeric selection that operates in this reaction. On the basis of a very large body of work by ourselves and numerous others, the reaction proceeds with total retention of the alkene configuration of the epoxide. We have already proposed[2] that this stereocontrol of the epoxidation derives from the potent 'lithium bonding' which ensures a chelate control of the epoxidation process (Scheme 1). For diastereocontrol of the process, a mechanism whereby a similar fixation of the geometry of the transition state is required. In order to achieve optimum diastereoselection we examined a series of homochiral secondary amines from which were made cinnamamides **1** (Scheme 2). These alkenes proved universally disappointing, giving diastereomeric ratios between 1.2 : 1 and 3 : 1 (Scheme 2). Clearly, the usual steric or geometric factors alone were not sufficient to generate a high diastereomeric excess (de).

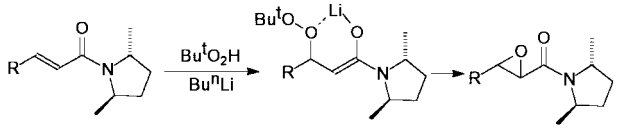

Scheme 1

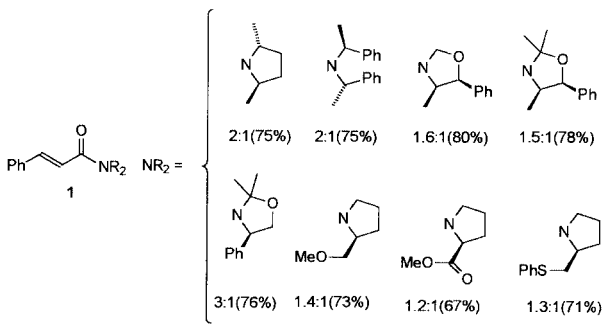

Scheme 2 Diastereomeric ratios and yields from epoxidation of homochiral cinnamamides.

We next examined the (*S*)-prolinol-derived cinnamamides **2**. These compounds reacted very rapidly and generated essentially enantiopure products in reasonable yield. However, the products were not the expected epoxides but the pyrrolidinooxazinones **3**. The structures were confirmed both by spectroscopy and by X-ray crystallography (Fig. 1)† which showed that the product had the (*S*,*S*,*S*)-configuration.

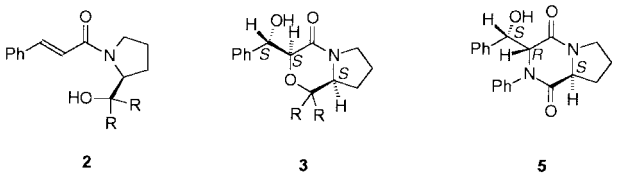

2 a, R = H; b, R = Ph

3 a; de >99:1, 65%; b, de >99:1, 61%

5

We then made a series of cinnamamides **4** based on (*S*)-proline, with the proline side-chain being varied. Using proline itself or prolinamide, epoxidation of the cinnamamide (**4**, R = H) gave complex mixtures, and thus derivatives were studied. Some remarkable variations in diastereomeric ratio were uncovered, the more surprising in that closely similar systems proved to be either highly effective or of little value (Scheme 3). In general, the de of the epoxidation increased with the steric bulk of the group R on the proline side-chain. However, spectacular ratios were observed using prolineanilide (> 99 : 1), the epoxide always being accompanied by an interesting bicyclic product. Spectroscopy and ultimately X-ray crystallography (Fig. 2)† confirmed that the product was the pyrrolidinopiperazinedione **5** but surprisingly with (*S*,*R*,*S*)-configuration.

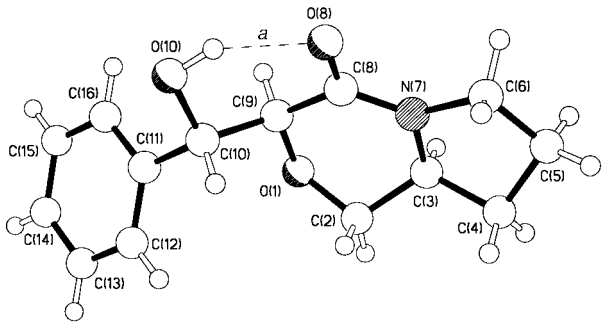

Fig. 1 The molecular structure of **3**. The hydrogen bonding geometry, (*a*) is O···O, H···O 2.66, 1.84 Å; O–H···O 149°.

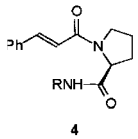

4

R	Me	Pr^i	$PhCH_2$	Ph	1-adamantyl	mesityl
de	1.5:1	2.5:1	3.5:1	>99:1	5:1	5:1
Yield (%)	48	62	61	48	58	64

Scheme 3 Diastereomeric ratios and yields from epoxidation of proline-derived cinnamamides.

DOI: 10.1039/b000520g

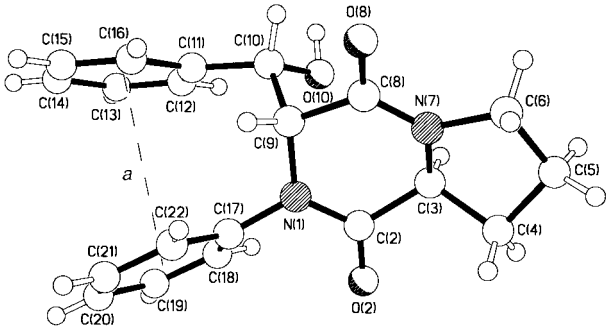

Fig. 2 The molecular structure of **5**. The ring-centroid ring-centroid separation (*a*) is 3.75 Å.

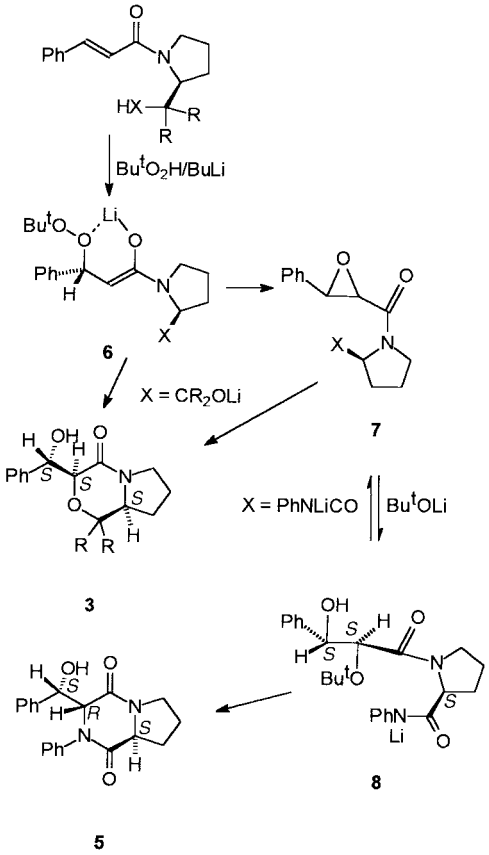

Scheme 4

Short reaction times gave primarily the epoxide (61%) while longer reaction time resulted in the sole formation of the potentially useful pyrrolidinopyrazinedione **5** (45%), both in >99% de. The related *p*-chloro-, *p*-cyano- and *p*-methoxy-anilides gave solely the bicyclic analogue of **5**, again essentially enantiopure (41–45%), while proline-*N*-methylanilide (CONMePh) gave only the corresponding epoxide **7** though with poor diastereo-discrimination (1.4:1, 68%). Both of these cyclic derivatives **3** and **5** are of considerable interest *per se*, being potential sources of novel homochiral amino acids and dihydroxy acids respectively. It should be underlined that while the *oxazine* derivative **3** shows (*S,S,S*)-stereochemistry the *piperazine* **5** is (*S,R,S*)!

A possible explanation for this stereochemical surprise is presented in Scheme 4. The prolinol-derived system **4** could arise either by direct interception of the hydroperoxide intermediate **6** *en route* to the epoxide **7** or by ring-opening of the epoxide **7**, in both cases by the pendant OLi group, both processes being highly enantioselective. The stereochemical inversion involved in the generation of the compound **5** suggests that a double inversion at the central chiral centre occurs. Thus, the *trans*-epoxide **7** is opened rapidly (and probably reversibly; this reversibility is probably a general, though degenerate process in all such epoxidations) firstly by LiOBu^t, the by-product of the epoxidation, followed by a slow attack by the considerably less nucleophilic CONPhLi side-chain. This would explain (a) the comparatively slow formation of this product compared to the oxygen analogue **3** and (b) the fact that brief reaction gives the epoxide while prolonged reaction generates the bicyclic product **5**. Treatment of the isolated epoxide **7** (X = CONHPh) with butyllithium does not yield the piperazine **5**.

As regards the remarkable diastereospecificity observed in the epoxidation of prolinol and prolineanilide derivatives (not in the case of NMePh, and other NHR derivatives of proline) we propose: (a) The preferred conformation of the cinnamamides prior to epoxidation is as shown (*e.g.* Scheme 4) to backside attack by the Bu^{t}O$_2$Li. This backside attack is further favoured by side-chain OLi or NLi 'lithium bonding' to the carbonyl oxygen. (b) As shown in the X-ray crystallographic study (Fig. 2) a π–π interaction between the two benzenoid rings of the prolinamide is favoured; this effect also tends to lock the preferred conformation for backside attack in the epoxidation, enhancing the otherwise weaker 'lithium bonding' between an NLi and the carbonyl oxygen. Presumably, this interaction is weakened by steric factors (*e.g.* as with the 2,4,6-trimethylanilide).

A fuller explanation of the specificities and mechanisms is clearly necessary and the application of these epoxidations and their the interesting downstream derivatives is under active study.

We thank the EPSRC for a grant that made this work possible.

Notes and references

† *Crystal data*: for **3**: $C_{14}H_{17}NO_3$, M = 247.3, monoclinic, space group $P2_1$ (no. 4), a = 6.269(1), b = 8.642(1), c = 12.173(2) Å, β = 104.16(2)°, V = 639.5(2) Å^3, Z = 2, D_c = 1.289 g cm^{-3}, μ(Mo-Kα) = 0.90 cm^{-1}, T = 293 K, F(000) = 264. For **5**: $C_{20}H_{20}N_2O_3$, M = 336.4, orthorhombic, space group $P2_12_12_1$ (no. 19), a = 6.271(1), b = 10.994(1), c = 24.771(5) Å, V = 1707.7(5) Å^3, Z = 4, D_c = 1.308 g cm^{-3}, μ(Cu-Kα) = 7.19 cm^{-1}, T = 293 K, F(000) = 712. For **3**, 2121 independent reflections, 2θ < 60°, were measured on a Siemens P4 diffractometer with Mo-Kα radiation, and for **5**, 1675 independent reflections, 2θ < 128°, were measured on a Siemens P4 rotating anode diffractometer with Cu-Kα radiation, using ω-scans. The structures were solved by direct methods and the non-hydrogen atoms were refined anisotropically by full-matrix least squares based on F^2 to give, for **3**, R_1 = 0.046, wR_2 = 0.117, and for **5**, R_1 = 0.066, wR_2 = 0.151, for 1674 and 1071 independent observed reflections [$|F_o| > 4\sigma(|F_o|)$], respectively. The absolute chiralities of both structures were determined by internal reference to the known centre at C(3). CCDC 182/1547. See http://www.rsc.org/suppdata/cc/b0/b000520g/ for crystallographic files in .cif format.

1 O. Meth-Cohn and Y. Chen, *Tetrahedron Lett.*, 1999, **40**, 6069.

2 O. Meth-Cohn, C. Moore and H. C. Taljaard, *J. Chem. Soc., Perkin Trans. 1*, 1988, 2663. For other diastereoselective epoxidation methods: see, *e.g.* S. Julia, J. Masana and J. C. Vega, *Angew. Chem., Int. Ed. Engl.*, 1980, **19**, 929; S. Watanabe, T. Arai, H. Sasai, M. Bougauchi and M. Shibasaki, *J. Org. Chem.*, 1998, **63**, 8090; B. Lygo and P. G. Wainwright, *Tetrahedron Lett.*, 1998, **39**, 1599; W. P. Chen and S. M. Roberts, *J. Chem. Soc., Perkin Trans. 1*, 1999, 103; C. L. Elston, R. F. W. Jackson, S. F. MacDonald and P. J. Murray, *Angew. Chem., Int. Ed. Engl.*, 1997, **36**, 410, and references in these papers.

Communication b000520g

The *N,N′*-bis(trimethylsilyl)pentafluorobenzamidinate ligand: enhanced ethene oligomerisation with a neutral V(III) bis(benzamidinate) alkyl catalyst†‡

Edward A. C. Brussee, Auke Meetsma, Bart Hessen* and Jan H. Teuben

Centre for Catalytic Olefin Polymerisation, Stratingh Institute of Chemistry and Chemical Engineering, University of Groningen, Nijenborgh 4, 9747 AG Groningen, The Netherlands. E-mail: hessen@chem.rug.nl

Received (in Basel, Switzerland) 20th December 1999, Accepted 18th February 2000

The pentafluorobenzamidinate ligand $[C_6F_5C(NSiMe_3)_2]^-$ is reported, together with its bis(benzamidinate) vanadium(III) methyl derivative; the latter is considerably more active in catalytic ethene oligomerisation than its non-fluorinated analogue.

Fluorination of ancillary ligands attched to catalytically active transition-metal centres leads in many cases to a significant improvement in catalytic properties relative to the non-fluorinated analogues. Examples of this can be found in the metathesis catalysts $[(CF_3)_nMe_{3-n}CO]_2W(CHCMe_3)(NAr)$ (n = 0, 1 2; Ar = 2,6-diisopropylphenyl)[1] and in the olefin polymerisation catalysts based on [2-pyridyl–$C(CF_3)_2O]_2Zr(CH_2Ph)_2$.[2] The electron withdrawing properties of the fluorinated ligand renders the metal centre more electrophilic and, for many reaction types, more reactive. In this contribution we present the synthesis of a new fluorinated derivative of a well known ancillary ligand, *N,N′*-bis(trimethylsilyl)benzamidinate, and show that this leads to a significant improvement in the catalytic performance of an ethene oligomerisation catalyst, bis(benzamidinate)vanadium alkyl.

The *N,N′*-bis(trimethylsilyl)benzamidinate monoanionic ancillary ligand, $[PhC(NSiMe_3)_2]^-$, is widely used in transition-metal chemistry and catalysis,[3] for example in the olefin polymerisation catalysts $[PhC(NSiMe_3)_2]_2MCl_2$/MAO (M = Ti, Zr, Hf; MAO = methylaluminoxane)[4] and Cp*M[PhC(NSi-$Me_3)_2]Cl_2$/MAO (M = Ti, Zr, Hf).[5] We recently reported the neutral paramagnetic (S = 1) 12-electron bis(benzamidinate)-vanadium(III) alkyls $[PhC(NSiMe_3)_2]_2VR$ (R = Me, Et).[6] This neutral alkyl system catalyses the oligomerisation of ethene to linear alkenes without the need for added cocatalysts. The productivity of the catalyst system is modest, which is likely to be due to the relatively low electrophilicity of the metal centre. We therefore sought to increase this electrophilicity by preparing a benzamidinate with a more electron-withdrawing aryl group, pentafluorophenyl, on the ligand backbone.

Lithium *N,N′*-bis(trimethylsilyl)benzamidinate is readily prepared by reacting benzonitrile with the bis(trimethylsilyl)amide $LiN(SiMe_3)_2$.[7] The reaction of pentafluorobenzonitrile with $LiN(SiMe_3)_2$ in THF was recently reported to lead to C–F activation of the nitrile rather than to formation of the pentafluorobenzamidinate $[C_6F_5C(NSiMe_3)_2]Li$.[8] We observed that changing the solvent from THF to diethyl ether suppresses this tendency towards C–F activation. Thus, addition of 1 equivalent of C_6F_5CN to a suspension of $Li[N(SiMe_3)_2]$ in diethyl ether at −40 °C and gradual warming to ambient temperature yields a clear, pale yellow solution of the desired pentafluorobenzamidinate that is ready for further use (Scheme 1). For spectroscopic analysis, small solid samples were obtained by simply evaporating the solvent from an aliquot of the solution. NMR spectroscopy (^1H, ^{13}C and ^{19}F)[9] showed clean formation of a single product with apparent composition $[C_6F_5C(NSiMe_3)_2]Li\cdot0.5Et_2O$ and IR spectroscopy showed no residual nitrile bands.

Reaction of 2 equivalents of $[C_6F_5C(NSiMe_3)_2]Li$ with $VCl_3(THF)_3$ in THF resulted in formation of the green bis(amidinate) complex $[C_6F_5C(NSiMe_3)_2]_2VCl(THF)$ **1** (Scheme 1), which was isolated in 58% yield. Removal of THF by heating solid **1** *in vacuo* at 120 °C for 5 h yields the orange base-free chloride $[C_6F_5C(NSiMe_3)_2]_2VCl$ **2**. The ^{19}F NMR spectrum of paramagnetic **2** shows a strong downfield shift of the *o*-F resonance (δ −106.8, $\Delta\nu_{1/2}$ 380 Hz), and less pronounced shifts for the *p*-F (δ −144.1, $\Delta\nu_{1/2}$ 85 Hz) and *m*-F (δ −155.3, $\Delta\nu_{1/2}$ 45 Hz) resonances.

It proved to be difficult to obtain single crystals of **2** that were suitable for X-ray diffraction. For structural characterisation the benzonitrile adduct $[C_6F_5C(NSiMe_3)_2]_2VCl(NCPh)$ **3a** was prepared by addition of benzonitrile to a pentane solution of **2** followed by recrystallisation from diethyl ether. Its molecular structure§ is shown in Fig. 1. For comparison a structure determination of the non-fluorinated analogue **3b** was also performed.§ This compound is essentially isostructural, and its

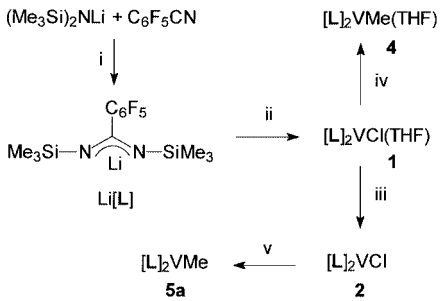

Scheme 1 *Reagents and conditions*: i, Et_2O, −40 to 20 °C, 16 h; ii, $VCl_3(THF)_3$ (0.5 equiv.), THF, −78 to 20 °C, 16 h; iii, 120 °C, vacuum, 5 h; iv, MeMgCl, THF, −78 to 20 °C, 1 h; v, MeLi, Et_2O, −78 to 20 °C, 1 h.

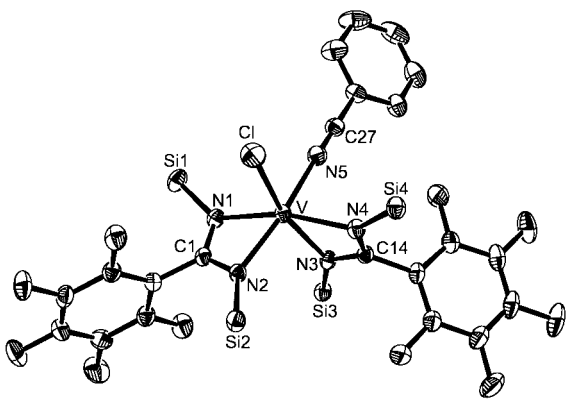

Fig. 1 Molecular structure of **3a** ($SiMe_3$ methyl groups omitted for clarity). Selected interatomic distances (Å) and angles (°): V–Cl 2.3060(9), V–N(1) 2.082(2), V–N(2) 2.067(2), V–N(3) 2.104(2), V–N(4) 2.121(2), V–N(5) 2.153(2), N(1)–C(1) 1.326(3), N(2)–C(1) 1.317(2), N(5)–C(27) 1.139(3); Cl–V–N(5) 91.33(5), N(1)–V–N(2) 65.59(6), V–N(5)–C(27) 177.5(2).

† Electronic supplementary information (ESI) available. Synthetic and spectroscopic details and ethene oligomerisation experiments. See http://www.rsc.org/suppdata/cc/b0/b000397m

‡ Netherlands Institute for Catalysis Research (NIOK) publication no. RUG 99-4-05.

DOI: 10.1039/b000397m

molecular structure is not shown here. The metal centre in **3a** has a distorted octahedral geometry, with two bidentate amidinate ligands and with the chloride and benzonitrile ligands being *cis* relative to each other. The pentafluorobenzamidinate exhibits a normal bidentate coordination mode, and the aryl substituent is perpendicular to the ligand NCN plane. In this respect it does not differ significantly from the non-fluorinated ligand in **3b**. The largest differences between the structures of the two complexes are found in the V–Cl distance and the Cl–V–N(5) and N(1)–V–N(4) angles [2.306(1) Å, 91.33(3) and 164.63(7)°, respectively, in **3a**; 2.350(1) Å, 86.01(8) and 168.6(1)° in non-fluorinated **3b**].

Unlike with the non-fluorinated analogue,[6] reaction of **1** with MeMgCl in THF followed by crystallisation from pentane yields a stable THF adduct of the methyl complex, $[C_6F_5C(NSiMe_3)_2]_2VMe(THF)$ **4** (Scheme 1). The stability of this adduct is an indication of the enhanced electrophilicity of the metal centre in the fluorinated benzamidinate complexes. Reaction of the base-free chloride **2** with MeLi in diethyl ether, followed by extraction with and crystallisation from pentane, affords the orange 12-electron methyl complex $[C_6F_5C(NSiMe_3)_2]_2VMe$ **5a** in 52% isolated yield. NMR spectra indicate that this alkyl compound (without β hydrogens) is thermally robust in benzene solution at 80 °C (no noticeable decomposition after 18 h).

To illustrate the effect of the fluorination of the amidinate ligand on the reactivity of the metal complexes, we compared the catalytic conversion of ethene by the neutral alkyl **5a** and its non-fluorinated analogue **5b**. Reactions on NMR tube scale had already shown that at 80 °C **5b** converts ethene to linear alkenes.[6] Initially, linear alk-1-enes are formed which are isomerised to internal alkenes when the system is starved of ethene. Autoclave experiments (80 °C, toluene, 4 or 8 bar ethene pressure) were performed using **5a** and **5b** as catalysts. Under these conditions, **5b** produces a Flory–Schultz distribution of linear alk-1-enes (>99% by GC) with $[C_{n+2}]/[C_n]$ = 0.87(2) over the range C_8–C_{32}, that is practically invariant with ethene pressure. The catalyst productivity for **5b** (as determined from isolated material precipitated with methanol) at 8 bar ethene (4 h run time) is 1.5 kg (mol V)$^{-1}$ h^{-1} of a material with M_n = 850 (by NMR). Under the same conditions, the fluorinated catalyst **5a** shows a productivity that is more than five times higher, 8.1 kg (mol V)$^{-1}$ h^{-1} giving a material with higher molecular weight (M_n = 1780, M_w/M_n = 2.3 by GPC).

A series of experiments with **5a** at 4 bar ethene pressure and run times of 2, 4 and 16 h shows that catalyst deactivation occurs, as the observed overall productivity drops from 7.4 to 4.5 and 1.3 kg (mol V)$^{-1}$ h^{-1}, respectively. As vanadium-based polymerisation catalysts are generally considered to deactivate through reduction of the metal centre to V(II),[10] it is likely that the electron-withdrawing nature of the fluorinated ligand accellerates this process.

In conclusion, we have prepared the new *N*,*N*′-bis(trimethylsilyl)pentafluorobenzamidinate ligand in a convenient manner, and have shown that the fluorination of the aryl substituent has a significant effect in the reactive properties of the metal centre in complexes with this ligand. Presently we are extending the chemistry of this ligand to other catalytically active metal centres. We are also using the synthesis route to prepare pentafluoro-derivatives of other trimethylsilylbenzamidinates (such as the amidinate–amine ligands reported recently by us[11]).

This investigation was carried out in connection with NIOK, the Netherlands Institute for Catalysis Research, and supported by the Department of Economic Affairs of the Netherlands.

Notes and references

§ *Crystallographic data*: for **3a**: $C_{33}H_{41}ClF_{10}N_5Si_4V$, M = 896.44, triclinic, space group $P\bar{1}$, a = 10.206(2), b = 13.176(2), c = 17.992(3) Å, α = 86.41(1), β = 74.73(1), γ = 67.63(1)°, U = 2148.1(7) Å, T = 130 K, Z = 2, D_c = 1.386 g cm^{-3}, μ = 4.8 cm^{-1}, Enraf Nonius CAD4-F diffractometer, λ(Mo-Kα) = 0.71073 Å, 8144 unique reflections, final residuals $wR(F^2)$ = 0.0986, $R(F)$ = 0.0356 for 7274 reflections with $F_o > 4\sigma(F_o)$ and 650 parameters. For **3b**: $C_{33}H_{51}ClN_5Si_4V$, M = 716.54, orthorhombic, space group *Pbca*, a = 20.778(1), b = 17.918(1), c = 21.623(1) Å, U = 8050.2(7) Å, T = 130 K, Z = 8, D_c = 1.182 g cm^{-3}, μ = 4.6 cm^{-1}, Enraf Nonius CAD4-F diffractometer, λ(Mo-Kα) = 0.71073 Å, 6975 unique reflections, final residuals $wR(F^2)$ = 0.109, $R(F)$ = 0.051 for 5016 reflections with $F_o > 4\sigma(F_o)$ and 601 parameters. CCDC 182/1548. See http://www.rsc.org/suppdata/cc/b0/b000397m/ for crystallographic files in .cif format.

1 R. R. Schrock, *Acc. Chem. Res.*, 1990, **23**, 158; R. R. Schrock, R. DePue, J. Feldman, C. J. Schaverien, J. C. Dewan and A. M. Lin, *J. Am. Chem. Soc.*, 1988, **110**, 1423.

2 T. Tsukehara, D. C. Swenson and R. F. Jordan, *Organometallics*, 1997, **16**, 3303.

3 F. T. Edelmann, *Coord. Chem. Rev.*, 1994, **137**, 403; J. Barker and M. Kilner, *Coord. Chem. Rev.*, 1994, **133**, 219; J. R. Hagadorn and J. Arnold, *J. Am. Chem. Soc.*, 1996, **118**, 893; R. Duchateau, C. T. van Wee, A. Meetsma, P. Th. Van Duijnen and J. H. Teuben, *Organometallics*, 1996, **15**, 2279; S. Hao, P. Berno, R. K. Minhas and S. Gambarotta, *Inorg. Chim. Acta*, 1996, **244**, 37.

4 D. Herskovics-Korine and M. S. Eisen, *J. Organomet. Chem.*, 1995, **503**, 307.

5 R. Gómez, R. Duchateau, A. N. Chernega, J. H. Teuben, F. T. Edelmann and M. L. H. Green, *J. Organomet. Chem.*, 1995, **491**, 153.

6 E. A. C. Brussee, A. Meetsma, B. Hessen and J. H. Teuben, *Organometallics*, 1998, **17**, 4090.

7 A. R. Sanger, *Inorg. Nucl. Chem. Lett.*, 1973, **9**, 351.

8 M. Shmulinson, A. Pilz and M. S. Eisen, *J. Chem. Soc., Dalton Trans.*, 1997, 2483.

9 $[C_6F_5C(NSiMe_3)_2]Li{\cdot}0.5Et_2O$: ^{1}H NMR (200 MHz, C_6D_6) δ 3.20 (q, 2H, J 7.1, OCH_2), 0.98 (t, 3H, J 7.1, ether Me), −0.02 (s, 18H, $SiMe_3$). ^{13}C{^{1}H} NMR (125.7 MHz, C_6D_6) δ 162.2 (NCN), 142.2 (d, J_{CF} 243.4, *m*-CF), 140.7 (d, J_{CF} 253.0, *p*-CF), 138.0 (d, J_{CF} 253.0, *o*-CF), 119.6 (br, C *ipso*), 65.7 (OCH_2), 14.4 (ether Me), 1.1 ($SiMe_3$). ^{19}F NMR (188 MHz, C_6D_6) δ −144.6 (dd, 2F, J 24.8, 7.9, *o*-F), −160.9 (t, 1F, J 24.8, *p*-F), −164.6 (td, 2F, J 24.8, 7.9, *m*-F).

10 See for example: Y. Ma, D. Reardon, S. Gambarotta, G. Yap, H. Zahalka and C. Lemay, *Organometallics*, 1999, **18**, 2773 and references therein.

11 M. J. R. Brandsma, E. A. C. Brussee, A. Meetsma, B. Hessen and J. H. Teuben, *Eur. J. Inorg. Chem.*, 1998, 1867.

Communication b000397m

ChemComm

Radical-chain deoxygenation of tertiary alcohols, protected as their methoxymethyl (MOM) ethers, using thiols as polarity-reversal catalysts

Hai-Shan Dang, Paola Franchi† and Brian P. Roberts*

Christopher Ingold Laboratories, Department of Chemistry, University College London, 20 Gordon Street, London, UK WC1H 0AJ. E-mail: b.p.roberts@ucl.ac.uk

Received (in Liverpool, UK) 19th January 2000, Accepted 14th February 2000

The deoxygenation of tertiary alcohols can be accomplished by heating their MOM ethers in the presence of a peroxide initiator and a thiol catalyst: the proposed radical-chain mechanism is supported by EPR spectroscopic studies.

Several free-radical based procedures are available for the deoxygenation of secondary alcohols (R^sOH). In particular, methods that involve radical-chain reactions of thiocarbonyl derivatives $R^sOC(=S)X$ with tributyltin hydride have found wide application in organic synthesis.[1] However, because of the thermal instability of many corresponding thiocarbonyl derivatives of tertiary alcohols, the number of methods available for the deoxygenation of the latter is more limited.[1] Conversion to an ether is commonly used to protect the alcohol functionality during chemical manipulations[2] and it would be convenient if appropriate ether derivatives of tertiary alcohols (generalised as R^tOCHR_2) could be induced to undergo radical-chain deprotection and deoxygenation in a single step to yield the deoxy compound R^tH, as shown in Scheme 1. Although the β-scission

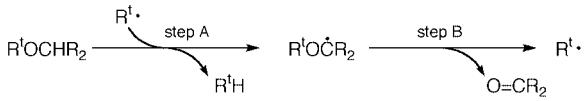

Scheme 1

step B is expected to be rapid above room temperature,[3] the hydrogen transfer step A will be close to thermoneutral and also suffer from adverse polar effects in the transition state (a nucleophilic radical R^t· is required to abstract hydrogen to give another nucleophilic radical $R^tO\dot{C}R_2$), making it a relatively slow process at moderate temperatures.[4] Consonant with this analysis, no 2-methyladamantane **2a** was formed after heating the methoxymethyl (MOM) ether of 2-methyl-2-adamantanol **1a** in refluxing octane for 2 h in the presence of the 2,2-di-*tert*-butylperoxybutane (DBPB, 2 × 3 mol%) as a thermal source of initiating alkoxyl radicals. We reasoned that step A should be subject to polarity-reversal catalysis[4] by a protic catalyst such as a thiol when, in the case of a MOM ether, it would be replaced by the cycle of polarity-matched reactions (1) and (2). Coupled with the β-scission reaction (3), this sequence would then provide a pathway for the thiol-catalysed deprotection and deoxygenation of the MOM ethers of tertiary alcohols to give R^tH and methyl formate.

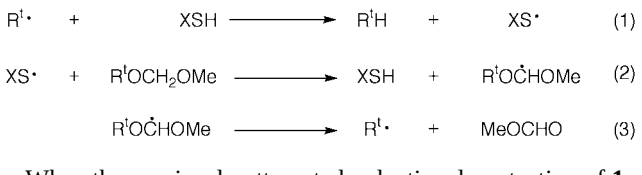

When the previously-attempted reductive deprotection of **1a** was repeated in the presence of tri-*tert*-butoxysilanethiol[5] (TBST; 2 × 3 mol%), the reaction now proceeded smoothly and 2-methyladamantane was isolated in 87% yield. Similar treatment of the tertiary alkyl MOM ethers **1b–d** gave the

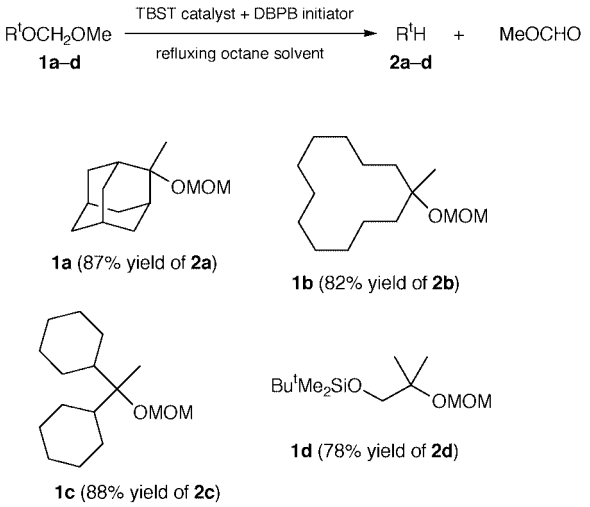

Scheme 2

corresponding deoxy compounds **2b–d** in good yields (Scheme 2); only traces of R^tH were formed in the absence of the thiol catalyst and most of the MOM ether could be recovered unchanged.‡

In order to explore its applicability to more complex systems, we made use of the procedure in the conversion of diacetone D-glucose **3** to 3-deoxy-1,2:5,6-di-*O*-isopropylidene-3-*C*-methyl-α-D-allofuranose **4** [eqn. (4)]. Swern oxidation followed by

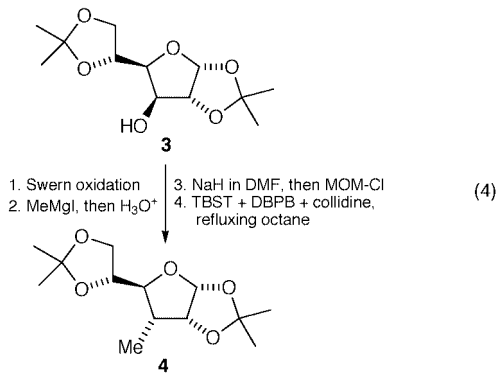

treatment of the derived ketone with methylmagnesium iodide afforded the tertiary alcohol **5**,[7] which was converted to the corresponding MOM ether **6**. The latter was heated under reflux in octane in the presence of TBST (3 × 3 mol%), DBPB (3 × 3 mol%) and 2,4,6-trimethylpyridine§ (collidine, 1 ×

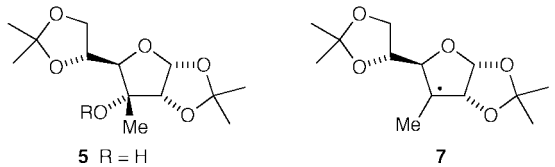

† On study leave from the University of Bologna, Italy.

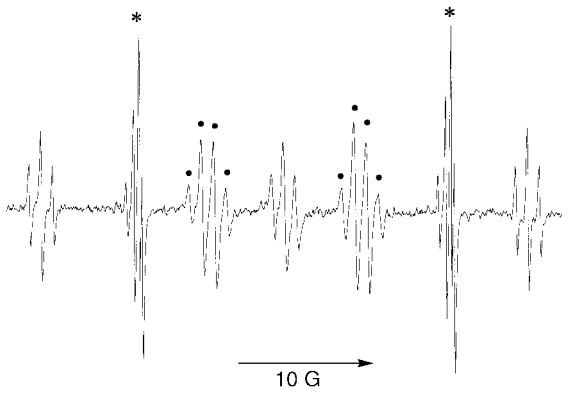

Fig. 1 EPR spectrum recorded during UV irradiation of a fluorobenzene solution containing Bu^tOCH_2OMe and di-*tert*-butyl peroxide at −61 °C. The two central 'lines' (showing second-order fine structure) from the *tert*-butyl radical are indicated by asterisks and the doublet of quartets from **8** by filled circles; the remaining lines arise from **9**. At −61 °C, the splitting constants for **8** (g = 2.0031) are 11.3 G (1 H_α) and 0.91 G (3 H_γ); for **9** (g = 2.0032) they are 18.0 G (2 $H_\alpha^{average}$) and 0.87 G (2 H_t). The central multiplet in the spectrum of **9** is broadened because rotation about the C_α–O bond is occurring at an intermediate rate on the EPR timescale.

10 mol%), to afford, after chromatography, a 91 : 9 mixture of **4**[9] and its C-3 epimer in a total isolated yield of 90%. The predominance of **4** in the epimeric product mixture is evidently a result of the preferential attack by TBST at the *exo*-face of the intermediate radical **7**.

In order to gain further insight into the mechanism of this redox process, the reaction of Bu^tOCH_2OMe with *tert*-butoxyl radicals was investigated by EPR spectroscopy. UV irradiation of a fluorobenzene solution containing Bu^tOCH_2OMe (1.4 M) and di-*tert*-butyl peroxide (*ca*. 20% v/v) at −61 °C, while the sample was in the microwave cavity of the spectrometer,[10] afforded the EPR spectrum shown in Fig. 1. The three radicals $Bu^tOCHOMe$ **8**, $Bu^tOCH_2OCH_2$ **9** and $Bu^{t\cdot}$ are present at this temperature, while above *ca*. −35 °C only the spectra of the last two were detectable. The rate constant (k_β) for β-scission of **8** to give *tert*-butyl radicals was determined relative to the rate constant ($2k_t$) for self-reaction of the latter, using the established 'steady-state' EPR method,[11] and the Arrhenius relation obtained from measurements in the temperature range −70 to −40 °C is given in eqn. (5), where $\theta = 2.303RT$ kJ mol^{-1}.¶

$$\log_{10}(k_\beta/s^{-1}) = (12.0 \pm 0.5) - (33.8 \pm 1.5)/\theta \qquad (5)$$

The value of k_β extrapolated to 126 °C (the boiling point of octane) is 3.8×10^7 s^{-1}. Even at +20 °C, there was no EPR evidence for the β-scission of **9** to give Bu^tOCH_2 although, because of line overlap, the latter radical could be difficult to detect in the presence of a higher concentration of the former. However, in similar experiments with $MeOCH_2OMe$, only the spectra of $MeOCHOMe$ and $MeOCH_2OCH_2$ were observed up to +72 °C; in particular $MeOCH_2$ was not detected, supporting the conclusion that β-scission of **9** to give Bu^tOCH_2 and formaldehyde must be *very* much slower than the cleavage of **8** to give $Bu^{t\cdot}$ and methyl formate. Although the selectivity of $Bu^tO^\cdot$ in hydrogen-atom abstraction from Bu^tOCH_2OMe will differ quantitatively from that of $(Bu^tO)_3SiS^\cdot$,‖ both radicals are electrophilic and it is probable that the thiyl radical would also abstract hydrogen to some extent from the *O*-methyl group of the mixed acetal. However, for the tertiary alkyl MOM ethers examined in this work, the major fate of any radicals of the type $R^tOCH_2OCH_2$ (or of radicals which might possibly be formed by abstraction of hydrogen from the R^t group)** must be 'repair' by hydrogen-atom transfer from the thiol to regenerate the starting MOM ether.

Financial support for this work was provided by the EPSRC. We thank Professors K. J. Hale and W. B. Motherwell for helpful discussions and we are grateful to Peroxid-Chemie GmbH for a gift of 2,2-di-*tert*-butylperoxybutane.

Notes and references

‡ *Representative procedure*: a solution containing the MOM ether **1a** (210 mg, 1.0 mmol), TBST (9 mg, 3 mol%) and DBPB (18 μl of a 50% w/w solution in mineral oil, 3 mol%) in dry octane (1.2 cm^3) was stirred and heated under gentle reflux (bath temperature 130 °C, pre-heated) under an atmosphere of argon. After 40 min, more initiator and thiol (3 mol% of each) were added and heating was continued for a further 2 h. The solvent was removed by evaporation under reduced pressure and the residue was subjected to flash chromatography on silica gel (hexane eluent) to give 2-methyladamantane **2a** (131 mg, 87%), mp 146–147 °C (lit.[6] mp 146–148 °C).

§ The yield was improved in the presence of collidine, probably because this acts as a scavenger of acid resulting from reactions between the initiator and the thiol.[8] Collidine was also present during the reductive deprotection of **1d** (Scheme 2).

¶ The value of ($k_\beta/2k_t$) at a given temperature is equal to ([$Bu^{t\cdot}$]/[**8**])\{[$Bu^{t\cdot}$] + [**8**] + [**9**]\}.[11] The Arrhenius relation for the self-reaction of *tert*-butyl radicals in fluorobenzene was taken[12] to be $\log_{10}(2k_t/M^{-1}\ s^{-1}) = 11.6 - 10.2/\theta$ and the rate constants for the diffusion-controlled reactions of $Bu^{t\cdot}$ with **8** and with **9** are assumed to be equal to $2k_t$.

‖ The relative molar rate constants (k_8/k_9) for hydrogen abstraction by $Bu^tO^\cdot$ from Bu^tOCH_2OMe to give **8** and **9** were determined by measuring relative radical concentrations in the temperature range −70 to −20 °C.[13] The value of k_8/k_9 is given by \{[**8**] + [$Bu^{t\cdot}$]\}/[**9**] and was shown to conform to the Arrhenius relation $\log_{10}(k_8/k_9) = -0.59 + 4.4/\theta$; the extrapolated value of k_8/k_9 at 126 °C is 0.97.

** Epimerisation[8] at C-5 did not compete with the reductive deprotection reaction of **6** to give **4**.

1 W. B. Motherwell and D. Crich, *Free Radical Chain Reactions in Organic Synthesis*, Academic Press, London, 1992, pp. 47–50, 54-58.
2 T. W. Green and P. G. M. Wuts, *Protective Groups in Organic Synthesis*, Wiley-Interscience, New York, 3rd edn, 1999,
3 M. J. Perkins and B. P. Roberts, *J. Chem. Soc., Perkin Trans. 2*, 1975, 77.
4 B. P. Roberts, *Chem. Soc. Rev.*, 1999, **28**, 25.
5 A. Herman, B. Becker and W. Wojnowski, *Z. Anorg. Allg. Chem.*, 1979, **450**, 178.
6 S. F. Nelsen, G. R. Weisman, E. L. Clennan and V. E. Peacock, *J. Am. Chem. Soc.*, 1976, **98**, 6893.
7 Z. Ali, S. Qureshi and G. Shaw, *J. Chem. Soc., Perkin Trans. 1*, 1990, 2627.
8 H.-S. Dang and B. P. Roberts, *Tetrahedron Lett.*, 1999, **40**, 4271.
9 O. R. Martin, R. C. Nabinger, Y. Ali, D. M. Vyas and W. A. Szarek, *Carbohydr. Res.*, 1983, **121**, 302.
10 J. A. Baban and B. P. Roberts, *J. Chem. Soc., Perkin Trans. 2*, 1981, 161; V. Diart and B. P. Roberts, *J. Chem. Soc., Perkin Trans. 2*, 1992, 1761.
11 D. Griller and B. P. Roberts, *J. Chem. Soc., Perkin Trans. 2*, 1972, 747; D. Griller and K. U. Ingold, *Acc. Chem. Res.*, 1980, **13**, 317.
12 H.-H. Schuh and H. Fischer, *Helv. Chim. Acta.*, 1978, **61**, 2130; J. C. Walton, *J. Chem. Soc., Perkin Trans. 2*, 1987, 231.
13 A. G. Davies, D. Griller and B. P. Roberts, *J. Chem. Soc. B*, 1971, 1823; D. Griller and K. U. Ingold, *Acc. Chem. Res.*, 1980, **13**, 193; H. Fischer and H. Paul, *Acc. Chem. Res.*, 1987, **20**, 200.

Communication b000533i

Important sedimentary sesterterpenoids from the diatom *Pleurosigma intermedium*

Simon T. Belt,*[a] Guy Allard,[a] Guillaume Massé,[ab] Jean-Michel Robert[b] and Steve Rowland[a]

[a] *Petroleum and Environmental Geochemistry Group, Department of Environmental Sciences, University of Plymouth, Drake Circus, Plymouth, UK PL4 8AA. E-mail: sbelt@plymouth.ac.uk*

[b] *ISOMer, Faculté des Sciences et des Techniques, Université de Nantes, 2 Rue de la Houssinière, 44027 Nantes Cedex 3, France*

Received (in Liverpool, UK) 8th December 1999, Accepted 16th February 2000

The new sesterterpenoids (5*E*,8*E*/*Z*)-3,9,13-trimethyl-6-(1,5-dimethylhex-4-enyl)tetradeca-1,5,8,12-tetraene have been isolated from the diatom *Pleurosigma intermedium* and characterised structurally by NMR spectroscopy.

Highly branched isoprenoid (HBI) C_{25} and C_{30} hydrocarbons are ubiquitous chemicals found in environmental matrices ranging from recent sediments to ancient oils.[1] The parent structures of these geochemicals (**1** and **2**, Fig. 1) were established by synthesis[1,2] during the 1980s, but it was not until 1994, that Volkman *et al.*[3] reported their occurrence in the diatoms *Haslea ostrearia* (C_{25}) and *Rhizosolenia setigera* (C_{30}) thus revealing the only known source organisms for these compounds. In our own studies, we have reported on the structures of the compounds in *H. ostrearia*, together with descriptions of some of the controls governing their unsaturation.[4–7] The most common HBIs possess between two and six double bonds, though pentaenes and hexaenes are relatively rare in *H. ostrearia*[5] (*e.g.* structures **3** and **4**, Fig. 1). In a recent report, *Rhizosolenia setigera* was shown to produce a C_{25} HBI pentaene rather than C_{30} compounds,[8] but to date, no further species or genus of diatoms have been shown to produce this class of widespread organic geochemicals. In terms of stereochemistry, HBIs exist as single geometric isomers in all cases (*E* where appropriate), though they are often reported as mixtures of configurational diastereoisomers.[4,9,10]

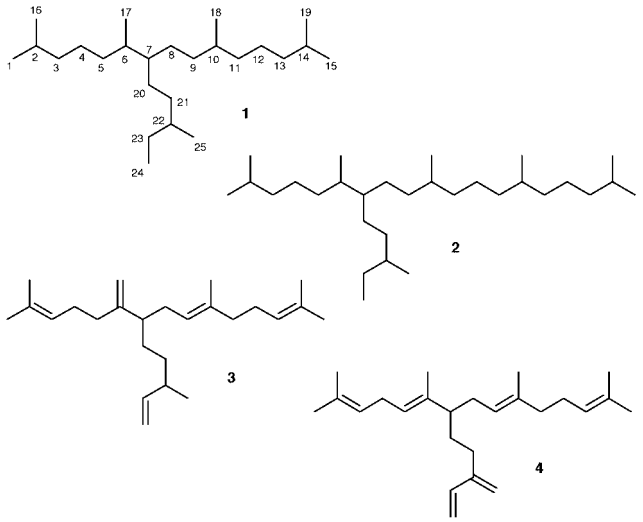

Fig. 1 C_{25} and C_{30} HBI parent structures and typical alkenes.

Here, we report the identification of an entirely different genus of diatom which biosynthesises C_{25} HBIs of a previously unreported structural type, which nonetheless appears to be common in sediments.

Pleurosigma intermedium is a benthic diatom measuring *ca.* 130 × 20 μm that is commonly found in estuarine muds. After large scale (400 L) culture of this species (Bay of Bourgneuf, France) followed by harvesting, centrifugation and freeze drying, we isolated a lipid fraction by extraction with hexane. Subsequent saponification (to remove triglyceride esters of fatty acids) and extraction (hexane) yielded a hydrocarbon fraction that was analysed by GC and GC–MS. Analysis of these chromatograms revealed the presence of *n*-$C_{21:5}$, *n*-$C_{21:6}$, squalene and eight compounds possessing related but different properties to previously reported HBIs.[4,5,7] Thus, hydrogenation of this mixture resulted in the formation of a single compound having identical GC–MS characteristics[1] to that of the authentic C_{25} alkane **1**. Following purification by column chromatography (SiO_2/hexane) and re-examination by GC–MS, the two major components (> 55%) of the hydrocarbon fraction were assigned as new HBI pentaenes ($C_{25:5}$, M^+ 342, RI 2126,2172 $_{HP\text{-}5}$; 2112,2159 $_{HP\text{-}1}$, relative abundance 1.6 : 1). The mass spectra of the two compounds were virtually identical, suggesting that that they were stereoisomers rather than positional isomers. Examination of the ^1H and ^{13}C NMR spectra† revealed the presence of four trisubstituted alkene moieties, together with a vinyl group, a structural feature common to all known HBIs. For all of these previously reported HBIs, the main branch point is at C-7, probably as the result of a biosynthetic coupling of geranyl and farnesyl type precursors.[9] However, for these new sesterterpenoids isolated from *Pleurosigma intermedium*, C-7 is unsaturated with a double bond between C-7 and C-20 (note: the numbering scheme for NMR assignments is shown for parent alkane **1**). The determination of this double bond position (C7–C20) and of the other trisubstituted double bonds was established using 2-D NMR methods (COSY, HMQC, HMBC) resulting in structures **5** and **6** (Fig. 2), namely 3,9,13-trimethyl-6-(1,5-dimethylhex-4-enyl)tetradeca-1,5,8,12-tetraene. Of particular note is the absence of any ^{13}C resonances in the 40–50 ppm region indicative of saturated, branched positions (C-7) observed for all previously reported HBIs.[4–10] Instead, alkenic C-7 resonates at δ 142.8 and 142.4 for **6** and **5**, respectively. To date, we have not been successful in separating the two $C_{25:5}$ isomers using further chromatography including argentation TLC. However, both spectroscopic (^{13}C NMR) and chromatographic (GC) separations of these compounds are most consistent with the presence of two geometric isomers (C9–C10). The mixed double bond stereochemistry of C9–C10 (and not C7–C20) was determined by careful examination of the NMR data. Specifi-

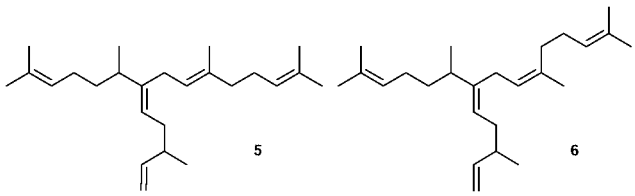

Fig. 2 Structures of C_{25} pentaenes isolated from *Pleurosigma intermedium.*

DOI: 10.1039/a909670a

cally, unique ^{1}H and ^{13}C (CH_3) resonances at δ 1.55, 1.69 (H-18) and δ 15.8, 23.4 (C-18) were observed for **5** and **6** (with **6** being the major isomer). Two further ^{13}C resonances for C-11, each of which correlated with the corresponding H-18 protons in the HMBC spectrum were also observed. Since the alternative position for geometric isomerism (C7–C20) does not possess a CH_3 substituent, the position of *E/Z* isomerism is limited to C9–C10. In order to determine the stereochemistry of the C7–C20 double bond, NOE data were obtained for **5** and **6**. Significantly, NOEs were observed between H-6 and H-20, indicating an *E* configuration. The remaining six HBIs consisted of two trienes ($C_{25:3}$) and four tetraenes ($C_{25:4}$) on the basis of their mass spectra (M^+ 346 and 344, respectively), though insufficient quantities of these compounds were present in the culture to allow for comprehensive NMR analysis.

HBIs in general have been proposed as potential biomarkers or palaeoenvironmental indicators.[11] However, to date, the environmental record of these compounds does not correlate well with those compounds structurally characterised from previous large scale cultures of diatoms including *Haslea ostrearia* and *Rhizosolenia setigera*.[4–10] The reason for this may be that HBIs from these two species undergo relatively mild diagenetic reactions (*e.g.* alkene isomerisation) but since the products of laboratory simulations of these processes do not produce the sedimentary isomers,[12] a more attractive explanation is that other diatoms such as *Pleurosigma intermedium* are the producers of many of the common sedimentary HBIs. To address this more fully, we now intend to isolate and characterise all of the HBIs produced by *Pleurosigma intermedium* under different culture conditions and to compare the mass spectra and chromatographic data (retention indices) of these with the numerous geochemical reports.[13] A preliminary investigation of this type indicates that two of the C_{25} pentaenes (RI 2124, 2169 $_{DB\text{-}5}$) reported from the Todos os Santos Bay, Brazil,[14] are HBIs **5** and **6**.

We would like to acknowledge the British Council (ALLIANCE program) and the University of Plymouth for funding (G. A. and G. M.).

Notes and references

† Selected NMR data for **5** and **6** at 270 and 400 MHz for ^{1}H in $CDCl_3$. (numbering shown for parent alkane **1**). ^{1}H, COSY: δ 5.74 (ddd, 1H, *J* 17.5, 10.0, 7.0 Hz, H-23), 5.10 (m, 4H, H-3,9,13,20), 4.93 (m, 2H, H-24), 2.58 (m, 3H, H-6,8), 2.01 (m, 9H, H-4,11,12,21,22), 1.69 (s, 3H, H-18, **6**), 1.65 (s, 6H, H-1,15), 1.58 (s, 3H, H-16/19), 1.55 (s, 6H, H-16/19,18, **5**), 0.95 (d, 3H, *J* 6.5 Hz, H-25), 0.94, 0.93 (2 × d, 3H, *J* 6.5 Hz, H-17).

^{13}C, DEPT, HMQC, HMBC: δ 144.5 (C-23), 142.8 (C-7, **6**), 142.4 (C-7, **5**), 135.6 (C-10), 131.4, 131.2, 131.1 (C-2,14), 124.9, 124.4, 123.9, 123.3, 123.0, 122.9, (C-3,9,13,20), 112.1 (C-24), 39.8 (C-11, **5**), 38.2 (C-22), 35.2 (C-5), 34.4 (C-21), 33.9 (C-6), 31.8 (C-11, **6**) 29.2 (C-8, **5**), 28.9 (C-8, **6**), 26.7, 26.6, 26.4 (C-4,12), 25.7 (C-1,15), 23.4 (C-18, **6**), 19.5 (C-25), 19.4 (C-17), 17.6 (C-16,19), 15.8 (C-18, **5**).

1 J. N. Robson and S. J. Rowland, *Nature*, 1986, **324**, 561.
2 J. N. Robson and S. J. Rowland, *Tetrahedron Lett.*, 1988, **29**, 3837.
3 J. K. Volkman, S. M. Barratt and G. A. Dunstan, *Org. Geochem.*, 1994, **21**, 407.
4 S. T. Belt, D. A. Cooke, J.-M. Robert and S. J. Rowland, *Tetrahedron Lett.*, 1996, **37**, 4755.
5 E. J. Wraige, S. T. Belt, C. A. Lewis, D. A. Cooke, J.- M. Robert, G. Massé and S. J. Rowland, *Org. Geochem.*, 1997, **27**, 497.
6 E. J. Wraige, S. T. Belt, L Johns, G. Massé, J.-M. Robert and S. J. Rowland, *Org. Geochem.*, 1998, **28**, 855.
7 E. J. Wraige, S. T. Belt, L. Johns, G. Massé, J.-M. Robert and S. J. Rowland., *Phytochemistry*, 1999, **15**, 69.
8 J. S. Sinninghe Damsté, W. I. C. Rijpstra, S. Schouten, H. Peletier, M. J. E. C. van der Maarel and W. W. C. Gieskes, *Org. Geochem.*, 1999, **30**, 95.
9 L. Johns, E. J. Wraige, S. T. Belt, C. A. Lewis, G. Massé, J.-M. Robert and S. J. Rowland, *Org. Geochem.*, 1999, **30**, 1471.
10 L. Johns, S. T. Belt, C. A. Lewis, S. J. Rowland, G. Massé, J.-M. Robert and W. König, *Phytochemistry*, 2000, **53**, 607.
11 D. A. Yon, G. Ryback and J. R. Maxwell, *Tetrahedron Lett.*, 1982, **23**, 2143.
12 S. T. Belt, G. Allard, J. Rintatalo, L. Johns, A. C. T. van Duin and S. J Rowland, *Geochim. Cosmochim. Acta*, 1999, submitted.
13 S. J. Rowland and J. N. Robson , *Mar. Environ. Res.*, 1990, **30**, 191.
14 C. Porte, D. Barceló, T. M. Tavares, V. C. Rocha and J. Albaigés, *Arch. Environ. Contam. Toxicol.*, 1990, **19**, 263.

Communication a909670a

A new synthetic approach to 1,2,3,4-tetrahydroisoquinoline-3-carboxylic acid (Tic) derivatives *via* enyne metathesis and the Diels–Alder reaction

Sambasivarao Kotha* and Nampally Sreenivasachary

Department of Chemistry, Indian Institute of Technology-Bombay, Mumbai, 400 076, India.
E-mail: srk@ether.chem.iitb.ernet.in

Received (in Cambridge, UK) 20th December 1999, Accepted 7th February 2000

Various subtituted 1,2,3,4-tetrahydroisoquinoline-3-carboxylic acid (Tic) derivatives are synthesized *via* enyne metathesis and the Diels–Alder reaction.

1,2,3,4-Tetrahydroisoquinoline-3-carboxylic acid (Tic) is a phenylalanine analogue in which the dihedral angle χ is limited to a very small range because of its bicyclic nature.[1] In connection with the design of topographically constrained peptides Tic has been utilized in several instances as a replacement of phenylalanine or tyrosine.[2] Moreover, the tetrahydroisoquinoline unit is an important structural element in several important alkaloids and other medicinally useful products.[3] Availability of synthetic methods for the preparation of various Tic derivatives with varying degrees of steric/electronic and hydrophobic properties are useful in receptor mapping and also in designing meaningful QSAR studies.[4] In connection with our building block approach for the preparation of constrained amino acid derivatives[5] we sought a Diels–Alder strategy to prepare various unknown Tic derivatives **1**–**3**. Most of the known methods such as Bischler–Napieralski[6a] Picter–Spengler[6b] and among others[6c] for Tic preparation starts with the preformed benzene derivatives while our methodology involves generation of a benzene ring *via* the cycloaddition reaction as a key step. Consequently, the present methodology provides a unique opportunity to efficiently enhance the molecular complexity of inaccessible Tic derivatives. Here, we report our preliminary results for the preparation of various Tic derivatives using enyne metathesis and the Diels–Alder reaction as key steps.

Retrosynthetic routes for various Tic derivatives *via* Diels–Alder strategy as a key step are shown in Fig. 1. Pathways a and b in Fig. 1 lead to angularly substituted and pathway c to linearly substituted Tic derivatives. In exploring the synthesis of inner–outer ring dienes such as **4** and **5** containing a dehydropipicolinic acid moiety, we conceived a relatively less explored enyne metathesis reaction as a viable option. Conceptually, cycloiosomerization of a suitably functionalised 1,7-enyne building block is expected to deliver the 4,5-dimethylene pipicolinic acid derivative (*e.g.* **6**).

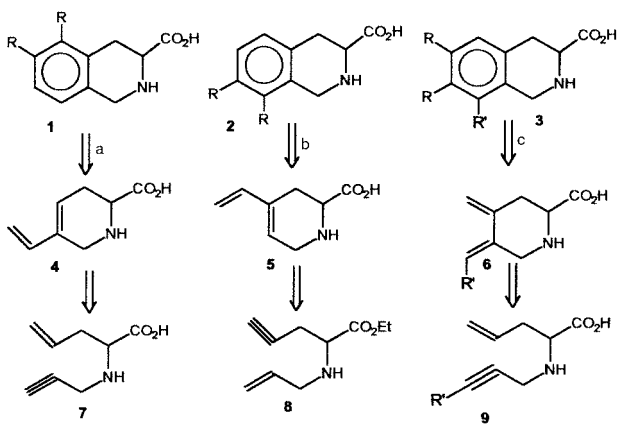

Fig. 1

Realization of the strategies shown in Fig. 1 require the preparation of key building blocks **7**, **8** and **9**. In this regard, ethyl *N*-(diphenylmethylene)glycinate **10**[7] was treated with allyl bromide in the presence of K_2CO_3 to give allylated product **11** (82%, Scheme 1). Hydrolysis of **11** with 1 M HCl in diethyl ether gave the amino ester which upon treatment with tosyl chloride in presence of triethylamine gave **12** in 78% yield [mp 43–44 °C, ^{13}C NMR ($CDCl_3$, 75 MHz) δ 170.7, 143.1, 137.4, 131.5, 129.5, 127.4, 119.6, 61.4, 55.2, 37.7, 21.6, 14.0]. Reaction of **12** with propargyl bromide in the presence of K_2CO_3 gave **13** in quantitative yield. Under similar reaction conditions, enyne **14** was prepared in 90% yield.

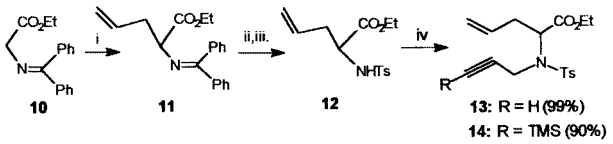

Scheme 1 *Reagents and conditions*: i, allyl bromide, K_2CO_3, MeCN, 82%; ii, 1 M HCl, diethyl ether, 85%; iii, TsCl, Et_3N, CH_2Cl_2, 78%; iv, K_2CO_3, RC≡CCH_2Br, MeCN.

Towards the preparation of building blocks related to **8**, sequential reaction of ethyl *N*-(diphenylmethylene)glycinate **10** with propargyl bromide and 3-bromo-1-trimethylsilylprop-1-yne in the presence of K_2CO_3 in acetonitrile gave **15** (86%) and **16** (88%) respectively (Scheme 2). Hydrolysis of **15** with 1 M HCl in diethyl ether gave amino ester **17** (88%) which was protected as a tosyl derivative using tosyl chloride/triethylamine in dichloromethane at room temperature to give **19** (mp 48–49 °C). The structure of **19** is established by ^{1}H and ^{13}C NMR spectral data. During the hydrolysis of compound **16**, a minor amount of desilylated product was obtained which was separated (11%) after a protection sequence. The required compound **20** was obtained in 77% yield. Then allylation of compounds **19** and **20** in the presence of K_2CO_3 with allyl bromide gave **21** and **22** in 98 and 90% yields, respectively.

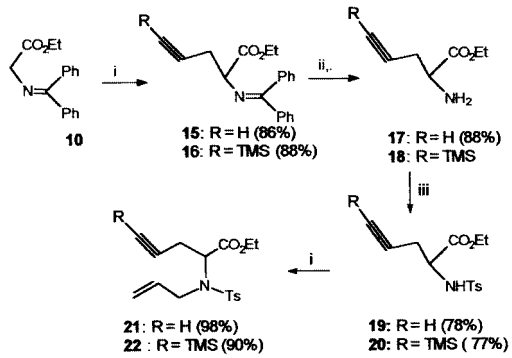

Scheme 2 *Reagents and conditions*: i, RC≡CCH_2Br, K_2CO_3, MeCN; ii, 1 M HCl, diethyl ether; iii, TsCl, Et_3N, CH_2Cl_2, 78%.

Having accomplished a high yielding synthesis of enyne building blocks **13** and **21**, we then focussed our attention towards the preparation of inner–outer ring dienes **24** and **25**.

DOI: 10.1039/a910217p

Table 1

Enyne	13	21	26	27
Reagents/ conditions	$(Cy_3P)Cl_2Ru{=}CHPh$/ 36 h	$(Cy_3P)Cl_2Ru{=}CHPh$/ 36 h	toluene/reflux	toluene/reflux
Diene	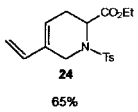 24 65%	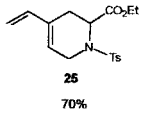 25 70%	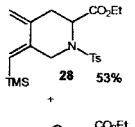 28 53% + 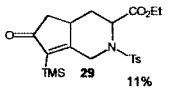 29 11%	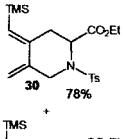 30 78% + 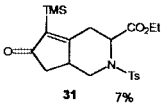 31 7%

Thus, treatment of **13** with Grubb's catalyst[8] in refluxing toluene gave **24** in 65% isolated yield after column chromatography. Under similar reaction conditions diene **25** was prepared (70%) from enyne **21** (Table 1). Attempts to convert enynes **14** and **22** to the corresponding dienes by enyne metathesis conditions were not rewarding.

Next we turned our attention towards the preparation of silylated dienes **28** and **30**. Towards this goal, enyne **14** was treated with dicobalt octacarbonyl in diethyl ether to give compound **26** in 83% yield.[9] Similarly, enyne **27** was prepared in 84% yield (Scheme 3).

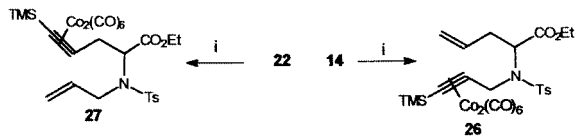

Scheme 3 *Reagents and conditions*: $Co_2(CO)_8$, diethyl ether, room temp.

Refluxing of enyne **26** in toluene followed by oxidative decomposition with *N*-methylmorpholine *N*-oxide yielded the 4,5-dimethylene pipicolinic acid derivative **28** in 53% yield along with a minor amount of Pauson–Khand product **29** (11%). The other diene **30** was obtained under similar reaction conditions in 78% yield along with the enone **31** (7%). It is worth mentioning that compound **31** is a useful precursor for tecomanine alkaloid.[10]

Having the dienes **24**, **25**, **28** and **30** in hand, we then examined their Diels–Alder chemistry with the readily available dienophiles (Table 2). The reaction of dienes **24** and **25** with different dienophiles and subsequent oxidation of Diels–Alder adducts with DDQ[11] gave angularly substituted Tic derivatives (**32**–**35**). Similarly, the Diels–Alder reaction of dienes **28** (or **30**) with dimethyl acetylenedicarboxylate (DMAD) and oxidation with DDQ gave desilylated product **36**.

In conclusion, for the first time we have demonstrated an exceptionally simple and versatile method for the synthesis of several Tic derivatives using enyne metathesis and the Diels–Alder reaction as key steps.

We gratefully acknowledge the DST for financial support and RSIC Mumbai, Professor A. Srikrishna for recording the spectral data. NS thanks CSIR, New Delhi for the award of research fellowship.

Table 2

Entry	Diene	Dienophile	DDQ product	Yield[a] (%)
1	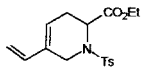 24		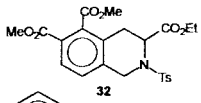 32	93
2	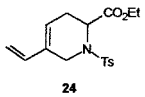 24	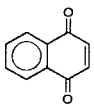	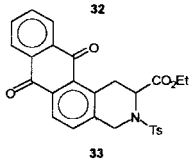 33	52
3	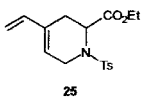 25		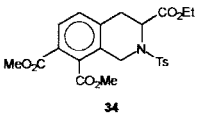 34	85
4	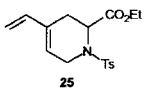 25	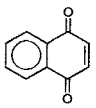	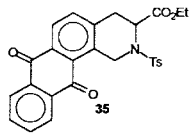 35	45
5	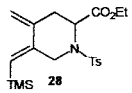 28		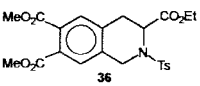 36	69
6	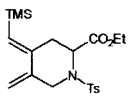 30		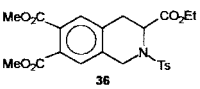 36	65

[a]Yields refer to combined isolated yields for both the Diels–Alder reaction and DDQ oxidation.

Notes and references

1 S. E. Gibson (nee Thomas), N. Guillo and M. J. Tozer, *Tetrahedron*, 1999, **55**, 585.

2 H. J. Mosberg, A. L. Lomize, C. Wang, H. Kroona, D. L. Heyl, K. Sobczyk-Kojiro, W. Ma, C. Mousigian and F. Porreca, *J. Med. Chem.*, 1994, **37**, 4371; H. Nakagawa, N. Nihonmatsu, S. Ohta and M. Hirobe, *Biochem. Biophys. Res. Commun.*, 1996, **225**, 1027; W. M. Kazmierski, Z. Urbanczyk-Lipkowska and V. J. Hruby, *J. Org. Chem.*, 1994, **59**, 1789; T. Tancredi, S. Salvadori, P. Amodeo, D. Picone, L. H. Lazarus, L. D. Bryant, R. Guerrini, R. Marzola and P. A. Temussi, *Eur. J. Biochem.*, 1994, **224**, 241; B. C. Wilkes and P. W. Schiller, *Biopolymers*, 1995, **37**, 391; V. J. Hruby, *Biopolymers*, 1993, **33**, 1073.

3 K. W. Bentley, *The Isoquinoline Alkaloids*, Harwood Academic, Singapore, 1998.

4 E. C. Griffiths, in *A Text Book of Drug Design and Development*, ed. Krogsgaard-Larsen and P. Bundgaard, Harwood Academic Publishers, Tokyo, 1992, pp. 487–528.

5 S. Kotha, N. Sreenivasachary and E. Brahmachary, *Tetrahedron Lett.*, 1998, **39**, 2805.

6 (*a*) W. Whaley and T. R. Govindachari, *Org. React.*, 1951, **VI**, 74–150; (*b*) W. J. Gensler, *Org. React.*, 1951, **VI**, 151–206; (*c*) E. A. Mash, L. J. Williams and S. S. Pfeiffer, *Tetrahedron Lett.*, 1997, **38**, 6977; C. Wang and H. I. Mosberg, *Tetrahedron Lett.*, 1995, **36**, 3623; D. Seebach, E. Dziadulewicz, L. Behrendt, S. Cantoreggi and R. Fitzi, *Liebigs. Ann. Chem.*, 1989, 1215.

7 M. J. O'Donnell and R. L. Polt, *J. Org. Chem.*, 1982, **47**, 2663.

8 M. Mori, in *Alkene Metathesis in Organic Synthesis*, ed. A. Fürstner, Springer, Berlin, 1998, pp. 133–154; R. H. Grubbs and S. Chang, *Tetrahedron*, 1998, **54**, 4413.

9 M. E. Krafft, A. M. Wilson, O. A. Dasse, L. V. R. Bonaga, Y. Y. Cheung, Z. Fu, B. Shao and I. L. Scott, *Tetrahedron Lett.*, 1998, **39**, 5911; D. Seyferth, M. O. Nestle and A. T. Wehman, *J. Am. Chem. Soc.*, 1975, **97**, 7415; D. Seyferth and A. T. Wehman, *J. Am. Chem. Soc.*, 1970, **92**, 5522.

10 T. Imanishi, N. Yagi and M. Hanaoka, *Tetrahedron Lett.*, 1981, **22**, 667.

11 P. P. Fu and R. G. Harvey, *Chem. Rev*, 1978, **78**, 317.

Communication a910217p

ChemComm

Electrogenerated chemiluminescence from Ru(II) bipyridylphosphonic acid complexes adsorbed to mesoporous TiO_2/ITO electrodes

Ann-Margret Andersson, Ralph Isovitsch, Divina Miranda, Seema Wadhwa and Russell H. Schmehl*

Department of Chemistry, Tulane University, New Orleans, LA 70118, USA. E-mail: russ@mailhost.tcs.tulane.edu

Received (in Columbia, MO) 7th October 1999, Accepted 30th November 1999

Ru(II) diimine complexes having phosphonic acid substituents adsorb to TiO_2 modified ITO electrodes and exhibit electrogenerated chemiluminescence when potentiostated at positive voltages in the presence of oxalate in buffered aqueous solutions.

Luminescence is often observed from chromophores excited by highly exoergic redox reactions that generate excited states without direct photonic excitation.[1] When the redox reaction is driven electrochemically the process (electrogenerated chemiluminescence, ECL) has several potential applications including electroactive display development and trace analysis.[2] Many potential applications of ECL can be optimized by using luminescent electroactive species that are immobilized at an electrode surface. A number of approaches to surface modification for ECL have been developed including (a) covalent or ionic attachment of the chromophore to a surface bound polymer,[3] (b) formation of thin polymer films from a monomer containing an ECL active chromophore,[4] (c) attachment of a chromophore to a substrate capable of binding to the surface *via* specific molecular recognition (*i.e.* antibody/antigen interaction)[5] and (d) direct incorporation of the redox active species into the electrode material.[6,7] For many applications it is desirable for the ECL active chromophore to be bound to a highly robust support which is also porous enough to allow for rapid ion and substrate uptake. This report describes ECL of Ru(II) diimine complexes adsorbed onto mesoporous TiO_2 films on optically transparent ITO electrode supports.

Among the chromophores most commonly used for ECL are Ru(II) diimine complexes.[8] They are stable upon one-electron oxidation and reduction and annihilation of the radical ions leads to formation of a metal-to-ligand (MLCT) charge transfer excited state. Electrogenerated luminescence can also be obtained from these complexes by reducing the complex in the presence of a species which can be reduced to produce a strong oxidizing agent (such as $S_2O_8^{2-}/SO_4^{\cdot -}$)[9] or oxidizing the complex in the presence of a species which can be oxidized to produce a strong reductant (such as $C_2O_4^{2-}/CO_2^{\cdot -}$).[10]

Several examples exist of ECL from surface bound Ru(II) diimine complexes[2–7] and recent work has shown the potential of these complexes in electroluminescent displays.[11] The most chemically flexible and durable of the modified surface ECL systems consists of ITO with a thin film of Nafion into which the Ru(II) diimine complex is adsorbed. This system involves a polymer support for which the porosity, solubility and ion transport characteristics are intimately dependent on the medium. The development of porous, insoluble, inert supports for ECL would expand the opportunities for applications of ECL in sensing and display development. Very recently Sykora and Meyer reported ECL from a polymer/SiO_2 sol–gel composite, which has the potential to meet the above criteria.[12] We report here, the observation of ECL from Ru(II) diimine complexes adsorbed onto mesoporous TiO_2 films deposited on ITO optically transparent electrodes. The TiO_2 films provide an inert, robust support for the ECL active Ru(II) complex. Gratzel and coworkers have recently observed ECL in a similar system involving reduction of $S_2O_8^{2-}$ in DMF at ITO/TiO_2 surfaces having an adsorbed Ru(II) diimine complex; the $SO_4^{\cdot -}$ radical ion produced oxidizes surface bound Ru(II) which then annihilates with conduction band electrons to yield luminescence.[7]

TiO_2 modified ITO electrodes were initially prepared as a means of increasing the photoactive surface area of electrodes used in dye sensitized photoelectrochemical cells.[13] Films are prepared by deposition of a colloidal suspension of TiO_2 onto ITO surfaces, evaporation and sintering of the subsequent film.[14] Surfaces prepared in this way are typically 1–10 μm thick and appear by SEM and AFM as packed spherical particles of the order of 20–50 nm in diameter.[15] The films are known to adsorb dyes having negatively charged substituents (carboxylates, phosphonates, *etc.*). In two electrode cells consisting of the dye modified ITO/TiO_2 electrode and a noble metal counter electrode excitation of particular dyes results in charge injection into the TiO_2 with high efficiency.[8] However, other dyes often exhibit strong photoluminescence when adsorbed.[16,17] The observation of luminescence from Ru(II) diimine complexes on ITO/TiO_2 photoelectrodes is believed to result from either (a) complex which has desorbed from the surface[16*b*] or (b) complex adsorbed to surfaces for which charge injection is thermodynamically unfavorable.[17]

The Ru(II) complex dyes used in this work are adsorbed to the surface through interaction of phosphonic acid moieties on 2,2′-bipyridyl ligands. The ligands used are $bpppH_2$ and $bpdpH_4$. The complexes prepared from these ligands are $[(bpy)_2Ru(bpppH_2)]^{2+}$, $[(bpy)_2Ru(bpdpH_4)]^{2+}$ and $[Ru(bpppH_2)_3]^{2+}$, having one, two and three phosphonic acid substituents, respectively. The ligand and complex syntheses are reported elsewhere.[18] The complexes were deposited on ITO/TiO_2 surfaces by immersion of electrodes in DMSO–H_2O (90 : 10) solutions of the complex for 12 h.

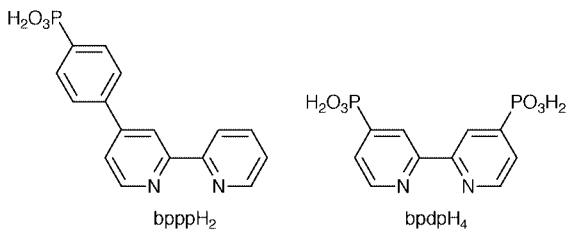

Observation of ECL from the dye modified ITO/TiO_2 surfaces requires that three conditions are met: (a) the adsorbed Ru(II) complex is oxidized by the electrode, (b) oxidation of the oxalate occurs in the film and (c) emission is observed from the adsorbed Ru(II) complex following reaction of Ru(III) with $CO_2^{\cdot -}$. Fig. 1 shows an oxidative cyclic voltammogram for a ITO/TiO_2/$[Ru(bpppH_2)_3]^{2+}$ modified electrode in aqueous pH 7 buffer. There is a large difference in peak potential between the oxidative and reductive waves reflecting limitations to charge transport in the thin film.[19,20]

Spectroelectrochemical studies indicate that nearly complete oxidation of the complexes in the film can be affected by potentiostating at voltages more positive than the one-electron oxidation potential; in addition, the process is reversible. However, complete oxidation of the complex in the films is extremely slow ($t_{1/2} \geqslant 15$ min). The implication is that only Ru(II) centers adsorbed near the ITO/TiO_2 interface are readily

DOI: 10.1039/a908148h

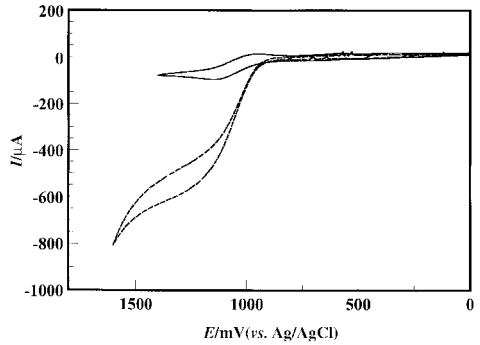

Fig. 1 Cyclic voltammogram of (—) $[Ru(bpppH_2)_3]^{2+}$ modified ITO/TiO_2 electrode in pH 7 buffer solution (0.1 M) and (----) the same modified electrode in the presence of sodium oxalate (0.002 M).

oxidized; oxidation of Ru(II) sites adsorbed away from the interfacial area must be affected by migration of Ru(III) in the TiO_2 thin film or, for films with high complex loading, charge percolation.[8] Cyclic voltammograms obtained following addition of oxalate exhibit a significant increase in current associated with the oxidative wave (Fig. 1). The process is completely irreversible, reflecting the decomposition of the oxidized oxalate. The result illustrates that oxalate is able to permeate the porous TiO_2 film and is oxidized on the cyclic voltammetric time scale [either directly at the electrode surface or by Ru(III) mediated oxidation].

When modified surfaces are potentiostated at > 0.9 V *vs.* Ag/AgCl in stirred solutions containing oxalate (0.02 M), luminescence is observed from all the Ru(II) complex modified electrodes.[21] No emission is observed in the absence of oxalate. The ECL spectrum of $[Ru(bpppH_2)_3]^{2+}$, shown in Fig. 2, is identical to that of the Ru(II) complex in aqueous buffer. The luminescence intensity increases with increasing potential until a maximum is reached at +1.25 V and falls off slightly at potentials above +1.4 V (inset). Thus, luminescence arises from the MLCT excited state of the complexes and the intensity is proportional to the relative steady state concentration of Ru(III) in the films. Whether luminescence arises in these systems from desorbed complex or from complex adsorbed to sites where charge injection is not thermodynamically favorable is not clear.

When the electrode potential is held at a potential positive relative to $E°[Ru(III/II)]$ in a stirred solution containing oxalate, the ECL intensity decreases with time. Both $[(bpy)_2Ru(bpppH_2)]^{2+}$ and $[(bpy)_2Ru(bpdpH_4)]^{2+}$ desorb from the TiO_2 support and dissolve in the buffer solution. Only the complex having three phosphonic acid substituents, $[Ru(bpppH_2)_3]^{2+}$, shows no evidence for desorption from the surface. However, even this complex exhibits a decrease in ECL intensity with time. The decrease in intensity is not related to depletion of oxalate in the solution. We are presently investigating the behavior of the $[Ru(bpppH_2)_3]^{2+}$ complex in greater detail, but preliminary results suggest that the oxidized form of the complex migrates in the film *via* desorption and readsorption processes which lead ultimately to depletion of the complex at the electrode surface.

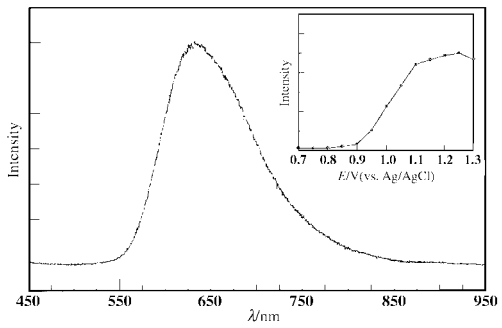

Fig. 2 Dispersed emission from a $[Ru(bpppH_2)_3]^{2+}$ modified ITO/TiO_2 electrode in pH 7 buffer containing sodium oxalate (0.02 M); 5 s exposure. Inset: integrated emission intensity as a function of applied potential.

In summary, ITO optically transparent electrodes modified with a clear ceramic thin film of mesoporous TiO_2 can serve as solid supports for generation of ECL from adsorbed Ru(II) diimine complexes. The Ru(II) complex dyes adsorb *via* interaction of phosphonic acid substituents on the diimine ligands with the surface sites on the TiO_2. Initial results suggest that the stability of the modified surfaces for generation of sustained ECL is dependent on the number of phosphonic acid substituents per chromophore. We are currently exploring covalent attachment of ECL active dyes to these robust, mesoporous thin film electrodes as a potential approach to making sensing devices with improved longevity.

We wish to thank the Department of Energy, Office of Basic Energy Sciences (Grant DE-FG-02-96ER14617) for support of this work. D. M. is grateful to the Louisiana Alliance for Minority Participation (LAMP) for a summer fellowship. The authors would like to thank Mr Jim Mellott of the D. K. Schwartz research group for AFM studies of ITO/TiO_2 surfaces.

Notes and references

1 See: M. A. DeLuca and W. D. McElroy, *Bioluminescence and Chemiluminescence*, Academic Press, New York, 1980, pp. 1–96; A. Zweig, *Adv. Photochem.*, 1968, **6**, 425.
2 A. W. Knight, *Trends Anal. Chem.*, 1999, **18**, 47; A. W. Knight and G. M. Greenway, *Analyst*, 1994, **119**, 879.
3 I. Rubenstein and A. J. Bard, *J. Am. Chem. Soc.*, 1980, **102**, 6641.
4 H. D. Abruna and A. J. Bard, *J. Am. Chem. Soc.*, 1982, **104**, 2641; K. M. Maness, R. H. Terrill, T. J. Meyer, R. W. Murray and R. M. Wightman, *J. Am. Chem. Soc.*, 1996, **118**, 10 609.
5 J. H. Kenten, J. Casadei, J. Link, S. Lupold, J. Willey, M. H. Powell, A. Rees and R. J. Massey, *Clin. Chem.*, 1991, **37**, 1626.
6 N. Egashira, H. Kumasaki and K. Ohga, *Anal. Sci.*, 1990, **6**, 903.
7 Y. Athanassov, F. P. Rotzinger, P. Pechy and N. Gratzel, *J. Phys. Chem. B*, 1997, **101**, 2558.
8 See: L. R. Faulkner and R. S. Glass, *Chemical and Biological Generation of Excited States*, Academic Press, New York, 1982, ch. 6.
9 H. S. White and A. J. Bard, *J. Am. Chem. Soc.*, 1982, **104**, 6891.
10 I. Rubenstein and A. J. Bard, *J. Am. Chem. Soc.*, 1981, **103**, 512.
11 C. H. Lyons, E. D. Abbas, J.-K. Lee and M. F. Rubner, *J. Am. Chem. Soc.*, 1998, **120**, 12100; K. M. Maness, H. Masui, R. M. Wightman and R. W. Murray, *J. Am. Chem. Soc.*, 1997, **119**, 3987.
12 M. Sykora and T. J. Meyer, *Chem. Mater.*, 1999, **11**, 1186.
13 See: T. Gerfin, M. Gratzel and L. Walder, *Prog. Inorg. Chem.*, 1997, **44**, 345.
14 C. J. Barbe, F. Arendse, P. Comte, M. Jirousek, F. Lenzmann, V. Shklover and M. Gratzel, *J. Am. Ceram. Soc.*, 1997, **80**, 3157.
15 SEM images obtained at the Advanced Materials Research Institute, University of New Orleans; AFM images obtained with instrumentation previously described, see: J. T. Woodward and D. K. Schwartz, *J. Am. Chem. Soc.*, 1996, **118**, 7861.
16 (*a*) P. V. Kamat, I. Bedja, S. Hotchandani and L. K. Patterson, *J. Phys. Chem.*, 1996, **100**, 4900; (*b*) B. I. Lemon and J. T. Hupp, *J. Phys. Chem. B*, 1999, **103**, 3797.
17 C. A. Kelly, F. Farzad, D. W. Thompson, J. M. Stipkala and G. J. Meyer, *Langmuir*, 1999, **15**, 7047.
18 M. Montalti, S. Wadhwa, W. Y. Kim, R. A. Kipp and R. H. Schmehl, *Inorg. Chem.*, in press.
19 S. A. Trammel and T. J. Meyer, *J. Phys. Chem. B*, 1999, **103**, 104.
20 A.-M. Andersson and R. H. Schmehl, manuscript in preparation.
21 The modified electrode is typically a 1 × 3 cm piece of ITO with the TiO_2 thin film containing the Ru(II) complex covering a 1 × 2 cm area. The electrode is mounted in the sample compartment of a SPEX fluorolog spectrofluorimeter at 45° relative to the emission collection optics. Emission spectra are observed using a spectrograph/CCD with 5–10 s exposure times. ECL is observed by potentiostating the ITO electrode at potentials more positive than 0.9 V in stirred solutions containing oxalate.

Communication a908148h

ChemComm

Electrogenerated poly(dendrimers) containing conjugated poly(thiophene) chains

Rosa-Maria Sebastian,[a] Anne-Marie Caminade,[a] Jean-Pierre Majoral,*[a] Eric Levillain,[b] Laurent Huchet[b] and Jean Roncali*[b]

[a] *Laboratoire de Chimie de Coordination, CNRS UPR 8241, 205 Route de Narbonne, 31077, Toulouse Cedex, France*

[b] *Ingénierie Moléculaire et Matériaux Organiques, CNRS UMR 6501,Université d'Angers, 2 Bd Lavoisier, 49045 Angers Cedex, France. E-mail: jean.roncali@univ-angers.fr*

Received (in Cambridge, UK) 18th January 2000, Accepted 15th February 2000

Electroactive conjugated polymers have been synthesized by electropolymerisation of increasing generations of dendrimers derivatized by peripheral bithiophene groups.

Dendrimer chemistry is a rapidly expanding field for both basic and applicative reasons.[1] Recently, the synthesis of dendrimers with conjugated oligomers introduced either at the periphery of the molecule,[2] or as a central rigid core,[3] has been reported by several groups. An interesting further development in this area involves the attachment of electropolymerisable groups at the periphery of a dendrimer taking advantage of the electropolymerisation process[4] to prepare electrodes modified by electroactive poly(dendrimers).

As a first step in this direction, we describe here the synthesis and electropolymerisation of dendrimers with peripheral bithiophene (BT) groups. The target structures are based on the association of neutral phosphorus containing dendrimers,[5] with bithiophenes having a linking site at an internal β-position. Such precursors are known for their better polymerisability compared to monomers in terms of applied potential, concentration and steric demand.[6]

Dendrimers with 3, 6, 12, 24 and 48 peripheral bithiophenes (**G_0b**–**G_4b**) were synthesized in 80–97% isolated yield† by a Wittig reaction between dendrimers with carbaldehyde end groups (**G_0a**–**G_4a**)[5] and the phosphonium salt derived from 3-(bromohexyl)-2,2′-bithiophene.[6c] All compounds were characterized by ^{1}H, ^{31}P and ^{13}C NMR and elemental analysis.

A single potential scan applied to solutions of **G_0b**–**G_4b** in 0.10 M $NBu^n_4PF_6$–CH_2Cl_2 shows an irreversible oxidation peak at 1.25 V typical for 3-alkyl-substituted BTs.[6] Upon application of recurrent potential scans, a broad redox system corresponding to the doping/undoping process of the growing polymer progressively develops in the region 0.50–1.10 V. The steady increase in the intensity of the waves with the number of scans indicates straighforward polymerisation, as confirmed by the formation of a dark blue film on the anode surface. A constant concentration of substrate (0.5 mM) leads to a steep increase in the intensity of the cyclic voltammetric (CV) waves

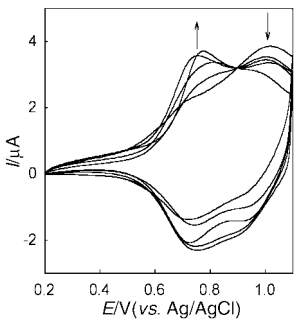

Fig. 1 Cyclic voltammograms of poly(**G_nb**) in 0.10 M NBu_4PF_6–MeCN, Pt electrodes, reference Ag/AgCl, scan rate 100 mV s^{-1}. The arrows indicate increasing generation number.

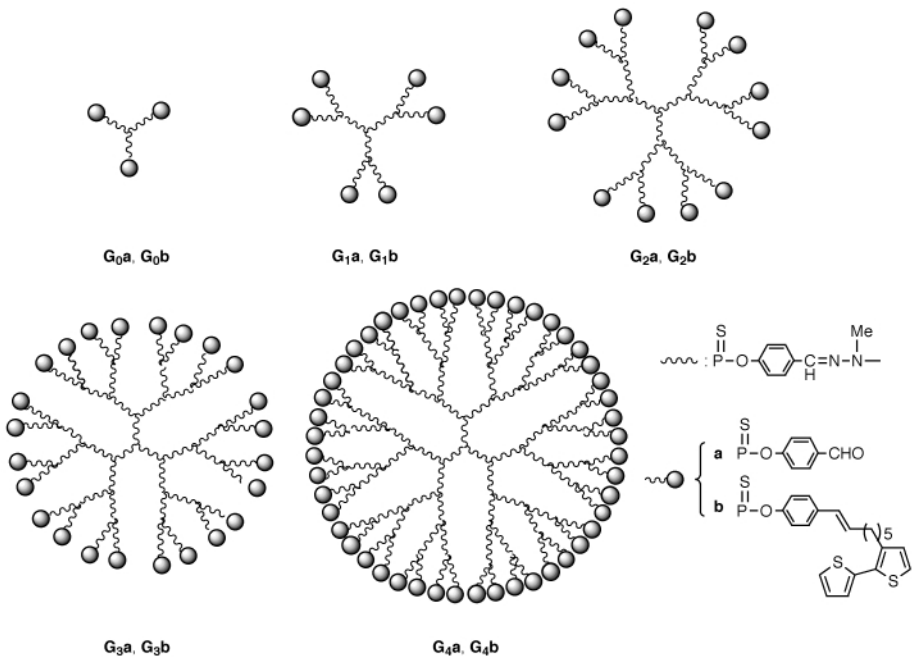

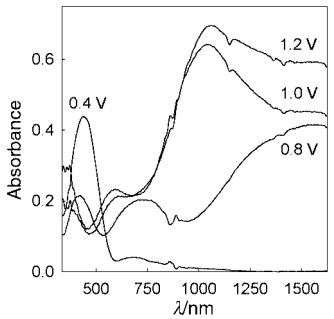

Fig. 2 Electronic absorption spectra of poly(**G_4b**) recorded *in situ* in 0.10 M NBu_4PF_6–MeCN, at various applied potentials.

with the generation number (**G_n**) owing to the rapid increase in the number of BT groups. Conversely, CV waves of similar intensity are obtained for all generations when using a constant BT concentration (1×10^{-2} M). Fig. 1 shows the CV of the five polymers in a precursor-free electrolyte. In each case two anodic waves occur around +0.75 and +1.00 V. Increasing **G_n** produces a slight negative shift of both waves and an intensification of the wave at 0.75 V to the detriment of the second one. This result suggests that raising **G_n** increases the number of longer conjugated segments in the polymer thus enhancing the effective conjugation. Such an evolution of the polymer structure could be related to the increasing probability of intra-dendrimer couplings of the BT units as **G_n** augments. Thus, whereas poly(**G_0b**) and poly(**G_1b**) essentially contain inter-dendrimer linkages subject to steric hindrance to planarity, the higher content of intra-dendrimer linkages in polymers of higher **G_n**, should limit intermolecular steric interactions in the poly(BT) chains. Consequently, the effective conjugation would approach an hypothetical limit determined by the bending imposed on the conjugated chains by the spherical shape of the underlying dendritic scaffolding.

The electrochemical behavior of the polymers has been analysed in more detail on films deposited potentiostatically under the same conditions (1×10^{-2} M equivalent BT, 1.30 V, deposition charge $Q_d = 50$ mC cm^{-2}). Under these conditions, the electroactivity expressed by the ratio Q_r/Q_d (where Q_r is the amount of charge reversibly exchanged upon cycling) increases from 5.2% for poly(**G_0b**) to 10.3% for poly(**G_4b**). While an increase in the doping level of the polymer cannot be totally excluded, these results strongly suggest a greater electropolymerization efficiency for high **G_n** precursors. This phenomenon could reflect the increasing proximity of the polymerizable BT groups.

The aqueous electroactivity of the polymers has been analysed in 0.10 M $LiClO_4$–H_2O. Whereas poly(BT) is almost inactive in this case, all poly(**G_n**) are highly electroactive in aqueous media. The electroactivity increases from 80% of its value in MeCN for poly(**G_0b**) to practically 100% for poly(**G_4b**). This enhancement may be related to the decrease in the relative weight of hydrophobic BT groups [and hence poly(BT) chains] from 45% for **G_0** to 30% for **G_4**.

Fig. 2 shows the *in situ* electronic absorption spectra of poly(**G_4**) at various applied potentials. The spectrum of the neutral polymer shows a broad band with λ_{max} around 450 nm. The 20–50 nm blue shift of λ_{max} compared to some highly conjugated functionalized poly(BTs),[6] indicates a less extended effective conjugation. Application of increasing potentials produces a gradual decrease of the π–π* absorption while two polaronic transitions develop around 700 and 1500 nm. At potentials higher than 1.00 V, these two bands merge into a broad band centered around 1050 nm assigned to the formation of bipolarons.

Attempts to solubilize the neutral polymers of higher **G_n** in CH_2Cl_2, THF or chlorobenzene remained unsuccesful. This behavior which contrasts with the good solubility of the starting dendrimers suggests that the outer poly(BT) chains form a barrier hindering the penetration of solvent molecules inside the dendrimer cavities.

While the formation, structure and properties of these new electroactive materials pose many complex problems requiring further investigation, these first examples of electrogenerated poly(dendrimers) open interesting perspectives in the field of modified electrodes for electrocatalysis or electroanalysis. A particularly exciting topic concerns the entrapment of guest molecules[7] during the electropolymerization process with possible electrochemical controlled release *via* the redox state of the poly(thiophene) outer layer. Work in this direction is now underway and will be reported in future publications.

R.-M. S. thanks the Fundación Ramón Areces for financial support.

Notes and references

† *Experimental procedure* for the synthesis of **G_4b**: to 0.15 g ($9.75\ 10^{-3}$ mmol) of **G_4a** and 0.011 g (0.471 mmol) of NaH was added THF (6 mL). Then, a solution of the phosphonium salt derived from 3-(bromohexyl)-2,2′-bithiophene[6c] (0.28 g, 0.471 mmol) in CH_2Cl_2 (6 mL) was added. The mixture was stirred at room temperature for 14 h, added to water (2 mL) and the solvent evaporated. The residue was extracted with 1 : 1 CH_2Cl_2–H_2O saturated with NaCl. Evaporation of the organic phase gave an oil which was washed with CH_2Cl_2 and pentane to yield **G_4b** (85%) as a yellow powder.

1 D. A. Tomalia, A. M. Naylor and W. A. Goddard, *Angew. Chem., Int. Ed. Engl.*, 1990, **29**, 138; G. R. Newcome, C. N. Moorefield and F. Vögtle, *Dendritic Molecules, Concepts Synthesis, Perspectives*, VCH, Weinheim, New York, 1996; M. Fischer and F. Vögtle, *Angew. Chem., Int. Ed.*, 1999, **38**, 885; A. W. Bosman, H. M. Janssen and E. W. Meijer, *Chem. Rev.*, 1999, **99**, 1665; J. M. J Fréchet, *Science*, 1994, **263**, 1710; J.-P. Majoral and A.-M. Caminade, *Chem. Rev.*, 1999, **99**, 845.

2 F. Wang, R. D. Rauh and T. L. Rose, *J. Am. Chem. Soc.*, 1997, **119**, 11 106; L. L. Miller, Y. Kunugi, A. Canavesi, S. Rigaut, C. N. Moorefield and G. R. Newkome, *Chem. Mater.*, 1998, **10**, 1751.

3 B. Karakaya, W. Claussen, K. Gessler, W. Saenger and A.-Dieter Schlüter, *J. Am. Chem. Soc.*, 1997, **119**, 3296; A. P. H. J. Schenning, R. E. Martin, M. Ito, F. Diederich, C. Boudon, J. P. Gisselbrecht and M. Gross, *Chem. Commun.*, 1998, 1013; P. R. L. Malenfant, L. Groenendaal and J. M. J. Fréchet, *J. Am. Chem. Soc.*, 1998, **120**, 10 990; I. Jestin, E. Levillain and J. Roncali, *Chem. Commun.*, 1998, 2655; P. R. L. Malenfant, M. Jayaraman and J. M. J. Fréchet, *Chem. Mater.*, 1999, **11**, 3420.

4 J. Roncali, *J. Mater. Chem.*, 1999, **9**, 1875.

5 N. Launay, A.-M. Caminade, R. Lahana and J.-P. Majoral, *Angew. Chem., Int. Ed. Engl.*, 1994, **33**, 1589; N. Launay, A.-M. Caminade and J.-P. Majoral, *J. Am. Chem. Soc.*, 1995, **117**, 3282.

6 (*a*) P. Bäuerle and S. Scheib, *Adv. Mater.*, 1993, **5**, 848; (*b*) P. Bäuerle and A. Emge, *Adv. Mater.*, 1998, **9**, 324; (*c*) L. Huchet, S. Akoudad and J. Roncali, *Adv. Mater.*, 1998, **10**, 541; (*d*) P. Blanchard, L. Huchet, E. Levillain and J. Roncali, *Electrochem. Commun.*, 1999, **2**, 1.

7 J. F. G. A. Jansen, E. M. M. de Brabander-van den Berg and E. W. Meijer, *Science*, 1994, **266**, 1220.

Communication b000523l

ChemComm

On-column derivatization of oligodeoxynucleotides with ferrocene†

Amy E. Beilstein and Mark W. Grinstaff*

Department of Chemistry, Paul M. Gross Chemical Laboratory, Duke University, Durham, North Carolina 27708, USA. E-mail: mwg@chem.duke.edu

Received (in Bloomington, IN, USA) 16th September 1999, Accepted 21st January 2000

The solid-phase synthesis and characteristics of ferrocenoyl propargylamide (FPA)-labeled oligodeoxynucleotides are described.

Site-specifically labeled DNA is of interest for hybridization assays, artificial nucleases, anticancer therapies, and DNA-mediated charge-transfer studies.[1–16] Current oligodeoxynucleotide (ODN) labels range from metal complexes[12,17] to organic dyes[10,11,18] that are covalently attached to DNA either at the ribose,[19] phosphate[20–22] or nucleobase[4–6,23–26] moieties. While synthetic strategies such as oligodeoxynucleotide post-modification and labeled nucleoside phosphoramidites afford modified ODNs, these methods are often hampered by extensive purification, side reactions and low yields. Furthermore, many of these approaches do not allow for systematic studies to be performed, as labeling is limited to the 3′- or 5′-terminus. Here, we report the *on-column derivatization* of ODNs with ferrocene at the nucleobase using a newly developed synthetic procedure in combination with standard automated DNA synthesis.[27] This site-specific on-column procedure requires an alkyne-terminated ferrocene and a halo-substituted nucleobase for Pd(0) cross-coupling.

Ferrocene was selected as the ODN label as it possesses high stability as well as reversible and tunable electrochemical and spectroscopic properties. In addition, ferrocene has been attached previously to other biomolecules of interest, including terminal-phosphate-labeled DNA oligomers,[3,28] as well as peptide nucleic acids[29] and amino acids.[30]

The ferrocene precursor for on-column derivatization (ferrocenoyl propargylamide or FPA) (Fig. 1) was synthesized by coupling ferrocene monocarboxylic acid to propargylamine hydrochloride in the presence of dicyclohexylcarbodiimide (94% yield). To further evaluate the physical properties of these novel FPA-modified ODNs, we also synthesized the corresponding FPA-labeled nucleobase, 3′,5′-dibenzoyl-5-(ferrocenoyl propargylamide) uridine, FPAU (Fig. 1). FPAU was synthesized by Pd(0) cross-coupling[31] FPA with 3′,5′-dibenzoyloxy-5-iodouridine. FPA displayed a reversible one-electron oxidation in the cyclic voltammogram, with $E_{\frac{1}{2}}$ = 0.243 V *vs.* Ag/Ag^+ (1.0 mM compound in $CDCl_3$, 0.1 M NBu_4PF_6), compared to 0.103 V for ferrocene. After attachment to uridine, $E_{\frac{1}{2}}$ shifts to 0.262 V *vs.* Ag/Ag^+.[30] The spectroscopic properties of ferrocene, FPA and FPAU were similar: all exhibited the characteristic weak (d–d) band at 444 mm.

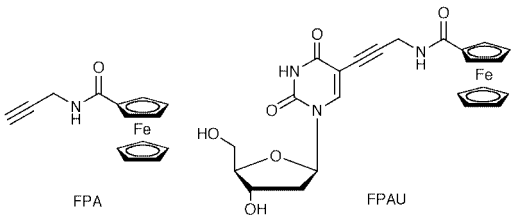

Fig. 1 Ferrocenoyl propargylamide (FPA) and 3′,5′-dibenzoyl-5-(ferrocenoyl propargylamide) uridine (FPAU).

† Electronic supplementary information (ESI) available: experimental procedures, melting profiles and CD spectra for the duplexes. See http://www.rsc.org/suppdata/cc/a9/a907568b/

The on-column derivatization method was used to site-specifically label an oligodeoxynucleotides with FPA at the nucleobase. As shown in Scheme 1, automated ODN synthesis was performed on an ABI 395 DNA synthesizer using a standard protocol. 5-Iodo-2′-deoxyuridine (5-IdU) phosphoramidite (Glen Research) was incorporated at the desired position on the ODN. Phosphoramidite couplings for the standard bases; dA, dC, dG and dT; as well as 5-IdU were > 95%. Synthesis was then paused,[32] and the column was removed from the synthesizer and dried by flushing with argon. The ferrocene precursor, FPA (20 mg), $Pd(PPh_3)_4$ (10 mg) and CuI (1 mg) were added to the column, which was then filled

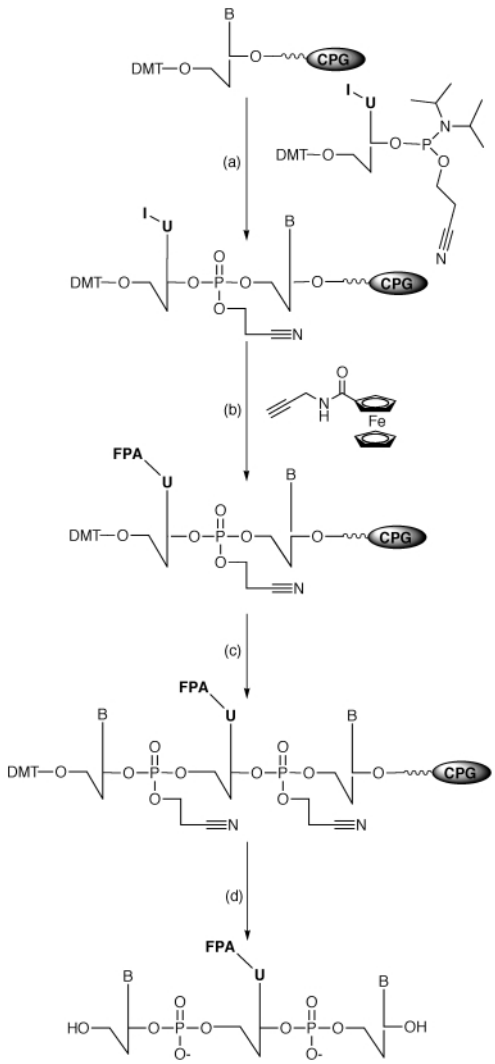

Scheme 1 Key: (a) Incorporation of 5-iodo-2′-deoxyuridine phosphoramidite (5-IdU) during standard ODN synthesis (B = A, C, G or T); (b) Pd(0) cross-coupling of FPA and the column-bound iodouridine; (c) normal ODN synthesis is resumed; (d) the synthesized site-specifically FPA-labeled ODN is cleaved from the column and protecting groups are removed by incubation in ammonia at 55 °C for 16 h.

DOI: 10.1039/a907568b

Table 1 Melting temperatures for FPA-labeled and unlabeled duplexes

Duplex		T_m/°C
1	5′-TGC TAC AAA CTG T**U**^{FPA}G A-3′	
4	5′-TCA ACA GTT TGT AGC A-3′	49.6 ± 0.1
2	5′-TGC TAC AAA C**U**^{FPA}G TTG A-3′	
4	5′-TCA ACA GTT TGT AGC A-3′	48.2 ± 0.2
3	5′-TGC TAC AAA CTG TTG A-3′	
4	5′-TCA ACA GTT TGT AGC A-3′	50.8 ± 0.3
5	5′-TGC TAC AAA C**U**^{FPA}G-3′	
7	5′-CAG TTT GTA GCA-3′	42.6 ± 0.3
6	5′-TGC TAC AAA CTG-3′	
7	5′-CAG TTT GTA GCA-3′	41.4 ± 0.4

(**U**^{FPA}) indicates the FPA-labeled uridine

with DMF–TEA (9:1). The column was shaken at room temperature for 6 h. It was then rinsed with DMF–TEA, dried and replaced on the synthesizer. Routine synthesis was resumed until the desired oligodeoxynucleotide was synthesized. A series of FPA-labeled ODNs were synthesized in this manner (Table 1). FPA-modified oligodeoxynucleotides were purified *via* reverse-phase HPLC; retention times for labeled and unlabeled ODNs differed by several minutes (18.8 *cf.* 14.8 min). Isolated yields of the labeled ODNs were typically 50%.[33]

The stabilities of FPA-labeled duplexes are evaluated by thermal denaturation of the duplexes.[34] Table 1 lists the melting temperatures of several FPA-labeled and unmodified duplexes. FPA-modified duplex **1**:**4** which is labeled at the third base from the 3′-terminus, exhibits similar stability to duplex **2**:**4**, labeled at the sixth base. These melting temperatures are only slightly lower than the T_m for the unmodified duplex, **3**:**4**. Duplex **5**:**7**, a dodecamer labeled at the second base, has a T_m of 42.6 *cf.* 41.4 °C for the analogous unmodified duplex **6**:**7**. The small changes in the melting temperatures of the labeled duplexes compared with the unmodified duplexes indicate that FPA derivatization causes minimal disruption of duplex structure. These data are consistent with previous reports that the 5-position of uridine tolerates a variety of modifications without disrupting the duplex.[26] CD spectra of the duplexes also indicate that the FPA-labeled duplexes retain the B-form DNA structure found in the unlabeled duplexes.

In summary, novel ODNs labeled with ferrocene are synthesized by solid-phase coupling of a ferrocene derivative to an ODN containing 5-iodouridine. This facile synthesis provides a simple method for labeling ODNs at the nucleobase with a spectroscopic or redox label in good yields, with minimal purification of the labeled ODN product. Melting profiles and CD spectra (see ESI) show that the FPA-labeled duplexes are stable at room temperature and have B-form DNA structure similar to unlabeled duplexes.

This work was supported in part by NSF (CAREER), Army Research Office, and Duke University.

Notes and references

1 U. Diederichsen, *Angew. Chem., Int. Ed. Engl.*, 1997, **36**, 2317.
2 M. W. Grinstaff, *Angew. Chem., Int. Ed.*, 1999, **38**, 3629 and references therein.
3 T. Ihara, M. Nakayama, M. Murata, K. Nakano and M. Maeda, *Chem. Commun.*, 1997, 1609.
4 G. B. Dreyer and P. B. Dervan, *Proc. Natl. Acad. Sci. USA*, 1985, **82**, 968.
5 R. Manchanda, S. U. Dunham and S. J. Lippard, *J. Am. Chem. Soc.*, 1996, **118**, 5144.
6 J. Schliepe, U. Berghoff, B. Lippert and D. Cech, *Angew. Chem., Int. Ed. Engl.*, 1996, **35**, 646.
7 R. E. Holmlin, P. J. Dandliker and J. K. Barton, *Angew. Chem., Int. Ed. Engl.*, 1997, **36**, 2714 and references therein.
8 A. M. Brun and A. Harriman, *J. Am. Chem. Soc.*, 1994, **116**, 10 383.
9 T. J. Meade and J. F. Kayyem, *Angew. Chem., Int. Ed. Engl.*, 1995, **34**, 352.
10 F. D. Lewis, R. Wu, Y. Zhang, R. L. Letsinger, S. R. Greenfield and M. R. Wasielewski, *Science*, 1997, **277**, 673.
11 S. M. Gasper and G. B. Schuster, *J. Am. Chem. Soc.*, 1997, **119**, 12762.
12 P. G. Sammes and G. Yahioglu, *Nat. Prod. Rep.*, 1996, 1.
13 A. Sigel and H. Sigel, *Probing of Nucleic Acids by Metal Ion Complexes of Small Molecules; Metal Ions in Biological Systems*, Marcel Dekker Inc., New York, 1996, vol. 33.
14 D. S. Sigman, *Acc. Chem. Res.*, 1986, **19**, 180.
15 T. L. Netzel, *Organic and Inorganic Photochemistry*, Marcel Dekker, New York, 1998.
16 M. J. Clarke, *Adv. Chem. Ser.*, 1997, **253**, 349.
17 R. E. Holmlin, R. T. Tong and J. K. Barton, *J. Am. Chem. Soc.*, 1998, **120**, 9724.
18 K. Fukui and K. Tanaka, *Angew. Chem., Int. Ed.*, 1998, **37**, 158.
19 E. Meggers, D. Kusch, M. Spichty, U. Wille and B. Giese, *Angew. Chem., Int. Ed.*, 1998, **37**, 460.
20 W. Bannwarth and D. Schmidt, *Tetrahedron Lett.*, 1989, **30**, 1513.
21 R. E. Holmlin, P. J. Dandliker and J. K. Barton, *Bioconjugate Chem.*, 1999, **10**, 1122.
22 S. I. Khan, A. E. Beilstein, M. Sykora, G. D. Smith, X. Hu and M. W. Grinstaff, *Inorg. Chem.*, 1999, **38**, 3922.
23 J. Telser, K. A. Cruickshank, K. S. Schanze and T. L. Netzel, *J. Am. Chem. Soc.*, 1989, **111**, 7221.
24 D. J. Hurley and Y. Tor, *J. Am. Chem. Soc.*, 1998, **120**, 2194.
25 S. I. Khan, A. E. Beilstein and M. W. Grinstaff, *Inorg. Chem.*, 1999, **38**, 418.
26 J. D. Kahl and M. M. Greenberg, *J. Am. Chem. Soc.*, 1999, **121**, 597.
27 S. I. Khan and M. W. Grinstaff, *J. Am. Chem. Soc.*, 1999, **121**, 4704.
28 R. C. Mucic, M. K. Herrlein, C. A. Mirkin and R. L. Letsinger, *Chem. Commun.*, 1996, 555.
29 A. Hess and N. Metzler-Nolte, *Chem. Commun.*, 1999, 885.
30 H. B. Kraatz, J. Lutsztyk and G. D. Enright, *Inorg. Chem.*, 1997, **36**, 2400.
31 K. Sonogashira, Y. Tohda and N. Hagihara, *Tetrahedron Lett.*, 1975, **50**, 4467.
32 Interruption of DNA synthesis to perform the coupling reaction resulted in higher yields than synthesizing the oligonucleotide in entirety before coupling to FPA (50 *cf.* 8% yield).
33 The labeled ODNs were confirmed by ESI-MS in the negative mode (**1**: (M − 2)/2, (M − 3)/3 and (M − 4)/4 ions found, with a reconstructed mass of 5132.84, compared to the calculated molecular mass of 5131.187).
34 Equimolar amounts of complimentary single strands were combined to give a duplex solution of absorbance of *ca.* 0.5. The mixture was heated to 80 °C for 15 min and was then cooled to ambient temperature over 3 h. After cooling, the following parameters were used for the melting experiment: (a) monitoring wavelength, 260 nm; (b) temperature range, 20–70 °C; (c) temperature step, 0.5 °C; (d) integration time 1 s; and wait time 1.0 min. Melting temperatures were determined by the first derivative of the melting profile and were repeated multiply for each duplex.

Communication a907568b

ChemComm

Self-assembly ultrathin films based on dendrimers

Jinfeng Wang, Jinyu Chen, Xinru Jia,* Weixiao Cao and Mingqian Li

College of Chemistry and Molecular Engineering, Peking University, Beijing 100871, China.
E-mail: xrjia@chemms.chem.pku.edu.cn

Received (in Cambridge, UK) 30th November 1999, Accepted 18th February 2000

A photosensitive ultrathin film with G1.5 PAMAM dendrimers (carboxylate salts) as polyanions and NDR (nitro-containing diazoresin) as polycations was fabricated *via* sequential deposition and subsequent UV irradiation which causes the linkage between the layers to change from ionic to covalent.

The large size and globular shape of PAMAM dendrimers make them suitable building blocks for self-assembled monolayer or multilayer ultrathin films. Watenabe and Regen[1] used the procedure of repeated deposition of amine terminated PAMAM dendrimers onto a Pt^{2+} bearing surface, followed by reactivation with K_2PtCl_4, which yielded multilayer films. Wells and Crooks[2] reported the first covalently bound dendrimer monolayer, which resulted from linking PAMAM dendrimers to a mercaptoundecanoic acid self-assembled monolayer *via* amide bond formation. Tsukruk's group fabricated composite molecular films by self-assembly of dendritic macromolecules of two adjacent generations using electrostatic layer-by-layer deposition.[3] All these examples showed the potential application of mono- or multi-layer films as chemical sensors,[4] size selective heterogeneous catalysts or a basis for optical filters and optical devices.[5–7] Recently, Cao and coworkers reported the formation of a stable ultra-thin multilayer film by converting hydrogen or ionic bonds to covalent bonds under ultraviolet irradiation.[8,9] This conversion of the bonding increases the resistance of films to etching by polar solvents.

Here, we describe, for the first time, the preparation of multilayer films constructed from poly(amidoamine) dendrimers (PAMAM) and nitro-containing diazoresin (NDR) *via* a layer-by-layer technique and the conversion of the linkage bonds under UV irradiation.

The PAMAM dendrimers were synthesized according to the literature.[10] The methyl-ester-terminated dendrimer (G = 1.5) was hydrolyzed with stoichiometric amounts of KOH in methanol to obtain external carboxylate groups associated with potassium ions. NDR was prepared according to the method described in ref. 11. Surface-negatively charged mica was used as the substrate. The freshly cleaved mica was immersed in an aqueous solution of 2 mg ml^{-1} NDR for 5 min, rinsed with deionized water and then dried under a stream of air. After being totally dried, the mica was dipped into an aqueous solution of 2 mg ml^{-1} hydrolyzed G1.5 PAMAM dendrimer for 5 min, followed by rinsing and drying. Repetition of this procedure six times yielded a 12-bilayer self-assembled ultrathin film. All stages of growth were carried out at room temperature in the dark.

The absorbance of NDR on mica after each cyclic deposition was recorded using a UV–VIS scanning spectrophotometer (Shimadazu UV-2101 PC) to monitor the self-assembly process (Fig. 1). The peak at 383 nm is assigned to the absorption of the diazonium group of NDR and increases linearly with increasing bilayer number. From Fig. 1, it can be seen that the absorbance increases by *ca.* 0.016 every two bilayers, indicating smooth step-by-step deposition.

The twelve bilayer film was then irradiated with UV light for different times and the resulting absorbances determined (Fig. 2). From the inset plot it can be seen that the photodecomposition of the film follows the kinetics of a first-order reaction,

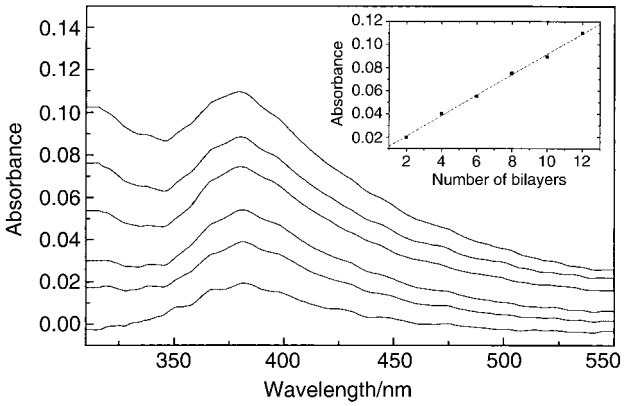

Fig. 1 Absorbance of multilayer films with different numbers of bilayers. Bilayer numbers (bottom to top): 0, 2, 4, 6, 8, 10 and 12. Inset: Relationship between the absorbance at 383 nm and the bilayer number.

where A_0 and A_t represent the absorbance of the film before and after irradiation for different times t, respectively. The absorbance at 383 nm (N_2^+ group absorption) decreases with irradiation, which indicates the formation of a covalent linkage. The conversion of the ionic bonds to covalent bonds is shown in Scheme 1. Before irradiation, the multilayer film is formed *via* electrostatic attraction between the diazonium groups and carboxyl groups. Under UV-irradiation, the diazonium groups decompose leading to phenyl cations, which combine with the carboxyl groups to produce covalent linkages.

The formation of covalent bonds was further verified by comparing the FTIR spectrum of the self-assembled film before and after irradiation. Distinct changes were the disappearance of the absorbances at 2162 and 1580 cm^{-1}, assigned to the stretching vibrations of the diazonium group and the carboxyl group, respectively. At the same time, the absorbance at 1738 cm^{-1} assigned to the carboxyl group of an ester bond increases.

From AFM measurements, the four-bilayer film (Fig. 3) is rather flat and the mean roughness only 1.4 nm which indicates

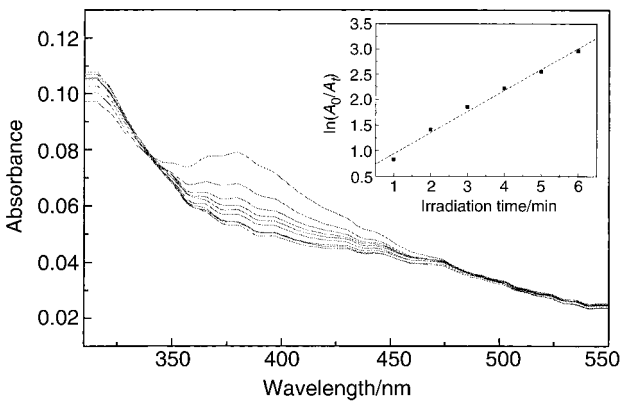

Fig. 2 UV–VIS spectra of a 12-bilayer film irradiated for different times. Irradiation intensity (360 nm): 230 μW cm^{-2}, irradiation time (top to bottom) 1, 2, 3, 4, 5, 6, 10, 20 and 30 min.

DOI: 10.1039/a909441e

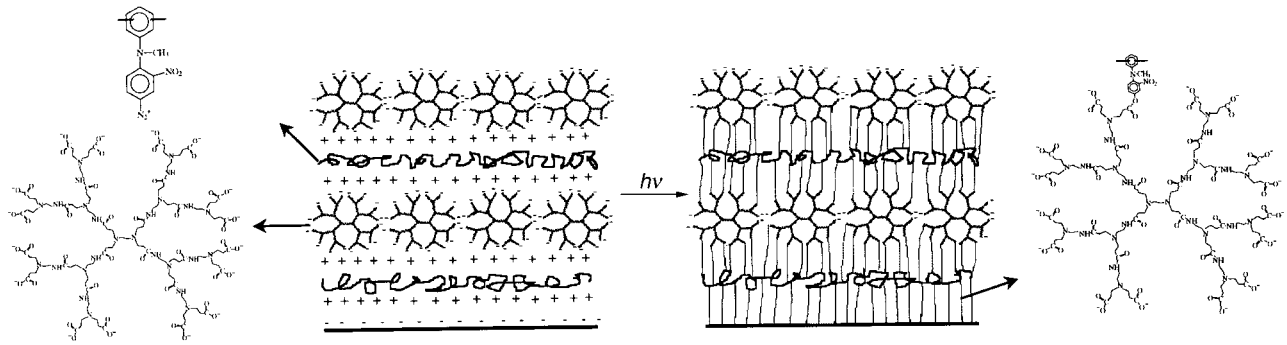

Scheme 1 The conversion of the linkage bonds from ionic to covalent in multilayer films fabricated from PAMAM and NDR.

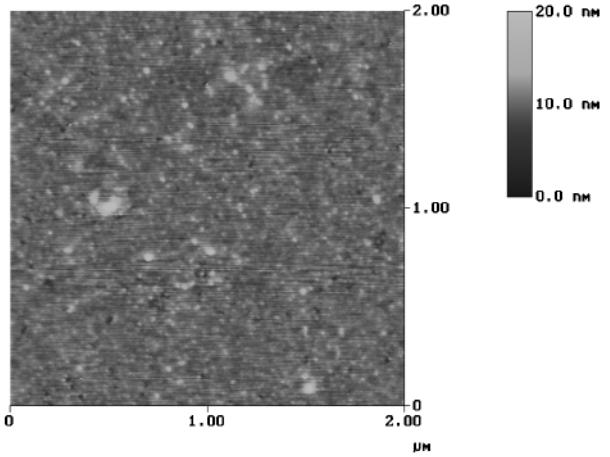

Fig. 3 Morphology of the 4-bilayer film fabricated from PAMAM and NDR. Mean roughness 1.4 nm.

the formation of a uniform multilayer film from PAMAM and NDR through the step-by-step technique.

The effect of UV irradiation on the stability of the film to polar solvents was also investigated. The absorbance of the unirradiated film decreases significantly after etching for 30 min in DMF, while the irradiated film showed no etching under the same conditions. This shows that the stability of the film towards polar solvents increases significantly after UV irradiation.

In order to determine the film thickness, X-ray diffraction measurements were performed on a Rigaku DMAX 2400 X-ray diffractometer. X-Ray data were collected within a scattering angle range of 1–8° using Cu-Kα radiation. A peak occurs at 2θ = 2.500 and 2.660 for the film before and after irradiation, respectively and suggests the film can be viewed as being ordered. According to the Bragg equation, the layer thickness of the film before and after irradiation is 3.5 and 3.3 nm, respectively. This change corresponds to the alteration in the bonding since the layers will become more compact when covalent bonds form.

In conclusion, an ultrathin multilayer film was fabricated from PAMAM dendrimers and NDR by a self-assembly technique. Under UV irradiation, the linkages change from ionic to covalent.

Studies in progress will focus on fabrication of the multilayer films by using different generation PAMAM dendrimers. We are also studying the characteristics of these unique films.

The authors gratefully acknowledge the NSFC (No. 59673010 and 29992590) for financial support of this work.

Notes and references

1 S. Watanabe and S. L. Regen, *J. Am. Chem. Soc.*, 1994, **116**, 8855.
2 M. Wells and R. M. Crooks, *J. Am. Chem. Soc.*, 1996, **118**, 3988.
3 V. V. Tsukruk, F. Rinderspacher and V. N. Bliznyuk, *Langmuir*, 1997, **8**, 13.
4 A. J. Ricco, *Electrochem. Soc. Interface*, 1994, **3**, 38.
5 Y. Lvov, G. Decher and G. Sukhorukov, *Macromolecules*, 1993, **26**, 5396.
6 H. B. Sunkara, J. M. Jethmalani and W. T. Ford, *Chem. Mater.*, 1994, **6**, 362.
7 S. A. Asher, J. Holtz, L. Liu and Z. Wu, *J. Am. Chem. Soc.*, 1994, **116**, 4997.
8 J.-Y. Chen and W.-X. Cao, *Chem. Commun.*, 1999, 1711.
9 J.-Y. Chen, L. Huang, L.-M. Ying, G.-B. Luo, X.-S. Zhao and W.-X. Cao, *Langmuir*, 1999, **15**, 7208.
10 D. A. Tomalia, A. M. Naylor and W. A. Goddard III, *Angew. Chem., Int. Ed. Engl.*, 1990, **29**, 138.
11 R.-X. Wang, J.-Y. Chen and W. X. Cao, *J. Appl. Polym. Sci.*, 1999, **74**, 189.

Communication a909441e

Organometallic models of catalytic hydrodesulfurization: $Re_2(CO)_{10}$-promoted cleavage of C–S bonds in benzothiophene

Michael A. Reynolds,[a] Ilia A. Guzei[b] and Robert J. Angelici*[a]

[a] *Ames Laboratory and the Department of Chemistry, Iowa State University, Ames, IA 50011, USA. E-mail: Angelici@iastate.edu.*

[b] *Molecular Structure Laboratory, Iowa State University, Ames, IA 50011, USA.*

Received (in Bloomington, IN, USA) 17th November 1999, Accepted 15th February 2000

Ultraviolet photolysis of hexanes solutions containing $Re_2(CO)_{10}$ and benzothiophene (BT) give the C–S cleavage product $Re_2(CO)_7[\eta^2(C2,C3)\text{-}\mu_2(C2,S)\text{-BT}]$ 1 which reacts with PMe_3 at room temperature to yield two phosphine-substituted products, 2 and 3, in which the fragmented BT ligand is partially displaced from the metals; molecular structures of 1, 2 and 3 are models for possible intermediates in the HDS of BT on catalyst surfaces.

Heterogeneous catalytic hydrodesulfurization (HDS), the commercial process used for the removal of sulfur from organosulfur compounds present in petroleum-based feedstocks, is important in industry and for the environment.[1,2] Typically, the sulfur in crude petroleum is present in the form of organic thiols, sulfides, disulfides and thiophenes. It is the thiophenic molecules, however, such as benzothiophene (BT) that are the most difficult to desulfurize under current hydrotreating conditions.[3] In order to improve the efficiency of current HDS catalytic systems, much needs to be learned about intermediates that are present on transition-metal sulfide-based catalysts during the HDS of benzothiophene.

The present paper reports preliminary results of reactivity studies of $Re_2(CO)_{10}$ with BT under mild conditions to produce the C–S cleavage product **1** containing a Re–Re backbone. Upon addition of PMe_3 to **1**, two unexpected phosphine substitution products are formed (**2** and **3**) in which both the C–S and Re–Re bonds have been cleaved (Scheme 1).

Complex **1** was prepared by UV photolysis (Hanovia 450 W, medium pressure Hg lamp) of a stirred hexanes solution containing $Re_2(CO)_{10}$ and 2 equiv. of BT in a quartz reaction vessel under nitrogen for 24–36 h at 10 °C. The progress of the reaction was monitored by IR spectroscopy of samples taken during the reaction. The IR bands corresponding to $Re_2(CO)_{10}$ [ν_{CO} (hexanes): 2071w, 2015s, 1977m cm^{-1}][4] were gradually replaced by those of **1** [ν_{CO} (hexanes): 2099m, 2043s, 2027s, 1981s, 1977s, 1957m, 1947s cm^{-1}]. Solvent removal, followed by extraction with CH_2Cl_2 and column chromatography on silica gel packed in hexanes, produced orange **1** in 30–45% yield.†‡

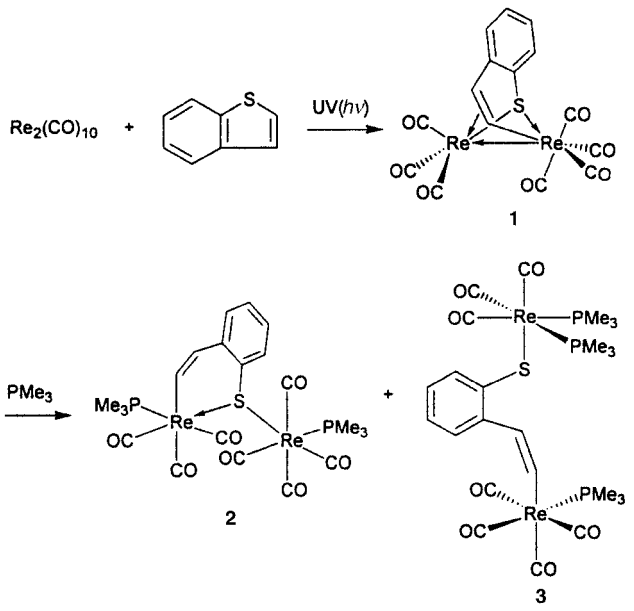

Scheme 1

The molecular structure of **1** was confirmed by single crystal X-ray structure analysis (Fig. 1). It contains a bridging BT ligand in which the vinylic C–S bond of the BT has been cleaved, and three CO ligands have been displaced from the $Re_2(CO)_{10}$. The sulfur bridges both Re atoms asymmetrically with distances of 2.506(2) Å for Re(1)–S and 2.431(3) Å for Re(2)–S. The vinyl carbon also bridges the two Re atoms asymmetrically acting as a η^1-ligand to Re(1) and η^2 to Re(2) with distances of 2.142(10) Å for Re(1)–C(8) and 2.208(10) Å for Re(2)–C(8). The Re–Re distance [2.8945(7) Å] is shorter than that in $Re_2(CO)_{10}$ [3.0413(11) Å].[5] Other previously reported dinuclear complexes, prepared by quite different methods, that contain a similar bridging BT ligand are $Fe_2(CO)_5(PPh_3)(C_8H_6S)$[6] and $[Cp^*Co]_2(\mu\text{-}C_8H_6S)$.[7]

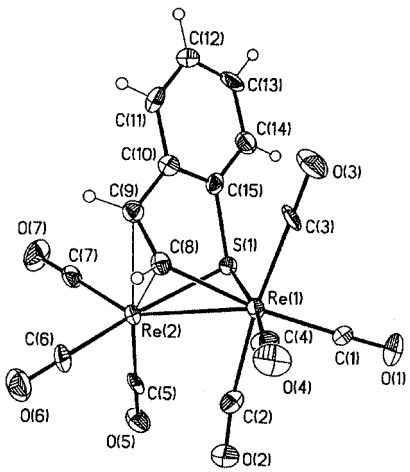

Fig. 1 Molecular structure of **1** in the solid state. Selected bond lengths (Å) and angles (°): Re(1)–Re(2) 2.8945(7), Re(1)–S, 2.506(2), Re(2)–S 2.431(3), Re(1)–C(8) 2.142(10), Re(2)–C(8) 2.208(10), Re(2)–C(9) 2.413(11), C(8)–C(9) 1.370(14), S–C(15) 1.805(11), Re(2)–S–Re(1) 71.77(7), Re(1)–C(8)–Re(2) 83.4(3), C(8)–Re(2)–S 82.8(3), C(8)–Re(1)–S 82.3(3), C(8)–C(9)–C(10) 126.6(10).

The addition of PMe_3 (1–5 equiv.) (1 M in toluene) to a toluene solution of **1** at room temperature causes an immediate change from orange to pale yellow with no evolution of CO. Solvent removal, extraction with CH_2Cl_2, and fractional crystallization of the crude residue produced yellow crystals of **2** and white **3**. Both complexes have been characterized spectroscopically‡ and by X-ray structure analysis of their single crystals.

DOI: 10.1039/a909161k

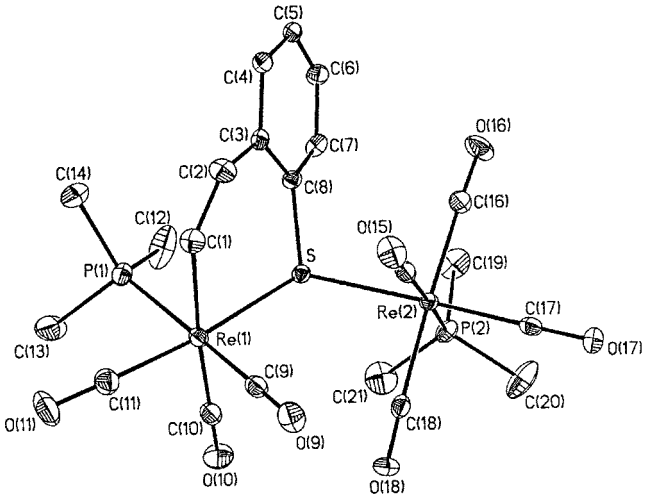

Fig. 2 Molecular structure of **2** in the solid state. Selected bond lengths (Å) and angles (°): Re(1)··Re(2) 4.2874(3), Re(1)–S 2.5027(9), Re(2)–S 2.5320(9), C(8)–S 1.796(3), Re(1)–C(1) 2.169(3), C(1)–C(2) 1.343(5), Re(1)–S–Re(2) 116.76(3), C(1)–Re(1)–S 86.51(10), Re(1)–S–C(8) 109.94(12), Re(2)–S–C(8) 105.40(12), P(1)–Re(1)–S 87.24(3), P(2)–Re(2)–S 88.04(3).

The X-ray structure of **2** (Fig. 2) shows that the C(1)–C(2) double bond is no longer η^2-coordinated and the Re–Re bond has been cleaved. Both Re atoms are pseudo-octahedral and each contains a PMe_3 ligand. The S bridges both Re atoms almost symmetrically with distances of 2.5027(9) Å for Re(1)–S and 2.5320(9) Å for Re(2)–S.

A single crystal X-ray analysis of **3** (Fig. 3) shows that there are no single atom bridges between the two Re centers nor is there a metal–metal bond. The Re centers are pseudo-octahedral with respect to the C–Re–C angles between Re and adjacent CO ligands. The Re(1)–C(1) distance is 2.205(3) Å which is longer than that in either **1** or **2**. The Re(2)–S distance is 2.5086(9) Å which is similar to those in both **1** and **2**.

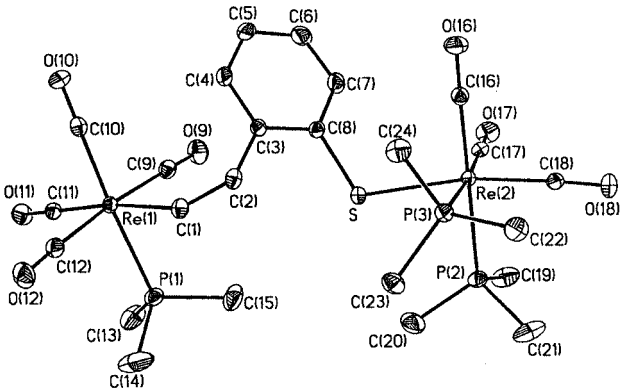

Fig. 3 Molecular structure of **3** in the solid state. Selected bond lengths (Å) and angles (°). Re(1)–C(1) 2.205(3), Re(2)–S 2.5086(9), C(1)–C(2) 1.327(4), S–C(8) 1.769(3), C(2)–C(3) 1.479(4), Re(1)–C(1)–C(2) 134.8(3), C(8)–S–Re(2) 113.18(12), P(2)–Re(2)–S 84.54(3), C(1)–C(2)–C(3) 129.8(3), C(1)–Re(1)–P(1) 82.44(8).

In the reaction (Scheme 1) of **1** with PMe_3, the relative amounts of **2** and **3** formed are the same whether 1 or 5 equiv. of PMe_3 are used. This means that the tri-phosphine product **3** is not formed from the bis-phosphine product **2** even in the presence of an excess of PMe_3. Therefore **2** and **3** must form by independent pathways. The structures of **2** and **3** are also fundamentally different from each other because the terminal vinyl carbon is bound to the $Re(CO)_3$ unit in **2** whereas in **3** it is coordinated to the $Re(CO)_4$ group. The formation of these products may be understood in terms of a mechanism that involves two forms of **1** resulting (Scheme 2) either from a "flip-flop" of the vinyl group from one Re to the other, as proposed for related bridging thiophene complexes $\{Fe_2(CO)_6(C_8H_6S)$,[6] $[(C_5Me_5)Co]_2(\mu\text{-}C_4H_4S)$[8] and $[(dippe)Ni]_2(\mu\text{-}C_8H_6S)$[9]}, or the migration of a CO group from one Re to the other.

1 **1′**

Scheme 2

The reaction of isomer **1′** with 2 equiv. of PMe_3 would lead to product **2** in which the olefin is displaced and the Re–Re bond is cleaved, leaving the terminal vinyl carbon coordinated to the $Re(CO)_3$ unit. On the other hand, the reaction of isomer **1** with 3 equiv. of PMe_3 would lead to product **3** with the vinyl carbon bonded to the $Re(CO)_4$ moiety while undergoing Re–olefin, Re–S and Re–Re bond cleavages. An attempt to detect the two isomers of **1** by low temperature (−50 °C, CD_2Cl_2 solvent) ^{1}H NMR spectroscopy showed only the same isomer that is present in the room temperature spectrum.‡ However, variable temperature ^{13}C NMR spectra of **1** (−50 °C to +20 °C) showed that the CO ligands are fluxional. Thus, while the two isomers are not detected by the NMR studies, a low concentration of the highly reactive **1′** would reasonably account for the formation of **2**.

The reactions in Scheme 1 are of special interest because they indicate the variety of ways that a bridging, C,S-cleaved BT ligand can bind to two metal centers. Were C–S cleavage to occur on a HDS catalyst, all three forms of BT represented in compounds **1**–**3** would be potential modes of BT adsorption on the catalyst surface.

The authors thank the U.S. Department of Energy, Office of Science, Office of Basic Energy Sciences, Chemical Sciences Division, under contract W-7405-Eng-82 with Iowa State University for financial support.

Notes and references

† Satisfactory elemental analyses were obtained for **1**–**3**.

‡ *Selected spectroscopic data*: for **1**: ^{1}H NMR (CD_2Cl_2, 300 MHz) δ 8.63 (d, 1 H, J = 11.4 Hz), 7.11 (m, 2 H), 7.05 (dt, 1 H, J_1 7.5, J_2 1.5 Hz), 7.00 (d, 1 H, J 11.4 Hz), 6.93 (dt, 1 H, J_1 7.2, J_2 1.5 Hz). IR (hexanes) ν_{CO}: 2099m, 2043s, 2027s, 1981s, 1977s, 1957m, 1947s cm^{-1}. For **2**: ^{1}H NMR (CD_2Cl_2, 300 MHz): δ 8.06 (dd, 1 H, J_1 14.1, J_2 2.4 Hz), 7.44 (dd, 1 H, J_1 14.1, J_2 3.6 Hz), 7.26 (d, 1 H, J 7.8 Hz), 7.00 (m, 2 H), 6.87 (m, 1 H), 1.87 (d, 9 H, PMe_3, J 9.3 Hz), 1.19 (d, 9 H, PMe_3, J 8.4 Hz). IR (CH_2Cl_2) ν_{CO}: 2100w, 2003s, 1953m, br, 1896m, br, 1873m, br cm^{-1}. For **3**: ^{1}H NMR (CD_2Cl_2, 300 MHz): δ 7.89 (dd, 1 H, J_1 13.5, J_2 3.9 Hz), 7.43 (dd, 1 H, J_1 7.8, J_2 1.2 Hz), 7.21 (d, 1 H, J 7.2 Hz), 6.99 (dt, 1 H, J_1 7.5, J_2 1.5 Hz), 6.92 (m, 2 H), 1.62 (m, 27 H, 3PMe_3). IR(CH_2Cl_2) ν_{CO} 2079w, 2018s, 1978s(sh), 1972s, 1933s, 1893s cm^{-1}.

CCDC 182/1551. See http://www.rsc.org/suppdata/cc/a9/a909161k/ for crystallographic files in .cif format.

1 H. Topsøe, B. S. Clausen and F. E. Massoth, *Hydrotreating Catalysts in Catalysis: Science and Technology*, ed. J. R. Anderson and M. Boudart, Springer-Verlag, Berlin, Heidelberg, 1996, vol. 11.
2 R. J. Angelici, in *Encyclopedia of Inorganic Chemistry*, ed. R. B. King, Wiley, New York, 1994, vol. 3, pp 1433–1443.
3 B. C. Gates, J. R. Katzer and G. C. A. Schuit, *Chemistry of Catalytic Processes*, MacGraw Hill, New York, 1979, pp. 390–447; G. D. Galpern, in *The Chemistry of Heterocyclic Compounds*, ed. S. Gronowitz, John Wiley and Sons, Inc., New York, 1985, vol. 44, Part 1, pp. 325–351.
4 N. Flitcroft, D. K. Huggins and H. D. Kaesz, *Inorg. Chem.*, 1964, **3**, 1123.
5 M. R. Churchill, K. N. Amoh and H. J. Wasserman, *Inorg. Chem.*, 1981, **20**, 1609.
6 A. E. Ogilvy, M. Draganjac, T. B. Rauchfuss and S. R. Wilson, *Organometallics*, 1988, **7**, 1171.
7 W. D. Jones, D. A. Vicic, R. M. Chin, J. H. Roache and A. W. Myers, *Polyhedron*, 1997, **16**, 3115.
8 W. D. Jones and R. M. Chin, *Organometallics*, 1992, **11**, 2698.
9 D. A. Vicic and W. D. Jones, *J. Am. Chem. Soc.*, 1999, **121**, 7606.

Communication a909161k

Synthetic dephosphorylation reagents: rate enhancement of phosphate monoester hydrolysis by Cu(II)-metallated adenine nucleobase polymers

S. G. Srivatsan and Sandeep Verma*

Department of Chemistry, Indian Institute of Technology-Kanpur, Kanpur-208016 (UP), India, E-mail: sverma@iitk.ac.in

Received (in Cambridge, UK) 11th January 2000, Accepted 17th February 2000

Significant rate enhancement of *p*-nitrophenyl phosphate hydrolysis, catalyst turnover and recycling has been observed for metallated, 9-allyladenine-containing cross-linked polymers.

Nucleic acids can coordinate to metal ions through the participation of base keto oxygen atoms, heterocyclic ring nitrogen atoms, sugar hydroxy groups and phosphate oxygen atoms.[1] The importance of metal ion binding is not simply limited to phosphate charge neutralization, but is also essential for stabilization of the nucleic acid structure and for RNA catalysis.[2,3] The design of our dephosphorylation agents has drawn inspiration from nucleic acids[4a–c] and we have invoked metal-ion coordination ability of purine nucleosides and nucleotides,[5a–h] for the synthesis of metallated, cross-linked nucleobase polymers. These polymeric molecules have been utilized for the hydrolysis of a model phosphate monoester and the kinetic parameters have also been determined.

Phosphate ester hydrolysis plays an important role in energy metabolism and in a variety of cellular signal transduction pathways in biological systems.[6a,b] The design of synthetic models of this reaction has been an attractive area of research and consequently, a wealth of information regarding artificial phosphatases and nucleases is available in literature.[7a–d] Most of these models utilize ligand bound transition and inner-transition metal ions for the catalysis of phosphate ester hydrolysis.[8a–k] It is assumed that metal ions play an important role in hydrolysis through the formation of metal–aqua complexes and by providing electrostatic neutralization of the negative charge on the phosphate group, thus making it more susceptible to nucleophilic attack.[8c] Owing to polarization effects, water molecules coordinated to metal ions can be substantially more acidic compared to free water molecules.[9]

The synthesis of our metallated nucleobase polymers involve AIBN-initiated polymerization of 9-allyladenine[10] with a cross-linking agent such as 1,4-divinylbenzene (DVB) or ethylene glycol dimethacrylate (EGDMA), in the presence of added metal ions. Adenine derivatives have been shown to coordinate to metal ions such as Cu^{2+}, Mn^{2+}, Zn^{2+} and Co^{2+}, predominantly through purine ring nitrogens.[5a–h] Keeping this fact in mind, we have prepared a polymeric matrix containing multiple adenine rings for extensive metal ion coordination. The metallated polymers so obtained were insoluble in common solvents and thus the present study is an example of heterogeneous catalysis of phosphate monoester hydrolysis. Atomic absorption spectroscopy and inductively coupled plasma analysis were used to estimate the amount of Cu(II) incorporated within the polymeric matrix (Table 1). It was found that incorporation of Cu(II) in EGDMA cross-linked polymer was 2.5 times that when compared to the DVB polymer. A much higher loading could be explained due to the presence of oxygen atoms in EGDMA, which can provide additional sites for metal ion coordination. Preliminary EPR studies have also been performed with these polymers.[11]

We have employed *p*-nitrophenyl phosphate (pNPP), a routinely used model monophosphate ester substrate, to evaluate the phosphatase activity of our adenine polymers and time-dependent release of *p*-nitrophenolate anion ($\varepsilon_{400} = 1.65 \times 10^4$ M^{-1} cm^{-1}) was used to determine kinetic constants. Remarkable rate enhancement was observed for pNPP hydrolysis in the presence of metallated polymers. The pseudo-first order rate constants (k_{obs}) were determined and it was found that polymers **1** and **2** displayed *ca.* 2,700- and 11,000-fold rate enhancement for pNPP hydrolysis (Table 1), respectively, as compared to the uncatalyzed reaction (4.92×10^{-7} min^{-1}, pH 7 at 25 °C[8h]). These observations prompted us to perform a more thorough kinetic evaluation and therefore, the Michaelis–Menten kinetic parameters for metallated adenine nucleobase polymers **1** and **2** were determined. Lineweaver–Burk plots (1/V *vs.* 1/[S], Fig. 1) were used to calculate Michaelis constants (K_m) and maximal velocities (V_{max}). For polymer **1**, containing DVB cross-linker, the K_m and V_{max} values were found to be 1.01 mM and 2.55×10^{-5} mM min^{-1}, respectively. While for polymer **2**, containing EGDMA cross-linker, the corresponding K_m and V_{max} values were found to be 0.21 mM and 4.6×10^{-5} mM min^{-1}, respectively (Table 2, Fig. 1).

Table 1 Estimated copper-loading and pseudo-first-order rate constants for pNPP hydrolysis in the presence of polymers **1** and **2**[a]

Polymer[b]	9-Allyladenine: cross-linker: Cu(II)	Mg of Cu(II) (g polymer)$^{-1}$ [c]	k_{obs}/min^{-1}	k_{rel}
1	DVB, 1:3:1	63.60	1.32×10^{-3}	2.7×10^3
2	EGDMA, 1:4:1	160.00	5.47×10^{-3}	1.1×10^4

[a] All hydrolytic reactions were performed in duplicate in 3 mL of 0.01 M *N*-ethylmorpholine buffer in 50% aqueous methanol (pH 8.0, 30 °C). [b] Polymer weights were 1 mg in 3mL of buffer, corresponding to 0.33 and 0.84 mM of Cu^{2+}, if polymers **1** and **2** were completely soluble in buffer and substrate concentrations were 3.3 and 8.4 mM, respectively. [c] Determined by AAS (AAS-300 Analyst, Perkin Elmer) and ICP (Integra XL, GBC) measurements.

We have also evaluated polymer **2** under turnover conditions[12e] by increasing the substrate concentration, while keeping the amount of polymer constant. Pseudo-first-order rates were determined and it was found that polymer **2** displayed efficient catalysis even in the presence of a 10-fold excess concentration of pNPP (Table 3). A unique feature of our

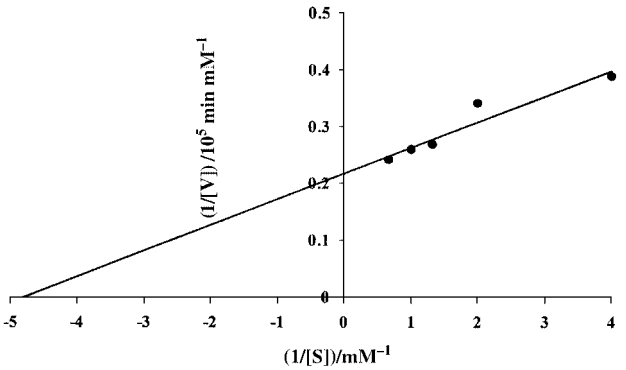

Fig. 1 Lineweaver–Burk plot of Cu(II)-metallated EGDMA cross-linked adenine nucleobase polymer **2**.

Table 2 Michaelis constants and maximal velocities of Cu(II)-containing adenine polymers for pNPP hydrolysis[a]

Polymer[b]	K_m/mM	V_{max}/mM min^{-1}
1	1.01	2.55×10^{-5}
2	0.21	4.6×10^{-5}

[a] All hydrolytic reactions were performed in duplicate in 5 mL of 0.01 M *N*-ethylmorpholine buffer in 50% aqueous methanol (pH 8.0, 30 °C), pNPP concentrations, [S]: 0.5–2.0 mM and 0.25–1.5 mM (for polymers **1** and **2**, respectively). [b] Polymer weights were 1 mg in 5 mL of buffer, corresponding to 0.2 and 0.5 mM of Cu^{2+}, for polymers **1** and **2** respectively, if the polymers were completely soluble in buffer.

Table 3 Turnover experiments[a]

Molar ratio of Cu(II) present in EGDMA adenine polymer[b]: pNPP	Pseudo-first-order rate constant k_{obs}/ min^{-1}
1:1	1.69×10^{-3}
1:3	2.39×10^{-3}
1:10	5.47×10^{-3}

[a] All hydrolytic reactions were performed in duplicate in 3 mL of 0.01 M *N*-ethylmorpholine buffer in 50% aqueous methanol (pH 8.0, 30 °C); [b] Polymer weights were 1 mg in 3 mL of buffer, corresponding to 0.84 mM of Cu^{2+}, if polymer **2** was completely soluble in buffer.

polymers is that they could be easily recycled. In a typical procedure, after pNPP hydrolysis, the reaction mixtures were centrifuged; polymers were filtered off and washed with copious volumes of 50% aqueous methanol. Washed and dried polymers were then reused for the catalysis of a subsequent hydrolytic reaction. Both of the polymers were reused thrice and the initial velocities, depending on the release of *p*-nitrophenolate anion, were found to be similar to the values obtained by using fresh polymeric catalysts (data not shown).

It is tempting to attribute a differential rate enhancement between the two polymers to the high loading of Cu(II) in polymer **2**. Unmetallated, cross-linked adenine polymers failed to catalyze pNPP hydrolysis over an extended period of time (data not shown), thereby indicating a crucial role of coordinated metal ion in accelerating the hydrolytic reaction. There are some literature reports that describe polymer-based, non-enzymatic hydrolysis of activated phosphate esters and RNA.[4c,12a–f] We have also introduced a novel matrix of cross-linked nucleobase polymers and have exploited metal coordination capability of adenine nucleobase for phosphate monoester hydrolysis. Turnover and recycling experiments indicate that these molecules are robust, possess high catalytic efficiency, and are amenable to recycling. Importantly, the heterogeneous nature of our catalyst can be utilized for its convenient removal at the completion of reaction.

The precise mechanism of monophosphate ester hydrolysis by metallated nucleobase polymers is unclear at the present time. Experiments are underway to elucidate the mechanism and to evaluate the catalytic assistance of these polymers for the hydrolysis of amides, esters, dinucleotides and nucleic acids. Moreover, we are also in the process of developing soluble, nucleobase containing polymeric matrices for effecting homogeneous catalysis of the above mentioned reactions.

We would like to thank Mr D. Saran for his contribution to the initial phase of this project and FEAT Lab, IIT-Kanpur, for AAS/ICP measurements. Financial support from the Council of Scientific and Industrial Research (CSIR) is gratefully acknowledged.

Notes and references

1 W. Saenger, in *Principles of Nucleic Acid Structure*, Springer Verlag, New York, 1984, p. 201.
2 A. M. Pyle, *Science*, 1993, **261**, 709.
3 T. M. Tarasow, S. L. Tarasow and B. E. Eaton, *Nature*, 1997, **389**, 54.
4 Other examples of nucleobase polymers: (*a*) P. M. Pitha and J. Pitha, *Biopolymers*, 1970, **9**, 965; (*b*) L. Maggiora, S. Boguslawski and M. P. Mertes, *J. Med. Chem.*, 1977, **20**, 1283; (*c*) T. Shiiba, M. Komiyama, E. Yashima and M. Akashi, *Nucleic Acids Symp. Ser.*, 1991, **25**, 71.
5 (*a*) S. A. Kazakov, in *Bioorganic Chemistry: Nucleic Acids*, ed. S. M. Hecht, Oxford University Press, New York, 1996, p. 244; (*b*) A. Schreiber, M. S. Lüth, A. Erxleben, E. C. Fusch and B. Lippert, *J. Am. Chem. Soc.*, 1996, **118**, 4124; (*c*) S. S. Massoud and H. Sigel, *Eur. J. Biochem.*, 1990, **187**, 387; (*d*) S. S. Massoud and H. Sigel, *Eur. J. Biochem.*, 1989, **179**, 451; (*e*) H. Sigel, *Biol. Trace Elem. Res.*, 1989, **21**, 49; (*f*) R. B. Martin, *Acc. Chem. Res.*, 1985, **18**, 32; (*g*) K. Maskos, *Acta. Biochim. Pol.*, 1978, **25**, 311; (*h*) L. G. Purnell and D. J. Hodgson, *Biochim. Biophys. Acta*, 1976, **447**, 117.
6 (*a*) J. B. Vincent, M. W. Crowder and B. A. Averill, *Trends Biochem. Sci.*, 1992, **17**, 105; (*b*) A. Fersht, in *Enzyme Structure and Mechanism*, W. H. Freeman and Company, New York, 1985, p. 235.
7 Reviews: (*a*) M. Komiyama, N. Takeda and H. Shigekawa, *Chem. Commun.*, 1999, 1443; (*b*) B. N. Trawick, A. T. Daniher and J. K. Bashkin, *Chem. Rev.*, 1998, **98**, 939; (*c*) J. Chin, *Curr. Opin. Chem. Biol.*, 1997, **1**, 514; (*d*) J. R. Morrow, *Met. Ions Biol. Syst.*, 1996, **33**, 561.
8 (*a*) K. Ichikawa, M. Khabir Uddin and K. Nakata, *Chem. Lett.*, 1999, 115; (*b*) S. Liu and A. D. Hamilton, *Chem. Commun.*, 1999, 587; (*c*) R. A. Moss, J. Zhang and K. Bracken, *Chem. Commun.*, 1997, 1639; (*d*) R. A. Moss, K. Bracken and J. Zhang, *Chem. Commun.*, 1997, 563; (*e*) M. Kalesse and A. Loos, *Bioorg. Med. Chem. Lett.*, 1996, **6**, 2063; (*f*) J. Rammo and H.-J. Schneider, *Liebigs Ann.*, 1996, 1757; (*g*) M. Wall, R. C. Hynes and J. Chin, *Angew. Chem., Int. Ed. Engl.*, 1993, **32**, 1633; (*h*) D. H. Vance and A. W. Czarnik, *J. Am. Chem. Soc.*, 1993, **115**, 12 165; (*i*) J. R. Morrow, L. A. Buttrey, V. M. Shelton and K. A. Berback, *J. Am. Chem. Soc.*, 1992, **114**, 1903; (*j*) R. Breslow and D. L. Huang, *Proc. Natl. Acad. Sci. USA*, 1991, **88**, 4080; (*k*) M. K. Stern, J. K. Bashkin and E. D. Sall, *J. Am. Chem. Soc.*, 1990, **112**, 5357.
9 E. Chaffee, T. P. Dasgupta and G. M. Harris, *J. Am. Chem. Soc.*, 1973, **95**, 4169.
10 9-Allyladenine was prepared by reacting adenine (1 equiv.) with allyl bromide (0.9 equiv.) in the presence of sodium hydride (1.2 equiv.), using anhydrous DMF as the solvent at 30 °C for 12 h. Silica gel column chromatography (R_f 0.31, ethyl acetate) afforded the pure compound, which was characterized by ^{1}H NMR and MS [EI] *m*/*z* 175 (M^+, base peak).
11 Preliminary EPR measurements, at liquid nitrogen temperature (77 K), suggest the presence of rhombic symmetry for the EGDMA cross-linked polymer **2**, while isotropic symmetry and indication of interacting Cu(II) centers were observed for DVB cross-linked polymer **1**. Detailed EPR-based structural investigations and determination of magnetic properties of these polymers are currently in progress.
12 (*a*) A. Bibillo, M. Figlerowicz and R. Kierzek, *Nucleic Acids Res.*, 1999, **27**, 3931; (*b*) A. Bibillo, K. Ziomek, M. Figlerowicz and R. Kierzek, *Acta Biochim. Pol.*, 1999, **46**, 145; (*c*) M. J. Han, K. S. Yoo, K. H. Kim, G. H. Lee and J. Y. Chang, *Macromolecules*, 1997, **30**, 5408; (*d*) J. Suh, J. Y. Lee and S. H. Hong, *Bioorg. Med. Chem. Lett.*, 1997, **7**, 2383; (*e*) F. M. Menger and T. Tsuno, *J. Am. Chem. Soc.*, 1989, **111**, 4903; (*f*) F. M. Menger, L. H. Gan, E. Johnson and D. H. Durst, *J. Am. Chem. Soc.*, 1987, **109**, 2800.

Communication b000348o

ChemComm

Entrapment of ferrocenes within supramolecular, deep-cavity resorcin[4]arenes†

Leonard R. MacGillivray,* Heather A. Spinney, Jennifer L. Reid and John A. Ripmeester

Steacie Institute for Molecular Sciences, National Research Council of Canada, Ottawa, Ontario, Canada, K1A 0R6. E-mail: lmacgil@ned1.sims.nrc.ca

Received (in Columbia, MO) 8th December 1999, Accepted 14th February 2000

Using a template-based method to molecular self-assembly, the ability of ferrocene (FcH) and two of its acetylated derivatives [FcAc, 1,1′-Fc(Ac)$_2$] to induce formation of a supramolecular deep cavity based upon *C*-methylcalix[4]resorcinarene 1 and 4,4′-bipyridine 2, 1·2(2), 3, is revealed; equatorial inclusion of 1,1′-Fc(Ac)$_2$ within 3 promotes a change in conformation of the guest.

Ferrocenes are attractive guests for studies involving facets of second sphere coordination in which molecular receptors serve as hosts.[1,2] The cyclopentadienyl (Cp) rings of such complexes can be readily derivatized and, upon interacting with the surface of a receptor, may adopt a conformation not exhibited by the free molecule which, in turn, may influence properties of the guest (*e.g.* reactivity).[3] Despite this realization, it is surprising that little structure information exists concerning the interaction of ferrocene (FcH) with most receptors designed to date, an observation likely related to the relatively large size of the complex. α-Cyclodextrin was the first receptor shown to assemble with FcH in the solid state, in the form of a 2:1 assembly [2(α-CD)·FcH],[4] while a hemicarcerand has been recently illustrated to encapsulate the molecule in a 1:1 host–guest complex (HC·FcH).[5] In each case, the included FcH is located within a symmetric cavity such that the Cp rings of the molecule are surrounded by identical chemical environments, which, in effect, prohibits any degree of discrimination, in terms of recognition, among the rings.[6]

Our approach to the construction of a host able to recognize FcH, and its derivatives (FcR), involves the use of a supramolecular cavity based upon Högberg's resorcin[4]arenes.[7] In particular, extensive work has demonstrated that co-crystallization of *C*-methylcalix[4]resorcinarene **1** with 4,4′-bipyridine **2** typically yields a one-dimensional, wave-like polymer, **1**·2(**2**), **3**, in which the cavity of **1** is deepened supramolecularly,[8] interacting with four stacking pyridine units of **2** by way of four O–H···N hydrogen bonds.[9] The cavity created by the five molecules, which may be induced to form by way of guest templation,[10] is flexible, being able to accommodate either single or multiple guests by way of a conformational reorganization of the network **3**.[9]

With the observation that hemicarcerands recognize FcH realized,[5] we sought to determine whether **3** may be exploited in a similar manner. In contrast to the cavities cited above, the cavity of **3** is polar and, therefore, may be used to control the orientation, and possibly the conformation, of a ferrocene guest in which the structure of the guest is dictated by the electron-rich, bowl-shaped cavity of **1**.[6] Here, we reveal the ability of **3** to serve as a host for FcR. In particular, using a template-based method to molecular self-assembly,[10] we demonstrate the ability of FcH in **3**·FcH, and its mono- (FcAc) and 1,1′-diacetylated [Fc(Ac)$_2$] derivatives in **3**·FcAc and **3**·Fc(Ac)$_2$, respectively, to assemble within **3** such that each FcH guest interacts with the cavity of **1** in a 'side-on', or equatorial fashion. For **3**·Fc(Ac)$_2$, the Cp rings of the complex adopt a 1,1′-eclipsed conformation[11] which contrasts a 1,3′-staggered structure for the free molecule.[12] To our knowledge, **3**·FcH, **3**·FcAc and **3**·Fc(Ac)$_2$ represent the first examples in which metallocenes have been isolated within a resorcin[4]arene in the solid state.‡

Addition of FcH (0.020 g) to a boiling aliquot of EtOH (5 mL) in the presence of an equimolar amount of **1** (0.058 g) and two molar equivalents of **2** (0.033 g) yielded, upon slow cooling, a microcrystalline powder with yellow–orange crystals of **3**·FcH suitable for X-ray analysis within a day. The formulation of **3**·FcH was confirmed by single crystal X-ray analysis§ and ^{1}H NMR spectroscopy.

A space-filling view of the X-ray crystal structure of **3**·FcH is shown in Fig. 1. The FcH guest, which lies across a crystallographic mirror plane, has assembled within the wave-like framework **3** [polymer wavelength (λ) 25.4 Å; amplitude (ampl.) 19.3 Å],[9] which is propagated along the crystallographic *b*-axis [O···N separations (Å): O(1)···N(1) 2.74(11), O(2)···N(2) 2.68(13)], such that the sandwich complex interacts with **1** in an equatorial fashion. In this arrangement, the Cp–Fe–Cp axis of the iron complex is pointed in a direction that runs approximately parallel to the direction of the hydrogen bonds of **3** such that the Cp ligands of the guest, which adopt an approximate eclipsed D_{5h} conformation,[13] interact with **1** and **2** by way of C–H···π interactions.[14] Notably, the fit displayed by **1** and FcH markedly contrasts that of HC·FcH in which the sandwich complex is included axially,[5] the principal rotation axes of host and guest being approximately coincident. In both 2(α-CD)·FcH[4] and HC·FcH,[5] the Cp rings of the FcH guest adopt a staggered D_{5d} conformation.[13]

The observation that **3** may host FcH in the solid state suggested that **3** may be used to host derivatives of the complex. Indeed, **3** has been shown to accommodate guests of various size by modifying the relative orientations of the components of the host which results in a conformational change of the network.[9] If achieved, we anticipated that it may be possible to control stereochemical features of a ferrocene guest in which the substituents of the Cp ligands, owing to their electronic nature, may be directed either in or out of the cavity of **1**.[6]

To test this hypothesis, **1** (0.040 g) was co-crystallized with two molar equivalents of **2** (0.023 g) from a boiling aliquot of EtOH (5 mL) in the presence of a molar equivalent of either

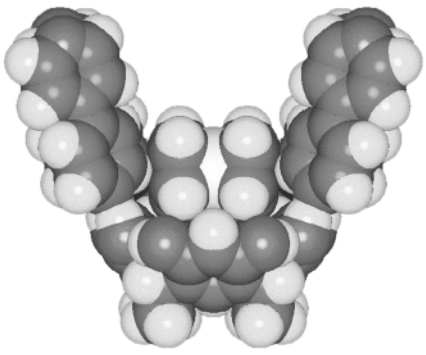

Fig. 1 Space-filling view of guest inclusion in the X-ray crystal structure of **3**·FcH.

† Published as NRCC no. 43832.

DOI: 10.1039/a909745g

FcAc or $Fc(Ac)_2$. Yellow and red crystals of **3**·FcAc and **3**·$Fc(Ac)_2$, respectively, suitable for X-ray analysis grew within a day. The formulations of **3**·FcAc and **3**·$Fc(Ac)_2$ were confirmed by single crystal X-ray analysis§ and ^{1}H NMR spectroscopy.

An ORTEP perspective of the X-ray crystal structure **3**·$Fc(Ac)_2$ is shown in Fig. 2(a). In a similar way to **3**·FcH, the guests have assembled within **3** such that both complexes lie within **1** in an equatorial fashion and the Cp rings of the guests, which run in a direction parallel to the hydrogen bonds of **3** [O···N separations for **3**·FcAc and **3**·$Fc(Ac)_2$ (Å): O(1)···N(1) 2.660(3), 2.705(3), O(2)···N(3) 2.710(3), 2.683(3), O(5)···N(2) 2.649(3), 2.762(3), O(6)···N(4) 2.758(3), 2.633(3), respectively], interact with **1** and **2** by way of C–H···π forces [**3**·FcAc and **3**·$Fc(Ac)_2$: polymer λ (Å): 27.0, 26.6; ampl. (Å): 18.4, 18.5, respectively]. In this arrangement, the electron-rich carbonyl substituents of the guests are directed away from the cavity of **1** such that the substituents, which, as in the free molecules,[12,18] are approximately co-planar with the Cp rings, lie above the wider rim of **1**. For **3**·$Fc(Ac)_2$, the acetyl groups of the disubstituted complex, in contrast to free $Fc(Ac)_2$ and most 1,1′-disubstituted ferrocenes which tend to crystallize in a 1,3′-conformation,[19] adopt a 1,1′-conformation such that the substituents are eclipsed [Fig. 2b].¶ Indeed, this latter observation may be attributed, in part, to the electron-rich nature of the cavity of **3** which, upon maximizing attractive non-covalent forces between host and guest, has induced the molecule, by way of second sphere coordination,[1,2] to adopt a structure of a less preferred conformer.[12,19]

In this report, we have revealed the ability of **1**, with a cavity deepened supramolecularly,[8] to entrap FcH, and two of its acetylated derivatives, in the solid state. Owing to the ability of **1** to interact with the complex in an equatorial fashion, we have shown that it is possible to effect the conformation of a ferrocene guest such that, for $Fc(Ac)_2$, the substituents of the complex lie eclipsed. With such observations realized, we plan to determine if more reactive derivatives of FcH may be entrapped within **3** such that the substituents of the Cp rings may undergo reaction in the solid state.[20] We are also investigating whether **3** may be used as a host for other transition-metal-based complexes in which the structure behaviours of such organic–organometallic host–guest materials are expected to be governed by the supramolecular properties of **3** by way of second-sphere coordination.[1,2]

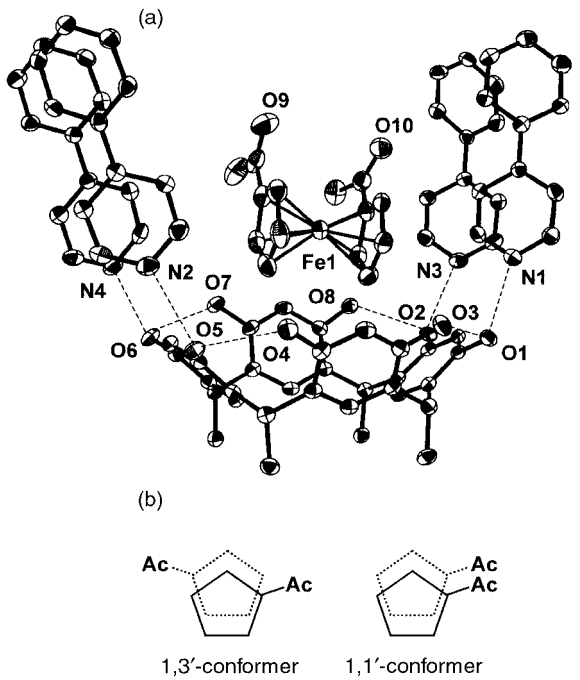

Fig. 2 (a) ORTEP perspective of the X-ray crystal structure of **3**·$Fc(Ac)_2$ and (b) schematic representation illustrating the conformation of $Fc(Ac)_2$ within the cavity of **3**. The guest adopts a 1,1′-conformation.

We are grateful for funding from the National Research Council of Canada (WES undergraduate scholarship, H. A. S.) and the Natural Sciences and Engineering Research Council of Canada (graduate scholarship, J. L. R.).

Notes and references

‡ To our knowledge, a metallocene has not been observed to assemble within a calix[4]arene in the solid state.

§ *Crystal data*: for **3**·FcH: monoclinic, space group, $P2_1/m$, a = 9.730(1), b = 25.440(3), c = 10.825(1) Å, β = 110.710(3)°, V = 2506.4(6) Å^3, D_c = 1.38 g cm^{-3}, Mo-Kα radiation (λ = 0.71070 Å) for Z = 2. Least-squares refinement based on 1527 reflections with $I_{net} > 2.0\sigma(I_{net})$ (out of 3370 unique reflections) led to a final value of R = 0.089.

For **3**·FcAc: monoclinic, space group, $P2_1/n$, a = 18.477(1), b = 11.742(1), c = 26.086(1) Å, β = 107.794(1)°, V = 5389.0(4) Å^3, D_c = 1.34 g cm^{-3}, Mo-Kα radiation (λ = 0.71070 Å) for Z = 2. Least-squares refinement based on 5416 reflections with $I_{net} > 2.0\sigma(I_{net})$ (out of 7041 unique reflections) led to a final value of R = 0.034.

For **3**·$Fc(Ac)_2$: monoclinic, space group, $P2_1/n$, a = 18.808(1), b = 11.948(1), c = 25.595(1) Å, β = 108.306(1)°, V = 5460.4(4) Å^3, D_c = 1.37 g cm^{-3}, Mo-Kα radiation (λ = 0.71070 Å) for Z = 2. Least-squares refinement based on 5676 reflections with $I_{net} > 2.0\sigma(I_{net})$ (out of 7141 unique reflections) led to a final value of R = 0.044. Intensity data for **3**·FcH, **3**·FcAc and **3**·$Fc(Ac)_2$ were collected at 173 K using the SMART system. Aromatic, methine, methyl and hydroxy hydrogen atoms were placed by modelling the moieties as rigid groups with idealised geometry, maximizing the sum of the electron density at the calculated hydrogen positions.

Structure solutions were accomplished using SHELXS-86[15] and refinements were conducted using SHELXL93[16] locally implemented on a pentium-based IBM compatible computer. Structure refinements and production of figures were accomplished with the aide of RES2INS.[17]

CCDC 182/1550. See http://www.rsc.org/suppdata/cc/a9/a909745g/ for crystallographic files in .cif format.

¶ We also note that the acetyl groups of free and entrapped $Fc(Ac)_2$ display *transoid* and *cisoid* relationships, respectively, while the Cp ligands in both complexes are eclipsed.

1 H. M. Colquhoun, J. F. Stoddart and D. J. Williams, *Angew. Chem., Int. Ed. Engl.*, 1986, **25**, 487.
2 S. J. Loeb, in *Comprehensive Supramolecular Chemistry: Volume 1, Second-Sphere Coordination*, ed. J. L. Atwood, J. E. D. Davies, D. D. MacNicol and F. Vögtle, Elsevier Science Inc., New York, 1996.
3 *Ferrocenes*, ed. A. Togni and T. Hayashi, VCH Publishers, New York, 1995.
4 Y. Odagaki, K. Hirotsu, T. Higuchi, A. Harada and S. Takahashi, *J. Chem. Soc., Perkin Trans. 1*, 1990, 1230.
5 D. J. Cram and J. M. Cram, in *Container Molecules and Their Guests*, ed. J. F. Stoddart, Royal Society of Chemistry, Cambridge, 1994.
6 C. Wieser-Jeunesse, D. Matt and A. De Cian, *Angew. Chem., Int. Ed.*, 1998, **37**, 2861.
7 A. G. S. Högberg, *J. Am. Chem. Soc.*, 1980, **102**, 6046.
8 D. M. Rudkevich and J. Rebek Jr., *Eur. J. Org. Chem.*, 1999, 1991.
9 L. R. MacGillivray and J. L. Atwood, *J. Am. Chem. Soc.*, 1997, **119**, 6931; L. R. MacGillivray and J. L. Atwood, in *Crystal Engineering: From Molecules and Crystals to Materials, NATO Science Series*, ed. D. Braga, F. Grepioni and A. G. Orpen, Kluwer Academic Publishers, Dordrecht, 1999.
10 L. R. MacGillivray, J. L. Reid and J. A. Ripmeester, *CrystEngComm*, 1999, 1.
11 B. M. O'Leary, R. M. Grotzfeld and J. Rebek Jr., *J. Am. Chem. Soc.*, 1997, **119**, 11701.
12 G. J. Palenik, *Inorg. Chem.*, 1970, **9**, 2424.
13 W. D. Luke and A. Streitwieser, Jr., *J. Am. Chem. Soc.*, 1981, **103**, 3241.
14 G. R. Desiraju and T. Steiner, *The Weak Hydrogen Bond in Structural Chemistry and Biology*, OUP, Oxford, 1999.
15 G. M. Sheldrick, *Acta. Crystallogr., Sect. A*, 1990, **46**, 467.
16 G. M. Sheldrick, SHELXL93, University of Göttingen, Germany, 1993.
17 L. J. Barbour, RES2INS, University of Missouri-Columbia, MO, 1997.
18 K. Sato, M. Iwai, H. Sano and M. Konno, *Bull. Chem. Soc. Jpn.*, 1984, **57**, 634.
19 L. Lin, A. Berces and H.-B. Kraatz, *J. Organomet. Chem.*, 1998, **556**, 11.
20 G. M. J. Schmidt, *Pure Appl. Chem.*, 1971, **27**, 647.

Communication a909745g

Typeset and printed by Black Bear Press Limited, Cambridge, England

ChemComm
FEATURE ARTICLE

Recent applications of olefin metathesis and related reactions in carbohydrate chemistry

René Roy* and Sanjoy Kumar Das

Department of Chemistry, University of Ottawa, Ottawa, Ontario, Canada K1N 6N5. E-mail: rroy@science.uottawa.ca

Received (in Cambridge, UK) 23rd September 1999, Accepted 4th November 1999
Published on the Web 1st March 2000

The potential use of olefin metathesis reactions in carbohydrate chemistry is discussed. In recent years, the use of olefin metathesis reactions for the construction of carbon–-carbon bonds has significantly expanded with the development of efficient and well-defined catalytic systems (1–7). These catalytic systems have found extensive use through cross-metathesis, ring-closing metathesis and ring-opening metathesis reactions for the syntheses of many carbohydrate-containing natural products. In some cases it has been shown that carbohydrate molecules can be synthesized from non-carbohydrate precursors using this simple but efficient procedure.

Professor René Roy was born in Sherbrooke, Québec, Canada in 1952. He received his Ph.D. degree in medicinal chemistry with Professor Stephen Hanessian in 1980 at the University of Montreal. He then obtained an NRC fellowship from 1980–1985 and worked in the Biological Sciences Division of the National Research Council in Ottawa, Ontario where he conducted immunological studies with Dr H. J. Jennings on bacterial polysaccharide vaccines. From 1985 onward, he joined the Department of Chemistry of the University of Ottawa were he moved to the rank of full Professor in 1995. During that time he also became adjunct Professor to the Department of Microbiology and Immunology. His research interests are centered around neoglycoconjugate syntheses and their applications in carbohydrate–protein interactions related to cancer vaccines and flu virus infections. He developed the first syntheses of glycodendrimers as potential antiadhesins. He made several contributions towards glycopolymer synthesis and their applications as coating antigens in ELISA assays. His recent interests lie in transition metal catalyzed reactions and phytomedicines. He has received the Hoffmann-La Roche Limited award in 1997.

Dr Sanjoy Kumar Das was born in Raiganj, India, in October 1967. He received his M.Sc. degree in Organic Chemistry from North Bengal University in 1991. After completing his Ph.D. degree under the supervision of Dr Mukund K. Gurjar at the Indian Institute of Chemical Technology, Hyderabad, India in 1996, he joined Professor Pierre Sinaÿ's laboratory at École Normale Supérieure, Paris as a postdoctoral fellow. After spending two years in Paris, he moved to Professor Roy's laboratory where currently he is working as a postdoctoral fellow. He is the recepient of several awards (awarded medals in B.Sc. and M.Sc. Exams. and selected as a best research scholar during his Ph.D. in 1995) including the most prestigious, Council of Scientific and Industrial Research, New Delhi, award. His research interests include the transition-metal catalyzed syntheses of neoglycoconjugates and the development of new methodologies in carbohydrate chemistry.

Introduction

The use of olefin metathesis in organic synthesis has grown considerably in recent years.[1,2] This simple procedure does not require the use of any additional reagents except for a catalytic amount of metal carbene, and the only by-product that forms is volatile ethylene gas. The importance of this carbon–carbon bond construction method is evident from the huge number of publications that have appeared within a short span of time.[3–5] Olefin metathesis can be categorized into three different sections: (1) cross-metathesis, in which two different alkenes undergo an intermolecular transformation to form a new olefinic product (eqn. 1); (2) ring-closing metathesis, a procedure which is useful for the formation of cyclic compounds (eqn. 2); and (3) ring-opening metathesis polymerization, which involves the metathetic opening of strained cyclic olefins to give polymeric compounds (eqn. 3).

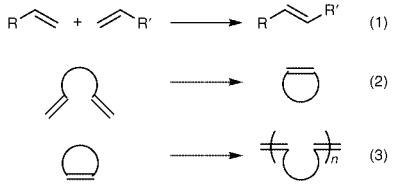

Although many examples of cross-metathesis, ring-closing metathesis and ring-opening metathesis reactions are available in the literature, only carbohydrate-related applications reported up to September 1999 will be discussed herein. Some interesting discoveries (cyclotrimerization, isomerization) from our laboratory using Grubbs' catalyst will also be discussed.

Catalyst development

The early examples of olefin metathesis employed classical catalysts which usually included a tungsten chloride or oxychloride and an alkyl metal species. These catalysts were less reactive to olefins due to their increased stability and yields were generally found to be low.[6–8] The other established catalyst is dichlorobis(2,6-dibromophenoxy)oxotungsten, $Cl_2(ArO)_2W{=}O$.[9] Although this system shows good functional group tolerance and has been used for many syntheses, it is considered to be unsuitable for industrial applications owing to its complexity and cost. Olefin metathesis began to receive more attention in 1993, when Basset and co-workers developed and applied the tungsten catalysts **1** and **2** for cross-metathesis reactions.[10,11] To date, these have been successfully shown to be remarkably tolerant to heteroatoms, including sulfur, silicon, phosphorus, and tin. Since the use of this catalyst is limited because of its steric demand toward shorter alkenes, such as allyl groups, researchers have searched for alternative catalytic systems for olefin metathesis reactions. One of the most useful catalysts for olefin metathesis reactions is the molybdenum catalyst (**3**) developed by Schrock *et al.*[12] Although the major advantage of **3** is its high reactivity towards a broad range of substrates with a variety of functional groups, this catalyst also

DOI: 10.1039/a907712j

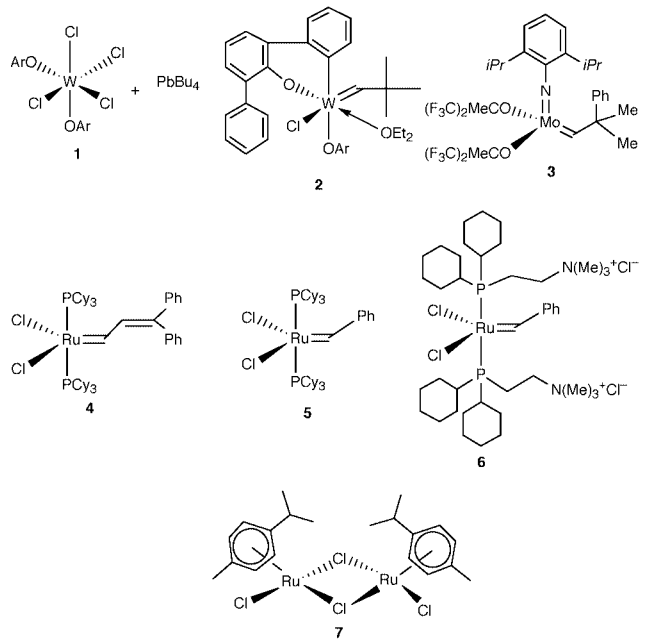

has some limitations. Its major drawbacks are that it is air sensitive and has moderate to poor functional group tolerance. Much work on the development of catalytic systems has been done by Grubbs and co-workers using two very important ruthenium-based catalysts, **4**[13] and **5**.[14] Although both catalysts benefit from the same impressive tolerance to air, moisture and various functional groups, catalyst **5** provides improved initiation rates and can be prepared easily. In addition to the catalytic systems discussed above, a few other transition metal catalysts have been prepared for olefin metathesis reactions. Among them, the water soluble ruthenium catalyst **6**,[15] also developed by Grubbs and co-workers, and a photoinducible dichloro(*p*-cymene)ruthenium(II) dimer (**7**), developed by Fürstner and Ackermann,[16] are noteworthy. Many applications of these catalysts have been recently reported in the literature. Although several metal carbenes have been mentioned, we have endeavoured to cover only the catalytic systems which have been used in carbohydrate chemistry.

Cross-metathesis

The cross-metathesis reaction, in which two different alkenes are used to form a new alkene, is shown in eqn. 1. This method has not found widespread application because of the fact that general conditions which give rise to high yields and stereoselectivity have not yet been discovered. With the development of new, well-defined metal alkylidenes and a better understanding of the nature of the reaction mechanisms involving these catalysts, some examples of selective cross-metathesis reactions have recently appeared in the literature. Thus, Blechert *et al.*[17] have shown that allyltributyl or allyltriphenyl stannane can undergo selective cross-metathesis reactions with allyl 2,3,4,6-tetra-*O*-acetyl-β-D-glucopyranoside (**8**) using Schrock's catalyst **3** (Scheme 1). The cross-metathesized

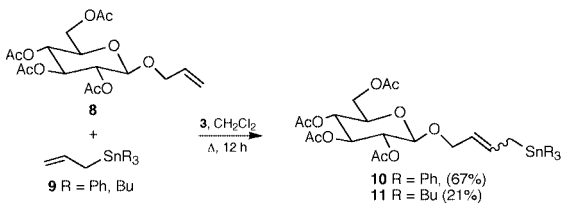

Scheme 1

product **10** could be very useful for nucleophilic additions to electrophilic carbon centres and for radical reactions.

Descotes *et al.*[18] have chosen this procedure as the most efficient method for the preparation of sugar bolaamphiphiles (**19**–**25**) in good yields (Scheme 2). Glucosides protected as

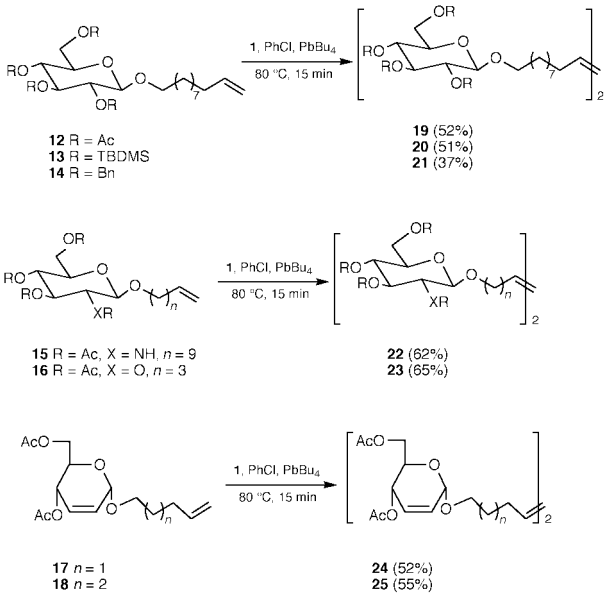

Scheme 2

acetates (**12**) or silyl ethers (**13**) were found to be superior substrates to benzyl-protected carbohydrates (**14**) in metathesis reactions. The same group has also successfully extended this methodology to the *N*-acetyl aminosugar **15**. Catalysts **1** and **2** were found to be active with pentenyl glycosides, whereas allyl glycosides did not afford any metathesis products; again the catalysts were deactivated by competitive coordination of the ether oxygen to the metallocarbenes. Metathesized products were synthesized in good yields, but the *cis*:*trans* ratios were not determined.

Recently, Grubbs *et al.*[19] have used the cross-metathesis reaction between *C*-allyl α-D-glucopyranoside and disubstituted olefins to supress the formation of self-metathesis products (Scheme 3). Homodimer **27** was subsequently used to function-

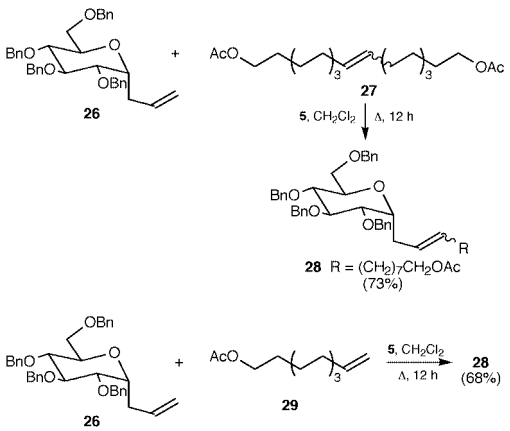

Scheme 3

alize *C*-allylglycoside (**26**) in 73% yield as a mixture of *cis* and *trans* isomers in a 3:1 ratio. In order to compare the yield and isomeric ratios, they performed the reaction with 4 equiv. of the terminal olefin **29**. The cross-metathesized product **28** was isolated in a marginally lower yield with slightly lower *trans*-selectivity (68%, 2.2:1 *E*:*Z*).

We have shown that peracetylated *O*-allyl β-galactoside (**30**) can be easily homodimerized in the presence of Grubbs' or Schrock's catalyst (Scheme 4).[20] Since, in both cases, the yields were found to be more or less the same, catalyst **5** was preferred

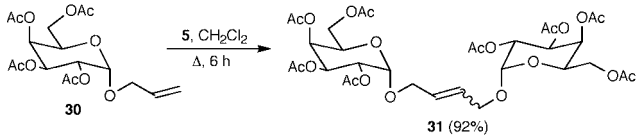

Scheme 4

because of its operational simplicity. Various other homodimers were synthesized using the same catalyst **5** (Table 1).

Table 1 Olefin self-metathesis of alkenyl *O*- and *C*-glycopyranosides

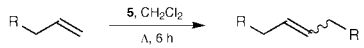

R	Product (*E*:*Z*)	Yield (%)
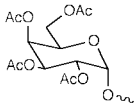	(5:1)	92
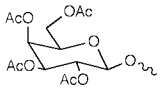	(4:1)	95
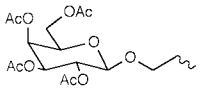	(5:1)	85
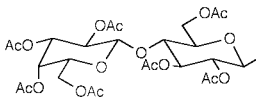	(4:1)	89
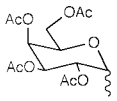	(2:1)	82
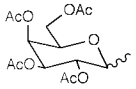	(1:1)	75
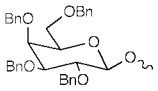	(3:1)	76

In order to investigate the influence of unprotected glycosides in metathesis reactions, we have shown[21] that the reaction proceeds smoothly with catalyst **5** at room temperature rather than under refluxing conditions, where *O*-allyl (**32**) and *O*-pentenyl mannopyranosides (**33**) gave homodimers **37** and **38** in good yields. Compounds **34** and **35** also provided homodimers, **39** and **40** in 95 and 66% yields, respectively (Scheme 5). The sterically more demanding C-vinyl glycoside (**36**) can undergo olefin metathesis reaction at elevated temperatures (70 °C) albeit slowly (Table 2).

Olefin metathesis has also been used for the synthesis of divalent sialoside derivatives.[22] Treatment of allyl *O*-α-sialoside (**42**) with 5 mol% of Grubbs' catalyst (**5**) in refluxing dichloromethane gave homodimer **44** in 82% yield. The corresponding thio-analogue, **43**, gave homodimer **45** in only 26% yield. Undoubtedly, the lower yield was due to catalyst-poisoning by the sulfide moiety (Scheme 6).

Synthesis of *O*- and *C*-glycosides **30** and **46** with differently functionalized spacers in the aglycon moiety was also carried out by cross-metathesis reactions from *O*-allyl and *C*-allyl glycosides in good yields (Table 3).[23] These extended glycosides can be further transformed by known methods into useful neoglycoconjugates including glycodendrimers and polymers. An interesting application of this reaction was the synthesis of

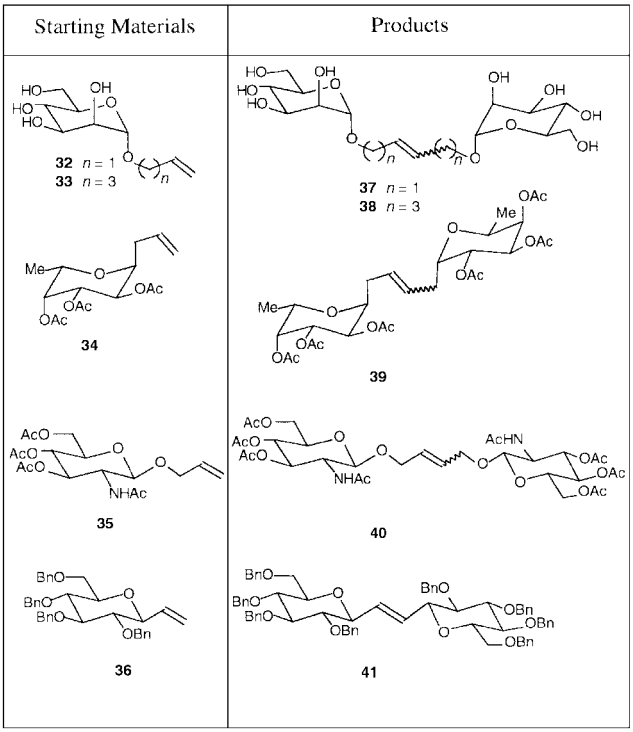

Scheme 5

Table 2 Olefin self-metathesis of alkenyl *O*- and *C*-glycopyranosides

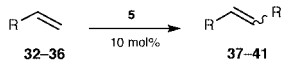

Substrate	Product	Reaction conditions	Yield (%)	*E*:*Z* Ratio
32	**37**	CH_2Cl_2:MeOH (3:1); rt	60	1.7:1
32	**37**	CH_2Cl_2:MeOH (3:1); 40 °C	34	1.4:1
33	**38**	CH_2Cl_2:MeOH (3:1); rt	67	1.3:1
33	**38**	CH_2Cl_2:MeOH (3:1); 40 °C	42	1.1:1
34	**39**	CH_2Cl_2; reflux	95	3:1
35	**40**	CH_2Cl_2; reflux	66	5:2
36	**41**	CH_2Cl_2; rt	n.r.	—
36	**41**	CH_2Cl_2; reflux	8	100:0
36	**41**	$ClCH_2CH_2Cl$; 70 °C	24	100:0

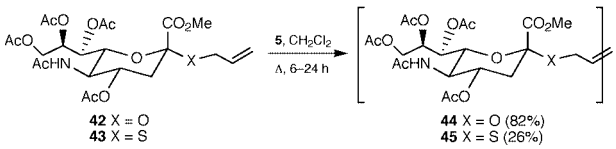

Scheme 6

C-linked pseudodisaccharides, which can be synthesized by the cross-metathesis between two different sugar moieties, using a head to tail condensation procedure (Scheme 7 and Table 4).

The cross-metathesis of *O*- or *C*-allyl glycosides and *N*-alkenyl-containing oligosaccharide derivatives (peptoids) has been reported by Hu and Roy.[24] The treatment of a GlcNAc derivative (**35**) with *N*-allylamine in the presence of Grubbs' catalyst (**5**) gave no cross-metathesis product, but dimerization of **35** was achieved in 30% yield. Alternatively, the use of amine **61** in the cross-metathesis reaction with **35** gave **62** in 41% yield. This was a surprising result, since free carboxylic acids are not considered to be good substrates for olefin metathesis reactions (Scheme 8).

The cross-metathesis reaction involving polymer-bound olefins has more potential benefits because product isolation should be easier. In an interesting application of the cross-metathesis reaction on a solid support, Blechert *et al.*[25] have

Table 3 Isolated yields and *E*:*Z* ratios of ruthenium catalyzed cross-metathesis of **30** with alkenes **47–54** to provide extended glycosides

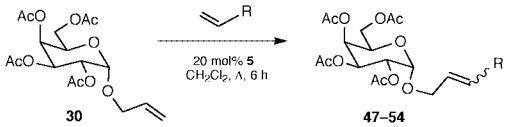

30 **47–54**

Entry	R	Equiv.	Reaction conditions	Product	Yield (%)	*E*:*Z* Ratio
1	CH_2SiMe_3	2	A	**47**	94	4:1
2	$CH_2CH_2CO_2Me$	2	A	**48**	67	2:1
3	CH_2OTBS	2	A	**49**	69	95:5
4	Ph	2	A	**50**	60	90:10
5	Ph	4	A	**50**	80	97:3
6	p-AcOPh	4	A	**51**	75	95:5
7	$(CH{=}CHCH_2OAc)_2$	2	A	**52**	70	5:1
8	CH_2NHBoc	2	A	**53**	30	4:1
9	CH_2NHBoc	2	B	**53**	57	4:1
10	CH_2NHCbz	2	A	**54**	39	4:1
11	CH_2NHCbz	2	B	**54**	65	4:1

Method A: CH_2Cl_2, reflux, 6 h; **Method B**: CH_2Cl_2; rt, 15 h

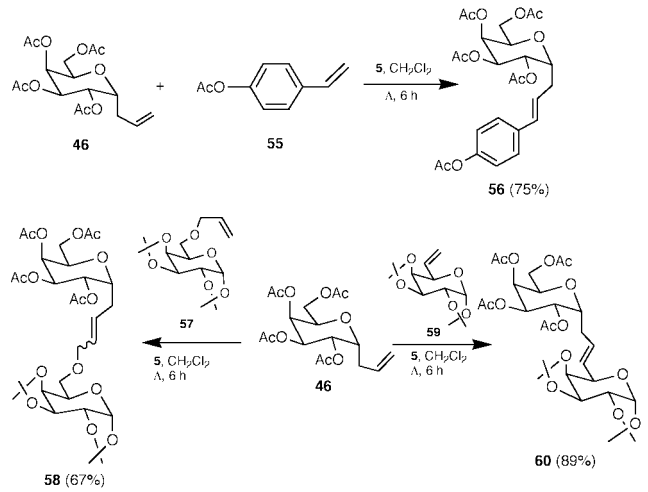

Scheme 7

Table 4 Isolated yields and *E*:*Z* ratios of ruthenium catalyzed cross-metathesis of a *C*-allyl galactoside derivative (**46**) with alkenes **55, 57** and **59**

Entry	Starting material	Equiv.	Product	Yield	*E*:*Z*ratio
1	**55**	2	**56**	50	100:0
2	**55**	4	**56**	75	100:0
3	**57**	2	**58**	67	4:1
4	**59**	2	**60**	89	2:1

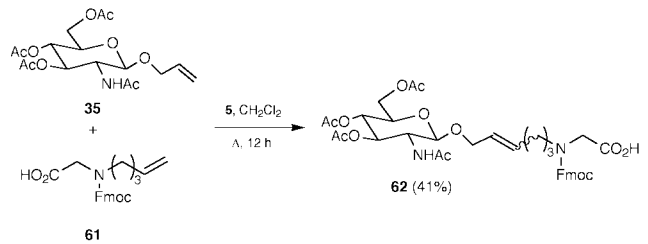

Scheme 8

reported the metathesis reaction between immobilized allyl silane **63** with various olefins (*e.g.*, **63a**) to give new immobilized olefins. Product **64** could be cleaved under acidic conditions to provide the homologated derivative **65** (Scheme 9).

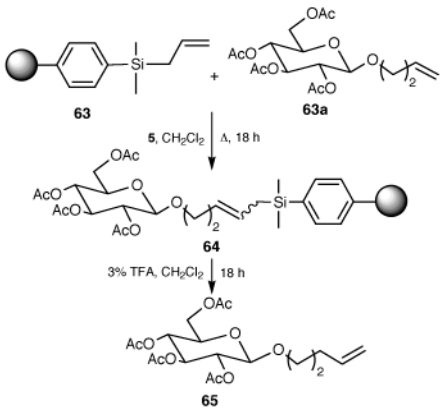

Scheme 9

In another solid-support application, Schuster and Blechert[26] have reported a catalytic cross-coupling reaction between the functionalized terminal alkynes **66** and allylsilyl polystyrene, **63**, *via* a more selective ruthenium-catalyzed crossed yne–ene metathesis reaction. Upon cleavage of **67** by 1.5% TFA, the procedure afforded the 1,3-diene **68** (Scheme 10).

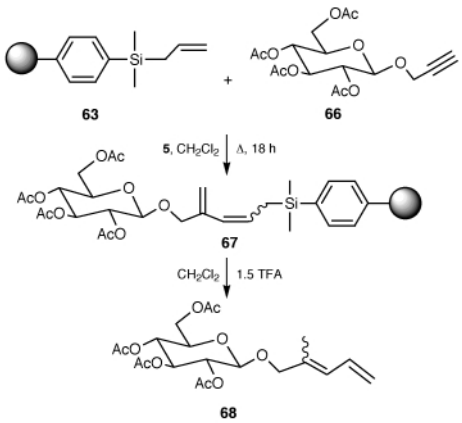

Scheme 10

Ring-closing metathesis

Among all the categories, ring-closing metathesis (RCM) reactions, which lead to cyclic products, have found the widest application in synthesis. With the advent of well-defined molybdenum- and ruthenium-based catalysts, high yielding

RCM of smaller ring systems was realized. It has been successfully used for the synthesis of a variety of carbo- and heterocyclic products and has also proven to be the key step for many total syntheses.

Huwe and Blechert[27] have chosen this novel strategy for the synthesis of azasugars from vinyl glycine methyl ester using catalyst **4**. They have shown that compound **69** is not suitable for olefin metathesis reactions (Scheme 11). Hydrolysis of **69** with NaOH in aqueous ethanol and subsequent treatment with di-*tert*-butyldicarbonate [$(Boc)_2O$] gave **71**. Olefin metathesis of **71** with 4 mol% of catalyst **4** gave a good yield of the RCM product **72** (95%). Compound **72**, on subsequent epoxidation and hydride opening of the epoxide, gave the 1,2-dideoxy sugar **76**.

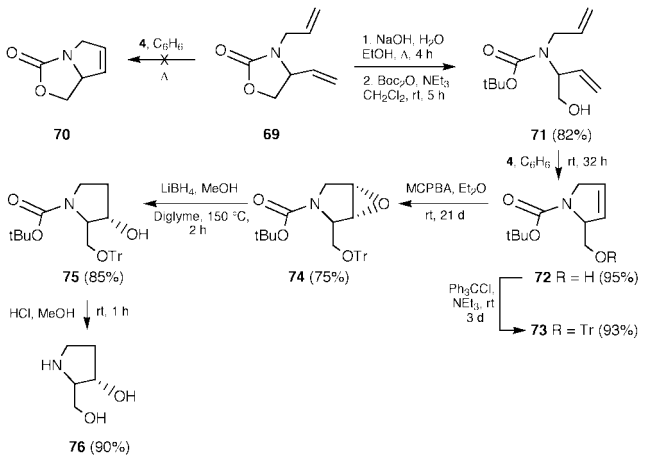

Scheme 11

In an another application, the same group[28] applied the Sharpless dihydroxylation method to obtain 1-deoxy azasugars (*e.g.*, **74** and **75**). They also used an analogous strategy toward the synthesis of the homoazasugar **79** from vinyl glycine methyl ester (Scheme 12).

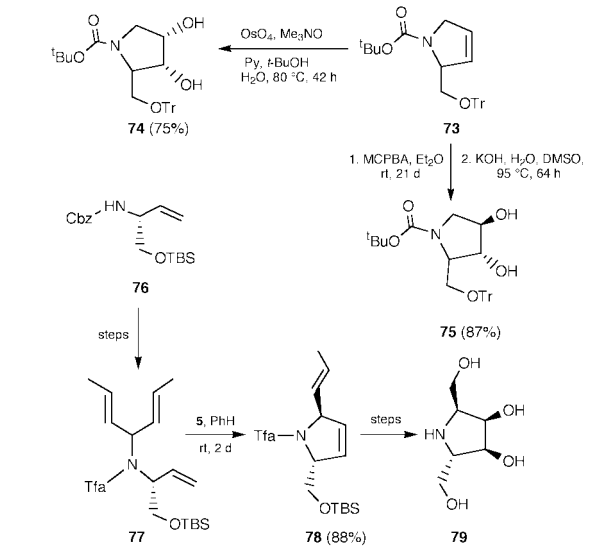

Scheme 12

Descotes *et al.*[29] have used catalysts **1** and **2** for an intramolecular carbohydrate macrocyclization. Thus, diluted solutions of the unsaturated substrates **80**–**83** in chlorobenzene when treated with 7 mol% of catalyst **1** at 80–85 °C afforded the cyclic products **84**–**87** in reasonable yields (56–73%). It has been observed that homodimerization of the starting material did not occur during the metathesis reaction. The results of the metathesis reaction are summarized in Scheme 13. The cyclization took place between the substituents at C1 and C6 which are in a *cis*-configuration. Thus, the chemoselectivity of the reaction could be controlled by the anomeric configuration.

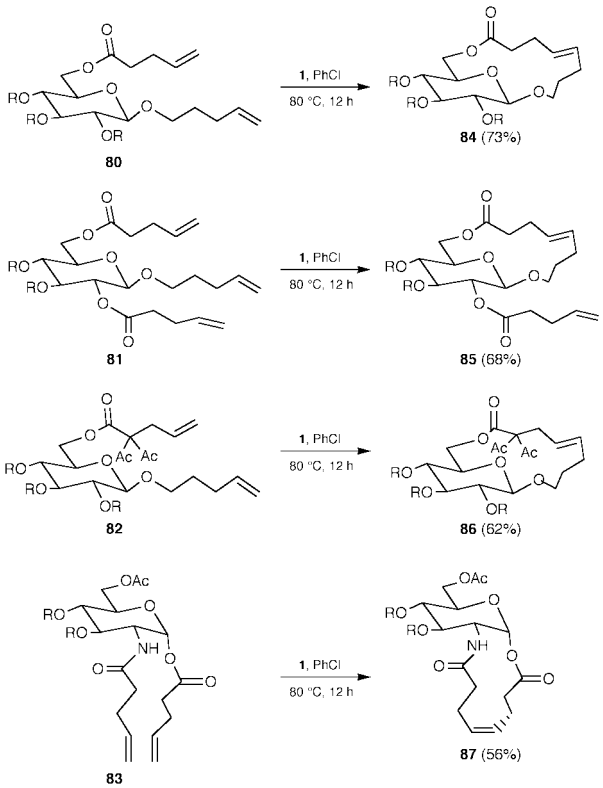

Scheme 13

Sturino and Wong[30] have made some interesting observations. They have reported the ring-closing metathesis of the vinyl ethers **89**, **91** and **93** with Grubbs' catalyst (**5**) (Scheme 14). Although compound **89** gave the cyclic product **90** in 69% yield, compound **91** was inert. They concluded that the presence of an allylic alkoxy substituent has a negative influence on the RCM reaction. As an exception to this finding, it was shown that compound **93** can give **94** due to the Thorpe–Ingold effect of the *gem*-dimethyl substituents.

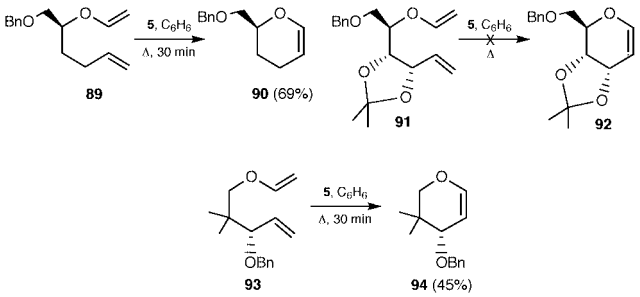

Scheme 14

A novel and versatile route to highly functionalized chiral oxepines, which is based on RCM of differently protected glycofuranoses,[31] has been developed by van Boom *et al.* Thus, treatment of **97**, which can be easily prepared from 2,3,5-tri-*O*-benzyl-D-arabinofuranose (**95**), with 5 mol% of the Ru-catalyst **5** in toluene at 50 °C for 24 h gave the expected cyclized product, **98** (Scheme 15). The success of this smooth cyclization of the vinyl-*O*-allyl derivatives encouraged this group to prepare interesting oxepanes, such as **100**. The RCM of **99** led to the formation of **100** as a mixture of diastereoisomers (1:1) in 55% yield. These compounds are potentially useful synthons for the construction of higher carbon sugars.

Recently, it has been shown[32] that the RCM reaction can be used as a highly stereoselective route to unsaturated spiroacetals

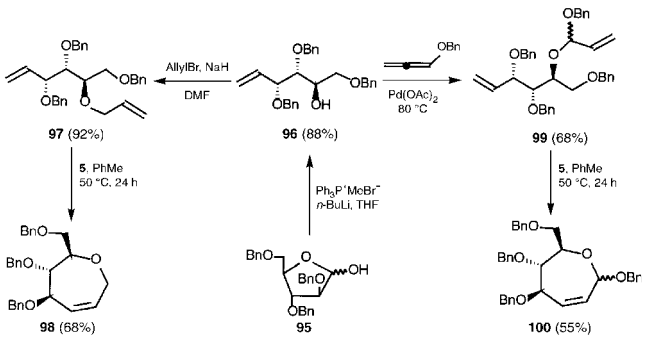

Scheme 15

starting from a terminal alkene–*O*–alkene arrangement at the anomeric centre of a sugar. Thus, the reaction of **102** in the presence of Grubbs' catalyst (**5**) (6 mol%) at 60 °C for 16 h gave the 1,6-dioxa-(5*R*)-spiro(4,5)dec-3-ene derivative **103** in excellent yield (95%) (Scheme 16). Interestingly, it has also been

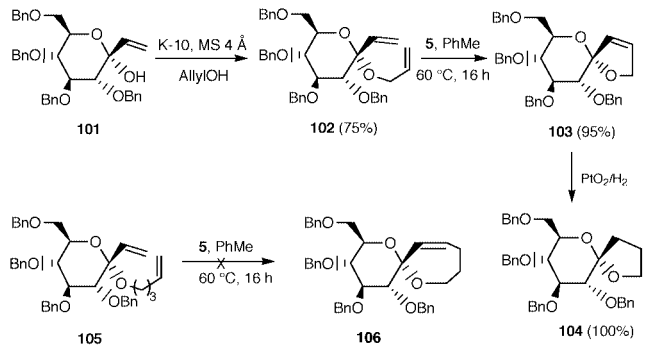

Scheme 16

shown that similar treatment of diene **105** did not lead to the expected spiro compound, **106**. Instead, a dimeric product was isolated. The formation of this dimer could not be prevented by lowering the concentration of the substrate with a larger amount of catalyst. It has been concluded that the RCM reaction depends on the site of the ring closure rather than the ring size.

The ring-closing metathesis of the acryloylated derivatives **111** and **108**, derived from allylic and homoallylic alcohols, appeared conveniently poised to provide five or six-membered α,β-unsaturated lactones (**109** and **112**). Unfortunately, this scenario did not happen to be operational. It could be postulated that this is due to the formation of unproductive six- (**114**) and seven-membered (**113**) metal chelates, formed between the ester carbonyl and the intermediate carbene species. These intermediates were apparently too stable for the subsequent olefin metathesis reactions to occur.[33]. However, Ghosh and his co-workers[34] have successfully overcome this problem by adding the external Lewis acid [Ti(^{i}OPr)$_4$], which can disrupt such inactive complexes and can provide effective cyclization. These methods provide convenient access to α,β-unsaturated, γ and δ-lactones (**109** and **112**) in good yields (Scheme 17).

The RCM reaction is an important method for the preparation of carbohydrate derivatives. Recently, Evans and Murthy[35] have developed an interesting silicon-tethered ring-closing metathesis procedure for the synthesis of C_2-symmetrical 1,4-diols (**115**) (Scheme 18). Dihydroxylation of the cyclic alkene by the Sharpless-protocol and removal of the protecting groups afforded the reduced carbohydrate D-altritol (**118**).

Overkleeft *et al*.[36] reported an efficient synthesis of pyrrolizidine (**121**) and quinolizidine (**125**) azasugar derivatives by using catalyst **4** or **5**. When γ-lactam **120**, derived from aldehyde **119** by Wittig olefination, was subjected to an RCM reaction with catalyst **4**, the expected 5/5 bicyclic pyrrolizidine azasugar (**121**) was formed (Scheme 19). Although the reaction required prolonged reaction time and elevated temperature (50 °C), compound **121** was still isolated in 66% yield. In other examples, the quinolizidine derivative **125** could be derived from either **122a** or **122b** using catalyst **4** or **5**.

The same group[37] has reported a formal total synthesis of the important glucosidase inhibitor castanospermine **130** using olefin metathesis as a key step. It is noteworthy that the cyclization of diene **126**, which contains an α,β-unsaturated ester (not usually suitable for metathesis reactions), reacted with catalyst **4** to give the bicyclic lactam **127** in 70% yield (Scheme 20).

In the synthesis of *C*-aryl glycosides, Schmidt and Sattelkau[38] have used the RCM strategy as the key step (Scheme 21). An interesting feature of their approach was that protecting

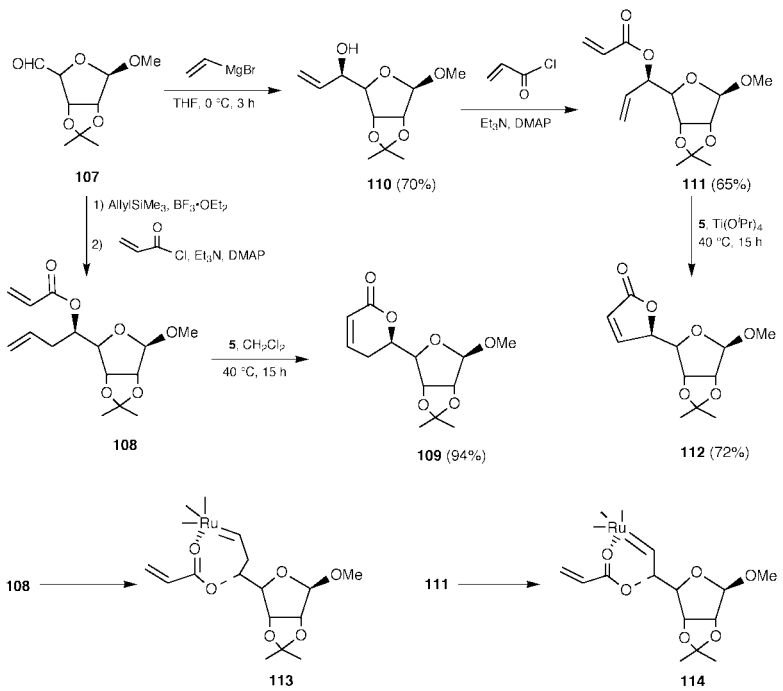

Scheme 17

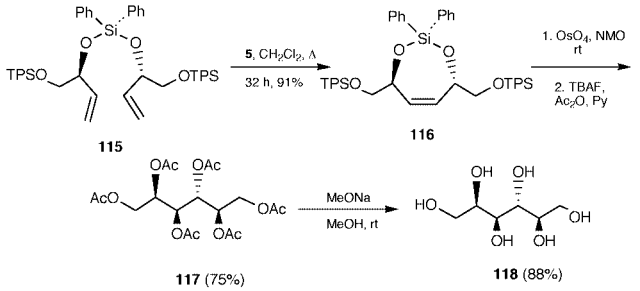

Scheme 18

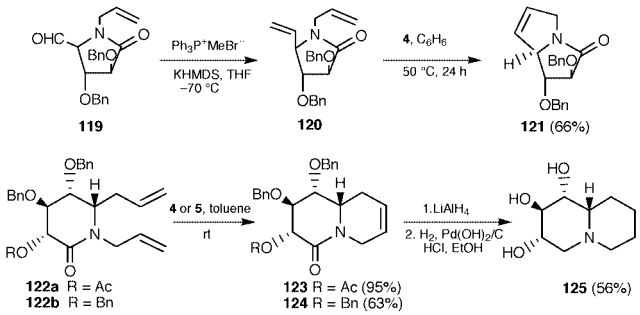

Scheme 19

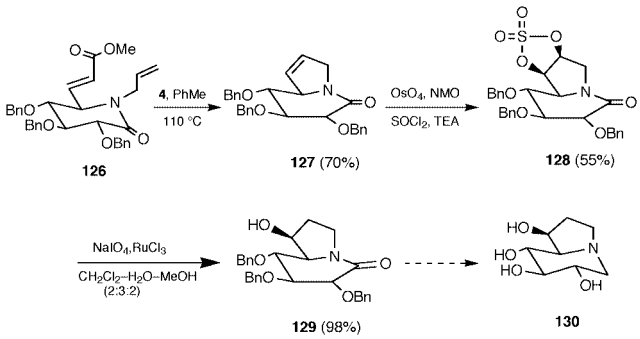

Scheme 20

groups, normally necessary for *C*-glycoside synthesis, were not required for the success of the reaction.

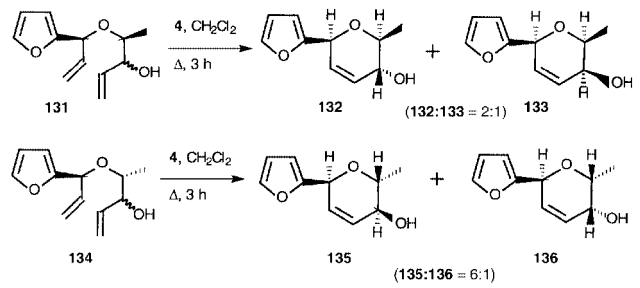

Scheme 21

Another approach toward the synthesis of *C*-glycosides was reported by Calimente and Postema,[39] in which RCM was employed as a key step for the intramolecular cyclization. The starting material, **138**, was prepared from the corresponding glycal, **137**, in a few steps. Exposure of the acyclic enol ether **138** to catalyst **3** in toluene solution produced the *C*-linked glycal **139** in 72% yield. It was further suggested by the authors[39] that glycal **139** could then be easily converted into a *C*-glycoside (**140**) by an oxidative hydroboration (Scheme 22).

An efficient and practical method for the preparation of valiolamine has been described.[40] The starting material, **141**, was easily prepared from a D-arabinose derivative and the ring-

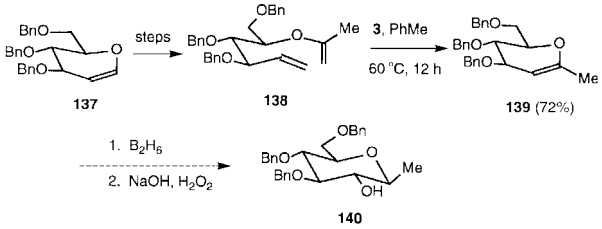

Scheme 22

closing metathesis reaction proceeded smoothly (92% crude yield) to provide the substituted cyclohexene derivatives **142** and **143** as a 7:3 mixture of stereoisomers that could be separated by HPLC (Scheme 23). Interestingly, when the

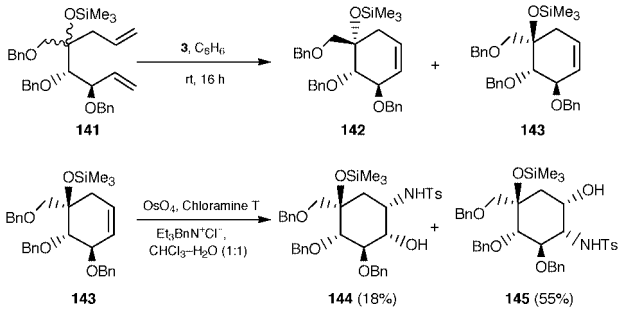

Scheme 23

reaction was subjected to the RCM conditions using Grubbs' catalyst, the reaction failed, but proceeded effectively using Schrock's catalyst at room temperature. After separation of both isomers, compound **143** was subjected to a *cis*-aminohydroxylation toward the synthesis of valiolamine (**144**) and its isomer (**145**).

An efficient synthesis of (+)-valienamine from commercially available D-glucose has been reported by Vasella *et al.*[41] using a ring-closing metathesis reaction as a key step. The ring-closing metathesis of **147**, derived by vinylation of ketone **146**, was performed in refluxing CH_2Cl_2 using catalyst **5**. Compound **148** was then converted into (+)-valienamine in three steps with a 47% overall yield (Scheme 24).

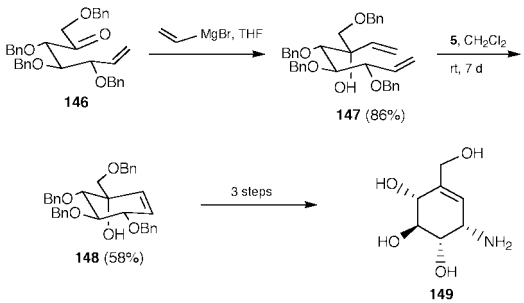

Scheme 24

Five-, six- and eight-membered annulated sugars along with spiro systems can also be prepared in good yields.[42] The Grignard reaction between **150** and vinylmagnesium chloride gave two stereoisomers, **151** and **152** (Scheme 25). The ring closing metathesis reaction of **151** with catalyst **5** gave the five-membered annulated sugar **153** in only 15% yield, due to the steric hindrance from the *trans*-fused 5-6 ring system in the product. For six-membered ring annulation, the starting materials (**154** and **155**) were prepared by the Grignard reaction of **150** with allylmagnesium chloride. Thus, the reaction of **155** and **5** involved ring-closing metathesis to produce the annulated sugar derivatives **156** in 80% yield. The structures were unambiguously determined by X-ray crystallography. Clearly, there was no steric impediment to the formation of the *cis* and *trans* 6-6

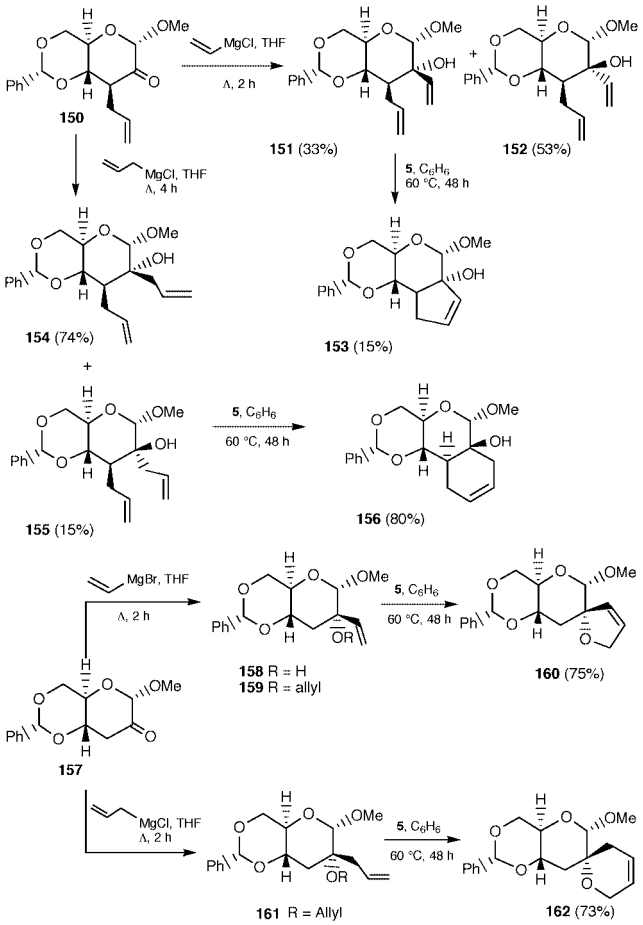

Scheme 25

ring system in both structures. Analogously, spiro-fused dihydropyran derivatives, such as **160** and **162** (Scheme 25) could also be obtained by efficient intramolecular ring-closing metathesis reactions involving allylic ethers **159** and **161**. Both derivatives were obtained from the same progenitor ketone (**157**) following the strategy described for **150** above.

In connection with the synthesis of annonaceous acetogenins and their analogs, ring-closing metathesis of unsaturated esters (**163**–**165**) has been used toward the synthesis of 9- to 15-membered-ring lactones (**166**–**168**) in moderate to good yields (Scheme 26).[43] The RCM reaction proceeded slowly and the corresponding lactones were isolated together with *ca.* 10% of the corresponding dimers. The yield was high in the case of **168** because of the formation of a 9-membered-ring lactone. Due to polymerization, the isolated yields of the 11- and 15-membered-ring lactones were moderate. When slow syringe pump addition was carried out, the yields were slightly better, but the formation of the corresponding dimers (**169** and **170**) was not prevented.

Recently, Fürstner and Muller[44] have synthesized the disaccharide fragment of tricolorin A (**173**) *via* ring-closing metathesis as the key step (Scheme 27). Tricolorin A exhibits significant cytotoxic properties against cultured P-388 and human breast cancer cell lines. The key intermediate was prepared *via* a multistep process. When disaccharide **171** was treated with catalyst **4**, the cyclized product **172** was formed. The free hydroxy group in the substrate did not interfere with the RCM, thus illustrating again the excellent compatibility and selectivity of Grubbs' catalyst. Hydrogenation of the crude 19-membered cycloalkene (*E*/*Z* mixture) afforded the desired cyclic disaccharide **173** in 77% yield (two steps) and completed the formal synthesis of tricolorin A.

Ziegler and Wang[45] completed the direct synthesis of (+)-cyclophellitol from a carbohydrate precursor, D-xylose (Scheme 28). Ru-catalyzed ring-closing metathesis of the diene

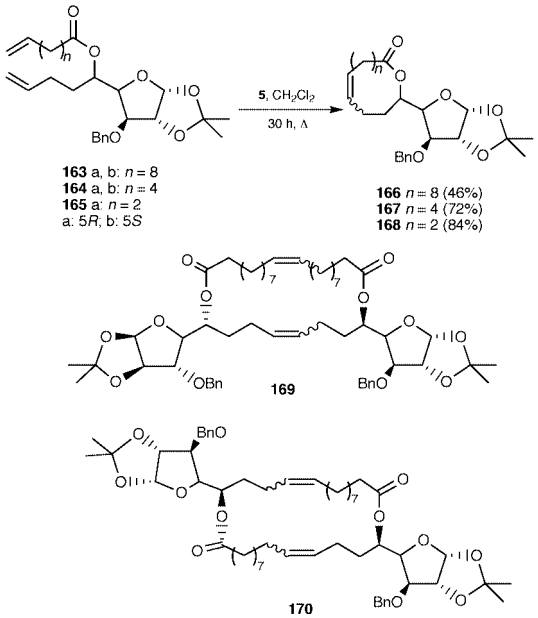

Scheme 26

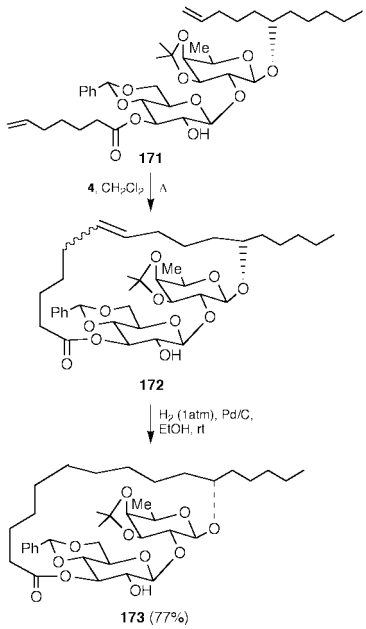

Scheme 27

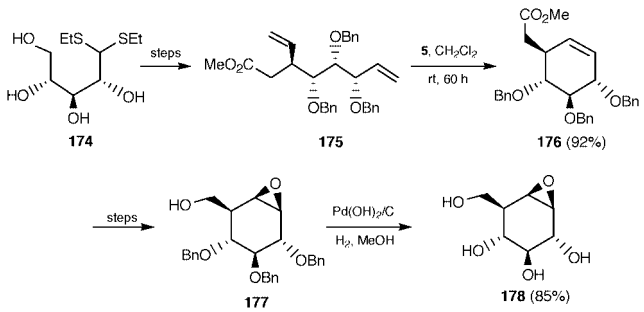

Scheme 28

175 led to the efficient formation of the cyclohexene **176** in 92% yield. Compound **176** was converted to the final target (+)-cyclophellitol **178** in a few further steps.

In the enantioselective total synthesis of the antifungal agent Sch 38516 (**180**), Houri *et al.*[46] have again used the RCM reaction as the crucial step (Scheme 29). The glycoside **179** was treated with Schrock's catalyst (**3**) to provide **180** as a single cycloalkene in 90% yield.

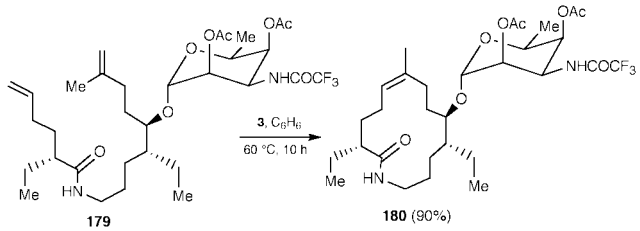

Scheme 29

Ring-opening metathesis

The ring-opening metathesis (ROM) reaction is a variation of the cross-metathesis reaction, where one of the olefin partners is a cyclic alkene and the driving force is the strain in the starting material that is released during the process (eqn. 3). Although this reaction is very useful in synthetic organic chemistry, the poor chemo-, stereo- and regio-selectivity have limited the synthetic utility of this reaction and, to the best our knowledge, there is no example of ROM in carbohydrate chemistry. On the other hand, in the absence of a second open-chain olefin, the metal-carbene intermediate formed by the reaction between the cyclic olefin and the catalyst can react with a series of cyclic olefins to give polymers. The application of this method (ROMP) has been greatly expanded by highly active and well-defined catalysts. Some examples of this method have appeared in the literature. A key advantage of the ROMP reaction is that the polymerization can be living, that is, the elongation can proceed more rapidly than termination or chain transfer. This living polymerization method offers new opportunities for oligomer synthesis.

Nomura and Schrock[47] have shown the formation of various kinds of norbornene-based homopolymers and multiblock copolymers (**182**, **184**) that contain protected sugars by ring-opening metathesis polymerizations of **181** and **183** using the Mo-catalyst **3**. The acetal groups in polymers containing 1,2:3,4-di-*O*-isopropylidene-α-D-galactopyranose residues can be hydrolyzed rapidly under acidic conditions to afford useful water-soluble 'sugar-coated' polymers (Scheme 30).

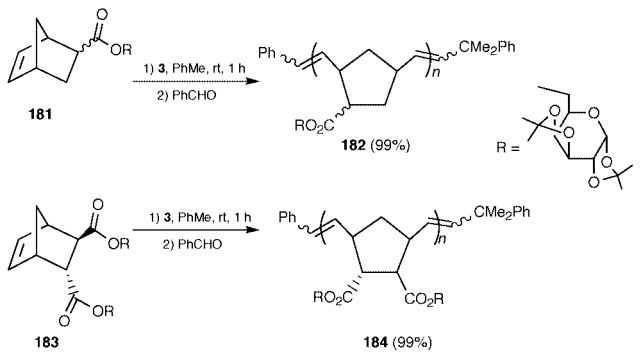

Scheme 30

The polymerization of an unprotected norbornene *N*-acylglucosamine derivative **185** has been reported in an aqueous–organic two phase system by Grubbs and Fraser[48] using catalyst **4**, since this catalyst is not sensitive to alcohol functionality (Scheme 31).

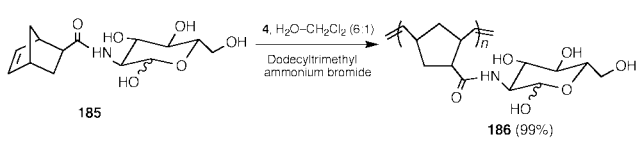

Scheme 31

Recently, Kiessling and co-workers[49] have shown that the ROMP reaction can be used to create a polyvalent carbohydrate-bearing polymer that can block protein-initiated cell agglutination. Thus, the treatment of **187** with $RuCl_3 \cdot H_2O$ in H_2O afforded a good yield of the glycopolymer **188** (Scheme 32). This novel application of ROMP to the synthesis of

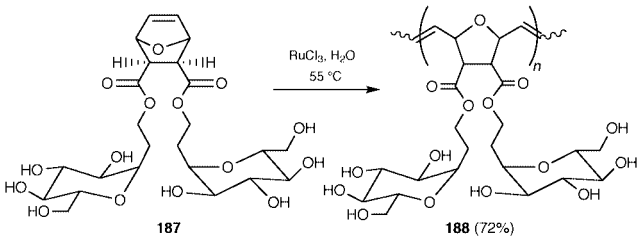

Scheme 32

polyvalent carbohydrate polymers offers new opportunities for the design of materials for modulation of cell adhesion, immobilization of particular cell types, and study of multivalency in extracellular interactions.

In an another application, Kiessling *et al.*[50] described ring-opening metathesis polymerization to generate collections of multivalent saccharide displays in which the number of repeat units within a set was systematically varied (Scheme 33).

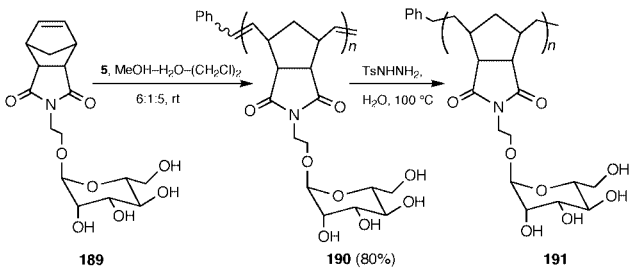

Scheme 33

Acetylene metathesis

We have recently found that 2-propynyl glycosides can undergo a cyclotrimerization reaction in the presence of Grubbs' catalyst to give a mixture of regioisomeric aryl glycosides (Scheme 34, Table 5).[51] As oligosaccharide mimetics, such molecules may find biological utility as 'cluster-type ligands' and may help to elucidate binding specificity in multiple carbohydrate–protein interactions.

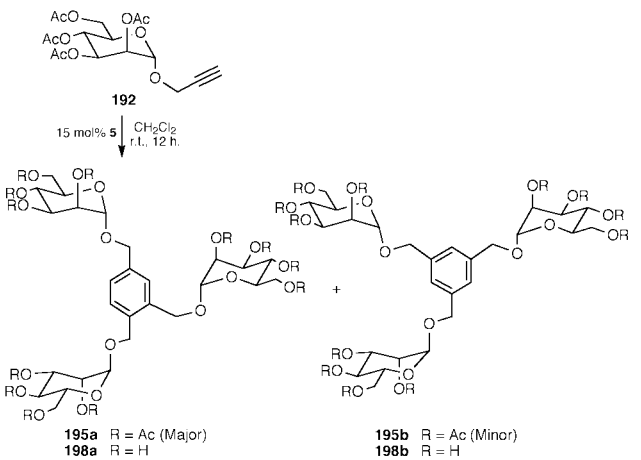

Scheme 34

Table 5 Cyclotrimerization of 2-propynyl derivatives

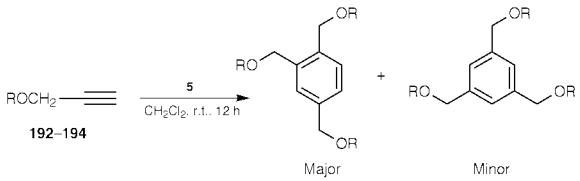

195–197

Entry	Substrate	R	Product	Yield (%)	Isomer Ratios
1	**192**	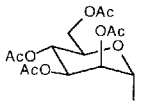	**195**	75	90 : 10
2	**193**	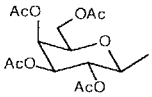	**196**	72	90 : 10
3	**194**	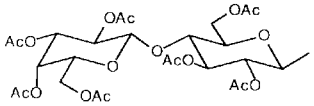	**197**	66	90 : 10

Isomerization

An unexpected[52] isomerization product, **198**, was isolated in 30% yield, instead of the anticipated cross-metathesis compound, when the cross-metathesis reaction between *N*-allyltritylamine and allyl 2,3,4,6-tetra-*O*-acetyl-α-D-galactopyranoside **30** was carried out with catalyst **5**. Furthermore, neither a sugar nor a *N*-allyltritylamine dimer could be detected. Treatment of **30** with 1,4-diazabicyclo[2,2,2]octane (DABCO) in the presence of Grubbs' catalyst (**5**) afforded only 4% of the isomerized product, **198**, together with 40% of allyl α-D-galactopyranoside homodimer. Similar results were obtained when triethylamine was used as base. Neither isomerization nor metathesis products were detected when diethylamine or pyridine were used. The isomerized product **198** was obtained with the highest yield when **30** was treated with diisopropylethylamine (DIPEA) in the presence of Grubbs' catalyst (**5**). However, all the isomerization yields of these reactions were still very low in the absence of *N*-allyltritylamine. When both *N*-allyltritylamine and 1 eq. of DIPEA were simultaneously used in the reaction, the isomerization yield was improved dramatically to 80%. Furthermore, no self-metathesis product could be detected. The new catalytic system offers a novel procedure for the cleavage of allyl ethers/acetals to provide reducing sugars such as **199** (Scheme 35).

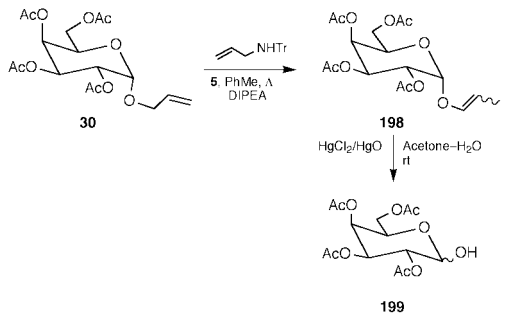

Scheme 35

Conclusions

The results outlined herein show that olefin metathesis has already proven to be an efficient method in synthetic organic chemistry. With the development of well-defined catalytic systems (**1**–**7**) and a better understanding of the nature of these catalysts, selective cross-metathesis, ring-closing metathesis and ring-opening metathesis reactions have started to appear in the literature. It has been shown that this efficient reaction provides diverse types of new alkenes, including some total syntheses of carbohydrate-containing natural products which can not be readily obtained by other known procedures, especially involving closure of large rings (macrocycles). While this review was under preparation, several other examples appeared in the literature[53–64] and we apologise to those investigators whose work could not be summarized herein. Ongoing work to search for even more active and tolerant metal complexes promises further interesting and useful work ahead.

Acknowledgements

We gratefully acknowledge financial support from NSERC for this work.

Notes and references

1 R. H. Grubbs, in *Comprehensive Organometallic Chemistry*, ed. G. Wilkinson, G. A. Stone and E. W. Abel, Pergamon, New York, 1982, vol. 8, p. 499; M. Leconte, J. M. Basset, F. Quignard and C. Larroche, in *Reactions of Coordinated Ligands*, ed. P. S. Braterman, Plenum, New York, 1986, vol. 1, p. 371; J. Feldman and R. R. Schrock, *Prog. Inorg. Chem.*, 1991, **39**, 2.

2 R. H. Grubbs, S. J. Miller and G. C. Fu, *Acc. Chem. Res.*, 1995, **28**, 446; R. R. Schrock, *The Strem Chemiker*, Strem Chemicals, Newburgport, 1992, vol. XIV, no. 1, p. 1; K. J. Ivin and J. C. Mol, in *Olefin Metathesis and Metathesis Polymerization*, Academic Press, San Diego, 1997; R. R. Schrock, *Acc. Chem. Res.*,1990, **23**, 158.

3 For recent reviews, see: M. Schuster and S. Blechert, *Angew. Chem., Int. Ed. Engl.*, 1997, **36**, 2036; R. H. Grubbs and S. Chang, *Tetrahedron*, 1998, **54**, 4413; S. K. Armstrong, *J. Chem. Soc., Perkin Trans. 1*, 1998, 371; M. L. Randall and M. L. Snapper, *The Strem Chemiker*, Strem Chemicals, Newburgport, 1998, vol. XVII, no. 1, p. 1; M. L. Randall and M. L. Snapper, *J. Mol. Catal. A*, 1998, **133**, 29.

4 D. J. O'Leary, H. E. Blackwell, R. A. Washenfelder, K. Miura and R. H. Grubbs, *Tetrahedron Lett.*, 1999, **40**, 1091; M. Scholl and R. H. Grubbs, *Tetrahedron Lett.*, 1999, **40**, 1425; A. G. M. Barrett, S. P. D. Baugh, D. C. Braddock, K. Flack, V. C. Gibson, M. R. Giles, E. L. Marshal, P. A. Procopiou, A. J. P. White and D. J. Williams, *J. Org. Chem.*, 1998, **63**, 7893; D. L. Boger and W. Chai, *Tetrahedron*, 1998, **54**, 3955;

S. C. G. Biagini, S. E. Gibson and S. P. Keen, *J. Chem. Soc., Perkin Trans. 1*, 1998, 2485.
5 J. F. Miller, A. Termin, K. Koch and A. D. Piscopio, *J. Org. Chem.*, 1998, **63**, 3158; J. S. Clark, O. Hamelin and R. Hufton, *Tetrahedron Lett.*, 1998, **39**, 8321; M. Lautens and G. Hughes, *Angew. Chem., Int. Ed.*, 1999, **38**, 129; A. Kinoshita, N. Sakakibara and M. Mori, *Tetrahedron*, 1999, **55**, 8155; H. E. Blackwell and R. H. Grubbs, *Angew. Chem., Int. Ed.*, 1998, **37**, 3281; J. Renaud and S. G. Ouellet, *J. Am. Chem. Soc.*, 1998, **120**, 7995; J. M. Campagne and L. Ghosez, *Tetrahedron Lett.*, 1998, **39**, 6175; T. Nishioka, Y. Iswabuchi, H. Irie and S. Hatakeyama, *Tetrahedron Lett.*, 1998, **39**, 5597; D. J. O'Leary, S. J. Miller and R. H. Grubbs, *Tetrahedron Lett.*, 1998, **39**, 1689; T. Oishi, Y. Nagumo and M. Hirama, *Chem. Commun.*, 1998, 1041; H. Sauriat-Dorizon and F. Guibe, *Tetrahedron Lett.*, 1998, **39**, 6711; T. R. Hoye and M. A. Promo, *Tetrahedron Lett.*, 1999, **40**, 1429; M. Week, B. Mohr, J. P. Sauvage and R. H. Grubbs, *J. Org. Chem.*, 1999, **64**, 5463.
6 J. Tsuji and S. Hashiguchi, *Tetrahedron Lett.*, 1980, **21**, 2955.
7 J. Tsuji and S. Hashiguchi, *J. Organomet. Chem.*, 1981, **218**, 69.
8 M. F. C. Plugge and J. C. Mol, *Synlett.*, 1991, 507.
9 W. A. Nugent, J. Feldman and J. C. Calabrese, *J. Am. Chem. Soc.*, 1995, **117**, 8992.
10 G. Descotes, J. Ramja, J.-M. Basset and S. Pagano, *Tetrahedon Lett.*, 1994, **35**, 7379.
11 J.-L. Couturier, K. Tanaka, M. Leconte, J.-M. Basset and J. Ollivier, *Angew. Chem., Int. Ed. Engl.*, 1993, **32**, 112.
12 R. R. Schrock, J. S. Murdzek, G. C. Bazan, J. Robbins, M. Dimare and M. O'Regan, *J. Am. Chem. Soc.*, 1990, **112**, 3875; G. C. Bazan, E. Khosravi, R. R. Schrock, W. J. Feast, V. C. Gibson, M. B. O'Regan, J. K. Thomas and W. M. Davis, *J. Am. Chem. Soc.*, 1990, **112**, 8378; G. C. Bazan, J. H. Oskam, H.-N. Cho, L. Y. Park and R. R. Schrock, *J. Am. Chem. Soc.*, 1991, **113**, 6899.
13 S. T. Nguyen, R. H. Grubbs and J. W. Ziller, *J. Am. Chem. Soc.*,1993, **115**, 9858.
14 P. Schwab, M. B. France, J. W. Ziller and R. H. Grubbs, *Angew. Chem., Int. Ed. Engl.*, 1995, **34**, 2039.
15 D. M. Lynn, B. Mohr and R. H. Grubbs, *J. Am. Chem. Soc.*, 1998, **120**, 1627.
16 A. Fürstner and L. Ackermann, *Chem. Commun.*, 1999, 95.
17 J. Feng, M. Schuster and S. Blechert, *Synlett.*, 1997, 129.
18 J. Ramja, G. Descotes, J. M. Basset and A. Mutch, *J. Carbohydr. Chem.*, 1996, **15**, 125.
19 D. J. O'Leary, H. E. Blackwell, R. A. Washenfelder and R. H. Grubbs, *Tetrahedron Lett.*, 1998, **39**, 7427.
20 R. Dominique, S. K. Das and R. Roy, *Chem. Commun.*, 1999, 2437.
21 S. K. Das, R. Dominique, C. Smith, J. Nahra and R. Roy, *Carbohydr. Lett.*, 1999, **3**, 361.
22 Z. Gan and R. Roy, *Tetrahedron*, in the press.
23 R. Roy, *Pure Appl. Chem.*, 1999, **71**, 565; R. Roy, R. Dominique and S. K. Das, *J. Org. Chem.*, 1999, **64**, 5408.
24 Y. J. Hu and R. Roy, *Tetrahedron Lett.*, 1999, **40**, 3305.
25 M. Schuster, N. Lucas and S. Blechert, *Chem. Commun.*, 1997, 823.
26 M. Schuster and S. Blechert, *Tetrahedron Lett.*, 1998, **39**, 2295.
27 C. M. Huwe and S. Blechert, *Tetrahedron Lett.*, 1995, **36**, 1621.
28 C. M. Huwe and S. Blechert, *Synthesis*, 1997, 61.
29 G. Descotes, J. Ramja, J.-M. Basset, S. Pagano, E. Gentil and J. Banoub, *Tetrahedron*, 1996, **52**, 10 903.
30 C. F. Sturino and J. C. Y. Wong, *Tetrahedron Lett.*, 1998, **39**, 9623.
31 H. Ovaa, M. A. Leeuwenburgh, H. S. Overkleeft, G. A. van der Marel and J. H. van Boom, *Tetrahedron Lett.*, 1998, **39**, 3025.
32 P. A. V. van Hooft, M. A. Leeuwenburgh, H. S. Overkleeft, G. A. van der Marel, C. A. A. van Boeckel and J. H. van Boom, *Tetrahedron Lett.*, 1998, **39**, 6061.
33 A. Fürstner and K. Langemman, *J. Am. Chem. Soc.*, 1997, **119**, 9130.
34 A. K. Ghosh, J. Cappiello and D. Shin, *Tetrahedron Lett.*, 1998, **39**, 4651.
35 P. A. Evans and V. S. Murthy, *J. Org. Chem.*, 1998, **63**, 6768.
36 H. S. Overkleeft, P. Bruggeman and U. K. Pandit, *Tetrahedron Lett.*,1998, **39**, 3869.
37 H. S. Overkleeft and U. K. Pandit, *Tetrahedron Lett.*, 1996, **37**, 547.
38 B. Schmidt and T. Sattelkau, *Tetrahedron*, 1997, **53**, 12 991.
39 D. Calimente and M. H. D. Postema, *J. Org. Chem.*, 1999, **64**, 1770.
40 O. Sellier, P. Van de Weghe, D. L. Nouen, C. Strehler and J. Eustache, *Tetrahedron Lett.*, 1999, **40**, 853.
41 P. Kapferer, F. Sarabia and A. Vasella, *Helv. Chim. Acta*, 1999, **82**, 645.
42 D. J. Holt, W. D. Barker, P. R. Jenkins, D. L. Davies, S. Garratt, J. Fawcett, D. R. Russell and S. Ghosh, *Angew. Chem., Int. Ed.*, 1998, **37**, 3298.
43 H. E. Sukkari, J. P. Gesson and B. Renoux, *Tetrahedron Lett.*, 1998, **39**, 4043.
44 A. Fürstner and T. Müller, *J. Org. Chem.*, 1998, **63**, 424.
45 F. E. Ziegler and Y. Wang, *J. Org. Chem.*, 1998, **63**, 426.
46 A. F. Houri, Z. Xu, D. A. Cogan and A. H. Hoveyda, *J. Am. Chem. Soc.*, 1995, **117**, 2943.
47 K. Nomura and R. R. Schrock, *Macromolecules*, 1996, **29**, 540.
48 C. Fraser and R. H. Grubbs, *Macromolecules*, 1995, **28**, 7248.
49 K. H. Mortell, M. Gingras and L. L. Kiessling, *J. Am. Chem. Soc.*, 1994, **116**, 12 053.
50 M. Kanai, K. H. Mortell and L. L. Kiessling, *J. Am. Chem. Soc.*, 1997, **119**, 9931.
51 S. K. Das and R. Roy, *Tetrahedron Lett.*, 1999, **40**, 4015.
52 Y. J. Hu, R. Dominique, S. K. Das and R. Roy, *Can. J. Chem.*, in the press.
53 C. M. Huwe, T. J. Woltering, J. Jiricek, G. W. Schmidt and C. H. Wong, *Bioorg. Med. Chem.*, 1999, **7**, 773.
54 O. M. Blanco and L. Castedo, *Synlett.*, 1999, 557.
55 A. Kirschning and G. W. Chen, *Tetrahedron Lett.*, 1999, **40**, 4665.
56 M. A. Leeuwenburgh, C. Kulker, H. I. Duynstee, H. S. Overkleeft, G. A. van der Marel and J. H. van Boom, *Tetrahedron*, 1999, **55**, 8253.
57 M. H. D. Postema and D. Calimente, *Tetrahedron Lett.*, 1999, **40**, 4755.
58 O. Dirat, T. Vidal and Y. Langlois, *Tetrahedron Lett.*, 1999, **40**, 4801.
59 H. Oguri, S. Y. Sasaki, T. Oishi and M. Hirama, *Tetrahedron Lett.*, 1999, **40**, 5405.
60 S. C. Schuster and S. Blechert, *Chem. Commun.*, 1999, 1203.
61 U. K. Pandit, H. S. Overkleeft, B. C. Borer and H. Bieraugel, *Eur. J. Org. Chem.*, 1999, 959.
62 H. Ovaa, J. D. C. Codee, B. Lastdrager, H. S. Overkleeft, G. A. van der Marel and J. H. van Boom, *Tetrahedron Lett.*, 1999, **40**, 5063.
63 O. Sellier, P. van de Weghe and J. Eustache, *Tetrahedron Lett.*, 1999, **40**, 5859.
64 N. L. Pohl and L. L. Kiessling, *Synthesis*, 1999, 1515.

Paper a907712j

The hydroxylation and amidation of equilenin acetate catalyzed by chloro[5,10,15,20-tetrakis(pentafluorophenyl)porphyrinato]manganese(III)

Jerry Yang, Richard Weinberg and Ronald Breslow*

Department of Chemistry, Columbia University, New York, NY 10027, USA. E-mail: rb33@columbia.edu

Received (in Corvallis, OR, USA) 11th January 2000, Accepted 14th February 2000
Published on the Web 13th March 2000

The aromatic steroid equilenin acetate undergoes regioselective and stereoselective hydroxylation and amidation catalyzed by a manganese porphyrin using iodosobenzene (PhIO) and *N*-tosyliminophenyliodinane (PhINTs) as the oxygen and nitrogen donor, respectively.

It is important to develop chemical methods for the regiospecific oxidation of natural products such as steroids to replace microbial fermentations that are currently used.[1] Biochemically, such oxidations are normally performed by the heme-containing cytochrome P-450 class of enzymes, and metalloporphyrins have been studied as models for these enzymes.[2] We have recently reported the regiospecific catalytic hydroxylation of steroids, using a water soluble porphyrin carrying hydrophobic binding units, that performs efficient and specific oxidations directed by the well defined geometry between the catalyst and substrates.[3–5] Herein, we report that the aromatic steroid equilenin acetate **1** can be hydroxylated and amidated at very specific positions with good catalytic turnover by iodosobenzene (PhI=O) and *N*-tosyliminophenyliodinane (PhI = NTs),[6] catalyzed by chloro[5,10,15,20-tetrakis(pentafluorophenyl)porphyrinato]manganese (III) **2**.

The metalloporphyrin-catalyzed oxidation of substituted arenes with several oxidants has been studied by the groups of Baciocchi[7] and Meunier.[8] Both groups found that quinones were the dominant products produced from these reactions, especially in the case of substituted naphthalenes. However, when we treated a 54 mM solution of equilenin acetate **1** with 270 mM PhI=O in the presence of 54 mM chloro[5,10,15,20-tetrakis(pentafluorophenyl)porphyrinato] manganese(III) **2**, no quinones were produced after 12 h. Instead, the major product isolated was the 6-hydroxylated product **3**, along with a smaller amount of the 11β-OH product **4** (Scheme 1). No starting material was recovered. Analytical HPLC studies using a catalyst:substrate:oxidant mole ratio of 1:50:250 (CH_2Cl_2, 23 °C, 12 h) resulted in a 57% conversion of **1** to 42% of **3** and 15% of **4**, indicating *ca*. 25 catalytic turnovers (Scheme 1).†

The products were characterized by MS and NMR spectra. Compound **3** had a ^{1}H NMR spectrum with one less aromatic proton than the starting material. COSY spectroscopy confirmed coupling between the 1, 2, and 4 protons as well as the allylic coupling between the 7 and 14 protons, indicating that hydroxylation occurred at C-6.

Compound **4** lacked the original C-11 benzylic methylene group signal at 3.3–3.4 ppm, and had a new peak at 5.77 ppm as expected for a downshifted C-11. The C-11 proton showed coupling to a methylene group with no other neighbors (C-12), and also showed NOE coupling to the C-1 proton. This coupling indicates that the H on C-11 is equatorial, so the OH is on the β face. This 11-β OH assignment is also consistent with an upfield shift of the angular methyl group from 0.80 ppm in **1** to 0.72 ppm in **4**. The remaining C-14, C-15, C-16 coupled protons and the aromatic protons were still present.

We first reported the metalloporphyrin catalyzed amidation of organic compounds in 1982.[9] Most recently, Che and coworkers reported the asymmetric amidation of substituted naphthalenes using chiral ruthenium and manganese porphyrins.[10] We find that such an amidation can also be performed on the equilenin steroid substrate **1** with good selectivity. A 60 mM solution of **1** was stirred for 12 h under argon in 1 ml of distilled CH_2Cl_2 containing metalloporphyrin **2** (60 mM), PhI=NTs (300 mM) and molecular sieves to produce the 11β-amidation product **5** and trace amounts of **3** and **4**, with complete conversion of starting material (Scheme 2).† In contrast to hydroxylation, the amidation reaction went completely to the 11β position of the steroid without any detectable amidation at the 6 position. A mole ratio of 1:50:250 catalyst:substrate:PhI=NTs afforded an 82% conversion of **1** to 30% **3**, 5% **4** and 47% **5**, as determined by HPLC assay, so there are *ca*. 40 turnovers.

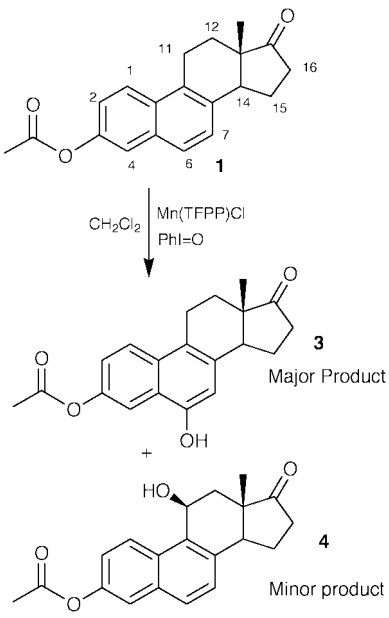

Scheme 1

Compound **5** had the expected MS, and again a downfield shifted C-11 proton at 5.43 ppm was coupled to the C-12 methylene and showed NOE coupling to the C-1 proton. Thus the tosylamide group is attached at the 11-β position. The

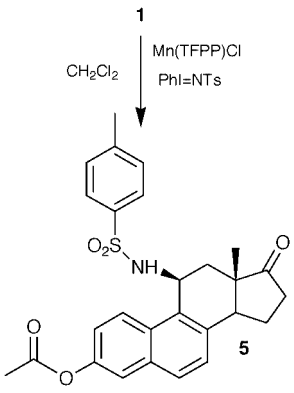

Scheme 2

DOI: 10.1039/b000463o

angular methyl group shifts strongly upfield from 0.80 ppm in **1** to 0.55 ppm in **5**.

The hydroxylation products **3** and **4** reflect hydrolysis of the Mn=NTs intermediate by traces of water in the small scale analytical runs, and they are minimally present in larger preparative scales. In previous work, we had found that the enzyme cytochrome P-450 could aminate cyclohexane with PhI=NTs, but that some hydroxylation also occurred in the water solution.[11] Since the relative amount of hydroxylation depended on the particular isoform of the enzyme used, hydrolysis of the metalloporphyrin intermediate was the most likely explanation. The finding that benzylic substitution in compounds **4** and **5** occurs on the beta face of the steroid must reflect the stereoelectronic control of the flat conjugated benzylic radical intermediate in these reactions.

The readily available manganese porphyrin **2** is able to catalyze the hydroxylation and amidation of an aromatic steroid. These reactions are especially interesting for their apparent differences in regiospecific oxidations. Although not explicitly stated in the literature, metalloporphyrin catalyzed oxidations of substituted naphthalene compounds have been reported to afford mostly quinones after aromatic ring hydroxylation in the presence of oxygen donors, whereas they tend to produce only amides at previously saturated carbon positions in the presence of PhINTs as the nitrogen donor.[7–10]

Apparently the oxidations involve preferential oxygen atom donation to the aromatic ring before hydrogen loss, while the tosylamidations involve initial hydrogen removal from a benzylic position. Perhaps aromatic ring addition is more sterically demanding, and thus more available to a small oxygen atom than to a large tosylamide group. We see that this difference generally holds true in the case of equilenin acetate and provides a method by which steroids of this class can be functionalized at different positions. Furthermore, the amidation of a steroid substrate can lead to the development of a novel class of nitrogen containing steroids that may have useful biological properties.

J. Y. acknowledges support from an NCERQA EPA Graduate Fellowship and a Bristol-Myers Squibb Graduate Fellowship. R. W. acknowledges support from a Goldwater Scholarship, a Pfizer Undergraduate Fellowship, a Perkin-Elmer Undergraduate Fellowship, and the Columbia University Rabi Scholars Program. This work was supported by the NIH and NSF.

Notes and references

† Equilenin acetate was synthesized by acylation of equilenin (Steraloids, Inc.) with acetic anhydride in pyridine using standard procedures. All products were isolated by column chromatography and characterized by ^{1}H-NMR, COSY, NOESY and CI-MS.

3: ^{1}H NMR ($CDCl_3$, 500 MHz): δ 7.86 (1H,d, C4-H), 7.82 (1H, d, C1-H), 7.41 (1H, dd, C2-H), 6.29 (1H, d, C7-H), 3.38 (1H, ddd, C14-H), 2.34 (3H, s, acetate Me), 0.76 (3H, s, C18-Me), 2.8–1.9 (8H, steroid envelope). CI-MS: m/z = 342 (M + 1 + NH_3), 323 (negative, M − 1). Product **3** in its ^{1}H NMR spectrum showed one less aromatic proton as compared to the starting material. COSY spectroscopy confirmed coupling between the 1, 2 and 4 protons as well as the allylic coupling between the 7 and 14 protons. All remaining aliphatic protons were identified by COSY, also confirming the identity of the product as C6-hydroxylated equilenin acetate.

4: ^{1}H NMR ($CDCl_3$, 500 MHz): δ 8.38 (1H, d, C1-H), 7.83 (1H, d, C6-H), 7.60 (1H, d, C4-H), 7.37–7.28 (2H, m, C7-H and C2-H), 5.77 (1H, br m, C11α-H), 3.43 (1H, m, C14-H), 2.39 (3H, s, acetate Me), 0.72 (3H, s, C18-Me), 2.83–1.91 (6H, steroid envelope). CI-MS: m/z 342 (M + 1 + NH_3). Product **4** COSY indicated coupling of both C15 hydrogens to the easily identifiable C14 proton at 3.43 ppm. The C15 protons were coupled to the C16 protons, indicating that oxidation must have occurred on the C11 or C12 steroid position. The C11 protons, originally at 3.3-3.4 ppm in **2**, were not present in product **4** and a new C*H*–OH appeared at 5.7 ppm, consistent with a benzylic oxidation. The relatively large upfield shift of the angular C18 methyl is inconsistent with C12 oxidation and is furthermore consistent only with oxidation occurring on the beta face of the last remaining steroid carbon position at C11 (most C11 α hydroxlations occur with large downfield shifts of the C18 methyl). Lastly, strong NOE coupling between the C1-H and the C11α-H indicated that compound **4** was indeed the 11β hydroxylated product.

In the analytical runs, the formation of products relative to starting material were monitored with 2-methoxynaphthalene as an internal standard, comparing NMR ratios and HPLC responses to calibrate the relative absorption coefficients of the products and starting material in the UV-VIS HPLC detector.

5: ^{1}H NMR ($CDCl_3$, 500 MHz): δ 7.81 (1H, d, C1-H), 7.77 (1H, dd, C6-H), 7.72 (2H, d, toluenesulfonamide), 7.52 (1H, d, C4-H), 7.31 (1H, dd, C7-H), 7.29(2H, d, toluenesulfonamide), 7.09 (1H, dd, C2-H), 5.43 (1H, ddd, C11α-H), 4.45 (1H, d, N–H), 3.36 (1H, m, C14-H), 2.45 (3H, s, toluene Me), 2.36 (3H, s, acetate Me), 0.55 (3H, s, C18-Me), 2.66–1.96 (6H, steroid envelope). CI-MS: m/z 495 (M + 1 + NH_3). The same COSY pattern was present as with product **4**. The C14 hydrogen was coupled to both C15 hydrogens, which in turn were coupled to both C16 hydrogens indicating oxidation at C11 or C12. Again, there was a large upfield shift of the angular C18 methyl, and the new CH-NH at 5.43 ppm is consistent with a benzylic oxidation. Also, strong NOE coupling between the C1-H and the C11α-H confirmed **5** as the 11β amidated product.

1 H. L. Holland, *Steroids*, 1999, **64**, 178.
2 M. J. Gunter and P. Turner, *Coord. Chem. Rev.*, 1991, **108**, 115; B. Meunier, *Chem. Rev.*, 1992, **92**, 1411.
3 R. Breslow, X. Zhang and Y. Huang, *J. Am. Chem. Soc.*, 1997, **119**, 4535.
4 R. Breslow, Y. Huang, X. Zhang and J. Yang, *Proc. Natl. Acad. Sci. USA*, 1997, **94**, 11 156.
5 R. Breslow, B. Gabriele and J. Yang, *Tetrahedron Lett.*, 1998, **39**, 2887.
6 Y. Yamada, T. Yamamoto and M. Okawara, *Chem. Lett.*, 1975, 361.
7 E. Baciocchi, O. Lanzalunga and A. Lapi, *Tetrahedron Lett.*, 1995, **36**, 3547.
8 R. Song, A. Sorokin, J. Bernadou and B. Meunier, *J. Org. Chem.*, 1997, **62**, 673.
9 R. Breslow and S. H. Gellman, *J. Chem. Soc., Chem. Commun.*, 1982, 1400.
10 X. G. Zhou, X. Q. Yu, J. S. Huang and C. M. Che, *Chem. Commun.*, 1999, 2377.
11 E. W. Svastits, J. H. Dawson, R. Breslow and S. Gellman, *J. Am. Chem. Soc.*, 1985, **107**, 6427.

Communication b000463o

ChemComm

Novel super-microporous silicate templating by ω-hydroxyalkylammonium halide bolaform surfactants

Stephen A. Bagshaw*[a] and Alan R. Hayman[b]

[a] *Advanced Materials Group, Industrial Research Limited, PO Box 31-310, Lower Hutt, New Zealand. E-mail: s.bagshaw@irl.cri.nz*

[b] *Department of Chemistry, University of Otago, PO Box 56, Dunedin, New Zealand. E-mail: hayman@alkali.otago.ac.nz*

Received (in Cambridge, UK) 14th January 2000, Accepted 21st February 2000
Published on the Web 13th March 2000

Templated silicate molecular sieves exhibiting templated super-micropores in the range 1.0–2.0 nm and interesting pore symmetries bearing similarity to the Lα, SBA-2 (*P6*$_3$/*mmc*) and Mα (*cmm*) phases have been prepared by exploiting the novel aggregation properties of a new family of ω-hydroxyalkylammonium bolaform surfactants.

Recently, a series of papers have described the formation of mesostructured silicates[1–3] and microporous transition metals oxides by exploiting the aggregation properties of bifunctional 'bolaform' surfactants.[4–8] These new templating systems have produced pillared-lamellar and M41S type mesostructures and most recently, an intermediate phase possessing the *cmm* space group. Unlike earlier work which focused on known surfactant systems,[1] Stucky and coworkers[6] exploited new design in surfactant molecular structure. Indeed mesostructures have been prepared that do not mimic any known surfactant liquid crystal phases.[6,9]

One of the synthetic goals identified early in the development of this field was the formation of materials possessing regular pores in the range 1.2–2.0 nm, that would allow shape selective catalysis of organic molecules too large to be accessed by zeolites. It is clear that while normal M41S materials exhibit great promise in the processing of long-chain and bulky hydrocarbons, they do not possess desirable shape selectivity.[2] The elegant preparation of extra-large pore crystalline aluminosilicate zeolite compositions such as UTD-1,[10] the PCH materials,[11] recent efforts at post-synthesis pore-mouth modification of MCM-41[12] and the ubiquitous pillared-clays[13] are among the somewhat few successful efforts at accessing the super-microporous region.

Here, we report preliminary results of the exploitation of a new family of ω-hydroxy-bolaform surfactants.[14,15] These surfactants have permitted the *a priori* design of templated super-microporous silicate structures. Primarily, the ω-hydroxy-bolaform surfactants form micelles in aqueous solution with low aggregation numbers and diameters approximately half those of the parent alkylammonium halide surfactants.[15] Secondly, it is implicit from the geometry of the aggregates that the polar ω-hydroxy groups be located near the micelle surface. Thus, the hydroxy group could conceivably be involved in additional H-bonding at the organic/water/inorganic interface thus modifying the effective surfactant headgroup area and thus the micelle packing and subsequent pore symmetries.

The bolaform surfactants $HO(CH_2)_{16}NR_3^+Br^-$ (R = Me or Et), were evaluated as potential templates. The materials we describe herein were prepared by substituting the new templates directly into existing M41S synthesis methods[16] from the following gel compositions: 4.0 SiO_2: *x* $HO(CH_2)_{16}NEt_3^+Br^-$: 3.0 NaCl : 2.0 NaOH : 0.34 $NH_3{\cdot}H_2O$: 236 H_2O (*x* = 0.40, 0.55, 0.70, 0.85). The high Krafft temperature, 63 °C,[16] of the trimethylammonium derivative precluded its use owing to poor solubility during the preliminary stages of the reaction. The triethyl surfactant has a much lower Krafft temperature, around room temperature, and hence an acceptable solubility.

Powder X-ray diffraction (XRD) patterns of selected samples prepared with different Si : surfactant ratios are presented in Fig. 1. The pattern in Fig. 1 of the as-prepared sample **A** (see Table 1), appears to describe a lamellar (Lα) phase, exhibiting strong d_{100} and weak d_{200} reflections. This material does not completely collapse upon calcination which suggests that a porous structure not based on a layered motif has been retained. The calcined material **B** (Fig. 1) produces a multireflection pattern that may possibly be indexed to a 3-D cubic (*P6*$_3$/*mmc*) array.[7] The XRD pattern of the calcined sample **C** (Fig. 1) is very similar to that described for the hexagonal Mα (*cmm*) liquid crystal phase.[18] The major Bragg reflections from all the materials formed were found at higher angles than those reported for M41S or SBA-8 type materials.[1,6] This is the first evidence that the repeat units formed are smaller than those of 'typical' mesostructured materials.

The formation of super-micropores was further supported by N_2 sorption isotherms (Fig. 2). Neither the Langmuir nor the

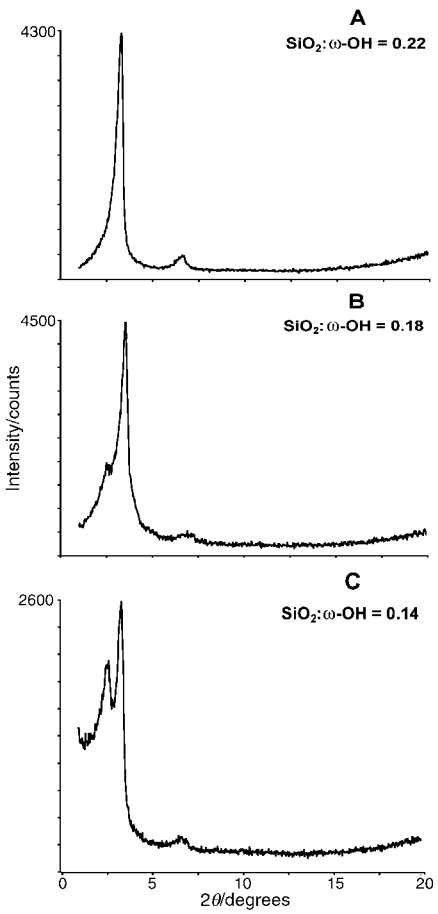

Fig. 1 XRD patterns of $HO(CH_2)_{16}NEt_3^+Br^-$ templated super-microporous silicas with different Si : surfactant ratios as indicated.

DOI: 10.1039/b000422g

Table 1 Physico-chemical characteristics of super-microporous silica samples

Sample	SiO_2 : ω-OH	d_{hk0}[a]/nm	Pore diameter[b]/nm		Surface area[c]/ $m^2\ g^{-1}$	Pore volume[d]/ $mL\ g^{-1}$
			BJH	HK		
A	1.0 : 0.22	4.7, 2.3	1.4	1.5	950	0.50
B	1.0 : 0.18	4.0, 2.9	1.6	2.1	1130	0.75
C	1.0 : 0.14	4.0, 3.1	1.6	2.1	870	0.65
D	1.0 : 0.10	n.o.[e]	1.4	1.4	550	0.75
E[f]	1.0 : 0.2	3.3	1.5	1.4	505	0.70

[a] ±0.1 nm; values taken from most intense XRD reflections. [b] ±0.1 nm. [c] ±10 $m^2\ g^{-1}$; surface areas calculated using the BET model. [d] ±0.05 mL g^{-1}; pore volumes calculated from p/p_0 = 0.98. [e] n.o. = Not observed. [f] Al incorporated at 2.0 mol% with respect to Si.

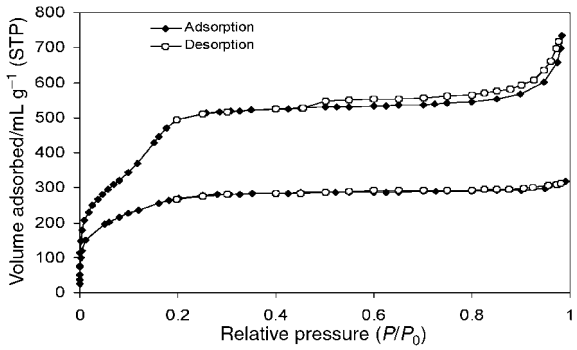

Fig. 2 Nitrogen adsorption–desorption isotherms of calcined samples corresponding to samples **B** (upper) and **E** (lower) in Table 1. Isotherm **B** has been offset along the Y axis for clarity.

BET model plots from the isotherms of these materials were linear thereby suggesting incompatabilities of the models with pores in this size regime. The BET model however, remains the most accessible and has thus been used here for indicative surface area determination. Surface areas and pore volumes (Table 1) of a selection of the materials prepared are relatively high, indicating that the pore structures of the new materials are well ordered and accessible. The isotherms of the most well defined materials *e.g.* **B** in Fig. 2 are typical reversible type IV curves[19] with small hysteresis of the desorption branch. The most interesting feature is the clear capillary condensation step at very low relative pressure (P/P_0 = 0.15). This is lower than any previously reported templated mesostructured material. The presence of an adsorption upturn at high partial pressures is suggestive of textural or indeed other non-specific meso-porosity. Pore diameters as calculated by the BJH method[19] centre around 1.6 nm, while HK calculations[19] centre around 2.0 nm (Table 1). However, the reliability of these common methods for pore size determination when applied to templated mesostructured materials has recently been questioned.[20]

Particle morphologies as determined by scanning electron micrographs (SEM) show particles of *ca*. 100 μm diameter that appear to be agglomerations of primary particles. Transmission electron micrographs (TEM) of micro-sectioned samples (Fig. 3) confirm the existence of pores of below 2.0 nm diameter. The TEM images are ambiguous with respect to the rigorous determination of pore symmetry and diameter, but do suggest the presence of hexagonal or similar symmetry among a generally disordered pore system. TEM data also indicated that the particles were not 'solid' but have highly open internal structures. This would explain the upturn in adsorption at higher nitrogen relative pressures. The reason for the formation of these particle morphologies however, is not known at this time.

We have been moderately successful, at this stage, in forming Al and Ti substituted materials with the goal of introducing catalytic function. As is often observed in M41S syntheses, the Al substituted materials were less ordered than the pure silica analogues and possessed smaller pore diameters as is evidenced in the type I nitrogen isotherm (sample **E**, Table 1, Fig. 2). The

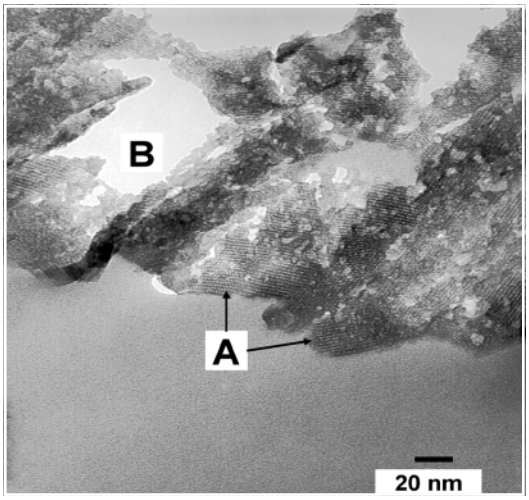

Fig. 3 Transmission electron micrograph of calcined sample **B** showing (*a*) ordered super-micropores and (*b*) open structure of the particles.

preparation of further novel super-microporous compositions from $HO(CH_2)_nNR_3^+Br^-$ surfactants where n = 12 or 14 and R = propyl and pyridyl is also continuing. It is anticipated that the reduction in the length of the alkyl chain of the surfactant from C_{16} will further reduce the pore diameters into the 1.2–1.5 nm region, although the increased solubility of these shorter surfactants may introduce new synthetic challenges. Indeed, early results indicate that ω-$HO(CH_2)_{12}NEt_3Br$ templated silicates do have pores in the range 1.0–1.2 nm, but are poorly ordered owing to the high solubility of the template. Further increasing the head group size will change the pore symmetries that are obtained due to packing parameter modification.

This work has been performed as part of a research contract with the New Zealand Foundation for Science Research and Technology, contract number CO 8512.7. We thank Karen Reader of the Victoria University of Wellington Electron Microscopy Facility for expert electron microscopic analysis, and Karl Lindsay of Otago University for preparation of surfactant samples.

Notes and references

1 C. T. Kresge, M. E. Leonowicz, W. J. Roth, J. C. Vartuli and J. S. Beck, *Nature*, 1992, **359**, 710.
2 A. Corma, *Chem. Rev.*, 1997, **97**, 2373.
3 U. Ceisla and F. Schüth, *Microporous Mesoporous Mater.*, 1999, **27**, 131.
4 P. T. Tanev and T. J. Pinnavaia, *Science*, 1996, **271**, 1267.
5 S. S. Kim, W. Zhang and T. J. Pinnavaia, *Science*, 1998, **282**, 1302.
6 D. Zhao, Q. Huo, J. Feng, J. Kim, Y. Han and G. D. Stucky, *Chem. Mater.*, 1999, **11**, 2668.
7 Q. Huo, R. Jeon, P. M. Petroff and G. D. Stucky, *Science*, 1995, **268**, 1324.
8 T. Sun and J. Y. Ying, *Angew. Chem., Int. Ed.*, 1998, **37**, 664.
9 D. Zhao, P. Yang, D. I. Margolese, B. F. Chmelka and G. D. Stucky, *Chem. Commun.*, 1998, 2499.
10 K. J. Balkus, A. G. Gabrielov and N. Sandler, *Mater. Res. Symp. Proc.*, 1995, **368**, 369.
11 A. Galarneau, A. Barodawalla and T. J. Pinnavaia, *Nature*, 1995, **374**, 529.
12 X. Song Zhao, G. Q. Lu and X. Hu, *Chem. Commun.*, 1999, 1391.
13 *Catal. Today*, 1988, **2** (ed. R. Burch).
14 T. W. Davey and A. R. Hayman, *Aust. J. Chem.*, 1998, **51**, 581.
15 T. W. Davey, W. A. Ducker and A. R. Hayman, *Langmuir*, in the press.
16 J. M. Kim, J. H. Kwak, S. Jun and R. Ryoo, *J. Phys. Chem.*, 1995, **99**, 16742.
17 T. W. Davey, W. A. Ducker, A. R. Hayman and J. Simpson, *Langmuir*, 1998, **14**, 3210.
18 V. Hassel, H. Ringsdorf, R. Laversanne and F. Nallet, *Recl. Trav. Chim. Pays-Bas*, 1993, **112**, 339.
19 S. J. Gregg and K. S. W. Sing, *Adsorption, Surface Area and Porosity*, Academic Press, London, 1982.
20 A. Galarneau, D. Desplantier, R. Dutartre and F. Di Renzo, *Microporous Mesoporous Mater.*, 1999, **27**, 297.

Communication b000422g

ChemComm

A new approach to cyclohexenes and related structures

Nathalie Cholleton,[a] Isabelle Gauthier-Gillaizeau,[b] Yvan Six[a] and Samir Z. Zard*[ab]

[a] *Institut de Chimie des Substances Naturelles, C. N. R. S., 91198 Gif-Sur-Yette, France. E-mail: sam.zard@icsn.cnrs-gif.fr*

[b] *Laboratoire de Synthèse Organique associé au CNRS, Ecole Polytechnique, 91128 Palaiseau, France*

Received (in Liverpool, UK) 9th February 2000, Accepted 25th February 2000
Published on the Web 15th March 2000

Intermolecular radical addition of a xanthyl phosphonoacetate to a γ,δ-enone gives rise to an adduct suitable for a base induced Horner–Emmons ring closure to a cyclohexene derivative, optionally after the reductive removal of the xanthate group.

The construction of rings often hinges on the ability to attach together two reacting partners, which are then made to undergo an intramolecular combination under suitable conditions.[1] In some cases, such as in the classical Robinson annelation, both the attachment and cyclisation require similar reaction conditions and can sometimes be accomplished concomittantly. This, however, imposes various constraints in terms of selectivity that must be addressed.[1b] More frequently, one or both of the reacting functions have to be protected and then unmasked just before the cyclisation step. A more concise approach would be to combine an intermolecular assembly process with a ring closure proceeding through two different mechanisms and operating under orthogonal sets of conditions: the two reacting units are thus rapidly brought together whilst avoiding cumbersome protection–deprotection steps. In view of the importance of ring structures in essentially all classes of natural products, numerous combinations of reactions have therefore been exploited to construct mono- and poly-cyclic derivatives.[1] Here, we describe the use of an intermolecular radical addition to an unactivated olefin in conjunction with an intramolecular Horner–Emmons reaction to rapidly access various cyclohexene containing architectures.

Unlike intermolecular C–C bond formation involving radical additions to activated (usually electrophilic) olefins, clean bimolecular additions to simple alkenes are not generally easy to accomplish using common radical processes.[2] The rate of the addition step is often too slow to allow it to compete successfully with other pathways open to the radical intermediate. In stannane based chemistry for example, premature hydrogen abstraction from the organotin hydride is difficult to avoid.[3] This limitation may be lifted to a large extent by using the dithiocarbonate (xanthate) transfer reaction we have developed over the past few years.[4] The main competing pathway is degenerate: the intermediate radicals acquire an extended effective lifetime and are thus able to interact with comparatively unreactive traps. For our present purpose, the reaction of xanthate **1**[5] derived from triethyl phosphonoacetate with a γ,δ-enone would provide in one step the desired combination of functionality for a subsequent intramolecular Horner–Emmons ring closure (Scheme 1). Indeed, heating 2-allyl-2-methylcyclohexanone **2a** (1.08 mmol) with xanthate **1** (2.17 mmol) in refluxing 1,2-dichloroethane (2 mL) in the presence of a small amount of lauroyl peroxide (16 mol%) as initiator under an inert atmosphere delivered the expected adduct **3a** in (80%) yield (Scheme 1). Reductive removal of the xanthate group with tributylstannane and base-induced (NaH/THF) cyclisation finally gave bicyclic derivative **5a** in high overall yield. The Horner–Emmons reaction may, if desired, be performed whilst keeping the xanthate group. In this way, **3a** was efficiently converted into **5b** by exposure to a combination of potassium carbonate and 18-crown-6 in toluene.[6] The initial NaH/THF system did not prove suitable in this case. The xanthate group in the final product represents a very useful handle since it provides an entry into the exceptionally rich chemistry of sulfur. The ring size of the starting cyclic ketone may of course be modified as illustrated by the conversion of cycloheptanone **2d** into bicyclo [5.4.0] derivative **5c**. Fused 6–7 ring systems are found in some terpene families, such as the sandresolides, the tiglianes (*e.g.* phorbol), and the daphnanes.[7]

One important feature of this approach is that the unsaturated ketone precursors are readily available, either by direct allylation of the corresponding enolate or through the powerful Claisen rearrangement. The latter route is especially interesting, since it can provide substituted substrates with controlled relative (and sometimes absolute) sterochemistry of adjacent chiral centres.[8] Compound **2d** was thus obtained by heating together 1-methoxy-2-methylcyclohexene and crotyl alcohol in the presence of trifluoroacetic acid.[8] Application of the same sequence gave **5d** with a defined relative stereochemistry, again in good overall yield (Scheme 1).

If a 2-allyl cyclopentanedione component is employed, the sequence now provides a ready access to the ubiquitous hydrindane backbone. This is illustrated by the conversion of **2e**, prepared by allylation of 2-methylcyclopentane-1,3-dione with allyl bromide[9] followed by ketalisation of one of the ketone groups, into **5e**, as outlined in Scheme 2. This route is significantly shorter than that previously reported for an analogue of **5e**.[10] The presence of the olefin allows access to the *trans*-hydrindane system through catalytic reduction.[10] For the ethyl derivative **2f**, the Horner–Emmons reaction was performed after acid mediated cleavage of the ketal group but

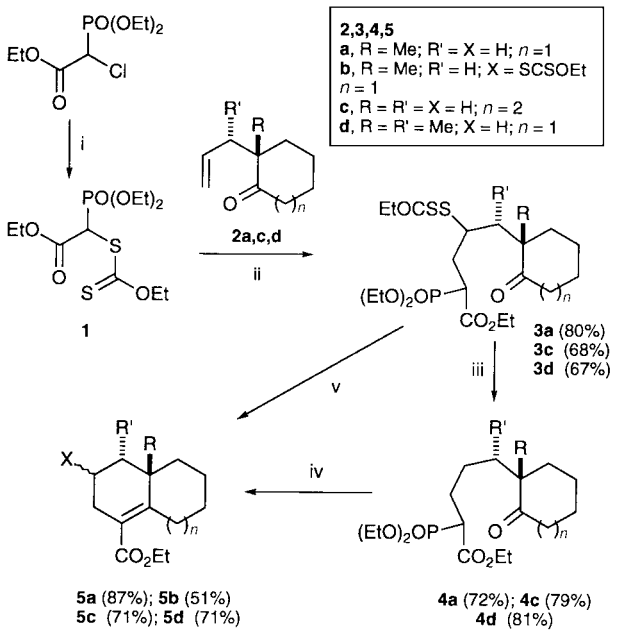

Scheme 1 *Reagents and conditions*: i, EtOCSSK, acetone; ii, lauroyl peroxide (0.1–0.2 equiv.), 1,2-dichloroethane, reflux; iii, Bu_3SnH (AlBN), toluene, reflux; iv, NaH, THF; v, K_2CO_3/18-crown-6, toluene, reflux.

DOI: 10.1039/b001119n

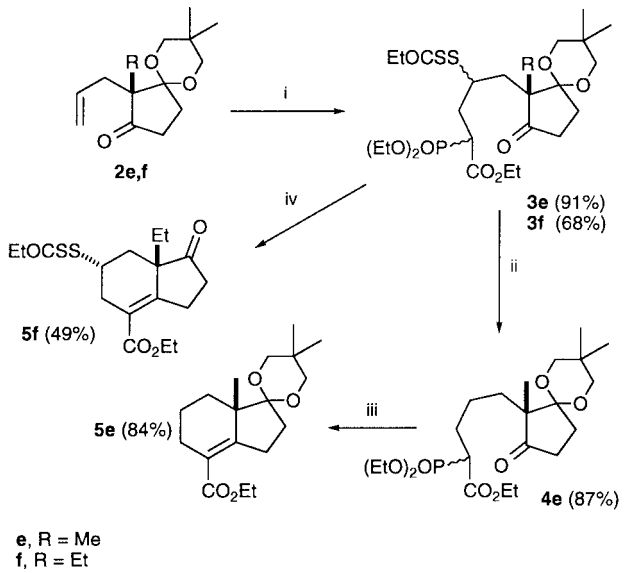

Scheme 2 *Reagents and conditions*: i, lauroyl peroxide (10–20 mol%) cyclohexane, reflux; ii, Bu_3SnH (AIBN), toluene, reflux; iii, NaH, THF; iv, (a) *p*-TSA, acetone; (b) K_2CO_3/18-crown-6, toluene, 80 °C.

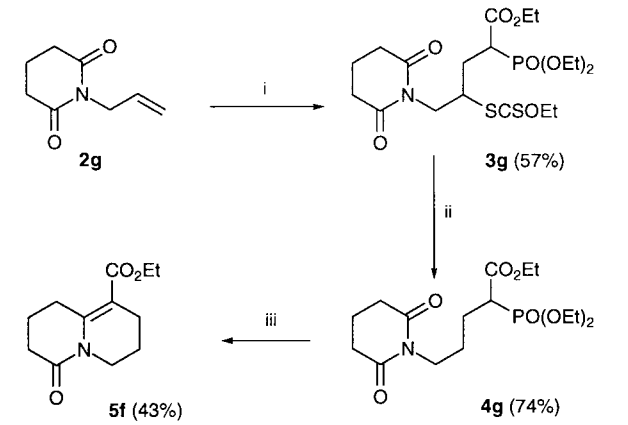

Scheme 3 *Reagents and conditions*: i, lauroyl peroxide (8 mol%), 1.2-dichloroethane, reflux; ii, lauroyl peroxide (1.46 mol. equiv.), isopropyl alcohol, reflux; iii, NaH (4.0 equiv.), THF, reflux.

without removal of the xanthate. Ring closure took place only on the ketone group leading to the least congested isomer, **5f**, with the xanthate in the equatorial orientation and in a location corresponding to the important C-11 position in steroids. There are several clinically useful steroid drugs with the unnatural C-13 ethyl group and some, such as the third-generation contraceptive Desogestrel, also contain a substituent at C-11.[11] Surprisingly, a Robinson-type annulation to construct the C-ring in this series was recently reported to fail.[12]

Finally, the possibility of performing a non-classical Horner–Emmons reaction[13] on an imide may be exploited as an entry to indolizidine and quinolizidine alkaloids. An example of the latter is displayed in Scheme 3. Addition of xanthate **1** to *N*-allylglutarimide followed by removal of the xanthate group using lauroyl peroxide/isopropyl alcohol gave the requisite adduct **4g** in 42% overall yield. We have previously described the use of this reagent combination as a an economical and ecologically more acceptable alternative to organotin hydides for reductively removing xanthates and related groups.[14] Treatment of **4g** with NaH/THF induced ring closure to furnish **5g** in 43% yield. This compound is in principle an immediate precursor of lupinine.[15] The moderate yield in the cyclisation step must be contrasted with the sole literature precedent of a Wittig–Horner-type cyclisation on a glutarimide motif, reported to proceed in only 19%.[16]

In summary, we have described a new, short and flexible strategy for accessing cyclohexenes and related structures. The key radical addition to the unactivated terminal olefin occurs under mild, *neutral* conditions, that are compatible with most functional groups encountered in modern synthesis.

We thank Dr Philippe Mackiewicz (Aventis, Romainville, France) for a generous gift of 2-ethylcyclopentane-1,3-dione.

Notes and references

1 A. Varmer and R. B. Grossman, *Tetrahedron*, 1999, **55**, 13 867; M. E. Jung, *Tetrahedron*, 1976, **32**, 1; R. E. Gawley, *Synthesis*, 1976, 777.
2 D. P. Curran, in *Comprehensive Organic Synthesis*, ed. B. M. Trost and I. Fleming, Pergamon Press, Oxford, 1991, vol. 4, pp. 715–831; B. Giese, *Radicals in Organic Synthesis: Formation of Carbon–Carbon Bonds*, Pergamon Press, Oxford, 1986; W. P. Neumann, *Synthesis*, 1987, 665; D. P. Curran, *Synthesis*, 1988, **417**, 489.
3 See, for example: D. P. Curran, J. Xu and E. Lazzarini, *J. Am. Chem. Soc.*, 1995, **117**, 6603.
4 For a review, see: S. Z. Zard, *Angew. Chem., Int. Ed. Engl.*, 1997, **36**, 672.
5 Xanthate **1** was obtained by reaction of ethyl potassium xanthate with triethyl phosphochloroacetate, itself obtained by chlorination of diethyl phosphonoacetate according to the procedure of C. E. McKenna and L. A. Khawli, *J. Org. Chem.*, 1986, **51**, 5467.
6 P. A. Aristoff, *J. Org. Chem.*, 1981, **46**, 1954.
7 A. D. Rodriguez, C. Ramirez and I. I. Rodriguez, *Tetrahedron Lett.*, 1999, **40**, 7621; P. A. Wender, K. D. Rice and M. E. Schnute, *J. Am. Chem. Soc.*, 1997, **119**, 7897; P. A. Wender, C. A. Jesudason, H. Nakahira, N. Tamura, A. L. Tebbe and Y. Ueno, *J. Am. Chem. Soc.*, 1997, **119**, 12 976 and references therein.
8 M. Sugiura and T. Nakai, *Tetrahedron Lett.*, 1996, **37**, 7991.
9 H. Schick, H. Schwarz and A. Finger, *Tetrahedron*, 1982, **38**, 1279.
10 T. Mandaï, T. Kojima and J. Tsuji, *J. Org. Chem.*, 1994, **59**, 5847.
11 S. Schwartz, S. Ring, G. Weber, G. Teichmüller, H.-J. Palure, C. Pfeiffer, B. Undeutsch, B. Erhart and D. Grawe, *Tetrahedron*, 1994, **50**, 10 709 and references therein.
12 E. J. Corey and A. X. Huang, *J. Am. Chem. Soc.*, 1999, **121**, 710.
13 For a recent review on non-classical Wittig-type reactions, see: P. Murphy and S. E. Lee, *J. Chem. Soc., Perkin Trans. 1*, 1999, 3049.
14 A. Liard, B. Quiclet-Sire and S. Z. Zard, *Tetrahedron Lett.*, 1996, **37**, 5877; B. Quiclet-Sire and S. Z. Zard, *Tetrahedron Lett.*, 1998, **39**, 9435.
15 For an approach to indolizidine and quinolizidine alkaloids using such intermediates, see: S. A. Miller and A. R. Chamberlain, *J. Am. Chem. Soc.*, 1990, **112**, 8100.
16 T. Minami, K. Watanabe and K. Hirakawa, *Chem. Lett.*, 1986, 2027.

Communication b001119n

The dinuclear manganese complex $Mn_2O(OAc)_2$(TPTN) as a catalyst for epoxidations with hydrogen peroxide†

Jelle Brinksma,[a] Ronald Hage,[b] Judith Kerschner[c] and Ben L. Feringa*[a]

[a] *Laboratory of Organic Chemistry, Stratingh Institute, University of Groningen, Nijenborgh 4, 9747 AG Groningen, The Netherlands. E-mail: B.L.Feringa@chem.rug.nl*
[b] *Unilever Research Laboratory Vlaardingen, PO Box 114, 3130 AC Vlaardingen, The Netherlands*
[c] *Unilever Research US, 45 River Road, Edgewater, New Jersey 07020, USA*

Received (in Cambridge, UK) 17th December 1999, Accepted 24th February 2000
Published on the Web 15th March 2000

In acetone and at ambient temperature, the dinuclear manganese complex of TPTN is able to catalyse the oxidation of several alkenes to the corresponding epoxides with high turnovers numbers (up to 900) using H_2O_2 as oxidant.

Selective oxidation of alcohols to aldehydes and the formation of epoxides from olefins are among the key reactions in organic chemistry. In the ongoing pursuit to develop environmentally benign synthetic methodology there is currently great interest in new and more efficient catalytic versions of these oxidations. Compared to catalytic methods that require oxidants like NaOCl and ammonium periodates the use of H_2O_2 offers the advantage that it is a cheap, environmentally friendly and a readily available reagent. Since water is the only expected byproduct, synthetic applications of this reagent are undoubtedly appealing provided efficient catalysis is accomplished.

Recently a number of metal complexes have been found to be suitable catalysts for selective epoxidation reactions with H_2O_2 as oxidant.[1–4] Noyori and coworkers reported a catalytic system based on Na_2WO_4 dihydrate for the epoxidation of terminal olefins and turnovers numbers (TON) were found in the range 150–200 per W atom by using 150 mol% H_2O_2 and 0.2–2 mol% of the catalyst.[1] Methyltrioxorhenium (MTO) is also emerging as a highly suitable epoxidation catalyst.[2] A remarkable acceleration effect on the epoxidation rate was found by Sharpless and coworkers by using pyridine and pyridine derivatives for the MTO catalysed epoxidation of terminal and internal olefins.[3] The Jacobsen catalyst[5] and the related Katsuki catalyst[6] are commonly applied for asymmetric epoxidation reactions of *cis*-olefins. However, with a few exceptions[7] NaOCl is used as oxidant for which TON values in the range of 35–40 were found. Recently it was found that a manganese(IV) complex based on the *N*,*N*′,*N*″-1,4,7-trimethyl-1,4,7-triazacyclononane (MeTACN) ligand is a highly active oxidation catalyst.[4]

This dinuclear manganese complex **1** is capable of the epoxidation of alkenes with TON usually below 100[8,9] but in some cases up to 1000 have been reported using H_2O_2 as oxidant.[10]‡ This complex was also shown by us to be a highly active and selective catalyst for the oxidation of benzyl alcohols to benzaldehydes (TON up to 1000).[11] Synthesis and modifications of the MeTACN ligand are, however, not easily accomplished due to lengthy and tedious preparation whereas the sensitivity of the corresponding metal complexes to changes in the MeTACN structure often leads to completely inactive Mn-complexes. Therefore a challenge is the design of novel dinucleating ligands featuring the three N-donor set for each Mn-site and retaining the high oxidation activity. We present here, high catalytic epoxidation activity for the manganese complex **2** based on the ligand TPTN† using H_2O_2 as oxidant.

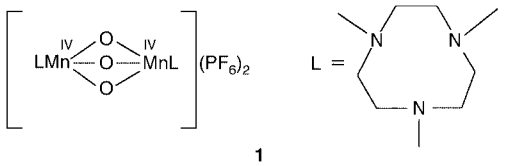

1

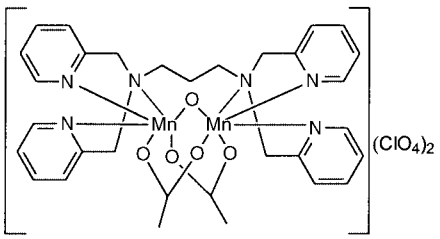

2

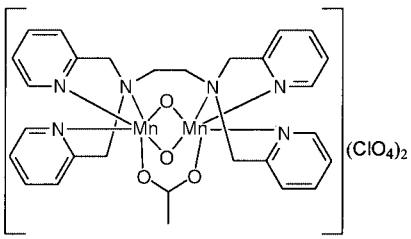

3

Advantages of this type of ligands are the accessibility and the possibility for ligand modification. The ligands and manganese complexes examined here were synthesised following literature procedures and complexes **2** (and **3**) have been reported as mimics for the photosystem II (PS II).[12–15] Preliminary screening in a number of different catalytic epoxidations showed that complex **3** based on TPEN,† featuring a two-carbon spacer between the three N-donor sets in the ligand, was unreactive in epoxidation reactions.§ In sharp contrast, complex **2**, based on TPTN with a three-carbon spacer, is able to catalyse the oxidation of various alkenes to the corresponding epoxides, with H_2O_2 as oxidant in acetone and at ambient temperature (Scheme 1).

Catalytic reactions were performed under a nitrogen atmosphere using 1 equiv. of complex **2**, 1000 equiv. substrate and H_2O_2 was used as oxidant (1 ml of 30% aqueous H_2O_2, 9.8 mM, 8 equiv. with respect to substrate).¶ During the oxidation reaction in acetone at room temperature gas bubbles developed rapidly when the excess of oxidant was added. As for the reactions using **1**[4,11] part of the H_2O_2 disproportionates to O_2. An increase of the catalyst TON was obtained by performing the

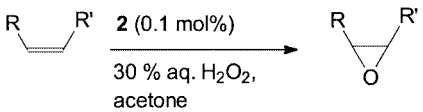

† Abbreviations TPTN = *N*,*N*,*N*′,*N*′-tetrakis(2-pyridylmethyl)propane-1,3-diamine, TPEN = *N*,*N*,*N*′,*N*′-tetrakis(2-pyridylmethyl)ethane-1,2-diamine.

DOI: 10.1039/a910232i

Table 1 Oxidation of selected olefins with $Mn_2O(OAc)_2$(TPTN) complex **2**[a]

Entry	Substrate	Product[b]	TON 2 h, 298 K[c]	TON 4 h, 298 K[d]	TON 2 h, 273 K[c]	TON 4 h, 273 K[d]
1	Styrene	Styrene oxide	157	208	176	271
		Benzaldehyde	5	75	2	14
	Cyclohexene	Cyclohexene				
2		oxide	247	563	328	868
	Cyclooctene	Cyclooctene				
3		oxide	193	636	262	575
		cis-Diol	49	93	61	48
4	Cinnamyl alcohol	Cinnamyl oxide	208	219	219	321
		Cinnamyl				
		aldehyde	69	85	70	86
		Benzaldehyde	22	47	21	46
	trans-2-Octene	*trans*-Oct-2-ene				
5		oxide	118	188	178	248
	trans-4-Octene	*trans*-oct-2-ene				
6		oxide	97	148	153	210
7	1-Decene	1-Decene oxide	28	34	80	97
8	*cis*-β-Methyl-	*trans*-oxide	19	84	23	115
	styrene	*cis*-oxide	43	104	44	147

[a] Experimental conditions, see text. [b] All products were identical to independent samples and identified by GC (HP 6890, column HP1 15 × 0.3 mm × 2.65 μm, polydimethylsiloxane) and ^{1}H NMR. [c] Turnover number = mol product per mol catalyst, 8 equiv. H_2O_2 with respect to substrate. [d] 16 equiv. H_2O_2 with respect to substrate.

catalytic reactions in acetone at 0 °C suppressing H_2O_2 decomposition. For the selected olefins generally up to 300 TONs were found. Addition of a further 1 ml of H_2O_2 (30% aqueous solution in water, 9.8 mmol, 8 equiv. with respect to substrate) resulted in an considerable increase in epoxide yield after 4 h (total TON up to 900, for cyclohexene). These results indicate that the catalyst is very robust under the conditions used. High selectivity is observed and it should be emphasized that in the epoxidation reaction of cyclic alkenes (especially for cyclohexene), besides the epoxides, no allylic oxidation products were found. In control experiments replacing $Mn_2O(OAc)_2$(TPTN) **2** with $Mn(OAc)_3{\cdot}3H_2O$, strong peroxide decomposition and no epoxide formation was found. Data for the conversion of various alkenes to the corresponding epoxides are compiled in Table 1. Styrene epoxidation is accompanied by the formation of a small amount of benzaldehyde; a feature commonly observed with epoxidation of this substrate. Cinnamyl alcohol also showed some cleavage and alcohol oxidation leading to benzaldehyde and cinnamyl aldehyde, respectively. A substantial amount of *trans*-epoxide is obtained in the reaction of *cis*-β-methylstyrene with H_2O_2 in the presence of catalyst **2** which is usually attributed to the formation of a radical intermediate with a lifetime sufficient for internal rotation before ring closure.[16] Excellent results were also found for internal alkenes *e.g.* entries 5 and 6 whereas slightly lower yields were found for terminal linear alkenes.

In conclusion, we have demonstrated that the manganese complex **2** based on TPTN is a promising catalyst in catalytic epoxidation procedures using H_2O_2 as the terminal oxidant. Main advantages of the new catalytic system are the facile synthesis and possibility for ligand modification. In acetone and at ambient temperature the manganese complex of TPTN is able to catalyse the selective oxidation of various alkenes to the corresponding epoxides, with H_2O_2 as oxidant. Further studies towards the elucidation of the mechanism and introduction of chirality in the ligand are in progress.

Notes and references

‡ Very recently a co-ligand effect was reported by the groups of De Vos and Berkessel, see: D. E. De Vos, B. F. Sels, M. Reynaers, S. Rao and P. A. Jacobs, *Tetrahedron Lett.*, 1998, **39**, 3221; A. Berkessel and C. A. Sklorz, *Tetrahedron Lett.*, 1999, **40**, 7965

§ L. Fraisse, J. J. Girerd, F. Perie, A. Rabion, D. Tetard, J. B. Verlhac and A. Nivorozhkin, PCT WO 97/18035 Elf-Aquitaine. Oxidation catalysis with various Mn and Fe complexes based on amine-heteroaromatic ligands has been claimed recently (*e.g.* cyclohexane oxidation, polyaromatic oxidation). No epoxidation activity was given however.

¶ Catalytic reactions were started by mixing 1.0 ml of a 1.2 μM stock solution of the manganese complex in acetone and 1.0 ml of a 1.2 mM stock solution of substrate at 25 °C under a nitrogen atmosphere. As an internal standard, bromobenzene or 1,2- dichlorobenzene (in the case of cyclooctene) were used. After stirring for 2 min, an excess of hydrogen peroxide (1.0 ml of 30% aqueous H_2O_2, 9.8 mM, 8 eq. with respect to substrate) was added. The progress of the reaction was monitored by GC, by removing small samples of the reaction mixture and filtering over a short column of silica. To establish the identity of the epoxides and other products unequivocally, the retention times and spectral data were compared to those of commercially available and independently synthesised compounds.

1 K. Sato, M. Aoki, M. Ogawa, T. Hashimoto and R. Noyori, *J. Org. Chem.*, 1996, **61**, 8310.
2 W. A. Herrmann, R. W. Fischer and D. W. Marz, *Angew. Chem., Int. Ed. Engl.*, 1991, **30**, 1638.
3 J. Rudolph, K. L. Reddy, J. P. Chiang and K. B. Sharpless, *J. Am. Chem. Soc.*, 1997, **119**, 6189.
4 R. Hage, J. E. Iburg, J. Kerschner, J. H. Koek, E. L. M. Lempers, R. J. Martens, U. S. Racherla, S. W. Russell, T. Swarthoff, M. R. P. van Vliet, J. B. Warnaar, L. van der Wolf and B. Krijnen, *Nature*, 1994, **369**, 637.
5 J. F. Larrow, E. N. Jacobsen, Y. Gao, Y. Hong, X. Nie and C. M. Zepp, *J. Org. Chem.*, 1994, **59**, 1939.
6 N. Hosoya, A. Hatayama, K. Yanai, H. Fujii, R. Irie and T. Katsuki, *Synlett*, 1993, 641.
7 P. Pietikäinen, *Tetrahedron*, 1998, **54**, 4319.
8 D. E. De Vos and T. Bein, *J Organomet. Chem.*, 1996, **520**, 195.
9 P. P. Knops-Gerrits, D. E. De Vos and P. A. Jacobs, *J. Mol. Catal. A.*, 1997, **117**, 57.
10 D. E. De Vos and T. Bein, *Chem. Commun.*, 1996, 917.
11 C. Zondervan, R. Hage and B. L. Feringa, *Chem. Commun.*, 1997, 419.
12 H. Toftlund and S. Yde-Andersen, *Acta Chem. Scand. Ser. A*, 1981, **35**, 575.
13 H. Toftlund, A. Markiewicz and K. S Murray, *Acta Chem. Scand.*, 1990, **44**, 443.
14 J .B. Mandel, C. Maricondi and B. E. Douglas, *Inorg. Chem.*, 1988, **27**, 2990.
15 S. Pal, J. W. Gohdes, W. Christian, A. Wilisch and W. H. Armstrong, *Inorg. Chem.*, 1992, **31**, 713.
16 W. Zhang, N. H. Lee and E. N. Jacobsen, *J. Am. Chem. Soc.*, 1994, **116**, 425.

Communication a910232i

Neutron powder and *ab initio* structure of *ortho*-xylene: the influence of crystal packing on phenyl ring geometry at 2 K†

Richard M. Ibberson,*[a] Carole Morrison[b] and Michael Prager[c]

[a] *ISIS Facility, CCLRC-Rutherford Appleton Laboratory, Chilton, Didcot, Oxfordshire, UK OX11 0QX. E-mail: rmi@isisa.rl.ac.uk*

[b] *Department of Chemistry, The University of Edinburgh, King's Buildings, West Mains Road, Edinburgh, UK EH9 3JJ*

[c] *Institut für Festköperforschung, Forschungszentrum Jülich, 52425 Jülich, Germany*

Received (in Oxford, UK) 27th October 1999, Accepted 24th February 2000
Published on the Web 15th March 2000

Crystal packing effects in the previously unknown structure of *ortho*-xylene are found to induce a high degree of strain to the phenyl ring which is not observed in high-level *ab initio* structure calculations or in the crystal structures of the *para* and *meta* isomers; the potential for aromatic hydrogen bonding in the structure is discussed.

One motive for performing crystallographic studies on simple model systems is to reveal structural motifs that may be applicable to whole classes of compound. The wealth and understanding of these crystallographic data has led to the development of crystal engineering[1] which is of increasing interest to organic and physical chemists. In addition such studies can be used in the derivation and testing of model potentials[2,3] which is the background to the present study. Though the three isomers of xylene are familiar laboratory compounds, until recently little was known about their structure in the solid state.[2,4,5] We now describe the crystal structure of *o*-xylene at low temperature which, in contrast to the other isomers, exhibits a strained ring conformation which we suggest may be attributed to weak intermolecular forces.

A 2 g powder sample of perdeuterated *o*-xylene was prepared by the method described in ref. 6 and neutron powder diffraction data‡ were collected at 2 K on the High Resolution Powder Diffractometer, HRPD, at the ISIS pulsed-neutron source, UK. The structure was solved§ routinely from the powder data using direct methods to reveal a monoclinic phase of cell volume 634 Å^3; space group $P2_1/a$. The four molecules in the unit cell are arranged in columns running along the unit cell *a* axis in a herring-bone configuration with D··Đ contact distances of *ca.* 2.4–2.8 Å.

Examination of the refined molecular conformation (Fig. 1) reveals the determination of bond lengths and bond angles to be both precise and accurate as is expected from a high-resolution study on a structure of this limited complexity. The conformation shows small but significant deviations from C_{2v} symmetry, but most striking is the deformation of the carbon skeleton of the phenyl ring between the two substituted carbon atoms C(1) and C(2). The observed bond length of 1.433(3) Å is considerably in excess of the distance expected on consideration of steric repulsion of the eclipsed methyl groups and possible conjugation effects due to the substituent methyl groups. This finding is in contrast to the minor ring deformation observed in the crystal structures of the *meta* and *para* isomers[5] determined from neutron powder diffraction data and, for example, the negligible deformation seen in the X-ray single crystal study of *ortho*-dinitrobenzene,[11] all of which are found to be in accord with expected conjugation effects. Accordingly, a series of high-level *ab initio* calculations¶ were undertaken in order to establish the minimum energy conformation of the *ortho, meta* and *para* isomers.

† Electronic supplementary information (ESI) available: neutron diffraction data and comparison of bond parameters from neutron and *ab initio* data. See http://www.rsc.org/suppdata/cc/a9/a908599h/

Calculations for *o*-xylene (Fig. 1), assuming overall ideal C_{2v} symmetry, show a significantly reduced distortion to the ring. In particular the C(1)–C(2) bond length is calculated at 1.412 Å—a discrepancy of 0.22 Å (> 7 standard deviations) as compared with the refined solid-state structure. Note, calculations were also made without the C_{2v} symmetry constraint and starting from the crystal structure coordinates, but the same minimum was obtained. Subsequent refinement of a model assuming C_{2v} symmetry against the neutron powder data, although resulting in a degraded fit to the pattern, was found to retain this discrepancy between the minimum-energy and solid-state conformation. Crystal packing effects in the structure of *o*-xylene thus appear to play a significant role in defining the molecular conformation.

In contrast, the calculated and experimentally determined solid-state conformations of the remaining isomers show excellent agreement. For *m*-xylene the discrepancies in bond lengths determined in each case were typically 0.004 Å (1 standard deviation) with a maximum discrepancy for one phenyl-ring bond of 0.007 Å. For *p*-xylene the discrepancies in

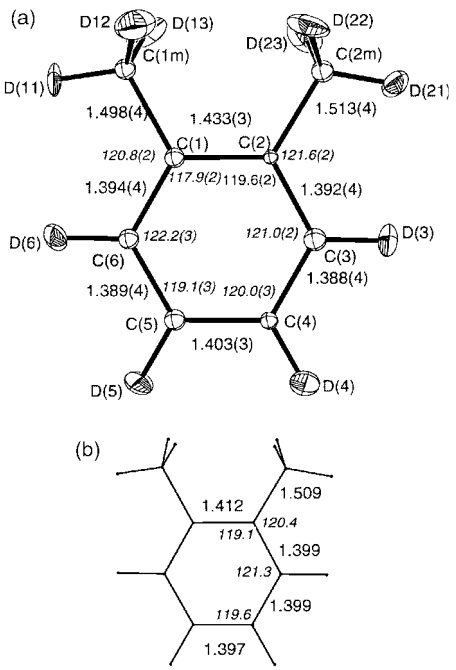

Fig. 1 (a) ORTEP[17] diagram of the molecular conformation of *o*-xylene at 2 K; thermal ellipsoids are drawn at the 50% probability level. Bond length (Å) and bond angle (°) values are shown with estimated standard deviations in parentheses determined from the neutron powder diffraction data. (b) Bond length (Å) and bond angle (°) values calculated *ab initio* using the MP2/6-311G* basis set. (Average values for bond lengths and bond angles around the methyl groups are: for C(1m) 1.093(3) Å, 110.85(3)°; for C(2m) 1.075(3) Å, 111.86(3) and from *ab initio* calculation 1.095 Å, 111.27°.)

DOI: 10.1039/a908599h

bond lengths determined in each case were typically 0.008 Å (2 standard deviations) with a maximum discrepancy for one phenyl-ring bond of 0.012 Å. The most significant differences in each case were observed for the torsions of the methyl groups. Rotations of 6 and 23° compared to the minimum-energy conformation are observed for *m*-xylene, and 6° (one clockwise, one anticlockwise) for *p*-xylene. However, as the vibrational frequencies calculated (b3pw91/6-31G*) for these low energy torsional modes are only 21 and 24 cm^{-1}, respectively, it is not surprising that crystal packing forces have distorted the ring substituents from their idealised torsional values.

The *o*-xylene crystal structure has, on inspection of the intermolecular contacts (Fig. 2), the potential for 'aromatic hydrogen bonding' (see for example ref. 12). The closest contact from the midpoint of the phenyl ring to a methyl, D(21), atom of a neighbouring molecule is 2.816(4) Å. The distances of this D(21) atom to the six individual C atoms lie in a broad range of 2.849–3.422 Å. The two shortest contacts with the C(1) and C(2) atoms are 2.849(4) and 2.908(5) Å, respectively, which is significantly less that the sum of the van der Waals radii at 3.05 Å, and, most notably the distance from the C(1)–C(2) bond midpoint to D(21) is only 2.789(4) Å, making an angle of 152.6(3)° with the methyl group C–D bond. No other significant contacts are made to C(1) and C(2), in contrast with the remaining four phenyl C atoms which typically have three or more contacts in the range 2.86–3.1 Å. The contact is made off-centre to the phenyl ring and in general would be regarded as less favourable for an interaction, however, in this case it is the apparent directional (as opposed to isotropic) nature of the contact which correlates well with the observed molecular conformation. It is this strong directional nature of the contact that leads us to suppose it to be a significant interaction.

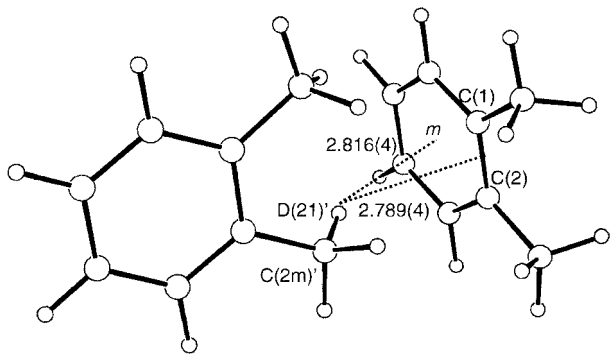

Fig. 2 Geometry of the aromatic ring–methyl group interactions. (Primed atoms denote symmetry code $\frac{1}{2}-x, -\frac{1}{2}+y, -z$; *m* denotes the midpoint of the phenyl ring.)

It is now generally recognised that C–H groups can act as weak hydrogen bond donors[13–16] and there is a growing literature on the subject particularly in the context of crystal engineering cited earlier. The documentation and characterization of these weak interactions is well advanced only in the case for bonds formed between C–H donors and oxygen acceptors. The interactions between other weak donor–acceptor combinations, especially as in the present case of such a weakly polarized donor group as Me with a π-acceptor, is considerably less well characterized. Nevertheless, electron donation from a Me group of a neighbouring molecule into an antibonding aromatic orbital seems the most plausible explanation for the unusual lengthening of the disubstituted C–C bond in the solid-state structure of *o*-xylene.

We thank Dr C. C. Wilson for helpful discussions during the course of this work. Acknowledgement is made to the EPSRC for the provision of beam time at the ISIS Facility and for the Edinburgh *ab initio* facilities (grant GR/K/04194).

Notes and references

‡ Data were recorded using a vanadium-tailed helium-flow 'orange' cryostat over a time-of-flight range of 30–230 ms corresponding to a *d*-spacing range of 0.6–4.6 Å at backscattering ($<2\theta>$ = 168°). Lower angle (90 and 30°) detector banks enabled *d*-spacings of, in this case, up to 6.0 Å to be recorded, albeit at lower resolution, for the purposes of unit cell indexing.

§ *Crystal data* for *ortho*-xylene: C_8D_{10}, M = 116.23, monoclinic, space group $P2_1/a$ (no.14), a = 12.5114(1), b = 6.0714(1), c = 8.8157(1) Å, β = 108.6847(4)°, U = 634.36(1) $Å^3$, T = 2 K, Z = 4. The unit cell was determined automatically from 36 low-order reflections $2.4 < d < 6.0$ Å using program ITO.[7] The structure was solved by direct methods (MITHRIL)[8] and refined without the use of bond length or bond angle constraints using the Rietveld method[9] implemented by program TF12LS.[10] Only the D atoms were refined anisotropically. R_e = 1.62%, R_p = 3.38%, R_{wp} = 3.90%, χ^2 = 3.63 for 6579 observations and 145 basic variables.

¶ All *ab initio* calculations were performed on a DEC Alpha APX 1000 workstation using the GAUSSIAN 94 program.[18] A graded series of calculations were undertaken for all three compounds using the standard gradient techniques at the SCF and b3pw91 levels of theory using the 6-31G* basis set. Vibrational frequencies calculated from analytic second derivatives at the b3pw91/6-31G* level confirmed the C_{2v} symmetry grouping for *o*-xylene, C_s for *m*-xylene and C_i for *p*-xylene as minimum on their respective potential energy surfaces. Further calculations were then undertaken for *o*-xylene: firstly, to confirm the C_{2v} structure as the global minimum an optimisation was performed (b3pw91/6-31G*) starting from the crystal structure coordinates with no symmetry constraints. From an observation of the absolute energies obtained it was clear that removal of the symmetry constraints resulted in exactly the same minima being obtained in the optimisation. Finally, for direct comparison with the crystal structure parameters one further higher level calculation (MP2/6-311G*) was undertaken. At this level all geometric parameters were observed to be effectively converged within the series of calculations performed, with *e.g.* C–C bond distances varying by <0.3 pm and all angles by $<0.2°$ for improvements in basis set at the MP2 level. It can therefore be concluded that any further higher level calculations are unlikely to result in significant changes in molecular geometry.

1 G. R. Desiraju, *Chem. Commun.*, 1997, 1475.
2 M. Prager, W. I. F. David and R. M. Ibberson, *J. Chem. Phys.*, 1991, **95**, 2473.
3 M. Prager, M. Monkenbusch, R. M. Ibberson, W. I. F. David and D. Cavagnat, *J. Chem. Phys.*, 1993, **98**, 5653.
4 H. van Koningsveld, A. J. van den Berg, J. C. Jansen and R. de Goede, *Acta Crystallogr., Sect. B.*, 1986, **42**, 491.
5 R. M. Ibberson, W. I. F. David, S. Parsons, M. Prager and K. Shankland, *J. Mol. Struct.*, 2000, in press.
6 R. M. Ibberson, *J. Appl. Crystallogr.*, 1996, **29**, 498.
7 J. W. Visser, Autoindexing program-ITO. Technisch Physische Dienst, P.O. Box 155, Delft, The Netherlands, 1988.
8 C. J. Gilmore, MITHRIL a computer program for the automatic solution of crystal structures from X-ray data (Version 1.0). Department of Chemistry, University of Glasgow, Glasgow, UK G12 8QQ, 1983.
9 H. M. Rietveld, *J. Appl. Crystallogr.*, 1969, **2**, 65.
10 W. I. F. David, R. M. Ibberson and J. C. Matthewman, Rutherford Appleton Laboratory Report, RAL-92-032.
11 F. H. Herbstein and M. Kapon, *Acta Crystallogr., Sect. B*, 1990, **46**, 567.
12 T. Steiner, S. A. Mason and M. Tamm, *Acta Crystallogr., Sect. B.*, 1997, **53**, 843.
13 G. R. Desiraju, *Acc. Chem. Res.*, 1996, **29**, 441.
14 T. Steiner, *Chem. Commun.*, 1997, 727.
15 T. Stenier and G. Desiraju, *Chem. Commun.*, 1998, 891.
16 G. Desiraju and T. Steiner, *The Weak Hydrogen Bond*, Oxford University Press/International Union of Crystallography, Oxford, 1999 and references therein.
17 ORTEP: M. N. Burnett and C. K. Johnson, ORTEP-III: Oak Ridge Thermal Ellipsoid Plot Program for Crystal Structure Illustrations, Oak Ridge National Laboratory, TN Report ORNL-6895, 1996.
18 GAUSSIAN 94 (Revision C.2), M. J. Frisch, G. W. Trucks, H. B. Schlegel, P. M. W. Gill, B. G. Johnson, M. A. Robb, J. R. Cheeseman, T. A. Keith, G. A. Petersson, J. A. Montgomery, K. Raghavachari, M. A. Al-Laham, V. G. Kakrezewski, J. V. Ortiz, J. B. Foresman, J. Cioslowski, B. B. Stefanov, A. Nanayakkara, M. Challacombe, C. Y. Peng, P. Y. Ayala, W. Chen, M. W. Wong, J. L. Andres, E. S. Replogle, R. Gomperts, R. L. Martin, D. J. Fox, J. S. Binkley, D. J. Defrees, J. Baker, J. P. Stewart, M. Head-Gordon, C. Gonzalez and J. A. Pople, Gaussian Inc., Pittsburgh, PA, 1995.

Communication a908599h

ChemComm

Restriction of guest rotation based on the distortion of a cyclodextrin cavity

Wen-Hua Chen,[a] Makoto Fukudome,[a] De-Qi Yuan,[a] Toshihiro Fujioka,[b] Kunihide Mihashi[b] and Kahee Fujita*[a]

[a] *Faculty of Pharmaceutical Sciences, Nagasaki University, 1-14 Bunkyo-Machi, Nagasaki 852-8521, Japan. E-mail: fujita@net.nagasaki-u.ac.jp*

[b] *Faculty of Pharmaceutical Sciences, Fukuoka University, Nakakuma, Jonan-ku, Fukuoka 814-0180, Japan*

Received (in Cambridge, UK) 10th December 1999, Accepted 18th February 2000
Published on the Web 15th March 2000

Significant restriction of the rotation of an intermolecular guest upon binding into a distorted cyclodextrin cavity has been observed for the first time.

Most enzymes bind substrates in their hydrophobic pockets and promote the reaction of bound substrates in a strictly controlled manner. It is not rare that enzymes control multiple reactants so exactly as to give only one isomeric product during the formation of multiple chiral centers. In the last three decades, bioorganic chemists have been investigating the main factors that predominate in enzyme reactions and have created artificial enzymes by mimicking the enzyme actions with synthetic model compounds.[1–3] In this endeavour, cyclodextrins (CDs) are the first and also the most profoundly studied class of apoenzyme mimics.[4,5] Cyclodextrins have a closed-up belt-type structure usually composed of 6–8 glucopyranose units. Their cavity can accommodate a variety of guest molecules of suitable size and shape, mainly *via* hydrophobic interactions. Since the hydrophobic binding force is non-directional, the C_n symmetry of the CD cavity leaves appreciable freedom for the bound substrates to rotate around the *z* axis (Scheme 1).[6] However, this rotation should be properly controlled in order to develop more efficient and sophisticated enzyme mimics. However, this problem has been essentially ignored up to now. The only work dealing with this problem appeared ten years ago, concluding that the hosts having larger binding constants restrict the molecular motion of guests more significantly.[7] Since the binding site of an enzyme is usually unsymmetrical rather than symmetrical, a cyclooligosaccharide with a distorted hydrophobic cavity may serve as a better model for enzymes than a C_n symmetrical CD. We found that distorting the hydrophobic cavity of β-CD remarkably reduces the rotation of bound 2-naphthalenesulfonate, but does not necessarily increase the binding strength. Herein, we describe NMR evidence for this first example of cavity-based restriction of guest rotation.

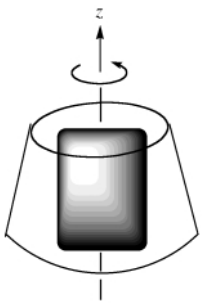

Scheme 1 In principle, a guest in a CD cavity has appreciable freedom to rotate around the *z* axis.

One glucose of β-CD can be readily converted to altrose.[8] The resultant mono-*altro*-β-CD **1** shows distinct NMR signals (Fig. 1, bottom) for all its protons. Though it no longer has C_n symmetry, the difference between the glucose units is not very significant. As a result, the signals of all the non-anomeric C–H protons are crowded in the narrow range of δ 3.9–3.5. However, significant changes occur in the NMR spectrum of **1** upon complexation with sodium 2-naphthalenesulfonate (Na–Nas). By following the spectral change upon addition of Na–Nas to the host solution, a binding constant of 176 M^{-1} can be derived, slightly smaller than that of β-CD–Nas.[9] In the NMR spectrum of 90% **1**–Nas complex and 10% **1** (Fig. 1), the originally overlapped signals in the range δ 3.9–3.5 are more widely dispersed over the range δ 4.2–2.69, and all the H-1 protons are clearly separated. Obviously, the guest Nas exercises a very strong anisotropic effect on each sugar unit of the host.

In order to further understand this phenomenon, the NMR spectrum of the complex has been assigned in detail with the aid of various techniques (the assignment is partially depicted in Fig. 1). As is clear from Fig. 1, inclusion complexation causes significant shifts for the inner-directed H-3 and H-5 protons. The drastic upfield shifts of protons 3C, 5C, 3D, 5D, 3G and 5G

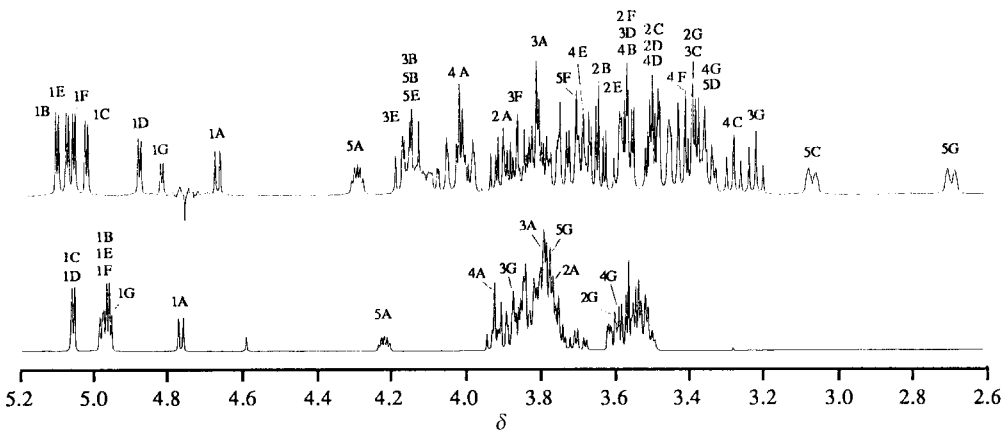

Fig. 1 500 MHz ^{1}H NMR spectra of mono-*altro*-β-CD **1** (bottom) and of its 2-naphthalenesulfonate inclusion complex **2** (top, 90% binding) in D_2O, assigned based on 1D TOCSY, 2D COSY, HMBC and NOE experiments. The sugar units are labeled clockwise A–G (viewed from the primary hydroxy side), starting from the altrose unit. The numbers denote the positions to which the corresponding protons are attached.

DOI: 10.1039/a909727i

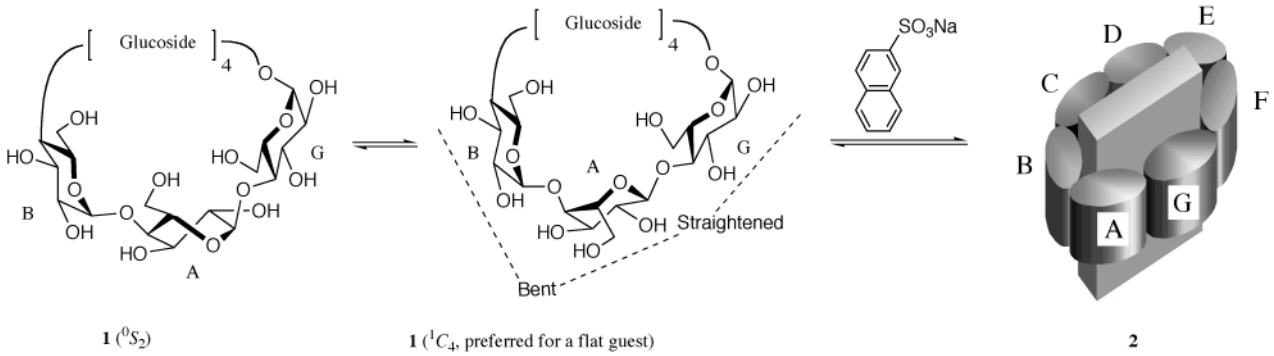

1 ($^0S_2$) **1** ($^1C_4$, preferred for a flat guest) **2**

Scheme 3 Mono-*altro*-β-CD **1** and its inclusion complex with sodium 2-naphthalenesulfonate. **2** is a sketch (view from the 6-OH side) for the proposed structure of the **1**–Nas complex: the cylinders denote pyranosides while the plate represents Nas.

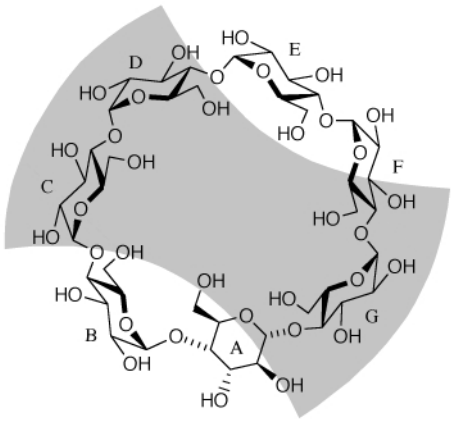

Scheme 2 The anisotropic effect that **1** experiences in the complex: the shaded region denotes a shielding field while the unshaded region represents a deshielding field.

imply that the sugar units C, D and G are under a strong shielding effect from Nas, while the large downfield shifts of protons 3B, 5B, 3E and 5E are indicative of a strong deshielding effect. Careful examination of the NMR data thus reveals that the host molecule in the complex is under an extremely unusual anisotropic effect, as represented in Scheme 2. The protons in the shaded region are shifted upfield while those in the non-shaded region are shifted downfield. Sugar G is located in the center of the lower right half of the shielding region and is subjected to the strongest shielding effect and the largest upfield shifts are for H-3 and H-5 of sugar G ($\Delta\delta$ −0.77 and −1.18 ppm, respectively). The effect becomes much weaker for the neighboring sugar units A and F, and gradually becomes deshielding when crossing the two units. On the opposite side of G, both C and D lie in the upper left half of the shielding region. Accordingly, protons H-4C and H-1D, although outward-directed, exhibit a remarkable upfield shift. The inward-directed H-3 and H-5 protons of the two sugar residues are still strongly shielded, but obviously to a smaller extent than the corresponding protons of sugar G. The shielding effect is weak for H-4D and H-1C and becomes deshielding for H-1E and H-4B. Both the sugar units B and E are fully under a deshielding effect with their inward-directed protons H-3 and H-5 being significantly shifted downfield. As a result, each pyranoside in the inclusion complex experience different anisotropic effects, which represents, to the best of our knowledge, an unprecedented strongly anisotropic effect of an intermolecular guest within a cyclooligosaccharide host.

Based on the above result, the structure of the complex (**2**) can be visualized as shown in Scheme 3. The pyranose G and disaccharide C–D are situated on either side of and nearly parallel to the naphthalene ring, while the naphthalene species directs its 1-9-8 and 4-10-5 rims towards between the sugar units B and A or E and F but much closer to the B and E units. Although Scheme 3 represents a static situation rather than a dynamic one, it probably represents the most probable rotamer, if indeed there is any rotation of the guest in the CD cavity, outweighing any others for the complex to a very large extent. Were mono-*altro*-β-CD not restricting the guest rotation, as in the case of β-CD, the ring-current effect of the guest would be averaged so that each sugar unit would be subjected to a similar shielding effect rather than the observed anisotropic effect, and the inward-oriented protons of all the sugar units would give NOE on irradiation at the naphthalene protons. Irradiation at the 1-H of the guest gave cross peaks at the frequencies corresponding to protons H-3 and H-5 of B and E whereas no cross peaks correlating with the protons of C, D and G were observed, which supports the above assertion.

It is not surprising that the rotation of the bound guest is substantially restricted as the host adopts a distorted conformation and **2** is the complex structure expected from the host conformation. The altrose portion of **1** is an equilibrium of the $^0S_2$ and $^1C_4$ conformers with an approximate 2 : 1 preponderance of the latter (Scheme 3).[10] The $^0S_2$ makes the overall shape of **1** closely resemble that of β-CD, while the $^1C_4$ conformer straightens the A–G disaccharide but bends the A–B disaccharide, and leads to a mussel-shaped ellipse shape for the cavity with its longer axis passing through residues B and E. It is reasonable to deduce that $^1C_4$ is the preferential conformer enabling the host to accommodate the flat guest Nas, by accommodating the guest plane along its longer axis. Indeed, the binding of Nas into the cavity of **1** increased the coupling constants $J_{1,2}$ and $J_{2,3}$ of the altroside, suggesting a significant enrichment of the $^1C_4$ conformer upon inclusion.

In conclusion, the introduction of an altrose unit to β-CD narrows the hydrophobic cavity and enables it to substantially reduce the rotation of the bound flat Nas guest. In this sense, the binding of mono-*altro*-β-CD **1** is more like an enzyme process than that of normal CDs.

We thank Japan Maize Products Co. Ltd. for a generous gift of CDs. D.-Q. Y. thanks the NSFC (project 29772023) and the State Education Ministry of China (project 380).

Notes and references

1 R. Breslow, *Pure & Appl. Chem.*, 1998, **70**, 267.
2 J. K. M. Sander, *Chem. Eur. J.*, 1998, **4**, 1378.
3 A. J. Kirby, *Angew. Chem., Int. Ed. Engl.*, 1996, **35**, 707.
4 *Comprehensive Supramolecular Chemistry*, ed. J. L. Atwood, J. E. Davies, D. D. MacNicol and F. Vogtle, Pergamon Elsevier, Oxford, UK, 1996, vol. 3, *Cyclodextrins.*
5 R. Breslow and S. D. Dong, *Chem. Rev.*, 1998, **98**, 1997.
6 J. P. Behr and J. M. Lehn, *J. Am. Chem. Soc.*, 1976, **98**, 1743.
7 Y. Kuroda, M. Yamada and I. Tabushi, *J. Chem. Soc., Perkin Trans. 2*, 1989, 1409.
8 K. Fujita, K. Ohta, Y. Ikegami, H. Shimada, T. Tahara, Y. Nogami, T. Koga, K. Saito and T. Nakajima, *Tetrahedron Lett.*, 1994, **35**, 9577.
9 J. Nishijo and Y. Ushiroda, *Chem. Pharm. Bull.*, 1998, **46**, 1790.
10 K. Fujita, W.-H. Chen, D.-Q. Yuan, Y. Nogami, T. Koga, T. Fujioka, K. Mihashi, S. Immel and F. Lichtenthaler, *Tetrahedron: Asymmetry*, 1999, **10**, 1689.

Communication a909727i

X-Ray crystal structure of the bis(dihydrogen) complex $RuH_2(H_2)_2(PCy_3)_2$

Andrzej F. Borowski,[a] Bruno Donnadieu,[b] Jean-Claude Daran,[b] Sylviane Sabo-Etienne[b] and Bruno Chaudret*[b]

[a] *Institute of Coal Chemistry, Polish Academy of Sciences, 5 Sowinskiego St., Gliwice, 44-121 Poland*
[b] *Laboratoire de Chimie de Coordination CNRS, 205 Route de Narbonne, F-31077 Toulouse Cedex 4, France. E-mail: Chaudret@lcc-toulouse.fr*

Received (in Basel, Switzerland) 25th October 1999, Accepted 17th December 1999
Published on the Web 15th March 2000

$RuH_2(H_2)_2(PCy_3)_2$, the first reported stable bis (dihydrogen) complex crystallizes in the *P*1 space group; the two dihydrogen ligands lie in the equatorial plane in a mutual *cis* position and are located *trans* to the hydride ligands; the H–H distances are *ca.* 0.85 Å, in agreement with the presence of unstretched dihydrogen ligands; these results are compared with previous theoretical calculations using density functional theory.

The chemistry of dihydrogen complexes has developed considerably since the first discovery of dihydrogen coordination without dissociation in 1984.[1] Many different compounds have now been isolated, characterized, in particular by X-ray crystallography, and have given rise to reactivity studies.[2]

The number of complexes containing more than one dihydrogen ligand remains, however, very limited.[3] No tris(dihydrogen) complex is known and only a few bis(dihydrogen) complexes have been isolated, namely $RuH_2(H_2)_2(PCy_3)_2$ **1**[4] and $LRuH(H_2)_2$ [L = hydridotris(3,5-dimethylpyrazolyl)borate, Tp*; L = hydridotris(3-isopropyl-4-bromopyrazolyl)borate, Tp'].[5] $RuH_2(H_2)_2(P^iPr_3)_2$ has been observed in solution following the same procedure as that used for preparing **1**[6] and recently isolated by Morris using a different procedure.[7] $Cr(CO)_4(H_2)_2$ has been observed in an argon matrix or in liquid xenon and characterized by IR spectroscopy.[8] Crabtree *et al.* have characterized the bis(dihydrogen) complex $[IrH_2(H_2)_2(PCy_3)_2]$+ in solution upon protonation of the neutral precursor $IrH_5(PCy_3)_2$.[9] Finally Caulton and coworkers have characterized a bis(dihydrogen) osmium derivative $[Os(H_2)_2(NCMe)_2(PPr^i_3)_2]^{2+}$ by protonation of $[OsH_3(NCMe)_2(P^iPr_3)_2]^+$.[10] A number of unstable bis(dihydrogen) ruthenium complexes have also been prepared when studying the reactivity of $RuH_2(H_2)_2(PCy_3)_2$.[11]

In a recent paper, we described the spectroscopic properties of $RuH_2(H_2)_2(PCy_3)_2$, in particular INS spectra demonstrating the presence of a low rotation barrier for the dihydrogen ligands and the results of DFT calculations showing that the most stable structure involved the presence of two mutually *cis* hydrides each of which was located *trans* to a dihydrogen ligand.[12] Complex **1** has proven to be important in ruthenium chemistry and has found applications as a starting material for a great variety of ruthenium dihydrogen complexes,[11,13,14] and complexes containing two σ-bonds.[15] It has also been used as a catalyst precursor for hydrogenation[13, 16] and silylation reactions[17] and as a precursor for carbene derivatives used in metathesis of alkenes, particularly ring closing metathesis.[18] Our synthesis involves the hydrogenation of Ru(cod)(cot) in the presence of the phosphine ligand PCy_3. This synthesis has proven over the years to be a high yield one, to be reproducible and to yield a very pure product.[4,13] An alternative synthesis has recently been proposed which is claimed to lead to a better yield but which produces a yellow complex, probably because of the presence of impurities mixed with **1**.[18]

We now describe the crystal structure of **1**, the first of a bis(dihydrogen) complex, including the location and refinement of all hydrogen atoms.

$RuH_2(H_2)_2(PCy_3)_2$ **1** was prepared as previously reported[13] by reacting a pentane solution of Ru(cod)(cot) and PCy_3 with dihydrogen (3 bar). After filtration, the white precipitate was dissolved in a minimum quantity of toluene by gentle warming under dihydrogen, concentrated in a dihydrogen stream and left standing at room temperature under a dihydrogen atmosphere. The resulting crystals were then mounted on a STOE diffractometer operating at 160 K under dinitrogen.†

The complex crystallizes in the *P*1 space group and the molecular structure is shown in Fig. 1. The environment of ruthenium consists of two phosphines located *trans* to each other [P–Ru–P 179.79(11)°] and displaying normal Ru–P distances (*ca.* 2.35 Å). In addition, two hydrides and two dihydrogen ligands are present in the equatorial plane. All Ru–H distances are within the range expected for such Ru–H and Ru–H_2 bonds (1.5–1.7 Å). The H–H distances within the

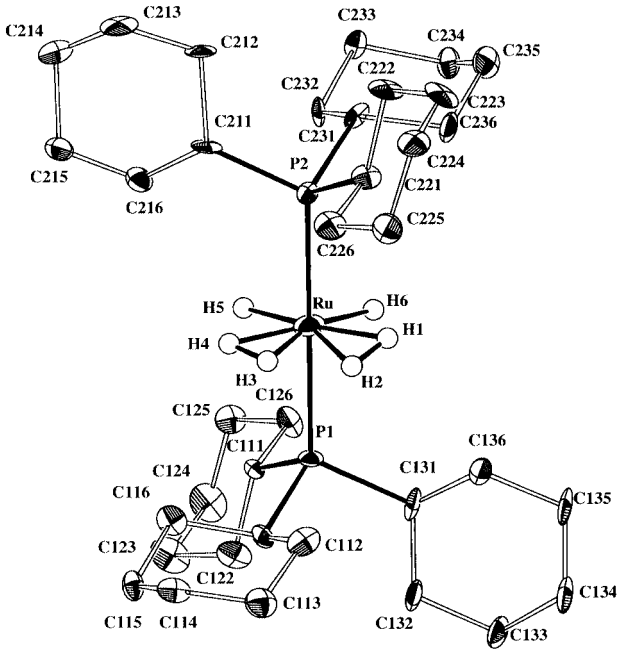

Fig. 1 Molecular structure of $RuH_2(H_2)_2(PCy_3)_2$. Selected bond lengths and interatomic distances (Å) : Ru1–H1 1.542(26), Ru1–H2 1.549(26), Ru1–H3 1.515(26), Ru–H4 1.529(26), Ru1–H5 1.708(38), Ru1–H6 1.687(37), H1–H2 0.848(37), H3–H4 0.864(38); H2–H3 1.405(65); H1–H6 2.152(57), H4–H5 2.080(55), Ru–P2 2.329(2); Ru–P1 2.347(2). Selected bond angles (°): P1–Ru1–P2 179.79(11), H1–Ru1–H2 31.84(14), H2–Ru1–H3 54.56(25), H3–Ru1–H4 32.96(14); H4–Ru1–H5 79.70(23); H5–Ru1–H6 78.92(24), H6–Ru1–H1 83.43(25).

DOI: 10.1039/a908567j

dihydrogen molecules are found to be *ca.* 0.85 Å, indicating the presence of an unstretched dihydrogen ligand (even taking into account the standard deviations, the H–H distances remain below 1 Å; see legend to Fig. 1)[2] and consistent with previous spectroscopic and theoretical studies carried out on this compound.[1,2] All the hydrogen atoms whether belonging to the hydride or dihydrogen ligands lie in the equatorial plane with no significant deviation from this plane. The distances between one hydride and the proton of the next dihydrogen molecule (*e.g.*; H6 ··H1 and H5··H4) are both > 2 Å and rule out the presence of any *cis*-interaction.[22] These data are consistent with the low rotation barrier found for the dihydrogen ligands in this complex by INS. However, it is interesting that the distance between the two dihydrogen ligands [H2··H3 1.405(65) Å] is relatively short, which may explain the structures found in the INS spectra, the origin of which was proposed to be the concerted rotation of both dihydrogen ligands.[1,2]

All these data are in complete agreement with previous DFT/B3LYP calculations.[1,2] In particular, the overall geometry of the complex, namely mutually *cis* disposition of the hydride and dihydrogen ligands, their coplanarity and the *trans* arrangement of the phosphines are well reproduced by the calculation. The Ru–P distances [2.311 Å by DFT/B3LYP calculations for the optimized most stable geometry *cf.* the experimental values of 2.329(2) and 2.347(2) Å] are very satisfactorily reproduced although the calculation was performed using PH_3 as a model for PCy_3. Steric interactions are presumably not important in this complex. The H–H distances within the dihydrogen molecule are also satisfactorily reproduced [0.853 Å by DFT/B3LYP; 0.848(37), 0.864(38) Å experimentally]. The only difference concerns the Ru–H distances which are found to be larger for the dihydrogen ligands than in the hydrides by X-ray diffraction, contrary to calculations. However, it is noteworthy that the X-ray technique only detects the electron density around the atoms. This density may be polarized towards ruthenium for these unstretched dihydrogen ligands which have a partially protonic character, much more than in the hydride ligands and may contribute to the present observation.

In conclusion, we report the first X-ray crystal structure of a bis(dihydrogen) complex with $RuH_2(H_2)_2(PCy_3)_2$ being first reported stable bis(dihydrogen) complex. It was originally formulated as a hexahydride and then correctly reformulated in 1988. Since its original preparation in 1982, this complex has proven to be very important in the chemistry of ruthenium. The confirmation of its structure by X-ray crystallography should induce a new interest for this bis(dihydrogen) complex and will provide renewed impetus for reactivity studies in our group.

The authors thank CNRS and the Polish Academy of Science/CNRS exchange program (CNRS/PAN/Projet 2722) for support.

Notes and references

† *Crystal data*: $C_{36}H_{72}P_2Ru$ **1**, M = 667.94, crystal size 0.5 × 0.2 × 0.1 mm, triclinic, space group $P1$, a = 9.1781(13, b = 9.9339(17), c = 11.7055(3) Å, α = 76.183(19), β = 110.690(17), γ = 69.386(18)°, V = 864.2(2) Å^3, Z = 1, D_c = 1.283 mg m^{-3}, μ = 0.569 mm^{-1}, $F(000)$ = 362. Data were collected at 160 K on a Stoe Imaging Plate Diffraction System (IPDS), equipped with an Oxford Cryosystems Cryostream cooler device. 8219 reflections were collected (6009 unique, R_{int} = 0.0451). The structure was solved by direct methods using SIR92,[19] and refined by least-squares procedures on F^2 with the the aid of SHELXL97;[20] largest electron density residue: $\Delta\rho_{max}$ = 0.358, $\Delta\rho_{min}$ = −0.257 e Å^{-3}; $R(F)$ = 0.0308 [$I > 2\sigma(I)$] and $wR(F^2)$ = 0.0760. All hydrogen atoms were located on a difference Fourier map and refined with an idealized model, except the hydrides H5, H6 and the hydrogen atoms H1, H2, H3, H4 of the two dihydrogen ligands which were refined with a fixed isotropic thermal parameter. All non-hydrogen atoms were anisotropically refined and in the last cycles of refinement a weighting scheme was used. A drawing of the molecule was generated with the program ZORTEP[21] with 50% probability displacement ellipsoids for non-hydrogen atoms. CCDC 182/1553. See http://www.rsc.org/suppdata/cc/a908567j/for crystallographic files in .cif format.

1 G. J. Kubas, R. R. Ryan, B. I. Swanson, P. J. Vergamini and H. J. Wasserman, *J. Am. Chem. Soc.*, 1984, **106**, 451.
2 For selected reviews on dihydrogen complexes chemistry: G. J. Kubas, *Acc. Chem. Res.*, 1988, **21**, 120; R. H. Crabtree, *Acc. Chem. Res.*, 1990, **23**, 95; P. G. Jessop and R. H. Morris, *Coord. Chem. Rev.*, 1992, **121**, 155; D. M. Heinekey and W. J. Oldham Jr., *Chem. Rev.*, 1993, **93**, 913; R. H. Crabtree, *Angew. Chem., Int. Ed. Engl.*, 1993, **32**, 789; M. A. Esteruelas and L. A. Oro, *Chem. Rev.*, 1998, **98**, 577.
3 S. Sabo-Etienne and B. Chaudret, *Coord. Chem. Rev.*, 1998, **178**–**180**, 381.
4 B. Chaudret, G. Commenges and R. Poilblanc, *J. Chem. Soc., Chem. Commun.*, 1982, 1388; B. Chaudret and R. Poilblanc, *Organometallics*, 1985, **4**, 1722; T. Arliguie, B. Chaudret, R. H. Morris and A. Sella, *Inorg. Chem.*, 1988, **27**, 598.
5 B. Moreno, S. Sabo-Etienne, B. Chaudret, A. Rodriguez, F. Jalon and S. Trofimenko, *J. Am. Chem. Soc.*, 1994, **116**, 2635; B. Moreno, S. Sabo-Etienne, B. Chaudret, A. Rodriguez, F. Jalon and S. Trofimenko, *J. Am. Chem. Soc.*, 1995, **117**, 7441.
6 T. Burrow, S. Sabo-Etienne and B. Chaudret, *Inorg. Chem.*,1995, **34**, 2470.
7 R. H. Morris, personnal communication.
8 R. L. Sweany, *J. Am. Chem. Soc.*, 1985, **107**, 2374; R. K. Upmacis, M. Poliakoff and J. J. Turner, *J. Am. Chem. Soc.*, 1986, **108**, 3645.
9 R. H. Crabtree and M. Lavin, *J. Chem. Soc. Chem. Commun.*, 1985, 1661; R. H. Crabtree, M. Lavin and L. Bonneviot, *J. Am. Chem. Soc.*, 1986, **108**, 4032.
10 K.-T. Smith, M. Tilset, R. Kuhlman and K. G. Caulton, *J. Am. Chem. Soc.*, 1995, **117**, 9473.
11 M. L. Christ, S. Sabo-Etienne and B. Chaudret, *Organometallics*, 1994, **13**, 3800.
12 V. Rodriguez, S. Sabo-Etienne, B. Chaudret, J. Thoburn, S. Ulrich, H.-H. Limbach, J. Eckert, J.-C. Barthelat, K. Hussein and C. J. Marsden, *Inorg. Chem.*, 1998, **37**, 3475.
13 A. F. Borowski, S. Sabo-Etienne, M. L. Christ, B. Donnadieu and B. Chaudret, *Organometallics*, 1996, **15**, 1427.
14 Y. Guari, S. Sabo-Etienne and B. Chaudret, *J. Am. Chem. Soc.*, 1998, **120**, 4228.
15 F. Delpech, S. Sabo-Etienne, B. Chaudret and J. C. Daran, *J. Am. Chem. Soc.*, 1997, **119**, 3167; F. Delpech, S. Sabo-Etienne, J. C. Daran, B. Chaudret, K. Hussein, C. J. Marsden and J.-C. Barthelat, *J. Am. Chem. Soc.*, 1999, **121**, 6668; K. Hussein, C. J. Marsden, J.-C. Barthelat, V. Rodriguez, S. Conejero, S. Sabo-Etienne, B. Donnadieu and B. Chaudret, *Chem. Commun.*, 1999, 1315.
16 R. P. Beatty and R. A. Paciello, U.S. Pat. WO 96/23803-4, 1996.
17 M. L. Christ, S. Sabo-Etienne and B. Chaudret, *Organometallics*, 1995, **14**, 1082; F. Delpech, S. Sabo-Etienne, B. Donnadieu and B. Chaudret, *Organometallics*, 1998, **17**, 4926.
18 T. R. Belderrain and R. H. Grubbs, *Organometallics*, 1997, **16**, 4001.
19 A. Altomare, G. Cascarano, G. Giacovazzo, A. Guagiardi, M. C. Burla, G. Polidori and M. Camalli, *J. Appl. Crystallogr.*, 1994, **27**, 435.
20 G. M. Sheldrick, SHELXL97. *Program for the Refinement of Crystal Structures*, University of Göttingen, Germany, 1997
21 L. Zolnaï, ZORTEP, *Graphical Program for X-Ray Structures Analysis*, University of Heilderberg, Germany, 1998.
22 L. S. Van der Sluys, J. Eckert, O. Eisenstein, J. H. Hall, J. C. Huffman, S. A. Jackson, T. F. Koetzle, G. J. Kubas, P. J. Vergamini and K. G. Caulton, *J. Am. Chem. Soc.*, 1990, **112**, 4831.

Communication a908567j

ChemComm

Al–Hg promoted chemoselective dehalogenation of halohydrin aldol adducts

Ying-Chuan Wang and Tu-Hsin Yan*

Department of Chemistry, National Chung-Hsing University, Taichung, Taiwan, ROC.
E-mail: thyan@mail.nchu.edu.tw

Received (in Cambridge, UK) 7th January 2000, Accepted 22nd February 2000
Published on the Web 15th March 2000

Al–Hg mediated chemoselective cleavage of the carbon–halogen bond of α-halocarboxylates allows for a facile and clean transformation of halohydrin aldol adducts into β-hydroxy acid derivatives with no evidence of dehydroxyhalogenation.

Chemoselective transformations of halohydrin aldol adducts into β-hydroxy acid derivatives are very important owing to the ready availability of the chiral starting materials[1] and the significance of the products as building blocks in the synthesis of drugs and natural products.[2] The recently reported catalytic hydrogenolysis (H_2/Pd–C) of α-bromo-β-hydroxy esters and tri-*n*-butyltin hydride mediated radical cleavage of carbon–bromo bonds provided β-hydroxy acid derivatives with the added benefit of good to excellent yields.[3]

However, their utilization is not unproblematic. Chemoselective hydrogenolysis of the C–Br bond in the presence of C=C double bonds is not possible while tributyltin hydride is relatively unstable, toxic and expensive. Furthermore, the tin byproducts are not always easy to separate. The invention and development of a new chemoselective procedure for removing the halogen from halohydrin aldol adducts would be of great synthetic value. A promising solution to this problem appeared to be metal-promoted reductive cleavage of carbon–halogen bonds. Although this process has been used in reductive elimination reactions such as zinc-mediated dehydroxybromination[4] and aluminium amalgam-mediated deacetoxybromination,[5] they leave open the question of whether these methodologies can be applied to the chemoselective cleavage of carbon–halogen bonds of halohydrin aldol adducts without concurrent elimination of the β-hydroxy group. We were attracted to the Al–Hg mediated process because of the mild neutral conditions.

Initial work centered on the debromination of various α-bromo-β-hydroxy esters **1** derived from aldolizations of bromoacetate enolates with isobutyraldehyde.[1] Treatment of *tert*-butyl ester **1a** with 3–5 equiv. of Al–Hg (mercury content *ca*. 2.5%) in aqueous acetonitrile (1:10) at 0 °C led to clean debromination within 30 min to give **2a** in 86% isolated yield [eqn. (1)]. Dehydroxybromination does not appear to compete with carbon–hydrogen bond formation, although products arising from elimination of hydroxy groups would not be isolable owing to their volatility. To quantify the potentially small degree of elimination that may be occurring, we chose to explore the related reductive cleavage of the C–Br bond using *p*-methoxybenzyl α-bromo-β-hydroxy ester **1b** derived from the transesterification of thioimide aldol.[6] The chemoselective debromination proceeded efficiently yielding the corresponding β-hydroxy ester **2b**† in excellent yield (96%) [eqn. (2)]. We were unable to detect any 4-methyl-2-pentenoate, a product of elimination, under careful analysis of the crude reaction mixture. In addition, allyl ester **1c**, which is particularly prone to hydrogenolysis, can also be cleanly converted to the correspopnding β-hydroxy ester **2c** under our standard conditions [eqn. (3)]. Switching the bromo ester from allyl to methyl had little effect. The debromination product **2d** was obtained in 80% isolated yield [eqn. (4)].

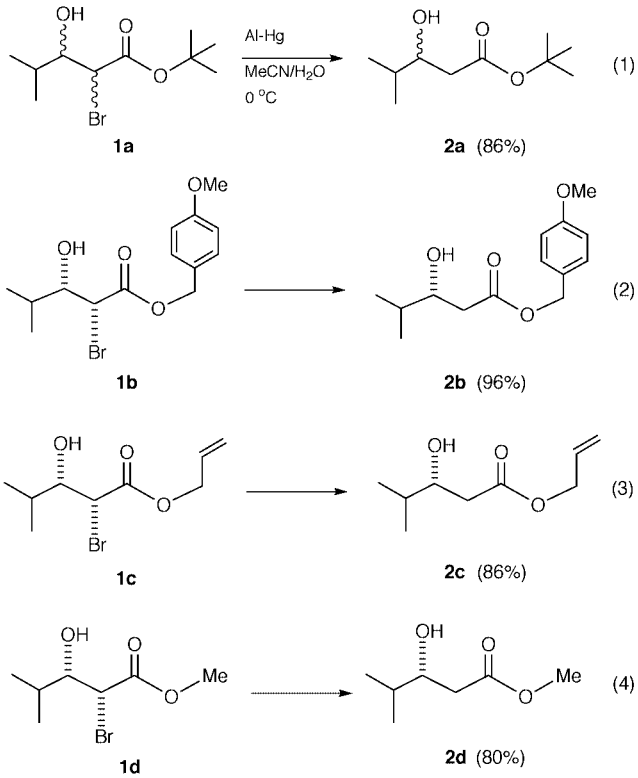

Variation of the halogen was briefly explored. Halohydrin aldols such as iodohydrin **3a**, bromohydrin **3b** and chlorohydrin **3c** were utilized to test the feasibility of Al–Hg promoted reductive cleavage. On exposure to an excess of Al–Hg in aqueous CH_2Cl_2 (1:10) at 0 °C for 2 min, the C–I bond in **3a** was completely cleaved (Scheme 1) while the same conditions effected complete debromination of **3b** within 30 min to afford β-hydroxy ester **4** in 94% isolated yield. Switching the halohydrin from bromo to chloro had a rate retardation effect while maintaining excellent yield. Thus, after 1 h at 0–25 °C, **3c** was cleanly converted to the ester **4** in 90% isolated yield with no evidence of dehydroxychlorination to the α,β-unsaturated ester.

Extension of these observations to other carboxylic acid derivatives confirms the generality of this procedure. We were

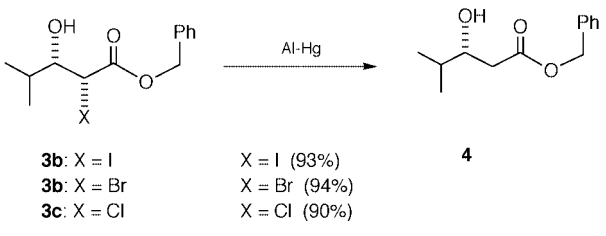

Scheme 1

DOI: 10.1039/b000335m

pleased to find that switching the α-bromo-β-hydroxy acid derivative from ester **3** to amide **5** had little effect. The debromination product **6** was obtained in 91% yield under the usual conditions in 30 min [eqn. (5)].

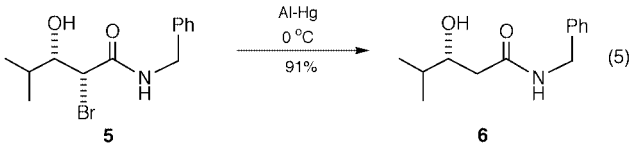

(5)

5 **6**

The broad scope of the reaction is illustrated by the additional examples provided below. A particularly interesting example illustrating the chemoselectivity of this process is the debromination of chiral bromohydrin aldol adduct **7**, which by virture of the sensitivity of allyl-type alcohol requires very mild methods. Using these standard reduction conditions, only reductive cleavage of the C–Br bond to give β-hydroxy ester **8** is observed, without concurrent reductive cleavage of the C–OH bond or dehydroxybromination [eqn. (6)]. Using an α-bromo ester bearing a benzyl-type alcohol **9**, the identical reaction gave the corresponding methyl β-hydroxy ester **10** in 90% isolated yield [eqn. (7)].[7]

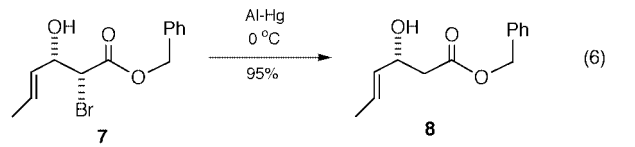

(6)

7 **8**

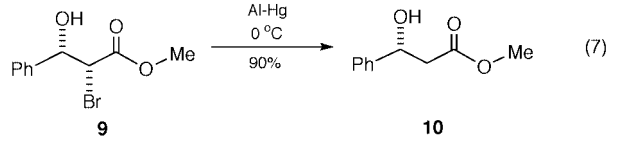

(7)

9 **10**

This Al–Hg mediated reductive cleavage of carbon–halogen bonds represents an extremely simple, practical and efficient elaboration of various halohydrin compounds into α-unsubstituted β-hydroxy acid derivatives. Its use in the reduction of halohydrin aldols to β-hydroxy acid derivatives compares very favorably with other methods such as catalytic hydrogenolysis or reduction with tri-*n*-butyltin hydride. Further studies on the reductive cleavage of isolated halohydrins and other α,β-difunctional aldol adducts such as α,β-epoxy esters and amides are currently underway and will be reported in due course.

We thank the National Science Council of the Republic of China for support of this work. (NSC 89-2113-M-005-003).

Notes and references

† *Selected data* for **2b**: δ_H(300 MHz, $CDCl_3$) 7.26–7.32 and 6.87–6.92 (m, 4 H, C_6H_4), 5.09 (s, 2 H, $OCH_2C_6H_4$), 3.74–3.82 (m, 4 H, OCH_3, C*H*OH), 2.53 (dd, *J* 16.5, 3.0 Hz, 1 H, HC*H*C = O), 2.43 (dd, *J* 16.5, 9.3 Hz, 1 H, *H*CHC = O), 1.70 [octet, *J* 6.3 Hz, *H*C$(CH_3)_2$], 0.94 and 0.91 [2 d, *J* 6.9 Hz, HC$(CH_3)_2$]; δ_C(75 MHz, $CDCl_3$) 173.34, 159.66, 130.14, 127.64, 113.94, 72.64, 66.33, 55.25, 38.47, 33.10, 18.28, 17.70; high-resolution MS (EI+) *m/z* calcd for $C_{14}H_{20}O_4$ 252.1362, found 252.1359; $[\alpha]_D^{25}$ +23.6° (*c* 0.6, CH_2Cl_2). For **6**: δ_H(300 MHz, $CDCl_3$) 7.24–7.36 (m, 5 H, C_6H_5), 6.48 (br s, 1 H, *H*NC=O), 4.42 (d, *J* 5.7 Hz, 2 H, HNCH_2Ph), 3.74–3.80 (m, 1 H, C*H*OH), 2.95 (br s, 1 H, O*H*), 2.38 (dd, *J* 15.0, 3.0 Hz, 1 H, HC*H*C=O), 2.29 (dd, *J* 15.0, 9.0 Hz, 1 H, *H*CHC=O), 1.69 [octet, *J* 6.6 Hz, *H*C$(CH_3)_2$], 0.93 and 0.91 [2 d, *J* 6.9 Hz, HC$(CH_3)_2$]; δ_C(75 MHz, $CDCl_3$) 172.76, 137.93, 128.69, 127.68, 127.51, 73.41, 43.44, 39.51, 33.44, 18.28, 17.72; high-resolution MS (EI+) Calc. for $C_{13}H_{19}NO_2$ *m/z* 221.1415, found 221.1412; $[\alpha]_D^{25}$ +38.7°° (*c* 0.5, CH_2Cl_2). For **10**: δ_H(400 MHz, $CDCl_3$) 7.18–7.31 (m, 5 H, C_6H_5), 5.05 (dd, *J* 8.8, 4.0 Hz, 2 H, HOC*H*CH_2), 3.64 (s, 3 H, H_3C–O), 2.70 (dd, *J* 16.4, 8.8 Hz, 1 H, HC*H*C=O), 2.63 (dd, *J* 16.4, 4.0 Hz, 1 H, *H*CHC=O); δ_C(100 MHz, $CDCl_3$) 172.46, 142.35, 128.40, 127.68, 125.50, 70.32, 51.87, 43.24; high-resolution MS (EI+) Calc. for $C_{10}H_{12}O_3$ *m/z* 180.0787, found 180.0788; $[\alpha]_D^{25}$ +36.1° (*c* 0.5, CH_2Cl_2).

1 D. A. Evans, E. B. Sjogren, A. E. Weber and R. E. Conn, *Tetrahedron Lett.*, 1987, **28**, 39; E. J. Corey, D.-H. Lee and S. Choi, *Tetrahedron Lett.*, 1992, **33**, 6735; Y.-C Wang, D.-W. Su, C.-M. Lin, H.-L. Tseng, C.-L. Li and T.-H. Yan, *J. Org. Chem.*, 1999, **64**, 6495.
2 G. I. Georg, J. Kant and H. S. Gill, *J. Am. Chem. Soc.*, 1987, **109**, 1129.
3 P. R. Fleming and K. B. Sharpless, *J. Org, Chem.*, 1991, **56**, 2869; E. J. Corey and S. Choi, *Tetrahedron Lett.*, 1991, **33**, 2857.
4 D. R. James, R. W. Rees and C. W. Shoppee, *J. Chem. Soc.*, 1955, 1370.
5 A. E. Greene, M. A. Teixeira, E. Barreiro, A . Cruz and P. Crabbe, *J. Org, Chem.*, 1982, **47**, 2553; S. Jain, S. N. Suryawanshi and D. S. Bhakuni, *Indian J. Chem., Sect. B*, 1987, **26**, 866.
6 D.-W. Su, Y.-C. Wang and T.-H. Yan, *Chem. Commun.*, 1999, 545.
7 New compounds have been satisfactorily characterized spectroscopically, and their elemental composition has been established by high-resolution mass spectrometry or combustion analysis.

Communication b000335m

ChemComm

Selective recognition of carbonic anhydrase using transition metal complexes†

Bidhan C. Roy, Md. Abul Fazal, Shuguang Sun and Sanku Mallik*

Department of Chemistry, North Dakota State University, Fargo, ND 58105, USA.
E-mail: sanku_mallik@ndsu.nodak.edu

Received (in Bloomington, IN, USA) 15th November 1999, Accepted 17th February 2000
Published on the Web 17th March 2000

A metal complex was designed to bind to the protein carbonic anhydrase strongly and selectively in aqueous medium.

Strong and selective binding to a pre-determined protein by synthetic receptors is of paramount importance for drug design,[1] protein purification[2] and protein sensing.[3] The recognition of active sites of enzymes leading to very effective inhibitors has been developed to a high level of sophistication. [4] Recognition of protein surface patterns by polypeptides has been used as a model system for studying protein–protein interactions[5] or to design enzyme inhibitors.[6] These studies employed multiple hydrogen bonding or ionic interactions as the basis of recognition. Herein, we report our results on selective recognition of a protein, carbonic anhydrase (CA, bovine erythrocyte) based on its *surface histidine pattern*, employing Cu^{2+}–histidine interactions in water (25 mM HEPES buffer, pH 7.0, 25 °C). To our knowledge, this is the first report of protein surface recognition using the surface histidine pattern of the protein. Metal–histidine interactions have been used for protein purification using immobilized metal affinity chromatography (IMAC).[2] However, in IMAC, the proteins are distinguished based on their surface histidine contents.

Metal–ligand interactions have several advantages in recognition compared to hydrogen bonding, ion-pair or other weak interactions. Metal–ligand interactions are stronger especially in aqueous media.[7] A variety of transition metal ions are available and are used by nature in biological systems for molecular recognition and catalysis.[8] This allows fine tuning of each of the interactions and opens the possibility of catalysis, following recognition. The spectroscopic properties of the metal ions can be utilized to monitor the binding process and to get structural information about the resultant complex.[9]

CA has five histidines (3, 10, 15, 17, 64) exposed on the surface (determined using the modeling software insight-II and discover, version 98.0, Molecular Simulations Inc., Burlington, MA).[10] The distance amongst the histidines 3, 10, 17 (or 15) are *ca*. 16 Å. This pattern was mapped into the pattern of Cu^{2+} ions by the tris–Cu^{2+} complex **2**. Another shorter tris–Cu^{2+} complex **3** (distance amongst the Cu^{2+} ions: *ca*. 12 Å) was synthesized for comparative studies. A mono-Cu^{2+} complex **1** served as the control for the recognition studies. Structures of the metal complexes **1**, **2** and **3** are shown in Fig. 1. These complexes were modeled using the software Spartan (version 5.0.3, Wavefunction Inc., Irvine) employing the Merck molecular mechanics force field. After energy minization, the resultant structures were subjected to systematic conformational searches to identify the lowest energy structures.

Two other proteins with different surface histidine patterns were used as controls for these studies, chicken egg albumin (CEA) and chicken egg lysozyme. CEA has six histidines on the surface (22, 23, 329, 332, 363, 371); lysozyme (chicken egg) has only one histidine (15) exposed to surface.[10] All of these three proteins are known to interact with transition metal ions through the surface exposed histidines.[11] CEA has a higher number of surface exposed histidines than the target protein (CA) but their distributions are different. If the recognition is based on the *contents* of surface exposed histidine residues (*e.g*. IMAC), then CEA is expected to bind more strongly compared to CA. Since the studies reported here rely on the histidine pattern, CEA was chosen as a control protein.

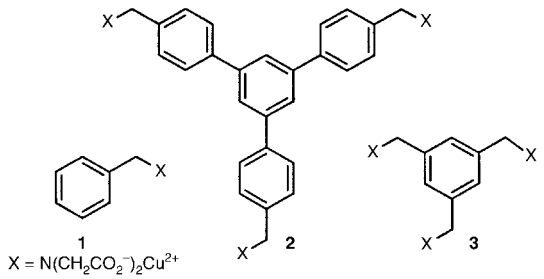

Fig. 1 Structures of the tris–Cu^{2+} complexes **2**, **3** and the control **1** used for recognition of carbonic anhydrase.

Complexes **2** and **3** were synthesized from the corresponding bromides and diethyl iminodicetate, using K_2CO_3 as the base in acetonitrile solvent. The ester groups were hydrolyzed by LiOH in methanol–water at 25 °C.[12] The complexes were found to be stable in aqueous buffer solution (25 mM HEPES buffer, pH 7.0), at room temperature, in air for more than a month. It is reported in the literature that the IDA–Cu^{2+} complex binds to proteins (pH 7.0) primarily through the surface exposed histidine residues of proteins. Primary amino groups and carboxylate residues on the protein surface only play weak, secondary roles.[13]

Binding studies were conducted in water (25 mM HEPES buffer, pH 7.0; [protein] = 100 μM, [**1**] = 0–1.2 mM; [**2**] or [**3**] = 0–500 μM, 25.0 °C) and were followed by isothermal titration microcalorimetry[14] (ITC-4200, Calorimetry Scientific Corporation, Provo, UT). The software provided by the instrument manufacturer (Bindworks 3.0) was used for data and error analysis. The raw data were corrected for the heat of dilution of the appropriate Cu^{2+}-complex before the curve fitting process (data for titrations are available as electronic supplementary information†).

Results for the binding experiments (stoichiometry, binding constant and enthalpy) are shown in Table 1. The control **1** showed low affinity ($K < 4000\ M^{-1}$) for the proteins tested. With the complex **2**, CA was found to bind tightly ($K \approx 300\,000\ M^{-1}$). CEA showed weak binding with complex **2** ($K < 1000\ M^{-1}$) under the experimental conditions. Lysozyme was found to precipitate when [**2**] > 25 μM. With the shorter complex **3**, the affinity for CA was found to decrease ($K \approx 75\,000\ M^{-1}$) compared to that of **2**. Both lysozyme and CEA bound weakly to complex **3** (no precipitation). Complex **2** bound CA more strongly compared to the control **1** (90 : 1) or the shorter tris–Cu^{2+} complex **3** (4 : 1). This slight selectivity of CA for **2** (over **3**) may be due to greater strain in binding for **3** ($\Delta H = -15.1$ kcal mol^{-1} for **2**; -12.2 kcal mol^{-1} for **3**) to the protein. Complex **2** also showed very good selectivity for CA when compared to CEA (300 : 1).

In order to demonstrate selective binding of **2** to CA, a mixture of the protein and the control **1** ([CA] = 100 μM; [**1**] = 100 μM) was titrated with **2** ([**2**] = 0–500 μM). No change in the binding constant of **2** with CA was observed. When a

† Electronic supplementary information (ESI) available: scheme for the synthesis of **2**, **3** and ITC titration data (raw and processed) for the results reported in Table 1. See http://www.rsc.org/suppdata/cc/a9/a909001k/

DOI: 10.1039/a909001k

Table 1 Binding parameters for the receptors **2**, **3** and control **1** with carbonic anhydrase, chicken egg albumin and lysozyme

Protein	Stoichiometry (n)	K/M^{-1}	$-\Delta H$/kcal mol^{-1}
Lysozyme	**1**: 1.2 ± 0.3	(1.6 ± 0.2) × 10^3	7.0 ± 0.5
	2: nd	Precipitation	—
	3: —	< 10^3	—
Carbonic anhydrase	**1**: 0.90 ± 0.03	(3.5 ± 0.7) × 10^3	39.2 ± 2.0
	2: 0.94 ± 0.006	(299 ± 30) × 10^3	15.1 ± 0.3
	2: 0.81 ± 0.02 (pH 6.0)	(199 ± 35) × 10^3 (pH 6.0)	10.8 ± 0.5 (pH 6.0)
	2: 0.82 ± 0.01 (pH 8.0)	(97 ± 16) × 10^3 (pH 8.0)	10.2 ± 0.3 (pH 8.0)
	3: 1.3 ± 0.01	(75 ± 6) × 10^3	12.7 ± 0.2
	3: 1.3 ± 0.04 (pH 6.0)	(27.5 ± 4) × 10^3 (pH 6.0)	12.2 ± 0.7 (pH 6.0)
	3: 1.3 ± 0.02 (pH 8.0)	(45 ± 5) × 10^3 (pH 8.0)	20.6 ± 0.6 (pH 8.0)
Albumin	**1**: —	< 10^3	—
	2: —	< 10^3	—
	3: 1.6 ± 0.07	(16 ± 2.5) × 10^3	20.9 ± 1.5

mixture of **2** and CA ([CA] = 100 μM; [**2**] = 100 μM) was titrated with control **1** ([**1**] = 0–1 mM), no binding was observed. Similar results were obtained with the complex **3**. When a mixture of the three tested proteins (100 μM each) was titrated with complex **2**, the binding constant remained unchanged (280 000 ± 30 000). If carbonic anhydrase was not included in the mixture (*i.e*. CEA and lysozyme, 100 μM each), very weak affinity (< 1000) was detected. The binding selectivity reported here (for complex **2**) is distinctly different compared to that observed with a random distribution of copper(II) ions (on chelating Sepharose fast flow with iminodiacetate–Cu^{2+}, pH 7.0, 22 °C, either in equilibrium binding experiments or in chromatograhy).[15]

To demonstrate the role of Cu^{2+}–histidine interactions in the recognition process, we have studied the binding between CA and complex **2** by EPR spectroscopy in the solution phase (9.4 GHz, [CA] = 1.2 mM; [**2**] = 600 μM, 25.0 °C). Upon addition of the protein, the $g_{\|}$ value of Cu^{2+} ions of **2** decreased from 2.290 to 2.261. These values match well with the reported $g_{\|}$ values of the iminodiacetate–Cu^{2+} complex, free and bound to myoglobin through the histidine residues (2.288 and 2.264, respectively).[16] Also ITC titrations failed to detect any binding between the metal-free ligands (for **1**, **2** and **3**) and the proteins.

The binding of CA with the metal complexes **2** and **3** were followed by UV–VIS spectrometry. Upon addition of CA to a solution **2** (or **3**, [**2** or **3**] = 0.5 mM; [CA] = 0.8 mM, 25 mM HEPES buffer, pH 7.0, 25 °C, 10 × 100 μL additions), the absorption maxima progressively shifted from 727 to 660 nm. This indicated the coordination of one imidazole group (of histidine residues) per copper(II) ion of the complexes.[17] Analyses[18] of the resultant titration curves corroborated the ITC results. Circular dichroism studies (80 μM protein, 0–500 μM of **2** or **3**, 25 mM phosphate buffer, pH 7.0, 23.0 °C) indicated that the proteins were not unfolding in presence of the control **1** or receptors **2** or **3**.

Thus these studies demonstrate that the tris–Cu^{2+}complex **2** binds carbonic anhydrase strongly and with good selectivity compared to two other proteins with different histidine patterns on the surface. It should be noted that the reported method of protein recognition is applicable to proteins of known structures possessing histidine residues on the surface. With rapidly increasing number of solved protein structures, the method has wide applicability.

This work was supported by NSF-CAREER award (CHE-9896083) and an NIGMS - AREA grant (1R15 59594-01, NIH). The microcalorimeter was purchased through an NSF-EPSCoR award to North Dakota. We thank Professor Kenton Rodgers for help with the EPR experiments.

Notes and references

1 H.-J. Bohm and G. Klebe, *Angew. Chem., Int. Ed. Engl.*, 1996, **35**, 2588; R. E. Baine and S. L. Bender, *Chem. Rev.*, 1997, **97**, 1359.

2 S. Vunnum, V. Natarajan and S. Cramer, *J. Chromatogr. A*, 1998, **818**, 31; K. M. Muller, K. M. Arndt, K. Bauer and A. Pluckthun, *Anal. Biochem.*, 1998, **259**, 54; J. Mahiou, J. P. Abastado, L. Cabanie and F. Godeau, *Biochem. J.*, 1998, **330**, 1051.

3 F. Loscher, T. Ruclestuhl and S. Seeger, *Adv. Mater.*, 1998, **10**, 1005; S. Okada, S. Peng, W. Spevak and D. Charych, *Acc. Chem, Res.*, 1998, **31**, 229; I. Vikham and W. M. Albers, *Langmuir*, 1998, **14**, 3865; D. Elbaum, S. K. Nair, M. W. Patchan, R. B. Thompson and D. W. Christainson, *J. Am. Chem. Soc.*, 1996, **118**, 8381.

4 A. C. Bishop, C. Kung, K. Shah, L. Witucki, K. M. Shokat and Y. Liu, *J. Am. Chem, Soc.*, 1999, **121**, 627; G. F. Short, M. Lodder, A. L. Laikhter, T. Arslan and S. M. Hecht, *J. Am. Chem. Soc.*, 1999, **121**, 478; M. Beuck, *Angew. Chem., Int. Ed.*, 1999, **38**, 631; R. Zutshi, M. Brickner and J. Chmielewski, *Curr. Opin. Chem. Biol.*, 1998, **2**, 62.

5 S. Hirota, M. Endo, K. Hayamizu, T. Tsukazaki, T. Takake, T. Kohzuma and O. Yamaguchi, *J. Am. Chem. Soc.*, 1999, **121**, 849.

6 H. S. Park, Q. Lin and A. D. Hamilton, *J. Am. Chem. Soc.*, 1999, **121**, 8; Y. Hamuro, C. Calama, H. S. Park and A. D. Hamilton, *Angew. Chem., Int. Ed. Engl.*, 1997, **36**, 2680.

7 P. A. Frey and W. W. Cleland, *Bioorg. Chem.*, 1998, **26**, 175.

8 S. J. Lippard and J. M. Berg, *Principles of Bioorganic Chemistry*, University Science Books, Mill Valley, CA, 1994, pp. 349–376; H. Dugas, *BioOrganic Chemistry: A Chemical Approach to Enzyme Action*, Springer, New York, NY, 1996, pp. 388–460.

9 M. J. Kendrick, M. T. May, M. J. Plishka and K. D. Robinson, *Metals in Biological Systems*, Ellis Horwood, New York, NY, 1992, pp. 17–56.

10 The pdb files were obtained from the pdb server. The URL on the internet is: http://www.rcsb.org/pdb/. The files used for modeling are: 1can.pdb (for carbonic anhydrase), 1ova.pdb (for albumin) and 1azf.pdb (for lysozyme).

11 P. J. Sadler and J. H. Viles, *Inorg. Chem.*, 1996, **35**, 4490; A. Singh, M. Markowitz, L.-I. Tsao and J. Deschapms, *ACS Symp. Ser.*, 1993, **556**, 252.

12 The synthetic scheme for the synthesis of **2** and **3** is available as electronic supplementary material.† The tribromides were prepared following reported procedures. Y. Kim and R. Beekerbauser, *Macromolecules*, 1994, **24**, 1968; W. P. Cochrane, P. L. Pauson and T. S. Stevens, *J. Chem. Soc. C*, 1968, 630. All new compounds gave satisfactory ^{1}H and ^{13}C NMR spectra. The Cu^{2+} complexes were characterized by elemental analysis. For **1**: Anal. Calc. for $C_{11}H_{11}CuNO_4$: C, 46.39; H, 3.89; N, 4.92. Found: C, 46.06; H, 3.58; N, 4.62. For **2**: Anal. Calc. for $C_{39}H_{33}Cu_3N_3O_{12}\cdot 3H_2O$: C, 49.60; H, 3.74; N, 4.45. Found: C, 49.68; H, 3.90; N, 4.52. For **3**: Anal. Calc. for $C_{21}H_{21}Cu_3N_3O_{12}\cdot 3H_2O$: C, 33.54; H, 3.62; N, 5.59. Found: C, 33.53; H, 3.59; N, 5.54%.

13 W. Jiang, B. Graham, L. Spiccia and M. T. W. Hearn, *Anal. Biochem.*, 1998, **255**, 47.

14 M. Doyle, *Curr. Opin. Biotech.*, 1997, **8**, 31; I. Wadso, *Chem. Soc. Rev.*, 1997, 79.

15 T. W. Hutchens, T.-P. Yip and J. Porath, *Anal. Biochem.*, 1988, **170**, 168.

16 D. R. Schnek, D. W. Pack, D. Y. Sasaki and F. H. Arnold, *Langmuir*, 1994, **10**, 2382.

17 P. K. Dhal and F. H. Arnold, *Macromolecules*, 1992, **25**, 7051.

18 K. A. Connors, *Binding Constants*, Wiley, New York, 1987.

Communication a909001k

ChemComm

Highly chemo- and regio-selective [2 + 2 + 2] cycloaddition of unsymmetrical 1,6-diynes with terminal alkynes catalyzed by Cp*Ru(cod)Cl under mild conditions†

Yoshihiko Yamamoto, Ryuji Ogawa and Kenji Itoh*

Department of Molecular Design and Engineering, Graduate School of Engineering, Nagoya University, Chikusa, Nagoya 464-8603, Japan. E-mail: Itohk@apchem.nagoya-u.ac.jp

Received (in Cambridge, UK) 17th January 2000, Accepted 24th February 2000
Published on the Web 17th March 2000

Ru(II)-catalyzed cycloaddition of unsymmetrical 1,6-diynes gives the desired cycloadducts in high yields with a regioselectivity *meta*:*ortho* = 88:12–98:2.

Transition-metal catalyzed [2 + 2 + 2] cyclotrimerizations of alkynes has been recognized as a straightforward route to substituted benzenes.[1] The control of both the chemo- and regio-chemistries in the cyclotrimerization of two or three different alkyne components, however, have been a crucial problem. Although the selective cyclocotrimerization of three different alkynes was achieved using stoichiometric zirconocene reagent,[2] the regiochemistry problem has remained unsolved. In addition, catalytic reactions are ideal from both the environmental and economical points of view. The intramolecular cyclization of triynes was pioneered as a completely chemo- and regio-selective process by Vollhardt in work on the catalytic reactions of $CpCo(CO)_2$,[3] and subsequently, many triyne cyclizations have been applied for the syntheses of complex polycyclic systems.[4] Intermolecular couplings between a diyne and a monoalkyne have also been realized as a successful method to construct bicyclic frameworks.[3,5] At the expense of the complete regio- and chemo-selections, this partially intermolecular approach becomes more advantageous than the triyne methodology, because a wide variety of readily accessible or commercially available diynes and monoalkynes could directly be used. The chemoselectivity can be improved using an excess amount of a monoalkyne, although a satisfactory level of regiocontrol has not been achieved in previous diyne–monoalkyne couplings. Herein, we report the first Ru-catalyzed regioselective cycloaddition between unsymmetrical 1,6-diynes and monoalkynes.

Recently, we have found that Cp*Ru(cod)Cl **1**: (Cp* = pentamethylcyclopentadienyl, cod = cycloocta-1,5-diene) effectively catalyzes the selective intermolecular coupling of 1,6-heptadiynes with 2,5-dihydrofuran.[6] In order to extend the catalytic utility of the ruthenium complex **1**, we further explored the catalyzed cross-cyclotrimerization of 1,6-diynes with monoalkynes. To the best of our knowledge, ruthenium-catalyzed [2 + 2 + 2] cyclotrimerizations of monoalkynes has scarcely been investigated so far,[7] and no example of co-cyclotrimerization of different alkynes was found in previous reports.[1,8] At the outset, dimethyl dipropargylmalonate **2a** [X = $C(CO_2Me)_2$] and 2 equiv. of hex-1-yne **3a** (R = Bu) were treated with 1 mol% of **1** in 1,2-dichloroethane at *ambient* temperature (Scheme 1). The

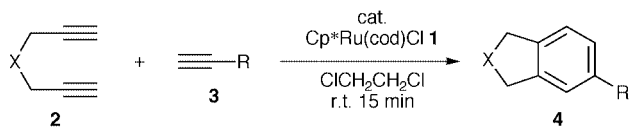

Scheme 1

† Electronic supplementary information (ESI) available: experimental procedures and analytical data for **4** and **6**. See http://www.rsc.org/suppdata/cc/b0/b000466i/

starting diyne **2a** was completely consumed within 15 min, and silica-gel column chromatography of the crude reaction mixture gave the desired indan derivative **4a** in 89% yield (TOF = 356 h^{-1}; Table 1, entry 1). The undesired competitive dimerization and trimerization of **2a** were effectively suppressed (11%), and the cyclotrimerization of **3a** was not detected in the crude reaction mixture by ^1H NMR spectroscopy. The yield and the selectivity were slightly improved using 4 equiv. of **3a** (entry 2). The reaction of phenyl acetylene **3b** (R = Ph) required a longer reaction time (14 h) even using 3 mol% of **1a** (entry 3). A biphenyl derivative **4b** was obtained in 74% yield. In contrast to these results, a terminal alkyne possessing a bulky substituent, *tert*-butyl acetylene **3c** (R = Bu^t) gave the corresponding cycloadduct **4c** only in low yield (entry 4). In this case, substantial amounts of the dimer and the trimer of **2a** were formed. In addition to terminal alkynes, the parent acetylene **3d** (R = H) was found to be an effective monoalkyne component for our catalyzed cycloaddition. The diyne **2a** was treated with **1** at 0 °C for 1 h under acetylene gas (balloon) to afford **4d** in 84% yield (entry 5).

Table 1 Cp*Ru(cod)Cl-catalyzed cycloaddition of 1,6-diynes **2a–c** with terminal alkynes **3**[a]

					Yield[b] (%)	
Entry	X	R	Catalyst (mol%)	*t*	**4**	Dimer + trimer
1	$C(CO_2Me)_2$	Bu	1	15 min	**4a**, 89	11
2	$C(CO_2Me)_2$	Bu[c]	1	15 min	**4a**, 94	5
3	$C(CO_2Me)_2$	Ph	3	14 h	**4b**, 74	21
4	$C(CO_2Me)_2$	Bu^t	1	30 min	**4c**, 21	53
5	$C(CO_2Me)_2$	H[d]	1	1 h	**4d**, 84	9
6	NTs	Bu	1	10 min	**4e**, 80	—
7	O	Bu	1	12 h	**4f**, 68	18

[a] All reactions were carried out with a terminal alkyne (2 equiv.) in 1,2-dichloroethane at r.t. [b] Isolated yield. [c] 4 equiv. [d] Under acetylene gas (balloon) at 0 °C.

Furthermore, this novel protocol using the Ru(II)-catalyst was successfully applied to other heterocyclic species. The cycloaddition of *N*,*N*-dipropargyl tosylamide **2b** (X = NTs) with hex-1-yne **3a** was complete within 10 min at ambient temperature to afford an isoindoline derivative **4e** as the sole product in 80% yield (entry 6). A phthalan derivative **4f** was obtained in 68% yield along with the dimer and trimer of **2c** (entry 7).

We next investigated the regiochemistry in the cycloaddition of a series of unsymmetrical 1,6-diynes **5** (Scheme 2). The regiochemistry of the cyclotrimerization key steps have been examined only to a limited degree: a few examples of regioselective cycloaddition using $ClRh(PPh_3)_3$ have been reported, but these were limited to alkynes possessing a hydroxyl group.[5f,k] In fact, the reaction of a malonate derivative **5a** [X = $C(CO_2Me)_2$, R^1 = Me] with hexyne **3a** at 60 °C for 3 days using 5 mol% $ClRh(PPh_3)_3$ gave a 5,7-disubstituted indan derivative *meta*-**6a** and its 5,6-disubstituted isomer *ortho*-**6a** in

DOI: 10.1039/b000466i

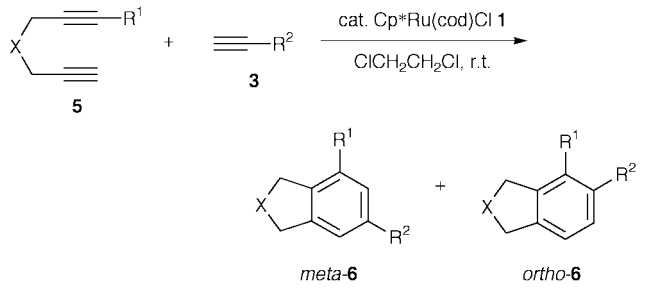

Scheme 2

Table 2 Cp*Ru(cod)Cl-catalyzed cycloaddition of 1,6-diynes **5a–c** with terminal alkynes **3**[a]

Entry	X	R^1	R^2	Catalyst (mol%)	Yield[b] (%) t	(*meta*:*ortho*)[c]
1	$C(CO_2Me)_2$	Me	Bu	1	1 h	**6a**, 85 (93:7)
2	$C(CO_2Me)_2$	Me	Me[d]	3	18 h	**6b**, 80 (94:6)
3	$C(CO_2Me)_2$	Me	CH_2OMe	1	3 h	**6c**, 86 (94:6)
4	$C(CO_2Me)_2$	Me	Ph	3	24 h	**6d**, 82 (88:12)
5	$C(CO_2Me)_2$	Ph	Bu	10	24 h	**6e**, 80 (95:5)
6	$C(CO_2Me)_2$	$SiMe_3$	Bu	5	7 h	**6f**, 94 (98:2)
7	NTs	Me	Bu	1	10 min	**6g**, 82 (93:7)
8	O	Me	Bu	1	30 min	**6h**, 75 (95:5)

[a] All reactions were carried out with a terminal alkyne (2 equiv.) in 1,2-dichloroethane at r.t. [b] Isolated yield. [c] Ratios in parentheses were determined by GC analyses of isolated products. [d] Under propyne gas (balloon).

61% total yield with a low regioselectivity *meta*:*ortho* = 65:35. In our hands, **5a** regioselectively reacted with 2 equiv. of **3a** in the presence of the catalyst **1** (1 mol%) to afford *meta*-**6a** and *ortho*-**6a** in 85% total yield with an excellent regioselectivity *meta*:*ortho* = 93:7 (Table 2, entry 1). The importance of the bulky Cp* ligand of **1** was clearly demonstrated by the fact that the reaction of **5a** and **3a** conducted using CpRu(cod)Cl bearing a smaller Cp ligand gave cycloadduct **6a** in 76% yield with lower selectivity (*meta*:*ortho* = 87:13). Similarly, the reaction of **5a** with propyne gas **3e** (R^2 = H; balloon) or propargyl methyl ether **3f** (R^2 = CH_2OMe) gave **6b** and **6c** in 80 and 86% yields, respectively with high *meta*-selectivities (entries 2 and 3). The ether functionality at the propargylic position in **3f** did not decrease both the yield and regioselectivity. Cycloaddition with the less reactive aromatic alkyne, phenylacetylene **3b**, was conducted using an increased amount of the catalyst, and biphenyl derivatives **6d** were obtained in a comparable total yield (82%) with somewhat lower selectivity (entry 4). Similar biphenyl derivatives **6e** were also obtained from the reaction of a 1,6-diyne possessing a phenyl group as a terminal substituent **5b** (entry 5). In this case, the increased amount of the catalyst (10 mol%) was again found to be effective. The highest yield and regioselectivity were achieved in the reaction of a diyne **5c** having a bulky trimethylsilyl substituent at the terminal position with **3a** (entry 6). The corresponding indan derivatives **6f** were obtained in 94% total yield with an isomer ratio of *meta*:*ortho* = 98:2. The regioselective syntheses of highly substituted heterocycles were also realized using nitrogen- or oxygen-tethered unsymmetrical diynes **5d** and **5e**. An isoindoline derivative **6g** and a phthalan derivative **6h** were obtained in 82 and 75% yields, respectively, with high *meta*-selectivities (entries 7 and 8).

The origin of the high *meta*-selectivity can be explained by the insertion mechanism depicted in Scheme 3. A ruthenacyclopentadiene **7** formed from **1** and **5** can be proposed as a key intermediate.[9] In order to avoid the steric interaction with the terminal substituent R^1, a monoalkyne **3** is selectively inserted into the less substituted Ru–C single bond to form ruthenacycloheptatriene intermediates **8** or **9**. At this stage, the bulky Cp* ligand directs formation of **8** because the steric repulsion between Cp* and R^2 is obviously greater in **9** and reductive elimination from **8** gives a *meta*-isomer *meta*-**6** as the major product.

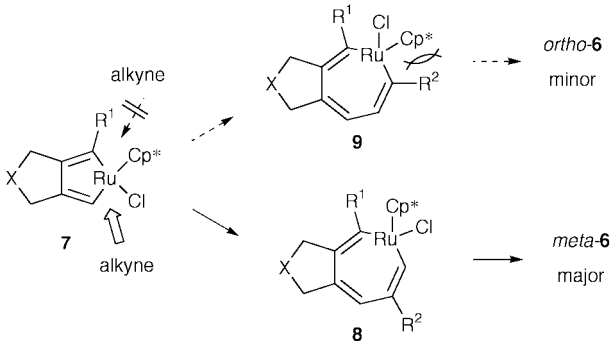

Scheme 3

In conclusion, an Ru(II) complex possessing a bulky planar ligand, Cp*Ru(cod)Cl, catalyzed the cycloaddition of 1,6-diynes with terminal alkynes at or below room temperature. Satisfactory chemoselectivity can be achieved using 2 equiv. of a monoalkyne. Excellent *meta*-selectivity was observed for the reaction of unsymmetrical diynes.

We gratefully acknowledge financial support (09305059, 10132222, and 11119223) from the Ministry of Education, Science, Sports, and Culture, Japan.

Notes and references

1 D. B. Grotjahn, in *Comprehensive Organometallic Chemistry II*, ed. L. S. Hegedus, E. W. Abel, F. G. A. Stone and G. Wilkinson, Pergamon, Oxford, 1995, vol. 12, p. 741; N. E. Shore, in *Comprehensive Organic Synthesis*, ed. B. M. Trost and I. Fleming, Pergamon, Oxford, 1991, vol. 5, p. 1037.
2 T. Takahashi, Z. Xi, A. Yamazaki, Y. Liu, K. Nakajima and M. Kotora, *J. Am. Chem. Soc.*, 1998, **120**, 1672.
3 K. P. C. Vollhardt, *Angew. Chem., Int. Ed. Engl.*, 1984, **23**, 539.
4 S. J. Neeson and P. J. Stevenson, *Tetrahedron*, 1989, **45**, 6239; P. Phansavath, C. Aubert and M. Malacria, *Tetrahedron Lett.*, 1998, **39**, 1561; I. G. Stará, I. Stary, A. Kollárovic, F. Teply, D. Saman and M. Tichy, *J. Org. Chem.*, 1998, **63**, 4046; I. G. Stará, I. Stary, A. Kollárovic, F. Teply, S. Vyskocil and D. Saman, *Tetrahedron Lett.*, 1999, **40**, 1993.
5 (*a*) E. Müller, *Synthesis*, 1974, 761; (*b*) R. Grigg, R. Scott and P. Stevenson, *J. Chem. Soc., Perkin Trans. 1*, 1988, 1357; (*c*) P. Bahataran and E. H. Smith, *J. Chem. Soc., Perkin Trans. 1*, 1990, 2603; (*d*) P. Bahataran and E. H. Smith, *J. Chem. Soc., Perkin Trans. 1*, 1992, 2163; (*e*) D. M. Duckworth, S. Lee-Wong, A. M. Z. Slawin, E. H. Smith and D. J. Williams, *J. Chem. Soc., Perkin Trans. 1*, 1996, 815; (*f*) F. E. McDonald, H. Y. H. Zhu and C. R. Holmquist, *J. Am. Chem. Soc.*, 1995, **117**, 6605; (*g*) Y. Sato, T. Nishimata and M. Mori, *Heterocycles*, 1997, **44**, 443; (*h*) Y. Sato, K. Ohashi and M. Mori, *Tetrahedron Lett.*, 1999, **40**, 5231; (*i*) S. Kotha and E. Brahmachary, *Tetrahedron Lett.*, 1997, **38**, 3561; (*j*) A. Bradley, W. B. Motherwell and F. Ujjainwalla, *Chem. Commun.*, 1999, 917; (*k*) B. Witulski and T. Stengel, *Angew. Chem., Int. Ed.*, 1999, **38**, 2426.
6 Y. Yamamoto, H. Kitahara, R. Ogawa and K. Itoh, *J. Org. Chem.*, 1998, **63**, 9610.
7 Ru-catalysed cyclotrimerization of electron-deficient alkynes has been reported, see: E. Lindner, R.-M. Jansen, H. A. Mayer, W. Hiller and R. Fawzi, *Organometallics*, 1989, **8**, 2355.
8 T. Naota, H. Takaya and S. Murahashi, *Chem. Rev.*, 1998, **98**, 2599; H. Butenschön, in *Organic Synthesis Highlights III*, ed. J. Mulzer, H. Waldman, Wiley-VCH, Weinheim, 1998, p. 96.
9 M. O. Albers, D. J. A. de Waal, D. C. Liles, D. J. Robinson, E. Singleton and M. B. Wiege, *J. Chem. Soc., Chem. Commun.*, 1986, 1680; B. K. Campion, R. H. Heyn and T. D. Tilley, *Organometallics*, 1990, **9**, 1106; M. I. Bruce and G. A. Koutsantonis, *Aust. J. Chem.*, 1991, **44**, 207; C. S. Yi, J. R. Torres-Lubian, N. Liu, A. L. Rheingold and I. A. Guzei, *Organometallics*, 1998, **17**, 1257; C. Ernst, O. Walter, E. Dinjus, S. Arzberger and H. Görls, *J. Prakt. Chem.*, 1999, **341**, 801.

Communication b000466i

Synthesis of a novel cationic water-soluble efficient blue photoluminescent conjugated polymer

Bin Liu,[a] Wang-Lin Yu,[b] Yee-Hing Lai*[a] and Wei Huang*[b]

[a] *Department of Chemistry, National University of Singapore, Singapore 119260, Republic of Singapore*
[b] *Institute of Materials Research and Engineering (IMRE), National University of Singapore, 3 Research Link, Singapore 117602, Republic of Singapore. E-mail: wei-huang@imre.org.sg*

Received (in Cambridge, UK) 24th January 2000, Accepted 23rd February 2000
Published on the Web 17th March 2000

A novel cationic conjugated polymer, poly[(9,9-dihexyl-2,7-fluorene)-*alt-co*-(2,5-bis{3-[(*N*,*N*-dimethyl)-*N*-ethylammonium]-1-oxapropyl}-1,4-phenylene)] dibromide, which is water-soluble and emits bright blue fluorescence both in solutions and as films, is synthesized through Suzuki coupling reaction and a post-polymerization treatment.

Water-solubility of conjugated polymers may offer many new application opportunities. Potential applications of water-soluble conjugated polymers include the construction of active layers in organic light-emitting diodes through a layer-by-layer self-assembly approach,[1] as buffer layer and emissive layer materials in inkjet printing fabricated organic LEDs,[2] and as highly sensitive fluorescent sensory materials in living bodies.[3] Such applications generally favor high molecular weights and high photoluminescence (PL) efficiencies and require different ionic types. Water-solubility of semiconducting conjugated polymers was first demonstrated in 3-substituted polythiophenes[4,5] and was then extended to poly(*para*-phenylene vinylene) (PPV)-based[6] and poly(*para*-phenylene) (PPP)-based polymers.[7,8] The water-solubility in such polymers was achieved by functionalizing the substituted side chains with terminal carboxylate or sulfonate groups. These polymers are, therefore, anionic polyelectrolytes. Until the most recent report on the synthesis of ammonium-functionalized PPPs from Reynolds' group,[9] there are no cationic water-soluble conjugated polymers available. Fluorene-based conjugated polymers have received considerable attention in the past few years for the high efficiencies both in PL and in electroluminescence (EL).[10] Moreover, we recently demonstrated that conjugated polymers based on alternating fluorene and phenylene backbones are promising efficient and stable blue luminescent materials.[11] This work presents the successful effort in developing a cationic water-soluble conjugated polymer based on the alternating fluorene and phenylene backbone, which represents the first example of fluorene-based water-soluble conjugated polymer and exhibits efficient blue light emission.

The chemical structure of the new water-soluble conjugated polymer, poly[(9,9-dihexyl-2,7-fluorene)-*alt-co*-(2,5-bis{3-[(*N*,*N*-dimethyl)-*N*-ethylammonium]-1-oxapropyl}-1,4-phenylene)] dibromide (PFP-NMe_2EtBr) and the synthetic route are depicted in Scheme 1. Monomer I, 9,9-dihexylfluorene-2,7-bis(trimethylene boronate), was synthesized from 2,7-dibromofluorene as the starting material.[11] Monomer II, 2,5-bis[3-(*N*,*N*-dimethylamino)-1-oxapropyl)-1,4-dibromobenzene], was prepared from 2,5-dibromohydroquinone by reaction with 2-chloroethyldimethylamine in refluxing acetone in the presence of an excess of anhydrous potassium carbonate.[9] The polymerization was carried out in a mixture of toluene and aqueous potassium carbonate solution (2 M) containing 1 mol% $Pd(PPh_3)_4$ under vigorous stirring at 85–90 °C for three days. The neutral polymer, polymer I, was obtained as a fibrous white solid with a yield of *ca*. 70% after purification and drying. Conversion of the neutral polymer to the final water-soluble polymer was achieved by treatment with bromoethane in dimethyl sulfoxide (DMSO) and tetrahydrofuran (THF) (1 : 4).

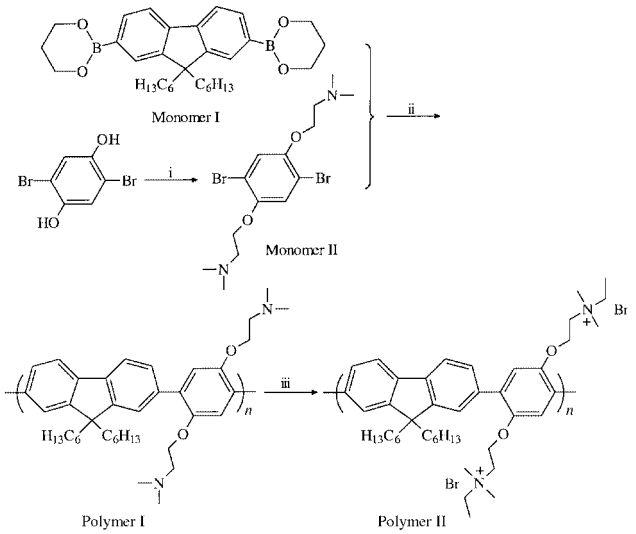

Scheme 1 Chemical structures and synthetic route towards the polymers. *Reagents and conditions*: i, 2-chlorotrimethylamine hydrochloride, anhydrous potassium carbonate, acetone, reflux, 3 days; ii, toluene/aqueous potassium carbonate solution (2 M), $Pd(PPh_3)_4$, 85–90 °C, 3 days; iii, bromoethane, DMSO–THF (1 : 4), 50 °C, 3 days.

The structures of both the neutral and the final water-soluble polymers were confirmed by NMR and elemental analysis.†

The characterization of molecular weight is often a problem for water-soluble conjugated polymers. The post-polymerization approach for the realization of water-solubility allows us to characterize the molecular weight at the stage of the neutral polymer. The neutral polymer, polymer I, can be readily dissolved in $CHCl_3$, THF, toluene and aqueous acid, but is insoluble in DMSO, methanol and water. Gel-permeation chromatography (GPC) measurement using THF as eluent and polystyrenes as the standards indicated the weight average molecular weight to be 47 000, with a polydispersity of 1.61. Another advantage of the post-polymerization approach is that the quaternization degree can be controlled and thus the water-solubility of the resultant polymer is tunable. The tunable solubility is useful for the application of such materials as buffer layers in inkjet printing fabrication of LEDs.[2] The degree of quaternization could be determined by ^{1}H NMR spectra. As shown in Fig. 1, the neutral polymer exhibits three peaks in the region δ 7.8–7.6 arising from the aromatic protons in fluorene and one peak at δ 7.15 due to the protons in the phenylene ring. The well resolved peaks at δ 4.09, 2.67 and 2.30 correspond to methylene groups adjacent to the oxygen ($-OCH_2-$) and nitrogen ($-CH_2N-$) atoms and the methylamino groups ($-NCH_3$), respectively. After the treatment with bromoethane, the peaks in the aromatic region remain almost unchanged, whereas all the signals corresponding to $-OCH_2-$, $-CH_2N-$, and $-NCH_3$ split into two peaks, which arise from the quaternarized (lower field) and un-quaternized components, respectively. The

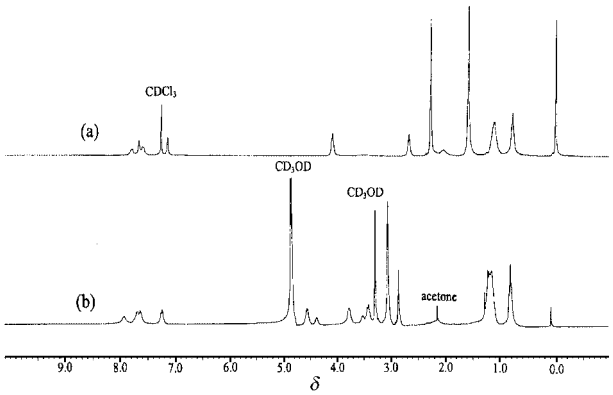

Fig. 1 ^{1}H NMR spectra of polymers I (a) and II (b).

relative integrals of each pair of the split peaks can thus be used to estimate the degree of quaternization. The highest degree of quaternization obtained in our experiments is *ca*. 80%. With this degree of quaternization, the resulting polymer shows solubility characteristics opposite to that of polymer I, being completely soluble in DMSO, methanol, and water but insoluble in $CHCl_3$ and THF.

Polymer II also possesses good thermal stability. The onset degradation temperature of this polymer is 300 °C in nitrogen, whereas it starts to decompose above 230 °C in air, with a small amount of water loss at lower temperatures. In air, no residue remained after heating to 800 °C.

The UV–VIS absorption spectra of polymer I in chloroform solution and as a film (on quartz plate, spin-cast from chloroform solution) are almost identical with the same maximum absorption at 366 nm. The PL spectrum of the polymer solution peaks at 414 nm, whereas the polymer film exhibits an emission maximum at 424 nm with a vibronic shoulder around 444 nm. The emission spectral feature of the polymer in the film state is very similar to that of the polymer having the same backbone structure and substitution on fluorene unit but without the terminal amino group in the phenylene side chains.[11] This implies that the terminal amino groups are unlikely to affect the conformation of the backbone in the film state. For the quaternized sample with the highest degree of quaternization (*ca*. 80%), the electronic spectra are remarkably dependent on the solvent, showing a bathochromic shift with a decrease in solvent polarity. As displayed in Fig. 2, the polymer shows absorption maxima at 343, 354 and 367 nm in water, methanol and DMSO, respectively. The corresponding PL maxima appear at 409, 409 and 419 nm, respectively. Uniform and transparent films of the polymer on quartz plates were prepared by spin-casting its aqueous solution. The UV–VIS absorption and PL spectra of the polymer film are also shown in Fig. 2. The absorption and emission peaks appear at 359 and 416 nm, respectively.

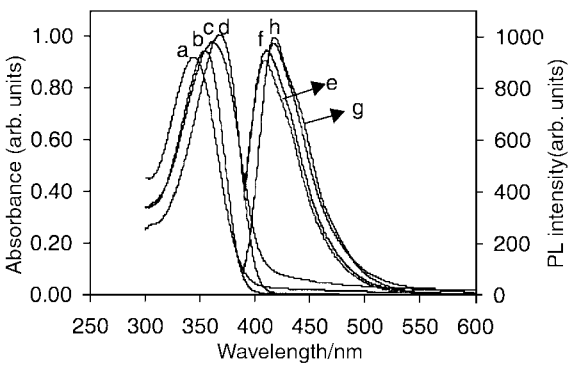

Fig. 2 UV–VIS absorption and photoluminescence spectra of polymer II in solutions and as films. (a) UV in aqueous solution, (b) UV in MeOH, (c) UV in film, (d) UV in DMSO, (e) PL in MeOH, (f) PL in aqueous solution, (g) PL as film and (h) PL in DMSO.

From the application point of view, one of the most attractive properties of the polymers is the relatively high PL quantum yield (Φ_{pl}). Both the neutral polymer and the quaternized polymers display strong blue fluorescence either in solutions or as films upon exposure to UV light. The Φ_{fl} of the neutral polymer (polymer I) is as high as 97% as measured from its dilute solution in chloroform.‡ For polymer II (with a degree of quaternization of 80%), the Φ_{pl} was measured to be 86% from its dilute solution in methanol. When the measurement was conducted in aqueous solution, the corresponding value of Φ_{pl} is 25%. The decrease of PL efficiency may be attributed to the aggregation of the polymer in aqueous solution. This was supported by a further reduced PL efficiency measured in the solid state (films on quartz plate cast from methanol solution), which is 4% compared with 9,10-diphenylanthracene as standard (dispersed in PMMA films with a concentration lower than 1×10^{-3} M, assuming a PL efficiency of 83%).[12]

In summary, we have synthesized a new cationic water-soluble conjugated polymer based on the alternating fluorene and phenylene backbone structure through a facile post-polymerization approach, which permits a full structural characterization of the polymer and control of the degree of cation formation. The polymer emits intense blue fluorescence both in solutions and in film states. The good water-solubility and high fluorescence quantum yield make it attractive for applications in fabricating organic LED devices and as fluorescent bio-sensory materials.

The work was partially supported by the National University of Singapore through a research grant (RP970610).

Notes and references

† *NMR and elemental analyses data* for polymers I and II: polymer I: δ(300 MHz, $CDCl_3$) 7.79 (br, 2H, Ar-H), 7.66–7.60 (br, 4H, Ar-H), 7.15 (s, 2H, Ar-H), 4.09 (br, 4H, $-OCH_2$), 2.67 (br, 4H, $-CH_2N$), 2.27 (s, 12H, NCH_3), 2.05 (br, 4H, fluorene 9-H), 1.12–0.78 (br, 22H, $-CH_2$, $-CH_3$). Calc. for $C_{39}H_{54}O_2N_2$: C, 80.41; H, 9.27; N, 4.81; Br, 0 (terminal group). Found: C, 79.60; H, 8.99; N, 4.90; Br, 0%.

Polymer II: δ(300 MHz, CD_3OD) 7.93 (br, 2H, Ar-H), 7.70–7.64 (br, 4H, Ar-H), 7.24 (br, 2H, Ar-H), 4.56 (br, 3.2H, $-OCH_2$), 4.38 (br, 0.8H, $-OCH_2$), 3.77 (br, 3.2H, $-CH_2N$), 3.52 (br, 0.8H, $-CH_2N$), 3.42 (br, 3.2H, NCH_2CH_3), 3.06 (br, 12H, NCH_3), 2.87 (br, 4.8H, NCH_2CH_3), 2.16 (br, 4H, fluorene 9-H), 1.28–0.80 (br, 22H, $-CH_2$, $-CH_3$). Calc. for $C_{39}H_{54}O_2N_2 \cdot 4H_2O \cdot 1.6C_2H_5Br$ (the amounts of H_2O and C_2H_5Br were based on TGA analysis and ^{1}H NMR): C, 61.10; H, 8.45; Br, 15.46; N, 3.38. Found: C, 60.63; H, 8.29; Br, 16.04; N, 3.52%.

‡ The quantum yields were measured using a Perkin Elmer LS 50B luminescence spectrometer with dilute solutions ($A < 0.2$) at room temperature.[13] Quinine sulfate solution (*ca*. 1.0×10^{-5} M) in 0.10 M H_2SO_4 (quantum yield, 55%) was used as a standard.

1 M. Ferreira and M. F. Rubner, *Macromolecules*, 1995, **28**, 7101; A. C. Fou, O. Onitsuka, M. Ferreira and M. F. Rubner, *J. Appl. Phys.*, 1996, **79**, 7501; J. W. Baur, S. Kim, P. B. Balanda, J. R. Reynolds and M. F. Rubner, *Adv. Mater.*, 1998, **10**, 1452.
2 J. Bharathan and Y. Yang, *Appl. Phys. Lett.*, 1998, **72**, 2660; S. C. Chang, J. Bharathan and Y. Yang, *Appl. Phys. Lett.*, 1998, **73**, 2561.
3 K Fäid and M. Leclere, *Chem. Commun.*, 1996, 2761; *J. Am. Chem. Soc.*, 1998, **120**, 5274.
4 A. O. Patil, Y. Ikenoue, F. Wudl and A. J. Heeger, *J. Am. Chem. Soc.*, 1987, **109**, 1858.
5 P. Pickup, *J. Electroanal. Chem.*, 1987, **225**, 273.
6 S. Shi and F. Wudl, *Macromolecules*, 1990, **23**, 2119.
7 T. I. Wallow and B. M. Novak, *J. Am. Chem. Soc.*, 1991, **113**, 7411.
8 A. D. Child and J. R. Reynolds, *Macromolecules*, 1994, **27**, 1975.
9 P. B. Balanda, M. B. Ramey and J. R. Reynolds, *Macromolecules*, 1999, **32**, 3970.
10 A. W. Grice, D. D. C. Bradley, M. T. Bernius, M. Inbasekaran, W. W. Wu and E. P. Woo, *Appl. Phys. Lett.*, 1998, **73**, 629.
11 W. L. Yu, J. Pei, Y. Cao, W. Huang and A. J. Heeger, *Chem. Commun.*, 1999, 1837.
12 J. N. Demas and G. A. Crospy, *J. Phys. Chem.*, 1971, **75**, 991.
13 H. S. Joshi, R. Jamshidi and Y. Tor, *Angew. Chem., Int. Ed.*, 1999, **38**, 2722.

Communication b000740o

Diastereoselective synthesis of α-substituted-γ-butyrolactones of nucleosides *via* [1,5]-C,H insertion reactions of α-diazomalonates of nucleosides†

Jinsoo Lim,[a] Dong-Joon Choo[b] and Yong Hae Kim*[a]

[a] *Department of Chemistry, Korea Advanced Institute of Science and Technology, Taejon, 305-701, Korea. E-mail: kimyh@sorak.kaist.ac.kr*

[b] *Department of Chemistry, College of Liberal Arts and Sciences, Kyung Hee University, Seoul, 130-701, Korea*

Received (in Cambridge, UK) 18th January 2000, Accepted 23rd February 2000
Published on the Web 17th March 2000

Diastereoselective and regioselective [1,5]-C,H insertion reactions of 2′-deoxy-3′-diazomalonate nucleosides afforded τ-butyrolactones of nucleosides as chiral synthons for the preparation of 2′-*C*-branched nucleosides.

Since oxetanocin[1] was isolated and turned out to show potent antiviral activity such as inhibition of HIV-1 antigens and infectivity, *C*-branched nucleosides bearing carbon–carbon bonds at the furanose rings have attracted considerable attention as clinically useful chemotherapeutic agents.[2] Moreover, the discovery of a positive correlation between inhibitory activity against ribonucleotide reductase and antitumor activity,[3] has led to rational drug design to find potent antitumor agents having C–C bonds at the 2′-positions.[4] The key step in the synthesis of *C*-branched nucleosides is stereocontrolled C–C bond formation at the branching site of the ribofuranose ring. However, it is especially difficult to construct C–C bonds at the 2′-position of nucleosides. Intramolecular cyclization is a facile and useful strategy for stereo- and regio-controlled C–C bond formation to provide γ-butyrolactones of nucleosides as a useful chiral synthon for the synthesis of *C*-branched nucleosides.[5] The γ-butyrolactones of nucleosides are important key intermediates to manipulate various 2′-*C*-branched nucleoside analogues. Recently Camarasa and coworkers reported that γ-butyrolactones of nucleosides were prepared by intramolecular radical cyclization in good diastereoselectivities but low yields[6] which might result from reductive deoxygenation, which is a feature of free radical cyclizations. Intramolecular [1,5]-C,H insertion reactions of α-diazocarbonyl compounds have been among the most attractive and effective methods for the construction of functionalized five membered rings.[7] Substrates can be smoothly cyclized without difficulty by dirhodium(II)-catalyzed C,H-insertion reactions. However, surprisingly, no successful C,H-insertion reactions in the modification of ribofuranose ring of nucleosides have been reported. Efficient construction of a C–C bond at the branching point has been a difficult task especially at the 2′-position of nucleosides by currently available methods. Here, we describe diastereoselective intramolecular C,H-insertion of 2′-deoxy-3′-α-diazoacetates of nucleosides in the presence of a catalytic amount of dirhodium tetraacetate to [3.3.0] fused lactones (γ-butyrolactones) of a series of nucleosides having a new chiral center at an off-template site of the ribofuranose ring, in high yields, as shown in Scheme 1.

For the synthesis of the fused γ-butyrolactones of nucleosides we chose 2′-deoxy-3′-diazoacetates of nucleosides (R^1 = H, MeCO, MeO_2C, EtO_2C) as templates for [1,5]-C,H insertion reactions. The general strategy is shown in Scheme 2.

The 5′-position of 2′-deoxynucleosides were protected with *tert*-butyldiphenylsilyl chloride in dried pyridine at room temperature. These 5′-*O*-protected-2′-deoxynucleoside derivatives **10a**–**e** undergo transesterification[8] by reaction with the corresponding methyl ester to give 3′-*O*-acetoacetyl-2′-deoxy-

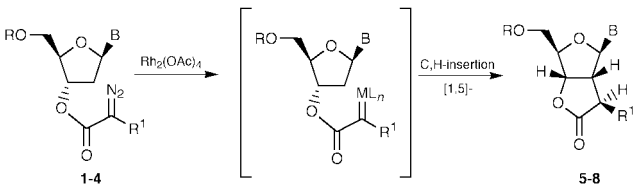

Scheme 1

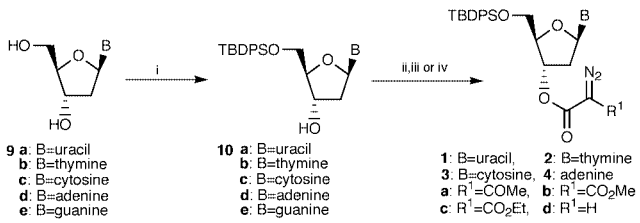

Scheme 2 *Reagents and conditions*: i, TBDPSCl, pyridine, rt; ii, $R^1C(N_2)CO_2Me$, DMAP, toluene, reflux; iii, (1) $EtO_2CCH_2CO_2H$, DCC, DMAP; (2) MsN_3, Et_3N, MeCN; iv, TsNHN=CHCOCl, Et_3N, MeCN.

nucleosides and 2′-deoxy-3′-*O*-α-(methoxycarbonyl)acetylnucleosides in moderate yields. Diazo transfer of these esters with methanesulfonyl azide and triethylamine in acetonitrile[9] afforded the corresponding 3′-diazoester derivatives **1a**–**4a** and **1b**–**4b** in poor yields (*ca.* 50%). These low yields might be due to steric hindrance by furanose rings. It was found, however, that the satisfactory yields (84–96%) of **1a**–**4a** and **1b**–**4b** could be smoothly obtained using methyl α-diazoacetate derivatives instead of methylacetate ones, and α-ethoxycarbonylacetates of nucleosides **1c** and **2c** were not formed by this procedure. The desired products **1c** and **2c** could be obtained by a coupling reaction of 5′-*O*-protected-2′-deoxynucleosides **10a**,**b** with monoethyl malonate followed by diazo transfer in moderate yields (56–71%), while 2′-deoxy-3′-α-diazoacetates of nucleosides **1d** and **2d** could be obtained in good yields (78–90%) using the modified House–Blankey procedure.[11]

Our initial studies on stereocontrolled C,H-insertion of 2′-deoxy-3′-α-diazoacetates of nucleosides were performed in the presence of dirhodium tetraacetate (1.0 mol%) in dichloromethane at room temperature. However, only a trace amount of product was obtained and starting material was recovered. To improve the yields, when the reaction mixture was refluxed, high yields of γ-butyrolactones of nucleosides **5**–**8** were obtained and results obtained are summarized in Table 1.

Moreover, the C,H-insertion of 2′-deoxy-3′-α-diazoacetates of nucleosides **1**–**4** afforded the γ-butyrolactones of nucleosides **5**–**8** with high diastereoselectivities. Through the J_{H-H} coupling constant ($J_{1''-2'}$ 8.8 Hz) between 1″-hydrogen and 2′-hydrogen of **6b**, the stereochemistry of 1″-position of γ-butyrolactone of nucleoside **6b** was determined as *exo*. Irradiation of the anomeric proton of **6b** caused enhancement of the signal for H-1″ (8%), indicating that the configuration at C-1″ of **6b** was (*S*). A possible mechanism for the stereochemical outcomes of γ-

† Electronic supplementary information (ESI) available: NMR data for **2b** and **6b**. See http://www.rsc.org/suppdata/cc/b0/b000524j/

Table 1 Dirhodium(II) tetraacetate catalyzed formation of **5**–**8**

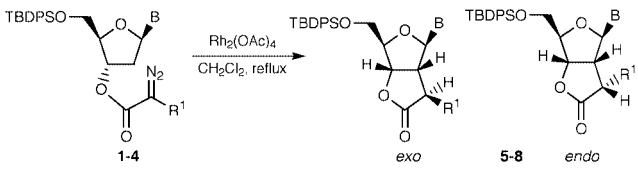

Run	Reactant	Product	*t*/h	Yield(%)[a]	*exo*:*endo*[b]
1	**1a**	**5a**	1.5	69	96:4
2	**1b**	**5b**	2	72	>98:2
3	**1c**	**5c**	2	70	>98:2
4	**1d**	**5d**	1	75	
5	**2a**	**6a**	1.5	64	95:5
6	**2b**	**6b**	1	70	>98:2
7	**2c**	**6c**	1	65	>98:2
8	**2d**	**6d**	1	71	
9	**3a**	**7a**	2.5	58	95:5
10	**3b**	**7b**	3	71	>98:2
11	**4a**	**8a**	5	66	97:3
12	**4b**	**8b**	5	80	>98:2

[a] Isolated yield. [b] Determined by ^{1}H NMR spectroscopy.

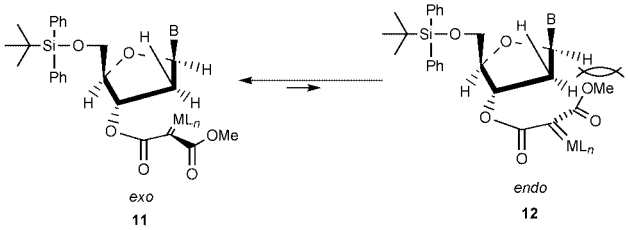

Scheme 3

butyrolactones of nucleosides **5**–**8** is proposed as shown in Scheme 3.

The unfavorable steric hindrance between the anomeric proton and the methyl ester in *endo* transition state **12** drives the equilibrium to the left to the *exo* transition state **11**, which gives the (*S*) conformer (*exo* adduct, **5**–**8**) stereoselectively. When pure **6b** was refluxed in CH_2Cl_2 for 10 h, no epimerization occurred.

The γ-butyrolactones of the nucleosides described above can be considered as useful chiral synthons for the synthesis of *C*-branched nucleosides. In connection with biologically interesting nucleosides containing the 2′-methylene moiety, for instance (*E*)-FMC[3] and (*E*)-2′-deoxy-2′-(carboxymethylene)-5′-*O*-trityluridine-3′,2′-γ-lactone **17**,[12] the synthesis of **17** was attempted by employing C,H-insertion of the 2′,5′-cyclouridine derivative **14** as shown in Scheme 4.

Cyclization of 5′-*O*-trityluridine **13** by basic diphenylcarbonate gave the 2′,5′-cyclouridine **14** in 81% yield. Exposure of **14** to the House–Blankey protocol afforded the corresponding diazo compound **15**, which could be converted to the γ-butyrolactone of uridine **16** in 65% yield. Product **17** could be smoothly obtained by an elimination reaction with sodium hydride in 85% yield.

In conclusion, we have achieved the new stereoselective syntheses of α-substituted-γ-butyrolactones of nucleosides *via* [1,5]-C,H insertion reactions of α-diazo-γ-butyrolactones of nucleosides.

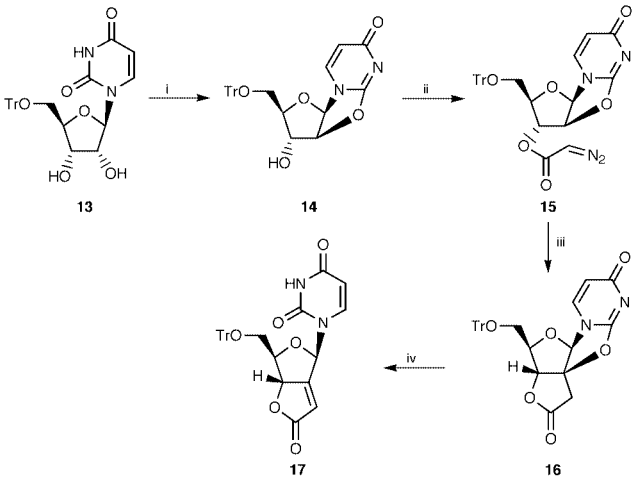

Scheme 4 *Reagents and conditions*: i, $(PhO)_2CO$, $NaHCO_3$, DMF; ii, TsHNN=CHCOCl, Et_3N, MeCN; iii, $Rh_2(OAc)_4$, CH_2Cl_2, reflux; iv, NaH, MeCN.

Furthermore, this reaction can be applied to the synthesis of (*E*)-2′-deoxy-2′-(carboxymethylene)-5′-*O*-trityluridine-3′,2′-γ-lactone **17**, a chiral synthon in the synthesis of 2′-*C*-branched nucleosides.

This work was supported by the Center for Molecular Design and Synthesis at Korea Advanced Institute of Science and Technology.

Notes and references

1 N. Shimada, S. Hasegawa, T. Harada, T. Tomisawa, A. Fujii and T. Takita, *J. Antibiot.*, 1986, **39**, 1623; H. Hoshino, N. Shimizu, N. Shimada, T. Takita and T. Takeuchi, *J. Antibiot.*, 1987, **40**, 1077.
2 A. Matsuda, A. Azuma, Y. Nakajima, K. Takenuki, A. Dan, T. Iino, Y. Yoshimura, N. Minakawa, M. Tanaka and T. Sasaki, in *Nucleosides and Nucleotides as Antitumor and Antiviral Agents*, ed. C. K. Chu, D. C. Baker, Plenum Press, New York, 1993, pp. 1–22 and references therein.
3 W. A. van der Donk, G. Yu, D. J. Silva, J. Stubbe, J. R. McCarthy, E. T. Jarvi, D. P. Mattews, R. J. Resvick and E. Wagner, *Biochemistry*, 1996, **35**, 8381.
4 H. L. Elford, M. Freese, E. Passamani and H. P. Morris, *J. Biol. Chem.*, 1970, **245**, 5228.
5 A. J. Lawrence, J. B. J. Pavey, M.-Y. Chan, R. A. Fairhurst, S. P. Collingwood, J. Fisher, R. Cosstick and I. A. O'Neil, *J. Chem. Soc. Perkin Trans. 1*, 1997, 2761.
6 S. Velazquez, M. L. Jimeno, S. Huss, J. Bazarini and M.-J. Camarasa, *J. Org. Chem.*, 1994, **59**, 7661.
7 A. Padwa and M. D. Weingarten, *Chem. Rev.*, 1996, **96**, 223; M. P. Doyle and D. C. Forbes, *Chem. Rev.*, 1998, **98**, 911.
8 D. F. Taber, J. C. Amedio, Jr. and Y. K. Patel, *J. Org. Chem.*, 1985, **50**, 3618.
9 J. B. Hendrickson and W. A. Wolf, *J. Org. Chem.*, 1968, **33**, 3608.
10 B. Neises and W. Steglich, *Org. Synth.*, 1990, **VII**, 93.
11 E. J. Corey and A. G. Myers, *Tetrahedron Lett.*, 1984, **25**, 3559.
12 A. E. A. Hassan, S. Shuto and A. Matsuda, *J. Org. Chem.*, 1997, **62**, 11.

Communication b000524j

ChemComm

Asymmetric synthesis of alkyl 5-oxotetrahydrofuran-2-carboxylates by enantioselective hydrogenation of dialkyl 2-oxoglutarates over cinchona modified Pt/Al_2O_3 catalysts

Katalin Balázsik,[a] Kornél Szöri,[a] Károly Felföldi,[b] Béla Török[a] and Mihály Bartók*[ab]

[a] *Organic Catalysis Research Group of the Hungarian Academy of Sciences and* [b] *Department of Organic Chemistry, József Attila University, H-6720 Szeged, Dóm tér 8, Hungary. E-mail: bartok@chem.u-szeged.hu*

Received (in Liverpool, UK) 12th January 2000, Accepted 22nd February 2000
Published on the Web 17th March 2000

The first direct asymmetric synthesis of chiral alkyl 5-oxotetrahydrofuran-2-carboxylates (up to 96% ee), which are important building blocks in the synthesis of natural products by heterogeneous cinchona-modified Pt-catalyzed hydrogenation of α-ketoglutaric acid esters and subsequent cyclization of hydroxy esters is described.

The growing interest in the synthesis of important chiral compounds provides significant impetus for asymmetric synthesis. Owing to the recent environmental considerations and safety concerns, the use of heterogeneous asymmetric methods such as enantioselective hydrogenation are especially preferable.[1] One of those, the cinchona alkaloid-modified platinum catalyst system, was found to be especially effective in the hydrogenation of α-ketoesters and ketoacids[1] and ketoacetals.[2] The most prominent substrates are ethyl pyruvate,[3] pyruvaldehyde dimethyl acetal,[2] ketopantolactone[4] and 1-ethyl-4,4-dimethylpirrolidine-2,3,5-trione,[5] which can all be hydrogenated with excellent enantioselectivity (91–98%) over cinchona-modified Pt/Al_2O_3 catalysts.

Here, we report a new successful enantioselective synthesis of alkyl (*R*)-5-oxotetrahydrofuran-2-carboxylates, *via* the asymmetric hydrogenation of α-ketoglutaric acid esters over cinchona-modified Pt/Al_2O_3 catalyst.

The target chiral esters are very frequently used synthons in the synthesis of natural products.[6] In addition, their utilization in the free acid form as chiral derivatizing agents[7] or as a template for acyclic stereoselection through asymmetric synthesis[8] is also well known. The enantioselective hydrogenation of dialkyl 2-ketoglutarates and the subsequent cyclization to alkyl 5-oxotetrahydrofuran-2-carboxylates are shown in Scheme 1.

The existing process for the preparation of the target compounds is a template synthesis based on the deamination of enantiopure glutamic acid.[9] Asymmetric pathways to their perparation are enzymatic resolution of the racemic mixtures or direct bioreduction of ketoglutaric acid esters.[10] The former process provides high enantiomeric excess, however, the yield is obviously does not exceed 50% in the best case. The bioreduction, however, is not an efficient method for the preparation of enantiomers of high purity, since the ee values (up to 67%) vary considerably and significant decarboxylation and byproduct formation may be observed. Heterogeneous hydrogenation carried out on camphor-modified Raney Ni was also inefficient (24% ee).[11] As a consequence, to the best of our knowledge, no satisfactory enantioselective reduction of α-ketoglutaric acid derivatives has been developed.

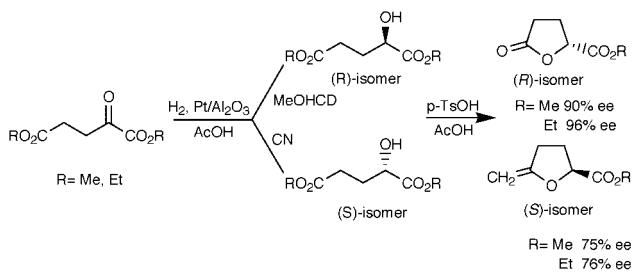

Scheme 1

In this study two well known Pt/Al_2O_3 reference catalysts (Engelhard 4759, denoted E4759 and Johnson Matthey 94, denoted JMC94) were used while the two modifiers [cinchonidine (CD) and cinchonine (CN)] and 2-ketoglutaric acid were all Fluka products. 9-Methoxy-10,11-dihydrocinchonidine (MeOHCD) was kindly donated by Dr Martin Studer (Novartis, Basel, Switzerland). The dimethyl and diethyl α-ketoglutaric acid esters were prepared on the basis of a literature procedure.[10] The hydrogenations were performed in an atmospheric batch reactor or in a Berghof Bar 45 autoclave at 20 °C as described previously.[2,3] After hydrogenation, the hydroxyester obtained was subjected to a cyclization reaction with *p*-toluenesulfonic acid according to the literature procedure.[10] During the reaction no racemization or inversion occured, as a result the ee of the cyclic products corresponded to that of the open chain hydroxy esters. Product identification was carried out by GC–MS (HP5890 GC-HP5970 MSD) and ^{1}H NMR spectroscopy (Bruker AM500), while the enantiomeric excesses $\{ee\% (|[R] - [S]|) \times 100/([R] + [S])\}$ were monitored by chiral gas chromatography [HP 5890 GC-FID, 30 m long Cyclodex-B (J&W Scientific) capillary column, carrier gas: He, 15 psi, 125 °C, retention time for (*S*)-isomer: 31.8 min, for (*R*)-isomer: 32.5 min]. The ee values were reproducible within 2%.

According to earlier findings[1–5] two well known 5% Pt/Al_2O_3 references catalysts (E4759 and JMC94) were highly efficient in the enantioselective hydrogenation of activated α-oxo-compounds. As a result, these samples were selected for the enantioselective hydrogenation of diethyl α-ketoglutarate. Taking into account that in the literature, toluene and acetic acid have mainly been applied as solvents in these systems, both of them were tested first to find the most suitable medium, catalyst and modifier for the hydrogenation. Although the enantioselectivity in toluene is only moderate (up to 63% ee), using acetic acid as solvent, the results are excellent (up to 93% ee) and comparable or even slightly higher than those obtained with ethyl pyruvate.[1,2] As generally found,[12] the ee was always higher with the CD modifier than with the CN modifier. The results obtained in the two solvents, including reaction rates and optical yields, are tabulated in Table 1.

In the light of the results shown in Table 1 it can be concluded that the JMC catalyst exhibited a slight but clear increase in both reaction rates and optical yields (5–6% ee increase) compared to E4759. It seems also clear that MeOHCD is the best modifier for the reaction, the ee values obtained mostly exceed by *ca.* 10% those achieved with cinchonidine.

Since the enantioselective hydrogenation of α-ketoesters over the Pt-cinchona catalyst system generally shows better performance (higher reaction rates and optical yields) under elevated hydrogen pressures, the effect of hydrogen pressure, on the present system was also studied. According to the literature[1] a wide hydrogen pressure (1–100 bar) was studied with acetic acid as solvent using the JMC94 catalyst and MeOHCD modifier.

DOI: 10.1039/b9000390p

Table 1 Enantioselective hydrogenation (and subsequent cyclization) of diethyl α-ketoglutarate to ethyl 5-oxotetrahydrofuran-2-carboxylate over 5% Pt/Al_2O_3 catalysts (E4759, JMC94) under 1 bar hydrogen pressure and at 20 °C (values are the average of three experiments)

Entry	Solvent	Catalyst	Modifier[a]	*r*/mmol $min^{-1}g_{cat}^{-1}$	Product configuration	ee (%)
1	Toluene	E4759	CD	0.51	(*R*)	53
2	Toluene	E4759	CN	0.34	(*S*)	25
3	Toluene	E4759	MeOHCD	0.53	(*R*)	47
4	Toluene	E4759	—	0.49	Racemic	—
5	AcOH	E4759	CD	0.50	(*R*)	78
6	AcOH	E4759	CN	0.37	(*S*)	60
7	AcOH	E4759	MeOHCD	0.55	(*R*)	87
8	AcOH	E4759	—	0.12	Racemic	—
9	AcOH	JMC94	CD	0.75	(*R*)	83
10	AcOH	JMC94	CN	0.46	(*S*)	66
11	AcOH	JMC94	MeOHCD	1.41	(*R*)	93
12	AcOH	JMC94	—	0.34	Racemic	—
13	Toluene	JMC94	MeOHCD	0.75	(*R*)	63

[a] CD = cinchonidine, CN = cinchonine, MeOHCD = 9-methoxy-10,11-dihydrocinchonidine.

The ee data indicate that the enantioselectivity of the reaction shows a slight hydrogen pressure dependence. Starting from 93% ee (1 bar H_2) the optical yields increased as a function of hydrogen pressure up to 96% ee. However, at 20 bar hydrogen pressure the enantiomeric excess seems to reach its maximum, and any further increase in hydrogen pressure does not result in higher optical yields. Under the same conditions (JMC94, MeOHCD, 20 bar) using dimethyl ester, the product was obtained in 90% ee. The (*S*)-isomer can also be prepared in 76% optical purity in the presence of CN-modified JMC94 catalyst at elevated hydrogen pressures (20–40 bar). Although the study currently is of an experimental nature, the kinetic data (Table 1)indicate that the mechanism is most likely similar to that proposed for ethyl pyruvate and other α-ketoesters. The cinchona-modified reactions all take place at higher rates than the modifier-free runs, resulting in a racemic product mixture. This phenomenon unambiguously indicates a ligand accelerated mechanism.[13] As a result, the highest enantioselectivity was obtained at the highest reaction rate (entry 11, Table 1).

Taking into account the practical importance of the products, one of them was prepared and isolated in preparative scale. Starting from 1.5 g of diethyl 2-ketoglutarate after the hydrogenation (20 bar) and cyclization, ethyl (*R*)-5-oxotetrahydrofuran-2-carboxylate was isolated in 80% yield and 94% ee optical purity.

In conclusion, the cinchona-modified Pt/Al_2O_3 catalytic system was found to be effective in the highly enantioselective hydrogenation of α-ketoglutaric acid esters providing the first satisfactory asymmetric synthetic route for the preparation of chiral alkyl 5-oxotetrahydrofuran-2-carboxylates which are frequently used as chiral building blocks. In addition, this work provides an opportunity to widen further the practical applications and potential of the Pt–cinchona catalytic system.

Financial support by Hungarian Academy of Sciences (AKP97-4 2,4) and Hungarian National Science Foundation (OTKA T031707) is highly appreciated.

Notes and references

1 A. Baiker and H.-U. Blaser, in *Handbook of Heterogeneous Catalysis*, ed. G. Ertl, H. Knözinger and J. Weitkamp, Wiley-VCH, New York, 1997, vol. 5, p. 2422.
2 B. Török, K. Felföldi, K. Balázsik and M. Bartók, *Chem. Commun.*, 1999, 1725; M. Studer, S. Burkhardt and H.-U. Blaser, *Chem. Commun*, 1999, 1727.
3 B. Török, K. Felföldi, G. Szakonyi, K. Balázsik and M. Bartók, *Catal. Lett.*, 1998, **52**, 81.
4 M. Schürch, N. Künzle, T. Mallat and A. Baiker, *J. Catal.*, 1998, **176**, 569.
5 N. Künzle, A. Szabó, M. Schürch, G. Wang, T. Mallat and A. Baiker, *Chem. Commun.*, 1998, 1377.
6 G. Fronza, G. Fuganti, P. Grasselli and S. Servi, *Chimia*, 1993, **47**, 43 and references therein; K. Mori, in *Techniques in Pheromone Research*, ed. H. H. Hummel and T. Miller, Springer-Verlag, New York, 1989, ch. 12.
7 R. E. Doolittle and R. R. Health, *J. Org. Chem.*, 1984, **49**, 5041; A. M. Riley and B. V. L. Potter, *Tetrahedron Lett.*, 1998, **39**, 6769.
8 S. Hanessian, S. P. Sahoo and M. Botta, *Tetrahedron Lett.*, 1987, **28**, 1143.
9 C. Herdeis, *Synthesis*, 1986, 232.
10 S. Drioli, P. Nitti, G. Pitacco, L. Tossut and E. Valentin, *Tetrahedron: Asymmetry*, 1999, **10**, 2713.
11 T. Isoda, A. Ichikawa and T. Shimamoto, *Rikagaku Kenkyusho Hokuku*, 1958, **34**, 134, (*Chem. Abstr.*, 1958, **54**, 285).
12 M. Bartók, K. Felföldi, Gy. Szöllösi and T. Bartók, *Catal. Lett.*, 1999, **61**, 1.
13 M. Garland and H.-U. Blaser, *J. Am. Chem. Soc.*, 1990, **112**, 7048.

Communication b000390p

ChemComm

Production and isolation of an ellipsoidal C_{80} fullerene

Chun-Ru Wang, Toshiki Sugai, Tsutomu Kai, Tetsuo Tomiyama and Hisanori Shinohara*

Department of Chemistry, Nagoya University, Nagoya 464-8602, Japan. E-mail: nori@chem2.chem.nagoya-u.ac.jp

Received (in Cambridge, UK) 12th January 2000, Accepted 23rd February 2000
Published on the Web 17th March 2000

We report the first successful production and isolation of a new C_{80} isomer together with ^{13}C NMR structural and UV–VIS–NIR spectroscopic studies of the purified sample; ^{13}C NMR results unambiguously suggest that the new C_{80} isomer has an ellipsoidal structure with D_{5d} symmetry.

C_{80} has seven structural isomers satisfying the isolated pentagon rule (IPR).[1,2] However, owing to its extremely low abundance in arc-burning soot, this fullerene has long been known as one of the three 'missing' fullerenes[3] between C_{70} and C_{96} (the other two fullerenes are C_{72} and C_{74}).[3] It was not until recently that a small quantity of $C_{80}(D_2)$ was isolated by Henrich *et al.*[4] Here, we report the production, isolation and ^{13}C NMR structural analysis of a new C_{80} isomer.

Fullerene soot containing C_{80} was produced by the dc arc discharge method. Graphite/iron composite rods (12.5 × 12.5 × 300 mm, 0.7 atom% Fe/C, Toyo Tanso Co.Ltd.) were used for the arc discharge at 350 A and 23 V under a 12 l min^{-1} He flow (90–100 Torr). The resulting soot was succesively extracted with carbon disulfide and pyridine for 20 h. The separation of C_{80} was achieved by a multi-stage HPLC method[5,6] using a Buckyprep column (nacalai Cosmosil, 25 × 250 mm, toluene eluent) at 16.5 ml min^{-1} flow rate and a Buckyclutcher column (Regis, 20 × 300 mm) at 10 ml min^{-1} flow rate. The first stage was performed on the Buckyprep column which roughly separates C_{80}(I) and C_{80}(II) from other fullerenes by collecting the corresponding C_{80}-containing fractions. In the second stage, the HPLC fractions collected in stage 1 were re-injected into a 5PYE column (nacalai Cosmosil, 25 × 250 mm, toluene eluent) and recycling HPLC was performed. The third stage was again a recycling HPLC process on the Buckyclutcher column which can finally isolate C_{80}(I) and C_{80}(II) obtained from stage 2. The purity of the isolated samples [C_{80}(I): > 98%, *ca.* 5 mg; C_{80}(II): > 98%, *ca.* 2 mg] was determined by both positive and negative laser-desorption time-of-flight (LD-TOF) mass spectrometry.

On the 5PYE column, the C_{80} isomers I and II have different HPLC retention times. C_{80}(I) appears immediately after C_{78}. A ^{13}C NMR spectrum of this fullerene has already been reported by Henrich *et al.*[4] to have 20 near-equal signals, suggesting D_2 symmetry. C_{80}(II) has a much longer retention time than C_{80}(I) and appeared after C_{86}. The relative abundance of C_{80}(I) to C_{80}(II) is *ca.* 30 : 1. C_{80}(II) is light green in carbon disulfide solution. Fig. 1 shows the VIS–NIR absorption spectra of C_{80}(II) together with that of $C_{80}(D_2)$ for comparison. Aside from the relative intensity, the band positions in the two absorption spectra are similar. The characteristic peaks of $C_{80}(D_2)$ are seen at 420(sh), 466(sh), 596, 775, 860, and 882 nm, whereas for C_{80}(II) the main peaks are observed at 446(sh), 484(sh), 589, 606, 845 and 880 nm. C_{80}(II) shows a strong absorption band at *ca.* 600 nm which accounts for the greenish color of this fullerene in CS_2 solution.

Fig. 2 shows a ^{13}C NMR spectrum of C_{80}(II) in carbon disulfide solution with chromium(III) tris(acetylacetonate) as a relaxant and benzene-d_6 as the internal lock. The spectrum consists of a series of three distinct lines of near-equal intensity (lines 1,2,3) and two additional lines at half the intensity (lines 4* and 5*). The position of line 1 (δ 128.9) is very close to that of benzene-d_6 (δ 128.5). However, its characteristic fullerene linewidth (*ca.* 0.02 ppm) unambiguously distinguishes it from other solvent signals (linewidth > 0.1 ppm). We also performed ^{13}C NMR measurements by using acetone-d_6 instead of benzene-d_6 as an internal lock. The results confirm the five NMR lines and show that no C_{80} resonant lines were hidden by the benzene signals. The five signals cover a wide chemical shift range (δ 128.9–163.9), suggesting that C_{80}(II) has an ellipsoidal shape. C_{80} has seven IPR isomers (D_2, D_{5d}, C_{2v}, C_{2v}', D_3, D_{5h} and I_h)[2,4]. The present ^{13}C NMR result unambiguously assigns C_{80}(II) as the D_{5d} isomer (3 × 20; 2×10), where (a × b) indicates (number of NMR lines × relative intensity).

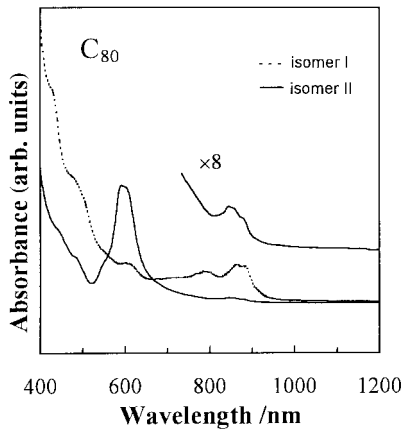

Fig. 1 VIS–NIR absorption spectra of C_{80}(I) and C_{80}(II) in CS_2 solution.

The most stable structure of C_{80} as D_{5d} is inferred from theoretical optimization by a nonlocal density function B3LYP/3-21G calculation using the Gaussian 98W program.[7] As shown in Fig. 3, $C_{80}(D_{5d})$ has an ellipsoidal structure with an aspect ratio (long axis/short axis) of *ca.*1.3. $C_{80}(D_{5d})$ can easily be obtained by adding one C_{10} ring on a half cap of $C_{70}(D_{5h})$ (*i.e.*, C_{30} or C_{40}) or adding two C_{10} rings successively on a $C_{60}(I_h)$ hemisphere (*i.e.*, C_{30}). As proposed by Curl,[8] $C_{70}(D_{5h})$ is formed by dissecting C_{60} into two C_{30} hemispheres along a suitable orientation (rotating one hemisphere 36° with respect to another hemisphere), and then by adding a ring of 10 carbon

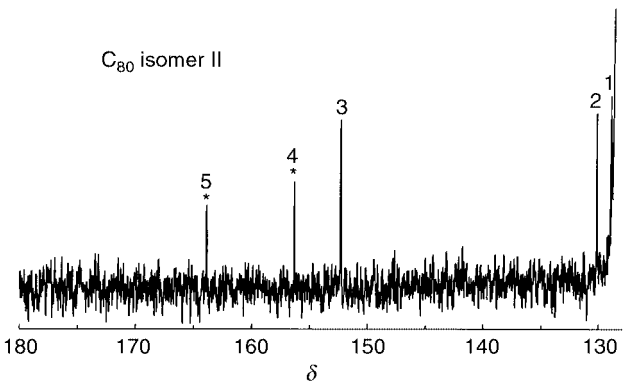

Fig. 2 ^{13}C NMR spectrum of purified C_{80}(II). The spectrum consists of five signals: 1(128.9, 13.9), 2(130.2, 12.7), 3(152.4, 12.2), 4*(156.3, 7.6), 5*(163.9, 6.0), in which (δ, I_{rel}) represent measured chemical shifts δ and relative intensity I_{rel}, and where lines indicated by * are half-intensity lines.

DOI: 10.1039/b000387p

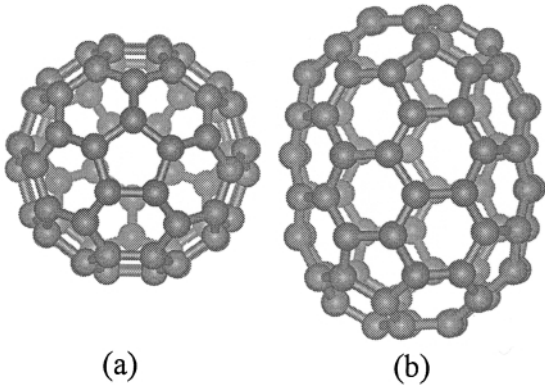

Fig. 3 The optimized structure of the $C_{80}(D_{5d})$ isomer based on *ab initio* calculation at the B3LYP/3-21G level by Gaussian 98W. (a) Top view along the main C_5 axis and (b) side view. The short/long axis ratio (a)/(b) is *ca.* 1/1.3.

atoms at the equator to combine the two hemispheres. The $C_{80}(D_{5d})$ fullerene is formed in a similar way by adding two C_{10} ring successively at the equator of C_{60} (*i.e.*, $C_{30} + C_{10} + C_{10} + C_{30}$). On going from $C_{60}(I_h)$ to $C_{70}(D_{5h})$ to $C_{80}(D_{5d})$, the fullerene structure, therefore, progressively acquires tubular and cap (hemisphere) parts, which leads to ^{13}C NMR lines spread over a wide range of chemical shift values.

The calculated energy ordering of the seven C_{80} isomers at the HF/Am1 level is: $D_5(D_{5d}) < D_2[+2.3] << C_{2v}[+23.6] < C_3(D_3)[+36] < C_s(C_{2v'})[+38.5] < C_s(D_{5h})[+49.9] << D_2(I_h)[+102$ kcal mol^{-1}], where the stabilization energies are given relative to the most stable $D_5(D_{5d})$ isomer.[4,9] The $D_5(D_{5d})$-C_{80} and D_2-C_{80} isomers are nearly isoenergetic and their relative energies are much smaller than those of the other five isomers. The currently isolated $C_{80}(D_{5d})$ is one of the most ellipsoidal fullerenes so far produced and isolated.

C. R. W. thanks JSPS for a Post Doctoral Fellowship for Foreigner Researchers. H. S. thanks JSPS for Future Program on New Carbon Nano-Materials for financial support of the present study.

Notes and references

1 H. W. Kroto, *Nature*, 1987, **329**, 529.
2 P. W. Fowler and D. E. Manolopoulos, *An Atlas of Fullerenes*, Clarendon, Oxford, 1995.
3 T. S. M. Wan, H. W. Zhang, T. Nakane, Z. Xu, M. Inakuma, H. Shinohara, K. Kobayashi and S. Nagase, *J. Am. Chem. Soc.*, 1998, **120**, 6806.
4 F. H. Henrich, R. H. Michel, A. Fischer, S. R. Schneider, S. Gilb, M. M. Kappes, D. Fuchs, M. Bürk, K. Kobayashi and S. Nagase, *Angew. Chem., Int. Ed. Engl.*, 1996, **35**, 1732.
5 T. J. S. Dennis and H. Shinohara, *Chem. Commun.*, 1998, 883.
6 C-R.Wang, M. Inakuma and H. Shinohara, *Chem. Phys. Lett.*, 1999, **300**, 379.
7 M. J. Frisch, G. W. Trucks, H. B. Schlegel, P. M. W. Gill, B. G. Johnson, M. A. Bobb, J. R. Cheeseman, T. Keith, G. A. Petersson, G. A. Montgomery, K. Raghavachari, M. A. Al-Laham, V. G. Zakrzewski, J. V. Ortiz, J. B. Foresman, J. Cioslowski, B. B. Stefanov, A. Nanayakkara, M. Challacombe, C. Y. Peng, P. Y. Ayala, W. Chen, M. W. Wong, J. L. Andres, E. S. Replogle, R. Gomperts, R. L.Martin, D. L. Fox, J. S. Binkley, D. J. DeFrees, J. Baker, J. P. Stewart, M. Head-Gordon, C. Gonzalez and J. A. Pople, *Gaussian 98W*, Gaussian, Pittsburgg, PA, 1998.
8 R. F. Curl, *Angew. Chem., Int. Ed. Engl.*, 1997, **36**, 1566.
9 K. Kbayashi, S. Nagase and T. Akasaka, *Chem. Phys. Lett.*, 1995, **245**, 230.

Communication b000387p

ChemComm

Modelling the enantioselectivity of subtilisin in water and organic solvents: insights from molecular dynamics and quantum mechanical/molecular mechanical studies†

Giorgio Colombo,*[a] Gianluca Ottolina,[a] Giacomo Carrea[a] and Kenneth M. Merz, Jr[b]

[a] *Istituto di Biocatalisi e Riconoscimento Molecolare, Via Mario Bianco, 9, 20131 Milano, Italy. E-mail: giorgio @ico.mi.cnr.it*

[b] *Department of Chemistry, 152 Davey Laboratory, Pennsylvania State University, University Park, Pennsylvania 16802, USA*

Received (in Cambridge, UK) 6th December 1999, Accepted 18th February 2000
Published on the Web 17th March 2000

Through molecular dynamics and quantum mechanical/molecular mechanical calculations we found that differential charge distributions due to the enzyme and to the different solvents can determine the reactivity of subtilisin in different media.

The possibility to use enzymes in organic media[1,2] has widened the range of applicability of proteins to almost all synthetic organic reactions. In these media, the absence of a continuous aqueous layer around the enzyme makes it possible for it to interact directly with the non-aqueous solvent, which results in modifications of the properties of the enzyme in terms of stability, activity and specificity/selectivity:[2] thus, enzymes like hydrolases and proteases can catalyse esterification and transesterification readily and with high product yields.[1] Serine proteases like subtilisin have also been the subject of many computational studies involving either the investigation of their structure–activity relationships[3–5] or of their catalytic mechanism using different theoretical approaches.[6–8] In a previous paper[9] we have examined the origin of enantioselectivity of the serine protease subtilisin in DMF through the use of molecular dynamics (MD) and free energy perturbation (FEP) simulations. As a model reaction we studied the resolution of a racemic mixture of *sec*-phenethyl alcohol by transesterification reaction with the acylating agent vinyl acetate in organic solvents (Scheme 1, ESI data†). The transition state (in which enantioselectivity is determined) leading to the ester formation in organic solvents is the same as the one leading to ester hydrolysis in water, and is represented by the tetrahedral intermediates (Figs. 1 and 2). A critical aspect of our previous study was the determination of the charge distribution on the two (*R* and *S*) tetrahedral intermediates and on the residues of the catalytic triad through the use of a combined quantum mechanical/molecular mechanical (QM/MM) electrostatic potential (ESP) fitting methodology. Our approach could reproduce the experimental $\Delta\Delta G^*_{(S-R)}$ value very well thanks to the application of a flexible charge model for the two diastereomeric intermediates. The experimental $\Delta\Delta G^*_{(S-R)}$ resulted 0.4 kcal mol^{-1}, while the calculated value was *ca.* 1 kcal mol^{-1}.[9]

We now extend the QM/MM treatment to other two solvents: water and hexane. The program ROAR 1.0[10] was used to carry out all the calculations, with all-atom AMBER parameters for the protein,[11] OPLS parameters for the organic solvents[12] and TIP3P parameters for water.[13] The QM region for QM/MM ESP calculations comprised the substrate and the residues involved in catalysis (Ser 221, Asp 32, His 64, Asn 155). The PM3[14,15] Hamiltonian was used for the minimisation stage, while MNDO[14,15] was used for the ESP stage. We used the MNDO Hamiltonian for ESP fitting because MNDO has been shown to give ESP fitted charges that are well correlated to HF/6-31G* ESP derived charges, while PM3 does not.[14,15] The systems (*R* and *S* complex in the three different environments) were MD equilibrated for 300 ps, and the structures for QM/MM calculations were saved every 15 ps over the last 180 ps of MD.

Two enantiomers in an achiral environment have the same physico-chemical properties, and hence, the same charge distribution on the corresponding atoms. The same enantiomeric substances bound or complexed to the enzyme, however, experience a chiral environment, which gives rise to two diastereoisomeric complexes. Lipkovitz *et al.*[16] pointed out that chiral auxiliaries can induce a desymmetrization of the frontier orbitals at the reaction site, making them chiral as well. This desymmetrization will be reflected in the electron (*i.e.* charge) distributions. In the tetrahedral complexes we have studied, the two substrates are perturbed by the chiral environment determined by the enzyme and thus by differential electrostatic fields, giving rise to differential charge distributions on analogous atoms of the substrate in the complex.

The concept of 'electrostatic stereodifferentiation',[9] together with steric factors, can be important in the determination of the energy difference between the two transition states leading to selectivity. The availability of QM/MM electrostatic potential fitting methods allows us to carefully take this aspect into consideration, by explicitly considering polarization and charge transfer effects due to the solvents (water, DMF, hexane).

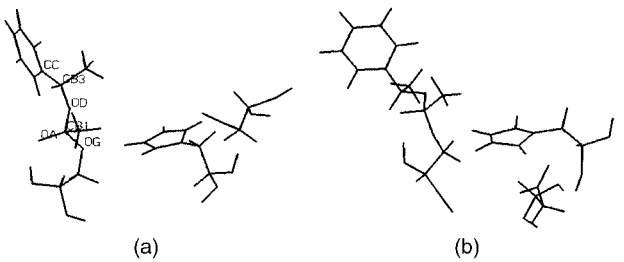

Fig. 1 Representation of the equilibrated *S* (a) and *R* (b) tetrahedral intermediates in organic solvents.

† Electronic supplementary information (ESI) available: average charge values for the reactive intermediate of Scheme 1. See http://www.rsc.org/suppdata/cc/a9/a909680i/

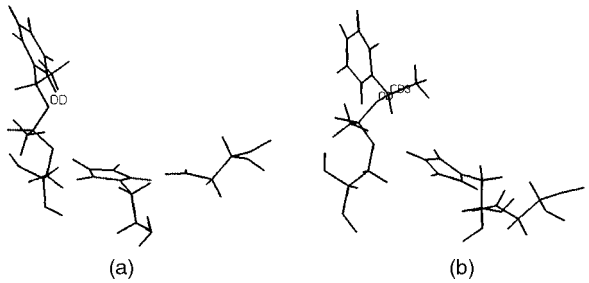

Fig. 2 Representation of the equilibrated *S* (a) and *R* (b) tetrahedral intermediates in water.

DOI: 10.1039/a909680i

The steric factors in the two organic solvents resulted very similar. Once the complex is equilibrated the phenyl group of the *S*-substrate fits very nicely into a hydrophobic pocket defined by residues 126, 127, 128 and Asn 155, in both DMF and hexane [Fig. 1(a)]. For the *R*-enantiomer [Fig. 1(b)] the phenyl ring is oriented towards the surrounding solvent, giving rise to favourable hydrophobic solvation interactions with the organic environment. The methyl group of the alcoholic moiety of the *R*-complex is now pointing into the hydrophobic pocket, and in total, these rearrangements contribute to disrupt the catalytically essential H-bonds (OD to HE2). We will show later on that this can have important consequences in terms of charge distribution.

In water, the phenyl ring tends to be removed from the unfavourable contact with the polar hydrogen bonding solvent, and resides in the hydrophobic pocket for both *R* and *S*-complexes. The methyl groups point towards the solvent. The difference in the two structures can be found in the conformation around the OD–CB3 bond. In the *S*-complex, the phenyl ring is in *anti*-conformation with respect to the rest of the bulky tetrahedral intermediate, while, for the *R*-complex, it assumes a more hindered and unfavourable *gauche*-conformation. The energetically unfavourable conformation of the *R*-complex will be a factor in depressing the reactivity of this enantiomer. The diastereoisomeric arrangement that determines the steric differences will be reflected in the charge distributions on the atoms which are directly involved in the formation (organic solvents) or disruption (water) of the tetrahedral intermediate (Table 1, ESI data†). Moreover, not only do we notice differences between enantiomers, but also on the same atoms of the same enantiomer in different solvents. In particular this is true for the stereogenic center CB3 and the atoms forming its environment. In fact, CB3 shows a charge value for the *S*-complex in water which is lower than in the two organic solvents. The same consideration applies also to CB3 in the *R*-complex, even if the charge differential among the solvents is less pronounced in this case. The case of CC (phenyl atom directly bound to the stereocenter) is also representative of this solvent effect for the *S*-complex: the charge on CC has a value of 0.11 in water and is negative for both hexane and DMF. For the *R*-complex the charges for this atom are very similar. Small but noticeable differences due to solvent effect can be noticed in HB3, as well. We believe that all these effects involving the differentiation of charges on analogous atoms of the same enantiomer in different solvents is mainly due to the differential polarising characteristics of the solvents.

When the same solvent environment is considered, the most dramatic differences between analogous atoms of the two enantiomers can still be noticed on the stereogenic (CB3) center and in the atoms around this center. This factor can be ascribed to the stereodifferentiating environment determined by the enzyme. In particular, we notice that the alcoholic OD has a higher charge concentration (*i.e.* more negative charge) in all solvents for the *S*-complex. On the other hand, a higher concentration of positive charge is localized on the tetrahedral carbon (CB1) in the *S*-complex in all solvents. This makes the CB1–OD bond (the one formed in organic solvents and cleaved in water) more highly polarised in the transition state leading to the *S*-product. A higher concentration of negative charge on the nucleophilic atom, coupled with a higher positive charge on the electrophilic carbon (CB1), will favour the approach between the alcoholic moiety and the acyl enzyme in the absence of other nucleophiles. Moreover, the higher negative charge concentration on OD will favour the formation of a stable hydrogen bond between OD and the acidic HE2 hydrogen on His 64 for the *S*-complex (the average distance between OD @Ser 221–HE2 @His 64 in this case is 2.6 ± 0.6). On the other hand, in the *R*-complex, the catalytically essential hydrogen bond is disrupted because of both steric and charge factors: OD is, in fact, less negative than in the *S*-complex case. These observations suggest that, in the transesterification reaction the *R*-alcohol cannot readily donate its proton to the catalytic residue His 64, which is essential for catalysis.[17] For hydrolysis this very factor will favour the cleavage of the reactive bond, by concentrating more negative charge on the more electronegative carbon (OD), in the tetrahedral intermediate for *S*-complex. A smaller polarization is found for the CB1–OD bond in the *R*-complex in all solvents. This will slow down the corresponding reaction leading to the preferential synthesis or hydrolysis of the compounds with *S* absolute configuration. By considering the charge distribution, we can garner deeper insights into how the electrostatically stereodifferentiating environment imposed by the enzyme can influence reactivity and selectivity. Our results are in agreement with, and help us rationalize, the experimental observation of reactivity in several environments.[18]

Summarising, we showed that steric and electrostatic factors play an important role in determining asymmetric induction and selectivity for enzymes in different environments. The application of QM/MM simulation techniques can be of valuable help in identifying the residues near the active site and of the binding pocket which are important for catalysis. The steric differentiation between two bound enantiomers can thus be magnified by mutating non-bulky residues of this region to sterically demanding ones. Maximising the charge differential between the two tetrahedral intermediates through mutations of non-polar to polar residues, which are involved in recognition, can also improve selectivity. Finally, focussing on the solvation patterns of the two simulated bound intermediates can help us find solvents which could better solvate the exposed parts of one of the two enantiomers.

We thank the Biotechnology Programme of the European Commission and the National Research Council of Italy (CNR) Target Project on Biotechnology for funding.

Notes and references

1 G. Carrea, G. Ottolina and S. Riva, *Trends. Biotechnol.*, 1995, 63.
2 A. Zaks and A. M. Klibanov, *Science*, 1984, 1249.
3 G. Colombo and K. M. Merz, Jr., *J. Am. Chem. Soc.*, 1999, **121**, 6895.
4 S. Toba, D. S. Hartsough and K. M. Merz, Jr., *J. Am. Chem. Soc.*, 1996, **118**, 6490.
5 S. Toba and K. M. Merz, *J. Am. Chem. Soc.*, 1997, **119**, 9939.
6 V. Daggett, S. Schröder and P. Kollman, *J. Am. Chem. Soc.*, 1991, **113**, 8926.
7 S. Schröder, V. Daggett and P. Kollman, *J. Am. Chem. Soc.*, 1991, **113**, 8922.
8 J. Bentzien, R. P. Muller, J. Florian and A. Warshel, *J. Phys., Chem. B*, 1998, **102**, 2293.
9 G. Colombo, S. Toba and K. M. Merz, Jr., *J. Am. Chem. Soc.*, 1999, **121**, 3486.
10 A. Cheng, R. S. Stanton, J. J. Vincent, K. V. Damodaran, S. L. Dixon, D. S. Hartsough, S. A. Best and K. M. J. Merz, *ROAR*; 1.0 edn.; ed. A. Cheng, R. S. Stanton, J. J. Vincent, K. V. Damodaran, S. L. Dixon, D. S. Hartsough, S. A. Best and K. M. J. Merz, The Pennsylvania State University, PA, 1997.
11 W. D. Cornell, P. Cieplak, C. I. Bayly, I. R. Gould, K. M. Merz, Jr., D. M. Ferguson, D. C. Spellmeyer, T. Fox, J. W. Caldwell and P. A. Kollman, *J. Am. Chem. Soc.*, 1995, **117**, 5179.
12 W. L. Jorgensen and J. Tirado-Rives, *J. Am. Chem. Soc.*, 1988, **110**, 1657.
13 W. L. Jorgensen, J. Chandrasekhar, J. Madura, R. W. Impey and M. L. Klein, *J. Chem. Phys.*, 1983, **79**, 926.
14 B. H. Besler, K. M. Merz, Jr. and P. A. Kollman, *J. Comput. Chem.*, 1990, **11**, 431.
15 S. C. Hoops, K.W. Anderson and K. M. Merz, Jr., *J. Am. Chem. Soc.*, 1991, **113**, 8262.
16 K. B. Lipkowitz, D. Gao and O. Katzenelson, *J. Am. Chem. Soc.*, 1999, **121**, 5559.
17 J. Uppenberg, N. Ohrner, M. Norin, K. Hult, G. J. Kleywegt, S. Patkar, V. Waagen, T. Anthonsen and T. Jones, *Biochemistry*, 1995, **34**, 16 838.
18 G. Colombo, G. Ottolina, G. Carrea, A. Bernardi and C. Scolastico, *Tetrahedron: Asymmetry*, 1998, **9**, 1205.

Communication a909680i

ChemComm

pH Modulation of the luminescence emission of a new europium cryptate complex

Carla Bazzicalupi,[a] Andrea Bencini,*[a] Antonio Bianchi,*[a] Claudia Giorgi,[a] Vieri Fusi,[b] Andrea Masotti,[a] Barbara Valtancoli,[a] Ana Roque[c] and Fernando Pina*[c]

[a] *Department of Chemistry, University of Florence, Via Maragliano 75/77, 50144 Florence, Italy. E-mail: benc@chim1.unifi.it*
[b] *Institute of Chemical Sciences, University of Urbino, Italy. E-mail: vieri@chim.uniurb.it*
[c] *Departamento de Química, Centro de Química-Fina e Biotecnologia, Faculdade de Ciências e Tecnologia, Universidade Nova de Lisboa, Quinta da Torre 2825, Monte de Caparica, Portugal. E-mail: fjp@dq.fct.unl.pt*

Received (in Cambridge, UK) 6th December 1999, Accepted 22nd February 2000
Published on the Web 17th March 2000

The luminescence emission of a new dipyridyl-containing Eu(III) cryptate complex is modulated by pH, due to protonation of the polyamine chain strategically inserted within the ligand backbone.

The use of europium and terbium complexes as luminescent labels in fluoroimmunoassay is limited by the fact that they have extremely low absorption coefficients.[1] This drawback can be overcome through encapsulation of the metal inside the cavity of phenanthroline or dipyridyl-containing cryptands.[2] These moieties contain two nitrogen donors which act as binding sites for the metal cation and can efficiently protect the metal from the solvent, especially in aqueous solution where metal-bound water molecules may act as quencher of the emission. In addition, these efficient chromophore units allow the collection and transfer of electronic energy to the metal.[1] A further development of this study is the design of water-soluble cryptate complexes whose fluorescence emission can be modulated by pH. To this purpose we have synthesized the new cryptand **L**.

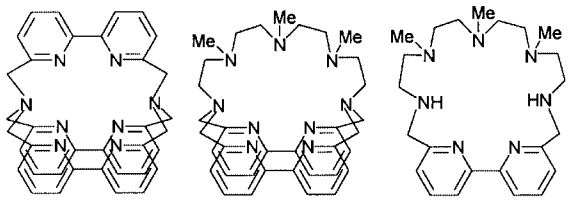

1 **L** **2**

The major difference from previously reported dipyridyl-containing cryptands, such as **1**,[1,2] is the strategic insertion in **L** of a polyamine chain within the ligand backbone, which connects the two dipyridyl chromophore units. We hoped that this ligand could be able to lead to a stable Eu(III) cryptate complex in aqueous solution. At the same time, the aliphatic amine groups, which are more basic than heteroaromatic nitrogens,[3] may be protonated, leading to protonated cryptate complexes.

Ligand **L** was obtained, as the sodium complex, [Na⊂**L**]ClO_4, by reaction of 2,2′-bis(bromomethyl)dipyridyl[4] with the macrocyclic precursor **2** (MeCN, Na_2CO_3, reflux). The latter was obtained by condensation of 2,2′-bis(bromomethyl)dipyridyl with 1,13-ditosyl-4,7,10-trimethyl-1,4,7,10,13-pentaazatridecane,[5] by using the procedure of Richman and Atkins.[6] Reaction of [Na⊂**L**]ClO_4 with $EuCl_3$ (1:1 molar ratio) in aqueous solution (pH 3, 100 °C, 24 h) affords the protonated complex [$EuCl_3$⊂$\mathbf{L}H_2$]$(ClO_4)_2 \cdot 4H_2O$ in 64% yield.†

The crystal structure of $[EuCl_3 \subset \mathbf{L}H_2]^{2+}$ **3** (Fig. 1)‡ shows the metal enclosed within the cryptand cavity, coordinated by the dipyridyl nitrogens N(2), N(3), N(5) and N(6) and by the two bridgehead amine groups N(1) and N(4). The polyamine chain N(7)–N(8)–N(9) is not coordinated, due to binding of the two acidic protons within this triamine subunit. The Eu(III) cation completes its coordination environment by binding three chloride anions. The coordination geometry is best described as a distorted tricapped trigonal prism, the two basal planes being defined by N(5), N(6) and Cl(1) and N(2), N(3) and Cl(2), respectively. The capped positions are occupied by the N(1), N(4) and Cl(3) donors. It is also of interest that, although the metal is lodged inside the cryptand cavity, the protonated ligand leaves free binding sites at the metal, available for the binding of exogenous species, such as chloride anions in the present structure. Most likely, water molecules replace these anions in aqueous solutions in the absence of chloride.

The Eu(III) cryptate complex can be obtained in aqueous solution by addition of $Eu(ClO_4)_3$ to [Na⊂**L**]ClO_4 (1:1 molar ratio, 60 °C, 12 h at pH 7); the luminescence spectrum of the europium cryptate in aqueous solution shows the characteristic visible emission of the complexed metal (λ_{max} = 617 nm) which mainly arises from intramolecular transfer to the metal ion from the highest energy triplet state of the cryptand.§ The

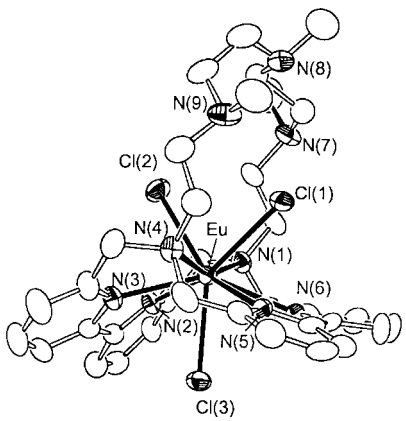

Fig. 1 ORTEP[11] drawing of $[EuCl_3 \subset H_2\mathbf{L}](ClO_4)_2 \cdot 4H_2O$. Selected bond lenghts (Å) and angles (°): Eu–N(3) 2.606(10), Eu–N(5) 2.607(10), Eu–N(6) 2.610(9), Eu–N(2) 2.632(10), Eu–N(4) 2.712(9), Eu–Cl(2) 2.713(4), Eu–N(1) 2.771(9), Eu–Cl(3) 2.800(4), Eu–Cl(1) 2.820(4), N(3)–Eu–N(5) 106.6(3), N(3)–Eu–N(6) 144.4(3), N(5)–Eu–N(6) 62.6(3), N(3)–Eu–N(2) 61.1(3), N(5)–Eu–N(2) 144.1(3), N(6)–Eu–N(2) 106.4(3), N(3)–Eu–N(4) 64.1(3), N(5)–Eu–N(4) 62.7(3), N(6)–Eu–N(4) 124.2(3), N(2)–Eu–N(4) 124.2(3), N(3)–Eu–Cl(2) 76.9(2), N(5)–Eu–Cl(2) 136.3(2), N(6)–Eu–Cl(2) 135.7(2), N(2)–Eu–Cl(2) 76.8(2), N(4)–Eu–Cl(2) 82.0(2), N(3)–Eu–N(1) 122.7(3), N(5)–Eu–N(1) 125.6(3), N(6)–Eu–N(1) 64.0(3), N(2)–Eu–N(1) 62.8(3), N(4)–Eu–N(1) 158.6(3), Cl(2)–Eu–N(1) 80.4(2), N(3)–Eu–Cl(3) 71.8(2), N(5)–Eu–Cl(3) 71.4(2), N(6)–Eu–Cl(3) 72.6(2), N(2)–Eu–Cl(3) 72.7(2), N(4)–Eu–Cl(3) 99.7(3), Cl(2)–Eu–Cl(3) 143.91(12), N(1)–Eu–Cl(3) 101.7(2), N(3)–Eu–Cl(1) 141.6(2), N(5)–Eu–Cl(1) 72.2(2), N(6)–Eu–Cl(1) 70.7(2), N(2)–Eu–Cl(1) 139.6(2), N(4)–Eu–Cl(1) 83.2(3), Cl(2)–Eu–Cl(1) 79.15(12), N(1)–Eu–Cl(1) 81.6(2), Cl(3)–Eu–Cl(1) 136.94(11).

DOI: 10.1039/a909581k

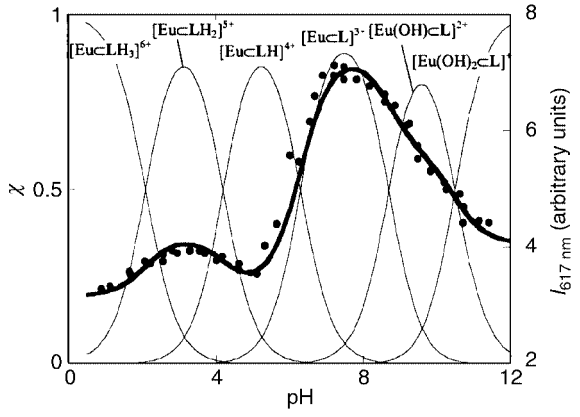

Fig. 2 Luminescence emission (●) of the Eu(III) complex with **L** (λ_{exc} = 260 nm; λ_{em} = 617 nm, [**L**] = [Eu^{3+}] = 5×10^{-5} M, T = 300 K) and calculated molar fractions of the Eu(III) complexes (——) as a function of pH.

luminescence emission, however, is strongly affected by pH, displaying a maximum at neutral pH and significant decreases both at acidic and alkaline pH, as shown in Fig. 2. pK_a values of 2.1, 4.2, 6.3, 8.7 and 10.5 for the Eu(III) complex can be derived from the titration curve in Fig. 2 by least-squares analysis using the bracketing technique.[7]¶ Most likely, the first three constants correspond to protonation of the complex to give [Eu⊂**L**H$_n$]$^{(n+3)+}$ (n = 1–3) species at acidic pH. This process involves the aliphatic polyamine chain, as strongly supported by the crystal structure of the [EuCl$_3$⊂**L**H$_2$]$^{2+}$ cation. Protonation does not allow the amine groups to bind to the Eu(III) cation, and, therefore, the ligand donors do not fulfill the coordination sphere of the metal. The resulting free binding sites at the metal are occupied by water molecules, which can quench the luminescence of the complex. This hypothesis is confirmed by the analysis of the lifetimes (τ) of the Eu(III) cryptate at different pH values in H_2O and D_2O at 300 K. For instance, at pH 2, τ = 0.39 ms in H_2O and 1.4 ms in D_2O, while, at pH 6.8, τ = 0.52 and 1.34 ms in H_2O and D_2O, respectively. These data account for the coordination of *ca*. two water molecules at pH 2 and just one at pH 6.8.[8] Binding of amine groups in the unprotonated [Eu⊂**L**]$^{3+}$ complex gives a more 'protected' metal cation from the solvent molecules, thus enhancing the luminescence emission, with a maximum at pH 7.2. Finally, the observed decrease of the emission at alkaline pH is due to the formation of the hydroxylated species [Eu(OH)⊂**L**]$^{2+}$ and [Eu(OH)$_2$⊂**L**]$^+$, with pK_a values of 8.7 and 10.5, respectively. Binding of hydroxide anions to Eu(III) gives rise to a quenching of the emission.

The spectral features of the present complex are similar to those reported for other dipyridyl-containing Eu(III) cryptate complexes.[1,2,9] At pH 6.8, the quantum yield (Φ = 0.014 at 300 K), the radiative rate constant (k_r = 746 s^{-1}), the non-radiative temperature independent rate constant due to the coupling with the high-energy O–H oscillators [k_{nr}(OH) = 1177 s^{-1}], and the temperature dependent decay rate constant [$k_{nr}(T) \cong 0$], are somewhat lower than those found for [Eu⊂**1**]$^{3+}$, as expected considering the replacement of a dipyridyl chromophore unit of **1** by an aliphatic polyamine chain in **L**. The present complex, however, still remains an efficient luminescent system. At the same time, the pH dependence of the emission intensity is a novel characteristic of our cryptate complex, which can be defined a 'pH modulated antenna device'.

Notes and references

† **2**: Elemental anal. Calc. for $C_{23}H_{37}N_7$: C, 67.12; H, 9.06; N, 23.82. Found: C, 66.9; H, 9.1; N, 23.7%. ^{1}H NMR (D_2O, pH = 11): δ 1.97 (s, 3H), 2.17 (s, 6H), 2.19 (t, 4H), 2.35 (t, 4H), 2.38 (t, 4H), 2.7 (t, 4H), 3.93 (s, 4H), 7.51 (dd, 2H), 7.98 (dd, 2H), 8.02 (dd, 2H).^{13}C NMR (D_2O, pH = 11): δ 42.26, 43.74, 45.51, 54.02, 54.66, 54.89, 56.54, 122.56, 125.49, 140.18, 156.54, 160.19.

[Na⊂**L**]ClO_4: Elemental anal. Calc. for $C_{35}ClH_{45}NaN_9O_4$: C, 58.86; H, 6.35; N, 17.65. Found: C, 58.9; H, 6.5; N, 17.5%. ^{1}H NMR ($CDCl_3$): δ 7.94 (dd, 4H), 7.85 (d, 4H), 7.36 (dd, 4H), 3.98 (d, 2H), 3.78 (d, 2H), 3.13 (m, 4H), 2.78 (t, 4H), 2.68 (m, 7H), 2.51 (m, 4H), 2.05 (s, 6H). ^{13}C NMR ($CDCl_3$): δ 42.26, 42.89, 53.84, 54.75, 61.06, 120.49, 124.59,138.75,154.61, 158.79.

[$EuCl_3$⊂**L**H$_2$]$(ClO_4)_2$·4H_2O. Elemental anal. Calc. for $C_{35}Cl_5EuH_{55}N_9O_{12}$: C, 37.43; H, 4.94; N, 11.22. Found: C, 37.4; H, 4.9; N, 11.3%.

‡ *Crystal data* for $C_{35}H_{55}Cl_5EuN_9O_{12}$: M = 1123.09, triclinic, $P\bar{1}$, a = 13.302(4), b = 13.306(6), c = 15.23(1) Å, α = 83.69(5), β = 64.46(4), γ = 66.14(3)°, V = 2218(2) Å^3, T = 298 K, Z = 2, μ(Mo-Kα) = 1.785 mm^{-1}, 5638 reflections collected, 5329 unique (R_{int} = 0.1189) which were used in all calculation, final R indices $R1$ = 0.0769 [$I > 2\sigma(I)$], $wR2$ = 0.2364 (all data).

The structure was solved using direct method (SIR92) and refined by full matrix least squares on F^2 (SHELXL-93).[10] An absorption correction was applied once the structure was solved (DIFABS).[10]

CCDC 182/1554. See http://www.rsc.olg/suppdata/cc/a9/a909581k/ for crystallographic files in .cif format.

§ Fluorescence emission spectra at different pH values were recorded on solutions with [**L**] = [Eu^{3+}] = 5×10^{-5} M using a SPEX F111 Fluorolog spectrofluorimeter.

¶ The total emission intensity at each pH value is given by $\Sigma_i c_i \chi_i$, where c_i is a constant proportional to the quantum yield and χ_i the molar fraction of the ith species. The c_i and χ_i values were calculated by least squares fitting of the emission data collected at different pH values. The pK_a values were then derived from the calculated χ_i. The fitting was carried out by using the emission intensity at 617 nm with an excitation wavelength of 260 nm. Absolute quantum yields were calculated by least squares fitting of the integrals of the emission spectra at each pH value, using the fluorescence emission of [Ru(bpy)$_3$]$^{2+}$ as reference: [Eu⊂**L**H$_3$]$^{6+}$, 0.0022; [Eu⊂**L**H$_2$]$^{5+}$, 0.0098; [Eu⊂**L**H]$^{4+}$, 0.00014; [Eu⊂**L**]$^{3+}$, 0.014; [Eu(OH)⊂**L**]$^{2+}$, 0.011; [Eu(OH)$_2$⊂**L**]$^+$, 0.0014.

1 N. Sabbatini, M. Guardigli and J.-M. Lehn, *Coord. Chem. Rev.*, 1993, **123**, 201; V. Balzani, A. Credi and M. Venturi, *Coord. Chem. Rev.*, 1998, **171**, 3 and references therein.

2 J.-C. Rodriguez-Ubis, B. Alpha, D. Plancherel and J.-M. Lehn, *Helv. Chim. Acta*, 1984, **67**, 2264; B. Alpha, J.-M. Lehn and G. Mathis, *Angew. Chem., Int. Ed. Engl.*, 1987, **26**, 266; I. Bkouche-waksman, J. Guilhem, C. Pascard, B. Alpha, R. Deschneaux and J.-M. Lehn, *Helv. Chim. Acta*, 1991, **74**, 1163; C. O. Paul-Roth, J.-M. Lehn, J. Guilhem and C. Pascard, *Helv. Chim. Acta*, 1995, **78**, 1895.

3 *Critical Stability Constants*, ed. R. M. Smith and A. E. Martell, Plenum, New York, 1975; C. Bazzicalupi, A. Bencini, A. Bianchi, C. Giorgi, V. Fusi, B. Valtancoli, M. A. Bernardo and F. Pina, *Inorg. Chem.*, 1999, **38**, 3806.

4 Z. Wang, J. Reibenspies and A. E. Martell, *J. Chem. Soc., Dalton Trans.*, 1995, 1511.

5 A. Bencini, A. Bianchi, E. Garcia-España, V. Fusi, M. Micheloni, P. Paoletti, J. A. Ramirez, A. Rodriguez and B. Valtancoli, *J. Chem. Soc., Perkin Trans. 2*, 1992, 1059.

6 J. E. Richman and T. J. Atkins, *J. Am. Chem. Soc.*, 1974, **96**, 2268.

7 W. H. Press, B. P. Flannery, S. A. Teukolsky and W. T. Vetterling, *Numerical Recipes. The Art of Scientific Computing*, Cambridge University Press, New York, 1991, **61**, 956.

8 W. DeW. Horrocks and D. R. Sudnick, *J. Am. Chem. Soc.*, 1979, **101**, 334; W. DeW. Horrocks and D. R. Sudnick, *Acc. Chem. Res.*, 1981, **14**, 384.

9 B. Alpha, V. Balzani, J.-M. Lehn, S. Perathoner and N. Sabbatini, *Angew Chem., Int. Ed. Engl.*, 1987, **26**, 1266.

10 SIR92: A. Altomare, G. Cascarano, C. Giacovazzo and A. Guagliardi, *J. Appl. Crystallogr.*, 1993, **26**, 343; SHELXL-93: G. M. Sheldrick, SHELXL-93, Göttingen, 1993; DIFABS: N. Walker and D. D. Stuart, *Acta Crystallogr., Sect. A*, 1983, **39**, 158.

11 C. K. Johnson, ORTEP: Report ORNL-3794; Oak Ridge National Laboratory, Oak Ridge, TN, 1971.

Communication a909581k

ChemComm

A novel alkoxide bridging motif between boron trifluoride and copper(II) in a crown thioether complex

Liam R. Sutton, Alexander J. Blake, Paul A. Cooke and Martin Schröder*

School of Chemistry, The University of Nottingham, Nottingham, UK NG7 2RD.
E-mail: m.schroder@nottingham.ac.uk

Received (in Cambridge, UK) 3rd November 1999, Accepted 19th January 2000

Reaction of 6-hydroxy-1,4,8,11-tetrathiacyclotetradecane (LH) with $Cu(BF_4)_2$ in THF yields $[Cu(LH)](BF_4)_2$; crystallisation of the complex from $MeNO_2/Et_2O$ gives brown crystals of $[Cu(LBF_3)](BF_4)$, the first example of alkoxide bridging between BF_3 and a metal centre.

The synthesis and coordination chemistry of crown thioethers has become well established over the past two decades[1] with many complexes of the transition metals, from titanium to mercury, having been reported.[2] We have been interested in the functionalisation of thioether crowns[3] in order to couple their coordination behaviour to desirable physical and/or chemical properties, with a particular interest in developing macrocyclic metallomesogens.[4] Because such modification must take place on the carbon backbone we have been studying the organic and coordination chemistry of a number of functionalised crown thioethers including 6-hydroxy-1,4,8,11-tetrathiacyclotetradecane (LH)[5] so that we might better understand the interplay between the macrocyclic core and the pendant functionality.

Addition of a colourless solution of LH in THF to a pale green solution of a slight excess of $Cu(BF_4)_2$ hydrate in THF immediately affords a fine dark green precipitate which was isolated in 85% yield (Scheme 1). IR spectroscopic, FAB mass spectrometric and microanalytical data for this product are in accord with the stoichiometry $[Cu(LH)](BF_4)_2$, **1**.† Compound **1** appears to be unstable in MeCN and $MeNO_2$ to give very dark brown solutions. Deep brown crystals suitable for X-ray diffraction were formed over several days by the diffusion of Et_2O vapour into a solution of **1** in $MeNO_2$ and a single crystal structural determination‡ was undertaken in order to confirm the structure of the product. The single crystal X-ray structure determination (Fig. 1) confirms the formation of $[Cu(LBF_3)]BF_4$, **2**, in which one of the BF_4^- anions from **1** has condensed with the $[Cu(LH)]^{2+}$ cation, eliminating HF. Presumably, HF goes on to combine with the glass walls of the vials used for crystallisation forming Si–F bonds which provide the thermodynamic driving force for the reaction. Interestingly, attempted crystallisation of $Ni(BF_4)_2$ with LH from MeOH–Et_2O resulted in the quantitative formation of $[Ni(MeOH)_6]SiF_6$ (confirmed by single crystal X-ray structural analysis) supporting the mechanism postulated.

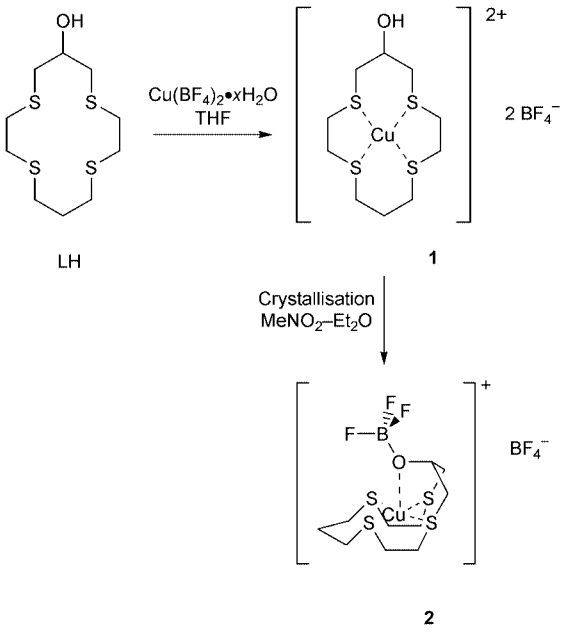

Scheme 1

Microanalytical data obtained from the sample of **2** from which the crystal was drawn, in concert with the difference in colour of **1** and **2**, indicate that conversion of **1** to **2** occurs quantitatively.§ Further evidence that **1** is different to **2** is provided by the powder X-ray diffraction pattern (Fig. 2) obtained from **1**, which is different to that calculated for **2**. Compound **2** is unstable in air, with hydrolysis *via* atmospheric moisture affording a product tentatively assigned as $[Cu(LH)](BF_4)(BF_3OH)$, which exhibits a similar electronic spectrum to **1**.

The monocation $[Cu(LBF_3)]^+$ in **2** adopts a square-pyramidal geometry at Cu(II) which is somewhat distorted by the steric restrictions imposed by the macrocyclic ligand, with Cu, B(1), O(6), C(6) and C(13) lying on a crystallographic mirror plane. The Cu–S distances of 2.2677(15) and 2.3312(15) Å in **2** are similar to those observed[6] in $[Cu([14]aneS_4)]^{2+}$, with the Cu–O(6) distance of 2.311(5) Å in the five coordinate complex **2**

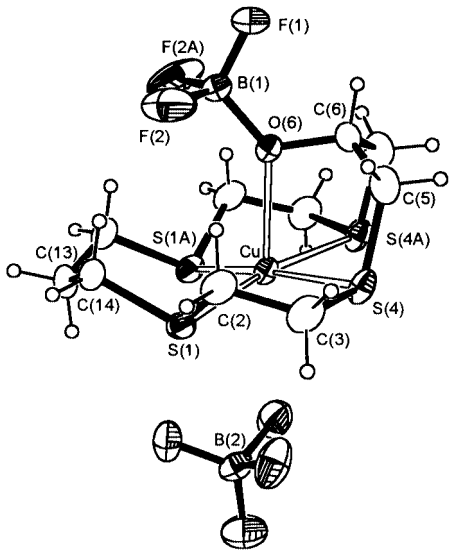

Fig. 1 View of the structure of **2** with numbering scheme adopted. Selected bond distances (Å) and angles (°): Cu–S(1) 2.2677(15), Cu–S(4) 2.3312(15), Cu–O(6) 2.311(5), B(1)–O(6) 1.441(10), O(6)–C(6) 1.419(9); S(1)–Cu–S(1A) 95.32(8), S(1)–Cu–S(4) 88.58(6), S(4)–Cu–S(4A) 86.43(8), S(1)–Cu–O(6) 103.29(9), S(4)–Cu–O(6) 83.71(10), Cu–O(6)–B(1) 139.2(4), Cu–O(6)–C(6) 100.0(4), B(1)–O(6)–C(6) 120.8(6). Minor parts of disorder omitted for clarity. Atoms carrying the suffix A are related to the corresponding unsuffixed atoms across a crystallographic mirror plane by $x, -y + 3/2, z$.

DOI: 10.1039/a908778h

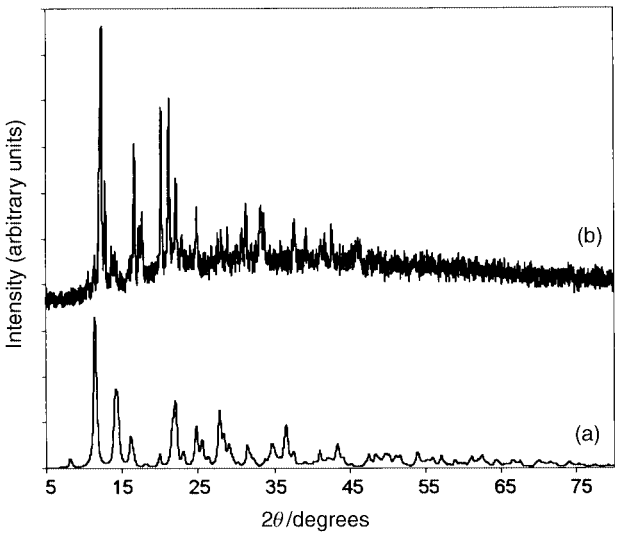

Fig. 2 Powder X-ray diffraction patterns: (a) calculated for **2** from crystal data[13] and (b) recorded for **1** (Philips X-pert diffractometer; PW3710 diffractometer control unit; Cu-*K*α radiation source at 40kV/40mA; step size 0.02° (0.4 s per step); 2θ range 5–80°; divergence slit 1° and receiving slit 2°).

some 0.131 Å shorter than in the related [Cu(*trans*-6,13-dihydroxy[14]aneS$_4$)](ClO$_4$)$_2$ where O atoms occupy the two axial sites of a Jahn–Teller distorted octahedral Cu(II) centre.[7] This reflects the greater electrostatic interaction expected for the five coordinate Cu(II) centre in **2** with an apical alkoxide ligand compared to the six coordinate analogue. The apical O-donor in **2** bridges to a disordered BF_3 moiety, O(6)–B(1) 1.441(10) Å which exhibits a rigorously planar geometry. The unconstrained B(1)–O(6)–C(6) angle of 120.8(6)° and the fact that the relevant atoms lie on a crystallographic mirror plane indicate sp^2 hybridisation at O(6), supporting the designation of this oxygen as a bridging alkoxide.[8]

Significantly, the structure of **2** represents the first example of an alkoxide bridge between BF_3 and a metal ion to be confirmed crystallographically. Hydrolysis of BF_4^- to give $BF_3(OH)^-$ is not uncommon and several examples of coordination of this anion *via* bridging hydroxide have been reported.[9] Alcoholysis has also been observed yielding, for example, the $BF_3(OEt)^-$ anion, which has not been seen to coordinate further.[10] A small number of adducts of BF_3 and carbonyl compounds have been isolated[11] due to the interest in the use of Lewis acids to activate such compounds. However, examples of trigonal oxygen in BF_3–alcohol adducts such as the MeOH·BF_3 are rare,[12] and the structure of **2** represents, to our knowledge, the first example of alkoxide bridging between BF_3 and a metal centre.

The short Cu–O(6) distance in **2** affords boat conformation for the Cu–S(4)–C(5)–C(6)–C(5A)–S(4A) chelate ring. We conclude that the stereochemistry and conformation of the complexed macrocycle is a key factor governing the formation of the novel bridging motif observed in **2**, the macrocyclic core allowing O(6) to adopt a position where stabilising interactions with both BF_3 and Cu(II) are possible. The crown thioether macrocycle, therefore, provides a covalently attached S_4-donor set which supports the close approach of Cu(II) to the alkoxytrifluoroborate O-centre, resulting in the unusual structure observed.

We thank the EPSRC for support and Dr David Rees for assistance with X-ray powder diffraction.

Notes and references

† *Analytical data* for **1**: found: C, 23.06; H, 3.83; N, 0.00. $C_{10}H_{20}B_2CuF_8OS_4$ requires C, 23.02; H, 3.86; N, 0%; ν_{max}/cm^{-1} (KBr disc) 3441s, 2920w, 1636m, 1419m, 1294w, 1084v, 1059v, 862w, 668w, 522m; λ_{max}/nm (ε/M^{-1} cm^{-1}): (DMF, 25 °C) 396 (330); *m*/*z* (FAB) 347 (M$^+$ −2BF_4).

‡ *Crystal data* for: **2**: $C_{10}H_{19}B_2CuF_7OS_4$, M = 501.65, monoclinic, space group $P2_1/m$ with a = 7.6090(5), b = 11.0873(10), c = 10.7640(9) Å, β = 91.687(7)°, U = 907.7 Å^3, Z = 2, μ = 1.728 mm^{-1}. Of 1783 reflections collected ($2\theta_{max}$ = 50°, $-9 \leqslant h \leqslant 9$, $-8 \leqslant k \leqslant 13$, $-9 \leqslant l \leqslant 12$), 1688 were unique and 1432 were used in all calculations. Disorder was modelled by rotation of 60° about the B(1)–O(6) bond in *ca.* 10%, and rotation of 60° about the B(2)–F(3) vector in *ca.* 34% of the asymmetric units, similarity restraints being placed on appropriate bond lengths, angles and anisotropic displacement parameters. At final convergence, $R1$[1432 $F \geqslant 4\sigma(F)$] = 0.0464 and $wR2(F^2$, all data) = 0.1325 and the final ΔF synthesis showed no peaks above 0.81 e Å^{-3}. CCDC 182/1527. See http://www.rsc.org/suppdata/cc/a9/a908778h/ for crystallographic files in .cif format.

§ *Analytical data* for **2**: found C, 24.00; H, 3.85; N, 0.00. $C_{10}H_{19}B_2CuF_7OS_4$ requires C, 23.94; H, 3.82; N, 0%; λ_{max}/nm (ε/M^{-1} cm^{-1}) (MeCN, 25°C) 571 (1200), 392 (7200).

1 A. J. Blake and M. Schröder, *Adv. Inorg. Chem.*, 1990, **35**, 1; S. R. Cooper, *Struct. Bonding (Berlin)*, 1990, **72**, 1.

2 For example see: P. J. Wilson, A. J. Blake, P. Mountford and M. Schröder, *Chem. Commun.*, 1998, 1007; M. Herceg and D. Matkovic-Calogovic, *Z. Kristallogr.*, 1995, **210**, 36; R. Schibli, R. Alberto, U. Abram, S. Abram, A. Egli, P. A. Schubiger and T. A. Kaden, *Inorg. Chem.*, 1998, **37**, 3509; L. R. Sutton, A. J. Blake, W.-S. Li and M. Schröder, *J. Chem. Soc., Dalton Trans.*, 1998, 279; A. F. Hill and J. D. E. T. Wilton-Ely, *Organometallics*, 1997, **16**, 1430; C. Landgrafe and W. S. Sheldrick, *J. Chem. Soc., Dalton Trans.*, 1996, 1237; A. J. Blake, Y. V. Roberts and M. Schröder, *J. Chem. Soc., Dalton Trans.*, 1996, 1885; A. J. Blake, V. Lippolis, S. Parsons and M. Schröder, *Chem. Commun.*, 1996, 2207; R. D. Adams, S. B. Fallon, J. L. Perrin, J. A. Queisser and J. H. Yamamoto, *Chem. Ber.*, 1996, **129**, 313; R. D. Adams, J. A. Queisser and J. H. Yamamoto, *J. Am. Chem. Soc.*, 1996, **118**, 10 674.

3 L. R. Sutton, A. J. Blake, P. A. Cooke, R. O. Gould, S. Parsons and M. Schröder, *Synlett.*, 1999, **S1**, 921; N. R. Champness, D. W. Bruce and M. Schröder, *New. J. Chem.*, 1999, **23**, 671.

4 A. J. Blake, D. W. Bruce, I. A. Fallis, S. Parsons and M. Schröder, *J. Chem. Soc., Chem. Commun.*, 1994, 2471; A. J. Blake, D. W. Bruce, I. A. Fallis, S. Parsons, H. Richtzenhain, S. A. Ross and M. Schröder, *Philos. Trans. R. Soc. London, Ser. A*, 1996, **354**, 395.

5 V. B. Pett, G. H. Leggett, T. H. Cooper, P. R. Reed, D. Situmeang, L. A. Ochrymowycz and D. B. Rorabacher, *Inorg. Chem.*, 1988, **27**, 2164; M. Tomoi, O. Abe, N. Takazu and H. Kakiuchi, *Makromol. Chem.*, 1983, **184**, 2431.

6 M. D. Glick, D. P. Gavel, L. L. Diaddario and D. B. Rorabacher, *Inorg. Chem.*, 1976, **15**, 1190.

7 N. E. Meagher, K. L. Juntunen, M. J. Heeg, C. A. Salhi, B. C. Dunn, L. A. Ochrymowycz and D. B. Rorabacher, *Inorg. Chem.*, 1994, **33**, 670.

8 M. H. Chisholm and I. P. Rothwell in *Comprehensive Co-ordination Chemistry*, ed. G. Wilkinson, Pergamon Press, Oxford, 1987, vol. 2.

9 For example, see: W. Beck, W. Sacher and U. Nagel, *Angew. Chem., Int. Ed. Engl.*, 1986, **25**, 270; E. Horn and M. Snow, *Aust. J. Chem.*, 1984, **37**, 35; D. Onggo, D. C. Craig, A. D. Rae and H. A. Goodwin, *Aust. J. Chem.*, 1991, **44**, 219; R. C. Kerber and K. P. Reis, *J. Org. Chem.*, 1989, **54**, 3550; S. Belanger and A. L. Beauchamp, *Inorg. Chem.*, 1997, **36**, 3640; B. Thiyagarajan, M. E. Kerr, J. C. Bollinger, V. G. Young and J. W. Bruno, *Organometallics*, 1997, **16**, 1331; K. W. Liang, W.-T. Li, S.-M. Peng, S.-L. Wang and R.-S. Liu, *J. Am. Chem. Soc.*, 1997, **119**, 4404; P. R. Sharp and J. R. Flynn, *Inorg. Chem.*, 1987, **26**, 3231.

10 For example, see: P. J. M. W. L. Birker, S. Gorter, H. J. M. Hendriks and J. Reedijk, *Inorg. Chim. Acta*, 1980, **45**, 63; P. J. M. W. L. Birker, H. M. J. Hendricks, J. Reedijk and G. C. Verschoor, *Inorg. Chem.*, 1981, **20**, 2408.

11 For example, see: A. Berkessel and R. Breslow, *Bioorg. Chem.*, 1986, **14**, 249; M. T. Reetz, M. Hullmann, W. Massa, S. Berger, P. Rademacher and P. Heymanns, *J. Am. Chem. Soc.*, 1986, **108**, 2405; T. E. Snead, C. A. Mirkin, K.-L. Lu, S. T. Nguyen, W-C. Feng, H. L. Beckman, G. L. Geoffroy, A. L. Rheingold and B. S. Haggerty, *Organometallics*, 1992, **11**, 2613; E. J. Corey, T-P. Loh, S. Sarshar and M. Azimiora, *Tetrahedron. Letts.*, 1992, **33**, 6945.

12 D. Mootz and M. Steffen, *Z. Anorg. Allg. Chem.*, 1981, **483**, 171.

13 W. Kraus and G. Nolze, PowderCell for Windows (v. 1.0), Federal Institute for Materials Research and Testing, Berlin, 1997.

Communication a908778h

The X-ray structure of a protonated hypervalent silanol

Alan R. Bassindale,*[a] David J. Parker,[a] Peter G. Taylor,*[a] Norbert Auner*[b] and Bernhard Herrschaft[b]

[a] *The Chemistry Department, The Open University, Walton Hall, Milton Keynes, Buckinghamshire, UK MK7 6AA. E-mail: P.G.Taylor@open.ac.uk*

[b] *Institut für Anorganische Chemie, Johann Wolfgang Goethe-Universitat, Marie-Curie Str. 11, 60439 Frankfurt am Main, Germany*

Received (in Basel, Switzerland) 29th November 1999, Accepted 23rd February 2000
Published on the Web 17th March 2000

Careful hydrolysis of a pentacoordinate chlorosilane gives a pentacoordinate protonated silanol that resembles the intermediate in the aqueous hydrolysis of silanes.

One of the key areas of organosilicon chemistry is the study of the mechanism of nucleophilic substitution and in particular the mechanism of hydrolysis of chlorosilanes.[1] Application of crystal structure correlation has shown that formation of the nucleophile–silicon bond is accompanied by lengthening of the silicon-leaving group bond and formation of a trigonal bipyramidal structure with the non-participating groups equatorial.[2] Many model pentacoordinate silicon species have now been prepared and characterised using X-ray crystallography.[1c,3] Although a range of ligands have been used to form hypervalent silicon species, we are unaware of any that contain a water molecule as a coordinating ligand. Such elusive species are highly desirable since they mimic the intermediate and/or activated complex for the hydrolysis of silanes.

Here we report the preparation and characterisation of a protonated hypervalent silanol, **1**. Careful hydrolysis of the quinoline derivative **2**[4] in acetonitrile followed by slow, partial evaporation of the solvent led to colourless, needle-like crystals of **1** (Scheme 1).

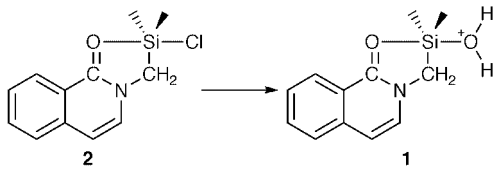

Scheme 1

The crystal structure (Fig. 1) shows that there is chloride in the crystal, but it is not bonded directly to the silicon.[5] The closest contact between the silicon and the chlorine atoms is 4.39 Å. By comparison, a typical Si–Cl bond distance is 2.03 Å and the sum of the van der Waals radii for Si and Cl is 3.85 Å. The Si–O bond length corresponding to the protonated silanol is 1.9114(14) Å. An additional oxygen atom (O3) is also present in the unit cell. The closest silicon atom to O3 is 3.97 Å away while a typical Si–O distance is 1.63 Å[6] and the sum of the van der Waals radii for Si and O is 3.62 Å.

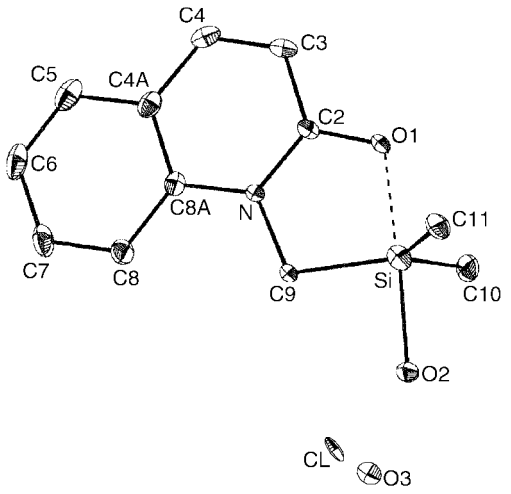

Fig. 1 Structure of **1** in the crystal. Selected bond distances (Å) and bond angles (°): Si–O1 1.9604(14), Si–O2 1.9114(14), Si–C9 1.8726(19), Si–C10 1.856(2), Si–C11 1.867(2), O1–Si–O2 174.62(7), N–C9–Si 106.54(13), O1–Si–C9 86.53(8), O2–Si–C9 88.14(8), C9–Si–C10 118.62(10), C9–Si–C11 119.43(10), C10–Si–C11 121.85(9).

The X-ray analysis revealed the positions of all the hydrogen atoms which show that O2 is part of a water molecule which is bonded to the silicon. This water molecule is hydrogen bonded to a second water molecule containing O3, which in turn is hydrogen bonded to a chloride ion, as shown in **3**. The other

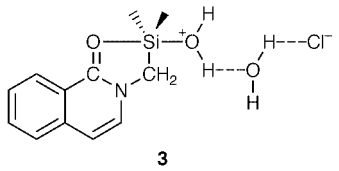

3

alternative involving a molecule of hydrogen chloride hydrogen bonded to a water molecule which in turn is hydrogen bonded to a hypervalent silanol is ruled out by the bond distances. The covalent O–H bond distances in **3** are between 0.82 and 0.99 Å, and the O···H hydrogen bond distances are between 2.6 and 3.1 Å.

Solid state silanol structures which do not involve any hydrogen bonding are known but are comparatively rare.[7] Thus, intermolecular hydrogen bonding in silanols has been extensively studied and shown to take many forms.[8] For example, diisopropylsilanediol,[9] exists as hydrogen bonded dimers which are linked together in ladder chains by further hydrogen bonds, and tris(trimethylsilyl)silylsilanetriol[10] forms hexameric cages of hydrogen bonds. As expected, there is extensive intermolecular hydrogen bonding throughout the crystal of **1**. Each of the hydrogen atoms associated with the two water molecules are involved in hydrogen bonding and each chlorine is hydrogen bonded to three hydrogens, as shown in Fig. 2. Effectively there are ladders of hydrogen bonding running through the structures.

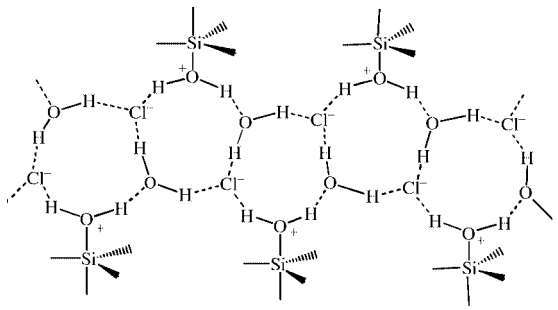

Fig. 2 The arrangement of hydrogen bonding within a crystal of **1**.

DOI: 10.1039/a909504g

These are made of puckered, fused 10-membered rings with hydrogen atoms in alternate positions. The chains extend indefinitely in parallel along the *y*-axis repeating every 7.22 Å. Along the *z* axis the chains stack one above the other in an 'AB' fashion, repeating every 21.45 Å. In the *x* direction the chains stack side by side in a repeating 'AA' manner every 9.13 Å. Hydrogen bonding is confined to within a chain.

The Si–O2 distance observed, [1.9114(14) Å] is, as expected, somewhat longer than that for a traditional Si–O bond. Reed and coworkers have recently reported the crystal structure of a protonated tetracoordinated silanol complex, $[Bu^t_3Si(OH_2)]^+[Br_6CB_{11}H_6]^-$[11]. The Si–O distance in this compound is 1.78 Å, which is longer than that of a standard Si–O bond, reflecting the fact that the silanol is protonated. The Si–O2 bond distance in the hypervalent species **1** is greater than that observed for the protonated silanol as a result of the axial bond length distortion that is expected in five-coordinate silicon complexes.[2]

The Si–O1 bond distance in **1** is 1.9604(14) Å, similar to that for Si-O2. This suggests that the structure resembles a point on the reaction profile where the extent of bond formation is equivalent to that of bond breaking. In the absence of ring strain the structure should be perfectly trigonal pipyramidal. This is confirmed by the fact that the three equatorial substituents and the silicon atom effectively all lie in the same plane. The sum of the three C_{eq}–Si–C_{eq} bond angles, 359.9°, is very close to the 360° expected. The sum of the C–Si–C bond angles in Reed's protonated silanol was 348°, that is, significantly distorted from a trigonal bipyramidal structure and moving towards a tetrahedral species. The larger value observed by Reed and coworkers suggests that the protonated silanol has some characteristics reminiscent of a silyl cation complexed by a water molecule.[12] In this context **1** has some of the features of a silyl cation complexed by two oxygen atoms, but is better described as a covalently bonded trigonal bipyramidal molecule.

Macharashvili and coworkers have used a series of pentacoordinate silicon species involving amide ligands to map nucleophilic substitution at silicon.[2b] The maximum extent of pentacoordination was observed for the chloride derivative where the carbonyl oxygen–silicon bond distance was *ca.* 1.95 Å. This is very close to the Si–O1 bond distance in **1**, confirming that maximum pentacoordination is achieved with two equivalent axial Si–O bond distances.

We thank the EPSRC for financial support for D. J. P.

Notes and references

1 (*a*) A. R. Bassindale, S. J. Glynn and P. G. Taylor, in *The Chemistry of Organosilicon compounds*, ed. Z. Rappoport and Y. Apeloig, Wiley, New York, 1998, vol. 2, ch 9, pp. 495–511; (*b*) R. R. Holmes, *Chem. Rev.*, 1990, **90**, 17; (*c*) C. Chuit, R. J. P. Corriu, C. Reye and J. C. Young, *Chem. Rev.*, 1993, **93**, 1371.

2 (*a*) M. J. Barrow, E. A. V. Ebsworth and M. M. Harding, *J. Chem. Soc., Dalton Trans.*, 1980, 1838; (*b*) A. A. Macharashvili, V. E. Shklover, Yu. T. Struchkov, G. I. Oleneva, E. P. Kramarova, A. G. Shipov and Yu. I Baukov, *J. Chem. Soc., Chem. Commun.*, 1988, 683; (*c*) V. F. Sidorkin, V. V. Vladimirov, M. G. Voronkov and V. A. Pestunovich, *J. Mol. Struct. (Theochem)*, 1991, **228**, 1; (*d*) Yu. E. Ovchinnikov, A. A. Macharashvili, Yu. T. Struchkov, A. G. Shipov and Yu. I. Baukov, *J. Struct. Chem.*, 1994, **35**, 91.

3 (*a*) D. Kost and I. Kalikhman, in *The Chemistry of Organosilicon Compounds*, ed. Z. Rappoport and Y. Apeloig, Wiley, New York, 1998, vol. 2, ch. 23, pp. 1339–1446; (*b*) R. R. Holmes, *Chem. Rev.*, 1996, **96**, 927.

4 A. R. Bassindale, M. Borbaruah, S. J. Glynn, D. J. Parker and P. G. Taylor, *J. Chem. Soc., Perkin Trans. 2*, 1999, 2099.

5 *Crystallographic data* for **1**·H_2O·HCl: colourless, dimensions 0.154 × 0.154 × 0.924 mm, monoclinic, space group, *P*21/*c* (no 14), $Z = 4$, $a = 9.126(2)$, $b = 7.223(1)$, $c = 21.450(4)$ Å, $V = 1413.4(5)$ Å^3, = 1.353 g cm^3; Mo-Kα radiation ($\lambda = 0.71073$ Å); 9552 total data, 2763 [$F > 4\sigma(F)$] observed independent reflections with $2.2 < \theta < 26.8°$ collected: $R = 0.0763$, $wR2 = 0.2336$. CCDC 182/1555. See http://www.rsc.org/suppdata/cc/a9/a909504g/ for crystallographic files in .cif format.

6 B. Csakvari, Z. Wagner, P. Gomory, I. Hargitta, B. Rozsonda and F. C. Mulhoff, *Acta. Chim. Acad. Sci. Hung.*, 1976, **90**, 149.

7 R. D. Brost, G. C. Bruce and S. R. Stobart, *J. Chem. Soc., Chem. Commun.*, 1986, 1580.

8 P. D. Lickiss, *Adv. Inorg. Chem.*, 1995, **42**, 147.

9 A. H. Buttrus, C. Eaborn, P. B. Hitchcock and P. D. Lickiss, *J. Organomet. Chem.*, 1986, **302**, 159.

10 S. S. Al-Juaid, A. H. Buttrus, R. I. Damja, Y. Derouiche, C. Eaborn, P. B. Hitchcock and P. D. Lickiss, *J. Organomet. Chem.*, 1989, **371**, 287.

11 Z. Xie, R. Bau and C. A. Reed, *J. Chem. Soc., Chem. Commun.*, 1994, 2519.

12 L. Olsson, C.-H. Ottosson and D. Cremer, *J. Am. Chem. Soc.*, 1995, **117**, 7460; M. Arshadi, D. Johnd, U. Edlund, C.-H. Ottosson and D. Cremer, *J. Am. Chem. Soc.*, 1996, **118**, 512.

Communication a909504g

ChemComm

The vitamin C route to the ciguatoxins: enantioselective synthesis of a ring F building block

Silas Bond and Patrick Perlmutter*

Department of Chemistry, Monash University, Clayton, Victoria 3168, Australia.
E-mail: Patrick.Perlmutter@sci.monash.edu.au

Received (in Cambridge, UK) 21st December 1999, Accepted 2nd February 2000
Published on the Web 17th March 2000

A ten-step enantioselective synthesis of an F ring lactone for CTX antibody assay development, employing vitamin C as a starting material, is described.

Ciguatera, a disease caused by consumption of ciguateric fish (*i.e.* those fish which have accumulated ciguatoxins (CTXs) in their flesh as a result of ingesting *Gambierdiscus toxicus*, a benthic dinoflagellate which synthesizes these toxins) is endemic throughout the tropics.[1] Consequently there is a need to develop a simple assay for the presence of these toxins in fish. Because of the very low concentrations (<0.1 ppb) of ciguatoxins in fish such an assay will need to be highly sensitive, such as an immunoassay.[2] Hence as part of a program[3] directed towards the synthesis of immunogenic domains of the CTXs, we report here, the enantioselective synthesis of a ring F building block.[4]

From a synthetic point of view, the ciguatoxins constitute one of the most synthetically challenging classes of naturally occurring marine toxins.[5] Each of these toxins consists of thirteen contiguous, fused cyclic ethers ranging in size from five to nine members. The structures of two potential targets, the Pacific ciguatoxins 2,3-dihydroxy-P-CTX-3C **1a**[6] and P-CTX-3C **1b**[7] are shown in Fig. 1.

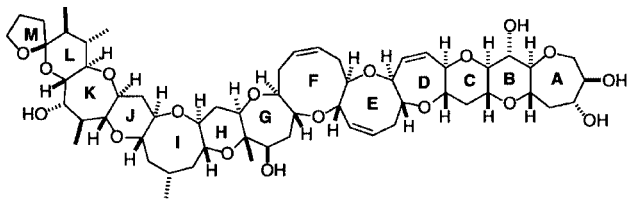

1a 2*R*,3*R*-Dihydroxy-P-CTX-3C

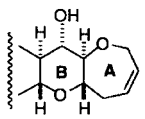

1b P-CTX-3C

Fig. 1 The structures of two Pacific ciguatoxins: P-CTX-3C and 2,3-dihydroxy-P-CTX-3C.

We envisaged the ring F target to be of general structure **4** (Fig. 2). This nine-membered lactone has the correct relative and absolute stereochemistry in place as well as a reactive lactone carbonyl. Related oxoninones have been shown to be valuable intermediates in natural product synthesis.[8–10] In principle **4** should be accessible from vitamin C **2** *via* bicyclic lactone **3** (Fig. 2). Indeed an intermediate bicyclic *ether*, similar to **3**, has recently been reported by Hirama's group to be a very useful intermediate in CTX synthesis.[11]

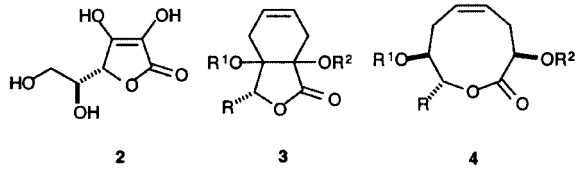

Fig. 2 The structures of vitamin C **2** and two key synthetic targets.

The synthesis of **4** is shown in the Schemes and begins with the cyclohexylidene acetal **5** of vitamin C (Scheme 1). (The corresponding acetonide[12] was employed initially, however it proved to be insufficiently robust in subsequent transformations). Selective *O*-allylation of the C4 hydroxyl of **5** in preference of the hydroxyl at C3, using potassium carbonate/THF–DMSO/allyl bromide, has been reported for vitamin C acetonide.[12] Unfortunately under these conditions we were not able to obtain **6** sufficiently pure for further reactions. Selective C4 *O*-allylation of **5** was ultimately achieved by treatment with allyl bromide in aqueous THF maintaining neutral to slightly alkaline pH. The corresponding *C*-allyl derivative **7** was obtained as a 4 : 1 mixture of diastereomers by heating a toluene solution of **6** at reflux for 6 h. Next it was necessary to generate a diene from **7** which could be closed under ring closing metathesis conditions. Addition of a variety of allyl nucleophiles to **7** gave mixtures of diastereomers which proved very difficult to purify. After considerable experimentation it was found that addition of allylzinc bromide to the *O*-trimethylsilyl derivative **8** (obtainable as a single diastereomer, after purification, by silylation of crude **7**) gave pure diene **9** in excellent yield and complete diastereoselectivity. The preference for attack from the *Si*-face at C4 is probably due to a combination of steric hindrance from the C3 allyl group and coordination to the oxygens at C3 and/or those contained in the side chain acetal. Although the stereochemistry at C3 and C4 is lost later it

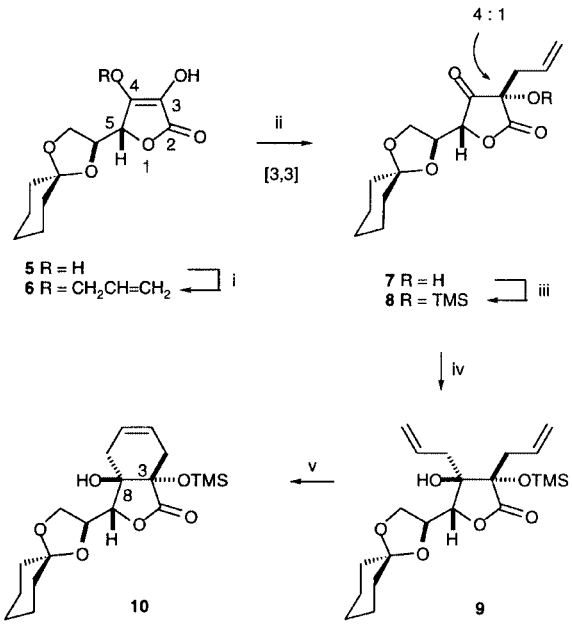

Scheme 1 *Reagents and conditions*: i, K_2CO_3, allyl bromide, DMSO–THF, r.t., 6 h or allyl bromide, 1 M NaOH–THF pH 7–8, r.t., 24 h; ii, toluene, reflux, 6 h; iii, TMSCl, imidazole, THF, r.t., 2 h, 20% as a single isomer from **5**; iv, allylzinc bromide, THF, r.t., 30 min, 94%; v, RuCHPh(P-$Cy_3)_2Cl_2$, toluene, 60–70 °C, 24 h, 69%.

DOI: 10.1039/a910163m

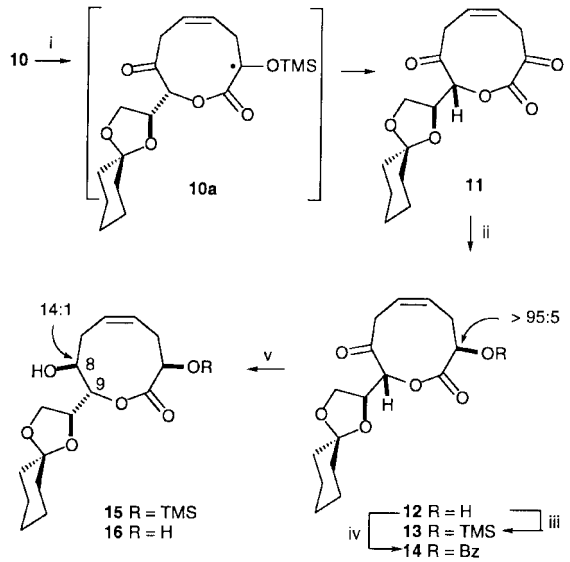

Scheme 2 *Reagents and conditions*: i, HgO, I_2, benzene, *hν*, reflux, 8 h; ii, $NaCNBH_3$, AcOH, *ca.* 13 °C, 20 min, 43% from **10**; iii, TMSCl, imidazole, THF, r.t., 12 h, 99%; iv, $(PhCO)_2O$, Et_3N, DMAP, THF, r.t., 2 h, 99%; v, 1 M LiB[CHMe(Et)]$_3$H, THF, *ca.* −130 °C, 30 min, 73%.

proved operationally more practicable to handle a single stereoisomer through the next sequence of reactions. Thus ring closing metathesis[13] of **9** gave bicyclic lactone **10** in excellent yield. This crystalline product was subjected to single crystal X-ray analysis and the relative stereochemistry of the new stereogenic centres at C3 and C8 was confirmed to be as shown.

Oxidative ring opening of **10**, following adaptations of the conditions of O'Dell *et al.*[14] and Ito *et al.*[15] yielded oxonintrione **11** in good yield (Scheme 2). We assumed that an intermediate such as **10a** would be generated under these conditions. Such intermediates have been proposed before for the oxidative cleavage of silyl ethers.[15] With the nine-membered lactone in hand it remained to reduce the two ketone carbonyls. We found that this was best achieved in a stepwise manner. Thus treatment with sodium cyanoborohydride regio- and stereo-selectively reduced **11** to alcohol **12**. The (*R*)-stereochemistry of the new centre was confirmed by single crystal X-ray analysis of the corresponding benzoate (**14**, R = benzoyl in Scheme 2 and Fig. 3).

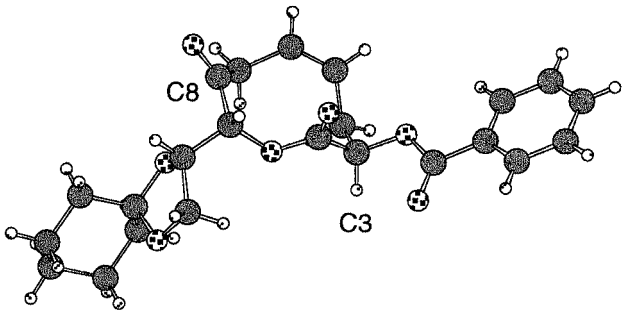

Fig. 3 Single crystals of $C_{23}H_{26}O_7$ **14** were recrystallised from diethyl ether–hexanes, mounted in inert oil and transferred to the cold gas stream of the diffractometer. *Crystal data*: $C_{23}H_{26}O_7$, M = 414.44, monoclinic, space group $P2_1$ (no. 4), a = 10.1336(2), b = 9.5207(2), c = 11.1957(2) Å, β = 104.750(1)°, U = 1044.55(4) Å^3, T = 123 K, Z = 2, μ(Mo-K) = 0.097 mm^{-1}, 14784 reflections measured, 4923 unique (R_{int} = 0.023) which were used in all calculations. The final $wR(F^2)$ was 0.074 (all data), and flack parameter χ = 0.1(6). CCDC 182/1556. See http://www.rsc.org/suppdata/cc/a9/a910163m/ for crystallograpic files in .cif format.

Treatment of **13** with L-selectride {LiB[CHMe(Et)]$_3$H} at −78 °C gave **15** as a 6:1 mixture of diastereomers. Lowering the reaction temperature to *ca.* −130 °C improved the selectivity to 14:1 in favour of the desired isomer. Reduction of **11** with 2 equivalents of L-selectride at *ca.* −130 °C resulted in a mixture of products consisting of 60% **16** and a 1:1:1 mixture of the other three possible diastereomers. The relative stereochemistry of **15** was established by examination of the coupling between H8 and H9 ($J_{8,9}$ 8.7 Hz). For closely related nine-membered cyclic ethers, typical coupling constants are J_{trans} 8.5 Hz, J_{cis} 2.2 Hz.[11] The reasons for the remarkably high diastereoselectivity in the first reduction remain unclear as initial molecular mechanics modelling failed to reveal a low-energy conformation likely to lead to the observed stereochemistry at C3. However, the source of the selectivity in the second reduction appears to be a folded conformation for **13** similar to that shown in Fig. 3 for crystalline **14**. If this conformation is maintained in solution then attack at the *Si* face of the ketone is clearly favoured, generating the observed sterochemistry at C8.

In conclusion, we have demonstrated the usefulness of vitamin C as an enantiomerically pure starting material for the synthesis of oxonins. Key steps included (i) a ring closing metathesis/oxidative cleavage sequence to form the nine-membered ring and (ii) a sequence of two highly diastereoselective reductions. Compounds such as oxonin **15** represent valuable intermediates for the synthesis of F-ring containing CTX domains as well as other naturally occurring oxonins such as obtusenyne and other nine-membered cyclic ethers of marine origin.[16]

We are grateful to Dr Gary D. Fallon for determining the X-ray structures of **10** and **15**. P. P. is grateful to the Australian Research Council for financial support. S. B. is grateful to the Australian Government for an Australian Postgraduate Award scholarship.

Notes and references

1 R. J. Lewis and M. J. Holmes, *Comp. Biochem. Physiol. C, Comp. Pharmacol.*, 1993, **106**, 615.
2 R. J. Lewis, *Mem. Queensland Museum*, 1993, **34**, 541.
3 L. Eriksson, S. T. Guy, P. Perlmutter and R. J. Lewis, *J. Org. Chem.*, 1999, **64**, 8396.
4 M. Inoue, M. Sasaki and K. Tachibana, *Tetrahedron*, 1999, **55**, 10 949.
5 E. Alvarez, M.-L. Candenas, R. Perez, J.-L. Ravelo and J. D. Martin, *Chem. Rev.*, 1995, **95**, 1953.
6 M. Satake, M. Fukui, A.-M. Legrand, P. Cruchet and T. Yasumoto, *Tetrahedron Lett.*, 1998, **39**, 1197.
7 M. Satake, M. Murata and T. Yasumoto, *Tetrahedron Lett.*, 1993, **34**, 1975.
8 J. G. Bendall, A. N. Payne, T. E. O. Screen and A. B. Holmes, *Chem. Commun.*, 1997, 1067.
9 K. Fujiwara, M. Tsunashima, D. Awakura and A. Murai, *Tetrahedron Lett.*, 1995, **36**, 8263.
10 K. Fujiwara, D. Awakura, M. Tsunashima, A. Nakamura, T. Honma and A. Murai, *J. Org. Chem.*, 1999, **64**, 2616.
11 T. Oishi, M. Maruyama, M. Shoji, K. Maeda, N. Kumahara, S. Tanaka and M. Hirama, *Tetrahedron*, 1999, **55**, 7471.
12 K. Wimalasena and M. P. D. Mahindarate, *J. Org. Chem.*, 1994, **59**, 3427.
13 M. Schuster and S. Blechert, *Angew. Chem., Int. Ed. Engl.*, 1997, **36**, 2036.
14 D. E. O'Dell, J. T. Loper and T. L. Macdonald, *J. Org. Chem.*, 1988, **53**, 5225.
15 Y. Ito, S. Fujii and T. Saegusa, *J. Org. Chem.*, 1976, **41**, 2076.
16 D. J. Faulkner, *Nat. Prod. Rep.*, 1998, **15**, 113 and earlier reports in this series.

Communication a910163m

Total synthesis of (+)-streptazolin

Shenlin Huang and Daniel L. Comins*

Department of Chemistry, North Carolina State University, Raleigh, North Carolina 27695-8204, USA. E-mail: daniel_comins@ncsu.edu

Received (in Cambridge, UK) 21st February 2000, Accepted 28th February 2000
Published on the Web 17th March 2000

The first chiral auxiliary mediated asymmetric synthesis of (+)-streptazolin has been accomplished in 13 steps and with a high degree of stereocontrol.

Streptazolin **1** was first isolated from cultures of *Streptomyces viridochromogenes* by Drautz *et al.* in 1981.[1] Streptazolin and a derivative, 3,9-dihydrostreptazolin, were found to exhibit antibacterial and antifungal properties.[1,2] Some naphthoquinone Diels–Alder adducts of **1** have been reported to have

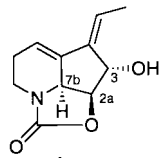

1
(+)-streptazolin

striking bactericidal, fungicidal and protozoacidal activities, as well as antitumor activity similar to adriamycin on leukemia L1210 cells.[3] The unique structure of the natural product, and its interesting biological activities, have stimulated synthetic efforts that resulted in three total syntheses. Kozikowski and Park[4] reported a racemic synthesis of **1**, and Flann and Overman[5] completed an enantioselective synthesis starting from L-tartaric acid. Recently, Kibayashi and coworkers[6] reported a total synthesis of (+)-streptazolin also starting from L-tartaric acid.

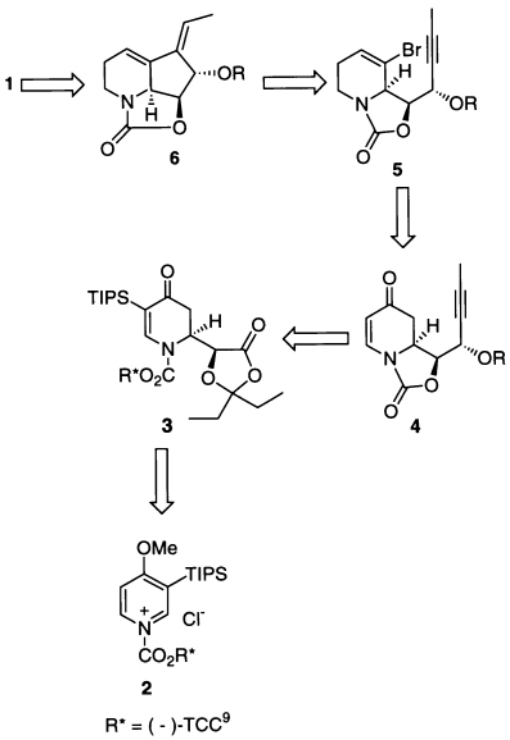

Scheme 1 Retrosynthetic analysis.

As part of a program directed at synthesizing alkaloids using enantiopure *N*-acyldihydropyridones as chiral building blocks,[7] we developed a strategy for the first chiral auxiliary mediated asymmetric synthesis of (+)-streptazolin. In addition to effectively installing the required stereocenters, the direct incorporation of the diene system of **1** in a regio- and stereo-controlled manner was given high priority. Metallo-enolate addition to chiral 1-acylpyridinium salts is a useful method for the enantioselective synthesis of 2-substituted piperidines containing functionality and stereocenters in the C-2 side chain[8] The piperidine core of streptazolin, with its highly functionalized cyclopentane apendage, seemed to be an attractive target for this recently developed methodology. We now report a concise and highly stereocontrolled asymmetric synthesis of **1**.

Our synthesis plan was based on the retrosynthetic analysis depicted in Scheme 1. The enantiopure *N*-acyldihydropyridone **3**, prepared from chiral pyridinium salt **2**, would be converted to bicyclic carbamate **4**. Through a bromination/reduction/elim-

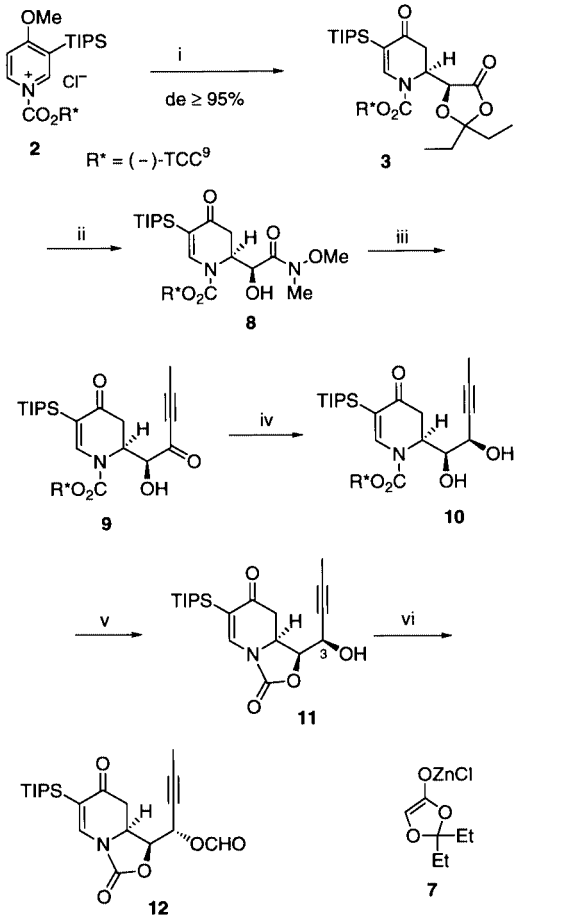

Scheme 2 *Reagents and conditions*: i, **7** (3 equiv.), THF, −78 °C, 3 h, then 10% HCl, 76%; ii, MeONHMe–HCl, $AlMe_3$, CH_2Cl_2, 25 °C, 1 h, 95%; iii, prop-1-ynyllithium (2.5 equiv.), THF, −78 → −15 °C, 1 h, 84%; iv, $NaBH_4/CeCl_3$, MeOH, −50 °C, 95%; v, NaH (2.2 equiv.), THF, 25 °C, 6 h, 81%; vi, formic acid, DEAD, PPh_3, THF, 64%.

DOI: 10.1039/b001425g

ination sequence, vinyl bromide **5** would be prepared from **4**. At this stage, an intramolecular palladium-catalyzed cyclization would be used to give streptazolin precursor **6**, which contains the diene in the proper position and with the required stereochemistry. Removal of the alcohol protecting group would provide **1**.

The 1-acylpyridinium salt **2**[9] was treated with zinc enolate **7**[8] to afford dihydropyridone **3** in 76% yield (Scheme 2).† Conversion of **3** to Weinreb's amide **8** proceeded in excellent yield using standard conditions.[8,10] Addition of propynyllithium[11] (2.5 equiv.) to **8** provided ketone **9**, which was reduced under Luche conditions to afford diol **10** (> 95% de) in high yield.[12] The presence of the bulky C-5 TIPS group allowed the previous three steps to be carried out without serious side reactions at the enone functionality. Treatment of **10** with sodium hydride (2.2 equiv.) effected cyclization to give bicyclic carbamate **11** with concomitant release of the chiral auxiliary, (−)-TCC[13] (93% recovery). The C-3 secondary alcohol in **11** has the wrong stereochemistry for the natural product. This stereogenic center was inverted using the Mitsunobu reaction to provide formate ester **12**. The key intermediate **14** was prepared in good yield from **12** in three steps by removing the TIPS group through protodesilylation using formic acid, cleaving the formate ester with refluxing methanol, and reprotecting the hydroxyl as its TBDMS ether (Scheme 3). At this stage, conversion of dihydropyridone **14** to vinyl bromide **17** was needed. Bromination of the lithium enolate of **14** with NBS gave exclusively the desired *trans*-bromide **15**. Reduction of the enone moiety with K-Selectride (2 equiv.) provided the *cis*-bromohydrin **16** *via* a one-pot reaction.[14] After considerable effort, conditions were found to convert **16** into vinyl bromide **17**. This was carried out by first forming the corresponding triflate and then effecting a regioselective anti-elimination *in situ* with DBU to afford a good yield of **17** as the only vinyl bromide isolated.[15] This intermediate contains three contiguous stereocenters with the correct configuration for the natural product, and the alkyne and vinyl bromide are properly positioned for a palladium-catalyzed cyclization. Subjection of **17** to Grigg's conditions[16] effected ring closure to give the desired diene **18**. Cleavage of the silyl protecting group with fluoride provided the labile natural (+)-streptazolin **1** in near quantitative yield. Our synthetic **1** exhibited spectral data in agreement with reported data for authentic material.[6] The optical rotation, $[\alpha]_D^{22}$ = + 20.6 (*c* = 0.15, $CHCl_3$), is also in agreement with the literature value, $[\alpha]_D^{23}$ = + 22 (*c* = 2.8, $CHCl_3$).[6]

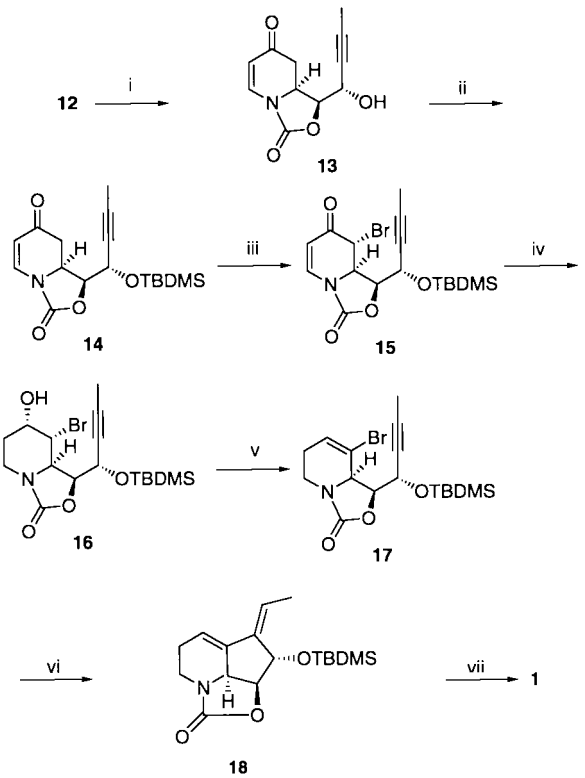

Scheme 3 *Reagents and conditions*: i, formic acid, reflux, 2 h, then MeOH, reflux, 3 d, 88%; ii, TBDMSCl, imidazole, DMF, 83%; iii, LiHMDS (1.1 equiv.), THF, −78 → −40 °C, NBS (1.1 equiv.), 84%; iv, K-Selectride (2 equiv.), THF, −78 °C, 30 min., 58%; v, Tf_2O (1.1 equiv.), CH_2Cl_2, pyridine (5 equiv.), 25 °C, 4 h, then DBU (5 equiv.), 25 °C, 10 h, 79%; vi, $Pd(OAc)_2$/TPP (cat.), sodium formate, THF, 130 °C (sealed tube), 20 h, 50%; vii, TBAF, THF, 0 °C, 30 min., 95%.

In summary, the first chiral auxiliary mediated asymmetric synthesis of (+)-streptazolin **1** has been accomplished in 13 steps and with a high degree of stereocontrol. The piperidine ring and two of the required stereocenters were introduced in one step using a metallo-enolate addition to chiral pyridinium salt **2**. Other key features are the use of a TIPS group to protect an enone moiety, and the regio- and stereo-specific construction of the diene system using a palladium-catalyzed vinyl bromide/alkyne cyclization.

We are grateful to the National Institutes of Health (GM-34442) for financial support of this research and to Dr C. Kabayashi for 400 MHz ^1H NMR and ^{13}C NMR spectra of streptazolin.

Notes and references

† Satisfactory IR, ^1H and ^{13}C NMR, HRMS or microanalyses were obtained for all compounds described.

1 H. Drautz, H. Zächner, E. Kupfer and W. Keller-Schierlein, *Helv. Chim. Acta*, 1981, **64**, 1752.
2 A. Karrer and M. Dobler, *Helv. Chim. Acta*, 1982, **65**, 1432.
3 S. Grabley, H. Kluge and H.-U. Hoppe, *Angew. Chem., Int. Ed. Engl.*, 1987, **26**, 664.
4 A. P. Kozikowski and P. Park, *J. Am. Chem. Soc.*, 1985, **107**, 1763; A. P. Kozikowski and P. Park, *J. Org. Chem.*, 1990, **55**, 4668.
5 C. J. Flann and L. E. Overman, *J. Am. Chem. Soc.*, 1987, **109**, 6115.
6 H. Yamada, S. Aoyagi and C. Kibayashi, *J. Am. Chem. Soc.*, 1996, **118**, 1054.
7 D. L. Comins, C. A. Brooks, R. S. Al-awar and R. R. Goehring, *Org. Lett.*, 1999, **1**, 229; D. L. Comins, A. H. Libby, R. S. Al-awar and C. J. Foti, *J. Org. Chem.*, 1999, **64**, 2184.
8 D. L. Comins, J. T. Kuethe, H. Hong, F. J. Lakner, T. E. Concolino and A. L. Rheingold, *J. Am. Chem. Soc.*, 1999, **121**, 2651 and references therein.
9 D. L. Commins, S. P. Joseph and R. R. Goehring, *J. Am. Chem. Soc.*, 1994, **116**, 4719.
10 S. Nahm and S. M. Weinreb, *Tetrahedron Lett.*, 1981, **22**, 3815; T. Shimizu, K. Osako and T. Nakata, *Tetrahedron Lett.*, 1997, **38**, 2685 and references therein.
11 Prop-1-ynyllithium was prepared from 1-bromoprop-1-ene and *n*-butyllithium in THF, see: D. Toussaint and J. Suffert, *Org. Synth.*, 1998, **76**, 214.
12 This highly stereoselective reduction is likely a result of a chelation-controlled addition mechanism.
13 D. L. Comins and J. M. Salvador, *J. Org. Chem.*, 1993, **58**, 4656.
14 A one-pot reduction of an *N*-alkyl-2,3-dihydro-4-pyridone to a C-4 axial alcohol using excess L-Selectride has been reported, see: G. Han, M. G. LaPorte, J. J. Folmer, K. M. Werner and S. M. Weinreb, *Angew. Chem.*, 2000, **39**, 237.
15 For an example of vinyl bromide formation from a β-bromo triflate, see: W. Ng and D. Wege, *Tetrahedron Lett.*, 1996, **37**, 6797.
16 R. Grigg, *J. Heterocycl. Chem.*, 1994, **31**, 631 and references therein.

Communication b001425g

ChemComm

Oxidation induced variation in polyelectrolyte multilayers prepared from sulfonated self-dopable poly(alkoxythiophene)

Jukka Lukkari,* Antti Viinikanoja, Janika Paukkunen, Mikko Salomäki, Mervi Janhonen, Timo Ääritalo and Jouko Kankare

Department of Chemistry, University of Turku, FIN-20014 Turku, Finland. E-mail: jukka.lukkari@utu.fi

Received (in Oxford, UK) 24th January 2000, Accepted 25th February 2000
Published on the Web 17th March 2000

Polyelectrolyte multilayers have been prepared using both the neutral and oxidised forms of a poly(alkoxythiophene) derivative with pendant sulfonate groups and it is shown that the oxidation state of the polymer affects multilayer formation.

The fabrication of polyelectrolyte multilayers by consecutive adsorption of polyanions and polycations on a charged surface is a facile method for the preparation of stable multicomposite thin films.[1] The strongly interpenetrating layers are held together principally by electrostatic interactions between multiple ion pairs in the oppositely charged chains. Multilayers of simple polyelectrolytes have been studied in detail but electrochemically active polyelectrolytes have received considerably less attention.[2,3] In particular, multilayers of conducting polymers carrying pendant ionic groups have scarcely been characterised at all,[4] although multilayers have been prepared using oxidised conducting polymers as polycations.[5] Owing to their special electrical and optical properties the polyelectrolyte films containing conducting polymers can have potential applications in the fields of, *e.g.*, sensors, electrooptics and LED technology.[1,6]

With weak polyelectrolytes the charge density can be controlled by pH with profound effects on the multilayer formation.[7] Analogously, the charge density of conducting polymers can be controlled by the oxidation state. We report here the formation and preliminary characterisation of multilayers prepared from the neutral or oxidised (referring to the polymer backbone) sodium salt of poly-3-(3′-thienyloxy)propanesulfonate (P3TOPS) as polyanion and poly(allylamine hydrochloride) (PAH, M_w = 5–6.5 × 10^4, Aldrich) or poly(diallyldimethylammonium chloride) (PDADMAC, M_w = 4–5 × 10^5, Aldrich) as polycation. The water-soluble polythiophene P3TOPS was prepared by iron(III) chloride oxidation of the monomer† in chloroform.[8] The crude polymer was fractionated with a Sephadex G-50 F column using water as eluent and the highest molecular weight fraction collected.[9] The neutral polymer is blue with λ_{max} at 620 nm and the oxidised form is bluish grey. The oxidation potential of P3TOPS is *ca.* +0.2 V *vs.* SSCE (sodium saturated calomel electrode) and it is easily oxidised by oxygen. In solution the polymer stays in the neutral state only by addition of a strong reducing agent, *e.g.*, hydrazine or $Na_2S_2O_4$. Polyelectrolyte adsorption was carried out from dilute polyelectrolyte solutions (1 or 10 mM with P3TOPS or PAH and PDADMAC, respectively) for 30 min followed by washing with water (3 × 1 min). The substrates were primed with a layer of physisorbed polycation, polyethyleneimine (PEI, M_w = 25 000, Aldrich; quartz and indium–tin oxide ITO), or chemisorbed 2-mercaptoethanesulfonic acid (MESA, Aldrich; gold). The ionic strength was set to 0.6 M with 0.2 M Na_2SO_4 or $Na_2S_2O_4$.

Neutral P3TOPS is a polyanion with one negative charge per monomer unit. Oxidation of the polymer introduces positive charges in the thiophene backbone and reduces the charge density. However, both forms can be used for the fabrication of polyelectrolyte multilayers. Fig. 1 shows the sequential build-up of P3TOPS/PAH bilayers on quartz. A linear increase of absorbance indicates a regular increase of adsorbed polymer. If the charge density of the oxidised polymer is too low multilayer formation would be hindered. However, oxidation of polythiophenes gives rise to a positive charge of *ca.* 0.25–0.4 per monomer unit, which itself is enough to render oxidised conducting polymers useful as polycations in multilayer fabrication.[5] The spectra of P3TOPS/PDADMAC multilayers on ITO are shown in Fig. 2. The film, which is electroactive owing to efficient interpenetration of the layers, displays behaviour similar to electrodeposited polythiophene films. As the potential is made more anodic, the π–π* transition of the neutral form decreases, and the absorbance increases above 800 nm. At high anodic potentials the absorbance at 900 nm again decreases and a new transition forms in the NIR region above 1000 nm. This implies that these multilayers can be oxidised to the metallic state in aqueous solutions.

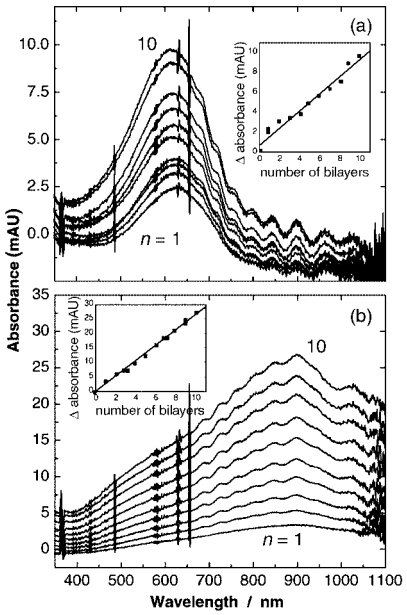

Fig. 1 Polyelectrolyte multilayer formation on quartz. Quartz/PEI/(P3TOPS/PDADMAC)$_n$ using (a) neutral (hydrazine added) and (b) oxidised P3TOPS. Insets show the increase of absorbance at 600 and 900 nm. [Ordinate values in milliabsorbance units (mAU).]

Sequential multilayer fabrication with the neutral and oxidised P3TOPS was carried out also on gold using a quartz crystal microbalance (QCM, Fig. 3). In the first case, the polyanion and polycation (PDADMAC) were adsorbed from 0.2 M $Na_2S_2O_4$ solutions in order to keep polythiophene in the neutral state. With oxidised P3TOPS, oxygen saturated 0.2 M Na_2SO_4 solutions were used. A regular build-up was observed after 2–4 bilayers, a common feature with polyelectrolyte

DOI: 10.1039/b000769m

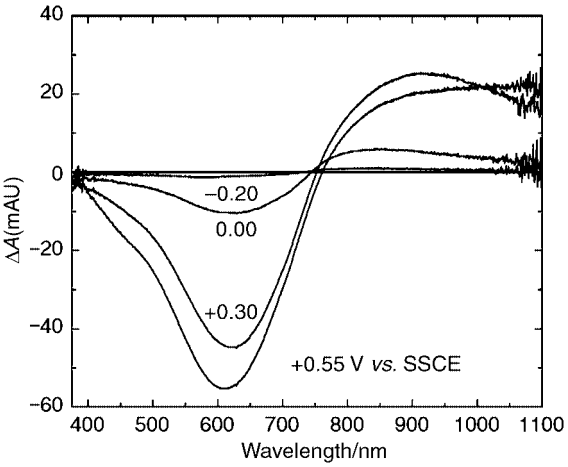

Fig. 2 Difference spectra of ITO/PEI/(P3TOPS/PDADMAC)$_5$ multilayers at potentials indicated (in 0.6 M $NaNO_3$; adsorbed using oxidised P3TOPS). Spectrum at –0.40 V *vs*. SSCE taken as reference.

multilayers.[1,2] QCM studies on polyelectrolyte layers have shown that viscoelastic properties are not important and data can be treated in a gravimetric manner.[10]

With oxidised P3TOPS the average mass increase per PDADMAC/P3TOPS bilayer was approximately half of that observed with neutral polymer, showing the effect of the charge density on multilayer formation. However, contrary to expectations, lower charge density results in the adsorption of less material. Lowering the charge density of weak polyelectrolytes by adjusting the pH of the adsorption solution yields thicker films because more polymer is needed to compensate the surface charge.[7] Closer inspection of Fig. 3 reveals a more complex behaviour with P3TOPS. Although irregular growth persists longer for the neutral (*cf.* also insets of Fig. 1; the more regular growth in that case can be attributed to the PEI underlayer) mass increase ($\Delta f < 0$) or decrease ($\Delta f > 0$) is observed after 3–4 bilayers upon addition of PDADMAC or

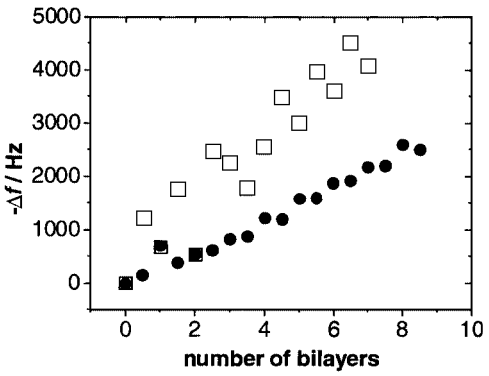

Fig. 3 QCM frequency changes (film side in contact with water) upon multilayer formation in the Au/MESA/(PDADMAC/P3TOPS)$_n$ system. Open and filled symbols refer to neutral and oxidised P3TOPS, respectively.

neutral P3TOPS, respectively. By contrast, the adsorption of oxidised P3TOPS leads to a mass increase and the mass stays constant when PDADMAC is added. Evidently, neutral P3TOPS, with high charge density, is able to remove some of the previously adsorbed polycation whereas PDADMAC does not adhere well to the surface of oxidised P3TOPS having low *surface* charge density. Therefore, even though more material is deposited when neutral P3TOPS is used, more electroactive polymer is adsorbed for the oxidised material. This conclusion is supported by electrochemical experiments, which show that the film oxidation current increases more rapidly with oxidised P3TOPS as the polyanion.

In summary, we have shown for the first time that electroactive polyelectrolyte multilayers can be prepared from ionically substituted polythiophenes using both neutral and oxidised polymer as a polyanion. The oxidation state changes the charge density of the polyanion and has a marked effect on multilayer formation. This behaviour is analogous to that of weak polyelectrolytes as a function of pH.

Financial support from the Academy of Finland (Grant no. 30579) is gratefully acknowledged.

Notes and references

† 3-(3-Bromo)propoxythiophene was synthesised from 3-methoxythiophene and 3-bromopropanol analogously as described in ref. 8. ^{1}H NMR ($CDCl_3$): δ 7.18 (1H, dd), 6.75 (1H, dd), 6.27 (1H, dd), 4.10 (2H, t), 3.58 (2H, t), 2.30 (2H, td). The product was refluxed with Na_2SO_3 in acetone–water (2:1), evaporated to dryness and the crude product dissolved in ethanol. Recrystallisation from ethanol yielded white crystals of sodium 3-(3′-thienyloxy)propanesulfonate. ^{1}H NMR (D_2O): δ 7.19 (1H, dd), 6.67 (1H, dd), 6.40 (1H, dd), 4.00 (2H, t), 2.90 (2H, t), 2.03 (2H, td).

1 G. Decher, *Science*, 1997, **277**, 1232.
2 M. Lösche, J. Schmitt, G. Decher, W. G. Bouwman and K. Kjaer, *Macromolecules*, 1998, **31**, 8893; K. Lowack and C. A. Helm, *ibid.*, 1998, **31**, 823.
3 D. Laurent and J. B. Schlenoff, *Langmuir*, 1997, **13**, 1552; J. B. Schlenoff, D. Laurent, H. Ly and J. Stepp, *Adv. Mater.*, 1998, **10**, 347.
4 M. Ferreira, J. H. Cheung and M. F. Rubner, *Thin Solid Films*, 1994, **244**, 806.
5 M. Ferreira and M. F. Rubner, *Macromolecules*, 1995, **28**, 7107; A. C. Fou and M. F. Rubner, *ibid.*, 1995, , **28**, 7115; J. H. Cheung, W. B. Stockton and M. F. Rubner, *ibid.*, 1997, **30**, 2712; W. B. Stockton and M. F. Rubner, *ibid.*, 1997, **30**, 2717; M. K. Ram, M. Salerno, M. Adami, P. Faraci and C. Nicolini, *Langmuir*, 1999, **15**, 1252.
6 P. K. H. Ho, M. Granström, R. H. Friend and N. C. Greenham, *Adv. Mater.*, 1998, **10**, 769.
7 D. Yoo, S. S. Shiratori andM. F. Rubner, *Macromolecules*, 1998, **31**, 4309.
8 M. Chayer, K. Faïd and M. Leclerc, *Chem. Mater.*, 1997, **9**, 2907.
9 This fraction was eluted practically at the void volume showing that the molecular weight is close to the fractionation range of the column (*ca.* 10000 for dextrans). Attempts to determine the molecular weight with analytical size-exclusion chromatography using sodium poly(styrene sulfonate) standards were not successful.
10 F. Caruso, K. Niikura, D. N. Furlong and Y. Okahata, *Langmuir*, 1997, **13**, 3422.

Communication b000769m

Molybdenum η^2-imine complex formation and the reductive coupling of imines†

Tom M. Cameron,[a] Carlos G. Ortiz,[a] Khalil A. Abboud,[a] James M. Boncella,*[a] R. Tom Baker[b] and Brian L. Scott[b]

[a] *Department of Chemistry, University of Florida, Gainesville, FL 32611, USA. E-mail: boncella@chem.ufl.edu*
[b] *Chemical Science and Technology Division, Los Alamos National Laboratory, MS J514, Los Alamos, NM 87545, USA*

Received (in Bloomington, IN, USA) 5th January 2000, Accepted 25th February 2000
Published on the Web 17th March 2000

Addition of imine PhN=C(Ar)R (Ar = Ph, R = Me; *p*-$MeOC_6H_4$, R = H) to (PhN)Mo(TMS-*o*-pda)(CH_2=CMe_2) 1 [TMS-*o*-pda = bis(trimethylsilyl)-*o*-phenylenediamide] affords the corresponding η^2-imine complexes (PhN)Mo(TMS-*o*-pda)[PhN=C(Ar)R] 2a and 2b; analogous reactions with aldimines RN=C(H)Ar (Ar = *p*-$MeOC_6H_4$, R = CH_2Ph, Et) afford products (PhN)Mo(TMS-*o*-pda)-[RNC(H)ArC(H)ArNR] 3a and 3b resulting from reductive imine coupling, providing the first example of facile and general Mo(IV) η^2-imine complex formation.

Current synthetic methodologies affording η^2-imine complexes (azametallacyclopropanes) consist of C–H activation from methylmetallocene amides,[1,2] rearrangements of iminoacyl complexes,[3] reaction between $Cp^*_2ZrH_2$ and ArNC,[4] reduction of a low-valent complex with phosphaazaallene,[5] and various *in situ* methods of η^2-imine complex formation.[6] Isolation and characterization of η^2-imine complexes generated by direct reaction of imines with metal reductants has for the most part been unsuccessful, and although two recent reports detail the isolation and characterization of ytterbium[6] and tantalum[7] η^2-imine complexes *via* such direct methods, examples with other early transition metals are, to our knowledge, non-existent. We report herein structural characterization and direct synthesis of molybdenum(IV) η^2-imine complexes obtained by treatment of the molybdenum(IV) olefin complex (PhN)Mo(TMS-*o*-pda)(CH_2=CMe_2) **1**[8] with appropriate aldimines and ketimines. Furthermore, aldimine reductive coupling products are isolated for less sterically demanding aldimines.

Reaction of the aryl amine derived aldimine PhN=C(H)Ar or ketimine PhN=C(Me)Ph with **1** affords the η^2-imine complexes **2a** and **2b**, respectively, as green crystals in 70% isolated yield (Scheme 1).‡ The molecular structure of **2b** was determined by an X-ray crystallographic study, and selected bond distances and angles for **2b** are shown in Fig. 1.§

Complex **2b** adopts a five-coordinate square pyramidal geometry with the imido ligand occupying the apical position.

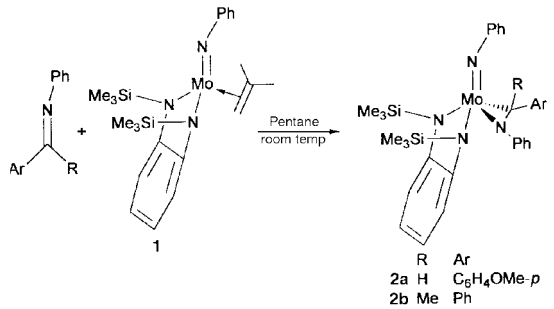

Scheme 1 The generation of molybdenum(IV) η^2-imine complexes.

† Electronic supplementary information (ESI) available: spectroscopic data for **1**, **2a**, **2b**, **3a** and **3b**. See http://www.rsc.org/suppdata/cc/b0/b000355g/

The short imido Mo(1)–N(3) bond length of 1.736(2) Å is typical of a Mo–N triple bond interaction.[9] The Mo(1)–N(4), Mo(1)–N(2) and Mo(1)–N(1) bond lengths of 1.944(2), 2.009(2) and 1.996(2) Å, respectively, are all consistent with Mo–N single bonds.[10] The C(31)-centered bond angles of the imine fragment are all < 120° and support a considerable amount of azametallacyclopropane character in **2b** as does the N(4)–C(31) bond length of 1.414(3) Å.[11]

Complete conversion of **2a** to the corresponding organic amine ($PhNHCH_2Ar$) was observed by ^{1}H NMR upon exposure of a solution of **2a** to an atmosphere of 15 psi H_2 at room temperature over a 1 week period.[12] Unfortunately no catalytic activity was observed upon treatment of **2a** with excess imine under low pressures (*ca.* 15 psi) of H_2 gas.

The reaction of aldimines derived from less hindered primary amines with **1** affords molybdenum(VI) bisdiamide imido complexes **3a** and **3b** from reductive imine coupling (Scheme 2).‡ Complexes **3a** and **3b** were isolated in 75% yield from cold pentane–toluene solutions. Interestingly, only the *rac*-coupled form of the metal complexes is isolated as ascertained from ^{1}H and ^{13}C NMR spectroscopy. An X-ray crystallographic study was performed on a single crystal of **3b**.

The molecular structure and selected bond lengths and angles are shown in Fig. 2.§ The complex adopts a distorted square pyramidal geometry around molybdenum with the imido ligand

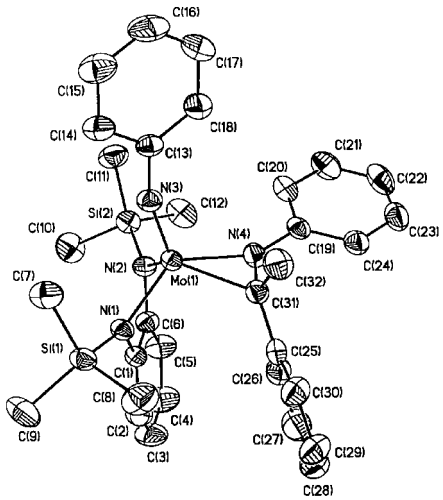

Fig. 1 Thermal ellipsoid plot of **2b**. Selected bond lengths (Å) and angles (°): Mo(1)–N(1) 1.996(2), Mo(1)–N(2) 2.009(2), Mo(1)–N(3) 1.736(2), Mo(1)–N(4) 1.944(2), Mo(1)–C(31) 2.200(3), N(3)–C(13) 1.409(3), N(4)–C(31) 1.414(3), C(31)–C(32) 1.518(4); Mo(1)–N(3)–C(13) 163.0(2), N(2)–Mo(1)–N(1) 85.28(9), N(4)–Mo(1)–C(31) 39.29(9), N(2)–Mo(1)–N(4) 100.09(9), N(1)–Mo(1)–C(31) 99.20(9), N(4)–C(31)–Mo(1) 60.55(13), N(4)–C(31)–C(32) 116.9(2), N(4)–C(31)–C(25) 116.6(2), C(32)–C(31)–C(25) 116.2(2).

DOI: 10.1039/b000355g

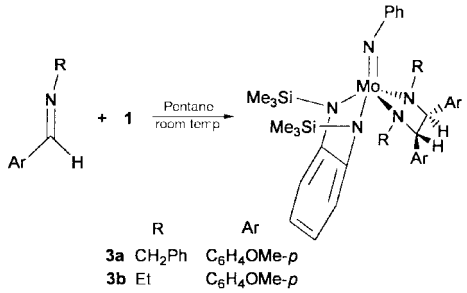

Scheme 2 The reductive coupling of imines.

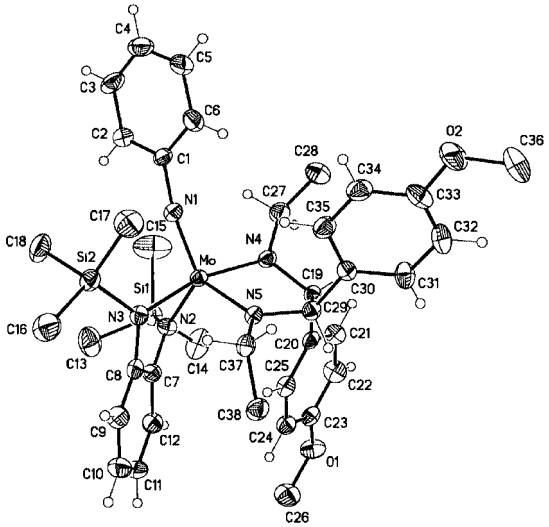

Fig. 2 Thermal ellipsoid plot of **3b** with 50% probability ellipsoids. Selected bond lengths (Å) and angles (°): Mo–N(1) 1.754(3), Mo–N(2) 2.008(3), Mo–N(3) 2.065(3), Mo–N(4) 1.996(3), Mo–N(5) 2.021(3), N(4)–C(19) 1.476(5), N(5)–C(29) 1.468(5), C(19)–C(29) 1.514(5); Mo–N(1)–C(1) 166.6(3), N(2)–Mo–N(3) 80.65(14), N(3)–Mo–N(5) 85.75(12), N(5)–Mo–N(4) 77.46(12), N(2)–Mo–N(4) 102.59(12).

occupying the apical position. The Mo–N(1) bond length of 1.754(3) Å is consistent with a molybdenum nitrogen triple bond interaction.[9] The Mo–N(2), N(3), N(4) and N(5) amide bond lengths of 2.008(3), 2.065(3), 1.996(3) and 2.021(3) Å, respectively, are within the range expected for Mo–N single bonds.[10] The hydrogen atoms located on the backbone of the newly formed diamide ligand are related by an H–C(19)–C(29)–H torsion angle of 90°. Consistent with this torsion angle there is no observed coupling between these protons in the solution ^{1}H NMR spectrum at 300 MHz. Complex **3a** displays similar characteristics in its ^{1}H NMR spectrum.

In summary, we have demonstrated that chelate-supported Mo(IV) η^2-imine complexes can be easily prepared *via* displacement of olefin from **1** upon reaction with *N*-aryl imines. In contrast, imine reductive coupling products were observed for sterically less demanding imines. We are currently investigating the reactivity of these η^2-imine complexes with unsaturated organic molecules.

J. M. B. thanks the National Science Foundation (CHE 9523279) for funding of this work. K. A. A. thanks the NSF and the University of Florida for funding X-ray equipment purchases, and R. T. B. thanks the Science and Technology Base programs at Los Alamos.

Notes and references

‡ All reactions and manipulations were carried out using standard Schlenk techniques or a dry box under atmospheres of nitrogen and argon. *Synthesis* of **2a** and **2b**: to a green solution of **1** (0.50 g, 1.05 mmol) in pentane at room temperature was added a pentane solution of the appropriate imine (0.20 g, 1.05 mmol). After stirring for 12 h the pentane solution was concentrated *in vacuo* and cooled, affording the appropriate metal complexes. The synthesis of **3a** and **3b** was similar but required the addition of 2 equivalents of the appropriate imine.

§ *Crystal data*: for **2b**: $C_{32}H_{40}N_4Si_2Mo$, M = 632.80, a = 9.8565(5), b = 18.8443(8), c = 17.9089(8) Å, β = 104.6520(1)°, V = 3218.2(3) Å^3, monoclinic, space group $P2_1/c$, Z = 4, T = 203(2) K, final $R1$ = 0.0431, $wR2$ = 0.0831, GOF (on F^2) = 1.225.

For **3b**: $C_{38}H_{53}MoN_5O_2Si_2$, M = 763.97, a = 9.9600(5), b = 19.0705(9), c = 10.2628(5) Å, β = 97.351(1)°, V = 1933.3(2) Å^3, monoclinic, space group $P2_1$, Z = 2, T = 173(2) K, final $R1$ = 0.0420, $wR2$ = 0.0775, GOF (on F^2) = 1.021.

Both structures were solved using the direct methods option of SHELXS. Full-matrix least-squares refinements based on F^2 were subsequently performed using SHELXL 97.[13] All non-hydrogen atoms were assigned anisotropic temperature factors, with corresponding hydrogen atoms included in calculated positions.

CCDC 182/1560. See http://www.rsc.org/suppdata/cc/b0/b000355g/ for crystallographic files in .cif format.

1 P. Berno and S. Gambarotta, *Organometallics*, 1995, **14**, 2159; D. A. Gately, J. R. Norton and P. A. Goodson, *J. Am. Chem. Soc.*, 1995, **117**, 986; L. Buchwald, B. T. Watson, M. W. Wannamaker and J. C. Dewan, *J. Am. Chem. Soc.*, 1989, **111**, 4486; J. A. Tunge, D. A. Gately and J. R. Norton, *J. Am. Chem, Soc.*, 1999, **121**, 4520.

2 A Mo(H)(η^2-imine) complex has been reported and presumably arises *via* C–H activation of an amide ligand. Y. Tsai, M. J. Johnson, D. J. Mindiola, C. C. Cummins, W. T. Klooster and T. F. Koetzle, *J. Am. Chem. Soc.*, 1999, **121**, 10 426.

3 M. J. Scott and S. J. Lippard, *Organometallics*, 1997, **16**, 5857; J. R. Clark, P. E. Fanwick and I. P. Rothwell, *Organometallics*, 1996, **15**, 3232; L. D. Durfee, J. E. Hill, P. E. Fanwick and I. P. Rothwell, *Organometallics*, 1990, **9**, 75; L. D. Durfee, P. E. Fanwick, I. P. Rothwell, K. Folting and J. C. Huffman, *J. Am. Chem. Soc.*, 1987, **109**, 4720; K. W. Chiu, R. A. Jones, G. Wilkinson, A. M. R. Galas and M. B. Hursthouse, *J. Chem. Soc., Dalton Trans.*, 1981, 2088; *J. Am. Chem. Soc.*, 1980, **102**, 7978.

4 P. T. Wolczanski and J. E. Bercaw, *J. Am. Chem. Soc.*, 1979, **101**, 6450.

5 J. B. Alexander, D. S. Glueck, G. P. A. Yap and A. L. Rheingold, *Organometallics*, 1995, **14**, 3603.

6 Y. Makioka, Y. Taniguchi, Y. Fujiwara, K. Takaki, Z. Hou and Y. Wakatsuki, *Organometallics*, 1996, **15**, 5476 and references therein.

7 K. Takai, T. Ishiyama, H. Yasue, T. Nobunaka, M. Itoh, T. Oshiki, K. Mashima and K. Tani, *Organometallics*, 1998, **17**, 5128.

8 We have recently prepared a variety of Mo(IV)(olefin) complexes (manuscript in preparation) from the corresponding dichloride species (C. G. Ortiz, K. A. Abboud and J. M. Boncella, *Organometallics*, 1999, **18**, 4253). Preparation of PhNMo(TMS-*o*-pda)(CH_2=CMe_2): To a −78 °C blue ethereal solution of PhNMo(TMS-*o*-pda)Cl_2•THF (1.0 g, 1.7 mmol) was added 2 equivalents of $ClMgCH_2CHMe_2$ (2.0 M in Et_2O, 1.7 ml) with stirring, which resulted in the emergence of a red-colored solution. Upon warming to room temperature (*ca*. 3 h) the reaction mixture turned green whereupon the solvent was removed *in vacuo*. The resulting green residue was extracted twice with 25 ml of pentane. The solvent was then removed *in vacuo* affording a green, waxy oil **1** in 65% yield.

9 P. W. Dyer, V. C. Gibson, J. A. K. Howard, B. Whittle and C. Wilson, *Polyhedron*, 1995, **14**, 103; P. W. Dyer, V. C. Gibson and W. Clegg, *J. Chem. Soc., Dalton Trans.*, 1995, 3313; P. W. Dyer, V. C. Gibson, J. A. K. Howard, B. Whittle and C. Wilson, *J. Chem. Soc., Chem. Commun.*, 1992, 1666; N. Bryson, M. T. Youinou and J. A. Osborn, *Organometallics*, 1991, **10**, 3389.

10 M. B. O'Donoghue, W. M. Davis and R. R. Schrock, *Inorg. Chem.*, 1998, **37**, 5149; Z. Duan and J. G. Verkade, *Inorg. Chem.*, 1995, **34**, 1576; N. C. Mösch-Zanetti, R. R. Schrock, W. M. Davis, K. Wanninger, S. W. Siedel and M. B. O'Donoghue, *J. Am. Chem. Soc.*, 1997, **119**, 11 037.

11 C–N single-bond length 1.45 Å and C–N double-bond length 1.27 Å: M. Burkr-Laing and M. Laing, *Acta. Crystallogr., Sect. B*, 1976, **32**, 3216.

12 (*a*) The identity of the amine produced by hydrogenolysis was confirmed *via* generation of the amine from the corresponding imine and LAH and comparison of ^{1}H NMR spectra after appropriate workup. At this time the nature of the metal containing products of this reaction are unknown, though we have isolated hydride complexes of closely related tungsten complexes;[12b] (*b*) J. M. Boncella, S.-Y. S. Wang and D. D. Van der Lende, *J. Organomet. Chem.*, 1999, **591**, 8.

13 SHELXTL/NT Version 5.10, Bruker Analytical X-Ray Instruments, Inc., Madison, Wisconsin 53719, 1997.

Communication b000355g

ChemComm

Highly ordered large caged cubic mesoporous silica structures templated by triblock PEO–PBO–PEO copolymer

Chengzhong Yu,[a,b] Yonghao Yu[a] and Dongyuan Zhao*[a]

[a] *Department of Chemistry, Fudan University, Shanghai, 200433, P. R. China. E-mail: dyzhao@fudan.edu.cn*
[b] *Department of Chemistry, Shanghai Medical University, Shanghai, 200032, P. R. China*

Received (in Cambridge, UK) 21st January 2000, Accepted 1st March 2000
Published on the Web 17th March 2000

Highly ordered, hydrothermally stable, caged cubic mesoporous silica structures ($Im\bar{3}m$) with unusually large pore size (120 Å) have been synthesized by using hydrophobic poly(butylene oxide) containing triblock PEO–PBO–PEO copolymer as a structure-directing agent.

Ordered large pore materials are in great demand because of their potential applications for catalysis, separation of large molecules, medical implants, semiconductors, magnetoelectric devices, *etc.*[1–8] Using triblock poly(ethylene oxide)–poly(propylene oxide)–poly(ethylene oxide) (PEO–PPO–PEO) copolymers as structure-directing agents, we have previously reported the synthesis of highly ordered hexagonal mesoporous silica structures (SBA-15) with large pore sizes of 50–300 Å.[2] Three-dimensional cubic mesoporous structures, such as MCM-48 ($Ia\bar{3}d$),[1] SBA-1 ($Pm\bar{3}n$)[7] and SBA-16 ($Im\bar{3}m$),[2] show advantages compared to hexagonal mesoporous structures with one-dimensional channels. However, such cubic structures could be synthesized only under strict conditions. Calcined SBA-16 synthesized with PEO–PPO–PEO triblock copolymers has the largest pore size (54 Å) among these cubic silica structures, but can only be synthesized with large PEO segment amphiphilic PEO–PPO–PEO block copolymers, such as F127 ($EO_{106}PO_{70}EO_{106}$) in a narrow range of reaction compositions at room temperature.[2b] The small differences of hydrophilicity/hydrophobicity between PEO and PPO chains at room temperature might be one of the reasons leading to such a small pore size.

Here, we report the synthesis of a highly ordered, ultra hydrothermally stable caged cubic mesoporous silica structure (FDU-1, $Im\bar{3}m$) with large, uniform pore size (120 Å) by using the more hydrophobic poly(butylene oxide) containing triblock copolymer PEO–PBO–PEO as the structure-directing agent.

Cubic mesoporous silica FDU-1 samples were synthesized by using the triblock copolymer $EO_{39}BO_{47}EO_{39}$ [B50-6600 (Dow) $\overline{M}_n$ = 6800] as the structure-directing agent under acidic conditions. In a typical experiment, 0.5 g of B50-6600 was dissolved in 30 g of 2 M HCl. To this homogeneous solution, 2.08 g (0.01 mol) of tetraethylorthosilicate (TEOS) was added with vigorous stirring for 24 h. The resulting solid was then aged at 100 °C for a further 24 h. The solid product was filtered off, washed, and dried *in vacuo* at room temperature. Calcination was carried out in an oven at 550 °C for 6 h in air.

Small angle X-ray diffraction (XRD) patterns of as-synthesized and calcined FDU-1 are shown in Fig. 1. As-synthesized FDU-1 shows a well resolved XRD pattern and the first diffraction peak appears at a low angle (2θ = 0.68). After calcination the first diffraction peak is shifted slightly (2θ = 0.73) due to shrinkage. Calcined FDU-1 shows nine well resolved Bragg peaks. Combined with TEM analysis (see below) we can index the diffraction peaks to 110, 200, 211, 220, 310, 222, 400, 411 and 420 reflections for space group $Im\bar{3}m$ (Q^{229}), respectively. The relative intensity of these observed peaks follows the trend reported in previous literature reports for surfactant–water systems.[9,10] The values of the cubic cell lattice parameter, *a*, are calculated to be 183 and 171 Å for as-synthesized and calcined FDU-1, respectively.

Transmission electron micrographs (TEM) of calcined FDU-1 are shown in Fig. 2. Although both simple (P) and centerd (I) cubic structures show a square lattice along the [100] direction and a hexagonal lattice along the [111] direction, the value of d_{100} relative to d_{111} is equal to 0.866 (I) and 1.224 (P), respectively, from geometrical calculations. From bright/dark TEM images [Fig. 2(a) and (b)] for calcined FDU-1, the value of d_{100}/d_{111} is estimated as 0.88, giving further evidence that the mesostructure is centered cubic with $Im\bar{3}m$ space group. The cell parameter, *a*, is estimated as 170 Å from TEM images, in good agreement with the value determined from the XRD data. Moreover, TEM measurements also reveal that all areas for calcined FDU-1 have well ordered mesoscopic arrays and a three-dimensional caged structure can be observed along the edge of the sample [Fig. 2(b)], indicating that calcined FDU-1 has a high quality caged cubic mesostructure.

Calcined cubic mesoporous silica FDU-1 synthesized using B50-6600 yields a type IV isotherm with a large type-H_1 hysteresis loop (Fig. 3).[11] A narrow pore-size distribution (FWHM *ca.* 10 Å) with a mean value of 120 Å (BJH model) is also obtained from the adsorption branch, indicating that FDU-1 has well defined uniform pore dimensions. The calcined cubic mesoporous silica has a pore volume of 0.77 $cm^3\ g^{-1}$ and a BET surface area of 740 $m^2\ g^{-1}$. Although the cell parameter for FDU-1 is similar to that of SBA-16 (176 Å), the pore size and pore volume for FDU-1 are much larger than those (54 Å, 0.45 $cm^3\ g^{-1}$, respectively) for SBA-16,[2b], suggesting that the pore size is very dependent on hydrophobic domains. More hydrophobic PBO segments relative to PPO segments yields a larger

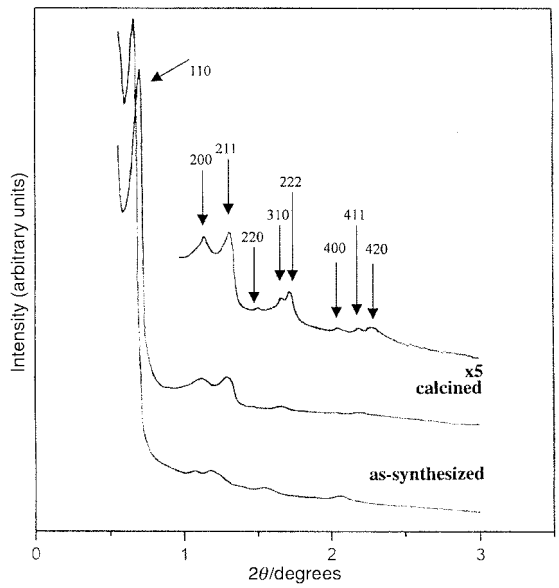

Fig. 1 XRD patterns of as-synthesized and calcined cubic mesoporous siica FDU-1 prepared using $EO_{39}BO_{47}EO_{39}$ triblock copolymer as the structure-directing agent at room temperature. XRD patterns were recorded with a Rigaku D/Max-IIA using Cu-Kα radiation.

DOI: 10.1039/b000603n

mesopore size. To the best of our knowledge, FDU-1 has the largest pore sizes among all reported cubic silica structures.

Cubic mesoporous silica can be synthesized over a relatively wide range of reaction mixture compositions at temperatures of 0–60 °C. At room temperature, the cubic structure can be synthesized over a range of PEO–PBO–PEO concentrations (0.6–2.4 wt%), with cell parameters (*a*) in the range 200 to 178 Å. Moreover, a low temperature such as 0 °C yields a large cell parameter (*a* up to 220 Å), but may lead to slight disorder for FDU-1 according to XRD and TEM. At higher temperatures, the cell parameter and crystalline quality for FDU-1 remain almost unchanged. Addition of swelling agents, such as 1,3,5-trimethylbenzene (TBM), can slightly enlarge the cell parameter (up to 220 Å) with a highly ordered mesostructure. Fig. 2(d) shows a TEM image of calcined FDU-1 obtained with TMB. The cell parameter is estimated as 220 Å, in agreement with that determined from XRD.

Despite of such large lattice dimensions, calcined cubic FDU-1 is hydrothermally stable. After calcined FDU-1 was heated in boiling water for more than 9 days, at least five diffraction peaks can be observed in the XRD pattern and the intensity for the (110) reflection was even increased after the treatment, indicating that large pore mesoporous FDU-1 is hydrothermally stable.

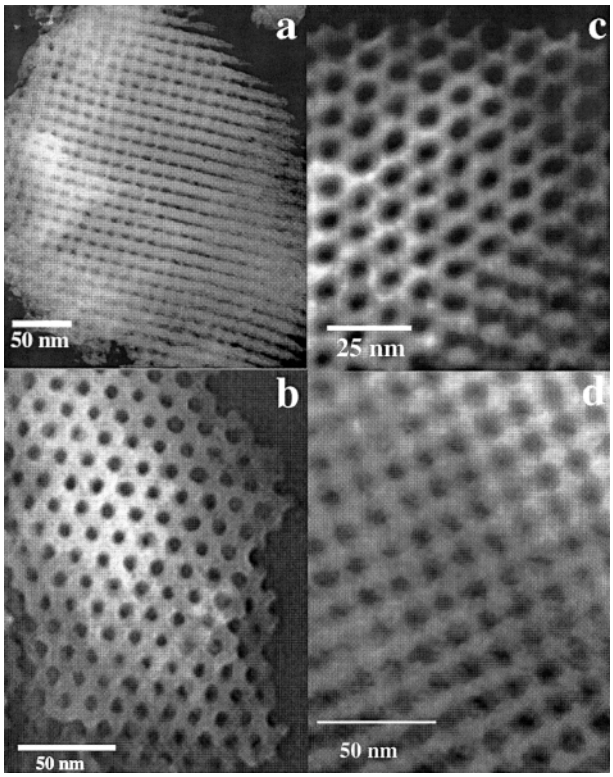

Fig. 2 TEM images of calcined cubic FDU-1 synthesized using $EO_{39}BO_{47}EO_{39}$ triblock copolymer without TMB at room temperature: (a) along the [100] direction, (b) along the [111] direction and (c) along the [110] direction; (d) calcined cubic FDU-1 synthesized with TMB as the swelling agent. TEM photographs were obtained with a JEM-1200EX microscope operated at 80 kV. For TEM measurements, the samples were ground, embedded in epoxy resin, and ultramicrotomed except the sample in Fig. 2(a), which was prepared by dispersing the powder products as a slurry in acetone and subsequently deposited and dried on a holey carbon film on a Cu grid.

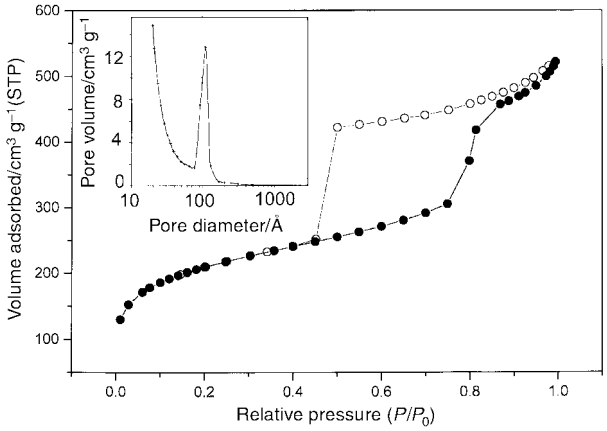

Fig. 3 Nitrogen adsorption–desorption isotherm plots and pore size distribution curve of calcined mesoporous silica FDU-1. N_2 adsorption measurements were performed at 77 K using a Micromeritics ASAP 2000 analyzer utilizing Barrett–Emmett–Teller (BET) calculations for surface area and Barrett–Joyner–Halanda (BJH) calculations for pore volume and pore size distributions for the adsorption branch of the isotherm.

In summary, highly ordered, large cage-structured cubic mesoporous silica FDU-1 has been synthesized with the hydrophobic PBO containing triblock PEO–PBO–PEO copolymer as a template. The new large cage structure and high hydrothermal stability for the resulting cubic mesoporous silica are expected to be of great value in electrochemistry, catalysis and separation for large moleculars.

This work was supported by the National Science Foundation of China (Grant No. 29925309 and 29873012) and National Education Ministry. We thank the Dow Company for providing block copolymer surfactants.

Notes and references

1 C. T. Kresge, M. E. Leonowicz, W. J. Roth, J. C. Vartuli and J. S. Beck, *Nature*, 1992, **359**, 710.
2 (*a*) D. Zhao, J. Feng, Q. Huo, N. Melosh, G. H. Fredrickson, B. F. Chmelka and G. D. Stucky, *Science*, 1998, **279**, 548; (*b*) D. Zhao, Q. Huo, J. Feng, B. F. Chmelka and G. D. Stucky, *J. Am. Chem. Soc.*, 1998, **120**, 6024.
3 I. A. Aksay, M. Trau, S. Manne, I. Honma, N. Yao, L. Zhou, P. Fenter, P. M. Eisenberger and S. M. Gruner, *Science*, 1996, **273**, 892; S. Schächt, Q. Huo, I. G. Voigt-Martin, G. D. Stucky and F. Schüth, *Science*, 1996, **273**, 768.
4 S. Mann and G. A. Ozin, *Nature*, 1996, **382**, 313; M. Trau, N. Yao, E. Kim, Y. Xia, G. M. Whitesides and I. A. Aksay, *Nature*, 1997, **390**, 674.
5 D. Zhao, P. Yang, Q. Huo, B. F. Chmelka and G. D. Stucky, *Curr. Opin. Solid Mater. Sci.*, 1998, **3**, 111.
6 H. Yang, N. Coombs and G. A. Ozin, *Nature*, 1997, **86**, 692; G. A. Ozin, H. Yang, I. Sokolov and N. Coombs, *Adv. Mater.*, 1997, **9**, 662.
7 Q. Huo, D. I. Margolese, U. Ciesla, D. G. Demuth, P. Feng, T. E. Bier, P. Sieger, A. Firouzi, B. F. Chmelka, F. Schüth and G. D. Stucky, *Chem. Mater.*, 1994, **6**, 1176; Q. Huo, R. Leon, P. M. Petroff and G. D. Stucky, *Science*, 1995, **268**, 1324.
8 C. Chen, H. Li and M. E. Davis, *Microporous Mater.*, 1993, **2**, 17.
9 P. Marian, V. Luzzati and H. Delacroix, *J. Mol. Biol.*, 1988, **204**, 165.
10 P. Alexandridis, U. Olsson and B. Lindman, *Langmuir*, 1997, **13**, 23.
11 W. Luckens, Jr., P. Schmidt-Winkel, D. Zhao, J. Feng and G. D. Stucky, *Langmuir*, 1999, **15**, 5403.

Communication b000603n

ChemComm

Switch-on luminescence detection of steroids by tris(bipyridyl)ruthenium(II) complexes containing multiple cyclodextrin binding sites†

Hubertus F. M. Nelissen,[a] Arnoldus F. J. Schut,[a] Fokke Venema,[b] Martinus C. Feiters*[a] and Roeland J. M. Nolte*[a]

[a] *Department of Organic Chemistry, NSR-Center, University of Nijmegen, Toernooiveld 1, NL-6525 ED, Nijmegen, The Netherlands. E-mail: nolte@sci.kun.nl*
[b] *Organon Teknika, P.O.-box 84, 5280 AB Boxtel, The Netherlands*

Received (in London, UK) 5th January 2000, Accepted 28th February 2000

A luminescent ruthenium(II) complex with six cyclodextrin binding sites is shown to switch off its emission upon binding of *N,N′*-dinonyl-4,4′-bipyridinium bromide and to recover luminescence upon displacement of the bipyridinium ion by a steroid.

The design of luminescent cyclodextrin sensor systems which are able to detect neutral organic compounds, *e.g.* steroids by a change in emission properties is an area which has attracted much interest over the last decade.[1] Most of these systems rely on a decrease in fluorescence intensity when a covalently linked fluorophore is displaced from the cyclodextrin cavity by a guest. Few systems exist in which the detection of a guest is accompanied by an increase in emission intensity.[2,3] Here, we describe the sensor properties of two novel cyclodextrin-based sensor compounds, containing a central luminescent tris(bipyridyl) ruthenium(II) complex,[4] to which six cyclodextrins are attached. One of these compounds (**2**) is able to detect steroids by first turning off the emission of the ruthenium complex by the binding of a quenching viologen in its cyclodextrin cavities, and then switching on the original luminescence by displacement of the viologen by the steroid.

The orange ruthenium complexes **1** and **2** were synthesised by reaction of $RuCl_3$ with 3 equivalents of the dimers **3**[5] and **4**,‡ respectively, in boiling water. The resulting mixtures were poured into acetone to precipitate the complexes as their chloride salts.‡ The UV–VIS spectra of **1** and **2** showed a characteristic metal-to-ligand charge transfer (MLCT) absorption centered at 465 nm and an intense ligand centered (LC) absorption around 300 nm. No quenching of the emission by oxygen was observed for either compound probably because the ruthenium centers are shielded by the cyclodextrins.[6]

Compound **1** was only weakly luminescent (95% less intense than **2**), probably because the bulky cyclodextrins prevent optimal coordination of the bipyridyl ligands to the ruthenium centers. Compound **2** displayed a bright luminescence, twice as intense as the reference compound $Ru(bpy)_3^{2+}$ (bpy = 2,2′-bipyridine). Compound **2** was, therefore, selected for binding studies with organic guest molecules. When ursodeoxycholic acid, lithocholic acid, cholesterol or 1-adamantanecarboxylic acid were added to a solution of **2** in water no change in the emission spectrum of **2** was observed. This means that there is no direct or indirect communication between the ruthenium complex and these guest molecules when they are bound. Since it is known[7] that covalently linked viologens (*N,N′*-dialkyl-4,4′-bipyridiniums) are able to quench the emission intensity of tris(bipyridyl)ruthenium(II) complexes very efficiently *via* an electron transfer process, we chose *N,N′*-dinonyl-4,4′-bipyridinium bromide as a guest molecule. The two long alkyl chains were attached to this molecule to increase its binding to the cyclodextrins.[8] Upon addition of the bipyridinium compound to an aqueous solution of **2** the emission intensity gradually dropped, resulting in 92% quenching at saturation (Fig. 1). Most importantly, when this guest was added to the reference compound $Ru(bpy)_3^{2+}$ under the same conditions (aereated solution, same concentrations) only a linear decrease of 15% in luminescence was observed. This implies that the bipyridinium compound is bound in the cyclodextrin cavities and thereby facilitates electron transfer.

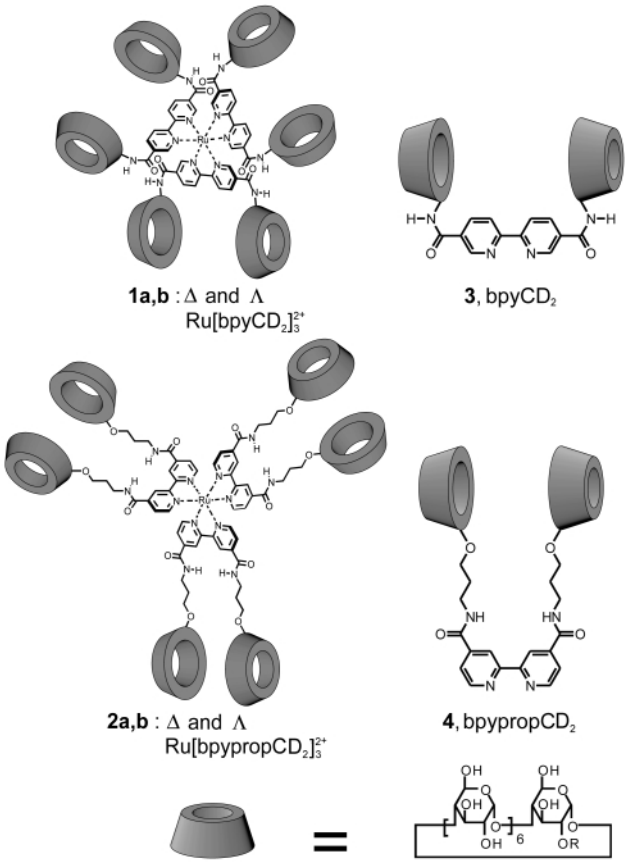

Analysis of the complex stoichiometry by constructing a Job-plot (see ESI†) suggested that a 1:1 complex was formed between **2** and the bipyridinium guest. The observed binding curve could be fitted to a 1:1 binding model and gave an apparent association constant (K_a) of 2.8×10^5 M^{-1}.

A microcalorimetric titration study of the binding of the bipyridinium guest in **2** revealed a different picture (Fig. 2). This time the observed titration curve could not be fitted to a 1:1 model, instead a second (**2**:bipyridinium = 1:2) equilibrium was needed to give a satisfactory fit (Fig. 2, inset). The data from this study are collected in Table 1. As can be seen the binding constant for the 1:1 complex matches within experimental error (15%) the observed value from the fluorimetric determination. Apparently, with the latter method, only the

† Electronic supplementary information (ESI) available: characterisation of compounds **2** and **4**, and a Job-plot for the binding of the *N,N′*-dinonyl-4,4′-bipyridinium bromide to **2**. See http://www.rsc.org/suppdata/cc/b0/b000271m/

DOI: 10.1039/b000271m

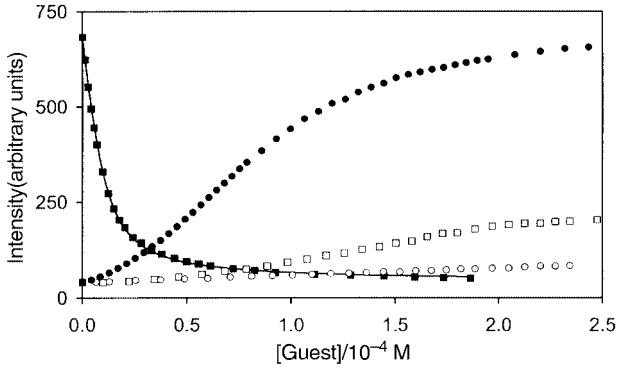

Fig. 1 Fluorimetric titration of (■) *N*,*N*′-dinonyl-4,4′-bipyridinium to **2** (1.0×10^{-5} M). The solid line shows the fitted curve assuming a 1:1 host(**2**):guest complex. Similar titration plots of (●) ursodeoxycholic acid, (□) lithocholic acid and (○) cholesterol to **2** (1.0×10^{-5} M) in the presence of 5.7×10^{-4} M of *N*,*N*′-dinonyl-4,4′-bipyridinium bromide. All titrations were performed in an aqueous 0.1 M Tris–HCl buffer at pH 7.0.

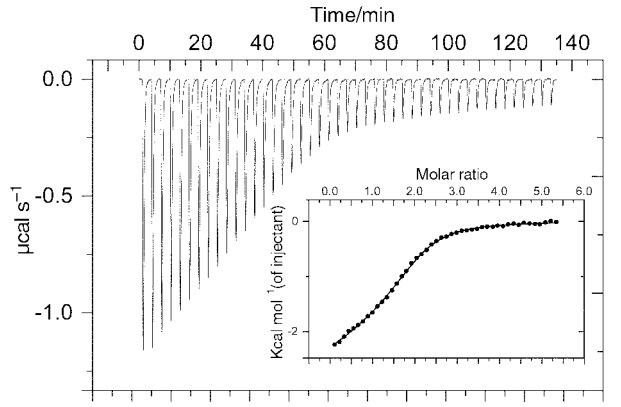

Fig. 2 Microcalorimetric titration of *N*,*N*′-dinonyl-4,4′-bipyridinium to **2** (1.0×10^{-4} M). For conditions see Table 1. The solid line (inset) shows the fitted curve according to a 1:2 (**2**:bipyridinium) model.

formation of the 1:1 complex can be detected. This implies that the binding of the first bipyridinium center results in almost complete quenching of the luminescence of **2** and that the second bipyridium unit has no effect on the luminescence.

Table 1 shows that $-T\Delta S$ of binding is the same for the 1:1 and the 1:2 complex. This parameter is probably related to the break up of solvent shells around the alkyl tails of the bipyridinium guest, which will be the same for the first and the second bipyridinium unit. By contrast ΔH of binding is different, being 1 kcal mol^{-1} smaller for the second step. We propose that two cyclodextrin moieties are involved in the complexation of a long chain bipyridinium guest.[8] Apparently, the binding of a second guest in **2** is disfavoured and the binding of a third guest completely absent, probably owing to a negative allosteric effect. Further studies are underway to substantiate this.

Having observed that bipyridinium compounds can quench the emission of **2** efficiently, we used this property to detect organic compounds. Displacement of the bipyridinium compound by other guests such as steroids should inhibit the quenching process and recover the luminescence of **2**. This would then give a sensor system which emits light when a guest is added. From a technological point of view this is an advantage since, in contrast to conventional systems, a luminescent signal is produced against a dark background, allowing a more sensitive detection in for instance a diagnostic test. When ursodeoxycholic acid was added to an aqueous solution of **2** and the bipyridinium ion, full recovery of the luminescence was observed (Fig. 1). A similar titration curve was recorded for lithocholic acid and cholesterol, showing the general applicability of the procedure. The curves for lithocholic acid and ursodeoxycholic acid displayed a sigmoidal shape suggesting that these steroids first displace one bipyridinium which will not result in a significant increase of the luminescence (*vide supra*), and only when the second bipyridinium ion becomes displaced the luminescence will be recovered.§

All steroids must have a binding constant of the same magnitude as the bipyridinium salt, *i.e.* 10^5 M^{-1} or slightly higher, in order for displacement in **2** to occur. The binding of ursodeoxycholic acid is strong enough to completely displace the bipyridinium salt and recover the full luminescence. Lithocholic acid only restores 30% of the emission, probably due to a weaker binding. The binding of cholesterol is too weak to even show a sigmoidal binding curve. Nevertheless, at a concentration of 2.3×10^{-4} M of cholesterol the luminescence has already doubled. Lithocholic acid shows a 5-fold increase at the same concentration, while for ursodeoxycholic acid the increase is 15-fold. This means that this sensor system is able to differentiate between different steroids which is a prerequisite for a selective diagnostic test. More detailed studies on this new sensor system are underway.

We thank the Netherlands Technology Foundation (STW) for financial support and M. R. de Jong and Dr J. Huskens (University of Twente) for stimulating discussions and their help with the microcalorimetry experiments.

Table 1 Thermodynamic data for the complexation of *N*,*N*′-dinonyl-4,4′ bipyridinium bromide in **2**[a]

Host–guest complex	K_a/M^{-1}	ΔH/kcal mol^{-1}	$-T\Delta S$/kcal mol^{-1}
1:1	2.4×10^5	−2.4	−4.8
1:2	4.0×10^5	−1.4	−4.9

[a] Obtained from a microcalorimetric titration of the bipyridinium guest with **2**. The data points were fitted assuming a two step (**2**:guest = 1:1 and 1:2) equilibrium. The titration was performed at 25.0 °C in an aqueous 0.1 M Tris–HCl buffer of pH 7.0, by adding small aliquots of a solution of the bipyridinium salt (3.09×10^{-3} M) to a solution of **2** (1.00×10^{-4} M). The data were corrected for the dilution heat of the bipyridinium ion.

Notes and References

‡ Compounds **1**, **2** and **4** were fully characterised by ^{1}H NMR, MS and elemental analysis.

§ In addition to compound **2** we also prepared a ruthenium complex with two unsubstituted bipyridines and one molecule of **4** as ligands. This mixed complex has only one binding site for the bipyridinium guest and therefore a single competition event should take place. The emission properties of this complex turned out to be much weaker than those of **2**, and, therefore, were not further investigated.

1 H. F. M. Nelissen, F. Venema, R. M. Uittenbogaard, M. C. Feiters and R. J. M. Nolte, *J. Chem. Soc., Perkin Trans. 2*, 1997, 2045 and references therein.
2 C. M. Rudzinski, W. K. Hartman and D. G. Nocera, *Coord. Chem. Rev.*, 1998, **117**, 115; S. Weidner and Z. Pikramenou, *Chem. Commun.*, 1998, 1473; S. Santra, P. Zhang and W. Tan, *Chem. Commun.*, 1999, 1301.
3 Some fluorophore appended γ-cyclodextrins show an increase in emission intensity upon co-inclusion of a small guest, see: Y. Wang, T. Ikeda, A. Ueno and F. Toda, *Chem. Lett.*, 1992, 863.
4 For other examples of bipyridyl appended cyclodextrins and their metal complexes, see: N. Brügger, R. Deschenaux, T. Ruch and R. Ziessel, *Tetrahedron Lett.*, 1992, **33**, 3871; R. Deschenaux, M. M. Harding and T. Ruch, *J. Chem. Soc., Perkin Trans. 2*, 1993, 1251; R. Deschenaux, A. Greppi, T. Ruch, H.-P. Kriemler, F. Raschdorf and R. Ziessel, *Tetrahedron Lett.*, 1994, **35**, 2165; R. Deschenaux, T. Ruch, P.-F. Deschenaux, A. Juris and R. Ziessel, *Helv. Chim. Acta*, 1995, **78**, 619; A. Nakamura, T. Imai, Y. Oda, S. Okutsu, A. Ueno and F. Toda, *J. Electroanal. Chem.*, 1997, **438**, 159.
5 F. Venema, H. F. M. Nelissen, P. Berthault, N. Birlirakis, A. E. Rowan, M. C. Feiters and R. J. M. Nolte, *Chem. Eur. J.*, 1998, **4**, 2237.
6 J. I. Cline III, W. J. Dressick, J. N. Demas and B. A. DeGraff, *J. Phys. Chem.*, 1985, **89**, 94.
7 P. D. Beer, N. C. Fletcher and T. Wear, *Inorg. Chim. Act.*, 1996, **251**, 335; P. R. Ashton, R. Ballardini, V. Balzani, E. C. Constable, A. Credi, O. Kocian, S. J. Langford, J. A. Preece, L. Prodi, E. R. Schofield, N. Spencer, J. F. Stoddart and S. Wenger, *Chem. Eur. J.*, 1998, **4**, 2413.
8 A. Diaz, P. A. Quintela, J. M. Schuette and A. E. Kaifer, *J. Phys. Chem.*, 1988, **92**, 3537.

Communication b000271m

ChemComm

A novel dodecanuclear chromium(III) cage: structural control by choice of leaving group

Simon Parsons, Andrew A. Smith and Richard E. P. Winpenny*

Department of Chemistry, The University of Edinburgh, West Mains Road, Edinburgh, UK EH9 3JJ
E-mail: repwol@holywood.ed.ac.uk

Received (in Basel, Switzerland) 8th February 2000, Accepted 25th February 2000
Published on the Web 17th March 2000

The synthesis and structural characterisation of a novel metal polyhedron is reported, involving chromium(III) and isobutyrate; comparison of this product with those obtained using different carboxylates suggests that the leaving group—which can be carboxylate, water or both—strongly influences the structure found.

Recent research on paramagnetic cages has been stimulated by the discovery of 'single molecule magnetism',[1,4] *i.e.* cages which have an energy barrier to reorientation of their magnetisation which is sufficiently high that at low temperature magnetisation is lost slowly when an external magnetic field is removed. We have been looking at new routes to high nuclearity cages, and found that heating small cages to high temperatures in an inert atmosphere can lead to oligomerisation.[5–7] Here we report a further reaction which gives a quite new metal polyhedron, but also which indicates that choice of carboxylate can control the structure of the resulting cage.

Reaction of $Cr(NO_3)_3{\cdot}9H_2O$ (0.050 mol) with $K(O_2CCHMe_2)$ (0.175 mol) in H_2O (100 cm^3) at *ca.* 80 °C gives a blue precipitate (> 90% yield) which is soluble in Pr^iOH. Analysis of this solid suggests formation of an oxo-centred chromium triangle, $[Cr_3O(O_2CCHMe_2)_6(H_2O)_3](NO_3)$ **1**.† Heating this precipitate at 400 °C under a stream of N_2 for 5 min gives a dark green solid which can be recrystallised from a mixture of Pr^nOH–CH_2Cl_2 to give green blocks suitable for X-ray study in 7 days. The yield of crude material is 84%. IR spectroscopy and elemental analysis confirm the crude and recrystallised compounds are identical.

Structural analysis‡ reveals a cage of stoichiometry $[Cr_{12}O_8(OH)_4(O_2CCHMe_2)_{16}(HO_2CCHMe_2)_4]$ **2** (Fig. 1). The cage consists of three face-sharing Cr_4O_4 heterocubanes, with the two terminal cubanes capped by further chromium centres attached to the external μ_4-oxides. The central cubane, containing Cr(3), Cr(4), Cr(5) and Cr(6), is held together exclusively through four μ_4-oxides [O(3), O(4), O(5) and O(6)]. These oxides have an unusual geometry, with one Cr–O–Cr angle *ca.* 164°, and five further Cr–O–Cr angles at between 90 and 101°. Therefore these four-coordinate oxygens have a 'saw-horse' geometry, rather than tetrahedral. This geometry may be found

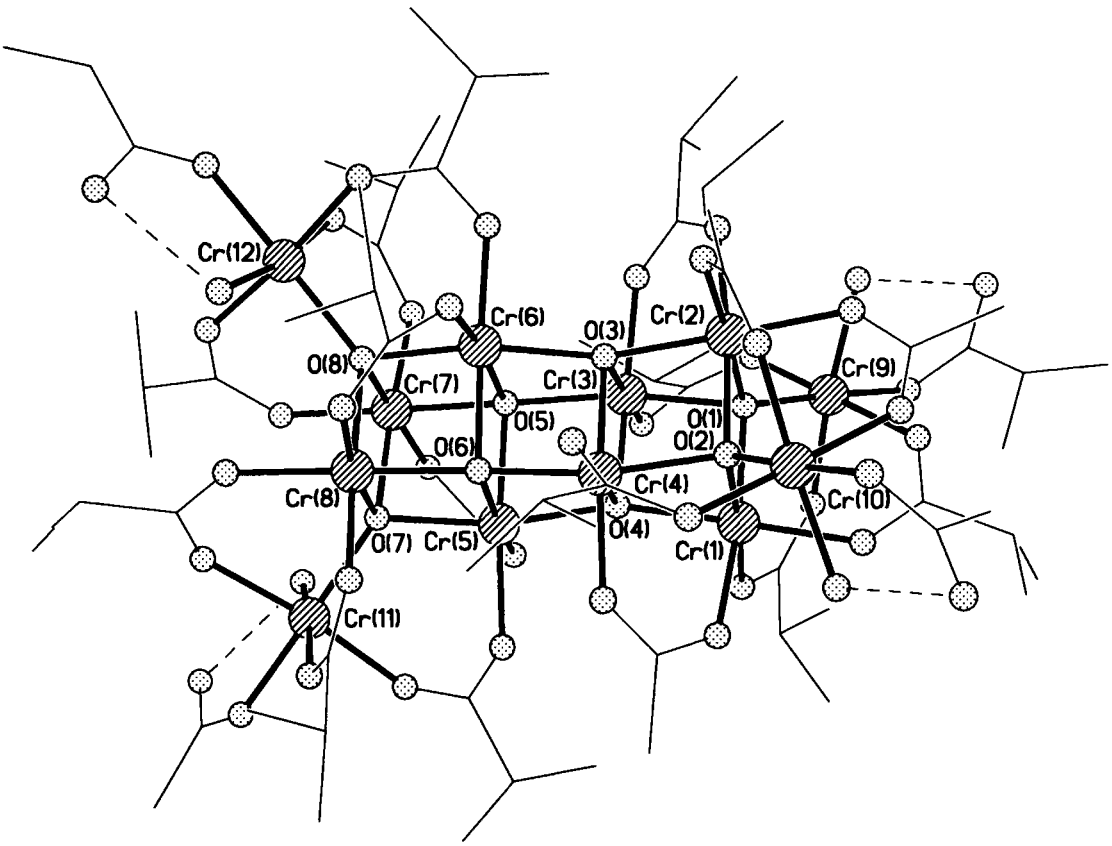

Fig. 1 The structure of **1**. The H-bonds between OH and protonated carboxylates are shown as dashed lines (see text). Bond length ranges: Cr–O(μ_4-O) 1.947–2.050, Cr–O(O_2CR) 1.943–1.997, Cr–O(OH) 1.966–1.986 Å. Av. esd. 0.008 Å. Bond angle ranges: *cis* O(μ_4-O)–Cr–O(μ_4-O) 78.8–89.3, *trans* O(μ_4-O)–Cr–O(μ_4-O) 163.7–166.1, *cis* O(μ_4-O)–Cr–O(O_2CR) 89.1–103.0, *trans* O(μ_4-O)–Cr–O(O_2CR) 169.6–179.2, *cis* O(O_2CR)–Cr–O(O_2CR) 81.7–90.8, *trans* O(O_2CR)–Cr–O(O_2CR) 173.0–173.9, *cis* O(OH)–Cr–O(μ_4-O) 92.6–93.4, *cis* O(OH)–Cr–O(O_2CR) 87.5–91.5, *trans* O(OH)–Cr–O(O_2CR) 170.1–171.4°. Av. esd. 0.4°.

DOI: 10.1039/b001140l

because this central Cr_8O_8 fragment can be considered to be a fragment of the NaCl structure.

The μ_4-oxides involved in the external heterocubanes have a more regular geometry, approximating to tetrahedral. The two Cr atoms in the face that is shared with the central heterocubane are each bridged to one of the two external Cr atoms [either Cr(1) and Cr(2) or Cr(7) and Cr(8)] by 1,3-bridging carboxylates. The final four Cr atoms [Cr(9), Cr(10), Cr(11) and Cr(12)] are found attached to the μ_4-oxides, and these are each further attached to the centre triple-cubane by bridging carboxylates. Two of these carboxylates bridge to Cr centres at the exterior of the triple-cubane [*e.g.* between Cr(9) and Cr(1)], and one bridges to a Cr centre in the shared-face [*e.g.* between Cr(9) and Cr(5)].

The chromium sites therefore fall into three groups. All are six-coordinate with regular octahedral geometries, but they vary in the groups attached to them. The Cr sites in the central cubane are each bound to four μ_4-oxides and two oxygen donors from carboxylate bridges. The Cr sites at the exterior of the triple-cubane are each bound to three μ_4-oxides and three O-atoms from carboxylates. The Cr sites capping the tricubane are each bound to one μ_4-oxide, three oxygens from bridging carboxylates and two terminal groups that can be described as a hydroxide and a HO_2CCHMe_2 group, or a water molecule and a $^-O_2CCHMe_2$. As there is a strong H-bond (O···O 2.47 to 2.53 Å) between these two groups, the exact description is perhaps unimportant.

The structure of **2** is new, but related to previous cages built of cubanes. The nearest relation is an octanuclear triple-cubane of cobalt(III), reported by Christou and coworkers,[10] which lacks the final four capping atoms. Three octanuclear cages, featuring Cr,[6] Fe[11] and Co,[12] contain a heterocubane capped on the μ_4-oxides. **2** combines features from both these previous structural types. There are also some similarities between **2** and Ni_{11} and Mn_{18} cages we have reported previously, which also feature face-sharing heterocubanes.[13]

It appears that the structure of **2** is largely maintained in solution. Two peaks, due to mono- and di-cationic species, dominate the electrospray mass spectrum.§ The mono-cationic species, at *m/z* 2351.4, can be assigned as ($\mathbf{2} - 2\ HO_2CCHMe_2 - 2H_2O)^+$ (calc. 2353.7), while the dication at *m/z* 1160.1 matches ($\mathbf{2} - 2\ HO_2CCHMe_2 - 2OH - 2H_2O)^{2+}$ (calc. 1159.8). Remaining peaks in the spectrum have less than 10% of the intensity of these peaks.

The reaction to form **2** gives quite different cages if the carboxylate present is benzoate[6] or pivalate (trimethylacetate).[7] As the yields are very good (approaching 90%) for all cages, it is worth discussing the difference in these three examples. For benzoate, assuming a stoichiometric reaction, a balanced equation for the reaction at 400 °C would give:

$$8\ [Cr_3O(O_2CPh)_6(H_2O)_2(OH)] \rightarrow 3\ [Cr_8(\mu_4\text{-}O)_4(O_2CPh)_{16}] + 20\ H_2O$$

This implies exclusive loss of water on heating. A balanced equation for the reaction involving pivalate is:

$$4[Cr_3O(O_2CCMe_3)_6(H_2O)_2(OH)] \rightarrow [Cr_{12}(\mu_4\text{-}O)_9(\mu_3\text{-}OH)_3(O_2CCMe_3)_{15}] + 9\ HO_2CCMe_3 + 4H_2O$$

This is mainly loss of carboxylic acid on heating, with some loss of water. The reaction which gives **2**, is intermediate between these two extremes:

$$4[Cr_3O(O_2CCHMe_2)_6(H_2O)_2(OH)] \rightarrow [Cr_{12}(\mu_4\text{-}O)_8(OH)_4(O_2CCHMe_2)_{16}(HO_2CCHMe_2)_4] + 4H_2O + 4HO_2CCHMe_2$$

It is noticeable that for benzoate, which has the lowest pK_a (4.19) of the three carboxylates, water is lost and the carboxylate is retained, while for both pivalate (pK_a 5.03) and isobutyric acid (pK_a 4.84) a mixture of acid and water are lost. This gives us a hypothesis to examine to see if further chromium cages with new metal polyhedra can be made from this simple route. It also implies an unusual means of influencing the structure of a cage by the pK_a of the leaving group.

Magnetic studies of **2** are disappointing.¶ The room temperature value of χ_mT (where χ_m is the molar magnetic susceptibility) of 18.1 emu K mol^{-1}, is below that expected for 12 non-interacting Cr^{III} centres (22.3 emu K mol^{-1}, for g = 1.99). This value indicates moderately strong antiferromagnetic exchange between metal centres. This is confirmed by the steady fall in χ_mT down to 25 K, where the value is 7.2 emu K mol^{-1}. Below 25 K the fall is more rapid, and at the lowest temperature studied (1.8 K) the cage is almost diamagnetic.

We thank the EPSRC(UK) for funding for a diffractometer, electrospray mass spectrometer and SQUID susceptometer, and for a studentship (to A. A. S.)

Notes and references

† Satisfactory elemental analyses were obtained for all compounds reported.

‡ *Crystal data* for $C_{80}H_{148}Cr_{12}O_{53}\cdot 3.5CH_2Cl_2$. **2**: triclinic, $P\bar{1}$, a = 16.770(5), b = 17.049(6), c = 24.405(9) Å, α = 88.12(3), β = 85.11(3), γ = 69.756(15)°, V = 6523(4) Å^3, M = 2755.15, Z = 2, T = 150.0(2) K, $R1$ = 0.0975. Data collection, structure solution and refinement were performed using programs DIRDIF[8] and SHELXL-97.[9] Only Cr and O atoms were refined anisotropically, and there is a disordered solvent region in the structure. CCDC 182/1559. See http://www.rsc.org/suppdata/cc/b0/b001140l/ for crystallographic files in .cif format.

§ Electrospray mass spectra were obtained on a Finnegan LCQ spectometer with the sample dissolved in CH_2Cl_2 which was added to MeOH prior to injection into the spectrometer.

¶ Variable-temperature magnetic measurements on **2** in the region 1.8–325 K were made using a SQUID magnetometer (Quantum Design) with samples sealed in gelatine capsules. Diamagnetic corrections for sample holders and samples were applied to the data.

1 R. Sessoli, H.-L. Tsai, A. R. Schake, S. Wang, J. B. Vincent, K. Folting, D. Gatteschi, G. Christou and D. N. Hendrickson, *J. Am. Chem. Soc.*, 1993, **115**, 1804; R. Sessoli, D. Gatteschi, A. Caneschi and M. A. Novak, *Nature*, 1993, **365**, 141.
2 S. M. J. Aubin, M. W. Wemple, D. M. Adams, H.-L. Tsai, G. Christou and D. N. Hindrickson, *J. Am. Chem. Soc.*, 1996, **118**, 7746.
3 C. Sangregorio, T. Ohm, C. Paulsen, R. Sessoli and D. Gatteschi, *Phys. Rev. Lett.*, 1997, **78**, 4645.
4 Z. Sun, C. M. Grant, S. L. Castro, D. N. Hendrickson and G. Christou, *Chem. Commun.*, 1998, 721.
5 E. K. Brechin, S. G. Harris, S. Parsons and R. E. P. Winpenny, *Chem. Commun.*, 1996, 1439.
6 I. M. Atkinson, C. Benelli, M. Murrie, S. Parsons and R. E. P. Winpenny, *Chem. Commun.*, 1999, 285.
7 F. E. Mabbs, E. J. L. McInnes, M. Murrie, S. Parsons and R. E. P. Winpenny, *Chem. Commun.*, 1999, 643.
8 P. T. Beurskens, G. Beurskens, W. P. Bosman, R. de Gelder, S. Garcia-Granda, R. O. Gould, R. Israel and J. M. M. Smits, DIRDIF-96 program system, University Crystallography Laboratory, University of Nijmegen 1996.
9 G. M. Sheldrick, University of Göttingen, 1997.
10 V. A. Grillo, Z. Sun, K. Folting, D. N. Hendrickson and G. Christou, *Chem. Commun.*, 1996, 2233.
11 R. G. Raptis, I. P. Georgakaki and D. C. R. Hockless, *Angew. Chem., Int. Ed.*, 1999, **38**, 1632.
12 K. Dimitrou, J.-S. Sun, K. Folting and G. Christou, *Inorg. Chem.*, 1995, **34**, 4160.
13 E. K. Breckin, W. Clegg, M. Murrie, S. Parsons, S. J. Teat and R. E. P. Winpenny, *J. Am. Chem. Soc.*, 1998, **120**, 7365.

Communication b001140l

ChemComm

Chemistry of M(allyl)$_3$ (M = Rh, Ir) compounds: structural characterization of tris(allyl)iridium complexes with phosphorus ligands†

Kevin D. John,[a] Kenneth V. Salazar,[b] Brian L. Scott,[a] R. Thomas Baker*[a] and Alfred P. Sattelberger*[a]

[a] *Los Alamos Catalysis Initiative, Chemical Science and Technology Division, Los Alamos National Laboratory, MS J514, Los Alamos, NM 87545, USA. E-mail: weg@lanl.gov; sattelberger@lanl.gov*

[b] *Materials Science and Technology Division, Los Alamos National Laboratory, MS E549, Los Alamos, NM 87545, USA*

Received (in Bloomington, IN, USA) 21st December 1999, Accepted 22nd February 2000

While addition of phosphorus ligands such as P(OPh)$_3$ to Rh(allyl)$_3$ gives monovalent Rh(allyl)L$_2$, the iridium analog gives stable mixed σ/π-tris(allyl) complexes, as evidenced by the structural characterization of mono-, bi-, and tri-dentate ligand complexes.

Recent efforts aimed at preparing and characterizing 'single-site' catalysts consisting of well defined, metal–oxide surface-bound, ligated transition metals have yielded exciting new catalytic systems for alkane metathesis and polyolefin depolymerization.[1,2] One particularly well-characterized class of such sites is derived from reactions of tris(allyl)rhodium, Rh(C$_3$H$_5$)$_3$, with carefully prepared, high-purity metal oxides.[3–5] The use of these systems for catalysis, however, is hampered by weak Rh–O bonds to the metal oxide surface and the proclivity of trivalent rhodium intermediates to undergo reductive elimination.[6] We are investigating the use of tris(allyl)iridium to prepare single-site catalysts with better thermal and reductive stability. In expanding the relatively unexplored[7] ligand addition chemistry of M(allyl)$_3$ compounds, we have developed an improved synthesis of the iridium analog and demonstrated that its reactions with a variety of phosphorus ligands all afford trivalent products, including a stable tris(σ-allyl) adduct.

The literature procedure[8] for preparing Ir(allyl)$_3$ from Ir(acac)$_3$ (acac = acetylacetonate) and (allyl)MgCl affords the desired product in *ca*. 20% yield. Ir(acac)$_3$ is itself prepared in *ca*. 10% yield from commercially available IrCl$_3$·*x*H$_2$O. We have found that the crystalline yellow tetrahydrothiophene adduct, IrCl$_3$(tht)$_3$, can be prepared from IrCl$_3$·*x*H$_2$O in *ca*. 90% yield *via* a slight modification of the original synthesis.[9] Reaction of IrCl$_3$(tht)$_3$ with allyllithium in benzene provides Ir(allyl)$_3$ in > 90% NMR yield [eqn 1)].[10]

$$IrCl_3(tht)_3 + 3\ LiC_3H_5 \xrightarrow[25\ °C]{\text{benzene}} Ir(C_3H_5)_3 + 3\ LiCl + 3\ tht \quad (1)$$

Removal of the solvent *in vacuo* followed by hexane extraction, filtration, solvent removal and sublimation of the brown residue affords colorless, microcrystalline Ir(allyl)$_3$ in *ca*. 45% yield. Treatment of isolated Ir(allyl)$_3$ with PPh$_3$ in toluene gives the 1:1 adduct Ir(σ-allyl)(π-allyl)$_2$(PPh$_3$) **1** in high yield (Scheme 1).‡ Alternatively, the hexane filtrate from the synthesis of Ir(allyl)$_3$ can be used directly to prepare **1** with comparable efficiency. Although complex **1** did not react further with excess PPh$_3$, even at 100 °C, smaller phosphorus ligands such as PMe$_3$ and P(OPh)$_3$ yielded 1:2 adducts Ir(σ-allyl)$_2$(π-allyl)L$_2$ **2a**,**b**. The chelating bis(phosphine) 1,2-(PPh$_2$)$_2$C$_6$H$_4$ gave a similar product **3**. Addition of the tridentate phosphine PhP(CH$_2$CH$_2$PPh$_2$)$_2$ to Ir(allyl)$_3$ gave the tris(σ-allyl) complex **4**. Complexes **2**–**4** were prepared in > 90% yield.

† Electronic supplementary information (ESI) available: preparative details and NMR data for **1**–**6** and crystallographic data for **1**, **3** and **4**. See http://www.rsc.org/suppdata/cc/a9/a910164k/

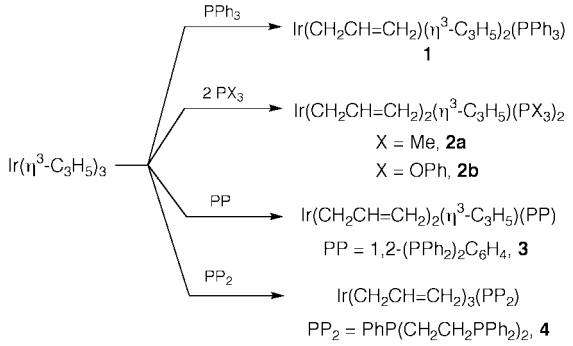

Scheme 1

The tris(allyl)iridium ligand adducts **1**–**4** were characterized by elemental analysis, NMR and IR spectroscopy, and, for **1**, **3** and **4** by single crystal X-ray diffraction (Fig. 1).§ IR analysis revealed that all phosphine adducts possess a characteristic C=C stretch in the region 1600–1610 cm^{-1}. ^{1}H and ^{13}C NMR spectra of **1** confirmed the presence of one σ-allyl and two *inequivalent* π-allyl groups, even at 100 °C. The PPh$_3$ ligand is located *trans* to a methylene group of one of the π-allyl groups, as evidenced by the large P–C coupling constant ($^2J_{PC}$ 38 Hz). Room temperature spectroscopic characterization of complexes **2a**,**b** was also consistent with an unsymmetrical structure, but a dynamic process leads to equivalent phosphorus ligands *and* σ-allyl groups at 40 °C. The P–C coupling constants for **2a**,**b** ($^2J_{PC}$ 32.6, 47.5 Hz, respectively) indicate that the phosphines are *trans* to the methylenes of the π-allyl group and the σ-allyls are thus mutually *trans*. By contrast, complex **3** has inequivalent σ-allyl groups, even at 100 °C, with the two phosphorus donors *trans* to one methylene of the π-allyl ($^2J_{PC}$ 39.4 Hz) and to one of the σ-allyl groups ($^2J_{PC}$ 79.5 Hz), respectively (Fig. 2). Adduct **4** has two sets of σ-allyl groups in a 1:2 ratio, consistent with C_s symmetry.

For compound **1**, the π-allyl ligand *trans* to P is symmetrically bound with typical Ir–C bond distances[11] (Ir–CH 2.143[5], Ir–CH$_2$ 2.201[5] Å). The other π-allyl ligand is unsymmetrically bound as a result of the *trans* influence of the σ-allyl {C(1)–Ir–C(7) 161.6[2]°; Ir–C(7) 2.268[4] *cf*. Ir–C(9) 2.196[4] Å}. A similar effect is seen in **3** {C(1)–Ir–C(7) 162.1(1)°; Ir–C(7) 2.270(2) *cf*. Ir–C(9) 2.202(3) Å}.

Reaction of Rh(allyl)$_3$[12] with PMe$_3$ afforded the 1:2 adduct **5** similar to **2a**. With triphenylphosphine[12] or better π-accepting ligands such as P(OPh)$_3$, however, only monovalent complexes, Rh(π-allyl)L$_2$ **6a**,**b** were obtained. Analogous complexes have been reported previously *via* alternative preparative routes.[11,13] The reaction leading to **6b** was accompanied by formation of the C$_6$ hydrocarbons *n*-hexane, hex-1-ene and 2-methylpentane.¶

In summary, our improved preparation of tris(allyl)iridium has enabled us to demonstrate that, in contrast to its rhodium analog, addition of a range of phosphorus ligands gives stable trivalent adducts which show no tendency to undergo hydro-

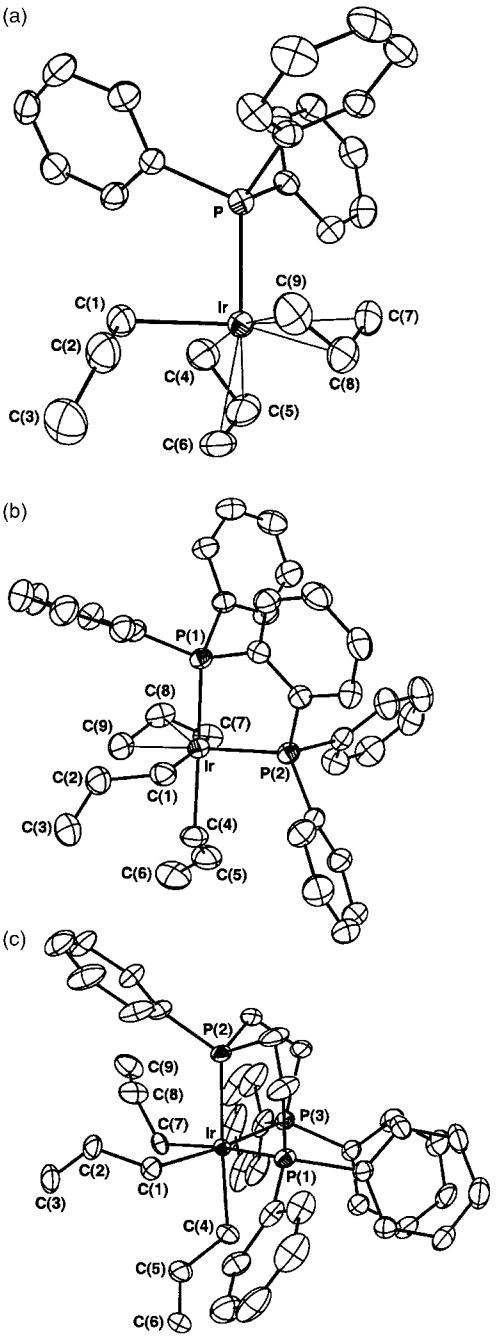

Fig. 1 Thermal ellipsoid representation of (a) **1**, (b) **3** and (c) **4** shown at the 50% probability level. For **1**, only one of the two molecules in the asymmetric unit is shown. For **1** and **4**, only one orientation of the disordered allyl group is shown.§ Hydrogen atoms have been omitted for clarity.

carbon elimination reactions. We are currently extending these findings to prepare trivalent, ligated iridium moieties on metal oxide surfaces for use in hydrocarbon functionalization.

We thank the Department of Energy's Laboratory Directed Research and Development (LDRD) program for financial support and Dr David Smith for preliminary experiments. This paper is dedicated to Professor John P. Fackler, Jr. on the occasion of his 65th birthday.

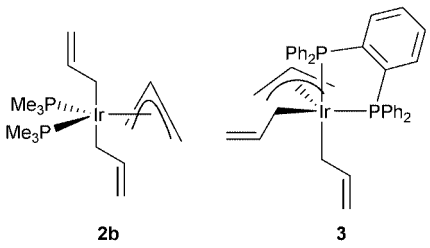

2b **3**

Fig. 2 Isomeric Ir(π-allyl)(σ-allyl)$_2$L$_2$ structures.

Notes and references

‡ *Preparation* of Ir(σ-allyl)(π-allyl)$_2$(PPh$_3$): to a room temperature solution of Ir(allyl)$_3$ (0.100 g, 0.32 mmol) in toluene (10 mL) was added triphenylphosphine (0.083 g, 0.32 mmol). The reaction mixture was stirred for 2 h and then filtered. The filtrate was concentrated to *ca*. 2 mL and allowed to sit at room temperature for 24 h to yield **1** as colorless crystals in 92.7% yield (0.170 g, 0.24 mmol). This procedure is representative of the syntheses of all of the phosphine complexes with the caveat that the preparation of **3** and **4** required brief heating (80 °C, 10 min) in order to dissolve the ligand.

§ CCDC 182/1552. See http://www.rsc.org/suppdata/cc/a9/a910164k/ for crystallographic files in .cif format.

¶ *Preparation* of Rh(π-allyl)[P(OPh)$_3$]$_2$: to a room temperature solution of Rh(allyl)$_3$ (0.031 g, 0.14 mmol) in toluene (5 mL) was added triphenyl phosphite (0.086 g, 0.28 mmol) with stirring. Approximately 30 min after the phosphite addition, a brilliant yellow precipitate was observed. The reaction mixture was stirred for an additional 2 h during which time the precipitate dissolved. The filtrate was then concentrated to *ca*. 2 mL and allowed to stand at −35 °C for 24 h to yield **2b** as yellow crystals in 96.7% yield (0.102 g, 0.13 mmol). GC–MS analysis of a portion of this reaction revealed that the organic products were *n*-hexane, 2-methylpentane and hex-1-ene.

1 F. Lefebvre, J. Thivolle-Cazat, V. Dufaud, G. P. Niccolai and J. M. Basset, *Appl. Catal. A: Gen.*, 1999, **182**, 1.
2 V. R. Dufaud and J. M. Basset, *Angew. Chem., Int. Ed.*, 1998, **37**, 806.
3 C. C. Santini, S. L. Scott and J. M. Basset, *J. Mol. Catal. A*, 1996, **107**, 263.
4 P. Dufour, C. Houtman, C. C. Santini, C. Nédez, J. M. Basset, L. Y. Hsu and S. G. Shore, *J. Am. Chem. Soc.*, 1992, **114**, 4248.
5 P. Dufour, C. Houtman, C. C. Santini and J. M. Basset, *J. Mol. Catal. A*, 1992, **77**, 257.
6 J. M. Basset, F. Lefebvre and C. Santini, *Coord. Chem. Rev.*, 1998, **178–180**, 1703.
7 The only reported reaction of Ir(allyl)$_3$ is with HCl to give [Ir(allyl)$_2$(μ-Cl)]$_2$: M. Green and G. J. Parker, *J. Chem. Soc., Dalton Trans.*, 1974, 333.
8 P. Chini and S. Martinengo, *Inorg. Chem.*, 1967, **6**, 837.
9 E. A. Allen and W. Wilkinson, *J. Chem Soc., Dalton Trans.*, 1972, 613.
10 For alkyl–metal complexes prepared analogously: R. S. Hay-Motherwell, G. Wilkinson, B. Hussain-Bates and M. B. Hursthouse, *Polyhedron*, 1990, **9**, 2071.
11 M. Manger, J. Wolf, M. Teichert, D. Stalke and H. Werner, *Organometallics*, 1998, **17**, 3210.
12 J. Powell and B. L. Shaw, *J. Chem. Soc. A*, 1968, 583.
13 S. Lange, K. Wittmann, B. Gabor, R. Mynott and W. Leitner, *Tetrahedron: Asymmetry*, 1998, **9**, 475.

Communication a910164k

ChemComm

Enantioselective synthesis of tetrahydroisoquinolines and benzazepines by silane terminated Heck reactions with the chiral ligands (+)-TMBTP and (*R*)-BITIANP

Lutz F. Tietze,*[a] Kai Thede,[a] Ralph Schimpf[a] and Franco Sannicolò[b]

[a] *Institut für Organische Chemie der Universität Tammannstraße 2, D-37077 Göttingen, Germany. Telefax: Int. + 551/39-9476, E-mail: ltietze@gwdg.de*

[b] *Dipartimento di Chimica Organica e Industriale, Università di Milano, Via Venezian 21, I-20133 Milano, Italy*

Received (in Cambridge, UK) 9th December 1999, Accepted 10th February 2000

The intramolecular Heck reaction of the iodoaryl compound 1 with a (*Z*)-allyl silane moiety in the presence of the chiral ligand (+)-TMBTP 13 leads to the benzazepine 5b with 92% ee, whereas 3 with an (*E*)-allyl silane moiety in the presence of the chiral ligand (*R*)-BITIANP 14 gives 5a with 91% ee; in a similar way, 9 and 10 were transformed in the presence of 13 into the tetrahydroisoquinolines 11b and 12b with 86 and 84% ee, respectively.

The Heck reaction,[1] the Pd(0) catalyzed coupling of an aryl or alkenyl halide or triflate with an alkene, is nowadays one of the most important C–C bond forming transformations and has been used in numerous syntheses of natural products;[2] extensive work has also been done in the enantioselective series.[3] Here, we describe the enantioselective intramolecular silane terminated Heck reaction[3g–i] of the substrates **1**–**4** and **7**–**10** with the novel chiral ligands (+)-4,4′-bis(diphenylphosphino)-2,2′,5,5′-tetramethyl-3,3′-bithiophene [(+)-TMBTP] **13**[4a] and (*R*)-(+)-2,2′-bis(diphenylphosphino)-3,3′-bibenzo[*b*]thiophene [(*R*)-BITIANP] **14**[4b] as well as, for comparison, also with the well known and widely used ligands (*R*)-MeO-BIPHEP **15**[5] and (*R*)-BINAP **16**,[6] to give the substituted benzazepines **5a**/**b** and **6a**/**b** and the tetrahydroisoquinolines **11a**/**b** and **12a**/**b** (Scheme 1). In addition, we have used phosphinooxazolines[3c,e] as chiral ligands, however, in our systems these ligands show low reactivity.

We have recently shown that one of the main disadvantages of the Heck reaction, namely the low selectivity in the elimination of the L_nPd–H species to form the double bond as the last step in the catalytic cycle, can be overcome by using allyl silanes as terminating alkenes.[3g–i] This allowed the selective formation of tertiary stereogenic centers starting from acyclic alkenes for the first time. However, the use of this procedure for the synthesis of chiral heterocyclic compounds such as benzazepines and tetrahydroisoquinolines with **16** as ligand was rather disappointing owing to its low enantioselectivity.[3i] By contrast, employing the novel chiral ligands **13** and **14** (Scheme 2) we are now able to synthesize these heterocycles with up to 92% ee.

13 had not been used successfully previously for enantioselective transformations, whereas **14** was employed with great success in the hydrogenation of C–C and C–O double bonds[4b] and in intermolecular Heck reactions.[3a] In our investigations we used (*E*)- and (*Z*)-allyl silanes as substrates, which not only gave different enantioselectivities using the various ligands, but also allowed us to control the formation of the different side chains in the products, namely a vinyl or a trimethylsilylvinyl group.

The selective formation of the (*Z*)-allyl silanes **1**, **2** and **9**, **10**, respectively, was performed by a Ni catalyzed hydrogenation of the corresponding propargyl silanes **17**–**20**. For the synthesis of the (*E*)-compounds **3**, **4** and **7**, **8**, respectively, the propargyl amine **21** was reduced with $LiAlH_4$, the obtained allyl amine **22** alkylated with **23**, **24**, **25** or **26** and finally treated with trifluoroacetyl anhydride (Scheme 3).

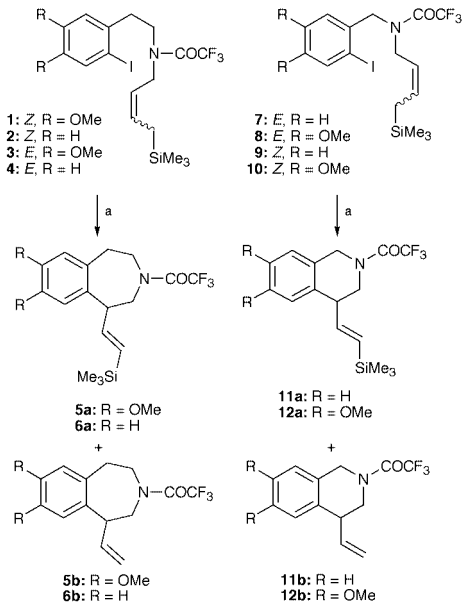

Scheme 1 Syntheses of benzazepines **5** and **6** and tetrahydroisoquinolines **11** and **12** by silane terminated enantioselective Heck reaction. *Reagents* a, $Pd_2dba_3{\cdot}CHCl_3$, ligand, Ag_3PO_4 (1.1 eq.), DMF.

The Heck reaction of the (*Z*)-allyl silane **1** in the presence of triphenylphosphane gave nearly exclusively the benzazepine **5b** with a vinyl side chain (Table 1, entry 1); using the chiral ligands **15** (entry 2) and **14** (entry 3), **5b** again was the main product, however, the enantioselectivity was < 50% ee; with (*S*)-BINAP *ent*-**16** (entry 4), **5b** was formed with 64% ee. In contrast, using **13**, the product **5b** could be obtained in good yield, with complete regioselectivity and 92% ee (entry 5). Similar results were found with the (*Z*)-allyl silane **2**, but here the highest ee value using **13** as chiral ligand was only 70% ee (entry 9). This could probably be ascribed to the lower ligand Pd ratio, which was necessary owing to the low reactivity using higher ratios. This, however, is a general problem in enantioselective Heck reactions.

Employing the (*E*)-allyl silane **3** again an excellent enantioselectivity of 91% ee was obtained (entry 10). For the first time in the enantioselective silane terminated Heck reation, **5a** with a

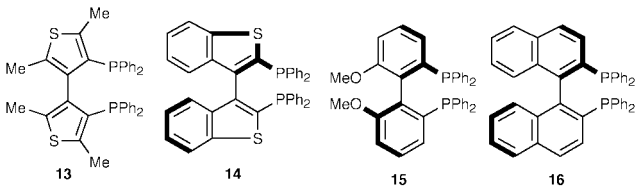

Scheme 2 Ligands for the enantioselective Heck reaction: (+)-TMBTP **13**, (*R*)-BITIANP **14**, (*R*)-MeO–BIPHEP **15** and (*R*)-BINAP **16**.

DOI: 10.1039/a909689b

Table 1 Enantioselective silane terminated Heck reactions of the allyl silanes **1**–**4** and **7**–**10** to give the benzazepines **5** and **6** and the tetrahydroisoquinolines **11** and **12**

Entry	Substrate (Config.)	R	Product	Pd Catalyst (mol%)	Ligand (mol%)	*t*/h	*T*/°C	Yield (%)		Ee[a] (%)	
								a	**b**	**a**	**b**
1	**1** (*Z*)	OMe	**5**	5[b]	PPh_3 (10)[c]	6	80	4	70	—	—
2	**1** (*Z*)	OMe	**5**	3	**15** (7)	65	80	15	42	< 5 (*S*)	< 25 (*R*)
3	**1** (*Z*)	OMe	**5**	3	**14** (7)	19	80	2	42	—[d]	< 20 (*R*)
4	**1** (*Z*)	OMe	**5**	3	*ent*-**16** (7)	40	80	7	72	< 18 (*R*)	64 (*S*)
5	**1** (*Z*)	OMe	**5**	1.5	**13** (15)	68	80	—	71	—	92 (*S*)
6	**2** (*Z*)	H	**6**	3	**16** (15)	27	90	4	73	—[d]	48 (*R*)
7	**2** (*Z*)	H	**6**	3	**15** (15)	168	90	6	49	—[d]	28 (*R*)
8	**2** (*Z*)	H	**6**	3	**14** (15)	24	90	—	72	—	42 (*R*)
9	**2** (*Z*)	H	**6**	3	**13** (15)	27	90	6	71	—[d]	70 (*S*)
10	**3** (*E*)	OMe	**5**	1.5	**14** (10)	24	80	66	21	91 (*S*)	≈ 60 (*S*)
11	**3** (*E*)	OMe	**5**	3	**13** (7)	45	80	57	33	8 (*R*)	≈ 45 (*S*)
12	**4** (*E*)	H	**6**	1.5	**14** (15)	26	80	42	41	86 (*S*)	22 (*S*)
13	**4** (*E*)	H	**6**	1.5	**13** (15)	16	80	25	43	12 (*R*)	64 (*R*)
14	**7** (*E*)	H	**11**	3	**16** (7)	20	80	40	32	2 (*R*)	67 (*R*)
15	**7** (*E*)	H	**11**	3	**14** (7)	14	70	14	51	0	50 (*R*)
16	**7** (*E*)	H	**11**	3	**13** (7)	46	80	38	35	< 5 (*R*)	< 5 (*S*)
17	**8** (*E*)	OMe	**12**	3	**14** (7)	48	80	42	24	30 (*R*)	34 (*R*)
18	**8** (*E*)	OMe	**12**	3	**13** (10)	48	80	9	56	76 (*R*)	56 (*R*)
19	**9** (*Z*)	H	**11**	1.5	**13** (10)	65	80	—	80	—	84 (*S*)
20	**9** (*Z*)	H	**11**	1.5	**13** (15)	63	90	—	61	—	86 (*S*)
21	**10** (*Z*)	OMe	**12**	3	**14** (7)	20	80	6	80	< 10 (*R*)	16 (*S*)
22	**10** (*Z*)	OMe	**12**	1	**13** (20)	64	80	—	73	—	84 (*S*)

[a] Determined by chiral HPLC (Baker CHIRALCEL OD-R). [b] $Pd(OAc)_2$ was used instead of $Pd_2dba_3{\cdot}CHCl_3$. [c] KOAc (4 eq.) and NPr_4Br (1 eq.) were used instead of Ag_3PO_4. [d] Not determined.

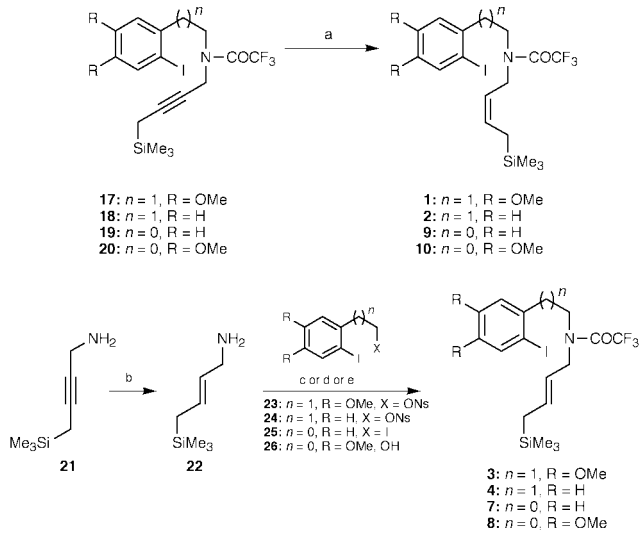

Scheme 3 Syntheses of the (*E*)- and (*Z*)-allyl silane precursors. *Reagents and conditions*: a, H_2, $Ni(OAc)_2$, $NaBH_4$, ethylenediamine, EtOH; **1**: 65%, **2**: 90%, **9**: 88%, **10**: 60%; b, $LiAlH_4$, THF, heat; 50%; c, 1. Pr^i_2NEt, MeCN–MeOH, 50 °C; 2. $(CF_3CO)_2O$, NEt_3, THF, 0 °C → r.t.; **3**: 42%, **4**: 40%; d, 1. $(CF_3CO)_2O$, NEt_3, THF, 0 °C → r.t.; 2. NaH, DMF, 0 °C → r.t.; **7**: 75%; e, 1. $(CF_3CO)_2O$, NEt_3, THF, 0 °C → r.t.; 2. MsCl, NEt_3, CH_2Cl_2, 0 °C → r.t.; NaH, DMF, 0 °C → r.t.; **8**: 39%.

trimethylsilylvinyl side chain is the main product, with **14** as the best ligand; thus, **13** gave **5a** with only 8% ee (entry 11). Interestingly, in the Heck reaction of the (*Z*)- and the (*E*)-allyl silanes with **14** and **13** the opposite enantiomers of **6b** were formed, whereas in the presence of **16** the double bond configuration had virtually no influence on the facial selectivity.

Astoundingly, the Heck reactions of the (*E*)-allyl silanes **7** and **8** were only marginally successful. Here the regio- and enantio-selectivity were rather low. However, the (*Z*)-compounds **9** and **10** gave much better results. Using **13** as chiral ligand, the vinyl substituted tetrahydroisoquinolines **11b** and **12b** were obtained with high enantioselectivities of 86 and 84% ee, and complete regioselectivity (entries 20 and 22).

These results together with the investigations of intermolecular Heck reactions[3a] clearly show that the novel ligands **13** and **14** are superior to known ligands, at least in the investigated transformations.

This work has been supported by the Fonds der Chemischen Industrie. We thank the Degussa AG for a generous gift of precious metals and the Hoffmann-La Roche AG for ligand **15**. We are also greatly indebted to Dr S. Console (Chemi SpA) for providing the new ligands.

Notes and references

1 Reviews: M. Beller, T. H. Riermeier and G. Stark, in *Transition Metals for Organic Synthesis*, ed. M. Beller and C. Bolm, Wiley–VCH, Weinham, 1998, p. 208; S. Bräse and A. de Meijere, in *Metal-Catalyzed Cross Coupling Reactions*, eds. P. J. Stang and F. Diederich, Wiley–VCH, Weinham, 1997, p. 99.

2 Reviews: J. T. Link and L. E. Overman, in *Metal-Catalyzed Cross Coupling Reactions*, ed. P. J. Stang and F. Diederich, Wiley–VCH, Weinheim, 1997, p. 231; L. F. Tietze, T. Nöbel and M. Spescha, *J. Am. Chem. Soc.*, 1998, **120**, 8971; L. F. Tietze and H. Schirok, *J. Am. Chem. Soc.*, 1999, **121**, 10 264; J. Jin and S. M. Weinreb, *J. Am. Chem. Soc.*, 1997, **119**, 5773; M. Brenner, G. Mayer, A. Terpin and W. Steglich, *Chem. Eur. J.*, 1997, **3**, 70.

3 (*a*) L. F. Tietze, K. Thede and F. Sannicolò, *Chem. Commun.*, 1999, 1811; (*b*) F. Miyazaki, K. Uotsu and M. Shibasaki, *Tetrahedron*, 1998, **54**, 13 073; (*c*) S. Y. Cho and M. Shibasaki, *Tetrahedron Lett.*, 1998, **39**, 1773; (*d*) review: M. Shibasaki, C. D. J. Boden and A. Kojima, *Tetrahedron*, 1997, **53**, 7371; (*e*) O. Loiseleur, M. Hayashi, N. Schmees and A. Pfaltz, *Synthesis*, 1997, 1338; (*f*) T. Ohshima, K. Kagechika, M. Adachi, M. Sodeoka and M. Shibasaki, *J. Am. Chem. Soc.*, 1996, **118**, 7108; (*g*) L. F. Tietze and T. Raschke, *Liebigs Ann. Chem.*, 1996, 1981; (*h*) L. F. Tietze and T. Raschke, *Synlett*, 1995, 597; (*i*) L. F. Tietze and R. Schimpf, *Angew. Chem., Int., Ed. Engl.*, 1994, **33**, 1089.

4 (*a*) P. Antognazza, T. Benincori, E. Brenna, E. Cesarotti, L. Trimarco and F. Sannicolò EP 0770085 to Chemi SpA; (*b*) T. Benincori, E. Brenna, F. Sannicolò, L. Trimarco, P. Antognazza, E. Cesarotti, F. Demartin and T. Pilati, *J. Org. Chem.*, 1996, **61**, 6244.

5 R. Schmid, J. Foricher, M. Cereghetti and P. Schönholzer, *Helv. Chim. Acta*, 1991, **74**, 370.

Communication a909689b

ChemComm

New effective synthons for supramolecular self-assembly of *meso*-carboxyphenylporphyrins

Yael Diskin-Posner, Sanjay Dahal and Israel Goldberg*

School of Chemistry, Sackler Faculty of Exact Sciences, Tel-Aviv University, 69978 Ramat-Aviv, Tel-Aviv, Israel. E-mail: goldberg@post.tau.ac.il

Received (in Oxford, UK) 10th February 2000, Accepted 28th February 2000

Tesselation of new supramolecular motifs of the tetra(4-carboxyphenyl)porphyrin building blocks by metal ion templates has been demonstrated in crystals, characterizing the square-planar $[Na^{+}\cdot(-COOH)_4\cdot X^{-}]$ and the tetrahedral $[Zn^{2+}\cdot(-COOH)_2\cdot(-COO^{-})_2]$ molecular recognition elements for effective multiporphyrin assembly.

The *meso*-tetra(4-carboxyphenyl)porphyrin (TCPP) framework turned out to be an extremely versatile building block for effective supramolecular self-assembly and fabrication of new materials.[1–4] We have reported previously the formation of interpenetrating as well as non-penetrating two-dimensional arrays of TCPP with large interporphyrin voids through cooperative hydrogen-bonding between the terminal carboxylic groups of adjacent porphyrin entities.[2,3] Noteworthy is a unique and remarkably stable molecular sieve structure with nanosized (15 Å wide) channels.[4] Here, we communicate the first formulations of extended TCPP networks sustained by metal ion templates through multiple coordination to the carboxylic substituents.[5] Such templates may provide higher enthalpic driving force for the self-assembly process than the soft hydrogen bonding interactions alone, by adding ion-pairing attractions between the assembling entities. They could be thus more helpful in efforts to tailor porous solids based on robust multiporphyrin architectures.

Mononuclear and binuclear metallo-carboxylic/carboxylate assemblies are quite abundant in crystallographic databases. Yet, these synthons have not been used thus far in the context of porphyrin supramolecular chemistry. The large and rigid TCPP is in fact an excellent building block to this aim containing four coordination sites, each one pointing in a different direction. Here, we describe two representative examples of TCPP networks tesselated by metal ion auxiliaries which provide the supramolecular organizing force by multiply coordinating to the carboxylic functions (compounds **1** and **2**).† The self-assembly process of the free-base TCPP in the presence of NaCl and benzoic acid leads to the formation of two-dimensional multiporphyrin arrays sustained by sodium ions. The resulting motif of the supramolecular organization, involving TCPP and sodium benzoate (associated with deprotonation of the benzoic acid and expulsion of HCl) is illustrated in Fig. 1. It charaterizes the $Na^{+}(-COOH)_4$ synthon (see also Fig. 3) in which every alkali metal cation is coordinated (at 2.318–2.360 Å) to the carboxylic groups of four surrounding porphyrin moieties. The O(=C) binding sites involved in these interactions form an approximate square planar arrangement around the central cation. The coordination sphere around each cation is supplemented on one side by a coordinating molecule of the ethyl benzoate solvent (at $Na^{+}\cdots O$ 2.261 Å). The benzoate anion provides another enforcement to the layered porphyrin structure by approaching the sodium cation from the opposite side, its carboxylate oxygens acting as effective proton acceptors for the four carboxylic groups of the converging porphyrins (this forces all O–H proton donors to point in the same direction, inducing a chiral polar structure in space group $P2_1$). The corresponding O···(H)O distances of these hydrogen bonds are within 2.57–2.68 Å, reflecting on a relatively strong

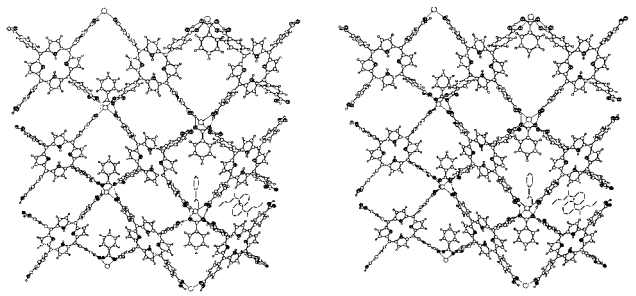

Fig. 1 Stereoview of the TCPP 'wavy' open networks formed in **1**, which are assembled by multiple coordination of the porphyrin units to the sodium benzoate template (*b* is horizontal and *a*–*c* is vertical). These layers stack tightly in the crystal along *a* + *c*. The interporphyrin channels thus formed are accommodated by molecules of the ethyl benzoate solvent (one of them coordinating to the sodium ion as well), as illustrated for clarity only in the lower right corner. The sodium ion is represented by a large uncrossed circle.

attraction. Every TCPP unit associates in this way with four different sodium benzoate entities (through four partly charged hydrogen bonds and four coordinative bonds to sodium), thus yielding a rather robust coordination polymer in two dimensions. Geometric optimization of these interactions results in the formation of corrugated ('wavy') porphyrin layers, adjacent units being related to each other either by pure lattice translation or by screw axis symmetry. van der Waals stacking of such layers one on top of the other in the normal direction (along *a* + *c*), at an average distance of *ca.* 4.21 Å between the corresponding porphyrin sections, composes the three-dimensional crystal structure. Additional molecules of the ethyl benzoate solvent fill effectively the channel voids which propagate in the lattice between the porphyrin columns of the stacked layers (Fig. 1).

The formation of the multiporphyrin networks in **2** is associated (in the absence of other acidic species in the crystallization environment) with double deprotonation of ZnTCPP to preserve neutrality. The observed assembly of the anionic porphyrin arrays templated by zinc ions is shown in Fig. 2. As commonly observed, the zinc ion residing within the porphyrin core is five-coordinated deviating outward from the porphyrin plane and attracting one molecule of the ethylene glycol solvent as an axial ligand. The external zinc cation is rather strongly coordinated (at 1.948–1.967 Å) to four different ZnTCPP units, maintaining an approximate tetrahedral geometry of coordination around it; it represents the $[Zn^{2+}\cdot(-COOH)_2\cdot(-COO^{-})_2]$ synthon (Fig. 3). This assembly mechanism *via* ion-pairing forces is assisted by additional intermolecular hydrogen bonding between the converging ZnTCPP units (involving the ethylene glycol axial ligand as well). Further coordination of any given ZnTCPP moiety to four different cations yields continuous diamondoid arrays consisting of chain-segments of nearly coplanar porphyrins which propagate in an alternating manner roughly in perpendicular directions. The resulting robust arrays thus extend in three dimensions, and the only way to pack them in a condensed

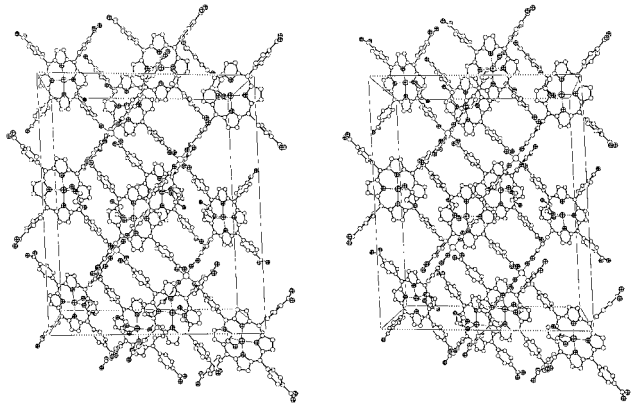

Fig. 2 Crystal structure of **2** (stereoview approximately down the *b*-axis; *a* is horizontal). It shows the diamondoid networks of $ZnTCPP^{2-}$ units templated by external Zn^{2+} cations, and the way they interpenetrate into one another. Large channel voids (*ca*. 7.5 Å in vdW diameter) centered at ($\frac{1}{2}$, 0, *z*) and (0, $\frac{1}{2}$, *z*) extend in the crystal along the *c*-axis between the concave surfaces of the porphyrin bands, explaining the large solvent content of this lattice. The zinc-ion template is represented by a large uncrossed circle. Hydrogen atoms are omitted for clarity.

crystalline phase must involve interpenetration.[6] Fig. 2 illustrates this feature, confirming that this is indeed the case. In the observed interwoven structure overlapping porphyrin bands of adjacent networks lie parallel to each other (at 4.33 and 4.62 Å) in the commonly observed offset stacked manner. The glycol–$ZnTCPP^{2-}$–Zn^{2+} networks occupy only about 40% of the crystal volume, reflecting on the geometric rigidity of this structure. Hexagonally shaped channels, which extend between the interpenetrating arrays, account for most of the remaining space. These channels propagate along the *c*-axis of the crystal between the concave surfaces of the porphyrin moieties, are centered at ($\frac{1}{2}$, 0, *z*) and (0, $\frac{1}{2}$, *z*), and have an average van der Waals diameter of 7.5 Å. They are filled in a diffused manner with numerous molecules (about 100 per unit cell) of the glycol solvent, which preserves the crystallinity of this open lattice.

The high significance of the metal ion templates to the formulation of TCPP-based networks with high structural rigidity has been demonstrated most recently by a successful crystal engineering of a stable metalloporphyrin zeolite analogue.[7] The latter represents three-dimensionally structured open arrays of interlinked $(ZnTCPP)^{2-}$ and 4,4′-bipyridyl units sustained by binuclear $[(Na^+)_2{\cdot}(-COOH)_6{\cdot}(-COO^-)_2]$ synthons (Fig. 3). It has been shown previously that cooperative hydrogen-bonding and coordination forces are sufficiently robust to direct concerted intermolecular organization and formation of stable nanostructures in solution as well.[5b,8]

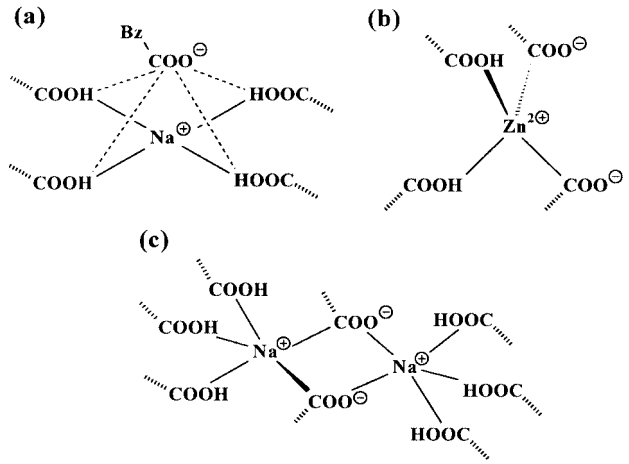

Fig. 3 The tesselation modes of TCPP supramolecular networks *via* metal ion templates in (a) **1**, (b) **2** and (c) the zeolite analogue reported in ref. 7. Every carboxylic or carboxylate group displayed here belongs to a different TCPP/ZnTCPP building block of the supramolecular aggregate.

Correspondingly, the above described molecular recognition algorithms can be also useful in the synthesis of *discrete* porphyrin-based supramolecular domains for the formulation of biomimetic photonic models and other molecular devices.[9]

This research was supported in part by the Israel Science Foundation administered by Israel Academy of Sciences and Humanities.

Notes and references

† Crystals of **1** were obtained by dissolving TCPP in a mixture of methanol, ethyl benzoate and benzoic acid in the presence of NaCl; those of **2**, by dissolving ZnTCPP in a hot mixture of methanol and ethylene glycol in the presence of $Zn(OAc)_2$. Both crystals turned out to contain a considerable amount of solvent in interporphyrin channels (see below).

Crystal data: **1,** $[(C_{48}H_{30}N_4O_8){\cdot}3(C_9H_{10}O_2){\cdot}(C_7H_5O_2)^-{\cdot}Na^+]$: M = 1385.4, monoclinic, space group $P2_1$, a = 9.854(1), b = 32.338(1), c = 11.358(1) Å, β = 110.52(1)°, V = 3389.6(2) Å^3, Z = 2, T = 110 K, D_c = 1.357 g cm^{-3}, μ(Mo-Kα) = 1.00 mm^{-1}, 10388 unique reflections ($2\theta_{max}$ = 51.5°). The final $R1$ = 0.065 for 7865 observations with $F_o > 4\sigma(F_o)$, $R1$ = 0.095 ($wR2$ = 0.178) for all unique data, $|\Delta\rho| \leqslant 0.74$ e Å^{-3}.

2, $[(C_{48}H_{26}N_4O_8Zn)^{2-}{\cdot}Zn^{2+}{\cdot}(C_2H_6O_2)_x]$: monoclinic, space group $C2/c$, a = 27.694(1), b = 19.510(1), c = 32.598(1) Å, β = 92.72(1)°, V = 17593.1(2) Å^3, Z = 8, T = 115 K, 13909 unique reflections ($2\theta_{max}$ = 50.0°). For x = 13 (see below) M = 1724.2, D_c = 1.302 g cm^{-3}, μ(Mo-Kα) = 0.63 mm^{-1}. This crystallographic refinement converged at $R1$ = 0.175 for 6785 reflections with $F > 4\sigma(F)$, $R1$ = 0.30 and $wR2$ = 0.42 for all the data. One molecule of ethylene glycol is coordinated to the five-coordinate zinc ion residing in the porphyrin center. The remaining solvent molecules incorporated the interporphyrin voids of the crystal lattice were found to be heavily disordered, and their structure could not be modeled. The contribution of the diffused solvent was thus subtracted from the diffraction pattern by the 'Squeeze' method.[10] This refinement converged smoothly at final $R1$ = 0.076 for 5931 observations with $F_o > 4\sigma(F_o)$, $R1$ = 0.150 ($wR2$ = 0.165) for all unique data, $|\Delta\rho| \leqslant 0.27$ e Å^{-3}. The integrated total residual electron density accounted for the presence of at least twelve additional molecules of ethylene glycol, or a corresponding combination of ethylene glycol and methanol (which represents about 45% of the overall electron count), in the asymmetric unit of this structure. CCDC 182/1562. See http://www.rsc.org/suppdata/cc/b0/b001189o/ for crystallographic files in .cif format.

1 For recent reviews on noncovalent assembly of porphyrin arrays and their potential applications see: J.-C. Chambron, V. Heitz and J.-P. Sauvage, *The Porphyrin Handbook*, ed. K. M. Kadish, K. M. Smith and R. Guilard, Academic Press, Orlando FL, 2000, vol. 6, ch. 40; J.-H. Chou, M. E. Kosal, H. S. Nalwa, N. A. Rakow and K. S. Suslick, *The Porphyrin Handbook*, ed. K. M. Kadish, K. M. Smith and R. Guilard, AP, Orlando FL, 2000, vol. 6, chap. 41.

2 P. Dastidar, Z. Stein, I. Goldberg and C. E. Strouse, *Supramol. Chem.*, 1996, **7**, 257.

3 Y. Diskin-Posner, R. Krishna Kumar and I. Goldberg, *New J. Chem.*, 1999, **23**, 885.

4 Y. Diskin-Posner and I. Goldberg, *Chem. Commun.*, 1999, 1961.

5 Successful tesselation of tetrapyridylporphyrin supramolecular aggregates by transion metal auxiliaries has been reported previously in the solid state (B. F. Abrahams, B. F. Hoskins, D. M. Michail and R. Robson, *Nature*, 1994, **369**, 727), as well as in solution (C. M. Drain and J.-M. Lehn, *J. Chem. Soc., Chem. Commun.*, 1994, 2313; C. M. Drain, F. Nifiatis, A. Vasenko and J. Batteas, *Angew. Chem., Int. Ed.*, 1998, **37**, 2344).

6 O. Ermer, *J. Am. Chem. Soc.*, 1988, **110**, 3747.

7 Y. Diskin-Posner, S. Dahal and I. Goldberg, *Angew. Chem., Int. Ed.*, 2000, **39**, in press.

8 H.-A. Klok, K. A. Jolliffe, C. L. Schauer, L. J. Prins, J. P. Spatz, M. Möller, P. Timmerman and D. N. Reinhoudt, *J. Am. Chem. Soc.*, 1999, **121**, 7154.

9 See, for example: C. M. Drain, S. Gentemann, J. A. Roberts, N. Y. Nelson, C. J. Medforth, S. Jai, M. C. Simpson, K. M. Smith, J. Fajer, J. A. Shelnutt and D. Holten, *J. Am. Chem. Soc.*, 1998, **120**, 3781; J. L. Sessler, B. Wang and A. Harriman, *J. Am. Chem. Soc.*, 1995, **117**, 704.

10 P. Van der Sluis and A. L. Spek, *Acta Crystallogr., Sect. A*, 1990, **46**, 194; A. L. Spek, *Acta Crystallogr., Sect. A*, 1990, **46**, C34. The 'Squeeze' method referred therein is widely used in crystallographic analysis of compounds containing substantial amounts of disordered solvent which cannot be located precisely from diffraction data.

Communication b001189o

ChemComm

Covalent coupling of an phospholipid monolayer on the surface of ceramic materials

Yikang Wang, Tsueu Ju Su, Rebecca Green, Yiqing Tang, Dmitrii Styrkas, Timothy N. Danks, Roger Bolton and Jian R. Lu*

Department of Chemistry, University of Surrey, Guildford, UK GU2 5XH. E-mail: j.lu@surrey.ac.uk

Received (in Oxford, UK) 13th January 2000, Accepted 28th February 2000

A new synthetic route to the covalent bonding of an organic monolayer bearing terminal phosphorylcholine (PC) groups onto the surface of silicon oxide is reported; such monolayers prohibit the deposition of enzymes and proteins and can be used to improve surface biocompatibility.

Phospholipids are a group of molecules with double acyl chains and zwitterionic head groups. Their existence in membrane walls is primarily responsible for creating a biocompatible environment so that proteins, enzymes and platelets in blood do not foul the surface of blood cells. The dominant phospholipids on the outer surface of membrane walls have phosphorylcholine (PC) head groups. The biocompatibility is therefore rendered by these lipid heads. The role played by these phospholipids has been known for decades and a great deal of endeavour has been made to mimic the natural behaviour of these phospholipids. Most of the activities have focused on creating polymeric materials containing pendent PC groups[1–3] although a great deal of work has explored other types of biocompatible polymers, *e.g.* polyurethane and polymethacrylate grafted with polyethylene oxide.[4] Literature results have shown that PC polymers are superior to other types of polymers in reducing protein deposition and the subsequent biological consequences.[1–5] Surfaces coated with PC polymers also show much better performance against thrombosis than heparin derivatized surfaces.[4]

An alternative approach to the coating of PC polymers is *via* covalent bonding of an organic monolayer bearing terminal PC groups onto a solid substrate. We report here, a new synthetic route to the construction of a PC monolayer onto silicon oxide. Covalent bonding of a PC monolayer should fulfil the same anti-fouling function as PC-incorporated polymers, and bring a number of improved features over polymer coating. First, although the coated layer is thin, its thickness can be reliably controlled to an accuracy around a few Å. Second, the coverage of the PC groups can be directly manipulated. The delicate chemical environment supporting the PC groups can also be engineered effectively. Third, the chemically grafted monolayer is robust and can withstand very harsh conditions. Leaching is therefore not a problem. These features are critical to a number of applications where small coating agents are desired. These include coating the surfaces of the inner pores of ceramic membranes and dialysis films. As the dimension of the inner pores within these membranes is usually between 1 and 100 nm and is comparable to the size of polymers, it is difficult to coat such pore surfaces with PC polymers. The incorporation of silyl groups in PC polymers can further intensify the blockage on the outer surface of membranes. For membranes with larger pore diameters, it is difficult to control the thickness of the coated films and the final dimensions of the coated pores will be poorly defined.

To our knowledge there is no literature work concerning the formation of a covalently bound PC monolayer on the surface of silicon oxide. The work of Hayward *et al.*[6,7] has demonstrated the potential of the formation of PC monolayers, but in their case the attached alkyl chain bearing terminal PC group is unstable as a result of the presence of an oxygen between carbon and silicon. The resulting alkyl silicate structure readily hydrolyses, with loss of the alkyl chain and its PC functionality. Our approach is similar to that of Hayward *et al.*, but we sought direct chemical bonding between the carbon and silicon so that stable chemical grafting is obtained. Because silica has a surface layer of hydroxide, a layer of organic compound can be grafted through silane cross-linking. In comparison with C–O–Si bonding, the formation of Si–O–Si connections at the end of the organic monolayer is much more stable. In fact, this part of the layer is identical to the structure of the underlying silica layer. The PC groups can be attached through reaction with hydroxy or amine groups in the outer surface of the organic layer. We show in the following a route (Scheme 1) *via* hydroxy groups as intermediate functionalities. Although different alkyl chain lengths can be used we choose the covalent binding of pentadecanol as an example.

The synthesis starts with 1,12-dibromododecane to which an allyl group is attached to one end and a silane group on the other *via* Grignard chemistry, resulting in the formation of 14-pentadecenyl trichlorosilane. The freshly cleaned silicon surfaces were treated with 1 mmol of 15-pentadecenyl trichlorosilane in dichloromethane–hexadecane (1 : 4, v/v) at 11 °C for 1.5 h. A number of studies have shown that the coverage and uniformity of the attached layer are strongly affected by temperature. Higher temperature tends to lower the surface coverage, possibly as a result of the thermal motions within the anchored layer.[8,9] In addition, the reaction time is also crucial; while insufficient time may not allow enough coating to proceed, immersion of the silicon surface in the solution for too long a period may lead to the formation of an inhomogeneous layer. The reaction conditions were optimised through a number of trial experiments, using spectroscopic ellipsometry to examine the quality of the coated surface layers. The advancing contact angle of the alkene surface was found to be 93 ± 2°, consistent with the value expected for an organic surface with double bond end groups. Structural information about the coated organic layer was obtained by fitting a uniform layer model to the two ellipsometric angles, Ψ and Δ measured at the air/solid interface, where Ψ measures the change in the amplitude of the

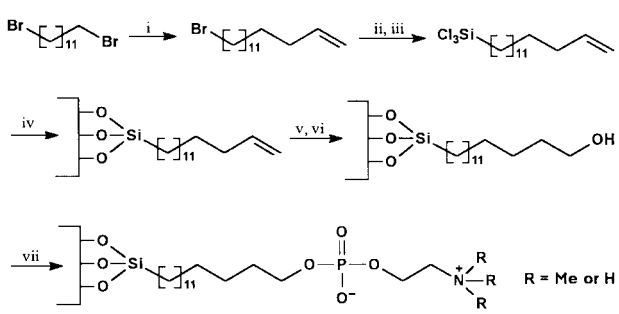

Scheme 1 The synthetic procedure for covalent bonding of an organic monolayer bearing terminal PC or PA groups. *Reagents and conditions*: i, allylmagnesium bromide, −10 to −20 °C; ii, Mg, THF, 20 °C; iii, $SiCl_4$; iv, silicon block, CH_2Cl_2–hexadecane (1 : 4), 11 °C, 1.5 h; v, BH_3·THF, 10 min, 20 °C; vi, H_2O_2/OH^-; vii, $POCl_3$, NEt_3, 10 to 20 °C.

DOI: 10.1039/b000419g

Table 1 Fragments detected by TOF-SIMS from the pentadecyl monolayer bearing terminal PC groups

Mass	Chemical formula	Chemical structure
59	$C_3H_9N^+$	NMe_3^+
73	$C_4H_{11}N^+$	$CH_2NMe_3^+$
87	$C_5H_{13}N^+$	$CH_2CH_2NMe_3^+$
103	$C_5H_{13}NO^+$	$OCH_2CH_2NMe_3^+$
168	$C_5H_{15}NO_3P^+$	$(HO)_2POCH_2CH_2NMe_3^+$
185	$C_5H_{16}NO_4P^+$	$(HO)_3POCH_2CH_2NMe_3^+$

beam before and after reflection and Δ measures the change in phases. In principle, the fitting directly leads to the thickness (τ) and volume fraction of the layer (ϕ). However, for such thin surface layers, there is little resolution to decouple τ and ϕ although the ellipsometric measurement is sensitive to the product of the two. For the layer coated under the optimised conditions, the fitting suggests a thickness of 17 ± 3 Å if the density of the layer is taken to be the same as liquid pentadecene. Thinner layers were detected when shorter reaction times were used. Under prolonged reaction conditions (*e.g.* a few days), layers were found to be well over 30 Å, suggesting the formation of multilayers. In contrast, the thickness of 17 ± 3 Å is a good indication of monolayer coating. The conversion of the double bond into the primary alcohol functions was achieved by reacting the grafted pentadecenes with BH_3·THF for 10 min, followed by alkaline hydrogen peroxide for 1 h.[9] This treatment did not alter the layer thickness within the quoted experimental error, as expected, but the contact angle was found to drop to 54 ± 3°, consistent with the presence of an organic layer containing terminal hydroxy groups on silicon oxide.

The subsequent connection of PC groups was achieved by reaction of the bound organic hydroxy groups with $POCl_3$ in the presence of triethylamine, leading to the attachment of phosphoric chloride systems, followed by a reaction with $HOCH_2CH_2NMe_3^+OAc^-$. A similar process using $HOCH_2CH_2NH_2$ in the final step, resulted in the formation of phosphorylamine (PA) groups. The ellipsometric measurement showed an increase in layer thickness by some 6 ± 3 Å after PC groups were attached and the contact angle with *ca.* 37 ± 2°. For PA, the layer was found to be thickened by some 8 ± 3 Å and the contract angle was 41 ± 2°. One would expect that the attachment of PC groups produces a thicker head group layer than that of PA groups, but the difference is within the experimental error.

The successful attachment of PC groups has been further confirmed using time-of-flight secondary ion mass spectrometry (TOF-SIMS). The results listed in Table 1 show the presence of a number of mass units (*e.g.* NMe_3^+, $CH_2NMe_3^+$) that match the characteristic fragments disintegrated from the PC monolayer. These fragments were not observed from the measurements on the surface coated with pentadecanol. Parallel SIMS experiments were also performed using the thin films of dipalmitoylglycerylphosphorylcholine (DPPC) and synthetic polymers grafted with PC head groups;[10–12] the results showed identical mass fragments characteristic of PC head groups, further confirming the presence of PC groups in the coated monolayer. Finally, the effectiveness of our C_{15}PC monolayer as a protein repellant interface has been characterised by performing ellipsometry measurement at the solid/solution interface at 25 °C. At a lysozyme concentration of 1 g dm^{-3} and at pH 7, the surface excess of lysozyme was found to be 0.5 ± 0.3 mg m^{-2}, as compared with 3.6 ± 0.3 mg m^{-2} at the bare silicon oxide/water interface.[13] The residual amount of lysozyme adsorption at the C_{15}PC surface is comparable to the values obtained on the surfaces of two PC polymers,[10–12] showing that the surfaces coated with PC monolayers are as effective as the PC polymers in their resistance to protein fouling.

We thank the EPSRC for a grant under the ROPA Scheme.

Notes and references

1 K. Iwasaki, A. Fujike, K. Kurita, K. Ishihara and N. Nakabayashi, *J. Biomater. Sci. Polym. Edn.*, 1996, **8**, 91.
2 K. Ishihara, K. H. Hanyuda and N. Nakabayashi, *Biomaterials*, 1995, **16**, 873.
3 E. J. Campbell, V. O'Byrne, P. Stratford, I. Quirk, T. A. Vick, M. C. Wiles and Y. P. Yianni, *Am. Soc. Artif. Int. Organ J.*, 1994, **40**, 853.
4 J. D. Andrade, *Surface and Interfacial Aspects of Biomedical Polymers*, Plenum, New York, 1998, vol. 2.
5 C. Pidgeon, S. Ong, H. S. Choi and H. L. Liu, *Anal. Chem.*, 1994, **66**, 2701.
6 J. A. Hayward, A. A. Durrani, C. Shelton, D. C. Lee and D. Chapman, *Biomaterials*, 1986, **7**, 126.
7 J. A. Hayward, A. A. Durrani, Y. Lu, C. R. Clayton and D. Chapman, *Biomaterials*, 1986, **7**, 252.
8 A. G. Richter, M. K. Durbin, C. J. Yu and P. Dutta, *Langmuir*, 1998, **14**, 5980.
9 J. Gun and J. Sagiv, *J. Colloid Interface Sci.*, 1996, **112**, 457.
10 E. F. Murphy, J. L. Keddie, J. R. Lu, J. Brewer and J. Russell, *Biomaterials*, 1999, **20**, 1501.
11 E. F. Murphy, J. R. Lu, J. Brewer, J. Russell and J. Penfold, *Langmuir*, 1999, **15**, 1313.
12 E. F. Murphy, J. R. Lu, A. L. Lewis, P. Stratford, J. Brewer and J. Russell, *Macromolecules*, submitted.
13 T. J. Su, J. R. Lu, R. K. Thomas, Z. F. Cui and J. Penfold, *Langmuir*, 1998, **14**, 438.

Communication b000419g

Oxazole–Carbonyl photocycloadditions: selectivity pattern and synthetic route to *erythro* α-amino, β-hydroxy ketones†

Axel G. Griesbeck,* Maren Fiege and Johann Lex

Institute of Organic Chemistry, University of Cologne, Greinstr. 4, D-50939 Köln, Germany. E-mail: griesbeck@uni-koeln.de

Received (in Liverpool, UK) 20th January 2000, Accepted 23rd February 2000

The photocycloaddition of aliphatic and aromatic aldehydes with 2,4,5-trimethyloxazole proceeds highly regio- and diastereoselectively to give bicyclic oxetanes; hydrolytic cleavage of these adducts gives selectively *erythro* α-amino, β-hydroxy methyl ketones.

The photocycloaddition of electronically excited carbonyl compounds to alkenes (Paternò–Büchi reaction, PBR) is *the* important synthetic route to oxetanes which can be subsequently transformed into polyfunctionalized products.[1] Concerning the regio- and especially diastereoselectivity of the PBR, recent experimental and theoretical work brought a remarkable increase in our understanding of triplet 1,4-biradical behaviour[2] which also improved the synthetic significance of this reaction.[3]

The regioselectivity of the PBR with unsymmetrically substituted cycloalkenes is only moderate but can be substantially increased by using cyclic enol ethers[4] and enamines,[5] respectively. The majority of these substrates show moderate simple diastereoselectivities with distinct preference for *endo*-products. This selectivity pattern is completely inverted for carbo- and heterocyclic 1,3-dienes. With respect to regio- and simple diastereoselectivity, furans have been most extensively investigated and *exo*/*endo*-selectivities of 212 : 1 (benzaldehyde addition to furan)[6] to 363 : 1 (mesitaldehyde addition to furan)[7] were determined. Similar reactivities and selectivities have been reported for pyrroles, thiophenes, thiazoles, imidazoles and pyrazoles as alkene components in Paternò–Büchi reactions.[8]

To the best of our knowledge, oxazoles have not been investigated until now. This class of heterocycles can be viewed as masked α-amino ketones or aldehydes (Fig. 1). Analogous to the furan–carbonyl photocycloaddition which equals a photo-Aldol process,[9] the oxazole-carbonyl process results in masked α-amino, β-hydroxy carbonyl compounds.

A similar concept has been evaluated already by the groups of Sekretar[10] and Scharf.[11] They used 2(3*H*)-oxazolones and 2,3-dihydrooxazoles, respectively, as alkene components and investigated the photocycloaddition with ketones and α-keto carboxylates. The simple stereoselectivity of these reactions was high, however, the regioselectivity was low with preferential formation of the 2-amino-substituted oxetanes in the case of 2,3-dihydrooxazoles. With phenylglyoxylic esters, the photocycloaddition proceeded efficiently and *endo*-phenyl (> 95%) selectively.[12]

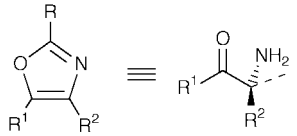

Fig. 1

† Regarded as Part 10 of the series 'Stereoselectivity of Triplet Photocycloadditions', Part 9: A. G. Griesbeck and M. Fiege, in *Molecular and Supramolecular Photochemistry*, ed. V. Ramamurthy and K. S. Schanze, Marcel Dekker, New York, 2000, vol. 6, in press.

We photolyzed 2,4,5-trimethyloxazole **1** together with several aliphatic and aromatic aldehydes. In all cases, only the regioisomers **2** were formed with very high (*exo*) diastereoselectivity (> 99 : 1) in near quantitative yields (Scheme 1).

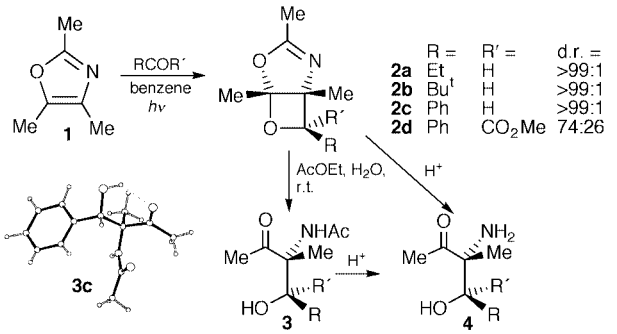

Scheme 1

Both regio- and diastereoselectivity are in accord with the rules reported by us for the carbonyl–furan photocycloaddition reaction,[6] but unusual for the oxazole derivatives mentioned above. The stereoselectivity decreased for the methyl ester of phenylglyoxylic acid: a 3 : 1 mixture of *exo*/*endo*-phenyl substituted oxetanes **2d** was isolated, however, still with high regioselectivity. This result is remarkable because not only has the stereoselectivity decreased in comparison with the results described by Scharf and coworkers,[12] but also the direction of stereocontrol was inverted. The resulting bicyclic oxetanes are thermally as well as hydrolytically labile products and were ring-opened during chromatography on silica or upon standing after several days at room temperature in moist solvents. For the benzaldehyde-derived *N*-acylated β-aminoalcohol **3c**, the primary product of this processes starting with **2c**, the *erythro* configuration was proven by means of an X-ray crystal structure determination.‡ The unprotected β-amino alcohols can be directly synthesized *via* treatment of the oxetanes **2** with trifluoroacetic acid or under milder conditions with acetic acid and conventional work-up.

From a mechanistic point of view, the stereoselectivity of the PBR with trimethyloxazole results from a combination of two factors: (1) the spin–orbit coupling controlled ISC-geometries favourable for spin inversion and transition to closed-shell products[2] and (2) the methyl-group effect which we have discovered for cyclic monoalkenes.[13] The three projections shown in Scheme 2 correspond to the three ISC-reactive

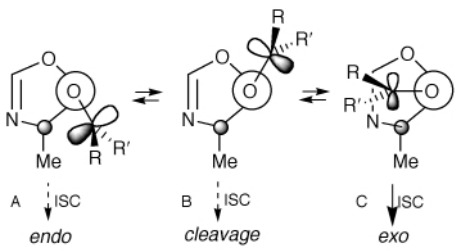

Scheme 2

DOI: 10.1039/b000578i

conformations which lead to cleavage reaction, *endo*- and *exo*-product formation, respectively.

Aldehydes (R′ = H) show strong preference for bond formation *via* structure **C** and thus give *exo* oxetanes with high stereoselectivities. For the unsubstituted furan, ketoesters (R = alkyl, aryl; R′ = CO_2R'') prefer structure **A** and give preferentially the *endo* diastereoisomers. If, however, the ring terminus of the triplet biradical is methyl substituted, additional steric interactions disfavor structure **A**. Methyl phenylglyoxylate addition to trimethyloxazole corresponds to such a case and a 3:1 *exo*/*endo* (with respect to the position of the phenyl group) mixture resulted.

In summary, we have shown that the oxazole–carbonyl photocycloaddition serves as an excellent method for the regio- and diastereoselective preparation of *erythro* β-amino alcohols from aldehydes and keto esters, respectively.

This work was supported by the Deutsche Forschungsgemeinschaft and the Fonds der Chemischen Industrie.

Notes and references

‡ *Crystal data*: $C_{13}H_{17}NO_3$ (from EtOAc, mp 128–129 °C) **3c**: M = 235.28, monoclinic, space group *Cc*, a = 15.632(1), b = 9.417(1), c = 9.668(1) Å, β = 111.10(1)°; Mo-Kα radiation, 1890 reflections measured, 1055 reflections with $I > 2\sigma(I)$ R_1 = 0.51, wR_2 = 0.076. CCDC 182/1557. See http://www.rsc.org/suppdata/cc/b0/b000578i/ for crystallographic files in .cif format.

1 A. G. Griesbeck, in *Handbook of Organic Photochemistry and Photobiology*, ed. W. M. Horspool and P.-S. Song, CRC Press, Boca Raton, FL, 1995, pp. 550 and 755.
2 A. G. Griesbeck, S. Stadtmüller and H. Mauder, *Acc. Chem. Res.*, 1994, **27**, 70.
3 T. Bach, *Synthesis*, 1998, 683; *Liebigs Ann.*, 1997, 1627.
4 A. G. Griesbeck and S. Stadtmüller, *J. Am. Chem. Soc.*, 1990, **112**, 1281.
5 T. Bach, J. Schröder, T. Brandl, J. Hecht and K. Harms, *Tetrahedron*, 1998, **54**, 4507; T. Bach and J. Schröder, *J. Org. Chem.*, 1999, **64**, 1265.
6 A. G. Griesbeck, S. Buhr, M. Fiege, H. Schmickler and J. Lex, *J. Org. Chem.*, 1998, **63**, 3848.
7 A. G. Griesbeck and M. Fiege, unpublished results.
8 C. Rivas and F. Vargas, in *Handbook of Organic Photochemistry and Photobiology*, ed. W. M. Horspool and P.-S. Song, CRC Press, Boca Raton, FL, 1995, p. 536.
9 S. L. Schreiber, *Science*, 1985, **227**, 857.
10 S. Sekretar, J. Kopecky and A. Martvon, *Collect. Czech. Chem. Commun.*, 1982, **47**, 1848.
11 M. Weuthen, H.-D. Scharf and J. Runsink, *Chem. Ber.*, 1987, **120**, 1023.
12 M. Weuthen, H.-D. Scharf, J. Runsink and R. Vaßen, *Chem. Ber.*, 1988, **121**, 971.
13 A. G. Griesbeck and S. Stadtmüller, *J. Am. Chem. Soc.*, 1991, **113**, 6923.

Communication b000578i

The first X-ray structurally characterized M_3L_2 cage-like complex with tetrahedral metal centres and its encapsulation of a neutral guest molecule

Hong-Ke Liu,[a] Wei-Yin Sun,*[a] De-Jian Ma,[a] Kai-Bei Yu[b] and Wen-Xia Tang[a]

[a] *Coordination Chemistry Institute, State Key Laboratory of Coordination Chemistry, Nanjing University, Nanjing 210093, China. E-mail: sunwy@netra.nju.edu.cn*

[b] *Analysis Center, Chengdu Branch of Chinese Academy of Science, Chengdu 610041, China*

Received (in Cambridge, UK) 4th January 2000, Accepted 28th February 2000

The first X-ray structurally characterized M_3L_2 cage-like complex with tetrahedral metal centres $[Zn_3(tib)_2(OAc)_6]\cdot xH_2O$ [tib = 1,3,5-tris(imidazol-1-ylmethyl)benzene, $x \approx 4$] obtained by reaction of zinc(II) acetate with the tripodal ligand tib exhibits guest inclusion properties of neutral molecule such as synthetic camphor in aqueous solution.

Metal-directed assembly has been proved to be a useful methodology in supramolecular chemistry.[1] Frameworks with specific topologies such as honeycomb grids and cages have been obtained by assembly of suitable metal ions with rationally designed tripodal ligands such as L[1], L[2] and L[3].[2–4] Among

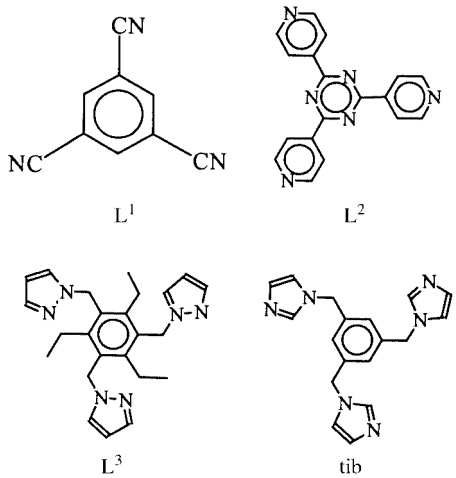

these, cage-like complexes have attracted much attention owing to their interesting properties and possible applications, *e.g.* molecular and chiral recognition.[5] The groups of Fujita, Steel, Robson, Stang and Raymond have performed outstanding work in the construction of cage-like complexes.[3–8] Most recently, an $M_{12}L_8$ type cage was obtained by assembly of a tri-bidentate ligand with Cu(II),[8] and larger cages with four organic moieties and eight-coordinate copper(III) centres have been reported by Beer's group.[9] However up to now, to our knowledge, no M_3L_2 cages have been isolated and characterized by X-ray structural analysis, although a guest-induced Pd_3L_2 cage-like complex [L = 1,3,5-tris(4-pyridylmethyl)benzene] and analogous cages have been reported.[6] Moreover, in reported M_6L_4 cage-like complexes, the metal ions are essentially square planar, *e.g.* Pd(II), Pt(II) or octahedral *e.g.* Ga(III), Fe(III),[3,4,6,7,10] with no case of the metal ion being tetrahedral being reported. Herein we report the assembly and X-ray crystal structure of an M_3L_2 cage-like complex formed between a novel tripodal ligand, 1,3,5-tris(imidazol-1-ylmethyl)benzene (tib), and zinc ion, which has tetrahedral configuration. The complex shows the interesting property of guest inclusion in aqueous solution.

The tib ligand was prepared from 1,3,5-tris(bromomethyl)benzene and imidazole in a molar ratio of 1 : 3 in dimethyl sulfoxide under strong alkali (KOH) conditions.† Its trinuclear zinc(II) complex $[Zn_3(tib)_2(OAc)_6]\cdot xH_2O$ ($x \approx 4$), was synthesized by self-assembly of the tib ligand with zinc acetate dihydrate in ethanol solution.‡ An X-ray crystal structural analysis provides direct evidence that the complex is an M_3L_2 cage.§ As shown in Fig. 1, two tib ligands that are both in *cis, cis, cis*-conformations adopt a face-to-face orientation and are joined together by three zinc atoms to generate an individual three-dimensional cage. Highly disordered water molecules may present in the cage as suggested by elemental analysis.‡ Each zinc atom is four-coordinate with two oxygen atoms from two acetate anions and two nitrogen atoms of imidazole from two different tib ligands. The coordination geometry of the zinc atoms is distorted tetrahedral with coordination angles ranging from 101.5(4) to 123.3(7)°. The distance between the zinc atoms are 9.10 Å and the two benzene ring planes are strictly parallel with each other with a separation of 9.49 Å.

It is clear from the X-ray structural analysis that the title complex has a large cavity inside the cage and therefore is

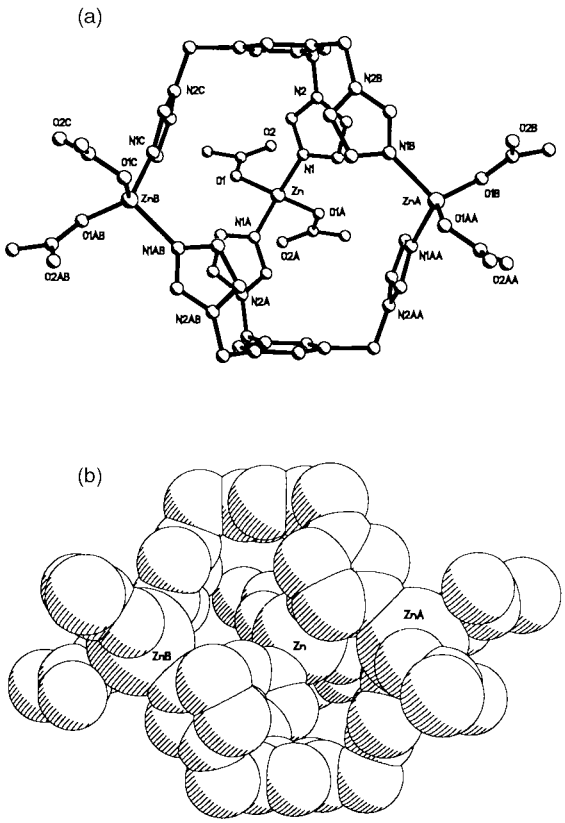

Fig. 1 Perspective view (a) and space-filling representation (b) of the X-ray crystal structure of $[Zn_3(tib)_2(OAc)_6]$. Selected bond lengths (Å) and angles (°): Zn–O1 1.84(2), Zn–N1 2.022(7); O1–Zn–O1A 123.3(7), O1A–Zn–N1A 110.3(4), O1–Zn–N1A 101.5(4), O1A–Zn–N1 101.5(4), O1–Zn–N1 110.3(4), N1A–Zn–N1 109.6(4).

DOI: 10.1039/b000259n

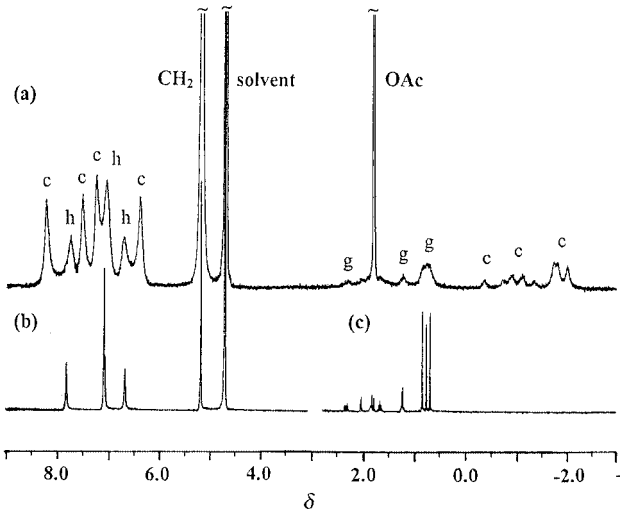

Fig. 2 ^{1}H NMR spectra in D_2O at 293 K: (a) camphor (3.0 mM) + $[Zn_3(tib)_2(OAc)_6]$ (3.0 mM); (b) downfield region for $[Zn_3(tib)_2(OAc)_6]$ (3.0 mM); (c) camphor (3.0 mM). c refers to complexed species; h to host species and g to guest species.

expected to have the ability to encapsulate guest molecules.[6] Thus we observed remarkable ability of the complex to encapsulate neutral molecules in its aqueous solution. It has been reported that ^{1}H NMR spectroscopy is a powerful method for investigation of host–guest complexation.[6,11] Fig. 2(a) shows the ^{1}H NMR spectrum of the complexation of the $[Zn_3(tib)_2(OAc)_6]$ with camphor in deuterated aqueous solution. Two kinds of signal were observed for both the host and guest species when the guest camphor was added to a D_2O solution of $[Zn_3(tib)_2(OAc)_6]$. One set remains unshifted compared with the corresponding signals of the host [Fig. 2(b)] and of the guest [Fig. 2(c)], *i.e.* the unshifted signals originate from uncomplexed species. The other set of upfield shifted signals are from the guest camphor molecules, while for the signals of the host molecule, both up- and down-field shifts were observed. These up- and down-field shifted signals for the host and guest species arise from complexed species.[11] The integration ratio of the host and guest signals in the ^{1}H NMR spectrum confirmed the 1 : 1 stoichiometry for the complexation between the cage complex and camphor and indicated that *ca.* 60% of the camphor was complexed [Fig. 2(a)]. The results indicate that the camphor molecule, which has a diameter of *ca.* 6 Å, is large enough so that species inside and outside of the cavity of the complex can be distinguished on the NMR time scale. The broadening of the signals as observed in Fig. 2(a) is due to slow exchange between the free and complexed species, since the signals become much broader when the temperature is raised. The kinetic process of the complexation of the cage with camphor was investigated by two-dimensional exchange spectroscopy (2D EXSY).¶ The rate constants for the forward (complexation) and reverse (decomplexation) process are 3.9×10^3 M^{-1} s^{-1} and 32.9 s^{-1}, respectively, giving an equilibrium constant of 117.6 M^{-1}. For chain-like molecules such as ethanol, ethyl acetate, diethyl ether or *n*-butyl alcohol, no complexation was observed.

In conclusion, the present study shows that an M_3L_2 cage is assembled from five small component molecules by the rational design of a suitable tripodal ligand and metal ions, and provides example of supramolecules with interesting properties such as guest inclusion.

We are grateful for funding from the National Nature Science Foundation of China for financial support of this work.

Notes and references

† The tib ligand was prepared from 1,3,5-tris(bromomethyl)benzene and imidazole in a molar ratio of 1 : 3 in dimethyl sulfoxide under strong alkali conditions and was isolated in 30% yield. ^{1}H NMR (D_2O): δ 5.08 (6H, s, CH_2), 6.93 (3H, s, $^4H_{im}$), 6.95 (3H, s, $^5H_{im}$), 6.96 (3H, s, H_{bz}), 7.63 (3H, s, $^2H_{im}$). H_{im} refers to imidazole protons and H_{bz} refers to benzene-ring protons.

‡ *Experimental*: a solution of tib (32 mg, 0.1 mmol) in ethanol (10 ml) was added to a ethanol (10 ml) solution of $Zn(OAc)_2{\cdot}2H_2O$ (33 mg, 0.15 mmol) at room temperature. The mixture was filtered after stirring for *ca.* 10 min and the filtrate was allowed to stand at ambient temperature for several days. Colorless crystals were collected in 56% yield. Single prismatic crystals suitable for X-ray diffraction analysis were obtained by slow evaporation of the filtrate. (Found: C, 45.94; H, 4.82; N, 13.24. $C_{48}H_{62}N_{12}O_{16}Zn_3$ $\{[Zn_3(tib)_2](OAc)_6{\cdot}(H_2O)_4\}$ requires C, 45.78; H, 4.96; N, 13.34%. ^{1}H NMR (D_2O, 298 K): δ 1.80 (18H, s, CH_3), 5.18 (12H, s, CH_2), 6.67 (6H, s, $^4H_{im}$), 7.07 (6H, s, $^5H_{im}$), 7.09 (6H, s, H_{bz}), 7.81 (6H, s, $^2H_{im}$).

§ *Crystal data* for $[Zn_3(tib)_2](OAc)_6$: M_w = 1187.14, rhombohedral, space group *R*32, a = 17.661(2), b = 17.661(2), c = 20.722(4) Å, γ = 120°, U = 5597.5(14) Å^3, Z = 3, D_c = 1.057 g cm^{-3}, μ = 1.007 mm^{-1}, $F(000)$ = 1836, T = 294(2) K. A single crystal with dimensions of 0.56 × 0.54 × 0.24 mm was mounted and data collection were performed on a Siemens-P4 four-circle diffractometer by the ω-scan technique using graphite-monochromated Mo-Kα radiation (λ = 0.71073 Å). 2385 reflections were collected of which 2081 are independent (R_{int} = 0.0231). The structure was solved by direct method with SHELXS-86 and refined by full-matrix least-squares calculations on F^2 with SHELXL-93. The final weighting scheme was $w = 1/[\sigma^2(F_o^2) + (0.1209P)^2 + 0.0000P]$ where $P = (F_o^2 + 2F_c^2)/3$; $R1$ = 0.0684 and $wR2$ = 0.1641 [$I > 2\sigma(I)$], max. min. residual density: +0.434, −0.282 e Å^{-3}. CCDC 182/1563. See http://www.rsc.org.suppdata/cc/b0/b000259n for crystallographic files in .cif format.

¶ ^{1}H NMR data were obtained from a Bruker AM 500 spectrometer. 2D EXSY spectral measurements were carried out using the phase-sensitive NOESY pulse sequence with a mixing time of 20 ms: R. R. Ernst, G. Bodenhausen and A. Wokau, *Principles of Nuclear Magnetic Resonance in One and Two Dimensions*, Oxford University Press, Oxford, 1983; G. Bodenhausen, H. Kogler and R. R. Ernst, *J. Magn. Reson.*, **1984**, *58*, 370.

1 See, for example: *Comprehensive Supramolecular Chemistry*, ed. J. L. Atwood, J. E. D. Davies, D. D. MacNicol, F. Vogtle and J. M. Lehn. Pergamon, Oxford, 1996, vol. 9.
2 G. B. Gardner, D. Venkataraman, J. S. Moore and S. Lee, *Nature*, 1995, **374**, 792.
3 M. Fujita, D. Oguro, M. Miyazawa, H. Oka, K. Yamaguchl and K. Ogura, *Nature*, 1995, **378**, 469.
4 C. M. Hartshorn and P. J. Steel, *Chem. Commun.*, 1997, 541.
5 P. J. Stang and B. Olenyuk, *Angew. Chem., Int. Ed. Engl.*, 1996, **35**, 732; B. Olenyuk, J. A. Whiteford and P. J. Stang, *J. Am. Chem. Soc.*, 1996, **118**, 8221.
6 M. Fujita, S. Nagao and K. Ogura, *J. Am. Chem. Soc.*, 1995, **117**, 1649; A. Ikeda, M. Yoshimura, H. Udzu, C. Fukuhara and S. Shinkai, *J. Am. Chem. Soc.*, 1999, **121**, 4296; S. Hiraoka and M. Fujita, *J. Am. Chem. Soc.*, 1999, **121**, 10 239; M. Fujita, N. Fujita, K. Ogata and K. Yamaguchi, *Nature*, 1999, **400**, 52.
7 C. M. Hartshorn and P. J. Steel, *Inorg. Chem.*, 1996, **35**, 6902; 1995, **48**, 1587; *Angew. Chem., Int. Ed. Engl.*, 1996, **35**, 2655.
8 B. F. Abrahams, S. J. Egan and R. Robson, *J. Am. Chem. Soc.*, 1999, **121**, 3535.
9 O. D. Fox, M. G. B. Drew and P. D. Beer, *Angew. Chem., Int. Ed.*, 2000, **39**, 136.
10 For example: T. N. Parac, D. L. Caulder and K. N. Raymond, *J. Am. Chem. Soc.*, 1998, **120**, 8003; P. Jacopozzi and E. Dalcanale, *Angew. Chem., Int. Ed. Engl.*, 1997, **36**, 613; S. Mann, G. Huttner, L. Zsolnai and K. Heinze, *Angew. Chem., Int. Ed. Engl.*, 1996, **35**, 2808.
11 T. Kusukawa and M. Fujita, *Angew. Chem., Int. Ed.*, 1998, **37**, 3142.

Communication b000259n

ChemComm

Do interstrand hydrogen bonds contribute to β-hairpin peptide stability in solution? IR analysis of peptide folding in water

Christopher S. Colley, Samuel R. Griffiths-Jones, Michael W. George* and Mark S. Searle*

Department of Chemistry, University Park, Nottingham, UK NG7 2RD. E-mail: mark.searle@nottingham.ac.uk; mike.george@nottingham.ac.uk

Received (in Cambridge, UK) 14th January 2000, Accepted 24th February 2000

The amide I carbonyl stretch in the IR spectrum, together with ^{1}H NMR Hα chemical shifts, have been used to investigate the folding of a 16-residue β-hairpin peptide in water: while Hα shifts are consistent with a significant population of the folded state (*ca.* 40%), we see no features in the IR spectrum in the amide I region to suggest a significant contribution from interstrand hydrogen bonds, although at high peptide concentration (≥10 mM) the appearance of a new band at 1616 cm^{-1} is consistent with the onset of irreversible peptide aggregation.

The question of how the compact, biologically active state of a protein can assemble reversibly from a relatively disordered polypeptide chain remains a cornerstone to our understanding of the relationship between amino acid sequence and three dimensional structure. One possible mechanism for the folding process proposes that short range interactions within the polypeptide chain are responsible for transient formation of elements of secondary structure (α-helix or β-sheet) which can subsequently act as nucleation sites for further collapse to the native folded state.[1] Protein fragments or designed peptides have proved useful in modelling these nucleation events. While α-helical peptides have been well studied,[2] short peptides that form β-structures, in particular β-hairpins, have been described only relatively recently.[3] There is still some debate as to which are the dominant factors in stabilising these model β-sheet structures, with contrasting opinions on the relative importance of interstrand hydrogen bonding interactions, hydrophobic burial of sides chains and amino acid conformational preferences arising from local steric interactions.[4] Although it is widely regarded that the hydrophobic effect contributes significantly to the folding of globular proteins,[5] thermodynamic evidence from simpler model systems is more difficult to obtain.

In several recent studies, we have investigated in detail the reversible temperature-dependent changes in the ^{1}H NMR Hα chemical shifts that accompany the folding of β-hairpin peptide **1** (Fig. 1) in aqueous solution.[4,6,7] Changes in Hα chemical shift deviations from random coil values indicate that the β-hairpin unfolds at temperatures both above and below *ca.* 298 K. A thermodynamic analysis of temperature-dependent effects on Hα chemical shifts shows that folding is entropy-driven at 298 K with a corresponding negative change in heat capacity.[4,6] Both of these thermodynamic signatures, including the observation of 'cold denaturation', point to the hydrophobic effect providing a key driving force for folding, at least in this model system. However, the contribution interstrand hydrogen bonding interactions make to the stability of the folded state is unclear.

The sensitivity of vibrational spectroscopy to protein structure is well documented, particularly the use of the amide I carbonyl stretch to monitor hydrogen bonding and secondary structure formation.[8–10] Variable temperature IR spectroscopy has been used to probe protein secondary structure in a model α-helix,[11] in β-sheet rich proteins,[12] other β-hairpin systems,[10] in intermolecular β-sheet formation,[13] and even in monitoring peptide aggregation and the onset of amyloid formation.[14,15] For the model α-helix, temperature-dependent changes in the IR spectrum show evidence for unfolding above 298 K with loss of intramolecular hydrogen bonding. Previous studies of β-hairpin peptides[10] have reported a characteristic amide I band at *ca.* 1617 cm^{-1} in aqueous solution at a significantly lower wavenumber than corresponding bands for unstructured random coil peptides.

We have investigated by FTIR spectroscopy the conformation in aqueous solution of the β-hairpin peptide **1**, and a truncated eight residue analogue **2** (Fig. 1). The latter represents the isolated C-terminal β-strand of the hairpin which we use as a reference state. FTIR spectra of peptide **2** at 2 mM concentration show an envelope of strong amide I bands centred around 1640 and 1670 cm^{-1} [Fig. 2(a)], which exhibit little temperature-dependence in the range 278–330 K, consistent with a monomeric, disordered 'random coil' conformation.[10]

Surprisingly, a 2 mM solution of β-hairpin peptide **1** gives a remarkably similar FTIR spectrum to peptide **2** [Fig. 2(b)]. These spectral features again show little temperature-dependence. Resolution enhancement techniques (derivative spectroscopy and Fourier self-deconvolution) reveal a very weak band at 1616 cm^{-1}, representing only a few percent of the total intensity of the amide I envelope. The temperature-dependent changes in the IR spectrum are very small and reversible, which we interpret in terms of temperature variation in band shape and position. To check the extent to which the hairpin is folded in aqueous solution we have repeated ^{1}H NMR experiments on the *exact same* sample used for FTIR analysis. Deviations of Hα chemical shifts from random coil values (ΔδHα values) are shown in Fig. 3 for both peptides **1** and **2**. While ΔδHα values for peptide **2** are very small, again supporting a random coil conformation, reasonably large deviations are apparent for peptide **1**, showing the characteristic pattern for a folded β-hairpin peptide, and ΔδHα values virtually identical to those previously described.[4]

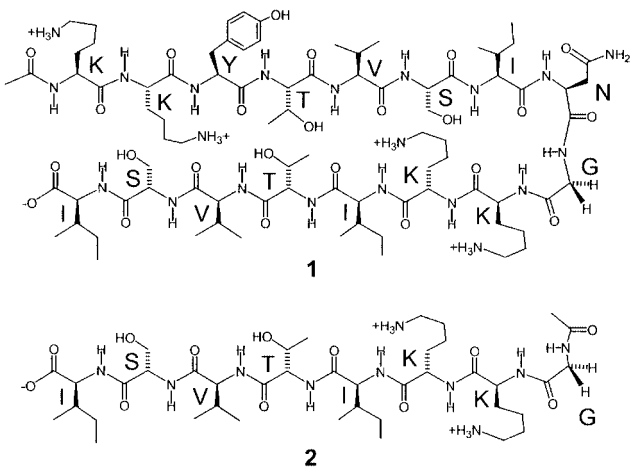

Fig. 1 Schematic representation of the amino acid sequences of peptides **1** and **2**, using the one letter amino acid code. The backbone alignment of the two strands of the β-hairpin peptide are shown to indicate the position of putative interstrand hydrogen bonding interactions.

DOI: 10.1039/b000426j

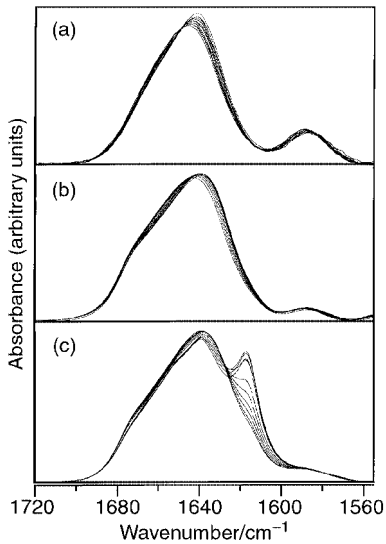

Fig. 2 Variable temperature FTIR spectra of (a) 2 mM aqueous solution of peptide **2**; (b) 2 mM solution of β-hairpin peptide **1**; (c) 10 mM solution of peptide **1**, all in the temperature range 278–330 K. FTIR spectra were collected using a Nicolet Nexus 670 FTIR spectrometer equipped with MCT detector. Circulating water bath controlled temperatures were measured with a J-type thermocouple inside the cell. All peptide solutions were made up in D_2O and the pH (uncorrected for the deuterium isotope effect) adjusted to 5.0 using D_2O solutions of NaOD and DCl. Typically IR spectra were collected as 1000 scans with a resolution of 2 cm^{-1} using a 100 μm cell with calcium fluoride windows. In (a) and (b), the signal intensity at 1640 cm^{-1} increases with increasing temperature, but in (c) decreases with increasing temperature in the range 278–330 K.

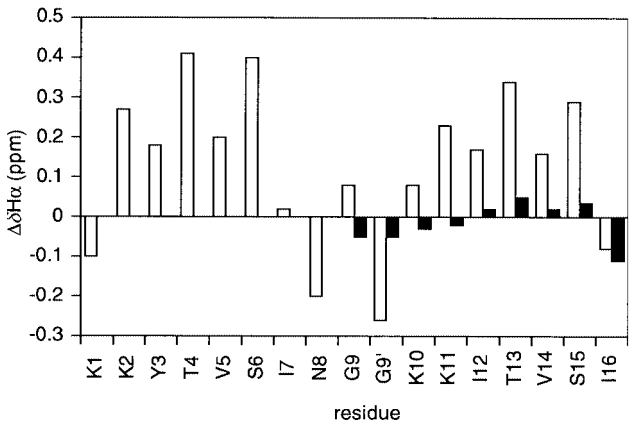

Fig. 3 Deviations of Hα chemical shifts from random coil values[18] (ΔδHα values) for β-hairpin peptide **1** and 8-mer peptide **2** (black bars) at 298 K. NMR data were collected at 500 MHz using reported procedures.[4]

Increasing the concentration of β-hairpin peptide **1** from 2 to 10 mM results in the appearance of a new band in the FTIR spectrum at *ca.* 1616 cm^{-1} [Fig. 2(c)], which is highly and irreversibly temperature-dependent, increasing in intensity initially as the temperature is increased. Integration of this band suggests that at its maximum intensity it corresponds to *ca.* 20% of the total concentration of the peptide. We readily attribute these concentration-dependent changes to irreversible peptide aggregation as reported for a number of model peptides,[10] and partially unfolded proteins that undergo amyloid formation.[14]

Despite previous IR studies of isolated β-hairpin peptides, that identify and assign an amide I band at *ca.* 1617 cm^{-1} to hydrogen bonding across the β-sheet,[10] such features are not a characteristic of the current system. The thermodynamic profile for the folding of peptide **1** has already indicated that hydrophobic contributions from the burial of non-polar side chains play an important part in stabilising the folded conformation.[4,6] The results presented in this study from FTIR analysis in aqueous solution suggest that direct interstrand hydrogen bonding plays, at best, a rather minor role in hairpin stabilisation, and that water molecules appear to compete effectively for hydrogen bonding sites. Significant effects on the amide I band only become apparent in the aggregated state at high concentrations, where arrays of intermolecular hydrogen bonds are co-operatively stabilised. There is, however, still some disagreement regarding the relative importance of the various contributions to the observed changes in the amide I band; hydrogen bonding interactions and other mechanisms involving adjacent oscillators coupled through the covalent framework, have already been discussed.[8,13,16,17]

Although hydrophobic side chains appear to be able to interact sufficiently to populate the folded state of the monomeric peptide, as evident from extensive NOE measurements,[4,6] the hydrophilic peptide backbone appears to remain sufficiently solvated that we can detect no significant changes in the amide I band between the single stranded reference peptide **2** and the folded hairpin **1**. Precise details of the nature of the 'folded state' remain unclear,[6] but explicit consideration of the role of solvent molecules in such models appears to be a necessity, with the possibility of water intercalated between the amide groups of opposing strands. Weakly stabilised β-hairpins ($\Delta G \approx 0$) undoubtedly adopt dynamic conformations in solution. Molecular dynamics simulations show that hydrophobic contacts between strands can be achieved without greatly restricting the orientation of the peptide backbone, while retaining some degree of solvent accessibility.[6] Measurements of backbone $^3J_{NH-H\alpha}$ values for peptides **1** and **2** demonstrate that the peptide backbone is no more ordered in the folded hairpin than in the reference peptide,[4] suggesting that the amino acid sequence predisposes the β-strand residues to adopt an extended conformation, with β-hairpin folding arising from coalescence of the two β-strand arms.

We are grateful to the EPSRC for studentships to C. S. C. and S. R. G.-J. and to Roche Discovery, Welwyn, UK for a CASE award to S. R. G.-J. We thank the Department of Chemistry for financial contributions to this work and John Keyte in the School of Biomedical Sciences for peptide synthesis.

Notes and references

1 P. S. Kim and R. L. Baldwin, *Annu. Rev. Biochem.*, 1990, **59**, 631.
2 A. Chakrabartty and R. Baldwin, *Adv. Protein Chem.*, 1995, **46**, 141; V. Munoz and L. Serrano, *J. Mol. Biol.*, 1995, **245**, 275; K. T. O'Neil and W. F. Degrado, *Science*, 1990, **250**, 646.
3 S. H. Gellman, *Curr. Opin. Chem. Biol.*, 1998, **2**, 717.
4 A. J. Maynard, G. J. Sharman and M. S. Searle, *J. Am. Chem. Soc.*, 1998, **120**, 1996.
5 R. L. Baldwin, *Proc. Natl. Acad. Sci. USA*, 1986, **83**, 8069; K. P. Murphy and S. J. Gill, *J. Mol. Biol.*, 1991, **222**, 699; K. P. Murphy, P. L. Privalov and S. J. Gill, *Science*, 1990, **247**, 559.
6 S. R. Griffiths-Jones, A. J. Maynard and M. S. Searle, *J. Mol. Biol.*, 1999, **292**, 1051.
7 M. S. Searle, S. R. Griffiths-Jones and H. Skinner-Smith, *J. Am. Chem. Soc.*, 1999, **121**, 11 615.
8 S. Krimm and J. Bandekar, *Adv. Protein Chem.*, 1986, **38**, 181.
9 J. L. R. Arrondo, A. Muga, J. Castresana and F. M. Goni, *Prog. Biophys. Mol. Biol.*, 1993, **59**, 23; D. M. Byler and H. Suoi, *Biopolymers*, 1986, **25**, 469; W. K. Surewicz, H. H. Mantsch and D. Chapman, *Biochemistry*, 1993, **32**, 389.
10 J. L. R. Arrondo, F. J. Blanco, L. Serrano and F. M. Goni, *FEBS Lett.*, 1996, **384**, 35.
11 S. Williams, T. P. Causgrove, R. Gilmanshin, K. S. Fang, R. H. Callender, W. H. Woodruff and R. B. Dyer, *Biochemistry*, 1996, **35**, 691.
12 R. Chehin, I. Iloro, M. J. Marcos, E. Villar, V. L. Shnyrov and J. L. R. Arrondo, *Biochemistry*, 1999, **38**, 1525.
13 J. W. Brauner, C. Dugan and R. Mendelsohn, *J. Am. Chem. Soc.*, 2000 **122**, 677.
14 F. Chiti, P. Webster, N. Taddei, A. Clark, M. Stefani, G. Ramponi and C. M. Dobson, *Proc. Natl. Acad. Sci. USA*, 1999, **96**, 3590.
15 K. Halverson, I. Sucholeiki, T. T. Ashburn and R. T. Lansbury, *J. Am. Chem. Soc.*, 1991, **113**, 6701.
16 T. Miyazawa, *J. Chem. Phys.*, 1960, **32**, 1647.
17 H. Torii and M. Tasumi, *J. Chem. Phys.*, 1992, **96**, 3379.
18 K. Wuthrich, *NMR of Proteins and Nucleic Acids*, Wiley, New York, 1986.

Communication b000426j

ChemComm

Synthesis and structure of zinc oxide clusters encapsulated in zeolite LTA

Jennifer E. Readman, Ian Gameson, Joseph A. Hriljac, Peter P. Edwards and Paul A. Anderson*

School of Chemistry, University of Birmingham, Edgbaston, Birmingham, UK B15 2TT.
E-mail: p.a.anderson@bham.ac.uk

Received (in Oxford, UK) 18th January 2000, Accepted 3rd March 2000

We report the synthesis and structure, obtained through Rietveld analysis of powder synchrotron X-ray diffraction data, of zinc oxide clusters encapsulated in zeolite LTA.

There is currently considerable interest in the study of zinc oxide nanoparticles and clusters formed within zeolite crystallites, which is based on potential applications in optics, electronics, sensors and photocatalysis.[1–4] Recent work has concentrated on the characterisation of the materials by spectroscopic methods such as UV–VIS and diffuse reflectance IR spectroscopy,[1–3] but to date there is no crystallographic information on the structure and location of such clusters. A variety of different synthetic routes have been used for the preparation of zinc oxide clusters in zeolites.[1–4] On account of our longstanding interest in metal-zeolite reactions,[5,6] we have adopted the method of Lee *et al.*,[3] who synthesised zinc oxide clusters in zeolite Y through oxidation of the zinc-loaded zeolite, and have applied it to a range of zeolites. As a first step we decided to examine the zinc-loaded zeolites prior to oxidation, and report that in zeolite A (LTA) oxygen-containing clusters are already present at this stage of the synthesis.

The zinc ion-exchanged form of zeolite A (Zn-A) was prepared from as-synthesised Na-A by conventional ion-exchange methods.[7] The zinc-loaded material was prepared through the reaction of dehydrated Zn-A (12 h, 500 °C under vacuum) with Zn powder in a sealed, evacuated (1×10^{-5} mbar) quartz tube. A homogeneous yellow powder was obtained after reaction for 7 days at 500 °C, with a small excess of zinc metal deposited on the ends of the tube. For structural studies to be carried out, a small amount of the sample was placed in a 0.7 mm diameter glass capillary and sealed with epoxy resin in an argon-filled glovebox. X-Ray powder diffraction data were collected at room temperature at station X3B1 at the National Synchrotron Light Source, Brookhaven National Laboratory, USA. The wavelength of the radiation (0.69884 Å) was chosen to minimise any sample absorption problems.

Least squares refinement of our structural model was carried out with the GSAS suite of programs.[8] The starting model was based on the framework coordinates for dehydrated Zn-A obtained by McCusker and Seff,[9] who used the primitive cubic space group $Pm\bar{3}m$ with a lattice constant of *ca*. 12.2 Å. A detailed justification for the use of $Pm\bar{3}m$ in the analysis of X-ray diffraction data from zeolite A has been given by Cruz *et al.*[10] There was no evidence in our data to suggest the need to use a doubled unit cell. After refinement of the background (automated linear interpolation), lattice parameter, peak profiles and framework atomic positions, difference Fourier maps were used to find the positions of three zinc sites. These sites were located at the centre of the sodalite cage (0, 0, 0), in the 6-ring (just inside the sodalite cage) (0.18, 0.18, 0.18) and inside the sodalite cage along the body diagonal (0.13, 0.13, 0.13). Refinement of the fractional occupancies of these sites gave a total zinc content of approximately nine ions per unit cell, three more than necessary to balance the negative charge of the framework.

Difference Fourier maps were used to check for any residual electron density. One peak was found inside the sodalite cage at (0, 0, 0.17). Examination of the bond distances between this site and the zinc site at the centre of the sodalite cage suggested that this new site was actually occupied by oxygen as the bond length of 2.08 Å would be much too short for a Zn–Zn interaction. No sites were found in the α-cage. After further refinement of atomic positions, isotropic thermal parameters and further fitting peak profiles, final difference Fourier maps were again calculated and showed no electron density due to further atomic positions. This refinement (labelled A) converged with $\chi^2 = 2.71$, $R_{wp} = 7.53\%$, $R_p = 5.83\%$, $D_{wd} = 0.807$ and $R_{F^2} = 8.41\%$. Owing to the pronounced asymmetry and large intensity of the first peak the refinement was carried out again with this peak excluded, to avoid excessive bias. This second refinement (B) converged with $\chi^2 = 1.83$, $R_{wp} = 7.32\%$, $R_p = 5.37\%$, $D_{wd} = 1.080$ and $R_{F^2} = 8.86\%$. There was little difference in the structural models obtained from each refinement; the atomic positions, fractional occupancies and isotropic thermal parameters were all within two standard deviations, except for the fractional occupancy of O(4) which was within four standard deviations. Final atomic coordinates, fractional occupancies and isotropic thermal parameters for refinement A are given in Table 1. Observed, calculated and difference plots are shown in Fig. 1. A close visual inspection indicates the main features in the difference plot can be attributed to imperfect modelling of the peak shapes, rather than a mismatch in intensities.

The presence of a non-framework oxygen site implies that a cluster comprising only zinc atoms has not been formed. McCusker and Seff[9] also found non-framework oxygen in Zn-A dehydrated at 600 °C, which was ascribed to water molecules coordinated to Zn^{2+}. In the present work the average unit cell composition[11] is approximately $Zn_{2.75}O_{2.7}/Zn_6[Al_{12}Si_{12}O_{48}]$. It

Table 1 Crystallographic data from refinement A

Atom	*x/a*	*y/a*	*z/a*	Occupancy	$10^2\ U_{iso}$/Å^2	Site Symmetry	Multiplicity
Si/Al	0	0.1839(2)	0.3630(2)	1	1.06(9)	*m*(100)	24
O(1)	0	0.1820(6)	0.5	1	1.2(3)	*mm*2(010)	12
O(2)	0	0.3109(5)	0.3109(5)	1	1.6(3)	*mm*1(011)	12
O(3)	0.1149(4)	0.1149(4)	0.3086(4)	1	2.2(2)	*m*(+ − 0)	24
Zn(1)	0.1346(2)	0.1346(2)	0.1346(2)	0.76(1)	2.3(1)	3*m*(111)	8
Zn(2)	0	0	0	0.74(1)	2.2(4)	*m*3*m*	1
Zn(3)	0.1835(9)	0.1835(9)	0.1835(9)	0.26(1)	4.7(6)	3*m*(111)	8
O(4)	0	0	0.175(3)	0.45(2)	5.8(17)	4*mm*(001)	6

$a = 11.9061(1)$ Å.

DOI: 10.1039/b000579g

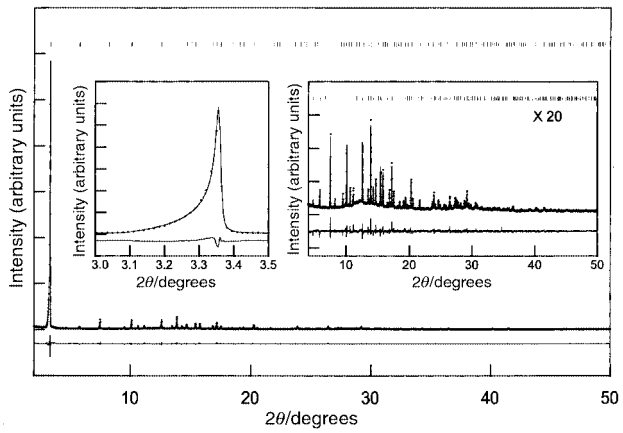

Fig. 1 Final Rietveld fits for refinement A (first peak included) showing observed (dots), calculated (solid line) and difference plots.

is unlikely the extra framework oxygens in this case are due to residual water molecules as the oxidation state of the added zinc atoms would then be close to zero. Likewise, if hydroxy groups were present, the oxidation state of the extra zinc atoms would be approximately +1. If O(4) is considered as O^{2-}, however, the extra zinc atoms can then be considered to be Zn^{2+}. Rittner *et al.*[12] have shown that zinc vapour reacts readily with zeolite H-Y to form a Zn^{2+}-exchanged product. For these reasons we propose that zinc oxide clusters have been formed as a result of the reaction of zinc metal with residual water molecules that remain coordinated to zinc ions within the zeolite after dehydration at 500 °C.

The model obtained from this refinement shows that clusters are formed in the sodalite cage of zeolite A (Fig. 2) as opposed to the larger α-cage as recently proposed by Lee *et al.*[3] The sum of the fractional occupancies of Zn(1) and Zn(3) is approximately unity, without the use of constraints. This is an expected consequence of the distance between the two sites, which is too short for both to be occupied simultaneously. Relatively short Zn–O bond distances supplemented by bond valence sum calculations[12] suggest that Zn(3), located at the centre of the 6-ring, can be considered as Zn^{2+} coordinated only to the oxygen atoms which form the 6-ring. McCusker and Seff[9] found a zinc site in approximately the same position in dehydrated Zn-A. In addition, the fractional occupancies of Zn(1) and Zn(2) are approximately equal, suggesting that each atom at Zn(2) is surrounded by eight at Zn(1). It seems logical to conclude that zinc atoms occupy Zn(1), recessed into the sodalite cage, only when bonded to O(4) atoms. We therefore propose that clusters are formed from Zn(1), Zn(2) and O(4) in approximately 75% of the sodalite cages, and the remaining 25% contain eight Zn^{2+} ions at Zn(3) coordinated to the 6-rings. As there is no evidence of a superstructure, the occupancy of the sodalite cages by the clusters must be random.

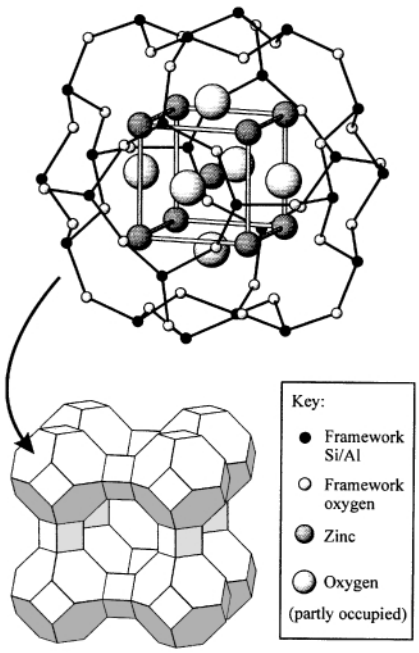

Fig. 2 Structure of zeolite LTA showing the proposed cluster arrangement in the sodalite cage. The oxygen sites are partially occupied.

The proposed cluster is illustrated in Fig. 2 with a zinc atom at the centre of the sodalite cage [Zn(2)] surrounded by eight zinc atoms [Zn(1)] at a distance of 2.78 Å. By symmetry there are six possible oxygen sites each at a distance of 2.08 Å from Zn(2) and 2.32 Å from four atoms at Zn(1). As the results indicate an average of three to four oxygen atoms per cluster, the exact geometry remains unknown. Although the difference between the extra zinc and oxygen contents obtained from the refinement is not significant, there is a possibility that the clusters are slightly oxygen deficient and this may account for the yellow colour of the compound. It is possible that the oxygen content is limited by the small number of water molecules remaining in the zeolite after high temperature dehydration.[9] Experiments aimed at varying the oxygen content are in progress.

One further interesting feature of the structure is that at 11.906 Å, the lattice parameter for this sample is one of the smallest reported for zeolite A. Depmeier has related the lattice parameters of a wide range of zeolite A samples to a framework distortion resulting in the O(3) atoms of the 6-ring being drawn into the sodalite cage and an approximately linear T–O(1)–T angle.[14] It is likely, therefore, that a range of unusual crystallographic parameters, such as the small lattice parameter and the T–O(1)–T angle of 178.5°, observed in this compound result from a framework distortion occasioned in part by cluster formation in the sodalite cage.

We would like to thank Peter Stephens for the synchrotron X-ray diffraction time at Brookhaven, USA.[15] We would also like to thank the Royal Society for the award of a University Research Fellowship (P. A. A.) and EPSRC (J. E. R.) for funding.

Notes and references

1 M. Wark, H. Kessler and G. Schulz-Ekloff, *Microporous Mater.*, 1997, **8**, 241.
2 V. B. Kazansky, V. Yu. Borovkov, A. I. Serykh, R. A. van Santen and P. J. Stobbelaar, *Phys. Chem. Chem. Phys.*, 1999, **1**, 2881.
3 H. B. Lee, H. M. Lim and C. S. Han, *Bull. Korean Chem. Soc.*, 1999, **19**, 1002.
4 L. Khouchaf, M. H. Tuilier, M. Wark, M. Soulard and H. Kessler, *Microporous Mesoporous Mater.*, 1998, **20**, 27.
5 P. P. Edwards, P. A. Anderson and J. M. Thomas, *Acc. Chem. Res.*, 1996, **29**, 23.
6 A. Goldbach, P. D. Barker, P. A. Anderson and P. P. Edwards, *Chem. Phys. Lett.*, 1998, **292**, 137.
7 I. J. Gal, O. Janković, S. Malčić, P. Radovanov and M. Todorovic, *Trans. Faraday Soc.*, 1971, **67**, 999.
8 A. C. Larson and R. B. Von Dreele, Generalised Structure Analysis System, MS-H805, Los Alamos, NM 87545, 1990.
9 L. B. McCusker and K. Seff, *J. Phys. Chem.*, 1981, **85**, 405.
10 W. V. Cruz, P. C. W. Leung and K. Seff, *J. Am. Chem. Soc.*, 1978, **100**, 6997.
11 Based on refinement A; total occupancy of Zn(1) and Zn(3) taken to be 1.
12 F. Rittner, A. Seidel and B. Boddenberg, *Microporous Mesoporous Mater.*, 1998, **24**, 127.
13 I. D. Brown and D. Altermatt, *Acta Crystallogr., Sect. B*, 1985, **41**, 244.
14 W. Depmeier, *Acta Crystallogr., Sect. B*, 1985, **41**, 101.
15 The NSLS at Brookhaven is supported by the US Dept. of Energy Division of Materials Sciences and Division of Chemical Sciences.

Communication b000579g

ChemComm

Artificial metallopeptidases: regioselective cleavage of lysozyme†

Challa V. Kumar,* Apinya Buranaprapuk, Abraham Cho and Anita Chaudhari

Department of Chemistry, U-60, University of Connecticut, Storrs, CT 06269-3060, USA. E-mail: C.V.Kumar@uconn.edu

Received (in Columbia, MO, USA) 10th September 1999, Accepted 30th October 1999

Pentammineaquocobalt(III) chloride and tetramminediaquocobalt(III) chloride cleave chicken hen egg lysozyme between Ala 110 and Trp 111 at neutral pH and 37 °C.

Metal complexes that can cleave proteins with a high specificity under mild conditions will be useful for structure–activity studies of proteins, investigation of protein structural domains, and in converting large proteins into smaller fragments that are more amenable for sequencing.[1–8] Such reagents are also useful for the chemical modification of proteins, or for heavy atom labeling.[2–3] Metal complexes have been attached to specific sites on proteins and subsequent activation resulted in protein fragmentation *via* oxidative or hydrolytic chemistry. Hydrolytic chemistry is preferred over oxidative chemistry as the latter can potentially damage the protein side chains and the resulting fragments may not be amenable to sequencing. Exopeptidase activities of pentammineaquocobalt(III) (CoPA) and tetramminediaquocobalt(III) (CoTA) ions (Scheme 1), under mild conditions, is demonstrated here for the first time.

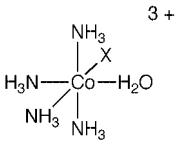

Scheme 1 Structure of the cobalt(III) metal complexes used to cleave lysozyme with high specificity. X = NH_3 for CoPA and H_2O for CoTA.

Metal complexes with labile ligands may bind to the side chains of amino acid residues such as Cys, His, Trp, Asp and Lys and such coordination may function as an anchor to position the reagent for the controlled hydrolysis of protein backbone.[2,3] In this context, Cu, Pt and Pd complexes showed significant artificial metallopeptidase activities.[3] Co(III) complexes are known to induce N-terminal hydrolysis of peptides (endopeptidase activity)[9,10] but the exopeptidase activity of Co(III) is not known. Hydrolysis of N-4(1-pyrenyl)butyroylphenylalanine by CoPA (hydrolysis occurs at the C-terminus) prompted us to investigate the catalytic hydrolysis of proteins by Co(III) complexes.[11] Chicken hen egg lysozyme was chosen for the current studies because lysozyme can bind a number of metal ions,[12] its three-dimensional structure is known[13] and catalytic activity of lysozyme provides a convenient handle to test if the protein cleavage results in the loss of activity.

Incubation of lysozyme (15 μM) with CoPA or CoTA (1 mM) at 37 °C for 21–26 h resulted in facile cleavage of the protein into two fragments as demonstrated in SDS PAGE experiments (6% acrylamide, 0.4% bisacrylamide, 13% glycerol; pH 8.4).[14] Two new bands with molecular weights of *ca.* 12 and 2 kDa are clearly visible in Fig. 1(a) (lanes 4 and 6). If the protein cleavage were to be random, one would have observed a smear in these lanes. Occasionally, the 2 kDa band was difficult to see in the gels (lane 2). The rate of protein cleavage increases with the concentration of CoTA (0.2, 0.5 and 1 mM) and similar activity was observed with CoPA [Fig. 1(b)].

† Electronic supplementary information (ESI) available: self cleavage of lysozyme at room temperature and 37 °C. See http://www.rsc.org/suppdata/cc/a9/a907477e/

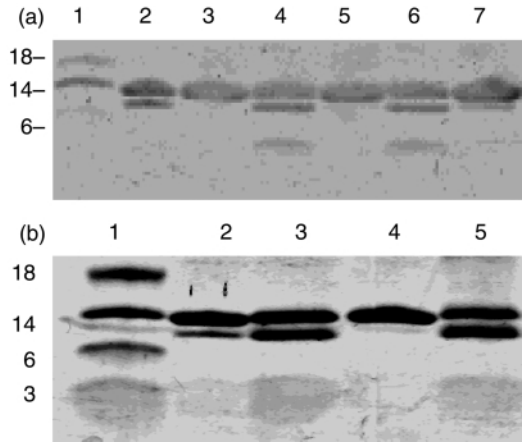

Fig. 1 (a) Lysozyme cleavage by CoTA at 37 °C. Lane 1 contains molecular weight markers at 18, 14 and 6 kDa. Lanes 2–7 contain lysozyme (15 μM) and increasing concentrations of CoTA (lanes 2, 3 contain 0.2 mM, lanes 4, 5 contain 0.5 mM and lanes 6, 7 contain, 1 mM CoTA, respectively). Lanes 2, 4 and 6 were kept at 37 °C (26 h) while lanes 3, 5, 7 were kept at room temperature (26 h). Two new bands corresponding to lower molecular weights than the native protein are indicated in lanes 4 and 6. (b) Lane 1 contains molecular weight markers at 18, 14, 6 and 3 kDa. Lanes 2–5 contain lysozyme (15 μM). Lane 2 contains protein treated with CoTA (1 mM, 22 °C); lane 3, CoTA (1 mM, 37 °C); lane 4, CoPA (1 mM, 22 °C) and lane 5, CoPA, 1 mM, 37 °C). Facile cleavage of lysozyme at 37 °C (26 h) by the aquo complexes is evident. In addition to the major new band in lanes 3, and 5, a faint band with a molecular weight around 2000 Da is also present.

No cleavage was observed when the protein was incubated with CoPA at room temperature (26 h, lane 4) while CoTA induced weak but detectable cleavage even at room temperaure (lane 2, 6%). The ratio of the major product band intensity to the sum of the intensities of the major product and the starting material in lanes 3 and 5 are 45 and 35%, respectively.

Even though the reaction does not proceed at room temperature with CoPA [Fig. 1(b), lane 4] and the reaction is very weak with CoTA [Fig. 1(b), lane 2] self cleavage of lysozyme at room temperature and at 37 °C was examined in the absence of the metal complexes (ESI†). No reaction occurs at 37 °C, 26 h (lane 3) or at room temperature (lane 2) indicating that the reaction is mediated by the metal complexes.

By contrast, no reaction was observed with the *cis* or *trans* isomers of bisethylenediaminediaquocobalt(III) bromide (Fig. 2, lanes 4, 5). Other cobalt complexes such as chloropentamminecobalt(III), chlorotetramminecobalt(III) or chlorotetramminecarbonatocobalt(III) also induced protein cleavage, although, at much slower rates (data not shown). These metal complexes can undergo hydrolysis under the reaction conditions to give rise to the corresponding aquo complexes which are active. Hexamminecobalt(III) chloride did not induce protein cleavage suggesting that the Co(III) center with one or more aquo ligands are needed for activity.

The reaction rate is accelerated with temperature and protein cleavage products could be detected within 5 h at 45 and 55 °C. The protein cleavage was optimal at pH 7 and was slowed down

DOI: 10.1039/a907477e

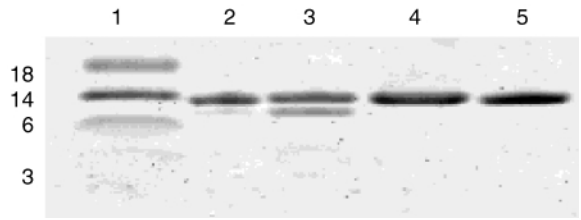

Fig. 2 Lane 1 contains molecular weight markers at 18, 14, 6 and 3 kDa. Lanes 2, 3, 4 and 5 contain lysozyme (15 μM) treated with the metal complexes (1 mM) under different conditions. Lane 2 contains CoTA at 25 °C; lane 3 contains CoTA at 37 °C; lane 4 contains *trans*-$[Co(en)_2Br_2]Br$ at 37 °C and lane 5 contains *cis*-$[Co(en)_2Br_2]Br$ (37 °C). An intense product band is evident in lane 3, and another faint band at 2000 Da is also present in this lane. No products were formed with the *cis*- or *trans*-ethylenediammine complexes treated at 37 °C or at 22 °C even after 21 h.

at pH 4.5 or 9. Protein cleavage proceeded smoothly when Tris–HCl buffer was replaced by acetate or phosphate.

The peptide fragments from the gels were isolated and their molecular weights have been determined from electrospray ionization mass spectrometry. The larger fragment had a molecular weight of 11998 Da while the smaller fragment had a molecular weight of 2343 Da. N-terminal sequencing by Edman degradation method revealed that the 12 kDa fragment had the sequence KVFGRCELAAAM, the known N-terminal sequence of lysozyme (Scheme 2). The N-terminus of the smaller fragment had the sequence, WRNRCK, a sequence internal to lysozyme. The cleavage thus occurs between Ala 110 and Trp 111, as inferred from the known sequence of lysozyme.[13] A minor product (< 3%) of molecular weight 3 kDa had the N-terminal sequence KVFGRCELAAAM, suggesting cleavage of lysozyme at a secondary site, in addition to the major cleavage site described above.

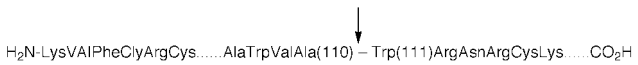

Scheme 2 Lysozyme sequence that has been targeted by the metal complex at neutral pH.

Catalytic activity of lysozyme was examined before and after the cleavage by CoTA, using glycol chitin as the substrate.[5b] The enzyme activity was unaffected by the protein cleavage reaction, and this observation is consistent with the location of the active site in the 12 kDa fragment. The major fragment thus retains the active site with little or no damage to the key residues involved in the enzyme catalysis. Preliminary ^{1}H NMR studies of lysozyme–CoPA solutions (2.9 mM lysozyme, 18 mM CoPA) indicate a number of shifts when compared to those of the protein (3 mM) in the absence of the metal complex. Further studies are needed to assign these changes but the resonances due to Trp 108 appears to have undergone significant changes. The known three-dimensional structure of lysozyme[13] indicates that Trp 108 is accessible to the aqueous medium and Trp108 could anchor the Co(III) reagent. Such coordination could position the metal complex proximate to the Ala 110 and Trp 111 peptide bond where the cleavage was observed.

The mechanism for protein cleavage by Co(III) is expected to be similar to that reported for amide hydrolysis by CoTA and CoPA.[15,16] The amide hydrolysis rates were higher for complexes with two open coordination sites.[15] Water molecules bound to the metal ion may participate in acid–base catalysis at the metal binding site, facilitating peptide bond cleavage. Size is also important as larger size may preclude the metal complex from reaching the peptide back bone (ethylenediamine complexes are not active). Current results demonstrate that Co(III) complexes can cleave internal peptide bonds, possibly *via* a hydrolytic mechanism. Chemical proteases derived from inorganic materials may prove to be useful as tools in molecular biology.

Financial support from the University of Connecticut Research Foundation, ACS Petroleum Research Fund and the Naional Science Foundation is gratefully acknowledged. We are grateful to Mary Moyer and William Burkhart of Glaxo Wellcome Inc., for the sequencing and mass spectral data.

Notes and references

1 A. Schepartz and B. Cuenoud, *J. Am. Chem. Soc.*, 1990, **112**, 3247; D. Hoyer, H. Cho and H. P. G. Schultz, *J. Am. Chem. Soc.*, 1990, **112**, 3249; T. M. Rana and C. F. Meares, *J. Am. Chem. Soc.*, 1990, **112**, 2457.
2 T. M. Rana and C. F. Meares, *Proc. Nat. Acad. Sci., USA*, 1991, **88**, 10 578; D. Rehder, *Angew. Chem., Int. Ed. Engl.*, 1991, **30**, 148; *Angew. Chem.*, 1991,**103**, 152; C. R. Cremo, J. A. Loo, C. G. Edmonds and K. M. Hatlelid, *Biochemistry*, 1993, **31**, 491.
3 L. Zhu, L. Qin, T. N. Parac and N. M. Kostic, *J. Am. Chem. Soc.*, 1994, **116**, 5218; L. Zhu and N. M. Kostic, *J. Am. Chem. Soc.*, 1993, **115**, 4566; E. L. Hegg and J. N. Burstyn, *J. Am. Chem. Soc.*, 1995, **117**, 7015; E. L. Hegg and J. N. Burstyn, *Coord. Chem. Rev.*, 1998, **173**, 133.
4 A. Buranaprapuk, S. P. Leach, C. V. Kumar and J. R. Bocarsly, *Biochem. Bioiophys. Acta: Protein Struct.*, 1998, **1387**, 309.
5 (*a*) C. V. Kumar and A. Buranaprapuk, *Angew. Chem., Int. Ed. Engl.*, 1997, **36**, 2085; *Angew. Chem.*, 1997, **109**, 2175; (*b*) C. V. Kumar, A. Buranaprapuk, M. Moyer, G. Opitek, S. Jockusch and N. J. Turro, *Proc. Natl. Acad. Sci.*, 1998, **95**, 10361; (*c*) C. V. Kumar and A. Buranaprapuk, *J. Am. Chem. Soc.*, 1999, **121**, 4264.
6 N. Ettner, G. A. Ellestad and W. Hillen, *J. Am. Chem. Soc.*, 1993, **115**, 2546; N. Ettner, J. W. Metzger, T. Lederer, J. D. Hulmes, C. Kisker, W. Hinrichs, G. Ellestad and W. Hillen, *Biochemistry*, 1995, **34**, 22.
7 K. Nagai and S. M. Hecht, *J. Biol. Chem.*, 1991, **266**, 3994.
8 B.-B. Jang, K.-P. Lee, D.-H. Min and J. Suh, *J. Am. Chem. Soc.*, 1998, **120**, 12 008.
9 J. P. Collman and E. Kimura, *J. Am. Chem. Soc.*, 1967, **89**, 6096.
10 R. M. Rhee and C. Storm, *J. Inorg. Biochem.*, 1979, **11**, 17; S. S. Isied, A. Vassilian and J. M. Lyon, *J. Am. Chem. Soc.*, 1982, **104**, 3900; P. A. Sutton and D. A. Buckingham, *Acc. Chem. Res.*, 1987, **20**, 357.
11 Attempts to coordinate CoPA to the carboxyl function of *N*-4(1-pyrenyl)butyroylphenylalanine resulted in the rapid hydrolysis of the peptide bond to give pyrenebutyric acid and 1-phenylalanine. Coordination of Co(III) to the carboxyl is suspected to activate the adjacent peptide bond for hydrolysis (unpublished results).
12 A. C. Awade, S. Moreau and G. Brule, *J. Agric. Food Chem.*, 1995, **43**, 883.
13 The reaction mixture was dried under reduced pressure and the residue was redissolved in sample buffer. The buffer contained glycerol (1 ml), sodium dodecyl sulfate (3 ml, 10% aqueous solution), Tris–HCl (1.25 ml, 0.5 M), bromophenol blue (0.6 ml, 0.1% solution) and deionized distilled water (4.5 ml). The gels were run by applying 60 V until the dye (Coomassie blue) passed through the stacking gel. The voltage was then increased (110 V) and the gels were run for a total of 2 h, as described in H. Schagger and G. V. Jagow, *Anal. Biochem.*, 1987, **166**, 368.
14 R. E. Dickerson and I. Geis, in *The Structure and Action of Proteins*, Benjamin, Melno Park, CA,, 1969.
15 B. K. Takasaki, J. H. Kim, E. Rubin and J. Chin, *J. Am. Chem. Soc.*, 1993, **115**, 1157.
16 L. M. Sayre, *J. Am. Chem. Soc.*, 1986, **108**, 1632.

Communication a907477e

ChemComm

Photoinduced energy transfer in a fullerene–oligophenylenevinylene conjugate†

Nicola Armaroli,*[a] Francesco Barigelletti,[a] Paola Ceroni,[b] Jean-François Eckert,[c] Jean-François Nicoud[c] and Jean-François Nierengarten*[c]

[a] *Istituto di Fotochimica e Radiazioni d'Alta Energia (FRAE) del CNR, via Gobetti 101, 40129 Bologna, Italy. E-mail: armaroli@frae.bo.cnr.it*

[b] *Dipartimento di Chimica 'G. Ciamician', Università di Bologna, via Selmi 2, 40126 Bologna, Italy*

[c] *Groupe des Matériaux Organiques, Institut de Physique et Chimie des Matériaux de Strasbourg, Université Louis Pasteur et CNRS, 23 rue du Loess, 67037 Strasbourg, France. E-mail: niereng@ipcms.u-strasbg.fr*

Received (in Cambridge, UK) 19th January 2000, Accepted 25th February 2000

A fullerene derivative in which two oligophenylenevinylene (OPV) groups are attached to C_{60} through a pyrrolidine ring has been prepared and photophysical studies in CH_2Cl_2 solution show that photoinduced energy transfer from the OPV moieties to C_{60} occurs, and not electron transfer.

Following the observation of electron transfer from conducting oligomers and/or polymers derived from poly(phenylenevinylene) or poly(thiophene),[1] and the successful preparation of photovoltaic cells from such bulk heterojunction materials,[2] several examples of covalent fullerene derivatives bearing a conjugated oligomer substituent have been synthesized in the past few years.[3,4] As a part of this research, we have recently shown that such hybrid compounds can be incorporated in photovoltaic devices.[4] Whereas the synthesis and applications of such hybrid compounds have been investigated, their electronic properties have been probed to a much lesser degree.

In this paper, we report on the preparation and the electronic properties of fullerene derivative **1** in which two OPV groups are attached to C_{60} through a pyrrolidine ring using the related OPV derivative **2** and the fulleropyrrolidine **FP**[4] as reference compounds. Interestingly, the photophysical studies of **1** in solution show that photoinduced energy transfer from the OPV moiety to C_{60} is the main pathway and not electron transfer.

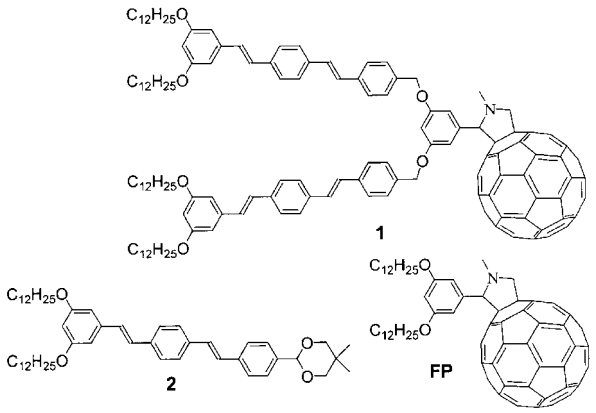

The synthesis of **1** is depicted in Fig. 1 and the functionalisation of C_{60} is based on the 1,3-dipolar cycloaddition[5] of the azomethine ylide generated *in situ* from aldehyde **7**.

The electrochemical properties of **1**, **2** and **FP** were investigated by cyclic voltammetry (CV) in CH_2Cl_2–0.1 M Bu_4NPF_6 solutions (Table 1). In the cathodic region, **1** shows three reversible one-electron processes followed by a bielectronic peak (IV_{red}), visible only at low temperature. A comparison of the $E_{1/2}$ potentials of **1** and **FP** clearly shows that the first three waves correspond to fullerene-centred reductions and the slightly negative shift observed for **1** compared to **FP** could be the result of a small interaction between the electron-accepting C_{60} unit and the electron-donating OPV groups. The fourth reduction process seen for **1** appears to be difficult to assign unambiguously as either fullerene- or OPV-based. In the anodic region, **1** presents two chemically irreversible and ill-defined peaks, corresponding to the transfer of three electrons. They can likely be attributed to the simultaneous oxidation of the two OPV groups and the bridging dialkyloxybenzene unit,[6] since these groups present in both model compounds **2** and **FP** are irreversibly oxidized in the same potential region.

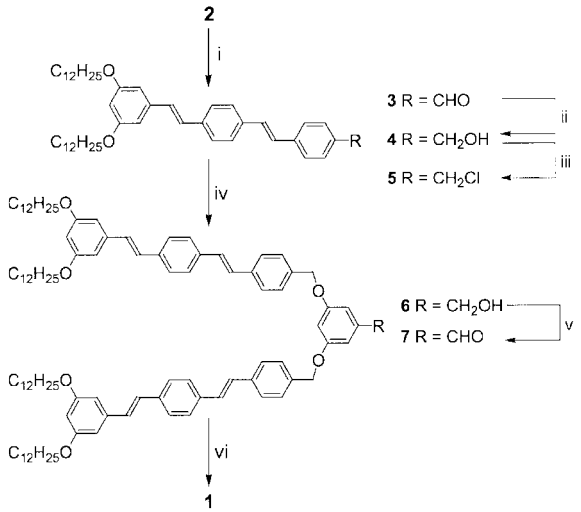

Fig. 1 *Reagents and conditions*: i, CF_3CO_2H, CH_2Cl_2, H_2O, room temp., 4 h (96%); ii, DIBAL-H, CH_2Cl_2, 0 °C, 1 h (90%); iii, TsCl, LiCl, DMAP, CH_2Cl_2, 0 °C to room temp., 12 h (80%); iv, 3,5-dihydroxybenzyl alcohol, K_2CO_3, KBr, 18-crown-6, acetone, Δ, 24 h (69%); v, MnO_2, CH_2Cl_2, room temp., 2 h (95%); vi, C_{60}, *N*-methylglycine, toluene, Δ, 16 h (40%).

The ground state electronic absorption spectrum of **1** is reported in Fig. 2 and, within the experimental error, it matches the profile obtained by summation of the spectra of the component units **FP** and **2**. Importantly, on each moiety of **1**, a fairly good excitation selectivity can be achieved. Indeed, at $\lambda >$

Table 1 $E_{1/2}$ or E_p values (V *vs.* SCE) determined by CV on a glassy carbon electrode at 298 K, unless otherwise noted,[b] of compounds **1**, **2** and **FP** in CH_2Cl_2–0.1 M Bu_4NPF_6 solutions

Compound	II_{ox}	I_{ox}	I_{red}	II_{red}	III_{red}	IV_{red}
1	+1.7[a,c]	+1.4[a,c]	−0.66	−1.04	−1.56	−1.98[b,d]
2	+1.82[a]	+1.28[a]	−1.88[b]	−2.11[a,b]		
FP	+1.60[a]	+1.38[a]	−0.62	−1.01	−1.54	−1.90[b]

[a] Chemically irreversible processes, peak potentials measured at 0.2 V s^{-1}. [b] T = 208 K. [c] Trielectronic process. [d] Bielectronic process.

† Electronic supplementary information (ESI) available: CV curves for **1**, **2** and **FP**, and calculation of energy transfer rate constants. See http://www.rsc.org/suppdata/cc/b0/b000564i/

DOI: 10.1039/b000564i

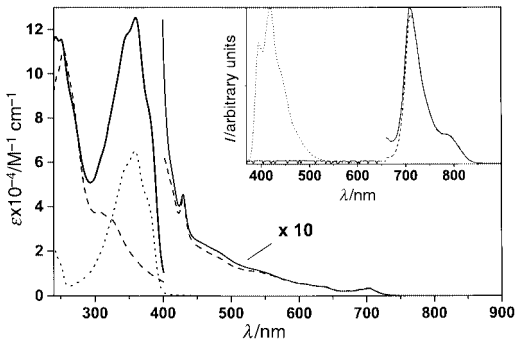

Fig. 2 Absorption spectra of **1** (full line), **FP** (dashed line) and **2** (dotted line) in CH_2Cl_2 at 298 K; above 400 nm a multiplying factor of 10 is used. Inset: fluorescence spectra of solutions of **2**, **FP** and **1** (for all samples, optical density = 0.50 at λ_{exc} = 360 nm). Above 660 nm the spectrofluorimeter sensitivity is increased by three orders of magnitude, due to the weakness of the **FP** fluorescence relative to that of **2**.

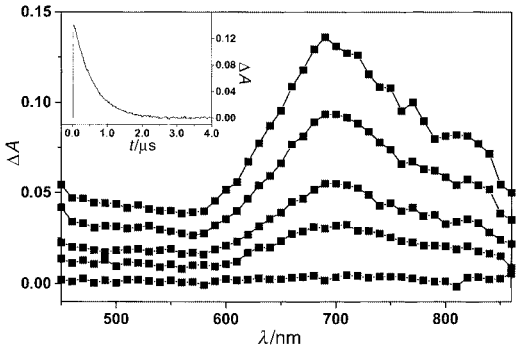

Fig. 3 Sensitized fullerene triplet–triplet transient absorption spectrum of **1** at 298 K in CH_2Cl_2 air equilibrated solution, upon laser excitation at 355 nm (energy = 5 mJ pulse^{-1}). The spectra were recorded at delays of 100, 300, 600, 900, 2000 ns following excitation (from top to bottom). The inset shows the time profile of ΔA (690 nm) from which the spectral kinetic data were obtained; the fitting is monoexponential and gives a lifetime of 540 ns.

530 nm light is exclusively directed to the fullerene fragment, whereas at λ = 360 nm at least 85% of the incident light is absorbed by the OPV moieties.

Upon selective excitation of **1** on the fullerene fragment, the typical fulleropyrrolidine fluorescence and triplet–triplet transient absorption spectra are observed.[6,7] This indicates that the excited state properties of the C_{60} fragment are not affected by the presence of the nearby OPV moieties. On the other hand, when excitation is directed to the latter (*e.g.* at λ = 360 nm, see above), intercomponent processes are evidenced. Under such conditions, the intense fluorescence band characteristic of the OPV moiety (Φ_{em} = 1.0, τ = 1.0 ns) is not observed (Fig. 2), whereas the typical fluorescence band of the fulleropyrrolidine fragment (λ_{max} = 710 nm, τ = 1.3 ns) is detected; in addition, the fullerene fluorescence quantum yields of **1** and **FP** obtained at λ_{exc} = 360 nm are identical (Φ_{em} = 5.5 × 10^{-4}), although in the former at least 85% of the incident light is absorbed by the OPV fragments. The excitation spectrum of **1**, taken at λ_{em} = 715 nm, matches the absorption profile throughout the UV–VIS, range including the diagnostic band of the OPV moieties around 360 nm. These findings are consistent with quantitative occurrence of singlet–singlet energy transfer from the OPV unit to the fullerene in the multicomponent array **1**.

In order to monitor the fate of the lowest triplet state centred on the fullerene moiety, following excitation of the OPV counterpart, we performed a series of transient absorption experiments by setting the excitation wavelength of an Nd:YAG laser to 355 nm. The reference compound **FP** displays a triplet–triplet transient absorption spectrum with λ_{max} = 690 nm and τ = 0.54 μs in air-equilibrated solution, which becomes 31 μs in deaerated solution due to the suppression of the well-known, very efficient quenching of fullerenes by dioxygen.[7,8] A quite similar behaviour is observed for **1**, which displays a fullerene triplet yield formation equal to that of **FP** and the same triplet lifetimes. In other words, preferential excitation of the OPV moieties (> 85%) quantitatively sensitizes the formation of the lowest fullerene singlet state, which then populates the lower lying triplet level (Fig. 3) *via* intersystem crossing.

From the electrochemical data one can place the energy of the charge separated state[9] of **1** at about 2 eV, *i.e.* well below the energy of the lowest singlet excited state of the OPV moieties (3.1 eV, as derived from the 77 K fluorescence spectrum). However, even if the population of the charge separated state following photoexcitation of the OPV units is thermodynamically allowed, this process is not evidenced in CH_2Cl_2 solution. The use of polar solvents does not change the observed pattern; for instance, quantitative evidence for OPV→C_{60} singlet–singlet energy transfer is also observed in benzonitrile solution. We have performed model calculations on the OPV→C_{60} singlet–singlet energy transfer step by following both the dipole–dipole and double-electron exchange approaches (for details, see supplementary data).† The spectral overlap between the luminescence spectrum of the donor OPV unit and the absorption spectrum of the fulleropyrrolidine acceptor unit allows calculation of the overlap integrals J^F = 1.4 × 10^{-14} cm^6 mol^{-1} and J^D = 1.4 × 10^{-4} cm for the two approaches, and results in estimated rate constants, k_{en}^F; $k_{en}^D \gg 10^{12}$ s^{-1} up to 10 Å of intercenter separation. These estimates suggest that the energy transfer step is so fast that the competing charge separation path is not effective.

In conclusion, **1** appears to be a multicomponent array containing a fullerene unit as a terminal receptor of excitation energy.[10] These results suggest the possibility of building up more complex arrays where a larger number of OPV fragments allow an even more pronounced excitation selectivity with an antenna effect, and the attachment of a suitable electron donor to the C_{60} unit would result in multicomponent artificial photosynthetic systems where light energy harvesting is followed by charge separation.[11]

Notes and references

1 L. Pasimeni, A. L. Maniero, M. Ruzzi, M. Prato, T. Da Ros, G. Barbarella and M. Zambianchi, *Chem. Commun.*, 1999, 429; R. A. J. Janssen, M. P. T. Christiaans, K. Pakbaz, D. Moses, J. C. Hummelen and N. S. Sariciftci, *J. Chem. Phys.*, 1995, **102**, 2628; R. A. J. Janssen, J. C. Hummelen, K. Lee, K. Pakbaz, N. S. Sariciftci, A. J. Heeger and F. Wudl, *J. Chem. Phys.*, 1995, **103**, 788; N. S. Sariciftci, L. Smilowitz, A. J. Heeger and F. Wudl, *Science*, 1992, **258**, 1474.

2 L. Ouali, V. V. Krasnikov, U. Stalmach and G. Hadziioannou, *Adv. Mater.*, 1999, **11**, 1515; L. S. Roman, M. R. Andersson, T. Yohannes and O. Inganäs, *Adv. Mater.*, 1997, **9**, 1164; G. Yu, J. Gao, J. C. Hummelen, F. Wudl and A. J. Heeger, *Science*, 1995, **270**, 1789.

3 S.-G. Liu, L. Shu, J. Rivera, H. Liu, J.-M. Raimundo, J. Roncali, A. Gorgues and L. Echegoyen, *J. Org. Chem.*, 1999, **64**, 4884; J. L. Segura and N. Martin, *Tetrahedron Lett.*, 1999, **40**, 3239; T. Yamashiro, Y. Aso, T. Otsubo, H. Tang, Y. Harima and K. Yamashita, *Chem. Lett.*, 1999, 443; F. Effenberger and G. Grube, *Synthesis*, 1998, 1372.

4 J.-F. Nierengarten, J.-F. Eckert, J.-F. Nicoud, L. Ouali, V. Krasnikov and G. Hadziioannou, *Chem. Commun.*, 1999, 617; J.-F. Nierengarten, J.-F. Eckert, D. Felder, J.-F. Nicoud, N. Armaroli, G. Marconi, V. Vicinelli, C. Boudon, J.-P. Gisselbrecht, M. Gross, G. Hadziioannou, V. Krasnikov, L. Ouali, L. Echegoyen and S.-G. Liu, *Carbon*, 2000, in press.

5 M. Prato and M. Maggini, *Acc. Chem. Res.*, 1998, **31**, 519.

6 M. Goez and G. Eckert, *J. Phys. Chem.*, 1991, **95**, 1179.

7 C. Luo, M. Fujitsuka, A. Watanabe, O. Ito, L. Gan, Y. Huang and C.-H. Huang, *J. Chem. Soc., Faraday Trans.*, 1998, **94**, 527.

8 F. Prat, R. Stackow, R. Bernstein, W. Qian, Y. Rubin and C. S. Foote, *J. Phys. Chem. A*, 1999, **103**, 7230.

9 V. Balzani and F. Scandola, *Supramolecular Photochemistry*, Ellis Horwood, Chichester, UK, 1991, p. 44.

10 D. M. Guldi, G. Torres-Garcia and J. Mattay, *J. Phys. Chem. A*, 1998, **102**, 9679.

11 H. Imahori and Y. Sakata, *Eur. J. Org. Chem.*, 1999, 2445; D. Kuciauskas, P. A. Liddel, S. Lin, T. E. Johnson, S. J. Weghorn, J. S. Lindsey, A. L. Moore, T. A. Moore and D. Gust, *J. Am. Chem. Soc.*, 1999, **121**, 8604.

Communication b000564i

ChemComm

Structural, electron paramagnetic resonance and electron spin echo envelope modulation studies of oxovanadium(IV)–amidate compounds containing monoanionic axial ligands: effect on the ^{51}V-hyperfine coupling constants†

Evangelos J. Tolis,[a] Kalliopi D. Soulti,[a] Catherine P. Raptopoulou,[b] Aris Terzis,[b] Yiannis Deligiannakis*[c] and Themistoklis A. Kabanos*[a]

[a] *Department of Chemistry, Section of Inorganic and Analytical Chemistry, University of Ioannina, 451 10 Ioannina, Greece. E-mail: tkampano@cc.uoi.gr*
[b] *NRCPS Demokritos, Institute of Materials Science, 15 310 Agia Paraskevi Attikis, Greece*
[c] *Department of Environmental and Natural Resources, Laboratory of Physical Chemistry, University of Ioannina, Pyllinis 9, Agrinio, Greece*

Received (in Basel, Switzerland) 29th September 1999, Revised manuscript received 1st January 2000, Accepted 23rd February 2000

Reaction of the amidate ligand *N*-{2-[(2-pyridylmethylene)amino]phenyl}pyridine-2-carboxamide (Hcapca) with $[VOCl_2(thf)_2]$ and MeONa in 1:1:1 molar ratio in MeCN affords the compound *trans*-[VOCl(capca)] 1, while reaction of 1 with NEt_4NCS, $MeCO_2NHEt_3$ and imidazole yields the complexes *trans*-[VO(NCS)(capca)] 2, *trans*-[VO(MeCO$_2$)(capca)] 3 and *trans*-[VO(im)(capca)]$^-$ 4 respectively; the X-ray crystal structure of 1 is reported; Cw EPR studies of compounds 1–3 reveal a novel phenomenon of the reduction of their A_z components by *ca*. 10% compared to N_4 reference compounds.

The oxovanadium(IV) cation, $V^{IV}O^{2+}$, has been successfully employed as a spin probe in EPR[1] and electron spin echo envelope modulation (ESEEM)[1] studies of naturally occurring vanadoproteins and in proteins where the divalent cations (Mg^{2+}, Ca^{2+}, *etc*.) have been substituted by $V^{IV}O^{2+}$. More specifically, the *z*-component of the ^{51}V(I = 7/2) hyperfine coupling tensor $\boldsymbol{A}$, has been extensively employed as a benchmark for the identification of the equatorial donor atom sets in oxovanadium(IV) complexes.[1a,2]

Oxovanadium(IV) compounds have usually square pyramidal or octahedral geometry with a weak sixth ligand in axial position. To the best of our knowledge, there are only two other structurally characterized $V^{IV}O^{2+}$ species with a monoanionic ligand (Cl^-)[3] in axial position and obviously the effect of the charged axial ligand on ^{51}V hyperfine coupling constants has not been systematically studied. The potentially tetradentate amidate ligand, *N*-{2-[(2-pyridylmethylene)amino]phenyl}pyridine-2-carboxamide (Hcapca), was chosen in an effort to force axial ligation of anionic as well as of neutral ligands. In this report, we describe the synthesis, the cw EPR, and ESEEM spectra of the oxovanadium(IV) compounds of the general formula *trans*-$[V^{IV}OX(capca)]^{0/+}$ (X = Cl^- **1**, SCN^- **2**, $MeCO_2^-$ **3** and imidazole **4**) as well as the X-ray crystal structure of **1**·MeOH with the view to studying the effect of the charged axial ligands on the ^{51}V-hyperfine coupling constants and in particular on the parallel component, A_z.

The mononuclear brick-red compound *trans*-[VOCl(capca)] **1** was prepared by refluxing an MeCN solution containing $[VOCl_2(thf)_2]$ (3 mmol), Hcapca (3 mmol) and MeONa (3 mmol) for *ca*. 24 h [eqn. (1)]. The brick-red precipitate was Soxhlet extracted (CH_2Cl_2) to remove NaCl and to obtain **1**·CH_2Cl_2.‡

$$[VOCl_2(thf)_2] + Hcapca + MeONa \rightarrow \textit{trans}\text{-}[VOCl(capca)] + MeOH + NaCl + 2thf \quad (1)$$

Crystals of **1**·$MeOH^+$ suitable for X-ray structure analysis§ were obtained by vapour diffusion of diethyl ether into a concentrated MeOH solution (at 4 °C) of the complex. **2**, **3** and **4** were prepared according to Scheme 1.‡

The continuous wave (cw) EPR parameters of the four oxovanadium(IV) compounds (Table 1) were determined by computer simulation of the experimental cw EPR spectra. The cw EPR spectrum of **1**·MeOH is typical of a monomeric oxovanadium(IV) ($S = \frac{1}{2}$, I = 7/2) species with no evidence for

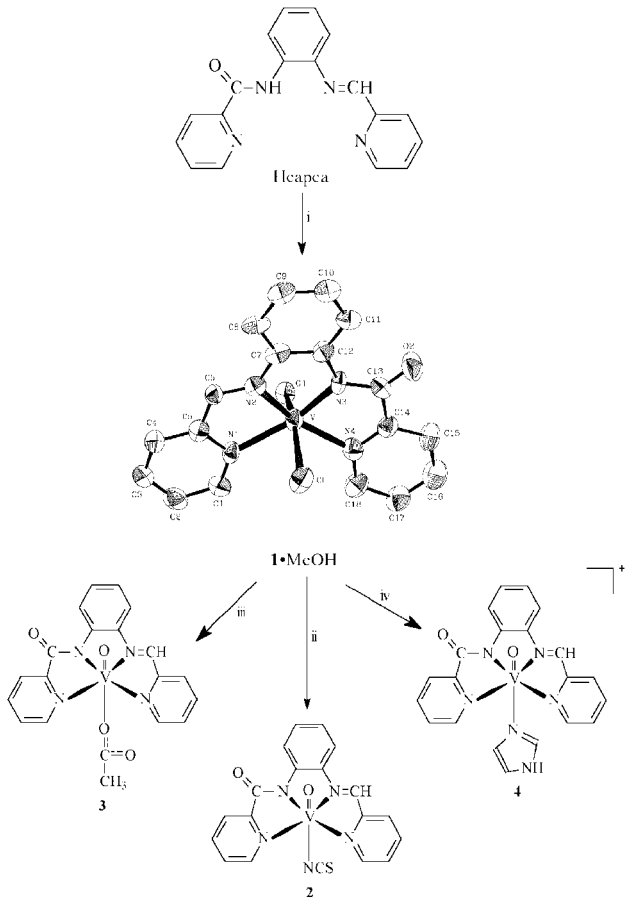

Scheme 1 Synthesis of the oxovanadium(IV) compounds **1** and **2**–**4** and X-ray crystal structure of **1**·MeOH. *Reagents and conditions*: i, MeCN, $[VOCl_2(thf)_2]$, MeONa, reflux, argon; ii, MeOH, NEt_4NCS; iii, MeCN, $MeCO_2H$, NEt_3, 0 °C; iv, $MeNO_2$, imidazole. Selected interatomic distances (Å) for **1**·MeOH: V–O(1) 1.626(5), V–N(1) 2.171(7), V–N(2) 2.079(6), V–N(3) 2.010(7), V–N(4) 2.120(7), V–Cl 2.569(3).

† Electronic supplementary information (ESI) available: reference oxovanadium(IV) compounds. See http://www.rsc.org/suppdata/cc/b0/b000399i/

Table 1 EPR parameters for the oxovanadium(IV) compounds **1**·MeOH, **2**, **3** and **4** in frozen $MeNO_2$ solutions (20 K) at X-band (microwave frequency 9.42 GHz, modulation amplitude 12.5 G, microwave power 3.2 mW)

					10^{-4} cm^{-1}			
Compound	g_x[a]	g_y[a]	g_z[a]	g_{iso}[a]	A_x[a]	A_y[a]	A_z[a]	A_{iso}[a]
1·MeOH	1.981	1.979	1.947	1.969	53.0	49.0	145.0	82.3
2	1.981	1.979	1.947	1.969	52.0	48.0	148.0	82.7
3	1.984	1.980	1.949	1.971	52.0	45.0	144.5	80.5
4	1.980	1.978	1.946	1.968	58.0	55.0	162.0	91.7

[a] Errors: g-values ± 0.002, $A_{x,y,z}$ values ± 0.5 × 10^{-4} cm^{-1}.

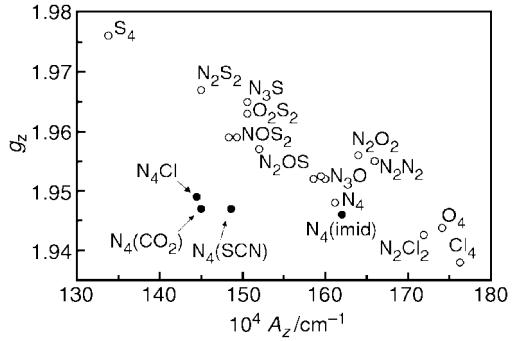

Fig. 1 A correlation plot of A_z *vs.* g_z for the $V^{IV}O^{2+}$ compounds **1**·MeOH and **2**–**4** (●) and a series of oxovanadium(IV) compounds (○) with various equatorial donor atoms.[2]

magnetic couplings between electron spins, *i.e.* line-broadening or splittings in the spectral features. $^{51}V(S = \frac{1}{2}, I = 7/2)$ EPR spectra of the oxovanadium(IV) compounds **2**, **3** and **4** are also typical of monomeric $V^{IV}O^{2+}$ compounds. The $\boldsymbol{g}$ and $\boldsymbol{A}$ tensors of **1**·MeOH and **2**–**4** were found to be rhombic (Table 1).

Fig. 1 (open circles) displays a correlation plot of g_z *vs.* A_z, for a series of known oxovanadium(IV) compounds with various equatorial donor atom sets.[2] The data lie approximately on a straight line with negative slope. This anti-correlation between g_z and A_z is well known and simply indicates that increased in-plane π- and σ-bonding results in decreased A_z values and increased g_z values.[2] Addition of the g_z and A_z values for compounds **1**·MeOH and **2**–**4** (filled circles) on the plot reveals that: (i) the points for compounds **1**·MeOH, **2** and **3** deviate substantially from the locus of the reference data. More specifically, compound **1**·MeOH[4] has an A_z value of 145 × 10^{-4} cm^{-1}, *ca.* 10% lower than the expected value of *ca.* 162 × 10^{-4} cm^{-1} for reference compounds[5] with an N_4 equatorial donor atom set. A similar reduction of the A_z values by *ca.* 8–10% is also observed for compounds **2** and **3**, (ii) in all cases, the g_z values seem to be unaltered, (iii) the A_z value for compound **4**, with imidazole in axial position, falls on the main locus as expected. The shift of the points for **1**·MeOH, **2** and **3** relative to **4**, as well as relative to the reference data, implies that the physical mechanism which determines the A_z values in compounds **1**·MeOH, **2** and **3** is not the same as in the reference compounds. In the same context, it is noted that the $A_{x,y}$ values (Table 1) in compounds **1**·MeOH, **2** and **3** are also lower than those of compound **4**.

The equatorial ligands in compounds **1**·MeOH and **2**–**4** were studied by electron spin echo envelope modulation (ESEEM) spectroscopy.[6] ESEEM is a pulsed EPR technique, eminently suited for measuring weak hyperfine couplings.[6] Orientation-selective ESEEM spectra recorded across the EPR spectrum of compound **1**·MeOH, were dominated by two sets of sharp features at 3–5 and 7–9.5 MHz. According to numerical simulations, performed as described in ref. 7, the ESEEM spectra are assigned to $^{14}N(I = 1)$-nuclei coupled to the electron spin $S = 1/2$. Two classes of almost isotropic ^{14}N-hyperfine couplings were resolved, with A_{iso} values of 5.2 and 6.1 MHz, respectively. These couplings are typical for $^{14}N(I = 1)$ atoms equatorially coordinated to $V^{IV}O^{2+}$.[1d,e] The ESEEM spectra recorded for **2**–**4** are comparable to those for **1**·MeOH, and this indicates that the equatorial coordination environment for compounds **2**–**4** is similar to the equatorial environment of **1**·MeOH, *i.e.* an N_4 donor-atom set for all complexes. Moreover, the ESEEM spectra show that in all four cases the $^{14}N(I = 1)$ hyperfine couplings are comparable, and this means that the bonding properties of the equatorial ligands in compounds **1**·MeOH and **2**–**4** are similar. Thus, the ESEEM spectra of compounds **1**·MeOH, **2** and **3** indicate that the reduction in their A_z values compared to N_4 reference complexes is not related to the nature of the equatorial ligands, but is rather due to the nature of the axial ligands.

In conclusion, a series of octahedral oxovanadium(IV) compounds, containing charged or neutral axial ligands, with the amidate molecule Hcapca was synthesized and structurally (**1**·MeOH) and spectroscopically characterized. The main effect of the monoanionic axial ligands on the A_z values of $V^{IV}O^{2+}$ compounds is their reduction by almost 10% compared to N_4 reference complexes. Thus, the present data reveal a novel phenomenon which bears strong relevance to the use of the A_z value as a predictive tool, in vanadoproteins, or $V^{IV}O^{2+}$ substituted proteins, *etc*. We are currently exploring analogous phenomena in $V^{IV}O^{2+}$-compounds with various combinations of symmetries/charges of the ligands.

Notes and references

‡ The compounds analysed satisfactorily (C, H, N, V) as **1**·CH_2Cl_2, **1**·MeOH(crystals), **2**, **3** and **4**. Compound **2** was prepared by addition of NEt_4NCS (0.4 mmol) to a stirred suspension of **1**·CH_2Cl_2 (0.4 mmol) in MeOH (5 mL). Compounds **3** and **4** were prepared in a similar way, except that MeCN and $MeNO_2$ were used as solvents for the preparation of **3** and **4**, respectively.

§ *Crystal data*: **1**·MeOH, $C_{19}H_{17}ClN_4O_3V$, M_r = 435.76, monoclinic, space group $P2_1/a$, a = 17.07(2), b = 9.82(1), c = 11.51(1) Å, β = 94.03(4)°, V = 1925(4) Å^3, Z = 4, D_C = 1.504 g cm^{-3}; T = 298 K; no. of unique reflections 2457; no. of parameters 310; $R1/wR2$ [1544 reflections with $I > 2\sigma(I)$] 0.0663/0.1453. CCDC 182/1558. See http://www.rsc.org/suppdata/cc/b0/b000399i/ for crystallographic files in .cif format.

1 (*a*) N. D. Chasteen, in *Biological Magnetic Resonance*, ed. L. Berliner and J. Reuben, Plenum, New York, 1981, vol. 3, pp. 53–119; (*b*) E. De Boer, C. P. Keijzers, A. A. K. Klaassen, E. J. Reijerse, D. Collison, C. D. Garner and R. Wever, *FEBS Lett.*, 1988, **235**, 93; (*c*) A. L. P. Houseman, L. Morgan, R. LoBrutto and W. D. Frasch, *Biochemistry*, 1994, **33**, 4910; (*d*) K. Fukui, H. Ohya-Nishiguchi and H. Kamada, *Inorg. Chem.*, 1998, **37**, 2326; (*e*) S. A. Dikanov, A. M. Tyryshkin, J. Hüttermann, R. Bogumil and H. Witzel, *J. Am. Chem. Soc.*, 1995, **117**, 4976; (*f*) R. LoBrutto, B. J. Hamstra, G. J. Colpas, V. L. Pecoraro and W. D. Frasch, *J. Am. Chem. Soc.*, 1998, **120**, 4410.

2 A. J. Tasiopoulos, A. N. Troganis, A. Evangelou, C. P. Raptopoulou, A. Terzis, Y. Deligiannakis, T. A. Kabanos, *Chem. Eur. J.*, 1999, **5**, 910 and references therein.

3 L. J. Calviou, J. M. Arber, D. Collison, C. D. Garner and W. Clegg, *J. Chem. Soc., Chem. Commun.*, 1992, 654; M. Mohan, M. R. Bond, T. Otieno and C. J. Carrano, *Inorg. Chem.*, 1995, **34**, 1233.

4 There are two compounds in the literature (ref. 3) containing the unit *trans*-[V(=O)Cl] and having N_4 equatorial donor atom sets, namely: $[VOCl(1\text{-vinylimidazole})_4)]^+$ and $[VOCl(pyrazole)_4]^+$ with A_z values of 162 and 176 × 10^{-4} cm^{-1}, respectively. The A_z value for compound $[VOCl(pyrazole)_4]^+$ is characteristic of an equatorial donor set dominated by oxygens, most likely indicating decomposition of the complex in the solvent system (water–glycerine) used. The A_z value for $[VOCl(1\text{-vinylimidazole})_4)]^+$ is in the expected range for an N_4 equatorial donor atom system.[5]

5 D. Sanna, G. Micera, L. S. Erre, M. G. Molinu and E. Garribba, *J. Chem. Res. S.*, 1996, 40; S. G. Brand, N. Edelstein, C. J. Hawkins, G. Shalimoff, M. R. Snow and E. R. T. Tiekink, *Inorg. Chem.*, 1990, **29**, 434.

6 S. A. Dikanov and Y. D. Tsvetkov, *Electron Spin Echo Envelope Modulation* (*ESEEM*) *Spectroscopy*, CRC Press, Boca Raton, FL, 1992.

7 Y. Deligiannakis and A. W. Rutherford, *J. Am. Chem. Soc.*, 1997, **119**, 4471.

Communication b000399i

ChemComm

Synthesis and gas permeation properties of an NaA zeolite membrane

Xiaochun Xu,[a] Weishen Yang,*[a] Jie Liu,[a] Xiaobo Chen,[a] Liwu Lin,[a] Norbert Stroh[b] and Herwig Brunner[b]

[a] *State Key Laboratory of Catalysis, Dalian Institute of Chemical Physics, Chinese Academy of Sciences, Dalian 116023, China. E-mail: yangws@ms.dicp.ac.cn*

[b] *Fraunhofer Institute for Interfacial Engineering and Biotechnology, Nobelstrasse 12, Stuttgart D-70569, Germany*

Received (in Cambridge, UK) 17th January 2000, Accepted 2nd March 2000

A high quality NaA zeolite membrane, which shows a H_2/n-C_4H_{10} permselectivity of 106, has been synthesized on a seeded α-Al_2O_3 support by a multistage synthesis method.

The synthesis of zeolite membranes and their application in separation and catalysis have attracted great interest in recent years.[1,2] For gas separation, most studies have concentrated on MFI type (silicalite-1 and ZSM-5) zeolite membranes. Although high separation factors were obtained for mixtures of organic gases,[3–6] MFI zeolite membranes do not show good separation performance for permanent gases or permanent gas/organic gas mixtures because of the large pore size and hydrophobic nature of the zeolite. Thus the investigation of zeolite membranes with small pore size has attracted much attention.[7–9] NaA zeolite has a smaller pore size (0.41 nm) than that of MFI zeolite (*ca.* 0.55 nm). However, most studies on NaA zeolite membranes focused on the dehydration of liquid mixtures by pervaporation[10,11] and few gas permeation results were reported.[9,12] Furthermore, it was shown, from the gas permeation results,[9,12] that the quality of these NaA zeolite membranes was poor. Here, a high quality NaA zeolite membrane has been synthesized on a seeded α-Al_2O_3 support by a multistage synthesis method.

A self-made porous α-Al_2O_3 disk (30 mm in diameter, 3 mm in thickness, 0.1–0.3 μm pore radius, *ca.* 50% porosity) was used as the support. Before synthesis, one side of the support was coated with NaA zeolite crystals as nucleation seeds by dipping the support in a 0.5 wt% NaA zeolite suspension in a single step for 30 s. The 0.5 wt% NaA zeolite suspension was prepared by peptizing 0.5 g NaA zeolite in 100 ml deionized water. In order to form a thin and uniform NaA zeolite membrane on the support surface and to inhibit the formation of zeolite in the pores of the support, a uniformly sized NaA zeolite of dimensions *ca.* 1 μm, larger than those of the pores of the support, was used as the seed. The synthesis mixture was prepared by mixing sodium aluminate, water glass, sodium hydroxide and water. The molar ratio of the resultant gel mixture was $3Na_2O:2SiO_2:Al_2O_3:200H_2O$. The synthesis was carried out at 90 °C for 24 h in a stainless steel autoclave with the seeded support held vertically in the synthesis mixture by a Teflon holder. After the synthesis, the composite membrane was washed several times with water until the pH of the washings was neutral, then dried at 150 °C for 3 h. In order to obtain a high quality NaA zeolite membrane, the synthesis was repeated twice more (in all, a three-stage synthesis). The as-synthesized membrane was characterized by X-ray diffraction (XRD), scanning electron microscopy (SEM) and gas permeation studies. The permeances of the gases were measured at different temperatures by a soap-film flowmeter under a pressure difference of 0.10 MPa. The permselectivity of A/B is defined as the permeance ratio of gas A to gas B.

The XRD pattern of the as-synthesized membrane prepared by the three-stage synthesis is shown in Fig. 1. The diffraction pattern of the as-synthesized membrane is represented by the sum of the peaks of the α-Al_2O_3 support and the NaA zeolite, which indicated that the membrane formed on the α-Al_2O_3 support is an NaA zeolite membrane. The variation of the intensity of the diffraction patterns of the NaA zeolite is possibly caused by the orientation of the zeolite crystals on the support surface. From the SEM images (Fig. 2), it can be seen that the surface of the α-Al_2O_3 support is completely covered with NaA zeolite crystals and the crystals are highly intergrown. A continuous membrane was formed on the support surface and the thickness of the zeolite membrane is *ca.* 18 μm. In addition, the zeolite membrane remained firmly bonded to the support surface even after 15 min of vigorous ultrasonic vibration. However, XRD and SEM characterization can only indicate

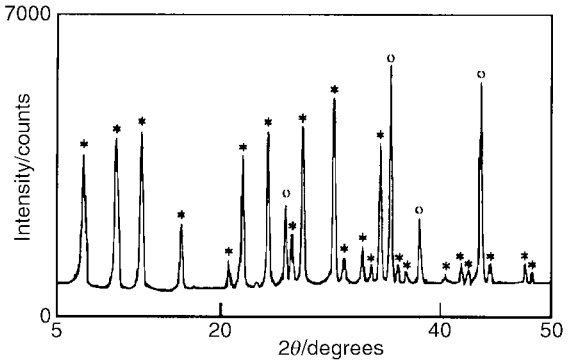

Fig. 1 XRD pattern of the NaA zeolite membrane: (○) α-Al_2O_3, (∗) NaA zeolite.

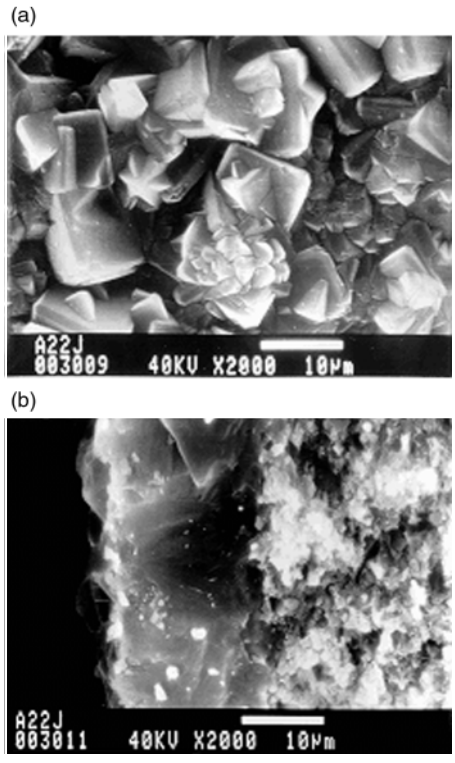

Fig. 2 SEM images of the NaA zeolite membrane: (a) top view, (b) cross-section.

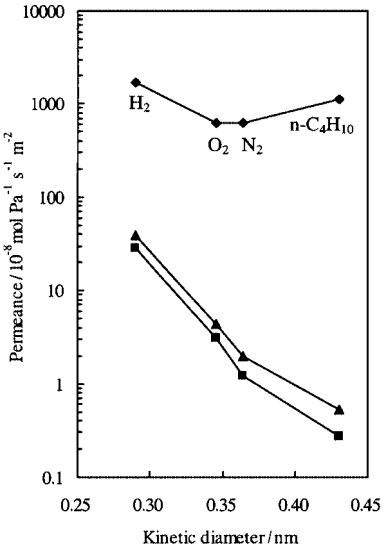

Fig. 3 Gas permeation properties of the seeded α-Al_2O_3 support (◆), the NaA zeolite membrane at 298 K (■) and the NaA zeolite membrane at 423 K (▲).

whether a continuous membrane is formed on the support, and can not confirm whether a defect-free zeolite membrane is formed. Such a property of the zeolite membrane can only be evaluated by gas permeation.[5] Taking into the consideration the opening pore size of the NaA zeolite channels and the hydrophilic nature of the NaA zeolite, the permselectivities of H_2/n-C_4H_{10} and O_2/N_2 were selected as the yardstick of the quality of the NaA zeolite membrane. Since the kinetic diameter of n-C_4H_{10} (0.43 nm) is larger than the pore size of the NaA zeolite (0.41 nm), n-C_4H_{10} should not permeate through a defect-free NaA zeolite membrane; the higher the permselectivity of H_2/n-C_4H_{10}, the more perfect is the NaA zeolite membrane. If the permselectivity of H_2/n-C_4H_{10} is near to or smaller than the Knudsen diffusion ratio of 5.39, large defects must be present in the NaA zeolite membrane. Since the kinetic diameter of O_2 (0.346 nm) is smaller than that of N_2 (0.364 nm), the permeance of O_2 should be higher than that of N_2 through a defect-free NaA zeolite membrane which is the reverse of the Knudsen diffusion ratio of 0.96 for a mesoporous membrane. Fig. 3 shows the gas permeation results of the NaA zeolite membrane. The permeances of H_2, N_2 and O_2 of the supported NaA zeolite membrane decreased by two orders of magnitude compared with those of the α-Al_2O_3 support, which indicated that a compact zeolite membrane was formed on the porous α-Al_2O_3 support. With an increase of the molecular kinetic diameter, the permeances of the gases decreased, which showed the molecular sieving effect of the NaA zeolite. At 298 K, the permeance of O_2 was 2.61 times higher than that of N_2, which is the reverse of that of the Knudsen diffusion ratio of 0.96. The permselectivity of H_2/n-C_4H_{10} was 106, a value much higher than that of the Knudsen diffusion ratio of 5.39, which indicated that a high quality NaA zeolite membrane was formed on the support surface. Compared with the gas permeation results of NaA zeolite membranes in the literature,[9,12] the NaA zeolite membrane synthesized in this study showed a very high H_2/n-C_4H_{10} permselectivity. The reason for the formation of the high quality NaA zeolite membrane may arise from the use of uniformly sized seeds and is still under investigation. With an increase of the permeation temperature, the permeance of the gases increased. However, the permselectivity of H_2/n-C_4H_{10} and O_2/N_2 at 423 K decreased to 73.2 and 2.22, respectively.

In conclusion, a high quality NaA zeolite membrane was successfully synthesized on a seeded α-Al_2O_3 support by a multistage synthesis method. The permeation of n-C_4H_{10} indicated that the NaA zeolite membrane had intercrystalline pores larger than those of the NaA zeolite channels. The permeance of the NaA zeolite membrane was also relatively low. Methods for the preparation of high permeance or virtually perfect NaA zeolite membranes are under investigation.

We gratefully acknowledge funding from the National Science Foundation of China (59789201) and the National Advanced Materials Committee of China (715-006-0120).

Notes and references

1 A. Tavolaro and E. Drioli, *Adv. Mater.*, 1999, **11**, 975.
2 J. C. Jansen, J. H. Koegler, H. van Bekkum, H. P. A. Calis, C. M. van den Bleek, F. Kapteijn, J. A. Moulijn, E. R. Geus and N. van der Puil, *Microporous Mesoporous Mater.*, 1998, **21**, 213.
3 Y. Yan, M. E. Davis and G. R. Gavalas, *Ind. Eng. Chem. Res.*, 1995, **34**, 1652.
4 Z. A. E. P. Vroon, K. Keizer, M. J. Gilde, H. Verweij and A. J. Burggraaf, *J. Membr. Sci.*, 1996, **113**, 293.
5 X. C. Xu, M. J. Cheng, W. S. Yang and L. W. Lin, *Sci. China Ser. B*, 1998, **41**, 325.
6 J. M. Van de Graaf, F. Kapteijn and J. A. Moulijn, *J. Membr. Sci.*, 1998, **144**, 87.
7 J. Dong and Y. S. Lin, *Ind. Eng. Chem. Res.*, 1998, **37**, 2404.
8 J. C. Poshusta, V. A. Tuan, J. L. Falconer and R. D. Noble, *Ind. Eng. Chem. Res.*, 1998, **37**, 3924.
9 K. Aoki, K. Kusakabe and S. Morooka, *J. Membr. Sci.*, 1998, **141**, 197.
10 J. J. Jafar and M. Budd, *Microporous Mesoporous Mater.*, 1997, **12**, 305.
11 H. Kita, K. Horii, Y. Ohtoshi, K. Tanaka and K.-I. Okamoto, *J. Mater. Sci. Lett.*, 1995, **14**, 206.
12 J. Wang, Y. Wang, S. Fan and X. Shi, *Proc. 3rd Int. Conf. Inorg. Membr.*, Worcester, MA, 1994.

Communication b000478m

ChemComm

A novel immobilised cobalt(III) oxidation catalyst†

Birinchi K. Das‡ and James H. Clark*

Clean Technology Centre, Department of Chemistry, University of York, York, UK YO10 5DD. E-mail: jhc1@york.ac.uk

Received (in Liverpool, UK) 19th January 2000, Accepted 25th February 2000

A complex form of cobalt(III) has been successfully immobilised on a chemically modified silica and proven to be an active catalyst for the selective oxidation of alkylaromatics using air as the source of oxygen and in the absence of solvent.

Cobalt salts are widely used as catalysts in the liquid phase oxidation of alkylaromatics.[1] Reactions are normally carried out in acetic acid as solvent and in the presence of a promoter such as a bromide. It has been reported that under such reaction conditions, the aerial oxidation of Co(II) to Co(III) is a slow process[2] although this can be accelerated by the addition of bases such as pyridine which stabilises the higher oxidation state of the metal.[3] The heterogenisation of catalysts and their use in the oxidation of neat substrates are subjects of considerable interest especially in these environmentally conscious days when solvent losses and catalyst losses on separation can lead to unacceptable levels of waste.[4] Several heterogeneous metal catalysts have been designed for aerial oxidation reactions[5] but limited activities and questionable stabilities[6] have delayed their commercial exploitation. It seemed to us that if we could design a heterogeneous system that favours and stabilises Co(III), this should enhance rates of reaction where the Co(II) to Co(III) step was rate limiting and should increase catalyst stability owing to the relative substitutional inertness of Co(III). Here, we report our preliminary results from designing such a catalyst that can indeed be successfully used to catalyse the aerial oxidation of alkylaromatics in the absence of solvents.

The novel catalyst is based on a chemically modified porous silica.[7,8] Cyanoethyl-silica was prepared from the sol–gel reaction of tetraethylorthosilicate (196 mmol) and cyanoethyltriethoxysilane (98 mmol) in aqueous ethanol in the presence of *N*-dodecylamine as the templating agent. The resulting precipitate was washed with boiling ethanol to remove the template and then treated with hot aqueous H_2SO_4 so as to hydrolyse the CN group to CO_2H.[9] The resulting silica-$(CH_2)_2CO_2H$ material was washed with water and ethanol and then dried at 110 °C before use as a support for the Co(III) complex. Pyridine (40 mmol) was added dropwise to a mixture of the silica material (5g), $Co(NO_3)_2{\cdot}6H_2O$ (20 mmol), and sodium acetate (40 mmol) in water (100 ml). Complexation of the cobalt to the support only occurs on addition of the pyridine as witnessed by the purple colour of the solid particles. After adding more water (50 ml), the mixture was heated to boiling and dilute hydrogen peroxide (80 mmol) was slowly added over 8 h. This resulted in the apparent oxidation of the immobilised cobalt with a change in colour of the solid particles from purple to olive green. It is necessary to treat the supported metal complex with peroxide so as to form the immobilised Co(III). This solid was separated by filtration, thoroughly washed with water and acetone and then dried at 110 °C.

While the precise structure of the surface-bound cobalt complex is as yet unknown we have carried out a number of analytical studies to gain information on the cobalt loading and distribution, the material structure and the surface species (Table 1). Atomic absorption analysis of the digested material gives a cobalt loading of 0.68 mmol g^{-1}. Optical and scanning electron microscopic studies on the material reveal a homogeneous mass with elemental analysis (EDAX) carried out at randomly selected spots showing a consistent Co : Si ratio of *ca.* 1 : 7. This suggests an evenly distributed cobalt complex rather than a simple mixture of a cobalt complex with the silica. The BET isotherms for the supported Co(III) complex and the intermediate silica-$(CH_2)_2CO_2H$ material have almost identical appearances and suggest a mixture of micropores and mesopores. The BJH pore size distributions of these materials show *ca.* 65 and 80%, respectively, of the pore volumes are due to pores with diameters of < 6 nm. The surface area is also reduced on going from the intermediate supported carboxylic acid to the final supported metal complex (from 1041 to 528 $m^2\ g^{-1}$) although it is still very high compared to more traditional supported reagents.[10,11] These results are consistent with a reasonably homogeneous build-up in the surface species as the metal complex is formed. The powder X-ray diffraction pattern of the supported Co(III) material shows a weak peak at < 2° with the strongest peak at 2θ *ca.* 22.5° consistent with a lack of long range order as expected for materials of this type.[8,10] Diffuse reflectance FTIR (DRIFTS) of the final material reveals bands characteristic of surface bound CO_2^-, pyridine and acetate. The difference in the wavenumbers of the symmetric and asymmetric stretching vibrations of the acetato ligand carboxyl group (125 cm^{-1}) is consistent with these ligands bonding in a bridging fashion. The diffuse reflectance UV–VIS spectrum of the final material shows an ill-defined absorption maximum at *ca.* 580 nm in contrast to the strong band at 545 nm for the material before treatment with hydrogen peroxide. This is consistent with a change from Co(II) to Co(III) on peroxide treatment. Furthermore, by carrying out a similar complex preparation but in the absence of the support material, the final cobalt complex, believed to contain the cation $[Co_3(\mu_3\text{-}O)(\mu\text{-}O_2CR)_6(py)_3]^+$ [12] (ClO_4^- as counter anion) gives an olive green complex with a very similar UV–VIS spectrum. The measured C : N ratio of 12 : 1 in the final material is consistent with the presence of a similar complex rather than a simple species containing two pyridines and two carboxylato ligands per cobalt atom (for which the C : N ratio would be 7 : 1)

Table 1 Physical data for the supported Co(III) complex

	HMS–Co(III) complex	HMS–CO_2H
BET surface area/$m^2\ g^{-1}$	528	1041
Pore volume/$cm^3\ g^{-1}$	0.315	0.688
Co : Si ratio (EDAX)	1 : 7	—
Co loading (AAS)/mmol g^{-1}	0.68	0
λ_{max}(UV–VIS)/nm	580	—

The supported cobalt(III) reagent was tested as a catalyst in the aerial oxidation of neat ethylbenzene, chlorotoluene and toluene as representative alkylbenzenes (Table 2). Reactions were carried out at atmospheric pressure with 400 ml of substrate and 0.8 g of the catalyst in a baffled glass reactor with a overhead stirrer operating at 700 rpm, an air feed at 400 ml min^{-1}, chilled water condensers and twin Dean–Stark separators to remove the water produced during the reactions. Reactions could be monitored both by the amount of water

† UK Patent application, 1999.

‡ Current address: Department of Chemistry, Gauhati University, Guwahati 781 014, India.

DOI: 10.1039/b000535p

Table 2 Catalytic oxidations of alkylaromatics using the supported Co(III) complex (0.8 g) in neat substrate (400 ml) at atmospheric pressure for 22 h

Substrate	*T*/°C	Product (isolated yield%)[a]
PhEt	130	PhCOMe (70)
4-ClC_6H_4Me	130	4-$ClC_6H_4CO_2H$ (25)
PhMe[b]	100	$PhCO_2H$ (6)

[a] Purified (> 99%) product. [b] 1% added PhCHO which remains constant.

produced and by GC/GC–MS. Ethylbenzene was converted to acetophenone at a rate of *ca*. 4% h^{-1} at 130 °C, and with no induction period (in contrast to other reports of heterogeneously catalysed aerial oxidations[13]). The absence of an induction period may be due to the metal existing in its higher oxidation state at the beginning of the reaction. After 22 h a remarkable 76% of the ethylbenzene had been oxidised with selectivity to acetophenone of 94%, the remainder being benzoic acid. An isolated yield of 70% acetophenone can be obtained. We believe that this is the highest reported yield of acetophenone obtained from a heterogeneous oxidation of ethylbenzene.[5,14] Previous reports have shown that conversions of > 60% are very difficult to achieve with neat substrate and this has been linked to the rate limiting adsorption of the relatively non-polar ethylbenzene from an increasingly acetophenone-rich mixture.[5,13] Here the rate of oxidation is almost linear up to *ca*. 70% conversion and this may be a result of the relatively organophilic surface of the new catalyst facilitating the adsorption–desorption processes. Under the same conditions a 25% isolated yield of pure 4-chlorobenzoic acid was obtained from the oxidation of neat 4-chlorotoluene after 22 h simply by filtering the solid product from the cooled final reaction mixture and washing it with light petroleum. No other products were observed. This oxidation occurred at over twice the rate of comparable reactions reported elsewhere.[5,13] We were also able to achieve a small but significant rate of oxidation for toluene itself. At 100 °C and in the presence of a small amount of benzaldehyde (1% by volume) as a promoter,[5] we obtained an isolated yield of recrystallised benzoic acid of 6% after 22 h reaction (the 1% benzaldehyde remains almost constant throughout the reaction). This is again a marked improvement in reaction rate compared to similar systems.[5] In none of these reactions was leached cobalt detectable by atomic absorption spectroscopy in the organic liquors and the amount of cobalt measured in the catalyst (after digestion) was always unchanged. However, our first attempts to reuse the catalysts failed. Closer analysis of the used catalysts showed that there had been a complete loss of pyridine during reaction although the cobalt was still present. By adding a small amount of pyridine (0.48 g) to any of the substrate–used catalyst reaction systems, or by treatment of recovered catalyst with pyridine, the rate of reaction returned to close to the original value and very similar levels of substrate oxidation and conversions to product were achieved. The facile loss of pyridine from the catalyst at elevated temperatures was confirmed from thermal analysis on the material under nitrogen which shows loss of pyridine at *ca*. 150–200 °C with decomposition of the remaining catalyst structure starting at > 300 °C. We are now investigating methods for stabilising the catalyst notably the replacement of pyridine by a less volatile nitrogen base.

We gratefully acknowledge the support of the Commonwealth Institute for a Fellowship to B. K. D. and the RAEng.-EPSRC for a Clean Technology Fellowship to J. H. C., as well as the support and advice of the York Green Chemistry group.

Notes and references

1 P. Raghavendrachar and S. Ramachandran, *Ind. Eng. Chem. Res. Dev.*, 1992, **31**, 453.
2 R. A. Sheldon and J. A. Kochi, *Metal Catalysed Oxidations of Organic Compounds*, Academic Press, New York, 1981.
3 M. Hronec and J. Ilavsky, *Oxid. Commun.*, 1983, **3**, 303.
4 J. H. Clark, *Green Chem.*, 1999, **1**, 1.
5 J. S. Rafelt and J. H. Clark, *Catal. Today*, 2000, in press.
6 H. E. Lempers and R. A. Sheldon, *J. Catal.*, 1998, **175**, 62.
7 J. H. Clark and D. J. Macquarrie, *Chem. Commun.*, 1998, 853.
8 P. M. Price, J. H. Clark and D. J. Macquarrie, *J. Chem. Soc., Dalton Trans.*, 2000, 101.
9 A. Butterworth, J. H. Clark, P. H. Walton and S. J. Barlow, *Chem. Commun.*, 1996, 1859.
10 D. J. Macquarrie, *Philos. Trans. A*, 2000, in press.
11 J. H. Clark, A. P. Kybett and D. J. Macquarrie, *Supported Reagents: Preparation, Analysis and Applications*, VCH, New York, 1992.
12 C. E. Sumner Jr. and G. R. Steinmetz, *Inorg. Chem.*, 1989, **28**, 4290.
13 I. C. Chisem, J. Rafelt, M. Tantoh Shieh, J. Chisem, J. H. Clark, R. Jachuck, D. J. Macquarrie, C. Ramshaw and K. Scott, *Chem. Commun.*, 1998, 1949.
14 I. C. Chisem, K. Martin, M. Tantoh Shieh, J. Chisem, J. H. Clark, R. Jachuck, D. J. Macquarrie, J. Rafelt, C. Ramshaw and K. Scott, *Org. Proc. Res. Dev.*, 1997, **1**, 365.

Communication b000535p

Rapid syntheses of difluorinated dihydropyrans

Jonathan M. Percy* and Stéphane Pintat

School of Chemistry, University of Birmingham, Edgbaston, Birmingham, UK B15 2TT.
E-mail: jmpercy@chemistry.bham.ac.uk

Received (in Liverpool, UK) 4th January 2000, Accepted 15th February 2000

A very short reaction sequence opens with metal-mediated addition of commercial bromodifluoropropene to aldehydes; allylation under phase transfer catalysed conditions sets the stage for a ring closing metathesis (RCM) in the presence of commercial Grubbs' catalyst to afford potentially useful difluorinated dihydropyrans.

Difluorinated carbohydrate analogues are normally prepared by DAST [(diethylamino)sulfur trifluoride] difluorination of highly protected precursors in which a ketonic carbonyl group has been isolated, chemistry which is highly vulnerable to stereoelectronic effects as demonstrated many times by Castillón and coworkers.[1] Even when such difficulties have been overcome, the hazardous nature of the DAST reagent precludes scale-up, while safer versions of the reagent sacrifice reactivity in the cause of thermal stability.[2] Building block chemistry then appears most attractive and the Reformatsky reaction of ethyl bromodifluoroacetate with aldehydes and other electrophiles is a well-worked and productive theme.[3] Our own approaches have relied on metallated difluoroenol derivatives fashioned *in situ* from trifluoroethanol but we were struck by the simplicity of a possible RCM-based approach.[4] Scheme 1 shows the analysis; the route closely follows that published recently by Carda *et al.*[5] but forms the first instance where RCM technology has been used for the synthesis of ring-fluorinated heterocycles.

Initially, we were interested in the reproducibility of the allylindium chemistry described by Momose and coworkers[6] in which bromodifluoropropene adds very smoothly to aldehydes. With the homoallyl alcohols in hand, we would perform an allylation and then expose the allyl homoallyl ether to an RCM catalyst. Both alkenes are made less electron rich by electron-withdrawing substitutents at the allyl position and we were concerned that the overall cycle would be slow and that metallo-[2 + 2] cycloaddition in the fluorinated allyl system could result in β-fluoride elimination with concomitant formation of a strong metal–fluorine bond destroying the catalyst.

In the event, our fears were groundless. The allylindium chemistry was highly reproducible and homoallyl alcohols **2a**–**d** were synthesised in moderate to high (57–80%) yield (Scheme 2).

The reactions worked best when the suspensions were shaken or sonicated, and purification was facile.[7] We also explored the replacement of the indium metal with 325-mesh zinc under the conditions described by Wilson and Guazzaroni (saturated NH_4Cl, THF).[8] The zinc-mediated reaction[9] was much more effective in the case of benzaldehyde, affording the homoallyl alcohol **2b** in 84% yield, but less effective (37%) when the more interesting and electrophilic benzyloxyacetaldehyde **1d** was present, despite our observation of an extremely clean ^{19}F NMR spectrum from the crude material. Pinacol coupling of the aldehyde may be responsible for the low yield though we did not isolate any products of this type.

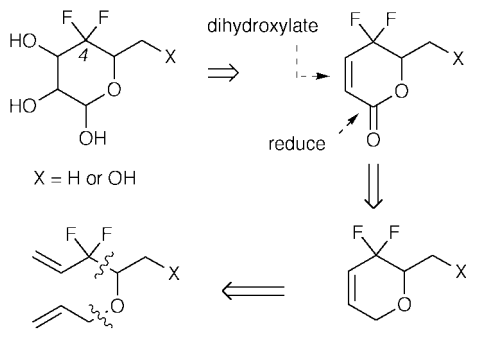

Scheme 1

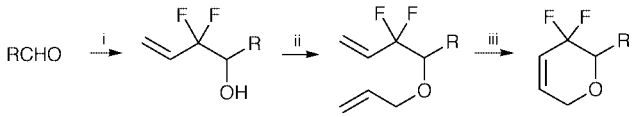

1a, R = Bu^n	**2a** 57%	**3a** 98%	**4a** 56%
1b, R = Ph	**2b** 57%	**3b** 99%	**4b** 57%
1c, R = 2-furyl	**2c** 77%	**3c** 99%	**4c** 81%
1d, R = CH_2OBn	**2d** 80%	**3d** 99%	**4d** 97%

Scheme 2 *Reagents and conditions*: i, $H_2C{=}CHCF_2Br$, In, DMF, sonication, room temp.; ii, $H_2C{=}CHCH_2Br$, NaOH, CH_2Cl_2, Bu_4NHSO_4, room temp.; iii, 5 mol% Grubbs' catalyst, CH_2Cl_2, rt, 24 h.

Allylation[10] was trouble-free as was the RCM reaction[11] at room temperature in dichloromethane, though reaction times of 24 h were required to consume the starting material entirely.

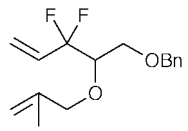

5

The methallyl ether **5** prepared by an analogous sequence failed to cyclise at all under these conditions suggesting that the additional steric hindrance imposed by a methyl group is enough to prevent coordination and stop the cycle. Dihydropyran **4d**, formed in a particularly high isolated and purified yield is of the type identified in the analysis, while **4c** is potentially interesting for the synthesis of higher sugars and related species; we are continuing to explore the scope of the reaction more fully. This short study clearly shows how potentially important oxygen heterocycles can be assembled in an extremely concise manner using off-the-shelf reagents.

We wish to thank the EPSRC (GR/K84882) and the University of Birmingham for financial support and Dr Philip Walker (Fluorochem Ltd.) for a generous gift of 1-bromo-1,1-difluoropropene.

Notes and references

1 M. I. Barrena, M. I. Matheu and S. Castillón, *J. Org. Chem.*, 1998, **63**, 2184; R. Fernández and S. Castillón, *Tetrahedron*, 1999, **55**, 8497.
2 G. S. Lal, G. P. Pez, R. J. Pesaresi, F. M. Prozonic and H. Cheng, *J. Org. Chem.*, 1999, **64**, 7048.
3 For a full discussion of two-carbon fluorinated building blocks, see: J. M. Percy, *Top. Curr. Chem.*, 1997, **193**, 131.
4 R. H. Grubbs and S. Chang, *Tetrahedron*, 1998, **54**, 4413. For a recent and most attractive approach to cyclitols, see: L. Hyldtoft, C. S. Poulsen and R. Madsen, *Chem. Commun.*, 1999, 2101.

5 M. Carda, E. Castillo, S. Rodríguez, S. Uriel and J. A. Marco, *Synlett*, 1999, 1639.
6 M. Kirihara, T. Takuwa, S. Takizawa and T. Momose, *Tetrahedron Lett.*, 1997, **38**, 2853.
7 *Preparation*: of **2d**: 1-bromo-1,1-difluoropropene (0.76 ml, 7.5 mmol) and benzyloxyacetaldehyde (0.70 ml, 5.0 mmol) were added to a sonicated suspension of indium powder (0.86 mg) in DMF (20 ml). The mixture was sonicated at room temperature for 5 h then quenched with 1 M HCl (10 ml). Extractive work up afforded a yellow oil which was purified by column chromatography [30% diethyl ether–light petroleum (bp 40–60 °C)] to afford **2d** as a pale yellow oil (0.91 g, 80%) (R_f = 0.23). ^{1}H NMR ($CDCl_3$, 300 MHz) δ 7.40–7.28 (m, 5H), 6.09–5.81 (m, 1H), 5.72 (dt, 1H, $^3J_{H-H_{trans}}$ 17.5, $^4J_{H-F}$ 2.6 Hz), 5.52 (d, 1H, $^3J_{H-H_{cis}}$ 11.0 Hz), 4.6 (s, 2H), 4.10–3.98 (m, 1H), 3.71 (dd, 1H, first half of an AB quartet, $^2J_{H-H}$ = 9.9, $^3J_{H-H}$ 3.3 Hz), 3.59 (dd, 1H, second half of an AB quartet, $^2J_{H-H}$ 9.9, $^3J_{H-H}$ 7.0 Hz), 2.76 (d, 1H, $^3J_{H-H}$ 5.2 Hz); ^{13}C NMR ($CDCl_3$, 75 MHz) δ 137.3, 129.9 (t, $^2J_{C-F}$ 25.5 Hz), 128.4, 127.9, 127.7, 120.9 (t, $^3J_{C-F}$ 9.5 Hz), 119.1 (t, $^1J_{C-F}$ 273.7 Hz), 73.6, 72.2 (t, $^2J_{C-F}$ 33.6 Hz), 68.6; ^{19}F NMR ($CDCl_3$, 282 MHz) δ −107.3 (dt, 1F, first half of an AB quartet, $^2J_{F-F}$ 251.8, $^3J_{F-H}$ 10.5 Hz), −111.3 (dt, 1F, second half of an AB quartet, $^2J_{F-F}$ 251.8, $^3J_{F-H}$ 11.1 Hz); *m/z* (ES) 251 (M + Na, 100); HRMS calc. for $C_{12}H_{14}O_2F_2Na$ 251.0860, found 251.0872.
8 S. R. Wilson and M. E. Guazzaroni, *J. Org. Chem.*, 1989, **54**, 3087.
9 For other difluoroallylation methods or building blocks, see: Z-Y. Yang and D. J. Burton, *J. Org. Chem.*, 1991, **56**, 1037; J. Gonzalez, M. J. Foti and S. Elsheimer, *Org. Synth.*, 1995, **72**, 225; M. Fujita, M. Obayashi and T. Hiyama, *Tetrahedron*, 1988, **44**, 4135.
10 M. Schlosser and S. Strunk, *Tetrahedron*, 1989, **45**, 2649.
11 *Preparation* of **4d**: a mixture of allyl homoallyl ether **3d** (403 mg, 1.5 mmol) and Grubbs' catalyst (62 mg, 5 mol%) in dry degassed DCM was stirred for 24 h under an atmosphere of nitrogen. The mixture was concentrated *in vacuo* to give a black oil. Purification by column chromatography using 5% diethyl ether–light petroleum ether (bp 40–60 °C) as eluent, afforded **4d** as a pale yellow oil (350 mg, 97%) (R_f = 0.30). ^{1}H NMR ($CDCl_3$, 300 MHz) δ 7.33–7.27 (m, 5H), 6.30–6.24 (m, 1H), 5.95–5.86 (m, 1H), 4.67 (d, 1H, first half of an AB quartet, $^2J_{H-H}$ 12.1 Hz), 4.59 (d, 1H, second half of an AB quartet, $^2J_{H-H}$ 12.1 Hz), 4.37, 4.18 (m, 2H), 3.98–3.94 (m, 1H), 3.90 (dd, 1H, first half of an AB quartet, $^2J_{H-H}$ 10.8, $^3J_{H-H}$ 2.4 Hz), 3.71 (dd, 1H, second half of an AB quartet, $^2J_{H-H}$ 10.8, $^3J_{H-H}$ 7.9 Hz); ^{13}C NMR ($CDCl_3$, 75 MHz) δ 137.8, 135.7 (t, $^3J_{C-F}$ 9.0 Hz), 128.5, 127.9, 121.4 (t, $^2J_{C-F}$ 28.0 Hz), 113.9 (dd, $^1J_{C-F}$ 243.0, 235.7 Hz), 77.0 (d, $^2J_{C-F}$, 30.5 Hz), 73.8, 67.1 (d, $^3J_{C-F}$, 5.7 Hz), 65.2; ^{19}F NMR ($CDCl_3$, 282 MHz) δ −105.6 (ddt, 1F, first half of an AB quartet, $^2J_{F-F}$ 274.0, $^3J_{F-H}$ 17.8, 8.9, $^4J_{F-H}$ = 8.9 Hz), −107.7 (br d, $^2J_{F-F}$ 274.0, $^3J_{F-H}$ 4.4 Hz); *m/z* (ES) 263 (M + Na, 100); HRMS calc. for $C_{13}H_{14}O_2F_2Na$ 263.0860, found 263.0853.

Communication b000006j

ChemComm

Synthesis and spectroscopic characterisation of *all* the intermediates in the Pd-catalysed methoxycarbonylation of ethene

Graham R. Eastham,[a] Brian T. Heaton,*[b] Jonathan A. Iggo,[b] Robert P. Tooze,[a] Robin Whyman[b] and Stefano Zacchini[b]

[a] *Ineos Acrylics, PO Box 90, Wilton, Middlesborough, Cleveland, UK TS90 8JE*
[b] *Chemistry Department, University of Liverpool, Liverpool, UK L69 7ZD. E-mail: amf@liv.ac.uk*

Received (in Cambridge, UK) 14th January 2000, Accepted 28th February 2000

The pathway of the palladium catalysed methoxycarbonylation of ethene to methyl propanoate has been shown to occur *via* a hydride rather than a methoxycarbonyl cycle and *all* the intermediates in this cycle have been unambiguously identified by multinuclear NMR spectroscopy and ^{13}C-labelling.

The alkoxycarbonylation of alkenes is of increasing scientific and technological importance. This reaction can give rise to a broad spectrum of products; for ethene, this can range from high melting thermoplastic polymers—the so called 'polyketones' to low boiling liquids such as methyl propanoate. The former materials have attracted more attention in the literature as they have been developed into commercial products.[1] Our work focuses on methyl propanoate, a key intermediate in the manufacture of methyl methacrylate, an important monomer produced annually on a multi-million tonne scale world wide.[2]

A new catalyst for the production of methyl propanoate (MeP) *via* the palladium catalysed methoxycarbonylation of ethene has recently been reported.[3] The catalyst, generated *in situ via* the reaction of [Pd(L–L)(dba)] [L–L = 1,2-$(CH_2PBu^t_2)_2C_6H_4$; dba = *trans*,*trans*-$(PhCH{=}CH)_2CO$] with *e.g.* methanesulfonic acid, gives MeP with a selectivity of 99.98% at a production rate of 50 000 mol product (mol Pd)$^{-1}$ h^{-1} under very mild conditions (353 K and 10 atm pressure of CO–C_2H_4). Two alternative mechanistic pathways have been proposed for this type of reaction, *i.e.* a hydride or a methoxy cycle (**A** and **B** respectively in Scheme 1).[1] Here, we report an investigation which provides unambiguous spectroscopic evidence for *all* the intermediates in the *hydride* catalytic cycle (**A** in Scheme 1).

The complex [Pd(L–L)(dba)] reacts in MeOH with HBF_4 or CF_3SO_3H in the presence of oxygen or benzoquinone (BQ) to give selectively a new compound, which can be formulated as either the neutral complex [Pd(L–L)HX] {X = $[BF_4]^-$ **1a**, X = $[CF_3SO_3]^-$ **1b**} or the solvento-cation [Pd(L–L)H(MeOH)]X {X = $[BF_4]^-$ **2a**, X = $[CF_3SO_3]^-$, **2b**}. We prefer the cationic formulation **2** since variable temperature ^{31}P and ^{1}H NMR spectra of the products resulting from the reaction with HBF_4 do not show any coupling to fluorine. Furthermore, the ^{31}P{^{1}H}, ^{31}P and ^{1}H NMR spectra of **2b** at room temperature in MeOH are very similar to those of **2a** and are entirely consistent with the proposed structure in which the anion is present only as a non-coordinating counter ion. Thus, the ^{31}P{^{1}H} NMR spectrum of **2b** consists of two resonances due to the inequivalent *cis*-P-atoms [δ 25.8 and 77.5; $^2J(P_A–P_B)$ 17 Hz] and the resonance at δ 25.8 is assigned to P_B since it shows additional coupling to the *trans*-hydride [$^2J(P_B–H)$ 179 Hz]. In order to avoid H/D exchange, the ^{1}H NMR spectrum was recorded in MeOH using the ^{1}H/^{31}P correlations measured *via* zero and double quantum coherences.[4] The hydride resonance consists of a doublet of doublets at δ −10 [^2J(P–H) 179 and 14 Hz], due to the *trans*- and *cis*-couplings respectively).

On carrying out the above reaction in CD_3OD, the new deuterides [Pd(L–L)D(CD_3OD)]X {X = $[BF_4]^-$ **2c**, X = $[CF_3SO_3]^-$ **2d**} can be isolated and their ^{31}P{^{1}H} NMR spectra are exactly in accord with their formulation; the resonance at δ 25.8 due to P_B is clearly a sextet [$^2J(P_A–P_B)$ 17 Hz and $^2J(P_B–D)$ 27 Hz].

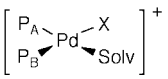

X	Solv	
H or D	MeOH	**2**
Et	MeOH	**3**
COEt	MeOH, THF	**4**

The hydride complex **2** reacts *immediately* with ethene at room temperature. Thus, addition of 1 equivalent of ethene to **2** results in the complete formation of the cationic complex [Pd(L–L)Et(MeOH)]X {X = $[BF_4]^-$ **3a**, X = $[CF_3SO_3]^-$ **3b**} and there is no further reaction on addition of more ethene. The ^{31}P{^{1}H} NMR spectra of **3a** and 3**b** in MeOH at 193 K consist of two doublets [δ 36.1 and 68.0; $^2J(P_A–P_B)$, 31 Hz] and $^2J(P_B–H)$ has completely disappeared. In order to confirm the formulation of **3**, the reaction of **2b** was repeated with $^{13}CH_2{=}CH_2$. In this case, there is a doublet at δ 68 [$^2J(P_A–P_B)$, 31 Hz] in the ^{31}P{^{1}H} NMR spectrum (at 193 K) and a more complicated multiplet at δ 36.1 (Fig. 1). As a result of using $^{13}CH_2{=}CH_2$, a 1 : 1 mixture of two isotopomers of **3b** is formed, *i.e.* [Pd(L–L)($CH_2{}^{13}CH_3$)(MeOH)]$^+$ **3c** and [Pd(L–L)($^{13}CH_2CH_3$)(MeOH)]$^+$ **3d**. For **3c**, the phosphorus *trans* to the ethyl group (P_B) couples only with the *cis*-phosphorus P_A [$^2J(P_A–P_B)$ 31 Hz] whereas in **3d**, P_B couples with both P_A and the *trans* carbon atom [$^2J(P_B–C)$ 38 Hz], resulting in a doublet of doublets (Fig. 1). The ^{13}C{^{1}H} NMR spectrum of the 1 : 1 mixture of the two isotopomers **3c** and **3d** at 193 K consists of a singlet at δ 8 (CH_3) and a doublet of doublets at δ 31 due to the CH_2 group [$^2J(P_A–C)$ 5 Hz, $^2J(P_B–C)$ 38 Hz]; the proton coupled ^{13}C NMR spectrum at 193 K shows the expected couplings due to the CH_3 and CH_2 groups [^1J(C–H) 124 and 158 Hz, respectively].

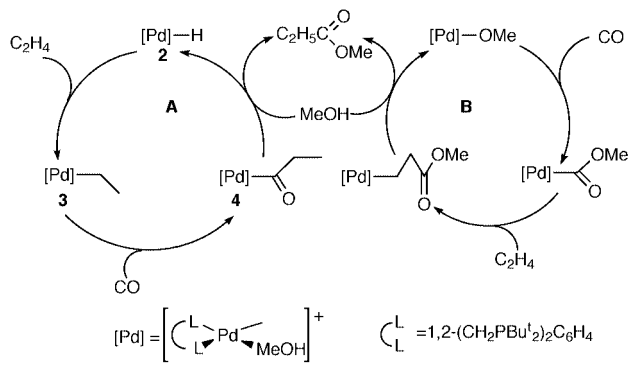

Scheme 1 Alternative reactive functional groups in the methoxycarbonylation of ethene (**A**, hydride cycle; **B**, methoxycarbonyl cycle).

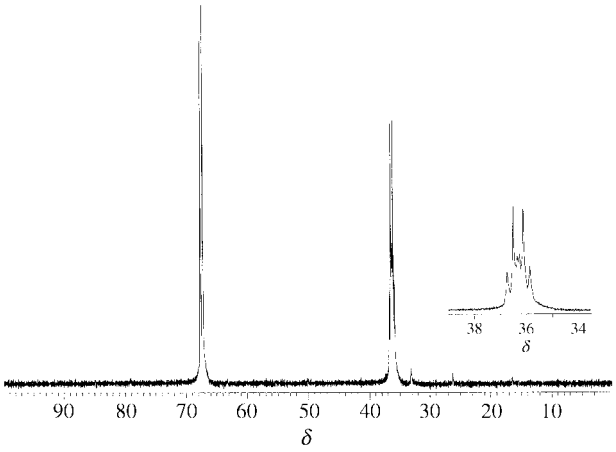

Fig. 1 ^{31}P NMR spectrum at 193 K of the two isotopomers **3c** and **3d** formed on reaction of $^{13}CH_2{=}^{12}CH_2$ with [Pd(L–L)H(MeOH)]$^+$ **2**, in MeOH.

The ethyl complex **3** is also quite stable in THF at low temperature. In this solvent the species [Pd(L–L)Et(THF)]$^+$ **3e** is present [in THF at 193 K, $\delta(P_A)$ 67.9, $\delta(P_B)$ 37.1; $^2J(P_A–P_B)$ 31.5 Hz]. On adding 1 equivalent of CO to **3e** in THF, [Pd(L–L)(COEt)(THF)]$^+$ **4** is formed *immediately* and the $^{31}P\{^1H\}$ NMR spectrum at 193 K consists of two doublets [δ 79.9 and 32.5; $^2J(P_A–P_B)$ 40 Hz]. On using ^{13}CO, both ^{31}P resonances become doublets of doublets owing to additional couplings [$^2J(P_B–C)$ 82.9 Hz, $^2J(P_A–C)$ 18.2 Hz] and, in the $^{13}C\{^1H\}$ NMR spectrum at 193 K, the $^{13}C(O)C_2H_5$ group is clearly identified at δ 232 as a doublet of doublets due to *cis* and *trans* $^2J(P–C)$.

On addition of a trace of MeOH to a THF solution of **4**, even at low temperature, there is an immediate reaction to regenerate the palladium hydride complex **2** with the formation of $EtCO_2Me$ (MeP). In methanol solution, **3** reacts immediately, even at low temperatures, with CO to give **2** and MeP, presumably *via* an acyl intermediate analogous to **4**.

The synthesis and reactivity of **2** provides important information on the mechanism involved in the methoxycarbonylation of ethene promoted by this particular class of catalyst. The nature of *all* the intermediates (**2**, **3** and **4**) involved in the hydride catalytic cycle (**A** in Scheme 1) has been determined and the chemical connections between these intermediates demonstrated.

It has been previously claimed that both the catalytic cycles, *i.e.* **A** and **B** in Scheme 1, are involved for the catalysts used for the synthesis of polyketones.[1,5] Moreover, it has been suggested that the methoxy cycle is the dominant cycle in the presence of oxidants (*e.g.* BQ).[1] These data have always been explained on the basis of the fact that Pd–hydrides are usually oxidised to give Pd–methoxy complexes in MeOH in the presence of oxidants.[1,6] However, we find that **2** is very stable in the presence of oxidants; oxygen can be bubbled through a methanol solution of **2** for 20–30 min at temperatures as high as 353 K without reaction; **2** is also stable in the presence of an excess of BQ (< 7 equivalents) on the timescale of the catalysis. In all cases, the only reaction observed on addition of further BQ is the metallation of the phosphine ligands[3] and there is no evidence for the formation of any methoxy complex. Hence, all the above data provide strong evidence in support of the hypothesis that the methoxycarbonylation of ethene promoted by [Pd(L–L)(dba)] follows the hydride catalytic cycle (**A** in Scheme 1).

We thank EPSRC for a CASE award (to S.Z.) and for funding the NMR equipment.

Notes and references

1 E. Drent and P. M. H. Budzelaar, *Chem. Rev.*, 1996, **96**, 663; E. Drent, J. A. M. van Broekhoven and P. H. M. Budzelaar, *Applied Homogeneous Catalysis with Organometallic Compounds*, ed. B. Cornils and W. A. Herrmann, VCH, 1996, p. 333.
2 Kirk Othmer, *Encyclopedia of Chemical Technology*, Wiley, New York, 4th edn, 1995, vol. 16, p. 487; *Chem. Week*, 1999, Nov. 10th, 14.
3 W. Clegg, G. R. Eastham, M. R. J. Elsegood, R. P. Tooze, X. L. Wang and K. W. Whiston, *Chem. Commun.*, 1999, 1877.
4 A. Bax, R. H. Griffey and B. L. Hawkins, *J. Magn. Reson.*, 1983, **55**, 301.
5 E. Drent, J. A. M. van Broekhoven and M. J. Doyle, *J. Organomet. Chem.*, 1991, **417**, 235; I. Toth and C. J. Elsevier, *Organometallics*, 1994, **13**, 2118.
6 A. Vavasori and L. Toniolo, *J. Mol. Catal. A*, 1996, **110**, 13.

Communication b001110j

ChemComm

Mechanistic studies on ruthenium-catalyzed hydrogen transfer reactions

Y. R. Santosh Laxmi and Jan-E. Bäckvall*

Department of Organic Chemistry, Arrhenius Laboratory, Stockholm University, SE-106 91 Stockholm, Sweden. E-mail: jeb@organ.su.se

Received (in Cambridge, UK) 19th January 2000, Accepted 1st March 2000

Ruthenium-catalyzed hydrogen transfer from (*S*)-α-deuterio-α-phenylethanol [(*S*)-1] to acetophenone with catalyst 3 occurs with retention of deuterium at the α-carbon of the alcohol product whereas H/D scrambling occurs with catalyst 2.

Hydrogen transfer reactions in which hydrogen is transferred from one organic molecule to another is of great importance in organic synthesis since one can avoid the use of molecular hydrogen.[1,2] In particular the reaction in which one equivalent of hydrogen is transferred from an alcohol to a ketone [eqn. (1)]

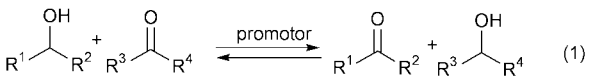

(1)

has become useful. This transformation has been known since 1925[3,4] and in the original version an aluminium alkoxide was employed as promotor [Meerwein–Ponndorf–Verley (MPV) reduction and Oppenauer oxidation].[1] In these reactions a direct transfer of a hydride is supposed to take place (Fig. 1, A).[5]

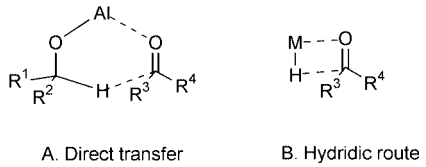

Fig. 1

More recently, transition metal-catalyzed versions of these reactions have been developed.[6,7] The latter reactions are supposed to involve metal hydride intermediates[7,8] (Fig. 1, B) and recently hydride intermediates were isolated from ruthenium–catalyzed hydrogen transfer reactions.[9,10] An interesting question is whether the metal hydride arises purely from the α-hydrogen of the secondary alcohol (path I, Scheme 1) or if hydride on the metal also originates from the OH group (path II, Scheme 1).

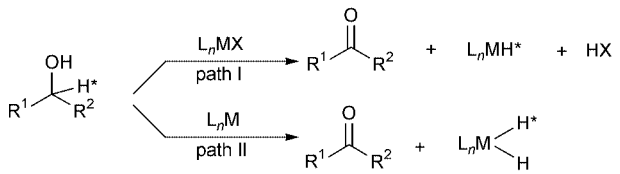

Scheme 1

To answer this question and to gain further insight into the mechanism of hydrogen transfer reactions we have studied the ruthenium-catalyzed hydrogen transfer from (*S*)-α-deuterated α-phenylethanol [(*S*)-**1**)] to acetophenone [eqn. (2)].

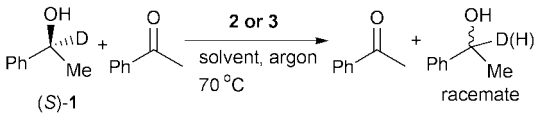

(2)

(*S*)-**1**

The use of enantiomerically pure α-deuterated alcohol (*S*)-**1** makes it possible to monitor the progress of the reaction since the hydrogen transfer catalyzed by the achiral catalyst should lead to racemization. The alcohol (*S*)-**1** is readily obtained from the enzymatic resolution of the corresponding racemic alcohol.[11] The latter was in turn obtained from $LiAlD_4$ reduction of acetophenone.

Ruthenium-catalyzed reaction of (*S*)-**1** with acetophenone resulted in moderate to slow racemization of the alcohol. Two different catalysts **2** and **3** were used in the present study. The

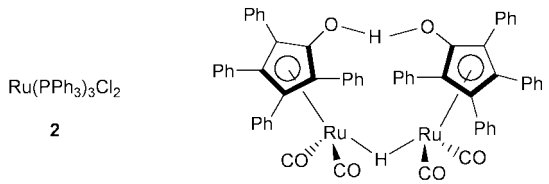

2

3

important question is to what extent deuterium is retained in the racemized alcohol. The racemization of (*S*)-**1** with both catalysts was carried out in aprotic as well as in protic solvents (Table 1). The reaction of (*S*)-**1** with **2** as the catalyst in THF in the presence of base and 0.5% of water resulted in complete racemization within 4 h (Table 1, entry 1). ^{1}H NMR and MS analyses showed that a significant loss of the deuterium had occurred and the deuterium content in the α-position was only 37%. In contrast, when **3** was employed as catalyst in the racemization of (*S*)-**1**, which took 24 h, essentially all of the deuterium was maintained in the α-position of the alcohol (entry 2). When the racemization experiment was carried out in a protic solvent (Bu^{t}OH) catalyst **2** gave a dramatic drop in the deuterium content to 15% (entry 3), whereas with catalyst **3** a high α-deuterium content was still maintained (91% D, entry 4). Interestingly, when catalyst **3** was employed in toluene, (*S*)-**1** gave a racemized product with 82% deuterium in the α-position. This suggests that slow aromatic activation of toluene by the active catalyst takes place leading to some H/D exchange.

The results from the racemization of (*S*)-**1**† suggest that catalysts **2** and **3** operate by two different mechanisms. With catalyst **2** it is evident that the hydride on the metal arises both from the α-position and the OH group of the alcohol (path II, Scheme 1), whereas with catalyst **3** the hydride arises only from the α-position (path I, Scheme 1). The former mechanism (path

Table 1 Racemization of (*S*)-**1** *via* Ru-catalyzed hydrogen transfer[a]

Entry	Catalyst	Base	Solvent	Water (%)	*t*/h	Result[b]
1	**2**	NaOH	THF	0.5	4	37% D
2	**3**	—	THF	—	24	95% D
3	**3**	—	Bu^{t}OH	0.5	72	91% D
4	**2**	NaOH	Bu^{t}OH	0.5	4	15% D
5	**3**	—	Toluene	—	24	82% D

[a] 2 mol% of the catalyst was employed together with 1 equiv. of acetophenone at 70 °C. [b] The deuterium content was determined by ^{1}H NMR and also by mass spectrometry and refers to the amount in the α-position.

DOI: 10.1039/b000530o

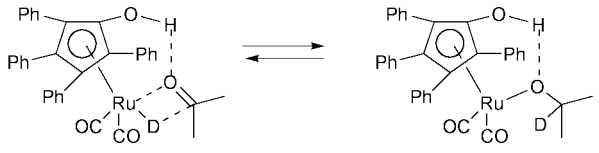

Fig. 2

II) is expected to give a H/D ratio of 50/50 in the α-position of the racemized alcohol from (*S*)-**1**. With path I (Scheme 1), (*S*)-**1** would give only ruthenium deuteride and as a result the α-position would be 100% deuterated in the racemized product.

The mechanism for catalyst **3**, which follows path 1, probably involves an intermediate in which the hydrogen transferred to the carbonyl carbon comes from the metal and the hydrogen transferred to the ketone oxygen arises from the OH group of the catalyst (Fig. 2). This may involve insertion of the ketone into a Ru–D bond followed by protonation of the ruthenium alkoxide by the OH group. In the reversed reaction a β-elimination from the alkoxide gives the ruthenium deuteride. This is in line with the mechanism proposed in our previous studies on ruthenium-catalyzed hydrogen transfer reactions with catalyst **3**.[12]

In the hydrogen transfer reaction with catalyst **2** it is known that the chlorides are eliminated under the formation of a ruthenium dihydride species.[9] With substrate (*S*)-**1** a di-deuterated complex **4** would be formed, which can react with the ketone to give a ruthenium(0) complex RuL_3 **5** after reductive elimination (Scheme 2). The latter complex should be in equilibrium with **4**.

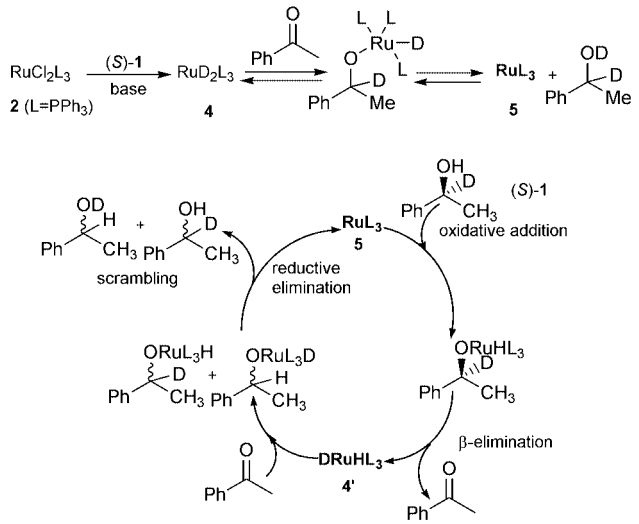

Scheme 2 Hydrogen transfer with catalyst **2**.

In the catalytic cycle (Scheme 2) oxidative addition of (*S*)-**1** to **5** would give a ruthenium alkoxide, which on β-elimination produces acetophenone and $DRuHL_3$ **4′**. The mixed hydride-deuteride species **4′** can now add to acetophenone, and after reductive elimination, the alcohol obtained would have deuterium scrambled between the α- and oxygen-positions. Any exchange with protons in the medium (*e.g.* a protic solvent) at this stage will lower the deuterium content of **1** by exchange of deuterium in the oxygen-position (*cf.* entry 4, Table 1). This is in contrast to catalyst **3** for which there will be no such H/D exchange since the hydride on the metal only arises from the α-position of the alcohol.

In conclusion, the results presented here show that quite different mechanisms may operate in ruthenium-catalyzed hydrogen transfer. Evidence is provided that catalyst **2** does not distinguish between the α-hydrogen and the OH hydrogen in hydrogen transfer from an alcohol to a ketone. In contrast, catalyst **3** selectively transfers the α-hydrogen to the carbonyl group and the OH hydrogen to the keto oxygen in the corresponding hydrogen transfer.

Financial support from the Swedish Natural Science Research Council and the Swedish Foundation for Strategic Research is gratefully acknowledged.

Notes and references

† *Typical procedure* for racemization of (*S*)-**1**: the ruthenium catalyst (2 mol%) and the base (10 mol%) were placed in a Schlenk tube, which was evacuated and filled with argon. Argon was bubbled through a solution of (*S*)-**1** (123 mg, 1 mmol) and acetophenone (120 mg, 1 mmol) in 1.25 ml of the appropriate solvent and transferred *via* a canula to the Schlenk tube containing the catalyst. The reaction mixture was heated to 70 °C (when THF was used as the solvent, the Schlenk tube was sealed with the help of a stopcock). The reaction was followed by chiral GC, worked up by filtration through a bed of Celite and purified by column chromatography. The racemized alcohol obtained was analyzed by ^{1}H NMR and MS for the deuterium content in the α-position.

1 C. F. de Graauw, J. A. Peters, H. Van Bekkum and J. Huskens, *Synthesis*, 1994, 1007.

2 M. J. Palmer and M. Wills, *Tetrahedron: Asymmetry*, 1999, 2045; S. Gladiali and G. Mestroni, in *Transition Metals for Organic Synthesis*, ed. M. Beller and C. Bolm, Wiley–VCH, Weinheim, 1998, p. 97.

3 H. Meerwein and R. Schmidt, *Liebigs Ann. Chem.*, 1925, **444**, 221; A. Verley, *Bull. Soc. Fr.*, 1925, **37**, 537; W. Ponndorf, *Angew. Chem.*, 1926, **39**, 138.

4 R. V. Oppenauer, *Recl. Trav. Chim. Pays-Bas.*, 1937, **56**, 137.

5 E. C. Assby, *Acc. Chem. Res.*, 1988, **21**, 414.

6 T. Naota, H. Takaya and S.-I. Murahashi, *Chem. Rev.*, 1998, **98**, 2599.

7 G. Zassinovich, G. Mestroni and S. Gladiali, *Chem. Rev.*, 1992, **92**, 1051; R. Noyori and S. Hashiguchi, *Acc. Chem. Res.*, 1997, **30**, 97; J. E. Bäckvall, R. L. Chowdhury, U. Karlsson and G.-Z. Wang, in *Perspectives in Coordination Chemistry*, ed. A. F. Williams, C. Floriani and A. E. Merbach, Verlag: Helv. Chem. Acta, Basel, 1992, p. 463.

8 S. Gladiali, L. Pinna, G. Delogu, S. de Martin, G. Zassinovich and G. Mestroni, *Tetrahedron: Asymmetry*, 1990, **1**, 635; M. A. Esteruelas, E. Sola, L. A. Oro, H. Werner and U. Meyer, *J. Mol. Catal.*, 1988, **45**, 1; R. Uson, L. A. Oro, R. Sariego and M. A. Esteruelas, *J. Organomet. Chem.*, 1981, **214**, 399.

9 A. Aranyos, G. Csjernyik, K. J. Szabó and J. E. Bäckvall, *Chem. Commun.*, 1999, 351.

10 K. J. Haack, S. Hashiguchi, A. Fujji, J. Takehera, T. Ikariya and R. Noyori, *Angew. Chem., Int. Ed. Engl.*, 1997, **36**, 285.

11 (*a*) To α-deuterated α-phenylethanol (0.625 g, 5 mmol) in toluene was added *p*-chlorophenyl acetate (0.844 g, 10 mmol) and enzyme N-435 (0.4 g) and the mixture stirred at 70 °C for 48 h.[11b] Workup followed by chromatography gave (*S*)-**1** (0.257 g, > 99% ee) and (*R*)-*O*-acetyl-α-deuterated α-phenylethanol (0.249 g, > 99% ee). (*b*) B. A. Persson, A. L. E. Larsson, M. L. Ray and J. E. Bäckvall, *J. Am. Chem. Soc.*, 1999, **121**, 1645.

12 M. L. S. Almeida, M. Beller, G-Z. Wang and J. E. Bäckvall, *Chem. Eur. J.*, 1996, **2**, 533.

Communication b000530o

ChemComm

Catalytic α-hydroxy carbon radical generation and addition. Synthesis of α-hydroxy-γ-lactones from alcohols, α,β-unsaturated esters and dioxygen

Takahiro Iwahama, Satoshi Sakaguchi and Yasutaka Ishii*

Department of Applied Chemistry, Faculty of Engineering & High Technology Research Center, Kansai University, Suita, Osaka 564-8680, Japan. E-mail: ishii@ipcku.kansai-u.ac.jp

Received (in Cambridge) 24th January 2000, Accepted 28th February 2000

A catalytic method for α-hydroxy carbon radical generation from alcohols has been developed and a convenient and synthetically useful approach to α-hydroxy-γ-lactones constructed.

Free radical reactions have attracted much attention in the synthesis of organic compounds because of their many advantages over ionic reactions, and therefore a variety of methodologies have been developed for the generation of carbon radicals.[1] To our knowledge, however, a limited number of methods, *e.g.* peroxide-[1,2] and photo-[1,3] initiated techniques and redox systems using metal ions,[1,4] have been used for the generation of carbon radicals from alcohols. Therefore, we believe that the catalytic carbon radical formation from alcohols and its use in organic synthesis are of interest and very useful as a synthetic tool. However, such a method has, as yet, not been realized.

Recently, we have shown that phthalimide *N*-oxyl (PINO), generated from *N*-hydroxyphthalimide (NHPI) and dioxygen, can abstract the hydrogen atom from alkanes to form alkyl radicals which are readily captured by O_2 to give oxygenated compounds such as alcohols, ketones and carboxylic acids.[5] As an application of this procedure, we report here, the first successful catalytic α-hydroxy carbon radical generation from alcohols using NHPI combined with cobalt species as the catalyst under O_2 (1 atm) and trapping the resulting α-hydroxy radicals by α,β-unsaturated esters leading to α-hydroxy-γ-lactones which are very difficult to obtain by conventional methods. Such lactones are very attractive as valuable synthetic precursors for species such as α,β-butenolides which have potent biological activity[6] as well as fine chemicals which are expected to be widely used in chemical industry.[7]

An outline of our approach is shown in Scheme 1: (i) *in situ* generation of an α-hydroxy carbon radical **Aa** from an alcohol assisted by NHPI/Co(II) under O_2; (ii) the addition of the radical **Aa** to an α,β-unsaturated ester; (iii) trapping of the radical **B** by O_2; (iv) the intramolecular cyclization of the resulting 1,3-diol **C** to yield α-hydroxy-γ-lactone **3**.

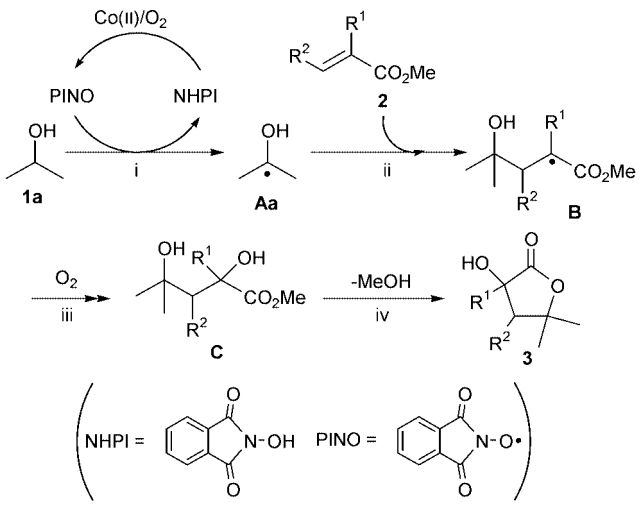

Scheme 1

Initially, the generation of an α-hydroxy carbon radical from isopropyl alcohol **1a** and the trapping of this radical by methyl acrylate **2a** were examined by the use of three different combined catalytic systems: NHPI/$Co(OAc)_2$ **I**, NHPI/$Co(acac)_3$ **II** and NHPI/$Co(OAc)_2$/$Co(acac)_3$ **III** under O_2 (1 atm) at 60 °C, leading to α-hydroxy-γ,γ-dimethyl-γ-butyrolactone **3a** in 27–78% yields (Fig. 1).† Inspection of Fig. 1 indicates that the reaction *via* catalyst **I** is terminated at an early stage and that catalyst **II** gives a higher yield of **3a**, although an induction period of 3 h was observed. The Co(III) ion is well known to be gradually reduced to Co(II) by organic substrates *via* a one-electron transfer process.[8] Therefore, it is thought that the induction period observed in the catalytic system **II** would correspond to the time required for the generation of Co(II) during the reaction. In order to shorten the induction period, we carried out the above reaction by adding a small amount of Co(II) ion [as $Co(OAc)_2$] to the NHPI/Co(III) system. As expected, a reduction of the induction period of the reaction was observed, and the best yield of **3a** (78%) was obtained by the use of the catalytic system **III**. On the basis of these results, a variety of alkenes were treated with **1a** under O_2 using the NHPI/$Co(OAc)_2$/$Co(acac)_3$ system (Table 1).

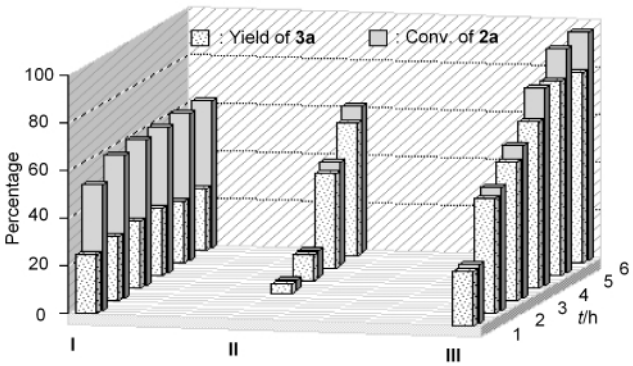

Fig. 1 Time dependence for the reaction of isopropyl alcohol **1a** with methyl acrylate **2a** to give **3a** under O_2 (1 atm) using NHPI/$Co(OAc)_2$ **I**, NHPI/$Co(acac)_3$ **II** and NHPI/$Co(OAc)_2$/$Co(acac)_3$ **III**. **2a** (3 mmol) was reacted with **1a** (10 equiv.) in the presence of NHPI (10 mol%) under O_2 (1 atm), 60 °C in MeCN (0.5 mL). **I**: $Co(OAc)_2$ (1 mol%), **II**: $Co(acac)_3$ (1 mol%), **III**: $Co(OAc)_2$ (0.1 mol%) and $Co(acac)_3$ (1 mol%).

Table 1 Reaction of various alkenes $CHR^2{=}CR^1CO_2Me$ with **1a**[a]

Run	R^1	R^2	Alkene	*T*/°C	Yield of **3b–d** (%)[b]	
1	Me	H	**2b**	70	71	(**3b**)
2	H	Me	**2c**	70	14 (74/26)[c]	(**3c**)
3[d,e]	H	CO_2Me	**2d**[f]	25	90 (76/24)[c]	(**3d**)
4[d]	H	CO_2Me	**2e**	25	86 (75/25)[c]	(**3d**)

[a] **2** (3 mmol) was reacted with **1a** (10 equiv.) under O_2 (1 atm) in the presence of NHPI (10 mol%), $Co(OAc)_2$ (0.1 mol%) and $Co(acac)_3$ (1 mol%) in MeCN (0.5 mL) for 8 h. [b] Isolated yield. [c] *trans*/*cis* ratio. [d] Reaction was carried out in the presence of $Co(OAc)_2$ (1 mol%) without $Co(acac)_3$. [e] 24 h. Air used. [f] Maleate.

DOI: 10.1039/b000707m

Table 2 Reaction of **2a** with various alcohols

Run[a]	Alcohol		t/h	Product[b](%)	
1	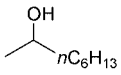	**1f**	5	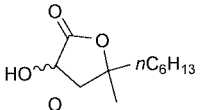	**3f** (74)[52/48][c]
2	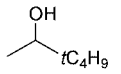	**1g**	8	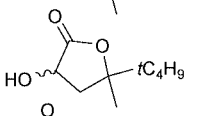	**3g** (71)[60/40][c]
3	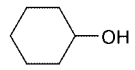	**1h**	3	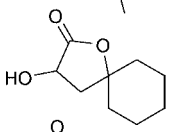	**3h** (83)
4[d]		**1h**	5		**3h** (76)
5	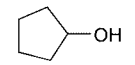	**1i**	8	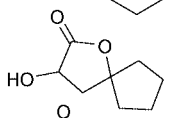	**3i** (80)
6	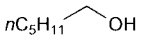	**1j**	5	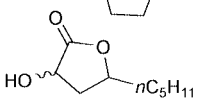	**3j** (41) [56/44][c]

[a] **2a** (3 mmol) was reacted with **1** (5 equiv.) in the presence of NHPI (10 mol%), $Co(OAc)_2$ (0.1 mol%) and $Co(acac)_3$ (1 mol%) under O_2 (1 atm) in MeCN (0.5 mL). [b] Isolated yield. [c] *trans/cis* ratio by GLC. [d] **1d** (3 equiv.) used.

From α- and β-methyl substituted acrylates, methacrylate **2b** and crotonate **2c**, the corresponding α-hydroxy-γ-lactones, **3b** and **3c**, were obtained in 71 and 14% yields, respectively. The lower reactivity of **2c** may be due to the β-CH_3 group which exerts steric hindrance towards the attacking radical **Aa**.[9] Reactions with methyl maleate **2d** and methyl fumarate **2e** proceeded smoothly even at 25 °C to afford α-hydroxy-β-carbomethoxy-γ-lactone **3d** in excellent yields, respectively. It is known that the incorporation of an electron-withdrawing substituent into the alkene decreases the SOMO–LUMO energy difference, and thus increases the rate of addition of alkyl radicals which possess nucleophilic reactivity.[9]

This new method for the construction of α-hydroxy-γ-lactones was quite general for a variety of alcohols (Table 2).‡ From cyclic alcohols, α-hydroxy-γ-spirolactones, which so far have been very difficult to synthesize, were obtained in high yields. Like secondary alcohols, the primary alcohol, hexa-1-nol **1j**, was found to generate the 1-hydroxyhexyl radical which then adds to **2a**, giving the corresponding γ-lactone **3j** (41%).

From viewpoints of low cost material, reaction efficiency and reaction simplicity, the present reaction is an innovative approach for the synthesis of α-hydroxy-γ-lactones which have considerable industrial potential.[10]

To gain further insight into the role of the cobalt species in the present reaction, the reaction of **1a** with **2a** by the NHPI/Co(II) system at room temperature was compared with that by the NHPI/Co(III) system [eqn. (1)]. The reaction *via* the NHPI/Co(II) system occurred at room temperature to give **3a** in excellent selectivity (92%) at 37% conversion, while the same reaction with the NHPI/Co(III) system was not observed even after 24 h. These results indicate that the presence of Co(II) is important to initiate the reaction. In a previous paper, we reported that a Co(III)–dioxygen complex derived from Co(II) species and O_2 accelerates the generation of PINO from NHPI.[5] Efforts to expand this method and to elucidate the reaction mechanisms are currently in progress.

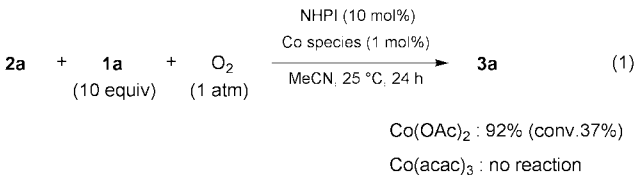

This work was supported by the Japan Society for the Promotion of Science under the Research for the Future program JSPS and a Grant-in-Aid for Scientific Research on Priority Areas from the Ministry of Education, Science and Culture, Japan.

Notes and references

† *Typical procedure* for the synthesis of α-hydroxy-γ-lactones **3a**: to a solution of alcohol **1a** (30 mmol), NHPI (0.3 mmol), $Co(OAc)_2$ (0.003 mmol) and $Co(acac)_3$ (0.03 mmol) in acetonitrile (0.5 mL) in a two-necked flask equipped a balloon filled with O_2 (1 atm) was added **2a** (3 mmol). After the mixture was vigorously stirred at 60 °C for 5 h, rotary evaporation of the solvent and unreacted alcohol followed by flash chromatography on silica gel afforded dihydro-3-hydroxy-5,5-dimethyl-2(3*H*)-furanone **3a** (78% yield).

‡ The present reaction resulted in concomitant formation of oxidation products, ketones or aldehydes, of the alcohols in the range of 0.6 to 1.2-fold of the resulting lactones.

1 B. Giese, *Radicals in Organic Synthesis: Formation of Carbon–Carbon Bonds*, Pergamon, Oxford, 1986; W. B. Motherwell and D. Crich, *Free-Radical Reactions in Organic Synthesis*, Academic Press, London, 1992.
2 W. H. Urry, F. W. Stacey, E. S. Huyser and O. O. Juveland, *J. Am. Chem. Soc.*, 1954, **76**, 450; K. Fukunishi, Y. Inoue, Y. Kishimoto and F. Mashio, *J. Org. Chem.*, 1975, **40**, 628.
3 D. Elad, *Organic Photochemistry*, ed. O. L. Chapman, Dekker, New York, 1969, vol. 2, pp. 168–186; G. O. Schenck, G. Koltzenberg and H. Grossmann, *Angew. Chem.*, 1957, **69**, 177.
4 F. Minisci, C. Giordano, E. Vismara, S. Levi and V. Tortelli, *J. Am. Chem. Soc.*, 1984, **106**, 7146.
5 Y. Yoshino, Y. Hayashi, T. Iwahama, S. Sakaguchi and Y. Ishii, *J. Org. Chem.*, 1997, **62**, 6810; S. Sakaguchi, T. Takase, T. Iwahama and Y. Ishii, *Chem. Commun.*, 1998, 2037 and references therein.
6 Y. S. Rao, *Chem. Rev.*, 1976, **76**, 625 and references therein.
7 S. Li and M. Vert, *Degradable Polymers*, ed. G. Scott and D. Gilead, Chapman & Hall, London, 1995, pp. 43–52.
8 A. Onopchenko and J. G. D. Schulz, *J. Org. Chem.*, 1973, **38**, 3729.
9 A β-alkyl substituent on acrylate is known to exert a powerful decelerating effect attributed to unfavorable steric interactions. The relative rate constant for the addition of a cyclohexyl radical to **2b** and **2c** is reported to be $k_{\mathbf{2b}}/k_{\mathbf{2c}}$ = *ca.* 90; B. Giese, *Angew. Chem., Int. Ed. Engl.*, 1983, **22**, 753.
10 There are a limited number of literatures on the synthesis of α-hydroxy-γ-lactones like **3a**. Mori *et al.* prepared **3a** *via* three steps from isobutene and trichloroacetaldehyde in 14% yield; K. Mori, T. Takigawa and T. Matsuo, *Tetrahedron*, 1979, **35**, 933; H. Laurent-Robert, C. Le Roux and J. Dubac, *Synlett*, 1998, 1138.

Communication b000707m

Heterogeneous asymmetric epoxidation of alkenes catalysed by a polymer-bound (pyrrolidine salen)manganese(III) complex

Choong Eui Song,*[a] Eun Joo Roh,[a] Byoung Mook Yu,[b] Dae Yoon Chi,[b] Su Chang Kim[c] and Kee-Jung Lee[c]

[a] *Life Sciences Division, Korea Institute of Science and Technology, PO Box 131, Cheongryang, Seoul, 130-650, Korea. E-mail: s1673@kistmail.kist.re.kr*
[b] *Department of Chemistry, Inha University, 253 Yonghyun-Dong, Nam-Ku, Inchon, 402-751, Korea*
[c] *Division of Chemical Engineering and Industrial Chemistry, Hanyang University, Seoul, 133-791, Korea*

Received (in Cambridge, UK) 1st February 2000, Accepted 6th March 2000

Excellent enantioselectivity (*e.g.* 92% ee for 2,2-dimethylchromene) has been achieved in heterogeneous asymmetric epoxidation using a polymer-bound (pyrrolidine salen)-manganese(III) complex; however, this polymeric catalyst underwent partial decomposition under epoxidation conditions.

Catalytic asymmetric epoxidation of alkenes presents a powerful strategy for the synthesis of enantiomerically enriched epoxides. Among several catalytic methods, the asymmetric epoxidation of unfuntionalised alkenes catalysed by chiral salen manganese complexes, *e.g.* the compound **1** developed by Jacobsen *et al*. is one of the most relevant methods.[1]

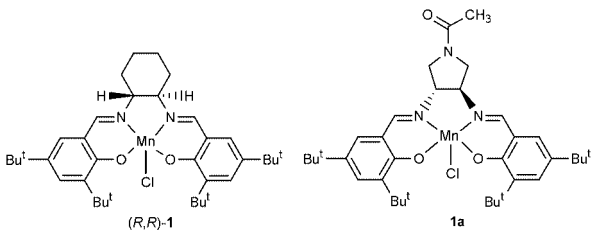

Recently, several attempts to build heterogeneous systems by the covalent attachment of Jacobsen-type catalysts to insoluble solid supports have been made.[2,3] Facilitation of catalyst separation, catalyst reuse and an increase in stability of the catalyst [*e.g.* minimisation of the possibility of formation of inactive μ-oxo-manganese(IV) species[4]] are the main objectives of such research. However, the results obtained so far are rather disappointing. This is perhaps not surprising since most of approaches have been focussed on copolymerisation of bis-styryl derivatives of chiral salen ligands.[2a–f] Such systems may show steric restriction for complex formation. Recently, Sherrington and coworkers[2g] have reported a series of polymer supported chiral (salen)Mn complexes, where the chiral catalytic unit was immobilised in a pendant fashion by only one of its aromatic rings to polymer supports to minimise local steric restriction. In one case, a very high ee (91%) was achieved in the epoxidation of 1-phenylcyclohexene, although the yield of the corresponding epoxide was relatively low (49%).

We now report the synthesis and application of a polymer-bound chiral (pyrrolidine salen)manganese(III) complex **2**, in which the (pyrrolidine salen)Mn moiety is attached by a single flexible linkage *via* the N-atom of the pyrrolidine moiety to the polymer support.

The dark brown polymeric complex **2** was prepared as shown in Scheme 1 by the reaction of NovaSyn® TG amino resin LL[5] with the chiral pyrrolidine salen derivative **4**, followed by treatment with $Mn(OAc)_2 \cdot 4H_2O$ in the presence of an excess of NaCl. In order to remove soluble (salen)Mn species which could interfere with the catalysis, the polymeric catalyst **2** was extracted in a Soxhlet device with MeOH for 24 h. Manganese analysis of **2** indicated that 0.11 mmol g^{-1} of the (salen)Mn complex was incorporated. The chiral pyrrolidine salen derivative **4** was readily prepared in 86% yield by the reaction of **3**[6] with glutaric anhydride in the presence of triethylamine and DMAP (CH_2Cl_2, 12 h, room temp.). To compare the catalytic efficiency in homogeneous and heterogeneous reactions, the homogeneous analogue **1a** was also prepared by a similar procedure.

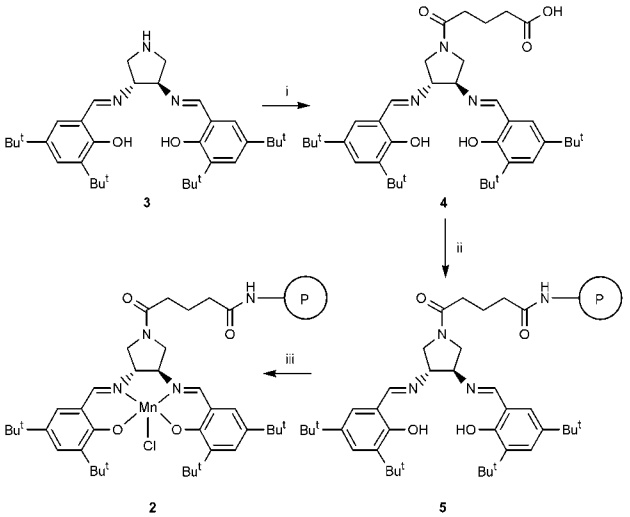

Scheme 1 *Reagents and conditions*: i, glutaric anhydride, NEt_3, DMAP, CH_2Cl_2, room temp., 12 h; ii, NovaSyn® TG amino resin LL (ref. 5), 1-hydroxybenzotriazole hydrate, $NEtPr^i_2$, 1.3-diisopropylcarbodiimide, DMF–CH_2Cl_2, room temp., 15 h; iii, $Mn(OAc)_2 \cdot 4H_2O$, EtOH–toluene, 85 °C, air, 12 h, then NaCl(aq).

Catalytic asymmetric epoxidations were carried out in the presence of 4 mol% of catalyst using NaOCl–PPNO (4-phenylpyridine *N*-oxide) or MCPBA–NMO as the oxidant system. The conditions were typical of those reported in the use of the soluble Jacobsen catalyst **1**[7] and the results obtained are shown in Table 1.

As a control experiment, we first investigated the catalytic efficiency (activity and enantioselectivity) of the monomeric analogue **1a** of the polymeric catalyst **2**. We were pleased to find that this catalyst was nearly as effective as Jacobsen's catalyst **1** (Table 1, entries 1 and 2). This result means that the chiral pyrrolidine salen moiety appears to be an appropriate chiral scaffold for the asymmetric epoxidation catalyst. With these results in hand, we turned to studying polymer-bound catalyst **2**. As shown in Table 1, the polymer-bound catalyst **2** exhibited quite satisfactory results, although the activity and enantioselectivity were still slightly lower than those obtained with its homogeneous analogue **1a**. In general, the reaction with MCPBA as the oxidant proceeded much faster than with NaOCl and afforded higher ee values. For example, the epoxidation of 2,2-dimethylchromene with MCPBA was completed in 1.5 h, affording the corresponding oxide with very high ee (92% ee, entry 4). On the other hand, the same reaction with NaOCl,

DOI: 10.1039/b000876l

Table 1 Asymmetric epoxidation of alkenes catalysed by polymer-bound chiral (salen)Mn^{III} complex **2** or its homogeneous analogue **1a**[a]

Entry	Catalyst	Substrate	Oxidant system	t/h	Yield (%)[b]	ee (%)[c]
1	**6**	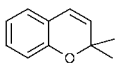	NaOCl –PPNO	4	90	95
2	**6**	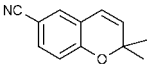	NaOCl –PPNO	5	96	90
3	**2**	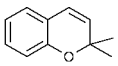	NaOCl –PPNO	24	84	87
4	**2**	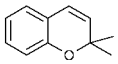	MCPBA –NMO	1.5	85	92
5	**2**	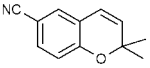	NaOCl –PPNO	50	82	87
6	**2**	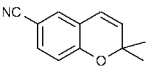	MCPBA –NMO	1.5	72	86
7	**2**		NaOCl –PPNO	24	82	78
8	**2**		MCPBA –NMO	2	76	68

[a] See footnote†. [b] Isolated yields. [c] Determined by chiral GC or chiral HPLC: see footnote† and ref. 7(*b*); major enantiomers: (3*R*,4*R*)-3,4-epoxy-2,2-dimethylchroman, (3*R*,4*R*)-3,4-epoxy-6-cyano-2,2-dimethylchroman and (1*R*,2*S*)-1-phenylcyclohexene oxide.

which was carried out under two-phase conditions, required 24 h for a comparable degree of conversion and gave the epoxide with 87% ee (entry 3). The polymeric catalyst **2** could be simply recovered by filtration so enabling catalyst recycling. However, the polymer-bound catalyst **2** underwent partial decomposition under epoxidation condition. The initially dark brown resin was more or less decolourised after the reaction. When MCPBA was used as oxidant, much more severe decolourisation was observed than when NaOCl was used. This result is in accord with results of Skarzewski *et al*., who also observed a fairly high resistance to degradation when NaOCl is used as an oxidant for salen complexes with *tert*-butyl groups at the 5- and 5′-positions.[8] This tendency of salen manganese catalysts to undergo decomposition under epoxidation conditions could limit successful recycling of immobilised catalyst.[9]

In summary, we have prepared a promising class of polymer-bound catalyst for heterogeneous asymmetric epoxidation of alkenes. Our results showed that polymeric catalyst **2** showed a comparable degree of enantioselectivity (92% ee for 2,2-dimethylchromene) in asymmetric epoxidation of alkenes to that obtained with its homogeneous analogue **1a**. However, the activity and enantioselectivity of the polymeric catalyst **2** are highly dependent on epoxidation conditions, and, moreover, the degree of decomposition of catalyst also seems to be highly influenced by oxidation conditions. Therefore, to carry out heterogeneous asymmetric epoxidation successfully, not only the design of supported catalysts, but also the selection of appropriate oxidation conditions are very important. More detailed studies concerning the optimisation of both catalyst structure (to increase activity and enantioselectivity by modifying the spacer length and resin morphology, *etc*.) and reaction conditions (to minimise catalyst decomposition) are currently in progress.

This research was supported by a grant from Ministry of Science and Technology in Korea.

Notes and references

† Asymmetric epoxidation using polymer-bound catalyst **2**.

Using NaOCl as the oxidant: resin beads of **2** (202 mg) were stirred in CH_2Cl_2 (2 mL) for 1 h. Alkene (0.54 mmol) and 4-phenylpyridine *N*-oxide (18.5 mg, 0.108 mmol) were then added and the mixture was cooled to 0 °C. To this mixture buffered NaOCl (0.81 mmol, pH = 11.3) was added and the reaction was stirred at 0 °C. At the end of the reaction, the suspension was filtered off and resin beads were washed with CH_2Cl_2. The filtrate was washed with brine and dried ($MgSO_4$). After removal of the solvent under reduced pressure, the residue was purified by column chromatography.

Using MCPBA as the oxidant: resin beads of **2** (202 mg) were poured into a solution containing 2.7 mmol (316 mg) of *N*-methylmorpholine *N*-oxide dissolved in CH_2Cl_2 (4 mL). Alkene (0.54 mmol) was then added and the mixture was cooled to −78 °C. Solid MCPBA (1.08 mmol, 186 mg) was then added as a solid in four roughly equal portions over a 2 min period. The reaction mixture was stirred at −78 °C and the progress of the reaction was monitored by TLC. At the end of the reaction, the suspension was filtered off and resin beads were washed with CH_2Cl_2. The filtrate was washed with 1 M NaOH, brine and dried. After removal of the solvent under reduced pressure, the residue was purified by column chromatography.

The ee values of products were determined by chiral HPLC or chiral GC: For 3,4-epoxy-2,2-dimethylchroman: Daicel Chiralpak AD, propan-2-ol–hexane (5:95), 0.8 mL min^{-1}; 9.30 min (3*R*,4*R*), 10.63 min (3*S*,4*S*); for 3,4-epoxy-6-cyano-2,2-dimethylchroman: Daicel Chiralcel OJ, propan-2-ol–hexane (30:70), 1 mL min^{-1}; 13.95 min (3*R*,4*R*), 26.88 min (3*S*,4*S*); for 1-phenylcyclohexene oxide: see ref. 7(*b*).

1 E. N. Jacobsen and M. H. Wu, *Epoxidation of Alkenes Other than Allylic Alcohols*, in *Comprehensive Asymmetric Catalysis II*, ed. E. N. Jacobsen, A. Pfaltz and H. Yamamoto, Springer Verlag, Berlin–Heidelberg–New York, 1999, p. 649.

2 (*a*) B. B. De, B. B. Lohray and P. K. Dhal, *Tetrahedron Lett.*, 1993, **34**, 2371; (*b*) B. B. De, B. B. Lohray, S. Sivaram and P. K. Dhal, *Macromolecules*, 1994, **27**, 2191; (*c*) B. B. De, B. B. Lohray, S. Sivaram and P. K. Dhal, *Tetrahedron: Asymmetry*, 1995, **6**, 2105; (*d*) B. B. De, B. B. Lohray, S. Sivaram and P. K. Dhal, *J. Polym. Sci., Polym. Chem. Ed.*, 1997, **35**, 1809; (*e*) F. Minutolo, D. Pini and P. Savadori, *Tetrahedron: Asymmetry*, 1996, **7**, 2293; (*f*) F. Minutolo, D. Pini, A. Petri and P. Savadori, *Tetrahedron Lett.*, 1996, **37**, 3375; (*g*) L. Canali, E. Cowan, H. Deleuze, C. L. Gibson and D. C. Sherrington, *Chem. Commun.*, 1998, 2561; (*h*) M. D. Angelino and P. E. Laibinis, *Macromolecules*, 1998, **31**, 7581; (*i*) M. D. Angelino and P. E. Laibinis, *J. Polym. Sci. Part A. Polym. Chem.*, 1999, **37**, 3888; (*j*) G.-J. Kim and J.-H. Shin, *Tetrahedron Lett.*, 1999, **40**, 6827; (*k*) D. Pini, A. Mandoli, S. Orlandi and P. Salvadori, *Tetrahedron: Asymmetry*, 1999, **10**, 3883.

3 Several other efforts to immobilize (salen)Mn-based epoxidation catalysts have been described: M. J. Sabater, A. Corma, A. Domenech, V. Fornés and H. García, *Chem. Commun.*, 1997, 1285; S. B. Ogunwumi and T. Bein, *Chem. Commun.*, 1997, 901; L. Frunza, H. Kosslick, H. Ladmesser, E. Hoft and R. Fricke, *J. Mol. Catal. A: Chem.*, 1997, **123**, 179; I. F. J. Vankelecom, D. Tas, R. F. Parton, V. Van de Vyver and P. A. Jacobs, *Angew. Chem., Int. Ed. Engl.*, 1996, **35**, 1346; K. B. M. Janssen, I. Laquiere, W. Dehaen, R. F. Parton, I. F. J. Vankelecom and P. A. Jacobs, *Tetrahedron: Asymmetry*, 1997, **8**, 3481; G. Pozzi, F. Cinato, F. Montanari and S. Quici, *Chem. Commun.*, 1998, 877.

4 K. Srinvasan, P. Michaud and J. K. Kochi, *J. Am. Chem. Soc.*, 1986, **108**, 2309.

5 NovaSyn® TG amino resin LL (0.29 mmol g^{-1}) was purchased from Calbiochem-Nova Biochem Japan Ltd.

6 R. G. Konsler, J. Karl and E. N. Jacobsen, *J. Am. Chem. Soc.*, 1998, **120**, 10780.

7 (*a*) For NaOCl: B. D. Brandes and E. N. Jacobsen, *J. Org. Chem.*, 1994, **59**, 4378; (*b*) for MCPBA: M. Palucki, G. J. McCormick and E. N. Jacobsen, *Tetrahedron Lett.*, 1995, **36**, 5457.

8 J. Skarzewski, G. Gupta and A. Vogt, *J. Mol. Catal. A: Chem.*, 1995, **103**, L63.

9 Very recently, the degradation of Mn-loaded polymeric salen ligands under epoxidation conditions was also noted by Angelino *et al.* [see ref. 2(*i*)].

Communication b000876l

ChemComm

Triply-bridged diphos disilver helical complexes $[Ag_2(\mu_2\text{-dppa-}P,P')_3(anion)_2]$ [dppa = bis(diphenylphosphino)acetylene]

Stuart L. James,* Elvira Lozano and Mark Nieuwenhuyzen

School of Chemistry, The Queen's University of Belfast, David Keir Building, Stranmillis Road, Belfast, Northern Ireland, UK BT9 6EQ. E-mail: s.james@qub.ac.uk

Received (in Basel, Switzerland) 6th December 1999, Accepted 18th February 2000

Triply-bridged disilver complexes $[Ag_2(\mu_2\text{-dppa-}P,P')_3(anion)_2]$ form selectively and are stabilised by many aromatic interactions.

Multimetallic 'coordination clusters' which assemble from metal ions and multidentate bridging ligands currently attract much interest.[1] In most cases, their structures can be predicted from the geometries of the rigid bridging ligand and the metal ion used (*e.g.* square planar or octahedral). By contrast, silver(I)–phosphine complexes exhibit varying coordination numbers, and often dissociative equilibria. Therefore more subtle 'secondary' factors might control product selectivity in the formation of a multisilver complex with bridging phosphines. Some known multisilver and -copper complexes with bridging phosphines[2] are shown in Fig. 1. Some of these have quite unexpected structures, *e.g.* the hexanuclear adamantanoid triphos cages **b**.[2j] With flexible diphosphines $Ph_2P(CH_2)_nPPh_2$, silver(I) or copper(I) salts with oxo-anions selectively form dinuclear (2:2) macrocycles, *e.g.* **a**. The larger rings of this type (up to 18-membered) are stabilised by bridging oxo anions. This stabilisation is enabled by the flexibility of the diphosphine, which allows the P lone pairs to point inwards, setting up the metals for anion bridging.

Bis(diphenylphosphino)acetylene ($Ph_2P–C\equiv C–PPh_2$, dppa), by contrast, cannot have inwardly pointing lone pairs owing to its rigidity. We were therefore interested to discover what type of stable non-dissociating structure, if any, this ligand would cause to form.

At room temperature, solutions of equimolar mixtures of dppa and AgX (X = SbF_6 or OTf) in $CDCl_3$–$MeNO_2$ (2:1) gave ^{31}P NMR spectra (121 MHz) which were broad and did not show Ag–P coupling, suggesting dissociation of the Ag–P bonds on the NMR timescale. At −60 °C, this process is slow on the NMR timescale and only sharp lines characteristic of coupling to ^{107}Ag and ^{109}Ag were seen. 95% of the spectral intensity was due to a mixture of three species, each with distinctly different coupling constants corresponding to AgP (767 Hz), AgP_2 (505 Hz) and AgP_3 (377 Hz) coordination centres.[3] The lowest nuclearity structures which could account for these coordination centres are indicated in Scheme 1. Therefore the rigid dppa ligand does not selectively produce a 2:2 macrocycle **2**, but instead favours some disproportionation to the 1:2 and 3:2 structures **1** and **3**.

We therefore investigated the selective formation of triply-bridged complex **3**, at the appropriate 3:2 ligand to metal ratio. The reaction of 3 equivalents of dppa with 2 equivalents of $AgSbF_6$ did indeed lead quantitatively to this product. This behaviour was further found to be general to the salts AgX (X = BF_4 **3a**, SbF_6 **3b** NO_3 **3c**, OTf **3d**).† Unusually for silver-phosphine complexes, **3a–d** show no evidence of Ag–P dissociation at room temperature on the NMR timescale (at 121 MHz). A $^{19}F\{^1H\}$-HOESY spectrum[4] in $CDCl_3$ reveals an interionic contact between the BF_4^- and the dppa *ortho* protons (of < 4.5–5 Å), showing that complex **3** exists as a tight ion-pair in this solvent.

Crystals obtained from chloroform–nitromethane–diethyl ether had the composition $[Ag_2(\mu_2\text{-dppa-}P,P')_3(BF_4)_2]\cdot 0.5CHCl_3\cdot 1.5MeNO_2$ as established by single crystal X-ray crystallography (Fig. 2).‡ Consistent with the NMR data, there is trigonal geometry at silver, although with pyramidal distortion toward the BF_4 anions (distances of Ag1 and Ag2 from their P_3 planes are 0.55 and 0.54 Å, respectively). The two Ag(I) centres are linked by three bridging dppa ligands with outwardly bent P–C≡C–P backbones, and C≡C–P angles lying in the range 171.3(4)–175.1(4)°. This strain results from the mismatch between distorted tetrahedral geometry at phosphorus and pseudo-cofacial silver coordination centres, and is partially alleviated by the pyramidal distortion at silver. There is a helical twist of *ca.* 27°, about the Ag···Ag axis, taken as the average of the torsion angles P(1)–Ag(1)–Ag(2)–P(2), P(3)–Ag(1)–Ag(2)–P(4) and P(5)–Ag(1)–Ag(2)–P(6). The crystalline material is achiral however, each unit cell containing two molecules of each enantiomer. There is small void at the centre (dimensions: Ag to molecular centroid 2.83 Å, typical C≡C centroid to molecular centroid 2.48 Å).

Perhaps importantly, there are sixteen intramolecular aromatic contacts of both stacking and C–H···π types in the range

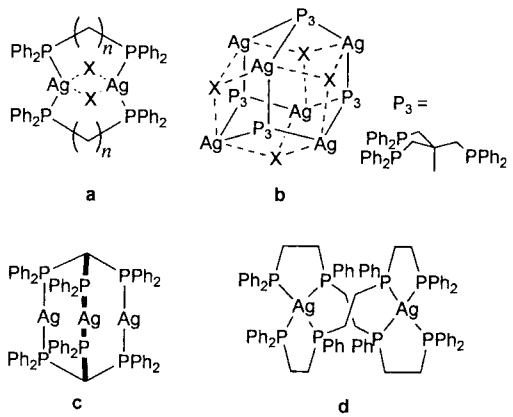

Fig. 1 Multisilver complexes with bridging multidentate phosphines: diphos macrocycles (**a**), triphosphine cages (**b** and **c**), and a tetraphosphine helicate (**d**).

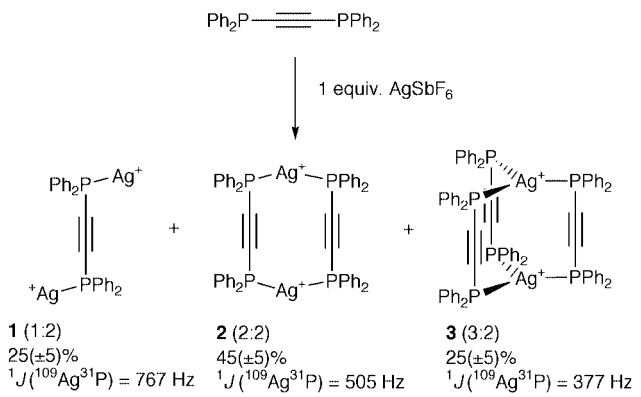

Scheme 1 The distribution of products from equimolar amounts of dppa and $AgSbF_6$.

DOI: 10.1039/a909683c

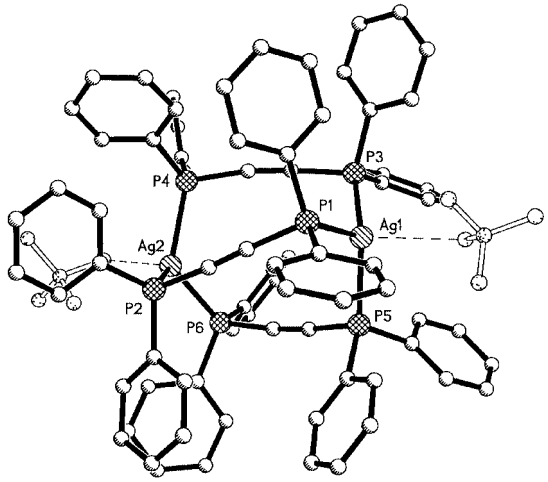

Fig. 2 The structure of complex **3a** in the solid state with H-atoms omitted.

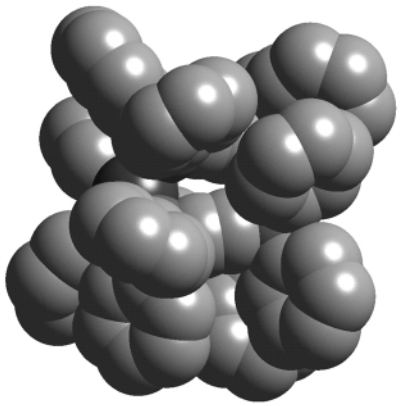

Fig. 3 Space-filling representation of complex **3a** to show the clustering of aromatic groups (H-atoms omitted).

3.5–3.8 Å (C–C distance) between the twelve phenyl groups. An impression of the clustering of aromatic groups can be gained from Fig. 3. Though individually weak, in combination these contacts may contribute significantly to the observed stability of complexes **3** in solution. Multiple aromatic interactions also occur in the triphos cage complexes $[Ag_6(triphos)_4(oxo\text{-}anion)]^{2+}$, and furthermore, may be responsible for their unexpected structure.[2j] The ^{1}H NMR spectrum of **3a** (−60 °C, 500 MHz) shows only one type of phenyl group suggesting that in solution it is either not helical or rapidly interconverts between enantiomers. Much interest has been shown in triple helicates,[4] and most are based on tris-chelate metal centres. Relevant exceptions are the Cu_3L_3 complex of Potts *et al.*[5a] with trigonal coordination, and the Ag_3L_3 toroidal triple helix with two-coordination at silver reported by Williams *et al*.[5b] We note with interest that the related dppa complexes $[(CO)_3Mo(\mu_2\text{-dppa-}P,P')_3Mo(CO)_3]$[6a] and [BuTeCu($\mu_2$-dppa-$P,P')_3$CuTeBu][6b] are also helical. In contrast to complex **3a**, as a consequence of their higher coordination numbers and correspondingly smaller P–M–P angles, these complexes have longer, narrower central voids (Mo–Mo distance 7.38 Å, Cu–Cu distance 6.40 Å).

In conclusion, complexes **3a**–**d** are a novel type of stable disilver complex with triply-bridging diphosphines. They assemble selectively from a 3:2 ligand to metal ratio, and unusually their Ag–P bonds do not dissociate on the NMR timescale at room temperature. Interesting structural features are the many intramolecular aromatic interactions, the central void and helical twist. The aromatic interactions may explain their selective assembly and stability in solution. This has implications for coordination-based self-assembly with flexible ligands or where the metal has no clearly preferred coordination number.

We are grateful to Dr Graham Saunders and Dr Graeme Hogarth for valuable discussions.

Notes and references

† To a solution of AgX (0.44 mmol) in nitromethane–acetonitrile or acetonitrile (8 ml) was added a solution of dppa (263 mg, 0.66 mmol) in $CHCl_3$ (10 ml). Layering with diethyl ether gave colourless prisms in > 90% yield. **3a** (X = BF_4) δ_P 19.4, $^1J(^{109}Ag^{31}P)$ 377 Hz, **3b** (X = SbF_6) $^1J(^{109}Ag^{31}P)$ 360 Hz, **3c** (X = NO_3) $^1J(^{109}Ag^{31}P)$ 336 Hz, **3d** (X = OTf) $^1J(^{109}Ag^{31}P)$ 336 Hz. $\delta_H(CDCl_3)$: **1a** (X = BF_4) 7.56 (m, 24H, H_{ortho}), 7.27 (t, 1.8 Hz, 12H, H_{para}), 7.10 (t, 1.8 Hz, 24H, H_{meta}).

‡ *Crystal data* for **3a**. $C_{80}H_{60}Ag_2B_2Cl_{1.50}F_8N_{1.50}O_3P_6$, M = 1718.65, monoclinic, space group $P2_1/n$ (no. 14), a = 22.1929(16), b = 14.8355(18), c = 23.8561(13) Å, β = 99.460(6)°, V = 7747.6(12) Å^3, Z = 4, D_c = 1.473 g cm^{-3}, μ = 0.749 mm^{-1}. Data collection ($2.21 \leqslant \theta \geqslant 25.00$) was performed at 153 K on a Bruker SMART diffractometer (Mo-Kα, λ = 0.71073 Å). The structure was solved by direct methods (SHELXS-97)[7] and refined with full matrix least squares to a final R_1 value of 0.0674, for 929 parameters and 13639 unique reflections with $I \geqslant 2\sigma(I)$ and wR_2 of 0.1067 for all 14014 reflections. The BF_4 anions are each disordered over two sites with occupancies of 65 and 60% for the major component of each anion. There are short fluorine contacts to the silver(I) centres and to some *ortho*-hydrogen atoms. For the major components, contacts shorter than the sum of the van der Waals radii (2.67 Å) between fluorine and hydrogen are F11–H62A 2.593, F21–H12B 2.589 and F22–H36B 2.507 Å. To the Ag centres, contacts shorter than the combined van der Waals radii (3.19 Å) are F21–Ag1 2.933(9), F22–Ag1 2.751(7), F11–Ag2 2.861(9) and F12–Ag2 2.656(9) Å. CCDC 182/1549. See http://www.rsc.org/suppdata/cc/a9/a909683c/ for crystallographic files in .cif format.

1 N. Takeda, K. Umemoto, K. Yamaguchi and M. Fujita, *Nature*, 1999, **398**, 794; B. Olenyuk, J. A. Whiteford, A. Fechtenkotter and P. J. Stang, *Nature*, 1999, **398**, 769; X. K. Sun, D. W. Johnson, D. L. Calder, R. E. Powers and K. N. Raymond, *Angew. Chem., Int. Ed.*, 1999, **38**, 1303; D. W. Johnson, J. D. Xu, R. W. Saalfrank and K. N. Raymond, *Angew. Chem., Int. Ed.*, 1999, **38**, 2882.

2 (*a*) S. Kitagawa, M. Kondo, S. Kawata, S. Wada, M. Maekawa and M. Munakata, *Inorg. Chem.*, 1995, **34**, 1455; (*b*) E. R. T. Tiekink, *Acta. Crystallogr., Sect. C*, 1990, **46**, 1933; (*c*) D. M. Ho and R. Bau, *Inorg. Chem.*, 1983, **21**, 4073; (*d*) S. P. Neo, Z.-Y. Zhou, T. C. W. Mak and T. S. A. Hor, *ibid.*, 1995, **34**, 520; (*e*) A. F. M. J. van der Ploeg, G. van Koten and A. L. Spek, *ibid.*, 1979, **18**, 1052; (*f*) A. F. M. J. van der Ploeg and G. van Koten, *Inorg. Chim. Acta*, 1981, **51**, 225; (*g*) Y. Ruina, Y. M. Hou, B. Y. Xue, D. M. Wang and D. M. Jin, *Transition Met. Chem.*, 1996, **21**, 28; (*h*) A. Cassel, *Acta Crystallogr., Sect B*, 1976, **32**, 2521; (*i*) F. Caruso, M. Camalli, H. Rimml and L. M. Venanzi, *Inorg. Chem.*, 1995, **34**, 673; (*j*) S. L. James, D. M. P. Mingos, A. J. P. White and D. W. Williams, *Chem. Commun.*, 1998, 2323; (*k*) A. L. Airey, G. F. Swiegers, A. C. Willis and S. B. Wild, *Inorg. Chem.*, 1997, **36**, 1588; (*l*) C. M. Che, H. K. Yip, V. W. W. Yam, P. Y. Cheung, T. F. Lai, S. J. Shieh and S. M. Peng, *J. Chem. Soc., Dalton Trans.*, 1992, 427.

3 *Methods in Stereochemical Analysis, Volume 8, Phosphorus-31 NMR Spectroscopy in Stereochemical Analysis*, ed. J. G. Verkade and L. D. Quin, VCH Publishers inc., Deerfield Beach, FL, 1987.

4 J. D. Xu, T. N. Parac and K. N. Raymond, *Angew. Chem., Int. Ed.*, 1999, **38**, 2878 and references therein; C. Piguet, G. Bernadinelli and G. Hopfgartner, *Chem. Rev.*, 1997, **97**, 2005; M. Albrecht, *Chem. Soc. Rev.*, 1998, **27**, 281.

5 (*a*) K. T. Potts, C. P. Horwitz, A. Fessak, M. Keshavarz-K, K. E. Nash and P. J. Toscano, *J. Am. Chem. Soc.*, 1993, **115**, 10 444; (*b*) C. Provent, S. Hewage, G. Brand, G. Bernadinelli, L. J. Charbonniere and A. F. Williams, *Angew. Chem., Int. Ed. Engl.*, 1997, **36**, 1287.

6 (*a*) G. Hogarth and T. Norman, *Polyhedron*, 1996, **15**, 2859; (*b*) M. Semmelmann, D. Fenske and J. F. Corrigan, *J. Chem. Soc., Dalton Trans.*, 1998, 2541.

7 G. M. Sheldrick, SHELXS-97, Program for X-Ray Crystal Structure Solution, University of Göttingen University, 1997.

Communication a909683c

Stereochemistry of the reaction of the inhibitor β-chloroalanine with mercaptoethanol, a β-substitution reaction catalysed by an aminotransferase

Benjamin Adams, Kenneth J. M. Beresford, Sheena M. Whyte and Douglas W Young*

Sussex Centre for Biomolecular Design and Drug Development, University of Sussex, Falmer, Brighton, UK BN1 9QJ. E-mail: d.w.young@sussex.ac.uk

Received (in Liverpool, UK) 17th January 2000, Accepted 12th February 2000

L-Aspartate aminotransferase, a member of the α-family of PLP mediated enzymes, which normally catalyses transamination, has been used to catalyse the β-substitution reaction of stereospecifically labelled samples of the enzyme inhibitor β-chloro-L-alanine with 2-mercaptoethanol; the stereochemistry of the products was assigned by independent synthesis, showing that the abnormal substitution reaction proceeds with overall retention of stereochemistry, the usual stereochemical consequence of reactions catalysed by enzymes of the β-family of PLP mediated enzymes which have low homology with enzymes of the α-family.

Pyridoxal phosphate (PLP) dependent enzymes catalyse a wide variety of different reactions, mainly involving amino acids. Early theories[1–3] to generalise and explain the chemical basis for these widely differing reactions have largely been confirmed. Dunathan and Voet[4] proposed that PLP-dependent enzymes evolved from a common ancestor protein, and there is evidence[5] that this is true for one of the three families of PLP mediated enzymes, the α-family, which contains a predominant number of enzymes. Homology studies have recently suggested that the α- and γ-families of enzymes may be distantly related but that enzymes of the β-family are not closely related to either of these families.[5]

L-Aspartate aminotransferase (EC 2.6.1.1) is an enzyme of the α-family, catalysing the transamination of L-aspartic acid to α-ketoglutaric acid giving oxaloacetic and glutamic acids. β-Chloro-L-alanine **1**[6,7] has been shown not only to inhibit this enzyme, but also to be converted to pyruvic acid by it. It has also been observed that introduction of thiosulfate during the inactivation of L-aspartate aminotransferase by L-serine-*O*-sulfate **2** reversed inhibition and caused production of L-cysteine-*S*-sulfonate **3**.[8] Further, inhibition of D-amino acid

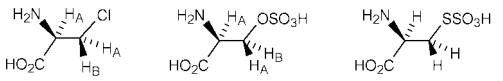

1 **2** **3**

aminotransferase by β-bromo-D-alanine was reversed by addition of thiols and, when β-mercaptoethylamine was used, *S*-(β-aminoethyl)-D-cysteine and Δ^1-thiomorpholine-2-carboxylic acid were products.[9] Thus these enzymes have catalysed β-substitution reactions typical of enzymes of the β-family, rather than transamination which is typical of α-family enzymes. This would suggest that the quinonoid form **4**, formed in the 'normal' reaction, instead of protonation at C-4′ by Lys258, converted to **5** in the inhibition reaction. This may be processed to pyruvate or an inhibitor complex in the absence of a thiol. In the presence of a thiol, however, the reaction presumably proceeds as shown in Scheme 1 eventually to give the final cysteine derivative **6**.

The change in role from catalyst for transamination to catalyst for β-substitution exhibited by aspartate aminotransferase on change of substrate from L-aspartate to β-chloro-L-alanine **1** was intriguing and we decided to examine the overall stereochemistry of the β-substitution reaction in the presence of thiol to see whether it was in keeping with the retention generally shown by reactions catalysed by the enzymes whose

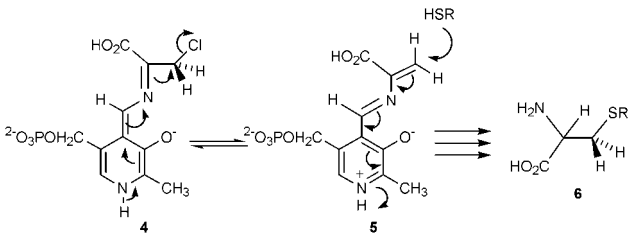

4 **5** **6**

Scheme 1

normal role this was.[10] We therefore prepared samples of β-chloro-L-alanine **1** which were stereospecifically labelled at C-3. This was achieved by first converting the labelled samples of methyl (2*S*)-*N*-tritylaziridine-2-carboxylate **7**(H_B = ^2H)[11] and **7**(H_A = ^2H)[11] to the corresponding urethanes **8**† by reaction with trifluoroacetic acid in chloroform to remove the trityl group, followed immediately by reaction with benzyl chloroformate under Schotten Baumann conditions (Scheme 2). β-Substitution with chloride ion was achieved by reaction with $TiCl_4$ in CH_2Cl_2–$CHCl_3$, and deprotection in refluxing 4 M H_2SO_4 then gave the enzyme inhibitors **1**.† The ^1H and ^2H NMR spectra indicated that the inhibitors **1** were unique diastereoisomers and, since substitution is accompanied by inversion of stereochemistry at the labelled β-position, these were assigned as (2*R*,3*S*)-[3-$^2H_1$]- and (2*R*,3*R*)-[2,3-$^2H_2$]-β-chloroalanine, **1**(H_B = ^2H) and **1**(H_A = ^2H), respectively.

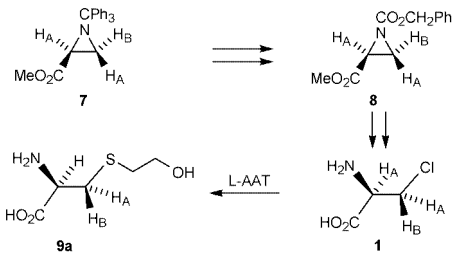

7 **8** **9a** **1**

Scheme 2

The enzyme L-aspartate aminotransferase (EC 2.6.1.1) was isolated by a standard purification protocol[12] from *E. coli* TY103[13] which was transformed with plasmid pKDHE19/AspC.[14] It had specific activity of 36.57 units mg^{-1} and appeared as one major band of molecular weight 43000 Da on SDS-PAGE. Incubation with (2*R*,3*R*)-[2,3-$^2H_2$]-β-chloroalanine **1**(H_A = ^2H) in the presence of a variety of thiols and under various conditions was now undertaken. The best results were obtained at pH 8.4 when mercaptoethanol was employed‡ and samples of labelled 3-(2-hydroxyethyl)cysteine **9a** were obtained in which the α-deuterium atom had exchanged as expected from the mechanism in Scheme 1. The β-deuterium atom also exchanged on prolonged incubation, an effect which had been previously noted in reactions with this enzyme.[15,16] However, when the incubation was stopped after 3 h, a sample of (2*R*)-3-(2-hydroxyethyl)cysteine **9a** was obtained with a ^1H NMR spectrum which showed that there was stereospecific

DOI: 10.1039/b000442l

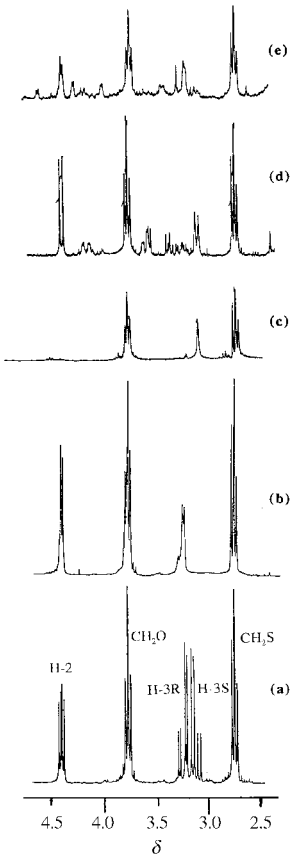

Fig. 1 ^{1}H NMR spectra in 10% ^{2}HCl–^2H_2O of (a) synthetic (2*R*)-3-(2-hydroxyethyl)cysteine **9**, (b) synthetic (2*R*,3*S*)-[3-$^2H_1$]-3-(2-hydroxyethyl)cysteine **9b**(H_B = ^{2}H), (c) synthetic (2*R*,3*R*)-[2,3-$^2H_2$]-3-(2-hydroxyethyl)cysteine **9b**(H_A = ^{2}H), (d) product from incubation of (2*R*,3*R*)-[2,3-$^2H_2$]-β-chloroalanine **1**(H_A = ^{2}H) with L-aspartate aminotransferase and (e) product from incubation of (2*R*,3*S*)-[3-$^2H_1$]-β-chloroalanine **1**(H_B = ^{2}H) with L-aspartate aminotransferase.

labelling at C-3 [Fig. 1(d)]. (2*R*,3*S*)-[3-$^2H_1$]-3-β-Chloroalanine **1**(H_B = ^{2}H) was therefore incubated for the same time when the ^{1}H NMR spectrum [Fig. 1(e)] of the product **9a** indicated that it was the C-3 epimer.

The trapping reaction was evidently stereospecific and it was now necessary to determine the absolute stereochemistry of the overall reaction. This was achieved by independent synthesis of samples of (2*R*)-3-(2-hydroxyethyl)cysteine **9b** which were labelled stereospecifically with deuterium at C-3 in an unambiguous manner. This is shown in Scheme 3, the labelled carbobenzyloxyaziridines **8** being reacted with mercaptoethanol containing a catalytic quantity of boron trifluoride etherate. Inversion of stereochemistry at the labelled atom, C-3, is expected and ^{1}H and ^{2}H NMR spectra showed that the labelled products† were single diastereoisomers. Hydrolysis in refluxing 4 M H_2SO_4 then gave the free amino acids **9b**.

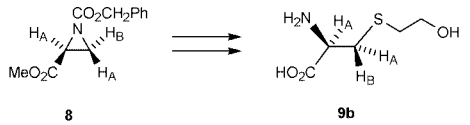

8 **9b**

Scheme 3

The ^{1}H NMR spectra of the synthetic samples of (2*R*,3*S*)-[3-$^2H_1$]-3-(2-hydroxyethyl)cysteine **9b**(H_B = ^{2}H)† [Fig. 1(b)] and (2*R*,3*R*)-[2,3-$^2H_2$]-3-(2-hydroxyethyl)cysteine **9b**(H_A = ^{2}H)† [Fig. 1(c)] allowed the 3-*pro-S* and 3-*pro-R* protons in the spectrum of 3-(2-hydroxyethyl)cysteine **9** to be assigned and therefore the absolute stereochemistry of the incubation products to be deduced. It was evident that the product from the incubation using (2*R*,3*S*)-[3-$^2H_1$]-3-β-chloroalanine **1**(H_B = ^{2}H) was (2*R*,3*S*)-[3-$^2H_1$]-3-(2-hydroxyethyl)cysteine **9a**(H_B = ^{2}H) [Fig. 1(e)] and that the product when (2*R*,3*R*)-[2,3-$^2H_2$]-3-β-chloroalanine **1**(H_B = ^{2}H) was used was (2*R*,3*R*)-[3-$^2H_1$]-3-(2-hydroxyethyl)cysteine **9a**(H_A = ^{2}H) [Fig. 1(e)].

These results imply that the β-replacement reaction, which in this case is catalysed by an enzyme of the α-family whose normal function is transamination, occurs with overall retention of stereochemistry. This is the general expectation[10] for the PLP-mediated enzymes of the β-family where β-replacement reactions are the norm and may imply a closer relationship between families than homology[5] suggests. Although X-ray structures are available for aspartate aminotransferase[17] and other α-family enzymes, tryptophan synthase (EC 4.2.1.20) is one of the few enzymes of the β-family whose tertiary structure has been defined by X-ray cystallography.[18] It is interesting that, in the presence of thiols, tryptophan synthase has been shown to catalyse transamination and β-replacement of L-serine by mercaptoethanol.[19] Further, the Lys87Thr mutant of tryptophan synthase will not turn over the natural substrate serine in the absence of NH_4^+ but it will turn over β-chloro-L-alanine.[20]

We thank the BBSRC (K. J. M. B.) and the Leukaemia Research Fund (B. A.) for fellowships and the EPSRC for a studentship (S. M. W.), Mr C. Dadswell for NMR experiments, the EPSRC National Mass Spectrometry Service, Swansea for accurate mass measurements and Professor H. Kagamiyama for *E. coli* TY103 and plasmid pKDHE19/AspC.

Notes and references

† These compounds had the expected analytical and spectroscopic properties.

‡ Incubation conditions: β-chloro-L-alanine: (0.08 mmol) and 2-mercaptoethanol (0.15 mmol) in sodium arsenate buffer (2 ml) containing 80 units of enzyme.

1 A. E. Braunstein and M. M. Shemyakin, *Biokhimya*, 1953, **18**, 393.
2 D. E. Metzler, M. Ikawa and E. E. Snell, *J. Am. Chem. Soc.*, 1954, **76**, 648.
3 H. C. Dunathan, *Proc. Natl. Acad. Sci. USA*, 1966, **55**, 712.
4 H. C. Dunathan and J. G. Voet, *Proc. Natl. Acad. Sci. USA*, 1974, **71**, 3888.
5 F. W. Alexander, E. Sandmeier, P. K. Mehta and P. Christen, *Eur. J. Biochem.*, 1994, **219**, 953.
6 Y. Morino, A. M. Osman and M. Okamoto, *J. Biol. Chem.*, 1974, **249**, 6684.
7 Y. Morino and S. Tanase, *J. Biol. Chem.*, 1978, **253**, 252.
8 D. Cavallini, G. Federici, F. Bossa and F. Granata, *Eur. J. Biochem.*, 1973, **39**, 301.
9 T. S. Soper and J. M. Manning, *Biochemistry*, 1978, **17**, 3377.
10 D. W. Young, *Top. Stereochem.*, 1994, **21**, 381.
11 K. J. M. Beresford and D. W. Young, *Tetrahedron*, 1996, **52**, 9891.
12 M. Herold and K. Kirschner, *Biochemistry*, 1990, **29**, 1907.
13 T. Yano, S. Kuramitsu, S. Tanase, Y. Morino, K. Hiromi and H. Kagamiyama, *J. Biol. Chem.*, 1991, **266**, 6079.
14 S. Kamitori, K. Hirotsu, T. Higuchi, K. Kondo, K. Inoue, S. Kuramitsu, H. Kagamiyama, Y. Higuchi, N. Yasuoka, M. Kusunoki and Y. Matsuura, *J. Biochem.*, 1987, **101**, 813.
15 U. Walter, H. Luthe, F. Gerhart and H.-D. Söling, *Eur. J. Biochem.*, 1975, **59**, 395.
16 U. M. Babu and R. B. Johnston, *Biochemistry*, 1976, **15**, 5671.
17 See for example: V. N. Malashkevich, M. D. Toney and J. N. Jansonius, *Biochemistry*, 1993, **32**, 13451.
18 T. R. Schneider, E. Gerhardt, M. Lee, P.-H. Liang, K. S. Anderson and I. Schlichting, *Biochemistry*, 1998, **37**, 5394.
19 E. W. Miles, M. Hatanaka and I. P. Crawford, *Biochemistry*, 1968, **7**, 2742.
20 Z. Lu, S. Nagata, P. McPhie and E. W. Miles, *J. Biol. Chem.*, 1993, **268**, 8727.

Communication b000442l

ChemComm

Molecular beacons attached to glass beads fluoresce upon hybridisation to target DNA

Lynda J. Brown,[a] Jon Cummins,[b] Alan Hamilton[b] and Tom Brown*[a]

[a] *Department of Chemistry, University of Southampton, Highfield, Southampton, UK SO17 1BJ*
[b] *Nycomed Amersham, Amersham Laboratories, White Lion Road, Amersham, UK HP7 9LL*

Received (in Liverpool, UK) 13th January 2000, Accepted 1st March 2000

Molecular beacons attached to glass beads have been synthesised which are non-fluorescent until exposed to a complementary target nucleic acid, whereupon they fluoresce, indicating hybridisation.

Tyagi and Kramer[1] have described a novel technology for the detection of specific nucleic acids in homogeneous solution. These probes, denoted 'molecular beacons', fluoresce upon hybridisation to their complementary DNA target. The essential feature of the probes is their stem–loop structure. The loop portion is an oligodeoxynucleotide probe for a complementary target nucleic acid. The stem is constructed of two short oligodeoxynucleotide arms, one which is terminally labelled with a fluorophore and the other with a quencher. Annealing of the arms causes intramolecular energy transfer from the fluorophore to the quencher. In this 'closed' conformation the probe is non-fluorescent. Hybridisation of the loop to its target causes the stem to open, the fluorophore and quencher are no longer in close proximity and fluorescence is emitted (Fig. 1).

Molecular beacons have been used in the detection of specific complementary sequences,[2–7] and the simultaneous detection of different pathogenic retroviruses has been reported.[8] Molecular beacons are able to distinguish between wild-type and single point mutations[3,9] and in real-time monitoring of the polymerase chain reaction (PCR) amplicon-specific probes lead to an increase in fluorescence intensity with increasing copy number of target DNA.

We have developed a modification of this technology that involves supporting the molecular beacons on solid glass particles (Fig. 2) and we have shown that glass-bound beacons exhibit similar properties to their soluble analogues. This technology could be harnessed in nucleic acid screening as hybridisation of CPG-bound beacons to target DNA or RNA generates fluorescent beads that can be isolated and analysed.

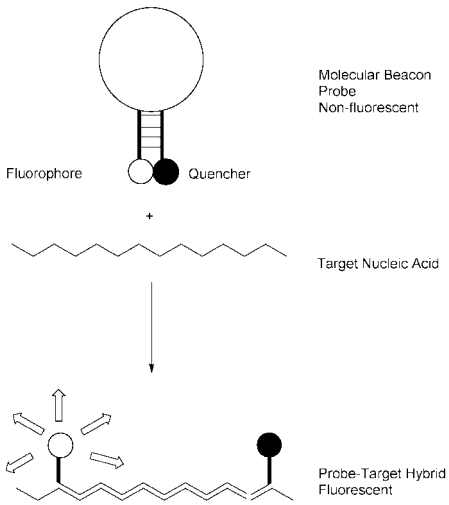

Fig. 1 Mechanism of action of molecular beacons in the presence of a complementary target nucleic acid.

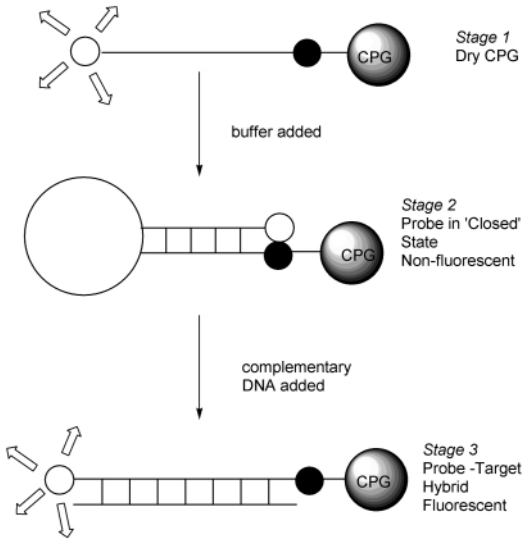

Fig. 2 Stages in assay of CPG-bound beacons.

Long chain alkyl amino-controlled pore glass (LCAA-CPG) was derivatised with a polyalkyl linker as shown in Scheme 1: first, the primary hydroxy group of 12-hydroxydodecanoic acid was protected as a 4,4′-dimethoxytrityl (DMT) ether.[10] Then, the carboxylic acid moiety was coupled to free amino groups on the CPG using DIC/HOBT (DIC = 1,3-diisopropylcarbodiimide, HOBT = 1-hydroxybenzotriazole) in 1% DIPEA–CH_2CCl_2 (DIPEA = *N*,*N*-diisopropylethylamine) to create a stable amide bond between the linker and CPG. The loading of the linker on the CPG was determined by acid-catalysed detritylation followed by quantitation at 495 nm using a UV–VIS spectrometer. The appropriate amount of CPG was used for 0.2 mmol scale oligonucleotide synthesis on a ABI 394 DNA synthesiser. Coupling efficiencies of > 98.5% were achieved by extending the coupling time from 45 s to 10 min.

In order to establish suitable conditions for the hybridisation of CPG-bound oligonucleotides to solution nucleic acids, an oligonucleotide, CGAGATACGGTTTTCACAGC (OG1), was assembled† on the LCAA-CPG. The CPG was heated (60 °C) in

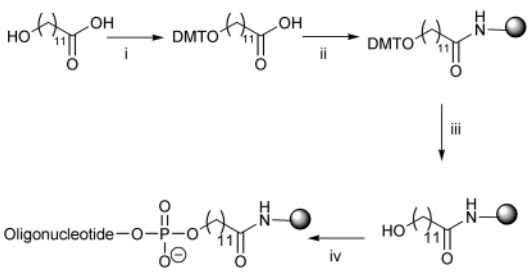

Scheme 1 Derivitisation of LCAA-CPG with a polyalkyl linker and oligonucleotide synthesis. *Reagents and conditions*: i, DMTCl, pyridine, room temp.; ii, LCAA-CPG, DIC, HOBT, DIPEA, CH_2Cl_2; iii, 5% CCl_3CO_2H, CH_2Cl_2; iv standard automated DNA synthesis.

DOI: 10.1039/b000389l

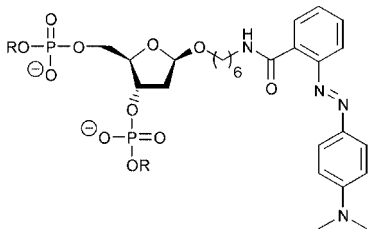

Fig. 3 Methyl Red phosphoramidite, the quencher used at the 3′ ends of CPG-bound probes.

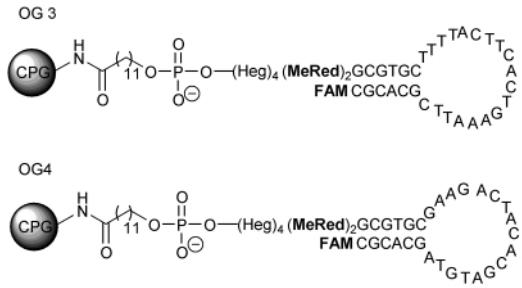

Fig. 4 Chemical structure of the CPG-bound molecular beacon probes.

conc. aqueous ammonia–ethanol (4 : 1 v/v) for 4 h and washed thoroughly with anhydrous CH_2Cl_2, to remove the cleaved protecting groups. An oligonucleotide GCTGTGAAAACCG-TATCTCG (OG2) of complementary sequence to the CPG-bound oligonucleotide (OG1) was synthesised and purified using standard methods. OG2 (0.22 OD) was mixed with the CPG-oligonucleotide (OG1) in 30 μL of an aqueous buffer of sodium hydrogenphosphate (10 mmol), EDTA (1 mmol) and NaCl (1 M) at pH 7.0, such that the CPG-bound oligonucleotide was in fourfold excess. The heterogeneous mixture was allowed to stand at room temperature for 3 h after which the absorbance (260 nm) of the CPG solution gave a reading of 0.035. This corresponds to a reduction of 84% of oligonucleotide in free solution. UV melting of the mixture gave a smooth transition as the oligonucleotide was released from the CPG into solution (T_m = 83.6 °C).

Two molecular beacons were assembled by solid phase DNA synthesis on the polyalkylamide LCAA-CPG previously described (Scheme 1). Both oligonucleotides were labelled at the 5′ end with fluorescein (FAM);

CGCACGCTTAAAGTCACTTCATTTTCGTGCG (OG3)

CGCACGATGTAGCACATCAGAAGCGTGCG (OG4).

Four hexaethylene glycol (Heg) spacers were incorporated between the CPG and the methyl red quencher (MeRed) to minimise steric interference from the solid support (Figs. 3, 4). Two complementary solution oligonucleotides were synthesised;

AAAATGAAGTGACTTTAAG (OG5), CTTCTGATGTGC-TACAT (OG6).

The molecular beacon-functionalised CPGs were heated (60 °C) in conc. aqueous ammonia–ethanol (4 : 1 v/v) for 4 h, to deprotect the oligonucleotides. Both solutions became fluorescent during this period implying loss of oligonucleotide from the CPG (*ca.* 70% loss of oligonucleotide from the resin). However subsequent thorough washing of the CPG afforded glass beads that remained fluorescent, indicating that some of the oligonucleotide was still present on the beads. Cleavage of a proportion of the silicon–oxygen bonds within the glass is inevitable under these strongly basic conditions. Alternative deprotection conditions or CPG material may be beneficial for future applications.

The heterogeneous beacon assay was carried out in two stages. First, the CPGs (OG3 and OG4, 2 mg) were placed in an aqueous buffer of sodium hydrogenphosphate (10 mmol), EDTA (1 mmol) and NaCl (1 M) at pH 7.0 to facilitate annealing. Then, the complementary oligonucleotides (OG5 and OG6) were added and after 2 h at room temperature any increase in fluorescence due to hybridisation (stem dissociation) was noted. Fluorescence was monitored under a fluorescence microscope (LEITZ DM IL) and photographed (ASHAI PENTAX K1000).

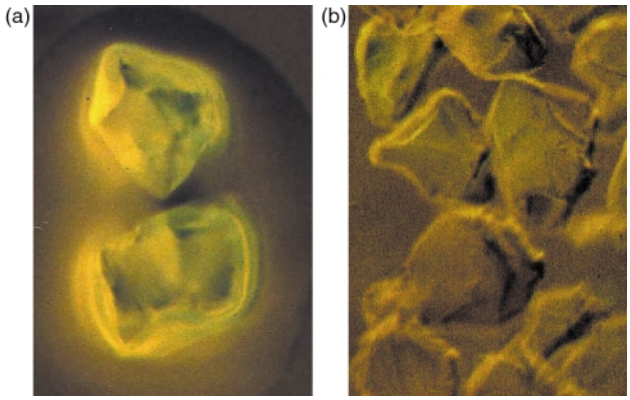

Fig. 5 (a) CPG-beacon in buffer and (b) CPG-beacon in buffer and complementary target nucleic acid.

Addition of a suitable annealing buffer causes the beads to become non-fluorescent [Fig. 5(a)], indicating the presence of a hairpin loop. Introduction of a complementary oligonucleotide in solution causes a significant increase in the fluorescence of the beads, due to the loop portion of the probe annealing to its target, allowing the solid-supported molecular beacons to exist in the fluorescent 'open' state [Fig. 5(b)]. Exposure of the CPG-beacons to a non-complementary oligonucleotide in the same buffer did not increase the level of fluorescence on the beads.

In summary, we have synthesised CPG-bound molecular beacon probes. These single-stranded probes have been shown to detect the presence of their target nucleic acids. At present, we are investigating the properties of alternative resins that have more uniform and spherical structures and we are applying the CPG-bound probes to the differentiation of nucleic acid sequences by variation of the fluorophore.

We thank the BBSRC and Nycomed Amersham for financial support of this work.

Notes and references

† All oligonucleotides were prepared in the Oswel Research Products Laboratory, Boldrewood, University of Southampton, Southampton, UK SO16 7PX.

1 S. Tyagi and F. R. Kramer, *Nat. Biotechnol.*, 1996, **14**, 303.
2 A. S. Piatek, S. Tyagi, A. C. Pol, L. P. Miller, F. R. Kramer and D. Alland, *Nat. Biotechnol.*, 1998, **16**, 359.
3 L. G. Kostrikis, S. Tyagi, M. M. Mhlanga, D. D. Ho and F. R. Kramer, *Science*, 1998, **279**, 1228.
4 L. G. Kostrikis, Y. Huang, J. P. Moore, S. M. Wolinsky, L. Zhang, Y. Guo, L. Deutsch, J. Phair, A. U. Neumann and D. D. Ho, *Nat. Med.*, 1998, **4**, 350.
5 R. Ehricht, T. Kirner, T. Ellinger, P. Foerster and J. S. McCaskill, *Nucleic Acids Res.*, 1997, **25**, 4697.
6 W. Gao, T. Tyagi, F. R. Kramer and E. Goldman, *Mol. Microbiol.*, 1997, **25**, 707.
7 B. A. J. Giesendorf, J. A. M. Vet, E. J. M. G. Mensink, F. J. M. Trijbels and H. J. Bolm, *Clin. Chem.*, 1998, **44**, 482.
8 J. A. M. Vet, A. R. Majithia, S. A. E. Marras, S. Tyagi, S. Dube, B. J. Poiesz and F. R. Kramer, *Proc. Natl. Acad. Sci. U.S.A.*, September 1998.
9 S. Tyagi, D. P. Bratu and F. R. Kramer, *Nat. Biotechnol.*, 1998, **16**, 49.
10 M. Smith, D. H. Rammler, I. H. Goldberg and H. G. Khorana, *J. Am. Chem. Soc.*, 1963, **84**, 430.

Communication b000389l

ChemComm

Formation of platinum nanosheets between graphite layers

Masayuki Shirai,* Koichi Igeta and Masahiko Arai

Institute for Chemical Reaction Science, Tohoku University, Katahira, Aoba, Sendai, 980-8577, Japan.
E-mail: mshirai@icrs.tohoku.ac.jp

Received (in Cambridge, UK) 13th August 1999, Accepted 3rd March 2000

Platinum nanosheets with thickness 2–3 nm containing hexagonal holes were formed between graphite layers by hydrogen reduction of platinum chloride–graphite intercalation compounds.

The size and shape of metal particles formed in a matrix are determined by its structural features. Platinum nanowires are formed in the mesotubes of FSM-16[1,2] and nanorods and nanoparticles are produced in the channels of carbon nanotubes.[3–6] Graphite has a layered structure, and each layer is a regular hexagonal net of carbon atoms. The interlayer spacing is equal to 0.335 nm with the layers interacting *via* van der Waals forces. Because the interaction between graphite layers is fairly weak, a variety of chemical substances can be inserted into the interlayer space to produce graphite intercalated compounds (GICs). Transition metal particles intercalated in graphite layers (M–GICs) are formed *via* the insertion of transition metal chlorides into graphite and subsequent reduction.[7–9] Commercially available M–GICs (Graphimet)[10] have numerous applications for catalytic reactions.[11–16] Graphimets are obtained by treating the graphite–metal chloride with lithium biphenyl at 223 K under a helium atmosphere and small metal particles (1–10 nm) were observed by HRTEM observations.[17] In the present work using different preparation procedures, we report the formation of platinum metal nanosheets containing hexagonal holes, intercalated within graphite layers.

Platinum(IV) chloride and graphite (KS6, Lonza) were mixed in a thick walled Pyrex reactor under nitrogen atmosphere and dried *in vacuo* at 423 K for 2 h. The intercalation reaction was performed in the reactor at 723 K for 2 weeks under 0.3 MPa of chlorine (Takachiho, 99.999%), to obtain the platinum chloride intercalated compounds ($PtCl_4$–GIC). The $PtCl_4$–GIC samples were reduced at 573 K for 1 h under 40 kPa hydrogen to produce the platinum metal intercalated compounds (Pt–GIC).

The XRD pattern of 5 wt% $PtCl_4$–GIC (platinum loading: 5 wt%) shows new peaks at 2θ = 10.0, 14.6 and 20.3°.† The peaks ascribed to platinum chloride disappeared and the (002) diffraction peak of graphite at 2θ = 26.57° was weakened after the reaction under chlorine atmosphere. The three new peaks remained unaltered after 12 days exposure to air, indicating that $PtCl_4$–GIC is stable in air. Peaks ascribed to platinum chloride and graphite were observed on XRD patterns of a reference mixture of platinum chloride and graphite [$PtCl_4$/G (mix)]. The platinum chloride peaks of $PtCl_4$/G(mix) changed after a few days exposure to air because of the hygroscopicity of platinum chloride. The diffraction peak positions calculated for (002), (003) and (004) reflections for $PtCl_4$–GIC of the repeat distance along the *c* axis (*c* = 1.76 nm) were 10.0, 15.1 and 20.2°, respectively, in good agreement with the experimental peaks. The distance of 1.76 nm corresponds to the sum of three graphite layers and one intercalated layer (0.75 nm). This result shows that platinum chloride is intercalated in every three graphite layers (stage three structure) in the 5 wt% $PtCl_4$–GIC sample. With an increasing amount of platinum chloride inserted from 1 to 15 wt% Pt loadings, the three peaks increased and the diffraction for (002) of graphite decreased. No other peaks except for the three peaks and graphite peaks were observed. The XRD results indicate that platinum chloride is intercalated in graphite layers with the stage three structure for 1–15 wt% Pt loading. The maximum amount of platinum chloride that can be intercalated is *ca.* 38 wt%, and thus platinum chloride intercalated compounds with the stage three structure are mixed with the graphite matrix at low platinum chloride loadings under our experimental conditions. EXAFS analysis showed the existence of Pt–Cl–Pt bonds in the 5 wt% $PtCl_4$–GIC sample, indicating that some platinum chloride molecules aggregate with each other within graphite layers at low platinum loadings.

Fig. 1(a) shows TEM image of 5 wt% Pt–GIC reduced at 573 K. This image reveals large sheets with a number of hexagonal holes with the edge angles of the large sheets being 120°. X-Ray microanalysis (XMA) results confirmed the dark images to be

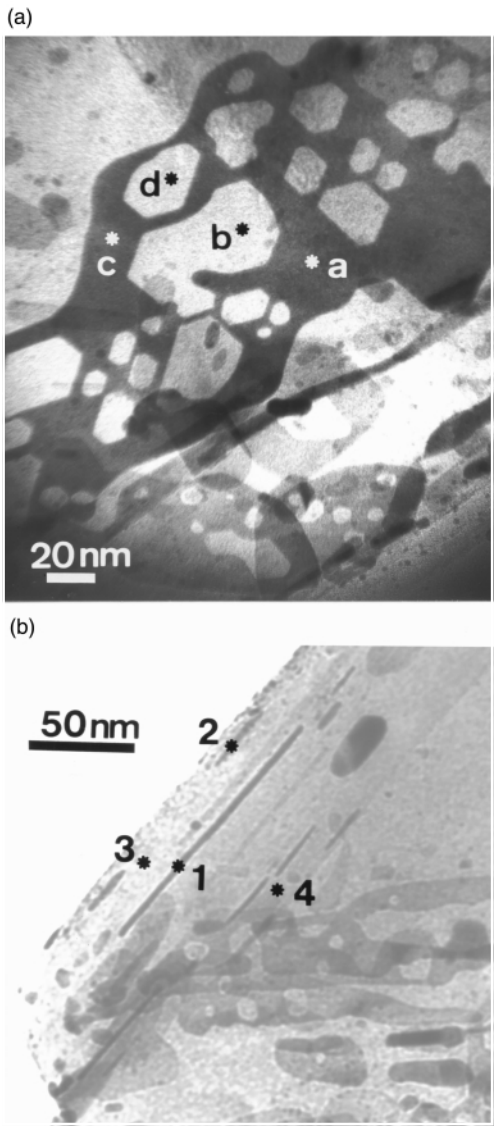

Fig. 1 TEM images of 5 wt% Pt–GIC showing Pt nanosheets; (a) top view and (b) side view.

DOI: 10.1039/a906596b

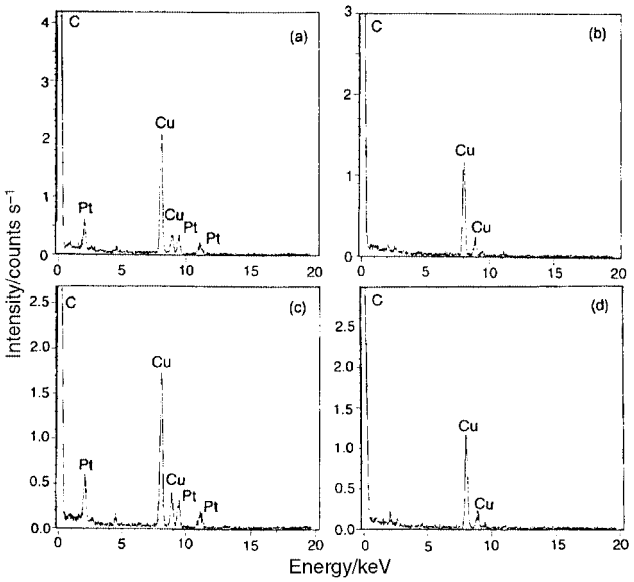

Fig. 2 XMA results of 5 wt% Pt–GIC at points a, b, c and d as indicated in Fig. 1(a).

platinum metal (Fig. 2).‡ Fig. 1(b) shows the presence of dark images in a parallel rod-like arrangement. XMA scans obtained from regions 1 and 2 showed that the dark material corresponded to platinum metal while XMA scans obtained from regions 3 and 4 indicated the absence of platinum metal, indicating that the dark features correspond to platinum layers. The TEM images show the structure of the platinum nanosheets, which are 2–3 nm thick and 5–300 nm wide. The observation of a number of sheets in parallel presumably indicates that platinum sheets exist between graphite layers. Platinum chloride can aggregate only two dimensionally between graphite layers during reduction because of the steric hindrance of graphite layers, so that the resulting platinum metal particles of Pt–GIC have two-dimensional structures. Platinum chloride molecules are reduced in a small area to produce small particles (1–10 nm) and do not move between graphite layers upon low temperature reduction at 223 K.[14,15,17] On the other hand, platinum atoms and/or platinum chloride molecules can migrate along a regular hexagonal net of carbon atoms during hydrogen reduction at 573 K. Movement during the reduction will determine the morphology of the resulting platinum nanosheets which have hexagonal holes. A number of nanosheets with hexagonal holes were also observed in TEM images of the 5 wt% Pt–GIC sample reduced at 773 K for 1 h after reduction at 573 K for 1 h. Large spherical particles still were not observed because the platinum nanosheets are still prevented from moving freely between graphite layers. For comparison, the mixture 5 wt% $PtCl_4$/G(mix) upon reduction at 573 K [Pt/G(mix)] led to spherical platinum particles according to TEM (Fig. 3).§ For $PtCl_4$/G(mix) samples platinum chloride molecules on the graphite surface can aggregate in a three dimensional manner and there is no interfering factor for the growth of metal particles, and so large platinum particles are formed.

In conclusion, platinum nanosheets can be prepared between graphite layers for Pt–GIC sample and such complex materials may show interesting properties owing to their structural features and metal–graphite interactions.

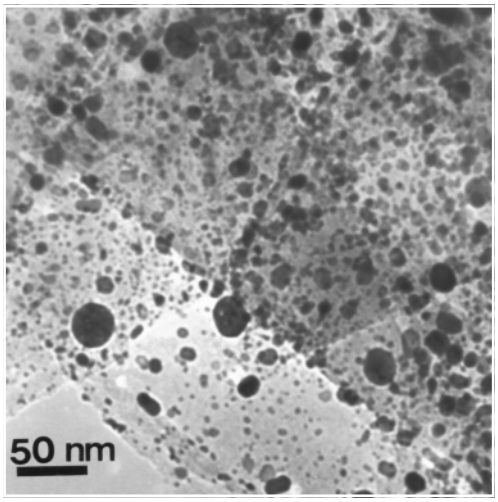

Fig. 3 TEM image of 5 wt% Pt/G(mix).

We thank Dr E. Aoyagi and Dr Y. Hayasaka (High Voltage Electron Microscope Laboratory of Tohoku University) for the TEM and XMA analysis.

Notes and references

† X-Ray diffraction measurements were performed on a Shimadzu XD-D1 instrument (30 kV, 20 mA) using a copper Kα source.
‡ TEM and XMA measurements were performed on a JEOL JEM-3010 instrument (300 keV) using copper grids.
§ TEM measurements were performed on a JEOL JEM-2000ExII instrument (200 keV) using copper grids.

1 M. Sasaki, N. Higashimoto, A. Fukuoka and M. Ichikawa, *Microporous Mesoporous Mater.*, 1998, **21**, 597.
2 M. Sasaki, M. Osada, N. Higashimoto, T. Yamamoto, A. Fukuoka and M. Ichikawa, *J. Mol. Catal. A*, 1999, **141**, 223.
3 T. Kyotani, L. Tsai and A. Tomita, *Chem. Commun.*, 1997, 701.
4 B. K. Pradhan, T. Toba, T. Kyotani and A. Tomita, *Chem. Mater.*, 1998, **10**, 2510.
5 Y. Li, J. Chen, Y. Ma, J. Zhao, Y. Qin and L. Chang, *Chem. Commun.*, 1999, 1141.
6 P. Chen, X. Wu, J. Lin and K. L. Tan, *J. Phys. Chem. B*, 1999, **22**, 4559.
7 M. E. Volpin, Y. N. Novikov, N. D. Lapkina, V. I. Kasatochkin, Y. T. Struchkov, M. E. Kazakov, R. A. Stukan, V. A. Povitskij, Y. S. Karimov and A. V. Zvarikina, *J. Am. Chem. Soc.*, 1975, **97**, 3366.
8 J. Tilquin, R. Cote, G. Veilleux, D. Guay, J. P. Dodelet and G. Denes, *Carbon*, 1995, **33**, 1265.
9 J. Walter and H. Shioyama, *Phys. Lett. A*, 1999, **254**, 65.
10 J. M. Lalancette, *US Pat.* 3847963 (November 12, 1974).
11 S. I. Chii, A. L. DeVera and M. C. Hawley, *Fuel*, 1986, **65**, 1432.
12 A. Frusta, F. Hoofer and H. Weidmann, *J. Catal.*, 1989, **118**, 502.
13 G. Sirokman, A. Mastalir, A. Molnar, M. Bartok, Z. Schay and L. Guczi, *J. Catal.*, 1989, **117**, 558.
14 G. Siroknam, A. Mastalir, A. Molnar, M. Bartok, Z. Schay and L. Guczi, *Carbon*, 1990, **28**, 35.
15 F. Notheisz, A. Mastalir and M. Bartok, *J. Catal.*, 1992, **134**, 608.
16 A. Mastalir, F. Notheisz, M. Bartok, T. Haraszti, Z. Kiraly and I. Dekany, *Appl. Catal. A*, 1996, **144**, 237.
17 D. J. Smith, R. M. Fisher and L. A. Freeman, *J. Catal.*, 1981, **72**, 51.

Communication a906596b

ChemComm

Iridium-catalyzed aziridination of aliphatic aldehydes, aliphatic amines and ethyl diazoacetate

Takashi Kubo, Satoshi Sakaguchi and Yasutaka Ishii*

Department of Applied Chemistry, Faculty of Engineering and High Technology Research Center, Kansai University, Suita, Osaka 564-8680, Japan. E-mail: ishii@ipcku.kansai-u.ac.jp

Received (in Cambridge, UK) 18th January 2000, Accepted 6th March 2000

Three-component coupling reactions of aliphatic aldehydes, aliphatic amines and ethyl diazoacetate to the corresponding aziridine derivatives has been achieved by the use of $[Ir(cod)Cl]_2$ as a catalyst under mild conditions; for instance, the reaction of *n*-butyraldehyde, *tert*-butylamine and ethyl diazoacetate in the presence of a catalytic amount of $[Ir(cod)Cl]_2$ in THF at −10 °C gave 1-*tert*-butyl-2-ethoxycarbonyl-3-propylaziridine in 85% yield in high stereoselectivity (*cis* : *trans* = 96 : 4).

Aziridines are versatile compounds as precursors for the synthesis of various types of nitrogen-containing compounds, which are biologically important, such as amino acids, amino alcohols and β-lactams, *etc.*[1] There are many reports on the synthesis of aziridines, *e.g.* trapping of nitrenes and carbenes by alkenes[2] and imines,[3] respectively, and Lewis acid-catalyzed reaction of imines with ethyl diazoacetate (EDA).[4] These methods are suitable for the synthesis of aziridines derived from aromatic imines and diazo compounds; however, aziridine synthesis from aliphatic imines and EDA has not yet been established. Recently, Nagayama and Kobayashi have reported a three-component coupling reaction of aldehydes, amines and EDA in the presence of $Ln(OTf)_3$, although 5 Å molecular sieves must be added to the reaction system.[5] Now we have found that the three-component coupling reaction of aliphatic aldehydes, aliphatic amines and EDA to aziridine derivatives proceeds smoothly using an iridium complex as a catalyst and without any dehydrating agents [eqn. (1)].

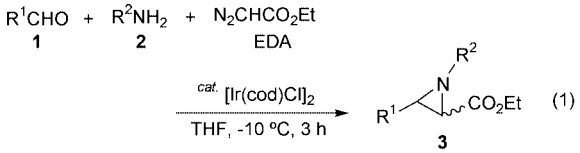

To a solution of $[Ir(cod)Cl]_2$ in THF was added *n*-butyraldehyde **1a** and *n*-butylamine **2a**. After stirring for 10 min, EDA was added and then the mixture was stirred at −10 °C for 3 h (standard conditions).† The reaction produced 1-butyl-2-ethoxycarbonyl-3-propylaziridine **3aa**‡ which consists of a *ca.* 1 : 1 stereoisomeric mixture of *cis*-**3aa** and *trans*-**3aa** in 71% yield (Table 1, run 1). Table 1 summarizes the results for various three-component coupling reactions of aldehydes, amines and EDA under selected reaction conditions. $[Ir(cyclooctene)_2Cl]_2$ also catalyzed the coupling reaction to form **3aa** in 75% yield, while $IrCl_3$ was inert (runs 2 and 3). Various solvents could be employed for this reaction. (runs 4–6).

On the basis of these results, the reaction of aldehydes, amines and EDA was examined in the presence of a catalytic amount of $[Ir(cod)Cl]_2$ in THF under standard conditions. The reaction led to the corresponding aziridines in fair to good yields (runs 7–11). Interestingly, the stereoselectivity of the resulting aziridines was found to be improved by the use of a bulky amine such as *tert*-butylamine **2f**. For instance, the reaction of **1a**, **2e** with EDA afforded 1-*tert*-butyl-2-ethoxycarbonyl-3-propylaziridine **3af** in 83% yield in excellent stereoselectivity (*cis* : *trans* = 96 : 4) (run 11).§ In this reaction, ethanol was also suitable as a solvent, and **3af** was obtained in almost the same yield and stereoselectivity as those in THF (run 12). No aziridine was detected in the reaction of benzaldehyde **1d**, aniline **2g**, and EDA under these reaction conditions (run 13). These results will be discussed later.

Table 1 Three-component coupling reaction of aldehyde **1**, amine **2** and EDA[a]

Run	Aldehyde	Amine	Adirizine	Yield (%)[b]	
1	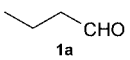 **1a**	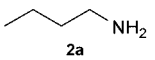 **2a**	**3aa**	71	(63/37)
2[c]	**1a**	**2a**	**3aa**	75	(52/48)
3[d]	**1a**	**2a**	**3aa**	No reaction	
4[e]	**1a**	**2a**	**3aa**	68	(46/54)
5[f]	**1a**	**2a**	**3aa**	74	(53/47)
6[g]	**1a**	**2a**	**3aa**	79	(63/37)
7	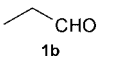 **1b**	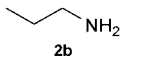 **2b**	**3bb**	52	(57/43)
8	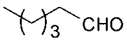 **1c**	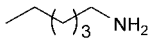 **2c**	**3cc**	54	(51/49)
9	**1a**	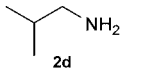 **2d**	**3ad**	76	(63/37)
10	**1a**	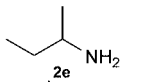 **2e**	**3ae**	83	(83/14)
11	**1a**	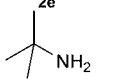 **2f**	**3af**	83	(96/ 4)
12[g]	**1a**	**2f**	**3af**	82	(96/ 4)
13	Ph—CHO **1d**	Ph—NH_2 **2g**	**3dg**	No reaction	

[a] Aldehyde (1 mmol), amine (1 mmol) and EDA (2 mmol) were allowed to react in the presence of $[Ir(cod)Cl]_2$ (0.05 mmol) in THF (1 mL) at −10 °C for 3 h under Ar atmosphere. [b] Parentheses indicate *cis*/*trans* ratio. [c] $[Ir(cyclooctene)_2Cl]_2$ (0.05 mmol) used as catalyst. [d] $IrCl_3$ (0.05 mmol) used as catalyst. [e] Dichloromethane (1 mL) used as solvent. [f] *n*-Hexane (1 mL) used as solvent. [g] Ethanol (1 mL) used as solvent.

The present Ir-catalyzed three-component coupling reaction seems to proceed *via* the formation of imine which then reacts with EDA. Indeed, *N*-butylidene-*n*-butylamine **4aa** prepared independently from **1a** and **2a** was allowed to react with EDA under standard conditions to form **3aa** (73%) as expected [eqn. (2)]. Although the $La(OTf)_3$-catalyzed three-component coupling reaction requires the presence of 5 Å molecular sieves,[5] the present three-component coupling reaction was performed without any dehydrating agents. It is noteworthy that the Ir-

DOI: 10.1039/b000518p

catalyzed aziridination was not affected by water in the reaction system. When the reaction of imine **4aa** with EDA was carried out in the presence of a small amount of water, **3aa** was obtained in almost the same yield as the reaction in the absence of water [(eqn. (2)].

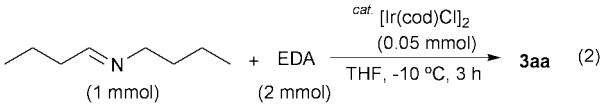

Additive	Yield (%)
–	73
H_2O (1 mmol)	69

Furthermore, the reaction of *N*-butylidene-*tert*-butylamine **4af** with EDA took place in high stereoselectivity, giving **3af** in 85% yield (*cis*:*trans* = 95:5) [(eqn. (3)]. For the reaction of *N*-benzylideneaniline **4dg** with EDA, however, diethyl maleate **5** and diethyl fumarate **6** were formed in 46% yield, and **4dg** was recovered unchanged.

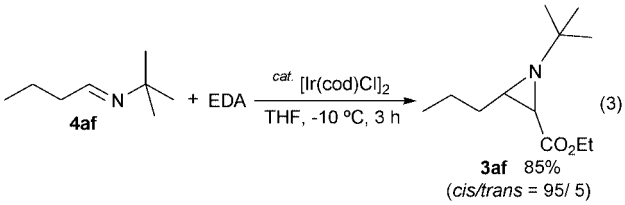

Addtionally, the reaction of a ketimine such as *N*-(1-ethylpropylidene)-*n*-butylamine with EDA led to 1-butyl-3,3-diethyl-2-ethoxycarbonylaziridine in 54% yield.

From the mechanistic point of view, it is of note that the selectivity of aziridine is affected by the order of the addition of substrates to the catalyst solution. When 1.0 mmol of imine **4aa** was added to a THF solution containing $[Ir(cod)Cl]_2$ (0.05 mmol) at −10 °C, the solution changed immediately from orange–red to light yellow, and EDA (2 mmol) was added to this solution to form aziridine **3aa** (73%). However, the addition of EDA (2.0 mmol) to a THF solution of $[Ir(cod)Cl]_2$ resulted in a change from orange–red to dark purple, and then **4aa** (1.0 mmol) was added to produce **3aa** in lower yield (59%) along with a homocoupling product of EDA, **5** and **6** (13%), the formation of which may be explained by *in situ* generation of carbene from EDA by the action of an Ir complex. Hence, it is probable that the present Ir-catalyzed aziridine synthesis proceeds *via* the formation of an Ir–imine complex rather than an Ir–carbene complex.

In addition, when imine **4dg** was added to a THF solution of $[Ir(cod)Cl]_2$, no color change was observed, and the aziridine expected was not obtained and instead, dimers of EDA, **5** and **6** as shown above. Therefore, it is reasonable to presume that the reaction of **4dg** with EDA is difficult to occur owing to the difficulty of the complexation of **4dg** with the Ir-complex.

The high stereoselectivity of the reaction of **1a**, **2f** and EDA (Table 1, run 11) may be explained by assuming a similar reaction path suggested in the $Yb(OTf)_3$-catalyzed reaction of *N*-benzylidene-*tert*-butylamine with EDA (Scheme 1).[4f] It is probable that the Ir complex $[Ir(cod)Cl]_2$ coordinates to imine **4af** to lead to a complex **A**.¶ The nucleophilic attack of EDA to the resulting complex **A** would take place from the direction to reduce the steric repulsion between the ester moiety of the incoming EDA and the *tert*-butyl group of the imine to form *cis*-**3af**.

In summary, various types of aziridine derivatives, which are difficult to prepare by the conventional methods, have been prepared by the three-component coupling reaction of aliphatic aldehydes, aliphatic amines and EDA, catalyzed by $[Ir(cod)Cl]_2$. High stereoselectivity was attained by the reaction of aldehyde, tertiary amine and EDA.

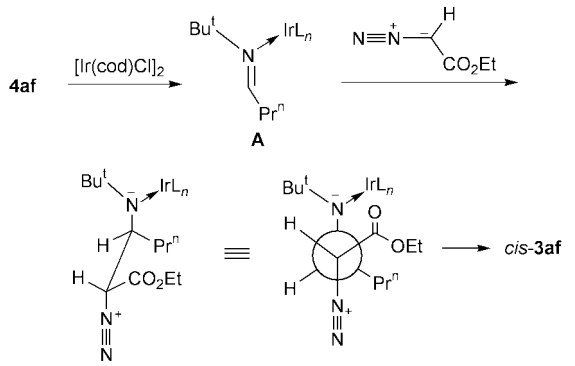

Scheme 1 A possible reaction pathway for reaction of **4af** with EDA.

Notes and references

† *Typical reaction procedure*: to a THF solution (1.0 mL) of dichlorobis(cycloocta-1,5-diene)diirdium {$[Ir(cod)Cl]_2$} (0.05 mmol) was added aldehyde (1.0 mmol) and amine (1.0 mmol) at −10 °C under Ar. After stirring for 10 min, EDA (2.0 mmol) was added, and then the reaction mixture was stirred at −10 °C for 3 h. The reaction was quenched with wet diethyl ether, and products were isolated by column chromatography [(230–400 mesh silica gel, ethyl acetate–hexane (1:12) eluent].

‡ *Spectral data* for **3aa**: ^{1}H NMR δ 4.25–4.15 (m, 2H), 2.42–2.06 (m, 2H), 2.09 (d, *J* 6.6 Hz, 1H), 1.72–1.69 (m, 1H), 1.60–1.30 (m, 6H), 1.31 (q, *J* 7.3 Hz, 2H), 1.27 (t, *J* 7.3 Hz, 3H), 0.92 (t, *J* 7.3 Hz, 3H), 0.90 (t, *J* 7.3 Hz, 3H); ^{13}C NMR δ 170.0, 60.8, 60.7, 46.6, 42.6, 31.4, 29.7, 20.6, 20.3, 14.3, 13.9, 13.7; IR (neat) 2959, 1747, 1183 cm^{-1}; MS, *m/z* = 213 (M^+), 198, 140, 84; Anal. Calc. for $C_{12}H_{23}NO_2$: C, 67.57; H, 10.87; N, 6.57. Found: C, 67.25, H, 10.52; N, 6.62%.

§ The stereochemistry of **3af** was determined by comparison of the coupling constant obtained from ^{1}H NMR spectral data for **3af** with that of 2-ethoxylcarbonyl-1,3-diphenylaziridine reported in the literature.[4a,f]

¶ NMR observation showed the formation of the complex **A** from $[Ir(cod)Cl]_2$ and imine; *i.e.* when $[Ir(cod)Cl]_2$ was added to 1.0 equiv. of **4af** in a NMR tube, the ^{13}C NMR signals at δ 164.5 (–CH=N–) and 61.0 (=NCH_2–) of **4af** were shifted to δ 171.6 and 63.6, respectively.

1 J. S. Brimacombe, R. Hanna and L. C. N. Tucker, *J. Chem. Soc., Perkin Trans. 1*, 1983, 2277; J. Martens and M. Scheunemann, *Tetrahedron Lett.*, 1991, **32**, 1417; D. Tanner, *Angew. Chem., Int. Ed. Engl.*, 1994, **33**, 599.

2 D. A. Evans, M. M. Faul and M. T. Bilodeau, *J. Am. Chem. Soc.*, 1994, **116**, 2742; Z. Li, K. R. Conser and E. N. Jacobsen, *J. Am. Chem. Soc.*, 1993, **115**, 5326; P. Muller, C. Baud and Y. Lacueier, *Tetrahedron*, 1996, **52**, 1543.

3 P. Baret, H. Buffet and J. L. Pierre, *Bull. Soc. Chim. Fr.*, 1972, 2493; A. J. Hubert, A. Feron, R. Warin and G. Mloston, *Tetrahedron Lett.*, 1976, 1317; R. Bartnik and G. Mloston, *Synthesis*, 1983, 924; V. K. Aggarwal, A. Thompson, R. V. H. Jones and M. C. H. Standen, *J. Org. Chem.*, 1996, **61**, 8368.

4 (*a*) K. B. Hansen, N. S. Finney and E. N. Jacobsen, *Angew. Chem., Int. Ed. Engl.*, 1995, **34**, 676; (*b*) Z. Zhu and J. H. Espenson, *J. Org. Chem.*, 1995, **60**, 7090; (*c*) Z. Zhu and J. H. Espenson, *J. Am. Chem. Soc.*, 1996, **118**, 9901; (*d*) L. Casarrubios, J. A Pérez, M. Brookhart and J. L. Templeton, *J. Org. Chem.*, 1996, **61**, 8358; (*e*) V. K. Aggarwal, A. Thompson, R. V. H. Jones and M. C. H. Standen, *J. Org. Chem.*, 1996, **61**, 8386; (*f*) K. G. Rasmuussen and K. A. Jørgensen, *J. Chem. Soc., Perkin Trans. 1*, 1997, 1287; (*g*) M. F. Mayer and M. M. Hossain, *J. Org. Chem.*, 1998, **63**, 6839; (*h*) K. Juhl, R. G. Hazell and K. A. Jørgensen, *J. Chem. Soc., Perkin Trans. 1*, 1999, 2293.

5 S. Nagayama and S. Kobayashi, *Chem. Lett.*, 1998, 685.

Communication b000518p

ChemComm

The role of neighbouring group participation in TTF-mediated 'radical-polar crossover' reactions: trapping of aliphatic radicals by $TTF^{+\bullet}$

Nadeem Bashir and John A. Murphy*

Department of Pure and Applied Chemistry, University of Strathclyde, 295 Cathedral Street, Glasgow, UK G1 1XL. E-mail: John.Murphy@strath.ac.uk

Received (in Cambridge, UK) 26th January 2000, Accepted 18th February 2000

Trapping of secondary alkyl radicals with tetrathiafulvalenium tetrafluoroborate ($TTF^{+\bullet}BF_4^-$) leads to *S*-alkyltetrathiafulvalenium tetrafluoroborate salts; the solvolysis of such salts is critically dependent on the presence of appropriately sited neighbouring groups.

The radical-polar crossover reaction[1] (Scheme 1) features a unique sequence of radical and polar steps in one pot. Tetrathiafulvalene (TTF) transfers an electron to an arenediazonium salt, dinitrogen is lost and the resulting radical can then cyclise before being trapped by the radical-cation of TTF to afford a sulfonium salt and terminate the radical chemistry. In the polar crossover step, solvolysis of the sulfonium salt occurs affording a useful functionalisation at the site of the ultimate radical. The reaction has recently been used as the key step in a novel route to (±)-aspidospermidine.[2]

The substitution (solvolysis) step is of particular interest. Whereas alcohols **8** and **9** were formed on treatment of diazonium salts **2** and **3** with tetrathiafulvalene **4** in undried acetone at room temperature, diazonium salt **1** proceeded only up to the tetrathiafulvalenium salt stage **5**. This strongly suggested that the solvolysis step involved an S_N1 substitution; solvolysis of the salt **5** would not be possible since it would require the intermediacy of a primary carbocation, while sulfonium salts **6** and **7** undergo solvolysis without difficulty. More recently, attempts to force the substitution of the sulfonium group of **5** uncovered a range of novel fragmentation reactions.[3]

Although **5** is resistant to solvolysis, the conversion[4] of the diallylamino diazonium salt **10** to the alcohol **13** suggested that matters could be more complex. Here, the powerful electron donating effect of the *ortho*-amino group must act through the aromatic ring to assist the departure of the TTF molecule from **11** *via* a cyclopropane intermediate **12**. However, the inability of the *ortho*-alkoxy group to trigger the solvolysis of **5** shows that there are strict demands for solvolysis at a primary carbon.[5] However, almost all examples of the radical-polar crossover reaction have involved substitution at secondary carbon. This paper provides experimental evidence that neighbouring group participation is mandatory for solvolysis at secondary carbon under our usual conditions and reveals the requirements for substrate structure in order for solvolysis to be observed.

To investigate whether solvolysis could occur at a secondary carbon in the absence of neighbouring groups, an alkyl radical free of other functionalities was required to be generated under radical-polar crossover conditions. This was achieved using intramolecular radical displacement at sulfur. This reaction has been investigated by the groups of Kampmeier,[6] Beckwith[7] and Schiesser.[8] More recently, Crich *et al.* have used this method to generate acyl radicals both from iodide[9] and diazonium salt[10] precursors. Accordingly, the cyclohexyl substrate **14** was prepared (all amines were prepared by reduction of the corresponding nitro compounds), diazotised and subjected to the radical-polar crossover conditions (Scheme 2). This afforded benzothiophene **16** (48%), (arising from facile elimination of methanol from methoxydihydrobenzothiophene **17** together with the salt **18** (32%) as major products. The S-coupled salt **18** was completely resistant to solvolysis under our conditions (room temperature, 2% water in acetone, 48 h), showing that a tetrathiafulvalenium salt linked *via* a secondary carbon could not of itself undergo solvolysis under these conditions.

Because the outcome of the experiment on the cyclohexyl radical differed from results found with all previously studied secondary radicals, there was some concern that the sulfur substitution reaction conditions might in some way have prevented the normal radical-polar crossover process from occurring. To test this, the intramolecular sulfur displacement reaction was used to generate a radical which had been previously studied under radical-polar conditions, namely **19**, the intermediate in the reaction of **2**. The required substrate, **20**, was prepared, diazotised and subjected to the radical-polar crossover reaction and afforded both dihydrobenzothiophene **21**

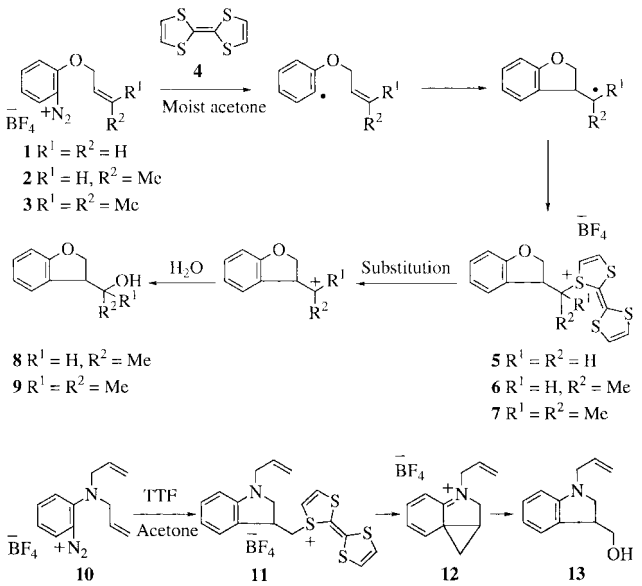

Scheme 1

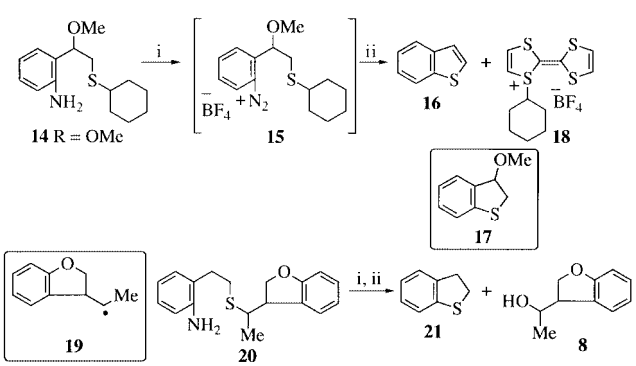

Scheme 2 *Reagents*: i, $NOBF_4$, CH_2Cl_2; ii, TTF, acetone, H_2O.

DOI: 10.1039/b000786m

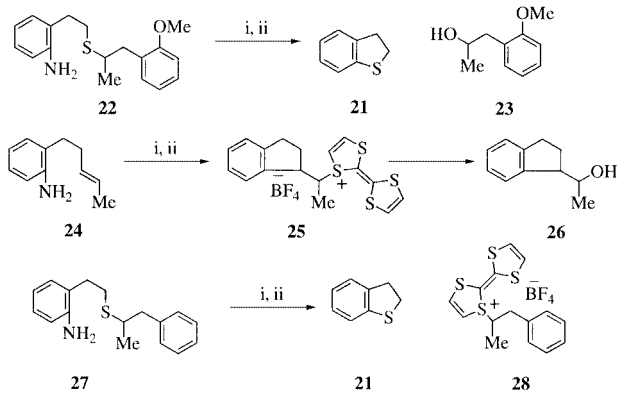

Scheme 3 *Reagents*: i, $NOBF_4$, CH_2Cl_2; ii, TTF, acetone, H_2O.

(52%) and the alcohol **8** (58%), showing that the radical **19** generated under these conditions was behaving exactly as it had in the reaction of **2**.

The contrast between cyclohexyl TTF salt **18** and salt **6** indicated that a solvolysis of a secondary TTF salt could not occur without some assistance from neighbouring groups. The nature and extent of the assistance were now probed directly. First, to investigate whether some special effect resulted from the dihydrobenzofuran ring system, amine **22** was prepared and diazotised to afford a diazonium salt analogue of **2** (Scheme 3). This duly cyclised to form dihydrobenzothiophene **21** (52%) and the alcohol **23** (53%). No TTF salts were detected after the solvolysis.

Next, amine **24**, lacking the electron-donating oxygen atom, was prepared and diazotised affording **25**. Surprisingly, the compound also afforded an alcohol product, *i.e.* **26** (24%), indicating that the oxygen atom is not essential for solvolysis.

In contrast, when the diazonium salt derived from **27** was subjected to the radical-polar crossover reaction, **21** was produced (45%) as well as the sulfur-coupled TTF salt **28** (21%). Intriguingly, this sulfur-coupled salt was stable to solvolysis. We deduce that there is a sharp demarcation between substrates that undergo solvolysis in acetone and those that do not. Salt **25** features an *ortho*-dialkylarene and so should be more electron-rich than the monosubstituted arene in **28**; hence it should more effectively promote neighbouring group participation.

The observation of neighbouring group assistance suggests an answer to one of the key questions on the mechanism of these reactions. Until now, solvolysis of TTF salts such as **29** (Scheme 4) was thought to involve intermediates such as the open secondary cation **30**. This cation should easily undergo rearrangement and/or fragmentation (*e.g.* to products **33** and **34**), but this was not observed. With neighbouring group participation, the delocalised cation **31** can be proposed as the true intermediate, and this involvement by the aryl ring can decelerate rearrangements by stabilising the cation and altering the orbital alignment from that required for rearrangement. (The delocalised cation could also control the stereochemistry of attack by the nucleophile water.)

The question now arose about whether groups other than an aromatic ring could assist the solvolysis step. An immediate answer was obtained from diazotisation of the silyl ether **35** and subjection of the product diazonium salt to reaction with TTF (Scheme 4). This afforded the perhydrobenzofuran **37** (23% from amine **35**) indicating that a side-chain oxygen can participate. Dihydrobenzothiophene **21** (56% from amine **35**) was also isolated from this reaction.

Summarising the findings: (i) for the first time, radicals have been produced under TTF-induced radical-polar crossover

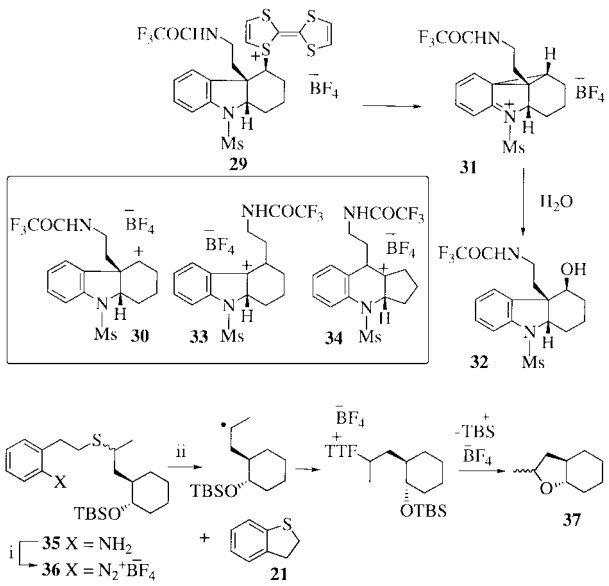

Scheme 4 *Reagents*: i, $NOBF_4$, CH_2Cl_2; ii, TTF, acetone, H_2O.

conditions which are totally aliphatic. Although we do not advocate the intramolecular sulfur displacement reaction as a synthetic route to aliphatic radicals, it allows us to determine the properties of such systems. The development of more powerful radical-polar crossover catalysts than TTF should lead to such products starting from *e.g.* alkyl and aryl halides, thus extending the scope of the reaction.

(ii) A TTF salt linked to a *secondary* carbon will undergo solvolysis with a little assistance from the arene—the arene needs to bear at least two alkyl functions to be sufficiently electron-rich to trigger the solvolysis in acetone under our conditions. This contrasts with the situation for *primary* carbon, where more powerful assistance is required. (The requirement for neighbouring group participation at a secondary carbon has important implications for stereochemical control.)

(iii) Groups other than arenes can participate in the solvolysis. This extends the scope of the radical-polar crossover reaction.

Notes and references

1 J. A. Murphy, C. Lampard and N. Lewis, *J. Chem. Soc., Chem. Commun.*, 1993, 295.
2 O. Callaghan, C. Lampard, A. R. Kennedy and J. A. Murphy, *J. Chem. Soc., Perkin Trans 1*, 1999, 995.
3 O. Callaghan, X. Franck and J. A. Murphy, *Chem. Commun.*, 1997, 1923.
4 C. Lampard, J. A. Murphy, F. Rasheed, N. Lewis, M. B. Hursthouse and D. E. Hibbs, *Tetrahedron Lett.*, 1994, **35**, 8675.
5 For a review of the extensive area of solvolysis of β-arylakyl substrates, see: J. C. Lancelot, D. J. Cram and P. von R. Schleyer, *Carbonium Ions*, ed. G. A. Olah and P. v. R. Schleyer, Wiley-Interscience, 1972, vol. 3, pp. 1347–1483.
6 J. A. Kampmeier and T. R. Evans, *J. Am. Chem. Soc.*, 1966, **88**, 4096.
7 A. L. J. Beckwith and S. A. M. Duggan, *J. Chem. Soc., Perkin Trans. 2*, 1994, 1509.
8 B. A. Smart and C. H. Schiesser, *J. Chem. Soc., Perkin Trans 2*, 1994, 2269; C. H. Schiesser, M. L. Styles and L. M. Wild, *J. Chem. Soc., Perkin Trans. 2*, 1996, 2257.
9 D. Crich and Q. Yao, *J. Org. Chem.*, 1996, **61**, 3566.
10 D. Crich and X. L. Hao, *J. Org. Chem.*, 1997, **62**, 5982.

Communication b000786m

Synthesis of medium-ring lactones *via* tandem methylenation/Claisen rearrangement of cyclic carbonates

James E. P. Davidson,[a] Edward A. Anderson,[a] Wilm Buhr,[a] Justin R. Harrison,[a] Paul T. O'Sullivan,[a] Ian Collins,[b] Richard H. Green[c] and Andrew B. Holmes*[a]

[a] *Department of Chemistry, University of Cambridge, Lensfield Road, Cambridge, UK CB2 1EW. E-mail: abh1@cus.cam.ac.uk*

[b] *Merck Sharp and Dohme Research Laboratories, Neuroscience Research Centre, Terlings Park, Harlow, UK CM20 2QR*

[c] *Exploratory Chemistry, Glaxo Wellcome Research & Development, Medicines Research Centre, Gunnels Wood Road, Stevenage, UK SG1 2NY*

Received (in Cambridge, UK) 6th January 2000, Accepted 4th February 2000

Tandem methylenation/Claisen rearrangement of cyclic carbonates derived from vinyl-substituted 1,3- and 1,4-diols afforded eight and nine-membered unsaturated lactones respectively.

Medium-ring oxacycles form the core of many natural products such as obtusenyne[1,2] and (+)-laurencin.[3] Our approach to systems of this type has used the ring-expansion Claisen rearrangement of a vinyl-substituted ketene acetal, generated *in situ* from the thermal elimination of a selenoxide precursor (in turn derived from the oxidation of a selenoacetal) to form a medium-ring lactone.[4] Whilst this methodology provides efficient access to many medium ring lactones, several limitations became evident when the vinyl group carried electron rich substituents. In addition to the toxicity associated with selenium reagents, the formation of the selenoacetal from a 1,3- or a 1,4-diol requires somewhat harsh conditions (refluxing toluene, PPTS). This can be a problem in cases where the allylic hydroxy group of the diol is prone to β-elimination. The selenoxide elimination product, benzeneselenenic acid **1**, has been shown to disproportionate under the reaction conditions to benzeneseleninic acid **2** and diphenyl diselenide **3**.[5] The latter is postulated to act as a reducing agent, converting the selenoxide (ketene acetal precursor **4**) back into the selenoacetal **5** (Scheme 1).

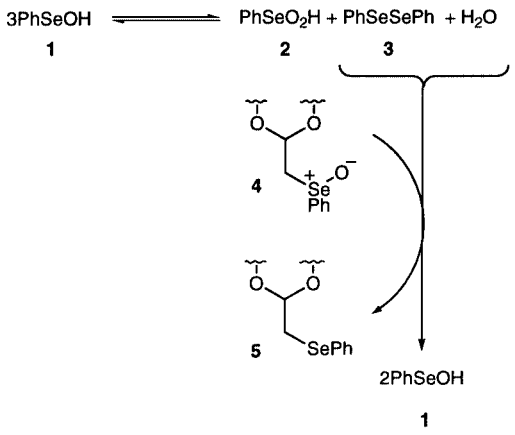

Scheme 1

The disproportionation of benzeneselenenic acid can be suppressed by the use of non-nucleophilic bases and a nucleophilic silyl ketene acetal as a selenium scavenger.[6] Even under these optimal conditions, oxygen transfer from **4** to produce **5** can be a significant side reaction. Finally, selenoxide elimination and rearrangement require high temperatures (sealed tube, up to 185 °C). These conditions and the need for high dilution could make large scale preparations more troublesome. Here we report the methylenation of cyclic carbonates derived from vinyl-substituted diols using the Petasis reagent (dimethyltitanocene)[7–9] and the subsequent *in situ* Claisen rearrangement of the presumed ketene acetal intermediate.

Preparation of the 1,3-diols **6a–f** (Scheme 2, Table 1) was carried out according to the methods described previously.[4] The carbonates **7a**,**c–f** were synthesised from the diols using carbonyldiimidazole.† Alternatively, the carbonates **7a–c** were prepared using a modification of a procedure with triphosgene.[10] Dimethyltitanocene was synthesised by the reported procedure,[11] and could be stored in the freezer as a solution in toluene for several months without degradation. Treatment of the carbonates **7a–f** with dimethyltitanocene in refluxing toluene provided the Claisen rearrangement eight-membered lactone products **9a–f** as single diastereomers (^{1}H NMR), in reasonable to good yields (Scheme 2, Table 1), presumably *via* the ketene acetal intermediates **8a–f**. Comparison of the yields over two steps with the combined yields for the analogous selenium route shows this method to be superior to the selenoxide route in many cases.[4]

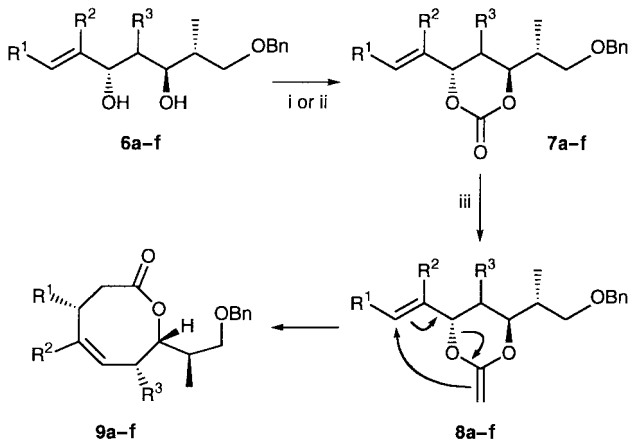

Scheme 2 *Reagents and conditions*: i, carbonyldiimidazole, toluene, reflux; ii, triphosgene, pyridine, Et_3N, −78 °C, 4 Å molecular sieves, CH_2Cl_2; iii, Cp_2TiMe_2, toluene, reflux in absence of light.

Nine-membered lactones may also be prepared. The 1,4-diols **10a–c** could be prepared from 2-deoxy-D-ribose in three steps. Treatment of the lactols derived from 2-deoxy-D-ribose by our previously reported route[12] with a variety of vinyl Grignard reagents provided mixtures of separable diastereomers of each of the diols **10a–c**. Exposure of the diols to triphosgene in dichloromethane and triethylamine–pyridine gave the carbonates **11a–c** which were converted into the lactones **13a–c**, as

DOI: 10.1039/b000299m

Table 1 Preparation of the carbonates **7a–f** and lactones **9a–f** from the diols **6a–f**

Substrate	R^1	R^2	R^3	Yield **7a–f** (%) (*t*/h)	Yield **9a–f** (%) (*t*/h)
6a	H	H	H	66[a] (48)	52 (3.5)
6a	H	H	H	45[b,c] (0.25)	52 (3.5)
6b	Me	H	H	77[b] (0.5)	52 (2.5)
6c	Me	Me	H	46[b] (1.0)	34 (4.5)
6c	Me	Me	H	32[a] (25)	34 (4.5)
6d	H	Me	(*R*)-Me	100[a] (23)	48 (3)
6e	H	Me	(*S*)-Me	91[a] (20)	67 (0.5)
6f	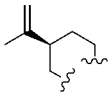		H	28[a] (24)	25 (24)

[a] *Conditions*: Scheme 1, i. [b] *Conditions*: Scheme 2, ii. [c] 33% Recovered **6a**.

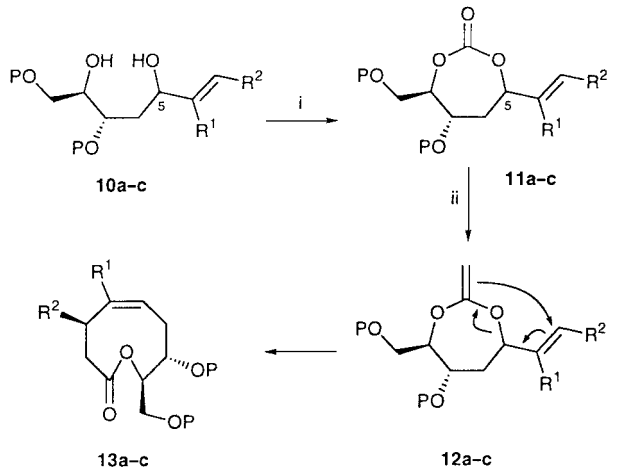

Scheme 3 *Reagents and conditions*: i, triphosgene, pyridine, Et_3N, −78 °C, 4 Å molecular sieves, CH_2Cl_2; ii, Cp_2TiMe_2, toluene, reflux in absence of light. P = TBDPS.

single diastereomers (^{1}H NMR), upon rearrangement of the *in situ* generated ketene acetals **12a–c** (Scheme 3, Table 2).

In summary, an alternative route to medium-sized lactones by a tandem methylenation/Claisen rearrangement has been developed. This milder route avoids the use of toxic selenium compounds and the problematic side reactions associated with certain selenoxides under elimination conditions. The application of this methodology to the synthesis of fused lactone derivatives is described in the following Communication.

Table 2 Preparation of carbonates **11a–c** and lactones **13a–c** from diols **10a–c**

Substrate	R^1	R^2	C-5 Configuration	Yield **11a–c** (%) (*t*/h)	Yield **13a–c** (%) (*t*/h)
10a	H	H	*R*	65 (1.75)	70 (1.2)
10b	H	H	*S*	69 (0.25)	49 (2)
10c	TMS	Me	*S*	91 (0.25)	51 (0.5)

We thank EPSRC for financial support and provision of the Swansea Mass Spectrometry Service, Merck Sharp and Dohme for the award of CASE studentships (to E. A. A. and J. R. H.), GlaxoWellcome for a studentship (to J. E. P. D.), the University of Cambridge (Robert Gardiner Memorial Scholarship), the Cambridge European Trust (awards to P. T. O'S.) and the Deutsche Forschungsgemeinschaft for a fellowship (to W. B.). We thank Dr J. W. Burton for his interest in this research.

Notes and references

† All new compounds exhibited spectroscopic and analytical (C, H, N) or exact mass data in accordance with the assigned structure.

1 N. R. Curtis and A. B. Holmes, *Tetrahedron Lett.*, 1992, **33**, 675.
2 N. R. Curtis, A. B. Holmes and M. G. Looney, *Tetrahedron Lett.*, 1992, **33**, 671.
3 J. W. Burton, J. S. Clark, S. Derrer, T. C. Stork, J. G. Bendall and A. B. Holmes, *J. Am. Chem. Soc.*, 1997, **119**, 7483.
4 J. R. Harrison, A. B. Holmes and I. Collins, *Synlett*, 1999, 972.
5 C. Paulmier, *Selenium Reagents and Intermediates in Organic Synthesis*, Pergamon Press, Oxford, 1987.
6 P. A. Evans, A. B. Holmes, R. P. McGeary, A. Nadin, K. Russell, P. J. O'Hanlon and N. D. Pearson, *J. Chem. Soc., Perkin Trans. 1*, 1996, 123.
7 N. A. Petasis and E. I. Bzowej, *J. Am. Chem. Soc.*, 1990, **112**, 6392.
8 N. A. Petasis and S. P. Lu, *Tetrahedron Lett.*, 1995, **36**, 2393.
9 N. A. Petasis, S. P. Lu, E. I. Bzowej, D. K. Fu, J. P. Staszewski, I. Akritopoulouzanze, M. A. Patane and Y. H. Hu, *Pure Appl. Chem.*, 1996, **68**, 667.
10 R. M. Burk and M. B. Roof, *Tetrahedron Lett.*, 1993, **34**, 395.
11 J. F. Payack, D. L. Hughes, D. W. Cai, I. F. Cottrell and T. R. Verhoeven, *Org. Prep. Proced.*, 1995, **27**, 707.
12 M. S. Congreve, A. B. Holmes, A. B. Hughes and M. G. Looney, *J. Am. Chem. Soc.*, 1993, **115**, 5815.

Communication b000299m

ChemComm

Synthesis of fused bicyclic medium-ring lactones *via* Claisen rearrangement

Jonathan W. Burton,*[a] Paul T. O'Sullivan,[a] Edward A. Anderson,[a] Ian Collins[b] and Andrew B. Holmes*[a]

[a] *Department of Chemistry, University of Cambridge, Lensfield Road, Cambridge, UK CB2 1EW. E-mail: abh1@cam.ac.uk; jwb1004@cam.ac.uk*

[b] *Merck Sharp and Dohme Research Laboratories, Neuroscience Research Centre, Terlings Park, Harlow, UK CM20 2QR*

Received (in Cambridge, UK) 6th January 2000, Accepted 4th February 2000

Fused bicyclic medium-ring lactones, carrying identical ring-fusion to that in the polyether toxins, are prepared by a Claisen rearrangement sequence.

The polyether neurotoxins have attracted enormous synthetic interest as a result of their unusual molecular architecture and biological activity.[1] Most recently Nicolaou *et al.* have described the total synthesis of brevetoxin A,[2,3] and there have been many contributions from others active in this field.[4] Here, we report the use of the Claisen rearrangement to prepare fused bicyclic medium-ring lactones having the precise structural features present in the medium-ring fused polyether segments of brevetoxin B and ciguatoxin.

Our approach to fused medium-ring lactones follows the methodology previously developed for the synthesis of obtusenyne[5,6] and (+)-laurencin.[7] Transformation of a 1,3-diol into a vinyl-substituted ketene acetal by selenoxide elimination or carbonate methylenation (see preceding Communication) provides the desired medium-ring fused bicyclic lactone after Claisen rearrangement.

Scheme 1† summarises the construction of the bicyclic lactone **1**. Methylenation (72%) of the monocyclic lactone **2**,‡ BOM deprotection (94%) and silylation with $(Me_2SiH)_2NH$ (100%) provided the silane **3**. Rhodium catalysed intra-

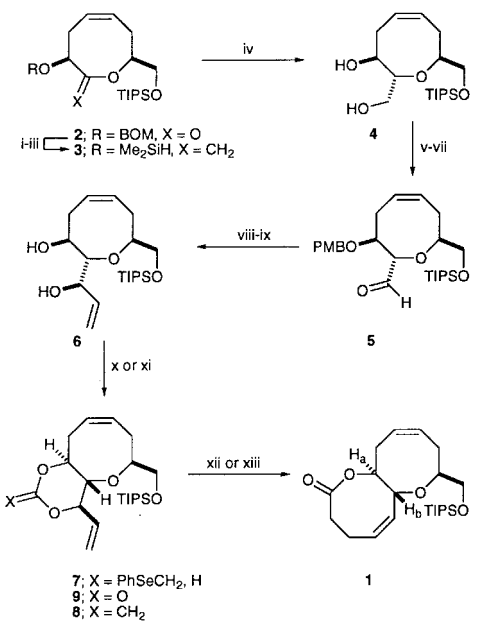

Scheme 1 Synthesis of the bicyclic lactone **1**. *Reagents and conditions*: i, Cp_2TiMe_2, toluene, reflux, 40 min, 72%; ii, LiDBB (excess), THF, −78 °C, 3 min, 94%; iii, 1,1,3,3-tetramethyldisilazane, NH_4Cl (cat.), 60 °C, 18 h, 100%; iv, (bicyclo[2.2.1]hepta-2,5-diene)[1,4-bis(diphenylphosphino)butane]rhodium(I) tetrafluoroborate (3 mol%), THF, 60 °C, 18 h, then $Na_2EDTA{\cdot}2H_2O$, 1 h, then 15% aqueous KOH, 30% aqueous H_2O_2, THF and methanol, 1 h, then $Na_2S_2O_3$, 86%; v, *p*-methoxybenzaldehyde, PPTS (cat.), benzene, Dean–Stark, 12 h, 85%; vi, DIBAL-H, toluene, CH_2Cl_2, $-78 \rightarrow -50 \rightarrow -30$ °C, 2.5 h, 80%; vii, IBX, Me_2SO, room temp., 18 h; viii, $CeCl_3$, THF, 18 h, then vinylmagnesium bromide, THF, −78 °C, 2 h, then **5**, −78 °C, 1.5 h, 74%; ix, CH_2Cl_2–TFA (5:1), −20 °C, 10 min, 90%; x, $PhSeCH_2CH(OEt)_2$, PPTS, toluene, reflux, 2 h, 94%, xi, triphosgene, pyridine, Et_3N, CH_2Cl_2, 4 Å molecular sieves, −78 °C → room temp., 89%; xii, $NaIO_4$, $NaHCO_3$, CH_2Cl_2, methanol, water, 2 h, then DBU, toluene, reflux, 18 h, 90%; xiii, Cp_2TiMe_2, toluene, reflux, 1.5 h, 63%. BOM = benzyloxymethyl; IBX = *o*-iodoxybenzoic acid; LiDBB = lithium di-*tert*-butylbiphenylide.

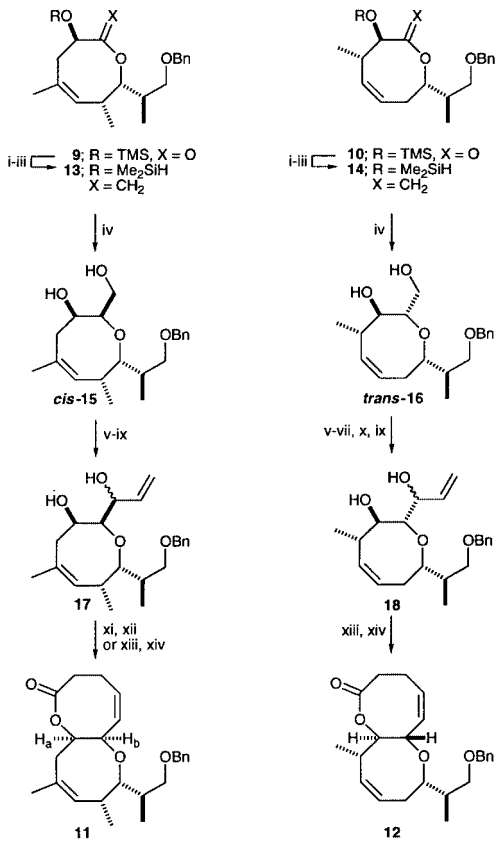

Scheme 2 Synthesis of the bicyclic lactones **11** and **12**. *Reagents and conditions*: i, Cp_2TiMe_2, toluene, reflux; ii, K_2CO_3, methanol, 85% from **9**, 76% from **10**; iii, 1,1,3,3-tetramethyldisilazane, NH_4Cl (cat.), 60 °C, 18 h, 99% for **13**, 98% for **14**; iv, (bicyclo[2.2.1]hepta-2,5-diene)[1,4-bis(diphenylphosphino)butane]rhodium(I) tetrafluoroborate (3 mol%), THF, 60 °C, 18 h, then $Na_2EDTA{\cdot}2H_2O$, 1 h, then 15% aqueous KOH, 30% aqueous H_2O_2, THF and methanol, 1 h, then $Na_2S_2O_3$, 61% for *cis*-**15**, 57% for *trans*-**16**; v, *p*-methoxybenzaldehyde, PPTS (cat.), benzene, Dean–Stark; vi, DIBAL-H, toluene, CH_2Cl_2; vii, IBX, Me_2SO, room temp., 18 h; viii, $CeCl_3$, THF, 18 h, then vinylmagnesium bromide, THF, −78 °C, 2 h, add aldehyde, −78 °C, 1.5 h; ix, CH_2Cl_2–TFA (5:1), −20 °C, 10 min, 58% from **15**, 24% from **16**; x, vinyl iodide, $CrCl_2$ 1% $NiCl_2$, Me_2SO, 72 h; xi, $PhSeCH_2CH(OEt)_2$, PPTS, toluene; xii, $NaIO_4$, $NaHCO_3$, CH_2Cl_2, methanol, water, 2 h, then DBU, toluene, reflux, 18 h, 58% from **17**; xiii, triphosgene, pyridine, Et_3N, CH_2Cl_2, 4 Å molecular sieves, −78 °C → room temp.; xiv, Cp_2TiMe_2, toluene, reflux, 1.5 h, 38% from **17**, 43% from **18**. IBX = *o*-iodoxybenzoic acid.

DOI: 10.1039/b000303o

molecular hydrosilation[5,7] followed by oxidation yielded the diol **4** (86%) as a single diastereomer (^{1}H NMR). *p*-Methoxybenzylidene acetal formation (85%), reduction with DIBAL-H (79%) and IBX oxidation[8] furnished the labile aldehyde **5**. Exposure of **5** to vinylmagnesium bromide in the presence of cerium(III) chloride, according to the procedure of Imamoto,[9] provided the corresponding allylic alcohols (85%, 5:1 mixture of diastereomers, Felkin control). The major diastereomer was deprotected with TFA to furnish the diol **6** (90%). Heating a solution of **6** and phenylselenoacetaldehyde diethyl acetal in acidic toluene provided the selenides **7** (94%, mixture of diastereomers) which were oxidised to the corresponding selenoxides. Pyrolysis of the selenoxides in toluene at reflux yielded the desired *trans*-fused bicyclic lactone **1** (90%, single diastereomer, $J_{a,b}$ 9.7 Hz) presumably *via* the intermediate ketene acetal **8**. Alternatively the diol **6** could be converted into the corresponding carbonate **9** (89%), which on heating with dimethyltitanocene provided **1** (63%). Thus the conversion of a medium-ring lactone into the corresponding *trans*-fused bicyclic lactone has been achieved in 11 synthetic steps and 25% overall yield.

In a similar manner the lactones **9**‡ and **10**‡ were converted into the corresponding bicyclic lactones **11** and **12** (Scheme 2†). The silanes **13** and **14** were synthesised from the lactones **9** and **10** by an analogous route to that depicted in Scheme 1. Rhodium catalysed intramolecular hydrosilation converted **13** into the diols **15** (61% combined yield, 6:1 mixture of *cis*:*trans* diastereomers, major diastereomer shown) after oxidative work-up. Similarly exposure of the silane **14** to the hydrosilation conditions provided the diols **16** after work-up (57% combined yield, 1.33:1, mixture of *trans*:*cis* diastereomers, major diastereomer shown). Conversion of the major diastereomers *cis*-**15** and *trans*-**16** into the corresponding allylic alcohols **17** and **18** proceeded without incident. The *cis*-fused bicyclic lactone **11** ($J_{a,b}$ 2.4 Hz) was accessed from the diols **17** *via* both the selenoacetal route (58% for three steps) and the carbonate route (38% for two steps) thus demonstrating the versatility of this method for the synthesis of bicyclic lactones. It also proved possible to convert the diols **18** into the *trans*-fused bicyclic lactone **12** *via* initial conversion to the corresponding carbonates (90%) followed by heating in the presence of dimethyltitanocene (48%).

The synthesis of the 8,9-*trans*-fused bicyclic lactone **19** was achieved *via* elaboration of the known nine-membered lactone-aldehyde **20** (Scheme 3†).[10] Treatment of **20** with vinyl iodide in the presence of chromium(II) chloride in Me_2SO[11] provided the allylic alcohols **21** (59%, 2:1 mixture of diastereomers, Felkin control, major diastereomer shown). The allylic alcohol **21-maj** was deprotected (50–69%) and converted into the crystalline carbonate **22** {78%, mp 126–127 °C (from hexane)}. Treatment of **22** with dimethyltitanocene in toluene at reflux provided the crystalline *trans*-fused bicyclic lactone **19**§ [25% unoptimised, mp 109–111 °C (from hexane)] and recovered starting material (75%).

In summary, we have shown that the Claisen rearrangement and hydrosilation methodology, developed for the synthesis of medium-ring oxygen-containing heterocycles, can readily be extended to the synthesis of *cis*- or *trans*-fused bicyclic medium-ring lactones which form the basis for the synthesis of members of the polyether toxin family.

We thank the EPSRC for financial support and provision of the Swansea MS service, Merck, Sharp and Dohme for a CASE award (to E. A. A.), the University of Cambridge (Robert Gardiner Memorial Scholarship), the Cambridge European Trust (awards to P. T. O'S) and Corpus Christi College, Cambridge (Research Fellowship, J. W. B.).

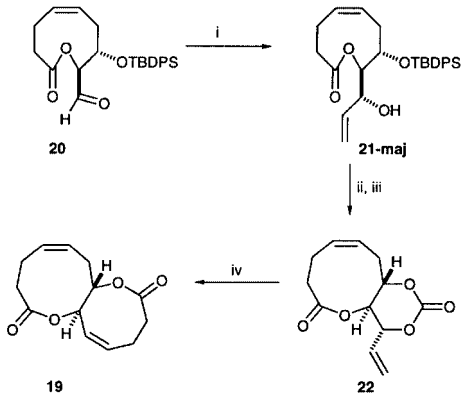

Scheme 3 Synthesis of the bicyclic lactone **19**. *Reagents and conditions*: i, vinyl iodide, $CrCl_2$ 1% $NiCl_2$, Me_2SO, 18 h, 59%; ii, HF·pyridine, pyridine, THF, 50–69%; iii, triphosgene, pyridine, Et_3N, CH_2Cl_2, 4 Å molecular sieves, −78 °C → room temp., 78%; iv, Cp_2TiMe_2, toluene, reflux, 1.5 h, 25%.

Notes and references

† All new compounds exhibited satisfactory spectroscopic and analytical and/or exact mass data.

‡ The synthesis of the lactones **2**, **9** and **10** will be reported in a separate paper.

§ *Selected data* for compound **19**: white crystalline solid; mp 109–111 °C (from hexane); R_f 0.6 (diethyl ether–hexane, 1:1); $[\alpha]_D^{16}$ −26.6 (*c* 0.165 in $CHCl_3$); $\nu_{max}(CHCl_3)/cm^{-1}$ 2947, 1744 (CO), 1737 (CO), 1340, 1149 and 1068; δ_H(800 MHz, $CDCl_3$) 5.88–5.82 (1H, m), 5.78–5.70 (3H, m), 5.70–5.62 (1H, m, H-6a), 4.65 (1H, br t, *J* 7.5, H-13a), 2.95–2.86 (1H, m), 2.84 (1H, dd, *J* 13.5, 6.4), 2.56–2.47 (2H, br), 2.46–2.36 (3H, m), 2.35–2.26 (2H, m) and 2.22–2.20 (1H, m); δ_C(100 MHz, $CDCl_3$) 175.9 and 174.7 (C-2 and C-8), 132.4, 131.6, 129.0 and 128.3 (C-11, C-12, C-5 and C-6), 78.6 (C-13a), 75.3 (C-6a), 37.6, 34.2, 30.9, 24.9 and 24.3 (C-3, C-4, C-13, C-10 and C-9); *m/z* (CI, NH_3) 254 [$(M + NH_4)^+$, 100%)] [Found: $(M + NH_4)^+$, *m/z* 254.1393. $C_{13}H_{20}O_4N$ requires *m/z* 254.1392].

1 E. Alvarez, M. L. Candenas, R. Perez, J. L. Ravelo and J. D. Martin, *Chem. Rev.*, 1995, **95**, 1953.
2 K. C. Nicolaou, Z. Yang, G. Q. Shi, J. L. Gunzner, K. A. Agrios and P. Gartner, *Nature*,1998, **392**, 264.
3 K. C. Nicolaou, J. L. Gunzner, G. Q. Shi, K. A. Agrios, P. Gartner and Z. Yang, *Chem. Eur. J.*, 1999, **5**, 646 and references therein.
4 M. C. Elliott, *J. Chem. Soc., Perkin Trans. 1*, 1998, 4175 and references therein.
5 N. R. Curtis and A. B. Holmes, *Tetrahedron Lett.*, 1992, **33**, 675.
6 N. R. Curtis, A. B. Holmes and M. G. Looney, *Tetrahedron Lett.*, 1992, **33**, 671.
7 J. W. Burton, J. S. Clark, S. Derrer, T. C. Stork, J. G. Bendall and A. B. Holmes, *J. Am. Chem. Soc.*, 1997, **119**, 7483.
8 M. Frigerio and M. Santagostino, *Tetrahedron Lett.*, 1994, **35**, 8019.
9 T. Imamoto, N. Takiyama, K. Nakamura, T. Hatajima and Y. Kamiya, *J. Am. Chem. Soc.*, 1989, **111**, 4392.
10 M. S. Congreve, A. B. Holmes, A. B. Hughes and M. G. Looney, *J. Am. Chem. Soc.*, 1993, **115**, 5815.
11 A. Fürstner, *Chem. Rev.*, 1999, **99**, 991.

Communication b000303o

ChemComm

Intramolecular conformational control in a cyclic peptide composed of alternating L-proline and substituted 3-aminobenzoic acid subunits†

Stefan Kubik*[a] and Richard Goddard[b]

[a] *Institut für Organische Chemie und Makromolekulare Chemie, Heinrich-Heine-Universität, Universitätsstr. 1, D-40225 Düsseldorf, Germany. E-mail: kubik@uni-duesseldorf.de*

[b] *Max-Planck-Institut für Kohlenforschung, Kaiser-Wilhelm-Platz 1, D-45470 Mülheim/Ruhr, Germany*

Received (in Liverpool, UK) 19th January 2000, Accepted 28th January 2000

Methoxycarbonyl groups in the 4-position of the aromatic subunits strongly influence the conformational behaviour and the receptor properties of cyclic peptides composed of alternating 3-aminobenzoic acid and L-proline

We recently showed that cyclic hexapeptides composed of alternating natural amino acids and 3-aminobenzoic acid subunits bind cations and anions with high affinity.[1,2] Cation–π interactions with the aromatic subunits of such cyclopeptides generally result in inclusion of cations into the shallow dish-shaped receptor cavity.[3] By contrast, anions are only bound when they are able to form hydrogen bonds to the peptide amide groups. This latter interaction induces a receptor conformation in which all NH groups of the peptide point towards the cavity centre.[4] In the absence of suitable anions, the amide groups are able to rotate more freely. We speculated that suitable substituents on the peptide subunits would also restrict amide rotation. Such an approach may have the additional advantage that the anion complexation could be completely prevented by locking the NH groups in an orientation unsuitable for interactions with these guests. Here we report our first results in this direction.

Inspired by the work of Hamilton and coworkers who have shown that methoxycarbonyl groups can be used for the conformational control in oligoanthranilamides,[5] we introduced these substituents at the 4-position of the aromatic subunits of **1**.

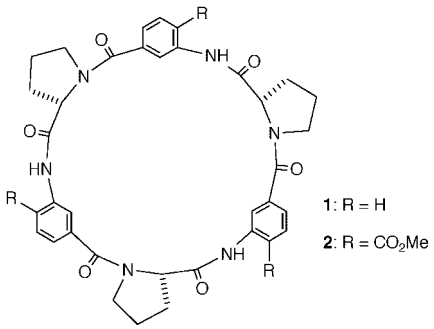

Methoxycarbonyl groups are able to form hydrogen bonds to adjacent NH protons and thus induce an amide orientation parallel to the aromatic rings. They also cause the NH protons to point away from the cavity centre and make the amides less available for anion complexation.

Peptide **2** was synthesised from the commercially available 2-aminoterephthalic acid 1-methyl ester by following a procedure similar to that used for **1**.[1] Whereas **1** possesses a simple ^{1}H NMR spectrum that represents an averaged C_3-symmetrical structure, the spectrum of **2** is more complicated [Fig. 1(a) and (c)]. Identical protons of **2** give two signals in most cases, and even the methyl ester signal is split. Since the spectrum is not significantly affected by varying the concentration of **2** in the region 2–0.2 mM, an intermolecular association of the peptide at these concentrations is unlikely. Instead, the spectrum more probably represents a non-symmetrical conformation of **2** or different slowly interconverting peptide conformers. Temperature-dependent ^{1}H NMR spectroscopy of **2** in $C_2D_2Cl_4$ shows that at 120 °C the flexibility of the peptide is still somewhat restricted. The rigidity of **2** is certainly caused by the effects of the additional methoxycarbonyl substituents. The unusually large downfield shift of the NH protons in the ^{1}H NMR spectrum of **2** in $CDCl_3$ at δ 11.1 [for **1** δ(NH) 9.2] and the strong N–H vibration band at 3303 cm^{-1} in the FTIR spectrum in $CDCl_3$ indicate that these groups are involved in hydrogen bonds. The crystal structure of **2** monohydrate (Fig. 2) shows that, as predicted, these hydrogen bonds are formed between the amide NH groups and the neighbouring methoxycarbonyl groups.‡ The overall peptide conformation in this structure is non-symmetrical, presumably caused by the water molecule, with one aromatic subunit tilted away from the others. As a result, one would expect a weak cation affinity of **2**.

Nevertheless, a significant upfield shift of the guest protons is observed upon addition of quaternary ammonium salts such as *n*-butyltrimethylammonium picrate (BTMA$^+$ picrate) to solutions of **2** in $CDCl_3$. This shift is generally interpreted in terms of an inclusion of the cation into a receptor cavity which brings the guest protons in close proximity to the aromatic subunits.[3] The spectrum of the peptide is also affected in the presence of the cation. On increasing the guest concentration, the spectrum becomes simpler until, after addition of 4 equivalents of BTMA$^+$ picrate to a 2 mM solution of **2** in $CDCl_3$, it represents a symmetrical conformation [Fig. 1(b)]. Complex formation

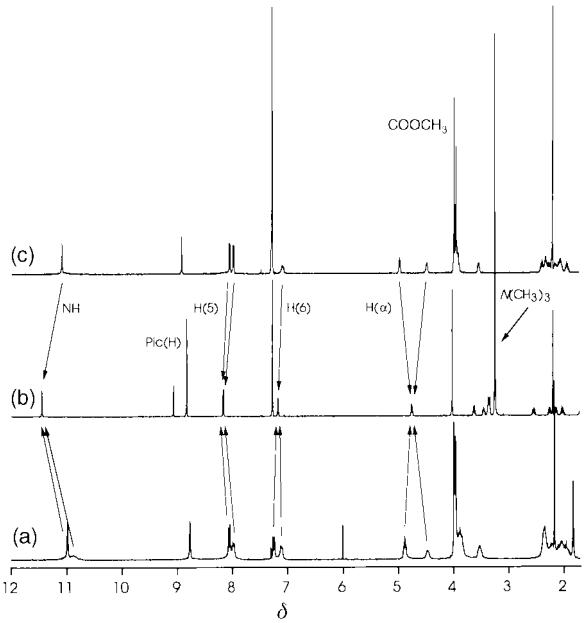

Fig. 1 ^{1}H NMR spectra of **2** (a) in $C_2D_2Cl_4$ (60 °C), (c) in $CDCl_3$ (25 °C) and (b) after addition of 4 equiv. of BTMA$^+$ picrate in $CDCl_3$ (25 °C).

† Electronic supplementary information (ESI) available: synthesis, IR and NMR data for **2**. See http://www.rsc.org/suppdata/cc/b0/b000568l/

DOI: 10.1039/b000568l

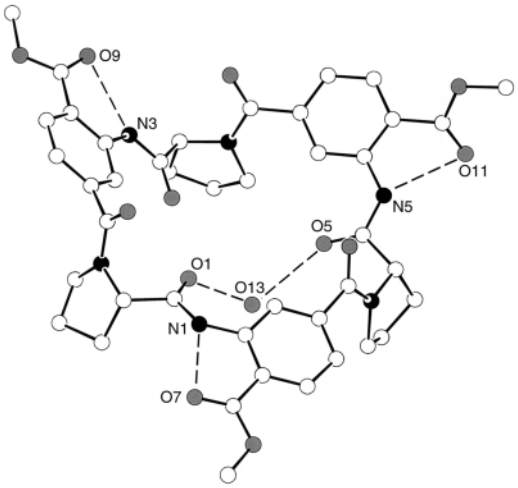

Fig. 2 Molecular structure of **2**·H_2O. Selected interatomic distances (Å): N1··O7 2.677(2), N3··O9 2.656(2), N5··O11 2.903(3).

obviously causes a shift of the conformational equilibrium of **2**. The NOESY NMR spectrum shows strong NOE effects between NH and H(α), which confirms that the NH groups are oriented towards the methoxycarbonyl substituents. As yet, we have not been able to obtain crystals of the **2**·BTMA$^+$ complex. However, **2** crystallises from acetone with one solvent molecule per peptide unit. X-Ray crystallography reveals that the solvent molecule is located inside the peptide cavity (Fig. 3). Moreover, the peptide conformation in this structure is more symmetrical than in **2**·H_2O. The three aromatic subunits are all tilted into the same direction with all hydrogen bonds between NH and the methoxycarbonyl substituents retained. These results indicate that suitable guest molecules can induce a symmetrical peptide conformation well suited for guest binding when they are included into the cavity of **2**. The NMR spectroscopic results demonstrate that certain cations induce a similar conformation in solution. This mechanism of complex formation is therefore consistent with an 'induced-fit'.

The upfield shift of the BTMA$^+$ protons in the presence of **2** can be used to quantitatively determine the complex stability by NMR titrations.[6] When the shifts of the cation protons of BTMA$^+$ picrate were followed in the titration, a stability constant K_a was obtained that is almost an order of magnitude larger than that of the corresponding complex of **1** (Table 1). This significant increase of cation complex stability can be attributed to the conformational rigidity of **2**.

Whereas a dramatic increase of the cation complex stability was observed for **1** with iodide or tosylate anions,[1] the BTMA$^+$

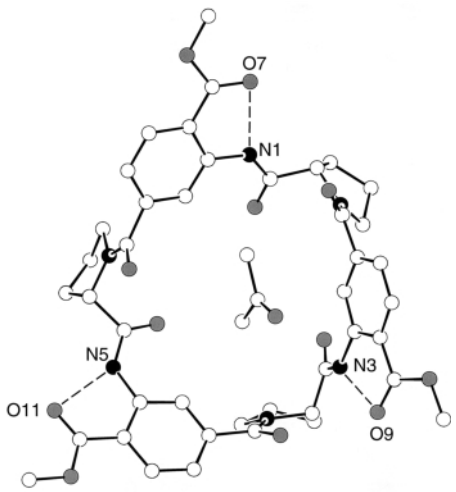

Fig. 3 Molecular structure of **2**·Me_2CO projected onto a plane through the three amide N atoms of **2** (tilt angles of the aromatic rings to this plane (°): at N1, +35; at N3, +57; at N5, +31). Selected interatomic distances (Å): N1··O7 2.668(3), N3··O9 2.692(3), N5··O11 2.678(2).

Table 1 BTMA$^+$ complex stabilities in $CDCl_3$ at 298 K (K_a = stability constant in M^{-1}, error limits of K_a < 20%; $\Delta\delta_{max}$ = maximum chemical shift in ppm; ΔG_H = Gibbs free energy of hydration of the anions in kJ mol^{-1})

	1		**2**		
Anion	K_a	$-\Delta\delta_{max}$	K_a	$-\Delta\delta_{max}$	$-\Delta G_H$
Picrate	1 260	0.70	10 800	0.54	197
Iodide	21 100	1.11	3 310	0.59	283
Tosylate	5 050 000	1.16	740	0.54	318

complex stabilities of **2** decrease when going from picrate to iodide and tosylate. A similar anion effect has also been reported for cation complexes of calixarenes.[7] Bartsch and coworkers have shown that the extraction efficiency of certain crown ether salt complexes correlates inversely with the hydration enthalpy of the anion.[8] In accordance with these findings, the stabilities of the BTMA$^+$ complexes of **2** decreases with increasing Gibbs free energy of hydration of the anion.[9] The dependence of the complex stabilities on the type of anion can therefore be attributed to an intrinsic property of the salts and not to possible peptide–anion interactions. Indeed, the FTIR spectrum of **2** is unaffected by the different anions, not even those that bind very strongly to **1**.

In summary, we have shown that the NH groups of **2** can be locked in a defined orientation by hydrogen bonds to methoxycarbonyl groups on the aromatic subunits. This results in a reduction of the conformational freedom of the cyclopeptide and in improved cation affinity as well as a complete loss of anion binding ability. Currently, we are investigating effects of other substituents. The fact that the conformation and hence the binding properties of these peptides can be influenced by non-covalent intramolecular interactions give them important advantages over many other artificial receptors.

S. K. thanks Professor G. Wulff, to whom this paper is dedicated on the occasion of his 65th birthday, for his generous support and Mrs D. Kubik for the preparative work.

Notes and references

‡ *Crystal data*: **2**·H_2O: $C_{42}H_{42}N_6O_{12}$·H_2O, M_r = 840.83, colourless prism, crystal size 0.44 × 0.54 × 0.58 mm, a = 13.2214(6), b = 17.0958(8), c = 18.0413(8) Å, U = 4077.9(3) Å^3, T = 100 K, orthorhombic, space group $P2_12_12_1$ (no. 19), Z = 4, D_c = 1.37 g cm^{-3}, μ = 0.10 mm^{-1}. Siemens SMART diffractometer, λ = 0.71073 Å. 44640 measured reflections, 15293 unique, 8260 with $I > 2.0\sigma(F_o^2)$. The structure was solved by direct methods and refined by full-matrix least squares on F^2 for all data with Chebyshev weights to R = 0.0595 [$I > 2\sigma(F_o^2)$], wR = 0.144 (all data), 553 parameters.

2·Me_2CO: $C_{42}H_{42}N_6O_{12}$·C_3H_6O, M_r = 880.89, colourless prism, crystal size 0.17 × 0.28 ×0.64 mm, a = 10.5607(6), b = 17.6047(10), c = 22.7991(13) Å, U = 4238.8(4) Å^3, T = 100 K, orthorhombic, space group $P2_12_12_1$ (no. 19), Z = 4, D_c = 1.38 g cm^{-3}, μ = 0.10 mm^{-1}. Siemens SMART diffractometer, λ = 0.71073 Å. 48668 measured reflections, 16532 unique, 9124 with $I > 2.0\sigma(F_o^2)$. Structure solution and refinement as above, R = 0.073 [$I > 2\sigma(F_o^2)$], wR = 0.172 (all data), 582 parameters.

CCDC 182/1564. See http://www.rsc.org/suppdata/cc/b0/b000568l/ for crystallographic files in .cif format.

1 S. Kubik and R. Goddard, *J. Org. Chem.*, 1999, **64**, 9475.
2 S. Kubik, *J. Am. Chem. Soc.*, 1999, **121**, 5846.
3 J. C. Ma and D. A. Dougherty, *Chem. Rev.*, 1997, **97**, 1303; P. Lhotak and S. Shinkai, *J. Phys. Org. Chem.*, 1997, **10**, 273.
4 See also: H. Ishida, M. Suga, K. Donowaki and K. Ohkubo, *J. Org. Chem.*, 1995, **60**, 5374.
5 Y. Hamuro, S. J. Geib and A. D. Hamilton, *J. Am. Chem. Soc.*, 1996, **118**, 7529.
6 K. A. Connors, *Binding Constants*, Wiley, New York, 1987; R. S. Macomber, *J. Chem. Educ.*, 1992, **69**, 375.
7 R. Arnecke, V. Böhmer, R. Cacciapaglia, A. Dalla Cort and L. Mandolini, *Tetrahedron*, 1997, **53**, 4901.
8 U. Olsher, M. G. Hankins Y. D. Kim and R. A. Bartsch, *J. Am. Chem. Soc.*, 1993, **115**, 3370.
9 Y. Marcus, *Ion Properties*, Marcel Dekker, New York, 1997.

Communication b000568l

ChemComm

Molecular recognition in the solid state: topology of experimental and theoretical charge densities for tetrasulfur tetranitride†

Wolfgang Scherer,*[a] Michael Spiegler,[a] Bjørn Pedersen,[a] Maxim Tafipolsky,[a] Wolfgang Hieringer,[a] Björn Reinhard,[a] Anthony J. Downs[b] and G. Sean McGrady*[c]

[a] *Anorganisch-chemisches Institut der Technischen Universität München, Lichtenbergstraße 4, Garching bei München, D-85747 Germany*
[b] *Inorganic Chemistry Laboratory, University of Oxford, South Parks Road, Oxford, UK OX1 3QR*
[c] *Department of Chemistry, King's College London, Strand, London UK WC2R 2LS. E-mail: sean.mcgrady@kcl.ac.uk*

Received (in Cambridge, UK) 20th December 1999, Accepted 6th March 2000

Topological analysis of experimental and theoretical charge densities in tetrasulfur tetranitride clarifies features of the intramolecular bonding; intermolecular charge concentrations reveal directional 'key–lock' interactions corresponding to molecular recognition in the solid state.

Tetrasulfur tetranitride, S_4N_4, is perhaps the most studied inorganic heterocycle, yet a full understanding of its bonding remains elusive. Thus, whilst S–S bonding interactions between *proximal* S atoms are established, the nature and extent of interaction remain unclear,[1–3] and the existence of *distal* S···S interactions is either claimed[1,4] or refuted.[2]

Two decades ago a low-temperature X-ray diffraction study provided the most accurate molecular geometry to date, and reported a preliminary analysis of the charge density distribution, $\rho(\boldsymbol{r})$, in S_4N_4.[1] With the subsequent advances in instrumentation, analytical methods and computing power, we have undertaken experimental and theoretical studies of $\rho(\boldsymbol{r})$ for S_4N_4[5] and a theoretical study of S_2N_2 for comparison. Our geometrical parameters for S_4N_4 are in good agreement with those of the earlier study.[1] We have clarified several inconsistencies still outstanding in the various bonding descriptions of S_4N_4, and observed distortions in the experimental charge density giving rise to directional *intermolecular* attractions corresponding to molecular recognition in the solid state.

Intramolecular bonding: in order to reveal both *gross* and *subtle* features of $\rho(\boldsymbol{r})$, we have analysed its Laplacian, $\nabla^2\rho(\boldsymbol{r})$, using the 'Atoms in Molecules' (AIM) approach of Bader.[6] By means of a topological analysis of $\rho(\boldsymbol{r})$, features such as bond critical points (CPs) and paths of maximum electron density can be used to construct a molecular graph representing the network of bond paths connecting linked atoms. As shown in Fig. 1(a), we find ten (3, −1) bond CPs,[6] corresponding to eight S–N and two S–S linkages, and four (3, +1) ring CPs,[6] in a tetrahedral array about a central (3, +3) cage CP.[6] These conclusions are in accord with an earlier theoretical study.[3] $\rho(\boldsymbol{r})$ at the cage CP is a minimum in all three dimensions, supporting the conclusions drawn from two theoretical deformation density studies,[2,7] and affording no evidence of significant distal S···S interactions. The value of ρ at the bond CPs, $\rho(\boldsymbol{r}_c)$, for the S–S bonds [$\rho(\boldsymbol{r}_c)_{av}$ = 0.37(1) e Å^{-3}; av = average] is significantly lower than that for the S–N linkages [$\rho(\boldsymbol{r}_c)_{av}$ = 1.54(1) e Å^{-3}], being about one-third that reported for an S–S single bond.[8] This, together with the long S–S distances[8] of 2.5995(2) and 2.5950(2) Å and a positive value of the Laplacian,[6] $\nabla^2\rho(\boldsymbol{r}_c)_{av}$ = 1.61(1) e Å^{-5}, may be interpreted in terms of a weak, closed-shell interaction between the two S atoms. However, analysis of both kinetic energy densities $G(\boldsymbol{r})$ and potential energy densities $V(\boldsymbol{r})$[10] of the electrons at the bond critical points suggests some covalent character for the S–S bond [$H(\boldsymbol{r}_c) = G(\boldsymbol{r}_c) + V(\boldsymbol{r}_c)$ = −0.116; $G(\boldsymbol{r}_c)$ = 0.228 hartree Å^{-3}].[9]

The shortness of the S–N bond [1.629(1) Å; on average] and its degree of ellipticity[6] [ε = 0.17; $\rho(\boldsymbol{r}_c)_{av}$ = 1.54(1) e Å^{-3}; $\nabla^2\rho(\boldsymbol{r}_c)_{av}$ = −10.60(3) e Å^{-5}] implies π-contributions. The bond paths are displaced, respectively, outwards and inwards for the S–S and S–N bonds, and the S–N bond CPs are located closer to the electropositive S atoms [Fig. 1(a)]. Calculated atomic charges[11] suggest transfer of *ca*. 1.3 electrons to N from S, although monopole charges based on the X-ray multipolar model suggest a lower figure of 0.3 electrons.

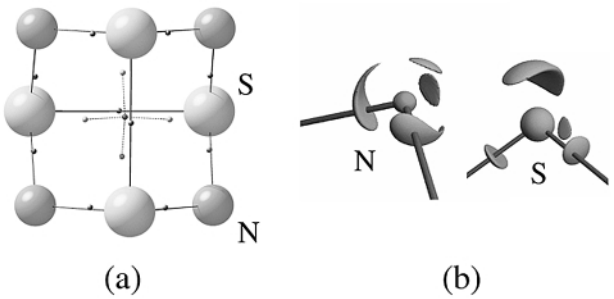

Fig. 1 (a) Location of the critical points denoted by closed circles in the S_4N_4 skeleton. The bond critical points along the S–N bonds are shifted towards the more electropositive sulfur atoms. Important distances (Å) and angles (°) (average values): S–N 1.629(1), S–S 2.598(1); N–S–N 104.5(1), S–N–S 112.7(1). (b) Isosurface maps at constant $-\nabla^2\rho(\boldsymbol{r})$ values indicating bonded and non-bonded charge concentrations on N(1) and S(2) [$-\nabla^2\rho(\boldsymbol{r})$ = 45 and 9 e Å^{-5}, respectively].

Intermolecular bonding. The solid-state structure of S_4N_4 consists of helical chains of molecular units along the crystallographic *b*-axis. The pronounced polarity of the S–N bonds orients neighbouring molecules such that electrostatic S···N contacts are formed [Fig. 2(a),(b)]. $\rho(\boldsymbol{r})$ at the intermolecular S···N bond CPs is rather small [$\rho(\boldsymbol{r}_c)_{av}$ = 0.085(1) e Å^{-3}], but is substantially greater than, for example, the S···S *intra*molecular interactions in 3,3,6,6-tetramethyl-*S*-tetrathiane [$\rho(\boldsymbol{r}_c)$ = 0.043(1) e Å^{-3}].[12] Despite the flatness of the $\rho(\boldsymbol{r})$ map, four *intermolecular* bond CPs, six ring CPs and one cage CP have been located; all experimental and theoretical topological parameters are in good agreement. A more detailed picture emerges from analysis of the Laplacian, $\nabla^2\rho(\boldsymbol{r}_c)$, in regions corresponding to these intermolecular bonding interactions. The results are depicted in Fig. 2 as contour plots for (a) the NNS′S′, and (b) the SNN′S′ interactions, respectively. Here maxima in $-\nabla^2\rho(\boldsymbol{r}_c)$ signal regions of local charge concentration and minima regions of local charge depletion. In accord with both the present and an earlier theoretical study,[3] we deduce that (i)

† Electronic supplementary information (ESI) available: experimental details; listing of geometrical and topological parameters; fractional atomic coordinates and mean square atomic displacement parameters; multipole population coefficients; expansion and contraction coefficients; description of the local coordinate systems and basis set information. See http://www.rsc.org/suppdata/cc/a9/a910209o/

DOI: 10.1039/a910209o

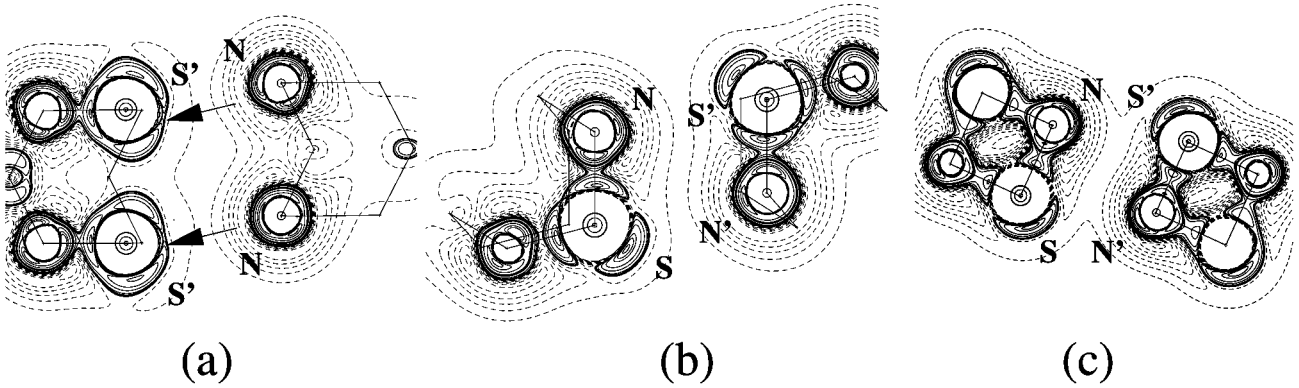

Fig. 2 Contour plots of charge concentrations determined experimentally and by calculation [B3LYP/6-311G(3df) level]. Negative values of $-\nabla^2\rho(\boldsymbol{r})$ are marked by broken lines. (a) $-\nabla^2\rho(\mathbf{r})_{exp}$ in the NNS′S′ plane and (b) $-\nabla^2\rho(\boldsymbol{r})_{exp}$ in the SNN′S′ plane. The relative orientations of the S_4N_4 molecules are indicated by solid lines. Salient distances (Å) and angles (°): S–N′ 3.0882(8); N–S···N′ 79.43(3); N···NS′ 100.00(3). (c) $-\nabla^2\rho(\boldsymbol{r})_{calc}$ in the SNN′S′ plane of the $(S_2N_2)_2$ dimer. In (a) the 'key–lock' interaction is marked by arrows.

two bonded and two non-bonded, and (ii) three bonded and one non-bonded charge concentrations, respectively, in the valence shells of the N and S atoms of S_4N_4 are retained in the solid state [Fig. 1(b)].

While the bonded charge concentrations constitute the intramolecular bonds, the *magnitude* and *location* of the non-bonded charge concentrations on the nitrogen and the local charge depletions on the sulfur atoms should be responsible for the orientation of the S_4N_4 molecules in the solid state.[3,13] According to a point charge model, optimal interaction should occur for closest contact of S···N′ pairs, giving a value of 90° for the NNS′ angle in the NNS′S′ plane. In fact, this angle is 100.00(3)° on account of the directionality of the interactions between the local charge concentrations in the valence shells of the N atom and the associated regions of charge depletion on the corresponding S′ atom. Fig. 2 clearly shows the resulting 'key–lock' principle of facing charge *concentrations* and charge *depletions* in the valence shells of the nitrogen and sulfur atoms in the intermolecular NNS′S′ plane of the $(S_4N_4)_2$ dimer. A similar pattern of charge tessellation is displayed by the Laplacian in the corresponding NSN′S′ plane of S_4N_4 and also in the structurally related model system $(S_2N_2)_2$,[12] as depicted in Fig. 2(c). For $(S_2N_2)_2$ the S···N′ contacts are significantly shorter than in $(S_4N_4)_2$ [2.890(1)[14] *cf.* 3.0882(8) Å], in accord with the proclivity of S_2N_2 to polymerise to $(SN)_x$ with the transformation of one S···N′ contact into a covalent S–N bond.

The 'key–lock' interaction based on the Laplacian goes beyond a point charge model which takes no account of the polarisation of the valence shell and the consequent formation of local charge concentrations and depletions. Whilst crystal architecture is often controlled by directional interactions like hydrogen bonding,[17] this appears to be the first experimental study to reveal a simple three-dimensional directional interaction involving facing charge concentrations and charge depletions as a transferable architectural principle in a molecular crystal. The transferability of the 'key–lock' pattern is remarkable since S_2N_2 and S_4N_4 display rather different geometries and electronic structures. These results suggest that similar architectural forces encoded in the Laplacian of the charge density may be more generally revealed by this type of experimental study. The ability to observe such intermolecular interactions is an important advance, for it demonstrates the response of the non-isolated molecule to its chemical environment, and so holds out the prospect of a better understanding not just of molecular structure, but of molecular *reactivity* and molecular *recognition* under appropriate conditions.

Notes and references

1 M. L. DeLucia and P. Coppens, *Inorg. Chem.*, 1978, **17**, 2336.
2 A. S. Brown and V. H. Smith, Jr., *J. Chem. Phys.*, 1993, **99**, 1837.
3 T.-H. Tang, R. F. W. Bader and P. J. MacDougall, *Inorg. Chem.*, 1985, **24**, 2047.
4 M. J. Almond, G. A. Forsyth, D. A. Rice, A. J. Downs, T. L. Jeffery and K. Hagen, *Polyhedron*, 1989, **8**, 2631.
5 *Crystal data* for S_4N_4: M_r = 184.32, yellow prisms; monoclinic, space group $P2_1/n$, a = 8.7286(4), b = 7.0783(4), c = 8.6377(4) Å, β = 93.722(2)°, V = 532.54(5) Å^3; T = 100(1) K; Z = 4, $F(000)$ = 368, D_c = 2.299 g cm^{-3}, μ = 16.6 cm^{-1}. 32220 (22404) Bragg reflections were collected on a Nonius kappa-CCD system with a rotating anode generator (Nonius FR591; Mo-K$_\alpha$, radiation (λ = 0.71073 Å); data for a second crystal in parentheses); 6887 (5488) independent reflections were observed. Both data sets were independently corrected for beam inhomogeneity and absorption effects and scaled together: 99.8% completeness in the data range $\sin\theta/\lambda_{max}$ = 1.10 Å^{-1}; R_{int} = 0.028 for 6108 unique reflections. The deformation density was described by a multipole model in terms of spherical harmonics multiplied by Slater-type radial functions with energy-optimised exponents (see ref. 16). The multipole expansion was terminated at the hexadecapolar level. The refinement of 105 parameters against 4849 observed reflections [$F > 3\sigma(F)$] converged to R_1 = 0.025, wR_2 = 0.033, GOF = 1.62, and a featureless residual $\rho(\boldsymbol{r})$. CCDC 182/1565. See http://www.rsc.org/suppdata/cc/a9/a910209o/ for crystallographic files in .cif format.
6 R. F. W. Bader, *Atoms in Molecules—A Quantum Theory*, Clarendon Press, Oxford, 1990.
7 Experimental deformation densities from this study also display a minimum in $\Delta\rho(\boldsymbol{r})$ at the centre of the S_4N_4 cage.
8 *Ab initio* molecular orbital calculations on H_2S_2 and S_2 suggest reference charge densities at the bond CP of 0.999 and 1.389 e Å^{-3} for single and double S–S bonds, respectively; see ref. 13.
9 $G(\boldsymbol{r})$ values are computed from experimental $\rho(\boldsymbol{r})$ values using the approach from Yu. A. Abramov, *Acta. Crystallogr., Sect. A.*, 1997, **53**, 264.
10 D. Cremer and E. Kraka, *Angew. Chem., Int. Ed. Engl.*, 1984, **23**, 627.
11 All calculations were performed at the B3LYP/6-311G(3df) level using Gaussian 98. The geometries of S_4N_4, $(S_4N_4)_2$ and $(S_2N_2)_2$ were fixed at the experimentally determined ones. The topology of $\rho(\boldsymbol{r})_{calc}$ was analysed using the AIM software package (ref. 15).
12 K. L. McCormack, P. R. Mallinson, B. C. Webster and D. S. Yufit, *J. Chem. Soc., Faraday Trans.*, 1996, **92**, 1709.
13 A similar key–lock situation based on an experimental charge density study has been observed in the case of the van der Waals interactions between two chlorine atoms in the (100) plane of solid Cl_2; see: V. G. Tsirelson, P. F. Zou, T.-H. Tang and R. F. W. Bader, *Acta Crystallogr., Sect. A.*, 1995, **51**, 143.
14 M. J. Cohen, A. F. Garito, A. J. Heeger, A. G. MacDiarmid, C. M. Mikulski, M. S. Saran and J. Kleppinger, *J. Am. Chem. Soc.*, 1976, **98**, 3844.
15 R. F. W. Bader, *Acc. Chem. Res.*, 1985, **18**, 9.
16 E. Clementi and C. Roetti, *At. Data Nucl. Data Tables*, 1974, **14**, 177; N. K. Hansen and P. Coppens, *Acta Crystallogr, Sect. A.*, 1978, **34**, 909; T. Koritsánszky, S. Howard, T. Richter, Z. W. Su, P. R. Mallinson and N. K. Hansen, *XD—A Computer Program Package for Multipole Refinement and Analysis of Electron Densities from Diffraction Data*, Free University of Berlin, Germany, 1995.
17 See, for example, D. Braga, F. Grepioni and G. R. Desiraju, *Chem. Rev.*, 1998, **98**, 1375.

Communication a910209o

Typeset and printed by Black Bear Press Limited, Cambridge, England

Host–guest chemistry of calixarene capsules

Julius Rebek, Jr.

The Skaggs Institute for Chemical Biology and Department of Chemistry, The Scripps Research Institute, 10550 North Torrey Pines Road, La Jolla, California USA. E-mail: jrebek@scripps.edu

Received (in Cambridge, UK) 24th December 1999, Accepted 27th January 2000
Published on the Web 7th March 2000

Reversible encapsulation is one of the more recent forms of molecular recognition. Small molecule targets are completely surrounded by larger molecular assemblies and steric barriers keep the guest from escaping the host. Calix[4]arenes make useful modules for capsule construction and the review traces their history. Applications in physical organic chemistry, materials science and spectroscopy are described.

Calixarenes are widely used modules in supramolecular chemistry but I was avoiding them. After all, there were (and still are) a good number of superbly capable research groups busy with these molecules. Their work has generated hundreds of original journal articles, extensive literature reviews and whole monographs; I did not intend to disappear in this avalanche of paper. But here I am, tossing another snowball on the heap, writing more about them. What changed my mind was the imagination and skill of a graduate student, Ken Shimizu. He presented me with an accomplished fact: a calixarene that formed an encapsulation complex. No one else could have arrived at the same molecules, we thought—but that was a colossal illusion.

Ken was working in aspects of molecular recognition chemistry involving cleft-like synthetic shapes and he possessed a keen eye for molecules with curvature. At that time more than half of the research group was involved in self-assembling systems, particularly hollow, pseudo-spherical structures, and he set out to invent his own version. Instead of carving up the sphere into a pattern of, say, a tennis ball, Ken felt that a simpler, hemispherical division would lead to a fertile formula for assembly. For this he needed a bowl-shaped molecule that could be usefully functionalized on its rim. He found it in calixarenes[1] when they are in the so-called 'cone' conformation (Fig. 1).

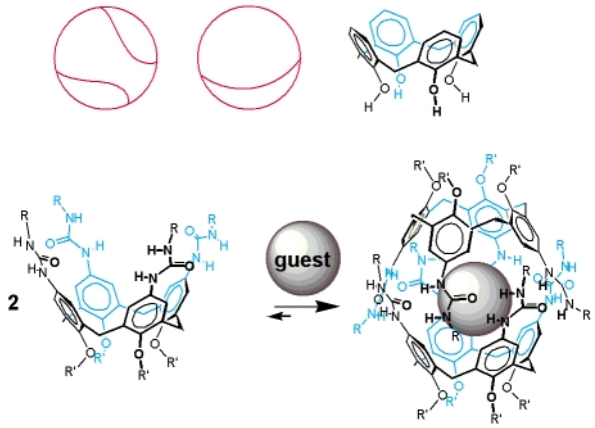

Fig. 1 *Top*. Ways of dividing a spherical surface and the curvature of a calix[4]arene in a cone conformation. *Bottom*. The calix[4]arene bearing ureas on the upper rim forms a dimeric capsule when an appropriate guest is present.

This conformation features a gentle curvature on its molecular surface that can be enforced and maintained by placing sizable groups on the lower rim, on the phenolic oxygens.[2] The cavity left by this shape is what matters; if the calixarene were constructed from CPK models then filled to the brim with, say, a quick-setting plaster,[3] then the hardened material, when removed, would resemble not so much a cone as it would (in miniature) the great pyramid at Giza. The cone descriptor was devised by Gutsche[1] whose heroic synthetic studies have resulted in calixarenes being articles of commerce. In addition, Böhmer,[4] Ungaro,[5] Shinkai,[6] de Mendoza[7] and others have worked out the synthetic protocols and the many conformational possibilities of calixarenes. I am grateful to the advantages their work gave us latecomers.

Shimizu's idea had been to bring two of these calixarenes together, rim-to-rim, and the enduring fashion in the group was to use hydrogen bonding patterns on self-complementary molecules to accomplish this. The moderate directionality and reversible formation of hydrogen bonds had been successful in other ongoing projects and Ken used the nature of ureas to nurture a seam of hydrogen bonds between the hemispheres. A circle of eight ureas, four from each hemisphere, assembled head-to-tail as shown in Fig. 1. This directionality leads to a reduction of symmetry (at least on the NMR timescale) and no planes of symmetry are present in the dimer: the two meta protons of the benzene units are now in different magnetic environments. It was the coupling constant between these protons that gave away the structure.

When I first lectured about this work at a conference in Jerusalem in the summer of 1995, I was disappointed to find that the calixarene capsule was greeted with some skepticism. Two other groups had already made molecules having all the functional aspects of Ken's, but had not recognized them to be dimeric capsules. Volker Böhmer proposed that we look for

Julius Rebek, Jr. was born in Hungary in 1944 and lived in Austria from 1945–49. He and his family then settled in the USA in Kansas. He received his undergraduate education at the University of Kansas in 1966, and obtained the PhD degree from the Massachusetts Institute of Technology (1970) for studies in peptide chemistry with Professor D. S. Kemp. As an Assistant Professor at the University of California at Los Angeles (1970–1976) he developed the 'three-phase test' for reactive intermediates. In 1976 he moved to the University of Pittsburgh where he rose to the rank of Professor of Chemistry and developed cleft-like structures for studies in molecular recognition. In 1989 he returned to the Massachusetts Institute of Technology, where he was the Camille Dreyfus Professor of Chemistry and devised synthetic, self-replicating molecules. In July of 1996, he moved his research group to The Scripps Research Institute to become the Director of The Skaggs Institute for Chemical Biology, where he continues to work in combinatorial chemistry and self-assembling systems.

DOI: 10.1039/a910339m

meta coupling in our systems, as predicted by a dimeric structure, and indeed, there was. Böhmer subsequently published his capsular system,[8] about which more later. David Reinhoudt favored a 'pinched cone' conformation but eventually described the cone conformation for anion detection with his urea and sulfonyl urea calixarenes.[9]

Even though the NMR spectra in solvents such as $CDCl_3$ were consistent with the formation of a dimeric capsule, it was not until Shimizu detected a guest inside the capsule that we were confident enough to publish this work.[10] First, it was necessary to solve the solvent problem and the solution was, well, in the solution. Still and Chapman[11] had shown that concave surfaces into which solvents do not fit tended to show high affinities for other small molecules that do. This scenario was staged by the use of solvents that are too large to be accommodated in the concavity, provided that they still dissolved the components of the system. These observations concerning solvent size *vs.* cavity size are generally applicable to encapsulation phenomena and we have used them extensively. For the case at hand, it meant that solvents such as $CDCl_3$ that are excellent guests for the cavities, are reluctant to leave the cavities to solutes. After all, the solvent at ~10 molar concentration has a seemingly insurmountable advantage. To make matters worse, trace impurities in the solvents can provide stoichiometric amounts of excellent guests. For example, a solvent like deuterated *p*-xylene, for which modeling suggested an uncomfortably tight fit, was easily displaced by simple aromatics. Benzene, for example, fits well and when it is added to such a solution a new resonance in the NMR spectrum appears, a sharp singlet at *ca.* 4 ppm. The benzene oozes into the cavity over the course of about an hour. But when the deuterated xylene solvent is subjected to fractional distillation to remove deuterated benzene contaminants, the added benzene guest enters rapidly.

A different approach to the dimeric nature of the capsule was provided by Böhmer. He showed that mixing two very similar calixarene dimers gave a heterodimeric system.[8] Shortly thereafter, Böhmer took all of the doubt out of things by providing an X-ray crystal structure[12] with the hydrogen bonds of the capsule clearly defined, and a benzene guest inside the capsule to boot.

Solubility is an ever-present issue for our self-assembling systems. For the calixarenes we enhanced it by attaching large groups, such as benzylic groups, to the lower rim and alkyl-substituted aromatics along the ureas of the upper rim. Nowadays, we use *p*-*n*-heptylphenyl, but in the early days the best peripherals were tolyl or even normal alkyl chains. Even with these appendages low solubility in our favorite (large) deuterated solvent, *p*-xylene and the pricey (largest) mesitylene often thwarted our encapsulation attempts. To this very day we suffer the neglect of commercial concerns for our need of larger, deuterated solvents.

Our studies centered around what types of guests could be ushered in. Because of the unusual shape of the cavity (two square pyramids rotated at 45° from each other) we tried some correspondingly exotic shapes (Fig. 2). Phil Eaton provided us with a generous sample of cubane and it proved to be an excellent guest. Halobenzenes, especially fluorobenzenes were also readily encapsulated and gave us some information about their orientation when trapped within. For example, in fluorobenzene the chemical shifts of the *ortho*, *meta* and *para* protons suggest a positioning in which the C–F bond and the *para* proton are along the equator (a polar microenvironment), directed at the seam of hydrogen bonds.[13] A semantically challenging situation arises in the description of these capsules since the 'poles' are not polar but the equator is! The resonance of the *para* proton of C_6H_5F was shifted only moderately upfield in the NMR spectrum, while the *ortho* and *meta* protons, directed at the eight aromatic faces in the poles of the cavity, experience the largest upfield shifts. Blake Hamann found that even the floppy pentane is encapsulated.[14] Its terminal methyl groups appear at higher field than −2 ppm. In any of these cases, it was possible to 'denature' the system, that is, by flooding the solution with competing ureas the hydrogen bonds were disrupted and the guest was liberated. Of course, the same result can be reached by adding a solvent such as DMSO that competes for the hydrogen bond acceptors. We will discuss those experiments in due course.

During this time, Christoph Schalley and Gary Siuzdak were intent on characterizing the capsules in the gas phase. Historically, it has not been easy to get evidence for hydrogen bonded assemblies through mass spectrometry, since the protic solvents required for protonation tend to disrupt the very hydrogen bonded aggregates that one wishes to detect. A number of static tactics have been used to overcome this problem: labeling with alkali ions by covalently attached crown ethers,[15] cation–π complexes with silver ions and suitably arranged aromatics,[16] and even anions[17] appended to the assemblies have been useful. Schalley tested various organic cations and found that the *N*-methylquinuclidinium ion was an excellent guest for the calixarene capsules, both in solution and in the gas phase. This ion acts simultaneously as a guest and an ion label. Moreover, this guest is one of the best for the calixarenes, it even competes with solvent chloroform for the interior of the capsule.[18] Cation–π interactions provide the driving force. Schalley used this ion in a number of contexts including heterodimerization experiments[19] and with a covalently bound capsule, discussed below.

A number of other functional groups were attached to the upper rims of the calixarenes then screened for capsule formation. One of these led to a discovery that had far-reaching consequences for our program. Ron Castellano and Professor Byeang Hyean Kim made a sulfonyl urea derivative,[20] similar to one earlier reported by Reinhoudt.[9] It was characterized as a capsule, but in the presence of a aryl urea capsule, disproportionation took place in an exclusive manner: only the heterodimeric system was observed by NMR! Probably the superior acidity of the sulfonyl urea finds its counterpart in the

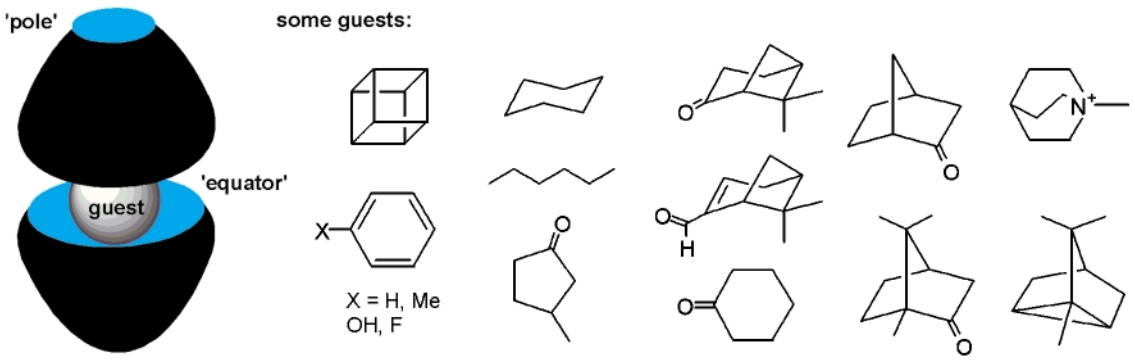

Fig. 2 *Left.* Cartoon representation of the calixarene capsules used elsewhere in this review. *Right*. Some of the many guests encapsulated by these dimers.

basicity of the aryl urea, but there must be other intermolecular forces involved since simple alkyl ureas do not show the same tendency to heterodimerize. Whatever the cause, this phenomenon helped us characterize a number of systems of increasing complexity (Fig. 3). For example, using a 1,3,5-trisubstituted aromatic spacer, we were able to observe an assembly in solution that was capped by three sulfonyl ureas.[21] This is one of the most complicated assemblies we have prepared to date; it consists of seven molecules – the centerpiece, three caps and three guests. It maintains its structure in solution and in the gas phase when quinuclidinium is the guest.

The calixarenes also allowed us to explore the practical differences between covalently bound molecules-within-molecules, carcerands[22] and reversibly formed capsules.[23] Independently, Sherman was pursuing this very line of inquiry using resorcinarene-based systems.[24] The question dealt with whether or not we could combine the best aspects of assembly—reversibility and stability—but side-step the worst aspects—lengthy syntheses and solubility problems—with capsules that were hybrids. In both approaches, the tactic was the same; to covalently attach two of the bowl-shaped molecules at their upper rims in such a way that they would still form a capsule. For the calixarenes, a tether was needed that was long enough to reverse the seemingly divergent directions, and yet short enough to minimize the problems posed by entropy. Marcus Brody arrived at the hexyl tether since it modeled well and provided the distance needed to span the two hemispheres without causing an undue amount of entropy loss from the methylenes of the chain. The synthesis was uneventful, following well-trodden paths.[25] Happily, he found enhanced stability for the new molecule (Fig. 4). It was loathe to miscengenate with other aryl substituted ureas at comparable concentrations; it neither dimerized nor polymerized, but it could be forced to heterodimerize with excess sulfonyl ureas. The product favored at equilibrium was a dumbbell-shaped assembly that featured five molecules. Again, it was characterized both in solution and in the gas phase as its quinuclidinium complex.

The capsule exists as a pair of enantiomers but we expected very little in the way of entantioselective recognition from such a system. After all, the chirality exists in the lining, in the seam of the hydrogen bonds, as a clockwise or counter-clockwise arrangement with respect to the tether. The tether is largely external and cannot reasonably be expected to influence binding events inside. The longer-term significance of this molecule is that the tether also provides a place for covalent attachment of an entire capsule-forming unit on, say, a solid surface. We have aims on a sensing device for appropriate guests, but this has not yet been brought to practice.

Polycaps

Self-complementary structures have fascinated us for some time as there is a certain economy, even dignity, in a molecule that recognizes itself in a predictable way. By predictable I include the contributions of crystal engineering,[26] but any molecule that enjoys a liquid or solid state does express some self-complementarity, intended or not. When the recognition surfaces are arranged in a way that all sites find their complements in a dimer, then additional possibilities arise: these self-complementary structures can give rise to the simplest molecular replicators.[27] Experiments in the Ghadiri lab have recently shown that trimeric peptide helix bundles are also capable of replication,[28] and there is no reason to exclude tetramers or higher order aggregates, even if no specific cases exist at this writing. What is certain is that recognition surfaces that diverge on self-complementary molecules lead to open-ended systems such as polymers. For some years we had been trying to realize this in the context of the capsular structures, and the calixarenes gave us the opening we were looking for.

Professor Dmitry Rudkevich and Ron Castellano used literature precedents to synthesize a calixarene tetraurea bearing

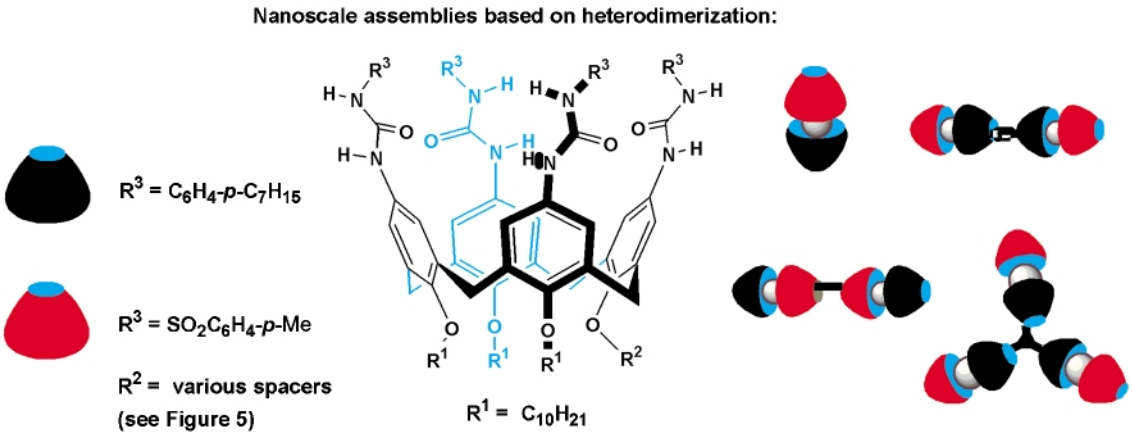

Fig. 3 Aryl and sulfonyl ureas further functionalized on their lower rims are converted into modules. Heterodimerization takes place exclusively to give predictable nanoscale assemblies.

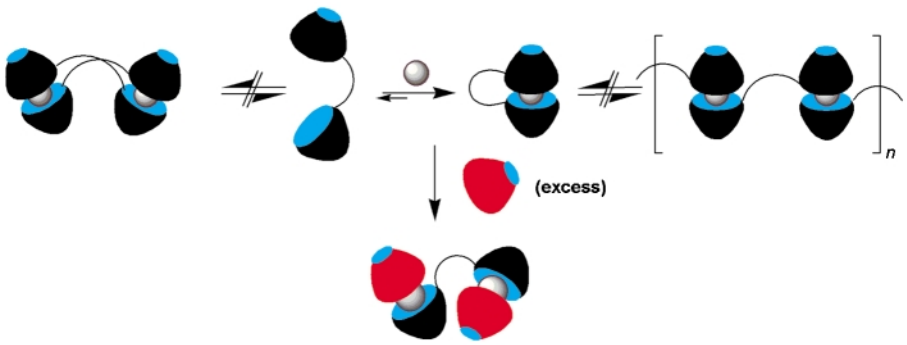

Fig. 4 Covalent connection of the two hemispheres at their upper rims now leads to capsules in an intramolecular sense. Neither 2+2 dimers (top left) nor polymers (top right) are formed. However, with excess sulfonyl functionalized calixarenes a dumbbell-like shape is favored (bottom).

a unique site for functionalization on the lower rim. This had already been accomplished elsewhere[29] to anchor alkali and alkaline earth ions to a calixarene platform. Dimerization of this molecule was as expected but gave us a taste of the complex flavors of isomerism that lay ahead. For example, two regioisomers of the capsules exist and there are unique environments for all 8 (downfield) N–H resonances in each! Nonetheless, they are not very different; these 16 urea resonances appear within 0.1 ppm of each other in the NMR spectrum. Two of the monomeric calixarenes were duly linked through amide bonds to relatively short spacers (Fig. 5).[30]

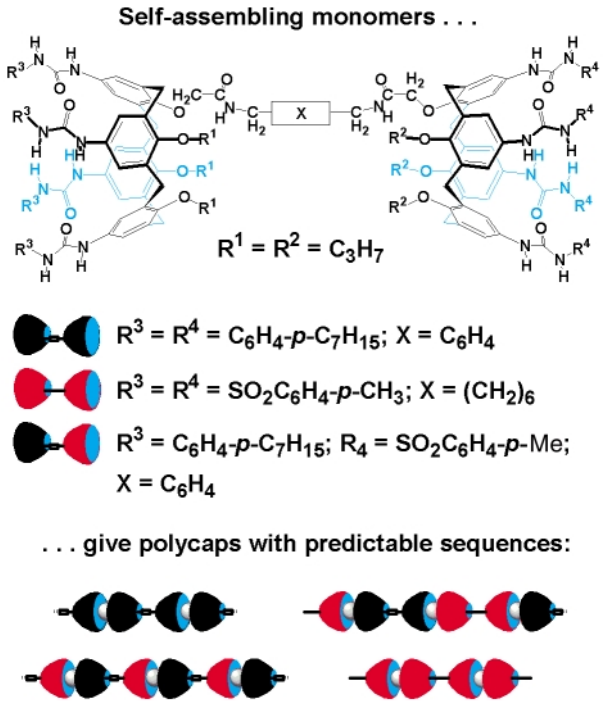

Fig. 5 Heterodimerization preferences lead to predictable polymer sequences from either complementary or self-complementary subunits.

Consider, now, the assembly of such a unit in a linear polymeric array. Capsules appear like beads on a string, and each site is at a characteristic distance from the end of the polymer. At first glance, one might think there is symmetry about the center of the supermolecule, but the two halves of each capsule are different, each cavity is chiral, that is, the head-to-tail arrangement of ureas is either clockwise or counterclockwise at each capsule. For a string of, say, 100 units the number of isomers due to chirality and regiochemistry approaches 4^{100}. This figure is many times greater than the total number of molecules in the sample (or on earth, for that matter). The symmetry must be broken as described by Eschenmoser.[31] That we were able to observe and interpret the signals for the polycaps and their encapsulated guests was a triumph of high resolution NMR.

The polymeric assemblies do show broadened NMR spectra but the positions of the resonances matched very closely those of simpler model (dimeric) capsules. Addition of guests resulted in the emergence of new signals, and the encapsulated species showed up right where we expected them. The reversibility of the polymerization was readily established: for example, a few % DMSO added to the $CDCl_3$ solvent gave a system that contained roughly equal amounts of monomer and polycap. When a good guest like *p*-difluorobenzene was then added, the growth of a new polycap species was evident at the expense of both the monomer and the original (solvent-filled) polycap.

A linear polymeric capsule can be of any length and we attempted to determine the length with size exclusion or gel-permeation chromatography. The polycaps proved to be at the limits of the sensitivity of our columns, and the technique, but we have been fortunate to recruit Professor George Benedek and Aleksey Lomakin to address some physical aspects of these systems. They are presently unraveling the complex questions regarding polymer length, individual association constants of the polycaps and their effect on reptation, that is, the entanglements often encountered in covalently bound polymers. The reversible formation of the polycaps may allow ideal, untangled arrangements to form. In the meantime, we note that there are not many examples of reversibly-formed, hydrogen bonded polymers.[32] The uniqueness of the systems at hand have to do with their ability to function as capsules as well as polymers.

The formation of heterodimeric systems was likewise explored by 'end capping' experiments. Specifically, the polycap rapidly broke down to a dumbbell-shaped assembly when treated with an excess of the simple dimeric capsule. The dumbbell featured a sharply resolved NMR spectrum that showed all of the expected resonances. A version capable of cross-linking was also prepared. This was based on a spacer derived from a symmetrical 1,3,5-trisubstituted benzene to which three of the monofunctionalized calixarenes described earlier[21] were attached. The polycap here was insoluble in all of the solvents in which it assembled, but the monomer proved useful in nucleating other complex assemblies.

Let me now describe the long-range order of these polycaps. Colin Nuckolls and Ron Castellano felt confident that the polycaps could be forced into increasing order, for example, into liquid crystalline phases, if the appropriate modifications were made on the surface of the structures. Accordingly, the monomers were outfitted with long alkyl chains that provided a liquid-like sheath around the polymer chains; this helps fill the space between the chains. The resulting polycaps (at high concentrations) showed birefringence patterns when viewed between crossed polarizers and gave typical Schlieren textures.[33] These textures reflect the morphology of the liquid crystals and were found to be a function of what guest was inside. Lyotropic, nematic liquid crystalline phases were generally observed with the polycaps. The characterization was done by our collaborators: Holger Eichhorn in Timothy Swager's lab at M.I.T. and Andrew Lovinger at the Bell Labs. Typically, molecules like difluorobenzene and nopinone were readily encapsulated in these liquid crystalline phases. Further characterization by X-ray diffraction patterns showed peaks at 2.4 and 1.6 nm that match well the repeat distances and the dimensions of the polycaps (Fig. 6).

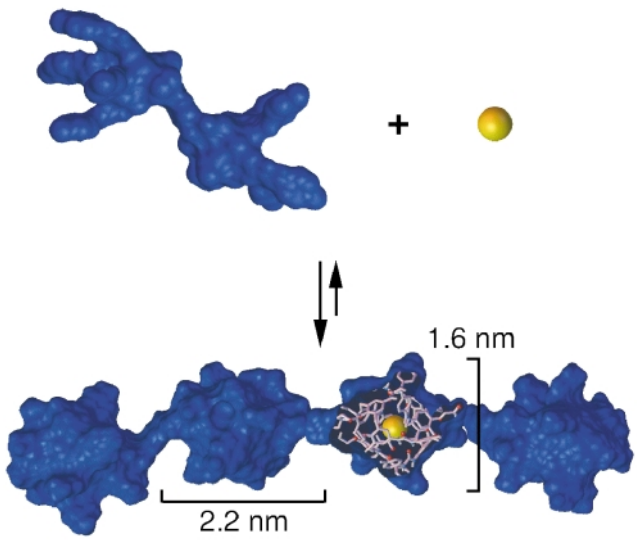

Fig. 6 Covalently-linked calixarenes form polycaps in the presence of a suitable guest.

It was also possible to show that external, mechanical forces can be used to further organize the liquid crystalline phases. For example, shearing gave fibers that showed a uniform width of about 6 μm when viewed through a confocal microscope. Macroscopic samples were also prepared. Specifically, fibers from liquid crystalline samples could be pulled to cm lengths. This ability to draw fiber structures from polymeric liquid crystals is also characteristic of other hydrogen bonded polymers.[34] In short, a hierarchical ordering of the molecules that ranges from the Å to the cm scale is at hand. Whether we are able to find applications for these liquid crystals that have encapsulated guests is not yet clear. After all, liquid crystals are a dime a dozen (or worse, a dime a pound) and our polymeric capsules cost a bit more.

While we started this discussion praising the virtues of self-complementarity, the heterodimerization that we discussed between the sulfonyl ureas and the aryl ureas took us a long way in ordering assemblies. There is another way heterodimerization became an advantage and that dealt with chiral derivatives. The calixarene tetraureas derived from norleucine in its optically active form showed a very high preference for forming heterodimers with the parent aryl urea. Within these the head-to-tail arrangement of the eight ureas appeared entirely to be oriented in one direction. In other words, the peripheral point chirality of the amino acid was being transmitted to the capsule's lining (Fig. 7). This heterodimerization was shown to

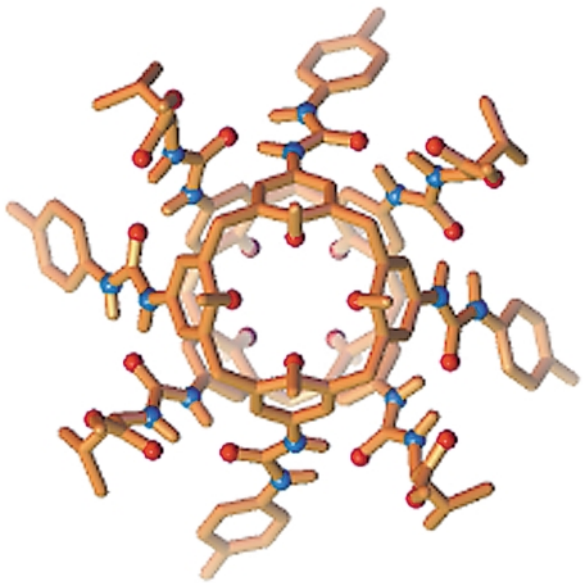

Fig. 7 The heterodimer formed between a tolyl urea and a chiral urea (L-valine) as viewed from one of its poles.

be exclusive with other amino acids that have β-branched side chains, like isoleucine and valine.[35] Circular dichroic spectroscopy was used to assign the absolute configuration of these capsules. The side chains of the amino acids provide contacts that are vital in the dimeric assembly and eventually lead to instruction of the clockwise or counter-clockwise arrangement of the ureas.

Do these asymmetric microenvironments distinguish between enantiomeric guests? They do, but to date only modestly. For example, with norcamphor as a racemic guest, the heterodimer shows two sets of assemblies and there is about a 15% excess of one diastereomeric complex. With smaller guests such as 3-methylcyclopentanone encapsulation occurs, but no enantioselective binding is observed. So the many asymmetric centers in these molecules do not necessarily translate into an outrageously chiral space. Rather, as is the case with cyclodextrins, the bumps and dimples of the lining of these capsules are smoothed over by the large number of their subunits. On the positive side, the heterodimerization systems that have emerged out of the studies of sulfonylureas and β-branched chiral ureas represent forms of molecular instruction. They have parallels in base pairing in double-stranded DNA. All of the bases can—and to some extent, do—homodimerize, but the appropriate heterodimers are far more stable.[36]

Polymeric systems based on heterodimerization capabilities of the capsules were also explored by Ron Castellano. For example, the alternating urea/sulfonyl urea polycap was made as was the system in which each subunit had one urea and one sulfonyl urea at each end. Both of these systems gave nearly the same NMR spectrum. The instructions for heterodimerization represent a vehicle for information in these systems, and it becomes possible to consider an informational polymer based on these molecules. For example, consider a backbone along which the calixarenes may be appended. One of the simplest constructs is an amino acid that has the calixarene as the side chain. Such a system was duly made[37] and is recognizable as a quite large amino acid (Fig. 8). The intent was to build a ladder-like polypeptide molecule capable of pairing, wherein the sequence of ureas and aryl ureas could be read by an opposite strand, very much like a sequence of a nucleic acid is read by the complementary strand. Would such a system show pairing? Our early characterization of the molecule answers this question in the affirmative. Specifically, the dipeptide analog was prepared and characterized as a self-complementary dimer, but the molecules have become so large that their characterization, even for the simplest cases, has become unmanageable by the conventional techniques we have at hand.

A third and independent means of establishing heterodimerization comes from Ron Castellano, Colin Nuckolls, and Stephen Craig's recent experiments with fluorescence resonance energy transfer, or FRET (Fig. 9). Two different dyes are placed on each of the lower rims of two different calixarenes and only when they are held in a heterodimeric capsule are the dyes close enough together to permit energy transfer.[38] Excitation of the donor ($h\nu$) results in two colors of emitted light: one fluorescence band at the donor emission wavelength ($h\nu'$), and a second at the acceptor emission wavelength ($h\nu''$) that signals the noncovalent union of three species—donor, acceptor and guest. By monitoring these wavelengths, assembly and dissociation processes can be observed in real time.

The FRET process allows for much more than just *detection* of the heterodimer; the kinetics and thermodynamics of the assembly can also be determined. We knew that a donor sulfonyl urea **1D** would heterodimerize exclusively with an acceptor aryl urea **2A** to give a predominance of the desired complex, **1D·2A**, capable of FRET. When these species are combined, the heterodimer **1D·2A** duly forms, FRET occurs, and the acceptor emission increases until essentially quantitative energy transfer is observed. By using different stoichiometries of donor and acceptor, as well as untagged derivatives, we were able to determine association and dissociation rates under pseudo first-order conditions. The corresponding K_A's are, as expected, high—just shy of 10^9 M^{-1} for **1D·2A** in benzene. By titrating these dimer solutions with a solvent that can effectively compete for the hydrogen bonds, such as DMSO, the assembly process can be reversed, and the donor emission is restored. We believe that energy transfer fluorescence techniques may be a general means to investigate the solution behavior of related assemblies wherein association constants are high and compound availability is low.

The assembly process shown in Fig. 9 can only occur in the presence of a suitable guest molecule. In our work published to date that role is played by the solvent itself, but when the solvent is not a viable guest, then the FRET system may be a sensitive method for small molecule detection. The analytes remain chemically unmodified because they are held in capsules by mechanical as well as intermolecular forces. In the sytem with heterodimers of calixarenes functionalized with aryl ureas and amino acid-derived ureas, our initial results are promising;

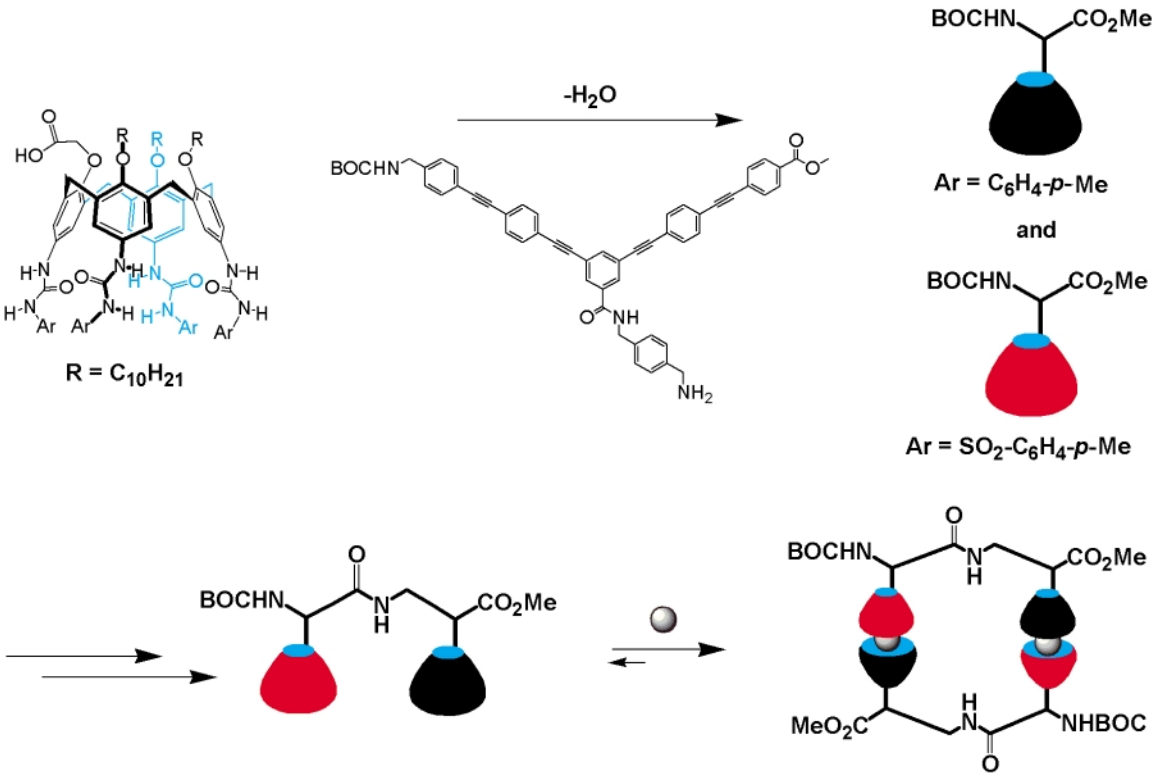

Fig. 8 A 'two bit' system. Hemispheres are placed on an extended amino acid. Heterodimerization preferences provide molecular instructions along the peptide backbone.

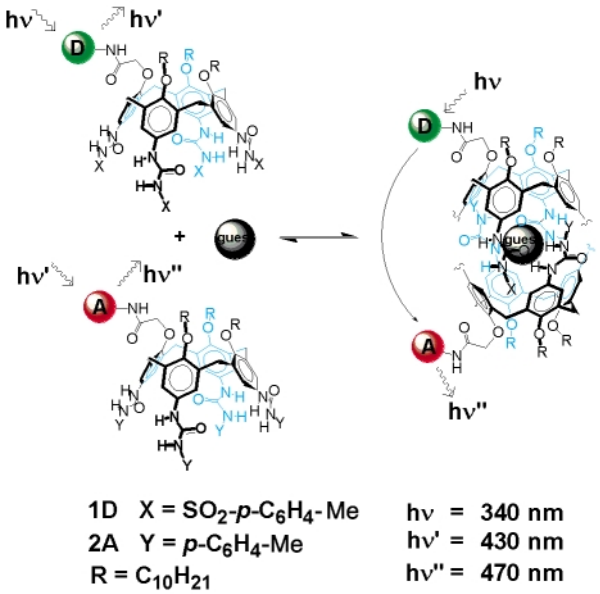

Fig. 9 The use of fluorescence resonance energy transfer (FRET) to monitor self-assembly. The two calixarene hemispheres are outfitted with energy transfer dyes; the presence of the guest nucleates the heterodimerization and allows the FRET to occur. Some ureas have been omitted for clarity.

energy transfer is observed only in the presence of the intended guest.

The molecular encounters described here are matters of timing and the timescales are huge. A normal diffusion complex lasts less than a billionth of a second, while molecules held within the carcerands[22] are confined for the lifetime of a covalent bond, typically a billion seconds. The reversible encapsulation complexes exist in the midrange of these extremes on a human-friendly timescale of 1 second, with three orders of magnitude on either side. Conventional kinetic studies concerning how guests get in and out of these capsules have been initiated and we have made some progress on the problem in the context of 'softballs'.[39] The calixarenes still pose a challenge that inspires our current efforts.

Acknowledgements

This work is supported by grants from the Skaggs Research Institute, National Institutes of Health (GM50174 and GM27932), and NASA. I am indebted to my co-workers whose names have appeared throughout this review: M. S. Brody, R. K. Castellano, S. L. Craig, B. C. Hamann, B. H. Kim, C. Nuckolls, D. M. Rudkevich, C. A. Schalley, K. D. Shimizu, G. Siuzdak and M. R. Wood. Their minds and laboratories are uncontrollably fertile.

References

1 Monographs: (*a*) C. D. Gutsche, *Calixarenes*, Royal Society of Chemistry, Cambridge, UK, 1989; (*b*) *Calixarenes. A Versatile Class of Macrocyclic Compounds*, ed. J. Vicens and V. Böhmer, Kluwer, Dordrecht, 1991; (*c*) C. D. Gutsche, *Calixarenes Revisited*, Royal Society of Chemistry, Cambridge, UK, 1998.
2 See, for example: I. Higler, P. Timmerman, W. Verboom and D. N. Reinhoudt, *Eur. J. Org. Chem.*, 1998, 2689.
3 C. N. Eid, Jr. and D. J. Cram, *J. Chem. Ed.*, 1993, **70**, 349.
4 V. Böhmer, *Angew. Chem., Int. Ed. Engl.*, 1995, **34**, 713.
5 A. Pochini and R. Ungaro, Calixarenes and Related Hosts, in *Comprehensive Supramolecular Chemistry*, ed. J. L. Atwood, J. E. D. Davies, D. D. Macnicol, F. Vögtle and J.-M. Lehn, Pergamon, Tarrytown, N.Y., 1996, vol. 2, pp. 103–142.
6 S. Shinkai, *Tetrahedron*, 1993, **49**, 8933.
7 C. Jaime, J. de Mendoza, P. Prados, P. M. Nieto and C. Sánchez, *J. Org. Chem.*, 1991, **56**, 3372.
8 O. Mogck, V. Böhmer and W. Vogt, *Tetrahedron*, 1996, **52**, 8489.
9 (*a*) J. Scheerder, R. H. Vreekamp, J. F. J. Engbersen, W. Verboom, J. P. M. van Duynhoven and D. N. Reinhoudt, *J. Org. Chem.*, 1996, **61**, 3476 and references cited therein; (*b*) J. Scheerder, J. P. M. van Duynhoven, J. F. J. Engbersen and D. N. Reinhoudt, *Angew. Chem., Int. Ed. Engl.*, 1996, **35**, 1090.
10 K. D. Shimizu and J. Rebek, Jr., *Proc. Natl. Acad. Sci. USA*, 1995, **92**, 12 403.
11 K. T. Chapman and W. Clark Still, *J. Am. Chem. Soc.*, 1989, **111**, 3075.

12 O. Mogck, E. F. Paulus, V. Böhmer, I. Thondorf and W. J. Vogt, *Chem. Commun.*, 1996, 2533.
13 B. C. Hamann, K. D. Shimizu and J. Rebek, Jr., *Angew. Chem., Int. Ed. Engl.*, 1996, **35**, 1326.
14 B. C. Hamann, Ph.D. thesis, M.I.T., 1996.
15 K. C. Russell, E. Leize, A. Van Dorsselaer and J.-M. Lehn, *Angew. Chem., Int. Ed. Engl.*, 1995, **34**, 209.
16 K. A. Jolliffe, M. Crego Calama, R. Fokkens, N. M. M. Nibbering, P. Timmerman and D. N. Reinhoudt, *Angew. Chem., Int. Ed.*, 1998, **37**, 1247.
17 X. Cheng, Q. Gao, R. D. Smith, E. E. Simanek, M. Mammen and G. M. Whitesides, *J. Org. Chem.*, 1996, **61**, 2204.
18 C. A. Schalley, R. K. Castellano, M. S. Brody, D. M. Rudkevich, G. Siuzdak and J. Rebek, Jr., *J. Am. Chem. Soc.*, 1999, **121**, 4568.
19 C. A. Schalley, J. M. Rivera, T. Martin, J. Santamaria, G. Siuzdak and J. Rebek, Jr., *Eur. J. Org. Chem.*, 1999, 1325.
20 R. K. Castellano, B. H. Kim and J. Rebek, Jr., *J. Am. Chem. Soc.*, 1997, **119**, 12 671.
21 R. K. Castellano and J. Rebek, Jr., *J. Am. Chem. Soc.*, 1998, **120**, 3657.
22 (*a*) D. J. Cram and J. M. Cram, *Container Molecules and Their Guests*, Royal Society of Chemistry, Cambridge, UK, 1994; (*b*) J. C. Sherman, *Tetrahedron*, 1995, **51**, 3395.
23 M. M. Conn and J. Rebek, Jr., *Chem. Rev.*, 1997, **97**, 1647.
24 R. G. Chapman, G. Olovsson, J. Trotter and J. C. Sherman, *J. Am. Chem. Soc.*, 1998, **120**, 6252.
25 M. S. Brody, C. A. Schalley, D. M. Rudkevich and J. Rebek, Jr., *Angew. Chem., Int. Ed.*, 1999, **38**, 1640.
26 G. R. Desiraju, *Crystal Engineering: The Design of Organic Solids*, Elsevier, New York, 1989.
27 M. M. Conn, E. A. Wintner and J. Rebek, Jr., *Acc. Chem. Res.*, 1994, **27**, 198.
28 D. H. Lee, K. Severin and M. R. Ghadiri, *Curr. Opin. Chem. Biol.*, 1997, **1**, 491.
29 E. Kelderman, L. Derhaeg, G. J. T. Heesink, W. Verboom, J. F. J. Engbersen, N. F. van Hulst, A. Persoons and D. N. Reinhoudt, *Angew. Chem., Int. Ed. Engl.*, 1992, **31**, 1075.
30 R. K. Castellano, D. M. Rudkevich and J. Rebek, Jr., *Proc. Natl. Acad. Sci. USA*, 1997, **94**, 7132.
31 M. Bolli, R. Micura and A. Eschenmoser, *Chem. Biol.*, 1997, **4**, 309.
32 N. Zimmerman, J. S. Moore and S. C. Zimmerman, *Chem. Ind.*, 1998, 604
33 R. K. Castellano, C. Nuckolls, S. H. Holger Eichorn, M. R. Wood, A. J. Lovinger and J. Rebek, Jr., *Angew. Chem., Int. Ed.*, 1999, **38**, 2603.
34 C. B. St. Pourcain and A. C. Griffin, *Macromolecules*, 1995, **28**, 4116.
35 R. K. Castellano, C. Nuckolls and J. Rebek, Jr., *J. Am. Chem. Soc.*, 1999, **121**, 11 156.
36 Y. Kyogoku, R. C. Lord and A. Rich, *Proc. Natl. Acad. Sci. USA*, 1967, **57**, 250.
37 R. K. Castellano, Ph.D. thesis, M.I.T., 2000.
38 R. K. Castellano, S. L. Craig, C. Nuckolls and J. Rebek, Jr., *J. Am. Chem. Soc.*, submitted.
39 J. Santamaría, T. Martín, G. Hilmersson, S. L. Craig and J. Rebek, Jr., *Proc. Natl. Acad. Sci. USA*, 1999, **96**, 8344.

ChemComm

Palladium–indium mediated Barbier-type allylation of aldehydes with allenes

Usman Anwar, Ronald Grigg,* Marcello Rasparini, Vladimir Savic and Visuvanathar Sridharan

Molecular Innovation, Diversity and Automated Synthesis (MIDAS) Centre, School of Chemistry, Leeds University, Leeds, UK LS2 9JT. E-mail: R.Grigg@chem.leeds.ac.uk

Received (in Cambridge, UK) 22nd February 2000, Accepted 6th March 2000
Published on the Web 27th March 2000

A new allylation reaction of carbonyl compounds using allenes is described; homoallylic alcohols were obtained in moderate to good yields from aryl iodides, allenes and carbonyl compounds and an excellent diastereoselection was exhibited when 2-hydroxycyclohexanone was employed.

In the last decade indium has emerged as the metal of choice to mediate the allylation of carbonyl compounds because of its environmentally benign properties allied with a high degree of *chemo-*, *regio-* and *diastereo*-selectivity especially in aqueous media.[1] Furthermore the reaction requires no activation of the carbonyl group and produces few by-products.

The indium mediated allylation reaction is an aldol-type reaction where the nucleophile is an allylindium(I) species usually generated from an allylic halide and indium(0).[2]

Here, we describe the formation of allylindium species by transmetallation[3] of π-allylpalladium(II) complexes generated from aryl iodides and allenes. The resultant allylindium species subsequently add to the carbonyl compound affording homoallylic alcohols (Scheme 1).

There are four synthetic variants of this Pd–In mediated reaction depending on whether the Pd or the In step are *intra-* or *inter*-molecular.

A first set of examples (class 1 processes) where both the Pd and the In steps are intermolecular is presented in Table 1. Aryl/heteroaryl iodides (1.5 mmol) react (DMF, 80 °C, 18 h, Schlenk tube) with allene (1.0 bar) and aldehydes (1.0 mmol) in the presence of indium (100 mesh powder, 1.5 mmol), $Pd(OAc)_2$ (0.1 mmol) and tris(2-furyl)phosphine (0.2 mmol). The use of triphenylphosphine resulted in an incomplete conversion of the starting materials.

Encouraged by these results we employed a substituted allene, *n*-octylallene[4] (1.5 mmol) in the process. A reaction time of 24 h was necessary to achieve complete conversion of the aldehyde. In both the cases so far explored (Table 2) only one geometric isomer was produced and their structures were assigned from NOE data.

A class 2 process (intermolecular π-allyl formation—intramolecular allylation[5]) was explored next. The increased rigidity of the transition state of the aldol-like addition (sub-optimal approach trajectory) may explain the lower yield observed in entry 1. The six membered product was obtained in a better yield (Table 3). The catalytic system comprised $Pd(PPh_3)_4$ (10 mol%) (entry 1) or $Pd_2(dba)_3$ (5.0 mol%) and tris(2-furyl)phosphine (20.0 mol%) (entry 2).

A class 3 process requires an aryl/heteroaryl iodide bearing an allenic side chain. The Pd catalysed step is then intramolecular and is combined with an intermolecular In mediated reaction. Allenyl (2-iodobenzyl) ether[7] (1.0 mmol) was reacted (DMF, 90 °C, 14 h) with aldehydes (1.05 mmol) in the presence of $Pd(PPh_3)_4$ (0.10 mmol) (Scheme 2).

We have briefly studied the effect of chelating groups α to the carbonyl group, such as nitrogen,[8] hydroxyl[9] and alkoxy,[10] on the stereochemical outcome (Table 4) of the reaction of iodobenzene and allene following the protocol described above.

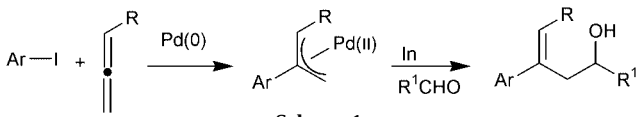

Scheme 1

Table 1

Aryl iodide	Aldehyde	Product	Yield (%)
	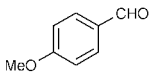	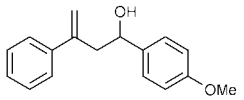	64
	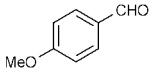	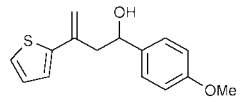	66
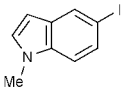	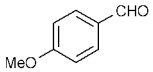	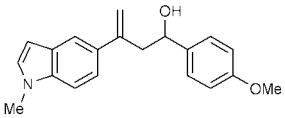	64
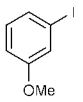	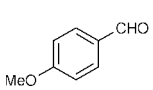	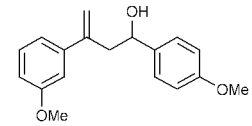	60
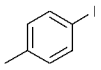	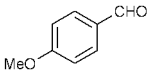	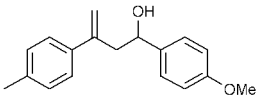	40
	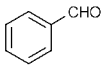	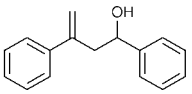	43
	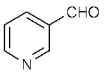	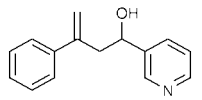	65
	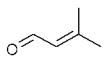	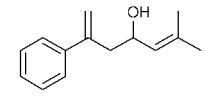	70[a]
	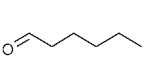	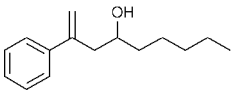	65
	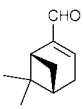	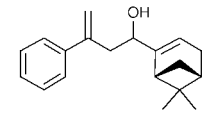	47[b]

[a] Alcohol : triene 2 : 1 (^{1}H NMR); [b] 1 : 1 Mixture of diastereoisomers (^{1}H NMR).

DOI: 10.1039/b001457p

Table 2

Aryl iodide	Aldehyde	Product	Yield (%)
	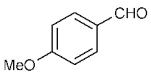	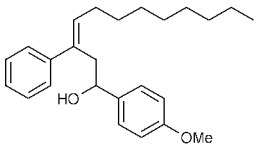	50
	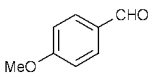	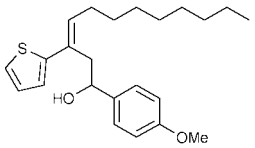	54

Table 3

Aldehyde	Product	Yield (%)
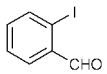	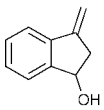	37
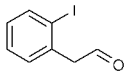	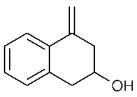	48[6]

The preliminary results (Table 4) show that the palladium–indium mediated allylation of carbonyl compounds using allenes provides easy access to homoallylic alcohols and that chelation clearly controls its diastereoselectivity.

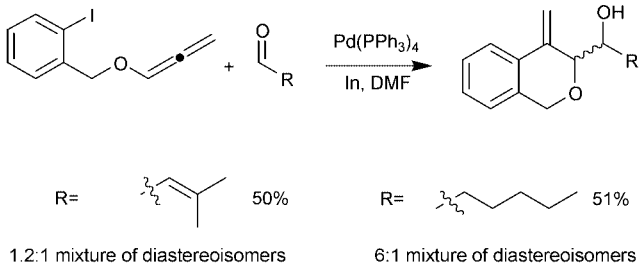

Scheme 2

Table 4

Reagent	Product	*Syn* : *Anti*[a]	Yield (%)
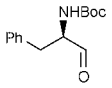	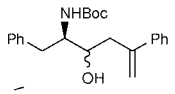	1 : 1	75
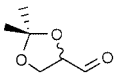	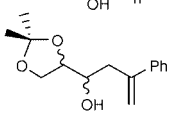	5 : 1[b]	55
	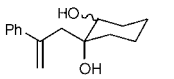	96 : 4	67

[a] Determined by ^{1}H NMR prior to purification. [b] X-Ray analysis on the major isomer in progress.

Further work on these and on the related class 4 processes (intramolecular π-allyl formation—intramolecular aldol-like condensation) are in hand.

We thank the EPSRC and Leeds University for support.

Notes and references

1 C. J. Li and. T. H. Chan, *Tetrahedron*, 1999, **55**, 11 149.
2 T. H. Chan and Y. Yang, *J. Am. Chem. Soc.*, 1999, **121**, 3228.
3 J. A. Marshall and C. M. Grant, *J. Org. Chem.*, 1999, **64**, 8214.
4 S. Searles, L. Yushun, B. Nassim, M. T. Robert-Lopes, P. Tran and P. Crabbè, *J. Chem Soc., Perkin Trans. 1*, 1984, 747.
5 To our knowledge this is the only example of In mediated intramolecular Barbier reaction: L. A. Paquette and J. L. Mendez-Andino, *J. Org. Chem.*, 1998, **63**, 9061.
6 S. E. Gibson, N. Guillo, R. J. Middleton, A. Thuilliez and M. J. Tozer, *J. Chem Soc., Perkin Trans. 1*, 1997, 447.
7 R. Grigg and J. M. Sansano, *Tetrahedron*, 1996, **52**, 13 441.
8 L. A. Paquette, T. M. Mitzel, M. B. Isaac, C. F. Crasto and W. W. Schomer, *J. Org. Chem.*, 1999, **62**, 4293.
9 L. A. Paquette and P. C. Lobben, *J. Org. Chem.*, 1998, **63**, 5604.
10 L. A. Paquette and P. C. Lobben, *J. Am. Chem. Soc.*, 1996, **118**, 1917.

The TpZn–OH/CS_2 reaction: theoretical and preparative visualization of an essential bioinorganic reaction path

Michael Bräuer,[a] Ernst Anders,*[a] Sebastian Sinnecker,[b] Wolfram Koch,[b] Michael Rombach,[c] Horst Brombacher[c] and Heinrich Vahrenkamp*[c]

[a] *Institut für Organische Chemie und Makromolekulare Chemie, Universität Jena, Humboldtstr. 10, D-07743 Jena, Germany. E-mail: ernst.anders@rz.uni-jena.de*
[b] *Institut für Organische Chemie, Technische Universität Berlin, Straße des 17. Juni 135, D-10623 Berlin, Germany*
[c] *Institut für Anorganische und Analytische Chemie, Universität Freiburg, Albertstr. 21, D-79104 Freiburg, Germany. E-mail: vahrenka@uni-freiburg.de*

Received (in Basel, Switzerland) 10th February 2000, Accepted 7th March 2000
Published on the Web 27th March 2000

The reaction between L_3Zn–OH complexes (L = N_3 based ligand) and CS_2 which is an analogue of the carbonic anhydrase functionality was computed at the B3LYP/6-311 + G* level to proceed *via* stable four-center intermediates [L_3Zn–SC(S)OH or L_3Zn–SC(O)SH] to give L_3Zn–SH and COS; in agreement with these calculations, the chemical reaction of $Tp^{Ph,Me}Zn$–OH with CS_2 resulted in the quantitative formation of $Tp^{Ph,Me}Zn$–SH and COS; in the presence of 1 equivalent of MeOH the reaction yielded $Tp^{Ph,Me}Zn$–SC(S)OMe, thus also supporting the existence of the four-center intermediate L_3Zn–SC(S)OH.

It is now generally accepted that hydrolytic zinc enzymes (carbonic anhydrase, peptidases, phosphatases, esterases, nucleases) owe their high efficiency to their double functionality, in that they allow electrophilic activation by metal coordination to a substrate oxygen (C=O, P=O) and they provide the attacking nucleophile in the form of the Zn–OH unit.[1] When only one zinc ion is present as in carbonic anhydrase or in the many matrix metalloproteases it performs both functions. This means that during the catalytic turnover zinc changes its coordination number from four to five and then back to four, and the essential intermediate for the general case of O=E–X [E = CR, $P(OR)_2$; X = OR, NHR] hydrolysis is a four-center species like **A**. Several computational studies have considered the details of this process,[2–4] and one of us has recently published structural evidence for the corresponding reaction trajectory.[5]

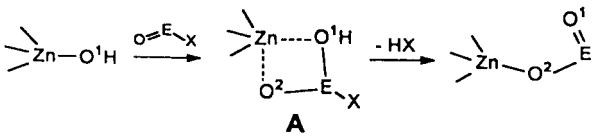

A

While one would assume that in passing through the intermediate **A**, the Zn–O^1 bond is broken and the Zn–O^2 bond is formed, *i.e.* hydroxide is the leaving group, experimental proof for this reaction course is still missing. Major obstacles to discerning O^1 and O^2 by isotopic labelling lie in the mobility of the OH proton, in the reversibility of the reactions, and in the high lability of zinc complexes, which for instance leads to rapid scrambling of ^{17}O from $C^{17}O_2$ over all positions in the TpZn–OH/CO_2 system [Tp = tris(pyrazolyl)borate].[6] It was therefore attractive to investigate a reaction system where homologous substitution, *i.e.* of O by S, renders distinguishable the atoms in question. We chose for this purpose the L_3Zn–OH/CS_2 system (L = N based ligand) based on previous experience in both the computational treatment of the L_3Zn–OH/CO_2 system[7] and reactivity studies of pyrazolylborate complexes TpZn–OH with CO_2 and similar heterocumulenes.[8] This has enabled us to present a case where the computational results came first and were only subsequently verified by the experiments.

The quantum chemical investigation on the B3LYP/6-311 + G* level of theory was carried out for the potential energy surface of the reaction system comprised of naked $[Zn–OH]^+$ and CS_2 (*cf.* Schemes 1 and 2). It confirmed what might have been expected from thermodynamic considerations, namely that the global energy minimum corresponds to $[Zn–SH]^+$ and COS, and it gave some insight into possible reaction mechanisms leading there. Scheme 1 presents the relevant intermediates of a reaction course which corresponds to the Lipscomb mechanism[9] of carbonic anhydrase action. It consists of subsequent proton transfers and implies that the oxygen of Zn–OH becomes part of O-bound COS (**P3**) which is then expelled. Scheme 2 shows a reaction sequence according to the Lindskog mechanism,[10] the essence of which is an internal rotation of the coordinated dithiocarbonate (**P1**) from the O,S- to the S,S-bound state without a proton transfer. A subsequent proton transfer then yields Zn–SH and COS which is now S-bound (**P5**) before it is expelled.

Our calculations have shown that both pathways are feasible because their steps have low to moderate activation barriers, and referred to the separated reactants the overall activation barrier is +2.4 (Scheme 2) or −3.9 (Scheme 1) kcal mol^{-1}. In order to corroborate the results obtained for this very simple model system we recalculated all minima of the potential energy surface for the two well accepted model systems $[(NH_3)_3ZnOH]^+$ and $[(Him)_3ZnOH]^+$ (Him = imidazole). A comparison of the relative energies of all three model complexes is given in Table 1. As expected, the inclusion of a complete ligand sphere levels the energy differences and yields no minimum for species like **P3** or **P5**. As compared with the results for the $[ZnOH]^+/CS_2$ system, the relative energies of the **P2**/**P4** intermediates change to a marked preference for the **P2** structures. Furthermore **P2** is now similar in energy to the separated reaction products L_3ZnSH and COS, as is **P1** to **P4**, supporting the notation that four-center intermediates like **P1**,

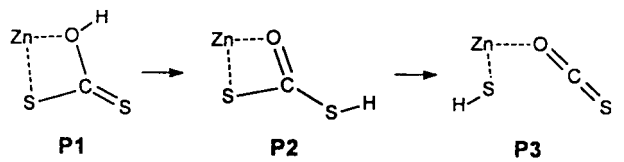

Scheme 1

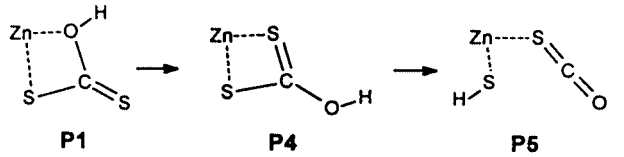

Scheme 2

DOI: 10.1039/b001149p

Table 1 Relative energies of the minima for the reaction of the three model complexes with CS_2 (energies in kcal mol^{-1})

	P1	P2	P4	Product(s)
$[ZnOH]^{+a}$	−28.49	−41.65	−46.87	−72.47/−69.90[c]
$[(NH_3)_3ZnOH]^{+a}$	−5.36	−20.61	−10.86	−21.82[d]
$[(Him)_3ZnOH]^{+b}$	−6.61	−20.84	−6.68	−24.80[d]

[a] B3LYP/6-311 + G*//B3LYP/6-311 + G*. [b] B3LYP/6-311 + G*//HF/6-311 + G*; Him = imidazole. [c] **P3**/**P5**. [d] L_3ZnSH + free COS.

P2 and **P4** are relevant entities in the reaction course for the CS_2 just like for the CO_2 reaction system.

The chemical investigation of this reaction system, carried out with the phenyl-substituted TpZn–OH complex **1**, resulted in full agreement between the calculated and observed reaction. In water-free dichloromethane **1** and a stoichiometric amount of

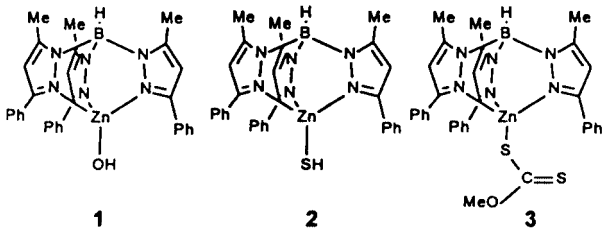

1 **2** **3**

CS_2 were converted quantitatively to the TpZn–SH complex **2** and COS within 12 h at room temperature.† The analysis of the gaseous reaction products† revealed that CO_2 had formed in addition to COS. This pointed to the fact that COS is capable of undergoing the same interconversion, as was verified subsequently by reacting **1** with COS.

An indication of possible reaction intermediates was found when MeOH was present accidentally in the reaction system: a 1:1:1 mixture of **1**, CS_2 and MeOH then yielded the xanthogenate complex **3**, again quantitatively.† The formation of **3** can be understood as a CS_2 addition to the methoxide complex TpZn–OMe (which can exist in very small quantities in equilibrium with **1** and methanol[11]), in analogy to the formation of alkali metal xanthogenates from alkali and CS_2. This proposal was verified by reacting TpZn–OMe, the methoxide derivative of **1**,[12] with CS_2 in dichloromethane, which produced **3** fast and quantitatively.† The corresponding intermediate, in analogy to **P1**, should be **P1a**. Alternatively, intermediate **P4** might be esterified with MeOH, yielding an intermediate **P4a**. We favor the insertion reaction *via* **P1a**,

P1a **P4a**

because we see no reason why **P4** should be esterified faster than being interconverted to **P5**. On the other hand, and in agreement with our calculations,[13] the methoxide in TpZn–OMe should be a stronger nucleophile than the hydroxide in TpZn–OH and hence capable of outracing the latter in the reaction with CS_2 even when present in much smaller

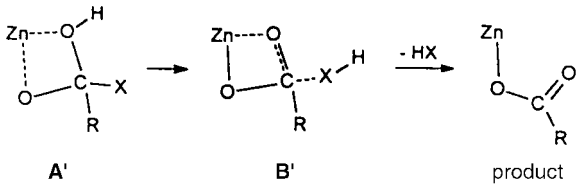

Scheme 3

concentrations. We have observed similar alcohol incorporations before when reacting the cumenyl substituted TpZn–OH with CO_2 and CS_2.[8]

The considerations applied and verified here for the CO_2/CS_2 system are applicable in the same way to the hydrolytic cleavage reactions of O=C(R)–X with intermediate **A** (Scheme 3). **A′** corresponds to **P1**, a conceivable proton transfer to X creates a possible intermediate **B′** corresponding to **P2**. Thereafter the course of events is different: HX is eliminated while HS in **P3** stays zinc-bound, and while OCS in **P3** leaves, its equivalent RCOO in **B′** becomes part of the reaction product, implying that the Zn–O^1 bond in **A** is broken. If one believes in the wisdom '*natura non facit saltus*' this means that the general pathway for all zinc-catalyzed hydrolytic reactions follows the mechanism in Scheme 1, *i.e.* the Lipscomb mechanism.

This work was supported by the Deutsche Forschungsgemeinschaft (Va 29/15 and GRK 307, Freiburg, and SFB 436, Jena) and by the Fonds der Chemischen Industrie. Financial support by the Thüringer Ministerium für Wissenschaft, Forschung und Kultur is gratefully acknowledged. Furthermore, we thank the Konrad-Zuse-Zentrum für Informationstechnik Berlin for generously providing us with computing time.

Notes and references

† The new complexes were characterized by elemental analyses, IR and NMR spectra in comparison with reference compounds.[8] COS and CO_2 were identified by GC–MS. An X-ray structure determination was carried out for **2**.

1 *Zinc Enzymes*, ed. T. G. Spiro, Wiley, New York, 1983; *Zinc Enzymes*, ed. I. Bertini, C. Luchinat, W. Maret and M. Zeppezauer, Birkhäuser, Boston, MA, 1986.
2 K. M. Merz, R. Hoffmann and M. J. S. Dewar, *J. Am. Chem. Soc.*, 1989, **111**, 5636; Z. Peng and K. M. Merz, *J. Am. Chem. Soc.*, 1992, **114**, 2733; Z. Peng and K. M. Merz, *J. Am. Chem. Soc.*, 1993, **115**, 9640.
3 O. Jacob, R. Cardenas and O. Tapia, *J. Am. Chem. Soc.*, 1990, **112**, 8692.
4 M. Sola, A. Lledos, M. Duran and J. Bertrán, *J. Am. Chem. Soc.*, 1992, **114**, 869; D. R. Garmer, *J. Phys. Chem. B*, 1997, **101**, 2945.
5 M. Rombach, C. Maurer, K. Weis, E. Keller and H. Vahrenkamp, *Chem. Eur. J.*, 1999, **5**, 1013.
6 A. Looney, R. Han, K. McNeill and G. Parkin, *J. Am. Chem. Soc.*, 1993, **115**, 4690.
7 M. Bräuer, J. L. Peréz-Lustres and E. Anders, manuscript in preparation.
8 M. Ruf and H. Vahrenkamp, *Inorg. Chem.*, 1996, **35**, 6571.
9 J.-Y. Liang and W. N. Lipscomb, *Int. J. Quantum Chem.*, 1989, **XXXVI**, 299.
10 D. N. Silverman and S. Lindskog, *Acc. Chem. Res.*, 1988, **21**, 30; M. Hartmann, K. M. Merz, T. Clark and R. v. Eldik, *J. Mol. Model.*, 1998, **4**, 355 and references therein.
11 C. Bergquist and G. Parkin, *Inorg. Chem.*, 1999, **38**, 422.
12 H. Brombacher and H. Vahrenkamp, unpublished work (*cf.* ref. 11).
13 M. Bräuer, Dissertation, Universität Jena, 2000.

ChemComm

Fluoridation of heteroaromatic iodonium salts—experimental evidence supporting theoretical prediction of the selectivity of the process‡

Sonsoles Martín-Santamaría,[a] Michael A. Carroll,†[a] Colm M. Carroll,†[a] Charles D. Carter,†[a] Victor W. Pike,[b] Henry S. Rzepa*[a] and David A. Widdowson*[a]

[a] *Department of Chemistry, Imperial College of Science, Technology and Medicine, London, UK SW7 2AY. E-mail: d.widdowson@ic.ac.uk and h.rezpa@ic.ac.uk*

[b] *Chemistry and Engineering Group, MRC Cyclotron Unit, Imperial College School of Medicine, Hammersmith Hospital, Ducane Road, London, UK W12 0NN*

Received (in Liverpool, UK) 1st February 2000, Accepted 1st March 2000
Published on the Web 27th March 2000

Theoretical prediction, that the nucleophilic substitution of a range of arylheteroaryliodonium salts by fluoride ion is regioselective for the aryl ring with the exception of benzo[*b*]furan, are borne out by experimental observation.

Iodine, like the other halogens, is found typically existing in monovalent form (oxidation state: −1), however owing to its large size and polarisability it is able to form stable polycoordinate, multivalent compounds. Compounds of this type, containing hypervalent iodine, have been known for over a century and have received considerable attention. The ability of these compounds to act as both selective reagents and intermediates has formed the basis for this interest.[1–3]

Our interest in the most numerous member of this group, the diaryliodinium salts, arose as it has been demonstrated that they are suitable precursors for the formation of fluoroarenes by the action of fluoride ion.[4,5] We have extended this methodology to the introduction of the fluorine-18 label ($t_{\frac{1}{2}}$ = 109.7 min) in the form of [^{18}F]fluoride.[6,7] This reagent has distinct advantages over the standard electrophilic procedures, which employ molecular [^{18}F]F_2 and derived reagents, as it is produced in higher amounts and higher specific radioactivity by several orders of magnitude.[8] This is an important consideration as ^{18}F-labelled organics are required at very high specific radioactivity as receptor radioligands in clinical research. Positron emission tomography (PET) is an imaging technique for the absolute measurement, *in vivo*, of positron emitters,[9] enabling their pharmacokinetics and biodistribution to be elucidated by non-invasive means. It is a well established technique; for example, L-6-[^{18}F]fluoro-DOPA[10,11] is used for the study of brain dopaminergic neuron density in movement disorders such as Parkinson's disease.

The ability to control/predict the regiochemical outcome of the aromatic nucleophilic substitution process is of paramount importance. Experimental observations, by us[7,12] and others,[13,14] suggest that it is the interplay of steric demand (the so called '*ortho* effect') and/or the electron deficiency of the aromatic rings that determines the site of nucleophilic substitution. It has been proposed[13,14] that the trigonal bipyramidal iodine(III) intermediates (see Fig. 1) in this process are fluxional and that the observations can be explained by the 'reactive' ring occupying the equatorial position *syn* to the nucleophile. This simple model does account for a large number of the reported observations for the nucleophilic aromatic substitution process. However, there are a number of examples where the outcome is not as predicted using this approach.[4,15] For arylheteroaryl iodonium salts (RR′I$^+$, R = phenyl, R′ = hereroaryl), the model predicts that the product will always be fluorobenzene, resulting from substitution of the relatively electron-poor phenyl ring (*i.e.* as in the equilibrium in Fig. 1).

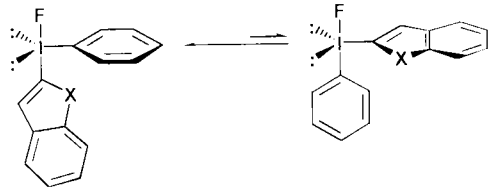

Fig. 1

We have recently applied computational modelling to the nucleophilic substitition of the structurally simpler dialkynyliodonium[16] and diphenyliodonium salts[15] in an attempt to gain a better understanding of the processes involved. This study established, *inter alia*, that the relative energies of the transition states for F–aryl extrusion, mediated by electron-withdrawing and electron-donating substituents, are the opposite of the axial/equatorial ground state equilibria, and that the latter cannot be reliably used to predict the regioselectivity of the process.

Here, we extend our model to the fluoridation of arylheteroaryliodonium salts in order to establish the method as a viable and accurate tool for predicting the outcome of such reactions. As before, quantitative models at the MNDO-d and at the Hartree-Fock *ab initio* level using the computationally efficient MIDI basis set (Table 1) were evaluated. Coordinate files for on-line viewing of the transition state models are available as ESI data.‡

The results reveal the phenyl group is more stable in the equatorial position for the ground state for all the pairs of isomers. Remarkably, the difference in energy grows along the heteroatom series N < S < O. However, the geometries and energies of the two possible transition states show significant variations from our original model. For the monocyclic systems, the transition state stability criterion is in the same sense as the ground state, which results in predicting fluorobenzene as the major product for all three heterocycles (Table 1, entries 1–3). The difference in energy between the two transition states grows in parallel with the aromaticity of the heterocycle. For the benzo-fused systems, all three ground states predict the phenyl group to be equatorial. At the transition state, however, we predict the 2-benzo[*b*]furyl group to be equatorial, resulting in 2-fluorobenzo[*b*]furan as the product. For benzo[*b*]thiophene this is reversed, and again fluorobenzene is predicted. For 1-methylindole, the energy differences are much smaller, and we predict a much less selective reaction, with fluoridation of both the phenyl and the indole rings.

As the prediction for the selectivity of the process did not appear to follow any simple trend, experimental data to assess the validity of the theoretical method was sought. Consequently, a range of arylheteroaryliodonium salts were prepared, in good yield, from the corresponding 2-trialkylstannyl derivatives by treatment with Koser's reagent [Ph(OH)OTs] (ESI‡)[17] (Scheme 1).

Fluoridation of the resultant iodonium tosylates was carried out by treatment with caesium fluoride in acetonitrile at 80 °C

† Undergraduate research participant.

‡ Electronic supplementary information (ESI) available: typical experimental and coordinate files for on line viewing of the transition state models. See http://www.rsc.org/suppdata/cc/b0/b000868k/

DOI: 10.1039/b000868k

Table 1 Fluoridation of iodonium tosylates

Entry	Diaryliodonium tosylate[a]	Product PhF[b]	Product HetF[b]	$E_{TS1} - E_{TS2}$[c] ($E_{GS1} - E_{GS2}$)[d]	Agrees with prediction	Prediction for 3-substituted systems $E_{TS1} - E_{TS2}$[c] ($E_{GS1} - E_{GS2}$)[d]
1	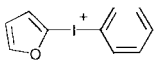	Yes	No	−0.1, *−2.6* (−4.1, *−9.7*)	Yes	−4.9 (0.0)
2	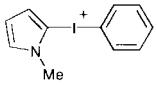	Yes	No	−3.4, *−3.6* (−1.3, *−3.1*)	Yes	−7.0 (+1.7)
3	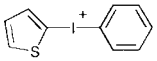	Yes	No	−6.1, *−6.2* (−2.4, *−4.6*)	Yes	−2.8 (0.0)
4	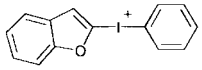	No	Yes	+2.0, *+0.8* (−4.8, *−10.2*)	Yes	−0.7 (−0.7)
5	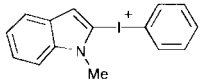	Yes[e]	Yes[e]	−0.3, *+1.7* (−2.4, *−3.8*)	Yes	−6.5 (+0.8)
6	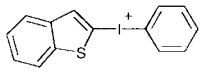	Yes	No	−4.5, *−3.5* (−3.1, *−4.6*)	Yes	−2.3 (−0.7)

[a] All diaryliodonium salts were characterised by ^1H, ^{13}C NMR, FTIR, mp, MS, HRMS and elemental analysis (except entry 2 which proved too labile for elemental analysis). [b] Typical radiochemical yields have already been reported for the process.[6,7] [c] E_{TS1} and E_{TS2} are the transition state energies for the generation of PhF and HetF, respectively (MNDO-d, *RHF/MIDI!*). [d] E_{GS1} and E_{GS2} are the ground state energies for the iodonium salts with the equatorial position occupied by Ph and Het, respectively (MNDO-d, *RHF/MIDI!*). [e] Ratio 7.7:1 fluorobenzene:2-fluoro-1-methylindole.

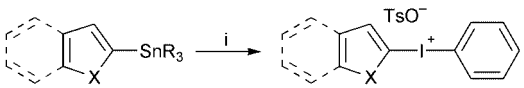

Scheme 1 *Reagents and conditions*: i, Ph(OH)OTs, DCM, room temp., 16 h. *Monocyclic series*: R = Bu^n, X = O, 77%; R = Me, X = NMe, 96%; R = Bu^n, X = S, 74%. *Bicyclic series*: R = Me, X = O, 98%; R = Me, X = NMe, 67%; R = Me, X = S, 96%.

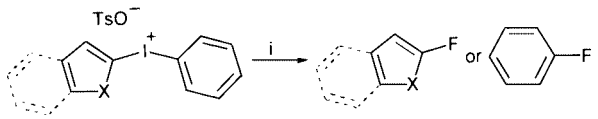

Scheme 2 *Reagents and conditions*: i, CsF, MeCN, 80 °C, 16 h.

overnight (Scheme 2) and the reaction mixture analysed by GC–MS (ESI‡).

The results from these reactions are summarised in Table 1. As expected the 2-substituted five-membered rings (Table 1, entries 1–3) gave fluorobenzene as the sole fluoroaromatic product. The small value for $E_{TS1} - E_{TS2}$ (−0.1, −2.6 kcal mol^{-1}) for the 2-furylphenyliodonium salt (Table 1, entry 1) suggests that 2-fluorofuran may also be a product. However, owing to the volatile nature of this material we are not able to discount its presence.

The fluoridation products from the reaction of the benzoheteroaromatics (Table 1, entries 4–6), with the exclusive formation of 2-fluorobenz[*b*]furan and the generation of 2-fluoro-1-methylindole, strikingly confirm our transition state model of stability, and not that adopted by the simple model[13,14] where the products should all be fluorobenzene.

We have also included predictions for the 3-substituted series of heteroaromatics (Table 1). In general, fluorobenzene is predicted as the product for all the systems. Specific differences from the 2-series include a much greater specificity predicted for the phenyl 3-(1-methylindolyl) system, and that the aromatic rings show little or no preference in the ground state for either the equatorial or axial position ($E_{GS1} - E_{GS2}$ values are small).

In summary, we have demonstrated, by the fluoridation of arylheteroaryliodonium salts, efficiency prepared from the corresponding aryltrialkylstannanes, that the computational techniques employed are a reliable way of predicting the outcome of the fluoridation process and that the process is therefore transition state and not ground state controlled.

We thank the EPSRC and the UROP scheme (C. D. C) for financial support. We also thank Mr J. Barton for GC–MS and Mr R. Sheppard for 2D NMR.

Notes and references

1 P. J. Stang and V. V. Zhdankin, *Chem. Rev.*, 1996, **96**, 1123.
2 A. Varvoglis, *Hypervalent Iodine in Organic Synthesis*, Academic Press, London, 1997.
3 A. Varvoglis and S. Spyroudis, *Synlett*, 1998, 221.
4 M. S. Ermolenko, V. A. Budylin and A. N. Kost, *J. Heterocyl. Chem. (Engl. Transl.)*, 1978, 752.
5 M. van der Puy, *J. Fluorine. Chem.*, 1982, **21**, 385.
6 V. W. Pike and F. I. Aigbirhio, *J. Chem. Soc., Chem. Commun.*, 1995, 2215.
7 A. Shah, V. W. Pike and D. A. Widdowson, *J. Chem. Soc., Perkin Trans. 1*, 1998, 2043.
8 M. Guillaume, A. Luxen, B. Nebeling, M. Argentini, J. C. Clark and V. W. Pike, *Appl. Radiat. Isot.*, 1991, **42**, 749.
9 M. J. Phelps, J. Mazziotta and H. Schelbert *Positron Emission Tomography and Autoradiography: Principles and Applications for the Brain and Heart*, Raven Press, New York, 1986.
10 A. Luxen, M. Guillaume, W. P. Melega, V. W. Pike, O. Solin and R. Wagner, *Nucl. Med. Biol.*, 1992, **19**, 149.
11 E. S. Garnett, G. Firnau and C. Nahmias, *Nature*, 1983, **305**, 137.
12 A. Shah, D. A. Widdowson and V. W. Pike, *J. Labelled Compds. Radiopharm.*, 1997, **39**, 65.
13 V. V. Grushin, *Acc. Chem. Res.*, 1992, **25**, 529 and references therein.
14 V. V. Grushin, I. I. Demkina and T. P. Tolstaya, *J. Chem. Soc., Perkin Trans. 2*, 1992, 505 and references therein.
15 M. A. Carroll, S. Martín-Santamaria, V. W. Pike, H. S. Rzepa and D. A. Widdowson, unpublished results.
16 M. A. Carroll, S. Martiń-Santamariá, V. W. Pike, H. S. Rzepa and D. A. Widdowson, *J. Chem. Soc., Perkin. Trans. 2*, 1999, 2707.
17 V. W. Pike, F. Butt, A. Shah and D. A. Widdowson, *J. Chem. Soc., Perkin Trans. 1*, 1999, 245.

Superlattices, polymorphs and solid-state NMR spin–lattice relaxation (T_1) measurements of 2,6-di-*tert*-butylnaphthalene

Arnold L. Rheingold,*[a] Joshua S. Figueroa,[a] Cecil Dybowski[a] and Peter A. Beckmann[b]

[a] *Department of Chemistry and Biochemistry, University of Delaware, Newark, DE 19716, USA. E-mail: arnrhein@udel.edu*

[b] *Department of Physics, Bryn Mawr College, Bryn Mawr, PA 19010, USA*

Received (in Columbia, MO, USA) 24th November 1999, Accepted 14th February 2000
Published on the Web 28th March 2000

Two polymorphs of 2,6-di-*tert*-butylnaphthalene, which differ by a factor of twelve in the number of crystallographically independent *tert*-butyl group environments, have been characterized by a synergistic combination of low-frequency ^{1}H NMR spin–lattice relaxation rate measurements and conventional crystallographic structure determinations.

When molecular materials crystallize, the symmetry-independent portion of the crystal lattice may consist of an ensemble of molecules that collectively form the *asymmetric unit*. This occurs in about 7–8% of molecular crystals.[1] Most often, the ensemble's organization has no symmetry relationships among its members, even though order is often created by hydrogen bonds or other weak interactions. However, in cases where the number of independent molecules is greater than two, it often happens that the molecules are arranged in a manner that almost, but not precisely, mimics a periodic translation. When such pseudo-periodic relationships exist among molecules, the diffraction patterns are commonly dominated by a subset of the reflections;[2] only the very minor differences among molecules contribute to superlattice (actually, the *true* lattice) reflections. Thus, superlattice reflections may be one to two orders of magnitude weaker than sublattice data and may be undetected during routine data collections.

Failure to recognize the presence of a superlattice results in one or more unit-cell dimensions being only $1/n$ as long as it actually is, where typically n ranges from 2 to 6. Hence, the determined 'structure' of the molecule will be a more or less malformed composite of n molecules in slightly different orientations. Based on our experience, we now believe that many structures reported to have bond parameters substantially outside of anticipated ranges (occasionally accompanied by bizarre chemical claims) may result from unrecognized superlattices.

Our current interest in superlattices was aroused by unusual results obtained in a ^{1}H solid-state NMR spin–lattice relaxation[3] study of 2,6-di-*tert*-butylnaphthalene (2,6-DTN).†

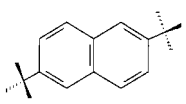

2,6-DTN

A dynamic process producing a local fluctuating magnetic field causes nuclear spin–lattice relaxation. For the molecular solid state, the spin–lattice interactions arise from rotational, and sometimes translational, motions. For molecular solids like 2,6-DTN, the primary process involves alkyl-group reorientation, either the *tert*-butyl group as a whole, the methyl groups individually, or a synchronized motion of both. Whatever process dominates relaxation in 2,6-DTN, its C_{2h} (2/*m*) symmetry suggests that the two *tert*-butyl groups will behave identically. Therefore, it was anticipated that a variable-temperature study of the nuclear spin relaxation rate ($R_1 = T_1^{-1}$) for 2,6-DTN would have the usual Debye form for a ln R_1 *vs.* $1/T$ plot, as has been recorded previously for several alkyl-substituted aromatics.[5] Instead, the very complex plots at Larmor frequencies of 8.50 and 22.5 MHz in Fig. 1 (labeled 'polymorph **E**') were obtained and found to be a composite of several, partially resolvable Debye relaxation curves.‡

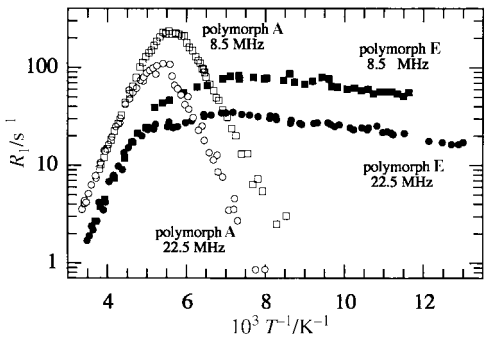

Fig. 1 Relaxation rate (R_1) *vs.* reciprocal temperature (T^{-1}) for **E** and **A** of 2,6-DTN at 8.5 and 22.5 MHz.

An X-ray diffraction study was initiated on a crystal of 2,6-DTN grown from ethanol (polymorph **E**).§ Using CCD detection, it was found that the reflection data contained a systematic weakness for $h \neq 3n$, with the $h = n$ set being approximately 20 times more intense. The unit-cell volume indicated that it contained 12 molecules ($Z = 12$). In the non-centrosymmetric space group, $P2_1$, the only symmetry operation is the 2_1 screw. There are, therefore, two equivalent positions in the unit cell and the asymmetric unit contains six independent molecules ($Z' = 6$). In the stereoview of the unit cell in Fig. 2(a), the arrangement of molecules appears to be repeated three times along the crystallographic *a* axis (horizontal), but if viewed from a perpendicular perspective [Fig. 2(b)], the aromatic planes of the three molecules are seen to be twisted by a few degrees along their long axis, one relative to the other. Fig. 2(b) also shows the herring-bone packing pattern formed by the 2,6-DTN molecules. These data for **E**, although very weak, were sufficient to explain the origin of the unusual relaxation data.

With $Z' = 6$, there are twelve symmetry independent *tert*-butyl groups and 36 independent methyl groups in **E**. Each slightly different environment has associated with it a different hindering potential and therefore a different mean reorientation rate. The localized pseudo-symmetry of the lattice suggests that similar environments might group into a smaller number of quasi-environments. The temperature dependence of ln R_1 at two Larmor frequencies for **E** can be fitted to a multiple-environment model, but the complexity of the curve makes a determination of the number of environments impossible. These environmentally sensitive relaxation studies confirm that the true repeat distance along *a* must be an integral multiple of some sublattice dimension, for only a large number of symmetry independent environments could account for the complex relaxation behavior observed.

DOI: 10.1039/a909449k

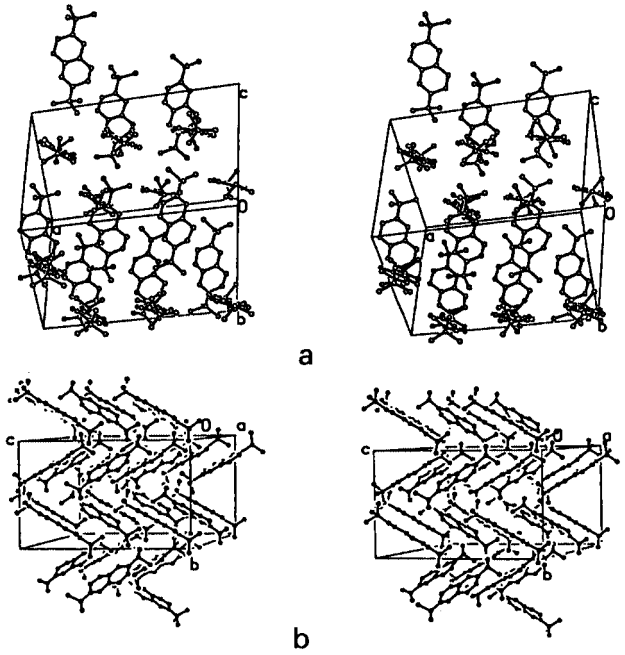

Fig. 2 Stereo drawings of the unit-cell packing for **E**. (a) As viewed with the *a* direction horizontal and (b) as rotated 90° with the *c* direction horizontal.

We then searched for other polymorphs of 2,6-DTN, assuming that the likelihood was strong that a more symmetrical form existed that would be thermodynamically favored at low temperature. Less symmetrical forms with more degrees of freedom may prevail at higher temperatures due to their higher vibrational entropies, but at lower temperatures denser packing arrangements with greater order commonly prevail.[7] Crystals were grown from 18 organic solvents and unit cells were obtained for each. **E** was recovered unchanged from 17 solvents, but a new polymorph (polymorph **A**) was obtained from acetone. It is *ca.* 4% denser, also monoclinic, and crystallizes in the centrosymmetric space group $P2_1/c$ with Z = 2 and Z' - 0.5. The unit-cell packing diagram for **A** is shown in Fig. 3. Thus, the asymmetric unit for **A** is half a molecule on a crystallographic inversion center, which requires all *tert*-butyl group environments to be chemically and crystallographically identical. As expected, the plot of ln R *vs.* $1/T$ plot for **A** Fig. 1) is the classical, single-environment Debye curve. When heated, samples of **A** irreversibly convert to **E** above 40 °C; no thermal events are seen on slowly lowering the temperature to 20 °C from above the transition temperature. The conversion is accompanied by a small, complex endotherm associated with the enthalpy of the conversion of **A** to **E**.

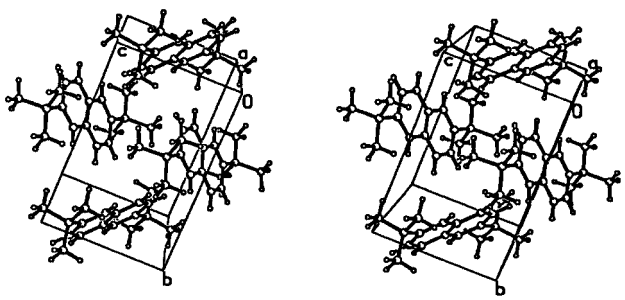

Fig. 3 Stereo drawing of the unit-cell packing for **A**.

That a single Debye process is observed in **A** (in marked contrast to **E**) shows that the motion is characterized by a single thermally activated correlation time τ_c (and only by a single τ_c). R_1 is given by $R_1 = A[J(\omega) + 4J(2\omega)]$, where $J(\omega) = 2\tau_c/(1 + \omega^2\tau_c^2)$ for Larmor frequency $\omega/2\pi$. The parameter A can be calculated from the geometry of a *tert*-butyl group and very reasonable assumptions about the motion.[8,9] The observation of a single Debye process coupled with the fitted value of A clearly shows that the *tert*-butyl groups and their methyl groups all reorient at the same rate τ_c, presumably due to some gearing process. The analysis shows, in addition, that there are no further motions on the NMR timescale.

^{13}C MAS NMR spectra for **E** and **A** reveal only small and random chemical shift differences of no more than 1.6 ppm at any site, and only minor differences in line width, despite the averaging of twelve *tert*-butyl group environments for **E**. Additionally, both agree closely with high-resolution solution chemical shift data.

Despite an obvious complementary relationship between the static, long-range information (translational order) available from X-ray diffraction data, and the dynamic, short-range information (especially spin–lattice relaxation rates, but also chemical shifts and coupling constants) available from solid-state NMR, surprisingly little effort has been made to exploit these potential synergies.[10] We have shown in this study of 2,6-DTN that crystallography and T_1 measurements can provide information essential to the complete understanding of the other, and that together they provide a very complete picture of both polymorphic and superlattice phenomena in these van der Waals molecular solids.

P. A. B. and C. D. acknowledge support of the ACS PRF Grant AC-33633 during this work.

Notes and references

† 2,6-DTN was prepared by literature methods[4] and purified by sublimation.

‡ R_1 rates was measured at 8.50 and 22.5 MHz with Spin–Lock CPS-2 Solid-State NMR spectrometers, one for each frequency. Measurements used a standard π–t–π/2 pulse sequence[6] with a recycle delay of at least $8T_1$. Temperature was varied by a controlled flow of cold nitrogen gas and measured by a calibrated copper–constantin thermocouple. Low frequencies are required to place the maxima in R_1 (corresponding to the motional correlation time being similar to the inverse Larmor frequency) in a convenient temperature region.

§ *Crystal data*: Siemens P4/CCD, Mo-Kα radiation. **E**: $C_{18}H_{24}$, colorless block, monoclinic, space group $P2_1$, a = 19.6636(1), b = 12.6712(3), c = 19.7853(1) Å, β = 104.4322(1)°, V = 4774.17(11) Å^3, Z = 12, Z' = 6, T = 173(2) K, $R(F)$ = 0.137, $R(wF^2)$ = 0.369, N_o/N_v = 10.2. The high residuals are associated with the extreme weakness of all 'superlattice' reflections, and not a result of diffuse scattering, an alternative raised by a reviewer. Spot shapes in the CCD images were found to be identical for both sub- and super-lattice data.

A: $C_{18}H_{24}$, colorless plate, monoclinic, space group $P2_1/c$, a = 11.3649(4), b = 9.9406(3), c = 6.6728(2) Å, β = 93.942(2)°, V = 752.07(4) Å^3, Z = 2, Z' = 1/2, T = 223(2) K, $R(F)$ = 0.058, $R(wF^2)$ = 0.126, N_o/N_v = 17.9. CCDC 182/1566. See http://www.rsc.org/suppdata/cc/a9/a909449k/ for crystallographic files in .cif format. Mp: **E**, 146–147° (lit.[4] 146 °C); **A**, 144–146 °C. DSC measurements show that **A** converts to **E** before melting.

1 (*a*) G. H. Stout and L. H. Jensen, *X-Ray Structure Determination*, MacMillan, New York, 1968, pp. 304–305; (*b*) G. R. Desiraju, J. C. Calabrese and R. L. Harlow, *Acta Crystallogr., Sect. B*, 1991, **47**, 77; (*c*) K. A. Wheeler, *Organized Molecular Assemblies in the Solid State*, ed. J. K. Whitesell, Wiley and Sons, New York, 1999, ch. 4.

2 D. Viterbo, *Fundamentals of Crystallography*, ed. C. Giacovazzo, Oxford Univ. Press, Oxford, 1992, ch. 5.

3 P. A. Beckmann, *Phys. Rep.*, 1988, **171**, 86 and references therein.

4 H. M. Crawford and M. C. Glesmann, *J. Am. Chem. Soc.*, 1954, **76**, 1108.

5 P. A. Beckmann, C. A. Buser, C. W. Mallory, F. B. Mallory and J. Mosher, *Solid State NMR*, 1998, **12**, 251.

6 C. P. Slichter, *Principles of Magnetic Resonance*, Springer, Berlin, 3rd edn., 1990.

7 G. Gilli, *Fundamentals of Crystallography*, ed. C. Giacovazzo, Oxford Univ. Press, 1992, ch. 7; J. Bernstein and A. T. Hagler, *J. Am. Chem. Soc.*, 1978, **100**, 673.

8 P. A. Beckmann, A. I. Hill, E. B. Kohler and H. Yu, *Phys. Rev. B, Solid State*, 1988, **11**, 98.

9 C. Palmer, A. A. Albano and P. A. Beckmann, *Physica B*, 1993, **190**, 267.

10 G. E. Maciel, N. R. Jagannathan and J. S. Frye, *NMR and X-Ray Crystallography: Interfaces and Challenges*, ed. M. C. Etter, *American Crystallographic Association*, Buffalo, NY, 1988, vol. 24.

A simple anion chemosensor based on a naphthalene–thiouronium dyad

Yuji Kubo,*[ab] Masahiko Tsukahara,[b] Shinji Ishihara[b] and Sumio Tokita[b]

[a] *PRESTO, Japan Science and Technology Corporation (JST), 255, Shimo-ohkubo, Urawa, Saitama 338-8570, Japan*
[b] *Department of Applied Chemistry, Faculty of Engineering, Saitama University, 255 Shimo-ohkubo, Urawa, Saitama 338-8570, Japan. E-mail: yuji@apc.saitama-u.ac.jp*

Received (in Cambridge, UK) 13th January 2000, Accepted 9th March 2000
Published on the Web 27th March 2000

A fluorescent-active molecular dyad comprising a naphthalene moiety covalently attached, *via* a methylene spacer, to a thiouronium receptor is described where selective anion-induced fluorescence changes make it of potential use as an anion chemosensor material.

Our ongoing program aimed at the synthesis of new easy-to-make optical sensors of biologically and/or chemically important anions leads us to explore a suitable anion-binding unit capable of efficient interaction with a built-in chromophore. A family of thiouronium salts, being known not only as synthetic intermediates for the conversion of alkyl halides to the corresponding mercaptans[1] but also as classical reagents for the identification of organic acids,[2] has potential as one of key functional groups for the purpose of molecular recognition of anion species in the area of supramolecular chemistry[3] because such groups would enhance the acidity of the NH moieties compared to the corresponding thiourea.[4] Indeed, quite recently, Yeo and Hong reported new thiouronium-derived systems for a carrier of 5′-AMP[5] and oxoanion recognition.[6] It occurred to us that a sophisticated combination of the above-mentioned functional entity and a suitable chromophore such as naphthalene would, therefore, allow production of a new type of chemosensor material. The design is mainly based on our idea that anion recognition events on the electron-deficient binding site of the thiouronium moiety would be efficiently communicated to the fluorescent property of naphthalene so that an easily detectable signalling effect would occur in the system. Surprisingly, to the best of our knowledge, although a number of optical read-out chemosensors of anions have been developed[7] a thiouronium-containing system towards this end is, as yet, unknown. Here, we report the intriguing aspects on the title system **1**.

The synthesis of **1** is shown in Scheme 1: 2-(bromomethyl)naphthalene **2** was converted to the corresponding thiourea **3** *via* amination using potassium phthalimide followed by $NH_2NH_2{\cdot}H_2O$, and then condensation with methyl isothiocyanate. Compound **3** was reacted with 1.1 equiv. of benzyl bromide followed by anion exchange treatment with $AgPF_6$. Purification by reversed phase column chromatography afforded the desired **1**† in excellent yield.

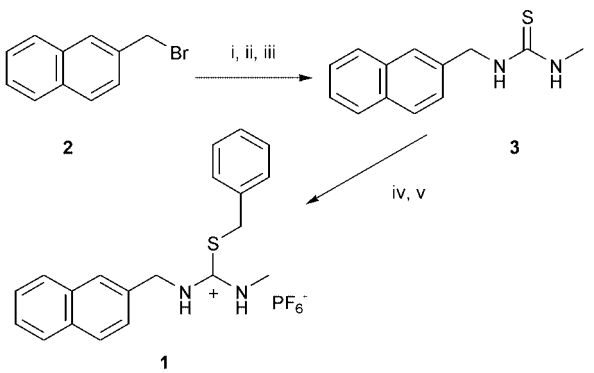

Scheme 1 *Reagents and conditions*: i, K^+ phthalamide$^-$ dry DMF; ii, $NH_2NH_2{\cdot}H_2O$, THF–EtOH; iii, MeNCS, $CHCl_3$; iv, benzyl bromide, dry EtOH; v, $AgPF_6$, dry EtOH.

System **1** showed very weak fluorescence in MeCN at 25 °C ([**1**] = 20 μM), the intensity of which was lower by a factor of 50 than that of 2-methylnaphthalene. This finding indicates that the electron-deficient thiouronium moiety acts as a quencher for the singlet state of the appended naphthalene. However, the addition of AcO^- as a putative response-induced anion was found to dramatically enhance the fluorescent intensity as illustrated in Fig. 1. Subsequently, 1 equiv. of AcO^- caused a remarkable intensity increase of up to *ca.* 350%. The acetate-induced signal effect is well explained by efficient emission retrieval upon an interaction between the anion and the thiouronium moiety of **1**. Further assessment of the receptor–anion complexation process came from a ^1H NMR titration; aliquots of the tetrabutylammonium salt of the anion were added to a CD_3CN solution of **1** (2 mM). Although NH resonances of the thiouronium moiety could not be detected in CD_3CN‡ because of the high acidity, significant upfield shifts (up to 0.2 ppm) of the resonances arising from two types of methylene (NaphCH_2NH– and PhCH_2S–) and methyl (–NHCH_3) protons, which are located in the periphery of the anion-binding site, were observed upon complexation with AcO^-. Judging from the titration, the strong binding of AcO^- allowed the mole ratio method[8] to be used in the determination of the binding stoichiometry, which was found to be 1 : 1 for the receptor–anion complex.

Fig. 2 shows the resulting titration curves for the fluorescent intensity when adding AcO^-, $(BuO)_2P(O)O^-$§ or Cl^- to an MeCN solution of **1** at 25 °C, supporting the formation of a 1 : 1 stoichiometry complex. The association constants (K_a)¶ could be calculated using nonlinear curve-fitting plots. As a result, interestingly, the fluorescent response of **1** was found to show a significant selectivity for the nature of anions in spite of the simple molecular system of **1** [K_a/M^{-1}: AcO^-, > 10^6; $(BuO)_2P(O)O^-$, 5.6 × 10^4; Cl^-, n.d.‖], being probably correlated with the guest basicity. Of particular note is that **1** shows not only a high susceptibility to AcO^- but also a

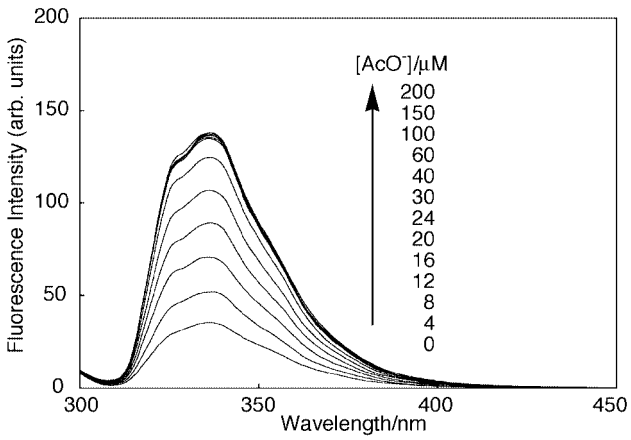

Fig. 1 Emission spectra of **1** (20 μM) in MeCN at 25 °C excited at 270 nm upon addition of AcO^- as a NBu_4 salt.

DOI: 10.1039/b000352m

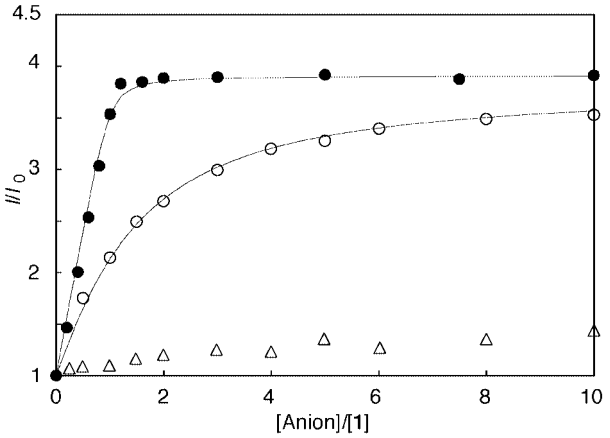

Fig. 2 Fluorescent intensity at 336 nm of **1** (20 μM) in MeCN at 25 °C excited at 270 nm as a function of anion concentration: (●) NBu_4OAc, (○) $NEt_4OP(O)(OBu)_2$, (Δ) NBu_4Cl.

discernible binding towards oxo-anions. Taken together, it could allow us to analyze AcO^- quantitatively[9] using an easy-to-detect fluorescent signal response. This would be most welcome to applications involving medical diagnostics.

As a control experiment, the interaction of AcO^- with 2-methylnaphthalene was investigated in the fluorescent spectra for which no change was observed. This insight supports the argument that the fluorescent enhancement of **1** induced by anions could be based on the significant change on the photoinduced charge transfer characteristics in system **1** where the anion binding event decreases the interaction between the naphthalene and thiouronium moieties.

We conclude that system **1** represents a simple, easy-to-make and hitherto unexplored class of luminescent chemosensors of anions. Owing to the unique sensing properties based on the naphthalene–thiouronium conjugate, the development of highly functional derivatives will represent an important synthetic challenge. Indeed, we are currently preparing more elaborate systems incorporating binaphthalene units.

This work is partly supported by a TORAY Award in Synthetic Organic Chemistry, Japan.

Notes and references

† δ_H(400 MHz, $CDCl_3$, TMS) 3.07 (s, 3H), 4.32 (s, 2H), 4.69 (s, 2H), 7.25–7.27 (m, 6H), 7.46–7.49 (m, 2H), 7.67 (br d, 1H), 7.76–7.80 (m, 3H); δ_C(100.7 MHz, $CDCl_3$) 31.07, 35.89, 48.52, 125.08, 126.63, 127.25, 127.68, 128.04, 128.96, 129.07, 129.17, 129.37, 131.80, 133.08, 133.16, 167.85; FAB-MS, *m*/*z* 321[M − PF_6]$^+$; Anal. Calc. for $C_{20}H_{21}N_2SPF_6$: C, 51.50; H, 4.54; N, 6.01. Found: C, 51.66; H, 4.53; N, 5.98%.

‡ The NH resonances were observed at δ 9.22–9.85 as a broad signal in d_6-DMSO.

§ The result of the titration by adding $H_2PO_4^-$ did not fit to curve based on a 1 : 1 host–guest stoichiometry complex, which may be due to a phosphate–phosphate dimerization.[7d,10]

¶ The K_a values were estimated by three individual fluorescent intensity titrations: λ_{max}(ex) = 270 nm, λ_{max}(em) = 336 nm in MeCN at 25 °C. The estimated error for the titration with $(BuO)_2P(O)O^-$ is < 3%.

‖ The response was too low to determine the K_a value.

1 J. March, *Advanced Organic Chemistry*, John Wiley & Sons, New York, 1985, p. 360.

2 J. J. Donleavy, *J. Am. Chem. Soc.*, 1936, **58**, 1004; B. T. Dewey and R. B. Sperry, *J. Am. Chem. Soc.*, 1939, **61**, 3251.

3 *Supramolecular Chemistry of Anions*, ed. A. Bianchi, K. Bowman-James and E. García-España, Wiley-VCH, New York, 1997.

4 For recent examples of anion receptors with thiourea units, see: S. Nishizawa, H. Kaneda, T. Uchida and N. Teramae, *J. Chem. Soc., Perkin Trans. 2*, 1998, 2325; Y. Tobe, S. Sasaki, M. Mizuno and K. Naemura, *Chem. Lett.*, 1998, 835; H. Boerrigter, L. Grave, J. W. M. Nissink, L. A. J. Chrisstoffels, J. H. van der Maas, W. Verboom, F. de Jong and D. N. Reinhoudt, *J. Org. Chem.*, 1998, **63**, 4174; T. Shioya, S. Nishizawa and N. Teramae, *J. Am. Chem. Soc.*, 1998, **120**, 11 534; H. Xie, S. Yi and S. Wu, *J. Chem. Soc., Perkin Trans. 2*, 1999, 2751.

5 W.-S. Yeo and J.-I. Hong, *Tetrahedron Lett.*, 1998, **39**, 3769.

6 W.-S. Yeo and J.-I. Hong, *Tetrahedron Lett.*, 1998, **39**, 8137.

7 (*a*) A. W. Czanik, *Acc. Chem. Res.*, 1994, **27**, 302; (*b*) A. P. de Silva, H. Q. N. Gunaratne, T. Gunnlaugsson, A. J. M. Huxley, C. P. McCoy, J. T. Rademacher and T. E. Rice, *Chem. Rev.*, 1997, **87**, 1515; (*c*) P. D. Beer, *Acc. Chem. Res.*, 1998, **31**, 71; For recent topics, see: (*d*) H. Miyaji, P. Anzenbacher Jr, J. L. Sessler, E. R. Bleasdale and P. A. Gale, *Chem. Commun.*, 1999, 1723; (*e*) P. D. Beer, V. Timoshenko, M. Maestri, P. Passaniti and V. Balzani, *Chem. Commun.*, 1999, 1755; (*f*) S. Nishizawa, Y. Kato and N. Teramae, *J. Am. Chem. Soc.*, 1999, **121**, 9463; (*g*) C. B. Black, B. Andrioletti, A. C. Try, C. Ruiperez and J. L. Sessler, *J. Am. Chem. Soc.*, 1999, **121**, 10 438; (*h*) H. Xie, S. Yi, X. Yang and S. Wu, *New J. Chem.*, 1999, 1105.

8 K. A. Conners, in *Binding Constants, The Measurement of Molecular Complex Stability*, Wiley, New York, 1987, pp. 24–28

9 For a review on receptors for carboxylates and other organic anions, see: C. Seel, A. Galán and J. de Mendoza, *Top. Curr. Chem.*, 1995, **175**, 102.

10 V. Král, H. Furuta, K. Shreder, V. Lynch and J. L. Sessler, *J. Am. Chem. Soc.*, 1996, **118**, 1595.

ChemComm

A high-nuclearity Ni–Sb carbonyl cluster displaying unprecedented metal stereochemistries: synthesis and X-ray structure of $[NEt_4]_6[Ni_{31}Sb_4(CO)_{40}]\cdot 2Me_2CO$

Cristina Femoni, M. Carmela Iapalucci, Giuliano Longoni* and Per H. Svensson

Dipartimento di Chimica Fisica ed Inorganica, Universita' di Bologna, viale Risorgimento 4, 40136 Bologna, Italy. E-mail: longoni@ms.fci.unibo.it

Received (in Basel, Switzerland) 21st January 2000, Accepted 10th March 2000
Published on the Web 3rd April 2000

The mild oxidation of $[NEt_4]_2[Ni_{15}Sb(CO)_{24}]$ in acetone solution with $SbCl_3$ in a *ca.* 3 : 1 molar ratio leads to the new high-nuclearity $[Ni_{31}Sb_4(CO)_{40}]^{6-}$ hexaanion, which displays two interstitial Ni and four semi-interstitial Sb atoms with unprecedented stereochemistries.

Several low-nuclearity Ni–Sb carbonyl clusters have been reported.[1–4] All adopt an icosahedral geometry which can be Sb-centred, *viz.* $[Ni_{15}(\mu_{12}\text{-Sb})(CO)_{24}]^{2-}$ $\mathbf{1}^{2-}$,[1] or Ni-centred, *viz.* $[Ni_{10}Sb_2(\mu_{12}\text{-Ni})(CO)_{18}]^{n-}$ $\mathbf{2}^{n-}$,[1] and $[Ni_{10}(Sb \rightarrow Ni(CO)_3)_2(\mu_{12}\text{-Ni})(CO)_{18}]^{n-}$ $\mathbf{3}^{n-}$, (n = 2–4),[2,3] as well as non-centred, *e.g.* $[Ni_{10}(SbR)_2(CO)_{18}]^{2-}$ $\mathbf{4}^{2-}$, (R = alkyl or aryl substituent).[4] Notably, only the Ni-centred $\mathbf{2}^{n-}$ and $\mathbf{3}^{n-}$ species are multivalent and display three stable oxidation states.[1–6] It has been later shown that the presence of interstitial or highly connected nickel or platinum atoms triggers multivalence in several carbonyl metal clusters.[5,6] Icosahedral species such as $\mathbf{1}^{2-}$, $\mathbf{2}^{n-}$ and $\mathbf{3}^{n-}$ are potential building blocks of poly-icosahedral *supra*-clusters,[7] related to $[Ag_{12}Au_{13}(PPh_3)_{10}Br_8]^-$,[8,9] $Ag_{20}Au_{18}[P(C_6H_4Me)_3]_{12}Cl_{14}$,[10] or $Pd_{59}(CO)_{32}(PMe_3)_{21}$.[11] The above consideration, as well as our interest in redox-active[5,6] and paramagnetic metal carbonyl clusters,[12] led us to investigate the chemical behaviour of $\mathbf{1}^{2-}$, $\mathbf{2}^{n-}$ and $\mathbf{3}^{n-}$ with the aim to synthesise polyicosahedral Ni–Sb carbonyl clusters of higher nuclearity. We now report our first result consisting in the synthesis and structural characterisation of the $[Ni_{31}Sb_4(CO)_{40}]^{6-}$ $\mathbf{5}^{6-}$, hexaanion, which displays unprecedented stereochemical features.

The $\mathbf{5}^{6-}$ salts were spectroscopically detected among the by-products of the synthesis of $\mathbf{1}^{2-}$ by reaction of $[Ni_6(CO)_{12}]^{2-}$ with $SbCl_3$. The best synthesis of $\mathbf{5}^{6-}$ consists in the mild oxidation of $[NEt_4]_2\mathbf{1}$ in acetone solution with $SbCl_3$ in a *ca.* 3 : 1 molar ratio. $[NEt_4]_6\mathbf{5}\cdot 2\,Me_2CO$ [ν_{CO} in acetonitrile at 2040vw, 2001s, 1980(sh), 1894m, 1861m, 1846m and 1812(sh) cm^{-1}; no hydride signal in the ^1H NMR spectrum in the range δ +25 to −50; diamagnetic] separates out from the reaction solution on standing as well shaped black crystals (yields up to 30% based on Sb) and has been characterised by X-ray diffraction studies.† The by-products of the above reaction are $[Ni(CO)_3Cl]^-$, $Ni(CO)_4$ and $[NEt_4]_3$ **3**. As shown by separated experiments, a mixture of $Ni(CO)_4$ and $[NEt_4]_3$ **3** also results from degradation of $\mathbf{5}^{6-}$ salts under a carbon monoxide atmosphere.

The overall structure of $\mathbf{5}^{6-}$ is shown in Fig. 1 and a formal reconstruction of its metal framework is given in Fig. 2(a). The central $Ni_{19}Sb_4$ moiety of the metal frame is based on two interpenetrating Ni-centred $Ni_{11}Sb_3(\mu_{14}\text{-Ni})$ 14-hedron displaying a distorted bicapped hexagonal antiprismatic geometry. One of the two 14-hedrons has been emphasised out with filled in bonds; its idealised C_6 axis is almost orthogonal to the plane of the paper and the in-plane idealised C_6 axis of the other moiety. Each of the two 14-coordinated nickel atoms behaves at the same time as an interstitial atom of one unit and as an *ortho* atom of the Ni_5Sb hexagonal ring of the second unit. The second hexagonal ring of the above 14-hedra displays a *para*-Sb_2Ni_4 geometry. The major deviation of the centred $Ni_{11}Sb_3(\mu_{14}\text{-Ni})$ 14-hedron from the idealised bicapped hexagonal antiprism is due to departure from the mid-point of the Sb–Sb diagonal of the Ni atoms capping the Ni_4Sb_2 hexa-rings. These caps become closer to one of the two pairs of nickel atoms and show Ni···Ni contacts with the second pair which are beyond the usually accepted limit for a Ni–Ni bond [3.350(2) and 3.426(2) Å].

The metal framework of $\mathbf{5}^{6-}$ is completed by condensing two Ni_6 moieties [Ni–Ni range 2.373(2)–2.944(2) Å], displaying a polytetrahedral metal arrangement having the architecture of the $Os_6(CO)_{18}$ prototype,[13,14] on two opposite sides of the central $Ni_{19}Sb_4$ kernel. These Ni_6 moieties bind to the two Sb and surrounding Ni atoms through their butterfly face. As

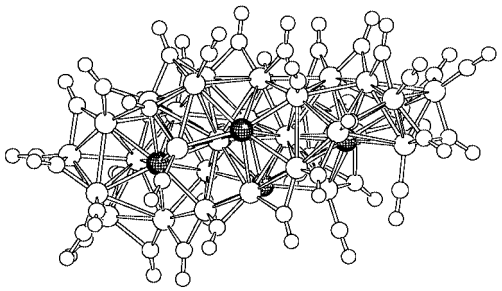

Fig. 1 The molecular structure of the $[Ni_{31}Sb_4(CO)_{12}(\mu\text{-}CO)_{24}(\mu_3\text{-}CO)_4]^{6-}$ $\mathbf{5}^{6-}$ ion. The Ni–Ni and Ni–Sb bonding interactions are spread over the ranges 2.357(1)–3.090(1) and 2.496(1)–2.782(1) Å respectively.

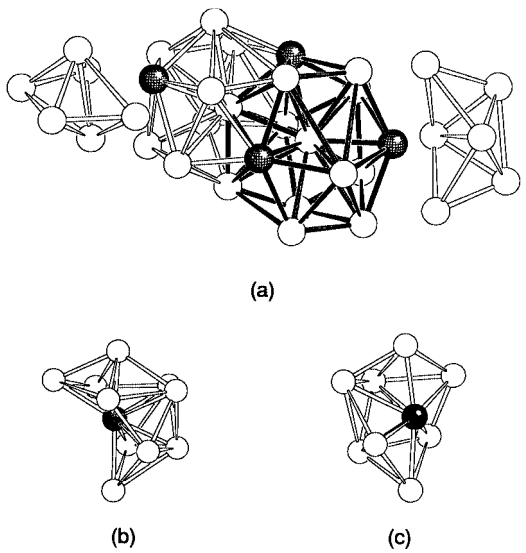

Fig. 2 Formal reconstruction of the metal framework of $\mathbf{5}^{6-}$ with omission of the bonds between the two outer Ni_6 moieties with the central $Ni_{19}Sb_4$ kernel (a) and the two coordination stereogeometries shown by the Sb atoms [(b) and (c)].

pointed out in Fig. 2(b) and (c), the four Sb atoms display two pairs of different stereogeometries, being semi-interstitially lodged in Ni_{10} and Ni_8 incomplete icosahedral moieties, which are related to the $[B_{10}H_{14}]^{2-}$ and B_8H_{14} *arachno*-boranes, respectively.[15,16] Semi-interstitial lodging of Sb atoms in a nickel cluster is not surprising because it has been shown that a Sb atom is oversized for a Ni_{12} icosahedral cage.[1] In contrast, the coordination of the two interstitial nickel atoms is more unexpected and unprecedented in molecular clusters. A metal coordination number of 14 has been found in intermetallic phases such as the Ni–V σ and Ni–Mo δ phases.[15] These alloys also involve 12-coordinated sites of icosahedral geometry, as partially displayed by $\mathbf{5}^{6-}$, as well as 15- and 16-coordinated sites. Besides, these intermetallic phases show a tendency to segregate the bulkiest metal atoms in the highest coordinated sites (14–16), while the other metal atoms occupy the 12- and 14-coordinated sites.[15] In this regard, an ideal 14-hedron having a bicapped hexagonal antiprismatic geometry provides two 6-fold vertices and the interstice as the most suitable sites for the bulkiest Sb atoms of a centred $Ni_{12}Sb_3$ moiety. Therefore, centring of the above by the least bulky nickel atom and segregation of Sb in the two hexagonal rings may appear odd. However, the segregation observed in $\mathbf{5}^{6-}$ could probably be due to its molecular nature and the need to accommodate the carbonyl ligand shell. The forty carbonyl ligands can be approximately classified as terminal (12), edge-bridging (24) and face-bridging (4).

In conclusion, the condensation of $\mathbf{1}^{2-}$ into $\mathbf{5}^{6-}$ does not lead to polyicosahedral *supra*-clusters, as for the Ag–Au system.[7–10] An alternative and unprecedented growth pathway has been observed, which shows that high nuclearity nickel carbonyl clusters can be stabilised not only by interstitially lodging small main group elements such as carbon, *e.g.* $[Ni_{32}C_6(CO)_{36}]^{6-}$ and $[Ni_{38}C_6(CO)_{42}]^{6-}$,[17] but also bulkier atoms such as antimony. Studies of the chemical and physical behaviour of $\mathbf{5}^{6-}$ are underway.

G. L. thanks the MURST (COFIN98) and the University of Bologna for funding. P. H. S. acknowledges The Wenner–Gren Foundation, Stiftelsen BLANCEFLOR Boncompagni-Ludovisi, född Bildt and Svenska Institutet for a grant.

Notes and references

† *Crystal data* for $[NEt_4]_6[Ni_{31}Sb_4(CO)_{40}]\cdot 2Me_2CO$: M = 4325, monoclinic, space group $P2_1/n$, a = 20.9876(6), b = 14.6084(4), c = 44.1418(11) Å, β = 93.707(1)°, U = 13505.4(6) Å^3, T = 298 K, Z = 4, μ(Mo-Kα) = 50.59 cm^{-1}, 94623 reflections measured, 23779 unique (R_{int} = 0.0492) which were used in all calculations. The final *wR*2 was 0.1166 [$I > 2\sigma(I)$]. CCDC 182/1573. See http://www.rsc.org/suppdata/cc/b0/b000783h/ for crystallographic files in .cif format.

1 V. G. Albano, F. Demartin, C. Femoni, M. C. Iapalucci, G. Longoni, M. Monari and P. Zanello, *J. Organomet. Chem.*, 2000, **593–594**, 325.
2 V. G. Albano, F. Demartin, M. C. Iapalucci, G. Longoni, A. Sironi and V. Zanotti, *J. Chem. Soc., Chem. Commun.*, 1990, 547.
3 V. G. Albano, F. Demartin, M. C. Iapalucci, F. Laschi, G. Longoni, A. Sironi and P. Zanello, *J. Chem. Soc., Dalton Trans.*, 1991, 739.
4 R. E. Des Enfants, J. A. Gavney, R. K. Hayashi, A. D. Rae and L. F. Dahl, *J. Organomet. Chem.*, 1990, **383**, 543.
5 G. Longoni, C. Femoni, M. C. Iapalucci and P. Zanello, in *Metal Clusters in Chemistry*, ed. P. Braunstein, L. Oro and P. Raithby, VCH, Weinheim, 1999, vol 2, p. 1137.
6 C. Femoni, M. C. Iapalucci, G. Longoni and P. Zanello, *Inorg. Chem.*, 1999, **38**, 3721.
7 B. K. Teo and H. Zhang, *J. Cluster Sci.*, 1990, **1**, 155.
8 B. K. Teo, X. Shi and H. Zhang, *J. Am. Chem. Soc.*, 1991, **113**, 4329.
9 B. K. Teo, X. Shi and H. Zhang, *J. Chem. Soc., Chem. Commun.*, 1992, 1195.
10 B. K. Teo, M. Hong, H. Zhang, D. Huang and X. Shi, *J. Chem. Soc., Chem. Commun.*, 1988, 204.
11 N. T. Tran, M. Kawano, D. R. Powell and L. F. Dahl, *J. Am. Chem. Soc.*, 1998, **120**, 10 986.
12 J. Sinzig, L. J. de Jongh, A. Ceriotti, R. Della Pergola, G. Longoni, M. Stener, K. Albert and N. Rösch, *Phys. Rev. Lett.*, 1998, **81**, 3211.
13 C. R. Eady, B. F. G. Johnson and J. Lewis, *J. Organomet. Chem.*, 1972, **37**, C39.
14 R. Mason, K. M. Thomas and D. M. P. Mingos, *J. Am. Chem. Soc.*, 1973, **95**, 3802.
15 A. F. Wells, *Structural Inorganic Chemistry*, Clarendon Press, Oxford, 1987, and references therein.
16 N. N. Greenwood and A. Earnshaw, *Chemistry of the Elements*, Pergamon Press, Oxford, 1990.
17 F. Calderoni, F. Demartin, F. Fabrizi de Biani, C. Femoni, M. C. Iapalucci, G. Longoni and P. Zanello, *Eur. J. Inorg. Chem.*, 1999, 663.

ChemComm

Novel room light-induced disproportionation reaction of organo-ditin and -dilead compounds with organic dichalcogenides: an efficient salt-free route to organo-tin and -lead chalcogenides

Farzad Mirzaei, Li-Biao Han and Masato Tanaka*

National Institute of Materials and Chemical Research, Tsukuba, Ibaraki 305-8565, Japan.
E-mail: mtanaka@home.nimc.go.jp

Received (in Cambridge, UK) 7th January 2000, Accepted 8th March 2000
Published on the Web 30th March 2000

Disproportionation of organo-ditin and -dilead compounds $(R_3M)_2$ (M = Sn, Pb) with organic dichalcogenides $(R'Z)_2$ (Z = S, Se, Te) is efficiently promoted by room light to produce the corresponding organo-tin and -lead chalcogenides R_3MZR' quantitatively.

Chalcogenides of heavier group 14 metals, R_3MZR' (M = heavier group 14 element; Z = chalcogen element) decompose upon heating to give composite metal chalcogenides which are useful for solar cells and other semiconductor applications.[1,2] They are also useful reagents in organic synthesis.[3] Conventional synthetic routes generally involve troublesome stoichiometric salt elimination reactions of R_3MX (X = halogen atom) with alkali metal chalcogenides.[3] However, the alkali metal salts concomitantly formed can be a serious contaminant that reduces the performance of the semiconductor materials derived *via* the MOCVD process of these metal chalcogenides as precursors.[2] Thus, an alternative, clean and salt-free route to R_3MZR' is highly desirable. During an extended research on the Pt-catalysed disproportionation of $(ArS)_2$ with $(SiCl_3)_2$[4] we accidentally came across a novel light-induced disproportionation.We disclose herein preliminary results of the light-induced disproportionation reaction of organic dichalcogenides $(R'Z)_2$ (Z = S, Se, Te; R′ = alkyl, aryl) with organo-ditin and -dilead compounds $(R_3M)_2$ (M = Sn, Pb) leading to R_3MZR' in excellent yields [eqn. (1)].[5]

$$(RZ)_2 + (R'_3M)_2 \xrightarrow{\text{room light}} 2RZMR'_3 \quad (1)$$

Z = S, Se, Te; M = Sn, Pb

In a typical experiment, an equimolar mixture of $(PhS)_2$ and $(Me_3Sn)_2$ in C_6D_6 (0.5 M) was placed in a Pyrex tube under nitrogen and exposed to room light at 35 °C.[6] As confirmed by ^{1}H NMR spectroscopy, the starting materials were completely consumed within 20 min and $PhSSnMe_3$ was obtained quantitatively as the sole product. Irradiation was essential for this disproportionation; a control experiment carried out in the dark under similar conditions did not lead to $PhSSnMe_3$ even after 2 h.[7,8] The reaction proceeded equally well in other solvents such as toluene and chloroform. Particularly noteworthy is that even in the *absence* of the solvent, the reaction took place as efficiently. Thus, a colourless liquid of analytically pure $PhSSnMe_3$ was obtained by simply stirring a heterogeneous mixture of 10 mmol of $(PhS)_2$ (2.18 g) and an equivalent amount of $(Me_3Sn)_2$ (3.28 g) for 1 h at 35 °C in room light.

Table 1 demonstrates the wide applicability of the present light-induced disproportionation reaction. Other aromatic disulfides such as $(4\text{-}MeC_6H_4S)_2$, $(4\text{-}ClC_6H_4S)_2$, $(2,4,5\text{-}Cl_3C_6H_2S)_2$ and $(2\text{-}pyS)_2$ all reacted efficiently with $(Me_3Sn)_2$ to afford the corresponding trimethyltin sulfides in quantitative yields. Primary aliphatic disulfides such as $(BuS)_2$ reacted similarly. However, as the alkyl group became bulkier,

Table 1 Light-induced disproportionation of $(R_3M)_2$ (M = Sn, Pb) with $(R'Z)_2$ (Z = S, Se, Te)[a]

Run	$(RZ)_2$	$(R'_3M)_2$	*t*/h	Product	Yield (%)
1	$(PhS)_2$	$(SnMe_3)_2$	< 0.5	$PhSSnMe_3$	quant.
2	$(4\text{-}MeC_6H_4S)_2$	$(SnMe_3)_2$	1.5	$4\text{-}MeC_6H_4SSnMe_3$	quant.
3	$(4\text{-}ClC_6H_4S)_2$	$(SnMe_3)_2$	1.5	$4\text{-}ClC_6H_4SSnMe_3$	quant.
4	$(2,4,5\text{-}Cl_3C_6H_2S)_2$	$(SnMe_3)_2$	1.5	$2,4,5\text{-}Cl_3C_6H_2SSnMe_3$	quant.
5	$(2\text{-}pyS)_2$	$(SnMe_3)_2$	1.5	$2\text{-}pySSnMe_3$	quant.
6	$(BuS)_2$	$(SnMe_3)_2$	1.5	$BuSSnMe_3$	quant.
7	$(CyS)_2$	$(SnMe_3)_2$	4	$CySSnMe_3$	60 (95)[b]
8	$(Bu^tS)_2$	$(SnMe_3)_2$	2.5	Bu^tSSnMe_3	8
9	$(PhS)_2$	$(SnPh_3)_2$	1.5	$PhSSnPh_3$	quant.
10	$(4\text{-}ClC_6H_4S)_2$	$(SnPh_3)_2$	3	$4\text{-}ClC_6H_4SSnPh_3$	quant.
11	$(4\text{-}FC_6H_4S)_2$	$(SnPh_3)_2$	1	$4\text{-}FC_6H_4SSnPh_3$	quant.
12	$(BuS)_2$	$(SnPh_3)_2$	2	$BuSSnPh_3$	quant.
13	$(PhS)_2$	$(PbPh_3)_2$	3.5	$PhSPbPh_3$	quant.
14	$(BuS)_2$	$(PbPh_3)_2$	6	$BuSPbPh_3$	quant.
15	$(PhSe)_2$	$(SnMe_3)_2$	< 0.5	$PhSeSnMe_3$	quant.
16	$(PhSe)_2$	$(SnPh_3)_2$	1.5	$PhSeSnPh_3$	quant.
17	$(PhSe)_2$	$(PbPh_3)_2$	1.5	$PhSePbPh_3$	96[c]
18	$(PhTe)_2$	$(SnMe_3)_2$	9	$PhTeSnMe_3$	93[c]
19[d]	$(PhTe)_2$	$(PbPh_3)_2$	3	$PhTePbPh_3$	98[c]

[a] Unless otherwise stated, the reaction was performed as follows: 0.03–0.5 M benzene solution in a Pyrex tube irradiated with a 40 W fluorescent lamp at 35 °C. [b] Yields in parentheses obtained after 7 h reaction time. [c] Traces of decomposition products were also formed. [d] Irradiation with a 200 W tungsten lamp at 50 °C.

DOI: 10.1039/b000309n

the reaction proceeded more slowly; the completion of the reaction between $(CyS)_2$ and $(Me_3Sn)_2$ required > 7 h and the formation of Bu^tSSnMe_3 in the reaction of $(Bu^tS)_2$ with $(Me_3Sn)_2$ under similar reaction conditions was only marginal. Although slower than $(Me_3Sn)_2$, $(Ph_3Sn)_2$ reacted with both aromatic and aliphatic disulfides to produce the corresponding triphenyltin sulfides in quantitative yields.

Similar disproportionation reactions did not take place with disilanes such as $(Me_3Si)_2$, $(MePh_2Si)_2$, $(Ph_3Si)_2$ or $(SiCl_3)_2$ under the same conditions. Digermanes such as $(Me_3Ge)_2$, $(ClMe_2Ge)_2$ and $(Ph_3Ge)_2$ did not react either. However, the reactions of $(Ph_3Pb)_2$ with $(PhS)_2$ and $(BuS)_2$ proceeded smoothly and quantitative yields of the products were obtained. $(PhSe)_2$ was as reactive as $(PhS)_2$ in the above disproportionation reactions. Similar reactions with $(PhTe)_2$ proceeded relatively slowly,[8] but ultimately afforded respectable yields.

$(Bu_3Sn)_2$ has no absorption maximum in the normal UV region. However, its λ_{max} at a wavelength < 215 nm displays strong end absorption that tails to 250–260 nm.[9] $(Ph_3Sn)_2$ and $(Ph_3Pb)_2$ display absorption maxima in the UV region (λ_{max} 248–260 nm for the former depending on the solvent and 294 nm for the latter).[9] Diphenyl dichalcogenides also have absorption maxima in the UV, near-UV or visible regions.[10] Because of these absorptions, various reactions involving ditins[11] or dichalcogenides[10] can very efficiently proceed under photolytic conditions by irradiation with a sunlamp through Pyrex.[12] With these precedents in mind, we envisioned that the present disproportionation reaction proceeds *via* a radical mechanism as shown in Scheme 1.[13] However, the initiation step is uncertain at the present time since precedents suggest that homolytic cleavage of both M–M[11] and Z–Z[10] bonds by light is possible to initiate the reaction. In agreement with the reactivity trends in other reactions of chalcogen-centered radicals (S > Se > Te),[10] the disproportionation of $(PhTe)_2$ proceeded most sluggishly. The decreasing trends in the reactivity of aliphatic disulfides, $(BuS)_2$ > $(CyS)_2$ > $(Bu^tS)_2$, appear to suggest that steric factors of the chalcogen-centered radicals also play an important role.[14]

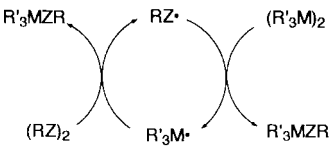

Scheme 1

In summary, a clean and salt-free route to single source precursors for semiconductors has been presented and the process does not require the use of the volatile organic solvents. These features appear to meet the requirement for 'green' chemistry, which is of contemporary public concern.[15]

Financial support from the Japan Science and Technology Corporation (JST) through the CREST (Core Research for Evolutional Science and Technology) program and a post-doctoral fellowship to F. M. are gratefully acknowledged.

Notes and references

1 G. A. Domrachev, V. K. Khamylov, M. Z. Bochkarev, B. V. Zhuk, B. S. Kaverin, B. A. Nesterov and A. I. Kirillov, *Ger. Pat.*, 2 703 873, 1977; H. Uchida, *Jpn. Pat.*, 01 298 010, 1989.

2 J. M. Fischer, W. E. Piers, S. D. P. Batchilder and M. J. Zaworotko, *J. Am. Chem. Soc.*, 1996, **118**, 283 and references therein.

3 For reviews, see: D. A. Armitage, in *The Silicon–Heteroatom Bond*, ed. S. Patai and Z. Rappoport, John Wiley and Sons, Chichester, 1991, pp. 213–243; *Comprehensive Organometallic Chemistry II*, ed. E. W. Abel, F. G. A. Stone and G. Wilkinson, Pergamon, Oxford, 1995, vol. 2, pp. 34–37, 166–174, 293–296; *Comprehensive Organometallic Chemistry*, ed. G. Wilkinson, F. G. A. Stone and E. W. Abel, Pergamon, Oxford, 1982, vol. 2, pp. 167–177, 443–447, 604–607. See also: Kosugi, T. Ogata, M. Terada, H. Sano and T. Migita, *Bull Chem. Soc. Jpn.*, 1985, **58**, 3657; Y. Nishiyama, S. Aoyama and S. Hatanaka, *Phosphorus, Sulfur Silicon Relat. Elem.*, 1992, **67**, 267; Y. Nishiyama, H. Ohashi, K. Itoh and N. Sonoda, *Chem. Lett.*, 1998, 159.

4 L.-B. Han and M. Tanaka, *J. Am. Chem. Soc.*, 1998, **120**, 8249.

5 Although photochemical disproportionation has not been documented, thermal disproportionation between $(Ph_3Pb)_2$ and $(PhS)_2$ in boiling aqueous benzene was reported to afford Ph_3PbSPh (60–76% yield); L. C. Willemsens and G. J. van der Kerk, *J. Organomet. Chem.*, 1968, **15**, 117; P. L. Clarke and J. L. Wardell, *J. Chem. Soc., Dalton Trans.*, 1974, 190. Disproportionation reactions of R_4E_2 (E = P, As, Sb, Bi) with dichalcogenides R'_2Z_2 (Z = S, Se, Te) are also known: R. S. Dickson and K. D. Heazle, *J. Organomet. Chem.*, 1995, **493**, 189; W. Uhl, M. Layh, G. Becker, K.-W. Klinkhammer and T. Hildenbrand, *Chem. Ber.*, 1992, **125**, 1547; H. J. Breuning and S. Guelec, *Z. Naturforsch., Teil B*, 1986, **41**, 1387; A. J. Ashe III and E. G. Ludwig, Jr., *J. Organomet. Chem.*, 1986, **308**, 289; W. W. du Mont, T. Severengiz and H. J. Breuning, *Z. Naturforsch., Teil B*, 1983, **38**, 1306.

6 Special irradiation apparatus is not necessary for the disproportionation of $(ArS)_2$ with $(Me_3Sn)_2$. Usually, mixing the two reagents in a flask placed about 2 m under a 40 W fluorescent lamp at room temperature for a few minutes leads to quantitative formation of the products. Only when the reactivity was low, was irradiation with a 200 W tungsten lamp performed.

7 $PhSSnMe_3$ was found to be formed only in *ca.* 15% yield by heating a benzene solution of $(PhS)_2$ and $(Me_3Sn)_2$ at 80 °C for 2 h in the dark.

8 Neither $(PhS)_2$ nor $(Me_3Sn)_2$ was detected by ^1H NMR spectroscopy when pure $PhSSnMe_3$ in benzene was exposed to the room light at room temperature, indicating the irreversibility of the disproportionation reaction. Similar phenomena were observed for $PhSeSnMe_3$ and $PhTeSnMe_3$, although decomposition of $PhTeSnMe_3$ (conversion 30%) to Ph_2Te and $(Me_3Sn)_2Te$ was found to have occurred after prolonged irradiation (44 h) at room temperature.

9 W. Drenth, M. J. Janssen and G. J. M. van der Kerk, *J. Organomet. Chem.*, 1964, **2**, 265.

10 UV absorption for $(PhZ)_2$: $(PhS)_2$, λ_{max} 250 nm; $(PhSe)_2$, λ_{max} 330 nm; $(PhTe)_2$, λ_{max} 406 nm. Radical additions of $(PhZ)_2$ to unsaturated carbon–carbon bonds under irradiation of visible light have been studied. For examples, see: A. Ogawa, I. Ogawa, R. Obayashi, K. Umezu, M. Doi and T. Hirao, *J. Org. Chem.*, 1999, **64**, 84; A. Ogawa, R. Obayashi, H. Ine, Y. Tsuboi, N. Sonoda and T. Hirao, *J. Org. Chem.*, 1998, **63**, 881; A. Ogawa, R. Obayashi, M. Doi, N. Sonoda and T. Hirao, *J. Org. Chem.*, 1998, **63**, 4277.

11 Irradiation with a sunlamp through Pyrex efficiently promotes $(Bu_3Sn)_2$-initiated radical chain reactions; see D. P. Curran, M.-H. Chen and D. Kim, *J. Am. Chem. Soc.*, 1989, **111**, 6265.

12 Curran *et al.* have reported that Pyrex shows 1–2.5% transmittance at 250–260 nm, which allows homolytic cleavage of $(Bu_3Sn)_2$. See ref. 11.

13 In agreement with the radical mechanism, heating an equimolar mixture of $(Me_3Sn)_2$ and $(PhS)_2$ in C_6D_6 at 80 °C in the dark in the presence of 10 mol% of AIBN led to 95% conversion after 2 h, whereas the same treatment in the absence of AIBN showed only 15% conversion.

14 $(BuS)_2$ is reported to be 14 times more reactive toward $Bu_3Sn^\cdot$ than $(Bu^tS)_2$, see: J. Spanswick and K. U. Ingold, *Int. J. Chem. Kinet.*, 1970, **2**, 157.

15 Note added at proof: We have found very recently that the December 20 issue of *Chemical Abstracts* has compiled a paper on a new method for the synthesis of stannyl selenides; see V. A. Potapov, S. V. Amosova, V. Svetlana, I. P. Beletskaya, A. A. Starkova, A. V. Martynov and L. Hevesi, *Sulfur Lett.*, 1999, **22**, 237; *Chem. Abstr.*, 1999, **131**, 337113u.

1,2,5-ortho esters of D-arabinose as versatile arabinofuranosidic building blocks. Concise synthesis of the tetrasaccharidic cap of the lipoarabinomannan of *Mycobacterium tuberculosis*

Toufiq Bamhaoud,[a] Sylvie Sanchez[b] and Jacques Prandi*[b]

[a] *Laboratoire de Chimie Organique et Bioorganique, Université Chouaib Doukkali, BP 20, El Jadida, Maroc*
[b] *Institut de Pharmacologie et de Biologie Structurale du CNRS, 205 route de Narbonne, 31077 Toulouse, France. E-mail: prandi@ipbs.fr*

Received (in Cambridge, UK) 1st February 2000, Accepted 7th March 2000
Published on the Web 31st March 2000

1,2,5-ortho esters of D-arabinose were found to be ideally suited building blocks for the stereoselective formation of α and β arabinofuranosidic linkages after nucleophilic opening of the orthoester with oxygen and sulfur nucleophiles; the tetrasaccharidic cap of the lipoarabinomannan of *Mycobacterium tuberculosis* was then synthesized in a highly convergent manner.

Lipoarabinomannans (LAMs) are highly antigenic polysaccharidic compounds isolated from the cell wall of various species of mycobacteria.[1] They share common structural features, a phosphatidyl *myo*-inositol anchor and a mannan core substituted by an arabinan domain, exclusively composed of D-arabinofuranosidic units.[1] At the ends of this arabinan domain, are found β-D-arabinofuranosides substituted on position 5 by small motifs, called caps, variable on the mycobacterial species.[2–5] Strong modulations of the biological properties of the LAMs were observed for LAMs isolated from different species of mycobacteria and these variations have been tentatively correlated to the structure of these caps.[2,4–8]

In light of the importance of these motifs for the biological properties of the LAMs in relation with the immunopathogenicity of *M. tuberculosis*, we now report the expeditious synthesis of **1** (Scheme 1) the major tetrasaccharide found at the ends of the LAMs of *M. tuberculosis* and *M. bovis* BCG in a form suitable for further conjugation with a protein.[9] Orthoesters **3** and **11** were found to be highly versatile precursors for the elaboration of the two different arabinofuranosidic rings and the construction of the crucial β-arabinofuranosidic linkage. The result is a rapid and convergent synthesis of **1**.

3-*O*-benzyl 1,2,5-benzylidene D-arabinofuranose **3** was readily obtained in 82% yield from the 1,2,5-benzylidene D-arabinofuranose **2** {$[\alpha]_D^{25}$ −28 (*c* 0.94, $CHCl_3$) lit.[10] +28 for the enantiomer} after treatment with benzyl bromide and sodium hydride in dimethylformamide (Scheme 1). $SnCl_4$ catalyzed opening of orthoester **3** with 5 equiv. of methyl 9-hydroxynonanoate[9] in CH_2Cl_2 gave the 2-*O*-benzoyl-α-D-arabinofuranoside **4** as the only isolated product in 76% yield. Complete regio- and stereo-selectivity were observed for the double orthoester opening[11] and none of the isomeric 5-*O*-benzoyl arabinofuranosidic compound was observed with this catalyst. In an analogous manner, ethyl 2-*O*-benzoyl-3-*O*-benzyl-1-thio-α-D-arabinofuranoside **5** was obtained in 80% yield from the opening of **3** with 1.1 equiv. of ethanethiol under $SnCl_4$ catalysis, once again with complete stereocontrol of the orthoester opening.[12,13] Unmasking of the hydroxy group on the 2-position of the arabinofuranosidic ring of thioglycoside **5** for later attachment of the *p*-methoxybenzyl tether[14] was carried out in two steps and gave alcohol **7** in 73% overall yield (Scheme 1).

We also looked at the reactions of 3-*O*-benzyl 1,2,5-dichloroethylidene D-arabinofuranose **11**, available in 90% yield (BnBr, NaH, DMF) from known compound **10**, prepared in only two steps from D-arabinose.[15] As was expected from electronic factors, nucleophilic opening of the orthoester function of **11**

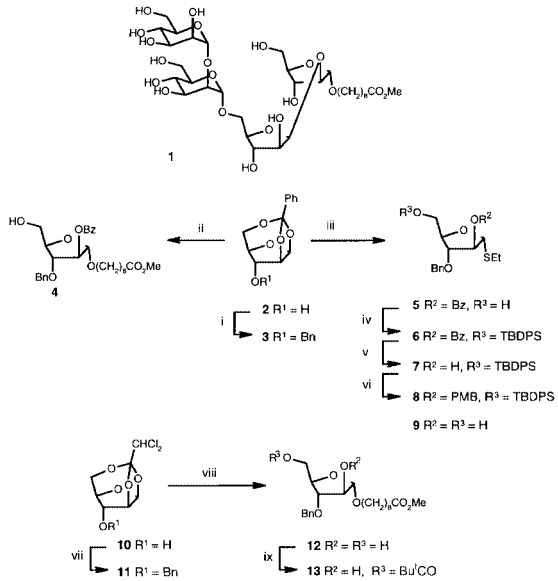

Scheme 1 *Reagents and conditions*: i, NaH, BnBr, DMF, room temp., 1 h, 82%; ii, 5 equiv. methyl 9-hydroxynonanoate, 0.1 equiv. $SnCl_4$, MS 4 Å, CH_2Cl_2, room temp., 15 min, 76%; iii, 1.1 equiv. EtSH, 0.1 equiv. $SnCl_4$, MS 4 Å, CH_2Cl_2, −18 °C, 30 min, 80%; iv, 1.5 equiv. Bu^tPh_2SiCl, 1.5 equiv. imidazole, DMF, room temp., 1 h, 92%; v, 0.1 equiv. MeONa, MeOH, room temp., 79%; vi, 2.5 equiv. BEMP, 2.5 equiv. *p*-MeOBnBr, MeCN, 0 °C to room temp., 1 h, 70%. vii, NaH, BnBr, DMF, room temp., 1 h, 90%; viii, 5 equiv. $HOCH_2(CH_2)_7C(O)OMe$, 2 equiv. $SnCl_4$, MS 4 Å, CH_2Cl_2, room temp., 3 h, then MeONa, MeOH, room temp., 1 h, 60%; ix, 1.5 equiv. Bu^tCOCl, 0.1 equiv. DMAP, pyridine, 0 °C, 1.5 h, 80%.

proved to be more difficult than for **3**. 2 Equiv. of $SnCl_4$ at room temperature were necessary to bring the reaction of **11** with methyl 9-hydroxynonanoate to completion and a mixture of 2-*O*- and 5-*O*-dichloroacetyl α-arabinofuranosides was obtained. α-Arabinofuranoside **12** was isolated in 60% yield after deacylation with sodium methoxide. Selective pivaloylation of the primary hydroxy group of **12** (0 °C, Bu^tCOCl, DMAP, pyridine) gave alcohol **13** ready for glycosylation (80%). Opening of **11** with ethanethiol was also obtained with 1.2 equiv. of EtSH and 0.2 equiv. $SnCl_4$ at 0 °C, deacylation of the mixture of dichloroacetates as above gave **9** in 64% overall yield from **11**. Selective silylation of the primary position of **9** with TBDPSCl and imidazole afforded 73% of the previously prepared **7**. Finally, the 4-methoxybenzyl group was introduced on the 2-position of **7** with 2.5 equiv. of 4-methoxybenzyl bromide[16] and 2.5 equiv. of 2-*tert*-butylimino-2-diethylamino-1,3-dimethylperhydro-1,3,2-diazaphosphorine[17] (BEMP) in acetonitrile to give thioarabinofuranoside **8** in 70% yield.

Coupling of the arabinofuranosidic units and elaboration of the β-arabinofuranosidic linkage were accomplished according to Ogawa's internal aglycon delivery approach.[14,18] Reaction of 1.1 equiv. of **8** with **13** and 1.5 equiv. of 2,3-dichloro-

DOI: 10.1039/b000873g

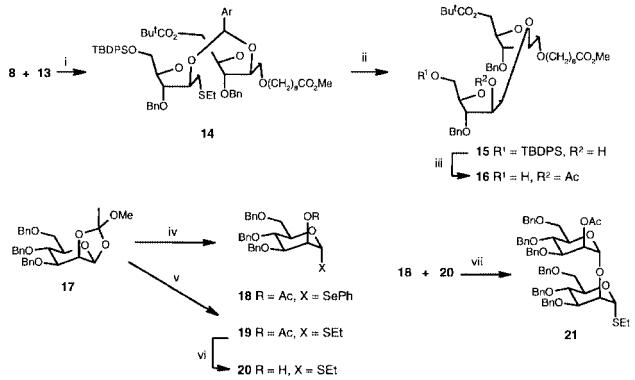

Scheme 2 *Reagents and conditions*: i, 1.1 equiv. **8**, 1 equiv. **13**, 1.5 equiv. DDQ, MS 4 Å, CH_2Cl_2, 0 °C to room temp., 2.5 h, 84%; ii, 1.2 equiv. IDCP, MS 4 Å, CH_2Cl_2, room temp., 1.5 h, 73%; iii, Ac_2O, pyridine, room temp., then 1.2 equiv. Bu^n_4NF, THF, room temp., 0.5 h, 75%, 2 steps; iv, 1.5 equiv. PhSeH, MS 4 Å, cat. $HgBr_2$, MeCN, room temp., 2 h, 75% ; v, 5.5 equiv. EtSH, MS 4 Å, cat. $HgBr_2$, MeCN, room temp., 48 h, 79% ; vi, MeONa, MeOH, room temp., 16 h, 91% ; vii, 1 equiv. **18**, 1.1 equiv. **20**, 1.1 equiv. NIS, 0.1 equiv. TMSOTf, MS 4 Å, CH_2Cl_2, −18 °C to room temp., 71%.

5,6-dicyano-1,4-benzoquinone in CH_2Cl_2 gave the mixed acetal **14** in 84% isolated yield after chromatography (Scheme 2). Intramolecular glycosylation was promoted with 1.2 equiv. of iodonium dicollidine perchlorate (IDCP)[19] in CH_2Cl_2 and gave a rewarding 73% yield of the β-linked disaccharide **15** as the only isolated product. The β-(D) configuration of the new anomeric center was firmly established from the ^1H and ^{13}C NMR data ($\delta_{H\text{-}1'}$ 5.15, $J_{H\text{-}1',H\text{-}2'}$ 4.5 Hz; $\delta_{C\text{-}1'}$ 101.48).[20] Acetylation (acetic anhydride, pyridine) and silyl ether deprotection with tetrabutylammonium fluoride in tetrahydrofuran gave the diarabinofuranoside **16** ready for further elongation (75% from **15**).

The dimannosidic glycosyl donor **21** was efficiently obtained from orthoester **17**[21] taking advantage of the higher reactivity of selenoglycosides over thioglycosides towards activation.[22,23] **17** was first opened with 1.5 equiv. of selenophenol[24] under $HgBr_2$ catalysis and gave (α-selenoglycoside **18** in 75% yield (Scheme 2). The known thioglycoside **19**,[25] obtained in 79% from **17** after $HgBr_2$-promoted ethanethiol opening, was deacetylated (MeONa, MeOH) to give glycosyl acceptor **20** in 91% yield. Selective activation of selenoglycoside **18** with 1.1 equiv. of *N*-iodosuccinimide (NIS) and 10% trimethylsilyl trifluoromethanesulfonate (TMSOTf),[26] and coupling with 1.1 equiv. of thioglycoside **20** in CH_2Cl_2 at −18 °C gave the expected α-linked dimannosidic compound **21** in 71% yield with complete control of the new anomeric center. **21** was isolated in slightly lower yield (64%) when the original silver trifluoromethanesulfonate/potassium carbonate combination[22] was used as promoter for the glycosylation of **20** with **18**.

Final coupling was done by glycosylation of disaccharide **16** with 1.5 equiv. of thiodisaccharide **21** under NIS/catalytic TMSOTf activation (Scheme 3). A 70% yield of tetrasaccharidic compounds **22** was obtained as a 4 : 1 α,β anomeric

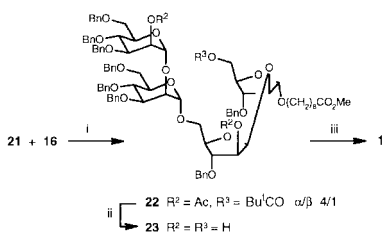

Scheme 3 *Reagents and conditions*: i, 1 equiv. **16**, 1.5 equiv. **21**, 1.7 equiv. NIS, 0.15 equiv. TMSOTf, MS 4 Å, CH_2Cl_2, −15 °C, 1 h, 70%; ii, 0.5 M MeONa, MeOH, room temp., 5 h, 75%; iii, H_2, $Pd(OH)_2$/C, MeOH, room temp., 1 h, 65%.

mixture on the H-1″ anomeric center. This mixture could not be separated at this stage, so the ester groups were removed with 0.5 M sodium methoxide solution in methanol (75%) and the mixture of triols was chromatographed to give pure **23**. Hydrogenolysis of the benzyl groups [H_2, $Pd(OH)_2$/C, MeOH] gave the target compound **1**[27] in 65% yield.

In conclusion, orthoester derivatives of arabinose and mannose were used for the efficient synthesis of **1**, the tetrasaccharidic cap of the lipoarabinomannan of *M. tuberculosis*, *via* a convergent route using minimal protecting groups manipulation and selective anomeric activation. Both α- and β-arabinofuranosides were obtained with complete stereocontrol from 3-*O*-benzyl-1,2,5-orthoesters of D-arabinose. Extension of this methodology to the elaboration of other complex polyarabinofuranosidic structures and synthesis of neoantigens from **1** for biological evaluation are currently under way.

Notes and references

1 D. Chatterjee and K. H. Khoo, *Glycobiology*, 1998, **8**, 113.
2 T. I. A. Roach, C. H. Barton, D. Chatterjee and J. M. Blackwell, *J. Immunol.*, 1993, **150**, 1886.
3 D. Chatterjee, K. Lowell, B. Rivoire, M. R. McNeil and P. J. Brennan, *J. Biol. Chem.*, 1992, **267**, 6234.
4 S. Prinzis, D. Chatterjee and P. J. Brennan, *J. Gen. Microbiol.*, 1993, **139**, 2649.
5 M. Gilleron, N. Himoudi, O. Adam, P. Constant, A. Venisse, M. Rivière and G. Puzo, *J. Biol. Chem.*, 1997, **272**, 117.
6 A. Vercellone, J. Nigou and G. Puzo, *Front. Biosci.*, 1998, **3**, e149.
7 P. A. Sieling, D. Chatterjee, S. A. Porcelli, T. I. Prigozy, R. J. Mazzaccaro, Y. Soriano, B. R. Bloom, M. B. Brenner, M. Kronenberg, P. J. Brennan and R. L. Modlin, *Science*, 1995, **269**, 227.
8 A. Venisse, J. J. Fournié and G. Puzo, *Eur. J. Biochem.*, 1995, **231**, 440.
9 R. U. Lemieux, D. R. Bundle and D. A. Baker, *J. Am. Chem. Soc.*, 1975, **97**, 4076.
10 N. K. Kochetkov, A. Y. Khorlin, A. F. Bochkov and I. G. Yazlovetskii, *Izv. Akad. Nauk. SSSR, Ser. Khim.*, 1966, 1966; A. F. Bochkov, Y. V. Voznyi, V. N. Chernetskii, V. M. Dashunin and A. V. Rodionov, *Izv. Akad. Nauk. SSSR, Ser. Khim.*, 1975, 348.
11 N. K. Kochetkov, A. F. Bochkov and I. G. Yazlovetsky, *Carbohydr. Res.*, 1969, **9**, 49.
12 Other catalysts gave mixtures of isomeric 2-*O*- and 5-*O*-benzoylated arabinofuranosides. For a related orthoester opening, see ref. 13.
13 F. Nakatsuko, H. Kamitakahara and M. Hori, *J. Am. Chem. Soc.*, 1996, **118**, 1677.
14 Y. Ito and T. Ogawa, *Angew. Chem., Int. Ed. Engl.*, 1994, **33**, 1765; A. Dan, Y. Ito and T. Ogawa, *J. Org. Chem.*, 1995, **60**, 4680.
15 Y. Gül Salman, Ö. Makinanakan and L. Yüceer, *Tetrahedron Lett.*, 1994, **35**, 9233.
16 N. Kornblum, R. A. Smiley, R. K. Blackwood and D. C. Iffland, *J. Am. Chem. Soc.*, 1955, **77**, 6229.
17 B. S. Sproat, B. Beijer and A. Iribarren, *Nucleic Acids Res.*, 1990, **18**, 41; C. H. Gotfredsen, J. P. Jacobsen and J. Wengel, *Tetrahedron Lett.*, 1994, **35**, 6941.
18 For other approaches to the synthesis of β-arabinofuranosides, see: H. B. Mereyala, S. Hotha and M. K. Gurjar, *Chem. Commun.*, 1998, 685; J. Désiré and J. Prandi, *Carbohydr. Res.*, 1999, **317**, 110.
19 P. Smid, G. A. de Ruiter, G. A. Van der Marel, F. M. Rombouts and J. H. Van Boom, *J. Carbohydr. Chem.*, 1991, **10**, 833.
20 K. Bock and C. Pedersen, *Adv. Carbohydr. Chem. Biochem.*, 1983, **41**, 27; R. C. Beier and B. P. Mundy, *J. Carbohydr. Chem.*, 1984, **3**, 253.
21 N. E. Franks and R. Montgomery, *Carbohydr. Res.*, 1968, **6**, 286.
22 S. Mehta and B. M. Pinto, *Tetrahedron Lett.*, 1991, **32**, 4435; *J. Org. Chem.*, 1993, **58**, 3269.
23 P. Grice, S. V. Ley, J. Pietruszka and H. W. M. Priepke, *Angew. Chem., Int. Ed. Engl.*, 1996, **35**, 197.
24 W. H. H. Gunther, *J. Org. Chem.*, 1966, **31**, 1202.
25 T. Peters, *Liebigs Ann. Chem.*, 1991, 135.
26 G. H. Veeneman, S. H. Van Leeuwen, H. Zuurmond and J. H. Van Boom, *J. Carbohydr. Chem.*, 1991, **9**, 783.
27 *Selected data* for **1**. $[\alpha]_D^{25}$ +18 (*c* 0.44, water); ^1H NMR (500 MHz, D_2O, 293 K): δ 5.16 (d, 1H, *J* 1.7 Hz, H-1″), 5.11 (d, 1H, *J* 4.5 Hz, H-1′), 5.10 (d, 1H, *J* 2 Hz, H-1), 5.02 (d, 1H, *J* 2 Hz, H-1‴). ^{13}C NMR (125.72 MHz, D_2O, 293 K) δ 106.09 (C-1), 103.01 (C-1‴), 101.05 (C-1′), 98.86 (C-1″), 87.48 (C-2), 80.40 (C-2″), 76.67 (C-2′).

Photoinduced energy transfer in mixed self-assembled monolayers of pyrene and porphyrin

Hiroshi Imahori,*[a] Yoshinobu Nishimura,[b] Hiroyuki Norieda,[c] Hironori Karita,[c] Iwao Yamazaki,*[b] Yoshiteru Sakata*[c] and Shunichi Fukuzumi[a]

[a] *Department of Material and Life Science, Graduate School of Engineering, Osaka University, CREST, JAPAN Science and Technology Corporation, Suita, Osaka 565-0871, Japan. E-mail: imahori@ap.chem.eng.osaka-u.ac.jp*
[b] *Department of Molecular Chemistry, Graduate School of Engineering, Hokkaido University, Sapporo 060-8628, Japan. E-mail: yamiw@eng.hokudai.ac.jp*
[c] *The Institute of Scientific and Industrial Research, Osaka University, 8-1 Mihoga-oka, Ibaraki, Osaka 567-0047, Japan. E-mail: sakata@sanken.osaka-u.ac.jp*

Received (in Cambridge, UK) 12th January 2000, Accepted 6th March 2000
Published on the Web 31st March 2000

Mixed self-assembled monolayers of pyrene and porphyrin have been prepared to mimic efficient energy transfer in the photosynthetic antenna complex.

X-Ray structural determination of the photosynthetic antenna complex[1] has stimulated many organic chemists to design covalently-linked multichromophores such as linear, circular and dendritic porphyrin oligomers for mimicry of efficient energy transfer (EN) process.[2,3] An alternative strategy involves molecular assembly of chromophores in organized media. Langmuir–Blodgett films and lipid bilayer membranes have been frequently employed to construct light-harvesting systems.[4–10] However, these systems seem to be inapplicable in terms of stability, uniformness and manipulation. In contrast, the use of self-assembled monolayers (SAMs)[11] may be a promising approach to organize chromophores on substrates because of their uniform and well ordered structures. Here, we report the first preparation of mixed SAMs of pyrene **1** and porphyrin **2** on a gold surface (Fig. 1) in which efficient singlet–singlet EN from **1** to **2** has been detected successfully.

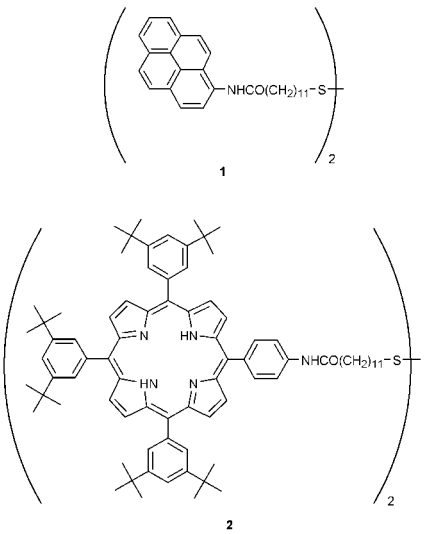

Fig. 1 Molecular structure of pyrene and porphyrin dimers **1** and **2**.

The synthetic route to **1** is shown in Scheme 1. Condensation of 1-aminopyrene with 12-bromododecanoic acid in the presence of 2-chloro-4,6-dimethoxy-1,3,5-triazine afforded **3** in 29% yield. Bromide **3** was converted to disulfide **1** *via* thioesterification with potassium thioacetate and subsequent base deprotection of **4**. Porphyrin disulfide **2** was prepared by following the same procedures as described previously.[12,13] The structures of **1** and **2** were verified by spectroscopic analyses including ^{1}H NMR and MALDI-TOF mass spectra.†

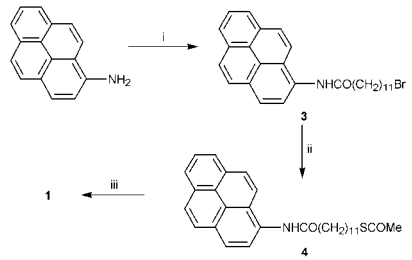

Scheme 1 *Reagents and conditions*: i, 12-bromododecanoic acid, 2-chloro-4,6-dimethoxy-1,3,5-triazine, THF, 29%; ii, potassium thioacetate,THF–EtOH, 52%; iii, KOH, THF–MeOH, 42%.

Monolayers of mixtures of **1** and **2** were formed by the coadsorption of **1** and **2** onto Au(111) mica substrates (denoted **1**–**2**/Au, where / represents an interface). The coadsorption onto the gold surface was carried out from CH_2Cl_2 solutions containing **1** and **2** with a total concentration of 10 μM [molar ratio of **1**:**2** = (a) 100:0, (b) 90:10, (c) 50:50, (d) 10:90, (e) 0:100] for 20 h to complete mixed SAM formation. After soaking, the gold substrate was washed well with CH_2Cl_2 and dried with a stream of argon. A cyclic voltammetric experiment using **1**–**2**/Au in CH_2Cl_2 containing 0.1 M $Bu^n_4NPF_6$ electrolyte with a sweep rate of 50 mV s^{-1} (electrode area, 0.48 cm^2) was performed to estimate the surface coverage (Fig. 2). The adsorbed amount of **1** and **2** on **1**/Au [**1**:**2** = (a) 100:0] and **2**/Au [**1**:**2** = (e) 0:100] was calculated from the charge of the anodic peak of the pyrene and the porphyrin moieties as 2.8×10^{-10} mol cm^{-2} (= 59 $Å^2$ $molecule^{-1}$)‡ and 1.5×10^{-10} mol cm^{-2} (= 110 $Å^2$ $molecule^{-1}$),[12] respectively. These values indicate the formation of the well packed structures of **1** and **2** on the gold surface. However, an attempt to determine the adsorbed amounts of **1** and **2** in the mixed SAMs was

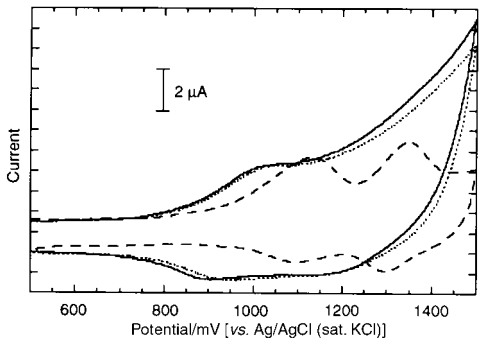

Fig. 2 Cyclic voltammograms of **1**/Au (—), **2**/Au (----), and a mixed SAM of **1** and **2** on a gold surface (·····) from CH_2Cl_2 solution using a molar ratio of 50:50.

unsuccessful because of the broad wave of the first oxidation due to the pyrene and porphyrin moieties.

Fig. 3 shows absorption spectra of **1** and **2** in CH_2Cl_2 and of **1**–**2**/Au [**1**:**2** = (c) 50:50] using the transmission mode in air.[12] The absorption band of **1** (λ_{max} = 337 nm) and **2** (λ_{max} = 424 nm) on the gold surface is blue- and red-shifted by 7 and 3 nm, respectively, as compared to that of **1** and **2** in CH_2Cl_2. Assuming that the relative ratio of the molar absorption coefficients of **1** and **2** in the mixed SAMs are the same as those in CH_2Cl_2 [**1**: 4.90×10^4 M^{-1} cm^{-1} (λ_{max} = 344 nm); **2**: 1.08×10^6 M^{-1} cm^{-1} (λ_{max} = 421 nm)], the relative ratios of **1**:**2** in the mixed SAMs are estimated as (a) 100:0, (b) 99:1, (c) 94:6, (d) 85:15 and (e) 0:100. The strong π–π interactions of the pyrene moieties compared with the relatively weak interaction between the porphyrin moieties (as a consequence of the bulky tert-butyl groups) may be responsible for the preference of adsorption of **1** over **2** on the gold surface. In addition, the fact that the pyrene molecules occupy about half the surface area of the porphyrins would lead to a thermodynamic preference for pyrene adsorption, since displacement of a porphyrin for two pyrenes results in an extra S–Au interaction.

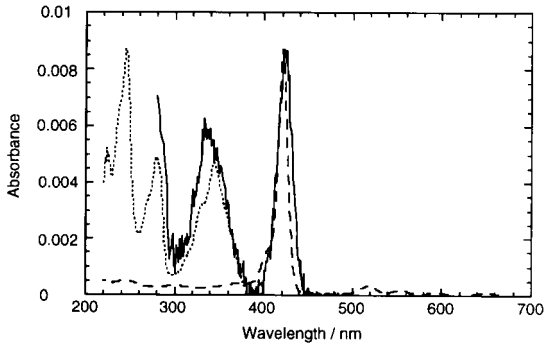

Fig. 3 Absorption spectra of **1** (⋯) and **2** (----) in CH_2Cl_2 and a mixed SAM of **1** and **2** on a gold surface (—) from CH_2Cl_2 solution using a molar ratio of 50:50. The spectra are normalized for comparison.

Steady-state corrected fluorescence spectra of **1** and **2** in CH_2Cl_2 were measured with the excitation wavelength at 340 and 427 nm, respectively, and were compared with those of **1**/Au and **2**/Au. The fluorescence spectrum of **2**/Au is essentially the same as that of **2** in CH_2Cl_2 as shown in Fig. 4.[12] Fluorescence emission of **1** in Fig. 4 overlaps well with absorption of **2** in Fig. 3. Thus, it is expected that excitation of the pyrene moiety as an antenna chromophore may lead to efficient singlet–singlet EN from the pyrene to the porphyrin in the SAMs. Unfortunately, however, the emission of **1**/Au was too weak to be detected. No detectable fluorescence from the pyrene or the porphyrin moiety was observed in **1**–**2**/Au under steady state irradiation. Then, time-resolved, single-photon counting fluorescence studies were made for **1**–**2**/Au§ [**1**:**2** = (a) 100:0, (b) 90:10, (c) 50:50, (d) 10:90, (e) 0:100) as well as for **1** and **2** in solutions with an excitation wavelength at 280 nm, where the light is mainly absorbed by the pyrene moiety. In each case the decay of the fluorescence intensity at 385 nm and/or 720 nm (due to the singlet excited states of the pyrene and the porphyrin, respectively) could be monitored. The decay curve could be fitted as single exponential except for **1** at 385 nm in CH_2Cl_2. The fluorescence lifetimes of **1**/Au at 385 nm (23 ps) and **2**/Au at 720 nm (40 ps) were much shorter than those of **1** [7.4 ns (30%), 3.2 ns (70%)] and **2** (8.1 ns) in CH_2Cl_2. This indicates that the excited singlet states of the pyrene and the porphyrin are quenched by the gold surface through EN, as reported previously.[12] The fluorescence lifetimes of the pyrene moiety in **1**–**2**/Au at 385 nm decreased with an increase in the relative ratio of the porphyrin to the pyrene [(a) 23 ps, (b) 20 ps, (c) 11 ps, (d) 8.8 ps].¶ The fluorescence lifetimes of the porphyrin moiety in **1**–**2**/Au at 720 nm also decreased with an increase in the relative ratio of the porphyrin to the pyrene [(b) 92 ps, (c) 88 ps, (d) 60 ps, (e) 40 ps]. A likely explanation for these observations is that efficient EN (> 62%) occurs from the excited singlet state of the pyrene to the porphyrin, followed by energy transfer among the porphyrins.[14]

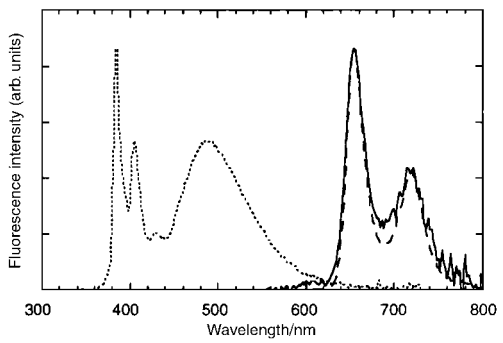

Fig. 4 Fluorescence spectra of **1** (⋯) and **2** (----) in CH_2Cl_2 and a SAM of **2** on a gold surface (—) with excitation at 340 nm for **1** and 427 nm for **2**. The spectra are normalized for comparison.

In conclusion, we have developed the first mixed self-assembled monolayers of pyrene and porphyrin in which efficient singlet–singlet EN takes place from the pyrene to the porphyrin. Further improvement on the ability of harvesting the light may be made by choosing a suitable couple of different chromophores which absorb visible light extensively.

This work was supported by Grant-in-Aids for COE Research and Scientific Research on Priority Area of Electrochemistry of Ordered Interfaces and Creation of Delocalized Electronic Systems from Ministry of Education, Science, Sports and Culture, Japan. H. I. thanks the Sumitomo Foundation for financial support.

Notes and references

† *Selected data* for **1**: δ_H(270 MHz; $CDCl_3$) 7.7–8.3 (m, 20H), 2.68 (t, *J* 8 Hz, 4H), 2.58 (t, *J* 8 Hz, 4H), 2.0–1.0 (m, 36H); *m/z* (MALDI-TOF; positive mode) 862 ($M + H^+$).

‡ Densely packed monolayer films are known to retard ion transport and electrochemical accessibility. Since pyrene is a planar aromatic molecule, the pyrene moiety of **1** may be densely packed owing to the strong π–π stacking in the monolayers. Thus, the real value of surface coverage may be larger, as compared to the estimated value using cyclic voltammetry.

§ For the time-resolved fluorescence measurements, gold substrates were prepared by a vacuum deposition technique with titanium (50–100 Å) and gold (200–1000 Å) in sequence onto a Si(100) wafer (Sumitomo Sitix Corp.).

¶ Monomer emission (*ca.* 400 nm) as well as excimer emission (*ca.* 500 nm) were observed for **1** in CH_2Cl_2, as shown in Fig. 4. The fluorescence lifetimes of **1**–**2**/Au at 500 nm also decreased with an increase in the relative ratio of the porphyrin to the pyrene.

1 G. Mcdermontt, S. M. Prince, A. A. Freer, A. M. Hawthornthwaite-Lawless, M. Z. Rapiz, R J. Cogdell and N.W. Isaacs, *Nature*, 1995, **374**, 517.
2 H. L. Anderson, *Chem. Commun.*, 1999, 2323.
3 P. F. H. Schwab, M. D. Levin and J. Michl, *Chem. Rev.*, 1999, **99**, 1863.
4 V. M. Agranovich and M. D. Galanin, *Electronic Excitation Energy Transfer in Condensed Matter*, North-Holland, New York, 1982.
5 I. Yamazaki, N. Tamai and T. Yamazaki, *J. Phys. Chem.*, 1990, **94**, 516.
6 J. A. Pescatore Jr. and I. Yamazaki, *J. Phys. Chem.*, 1996, **100**, 13 333.
7 A. K. Dutta, H. Lavoie, K. Ohta and C. Salesse, *Langmuir*, 1997, **13**, 801.
8 E. Vuorimaa, H. Lemmetyinen, P. Ballet, M. Van der Auweraer and F. C. De Schryver, *Langmuir*, 1997, **13**, 3009.
9 K. K. Jensen, B. Albinsson, M. Van der Auweraer, E. Vuorimaa and H. Lemmetyinen, *J. Phys. Chem. B*, 1999, **103**, 8514.
10 T. Morita, S. Kimura and Y. Imanishi, *J. Am. Chem. Soc.*, 1999, **121**, 581.
11 A. Ulman, *Introduction to Ultrathin Organic Films*, Academic Press, San Diego, 1991.
12 H. Imahori, H. Norieda, Y. Nishimura, I. Yamazaki, K. Higuchi, N. Kato, T. Motohiro, H. Yamada, K. Tamaki, M. Arimura and Y. Sakata, *J. Phys. Chem. B*, 2000, **104**, 1253.
13 H. Imahori, H. Norieda, S. Ozawa, K. Ushida, H. Yamada, T. Azuma, K. Tamaki and Y. Sakata, *Langmuir*, 1998, **14**, 5335.
14 K. Hirakawa and H. Segawa, *J. Photochem. Photobiol. A, Chem.*, 1999, **123**, 67.

H/D exchange between CH_4 and CD_4 catalysed by a silica supported tantalum hydride, $(\equiv SiO)_2Ta–H$

Laurent Lefort, Christophe Copéret, Mostafa Taoufik, Jean Thivolle-Cazat* and Jean-Marie Basset*

Laboratoire de Chimie OrganoMétallique de Surface UMR 9986 CNRS-CPE Lyon 43, boulevard du 11 Novembre 1918 F-69616 Villeurbanne Cedex, France. E-mail: basset@mulliken.cpe.fr

Received (in Cambridge, UK) 22nd December 1999, Accepted 1st March 2000
Published on the Web 30th March 2000

The silica supported tantalum hydride $(\equiv SiO)_2Ta–H$ 1, catalyses the H/D exchange reaction between CH_4 and CD_4 at 150 °C producing the statistical distribution of all methane isotopomers.

Methane is the most thermodynamically stable alkane. Its activation necessarily requires the cleavage of a C–H bond and, for example, the H/D exchange reaction between CH_4 and a deuterium source (D_2, D_2O or a deuterated alkane or arene) is a typical process involving C–H bond activation.[1] Some of the first examples were observed in the 1930s and 1940s using metal surfaces.[2] Numerous examples have appeared since in heterogeneous catalysis,[3] while only few homogeneous systems are known to perform the catalytic H/D exchange with CH_4.[4]

Surface OrganoMetallic Chemistry (SOMC) lies at the interface between homogeneous and heterogeneous catalysis and consists in grafting a molecular organometallic complex onto an oxide or metal surface to generate ultimately single site catalysts.[5] This strategy has led to the synthesis and the characterization of a silica supported tantalum hydride, $(\equiv SiO)_2Ta–H$ **1**, a highly electrophilic complex (formally a eight electron complex).[6] It can activate the C–H bond of cyclic alkanes, to form a tantalum cycloalkyl species, $(\equiv SiO)_2Ta–C_nH_{2n-1}$.[7] It also catalyses both the low temperature hydrogenolysis of alkanes[8] and the new reaction of alkane metathesis,[9] which transforms acyclic alkanes into their higher and lower homologues. Here, we report that **1** also catalyses the H/D exchange reaction between CH_4 and CD_4, leading to the statistical formation of all possible isotopomers.

When a 55:45 mixture of CH_4/CD_4 was contacted with **1** at 150 °C for 10 h, it was converted into a mixture of all the isotopomers of methane as a statistical distribution (Fig. 1).† At low conversion, d_1- and d_3-methanes were formed faster than d_2-methane, suggesting that the H/D exchange was stepwise *via* the exchange of one H/D atom at a time [Fig. 1(a)]. This initial CH_4/CD_4 mixture gave a mixture of methane isotopomers, of which CD_2H_2 was the major product. If a 65:35 mixture of CH_4/CD_4 was contacted with **1** under identical conditions, the evolution toward a different statistical distribution of all isotopomers was observed. The composition of the equilibrated mixture according to GC–MS was 24, 40, 24, 12, 0% of d_0-, d_1-, d_2-, d_3- and d_4-methanes, respectively, in good agreement with the calculated statistical distribution (18, 38, 31, 11, 1.5%), which was no longer centered on CD_2H_2 since there was an excess of H- over D-atoms in the initial mixture.

The number of turnovers for this exchange reaction can be estimated according to eqn. (1) if considering that (a) the formation of CDH_3 and CD_3H requires at least one C–H(D) bond cleavage and formation from CH_4 and CD_4, respectively, and that (b) the formation of CD_2H_2 necessitates at least two C–H bond cleavages and formations from either CH_4 or CD_4

$$\text{TON} = [Q(CDH_3) + Q(CD_3H) + 2\,Q(CD_2H_2)]/Q(\text{Ta}) \quad (1)$$

Q(X) represents the amount (in mol) of the compound X.

The number of turnovers as defined in eqn. (1) is underestimated since it does not take into account degenerate processes such as the exchange of a D atom with another D atom. The calculated TON for the H/D exchange is therefore *ca.* 200 after 6 h of reaction. For a comparison, the metathesis of ethane catalysed by the same surface complex **1** under similar experimental conditions has reached a TON of *ca.* 4 after 6 h.[9] The higher activity of **1** for H/D exchange reaction is however not surprising since this process involves C–H in place of C–C bond cleavage for alkane metathesis.

A similar H/D-exchange also occurs between deuterated methane and hydrogen. When a 1:2 mixture of CD_4/H_2 (P_{tot} = 200 Torr) was contacted with **1** (52 mg, 5.2 wt% Ta) at 150 °C, the formation of d_0-, d_1-, d_2-, d_3-methanes could be detected after 40 min by IR spectroscopy. A new stable composition of the gas mixture, containing all the deuterated methanes, was reached after several hours, which corresponded to the statistical distribution of all H/D atoms (7.6, 15.8, 35.8, 26.6, 14.2% of d_0-, d_1-, d_2-, d_3- and d_4-methanes, respectively, *cf.* the calculated theoretical composition of 6, 25, 37.5, 25, 6%). The initial rates obtained in the exchange of CH_4/CD_4 and CD_4/H_2 do not appear to be significantly different, which is in agreement with the cleavage of the C–H bond being the rate-determining step for both transformations.

During the reaction with CH_4/CD_4 mixtures, the evolution of **1** could be followed by *in situ* IR spectroscopy. The addition at room temperature of a mixture of d_0- and d_4-methanes to **1** did not lead to a significant decrease in intensity of the ν(Ta–H) band, centered at 1825 cm^{-1}.[6] However, after 45 min at 150 °C, the ν(Ta–H) band was reduced to about half its initial intensity, and a new band at 1323 cm^{-1} was observed, which corre-

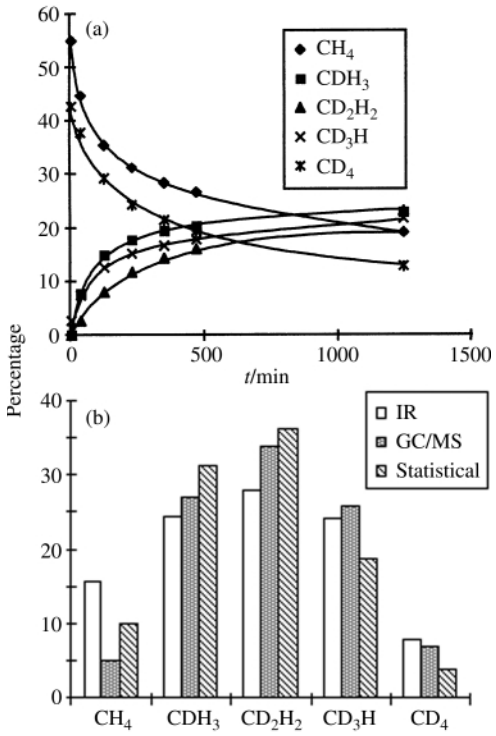

Fig. 1 CH_4/CD_4 exchange reaction (CH_4/CD_4 = 55:45; P_{tot} = 200 Torr; 150 °C, 36 mg of **1** (6.1 wt% Ta)). (a) Isotopomeric composition of the gas phase *vs.* time. (b) Distributions of the different isotopomers at the end of the reaction (2500 min).

DOI: 10.1039/a910239f

sponded to a ν(Ta–D) vibration.‡ No peaks associated with Ta–CH_3 or Ta–CD_3 were detected, but these types of surface species are usually difficult to observe by IR spectroscopy.[7] In fact, independent experiments showed that hydrolysing the surface species formed after reacting **1** with CH_4 (P = 200 Torr, T = 150 °C, 2 days) gave methane in the gas phase, which probably arose from the hydrolysis of a surface tantalum methyl, $(\equiv SiO)_2Ta–CH_3$ **2**. This consequently shows that **1** can be converted into **2** under the H/D exchange experimental conditions although the complete disappearance of both the Ta–H and Ta–D vibration bands has never been observed.

Two mechanisms for the H/D exchange reaction between CH_4 and CD_4 can be proposed. Both rely on a σ-bond metathesis C–H activation step and involve different active species, *i.e.* **1** or **2** (Scheme 1).

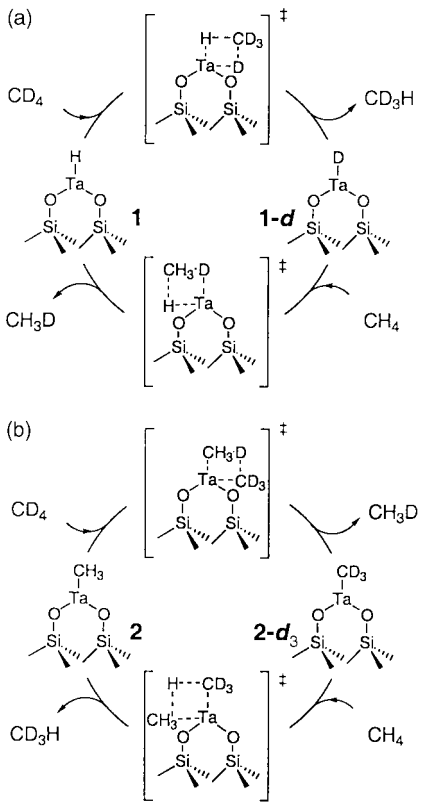

Scheme 1

A two-step experiment, in which **1** is first contacted with CD_4 (step 1) and then with CH_4 (step 2) under the same conditions, should provide a different isotopomeric distribution depending on the reaction mechanism (Scheme 2).

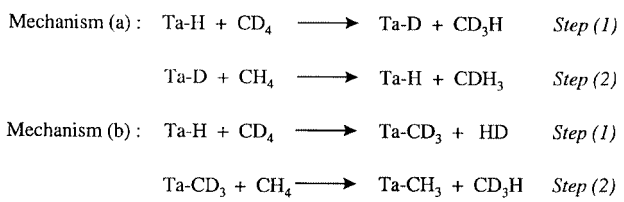

Scheme 2

Therefore, the reaction of CD_4 (30 Torr) with **1** at 150 °C for 3 h (step 1) led to the formation of CD_3H as the sole methane isotopomer in the gas phase. After removing the gas phase, the addition of 20 Torr of CH_4 (step 2) followed by a 3 h reaction at 150 °C gave CDH_3 as the only deuterated product present in the gas phase. This shows that despite the probable formation of Ta–CD_3 species in step 1 (*vide supra*), it does not participate efficiently in the H/D exchange process since CD_3H has not been observed [mechanism (b), step 2]. Consequently, mechanism (a) which only involves Ta–H bonds instead of Ta–C bonds [mechanism (b)] appears to be the most consistent to describe the H/D exchange between methanes. This observation also agrees with previous data relative to the stability of four-center intermediates, in which a carbon atom opposite to the metal [Scheme 1(a)] instead of a hydrogen/deuterium atom [Scheme 1(b)] is preferred.[4e]

In summary, the silica supported tantalum hydride **1** catalyses the H/D exchange reaction in CH_4/CD_4 mixtures. This reaction proceeds under mild conditions and leads to the formation of the statistical distribution of all isotopomers of methane. Its rate is approximately two orders of magnitude faster than that of the alkane metathesis reaction. A mechanism in which the tantalum hydride species is the active intermediate in the catalytic cycle rather than the Ta–CH_3 species is consistent with the experimental observations.

We are grateful to CNRS and ESCPE Lyon for financial support. We would also like to thank Dr O. Maury, Professors I. P. Rothwell (Purdue University) and R. A. Andersen (UC Berkeley) for fruitful discussions.

Notes and references

† A statistical distribution corresponds to a random distribution of all hydrogen and deuterium atoms among the five possible isotopomers of methane and can be calculated by the coefficients of the polynom: $(d_0 + d_4)^4$, where d_0 and d_4 represent the initial amount of non-deuterated and perdeuterated methane, respectively. The consumption of CH_4 and CD_4 as well as the formation of the different isotopomers of methane (d_1, d_2, d_3) were monitored by IR spectroscopy. CH_4, CDH_3, CD_2H_2, CD_3H and CD_4 show characteristic IR bands at 1347 cm^{-1} (CH_4), 1156 cm^{-1}, (CDH_3), 1090 cm^{-1} (CD_2H_2), 1034 cm^{-1} (CD_3H) and 994 cm^{-1} (CD_4). The isotopomeric composition of the gas phase was also measured by GC–MS at the end of the reaction. The determination of the isotopomeric distribution was evaluated by minimizing the sum of the square difference of the respective peaks of calculated theoretical and experimental spectra. The calculated theoretical spectra were generated by incrementing the selectivity of various relative amounts of d_0-, d_1-, d_2-, d_3- and d_4-methanes, which fragmentation patterns were taken from *Compilation of mass spectral data*, ed. A. Cornu and R. Massot, Heyden & Son Limited, London, 1966. The mass spectrum of a mixture of variously labelled methanes was considered according to a peak distribution in the range *m/z* 13–20.

‡ Changes in the intensity of the Ta–D vibration band are not easily observed since this band appears at the border of the spectral window of silica and is partially truncated.

1 R. H. Crabtree, *Chem. Rev.*, 1995, **95**, 987.
2 K. Morikawa, W. S. Benedict and H. S. Taylor, *J. Am. Chem. Soc.*, 1936, **58**, 1445; G. Parravano, E. F. Hammel and H. S. Taylor, *J. Am. Chem. Soc.*, 1948, **70**, 2269.
3 C. Kemball, *Adv. Catal.*, 1959, **11**, 223; L. Guczi and Z. Karpinski, *J. Catal.*, 1979, **56**, 438; J. A. Dalmon and C. Mirodatos, *J. Catal.*, 1984, **25**, 161; L. Quanzhi and Y. Amenomiya, *Appl. Catal.*, 1986, **23**, 173; V. Ponec and G. C. Bond, *Stud. Surf. Sci. Catal.*, 1995, **95**, 464; D. Profilet, A. P. Rothwell and I. P. Rothwell, *J. Chem. Soc., Chem. Commun.*, 1993, 42; I. P. Rothwell, personal communication.
4 (*a*) A. E. Shilov, *Activation and Functionalization of Alkanes*, ed. C. L. Hill, Wiley Interscience, New York, 1989; (*b*) W. D. Jones and J. A. Maguire, *Organometallics*, 1986, **5**, 590; (*c*) P. L. Watson, *J. Chem. Soc., Chem. Commun.*, 1983, 276; (*d*) P. L. Watson and G. W. Parshall, *Acc. Chem. Res.*, 1985, **18**, 51; (*e*) M. E. Thompson, S. M. Baxter, A. R. Bulls, B. J. Burger, M. C. Nolan, B. D. Santarsiero, W. P. Schaefer and J. E. Bercaw, *J. Am. Chem. Soc.*, 1987, **109**, 203.
5 S. L. Scott, J.-M. Basset, G. P. Niccolai, C. C. Santini, J.-P. Candy, C. Lécuyer, F. Quignard and A. Choplin, *New. J. Chem.*, 1994, **18**, 115.
6 V. Vidal, A. Théolier, J. Thivolle-Cazat, J.-M. Basset and J. Corker, *J. Am. Chem. Soc.*, 1996, **118**, 4595.
7 V. Vidal, A. Théolier, J. Thivolle-Cazat and J.-M. Basset, *J. Chem. Soc., Chem. Commun.*, 1995, 991.
8 M. Chabanas, V. Vidal, C. Copéret, J. Thivolle-Cazat and J.-M. Basset, *Angew. Chem., Int. Ed.*, 2000, in press.
9 V. Vidal, A. Théolier, J. Thivolle-Cazat and J.-M. Basset, *Science*, 1997, **276**, 99; V. Vidal, A. Théolier, J. Thivolle-Cazat and J.-M. Basset, CNRS, Fr. Pat. No. 96 09033, 1996 (*Chem. Abstr*. 1998, **128**, 129483a); O. Maury, L. Lefort, V. Vidal, J. Thivolle-Cazat and J. M. Basset, *Angew. Chem., Int. Ed.*, 1999, **38**, 1952.

ChemComm

Synthesis of a chiral adamantoid network— the role of solvent in the construction of new coordination networks with silver(I)

Alexander J. Blake, Neil R. Champness,* Paul A. Cooke and James E. B. Nicolson

School of Chemistry, The University of Nottingham, University Park, Nottingham, UK NG7 2RD. E-mail: Neil.Champness@nottingham.ac.uk

Received (in Cambridge, UK) 15th December 1999, Accepted 6th March 2000
Published on the Web 3rd April 2000

Depending on the crystallisation solvent used, reaction of 2,2′-bipyrazine with $AgBF_4$ results in the formation of either a chiral three-dimensional adamantoid coordination network or a two-dimensional sheet incorporating five coordinate Ag(I) ions.

Inorganic supramolecular chemistry and in particular the construction of polymeric coordination networks is an extremely topical area of research.[1] Chiral coordination polymers are particularly intriguing as such systems have potential future applications as stereoselective hosts for the separation of racemic mixtures. One of the most obvious methods of introducing chirality into coordination polymers is to use polymeric helicates and this method has been exploited to generate one-dimensional polymers.[2–4] Some of these polymeric helices spontaneously resolve through weak π–π[3] or H-bonding[4] interactions to give chiral three-dimensional structures within a given crystal. Structures formed through stronger metal–ligand bonds are rare[5] and resolution often relies upon weaker interactions[6] to induce the chirality within the system. We are interested in developing a strategy for preparing three-dimensional coordination polymers in which the chirality of the system is introduced *via* these more robust metal–ligand interactions, an integral feature of the network itself. We have targeted one of the most commonly studied structural motifs in coordination polymer chemistry, namely the adamantoid or super-diamondoid structure.[7,8] Such compounds, formed by the reaction of tetrahedral metal ions [*e.g.* Cu(I) or Ag(I)] with linear connecting units (*e.g.* 4,4′-bipyridyl), may not, at first, be an obvious choice. However, although conventionally considered to be built from edge-sharing adamantane units, such networks may also be thought of in terms of fused 4_1 and 4_3 helices.[8] These helices display opposing hands so that the conventional adamantoid structure does not exhibit chirality.

Our strategy was to see whether we could perturb the balance of these helices in order to remove the racemic nature of their orientation. In an attempt to achieve this, we have targeted a ligand system [2,2′-bipyrazine (bpyz)] which provides two different modes by which it can bridge adjacent metal centres. This ligand provides not only two independent types of binding sites, the chelating bidentate site and the two monodentate N-donor sites, but also two possible modes for bridging metal centres (Scheme 1). These two bridging modes provide a possible mechanism for generating two independent helices when reacted with a suitable metal centre and thus, potentially, an asymmetric adamantoid network. Two ligands which have a similar combination of one bidentate and two monodentate donor sites, 2,2′-bi-1,6-napthyridine and 5,5′-dicyano-2,2′-bipyridine, have previously been shown to generate one-dimensional helical structures with Cu(I)[9] and Ag(I)[10] in the elegant work of Janiak and coworkers but no examples of three-dimensional helical structures were prepared.

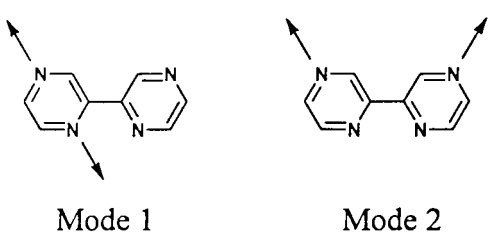

Scheme 1 Two possible bridging modes demonstrated by 2,2′-bipyrazine.

Single crystals of $\{[Ag(bpyz)](BF_4)\}_\infty$ were prepared by slow mixing of solutions of $AgBF_4$ and the ligand in $MeNO_2$, followed by diffusion of diethyl ether vapour into the homogeneous reaction solution.† Single crystal X-ray diffraction experiments‡ revealed that $\{[Ag(bpyz)](BF_4)\}_\infty$ crystallises in the chiral tetragonal space group $P4_32_12$ and that the Ag(I) centre is coordinated by one chelating ligand and by two monodentate N-donors from two further bpyz ligands in a distorted tetrahedral geometry. Each Ag(I) centre is linked to four nearest-neighbour Ag(I) centres, two *via* the chelating ligand and two more through the two monodentate pyrazine-like donors forming a distorted adamantoid array. Inspection of the extended lattice viewed down the *c*-axis confirms that the structure forms two distinct channels (A and B) which represent different helices running through the network (Fig. 1). The square-shaped channel, A (*ca.* 4.9 Å cross-section), runs through a 4_3 helix in which each Ag(I) centre is linked to the next Ag(I) centre along the helix through a pyrazine unit (bridging mode 1, Scheme 1) [Fig. 2(a)]. In contrast, the rhomboid-shaped channel, B (*ca.* 3.5 Å cross-section), runs through a 2_1 helix in which adjacent Ag(I) centres are linked through bridging mode 2 (Scheme 1) *via* two monodentate N-donor ligands [Fig. 2(b)]. Whereas in a conventional adamantoid lattice, adjacent helices which have opposing hands are chemically identical, in $\{[Ag(bpyz)](BF_4)\}_\infty$ adjacent anti-parallel helices are chemically distinct, displaying different bridging modes and different pitches. Therefore the structure of $\{[Ag(bpyz)](BF_4)\}_\infty$ has an overall chirality and represents the

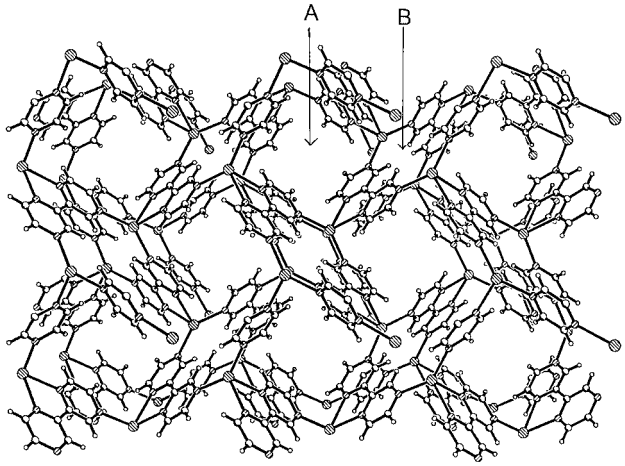

Fig. 1 View of the two different channels formed in $\{[Ag(bpyz)](BF_4)\}_\infty$. The square-shaped channels (A) are surrounded by the 4_3 helices and the rhomboid-shaped channels (B) by 2_1 helices (silver, left-hatch; nitrogen, right-hatch).

DOI: 10.1039/a909868b

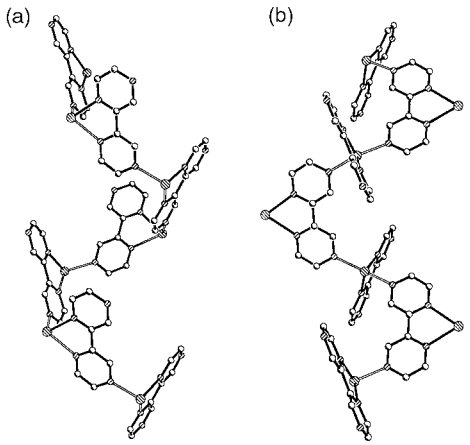

Fig. 2 (a) View, perpendicular to channel A, showing the 4_3 helix and illustrating the propagation of the channel periphery through bridging mode 1; (b) view, perpendicular to channel B, showing the 2_1 helix and illustrating propagation through bridging mode 2 (silver, left-hatch; nitrogen, right-hatch).

first example of a chiral adamantoid network. The channels are filled by BF_4^- counter-anions and $MeNO_2$ solvent molecules. Interestingly the BF_4^- anions sit exclusively in the channel generated by the 2_1 helix (channel B) leaving the more open channels generated by the 4_3 helix (channel A) open for solvent inclusion. This channel represents some 45.2%[11] of the total crystal volume and therefore this system appears promising for potential use as a chiral host material.

When single crystals were grown in an analogous manner but replacing non-coordinating $MeNO_2$ with the co-ordinating solvent MeCN, a different product, $\{[Ag(bpyz)(MeCN)](BF_4)\}_\infty$, was isolated. Single crystal X-ray diffraction experiments‡ show that this network adopts an entirely different structure. In this case, each Ag(I) centre coordinates a MeCN ligand leading to a distorted trigonal-bipyramidal Ag(I) environment. As with $\{[Ag(bpyz)](BF_4)\}_\infty$ each Ag(I) centre is coordinated by one chelating and two monodentate bpyz ligands resulting in each Ag(I) being linked to four nearest-neighbour Ag(I) junctions. However, in this case, the coordination of the MeCN ligand flattens the extended lattice to give a two-dimensional (4,4) sheet (Fig. 3). Each of these sheets undulates, with the MeCN ligands protruding from its surface resulting in interdigitation of adjacent $\{[Ag(bpyz)(MeCN)](BF_4)\}_\infty$ layers. The five-coordinate geometry observed here is rare for Ag(I), which prefers linear or tetrahedral coordination, and has only been observed three times before within coordination networks.[12]

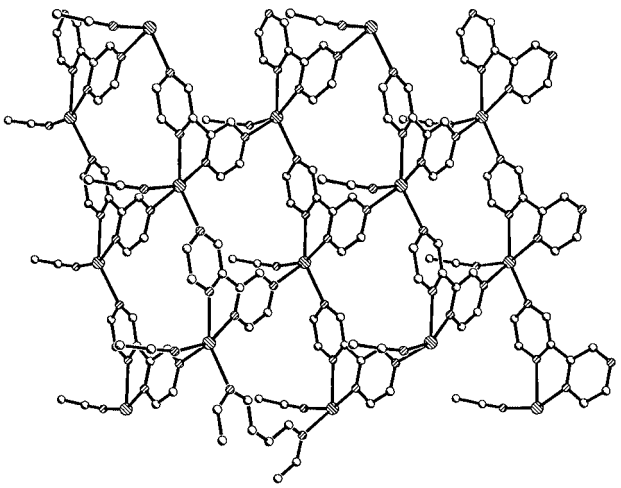

Fig. 3 View of the (4,4) two-dimensional sheet formed by $\{[Ag(bpyz)(MeCN)](BF_4)\}_\infty$ (silver, left-hatch; nitrogen, right-hatch).

In conclusion, we have shown that by using a ligand that can exhibit different bridging modes we can induce the formation of a chiral adamantoid network. The effect of solvent of crystallisation upon network structure has also been demonstrated by the formation of an extended two-dimensional lattice which incorporates five-coordinate Ag(I) centres. We are currently investigating whether the chirality of the adamantoid lattice can be controlled by the use of chiral anions.

We would like to thank the University of Nottingham (J. E. B. N.) and the EPSRC for support.

Notes and references

† *Experimental*: $\{[Ag(bpyz)](BF_4)\}_\infty$: a solution of $AgBF_4$ (10 mg, 0.05 mmol) in $MeNO_2$ (10 cm^3) was slowly diffused into a solution of 2,2′-bipyrazine {bpyz} (8 mg, 0.05 mmol) in $MeNO_2$ (10 cm^3) to give a homogeneous reaction solution. Diethyl ether was then diffused into the reaction solution affording colourless block crystals. Yield (8 mg, 44%). $\{[Ag(bpyz)(MeCN)](BF_4)\}_\infty$ was prepared analogously but replacing $MeNO_2$ with MeCN. Yield (54%). Satisfactory spectroscopic and analytical data were obtained.

‡ *X-Ray experimental, general procedures*: data for both compounds were collected on a Stoe Stadi-4 four-circle diffractometer using graphite monochromated Mo-Kα radiation (λ = 0.71073 Å). Hydrogen atoms were placed in geometrically calculated positions and allowed to ride on their parent atoms.

Crystal data: $\{[Ag(bpyz)](BF_4)\cdot 2MeNO_2\}_\infty$: $C_{10}H_{12}AgBF_4N_6O_4$, M = 474.94, tetragonal, space group $P4_32_12$ (no. 96), a = 11.396(7), c = 13.913(9) Å, U = 1807(2) $Å^3$, Z = 4, D_c = 1.746 g cm^{-3}, μ(Mo-Kα) = 1.183 mm^{-1}, T = 150(2) K. 1595 unique reflections (R_{int} = 0.0852) [1391 with $I > 2\sigma(I)$]. Final R = 0.0549, wR_2(all data) = 0.1262. Flack parameter = −0.12(12).

$\{[Ag(bpyz)(MeCN)](BF_4)\}_\infty$: $C_{10}H_9AgBF_4N_5$, M = 393.90, monoclinic, space group $P2_1/n$ (no. 14), a = 7.326(3), b = 18.423(6), c = 10.218(4) Å, U = 1356.7(9) $Å^3$, Z = 4, D_c = 1.531 g cm^{-3}, μ(Mo-Kα) = 1.531 mm^{-1}, T = 150(2) K. 2384 unique reflections, [1794 with $I > 2\sigma(I)$]. Final R = 0.0531, wR_2(all data) = 0.0913.

CCDC 182/1569. See http://www.rsc.org/suppdata/cc/a9/a909868b/ for crystallographic files in .cif format.

1 S. R. Batten and R. Robson, *Angew. Chem., Int. Ed.*, 1998, **37**, 1460; A. J. Blake, N. R. Champness, P. Hubberstey, W-S. Li, M. Schröder and M. A. Withersby, *Coord. Chem. Rev.*, 1999, **183**, 117.

2 P. K. Bowyer, K. A. Porter, A. D. Rae, A. C. Willis and S. B. Wild, *Chem. Commun.*, 1998, 1153; S. R. Batten, B. F. Hoskins and R. Robson, *Angew. Chem., Int. Ed. Engl.*, 1997, **36**, 636; C. Kaes, M. W. Hosseini, C. E. F. Rickard, B. W. Skelton and A. H. White, *Angew. Chem., Int. Ed.*, 1998, **37**, 920; B. Wum, W-J. Zhang, S-Y. Yu and X-T Wu, *J. Chem. Soc., Dalton Trans.*, 1997, 1795; O. J. Gelling, F. van Bolhuis and B. L. Feringa, *J. Chem. Soc., Chem. Commun.*, 1991, 917; Y. Dai, T. J. Katz and D. A. Nichols, *Angew. Chem., Int. Ed. Engl.*, 1996, **35**, 2109.

3 K. Biradha, C. Seward and M. J. Zaworotko, *Angew. Chem., Int. Ed.*, 1999, **38**, 492.

4 T. Ezuhara, K. Endo and Y. Aoyama, *J. Am. Chem. Soc.*, 1999, **121**, 3279.

5 K. Nakayama, T. Ishida, R. Takayama, D. Hashizume, M. Yasui, F. Iwasaki and T. Nogami, *Chem. Lett.*, 1998, 497; B. F. Abrahams, S. R. Batten, M. J. Grannas, H. Hamit, B. F. Hoskins and R. Robson, *Angew. Chem., Int. Ed.*, 1999, **38**, 1475; L. Carlucci, G. Ciani, P. Macchi and D. M. Proserpio, *Chem. Commun.*, 1998, 1837.

6 M. A. Withersby, A. J. Blake, N. R. Champness, P. Hubberstey, W-S. Li and M. Schröder, *Angew. Chem., Int. Ed. Engl.*, 1997, **36**, 2327.

7 A J. Blake, N. R. Champness, S. S. M. Chung, W.-S. Li and M. Schröder, *Chem. Commun.*, 1997, 1005, and references therein.

8 K. A. Hirsch, S. R. Wilson and J. S. Moore, *Chem. Eur. J.*, 1997, **3**, 765.

9 H-P. Wu, C. Janiak, L. Uehlin, P. Klüfers and P. Mayer, *Chem. Commun.*, 1998, 2637.

10 H-P. Wu, C. Janiak, G. Rheinwald and H. Lang, *J. Chem. Soc., Dalton Trans.*, 1999, 183; C. Janiak, L. Uehlin, H-P. Wu, P. Klüfers, H. Piotrowski and T. G. Scharmann, *J. Chem. Soc., Dalton Trans.*, 1999, 3121.

11 A. L. Spek, PLATON, *Acta Crystallogr., Sect. A*, 1990, **46**, C-34.

12 K. A. Hirsch, S. R. Wilson and J. S. Moore, *Inorg. Chem.*, 1997, **36**, 2960; L. Carlucci, G. Ciani, D. M. Proserpio and A. Sironi, *Angew. Chem., Int. Ed. Engl.*, 1995, **34**, 1895; G. K. H. Shimizu, G. D. Enright, C. I. Ratcliffe, J. A. Ripmeester and D. D. M. Rayner, *Angew. Chem., Int. Ed. Engl.*, 1997, **37**, 1407.

Bis(pentafluorophenyl)boron azide: synthesis and structural characterization of the first dimeric boron azide

Wolfgang Fraenk, Thomas M. Klapötke,* Burkhard Krumm and Peter Mayer

Department of Chemistry, Ludwig-Maximilians-University, Butenandtstr. 5-13 (D), D-81377 Munich, Germany. E-mail: tmk@cup.uni-muenchen.de

Received (in Cambridge, UK) 9th February 2000, Accepted 6th March 2000
Published on the Web 3rd April 2000

The reaction of $(C_6F_5)_2BCl$ with trimethylsilyl azide results in the formation of $(C_6F_5)_2BN_3$ 1; evaporation of the stabilizing solvent results in irreversible dimerization yielding $[(C_6F_5)_2BN_3]_2$ 1a as the first example of a dimeric boron azide; in the presence of pyridine a stable adduct $(C_6F_5)_2BN_3$·py 2 is isolated.

Extending the first report in boron azide chemistry by Wiberg and Michaud in 1954, Paetzold *et al*. has made remarkable contributions on this field.[1,2*a–e*] To our knowledge all of the liquid or solid boron azides reported in the literature are monomeric except for the trimeric boron dihalide azides $(BX_2N_3)_3$ (X = F, Cl, Br) and dimethylboron azide which shows a temperature dependent oligomerization.[3*a,b*] The structure of boron dichloride azide was determined by Müller in 1971, confirming the six-membered boron nitrogen heterocycle with diazo groups bound to nitrogen.[4] Here, we report on the synthesis and structural characterization of a novel dimeric boron azide, which can be considered as a *N*,*N*′-diazodiazadiboratacyclobutane.

Bis(pentafluorophenyl)boron chloride was reacted with trimethylsilyl azide in a toluene solution and the resulting mixture was monitored by NMR spectroscopy.† A single resonance was observed in the ^{11}B NMR spectrum at δ 43.9, in the region typical for three-coordinate boron. The ^{19}F NMR spectrum shows three signals for the pentafluorophenyl substituents at δ −131.4 (*o*-F), −146.4 (t, *p*-F, $^3J_{FF}$ 20.8 Hz) and −161.0 (*m*-F). In the ^{14}N NMR spectrum three resonances for covalent azide nitrogens are observed δ −144 (N_β), −160 (N_γ) and −322 (N_α).[5] The NMR data clearly indicate the formation of monomeric bis(pentafluorophenyl)boron azide **1**. After removal of the solvent, **1a** was obtained as a colorless solid which is insoluble in common organic solvents. For the NMR study of **1**, the reaction had to be performed in toluene or benzene as a solvent. In other solvents such as hexane, dichloromethane or chloroform, **1a** precipitated immediately.

The IR spectrum of solid **1a** shows a strong absorption at 2202 cm^{-1} which is the typical region for the asymmetric stretching vibration of azides.[6] However, in comparison to the corresponding asymmetric stretching vibration found for diphenylboron azide (2120 cm^{-1}), this vibration is significantly shifted to a higher wavenumber and is almost identical with that found for trimeric boron dichloride azide $(BCl_2N_3)_3$ (2210 cm^{-1}) which has bridging azides.[2*e*,7] In the Raman spectrum, $\nu_{as}(N_3)$ was found at 2209 cm^{-1} as a peak of medium intensity (Fig. 1).

A mass spectrum of **1a** recorded in the EI mode did not show a molecular ion peak M^+ and is therefore not expressive regarding a dimeric structure. The monomer **1** is visible, *m*/*z* = 387 (^{11}B), but N_2-abstraction of this fragment (**1** − N_2), typical for azides, is not observed.

The findings of the vibrational data indicate that **1a** is not monomeric in the solid state, which is in contrast to the structure of the starting material $(C_6F_5)_2BCl$ as determined by single X-ray diffraction techniques.[8] The solid state structure of **1a** (dimeric) has been determined by single crystal X-ray diffraction and confirmed the oligomeric skeleton proposed on the basis of vibrational (IR, Raman) spectroscopy (Fig. 2).‡

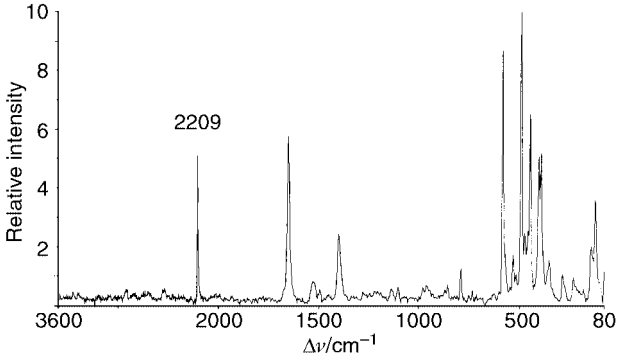

Fig. 1 Raman spectrum of **1a**.

Single crystals suitable for X-ray diffraction studies were obtained by cooling a concentrated solution of **1** in toluene. **1a** crystallized in the space group *C2/c* with four formula units in the unit cell. The B_2N_2 ring is planar with a B–N–B angle of 97.2(1)° and a N–B–N angle of 82.8(1)°. The B–N distances of 1.59/1.60 Å have typical B–N single bond character. The azide group is slightly bent with a N–N–N angle of 177.5(2)° which is in accord with the structures of other covalent boron azides previously determined.[2*b*,4,9*a,b*] The N1–N2 bond distance is 1.241(2) Å and comparable with the corresponding N–N distance found in $(BCl_2N_3)_3$ (1.25 Å); the N2–N3 distance is 1.113(3) Å indicating considerable triple bond character (N≡N 1.098 Å).[4,10*a–c*]

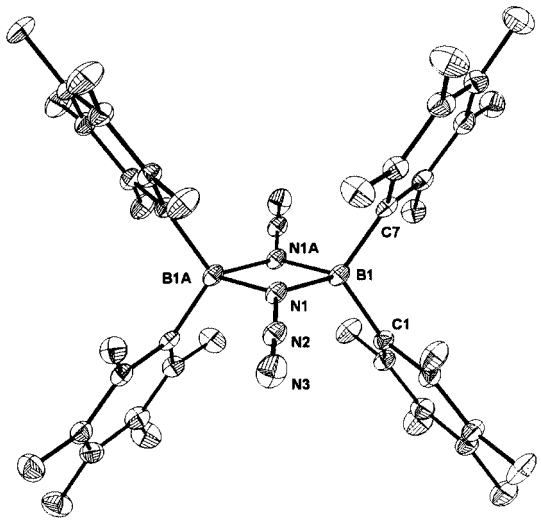

Fig. 2 ORTEP plot of the molecular structure of **1a** with thermal ellipsoids drawn at the 25% probability level. Selected bond lengths (Å) and angles (°): B(1)–N(1) 1.591(3), B(1A)–N(1) 1.601(2), N(1)–N(2) 1.241(2), N(2)–N(3) 1.113(3), B(1)–C(1) 1.607(3), C–F 1.33–1.35; N(1)–N(2)–N(3) 177.5(2), N(2)–N(1)–B(1) 130.3(2), N(1)–B(1)–N(1A) 82.8(1), B(1)–N(1)–B(1A) 97.2(1), C(7)–B(1)–C(1) 113.5(2), C(7)–B(1)–N(1) 115.2(2), C(1)–B(1)–N(1) 114.3(2), C(7)–B(1)–N(1A) 113.4(2).

DOI: 10.1039/b001103g

The results of the X-ray analysis, Raman and IR spectroscopy prove **1a** as the first example of a *N*,*N*′-diazodiazadiboratacyclobutane. The dimerization can be explained by the electronic character of the boron atom in **1**. The electron-withdrawing pentafluorophenyl substituents create a highly electron deficient boron atom which stabilizes itself to a borate **1a** with the formation of a σ-bond to the α-nitrogen atom of another molecule **1**.

The reaction was also carried out in the presence of pyridine yielding the new adduct $(C_6F_5)_2BN_3$·py **2** as a colorless solid [eqn. (1)].†

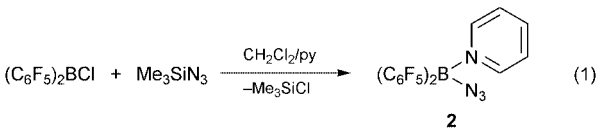

(1)

2

This adduct **2** is soluble in toluene, dichloromethane, diethyl ether and chloroform but insoluble in hexane. The IR spectrum shows a very strong absorption at 2137 cm^{-1} and the Raman spectrum shows a weak peak at 2138 cm^{-1} which can be assigned to the asymmetric stretching vibration of the azide group, and is comparable with those found in other reported adducts of this type [Ph_2BN_3·py $\nu_{as}(N_3)$ = 2110 cm^{-1}].[2e] The NMR data and elemental analysis are consistent with the product proposed in eqn. (1). The chemical shift for **2** [$\delta(^{11}B)$ −0.5] is in the region of four-coordinate boron, the ^{14}N NMR shows four resonances at δ −144 (N_β), −159 (N-py), −204 (N_γ) and −308 (N_α).

Further investigations of the chemistry of pentafluorophenyl substituted boron azides are in progress and will be reported in a full paper.

Financial support of this work by the University of Munich and the Fonds der Chemischen Industrie is gratefully acknowledged.

Notes and references

† *Experimental procedures*: **CAUTION** covalent azides are potentially explosive and safety precautions should be taken during work with azides. All manipulations were performed under an inert atmosphere of dry nitrogen using standard Schlenk techniques. All solvents were dried prior to use. Higher deviations from the theoretical values of the elemental analyses are common for boron azides [see refs. 9(*a*) and (*b*)].

1, **1a**: trimethylsilyl azide (1.0 mmol) was added to a solution of $(C_6F_5)_2BCl$ (1.0 mmol) in toluene (10 mL) at −78 °C. After stirring for 12 h at ambient temperature the solution was concentrated and cooled to −25 °C. The crystals of **1a** which formed, were found to be suitable for X-ray diffraction studies, were isolated and dried *in vacuo*. Yield 0.25 g, 65%, mp 73–76 °C (decomp.). Found: C, 38.6; N, 9.9. Calc. for $C_{24}B_2F_{20}N_6$: C, 37.3; N, 10.9%. IR/Raman: 2202vs/2209m [$\nu_{as}(N_3)$] cm^{-1}. ^{19}F NMR (376 MHz, toluene) δ −131.4 (m, *o*-F, 2F), −146.4 (t, *p*-F, 1F, $^3J_{FF}$ 20.8 Hz), −161.0 (m, *m*-F, 2F). ^{11}B NMR (128 MHz, toluene) δ 43.9. ^{14}N NMR (29 MHz, toluene, $\Delta\nu_{1/2}$/Hz) δ −144 (N_β, 220), −160 (N_γ, 300), −322 (N_α, 600).

2: compound **2** was prepared from $(C_6F_5)_2BCl$ (1.0 mmol), trimethylsilyl azide (1.0 mmol) and pyridine (1.0 mmol) in CH_2Cl_2 (10 mL) solution following the method described for **1**. Yield 0.37 g, 80%, mp 76–80 °C. Found: C, 43.2; H, 1.4; N, 11.3. Calc. for $C_{17}H_5BF_{10}N_4$: C, 43.8; H, 1.1; N, 12.0%. IR/Raman 2137vs/2138w [$\nu_{as}(N_3)$] cm^{-1}. ^{19}F NMR (376 MHz, $CDCl_3$) δ −134.1 (m, *o*-F, 2F), −154.7 (t, *p*-F, 1F, $^3J_{FF}$ 20.8 Hz), −162.3 (m, *m*-F, 2F). ^{11}B NMR (128 MHz, $CDCl_3$) δ −0.5. ^{14}N NMR (29 MHz, $CDCl_3$, $\Delta\nu_{1/2}$/Hz) δ −144 (N_β, 200), −159 (N-py, 350), −204 (N_γ, 300) −308 (N_α, 800).

‡ *Crystal data*: $C_{24}B_2F_{20}N_6$ **1a** M = 773.89, monoclinic, space group $C2/c$, a = 15.222(1), b = 10.6024(8), c = 16.895(2) Å, β = 99.73(1)°, V = 2687.4 (4) Å^3, Z = 4, μ(Mo-Kα) = 0.214 mm^{-1}, λ = 0.71073 Å, T = 200 K, 9071 reflections measured, 2545 unique (R_{int} = 0.107) which were used in all calculations. Final R indices [$I > 2\sigma(I)$], $R1$ = 0.055, $wR2$ = 0.135. The structure was solved using direct methods and refined by full-matrix least-squares on F^2. CCDC 182/1568. See http://www.rsc.org/suppdata/cc/b0/b001103g/ for crystallographic files in .cif format.

1 E. Wiberg and H. Michaud, *Z. Naturforsch.*, 1954, **96**, 497.
2 (*a*) P. I. Paetzold, *Z. Anorg. Allg. Chem.*, 1963, **326**, 47; (*b*) J. Mueller and P. I. Paetzold, *Heteroat. Chem.*, 1990, **1**, 461; (*c*) P. I. Paetzold, P. P. Habereder and R. Müllbauer, *J. Organomet. Chem.*, 1967, **7**, 45; (*d*) R. Hausser-Wallis, H. Oberhammer, W. Einholz and P. I. Paetzold, *Inorg. Chem.*, 1990, **29**, 3286; (*e*) P. I. Paetzold, *Fortsch. Chem. Forsch.*, 1967, **8**, 437.
3 (*a*) N. Wiberg, W.-Ch. Joo and K. H. Schmid, *Z. Anorg. Allg. Chem.*, 1972, **394**, 197; (*b*) P. I. Paetzold and H. J. Hansen, *Z. Anorg. Allg. Chem.*, 1966, **345**, 79.
4 U. Müller, *Z. Anorg. Allg. Chem.*, 1971, **382**, 110.
5 M. Witanowski, L. Stefaniak and G. A. Webb, *Annu. Rep. NMR Spectrosc.*, 1986, **18**, 486.
6 A. Schulz, I. C. Tornieporth-Oetting and T. M. Klapötke, *Inorg. Chem.*, 1995, **34**, 4343.
7 P. I. Paetzold, M. Gayoso and K. Dehnicke, *Chem. Ber.*, 1965, **98**, 1173.
8 W. E. Piers, R. E. von H. Spence, L. R. MacGillivray and M. J. Zaworotko, *Acta Crystallogr., Sect. C*, 1995, **51**, 1688.
9 (*a*) W. Fraenk, T. Habereder, T. M. Klapötke, H. Nöth and K. Polborn, *J. Chem. Soc., Dalton Trans.*, 1999, 4283; (*b*) R. T. Paine, W. Koestle, T. T. Borek, E. N. Duesler and M. A. Hiskey, *Inorg. Chem.*, 1999, **38**, 3738.
10 (*a*) T. M. Klapötke, *Chem. Ber.*, 1997, **130**, 443; (*b*) I. C. Tornieporth-Oetting and T. M. Klapötke, *Angew. Chem., Int. Ed. Engl.*, 1995, **34**, 511; (*c*) P. S. Ganguli and H. A. Mc Gee, Jr., *Inorg. Chem.*, 1972, **11**, 3072.

Facile synthesis of α-amino phosphonates in water using a Lewis acid–surfactant-combined catalyst

Kei Manabe and Shū Kobayashi*

Graduate School of Pharmaceutical Sciences, The University of Tokyo, CREST, Japan Science and Technology Corporation (JST), Hongo, Bunkyo-ku, Tokyo 113-0033, Japan. E-mail: skobayas@mol.f.u-tokyo.ac.jp

Received (in Cambridge, UK) 7th January 2000, Accepted 6th March 2000
Published on the Web 30th March 2000

Three-component reactions of aldehydes, amines and triethyl phosphite were efficiently catalyzed by scandium tris(dodecyl sulfate) at ambient temperature in water to give various α-amino phosphonates in high yields.

α-Amino phosphonates constitute an important class of biologically active compounds, and their synthesis has been a focus of considerable attention in synthetic organic chemistry as well as in medicinal chemistry.[1] Most synthetic methods reported utilize reactions of imines with phosphorus nucleophiles. Recently, it has been shown that three-component reactions of aldehydes (or ketones), amines, and diethyl phosphite [HOP(OEt)$_2$] were efficiently promoted by catalytic amounts of Lewis acids such as ytterbium triflate[2] and indium chloride[3] in dichloromethane (CH_2Cl_2) or THF at ambient temperature. Although these procedures do not require the isolation of the unstable imines prior to the reactions, reaction times of longer than 10 h are necessary to obtain the desired products in good yields at room temperature. In addition, the use of harmful organic solvents such as CH_2Cl_2 is undesirable from the viewpoint of today's environmental consciousness.

In the course of our investigations to develop environmentally friendly synthetic methods, we have found that surfactant-type Lewis acids function as effective catalysts for aldol reactions in water without using organic solvents.[4] The catalysts, which we denote Lewis acid–surfactant-combined catalysts (LASCs), consist of Lewis acidic metal cations such as scandium(III) and amphiphilic anions such as dodecyl sulfate, and form stable colloidal dispersions in the presence of organic substrates in water. Here we report that scandium tris(dodecyl sulfate) **1**, a representative LASC, effectively catalyzes three-component reactions of aldehydes, amines and triethyl phosphite [P(OEt)$_3$] in water to give α-amino phosphonates in high yields.

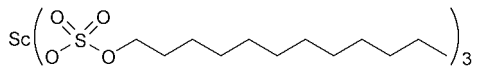

1

First, the reaction of benzaldehyde, benzhydrylamine and P(OEt)$_3$ was tested as a model reaction in the presence of various catalysts in water (Table 1). When LASC **1** was used as a catalyst, the reaction proceeded smoothly to afford the desired product **2** in good yield (entry 1). On the other hand, sodium dodecyl sulfate (SDS) or scandium triflate gave **2** in very low yields (entries 2 and 3). These results indicate that both the Lewis acidic cation and the anionic surfactant are indispensable for the efficient catalysis. LASC **1** was much superior to dodecylbenzenesulfonic acid (DBSA, entry 4), a surfactant-type Brønsted acid which has been successfully used for three-component Mannich-type reactions in water.[5] Furthermore, the reaction under neat conditions without any solvents proceeded slowly (entry 5), indicating that water as a solvent plays an essential role for acceleration of the reaction. It was interesting to find that a reaction with HOP(OEt)$_2$, which has been used as a phosphorus nucleophile in the Lewis acid-catalyzed synthesis of α-amino phosphonates in organic solvents,[2,3] scarcely proceeded (entry 6). Thus, the use of P(OEt)$_3$ instead of HOP(OEt)$_2$ is a characteristic of our system. Mechanistically, P(OEt)$_3$ attacks an imine, which is formed from an aldehyde and an amine *in situ* and then activated by the Lewis acid, to generate phosphonium intermediate **3**. In contrast to the reactions in organic solvents, hydrolysis of **3** to the corresponding phosphonate should occur rapidly in water without causing any side reactions. This rapid hydrolysis makes the use of P(OEt)$_3$ possible in the present catalytic system. Unfortunately, an excess of P(OEt)$_3$ is needed at the present stage, since it is gradually hydrolyzed to HOP(OEt)$_2$ in water. Under the same reaction conditions as those in entry 1, the reaction in the absence of the amine afforded only a trace amount of diethyl 1-hydroxy-1-phenylmethylphosphonate. This result indicates that imines are activated by **1** more effectively than aldehydes.

Table 1 Three-component synthesis of α-amino phosphonate **2** in water

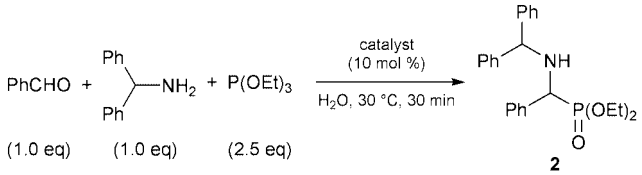

Entry	Catalyst	Yield(%)
1	**1**	71
2	SDS (30 mol %)	8
3	Sc(OTf)$_3$	6
4	DBSA	18
5[a]	**1**	31
6[b]	**1**	Trace

[a] Under neat conditons. [b] HOP(OEt)$_2$ (2.5 eq.) was used instead of P(OEt)$_3$.

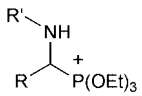

3

The reactions of various aldehydes and amines with P(OEt)$_3$ in the presence of **1** in water gave the corresponding α-amino phosphonates in high yields as shown in Table 2.† Not only benzaldehyde (entries 1–6) but also other aromatic (entries 7 and 8), heteroaromatic (entry 9) and aliphatic aldehydes (entries 10 and 11) worked well to give the phosphonates in high yields, although α,β-unsaturated aldehydes such as cinnamaldehyde (entry 12) afforded the desired products in lower yields. A characteristic point of these reactions is the extremely short reaction time. When using aniline-type amines such as aniline

Table 2 Three-component synthesis of α-amino phosphonates in water

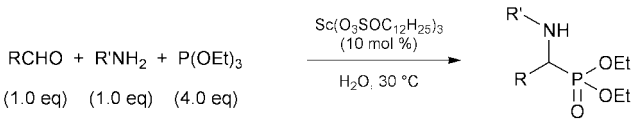

Entry	RCHO	R'NH$_2$	*t*/min	Yield (%)
1	PhCHO	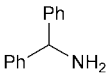	60	83
2	PhCHO	PhNH$_2$	20	88
3	PhCHO	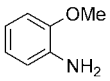	20	86
4	PhCHO	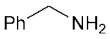	60	84
5	PhCHO	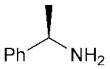	60	78[a]
6	PhCHO	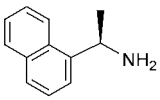	60	80[b]
7	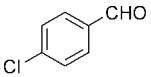	PhNH$_2$	30	85
8	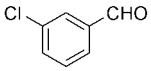	PhNH$_2$	20	80
9	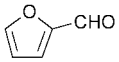	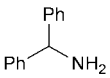	120	78
10	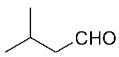	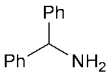	60	83
11	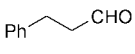	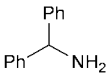	60	95
12	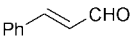	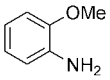	20	53

[a] 56% de. [b] 61% de.

and *o*-anisidine, the reaction proceeded rapidly, and > 80% yields of the products were attained in 20–30 min (entries 2, 3, 7, and 8). Thus, the turnover frequencies (TOFs) for these reactions are 17–26 h^{-1}, in contrast to the reported procedures in organic solvents, in which the TOFs are < 1 h^{-1}.[2,3] While several organic reactions in water have been developed so far,[6] most of them proceeded slowly in water compared with the corresponding synthetic methods in organic solvents. It is noted that the use of an LASC, a new type of Lewis acid, creates excellent hydrophobic reaction fields to realize the rapid three-component reactions in water. Use of chiral amines, (*R*)-1-phenylethylamine and (*R*)-1-(1-naphthyl)ethylamine, resulted in modest diastereoselectivities (entries 5 and 6).

In conclusion, three-component reactions of aldehydes, amines and triethyl phosphite were effectively catalyzed by LASC **1** to give various α-amino phosphonates in high yields. It should be noted that these high yields were obtained in water, at ambient temperature, and at high reaction rates. This reaction system not only provides a novel method for the synthesis of biologically important α-amino phosphonates but also extends the applicability of LASCs in organic synthesis in water to lead to environmentally friendly chemical processes.

Notes and references

† *General procedure* for the synthesis of α-amino phosphonates: an amine (0.25 mmol), an aldehyde (0.25 mmol) and $P(OEt)_3$ (1.0 mmol) were successively added to a mixture of LASC **1** (0.025 mmol, 10 mol%) in water (1.5 mL) at 30 °C. The mixture was stirred at the same temperature for 20–120 min, and then 1 M NaOH (5 mL) was added. After stirring at room temperature for 15–30 min, brine (5 mL) was added, the mixture extracted with ethyl acetate (30 mL), dried over Na_2SO_4, and concentrated. Purification by silica gel chromatography afforded the desired product.

1 F. Heaney, in *Comprehensive Organic Functional Group Transformations*, ed. A. R. Katritzky, O. Meth-Cohn and C. W. Rees, Elsevier Science, Oxford, 1995, vol. 4, ch. 4, 10; S. C. Fields, *Tetrahedron*, 1999, **55**, 12 237; E. K. Fields, *J. Am. Chem. Soc.*, 1952, **74**, 1528; R. Tyka, *Tetrahedron Lett.*, 1970, 677; G. H. Birum, *J. Org. Chem.*, 1974, **39**, 209; I. J. W. Huber and M. Middlebrooks, *Synthesis*, 1977, 883; D. Redmore, *J. Org. Chem.*, 1978, **43**, 992; K. Afarinkia, J. I. G. Cadogan and C. W. Rees, *Synlett*, 1990, 415; C. Yuan and S. Chen, *Synthesis*, 1992, 1124; S. Laschat and H. Kunz, *Synthesis*, 1992, 90.

2 C. Qian and T. Huang, *J. Org. Chem.*, 1998, **63**, 4125.

3 R. C. Ranu, A. Hajra and U. Jana, *Org. Lett.*, 1999, **1**, 1141.

4 S. Kobayashi and T. Wakabayashi, *Tetrahedron Lett.*, 1998, **39**, 5389; K. Manabe and S. Kobayashi, *Synlett*, 1999, 547; K. Manabe, Y. Mori and S. Kobayashi, *Tetrahedron*, 1999, **55**, 11 203; K. Manabe and S. Kobayashi, *Tetrahedron Lett.*, 1999, **40**, 3773.

5 K. Manabe, Y. Mori and S. Kobayashi, *Synlett*, 1999, 1401; K. Manabe and S. Kobayashi, *Org. Lett.*, 1999, **1**, 1965.

6 *Organic Synthesis in Water*, ed. P. A. Grieco, Blacky Academic and Professional, London, 1998.

ChemComm

Site-directed mutagenesis of dienelactone hydrolase produces dienelactone isomerase

Ian Walker, Christopher J. Easton* and David L. Ollis*

Research School of Chemistry, Australian National University, Canberra ACT 0200, Australia.
E-mail: easton@rsc.anu.edu.au; ollis@rsc.anu.edu.au

Received (in Cambridge, UK) 10th January 2000, Accepted 6th March 2000
Published on the Web 31st March 2000

Replacing the active site Cys-123 of dienelactone hydrolase with Ser completely changes the catalysis displayed by the protein, from hydrolysis of the substrate *E*- and *Z*-dienelactones to maleylacetate by the native enzyme, to interconversion of the substrates by the mutant, dienelactone isomerase.

Dienelactone hydrolase (EC 3.1.1.45) from *Pseudomonas* sp. B13 (DLH Type III) catalyses the hydrolysis of the *E*- and *Z*-dienelactones **1** and **2** to give maleylacetate **3** (Scheme 1),[1] as part of the chlorocatechol branch of the β-ketoadipate pathway for the biodegradation of toxic aromatic compounds.[2] The activity of DLH derives from a catalytic triad of amino acids at its active site, comprising Cys-123 aligned for nucleophilic attack on the substrates by the adjacent His-202 and Asp-171 residues.[3,4] This triad is a hybrid of those found in cysteine (Cys-His-Asn)[5] and serine (Ser-His-Asp)[6] proteases, and has been observed in human and yeast ubiquitin *C*-terminal hydrolase[7] and engineered in mutant serine proteases such as thiol-subtilisin[8] and thiol-trypsin.[9] The mechanism of catalysis by DLH has been elucidated primarily through crystallographic analysis of both the native protein and several of its site specific mutants.[10] In one mutant (C123S), Cys-123 was replaced with Ser, to produce the catalytic triad found in serine proteases. We now report that this mutation completely changes the catalysis displayed by the protein, from hydrolysis of the substrates **1** and **2** by DLH to catalysis of their isomerisation by the mutant protein, dienelactone isomerase (DLI).

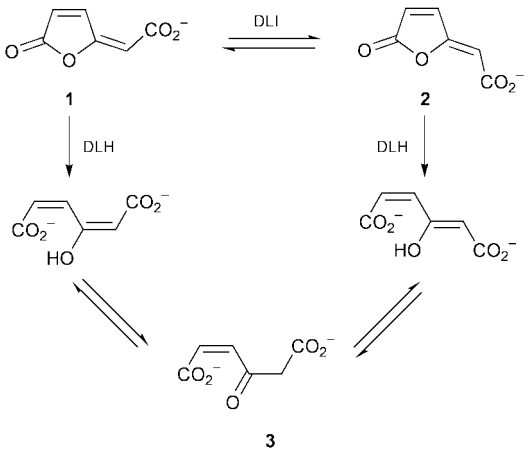

Scheme 1

The synthesis of the lactones **1** and **2**[11] and the procedures used to obtain the native and mutant proteins, DLH and DLI,[3,4,10] have been reported previously. The reactions of the proteins with the substrates **1** and **2** were examined in 0.02 mol dm^{-3} HEPES buffer containing 0.001 mol dm^{-3} EDTA, at pH 7.0 and 298 K. The products were characterised using HPLC and a diode array detector, thin layer chromatography and ^{1}H NMR spectrometry, by comparison with authentic samples. The kinetics of the reactions were studied by HPLC and by monitoring changes in absorbance at 280 nm by UV spectroscopy. The lactones **1** and **2** have λ_{max} values of 276 (ε 17200) and 277 (ε 17550 dm^3 mol^{-1} cm^{-1}) nm, and ε values of 17000 and 15625 dm^3 mol^{-1} cm^{-1} at 280 nm, respectively, while maleylacetate **3** shows negligible absorbance in this region.[1,12]

The effects of DLH and DLI on the dienelactones **1** and **2** are illustrated in Fig. 1 and the K_m and k_{cat} values characterising these interactions are summarised in Table 1. Hydrolysis of each of the lactones **1** and **2** is catalysed efficiently by DLH and there is no evidence of isomerisation of the substrates in the presence of this enzyme. In complete contrast, DLI catalyses the interconversion of the lactones **1** and **2**, to the equilibrium mixture where they are present in the ratio 53 : 47, and little hydrolysis of either substrate **1** or **2** is discernible, even long after equilibration of the substrates **1** and **2** is complete. On this basis, the k_{cat} values for hydrolysis of the lactones **1** and **2** by DLI are at least 100-fold less than those for substrate isomerisation.

Table 1 Kinetic parameters for interaction of DLH and DLI with the lactones **1** and **2**[a]

Enzyme	Substrate	k_{cat}/s^{-1}	10^3 K_m/mol dm^{-3}
DLH	**1**	14 ± 1 (9.2)[b]	0.20 ± 0.015 (0.17 ± 0.007)[b]
DLH	**2**	19 ± 0.2 (30)[c]	0.011 ± 0.001 (0.016)[c]
DLI	**1**	0.63 ± 0.03	4.4 ± 0.10
DLI	**2**	0.18 ± 0.003	2.7 ± 0.13

[a] In 0.02 mol dm^{-3} HEPES buffer containing 0.001 mol dm^{-3} EDTA, at pH 7.0 and 298 K. [b] Data from ref. 4. [c] Data from refs. 1 and 13.

The contrasting behaviour of DLH and DLI is not due simply to substrate isomerisation and hydrolysis by DLH and substrate isomerisation without hydrolysis by DLI. Hydrolysis of the *Z*-lactone **2** by DLH is catalysed *ca.* 25 times more efficiently (k_{cat}/K_m) than that of the *E*-isomer **1** under the conditions of this study. Isomerisation accompanying hydrolysis of the *E*-lactone **1** by DLH would therefore be expected to result in a build-up in the concentration of the *Z*-isomer **2**, until its proportion of the residual lactones **1** and **2** approached at least 4%. Isomerisation

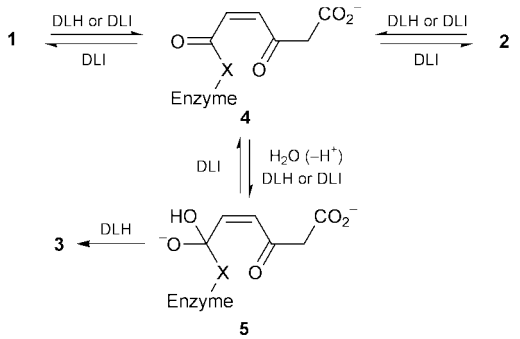

Scheme 2 (a) DLH, X = S; (b) DLI, X = O.

DOI: 10.1039/b000365o

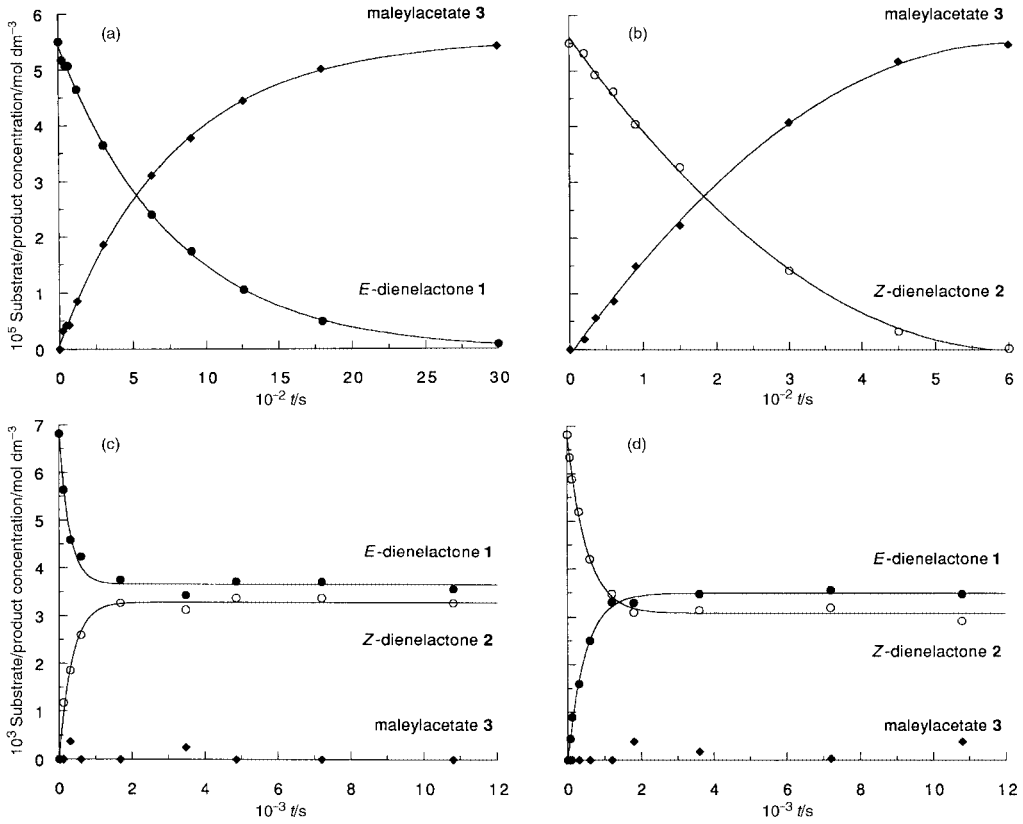

Fig. 1 Concentrations[a] of the *E*-dienelactone **1** (●), the *Z*-isomer **2** (○) and maleylacetate **3** (◆) in mixtures obtained by treatment[b] of (a) the lactone **1** with DLH (2×10^{-8} mol dm^{-3}), (b) the lactone **2** with DLH (1.2×10^{-8} mol dm^{-3}), (c) the lactone **1** with DLI (1.07×10^{-5} mol dm^{-3}), and (d) the lactone **2** with DLI (1.07×10^{-5} mol dm^{-3}). [a] Determined by HPLC. [b] In 0.02 mol dm^{-3} HEPES buffer containing 0.001 mol dm^{-3} EDTA, at pH 7.0 and 298 K.

of the *Z*-lactone **2** by DLH would be expected to lead to the accumulation of an even larger proportion of the *E*-isomer **1**, at least up to the equilibrium value of 53%. Such proportions (even the 4%) are well above the limits of detection, so there is no indication that DLH catalyses substrate isomerisation, only substrate hydrolysis. With DLI, substrate isomerisation occurs without hydrolysis.

The reactions of the lactones **1** and **2** with DLH involve formation of the thioester intermediate **4a** (Scheme 2).[10] In principle, DLI could react in a quite different manner, by reversible Michael addition of the enzyme's active site serine to the enolic carbon of the substrates **1** and **2**, with isomerisation. However, this mechanism seems implausible, since a similar process involving the thiolate of DLH would be more likely to lead to isomerisation if that was the case, and the distance between the serine oxygen of DLI and the enolic carbon of the substrates **1** and **2** is likely to be too great. The crystal structure of the lactam analogue of the lactone **2** bound in the active site of DLI indicates that this distance is 4.2 Å.[10] Thus it seems more reasonable that DLI reacts *via* the ester intermediate **4b** (Scheme 2). The lack of hydrolysis of this species may indicate that water is not available, at least in the necessary orientation, in the active site of the mutant protein. Alternatively, it could be due to non-productive collapse of the tetrahedral intermediate **5b**.[14] Whereas the intermediate **5a** will readily collapse with loss of the thiolate group, to give maleylacetate **3**, the analogous serine derivative **5b** should most readily lose hydroxide to revert to the ester **4b**, which could then recyclise. By analogy, with UDP-glucose dehydrogenase it has been found that the Ser mutant, obtained by displacing the active site Cys-260, reacts with the substrate to give an acyl enzyme, that is less labile towards hydrolysis than the corresponding putative thioester formed from the native protein.[15] However, the UDP-glucose dehydrogenase mutant is not active catalytically, unlike the situation with DLH and DLI, where both proteins are catalysts but of different processes. Irrespective of the mechanism, this difference between DLH and DLI is clear. The reaction of DLI with the lactone **1** affords ready access to the isomer **2**, and the general utility of this interconversion is currently being explored.

We are grateful to J. B. Kelly for assisting with the preparation of the *Z*-lactone **2**.

Notes and references

1 E. Schmidt and H.-J. Knackmuss, *Biochem. J.*, 1980, **192**, 339.
2 L. N. Ornston and W.-K. Yeh, in *Biodegradation of Environmental Pollutants*, ed. A. M. Chakrabarty, CRC Press, Boca Raton FL, 1982, pp. 105–126.
3 D. Pathak and D. Ollis, *J. Mol. Biol.*, 1990, **214**, 497.
4 D. Pathak, G. Ashley and D. Ollis, *Proteins: Struct. Funct. Genet.*, 1991, **9**, 267.
5 J. Drenth, J. N. Jansonius, R. Koekoek and B. G. Wolthers, *Adv. Protein Chem.*, 1971, **25**, 79; I. G. Kamphuis, K. H. Kalk, M. B. A. Swarte and J. Drenth, *J. Mol. Biol.*, 1984, **179**, 233.
6 C. S. Wright, R. A. Alden and J. Kraut, *Nature (London)*, 1969, **221**, 235; D.M. Blow, J. J. Birktoft and B. S. Hartley, *Nature (London)*, 1969, **221**, 337.
7 S. C. Johnston, C. N. Larsen, W. J. Cook, K. D. Wilkinson and C. P. Hill, *EMBO J.*, 1997, **16**, 3787; S. C. Johnson, S. M. Riddle, R. E. Cohen and C. P. Hill, *EMBO J.*, 1999, **18**, 3877.
8 L. Polgar and M. L. Bender, *J. Am. Chem. Soc.*, 1966, **88**, 3153; K. E. Neet and D. E. Koshland, *Proc. Natl. Acad. Sci. USA*, 1966, **56**, 1606.
9 H. Yokosawa, S. Ojima and S. Ishii, *Biochemistry J. Jpn.*, 1977, **82**, 869; J. N. Higaki, L. B. Evnin and C. S. Craik, *Biochem.*, 1989, **28**, 9256.
10 E. Cheah, C. Austin, G. W. Ashley and D. Ollis, *Protein Eng.*, 1993, **6**, 575; E. Cheah, G. W. Ashley, J. Gary and D. Ollis, *Proteins: Struct. Funct. Genet.*, 1993, **16**, 64.
11 R. A. Massy-Westropp and M. F. Price, *Aust. J. Chem.*, 1980, **33**, 333.
12 M. Schlömann, E. Schmidt and H.-J. Knackmuss, *J. Bacteriol.*, 1990, **172**, 5112.
13 K.-L. Ngai, M. Schlömann, H.-J. Knackmuss and L. N. Ornston, *J. Bacteriol.*, 1987, **169**, 699.
14 M. E. Wilke, J. N. Higaki, C. S. Craik and R. J. Fletterick, *J. Mol. Biol.*, 1991, **219**, 511.
15 X. Ge, R. E. Campbell, I. van de Rijn and M. E. Tanner, *J. Am. Chem. Soc.*, 1998, **120**, 6613.

trans-Dichloro(stilbazole)(methyl *n*-alkyl sulfoxide)platinum(II) complexes: the first examples of metallomesogens containing chiral centres directly bonded to the metal

Francesco Paolo Fanizzi,*[a] Vincenzo Alicino,[a] Cosimo Cardellicchio,[b] Paolo Tortorella[b] and Jonathan P. Rourke*[c]

[a] *Dipartimento Farmaco-Chimico, Università di Bari, via E. Orabona 4, I-70125, Bari, Italy. E-mail: fanizzi@farmchim.uniba.it*
[b] *CNR Centro di Studio sulle Metodologie Innovative di Sintesi Organica, Dipartimento di Chimica, Università di Bari, via G. Amendola 173, I-70126, Bari, Italy*
[c] *Department of Chemistry, University of Warwick, Coventry, UK CV4 7AL. E-mail: j.rourke@warwick.ac.uk*

Received (in Cambridge, UK) 21st January 2000, Accepted 8th March 2000
Published on the Web 31st March 2000

The first examples of enantiomerically pure metallomesogens containing the chiral centre directly bonded to the metal are reported; the chiral complexes show different phase behaviour to the racemic modifications.

There are many examples of chiral liquid crystals. Since the properties that chirality can confer to liquid crystals, such as ferroelectricity, are very attractive for technological applications, interest in chiral liquid crystals is more than purely academic. Whilst there has been an upsurge of interest in metal containing liquid crystals (metallomesogens) over the last two decades,[1–3] there have been relatively few examples of chiral metallomesogens. Most of these metallomesogens have relied on a chiral centre remote from the central core of the molecule to induce the asymmetry.[4–8] To date, no-one has fully investigated the effect of directly bonding a chiral centre to a metal within the metallomesogen. Early examples include a family of platinum stilbazole alkene complexes which proved to be unresolvable,[9,10] and a family of ruthenium bipyridyl compounds, where no attempt was made to separate enantiomers.[11]

Sulfoxides are widely used as ligands in platinum chemistry, normally bonding through the sulfur. Chiral sulfoxides with two different substituents are configurationally stable, and can be resolved into enantiomers.[12,13] Thus chiral sulfoxides, with two different alkyl chains, present themselves as ideal ligands for platinum based metallomesogens. By using a stilbazole ligand to complete the coordination sphere of the platinum, we can prepare direct analogues of the alkene complexes reported earlier.[9,10] It has been shown that such a highly unsymmetrical structure can be very beneficial, with reductions in the melting and clearing points of up to 100 K.

Enantiomerically pure methyl(*n*-alkyl)sulfoxides are available[14] and the methodology for the synthesis of appropriate platinum complexes is well understood. Crucially, the chirality at the sulfur has been shown to be configurationally stable on coordination to platinum with no racemisation observed even on ligand displacement.[15] Thus, using both racemic and enantiomerically pure sulfoxides we were able to isolate the required neutral complexes in a simple two step procedure, in effectively quantitative yield (Scheme 1).† Recrystallization of the products in diethyl ether–chloroform gave analytically pure samples which were analysed by NMR,‡ elemental analysis,§ polarimetry,¶ DSC and hot-stage polarised optical microscopy (Table 1).

All the new complexes reported here showed mesogenic behaviour at accessible temperatures. The phase behaviour of the new complexes is listed in Table 1 and summarised in Fig. 1. Thus it can be seen that all the complexes showed a melting transition into a mesophase at around 70 °C and cleared into the isotropic between 120 and 135 °C.

The most significant observation is the difference between the thermal behaviour of the racemic and chiral forms. The racemic compounds clearly exhibit two mesophases: a highly

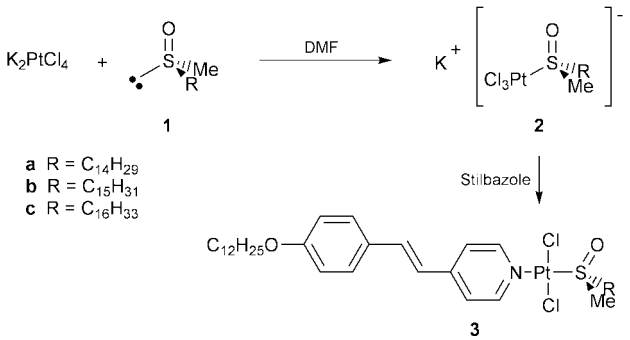

Scheme 1

Table 1 Thermal behaviour of compounds **3**

	Racemic	*T*/°C	Δ*H*/J g^{-1}	Chiral	*T*/°C	Δ*H*/J g^{-1}
3a	K–SmG	69.9	25.9	K–SmF	87.2	31.6
	SmG–SmF	72.5	25.7	K–I	128.3	38.6
	SmF–I	124.5	101.3			
3b	K–SmG	80.9	20.8	K–K′	75.4	5.4
	SmG–SmF	84.4	20.0	K′–SmF	92.6	24.6
	SmF–I	126.1	76.7	SmF–I	129.3	40.9
3c	K–SmG	74.8	17.6	K–K′	72.3	2.3
	SmG–SmF	85.1	17.4	K′–SmF	84.3	25.4
	SmF–I	118.6	63.3	SmF–I	121.7	28.5

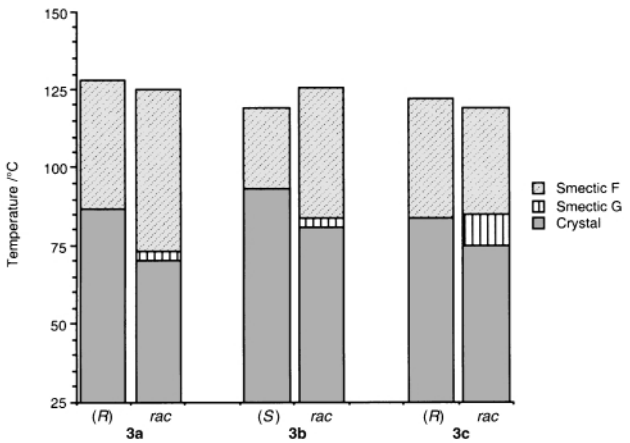

Fig. 1 Phase behaviour of compounds **3**.

DOI: 10.1039/b000594k

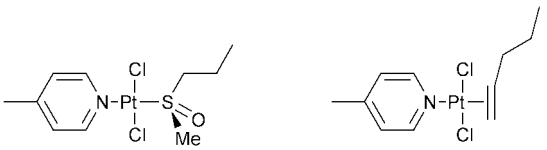

Fig. 2

ordered crystal smectic G followed by a smectic F‖ at higher temperatures, whereas the enantiomerically pure compounds only exhibit the smectic F phase. The melting points of the enantiomerically pure compounds are all about 10 K higher than the racemic compounds, though the clearing points are much more similar.

That the melting points of the chiral and racemic forms show a large difference is not totally unexpected: the packing arrangements within the crystal forms (assuming that the racemic form crystallises with both enantiomers present in the unit cell) must be substantially different—thus the melting points must be different. The presence of a short lived crystal smectic G for the racemic form at a temperature before the enantiomerically pure compound even melts can also be attributed to the differing crystal forms. At higher temperatures the molecules are much more mobile, therefore the intermolecular forces are more of an average, and thus less dependent on the precise structure of the molecule. Hence, the effect of enantiopurity on thermal behaviours is reduced and the final transition to the isotropic liquid is much the same for both racemic and enantiomerically pure compounds.

This type of effect has been seen on a number of occasions with organic compounds, with perhaps the most graphic demonstration being the existence of the so-called twist grain boundary phases,[16] though such a large effect has never been observed before with metallomesogens. This is almost certainly due to the presence of the chiral centre directly bonded to the mesogenic core, rather than remote on a chain. One group have reported the use of chiral carboxylates to bridge palladium centres within a dimeric metallomesogen, which gives rise to blue phases which would not have been present in the racemic mixtures.[8]

The alkene complexes reported earlier[9,10] typically melt into a smectic A phase at around 50 °C which persists until clearing at a temperature of around 90 °C. Thus the mesogenic range of the new sulfoxide complexes is greater than that of alkene complexes reported earlier, albeit at a slightly higher temperature. However, the major difference is the observation of the more ordered smectic F phases with the sulfoxide complexes, compared to the relatively disordered smectic A phase for the alkene complexes. This difference is highly significant, as it implies much stronger lateral interactions between the sulfoxide complexes than between the alkene complexes. Simplistically, one could ascribe this difference to one or both of two factors: the steric arrangement around the platinum, or the electronic effects of the different ligands. The geometry of a coordinated sulfoxide at platinum is known to approximate to a tetrahedral sulfur,[17] thus resulting in a compact arrangement and allowing the long chains to freely lie along the main axis of the molecule. In contrast, a coordinated alkene bonds *via* a face-like interaction, resulting in the alkyl chain being forced away from the main axis of the molecule (Fig. 2). Thus these steric factors would suggest the sulfoxide complexes would be able to achieve the greater lateral interactions necessary for the smectic F phase, whereas the alkene complexes could not. The major electronic difference between the two families relates to the sulfur–oxygen double bond. However since this bond is known to only be weakly polarised, any dipole that arises is almost certainly insignificant. Changing the sulfoxide for the alkene also has some effect on the melting point—the octadecene (effectively a 16 carbon chain) complex has a melting point of 64 °C compared with 75 °C for the racemic C-16 sulfoxide **1c** and 84 °C for the chiral analogue. The corresponding clearing points are 88 °C for the octadecene, and 119 and 122 °C for the racemic and chiral sulfoxides, respectively. Once again the most probable cause of the variation is the steric effect of the alkene which will destabilise both the crystal and the mesophase, resulting in lower transition temperatures.

We are now investigating the full range of platinum sulfoxide complexes over the full range of enantiopurity in order to see if the effects we observe are accentuated with longer or shorter chain lengths and to fully characterise the effect of enantiopurity on phase behaviour.

We would like to thank the British Council and MURST for a joint project grant.

Notes and references

† Methyl alkyl sulfoxide **1** (0.30 mmol) dissolved in DMF (4 ml) was added to a suspension of potassium tetrachloroplatinate (0.30 mmol) in DMF (1 ml). The mixture was stirred (40 °C, 16 h) giving a deep yellow solution. The solution was filtered to remove KCl and **2** precipitated as a yellow compound upon addition of diethyl ether (20 ml) followed by hexane (20 ml).

Alkoxy stilbazole (0.10 mmol) dissolved in acetone (5 ml) was added to a solution of **2** (0.10 mmol) in acetone (50 ml). The solution was stirred (1 h) by which time it had changed to a paler yellow colour. The solution was concentrated to one third of the original volume and **3** precipitated by addition of diethyl ether. The product was collected by filtration, washed with diethyl ether, then methanol and dried in air. Yield: 95% (0.095 mmol).

The chiral sulfoxides used were (*S*)-**1a**, (*R*)-**1b** and (*S*)-**1c**. Note that the priority at sulfur reverses on coordination to platinum, thus an (*R*)-sulfoxide becomes an (*S*)-platinum complex.

‡ $\delta_H(CDCl_3$, 400.0 MHz): 8.61 (2H, AA′XX′, ^3J 8 Hz), 7.50 (2H, AA′XX′, ^3J 8 Hz), 7.40 (2H, AA′XX′, ^3J 8 Hz), 7.34 (1H, d, ^3J 16 Hz), 6.93 (1H, AA′XX′, ^3J 8 Hz), 6.87 (2H, d, ^3J 16 Hz), 4.00 (2H, t, ^3J 7 Hz), 3.69 (1H, m), 3.40 (3H, s), 3.38 (1H, m), 2.11 (2H, m), 1.79 (2H, m), 1.4–1.3 (m), 0.87 (6H, t, ^3J 7 Hz).

§ Elemental analysis found (calc.): *rac*-**3a**: C 54.2 (53.9), H 7.7 (7.6), N 1.5 (1.6); (*R*)-**3a**: C 53.8 (53.9), H 7.6 (7.6), N 1.6 (1.6); *rac*-**3b**: C 54.0 (54.4), H 7.6 (7.7), N 1.8 (1.6); (*S*)-**3b**: C 54.4 (54.4), H 7.8 (7.7), N 1.4 (1.6); *rac*-**3c**: C 54.6 (54.8), H 7.4 (7.8), N 1.2 (1.5); (*R*)-**3c**: C 55.0 (54.8), H 7.7 (7.8), N 1.6 (1.5)%.

¶ $[\alpha]_D$ values at 20 °C: **3a** − 12.2°; **3b** + 12.5°; **3c** −12.4°

‖ Phases were identified by their optical textures: the smectic F was distinguished from the smectic I by the lack of point disclinations.

1 S. A. Hudson and P. M. Maitlis, *Chem. Rev.*, 1993, **93**, 861.
2 D. W. Bruce, in *Inorganic Materials*, ed. D. W. Bruce and D. O'Hare, Wiley, Chichester, 2nd edn., 1996.
3 J. L. Serrano, *Metallomesogens*, VCH, Weinheim, 1996.
4 P. Espinet, J. Etxebarria, M. Marcos, J. Pérez, A. Remón and J. L. Serrano, *Angew. Chem., Int. Ed. Engl.*, 1989, **28**, 1065.
5 M. J. Baena, J. Buey, P. Espinet, H.-S. Kitzerow and G. Heppke, *Angew. Chem., Int. Ed. Engl.*, 1993, **32**, 1201.
6 M. Ghedini, D. Pucci, E. Cesarotti, P. Antogniazza, O. Francescangeli and R. Bartolino, *Chem. Mater.*, 1993, **5**, 883.
7 N. J. Thompson, J. L. Serrano, M. J. Baena and P. Espinet, *Chem. Eur. J.*, 1996, **2**, 214.
8 J. Buey, P. Espinet, H.-S. Kitzerow and J. Strauss, *Chem. Commun.*, 1999, 441.
9 J. P. Rourke, F. P. Fanizzi, N. J. S. Salt, D. W. Bruce, D. A. Dunmur and P. M. Maitlis, *J. Chem. Soc., Chem. Commun.*, 1990, 229.
10 J. P. Rourke, F. P. Fanizzi, D. W. Bruce, D. A. Dunmur and P. M. Maitlis, *J. Chem. Soc., Dalton Trans.*, 1992, 3009.
11 D. W. Bruce, J. D. Holbrey, A. R. Tajbakhsh and G. J. T. Tiddy, *J. Mater. Chem.*, 1993, **3**, 905.
12 K. K. Andersen, *Tetrahedron Lett.*, 1962, 93.
13 S. Patai, Z. Rappoport and C. Stirling, *The Chemistry of Sulphones and Sulphoxides*, Wiley, New York, 1988.
14 M. A. M. Capozzi, C. Cardellicchio, G. Fracchiolla, F. Naso and P. Tortorella, *J. Am. Chem. Soc.*, 1999, **121**, 4708.
15 D. R. Rayner, E. G. Miller, P. Bickart, A. J. Gordon and K. Mislow, *J. Am. Chem. Soc.*, 1966, **88**, 3138.
16 J. W. Goodby, A. J. Slaney, C. J. Booth, I. Nishiyama, J. D. Vuijk, P. Styring and K. J. Toyne, *Mol. Cryst. Liq. Cryst.*, 1994, **243**, 231.
17 G. W. V. Cave, N. W. Alcock and J. P. Rourke, *Organometallics*, 1999, **18**, 1801.

Azafulvenium methides: new extended dipolar systems

Oliver B. Sutcliffe,[a] Richard C. Storr,*[a] Thomas L. Gilchrist,[a] Paul Rafferty[b] and Andrew P. A. Crew[b]

[a] *Department of Chemistry, University of Liverpool, Liverpool, UK L69 7ZD. E-mail: rcstorr@liv.ac.uk*
[b] *Department of Medicinal Chemistry, Knoll Ltd., Nottingham, UK NG1 1GF*

Received (in Cambridge, UK) 24th February 2000, Accepted 7th March 2000
Published on the Web 30th March 2000

The transient 8π 1,7-dipolar azafulvenium methides 5 and 8 undergo sigmatropic [1,8] H shifts and the acyl derivatives 12 electrocyclise to give novel pyrrolooxazines 13; the related diazafulvenium methide 15 can be intercepted in 8π + 2π cycloadditions with silylated acetylenes.

1,3-Dipolar cycloaddition is an allowed 4π + 2π pericyclic process and has been of considerable value in organic synthesis.[1] 1,4-Sigmatropic shifts[2] and electrocyclic reactions[3] in 1,3-dipoles are also well established. However, although 1,5[4] and 1,7[5]-dipolar cyclisation are well recognised reactions, other pericyclic reactions of extended dipoles (those with more than 4π electrons) are less familiar.[6] In designing an extended dipole suitable for cycloaddition, competing electrocyclisation has to be prevented and the termini of the dipole must be a convenient distance apart for bonding to an appropriate cycloaddend. These principles are illustrated in the oxidopyridinium betaines, studied by Katritzky *et al.*,[6,7] which function as 4π 1,3-dipoles with 2π systems but as 6π 1,5-dipoles with dienes. We report here, our preliminary studies with the novel aza- and diaza-fulvenium ylide systems **1** (X = CR, N) which, in principle, can act as 4π 1,3-dipoles or as 8π 1,7-dipoles.

Initial, unsuccessful approaches towards the azafulvenium methides and imides **1** (X = CR) involved attempted base catalysed elimination from the pyrrole derivatives **2**. Earlier, an analogous elimination approach to systems of type **1** (X = CR)

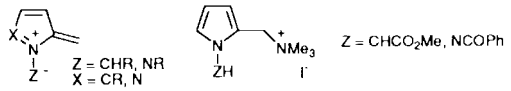

1 **2**

by Padwa *et al.*[8] also failed. Padwa had also considered the thermal extrusion of SO_2 from the dihydrothienopyrrole *S,S*-dioxide **3** (R = H) but found it to be too thermally stable. Our own experience with extrusion of SO_2 from heterocyclic sulfones and with flash vacuum pyrolysis (FVP)[9] led us to reinvestigate this thermolysis. The sulfone **3** (R = H) did not extrude SO_2 when heated in solution at 300 °C. However, on FVP at 700 °C/10^{-3} mm SO_2 was eliminated although no identifiable products arising from the dipole were detected on the cold receiver. Intermolecular trapping was attempted by cocondensation of the pyrolysate at −180 °C with methyl vinyl ketone or by condensation in a matrix with dichloromethane, which was allowed to thaw and mix with a solution of *N*-phenylmaleimide or dimethyl acetylenedicarboxylate below −100 °C. No evidence was obtained for the formation of adducts.

Encouraged by the extrusion of SO_2 we designed derivatives for which the formation of the dipole might be revealed by intramolecular trapping in the FVP experiment. Introduction of aryl groups (phenyl, 4-anisyl and 2-thienyl) at the 3-position was accomplished using the appropriate aldehyde in the synthesis of the thienopyrrole (Scheme 1). However, on FVP, there was no evidence for electrocyclisation of the type seen with *ortho*-quinodimethanes.[9] On the other hand, introduction of methyl groups at both the 1- and the 3-positions led to vinylpyrroles **6** and **9**, respectively, on FVP. Their formation

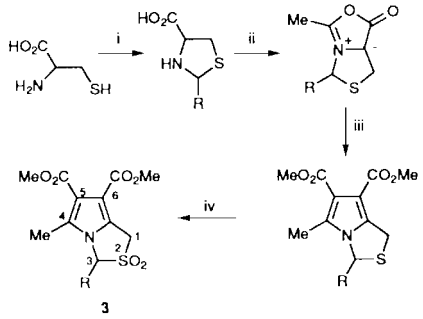

3

Scheme 1 *Reagents and conditions*: i, RCHO; ii, Ac_2O/heat; iii, DMAD; iv, MCPBA.

can be explained by allowed, suprafacial [1,8] H shifts in the 8π, 1,7-dipolar systems **5** and **8**, respectively. Synthesis of the 3-methyl derivative **4** was achieved by use of acetaldehyde in the route to the thienopyrrole (Scheme 1) and the 1-methyl derivative **7** was obtained from sulfone **3** (R = H) by methylation using LHMDS and iodomethane. Subsequent methylation of the 1-methyl compound **7** gave the 1,1-dimethyl derivative **10**. As expected the 1-proton in **3** (R = H) is more acidic than the 3-proton since it is activated by the 6-ester group.

The reaction of the 3-methyl derivative **4** to give the *N*-vinylpyrrole **6** was clean but the 1-methyl compound **7** gave the 2-vinylpyrrole **9** contaminated with an unidentified product showing vinylic H in the NMR spectrum. For sigmatropic shifts to occur the methyl groups must adopt an inward configuration. In a delocalised dipolar system there will be a barrier to rotation around the partial double bonds but rotation at the high temperatures of the FVP is not unreasonable. The difference between the two derivatives **4** and **7** may reflect the differing ease with which the dipoles can attain the required configurations having inward methyl groups (only the inward configurations are illustrated in Scheme 2). Significantly, the reaction of

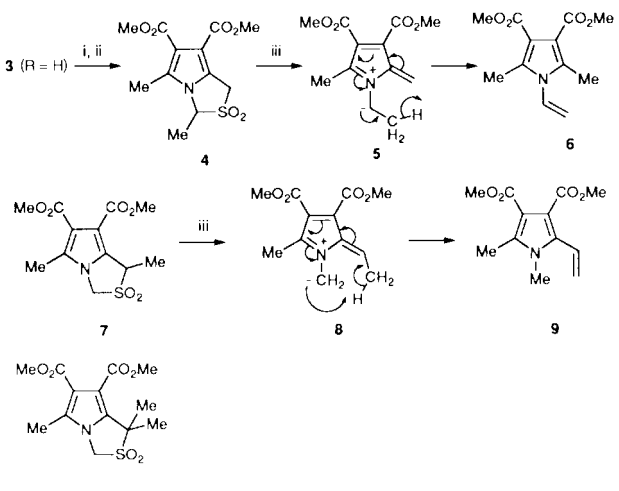

4 **5** **6** **7** **8** **9** **10**

Scheme 2 *Reagents and conditions*: i, LHMDS; ii, MeI; iii, 700 °C/10^{-3} mm.

DOI: 10.1039/b001521k

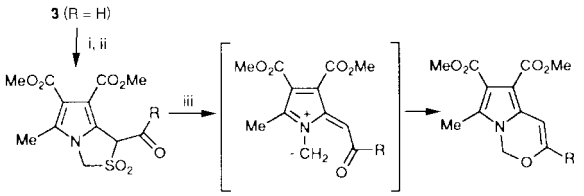

R	% yield 11	% yield 13
Me	40	52
MeO	38	–
Ph	69	86
4-MeC_6H_4	79	85
4-ClC_6H_4	40	76
3,4-$F_2C_6H_3$	51	60
2-furyl	64	72
cyclohexyl	88	68

Scheme 3 *Reagents and conditions*: i, LHMDS; ii, RCOCl; iii, 200 °C/1,2,4-trichlorobenzene.

the 1,1-dimethyl derivative **10** where one of the methyl groups must necessarily be inward was cleanest.

A series of 1-acyl derivatives **11**† (Scheme 3) was also obtained by treatment of sulfone **3** (R = H) with LHMDS followed by an acyl chloride. Optimum conditions involved sequential treatment with base (1 equivalent), acyl chloride (1 equivalent) followed by further equivalents of base and acyl chloride. On FVP (600 °C/10^{-3} mm) the benzoyl derivative **11** (R = Ph) gave the pyrrolooxazine **13** (R = Ph), the first example of this new ring system and further strong evidence for generation of the desired dipolar system. Introduction of the acyl group lowers the temperature required for extrusion of SO_2 and the reaction, which can be carried out in solution at 200 °C, is general for all the acyl derivatives (Scheme 3).† The ability to generate the dipole in solution opened up the possibility of intermolecular trapping in a cycloaddition but extrusion of SO_2 in the presence of *N*-phenylmaleimide, dimethyl acetylenedicarboxylate or bis(trimethylsilyl)acetylene gave only the oxazine and no trace of cycloadduct. Prolonged heating of the oxazine in the presence of the dipolarophiles gave only recovered starting material and there was no evidence for reversibility in the electrocyclic ring closure.

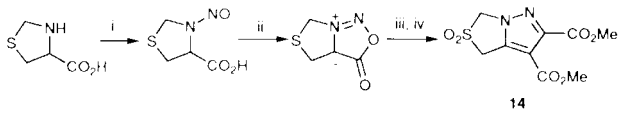

Scheme 4 *Reagents and conditions*: i, $NaNO_2$/HCl; ii, TFAA/Et_2O; iii, DMAD; iv, MCPBA.

The pyrazole analogue **14** was obtained as shown (Scheme 4). Alkylation and acylation of **14** proved difficult but extrusion of SO_2 from this unsubstituted sulfone occurs more easily and can be achieved in solution. The extra pyrazole ring N thus appears to exert the same effect as an electron withdrawing acyl group at the 1-position of the pyrrole system. Extrusion of SO_2 in refuxing 1,2,4-trichlorobenzene in the presence of *N*-phenylmaleimide or dimethyl acetylenedicarboxylate gave no adducts but in the presence of bis(trimethylsilyl)acetylene (a reactive electron rich dienophile at high temperatures[10]) a cycloadduct **16** was obtained in 34% yield providing the first evidence for formation of these dipolar systems by intermolecular trapping (Scheme 5).† When the reaction was carried

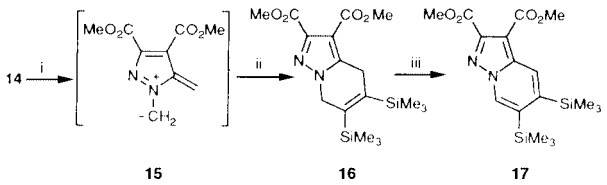

Scheme 5 *Reagents and conditions*: i, 230–300 °C; ii, bis(trimethylsilyl)-acetylene; iii, prolonged heating.

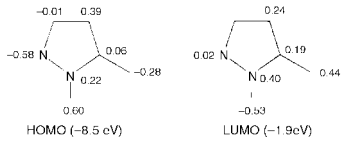

Fig. 1 MO coefficients of diazafulvenium methide.

out in a sealed tube with prolonged heating the aromatised adduct **17** was isolated (24%) (Scheme 5)†. Under similar conditions trimethylsilylacetylene gave a mixture of regioisomers. It may be significant that the dipolar systems undergo cycloaddition only with the electron rich dipolarophile and that addition occurs across the 1,7 and not the 1,3 positions. Molecular orbital calculations[11] for the pyrazole derivative (Fig. 1) indicate that dipole LUMO–dipolarophile HOMO interactions are dominant and that the MO coefficients are larger at the 1 and 7 positions than at the 3 position.

Notes and references

† *Selected data*: **11** (R = Ph): mp 221–222 °C, $\delta_H(CDCl_3)$ 2.47 (s, 3H, 5-Me), 3.58 and 3.86 (2 × s, 2 × 3H, ester Me), 4.99 (d, 1H, *J* 11 Hz, H-3) 5.07 (d, 1H, *J* 11 Hz, H-3′), 6.46 (s, 1H, H-1), 7.57–8.09 (m, 5H, aromatic H). **13** (R = Ph): oil, $\delta_H(CDCl_3)$ 2.41 (s, 3H, 7-Me), 3.85 and 3.86 (2 × s, 2 × 3H, ester Me), 5.66 (s, 2H, CH_2), 6.96 (s, 1H, CH), 7.33–7.71 (m, 5H, aromatic H). **16**: oil, $\delta_H(CDCl_3)$ 0.24 and 0.26 (2 × s, 2 × 9H, $SiMe_3$), 3.75 (t, 2H, *J* 5 Hz, CH_2), 3.82 and 3.92 (2 × s, 2 × 3H, ester Me) and 4.73 (t, 2H, *J* 5 Hz, CH_2). **17**: oil, $\delta_H(CDCl_3)$ 0.42 and 0.43 (2 × s, 2 × 9H, $SiMe_3$), 3.94 and 4.03 (2 × s, 2 × 3H, ester Me), 8.45 and 8.59 (2 × s, 2 × 1H, aromatic H).

1 *1,3-Dipolar Cycloaddition Chemistry*, ed. A. Padwa, Wiley, New York, 1984, vol. 1 and 2.
2 E. Grovenstein, *Angew. Chem., Int. Ed. Engl.*, 1978, **17**, 313; M. G. Pleiss and J. A. Moore, *J. Am. Chem. Soc.*, 1968, **90**, 4738.
3 R. Huisgen, *Angew. Chem., Int. Ed. Engl.*, 1977, **16**, 572.
4 R. Huisgen, *Angew. Chem., Int. Ed. Engl.*, 1980, **19**, 947; E. C. Taylor and I. Turchi, *Chem. Rev.*, 1979, **79**, 181.
5 G. Zecchi, *Synthesis*, 1991, 181; P. W. Groundwater and M. Nyerges, *Adv. Heterocycl. Chem.*, 1999, **73**, 97.
6 J. N. Crabb and R. C. Storr, in *1,3-Dipolar Cycloaddition Chemistry*, ed. A. Padwa, Wiley, New York, 1984, vol. 2, pp. 543–595.
7 A. R. Katritzky and N. Dennis, *Chem. Rev.*, 1989, **89**, 827; A. R. Katritzky, M. Karelson and G. J. Hitchings, *Rev. Heteroat. Chem.*, 1991, 43.
8 A. Padwa, G. E. Fryxell, J. R. Gasdaska, K. Venkatramanan and G. S. K. Wong, *J. Org. Chem.*, 1989, **54**, 644.
9 S. J. Collier and R. C. Storr, *Prog. Heterocycl. Chem.*, 1998, **10**, 25.
10 J. Sauer, D. K. Heldmann, J. Hetzenegger, J. Krauthan, H. Sichert and J. Schuster, *Eur. J. Org. Chem.*, 1998, 2885.
11 Calculations were carried out using the semi-empirical molecular orbital package MOPAC/PM3: M. J. S. Dewar and W. Thiel, *J. Am. Chem. Soc.*, 1977, **99**, 4899; J. P. Stewart, *J. Comput. Chem.*, 1989, **10**, 209.

ChemComm

Direct spectroscopic evidence for vanadium species in V-MCM-41 molecular sieve characterized by UV resonance Raman spectroscopy

Guang Xiong, Can Li,* Hongyuan Li, Qin Xin and Zhaochi Feng

State Key Laboratory of Catalysis, Dalian Institute of Chemical Physics, Chinese Academy of Sciences, P. O. Box 110, Dalian 116023, China. E-mail: canli@ms.dicp.ac.cn

Received (in Cambridge, UK) 19th January 2000, Accepted 6th March 2000
Published on the Web 30th March 2000

Vanadium species in tetrahedral and octahedral coordination in V-MCM-41 molecular sieve are characterized by UV resonance Raman bands at 1070 and 930 cm^{-1} respectively.

Vanadium-substituted molecular sieves have been found to be excellent catalysts for many selective oxidation reactions.[1–3] In particular, V-MCM-41 has drawn much interest owing to its large pore diameter which is suitable for selective oxidation of large organic compounds.[4–6]

The catalytic activity and selectivity of vanadium-substituted molecular sieves are directly related to the coordination structures of the vanadium species in the molecular sieves. In general, three forms of vanadium species, isolated tetrahedral, two-dimensional octahedral species and crystalline V_2O_5, are believed to be present.[4,5,7,8] The coordination structure of vanadium species in V-MCM-41 has been investigated by ^{51}V NMR, UV–VIS absorption spectroscopy and many other techniques,[4,5,8] but identification of vanadium species in tetrahedral or octahedral coordination environments is not straightforward. Raman spectroscopy is a potentially viable technique for the study of the structure of vanadium species in V-MCM-41, since it has been used to characterize supported vanadium oxides with both tetrahedral and octahedral coordination structures.[9,10]

However, there have been relatively few Raman studies on vanadium-substituted MCM-41,[8] mainly because of fluorescence interference and the low sensitivity of conventional Raman spectroscopy. The limited amount of substituted vanadium atoms also hinders the application of Raman spectroscopy in characterization of vanadium atoms in V-MCM-41.

UV Raman spectroscopy has been proved to be a powerful technique for the study of catalysts and other solids,[11,12] especially, for the identification of isolated transition metal atoms substituted in the framework of molecular sieves[13] or grafted on metal oxides.[14] An increase in the intensity of Raman signal and decrease in the intensity of fluorescence background help to increase the sensitivity of the Raman spectra. Moreover, the resonance Raman effect will selectively enhance the intensity of the Raman signal by several orders of magnitude when the excitation laser line is close to the electronic transition absorption of the samples.

In this work, for the first time, we study the different vanadium species in V-MCM-41 using UV resonance Raman spectroscopy. Based on the UV resonance Raman effect the vanadium species in tetrahedral and octahedral environments in V-MCM-41 can be successfully identified by UV resonance Raman spectroscopy.

MCM-41 and V-MCM-41 were synthesized according to the method reported in the literature.[4] V-MCM-41 samples which possess Si/V ratios of 250, 125 and 60 are denoted V-MCM-41 (250), V-MCM-41 (125) and V-MCM-41 (60), respectively. The as-synthesized samples show XRD patterns matching well with these reported in the literature.[4,5,15] UV Raman spectra were recorded on a homemade UV Raman spectrometer.[12] 244 and 488 nm lines from a Innova 300 FRED (Coherent) laser were chosen as the excitation sources. The laser power at the samples were kept below 2.0 mW for the 244.0 nm line and 100 mW for the 488 nm line. The spectral resolution is estimated to be 2.0 cm^{-1} for UV Raman spectra and 1.0 cm^{-1} for visible Raman spectra.

Fig. 1 shows Raman spectra of V-MCM-41 and MCM-41 samples excited by the 488 nm line. The signal to noise ratio of visible Raman spectra is very poor because of both fluorescence interference and the inherently low sensitivity of visible Raman spectroscopy. The MCM-41 sample excited by the 488 nm line showed weak Raman bands at 490, 610, 810 and 970 cm^{-1}. Bands at 490 and 610 cm^{-1} are attributed to the 3 and 4 Si siloxane rings, respectively,[10] while the bands at 810 and 970 cm^{-1} are assigned to the siloxane bridges (Si–O–Si) and surface silanol groups of MCM-41.[8,10] The visible Raman bands of V-MCM-41 are similar to that of MCM-41 in that no additional bands of V-MCM-41 due to vanadium species are observed. This means that the Raman bands associated with vanadium species in MCM-41 are too weak for detection by visible Raman spectroscopy.

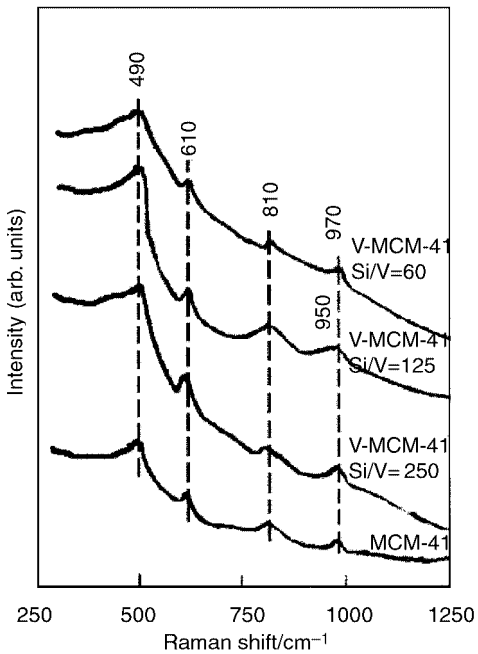

Fig. 1 Visible Raman spectra of V-MCM-41 and MCM-41 excited by 488 nm line radiation.

Compared with visible Raman spectra, UV Raman spectroscopy gives significantly different spectra, (Fig. 2). Besides the Raman bands at 490, 610 and 810 cm^{-1} which appear in the visible Raman spectra, Raman bands in the region 900–1200 cm^{-1} are present in the UV Raman spectra of MCM-41 and V-MCM-41 samples. The band at 970 cm^{-1} of MCM-41 is assigned to surface silanol stretching vibrations while weak bands in the region 1000–1200 cm^{-1} of MCM-41 are attributed to the asymmetric stretching modes of Si–O–Si bridges. These

DOI: 10.1039/b000557f

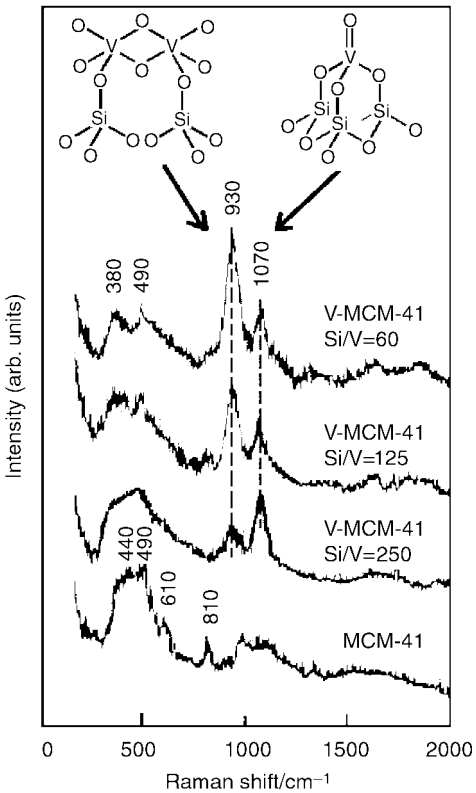

Fig. 2 UV Raman spectra of V-MCM-41 and MCM-41 excited by 244 nm line radiation.

bands become observable owing to reduced fluorescence interference when the excitation is changed from 488 to 244 nm. It is significant that two new bands at 930 and 1070 cm^{-1} are detected in UV Raman spectrum of V-MCM-41. Taking into account that the laser line at 244 nm is close to the charge transfer absorption of the vanadium species in V-MCM-41, the high intensity of the 930 and 1070 cm^{-1} bands must be a result of enhancement by the resonance Raman effect.

Two main absorptions bands are present at 275 and 340 nm in the UV–VIS diffuse reflectance spectrum of V-MCM-41.[15] These bands are assigned to low energy charge-transfer (CT) associated with framework vanadium species in tetrahedral coordination.[8,15] The band centered at 275 nm is very broad covering the range 230–300 nm. Thus the 244 nm laser line is within the electronic transition band of tetrahedral vanadium species. The UV–VIS absorption bands also appear in a similar region for polymerized vanadium oxides supported on SiO_2.[16] A band at 250 nm together with a shoulder at 320 nm is observed in the UV–VIS absorption spectrum of vanadium oxide. Therefore, the 244 nm laser line can excite both the band centered at 275 nm associated with the isolated vanadium species and the band centered at 250 nm of polymerized vanadium oxides. In other words, the 244 nm laser line can excite the electronic absorptions of vanadium species in tetrahedral and octahedral coordination simultaneously. Obviously the 488 nm laser line (visible Raman spectroscopy) lies outside of the UV–VIS absorption region for vanadium species in V-MCM-41.

The absence of a typical band at *ca.* 1000 cm^{-1} of V_2O_5 in Fig. 1 and 2 implies that no crystalline V_2O_5 is formed in V-MCM-41. This suggests that the vanadium species in V-MCM-41 are isolated or, at least, are highly dispersed on the surface. The Raman bands in the 900–1000 cm^{-1} region of supported vanadium oxides are usually attributed to hydrated polymerized vanadium oxides.[9,17] Thus the band at 930 cm^{-1} can be attributed to the V=O symmetric stretching mode of polymerized vanadium oxides.[9] The band at *ca.* 1030 cm^{-1} has been assigned to the V=O stretching vibration of monometric vanadyl species bound directly to the support. [8,9,10] The V=O stretching frequencies of VOF_3, $VOCl_3$ and $VOBr_3$ occur at 1053, 1035 and 1028 cm^{-1}, respectively.[18–20] Therefore the band at 1070 cm^{-1} is reasonably assigned to a tetrahedral V=O group bonded to the MCM-41 host. It should be noted that the band position (1070 cm^{-1}) of V-MCM-41 is higher than that of tetrahedral vanadate in the literature (*ca.* 1030 cm^{-1}).[10] An empirical relationship between V–O bond lengths and Raman stretching frequencies has been assumed based on vanadium oxides.[21] According to this assumption, a higher frequency position corresponds to shorter V–O bonds; the highest frequency position at 1070 cm^{-1} thus corresponds to the shortest V=O bond distance. This result provides evidence for the isolated mono–oxo vanadate species in V-MCM-41 molecular sieve being of tetrahedral structure with strong structural tension. This structure is metastable and aggregates into the octahedral vanadium species at high temperature as indicated by the disappearance of the band at 1070 cm^{-1} and the growth of the band at 930 cm^{-1} after calcination at high temperatures.

In summary, UV resonance Raman bands of V-MCM-41 at 1070 and 930 cm^{-1} are detected for the first time. These bands provide direct spectroscopic evidence for vanadium species in tetrahedral and octahedral environments, respectively. The vanadium species in tetrahedral coordination is an isolated species with strong structural tension, while that in the octahedral form corresponds to highly dispersed polymerized oxides. This study also demonstrates that UV resonance Raman spectroscopy is a powerful technique to selectively identify transition metal species in molecular sieves or on supports.

This work was supported by the National Natural Science Foundation of China (NSFC) for Distinguished Young Scholars (Grant 29625305).

Notes and references

1 M. S. Rigutto and H. Van Bekkum, *Appl. Catal.*, 1991, 68.
2 B. M. Weckhuysen, I. P. Vannijvel and R. A. Schoonheydt, *Zeolites*, 1995, **15**, 482.
3 S. Lim and G. L. Haller, *Appl. Catal. A: Gen.*, 1999, **188**, 277.
4 K. M. Reddy, I. Moudrakovskij and A. Sayasi, *J. Chem. Soc., Chem. Commun.*, 1994, 1059.
5 J. S. Reddy and A. Sayari, *J. Chem. Soc., Chem. Commun.*, 1995, 2231.
6 S. Gontier and A. Tuel, *Microporous Mater.*, 1995, **5**, 161.
7 T. Sen, V. Ramaswamy, S. Ganapathy, P. R. Rajamohanan and S. Sivasanker, *J. Phys. Chem.*, 1996, **100**, 3809.
8 K. J. Chao, C. N. Wu, H. Chang, L. J. Lee and S. F. Hu, *J. Phys, Chem.*, 1997, **101**, 6341.
9 M. A. Vuurman and I. E. Wachs, *J. Phys. Chem.*, 1992, **96**, 5008.
10 Zh. Luan, P. A. Meloni, R. S. Czernuszewicz and L. Kevan, *J. Phys. Chem.*, 1997, **101**, 9046.
11 P. C. Stair and C. Li, *J. Vac. Sci. Technol. A*, 1997, **15**, 1679.
12 G. Xiong, C. Li, Z. Feng, P. Ying, Q. Xin and J. Liu, *J. Catal.*, 1999, **186**, 234.
13 C. Li, G. Xiong, Q. Xin, J. Liu, P. Ying, Z. Feng, J. Li, W. Yang, Y. Wang, G. Wang, X. Liu M. Lin, X.Wang and E. Min, *Angew. Chem., Int. Ed.*, 1999, **38**, 2220.
14 Q. Yang, S. Wang, J. Lu, G. Xiong, Z. Feng, Q. Xin and C. Li, *Appl. Catal.: A*, 2000, **194–195**, 507.
15 Z. H. Luan, J. Xu, H. Y. He, J. Klinowski and L. Kevan, *J. Phys. Chem.*, 1996, **100**, 19595.
16 G. Centi, S. Perathoner, F. Trifiró, A. Aboukais, C. F. Aissi and M. Guelton, *J. Phys. Chem.*, 1992, **96**, 2617.
17 C. Cristiani, P. Forzatti and G. Busca, *J. Catal.*, 1989, **116**, 586.
18 H. Selig and H. H. Claassen, *J. Chem. Phys.*, 1966, **44**, 1404.
19 F. A. Miller and L. R. Cousins, *J. Chem. Phys.*, 1957, **26**, 329.
20 F. A. Miller and W. K. Baer, *Spectrochim. Acta.*, 1961, **17**, 112.
21 F. D. Hardcastle and I. E. Wachs, *J. Phys. Chem.*, 1991, **95**, 5031.

Ag_2HgO_2: the first silver mercurate

Stephan Deibele, Jan Curda, Eva-Maria Peters and Martin Jansen*

Max-Planck Institut für Festkörperforschung, Heisenbergstrasse 1, D-70569 Stuttgart, Germany. E-mail: martin@jansen.mpi-stuttgart.mpg.de

Received (in Basel, Switzerland) 1st January 2000, Accepted 10th March 2000
Published on the Web 3rd April 2000

The silver mercurate Ag_2HgO_2 is accessible by oxygen high pressure synthesis; the compound crystallizes in a novel structure type with three interpenetrating Ag–O–Hg (10, 3) nets.

Following research into high-T_c superconductivity the Hg-based copper oxides have been found to represent a remarkable group among the cuprate HTSCs: the highest transition temperature so far has been found in the system $HgBa_2Ca_{n-1}Cu_nO_{2n+2+\delta}$ at *ca*. 133.5 K. Within a short period it has been possible to synthesize series of Hg-based homologues, which differ in the number of CuO_2 layers per unit cell.[1–4] Compared to the related group of superconducting Tl-based copper oxides[5,6] the differences in the oxidation states and coordination chemistry of Tl and Hg are significant. Whereas Tl^{3+} cations prefer a distorted octahedral oxygen environment, Hg^{2+} cations are usually coordinated by two oxygen ions in a linear 'dumb-bell' like arrangement. The higher T_c of $HgBa_2CuO_{4+\delta}$ relative to $TlBa_2CuO_{5-\delta}$ could be a result of this difference in the coordination chemistry, which influences the oxygen stoichiometry in the HgO_δ and $TlO_{1-\delta}$ layers. Oxygen depletion in the mercury compound is possible, whereas the coordination of Tl^{3+} in the thallium compound only allows a small amount of oxygen depletion.

As a consequence of the presence of toxic heavy metal cations in the above mentioned superconducting phases, many attempts have been made to replace them by non-toxic cations. A promising candidate for the substitution of mercury in these layered oxides is silver, owing to its preference to linear coordination in silver oxides. However, all attemps to synthesize superconducting layered oxides containing silver instead of mercury have so far failed. As a first step towards Ag-based superconductors we have investigated the synthesis of ternary silver mercurates that might allow a partial substitution of silver for mercury by proceeding *via* solid state reactions of oxide mixtures, *e.g.* Ag_xHgO_y/BaO/CuO. The novel material Ag_2HgO_2 represents such a precursor, containing Ag^+ and Hg^{2+} cations in the characteristic oxygen 'dumb-bell' coordination mode.

Black crystals of Ag_2HgO_2 were prepared by solid state reaction of Ag_2O (precipitated from an aqueous $AgNO_3$ solution by adding 3 M NaOH solution) and HgO (Aldrich, 99%) under oxygen pressure. The binary oxides were mixed in a molar ratio of 1:1 and then annealed for 3–5 days in gold crucibles placed in stainless steel autoclaves. The optimized reaction temperature and oxygen pressure were 310 °C and 150 MPa, respectively. As an accelerator 3 ml water or 1 ml 1 M KOH solution for single crystalline products were added.

According to the structure determination using single-crystal diffractometer data, Ag_2HgO_2 shows a novel structure type.† Both cations are in d^{10} configuration exhibiting characteristic linear oxygen coordination (Table 1). The O–Ag–O units (Ag–O distances: 211.7 and 212.1 pm; O–Ag–O angle: 178.5°) form zigzag chains along [100] and [010]. These chains are connected *via* O–Hg–O units (Hg–O distance: 202.6 pm; O–Hg–O angle: 165.6°) to a three-dimensional net, consisting of decagons with oxygen atoms forming the knots (Fig. 1). As a consequence of these connectivities oxygen attains a threefold coordination (2 × Ag, 1 × Hg). The (10, 3) net is topologically identical to the net formed by silicon in $ThSi_2$ or by boron in α-B_2O_3.[7] In this respect, Ag_2HgO_2 can be regarded as antitypic to boronoxide. The crystal structure consists of three such identical (10, 3) nets, interpenetrating each other.

The silver partial structure in Ag_2HgO_2 shows a structural feature which is very common to silver-rich oxides: in spite of their positive charges, the silver cations form cluster-like agglomerates[8,9] with Ag–Ag distances ranging in general from *ca*. 280 to 330 pm, some may even be shorter than the distance in silver metal (289 pm). In Ag_2HgO_2 the presence of two different cations in d^{10} configuration yields an unprecedented situation. The shortest Ag–Hg distances of *ca*. 333.4 pm are somewhat larger than the Ag–Ag contacts, which range between 297.4 and 308.7 pm, however, they are still less than the van der Waals distance. This suggests the presence of weak bonding interactions between all d^{10} configurated cations in Ag_2HgO_2. Considering all Ag–Ag contacts up to the van der Waals distance for silver of *ca*. 340 pm, the silver atoms form a three dimensional network of corner-sharing tetrahedra. Includ-

Table 1 Selected bond lengths (pm) and angles (°) for Ag_2HgO_2

Hg–O^{i}	202.6(9)	Ag–Ag^{vii}	305.6(1)
Hg–O^{ii}	202.6(9)	Ag–Ag^{viii}	305.6(1)
Ag–O^{iii}	211.7(10)	Ag–Ag^{ix}	308.7(1)
Ag–O^{iv}	212.1(10)	Ag–Ag^{x}	308.7(1)
Ag–Ag^{v}	297.4(2)	Ag–Hg	333.4(2)
Ag–Ag^{vi}	304.6(2)		
O–Hg–O	165.6(6)	O–Ag–O	178.5(1)

Symmetry codes: (i) 0.5 + *x*, 1.5 − *y*, 0.25 − *z*; (ii) 1.5 − *y*, 0.5 + *x*, −0.25 + *z*; (iii) −1 + *y*, *x*, −*z*; (iv) −0.5 + *y*, 0.5 − *x*, 0.25 + *z*; (v) *y*, *x*, −*z*; (vi) −*y*, −*x*, 0.5 − *z*; (vii) −0.5 + y, 0.5 − *x*, 0.25 + *z*; (viii) 0.5 − *y*, 0.5 + *x*, −0.25 + *z*; (ix) −0.5 + *x*, 0.5 − *y*, 0.25 − *z*; (x) 0.5 + *x*, 0.5 − *y*, 0.25 − *z*.

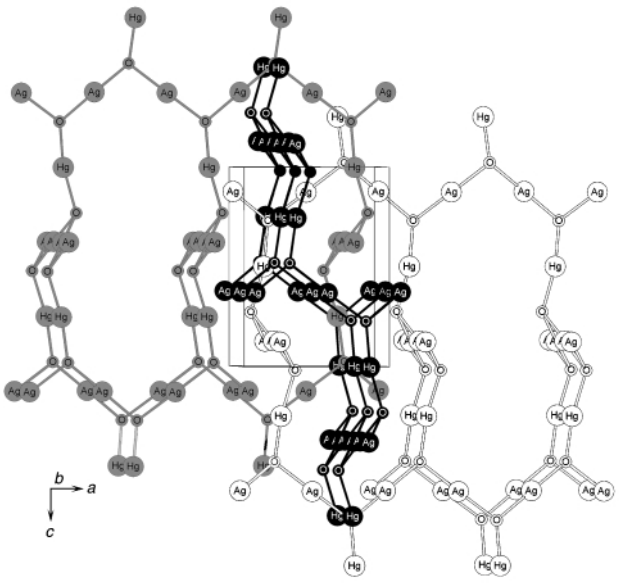

Fig. 1 Perspective view of the crystal structure of Ag_2HgO_2: the three identical interpenetrating Ag–O–Hg (10, 3) nets are colored white, gray and black.

DOI: 10.1039/b000400f

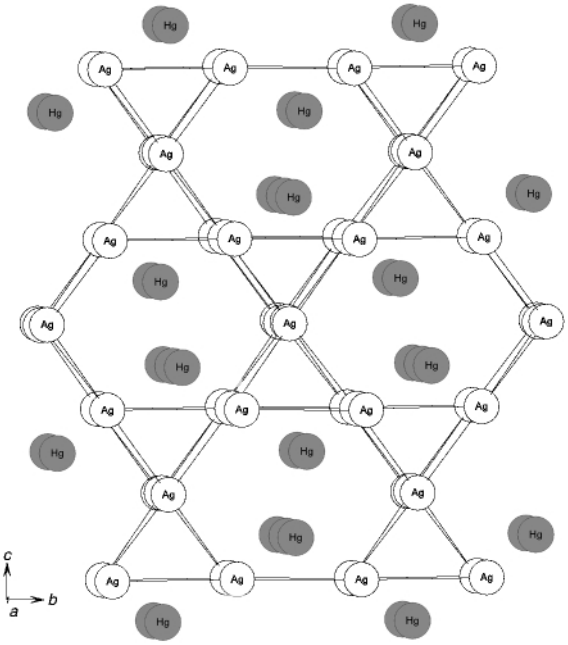

Fig. 2 The cation partial structure of Ag_2HgO_2.

ing mercury the resulting arrangement closely corresponds to Laves phase $MgCu_2$. In this description the silver cations occupy the Cu positions, whereas the mercury cations are located on the Mg positions in $MgCu_2$ (Fig. 2). Thus, the approach of describing crystal structures of extended non-metallic solids starting with the partial structures of the constituting metals applies well to Ag_2HgO_2.[10, 11]

The title compound decomposes at 340 °C in one step into its elements. According to EDX analyses (average of 20 spots), the Ag/Hg ratio is 1.95:1 and the samples are free of potassium. Measurements of the magnetic susceptibility show temperature independent diamagnetic behavior ($\chi_{obs} = -127 \times 10^6$ cm^3 mol^{-1}; $\chi_{cal} = -109 \times 10^6$ cm^3 mol^{-1}). In the temperature range investigated, 50–300 K, Ag_2HgO_2 is semiconducting ($\Delta E_{gap} = 0.24$ eV).

In our view the novel silver mercurate Ag_2HgO_2 might be of significant importance in the field of superconductivity either after doping or for use as a starting material for the synthesis of Ag/Hg/Ca/Ba/Cu/O phases.

Notes and references

† *Crystal data* for Ag_2HgO_2: $M = 448.33$, tetragonal, space group $P4_32_12$ (no. 96), $a = 617.4(1)$, $c = 842.2(1)$ pm, $U = 321.1(1) \times 10^6$ pm^3, $Z = 4$, $\mu = 59.54$ mm^{-1}, 2006 reflections measured, 388 unique ($R_{int} = 0.075$), no. of parameters 25. Final R-values for all data: $R1 = 0.032$ and $wR2 = 0.083$.

X-Ray data were collected on a single-crystal diffractometer with a CCD area detector and graphite monochromated Mo-Kα radiation at room temperature. The structure was solved using the Patterson technique and refined by full-matrix least squares on F^2. An absorption correction with the program HABITUS[12] was applied. Atomic parameters are listed in Table 2.

Table 2 Positional and isotropic displacement (U_{eq})[a] parameters for Ag_2HgO_2

Atom	x	y	z	$U_{eq}/10^{-1}$ pm^2
Hg	0.7825(1)	0.7825(1)	0	23(1)
Ag	0.0023(2)	0.2464(2)	0.1232(1)	28(1)
O	0.3756(16)	0.7525(16)	0.0207(11)	24(2)

[a] $U_{eq} = 1/3(U_{11} + U_{22} + U_{33})$.

CCDC 182/1572. See http://www.rsc.org/suppdata/cc/b0/b000400f/ for crystallographic files in .cif format.

1 S. N. Putilin, E. V. Antipov, O. Chmaissem and M. Marezio, *Nature*, 1993, **362**, 226.
2 A. Schilling, M. Cantoni, J. D. Guo and H. R. Ott, *Nature*, 1993, **363**, 56.
3 E. V. Antipov, S. M. Loureiro, C. Chaillout, J. J. Capponi, P. Bordet, J. L. Tholence, S. N. Putilin and M. Marezio, *Physica C*, 1993, **215**, 1.
4 S. N. Putilin, E. V. Antipov and M. Marezio, *Physica C*, 1993, **212**, 266.
5 S. S. P. Parkin, V. Y. Lee, A. I. Nazzal, R. Savoy, R. Beyers and S. J. La Placa, *Phys. Rev. Lett.*, 1988, **61**, 759.
6 I. K. Gopalakrishnan, J. V. Yakhimi and R. M. Iyer, *Physica C*, 1991, **175**, 183.
7 A. F. Wells, *Structural Inorganic Chemistry*, Clarendon Press, Oxford, 4th edn., 1975, p. 96.
8 M. Jansen, *J. Less-Common Met.*, 1980, **76**, 285.
9 M. Jansen, *Angew. Chem.*, 1987, **99**, 1136; *Angew. Chem., Int. Ed. Engl.*, 1987, **26**, 1098.
10 M. O'Keeffe and B. G. Hyde, *Struct. Bonding (Berlin)*, 1985, **61**, 77.
11 A. Vegas and R. Isea, *J. Solid State Chem.*, 1997, **131**, 358.
12 W. Herrendorf and H. Bärnighausen, HABITUS, University of Karlsruhe, Germany, 1993.

A novel triarylamine-based conjugated polymer and its unusual light-emitting properties

Wang-Lin Yu,[a] Jian Pei,[a] Wei Huang*[a] and Alan J. Heeger[b]

[a] *Institute of Materials Research and Engineering, National University of Singapore, 3 Research Link, Singapore 117602, Republic of Singapore*

[b] *Institute for Polymers and Organic Solids, University of California at Santa Barbara, Santa Barbara, CA 93106-5090, USA*

Received (in Cambridge, UK) 15th December 1999, Accepted 10th March 2000
Published on the Web 30th March 2000

A new soluble triphenylamine-based conjugated polymer, poly[*N*-(4′-butylphenyl)imino(1,1′:4′,1″-terphenyl-4′4″-ylene)], (PBPITP), has been synthesized, which emits blue photoluminescence (PL) with high absolute PL quantum efficiency (45 ± 3%) but exhibits red electroluminescence (red shifted by as much as 157 nm from the PL spectrum).

In the last two decades, conjugated polymers have attracted considerable attention because of their promising applications in optoelectronic devices.[1] In particular, significant progress has been achieved in the development of light-emitting diodes (LEDs) based on conjugated polymers.[2] The important molecular structures for light-emitting applications have been reviewed recently.[3,4] In the past few years, some effort has also been devoted to introducing group 13 and 15 elements, such as boron and nitrogen, into backbones of conjugated polymers to explore new functional materials.[5–8] Although the conjugation is limited because of the introduction of B or N atoms, in which the B or N atoms are connected with C atoms with three σ covalent bonds, extension of π-conjugation along the backbones *via* the vacant p-orbitals of boron atoms or the lone-paired electrons of nitrogen atoms is observed. Some attractive properties, such as improved solubility, high PL efficiency and high stability toward air oxidation, have been demonstrated in such polymers.[5,6] Among the new developed polymers, triarylamine-based ones are particularly interesting because they have low ionization potentials (I_p) and exhibit good hole transporting properties in organic LEDs.[9,10] Here, we report the synthesis of a new triarylamine-based conjugated polymer, poly[*N*-(4-butylphenyl)imino(1,1′:4′,1″-terphenyl-4′,4″-ylene)](PBPITP), and its unusual light-emitting properties.

The chemical structure and the synthetic route to the new polymer PBPITP are depicted in Scheme 1. Monomer **1** was synthesized (30% yield) through a modified Hartwig–Buchwald coupling reaction between 4-butylaniline and a 5-fold excess of 1,4-dibromobenzene in toluene in the presence of tris(dibenzylideneacetone)dipalladium [$Pd_2(dba)_3$], 1,1′-bis(diphenylphosphino)ferrocene (dppf) and $NaOBu^t$.[11,12] Monomer **2** was synthesized (overall yield 60%) in two steps from 1,4-dibromobenzene. 1,4-Dibromobenzene was first converted to *p*-phenylenediboronic acid following the procedure in the literature.[13] *p*-Phenylenediboronic acid was then refluxed with propane-1,3-diol in toluene to afford monomer **2**. Polymerization was performed by a Suzuki coupling reaction using K_2CO_3 as base and toluene as solvent. The polymer was isolated by pouring the hot (*ca.* 60 °C) reaction mixture into stirred methanol and was washed with water, methanol and acetone successively. The polymer was further purified by re-dissolving in THF and then precipitated from methanol twice prior to drying *in vacuo* at room temperature. The polymer was finally obtained as a pale yellow powder (yield 36%). The structure of the polymer was confirmed by ^1H and ^{13}C NMR and elemental analysis.†

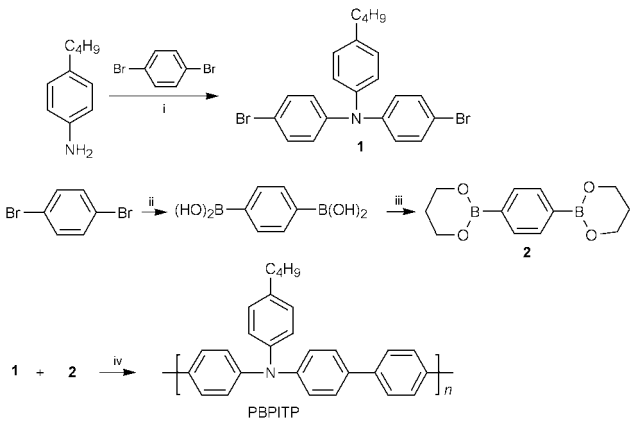

Scheme 1 Synthetic route to PBPITP. *Reagents and conditions*: i, $Pd_2(dba)_3$, dppf, toluene, $NaOBu^t$, 90 °C; ii, (1) Mg, THF, (2) $B(OMe)_3$, THF, −78 °C, (3) H^+, 0 °C; iii, $HO(CH_2)_3OH$, toluene, reflux; iv, $Pd(0)(PPh_3)_4$, K_2CO_3(aq), toluene, *ca.* 100 °C.

The polymer readily dissolves in highly polar solvents, such as THF, chlorobenzene and 1,3-dichlorobenzene, but shows low solubility in low polar solvents, such as toluene and xylene (dissolves upon heating). Uniform and pinhole-free thin films on substrates can be obtained by spin-coating chlorobenzene solutions of the polymer. Poor solubility in toluene and xylene allows the deposition of additional polymer on such films from these solvents. The molecular weight of the polymer was measured by gel permeation chromatography (GPC), using polystyrenes as standard and THF as eluent. The number-average molecular weight (M_n) and polydispersity (PD) were determined as 6400 and 1.75, respectively.

Polymer films on a variety of substrates (micro slides, ITO-coated glasses and quartz plates) emit intense blue light upon exposure to UV light. Fig. 1 shows the UV-VIS absorption and fluorescence (excited at 375 nm) spectra (curves 1 and 2) of the polymer measured from a film on a quartz plate at room temperature. The absorption spectrum peaks at 375 nm and onsets at 448 nm. The π–π* band gap, E_g, is estimated from the

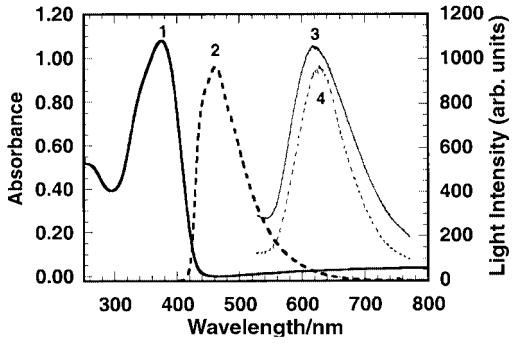

Fig. 1 UV–VIS absorption (1) and photoluminescence (excitation at 375 nm) (2) spectra of PBPITP, and EL spectra recorded from ITO/PBPITP/Ca (3) and ITO/PBPITP/PDHFDDOP/Ca (4).

DOI: 10.1039/a909857g

onset wavelength as 2.77 eV. The fluorescence spectrum exhibits a maximum at 461 nm with a shoulder around 440 nm. The absolute PL efficiency of the polymer as a neat film was measured in an integrating sphere as 45 ± 3%. These results indicate that PBPITP is an efficient blue emissive polymeric PL material.

The redox behavior of the polymer was investigated by cyclic voltammetry (CV) with a standard three-electrode electrochemical cell in a 0.10 M tetrabutylammonium perchlorate solution in acetonitrile at room temperature. The anodically scanned cyclic voltammogram is shown in Fig. 2. The oxidative process starts at *ca.* 0.6 V (*vs*. standard calomel electrode, SCE) and gives a sharp oxidative peak at 1.04 V. The oxidation is highly reversible, and the corresponding reduction peak appears at 0.77 V. The energy level of the highest occupied molecular orbital (HOMO) of the polymer, E_{HOMO}, can be estimated from the oxidative onset potential, to be −5.0 eV.[14] In the cathodic scan, no reduction peak (down to −2.5 V *vs*. SCE was observed). The energy level of the lowest unoccupied molecular orbital (LUMO), E_{LUMO}, can be estimated by subtracting the optical band gap energy, E_g, from E_{HOMO} as determined by the electrochemistry. This leads to an estimate of E_{LUMO} of −2.17 eV.

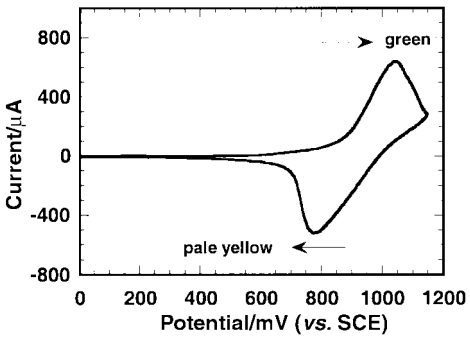

Fig. 2 Cyclic voltammogram of PBPITP. Working electrode: PBPITP film-coated platinum plate (square, *ca.* 1 cm^2); counter electrode: platinum wire; reference electrode: $Ag/AgNO_3$ (0.10 M). Scan rate: 20 $mV.s^{-1}$ room temperature. The arrows indicate the film color change during scan.

Single-layered electroluminescent (EL) cells, ITO|PBPITP(1000 –1500 Å)|Ca (1500 Å), were fabricated. The devices emitted bright red light above *ca.* 15 V under a forward bias (ITO wired positive). The EL spectrum is shown in Fig. 1 (curve 3) and exhibits a maximum at 618 nm. The EL spectrum is red-shifted by 157 nm (0.7 eV) in comparison with the PL spectrum. A layer (1000–1500 Å) of poly(9,9-dihexylfluorene-*alt*-*co*-2,5-didecyloxy-*para*-phenylene) (PDHFDDOP), an efficient blue EL polymer,[10] was further deposited on the PBPITP film to fabricate double polymer-layer ITO|PBPITP|PDHFDDOP|Ca devices, in which the PBPITP film was kept from direct contact with the calcium electrode by the PDHFDDOP layer. The double-layered devices also emitted red light. The EL spectrum (curve 4 in Fig. 1) is almost the same with that recorded from the single-layered devices. The results reveal that an interface effect is not the cause of the large red-shift of EL compared with PL. In addition, the threshold voltages for current flow and light emission were dramatically decreased to *ca.* 5 V upon addition of the PDHFDDOP layer. The external EL quantum efficiency was increased from *ca.* 0.01 to *ca.* 0.025% by the addition of the PDHFDDOP layer. It is evident that the role of the PDHFDDOP film is to serve as an electron-transporting rather than as an emissive layer. The improved EL performance can be attributed to the lower LUMO energy level of PDHFDDOP (− 2.6 eV)[15] compared with that of PBPITP, which results in a smaller energy barrier for electron injection. Also, the improved EL demonstrates the good hole transporting property of PBPITP.

It can be concluded from the results that PBPITP is a promising red EL polymeric material.

In conventional conjugated polymers, PL and EL normally originate from the same molecular excitation, *i.e.* singlet excitons. This results in the EL emission spectrum of a conjugated polymer closely resembling its PL spectrum. The large difference between the PL and EL spectra here implies that the recombination mechanisms of charge carriers for PL and EL in PBPITP are different. A similar phenomenon was reported most recently in a binaphthalene-containing conjugated polymer.[16] Excimer emission might be responsible for the unusual emissive phenomenon.[17] Further investigation is required in order to understand the origin of the unusual emissive phenomenon and what mechanisms are responsible for it, and are actively being pursued.

In summary, a new soluble triarylamine-containing conjugated polymer has been synthesized through a Suzuki coupling reaction. The polymer in the form of a film exhibits high absolute PL efficiency and good hole transporting properties. The PL emission of the polymer is blue whereas its EL emission is red. The wavelength difference between the PL and EL spectrum is as large as 157 nm. It is evident that the PL and EL spectrum correspond to different molecular excitations. Such a polymer provides a good opportunity to understand the PL and EL processes in conjugated polymers.

Part of the work was carried out in the University of California, Santa Barbara (UCSB). We would like to thank Dr Vojislav Srdanov (UCSB) for his kind help in the measurement of PL quantum efficiency.

Notes and references

† *Selected data* for PBPITP: $\delta_H(CDCl_3)$ δ 7.76–7.44 (m, 10H), 7.22–7.01 (m, 6H), 2.75–2.49 (t, 2H), 1.74–1.49 (m, 2H), 1.49–1.24 (m, 2H), 1.03–0.86 (t, 3H). $\delta_c(CDCl_3)$ 147.06, 144.88, 138.91, 138.23, 134.33, 129.27, 128.97, 128.16, 127.27, 126.81, 125.06, 123.67, 35.04, 33.61, 22.39, 13.95. Anal. Calc. for $C_{28}H_{25}N$: C, 89.56; H, 6.71; N, 3.73. Found: C, 88.17; H, 6.84; N, 3.46%.

1 A. J. Heeger, *Solid State Commun.*, 1998, **107**, 673.
2 R. H. Friend, R. W. Gymer, A. B. Holmes, J. H. Burroughes, R. N. Markes, C. Taliani, D. D. C. Bradley, D. A. Dos Santos, J. L. Brédas, M. Lögdlund and W. R. Salaneck, *Nature*, 1999, **397**, 121.
3 J. L. Segura, *Acta Polym.*, 1998, **49**, 319.
4 A. Kraft, A. C. Grimsdale and A. B. Holmes, *Angew. Chem., Int. Ed.*, 1998, **37**, 402.
5 N. Matsumi, K. Naka and Y. Chugo, *J. Am. Chem. Soc.*, 1998, **120**, 5112.
6 G. Yu, Y. Liu, X. Xu, M. Zheng, F. Bai and D. Zhu, *Appl. Phys. Lett.*, 1999, **74**, 2295.
7 Y. Kunugi, I. Tabakovic, A. Canavesi and L. L. Miller, *Synth. Met.*, 1997, **89**, 227.
8 F. E. Goodson and J. F. Hartwig, *Macromolecules*, 1998, **31**, 1700.
9 E. Bellmann, S. E. Shaheen, R. H. Grubbs, S. R. Marder, B. Kippelen and N. Peyghambarian, *Chem Mater.*, 1999, **11**, 399.
10 A. Yamamori, C. Adachi, T. Koyama and Y. Taniguchi, *Appl. Phys. Lett.*, 1998, **72**, 2147.
11 F. Paul, J. Patt and J. F. Hartwig, *J. Am. Chem. Soc.*, 1994, **116**, 5969.
12 A. S. Guram, R. A. Rennels and S. L. Buchwald, *Angew. Chem., Int. Ed. Engl.*, 1995, **34**, 1348.
13 I. G. C. Coutts, H. R. Goldschmid and O. C. Musgrave, *J. Chem. Soc. C*, 1970, 488.
14 J. C. de Mello, M. M. J. Simenon, A. R. Brown and R. E. F. Einerhand, *Synth. Met.*, 1997, **87**, 53.
15 W.-L. Yu, J. Pei, Y. Cao, W. Huang and A. J. Heeger, *Chem. Commun.*, 1999, 1837.
16 A. K.-Y. Jen, Y. Liu, Q.-S. Hu and L. Pu, *Appl. Phys. Lett.*, 1999, **75**, 3745.
17 S. A. Jenekhe and J. A. Osaheni, *Science*, 1994, **265**, 765.

IR spectroscopy as a high-throughput screening-technique for enantioselective hydrogen-transfer catalysts†

Daniëlle G. I. Petra, Joost N. H. Reek, Paul C. J. Kamer, Hans E. Schoemaker and Piet W. N. M. van Leeuwen*

Institute of Molecular Chemistry, University of Amsterdam, Nieuwe Achtergracht 166, 1018 WV Amsterdam, The Netherlands. E-mail: pwnm@anorg.chem.uva.nl

Received (in Basel, Switzerland) 17th January 2000, Accepted 10th March 2000
Published on the Web 30th March 2000

A new high-throughput screening-technique based on IR spectroscopy has been developed for ruthenium catalysed asymmetric transfer-hydrogenation by comparing the reaction rate of the reduction of ketones using (*R*)- *vs.* (*S*)-secondary alcohol as the hydrogen donor.

Combinatorial chemistry and rapid screening techniques are widely recognised as very promising tools in the development of novel catalysts.[1] Recent research has been focussed on two important aspects, *viz.* the parallel synthesis of new catalysts and the development of new rapid screening techniques. Most of the screening methods developed so far are based on UV–VIS, fluorescence spectroscopy and more recently also IR thermography[2] and involve screening of the activity of the catalyst only. The number of screening methods that have been reported involving enantioselective catalysis is rather small.[3–5] Here we report on a novel technique based on IR spectroscopy for the rapid screening of enantioselective transfer-hydrogenation catalysts.

Asymmetric transfer-hydrogenation is an efficient, mild and clean method for the synthesis of chiral alcohols.[6] Only a few examples are known of the enantioselective transfer-hydrogenation of functionalised ketones,[7] dialkyl ketones[8] and imines[9] that finally may lead to useful intermediates for the fine-chemical industries. Therefore, a combinatorial approach to develop efficient chiral transition metal catalysts for the transfer-hydrogenation of different substrates and a method to rapidly screen and optimise these catalysts is pivotal.

In order to test our proposed new rapid screening technique we used a known reaction: the reduction of acetophenone in propan-2-ol (Scheme 1) using (1*R*, 2*S*)-ephedrine **1** on (*R*)-phenylglycinol **2** in combination with ruthenium(II) as the catalyst.[10] The use of **1** gives rise to a high enantioselectivity (89%), whereas the use of **2** as the amino alcohol ligand results in a much lower enantioselectivity (24%) (Table 1).

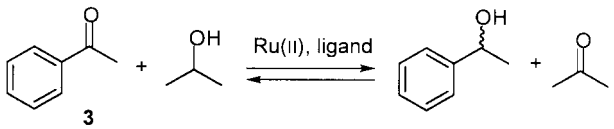

3

Scheme 1

The carbonyl of the aryl alkyl ketone absorbs at a different wavenumber in the IR than the dialkyl ketone (1682 and 1707 cm-1, respectively) which allows the reaction to be monitored by IR spectroscopy (Fig. 1). We performed a test reaction (reduction of acetophenone using propan-2-ol as the H-donor) that was followed both by IR and gas chromatography (GC) giving identical results. This indicates that IR is a reliable technique (Fig. A, ESI†).

A drawback of the transfer-hydrogenation reaction using an alcohol as the hydrogen source is its reversibility. At the same time, however, this property can be utilised for the kinetic resolution of secondary alcohols.[11] When the reduction of acetophenone occurs with an enantiofacial differentiation of $k_{Si}/k_{Re} \approx 100$, the dehydrogenation of (*R*)-1-phenylethanol is also *ca.* 100 times faster than that of (*S*)-phenylethanol. Here, we use the reversibility of the reaction to set up a rapid screening technique for enantioselective hydrogen transfer catalysts. Instead of monitoring the transfer-hydrogenation reaction we screen on the reverse reaction by determining the difference in dehydrogenation rate using (*R*)- and the (*S*)-1-phenylethanol. The difference in *dehydrogenation rate* between the (*R*)- and the (*S*)-alcohol is a measure of the enantioselectivity of the reaction and can be determined rapidly by IR spectroscopy. Table 1 shows the results of the ruthenium(II)-amino alcohol catalysts, containing ligands **1** and **2**, in the dehydrogenation of (*R*)- and (*S*)-1-phenylethanol (entries 3–6). These reactions were monitored with time by IR spectroscopy and Fig. 2 shows the results of experiments with **1** as ligand whereas Fig. B (ESI†) shows the results for ligand **2**.

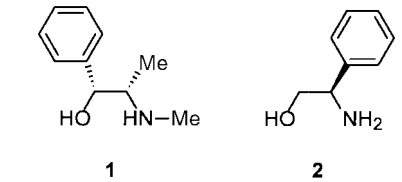

1 **2**

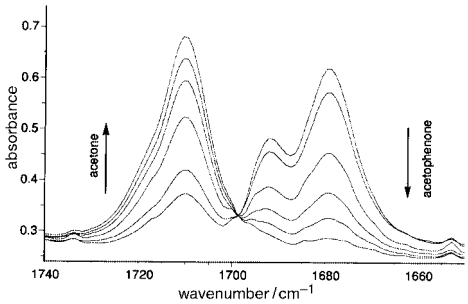

Fig. 1 The hydrogen transfer reaction followed by IR spectroscopy.

The reaction rate for the dehydrogenation of (*R*)-1-phenylethanol is much faster than the dehydrogenation of (*S*)-1-phenylethanol. The initial reaction rate calculated from the IR data is *ca.* 15 times higher for (*R*)-*cf.* (*S*)-1-phenylethanol (k_R/k_S = 15). This is in very good agreement with the k_{Si}/k_{Re} ratio of 17 calculated from the enantioselectivity in the hydrogenation reaction (entries 1 and 2). A smaller difference in dehydrogenation rate is observed for the Ru(II)–phenylglycinol catalyst (Table 1, Fig. B, ESI†). The much smaller k_R/k_S ratio of 2, calculated from the IR data, was again in very good agreement with the k_{Si}/k_{Re} ratio calculated from the enantioselectivity in the hydrogenation reaction.

To use this technique for rapid screening of novel chiral catalysts, a single measurement per reaction mixture should suffice to determine an approximate ee value. Therefore the

† Electronic supplementary information (ESI) available: Fig. A, B and C; IR, GC, UV–VIS data and Experimental details (see text). See http://www.rsc.org/suppdata/cc/b0/b000479k/

DOI: 10.1039/b000479k

Table 1 Ru(II)-amino alcohol catalysed transfer hydrogenation[a]

Entry	Ligand	Ketone	H-donor	Conv. of ketone (%)[b]	Ee (%) alcohol[c,d]	k_{Si}/k_{Re}[e]	k_R/k_S[f]
1	**1**	**3**	Propan-2-ol	96	89	17	
2	**2**	**3**	Propan-2-ol	94	24	1.6	
3	**1**	**4**	(*R*)-1-Phenylethanol	95	—		15
4	**1**	**4**	(*S*)-1-Phenylethanol	15	—		
5	**2**	**4**	(*R*)-1-Phenylethanol	93	—		2
6	**2**	**4**	(*S*)-1-Phenylethanol	60	—		

[a] Reactions were carried out at room temperature using a 0.1 M ketone solution (33.3 mmol) in alcohol. Substrate : [$RuCl_2$(*p*-cymene)]2 : ligand : Bu^tOK = 400 : 1 : 5: 12.5. [b] Conversions were determined after 40 min by GLC analysis and/or IR spectroscopy. [c] Determined by capillary GLC analysis using a chiral cycloSil-B column. [d] The product configurations are (*R*). [e] k_{Si}/k_{Re} = (100 − *x*)/*x*; *x* = (100 − ee)/2. [f] Determined by IR spectroscopy after 5 min.

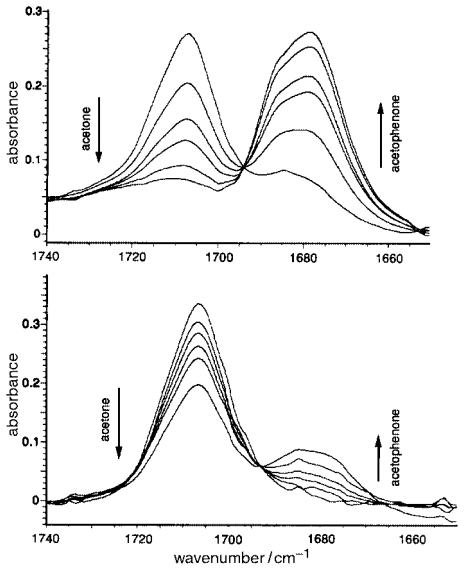

Fig. 2 Dehydrogenation of (*R*)- (top) and (*S*)-1-phenylethanol (bottom) using ligand **1**.

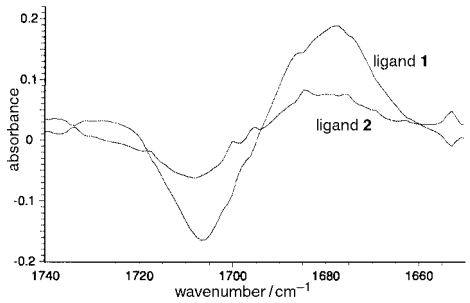

Fig. 3 IR-difference spectra of the dehydrogenation of (*R*)- and (*S*)-1-phenylethanol taken after 30 min reaction time, using **1** and **2** as the ligand.

difference in dehydrogenation rate between (*R*)- and (*S*)-1-phenylethanol was measured after 30 min and visualised as a difference spectrum (Fig. 3). Catalysts that give no chiral induction will give a flat line, whereas active and highly enantioselective catalysts will result in large peaks. Indeed the difference in reaction rate between the oxidation of (*R*)- and (*S*)-1-phenylethanol is much larger when Ru(II)–**1** is used than when Ru(II)–**2** is used as the catalyst. A good estimation of the enantioselectivity can be made simply from two IR measurements. Using an automated set up one could easily measure 100 IR spectra per hour,[12] which makes this rapid screening technique an order of magnitude faster than the known techniques as GC, HPLC and NMR.

Screening catalysts for reduction of dialkyl ketones using propan-2-ol as the donor using the above method is troublesome since the signals of acetone **4** and other dialkyl ketones overlap in the IR spectrum. Therefore acetophenone **3** and benzophenone **5** were used as substrates, using (*R*)- and (*S*)-hexan-2-ol as the H-donor, allowing the reaction to be followed by IR spectroscopy (Fig. C, ESI†). The k_{Si}/k_{Re} ratio calculated from the IR data was between 1 and 2 for both experiments, *i.e.* using ligands **1** and **2**. This is again in full agreement with the hydrogen transfer experiment, since only low ee values were obtained in the transfer-hydrogenation of hexanon using either ligand **1** or **2**.

In conclusion, IR spectroscopy proved to be a very useful technique to determine the performance of enantioselective transfer-hydrogenation catalysts. The reaction can be followed with time by performing it in the IR cell, or samples can be taken from a reaction mixture and subsequently analysed. The former method is especially interesting if non-linear effects are involved, whereas the single point measurements are more suited for rapid screening techniques. The difference in dehydrogenation rate between the (*R*)- and (*S*)-alcohol, *i.e.* the ratio k_R/k_S, serves as a reliable prefatory measure for the enantioselectivity of the transfer-hydrogenation of both aryl alkyl and dialkyl ketones.

The Innovation Oriented Research Programme (IOP-Katalyse) is gratefully acknowledged for their financial support of this research.

Notes and references

1 B. Jandeleit, H. W. Turner, T. Uno, J. A. M. van Beek and W. H. Weinberg, *CatTech*, 1998, **2**, 101; R. H. Crabtree, *Chem. Commun.*, 1999, 1611; B. Jandeleit, D. J. Schaefer, T. S. Powers, H. W. Turner and W. H. Weinberg, *Angew. Chem., Int. Ed.*, 1998, **38**, 2494.
2 S. J. Taylor and J. P. Morken, *Science*, 1998, **280**, 267; A. Holtzwarth, H.-W. Schmidt and W. F. Maier, *Angew. Chem., Int. Ed.*, 1998, **37**, 2644.
3 X. Gao and H. B. Kagan, *Chirality*, 1998, **10**, 120 and references therein.
4 M. T. Reetz, M. H. Becker, K. M. Kühling and A. Holtzwarth, *Angew. Chem., Int. Ed.*, 1998, **37**, 2647; M. T. Reetz, M. H. Becker, H.-W. Klein and D. Stöckigt, *Angew. Chem., Int. Ed.*, 1999, **38**, 1758; M. T. Reetz and K.-E. Jaeger, *Top. Curr. Chem.*, 1999, **200**, 31.
5 M. T. Reetz, A. Zonta, K. Schimossek, K. Liebeton and K.-E. Jaeger, *Angew. Chem., Int. Ed.*, 1997, **36**, 2830.
6 M. J. Palmer and M. Wills, *Tetrahedron: Asymmetry*, 1999, **10**, 2045.
7 K. Matsumura, S. Hashiguchi, T. Ikariya and R. Noyori, *J. Am. Chem. Soc.*, 1997, **119**, 8738; D. J. Bayston, C. B. Travers and M. E. C. Polywka, *Tetrahedron: Asymmetry*, 1998, **9**, 2015.
8 T. Langer and G. Helmchen, *Tetrahedron Lett.*, 1996, **37**, 1381; Y. Jiang, Q. Jiang, G. Zhu and X. Zhang, *Tetrahedron Lett.*, 1997, **38**, 215.
9 N. Uematsu, A. Fujii, S. Hashiguchi, T. Ikariya and R. Noyori, *J. Am. Chem. Soc.*, 1996, **118**, 4916.
10 J. Takehara, S. Hashiguchi, A. Fujii, I. Shin-ichi, T. Ikariya and R. Noyori, *Chem. Commun.*, 1996, 233; D. G. I. Petra, P. C. J. Kamer, P. W. N. M. van Leeuwen, K. Goubitz, A. M. van Loon, J. G. de Vries and H. E. Schoemaker, *Eur. J. Inorg. Chem.*, 1999, **12**, 2335; M. Palmer, T. Walsgrove and M. Wills, *J. Org. Chem.*, 1997, **62**, 5226.
11 R. Noyori and S. Hashiguchi, *Acc. Chem. Res.*, 1997, **30**, 97.
12 IR set-ups equipped with an autosampler that can handle between 100 and 180 samples per hour are nowadays commercially available.

ChemComm

Characterisation and kinetic behaviour of $H_2Rh(PPh_3)_2(\mu\text{-}Cl)_2Rh(PPh_3)$(alkene) and related binuclear complexes detected during hydrogenation studies involving parahydrogen induced polarisation

Simon A. Colebrooke,[a] Simon B. Duckett*[a] and Joost A. B. Lohman[b]

[a] *Department of Chemistry, University of York, Heslington, York, UK YO10 5DD. E-mail: sbd3@york.ac.uk*
[b] *Bruker UK Limited, Coventry, UK*

Received (in Cambridge, UK) 21st January 2000, Accepted 14th March 2000
Published on the Web 31st March 2000

When parahydrogen induced polarisation is used to examine hydrogenation reactions involving $[Rh(\mu\text{-}Cl)(PPh_3)_2]_2$ and $RhCl(CO)(PMe_3)_2$, binuclear dihydride complexes are detected, characterised, and shown to be capable of alkene hydrogenation.

The *in situ* study of H_2 oxidative addition reactions using NMR spectroscopy in conjunction with para-enriched hydrogen (p-H_2)[1] has led to the detection of many new dihydride complexes.[2,3] This phenomenon enables the generation of a non-Boltzmann spin population for the ensemble of nuclei originally in p-H_2 which in turn allows their detection *via* signal strengths that often exceed the norm by 1000 times.[2] Prior work in this area has shown that monitoring the oxidative addition of p-H_2 to $RhCl(CO)L_2$ and $RhClL_3$ (L = PPh_3, PMe_3) enables the detection of binuclear dihydride species.[4] Here, we demonstrate how p-H_2 can be used to monitor the hydrogenation process directly and facilitate the detailed characterisation of species such as $(H)_2Rh(PPh_3)_2(\mu\text{-}Cl)_2Rh(PPh_3)$(alkene). We also show that the addition of a sacrificial alkene can facilitate the characterisation of previously uncharacterised dihydrides.

Initially, a series of C_6D_6 solutions containing *ca.* 1 mg of $[Rh(\mu\text{-}Cl)(PPh_3)_2]_2$ and varying amounts of styrene were monitored by ^1H NMR spectroscopy at 295 K while under 3 atm of p-H_2. At early reaction times these solutions immediately yielded polarised hydride resonances at δ −18.72 and −19.51, arising from the previously reported complex $(H)_2Rh(PPh_3)_2(\mu\text{-}Cl)_2Rh(PPh_3)$(styrene) **2a**.[4] A 2D-^1H–^{31}P HMQC experiment [Fig. 1(a)] revealed that this product contains two mutually coupled phosphorus resonances separated by 1210 Hz, at δ 35.23 and 42.73.† The large J_{PP} coupling of 427 Hz confirms that the two detected phosphines are located in a *trans* arrangement in the product.[7] The analogous species formed with hex-1-ene, **2b**, also possesses inequivalent phosphines, although the separation between the ^{31}P signals is reduced to 590 Hz. However, the corresponding species with *cis*-stilbene, **2c**, yields a single ^{31}P resonance in the same experiment which requires the two phosphines to be equivalent.†

Hence for **2a** and **2b** the alkene substituents are unsymmetrically displaced about the plane containing the Rh centres and thereby render the PPh_3 ligands inequivalent. For the *cis*-stilbene complex **2c** the presence of a mirror plane makes the phosphines equivalent. These experimental results are consistent with calculations that show it is favourable for an alkene to bind to a ML_3 fragment with the C=C bond arranged perpendicular to the plane containing the framework atoms.[5] Surprisingly, when 1,2 diphenylethene is employed, the analogous product **2d** also contains equivalent phosphines. This suggests that steric interactions can force the alkene to bind with the C=C bond arranged in the plane of the two metal centres.

In these studies, the observed hydride signals for species of type **2** decay rapidly as the hydrogen present in solution is consumed by alkane formation. However, the absolute intensity of the hydride signals for **2** increased consistently when solutions were examined which contain lower alkene, and identical rhodium and p-H_2, concentrations. In order to learn more about this effect we adapted the 1D NOE sequence of Keeler for use with p-H_2.[6] Selective pulses were used in conjunction with a suitable mixing time (for chemical exchange and NOE build-up) to probe the behaviour of a single, pre-selected, hydride resonance. We note that there are several possibilities for dynamic behaviour involving the hydride

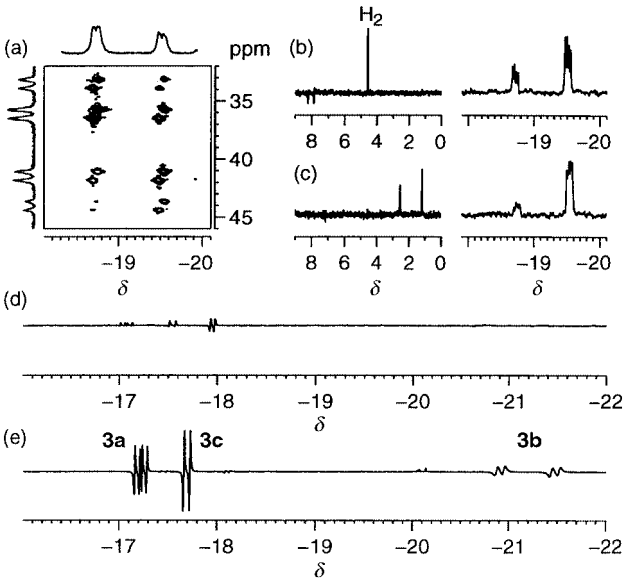

Fig. 1 (a) Selected cross peaks (absolute value display) and projections of the ^1H–^{31}P HMQC spectrum of **2a** showing hydride and phosphorus connectivity. (b) $^1H\{^{31}P\}$ 1D-NOE spectrum of p-H_2 enhanced **2a** at 295 K with resonance selection at δ −19.51 and a mixing time of 400 ms. Intramolecular hydride interchange is indicated. (c) $^1H\{^{31}P\}$ 1D-NOE spectrum of parahydrogen enhanced **2a** at 295 K with resonance selection at δ −19.51, mixing time of 200 ms, and *ca.* 20-fold reduction in [styrene]. Peaks indicate intramolecular hydride interchange, conversion to ethylbenzene and exchange with free H_2. (d) ^1H NMR spectrum showing the hydride region of a sample containing $RhCl(CO)(PMe_3)_2$ and p-H_2 in C_6D_6 at 295 K. (e) ^1H NMR spectrum at 295 K showing the same sample used in recording (d) but after introducing styrene in addition to the p-H_2.

DOI: 10.1039/b000607f

ligands of **2**: (i) intramolecular hydride interchange (ii) exchange with free hydrogen and (iii) transfer into the alkene (bound or free).

When the hydride resonances of **2a** at δ −18.72 or −19.51 were probed in separate experiments, NOE connections were visible, with both selections, to two *ortho* phenyl resonances at δ 8.20 and 7.85, supporting the conclusion that the two phosphines of the Rh(III) centre are inequivalent. The spectrum shown in Fig. 1(b) illustrates the result for the δ −19.51 hydride resonance of **2a**. The presence of the second peak, at δ −18.72, indicates that hydride interchange occurs during the mixing time. The magnitude of this exchange peak, for a given mixing time, proved to be independent of the concentration of styrene, and catalyst, which suggests that the hydride interchange process is intramolecular. Eyring analysis of the resulting rate data yielded activation parameters for hydride interchange, $\Delta H^{\ddagger}$ = 42 ± 4 kJ mol^{-1} and $\Delta S^{\ddagger}$ = −100 ± 12 J K^{-1} mol^{-1}. A process involving halide bridge rupture, followed by rotation about the remaining Rh–Cl bridge, and bridge re-establishment is consistent with this information (Scheme 1).[7]

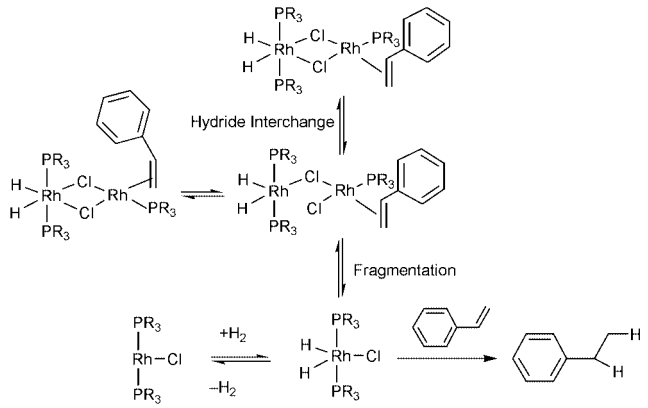

Scheme 1 (R = Ph).

The overall situation is complicated by the fact that the hydride resonances of **2** also connect to the resonance of free H_2. Surprisingly, as the concentration of alkene in solution falls both the proportion (rate) of reductive elimination of H_2 from **2** and the relative signal intensities of the two hydride resonances increase. For example, when the alkene concentration was reduced by a factor of 16, the associated hydride signals of **2a** increased by over 100 times. Significantly, at even lower alkene concentrations magnetisation transfer from the hydrides of **2a** to the alkyl protons of the hydrogenation product ethylbenzene is observed [Fig. 1(c)]. This corresponds to direct evidence for the binuclear metal dihydride complexes themselves being linked to alkene hydrogenation. In order to account for this complex kinetic behaviour the hydrogenation process cannot simply involve bridge opening followed by alkene binding. A logical option would be for hydrogenation to proceed *via* binuclear complex fragmentation with trapping of the resultant $RhClH_2(PR_3)_2$ fragment by alkene, rather than halide of a mononuclear rhodium centre, being productive in this regard. We therefore examined the hydrogenation activity of $RhCl(CO)(PMe_3)_2$. As a control, a benzene solution of $RhCl(CO)(PMe_3)_2$ was first reacted with p-H_2 at 295 K. The corresponding 1024 scan ^{1}H spectrum, shown in Fig. 1(d), contained polarised signals due to $(H)(Cl)Rh(PMe_3)_2(\mu\text{-}H)(\mu\text{-}Cl)Rh(CO)(PMe_3)$ **3a**.[7] When an identical sample was prepared and monitored in the presence of a 1.5 fold excess of styrene relative to $RhCl(CO)(PMe_3)_2$, the spectrum shown in Fig. 1(e) was obtained. Now the new species $(H)_2Rh(PMe_3)_2(\mu\text{-}Cl)_2Rh(CO)(PMe_3)$ **3b** and $HRh(PMe_3)_2(\mu\text{-}H)(\mu\text{-}Cl)_2Rh(CO)(PMe_3)$ **3c** are clearly visible, and there is a dramatic 16 fold increase in size of the associated hydride signal intensities of **3a**; the spectral features of these species are

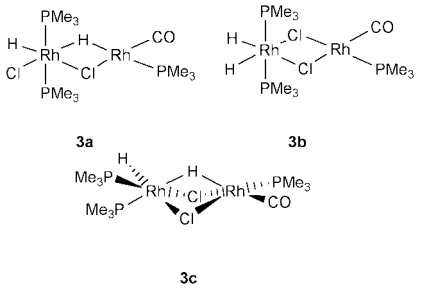

similar to those of their iodide derivatives.[7] These additional complexes are visible because p-H_2 cycling in **3** is enhanced by the hydrogenation pathway (in addition to simple reversible H_2 exchange).

In summary, these studies have demonstrated that there is a role for binuclear dihydride species as a 'hydrogen store' during hydrogenation catalysis. For **2**, this corresponds to direct evidence for H_2 transfer from the binuclear complex to the substrate *via* initial fragmentation to $RhH_2Cl(PPh_3)_2$. Significantly, we have shown that (metal–dihydride)–p-H_2 exchange reactions can be promoted by the addition of a sacrificial alkene with the result that previously unseen species become observable with this technique.

Financial support from the EPSRC, Bruker UK (Spectrometer, CASE award S. A. C.), the Royal Society, NATO, and discussions with Prof. R. Eisenberg, Prof. R. N. Perutz, Dr B. A. Messerle, and Dr R. J. Mawby are gratefully acknowledged.

Notes and references

† *Selected spectroscopic data* at 400.13 MHz (^{1}H) and 161.45 MHz (^{31}P) and 100.2 MHz (^{13}C) in benzene-d_6 (couplings Hz): **2a**: ^{1}H, δ −18.72 (ddt, $^2J_{HH}$ −10.9, $^1J_{RhH}$ 22.1, $^2J_{PH}$ 17), −19.51 (ddt, $^2J_{HH}$ −10.9, $^1J_{RhH}$ 22.7, $^2J_{PH}$ 17), 8.20 (m, *o*-Ph), 7.85 (m, *o*-Ph); ^{31}P, δ 42.73 ($^1J_{RhP}$ 127, $^2J_{PP}$ 417); 35.23 ($^1J_{RhP}$ 127, $^2J_{PP}$ 417); ^{103}Rh, δ 900. **2b**: ^{1}H, δ −18.66 (ddt, $^2J_{HH}$ −11.0, $^1J_{RhH}$ 22.6, $^2J_{PH}$ 17), −19.46 (ddt, $^2J_{HH}$ −11.0, $^1J_{RhH}$ 22.4, $^2J_{PH}$ 17), 8.24 (m, *o*-Ph), 8.09 (m, *o*-Ph); ^{31}P, δ 40.42 ($^1J_{RhP}$ 127, $^2J_{PP}$ 417), 36.78 ($^1J_{RhP}$ 127, $^2J_{PP}$ 417). **2c**; ^{1}H, δ −18.73 (ddt, $^2J_{HH}$ −10.8, $^1J_{RhH}$ 23.4, $^2J_{PH}$ 17), −19.46 (ddt, $^2J_{HH}$ −10.8, $^1J_{RhH}$ 23.0, $^2J_{PH}$ 17); ^{31}P, δ 39.6 ($^1J_{RhP}$ 126.6). **2d**: ^{1}H, δ −19.12 (ddt, $^2J_{HH}$ −10.5, $^1J_{RhH}$ 23.7, $^2J_{PH}$ 16), −19.43 (ddt, $^2J_{HH}$ −10.5, $^1J_{RhH}$ 23.8, $^2J_{PH}$ 16); ^{31}P, δ 41.2 ($^1J_{RhP}$ 132.9). **3a**: ^{1}H, δ −17.09 (ddddt, $^2J_{HH}$ −3.2, $^1J_{RhH}$ 29, $^1J_{RhH}$ 19, $^2J_{PH}$ 15.5, $^2J_{PH}$ 30), −17.57 (ddt, $^2J_{HH}$ −3.2, $^1J_{RhH}$ 24.8, $^2J_{PH}$ 15.5). **3b**: ^{1}H, δ −20.75 (ddt, $^2J_{HH}$ −11, $^1J_{RhH}$ 30.9, $^2J_{PH}$ 19), −21.3 (ddt, $^2J_{HH}$ −11, $^1J_{RhH}$ 30.0, $^2J_{PH}$ 22). **3c**: ^{1}H δ −10.1 (ddddt, $^2J_{HH}$ −7, 2 × $^1J_{RhH}$ 20.2, $^2J_{PH}$ 115, $^2J_{PH}$ 20, 17), −17.95 (ddt, $^2J_{HH}$ −7, $^1J_{RhH}$ 18.5, $^2J_{PH}$ 19, 11).

1 C. R. Bowers and D. P. Weitekamp, *J. Am. Chem. Soc.*, 1987, **109**, 5541; R. Eisenberg, *Acc. Chem. Res.*, 1991, **24**, 110; J. Natterer and J. Bargon, *Prog. Nucl. Magn. Reson. Spectrosc.*, 1997, **31**, 293.

2 C. J. Sleigh and S. B. Duckett, *Prog. Nucl. Magn. Reson. Spectrosc.*, 1999, **34**, 71; S. Hasnip, S. B. Duckett, D. R. Taylor and M. J. Taylor, *Chem. Commun.*, 1998, 923; S. Hasnip, S. B. Duckett, D. R. Taylor, G. K. Barlow and M. J. Taylor, *Chem. Commun.*, 1999, 889; A. Harthun and J. Bargon, *Angew. Chem., Int. Ed. Engl.*, 1997, **109**, 1103.

3 S. B. Duckett, C. L. Newell and R. Eisenberg, *J. Am. Chem. Soc,*, 1994, **116**, 10 548.

4 S. B. Duckett and R. Eisenberg, *J. Am. Chem. Soc.*, 1993, **115**, 5292; S. B. Duckett, R. Eisenberg and A. S. Goldman, *J. Chem. Soc., Chem. Commun.*, 1993, 1185; P. D. Morran, S. A. Colebrooke, S. B. Duckett, J. A. B. Lohmann and R. Eisenberg, *J. Chem. Soc., Dalton. Trans.*, 1998, 3363.

5 T. A. Albright, R. Hoffmann, J. C. Thibeault and D. L. Thorn, *J. Am. Chem. Soc.*, 1979, **107**, 3801.

6 K. Stott, J. Stonehouse, J. Keeler, T. L. Hwang and A. J. Shaka, *J. Am. Chem. Soc.*, 1995, **117**, 4199.

7 P. D. Morran, S. B. Duckett, P. R. Howe, J. E. McGrady, S. A. Colebrooke, R. Eisenberg, M. G. Partridge and J. A. B. Lohman, *J. Chem. Soc., Dalton Trans.*, 1999, 3949.

First observation of high-resolution solid-state ^{73}Ge NMR spectra of organogermanium compounds

Yoshito Takeuchi,*[a] Miki Nishikawa,[a] Katsumi Tanaka,[a] Toshio Takayama,[b] Mamoru Imanari,[c] Kenzou Deguchi,[c] Teruaki Fujito[c] and Yasushi Sugisaka[c]

[a] *Department of Chemistry, Faculty of Science, Kanagawa University, 2946 Tsuchiya, Hiratsuka-shi, Japan 259-1293. E-mail: yoshito@info.kanagawa-u.ac.jp*
[b] *Department of Applied Chemistry, Faculty of Engineering, Kanagawa University, 3-27-1 Rokkakubashi, Kanagawa-ku, Yokohama-shi, Japan 221-8686*
[c] *NMR Application Laboratory, JEOL Ltd., 3-1-2 Musashino, Akishima-shi, Tokyo, Japan 196-8558*

Received (in Cambridge, UK) 7th February 2000, Accepted 15th March 2000
Published on the Web 30th March 2000

High-resolution solid-state MAS ^{73}Ge NMR spectra of organogermanium compounds have been observed for the first time; the chemical shifts and half-widths of tetraphenylgermane and tetrabenzylgermane were recorded with and without high-power decoupling.

Though the natural abundance is comparaable with the ^{29}Si isotope, recording of ^{73}Ge resonances is known to be very difficult because of the low value of γ, along with its nuclear spin of $-9/2$ and large quadrupolar moment. These cause distortion of the electric field gradient around the germanium nucleus leading to excessive broadening of the signals. In solution ^{73}Ge NMR spectroscopy, it was observed that when the symmetry of the structure around the germanium atom is high, a sharp signal can be observed (as found for ^{14}N NMR) while the signal tends to broaden as the symmetry is lost. For instance the half-width of tetramethylgermane, a compound with the highest symmetry, is only 1,4 Hz[1] while corresponding values of germacyclohexane, 1-methylgermacyclohexane and 1,1-dimethylgermacyclohexane are 15.4, 22.3 and 15.6 Hz, respectively.[2] It was also observed that when either halogen or oxygen atoms are unsymmetrically substituted, as found in 1-bromo-1-methylgermacyclohexane, an excessive broadening took place to such an extent that observation of signals was impossible.

Given these factors, it has generally been accepted that observation of ^{73}Ge signals in the solid state would be even more difficult, and to the best of our knowledge, there have been no reports on ^{73}Ge signals of organogermanium compounds in the solid state.

In a series of papers on solution ^{73}Ge NMR spectra over the last 15 years we have accumulated data for a variety of organogermanium compounds.[3] We noted that the rapid development of NMR hard- and soft-ware has made observation of ^{73}Ge signals more feasible. We thought that by an appropriate modification of hardware it might be possible to observe solid-state high-resolution ^{73}Ge NMR spectra of organogermanium compounds with the aid of high-field instruments. Thus, we initiated an investigation to observe ^{73}Ge NMR spectra of solid-state samples.

We chose tetraphenylgermane **1** and tetrabenzylgermane **2** for over first attempt because of their high symmetry.[4] To our surprise, **1** gave an unexpectedly sharp signal, even without high-power proton decoupling, after an accumulation of a few hundred FIDs. Under similar measurement conditions, the half-width of the signal of 2 is much broader, and required much more accumulation for signal recording. ^{73}Ge chemical shifts and the half-width of the signals for **1** and **2** are given in Table 1. There is a small shift, in comparison to values in solution, arising from a solid-state effect. When high-power proton decoupling was applied to **1**, the half-width became slightly smaller. Fig. 1 shows the^{73}Ge NMR spectra of **1** and **2**.

As is always the case for NMR signals for low-γnuclei, there is some possibility that the observed signal may be an artifact. We eliminated this possibility by several means: (i) the FID shows a clear ringing pattern; (ii) a systematic change of irradiation frequency yields a corresponding change of resonance frequency; (iii) removal of the sample tube caused the disappearance of the signal.

It is unusual that there is such a large difference in the half-width for the two compounds since X-ray crystallographic analysis indicated a very high symmetry around germanium atom for both **1** and **2**.[6] There is, however, a small difference in the structures (**2** exhibits four independent phenyl rings while **1** exhibits only one in the asymmetric unit), which may be the reason for the difference in half-width.

Given the above encouraging results it will be important and interesting to delineate the scope and limitation of high-resolution solid-state ^{73}Ge NMR spectroscopy for organogermanium compounds. We believe that most if not all

Table 1 Chemical shifts and half-width of ^{73}Ge signals for **1** and **2** in the solid state [a]

Compound	δ[b]	Half-width/Hz
1 (proton decoupled)	−31.0 (−3.6)[c]	40 (6)[c]
1 (proton coupled)	−31.0	49
2 (proton decoupled)	0.14 (0.04)	*ca.* 350 (24)

[a] Values in parentheses are solution data for the same compounds. [b] We measured the ^{17}Ge NMR spectrum for tetraethylgermane (liquid) filled in a cell without rotation and assumed that the chemical shift under this measurement condition was δ 17.3 (the same value as in solution). The chemical shifts of **1** and **2** in the solid state were referenced to this value. [c] Data taken from ref. 1.

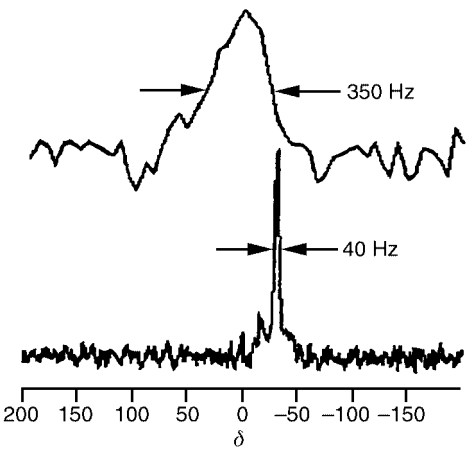

Fig. 1 Solid-state high-resolution ^{73}Ge NMR spectra of **1** (lower) and **2** (upper).

DOI: 10.1039/b001011l

symmetrically substituted germanes will give signals. It will also be of interest whether asymmetrically substituted germanes can also rise to signals. A study along such lines is under progress in our laboratories.

Notes and references

1 Y. Takeuchi, T. Harazono and N. Kakimoto, *Inorg. Chem.*, 1984, **23**, 3835.
2 Y. Takeuchi, M. Shimoda and S. Tomoda, *Magn. Reson. Chem.*, 1985, **23**, 580.
3 Y. Takeuchi, *Main Group Met. Chem.*, 1989, **13**, 323.
4 The ^{73}Ge NMR spectra were recorded with JEOL ECP 300 spectrometer operating at 10.48 MHz, equipped with a probe modified for this purpose. The design of the probe is essentially the same as that used for observation of ^{107}Ag. To obtain the best matching, a dummy condenser was attached in series. Cross polarization was not applied. Typically, 208 mg of **1** was packed in a 7 mm (o.d.) cell which was rotated at 4600 kHz. Pulse width, 45°; pre-delay, 1 s; delay; 5 s; number of accumulation, 1000 for **1** and 400 000 for **2**; sweep width, 20 kHz; high-power decoupling, 30 W.
5 A. Karipides and D. A. Haller, *Acta Crystallogr., Sect. B*, 1972, **28**, 2889; P. C. Chieh, *J. Chem. Soc. A.*, 1971, 3243.
6 G. Ferguson and C. Glidewell, *Acta Crystallogr., Sect. C*, 1996, **52**, 1889.

ChemComm

Direct determination of single-to-double stranded DNA ratio in solution applying time-resolved fluorescence measurements of dye–DNA complexes

G. Cosa,[a] K.-S. Focsaneanu,[a] J. R. N. McLean[b] and J. C. Scaiano*[a]

[a] *Department of Chemistry, University of Ottawa, Ottawa, K1N 6N5, Canada. E-mail: tito@photo.chem.uottawa.ca*
[b] *Radiation Protection Branch, Health Canada, Ottawa, K1A 1C1, Canada*

Received (in Corvallis, OR, USA) 28th December 1999, Accepted 3rd March 2000
Published on the Web 30th March 2000

We report the fluorescence lifetimes of the DNA-stain dye PicoGreen and discuss the difference exhibited in the upon binding to single-stranded *vs.* double-stranded DNA; we here developed a direct method for determining single-to-double stranded DNA ratios in solution by measurement of the pre-exponential factors in the fluorescence decay traces of dye–DNA complexes.

The search for new non-radioactive analytical techniques to determine minute amounts of DNA in solution and gels brought about the development of a family of new fluorescent probes.[1,2] Many studies have been concerned with determining the properties of these dyes free in solution,[3] and when complexed to dsDNA.[2,4–6] These recently patented[7,8] fluorescent stains derived from unsymmetric cyanine dyes (Scheme 1) exhibit a high increase (*ca*. 1000 fold) in their fluorescence quantum yields upon binding to double-stranded DNA (dsDNA) as compared to free in solution, making them sensitive probes for DNA detection. These dyes are free to rotate about their central methine bridge while in solution, but this non-radiative deactivation pathway is closed when the dye intercalates between the DNA base-pairs. This explains their high sensitivity as dsDNA sensors.[4,6]

We have explored the possibility that in a complex with single-stranded DNA (ssDNA) a less rotationally restricted dye should be present, as compared to that with dsDNA and that this difference can be reflected in the fluorescence lifetimes. Thus, we have studied the complexes formed with PicoGreen (PG), a representative of the family of cyanine dyes of Scheme 1 which exhibits the greatest sensitivity for selective detection of dsDNA in solution.[7–10] Our results show not only that the dye–ssDNA complexes are more prone to deactivate non-radiatively, but also that the different lifetimes characteristic for each of the complexes (*i.e.* dye–dsDNA and dye–ssDNA) allow a simple approach to quantify their relative amount in solution by determining the pre-exponential factors for the fluorescence decay in a mixture containing both types of DNA. The choice of PG is not accidental, preliminary screening of a range of common dyes showed PG to be that with the best lifetime discrimination between ssDNA and dsDNA.

Our work was performed on calf thymus DNA (type I) (CT DNA) and salmon testes DNA (type III) (ST DNA) suspensions prepared on a TRIS (10 mM) buffer (pH 7.4) solution consisting of distilled and deionized water with Trizma Pre-set crystals, Na_2H_2EDTA (1 mM) and (NaCl) 100 mM. The ssDNA was obtained after boiling a dsDNA solution for 30 min followed by immersion in an ice bath. The fluorescence enhancement of PG upon binding to CT dsDNA, as compared to CT ssDNA was *ca*. 1.89, measured on a PTI 1.2 X luminescence spectrometer. This value is slightly higher than the reported one of 1.56.[9] We also noticed a broader fluorescence band for the dye–ssDNA complex (data not shown), with the maximum red shifted by 3 nm. The unbound dye fluorescence band is also broader than that of the dye–dsDNA complex, though it is hard to quantify this shift since the spectrum in the absence of DNA is very noisy. While the broadening had been previously reported, it was measured at high dye–DNA base pair ratios (*i.e.* 1:1); under this conditions, not only intercalation but groove binding can occur.[5,11] In our work we kept dye/DNA base-pair ratios always lower or around 1/7 to ensure that the predominant binding mode would be that of intercalation.[5] Specifically, the preferred concentrations were 11 mM for PG, and 70 and 150 mM for CT and ST DNA, respectively, both expressed as base pairs.

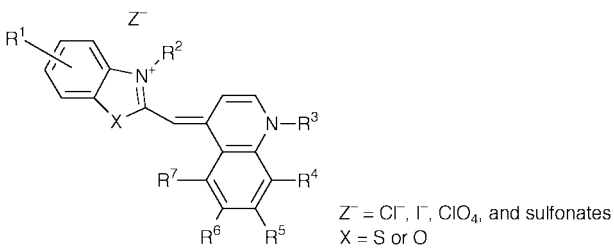

Scheme 1

Assuming that there is only one kind of complex for each ssDNA and dsDNA, and considering that, for other dyes of the same family, there exists a single lowest energy excited singlet state,[4] we would anticipate that the lifetimes for each of these complexes should be monoexponential. Thus, we measured the lifetimes following picosecond laser excitation using streak camera detection.[12] The results obtained following 355 nm irradiation of the sample with a $\leqslant$50 ps pulse show a virtually pure monoexponential decay with a lifetime of 4.5 ns for dye–dsDNA (for both CT or ST type DNA). The decay obtained for the complex formed with ssDNA was biexponential, with lifetimes of 1.16 ns (51%) and 3.09 ns (49%), where the weight of each exponential is given in parentheses (Fig. 1). The fact that the trace is biexponential may reflect two different phenomena. We are either dealing with two types of binding of the dye (*vide supra*), or there exists some DNA that renatured before data acquisition took place. The dye/DNA ratio employed was low enough as to have only intercalation in the case of dsDNA; however, ssDNA, that may have a lower binding constant,[10,13–15] might show other forms of dye interaction. In relation to the possibility that some DNA may have renatured, we tested our method of DNA denaturation by comparing the absorbance at 260 nm, immediately after the denaturation process, for a treated sample and an untreated one. We determined that within the experimental error, all of the sample had been denatured.[16] In principle, some DNA could renature before data acquisition, however this delay was kept to only 15 min. We cannot rule out either of the two possibilities described, and, conceivably, we may be dealing with a system presenting both some traces of renatured DNA, and some non-intercalated bound dye. This uncertainty does not influence our ability to discriminate between ssDNA and dsDNA.

The fluorescence broadening does not develop over time; rather it is evident immediately after excitation (data not shown). In any event, from the calculated fluorescence lifetime of the free dye in solution, *i.e.* shorter than *ca*. 5 ps, we assume that rotation takes place too fast for our acquisition setup to detect it.

DOI: 10.1039/b000473l

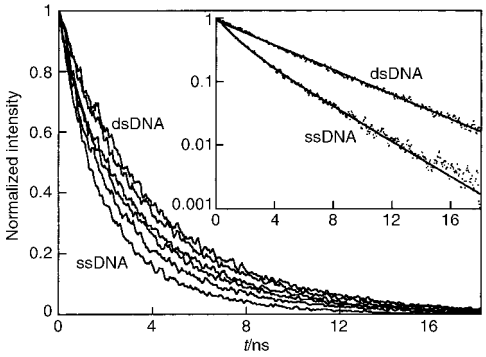

Fig. 1 Normalized fluorescence decay profiles measured on static 2 ml quartz cells in air equilibrated solutions of DNA in TRIS buffer (pH = 7.4) following 355 nm laser excitation; ST DNA base-pair concentration = 150 μM, PG = 11 μM, for 100, 80, 60, 40 and 20% dsDNA and of dsDNA alone. Insert: semi-log plot and fit for dsDNA (single exponential) and ssDNA (double exponential).

In view of the noticeable difference in fluorescence lifetimes between dye–ssDNA complex and dye–dsDNA complex, we attempted and succeeded in developing an analytical technique that would enable us to monitor in solution the ssDNA/dsDNA ratio with a simple method devoid of any operator subjectivity. To that effect, we determined the fluorescence lifetimes in different mixtures containing known amounts of ssDNA, dsDNA (we employed both CT DNA and ST DNA) and PG. From the previous analysis (*vide supra*), we expect a triexponential decay in this system [eqn. (1)]; *i.e.* dye–dsDNA decays with its characteristic rate constant, and ssDNA complexes exhibit their biexponential decay.

$$I = a_{ds}e^{-k_{ds}t} + a_2e^{-k_2t} + a_3e^{-k_3t} \quad (1)$$

where a_{ds} is the preexponential factor for dsDNA, and k_{ds} the reciprocal of its lifetime, while a_2, a_3, k_2 and k_3 are the corresponding parameters for ssDNA, and t is the time.

Though complicated in appearance, we know the three decay rate constants for this system (that of dsDNA, and each of the two for ssDNA); on the other hand, the addition of the preexponential factors for the decays has to be equal to unity for the normalized profile. At this point a six-variable function initially needed to fit this decay (three pre-exponential values, and three decay rate constants), is now reduced to one with two parameters, *i.e.* the two pre-exponential values. Further, since the relative values for the two pre-exponential values for the ssDNA decay are known, and coincidentally they are about equal, *i.e.*

$$a_{ds} + a_2 + a_3 = 1$$
$$a_2 \cong a_3$$

Combined these factors lead to a one-parameter fit according to eqn. (2):

$$I = a_{ds}e^{-0.22t} + [1 - a_{ds}) (e^{-0.86t} + e^{-0.32t})/2] \quad (2)$$

When we plot the recovered pre-exponential value (a_{ds}) corresponding to the dsDNA rate constant *vs.* the fraction of dsDNA in the sample (see inset in Fig. 2) for CT DNA and for ST DNA, a straight line is obtained with a slope of 0.80 and an intercept of 0.048. The theoretical line should go through the origin and have a slope of 1.0. The difference is not surprising; analysis according to eqn. (2) of computer simulated data shows that only perfect data (*i.e.* noise-free) leads to perfect recovery of the pre-exponential factors, particularly for the pure forms, dsDNA and ssDNA; addition of random noise always leads to apparent small weights for other DNA components. Effectively, the percentage of dsDNA present in a sample can be calculated according to eqn. (3), although we note that different instruments may lead to slightly different deviations from the ideal equation; in this sense a recalibration may be desirable.

$$\%(\text{dsDNA}) = 100(a_{ds}^{\text{recovered}} - 0.048)/0.80 \quad (3)$$

It is worthwhile noting that for the fittings, the rate constants used corresponding to ssDNA (0.32 and 0.86 × 10^9 s^{-1}) and dsDNA (0.22 × 10^9 s^{-1}) where those determined in the absence of the other form of DNA, and are the same for CT or ST DNA, and are not adjustable parameters. We believe this new method

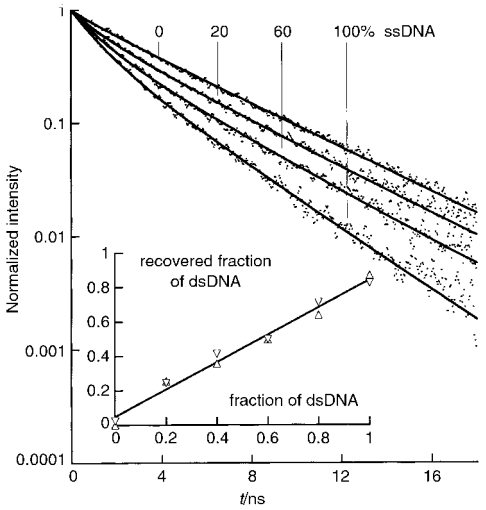

Fig. 2 Normalized fluorescence decay profiles measured on static 2 ml quartz cells in air equilibrated solutions of DNA in TRIS buffer (pH = 7.4) following 355 nm laser excitation; ST DNA base-pair concentration = 150 μM, PG = 11 μM, for various percentages of dsDNA, showing the fit of the data to the one-parameter function of eqn. (2); Insert: linear plot of the recovered dsDNA fraction as a function of the actual fraction in the sample for (△) CT DNA and for (▽) ST DNA.

may find application not only in solution, but also in gels where this information may prove useful for methods such as the comet assay.[17] Finally, we note that while our work involved a sophisticated picosecond fluorescence system, similar measurements could be developed around less expensive light sources, such a short pulse diodes.

J. C. S. thanks the Natural Sciences and Engineering Research Council of Canada for support, and the Instituto de Tecnología Química (Valencia) where this article was completed while J. C. S. was a guest under the auspices (grant SAB1998-0121) of the Ministerio de Educación y Ciencia (Spain). G. C. thanks the Ontario Graduate Scholarship Program for a post-graduate scholarship.

Notes and references

1 P. Selvin, *Science*, 1992, **257**, 885.
2 H. S. Rye, S. Yue, D. E. Wemmer, M. A. Quesada, R. P. Haugland, R. A. Mathies and A. N. Glazer, *Nucleic Acid Res.*, 1992, **20**, 2803.
3 B. Sauerwein, S. Murphy and G. B. Schuster, *J. Am. Chem. Soc.*, 1992, **114**, 7920.
4 C. Carlsson, A. Larsson, M. Jonsson, B. Albinsson and B. Nordén, *J. Phys. Chem.*, 1994, **98**, 10313.
5 A. Larsson, C. Carlsson, M. Jonsson and B. Albinsson, *J. Am. Chem. Soc.*, 1994, **116**, 8459.
6 T. L. Netzel, K. Nafisi, M. Zhao, J. R. Lenhard and I. Johnson, *J. Phys. Chem.*, 1995, **99**, 17936.
7 *US Pat.*, US5436134, R. P. Haugland, S. T. Yue, P. J. Millard and B. L. Roth, *Cyclic Substituted Unsymmetrical Cyanine Dyes*, 25 Jul, 1995.
8 *WO Pat.*, WO96/13552, S. T. Yue, V. L. Singer, B. L. Roth, T. J. Mozer, P. J. Millard, L. J. Jones, J. Xiaokui and R. P. Haugland, *Substituted Unsymmetrical Cyanine Dyes with Selected Permeability*, 9 May, 1996.
9 V. L. Singer, L. J. Jones, S. T. Yue and R. P. Haugland, *Anal. Biochem.*, 1997, **249**, 228.
10 K. R. Rogers, A. Apostol, S. J. Madsen and C. W. Spencer, *Anal. Chem.*, 1999, **71**, 4423.
11 T. Stokke and H. B. Steen, *J. Hystochem. Cytochem.*, 1985, **33**, 333.
12 N. Mohtat, F. L. Cozens and J. C. Scaiano, *J. Phys. Chem. B*, 1998, **102**, 7557.
13 J. Kapuscinski, Z. Darzynkiewickz and M. R. Melamed, *Cytometry*, 1982, **2**, 201.
14 D. J. Arndt-Jovin and T. M. Jovin, *Methods in Cell Biology*, Academic Press, Inc., New York, 1989, vol. 30, p. 417.
15 K. Elmendorff-Dreikorn, C. Chauvin, H. Slor, J. Kutzner, R. Batel, W. E. Muller and H. C. Schroder, *Cell. Mol. Biol.*, 1999, **45**, 211.
16 S. R. Gallagher, in *Current Protocols in Molecular Biology*, ed. F. M. Ausubel, R. Brent, R. E. Kingston, D. D. Moore, J. G. Seidman, J. A. Smith and K. Struhl, Greene Pub. Associates and Wiley-Interscience, New York, 1987, vol. 3; suppl. 28. p. A3.D1.
17 W. Böcker, W. Rolf, T. Bauch, W.-U. Müller and C. Streffer, *Cytometry*, 1999, **35**, 134.

ChemComm

The first structurally characterised σ-bonded organonickel(I) compound. Crystal structures of [Ni{C(SiMe$_3$)$_2$(SiMe$_2$C$_5$H$_4$N-2)}(PPh$_3$)], [Ni{C(SiMe$_3$)(SiMe$_2$C$_5$H$_4$N-2)(SiMe$_2$O)}]$_2$ and [Pd(μ-Cl){C(SiMe$_3$)$_2$(SiMe$_2$C$_5$H$_4$N-2)}]$_2$

Colin Eaborn,* Michael S. Hill, Peter B. Hitchcock and J. David Smith*

School of Chemistry, Physics and Environmental Science, University of Sussex, Brighton, UK BN1 9QJ. E-mail: j.d.smith@sussex.ac.uk;c.eaborn@sussex.ac.uk

Received (in Basel, Switzerland) 20th December 1999, Accepted 5th March 2000
Published on the Web 3rd April 2000

The reaction between [NiCl$_2$(PPh$_3$)$_2$] and [Li{C(SiMe$_3$)$_2$(SiMe$_2$C$_5$H$_4$N-2)}] in tetrahydrofuran gave the monomeric Ni(I) compound [Ni{C(SiMe$_3$)$_2$(SiMe$_2$C$_5$H$_4$N-2)}(PPh$_3$)], which shows planar coordination at Ni with Ni–C 2.025(4) Å, together with the Ni(II) silanolato compound [Ni{C(SiMe$_3$)(SiMe$_2$C$_5$H$_4$N-2)(SiMe$_2$O)}]$_2$ as a minor product, however, the corresponding reaction with [PdCl$_2$(PPh$_3$)$_2$] gave [Pd(μ-Cl){C(SiMe$_3$)$_2$(SiMe$_2$C$_5$H$_4$N-2)}]$_2$, which has a chloride-bridged structure with an unusual fold angle of 60° at the Cl···Cl axis.

Organonickel compounds have been widely studied, particularly because of their applications as catalysts.[1] Some catalytic processes are thought to involve Ni(I) intermediates[2] but, although triorganophosphine and amine complexes have been obtained,[3] attempts to isolate organo–Ni(I) compounds commonly lead to precipitation of elemental nickel.

We have previously isolated organometallic compounds of the s-, p- and f-elements containing ligands C(SiMe$_3$)$_n$(SiMe$_2$X)$_{3-n}$ in which the groups X have lone pairs of electrons.[4] We reasoned that, if the substituents X had π-acceptor properties, it might be possible to obtain compounds of d-block elements without unwanted reduction. Reactions of the precursor Li{C(SiMe$_3$)$_2$(SiMe$_2$C$_5$H$_4$N-2)} **1** to give the novel derivatives **2**–**4**, show that this is indeed the case.

The Ni(I) compound **2** (the first structurally characterised compound to contain a Ni(I)–C σ-bond, and, apart from the electrochemically characterised dimeric species [Cu$_2$R$_2$]$^{2+}$ [R = C(SiMe$_3$)$_2$(C$_5$H$_4$N-2)],[5a] the first d^9 σ-bonded organometallic compound) was obtained from the reaction of NiCl$_2$(PPh$_3$)$_2$ with 2 equivalents of **1**,† and crystals suitable for an X-ray study‡ (Fig. 1) were isolated from hexane. Compound **2** appeared to be stable in the solid state under Ar, but solutions in hexane deposited metallic nickel. The EPR spectrum in toluene at 298 K (g = 2.239) was broad but similar to that of [NiCl(PPh$_3$)$_3$],[6] and the magnetic moment of 1.55 μ_B at room temperature was as expected for a d^9 complex with one unpaired electron. The coordination at Ni is planar (sum of angles 360°) with a bite angle of 98° for the bidentate ligand and a wide C–Ni–P angle, reflecting the repulsion between the SiMe$_3$ groups and the phosphine ligand. The dihedral angle between the pyridine ring and the NiCNP coordination plane is 22°, the Ni–P bond distance is normal, and the Ni–C and Ni–N distances, 2.025(4) and 2.007(3) Å, suggest that the covalent radius for Ni(I) is *ca.* 1.25 Å. Longer Ni–C and shorter Ni–N distances are found in [Ni{C(SiMe$_3$)$_2$(C$_5$H$_4$N-2)}Cp] and [Ni{C(SiMe$_3$)$_2$(C$_5$H$_4$N-2)}$_2$],[7] reflecting the greater strain in the four-membered metallacycles than in the five-membered ring of **2**.

We have found no evidence for the presence of an alkylnickel(II) chloride in the products from the reaction between [NiCl$_2$(PPh$_3$)$_2$] and **1**. Nevertheless such a species is probably formed at the surface of the sparingly soluble [NiCl$_2$(PPh$_3$)$_2$] and rapidly reduced to **2** by the excess of **1**. Compound **2** is probably prevented by the steric requirements of the ligand from giving aggregates with Ni–Ni bonds and ultimately metallic nickel, and remains in solution as a Ni(I) species stabilised by the soft PPh$_3$ and C$_5$H$_4$N ligands. Compound **2** was also the principal product from a 1:1 [NiCl$_2$(PPh$_3$)$_2$]:**1** mixture but in this case we isolated a few crystals of a second compound identified‡ as the silanolato compound **3** (Fig. 2). Our [NiCl$_2$(PPh$_3$)$_2$] probably contained a trace of hydroxide and intra- or inter-molecular elimination of CH$_4$ from [Ni(OH){C(SiMe$_3$)$_2$(SiMe$_2$C$_5$H$_4$N-2)}] could lead to compound **3**. Cleavage of C–Si bonds under mild conditions is highly unusual, but a few examples are known where an OH group is held in a favourable position with respect to an SiMe$_3$ group.[5b,8] Trialkylsilanolatonickel derivatives have not apparently been reported before.

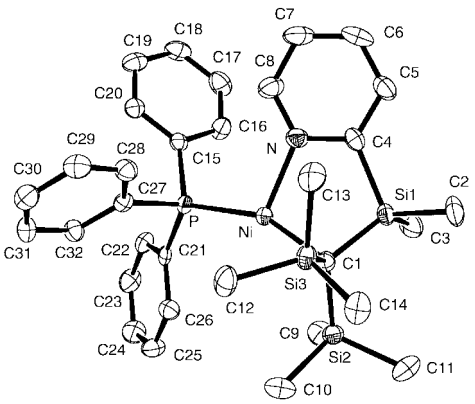

Fig. 1 The molecular structure of **2**. Selected bond lengths (Å) and angles (°). For mean values, e.s.d's of individual measurements are given in parentheses: Ni–N 2.007(3), Ni–C 2.025(4), Ni–P 2.200(1), Si(1)–C(1) 1.826(4), Si(2,3)–C(1) 1.857(4), mean Si–Me 1.880(4); N–Ni-C(1) 98.28(14), N–Ni–P 105.81(10), C(1)–Ni–P 155.67(11), mean Si–C–Si 114.1(2), mean Me–Si–Me 105.4(2), mean C–Si–Me 113.2(2), C(1)–Si–C(4) 105.36(18), Si–C(4)–N 114.0(3), C(4)–N–Ni 111.8(3), Ni–C(1)–Si 97.20(17), Ni–C(1)–Si(3) 102.52(18), Ni–C(1)–Si(2) 112.85(18).

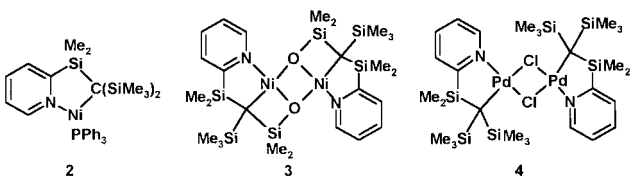

DOI: 10.1039/b000374n

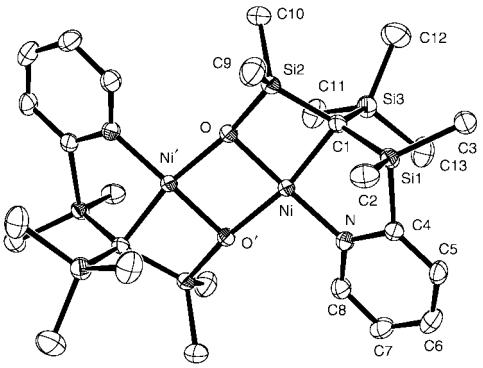

Fig. 2 The molecular structure of **3**. Selected bond lengths (Å) and angles (°): Ni–N 1.881(5), Ni–O 1.891(45), Ni–O′ 1.918(4), Ni–C(1) 1.980(6), mean Si–C(1) 1.852(6), Si–Me 1.875(7), Si–O 1.651(4); O–Ni–O 84.00(18), Si–O–Ni 93.2(2), Ni–O–Ni′ 96.00(18), Si–C(1)–Si 126.0(3), 115.0(3), 115.6(3), Ni–C–Si(2) 84.5(2), C(1)–Ni–O 84.2(2), Ni–O–Si(2) 93.2(2), Si(2)–C(1)–Ni 84.5(2).

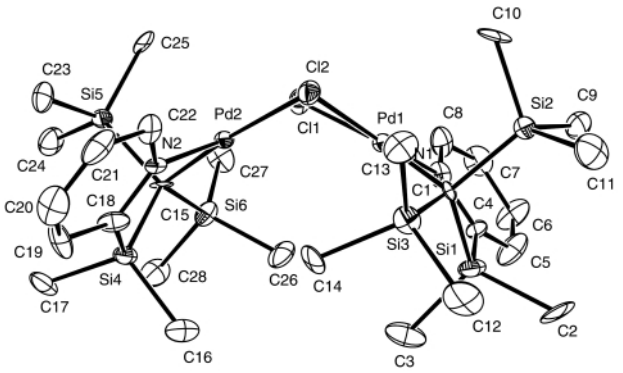

Fig. 3 The molecular structure of **4**. Selected mean bond lengths (Å) and angles (°): Pd··Pd 3.1433(15), Pd–N 2.026(10), Pd–C 2.123(12), Pd–Cl 2.325(3), 2.465(3), Si–C(1,15) 1.877(12), Si–Me 1.873(13), Si–C(py)1.864(15), N–C(Si) 1.362(16); N–C(C) 1.329(16), N–Pd–C 89.9(4), N–Pd–Cl 92.0(3), Cl–Pd–Cl, 82.62(11), C-Pd-Cl, 95.6(3); Pd–Cl–Pd 81.95, Pd–C–Si(py) 100.0(5), C–Si–C(py) 102.6(6), Si–C–N 113.6(8), C(py)–N–Pd 118.7(8), Si–C–Si 112.8(6), Me–Si–Me 106.4(6). Angles between pyridyl and Pd coordination planes 26.5, 30°.

The palladium compound **4** is obtained from equimolar quantities of **1** and $[PdCl_2(PPh_3)_2]$.§ It is stable in the solid state under Ar but Pd metal is deposited slowly from solutions in hexane at room temperature. The dimer‡ (Fig. 3) shows no crystallographic symmetry but there is an approximate C_2 axis perpendicular to and bisecting the Pd··Pd and Cl··Cl vectors. The coordination at Pd is square planar and the Pd–Cl bonds *trans* to C [2.465(3) Å] are longer than those *trans* to N [2.325(3) Å], as in similar compounds containing the NCPd(μ-Cl)$_2$PdCN core. The Pd–N bond lengths are normal and the Pd–C lengths are at the upper end of the usual range. The most intriguing feature of the structure is the large fold angle (60°) at the Cl··Cl axis since most Cl-bridged Pt(II) dimers with bidentate *C,N*-ligands are planar or nearly so. Two compounds with fold angles of 37–39°, and one with a fold angle of 58°, have been reported.[9,10] That the palladium compound **4** is much more easily isolated than the nickel analogue is in accord with the generalisation that the stabilities of M(II) organometallic compounds increase in the series from Ni to Pt.

We thank the EPSRC for financial support.

Notes and references

† *Formation of complexes* **2** *and* **3**: $(Me_3Si)_2[(C_5H_4N)Me_2Si]CH$ (0.63 g, 2.13 mmol) in thf (15 cm³) was treated with a solution of LiMe (2.16 mmol) in thf (10 cm³). The resulting solution of **1** was then added to a slurry of $[NiCl_2(PPh_3)_2]$ (0.70 g, 1.07 mmol) in thf (20 cm³) at −78 °C. The solution became dark brown as it was allowed to warm to room temperature. The solvent was then removed, the solid residue extracted with hexane (40 cm³), and the extract filtered. The filtrate was reduced to 20 cm³ and kept at −30 °C, and the brown solid that separated was filtered off and recrystallised three times from hexane at −30 °C to give bright orange–red crystals of **2** (0.20 g, 30%), mp 167–168 °C (Found: C, 62.5; H, 7.1; N, 2.2. $C_{32}H_{43}NNiPSi_3$ requires C, 62.4; H, 7.0; N, 2.2%); *m/z* 614 (12, *M*); 599 (4, *M* − Me), 352 [43, *M* − PPh_3 (RNi)], 337 (30, RNi − Me), 322 (32, RNi − 2Me), 294 (35, R), 279 (65, R − Me), 262 (100, PPh_3), 221 (45, R − $SiMe_3$). The reaction between **1** (2.14 mmol), prepared as above, and $[NiCl_2(PPh_3)_2]$ (2.14 mmol) in thf also gave mainly **2** but a few deep red crystals observed in the products were separated manually and shown to be **3** (*m/z* 706.1181. $C_{26}H_{50}N_2Ni_2O_2Si_6$ requires 706.1195).

‡ *Crystal data*: for **2**: *M* = 615.6; monoclinic, space group $P2_1/n$; *a* = 16.476(2), *b* = 9.142(3), *c* = 21.687(5) Å, *β* = 91.22(2)°, *U* = 3266(1) Å³, *Z* = 4, *μ* = 0.77 mm⁻¹; 5932 reflections collected, 5732 unique (R_{int} = 0.038), 3974 with $I > 2\sigma(I)$; *R*1, *wR*2 0.049, 0.102 [$I > 2\sigma(I)$] and 0.089, 0.118 (all data). For **3**: *M* = 708.64; triclinic, space group $P\bar{1}$; *a* = 8.8600(8), *b* = 10.1220(10), *c* = 10.6164(11) Å, *α* = 91.437(6), *β* = 111.283(7), *γ* = 92.595(5)°, *U* = 885.4 Å³, *Z* = 1; *μ* = 1.29 mm⁻¹; 8262 reflections collected, 3091 unique (R_{int} = 0.058); 2618 with $I > 2\sigma(I)$; *R*1, *wR*2 0.066, 0.154 [$I > 2\sigma(I)$], 0.079, 0.160 (all data). For **4**: *M* = 873.0; orthorhombic, space group *Pbca*; *a* = 13.465(5), *b* = 23.390(12), *c* = 25.032(9) Å, *U* = 7884(6) Å³, *Z* = 8, *μ* = 1.25 mm⁻¹; 13619 reflections collected, 6907 unique (R_{int} = 0.128), 3750 with $I > 2\sigma(I)$; *R*1, *wR*2 0.082, 0.187 [$I > 2\sigma(I)$] and 0.154, 0.226 (all data). A CAD4 diffractometer was used for **2** and **4** and a Kappa CCD diffractometer for **3**. Structures were refined by full matrix least squares refinement (SHELXL-97) with non-H atoms anisotropic and H atoms in riding mode. For **4** the structure was disordered 80:20 with only Pd sites located for the low occupancy orientation.

CCDC 182/1571. See http://www.rsc.org/suppdata/cc/b0/b000374n/ for crystallographic files in .cif format.

§ A solution of **1** (1.22 mmol) in thf (30 cm³) was added to a slurry of $[PdCl_2(PPh_3)_2]$ (0.86 g, 1.22 mmol) in thf (25 cm³) at −78 °C and the resulting solution allowed to warm to room temperature. The solvent was pumped away, the dark brown residue extracted with hexane (3 × 25 cm³), and the extract filtered. The filtrate was reduced to 25 cm³ and kept at 5 °C to give pale yellow crystals of **4** (0.28 g, 53%), mp 193–195 °C (decomp.), darkens 104 °C (Found: C, 38.7; H, 6.4; N, 3.2. $C_{28}H_{56}Cl_2N_2Pd_2Si_6$ requires C, 38.7; H, 6.5; N, 2.8%.); $\delta_H(C_6D_6)$ 0.07 (18 H, s, $SiMe_3$), 0.43 (6 H, s, $SiMe_2$), 6.70 (1 H, m, 4-H), 7.09 (1 H, t, 5-H), 7.23 (1 H, d, 3-H), 8.63 (1 H, d, 6-H); $\delta_C(C_6D_6)$ 1.3 ($^1J_{SiC}$ 51.8 Hz, $SiMe_2$), 3.4 ($^1J_{SiC}$ 51.2 Hz, $SiMe_3$), 15.9 ($^1J_{SiC}$ 37.1 Hz, CSi_3), 122.3 (4-C), 128.4 (5-C), 133.6 (3-C), 150.9 (6-C), 170.2 ($^1J_{SiC}$ 77.4 Hz, 2-C); δ_{Si} (C_6D_6) −6.1 ($^1J_{SiC}$ 39.4, 52.2, 77.8 Hz, $SiMe_2$), −0.09 ($^1J_{SiC}$ 37.4, 50.7 Hz, $SiMe_3$); *m/z* 857, (30, *M* − Me), 764 (15, *M* − $SiMe_3Cl$), 402, (12, RPd), 385 (22, RPd − Me), 370, (27, RPd − 2Me), 312 (100, RPd − $SiMe_4$), 206 (80, R − $SiMe_4$) [R = $C(SiMe_3)_2(SiMe_2C_5H_4N)$].

1 A. K. Smith in *Comprehensive Organometallic Chemistry II*, ed. E. W. Abel, F. G. A. Stone and G. Wilkinson, Pergamon, Oxford, 1995, vol. 9, pp. 29–106; P. W. Jolly in *Comprehensive Organometallic Chemistry*, ed. G. Wilkinson, F. G. A. Stone and E. W. Abel, Pergamon, Oxford, 1982, vol. 6, pp. 37–100 and vol. 8, pp. 613–797.

2 T. T. Tsou and J. K. Kochi, *J. Am. Chem. Soc.*, 1979, **101**, 7547.

3 L. Sacconi, F. Mani and A. Bencini, in *Comprehensive Coordination Chemistry*, ed. G. Wilkinson, R. D. Gillard and J. A. McCleverty Pergamon, Oxford, 1987, vol. 5, pp. 1–347.

4 C. Eaborn, P. B. Hitchcock, J. D. Smith and S. E. Sözerli, *Organometallics*, 1997, **16**, 5653; 1998, **17**, 4322; S. S. Al-Juaid, C. Eaborn, S. M. El-Hamruni, P. B. Hitchcock and J. D. Smith, *Organometallics*, 1999, **18**, 45 and references therein.

5 (*a*) R. I. Papasergio, C. L. Raston and A. H. White, *J. Chem. Soc., Chem. Commun.*, 1983, 1419; *J. Chem. Soc., Dalton Trans.*, 1987, 3085; (*b*) L. M. Engelhardt, R. I. Papasergio, C. L. Raston and A. H. White, *J. Chem. Soc., Dalton Trans.*, 1984, 311.

6 M. J. Nilges, E. K. Barefield, R. L. Belford and P. H. Davis, *J. Am. Chem. Soc.*, 1977, **99**, 755.

7 W.-P. Leung, H.-K. Lee, Z.-Y. Zhou and T. C. W. Mak, *J. Organomet. Chem.*, 1993, **462**, 7; 1998, **564**, 193 and references therein.

8 C. Eaborn and P. B. Hitchcock, *J. Chem. Soc., Perkin Trans. 2*, 1991, 1137.

9 A. Crispini, G. De Munno, M. Ghedini and F. Neve, *J. Organomet. Chem.*, 1992, **427**, 409; M. Ghedini, S. Armentano, G. De Munno, A. Crispini and F. Neve, *Liq. Cryst.*, 1990, **8**, 739.

10 A. G. Constable, W. S. McDonald, L. C. Sawkins and B. L. Shaw, *J. Chem. Soc., Dalton Trans.*, 1980, 1992; S. Armentano, A. Crispini, G. De Munno, M. Ghedini and F. Neve, *Acta Crystallogr., Sect. C*, 1991, **47**, 966.

ChemComm

Carbon dioxide gas accelerates solventless synthesis†

Philip Jessop,* Dolores C. Wynne, Scott DeHaai and Denise Nakawatase

Department of Chemistry, University of California, Davis, CA, 95616 USA. E-mail: jessop@chem.ucdavis.edu

Received (in Covallis, OR, USA) 8th December 1999, Accepted 8th March 2000
Published on the Web 30th March 2000

Some solventless reactions involving solid reactants or products can be accelerated by the influence of subcritical gaseous CO_2.

Although the utility of supercritical carbon dioxide for solventless synthesis has been well publicized,[1] it is less well known that *subcritical gaseous* CO_2 can promote such reactions. At temperatures above 31 °C and pressures below 74 bar, carbon dioxide exists as a gas and not a supercritical fluid. It therefore does not dissolve organic solids or liquids to a significant extent. However, it is capable of dissolving *into* organics, and in so doing can affect the properties of the organic material such as its viscosity, diffusion coefficient,[2] dielectric constant, melting point,[3] glass transition temperature,[4] or ability to dissolve hydrogen.[5] In each of these ways, the presence of gaseous CO_2 could affect a reaction taking place in the organic phase. These possibilities have not been much explored. We now present examples of the effect of gaseous CO_2 on reactions involving organic solids.

Three reactions are offered as examples of the accelerating effect of CO_2. In each case, the reaction performance under gaseous CO_2 is compared to the performance in the absence of CO_2. In the first example, the starting material is a solid at the reaction temperature, while the product is a liquid. In the second example, the product is the solid. In the last example, both the starting material and the product are solids.

The first example is the hydrogenation of 2-vinylnaphthalene (lit.[6] mp 65–66 °C, mp of commercially available sample 62–65 °C) catalysed by $RhCl(PPh_3)_3$ (Scheme 1). In the absence of CO_2, this reaction can be performed at temperatures of 36 °C or higher (entry 4 in Table 1). The fact that it can proceed at temperatures somewhat below the melting point of 2-vinylnaphthalene is probably a result of a slow surface reaction

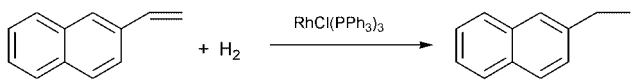

Scheme 1

Table 1 Hydrogenation of 2-vinylnaphthalene in the absence of added solvent[a]

Entry	*T*/°C	P_{CO_2}[b]/bar	*t*/h	Conv. (%)	TOF[c]/h^{-1}
1	33	0	0.5	0	0
2	33	56	0.5	52[d]	310
3	33	0[e]	0.5	16	96
4	36	0	0.5	5[d]	33
5	36	56	0.5	73[d]	430
6	36	56	1.5	100	200

[a] 7 mg (7.6 μmol) $RhCl(PPh_3)_3$, 350 mg (2.27 mmol) 2-vinylnaphthalene, 10 bar H_2, vessel size 160 mL. [b] Calculated as $P_{total} - P_{H_2}$. [c] Turnover frequency = mol product per mol catalyst per hour. [d] Average of two runs. [e] H_2 pressure 66 bar.

† Electronic supplementary information (ESI) available: experimental procedures for the hydrogenation of 2-vinylnaphthalene and oleic acid, and the hydroformylation of 2-vinylnaphthalene See http://www.rsc.org/suppdata/cc/a9/a909703a/

generating a small quantity of the product, 2-ethylnaphthalene (mp −7.4 °C),[7] which acts as a liquid solvent for further reaction. Thus one would expect the reaction to proceed very slowly until enough liquid product has formed, at which point the system would accelerate. However, at 33 °C no conversion is observed in 30 min (entry 1).

In the presence of subcritical gaseous CO_2, the reaction proceeds more rapidly.† At 36 °C, the enhancement of the rate over that observed in the absence of CO_2 is at least an order of magnitude (entries 4 and 5). Complete conversion is obtained within 90 min (entry 6). At 33 °C, the yield after 30 min is obviously superior to that in the absence of CO_2 (compare entries 1 and 2). Hydrogen gas seems to be less effective than CO_2 in enhancing the rate (entry 3). Note that in all of the experiments, the pressure of CO_2 (56 bar) is below the critical pressure of CO_2 (73.9 bar),[8] while the total pressure of the H_2/CO_2 mixture (P_{tot} = 66 bar) is below the mixture critical pressure.‡ Thus one can be certain that the gaseous phase is not supercritical. It is unlikely that the reaction takes place in the gaseous phase because: (a) at the pressure used, the density of the gaseous CO_2 is so low (*ca.* 0.14 g mL^{-1} at 36 °C and 56 bar of CO_2)[8] that it can dissolve neither the substrate nor catalyst to any significant extent, (b) the catalyst used here has not been modified to render it soluble in CO_2, and (c) all of the product mixture was found inside the glass liner at the end of the reaction. The most likely explanation of the rate enhancement is the effect of gaseous CO_2 on the melting point of 2-vinylnaphthalene.

This explanation involves the phenomenon of gas-induced melting (or gas-induced melting point lowering) of organic solids. Melting of a solid compound A can not normally be achieved below the temperature of its triple point. However, in the presence of a gas B, the melting temperature of A becomes a function of the pressure of B. The melting temperature of A can be significantly lowered from its triple point, especially at pressures approaching the critical pressure of gas B. The degree of melting point lowering depends on the solubility of B in molten A, and can be limited by the occurrence of a critical end point in the binary phase diagram.§ The end result of this phase behaviour is that solid organic compounds can be made to melt even at temperatures well below their normal melting points. This phenomenon is the basis of the recently-developed PGSS (Particles from Gas Saturated Solution) process for the micronization of solids.[9–11] Note, however, that this effect alone can not bring the melting point of 2-vinylnaphthalene to as low as 36 or 33 °C; a combination of the induced-melting effect and some initial surface reaction is required to explain the rapid rate at these temperatures.

The hydrogenation of oleic acid to stearic acid, catalysed by 5% Pt/C (Scheme 2), is also affected by the induced-melting effect. Oleic acid is a model compound for the unsaturated fatty acids in vegetable oils.[12] While oleic acid is a liquid (mp 13–16 °C),[13] the hydrogenation product stearic acid (mp 69–70 °C)[14] is a solid at room temperature. Therefore, one would expect that the solventless hydrogenation would proceed

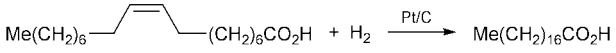

Scheme 2

DOI: 10.1039/a909703a

Table 2 Hydrogenation of oleic acid in the absence of added solvent[a]

Entry	*T*/°C	*t*/h	Conv. (%) P_{CO_2} = 0 bar	Conv. (%) P_{CO_2} = 60 bar
1	35	1	90	97
2	35	4	90	97
3	35	25	90	—
4	50	1	94	98
5	50	4	95	99
6	50	25	95	—

[a] 100 mg (0.35 mmol) oleic acid, 3.5 μmol Pt (as 5% Pt/C), 10 bar H_2, vessel size 160 mL, vial diameter 12 mm. P_{CO_2} calculated as $P_{total} - P_{H_2}$.

readily at temperatures above 4 °C, but the reaction should stop short of completion because at high conversions the melting point of the reaction mixture would climb above the ambient temperature; the conversion at which the reaction 'stalls' should be a function of the reaction temperature. At 50 °C, for example, the conversion climbs no higher than 95% even after 25 h (Table 2). The reaction in the presence of subcritical gaseous CO_2 attains 99% conversion within 4 h.† At 35 °C, the reaction in the absence of CO_2 climbs no higher than 90% even after 25 h, while it reaches 97% after 1 h in the presence of CO_2. Thus gaseous CO_2 has a strong effect on this reaction at high conversions.

The third reaction to be described is the solventless hydroformylation of 2-vinylnaphthalene catalysed by $RhH(CO)(PPh_3)_3$ (Scheme 3). This reaction generates 2-(2-naphthyl)propanal (mp 53 °C),[15] plus traces of 3-(2-naphthyl)propanal (mp 42 °C).[16] In the absence of CO_2, the melting point of the reaction mixture starts at 65 °C (the melting point of 2-vinylnaphthalene), drops after partial conversion (because a mixture forms), and rises up towards the melting point of the product as the reaction approaches completion. Thus in the absence of CO_2 and at temperatures below 50 °C, one would predict that the reaction would start slowly, accelerate after some product is formed, and become slow again at high conversions. Indeed, the presence of subcritical gaseous CO_2 was found to make the reaction start more quickly (Table 3, entries 1, 2, and 4) and reach completion more readily (entries 6–8).†

There are many advantages to performing a reaction by induced-melting rather than in a SCF: (1) the pressure of the SCF/gas is lower, (2) the volume of vessel required is lower, (3) the concentration of reagent in the reaction phase is much higher, which could lead to greater rates, (4) homogeneous catalysts do not have to be designed to be CO_2-soluble, and (5) depending on the substrate, the polarity of the reaction phase may be much higher than the very low polarity of $scCO_2$. The disadvantage of the induced-melting option is that it is only effective for organic solids which have melting points within 30–40 °C of the reaction temperature. Even for those reactions, one could perform the reaction by melting the reagent in the usual manner of raising the temperature, but this may not always be an option, depending on the temperature dependence of the selectivity (particularly for enantioselective reactions).

In conclusion, we have demonstrated, with three examples, the acceleration of solventless synthesis by the application of subcritical (gaseous) CO_2. The hydrogenation and hydroformylation reactions of 2-vinylnaphthalene are accelerated by CO_2 pressure, while the conversions obtained from the hydrogenation of oleic acid and hydroformylation of 2-vinylnaphthalene are improved by CO_2 pressure. The use of gaseous CO_2 can thus extend the range of temperatures at which 'neat' reactions can be performed. Future work will include the testing of other gases and other reactions.

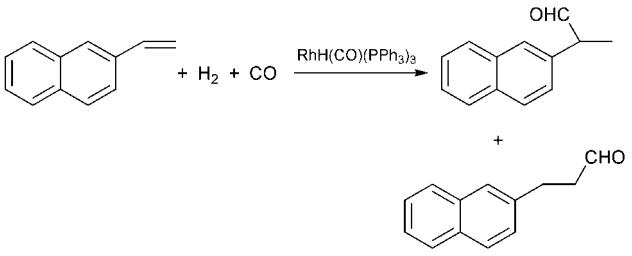

Scheme 3

Table 3 Hydroformylation of 2-vinylnaphthalene in the absence of added solvent.[a]

Entry	*T*/°C	*t*/h	Conv. (%) P_{CO_2} = 0 bar	Conv. (%) P_{CO_2} = 55 bar
1	33	0.5	0	8.5
2	33	2	9.6	24
3	33	16	—	88
4	36	2	14	44
5	43	1	—	74
6	43	2	93	96
7	43	4	—	100
8	43	11	98	—

[a] 12 mg (13 μmol) $RhH(CO)(PPh_3)_3$, 400 mg (2.6 mmol) 2-vinylnaphthalene, 10 bar each of CO and H_2, vessel size 160 mL, vial diameter 22 mm. P_{CO_2} calculated as $P_{total} - P_{H_2} - P_{CO}$. The selectivity of the reaction is high (14 : 1) for the desired[17] branched aldehyde.

This material is based upon work supported by the EPA/NSF Partnership for Environmental Research under NSF Grant No. 9815320. We also acknowledge useful discussions with Dr Charles Eckert of the Georgia Institute of Technology and experimental assistance from Mr Philip Stalcup.

Notes and references

‡ The mixture critical pressure curve starts at 73.9 bar for pure CO_2 and rises with increasing H_2 mol fraction.[18]

§ Not all binary solid/SCF mixtures have such an end point. For example, the systems *p*-dichlorobenzene/ethene and menthol/ethene do not. In these systems, the induced lowering of the melting temperature can be significantly greater: G. A. M. Diepen and S. E. C. Scheffer, *J. Am. Chem. Soc.*, 1948, **70**, 4081.

1 *Chemical Synthesis using Supercritical Fluids*, ed. P. G. Jessop and W. Leitner, VCH/Wiley, Weinheim, 1999.
2 C. Dariva, L. A. F. Coelho and J. V. Oliveira, *Fluid Phase Equilib.*, 1999, **160**, 1045.
3 M. A. McHugh and T. J. Yogan, *J. Chem. Eng. Data*, 1984, **29**, 112.
4 R. G. Wissinger and M. E. Paulaitis, *J. Polym. Sci., Part B: Polym. Phys.*, 1987, **25**, 2497.
5 N. P. Freitag and D. B. Robinson, *Fluid Phase Equilib.*, 1986, **31**, 183.
6 D. T. Mowry, M. Renoll and W. F. Huber, *J. Am. Chem. Soc.*, 1946, **68**, 1105.
7 T. Ohno and S. Kato, *Bull. Chem. Soc. Jpn.*, 1981, **54**, 1517.
8 *International Thermodynamic Tables of the Fluid State: Carbon Dioxide*, ed. S. Angus, B. Armstrong and K. M. de Reuck, IUPAC, Pergamon Press, Oxford, 1976.
9 E. Weidner, R. Steiner and Z. Knez, in *High Pressure Chemical Engineering*, ed. P. R. von Rohr and C. Trepp, Elsevier, Amsterdam, 1996.
10 A. Bertucco, in *Chemical Synthesis using Supercritical Fluids*, ed. P. G. Jessop and W. Leitner, Wiley–VCH, Weinheim, 1999.
11 I. Kikic, M. Lora and A. Bertucco, *Ind. Eng. Chem. Res.*, 1997, **36**, 5507.
12 H. B. W. Patterson, *Hydrogenation of Fats and Oils*, Applied Science, London, 1983.
13 N. Yoshimoto, T. Nakamura, M. Suzuki and K. Sato, *J. Phys. Chem.*, 1991, **95**, 3384.
14 *Merck Index*, ed. S. Budavari, M. J. O'Neil, A. Smith, P. E. Heckelman and J. F. Kinneary, Merck & Co., Inc., Whitehouse Station, NJ, 1996.
15 G. Darzens, *C. R. Hebd. Seances Acad. Sci.*, 1907, **145**, 1342.
16 T. Lee and J. B. Jones, *J. Am. Chem. Soc.*, 1997, **119**, 10 260.
17 D. Neibecker, R. Réau and S. Lecolier, *J. Org. Chem.*, 1989, **54**, 5208.
18 C. Y. Tsang and W. B. Streett, *Chem. Eng. Sci.*, 1981, **36**, 993.

ChemComm

A novel caesium selective fluorescent chemosensor

Wen-Sheng Xia, Russell H. Schmehl* and Chao-Jun Li*

Department of Chemistry, Tulane University, New Orleans, Louisiana 70118, USA.
E-mail: cjli@mailhost.tcs.tulane.edu

Received (in Corvallis, OR, USA) 9th February 2000, Accepted 8th March 2000
Published on the Web 30th March 2000

A novel caesium selective fluorescent chemosensor has been designed and synthesized; the chemosensor exhibited a selective fluorescent enhancement in the presence of other alkali metal ions.

The rapid and selective measurement of trace ions *in situ* has significant environmental and biological applications.[1] The selective sensing of trace amounts of caesium is important in detecting leaks from nuclear waste storage tanks (^{137}Cs in particular), which may cause serious problems to the environment.[2] Currently, there is no method available for *in situ* quantitative determination of Cs^+ in nuclear solutions. Very recently, Dabestani and coworkers developed a first-generation caesium selective fluorescent chemosensor based on a calix-[4]arene derivative.[3] Nevertheless, it is still necessary to develop more sophisticated and more selective caesium chemosensors that can be easily handled.

Recently, we reported a highly selective fluorescent chemosensor for potassium, a dicyano-substituted distyrylbenzene derivative containing two 15-crown-5 rings which has a low emission quantum yield in acetonitrile ($\phi = 0.001$).[4] Studies showed that the high potassium selectivity of the sensor upon the complexation of potassium ions results from formation of a sandwich complex between the 15-crown-5 and a potassium ion that leads to a large enhancement of the fluorescence of the disytrylbenzene derivative. We have denoted this type of fluorescence enhancement Self-Assembling Fluorescent Enhancement (SAFE) since the luminescence is believed to result from formation of a structure in which each crown of the fluorophore is part of a sandwich complex.[5] Herein, we report a novel caesium-selective fluorescent chemosensor **1** that consists of a dicyano-substituted distyrylbenzene derivative and two 18-crown-6 rings.[6]

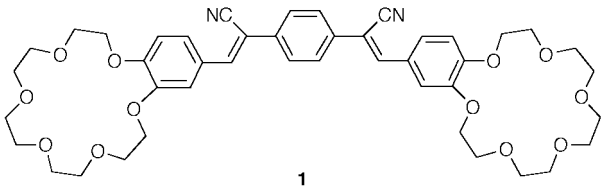

1

In acetone solution, **1** shows a broad absorption at 380 nm. With the addition of Cs^+ ion [$Cs(CF_3CO_2)$ in acetonitrile], a slight decrease of the absorption is observed. However, a significant change is observed in fluorescence spectra of **1** when Cs^+ ions are added as shown in Fig. 1. The fluorescence intensity is enhanced significantly and the fluorescent peak red-shifts from 482 to 526 nm. The insert in Fig. 1 shows the titration curve of **1** with Cs^+. Stoichiometry studies indicate that **1** forms a 1:1 complex with caesium ion, indicating that each Cs^+ ion coordinates to two 18-crown-6 moieties. At saturation in acetone solution the maximum fluorescence intensity of **1** complexed with Cs^+ is about 20 times that of free **1**. Other alkali metal ions such as Li^+, Na^+ and K^+ were also examined. No significant fluorescent enhancement was observed with any of these, even though 18-crown-6 is known to bind K^+ strongly.[7] The results strongly suggest the formation of a sandwich complex consisting of two 18-crown-6 substituents and Cs^+. A similar fluorescence enhancement of *ca.* 12–15 times was also observed when CsF was used as a cation source. Stability constants, expressed as log *K*, determined assuming 1:1 complex formation are 4.3 in acetone and 5.7 M^{-1} in chloroform–acetonitrile (9:1, v/v).

The fluorescence behavior of **1** in the presence of Cs^+ is strongly dependent on solvent. In acetonitrile, sensor **1** shows a similar fluorescent enhancement when Cs^+ ions are added, but the enhancement is significantly lower than that in acetone. The saturation enhancement is only a factor of 4 in acetonitrile. The diminished enhancement could be due to a variety of factors such as differences in the emission quantum yield of the $Cs(\mathbf{1})_2$ sandwich complex in the two solvents or competitive formation of other Cs^+/**1** complexes involving acetonitrile displacement of a crown [*i.e.* formation of $Cs(\mathbf{1})(MeCN)_n$ complexes]. The use of mixed solvents containing chloroform and a small amount of acetonitrile (9:1, v/v) results in a much larger fluorescence enhancement than observed in pure acetonitrile. The titration curve, monitoring emission at 512 nm, is shown in Fig. 2. An enhancement of a factor of 20 is observed when two equivalents of Cs^+ ion are added to solutions containing 20 μM **1**. However, the luminescence intensity *decreases* with increasing Cs^+ concentration above Cs^+/**1** ratios of 2 (no new emission with a different maximum is observed). The decrease may result from break-up of the sandwich structure to form 1:1 (Cs^+:18-crown-6) complexes with the excess Cs^+ present. Results from ^1H NMR measurements support this hypothesis.[8] It should be noted that the fluorescence enhancement observed in acetone in greatly diminished upon addition of water as a cosolvent. For instance, acetone–water (9:1, v/v) little change in luminescence occurs with less than a ten-fold excess of Cs^+ and the maximum enhancement observed is only a factor of 3.5.

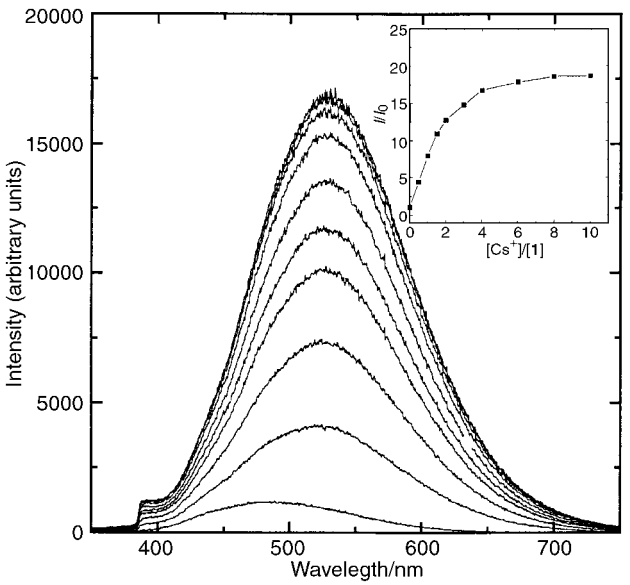

Fig. 1 Fuorescence spectral change upon the addition of caesium ions in acetone, [**1**] = 2×10^{-5} M. The insert shows the titration curve of Cs^+ in acetone (monitored at 526 nm, excited at 350 nm).

DOI: 10.1039/b001139h

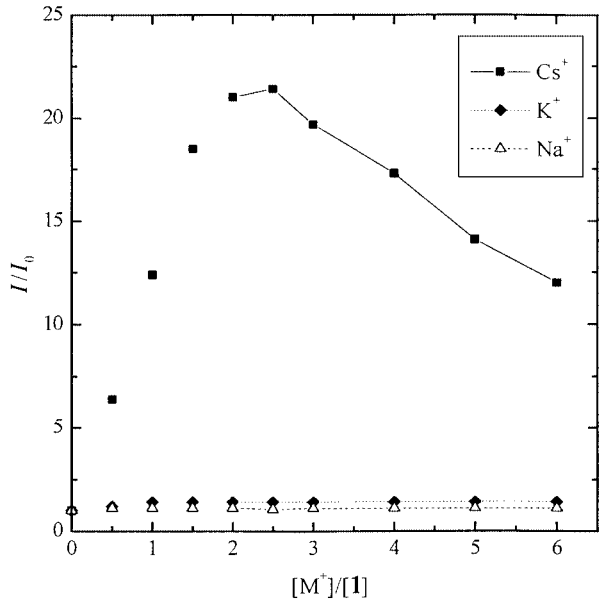

Fig. 2 Titration curve of **1** with metal ions ([**1**] = 2 × 10^{-5} M) monitored at 512 nm.

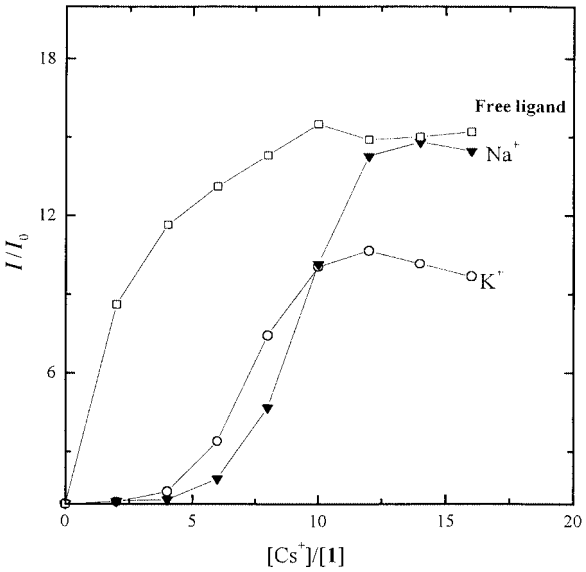

Fig. 3 The fluorescence intensity change upon the addition of Cs^+ ion in acetone in the presence of K^+ and Na^+ ([K^+] = 3.75 ×10^{-4} M, [Na^+] = 3.75 × 10^{-4} M). The intensity was monitored at 526 nm; [**1**] = 2 × 10^{-5} M.

The selectivity of this novel sensor for Cs^+ was also examined by competition experiments. Fig. 3 shows fluorescence intensity changes upon addition of Cs^+ when either K^+ or Na^+ is also present. Although K^+ and Na^+ each cause some interference to the fluorescence response at the beginning stage of the addition of Cs^+ ions, the fluorescence is turned on when [Cs^+]/[K^+] or [Cs^+]/[Na^+] reaches *ca.* 1:4. Further increases in the Cs^+ ion concentration lead to increases in the fluorescence intensity until a plateau in the emission is reached at [Cs^+]/[M^+] and [Cs^+]/[**1**] ratios of 1:3 and 5:1, respectively. Competition studies between the Cs^+ ion and K^+ or Na^+ ions are also consistent with the assumption that only the formation of a sandwich structure will result in the turn-on of the fluorescence.

We are grateful to the Tulane/Xavier Center for Bio/Environmental Research (DOD/ONR) for partial support of this research.

Notes and references

1 B. Eggins, *Biosensor: An Introduction*, John Wiley & Sons, Chichester, 1996.
2 *Chem. Eng. News*, 1998, **67**, 37.
3 H.-F. Ji, G. M. Brown and R. Dabestani, *Chem. Commun.*, 1999, 609.
4 W.-S. Xia, Russel H. Schemhl and C.-J. Li, *J. Am. Chem. Soc.*, 1999, **121**, 5599.
5 Results from MALDI-TOF mass spectrometry and ^{1}H NMR suggest a 2:2 complex is formed.
6 Sensor **1** was synthesized by the following procedure: a mixture of 4′-formyl-benzo-18-crown-6 (100 mg), 1,4-phenyldiacetonitrile (22 mg) and three drops of tetrabutylammonium hydroxide in methanol was refluxed for 12 h. The reaction mixture was then filtered hot, and the recovered yellow solid was washed with ethanol several times. Further purification by recrystallization from a mixture of chloroform and methanol (2:8) gave **1** (100 mg, 40%) as yellow solid. δ_H($CDCl_3$) 7.71(m, 3H), 7.49 (s, 1H), 7.4 (m, 1H), 6.92 (d, 1H, *J* = 12 Hz), 4.27 (m, 4H), 3.97 (m, 4H), 3.83–3.67 (m, 12H). δ_C($CDCl_3$) 151.9, 149.8, 135.5, 127.7, 126.6, 125.3, 118.7, 113.8, 113.5, 108.1, 71.4, 71.2, 71.1, 69.9, 69.8, 69.6, 69.4. Elemental analysis. Calc. for $C_{44}H_{52}N_2O_{12}$: C, 66.00; H, 6.50; N, 3.50. Found: C, 65.46; H, 6.56; N, 3.39%.
7 P. Buhlmann, E. Pretsch and E. Bakker, *Chem. Rev.*, 1998, **98**, 1609.
8 ^{1}H NMR titration of caesium trifluoroacetate in CD_3CN and **1** in $CDCl_3$–CD_3CN (9:1, v/v) shows that with the addition of caesium ions, the chemical shift first shifts upfield and then shifts downfield when the ratio of caesium to **1** is *ca.* 2:1.

ChemComm

Synthesis and structural characterization of a silacycloheptadiene

Honglae Sohn,*[a] Hee-Gweon Woo*[b] and Douglas R. Powell[c]

[a] *Department of Chemistry and Biochemistry, University of California, San Diego, CA 92093, USA. E-mail: hsohn@ucsd.edu*
[b] *Department of Chemistry, Chonnam National University, Kwangju 500-757, Korea*
[c] *Department of Chemistry, University of Wisconsin, Madison, WI 53705, USA*

Received (in Corvallis, IR, USA) 18th January 2000, Accepted 8th March 2000

The dilithium salt of tetraphenylbutadiene (1) reacts normally with phenylethynyltrichlorosilane to give 1-chloro-1-phenylethynyl-2,3,4,5-tetraphenylsilole (3), but with vinyltrichlorosilane the unexpected product is the silacycloheptadiene 2, and X-ray crystal structures were obtained for 2 and 3; the seven-membered ring in 2 adopts a boat conformation, and a possible mechanism for the formation of 2 is suggested.

The reaction of vinylchlorosilanes with a bulky organolithium compound such as *tert*-butyllithium has been reported by Jones and Lim[1] and later extensively studied by Auner[2] for almost 20 years. However only one report, by Balasubramanian and George,[3] for the reaction of 1,2,3,4-tetraphenylbuta-1,3-diene dianion **1** with an alkenylchlorosilane, $Me(CH_2{=}CH)SiCl_2$, to give 1-methyl-1-vinyltetraphenylsilole has been published.[3]

Here, we report the reactions of **1** with phenylethynyltrichlorosilane and vinyltrichlorosilane. Although many synthetic routes for siloles have been reported,[4] siloles can often be synthesized in high yield by using our previously reported method[5] in which a solution of the dilithio compound **1** is frozen with liquid nitrogen, an excess of a chlorosilane is added *via* a syringe in one portion and the mixture is slowly warmed. However, the reaction of **1** with vinyltrichlorosilane using the method described above gave, surprisingly, a reaction involving two molecules of the chlorosilane yielding silacycloheptadiene **2** (Scheme 1).† No evidence for the formation of the expected silole $C_4Ph_4SiCl(CH{=}CH_2)$ was observed. Even preparative scale reactions of **1** with just 1 equiv, rather than an excess of vinyltrichlorosilane, gave only **2** in 50% yield, leaving 50% of **1** unreacted**.** The reaction produced two enantiomers which could result from the chiral carbon C(6).

The X-ray crystal structure of **2** was determined and is shown in Fig. 1.‡ The molecule has two localized double bonds, and the vinyldichlorosilyl substituent group is attached to carbon atom C(6), as shown. The conformation of the seven-membered ring is boat like. The silicon atom Si(1) and carbon atoms C(1), C(2), C(3) are nearly coplanar, as are carbon atoms C(2), C(3), C(4), C(5), but there is a twist (51.3°) between C(2) and C(3), and a strong bend at the C(4)–C(5) junction (−89.8°). The result is that the silyl substituent group is moved away from the hindering phenyl groups on the ring.

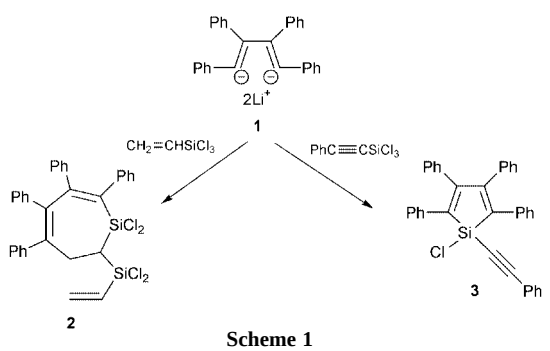

Scheme 1

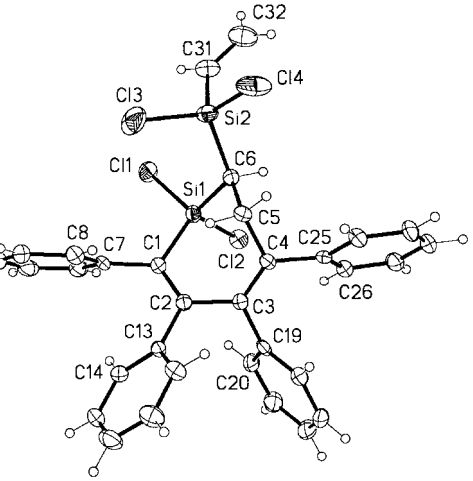

Fig. 1 Thermal ellipsoid diagram of structure of **2**. Selected bond lengths, (pm): Si1–C1 187.2(4), Si1–C6 186.8(4), Si1–Cl1 205.23(13), Si1–Cl2 207.01(13), Si2–C6 186.7(4), Si2–C31 183.5(4), C1–C2 136.1(5), C2–C3 150.7(5), C3–C4 135.3(5), C4–C5 152.0(5), C5–C6 156.2(5), C31–C32 131.5(6), Intramolecular angles, (°): C1–Si1–C6 111.8(2), Si1–C1–C2 118.8(3), Si1–C6–C5 105.9(2), C1–C2–C3 121.5(3), C2–C3–C4 122.7(3), C3–C4–C5 122.2(3), C4–C5–C6 110.4(3), Si1–C6–Si2 118.4(2), C6–Si2–C31 115.0(2), Si2–C31–C32 123.4(4), Cl1–Si1–Cl2 103.83(6), Cl3-Si2–Cl4 107.32(8). Selected torsion angles, (°): C1–C2–C3–C4 51.3(5), Si1–C1–C2–C3 −0.7(5), C2-C3–C4–C5 3.9(5), C3–C4–C5–C6 −89.8(4), C4–C5–C6–Si1 55.5(4), C4–C5–C6-Si2 −172.9(2), C7–C1–C2–C13 7.5(5), C13–C2–C3–C19 51.2(4), C19–C3–C4–C25 7.8(5).

A possible mechanism for the formation of **2** is shown in Scheme 2. Nucleophilic reaction of the butadiene anion in **4** with the β-carbon atom of the vinyldichlorosilane moiety could give an intermediate which could close to give the dichlorosilacycloheptadienyl anion **5**. This anion could react with another molecule of vinyltrichlorosilane to give **2**. An alternative mechanism would involve loss of LiCl from the anion of **5** to give a Si=C bond. This would then be followed by Si–Cl addition across the Si–C double bond to give the product **2**. However, the reaction of **1** with 1 equiv. of vinyltrichlorosilane

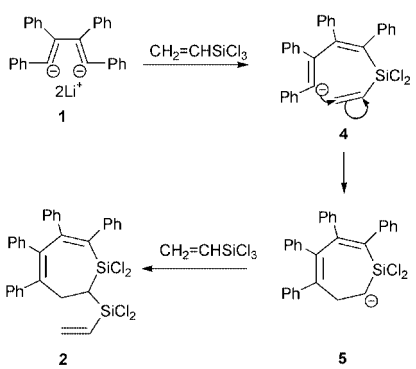

Scheme 2

DOI: 10.1039/b000585l

in the presence of a trapping reagent such as a 2,3-dimethylbutadiene gave only **2** without any addition product of buta-1,3-diene across the Si=C bond. This result argues against the alternative mechanism.

In contrast to the reaction described above, the reaction of **1** with phenylethynyltrichlorosilane proceeded normally to give the silole **3**,§ with no indication of formation of a seven-membered ring, even when an excess of $PhC{\equiv}CSiCl_3$ was present. The crystal structure of **3**, shown in Fig. 2,‡ is very similar to that for previously known siloles.[6] The ring is nearly planar, with a torsion angle C(1)–C(2)–C(3)–C(4) for the butadiene moiety of 5.3°. The Si(1)–C(29) bond distance of 181.6 pm for **3** is shorter by *ca.* 3.6–4.6 pm than intra ring bond distances of Si(1)–C(1) and Si(1)–C(4). The angle Si(1)–C(29)–C(30) of 174.3° and the torsion angle Si(1)–C(29)–C(30)–C(31) of 25.0° show that the Si–C≡C–C moiety is non-linear; this distortion may result from crystal packing forces.

Tetraphenylsilole and its polymers have been reported to exhibit interesting photophysical properties.[7] Surprisingly, silacyclohepta-2,4-diene **2** is also photoluminescent. Compound **2** and **3** exhibit two broad bands at *ca.* 300 and 380 nm in their electronic absorption spectra, assignable to the butadiene moiety. As shown in Fig. 3, both **2** and **3** have a broad emission band at *ca.* 380 nm in the fluorescence spectra.

Although several silacyclohepta-2,4,6-trienes[8] and silacycloheptenes[9] are known, as are some dihydrobenzosilepins,[10] **2** appears to be the first example of a silacycloheptadiene. We plan to extend the method used for the synthesis of **2** to prepare other new silacycloheptadiene compounds and their polymers.

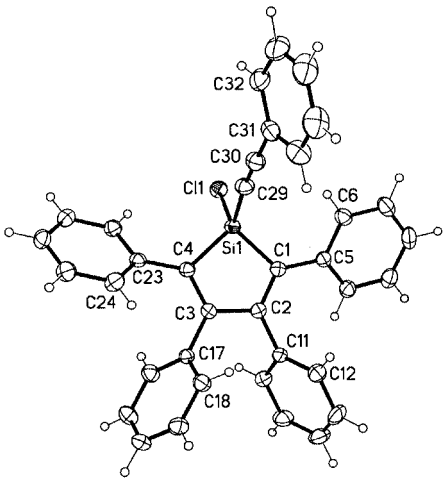

Fig. 2 Thermal ellipsoid diagram of structure of **3**. Selected bond lengths, (pm): Si1–C1 186.2(2), Si1–C4 185.2(2), Si1–Cl1 205.89(5), Si1–C29 181.6(2), C1–C2 136.1(2), C2–C3 151.4(2), C3–C4 135.9(2), C29–C30 120.5(2), C30–C31 144.1(2). Intramolecular angles (°): C1-Si1–C4 95.35(7), Si1–C29–C30 174.3(2), Si1–C1–C2 105.19(11), Si1–C4–C3 105.34(11), C1–C2–C3 116.80(13), C2–C3–C4 116.95(13), C1–Si1–C29 115.11(7), C29–C30–C31 177.5(2).

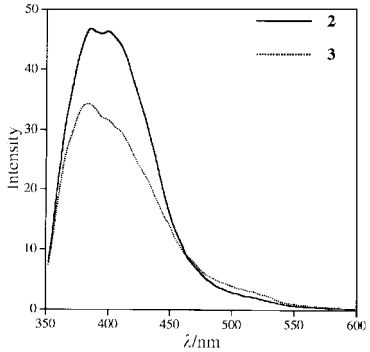

Fig. 3 Fluorescence spectra of **2** and **3** at 10^{-5} M in THF. Excitation was at 340 nm.

This research and the purchase of X-ray equipment and computers used in this research were supported by grants from the National Science Foundation. H. G. W. is grateful to the Korea Science and Engineering Foundation (1999). The author greatly acknowledges the advice and useful discussions provided by Professor Robert West (University of Wisconsin–Madison).

Notes and references

† *Synthesis* of **2**: diphenylacetylene (4.5 g, 25 mmol) and lithium (0.35 g, 50 mmol) were stirred in diethyl ether (50 mL) at room temperature for 3.5 h. The solution was cannulated to remove the residual lithium metal and frozen with a bath of liquid nitrogen. Vinyltrichlorosilane (3.2 mL, 25 mmol) was added by a syringe in one portion. The mixture was kept at −196 °C for 5 min before the cooling bath was removed, then the solution was allowed to warm up slowly to room temperature and stirred for 4 h to give a yellow solution. The solution was cannulated, concentrated, and crystallized at −20 °C to give product as yellowish-green crystals (19.2 g, 63%); mp 178-–180 °C. Selected data ^{1}H NMR (300.133 MHz, $CDCl_3$), δ 6.70–7.55 (br m, 20H, Ph), 6.05–6.35 (br m, 3H, vinyl H), 3.77 (dd, 1H, *J* 14.0, 12.5 Hz), 3.28 (dd, 1H, *J* 15.4, 3.3 Hz), 2.17 (dd, 1H, *J* 14.0, 3.7 Hz); ^{13}C{H} NMR (75.403 MHz, $CDCl_3$), δ = 158.61, 140.70, 139.94, 138.89, 138.68, 138.51, 138.21, 131.60, 131.47, 130.62, 129.89, 129.51, 128.33, 128.00, 127.79, 127.68, 127.32, 127.23, 127.05, 126.52, 35.31, 33.26; ^{29}Si NMR (71.548 MHz, $CDCl_3$), δ = 10.58, 8.53; MS(EI): *m/z* (%): 608 (100) [M^+], 481 (5) [$M^+ - Si(CH{=}CH_2)Cl_2$]. High-resolution MS: calc. for $C_{32}H_{26}Si_2Cl_4$, 608.0303; found, 608.0313.

‡ *Crystal data*: for **2**: $C_{32}H_{26}Si_2Cl_4$, M_r = 608.51, monoclinic, $P2_1/n$, a = 6.8402(3), b = 20.6247(9), c = 21.2353(10) Å, β = 92.484(2)°, V = 2993.0(2) Å^3, Z = 4, D_c = 1.350 Mg m^{-3}, F(000) = 1256, λ = 0.71073 Å, T = 133(2) K, crystal size 0.35 × 0.25 × 0.03 mm. Intensity data were collected by the ϕ-scan method (1.38 < θ < 26.01°) on a Siemens P4 diffractometer equipped with a CCD area detector. From a total of 11579 measured data, 4952 were independent (R_{int} = 0.0377). The structure was solved by direct methods and refined by the full-matrix least-squares method on F^2 using the SHELXTL+ program. $R(F_o)$ = 0.0516, $wR(F^2$, all) = 0.1215, S = 1.204 for 4949 data and 343 variables.

For **3**: $C_{36}H_{25}SiCl$, M_r = 521.10, monoclinic, $P2_1/n$, a = 9.1677(3), b = 16.5631(4), c = 18.6634(6) Å, β = 101.333(2)°, V = 2778.70(14) Å^3, Z = 4, D_c = 1.246 Mg m^{-3}, F(000) = 1088, λ = 0.71073 Å, T = 133(2) K, crystal size 0.20 × 0.20 × 0.20 mm. Data were collected by the ϕ-scan method (2.54 < θ < 29.17°) on a Siemens P4 diffractometer equipped with a CCD area detector. From a total of 13288 measured data, 6555 were independent (R_{int} = 0.0204). The structure was solved by direct methods and refined by the full-matrix least-squares method on F^2 using the SHELXTL+ program. $R(F_o)$ = 0.0394, $wR(F^2$, all) = 0.1059, S = 1.022 for 6555 data and 343 variables.

CCDC 182/1574. See http://www.rsc.org/suppdata/cc/b0/b000585l/for crystallographic files in .cif format.

§ *Synthesis* of **3**: the method described for **2** was followed, using $PhC{\equiv}CSiCl_3$ (5.1 g, 25 mmol). **3** was crystallized from diethyl ether as yellow crystals (4.9 g, 76%) at −20 °C, mp187–188 °C. Selected data; ^{1}H NMR (300.133 MHz, $CDCl_3$), δ = 6.82–6.89 and 7.00–7.54 (br m, 25H, Ph); ^{13}C{H} NMR [75.403 MHz, $CDCl_3$ (δ = 77.00)], δ 155.84, 137.56, 136.57, 133.90, 132.48, 129.83, 129.54, 129.39, 128.32, 128.06, 127.71, 127.02, 126.66, 121.37, 109.63, 85.42; ^{29}Si NMR (71.548 MHz, $CDCl_3$), δ −17.15; Anal. Calc. for $C_{36}H_{25}SiCl$: C, 82.97; H, 4.84. Found: C, 82.28; H, 4.99%. MS(EI): *m/z* (%): 520 (6) [M^+]. High-resolution MS: calc. for $C_{36}H_{25}SiCl$, 520.1414; found, 520.1390.

1 P. R. Jones and T. F. O. Lim, *J. Am. Chem. Soc.*, 1977, **99**, 2013.
2 Review: N. Auner, *J. Prakt. Chem.*, 1995, **337**, 79.
3 R. Balasubramanian and M. V. George, *Tetrahedron*, 1973, **29**, 2395.
4 J. Dubac, A. Laporterie and G. Manuel, *Chem. Rev.*, 1990, **90**, 215.
5 U. Bankwitz, H. Sohn, D. R. Powell and R. West, *J. Organomet. Chem.*, 1995, **499**, C7; R. West, H. Sohn, D. R. Powell, T. Mueller and. Y. Apeloig, *Angew. Chem., Int. Ed. Engl.*, 1996, **35**, 1002.
6 B. Goldfuss, P. v. R. Schleyer and F. Hampel, *Organometallics*, 1996, **15**, 1755.
7 H. Sohn, R. R. Huddleston, D.R. Powell and R. West, *J. Am. Chem. Soc.*, 1999, **121**, 2935.
8 Review: Y. Nakadaira, in *Organosilicon and Bioorganosilicon Chemistry*, ed. H. Sakurai, Horwood, Chichester, UK, 1985, pp. 145–156.
9 N. Auner, I. M. T. Davidson and S. Ijadi-Maghsoodi, *Organometallics*, 1985, **4**, 2210.
10 L. D. Lange, J. Y. Corey and N. P. Rath, *Organometallics*, 1991, **10**, 3189.

A ring-closing metathesis-mediated route to novel enantiopure conformationally restricted cyclic amino acids†

Kim C. M. F. Tjen,[a] Sape S. Kinderman,[a] Hans E. Schoemaker,[b] Henk Hiemstra[a] and Floris P. J. T. Rutjes*[ac]

[a] *Institute of Molecular Chemistry, University of Amsterdam, Nieuwe Achtergracht 129, 1018 WS Amsterdam, The Netherlands*
[b] *Department of Organic Chemistry and Biotechnology, DSM Research, P.O. Box 18, 6160 MD Geleen, The Netherlands*
[c] *Department of Organic Chemistry, University of Nijmegen, Toernooiveld 1, 6525 ED Nijmegen, The Netherlands*

Received (in Cambridge, UK) 15th February 2000, Accepted 15th March 2000

A combination of palladium-catalysed *N,O*-acetal formation, ruthenium-catalysed ring-closing metathesis and *N*-sulfonyliminium ion-mediated C–C bond formation constitutes an efficient and versatile route to a set of enantiomerically pure 2,6-disubstituted unsaturated pipecolic acid derivatives.

The pipecolic acid derivatives **1**, heterocycles containing a variety of functional groups, constitute an interesting compound class. They are rigid amino acids and may therefore be used to introduce conformational restriction in peptides.[1] Furthermore, this class of cyclic amino acid derivatives is a versatile starting point for the construction of (libraries of) biologically active compounds and for the synthesis of naturally occurring alkaloids.[2] Although a few approaches towards the synthesis of such systems are known,[3] general access to a wide range of these types of amino acids is still rather limited. Here we present an efficient and flexible route to the unsaturated 2,6-disubstituted pipecolic acid derivatives **1** consisting of (i) a novel amidopalladation reaction of an alkoxy-substituted allene to form the allylic *N,O*-acetals **2a** and **2b**, (ii) Ru-mediated ring-closing metathesis of these intermediates and (iii) selective functionalisation at the 6-position *via* allylic *N*-sulfonyliminium ion chemistry (Scheme 1).[4] The starting material is enantiomerically pure allylglycine (**3**), which is commercially available but alternatively can be efficiently prepared in both enantiomeric forms.[5]

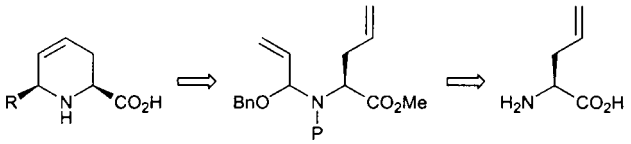

1 **2a**: P = Ts; **2b**: P = Ns **3**

Scheme 1 Retrosynthesis.

This route was inspired by previous work in our group on the synthesis of oxygen heterocycles, where one of the key steps consisted of a highly efficient acetal formation *via* oxypalladation of methyl propadienyl ether.[6] We envisioned that formation of the corresponding *N,O*-acetals should be possible in a similar fashion.[7] However, treatment of Ts-protected allylglycine methyl ester (**4**) with methyl propadienyl ether in the presence of $Pd(OAc)_2$ at 80 °C surprisingly led to the undesired enol ether **5**, formed by reaction of the tosylamide at the least hindered γ-position of the allene (Scheme 2). Interestingly, a similar reaction with benzyl propadienyl ether[8] did not require these refluxing conditions to proceed, but instead

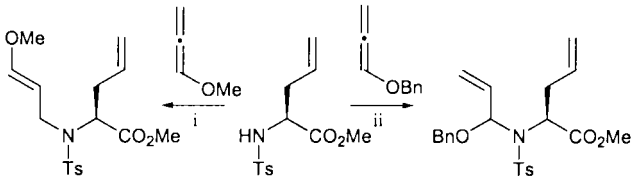

5 **4** **2a**

Scheme 2 *Reagents and conditions*: i, methyl propadienyl ether, $Pd(OAc)_2$, dppp, Et_3N, MeCN, sealed tube, reflux, 50%; ii, benzyl propadienyl ether, $Pd(OAc)_2$, dppp, Et_3N, MeCN, room temperature, 85%.

went to completion in one hour at room temperature to selectively give the desired *N,O*-acetal **2a** in 85% yield.[9] Most probably, at higher temperatures the thermodynamic product is formed, whereas at room temperature the kinetic product is produced.

The *N,O*-acetal formation proceeded well for both the Ts- and Ns (4-nitrobenzenesulfonyl)-protected allylglycine derivatives (yield of **2b**: 84%; both **2a** and **2b** were obtained as *ca.* 1:1 mixtures of diastereomers), but did not work satisfactorily for the corresponding carbamates. It should be stressed that this amidopalladation of benzyl propadienyl ether represents a novel method of generating *N,O*-acetals. More general application of this smooth reaction to convert sulfonylamides into the corresponding *N,O*-acetals[10] in principle paves the way to a large variety of *N*-sulfonyliminium ion precursors.[4]

Having these stable diolefins in hand, the compounds were subjected to standard ring-closing metathesis conditions using the well-established Grubbs Ru–benzylidene catalyst[11] to give the desired cyclic *N,O*-acetals **6a** and **6b** in excellent yields as *ca.* 1:1 mixtures of *cis/trans*-isomers (Scheme 3)

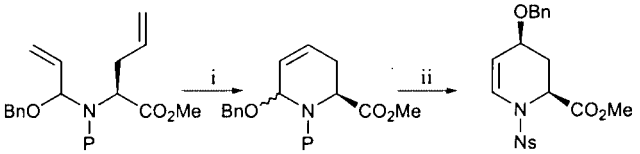

2a: P = Ts; **2b**: P = Ns **6a**: 95%; **6b**: 90% **7**

Scheme 3 *Reagents and conditions*: i, $Cl_2(Cy_3P)_2Ru{=}CHPh$, CH_2Cl_2, room temperature; ii, $BF_3{\cdot}OEt_2$, CH_2Cl_2, −78 °C, 90%.

Treatment of this mixture with $BF_3{\cdot}OEt_2$ at −78 °C led to isomerisation of **6b** to the thermodynamically more stable vinylogous *N,O*-acetal **7**,† which consisted of an 8:1 mixture of *cis/trans* isomers. After comparison with literature data[3c] and based on the observed NOE signals in the ^1H NMR spectrum, the major isomer was identified as the *cis*-product. This isomerisation was a useful indication of the feasibility of cationic reactions *via* such types of *N*-sulfonyliminium ions.

To establish CC-bond formation, precursors **6a** and **6b** where treated with a variety of nucleophiles in the presence of different Lewis acids. In Table 1, the results with $BF_3{\cdot}OEt_2$ are shown,

† Electronic supplementary information (ESI) available: characterisation data for compounds **7**, **9** and **16**. See http://www.rsc.org/suppdata/cc/b0/b001253j/

Table 1 *Reagents and conditions*: i, nucleophile, $BF_3{\cdot}OEt_2$, CH_2Cl_2, −78 °C → room temperature; yields were determined after flash column chromatography. The enantiopurity of the products was checked by chiral HPLC (Chiracel OD, heptane–isopropyl alcohol = 80:20)

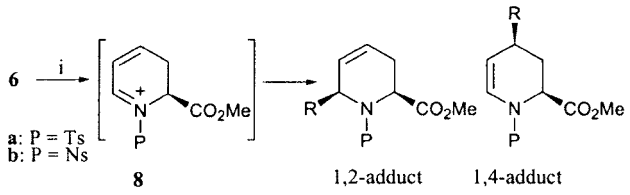

8

Entry	Substrate	Nucleophile	Product	Ratio (1,2:1,4)	Yield (%)
1	**6b**	Et_3SiH	**9** (R = H)	100:0	88
2	**6a**	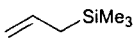	**10** (R = Allyl)	90:10	62
3	**6b**	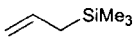	**11** (R = Allyl)	75:25	79
4	**6b**	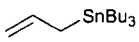	**11** (R = Allyl)	98:2	94
5	**6a**	$Me_3Si{-}C{\equiv}N$	**12** (R = CN)	100:0	70
6	**6b**	$Me_3Si{-}C{\equiv}N$	**13** (R = CN)	100:0	89
7	**6b**	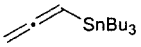	**14** (R = Propargyl)	100:0	75
8	**6b**	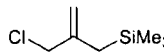	**15** (R = 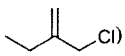)	80:20	67

since this Lewis acid appeared superior in terms of selectivity and yield. The most simple nucleophile (Et_3SiH, entry 1) provided selectively the unsaturated pipecolic acid **9** in 88% yield. The enantiopurity of the product was checked by analysis of the enantiopure and the racemic product with chiral HPLC (as in all other entries) to confirm that racemisation during the *N*-sulfonyliminium ion reaction does not take place. With allyltrimethylsilane as the nucleophile (entries 2 and 3), mixtures of 1,2- and 1,4-addition products were obtained, both as single diastereoisomers. The stereochemistry of the 1,2-adduct was assigned on the basis of ^1H NMR NOE studies after deprotection to the free amino acid (10% enhancement of H6 upon irradiation of H2 and *vice versa*) and was in accordance with previously published observations.[3a] The *cis*-configuration of the 1,4-adduct was concluded *via* comparison with ^1H NMR data of **7**. The regioselectivity of this reaction could not be influenced by using different Lewis acids, but instead by applying the more reactive nucleophile allyltributyltin a highly selective reaction took place at the six-position. In addition, both trimethylsilylcyanide and 1,2-propadienyltributyltin[12] (entries 5–7) reacted solely and with complete diastereoselectivity at the six-position to give the corresponding cyanide- and propargyl-substituted product, respectively. Inversely, the chloromethyl-substituted allylsilane (entry 8) provided again a mixture of regioisomers.

Eventually, most of the Ns-protected products were converted into the corresponding free pipecolic acid derivatives (Scheme 4). A straightforward sequence involving (i) cleavage of the sulfonamide with K_2CO_3 and PhSH, (ii) LiOH-mediated hydrolysis of the ester and (iii) purification by ion exchange chromatography yielded the cyclic amino acids in good to moderate yields over these two steps without detectable epimerisation of the stereocentres. Thus, a number of differently substituted amino acid building blocks were obtained, including the natural product baikiain (**17**: $[\alpha]_D$ = −182.6 (*c* 0.3, H_2O); lit.,[13] −201.6 (*c* 1, H_2O)) and the allylic sulfide **19**, which arose from nucleophilic substitution of the chloride during the deprotection.

In summary, we developed a practical and concise transition metal-catalyzed route to a variety of substituted pipecolic acid

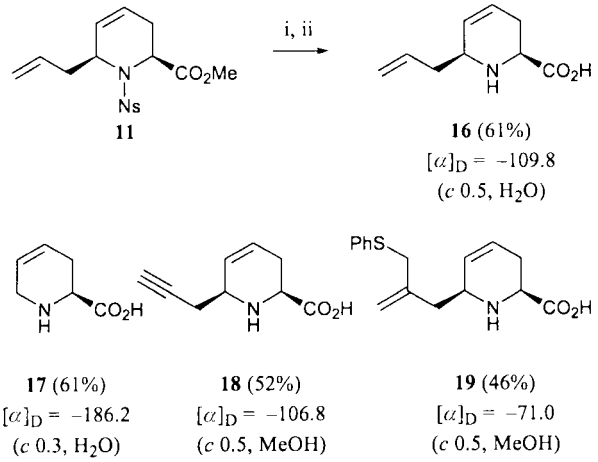

Scheme 4 *Reagents and conditions*: i, PhSH, K_2CO_3 DMF, room temperature; ii, LiOH, MeOH–H_2O (1:1), room temperature.

derivatives including the natural product baikiain. At present, we are further extending the scope of the cyclic *N,O*-acetals as synthetic intermediates in different (metal-catalysed) types of C–C bond forming reactions and are also exploring the possibilities to apply these building blocks in natural product synthesis.

DSM Research is kindly acknowledged for providing a research grant to K. C. M. F. T. This research has been financially supported by the Council for Chemical Sciences of the Netherlands Organisation for Scientific Research (CW-NWO).

Notes and references

1 For a review, see: S. Hanessian, G. McNaughton-Smith, H.-G. Lombart and W. D. Lubell, *Tetrahedron*, 1997, **53**, 12 789.
2 For some recent examples, see: (*a*) J. Åhman and P. Somfai, *Tetrahedron Lett.*, 1995, **36**, 303; (*b*) S. A. Angle and J. G. Breitenbucher, *Tetrahedron Lett.*,1993, **34**, 3985; (*c*) T. Hamada, T. Zenkoh, H. Sato and O. Yonemitsu, *Tetrahedron Lett.*, 1991, **32**, 1649.
3 For some recent examples, see: (*a*) D. Craig, R. McCague, G. A. Potter and M. R. V. Williams, *Synlett*, 1998, 55; (*b*) J. Åhman and P. Somfai, *J. Am. Chem. Soc.*, 1994, **116**, 9781; (*c*) Y. Matsumura, Y. Yoshimoto, C. Horikawa, T. Maki and M. Watanabe, *Tetrahedron Lett.*, 1996, **37**, 5715; (*d*) P. D. Bailey, R. D. Wilson and G. R. Brown, *J. Chem. Soc., Perkin Trans. 1*, 1991, 1337; (*e*) S. R. Angle, J. G. Breitenbucher and D. O. Arnaiz, *J. Org. Chem.*, 1992, **57**, 5947.
4 For a review on related *N*-acyliminium ion chemistry, see: H. Hiemstra and W. N. Speckamp, in *Comprehensive Organic Synthesis*, ed. B. M. Trost and I. Fleming, Pergamon, Oxford, 1991, vol. 2, p. 1047.
5 (*a*) H. E. Schoemaker, W. H. J. Boesten, Q. B. Broxterman, E. C. Roos, B. Kaptein, W. J. J. van den Tweel, J. Kamphuis and F. P. J. T. Rutjes, *Chimia*, 1997, **51**, 308; (*b*) F. P. J. T. Rutjes and H. E. Schoemaker, *Tetrahedron Lett.*, 1997, **38**, 677.
6 F. P. J. T. Rutjes, T. M. Kooistra, H. Hiemstra and H. E. Schoemaker, *Synlett*, 1998, 192.
7 For a review on metal-catalyzed amination, see: T. E. Müller and M. Beller, *Chem. Rev.*, 1998, **98**, 675.
8 For the use of benzyl propadienyl ether in allylic acetal formation, see: H. Ovaa, M. A. Leeuwenburgh, H. S. Overkleeft, G. A. van der Marel and J. H. van Boom, *Tetrahedron Lett.*, 1998, **39**, 3025.
9 A similar mild reacton was previously observed in our lab upon oxypalladation of benzyl propadienyl ether. The remarkable difference in reactivity with methyl propadienyl ether is not yet understood. R. Doodeman, unpublished work.
10 For example, *N*-tosylallylamine and its homologue give comparable yields for the reaction with benzyl propadienyl ether.
11 For a recent review on ring-closing metathesis, see: *Alkene Metathesis in Organic Synthesis in Topics in Organometallic Chemistry*, ed. A. Fürstner, Springer, Berlin, 1998.
12 J. S. Prasad and L. S. Liebeskind, *Tetrahedron Lett.*, 1988, **29**, 4257.
13 Isolation: F. E. King, T. J. King and A. J. Warwick, *J. Chem.Soc.*, 1950, 3590. For an entry into recent syntheses of baikiain, see: A. Mazon and C. Najera, *Tetrahedron: Asymmetry*, 1997, **11**, 1855.

Competition between photosensitization and charge transfer in soluble oligo(naphthylenevinylene)–fullerene dyads

José L. Segura,[a] Rafael Gómez,[a] Nazario Martín,*[a] Chuping Luo[b] and Dirk M. Guldi*[b]

[a] *Departamento de Química Orgánica, Facultad de Ciencias Químicas, Universidad Complutense, E-28040-Madrid, Spain. E-mail: Nazmar@eucmax.sim.ucm.es*

[b] *Radiation Laboratory, University of Notre Dame, Indiana, USA*

Received (in Liverpool, UK) 5th January 2000, Accepted 14th February 2000

In a novel series of soluble C_{60}–oligo(naphthylenevinylene) dyads both singlet–singlet energy transfer and intramolecular electron transfer were found to take place and to compete with each other.

Conjugated, polymeric semiconductors are effective and stable electron-donor materials. Upon illumination of the polymer, a valence band electron is excited across the band-gap into the conduction band and generates a highly reactive donor state. Charge separation evolving from the latter process is facilitated by a possible charge delocalization within the polymer or by structural relaxation. On the other hand, fullerenes also display strong electron-acceptor properties in their ground and excited states. In mixed composites of these two donor acceptor materials ultrafast photoinduced electron transfer can occur with high quantum efficiency.[1] This feature attracted interdisciplinary effort to utilize conjugated polymer/C_{60} blends as novel materials for photovoltaic cells (*i.e.* the conversion of photon energy into electricity).[2]

The tendency of C_{60} to phase-separate and crystallize limits its solubility in conjugated polymers. However, uniformity and high quality of conjugated polymer/C_{60} thin films are essential requirements for opto-electronic device applications. Thus, soluble functionalized C_{60} derivatives have been synthesized in an attempt to suppress the phase separation once these derivatives are blended with the conjugated polymers.[3]

A viable alternative for fabricating stable bicontinuous networks is the synthesis of molecular dyads[4] and triads[5] bearing conjugated oligomer moieties covalently linked to an electron acceptor, such as a fullerene.[6] Well structured oligomers allow the possibility for mimicking the basic structural and electronic properties of the related polymers and, therefore, have emerged as interesting materials for opto-electronic applications.[7,8]

Here, we report the preparation of a covalently linked [60]fullerene–oligo-2,6-naphthylenevinylene (ONV) derivative **4** as well as that of the [60]fullerene–monomer analogue **6**. Furthermore, a detailed investigation of intramolecular energy and electron transfer reactions in both dyads is presented.

Among the suitable procedures for the functionalization of fullerenes, the 1,3-dipolar cycloaddition of azomethine ylides to C_{60} emerged as an important methodology for the production of stable fullerene derivatives.[9] We have adapted this synthetic approach for the preparation of dyad **4** which was obtained in 63% yield (*i.e.* based on recovered C_{60}) by reacting sarcosine, C_{60} and the formylsubstituted trimeric material **3** in refluxing toluene for 24 h. Oligomer **3** was obtained from the dibromoderivative **1**[10] by using a two step reaction pathway. Treatment of **1** with copper cyanide in dimethylformamide[11] under stoichiometric control led to a mixture of the monocyanoderivative **2** (49%) and dicyano derivative (21%) which were subsequently separated by column chromatography. Reduction with DIBAL-H at −78 °C of oligomer **2** yielded the aldehyde **3** in a 40% yield (Scheme 1).

Reaction of 2-bromo-6-formyl-1,5-dihexyloxynaphthalene[10] with [60]fullerene and sarcosine in refluxing toluene for 24 h yielded dyad **6** (Scheme 1). The good solubility afforded by the alkoxy chains allowed full spectroscopic and electrochemical characterization of both dyads (**4** and **6**).

The redox properties of the fullerene-linked oligomers were studied by cyclic voltammetry in toluene–acetonitrile (5 : 1 v/v) at room temperature. Dyads **4** and **6** both exhibit an amphoteric redox-active behaviour. In particular, they show an oxidation wave at $E_{1/2}$ *ca.* 1.4 V, (1.48 V for **3** *vs.* SCE) due to the oxidation of the oligomer, and three quasireversible waves at $E_{1/2}$ = −0.59, −1.04 and −1.66 V corresponding to the fullerene reduction.

The absorption spectra of dyads **4** and **6** in dichloromethane solution disclose superimposed features of the C_{60} and the trimeric or monomeric unit, respectively. Taking the electrochemical data and the absorption features into consideration, we reached the conclusion that no significant interactions arise between the two redox-active moieties in the ground state of the combined units.

Relative to the strong emission of the oligomer references [*i.e. ca.* 400 nm (**5**) and 430 nm (**3**)], the trimer and monomer emission in dyads **4** and **6** is nearly quantitatively quenched.[5] Instead, a familiar fullerene fluorescence spectrum was found with a strong 0→0 emission at 715 nm, despite exclusive excitation of the oligomer moiety (Table 1).[12] To unravel the mechanism of producing the emission, an excitation spectrum was measured. The excitation spectra of dyads **4** and **6** were exact matches of the ground state absorption of the oligomer (**3**) and monomer (**5**) moieties with maxima at 412 and 360 nm respectively. This implies that there is a rapid transfer of singlet excited state energy from the photoexcited oligomer to the covalently linked fullerene.

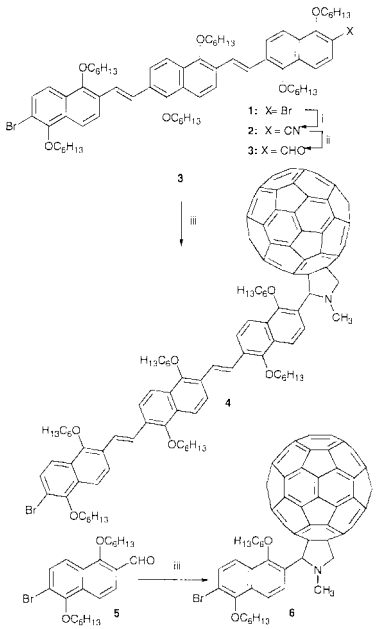

Scheme 1 *Reagents and conditions*: i, CuCN, NaI, DMF ; ii, DIBAL-H, Et_2O ; iii, C_{60}, $CH_3NHCH_2CO_2H$, Tol, heat.

DOI: 10.1039/b000289p

Table 1 Photophysical data of oligo(naphthylenevinylene)–fullerene dyads

	Fulleropyrrolidine	Dyad **4**	Dyad **6**
Fluorescence max/nm	715,[a] 715[b]	715,[a] 715[b]	715,[a] 715[b]
$\Phi_{\text{fluor. } C_{60}}$ (Tol)	6.0×10^{-4}	4.68×10^{-4}	4.98×10^{-4}
$\Phi_{\text{fluor } C_{60}}$ (THF)	6.0×10^{-4}	3.56×10^{-4}	4.59×10^{-4}
$k_{\text{energy}}/\text{s}^{-1}$	—/—	1.51×10^{10}[c]	1.89×10^{10}[c]
		2.04×10^{10}[d]	2.22×10^{10}[d]
ISC (Tol)/ns	1.35	1.21	1.2
Triplet max/nm	700	700	700
Φ_{triplet}(Tol)	0.98	0.636	0.83
Φ_{triplet} (THF)	—	0.595	0.748
Φ_{triplet}(PhCN)	—	0.570	0.72

[a] In toluene. [b] In THF. [c] Measured at 550 nm. [d] Measured at 880 nm.

In ps-resolved transient absorption measurements, oligomer **3** and monomer **5** gave rise to a broadly absorbing transient with a maximum at *ca.* 550 nm. On the ps timescale (*i.e.* up to 6000 ps), no significant decay of the excited state absorption was observed. C_{60}-oligomers **4** and **6**, on the other hand, displayed a drastically different behavior. The spectral features recorded immediately after the laser pulse (*i.e.* maximum at *ca.* 550 nm) clearly confirmed the excitation of the oligomer moieties. In contrast to reference compounds **3** and **5**, the excited state absorption was short-lived. In particular, lifetimes of 66 and 53 ps for dyads **4** and **6** (Table 1), respectively, corroborated the efficient emission quenching.

Once the rapid disappearance of the excited oligomer absorption comes to an end (*i.e. ca.* 200 ps after the laser pulse), only characteristics of the fullerene singlet excited state absorption remain. The noted maximum (880 nm) is reminiscent of that found for a reference fulleropyrrolidine.[13] In line with an energy transfer mechanism the singlet–singlet absorption revealed a two step grow-in dynamics. The faster process stems from the direct excitation of the fullerene core, while the slower component is ascribed to the actual transfer of excited state energy. The latter assignment is based on the nearly identical dynamics [49 ps (**4**) and 45 ps (**6**)] observed for the second components relative to those of the decays at 500 nm.

Another process follows the conclusion of the energy transfer reaction, the outcome of which on the timescale of a few thousand ps is the formation of a distinct, new maximum at 700 nm. This absorption is in excellent agreement with the triplet excited state absorption of a fulleropyrrolidine reference, which infers that the underlying reaction is an intersystem crossing (ISC) from the fullerene singlet to the energetically lower-lying triplet excited state.

In order to quantify the energy transfer, and to probe a possible contribution from an electron transfer channel, triplet quantum yields were measured in different solvents. The quantum yields deviate substantially from unity (Table 1) and are in the range of 57–63% for **4** and 72–83% for **6**. It is noteworthy that the values are particularly low in polar solvents.

Taking the redox potential of the electron accepting fullerene and those of the two oligomers into account (see above), the possibility of electron transfer is thermodynamically feasible, especially considering the high energies of the photoexcited trimer (**3**; E_{singlet} = 2.88 eV) and monomer (**5**; E_{singlet} = 3.09 eV). None of the photoexcited fullerene states (*i.e.* E_{singlet} = 1.76 eV; E_{triplet} = 1.50 eV) should, however, be powerful enough to initiate the intramolecular electron transfer and to yield the charge-separated radical pair ($E_{\text{charge-separated}}$ *ca.* 2 eV).

In the context of confirming the electron transfer mechanism, the strong triplet–triplet absorptions ($\varepsilon_{700\text{ nm}}$ = 16 100 $\text{M}^{-1}\text{cm}^{-1}$) should be noted, which dominate in large the ps and ns spectra. Consequently, to obtain direct evidence in support of the weaker absorbing radical pair ($\varepsilon_{1000\text{ nm}}$ *ca.* 8000 $\text{M}^{-1}\text{ cm}^{-1}$) subtraction of the triplet absorption features from, for example, the ns spectrum became necessary. The resulting differential absorption changes reveal a near IR-maximum at 1000 nm and a visible-doublet at 660 and 800 nm, characteristics of the reduced fullerene moiety and the oxidized oligomer,[14] respectively. Another argument for an intramolecular electron transfer is the solvent dependence on the triplet quantum yields mentioned above. Lower Φ-values in polar solvents correlate with larger free energy changes ($-\Delta G°$) for the associated electron transfer and, in turn, indicate a stronger competition to the energy transfer.

In summary, with a novel series of fullerene oligomer composites, we have demonstrated that an intramolecular electron transfer competes with the dominant singlet–singlet energy transfer. This observation is in good agreement with the thermodynamics of the investigated systems that predict a highly exergonic energy transfer ($-\Delta G°$ *ca.* 1.25 eV) and a less exergonic electron transfer reaction ($-\Delta G°$ *ca.* 1.0 eV). More important, lowering the energy of the charge-separated radical, by means of increasing the solvent polarity, enhances the efficiency of the electron transfer channel.

We are indebted to the DGICYT of Spain (Project PB98-0818) for financial support. Part of this work has been supported by the Office of Basic Energy Sciences of the US Department of Energy. This is document NDRL-4216 from the Notre Dame Radiation Laboratory. We are also indebted to Centro de Espectroscopia de la UCM.

Notes and references

1 N. S. Sariciftci, *Prog. Quantum Electron.*, 1995, **19**, 131.
2 G. Yu, J. Gao, J. C. Hummelen, F. Wudl and A. J. Heeger, *Science*, 1995, **270**, 1789.
3 J. C. Hummelen, B. W. Knight, F. LePeq, F. Wudl, J. Yao and C. L. Williams, *J. Org. Chem.*, 1995, **60**, 532.
4 F. Effenberger and G. Grube, *Synthesis*, 1998, 1372; S. Knorr, A. Grupp, M. Mehring, G. Grube and F. Effenberger, *J. Chem. Phys.*, 1999, **110**, 3502; J.-F. Nierengarten, J.-F. Eckert, J.-F. Nicoud, L. Ouali, V. Krasnikov and G. Hadziioannou, *Chem. Commun.*, 1999, 617; S.-G. Liu, L. Shu, J. Rivera, H. Liu, J.-M. Raimundo, J. Roncali, A. Gorgues and L. Echegoyen, *J. Org. Chem.*, 1999, **64**, 4884; T. Yamashiro, Y. Aso, T. Otsubo, H. Tang, Y. Harima and K. Yamahita, *Chem. Lett.*, 1999, 443.
5 J. L. Segura and N. Martín, *Tetrahedron Lett.*, 1999, **40**, 3239; R. A. Janssen, P. A. van Hal, J. Knol, J. K. Hummelen, communication presented to the European Conference on Organic solar cells, *ECOS, Cadarache, France*, 1998.
6 N. Martín, L. Sánchez, B. Illescas and I. Pérez, *Chem. Rev.*, 1998, **98**, 2527; H. Imahori and Y. Sakata, *Adv. Mater.*, 1997, **9**, 537; *Eur. J. Org. Chem.*, 1999, 2445.
7 *Electronic Materials. The Oligomer Approach*, ed. K. Müllen and G. Wegner, Wiley-VCH, Weinheim, 1998.
8 *Acc. Chem. Res.*, 1999, **32(3)**. Special issue dedicated to *Molecular Materials in Electronic and Optoelectronic Devices*.
9 M. Prato and M. Maggini, *Acc. Chem. Res.*, 1998, **31**, 519.
10 J. L. Segura, N. Martín and M. Hanack, *Eur. J. Org. Chem.*, 1999, 643.
11 G. P. Ellis and T. M. Romney-Alexander, *Chem. Rev.*, 1987, **87**, 779.
12 D. M. Guldi and K.-D. Asmus, *J. Phys. Chem. A*, 1997, **101**, 1472.
13 D. M. Guldi, M. Maggini, G. Scorrano and M. Prato, *J. Am. Chem. Soc.*, 1997, **119**, 974.
14 The spectral fingerprint of the oligomer radical cation was obtained from a complementary oxidation experiment performed with a time-resolved pulse radiolysis equipment in oxygen-saturated dichloromethane.

Clean catalytic combustion of nitrogen-bearing gasified biomass

Robert Burch and Barry W. L. Southward*

Catalysis Research Group, Department of Chemistry, The Queen's University of Belfast, Belfast BT9 5AG, Northern Ireland. E-mail: b.w.l.southward@qub.ac.uk

Received (in Cambridge, UK) 24th January 2000, Accepted 15th March 2000

Zero NO_x emissions are obtained in the catalytic combustion of simulated biomass mixtures containing substantial amounts of ammonia by optimisation of NH_3 oxidation and NO_x reduction using a 2%Rh–Al_2O_3 catalyst.

Renewable energy sources will be of increasing importance for power generation in the future. Attempts have been made to harness biomass-derived fuels for combined heat and power generation.[1–3] However, gasified biomass contains significant quantities of NH_3 (600–4000 ppm) in addition to substantial amounts of CO (9.8–17.2%), H_2 (9.8–13.2%) as well as CH_4, CO_2, H_2O and N_2.[3] The NH_3 represents a particular challenge since its combustion in the gas phase results in the formation of an equivalent amount of NO_x.

The environmental benefits of cleaner power generation has prompted much interest in catalytically stabilised combustion to reduce harmful emissions of nitrogen oxides (NO_x) and unburnt fuels.[1,2,4] A key question is whether catalytic combustion of biomass-derived gases can be controlled so as to avoid the conversion of ammonia into NO_x. The novel solution to this problem which we have discovered,[5] and which is reported here, is to first oxidise all the ammonia to NO_x and then utilise the large excess of CO and H_2 in the gas stream to reduce the NO_x to N_2 through the NO/CO and NO/H_2 reactions.

The catalyst used was 2%Rh–Al_2O_3 prepared by incipient wetness impregnation of CK300 Al_2O_3 (ex Akzo, surface area 200 $m^2\ g^{-1}$). The dried Al_2O_3 (120 °C, 24 h) was impregnated with Rh III nitrate (ex Johnson Matthey) and dried at room temperature for 24 h, then at 120 °C for a further 24 h prior to calcination at 700 °C in flowing O_2/He for 12 h. A second catalyst comprising 2%Rh–10%CeO_2–Al_2O_3 was prepared by sequential impregnation/calcination of $Ce(NO_3)_3{\cdot}6H_2O$ followed by $Rh(NO_3)_3$. Catalyst testing (60 mg, prereduced for 4 h at 700 °C in CO/H_2/He) was performed in a standard quartz flow microreactor at a GHSV of 240000 h^{-1}. Product analysis was by mass spectrometry (Hiden DSMS) with NO_x emissions and residual NH_3 levels being corroborated using an external NH_3 oxidation reactor (with independent oxygen supply) coupled with a NO_x chemiluminescence detector (Signal series 4000).

A conventional direct oxidation of NH_3 over 2%Rh–Al_2O_3 at typical gasifier output temperatures (Fig. 1) shows a low conversion initially but with a high selectivity to N_2. However, whilst both conversion and N_2 yields increase with temperature, N_2O and NO are also formed. N_2O and N_2 concentrations peak at *ca.* 375 °C (*ca.* 85–90% N_2) before decreasing, consistent with previous results,[2,6] whilst NO formation is seen to increase steadily with temperature to become the major product at $T >$ 500 °C. Fig. 1 therefore illustrates the difficulty of selectively oxidising NH_3 by conventional methods.

However, such problems may be overcome by making use of the other components of the biomass gas, namely CO and H_2 and by controlling the process conditions. Thus, catalytic reduction of NO by CO is very facile,[7] and the reduction of NO_x by H_2 has also been demonstrated.[8] Therefore, if NH_3 is first oxidised to NO_x, the other components of the biomass gas (CO and H_2) could be used for the catalytic reduction of NO_x to N_2. Hence by coupling NH_3 oxidation with NO_x reduction in an oxygen-limited environment it should be possible to convert NH_3 completely to N_2 in a pseudo-two-stage process. Thus, the strategy we propose is to first catalyse the complete oxidation of the NH_3 to NO_x in a limited amount of O_2, followed by catalytic reduction of NO_x by the CO or H_2 present in the biomass gas.

The main challenge is to selectively oxidise NH_3 in the presence of a large excess of CO and H_2. Our success in achieving this with a Rh catalyst is illustrated in Fig. 2. This shows that conversion of NH_3, rather than reaction selectivity, is the limiting factor for the selective oxidation. Thus, at low temperatures NH_3 does not react but H_2 and CO are very reactive. In contrast, at higher temperatures, the NH_3 begins to react and by around 600 °C the conversion of ammonia is effectively 100% whereas the combustion of H_2 has dropped to close to zero. Of course, the overall levels of oxidation are limited, deliberately, by controlling the O_2 concentration. Clearly, with this catalyst the selective oxidation of NH_3 to NO_x in the presence of a large excess of CO and H_2 has been achieved. The second stage, namely, the reduction of the NO_x

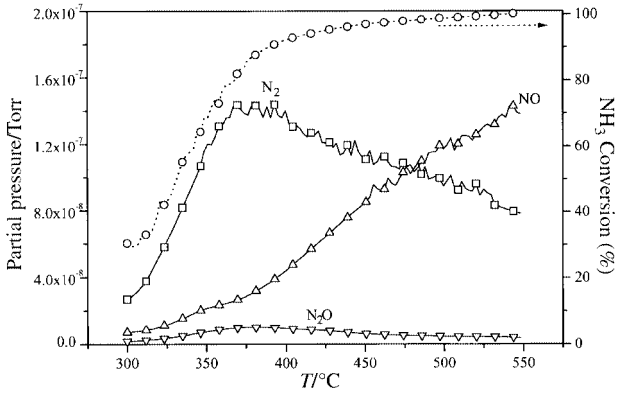

Fig. 1 Nitrogen-bearing products and NH_3 conversion for the selective catalytic oxidation of NH_3 over 2%Rh–Al_2O_3 (1000 ppm NH_3, 18% O_2, balance He). Key: □, N_2; ▽, N_2O; Δ, NO; ○, NH_3 conversion.

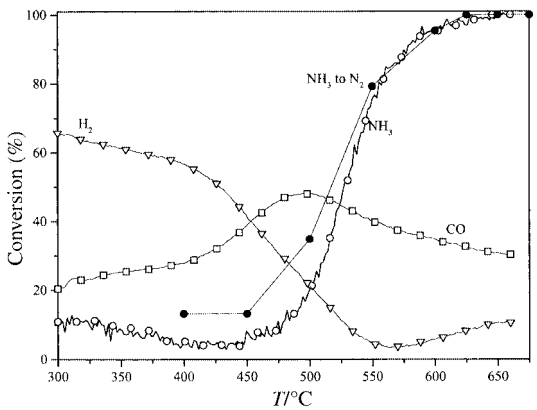

Fig. 2 Conversion profiles for the O_2 lean combustion of simulated biomass over 2%Rh–Al_2O_3 (1000 ppm NH_3, 0.275% O_2, 1.02% CO, 0.68% H_2, balance He). Key: ○, NH_3; □, CO; ▽, H_2, ●, NH_3 as determined by external oxidation reactor/chemiluminescence.

DOI: 10.1039/b000775g

Table 1 Lifetime performance of (1) 2%Rh–Al_2O_3 and (2) 2%Rh–10%CeO_2–Al_2O_3

Entry	$\%O_2:CO/H_2:H_2O$	$\%N_2$ at 1 h	$\%N_2$ at 2 h	$\%N_2$ at 3 h	$\%N_2$ at 4 h	$\%N_2$ at 5 h
1	0.275:1.7:0	98.3	97.5	96.7	96.6	96.6
2	0.275:8.9:2.5	100	100	100	99.9	99.8

by residual CO and/or H_2 occurs sequentially within the same bed of catalyst because the only nitrogen-containing product detected is N_2. This methodology has also been examined for its efficacy under more severe conditions for extended periods with minimal loss of activity (Table 1) underlining its potential for commercial application. Moreover it should be stressed that in case of the 2%Rh–10%CeO_2–Al_2O_3 catalyst, a significantly higher CO/H_2 concentration was employed, which in theory should mitigate *against* the activation of the NH_3 due to significantly enhanced competition for active sites, when in fact this sample exhibited almost no deactivation over the duration of the experiment.

In conclusion, we have developed a strategy for the complete removal of NH_3 from biomass-derived gases by coupling the total oxidation of NH_3 with the reduction of NO_x by CO and/or H_2. Experiments have demonstrated that the concept is viable and provides a novel way to overcome the environmenal problems associated with the direct combustion of biomass-derived gas. The strategy is equally applicable to any comparable gasification gas (from coal, or from other renewable sources). Future work will examine the potential poisoning effects of sulfur, alkali metals and chloride ions on activity, although given the net reducing conditions employed in this new process the impact of the former is expected to be limited given previous experience of the negligible effect of sulfur on 3-way catalysts.[9]

We are pleased to acknowledge the financial support of ABB-Alstom power, the DTI and the EPSRC through the FORESIGHT Challenge initiative. Helpful discussions with colleagues at Lens (Dr Matthieu Amblard), Cranfield University (Mr J. J. Witton, Professor B. Moss, Mr J. M. Przybylski and Dr E. Noordally) and at ABB-Alstom Power (Mr M. Cannon, G. J. Kelsall) are gratefully acknowledged.

Notes and references

1 M. F. M. Zwinkels, G. M. Eloise Heginuz, B. H. Gregertsen, K. Sjöström and S. G. Järås, *Appl. Catal. A*, 1997, **148**, 325.
2 L. Lietti, C. Groppi and C. Ramella, *Catal. Lett.*, 1998, **53**, 91.
3 *Development of Improved Stable Catalysts and Trace Element Capture for Hot Gas Cleaning*, DTI/ETSU/Clean Coal Power Generation Group, Project Profile 178, 1996.
4 W. C. Pfefferle, *Belg. Pat.*, 814572, 1974.
5 R. Burch and B. W. L. Southward, *Br. Pat. Appl.*, 98238879.3, 1998.
6 Y. Li and J. N. Armor, *Appl. Catal. B*, 1997, **13**, 131.
7 A. Fritz and V. Pitchon, *Appl. Catal. B*, 1997, **13**, 1.
8 D. Ferri, L. Forni, M. A. P. Dekkers and B. E. Nieuwenhuys, *Appl. Catal. B*, 1998, **16**, 339.
9 R. J. Farrauto and R. M. Heck, *Catal. Today*, 1999, **51**, 351.

ChemComm

Ab initio simulation of the interaction of hydrogen with the {111} surfaces of platinum, palladium and nickel. A possible explanation for their difference in hydrogenation activity

Graeme W. Watson,*† Richard P. K. Wells, David J. Willock and Graham J. Hutchings

Department of Chemistry, Cardiff University, PO Box 912, Cardiff, UK CF10 3TB

Received (in Oxford, UK) 25th January 2000, Accepted 14th March 2000

Density functional theory calculations have been performed on Pt, Pd and Ni {111} surfaces showing a considerable difference in adsorption energies for different sites on Pd and Ni while Pt shows an almost uniform adsorption energy which may be linked to the difference in activity of the these metals for hydrogenation.

Platinum, palladium and nickel, despite their close structural relationship and their proximity in the periodic table, show several significant differences in their chemistry. For example, for a given olefin the ease of hydrogenation over metal catalysts decreases in the order Pd > Rh > Pt > Ni >> Ru.[1] Under low hydrogen pressure conditions olefin isomerisation can also occur. Pt shows little isomerisation activity while Pd (together with Ni) promotes double bond migration *via* the formation of π-allyl intermediates. The degree of isomerisation over metal catalysts tends to decrease in the following order: Pd > Ni > Rh > Ru > Os ≅ Pt .[2,3] From this data it is clear that there are significant differences in the interaction of olefins and/or hydrogen with the metal surfaces. In this study we focus on one aspect of these differences, the interaction of hydrogen.

Molecular hydrogen adsorbs dissociatively on most transition metal surfaces with heats of chemisorption of between 30 and 60 kJ mol^{-1} (per H atom). Owing to its small size it can enter a metal surface fairly deeply leading to strong perturbations of the electronic structure. In most cases, including Pt and Ni, this only results in a relaxation of the first few atomic layers. However, some metals, including Pd, undergo a surface reconstruction which can lead to bulk absorption and the formation of PdH. The presence of sub-surface hydrogen in Pd has been illustrated by both temperature programmed desorption (TPD)[4] and H–D exchange reactions.[5]

Here, we consider the energetic differences between hydrogen atoms adsorbed at alternative sites of the clean {111} surfaces of Ni, Pd and Pt. We have employed the periodic plane wave pseudopotential density functional theory (DFT) method as implemented in the code VASP (Vienna *Ab initio* Simulation Program).[6] The Kohn–Sham equations are solved self consistently within the generalised gradient approximation, using the parameterisation derived by Perdew *et al.*[7] *k*-Point sampling, obtained using the Monkhorst–Pack scheme,[8] was used to treat the extended electronic states of the metal band structure with convergence accelerated using second order Methfessel–Paxton smearing[9] with a width of 0.1 eV. In this study a *k*-point grid of 5 × 5 × 1 was used which has been shown to provide accurate results.[10]

The {111} surfaces were constructed using the calculated equilibrium lattice constants of 3.990 Å (Pt), 3.950 Å (Pd) and 3.526 Å (Ni). These compare well with the experimental values of 3.924 Å (Pt), 3.891 Å (Pd) and 3.524 Å (Ni). A p(2 × 2) surface unit cell with three atomic layers, containing 12 metal atoms, was constructed. A vacuum gap equivalent to three layers was introduced to create the surfaces (one each side of the slab) with one hydrogen atom placed on one side of the slab corresponding to a surface coverage of 0.25 of a monolayer. The position of the hydrogen atom at each adsorption site was optimised with the metal surface held rigid. The adsorption energy is defined as the energy released on adsorption and is given by

$$E_{ads} = -[E(M + H) - E(M) - \tfrac{1}{2} E(H_2)]$$

Where E(M + H) is the energy of the hydrogen adsorbed on the metal, E(M) is the energy of the bare metal slab and $E(H_2)$ is the energy of a gas phase H_2 molecule. A positive value of E_{ads} implies that chemisorption from gas phase H_2 is thermodynamically favourable.

Fig. 1 shows a plan view of the {111} surface illustrating the four adsorption sites examined, the atop, bridge, fcc hollow and hcp hollow. Table 1 lists the adsorption energies and structures of hydrogen adsorbed onto each on these sites on the {111} surfaces of Ni, Pd and Pt. The differences in the influence of the H coordination on the adsorption energy for different metals is striking.

The adsorption onto the {111} surface of Ni increase with the coordination number of the hydrogen atom. The most stable site is the three-fold hcp hollow site (63.8 kJ mol^{-1}) closely followed by the three-fold fcc site (63.6 kJ mol^{-1}). The least stable is the atop site (10.1 kJ mol^{-1}) with the two-fold bridge site having an intermediate value (51.4 kJ mol^{-1}). The Ni–H bond lengths also follows the coordination number with the singularly coordinated atop site having the shortest bond and the three-fold hollow sites the longest bonds. Table 1 also lists the height Z(h) of the H atom above the first surface layer, clearly demonstrating that the atop hydrogen is significantly above the surface.

The results for Ni are in good agreement with experiment. Christmann *et al.*[11] found an adsorption energy of 49 kJ mol^{-1} while the stability of the hcp and fcc sites is consistent with the observed c(2 × 2)-2H structure.[12] Previous *ab initio* calculations[13] at a coverage of $\theta = 1$, gave rise to the same trend in the adsorption energy with the higher coordinated sites having the largest adsorption energies.

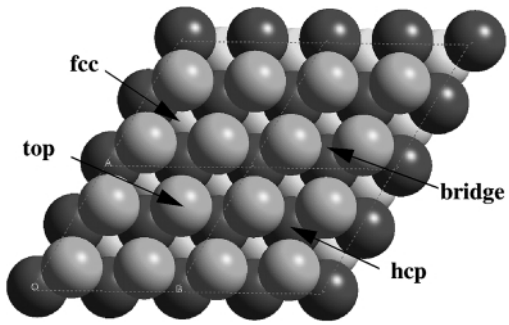

Fig. 1 Schematic illustration of the four adsorption modes for hydrogen investigated on the {111} surfaces of nickel, palladium and platinum. The one-fold atop site, the two-fold bridge site and the three-fold hollow sites (hcp and fcc) with the metal atoms not shown to scale so that the top, second (dark) and third (light) metals layers are clearly visible.

† Current address: Department of Chemistry, Trinity College, Dublin 2, Ireland. E-mail: watsong@tcd.ie

DOI: 10.1039/b000772m

Table 1 Comparison of the adsorption energies, bond lengths and height of the hydrogen atom above the surface for hydrogen adsorption on the {111} surfaces of nickel, palladium and platinum. The numbers in parentheses indicate the coordination number of the hydrogen atoms in each case

	Nickel			
	Atop	Bridge	hcp hollow	fcc hollow
E_{ads}/kJ mol^{-1}	10.1	51.4	63.8	63.6
Ni–H distance/Å	1.469 (×1)	1.626 (×2)	1.708 (×3)	1.708 (×3)
Z(H)/Å	1.47	1.04	0.92	0.92
	Palladium			
E_{ads}/kJ mol^{-1}	3.1	36.4	45.2	49.1
Pd–H distance/Å	1.552 (×1)	1.725 (×2)	1.818 (×3)	1.818 (×3)
Z(H)/Å	1.552	1.012	0.840	0.838
	Platinum			
E_{ads}/kJ mol^{-1}	44.8	42.4	43.2	43.9
Pt–H distance/Å	1.565 (×1)	1.772 (×2)	1.876 (×3)	1.875 (×3)
Z(H)/Å	1.565	1.071	0.927	0.922

Adsorption on the Pd {111} surface follows closely the results obtained for Ni {111} but with slightly lower adsorption energies. In this case the fcc hollow site (49.1 kJ mol^{-1}) is slightly more stable than the hcp hollow site (45.2 kJ mol^{-1}). The bridge site is again slightly less stable (36.4 kJ mol^{-1}) and the atop site the least stable (3.1 kJ mol^{-1}). These results are consistent with thermal desorption spectroscopy,[14] which gave an adsorption energy of 43.4 kJ mol^{-1}, and low energy electron diffraction[15] (LEED) which suggests that the hydrogen occupies the fcc hollow site with a Pd–H distance of 1.78–1.80 Å. Previous calculations[13,16,17] also identified the hcp hollow site as the most stable with the stability reducing as a function of the coordination of the hydrogen. In the previous computational studies, the effect of surface relaxation was also investigated and found to be very small thus justifying our use of rigid surfaces.

For the Pt {111} surface the results are significantly different. All four adsorption sites have very similar energies, around 44 kJ mol^{-1} which is also in good agreement with microcalorimetric experiments on hydrogen adsorption to Pt powders[18] (45 kJ mol^{-1}). Although there is no relationship between the adsorption energy and the coordination number, surprisingly, the Pt–H distance follows the same trend as for the Ni and Pd with the atop site the shortest and the hollow sites the longest. For Pt {111} there are no previous *ab initio* calculations with which to compare.

From this it is clear that the interaction of hydrogen with the surface of Pt is significantly different to Pd and Ni. This is likely to have significant implications for reactions involving hydrogen on the surfaces of these metals. The atop will be more accessible for reacting with other adsorbed species and for Pd and Ni it is clear that hydrogen will not occupy this site. For Pt the atop site is in fact the most stable (although only marginally) implying that both the atop site and the hollow sites will be significantly populated and thus hydrogen will be more accessible for reaction.

More significantly the similar adsorption energies for all sites on Pt imply that the diffusion of hydrogen across the surface will be more rapid than for the other two metals. Recent experimental evidence to this effect has been obtained from quasi-elastic helium scattering.[19] If a hydrogen atom is located on a fcc hollow site on the {111} surface it will have to pass through either an atop or bridge site to diffuse across the surface. For Pt {111}, the energy of these sites is almost identical, and thus the energy barriers to diffusion are likely to be small. For Pd and Ni, the lowest energy pathway is through the bridge site, which is less stable than the fcc hollow site by 12 kJ mol^{-1} for Ni and 13 kJ mol^{-1} for Pd, compared to a difference of only 1.5 kJ mol^{-1} on Pt {111}. Diffusion over the Pd and Ni {111} surfaces will thus be hindered since H adsorbates have to pass through the bridge site creating a significant energy barrier compared to that on Pt. Evidence for this effect can be found in the isomerisation data presented earlier. At low partial pressure of hydrogen Pd and Ni allow olefin isomerisation while Pt does not. This can be explained by the rate of the hydrogenation reaction on Pd and Ni being limited by the transport of hydrogen to the reaction site. On Pt, owing to the faster diffusion, hydrogen transport will not be a significant factor.

The results presented indicate that there are fundamental differences in the interaction of hydrogen on the surfaces of platinum, paladium and nickel, and that these differences may contribute to the differences in the hydrogenation activity. While we have not considered sub-surface hydrogen in our calculations on Pd, the similarity of our results for Pd and Ni, where sub-surface hydrogen is known to be less important, suggest that our conclusions regarding the surface hydrogen species are valid.

We would like to thank the EPSRC IMI, Synetix, Johnson Matthey, BP-Amoco, Cambridge Reactor Design, Molecular Simulations Inc and OCF for financial support.

References

1 R. L. Augustine, in *Heterogeneous Catalysis for the Synthetic Chemist*, Marcel Decker, New York, 1995.
2 G. C. Bond and J. S. Rank, *Proc. 3rd Int. Cong. Catalal.*, 1965, **2**, 1225.
3 G. C. Bond and P. B. Wells, *Adv. Catal.*, 1964, **15**, 91.
4 H. Conrad, G. Ertl and E. E. Latta, *Surf. Sci.*, 1974, **41**, 435.
5 T. Engel and H. Kuipers, *Surf. Sci.*, 1979, **90**, 162.
6 G. Kresse and J. Furthmüller, *Phys. Rev. B*, 1996, **54**, 11 169.
7 J. P. Perdew, J. A. Chevary, S. H. Vorto, K. A. Jackson, M. R. Pedersen, D. J. Singh and C. Frolhais, *Phys. Rev. B*, 1992, **46**, 6671.
8 H. J. Monkhurst and J. D. Pack, *Phys. Rev. B*, 1976, **13**, 5188.
9 M. Methfessel and A. Paxton, *Phys. Rev. B*, 1989, **49**, 3616.
10 G. W. Watson, R. P. K. Wells, D. J. Willock and G. J. Hutchings, *J. Phys. Chem.*, submitted.
11 K. Christmann, R. J. Behm, G. Ertl, M. A. van Hove and W. H. Weinberg, *J. Chem. Phys.*, 1979, **70**, 4168.
12 K. Christmann, O. Schober, G. Ertl and M. Neumann, *J. Chem. Phys.*, 1974, **70**, 4528.
13 J.-F. Paul and P. Sautet, *Surf. Sci.*, 1996, **356**, L403.
14 H. Conrad, G. Ertl and E. E. Latta, *Surf. Sci.*, 1974, **41**, 435.
15 T. E. Felter, E. C. Sowa and M. A. van Hove, *Phys. Rev. B*, 1989, **40**, 891.
16 W. Dong, V. Ledentu, P. Sautet, A. Eichler and J. Hafner, *Surf. Sci.*, 1998, **411**, 123.
17 O. M. Løvvik and R. A. Olsen, *Phys. Rev. B*, 1998, **58**, 10 890.
18 B. E. Spiewak, R. D. Cortright and J. A. Dumesic, *J. Catal.*, 1998, **176**, 405.
19 A. P. Graham, A. Menzel and P. Toennies, *J. Chem. Phys.*, 1999, **111**, 1676.

ChemComm

Controllable pH modulation of lanthanide luminescence by intramolecular switching of the hydration state†

Mark P. Lowe and David Parker*

Department of Chemistry, University of Durham, South Road, Durham, UK DH1 3LE.
E-mail: David.Parker@durham.ac.uk

Received (in Cambridge, UK) 28th February 2000, Accepted 16th March 2000

The pH dependent ligation of a pendant arylsulfonamide group allows switching between the $q = 0$ and $q = 2$ states to be reported by changes in lanthanide luminescence emission over the pH range 5.5–7.5 and in the presence of serum albumin.

The behaviour of responsive luminescent lanthanide complexes is being studied actively at present, in which changes in the lanthanide emission intensity, lifetime or polarisation are used to signal selectively concentration variations of a target analyte.[1,2] Particular attention has focused on well-defined, kinetically stable Eu and Tb complexes, and examples of pH,[3] pO_2[4] and pX[5] dependent luminescence have been reported in high salt aqueous media. These cases rely upon a perturbation either of the singlet or triplet excited states of the sensitising chromophore or the longer-lived $^5D_0$ and $^5D_4$ states of Eu and Tb respectively (Scheme 1). In the latter case, the lifetime and emission intensity are primarily determined by the nature and proximity of energy-matched XH oscillators, which quench the lanthanide excited state by vibrational energy transfer.[6] Thus reversible binding of HCO_3^- to di-aqua Eu or Tb complexes of chiral heptadentate ligands, causes displacement of the bound water molecules and an enhancement in emission intensity and lifetime as well as marked changes in emission polarisation.[5b] We now report a new example of controllable modulation of lanthanide luminescence, whereby variations in pH allow a switching between $q = 0$ and $q = 2$ states associated with the on/off ligation of an arylsulfonamide group (Fig. 1). Furthermore, by varying the structure of the macrocyclic ligand, competitive binding by endogenous anions and proteins may be suppressed, thereby paving the way for the development of complexes which operate directly in 'biological' samples (*e.g.* serum).

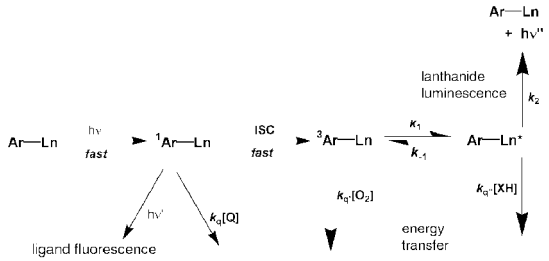

Scheme 1

For the preparation of the initial target complexes (Fig. 1), advantage was taken of the ring opening reaction of *N*-*p*-methoxyphenylsulfonylaziridines with secondary amines.[7] For example, reaction of *N*-*p*-trifluoromethylphenylsulfonyl-aziridine with 1,4,7-tris(*tert*-butoxycarbonylmethyl)-1,4,7,10-tetraazacyclododecane in MeCN followed by TFA deprotection and metal complexation ($LnCl_3$, H_2O, pH 6) yielded the desired complexes.[8] The rate constants for decay of the Eu (and Tb) complexes were measured at pH 10 and 4 (λ_{exc} = 270 or 397 (Eu)/355 (Tb); 295 K) and gave values (Table 1) that are consistent with hydration states *q*, of 0.2 at pH 10 and 1.6 at pH 4. Profound changes in the form and intensity of the Eu emission spectra, especially the hypersensitive $\Delta J = 2$ and $\Delta J = 4$ transitions also characterised this pH change. In addition the Eu and Tb spectra, following sensitised excitation, were much more intense in the $q = 0$ régime, as not only the quenching bound OH oscillators have been displaced but also the aryl chromophore is much closer to the Ln centre, enhancing the efficiency of the intramolecular energy transfer step (Scheme 1). In accord with the hypothesis, quantum yields following excitation at 270 nm of 0.39% (pH 10) and 0.11% (pH 4) were recorded for [Eu·**1**] (R = OMe; 295 K, H_2O), and the corresponding values for [Tb·**2**] were 3.5% (pH 10) and 0.17% (pH 4).

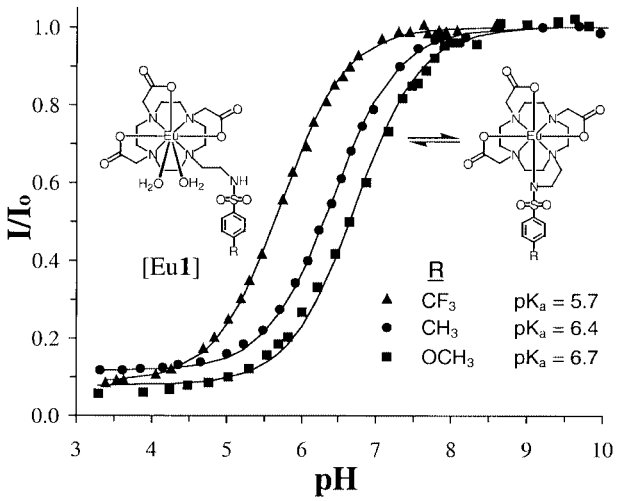

Fig. 1 pH Dependence of the europium luminescence (I/I_0) of [Eu·**1**] at 295 K (1 mM complex, 295 K, 0.1 M NaCl; λ_{exc} = 270 nm; λ_{em} = 612 nm ($\Delta J = 2$); solid lines show the fit to the experimental data).

Table 1 Rate constants *k* (ms^{-1}) and hydration states *q*, for decay of the lanthanide luminescence at limiting pH values (295 K, *I* = 0.1 M NaCl)

	pH/D 4			pH/D 10		
Complex	k_{H_2O}	k_{D_2O}[a]	q[a]	k_{H_2O}	k_{D_2O}	q
[Eu·**1**](*p*CF$_3$)	2.35	0.76	1.6	1.09	0.74	0.1
[Eu·**1**](*p*Me)	2.27	0.70	1.6	1.20	0.80	0.2
[Eu·**1**](*p*OMe)	2.32	0.66	1.7	1.43	0.93	0.3
[Eu·**2**]	2.21	0.65	1.6	1.11	0.72	0.2
[Tb·**2**]	0.90	0.56	1.4	0.45	0.40	0

[a] *q* Values were estimated using the equations $q^{Eu} = 1.2 (k_{H_2O} - k_{D_2O} - 0.25)$, $q^{Tb} = 5 (k_{H_2O} - k_{D_2O} - 0.06)$, which allow for contribution of unbound water molecules.[6a] Non-integral values may reflect the presence of a coordination equilibrium between the $q = 1$ and 2 states[6b] or the presence of a relatively 'long' Ln-OH_2 bond.[6a]

† Electronic supplementary information (ESI) available: examples of representative spectra of Eu and Tb complexes and their pH dependence. See http://www.rsc.org/suppdata/cc/b0/b001629m/

DOI: 10.1039/b001629m

Variation of the *p*-substituent in the arenesulfonyl group determines the basicity of the sulfonyl nitrogen and hence the pH at which protonation of the complex occurs. The pH dependence of the luminescence emission intensity was measured (295 K, I = 0.1 M, NaCl) for the series of terbium and europium complexes, (Fig. 1), showing behaviour in accord with the change in basicity at N. Thus the *p*-CF_3 europium complex gave a pK_a of 5.7 (±0.05) and the *p*-Me/*p*-OMe analogues yielded values of 6.4 and 6.7 respectively. The large pH-dependent changes in the form and intensity of the Eu emission allows the precise definition of pH (amenable in principle to multivariate calibration) with an estimated tolerance of ±0.1 pH units.

A limitation to the application of such complexes in a mixed salt or 'biological' background is the competititve binding of oxyanions (*e.g.* HCO_3^-, HPO_4^{2-} and lactate/citrate) or proteins (*e.g.* human serum albumin) to the q = 2 complex.[9] In order to obviate this problem, polyanionic analogues of the macrocyclic ligand were prepared by introduction of a carboxyethyl substituent α to three of the ring nitrogens.[8,10] The resultant complexes are tri- or tetra-anionic, inhibiting intermolecular anion binding to the q = 2 state. The pH-dependence of the terbium emission intensity (Fig. 2) was the same in 0.1 M NaCl and in a simulated 'clinical-anion' background—with an apparent pK_a of 6.7 (295 K). Moreover in the presence of an excess of human serum albumin (0.2 mM complex; 2 mM HSA) there was no change in the form and relative intensity of the Eu complex emission spectrum at pH 7.4, 6.9 and 5.5; the emission decay curves were also identical for each of these pH values.

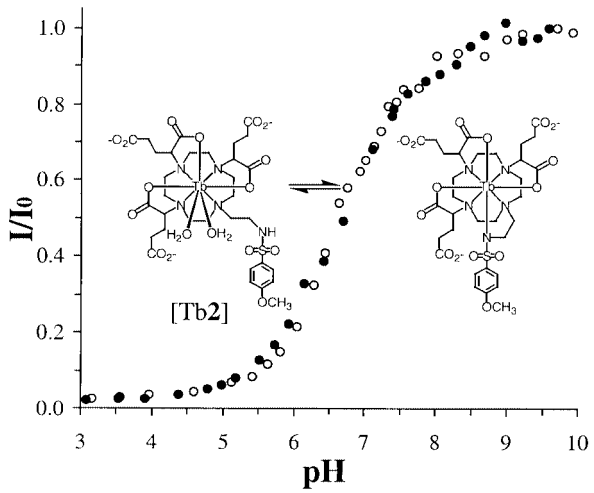

Fig. 2 pH Dependence of the terbium luminescence (I/I_0) of [Tb·**2**] at 295 K [1 mM complex; filled circles: 0.1 M NaCl, 30 mM $NaHCO_3$, 2.3 mM Na lactate, 0.13 mM citrate, 0.9 mM NaH_2PO_4; λ_{exc} = 272 nm, λ_{em} = 541 nm (ΔJ = 1); open circles: 0.1 M NaCl only; pK_a = 6.7 (±0.06)].

Such behaviour augurs well for the application of such complexes in the pH determination of serum samples, for which longer wavelength excitation (*e.g.* λ_{exc} = 355 nm) may be achieved by using a 6-phenanthridinesulfonyl group as an antenna chromophore. Moreover, the characteristics of the Eu/Tb complexes strongly suggest that the corresponding Gd complexes may be used as contrast agents to report pH changes *in vivo*. This aspect will be reported in a subsequent communication.

We thank the EPSRC, BBSRC and the COST-D18 action for support and Professor Silvio Aime for discussions on parallel work on Gd complexes of alkylated DO3A ligands.

Notes and references

1 D. Parker, K. Senanayake and J. A. G. Williams, *J. Chem. Soc., Perkin Trans. 2*, 1998, 2129; A. P. de Silva, D. B. Fox, A. J. M. Huxley, N. D. McClenaghan and J. Roiron, *Coord. Chem. Rev.*, 1999, **185/6**, 297.

2 (*a*) R. S. Dickins, T. Gunnlaugsson, D. Parker and R. D. Peacock, *Chem. Commun.*, 1998, 1643; (*b*) N. Sabbatini, M. Guardigli and J.-M. Lehn, *Coord. Chem. Rev.*, 1993, **123**, 201.

3 T. Gunnlaugsson and D. Parker, *Chem. Commun.*, 1998, 511; T. Gunnlaugsson, D. Parker and D. A. McDonnaill, *Chem. Commun.*, 2000, 93.

4 D. Parker and J. A. G. Williams, *Chem. Commun.*, 1998, 245. For other examples of non-lanthanide luminescent pO_2 sensors see: J. N. Demas, B. A. DeGraff and P. B. Coleman, *Anal. Chem.*, 1999, 793A.

5 (*a*) For halide anion dependent luminescence, see: D. Parker, K. Senanayake and J. A. G. Williams, *Chem. Commun.*, 1997, 1777; (*b*) For dependence on [HCO_3^-] in competitive media see refs. 2(*a*) and: S. Aime, A. Barge, M. Botta, J. A. K. Howard, R. Kataky, M. P. Lowe, J. M. Moloney, D. Parker and A. S. de Sousa, *Chem. Commun.*, 1999, 1047.

6 (*a*) A. Beeby, I. M. Clarkson, R. S. Dickins, S. Faulkner, D. Parker, L. Royle, A. S. de Sousa, J. A. G. Williams and M. Woods, *J. Chem. Soc., Perkin Trans. 2*, 1999, 493; (*b*) E. Toth, O. M. Ni, M. Dhubhghaill, G. Besson, L. Helm and A. E. Merbach, *Magn. Reson. Chem.*, 1999, **37**, 701.

7 A. E. Martin, T. M. Ford and J. E. Bulkowski, *J. Org. Chem.*, 1982, **47**, 412; the *N*-ligation of *N*-arylsulfonamides to macrocyclic Zn^{2+} complexes has been defined: T. Koike, E. Kimura, I. Nakamura, Y. Hashimoto and M. Shiro, *J. Am. Chem. Soc.*, 1992, **114**, 7338.

8 Each complex gave ^{1}H NMR and accurate mass negative ion ESMS data consistent with the proposed structures *e.g.* [Eu·**1**] (*p*-OMe); calc. for [$C_{23}H_{33}N_5O_9SEu$] 708.1211 found: 708.1210; δ_H(pD 10, 277 K) 37.5, 30.7, 27.9, 18.9 (ring H axial) typical of a square-anti-prismatic geometry about Eu. IR (KBr and CH_3OH) revealed no changes in ν_{SO} in the q = 0 and q = 2 states (ν_{SO} = 1329 (asymm.) and 1159 (symm) cm^{-1}) consistent with *N*-coordination only.

9 L. Burai, V. Hietopelto, R. Király, E. Toth and E. Brücher, *Magn. Reson. Inorg.*, 1997, **38**, 146; S. Aime, E. Gianolio, E. Terreno, G. B. Giovenzana, R. Pogliarin, M. Sisti, G. Palmisano, M. P. Lowe, D. Parker and M. Botta, *J. Bioinorg. Chem.*, 2000, in press.

10 M. Woods, J. A. K. Howard, J. M. Moloney, M. Navet, D. Parker, M. Port and O. Rousseau, *Chem. Commun.*, 1998, 1381. The Eu and Tb complexes were isolated as a 70:30 diastereoisomeric mixture of the *RRR* (major) and *RRS* isomers.

Nematic mesomorphism in laterally substituted palladium complexes of alkoxystilbazoles

Carsten P. Roll,[ab] Bertrand Donnio,[a]† Wolfgang Weigand[b] and Duncan W. Bruce*[a]

[a] *School of Chemistry, University of Exeter, Stocker Road, Exeter, UK EX4 4QD. E-mail: d.bruce@exeter.ac.uk*
[b] *Institut für Anorganische und Analytische Chemie, Friedrich-Schiller-Universität Jena, August-Bebel-Str. 2, 07443 Jena, Germany*

Received (in Cambridge, UK) 15th February 2000, Accepted 17th March 2000

Attachment of lateral carboxylate chains to polycatenar stilbazole complexes of palladium(II) unexpectedly leads to a series of materials with only nematic phases.

In the study of liquid crystals in general, a major objective is to be able to control the liquid-crystalline properties of a material *via* control of the molecular structure. As the subject advances and new types of molecules showing liquid-crystal properties appear, so there is a need to establish whether new structure–property relationships apply or whether existing principles are sufficient to understand the observed behaviour. Two of the more exciting areas of development in recent years have been the emergence of liquid crystals based on metal complexes[1] and the synthesis of polycatenar mesogens.[2]

In the former case, the field has developed rather rapidly in the last 10 years and mesogens based on metals with coordination numbers from 2 to 9 are known showing all the major phase types and exhibiting phase types and properties known for organic systems, such as ferroelectricity.[3] In addition, it is interesting to note that because of the presence of the metal centre in the molecule, the substitutional possibilities are enhanced over those offered by purely organic systems leading to materials with interesting geometric arrangements. Polycatenar liquid crystals can be defined as those with a rod-like core which possess three or more terminal chains. Much of the interest arises as these systems can show the nematic and lamellar mesomorphism characteristic of calamitic mesogens as well as the columnar mesomorphism characteristic of disk-like systems. This is best shown in systems where there are four terminal chains (tetracatenar mesogens) with each end of the molecule carrying two of these in the 3- and 4-positions of the terminal phenyl rings. In such a case, an individual mesogen can show either nematic or smectic C mesophases at short chain lengths and columnar phases at long chain lengths, with cubic phases sometimes being seen at intermediate chain lengths. A good example of this progression across a phase diagram is provided by some 5,5′-disubstituted-2,2′-bipyridines which we reported in 1998.[4]

We have for some time been interested in metal complexes of alkoxystilbazoles and have reported mesomorphic systems based on Ag(I),[5] Ir(I) and Rh(I),[6] Pd(II) and Pt(II).[7,8] In particular, we draw attention to a comparison which can be made between some complexes of Ag(I) and related systems based on Pd(II) (Fig. 1). Thus, we have reported[9] that Ag(I) complexes of 3,4-dialkoxystilbazoles bearing dodecylsulfate counter-anions (Fig. 1, **1**) show either a cubic or columnar phase depending on the chain length of the stilbazole. We have interpreted this behaviour in terms of the mesomorphism of polycatenar mesogens, but we notice that in the phase diagram, there is no sign of a smectic C phase which would be expected at shorter chain lengths. This may well be due to the presence of the dodecylsulfate anion acting as a lateral chain. Analogous complexes of 3,4-dialkoxystilbazoles have also been synthesised on palladium(II)[8] (Fig. 1, **2**) and this time we found a smectic C phase at shorter chain lengths and a columnar phase at longer chain lengths, but with no complexes showing both phases and no cubic phase at intermediate chain lengths.

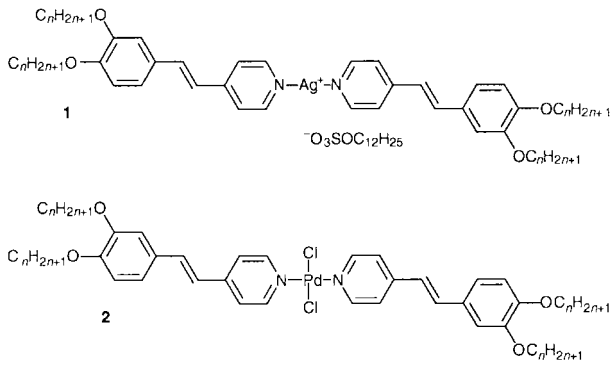

Fig. 1 Structure of dialkoxystilbazole complexes of Ag(I) and Pd(II).

We were interested, therefore, to see whether we could understand these differences in purely structural terms and so we set out to synthesise some stilbazole complexes of palladium(II) bearing lateral chains. In order to do this, we adopted an approach which we had used previously, namely to react the stilbazole with palladium carboxylates, $[Pd(O_2C–C_mH_{2m+1})_2]$, obtained from $[Pd(OAc)_2]_3$ and the carboxylic acid.[10] A number of palladium carboxylates can be obtained in this way and so reaction with 2 equiv. of dialkoxystilbazole will lead to the complexes shown in Fig. 2.

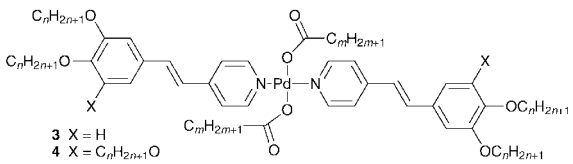

Fig. 2 Structure of the palladium complexes with lateral chains.

The reasons we adopted this approach were to do with ideas about the factors controlling the formation of lamellar, cubic and columnar phases in polycatenar mesogens. Thus, arguments are presented in which the curvature at the interface between the rigid core and the alkyl chains (Fig. 3) determine the mesophase formed in a manner analogous to that described for lyotropic systems.[11] Thus, at short chain lengths, there is no imbalance between the volumes of the core and the chains, no interfacial curvature and hence no barrier to the formation of a lamellar phase. However, at longer chain lengths, the volume required by the chains becomes much greater than that required by the core and so an interfacial curvature is established. When this curvature is large, the smectic layers are disrupted and columnar phases can form, with the columnar repeat unit being an aggregate of typically three or four molecules as shown in Fig. 4. At intermediate curvatures, cubic phases may form. Thus, it

† Present address: IPCMS, Groupe des Materiaux Organiques, 23 rue du Loess, BP 20CR, 67037 Strasbourg cedex, France.

DOI: 10.1039/b001268h

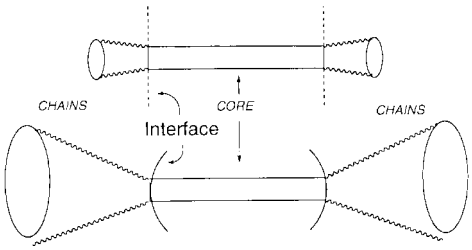

Fig. 3 Schematic to show the origin of the interfacial curvature in polycatenar mesogens.

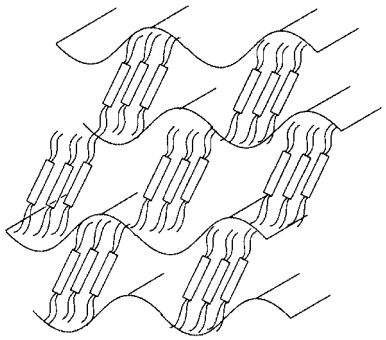

Fig. 4 Schematic to show the break-up of a lamellar structure into columnar units.

is possible to view phase formation as being dependent on the balance between the volume of the mesogen core and its chains.

We therefore speculated that in the case of the palladium mesogens, the rate of change of the volume of the chains (four methylene groups per homologue – *i.e.* about 108 Å^3) was quite rapid for the size of the core and so the transition from lamellar to columnar behaviour would be rather rapid as a function of the chain length accounting for the fact that this transition happens at a given chain length. Therefore, we reasoned that we could influence the volume of the core by introducing lateral substituents, and so modulate the effect of the increase in the chain volume. To this end, we synthesised a number of complexes **3** (Fig. 2) in which we varied the stilbazole chain length and the carboylate chain length.

The results are summarised in Table 1 and show somewhat unexpected phase behaviour. Thus, for all dialkoxystilbazoles examined with all carboxylates from butanoate upwards (shorter carboxylates did not give mesomorphic materials), only a nematic phase was seen. Previously, Maitlis and coworkers[7a] had shown that palladium complexes of *mono*alkoxystilbazoles with lateral carboxylates gave nematic phases, consistent with the known behaviour of organic systems where the introduction of lateral chains suppresses smectic phase formation.[12] Other examples of lateral substitution in metallomesogens may be found as compounds **24**–**39** in ref. 1*a*. However, here we are dealing with a polycatenar mesogen and so we might expect the lateral chains to behave differently, particularly when the chain length on the stilbazole was long. Thus, we might have expected to see a smectic C or columnar phase depending on whether the chains added to the core or radiated out, respectively. Curious then to pursue this further, we extended the approach by accessing the complexes **4** in whch we used a 3,4,5-trialkoxystilbazole ligand. All of the palladium dichloride complexes of these ligands which were mesomorphic showed a columnar mesophase[8] and so we reasoned here that by increasing the volume of the core with the lateral chains, it would be possible to find smectic C or even cubic phases. Alternatively and perhaps most likely, the complex would simply behave as a classical discotic mesogen with eight peripheral chains and continue to show a columnar phase. Table 1 shows that even these thoughts were misplaced and once more we found

Table 1 Thermal data for the new complexes

n	*m*	Transition	*T*/°C
Compound **3**			
6	3	Crys–I	181 (decomp)
12	3	Crys–N	111
		N–I	123
6	5	Crys–N	125
		N–I	131
12	5	Crys–N	95
		N–I	109
6	7	Crys–N	115
		N–I	123
12	7	Crys–N	90
		N–I	100
Compound **4**			
14	3	Crys–N	69
		N–I	77
14	7	Crys–I	55
		(N–I)	(53)

complexes which showed only the nematic phase. Thus, for compounds of this type with six or eight peripheral chains to show only nematic phases is, we believe, unprecedented.

The questions now arise as to the nature of the nematic phases of these complexes and why they arise. Are the nematic phases of complexes **4** 'discotic nematic' or are they composed of more rod-like systems, *i.e.* how are the chains arranged? What is the behaviour of the lateral chains in these systems which causes the formation of only nematic phases irrespective of the nature of the ligands and unrelated to the phases formed by the parent dichloride systems? These are clearly quite unique materials which require further detailed study both to ascertain why nematic phases are formed exclusively and how their mesomorphism contributes to the understanding of the mesomorphism of polycatenar liquid crysals. It is also important to note that a study of this type is greatly facilitated by the substitutional possibilities offered by the metal centre.

We thank the University of Exeter and the DAAD for support and Johnson Matthey for generous loans of precious metal salts.

Notes and references

1 (*a*) B. Donnio and D. W. Bruce, *Struct. Bonding* (*Berlin*), 1999, **95**, 193; (*b*) *Metallomesogens*, ed. J.-L. Serrano, Wiley-VCH, Weinheim, 1996.
2 J. Malthête, H. T. Nguyen and C. Destrade, *Liq. Cryst.*, 1993, **13**, 171; H. T. Nguyen, C. Destrade and J. Malthête, *Adv. Mater.*, 1997, **9**, 375.
3 M. J. Baeña, J. Barbera, P. Espinet, A. Ezcurra, M. B. Ros and J.-L. Serrano, *J. Am. Chem. Soc.*, 1994, **116**, 1899; P. Espinet, J. Etxebarria, M. Marcos, J. Pérez, A. Rémon and J.-L. Serrano, *Angew. Chem., Int. Ed. Engl.*, 1989, **28**, 1065.
4 K. E. Rowe and D. W. Bruce, *J. Mater. Chem.*, 1998, **8**, 331.
5 See *e.g.* B. Donnio and D. W. Bruce, *New J. Chem.*, 1999, **23**, 275 and references therein.
6 D. W. Bruce, D. A. Dunmur, M. A. Esteruelas, S. E. Hunt, R. Le Lagadec, P. M. Maitlis, J. R. Marsden, E. Sola and J. M. Stacey, *J. Mater. Chem.*, 1991, **1**, 251.
7 (*a*) J. P. Rourke, F. P. Fanizzi, N. J. S. Salt, D. W. Bruce, D. A. Dunmur and P. M. Maitlis, *J. Chem. Soc., Chem. Commun.*, 1990, 229; (*b*) J. P. Rourke, F. P. Fanizzi, D. W. Bruce, D. A. Dunmur and P. M. Maitlis, *J. Chem. Soc., Dalton Trans.*, 1992, 3009.
8 B. Donnio and D. W. Bruce, *J. Chem. Soc., Dalton Trans.*, 1997, 2745.
9 B. Donnio, D. W. Bruce, B. Heinrich, D. Gullion, H. Delacroix and T. Gulik-Krzywicki, *Chem. Mater.*, 1997, **9**, 2951.
10 N. J. S. Salt, *PhD Theses*, University of Sheffield, 1989.
11 These ideas are discussed in: A. Skoulios and D. Guillon, *Mol. Cryst. Liq. Cryst.*, 1988, **165**, 317; Y. Hendrikx and A.-M. Levelut, *Mol. Cryst. Liq. Cryst.*, 1988, **165**, 233; J. Charvolin, *J. Chim. Phys.*, 1983, **80**, 15; C. Tschierske, *J. Mater. Chem.*, 1998, **8**, 1485.
12 D. Demus, *Mol. Cryst. Liq. Cryst.*, 1988, **165**, 45.

Bisphosphonate prodrugs: unusual dimerisation of clodronic acid trimethyl ester to a cyclic bis(bisphosphonate)

Marko J. Ahlmark,*[a] Markku Ahlgrén,[b] Riku Niemi,[c] Hannu Taipale,[c] Tomi Järvinen[c] and Jouko J. Vepsäläinen[a]

[a] *Department of Chemistry, University of Kuopio, PO Box 1627, FIN-70211 Kuopio, Finland. E-mail: Marko.Ahlmark@uku.fi*
[b] *Department of Chemistry, University of Joensuu, PO Box 111, FIN-80101 Joensuu, Finland*
[c] *Department Pharmaceutical Chemistry, University of Kuopio, PO Box 1627, FIN-70211 Kuopio, Finland*

Received (in Liverpool, UK) 19th January 2000, Accepted 15th March 2000

$Cl_2C[P(O)(OMe)_2P(O)(OMe)(O^-Z^+)]$ selectively reacts with acetyl chloride to provide a new enzymatically stable heterocyclic bis(bisphosphonate); the structure is confirmed by X-ray crystallography.

Methylenebisphosphonates (MBP), such as clodronate (Cl_2MBP), are an important class of drugs which have proven to be effective in the treatment of various diseases of bone and calcium metabolism including Paget's disease, non tumor-induced hypercalcaemia, and osteoporosis.[1] Recently, we reported[2] the synthesis and *in vitro* evaluation of clodronic acid dianhydrides as bioreversible prodrugs of clodronate. Exploration[3] of new strategies to prepare clodronate anhydrides lead us to a discovery of the selective synthesis of a new cyclic bis(bisphosphonate) anion **2**. The prepared dimer is the first approach to the self-prodrug of clodronate in which the number of promoities are minimised. We report here the selective synthesis and the X-ray structure of a stable cyclic dimer of clodronate, and its stability in aqueous buffer and human plasma.

Triester **1** (0.206 mmol), prepared by known method,[4] reacted selectively with acetyl chloride (2.196 mmol) in dry acetonitrile (4.0 ml) under reflux for 2 h to give a cyclic bis(bisphosphonate). The mixture was concentrated *in vacuo*, dissolved in CH_2Cl_2 and extracted once with cold water to give $[NMeBu_3]_2$**2**† as a colourless oil in 92% yield after evaporation of the aqueous phase (Scheme 1). The backbone structure was assigned by ^{31}P NMR spectroscopy, where peaks with intensities of 1:2:1 appeared as two doublets at δ 1.78 ($^2J_{PP}$ 16.9 Hz) and −2.17 ($^2J_{PP}$ 42.6 Hz), and a triplet of doublets at δ −17.58 (ring phosphorus). This structure was confirmed by X-ray crystallography‡ (Fig. 1).

This type of selective and quantitative cyclisation reaction is rather unusual.[5–8] According to NMR studies, the reaction starts with the removal of the methyl group (first step) as MeCl from the anionic phosphorus **1** to form monoacetyl compound **3**. The formation of anionic bisphosphonates **4**–**9** was also detected during the reaction by 2D ^{31}P NMR P,P-COSY. However, all these species led to selective formation of **2**.

X-Ray diffraction study of $[NMeBu_3]_2$**2** showed a strained six-membered ring as a consequence of the O13–P1–C1 and O23–P2–C1 angles of 98.8°, 6° smaller than for acyclic derivatives.[9] The bond angle distortion of P1–O13–P3 is *ca.* 15° wider than in non-cyclic derivatives.[9] The stability of the cyclic structure is likely due to the short hydrogen bonds between

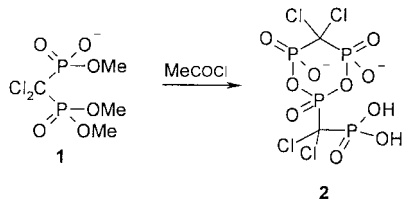

1 **2**

Scheme 1 Preparation of **2**.

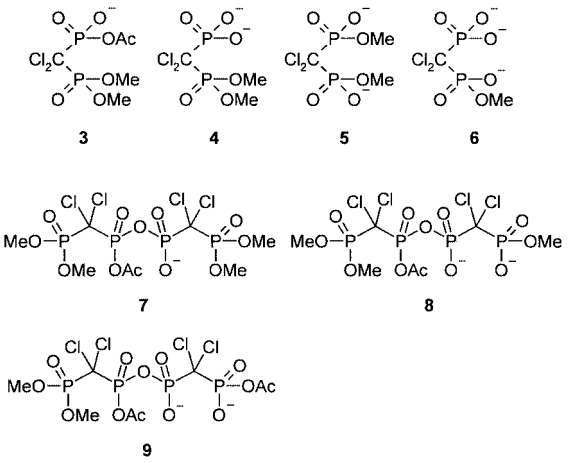

3 **4** **5** **6** **7** **8** **9**

O12–O43 and O21–O42. Moreover, the two oxygens bonds, O11(O22) and O12(O21) at P1(P2), are short (1.466 and 1.490 Å) indicating a strong double bond character for both bonds. Other bond lengths are within normal ranges.

The usefulness of the cyclic structure as a prodrug was investigated in aqueous buffer and human plasma. Ring **2** was cleaved to an acyclic dimer **10** (Scheme 2) in 50 mM aqueous

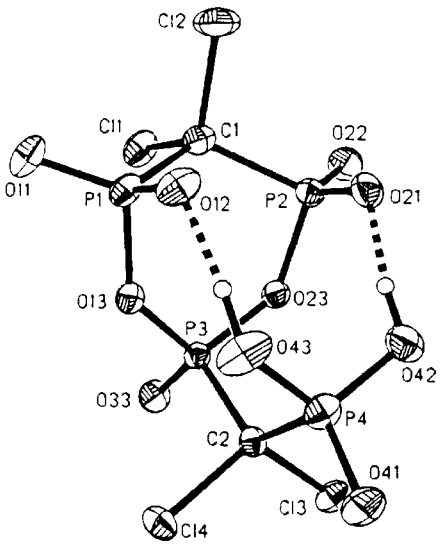

Fig. 1 Crystal structure of the anion **2**.

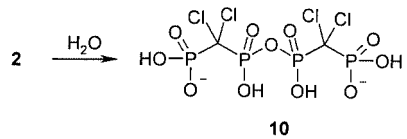

10

Scheme 2

DOI: 10.1039/b000558o

phosphate buffer solution at 37 °C. The half-lives for chemical degradation of **2** were 60 min (pH 5.0) and 63 min (pH 7.4). Further hydrolysis of dimer **10** to clodronate was not observed during 9 h at pH 7.4. Compounds **2** and **10** are resistant to enzymatic hydrolysis, probably because the bridging carbon prevents[10] stepwise hydrolysis, which is generally observed for terminal phosphates.

Notes and references

† *Spectroscopic data* for 1,1-dichloro-1-(5,5-dichloro-4,6-dihydroxy-2,4,6-trioxo-2λ^5,4λ^{5}6λ^5-[1,3,2,4,6]dioxatriphosphinan-2-yl)methylphosphonic acid bis(tributyl(methyl)ammonium) salt $[NMeBu_3]_2$**2**: δ_H(400.1 MHz, CD_3COCD_3): 3.48 (m, 12H, NCH_2), 3.24 (s, 6H, NCH_3), 1.83 (m, 12H, NCH_2CH_2), 1.44 (m, 12H, CH_2CH_3), 0.99 (t, 18H, *J* 7.2 Hz, CH_2CH_3); δ_P(162.0 MHz, CD_3COCD_3): 1.78 (d, $^2J_{PP}$ 16.9 Hz), −2.17 (d, $^2J_{PP}$ 42.6 Hz), −17.58 (td, $^2J_{PP}$ 16.9, $^2J_{PP}$ 42.6 Hz); δ_C(100.6 MHz, CD_3COCD_3): 62.16 (CH_2), 48.95 (CH_3) 24.84 (CH_2), 20.39 (CH_2) 14.00 (CH_3); ES-MS *m/z* 435.1 (M − 2MeN$^+$Bu$_3$ − H_2O + 2H$^+$). Anal. calc. for $C_{28}H_{62}Cl_4N_2O_{10}P_4 \cdot 0.25H_2O$: C, 39.62; H, 7.41; N 3.24. Found: C, 39.84; H, 7.46; N 3.26%.

‡ *Crystal data* for $C_{28}H_{62}Cl_4N_2O_{10}P_4 \cdot 0.25H_2O$, $[NMeBu_3]_2$**2**$\cdot 0.25H_2O$: colorless single crystals were obtained by slow air evaporation of ethyl acetate–acetone solution, M = 856.98, triclinic, space group $P\bar{1}$, a = 11.3054(4), b = 11.5193(4), c = 17.8036(7) Å, U = 2067.68(13) Å^3, T = 120 K, Z = 2, λ = 0.71073 Å, μ(Mo-Kα) = 0.492 mm^{-1}, 17 094 reflections measured, 8667 unique (R_{int} = 0.0326). Final R_1 = 0.0371, wR_2 = 0.0828 (for 8667 data). CCDC 182/1575. See http://www.rsc.org/suppdata/cc/b0/b000558o/ for crystallographic data in .cif format.

1 H. Fleisch, *Bisphosphonates in Bone Disease: From the Laboratory to the Patient*, The Parthenon Publishing Group Inc., New York, 1995.
2 M. Ahlmark, J. Vepsäläinen, H. Taipale, R. Niemi and T. Järvinen, *J. Med. Chem.*, 1999, **42**, 1473.
3 M. Ahlmark and J. Vepsäläinen, *Tetrahedron*, submitted.
4 J. Vepsäläinen, J. Kivikoski, M. Ahlgrén, H. Nupponen and E. Pohjala, *Tetrahedron*, 1995, **51**, 6805.
5 D. A. Nicholson, W. A. Cilley and O. T. Quimby, *J. Org. Chem.*, 1970, **35**, 3149.
6 A. J. Collins, G. W. Fraser and P. G. Perkins, *J. Chem. Soc., Dalton Trans.*, 1974, 960.
7 K. W. Pankiewicz, K. Lesiak and K. A. Watanabe, *J. Am. Chem. Soc.*, 1997, **119**, 3691.
8 K. Lesiak, K. A. Watanabe, J. George and K. W. Pankiewicz, *J. Org. Chem.*, 1998, **63**, 1906.
9 J. Vepsäläinen, H. Nupponen, E. Pohjala and M. Ahlgrén, *J. Chem. Soc., Perkin Trans. 2*, 1992, 835.
10 L. A. Welford, N. J. Cusack and S. M. O. Hourani, *Eur. J. Pharmacol.*, 1986, **129**, 217.

Crystal structure and magnetic properties of a new two-dimensional cyano-bridged bimetallic assembly $[NiL']_3[Cr(CN)_5(NO)]_2\cdot 10H_2O$ (L′ = 3,10-dimethyl-1,3,5,8,10,12-hexaazacyclotetradecane)

Hui-Zhong Kou,[a] Song Gao,*[a] Bao-Qing Ma[a] and Dai-Zheng Liao[b]

[a] *State Key Laboratory of Rare Earth Materials Chemistry and Applications, College of Chemistry, Peking University, Beijing 100871, P.R. China. E-mail: gaosong@chemms.chem.pku.edu.cn*
[b] *Department of Chemistry, Nankai University, Tianjin 300071, P.R. China*

Received (in Cambridge, UK) 7th February 2000, Accepted 20th March 2000

A new cyano-bridged Ni(II)–Cr(I) complex, $[NiL']_3[Cr(CN)_5(NO)]_2\cdot 10H_2O$ (L′ = 3,10-dimethyl-1,3,5,8,10,12-hexaazacyclotetradecane) with a honeycomb molecular structure, displays a long-range magnetic ordering at T_c = 4.5 K.

In the area of molecule-based magnets, many chemists have been interested in the topologies leading to ferromagnetic interactions between paramagnetic metal ions. The approach of the strict orthogonality of magnetic orbitals has been most frequently utilized. On this basis, cyanide-bridged bimetallic assemblies derived from low-spin $[M(CN)_6]^{3-}$ (M = Cr^{III}, Mn^{III}, Fe^{III}) and high-spin $[ML]^{2+}$ (M = Cu^{II}, Ni^{II}, L = neutral ligand) are anticipated to be ferromagnetic, which has been verified by many experimental results.[1] Some of them exhibit spontaneous magnetization owing to the efficient propagation of magnetic coupling through the cyanide bridges and the hydrogen bonds.

Very recently, square-planar macrocyclic Ni(II) complexes have been employed to construct cyano-bridged 2D Ni_3M_2 (M = Cr^{III}, Fe^{III}) assemblies that exhibit ferromagnetic behaviour.[1j–m] In order to construct new molecule-based magnetic materials it is desirable to explore alternative building blocks containing cyanide groups. Most recently, Holmes and Girolami have presented some Prussian blue analogues containing $[Cr^{I}(CN)_5(NO)]^{3-}$, and found that the complex $K_{0.5}Mn[Cr(CN)_5(NO)]_{0.83}\cdot 4H_2O\cdot 1.5MeOH$ possesses a cubic structure based on powder XRD analysis, and that the NO^+ group in $[Cr(CN)_5(NO)]^{3-}$ is involved in bridging on the basis of the IR spectrum in which the N=O stretching frequency is *ca.* 60 cm^{-1} higher than that in $K_3[Cr(CN)_5(NO)]$ (1630 cm^{-1}).[2] In order to gain further evidence on the binding modes of $[Cr(CN)_5(NO)]^{3-}$ with transition metal complexes, we have studied the reaction of $[NiL']^{2+}$ (L′ = 3,10-dimethyl-1,3,6,8,10,12-hexaazacyclooctadecane) with $[Cr(CN)_5(NO)]^{3-}$, and obtained a new two-dimensional honeycomb assembly, $[NiL']_3[Cr(CN)_5(NO)]_2\cdot 10H_2O$ **1**. The adoption of $[Cr(CN)_5(NO)]^{3-}$ is due to the electronic configuration [$3d^5$, $(3d_{xz})^2(3d_{yz})^2(3d_{xy})^1$] of low-spin Cr(I) ion together with the approximate C_{4v} symmetry of $[Cr(CN)_5(NO)]^{3-}$ that is quite different from the O_h symmetry of $[Fe(CN)_6]^{3-}$.[3] The magnetic coupling between the magnetic orbitals of the neighbouring nickel(II) and chromium(I) ions is expected to be ferromagnetic. Here, we present the synthesis, single crystal structure analysis and magnetic properties of the new complex.

To an aqueous solution (15 mL) of $[NiL'](ClO_4)_2$[4] (0.3 mmol) was added dropwise, with stirring, a solution of $K_3[Cr(CN)_5(NO)]\cdot H_2O$[5] (0.2 mmol) in 10 mL of water. This led to the immediate precipitation of yellow microcrystals that were collected by suction filtration, washed with water and dried in air.† The complex is insoluble in most organic and inorganic solvents and stable in air.

The IR spectrum of the complex shows two sharp bands in the range 2000–2200 cm^{-1} which are attributed to C≡N stretching modes. The shift of ν(C≡N) to higher wavenumber (2140 cm^{-1}) compared with that of $K_3[Cr(CN)_5(NO)]$ (2120 cm^{-1})[6] suggests the formation of CN^- bridges, as observed for other cyano-bridged systems.[1] Further, the blue shift of ν(N=O) with respect to that of $K_3[Cr(CN)_5(NO)]$ (1630 cm^{-1})[6] also suggests the distortion of $[Cr(CN)_5(NO)]^{3-}$ from C_{4v} symmetry as a result of the formation of Cr–C≡N–Ni linkages and that the cyanide ligand *trans* to the NO ligand has been involved in bridging.

The structure of **1** was determined by single crystal X-ray crystallography (Fig. 1).‡ It consists of a neutral stair-shaped layer network with the stoichiometry $[NiL']_3[Cr(CN)_5(NO)]_2$. Each $[Cr(CN)_5(NO)]^{3-}$ unit uses three *cis*-C≡N groups to connect with three $[NiL']^{2+}$ groups, whereas the two remaining CN^- and the NO^+ groups are monodentate. The adjacent Cr···Ni distances are 5.293(2) Å for Cr···Ni(1), 5.300(1) Å for Cr···Ni(2) and 5.270(1) Å for Cr···Ni(2a), respectively (a denotes the symmetry operation $-x + 0.5$, $y - 0.5$, $-z + 0.5$). Each NiL′ unit is linked to two $[Cr(CN)_5(NO)]^{3-}$ ions in *trans* positions. Four secondary amine nitrogen atoms of the macrocycle coordinate to the nickel center with an average Ni–N distance of 2.097(4) Å for Ni(1), 2.074(4) Å for Ni(2). Two nitrogen atoms of the bridging C≡N ligands axially coordinate to the Ni(II) ions with Ni–N_{ax} contacts of 2.153(3) Å for Ni(1)–N(3) and 2.105(4) Å (average) for Ni(2)–N, respectively, which are slightly larger than those of the corresponding Ni–N_{eq} bonds. The bridging cyanide ligands coordinate to the nickel(II) ions in a bent fashion with the Ni–N≡C bond angles ranging from 164.3(3) to 172.8(4)°. The coordination symmetry about the Cr atom is C_{4v} or distorted octahedron, and the Cr–N–O and Cr–C–N groups are nearly linear. The Cr–C distances range from 1.926(5) to

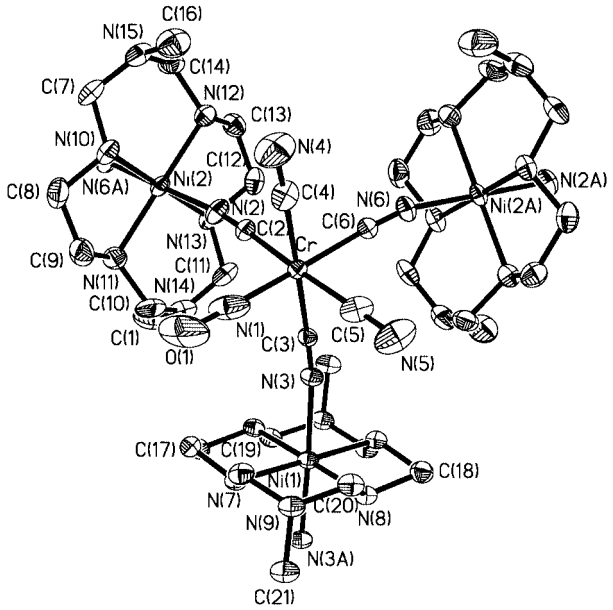

Fig. 1 ORTEP plot of **1** (hydrogen atoms are omitted for clarity).

DOI: 10.1039/b001005g

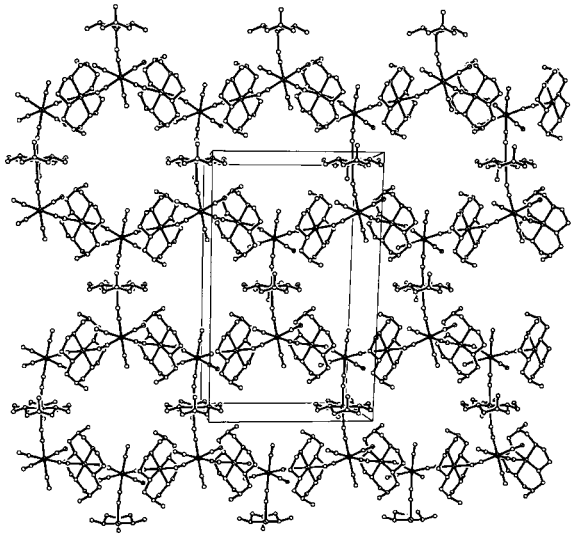

Fig. 2 Projection showing the 2D honeycomb-like layer containing Cr_6Ni_6 hexagons.

2.083(5) Å, whereas the Cr–N distance of 1.866(5) Å is comparatively long. These compare with the structural results for the double salt $[Co(en)_3][Cr(CN)_5(NO)]\cdot 2H_2O$.[7] The particular local molecular disposition leads to a honeycomb-like layered structure (Fig. 2). The shortest interlayer metal–metal distance is 6.910 Å for Cr··Ni(2m) (m: x, $1 - y$, $-0.5 + z$).

The magnetic susceptibilities of **1** have been measured on a Model Maglab System2000 magnetometer in the temperature range 2.0–280 K. A plot of $\chi_m T$ *vs.* T for **1** (H = 1 T) is shown in Fig. 3, where χ_m is the magnetic susceptibility per Ni_3Cr_2 unit. The $\chi_m T$ value at 280 K is *ca.* 4.8 emu K mol^{-1} (6.2 μ_B), higher than expected (3.75 emu K mol^{-1}) for three high spin nickel(II) ions (S = 1, g = 2.0) and two low-spin chromium(I) ions (S = 1/2,[5] g = 2.0) in a dilute system, and equal to that calculated assuming the g_{Ni} value of 2.32. With a decrease of the temperature, $\chi_m T$ increases smoothly down to *ca.* 50 K and then sharply reaches a maximum value of 14.2 emu K mol^{-1} (10.66 μ_B) at 6.4 K, which is much larger than the spin-only value of 10.0 emu K mol^{-1} (8.9 μ_B) for S_T = 4 resulting from the ferromagnetic coupling of three nickel(II) ions (S = 1, g = 2.0) and two low-spin chromium(I) ions (S = 1/2, g = 2.0), suggestive of the occurrence of magnetic ordering. Below 6.4 K, $\chi_m T$ decreases rapidly, which indicates the presence of interlayer antiferromagnetic interaction and/or the zero-field splitting effect of the nickel(II) ions. The magnetic susceptibility above 6 K obeys the Curie–Weiss law with a positive Weiss constant θ = + 10.0 K, which also proves the presence of ferromagnetic coupling within the Ni_3Cr_2 sheet of **1**. The abrupt increase in M at *ca.* 11 K suggests a phase transition in the complex (Fig. 3).

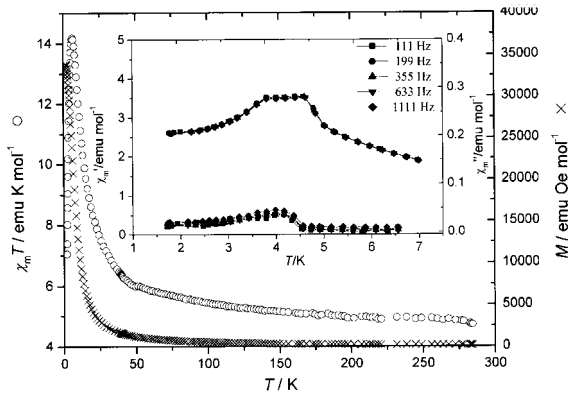

Fig. 3 Temperature dependences of $\chi_m T$ and M for **1**. Inset: real, χ' (top), and imaginary χ'' (bottom) ac magnetic susceptibilities as a function of temperature taken at 111, 199, 355, 633 and 1111 Hz for **1**.

The onset of a long-range magnetic phase transition is further confirmed by the temperature dependence of ac molar magnetic susceptibilities displayed in the inset of Fig. 3. The real part of the zero field ac magnetic susceptibility, $\chi'(T)$, has a maximum at *ca.* 4.5 K for frequencies of 111, 199, 355, 633 and 1111 Hz, suggesting that T_c of complex **1** is about 4.5 K. The frequency independence of χ_{ac}' and χ_{ac}'' suggests a non-glassy ground state. The field dependence of the magnetization at 1.75 K reveals a hysteresis loop with a coercive field of 170 Oe and a remnant magnetization of *ca.* 0.19 $N\mu_B$.

The ferromagnetic interaction between the chromium(I) and nickel(II) ions is due to the strict orthogonality of the magnetic orbitals of the low-spin Cr(I) [d^5, $(3d_{xy})^1$] and high-spin Ni(II) [d^8, $(d_{x^2-y^2})^1(d_{z^2})^1$] ions. According to ligand field theory, the high-spin nickel(II) ion in octahedral surroundings has two unpaired electrons in $d_{x^2-y^2}$ and d_{z^2} orbitals that interact with the MOs of the cyano bridge with the same symmetry producing a magnetic orbital with σ-character. The low-spin chromium(I) ion in distorted octahedral surroundings has an unpaired electron in the d_{xy} orbital[3] that interacts with the MOs of the cyano bridge with the right symmetry generating a magnetic orbital with π-character. Consequently, strict orthogonality is obeyed and the interaction between Ni(II) and Cr(I) ions through the cyano bridge should be ferromagnetic.

Notes and references

† Calc. for $C_{40}H_{98}N_{30}O_{12}Cr_2Ni_3$: C, 32.65; N, 28.6; H, 6.7. Found: C, 32.8; N, 27.9; H, 6.6%. IR (KBr, cm^{-1}): ν(C≡N), 2140, 2116; ν(O = N), 1678. Well shaped yellow crystals suitable for X-ray structure analysis are grown at room temperature by the slow diffusion of an orange MeCN solution (30 mL) of $[NiL'](ClO_4)_2$ (0.15 mmol) and a yellow aqueous solution (30 mL) of $K_3[Cr(CN)_5(NO)]\cdot H_2O$ (0.15 mmol) in an H-tube.

‡ *Crystal data for* **1**: $[NiL']_3[Cr(CN)_5(NO)]_2\cdot 10H_2O$, $C_{40}H_{98}N_{30}O_{12}Ni_3Cr_2$: M_w = 1471.61, yellow platelet (0.17 × 0.13 × 0.08 mm), monoclinic, space group $C2/c$, a = 25.836(5), b = 15.369(3), c = 19.478(4) Å, β = 105.15(3)°, U = 7466(3) Å^3, Z = 4, D_c = 1.313 g cm^{-3}, D_m = 1.31(1) g cm^{-3}, μ(Mo-Kα) = 1.092 mm^{-1}, T = 293 K. A total of 8871 unique reflections were collected in the range $3.47 < \theta < 25°$, of which 6257 were considered observed [$I \geqslant 2\sigma(I)$] and used in the calculations. The structure was solved by the direct method. All non-hydrogen atoms were refined anisotropically. All hydrogen atoms were added geometrically and refined using a riding model. The refinement on F^2 converged to $R1$ = 0.0605, $wR2$ = 0.191 (all data).

CCDC 182/1578. See http://www.rsc.org/suppdata/cc/b0/b001005g/ for crystallographic files in .cif format.

1 (*a*) K. V. Langenberg, S. R. Batten, K. J. Berry, D. C. R. Hockless, B. Moubaraki and K. S. Murray, *Inorg. Chem.*, 1997, **36**, 5006; (*b*) M. Ohba, N. Maruone, H. Okawa, T. Enoki and J.-M. Latour, *J. Am. Chem. Soc.*, 1994, **116**, 11 566; (*c*) M. Ohba, N. Fukita and H. Okawa, *J. Chem. Soc., Dalton Trans.*, 1997, 1733; (*d*) H. Okawa and M. Ohba, *ACS Symp. Ser.*, 1996, **644**, 319; (*e*) M. Ohba, N. Usuki, N. Fukita and H. Okawa, *Inorg. Chem.*, 1998, **37**, 3349; (*f*) M. Ohba, H. Okawa, T. Ito and A. Ohto, *J. Chem. Soc., Chem. Commun.*, 1995, 1545; (*g*) M. Ohba, H. Okawa, N. Fukita and Y. Hashimoto, *J. Am. Chem. Soc.*, 1997, **119**, 1011; (*h*) H.-Z. Kou, W.-M. Bu, D.-Z. Liao, P. Cheng, Z.-H. Jiang, S.-P. Yan, Y.-G. Fan and G.-L. Wang, *J. Chem. Soc., Dalton Trans.*, 1998, 4161; (*i*) M. S. El Fallah, E. Rentschler, A. Caneschi, R. Sessoli and D. Gatteschi, *Angew. Chem., Int. Ed. Engl.*, 1996, **35**, 1947; (*j*) S. Ferlay, T. Mallah, J. Vaissermann, F. Bartolome, P. Veillet and M. Verdaguer, *Chem. Commun.*, 1996, 2481; (*k*) E. Colacio, J. M. Dominguez-Vera, M. Ghazi, R. Kivekas, F. Lloret, J. M. Moreno and H. Stoeckli-Evans, *Chem. Commun.*, 1999, 987; (*l*) B. Nowicka, M. Hagiwara, Y. Wakatsuki and H. Kisch, *Bull. Chem. Soc. Jpn.*, 1999, **72**, 441; (*m*) H.-Z. Kou, S. Gao, W.-M. Bu, D.-Z. Liao, B.-Q. Ma, Z.-H. Jiang, S.-P. Yan, Y.-G. Fan and G.-L. Wang, *J. Chem. Soc., Dalton Trans.*, 1999, 2477; (*n*) D. G. Fu, J. Chen, X. S. Tan, L. J. Jiang, S. W. Zhang and W. X. Tang, *Inorg. Chem.*, 1997, **36**, 220; (*o*) H.-Z. Kou, D.-Z. Liao, P. Cheng, Z.-H. Jiang and G.-L. Wang., *Transition Met. Chem.*, 1996, **21**, 349.

2 S. M. Holmes and G. S. Girolami, *Mol. Cryst. Liq. Cryst. A*, 1997, **305**, 279.

3 P. T. Manoharan and H. B. Gray, *J. Am. Chem. Soc.*, 1965, **87**, 3340.

4 M. P. Suh and S.-G. Kang, *Inorg. Chem.*, 1988, **27**, 2544.

5 W. P. Griffith, J. Lewis and G. Wilkinson, *J. Chem. Soc.*, 1959, 872.

6 P. Gans, A. Sabatini and L. Sacconi, *Inorg. Chem.*, 1966, **5**, 1877.

7 J. H. Enemark, M. S. Quinby, L. L. Reed, M. J. Steuck and K. K. Walthers, *Inorg. Chem.*, 1970, **9**, 2397.

ChemComm

Hydrothermal growth of β-Ag_2Se tubular crystals

Junqing Hu,[ab] Bin Deng,[b] Qingyi Lu,[ab] Kaibin Tang,*[ab] Rongrong Jiang,[b] Yitai Qian,*[ab] Guien Zhou[a] and Hao Cheng[a]

[a] *Structure Research Laboratory, University of Science and Technology of China, Hefei 230026, P.R. China. E-mail: kbtang@ustc.edu.cn*

[b] *Department of Chemistry, University of Science and Technology of China, Hefei 230026, P.R. China*

Received (in Cambridge, UK) 14th December 1999, Accepted 21st March 2000

Millimeter-sized tubular crystals of Ag_2Se are successfully grown for the first time *via* a hydrothermal reaction route from AgCl, Se and NaOH at 155 °C.

The synthesis of large three-dimensional (3D) mesoscale (millimeter- to centimeter-scale) objects has recently been the focus of much attention.[1–3] Existing technologies for making 3D microstructures are the limited stereolithography,[4] free-form laser sintering (slow)[5] and traditional casting, machining and assembly which are difficult with a complex or porous structure. Whitesides and coworkers reported the fabrication of open regular 3D mesostructures by self-assembly.[1–3] The newly discovered fullerene-like nest polyhedra (NP) and nanotubules have been observed for metal dichalcogenides[6–8] and micrometer-sized hexagonal, hollow needles of CdSe have been prepared by electrodeposition from molten salts.[9] However, a mesoscale crystal with open structure is, to the best of our knowledge, hitherto unknown for Ag_2Se. Here we report for the first time the growth of millimeter-sized tubular Ag_2Se crystals by a known hydrothermal reaction route.

The synthesis was carried out in an autoclave and was based on the disproportionation reaction of Se:

$$4AgCl + 3Se + 6NaOH \rightarrow 2Ag_2Se + Na_2SeO_3 + 4NaCl + 3H_2O \quad (1)$$

An appropriate amount of AgCl (0.383 g), Se (0.160 g) and NaOH (0.20 g) was put into a Teflon-lined autoclave (50 mL capacity). The autoclave was then filled with distilled water to 80% of the total volume, maintained at 155 °C for 10 h and then allowed to cool to room temperature. The products were filtered off and washed sequentially with distilled water and absolute ethanol to remove the residual impurities. After drying in a vacuum at 70 °C for 2 h, metallic-gray crystals were obtained.

Fig. 1 shows the X-ray diffraction (XRD)† pattern of several Ag_2Se crystals that were crushed. All the reflections could be indexed to the orthorhombic Ag_2Se phase with lattice constants a = 4.333, b = 7.062, c = 7.764 Å, in agreement with the reported data for Ag_2Se (JCPDS Card File, 24-1041). No characteristic peaks of other impurities such as Ag_2O, Se or AgCl were observed.

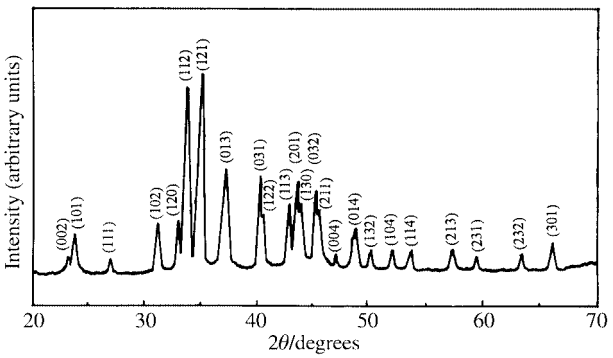

Fig. 1 X-Ray powder diffraction pattern of several Ag_2Se crystals that were crushed.

Fig. 2 shows the scanning electron microscopy (SEM)‡ images of as-grown Ag_2Se crystals. It can be seen that Ag_2Se crystals show tubular hexagonal prism structure. Typically, this structure is 10–15 mm in length, 80–120 μm in diameter and 20–25 μm in thickness. It is of considerable interest that some tubes appear to have one closed-round end [Fig. 2(*b*)], and others show hollow cavities which run through the whole length [Fig. 2(*c*) and 2(*d*) are two undersides of one prism crystal]. From these SEM images, we can see that the as-grown tubular Ag_2Se crystals may show near single crystal nature.

To confirm that single crystals of Ag_2Se were obtained, we recorded the transmission X-ray Laue§ photographs of the tubular crystals. Fig. 3 shows one of these Laue photographs of the Ag_2Se samples. It revealed that the crystal obtained was nearly a single crystal. From the eight-fold symmetrical patterns of the X-ray Laue photographs, we can deduce it is due to the (121) patterns of the characteristic X-ray (Cu-Kα and Cu-Kβ) diffraction. This result was in good agreement with the strong (121) reflection in the XRD pattern.

To provide further evidence for the formation of Ag_2Se crystals, the samples were also characterized by X-ray photoelectron spectra (XPS).¶ The two strong peaks in the spectra (spectra not shown) at 368.00 and 53.65 eV corresponding to Ag 3d and Se 3d binding energy, respectively, are consistent with the formation of Ag_2Se.[10] Quantification of the XPS peak intensities gave elements with a stoichiometry of $Ag_2Se_{1.03}$. No

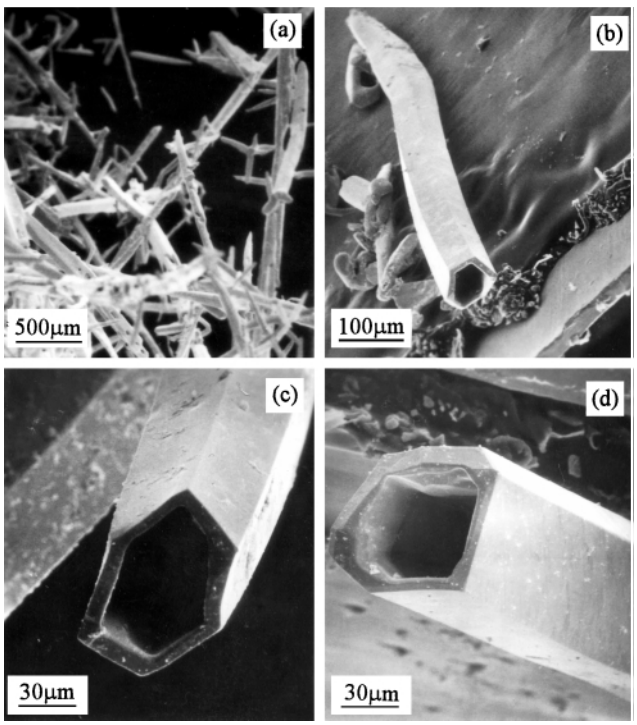

Fig. 2 Scanning electron microscopy images of the as-grown Ag_2Se crystals.

DOI: 10.1039/a909785f

Fig. 3 Transmission X-ray Laue photograph of the single crystal Ag_2Se as in Fig. 2(*c*).

obvious peaks for silver or selenium oxides were detected, which indicated a high purity of the Ag_2Se crystals produced.

Although the growth mechanism for the tubular crystals is unclear, the reaction temperature and the change of pH were critical factors in the formation of this morphology. Structural studies indicate that Ag_2Se exists as a low-temperature phase β-Ag_2Se (orthorhombic structure) and a high-temperature phase α-Ag_2Se (cubic structure) and the transition from β to α takes place at *ca.* 136 °C.[11] In our hydrothermal route, the essential temperature range for the tubular form was at 150–160 °C. However, the tubular Ag_2Se crystals existed as the low-temperature phase. It may be concluded that the temperature condition falls into the growth thermodynamic stability range of the tubular morphology. According to Korczynski *et al.*,[12] we first prepared the Na_2Se solution (pH 8–9) through the reaction: $3Se + 6NaOH \rightarrow 2Na_2Se + Na_2SeO_3 + 3H_2O$, and then obtained Ag_2Se by the reaction of AgCl with Na_2Se in aqueous media at 150–160 °C. However, the Ag_2Se obtained deviated from its theoretical composition and did not show the tubular morphology. For the growth of tubular crystals of Ag_2Se, we selected a one step hydrothermal reaction from AgCl, Se and NaOH. An initial feedstock pH (NaOH solution) above 13 was needed. In the hydrothermal process, the pH value of the reaction system decreased. So, it is believed that the change of pH value was matched with the nucleation and growth of crystalline Ag_2Se. This matching effect may be beneficial to the formation of the tubular morphology.

In summary, tubular β-Ag_2Se crystals were synthesized successfully for the first time through a hydrothermal reaction at 155 °C. Group 11 chalcogenides have wide applications in semiconductors, pigments,[13] luminescence devices,[14] solar cells, IR detectors and optical fiber communication.[15] It is believed that hollow tubular crystals should be expected to have novel properties, and may offer exciting opportunities for both fundamental research and technological applications. Deeper understanding of the growth mechanism of tubular Ag_2Se crystals and controlling the reaction kinetics are clearly needed.

Financial support of this work by the National Natural Science Research Foundation of China is gratefully acknowledged.

Notes and references

† XRD patterns were obtained on a Japan Rigaku Dmax-γA X-ray diffractometer with graphite-monochromatized Cu-Kα radiation (λ = 1.5418 Å).

‡ SEM images were taken with a Hitachi X-650 scanning electron microscope, using a Ni–Co alloy plate.

§ Transmission X-ray Laue photographs were obtained from a China JF-1 X-ray generator equipped with a Cu target with films 31 mm from the sample.

¶ XPS spectra were recorded on an ESCALAB MKII X-ray photoelectron spectrometer, using non-monochromatized Mg-Kα ($h\nu$ = 1253.6 eV) radiation as the excitation source.

1 T. L. Breen, J. Tien, S. R. J. Oliver, T. Hadzic and G. M. Whitesides, *Science*, 1999, **284**, 948.
2 J. Tien, T. L. Breen and G. M. Whitesides, *J. Am. Chem. Soc.*, 1998, **120**, 12 670.
3 A. Terfort, N. Bowden and G. M. Whitesides, *Nature*, 1997, **386**, 162.
4 J. J. Clair, *J. Mater. Proc. Technol.*, 1991, **57**, 393.
5 F. E. DeAngelis, *Proc. SPIE*, 1991, **1598**, 61.
6 K. Chihiro, S. Yoshio and F. Kazuo, *J. Cryst. Growth*, 1989, **94**, 967.
7 R. Tenne, L. Margulis, M. Genut and G. Hodes, *Nature*, 1992, **360**, 444.
8 M. Hershfinkel, L. A. Gheber, V. Volterra, J. L. Hutchison, L. Margulis and R. Tenne, *J. Am. Chem. Soc.*, 1994, **116**, 1914.
9 H. Minoura, T. Negoro, M. Kitakata and Y. Ueno, *Sol. Ener. Mater.*, 1985, **12**, 335.
10 C. D. Wagner, *Handbook of X-Ray Photoelectron Spectroscopy*, Perkin-Elmer Corporation, Minnesota, 1979.
11 V. D. Das and D. Karunakaran, *Phys. Rev. B*, 1989, **39**, 10 872.
12 A. Korczynki, I. Lauomirska and T. Sobierajski, *Chem. Stosow.*, 1981, **25**, 391.
13 G. Henshaw, I. P. Parkin and G. Shaw, *Chem. Commun.*, 1996, 1095.
14 N. N. Greenwood and E. A. Earnshaw, *Chemistry of the Elements*, Pergamon, Oxford, 1990, p. 1403.
15 A. J. Strausse, *Phys. Rev. Lett.*, 1966, **16**, 1193.

Two dimensional stair-shaped coordination polymer exhibiting three-dimensional structure with cavities

Lei Zhang,[a] Peng Cheng,*[a] Liang-Fu Tang,[a] Lin-Hong Weng,[b] Zong-Hui Jiang,[a] Dai-Zheng Liao,[a] Shi-Ping Yan[a] and Geng-Lin Wang[a]

[a] *Department of Chemistry, Nankai University, Tianjin 300071, P.R. China. E-mail: pcheng@nankai.edu.cn*
[b] *Institute of Elemento-Organic Chemistry, Nankai University, Tianjin 300071, P.R. China*

Received (in Cambridge, UK) 14th January 2000, Accepted 7th March 2000

The crystal structure of {[NaCr(2,2'-bipy)(ox)$_2$]$_2$[bis(1-pyrazolyl)methane]•2H$_2$O}$_n$ reveals the first 2-D stair-shaped architecture which constructs a 3-D network *via* interlayer π–π interactions with guest water molecules present in the cavities.

The synthesis and characterization of 2- or 3-D coordination polymers with well defined pores have been an area of rapid growth and will continue to grow, especially with development of materials of new compositions, predetermined structures and useful properties, *e.g.* catalysis, magnetism, electronics and chemical separation.[1] In recent years the preparation of porous materials whose host frameworks can facilitate the removal/addition of guest molecules has been explored largely owing to their potential applications.[2] In particular, the incorporation of transition metals into coordination polymers is significant in the crystal engineering of novel heterogeneous catalytic systems,[3] as well as non-linear optical, conducting and ferromagnetic materials.[4] Supramolecular synthons are bridged mainly by two types of modules **a** and **b**. Developments in crystal engineering

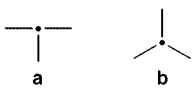

have also shown that hydrogen-bonding and π–π stacking interactions have enormous potential for assembling multi-component inorganic–organic molecules into well organized architectures.[5] It is clear that the strategy of utilizing transition metals with rigid or flexible bifunctional ligands affords an array of new network architectures through self-assembly.[6] However, little attention has been paid to alkaline ions acting as both counter ions and structural elements toward the synthesis of new multidimensional structure.[7] In this contribution, we report the first 2-D stair-shaped network containing hetero-bimetallic Cr^{III}–Na^{I} centers, [NaCr(bipy)(ox)$_2$]$_2$(bpm)·2H$_2$O **1** [bipy = 2,2'-bipyridine, ox = oxalate dianion, bpm = bis(1-pyrazolyl)methane], which forms a 3-D structure containing cavities which can incorporate small molecules.

The reaction of [NaCr(bipy)(ox)$_2$(H$_2$O)]·2H$_2$O and bpm in methanol leads to formation of red plates of [NaCr(bipy)(ox)$_2$]$_2$(bpm)·2H$_2$O, suitable for single X-ray diffraction.† The fundamental tetranuclear unit is shown in Fig. 1. The coordination geometry around the Cr(III) ion is a six-coordinate distorted octahedron, and is similar to those in related complexes.[8] The sodium atoms are also six-coordinate distorted octahedral with larger differences in bond lengths (shown in Fig. 1). Although only the coordinated water molecule has been replaced by the pyrazole nitrogen atom of bpm, the structure has changed significantly. Fig. 2(a) shows that the compound exists as an open railroad framework polymer with channels of 15.0 × 7.3 Å, and shows that the complex molecule is located on a crystallographic two-fold screw axis along the ox bridge ligands. The structure can be represented schematically as a stair-shaped supramolecular architecture as illustrated in Fig. 2(b). This particular supramolecular structure is unprecedented among molecular frameworks.[1b,6c,9]

Within a layer, hydrophilic nitrogen atoms (head or tail) interact with two 1-D inorganic precursors to form two natural hydrophilic–hydrophobic domains. It is interesting that the ligand, bpm, acts as a bidentate bridging ligand rather than as a chelating ligand.[10] In particular, between the layers, the stair-shaped frameworks stack the 2-D structure together *via* interlayer π–π interactions of pyridine rings to form a quasi-3-D structure containing small-pore channels. The narrowest interplanar distance of the aromatic moieties (bipy) is *ca.* 3.560 Å. The π–π interactions enhance the stability of the complex and result in a higher dimensional structure with the channels parallel to the *b* axis. The effective void size of the channels is 18.6 × 9.3 Å. The cavities are filled with guest water molecules which are hydrogen bonded to oxalato oxygen atoms (2.911 Å) (Fig. 3).

Mixed solvents (V_{MeOH}/V_{H_2O} = 1:1, V_{EtOH}/V_{H_2O} = 1:1, V_{EtOH}/V_{H_2O} = 9:1) were also employed instead of water in the synthesis, but no alcohol molecules were found in the solids obtained.

In conclusion, the design of metal-containing coordination polymers by self-assembly is of great promise. The sizes of the channels offer appreciable potential for guest molecule uptake, and the formation of this type of porous metal–organic

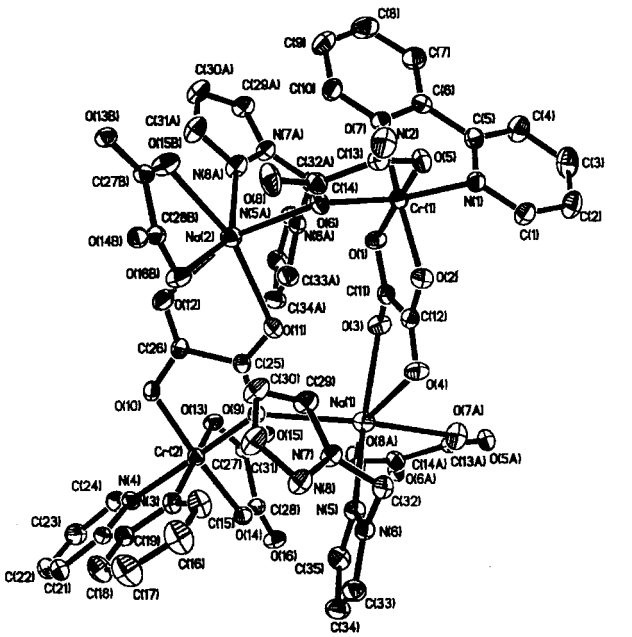

Fig. 1 ORTEP view of the tetranuclear unit of **1** in the crystal. Selected bond lengths (Å): Na1–N5 2.505, Na1–O3 2.424, Na1–O4 2.416, Na1–O7a 2.498, Na1–O8a 2.360, Na1–O9 2.595, Na2–N8a 2.642, Na2–O11 2.362, Na2–O12 2.478, Na2–O15b 2.366, Na2–O16b 2.472, Na2–O6 2.504, Na1–Cr1 5.551, Na1–Cr2 4.202, Na1–Na2 5.521, Na2–Cr1 3.980, Na2–Cr2 5.668, Cr1–Cr2 8.118.

DOI: 10.1039/b000588f

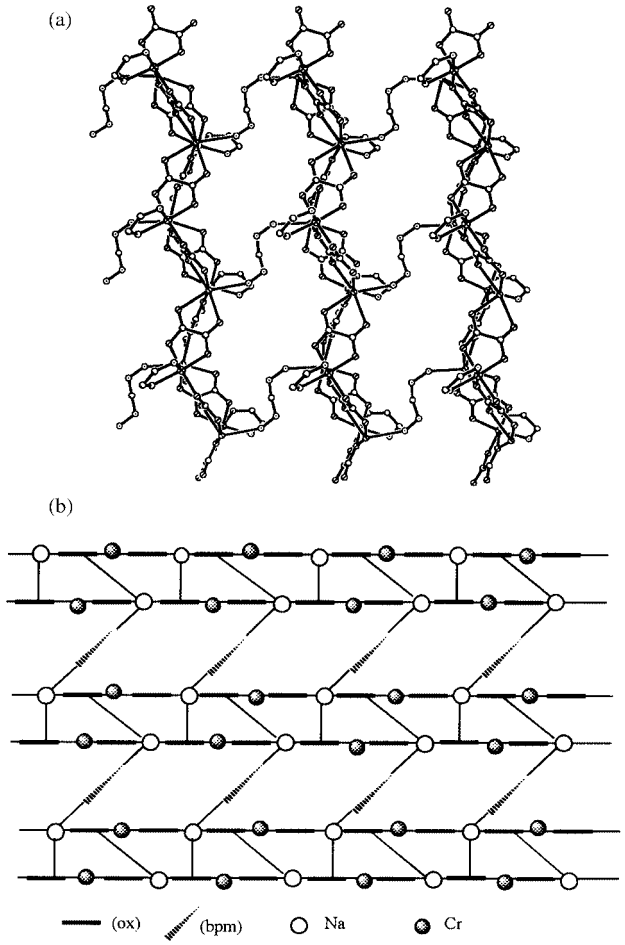

Fig. 2 (a) The helical structure viewed along the crystallographic *ab* plane and (b) a schematic representation of stair-shaped network architecture.

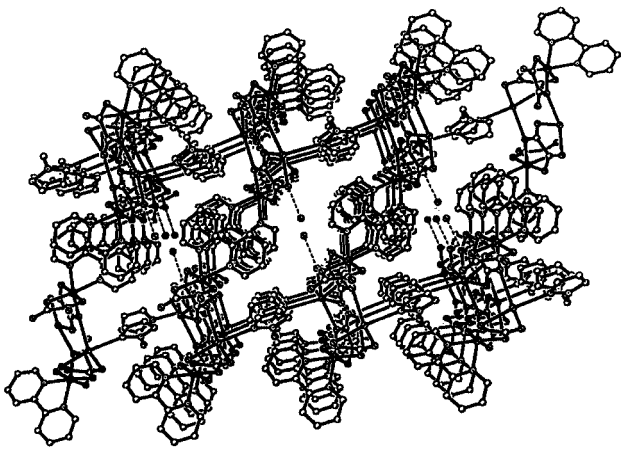

Fig. 3 View of π–π interactions of the pyridyl rings and water molecules in the channels.

compound demonstrates that this aspect of crystal engineering has many potential implications for materials science as new candidates for catalysis or separation processes. We expect that many new functional solid coordination polymers will be synthesized and applied based on these results.

We authors gratefully acknowledge the National Natural Science Foundation of China (29401004 and 29631040) and Ministry of Education of China for support of this work.

Notes and references

† *Crystal data*: $C_{35}H_{28}N_8O_{18}Cr_2Na_2$: M_r = 998.63, triclinic, $P\bar{1}$, a = 9.3366(15), b = 9.5519(15), c = 22.527(4) Å, α = 96.259(3), β = 95.649(3), γ = 95.673(3)°, U = 1975.1(5) Å^3, Z = 2, D_c = 1.679 g cm^{-3}, μ(Mo-K$_\alpha$) = 0.664 mm^{-1}, T = 293(2) K. 11435 Reflections of which 7968 with $I > 2\sigma(I)$ were measured (2.21 < θ < 26.44°) on a Siemens SMART/CCD area detector using the ω-scan mode. The structure was solved by direct methods, and refined by least-squares treatment on F^2 using the SHELXS-97 and the SHELXL-97 programs, R_1 = 0.0442 and R_w = 0.0950 with GOF = 0.973 (R_1 = 0.0783 and R_w = 0.1066 for all data). Non-hydrogen atoms were refined anisotropically, and hydrogen atoms were fixed at calculated positions and refined using a riding model. CCDC 182/1567. See http://www.rsc.org/suppdata/cc/b0/b000588f/ for crystallographic files in .cif format.

1 (*a*) R. Bishop, *Chem. Soc. Rev.*, 1996, 311; (*b*) M. Fujita, Y. J. Kwon, O. Sasaki, K. Yamaguchi and K. Ogura, *J. Am. Chem. Soc.*, 1995, **117**, 7287; (*c*) P. Brunet, M. Simard and J. D. Wuest, *J. Am. Chem. Soc.*, 1997, **119**, 2737; (*d*) O. M. Yaghi, G. Li and H. Li, *Nature*, 1995, **378**, 703; (*e*) D. Venkataraman, G. B. Gardner, S. Lee and J. S. Moore, *J. Am. Chem. Soc.*, 1995, **117**, 11600; (*f*) S. Decurtins, H. W. Schmalle, R. Pellaux, P. Schneuwly and A. Hauser, *Inorg. Chem.*, 1996, **35**, 1451.

2 H. Li, M. Eddaoudi, T. L. Groy and O. M. Yaghi, *J. Am. Chem. Soc.*, 1998, **120**, 8571; C. Janiak, *Angew. Chem., Int. Ed. Engl.*, 1997, **36**, 1431; G. B. Gardner, D. Venkataraman, J. S. Moore and S. Lee, *Nature*, 1995, **374**, 792.

3 I. W. C. E. Arends, R. A. Sheldon, M. Wallau and U. Schuchardt, *Angew. Chem., Int. Ed. Engl.*, 1997, **109**, 1144.

4 A. D. Burrows, C.-W. Chan, M. M. Chowdhry, J. E. McGrady and D. M. P. Mingos, *Chem. Soc. Rev.*, 1995, 329; A. D. Burrows, D. M. P. Mingos, A. J. P. White and D. J. Williams, *Chem. Commun.*, 1996, 97; S. Decurtins, H. W. Schmalle, P. Schneuwly, J. Ensling and P. Gutlich, *J. Am. Chem. Soc.*, 1994, **116**, 9521.

5 S. Kawata, S. R. Breeze, S. Wang, J. E. Greesan and N. P. Raju, *Chem. Commun.*, 1997, 717; R. H. Groeneman, L. R. MacGillivray and J. L. Atwood, *Inorg. Chem.*, 1999, **38**, 208; C. C. Evans, L. Sukarto and D. Ward, *J. Am. Chem. Soc.*, 1999, **121**, 320.

6 (*a*) M. Fujita, Y. J. Kwon, S. Washizu and K. Ogura, *J. Am. Chem. Soc.*, 1994, **116**, 1151; (*b*) S. Subramanian and M. Zaworotko, *Angew. Chem., Int. Ed. Engl.*, 1995, **34**, 2127; (*c*) I. Losier and M. J. Zaworotko, *Angew. Chem., Int. Ed. Engl.*, 1996, **35**, 2779; (*d*) D. M. L. Goodgame, S. Menzer, A. M. Smith and D. J. Williams, *Angew. Chem., Int. Ed. Engl.*, 1995, **34**, 574.

7 E. K. Berchin, L. M. Gilby, R. O. Gould, S. G. Harris, S. Parsons and R. E. P. Winpenny, *J. Chem. Soc., Dalton Trans.*, 1998, 2657; E. K. Berchin, R. O. Gould, S. G. Harris, S. Parsons and R. E. P. Winpenny, *J. Am. Chem. Soc.*, 1996, **118**, 11293; H. Bock, J.-M Lehn, J. Pauls, S. Holl and V. Krenzel, *Angew. Chem., Int. Ed.*, 1999, **38**, 952.

8 M. C. Muñoz, M. Julve, F. Floret, J. Faus and M. Andruh, *J. Chem. Soc., Dalton Trans.*, 1998, 3125.

9 M. Kondo, T. Yoshitomi, K. Seki, H. Matsuzaka and S. Kitagawa, *Angew. Chem., Int. Ed. Engl.*, 1997, **36**, 1725; H. Gudbjartson, K. Biradha, K. M. Poirier and M. J. Zaworotko, *J. Am. Chem. Soc.*, 1999, **121**, 2599; S. R. Batten and R. Robson, *Angew. Chem., Int. Ed.*, 1998, **37**, 1460; M. J. Zaworotko, *Angew. Chem., Int. Ed.*, 1998, **37**, 1211.

10 K. Langenberg, S. R. Batten, K. J. Berry, D. C. R. Hockless, B. Moubaraki and K. S. Murray, *Inorg. Chem.*, 1997, **36**, 5006; L.-F. Tang, L. Zhang, L.-C. Li, P. Cheng, Z.-H. Wang and J.-T. Wang, *Inorg. Chem.*, 1999, **38**, 6326.

Nucleobase dendrimer as a multidentate ligand for a rare-earth metal ion

Masahide Tominaga, Jun Hosogi, Katsuaki Konishi* and Takuzo Aida*

Fields and Reactions, Precursory Research for Embryonic Science and Technology, Japan Science and Technology Corporation, and Department of Chemistry and Biotechnology, Graduate School of Engineering, The University of Tokyo, 7-3-1 Hongo, Bunkyo-ku, Tokyo 113-8656, Japan. E-mail: aida@macro.t.u-tokyo.ac.jp

Received (in Cambridge, UK) 5th January 2000, Accepted 15th March 2000

Novel dendritic macromolecules consisting of uracil units (L*n*U-OBn) with the numbers of the nucleobase layers (*n*) of 2–4 were synthesized; L3U-OBn and L4U-OBn both formed 1:1 complexes with La^{3+}, where the L4U-OBn–La^{3+} complex, in particular, was highly robust towards methanolysis.

Dendrimers are hyperbranched, three-dimensional macromolecules with a pseudo network structure,[1] and have a potential for trapping of guest molecules.[2] In particular, dendritic molecules bearing binding sites for metal ions have attracted great attention.[3–5] Herein, we report the synthesis of the first dendritic polynucleobase, and highlight its very high activity for multidentate ligation with lanthanum ion.[6]

For the synthesis of the dendritic architecture, we chose uracil as a building block. Synthesis of the dendritic polyuracils (L*n*U-OBn; *n* = number of the nucleobase layers) was carried out by the convergent approach (Scheme 1) starting from (i) bromination of 1,3-dibenzyl-5-benzyloxymethyluracil (L1U-OBn) with HBr–AcOH,[7] followed by (ii) an alkaline-mediated coupling reaction of the resulting 5-bromomethyl derivative (L1U-Br) with 5-benzyloxymethyluracil **1**, to give L2U-OBn. Repetition of these two steps allowed formation of higher-generation L*n*U-OBn (*n* = 3, 4).[8] The absence of structural defects in L*n*U-OBn (*n* = 2–4) was confirmed by ^{1}H NMR, MALDI-TOF-MS and SEC analyses. For example, L*n*U-OBn (*n* = 2–4) all showed a single MALDI-TOF-MS peak due to $[M + Na]^+$ [Fig. 1(a) (I)–(III)] and a unimodal SEC chromatogram [Fig. 1(b)]. L*n*U-OBn (*n* = 2–4) were highly soluble in common organic solvents such as CH_2Cl_2, $CHCl_3$, benzene, acetone, MeCN and DMF, but scarcely soluble in protic solvents such as MeOH and water. In the electronic absorption spectra in MeCN, L*n*U-OBn (*n* = 2–4) showed an absorption band due to the uracil units at 274.8–275.6 nm, which is red-shifted from that of non-dendritic L1U-OBn (270.0 nm), indicating some intramolecular electronic interactions among the dendritic uracil units.

Dendritic polyuracils bear many heteroatoms and are expected to show potential for trapping of multi-coordinate metal ions. La^{3+} was chosen as a substrate, which is characterized by the largest ionic radius among rare-earth metal ions, and its preference to adopt a high coordination number (up to 12).[9] Typically, upon titration of an MeCN solution of L3U-OBn (10 μM) with $La(OTf)_3$ at 25 °C, the absorption band of the uracil units red-shifted from 275.2 to 281.4 nm with clear isosbestic points at 248.4 and 275.0 nm (Fig. 2, inset). Plots of the absorbance at 296.6 nm *vs.* $[La(OTf)_3]_0$ showed a clear inflection point at a mole ratio $[L3U\text{-}OBn]_0/[La(OTf)_3]_0$ of unity (Fig. 2). Job plots of ΔA at 296.6 nm also exhibited a maximum at a mole ratio $[L3U\text{-}OBn]_0/[La(OTf)_3]_0$ of unity. Furthermore, MALDI-TOF-MS spectrometry of a mixture of L3U-OBn and $La(OTf)_3$ (1:2) showed a peak at 2133 due to $[L3U\text{-}OBn\text{–}La(OTf)_2]^+$ (calc. *m/z* 2134) in addition to that of a Na^+ adduct [Fig. 1(a) (ii)]. These observations indicate a strong one-to-one complexation between L3U-OBn and La^{3+} with an association constant $> 10^7$ M^{-1}.[10] Likewise, titration of one-generation larger L4U-OBn with $La(OTf)_3$ (Fig. 2) showed a similar red shift (275.6 to 281.0 nm) with two isosbestic points (246.8, 271.8 nm), and a Job plot again indicated a 1:1 complexation of L4U-OBn with La^{3+}. Furthermore, a MALDI-TOF-MS peak due to the one-to-one adduct $[L4U\text{-}OBn\text{–}La(OTf)_2]^+$ (calc. *m/z* 3847) was observed [Fig. 1(a) (iii)].

An MeCN solution of L3U-OBn (2.5 mM) at 25 °C showed two C=O stretching vibrational bands at 1708 [C(2)=O] and 1665 cm^{-1} [C(4)=O] [Fig. 3(a)].[11] On the other hand, when $La(OTf)_3$ (5.0 mM) was added to the solution, a new IR band at 1609 cm^{-1}, assignable to the coordinated C=O functionality,

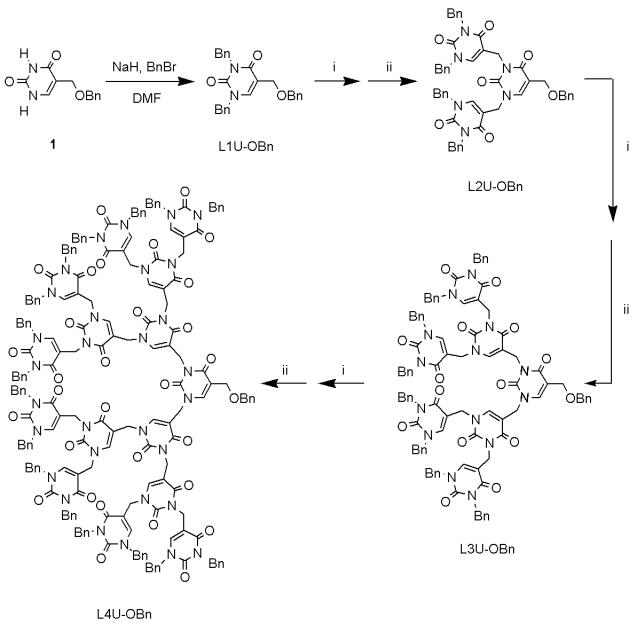

Scheme 1 Synthetic approach to dendritic polyuracils L*n*U-OBn (*n* = 2–4). *Reagents and conditions*, i, HBr, AcOH, dioxane, r.t., 12 h; ii, **1**, K_2CO_3, DMF, r.t., 12 h.

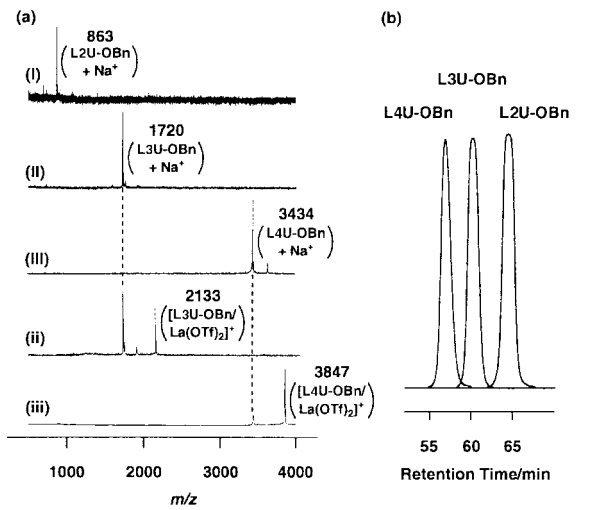

Fig. 1 (a) MALDI-TOF-MS spectra of (I) L2U-OBn, (II) L3U-OBn, (III) L4U-OBn, (ii) a 1:2 mixture of L3U-OBn and $La(OTf)_3$ and (iii) a 1:2 mixture of L4U-OBn and $La(OTf)_3$. (b) SEC profiles of dendritic polyuracils L*n*U-OBn (*n* = 2–4).

DOI: 10.1039/b000318m

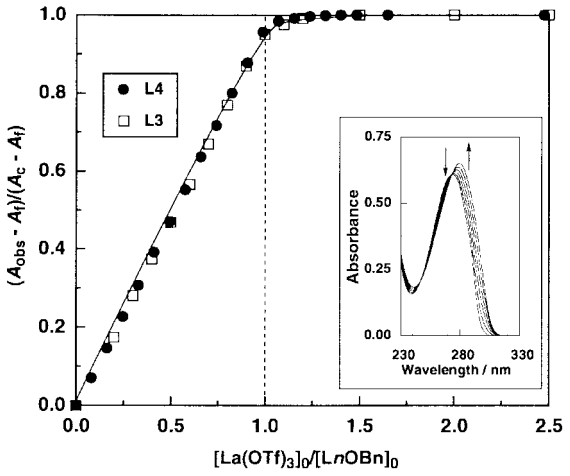

Fig. 2 Spectroscopic titration of MeCN solutions of L*n*U-OBn (10 μM) (*n* = 3 [□], 4 [●]) with $La(OTf)_3$ at 25 °C monitored at 296.6 nm. Plots of $(A_{obs} - A_f)/(A_c - A_f)$ *vs.* $[La(OTf)_3]_0/[LnU\text{-}OBn]_0$. A_{obs} represents the observed absorbance, while A_f and A_c denote the absorbances of free and complexed uracil units, respectively. Inset: absorption spectral change.

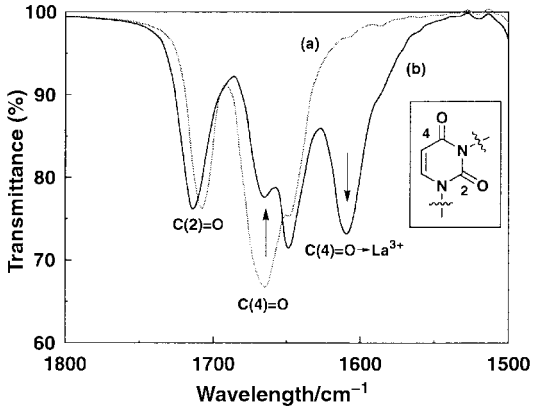

Fig. 3 IR spectra of (a) L3U-OBn (2.5 mM) and (b) a 1 : 2 mixture of L3U-OBn and $La(OTf)_3$ (2.5, 5.0 mM) in MeCN at 20 °C.

appeared at the expense of the non-coordinated C(4=O band [Fig. 3(b)]. Considering also a small shift due to the C(2)=O frequency (1708 to 1714 cm^{-1}), the C(4)=O functionality is likely involved predominantly in the complexation with La^{3+}.[12] As estimated from the decrease in integral area of the free C(4)=O band at 1665 cm^{-1},[13] an La^{3+} ion accommodates four out of seven C(4)=O groups in L3U-OBn for complexation. On the other hand, in the complexation with higher-generation L4U-OBn having fifteen C(4)=O groups, seven C(4)=O groups were estimated to coordinate to a La^{3+} ion.

From the above results, it is expected that La^{3+} ion is trapped by L4U-OBn more strongly than lower-generation L3U-OBn. In fact, the L4U-OBn–La^{3+} complex was highly robust towards methanolysis: when an MeCN solution of a mixture of L3U-OBn (10 μM) and $La(OTf)_3$ (20 μM) was titrated with MeOH (Fig. 4), the absorption spectral change at 296.6 nm showed a complete dissociation of La^{3+} from L3U-OBn at a MeOH content of 40%. On the other hand, the L4U-OBn–La^{3+} complex showed a spectral profile of only 30% dissociation under the same conditions (Fig. 4).

The high activity of L*n*U-OBn for the complexation with La^{3+} is considered to take great advantage of the multidentate coordination characteristics of the dendritic polyuracil architecture, since non-dendritic L1U-OBn did not show any substantial spectral changes upon mixing with $La(OTf)_3$. Spectral changes were also small when L*n*U-OBn (*n* = 3, 4) were mixed (1 : 1 mol ratio; in MeCN) with metal ions such as

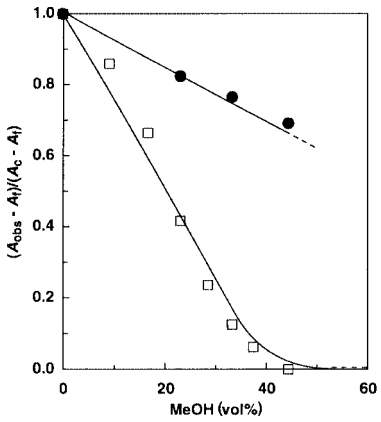

Fig. 4 Spectroscopic titration of an MeCN solution of a 1 : 2 mixture of L*n*U-OBn (10 μM) (*n* = 3 [□], 4 [●]) and $La(OTf)_3$ (20 μM) with MeOH at 25 °C monitored at 296.6 nm. Plots of $(A_{obs} - A_f)/(A_c - A_f)$ *vs.* vol.% of MeOH.

Na^+, K^+, Zn^{2+}, Cu^+, Cu^{2+} or Ag^+ (triflate salts) having a preference for lower coordination numbers.

Dendrimer complexes of lanthanide ions have attracted attention as luminescent materials[4] and have also been applied as MRI contrast agents.[5] On the other hand, a nucleobase complex of a transition metal such as platinum has been studied for biomedical applications.[14] The new metal-ligating nucleobase dendrimer consisting of uracil units may therefore have good potential for a variety of applications in materials science and medicinal chemistry.

Notes and references

1 Reviews on dendrimers, see: D. A. Tomalia, *Adv. Mater.*, 1994, **6**, 529; J. M. J. Fréchet, *Science*, 1994, **263**, 1710; F. Zeng and S. C. Zimmerman, *Chem. Rev.*, 1997, **97**, 1681; M. Fischer and F. Vögtle, *Angew. Chem., Int. Ed.*, 1999, **38**, 884.

2 M. W. P. L. Baars, P. E. Froehling and E. W. Meijer, *Chem. Commun.*, 1997, 1959; A. I. Cooper, J. D. Londono, G. Wignall, J. B. McClain, E. T. Samulski, J. S. Lin, A. Dobrynin, M. Rubinstein, A. L. C. Burke, J. M. J. Fréchet and J. M. DeSimone, *Nature*, 1997, **389**, 368.

3 L. Balogh and D. A. Tomalia, *J. Am. Chem. Soc.*, 1998, **120**, 7355; M. Zhao and R. M. Crooks, *Angew. Chem., Int. Ed.*, 1999, **38**, 364.

4 M. Kawa and J. M. J. Fréchet, *Chem. Mater.*, 1998, **10**, 286.

5 E. Tóth, D. Pubanz, S. Vauthey, L. Helm and A. E. Merbach, *Chem. Eur. J.*, 1996, **2**, 1607.

6 Examples of complexation of rare-earth metal ions, see: H. Maumela, R. D. Hancock, L. Carlton, J. H. Reibenspies and K. P. Wainwright, *J. Am. Chem. Soc.*, 1995, **117**, 6698; Y. Liu, B.-H. Han, Y.-M. Li, R.-T. Chen, M. Ouchi and Y. Inoue, *J. Phys. Chem.*, 1996, **100**, 17361; J. M. Harrowfield, M. Mocerino, B. J. Peachey, B. W. Skelton and A. H. White, *J. Chem. Soc., Dalton Trans.*, 1996, 1687 and references therein; F. Renaud, C. Piguet, G. Bernardinelli, J.-C. G. Bünzli and G. Hopfgartner, *J. Am. Chem. Soc.*, 1999, **121**, 9326.

7 L. Bérillon, R. Wagner and P. Knochel, *J. Org. Chem.*, 1998, **63**, 9117.

8 Full synthetic and spectroscopic details will be reported elsewhere.

9 R. Anwander and W. A. Herrmann, *Top. Curr. Chem.*, 1996, **179**, 1.

10 Owing to the strong complexation, the titration profiles did not allow determination of the association constants: K. A. Connors, *Binding Constants: the measurement of molecular complex stability*, Wiley, New York, 1987.

11 Y. Kyogoku, R. C. Lord and A. Rich, *J. Am. Chem. Soc.*, 1967, **89**, 496.

12 This is possibly due to a high coordination ability of the C(4)=O oxygen due to the presence of a conjugated vinyl group (M. Tominaga, K. Konishi and T. Aida, *J. Am. Chem. Soc.*, 1999, **121**, 7704).

13 The spectra at 1500–1800 cm^{-1} were analysed with curve-resolving software by combination of Lorenz and Gaussian curves. A vibrational band centered at 1647 cm^{-1} is likely to include C=C stretching frequencies of the uracil and benzyl moieties.

14 S. J. Lippard and J. M. Berg, *Principles of Bioinorganic Chemistry*, University Science Books, Mill Valley, CA, 1994; B. Lippert,, *Biometals*, 1992, **5**, 195; H. Sigel, *Chem. Soc. Rev.*, 1993, **22**, 255.

ChemComm

Homologations of boronate esters: the first observation of sequential insertions

Li Ren and Cathleen M. Crudden*

Department of Chemistry, University of New Brunswick, Fredericton, New Brunswick, Canada, E3B 6E2. E-mail:cruddenc@unb.ca

Received (in Corvallis, OR, USA) 10th January 2000, Accepted 2nd March 2000

By employing dibromo or diiodomethane as halomethyllithium precursors, the *in situ* double and triple homologation of boronate esters has been obtained for the first time.

Homologation reactions of boronate esters and other borane species have been well explored, most notably by Brown *et al.*[1] and Matteson *et al.*[2] We have recently reported a variant in which the chirality is introduced *catalytically via* a Rh–binap-mediated hydroboration with catechol borane.[3,4] Homologation of the intermediate boronate ester with CH_2Cl_2 or CH_2BrCl in the presence of Bu^nLi yields either 2-arylpropionic acids **1** or 2-arylpropanols **2** respectively [eqn. (1)]. This asymmetric hydroboration–homologation (AHH) reaction was used in the synthesis of enantiomerically enriched 2-arylpropionic acids, such as Ibuprofen™ [eqn. (1)].

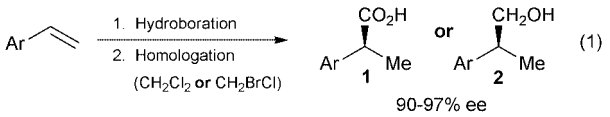

(1)

During our study of the latter reaction, we were intrigued by the observed chemoselectivity. In both cases, the products of the homologation reaction, prior to oxidation, are also boronate esters and might be expected to undergo homologation themselves. The boronate ester resulting from homologation with $LiCHCl_2$ is sufficiently distinct from the starting boronate ester **3** [eqn. (2)] by virtue of the chlorine substituent. However, the boronate ester from homologation with $LiCH_2Cl$ **7** [eqn. (5)] should be susceptible to further homologation. Despite this fact, no such sequential homologation with halomethane reagents has been reported to the best of our knowledge. Brown *et al.* have reported a ring-expansive sequential homologation reaction using halomethane reagents, in which the halomethane reagent was added in successive portions after isolation of the previously generated boracycle.[5] Shea *et al.*[6] have reported that sulfur ylides can homologate triorganoboranes sequentially in the same pot to yield long chain aliphatic alcohols after oxidation but such a reaction has not been observed with boronate esters. We wish to report that by adjusting the leaving group ability of the halomethane reagent, double and triple homologations can be achieved.

Using our standard protocol, boronate ester **3** is generated by hydroboration of styrene with catechol borane in the presence of $[Rh(cod)_2]^+BF_4^-$ and dppb,† followed by transesterification with pinacol which permits isolation of the boronate ester by chromatography [eqn. (2)].[4]

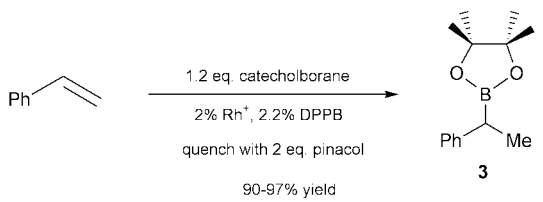

(2)

Treatment of **3** with $LiCH_2Cl$ provided, after oxidation, the expected product **2** (Table 1).‡§ The nature of the halogen which is transmetallated to generate $LiCH_2Cl$ has little effect on the outcome of the homologation. Thus ICH_2Cl gave 79% homologation while $BrCH_2Cl$ gave 88%. However, the nature of the leaving group was significant. Using $BrCH_2Br$ as the precursor to the homologation reagent, a new product **4** was observed which resulted from the incorporation of two CH_2 units. Diiodomethane also gave the product of double homologation, but with lower overall conversion (entry 4). This is presumably due to the decreased stability of $LiCH_2I$.[7] (Note that any unreacted boronate ester **3** is converted into **5** after oxidation with $NaOH/H_2O_2$.) Although the amount of the doubly homologated alcohol could be increased by increasing the amount of $LiCH_2Br$ (see below), no double homologation was observed with $LiCH_2Cl$ even when it was used in excess (entry 5).

Table 1 Observation of single and double homologation

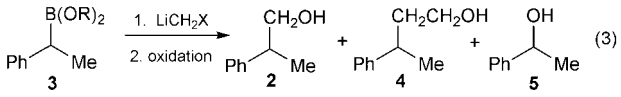

(3)

Entry	Reagent precursor	Homologation reagent	Equiv.	Single insertion **2**[a]	Double insertion **4**	Unreacted **5**
1	$BrCH_2Cl$	$LiCH_2Cl$	1.1	88%	0%	12%
2	ICH_2Cl	$LiCH_2Cl$	1.1	79%	0%	21%
3	$BrCH_2Br$	$LiCH_2Br$	1.1	74%	15%	11%
4	ICH_2I	$LiCH_2I$	1.1	43%	17%	40%
5	$BrCH_2Cl$	$LiCH_2Cl$	2.0	83%	0%	17%

[a] Relative ratios determined by integration of appropriate resonances in NMR; NMR yield calculated by use of internal standard is within several percent of quoted ratios.

Using dibromomethane as the candidate for further study, the effect of increasing the amount of the homologating reagent was examined. As shown in Table 2, the percentage of doubly homologated alcohol **4** which was formed in the reaction increased when the amount of $LiCH_2Br$ was increased above 1 equivalent. A significant increase was not, however, observed as the amount of $LiCH_2Br$ was increased further. It should be noted that a 5–10% variance was generally observed in the relative ratios reported in Table 2, which may be attributable to

Table 2 Effect of increasing amounts of $LiCH_2Br$

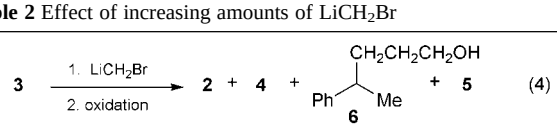

(4)

Entry	Equiv. of $LiCH_2Br$	Single insertion **2**[a]	Double insertion **4**	Triple insertion **6**	Unreacted **5**
1	1.1	74%	15%	0%	11%
2	2.0	34%	34%	10%	22%
3	4.0	29%	40%	10%	21%
4	6.0	35%	28%	7%	31%
5	10.0	22%	30%	19%	29%

[a] Relative ratios determined by integration of appropriate resonances in NMR; NMR yield calculated by use of internal standard is within several percent of quoted ratios.

DOI: 10.1039/b000243g

differences in rates of addition of Bu^nLi, especially as we attempted to generate increasing amounts of $LiCH_2Br$. At these higher loadings, we also observed alcohol **6**, resulting from incorporation of *three* CH_2 units. One interesting trend which can be gleaned from Table 2 is that as the amount of $LiCH_2Br$ used is increased, there is a concomitant increase in the amount of alcohol **5** resulting from unreacted starting material (compare entry 1 with 4 and 5).

This observation led us to postulate that homologated boronate esters such as **7** were more reactive than the seondary boronate esters **3**. This reactivity difference could be rationalized by the different steric requirements of **3** *cf.* primary homologated derivatives such as **7**. To test this hypothesis, we prepared and isolated **7** and also prepared boronate ester **3′** by hydroboration of *p*-methylstyrene. A *ca.* 1 : 1 mixture of **7** and **3′** was then treated with $LiCH_2Cl$ [eqn. (5)]. This homologating reagent was chosen for two reasons. Firstly, its use would obviate complications due to double homologations observed with $LiCH_2Br$; and secondly, as $LiCH_2Cl$ is the least reactive of the homologating reagents, it would presumably be the best probe of reactivity differences.

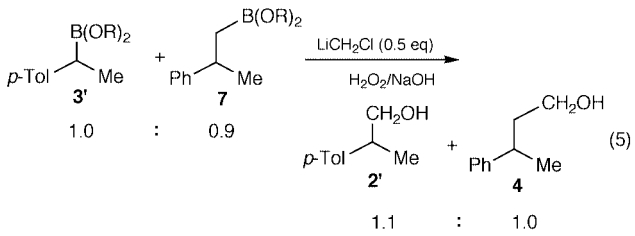

Much to our surprise, in the presence of a limiting quantity of $LiCH_2Cl$ (50%), boronate esters **7** and **3′** gave equal amounts of homologated products **4** and **2′** (19 and 21% respectively) indicating no difference in the reactivity of the secondary and primary boronate esters under these conditions. It should be noted that the introduction of the *para* methyl substituent will skew the results somewhat as it alters the electronic nature of the migrating group. An isotopically labeled analog of **3** is currently being prepared and the results of this study will be reported in due course. Experiments are also underway to elucidate the reason for the remarkable differences in the reactivity of $LiCH_2Cl$ and $LiCH_2Br$.

In conclusion, we have shown that the homologation of boronate esters derived from the hydroboration of styrene and its derivatives can be carried out in a sequential, one-pot manner depending on the nature of the homologating reagent used. Homologation with $LiCH_2Cl$ yields only the product of single homologation regardless of the number of equivalents used, and $LiCH_2Br$ yields the doubly homologated product even at 1 equivalent loading. Increasing the amount of this reagent leads to the incorporation of three CH_2 units in a single reaction.

The Natural Sciences and Engineering Research Council of Canada (NSERC) is gratefully acknowledged for support of this research in terms of research and equipment grants to CMC. The Department of Chemistry at UNB is thanked for providing a Wiesner award to Li Ren.

Notes and references

† cod = Cycloocta-1,5-diene, dppb = 1,4-bis(diphenylphosphino)butane. Note that the asymmetric version of this reaction employs binap [2,2'-bis(diphenylphosphino)-1,1'-binapthyl]. See ref. 4 for appropriate experimental procedures.

‡ The following procedure is representative. *Double homologation with* $LiCH_2X$: in a 10 mL flame dried round bottomed flask, (1-phenethyl)pinacolboronate **3** (229.8 mg, 1.0 mmol) and $BrCH_2Br$ (0.077 mL, 1.1 mmol) were dissolved in 2.0 mL of THF. After cooling to −78 °C using a N_2/isopropyl alcohol bath (bath temperature monitored by a low temp. thermometer), Bu^nLi (2.17 M in hexane, 0.50 mL, 1.1 mmol) was added dropwise over 15 min to the center of the flask with vigorous stirring. The reaction mixture was then allowed to warm gradually to room temperature overnight under N_2. The solvent was removed *in vacuo*, and the resulting residue diluted with 10 mL of saturated aqueous NH_4Cl. The aqueous layer was extracted with light petroleum (bp 30–60 °C, 20 mL × 4), and the combined organic layers dried over $MgSO_4$. After filtration and removal of solvent *in vacuo*, crude (1-phenylpropyl)pinacolboronate (231 mg) **7** was obtained.

Boronate ester **7**, (231 mg), was dissolved in 10 mL of diethyl ether, 2.0 mL of methanol and 4.0 mL of 1 M NaOH (8.0 mmol). The flask was flushed with nitrogen and 0.285 mL of H_2O_2 (30% w/v in H_2O, 2.27 mmol) was added slowly at room temperature. The reaction mixture was left at room temperature under N_2 overnight. The ether layer was separated and the aqueous layer washed with diethyl ether (20 mL × 3). The combined organic layers were dried over $MgSO_4$. After filtration and removal of solvent *in vacuo*, a mixture of 1-phenethanol **5** (11%), 2-phenylpropanol **2** (74%) and 3-phenylbutanol **4** (15%) was obtained. The ratio was determined by 400 MHz ^1H NMR. The NMR yields (11, 74 and 15%, respectively) of the aforementioned products were determined by integration of the peaks of interest *vs*. added internal standard (*p*-nitrotoluene).

§ For spectral data of compound **2**, see ref. 4; compound **4** is commercially available (Aldrich); and for compound **6**, the data are as follows: ^1H NMR (400 MHz, $CDCl_3$) δ 7.35–7.19 (m, 5H, C_6H_5), 3.62 (t, *J* 6.8 Hz, 2H, CH_2OH), 2.72 (m, 1H, C*H*), 1.70–1.63 (m, 2H, $CH_2CH_2CH_2$), 1.55–1.40 (m, 2H, $CH_2CH_2CH_2$), 1.28 (d, *J* 7.2 Hz, 3H, CH_3), 1.18 (br s, 1H, O*H*). ^{13}C NMR (100 MHz, $CDCl_3$) δ 147.5, 128.6, 127.2, 126.2, 63.3, 40.0, 34.6, 31.2, 22.6.

1 H. C. Brown, *Organic Syntheses via Boranes*, John Wiley and Sons, London, 1975; H. C. Brown, S. M. Singh and M. V. Rangaishenvi, *J. Org. Chem.*, 1986, **51**, 3150; H. C. Brown, N. N. Joshi, C. Pyun and B. Signaram, *J. Am. Chem. Soc.*, 1989, **111**, 1754; M. V. Rangaishenvi, B. Singaram and H. C. Brown, *J. Org. Chem.*, 1991, **56**, 3286; H. C. Brown, A. S. Phadke and N. G. Bhat, *Tetrahedron Lett.*, 1993, **34**, 7845.

2 D. S. Matteson and D. Majumdar, *J. Am. Chem. Soc.*, 1980, **102**, 7590; D. S. Matteson, R. Ray, R. R. Rocks and D. J. Tsai, *Organometallics*, 1983, **2**, 1536; D. S. Matteson and E. Erdlik, *Organometallics*, 1983, **2**, 1083; D. S. Matteson, K. M. Sadhu and M. L. Peterson, *J. Am. Chem. Soc.*, 1986, **108**, 810; D. S. Matteson, R. P Singh, B. Schafman and J.-J. Yang, *J. Org. Chem.*, 1998, **63**, 4466.

3 A. C. Chen, L. Ren and C. M. Crudden, *Chem. Commun.*, 1999, 611.

4 A. C. Chen, L. Ren and C. M. Crudden, *J. Org. Chem.*, 1999, **64**, 9704.

5 H. C. Brown, A. S. Phadke and M. V. Rangaishenvi, *J. Am. Chem. Soc.*, 1988, **110**, 6263.

6 K. J. Shea, B. B Busch and M. M. Paz, *Angew. Chem., Int. Ed.*, 1998, **37**, 1391.

7 Decreased yields were also reported with $LiCH_2I$ compared with the bromo and chloro derivatives, but double homologation was not observed: R. Soundararajan, G. Li and H. C. Brown, *Tetrahedron Lett.*, 1994, **35**, 8957.

Typeset and printed by Black Bear Press Limited, Cambridge, England

Single-molecule magnets based on iron(III) oxo clusters†

Dante Gatteschi,*[a] Roberta Sessoli[a] and Andrea Cornia[b]

[a] *Department of Chemistry, University of Florence, Florence, Italy*
[b] *Department of Chemistry, University of Modena and Reggio Emilia, Modena, Italy. E-mail: gattesch@blu.chim1.unifi.it*

Received (in Cambridge, UK) 14th October 1999, Accepted 15th December 1999
Published on the Web 9th February 2000

Polynuclear compounds of magnetic transition metal ions are attracting large interest after the discovery that their magnetisation may relax very slowly at low temperature. Since their behaviour is similar to that of bulk magnets they may be called single molecule magnets. Here we review the magnetic properties of iron(III) clusters showing such features which may be interesting for future applications, as well as strategies for designing new molecules with increased performances.

Introduction

The magnetic properties of large polynuclear compounds containing transition metal and/or rare earth ions have become the focus of much attention in the last few years,[1–4] after the discovery that the magnetisation of a cluster comprising twelve manganese ions, $[Mn_{12}O_{12}(MeCO_2)_{16}(H_2O)_4]\cdot 2MeCO_2H\cdot 4H_2O$.[5] Mn12Ac, relaxes so slowly at low temperature that the individual molecules behave in manner reminiscent of bulk magnets.[6] In fact if a molecule is magnetised at 2 K by applying a magnetic field, after 2 months the magnetisation is still *ca*. 40% of the saturation value, if the sample is kept at that temperature. In order to achieve the same result at 1.5 K it will be necessary to wait for *ca*. 40 years! Clusters, which behave like Mn12Ac, have been called single-molecule magnets.[1] In a sense this is a misnomer, because the term magnet must rigorously apply only to systems in which the spin correlation length diverges, *i.e.* goes to infinite, and this is clearly not possible in a cluster with a finite size. However the term is evocative, and in our opinion it can be used, provided its true meaning is understood.

One of the features of Mn12Ac which has attracted much interest is that the slow relaxation of the magnetisation gives rise to hysteresis effects, similar to those observed in bulk magnets, but of molecular origin: therefore it becomes in principle possible to store information in one single molecule.[6] The second appealing feature of Mn12Ac is that the relaxation of its magnetisation shows clear quantum effects, and the single molecule magnets can be used to investigate the macroscopic range in which quantum and classical behaviour coexist.[7,8] In principle these features can be exploited for developing new classes of computers in which quantum coherence is used to store and elaborate information. Currently the most promising results seem to be achieved using NMR techniques in solution,[9] but also Josephson junctions and magnetic nanoparticles can be taken into consideration.

In order to be considered for real applications, single molecule magnets must have the highest possible blocking temperature. The blocking temperature is that below which the relaxation of the magnetisation becomes slow compared to the time scale of a particular investigation technique. For instance for NMR the time scale is 10^{-8}–10^{-9} s, while for ac susceptibility measurements it is 10^{-2}–10^{1} s. Therefore the magnetisation of a molecule may appear as blocked in NMR but still dynamic in ac susceptibility measurements. Further it is also important that the molecules show clearly observable quantum effects.

After Mn12Ac, many attempts have been made in order to increase the blocking temperature of the single molecule magnets. In order to reach this goal it is necessary to build molecules which have the largest possible value of the total spin S in the ground state. Mn12Ac itself has $S = 10$ in the ground state, with the magnetisation corresponding to that of an atom with twenty unpaired electrons,[10] but molecules with up to 33 unpaired electrons have been reported.[11] We must emphasize that in general these molecules have many spin states which are thermally populated, therefore the properties associated to the ground state will only show up at low temperatures, when the excited states are depopulated. Clearly in order to increase the blocking temperature it is required that the ground state is the only populated one at relatively large temperatures.

The second requisite for observing single molecule magnet behaviour is that the ground state must have a high magnetic anisotropy of the easy-axis (Ising) type. This means that the magnetisation at low temperature may be stable either parallel or antiparallel to a given axis, and that an energy barrier must be overcome during the reversal of the magnetisation, passing for instance from the orientation 'up' to the orientation 'down'. In

Dante Gatteschi, born in Florence, Italy, in 1945 studied Chemistry at the University of Florence, and he is now Professor of General and Inorganic Chemistry at the same University. His research interests range from the use of spectroscopic techniques, particularly EPR and recently high frequency EPR, for the investigation of metal ion compounds to molecular magnetism. In the latter area his main achievements have been in the field of system comprising metal ions interacting with stable organic radicals and recently in the development of single molecule magnets.

Roberta Sessoli graduated in 1987 and obtained her PhD in Chemistry in 1992 studying the magnetism of molecular materials based on organic stable radicals and transition metal or rare earth ions. Since 1997 she has been an associate researcher at the University of Florence. Her main interests are presently in the magnetism of mesoscopic systems like clusters of magnetic metal ions or nanostructured materials.

Andrea Cornia, born in Modena, Italy, studied Chemistry and graduated in 1992. He obtained his PhD in Chemistry in 1996 under the supervision of D. Gatteschi and A. C. Fabretti. His research interests range from the supramolecular synthesis and structural investigation of nanomagnetic materials to the application of physical techniques in molecular magnetism and solid-state inorganic chemistry.

† Dedicated to the memory of Professor Olivier Kahn.

a system with spin S this occurs when the components with $M = \pm S$ lie lowest ($-S \leq M \leq S$). For axially distorted systems the energies of the M components are given by $E(M) = M^2D$, where D is the axial zero-field splitting (zfs) parameter. Therefore an Ising type anisotropy will be observed when D is negative. For Mn12Ac this condition is met and the barrier for the re-orientation of the magnetisation has been observed to be *ca.* 44 cm^{-1} or 64 K.

Beyond the obvious chemical variants of Mn12Ac,[12–14] other manganese complexes[13,15–17] have been found to behave as single molecule magnets. A few iron,[18–20] chromium[21–23] and vanadium[24] clusters also exhibit similar properties. Certainly the goal of a large ground spin state can be most easily achieved by assembling individual ions with a large ground spin state. Two ions with $S = 5/2$ ferromagnetically coupled have a ground state with $S = 5$, while it is necessary to assemble a cluster of ten $S = 1/2$ ions in order to achieve the same result. This is the reason why ions with large spin, like high spin iron(III) ($S = 5/2$), manganese(III) and iron(II) ($S = 2$), have been largely used.

Iron is certainly a very interesting ion in order to prepare single molecule magnets, not only because of the large spin state, but also because ferritin, the iron-storage protein in most living organisms, can be considered itself as a nanosize magnetic particle. In fact ferritin has been investigated for quantum tunnelling effects of the magnetisation.[25] Many large iron clusters have been reported, ranging from binuclear up to thirty nuclear species. We want to show here how several clusters containing iron behave as single molecule magnets, and discuss which conditions may favour this behaviour. All the clusters of this type so far reported are characterised by antiferromagnetic coupling between the iron(III) ions so that large spin in the ground state can only arise if the number of 'up' spins is different from that of 'down' spins. Therefore the clusters behave as single-molecule ferrimagnets. An example of a bulk ferrimagnet with a similar type of non-compensation of magnetic moments is maghemite, γ-Fe_2O_3. Ferrimagnetic iron–oxo clusters can indeed be considered as models of this prototype mineral.

Properties of iron(III) ions and exchange interactions in pairs

In order to understand which are the best strategies for obtaining single molecule magnets using iron(III) it is necessary to understand which are the conditions favouring both a strong magnetic coupling between the iron ions and a large magnetic anisotropy. The exchange interactions in oxo-bridged iron(III) pairs have been much investigated both theoretically and experimentally, also due to the relevance of these systems to non–heme metallo-proteins containing binuclear iron units in their active site.[26,27] The simplest approach considers two parameters, the average metal–oxygen distance, P, and the metal–oxygen–metal angle, α. Magnetic data recorded on a large series of iron complexes suggest that the P-dependence of the exchange coupling constant, J, is well represented by eqn. (1):[27]

$$J = 1.753 \times 10^{12} \exp(-12.663P) \quad (1)$$

where J is expressed in cm^{-1}, P in Å, and the exchange Hamiltonian is in the form $H = JS_1 \cdot S_2$. The coupling constant is largely insensitive to the Fe–O–Fe angle for $\alpha > 120°$. For smaller angles an effect is clearly observed, J becoming smaller as the angle α is reduced. A systematic study has been performed in a series of binuclear complexes with two alkoxo bridges[28] and similar Fe–O distances. The values of α range from 102 to 106°, while J varies between *ca.* 15 and 21 cm^{-1}. The simplest correlation was found to be of the type given by eqn. (2):

$$J = 1.48\,\alpha - 135 \quad (2)$$

with J in cm^{-1} and α in degrees. An extrapolation of eqn. (2) suggests that for $\alpha \approx 90°$ the coupling should become ferromagnetic. A justification for these experimental results was found on the basis of extended Hückel calculations, which however indicate that for small angles ($\alpha \approx 90°$) the coupling should become antiferromagnetic again, due to the importance of direct overlap between the iron(III) magnetic orbitals. In fact if the Fe–O bond distances are kept constant while the α angle is progressively reduced, the shortening of the Fe–Fe distance favours direct exchange. More experimental data are certainly needed to check this prediction. It should be remarked that the decrease in the antiferromagnetic coupling constant for a < 120° has been predicted also by a complete exchange model recently suggested by Güdel and Weihe.[29]

The anisotropy of the pairs depends on the anisotropy of the individual ions, and on an additional term that is brought about by the interaction between the two iron ions.[30] The former contribution is referred to as single-ion anisotropy, while the latter is known as spin–spin anisotropy. High spin iron(III) has a d^5 configuration, which yields an orbital singlet ^6S ground term for the free ion. The ground state of the complexed ion is also orbitally non-degenerate, therefore the Zeeman anisotropy is very low, with $g_x \approx g_y \approx g_z \approx 2.0023$. However some admixture with excited states of lower spin multiplicity is allowed by spin–orbit coupling and the ground $S = 5/2$ state does show zero field splitting, which may easily be of the order of 1 cm^{-1}. This splitting determines the single ion anisotropy.

Single ion contributions to the anisotropy cannot be rigorously calculated, and so far even the experimental data are lacking in the sense that no significant correlation between structural features and values of D has been established. Recently Neese and Solomon have suggested[31] that it is possible to calculate the zfs parameters by using a MO approach, while traditional ligand field models have been implemented in the Angular Overlap Model, AOM, formalism.[32] For instance it has been found that a trigonal distortion from octahedral geometry yields a negative zfs parameter D for elongation, and positive for compression. In order to have direct information on the zfs in model compounds the HF-EPR spectra of a tris ß-diketonate complex, $Fe(dpm)_3$, where dpm = 2,2,6,6-tetramethylheptane-3,5-dionate, were recorded.[20] The spectra yielded $D = -0.18\ cm^{-1}$ and $E/D = 0.25$. These values were reproduced in a reasonable way by using the AOM. However, more experimental and theoretical work is needed in order to establish useful correlations between structure and zfs of iron(III) ions. Given their relevance also for biological systems this seems to be indeed an important task.

The anisotropy associated with the spin–spin interaction can be described to a good approximation by the interaction between the magnetic point dipoles centred on the two iron ions. For a pair of antiferromagnetically coupled ions the dipolar interaction orients the two spins orthogonal to the vector $\boldsymbol{r}$ connecting the two centres. In fact the poles of the same sign would be in contact for an orientation parallel to $\boldsymbol{r}$. Therefore the plane perpendicular to $\boldsymbol{r}$ [Fig. 1(a)] is a hard plane for the magnetisation of the antiferromagnetic dimer, which is more easily magnetised when the field is applied parallel to the axis connecting the two spins. Dipolar interactions thus provide an Ising-type contribution to the magnetic anisotropy.

These considerations can be extended to polynuclear systems as well. In particular, when antiferromagnetically coupled metal ions are arranged in a planar structure with axial symmetry, like in some of the iron(III) clusters described in the forthcoming sections, nearest-neighbour dipolar interactions determine a *XY*-anisotropy with an easy plane of magnetisation when the ground state has $S = 0$ [Fig. 1(b)]. In fact, in the lowest-energy configuration, the individual spins are antiparallel to their nearest neighbours (owing to exchange interactions) *and* perpendicular to the average plane through the metal array

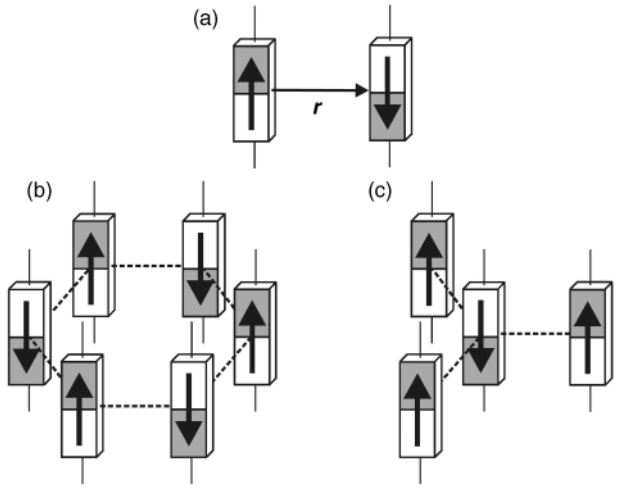

Fig. 1 Schematic view of the preferred spin orientation due to the dipolar interaction in an antiferromagnetic dimer (a), in a cyclic antiferromagnetic cluster (b), and in a ferrimagnetic tetrameric cluster (c).

(owing to dipolar interactions). By contrast, when the ground state has *S* different from zero, *i.e.* in ferrimagnetic clusters, the system exhibits an Ising-type anisotropy [Fig. 1(c)]. It is noteworthy that dipolar interactions alone lead to an Ising-type anisotropy in planar ferrimagnetic clusters, thus giving the possibility to observe single molecule magnet behaviour. The topology of the metal ions can thus strongly influence magnetic anisotropy *via* dipole–dipole interactions, establishing a direct connection between the shape of the cluster and its magnetic properties.

Iron rings: quantum size effects and anisotropy

Using alkoxides or carboxylates as bridging ligands it has been possible to synthesise six-,[33,34] eight, ten-[35] and twelve-[36] membered iron(III) rings. In all the cases the iron–iron interaction is antiferromagnetic, yielding a ground $S = 0$ state. The energies of the lowest lying *S* states can be expressed by eqn. (3):

$$E(S) = J_{\text{eff}}S(S + 1) \qquad (3)$$

where $J_{\text{eff}} = 4J/N$, with *N* the number of iron ions in the ring. Below 1 K the rings are in the non-magnetic ground state, and consequently under low field conditions the magnetisation is zero. However, on increasing the field, the excited magnetic states are stabilised, until eventually they become the ground state. This gives rise to a typical stepped magnetisation, with a first jump at the field where the lowest lying $S = 1$ state becomes the ground state, then where the $S = 2$ crosses over to become the ground state, and so on.[35,37] These observations are clear evidence for quantum effects, corresponding to the fact that the lowest $S = 0$ level is separated by a gap from the first excited level. The larger the ring the smaller the gap, until eventually the levels must merge in a continuum. In fact the magnetisation of one-dimensional magnetic materials, that can be considered as the extrapolation of rings to infinite, does not show steps.[38] Therefore it would be extremely important to make available larger and larger rings in order to follow the passage from microscopic to bulk. In fact the thermodynamic properties calculated for finite rings have long been used to extrapolate the properties of the infinite chains. Another interesting goal is that of synthesising odd membered rings of half integer spins, which should show spin frustration effects.[39]

All the measurements referred to above are static measurements, which do not provide any information on the dynamics of the magnetisation and on possible tunnelling phenomena. Dynamic measurements can in principle be made with a variety of techniques, ranging from ac susceptometry to magnetic resonance. In this respect NMR is particularly appealing, because it can monitor the variations in the relaxation rate of the nuclear moments under the influence of the electron magnetisation. In fact, it can be expected that when two levels cross, the electron relaxation at low temperature is drastically influenced. Therefore the field dependence of the nuclear relaxation rate should show anomalies corresponding to the crossover fields. This has been recently observed[40] in a decanuclear ring, the so-called ferric wheel, whose structure is shown in Fig. 2. All the methods exploiting NMR have potential interest for quantum computing applications, given the recent implementation of NMR techniques in solution.[9]

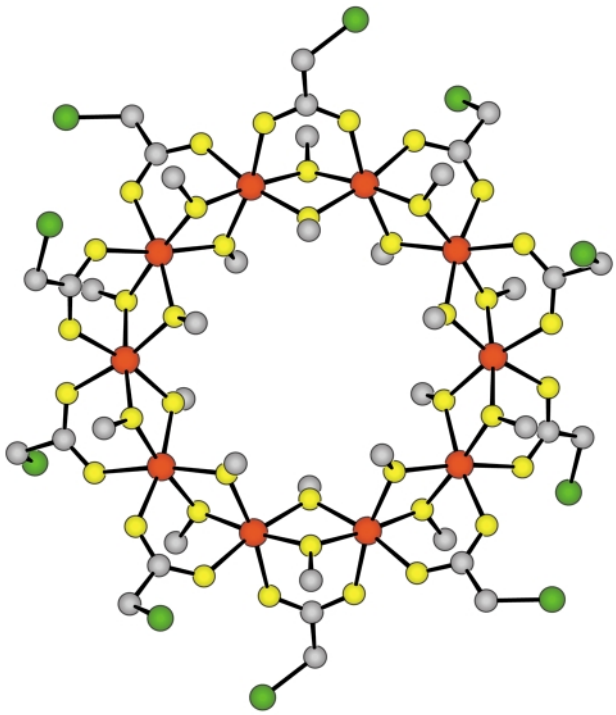

Fig. 2 View of the structure of the cluster $[Fe(OMe)_2(O_2CCH_2Cl)]_{10}$, the so-called 'ferric wheel'. The iron atoms are in red, oxygen in yellow, carbon in grey and chlorine in green. The ten iron atoms lie in a plane within ±0.009 Å and the diameter of the cluster, defined as the longest Fe···Fe distance, is 9.80 Å.

Stepped magnetisation has been observed also in smaller iron(III) rings, like LiFe6 and NaFe6, whose structure is depicted in Fig. 3 The alkali-metal ion, Li^+ or Na^+, is hosted in the. centre of the ring, which behaves like an inorganic crown ether.[34] Solution studies have shown that the affinity of the Fe6 ring is higher for sodium than for lithium ions. Further, LiFe6 and NaFe6 can be neatly obtained by adding lithium or sodium ions to a solution of a twelve-membered iron(III) ring which does not host any alkali-metal ion.[36]

The magnetisation of small single crystals of LiFe6 and NaFe6 was investigated through new torque magnetometers using a sensitive cantilever which directly provided the magnetic anisotropy of the excited *S* states.[41] The central alkali-metal ion strongly influences not only the isotropic exchange interaction, which passes from 14 to 20 cm^{-1} by replacing Li^+ with Na^+, but also the magnetic anisotropy. In fact the zero-field splitting of the first excited $S = 1$ state is $D = 1.16$ cm^{-1} for the lithium derivative and $D = 4.32$ cm^{-1} for the sodium derivative. The former value corresponds almost exactly to the calculated dipolar contribution. By contrast, the magnetic anisotropy of the sodium derivative points to the presence of large single ion contributions. Minor differences in the environment of the individual iron(III) centers, such as those induced by the different size of the guest ion, may thus induce

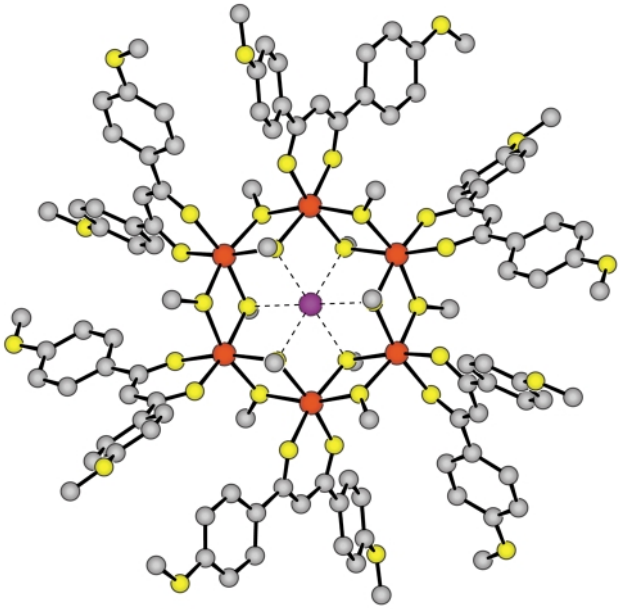

Fig. 3 View of the structure of the hexanuclear iron cluster $[NaFe_6(OMe)_{12}(pmdbm)_6]^+$, where pmdbm = 1,3-di(4-methoxyphenylpropane)-1,3-dionate (colour code as in Fig. 2). Li^+ can replace the Na^+ cation in the centre with significant changes in the intracluster magnetic exchange interaction and in the magnetic anisotropy.

large zfs variations. This clearly indicates that the control of the magnetic anisotropy of the clusters is a difficult task.

Iron-containing single molecule magnets

The smallest iron cluster showing slow relaxation effects in the magnetisation at low temperature is $[Fe_4(OMe)_6(dpm)_6]$, Fe4.[20] The structure of Fe4 is shown in Fig. 4. A central iron ion is

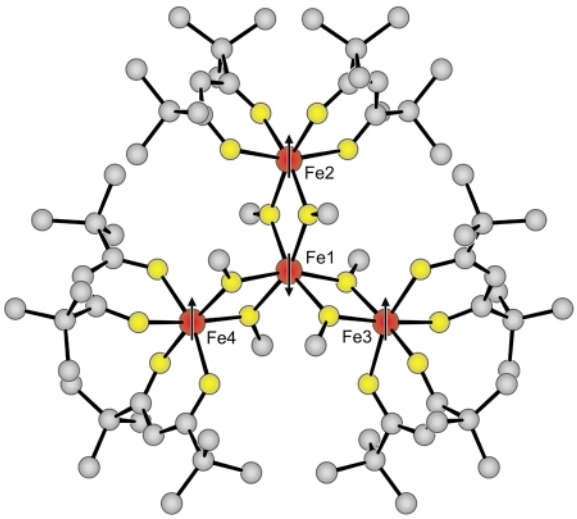

Fig. 4 Structure of the ferrimagnetic cluster $[Fe_4(OMe)_6(dpm)_6]$ where dpm = 2,2,6,6-tetramethylheptane-3,5-dionate (colour code as in Fig. 2). The arrows correspond to the spin structure in the ground $S = 5$ state.

connected to three terminal ions by three double μ-alkoxo bridges. Crystal symmetry requires a C_2 axis in the cluster passing through Fe1 and Fe2. The three external iron(III) ions define an almost equilateral triangle. In this case the spin topology, which for antiferromagnetic coupling orients the central spin 'down' and the external ones 'up' determines the non-compensation of the spins. The ground state has $S = 5$, and the ferrimagnetic nature of the cluster is clearly shown by the χT *vs.* T curve which goes through a broad minimum at *ca.* 150 K and then reaches 14.6 emu K mol^{-1} at low temperature, in reasonable agreement with an $S = 5$ state ($\chi T = 15$ emu K mol^{-1}, for $g = 2.00$). The temperature dependence of χT has been successfully reproduced calculating the energies of the total spin states using the spin Hamiltonian eqn. (4):

$$H = J\,(\boldsymbol{S_1}\bullet\boldsymbol{S_2} + \boldsymbol{S_1}\bullet\boldsymbol{S_3} + \boldsymbol{S_1}\bullet\boldsymbol{S_4}) + J'\,(\boldsymbol{S_2}\bullet\boldsymbol{S_3} + \boldsymbol{S_3}\bullet\boldsymbol{S_4} + \boldsymbol{S_2}\bullet\boldsymbol{S_4}) \quad (4)$$

The best-fit values are: $J = 21.1$ cm^{-1}, $J' = -2.1$ cm^{-1}, in reasonable agreement with the values expected using eqns. (1) and (2).

The anisotropy of the ground state has been determined using high field EPR spectroscopy, and it has been shown to be quasi axial, and of the Ising type, with $D = -0.20$ cm^{-1}. This means that the ground $S = 5$ state is split in such a way that the $M = \pm5$ levels lie lowest, with $M = \pm 4$ at 1.8 cm^{-1}, $M = \pm3$ at 3.2 cm^{-1}, $M = \pm2$ at 4.2 cm^{-1} and $M = 0$ at 5 cm^{-1}. If the system is magnetised at low temperature, the $M = -S$ state will be selectively populated. On switching the field off, the system will revert to thermal equilibrium, *i.e.* it will equalise the populations of the $M = -S$ and $M = +S$ states. At the simplest level of approximation this cannot occur directly, but the system must climb all the levels, one at a time, up to $M = 0$, and then descend.[42] Under this simplifying approximation the barrier for the re-orientation of the magnetisation is given by the difference in energy between the lowest $M = +S$ and the top $M = 0$ level [eqn. (5)]:

$$\Delta = |D|\,S^2 \quad (5)$$

and the relaxation of the magnetisation is expected to follow the Arrhenius law:

$$\tau = \tau_0 \exp(\Delta/kT) \quad (6)$$

where τ_0 is expected to be proportional to S^6/Δ^3. Eqn. (6) is the same as that appropriate to classical superparamagnets.[43]

Below 1 K Fe4 shows slow relaxation of the magnetisation in ac susceptibility measurements. The relaxation time follows the Arrhenius law with $\tau_0 = 1.1 \times 10^{-6}$ s and $\Delta/k = 3.5$ K. This means that at 0.2 K, the lowest measurement temperature, the relaxation time is of the order of one minute. This relaxation is much faster than that of Mn12Ac,[6] as it should be expected given the smaller S and the lower barrier.

The height of the barrier, calculated with eqn. (5), is larger than the experimental value. This has been found to be the case in all systems showing slow relaxation of the magnetisation investigated so far. It must be concluded that eqn. (5) is only a loose approximation. In particular, the simplified model does not take into account direct tunnelling within a formally degenerate $\pm M$ pair. This point will be addressed in detail in the following section on Fe8.

Given the small number of magnetic ions in Fe4, detailed calculations were performed of the energies of the spin levels. Attempts were made also to rationalise the anisotropy of the ground state. As outlined in a previous section, the dipolar contribution has the same sign as the observed anisotropy, although spin–spin interactions alone can not quantitatively account for it. Attempts were made to calculate the single ion contributions, using the AOM, but no really acceptable results were achieved.[20] More efforts are needed in this field.

Fe8, the quantum magnet

The structure of $[Fe_8O_2(OH)_{12}(tacn)_6]^{8+}$, Fe8, where tacn = 1,4,7-triazacyclononane, which Wieghardt *et al.* originally reported as the bromide salt,[44] Fe8Br, is shown in Fig. 5. The analysis of the temperature dependence of the magnetic susceptibility,[45] provided evidence for a ground $S = 10$ state, which can occur if six spins are up and two down. Since there are several triangles in the exchange pathways connecting the iron(III) ions spin, frustration effects[39] can be anticipated. This means that the ground state is not correctly described by simply putting the spins up or down on different metal ions. However

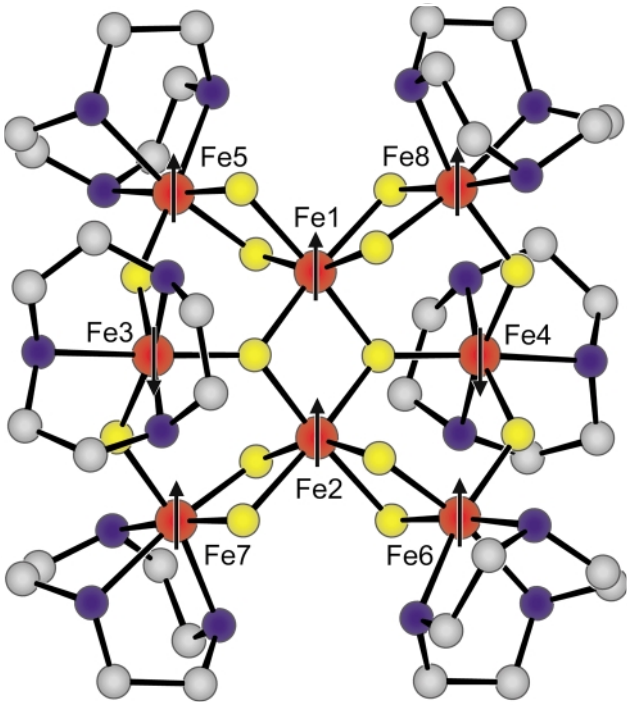

Fig. 5 View of the cluster $[Fe_8O_2(OH)_{12}(tacn)_6]^{8+}$ where tacn = 1,4,7-triazacyclononane. The arrows correspond to the spin structure previously suggested by the analysis of the magnetic susceptibility and then determined from single crystal polarised neutron diffraction experiments (see ref. 46).

it was possible to obtain a direct picture of the spin density by using polarised neutron diffraction techniques.[46] These showed that the spin density on Fe3 and Fe4 is negative, and that on all the other iron ions is positive. These data are in qualitative agreement with the values obtained from the fit of the temperature dependence of the magnetic susceptibility. The spin density however does not correspond to five unpaired electrons on each iron ion, confirming that the 'up-down' description is an oversimplification.

The ground state is largely split in zero field, as evidenced by HF-EPR[19] and inelastic neutron scattering, INS,[47] experiments. When neutrons interact with the clusters they may induce transitions between the M levels of S multiplets, according to the selection rules $\Delta M = 0, \pm 1$. Therefore, by measuring the INS it is possible to obtain detailed information on the spectrum of the M energy levels. The INS of Fe8Br is particularly rich, and it has shown, for the first time, how the technique can be fruitfully used also on systems with many protons in the energy window up to 60 cm^{-1}. In fact, after the spectra of Fe8Bt, recently the spectra of Mn12Ac have been reported[48] showing a similar abundance of absorptions. The INS spectra of Fe8Br are shown in Fig. 6, together with the assignment of the peaks to the transitions within the lowest $S = 10$ multiplet.

The HF-EPR and the INS spectra have provided essentially the same sets of parameters to describe the splitting of the ground $S = 10$ state. In particular, they agree on the fact that the spin Hamiltonian for describing the zero field splitting requires the inclusion of both second order and fourth order terms. This means that the splitting of the ground state is determined by both quadrupolar terms, described by the parameters D and E, and hexadecupolar terms described by the B_4^0, B_4^2 and B_4^4 parameters. Single crystal EPR spectra have also provided the principal directions of the zero field splitting tensors, and consequently the principal directions of the magnetic anisotropy. The easy axis, *i.e.* that of prevailing orientation of the individual spins, makes a small angle, *ca.* 10°, with the perpendicular of the plane of the iron ions, while the hard axis

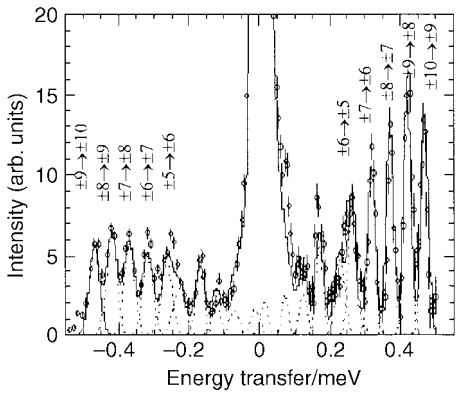

Fig. 6 Inelastic neutron scattering spectrum recorded at 10 K on Fe8Br cluster microcrystalline powder. The large peak at zero energy corresponds to the elastic contribution. On the left side the emission spectrum is reported while on the right side are the absorption lines. The transitions at the extremes of the spectrum can be easily assigned as shown in the picture using the basis of the eigenvalues of $\boldsymbol{S}_z$ (1 meV = 8.065 cm^{-1}).

passes through the Fe1 and Fe2 ions. The energies of the M levels of Fe8Br are shown in Fig. 7. The lowest lying levels

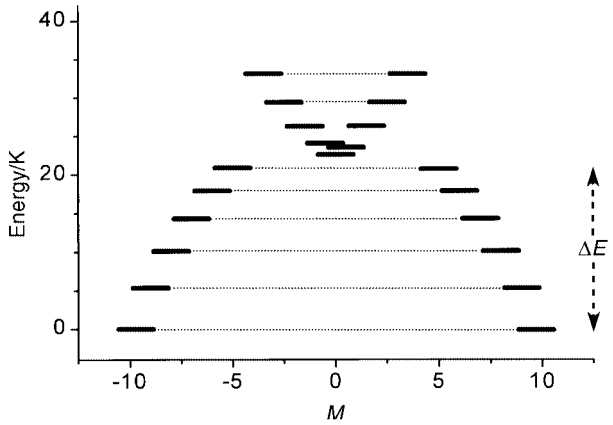

Fig. 7 Schematic view of the splitting in zero field of the $S = 10$ ground manifold of Fe8Br using the spin Hamiltonian parameters of ref. 47. The height of the classical energy barrier is shown. Underbarrier transitions dominate at low temperature. The levels above *ca.* 22 K cannot be labelled with M and their assignment on the graph is arbitrary.

correspond to $M = \pm S$, and on increasing temperature, the levels are progressively more admixed. This is essentially determined by the non-zero E parameter that admixes levels differing in M by ±2. In particular from Fig. 7 we learn that at the top of the manifold there is not a unique level corresponding to $M = 0$. Therefore the meaning of eqn. (5) for defining the barrier for the reorientation of the magnetisation is completely lost and the barrier is significantly reduced.[49] However, if it is used in a first approximation, Δ/k is calculated to be 29 K, and therefore slow relaxation effects are expected at low temperature.

In Mössbauer experiments, which have a time scale of 10^{-8}–10^{-9} s slow relaxation of the magnetisation of Fe8Br is observed[19] below 20 K, while the same effect can be detected by ac susceptibility measurements only below 3 K. The relaxation times however do not rigorously obey an Arrhenius type relation (6). The relaxation time of the magnetisation becomes so slow below 1 K that hysteresis loops of molecular origin can be observed.[50] The hysteresis, shown in Fig. 8, has a dynamic nature, as revealed by the strong dependence on the rate of the field sweep, and the same stepped appearance first reported for Mn12Ac.[7,8] The flat regions correspond to fields at which the relaxation is slow, while the steps correspond to fields at which a rapid increase of the relaxation rate is observed. This behaviour has been attributed to thermally assisted quantum tunnelling. In a magnetic quantum system the relaxation of the magnetisation may occur either with the mechanism described

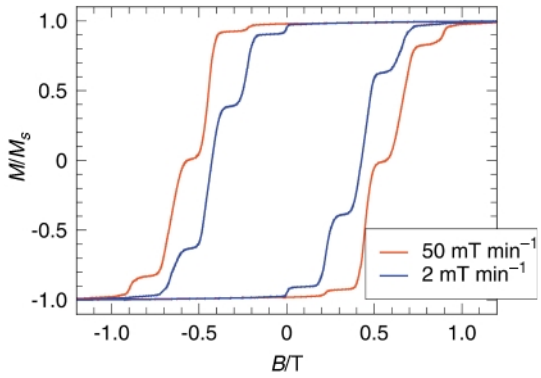

Fig. 8 Hysteresis loops recorded for Fe8Br at 0.30 K and two different field scan speeds. The dynamic nature of the hysteresis is revealed by the strong dependence on the sweep rate. The stepped shape is due to the tunnelling of the magnetisation, which occurs when two levels on the opposite sides of the barrier are brought in coincidence by sweeping the field, which accelerates the magnetic relaxation giving rise to the jumps in the magnetisation.

above, where the absorption or emission of a phonon allow the transition from the M to the $M \pm 1$ level, or by tunnelling between pairs of degenerate levels. In zero field the lowest lying pairs of M levels meet the tunnelling condition, and the relaxation is comparatively fast. In the presence of an external field the energy of the $+M$ level increases and that of the $-M$ level decreases, making quantum tunnelling impossible, as shown schematically in Fig. 9. However the condition for

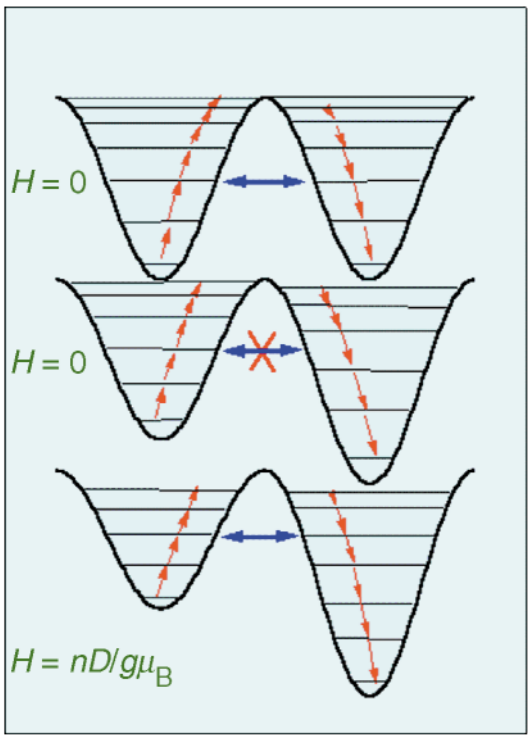

Fig. 9 Schematic drawing of the energy barrier for the reversal of the magnetisation generated by the magnetic anisotropy. The levels correspond to the M states of the ground spin multiplet and for the sake of clarity an axial zero field splitting has been considered. In zero applied field the $\pm M$ states are degenerate allowing a shortcut of the barrier through a tunnelling process. An external magnetic field removes the energy correspondence of the states on the opposite sides of the barrier, thus hampering the underbarrier mechanism of relaxation, except for critical values of the field for which the energy correspondence is re-established.

tunnelling are restored for fields at which the $+M$ level has the same energy as of the $-M + n$ level, where $n = 1,2,\ldots$*etc*. The fields where these conditions are met can be calculated using the spin Hamiltonian parameters obtained from HF-EPR and INS experiments. The calculated fields correspond to the fields where steps are observed in the hysteresis. These tunnelling processes occur not only between the lowest levels, but also between the higher thermally populated levels. Therefore the overall mechanism has been described as thermally assisted quantum tunnelling.

Direct measurements of the relaxation time of Fe8Br can be performed at low temperature by first saturating the magnetisation and then monitoring its time decay.[50] In this way it is observed that below 350 mK the relaxation becomes temperature independent, thus confirming the quantum tunnelling effects. Under these conditions only the lowest $M = 10$ levels are populated, and tunnelling occurs between them. This has been the first experimental evidence of pure quantum tunnelling in a magnetic nanoparticle. Attempts to observe this behaviour in particles obtained by techniques other than molecular chemistry had failed, essentially because it was impossible to have absolutely monodisperse particles.

The way the molecules undergo tunnelling is still a matter of debate, but evidence is accumulating in favour of the mechanism to be discussed below. The $M = \pm 10$ levels are degenerate in axial symmetry. If a transverse anisotropy is present, *i.e.* a matrix element different from zero, $\Delta/2$, connects the two states, then tunnelling is possible. The two levels are split by the transverse field, $H_t = \Delta/g\mu_B$, and the magnetisation can fluctuate with a frequency proportional to Δ, the tunnel splitting. This picture is correct if no additional fields are present. These however cannot be avoided because the molecule is embedded in a lattice with other magnetised molecules that generate a dipolar field, H_d. If this is larger than H_t the effect of the matrix element is quenched and no tunnelling is observed. In Fe8Br, H_d is of the order of 1–10 mT, while H_t is of the order of 10^{-9} T, therefore the condition for tunnelling is not met at this level of approximation. However the above picture neglects the role of the magnetic nuclei present in the cluster. The ^{1}H ($I = 1/2$), ^{14}N ($I = 1$), and ^{79,81}Br ($I = 3/2$) nuclei generate a fluctuating hyperfine field, H_{hy}, at the magnetic centres broadening the $M = \pm 10$ levels. The broadening is of the order of 1 mT and it may restore the tunnelling conditions for the molecules for which $H_d < H_{hy}$. However, since the distribution of dipolar fields is broader than that of hyperfine fields, the process should stop soon. In order to justify the observed continuous quantum relaxation to thermal equilibrium it must be considered that when a molecule tunnels it changes its magnetisation. Consequently, the dipolar field felt by the neighbouring molecules also changes, creating regions in the sample where the condition $H_d < H_{hy}$ is met.

Another way of imposing the condition that the tunnel splitting is larger than the local fields is to apply a field perpendicular to the easy axis. The applied field will increase the tunnel splitting which then can be more easily measured.

Using micro SQUID techniques it was also possible to measure the intrinsic width of the tunnel splitting.[51] This has been experimentally shown to be proportional to the hyperfine field in Fe8Br.[52] In fact when the naturally occurring non-magnetic Fe isotopes have been substituted with the magnetic ^{57}Fe ($I = 1/2$) the width of the splitting has been measured to increase from 0.8 to 1.2 mT as shown in the inset of Fig. 10. When the ^{1}H nuclei are partially substituted with the less magnetic ^{2}H nuclei the width decreased to 0.6 mT. The hyperfine field generated by the nuclei also strongly affects the relaxation rate of the macroscopic magnetisation, which is fastest in ^{57}Fe-enriched samples and slowest in the partially deuterated ones. This is shown in Fig. 10, where the time needed to relax 1% of the saturation magnetisation is plotted as a function of the temperature. These results showed the fundamental role of nuclei for the relaxation of the magnetisation of Fe8Br in the quantum regime and open the possibly of controlling the dynamics of the magnetisation by acting on the nuclei.

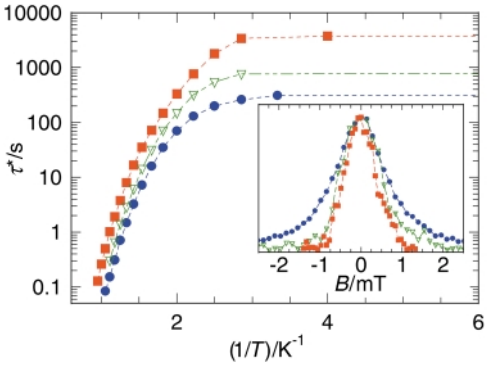

Fig. 10 Isotopic effect on the relaxation of the magnetisation and on the intrinsic line-width of the resonant tunnelling process (inset). τ^* corresponds to the time needed to relax 1% of the saturation magnetisation and its temperature dependence is studied for three isotopic samples of Fe8Br: natural sample (green),^{57}Fe enriched sample (blue), partially deuterated sample (red). In the inset the resonance line, estimated from the field dependence of the relaxation rate, is reported for the three isotopic samples. In order to study the intrinsic linewidth and to avoid the broadening due to dipolar interaction a hole-burning technique has been employed (see ref. 51).

Chemical modifications to Fe8Br have been also attempted. So far the most successful has been the partial substitution of bromide anions with perchlorate anions. $[Fe_8O_2(OH)_{12}(tacn)_6]Br_4(ClO_4)_4$, Fe8ClO4, has been shown to behave similarly to Fe8Br, with a ground $S = 10$ state. However the zfs of the ground state is slightly different in the two compounds. In particular the E/D ratio, which determines the rhombic splitting of the magnetic anisotropy, is larger than that of Fe8Br. Therefore the blocking temperature and the onset of quantum regime are different. It may be hoped that these small variations may provide additional handles to test the theories of quantum tunnelling.

Perspectives

The field of molecular nanomagnetism is just at the beginning. The advantage of molecular clusters, compared to all the other types of magnetic nanoparticles, is that they are all identical to each other and their structure is known. Further, intermolecular interactions in the crystal lattice are so weak that in most cases the response of the crystal is the same as that of an individual molecule. Therefore it is possible to measure a molecular response by using traditional macroscopic techniques. On the other hand, the fact that the molecules are bistable makes them interesting objects to be addressed individually. Therefore it can be foreseen that in the next few years techniques to address single molecules will be developed. Another important development to be expected is the synthesis of larger clusters, which will be investigated for a large number of different properties, such as those related with biocompatibility (for MRI contrast agents, or for magnetic drug delivery) and for the development of new physics. In fact the results already obtained have shown that these materials open exciting new perspectives in mesoscopic physics. For instance Fe8Br has for the first time provided an experimental confirmation of the so-called Berry phase in magnets,[53] a phenomenon long looked for. There are high expectations for the fundamental contributions that this highly interdisciplinary area can bring.

Acknowledgements

The financial support of MURST, CNR and PFMSTAII is gratefully acknowledged. We gratefully acknowledge G. Amoretti, R. Caciuffo, A. Caneschi and W. Wernsdorfer.

Notes and references

1 G. Aromi, S. M. J. Aubin, M. A. Bolcar, G. Christou, H. J. Eppley, K. Folting, D. N. Hendrickson, J. C. Huffman, R. C. Squire, H. L. Tsai, S. Wang and M. W. Wemple, *Polyhedron*, 1998, **17**, 3005.
2 B. Barbara, L. Thomas, F. Lionti, A. Sulpice and A. Caneschi, *J. Magn. Magn. Mater.*, 1998, **177**, 1324.
3 D. Gatteschi, A. Caneschi, L. Pardi and R. Sessoli, *Science*, 1994, **265**, 1054.
4 A. Muller, F. Peters, M. T. Pope and D. Gatteschi, *Chem. Rev.*, 1998, **98**, 239.
5 A. Caneschi, D. Gatteschi, R. Sessoli, A.-L. Barra, L. C. Brunel and M. Guillot, *J. Am. Chem. Soc.*, 1991, **113**, 5873.
6 R. Sessoli, D. Gatteschi, A. Caneschi and M. A. Novak, *Nature (London)*, 1993, **365**, 141.
7 L. Thomas, F. Lionti, R. Ballou, D. Gatteschi, R. Sessoli and B. Barbara, *Nature (London)*, 1996, **383**, 145.
8 J. R. Friedman, M. P. Sarachik, J. Tejada and R. Ziolo, *Phys. Rev. Lett.*, 1996, **76**, 3830.
9 I. L. Chuang, N. Gershenfeld and M. Kubinec, *Phys. Rev. Lett.*, 1998, **80**, 3408.
10 R. Sessoli, H. L. Tsai, A. R. Schake, S. Wang, J. B. Vincent, K. Folting, D. Gatteschi, G. Christou and D. N. Hendrickson, *J. Am. Chem. Soc.*, 1993, **115**, 1804.
11 A. K. Powell, S. L. Heath, D. Gatteschi, L. Pardi, R. Sessoli, G. Spina, F. Del Giallo and F. Pieralli, *J. Am. Chem. Soc.*, 1995, **117**, 2491.
12 Z. M. Sun, D. Ruiz, E. Rumberger, C. D. Incarvito, K. Folting, A. L. Rheingold, G. Christou and D. N. Hendrickson, *Inorg. Chem.*, 1998, **37**, 4758.
13 S. M. J. Aubin, S. Spagna, H. J. Eppley, R. E. Sager, G. Christou and D. N. Hendrickson, *Chem. Commun.*, 1998, 803.
14 Z. M. Sun, C. M. Grant, S. L. Castro, D. N. Hendrickson and G. Christou, *Chem. Commun.*, 1998, 721.
15 E. K. Brechin, J. Yoo, M. Nakano, J. C. Huffman, D. N. Hendrickson and G. Christou, *Chem. Commun.*, 1999, 783.
16 B. Pilawa, M. T. Kelemen, S. Wanka, A. Geisselmann and A. L. Barra, *Europhys. Lett.*, 1998, **43**, 7.
17 A. L. Barra, A. Caneschi, D. Gatteschi, D. P. Goldberg and R. Sessoli, *J. Solid State Chem.*, 1999, **145**, 484.
18 K. L. Taft, G. C. Papaefthymiou and S. J. Lippard, *Science*, 1993, **259**, 1302.
19 A. L. Barra, P. Debrunner, D. Gatteschi, Ch. E. Schulz and R. Sessoli, *Europhys. Lett.*, 1996, **35**, 133.
20 A. L. Barra, A. Caneschi, A. Cornia, F. Fabrizi de Biani, D. Gatteschi, C. Sangregorio, R. Sessoli and L. Sorace, *J. Am. Chem. Soc.*, 1999, **121**, 5302.
21 S. Ferlay, T. Mallah, R. Ouahes, P. Veillet and M. Verdaguer, *Inorg. Chem.*, 1999, **38**, 229.
22 T. Mallah, C. Auberger, M. Verdaguer and P. Veillet, *J. Chem. Soc., Chem. Commun.*, 1995, 61.
23 A. Scuiller, T. Mallah, M. Verdaguer, A. Nivorozkhin et al., *New J. Chem.*, 1996, **20**, 1.
24 S. L. Castro, Z. M. Sun, C. M. Grant, J. C. Bollinger, D. N. Hendrickson and G. Christou, *J. Am. Chem. Soc.*, 1998, **120**, 2365.
25 E. M. Chudnovsky, *J. Magn. Magn. Mater.*, 1998, **185**, 267.
26 D. M. Kurtz, *Chem. Rev.*, 1990, **90**, 585.
27 S. M. Gorun and S. J. Lippard, *Inorg. Chem.*, 1991, **30**, 1625.
28 F. Le Gall, F. Fabrizi de Biani, A. Caneschi, P. Cinelli, A. Cornia, A. C. Fabretti and D. Gatteschi, *Inorg. Chim. Acta*, 1997, **262**,123.
29 H. Güdel and H. U. Weihe, *J. Am. Chem. Soc.*, 1998, **120**, 2870.
30 A. Bencini and D. Gatteschi, *EPR of Exchange Coupled Systems*, Springer-Verlag, Berlin, 1990.
31 F. Neese and E. I. Solomon, *Inorg. Chem.*, 1998, **37**, 6568.
32 A. Bencini, I. Ciofini and M. G. Uytterhoeven, *Inorg. Chim. Acta*, 1998, **274**, 90.
33 R. W. Saalfrank, I. Bernt, E. Uller and F. Hampel, *Angew. Chem., Int. Ed. Engl.*, 1997, **36**, 2482.
34 A. Caneschi, A. Cornia and S. J. Lippard, *Angew. Chem., Int. Ed. Engl.*, 1995, **34**, 467.
35 K. L. Taft, C. D. Delfs, G. C. Papaefthymiou, S. Foner, D. Gatteschi and S. J. Lippard, *J. Am. Chem. Soc.*, 1994, **116**, 823.
36 A. Caneschi, A. Cornia, A. C. Fabretti and D. Gatteschi, *Angew. Chem., Int. Ed.*, 1999, **38**, 1295.
37 A. Caneschi, A. Cornia, A. C. Fabretti, S. Foner, D. Gatteschi, R. Grandi and L. Schenetti, *Chem. Eur. J.*, 1996, **2**, 1379.
38 J. Sinzig, L. J. De Jongh, A. Ceriotti, R. Della Pergola, G. Longoni, M. Stener, K. Albert and N. Rosch, *Phys. Rev. Lett.*, 1998, **81**, 3211.
39 C. A. Christmas, H. L. Tsai, L. Pardi, J. M. Kesselman, P. K. Gantzel, R. K. Chadha, D. Gatteschi, D. F. Harvey and D. N. Hendrickson, *J. Am. Chem. Soc.*, 1993, **115**, 12483.

40 M. H. Julien, Z. H. Jang, A. Lascialfari, F. Borsa, M. Horvatic, A. Caneschi and D. Gatteschi, *Phys. Rev. Lett.*, 1999, **83**, 227.
41 A. Cornia, M. Affronte, A. G. M. Jansen, G. L. Abbati and D. Gatteschi, *Angew. Chem., Int. Ed.*, 1999, **38**, 2264.
42 F. Hartmann-Boutron, P. Politi and J. Villain, *Int. J. Mod. Phys. B*, 1996, **10**, 2577.
43 R. Morrish, Wiley, New York, 1966.
44 K. Wieghardt, K. Pohl, I. Jibril and G. Huttner, *Angew. Chem., Int. Ed. Engl.*, 1984, **23**, 77.
45 C. Delfs, D. Gatteschi, L. Pardi, R. Sessoli, K. Wieghardt and D. Hanke, *Inorg. Chem.*, 1993, **32**, 3099.
46 Y. Pontillon, A. Caneschi, D. Gatteschi, R. Sessoli, E. Ressouche, J. Schweizer and E. Lelievre-Berna, *J. Am. Chem. Soc.*, 1999, **121**, 5342.
47 R. Caciuffo, G. Amoretti, A. Murani, R. Sessoli, A. Caneschi and D. Gatteschi, *Phys. Rev. Lett.*, 1998, **81**, 4744.
48 I. Mirebeau, M. Hennion, H. Casalta, H. Andres, H. U. Gudel, A. V. Irodova and A. Caneschi, *Phys. Rev. Lett.*, 1999, **83**, 628.
49 J. R. Friedman, *Phys. Rev. B: Condens. Matter*, 1998, **57**, 10291.
50 C. Sangregorio, T. Ohm, C. Paulsen, R. Sessoli and D. Gatteschi, *Phys. Rev. Lett.*, 1997, **78**, 4645.
51 W. Wernsdorfer, T. Ohm, C. Sangregorio, R. Sessoli, D. Mailly and C. Paulsen, *Phys. Rev. Lett.*, 1999, **82**, 3903.
52 W. Wernsdorfer, A. Caneschi, D. Gatteschi, R. Sessoli, A. Villar and C. Paulsen, *Phys. Rev. Lett.*, in press.
53 W. Wernsdorfer and R. Sessoli, *Science*, 1999, **284**, 133.

On-chip catalysis using a lithographically fabricated glass microreactor—the dehydration of alcohols using sulfated zirconia

Natalie G. Wilson and Tom McCreedy*

Department of Chemistry, University of Hull, Hull, UK HU6 7RX. E-mail: T.McCreedy@chem.hull.ac.uk

Received (in Cambridge, UK) 2nd March 2000, Accepted 22nd March 2000
Published on the Web 13th April 2000

A heated microreactor has been fabricated for heterogeneous catalysis, employing channels microfabricated in glass using photolithography and wet chemical etching; the demonstration reaction is the dehydration of alcohols.

There remains growing interest in miniaturised systems for chemical analysis and synthesis. These chemical analysis devices are commonly referred to as micro total analytical systems (μTAS), and have been reported for a diverse range of applications. Hadd *et al.*[1] employed laser induced fluorescence detection to determine a number of acetycholinesterase inhibitors after electrophoretic separation on a glass chip. A polymeric microchip was employed for the analysis of PCR products of the hepatitis C virus,[2] again laser induced fluorescence detection was employed. Fibre optically linked spectrophotometric detection of analytes on chip provides a convenient detection method for on-chip measurements, including the determination of nitrite *via* the formation of an azo dye,[3] and orthophosphate *via* the molybdenum blue reaction.[4] The integration of microfabricated devices with mass spectrometry offers a potentially powerful analytical tool, for example in the rapid analysis of proteolytic digests.[5] While electrophoretic processes prove vital for separations on chip, electroosmotic flow offers a very convenient pumping mechanism for fluidic manipulation, such as for moving solutions through micromachined filters.[6]

However, while great interest exists in μTAS, the application of similar devices to synthetic applications is deriving much interest. One only has to look through the proceedings of recent conferences (such as IMRET 3, Frankfurt, April 1999) to see the potential applications of such devices. These include highly exothermic reactions, *e.g.* the direct fluorination of aromatic compounds, the *in situ* generation of hazardous compounds, *e.g.* phosgene, and rapid energy transfer systems, *e.g.* fuel pumps. However, one area of interest to us is on chip heterogeneous catalysis. This represents an important area in organic synthesis, and there are many potential applications for miniaturised synthetic reactors able to utilise small amounts of catalysts in conjunction with very limited reaction volumes. This latter feature permits very rapid mass transfer and control of reaction conditions. In addition, the potential to employ electroosmotic pumping with such devices represents a very attractive feature, permitting reagents to be pumped by a device with no moving parts. Within the Hull group, much extensive work is on-going in the area of microreactors employing catalyst mediation, but the work reported here is the first in a heated system. Miniaturised catalytic devices can be used to conveniently gain kinetic and thermodynamic data for reactions. They are also convenient for screening new reactions and catalysts. The screening can either be with respect to the catalyst, *i.e.* to determine which catalysts show activity, or with respect to the reaction, *i.e.* which reaction shows promise on a certain catalyst.

Here, we report the dehydration of hexanol to hexene, and ethanol to ethene (with some degree of cracking). The catalyst used was sulfated zirconia (zirconia treated with sulfuric acid). This catalyst is known as a super acid catalyst with well documented reactions including the conversion of methanol to hydrocarbons,[7] isobutane/but-1-ene alkylation,[8] and the methoxymethylation of alcohols.[9] It has also been reported for the dehydration of alcohols to the associated alkene, with the added advantage that the reaction conditions are significantly milder than those required for other acid catalysts, such as silica-alumina. In a previous paper,[10] a 1 mm diameter reactor was reported to offer conversion efficiencies of only 3% for the conversion of hexanol to hexene, however in this paper, conversion efficiencies approaching 100% are reported (compared to the industrial process that only gives *ca.* 30% conversion).

Sulfated zirconia (ZrO_2/SO_4^{2-}) catalyst (MEL Chemicals, Swinton, Manchester, UK) was first activated by heating to 600 °C for 1 h in a microwave furnace (CEM). The microreactor used with syringe pumping was constructed from two plates. The base plate was produced by photolithography and wet chemical etching. The mask was produced in house and used to transfer the pattern onto glass coated with chrome and photo resist layers (Alignrite, Bridgend, South Wales). After etching in 1% $HF{\cdot}NH_3$(aq) for 1 h at 70 °C, the remaining photo-resist and chrome was removed. The channel dimensions were 200 μm wide by 80 μm deep and 30 mm long (in a 'Z' shaped configuration). The top plate was prepared from Sylgard 184 (ISL, West Midlands, UK), a polydimethylsiloxane (PDMS) resin and cast in a mould containing inserts to form the reservoirs. After baking for 1 h at 100 °C, the resin was released from the mould and the inserts removed. The mating face was then coated with a thin layer of PDMS and activated catalyst dusted over the surface; it was then baked at 100 °C for 1 h. The effect of this step was to give a high surface area for the catalyst reactor, but with the catalyst firmly immobilised. When these two surfaces were clamped together, the effect was to produce a reactor with one wall of the channel being catalytically active. The *in situ* heater was fabricated from Nichrome wire (Ni90/Cr10) 0.25 mm o.d. (Goodfellows, Cambridge, UK) immobilised in the PDMS top plate. The heating wire was inserted into the mould near to the mating face before the liquid PDMS was poured into the mould. The PDMS was stable to heating up to 175 °C (this temperature was not exceeded so no data exists beyond this point). Heating was achieved by a potentiostat (0–270 V) and monitored *via* a digital thermometer (Jencons model 2003) with the temperature probe (RS components) located close to the reaction channel. Where electroosmotic flow was used as a pumping method, a 2 cm long tube (0.5 mm i.d.) was inserted into the base plate, butting up to the start of the reaction channel. On-chip electroosmotic pumping is at present unreliable owing to vapourisation of the ethanol on the heated chip, however, this limitation is being overcome with the aid of a heat sink.

The hexan-1-ol was obtained from Avocado Research Chemicals (Heysham, UK), while other alcohols were obtained from supplies bottled in-house. Alcohols were purged with nitrogen for 10 min prior to use in order to minimise coking in the reactor; a frequent problem at high temperatures when trace oxygen is present. Pumping was achieved using a syringe pump (Baby Bee, BAS) or an electroosmotic pump fabricated as previously reported.[10]

The effect of temperature on the dehydration of hexan-1-ol to hexene has been studied in prior work, and an optimum conversion occurred at a temperature of 155–160 °C. This was

DOI: 10.1039/b001705l

used in this work. Currently, no optimisation of the ethanol temperature has been undertaken.

Hexan-1-ol was pumped through the reactor chip at a flow rate of 3 μL min^{-1} and a reaction temperature of 155 °C. The products were collected and analysed by gas chromatography using a Porapak Q column at 220 °C. From the gas chromatogram, a hexan-1-ol to hexene conversion on average between 85 and 95% could be determined. No additional products were detected, and the reaction was specific to hexene. The conversion efficiency is favourable compared to that observed with large-scale reactors, where 30% is common. The reactor was used constantly over three working days, and no degradation of the performance was observed.

Ethanol has been pumped by both electroosmotic flow and by means of a syringe pump. Initially, ethanol was pumped through the chip at a flow rate of 3 μL min^{-1} using a syringe pump and a reaction temperature of 155 °C. The products were collected and analysed by gas chromatography using a Porapak Q column at 50 °C. Only trace amounts of ethanol were detected, with most of the feedstock converted to ethene (68%), ethane (16%), and methane (15%). The electroosmotic pump produced repeatable flow rates of 0.9–1.1 μL min^{-1} at a field strength of 200 V cm^{-1}, giving a significantly greater residence time for ethanol in the reactor. The effect of this could clearly be seen in the GC results obtained where the only detectable product was methane. This indicates that the reaction has gone beyond dehydration to complete cracking of the feedstock. Trace amounts of methanol were also detected.

In conclusion, open channel on-chip microreactors have been demonstrated for the dehydration of alcohols to the associated alkene. While excellent results have been obtained with mechanical pumping, electroosmotic pumping appears to offer a significant advantage over other types of pumping, namely a very slow flow rate resulting in long residence times in the reactor. This can lead to a significant decrease in the required path length for reaction. Electroosmotic flow has a disadvantage since many liquids, *e.g.* hexanol exhibit no flow under applied potential, indeed the volume flow rate is inversely proportional to carbon chain length. The obvious outcome of this will be the further miniaturisation of reactors, and the potential for *in situ* production of chemicals.

We express thanks to Mel Chemicals (Manchester) for the donation of the sulfated zirconia. N. G. W. was funded by the Department of Chemistry, University of Hull.

Notes and references

1 A. G. Hadd, S. C. Jacobson and J. M. Ramsey, *Anal. Chem.*, 1999, **71**, 5206.
2 Y. H. Chen, W. C. Wang, K. C. Young, T. T. Chang and S. H. Chen, *Clin. Chem.*, 1999, **45**, 1938.
3 G. M. Greenway, S. J. Haswell and P. H. Petsul, *Anal. Chim. Acta*, 1999, **387**, 1.
4 G. N. Doku and S. J. Haswell, *Anal. Chim. Acta*, 1999, **382**, 1.
5 J. Li, P. Thibault, N. H. Bings, C. D. Skinner, C. Wang, C. Colyer and J. Harrison, *Anal. Chem.*, 1999, **71**, 3036.
6 B. He, L. Tan and F. Regnier, *Anal. Chem.*, 1999, **71**, 1464.
7 M. Nitta, H. Sakoh and K. Aomura, *App. Catal.*, 1984, **10**, 215.
8 D. Das and D. K. Chakbrabarty, *Energy Fuels*, 1998, **12**, 109.
9 A. Sarkar, *Indian J. Chem., Sect. B*, 1996, **35**, 862.
10 P. D. Christensen, S. W. P. Johnson, T. McCreedy, V. Skelton and N. G. Wilson, *Anal. Commun.*, 1998, **35**, 341.

Synthesis and structural characterization of a volatile, intramolecularly coordinated monomeric homoleptic magnesium alkylamide

William S. Rees Jr.,* Henry A. Luten and Oliver Just

School of Chemistry and Biochemistry and School of Materials Science and Engineering and Molecular Design Institute, Georgia Institute of Technology, Atlanta, GA 30332-0400, USA. E-mail: will.rees@chemistry.gatech.edu

Received (in Columbia, MO, USA) 2nd December 1999, Accepted 16th December 1999

The design, synthesis and X-ray crystal structure of the first intramolecularly coordinated homoleptic, monomeric and highly volatile magnesium alkylamide example, $Mg\{N[Si(CH_3)_3](CH_2)_3N(CH_3)_2\}_2$, are described.

The majority of structurally characterized magnesium–amide complexes, monomeric[1] or dimeric,[2] contain three- or four-coordinate metal centers, with a few compounds reported containing two-[3] or six-coordinate[4] magnesium. Numerous examples exist with intermolecular Lewis-base complexation, however, an intramolecular coordination motif for the central atom is uncommon for magnesium amides. Monomeric magnesium complexes possessing bidentate monoanionic ligands also are rather rare. In an ongoing effort to design and synthesize precursors for electronic materials, we have focused on developing highly volatile, thermally robust, ambient atmosphere stable, coordinatively saturated, oxygen-free magnesium alkylamide compounds as potential dopant sources for the CVD of GaN:Mg.[5] The synthesis and structural examination of the first intramolecularly coordinated monomeric magnesium alkylamide, which concomitantly possesses both substantial volatility and vapor phase integrity, are described herein.[6]

Magnesium bis[(γ-dimethylaminopropyl)trimethylsilylamide] **1**,† was prepared by reaction of the new secondary amine, γ-dimethylaminopropyl(trimethylsilyl)amine **2**‡ with dibutyl magnesium in hexane. This white solid has a high vapor pressure (intact sublimation at 80 °C and 10^{-2} Torr),[7] substantial vapor phase stability, and has been demonstrated, by TGA to have exceptionally clean transport characteristics (Fig. 1). The rather unusual combination of heightened vapor phase robustness and mild vaporization conditions are, to our knowledge, unique among magnesium compounds.

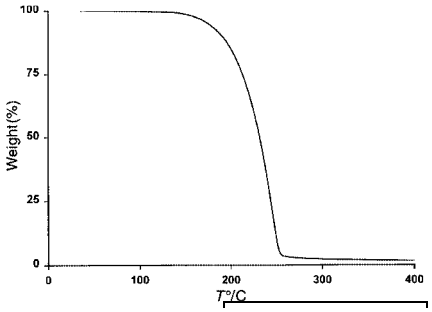

Fig. 1 Thermogravimetric analysis of $Mg\{N[Si(CH_3)_3](CH_2)_3N(CH_3)_2\}_2$, heating rate 10 °C min^{-1}, 1 atmosphere Ar.

A single crystal of suitable quality, obtained from a hexane solution at −80 °C, was mounted on a diffractometer under a cooled argon stream. The solid state structure of **1**, determined by X-ray diffraction,§ contains two crystallographically independent molecules in the asymmetric unit. Compound **1** is monomeric, has a four-coordinate distorted tetrahedral magnesium center, composed of four nitrogen atoms, two of which form covalent metal–amide interactions (ORTEP plot: Fig. 2). Nitrogen atoms bearing three fully saturated aliphatic groups and available lone pairs intramolecularly coordinate with the magnesium center, occupying the remaining two coordination sites.[8] The N1–Mg1–N3 (N5–Mg2–N7) interatomic angles of 137.57° (136.01°) are considerably wider than analogous angles present in di-solvated, four-coordinate, monomeric magnesium bis(amide) species $Mg\{N[Si(CH_3)_3]_2\}_2(THF)_2$[1a] (127.9°), $Mg\{N[Si(CH_3)_3]_2\}_2((2,3,5\text{-collidine})_2$[1c] (120.9) and $Mg\{N[Si(CH_3)_3]_2\}_2(4\text{-picoline})_2$[1c] (125.5). A similar trend is observed for the N2–Mg1–N4 and N6–Mg2–N8 angles (109.71 and 109.07°), which are substantially larger than the corresponding angles for the O(N)–Mg–O(N) donor interactions present in the compounds mentioned above: 89.9,[1a] 87.9[1c] and 86.8°.[1c] This may be explained by the diminished steric constraints imposed on the overall geometry of the complex by the newly designed, flexible, intramolecularly coordinated γ-dimethylaminopropyl(trimethylsilyl)amine ligand. A comparably disordered tetrahedral environment around the central metal atom (covalent N–Mg–N angles of 135.1 and 138.7°; dative N→Mg←N angles of 116.8 and 117.8°) also is encountered for the intramolecularly coordinated complex $Mg[N(8\text{-quinolyl})(SiMe_3)]_2$,[1d] which contains the rigid aromatic quinolyl ligand.

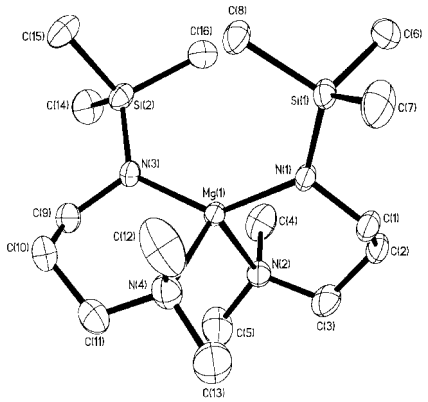

Fig. 2 ORTEP Representation of $Mg\{N[Si(CH_3)_3](CH_2)_3N(CH_3)_2\}_2$ with 30% probability thermal ellipsoids, and all hydrogen atoms omitted for clarity in viewing. Selected interatomic distances (Å) and angles (°) for compound **1**: Mg1–N1 1.988(2), Mg1–N2 2.190(2), Mg1–N3 1.982(2), Mg1–N4 2.185(2); N1–Mg1–N2 97.20(8), N1–Mg1–N3 137.57(9), N2–Mg1–N4 109.71(10), N3–Mg1–N4 98.19(9), Mg1–N1–Cl 116.64(15), Mg1–N2–C3 114.31(17), Mg1–N3–C9 117.52(16), Mg1–N4–C11 113.23(18).

The interatomic angles present within the rings formed as a consequence of N:→Mg intramolecular coordination for **1** (114.3–115.4°), well within standard data,[9] are evidence of lack of significant molecular strain, imposed as a consequence of ring formation. The N3–Mg–N4 plane forms an angle of 80.08(8)° with the Ni–Mg–N2 plane (80.71° for N5–Mg2–N6 and N7–Mg2–N8), thereby lending **1** a pseudo spiro geometry.

The magnesium–nitrogen interatomic distances found for **1** can be placed into two categories. Dative bond distances, resulting from interactions between tertiary nitrogen atoms and Lewis-acid sites on Mg^{2+}, Mg1–N2 and Mg1–N4 (Mg2–N6 and

DOI: 10.1039/a909746e

Mg2–N8) 2.190(2) and 2.185(2) Å [2.188(2) and 2.198(2) Å] agree well with previously reported values ranging between 2.096 and 2.259 Å.[1,2] The metal–amide distances Mg1–N1 and Mg1–N3 (Mg2–N5 and Mg2–N7) of 1.988(2) and 1.982(2) Å [1.977(2) and 1.983(2) Å] represent relatively short interactions, compared with corresponding data for other magnesium–amide compositions, which fall into the range of 1.959–2.188 Å.[1,2] In the present structure, no significant perturbation is evidenced in either type of Mg–N interaction for **1**, as compared with earlier work involving non-intramolecularly coordinating ligands, be they anionic or neutral in character. It is suggested that, to a great degree, the observed combination of high vapor pressure and high vapor phase molecular integrity for **1** has its origin in these structural details. The design of an appropriate (*i.e.* flexible arm on a saturated alkyl tether) pendant amine to intramolecularly coordinate the metal center fulfills its requirements as manifested by the 'normalcy' of the metrical and geometrical data measured for **2**. As clearly demonstrated in the TGA (Fig. 1), **2** is quite volatile, even at 1 atm. Unlike simple organic compounds, where vapor pressure, to a first order, inversely follows molecular weight, organometallic compounds show not only simple van der Waals interactions in the condensed state. The dominant intermolecular forces for organometallic compounds in the condensed state are dipole–dipole interactions. Thus, the unusually high vapor pressure exhibited by **2** would seem to indicate that it might have a relatively small dipole moment. In related work, we have shown recently that such trends serve some predictive role for zinc bis(amide) compounds.

One interesting feature of **1** emerges upon examination of the ^{1}H and ^{13}C solution state NMR data. The methyl groups represented by C4, C5, C12 and C13 are magnetically inequivalent in this environment. This is understood best by examination of the plane represented by N3–Mg–N4 (or N1–Mg–N2), and noting that C12 resides on the side of the plane containing N2, while C13 resides on the N1-containing side. This is evidenced by a ^{1}H NMR chemical shift difference of 0.44 ppm for the methyl groups, and a 2.0 ppm ^{13}C NMR chemical shift difference. As expected, the ambient temperature solution dynamic structure portrays a single environment for the TMS methyl groups; however, ^{1}H inequivalence also is exhibited at C3 and C11 (difference of 0.38 ppm) and C1 and C9 (difference of 0.29 ppm), while C2 and C10 experience equivalence under these conditions. Apparently, ring flip motion equilibrates the later, while the methylene positions α to each nitrogen, both amide and amine, bear the influence of asymmetry. This may be compared with an extremely recent example of a Mg bis(1-azaalkyl) compound, which has a rigid chair skeletal conformation in the solid state, yet has solution NMR data reported which indicate dynamic behavior at ambient spectrometer conditions on the observational time scale.[10]

In summary, the first example of intramolecular coordination for a monomeric magnesium alkylamide has been designed, prepared and structurally characterized.[12] The two nearly perpendicular rings, exhibiting negligible strain, as evidenced by typical interatomic angles, are formed by the simultaneous occurrence of both tertiary amine donation at the end of a flexible alkyl tether and ionic amide attachment to the metal center. Compound **1**, highly stable in the vapor phase and portraying substantial vapor pressure, differs from earlier intermolecular adducts,[2d] which can irreversibly dissociate free Lewis base, penultimately producing lower coordinate transients that subsequently oligomerize into low vapor pressure species.[12]

We gratefully acknowledge the ONR for financial support. W. S. R. was awarded an Alexander von Humboldt Fellowship with Prof. H. Schumann at the TU Berlin in 1998–1999.

Notes and references

† *Selected data* for **1**: sublimation conditions: 80 °C/10^{-2} Torr, mp = 106 °C; ^{1}H NMR [400 MHz, C_6D_6, 25 °C] δ 3.41 (m, 2 H, C$H_{2(a)}$N(CH$_3$)$_2$), 3.03 (m, 2 H, C$H_{2(b)}$N(CH$_3$)$_2$), 2.15 (s, 6 H, N(C$H_{3(a)}$)$_2$), 2.05 (m, 4 H, NCH$_2$CH_2CH$_2$), 1.71 (m, 6 H, N(C$H_{3(b)}$)$_2$), 1.57 (m, 2 H, NC$H_{2(a)}$), 1.28 (m, 2 H, NC$H_{2(b)}$), 0.49 (s, 9 H, Si(CH_3)$_3$); ^{13}C NMR [75.43 MHz, C_6D_6, 25 °C] δ 62.91 (s, *C*H$_2$NMe$_2$), 49.11 (s, N*C*H$_2$), 47.78 (s, N(*C*H$_{3(a)}$)$_2$), 45.82 (s, N(*C*H$_{3(b)}$)$_2$), 32.70 (s, NCH$_2$*C*H$_2$), 2.37 (s, Si(*C*H$_3$); ^{29}Si NMR [59.59 MHz, C_6D_6, 25 °C] δ −5.87 (s, *Si*(CH$_3$)$_3$). Anal calc. for **1**: C, 51.79; H, 11.41; N, 15.10. Found: C, 51.74; H, 11.14; N, 15.89. MS [EI, 70 eV, 188 °C] 370 [M$^+$], 355 [M$^+$ − CH$_3$], 197 [M$^+$ − Me$_2$N(CH$_2$)$_3$NSi(CH$_3$)$_3$].

‡ *Selected data* for **2**: bp = 177 °C (determined by DSC); ^{1}H NMR [400 MHz, C_6D_6, 25 °C] δ 2.72 (d/tr, 2H, HNCH_2CH$_2$), 2.24 (tr, 2H, CH$_2$CH_2N(CH$_3$)$_2$), 2.20 (s, 6H, N(CH_3)$_2$), 1.54 (m, 4H, HNCH$_2$CH_2CH$_2$), 0.34 (br s, *H*N), 0.02 (s, 9H, Si(CH_3)$_3$); ^{13}C NMR [75.43 MHz, C_6D_6, 25 °C] δ 57.45 (s, *C*H$_2$N(CH$_3$)$_2$), 45.40 (s, N(*C*H$_3$)$_2$), 40.00 (s, N*C*H$_2$), 32.66 (s, NCH$_2$*C*H$_2$), 0.20 (s, Si(*C*H$_3$)$_3$); ^{29}Si NMR [59.59 MHz, C_6D_6, 25 °C] δ 2.10 (s, *Si*(CH$_3$)$_3$); ^{14}N NMR [21.61 MHz, C_6D_6, 25 °C] δ − 316 (s, *N*(CH$_3$)$_2$), −353 (s, *N*Si(CH$_3$)$_3$). Anal. calc. for **1**: C, 55.10; H, 12.72. Found: C, 55.16; H, 12.63. MS [EI, 70 eV] 174 [M$^+$], 159 [M$^+$ − CH$_3$], 85, 73, 58.

§ *Crystal data* for **1**: $Mg_1N_4C_{16}H_{42}$, M_r = 371.03, crystal dimensions 0.850 × 0.238 × 0.102 mm, triclinic, space group $P\bar{1}$, a = 10.327(2), b = 15.066(3), c = 16.698(4) Å, α = 110.738(4), β = 92.948(4), γ = 92.182(4)°; V = 2422.1(9) Å^3, Z = 4, D_c = 1.017 g cm^{-3}, Siemens SMART CCD diffractometer, 1.31 < θ < 25.00°, MoKα radiation (λ = 0.71073 Å), ω scans, F(000) = 824, μ = 0.177 mm^{-1}, T = 173(2) K; of 18267 measured reflections, 8489 were independent and 5688 observed with $I > 2\sigma(I)$, −12 < h < 12, −17 < k < 17, −19 < l < 19; R = 0.0443, wR = 0.1111, GOF = 1.021 for 467 parameters, $\Delta\rho_{max}$ = 0.492 e Å^{-3}. The structure was solved by direct methods (SHELXS-97) and refined by full-matrix least-squares procedures (SHELXL-97). The hydrogen atoms coordinates were calculated in SHELXL using an appropriate riding model with varied thermal parameters. CCDC 182/1577. See http://www.rsc.org/suppdata/cc/a9/a909746e/ for crystallographic files in .cif format.

1 (*a*) D. C. Bradley, M. B. Hursthouse, A. A. Ibrahim, K. M. Abdul Malik, M. Motevalli, R. Möseler, H. Powell, J. D. Runnacles and A. C. Sullivan, *Polyhedron*, 1990, **9**, 2959; (*b*) W. S. Rees, Jr., J. S. Matthews and O. Just, unpublished results; (*c*) J. L. Sebestl, T. T. Nadasdi, M. J. Heeg and C. H. Winter, *Inorg. Chem.*, 1998, **37**, 1289; (*d*) L. M. Engelhardt, P. C. Junk, W. C. Patalinghug, R. E. Sue, C. L. Raston, B. W. Skelton and A. H. White, *J. Chem. Soc., Chem. Commun.*, 1991, 930.

2 (*a*) B. Goldfuss, P. v. R. Schleyer, S. Handschuh, F. Hampel and W. Bauer, *Organometallics*, 1997, **16**, 5999; (*b*) V. R. Magnusson and G. D. Stucky, *Inorg. Chem.*, 1969, **8**, 1427; (*c*) M. Westerhausen and W. Schwarz, *Z. Anorg. Allg. Chem.*, 1992, **609**, 39; (*d*) D. Pfeiffer, M. J. Heeg and C. Winter, *Angew. Chem., Int. Ed.*, 1998, **37**, 2517; (*e*) A. W. Duff, P. B. Hitchock, M. F. Lappert, R. G. Taylor and J. A. Segal, *J. Organomet. Chem.*, 1985, **293**, 271; (*f*) M. Veith, W. Frank, F. Töllner and H. Lange, *J. Organomet. Chem.*, 1987, **326**, 315; (*g*) K. W. Henderson, R. E. Mulvey, W. Clegg and P. A. O'Neill, *J. Organomet. Chem.*, 1992, **439**, 237; (*h*) K. W. Henderson, R. E. Mulvey, W. Clegg and P. A. O'Neill, *Polyhedron*, 1993, **12**, 2535.

3 R. A. Bartlett, M. M. Olmstead and P. P. Power, *Inorg. Chem.*, 1994, **33**, 4800.

4 (*a*) T. E. Glassman, A. H. Liu and R. R. Schrock, *Inorg. Chem.*, 1991, **30**, 4723; (*b*) W. S. Rees, Jr., J. S. Matthews and O. Just, *Chem. Vap. Deposition*, in press.

5 (*a*) W. S. Rees, Jr. and A. Barron, *Adv. Mater. Opt. Electron.*, 1993, **2**, 271; (*b*) W. S. Rees, in *CVD of Nonmetals*, VCH New York, 1996.

6 The use of the nomenclature magnesium(alkylamide) is standard to differentiate the organic substituent present on the amide. For an example of a magnesium(arylamide) see ref. 1(*d*).

7 Compounds with intermolecular coordination have been reported recently; however, little data related to vapor phase stability was provided.

8 To our knowledge, the only other reported example of a structurally characterized intramolecular coordination in a magnesium amide involved the aromatic amine quinoline.

9 F. A. Cotton and G. Wilkinson, *Advanced Inorganic Chemistry*, Wiley, 5th edn., 1988, p. 144.

10 C. F. Caro, P. B. Hitchcock and M. F. Lappert, *Chem. Commun.*, 1999, 1433.

11 It is noted that an intramolecular agostic Si-H interaction recently has been observed for a dimeric species [see ref. 2(*a*)].

12 W. S. Rees, Jr., M. W. Carris and W. Hesse, *Inorg. Chem.*, 1991, **30**, 4479.

Polymerisation of 1-iodohexa-1,3,5-triyne and hexa-1,3,5-triyne: a new synthesis of carbon nanotubes at low temperatures

Jaromír Hlavatý,*[a] Ladislav Kavan,[a] Naoto Kasahara[b] and Asao Oya[b]

[a] *J. Heyrovský Institute of Physical Chemistry, Dolejškova 3, CZ 182 13 Prague 8, Czech Republic. E-mail: hlavaty@jh-inst.cas.cz*

[b] *Faculty of Engineering, Gunma University, Kiryu, Gunma 376-8515, Japan*

Received (in Oxford, UK) 31st January 2000, Accepted 15th March 2000
Published on the Web 13th April 2000

1-Iodohexa-1,3,5-triyne (I) and hexa-1,3,5-triyne (II) spontaneously polymerise in aprotic solution to form a solid carbonaceous product which contains polyyne-like structures and multi-walled carbon nanotubes with outer diameter *ca.* 10–20 nm and length 100–200 nm.

Carbon nanotubes are conventionally produced by high-temperature (T > 1000 °C) catalytic processes. Nanotubes and fullerenes can also be prepared, albeit in low yield, at room temperature by chemical defluorination of perfluorocyclopentene, perfluorodecalin and perfluoronaphthalene.[1] Kawase *et al*.[2] have shown that a totally defluorinated poly(tetrafluoroethylene) (PTFE) can be partly transformed into carbon nanotubes (10–50 nm diameter, 1 μm length) by irradiation with fast electrons (100 kV; 103 C cm^{-2}) at 800 °C. The process assumes the presence of reactive polyyne, which is formed by electrochemical reductive defluorination of PTFE,[2] Scheme 1.

$$(-CF_2CF_2-)_n \xrightarrow[-4n\ F^-]{4n\ e^-} (-C{\equiv}C-)_n \xrightarrow{800\ °C,\ e^-} \text{C-nanotubes}$$

Scheme 1

However, the polyyne, $(-C{\equiv}C-)_n$ hardly exists in the pure state.[3] The actual precursor of nanotubes in Scheme 1 is, probably, a disordered graphitic carbon containing some chemically bound oligoyne segments with conjugation lengths less than 16 C-atoms.[3,4] If the electron/heat treatment in Scheme 1 was omitted, no nanotubes grew.[2] Also, no defined carbonaceous nanoclusters were found in PTFE defluorinated by alkali metal amalgams.[1]

To avoid the poorly defined precursor in Scheme 1, we have explored whether carbonaceous nanoparticles can be synthesised as in Scheme 1, but from chemically defined low-molecular-weight oligoynes. The reactants of choice seem to be hexatriyne derivatives: butadiyne is almost inert against chemical carbonization,[5] but higher homologues are too reactive to be handled safely.

Hexa-1,3,5-triyne (**II**), was prepared from prop-2-ynylol.[6] 1-Iodohexa-1,3,5-triyne (**I**) was synthesised from hexa-1,3,5-triyne according to a procedure developed by ourselves[5] Briefly, **II** was monolithiated by a stoichiometric amount of MeLi in THF at −30 to −40 °C, and Li was subsequently substituted with iodine.[5,7] Both precursors **I** and **II** are ultimately stable only in solution at low temperatures.

'Poly(iodohexatriyne)' was prepared as follows: a freshly made 0.3–0.4 M solution of **I** in *n*-hexane–diethyl ether (*ca.* 1 : 1 *v/v*; water concentration < 50 ppm; stored under Ar) was vacuum evaporated at room temperature over several minutes, while an insoluble, explosive, brown solid remained. Its composition was not too far from that of the precursor. (Elemental analysis: C 39.65, H 1.23, I 57.20%. Calc. for C_6HI: C 36.04, H 0.50, I 63.46%). The solid was, presumably, produced as a result of radical polymerisation of **I**, which progressed according to a *brutto* scheme (Scheme 2) A more stable, non-explosive material was prepared by slow polymerisation of **I**. This occurred simply after storing the solution

$$n\ IC{\equiv}C-C{\equiv}C-C{\equiv}CH \longrightarrow {=}(IC-C{\equiv}C-C{\equiv}C-CH)_n{=} \Longleftrightarrow -(IC{=}C{=}C{=}C{=}C{=}CH)_n-$$

Scheme 2

under Ar for 1–2 d at room temperature. During this time, a dark brown powder precipitated, and a brown-yellow film deposited on the walls of the reaction vessel. When the reaction progressed, the film tended to peel off and roll into fine tubes. The addition of a small amount of *n*-undecane to the solution impeded the film formation and the product was mostly powder. On the contrary, the film formation was promoted by the addition of THF or ethyl acetate. The product was isolated by filtration, washed with hexane and diethyl ether, dried in vacuum at room temperature and stored under Ar. Elemental analysis evidenced some carbonisation, as the iodine content decreased: C 53.50, H 1.17, I 45.20%. [The difference from 100% mostly corresponds to adsorbed Ar (*vide infra*)]. The loss of iodine was further promoted by illumination with UV light (100 W high-pressure Hg lamp). The photo-assisted polymerisation–carbonisation of **I** gave a product containing: C 57.27, H 1.55, I 38.90%. Infrared spectra of 'poly(iodohexatriyne)' (both powder and film) exhibited comparable features with a characteristic intense band of conjugated sp-bonded carbon atoms (polyyne-like) between 2184–2194 cm^{-1}.

The polymerisation of hexatriyne **II** in *n*-undecane or *n*-hexane (water concentration < 50 ppm) was considerably faster compared to that of iodohexatriyne. It occurred within *ca.* 1 h at room temperature or within 1 d at 0 °C. The reaction accelerated with temperature (from 0–60 °C) and the concentration of **II** (up to 0.8 M). The addition of THF, diethyl ether or benzene promoted the formation of a yellow-brown film at the walls of the reaction vessel. Methanol, on the other hand, blocked any precipitation, and only soluble products were formed. Elemental analysis of a solid 'poly(hexatriyne)' gave: C 88.21, H 3.37%. The sample reversibly lost about 10% of its weight at 250 °C in vacuum, but this was almost completely re-captured if the outgased sample was exposed to Ar (weight increase 9.2%). This roughly accounts for the difference of analytical data from 100%, if we assume that Ar adsorbs from the sample's environment (calculated for C_6H_2: C 97.28, H 2.72%). The 'poly(hexatriyne)' exhibited two IR bands at 2110 and 2188 cm^{-1}, whose intensity was much smaller compared to those of 'poly(iodohexatriyne)'.

A pure 'one-dimensional' polymerisation (Scheme 2) seems to take place only after a fast rise of the concentration of **I**. Slow reactions in the solution are dominated be 'two-dimensional' polymerisation, which occurs *via* cross-linking of oligoyne sections in the precursor and/or in the primary chain-like polymer (*cf.* Scheme 2). The cross-linking of hexatriyne to yield graphene segments is shown in Scheme 3, where R = I, H. There are numerous theoretical[8] and experimental[3] arguments that the two-dimensional polymerisation (Scheme 3) is highly favoured, while it may produce extended graphite-like structures. The graphitisation (Scheme 3) seems to also provide a driving force for the partial splitting off of iodine and hydrogen

DOI: 10.1039/b000895h

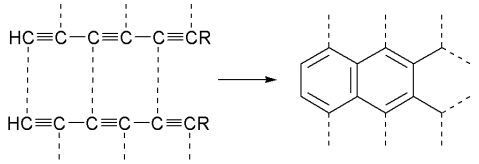

Scheme 3

from the precursor. However, the mechanism of propagation of the extended graphene is unknown.

The presence of iodine in the precursor **I** retards the polymerisation–carbonisation and stabilises the chain-like structure (Scheme 2). Hence, hexatriyne **II** exhibits a larger tendency towards the two-dimensional polymerisation (Scheme 3). Analogously, iodobutadiyne and 1,4-diiodobutadiyne[5] are inert in *n*-hexane (they polymerise only after UV excitation).[5] Butadiyne in *n*-hexane exhibited a very slow spontaneous polymerisation at room temperature in the dark, yielding solely a thin film at the walls, but the film showed a strong IR band at 2246 cm^{-1}. These results match the general conclusion that the stability of sp-bonded all-carbon chains against cross-linking increases when the chains contain bulky substituents at defect sites.[3]

Transmission electron microscopy (TEM) of both 'poly(iodohexatriyne)' and 'poly(hexatriyne)' revealed a presence of multi-walled carbon nanotubes (Fig. 1). The nanotubes were found in all the studied samples except 'poly(hexatriyne)' generated at temperatures ⩾40 °C. (At higher temperatures, the hexatriyne conversion to planar graphene (graphite) seems to prevail). The highest content of nanotubes was found in 'poly(hexatriyne)' polymerised at 0 °C. The nanotubes were not spread statistically in the sample: they formed agglomerates (as in Fig. 1) embedded in a material with an amorphous shape. Hence, the yield of nanotubes cannot be precisely determined. By comparison with many TEM pictures, we estimate the yield of nanotubes to be roughly 1% in good samples. Some products showed also a casual occurrence of spherical onion-like nanoparticles (*cf.* Fig. 1). The nanotubes in 'poly(hexatriyne)' and 'poly(iodohexatriyne)' resemble those generated by reductive defluorination of perfluorocyclopentene.[1] Typically, the nanotubes, are straight, multi-walled, with diameter 10–20 nm and length 100–200 nm, and they are capped by onion-like hemispheres. The presence of curved moieties (onions, nanotube-caps) requires that some five-membered carbon rings are also formed *via* the interchain reaction (Scheme 3). However, the mechanism of pentagon-formation is again unclear. Our nanotubes (grown at low temperature both from hexatriyne and fluorocarbons[1]) are narrower and shorter than those grown from ex-PTFE 'polyyne' by electron bombardment at 800 °C.[2]

Raman spectra of the nanotube-rich 'poly(hexatriyne)' displayed only two broad bands at 1350 and 1600 cm^{-1}, which can be assigned to polycrystalline graphite and/or multi-walled carbon nanotubes. (These two structures are difficult to distinguish by Raman spectroscopy). If we assign the Raman bands at 1350 and 1600 cm^{-1} to the graphite D and G lines, respectively,[4] their intensity ratio (0.43) allows the size of graphite crystals to be estimated at about 10 nm. (Similar-size graphite nanocrystals result also from cross-linking of PTFE-borne 'polyyne'.[3,4]) In accord with TEM, no single-walled carbon nanotubes were detectable in the region of the radial breathing mode (*ca.* 200 cm^{-1}).

In conclusion, hexatriyne derivatives show a pronounced tendency towards conversion into disordered graphene-like nanostructures, *viz* multi-walled carbon nanotubes. The production of nanotubes from hexatriyne seems to be more facile and more efficient, compared to the processes based on defluorination of octafluorocyclopentene and similar precursors.[1] Further effort should concentrate on the understanding and optimisation of the chemical synthesis of nanotubes. This knowledge might also help us to understand the mechanism of production of carbon nanotubes in the common high-temperature catalytic processes.

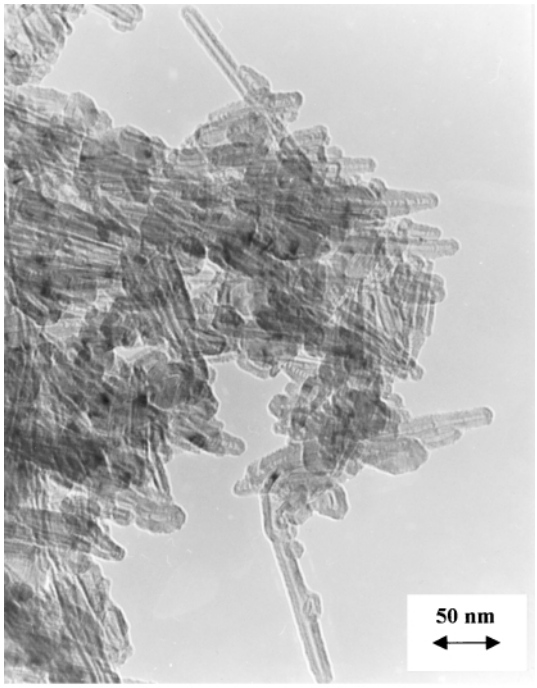

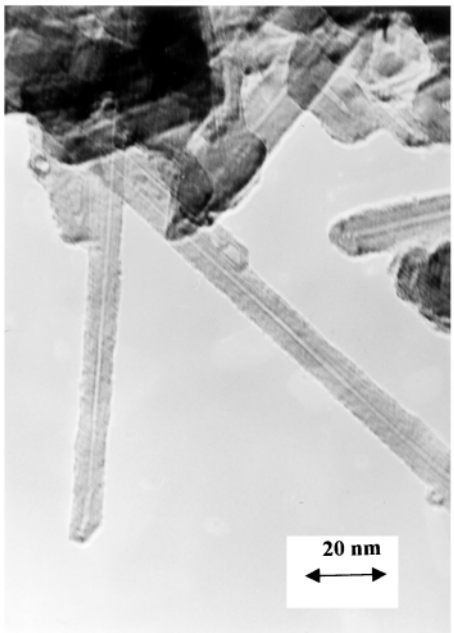

Fig. 1 Transmission electron microscopy of carbonaceous material prepared by spontaneous polymerization of hexatriyne at 0 °C.

This work was supported by The Grant Agency of the Czech Republic (contracts Nos. 203/98/1168 and 203/98/1181) and by the Ministry of Education of the Czech Republic (Czech-Japanese cooperation project No. ME164).

Notes and references

1 L. Kavan and J. Hlavatý, *Carbon*, 1999, **37**, 1863.
2 N. Kawase, A. Yasuda, T. Matsui, C. Yamaguchi and H. Matsui, *Carbon*, 1999, **37**, 522.
3 L. Kavan, *Chem. Rev.*, 1997, **97**, 3061.
4 L. Kavan, F. P. Dousek, P. Janda and J. Weber, *Chem. Mater.*, 1999, **11**, 329.
5 J. Hlavatý, J. Rathouský, A. Zukal and L. Kavan, *Carbon*, in press.
6 L. Brandsma and H. D. Verkruijsse, *Preparative Polar Organic Chemistry*, Springer Verlag, 1987, vol. I.
7 GC-MS, *m/z* (intensity): 201(6), 200 (M^+ 100), 128 (25), 100 (5.5), 74 (10), 73 (53), 72 (12), 37 (25), 36 (8). FTIR (*n*-hexane–diethyl ether): υ 625 (m), 2125 (w), 2150 (w), 2190 (w), 3211 (m), 3207 (m) cm^{-1}. UV–VIS λ (toluene): 287, 304, 322, 344 and 392 nm.
8 M. Springborg and L. Kavan, *Chem. Phys.*, 1992, **168**, 249.

Mesoscopic string structures of thiacyanine J aggregates in solution

Hiroshi Yao,*† Mayumi Omizo and Noboru Kitamura

Division of Chemistry, Graduate School of Science, Hokkaido University, Nishi 8, Kita 10, Kita-ku, Sapporo 060-0810, Japan

Received (in Cambridge, UK) 19th January 2000, Accepted 28th March 2000
Published on the Web 13th April 2000

Mesoscopic string structures of single 5,5′-dichloro-3,3′-disulfopropyl thiacyanine J aggregates produced in an aqueous solution were observed directly by both fluorescence microscopy and microspectroscopy.

J aggregates are specific organic dye assemblies discovered by Jelley and Scheibe,[1,2] and characterized by a narrow and intense absorption band that shows a bathochromic shift compared to the relevant monomer band.[3] On the basis of such optical characteristics, the aggregates have been often used as spectral sensitizers in photography.[4] Recent interest has also focused on the ability of J aggregates to exhibit coherent excitation phenomena which provide large optical nonlinearities.[5,6] Since the aggregate structure reflects highly on its spectroscopic properties such as the spectral line shape and peak energy, detailed investigations of the structures and/or morphologies of *single* aggregates are of primary importance. Previous studies demonstrated that a pseudoisocyanine (PIC) dye produces J aggregates at a mica/solution interface, and the single aggregate has a three-dimensional disk-like island structure in the mesoscopic size range as elucidated by tapping mode AFM (atomic force microscopy) in solution.[7,8] On the other hand, although structural and/or morphological differences are expected between the J aggregates at a solid/liquid interface and those produced in bulk solution,[9] details have been poorly understood since a real structure of the aggregates in solution have not been observed *in situ*. In this study, we report a direct observation of single thiacyanine J aggregates in an aqueous solution by both fluorescence microscopy and microspectroscopy.

Sample solutions were prepared by dissolving a 5,5′-dichloro-3,3′-disulfopropyl thiacyanine sodium salt [abbreviated as TC; chemical structure shown in the inset of Fig. 1; Nippon Kankoh-Shikiso Kenkyusho (99%)] in an aqueous NaCl (5.0 mM) solution under moderate heating (< 60 °C). Fluorescence microscope images were obtained by using a CCD camera (Hitachi, Remote Eye) set on an optical microscope (Nikon, Optiphoto-2). Fluorescence spectroscopy under the microscope was conducted by using a polychromator–multichannel photodetector set (Hamamatsu Photonics, PMA-11) equipped on the microscope.[10] An Xe beam (Hamamatsu Photonics, L2273) passed through an interference filter (KL-45, Toshiba Glass) or an Ar^+ laser beam (Coherent, Innova 70) at 454.5 nm were used as the excitation sources for fluorescence imaging and spectroscopy, respectively. A sharp-cut filter (Y-47, Toshiba Glass) was mounted in front of the CCD camera–photodetector set to eliminate scattering light of the excitation beam. Measurements were performed at room temperature.

Fig. 1 shows the absorption and fluorescence spectra of TC in aqueous NaCl solutions at different concentrations ([TC] = 0.2, 0.1, 0.05 and 0.03 mM) with a set optical path length of 300 μm. When the concentration of TC is > 0.05 mM, the absorption spectrum [Fig. 1(a)] showed a sharp and intense J band at *ca.* 464 nm in addition to the monomer (430 nm) and dimer bands (408 nm). The peak position and line width of the J band was constant under these concentrations, indicating that the internal structure of the J aggregate was unchanged. The fluorescence spectrum [Fig. 1(b)] does not show a Stokes shift, which is characteristic of J aggregates.[11]

In concentrated solutions, distinctive opalescence was observed. Therefore, fluorescence microscopy was conducted to examine the microstructures of the TC J aggregates. Fig. 2 shows fluorescence microscope images at [TC] $\geqslant$ 0.05 mM, above which the J band appears and mesoscopic string structures were clearly observed. Since a characteristic fluorescence image was not detected below 0.05 mM, the strings distributed in solution were considered to be J aggregates of TC. To the best of our knowledge, this is the first observation of mesoscopic J aggregates in a solution phase. The length of the string was several tens of μm while the width was very narrow; sub- or a few μm. This string structure of the J aggregate is probably due to anisotropic interactions between TC molecules in solution (*i.e.* quasi-one-dimensional stacking interactions), different from that of PIC J aggregates observed at a solid/liquid interface.[7,8] A single string is likely to bend in an arc form, suggesting that the mesoscopic J aggregate is flexible and polycrystalline-like. The fluorescence images also show that morphologies of the aggregates were dependent on the TC concentration. With a decrease in the concentration, the density of the string decreased while the length of the aggregate was slightly increased. The results are probably due to lower supersaturation at a low concentration which leads to generation of fewer nuclei, and the string would grow to a larger size; *cf.* microcrystallite formation processes. It is worth noting, furthermore, tha single J aggregates could be optically trapped by

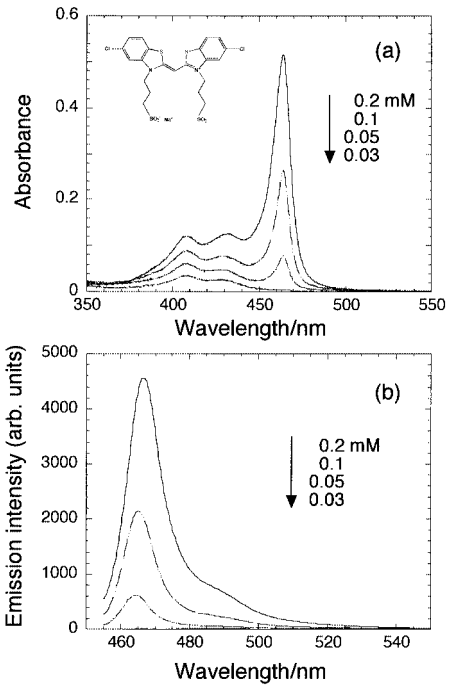

Fig. 1 Absorption (a) and fluorescence (b) spectra of TC in an aqueous NaCl solution ([NaCl] = 5 mM): optical path length = 300 μm.

† Present address: Department of Material Science, Faculty of Science, Himeji Institute of Technology, 3-2-1 Koto, Kamigori-cho, Ako-gun, Hyogo 678-1297, Japan. E-mail: yao@sci.himeji-tech.ac.jp

DOI: 10.1039/b000548g

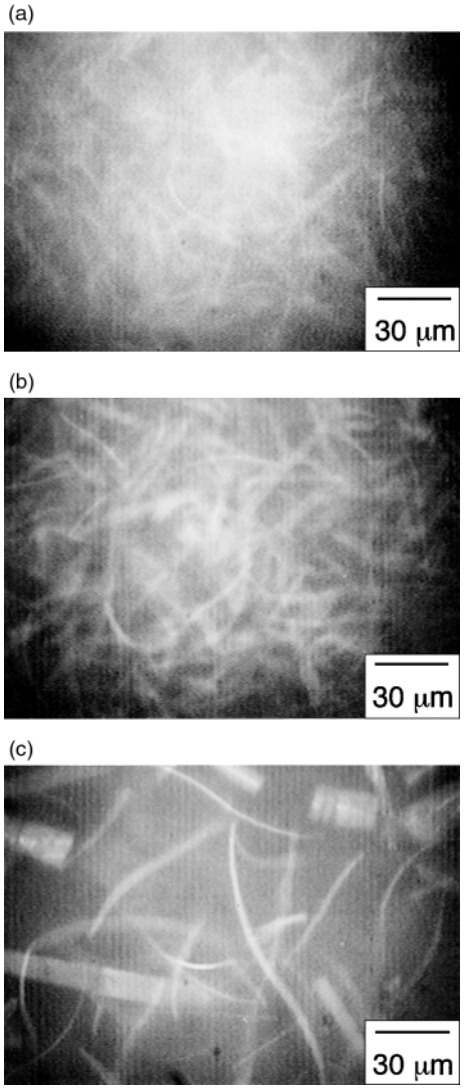

Fig. 2 Fluorescence microscope images of the TC J aggregates in aqueous NaCl solutions. (a), (b) and (c) show images at [TC] = 0.2, 0.1 and 0.05 mM, respectively. The mesoscopic strings correspond to the TC J aggregates.

a focused laser beam at 1064 nm (optical tweezers) and details will be described elsewhere.[12]

Fig. 3 shows fluorescence spectra observed for a single string and at the periphery of the string {[TC] = 0.05 mM, corresponding to Fig. 2(c)}. The excitation beam diameter was *ca.* 10 μm, and the measurements were conducted at various positions in the string. However, the spectral band shape did not change with the observation position in the string. Since the spectrum was quite similar to that in Fig. 1(b), the strings seen in Fig. 2 were concluded to be TC J aggregates.[13] It is noteworthy that fluorescence was scarcely observed at the outer periphery of the strings, indicating that TC in an aqueous solution produces exclusively mesoscopic-size J aggregates.

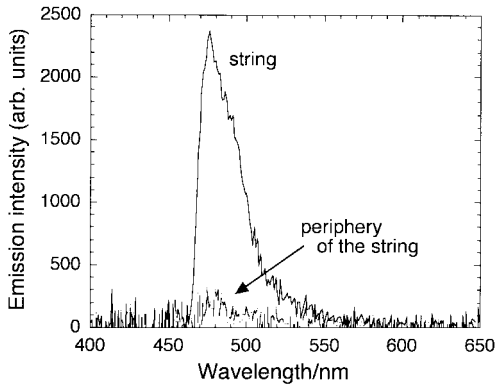

Fig. 3 Fluorescence spectra observed for a *single* string of TC J aggregates and at the periphery of the string: concentration of TC = 0.05 mM.

Recently, the structures of TC J aggregates with different counter cations in solution have been studied by synchrotron XRD and NMR spectroscopy by Tiddy *et al.*[14,15] The results suggested that the J aggregates involve thousands of molecules, which generate a liquid-crystalline lamellar phase composed of ordered dyes and water layers in an aqueous solution. If similar morphologies are also expected in our system, the observed single string could show a lamellar phase, and the water content could be more than *ca.* 95%, which would probably be the origin of the flexibility of the aggregates. Thus, detailed microstructures of the J aggregates are worth studying by various local sensing tools such as AFM and SNOM (scanning near-field optical microscopy), and work along such lines is now in progress.

Notes and references

1 E. E. Jelley, *Nature*, 1936, **138**, 1009; 1937, **139**, 631.
2 G. Scheibe, *Angew. Chem.*, 1936, **49**, 563; 1937, **50**, 212.
3 K. Norland, A. Ames and T. Taylor, *Photogr. Sci. Eng.*, 1970, **14**, 296.
4 A. H. Herz, *The Theory of the Photographic Process*, ed. T. H. James, Macmillan, New York, 4th edn., 1977, ch. 10.
5 E. Hanamura, *Phys. Rev. B*, 1988, **37**, 1273.
6 F. C. Spano, J. R. Kuklinski and S. Mukamel, *J. Chem. Phys.*, 1991, **94**, 7534.
7 H. Yao, S. Sugiyama, R. Kawabata, H. Ikeda, O. Matsuoka, S. Yamamoto and N. Kitamura, *J. Phys. Chem. B*, 1999, **103**, 4452.
8 S. S. Ono, H. Yao, O. Matsuoka, R. Kawabata, N. Kitamura and S. Yamamoto, *J. Phys. Chem. B*, 1999, **103**, 6909.
9 V. Czikkely, H. D. Försertling and H. Kuhn, *Chem. Phys. Lett.*, 1970, **6**, 11.
10 H. Yao, H. Ikeda and N. Kitamura, *Langmuir*, 1997, **13**, 1996.
11 A slight red-shift of the fluorescence peak wavelength of the J aggregate was observed depending on the TC concentration. The result is due to re-absorption effects of the fluorescence.
12 H. Yao, M. Omizo and N. Kitamura, to be submitted.
13 Since a Y-47 filter was mounted in front of the photodetector set, the fluorescence spectrum in the shorter wavelength region was somewhat distorted.
14 G. J. T. Tiddy, D. L. Mateer, A. P. Ormerod, W. J. Harrison and D. J. Edwards, *Langmuir*, 1995, **11**, 390.
15 W. J. Harrison, D. L. Mateer and G. J. T. Tiddy, *J. Phys. Chem.*, 1996, **100**, 2310.

ChemComm

A novel biosensor using electrochemical surface plasmon resonance measurements

Satoshi Koide,[a] Yuzuru Iwasaki,*[b] Tsutomu Horiuchi,[b] Osamu Niwa,[b] Eiichi Tamiya[a] and Kenji Yokoyama[a]

[a] *School of Materials Science, Japan Advanced Institute of Science and Technology Tatsunokuchi, Ishikawa 923-1292, Japan. E-mail: iwasaki@with.brl.ntt.co.jp*

[b] *NTT Lifestyle and Environmental Technology Laboratories, 3-1 Morinosato Wakamiya Atsugi-shi Kanagawa, 243-0198 Japan*

Received (in Cambridge, UK) 31st January 2000, Accepted 27th March 2000
Published on the Web 13th April 2000

Surface plasmon resonance measurements have been conducted to construct a unique electrochemical enzyme sensor which detected the reversible change in the refractive index of a redox film containing an enzyme.

A number of electrochemical biosensors have been constructed based on the enzymatic consumption of substrates and the electrochemical regeneration of an active enzyme by electron mediators. These electrochemical biosensors convert the analyte concentration to faradic current and this current is proportional to the concentration gradient of the electrochemically active molecules on the electrode surface. Meanwhile, surface plasmon resonance (SPR) has been used to measure biological reactions in real time. For instance, DNA elongation by polymerase has been measured in real time using SPR.[1] We have shown that SPR measurements can be used to detect certain electrochemical reactions.[2,3] The combination of SPR and electrochemical measurements will make it possible to detect the refractive index of an electrochemically activated enzyme-mediator film. Here we describe our SPR-based analysis of immobilized enzyme films for electrochemical biosensor applications, and propose a novel transducer element.

Thin gold film electrodes were coated with a horseradish peroxidase (HRP)–osmium redox polymer solution and dried for immobilization.[4] It is expected that reduced and oxidized HRP–osmium films in an electrolyte will have different refractive indices, and that the refractive index will change with the electrode potential and can be used to indicate an enzymatic reaction. However, the refractive index may also depend on the redox reaction of HRP, osmium ions and their ionic environment, the substrate/product concentration, and the packing of the film. When the redox reaction chain is working, all these values change and this affects the minimum reflection angle in SPR measurements (θ_{SPR}). We investigated the effect of catalytic electrochemical reactions on θ_{SPR} values. First, we measured θ_{SPR} for the HRP–osmium redox polymer immobilized electrode simultaneously with cyclic voltammetry without the HRP substrate. The cyclic voltammogram (CV) showed a narrow peak separation and symmetric waves which are characteristics of reactions of an immobilized species.[5] In the absence of hydrogen peroxide (substrate of HRP), Os^{3+} ions are not regenerated by chemical reaction. Therefore, the θ_{SPR} change in the CV was the result of the redox reaction of the osmium film. The θ_{SPR} response showed a bimodal change with potential (similar to that in Fig. 1). We also observed similar θ_{SPR} changes in a solution containing 1 M $NaClO_4$. The value of θ_{SPR} increased at lower potentials, and the potential at which the θ_{SPR} value showed the steepest change was the same as the CV peak potential. This is because of the change in the concentration of ions in the film to compensate the charge neutrality which depends on the valence state of the osmium ions.[6]

In the presence of the HRP substrate the CV shown in Fig. 1 was obtained. In this CV, the hydrogen peroxide was reduced by HRP and a catalytic current was observed. The dependence of θ_{SPR} on the potential was flat in the potential region far from the formal potential, indicating that θ_{SPR} changes from other factors is small. In the potential range in which the catalytic current was observed, oxidized osmium ions (Os^{3+}) were regenerated by the enzymatic reaction. However, the curve of θ_{SPR} *vs.* potential showed a bimodal change, and the graph was almost the same as that obtained without hydrogen peroxide. Therefore, the effect of the redox state of the enzyme and hydrogen peroxide on the θ_{SPR} was far less than that of the mediator film. In the above experiments, the maximum concentration gradient in the film was at the electrode surface when a catalytic current was observed. When the electrode potential is not controlled, the mediator will be oxidized chemically by the enzyme until it is fully oxidized. The concentration ratio of the reduced and oxidized mediator at the electrode surface can be monitored in terms of the electrode potential by means of a potentiometric experiment.

Next, we carried out chronopotentiometry for the catalytic electrochemical reaction as shown in Fig. 2A. Before the chronopotentiometry was started (E = 0 mV), θ_{SPR} increased because of reduction of the film. At zero time, the working electrode was set in the potentiometer mode and θ_{SPR} remained unchanged in the absence of hydrogen peroxide (0 M). In the presence of hydrogen peroxide, θ_{SPR} began to decrease with this being more marked with an increase in hydrogen peroxide concentration. This indicates that the ratio of the reduced form of the film (Os^{2+}) near the electrode surface decreased through the enzymatic consumption of hydrogen peroxide by HRP. The rate of change of θ_{SPR} can thus be used to determine the substrate concentration. Moreover, this method does not require electrochemical instrumentation; we can simply employ the chemical reduction of a mediator using a flow system. Fig. 2B shows the potential change measured by chronopotentiometry. As with the SPR measurement, a potential change was observed in the presence of hydrogen peroxide owing to a decrease in the reduced form of the film. At low hydrogen peroxide concentra-

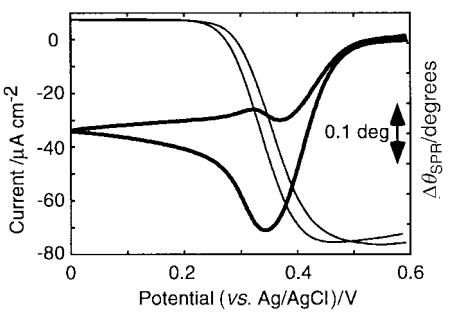

Fig. 1 θ_{SPR} (thin line) dependence of the electrode potential measured simultaneously with cyclic voltammetry (thick line) for an HRP–osmium redox polymer immobilized electrode in 0.1 M phosphate buffer (pH 7) with 10 mM hydrogen peroxide: scan rate 10 mV s^{-1}, geometric surface area = 0.16 cm^2.

DOI: 10.1039/b000866o

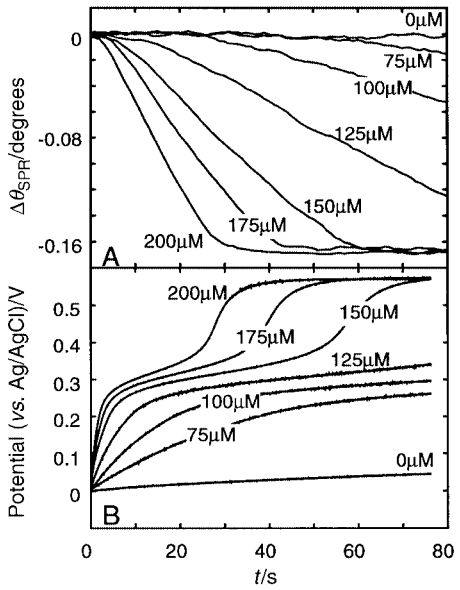

Fig. 2 Time course of θ_{SPR} (A) and equilibrium potential (B) in the chronopotentiometry of an HRP–osmium film with various substrate concentrations. The SPR measurement was initially held a potential at 0 mV for 1 min and then the working electrode was set in the potentiometer mode (t = 0) and simultaneous chronopotentiometry was started. The formal potential ($E^{0\prime}$) was evaluated from the peak potentials of the CV in the absence of the substrate, F is the Faraday constant, R is the gas constant and T is the measuring temperature.

tions, the potential change was also smaller than at higher hydrogen peroxide concentrations. As the concentration ratio of reduced Os ions (Os^{2+}) approached 0.5, the electrode potential change became slower, and a potential plateau (Fig. 2B) was observed.

Fig. 3 shows the relation between θ_{SPR} and the electrode potential of the experiment in Fig. 2. The fraction of reduced film was calculated from the measured potential (Fig. 2B) based on the Nernst equation, and θ_{SPR} was plotted. Despite the

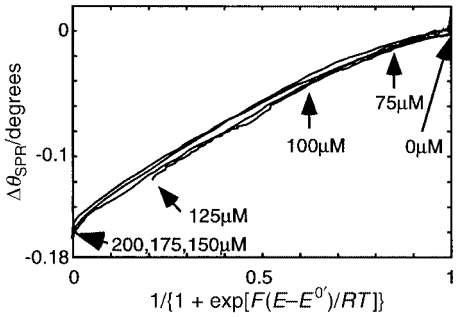

Fig. 3 Relation between θ_{SPR} and surface concentration ratio in the experiment shown in Fig. 2. The arrows indicate the position at 80 s for each substrate concentration.

different substrate concentrations, the trajectories traced the same curve. This implies that the film reacted uniformly and θ_{SPR} represented the redox state of the mediator film in real time. The SPR detection of an enzyme containing redox film can provide a new method of enzyme sensor detection. The physical sensing space can be greatly reduced because of the nature of SPR, and a small dead volume sensor can be constructed. The time response of this method can be improved using a higher sampling rate for the SPR signal. In addition, kinetic information on the multistage enzyme reaction can be obtained. We are currently constructing enzyme sensors using glucose oxidase.

This work was completed while S. K. was staying at NTT.

Notes and references

1 M. Buckle, R. M. Williams, M. Negroni and H. Buc, *Proc. Natl. Acad. Sci. USA*, 1996, **93**, 889.
2 Y. Iwasaki, T. Horiuchi, M. Morita and O. Niwa, *Electroanalysis*, 1997, **9**, 1239.
3 Y. Iwasaki, T. Horiuchi, M. Morita and O. Niwa, *Sens. Actuators, B*, 1998, **50**, 145.
4 O. Niwa, K. Torimitsu, M. Morita, P. Osborne and K. Yamamoto, *Anal. Chem.*, 1996, **68**, 1865.
5 M. Vreeke, R. Maidan and A. Heller, *Anal. Chem.*, 1992, **64**, 3084.
6 T. Tjaernhage and M. Sharp, *Electrochim. Acta*, 1994, **39**, 623.

ChemComm

Unique sodium-caged structure of a potent endothelin-1 inhibitor: crystal structure of BQ123 sodium salt, *cyclo*(-D-Trp-D-Asp$^-$-Pro-D-Val-Leu-)·Na$^+$

Mitsunobu Doi,*[a] Toshimasa Ishida,[a] Yoshio Katsuya,[b] Yoshihiro Mezaki,[b] Masahiro Sasaki,[c] Akira Terashima,[c] Taizo Taniguchi,[c] Hiroshi Hasegawa[c] and Masaaki Shiono[d]

[a] *Osaka University of Pharmaceutical Sciences, 4-20-1 Nasahara, Takatsuki, Osaka 569-1094, Japan. E-mail: doit@oysun01.oups.ac.jp*
[b] *Hyogo Prefectural Institute of Industrial Research, 3-1-12 Yukihira-cho, Suma, Kobe 654-0037, Japan*
[c] *Hyogo Institute for Aging Brain and Cognitive Disorders, 520 Saisho-ko, Himeji 670-0981, Japan*
[d] *Kyushu University, Hakozaki, Higashi-ku, Fukuoka-shi 812-8581, Japan*

Received (in Cambridge, UK) 28th November 1999, Accepted 20th March 2000

The crystal structure of *cyclo*(D-Trp-D-Asp$^-$-Pro-D-Val-Leu-)·Na$^+$, a potent endothelin-1 antagonist, showed four conformational isomers and two Na$^+$-caged structures in pairs.

Endothelin (ET) is an endogenous vasoconstrictor peptide with 21 amino acid residues.[1] Two cyclic peptapeptides of BE18257A and B, isolated from *Streptomyces misakiensis*,[2,3] antagonize the ET induced vasoconstriction by binding to the ET-A receptor subtype.[4] The peptide BQ123, *cyclo*(-D-Trp-D-Asp-Pro-D-Val-Leu-), was designed from these leading peptides (Scheme 1).[5,6] Many NMR studies have been carried out on ET,[7–11] and it was recently suggested[11] that BQ123 partially resembles the structure of ET-1 determined by X-ray diffraction.[12,13] In spite of such intensive approaches, no structures of ET antagonists have been elucidated in the solid state. We reported here, the crystal structure of the sodium salt of BQ123.† This is the first X-ray structural analysis of an ET antagonist.

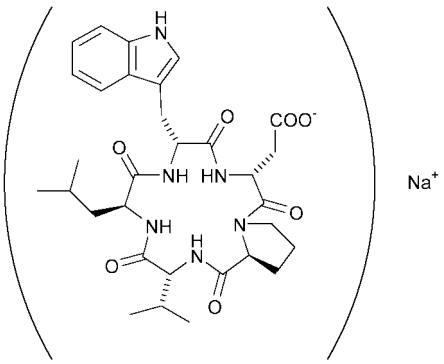

Scheme 1

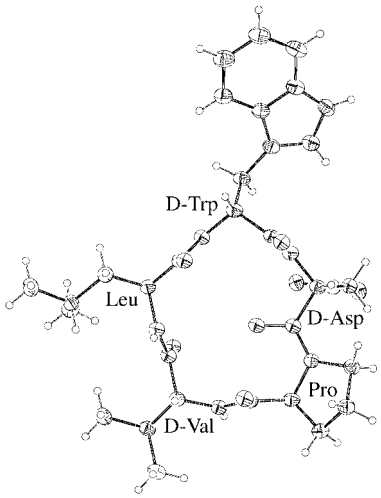

Fig. 1 Molecular conformation of BQ123. Since the conformations of four independent molecules are very similar to each other, only molecule 1 is drawn.

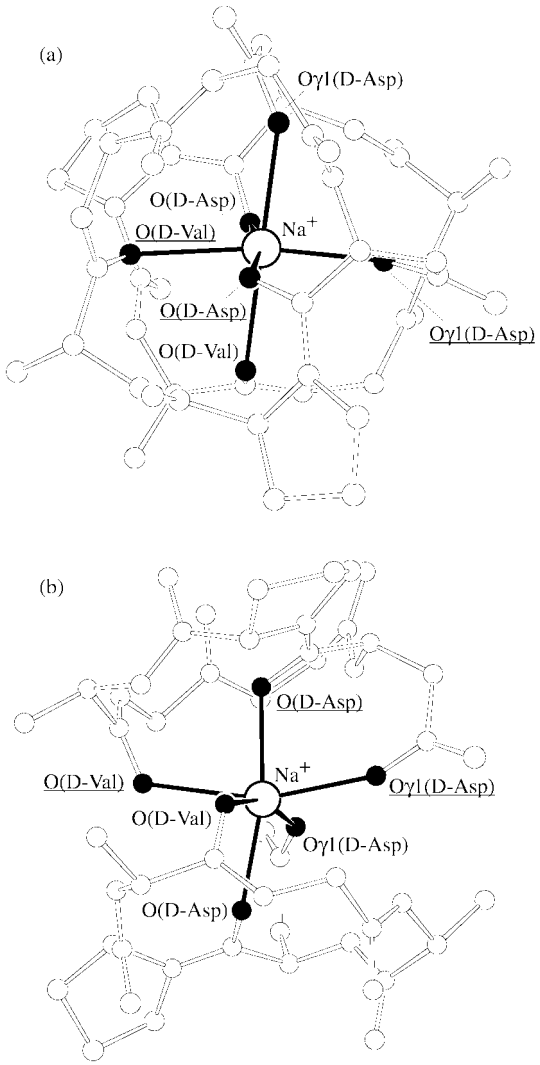

Fig. 2 A caged structure composed of two peptides and a Na$^+$ ion. (a) Top and (b) orthogonal side (rotated −90° for horizontal axis) views. Hydrogens and side chains of D-Val, Leu and D-Trp are omitted for clarity. Filled bonds and balls represent Na–O bonds and coordinated oxygen atoms, respectively. Oxygen atoms of independent molecules 1 and 2 are distinguished by underlined labels. This structure corresponds to one of two similar caged structures in the crystal.

DOI: 10.1039/a909413j

Four independent peptide molecules are located in an asymmetric unit. Conformational differences are observed in the side chain rotation of Trp and the puckering of Pro among the independent molecules, although their overall conformations are similar to each other; the rms deviations are 0.10–0.17 Å in the main chains. Fig. 1 shows the conformation of a single peptide molecule. The conformation of BQ123 is similar to the solution structure of the Na^+-free form in methanol and chloroform,[10] though some local differences are induced *via* the interactions with ions. The most prominent feature in the crystal is the Na^+-coordinated form sandwiched between two independent peptides in pairs, as shown in Fig. 2. The carbonyl oxygens (C=O) of D-Asp and D-Val and the carboxyl oxygens (COO^-) of D-Asp are coordinated to the Na^+ ion, forming an octahedral structure. In this form, the carboxyl and the carbonyl oxygens of the Asp residues are coordinated at the *cis* and *trans* positions, respectively, and these six Na–O bonds range in distance from 2.2 to 2.5 Å. Intermolecular hydrogen bonds are formed between the two BQ123 molecules wrapping the Na^+ ion (not shown in Fig. 2), and thus the peptide molecules form a unique caged structure specific for the Na^+ ion. Two similar caged structures are formed in the crystal, and are distinguished based on interaction modes with the solvents and the two remaining Na^+ ions forming either five- or six-coordinate bonds.

Although we surveyed the characteristics of the structures of ET-1 and the Na^+-ion and BQ123 complexes, no similarities were found, except for a number of amino acids (ET-1 is composed of 21 amino acids, and the total residue number of the four independent cyclic pentapeptides is 20). However, considering that both peptides selectively bind to the ET-A receptor, such differences and the unique structure of the sodium salt of BQ123 are important information for identifying the stereospecificity of the ET-A receptor.

Notes and references

† *Crystal data* for BQ123·Na: $4C_{31}H_{41}N_6O_7Na{\cdot}10H_2O{\cdot}8C_3H_7OH$, M = 3192.6, orthorhombic, space group $P2_12_12_1$, a = 25.3987(3), b = 34.7167(3), c = 25.7365(3) Å, V = 22693.4(24) Å^3, Z = 4, D_c = 0.934 g cm^{-3}, $F(000)$ = 6864, μ = 0.076 mm^{-1}, λ = 0.834 Å, T = 100 °K, 35804 independent reflections were used, θ_{max} = 31.42° (0.80 Å resolution). The molecular weight of BQ123·Na is > 3000 Da, and all attempts to solve the structure using the intensity data collected using commercial X-ray generators (Rigaku RU200/300) failed. The data were, therefore, measured using a Rigaku RAXIS-4 on a synchrotron, SPring-8/BL24XU-A (the figure-eight undulator and double-crystal monochromator system), with the approval of Hyogo prefecture and the Japan Synchrotron Radiation Research Institute (Approval No. C99A24XU-005N and 006N). The structure was finally solved by the electron density modification method using LODEM[14] and refined using SHELXL-97.[15] The solvent molecules were located by difference Fourier syntheses, and 8 isopropyl alcohol and 16 water molecules were found between the peptides. Some solvent sites were disordered: the calculated occupancies of two isopropyl alcohol molecules were 0.55 and 0.75, and those of 8 water molecules ranged from 0.16 to 0.36. Hydrogens of peptides were calculated in geometrically ideal positions by the 'ride on' method, and the hydrogens of solvent molecules were found from the Fourier map considering hydrogen-bonding networks. All hydrogens were included in the calculation of structure factors with isotropic temperature factors. A total of 2088 refinement parameters were divided into three blocks, and the positions and temperature factors were refined in a single refinement cycle. The $R1$ and wR values converged to 0.0845 and 0.2146, respectively, and goodness of fit = 1.044, $\Delta\rho_{max}$ = 0.572 e Å^3 and $\Delta\rho_{min}$ = −0.383 e Å^3.

CCDC 182/1579. See http://www.rsc.org/suppdata/cc/a9/a909413j/ for crystallographic files in .cif format.

1 M. Yanagisawa, H. Kurihara, S. Kimura, Y. Tombe, M. Kobayashi, Y. Mitsui, Y. Yazaki, K. Goto and T. Masaki, *Nature (London)*, 1988, **332**, 411.
2 K. Kojiri, M. Ihara, S. Nakajima, K. Kawamura, K. Funaishi, M. Yano and H. Suda, *J. Antibiot.*, 1991, **44**, 1342.
3 S. Nakajima, K. Niiyama, M. Ihara, K. Kojiri and H. Suda, *J. Antibiot.*, 1991, **44**, 1348.
4 K. Ishikawa, T. Fukami, T. Nagase, K. Fujita, T. Hayama, K. Niiyama, T. Mase, M. Ihara and M. Yano, *J. Med. Chem.*, 1992, **35**, 2139.
5 M. Ihara, K. Noguchi, T. Saeki, T. Fukuroda, S. Tsuchida, S. Kimura, T. Fukami, K. Ishikawa, M. Nishikibe and M. Yano, *Life Sci.*, 1992, **50**, 247.
6 T. Fukami, T. Nagase, K. Fujita, T. Hayama, K. Niiyama, T. Mase, S. Nakajima, T. Fukuroda, T. Saeki, M. Nishikibe, M. Ihara, M. Yano and K. Ishikawa, *J. Med. Chem.*, 1995, **38**, 4309.
7 S. Endo, H. Inooka, Y. Ishibashi, C. Kitada, E. Mizuta and M. Fujino, *FEBS Lett.*, 1989, **257**, 149.
8 V. Saudek, J. Hoflack and J. T. Pelton, *Int. J. Pept. Protein Res.*, 1991, **37**, 174.
9 M. Coles, V. Sowemimo, D. Scanlon, S. L. Munro and D. J. Craik, *J. Med. Chem.*, 1993, **36**, 2658.
10 J. W. Bean, C. E. Peishoff and K. D. Kopple, *Int. J. Pept. Protein Res.*, 1994, **44**, 223.
11 C. E. Peishoff, R. W. Janes and B. A. Wallace, *FEBS Lett.*, 1995, **374**, 379.
12 M. Wolff, J. Day, A. Greenwood, S. Larson and A. McPherson, *Acta Crystallogr. Sect. B*, 1992, **48**, 239.
13 R. W. Janes, D. H. Peapus and B. A. Wallace, *Nat. Struct. Biol.*, 1997, **1**, 311.
14 N. Matsugaki and M. Shiono, LODEM, A Density Modification Program for *ab initio* Solution of Crystal Structures from X-ray Diffraction Data, Kyushu University, Kyushu, 1998.
15 G. M. Sheldrick, SHELXL-97. Program for the Refinement of Crystal Structures from Diffraction Data. University of Göttingen, Göttingen, 1997.

Selective catalytic reduction of N_2O with methane in the presence of excess oxygen over Fe-BEA zeolite

S. Kameoka,*[a] T. Suzuki,[a] K. Yuzaki,[a] T. Takeda,[a] S. Tanaka,[a] S. Ito,[a] T. Miyadera[b] and K. Kunimori*[a]

[a] *Institute of Materials Science, University of Tsukuba, 1-1-1 Tennodai, Tsukuba, Ibaraki 305-8573, Japan. E-mail: kameoka@ims.tsukuba.ac.jp, kunimori@ims.tsukuba.ac.jp*

[b] *National Institute for Resources and Environment, 16-3 Onogawa, Tsukuba, Ibaraki 305-8569, Japan*

Received (in Cambridge, UK) 17th February 2000, Accepted 21st March 2000

An Fe ion-exchanged BEA zeolite (Fe-BEA), which effectively performs selective catalytic reduction of N_2O with methane in the presence of excess oxygen, is much more active than Fe-MFI zeolite reported in the literature.

Nitrous oxide (N_2O) and methane (CH_4) are strong greenhouse-effect gases with a global warming potential (GWP) per molecule of *ca.* 300 and 30 times that of carbon dioxide (CO_2), respectively.[1] N_2O is also identified as a contributor to the destruction of ozone in the stratosphere.[2] From the point of view of the environment, therefore, it is of interest to study selective catalytic reduction (SCR) of N_2O by CH_4 which can lead to simultaneous abatement of N_2O and CH_4 in emission gases. Recently, the groups of Segawa[3,4] and Turek[5,6] reported that the SCR of N_2O by hydrocarbons such as C_3H_6 and C_3H_8 took place effectively over Fe-MFI catalysts even in the presence of coexistent gases such as excess O_2 and H_2O. However, little detailed work with respect to other catalysts and/or reductants in the SCR of N_2O has been performed. We have been studying the SCR of N_2O with hydrocarbons over different Fe ion-exchanged zeolite catalysts (*e.g.* Fe-MFI, Fe-MOR, Fe-NaY, *etc.*).[7] During the course of this study, an Fe ion-exchanged BEA (Fe-BEA) catalyst was found to be much more active for the SCR of N_2O than Fe-MFI zeolite reported in the literature. We report here that the Fe-BEA catalyst performs effectively for the SCR of N_2O with CH_4 even in the presence of an excess of oxygen.

Fe-BEA (SiO_2/Al_2O_3 = 27.3) catalyst was prepared by ion-exchange with a dilute solution of $Fe(SO_4)$ at 50 °C for 20 h under a nitrogen atmosphere, and calcined in air for 12 h at 500 °C.[3,4] For comparison, Fe-MFI (SiO_2/Al_2O_3 = 23.8) was also prepared by the same procedures as Fe-BEA. The zeolite supports (H-BEA, Na-MFI) were supplied by TOSOH Co. The loading weight of Fe on BEA and MFI supports was 0.77 wt% (25 % exchanged with Fe^{2+}) and 2.90 wt% (80% exchanged with Fe^{2+}), respectively. The reaction was carried out in a standard fixed-bed flow reactor by passing a gaseous mixture of N_2O (950 ppm), CH_4 (500 or 3000 ppm) and O_2 (10%) in an He flow at a total flow rate of 50 cm^3 min^{-1} over 50 mg of catalyst [total pressure: 1 atm; space velocity (SV): 60 000 h^{-1}]. The samples were pretreated at 500 °C with O_2 for 1 h in a flow reactor, followed by a He purge at the initial reaction temperature. Catalytic experiments on various reaction systems were performed as detailed in Table 1. The products were monitored by an on-line gas chromatograph (Shimadzu GC-8A) equipped with Molecular Sieve 5A (N_2, CH_4, CO) and Porapak Q (N_2O, CO_2, H_2O) columns. The catalytic activity for the reduction of N_2O with CH_4 was evaluated by the percentage conversion of N_2O and CH_4 to N_2 and CO_x (CO_2 and/or CO), respectively.

Figs. 1 and 2 show N_2O and CH_4 conversions in the different reaction systems (over Fe-BEA and Fe-MFI catalysts), respectively. As shown in Fig. 1, the catalytic activities of N_2O decomposition on both Fe-BEA and Fe-MFI catalysts were significantly promoted by adding CH_4, while N_2O decomposition was inhibited in the presence of O_2. Compared with the N_2O (950 ppm)/O_2 (10 %)/CH_4 (500 ppm) system, the N_2O conversion curve shifted to lower temperature in the absence of O_2 (O_2: 10 → 0%: **No. 3** and **4** in Fig. 1), while the N_2O conversion was scarcely affected by the composition of CH_4 in this range (CH_4: 500 → 3000 ppm: **No. 4** and **5** in Fig. 1). For both Fe-BEA and Fe-MFI, increases of CH_4 conversions correlated well with that of N_2O conversions. N_2, H_2O and CO_2 were observed as the main products in the $N_2O/CH_4/O_2$ system for both catalysts. Moreover, it was found that there was a plateau in CH_4 conversion after N_2O conversion reached 100% (*ca.* 350–450 °C, Fig. 2). This is due to the fact that N_2O in the mixture gas was completely consumed by reaction with CH_4 at such temperatures. It should be noted that oxidation of CH_4 by O_2 over the Fe-BEA catalyst began above 450 °C (**No. 6** in Fig. 2). These results indicate that the reduction of N_2O and the oxidation of CH_4 in this reaction system ($N_2O/CH_4/O_2$) concomitantly take place at much lower temperature than each of original reaction temperatures in the N_2O decomposition (N_2O alone: **No. 1** in Fig. 1) and the CH_4 oxidation (CH_4/O_2

Table 1 List of the reaction systems on the catalytic experiments

Reaction No.	Catalyst	Feed composition in mixture gases		
		N_2O (ppm)	O_2 (%)	CH_4 (ppm)
1	Fe-BEA	950	0	0
2	Fe-BEA	950	10	0
3	Fe-BEA	950	0	500
4	Fe-BEA	950	10	500
5	Fe-BEA	950	10	3000
6	Fe-BEA	0	10	500
7	Fe-MFI	950	0	0
8	Fe-MFI	950	10	0
9	Fe-MFI	950	10	500

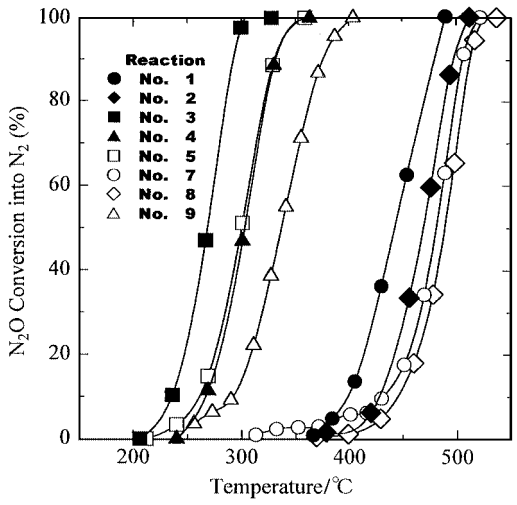

Fig. 1 N_2O conversion to N_2 over Fe-BEA and Fe-MFI. Reaction conditions (**No.**) are described in Table 1.

DOI: 10.1039/b001321h

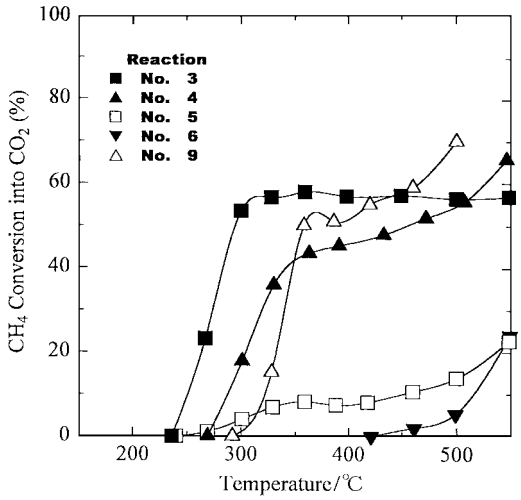

Fig. 2 CH_4 conversion to CO_2 over Fe-BEA and Fe-MFI. Reaction conditions (**No.**) are described in Table 1.

mixture: **No. 6** in Fig. 2). Therefore, O atoms from N_2O molecules are much more efficient in activating CH_4 than O atoms from O_2 molecules at low temperature (< 400 °C).

As also shown in Fig. 1, catalytic activities (per g cat) for the decomposition of N_2O and the selective catalytic reduction (SCR) of N_2O by CH_4 over the Fe-BEA catalyst are much higher than those over the Fe-MFI catalyst. Table 2 shows TOF values based on the catalytic activities in N_2O (**No. 1** and **7**) and $N_2O/O_2/CH_4$ (**No. 4** and **9**) systems over Fe-BEA and Fe-MFI. The TOF values were estimated by assuming that all of loaded Fe (exchanged with Fe^{2+}) act as active sites. These TOF values, of both the decomposition of N_2O and the SCR of N_2O by CH_4 over Fe-BEA are more than one order of magnitude higher than those over Fe-MFI. From the above results, it is strongly suggested that Fe-BEA zeolite is much more active than Fe-MFI zeolite. The difference in the catalytic activities between Fe-BEA and Fe-MFI suggests that the decomposition of N_2O and the SCR of N_2O by CH_4 may be influenced by the structure of zeolite and/or states of the Fe ions.[7] On the other hand, the TOF values of N_2 formation on the SCR of N_2O by CH_4 were significantly higher than those for the decomposition of N_2O over both zeolites. This result indicates that the reaction mechanism for the SCR of N_2O by CH_4 is substantially different from that for the decomposition of N_2O.

Table 2 Comparison of TOF values for N_2O decomposition and SCR of N_2O

	10^{-4} TOF[a]/s^{-1}		
		SCR of N_2O by CH_4[c]	
Catalyst	Decomposition of N_2O[b] N_2 formation	N_2 formation	CO_2 formation
Fe-BEA	16.8	21.8	4.35
Fe-MFI	1.19	1.73	0.07

[a] Turnover frequency (TOF: s^{-1}): number of product molecules per number of Fe ions s^{-1}. [b] At 430 °C (reaction **No. 1** and **7**). [c] At 300 °C (reaction **No. 4** and **9**).

The present results have demonstrated that the SCR of N_2O by CH_4 in the presence of an excess of O_2 occurs effectively over the Fe-BEA catalyst. Interestingly, the reaction temperatures for the SCR of N_2O by CH_4 and the selective oxidation of CH_4 by N_2O over Fe-BEA are much lower than those for N_2O decomposition ($2N_2O \rightarrow 2N_2 + O_2$) or CH_4 combustion ($CH_4 + 2O_2 \rightarrow CO_2 + 2H_2O$) even in the presence of excess O_2. We are currently undertaking further investigations in our laboratory with respect to the detailed mechanism, the effect of coexistent gases (SO_2, NO, H_2O, *etc.*) and the characterization of active sites (Fe ion states *etc.*).

Notes and references

1 H. Rodhe, *Science*, 1990, **248**, 1217.
2 F. Kapteijn, J. Rodriguez-Mirasol and J. A. Moulijn, *Appl. Catal. B*, 1996, **9**, 25.
3 C. Pophal, T. Yogo, K. Yamada and K. Segawa, *Appl. Catal. B*, 1998, **16**, 177.
4 K. Yamada, C. Pophal and K. Segawa, *Microporous Mesoporous Mater.*, 1998, **21**, 549.
5 M. Kögel, V. H. Sandoval, W. Schwieger, A. Tissler and T. Turek, *Catal. Lett.*, 1998, **51**, 23.
6 M. Kögel, R. Mönnig, W. Schwieger, A. Tissler and T. Turek, *J. Catal.*, 1999, **182**, 470.
7 T. Takeda, K. Yuzaki, S. Ito, S.Kameoka, T. Miyadera and K. Kunimori, *The 84th Annual Meeting Catal. Soc. Jpn.*, 1999, 4G07.

ChemComm

Bipyridine–porphyrin conjugates with a conjugated connection†

Jacinda L. Allwood,[a] Anthony K. Burrell,*[a] David L. Officer,*[a] Sonya M. Scott,[a] Kirstie Y. Wild[a] and Keith C. Gordon[b]

[a] *IFS-Chemistry, Massey University, Private Bag 11222, Palmerston North, New Zealand. E-mail: a.k.burrell@massey.ac.nz*
[b] *Department of Chemistry, University of Otago, P.O. Box 56, Dunedin, New Zealand*

Received (in Cambridge, UK) 11th January 2000, Accepted 22nd March 2000
Published on the Web 13th April 2000

A bisporphyrin substituted bipyridine ligand and several metal derivatives are described.

There has been great interest in recent years in the photochemical and electrochemical properties of supramolecular assemblies composed of mononuclear metal polypyridyl complexes.[1] Such systems have applications in solar energy harvesting[2] and in molecular device technology.[3] These functions may be achieved by programming such assemblies, through molecular design, so they transduce energy in one particular direction. This is possible by using binuclear complexes with different metals or by having different terminal ligand substituents.[4]

We have a particular interest in the assembly of polychromophore systems, especially those involving porphyrins.[5] More recently we have been investigating the chemistry of porphyrins that have pendant groups such as pyridine capable of acting as ligands.[6] Here, we report the expansion of this work to include the bipyridyl ligand.

Treatment of 4,4′-diformyl-2,2′-bipyridine **1** with 1 equivalent of tetraxylylporphyrin phosphonium salt (TXP-CH_2PPh_3Cl) **2** proceeds to give the porphyrin functionalised bipyridine **3** in 91% yield (Scheme 1). The remaining aldehyde group can be treated with a further equivalent of **2** to give the bisporphyrin–bipyridine compound **4**. Alternatively, **3** can be treated with other Wittig reagents such as the tetraphenylporphyrin or variants[7] of **2** such as tetra(di-*tert*-butylphenyl)porphyrin[5] to give the hetero-bisporphyrin–bipyridines **5** and **6**. All of the compounds **3**–**6** are insoluble in hexane or alcohols but are very soluble in most other organic solvents.

The ^{1}H NMR spectrum of **4** is consistent with a symmetrical compound. In particular the symmetry is demonstrated by the presence of only three signals associated with the bipyridyl group. A doublet at δ 7.30 (^3J 5.2 Hz) identified as the two equivalent 5-position protons ($H_{5,5'\text{-bpy}}$), the two 3-position bipyridine protons ($H_{3,3'\text{-bpy}}$) appear as a singlet at δ 8.41 while protons of the 6-position ($H_{6,6'\text{-bpy}}$) give rise to a doublet (^3J 5.2 Hz) at δ 8.81. The lack of steric restrictions apparent from the spectrum of **4** is confirmed by its CPK model with no unfavorable steric interactions being apparent.

Treatment of **4** with suitable transition metal complexes results in the formation of stable coordination complexes where it acts as a bidentate ligand. Thus, heating $ReCl(CO)_5$ and **4** in benzene at reflux temperature gives the rhenium complex **7** in

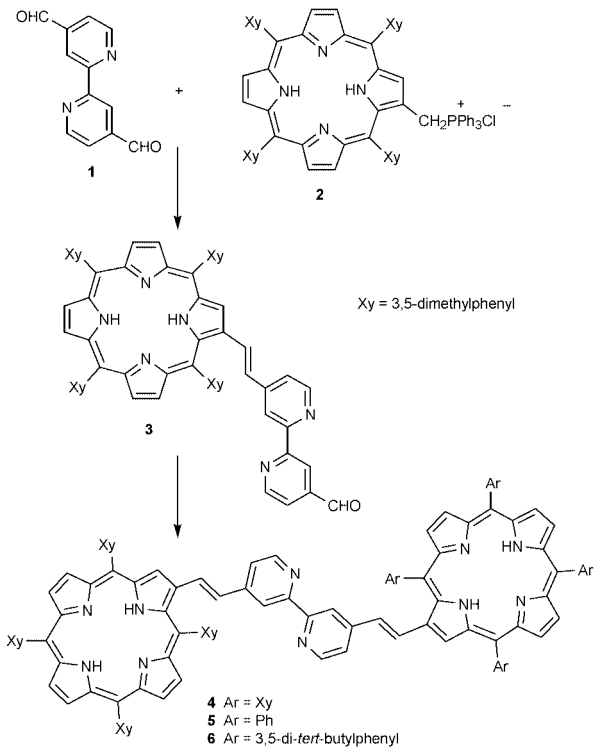

Scheme 1

† Electronic supplementary information (ESI) available: characterisation data for **3**–**10**. See http://www.rsc.org/suppdata/cc/b0/b000364f/

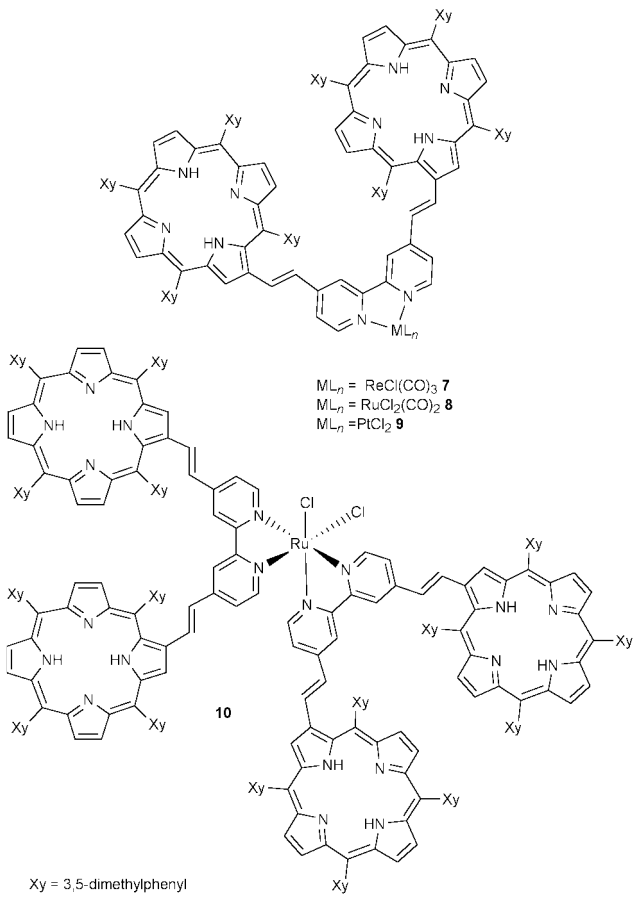

Fig. 1 Molecular structures of compounds.

DOI: 10.1039/b000364f

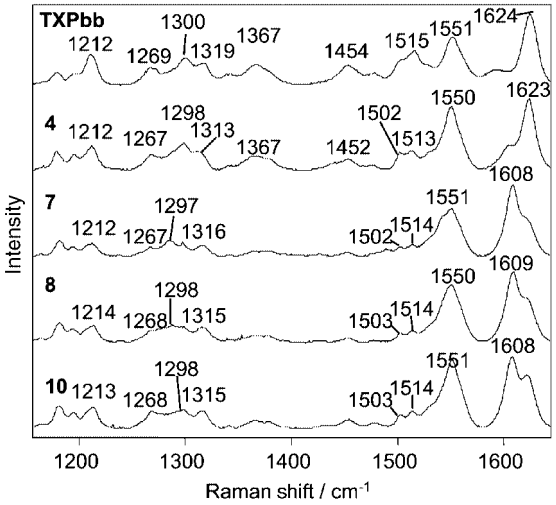

Fig. 2 Resonance Raman spectra of **4**, **7**, **8** and **10** in dichloromethane (1 mM). Excitation wavelength was 457.9 nm (20 mW).

74% yield. Similar complexes of ruthenium **8** and platinum **9** can be obtained by treating **4** with $[Ru(CO)_2Cl_2]_n$ and $PtCl_2(Me_2SO)_2$, respectively (Fig. 1). The ^{1}H NMR spectra for **7**–**9** are little changed from **3**, with only slight shifts observed in the positions of the resonances.

The reaction of **4** with $RuCl_2(Me_2SO)_4$ results in the formation of a complex **10** where 2 equivalents of **4** are coordinated. The yield is 28%, but all of the unreacted **4** can be recovered and reused. The ^{1}H NMR spectrum of **10** is particularly interesting as it enables the geometry of the metal complex to be established unequivocally. In contrast to **4** and the complexes **7**–**9** where the resonances of the protons attached to the bipyridyl rings give only three signals as expected for symmetrical coordination, six signals are observed for these protons in the ^{1}H NMR spectrum of **10**. This indicates that the chloride ligands must be *cis* to each other, imposing an asymmetry in the bipyridine ligand.

The electronic absorption spectra of the ligands **4**–**6** show porphyrin character with the $\pi \rightarrow \pi^*$ band of the bpy evident at 299 nm in **4**. The metal complexes **7**, **8** and **10** appear to possess only porphyrin character in their visible spectra but close examination of the spectra shows a broadening and asymmetry in the Soret band owing to the presence of the metal to ligand charge transfer under the Soret. The spectra are effectively the sum of the spectra of the porphyrin and $M(bpy)_3$ components.[8] Emission studies on these systems show similar results to other bpy–porphyrin complexes[8] with significantly reduced porphyrin emission, and no emission attributable to the M(bpy) portion of the system observed. The emission quenching observed in these systems is thought to be energy transfer similar to that observed in terpy based systems by Flamigni *et al.*[8b,c] The resonance Raman spectra of **4**, **7**, **8** and **10** are shown in Fig. 2. Also present is the spectrum of TXPbb, which is a vinyl-phenyl substituted tetraxylyl porphyrin, for comparative studies. The spectra for **4**, **7**, **8** and **10** are largely porphyrin in nature, with the only feature attributable to the MLCT transition the band at 1608 cm^{-1} in **7**, **8** and **10**. In **7** a band due to the carbonyl can be observed at 2020 cm^{-1}. An investigation of systems such as these in solar energy conversion is currently underway in our laboratory.

We are grateful to The Public Good Science Fund (MAU602 and MAU809), the Massey University Research Fund, the Research Institute of Innovative Technology for the Earth, and the Marsden Fund of New Zealand (MAU810) for support of this work.

Notes and references

1 F. Scandola, M. T. Indelli, C. Chiorboli and C. A. Bignozzi, *Top. Curr. Chem.*, 1990, **158**, 73; V. Balzani, S. Campagna, G. Denti, A. Juris, S. Serroni and M. Venturi, *Acc. Chem. Res.*, 1998, **31**, 26; K. Kalyanasundaram, *Photochemistry of Polypyridine and Porphyrin Complexes*, Academic Press Ltd, London, 1992.

2 M. K. Nazeeruddin, A. Kay, I. Rodicio, R. Humphrey-Baker, E. Mueller, P. Liska, N. Vlachopoulos and M. Gratzel, *J. Am. Chem. Soc.*, 1993, **115**, 6382; R. Argazzi, C. A. Bignozzi, T. A. Heimer and G. J. Meyer, *Inorg. Chem.*, 1997, **36**, 2; I. Willner, E. Kaganer, E. Joselevich, H. Durr, H. E. David, M. J. Gunter and M. R. Johnston, *Coord. Chem. Rev.*, 1988, **171**, 261.

3 F. Scandola, R. Argazzi, C. A. Bignozzi, C. Chiorboli, M. T. Indelli and M. A. Rampi, in *Supramolecular Chemistry*, ed. V. Balzani and L. DeCola, Kluwer Academic Publishers, Netherlands, 1992, p. 235; V. Grosshenny, A. Harriman and R. Ziessel, *Angew. Chem., Int. Ed. Engl.*, 1996, **34**, 2705.

4 K. Kalyanasundaram and Md. K. Nazeeruddin, *Inorg. Chim. Acta*, 1994, **226**, 213; R. Ziessel, M. Hissler, A. El-Ghayoury and A. Harrimann, *Coord. Chem. Rev.*, 1998, **180**, 1251.

5 A. K. Burrell and D. L. Officer, *Synlett*, 1998, **12**, 1297.

6 A. K. Burrell, D. L. Officer, D. C. W. Reid and K. Y. Wild, *Angew. Chem., Int. Ed.*, 1998, **37**, 114.

7 E. E. Bonfantini and D. L. Officer, *Tetrahedron Lett.*, 1993, **34**, 8531.

8 (*a*) J. L. Sessler, V. L. Capuano and A. K. Burrell, *Inorg. Chim. Acta*, 1993, **204**, 93; (*b*) L. Flamigni, F. Barigelletti, N. Armaroli, B. Ventura, J.-P. Collin, J.-P. Sauvage and J. A. G. Williams, *Inorg. Chem.*, 1999, **38**, 661; (*c*) L. Flamigni, N. Armaroli, F. Barigelletti, V. Balzani, J.-P. Collin, J.-O. Dalbavie, V. Heitz and J.-P. Sauvage, *J. Phys. Chem. B*, 1997, **101**, 5936; (*d*) A. D. Hamilton, H.-D. Rubin and A. B. Bocarsly, *J. Am. Chem. Soc.*, 1984, **106**, 7255.

The paramagnetic, heterometallic manganese cubanes [{$E_2(NCy)_4$}$(MnCp)_2$] (Cy = C_6H_{11}, Cp = C_5H_5, E = As, Sb)†

Alan Bashall,[a] Michael A. Beswick,[b] Helmut Ehlenberg,[c] Sara J. Kidd,[b] Mary McPartlin,[a] Julie S. Palmer,[b] Paul R. Raithby,[b] Jeremy M. Rawson[b] and Dominic S. Wright*[b]

[a] *School of Chemistry, University of North London, London, UK N7 8DB*
[b] *Chemistry Department, University of Cambridge, Lensfield Road, Cambridge, UK CB2 1EW. E-mail: dsw1000@cus.cam.ac.uk*
[c] *Department of Physics, Cavendish Laboratory, University of Cambridge, Madingley Road, Cambridge, UK CB3 OHE*

Received (in Cambridge, UK) 17th December 1999, Accepted 23rd March 2000
Published on the Web 13th April 2000

The heterometallic cubanes [{$E_2(NCy)_4$}$(MnCp)_2$] (E = Sb 1, As 2; Cy = C_6H_{11}, Cp = C_5H_5) are the first examples of complexes in which a paramagnetic metal ion has been incorporated into a p block ligand framework.

The coordination chemistry of ligand systems based on *p* block element imido frameworks has become increasingly studied in recent years.[1,2] Species such as the homologous group 15 dianions $[E_2(NR)_4]^{2-}$ (E = P–Bi)[1,3] offer readily accessible building blocks for the assembly of cage complexes containing a broad variety of mixed p block element/main group and transition element compositions.[1a] However, so far studies of the coordination chemistry of imido p block ligands have only involved main group and transition metal ions which possess closed-shell electronic configurations (for the transition metals d^0 or d^{10} only have been reported).[1,4,5] A current interest of ours involves utilising the differing geometric and bonding demands in homologous ligands of this type to control the degree of magnetic and/or bonding interactions between the ligand-supported metal frameworks present in these species.[4c] The heterometallic complexes [{$Sb_2(NCy)_4$}$(MnCp)_2$] **1** and [{$As_2(NCy)_4$}$(MnCp)_2$] **2**, presented here, provide the first opportunity to investigate ligand control of magnetic properties in these systems.

[{$Sb_2(NCy)_4$}$(MnCp)_2$] **1** and [{$As_2(NCy)_4$}$(MnCp)_2$] **2** were prepared by the nucleophilic substitution reactions of $MnCp_2$[6] with [{$E_2(NCy)_4$}$_2M_4$] (E = Sb, M = Na;[6] E = As, M = Li[3b]), with the elimination of CpM (Scheme 1.‡ ^{1}H NMR studies of both showed only broad ill defined resonances which are consistent with paramagnetic materials.

The low-temperature X-ray structures of **1** (Fig. 1) and **2** (Fig. 2)§ reveal that both complexes have similar pseudo-cubane structures in the solid state, which are composed of two (formally 17e) $CpMn^+$ fragments[7] complexed by $[Sb_2(NCy)_4]^{2-}$ and $[As_2(NCy)_4]^{2-}$ dianions. The similarity of the endo- and exo-cyclic Sb–N and As–N bonds of their $[Sb_2(NCy)_4]^{2-}$ and $[As_2(NCy)_4]^{2-}$ anions with those observed in the precursor Na complexes [{$Sb_2(NCy)_4$}$_2Na_4$][8] and [{$As_2(NCy)_4$}$_2Na_4$][4c] illustrates that, like these complexes, the anion units have the primary role in dictating the overall structures of **1** and **2**. The reduction in the endo-cyclic Sb–N and As–N bond lengths from **1** to **2** (of *ca.* 0.19 Å) has a major affect on the Mn_2N_2 rings in both complexes. In order to retain similar Mn–N bond lengths within these units (*ca.* 2.20 Å in both complexes[9]), this ring is far more puckered in **2** (the angle between the MnN_2 planes being 161.9° in **1** and 142.6° in **2**).

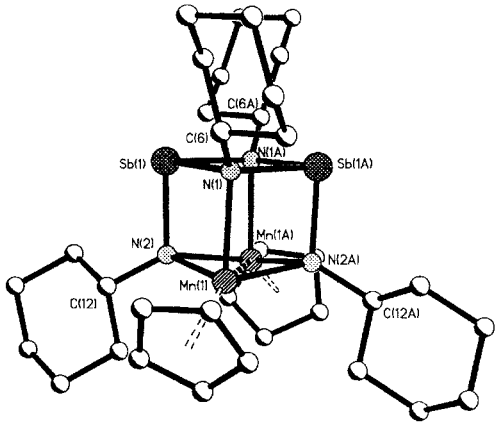

Fig. 1 Structure of the Sb_2Mn_2 cubane **1** with H-atoms omitted for clarity. Key bond lengths (Å): Sb(1)–N(1) 2.109(5), Sb(1)–N(1A) 2.128(5), Sb(1)–N(2) 2.039(5), N(1)–Mn(1) 2.269(6), N(2)–Mn(1) 2.215(5), N(2)–Mn(1A) 2.217(5), Mn(1)–Mn(1A) 3.041(2), Mn–C range 2.421(7)-2.615(8) ($Cp_{centroid}$–Mn 2.16). Bond angles (°); N(1)–Sb(1)–N(1A) 80.1(2), Sb(1)–N(1)–Sb(1A) 99.9(2), N(1,1A)–Sb(1)–N(2) mean 88.2, Sb(1)–N(2)–Mn(1,1A) mean 97.6, Sb(1,1A)–N(1)–Mn(1) mean 93.2, N(1)–Mn(1)–N(2,2A) mean 80.7, Mn(1)–N(2)–Mn(1A) 87.6(2), N(2)–Mn(1)–N(2A) 91.0(2). Dihedral angles (°) between planes; MnN_2 161.9, SbN_2 178.4.

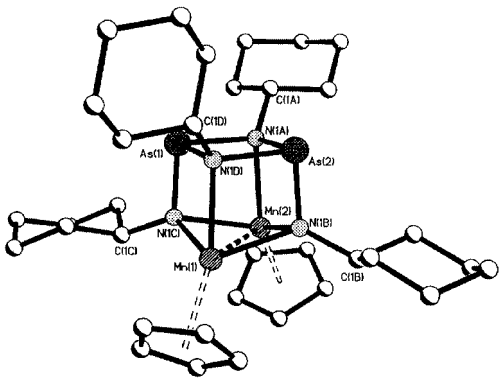

Fig. 2 Structure of the As_2Mn_2 cubane **2** with H-atoms omitted for clarity. Key bond lengths (Å): As(1)–N(1A) 1.940(8), As(1)–N(1C) 1.816(7), As(1)–N(1D) 1.912(7), As(2)–N(1A) 1.923(7), As(2)–N(1B) 1.820(7), As(2)–N(1D) 1.935(7), Mn(1)–N(1B) 2.202(7), Mn(1)–N(1C) 2.170(7), Mn(1)–N(1D) 2.264(7), Mn(2)–N(1A) 2.278(7), Mn(2)–N(1B) 2.199(7), Mn(2)–N(1C) 2.253(7), Mn(1)···Mn(2) 2.934(2), Mn–C range 2.39(1)–2.53(1) ($Cp_{centroid}$–Mn 2.16). Mean angles (°): N(1A)–As(1,2)–N(1D) 83.0, N(1C)–As(1)–N(1A,1D) 91.9, N(1B)–As(2)–N(1A,1D) 91.3, Mn(1)–N(1B,1C)–Mn(2) 83.4, N(1C)–Mn(1,2)–N(1B) 90.8. Dihedral angles (°) between planes; MnN_2 142.6, AsN_2 176.2.

Scheme 1

† Electronic supplementary information (ESI) available: plots of the effective magnetic moments of **1** and **2** as a function of temperature. See http://www.rsc.org/suppdata/cc/a9/a910196i/

Although this distortion has only a small affect on the Mn–N–Mn and N–Mn–N angles within the Mn_2N_2 ring units, a consequence of the presence of the more compact $[As_2(NCy)_4]^{2-}$ ligand in **2** is a large reduction in Mn···Mn separation [from 3.041(2) Å in **1** to 2.934(2) Å in **2**]. The Mn···Mn separation in **2** is almost identical to that in $Mn_2(CO)_{10}$ (2.93 Å).[10]

Whilst Mn(II) ions are almost invariably high spin, the large ligand field associated with the π-donor Cp^- ligand makes the high- and low-spin electronic configurations energetically similar. Indeed, for manganocenes ($MnCp^R_2$; Cp^R = substituted Cp) examples of pure low-spin, pure high-spin and high-/low-spin equilibria have been observed (depending on the donor or acceptor character and steric demands of ring substituents).[11,12] For the half-sandwich ($MnCp^R$) derivatives, pure high-spin behaviour has been observed.[13] For **1** and **2**, the possibility of high-/low-spin equilibria is complicated by the potential for superexchange *via* the bridging imido ligands. Preliminary magnetic studies of **1** and **2** (5.5–380 K) show a marked temperature dependence of μ_{eff} (ESI†). Even at 380 K, the observed moments (6.0 and 6.6 μ_B for **1** and **2**, respectively) are significantly less than that expected for two high-spin Mn(II) ions per molecule (8.37 μ_B). The value of μ_{eff} decreases steadily on cooling, reaching 2.6 μ_B for **1** and 1.9 μ_B for **2** at 5.5 K. While the value for **1** is consistent with two non-interacting low-spin Mn(II) ions (2.5 μ_B), the significantly lower value for **2** may indicate intramolecular exchange between the Mn ions.

Attempts to model the data for **1** and **2** have so far proved inconclusive.¶ The suggestion that a high-/low-spin equilibrium may be occurring over a wide temperature range for both complexes is apparently inconsistent with the long Mn–C bond lengths in **1** and **2** [range 2.389(10)–2.615(8) Å], which are typical of high-spin manganocenes (*cf. ca.* 2.11–2.14 Å in low-spin species).[12] Although some shortening of the Mn–C bonds is anticipated for the high-/low-spin equilibrium at the temperatures at which the structures of the complexes were obtained (180 K for **1** and 223 K for **2**), a possible reason for the maintenance of long metal–ligand bonds in both complexes is the sterically congested nature of the $[E_2(NCy)_4]^{2-}$ ligand frameworks (making closer approach of the Cp ligands unfavourable[12*b*]). A detailed study of the magnetic behaviour (EPR and solid-state susceptibility) and variable-temperature X-ray diffraction studies of **1** and **2** will be the subject of a full paper.

We gratefully acknowledge the EPSRC (A. B., S. J. K., J. S. P., M. McP., P. R. R., D. S. W.) and The Leverhulme Trust (M. A. B.) for financial support. We also thank Dr J. E. Davies for collecting X-ray data on **1**. We are also particularly grateful to the referees for their helpful comments regarding the magnetic behaviour of **1** and **2**.

Notes and references

‡ *Syntheses*: **1**: solid $MnCp_2$ (0.273g, 1.48 mmol) and $[\{Sb_2(NCy)_4\}_2Na_4]$ (0.676 g, 0.74 mmol) were mixed together in a glove box under argon. The mixture was dissolved in toluene (20 ml) and brought to reflux, producing a fine gelatinous solid of CpNa which was separated by the addition of thf (10 ml) followed by filtration. The red filtrate was reduced to dryness under vacuum and the solid residue dissolved by the addition of hexane (10 ml) and toluene (10 ml) and gentle heating. Storage (25 °C, 12 h) gave red plates of **1**. Yield 0.520 g (81%). Decomp. *ca.* 200 °C. δ_H(+25 °C, thf-d_8, 250 MHz), 4.75 (Cp), 1.8–0.7 (Cy groups) (Found: C 46.2; H 6.0; N 5.3. Calc. for **1**: C, 46.8; H, 6.2; N, 6.4%).

2: $[\{As_2(NCy)_4\}_2Li_4]$ was prepared *in situ* by the reaction of $As(NMe_2)_3$ (5.0 ml, 2.43 mol dm^{-3} solution in toluene, 12.15 mmol) with a solution of $CyNH_2$ (1.39 ml, 12.15 mmol) in toluene (8 ml), followed by the addition of a suspension of CyNHLi (12.15 mmol) in toluene (8 ml). $MnCp_2$ (2.25 g, 12.15 mmol) in thf (10 ml) was added to this mixture and a white precipitate of CpLi was formed after bringing to reflux. Filtration gave a yellow solution which was stored (25 °C, 12 h) to give yellow plates of **2**. Yield 1.62 g (34%). Decomp. *ca.* 210 °C. δ_H(+25 °C, thf-d_8, 250 MHz), *ca.* 6.5 (Cp), 2.5–0.5 (Cy groups) (Found: C, 51.5; H, 6.6; N, 6.2. Calc. for **2**: C, 52.4; H, 6.9, N, 7.2%).

§ *Crystal data*: for **1**: $C_{34}H_{54}Mn_2N_4Sb_2$, M = 872.20, tetragonal, space group $P4_12_12$, Z = 4, a = 11.775(2), c = 26.095(5) Å, U = 3618.1(11) Å^3, D_c = 1.601 g cm^{-3}, $F(000)$ = 1752, μ(Mo–Kα) = 2.187 mm^{-1}, T = 180(2) K. Data in the θ range 1.90–25.06° were collected on a Nonius Kappa CCD diffractometer. The structure was solved by direct methods. Full-matrix least-squares refinement on F^2 with 190 parameters was based on 3156 independent data (total collected 5231, R_{int} = 0.044). Final R_1 = 0.028 [$I > 2\sigma(I)$], wR_2 = 0.126 (all data).[14] Largest peak and hole in the final difference map 0.808 and −1.750 e Å^{-3}. Absolute structure parameter −0.09(6).

For **2**: $C_{34}H_{54}As_2Mn_2N_4$, M = 778.53, monoclinic, space group $P2_1/c$, Z = 4, a = 10.336(2), b = 17.095(6), c = 20.506(5) Å, β = 103.99(2)°, U = 3516(2) Å^3, D_c = 1.471 g cm^{-3}, $F(000)$ = 1608, μ(Mo-Kα) = 2.615 mm^{-1}, T = 223(2) K. Data in the θ range 2.03–23.01° were collected on a Siemens P4 difractometer, and corrected for absorption effects using Ψ scans. The structure was solved by direct methods. Full-matrix least-squares refinement on F^2 with 379 parameters was based on 4893 independent data (total collected 6294, R_{int} = 0.0509). Final R_1 = 0.054 [$I > 2\sigma(I)$], wR_2 = 0.156 (all data).[14] Largest peak and hole in the final difference map 0.868 and −0.877 e Å^{-3}.

CCDC 182/1581. See http://www.rsc.org/suppdata/cc/a9/a910196i/ for crystallographic files in .cif format.

¶ *Magnetic behaviour* of **1** and **2**: solid samples were measured between 5.5 and 380 K using a SQUID magnetometer in fields of 100 (for **1**) and 1000 G (for **2**). They were corrected for diamagnetism using Pascals' constants. Attempts to model the magnetic behaviour as a low-spin ground state with a thermally accessible high-spin state were unsuccessful as was an attempt to fit the data to two interacting Heisenberg S = ⅝ ions. For **1**, a high-spin/low-spin thermal equilibrium fits the data throughout the temperature range 5.5-380 K, and also for the range 25–380 K for **2**.

1 (*a*) M. A. Beswick and D. S. Wright, *Coord. Chem. Rev.*, 1998, **176**, 373; (*b*) M. A. Beswick, M. E. G. Mosquera and D. S. Wright, *J. Chem. Soc., Dalton Trans.*, 1998, 2437, and references therein.
2 For related Group 16 examples, see: R. Fleischer, S. Freitag, F. Pauer and D. Stalke, *Angew. Chem., Int. Ed. Engl.*, 1996, **35**, 204; T. Chivers, X. Gao, M. Parvez and G. Schatte, *Inorg. Chem.*, 1996, **35**, 4094.
3 I. Schranz, L. Stahl and R. J. Staples, *Inorg. Chem.*, 1998, **37**, 1493.
4 Group 15 examples, see (*a*) D. F. Moser, I. Schranz, M. C. Gerrety, L. Stahl and R. J. Staples, *J. Chem. Soc., Dalton Trans.*, 1999, 751; (*b*) L. Grocholl, V. Huch, L. Stahl, R. Staples, P. Steinhart and A. Johnson, *Inorg. Chem.*, 1997, **36**, 4451; (*c*) A. Bashall, M. A. Beswick, E. A. Harron, A. D. Hopkins, S. J. Kidd, M. McPartlin, P. R. Raithby, A. Steiner and D. S. Wright, *Chem. Commun.*, 1999, 1145; (*d*) L. Grocholl, I. Schranz, L. Stahl and R. J. Staples, *Inorg. Chem.*, 1998, **37**, 2496.
5 Group 16 examples, see: T. Chivers, T. Parvez, M. Schatte and G. P. A. Yap, *Inorg. Chem.*, 1999, **38**, 1380;
6 For further aspects of the nucleophilic substitution of Cp_2Mn, see: K. Jonas, *Angew. Chem., Int. Ed. Engl.*, 1985, **24**, 295.
7 Electron count for **1** and **2**, viewed as $[E_2(NCy)_4]^{2-}\cdot 2Mn^{2+}$; Mn(II) (5e), Cp^- (6e), E–(μ-N)–E (2e), Mn–(μ-N)–Mn (4e).
8 A. Bashall, M. A. Beswick, C. N. Harmer, A. D. Hopkins, M. McPartlin, M. A. Paver, P. R. Raithby and D. S. Wright, *J. Chem. Soc., Dalton Trans.*, 1998, 1389.
9 These Mn–N bonds are considerably longer than in related Mn(II) complexes, for example see N. Wiberg, H.-W. Häring, G. Gottfried and P. Friedrich, *Chem. Ber.*, 1978, **111**, 2708; W. J. Grigsby and P. P. Power, *J. Chem. Soc., Dalton Trans.*, 1996, 4613.
10 M. R. Churchill, K. N. Amoh and H. J. Wasserman, *Inorg. Chem.*, 1981, **20**, 1609; M. Martin, B. Rees and A. Mitschler, *Acta Crystallogr., Sect. B*, 1982, **38B**, 6.
11 N. Hebendanz, F. Köhler, G. Müller and J. Riede, *J. Am. Chem. Soc.*, 1986, **108**, 3281.
12 (*a*) M. E. Switzer, R. Wang, M. F. Rettig and A. H. Maki, *J. Am. Chem. Soc.*, 1974, **96**, 7669; (*b*) M. L. Hays, D. J. Burkey, J. S. Overby, T. P. Hanusa, S. P. Sellers, G. T. Yee and V. G. Young, Jr., *Organometallics*, 1998, **17**, 5521 and references therein.
13 F. H. Köhler, N. Hebendanz, U. Thewalt, B. Kanellakopulus and R. Klenze, *Angew. Chem., Int. Ed. Engl.*, 1984, **23**, 721; J. Heck, W. Massa and P. Weinig, *Angew. Chem., Int. Ed. Engl.*, 1984, **23**, 722; F. H. Köhler, N. Hebendanz, G. Müller and U. Thewalt, *Organometallics*, 1987, **6**, 115.
14 SHELXTL PC version 5.03, Siemens Analytical Instruments, Madison, WI, 1994.

Paramagnetic NMR studies of copper-containing nitrite reductases

Christopher Dennison,*[a] Kenji Oda[b] and Takamitsu Kohzuma[b]

[a] *Department of Chemistry, University of Newcastle, Newcastle-upon-Tyne, UK NE1 7RU. E-mail: christopher.dennison@ncl.ac.uk*

[b] *Department of Chemistry, Ibaraki University, Mito, Ibaraki 310, Japan*

Received (in Cambridge, UK) 8th February 2000, Accepted 27th March 2000
Published on the Web 13th April 2000

Paramagnetic signals have been observed in the ^{1}H NMR spectra of copper-containing nitrite reductases ($M_r \approx 110$ kDa), which provide a detailed fingerprint of the type 1 centres in these proteins.

Copper-containing nitrite reductases (NiRs) function in the dissimilatory denitrification pathway of certain micro-organisms, reducing nitrite to nitric oxide.[1] Structural studies have shown that these proteins are trimeric[2–4] with each subunit ($M_r \approx 36$ kDa) possessing a type 1 copper site. In addition, the protein possesses three inter-subunit type 2 copper centres (sites of nitrite binding) in close proximity to the type 1 centres. The arrangement of the two copper centres in one of the monomers of nitrite reductase is shown in Fig. 1. The presence of type 1 centres in NiRs results in them having unique spectroscopic features, including intense LMCT bands in their visible spectra. NiRs can be either green or blue, with the distinction due to differences at the type 1 centre.[4–7] Herein, we investigate the differences at the type 1 centres of the green NiR from *Achromobacter cycloclastes* and the blue NiR from *Alcaligenes xylosoxidans* using paramagnetic ^{1}H NMR spectroscopy.

Recent studies have demonstrated that isotropically shifted ^{1}H NMR resonances can be observed and assigned for simple, low molecular weight ($M_r \approx 12$ kDa), type 1 copper proteins (cupredoxins).[8,9] In all cases, a number of broad resonances can be observed and assigned. The assigned spectra provide a detailed fingerprint of the active sites of the various cupredoxins. We now show that similar resonances can be observed for the type 1 centre in the more complex copper-containing nitrite reductases. This is possibly the largest copper protein that has been studied to date using paramagnetic NMR spectroscopy. Interpretation of the isotropic shifts experienced by these resonances provides details of the structure of the type 1 copper centres in these proteins and highlights differences between blue and green NiRs.

The paramagnetic ^{1}H NMR spectrum[10] of the type 2 depleted (T2D, *i.e.* with copper removed from the type 2 centres) green NiR from *A. cycloclastes*[12] is presented in Fig. 2A. Also shown (Fig. 2B) is the spectrum of the protein which possesses > 80% Cu(II) at its type 2 centre.[14] The spectrum of the T2D blue NiR from *A. xylosoxidans*[15] is shown in Fig. 2C. The chemical shifts of the observed resonances are listed in Table 1 along with spin–lattice (T_1) relaxation times.

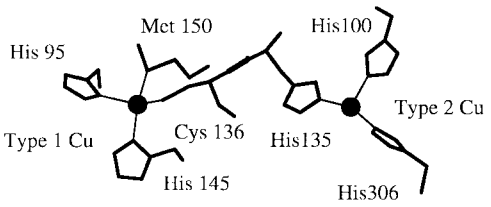

Fig. 1 Structure of the Cu(II) sites in one of the monomers of NiR (the His306 ligand of the type 2 copper centre originates from the adjacent monomer). Black spheres indicate the copper ions. This picture was produced using the coordinates of the crystal structure of the protein from *A. cycloclastes*.[3]

The spectra of the green NiR and the corresponding T2D enzyme show no significant differences in chemical shift values and relaxation times (see Table 1). This clearly demonstrates that all of the observed resonances are due to protons associated with the type 1 centre, and that the binding of Cu(II) to the type 2 centre has no effect on the structure, or electronic properties, of the type 1 site.[16,17] The temperature dependence of the chemical shifts of the resonances observed in Fig. 2A has been investigated in the range 292–328 K, and in all cases they exhibit Curie-type behaviour (data not shown).

In previous paramagnetic ^{1}H NMR studies on the oxidised forms of the cupredoxins amicyanin[8] and plastocyanin,[9] the assignment of paramagnetic resonances has relied upon the ability to correlate these peaks to their counterparts in the spectrum of the reduced (diamagnetic) protein, utilising the electron self-exchange reaction. This is clearly not possible in the case of NiRs. However, a comparison to the assigned cupredoxin spectra provides a very reliable initial analysis of the NiR spectra.

The exchangeable resonance d arises from one of the N$^{\varepsilon 2}$H of the two His ligands. Spectra were acquired of the proteins in H_2O–D_2O (9 : 1, v/v) at lower pH values, but there was no evidence for a second such resonance.[18] These observations

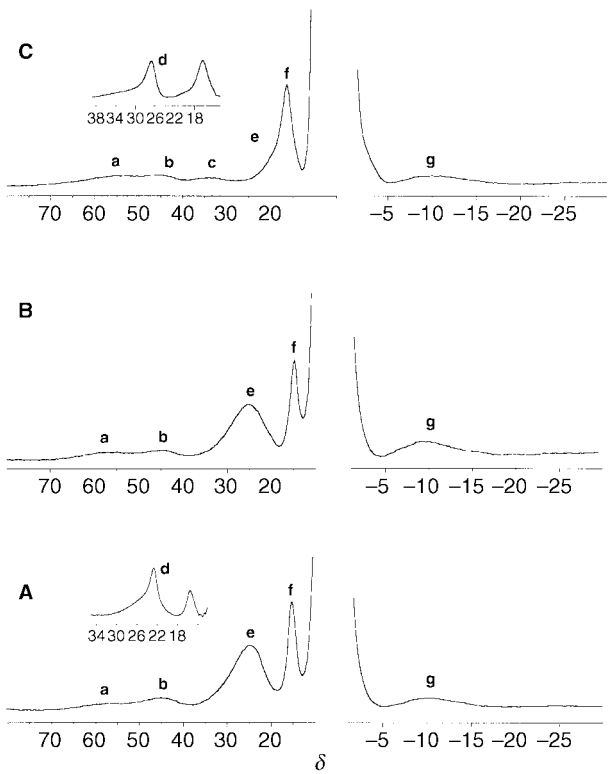

Fig. 2 ^{1}H NMR spectra of Cu(II) NiRs (500 MHz, 25 °C): A, T2D green NiR in D_2O at pH 7.5 with the inset showing part of the spectrum in H_2O at pH 7.5; B, green NiR in D_2O at pH 7.0; **C**, T2D blue NiR in D_2O at pH 7.5 with the inset showing part of the spectrum in H_2O at pH 7.5.

DOI: 10.1039/b001067g

Table 1 Hyperfine shifted resonances in the 500 MHz ^{1}H NMR spectrum of Cu(II) NiRs at 25 °C

	T2D green[a] NiR		Green[a] NiR		T2D Blue[b] NiR		
Resonance	δ_{obs}[c]	T_1[d]/ms	δ_{obs}[c]	T_1[d]/ms	δ_{obs}[c]	T_1[d]/ms	Assignment[e]
a	~58	n.d.[f]	~58	n.d.	~54	n.d.	His C$^{\delta 2}$H
b	~45	n.d.	~45	n.d.	~44	n.d.	His C$^{\delta 2}$H
c					~33	n.d.	His C$^{\varepsilon 1}$H
d	22.7	2.9			26.6	2.6	His95 N$^{\varepsilon 2}$H
e	25.1	0.46	25.3	0.40	< 18	n.d.	Met150 C$^{\gamma}$H
f	15.3	6.3	15.1	6.0	16.3	4.8	Asn96 C$^{\alpha}$H
g	−10.8	n.d.	−10.5	n.d.	−10.5	n.d.	Cys136 C$^{\alpha}$H

[a] *A. cycloclastes.* [b] *A. xylosoxidans.* [c] Estimated error ±0.1 for sharp resonances and ±0.3–0.5 for broader peaks. [d] Estimated error is ±5%; this is larger for the very fast relaxing signals. [e] The numbering of the residues is as found in NiR from *A. cycloclastes*. [f] n.d. = not determined.

point to peak d belonging to the N$^{\varepsilon 2}$H of the more buried His95 ligand in both proteins.[19] The corresponding resonance of the exposed His145 ligand is broadened beyond detection owing to fast exchange with the bulk solvent.

The two very broad resonances a and b have counterparts in the spectra of amicyanin[8] and plastocyanin,[9] and can be assigned to the two C$^{\delta 2}$ protons of the histidine ligands. Resonance e has an apparent T_1 value of 0.46 ms in the T2D green NiR and is most likely due to one or both of the C$^{\gamma}$H signals of the axial Met150 ligand. In the paramagnetic ^{1}H NMR spectra of other cupredoxins a very broad peak, comprised of the two C$^{\varepsilon 1}$H resonances of the two histidine ligands, has been found at δ *ca.* 30–35, which could also be present in the spectrum in Fig. 2A overlapping with one, or both, of the Met C$^{\gamma}$H signals. The histidines C$^{\varepsilon 1}$H peak is present in the spectrum of the blue NiR (peak c), whilst peak e (Met150 C$^{\gamma}$H) now overlaps with peak f (*vide infra*).

Resonance f is the least paramagnetic signal in the spectra of the two T2D NiRs (see Table 1). A corresponding resonance has been found in the region δ *ca.* 12–18 in all such studies on proteins possessing type 1 centres. In the published study on Cu(II) amicyanin[8] this resonance was assigned to the C$^{\alpha}$H of the coordinated Cys ligand. However, in the Cu(II) plastocyanin work[9] the corresponding resonance has been assigned to the C$^{\alpha}$H of Asn38, the backbone amide group of which makes a strong hydrogen bond to the thiolate sulfur of the coordinated Cys ligand (the Cys C$^{\alpha}$H is upfield shifted and has a T_1 value of < 1 ms in plastocyanin, *vide infra*). The long spin–lattice relaxation time and relatively small linewidth of peak f clearly point to it belonging to the C$^{\alpha}$H of Asn96 in the NiRs, whose backbone amide makes a hydrogen bond with the S$^{\tau}$ of the ligand Cys136.

Finally, resonance g is the only upfield shifted signal observed in the spectra of the NiRs. In studies on amicyanin and plastocyanin two upfield shifted resonances have been observed. For the former, these have been assigned as the two C$^{\beta}$ protons of one of the His ligands.[8] For plastocyanin, the most upfield shifted resonance has been assigned to the C$^{\alpha}$H of the Cys ligand with the other upfield shifted resonance due to a His C$^{\beta}$H.[9] Due to the assignment of peak f as the C$^{\alpha}$H of Asn96 we conclude that peak g must belong to the C$^{\alpha}$H of Cys136.

The hyperfine shifts of the ^{1}H NMR signals associated with type 1 copper centres are made up mainly of a Fermi-contact contribution, and therefore directly provide information about the spin density distribution of the unpaired electron. The shifts observed for the two NiRs are, on the whole, very similar and are also reminiscent to those observed in the published studies on type 1 copper centres.[8,9] This is especially so for the signals derived from the two histidines, the Cys C$^{\alpha}$H and the Asn C$^{\alpha}$H resonances, consistent with very similar type 1 architectures in the various proteins. The major difference between the spectra of the blue and green NiRs lies in the shifts experienced by the Met C$^{\gamma}$H resonances (peak e). This signal in the green NiR lies at δ = 25.1, *cf.* δ < 18 in the blue enzyme. This indicates *ca.* 1.5 times more spin density on this proton in the green protein, which cannot be due to differences in the Cu–S(Met) distances as structural studies have shown this bond length (precision *ca.* 0.1 Å) to be very similar in the green (2.56 Å)[3] and blue (2.64 Å)[4] NiRs. These variations are therefore probably due to differences in the Cu–S$^{\delta}$–C$^{\gamma}$–H$^{\gamma}$ dihedral angles in the two proteins.[20] Further paramagnetic NMR studies on Co(II)-substituted NiRs are currently underway to clarify this issue.

Notes and references

1 S. J. Ferguson, *Curr. Opin. Chem. Biol*., 1998, **2**, 182.
2 J. G. Grossmann, Z. H. L. Abraham, E. T. Adman, M. Neu, R. R. Eady, B. E. Smith and S. S. Hasnain, *Biochemistry*, 1993, **32**, 7360.
3 E. T. Adman, J. W. Godden and S. J. Turley, *J. Biol. Chem.*, 1995, **270**, 27 458.
4 F. E. Dodd, J. Van Beeumen, R. R. Eady and S. S. Hasnain, *J. Mol. Biol.*, 1998, **282**, 369.
5 C. R. Andrew, H. Yeom, J. S. Valentine, B. G. Karlsson, N. Bonander, G. van Pouderoyen and G. W. Canters, *J. Am. Chem. Soc.*, 1994, **116**, 11489.
6 L. B. LaCroix, S. E. Shadle, Y. Wang, B. A. Averill, B. Hedman, K. O. Hodgson and E. I. Solomon, *J. Am. Chem. Soc.*, 1996, **118**, 7755.
7 K. Pierloot, J. O. A. De Kerpel, U. Ryde, M. H. Olsson and B. O. Roos, *J. Am. Chem. Soc.*, 1998, **120**, 13 156.
8 A. P. Kalverda, J. Salgado, C. Dennison and G. W. Canters, *Biochemistry*, 1996, **35**, 3085.
9 I. Bertini, S. Ciurli, A. Dikiy, R. Gasanov, C. Luchinat, G. Martini and N. Safarov, *J. Am. Chem. Soc.*, 1999, **121**, 2037.
10 Samples (2–3 mM) for NMR were prepared in 20 mM phosphate buffer in both D_2O and H_2O–D_2O (9:1, v/v) usually at pH 7.5. ^{1}H NMR spectra were acquired on a Varian Unity 500 and a JEOL Lambda 500 spectrometer usually at 25 °C using the super-WEFT pulse sequence,[11] typically with a spectral width of 100 kHz. The data were processed using 20–50 Hz exponential line broadening as apodization.
11 T. Inubushi and E. D. Becker, *J. Magn. Reson.*, 1983, **51**, 128.
12 The green NiR from *A. cycloclastes* was isolated and purified as described previously.[13] The isolated enzyme possesses *ca.* 10% copper at its T2 centre and this sample was used for the T2D spectra.
13 S. Suzuki, S. Deligeer, K. Yamaguchi, K. Kataoka, K. Kobayashi, S. Tagawa, T. Kohzuma, S. Shidara and H. Iwasaki, *J. Biol. Inorg. Chem.*, 1997, **2**, 265.
14 The incorporation of copper at the T2 centre of *A. cycloclastes* NiR was achieved by dialysing (Spectra/Por CE DispoDialyzer, MWCO 10000) the protein in 50 mM Tris buffer at pH 7.0 against a similar buffer solution containing 1 mM $Cu(NO_3)_2$. Dialysis was carried out over 4–7 days immediately prior to the acquisition of NMR spectra. The excess copper was dialysed out of the protein solution against 50 mM Tris at pH 7.0.
15 The blue NiR from *A. xylosoxidans* was isolated and purified according to a literature method.[13] The isolated enzyme possesses *ca.* 70% copper at its T2 centre. The T2D protein was obtained as described in the literature[13] and contained < 10% copper at the type 2 centre.
16 Spectra of green NiR in the presence of nitrite were also obtained, and exhibited very little difference to those of either NiR or of the T2D enzyme. This shows that binding of the substrate at the type 2 centre has very little effect on the structure and electronic properties of the type 1 site.
17 Spectra were obtained of the blue NiR with and without Cu(II) at its type 2 centre. No significant differences were observed between these spectra. For example the δ_{obs} and T_1 values of peak d in blue NiR are 26.5 and 2.9 ms, respectively.
18 In the spectrum of the T2D blue NiR in H_2O–D_2O (9:1, v/v) there is an indication of a second exchangeable resonance at δ *ca.* 46. However, this peak appears to be quite broad and overlaps with resonances a and b making any definite conclusions impossible.
19 The type 1 ligands are numbered as in *A. cycloclastes* NiR. The corresponding residues in *A. xylosoxidans* NiR are His89, Cys130, His139 and Met144.
20 Analysis of the crystal structures of the green and blue NiRs reveals that one of the Cu–S$^{\delta}$–C$^{\gamma}$–H$^{\gamma}$ dihedral angles is in the region 50°–60°. If the contact shift of the Met C$^{\gamma}$H$_2$ protons follow a $\cos^2\theta$ Karplus law, where θ is the Cu–S$^{\delta}$–C$^{\gamma}$–H$^{\gamma}$ dihedral angle, then small changes in this angle could result in quite large differences in the observed shift. It should be noted that in the crystal structures of *A. cycloclastes* NiR small differences (greater than the estimated precision of 3°) are observed in these dihedral angles for the type 1 sites in the different monomers, and also in the proteins crystallised under different conditions (see ref. 3).

Negative solvatochromism of azo dyes derived from (dialkylamino)thiazole dimers

Jae Joon Kim,[a] Kazumasa Funabiki,[a] Hiroshige Muramatsu,[a] Katsuyoshi Shibata,[a] Sung Hoon Kim,[b] Hisayoshi Shiozaki,[c] Horst Hartmann[d] and Masaki Matsui*[a]

[a] *Department of Chemistry, Faculty of Engineering, Gifu University, Yanagido, Gifu 501-1193, Japan. E-mail: matsui@apchem.gifu-u.ac.jp*
[b] *Department of Dyeing and Finishing, College of Engineering, Kyungpook National University, Taegu, 702-701, Korea*
[c] *Technology Research Institute of Osaka Prefecture, Kishibe-naka 1-18-13, Suita 564-0002, Japan*
[d] *Fachhochschule Merseburg, Fachbereich Chemie, D-06217 Merseburg, Germany*

Received (in Cambridge, UK) 1st March 2000, Accepted 23rd March 2000
Published on the Web 13th April 2000

The first examples of negative solvatochromism in neutral azo dyes containing both strongly electron-donating bis-(dialkylamino)thiazolyl and electron-withdrawing 4-(trifluoromethylsulfonyl)phenyl or 2-thiazolyl moieties are reported.

The absorption bands of azo dyes depend on the combination of electron-donating and -withdrawing moieties in the molecules.[1] Recently, (dialkylamino)thiazole dimers, assumed to be very electron-rich substrates, have been synthesized.[2] It was of interest to examine the solvatochromic behavior of azo dyes having both strong electron-donating and -withdrawing moieties in a molecule. We report here, the solvatochromism of azo dyes derived from (dialkylamino)thiazole dimers.

The azo dyes **1a**–**d** and **1a′** derived from (dialkylamino)thiazole dimers were synthesized in low to good yields by the diazotisation-coupling reaction shown in Scheme 1.[3,4] The absorption spectrum of **1a** is shown in Fig. 1. The azo dye **1a** showed absorption bands at 637 nm (ε = 82 000 dm^3 mol^{-1} cm^{-1}) and 449 (25 000) in dichloromethane, while the absorption spectra of the other azo dyes are summarized in

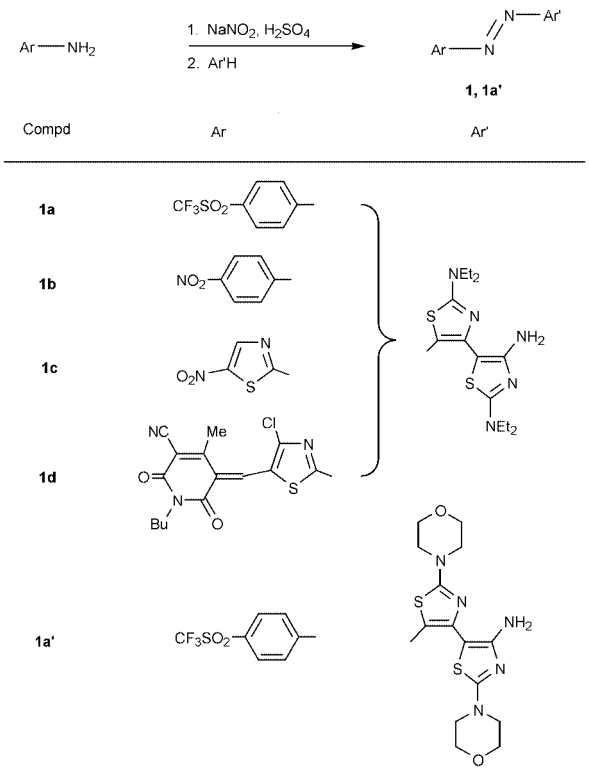

Scheme 1

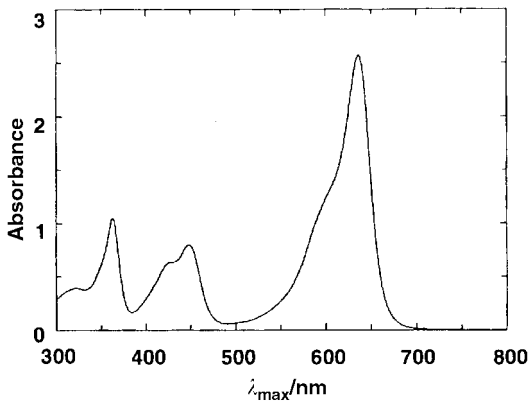

Fig. 1 Absorption spectrum of **1a** in dichloromethane.

Table 1. The lower energy absorption band of **1d**, containing a very strong electron-withdrawing moiety, was most bathochromic among the azo dyes **1**.

Neutral azo dyes have been reported to show a positive solvatochromism[5–12] while two types of ionic azo dyes, 4-[2-(triphenylphosphonio)phenylazo]phenolates and 2-(1-methylpyridiniumazo)- and 2-(1-methylqunoliniumazo)-tetracyanocyclopentadienides, have been reported to reveal negative solvatochromic behavior.[13,14]

Interestingly, the azo dyes **1** showed either positive and negative solvatochromism depending on the diazo components. Typical solvatochromism is shown in Fig. 2 where the λ_{max} values of the first (lower energy) absorption band are plotted against the molar electronic transition energy (E_T) of the solvent.[15] Azo dyes **1a**, **1c** and **1d** showed negative solvatochromism, especially, so for **1d**. While azo dye **1b** showed a positive solvatochromic behavior, azo dye **1a′** also showed negative solvatochromic behavior.[16] Thus the azo dyes containing very strong electron-withdrawing moieties such as 4-(trifluoromethylsulfonyl)phenyl and 2-thiazolyls showed negative solvatochromism. This result is in contrast to a positive

Table 1 Absorption spectra of **1a**–**d** and **1a′** in dichloromethane

Compound	λ_{max}/nm	ε/dm^3 mol^{-1} cm^{-1}
1a	449	25 000
	637	82 000
1b	431	29 000
	669	64 000
1c	441	35 000
	665	48 000
1d	457	51 000
	737	24 000
1a′	445	22 000
	641	69 000

DOI: 10.1039/b001697g

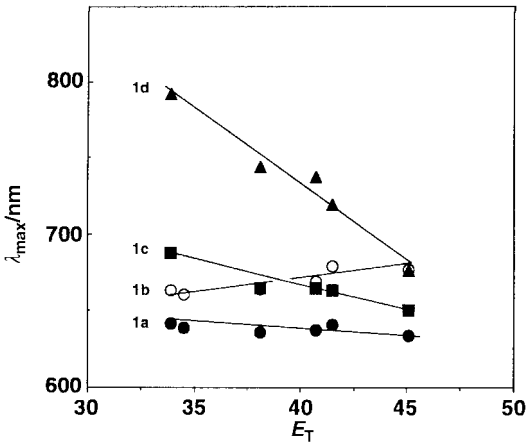

Fig. 2 Solvatochromism of azo dyes **1**. The absorption spectra were measured in toluene (E_T: 33.9 kcal mol^{-1}), diethyl ether (34.5), ethyl acetate (38.1), dichloromethane (40.7), benzonitrile (41.5), dimethyl sulfoxide (45.1). Azo dyes **1c** and **1d** were insoluble in diethyl ether.

solvatochromism of the near-IR absorbing push–pull 5-acetylamino-4-[2-(4-chloro-5-substituted thiazolylazo)]-2-methoxy-*N*-(2-hexyl)aniline derivative.[17] The structures of the azo dyes were optimized by a MOPAC AM-1 program and the dipole moment (μ) of the azo dyes in the excited and ground states were calculated by a CNDO/S program. The μ values of **1b** in the ground and excited states were calculated to be 14.58 and 18.98 D, respectively. This calculation is consistent with the positive solvatochromic behavior of **1b**. Interestingly, the electron-withdrawing nature of the nitro group [$\sigma_p(NO_2)$ = 0.78] was not strong enough to cause a negative solvatochromism in the azo dyes **1**. The ground state of the 4-(trifluoromethylsulfonyl) derivative **1a** [$\sigma_p(CF_3SO_2)$ = 0.93][18] was calculated to be slightly more polar (μ = 15.96 D) than the excited state (15.85 D). The ground state of **1d** was also calculated to be more polar (24.67 D) than the excited state (23.26 D). These results support the negative solvatochromism of **1a** and **1d**.[19]

The possible structures of **1a** in the ground and excited states are depicted in Fig. 3.

More polar charge-separated diazamerocyanine structures **A**, **A′** and **A″** could be predominant in the ground state and with a less polar neutral azo form **B** in the excited state. The other azo

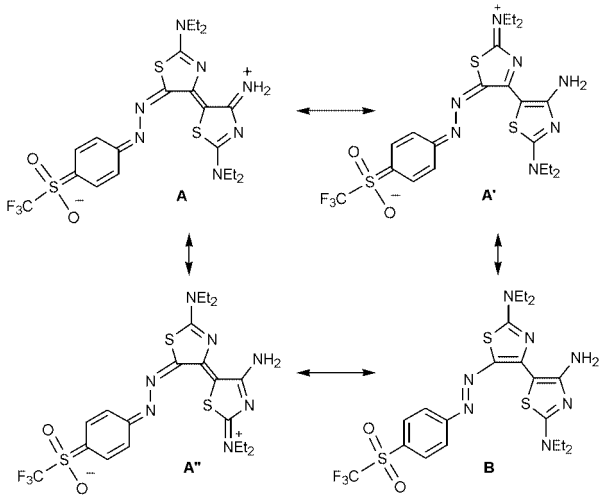

Fig. 3 Possible structures in **1a**.

dyes **1c**, **1d** and **1a′** which showed negative solvatochromism can also have charge-separated diazamerocyanine structures. This is different from the reported negatively solvatochromic azo compounds, which can have charge-separated azo and neutral diazamerocyanine structures in the ground and excited states, respectively.[13,14]

In conclusion, we have synthesized azo dyes derived from strong electron-donating coupling components, (dialkylamino)thiazole dimers. The azo dyes derived from diazo components with strong electron-withdrawing substituents such as 4-(trifluoromethylsulfonyl)aniline and 2-aminothiazoles showed a negative solvatochromism, owing to the ground state having a predominantly charge-separated polar diazamerocyanine structure.

This work was supported by Grant-in-aid for Scientific Research (No. 11650869) from the Ministry of Education, Science, Sport and Culture. The authors are grateful to Dr Kazuko Shirai and Professor Dr Masaru Matsuoka for the elemental analysis measurement and useful discussions.

Notes and references

1 J. Fabian and H. Hartmann, in *Light Absorption of Organic Colorants*, Springer-Verlag, Berlin, 1980.
2 R. Flaig and H. Hartmann, *J. Heterocycl. Chem.*, 1997, **34**, 1291.
3 *Typical procedure* for the synthesis of **1**: to a DMF solution (5 mL) of arylamines (1.5 mmol) were added sodium nitrite (1.5 mmol) and concentrated sulfuric acid (0.5 mL), and the mixture was stirred at 0 °C for 3 h. To the mixture was added a DMF solution (15 mL) of coupling components (1.5 mmol), and the mixture was stirred at room temperature overnight. After the reaction was completed, the mixture was poured into water, neutralized and extracted with dichloromethane (200 mL × 2). After evaporation of the solvent *in vacuo*, the product was isolated by column chromatography (SiO_2, AcOEt) and recrystallized from chloroform–hexane. All the products showed satisfactorily spectral and elemental analysis data. **1a**: yield 30 %; mp 218–220 °C (Found: C, 45.16; H, 4.69: N, 17.03. $C_{21}H_{26}F_3N_7O_2S_3$ requires C, 44.91; H, 4.67: N, 17.46%); δ_H(400 MHz, $CDCl_3$) 1.36 (12H, t, *J* 7.1 Hz), 3.50–3.78 (8H, m), 7.61 (2H, d, *J* 9.0 Hz), 7.83 (2H, d, *J* 9.0 Hz); *m/z* (EI, 70 eV) 561 (M^+; 100), 444 (14), 428 (19), 398 (32), 263 (30), 226 (17), 135 (53), 99 (29), 77 (34), 72 (56).
4 Compound **1d** was prepared by diazotisation-coupling reaction followed by condensation with a pyridone derivative: yield 30%; mp 269 °C (decomp.) (Found: C, 50.25; H, 5.27; N, 20.20. $C_{29}H_{35}ClN_{10}O_2S_3$ requires C, 50.68; H, 5.13; N, 20.38%); δ_H(400 MHz, $CDCl_3$) 0.90 (3H, t, *J* 7.3 Hz), 1.29–1.47 (16 H, m), 2.46 (3H, s), 3.74–3.86 (8H, m), 3.94 (2H, t, *J* 7.3 Hz), 7.83 (1H, s).
5 M. G. Hutchings, P. Gregory, J. S. Campbell, A. Strong, J.-P. Zamy, A. Lepre and A. Mills, *Chem. Eur. J.*, 1997, **3**, 1719.
6 C. Machado, M. G. Nascimento and M. C. Rezende, *J. Chem. Soc., Perkin Trans. 2*, 1994, 2539.
7 A. T. Peters and A. Gbadamosi, *J. Chem. Technol. Biotechnol.*, 1992, **53**, 301.
8 D.-M. Shin, K. S. Schanze and D. G. Whitten, *J. Am. Chem. Soc.*, 1989, **111**, 8494.
9 D.-M. Shin and D. G. Whitten, *J. Am. Chem. Soc.*, 1988, **110**, 5206.
10 S. Kobayashi, H. Yokoyama and H. Kamei, *Chem. Phys. Lett.*, 1987, **138**, 333.
11 N. Nishimura, T. Tanaka, M. Asano and Y. Sueshi, *J. Chem. Soc., Perkin Trans. 2*, 1986, 1893.
12 H. Mustroph and J. Epperlein, *J. Prakt. Chem.*, 1980, **322**, 305.
13 D. W. Allen and X. Li, *J. Chem. Soc., Perkin Trans. 2*, 1997, 1099.
14 H. Quast and E. Schmitt, *Liebigs Ann. Chem.*, 1970, **732**, 43.
15 C. Reichardt, *Chem. Rev.*, 1994, **94**, 2319.
16 **1a′**: 642 (toluene), 641 (dichloromethane), 639 nm (Me_2SO).
17 K. A. Bello and J. Griffiths, *J. Chem. Soc., Chem. Commun.*, 1986, 1639.
18 L. M. Yagupol'skii and L. Z. Gandel'sman, *J. Gen. Chem. USSR.*, 1965, **35**, 1259.
19 **1c**: ground state: 14.99 D, excited state: 14.86 D. **1a**: ground state: 14.50 D, excited state: 12.89 D.

Positioning dependent anion recognition by thiourea-based chromoionophores *via* hydrogen bonding in aqueous vesicle solutions†

Takashi Hayashita,* Tsunenobu Onodera, Ryo Kato, Seiichi Nishizawa and Norio Teramae*

Department of Chemistry, Graduate School of Science, Tohoku University, Aramaki, Sendai 980-8578, Japan. E-mail: tera@anal.chem.tohoku.ac.jp

Received (in Cambridge, UK) 13th December 1999, Accepted 28th March 2000
Published on the Web 13th April 2000

A cationic vesicle interface exhibited a filter function for less hydrophobic anions, and highly selective anion recognition *via* hydrogen bonding was achieved by thiourea-based chromoionophores (C_n-TU) located deep inside the vesicle.

Selective recognition and *in situ* sensing of biologically important anions are of current interest in host-guest chemistry.[1,2] Several synthetic neutral receptors possessing amide,[3] urea[4] and thiourea moieties[5] as a binding site for anion recognition have been reported, in which the binding takes place exclusively *via* hydrogen bonding interaction. Recently we have shown that thiourea-based chromoionophore (C_1-TU) interacts strongly with anions *via* formation of hydrogen bonds in non-aqueous media (Fig. 1) and produces a readily observable color change with a selectivity of $MeCO_2^-$ > $H_2PO_4^-$ > Cl^- >> ClO_4^-, reflecting anion basicity.[6] For anion sensing in aqueous media, however, the hydrogen bonding interaction of the binding site encounters significant interference from anion hydration. In biological systems, hydrophobic microenvironments produced by the supramolecular structure of receptors are cleverly utilized for ion recognition.[7] Thus, a simple strategy to achieve anion recognition in water is to incorporate the chromoionophore into hydrophobic regions, such as vesicle media, to shield their binding site from water.[8–10]

To develop an anion sensing system in water using a chromoionophore/vesicle complex as a mimic of a biological system, two factors are important: (i) the positioning of the thiourea binding site inside the vesicle, and (ii) the role of the cationic vesicle interface in anion recognition. To elucidate these factors, we have designed novel thiourea-based chromoionophores having various length of alkyl chains (C_n-TU)[11] and examined their anion recognition function in cationic vesicle solutions. We report here, the first positioning-dependent anion recognition by C_n-TU chromoionophore/vesicle complexes in water.

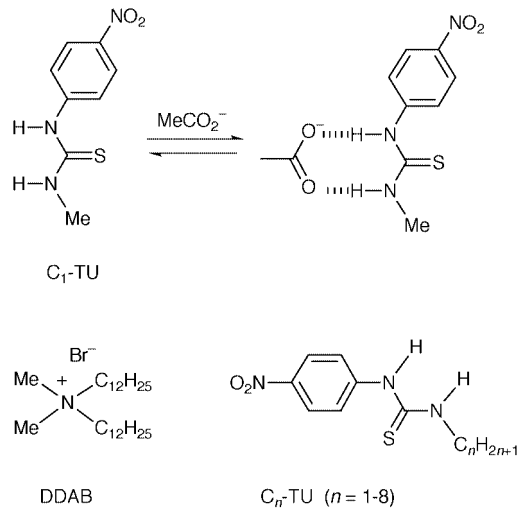

Fig. 1 Anion recognition by thiourea-based chromoionophores.

As a well known cationic amphiphile which forms single lamellae vesicles in water, didodecyldimethylammonium bromide (DDAB) was selected.[12] Films of C_n-TU/DDAB (1:10 mol%) were prepared by evaporation of a chloroform solution containing 1.0×10^{-5} mol C_n-TU and 1.0×10^{-4} mol DDAB on the inside of 100 mL-round bottomed flask. The films were left under vacuum for 1 day, followed by hydration with 10 mL of pure water at 40 °C by vortex mixing. The solution temperature was maintained at 40 °C while being probe-sonicated for 3 min using a power of 30–40 W. The resultant clear solution of C_n-TU/DDAB was diluted 20× with 0.01 M 2-[4-(2-hydroxyethyl)-1-piperazinyl]ethanesulfonic acid buffer (HEPES, pH 7.50) containing guest anions as sodium salts.

In acetonitrile, all C_n-TU show the same UV-VIS spectra with λ_{max} at 340 nm ($\varepsilon = 1.4 \times 10^4$ M^{-1} cm^{-1}), which can be assigned as an intramolecular charge transfer (CT) absorption band, despite the difference in their alkyl chain lengths (n = 1–8). However in DDAB solution, the λ_{max} of C_n-TU shifts monotonously to higher wavelengths with an increase in alkyl chain lengths from 338 nm (ε = 1.1 x10^4 $M^{-1}cm^{-1}$) for C_1-TU to 361 nm (ε = 1.5 x10^4 M^{-1} cm^{-1}) for C_8-TU (Fig. 2). The CT absorption bands generally show a bathochromic shift when the solvent polarity is increased.[13] Thus the results in Fig. 2 clearly reveal that the positioning of chromophore binding sites is controlled by the alkyl chain length of C_n-TU; the binding site of C_n-TU bearing a long alkyl chain is located on the surface of the cationic vesicle (hydrophilic microenvironment), whereas that of C_n-TU bearing a short alkyl chain is positioned deep within the vesicle (hydrophobic microenvironment).

The thiourea proton associated with the *p*-nitrophenyl unit dissociates under basic conditions and a new peak in the UV–VIS spectrum appears at 450 nm. Thus the apparent pK_a of C_n-TU in DDAB solution can be assessed by pH titration analysis.[14] Observed pK_a values are 9.9 ± 0.1 for C_1-TU and 9.5 ± 0.1 for C_8-TU. The larger pK_a value observed for C_1-TU supports the finding that the binding site of C_1-TU is located in the hydrophobic microenvironment. In DMSO-d_6, the ^{1}H NMR spectra of the vicinal phenyl protons in all C_n-TU show the same chemical shifts at δ 7.80/8.16. However in DDAB–D_2O solution, the chemical shifts of these phenyl protons are δ 8.00/8.21 for C_1-TU and δ 8.22/8.39 for C_8-TU. The chemical shifts of C_1-TU observed at higher magnetic fields are ascribed

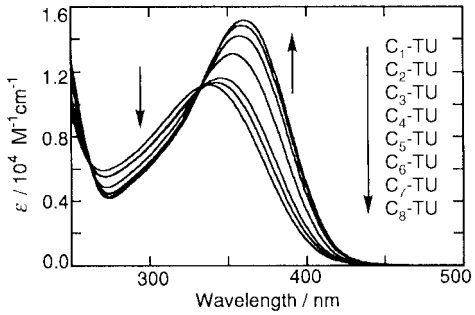

Fig. 2 UV-VIS spectra of C_n-TU in DDAB; [C_n-TU] = 5.0×10^{-5} M in 5.0×10^{-4} M DDAB solution, pH = 5.5–6.0 at 25 °C.

† Electronic supplementary information (ESI) available: response profiles of C_n-TU in DDAB upon addition of Cl^- and their equilibrium analysis. See http://www.rsc.org/suppdata/cc/a9/a909758i/

DOI: 10.1039/a909758i

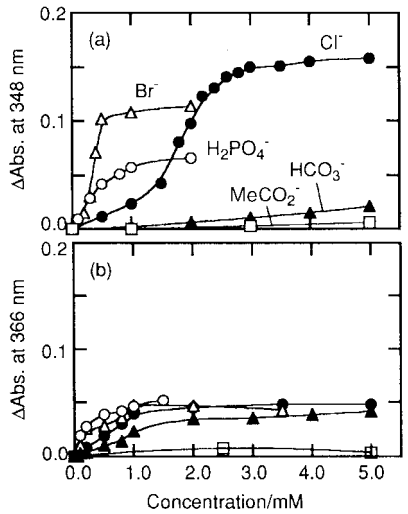

Fig. 3 Effect of anion concentration upon the spectral response of (a) C_1-TU and (b) C_8-TU in DDAB. (○) $H_2PO_4^-$, (△) Br^-, (●) Cl^-, (▲) HCO_3^-, (□) $MeCO_2^-$. [C_n-TU] = 5.0×10^{-5} M in 5.0×10^{-4} M DDAB solution. pH = 7.5 (adjusted by HEPES buffer at 25 °C).

to the hydrophobic effect,[15] which is additional evidence that C_1-TU is present deep within the vesicle.

The spectral responses of C_n-TU/DDAB complexes in water upon addition of anions were examined at pH 7.5 (Fig. 3). Increasing the anion concentration produced a bathochromic shift in λ_{max} with an enhanced molar absorptivity. These spectral changes are ascribed to (i) complex formation of anions with the thiourea moiety *via* hydrogen bonding as reported in acetonitrile,[6] and/or (ii) changes in the location of the chromophore within the vesicle due to the hydrophilic nature of the anion complexes. It is interesting that C_n-TU/DDAB complexes in water exhibit no response for $MeCO_2^-$, which differs from the response selectivity recorded in acetonitrile.[6] Since $MeCO_2^-$ is strongly hydrated in water,[16] the low binding affinity of $MeCO_2^-$ on the surface of DDAB vesicle may cause this poor response. This is a unique filter function of the cationic vesicle interface. The observed selectivity for C_1-TU/DDAB complex is Br^- > $H_2PO_4^-$ > Cl^- >> HCO_3^-, $MeCO_2^-$, reflecting a Hofmeister series [Fig. 3(a)].[16] On the other hand, no distinct selectivity is recorded for the C_8-TU/DDAB complex [Fig. 3(b)]. The spectral change (ΔAbs) upon addition of HCO_3^- is even larger for C_8-TU than for C_1-TU. This indicates that the binding of fewer hydrophobic anions takes place mainly on the vesicle surface. For C_n-TU with alkyl chain lengths from n = 2 to 7, an intermediate response between those of C_1-TU and C_8-TU is clearly observed.†

Thus it is apparent that the response selectivity is strongly affected by the positioning of C_n-TU in DDAB vesicles (Fig. 4).

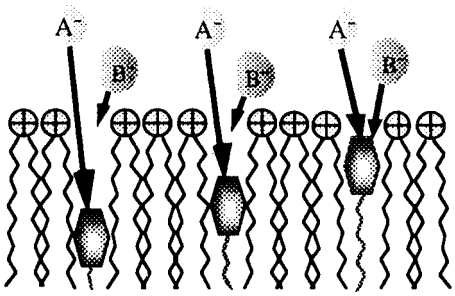

Fig. 4 Positioning-dependent anion recognition by C_n-TU in DDAB.

This is the first report that positioning dependent anion recognition can be carried out in aqueous vesicle solution.

In summary, the shifts in λ_{max}, pK_a, and ^{1}H NMR resonances revealed that the positioning of chromophore binding sites in DDAB was successfully controlled by the alkyl chain length of C_n-TU. This first report of positioning-dependent anion recognition *via* hydrogen bonding has been achieved by use of C_n-TU/DDAB complexes in water. Based on the filter function of the vesicle interface as well as the depth dependent distribution of the chromoionophores, this molecular assembled system should provide a new methodology for specific ion and molecule recognition in aqueous solutions.

This work was supported by a Grant-in-Aid for Scientific Research (No. 11304054) from the Ministry of Education, Science, Sports, and Culture, Japan.

Notes and references

1 P. D. Beer and D. K. Smith, *Prog. Inorg. Chem.*, 1997, **46**, 1.
2 F. P. Schmidtchen and M. Berger, *Chem. Rev.*, 1997, **97**, 1609.
3 R. C. Jagessar and D. H. Burns, *Chem. Commun.*, 1997, 1685; J. E. Redman, P. D. Beer, S. W. Dent and M. G. B. Drew, *Chem. Commun.*, 1998, 231; S. Watanabe, O. Onogawa, Y. Komatsu and K. Yoshida, *J. Am. Chem. Soc.*, 1998, **120**, 229.
4 T. R. Kelly and M. H. Kim, *J. Am. Chem. Soc.*, 1994, **116**, 7072; J. Scheerder, J. P. M. Duynhouen, J. F. J. Engbersen and D. N. Reinhoudt, *Angew. Chem., Int. Ed. Engl.*, 1996, **35**, 1090; R. C. Jagessar, M. Shang, W. R. Scheidt and D. H. Burns, *J. Am. Chem. Soc.*, 1998, **120**, 11 684.
5 C. S. Wilcox, E.-I. Kim, D. Romano, L. H. Kuo, A. L. Burt and D. D. Corrain, *Tetrahedron*, 1995, **51**, 621; S. Nishizawa, P. Bühlmann, M. Iwao and Y. Umezawa, *Tetrahedron Lett.*, 1995, **36**, 6483; K. P. Xiao, P. Bühlmann and Y. Umezawa, *Anal. Chem.*, 1997, **69**, 1038; S. Nishizawa and N. Teramae, *Anal. Sci.*, 1997, **13** (suppl.), 485; S. Nishizawa, H. Kaneda, T. Uchida and N. Teramae, *J. Chem. Soc., Perkin Trans. 2*, 1998, **2**, 2325; Y. Tobe, S. Sasaki, M. Mizuno and K. Naemura, *Chem. Lett.*, 1998, 835.
6 S. Nishizawa, R. Kato, T. Hayashita and N. Teramae, *Anal. Sci.*, 1998, **14**, 595.
7 See, for example: H. Luecke and F. A. Quiocho, *Nature*, 1990, **347**, 402.
8 For micelle and vesicle systems, see: J. S. Nowick and J. C. Chen, *J. Am. Chem. Soc.*, 1992, **114**, 1107; J. S. Nowick, J. S. Chen and G. Noronha, *J. Am. Chem. Soc.*, 1993, **115**, 7636; M. Onda, K. Yoshihara, H. Koyano, K. Ariga and T. Kunitake, *J. Am. Chem. Soc.*, 1996, **118**, 8524.
9 For monolayer/water system, see: K. Kurihara, K. Ohto, Y. Tanaka, Y. Aoyama and T. Kunitake, *J. Am. Chem. Soc.*, 1991, **113**, 444; K. Kurihara, K. Ohto, Y. Honda and T. Kunitake, *J. Am. Chem. Soc.*, 1991, **113**, 5077; D. Y. Sasaki, K. Kurihara and T. Kunitake, *J. Am. Chem. Soc.*, 1992, **114**, 10 994.
10 For solvent extraction and transport, see: D. M. Rudkevich, J. D. Mercer-Chalmers, W. Verboom, R. Ungaro, F. D. Jong and D. N. Reinhoudt, *J. Am. Chem. Soc.*, 1995, **117**, 6124; P. D. Beer, P. K. Hopkins and J. D. McKinney, *Chem. Commun.*, 1999, 1253; M. M. Murad, T. Hayashita, K. Shigemori, S. Nishizawa and N. Teramae, *Anal. Sci.*, 1999, **15**, 1185.
11 The structures were fully characterized by ^{1}H NMR spectroscopy and elemental analyses.
12 T. Kunitake and Y. Okahata, *J. Am. Chem. Soc.*, 1977, **99**, 3860; T. Kajiyama, A. Kumano, M. Takayanagi, Y. Okahata and T. Kunitake, *Chem. Lett.*, 1979, 645; Y. Okahata, R. Ando and T. Kunitake, *Ber. Bunsenges. Phys. Chem.*, 1981, **85**, 789.
13 C. Reichardt, *Solvents and Solvent Effects in Organic Chemistry*, VCH, Weinheim, 2nd edn., 1988; R. Helburn, Y. Dijiba, G. Mansour and J. Maxka, *Langmuir*, 1998, **14**, 7147.
14 T. Hayashita, K. Kunogi, H. Yamamoto and S. Shinkai, *Anal. Sci.*, 1997, **13** (Suppl.), 161.
15 A. A. Ribeiro and E. A. Dennis, *Biochemistry*, 1975, **14**, 3746; F. Podo, A. Ray and G. Nemethy, *J. Am. Chem. Soc.*, 1973, **95**, 6164.
16 D. Wegmann, H. Weiss, D. Ammann, W. E. Morf, E. Pretsch, K. Sugahara and W. Simon, *Mikrochim. Acta*, 1984, **3**, 1; F. Hofmeister, *Arch. Exp. Pathol. Pharmakol.*, 1888, **24**, 247.

ChemComm

Unusual reaction of azetidine-2,3-diones with primary amines. Straightforward asymmetric synthesis of α-amino acid and peptide derivatives

Benito Alcaide,* Pedro Almendros and Cristina Aragoncillo

Departamento de Química Orgánica I, Facultad de Ciencias Químicas, Universidad Complutense, 28040-Madrid, Spain. E-mail: alcaideb@eucmax.sim.ucm.es

Received (in Cambridge, UK) 9th December 1999, Accepted 27th March 2000
Published on the Web 13th April 2000

An unprecedented one-step synthesis of unnatural α-amino acid and peptide derivatives, in both the racemic and optically pure forms, using azetidine-2,3-diones as building blocks has been developed by treatment with primary amines.

As the defining subunit of peptides and proteins, α-amino acids play a central role in chemistry and biology, and the development of new stereoselective strategies for the synthesis of α-amino acids has evolved in a very active field in recent years.[1] In addition to the need for large-scale preparation of the 20 common proteinogenic α-amino acids, there is an ever increasing demand for the much rarer nonproteinogenic α-amino acids. Peptides containing α-amino acids that are not naturally occurring can also be used in biological studies, either to provide information on the active conformation of related peptides,[2] or as enzyme inhibitors.[3] On the other hand, while the chemistry of 6-oxopenicillanates and 7-oxocephalosporanates has been the focus of intense effort,[4] little was known about the synthesis and application of monocyclic azetidine-2,3-diones[5] and even less on their optically active derivatives,[6] until Palomo *et al.* elegantly merged into this field.[7] In our ongoing project directed toward the asymmetric synthesis and synthetic applications of functionalised 2-azetidinones,[8] we have recently described both the allylation and the stereoselective Baylis–Hillman reaction of enantiopure azetidine-2,3-diones.[9] In connection with this work, we report here, the unexpected manner in which azetidine-2,3-diones **1** and a variety of primary amines undergo reaction to give novel α-amino acid and peptide derivatives **2** (Scheme 1). The concise and convergent approach described herein presents a practical opportunity to connect the rapidly expanding fields of β-lactam chemistry and α-amino acid and peptides.[10]

Starting substrates, azetidine-2,3-diones **1**, were prepared both in racemic and in optically pure forms following our previously reported methods. Racemic compound **1a** was obtained from 3-methylidene-4-phenyl-2-azetidinone by dihydroxylation followed by oxidative cleavage with $NaIO_4$.[11] Enantiopure azetidine-2,3-diones (+)-**1b** and (−)-**1c** were available in high yield by Swern oxidation of the corresponding 3-hydroxy-β-lactam.[9] We sought to explore the reactivity of azetidine-2,3-diones **1** with various primary amines. To our surprise, under the usual conditions utilized for imine formation,† α-amino acid derivatives **2** can be smoothly prepared in both the racemic and enantiopure forms, instead of the expected imino-β-lactams (Table 1).‡ This result is in sharp contrast with the smooth reaction of related indoline-2,3-diones with primary amines to afford imino-γ-lactams.[12] Of particular interest was the reaction of azetidine-2,3-diones **1** with α-amino esters such as methyl glycinate or methyl alaninate, showing the utility of this approach in the rapid synthesis of optically pure peptides (Table 1, entries 4, 8 and 9).§ Treatment of azetidine-2,3-dione (+)-**1b** with (*S*)-alanine methyl ester forms in 55% yield the peptide **(–)-2i**, bearing three chiral centers.¶ Compound (−)-**2i** showed a single set of signals in ^{1}H NMR spectrum, thus proving that this transformation proceeded without detectable racemization.

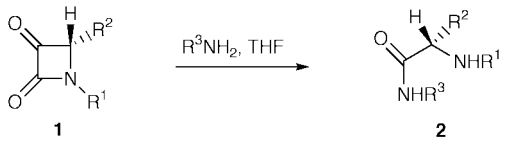

1 **2**

Scheme 1

Palomo *et al.* have reported the synthesis of some α-amino acid derivatives from *N*-carboxy anhydrides (NCA), with NCAs being obtained through Baeyer–Villiger oxidation of azetidine-2,3-diones.[7] However, our one-step flask synthesis of α-amino acid derivatives starting from azetidine-2,3-diones is significant and should have application in organic synthesis.

This process could be rationalized through an initial nucleophilic addition of the amine to the ketone moiety of the azetidine-2,3-dione **1**, forming an intermediate carbinolamine **3**. This intermediate **3** may react through two different pathways to give the expected 3-imino-β-lactam **4** or the intermediate **5**, but presumably evolves to the fused aziridine-β-lactam **5**. We believe that the N1–C2 bond of intermediate **5** should be very labile, evolving to aziridinone **6**. Compound **6** under the reaction conditions furnish *N*-formylamide **7**. Intermediate **7** appears as the final, not isolable product, in the reaction. It is well known that *N*-formylamides, related to **7** smoothly lose CO under basic conditions to give the corresponding NH-amides.[13] Furthermore, heating in a sealed tube at 90 °C may well favour

Table 1 Synthesis of *α*-amino acid and dipeptide derivatives **2**

Entry	Substrate	R^1	R^2	R^3	Product	Yield(%)[b]	$[\alpha]_D$[c]
1	(±)-**1a**	PMP[a]	Ph	$PhCH_2$	(±)-**2a**	45	-
2	(±)-**1a**	PMP	Ph	allyl	(±)-**2b**	77	-
3	(±)-**1a**	PMP	Ph	propargyl	(±)-**2c**	49	-
4	(±)-**1a**	PMP	Ph	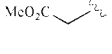	(±)-**2d**	60	-
5	(+)-**1b**	PMP	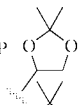	$PhCH_2$	(+)-**2e**	50	41.7
6	(+)-**1b**	PMP	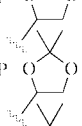	allyl	(+)-**2f**	45	17.0
7	(+)-**1b**	PMP	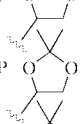	propargyl	(+)-**2g**	48	8.5
8	(+)-**1b**	PMP	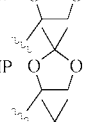	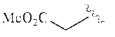	(−)-**2h**	50	−2.4
9	(+)-**1b**	PMP	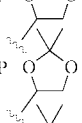	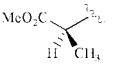	(+)-**2i**	55	18.7
10	(−)-**1c**	Allyl	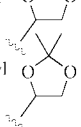	$PhCH_2$	(−)-**2j**	58	−34.0

[a] PMP = 4-$MeOC_6H_4$. [b] Yield of pure, isolated product with correct analytical and spectral data. [c] Specific rotation is given in degrees dm^{-1} at 20 °C (*c* 1.0, $HCCl_3$).

DOI: 10.1039/a909688d

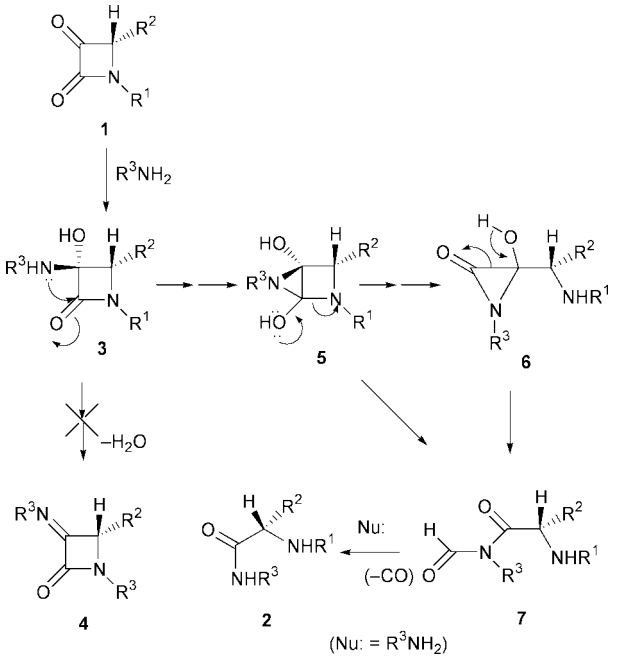

Scheme 2

the suggested CO extrusion and hence the shorter time needed for the thermal process in comparison with the reaction at room temperature (Scheme 2).

The suggestion that the reactive species involved in the reaction is the aziridine **5**, is presently made to explain the formation of α-amino acid derivatives rather that of the expected 3-imino-β-lactams. The different behaviour of azetidine-2,3-diones and pyrroline-2,3-diones may be due to differences in the carbinolamine presumably involved in the reaction, perhaps in the easier opening tendecy of the more strained four-membered ring.

In conclusion, a rapid one-step synthesis of unnatural α-amino acid and peptide derivatives both in racemic and in optically pure forms, starting from azetidine-2,3-diones has been developed. Furthermore, as far as we know, this unusual reaction of azetidine-2,3-diones with primary amines to afford α-amino acid derivatives is unprecedented, allowing structure variability and facile incorporation of functional groups. Studies concerning the scope and generality of this methodology are underway in our laboratory, and further details will be reported in due course.

We would like to thank the DGES (MEC-Spain, grant PB96-0565) for financial support. P. Almendros thanks the DGES (MEC, Spain) for a 'Contrato de Incorporación'. C. Aragoncillo thanks the DGI (CEC-Comunidad de Madrid-Spain) for a fellowship.

Notes and references

† Preliminary experiments were carried out under the usual anhydrous conditions utilized for the formation of imines, using $MgSO_4$, but we then realised that this was not necessary. Also, initial experiments with the most volatile amines were carried out in large excess (10 equiv.), however we later performed the reaction using equimolecular amounts of amine/substrate obtaining the same results as previously. Besides, we have carried out the experiments either with or without argon and with or without rigurously dry and degassed THF, obtaining similar results in all cases.

‡ No loss of optical purity was evident by ^{1}H NMR spectroscopy in presence of a chiral shift reagent of europium(III).

§ *Representative experimental procedures* for the synthesis of α-amino acid and dipeptide derivatives **2**: *method A* [Compounds **2a**–**c**, (−)-**2f**–**g**]: A solution of the appropriate amine (0.5 mmol) in tetrahydrofuran (1 mL) was added to a solution of the azetidine-2,3-dione **1** (0.5 mmol) in tetrahydrofuran (5 mL) and the solution was heated in a sealed tube at 90 °C for 2–6 h. The reaction mixture was allowed to cool to room temperature, the solvent removed under reduced pressure and after flash chromatography eluting with hexanes–ethyl acetate or dichloromethane–ethyl acetate, compounds **2** were obtained in analytically pure form.

Method B [Compounds **2a**, (−)-**2d**–**e**, (−)-**2h**–**j**]: a solution of the appropriate amine (0.5 mmol) in tetrahydrofuran (0.1 mL) was added to a solution of the azetidine-2,3-dione **1** (0.5 mmol) in tetrahydrofuran (5 mL) and the solution stirred at room temperature for 2–24 h. Compound (−)-**2j** required more prolonged reaction time (4 days). The solvent was removed under reduced pressure and after flash chromatography eluting with hexanes–ethyl acetate or dichloromethane–ethyl acetate, compounds **2** were obtained in analytically pure form.

¶ All new compounds were fully characterised by spectroscopic data and microanalysis and/or HRMS.

1 For reviews, see: R. O. Duthaler, *Tetrahedron*, 1994, **50**, 1539; R. M. Williams, *Synthesis of Optically Active α-Amino Acids*, Pergamon, Oxford, 1989; G. M. Coppola and H. F. Schuster, *Asymmetric Synthesis. Construction of Chiral Molecules Using Amino Acids*, Wiley, New York, 1987.

2 For selected examples, see: M. D. Struthers, R. P. Cheng and S. Imperiali, *Science*, 1995, **271**, 342; J. W. Bryson, S. F. Betz, H. S. Lu, D. J. Suich, H. W. Zhou, R. T. O'Neil and W. F. Degrado, *Science*, 1995, **270**, 935; M. W. Nowak, P. C. Kearney, J. R. Sampson, D. A. Dougherty and H. A. Lester, *Science*, 1995, **268**, 439.

3 For reviews, see: A. Nangia and P. S. Chandrakala, *Current Science*, 1995, **68**, 699; R. B. Silverman, *Mechanism Based Enzyme Inactivation: Chemistry and Enzymology*, CRC Press, Boca Raton, FL, 1988.

4 For representative examples, see: Y. S. Cho, J. E. Lee and H. Y. Koh, *Tetrahedron Lett.*, 1999, **40**, 1725; J. D. Buynak, H. B. Borate, G. W. Lamb, D. D. Khasnis, C. Husting, H. Isom and U. Sriwardane, *J. Org. Chem.*, 1993, **58**, 1325; D. G. Brenner, *J. Org. Chem.*, 1985, **50**, 18.

5 L. A. Paquette and M. B. Isaac, *Heterocycles*, 1998, **47**, 107; M. Jayaraman, M. S. Manhas and A. K. Bose, *Tetrahedron Lett.*, 1997, **38**, 709.

6 L. A. Paquette, R. R. Rothhaar, M. Isaac, L. M. Rogers and R. D. Rogers, *J. Org. Chem.*, 1998, **63**, 5463; S. T. Hodgson, D. M. Hollinshead, S. V. Ley, C. M. R. Low and D. J. Willians, *J. Chem. Soc., Perkin Trans. 1*, 1985, 2375.

7 For selected examples of the potential of β-lactams as intermediates for the access to α- and β-amino acid-derived peptides, see: C. Palomo, J. M. Aizpurua, I. Ganboa and M. Oiarbide, *Amino Acids*, 1999, **16**, 321; C. Palomo, M. Oiarbide, A. Esnal, A. Landa, J. I. Miranda and A. Linden, *J. Org. Chem.*, 1998, **63**, 5838; C. Palomo, I. Ganboa, B. Odriozola and A. Linden, *Tetrahedron Lett.*, 1997, **38**, 3093; C. Palomo, M. Oiarbide and A. Esnal, *Chem. Commun.*, 1997, 691; C. Palomo, J. M. Aizpurua, I. Ganboa, F. Carreaux, C. Cuevas, E. Maneiro and J. M. Ontoria, *J. Org. Chem.*, 1994, **59**, 3123; F. P. Cossio, C. López, M. Oiarbide, C. Palomo, D. Aparicio and G. Rubiales, *Tetrahedron Lett.*, 1988, **29**, 3133.

8 B. Alcaide, P. Almendros and C. Aragoncillo, *Chem. Commun.*, 1999, 1913; B. Alcaide, I. M. Rodríguez-Campos, J. Rodríguez-López and A. Rodríguez-Vicente, *J. Org. Chem.*, 1999, **64**, 5377; B. Alcaide and P. Almendros, *Tetrahedron Lett.*, 1999, **40**, 1015; B. Alcaide, J. M. Alonso, M. A. Aly, E. Sáez, M. P. Martínez-Alcázar and F. Hernández-Cano, *Tetrahedron Lett.*, 1999, **40**, 5391.

9 B. Alcaide, P. Almendros and C. Aragoncillo, *Tetrahedron Lett.*, 1999, **40**, 7537.

10 Ojima *et al.* have developed a smart methodology for the synthesis of peptides and peptidomimetics starting from enantiopure 2-azetidinones by means of the β-lactam synthon method. See: I. Ojima and F. Delaloge, *Chem. Soc. Rev.*, 1997, **26**, 377; I. Ojima, *Adv. Asymmetric Synth.*, 1995, **1**, 95.

11 B. Alcaide, G. Esteban, Y. Martín-Cantalejo, J. Plumet, J. Rodríguez-López, A. Monge and V. Pérez-García, *J. Org. Chem.*, 1994, **59**, 7994.

12 J. W. Skiles and D. McNeil, *Tetrahedron*, 1990, **31**, 7277.

13 In the β-lactam series, it has been reported that *N*-formyl-β-lactams gives *NH*-β-lactams on treatment with Et_3N (cat.) in methanol: J. M. Aizpurua, F. P. Cossío and C. Palomo, *Tetrahedron Lett.*, 1986, **27**, 4359. According to the proposed mechanism some evolution of CO is expected in the course of the process. However, we believe that the reaction is carried out on a small scale (0.5 mmol) and is too slow to observe any appreciable gas evolution.

ChemComm

Acyclic imidoselenium(II) dihalides: synthesis and X-ray structures of $ClSe[N(Bu^t)Se]_nCl$ (n = 1, 2)

Tiina Maaninen,[ab] Tristram Chivers,*[a] Risto Laitinen*[b] and Elina Wegelius[c]

[a] *Department of Chemistry, University of Calgary, 2500 University Drive, N.W., Calgary, Alberta, Canada T2N 1N4. E-mail: chivers@ucalgary.ca*
[b] *Department of Chemistry, University of Oulu, PO Box 3000, FIN-90401 Oulu, Finland*
[c] *Department of Chemistry, University of Jyväskylä, PO Box 35, 40351 Jyväskylä, Finland*

Received (in Cambridge, UK) 7th February 2000, Accepted 29th March 2000

The reaction of $SeCl_2$ with *tert*-butylamine in THF yields the acyclic imidoselenium(II) dichlorides $ClSeN(Bu^t)NSeCl$ and $ClSeN(Bu^t)SeN(Bu^t)SeCl$, in addition to the six-membered ring $Se_3(NBu^t)_3$.

Numerous selenium–nitrogen (Se–N) compounds have been discovered in the past decade.[1–3] These include a number of nitride halides of Se(III) and Se(IV), *e.g.* the cyclic system $Se_3N_2Cl^+$,[4] the acyclic cations $N(SeCl)_2^+$ and $N(SeCl_2)_2^+$,[5,6] and the anion $N(SeCl_3)_2^-$.[7] Transient selenonitroso derivatives ArN=Se (Ar = 4-XC_6H_4, X = Br, Me; Ar = 2-XC_6H_4, X = SMe, SeMe) have been trapped as Diels–Alder adducts with dimethylbutadiene,[8] but oligomers of this unit [cyclic Se(II) imides] have not been described. The only known cyclic Se(II) imides, $Se_6(NBu^t)_2$ and $Se_9(NBu^t)_6$, contain Se–Se linkages.[9] We report here, the preparation and X-ray structures of $ClSe[N(Bu^t)Se]_nCl$ (**1**, n = 1; **2**, n = 2), the first two members of a homologous series of imidoselenium(II) dihalides, which represent a new class of SeN compounds, and $Se_3(NBu^t)_3$ **3**, the first cyclic oligomer of an SeNR unit. There are no sulfur or tellurium analogues of **1** and **2**.

The reaction of $SeCl_2$[10] with Bu^tNH_2 in a 2:3 molar ratio in THF at −80 °C yields a mixture of **1** and **2**,† in addition to the cyclic Se(II) imide **3**. The lower solubility of the imidoselenium(II) dihalides allows them to be isolated as red crystals by fractional crystallization. Both **1** and **2** are extremely moisture-sensitive and the crystals of **1** melt below room temperature. Compound **2** can be isolated in 34% yield when the reaction of $SeCl_2$ with Bu^tNH_2 is conducted in a 1:2 molar ratio. The identities of **1** and **2** were established by X-ray crystallography.

The X-ray analysis of **1**‡ revealed an acyclic ClSeNSeCl arrangement with planar geometry at the nitrogen atom [Σ < N(1) = 359.7°] (Fig. 1). The two Cl substituents are in similar orientations above the SeNSe plane as indicated by the ClSeNSe torsion angles of 84.8(4) and −92.9(4)°. By contrast, the related Se(III) system $[ClSeNSeCl]^+$ is planar and both *cis*,*cis* and *cis*,*trans* isomers have been observed in the solid state.[5] Presumably the rotation of the Se–Cl bonds away from planarity in **1** minimises lone pair–lone pair repulsions between Se and N. The mean Se–N bond distance of 1.810 Å in **1** is slightly shorter than the value of 1.869 Å found for $Se[N(SiMe_3)_2]$[11] and the predicted Se(II)–N single bond value of 1.86 Å.[12] The mean Se–Cl bond length of 2.219 Å is, as expected, somewhat longer than the corresponding value of *ca.* 2.15 Å found for the cation $[ClSeNSeCl]^+$.[5]

An X-ray structural determination‡ showed that **2** consists of a U-shaped SeNSeNSe unit terminated by Cl atoms, which adopt very different orientations (Fig. 2). The torsion angles Cl(1)–Se(1)–N(1)–Se(3) and Cl(2)–Se(2)–N(2)–Se(3) are 83.0(2) and −116.5(1)°, respectively. The SeNSeNSe unit is distinctly non-planar with torsion angles of 40.8(2) and -69.4(2)° for Se(1)–N(1)–Se(3)–N(2) and N(1)–Se(3)–N(2)–Se(2), respectively. The marked difference in torsion angles is apparently reflected in a variation in the Se–N bond lengths. Those involving N(2) are almost equal, 1.803(3) and 1.822(3) Å, while the values for the two Se–N(1) bonds differ by 0.19 Å. The geometry at the nitrogen atoms is approximately planar [Σ < N(1) = 355.2°, Σ < N(2) = 357.0°]. The Se–Cl bond distances are 2.269(1) and 2.312(1) Å in **2** *cf.* 2.219 Å for **1**. Negative hyperconjugation [lp(N) → σ*(Se–Cl)] may contribute to a lengthening of the Se–Cl bonds.[5b]

The NMR data for **1** and **2** are consistent with their solid-state structures.† Single NBu^t environments are observed in both the ^1H and ^{13}C NMR spectra. The ^{77}Se NMR spectrum of **1** in toluene exhibits a singlet at δ 1854 and that of **2** shows two resonances at δ 1620 and 1613, which are assigned to NSeCl and NSeN, respectively, on the basis of their relative intensities.

The formation of **1** and **2** can be envisaged to occur *via* the intermediate $[Bu^tN(H)SeCl]$ **4** (Scheme 1). When the molar ratio $SeCl_2$:Bu^tNH_2 is increased to 1:3 a complex mixture of selenium(II) imides is produced, including the known cyclic systems $Se_6(NBu^t)_2$ and $Se_9(NBu^t)_6$[9] and a new SeN heterocycle $Se_3(NBu^t)_3$, **3**, which was isolated in *ca.* 10% yield as yellow crystals by fractional crystallization from *n*-hexane. An X-ray structural determination showed that **3** is a six-membered ring [|*d*(Se–N)| = 1.833 Å] in a chair conformation analogous

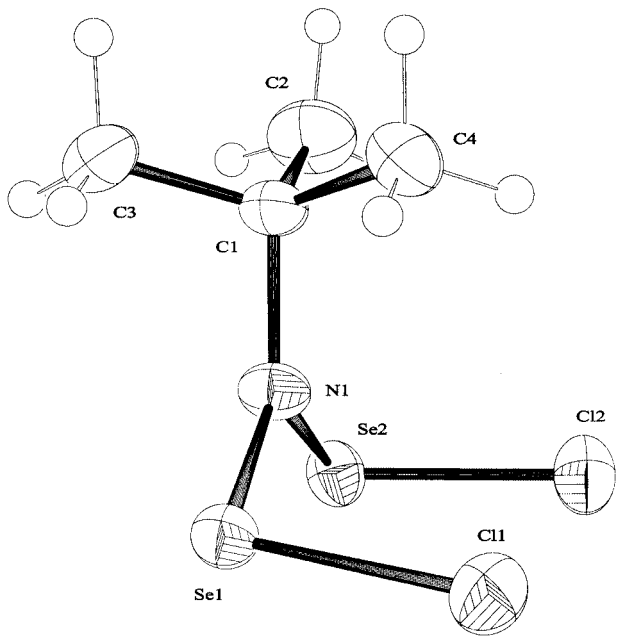

Fig. 1 ORTEP view (50% probability ellipsoids) of $ClSeN(Bu^t)SeCl$ **1**. Selected bond lengths (Å) and angles (°): Se(1)–N(1) 1.804(6), Se(2)–N(1) 1.816(7), Se(1)–Cl(1) 2.223(2), Se(2)–Cl(2) 2.215(2), N(1)–Se(1)–Cl(1) 103.9(2), N(1)–Se(2)–Cl(2) 103.8(2); C(1)–N(1)–Se(1) 119.9(5), C(1)–N(1)–Se(2) 123.1(5), Se(1)–N(1)–Se(2) 116.7(4).

DOI: 10.1039/b001002m

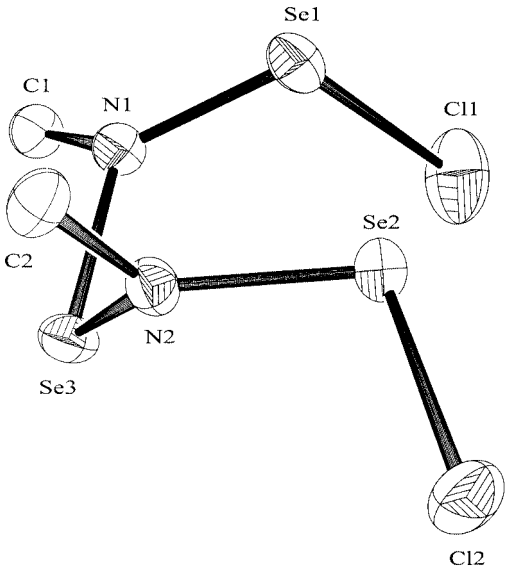

Fig. 2 ORTEP view (50% probability ellipsoids) of ClSeN(Bu^t)SeN=(Bu^t)SeCl **2**. For clarity, only α-carbon atoms of Bu^t groups are shown. Selected bond lengths (Å) and angles (°): Se(1)–N(1) 1.758(3), Se(2)–N(2) 1.822(3), Se(3)–N(1) 1.948(3), Se(3)–N(2) 1.803(3), Se(1)–Cl(1) 2.269(1), Se(2)–Cl(2) 2.312(1); Cl(1)–Se(1)–N(1) 109.24(10), Cl(2)–Se(2)–N(2) 98.93(8), Se(1)–N(1)–Se(3) 118.03(14), Se(2)–N(2)–Se(3) 112.97(16), N(1)–Se(3)–N(2) 96.54(12).

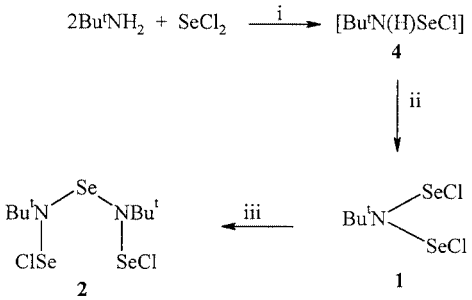

Scheme 1 *Reagents and conditions*: i, −[Bu^{t}NH$_3$]Cl, THF, −80 °C; ii, SeCl$_2$, Bu^{t}NH$_2$, −[Bu^{t}NH$_3$]Cl, THF, −80 °C; iii, 3Bu^{t}NH$_2$, SeCl$_2$, −2[Bu^{t}NH$_3$]Cl, THF, −80 °C.

to that of the tellurium analogue.[13] Details of this structure and our ^{77}Se NMR investigations of these systems will be given in a full account of this work.

In summary, we have isolated and structurally characterized the first two members of a novel class of Se(II)–N compound, the imidoselenium(II) dihalides, **1** and **2**, as well as the first example of a cyclic oligomer of a selenonitroso compound, **3**. The acyclic systems are potentially versatile reagents for the synthesis of Se(II)–N macrocycles, while **3** can be viewed as a tridentate Se(II) ligand.

Financial support from the Natural Sciences and Engineering Research Council (Canada), the Academy of Finland and the Finnish Cultural Foundation (T. M.) is gratefully acknowledged.

Notes and references

† A solution of SeCl$_2$ (15 mmol)[10] in THF (10 mL) was added to a solution of Bu^{t}NH$_2$ (2.2 mL, 22.5 mmol) in THF (40 mL) at −80 °C. The reaction mixture was stirred for 1 h at −80 °C and then for a further 1 h at 23 °C. The precipitate of [Bu^{t}NH$_3$]Cl was removed by filtration and solvent was evaporated under vacuum to give a dark red oil. A hexane solution of this oil at −22 °C deposited X-ray quality dark red crystals of **1** and red crystals of **2**, which were separated manually. The total yield of **1** and **2** was estimated to be *ca.* 50% from the ^{77}Se NMR spectrum of the reaction mixture.

NMR characterization data: **1** δ (^{1}H) (C$_7$D$_8$, 25 °C) 1.10 [*s*, C(CH$_3$)$_3$]; δ (^{13}C) (C$_7$H$_8$, 25 °C) 74.1 [*C*(CH$_3$)$_3$], 31.4 [C(*C*H$_3$)$_3$]; δ (^{77}Se) (C$_7$D$_8$, 25 °C) 1857 (NSeCl) (referenced to an external saturated solution of SeO$_2$ at 25 °C); chemical shifts are reported relative to Me$_2$Se(l) at 25 °C [δ(Me$_2$Se) = δ(SeO$_2$) + 1302.6].

2 δ (^{1}H) (C$_7$D$_8$, 25 °C) 1.16 [*s*, C(CH$_3$)$_3$]; δ (^{13}C) (C$_7$H$_8$, 25 °C) 26.8 [C(*C*H$_3$)$_3$], not observed [*C*(CH$_3$)$_3$]; δ (^{77}Se) (C$_7$H$_8$, −30 °C) 1620 (NSeCl), 1613 (NSeN).

3 δ (^{1}H) (C$_7$D$_8$, 25 °C) 1.23 [*s*, C(CH$_3$)$_3$]; δ (^{13}C) [C$_7$H$_8$–C$_7$D$_8$ (4:1), 25 °C] 64.8 [*C*(CH$_3$)$_3$], 30.7 [C(*C*H$_3$)$_3$]; δ (^{77}Se) [C$_7$H$_8$–C$_7$D$_8$ (4:1), 25 °C] 1396 (NSeN).

‡ *Crystal data*: for **1**: C$_4$H$_9$Cl$_2$NSe$_2$, M = 299.94, monoclinic, space group $P2_1/c$, a = 7.263(1), b = 10.282(1), c = 12.312(1) Å, β = 92.06(1)°, V = 918.8(2) Å^3, Z = 4, D_c = 2.168 g cm^{-3}, F(000) = 568, μ = 8.553 mm^{-1}, T = 173 K, crystal dimensions 0.30 × 0.25 × 0.15 mm. Data were collected on a Nonius Kappa CCD diffractometer using graphite monochromated radiation (λ = 0.71073 Å). Total no. of reflections was 4419 of which 2076 had $I > 2.00\sigma(I)$. The structure was solved by direct methods[14a] and refined on F^2, R_1 = 0.0753, wR_2 = 0.1947.

For **2**: C$_8$H$_{18}$Cl$_2$N$_2$Se$_3$, M = 450.02, monoclinic, space group $P2_1/c$, a = 9.989(2), b = 9.643(2), c = 16.124(3) Å, β = 101.81(3)°, V = 1520.2(5) Å^3, Z = 4, D_c = 1.966 g cm^{-3}, F(000) = 864, μ = 7.586 mm^{-1}, T = 173 K, crystal dimensions 0.20 × 0.10 × 0.10 mm. Data were collected on a Nonius Kappa CCD diffractometer using graphite monochromated Mo-Kα radiation (λ = 0.71073 Å). Total no. of reflections was 10 567 of which 2629 had $I > 2.00\sigma(I)$. The structure was solved by direct methods[14a] and refined on F^2,[14b] R_1 = 0.0262, wR_2 = 0.0792.

CCDC 182/1587. See http://www.rsc.org/suppdata/cc/b0/b001002m/ for crystallographic files in .cif format.

1 For binary compounds and ternary NSeCl systems, see: T. Chivers, *Main Group Chem. News*, 1993, **1**, 6; T. M. Klapötke, in *The Chemistry of Inorganic Ring Systems*, ed. R. Steudel, Elsevier, Amsterdam, 1992, ch. 20, p. 409.
2 For CNSe cations and radicals, see: A. W. Cordes, R. C. Haddon and R. T. Oakley, in *The Chemistry of Inorganic Ring Systems*, ed. R. Steudel, Elsevier, Amsterdam, 1992, ch. 16, p. 295.
3 For transition-metal complexes, see: P. F. Kelly, A. M. Z. Slawin, D. J. Williams and J. D. Woollins, *Chem. Soc. Rev.*, 1992, **21**, 245.
4 J. Siivari, T. Chivers and R. S. Laitinen, *Angew. Chem., Int. Ed. Engl.*, 1992, **31**, 1518; J. Siivari, T. Chivers and R. S. Laitinen, *Inorg. Chem.*, 1993, **32**, 4391; R. Wollert, B. Neumüller and K. Dehnicke, *Z. Anorg. Allg. Chem.*, 1992, **616**, 191; C. Lau, B. Neumüller and K. Dehnicke, *Z. Naturforsch. Teil. B*, 1997, **52**, 543.
5 (*a*) R. Wollert, A. Höllwarth, G. Frenking, D. Fenske, H. Goesmann and K. Dehnicke, *Angew. Chem., Int. Ed. Engl.*, 1992, **31**, 1251; (*b*) M. Broschag, T. M. Klapötke, A. Schulz and P. S. White, *Inorg. Chem.*, 1993, **32**, 5734; (*c*) M. Broschag, T. M. Klapötke, A. Schulz and P. S. White, *Chem. Ber.*, 1994, **127**, 2177.
6 M. Broschag, T. M. Klapötke, I. C. Tornieporth-Oetting and P. S. White, *J. Chem. Soc., Chem. Commun.*, 1992, 1390; A. Schulz, P. Buzek, P. von R. Schleyer, M. Broschag, I. C. Tornieporth-Oetting, T. M. Klapötke and P. S White, *Chem. Ber.*, 1995, **128**, 35.
7 C. Lau, B. Neumüller, W. Hiller, M. Herker, S. F. Vyboishchikov, G. Frenking and K. Dehnicke, *Chem. Eur. J.*, 1996, **2**, 1373.
8 M. R. Bryce and A. Chesney, *J. Chem. Soc., Chem. Commun.*, 1995, 195.
9 H. W. Roesky, K.-L. Weber and J. W. Bats, *Chem. Ber.*, 1984, **117**, 2686.
10 Pure SeCl$_2$ is generated by the reaction of elemental selenium with SO$_2$Cl$_2$ in THF: A. Maaninen, T. Chivers, M. Parvez, J. Pietikäinen and R. S. Laitinen, *Inorg. Chem.*, 1999, **38**, 4093.
11 M. Björgvinsson, H. W. Roesky, F. Pauer, D. Stalke and G. M. Sheldrick, *Inorg. Chem.*, 1990, **29**, 5140.
12 M. Björgvinsson and H. W. Roesky, *Polyhedron*, 1991, **10**, 2353.
13 T. Chivers, X. Gao and M. Parvez, *J. Am. Chem. Soc.*, 1995, **117**, 2359.
14 (*a*) G. M. Sheldrick, SHELXS-97, University of Göttingen, Germany, 1997; (*b*) G. M. Sheldrick, SHELXL-97, University of Göttingen, Germany, 1997.

Synthesis and catalytic activity of Ti-ITQ-7: a new oxidation catalyst with a three-dimensional system of large pore channels

María-José Díaz-Cabañas, Luis A. Villaescusa† and Miguel A. Camblor*

Instituto de Tecnología Química (CSIC-UPV), Avda. Los Naranjos s/n, 46022 Valencia, Spain. E-mail: macamblo@itq.upv.es

Received (in Oxford, UK) 18th January 2000, Accepted 28th March 2000

Isomorphous substitution of Si by Ti in the framework of ITQ-7, the crystalline silica polymorph of lowest density, has been achieved by direct synthesis, affording its three dimensional system of large pore channels to be used in selective oxidation reactions.

After the discovery of the medium pore zeolite TS-1[1] and of its outstanding properties as a catalyst for the selective oxidation of organic compounds with aqueous hydrogen peroxide,[2] the isomorphous substitution of Si by Ti in zeolites has received much attention.[3] Aside from a fundamental interest in understanding the remarkable catalytic properties of TS-1, there has been a considerable effort in making new Ti-zeolites that could enlarge the field of application of these materials in industrially important oxidation reactions. Within this aim, the search for catalysts with larger pores allowing processing of larger molecules and/or the use of oxidising agents larger than H_2O_2 has been particularly relevant. New materials with larger pores such as zeolite Ti-beta[4] and the non-zeolite mesoporous Ti-MCM-41[5] have been developed and their catalytic properties tested. Although those materials, particularly Ti-beta, have clear advantages from the point of view of pore size, they are also intrinsically less active than TS-1. Very interestingly, Ti-beta presents peculiar differences in catalytic properties when compared to TS-1 (with regard to catalytic behaviour in different solvents and selectivity in the epoxidation of olefins and in the hydroxylation of phenol) which appear to be due to the different crystalline structure of both materials[6] rather than to differences in their hydrophobicity, Al content or degree of isolation of Ti in tetrahedral positions as initially assumed. Unfortunately, a detailed structural investigation of those differences is hindered by the very complex, severely intergrown nature of the structure of zeolite beta.[7] Here, we present Ti-ITQ-7 (structure code ISV), a new three dimensional large pore zeolite which presents a more ordered structure than zeolite beta.[8] In addition to the opportunities that Ti-ITQ-7 may offer in the investigation of the structure/activity/selectivity relationships in Ti-zeolites, its distinct pore architecture could give rise to differences in its catalytic performance when compared to Ti-beta.

Ti-ITQ-7 can be prepared in conditions similar to those described for the pure silica polymorph,[8] by first cohydrolyzing tetraethylorthotitanate (TEOTi) and tetraethylorthosilicate (TEOS) in an aqueous solution of the hydroxide form of the structure directing agent (SDA) 1,3,3-trimethyl-6-azonium-tricyclo[3.2.1.4[6,6]]dodecane. Crystallites of ITQ-7 may be added as seeds to promote the crystallisation. In a typical synthesis, 0.76 g TEOTi and 13.87 g TEOS were hydrolysed in 27.77 g of a solution of the hydroxide form of the SDA (1.0 mol kg^{-1}). Then, 0.65 g H_2O_2 (aq. 35 wt.%) were added and the mixture was stirred at room temperature allowing evaporation of all the ethanol and of the water needed to obtain the final composition given below. Then, 1.38 g HF (aq. 48 wt.%) were added before the final addition of a suspension of SiO_2 ITQ-7 crystallites in water (0.20 g zeolite, 2.50 g water). The final composition of the gel was SiO_2 : 0.05 TiO_2 : 0.10 H_2O_2 : 0.5 SDAOH : 0.50 HF : 3 H_2O. The mixture was poured into Teflon-lined stainless steel autoclaves and crystallised under rotation at 150 °C for 12 days (yield: 27.48 g Ti-ITQ-7 per 100 g synthesis mixture; Si/Ti ratio of Ti-ITQ-7 : 120). The solid presents an XRD pattern characteristic of zeolite ITQ-7 and, in order to remove its guest species, it can be calcined to 580 °C without structural damage (Fig. 1).

In the absence of seeds, the crystallisation of Ti-ITQ-7 in the presence of relatively high Ti contents (Si/Ti $\leq$ 30) does not proceed to completion: while the zeolite nucleates and starts growing, the crystallisation stops at certain point and the partially crystallised solid remains essentially unchanged by powder XRD even if heating is extended for an additional month. At present we do not have a clear explanation for this observation, which appears difficult to rationalise given that Ti-ITQ-7 may be crystallised from gels with even higher Ti contents if seeds are used (see example above). For Si/Ti ratios of 50 or above in the starting gel, no seeds are required.

The isomorphous substitution of Si by Ti in the framework of ITQ-7 (the crystalline silica polymorph of lowest density known to date)[8] has been confirmed by the usual techniques. The diffuse reflectance UV spectra of calcined Ti-ITQ-7 sample (Fig. 2) show a band at 205–220 nm, typically assigned to a electronic transition with ligand to metal charge transfer character involving isolated Ti in the framework of zeolites.[9] Only for TiO_2 contents of 1.1% or above, does the band have a tail at high wavelength which suggests the presence of a small amount of TiO_2 anatase. The IR spectra of the calcined materials in the region of framework vibrations show a band at 960 cm^{-1}, characteristic of Ti-zeolites and assigned to the Si–O stretching in Si–O–Ti groups.[10]

The activity and selectivity of Ti-ITQ-7 in the selective epoxidation of hex-1-ene with H_2O_2 was tested and compared to the performance of aluminium-free Ti-beta synthesised in fluoride media[6] (Table 1). Three main conclusions may be derived from the results in Table 1. First, the activity and selectivity of Ti-ITQ-7 for the oxidation of this alkene is equivalent to that of Ti-beta with similar Ti content. Second, the

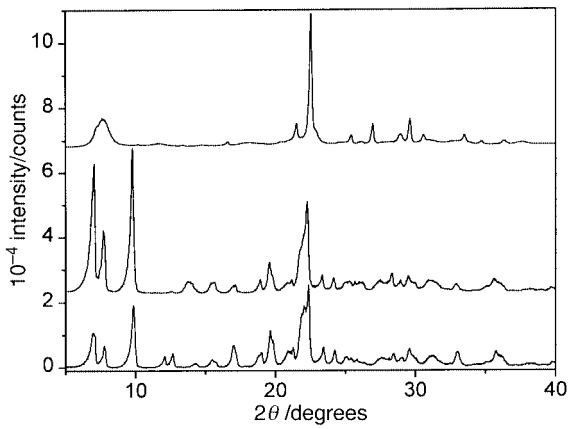

Fig. 1 X-Ray diffractograms of (from bottom to top) as-made and calcined Ti-ITQ-7 and as-made Ti-beta (TiO_2 contents: 1.24, 1.24 and 1.40%).

† Current address: School of Chemistry, University of St. Andrews, St. Andrews, UK KY16 9ST.

DOI: 10.1039/b000539h

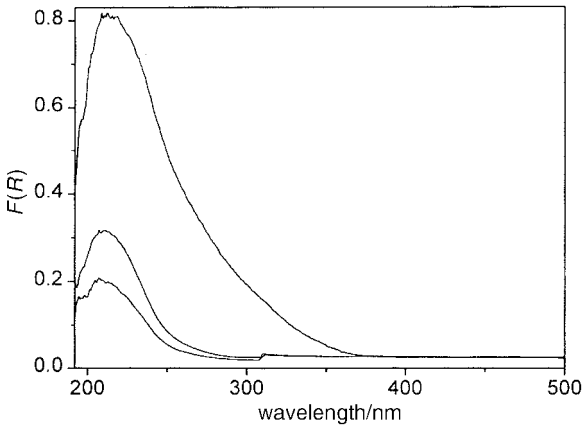

Fig. 2 Diffuse reflectantance UV–VIS absorption spectra of calcined Ti-ITQ-7 with (from bottom to top) 0.15, 0.31 and 1.24 % TiO_2.

Table 1 Results of the selective oxidation of hex-1-ene with H_2O_2 over Ti-ITQ-7 and Ti-Beta[a]

Material	%TiO_2	Solvent	Hex-1-ene conversion (%)	Selectivity (%)	
				Epoxide	H_2O_2[b]
Ti-ITQ-7	0.30	MeOH	1.7	100	76
Ti-ITQ-7	0.30	MeCN	8.8	100	100
Ti-ITQ-7	1.14	MeCN	27.1	100	89
Ti-beta	0.76	MeOH	7.6	91	100
Ti-beta	0.76	MeCN	12.9	100	100
Ti-beta	1.40	MeOH	20.0	50	98
Ti-beta	1.40	MeCN	39.2	100	100

[a] Batch reactor, 50 °C, 17 mmol hex-1-ene, 11.8 g solvent, 0.4 g H_2O_2 (35 wt%), 100 mg catalyst, 7 h. The Ti-beta catalysts were prepared according to ref. 6. [b] H_2O_2 selectivity is defined in terms of mol of oxidized products (epoxide and glycols) per 100 mol of H_2O_2 consumed in the reaction.

activity of Ti-ITQ-7 is much higher in acetonitrile than in methanol, in contrast to the known behaviour of TS-1, for which protic solvents work better,[11] and much alike that of Ti-beta. The better defined XRD pattern of ITQ-7 (Fig. 1) compared to Ti-beta might allow a more detailed structural study of the striking observation that Ti-zeolites with different structures perform much differently when used as catalysts in different solvents. Finally, the catalytic results support the conclusion, primarily derived from the characterisation results described above, that Ti has been successfully substituted for Si in the zeolite ITQ-7 framework.

Ti-ITQ-7 is the first high-silica zeolite catalyst with a three dimensional system of large pore channels circumscribed by windows of 12 tetrahedra since the discovery 30 years ago of the aluminosilicate zeolite beta,[12] and follows the very recent publication of the non-catalyst all-SiO_2 zeolite ITQ-7.[8] Despite the very similar catalytic performance of Ti-ITQ-7 and Ti-beta in the epoxidation of a small alkene such as hex-1-ene, the different pore architecture of both materials, especially in the crystallographic *c* direction (Fig. 3), might give rise to differences in shape selectivity if a different, larger substrate of particular shape is used.

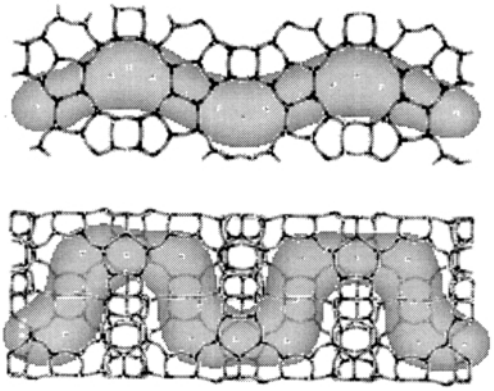

Fig. 3 Comparison of the non-linear large pore channels running along the [001] direction of ITQ-7 (ISV, bottom) and one of the polymorphs of zeolite beta (*BEA, top). The frameworks, depicted in a stick model, are viewed in projection down the [110] (ISV) or [100] direction (BEA) to show the largest deviation from linearity of the [001] channels, which are drawn as gray tubes. Both structures show linear large pore channels (not emphasized in the figure) running along the [100] and [010] crystallographic directions.

We gratefully acknowledge financial support by the Spanish CICYT (project MAT97-0723).

Notes and references

1 M. Taramasso, G. Perego and B. Notari, *US Pat.* 4410501, 1983.
2 D. R. C Huybrechts, L. De Bruycker and P. A. Jacobs, *Nature*, 1990, **345**, 240; B. Notari, *Stud. Surf. Sci. Catal.*, 1991, **67**, 243.
3 G. Bellussi and M. S. Rigutto, *Stud. Surf. Sci. Catal.*, 1994, **85**, 177.
4 M. A. Camblor, A. Corma, A. Martínez and J. Pérez-Pariente, *J. Chem. Soc., Chem. Commun.*, 1992, 589; M. A. Camblor, A. Corma, A. Martínez, J. Pérez-Pariente and S. Valencia, *Stud. Surf. Sci. Catal.*, 1994, **82**, 531; M. A. Camblor, M. Costantini, A. Corma, L. Gilbert, P. Esteve, A. Martínez and S. Valencia, *Chem. Commun.*, 1996, 1339.
5 P. T. Tanev, M. Chibne and T. J . Pinnavaia, *Nature*, 1994, **368**, 321; A. Corma, M. T. Navarro and J. Pérez-Pariente, *J. Chem. Soc., Chem. Commun.*, 1994, 147.
6 T. Blasco, M.A. Camblor, A. Corma, P. Esteve, J. M. Guil, A. Martínez, J. A. Perdigón-Melón and S. Valencia, *J. Phys. Chem. A*, 1998, **102**, 75.
7 J. M. Newsam, M. M. J. Treacy, W. T. Koetsier and C. B. de Gruyter, *Proc. R. Soc. London, Ser. A*, 1988, **420**, 375; J. B. Higgins, R. B. LaPierre, J. L. Schlenker, A. C. Rohrman, J. D. Wood, G. T. Kerr and W. J. Rohrbaugh, *Zeolites*, 1988, **8**, 446.
8 L. A. Villaescusa, P. A. Barrett and M. A. Camblor, *Angew. Chem., Int. Ed.*, 1999, **38**, 1997.
9 A. Zecchina, G. Spoto, S. Bordiga, A. Ferrero, G. Petrini, G. Leofanti and M. Padovan, *Stud. Surf. Sci. Catal.*, 1991, **69**, 251.
10 M. R. Boccuti, K. M. Rao, A. Zecchina, G. Leofanti and G. Petrini, *Stud. Surf. Sci. Catal.*, 1989, **48**, 133.
11 M. G. Clerici, G. Bellussi and U. Romano, *J. Catal.*, 1991, **129**, 159; M. G. Clerici and P. Ingallina, *J. Catal*, 1993, **140**, 71.
12 R. L. Wadlinger , G. T. Kerr, E. J. Rosinski, *US Pat.*, 3308069, 1967.

ChemComm

13*H*-benzo[6-7]indolo[3,2-*c*]quinolines (B[6,7]IQ): optimization of their DNA triplex-specific stabilization properties†

Philippe Schmitt,[ab] Chi Hung Nguyen,[b] Jian-Sheng Sun,*[a] David S. Grierson,[b] Emile Bisagni,[b] Thérèse Garestier[a] and Claude Hélène[a]

[a] *Laboratoire de Biophysique, UMR 8646 CNRS-Muséum National d'Histoire Naturelle, INSERM U201, 43 rue Cuvier, 75231 Paris Cedex 05, France. E-mail: sun@mnhn.fr*

[b] *UMR 176 CNRS-Institut Curie, Section Recherche, Batiment 110, Centre Universitaire, 91405 Orsay, France*

Received (in Liverpool, UK) 17th February 2000, Accepted 28th March 2000

The triple helix stabilization property of 13*H*-benzo[6-7]indolo[3,2-*c*]quinoline was significantly improved by changing the electron-donor acceptor properties of the substituent at position 10 or 11.

Sequence-specific recognition of double-stranded DNA (dsDNA) by triplex-forming oligonucleotides (TFOs) offers a promising strategy to control the expression of genetic information and to develop new molecular tools.[1–3] TFOs bind to the major groove of dsDNA through formation of Hoogsteen or reverse Hoogsteen hydrogen bonds with the purines already engaged in Watson–Crick base pairs.[2] For this reason, triplex helix formation is mainly restricted to oligopyrimidine–oligopurine tracts of dsDNA. As a triple helix is generally thermodynamically less stable than a double helix, considerable efforts have been made to stabilize triple helices, and thus to extend the scope of dsDNA targeting by TFOs to shorter and therefore more numerous oligopyrimidine–oligopurine sequences. A number of triplex-specific ligands have thus been developed to promote the formation of triple helices, which would be otherwise unstable under physiological conditions.[4]

Recently, we have designed and synthesized a series of 13*H*-benzo[6-7]indolo[3,2-*c*]quinolines (B[6,7]IQ) which are pentacyclic crescent-shaped aromatic molecules.[5] Characteristic of the B[6,7]IQ compounds is their great efficacy for triplex stabilization, and weak binding towards duplexes. Possessing an extended aromatic surface, B[6,7]IQ derivatives are able to intercalate into triplexes, and to provide large π orbital overlap with the neighboring triplets at the intercalation site. In an effort to further optimize the design of an efficient triplex stabilizer, we report herein, the synthesis and DNA binding behavior of B[6,7]IQ derivatives **1**–**4**, bearing either an electron-donating or an electron-withdrawing functionality at the C–10 or C–11 center.

B[6,7]IQs **1**–**4** were obtained according to adaptations of the procedure reported for compound **5**[5] (Scheme 1). The tetralones **6a**–**d**, either commercially available, or obtainable through reported syntheses,[6] were reacted with 4-hydrazinoquinolin-2-(1*H*)-one **7** in acetic acid to form the corresponding hydrazones **8a**–**d**. Compounds **8b**–**d** were subsequently converted directly to the benzoindoloquinolones **9b**–**d** in a 'one pot' process involving thermal Fisher indolization, followed by addition of palladium/carbon (large excess) to effect aromatization of the dihydro intermediate formed. For **8a**, the treatment with Pd/C was accompanied by a further palladium-promoted reaction of the nitro group by the molecular hydrogen generated *in situ*. To circumvent this problem, compound **9a** was obtained by reaction of the isolated Fisher indolization product with a stoichiometric amount of 2,3-dichloro-5,6-dicyano-1,4-benzoquinone (DDQ) in DMF. Conversion of benzoindoloquinolin-6-ones **9a**–**d** to the corresponding 6-chloro derivatives **10a**–**d** was then achieved through reaction with benzyltriethylammonium chloride, *N*,*N*-diethylamine and phosphorus oxychloride.[7] These intermediates were then reacted with *N*,*N*-dimethyl-1,3-propanediamine under reflux. This latter reaction proceeded smoothly for the methoxy-substituted substrates **10c**,**d** yielding products **4** and **5** in 64 and 93% yields, respectively.[5] In a similar way the acetamido derivative **10b** was converted directly to compound **3** in 75% yield. However, for the nitro-containing substrate **10a** a mixture of both nitro (**1**) and amino-containing (**2**) substitution products (15 and 9%, respectively) was obtained. Even though the yield of this reaction was poor, it produced enough material to permit study of both compounds **1** and **2** for their ability to stabilize triple helices.

Triple helix stabilization by ligands **1**–**4** and **5**[5] was investigated by thermal denaturation experiments while monitoring the absorbance of double- or triple-helical DNA complexes at 260 nm (Fig. 1). The extent of duplex and triplex stabilization was estimated by measuring the melting temperature of the corresponding nucleic acid structures in the presence and absence of ligands **1**–**5**.

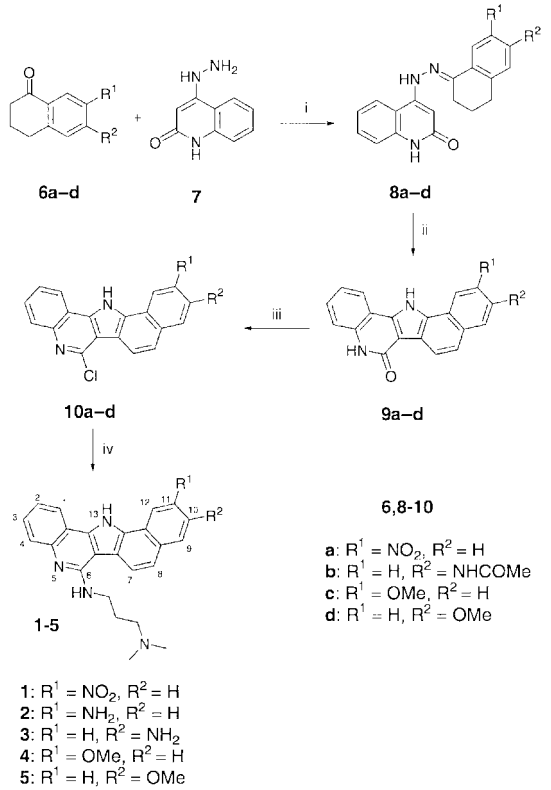

Scheme 1 Synthetic pathway and conditions of B[6,7]IQ derivatives (see text and ESI† for details): i, HOAc, room temp. 18–36 h, 79–99%; ii, for **9a**: (1) Ph_2O, reflux 4.5 h, (2) DDQ, DMF, reflux 2 h, 69%; for **9b**–**d**: Ph_2O, reflux 2–3.5 h, then 10% Pd/C, reflux 1–2 h, 44–76%; iii, $C_6H_5NEt_2$, $PhCH_2NEt_3Cl$, MeCN, $POCl_3$, reflux 24–48 h, 42–95%; iv, $NH_2(CH_2)NMe_2$, reflux 3 h, 9–93%.

† Electronic supplementary information (ESI) available: experimental. See http://www.rsc.org/suppdata/cc/b0/b001318h/

DOI: 10.1039/b001318h

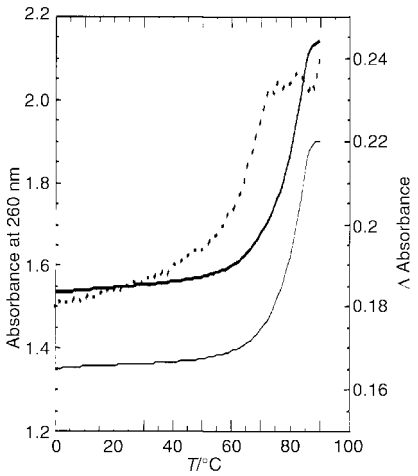

Fig. 1 Melting curves of 1.5 μM double- and triple-helices 14C3 (thin and thick lines, respectively) in the presence of 15 μM compound **5**. The triplex–duplex transition is better shown by subtracting the duplex melting curve from the triplex one (dashed thick line, scaled to the right) than by usual first derivative plot, owing to closely overlapped transitions. All thermal denaturation experiments were carried out in 10 mM sodium cacodylate buffer (pH 6.2) containing 100 mM sodium chloride.

In agreement with previously reported studies, it was determined that all five ligands, which share a common extended aromatic ring system, are able to stabilize the triplex more strongly than the duplex. Regardless of the ligand and the sequence, the differences in melting temperatures for the transition from duplex to single strands exhibited only modest variations (+13 to +19 °C). In contrast, the changes in the triplex-to-duplex melting temperatures were much higher (between +38 and +65 °C for the 14C3 triplex, or between +29 and +45 °C for the 14C5 triplex) and showed marked susceptibility to the nature of the R^1 and R^2 functional groups (Scheme 1). Thus, whereas the amino-bearing ligands **2** and **3** showed significant stabilization, with a $\Delta T_m^{3\rightarrow2}$ of +38 and +43 °C, respectively, in the presence of the 14C3 triplex sequence, and +29 and +35 °C in the presence of the 14C5 sequence, the methoxy-bearing ligands **4** and **5** induced significantly better triplex stabilization (+51 and +50 °C for the 14C3 sequence, and +39 and +41 °C for the 14C5 sequence).

The nitro-containing ligand **1** shows unprecedented triplex-promoting properties with a $\Delta T_m^{3\rightarrow2}$ of +65 and +45 °C in the presence of the 14C3 and 14C5 sequences, respectively. Furthermore, this ligand shows only modest affinity for double-helical structures (the $\Delta T_m^{2\rightarrow1}$ for the 14C3 and 14C5 sequences are +15 and +16 °C, respectively: Table 1). Thus, compound **1** presents a significantly greater specificity for triplexes as compared to duplexes.

To rationalize the trends that we observed, at least two parameters need to be taken into account: (i) the electron withdrawing capacity of the substituent group at position 11: triplex stabilization increases in the order NH_2 < OMe < NO_2, and (ii) the position of the substituent : substitution at position 10 appears to be more stabilizing than at position 11 (at least for the 14C5 sequence).

According to molecular models,[5] substitution at position 10 or 11 occurs in a region which is supposed to interact with Hoogsteen bases in base triplets. As a consequence, these substitutions should have a smaller effect on duplex than on triplex stabilization. The complete set of data is reported in Table 1.

The observations reported herein show that a significant part of the binding energy for intercalation of B[6,7]IQ derivatives into a triplex can be ascribed to the electron-donor acceptor (EDA) properties of the substituent at position 10 or 11. This leads us to the conclusion that further improvements in the design of triplex-stabilizers could take advantage of the fact that electron-withdrawing groups provide triplex-specific intercalators with both improved efficiency and selectivity. Polynitrated or polycyanated structures which not only expand the hyper-conjugated surface, but also increase the electron-withdrawing capabilities of intercalator might represent interesting candidates to explore for their triplex stabilizing properties. Synthetic studies toward such molecules are currently in progress.

Table 1 Sequences of the triple helices studied in this work (14C3 and 14C5) and the increased melting temperatures of triple- and double-helices ($\Delta T_m^{3\rightarrow2}$ and $\Delta T_m^{2\rightarrow1}$, respectively) in the presence of the B[6,7]IQ derivatives (see the legend of Fig. 1 for experimental conditions). The oligopyrimidine–oligopurine sequence for triplex formation in the double-stranded DNA fragment is in bold letters. In the absence of ligands, the $T_m^{3\rightarrow2}$ of the triplexes 14C3 and 14C5 are 16 and 17 °C, respectively, whereas the $T_m^{2\rightarrow1}$ of the corresponding duplexes are 62 and 63 °C, respectively. The accuracy of T_m values is *ca.* ±1 °C

14C3

5′ CTATCAGCTCAA**TCTTTTTTCTTCTT**AACTCGTATC 3′
3′ GATAGTCGAGTT**AGAAAAAAGAAGAA**TTGAGCATAG 5′
3′ **TCTTTTTTCTTCTT** 5′

14C5

5′ CTATCAGCTCAA**TCTTTCCTCTTCTT**AACTCGTATC 3′
3′ GATAGTCGAGTT**AGAAAGGAGAAGAA**TTGAGCATAG 5′
3′ **TCTTTCCTCTTCTT** 5′

	Triplex			
	14C3		14C5	
Compound	$\Delta T_m^{3\rightarrow2}$	$\Delta T_m^{2\rightarrow1}$	$\Delta T_m^{3\rightarrow2}$	$\Delta T_m^{2\rightarrow1}$
1	+65	+15	+45	+16
2	+38	+13	+29	+16
3	+43	+14	+35	+15
4	+51	+16	+39	+18
5	+50	+18	+41	+19

Notes and references

1 T. Le Doan, L. Perrouault, D. Praseuth, N. Habhoub, J. L. Decout, N. T. Thuong, J. Lhomme and C. Hélène, *Nucleic Acids Res.*, 1987, **15**, 7749; H. E. Moser and P. B. Dervan, *Science*, 1987, **238**, 645.

2 Reviews: C. Hélène, *Anticancer Drug Des.*, 1991, **6**, 569; N. T. Thuong and C. Hélène, *Angew. Chem., Int. Ed. Engl.*, 1993, **32**, 666; M. D. Frank-Kamenetskii and S. M. Mirkin, *Annu. Rev. Biochem.*, 1995, **64**, 65; J. S. Sun, T. Garestier and C. Hélène, *Curr. Opin. Struct. Biol.*, 1996, **6**, 327.

3 Applications and biological aspects of the triplex strategy: C. Giovannangeli and C. Hélène, *Antisense Nucleic Acid Drug Dev.*, 1997, **7**, 413; P. P. Chan and P. M. Glazer, *J. Mol. Med.*, 1997, **75**, 267; L. J. Maher, *Cancer Invest.*, 1996, **14**, 66.

4 Triplex helix-stabilizing ligands: J. L. Mergny, G. Duval-Valentin, C. H. Nguyen, L. Perrouault, B. Faucon, M. Rougée, T. Montenay-Garestier, E. Bisagni and C. Hélène, *Science*, 1992, **256**, 1681; J. S. Lee, L. J. P. Latimer and K. J. Hampel, *Biochemistry*, 1993, **32**, 5591; W. D. Wilson, F. A. Tanious, S. Mizan, S. Yao, A. S. Kiselyov, A. S. Zon and G. L. Strekowski, *Biochemistry*, 1993, **32**, 10 614; K. R. Fox, P. Polucci, T. C. Jenkins and S. Neidle, *Proc. Natl. Acad. Sci. USA*, 1995, **92**, 7887; C. Escude, C. H. Nguyen, J. L. Mergny, J. S. Sun, E. Bisagni, T. Garestier and C. Hélène, *J. Am. Chem. Soc.*, 1995, **117**, 10 212; S. K. Kim, J. S. Sun, T. Garestier, C. Hélène, E. Bisagni, A. Rodger and B. Norden, *Biopolymers*, 1997, **42**, 101; C. Escudé, C. H. Nguyen, S. Kukreti, Y. Janin, J. S. Sun, E. Bisagni, T. Garestier and C. Hélène, *Proc. Natl. Acad. Sci. USA*, 1998, **95**, 3591.

5 C. H. Nguyen, C. Marchand, S. Delage, J. S. Sun, T. Garestier, C. Hélène and E. Bisagni, *J. Am. Chem. Soc.*, 1998, **120**, 2501.

6 7-Nitro-1-tetralone and 7-methoxy-1-tetralone were purchased from Aldrich Chemicals. 6-acetamino-1-tetralone was prepared according to: N. L. Allinger and E. S. Jones, *J. Org. Chem.*, 1962, **27**, 70.

7 M. J. Robins and B. Uznanski, *Can. J. Chem.*, 1981, **59**, 2601.

Replacement of the phosphodiester linkage in DNA with sulfamide and 3′-*N*-sulfamate groups†

Kevin J. Fettes,[a] Nigel Howard,[a] David T. Hickman,[a] Steven A. Adah,[b] Mark R. Player,[b] Paul F. Torrence[c] and Jason Micklefield*[d]

[a] *Department of Chemistry, Birkbeck College, University of London, 29 Gordon Square, London, UK WC1H 0PP*
[b] *Laboratory of Medicinal Chemistry, NIDDK, NIH Bethesda, MD, 20892–0805, USA*
[c] *Department of Chemistry, Northern Arizona University, Flagstaff, AZ, 86011-5698, USA*
[d] *Department of Chemistry, Faraday Building, UMIST, PO Box 88, Manchester, UK M60 1QD. E-mail: jason.micklefield@umist.ac.uk*

Received (in Liverpool, UK) 25th February 2000, Accepted 27th March 2000

Replacing phosphodiester linkages in DNA with neutral 3′-*N*-sulfamate groups has little effect on the binding affinity for complementary DNA or RNA, whereas incorporation of sulfamide groups into DNA results in considerable destabilisation of isosequential duplexes.

Modified oligonucleotides with neutral linkages replacing the native phosphodiester groups are of interest in the development of improved antisense and antigene agents.[1] Methylphosphonates, one of the earliest examples of this class, can only be efficiently prepared at present as a mixture of diastereoisomers at the phosphorus atom and have low affinity for complementary nucleic acids.[2] More recently neutral methylene(methylimino) (MMI),[3] amide[1] and 3′-thioformacetal[4] modified oligonucleotides have been developed which exhibit improved affinity for complementary nucleic acids. Furthermore, neutral formacetal[5] and dimethylenesulfone[6] linkages have been used effectively in the development of modified DNA aptamers[5] and dsDNA transition state analogues[6] that can bind to specific protein targets.

Earlier we reported the synthesis of dinucleotide analogues in which the phosphodiester linkage is exchanged for a neutral sulfamide group.[7] Here, the effects of the sulfamide **1** and 3′-*N*-sulfamate **2** (Scheme 1) internucleoside linkages on nucleic acid conformation and duplex stability are described. It was envisaged that the block synthesis approach could be used to synthesise chimeric oligodeoxynucleotides in which one or more of the phosphodiester groups are replaced by the neutral linkages. With the sulfamide phosphoramidite **10** in hand[7] a route to the 3′-*N*-sulfamate dinucleosides was required. Although isomeric 5′-*N*-sulfamate dinucleosides have been prepared before, the synthesis uses explosive sulfuryl chloride azide ($ClSO_2N_3$) and the overall yields are low.[8] Therefore, the development of an alternative method was necessary. Initially the coupling of 2–hydroxyphenyl sulfamate **5**[7] with the 5′-alcohol **8** was investigated. However, compound **5** proved insufficiently reactive and failed to give any of the sulfamate dinucleoside **11** despite the earlier observation that **5** reacts smoothly, albeit at high temperature, with the 5′-amine **7** to give the sulfamide dinucleoside **9**. In light of this, the more reactive 4–nitrophenyl sulfamate **6** was prepared by treating the 3′-amine **3** with 4–nitrophenyl chlorosulfate **4**.[9] Coupling of **6** with 5′-alcohol **8** was successful resulting in the sulfamate dinucleoside **11** in excellent yield at room temperature. Similarly the sulfamide dinucleoside **9** could also be prepared more effectively at room temperature from **6** and the 5′-amine **7**. Desilylation of dinucleoside **11** and 3′-phosphitylation gave the required phosphoramidite **12**.

The sulfamate dinucleoside d(TnsoT) **2** was also prepared and its conformation compared with d(TnsnT) **1**, and the native dinucleoside phosphate d(TpT) using NMR spectroscopy. As expected the sum of the $J_{1'2'}$ and $J_{1'2''}$ vicinal coupling constants ($\Sigma 1'$) for the 5′-terminal ribose ring of d(TnsoT) revealed a higher proportion of the C3′-*endo*, or northern (N), sugar conformation (69% N at 30 °C) than the native d(TpT) which exists predominantly in the C2′-*endo*, southern, conformation (36% N).[7] This can be attributed to the lower electronegativity of the 3′–amino substituent of d(TnsoT) and a reduced *gauche* effect between this substituent and the deoxyribose O4′ atom. Furthermore, the shift in the % of N-conformer with change in temperature for both deoxyribose rings of d(TnsoT) was virtually the same as that observed for d(TnsnT),[7] with the largest change occurring in the 5′-terminal ring (63% N at 70 °C increasing to 78% at 10 °C). The native d(TpT) shows little or no variation in sugar pucker with change in temperature. To investigate if this effect is due, in part, to an increase in base stacking of the modified dimers circular dichroism (CD) spectra of d(TnsoT) d(TnsnT) and d(TpT) were recorded at various temperatures. All spectra revealed the same basic characteristics

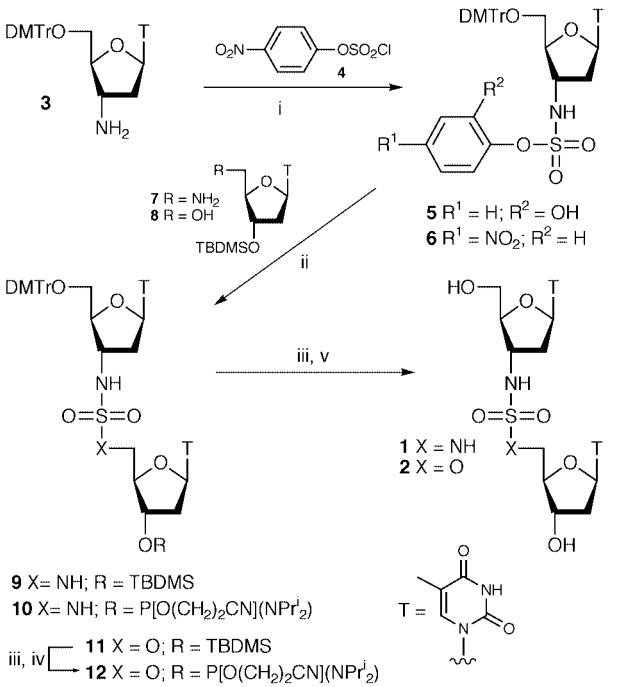

Scheme 1 *Reagents and conditions*: i, 4–nitrophenyl chlorosulfate **4**,[9] 4–nitrophenol, Et_3N, CH_2Cl_2; ii, alcohol **8** (2 equiv.), Et_3N, 4Å molecular sieves, CH_2Cl_2; iii, TBAF, THF; iv, 2–cyanoethyl–*N*,*N*,*N*′,*N*′–tetraisopropylphosphorodiamidite, 4,5–dicyanoimidazole, CH_2Cl_2; v, 2% $CHCl_2CO_2H$, CH_2Cl_2. 4,4′–Dimethoxytrityl is abbreviated to DMTr.

† Electronic supplementary information (ESI) available: Experimental details for oligonucleotide synthesis and duplex denaturation experiments. See http://www.rsc.org/suppdata/cc/b0/b001586p/

DOI: 10.1039/b001586p

Table 1 Electrospray mass spectrometry data and duplex melting temperatures for oligonucleotides **13**–**18**

			T_m[a] (ΔT_m/mod.)[b]/°C			
	Electrospray MS/Da		DNA d(CGCA$_{10}$CGC)			RNA r(CGCA$_{10}$CGC)
	M^+ (calc.)	M^+ (found)	0.02 M [Na^+]	0.1 M [Na^+]	1.0 M [Na^+]	0.1 M [Na^+]
13 d(GCGT$_{10}$GCG)	4875.2	4875.3	43.2	55.0	66.4	49.0
14 d(GCGT$_4$TnsnTT$_4$GCG)	4873.3	4872.8	40.0 (−3.2)[b]	51.7 (−3.3)	60.9 (−5.5)	45.9 (−3.1)
15 d(GCGTnsnTTTTnsnTTTTnsnTGCG)	4869.5	4869.7	33.7 (−3.2)	45.0 (−3.3)	54.6 (−3.9)	41.0 (−2.7)
16 d(GCGT$_4$TnsoTT$_4$GCG)	4874.3	4874.2	43.6 (+0.4)	55.1 (+0.1)	66.0 (−0.4)	47.8 (−1.2)
17 d(GCGTnsoTTTTnsoTTTTnsoTGCG)	4872.5	4872.5	44.0 (+0.3)	55.5 (+0.2)	N.D.[c]	48.0 (−0.3)
18 d(GCGTnsoTTnsoTTnsoTTnsoTTnsoTGCG)	4870.7	4870.6	44.8 (+0.3)	53.3 (–0.3)	N.D.[c]	46.0 (−0.6)

[a] T_m values are accurate to within ± 0.5 °C. [b] The changes in T_m per modification (ΔT_m/mod.) are shown in parentheses.[c] T_m was not determined.

of strong and weak positive bands at 280 and 225 nm, respectively, as well as a negative band at 255 nm, suggesting that the native and the modified dimers are adopting similar overall conformations. Upon increasing temperature all showed a significant decrease in the intensity of the bands at 280 and 255 nm. Notably the change in band intensity for d(TnsoT) was twice the magnitude of that observed for d(TnsnT) and d(TpT) which were virtually identical. This suggests that d(TnsoT) has an higher propensity to adopt a base stacked helical conformation than d(TnsnT) and d(TpT), which base stack to a lesser extent.[10]

Solid phase synthesis of 16-mer chimeric oligodeoxynucleotides, incorporating 3′–*N*-sulfamate or sulfamide linkages, was carried out under standard conditions using the modified dimer phosphoramidites **10** and **12**. The oligonucleotides prepared, **13**–**18**, were characterised by electrospray mass spectrometry and all have the same sequence GCGT$_{10}$GCG[11] (Table 1). The duplex melting temperatures (T_m) of modified oligonucleotides with complementary DNA were then determined by variable temperature UV spectroscopy and compared with the T_m for the native duplex. Modified oligonucleotides with one and three central sulfamide linkages, **14** and **15**, both show a similar change in T_m per modification (ΔT_m/mod.), compared with the native duplex, of −3.2 °C at 0.02 and 0.1 M salt concentration [Na^+]. At 1.0 M salt concentration the modification was even more destabilising. In contrast incorporation of one, three and five sulfamate groups, **16**, **17** and **18**, has little effect on duplex stability with complementary DNA and is even moderately stabilising at low salt concentration with an observed increase in T_m of 0.3 °C per modification. Upon increasing salt concentration the T_m dropped by 0.4 °C for one sulfamate modification. It is likely that the neutral linkages reduce the electrostatic repulsion between strands which is more evident at low salt concentration when fewer cations are present to mask the negatively charged phosphodiester groups. With complementary RNA at 0.1 M salt concentration, the sulfamide group had a similar effect on duplex stability with a drop in T_m of *ca.* 3.0 °C per modification. However the 3′-*N*-sulfamate modified oligonucleotides formed slightly less stable duplexes with RNA than DNA with a drop in T_m of 1.2 °C for one modification and a more moderate drop in ΔT_m/mod of 0.3 and 0.6 °C for three and five modifications respectively. It is probable that oligonucleotides with more 3′-*N*-sulfamate linkages have an higher proportion of C3′-*endo* sugar rings and are therefore more likely to adopt an A–type conformation which is preferred for binding to RNA.

From these results it is clear that 3′-*N*-sulfamate modified oligonucleotides hybridise with complementary nucleic acids with similar binding affinity as native DNA, whereas the sulfamide congeners have significantly lower affinity. It is possible in light of the CD spectra that the sulfamate modified oligonucleotides are more preorganised into a base stacked helical conformation, in the single stranded state, which would reduce the loss of entropy on binding to complementary RNA and DNA and account for the greater stability of the resulting duplexes. Furthermore, the 3′-*N*-sulfamate modified oligonucleotides appear to form more stable duplexes than DNA incorporating the isomeric 5′-*N*-sulfamate modification, which is reported to result in a drop in T_m of 1.5 °C per modification.[8] The destabilisation of duplexes by sulfamide and 5′-*N*-sulfamate modifications may be accounted for by the 5′-amino substituent common to both. In the case of isosteric and isoelectronic N5′→P3′ phosphoramidate DNA, the presence of a 5′-NH group completely abolishes base pairing with complementary nucleic acids.[12] This is attributed to poor hydration and steric clashes between the 5′-amino hydrogen atom and either the H2′ atom of an adjacent deoxyribose ring in an A–type conformation, or the pyrimidine H6 and deoxyribose O4′ atoms in a B-type conformation.[12]

The data reported here suggest that the 3′-*N*-sulfamate modification may be of use in the development of improved antisense or antigene agents. Moreover, given that the 3′-*N*-sulfamate group causes minimal disruption of nucleic acid duplexes, is sterically and electronically more similar to the phosphodiester group than other neutral linkages so far developed, it might also be useful as a general phosphodiester replacement for other applications. For example, one can envisage probing nucleic acid–protein interactions using this modification to determine which phosphodiester groups are involved in electrostatic contacts with protein residues. Alternatively 3′-*N*-sulfamate groups might be used to stabilise aptamers, or hammerhead ribozymes for use *in vivo*.

We thank the EPSRC for studentships to K. J. F. and D. T. H., Polkit Sangvanich for assistance with electrospray mass spectrometry and the EPSRC National Chiroptical Spectroscopy Service.

Notes and references

1 A. De Mesmaeker, R. Häner, P. Martin and H. E. Moser, *Acc. Chem. Res.*, 1995, **28**, 366.
2 M. A. Reynolds, R. I. Hogrefe, J. A. Jaeger, D. A. Schwartz, T. A. Riley, W. B. Marvin, W. J. Daily, M. M. Vaghefi, T. A. Beck, S. K. Knowles, R. E. Klem and L. J. Arnold Jr., *Nucleic Acids Res.*, 1996, **24**, 4584.
3 F. Morvan, Y. S. Sanghvi, M. Perbost, J.–J. Vasseur and L. Bellon, *J. Am. Chem. Soc.*, 1996, **118**, 255.
4 J. Zhang, J. T. Shaw and M. D. Matteucci, *Bioorg. Med. Chem. Lett.*, 1999, **9**, 319.
5 G.-X. He, J. P. Williams, M. J. Postich, S. Swaminathan, R. G. Shea, T. Terhorst, V. S. Law, C. T. Mao, C. Sueoka, S. Coutré and N. Bischofberger, *J. Med. Chem.*, 1998, **41**, 4224.
6 M. O. Blättler, C. Wenz, A. Pingoud and S. A. Benner, *J. Am. Chem. Soc.*, 1998, **120**, 2674.
7 J. Micklefield and K. J. Fettes, *Tetrahedron*, 1998, **54**, 2129.
8 M. E. Huie, M. R. Kirshenbaum and G. L. Trainor, *J. Org. Chem.*, 1992, **57**, 4569.
9 J. Charalambous, M. J. Frazer and W. Gerrard, *J. Chem. Soc.*, 1964, 5480.
10 M. Weinfeld, A. F. Drake, R. Kuroda and D. C. Livingston, *Anal. Biochem.*, 1989, **178**, 93.
11 S. M. Freier and K.-H. Altmann, *Nucleic Acids Res.*, 1997, **25**, 4429.
12 V. Tereshko, S. Gryaznov and M. Egli, *J. Am. Chem. Soc.*, 1998, **120**, 269.

De novo synthesis of artificial ribonucleases with benign metal catalysts

William C. Putnam† and James K. Bashkin*‡

Department of Chemistry, Washington University, St. Louis, MO 63130-4899, USA.
E-mail: bashkin@wuchem.wustl.edu

Received (in Bloomington, IN, USA) 11th November 1999, Accepted 13th March 2000

A zinc(II)–neocuproine based ribozyme mimic has been constructed for the sequence-selective transesterification of RNA using a begin metal catalyst.

We report the *de novo* synthesis of a Zn-based ribozyme mimic that can cleave HIV mRNA in a sequence-specific manner, with excellent activity. The design of artificial ribonucleases that are both biocompatible and sequence-specific has attracted much attention for their potential use as catalytic, gene-specific therapeutics.[1–8] Many of the artificial ribonucleases prepared thus far are constructs that contain chelates of copper or chelates of heavy metals. Two of our goals in the construction of artificial ribonucleases are: (i) the use of bioavailable, innocuous metals such as zinc, and (ii) the optimization of activity. The most specific artificial ribonucleases are referred to as 'ribozyme mimics' owing to the fact they mimic the Watson–Crick derived sequence-specific activity of some ribozymes. With ribozyme mimics, the large catalytic domain of a natural ribozyme is replaced by a small-molecule catalyst.

The RNA cleavage ability of free mononuclear and dinuclear zinc complexes and conjugates has been demonstrated in previous work from our lab and from other groups, but the cleavage activity of Zn reagents has generally been low. In 1995, sequence-specific cleavage of RNA was demonstrated by Lönnberg and coworkers[9] when they used a 5′-imidazole DNA conjugate in concert with free zinc ions to form an active artificial ribonuclease that cleaved 2–5% of the target RNA in 19 h at room temperature. It was followed by a 1998 communication by Matsuda *et al.* where a novel dinuclear Zn(II)–DNA conjugate was used to effect sequence-specific cleavage of RNA.[10] The dinuclear construct cleaved 5% of the RNA after 3 h at 37 °C ([RNA] = 0.2 μM; [cleavage agent] = 5 μM). Here we report the *de novo* construction of an active, sequence-specific artificial ribonuclease containing an internal serinol-neocuproine residue embedded in a DNA 17-mer (Fig. 1).

We have previously reported the synthesis and activity of a ribozyme mimic derived from serinol and copper(II)–terpyridine (Cu–terpy) (Probe 1, Fig. 1).[1,11] The serinol residue introduced an abasic site into the ribozyme mimic–RNA duplex, and was shown to be three times more efficient at RNA cleavage than a fully duplexed Cu(II)–terpy derived ribozyme mimic. The phosphoramidite **1**, a serinol-neocuproine conjugate, was synthesized according to Scheme 1 and incorporated into a DNA 17-mer (Probe 2) using standard automated DNA synthesis.§ This 17-mer is complimentary to a region of the mRNA from the HIV *gag*-gene. Probe 3 (Fig. 1), which contains a three-carbon spacer produced from a commercially available (Glen Research) phosphoramidite, was used to test for cleavage associated with the presence of an abasic site in the RNA/DNA duplex.

The modified DNA conjugates that were synthesized are shown here where X indicates the modified position. RNA cleavage reactions were conducted with two RNA substrates: a 159-mer from a relatively well conserved sequence from the *gag* mRNA of HIV (775-933), and a 28-mer that contains the same 17-mer recognition sequence (Fig. 2). The 28-mer substrate allowed identification of cleavage products and the 159-mer allowed assessment of the sequence-specificity of the ribozyme mimic in the presence of numerous binding sites. Reactions were conducted at both 37 and 45 °C, at pH 7.4 (HEPES Buffer).

High-resolution polyacrylamide gel-electrophoresis was used to analyse the RNA cleavage, and a typical image of the 28-mer reaction mixture is shown in Fig. 1. No sequence-specific cleavage was observed with probe 2 in the absence of added metal. In the presence of EDTA, probe 1 gave no

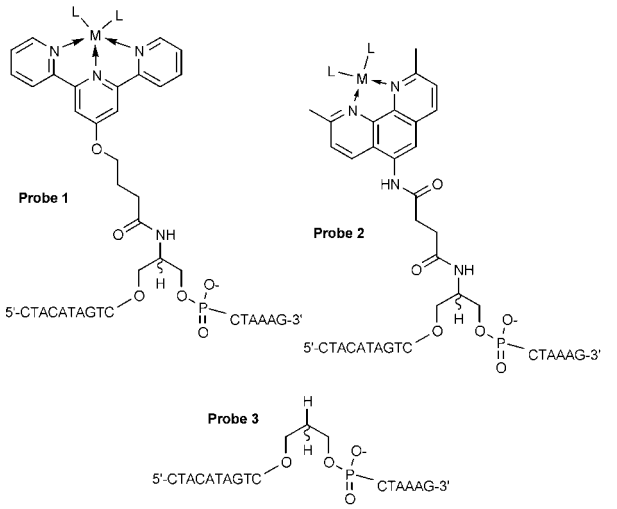

Fig. 1 Ribozyme mimic probes.

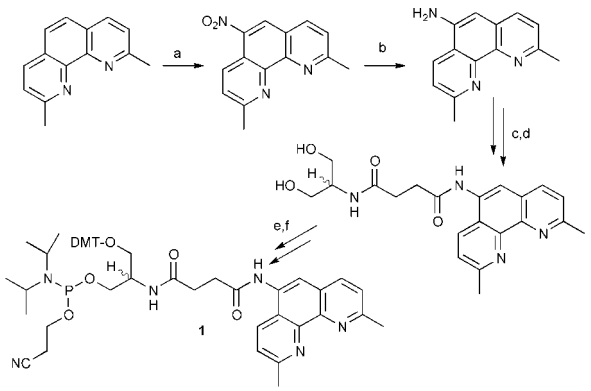

Scheme 1 Synthesis of phosphoramidite **1**. *Reagents and conditions*: (a) H_2SO_4, fuming HNO_3, reflux, 5 h, 23%; (b) NH_2NH_2, Pd/C, EtOH, reflux, 5 h, 81%; (c) succinic anhydride, pyridine, room temp., 12 h, 59%; (d) EDC–HCl, serinol, DMF, room temp., 12 h, 63%; (e) DMTCl, pyridine, room temp., 12 h, 51%; (f) 2-cyanoethyl-*N*,*N*-diisopropylphosphoramidite, room temp., 1 h, 82%.

† William Putnam was a 1998 NSF-GOALI fellow at Reliable Biopharmaceutical Company. Current address: Midwest Research Institute, 425 Volker Boulevard, Kansas City, Missouri 64110, USA. E-mail: wputnam@mriresearch.org

‡ Current address: Monsanto Company R3A, 800 N. Lindbergh Blvd., St. Louis, MO 63167, USA. E-mail: james.k.bashkin@monsanto.com

DOI: 10.1039/a908783d

(a)
5′-^{1}(775)GGAGAA^{6} AUUUAUAAAA^{16} GAUGGAUAAU^{26} CCUGGGAUUA^{36} AAUAAAAUAG^{46}
UAAGAAUGUA^{56} UAGCCCUACC^{66} CAGCAUUCUG^{76} GACAUAAGAC^{86} AAGGACCAAA^{96}
GGAACCUUUA^{106} GAGACUAUGU^{116} AGACCGGUUC^{126} UAUAAAACUC^{136} UAAGAGCCGA^{146}
GCAAGCUUCA^{156} CAG^{159} (933)-3′

(b)
5′-A^{1}A^{2}A^{3}C^{4}C^{5}A^{6}A^{7}C^{8}C^{9}C^{10}U^{11}U^{12}U^{13}A^{14}G^{15}A^{16}G^{17}A^{18}C^{19}U^{20}A^{21}U^{22}G^{23}U^{24}A^{25}G^{26}A^{27}C^{28}-3′

Fig. 2 RNA Substrates. (a) The 159-mer target RNA strand, a relatively well-conserved sequence from the *gag* mRNA of HIV (775-933 HIVHXB2R), is shown, with the 17-mer target region underlined. (b) The 28-mer target RNA strand containing the same 17-mer recognition sequence from the *gag*-mRNA of HIV (HIVHXB2R), is shown, with the 17-mer target region underlined.

Table 1 Sequence-specific cleavage of 28-mer and 159-mer RNA targets by ribozyme mimics derived from Cu(II) and Zn(II) with probes 1–3 (exact reaction conditions given in experimental)

Probe no. (metal)	Cleavage (%) (28-mer, 15 h 37 °C)	Cleavage site (28-mer)	Cleavage (%) (159-mer, 10 h, 37 °C	Cleavage site (159-mer)
1 (Cu)	14	A^{16}	8	A^{108}
2 (Cu)	65	G^{15}, A^{16}	80	G^{109}, A^{108}
2 (Zn)	25	G^{15}, A^{16}	18	G^{109}, A^{108}
3	0	n/a	0	n/a

sequence-specific RNA cleavage. In accordance with previous reports, EDTA treatment is necessary to suppress cleavage in the case of probe 1 because of the high binding constant of terpy for copper. This extremely high affinity allows ribozyme mimics that contain pendant terpy ligands to scavenge trace amounts of Cu(II) from commercial buffer salts.[11] In the presence of copper, both probe 1 and 2 form active ribozyme mimics, and in the presence of zinc, probe 2 forms an active ribozyme mimic. The products of all of the cleavage reactions co-migrate with alkaline hydrolysis and Ribonuclease T_1 (G specific) digestion products, which lends strong evidence that, in the presence of either metal, these ribozyme mimics react *via* a biomimetic pathway of transesterification and hydrolysis.

The extent of cleavage is shown in Table 1. The major site of RNA scission by probes 1 and 2 varies by one base. Probe 1 induces nucleophilic cleavage of the RNA at the 3′ side of A^{16} while probe 2 cleaves on the 5′ side of this nucleotide. No sequence-specific cleavage is observed in the presence of Cu(II) or Zn(II) alone (with no DNA probe). Probe 3, the control oligonucleotide containing the abasic site and no pendant ligand, is completely inactive for RNA cleavage in the presence of Cu(II) and Zn(II) (data not shown for Zn). This control tested for any site-specific cleavage derived solely from the presence of metal ions and an abasic site.

The Zn(II) conjugate of probe 2 is only the third example of a zinc based artificial ribonuclease derived from Zn(II), and the second mononuclear example. Direct comparisons of sequence-specific RNA cleavage efficiencies are very difficult because of differences in reaction time and temperature, but the zinc–neocuproine-mediated cleavage reported here is higher than the sequence-specific cleavage previously reported. We have demonstrated that high cleavage efficiencies that can be attained using benign inorganic chemistry. The extent of cleavage by ribozyme mimics observed in these studies is as follows:

Cu(II)–neocuproine > Zn(II)–neocuproine > Cu(II)–terpy.

The observed trends result predominately from two phenomena: (i) The speciation between metal-bound water and metal bound hydroxide (the most probable active species) *i.e.* the trends in the pK_a of the coordinated waters and (ii) the suppression of bis(μ-hydroxide) dimers by the methyl groups of neocuproine.[12]

The *in vivo* concentration of zinc in human serum is 17.2 μM,[13] three times greater than the concentration of zinc used in these *in vitro* experiments. There remains controversy over the amount of free zinc in the cell. Note also that the free copper concentration *in vivo* has recently been determined to be approximately zero.[14] The large cleavage efficiency of the zinc

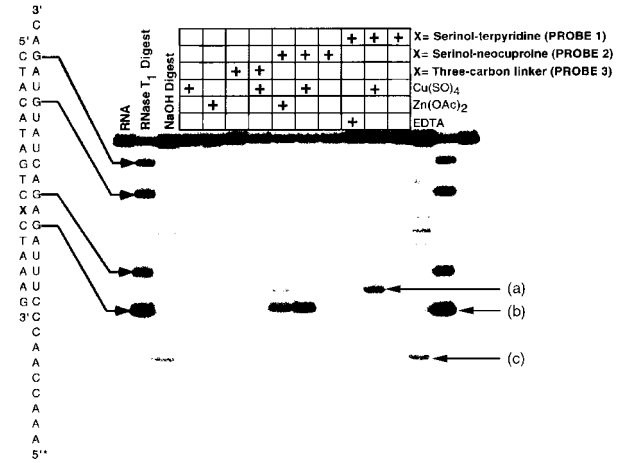

Fig. 3 Audioradiogram of the sequence-specific cleavage of the 5′-end labeled 28-mer RNA substrate 5′-CTA CAT AGT CXC TAA AG-3′ by ribozyme mimics; (a) sequence-specific cleavage by probe 1 (minor site probe 2), (b) sequence-specific cleavage by probes 2, (c) hot spot for RNA cleavage.

based ribozyme mimic bodes well for the production of biocompatible sequence-specific artificial ribonucleases.

Acknowledgment for partial support of this research is made to NSF GOALI Grant CHE-9802660, Reliable Biopharmaceutical Inc., and to the donors of The Petroleum Research Fund, administered by the American Chemical Society.

Notes and references

§ The compounds synthesized in Scheme 1 were fully characterized by ^{1}H, ^{13}C and ^{31}P(phosphoramidite **1**) high-resolution NMR spectroscopy and high-resolution fast-atom-bombardment (HR-FAB) mass spectrometry (MS). All probes were characterized by matrix-assisted laser desorption ionization time-of-flight (MALDI-TOF) mass spectrometry and electrospray mass spectrometry.(Mass spectrometry was provided by the Washington University Mass Spectrometry Resource, an NIH Research Resource (Grant No. P41RR0954)).

The 159-mer RNA was synthesized by runoff transcription and 5′ end labeled with ^{32}P (We thank Dr Lee Ratner for the plasmid containing the HIV *gag*-gene fragment). The 28-mer RNA was purchased (Oligo's *etc.*) and ^{32}P 5-end labeled in a similar fashion. RNA cleavage reactions were carried out in 10 mM *N*-(2-Hydroxyethyl)piperazine-*N*′-(2-ethanesulfonic acid) (HEPES) buffer pH 7.4, with 0.1 M $NaClO_4$, [0.1 μM RNA (28-mer) and 0.01 μM RNA (159-mer), 5 μM probe, and 5 μM metal (total reaction volume = 10 μL. The reactions were heated to the desired temperature and time. The reactions were quenched by the addition of 5 μL loading buffer, and loaded on a denaturing polyacrylamide gel (20% 28-mer and 6% 159-mer). The gel image was quantified using a Molecular Dynamics PhosphorImager™ and the ImageQuant™ software package.

1 J. K. Bashkin, J. Xie, A. T. Daniher, L. A. Jenkins and G. C. Yeh, *Nato ASI Ser., Ser. C*, 1996, **479**, 355.
2 T. R. Cech, *JAMA*, 1988, **260**, 3030.
3 J. S. Cohen, *Oligodeoxynucleotides: Antisense Inhibitors of Gene Expression*, CRC Press, Boca Raton, FL, 1989.
4 R. Haner and J. Hall, *Antisense Nucleic Acid Drug Dev.*, 1997, **7**, 423.
5 J. R. Morrow, L. A. Buttrey, V. M. Shelton and K. A. Berback, *J. Am. Chem. Soc.*, 1992, **114**, 1903.
6 K. Matsumura, M. Endo and M. Komiyama, *J. Chem. Soc., Chem. Commun.*, 1994, 2019.
7 D. Magda, S. Crofts, A. Lin, D. Miles, M. Wright and J. L. Sessler, *J. Am. Chem. Soc.*, 1997, **119**, 2293.
8 D. Magda, M. Wright, S. Crofts, A. Lin and J. L. Sessler, *J. Am. Chem. Soc.*, 1997, **119**, 6947.
9 J. Hovinen, A. Guzaev, E. Azhayeva, A. Azhayev and H. Lönnberg, *J. Org. Chem.*, 1995, **60**, 2205.
10 S. Matsuda, A. Ishikubo, A. Kuzuya, M. Yashiro and M. Komiyama, *Angew. Chem., Int. Ed.*, 1998, **37**, 3284.
11 A. T. Daniher and J. K. Bashkin, *Chem. Commun.*, 1998, 1077.
12 B. Linkletter and J. Chin, *Angew. Chem., Int. Ed. Engl.*, 1995, **34**, 472.
13 I. Bernini, H. B. Gray, S. J. Lippard and J. S. Valentine, *Bioinorganic Chemistry*, University Science Books, Mill Valley, CA, 1994.
14 T. D. Rae, P. J. Schmidt, R. A. Pufahl, V. C. Culotta and T. V. O'Halloran, *Science*, 1999, **284**, 805.

ChemComm

Low-density hydrogen-bonded networks in crystals and at the air/water interface

David J. Plaut, Kristian M. Lund and Michael D. Ward*

Department of Chemical Engineering and Materials Science, University of Minnesota, Minneapolis, MN, USA. E-mail: wardx004@tc.umn.edu

Received (in Columbia, MO, USA) 13th December 1999, Accepted 9th March 2000

Trimesic acid and various alkylamines assemble into ordered two-dimensional hexagonal hydrogen-bonded networks in both bulk crystals and at the air/water interface.

Interest in low-density open organic frameworks, assembled by non-covalent interactions, has increased significantly owing to their potential application as designer solids for separations, catalysis, and electronic materials.[1] Controlling the structure of porous networks can be complicated by interpenetration of equivalent frameworks[2] and the influence of guest or solvent molecules on structural isomerism of the framework.[1d,3] A recent study of a single crystal of a 3:1 complex consisting of dicyclohexylamine and trimesic acid (H_3TMA), crystallized from a 1:1 mixture of butan-1-ol and methanol,[4] revealed a low-density hydrogen-bonded network with the 'chicken-wire' motif A, rather than the more symmetrical structural isomer based on motif B. We report herein, three new compounds that

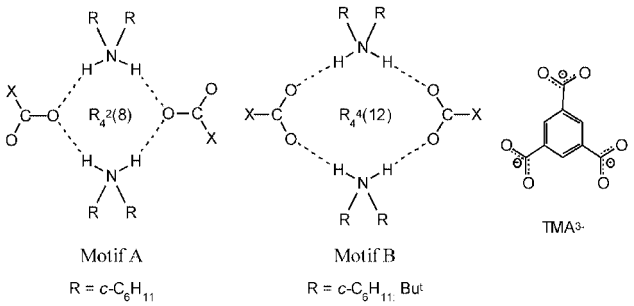

contain the cyclic $R_4^4(12)$ motif B,[5] in which both carboxylate oxygen atoms form hydrogen bonds with the dialkylammonium protons. The formation of these compounds illustrates the sensitivity of structural isomerism to different guest molecules. We also demonstrate that these hydrogen-bonded motifs can be generated at the air/water interface from long chain aliphatic amines and H_3TMA.

Vapor diffusion of acetone into methanol or isopropyl alcohol solutions containing H_3TMA and dicyclohexylamine afforded single crystals of $[NH_2(c\text{-}C_6H_{11})_2^+]_3[TMA^{3-}]\cdot Me_2CO\cdot 0.5MeOH$ **1** and $[NH_2(c\text{-}C_6H_{11})_2^+]_3[TMA^{3-}]\cdot 2.5\ Me_2CHOH$ **2**, respectively. Similarly, vapor diffusion of acetone and di-*tert*-butylamine into an isopropyl alcohol solution of H_3TMA afforded single crystals of $[NH_2(Bu^t)_2^+]_3[TMA^{3-}]\cdot Me_2CO$ **3**. Single crystal X-ray diffraction reveals 2D hydrogen-bonded 'honeycomb' networks in each of these materials.† These networks can be viewed as expanded versions of the 'chicken-wire' motif reported for H_3TMA alone.[2] Pairs of ammonium cations acts as 'spacer' molecules between pairs of carboxylate substituents on the TMA^{3-} anions as depicted in motif B. The 2D sheets pucker to different extents in these structures, reflecting an intrinsic flexibility that enables this network architecture to persist despite the differently sized alkyl groups and solvent molecules included within the networks. Nevertheless, the formation of motif B apparently is quite sensitive to the crystallization solvent, given that motif A was observed in methanol solvated crystals grown from butan-1-ol–methanol solutions.

Compound **1** crystallizes in the space group $P\bar{1}$ and exhibits two crystallographically independent flat 2D hydrogen-bonded layers (Fig. 1). The cyclohexyl substituents of one of these layers project into the hexagonal pores, with six cyclohexyl groups lying in the midplane of the pore, three projecting above the plane, and the remaining three projecting below the plane. The second layer (not shown) also has the identical honeycomb motif but the cyclohexyl substituents are twisted out of the layer plane to a greater extent. These layer structures reflect the flexibility of the hydrogen bonds and the ability of the carboxylate groups to rotate around the C–C bond. The two independent layers alternate along the *a* axis with the pores overlapping, creating a continuous channel along this direction. This contrasts with the previously reported methanol solvate, which crystallized in the hexagonal space group $P6_3$ and exhibited 2D hydrogen-bonded sheets that were organized along the six-fold screw axis such that pores were not continuous. Disordered acetone and methanol molecules occupy the pores in **1**, filling the void space not occupied by the cyclohexyl groups. The guest stoichiometry was determined by thermal gravimetric analysis and ^1H NMR spectroscopy.

Compound **2** crystallizes in space group $P\bar{1}$ and exhibits hydrogen-bonding motif B. However, two carboxylate groups of each TMA^{3-} anion each have one oxygen that is hydrogen bonded to the dialkylammonium protons as well as an isopropyl alcohol molecule that resides below the plane of the 2D hydrogen-bonded sheet. Each puckered 2D sheet can be described as interconnected hexagons with chair-like conformations. If the hexagon is defined by the centroids of the TMA^{3-}

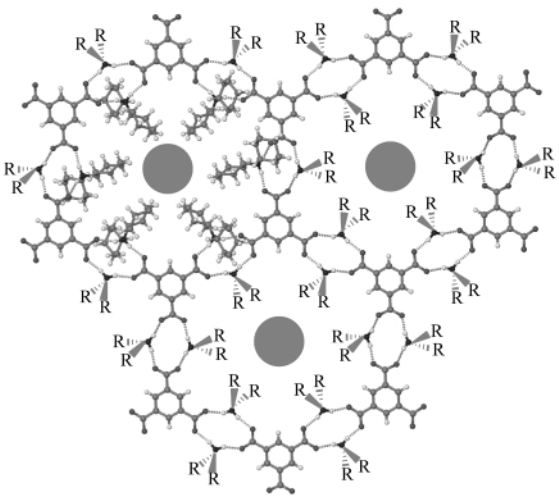

Fig. 1 A portion of one of the two unique 2D hydrogen-bonded networks in **1**. Of the twelve cyclohexyl substituents on the interior of each pore, six project along the midplane of the pore while the remaining six project above or below the plane. The pore at the upper left is depicted with all its cyclohexyl substituents; in the remaining two pores these have been denoted as R for simplicity. The disordered guest molecules are depicted by the circles in the center of the pores.

DOI: 10.1039/a910252n

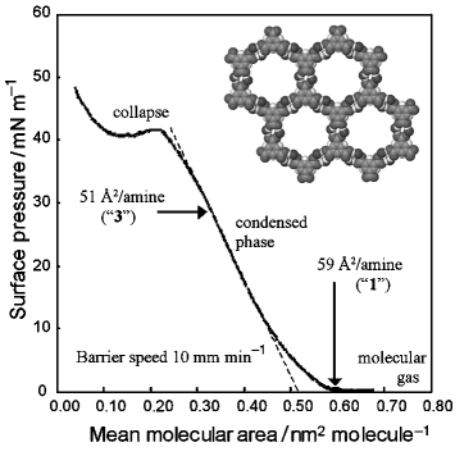

Fig. 2 Pressure–area isotherm of ODA over an aqueous H_3TMA subphase, indicating a molecular area of *ca.* 59 Å^2/amine at lift-off, and 51 Å^2/amine before collapse. The insert depicts the *bc* plane of compound **1** (cyclohexyl groups and guest molecules omitted for clarity), which has a calculated area matching that obtained from the Langmuir isotherm.

anions, the torsion angles associated with the chair-like conformations are 19.1, 16.2 and 18.4°. The hexagonal pores in adjacent sheets are slightly offset but still create a continuous channel, along the *a* axis, that is filled with disordered isopropyl alcohol guests.

Compound **3** crystallizes in the space group $P2_1/n$, and exhibits motif B with hydrogen-bonded sheets consisting of chair-like hexagons that are more severely puckered than in **2**, with torsion angles measuring 22.9, 23.9 and 25.5°. Two acetone molecules occupy the void space not occupied by the *tert*-butyl groups of the amines within each pore.

The bulk structure of organic crystals can often be described as 2D molecular layers that stack in the remaining third dimension. Consequently, these layer motifs can be used as models for the design of monolayers on solid substrates and at the air/water interface. The latter requires amphiphiles with polar head groups capable of organizing at the air/water interface into motifs that mimic the structure of the 2D layers in the bulk crystals.[3a,6]

The pressure–area isotherm measured for the long chain amphiphile octadecylamine (ODA), spread over an aqueous subphase of H_3TMA, exhibits lift-off at a molecular area of 59 Å^2/amine. Extrapolation of the linear compression regime afforded a molecular area of 51 Å^2/amine (Fig. 2). In contrast, a molecular area of *ca.* 20 Å^2/amine was measured when ODA was spread over a basic subphase without H_3TMA.[7] Similar isotherms were collected for methyloctadecylamine (MODA) and dioctadecylamine (DODA), both exhibiting linear compression regimes that were consistent with an area of 54 Å^2/amine.‡ The molecular areas measured from the isotherms collected over H_3TMA lie within the range of the molecular areas occupied by the 2D hydrogen-bonded networks in **1**–**3** (58.6, 56.6 and 51.5 Å^2/amine, respectively). This strongly supports the formation of a 2D porous hydrogen-bonded monolayer at the air/water interface having motif B. Notably, the molecular area for the methanol solvate of **1** and **2** (motif A), based on the reported crystal structure, is only 45 Å^2/amine. Furthermore, the range of lift-off and extrapolated values reflected by the different isotherms, suggests that the monolayers possess the flexibility evident from the bulk crystalline networks.

We anticipate that porous Langmuir monolayers can serve as structural mimics of isostructural porous 2D networks in crystalline solids. These monolayers, for which interpenetration is not possible, may promote the nucleation and growth[6,8] of crystalline phases containing such networks. Porous monolayers, transferred to permeable solid substrates by the Langmuir–Blodgett method, may also be useful as size exclusion membranes in which the pore sizes can be adjusted by molecular design.

We gratefully acknowledge Maren Pink and Victor J. Young of the X-ray Crystallographic Laboratory at the University of Minnesota for the acquisition of crystallographic data. Financial support was provided by the National Science Foundation and the University of Minnesota Industrial Partnership in Interfacial and Materials Engineering (IPRIME).

Notes and references

† *Crystal data*: for **1**: $C_{45}H_{75}N_3O_6\cdot(CH_3)_2CO\cdot0.5CH_3OH$, triclinic, $P\bar{1}$, a = 16.9805(3), b = 19.5242(4), c = 20.0428(4) Å, α = 116.268(1), β = 111.491(1), γ = 95.189(1)°, U = 5284.2(2) Å^3, T = 173 K, Z = 4, μ(Mo-Kα) = 0.062 mm^{-1}, 35303 reflections measured, 17825 unique (R_{int} = 0.0289) which were used in all calculations. There is disordered solvent present in this structure. Attempts were made to model this, but were unsuccessful since there were no obvious major sire occupations for the solvent molecules. PLATON/SQUEEZE[9] was used to correct the data for the presence of the disordered solvent. A potential solvent volume of 1091.1 Å^3 was found. 300 electrons per unit cell worth of scattering were located in the void. The stoichiometry of solvent was calculated independently by NMR and TGA to be one molecule of MeOH and two molecules of acetone per unit cell, which results in 228 electrons per unit cell. The modified dataset improved the *R*1 value by *ca.* 10%; final *R*1 = 0.0563, *wR*2 = 0.1379.

For **2**: $C_{45}H_{75}N_3O_6\cdot2.5(CH_3)_2CHOH$, triclinic, $P\bar{1}$, a = 10.5401(6), b = 15.815(1), c = 18.711(1) Å, α = 107.648(1), β = 105.627(1), γ = 97.211(1)°, U = 2788.3(3) Å^3, T = 173 K, Z = 2, μ(Mo-Kα) = 0.074 mm^{-1}, 22227 reflections measured, 9779 unique (R_{int} = 0.0385) which were used in all calculations. Two isopropyl alcohol molecules were found and refined in the structure. The structure contains disordered solvent in a channel along (*x*,1/2,1/2). Attempts to model this were unsuccessful. PLATON/SQUEEZE was used to correct the data for the presence of the disordered solvent. A potential solvent volume of 246.9 Å^3 located in the above mentioned channel was found. 38 electrons per unit cell worth of scattering were located in the void. The electron count suggests the presence of *ca.* one isopropyl alcohol molecule per unit cell. The modified dataset improved the *R*1 value by *ca.* 6%; final *R*1 = 0.0642, *wR*2 = 0.1895.

For **3**: $C_{45}H_{75}N_3O_6\cdot(CH_3)_2CO$, monoclinic, $P2_1/n$, a = 9.745(1), b = 18.486(2), c = 23.157(2) Å, β = 101.644(3)°, U = 4090.0(5) Å^3, T = 173 K, Z = 4, μ(Mo-Kα) = 0.073 mm^{-1}, 30377 reflections measured, 7227 unique (R_{int} = 0.0828) which were used in all calculations; final *R*1 = 0.0600, *wR*2 = 0.1752. The dataset was checked for twinning and disordered solvent, however, no evidence for either was found.

CCDC 182/1580. See http://www.rsc.org/suppdata/cc/a9/a910252n/ for crystallographic files in .cif format.

‡ Interestingly, the isotherm of DODA initially reveals a linear compression feature corresponding to 94 Å^2/amine, but collapses at 23 mN m^{-1} to the linear region associated with the 54 Å^2/amine value. We surmise that this value corresponds to a condensed phase in which one of the alkyl chains lies at the air/water interface until increased compression drives both alkyl chains away from the air/water interface to form a 2D structure similar to the monoalkylamine layers.

1 (*a*) D. D. MacNicol, J. J. McKendrick and D. R. Wilson, in *Inclusion Compounds*, ed. J. L. Atwood, J. E. Davies and D. D. MacNicol, Academic Press, London, 1984, vol. 2; (*b*) M. Simard, D. Su and J. D. Wuest, *J. Am. Chem. Soc.*, 1991 **113**, 4696; (*c*) O. Ermer and L. Lindenberg, *Helv. Chim. Acta*, 1991, **74**, 825; (*d*) K. Endo, T. Ezuhara, M. Koyonagi, M. Hideki and Y. Aoyama, *J. Am. Chem. Soc.*, 1997, **119**, 499.
2 F. H. Herbstein, *Top. Curr. Chem.*, 1987, **140**, 108.
3 (*a*) V. A. Russell, C. C. Evans, W. Li and W. D. Ward, *Science*, 1997, **276**, 575; (*b*) J. A. Swift, A. M. Pivovar, A. M. Reynolds and M. D. Ward, *J. Am. Chem. Soc.*, 1998, **120**, 5887.
4 R. E. Melendez, C. V. K. Sharma, M. J. Zaworotko, C. Bauer and R. D. Rogers, *Angew. Chem., Int. Ed. Engl.*, 1996, **35**, 2213.
5 M. C. Etter, *Acc. Chem. Res.*, 1990, **23**, 120; M. C. Etter, *J. Phys. Chem.*, 1991, **95**, 4601.
6 D. Jacquemain, S. G. Wolf, F. Leveiller, M. Deutsch, K. Kjaer, J. Als-Nielsen, M. Lahav and L. Leiserowitz, *Angew. Chem., Int. Ed. Engl.*, 1992, **31**, 130.
7 G. L. Gaines, Jr., *Insoluble Monolayers at Liquid–Gas Interfaces*, Interscience Publishers, New York, 1966.
8 L. M. Frostman and M. D. Ward, *Langmuir*, 1997, **13**, 330; S. Mann, B. R. Heywood, S. Rajam and J. B. A. Walker, *J. Phys. D: Appl. Phys.*, 1991, **24**, 154.
9 A. L. Spek, *Acta Crystallogr., Sect. A*, 1990, **46**, C34.

A two-step, catalytic synthesis of δ-hydroxy-γ-lactones from allylic acetates and bis(trimethylsilyl)ketene acetals

Henri Rudler,*[a] Andrée Parlier,[a] Frederic Cantagrel,[a] Paul Harris[a] and Moncef Bellassoued[b]

[a] *Laboratoire de Synthèse Organique et Organométallique, UMR 7611, Université Pierre et Marie Curie, T 44-45, 4 place Jussieu, 75252 Paris Cedex 5, France. E-mail: rudler@ccr.jussieu.fr*

[b] *Laboratoire de Synthèse Organométallique associé au CNRS, Université de Cergy-Pontoise, 5 Mail Gay Lussac, Neuville-sur-Oise, 95031 Cergy-Pontoise Cedex, France*

Received (in Liverpool, UK) 11th February 2000, Accepted 21st March 2000

Bis(trimethylsilyl) ketene acetals react successively with allylic acetates, in the presence of Pd(0) then with H_2O_2, in the presence of methyltrioxorhenium, to give δ-hydroxy-γ-lactones *via* γ-unsaturated carboxylic acids.

η³-allyl palladium complexes, formed upon oxidative addition of allylic compounds to Pd(0), have found wide applications, as intermediates, in their reaction with nucleophiles.[1] Much effort has been devoted to the modification of the structure of the allylic moiety, the ligands around the metal, and also of the nucleophiles. It is this last point on which will focus our attention. Indeed, we have shown recently that bis(trimethylsilyl) acetals of ketenes could be used either as nucleophiles or versatile precursors of nucleophiles, when suitably activated, in reactions with a large variety of electrophiles such as carbonyl compounds, organic and organometallic peroxo derivatives,[2] and arene tricarbonyl chromium complexes.[3] These acetals lead *directly*, in contrast to other precursors, to functionalized carboxylic acids in high yield. Moreover, for chromium complexes, a direct double nucleophilic addition of potassium enolates originating from these acetals on a carbon–carbon double bond of anisole (and its derivatives) has been brought to the fore. This one pot reaction leads to functionalized lactones (Scheme 1).

Alkoxy monotrimethylsilyl ketene acetals have already been used in palladium(0) catalyzed alkylations in conjunction with allylic acetates for the preparation of unsaturated esters.[4–6] Under the same conditions, bis(trimethylsilyl) ketene acetals might thus lead to unsaturated carboxylic acids. Moreover, we have shown[7] that γ-unsaturated hydroxyalkenes underwent a high yield catalytic oxidative cyclization to lactols promoted by the system H_2O_2/MTO (methyltrioxorhenium),[8] a reaction which has recently been applied to the transformation of γ-unsaturated carboxylic acids into hydroxylactone (Scheme 2).[9]

Taken together, the interaction of bis(trimethylsilyl) ketene acetals first with allylic acetates to give unsaturated carboxylic acids, then with MTO/H_2O_2 to give hydroxylactones (Scheme 3) would constitute a means for the catalytic addition of two nucleophiles on a carbon–carbon double bond,[10] and would thus

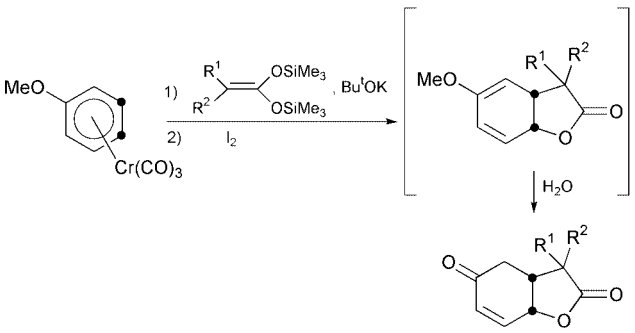

Scheme 1

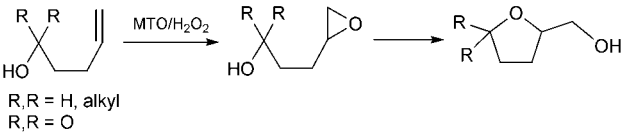

Scheme 2

parallel, on a formal point of view, the transformation of anisole depicted in Scheme 1. And this indeed turned out to be the case.

Depending on the nature of the starting ketene acetals, cyclopropane carboxylic acids could be isolated as secondary products, and epoxycarboxylic acids detected by NMR as intermediates in the lactonization reactions.

Thus, a mixture of allyl acetate (10 mmol) and bis-(trimethylsilyl)ketene acetal **1a**† (11 mmol) was heated in THF (70 mL) for 24 h in the presence of $Pd(PPh_3)_4$ (0.2 mmol, 2%). Evaporation of the volatiles, under vacuum, left a residue which was diluted in dichloromethane and filtered through a pad of silica gel. Extraction with aqueous sodium hydroxide followed by acidification and extraction with dichloromethane gave a mixture of acids. After cooling the solution to 0 °C, MTO (5% with respect to the unsaturated acids) was added followed by a 30% solution of hydrogen peroxide (1.1 equiv. with respect to the acids). The biphasic mixture was then stirred for three days at room temperature, the excess oxidant destroyed with aqueous sodium bisulfite, and the organic products extracted with dichloromethane. Treatment of the organic layer with dilute sodium hydroxide left an organic phase containing the hydroxy-lactone (5 mmol). Acidification of the aqueous layer followed by extraction with diethyl ether gave, after evaporation of the solvents, the cyclopropyl acid (1.5 mmol).

The same reactions were carried out on a series of bis(trimethylsilyl) ketene acetals and two allylic acetates.† They led to hydroxylactones and, for the more substituted ketene acetals, to mixtures of lactones and cyclopropyl acids (Table 1).‡

For cinnamyl acetate **2a** (R^3 = Ph) and the ketene acetal **1a** (R^1 = R^2 = Me), the two acids **3a** and **4a** resulting, respectively, from S_N2 and S_N2' reactions, were separated by crystallization and by silica gel chromatography. Their oxidation led, respectively, to the lactones **6a** and **7a** (Scheme 4). Whereas the transformation of **3a** into **6a**, obtained as a single isomer was complete within 6 h, the conversion of **4a** into **7a** took three days. This result is in agreement with the difference of epoxidation rate observed for substituted and terminal olefins with the system H_2O_2/MTO.[8]

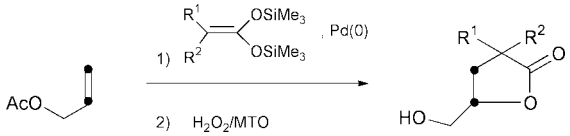

Scheme 3

DOI: 10.1039/b001175o

Table 1 Lactones and cyclopropyl carboxylic acids from allylic acetates and bis(trimethylsilyl) ketene acetals. The ratios were obtained from ^{1}H NMR (400 MHz) data, after oxidation. The ratios of **8** *vs.* **6** and **7** was also determined upon isolation of **8**

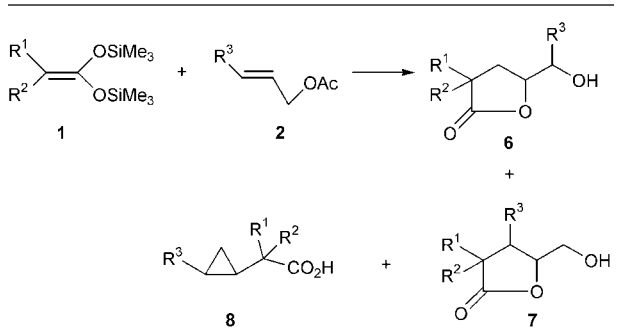

Entry	1	2	R^1	R^2	R^3	Yield (%)	6	7	8
1	**1a**	**2a**	Me	Me	Ph	69.5	49	27	24
2	**1a**	**2b**	Me	Me	H	26	76	—	24
3	**1b**	**2a**	$(CH_2)_5$		Ph	23.5	50	27	23
4	**1b**	**2b**	$(CH_2)_5$		H	66	76.5	—	23.5
5	**1c**	**2a**	H	*t*Bu	Ph	29	80	20	—
6	**1d**	**2a**	Ph	Ph	Ph	65	100	—	—
7	**1e**	**2a**	OPh	H	Ph	50	50	50	—

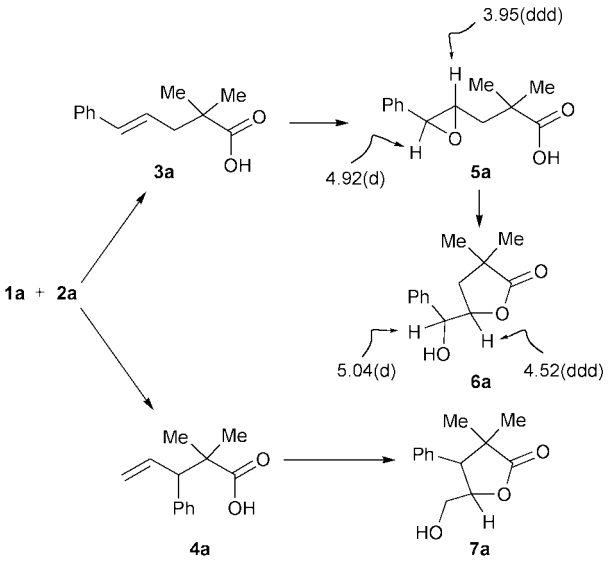

Scheme 4

That indeed epoxides were formed as intermediates in these oxidation reactions as for γ-hydroxyalkenes[7] was demonstrated as follows: when the acid **3a** was subjected to the oxidation reaction, a labile precursor could be detected by ^{1}H NMR spectroscopy after 2 h giving a doublet and a multiplet at δ 4.92 and 3.95, respectively attributable to the two hydrogens of the epoxide **5a** (Scheme 4). These signals disappeared progressively in favour of those due to the hydroxylactone **6a** at δ 5.04 (doublet), and δ 4.52 (multiplet). Attempts to isolate the epoxide **5a** by silica gel chromatography failed however, a result which is reminiscent of previous observations.[7]

The results described herein allow the following comments to be made.

As for mono(trialkylsilyl) ketene acetals, no base was required for the interaction with the allylic acetates: the ketene acetals are thus nucleophilic enough to interact as such with the π-allyl complexes of palladium.[6,10]

In addition, these transformations are interesting from a double point of view. First, highly substituted, unsaturated carboxylic acids can be obtained *directly* in the first step of the process. Second, for the disubstituted ketene acetals, cyclopropyl acids are formed, yet, up to now, in rather low yield. Their purification, without the need of chromatography, can easily be achieved by the use of the second step of the process; indeed, the separation of the lactones from the cyclopropyl acids, whenever formed, is possible by a simple extraction process.

The interaction of mono(trialkylsily) ketene acetals with allylic acetates in the presence of complexes of palladium had already been shown to give, besides unsaturated esters, cyclopropyl esters in variable amounts.[5] The reasons behind this dual reactivity of the intermediate π-allyl complexes with the nucleophiles (central *vs.* terminal addition) have not been clearly established since contrasting results have been found in the literature.[12–15] Up to now, no attempts have been made in order to optimize the yields of the reactions described above by modifying the nature of the catalyst and the experimental conditions, or to drive them in one or the other direction. It seems nevertheless likely that steric factors are important both as far as the ligands around the metal and the substituents on the ketene acetals are concerned.

Notes and references

† *Selected data* for **6** [R^{1}R^2 = $(CH_2)_5$, R^3 = H], colorless oil; IR(Nujol), 1750 cm^{-1}; δ_H($CDCl_3$, 400 MHz) 4.52 (m,1H, C*H*O), 3.89 (dd, *J* 12, 2.5 Hz, 1H, C*H*OH), 3.61 (dd, *J* 12, 5.1 Hz, 1 H, C*H*OH), 2.77 (1H, O*H*), 2.24 (dd, *J* 13 and 6.6 Hz, 1H, C*H*H), 1.88 (dd, 1H, *J* 13 and 8 Hz, 1H, CH*H*), 1.81–1.52 (m, 10H, 5 CH_2); δ_C($CDCl_3$, 100 MHz) 182.0, 77.84, 63.9, 44.9, 34.1, 34.0, 32.1, 25.26, 22.2, 22.1; HRMS: 185.1178 (M$^+$). For **8** [R^{1}R^2 = $(CH_2)_5$, R^3 = H]: colorless oil; δ_H($CDCl_3$) 2.1–1.07 (m, 10H), 0.87 (m, 1H), 0.18 (m, 4H); δ_C($CDCl_3$) 183.2, 45.14, 32.18, 25.8, 23.5, 20.9, 0.85; HRMS: 169.122 (M$^+$). For **3a**: white crystals, mp 38 °C, δ_H($CDCl_3$) 7.11–7.31 (m, 5H, ArH); 6.16 (d, *J* 16 Hz, 1H, PhC*H*=), 6.11 (dt, *J* 16, 7.5 Hz, 1H, =C*H*CH_2), 2.39 (d, *J* 7.5 Hz, 2H), 1.17 (s, 6H, 2 Me), δ_C($CDCl_3$) 184.3, 137.7, 133.7, 128.9, 127.6, 126.5, 126.0, 43.9, 43.0, 25.1. Anal. Calc. For $C_{13}H_{14}O_3$: C, 70.91; H, 7.27. Found: C, 70.71; H, 7.31%.

‡ Satisfactory elemental analyses or HRMS were obtained for the various carboxylic acids and hydroxylactones.

1 B. M. Trost and T. R. Verhoeven, *Organometallic Compounds in Organic Synthesis and in Catalysis, in Comprehensive Organometallic Chemistry*, ed. G. Wilkinson, F. G. A. Stone and E. W. Abel, Pergamon Press, New York, 1982, vol. 8, ch. 57; J. Tsuji, *Organic Synthesis with Palladium Compounds*, Springer, Berlin, 1980, pp. 45–51.
2 Unpublished results from this Laboratory, manuscript in preparation.
3 M. Bellassoued, E. Chelain, J. Collot, H. Rudler and J. Vaissermann, *Chem. Commun.*, 1999, 187.
4 J. Tsuji, K. Takahashi, I. Minami and I. Shimizu, *Tetrahedron Lett.*, 1984, **25**, 4783.
5 A. Satake and T. Nakata, *J. Am. Chem. Soc.*, 1998, **120**, 10 391.
6 A. Saitoh, K. Achiwa and T. Morimoto, *Tetrahedron: Asymmetry*, 1998, **9**, 741.
7 H. Rudler, J. Ribeiro Gregorio, B. Denise, J.-M. Brégeault and A. Deloffre, *J. Mol. Catal. A: Chem.*, 1998, **133**, 255.
8 W. A. Herrmann, R. W. Fischer and D. W. Marz, *Angew. Chem., Int. Ed. Engl.*, 1991, **30**, 1638.
9 H. Tan and J. H. Espenson, *J. Mol. Catal. A: Chem.*, 1999, **142**, 333.
10 For consecutive nucleophilic additions on olefins, see: Y.-S. Lin, S. Takeda and K. Matsumoto, *Organometallics*, 1999, **18**, 4897 and references therein.
11 O. Kühn and H. Mayr, *Angew. Chem., Int. Ed.*, 1999, **38**, 333.
12 A. Wilde, A. P. Lotte and H. M. R. Hoffmann, *J. Chem. Soc., Chem. Commun.*, 1993, 615.
13 L. S. Hegedus, W. H. Darlington and C. E. Russell, *J. Org. Chem.*, 1980, **45**, 5193.
14 C. Carfagna, L. Mariani, A. Musco, G. Sallese and R. Santi, *J. Org. Chem.*, 1991, **56**, 3925.
15 E. B. Tjaden and J. M. Stricker, *Organometallics*, 1992, **11**, 16.

ChemComm

In situ Brewster angle microscopy and surface pressure studies on the interfacial growth of mesostructured silica thin films

Karen J. Edler,*[a] Steve J. Roser*[a] and Stephen Mann[b]

[a] *Department of Chemistry, University of Bath, UK BA2 7AY. E-mail: K.Edler@bath.ac.uk; S.J.Roser@bath.ac.uk*
[b] *School of Chemistry, University of Bristol, Bristol, UK BS8 1TS. E-mail: S.Mann@bristol.ac.uk*

Received (in Oxford, UK) 4th January 2000, Accepted 28th March 2000

Growth of a mesostructured silica thin film at the air/water interface was observed *in situ* using Brewster angle microscopy and surface pressure measurements allowing real time observation of nucleation of the film and its rapid growth to full surface coverage at the end of the induction period.

Mesoporous inorganic materials, such as the hexagonally ordered silica MCM-41, can be synthesized by template-directed reactions using surfactant or block copolymer self-assembled templates. Although much work has been carried out on the preparation of these materials in bulk, powdered forms, many applications particularly in the fields of filtration, separation and catalysis, require thin film geometries. Several groups have reported films formed by dip[1,2] or spin coating,[3] or by growth at the air/water,[4,5] mica/water,[6] and graphite/water interfaces.[7] Although films have been studied by X-ray and neutron reflectivity,[8–10] TEM and SEM,[11] AFM and optical microscopy,[12,13] none of these techniques have allowed detailed examination of the *in situ* growth of the silicate film. Here, we report the use of Brewster angle microscopy (BAM) and surface pressure measurements to trace the real-time evolution of growing films of mesostructured silica at the air/water interface. The data provide new insights into the formation mechanism and growth kinetics of such films as the measurements can be made on a much finer timescale than was previously possible. From these measurements it seems that the film is nucleated at many points across the surface and grows together from nuclei that are only a few microns across.

The growth of mesostructured silica thin films at the air/water interface of a synthesis solution† in a Langmuir trough showed three distinct stages observable by BAM: an induction period; a period of rapid film growth to cover the interface; and a period of coarsening of the surface film. The induction period (*ca.* 330 min from mixing), was characterized by a relatively constant value in the surface pressure measurements‡ (Fig. 1). The length of this period decreased with higher concentrations of CTAB and TMOS but was reproducible to within 10 min for a given set of conditions. A reproducible fluctuation in the surface pressure was observed during the induction period that consisted of a pressure increase followed by a decrease of *ca.* 1 mN m^{-1} between 125 and 285 min after mixing (Fig. 1).

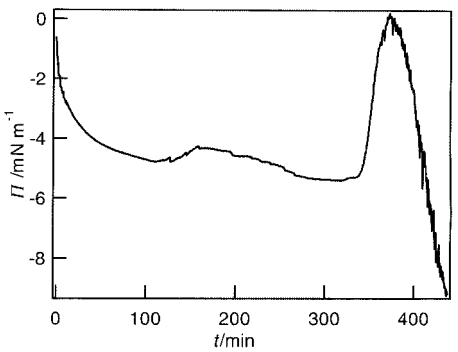

Fig. 1 Surface pressure changes with time during growth of a surfactant–silica mesostructured film at the air/water interface.

Corresponding BAM images§ taken during the induction period showed a uniform background with randomly distributed high-contrast point features, 5–10 μm in size [Fig. 2(a)]. These features increased slightly in number with time and moved across the interface owing to convection currents in the sub-phase. On the surface of a similar solution, CTAB in 0.2 M HCl with no TMOS present, such features are visible but are much less numerous and do not increase in number with time. Degassing the acid solution prior to adding CTAB and TMOS did not affect the appearance of the point features, indicating that they were not gas bubbles.

Taken together, the surface pressure measurements and BAM images indicate significant changes in the surface behaviour of the synthesis solutions prior to film formation. The results suggest that surfactant molecules are partitioned at the air/water boundary as a surface excess in the form of a continuous monolayer. Polysilicate binding to the cationic headgroups of the surfactant then gives rise to domains with modified thickness or molecular orientation. This is consistent with a model in which silicate binding in discrete regions under the monolayer is responsible for preferential nucleation of the silica–surfactant mesophase at the air/water interface, rather than bulk deposition in solution, although some precipitation from the bulk also occurs. An interaction between silica and surfactant at the surface of a CTAB/tetraethoxysilane solution has been proposed on the basis of X-ray and neutron reflectometry measurements.[4,9] These showed a slight decrease in the thickness of the surfactant monolayer from 3 to 2.7 nm and an increased scattering length density prior to film growth, indicating silica gathering at the interface. Reflectometry measurements, however cannot distinguish a low density, uniform silica/surfactant film from local regions of higher

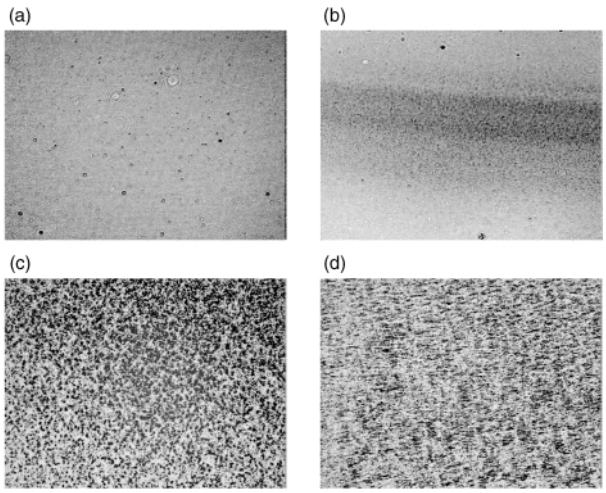

Fig. 2 Brewster angle microscope images following the evolution of a silica–surfactant composite film at the air/water interface (a) during the induction period, (b) just after the onset of film growth, 331 min after mixing of the reagents, (c) 350 min after mixing and (d) 407 min after mixing, showing growth and coarsening of the film at the interface. The horizontal edge of each image corresponds to 430 microns.

DOI: 10.1039/b000375l

density silica at nucleation sites scattered over the surfactant monolayer as is observed in the BAM.

The end of the induction period (330 min after mixing) was marked by a rapid increase in surface pressure over a period of 50 min (Fig. 1) owing to the formation of a densely packed surface film of mesostructured silica. Further growth resulted in an apparent decrease in pressure owing to the attachment of the film to and consequent increase in weight of the Wilhelmy plate. Corresponding BAM images showed an increase in the homogeneity of the surface film just prior to the rapid increase in surface pressure. Many of the point features in the BAM images became less distinct and merged with the background to give a lower contrast continuous texture that was still mobile on the liquid surface. Some point features were still visible, but their movement became associated with that of the continuous phase. The onset of film formation was associated with an increased density of the low contrast texture and a cessation of individual motion of the points over the whole region [Fig. 2(b)]. The texture then coarsened and became more distinct with growing visual contrast between dark and light regions, producing a dense coverage of 5–10 μm dots over the surface which began to merge [see Fig. 2(c)]. The lighter coloured horizontal bands across the image [Fig. 2(b)] were seen in most film forming preparations, appearing just prior to visible film formation in the BAM. They move across the surface in the same manner as the point features, so are connected with the surface, rather than the sub-phase. They do not appear in CTAB-only solutions and may be related to formation of oriented domains of the porous mesostructure in the growing surface film. Further evolution of the film, over 75 min from its first appearance, produced a network of strands with none of the original dots or the horizontal bands visible [Fig. 2(d)]. Similar fibrous structures in the final film have been reported using laser scanning confocal microscopy.[5]

The existence of point features with distinct contrast from the surrounding surface early in the induction period suggests that the film development process occurs *via* nucleation at many discrete points on the surface, rather than as a gradual building up of more or less uniform structures over the whole surface. During the induction period gradual condensation of the hydrolysed TMOS molecules proceeds, resulting in silica polyanions which interact with the surfactant monolayer at the interface causing nucleation of domains 5–10 μm across. These point features observed from the beginning the induction period are however, large compared to the coherence length expected from peak width studies of bulk hexagonal phase surfactant templated materials (several hundred nanometers[14]). Encouraging the growth of such domains may be a route to increasing long range homogeneity in these films. Once favourable conditions are achieved, possibly through concentration of the reacting species after evaporation of methanol, or by optimisation of headgroup spacing for the surfactant template by charge interaction with the polysilicates, the film forming process accelerates and full surface coverage is reached in a few minutes. Further condensation of the silica in the local environment and continuing addition of material from the sub-phase have been suggested to cause such films[5] to warp and buckle and are probably the cause of the development of ridges and the fibrous texture ultimately observed here.

Overnight, the film developed to a thickness of *ca*. 0.1 mm and showed macroscopic wrinkling, presumably induced by the confined area of the trough and from microscopic stresses such as local shrinkage of the system during polymerisation. *In situ* X-ray reflectometry on the final film showed two well developed broad Bragg peaks at Q = 0.132 and 0.257 Å^{-1} indicating formation of an ordered silica–surfactant mesophase. Reflectometry measurements however were too slow to follow the growth of the film during the induction period. Further work on the structural characterization of this material is in progress.

We thank Arach Goldar for assistance with the X-ray reflectometry. The financial support of the EPSRC Materials Committee (Grant no. GR/M15989) is gratefully acknowledged.

Notes and references

† Thin films of mesostructured silica were prepared using a molar ratio of CTAB : water : HCl : TMOS of 1.53×10^{-3} : 1 : 3.63 $\times 10^{-3}$: 0.011. The surfactant template, cetyltrimethylammonium bromide (CTAB, Sigma 99%) was dissolved in 0.2 M HCl and tetramethoxysilane (TMOS, Merck 98%) was added dropwise. This clear solution was transferred to a Teflon Langmuir trough 3.5 mm deep, surface area *ca.* 40 cm^2, so that the liquid formed a raised meniscus. Other experiments on this system have shown that at these reactant concentrations, films will grow in sealed containers where no evaporation can occur, however during these experiments, evaporation did occur and this undoubtedly affects film growth. Film formation was nevertheless highly reproducible with respect to induction time, morphology and surface pressure behaviour.

‡ Surface pressure measurements were made at 30 s intervals by a Wilhelmy plate method using a Nima surface pressure sensor. The measurements began 7 min after mixing, during which time the solution was poured into the trough and initial wetting of the Wilhelmy plate occurred. Evaporation of methanol generated by TMOS hydrolysis led to a change in plate buoyancy and an initial decrease in surface pressure; however this leveled off *ca.* 100 min after mixing. A similar although less rapid decrease in surface pressure of 0.7 mN m^{-1} owing to evaporation of water from the sub-phase was noted for a solution of CTAB in 0.2 M HCl with the same surface area in the absence of TMOS, over a 90 min period.

§ The Langmuir trough was mounted under a Brewster angle microscope (BAM2, Nanofilm Technologie GmbH) so that the surface structure and surface pressure of the synthesis solution could be monitored simultaneously. Light from a diode pumped frequency doubled Nd : YAG laser at 532 nm was used. At the Brewster angle, the reflectivity of polarised light at the interface is zero, so any small changes in interfacial refractive index, such as the presence of a surface film, are clearly visible. BAM images were taken every 30 s during the rapid growth phase of the film and every 5–10 min during the induction period. Evolution of the film structure was monitored in real time with the aid of a video camera attached to the BAM.

1 D. Zhao, P. Yang, N. Melosh, J. Feng, B. F. Chmelka and G. D. Stucky, *Adv. Mater.*, 1998, **10**, 1380.
2 Y. Lu, R. Ganguli, C. A. Drewien, M. T. Anderson, C. J. Brinker, W. Gong, Y. Guo, H. Soyez, B. Dunn, M. H. Huang and J. I. Zink, *Nature*, 1997, **389**, 364.
3 M. Ogawa, H. Ishikawa and T. Kikuchi, *J. Mater. Chem.*, 1998, **8**, 1783.
4 A. S. Brown, S. A. Holt, T. Dam, M. Trau and J. W. White, *Langmuir*, 1997, **13**, 6363.
5 H. Yang, N. Coombs, O. Dag, I. Sokolov and G. A. Ozin, *J. Mater. Chem.*, 1997, **7**, 1755.
6 H. Yang, A. Kuperman, N. Coombs, S. Mamiche-Afara and G. A. Ozin, *Nature*, 1996, **379**, 703.
7 H. Yang, N. Coombs, I. Sokolov and G. A. Ozin, *J. Mater. Chem.*, 1997, **7**, 1285.
8 J. L. Ruggles, S. A. Holt, P. A. Reynolds, A. S. Brown, D. C. Creagh and J. W. White, *Phys. Chem. Chem. Phys.*, 1999, **1**, 323.
9 A. S. Brown, S. A. Holt, P. A. Reynolds, J. Penfold and J. W. White, *Langmuir*, 1998, **14**, 5532.
10 S. Roser, H. M. Patel, M. R. Lovell, J. E. Muir and S. Mann, *Chem. Commun.*, 1998, 829.
11 S. H. Tolbert, T. E. Schaffer, J. Feng, P. K. Hansma and G. D. Stucky, *Chem. Mater.*, 1997, **9**, 1962.
12 H. Yang, N. Coombs, I. Sokolov and G. A. Ozin, *Nature*, 1996, **381**, 589.
13 H. Yang, N. Coombs and G. A. Ozin, *J. Mater. Chem.*, 1998, **8**, 1205.
14 K. J. Edler and J. W. White, *Chem. Mater.*, 1997, **9**, 1226.

ChemComm

Synthesis of nanometer-sized hollow polymer capsules from alkanethiol-coated gold particles

Minglang Wu, Stacy A. O'Neill, Louis C. Brousseau, Wyatt P. McConnell, David A. Shultz,* Russell J. Linderman* and Daniel L. Feldheim*

Department of Chemistry, North Carolina State University, Raleigh, NC 27695, USA.
E-mail: Dan_Feldheim@NCSU.edu; Russell_Linderman@NCSU.edu; David_Shultz@NCSU.edu

Received (in Columbia, MO, USA) 17th January 2000, Accepted 13th March 2000

A tripodal alkythiolate ligand has been assembled on gold nanoparticles, which upon metathesis polymerization and particle etching, yields crosslinked spherical hollow polymer capsules.

In previous reports, we have shown that gold particles are useful templates for the synthesis of hollow nanoscopic poly(pyrrole) and poly(*N*-methylpyrrole) capsules.[1] In that work, polymerization was initiated in an aqueous suspension of gold particles. Owing to the insolubility of pyrrole-based polymers in water, a polymer shell formed around the particle, which upon gold etching could be converted to a hollow capsule (Scheme 1). The hollow core volume and shell thickness were easily tuned *via* template diameter and polymerization time, respectively; guest entrapment within the host polymer capsule was demonstrated by attaching the guest to the gold particle prior to polymer formation and particle etching.

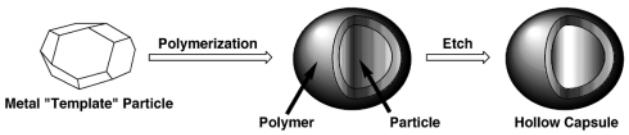

Scheme 1

Here, we demonstrate an alternative strategy for the formation of hollow polymer capsules. The strategy is similar to that reported by Mirkin and coworkers recently in which a surface-bound ω-substituted alkanethiol was polymerized to form polymer/gold composite particles.[2] In our work, the alkene-terminated tripodal ligand **A** was designed and synthesized in order to maximize polymer crosslinking. Crosslinking is important in forming structurally rigid hollow capsules following removal of the gold particle. Moreover, as demonstrated below, polymerization of **A** leaves alkene functionalities that may be further modified to manipulate the chemical properties of the resulting polymer capsule (Scheme 2).

The tripodal ligand was prepared in seven steps from 1-decen-1-ol and 11-bromo-1-undecanol.[3] Selective hydrolysis of the ester/thioacetate intermediate using methanolic potassium hydroxide in the presence of air gave high yields of the triene functionalized disulfide. Formation of triene functionalized thiol derivatized gold nanoparticles was then accomplished directly from the disulfide using procedures reported previously.[4] The thiol derivatized nanoparticle was purified by precipitation from toluene with ethanol–methanol followed by filtration. TEM images revealed spherical nanoparticles, *ca.* 5 nm in diameter. IR spectral analysis of the thiol-derivatized nanoparticle clearly indicated the presence of the ester at 1725 cm^{-1} (compared to 1731 cm^{-1} in the free ligand) and, as shown in Fig. 1(a), the terminal alkene CH bending modes at 908 cm^{-1} (compared to 908 cm^{-1} in the free ligand) and C=C stretching modes (1632 cm^{-1}) are observed. The free disulfide ligand exhibited a triplet in its ^{1}H NMR spectrum at δ 2.67 for the methylene protons adjacent to sulfur. However, upon complexation to the gold nanoparticle, the signal at δ 2.67 was no longer observed, as expected.[4b] As shown in Fig. 2(a), the terminal alkene protons were observed in the ^{1}H NMR spectrum of the thiol derivatized nanoparticle as very broad multiplets

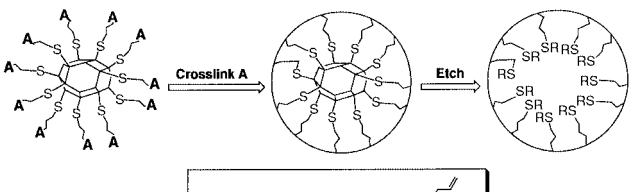

Scheme 2

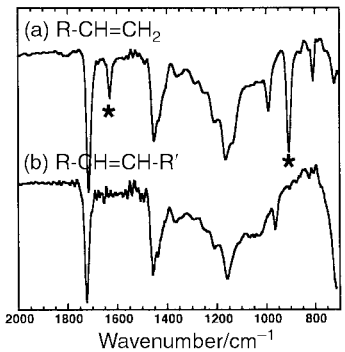

Fig. 1 (a) IR spectrum (neat film) of alkene-terminated thiol-derivatized gold nanoparticles. * Indicates terminal C=C stretching and alkene CH bending modes. (b) IR spectrum (neat film) of thiol-derivatized nanoparticles after reaction with Grubbs catalyst. Note lack of terminal C=C stretching and alkene CH bending modes, while other spectral features remain intact.

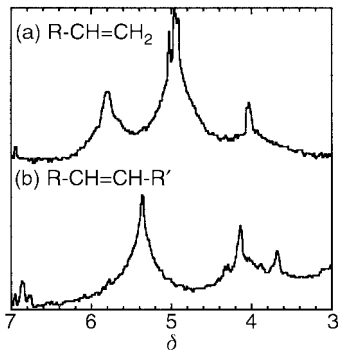

Fig. 2 (a) ^{1}H NMR spectrum (alkene region) of alkene-terminated thiol-derivatized gold nanoparticles. Alkene resonances appear as broad signals at δ *ca.* 4.9 and 5.9. (b) ^{1}H NMR spectrum (alkene region) of thiol-derivatized nanoparticles after reaction with Grubbs catalyst. Note new alkene resonances at δ *ca.* 5.3.

DOI: 10.1039/b001019g

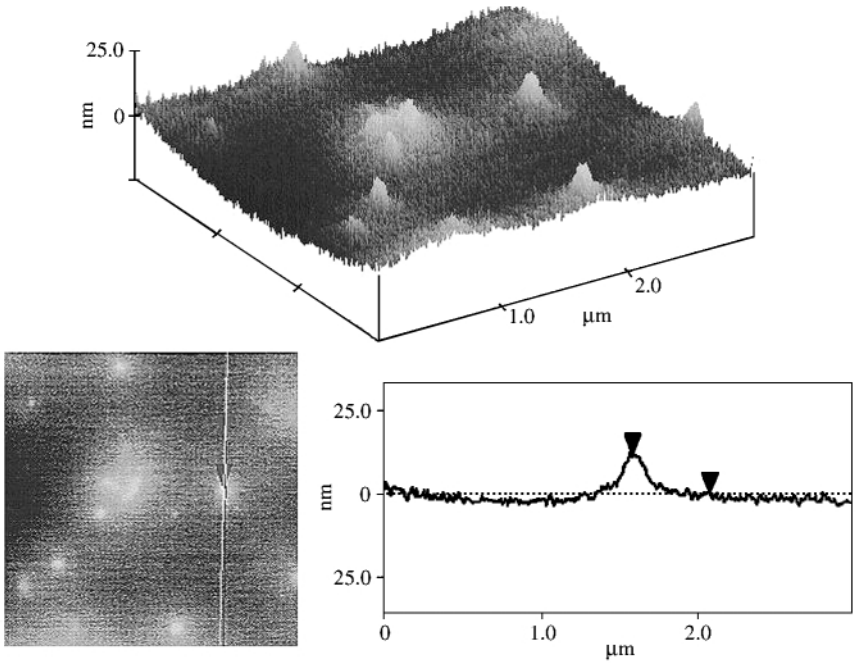

Fig. 3 Atomic force images of hollow polymer capsules. See text for details.

centered at δ *ca.* 5.9 and 4.9 which corresponded very well with the chemical shifts observed in the free triene ligand.

Metathesis of the thiol derivatized nanoparticles was then carried out using *ca.* 7 mol% of Grubbs catalyst[5] per alkene in benzene at room temp. Precipitation of the product from benzene by the addition of ethanol provided a purple waxy solid. The assumption that intramolecular polymerization to form a highly crosslinked polymeric surface occurred is strongly supported by the spectral data of the polymerized nanoparticles. As shown in Fig. 1(b), the IR spectrum shows a lack of *both* the C=C terminal alkene stretches at 1632 cm^{-1} and the alkene CH bending modes at 908 cm^{-1} for the polymerized particles. The changes in the IR spectrum are paralleled by the changes in the ^{1}H NMR spectrum: the signals for the terminal alkene protons collapsed to a single broad peak at δ *ca.* 5.3, as shown in Fig. 2(b). The signals for the terminal alkene protons collapsed to a single broad peak at δ 5.4.

Removal of the gold from the thiol derivatized particles under the same conditions used for the polypyrrole capsules [0.1 M KCN, 0.002 M $K_3Fe_2(CN)_3$] was not possible. However, sonication of a THF–water solution of KCN, $K_3Fe_2(CN)_3$ and the particles produced a change from purple to brown, indicative of particle etching. Treatment of the brown particles with hydrogen peroxide was necessary to effect complete removal of the gold. ^{1}H NMR spectra of the hollow polymerized tripodal ligand also indicated the absence of gold by virtue of the now sharp and well defined spectrum.[4b] Treatment of the nanoparticles with hydrogen peroxide efficiently oxidized the polyalkene particle to a polyol particle as evidenced by signals in the range δ 3.6–4.2 in the ^{1}H NMR spectra.

The fate of the sulfur atoms in the linker is unclear from the data in hand although it is very likely that the sulfur has been oxidized along with the alkenes. In addition, the internal ester linkage may have been partially cleaved. IR data shows hydroxy groups at 3350 cm^{-1}, and a significantly diminished CO stretch at 1723 cm^{-1}.

Atomic force microscopy confirmed that the structural integrity of the polymer capsules was maintained following gold dissolution (Fig. 3).[6] Qualitatively, AFM revealed the presence of spherical capsules, which were relatively impressible compared to gold particles or hollow polypyrrole capsules. Quantitatively, the dimensions of the capsules were 10.47 ± 2.54 nm based on the relative height of 25 capsules. This value agrees well with the diameter expected based on the size of the template gold particle (*ca.* 5 nm) and the length of alkythiol spacer.

In summary, a method has been described for converting alkylthiolate monolayers on gold particles into hollow polymer capsules. The synthetic design of the tripodal ligand provides the potential to ultimately control the functionality present on the surface of the particle as well as that present internally.

This work was supported in part by grants from the North Carolina Biotechnology Center and the NSF (DMR-9900073).

We thank Professor Christopher Gorman for helpful discussions.

Notes and references

1 S. M. Marinakos, J. P. Novak, L. C. Brousseau III, A. B. House, E. M. Edeki, J. C. Feldhaus and D. L. Feldheim, *J. Am. Chem. Soc.*, 1999, **121**, 8518; S. M. Marinakos, D. A. Shultz and D. L. Feldheim, *Adv. Mater.*, 1999, **11**, 34.

2 K. J. Watson, J. Zhu, S. T. Nguyen and C. A. Mirkin, *J. Am. Chem. Soc.*, 1999, **121**, 462.

3 M. Wu, M. Rodriguez, H. J. Carpenter, A. C. deBaille, N. P. Mehta, D. A. Shultz, D. L. Feldheim and R. J. Linderman, manuscript in preparation.

4 (*a*) M. Brust, M. Walker, D. Bethell, D. J. Schiffrin and R. Whyman, *J. Chem. Soc., Chem. Commun.*, 1994, 801; (*b*) A. C. Templeton, W. P. Wuelfing and R. W. Murray, *Acc. Chem. Res.*, 2000, **33**, 27.

5 P. Schwab, M. B. France, R. H. Grubbs and J. W. Ziller, *Angew. Chem., Int. Ed. Engl.*, 1995, **34**, 2039.

6 AFM samples were prepared by drop casting a THF solution of capsules onto a freshly cleaned gold-coated glass slide and allowing the solvent to evaporate. Gold substrates were cleaned by dipping in H_2SO_4–H_2O_2 (3:1) for *ca.* 2 min followed by sonication in deionized H_2O.

New structurally rigid palladium catalysts for the alternating copolymerization of carbon monoxide and ethene†

Claudio Bianchini,*[a] Hon Man Lee,[a] Andrea Meli,[a] Werner Oberhauser,[a] Francesco Vizza,[a] Peter Brüggeller,[b] Rainer Haid[b] and Christoph Langes[b]

[a] *Istituto per lo Studio della Stereochimica ed Energetica dei Composti di Coordinazione, ISSECC-CNR, 50132 Firenze, Italy. E-mail: bianchin@fi.cnr.it*

[b] *Institut fuer Allgemeine, Anorganische und Theoretische Chemie der Universitaet Innsbruck, Innrain 52a, Innsbruck, Austria*

Received (in Cambridge, UK) 20th December 1999, Accepted 28th March 2000

Decreasing the flexibility of the $Ph_2PCH_2CH_2PPh_2$ (dppe) backbone by making the central carbon atoms part of a cyclobutane ring leads to the formation of Pd(II) catalysts for CO/ethene copolymerization that are more efficient than those of dppe by a factor of ten.

Polyketones obtained by alternating copolymerization of carbon monoxide and olefins are important innovative materials prepared on industrial scale by homogeneous palladium catalysis [eqn. (1)].[1]

$$n C_2H_4 + n CO + MeOH \xrightarrow{cat} Et\text{-}(CCH_2CH_2)_{n-1}\text{-}C(=O)\text{-}OMe \quad (1)$$

The diphosphine 1,3-bis(diphenylphosphino)propane (dppp) is the ligand of choice for the copolymerization of CO and ethene;[2,3] indeed, dppp forms Pd(II) catalysts that are more efficient than those with the lower homologue 1,2-bis(diphenylphosphino)ethane (dppe) by almost one order of magnitude.[1–3] The ability of the chelate ring size (as determined by the number of carbon atoms separating the PPh_2 groups) to modulate the flexibility of the Pd(P–P) moiety is the factor that, most commonly, is invoked to account for the dramatically different activity of the dppp and dppe catalysts.[3–5] In particular, several studies have tried to correlate the greater catalytic activity of the dppp complexes to the higher flexibility of the dppp backbone as compared to that of dppe.[3–5]

In this work, we prove experimentally that efficient Pd catalysts are formed also with diphosphine ligands containing two carbon atoms between the PPh_2 donors on the condition, however, that ligand *flexibility* is substantially *reduced*.

Reaction of the tetraphosphine *cis*,*trans*,*cis*-1,2,3,4-tetrakis(diphenylphosphino)cyclobutane[6] (*cyclo*-tetraphos) with 2 equiv. of either $Pd(CO_2Me)_2$ or $PdCl_2$ in CH_2Cl_2 yielded the bimetallic complexes Pd_2(*cyclo*-tetraphos)$(OCOMe)_4$ **1** and

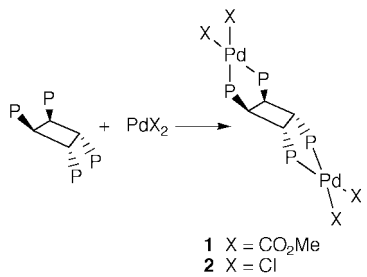

1 X = CO_2Me
2 X = Cl

Pd_2(*cyclo*-tetraphos)Cl_4 **2**, respectively.‡ The latter complex was quantitatively transformed into the acetonitrile derivatives $[Pd_2$(*cyclo*-tetraphos)$(MeCN)_4]Y_4$, **3** Y_4 (Y = PF_6 or BF_4) by treatment with AgY in acetonitrile solution.

† Electronic supplementary information (ESI) available: experimental section. See http://www.rsc.org/suppdata/cc/b0/b000376j/ for crystallographic data in .cif format.

Under standard copolymerization conditions (Table 1),[2,3] **1** and **3** $(PF_6)_4$ give rise to the same catalyst system with a productivitiy of 10 kg of polyketone (g of Pd)$^{-1}$ (entry 2). This productivity value is higher than that obtained with Pd(dppe)$(OCOMe)_2$ **4** by a factor of *ten* (entry 1) and is comparable with that of the industrial catalyst Pd(dppp)$(OCOMe)_2$.[2,3] The increase in productivity using either **1** or **3**$(PF_6)_4$ in the place of **4** is not accompanied by a change in the average molecular weights of the copolymers (*ca.* 6 kg mol^{-1}).[3,7]

A single-crystal X-ray analysis has been carried out on **3**$(BF_4)_4 \cdot 2MeCN \cdot 3.4CH_2Cl_2$.§ As is shown in Fig. 1, a perfectly planar cyclobutane ring connects two equivalent $(-PPh_2)_2Pd(NCMe)_2$ moieties in each of which the Pd(II) centres adopts a slightly distorted square-planar coordination. The bond angles and distances in the cyclobutane ring are close to those of an ideal square. The P–Pd–P chelate angle and the Pd–P distances are in the usual range for dppe Pd(II) complexes with nitrogen ligands.[8] The two symmetry-related metalla-rings in **3** adopt an envelope conformation. As a consequence, each phosphorous centre of the asymmetric unit exhibits one equatorial and one axial phenyl group with the two axial phenyl rings being related by a mirror plane. The conformation of the metalla-ring and the mutual disposition of the phenyl substituents represent the most striking difference between **3** and square-planar dppe complexes in which the ligand generally assumes a twisted conformation and the phenyl groups can be all equatorial.[8,9] Therefore, in terms of steric hindrance (quadrant effect),[10] each palladium centre in **3** has a larger space for coordination and reactivity than in dppe complexes.

Since the envelope conformation of each metalla-ring is maintaned in solution, at least on the NMR time scale, the remarkable increase in catalytic activity of the *cyclo*-tetraphos

Table 1 Alternating CO/C_2H_4 copolymerization catalyzed by Pd(P–P)$(OCOMe)_2$[a]

Complex	P–P Ligand	Entry	Copolymer productivity[b]
4		1	1.1
1, **3**		2	9.8
5		3	6.4
6		4	5.5

[a] *Conditions*: catalyst (0.01 mmol based on Pd), MeOH (100 mL), 1,4-benzoquinone (0.8 mmol), *p*-toluenesulfonic acid (0.2 mmol), initial $p(C_2H_4)$ (300 psi), initial $p(CO)$ (300 psi), temperature (85 °C), time (3 h), stirring rate (1400 rpm). [b] Productivity expressed as kg of polymer (g Pd)$^{-1}$.

DOI: 10.1039/b000376j

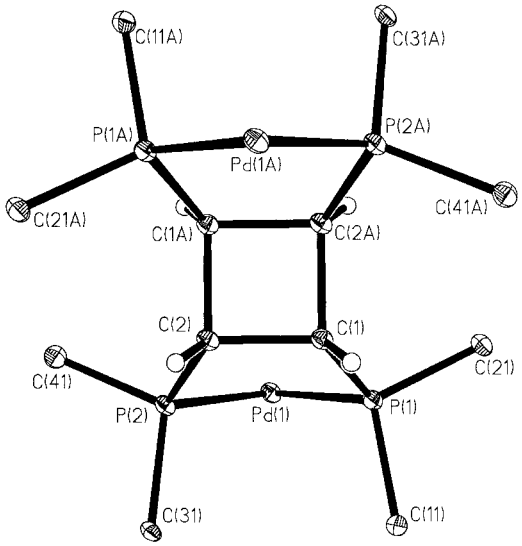

Fig. 1 ORTEP drawing of $\mathbf{3}(BF_4)_4{\cdot}2MeCN{\cdot}3.4CH_2Cl_2$ (coordinated MeCN ligands are omitted for clarity). Selected bond lengths (Å) and angles (°): Pd–P(1) 2.2484(8), Pd–N(1) 2.070(3), Pd–P(2) 2.2505(8), Pd–N(2) 2.077(3), P(1)–Pd–P(2) 82.81(3), N(1)–Pd–N(2) 89.35(12), N(1)–Pd–P(1) 93.94(9), N(2)–Pd–P(1) 174.63(9), N(1)–Pd–P(2) 176.72(9), N(2)–Pd–P(2) 93.85(9).

complex as compared to the dppe derivative may reasonably be associated to the substantial rigidity of the former that ultimately controls the steric hindrance at the metal centre. In an attempt to verify this hypothesis, the structurally rigid complexes Pd(*o*-dppbe)$(OCOMe)_2$ **5** and Pd(*cis*-dppen)$(OCOMe)_2$ **6** have been prepared and employed as catalyst precursors for CO/C_2H_4 copolymerization under the same experimental conditions [*o*-dppbe = *o*-bis(diphenylphosphino)benzene, *cis*-dppen = *cis*-bis(diphenylphosphino)ethylene].‡ Neither **5** and **6** are as efficient as **1** or **3** in the copolymerization reaction (likely due to the different electronic nature of the phosphine donors), but still the productivities are *ca*. six times higher than that of the dppe precursor **4**, yielding copolymers with comparable chain lengths.[3,7]

In conclusion, we have shown here that high rigidity of the control ligand is a structural feature that improves CO/olefin copolymerization Pd(II) catalysts. Recent studies with dppp-based catalysts are consistent with the present results as it has been found that the introduction of methyl substituents into the dppp backbone has beneficial effects on the copolymerization rate.[11] Conformational rigidity has also been invoked to account for the higher activity of the C_4-bridged bis(tetramethylphosphole) complex $[(Me_4C_4P)_2X]Pd(CO_2Me)_2$ [X = $CH_2(C_6H_4)CH_2$] as compared to C_2- [X = $(CH_2)_2$] and C_3-bridged [X = $(CH_2)_3$] analogs. The copolymerization activity of the *o*-xylene-bridged bis(phosphole)-based complex is, however, quite low [300 g of polymer (g Pd)$^{-1}$ h^{-1}].[12]

Shell International Chemicals B. V. (Amsterdam) is gratefully acknowledged for financing a post-doctoral program to H. M. L. at ISSECC-CNR.

Notes and references

‡ *Selected spectroscopic data*: **1**: $\delta_P(CD_2Cl_2$, 81.01 MHz) 67.0 (s). $\delta_H(CD_2Cl_2$, 200.13 MHz) 1.46 (s, 12H, $OCOCH_3$), 4.26 (pseudo t, $^2J_{HP}$ 7.0 Hz, 4H, CH), 7.15–7.64 (m, 40H, aromatic protons). $\delta_C(CD_2Cl_2$, 50.32 MHz) 24.0 (s, $OCOCH_3$), 38.7 (s, CH), aromatic carbons [129.9 (s), 132.6 (s), 134.7 (s), 135.4 (s)], 177.1 (s, $OCOCH_3$). **3**$(PF_6)_4$: $\delta_P(CD_3CN$, 81.01 MHz) 79.3 (s). $\delta_H(CD_3CN$, 200.13 MHz) 4.6 (s, 4H, CH), 3.0 (s, 12H, CH_3CN), 7.3–8.2 (m, 40H, aromatic protons). IR ν(KBr)/cm^{-1} 1656s (C–N). **4**: $\delta_P(CD_2Cl_2$, 81.01 MHz) 58.9 (s). $\delta_H(CD_2Cl_2$, 200.13 MHz) 1.66 (s, 6H, $OCOCH_3$), 2.23 (d,$^2J_{HP}$ 22.0 Hz, 4H, CH_2), 7.52–7.83 (m, 20H, Ph). $\delta_C(CD_2Cl_2$, 50.32 MHz) 23.5 (s, $OCOCH_3$), 27.5 (AXX′ system, $^1J_{CP}$ 36.6, $^2J_{CP}$ 12.8 Hz, CH_2), aromatic carbons [129.6 (s), 131.4 (s), 132.8 (s), 134.1 (s)], 176.6 (s, $OCOCH_3$). **5**: $\delta_P(CD_2Cl_2$, 81.01 MHz) 56.9 (s) $\delta_H(CD_2Cl_2$, 200.13 MHz) 1.60 (s, 6H, $OCOCH_3$), 7.18–7.80 (m, 24H, aromatic protons). $\delta_C(CD_2Cl_2$, 50.32 MHz) 23.5 (s, $OCOCH_3$), aromatic carbons (128.9–134.6), 176.5 (s, $OCOCH_3$). **6**: $\delta_P(CD_2Cl_2$, 81.01 MHz) 65.5 (s). $\delta_H(CD_2Cl_2$, 200.13 MHz) 1.70 (s, 6H, $OCOCH_3$), 7.08 (AA′XX′ system, $^2J_{HP}$ 60.0, $^3J_{HP}$ 13.0 Hz, 2H, CH), 7.44–7.84 (m, 20H, aromatic protons). $\delta_C(CD_2Cl_2$, 50.32 MHz) 23.4 (s, $OCOCH_3$), aromatic carbons [129.7 (s), 129.9 (s), 132.8 (s), 133.7 (s), 133.9 (s)], 146.2 (dd, $^1J_{CP}$ 48.4, $^2J_{CP}$ 27.0 Hz, CH), 176.4 (s, $OCOCH_3$).

§ *Crystal data* for $\mathbf{3}(BF_4)_4{\cdot}2MeCN{\cdot}3.4CH_2Cl_2$: M = 1889.65, triclinic, space group $P\bar{1}$, a = 12.180(2), b = 12.702(2), c = 15.338(3) Å, α = 110.35(1), β = 105.72(1), γ = 101.78(1)°, U = 2021.2(6) Å^3, T = 173 K, Z = 1, D_c = 1.552 g cm^{-3}, μ = 0.863 mm^{-1}, λ(Mo-Kα) = 0.71069 Å, F(000) 947, Crystal size 1.0 × 0.8 × 0.6 mm, 8779 independent reflections (R_{int} = 0.0186), 10 006 reflections collected. Refinement method: full-matrix least squares on F^2, Goodness-of-fit on F^2 = 1.052, Final R indices [$I > 3\sigma(I)$] R_1 = 0.0454, wR_2 = 0.1251. CCDC 182/1583.

1 A. Sen, *Acc. Chem Res.*, 1993, **26**, 303; C. E. Ash, *J. Mater. Educ.*, 1994, **16**, 1; E. Drent and P. Budzelaar, *Chem Rev.*, 1996, **96**, 663; A. Sommazzi and F. Garbassi, *Prog. Polym. Sci.*, 1997, **22**, 1547.

2 E. Drent, EP-A 121965, 1984; E. Drent, EP-A 181014, 1986; J. A. M. van Broekhoven, E. Drent and E. Klei, EP-A 213671, 1987; J. A. M. van Broekhoven, E. Drent and E. Klei, EP-A 235865, 1987.

3 E. Drent, J. A. M. van Broekhoven and M. J. Doyle, *J. Organomet. Chem.*, 1991, **417**, 235.

4 F. Y. Xu, A. X. Zhao and J. C. W. Chien, *Macromol. Chem.*, 1993, **194**, 2579; Y. Koide, S. G. Bott and A. R. Barron, *Organometallics*, 1996, **15**, 2213.

5 G. P. C. M. Dekker, C. J. Elsevier, K. Vrieze, P. W. N. M. van Leeuwen and C. F. Roobeek, *J. Organomet. Chem.*, 1992, **430**, 357; G. P. C. Dekker, C. J. Elsevier, K. Vrieze and P. W. N. M. van Leeuwen, *Organometallics*, 1992, **11**, 1598.

6 W. Oberhauser, C. Bachmann, T. Stampfl, R. Haid, C. Langes, H. Kopacka, A. Rieder and P. Brüggeller, *Inorg. Chim. Acta*, 1999, **290**, 167.

7 The average molecular weights (M_n) were calculated by means of ^{1}H NMR spectroscopy in 1,1,1,3,3,3-hexafluoropropan-2-ol-d_2.

8 G. J. Palenik, M. Mathew, W. L. Steffen and G. Beran, *J. Am. Chem. Soc.*, 1975, **97**, 97.

9 W. L. Steffen and G. J. Polenik, *Inorg. Chem.*, 1976, **15**, 2432; W. A. Hermann, W. R. Thiel, C. Brosman, K. Ofile, T. Piermeier and W. Scherer, *J. Organomet. Chem.*, 1993, **461**, 51.

10 J. Bakos, I. Toth, B. Heil, G. Szalontai, L. Párkányi and V. Fülöp, *J. Organomet. Chem.*, 1989, **370**, 263; N. Rahmouni, J. A. Osborne, A. De Cian, J. Fischer and A. Ezzamarty, *Organometallics*, 1998, **17**, 2470.

11 C. Bianchini, H. M. Lee, A. Meli, S. Moneti, F. Vizza, M. Fontani and P. Zanello, *Macromolecules*, 1999, **32**, 4183.

12 S. Doherty, G. R. Eastham, R. P. Tooze, T. H. Scanlan, D. Williams, M. R. J. Elsegood and W. Clegg, *Organometallics*, 1999, **18**, 3558.

ChemComm

Weakly-coordinating anions stabilise the unprecedented monovalent and divalent η-benzene nickel cations $[(\eta\text{-}C_5H_5)Ni(\eta\text{-}C_6H_6)Ni(\eta\text{-}C_5H_5)]^{2+}$ and $[Ni(\eta\text{-}C_6H_6)_2]^{2+}$

José L. Priego, Linda H. Doerrer, Leigh H. Rees and Malcolm. L. H. Green*

Inorganic Chemistry Laboratory, South Parks Road, Oxford, UK OX1 3QR. E-mail: malcolm.green@chem.ox.ac.uk

Received (in Cambridge, UK) 9th March 2000, Accepted 15th March 2000

Nickelocene in benzene reacts with the Brønsted acid H_2O–$B(C_6F_5)_3$ to give the salt $[(\eta\text{-}C_5H_5)Ni(\eta\text{-}C_6H_6)Ni(\eta\text{-}C_5H_5)][B_3(\mu\text{-}O)_3(C_6F_5)_5]$ which is the first example of a triple-decker nickel sandwich with a bridging η-benzene ligand; the borate anion is also unprecedented; treatment of $Ni(\eta\text{-}C_5H_5)_2$ with Brookhart's acid $[H(OEt_2)_2][B(3,5\text{-}(CF_3)_2C_6H_3)_4]$ in benzene gives the paramagnetic bis(η-benzene)nickel derivative $\{[Ni(\eta\text{-}C_6H_6)_2][B(3,5\text{-}(CF_3)_2C_6H_3)_4]_2{\cdot}Ni(\eta\text{-}C_5H_5)_2\}$ in which nickelocene is present as a molecule of crystallisation.

Large and very weakly coordinating anions $[BR_4]^-$ [R = 3,5-$(CF_3)_2C_6H_3$, C_6F_5] have recently attracted interest owing to their ability to stabilise highly electrophilic metal cations.[1] The strong Lewis acid $B(C_6F_5)_3$, is currently of interest as a methyl abstracting agent and activator of early transition metal Ziegler–Natta polymerisation systems.[2] Recently the mono-aquo adduct H_2O–$B(C_6F_5)_3$ was reported, and the solution behaviour as a Brønsted acid was described.[3,4]

Here, we report reaction between nickelocene and the Brønsted acids H_2O–$B(C_6F_5)_3$ or $[H(OEt_2)_2][B(3,5\text{-}(CF_3)_2C_6H_3)_4]$ (Brookhart's acid) which give unexpected new chemistry.

Treatment of nickelocene with Brookhart's acid $[H(OEt_2)_2][B(3,5\text{-}(CF_3)_2C_6H_3)_4]$ in toluene gives green–blue crystals of the Ni(III) compound $[Ni(\eta\text{-}C_5H_5)_2][B(3,5\text{-}(CF_3)_2C_6H_3)_4]$ **1**†. The nickelocenium cation has been isolated previously as the BF_4^- salt,[5] but no crystal structure was reported. The cation $[Ni(\eta\text{-}C_5Me_5)_2]^+$ has been structurally characterised as C_{60}^- and $[HTCNQF_4]^-$ salts.[6] The crystal structure of **1** has been determined and the ORTEP of $[Ni(\eta\text{-}C_5H_5)_2]^+$ (Fig. 1) shows eclipsed cyclopentadienyl rings as observed in $[Ni(\eta\text{-}C_5H_5)_2]$.[7] The average Ni–C distance of 2.075 Å is slightly shorter than in $[Ni(\eta\text{-}C_5H_5)_2]$ (2.178 Å). The magnetic moment of **1** at room temperature is 1.69 μ_B and corresponds to one unpaired electron, consistent[8] with the ground state configuration $\delta^4\sigma^2\pi^1$.

Treatment of nickelocene with H_2O–$B(C_6F_5)_3$ in CH_2Cl_2–benzene, gave brown crystals of the triple-decker sandwich compound $[(\eta\text{-}C_5H_5)Ni(\eta\text{-}C_6H_6)Ni(\eta\text{-}C_5H_5)][B_3(\mu\text{-}O)_3(C_6F_5)_5]$ **2**. In contrast, the reaction between nickelocene and the Brønsted acid $HBF_4{\cdot}Et_2O$ gave the cation $[Cp_3Ni_2]^+$.[9] We envisage the cation $[(\eta\text{-}C_5H_5)Ni(\eta\text{-}C_6H_6)Ni(\eta\text{-}C_5H_5)]^{2+}$ is formed by the addition of two intermediate $[Ni(\eta\text{-}C_5H_5)]^+$ fragments to a benzene molecule. Each nickel centre is formally equivalent to the 18-electron centres in $[Ni(\eta\text{-}C_5H_5)(\eta^3\text{-allyl})]$.[10] The crystal structure of **2** (Fig. 2) shows the rings are eclipsed with an average Ni–C_{Cp} distance of 2.121 Å, and the C–C–C angles lie between 106.6(5) and 109.2(4)°; the corresponding Ni–$C_{benzene}$ distance is 2.168 Å, with the C–C–C angles between 118.5(6) and 121.8(5)°. This compound is the first η-benzene–nickel(II) sandwich compound to be structurally characterised. The only other η-benzene–nickel compound is the Ni(0) phosphine compound, $[Ni(\eta\text{-}C_6H_6)(Bu^t_2PCH_2PBu^t_2)]$.[11] Nickel(II) compounds with one η-toluene or η-mesitylene ligand have been structurally characterised.[12]

The counter ion in **2** is a new dianion. The six-membered B_3O_3 ring is surrounded by five C_6F_5 groups, giving one neutral, three-coordinate boron, B(1), and two anionic tetrahedral boron centres, B(2) and B(3). There are only two non-solvent moieties present in the crystal structure, and to maintain electrostatic balance we assign a charge of −2 to the anion. The average B–O bond distance is 1.448 Å and the average B–O–B angle is 120.9°. The anion likely results from acidic decomposition and aryl group loss in H_2O–$B(C_6F_5)_3$.

Treatment of nickelocene with Brookhart's acid in benzene gives red–brown crystals of **3** and the crystal structure of **3** shows the presence of $Ni(\eta\text{-}C_5H_5)_2$, $Ni(\eta\text{-}C_6H_6)_2$ and two

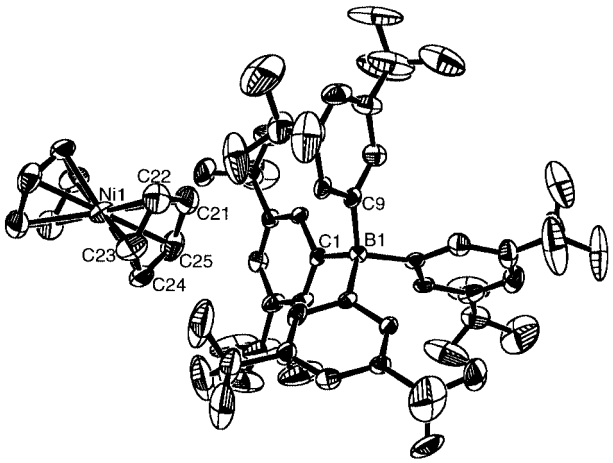

Fig. 1 Crystal structure of **1**. Selected bond lengths (Å) and angles (°): Cp_{cent}–Ni(1) 1.70, B(1)–C(1) 1.631(8), B(1)–C(9) 1.636(8); C(23)–C(22)–C(21) 109.3(8), C(22)–C(21)–C(25) 105.3(7), C(23)–C(24)–C(25) 106.6(7), C(22)–C(23)–C(24) 108.4(7), C(24)–C(25)–C(21) 109.1(7).

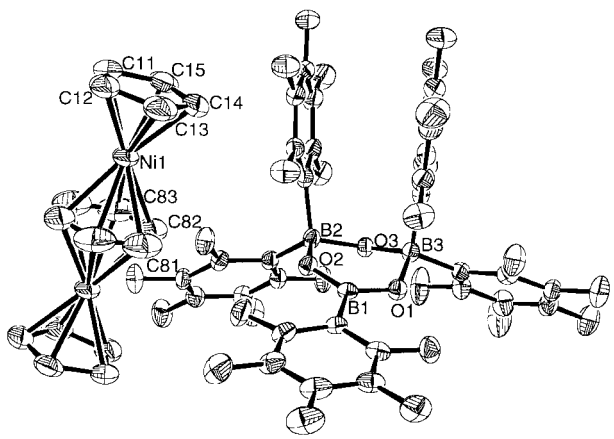

Fig. 2 Crystal structure of **2**. Selected bond lengths (Å) and angles (°): Cp_{cent}–Ni(1) 1.744, $benzene_{cent}$–Ni(1) 1.795, B(1)–O(1) 1.349(4), B(2)–O(2) 1.438(4), B(3)–O(3) 1.549(4); O(1)–B(1)–O(2) 123.8(3), O(2)–B(2)–O(3) 108.0(2), O(1)–B(3)–O(3) 107.6(2).

DOI: 10.1039/b001190h

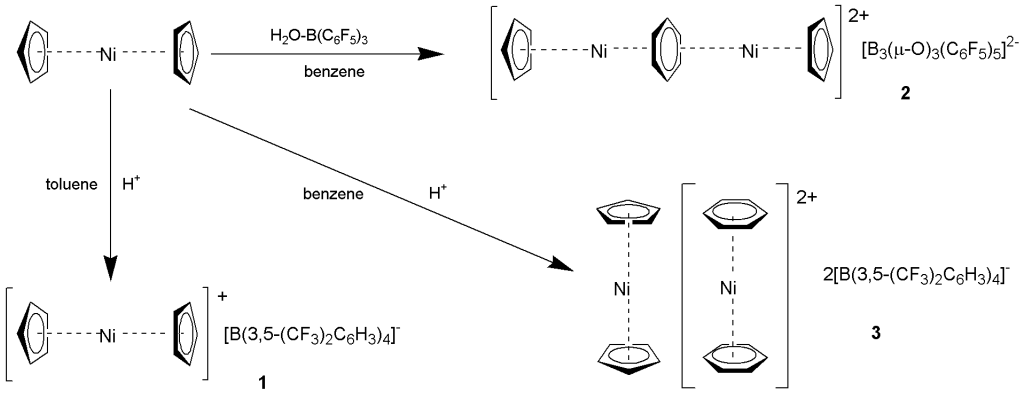

Scheme 1

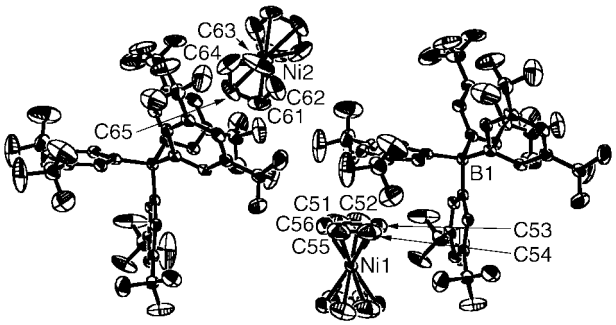

Fig. 3 Crystal structure of **3**. Selected bond lengths (Å) and angles (°): benzene$_{cent}$–Ni(1) 1.713, Cp$_{cent}$–Ni(2) 1.710, C(51)–C(52)–C(53) 124.2(15), C(56)–C(55)–C(54) 113.8(9), C(52)–C(51)–C(56) 126.2(16), C(63)–C(62)–C(61) 109.7(7), C(61)–C(65)–C(64) 107.0(7).

$[B(3,5\text{-}(CF_3)_2C_6H_3)_4]^-$ anions. The room temperature magnetic moment of **3** is 4.26 μ_B, corresponding to four unpaired electrons. These data are consistent with the presence in the crystal of neutral $Ni(\eta\text{-}C_5H_5)_2$ and dicationic $[Ni(\eta\text{-}C_6H_6)_2]^{2+}$; therefore we formulate this compound as $\{[Ni(\eta\text{-}C_6H_6)_2][B(3,5\text{-}(CF_3)_2C_6H_3)_4]_2\cdot Ni(\eta\text{-}C_5H_5)_2\}$, and the nickelocene is present as a molecule of crystallisation (Fig. 3). The average Ni–C distance in the dication $[Ni(\eta\text{-}C_6H_6)_2]^{2+}$ is 2.079 Å and the C–C–C angles are between 113.8(9) and 126.2(16)°. Bis(η-hexamethylbenzene)nickel(II) has been reported,[13] but not structurally characterised.

The new and often surprising reactions are summarised in Scheme 1.

J. L. P. thanks the Spanish Goverment for financial support. L. H. D thanks St. John's College Oxford for a Junior Research Fellowship.

Notes and references

† *Crystal data*: **1**: $C_{42}H_{22}BF_{24}Ni$, M_w = 1052.12, monoclinic, space group *C*2/*c*, *a* = 15.792(3), *b* = 12.679(3), *c* = 21.434(4) Å, β = 91.52(3), *U* = 4290.1(15) Å^3, *Z* = 4, μ(Mo-Kα) = 0.588 mm^{-1}. *T* = 150 K, 2802 independent reflections were collected (R_{int} = 0.0000); *R* = 0.0948 and R_w = 0.1973. The fluorine atoms of the CF_3 groups were found to be disordered and modelled as occupying staggerred positions (F121–F123 s.o.f. 84%; F151–F153 s.o.f. 87% and F41–F43 s.o.f. 84%).

2·CH_2Cl_2: $C_{47}H_{18}B_3Cl_2F_{25}Ni_2O_3$, M_w = 1326.37, triclinic, space group *P*1, *a* = 11.873(7), *b* = 13.526(8), *c* = 16.304(8) Å, α = 73.658(6), β = 75.969(6), γ = 71.607(6)°, *U* = 2350.0(5) Å^3, *Z* = 2, μ(Mo-Kα) = 1.06 mm^{-1}. *T* = 150 K; 8130 independent reflections were collected (R_{int} = 0.03); *R* = 0.0462 and R_w = 0.0572.

3: $C_{43}H_{23}BF_{24}Ni$, M_w = 1065.13, triclinic, space group $P\bar{1}$, *a* = 12.889(5), *b* = 13.191(6), *c* = 14.420(4) Å, α = 86.902(6), β = 90.131(6), γ = 61.171(6)°, *U* = 2143.55(14) Å^3, *Z* = 2, μ(Mo-Kα) = 0.590 mm^{-1}. *T* = 150 K; 7199 independent reflections were collected (R_{int} = 0.0000); *R* = 0.0797 and R_w = 0.2037. The fluorine atoms of the CF_3 groups have been modelled as disordered over two staggerred positions (F171–F173 s.o.f 49%, F341–F343 s.o.f 72% and F472–F473 s.o.f 74%).

CCDC 182/1576. See http://www.rsc.org/suppdata/cc/b0/b001190h/ for crystallographic files in .cif format.

1 C. A. Reed, *Acc. Chem. Res.*, 1998, **31**, 133.
2 M. Bochmann, *J. Chem. Soc., Dalton Trans.*, 1996, 255.
3 A. A. Danopoulos, J. R. Galsworthy, M. L. H. Green, S. Cafferkey, L. H. Doerrer and M. B. Hursthouse, *Chem. Commun.*, 1998, 2529.
4 L. H. Doerrer and M. L. H. Green, *J. Chem. Soc., Dalton Trans.*, 1999, 4325.
5 H. Werner and B. Ulrich, *J. Organomet. Chem.*, 1977, **141**, 339; J. D. Gribble and S. Wherland, *Inorg. Chem.*, 1990, **29**, 1130.
6 W. C. Wan, X. Liu, G. M. Sweeney and W. E. Broderick, *J. Am. Chem. Soc.*, 1995, **117**, 9580; X. Wang, L. M. Liable-Sands, J. L. Manson, A. L. Rheingold and J. S. Miller, *Chem. Commun.*, 1996, 1979.
7 P. Seiler and J. D. Dunitz, *Acta Crystallogr., Sect. B.*, 1980, **36**, 2255.
8 K. D. Warren, *Inorg. Chem.*, 1974, **13**, 1317.
9 H. Werner and A. Salzer, *Synth. Inorg. Met-org. Chem.*, 1972, **2**, 239; A. Salzer and H. Werner, *Angew. Chem., Int. Ed. Engl.*, 1972, **2**, 249; E. Dubler, M. Textor, H.-R. Oswald and A. Salzer, *Angew. Chem., Int. Ed. Engl.*, 1974, **13**, 135; E. Dubler, M. Textor, H. R. Oswald and G. B Jameson, *Acta Crystallogr., Sect. B.*, 1983, **39**, 607.
10 A. E. Smith, *Inorg. Chem.*, 1972, **11**, 165.
11 T. Nickel, R. Goddard, C. Krüger and K. Pörschke, *Angew. Chem., Int. Ed. Engl.*, 1994, **33**, 879.
12 L. J. Radonovich, K. J. Klabunde, C. B. Behrens, D. P. McCollor and B. B. Anderson, *Inorg. Chem.*, 1980, **19**, 1221; L. J. Radonovich, F. J. Koch and T. A. Albright, *Inorg. Chem.*, 1980, **19**, 3373.
13 H. H. Kinder and E. O. Fischer, *J. Organomet. Chem.*, 1968, **12**, P18.
14 A. Altomare, G. Cascarano, C. Giacovazzo and A. Guagliardi, SIR92, Program for crystal structure solution, *J. Appl. Crystallogr.*, 1993, **26**, 343.

ChemComm

Bacterial templating of zeolite fibres with hierarchical structure

Baojian Zhang,[a] Sean A. Davis,[a] Neil H. Mendelson[b] and Stephen Mann*[a]

[a] *School of Chemistry, University of Bristol, Bristol, UK BS8 1TS. E-mail: s.mann@bris.ac.uk*
[b] *Department of Molecular and Cellular Biology, University of Arizona, Tucson, Arizona 85721, USA*

Received (in Oxford, UK) 22nd February 2000, Accepted 27th March 2000

Ordered macroporous zeolite fibres are prepared from the infiltration of swollen bacterial supercellular threads with as-synthesized silicalite nanoparticles.

There is considerable interest in the production of inorganic materials containing frameworks with well defined pore networks. In general, strategies for synthesising these materials rely on the use of templates, the size and nature of which dictate the pore dimensions and architecture. Microporous (nanoporous) materials, such as zeolites, are prepared using molecular templates[1] whilst mesoporous solids, for example MCM-41 silicas, are structured by supramolecular aggregates.[2] We have previously demonstrated how supercellular templates can be used to extend the length scale of 3D inorganic patterning into the micrometre dimension.[3,4] For example, we were able to prepare MCM-41 silica-based fibres containing hierarchically organized pore structures at the meso- and micro-metre scale.[3] Subsequently, various other strategies, most notably the use of colloidal crystal templates,[5] have been employed to prepare ordered macroporous inorganic oxide structures by infiltration of the void spaces with alkoxide or inorganic precursors.[6] Both meso-[6] and micro-scopic[7] pores have been introduced into the macroporous architecture using a dual templating procedure.

Here, we report the synthesis and characterization of hierarchically structured zeolite fibres containing ordered pores at the nano- and micro-scopic length scale. In contrast to our previous work, in which we used *in situ* precipitation from a MCM-41 synthesis mixture,[3] here we use a stable aqueous dispersion of preformed zeolite nanoparticles as building blocks for the infiltration of a bacterial supercellular thread by reversible swelling. Silicalite nanoparticles are aggregated specifically within the organized micro-architecture, which consists of long multicellular filaments (0.5 μm in diameter) aligned parallel to the thread axis and arranged in a pseudo-hexagonally packed configuration.[8] Subsequent thermal decomposition of the bacterial template produces an intact zeolite fibre with ordered macroporous channels lined by 100-nm wide walls of coalesced silicalite nanoparticles. Because each nanoparticle consists of a periodic structure of intersecting nanoporous channels, the porous architecture is hierarchically ordered.

TPA-silicalite-1 nanoparticles were synthesized from clear solution by reflux of an aqueous solution containing tetraethylorthosilicate (TEOS) and tetrapropylammonium hydroxide (TPAOH) followed by repeated centrifugation and washing.† The resulting colloidal suspension was stable in deionized water at pH values between 10 and 11. Dynamic light scattering gave a mean hydrodynamic radius of 57 nm for the as-synthesized TPA-silicalite. This was in close agreement with transmission electron microscopy (TEM) which showed that the sample consisted of discrete nanoparticles with irregular surface texture and narrow particle size distribution (47 ± 10 nm) (Fig. 1). Significantly, the mean particle size was lower than that previously reported (95 nm),[9] possibly due to the reduced temperature (80 *cf.* 98 °C) and water content used in our synthesis mixture. High magnification TEM images suggested that the individual nanoparticles were constructed from aggregates of smaller primary clusters, and this was consistent with TEM analysis of the early stages of crystallization, which showed a predominance of 10 nm-size silicalite particles in samples extracted 24 h after the start of the reaction.

The crystallinity of the particles was confirmed by electron diffraction, XRD and FTIR spectroscopy. Powder X-ray diffraction (PXRD) patterns of the as-synthesized-TPA-silicalite-1 samples showed an orthorhombic lattice with broadened reflections and *d* spacings (d_{hkl} = 1.13 nm {011}, 1.00 nm {200}, 0.385 nm {501}, 0.373 nm {033}, 0.366 nm {133}) consistent with the PDF data base.[10] Corresponding FTIR spectra showed typical Si–O–Si framework bands, including the characteristic double ring vibration at *ca.* 550 cm^{-1}.[11] The sample also showed a shoulder at 960 cm^{-1} and bands at 2980 and 1380–1470 cm^{-1}, attributable to Q^3 Si–OH groups and TPA^+, respectively.[11,12] Thermogravimetric analysis gave a total weight loss of 20% that included the desorption of water and TPAOH (< 260 °C). The weight loss between 260 and 600 °C was 12% owing to decomposition of occluded TPA–OSi and loss of TPA^+ framework counter ions. This value was consistent with a theoretical value of 11.7 wt% for four TPA^+ cations per unit cell.

Bacterial threads‡ were swollen without loss of structural integrity in silicalite sols and air-dried to produce composite fibres consisting of a semi-ordered matrix of multicellular filaments embedded in a continuous framework of zeolite nanoparticles. The reversible swelling procedure gave good infiltration of the inter-filament spaces throughout the macroscopic fibre, and produced a highly compacted network of silicalite nanoparticles after air-drying. The composite fibres were calcined at 600 °C to remove the molecular (TPAOH) and supercellular (bacteria) templates. Thermogravimetric analysis gave a total weight loss of 75%, corresponding to removal of water, TPAOH and the bacteria template. The remaining inorganic phase was in the form of an intact white silicalite fibre with a macroporous internal structure (Fig. 2). Significantly, the replica consisted of an organized array of *ca.* 0.5 μm-wide channels that were oriented approximately parallel to the fibre axis [Fig. 2(c)]. The channel walls were *ca.* 100 nm thick as

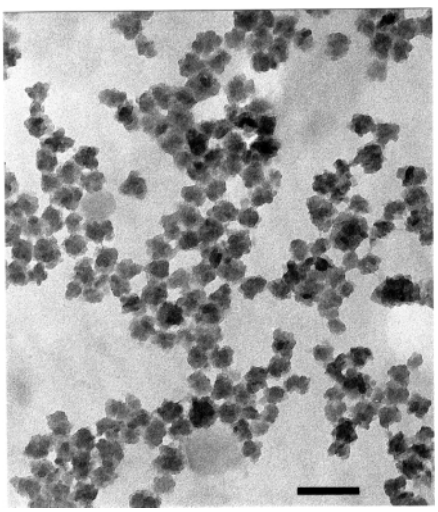

Fig. 1 TEM image of as-synthesized silicalite nanoparticles used as building blocks for the construction of porous zeolite fibres, scale bar = 100 nm.

DOI: 10.1039/b001528h

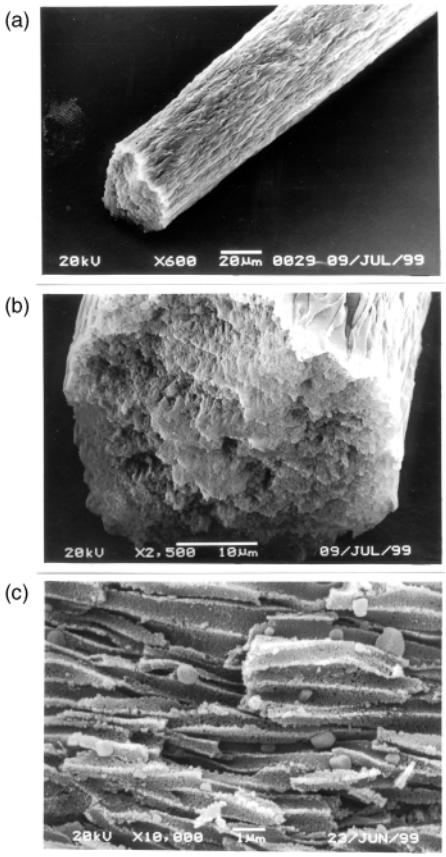

Fig. 2 SEM micrographs of silicalite-infiltrated bacterial thread after calcination at 600 °C: (a) intact zeolite replica, scale bar = 20 μm. (b) Fractured fibre tip showing the channel-like architecture, scale bar = 10 μm. (c) High magnification image of a thread fractured longitudinally, showing the continuous zeolite wall structure enclosing co-aligned channels, 0.5 μm in width, scale bar = 1 μm.

determined by SEM measurements. TEM images of lightly ground samples indicated that the wall structure consisted of closely packed aggregates of 50 nm sized silicalite nanoparticles. Corresponding electron diffraction data on the particles were consistent with crystalline silicalite. XRD patterns on the bulk calcined thread showed reflections with increased intensities, indicating an increase in the crystallinity of the nanoparticles compared with the as-synthesized zeolite. FTIR spectroscopy showed the characteristic double-ring vibration band at *ca.* 550 cm^{-1}, but no shoulder at 960 cm^{-1}, indicating almost complete condensation of the Si–OH groups in the calcined product.

Our results indicate that silicalite nanoparticles can be infiltrated into the ordered void spaces of a bacterial template where they can be used as building blocks for the construction of a macroporous inorganic framework. The mechanism responsible for high-fidelity inorganic replication of the bacterial superstructure has been described previously for macroporous fibres prepared from amorphous silica colloids.[3] The same considerations, such as surface-charge repulsion between the bacterial cell walls and the silicalite nanoparticles at high pH, and ionic strength-induced aggregation on deswelling, are likely to be responsible for the irreversible coalescence and compaction of the zeolite nanoparticles into the patterned architecture. Removal of both molecular (TPA^+) and micrometre-scale (multicellular filaments) templates by thermal degradation affords a zeolite fibre with hierarchical porosity that might have technological advantages owing to the high surface area and unidirectionality of the patterned architecture. Porous zeolite threads could also be aligned in thin films or flow tubes for separation processes or catalysis. By changing the template, it should also be possible to produce more complex macroporous zeolite monoliths by nanoparticle infiltration of patterned organic materials exhibiting reversible swelling. For example, recent studies indicate that sponge-like block copolymer gel templates can be used to prepare interconnected macroporous frameworks of coalesced magnetite or titania nanoparticles.[13]

We thank the EPSRC and the University of Bristol for financial support to S.A.D and B. Z, respectively.

Notes and references

† TPA-silicalite nanoparticles were synthesized from clear solutions following a modified version of the method described by Persson *et al*.[9] Tetraethylorthosilicate (16.0 g; Aldrich, > 98%) was added to 27.32 g of 1.0 M aqueous solution of tetrapropylammonium hydroxide (TPAOH; Aldrich) in a polypropylene bottle. The reactant mixture (molar composition: 9 TPAOH : 25 SiO_2 : 354 H_2O : 100 EtOH) was stirred for 24 h at room temp. to allow hydrolysis of the TEOS. The colourless solution obtained was heated under reflux in a preheated paraffin oil bath at 80 °C for 96 h without stirring. The colloidal particles produced were sedimented by centrifugation (12000 rpm) and washed by resuspending in deionized water. This process was repeated until the final pH of the suspension was 10–11. At this pH the particles have a net negative surface charge, and the dispersion is stable for several months. Dynamic light scattering and zeta potential measurements were performed on suitably diluted solutions, using a Brookhaven Instruments ZetaPlus particle sizer. Specimens for TEM were prepared by depositing a drop of the suspension onto carbon-coated, formvar-covered copper grids. Powder samples for XRD, FTIR and TGA were prepared by air drying the suspension.

‡ Macroscopic bacterial threads were produced from cell cultures of mutant FJ7 strain of *Bacillus subtilis* by methods described elsewhere.[8] Infiltration of the bacterial superstructure was achieved as follows. The tip of a 3–5 cm long prewashed bacterial thread was held by reverse tweezers and the fibre dipped into the washed silicalite colloidal solution (pH 10–11, 1–4% w/w) for at least 3 h at room temp. The swollen fibre was then very slowly withdrawn from the colloidal solution and allowed to dry in air. During the dipping process, the tweezers were held so that the tip of the thread was not immersed in the colloidal solution. This aided recovery of the intact mineralized fibre. Calcined materials were prepared by heating the composite fibres in a Carbolite furnace to a temperature of 600 °C at a rate of 2 °C min^{-1}. Samples were kept at 600 °C for at least 2 h before cooling to room temperature.

SEM and EDXA were carried out using a JEOL JSM5600LV instrument operated at 5 keV for uncoated samples or at 20 keV for gold-coated samples. The samples were mounted onto Al stubs, using carbon sticky pads. TGA was performed on a Netzsch TG209 instrument at a heating rate 5 °C min^{-1} from room temperature to 800 °C in a nitrogen atmosphere with flow rate 90 ml min^{-1}. The TGA residues were collected and used for PXRD and FTIR measurements. Powder X-ray diffraction studies were carried out on a Siemens D500 diffractometer with Cu-Kα_1 radiation, in the 2θ range 5–60°. FTIR spectra were recorded on a Bruker IFS 25 spectrophotometer using KBr pellets in the range 400–4000 cm^{-1}. For TEM and SAED analysis the calcined fibres were ground, dispersed in deionized water and then deposited on carbon-coated, formvar-covered copper grids.

1 M. E. Davis, *Chem. Eur. J.*, 1997, **3**, 1745.
2 C. G. Goeltner and M. Antonietti, *Adv. Mater.*, 1997, **9**, 431.
3 S. A. Davis, S. L. Burkett, N. H. Mendelson and S. Mann, *Nature*, 1997, **385**, 420.
4 S. A. Davis, H. M. Patel, E. L. Mayes, N. H. Mendelson, G. Franco and S. Mann, *Chem. Mater.*, 1998, **10**, 2516.
5 O. D. Velev, T.A. Jede, R. F. Lobo and A. M. Lenhoff, *Nature*, 1997, **389**, 447; O. D. Velev, T. A. Jede, R. F. Lobo and A. M. Lenhoff, *Chem. Mater.*, 1998, **10**, 3597.
6 B. T. Holland, C. F. Blanford and A. Stein, *Science*, 1998, **281**, 538; B. T. Holland, C. F. Blanford, T. Do and A. Stein, *Chem. Mater.*, 1999, **11**, 795.
7 B. T. Holland, L. Abrams and A. Stein, *J. Am. Chem. Soc.*, 1999, **121**, 4308.
8 N. H. Mendelson, *Proc. Natl. Acad. Sci. USA*, 1976, **73**, 1740.
9 A. E. Persson, B. J. Schoeman, J. Sterte and J. E. Otterstedt, *Zeolites*, 1994, **14**, 557.
10 PDF file 44-696 JCPDS-ICDD 1995.
11 R. Ravishankar, C. Kirschhock, B. J. Schoeman, P. Vanoppen, P. J. Grobet, S. Storck, W. F. Maier, J. A. Martens, F. C. De Schryver and P. A. Jacob, *J. Phys. Chem. B*, 1998, **102**, 2633.
12 E. R. Geus, J. C. Jansen and H. van Bekkum, *Zeolites*, 1994, **14**, 82.
13 M. Breulmann, S. A. Davis, S. Mann, H. P. Hentze and M. Antonietti, *Adv. Mater*, 2000, **12**, 502.

ChemComm

Extension of a π-stacked N_2S ligand to form bi- and tri-nuclear silver(I) complexes†

Paula L. Caradoc-Davies, Lyall R. Hanton* and Kitty Lee

Department of Chemistry, University of Otago, PO Box 56, Dunedin, New Zealand.
E-mail: lhanton@alkali.otago.ac.nz

Received (in Cambridge, UK) 24th December 1999, Accepted 27th March 2000

Reactions of tri- and penta-dentate thio-substituted oligopyridines with Ag(I) yielded two differently coded bi- and tri-nuclear structures containing strong intraligand π stacking of the heterocycles.

The design and construction of helicates from ligand threads and metal-ion induced self assembly has been much investigated.[1,2] However, alternatives to helicates exist, such as side-by-side arrangements which represent limiting non-helical structures formed by metal centres fixed between adjacent ligand threads.[1] These have been theoretically predicted and discussed in detail[2] but their observation is rare.[3] Such side-by-side structures offer the same opportunities for the development and understanding of the underlying construction principles of supramolecular chemistry. Both arrangements are driven by coding requirements, namely, the need to match ligand domains to the coordination preferences of the transition metal centres. Typically domains have been linked by non-coordinating species.[1] Incorporation of thioether donors into the linkers decreases the distance between the potential ligand domains thus bringing the metal centres closer together. Compressed conformations of this nature are more likely to favour side-by-side rather than helical arrangements about metal centres. With such an array of donors, ambiguity in coding may arise because of a mismatch of the number of donor atoms to metal-acceptor sites or a mis-allocation of the ligand domains to the metal centres. In such circumstances, the metal centres are required to compensate for this ambiguity. Hence, coordinatively flexible metal ions such as Ag(I) rather than Cu(I) are more likely to succeed in complex formation.

As part of our investigation of thio-substituted oligopyridines we found that the tridentate ligand **1** formed a side-by-side

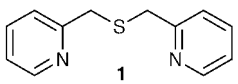

1

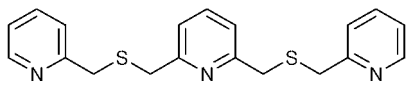

2

dimeric silver complex $[Ag_2(\mathbf{1})_2]^{2+}$ with strong intraligand π stacking of the pyridine rings. The coordinatively flexible Ag(I) ions adopted a three-coordinate planar geometry to code as a [3 + 3] rather than a [4 + 2] complex. It was of interest to see if on extending the ligand from the tridentate **1** to the related pentadentate **2** the same important features of intraligand π stacking and coding information were retained on complex formation.

Equimolar reaction of **1**[4] with $AgNO_3$ in MeCN, followed by treatment with NH_4PF_6, led to isolation of a cream complex in 46% yield, which analysed with a 1:1 ligand:metal ratio and gave ^{1}H and ^{13}C NMR spectra consistent with a symmetrical but dynamic complex.‡ The ^{1}H NMR spectra measured in CD_3CN and d_6-acetone remained unchanged down to the temperature limit for each solvent. Reaction of a related ligand di-2-pyridyl sulfide with Ag(I) produces a binuclear dimer containing two ligands.[5] This work would suggest **1** may not be ideally suited to forming mononuclear Ag(I) complexes. Electrospray mass spectrometry under normal operating conditions showed parent ions with appropriate isotope patterns for $\{[Ag_2(\mathbf{1})_2]PF_6\}^+$ at *m/z* 790.8 and $[Ag_2(\mathbf{1})_2]^{2+}$ at *m/z* 323.5. In addition using the Onsager equation,[6] dilution conductivity measurements in MeCN confirmed the presence of a 2:1 electrolyte‡ indicating the dimer remains intact in solution.

X-Ray crystal structure analysis§ showed the dimer is constructed from two ligands related by a crystallographic two-fold axis at the mid-point between the two Ag atoms. Each ligand experiences strong π-stacking interactions (3.41 Å) leading to an *endo-syn* conformation where the pyridine rings are tilted by 16.4° with respect to each other. The Ag atoms adopt a distorted trigonal planar geometry (Fig. 1), which links the two symmetry-related ligands by N,S chelation from one ligand and N′ donation from the other, giving rise to a folded side-by-side arrangement. This is in contrast to the centrosymmetric dimer of di-2-pyridyl sulfide in which the four-coordinate Ag atoms are bound in a NNS′ fashion with an O from a NO_3^- ion completing the coordination sphere.[5] In $[Ag_2(\mathbf{1})_2]^{2+}$ the Ag ions are separated by a short Ag···Ag distance of 3.052 Å which lies in the middle of the range (2.86–3.22 Å) found for similar systems.[3,5,7] The Ag(I) ions diverge by 0.159 Å from the trigonal planes which are tilted at 61.0° with respect to each other. As a consequence of the packing, chains of alternating intra- and inter-molecular (3.56 Å) π-stacked rings run along the *c* axis.

Reaction of **2**[8] with $AgNO_3$ in a 1:1 molar ratio in MeCN gave an off-white powder which analysed as $[Ag_3(\mathbf{2})_2](NO_3)_3$. Subsequently, the same compound was obtained in 76% yield using a 2:3 molar ratio.‡ A ^{1}H NMR spectrum measured in CD_3CN was consistent with a symmetrical structure. Previously, **2** was found to act as a pentadentate ligand in the monomeric complex $[Co(\mathbf{2})Cl]^+$.[8] Such a coordination preference is seemingly inconsistent with the analytical data for the Ag(I) complex.

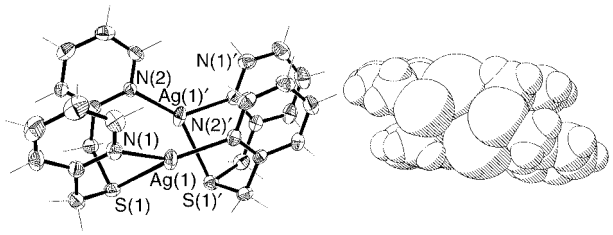

Fig. 1 Views of the binuclear $[Ag_2(\mathbf{1})_2]^{2+}$ cation, with the non-coordinating PF_6^- anions omitted: (left) Perspective view with thermal ellipsoids drawn at the 50% level. Selected distances (Å) and angles (°): Ag(1)–N(1) 2.263(3), Ag(1)–S(1) 2.5997(11), Ag(1)–N(2)′ 2.190(3); N(2)′–Ag(1)–N(1) 137.61(11), N(2)′–Ag(1)–S(1) 140.92(7), N(1)–Ag(1)–S(1) 79.77(8); (right) Space–filling view emphasising the π stacking of the ligands.

† Dedicated to Dr Charles R. Clark on the occasion of his 60th birthday.

DOI: 10.1039/a910342m

The trinuclear nature of the complex was confirmed by X-ray structural analysis (Fig. 2).§ The structure consists of three non-equivalent Ag(I) ions held in a linear chain (Ag···Ag···Ag 175.3°) by two folded ligands arranged in a side-by-side fashion 11.6 Å wide and 8.3 Å long. This linear silver core is particularly rare in both helicate[9] and side-by-side structures[10] where to date in helicate formation Cu(I) predominates.[11] The Ag(I) ions adopt [4 + 4 + 2] coordination rather than the anticipated [3 + 3 + 4], with Ag···Ag distances of 3.204 and 3.232 Å, respectively, lying at the long end of the range for similar systems.[3,5,7] The four-coordinate Ag(I) ions have distorted-tetrahedral geometries (NSN′S′) while the two-coordinate Ag(I) ion has a bent structure (NN′). In addition, two NO_3^- anions interact weakly with the two-coordinate Ag(I) centre [Ag(3)···O(23) 2.698 Å, Ag(3)···O(31) 2.712 Å]. The folding of the ligand is determined by strong intramolecular π stacking, as in $[Ag_2(\mathbf{1})_2]^{2+}$. The pyridine rings are separated from each other with values in the range 3.29–3.72 Å and are inclined with respect to each other with values in the range 13.4–26.0°.

Both pentadentate ligands have the same chirality, which causes the S donors attached to the four coordinate Ag(I) ions to be diametrically opposite each other. This contrasts with the structure of $[Ag_2(\mathbf{1})_2]^{2+}$ in which the S donors are adjacent. In the trinuclear complex, such an arrangement would require the two ligands to have opposite chirality. Chains of alternating enantiomers are arranged head-to-head and form intermolecular π-stacked chains (3.42 and 3.61 Å) along the diagonal axes [1 1 0] and [1 1 0].

The symmetrical nature of the ^{1}H NMR spectrum was at odds with the unsymmetrical [4 + 4 + 2] coding. Thus in solution either the complex is symmetrical or is undergoing rapid dynamic processes which may include equilibria between species of differing nuclearities. Electrospray mass spectrometry showed peaks which could be assigned to a number of species including a parent ion $\{[Ag_3(\mathbf{2})_2](NO_3)_2\}^+$ at *m/z* 1154.8, $\{[Ag_2(\mathbf{2})_2](NO_3)\}^+$ at *m/z* 983.9, $\{[Ag_2(\mathbf{2})](NO_3)\}^+$ at *m/z* 630.9 and $[Ag(\mathbf{2})]^+$ at *m/z* 459.9. However using the Onsager equation,[6] dilution conductivity measurements in $MeNO_2$ strongly indicated a 1:1 electrolyte‡ suggesting the trimer does not maintain its integrity in solution. Results from variable-temperature ^{1}H NMR spectra measured in d_6-acetone–10% CF_3CO_2D were inconclusive. They showed no changes other than significant broadening and collapse of peaks down to 188K.

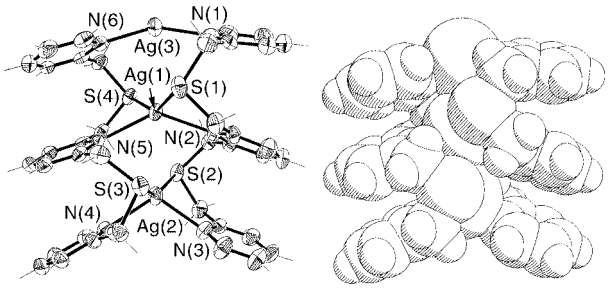

Fig. 2 Views of the trinuclear $[Ag_3(\mathbf{2})_2]^{3+}$ cation with NO_3^- anions, two weakly coordinating and one non–coordinating, omitted: (left) Perspective view with thermal ellipsoids drawn at the 50% level. Selected distances (Å) and angles (°): Ag(1)–N(2) 2.408(6), Ag(1)–N(5) 2.491(6), Ag(1)–S(4) 2.609(2), Ag(1)–S(1) 2.667(2), Ag(2)–N(4) 2.332(6), Ag(2)–N(3) 2.357(6), Ag(2)–S(2) 2.584(2), Ag(2)–S(3) 2.652(2), Ag(3)–N(1) 2.213(7), Ag(3)–N(6) 2.228(6); N(2)–Ag(1)–N(5) 133.8(2), N(2)–Ag(1)–S(4) 121.7(2), N(5)–Ag(1)–S(4) 75.9(2), N(2)–Ag(1)–S(1) 75.5(2), N(5)–Ag(1)–S(1) 114.7(2), S(4)–Ag(1)–S(1) 146.35(7), N(4)–Ag(2)–N(3) 112.7(2), N(4)–Ag(2)–S(2) 126.6(2), N(3)–Ag(2)–S(2) 79.0(2), N(4)–Ag(2)–S(3) 77.2(2), N(3)–Ag(2)–S(3) 111.5(2), S(2)–Ag(2)–S(3) 149.44(7), N(1)–Ag(3)–N(6) 150.6(2); (right) Space–filling view emphasising the extensive π stacking of the ligands.

We have shown that side-by-side structures can offer the diversity found in helicate structures. The intramolecular π stacking of the ligands was maintained in both complexes despite the ambiguity of coding being resolved in different ways to give different structural arrangements of side-by-side complexes.

We thank Professor Ward T. Robinson and Dr Jan Wikaira (University of Canterbury) for X-ray data collection and Dr Bill Henderson (University of Waikato) for electrospray MS data and the University of Otago for financial support.

Notes and references

‡ *Selected data*: for $[Ag_2(\mathbf{1})_2](PF_6)_2$: δ_H(300 MHz; CD_3CN) 8.42 (d, 4H, ^3J 7.5 Hz), 7.72 (dt, 4H, ^3J 7.5, ^4J 1.8 Hz), 7.33 (d, 4H, ^3J 7.8 Hz), 7.27 (m, 8H), 4.03 (s, 8H). Anal. Calc. for $C_{24}H_{24}N_4S_2Ag_2P_2F_{12}$: C, 30.73; H, 2.58; N, 5.97; S, 6.84. Found: C, 30.47; H, 2.47; N, 6.25; S, 6.72%. Slope of the linear variation of $\Lambda_0 - \Lambda_{eq}$ *vs.* $\sqrt{C_{eq}}$ (MeCN): $[Ag_2(\mathbf{1})_2](PF_6)_2$ 365 ± 85 Ω^{-1} $L^{1/2}$ equiv.$^{-1/2}$, standard: $[Cu(H_2O)_6](ClO_4)_2$ 353 ± 19 Ω^{-1} $L^{1/2}$ equiv.$^{-1/2}$. Colourless crystals were grown from slow evaporation of an acetonitrile solution.

For $[Ag_3(\mathbf{2})_2](NO_3)_3$: δ_H(300 MHz; CD_3CN) 8.55 (d, 4H, ^3J 4.8 Hz), 7.88 (dt, 4H, ^3J 7.8, ^4J 1.8 Hz), 7.58 (t, 2H, ^3J 7.5 Hz), 7.53 (d, 4H, ^3J 7.8 Hz), 7.38 (m, 4H), 7.18 (d, 4H, ^3J 7.5 Hz), 4.19 (s, 8H), 4.02 (s, 8H). Anal. Calc. for $C_{38}H_{38}N_9S_4Ag_3O_9$: C, 37.51; H, 3.15; N, 10.36; S, 10.54. Found: C, 37.45; H, 3.36; N, 10.32; S 10.23%. Slope of the linear variation of $\Lambda_0 - \Lambda_{eq}$ *vs.* $\sqrt{C_{eq}}$ ($MeNO_2$): $[Ag_3(\mathbf{2})_2](NO_3)_3$ 272 ± 11 Ω^{-1} $L^{1/2}$ equiv.$^{-1/2}$, standard: (NEt_4ClO_4 277 ± 42 Ω^{-1} $L^{1/2}$ equiv.$^{-1/2}$. Colourless crystals were grown from slow diffusion of diethyl ether in an acetonitrile solution.

§ *Crystal data*: $[Ag_2(\mathbf{1})_2](PF_6)_2$: $C_{12}H_{12}AgF_6N_2PS$, M = 469.14, monoclinic, space group $P2/n$ (no. 13), a = 13.657(4), b = 8.278(3), c = 14.071(4) Å, β = 103.063(4)°, U = 1549.7(8) Å^3, T = 173(2) K, Z = 4, μ(Mo-Kα) = 1.599 mm^{-1}, 19 328 reflections measured, 3176 independent reflections (R_{int} = 0.032), [2720, $I \geqslant 2\sigma(I)$], R_1 = 0.0353, 0.0426 (all data), wR_2 = 0.0899, 0.0940 (all data).

$[Ag_3(\mathbf{2})_2](NO_3)_3{\cdot}1.5CH_3CH_2OCH_2CH_3$: $C_{44}H_{53}Ag_3N_9O_{10.5}S_4$, M = 1317.72, monoclinic, space group $P2_1/n$ (no. 14), a = 18.749(7), b = 12.780(5), c = 21.716(8) Å, β = 99.729(4)°, U = 5128(3) Å^3, T = 170(2) K, Z = 4, μ(Mo-Kα) = 1.362 mm^{-1}, 63 340 reflections measured, 10 233 independent reflections (R_{int} = 0.11), [5676, $I \geqslant 2\sigma(I)$], R_1 = 0.0588, 0.1380 (all data), wR_2 = 0.1196, 0.1512 (all data). A disordered diethyl ether solvent molecule was refined isotropically without H-atoms. CCDC 182/1584. See http://www.rsc.org/suppdata/cc/a9/a910342m/ for crystallographic files in .cif format.

1 E. C. Constable, in *Polynuclear Transition Metal Helicates*, ed. J.-P. Sauvage and M. W. Hosseini, Pergamon, Oxford, 1996.
2 C. Piguet, G. Bernardinelli and G. Hopfgartner, *Chem. Rev.*, 1997, **97**, 2005.
3 S.-M. Kuang, Z.-Z. Zhang, Q.-G. Wang and T. C. W. Mak, *J. Chem. Soc., Dalton Trans.*, 1998, 2927; C. M. Hartshorn and P. J. Steel, *Inorg. Chem.*, 1996, **35**, 6902; A. Bilyk, M. M. Harding, P. Turner and T. W. Hambley, *J. Chem. Soc., Dalton Trans.*, 1995, 2549.
4 H. J. J.-B. Martel and M. Rasmussen, *Tetrahedron Lett.*, 1971, **41**, 3843.
5 R. J. Anderson and P. J. Steel, *Acta Crystallogr., Sect. C*, 1998, **54**, 223.
6 D. P. Rillema, R. Sahai, P. Matthews, A. K. Edwards, R. J. Shaver and L. Morgan, *Inorg. Chem.*, 1990, **29**, 167; R. K. Boggess and D. A. Zatko, *J. Chem. Educ.*, 1975, **52**, 649; R. D. Feltham and R. G. Hayter, *J. Chem. Soc.*, 1964, 4587.
7 J. Zank, A. Schier and H. Schmidbaur, *J. Chem. Soc., Dalton Trans.*, 1999, 415.
8 G. R. Newkome, V. K. Gupta, F. R. Fronczek and S. Pappalardo, *Inorg. Chem.*, 1984, **23**, 2400.
9 W. K. Wong, L. L. Zhang, F. Xue and T. C. W. Mak, *Chem. Commun.*, 1997, 1525; J. de Mendoza, E. Mesa, J.-C. Rodriguez-Ubis, P. Vázquez, F. Vögtle, P.-M. Windscheif, K. Rissanen, J.-M. Lehn, D. Lilienbaum and R. Ziessel, *Angew. Chem., Int. Ed. Engl.*, 1991, **30**, 1331; T. M. Garrett, U. Koert, J.-M. Lehn, A. Rigault, D. Meyer and J. Fischer, *J. Chem. Soc., Chem. Commun.*, 1990, 557.
10 R.-H. Uang, C.-K. Chan, S.-M. Peng and C.-M. Che, *J. Chem. Soc., Chem. Commun.*, 1994, 2561; C.-M. Che, H.-K. Yip, D. Li, S.-M. Peng, G.-H. Lee, Y.-M. Wang and S.-T. Liu, *J. Chem. Soc., Chem. Commun.*, 1991, 1615.
11 M. Greenwald, D. Wessely, I. Goldberg and Y. Cohen, *New J. Chem.*, 1999, 337.

Synthesis of carbonyl-bridged peptides containing an α-fluoroglycine residue†

Yoshio Takeuchi,*[a] Kiyotoshi Kirihara,[a] Kenneth L. Kirk[b] and Norio Shibata[a]

[a] *Faculty of Pharmaceutical Sciences, Toyama Medical and Pharmaceutical University, Sugitani 2630, Toyama 930-0194, Japan. E-mail: takeuchi@ms.toyama-ac.jp*

[b] *Laboratory of Bioorganic Chemistry, National Institute of Diabetes and Digestive and Kidney Disease, National Institutes of Health, Bethesda, MD 20892, USA*

Received (in Cambridge, UK) 15th February 2000, Accepted 29th March 2000

Gabriel reaction of hydantoins with bromofluoroacetate provides a general method for the synthesis of carbonyl-bridged peptides containing an α-fluoroglycine residue.

Introduction of fluorine atoms into amino acids is a powerful and reliable strategy for the design of potent biologically active amino acid and peptide derivatives.[1] Numerous fluorinated analogues encompassing essentially every class of amino acid have been synthesized and examined for biological activity. As part of an ongoing research program committed to preparation of multifunctional carbon compounds,[2] we have selected the α-fluoro α-amino acids **1** as synthetic targets. Fluorine substitution at the α-position of α-amino acids is of great interest because of the profound influence this has on the chemical properties of the carbonyl carbon and, in particular, the α-amino group, and the expected accompanying consequences on biological activity. However, there are few reports for the synthesis of α-fluoro α-amino acids. Bailey *et al.* developed pioneering work for this study in 1989.[3] They carried out an asymmetric synthesis of protected α-fluoroglycines utilizing the Gabriel reaction of chiral fluoroiodoacetamides with potassium phthalimide. We also independently reported the synthesis of a protected α-fluoroglycine in the following year[4] and recently applied our method to the preparation of protected α-fluoroglycine containing dipeptides.[5] Despite considerable effort, however, neither free α-fluoroglycine nor free fluorine-containing dipeptides have ever been isolated because of rapid dehydorofluorination under ambient conditions. Whereas we recognized the importance of a more recent report by Bailey *et al*. on the first isolation of a free α-fluoroglycine derivative, α-fluorobetaine,[6] it is obviously impossible to incorporate this structure into peptides. We herein disclose a general method for a synthesis of carbonyl-bridged peptides containing the α-fluoroglycine residue **2** using the Gabriel reaction of hydantoins **3** with bromofluoroacetate.

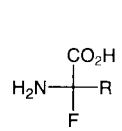

1

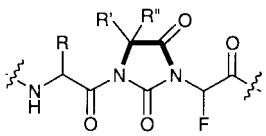

2

The design of the target carbonyl-bridged peptides **2** was based on the following strategies. First, the carbon–fluorine bond of **2** is stabilized to loss of fluoride by virtue of the electron attracting effect of the imide carbonyl groups. Second, peptides in a conformationally restricted environment are important structural features used in the field of peptidomimetics.[7] In addition, hydantoins are known to possess a broad range of biological activities, including antiviral, antibacterial, antifungal and herbicidal activity.[8] We first examined the synthesis of hydantoin-α-fluoroglycine-containing dipeptides **4** that are the key component parts of **2**. The Gabriel-type reaction of the commercially available diphenylhydantoin **3a** was performed by deprotonation, using NaH in DMF, followed by the addition of ethyl bromofluoroacetate (Table 1, entry 1). Although the desired **4a** was the predominant product, obtained in moderate yield, this procedure resulted in the formation of a mixture of **4a** and bis-alkylated product **5** along with recovered starting material **3a**. In an attempt to overcome this problem of selectivity in the alkylation reaction, optimization of the

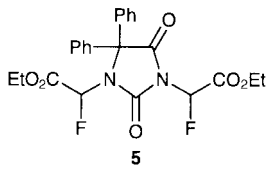

5

Table 1 Synthesis of hydantoin-fluoroglycine-containing dipeptides

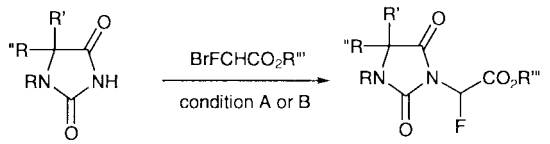

3 **4**

Entry	3	R	R'	R"	Condition	R"'	4	Yield[a] (%)
1	**3a**	H	Ph	Ph	A	Et	**4a**	46
2	**3a**	H	Ph	Ph	B	Et	**4a**	53
3	**3a**	H	Ph	Ph	C	Et	**4a**	91
4	**3a**	H	Ph	Ph	C	Bu^t	**4b**	67
5	**3b**	H	Me	Me	C	Et	**4c**	42
6	**3c**[b]				C	Et	**4d**[c]	74
7	**3c**[b]				C	Bu^t	**4e**[c]	65
8	**3d**[b]	H	Ph	H	C	Bu^t	**4f**[c]	31
9	**3e**[b]	H	Bn	H	C	Et	**4g**[c]	51
10	**3f**[b]	H	Pr^i	H	C	Et	**4h**[c]	20
11	**3g**[b]	H	H	H	C	Et	**4i**[c]	32
12	**3h**[b]	Boc	Ph	H	C	Et	**4j**[c]	97
13	**3i**[b]	Boc	Bn	H	C	Et	**4k**[c]	69
14	**3j**[b]	Boc	Pr^i	H	C	Et	**4l**[c]	57
15	**3k**	Boc	H	H	C	Et	**4m**	55

Condition A: NaH, DMF 80 °C, 1 h; B: NaH, NBu_4Br, DMF, room temp., 12 h; C: NaH, NBu_4Br, THF, room temp., 12 h. [a] Isolated yield. [b] Racemic hydantoins **3c**–**j** used. [c] Mixture of diastereoisomers (1 : 1).

† Part 4 of series: Synthetic studies for novel structure of α-nitrogenousyl functionalized α-fluorocarboxylic acids.

DOI: 10.1039/b001265n

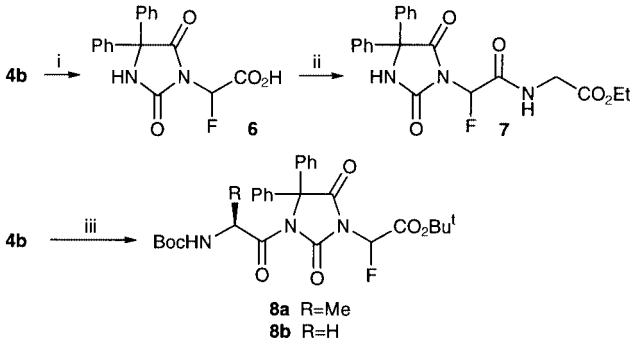

Scheme 1 *Reagents and conditions*: i, TFA, CH_2Cl_2, room temp. (quant.); ii, H-Gly–OEt, DCC, HOBT, Et_3N, DMF, room temp. 12 h (76%); iii, isobutyl chloroformate, Et_3N, DMAP, DMF, THF, then Boc-Ala–OH or Boc-Gly–OH, −15 °C to room temp., 3 h (91% for **8a**, 79% for **8b**).

conditions was investigated by examining several bases and additives in several solvents at different temperatures. The best result was obtained in the reaction of **3a** with NaH, NBu_4Br and ethyl bromofluoroacetate in THF at room temperature to give **4a** in 91% yield (entry 3).[9] Other hydantoins **3b**,**c** having different substituents at the 5 position were treated with ethyl or *tert*-butyl bromofluoroacetate under the same conditions to give **4b**–**d** in moderate to good yields (entries 4–7). Lower yields (31–51%) of **4** were observed when unsubstitutued or 5-mono-substituted hydantoins **3d**–**g** derived from naturally occurring α-amino acids were used as starting materials (entries 8–11). However, the yields using these substrates were improved to 55–97% by the use of Boc protected hydantoins **3h**–**k** (entries 12–15) (Table 1).[10]

With the development of a general method for the synthesis of hydantoin-α-fluoroglycine-containing peptides **4**, we next demonstrated that **4** could be incorporated into the oligopeptide **2** by normal peptide coupling techniques. Deprotection at the *C*-terminus of **4b** was nicely achieved with TFA–CH_2Cl_2 to give free dipeptide **6** quantitatively. As expected, the free acid **6** is sufficiently stable for subsequent chemical manipulation under ambient conditions. Coupling of the carboxylic acid **6** obtained with glycine ethyl ester in the presence of DCC/HOBT furnished the tripeptide **7** in 76% yield. Furthermore, *N*-terminal chain elongation was achieved by coupling **4b** with Boc-Ala–OH or Boc-Gly–OH using the mixed anhydride method to give the tripeptides **8** in good yield (Scheme 1).

In summary, we have described the design and synthesis of fluoroglycine-containing peptides.[2] Neither free α-fluoroglycine nor free fluorine-containing dipeptides have been previously isolable.[3–6] The carbonyl-bridged strategy employed in the present work offers one solution to this problem.[11] Oligomerization of hydantoin-α-fluoroglycine-containing dipeptides **4** will be presented in the near future.

We thank the Ministry of Education, Science, Sports and Culture, Japan for a Grant-in Aid for Scientific Research and for Encouragement of Young Scientists. Y. T. thanks the Grant from Asahi Glass Foundation.

Notes and references

1 V. P. Kukhar and V. A. Soloshonok, *Fluorine-containing Amino Acids*, John Wiley & Sons Ltd, Chichester, West Sussex, England, 1995.
2 Y. Takeuchi, *Yuki Gousei Kagaku Kyokai-shi*, 1997, **55**, 886.
3 P. D. Bailey, A. N. Boa, G. A. Crofts, M. van Diepen, M. Helliwell, R. E. Gammon and M. J. Harrison, *Tetrahedron Lett.*, 1989, **30**, 7457.
4 Y. Takeuchi, M. Nabetani, K. Takagi, T. Hagi and T. Koizumi, *J. Chem. Soc., Perkin Trans. 1*, 1991, 49.
5 Y. Takeuchi, M. Kamezaki, K. Kirihara, G. Haufe, K. W. Laue and N. Shibata, *Chem. Pharm. Bull.*, 1998, **46**, 1062.
6 P. D. Bailey, S. R. Baker, A. N. Boe, J. Clayson and G. M. Rosair, *Tetrahedron Lett.*, 1998, **39**, 7755.
7 A. Abell, *Advances in Amino Acid Mimetics and Peptidomimetics*, JAI Press Inc., London, UK, 1997, vol. 1; M. D. Fletcher and M. M. Campbell, *Chem. Rev.*, 1998, **98**, 763.
8 C. A. Lo'pez and G. G. Trigo, *Adv. Heterocycl. Chem.*, 1985, **38**, 177; N. Nakajima, K. Itoi, Y. Takamatsu, H. Okazaki, T. Kinishita, M. Shindou, K. Kawakubo, T. Honma, M. Toujigmor and T. Haneishi, *J. Antibiot.*, 1991, **44**, 293.
9 General procedure; to a stirred mixture of **3a** (100 mg, 0.40 mmol) and NBu_4Br (129 mg, 0.48 mmol) in THF (1.0 ml) was added NaH (60%, 19 mg, 0.48 mmol) at 0 °C. After 30 min stirring at room temperature, ethyl bromofluoroacetate (73.4 mg, 0.40 mmol) was added to the mixture which was stirred for 12 h. The reaction was stopped by addition of a saturated solution of NH_4Cl (1 ml) and the mixture was diluted with ethyl acetate (100 ml). The organic phase was washed with water (20 ml), brine (20 ml) and dried over $MgSO_4$. The solvent was removed under reduced pressure to give an oil that was purified by column chromatography on silica gel eluting with 60% ethyl acetate in hexane to give **4a** (128 mg, 91%) as a colorless oil.
10 Dipeptides **4d–l** were the 1 : 1 mixtures of diastereomers, which were not separated.
11 A recent publication of similar types of bridged compounds; P. D. Bailey, A. N. Boe, S. R. Baker, J. Clayson, E. J. Murray and G. M. Rosair, *Tetrahedron Lett.*, 1999, **40**, 7557.

CFTA, a new efficient agent for determination of absolute configurations of chiral secondary alcohols

Tamiko Takahashi,[a] Aki Fukuishima,[a] Yuki Tanaka,[a] Yoshio Takeuchi,*[a] Kuninobu Kabuto*[b] and Chizuko Kabuto[b]

[a] *Faculty of Pharmaceutical Sciences, Toyama Medical and Pharmaceutical University, Sugitani 2630, Toyama 930-0194, Japan*

[b] *Graduate School of Chemistry, Tohoku University Aoba-ku Aramaki, Sendai 980-8578, Japan. E-mail: takeuchi@ms.toyama-mpu.ac.jp*

Received (in Cambridge, UK) 10th March 2000, Accepted 29th March 2000

The CFTA method using α-cyano-α-fluoro-*p*-tolylacetic acid (CFTA) can be reliable in assigning absolute configurations of chiral secondary alcohols based on both ^{1}H and ^{19}F NMR spectroscopy, and the most stable and most predominant conformer of the CFTA esters that can explain the ^{1}H and ^{19}F NMR data were supported by X-ray analysis and *ab initio* calculations.

Recent advances in enantioselective synthesis have produced an increasing demand for convenient and reliable techniques for assigning the absolute configuration of chiral molecules. A number of methods using chiral derivatizing agents (CDAs), such as α-methoxyarylacetic acids and α-methoxy-α-trifluoromethylphenylacetic acid (MTPA, Mosher's agent) by ^{1}H NMR spectroscopy have been developed for this purpose.[1] Among them, the well known modified Mosher method[2] using MTPA is one of the most reliable and widely applicable techniques to general secondary alcohols except sterically hindered ones. On the other hand, fluorine-containing CDAs are very useful with respect both to general applicability and convenience for the ee determination.[1c] In this case, the ^{19}F NMR spectroscopy is particularly useful because the shift differences are usually larger than those in the ^{1}H NMR spectra and there is seldom an overlap of signals. However, the ^{19}F-chemical shifts observed with MTPA[2] and fluorinated CDAs[3] can not be used for configuration determination because no general trend is observed. In the course of our continuing research to improve the utility of CDAs,[4] we have developed α-cyano-α-fluoro-*p*-tolylacetic acid (CFTA).[5] This agent far surpasses the capabilities of MTPA with respect to both reactivity and signal resolution ability. We report here, that the ^{19}F NMR-based CFTA method is promising for the determination of absolute configuration of chiral secondary alcohols. In addition, the CFTA method using ^{1}H NMR is not only of higher reliability but also of broader applicability compared to the modified Mosher method.

By a procedure similar to that used in the modified Mosher method,[2] we obtained the chemical shift difference, $\Delta\delta_H$ ($\delta_S - \delta_R$), for the corresponding protons in the diastereomeric (*S*)- and (*R*)-CFTA esters prepared from ten chiral secondary alcohols with known absolute configurations (Fig. 1). The results are as follows: (i) For all CFTA esters examined, the magnitude of $\Delta\delta_H$ was larger than that of the MTPA esters.[6] (ii) The signs of $\Delta\delta_H$ are distributed symmetrically with respect to the plane containing the carbinyl proton and the ester carbonyl (designated as the CFTA plane, Scheme 1). The $\Delta\delta_H$ values on the left side of the CFTA plane are positive and those on the right side negative. (iii) One of the most striking features of the CFTA method can be seen for the results for isomenthol. The signs of $\Delta\delta_H$ for the CFTA esters followed a regular plus order, while those for the MTPA esters did not. (iv) Another feature of the CFTA method can be seen for the application to 10-bromoisoborneol.[7] The CFTA esters were obtained, while the MTPA esters of this alcohol were not. These results validate the

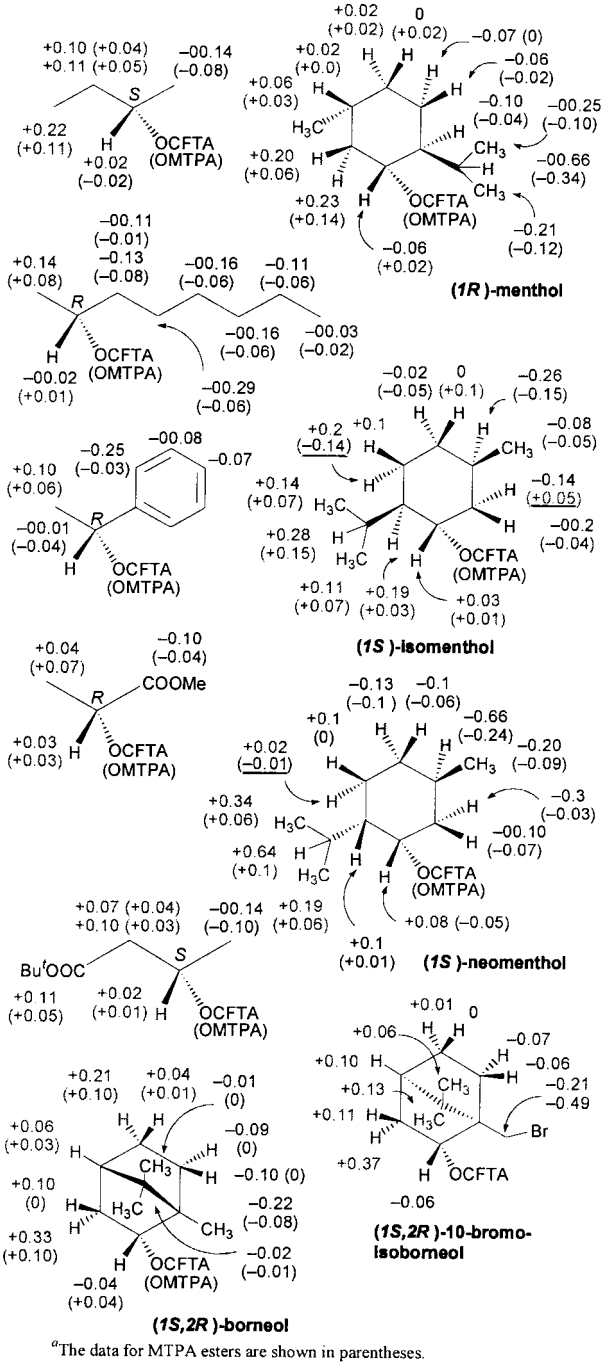

[a]The data for MTPA esters are shown in parentheses.

Fig. 1 $\Delta\delta_H$ values obtained for the CFTA and MTPA esters[a] [$\Delta\delta_H$/ppm = $\delta_S - \delta_R$].

Table 1 $\Delta\delta_F$ values obtained for the CFTA and MTPA esters

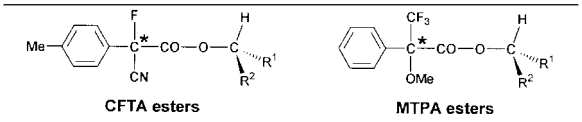

CFTA esters MTPA esters

		$\Delta\delta_F$/ppm = $\delta_{SR} - \delta_{RR}$ or $\delta_{RS} - \delta_{SS}$	
R^1	R^2	CFTA ester	MTPA ester
Me	Et	+0.08	+0.00
Me	Hex	+0.32	−0.05
Me	Ph	+0.87	−0.20
Me	COOMe	+1.28	−0.48
Me	CH_2COOBu^t	+0.59	+0.01
	Bornyl	+0.74	+0.10
	10-Bromoisobornyl	+0.92	—
	Menthyl	+0.59	−0.11
	Isomenthyl	+0.11	+0.02
	Neomenthyl	+0.79	+0.22

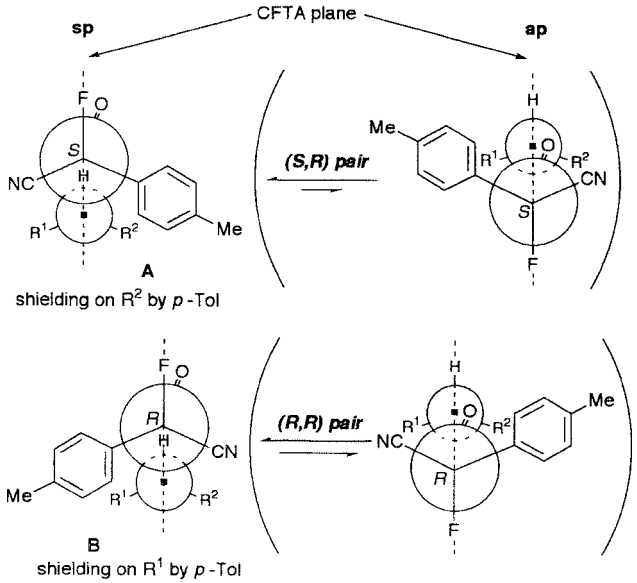

Scheme 1

usefulness of the CFTA method to elucidate the absolute configuration of the secondary alcohols. Owing to the larger and more predictable signs of the $\Delta\delta_H$ values, as well as the higher reactivity of CFTA chloride compared to MTPA chloride, the CFTA method based on ^{1}H NMR spectroscopy should be more widely applicable than the modified Mosher procedure using MTPA esters.

In addition to the satisfactory results in ^{1}H NMR, the ^{19}F NMR-based CFTA method is promising. By a procedure similar to that used in the MTPA method,[2] we obtained the chemical shift difference, $\Delta\delta_F$ ($\delta_{SR} - \delta_{RR}$ or $\delta_{RS} - \delta_{SS}$)[8] in the diastereomeric (*S*)- and (*R*)-CFTA esters (Table 1). The larger $\Delta\delta_F$ values of the CFTA esters compared with the MTPA esters showed correlations to the absolute configuration of the alcohols. In contrast, no consistent correlation was found with the MTPA esters.

The relationship between the sign of $\Delta\delta_H$ and absolute configuration observed for the CFTA esters can be explained by the correlation model[1d,e,2] depicted in Scheme 1. In the model, the C–F is *synperiplanar* (sp) to the C=O bond, to which the carbinyl C–H is *syn*. The sp conformer was seen by the X-ray structure of (*R*)-CFTA ester of (1*S*)-neomenthol.[9] The signals due to the substituents that confront the aromatic ring (R^2 and R^1 groups in the diastereomers A and B, respectively) are always shifted upfield by the aromatic ring. Accordingly, the $\Delta\delta_H$ values for each proton in the R^1 group should be plus and those in the R^2 group minus. This model was supported by *ab initio* calculations [GAUSSIAN 98, RHF/6-31+G(d)] on the ground state geometry and energy of the diastereomeric pair of (*R*)-α-cyano-α-fluorophenylacetic acid (CFPA)[4] esters of (1*S*)- and (1*R*)-menthol.[10] Two predominant rotamers regarding the C_α–CO bond were found: one is the sp described above and the other is *antiperiplanar* (ap) with the C–F and C=O bonds. Calculations predicted a preference of the sp rotamers that can explain the signs of $\Delta\delta_H$ over the ap ones by *ca.* 0.94 and 0.55 kcal mol^{-1} for (*R*,*S*)- and (*R*,*R*)-esters, respectively. The signs of $\Delta\delta_F$ can be explained on the basis of the calculated chemical shifts of ^{19}F nuclei in the two rotamers[11] and the conformational bias between these. Since the observed chemical shifts were averaged between the sp and the ap, and the conformational equilibrium is more biased to the sp in the (*R*,*S*) ester than in the (*R*,*R*) ester, the ^{19}F signal in the (*R*,*S*) ester is expected to appear at lower field than that in the (*R*,*R*) ester, as observed.

In order to ensure the reliability of our method and to extend the range of applications, further investigations are currently underway.

This work was supported by Grants-in-Aid for Scientific Research from the Ministry of Education, Science, Sports and Culture, Japan and partially by grants from Uehara Foundation and The Mitsubishi Foundation.

Notes and references

1 For reviews, see: (*a*) S. Yamaguchi, in *Asymmetric Synthesis*, ed. J. D. Morrison, Academic Press, New York, 1983, vol. 1, p. 125; (*b*) D. Parker, *Chem. Rev.*, 1991, **91**, 1441; (*c*) Y. Takeuchi and T. Takahashi, in *Enantiocontrolled Synthesis of Fluoro-organic Compounds*, ed. V. A. Soloshonok, Wiley, Chichester, 1999, p. 497. For CDAs for determination of absolute configuration of chiral secondary alcohols: (*d*) J. A. Dale and H. S. Mosher, *J. Am. Chem. Soc.*, 1973, **95**, 512; (*e*) B. M. Trost, J. L. Belletire, S. Godleski, P. G. McDougal and J. M. Balkovec, *J. Org. Chem.*, 1986, **51**, 2370; (*f*) J. M. Seco, Sh. Latypov, E. Quiñoá and R. Riguera, *Tetrahedron Lett.*, 1994, **35**, 2921; (*g*) I. Chataigner, J. Lebreton, D. Durand, A. Guingnant and J. Villiéras, *Tetrahedron Lett.*, 1998, **39**, 1759 and references therein.

2 I. Ohtani, T. Kusumi, Y. Kashman and H. Kakisawa, *J. Am. Chem. Soc.*, 1991, **113**, 4092; T. Kusumi, *Synth. Org. Chem.*, 1993, **51**, 462 and references therein.

3 H. Kawa, F. Yamaguchi and N. Ishikawa, *J. Fluorine Chem.*, 1982, **20**, 475; S. Hamman, *J. Fluorine Chem.*, 1989, **45**, 377; M. Barrele and S. Hamman, *J. Chem. Res. (S)*, 1990, 100; 1995, 316.

4 Y. Takeuchi, N. Itoh, T. Satoh, T. Koizumi and K. Yamaguchi, *J. Org. Chem.*, 1993, **58**, 1812 and references therein.

5 Y. Takeuchi, M. Konishi, H. Hori, T. Takahashi, T. Kometani and K. L. Kirk, *Chem. Commun.*, 1998, 365; Y. Takeuchi, M. Konishi, H. Hori, T. Takahashi and K. L. Kirk, *Enantiomer*, 1999, **4**, 339.

6 The magnitude of $\Delta\delta_H$ of the CFTA esters was similar to that of the methoxyphenylacetic acid esters (MPA esters).[1f] However, MPA chloride did not react with 10-bromoisoborneol.

7 N. Poth, *Rev. Tech. Luxemb.*, 1976, **68**, 195 (*Chem. Abstr.*, 1977, **87**, 135965k).

8 The esters of (*S*)-acids with (*R*)-alcohols are designated *SR* and those of (*R*)-acids with (*R*)-alcohols are designated *RR*.

9 *Crystal data* for the (*R*)-CFTA ester of (1*S*)-neomenthol: $C_{20}H_{26}NO_2F$, M = 331.43, colorless, crystal size = 0.01 × 0.02 × 0.03 mm, triclinic, space group *P*1 (no. 1), a = 8.739(9), b = 9.404(9), c = 6.411(8) Å, α = 103.23(8), β = 97.33(9), γ = 111.00(8), V = 465(1) Å^3, Z = 1, D_c = 1.181 g cm^{-3}, no. of measured unique reflections = 2143 (2θ = 55°), T = 150 K, Mo-Kα radiation (λ = 0.71069 Å), Full-matrix least squares (teXan), R = 0.061 for 1570 observed F_o data [$I_o > 4.10\sigma(I_o)$], R_w = 0.062, GOF = 2.01, $\Delta\rho_{max}$ = 0.22 e Å^{-3}. At least one of the methyl hydrogens was located using a difference Fourier map and then the others were calculated geometrically on the basis of the observed hydrogen atoms. CCDC 182/1586. See http://www.rsc.org/suppdata/cc/b0/b001962n/ for crystallographic files in .cif format.

10 The tolyl group of CFTA was replaced by a phenyl group to reduce the number of atoms. The relative configuration of the (*R*,*S*) diastereomer is the same as that of the (*S*,*R*) diastereomer.

11 The ^{19}F chemical shifts of the two rotamers in each diastereomeric ester were calculated using GAUSSIAN 98 on the calculated structures described above: δ_F (δ_{CFCl_3} = 0) − 128.59 (sp) and −145.33 (ap) for the (*R*,*S*) ester; −133.05 (sp) and −146.47 (ap) for the (*R*,*R*) ester.

Highly effective and recyclable dendritic BINAP ligands for asymmetric hydrogenation†

Qing-Hua Fan,*[a] Yong-Ming Chen,[a] Xiao-Min Chen,[a] Da-Zhi Jiang,[a] Fu Xi[a] and Albert S. C. Chan*[b]

[a] *LMRSS, Center for Molecular Science, Institute of Chemistry, The Chinese Academy of Sciences, Beijing 100080, P.R. China. E-mail: fanqh@infoc3.icas.ac.cn*

[b] *Open Laboratory of Chirotechnology and Department of Applied Biology and Chemical Technology, The Hong Kong Polytechnic University, Hong Kong, P.R. China*

Received (in Cambridge, UK) 23rd February 2000, Accepted 29th March 2000

A series of dendritic BINAP ligands have been synthesised and their ruthenium complexes used as catalysts in asymmetric hydrogenation.

In recent years, the attachment of homogeneous catalysts to soluble polymer supports has been attracting considerable attention owing to its potential combination of the advantages, and minimization of the disadvantages, of homogeneous and heterogeneous catalysis.[1–3] Unlike traditional cross-linked polymer-supported catalysts in which the structure is usually not clear, soluble polymer-supported catalysts also offer opportunities for the study of polymer–catalyst interactions to fine-tune both catalytic activity and stereoselectivity through systematically adjusting the microstructure of the catalytic sites in the polymer supports. Recently, we have developed a soluble chiral polyester-supported Ru(BINAP) catalyst which offered a higher rate of reaction than the corresponding monomeric homogeneous catalyst while retaining high stereoselectivity.[4] Most recently, dendritic organometallic catalysts have become a very active field of research.[5–7] The dendrimer architecture might offer a means of better controlling the disposition of the catalytic species in soluble polymer-based catalysts. Such novel catalysts are well defined and highly branched three-dimensional macromolecules on the nano-scale size, which may aid the recycling of catalysts simply by supra-filtration or solvent precipitation methods.‡ For asymmetric catalysis, chiral dendrimers are required, however, so far, very few dendritic chiral catalysts have been described.[8–14] Two general strategies for the construction of chiral dendritic catalysts can be applied: multiple chiral metal complexes employed at the periphery of the dendrimer, or chiral metal complexes incorporated in the core of the dendrimer. For the second strategy the space-filling nature of the dendritic wedges near the metal center would alter the structure of the metal complex, and thus possibly influence the reactivity of the catalyst and/or the substrate selectivity of the catalytic reaction with increasing generations. This kind of dendritic catalyst has been thus termed 'dendrizyme'.[6] For chiral diphosphine-containing catalysts, such as Ru(BINAP), chiral information is transferred from the ligand to the catalytically active center *via* the arrangement of the four phenyl rings of the diphenylphosphino groups.[15] Therefore, upon incorporation of a chiral diphosphine-containing catalyst into the core of a dendrimer, the chiral information might be enhanced by the steric bulk of the dendritic wedges and forced towards the pocket of the catalyst, in which the enantioselective reaction takes place.

Here, we report the first use of chiral diphosphine ligands bearing dendritic wedges for asymmetric hydrogenation.[16] BINAP was chosen as a model ligand for this study, since it is probably the most versatile and effective ligand among all the chiral phosphine ligands which have been studied for asymmetric catalysis.[15] Both rhodium and ruthenium BINAP complexes have been extensively studied and several commercial processes based on these catalysts have been developed.[17] BINAP itself cannot be easily attached to a dendrimer so (*R*)-5,5′-diamino-BINAP (*R*-**1**) was synthesized according to the literature.[18] A polyether dendrimer was chosen owing to its inertness to catalytic reaction. Polyether dendritic wedges **2**–**4** with carboxyl groups located at the focal point were synthesised by the convergent-growth approach introduced by Hawker and Fréchet.[19] The chiral dendritic BINAP ligands **5**–**7** were synthesised in > 85% yield by condensation of the wedges **2**–**4** with *R*-**1** in the presence of triphenylphosphite, pyridine and calcium chloride in *N*-methyl-2-pyrrolidone (NMP) at 100 °C (Scheme 1). These ligands were purified by fast column chromatography and characterized by ^{1}H and ^{31}P NMR spectroscopy, MALDI-TOF mass spectrometry and elemental analysis. All results are in full agreement for the proposed structures.

Asymmetric hydrogenation of 2-[*p*-(2-methylpropyl)phenyl]acrylic acid **8** was used as the model reaction for the investigation of the catalytic activity and enantioselectivity of these dendritic Ru(BINAP) catalysts. *In situ* catalyst preparation was attained by mixing a dendritic BINAP ligand with $[Ru(cymene)Cl_2]_2$ in methanol–toluene (1 : 1, v/v) and stirring for *ca.* 40 min at 50 °C. Various generations (**5**–**7**) of these dendritic Ru(BINAP) catalysts were tested, and complete conversions of **8** were obtained with high enantioselectivities in 24 h with preliminary results summarised in Table 1. For

† Electronic supplementary information (ESI) available: (A) characterisation of dendritic ligands and *in situ* catalysts; (B) time-dependent conversion of **8** catalysed by dendritic catalysts. See http://www.rsc.org/suppdata/cc/b0/b001503m/

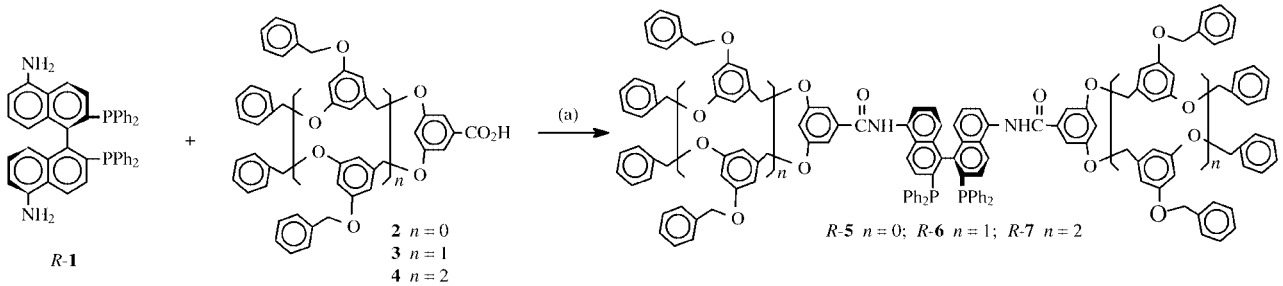

Scheme 1 Synthesis of BINAP ligands with polyether dendritic wedges. *Reagents and conditions:* (a) NMP, $CaCl_2$, $P(OPh_3)$, pyridine, 100 °C, 2 h.

Table 1 Activity and enantioselectivity in the asymmetric hydrogenation of **8** catalyzed by dendritic Ru(BINAP) complexes[a]

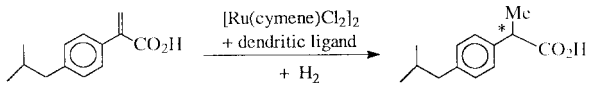

8 ibuprofen

Entry	Ligand	*t*/h	Conv.[b] (%)	TOF[c]/ h^{-1}	Ee[d] (%)	Abs. config.[e]
1	(*S*)-BINAP	2	10.2	6.3	89.8	(*S*)
2	**5**	2	10.4	6.5	91.8	(*R*)
3	**6**	2	13.2	8.3	92.6	(*R*)
4	**7**	2	34.3	21.4	91.6	(*R*)
5	**7**	5	69.3	17.3	91.6	(*R*)
6	**7** (cycle 1)[f]	5	67.3	16.8	91.4	(*R*)
7	**7** (cycle 2)[f]	5	68.9	17.2	91.8	(*R*)
8	**7** (cycle 3)[f]	5	66.6	16.6	90.9	(*R*)

[a] Hydrogenations were carried out using a 0.06 M solution of **8** in methanol–toluene (1:1, v/v) as solvent under the following reaction conditions: *in situ* catalyst = $[Ru(cymene)Cl_2]_2$ + dendritic ligand or (*S*-BINAP); substrate/catalyst = 125 (mol/mol); NEt_3/substrate = 3:2 (mol/mol); H_2 = 80 atm, room temperature. [b] Based on GC analysis and ^1H NMR; all catalytic reactions reached 100% conversion in 24 h. [c] Average TOFs calculated over the quoted reaction time. [d] Ee values at 100% conversion of **8** were determined by GC with a Chrompack Chirasil-dex column (25 m × 0.25 mm). [e] Determined by comparison of optical rotations with literature values. [f] Recovered catalyst used.

example, with 0.8 mol% Ru(*R*-**6**) catalyst, hydrogenated product (ibuprofen) was obtained with 92.6% ee and 100% conversion in 20 h. Confirming the worth of designing Ru(BINAP) catalysts with dendritic wedges, all of the dendritic catalysts performed better compared to the parent BINAP complex. These catalysts showed higher ee values than Ru(BINAP), although the highest-generation catalyst Ru(*R*-**7**) gave slightly lower enantioselectivity (Table 1, entries 1–4).§ Most interestingly, the size of the dendritic wedges influenced the reactivity of these catalysts. Unlike common dendritic catalysts,[7a] the rate of the reaction increased using higher generation catalysts. This effect is most pronounced when going from generation 1 to 2 (Table 1, entries 2–4). The profound size effect is probably due to the steric bulk of the dendritic wedges which affects the dihedral angle of the two naphthalene rings in the Ru(BINAP) complex, and thus leads to a faster rate and/or better enantioselectivity of reaction. Similar acceleration effects have been observed in the asymmetric hydrogenation of unsaturated carboxylic acids catalyzed by Ru(II) catalysts containing polyester-supported BINAP,[4] H_8-BINAP[20] or a bis-steroidal phosphine,[21] which possess a larger steric bulk than BINAP itself.

The large molecular size and different solubilities of the dendritic Ru(BINAP) catalysts in various solvents provided a convenient and reliable method for the separation and reuse of the catalysts. For example, upon completion of the reaction, methanol was added to the reaction mixture and the catalyst Ru(*R*-**7**) was quantitatively precipitated and recovered *via* filtration. The recovered catalyst was reused for at least three cycles with the same activity and enantioselectivity (Table 1, entries 5–8).

In summary, we have demonstrated the importance of the dendritic wedges on the catalytic activity and enantioselectivity of dendritic Ru(BINAP) complexes. This study opens up a new frontier for the development of highly effective and easily separable chiral catalysts. Current work is aiming at a detailed insight of the nature of the dendritic effect and the exploration of these catalysts in other reactions.

We are grateful to the Foundation of the President of The Chinese Academy of Sciences and the Foundation of the Director of Institute of Chemistry, CAS, the National Natural Science Foundation for Youth of China (projects 29604009 and 29904009) and The Hong Kong Polytechnic University for financial support.

Notes and references

‡ Supra-filtration or solvent precipitation methods are suitable procedures for small scale high-value processes, but are not viable options for larger scale lower cost processes.

§ In three-times repeated experiments, the catalysts showed very similar ee values [experimental error (on a computer-controlled VISTA 6000 gas chromatograph) is ≤ ±0.5%]. Further demonstration of the 'dendrimer effect' on enantioselectivity is under way in our laboratory, by using higher generation dendritic BINAP ligands and exploring the catalysts in other reactions in which Ru(BINAP)-type catalysts are less effective.

1 For pioneering work using soluble supports, see: E. Bayer and M. Mutter, *Nature*, 1972, **237**, 512; V. Schurig and E. Bayer, *Chemtech*, April, 1976, 212; V. N. R. Pillai and M. Mutter, *Acc. Chem. Res.*, 1981, **14**, 122.
2 For later reviews on soluble polymer-supported catalysts, see: P. Wentworth and K. D. Janda, *Chem. Commun.*, 1999, 1917; L. Pu, *Chem. Eur. J.*, 1999, **5**, 2227.
3 For later examples of soluble polymer-supported chiral ligand or chiral catalysts, see: L. Canali, J. K. Karjalainen, D. C. Sherrington and O. Hormi, *Chem. Commun.*, 1997, 123; H. Han and K. D. Janda, *J. Am. Chem. Soc.*, 1996, **118**, 7632; C. Bolm and A. Gerlach, *Angew. Chem., Int. Ed. Engl.*, 1997, **36**, 741; W.-S. Huang, Q.-S. Hu, X.-F. Zheng, J. Anderson and L. Pu, *J. Am. Chem. Soc.*, 1997, **119**, 4313.
4 Q.-H. Fan, C.-Y. Ren, C.-H. Yeung, W.-H. Hu and A. S. C. Chan, *J. Am. Chem. Soc.*, 1999, **121**, 7407.
5 J. W. J. Knapen, A. W. van der Made, J. C. de Wilde, P. W. N. M. van Leeuwen, P. Wijkens, D. M. Grove and G. van Koten, *Nature*, 1994, **372**, 659.
6 For reviews on organometallic dendrimers, see: M. A. Hearshaw and J. R. Moss, *Chem. Commun.*, 1999, 1; G. R. Newkome, E. He and C. N. Moorefield, *Chem. Rev.*, 1999, **99**, 1689.
7 For later examples of *achiral* dendritic catalysts, see: (*a*) G. E. Oosterom, R. J. van Haaren, J. N. H. Reek, P. C. J. Kamer and P. W. N. M. van Leeuwen, *Chem. Commun.*, 1999, 1119; (*b*) D. de Groot, E. B. Eggeling, J. C. de Wilde, H. Kooijman, R. J. van Haaren, A. W. van der Made, A. L. Spek, D. Vogt, J. N. H. Reek, P. C. J. Kamer and P. W. N. M. van Leeuwen, *Chem. Commun.*, 1999, 1623; (*c*) S. C. Bourque, F. Maltais, W.-J. Xiao, O. Tardif, H. Alper, P. Arya and L. E. Manzer, *J. Am. Chem. Soc.*, 1999, **121**, 3035; (*d*) N. J. Hovestad, E. B. Eggeling, H. J. Heidbüschel, J. T. B. H. Jastrzebski, U. Kragl, W. Keim, D. Vogt and G. van Koten, *Angew. Chem., Int. Ed.*, 1999, **38**, 1655.
8 H. Brunner, *J. Organomet. Chem.*, 1995, **500**, 39; H. Brunner and S. Altmann, *Chem. Ber.*, 1994, **127**, 2285; H. Brunner and G. Net, *Synthesis*, 1995, 423; H. Brunner, S. Stefaniak and M. Zabel, *Synthesis*, 1999, 1776.
9 M. S. T. H. Sanders-Hovens, J. F. G. A. Jansen, J. A. J. M. Vekemans and E. W. Meijer, *Polym. Mater. Sci. Eng.*, 1995, **73**, 338.
10 D. Seebach, R. E. Marti and T. Hintermann, *Helv. Chim. Acta*, 1997, **79**, 1710; P. B. Rheiner, H. Sellner and D. Seebach, *Helv. Chim. Acta*, 1997, **80**, 2027; P. B. Rheiner and D. Seebach, *Polym. Mater. Sci. Eng.*, 1997, **77**, 130; H. Sellner and D. Seebach, *Angew. Chem., Int. Ed.*, 1999, **38**, 1918; P. B. Rheiner and D. Seebach, *Chem. Eur. J.*, 1999, **5**, 3221.
11 C. Bolm, N. Derrien and A. Seger, *Synlett*, 1996, 387.
12 T. Suzuki, Y. Hirokawa, K. Ohtake, T. Shibata and K. Soai, *Tetrahedron: Asymmetry*, 1997, **8**, 4033.
13 S. Yamago, M. Furukawa, A. Azuma and J.-I. Yoshida, *Tetrahedron Lett.*, 1998, **39**, 3783.
14 Q.-S. Hu, V. Pugh, M. Sabat and L. Pu, *J. Org. Chem.*, 1999, **64**, 7528.
15 R. Noyori and H. Takaya, *Acc. Chem. Res.*, 1990, **23**, 345.
16 For chiral diphosphine employed at the periphery of the dendrimer, see: C. Köllner, B. Pugin and A. Togni, *J. Am. Chem. Soc.*, 1998, **120**, 10274; R. Schneider, C. Köllner, I. Weber and A. Togni, *Chem. Commun.*, 1999, 2415.
17 R. Noyori, *Chemtech*, 1992, 360.
18 T. Okano, H. Kumobayashi, S. Akutagawa, J. Kiji, H. Konishi, K. Fukuyama and Y. Shimano, *US Pat.*, 1987, 4 705 895.
19 C. J. Hawker and J. M. J. Fréchet, *J. Am. Chem. Soc.*, 1990, **112**, 7638.
20 T. Uemura, X. Zhang, K. Matsumura, N. Sayo, H. Kumobayashi, T. Ohta, K. Nozaki and H. Takaya, *J. Org. Chem.*, 1996, **61**, 5510.
21 V. Enev, C. L. J. Ewers, M. Harre, K. Nickisch and J. T. Mohr, *J. Org. Chem.*, 1997, **62**, 7092.

An assignment of the ^{23}Na MAS NMR spectrum of $Na_5P_3O_{10}\cdot6H_2O$ using a general *ab initio* method

Clive Johnson, Elaine A. Moore and Michael Mortimer*

Department of Chemistry, The Open University, Milton Keynes, UK MK7 6AA. E-mail: m.mortimer@open.ac.uk

Received (in Cambridge, UK) 2nd March 2000, Accepted 30th March 2000

A new assignment method based on the periodic *ab initio* calculation of ^{23}Na quadrupole coupling information using the CRYSTAL95 code is described and applied to the multi-site problem posed by $Na_5P_3O_{10}\cdot6H_2O$.

Modern solid-state NMR techniques for non-integer quadrupolar nuclei, particularly those based on MAS NMR techniques, are now commonly used in the characterisation of a wide range of materials including simple inorganic salts and complexes, zeolites, catalysts, minerals and ceramics.[1] In the particular case of the ^{23}Na nucleus (I = 3/2) an extensive body of experimental information for the quadrupole parameters, that is the quadrupole coupling constant ($C_Q = e^2qQ/h$) and the asymmetry parameter (η), has now been established. The assignment of ^{23}Na spectra, however, still remains problematic even in cases for which a crystal structure is available. One approach has been to use classical electrostatic modelling methods, although these are not always reliable.[2] Here we describe an *ab initio* approach which is specifically designed to be used in a routine manner for assignment purposes. It is based on the CRYSTAL95 code.[3] This package performs *ab initio* calculations of the properties of periodic systems taking into account the symmetry of the crystal lattice to form crystalline orbitals from a linear combination of atomic orbitals.

The ability to assign quadrupole parameters to individual sodium sites in a known crystal structure is important. This is because the magnitudes of these parameters are directly related to the nature of the electronic charge distribution surrounding a given sodium site. A more detailed understanding of this relationship can provide information on the electronic structure of a solid as a whole. At a more practical level, the knowledge gained is useful for more complex assignment problems such as those associated with glassy and amorphous materials.

We have selected as an example the hydrate of pentasodium triphosphate, $Na_5P_3O_{10}\cdot6H_2O$[4] since this material is recognised as presenting a particularly difficult assignment problem.[5] It crystallises in the triclinic space group $P\bar{1}$ with all atoms in general positions so that there are five different sodium sites with equal multiplicities.[6] The experimental ^{23}Na MAS NMR spectrum[7] is shown in Fig. 1 and, as expected, is complex with overlapping second-order quadrupolar lineshapes. Using our periodic *ab initio* approach we are able to provide a reasonable interpretation of this spectrum. In principle, MQMAS methods,[8] although experimentally demanding, could provide better spectral resolution and so comparison between the present work and any subsequent MQMAS investigation would be of direct interest.

We have used CRYSTAL95 to calculate the C_Q values for ^{23}Na for a wide range of sodium compounds with known crystal structures (19 in all involving 27 different sodium sites).[9] The Hartree–Fock calculations were based on the relatively small 3-21G molecular basis set of Pople and co-workers[10] and the basis sets for individual atoms were applied consistently across the whole range of compounds investigated. Only modest computer resources were required.[11] A key criterion was to obtain a good linear fit between calculated and experimental values of C_Q; exact agreement for each compound was not required. It can be noted that this approach is independent of the variability in the published values[12] of the nuclear quadrupole moment for ^{23}Na; in this work we use $Q = 0.1089 \times 10^{-28}$ m^2. For sodium, the 3-21G basis set was modified in the manner usually[3] adopted for alkali metal cations by replacing the valence orbitals by a single sp shell; we used an exponent of 0.18. Unmodified 3-21G basis sets were used for oxygen, sulfur and chlorine atoms, whereas some modifications to the values of the exponents for the outermost shells of hydrogen (0.183), nitrogen (0.273) and carbon (0.132) were required. In the case of aluminium, the outermost valence orbital of the 3-21G set is diffuse and this is known to cause convergence problems in periodic calculations.[3] Consequently, this orbital was removed giving a 3-2G set. The same modification of basis set was also found to be of benefit for silicon and phosphorus.

Fig. 2 shows a plot of experimental *versus* calculated C_Q values for ^{23}Na for all of the compounds that we have investigated.[13] The straight line in this figure represents the best linear fit to the data (R^2 = 0.977): the slope of the line is 0.979 ± 0.030 and the intercept is 0.084 ± 0.064 MHz. Since the sign of C_Q is usually not obtained in NMR experiments, it is assumed in Fig. 2 that the experimental value of C_Q takes the calculated sign. Overall we conclude that CRYSTAL95 calculations, based on the relatively simple 3-21G basis set, can calculate ^{23}Na C_Q values with sufficient accuracy to be useful for assignment purposes in multi-site problems.

In the case of $Na_5P_3O_{10}\cdot6H_2O$ the calculated values of the ^{23}Na C_Q for each of the five different sodium sites in the crystal structure are given in Table 1. These values provide a powerful starting point, along with the knowledge that the individual resonances must be of equal intensity, for the simulation of the experimental ^{23}Na MAS NMR spectrum shown in Fig. 1. The results of this simulation[15] are summarised in Table 1 and the simulated MAS NMR spectrum is compared with experiment in Fig. 1.

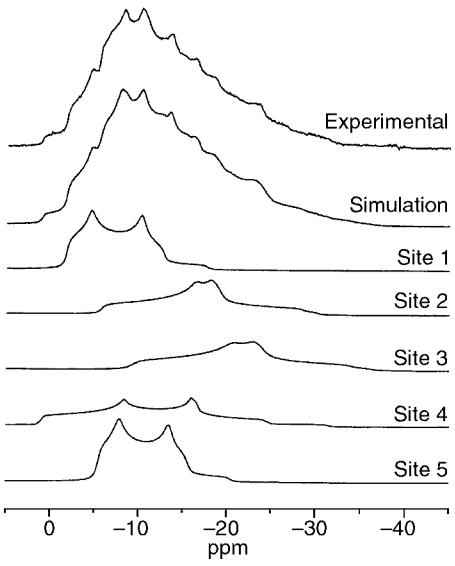

Fig. 1 Experimental (proton-decoupled) and simulated ^{23}Na MAS NMR spectrum of $Na_5P_3O_{10}\cdot6H_2O$. Individual contributions to the simulated spectrum are also shown.

DOI: 10.1039/b001724h

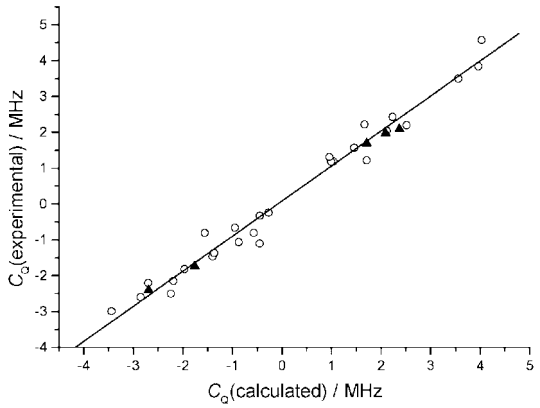

Fig. 2 A plot of experimental *versus* calculated ^{23}Na C_Q values for (i) sodium compounds involving oxyanions of silicon, sulfur, phosphorus, nitrogen, carbon, aluminium, chlorine and hydrogen (○) and (ii) the different sodium sites in $Na_5P_3O_{10}·6H_2O$ (▲): see Table 1.

Table 1 Information from both *ab initio* calculation and simulation of the experimental ^{23}Na MAS NMR spectrum for the different sodium sites in $Na_5P_3O_{10}·6H_2O$

	Calculation	Simulation			
Site[a]	^{23}Na C_Q/MHz	^{23}Na C_Q/MHz[b]	η	$\delta_{iso,cs}$(^{23}Na)[c]	Intensity[d]
1	−1.76	1.74	0.29	−0.55	0.21
2	2.09	1.97	0.85	−5.71	0.18
3	2.37	2.09	0.81	−9.09	0.19
4	−2.69	2.40	0.51	2.20	0.22
5	1.71	1.69	0.26	−4.20	0.21

[a] The labels correspond to those used in ref. 6. [b] The sign of these values cannot be determined from the ^{23}Na MAS NMR spectrum. [c] Isotropic chemical shift relative to external solid NaCl. [d] These values have been corrected using the method of Massiot *et al.*[14]

The assignment of the individual sodium sites (1–5) in Table 1 is based on the general linear relationship shown in Fig. 2; individual points corresponding to the assignment are plotted in this figure. The relatively small differences between the simulated ^{23}Na C_Q values does introduce some uncertainty into the assignment. Nonetheless, by using a consistent approach for all 5 sites we obtain, in the absence of any other information, a reasonable assignment. Potentially, the results also provide a very good starting point for a more detailed MQMAS investigation. It is worth noting that the sign of C_Q, if available experimentally, is an important assignment parameter; for example, in the present work it would resolve any ambiguity in the assignment of sodium sites 1 and 5.

In a wider context we have found the periodic *ab initio* approach described in this communication to be useful in a number of assignment problems in ^{23}Na solid-state NMR spectroscopy. In some cases it is sufficiently robust to indicate errors in published crystal structures.[16] In addition, we have found that it can be applied equally well to other widely-studied quadrupolar nuclei such as ^{17}O and ^{27}Al.

Acknowledgement is made to the EPSRC for the award of a studentship (C. J.) and for the use of the Chemical Database Service at Daresbury, UK.

Notes and references

1 M. E. Smith and E. R. H van Ecke, *Prog. NMR Spectrosc.*, 1999, **34**, 159.
2 H. Koller, G. Engelhardt, A. P. M. Kentgens and J. Sauer, *J. Phys. Chem.*, 1994, **98**, 1544.
3 R. Davies, V. R. Saunders, C. Roetti, M. Causà, N. M. Harrison, R. Orlando and E. Aprà, *CRYSTAL95 User's Manual*, University of Torino, Torino, 1996.
4 Anhydrous $Na_5P_3O_{10}$ was obtained from Fluka Chemicals. The hexahydrate was prepared by slow evaporation of a concentrated solution of $Na_5P_3O_{10}$.
5 C. A. Fyfe, H. M. zu Altenschildesche and J. Skibsted, *Inorg. Chem.*, 1999, **38**, 84.
6 D. M. Wiench, M. Jansen and R. Z. Hoppe, *Anorg. Allg. Chem.*, 1982, **488**, 80.
7 ^{23}Na MAS NMR spectra in this work were recorded at 105.8 MHz, with spinning speeds in the range 8–10 kHz, using a Doty Scientific 5 mm probe in a JEOL EX-400 spectrometer. A pulse length of 1 μs (less than π/8) was used with high-power proton decoupling where necessary.
8 A. Medek, J. S. Harwood and L. Frydman, *J. Am. Chem. Soc.*, 1995, **117**, 12 779.
9 All crystallographic data were taken from: The United Kingdom Chemical Database Service, D. A. Fletcher, R. F. McMeeking and D. Parkin, *J. Chem. Inf. Comput. Sci.*, 1996, **36**, 746.
10 W. J. Hehre, L. Radom, P. V. R. Schleyer and J. A. Pople, *Ab Initio Molecular Orbital Theory*, John Wiley and Sons, New York, 1986.
11 All calculations were carried out using a DEC alpha-600 cluster; typically computational times were of the order of a few hours for compounds with unit cells containing *ca*. 30 atoms.
12 P. Jönsson, A. Ynnerman, C. F. Fischer, M. R. Gudefroid and J. Olsen, *Phys. Rev. A.*, 1996, **53**, 4021.
13 The compounds investigated and the sources of the experimental ^{23}Na C_Q data are as follows: Na_2SiO_3, α- and β-$Na_2Si_2O_5$, Na_2SO_4, $NaH_2PO_4·H_2O$, $NaH_2PO_4·2H_2O$, $Na_3P_3O_9$, $NaAlO_2$, $NaClO_4$, NaOH, $NaOH·H_2O$: ref. 2 and references therein; Na_2SO_3: W. P. Power, *Magn. Reson. Chem.*, 1995, **33**, 220; Na_2HPO_4: ref. 8; $Na_5P_3O_{10}$ (II): ref. 5; $NaNO_2$, $NaNO_3$, $NaHCO_3$, $Na_2C_2O_4$: this work; $NaClO_3$: R. Bersohn, *J. Chem. Phys.*, 1958, **29**, 326.
14 D. Massiot, C. Bessada, J. P. Coutures and F. Taulelle, *J. Magn. Reson.*, 1990, **90**, 231.
15 The Bruker WINFIT module (included in the Bruker WINNMR program suite for PCs) for simulating the central transitions of MAS NMR lineshapes was used.
16 For example, we have found that the reported location of the Na(2) sodium site in the structure of phase I of $Na_5P_3O_{10}$ is in error. We have confirmed this by analysis of the X-ray powder diffraction pattern.

ChemComm

Infinite molecular tubes: structure and magnetism of $M(dca)_2(apym)$ [M = Co, Ni, apym = 2-aminopyrimidine, dca = dicyanamide, $N(CN)_2^-$]

Paul Jensen, Stuart R. Batten, Boujemaa Moubaraki and Keith S. Murray*

Department of Chemistry, Monash University, Clayton, Victoria 3168, Australia. E-mail: Keith.S.Murray@sci.monash.edu.au

Received (in Cambridge, UK) 18th November 1999, Accepted 28th March 2000

The title compounds have a molecular tube-like structure topologically related to the α-$M(dca)_2$ rutile structure, and display unusual field-dependent magnetic moments at low temperature but without long-range order.

Since our initial report on the unusual molecule-based magnetism of α-$M(dca)_2$ [dca = dicyanamide, $N(CN)_2^-$],[1] a great deal of attention has focussed on the structural and magnetic properties of coordination polymers containing the dca ligand.[2–4] In the α-$M(dca)_2$ series of compounds, M = Co and Ni behave as ferromagnets while M = Cr, Mn and Fe behave as spin-canted antiferromagnets and M = Cu is a paramagnet. All these compounds are isostructural and possess a rutile-like topology, with the octahedral metal ions bridged by dca anions which coordinate through all three nitrogen atoms.

We report here the structural and magnetic properties of a series of polymeric complexes, $M(dca)_2(apym)$ (M = Co **1** or Ni **2**, apym = 2-aminopyrimidine), which form novel 'molecular tubes' that are structurally related to the rutile networks formed by the α-$M(dca)_2$ compounds, and which contain both two- and three-connecting dca ligands.

Reaction of apym, sodium dicyanamide and the corresponding metal nitrate in water resulted in formation of **1** or **2**.† These compounds are formed from the 1 : 2 adducts $M(dca)_2(apym)_2$, (M = Co, Ni). The $M(dca)_2(apym)_2$ compounds exhibit chain structures similar to those of $M(dca)_2L_2$, (L = MeOH, pyridine, DMF)[2,4b,c] full details of which will be published elsewhere.‡ Single crystals of **1** or **2** suitable for X-ray diffraction were grown by slow transformation of $M(dca)_2(apym)_2$ left in the reaction mixture for several months, and their structures were determined by X-ray crystallography.§ The IR spectra of **1** and **2** indicated the presence of both bidentate and tridentate dca ligands. X-Ray powder diffraction was used to prove that the bulk samples of **1** and **2** had the same structure as the single crystals, and were free from contamination.

Both structures are isomorphous (identical space groups), and the structure of **1** is shown in Fig. 1(a). It consists of infinite 1D 'molecular tubes' of square cross-section, with metal atoms occupying the edges and three-connecting dca ligands forming the sides of the tube. The octahedral coordination of the metal atoms is completed by chains of two-connecting dca ligands (with the amide nitrogens uncoordinated) which occupy the outside of each edge, and monodentate apym ligands. The sides of the tubes are 4.864 Å wide (4.821 Å in **2**).

The structure of the square tubes can be related back to the rutile-like structures of α-$M(dca)_2$. Fig. 1(b) shows the (distorted) rutile-like net of α-$Co(dca)_2$, with one of the channels of the structure highlighted. This highlighted channel has the same topology as the tubes. In effect, we have isolated a polymeric 1D section of the rutile-like network of α-$M(dca)_2$. Interestingly, while the channels in α-$M(dca)_2$ are buckled, the molecular tubes are not.

The tubes (all of which are crystallographically equivalent) pack in the crystal structure with extensive hydrogen bonding between the tubes *via* the apym ligands, as shown in Fig. 2. The apym groups form dimeric hydrogen bonded pairs with apym ligands in adjoining tubes, such that the amino group of one

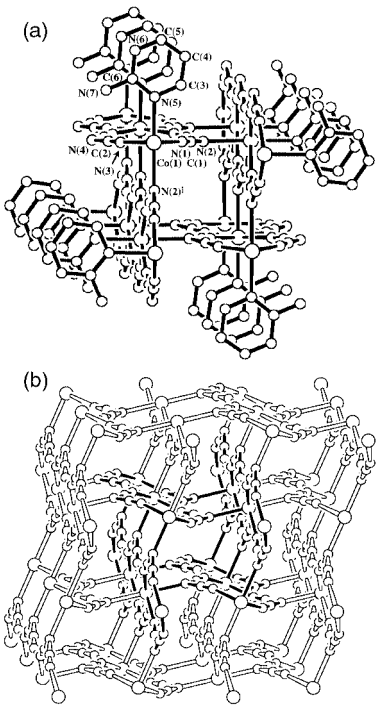

Fig. 1 (a) Structure of a single molecular tube in $Co(dca)_2(apym)$ **1**. Selected bond lengths (Å) for **1** (**2** in parentheses): Co(1)–N(1) 2.110(1) (2.074(3)), Co(1)–N(3) 2.089(1) (2.048(3)), Co(1)–N(5) 2.149(2) (2.126(4)), Co(1)–$N(2)^i$ 2.224(2) (2.201(4)). (b) The rutile-like network of α-$Co(dca)_2$ with a single channel with the same topology as the tubes highlighted.

ligand hydrogen bonds to the pyrimidine nitrogen of the adjoining ligand, and *vice versa*. These hydrogen bonding interactions (N(7)–H(1)···N(6) 178.6(3)° for**1** [177.4(5)° for **2**], H(1)···N(6) 2.200(3) Å [2.227(5) Å]) connect every alternate tube in the structure (black tube to black tube and white tube to white tube in Fig. 2), giving two separate sets of tubes. The two

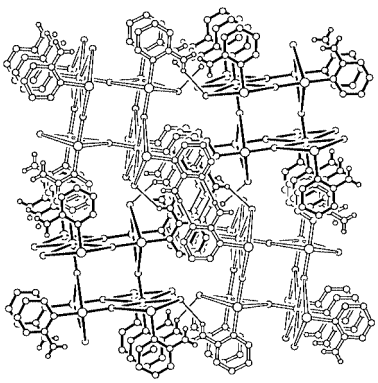

Fig. 2 Hydrogen bonding interactions between four tubes in the crystal lattice. For clarity, only the amino protons are shown. Hydrogen bonding interactions are shown by thin lines.

DOI: 10.1039/a909067c

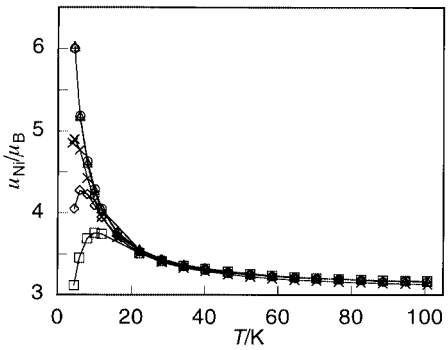

Fig. 3 Plots of the effective magnetic moment μ_{eff}, per Ni, *vs*. temperature for Ni(dca)$_2$(apym) **2**. Applied-field values are 20 Oe (Δ), 200 Oe (+), 10000 Oe (×), 20000 Oe (◇) and 40000 Oe (□). The μ_{eff} values are independent of field and essentially constant between 100 and 300 K.

sets of tubes are then connected by weaker hydrogen bonding interactions between the amino group of the apym ligands and the amide nitrogens of the two-connecting dca anions (N(7)–H(2)··N(4) 136.1(3)° for **1** [135.8(5)° for **2**], H(2)··N(4) 2.539(3) Å [2.517(5) Å]), white tubes to black tubes in Fig. 2.

Another feature of the packing is the interdigitation of the apym ligands of adjoining tubes into infinite π-stacked columns (Fig. 2). The mean planes of the ligands are separated by $c/2$ = 3.691 (for **1**) and 3.655 (for **2**) Å.

The magnetic data for **2** will be emphasised briefly here. The samples measured were shown to be free from any contaminant by checking the powder X-ray diffraction patterns. It can be seen in Fig. 3 that μ_{eff}, per Ni, remains constant at 3.1 μ_B between 300 and 100K in a field of 1 T as expected for octahedral Ni(II) centres. A gradual increase then occurs before reaching a maximum of 4.9 μ_B at 3.6K, behaviour indicative of ferromagnetic coupling. The corresponding χ^{-1}_{Ni} *vs*. temperature data are Curie–Weiss like, with θ = +3.1K. As the applied field is increased to 4 T, the μ_{max} region becomes broader in shape, with μ_{max} values lower and moving to higher temperatures. Magnetisation isotherms (*M vs. H*; 2–10 K) show rapid increases in *M* at low *H* and are indicative of ferromagnetic coupling, with a saturation value M_{sat} of 2.1 $N\beta$ noted at 2 K. Since μ_{eff} is a derived quantity (μ_{eff}^2 = 7.997 *M*T/*H*) the unusual shape of μ_{eff} at high fields and low temperatures to some extent will reflect this derivation since *M* is not linear with *H*. The shapes are also reminiscent of Zeeman level (M_S) depopulation effects noted in ferromagnetically coupled clusters.[6]

Measurements in low applied fields also lead to unusual behaviour. In Fig. 3 it can be seen that μ_{eff} increases sharply as *H* is decreased, then attenuates to a value of 6 μ_B for *H* = 200 or 20 Oe. The corresponding *M vs*. temperature plots are Curie–Weiss like with no sharp rise which would be indicative of a transition to long-range order. Other tests for long-range order such as measuring ac susceptibilities, χ' and χ'' (2–20 K), where χ'' was found to be zero at all temperatures between 4 and 20 K, or dc magnetisation in field-cooled or zero-field cooled modes, proved negative. In contrast to these puzzling features observed for **2**, the magnetic behaviour of the linear chain precursor, Ni(dca)$_2$(apym)$_2$, gives quite normal *S* = 1 behaviour with very weak antiferromagnetic coupling and/or zero-field splitting evident at low temperatures, and independent of *H*.

Further experimental and theoretical work is in progress on these novel tube-like materials to try and explain these magnetic anomalies, which are also present in the Co complex. Preliminary Heisenberg-type calculations made in collaboration with Kurmoo,[7] using a Ni_8 fraction of a tube, reproduce the 20 Oe data very well.

This work was supported by an Australian Research Council (Large) Grant (to K. S. M.) and an Australian Postdoctoral Research Fellowship (to S. R. B.). We thank Professor M. Kurmoo for stimulating discussions.

Notes and references

† *Preparative details*: **1**: an aqueous solution (7 ml) of Co(NO$_3$)$_2$·6H$_2$O (368 mg, 1.26 mmol) was added to an aqueous solution (3 ml) of Na(dca) (200 mg, 2.25 mmol) and apym (107 mg, 1.13 mmol) at room temperature yielding an instant pale pink precipitate [Co(dca)$_2$(apym)$_2$]. 10 ml H$_2$O was added and the reaction mixture boiled to dissolve the pink precipitate. Boiling was continued and the volume of the solution reduced to *ca.* 10 ml. A pink–purple microcrystalline powder formed and was filtered off (255 mg, 0.891 mmol, 79%). Found: C, 33.7; H, 1.5; N, 44.2. Calc. for $C_8H_5CoN_9$: C, 33.6; H, 1.8; N, 44.1%. Selected IR (dca) (cm^{-1}, Nujol): ν_{as}(C≡N) 2268m, 2260m; ν_s(C≡N) 2192s, 2182s(sh); ν_{as}(C–N) 1356, 1317. Crystals suitable for X-ray study were obtained by allowing the initial pink precipitate to transform in solution over several months.

2: a hot aqueous solution (10 ml) of Ni(NO$_3$)$_2$·6H$_2$O (375 mg, 1.29 mmol) was added to a hot aqueous solution (10 ml) of Na(dca) (200 mg, 2.25 mmol) and apym (110 mg, 1.16 mmol). The solution was boiled and the volume reduced to *ca.* 15 ml yielding a blue microcrystalline powder (245 mg, 0.857 mmol, 76%). Found: C, 33.6; H, 1.6; N, 43.9. Calc. for $C_8H_5NiN_9$: C, 33.6; H, 1.8; N, 44.1%. Selected IR (dca) (cm^{-1}, Nujol): ν_{as}(C≡N) 2274m, 2268m; ν_s(C≡N) 2198s; ν_{as}(C–N) 1354, 1314.

‡ Reedijk and coworkers[5] have just reported the crystal structure of Cu(dca)$_2$(apym)$_2$. It is the same as those of Ni and Co except for small symmetry differences owing to Jahn–Teller distortions.

§ *Crystal data*: **1**: $C_8H_5CoN_9$, *M* = 286.14, tetragonal, space group $P4_2/mbc$, *a* = 17.1243(2), *c* = 7.3816(1) Å, *U* = 2164.59(5) Å^3, *T* = 123 K, *F*(000) = 1144, *Z* = 8, D_c = 1.756 g cm^{-3}, μ(Mo-Kα) = 1.582 mm^{-1}, red needle, 31921 reflections measured, 1695 unique (R_{int} = 0.050), 102 parameters, R_1 = 0.0279 for 1471 reflections with $I > 2\sigma(I)$, wR_2 = 0.0626 (all data), *S* = 1.099. The structure of **1** was also solved at 295 K.

2: $C_8H_5NiN_9$, *M* = 285.92, *a* = 17.0863(6), *c* = 7.3099(2) Å, *U* = 2134.1(1) Å^3, *T* = 297 K, *F*(000) = 1152, D_c = 1.780 g cm^{-3}, μ(Mo-Kα) = 1.815 mm^{-1}, blue needle, 15738 reflections measured, 1653 unique (R_{int} = 0.113), 97 parameters, R_1 = 0.0530 for 1127 reflections with $I > 2\sigma(I)$, wR_2 = 0.1010 (all data), *S* = 1.092. CCDC 182/1585. See http://www.rsc.org/suppdata/cc/a9/a909067c/ for crystallographic files in .cif format.

1 S. R. Batten, P. Jensen, B. Moubaraki, K. S. Murray and R. Robson, *Chem. Commun.*, 1998, 439.
2 S. R. Batten, P. Jensen, C. J. Kepert, M. Kurmoo, B. Moubaraki, K. S. Murray and D. J. Price, *J. Chem. Soc., Dalton Trans.*, 1999, 2987.
3 (*a*) M. Kurmoo and C. J. Kepert, *New J. Chem.*, 1998, **22**, 1515; (*b*) J. L. Manson, C. R. Kmety, Q. Huang, J. W. Lynn, G. M. Bendele, S. Pagola, P. W. Stephens, L. M. Liable-Sands, A. L. Rheingold, A. J. Epstein and J. S. Miller, *Chem. Mater.*, 1998, **10**, 2552.
4 (*a*) P. Jensen, S. R. Batten, G. D. Fallon, D. C. R. Hockless, B. Moubaraki, K. S. Murray and R. Robson, *J. Solid State Chem.*, 1999, **145**, 387; (*b*) J. L. Manson, A. M. Arif and J. S. Miller, *J. Mater. Chem.*, 1999, **9**, 979; (*c*) J. L. Manson, A. M. Arif, C. D. Incarvito, L. M. Liable-Sands, A. L. Rheingold and J. S. Miller, *J. Solid State Chem.*, 1999, **145**, 369.
5 G. A. van Albada, M. E. Quiroz-Castro, I. Mutikainen, U. Turpeinen and J. Reedijk, *Inorg. Chim. Acta*, 2000, **298**, 221.
6 P. E. Kruger, G. D. Fallon, B. Moubaraki, K. J. Berry and K. S. Murray, *Inorg. Chem.*, 1995, **34**, 4808.
7 M. Kurmoo, personal communication, Nov. 1999.

Unusual high nuclearity and pseudo-tetrahedral Zn_8O_{13} core found in a self-assembled complex

Jesús Sanmartín,[a] Manuel R. Bermejo,*[a] Ana M. García-Deibe[a] and Antonio L. Llamas-Saiz[b]

[a] *Departamento de Química Inorgánica, Facultade de Química, Campus Sur, Universidade de Santiago de Compostela, E-15706 Santiago de Compostela, Galicia, Spain. E-mail: qimb45@uscmail.usc.es*

[b] *Unidade de Raios X. Vicerrectorado de Investigación, Universidade de Santiago de Compostela, Campus Sur, E-15706 Santiago de Compostela, Galicia, Spain*

Received (in Cambridge, UK) 18th February 2000, Accepted 23rd March 2000

An electrochemical synthesis yielded powdery $[Zn_2(L)(H_2O)]_n$ [H_4L = *N*,*N*′-bis(3-hydroxysalicylidene)-1,4-diaminobutane] and crystals of $[Zn_8(L)_4(H_2O)_3]\cdot H_2O\cdot 0.25MeCN$, whose X-ray crystal structure shows an unusual pseudo-tetrahedral Zn_8O_{13} core assembled by thirteen μ-phenoxo bridges, where Zn(II) ions are pentaco-ordinated.

A large number of S-bridged polynuclear zinc complexes are described in the literature,[1] but not so many examples of high nuclearity are found containing O- and N-donor ligands. An interesting approach to design these compounds is the assembly of simple units into polynuclear molecules.[2] The ability of compartmental or polynucleating ligands to hold closely metal ions is useful for this.[3,4] Therefore, the behaviour of the hexadentate Schiff base H_4L has been studied here. This ligand was prepared by condensation of 2,3-dihydroxybenzaldehyde and 1,4-diaminobutane in a 2 : 1 molar ratio.

The synthesis of the complexes was performed by using an electrochemical method,[4,5] with the cell summarised as: $Zn_{(+)}|MeCN + H_4L|Pt_{(-)}$. An acetonitrile solution of H_4L (0.10 g) was electrolysed (V = 14.5 V) for a calculated time (195 min) according to: $2Zn_{(s)} + H_4L \rightarrow Zn_2(L)(H_2O)_x + 2H_{2(g)}$. Anodic zinc was dissolved during the reaction (0.065 g), whilst hydrogen was evolved at the Pt cathode. An insoluble product $[Zn_2(L)(H_2O)]_n$,† was easily isolated from solution (yield: 90%). The brown solution obtained was slowly evaporated and small crystals were collected and later crystallographically identified as $Zn_8(L)_4(H_2O)_3\cdot H_2O\cdot 0.25MeCN$.‡

The study of the free ligand and both complexes by IR spectroscopy indicates that the Schiff base is behaving as hexadentate, through its potential oxygen and nitrogen donor atoms.[4–7] Positive ion ES mass spectrometry shows for $[Zn_2(L)(H_2O)]_n$ two peaks related to fragments of the type $Zn_2(L)^{2+}$ and $Zn_3(L)_2^{2-}$ at *m/z* (abundance) 453 (4×10^3) and 847 (2×10^3), respectively. This seems to be in accordance with a polymeric nature for the complex.

X-Ray diffraction studies of $Zn_8(L)_4(H_2O)_3\cdot H_2O\cdot 0.25MeCN$ revealed its molecular structure as a neutral octanuclear

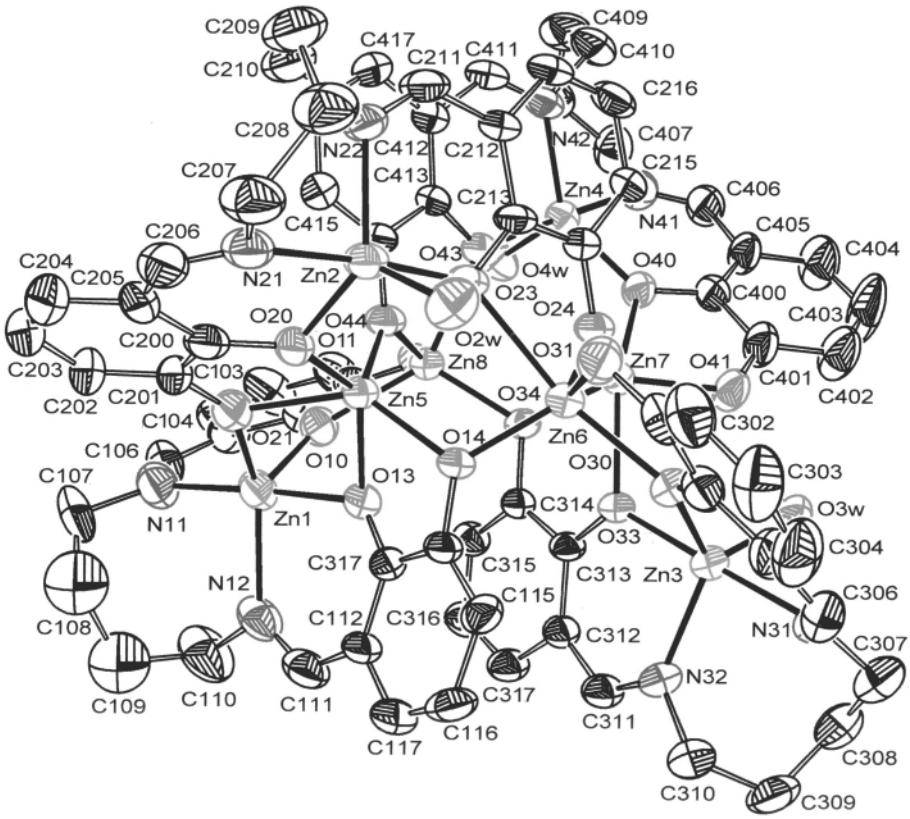

Fig. 1 ORTEP plot of $Zn_8(L)_4(H_2O)_3$. Atoms are represented by their 30% probability ellipsoids. Disordered atoms, H atoms, parentheses and some C atom labels are omitted for clarity. Angle ranges: Zn–O–Zn 126.8(3)–99.5(2)°; around Zn(1) 78.1(2)–176.8(3)°; around Zn(2) 87.5(2)–175.3(3)°; around Zn(3) 88.1(2)–178.3(3)°; around Zn(4) 88.0(2)–176.0(3)°; around Zn(5) 79.1(2)–137.3(2)°; around Zn(6) 76.5(2)–162.3(2)°; around Zn(7) 76.8(2)–155.5(2)°; around Zn(8) 77.5(2)–146.4(3)°.

complex (Fig. 1), where all the Zn ions are pentacoordinated. Four tetradeprotonated ligand units, L^{4-}, assemble the metal ions in a pseudo-tetrahedral arrangement by means of thirteen μ-phenoxo bridges. This is an interesting example of three-dimensional supramolecular architecture.

Atoms Zn(1), Zn(2), Zn(3) and Zn(4) lie on the pseudo-tetrahedron vertexes, having three water molecules bonded to three of them (Fig. 2). The other four inner Zn atoms [Zn(5)–Zn(8)] lie on four of the tetrahedron edges, and so they almost form a square. Additionally, the crystal contains encapsulated water (one molecule dispersed in five different positions with occupation factors of 20%) and acetonitrile (25% occupation factor) in the asymmetric unit.

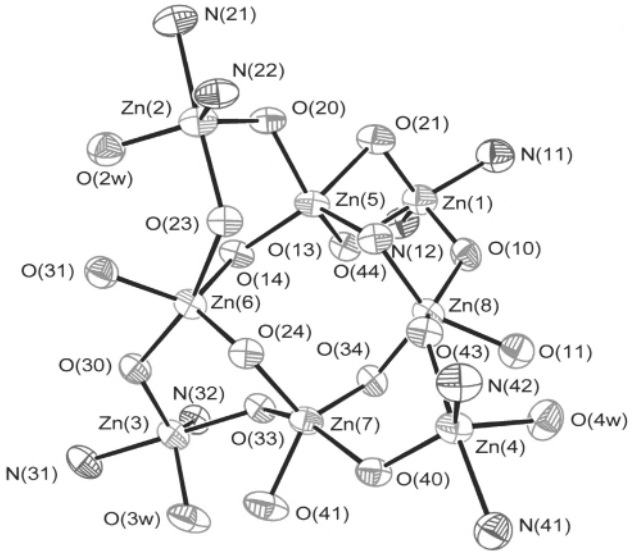

Fig. 2 A drawing of the coordination environments for $Zn_8(L)_4(H_2O)_3$. Dotted lines highlight the pseudo-tetrahedral shape.

Zn(*x*) (*x* = 1–4), are in N_2O_3 environments, which are formed by the inner N_2O_2 compartment of each L^{4-} unit and an additional O atom. This corresponds to a coordinated water molecule O(*x*w) for Zn(*x*) (*x* = 2–4), whilst for Zn(1) a μ-phenoxo bridge to Zn(5), through O(21), completes its coordination polyhedron. These environments can be described as slightly distorted trigonal-bipyramidal,[8] where Zn(1) is the most distorted. An imino N atom and its opposite inner phenolic O atom are occupying the axial positions in all cases.

Likewise, each one of these four outer metal centres is bound to two other inner Zn ions by two μ-$O_{phenolate}$ bridges through the inner oxygen atoms of their corresponding ligand units [O(*x*0) and O(*x*3)] for Zn(*x*) (*x* = 1–4). Additionally, Zn(1) is also bound through the outer O(21). Thus, Zn(1)···Zn(5) [3.182(2) Å] is the shortest Zn···Zn distance, the longest being 3.901(2) Å. These values are in the range found for other polynuclear zinc complexes containing imino or amino ligands with μ-oxo bridges.[2,9–11]

For the other four inner metal centres, Zn(5)–Zn(8), O_5 environments are formed exclusively by the sixteen phenolic donor atoms, with each metal ion simultaneously bound to three different ligand units. The polyhedron around Zn(6) can be also described as trigonal bipyramidal, with two inner O atoms in axial positions, and three outer phenolic O atoms in the equatorial plane. By contrast, the environments of Zn(5), Zn(7) and Zn(8) can be considered as distorted square pyramids.[8]

Zn–N and Zn–O distances [2.021(7)–2.156(9) and 1.910(6)–2.328(5), respectively], lie within the ranges found for other polynuclear complexes with N- and O-donor ligands.[9,12,13]

Some related Schiff bases had been previously designed as potentially compartmental and binucleating, being able to accommodate, two metal ions (d + f or less commonly d + d) in different modes.[6,7] Here, the intricate bridging behaviour of L^{4-} leads to much higher polynucleating ability. Thus, the ligand unit containing Zn(2) in its inner compartment is also coordinated to Zn(1), Zn(5), Zn(6) and Zn(7), whilst the other three ligand units are each bonded to four metal ions.

This structure is very unusual and one of the rare and recent examples of oxygen bridged octanuclear Zn(II) complexes.[9,14] No Schiff base ligands are present in these two cores, which are significantly different and contain additional bridging oxo or hydroxo groups.

Therefore, to our knowledge, this is the first example of an octanuclear μ-phenoxo bridged zinc complex containing Schiff base ligands. The long methylene chain of L^{4-} appears to provide enough flexibility to achieve such high nuclearity. This factor seems to be important. Thus, in the case of an amino octanuclear complex,[9] high nuclearity could not be observed when the more rigid imino ligand derivative was employed.

We would like to thank the Xunta de Galicia (Spain) for financial support (XUGA 20903B99).

Notes and references

† Elemental analyses: found(calc.) for $[Zn_2(L)(H_2O)]_n$: C, 45.4(45.7); H, 4.0(3.8); N, 6.0(5.9); O, 16.5(16.9)%.

‡ *Crystal data* for $Zn_8(L)_4(H_2O)_3{\cdot}H_2O{\cdot}0.25MeCN$: $C_{72.5}H_{72.75}N_{8.25}O_{20}Zn_8$; M_r = 1902.60; monoclinic, space group $P2_1/n$ (no. 14), a = 13.606(2), b = 17.608(3), c = 32.497(4) Å, β = 91.698(6), V = 7782.3(19) Å^3, T = 293(2) K, Z = 4; μ(Cu-Kα) = 3.310 mm^{-1}; 33 682 reflections measured, 16 195 reflections unique (R_{int} = 0.12); $R1$ = 0.0895, $wR2$ = 0.2625 ($F > 4\sigma(F)$; for all data $R1$ = 0.2279, $wR2$ = 0.3450.[15] One C atom of a methylene chain was found in two disordered positions [C(408) and C(48′)]. Their occupancy parameters were fixed and refined anisotropically and isotropically, respectively. Disperse electronic density could be found around C108 and C109, but a satisfying disorder model was not established. Both atoms have been isotropically refined due to the high values found for the anisotropic thermal parameters. Hydrogen atoms were included, using a riding model, except for the coordinated water molecules, where H atoms could be located, fixed and given isotropic displacement parameters of 0.1 Å^2. Five water molecules were also located with occupancy parameters fixed to 0.2. In addition, a MeCN molecule was found and fixed with an occupancy parameter of 0.25. Disordered atoms and solvent molecules were treated with some restraints.

CCDC 182/1582. See http://www.rsc.org/suppdata/cc/b0/b001368o/ for crystallographic files in .cif format.

1 B. Krebs and G. Henkel, *Angew. Chem., Int. Ed. Engl.*, 1991, **30**, 769.
2 M. Mikuriya and S. Tashima, *Polyhedron*, 1998, **17**, 207.
3 P. A. Vigato, S. Tamburini and D. E. Fenton, *Coord. Chem. Rev.*, 1990, **106**, 25.
4 J. Sanmartín, M. R. Bermejo, A. M. García-Deibe, O. Piro and E. E. Castellano, *Chem. Commun.*, 1999, 1953.
5 J. Sanmartín, M. R. Bermejo, A. M. García-Deibe, M. Maneiro, C. Lage and A. J. Costa-Filho, *Polyhedron*, 2000, **19**, 185.
6 U. Casellato, P. Guerriero, S. Tamburini, S. Sitran and P. A. Vigato, *J. Chem. Soc., Dalton Trans.*, 1991, 2145.
7 P. Guerriero, S. Tamburini, P. A. Vigato, U. Russo and C. Benelli, *Inorg. Chim. Acta*, 1993, **213**, 279.
8 C. Bolos, P. C. Christidis, G. Will and L. Wiehl, *Inorg. Chim. Acta*, 1996, **248**, 209.
9 M. Mikuriya, N. Tsuru, S. Ikemi and S. Ikenoue, *Chem. Lett.*, 1998, 879.
10 E. Asato, H. Furutachi, T. Kawahashi and M. Mikuriya, *J. Chem. Soc., Dalton Trans.*, 1995, 3897.
11 F. A. Cotton, L. M. Daniels, L. R. Falvello, J. H. Matonic, C. A. Murillo, X. Wang and H. Zhou, *Inorg. Chim. Acta*, 1997, **266**, 91.
12 N. Latioly, C. P. Raptopoulou, A. Terzis, A. E. Aliev, S. P. Perlepes, I. P. Gerotanassis and E. Manessi-Zoupa, *Chem. Commun.*, 1998, 1513.
13 E. V. Rybak-Akimova, N. W. Alcock and D. H. Busch, *Inorg. Chem.*, 1998, **37**, 1563.
14 R. W. Saafrank, N. Low, S. Trummer, G. M. Sheldrick, M. Teichert and D. Stalke, *Eur. J. Inorg. Chem.*, 1998, 559.
15 G. M. Sheldrick, *SHELX97, Programs for Crystal Structure Analysis*, University of Göttingen, 1997.

ChemComm

Synthesis of hammer-like macromolecules of C_{60} with well-defined polystyrene chains *via* atom transfer radical polymerization (ATRP) using a C_{60}-monoadduct initiator

Peng Zhou, Guang-Qiang Chen, Chun-Zhao Li, Fu-Sheng Du, Zi-Chen Li and Fu-Mian Li*

Department of Polymer Science and Engineering, College of Chemistry, Peking University, Beijing 100871, China. E-mail: fmli@chemms.chem.pku.edu.cn

Received (in Cambridge, UK) 12th January 2000, Accepted 14th March 2000

A new preparation of uniform hammer-like macromolecules of C_{60} with designed molecular weight and narrow molecular weight distributions in the range of 1.13–1.37 is developed by using C_{60}-monoadduct initiator (I) in a copper-mediated atom transfer radical polymerization (ATRP).

Recently, C_{60} (fullerene) has attracted much interest in the field of chemistry, physics and materials owing to its uniquely caged shape and intriguing properties. The structure, physical properties and photophysical behavior of C_{60} have been extensively studied.[1] Since the large-scale preparation of C_{60} was developed, there have been considerable reports on the macromolecular modification of C_{60} for practical purposes.[2–6,9–12] Since block polymers whose segments with different properties can be used as building units for aggregates,[7,8] it can be expected that an asymmetric hammer-like polymer containing C_{60} would self-assemble into a highly ordered supramolecular architecture with special electrical and optical properties. On the other hand, in order to establish the structure–property relationship of C_{60}-containing polymers, it is necessary to know the accurate content of C_{60} in the polymers. However, this has been proven to not be an easy task. The amount of C_{60} present estimated by thermogravimetry (TG), UV–VIS spectroscopy and gel permeation chromatography (GPC) do not agree well. In general, the actual amount of C_{60} incorporated in the polymer is usually much less than that in the feed.[5] Thus, there is an increasing need to synthesize well-defined C_{60}-containing polymers. This goal has been achieved partially by using different methods.[9–12] Recently, we tried an approach to synthesise well-defined C_{60}-containing polymers. In previous work,[12] well-defined bromo-terminated polymers obtained by ATRP[13] were treated with C_{60} under ATRP conditions to yield C_{60}-end-bonded PSt (PSt-C_{60}-Br) and PMMA (PMMA-C_{60}-Br). The final products were characterized to be mainly monoadducts and had controlled molecular weight with narrow molecular weight distributions, however, it was difficult to separate them from homopolymers. Here, we synthesized C_{60}-monoadduct **I** first, then it was used as an initiator for the ATRP of styrene to obtain uniform hammer-like macromolecules of C_{60} with designed molecular weight and narrow molecular weight distributions, Scheme 1.

Shown in Fig. 1 is the $\ln([M_0]/[M])$ *vs.* polymerization time plot. It can be seen that when the polymerization conversion was lower than 5%, it showed a linear relationship, meaning that the number of active species during the polymerization is constant under these conditions. This observation together with the linear evolution of molecular weight with conversion (as shown in Fig. 2) indicates that the initiation is fast so the contribution of chain breaking, transfer and termination is negligible; thus, when the conversion is lower than 5%, the process is controlled. When the conversion is higher than 5%, there is a deviation from the semilogarithmic kinetic plot, the consumption of styrene is faster than the initial stage, thus the termination on the C_{60} core can not be neglected, and the product obtained is no more well defined. The reason can be traced to the mechanism of ATRP. The initial stage of ATRP that generates radicals is a rate-determining step. In this step, a catalytic amount of the CuBr/bipy coordination complex reversibly abstracts the bromine atoms from the C_{60}-monoaduct initiator **I**, switching them from a dormant state to an active state, and generates a low concentration of C_{60}-based radicals. Since the concentration of

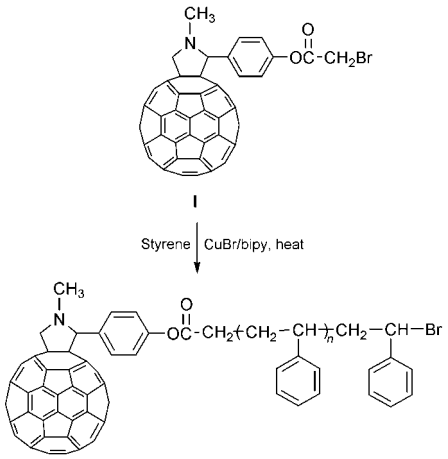

Scheme 1

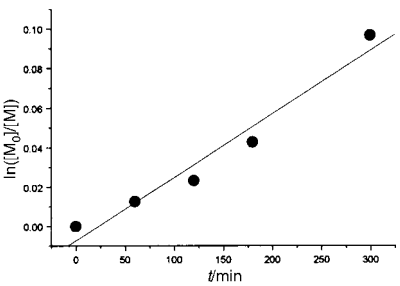

Fig. 1 Semilogarithmic kinetic plot of the preparation of C_{60}-end-bonded polystyrene *via* ATRP using C_{60}-monoadduct **I** as an initiator.

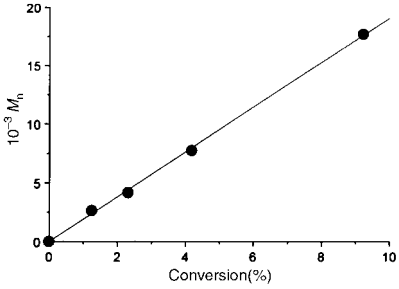

Fig. 2 Dependence of molecular weight on conversion of the preparation of C_{60}-end-bonded polystyrene *via* ATRP using C_{60}-monoadduct **I** as an initiator.

DOI: 10.1039/b000278j

Table 1 A summary of the conversion, molecular weight and molecular weight distribution of C_{60}-end-bonded polystyrene prepared *via* ATRP using C_{60}-monoadduct **I** as initiator

Run	Polymerization time/min	Conversion (%)	$M_{n,\,th}$ $(10^{-3})^a$	$M_{n,\,GPC}{}^b$ (10^{-3})	$M_w/M_n{}^b$
1	60	1.3	2.57	2.64	1.37
2	120	2.3	4.75	4.18	1.18
3	180	4.2	8.61	7.75	1.13
4	300	9.2	19.0	17.7	1.32

[a] Polymerization conditions for the bulk ATRP of St at 110 °C using C_{60}-monoadduct **I** as an initiator: $[St]_0$ = 9.26 M, $[CuBr]_0 = [bipy]_0/2 = [\mathbf{I}]_0 = 4.63 \times 10^{-2}$ M. [b] As determined by GPC in THF, low distribution polystyrenes were used as standards.

styrene is much higher than C_{60}-monoadduct initiator **I**, the addition of radicals to styrene double bonds occurs almost exclusively. As the polymer chains propagate, the relative concentration of styrene against C_{60}-monoadduct initiator **I** decrease, and the possibility of termination on the double bonds of C_{60} increase, thus making the molecular weight distribution broader. From the above observation, it is concluded that hammer-like macromolecules of C_{60} with designed molecular weight could be obtained by this method with low conversion.

The presence of C_{60} in polymers can be characterized by UV–VIS, DSC and NMR *etc*. Here we use 2-aminoacetonitrile (AAN) as an IR label of C_{60} in the polymers as we had reported previously.[15] Since the reaction between C_{60} and the aliphatic primary amino group of AAN proceeded smoothly under mild conditions *via* single electron transfer, the cyano group would display a characteristic peak at around 2250 cm^{-1}, while both PSt and PSt-C_{60} do not exhibit any absorption peak in the range 2000–2600 cm^{-1}. In the IR spectrum of NH_2CH_2CN-labeled PSt-C_{60}, an apparent new absorption peak appears at 2369 cm^{-1}. In a control experiment, the reaction product of pure PSt with NH_2CH_2CN does not absorb in this region. The result thus confirmed that C_{60} had been covalently bonded to PSt and this method can be extended to label other C_{60} derivatives.

Table 1 demonstrates that narrow molecular weight distribution C_{60}-bonded polystyrenes with high content of C_{60} can be obtained *via* this method. Since in ATRP, the molecular weight depends on the polymerization conversion, and the change of polymer chain length lead to the change of C_{60} content in the polymers, then by tailoring the polymer chain length, the content of C_{60} in the polymers can be well controlled.

Fig. 3(a) shows the GPC profiles of PSt-C_{60} with different molecular weight prepared by using C_{60}-monoadduct initiator **I** in THF. In all the GPC profiles the shapes are symmetrical, and there is no shoulder peak on the profiles of the PSt-C_{60} samples 2, 3 and 4 obtained by this method as compared to those obtained by preformed PSt which reacts with C_{60}.[15] This indicates that the sample possesses the designed hammer-like structure, not a mixture of PSt-C_{60} and PSt homopolymer.

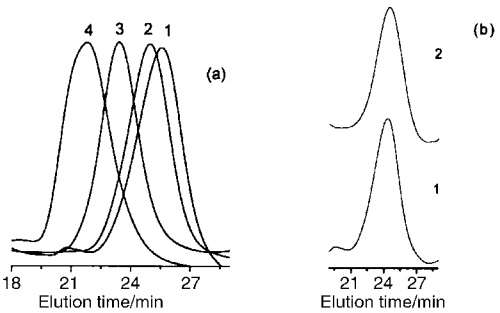

Fig. 3 (a) GPC profiles of C_{60}-end-bonded PSt prepared by using C_{60} monoadduct initiator (**I**) *via* ATRP (sample 1: $M_n = 2.64 \times 10^3$, sample 2: $M_n = 4.18 \times 10^3$, sample 3: $M_n = 7.75 \times 10^3$, sample 4: $M_n = 17.7 \times 10^3$) (b) GPC profiles of C_{60}-end-bonded polystyrene (sample 1, $M_n = 2.64 \times 10^3$) obtained by refractive index (1) and UV–VIS (2) dual detector, the working wavelength for the UV detector was set at 350 nm.

Fig. 3(b) shows the GPC profiles of C_{60}-end-bonded polystyrene (sample 1, $M_n = 2.64 \times 10^3$) obtained by UV and RI dual detector. The working wavelength of the UV detector was set at 350 nm where the PSt could not be detected and only derivatives of C_{60} can be recorded. Comparing the GPC profiles of C_{60}-end-bonded polystyrene, the profiles thus obtained are almost the same. The slight difference between the peaks at elution time is due to the different distance that the polymers passed from the pump to the detectors. This result indicates that C_{60} is bonded evenly in the polymers and the C_{60}-end bonded polystyrenes are monoadducts with well-defined structure.

Since the structure of C_{60}-end-bonded polystyrene obtained was defined with one C_{60} per polymer chain end, *i.e*. hammer shaped, by controlling the polymer chain length, the content of C_{60} in the polymers can be altered and the quantification of C_{60} in the polymers can be achieved thus aiding to establish the structure–property relationship of the C_{60}-containing polymers.

The preparation and the study of self-assembled aggregation behavior of these hammer-like macromolecules with well-defined flexible polymer chains including hydrophilic and amphiphilic chains are underway.

This work was financially supported by the National Natural Science Foundation of China (Nos. 59283032 and 29671030).

Notes and references

The C_{60}-monoadduct initiator **I** was synthesized according to the literature[14,15] as shown in Scheme 1. In a typical run, a mixture of *N*-methylglycine and 4-bromoacetoxybenzaldehyde was refluxed in toluene in the presence of C_{60}. The reaction proceeded readily over 8 h, affording the monoadduct **I** of the C_{60} *N*-methylpyrrolidine derivative in 35% yield after chromatography and recrystallization (70% based on C_{60} conversion). ^1H NMR of C_{60} monoadduct ($CDCl_3/CS_2$) δ 7.82 (br, 2H), 7.12 (d, 2H), 4.94 (s, 1H), 4.84 (d, 1H), 4.18 (d, 1H), 3.99 (s, 2H), 2.69 (s, 3H). UV–VIS (cyclohexane): 213.8, 257.2, 317.4, 430.5 nm.

The polymerizations of styrene were conducted in bulk in sealed glass tubes. The feed molar ratio was **I** : CuBr : bipy = 1 : 1 : 2. After the mixture was degassed three times, the tube was sealed under vacuum, and the polymerization was carried out in an oil bath of 110 °C for given times. The crude polymer was obtained by precipitation from methanol, dissolved in $CHCl_3$, and the solution then passed through a silica column to remove the catalysts. The polymer was recovered by precipitation from a large excess of methanol, and then dried under vacuum. A yellow to brown fine powdery polymer was obtained. UV–VIS (cyclohexane): 215.2, 259.3 nm.

1 *The Chemistry of Fullerenes*, ed A. Hirsch, Thieme, New York, 1994.
2 E. T. Samuski, J. M. DeSimone, M. O. Hunt, Y. Z. Menceloglu, R. C. Jarnagin, K. B. Labat and H. Wang, *Chem. Mater*., 1992, **4**, 1153.
3 C. E. Bunker, G. E. Lawson and Y.-P. Sun, *Macromolecules*, 1995, **28**, 3744.
4 T. Cao and S. E. Webber, *Macromolecules*, 1996, **29**, 3826.
5 C. Weis, C. Friedrich, R. Mulhaupt and H. Frey, *Macromolecules*, 1995, **28**, 403.
6 E. Clouet, Y. Gnanou, J.-L. Fillaut and D. Astruc, *Chem. Commun.*, 1996, 1565.
7 I. Stupp, V. LeBonheur, K. Walker, S. Li, K. E. Huggins, M. Keser and A. Amstutz, *Science*, 1997, **276**, 384.
8 Z. C. Li, Y. Z. Liang and F. M. Li, *Chem. Commun.*, 1999, 1557
9 C. Wang, J. He, S. Fu, K. Jiang, H. Chang and M. Wang, *Polym. Bull. (Berlin)*, 1996, **37**, 305; H. Okamura, N. Ide, M. Minoda, K. Komatsu and T. Fukuda, *Macromolecules*, 1998, **31**, 1859
10 D. Taton, S. Angot, Y. Gnanou, E. Wolert, S. Setz and R. Duran, *Macromolecules*, 1998, **31**, 6030.
11 Z. Y. Wang, L. Kuang, X. S. Meng and J. P. Gao, *Macromolecules*, 1998, **31**, 5556.
12 P. Zhou, G. Q. Chen, F. S. Du, Z. C. Li and F. M. Li, *Acta Polym. Sin.*, 1999, **6**, 757.
13 J. S. Wang and K. Matyjaszewski, *J. Am. Chem. Soc.*, 1995, **117**, 5614.
14 M. Maggini, G. Scorrano and M. Prato, *J. Am. Chem. Soc.*, 1993, **115**, 9798; L. B. Gan, D. J. Zhou, C. P. Luo, H. S. Tan, C. H. Huang, M. J. Lu, J. Q. Pan and Y. Wu, *J. Org. Chem.*, 1996, **61**, 1954.
15 P. Zhou, G. Q. Chen, F. S. Du, Z. C. Li and F. M. Li, *Macromolecules*, in press.

Tribochromic compounds, exemplified by 3-dicyclopropylmethylene-5-dicyanomethylene-4-diphenylmethylenetetrahydrofuran-2-one

Abdullah M. A. Asiri, Harry G. Heller,* Michael B. Hursthouse and Alexander Karalulov

Chemistry Department, Cardiff University, PO Box 912, Cardiff, UK CF1 3TP. E-mail: heller@cardiff.ac.uk

Received (in Cambridge, UK) 25th February 2000, Accepted 30th March 2000

The title compound 2 is obtained as bright yellow metastable crystals, which on mechanical grinding change to the dark red stable form; unlike piezochromic compounds, the reverse colour change does not occur; X-ray crystallographic analyses shows that the yellow form has a folded structure while the red form has a twisted structure.

We introduce the term 'tribochromism' (Greek tribos rubbing, khroma colour) to describe the new phenomenon of metastable crystals that undergo a major and irreversible colour change on mechanical grinding. The coloured form is stable and does not undergo the reverse change when kept in the dark, on heating or when dissolved in an organic solvent. In contrast, piezochromism[1] defines stable crystals, which give highly coloured metastable forms on fracture, which undergo the reverse colour change under the conditions described above.

As part of our studies[2] on photochromic dicyanomethylene derivatives, the severely overcrowded 3-dicyclopropylmethylene-5-dicyanomethylene-4-diphenylmethylenetetrahydrofuran-2-one **2** was prepared by reaction of dicyclopropylmethylene(diphenylmethylene)succinic anhydride **1** with malononitrile in THF in the presence of diethylamine (2 equiv.) at room temperature. The resulting colourless salt was filtered off and treated with acetyl chloride in dichloromethane. Solvent and acetyl chloride were removed and the residue purified by chromatography on silica gel using ethyl acetate and light petroleum (bp 60–80 °C) as eluent. The deep red solution, on concentration, gave a first crop of bright yellow crystals **2y** (*ca*. 0.3 g) and a second crop of dark red crystals **2r** (*ca*. 0.1 g). Red crystals and yellow crystals gave red solutions that showed identical NMR and UV/visible spectra. Repeat experiments with recrystallisation from different solvents gave only red crystals. The deep red solutions gave only red crystals when seeded with yellow crystals. X-Ray crystallographic analysis (which presented difficulties with refinement) on the best of the crude yellow crystals **2y** showed that the diphenylmethylene group is folded (one phenyl lies above a cyclopropyl group and the other above a cyano group). [X-Ray crystallographic analyses on compound **3c(y)**, which was obtained only as tribochromic yellow crystals, showed a folded structure also.] X-Ray crystallographic analysis† of dark red crystals **2r** showed that the diphenylmethylene group is twisted (one phenyl lies above a cyclopropyl group and the other below a cyano group) (Fig. 1).

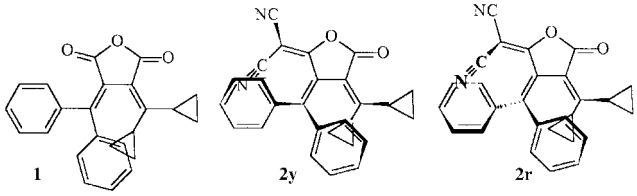

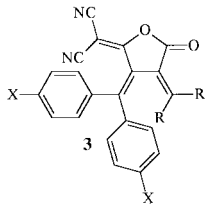

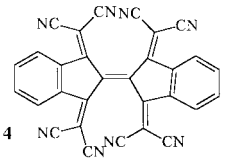

Gompper[3] has reported that di[1,1-bis(dicyanomethylene)-indan-2-ylidene] **4** exists in yellow and in red crystal modifications and that X-ray crystallographic analysis showed that in yellow crystals, molecules have a folded structure whereas in red crystals, molecules have a twisted structure.

The tribochromic properties were discovered accidentally. Since yellow crystals **2y** gave deep red solutions, it was not possible to observe whether compound **2y** was photochromic in solution. To produce a greater surface area to test for

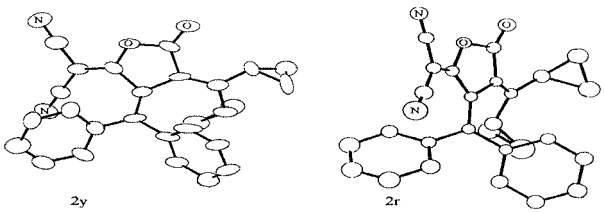

Fig. 1 X-Ray structures of yellow crystals **2y** and red crystals **2r**.

Table 1 Melting points, yields, and λ_{max} values of long wavelength absorption bands for solutions measured in toluene for overcrowded molecules **2** and **3a**–**i**, indicating whether they are obtained as yellow tribochromic crystals (**y**) or dark red stable crystals (**r**)

Compound	R_2C=	X	Mp/°C[a]	Yield(%)	λ_{max}/nm
2(y)[c]	dicyclopropylmethylene	H	183–4	21[b]	503
2(r)[c]	dicyclopropylmethylene	H	188–9	7	503
3a(y)	dicyclopropylmethylene	F	203–5	59	510
3b(y)	dicyclopropylmethylene	Cl	197–8	42	514
3c(y)[c]	isopropylidene	H	182–3	55	479
3d(r)	isopropylidene	F	185–8	45	484
3e(r)	isopropylidene	Cl	193–4	66	484
3f(y)	adamantylidene	H	213–5	56	486
3g(y)	adamantylidene	F	235–7	36	495
3h(y)	adamantylidene	Cl	245–7	48	503
3i(r)[c]	cyclopentylidene	H	162–4	41	489

[a] Gave deep red melts. [b] An unrepeatable reaction. [c] X-Ray analysis showed that yellow forms **2(y)** and **3c(y)** have folded structures and red forms **2(r)** and **3i(r)** have twisted structures.

DOI: 10.1039/b001567i

photochromism in the solid state by irradiation with ultraviolet light, yellow crystals were ground with a spatula. On grinding, they turned dark red.

A range of related compounds **3a**–**i** has been prepared in which the dicyclopropylmethylene group was replaced by 2-propylidene, adamantylidene and cyclopentylidene groups and in which 4-hydrogens on the phenyl groups were replaced by chloro and fluoro groups. Compounds were obtained either as yellow or dark red crystals (see Table 1) but never in both forms with the exception of **2y** and **2r**. All compounds obtained as yellow crystals were tribochromic.

We thank King Abdul Aziz University, Saudi Arabia for financial support (to A. M. A. A.) and the EPSRC for support for the X-ray crystallographic work.

Notes and references

† *Crystal data* for **2y**: $C_{27}H_{20}N_2O_2$, M = 404.4, monoclinic, space group $C2/c$, a = 10.07(3), b = 23.91(5), c = 9.50(5) Å, β = 110.4(2)°, V = 2144(13) Å^3, T = 293(2) K, Z = 4, D_c = 1.253 g cm^{-3}, R_1 = 0.0897, wR_2 = 0.2076 for all 2629 data and 257 parameters. For **2r**: $C_{27}H_{20}N_2O_2$, M = 404.4, monoclinic, space group $P2_1/c$, a = 20.349(2), b = 10.095(2), c = 21.338(2) Å, β = 99.06(2)°, V = 4328.6(13) Å^3, T = 293(2) K, Z = 8, D_c = 1.241 g cm^{-3}, R_1 = 0.0640, wR_2 = 0.1743 for all 5500 data and 282 parameters. Data were recorded using a FAST TV area detector diffractometer and Mo-Kα radiation. CCDC 182/1589. See http://www.rsc.org/suppdata/cc/b0/b001567i/ for crystallographic files in .cif format.

1 H. Meyer, *Chem. Ber.*, 1909, **42**, 143; A. Schönberg, F. A. Ismail and W. Asker, *J. Chem. Soc.*, 1942, 272; 1946, 442; A. Schönberg, M. Elkaschef, M. Nosseir and M. M. Sidky, *J. Am. Chem. Soc.*, 1958, **80**, 6312; G. Kortum, W. Theilhacker and G. Schreyer, *Z. Phys. Chem.*, 1957, **11**, 182; K. Maeda and T. Hayashi, *Bull. Chem. Soc., Jpn.*, 1960, **33**, 556; 1962, **35**, 2057; 1965, **38**, 685 and 2203; 1970, **43**, 429; T. Hayashi and M. Moringa, *Bull. Chem. Soc. Jpn.*, 1964, **37**, 1563; K. Maeda, T. Hayashi and T. Kanaji, *Bull. Chem. Soc. Jpn.*, 1965, **38**, 857; K. Maeda, A. Chinone and T. Hayashi, *Bull. Chem. Soc. Jpn.*, 1970, **43**, 1431; D. M. White and J. Sonnenberg, *J. Org. Chem.*, 1964, **29**, 1925; D. M. White and J. Sonnenberg, *J. Am. Chem. Soc.*, 1966, **88**, 3825; S. M. Blinder, M. L. Peller, N. W. Lord, L. C. Aamodt and N. S Invanchukov, *J. Chem. Phys.*, 1962, **36**, 540; F. Kehrmann and Zd. Matusinsky, *Chem. Ber.*, 1912, **45**, 3498; N. Campbell and A. G. Cairns, *J. Chem. Soc.*, 1961, 1191; M. Matsui, K. Shibata and H. Muramatsu, *Bull. Chem. Soc. Jpn.*, 1990, **63**, 1845.

2 H. G. Heller, D. S. Hughes, M. B. Hursthouse and K. V. S. Koh, *J. Chem. Soc., Chem. Commun.*, 1994, 2713.

3 A. Beck, R. Gompper, K. Polborn and H.-U. Wagner, *Angew. Chem., Int. Ed. Engl.*, 1993, **32**, 1352.

Weak hydrogen bonds: theoretical studies

Maria José Calhorda

ITQB, Quinta do Marquês, EAN, Apart. 127, 2781-901 Oeiras and Departamento de Química e Bioquímica, Faculdade de Ciências, Universidade de Lisboa, 1749-016 Lisboa, Portugal. E-mail: MJC@ITQB.UNL.PT

Received (in Cambridge, UK) 7th January 1999, Accepted 16th February 2000
Published on the Web 29th March 2000

Hydrogen bonds A–H···A′, where A and A′ are electronegative atoms have been widely discussed. Weak hydrogen bonds involving such different arrangements as X–H···A, where X can be C; X–H···π, with phenyl rings, C≡C bonds; X–H···M, where M is a transition metal; X–H···H–M and X–H···H–B, have also been described in recent years. While the first types are typical of organic and inorganic compounds, as well as biological molecules, those involving transition metal atoms are special to organometallic chemistry. Theoretical calculations of different kinds and at several levels have been performed for many systems, revealing that a similar geometrical arrangement can hide another type of interaction. This happens for N–H···M close contacts which can be agostic interactions or hydrogen bonds, not so easily distinguishable for 16-electron complexes. M–H···H–X interactions also exhibit a different behavior, depending on whether the complexes are neutral or ionic. The AIM approach, by analysing the topological properties of the charge density with the determination of critical points, provides another way of looking for bonds, as discussed in several examples.

Introduction

Hydrogen bonds have been known since the beginning of this century, but were brought into the common body of knowledge by Pauling in 1939, in his book *The Nature of the Chemical Bond*.[1] Strong and weak hydrogen bonds are discussed by Jeffrey and Saenger, in *Hydrogen Bonding in Biological Structures*.[2] They consider as strong hydrogen bonds only those of the types F–H···F$^-$, O–H···O$^-$, and O$^+$–H···O, which are always two-center bonds, involving short distances and strongly directional, with typical energies higher than 41 kJ mol^{-1}. On the other hand, the normal or weak hydrogen bonds would be X–H···A, where the acceptor A is an electronegative atom. Multicentered bonds start to appear, directionality is lost, and the bond energies drop to below 20 kJ mol^{-1}. The common feature to all of these bonds is the presence of an electronegative atom A as acceptor. More recently, other types of hydrogen bonds were identified. The acceptor can be a π system, usually a ring, and these are denoted X–H···π hydrogen bonds.[3] More interesting for the inorganic chemist are those involving a transition metal, either directly in X–H···M interactions,[4] or as a metal hydride, to form X–H···H–M groups.[5] A similar environment can be found when boron takes the place of the transition metal, giving rise to X–H···H–B interactions.[6] This latter type, where the hydrogen attached to X acts as a proton and the other as a hydride, has been denoted the dihydrogen bond, emphasizing the proximity of the two hydrogen atoms (Scheme 1).[6]

O-H---O$^-$		X-H---π
O$^-$-H---O	X-H---A	X-H---M
F-H---F$^-$		X-H---H-M
		X-H---H-B
Strong hydrogen bonds	Normal or weak hydrogen bonds	Non classical hydrogen bonds

Scheme 1

As the hydrogen bonds become weaker, the difficulty of distinguishing between hydrogen bonds and van der Waals interaction becomes relevant and has been discussed.[7] The role of hydrogen bonds in supramolecular chemistry and solid design is extremely important, as well as in biochemical environments, namely in protein folding, and many publications deal with these themes.[8]

In this work, theoretical studies of the different types of weak interactions will be addressed, after a brief introduction to the computational methods that have been used for this purpose, with more or less success and limitations. Our interest lies mainly on the study of hydrogen bonds in systems containing transition metal organometallic complexes. They therefore constitute the main objective of this review, which is organized by type of bond, starting from weak X–H···A hydrogen bond, and moving on to X–H···π, X–H···M, and X–H···H–M(B). In some systems, the hydrogen bond takes place at the periphery of the molecules or ions, and the role of the metal is minimum. In such cases, results involving only main group elements are comparable. The X–H···H–B interaction also does not necessarily involve transition metals, but is very interesting to compare with X–H···H–M, in view of the differences between boron and a transition metal.

Computational methods

Many different approaches have been used to study weak hydrogen bonds, ranging from semiempirical calculations (extended Hückel,[4a,9] MNDO[10]) to *ab initio* studies (HF/MP2,[5c] B3LYP,[6,11] DFT[12]). These methods allow either a qualitative interpretation of the bond (extended Hückel), or geometry optimization, determination of binding energies, and calculation of charges and other relevant parameters. MP2 and B3LYP approaches are compared in a detailed study of formation of hydrogen bonded complexes of small molecules with water, where water can behave as donor or acceptor,

Maria José Calhorda is Professor of Inorganic Chemistry at the Department of Chemistry and Biochemistry of the Faculty of Sciences, University of Lisbon, since 1996, and has her research group at the Instituto de Tecnologia Química e Biológica, Oeiras, since 1990. She received her PhD from Instituto Superior Técnico, Lisbon (1980), and spent one year as a post-doc in Oxford (ICL) with D. M. P. Mingos. A sabbatical leave at Cornell University with R. Hoffmann and a later one at the MPI für Festkörperforschung, Stuttgart, with A. Simon contributed to a wide range of scientific interests, dealing essentially with the theoretical study of electronic structure and reactivity of inorganic systems, and a more recent one in the design of solids.

DOI: 10.1039/a900221i

depending on the type of molecule. B3LYP was found, by some authors,[11d] superior to MP2 in what concerns the quality of the results, and has the advantage of a much lower computational cost. In order to consider short-range, electrostratic, induction, and dispersion interactions, reliable quantitative calculations should include correlation effects, which are only taken into account by DFT and *n*th order Møller–Plesset methods, the lowest being MP2.[13a,b] Correlation determines dispersion interactions, and influences the others. There is much discussion about to what extent DFT methods can indeed be used when dispersion forces are significant, and the accepted view is that MP2 is better.[13] Another difficulty present in the determination of weak interaction energies is the basis set superposition error (BSSE). It can significantly reduce the magnitude of a weak interaction and eventually destroy it. Although its contribution should always be calculated, it has not been done, especially in less recent works and the results must be critically considered.[13a–c]

The theory of 'atoms in molecules' (AIM)[14] has been used to extract chemical bond information from wave functions (and therefore its 'value' depends on the theoretical calculations behind). An analysis of the topological properties of the charge density with the determination of critical points can help determine the presence of a bond and this reasoning has been applied to the study of hydrogen bonds.[15] Carroll and Bader studied, among others, the hydrogen bond formation between HF and a series of bases. They calculated critical points of the charge density, ρ, corresponding to open shell interactions (covalent bonds) and compared them with those resulting from closed shell interactions (Fig. 1).

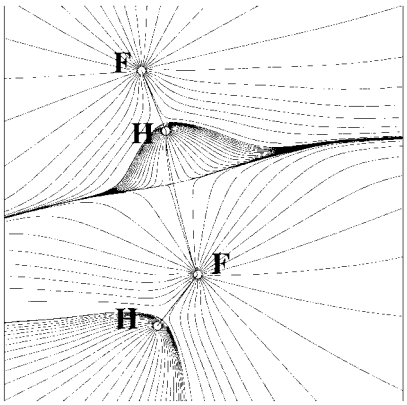

Fig. 1 Display of the gradient vector field of the charge density ρ for $(HF)_2$. Each line represents a trajectory of $\nabla\rho$. A nucleus acts as an attractor of the $\nabla\rho$ field, that is, all the trajectories in some open neighbourhood of a nucleus terminate at that nucleus. These trajectories are lines of steepest ascent through the charge density. An atom is the union of an attractor and its basin. Basins of neighbouring atoms are separated by trajectories that terminate at a bond critical point (denoted by a black dot). A pair of lines of steepest ascent (also shown as bold lines) originate at each critical point and terminate, one to each, at the neighbouring nuclei. They define the atomic interaction lines—lines along which ρ is a maximum with respect to any neighbouring line. If the system is at its equilibrium geometry, these lines are called bond paths.

In the first case, covalent bonds, the laplacian of the charge density, $\nabla^2\rho$, is negative at the critical point, while $\nabla^2\rho$ is positive for closed shell interactions, such as hydrogen bonds.[14b] The determination of critical points in the charge density and the signal of $\nabla^2\rho$ can therefore help in identifying bonds.

Weak hydrogen bonds of the type X–H···A

Weak hydrogen bonds, where X and A are not simultaneously very electronegative atoms, are important in organic and in organometallic chemistry, and a large group comprises C–H···A interactions, where A is an electronegative atom, such as oxygen. The use of the Cambridge Crystallographic Data Base (CSD)[16] has been of major importance in their detection. C–H···O short distances have been identified in organic[17] and organometallic compounds,[18] and also in nucleic acid molecules.[19]

The general properties of the C–H···O interactions were studied in detail, with an emphasis on the application of crystal correlation studies.[17] Calculated bond energies of organic C–H···O bonded dimers in vacuum led to values between *ca.* 2.1 and 15.8 kJ mol^{-1}, with an exceptionally high 38.9 kJ mol^{-1} for NH_3^+–CH_3···OH_2. Of course these values will be changed in solution, solvation being an important factor, but it is thought that the energies are essentially below 8.4 kJ mol^{-1}. The shortest contacts are *ca.* 3.0 Å (C···O) and *ca.* 2.0 Å (H···O).[17a]

C–H···O interactions are very much present in organometallic chemistry, namely in the crystal structures of carbonyl complexes simultaneously containing cyclopentadienyl, benzene, carbene, or any other group with a C–H group.[18] Electrostatic effects are determining in allowing the approach of C–H to an oxygen atom, and so the charges (positive in the hydrogen, negative in the oxygen) will play a major role. It is well known that the amount of back donation from metal centres to carbonyl ligands increases from terminal, to doubly bridging, to triply bridging carbonyls, leading to an increasing negative charge on the oxygen atom. Several families of compounds, obtained from a search in the CSD, were analysed in a molecular orbital study.[20] Triply bridging carbonyls should be the best at establishing strong hydrogen bonded networks in the solids. Would this effect overcome the natural preferences for carbonyl bonding in each complex? As a matter of fact, it does not, as covalent bonds are much stronger. Carbonyls bind in their preferred way to each metal, the trend being that the lighter the metal, the larger can be the number of bridging carbonyls. For instance, for the $(Cp^R)_3M_3(CO)_3$ clusters (M = Co, Rh, Ir), one finds, among other structures, $(Cp)_3Co_3(\mu_3\text{-}CO)_3(\mu\text{-}CO)_2$ and $(Cp)_3Ir_3(CO)_3$, bridges being observed for the lighter element clusters.[20b] Once the number and type of carbonyl is defined, the tendency to form stronger hydrogen bonds (defined here as having shorter distances and angles closer to 180°) lies with the triply bridging carbonyls.[20]

C–H···N hydrogen bonds with an estimated short H···N distance of 2.33 Å and an almost linear C-H···N arrangement are responsible for the packing in the crystals of bis(2,2′-dipyridylamido)cobalt(II).[7b] The authors question that many not so short C–H···X distances, along with not so linear C–H···X arrangements, are not indicative of hydrogen bonds, and sustain that most of them are indeed only classical van der Waals interactions. A reply has recently come out, giving more examples from the CSD.[7d]

A CSD search of hydrogen bonds to halides in organic and organometallic structures was recently reported, along with a statistical study, but no theoretical interpretations were attempted. One example of N–H···Cl interactions is found in 2,6-diphenylpyridinium tetrachloroaurate(III), where the Cl atom is coordinated to gold, and there is a bifurcated interaction between the N–H of the cation and two chlorides of the anionic complex.[21] The hydrogen bond between the chlorine atom in $OsHCl(CO)(PBu^t_2Me)_2$ and the hydrogen atom of alcohols was studied by NMR and computational methods (B3LYP and IMOMM, the integrated molecular orbital/molecular mechanics approach).[22] The bulk of the phosphines plays a significant role, preventing the formation of a Os←O bond, and only the IMOMM method, including a good basis set in the B3LYP part, provides a good reproduction of the experimental results. The role of fluorine in X–H···F hydrogen bonds has been discussed. Dunitz and Taylor demonstrated that, when covalently bound to carbon, fluorine does not participate in hydrogen bonds.[23] On

the other hand, fluorine in the PF_6^- anion, a very popular ion in organometallic chemistry, is observed in many X–H···F–P interactions, believed to be hydrogen bonds.[8]

Hydrogen bonds of the X–H···π type

Suzuki *et al.* investigated the benzene–water dimer using MP2 calculations with BSSE corrections and found that the water molecule stood over the benzene ring, with its centre of mass on the sixfold symmetry axis. The ring acted as a hydrogen-bond acceptor toward the two hydrogens. The dissociation energy was calculated as 7.4 kJ mol^{-1}.[24a] A similar study of the ammonia–benzene dimer was also carried out. The ammonia molecule also preferred a position such that its centre of mass coincided with the sixfold symmetry axis, but in the lowest energy arrangement only one hydrogen pointed toward the benzene ring.[24b] The energy difference to the next arrangement with two hydrogen atoms pointing toward the ring was very small.

The observation of X–H···π hydrogen bond has become frequent in recent years, as more examples of their presence in organic and organometallic crystals have been reported.[25] The first neutron diffraction study of an O–H···π hydrogen bond appeared in 1996.[25c]

A statistical study of these bonds, taking as donors O–H, N–H, $N–H^+$, sp^2 C–H, sp C–H, and S–H, and as acceptors phenyl or substituted phenyl rings, used the April 1996 version of the CSD and led to 1537 occurrences, in 530 of which the C_6H_5 ring participated.[10] The X–H approaches to the ring were classified in six groups. In group I, the hydrogen atom pointed at the centre and the X–H bond was perpendicular to the ring, while in group II X–H was no longer vertical. The other four groups included X–H bonds more or less near a carbon atom, rather than the centre, and more or less vertical. Types III and V were preferred by almost all donors, type I being significant for only $N–H^+···C_6H_5$. The authors performed semiempirical calculations (AM1, PM3) in a wide range of systems and *ab initio* calculations [HF with MP2, BSSE, ZPE (zero point energy) corrections] in a few. The interactions were always found to be attractive, with binding enthalpies decreasing in the order $N–H^+$ > O–H > N–H > sp^2 C–H > sp C–H. The interactions are described by shallow potentials allowing many binding arrangements (for instance, ammonia pointing with one, two, or three hydrogen atoms at the centre of the ring) and exhibit a long range nature.[10]

Theoretical calculations (GAUSSIAN92/DFT) were also performed on 5-ethynyl-5*H*-dibenzo[*a*,*d*]cyclohepten-5-ol, a molecule which dimerizes in the solid (Fig. 2) and exhibits C–H···π and O–H···π interactions.

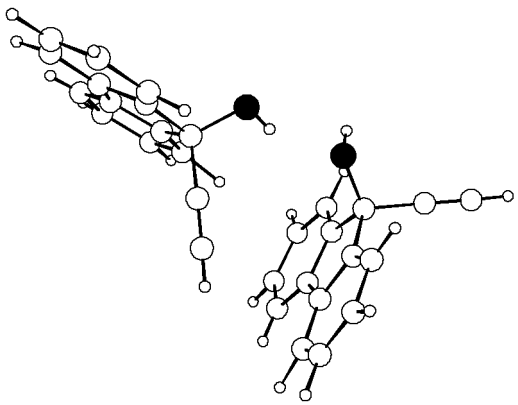

Fig. 2 The dimer of 5-ethynyl-5*H*-dibenzo[*a*,*d*]cyclohepten-5-ol (the black circle represents the oxygen). Hydrogen bonds are intermolecular and not seen.

In C–H···π, the hydrogen is close to the centre of the ring and almost vertical, while the O–H in O–H···π is much closer to one of the carbon atoms. The interaction energies were calculated at *ca.* 1.3 kcal mol^{-1} for both types.[25a] The authors also point out the softness of the interaction, which allows many different geometric arrangements with similar energies, although the minimum energy is observed for the face-on bonds.

Other π bonds have been shown to participate in hydrogen bonding.[26] Philp and Robinson[26a] searched the occurrence of C≡C–H···π(C≡C) short contacts in the CSD (October 1997) and found 37 hits. They performed *ab initio* calculations (MP2) in order to determine cooperative effects when hydrogen bond networks were found. The energy determined for a C–H···π(C≡C) interaction was 1 kcal mol^{-1}, close to that of an O–H···π(C≡C) interaction (1.5 kcal mol^{-1}). Cooperative effects turned out not to be significant, while the 'independence' of the interaction energy from the interaction geometry was again noted, as well as the poor capabilities of the C≡C bond as a hydrogen bond acceptor. Mingos and coworkers[26b] also studied theoretically, using different approaches, the interactions between HC donors (HCN, $C_{4-n}H_n$) and C_2R_2 acceptors (R = H, Na, H_3PAu) in a T shaped geometry. They are very weak for ethyne (< 10 kJ mol^{-1}), but become much stronger (stronger than most hydrogen bonds) in the gold derivative (10 kJ mol^{-1}) and in C_2Na_2. Another conclusion of the study was that DFT methods, of the best quality, always underestimated weak interaction energies by failing to describe accurately the dispersion force,[26b] as pointed out above.[13]

X–H···π hydrogen bonds with X = Cl, F and the π bond a C=C or a C≡C bond, were studied using the formalism of AIM,[14] and HF/MP2 calculations.[27] Their energies ranged from 3.09 kcal mol^{-1} for Cl–H···π(HC≡CH), to 4.87 kcal mol^{-1} in other systems (HF with MP2 corrections) and the values of $\nabla^2\rho$ at the hydrogen bond critical point were all negative, reflecting an interaction between closed shells.[27]

The participation of a pyrazole ring as a hydrogen bond acceptor was reported for the first time recently and was observed in the $[Re_3(\mu\text{-}H)_3(\mu\text{-}\eta^2\text{-}pz)(CO)_9(Hpz)]^-$ complex. In the crystal structure, one N–H bond points perpendicularly toward the centre of the ring, and NMR data show that this interaction remains in solution.[25d]

Recently, we came across C–H···π intramolecular hydrogen bonds involving fluorenyl rings. One example is given by $[(C_{13}H_9)_2ZrCl_2]$, where Zr exhibits the pseudo tetrahedral coordination environment typical of bent metallocenes. The two rings are coordinated in a rather asymmetric fashion, one of them being a characteristically η^5 bound ring, while the second is slipped to an extent that made the authors call it a η^3-fluorenyl, as two Zr–C bonds are 2.8 Å long (the others range between *ca.* 2.39 and 2.64 Å).[28] There is considerable steric crowding around the metal. The slippage of the ring can be compensated by more π-donation from the chlorine atoms to the metal, and a small stabilization is in principle gained by the formation of the C–H···π hydrogen bond (Fig. 3).

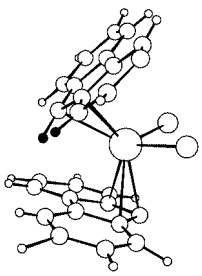

Fig. 3 The C–H···π hydrogen bonds in $[(C_{13}H_9)_2ZrCl_2]$.

A similar interaction is observed in $[(C_{13}H_9)(C_9H_7)_2Mo(CO)_2]$, a complex having one η^3-fluorenyl and one η^5-indenyl ring. Both in the experimentally determined structure and in the optimized geometry (DFT calculations, ADF program, with nonlocal and correlations corrections included in the calculation of gradients),[29] C–H groups from the indenyl are

involved in intramolecular hydrogen bonds with carbon atoms of the fluorenyl groups.[30]

X–H···M interactions

Short distances between a hydrogen atom attached to nitrogen or carbon and a metal have been known for a while, but were often interpreted as a manifestation of agostic hydrogens.[31] They were mainly observed in square planar Group VIII complexes, formally 16-electron species, where the X–H bond approached the metal from one of the axial positions.[32] Brammer *et al.* were among the first to assign X–H···M short contacts as intermolecular hydrogen bonds, in the study of $[NPr^n_4][PtCl_4][PtCl_2(NH_2Me)_2]$.[4a] The structure of this compound was determined at 4 K by neutron diffraction and showed a short N–H···Pt distance of 2.262(11) Å, with an N–H···Pt angle of 167.1(9)°. NMR evidence did not agree with the typical behavior of agostic hydrogens. As similar X–H···M distances had also been observed in d^{10} 18-electron complexes,[33] and agostic hydrogens were not expected, they were thought to be ideal systems worth further study. $[NHEt_3][Co(CO)_4]$ was chosen,[33a] and a neutron diffraction study at 15 K revealed a Co···H–N distance of 2.613 Å, C–H 1.054 Å, and an angle N–H···Co 180°.[4b] The authors performed EH calculations, but the results were not conclusive.[4b] Previous EH calculations on a related model $[NH_4][Ni(CO)(PPh_3)_3]^+$, had indicated a weak attractive interaction, made possible by mixing N–H σ* in the otherwise four-electron repulsive interaction between Ni d_{z^2} and N–H σ.[33b] The strength of the N–H···Co hydrogen bonds was further investigated by modifying ligands (to modify the basicity of the metal centre) or the cation. Indeed, replacing $[NHEt_3]^+$ by protonated DABCO (1,4-diazobicyclooctane), a less bulky cation, favouring the approach to the metal, the N···Co distance is reduced from 3.648 to 3.437 Å. Substitution of a carbonyl by a phosphine in the *trans* position relative to the N–H bond, leads to an N···Co distance of 3.294 in $(DABCO)H^+Co(CO)_3(PPh_3)$. The authors performed *ab initio* calculations (HF) on these systems, and found that transfer of hydride to cobalt was energetically preferred. The energy minimum for $(DABCO)[HCo(CO)_3(PPh_3)]$ was deeper than the minimum for $(DABCO)H^+Co(CO)_3(PPh_3)$, a result understandable by the fact that solvent effects were not considered.[34]

These weak X–H···M interactions are thus important in the context of metal protonation and reactivity, especially when square planar metal centres are involved.[35] The complex [*trans*-$Rh(CO)(8\text{-methylquinoline})(PPh_3)_2][BF_4]$, for instance, is a 16-electron complex containing a square planar d^8 species and exhibits a short C–H···Rh distance 2.21 Å. The authors were looking for agostic hydrogens, but the weak interaction detected between the axial methyl and the metal was not unambiguously an agostic hydrogen.[36]

In a typical agostic interaction, the metal centre is electron deficient and receives electrons from a C–H σ bond, back donation from the metal to the σ* C–H bond being possible. As a result, the C–H bond becomes weaker and relatively short metal···hydride (though much longer than metal–hydride) distances develop. Such bonds can be described as three-centre–two-electron bonds (C–H→M), as sketched in the left of Scheme 2.[37]

The agostic bond was theoretically studied using the AIM formalism,[38] and it was found that the criteria used to define hydrogen bonds did not apply in the systems studied ($CH_3TiCl_2^+$, $C_2H_5TiCl_2^+$, $C_3H_7TiCl_2^+$), emphasizing the difference between the two types of bonds. Indeed, in a hydrogen bond, the metal is not necessarily electron deficient, and the interaction is a three-centre–four-electron one (Scheme 2, right).[35]

NMR was used to distinguish between agostic and hydrogen bond interactions in 16-electron square planar complexes, as the proton resonance was shifted upfield for the first case, and

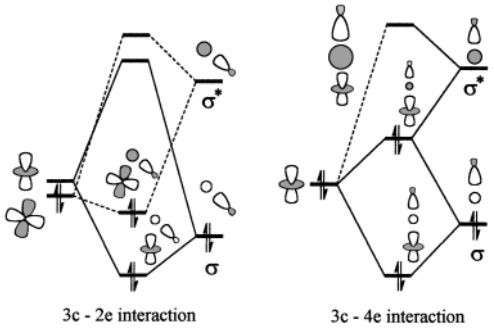

Scheme 2

downfield for the second, compared to the free ligand.[35] More recently, the CSD was searched for examples of complexes containing the X–H···M arrangement.[4c] The 50 hits included d^8 square planar complexes, d^6 square pyramidal complexes (the sixth position of the octahedron being taken by the H–X) and other systems. Only N–H and C–H bonds were found to interact with d^8 square planar centres. All the N–H groups were oriented perpendicularly to the plane of the complex, so that the orbitals of the metal which can overlap are d_{z^2} and p_z. As this last orbital has a very high energy, the interaction belongs to the three-centre–four-electron type (Scheme 2, right), namely a hydrogen bond, as in the 18-electron systems. The C–H···M arrangements were not so clearly cut, as many were not perpendicular and a final conclusion was not reached. The doubt remains as to whether a hydrogen or an agostic bond is present, but a weak hydrogen bond is favored.[4c]

The dihydrogen bond: X–H···H–M and X–H···H–B

The term dihydrogen bond was introduced by Crabtree and coworkers[6] to describe X–H···H–M bonds, where X is an electronegative atom and the metal–hydride σ bond behaves as an acceptor. The complex *cis*-$[IrH(OH)(PMe)_4][PF_6]$[39] was the compound where such an arrangement was seen for the first time in 1986.[39a] A low temperature neutron diffraction study was carried out later,[39b] showing a short O–H···H–Ir distance of 2.40(1) Å and a short Ir–O–H angle of 104.4(7)°. This weak interaction was assigned to a dipole–dipole interaction.[5e] Another O–H···H–Ir interaction was discovered by Crabtree and coworkers[5a] in the iridium complex **a** shown in Scheme 3, based on NMR evidence, as no hydrogen atoms could be detected in the X-ray crystal structure. The H···H distance was estimated as *ca.* 1.8 Å from the NMR data. Other related complexes were prepared and the first N–H···H–Ir (Scheme 3, **b**) interaction was observed.[5b]

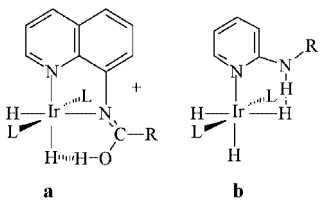

Scheme 3

Calculations (HF, GAUSSIAN92) were performed on a model of complex **b**.[5c] The energy of the model $IrH_3(PH_3)_2(HNCHNH_2)$ was lower by 60.3 kJ mol^{-1} when the N–H group was in the same plane as IrH_3, as in **b**, showing a barrier to rotation due to breaking the N–H···H–Ir interaction. This value was corrected to 41.5 kJ mol^{-1} to account for the difference between formamidine (model) and 2-aminopyridine,

in good agreement with the experimental value of 45.1 kJ mol^{-1}. The strength of the hydrogen bond was estimated as 29.7 kJ mol^{-1}. The ligand *trans* to the hydride participating in the hydrogen bond may affect the bond; a poorer σ donor will cause a less negative charge on the hydride, decreasing the electrostatic interaction between the H^- and the H^+, and therefore leading to a weaker hydrogen bond.[5c]

Another interesting system, dealing also with N–H···H–Ir interactions, was reported in 1994. Morris and coworkers synthesized iridium hydride complexes containing aminothiolate ligands and exhibiting N–H···H(Ir)···H–N[5g] or two N–H···H–Ir interactions.[5h] The H···H interactions were detected by NMR experiments, as the position of the hydrogen atoms could not be located in the X-ray crystal structures. Liu and Hoffmann studied [Ir{H(η^1-SC_6H_4NH)(PH_3)}$_2$] (PH_3 instead of PCy_3, in the model) using EH calculations,[9] starting by locating the two hydrides. They found a positive, though small, overlap population for the H···H interaction and also noticed the increase in energy upon rotation of the aminothiolate and consequent disruption of the hydrogen bond. The bond was found to be weakly attractive and with a significant electrostatic contribution. Smaller related systems, where similar interactions could arise from intermolecular approaches, such as H–F···H–Li and H–F···$HMn(CO)_5$, were also studied (HF calculations). For H–F···$HMn(CO)_5$, an energy minimum (27.4 kJ mol^{-1}) at a distance of 1.683 Å was determined.

The search for H···H intermolecular dihydrogen bonds[40] had the first result in the cocrystallization of the complex $ReH_5(PPh_3)_3$ with indole. A neutron diffraction structure showed that two of the hydrides were interacting with the N–H bond of the indole (H···H distances 1.75 and 2.25 Å). B3LYP calculations led to a relatively good reproduction of the geometrical features (H···H distances 1.92 and 2.48 Å) and gave an interaction energy of 33.4 kJ mol^{-1}.[40a] Reaction of the Re precursor with imidazole afforded $ReH_5(PPh_3)_2$(imidazole), where two of the hydrides were involved in hydrogen bonding with the N–H of a free imidazole molecule (H···H distances 1.68 and 1.99 Å).[40b] The strength of the interaction was estimated from IR data to be 22.6 kJ mol^{-1}.

The related derivatives containing pyridine[40c] and *o*- or *p*-NHR substituted pyridine, were prepared and the hydride fluxionality studied by NMR[40d] and theoretically (B3LYP).[40e] The rate was accelerated with the introduction of the *o*-NHR substituent in pyridine, and ascribed to intramolecular dihydrogen bond formation. Comparisons were made with the *p*-NHR derivative as this substituent cannot form intramolecular hydrogen bonds but electronic substituent effects are similar. The turnstile mechanism, with simultaneous rotation of three hydrides, was found to be the preferred both from experimental and theoretical results, leading to comparable barriers. A detailed study of the reaction mechanism showed that, for the 2-aminopyridine complex, strong hydrogen bonding was found in an intermediate along the reaction pathway. There was a barrier before reaching the transition state, owing to repulsion between two hydrides, and this prevented more powerful consequences of hydrogen bond toward lowering the activation barrier for hydride rotation.

Reviews about these non-classical hydrogen bonds appeared[5d–f] and several searches in the CSD for crystals exhibiting short intra- and inter-molecular H···H contacts were made.[12,41,42] Many of the examples refer to intramolecular interactions involving X–H···H–M, where X is an electronegative atom (O, N, S), starting with the already mentioned *cis*-[IrH(OH)(PMe_3)$_4$][PF_6].[39] Other cationic mononuclear complexes belong to this group, such as [IrH_2(CO)(PPh_3)$_2$(pzH-*N*)][BF_4]·C_6H_5Me with H···H 1.998 Å,[43] [IrH(Cl)(L)][PF_6] (L = 7-methyl-3,7,11,17-tetraazabicyclo[11.3.1]heptadeca-1(17),13,15-triene) with H···H 2.335 Å,[44] as well as the neutral compounds IrH(Cl)(PEt_3)$_2$[NHPh(C_7H_{10})] with H···H 2.242 Å,[45] Ru(H)$_2$($CO)_2$($PHPh_2$)(PPr^i_3)$_2$, with H···H 2.63 Å, and the *cis*-dicarbonyl [OsH($CO)_2$($PHPh_2$)(PPr^i_3)$_2$][BF_4] with H···H 3.04 and 2.83 Å.[46] Spectroscopic evidence suggested the presence of M–H···H–N interactions in Ru complexes (NMR),[47] although no crystals of the product could be obtained. Polynuclear complexes and clusters also exhibit short H···H distances between a hydride and a X–H hydrogen. Examples are given by Cp_2Zr(NHAr)(μ-H)(μ-NBu^t)IrCp*, with an H···H distance of 1.717 Å,[48] the two related complexes [Rh_2H_2(μ-SH_2)$_2${$MeC(CH_2PPh_2)_3$}][BPh_4]·$HCONMe_2$[49] and [(μ-H)$_2$$Ir_2$-(μ-$NH_2$)$_2$($PEt_3$)$_4$($NH_3$)$_2$]·$Me_2CO$,[50] with H···H 1.891 Å and 2.260, 2.189 Å, respectively for the Rh and the Ir complex, (μ-H)Ru_3($CO)_9$(μ-C_6H_2-1-NH-2-NH_2-4,5-Me_2), with H···H 2.383 Å,[51] [Ru_6(μ-H)$_6$(μ^3-η^2-ampy)($CO)_{14}$] (ampy = 2-aminopyridine), with H···H 2.064 Å.[52] N–H···H–M interactions have also been detected in compounds without structural characterization, such as $OsH(NH_3)(CO)_9$,[53a] and [{η^5-$C_5H_4CH(CH_2)_4NMe$}Ir(PPh_3)H_2].[53b] The observation of these interactions in the polynuclear complexes containing bridging hydrides is particularly interesting, as these hydrides often behave like acids. A close observation of the structure, however, suggests that steric constraints are responsible for the observed short H···H contacts.[12a] The M–H bond can also participate in M–H···O hydrogen bonding,[18a] as seen from many structures, but most of the hydrides involved are doubly or triply bridging hydrides which are very likely to carry a positive charge, so that the situation is not so surprising from an electrostatic point of view. Theoretical studies (DFT) were performed on some of the complexes, the most interesting results relating to the two cationic species, *cis*-[IrH(OH)(PMe_3)$_4$][PF_6] and [IrH_2-($CO)($PPh_3$)$_2$(pzH-*N*)][$BF_4$].[12] The geometries of the cations were optimised (using PH_3 instead of PMe_3 or PPh_3) and the agreement with the experimental structures was not particularly good. Introduction of the counter ion (PF_6^- or BF_4^-) in the calculations led to a better geometry. The charge distribution in these complexes is compatible with an electrostatic interaction between the negatively charged hydride and the positive hydrogen attached to N or O. The relevant geometric features can be seen in Scheme 4 for *cis*-[IrH(OH)(PH_3)$_4$][PF_6].

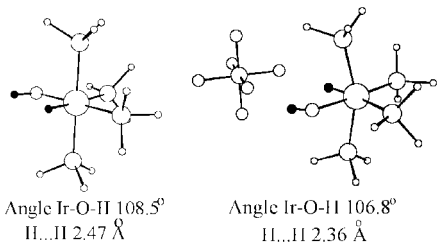

Scheme 4

The energy increases by 20.8 kJ mol^{-1} when the torsion angle H–Ir–O–H changes from 0 to 180° in the cation. As the angle varies, the H···H interaction vanishes. The corresponding energy difference is 44.1 kJ mol^{-1} when the PF_6^- anion is present. The relevant conclusion is of a non-negligible role of the counter ion in helping to stabilize the short H···H arrangements. In order to understand more about these interactions, the AIM approach was used to detect the hydrogen bonds.[54] *cis*-[IrH(OH)(PH_3)$_4$][PF_6][39] and the neutral complex $IrH_3(PH_3)_2(HNCHNH_2)$, theoretically studied by Eisenstein and coworkers,[5c] were chosen, to allow a direct comparison between neutral and charged species. These two complexes have iridium as the metal, which is also an advantage, as all the calculations can be done under the same conditions. The gradient vector fields and the bond critical points (black circles) are shown in Fig. 4, in the plane containing the X–H···H–Ir bonds.

For the neutral $IrH_3(PH_3)_2(HNCHNH_2)$ there is a critical point between the hydride and the N–H hydrogen. The values

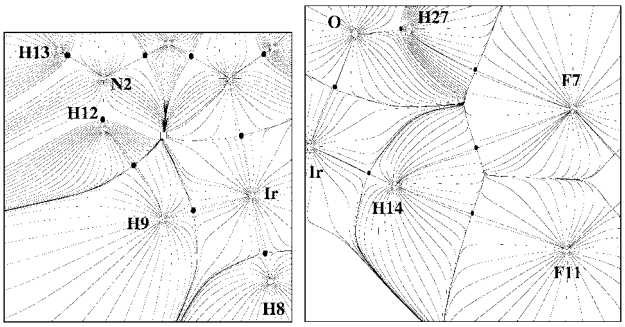

Fig. 4 The gradients of charge density and the critical points (black dots) along bonds in the Ir–H···H–N plane for $IrH_3(PH_3)_2(HNCHNH_2)$ (left) and *cis*-$[IrH(OH)(PMe_3)_4][PF_6]$ (right).

shown in Table 1 for the density ρ and the laplacian $\nabla^2\rho$ are typical for hydrogen bonds,[15] with positive $\nabla^2\rho$. For comparison, the critical points describing some relevant covalent bonds are also given. $\nabla^2\rho$ is now negative and the different values indicate, for instance, how the participation of H12 in the hydrogen bond with the hydride modifies the N2–H12 bond relative to N2–H13.

The cationic complex is different, because no critical point exists between the two hydrogen atoms. Instead, there are hydrogen bonds to the fluorine atoms in the PF_6^- anion. The H27(O) atom makes one hydrogen bond with F7, while the hydride is involved in hydrogen bond with the two fluorines, F7 and F11. The first hydrogen bond, H27–F7 is not surprising, as H27 carries a positive charge and F7 is negative. On the other hand, both the hydride H14 and the two fluorines F7 and F11 are negative. The values of $\nabla^2\rho$ and ρ for the bonds given in Table 1 are characteristic of covalent bonds (N–H, O–H) and hydrogen bonds (H···F). If this interpretation is indeed correct, the role of the counter ion is even greater than was thought.

The effect of charges in hydrogen bonds has also been assessed in the study of O–H$^-$···O$^-$ interactions in chains of oxalate anions (UHF). These are repulsive interactions. The reason why the atoms hold together is that they simultaneously participate in attractive interactions with the counter ion, K^+.[55] This is a situation where a short O–H$^-$···O$^-$ distance does not indicate a hydrogen bond.[18e] The point is controversial,[56] and brings forward the question whether distances by themselves provide an answer to the existence of a bond. As the previous example shows, short distances in O–H$^-$···O$^-$ chains can coexist with repulsive interactions, because a stronger cation–anion electrostatic attraction holds all ions in their place. A similar effect seems to take place in *cis*-$[IrH(OH)(PH_3)_4][PF_6]$.

Besides the previous examples, which include the oldest known systems, other intramolecular and intermolecular hydrogen bonds have been studied. Sometimes, they may be considered as the first step in the formation of a H–H bond, to give M–H_2 complexes, for instance. The $ReH_5(PPh_3)_3$·indole·C_6H_6 compound,[40] where two hydrides approach the N–H bond of indole, has already been mentioned. More recently, an equilibrium between the Ir–H_2 complex of $IrH(L)_2(bq\text{-}NH_2)$ (L = phosphine, bq-NH_2 = 2-amino-10-methylbenzo[*h*]quinoline) and the Ir–H···H_3N species was found to take place, its extent depending on the phosphine. Theoretical calculations (B3PW91) reproduce the trend: more basic phosphines lead to formation of the Ir–H_2 complex. An accurate modeling of the phosphine was critical and surprisingly PH_3 was not a good model for PPh_3.[5i]

A hydrogen bond between the H–O group in acidic alcohols and W hydrido complexes $WH(CO)_2(NO)L_2$ (L = phosphine) was detected by IR and NMR data and the H···H distance estimated as 1.77 Å, for L = PMe_3.[57] $Ru(dppm)_2H_2$ interacts with PhOH or 1,1,1,3,3,3-hexafluoroisopropyl alcohol, *via* Ru–H···H–O hydrogen bonds and forms the dihydride complex.[58] $ReH_2(CO)(NO)L_2$ (L = phosphine) also interacts with alcohols,[59] but both O–H···H–Re and O–H···O–N–Re hydrogen bonds may be formed, the latter becoming predominant when the phosphine is bulky (PPr^i_3). Theoretical calculations (DFT) were performed in the model compound $ReH_2(CO)(NO)(PH_3)_2\cdots OH_2$, allowing both types of approach to take place (to the M–H or to the O–N bond). The O–H···H–Re bond type is electronically favoured by 12.5–14.6 kJ mol^{-1}, but forces the OH carrying molecule to be very close to the metal, and this becomes difficult when two bulky axial phosphines are present. O–H···O–N–Re hydrogen bonds are then formed for steric reasons.[59]

Orlova and Scheiner performed calculations of different types (HF/3-21G, B3LYP, BLYP, B3PW91) to study the intermolecular bonding of molybdenum and tungsten hydrides with HR (R = F, OH, H_2O^+) complexes.[11a] The study of the interaction of HF with $Mo(CO)_2(NO)(PH_3)H$ led to the conclusion that the DFT/B3PW91 method was the best, even taking into account that all DFT methods tend to afford distances that were too long, and it was chosen for most studies. The Mo–H···H–F hydrogen bond energy was estimated as *ca.* 46 kJ mol^{-1}. Substitution of the *cis* ligand PH_3 by the better σ donor NH_3 increases the strength of the hydrogen bond, while changing the metal to W does not afford any major change. A greater acidity of the HR species also leads to a stronger hydrogen bond and formation of H_2-complexes, while, as expected, bulkier ligands have the opposite effect. The authors notice the inadequacy of Mulliken charges to adequately describe the system, but they rely on a Mulliken-type analysis (overlap populations) to interpret relative trends. The competition of formation of other bonds, such as F–H···O–N–Mo was investigated,[11a] as done previously for Re complexes.[59]

Orlova and Scheiner[11b] also addressed the interactions of CpReH(CO)(NO), $CpReH(NO)(PH_3)$ and $CpRuH(CO)(PH_3)$ with several proton donors (H_2O, $HOCF_3$, H_3O^+) with B3PW91 methods. The formation of H_2-complexes as a result of H···H hydrogen bonding and the alternative protonation at the metal to form dihydride complexes are discussed. $CpReH(NO)(PH_3)$ has a very strong nucleophilic centre at the metal and only the dihydride forms, while for $CpRuH(CO)(PH_3)$ only the H_2-complex forms with strongly acidic HR. When a weaker acid such as CF_3OH is considered, the R–H···H–Ru interaction also becomes a minimum on the potential energy surface. For the third complex, CpReH(CO)(NO), the three species (the dihydrogen complex, the dihydride complex and the hydrogen bonded complex with R–H··H–M) can be obtained from the calculations. The basicity of the metal is therefore an important factor in determining the formation of hydrogen bonds where the M–H bond behaves as acceptor.[11b]

The C–H bond can also engage in weak intra- and intermolecular hydrogen bonds of the type C–H···H–M. They were seen in some of the complexes referred to above, such as $[(\mu\text{-}H)_2Ir_2(\mu\text{-}NH_2)_2(PEt_3)_4(NH_3)_2]\cdot Me_2CO$,[50] with H···H 2.105 Å, and $ReH_5(PPh_3)_3$·indole,[40] with H···H 1.903, 1.929 Å. These and other complexes were hits in a CSD search for short C–H···H–M distances and the observation of the data suggested a new mechanism for cyclometallation.[60] Some other examples have been reported since then and structurally characterized.[61]

Table 1 The charge density and the laplacian of the charge density at some critical points between bonds in model complexes $IrH_3(PH_3)_2(HNCHNH_2)$ and *cis*-$[IrH(OH)(PH_3)_4][PF_6]$

$IrH_3(PH_3)_2(HNCHNH_2)$			*cis*-$[IrH(OH)(PH_3)_4][PF_6]$		
Bond	ρ	$\nabla^2\rho$	Bond	ρ	$\nabla^2\rho$
N2–H12	0.352	−0.2129	H27···F7	0.193	0.714
N2–H13	0.366	−0.2175	H14···F11	0.252	0.782
H9···H12	0.168	0.4251	O1–H27	0.376	−0.234
			Ir2–H14	0.169	0.344

Intermolecular C–H···H–M hydrogen bonds are very weak and normally coexist with other types of not so weak hydrogen bonds involving N–H or O–H, especially if they are intramolecular. Intermolecular C–H···H–M hydrogen bonds are sometimes alone in holding together two molecules, as seen in many of the examples taken in CSD search (October 1996).[41]

$[N(PPh_3)_2]_2[W_2H_2(CO)_8]$ offers an interesting situation, where one C–H bond of a phenyl group approaches a bridging hydride on each side of the molecule.[62] EH calculations[41] indicate that the bridging hydride carries a negative charge, owing to the large electron richnness of the metal centres. Therefore, an electrostatic interaction between the negative hydride and the positively charged H–C is responsible for the short H···H distances. Only a very small positive overlap population of 0.01 is found between the hydrogen atoms. In *mer*-$[(Me_3P)IrH(Cl)(C_5H_4N)]$,[63] each hydride enters an interaction with a C–H bond of the pyridine ring of the adjacent molecule. These two Ir–H···H–C bonds hold together the dimer (data taken from CSD). Rotating the pyridine out of the plane disrupts the bond and increases the energy by *ca.* 58 kJ mol^{-1}.[41] In the other representative compounds of the group,[64] small positive overlap populations were found, and a charge distribution consistent with an electrostatic interaction.[41]

B–H bonds can replace M–H as hydrogen bond acceptors. This was recognized in 1995 and confirmed with a CSD search which gave 22 structures with H···H distance < 2.2 Å. The average H···H distance was 1.96 Å, in a range between 1.7 and 2.2 Å.[6]

The B–H···H–X bond was studied (PCI-80/B3LYP method) in the $[H_3BNH_3]_2$ dimer (Scheme 5, left) and although there is no available structure of this compound, the features seen in the optimized geometry are typical of other boron compounds.[6]

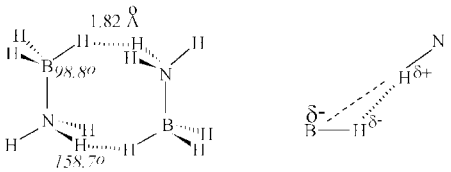

Scheme 5

A particularly interesting aspect of these bonds with boron is that a linear B–H···H–X arrangement is an exception. In $[H_3BNH_3]_2$, the calculated B–H–N angle is 98.8° and N–H–H is 158.7°. Although bent bonds were observed in other cases for weak bonds, here they seem to be rule. An explanation lies in the large negative charge carried by the boron atom, compared to the small negative charge carried by the hydrogen. In order to take advantage of the charge distribution, the H–N points toward the B–H bond rather than toward H (Scheme 5, right).[6]

Epstein *et al.*[65] studied these interactions theoretically (HF) and spectroscopically, using as models $BH_4^+\cdots OH_2$, $BH_4^+\cdots HOCH_3$, $H_3NBH_3\cdots HOCH_3$, $[H_3BNH_3]_2$. They determined minima for the approach of the B–H bond to the donor, for distances 1.836–2.209 Å, always smaller than the sum of van der Waals radii (2.4 Å), and small positive overlap populations between the hydrogen atoms. Contrary to the results of Siegbahn and coworkers,[6] a positive charge is assigned to boron.

Alkorta *et al.*[66] studied dihydrogen bonds for a variety of combinations of acid hydrogen atoms (NH_4^+, HCN, HC≡CH), basic hydrogen atoms (BH_4^-, LiH, BeH_2), and an amphoteric (CH_4), using several methods (HF, MP2) and correcting for BSSE. Frequency calculations were used to check the minima. The charge density at the critical points and the positive values of $\nabla^2\rho$, within the AIM approach, indicated strong hydrogen bonds. The geometries obtained were compared with structures taken from the CSD, which included B–H···H–N, B–H···H–O, B–H···H–C, Al–H···H–C, besides the ones described earlier in ref. 6.

The homonuclear dihydrogen bond?

The CSD searches for short H···H distances also afforded structures not belonging to any of the previous type, namely dimeric species, where both hydrogens must have the same charge and the electrostatic features of hydrogen bonds are not present.[41] The prototype is the dimer of $HMn(CO)_5$.[67] The structure has been determined both by X-ray and neutron diffaraction,[67a] and later by electron diffraction in the gas phase.[67b] There are two polymorphs in the solid, α and β, differing in the packing. In α, the hydride was not located. β-$HMn(CO)_5$ contains dimers with an H···H distance of 2.292 Å, approaching each other in a non linear way, as seen in Fig. 5.

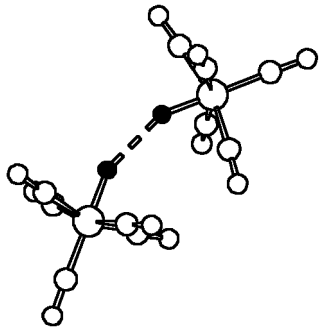

Fig. 5 The $HMn(CO)_5$ dimer, showing the short H···H distance.

The monomer, which exhibits a distortion of the equatorial carbonyls toward the hydride, had been the object of an earlier theoretical study.[68] The approach geometry of the dimer was optimized using DFT calculations.[41] The H···H distance was found to be 2.008 Å, the Mn–H 1.559 Å and the angle between Mn–H bonds 147°. The experimental values are 2.292 Å, 1.601(16) Å, and 155.8°, respectively. The interaction energy was calculated as 0.4 kcal mol^{-1}. A qualitative EH analysis showed that there was some residual bonding character between the two hydrogens, as if an activated H_2 molecule was bridging the two manganese atoms. This same interaction has been suggested by other authors.[5d] A BSSE correction should be performed before giving a final answer to this problem.

The other example of M–H···H–M interaction is provided by the dimer $[(\eta^5\text{-}C_5H_5)_2Zr(\mu\text{-}H)(OSO_2CF_3)]_2\cdot 0.5THF$ with an H···H separation of 2.122 Å.[69] EH calculations indicated a repulsive interaction between the hydrogens. The monomer would be $[(\eta^5\text{-}C_5H_5)_2Zr(H)(OSO_2CF_3)]$, a 16-electron bent metallocene (Scheme 6).

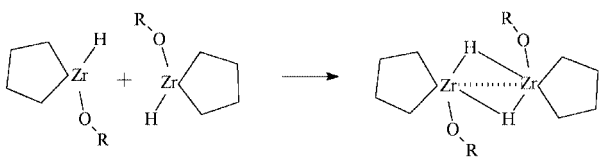

Scheme 6

Two monomers interlock, allowing the hydride of each unit to engage in a bond with the other Zr atom. Although this is a longer bond, it is a covalent bond. The interaction can be termed agostic, as one Zr–H bond donates electrons into the empty orbital of the other Zr.[41]

C–H···H–C interactions in the methane dimer were studied at several levels of theory. MP2 provided the best method to study the approach of two methane molecules. All possible H···H contact arrangements were atractive, and the stabilization energy increases with the number of H···H contacts.[70]

Attractive interactions between identical hydrogen atoms can therefore exist in different contexts, either in organic molecules involving C–H bonds, or in organometallic complexes through M–H bonds.

Conclusions

Theoretical calculations of different types have been performed to study weak hydrogen bonds. Small attractive energies were determined in many cases, but owing to the size of the systems, BSSE corrections were not performed routinely, especially for organometallic systems. On the other hand, many studies rely on DFT (rather than MP2) calculations, which appear to lead to long distances and weak bonds, in spite of consideration of correlation effects. There is still much to be done to reproduce quantitatively these weak interactions: good models, high levels of theory and good basis sets are required. In ionic systems, the role of the counter ion is determining, therefore making calculations even larger and more difficult. The dihydrogen bond M–H···H–X in cationic complexes is one of such systems where the interaction appears to be dependent on the counter ion, as its introduction in the calculation leads to a better geometrical agreement with experimentally determined structures. The 'atom in molecules' approach appears to be very promising to study these weak bonds and to determine their origin, allowing one to distinguish between agostic and hydrogen bonds in some ambiguous situations. The quality of the results depends, however, on the level of theory used in calculating the electron density.

Acknowledgements

Dario Braga and Fabrizia Grepioni (Bologna, Italy) are thanked for having introduced me to the field of weak hydrogen bonds in organometallic compounds, as well as Emilio Tedesco who worked as a PhD student in Bologna and for some periods in Portugal. JNICT, FCT/CNR funding for this collaboration, extending over a couple of years, is acknowledged. I also want to thank, among other collaborators, Pedro E. M. Lopes who, as a PhD student, performed our first DFT calculations in some of the systems described, and whose enthusiasm and persistence led to the AIM pictures of M–H···H–X bonds, and Luis Veiros (IST, Portugal) for many discussions and unlimited help.

Notes and references

1 L. Pauling, *The Nature of the Chemical Bond*, Cornell University Press, Ithaca, NY, 1939.
2 G. A. Jeffrey and W. Saenger, *Hydrogen Bonding in Biological Structures*, Springer-Verlag, Berlin, 1991.
3 M. Nishio and M. Hirota, *Tetrahedron*, 1989, **45**, 7201; M. Nishio, Y. Umezawa, M. Hirota and Y. Taceuchi, *Tetrahedron*, 1995, **51**, 8665; L. R. Hanton, C. A. Hunter and D. H. Purvis, *J. Chem. Soc., Chem. Commun.*, 1992, 1134.
4 (*a*) L. Brammer, J. M. Charnock, P. L. Goggin, R. J. Goodfellow, A. G. Orpen and T. F. Koetzle, *J. Chem. Soc., Dalton Trans.*, 1991, 1789; (*b*) L. Brammer, M. C. McCann, R. M. Bullock, R. K. McMullan and P. Sherwood, *Organometallics*, 1992, **11**, 2339; (*c*) W. Yao, O. Eisenstein and R. H. Crabtree, *Inorg. Chim. Acta*, 1997, **254**, 105.
5 (*a*) J. C. Lee Jr., A. L. Rheingold, B. Muller, P. S. Pregosin and R. H. Crabtree, *J. Chem. Soc., Chem. Commun.*, 1994, 1021; (*b*) J. C. Lee Jr., E. Peris, A. L. Rheingold and R. H. Crabtree, *J. Am. Chem. Soc.*, 1994, **116**, 110 145; (*c*) E. Peris, J. C. Lee Jr., J. R. Rambo, O. Eisenstein and R. H. Crabtree, *J. Am. Chem. Soc.*, 1995, **117**, 3485; (*d*) R. H. Crabtree, O. Eisenstein, G. Sini and E. Peris, *J. Organomet. Chem.*, 1998, **567**, 7; (*e*) R. H. Crabtree, P. E. M. Siegbhan, O. Eisenstein, A. L. Rheingold and T. F. Koetzle, *Acc. Chem. Res.*, 1996, **29**, 348; (*f*) R. H. Crabtree, *J. Organomet. Chem.*, 1998, **577**, 111; (*g*) S. Park, R. Ramachandran, A. L. Lough and R. H. Morris, *J. Chem. Soc., Chem. Commun.*, 1994, 2201; (*h*) A. L. Lough, S. Park, R. Ramachandran and R. H. Morris, *J. Am. Chem. Soc.*, 1994, **116**, 8356; (*i*) D.-H. Lee, B. P. Patel, E. Clot, O. Eisenstein and R. Crabtree, *Chem. Commun.*, 1999, 297.
6 T. R. Richardson, S. Gala, R. H. Crabtree and P. E. M. Siegbahn, *J. Am. Chem. Soc.*, 1995, **117**, 12 875.
7 (*a*) T. Steiner and G. Desiraju, *Chem. Commun.*, 1998, 891; (*b*) F. A. Cotton, L. M. Daniels, G. T. Jordan IV and C. A. Murillo, *Chem. Commun.*, 1997, 1673; (*c*) R. G. A. Bone and R. F. W. Bader, *J. Phys. Chem.*, 1996, **100**, 10 892; (*d*) M. Mascal, *Chem. Commun.*, 1998, 303.
8 J. D. Dunitz, *Chem. Eur. J.*, 1998, **4**, 74; D. Braga, A. Angeloni, F. Grepioni and E. Tagliavini, *Organometallics*, 1997, **16**, 5485; F. Grepioni, G. Cojazzi, S. M. Draper, N. Scully and D. Braga, *Organometallics*, 1998, **17**, 296; Z. N. Chen, H.-X. Zhang, K.-B. Yu, K.-C. Zheng, H. Cai and B.-S. Kang, *J. Chem. Soc., Dalton Trans.*, 1998, 1133; A. J. Amoroso, A. M. Arif and J. A. Gladysz, *Organometallics*, 1997, **16**, 6032; A. D. Burrows, C.-W. Chan, M. M. Chowdhry, J. E. McGrady and D. M. P. Mingos, *Chem. Soc. Rev.*, 1995, 331; S. L. James, D. M. P. Mingos, X. Xu, A. J. P. White and D. J. Williams, *J. Chem. Soc., Dalton Trans.*, 1998, 1335; G. R. Desiraju, *Angew. Chem., Int. Ed. Engl.*, 1995, **34**, 2311; S. Coe, J. J. Kane, T. L. Nguyen L. M. Toledo, E. Wininger, F. W. Fowler and J. W. Lauher, *J. Am. Chem. Soc.*, 1997, **119**, 86; C. B. Aakeröy and K. R. Seddon, *Chem. Soc. Rev.*, 1993, 397; D. Braga and F. Grepioni, *J. Chem. Soc., Dalton Trans.*, 1999, 1; D. Braga and F. Grepioni, *Coord. Chem. Rev.*, 1999, **183**, 19; R. Atencio, L. Brammer, S. Fang and F. C. Pigge, *New J. Chem.*, 1999, **23**, 461.
9 Q. Liu and R. Hoffmann, *J. Am. Chem. Soc.*, 1995, **117**, 10 108.
10 J. F. Malone, C. M. Murray, M. H. Charlton, R. Docherton and A. J. Lavery, *J. Chem. Soc., Faraday Trans.*, 1997, 3429.
11 (*a*) G. Orlova and S. Scheiner, *J. Phys. Chem.*, 1998, **102**, 260; (*b*) G. Orlova and S. Scheiner, *J. Phys. Chem.*, 1998, **102**, 4813; (*c*) D. Adotöledo, V. Aviyenta, J. M. L. Martin and C. Lifshitz, *J. Phys. Chem. A*, 1998, **102**, 6357; (*d*) P. R. Rablen, J. W. Lockman and W. L. Jorgensen, *J. Phys. Chem. A*, 1998, **102**, 3782; (*e*) G. Chung, O. Kwon and Y. Kwon, *J. Phys. Chem. A*, 1998, **102**, 2381; (*f*) I. Alkorta, I. Rozas and J. Elguero, *Theor. Chem. Acc.*, 1998, **99**, 116.
12 (*a*) D. Braga, F. Grepioni, E. Tedesco, M. J. Calhorda and P. E. M. Lopes, *New J. Chem.*, 1999, **23**, 129; (*b*) J. E. McGrady and D. M. P. Mingos, *J. Chem. Soc., Perkin Trans. 2*, 1996, 355.
13 (*a*) P. Pyykkö, *Chem. Rev.*, 1997, **97**, 524; (*b*) P. Pyykkö, in *Crystal Engineering: From Molecules to Crystals to Materials*, ed. D. Braga, F. Grepioni and A. G. Orpen, Kluwer Academic Publishers, Dordrecht, 1999, and references therein; (*c*) E. Ruiz, D. R. Salahub and A. Vela, *J. Phys. Chem.*, 1996, **100**, 12 265; (*d*) A. C. Cooper, E. Clot, J. C. Huffman, W. E. Streib, F. Maseras, O. Eisenstein and K. G. Caulton, *J. Am. Chem.Soc.*, 1999, **121**, 97.
14 (*a*) R. F. W. Bader, *Atoms in Molecules—A Quantum Theory*, Oxford Science Publications, Oxford, 1990; (*b*) R. F. W. Bader, *Chem. Rev.*, 1991, **91**, 893.
15 (*a*) M. T. Carroll, C. Chang and R. F. W. Bader, *Mol. Phys.*, 1988, **63**, 387; (*b*) M. T. Carroll and R. F. W. Bader, *Mol. Phys.*, 1988, **65**, 695.
16 F. H. Allen, J. E. Davies, J. J. Galloy, O. Johnson, O. Kennard, C. F. Mcrae and D. G. Watson, *J. Chem. Inf. Comput. Sci.*, 1991, **31**, 204.
17 T. Steiner, *Chem. Commun.*, 1997, 727; J. Bernstein, R. E. Davis, L. Shimoni and N.-L. Chang, *Angew. Chem., Int. Ed. Engl.*, 1995, **34**, 1555; T. Steiner, *J. Chem. Soc., Perkin Trans. 2*, 1995, 1315; T. Steiner, E. B. Starikov, A. M. Amado and J. J. C. Teixeira-Dias, *J. Chem. Soc., Perkin Trans. 2*, 1995, 1321; G. R. Desiraju, *Acc. Chem. Res.*, 1991, **24**, 290; Y. Gu, T. Kar and S. Scheiner, *J. Am. Chem. Soc.*, 1999, **121**, 9411; T. Steiner, *Chem. Commun.*, 1999, 313.
18 (*a*) D. Braga, K. Biradha, F. Grepioni, V. R. Pedireddi and G. R. Desiraju, *J. Am. Chem. Soc.*, 1995, **117**, 3156; (*b*) D. Braga, F. Grepioni, E. Tedesco, H. Wadepohl and S. Gebert, *J. Chem. Soc., Dalton Trans.*, 1997, 1727; (*c*) D. Braga, P. J. Dyson, F. Grepioni, B. F. G. Johnson and M. J. Calhorda, *Inorg. Chem.*, 1994, **33**, 3218; (*d*) D. Braga, A. L. Costa, F. Grepioni, L. Scaccianoce and E. Tavigliani, *Organometallics*, 1997, **16**, 2070; (*e*) D. Braga, F. Grepioni, E. Tavigliani, J. J. Novoa and F. Mota, *New J. Chem.*, 1998, **22**, 775; (*f*) D. Braga and F. Grepioni, *New J. Chem.*, 1998, **22**, 1159; (*g*) D. Braga, F. Grepioni, P. Sabatino and G. Desiraju, *Organometallics*, 1994, **13**, 3532.
19 I. Berger and M. Egli, *Chem. Eur. J.*, 1997, **3**, 1400.
20 (*a*) D. Braga, F. Grepioni, M. J. Calhorda and L. F. Veiros, *Organometallics*, 1995, **14**, 1992; (*b*) D. Braga, F. Grepioni, H. Wadepohl, S. Gebert, M. J. Calhorda and L. F. Veiros, *Organometallics*, 1995, **14**, 5350; (*c*) D. Braga, F. Grepioni, J. J. Byrne and M. J. Calhorda, *J. Chem. Soc. Dalton Trans*, 1995, 3287.
21 G. P. A. Yap, A. L. Rheingold, P. Das and R. H. Crabtree, *Inorg. Chem.*, 1995, **34**, 3474.
22 D. Y. Yandulov, K. G. Caulton, N. V. Belkova, E. S. Shubina, L. M. Epstein, D. V. Khoroshun, D. G. Musaev and K. Morokuma, *J. Am. Chem. Soc.*, 1998, **120**, 12553.

23 J. Dunitz and R. Taylor, *Chem. Eur. J.*, 1997, **3**, 89.
24 (*a*) S. Suzuki, P. G. Green, R. E. Bumgarner, S. Dasgupta, W. A. Goddard III and G. A. Blake, *Science*, 1992, **257**, 942; (*b*) D. A. Rodham, S. Suzuki, R. D. Suenram, F. J. Lovas, W. A. Goddard III and G. A. Blake, *Nature*, 1993, **362**, 735.
25 (*a*) T. Steiner, E. B. Starikov and M. Tamm, *J. Chem. Soc., Perkin Trans. 2*, 1995, 67; (*b*) N. N. L. Madhavi, A. K. Katz, H. L. Carrell, A. Nangia and G. R. Desiraju, *Chem. Commun.*, 1997, 1953; (*c*) F. H. Allen, J. A. K. Howard, V. J. Hoy, G. R. Desiraju, D. S. Reddy and C. C. Wilson, *J. Am. Chem. Soc.*, 1996, **118**, 4081; (*d*) T. Beringhelli, G. D'Alfonso, M. Panigati, F. Porta, P. Mercandelli, M. Moret and A. Sironi, *Organometallics*, 1998, **17**, 3282; (*e*) F. H. Allen, V. J. Hoy, J. A. K. Howard, V. R. Thalladi, G. R. Desiraju, C. C. Wilson and G. J. McIntyre, *J. Am. Chem. Soc.*, 1997, **119**, 3477.
26 (*a*) D. Philp and J. M. A. Robinson, *J. Chem. Soc., Perkin Trans. 2*, 1998, 1643; (*b*) M.-F. Fan, Z. Lin, J. E. McGrady and D. M. P. Mingos, *J. Chem. Soc. Perkin Trans. 2*, 1996, 563.
27 T.-H. Tang and Y.-P. Cui, *Can. J. Chem.*, 1996, **74**, 1162.
28 C. Kowala and J. A. Wunderlich, *Acta Crystallogr., Sect. B*, 1976, **32**, 820.
29 *Amsterdam Density Functional (ADF) program*, release 2.3, Vrije Universiteit, Amsterdam, The Netherlands, 1995.
30 M. J. Calhorda, I. S. Gonçalves, E. Herdtweck, C. C. Romão, B. Royo and L. F. Veiros, *Organometallics*, 1999, **18**, 3956.
31 M. Brookhart and M. L. H. Green, *J. Organomet. Chem.*, 1983, **250**, 395.
32 A. D. Ryabov, G. M. Kazankov, A. K. Yatsimirsky, L. G. Kuz'mina, O. Yu. Burtseva, N. V. Dvortsova and V. A. Polyakov, *Inorg. Chem.*, 1992, **31**, 3083; A. D. Ryabov, *Chem. Rev.*, 1990, **90**, 403; D. Drago, P. S. Pregosin, M. Tschoerner and A. Albinati, *J. Chem. Soc., Dalton Trans.*, 1999, 2279.
33 (*a*) F. Calderazzo, G. Fachinetti, F. Marchetti and P. F. Zanazzi, *J. Chem. Soc., Chem. Commun.*, 1981, 181; (*b*) F. Cecconi, C. A. Guilardi, P. Innocenti, C. Mealli, S. Midollini and A. Orlandini, *Inorg. Chem.*, 1984, **23**, 922.
34 D. Zhao, F. T. Ladipo, J. Braddock-Wilking, L. Brammer and P. Sherwood, *Organometallics*, 1996, **15**, 1441.
35 A. J. Canty and G. van Koten, *Acc. Chem. Res.*, 1995, **28**, 406.
36 F. Neve, M. Ghedini and A. Crispini, *Organometallics*, 1992, **11**, 3324.
37 O. Eisenstein and Y. Jean, *J. Am. Chem. Soc.*, 1985, **107**, 1177; A. Demolliens, Y. Jean and O. Eisenstein, *Organometallics*, 1986, **5**, 1457.
38 P. L. A. Popelier and G. Logothetis, *J. Organomet. Chem.*, 1998, **555**, 101.
39 (*a*) D. Milstein, J. C. Calabrese and I. D. Williams, *J. Am. Chem. Soc.*, 1986, **108**, 6387; (*b*) R. C. Stevens, R. Bau, D. Milstein, O. Blum and T. F. Koetzle, *J. Chem. Soc., Dalton Trans.*, 1990, 1429.
40 (*a*) J. Wessel, J. C. Lee Jr., E. Peris, G. P. A. Yap, J. B. Fortin, J. S. Ricci, G. Sini, A. Albinati, T. F. Koetzle, O. Eisenstein, A. L. Rheingold and R. H. Crabtree, *Angew. Chem., Int. Ed. Engl.*, 1995, **34**, 2507; (*b*) B. P. Patel, W. Yao, G. P. A. Yap, A. L. Rheingold and R. H. Crabtree, *Chem. Commun.*, 1996, 991; (*c*) J. C. Lee Jr., W. Yao, R. H. Crabtree and H. Rüegger, *Inorg. Chem.*, 1996, **35**, 695; (*d*) B. P. Patel, K. Kavallieratos and R. H. Crabtree, *J. Organomet. Chem.*, 1997, **528**, 205; (*e*) R. Bosque, F. Maseras, O. Eisenstein, B. P. Patel, W. Yao and R. H. Crabtree, *Inorg. Chem.*, 1997, **36**, 5505.
41 D. Braga, P. DeLeonardis, F. Grepioni, E. Tedesco and M. J. Calhorda, *Inorg. Chem.*, 1998, **37**, 3337.
42 E. S.Shubina, N. V. Belkova and L. M. Epstein, *J. Organomet. Chem.*, 1997, **536**, 17.
43 A. L Bandini, G. Banditelli, F. Bonati, G. Minghetti, F. Demartin and M. Manassero, *Inorg. Chem.*, 1987, **26**, 1351.
44 A. J. Blake, T. J. Hyde and M. J. Schroder, *J. Chem. Soc., Dalton Trans.*, 1988, 1165.
45 A. L. Casalnuovo, J. C. Calabrese and J. D. Milstein, *J. Am. Chem. Soc.*, 1988, **110**, 6738.
46 M. L. Buíl, M. A. Esteruelas, E. Oñate and N. Ruiz, *Organometallics*, 1998, **17**, 3346.
47 H. S. Chu, C. P. Lau, K. Y. Wong and W. T. Wong, *Organometallics*, 1998, **17**, 2768.
48 A. M. Baranger, F. J. Hollander and R. G. Bergman, *J. Am. Chem. Soc.*, 1993, **115**, 7890.
49 C. Bianchini, C. Mealli, A. Meli and M. Sabat, *Inorg. Chem.*, 1986, **25**, 4617.
50 A. L. Casalnuovo, J. C. Calabrese and J. D. Milstein, *Inorg. Chem.*, 1987, **26**, 971.
51 J. A. Cabeza, V. Riera, M. A. Pellinghelli and A. Tiripicchio, *J. Organomet. Chem.*, 1989, **376**, C23.
52 J. A. Cabeza, I. Rio, J. M. Fernández-Colinas, A. Llamazares and V. Riera, *J. Organomet. Chem.*, 1995, **494**, 169.
53 (*a*) S. Aime, R. Gobetto and E. Valls, *Organometallics*, 1997, **16**, 5140; (*b*) M. M. Abad, I. Atheaux, A. Maisonnat and B. Chaudret, *Chem. Commun.*, 1999, 381.
54 P. E. M. Lopes and M. J. Calhorda, *J. Organomet. Chem.*; in press.
55 D. Braga, F. Grepioni and J. J. Novoa, *Chem. Commun.*, 1998, 1959.
56 T. Steiner, *Chem. Commun.*, 1999, 2299.
57 E. S. Shubina, N. V. Belkova, A. N. Krylov, E. V. Vorontsov, L. M. Epstein, D. G. Gusev, M. Niedermann and H. Berke, *J. Am. Chem. Soc.*, 1996, **118**, 1105.
58 J. A. Ayllón, C. Gervaux, S. Sabo-Etienne and B. Chaudret, *Organometallics*, 1997, **16**, 2000.
59 N. V. Belkova, E. S. Shubina, A. V. Ionidis, L. M. Epstein, H. Jacobsen, A. Messmer and H. Berke, *Inorg. Chem.*, 1997, **36**, 1522.
60 T. B. Richardson, T. F. Koetzle and R. H. Crabtree, *Inorg. Chim. Acta*, 1996, **250**, 69.
61 W. Xu, A. J. Lough and R. H. Morris, *Can. J. Chem.*, 1997, **75**, 475; L.-Y. Huang, U. R. Aulwurm, F. W. Heinemann, F. Knoch and H. Kisch, *Chem. Eur. J.*, 1998, **4**, 1641.
62 C.-H. Wei, M. W. Marks, R. Bau, S. W. Kirtley, D. E. Bisson, M. E. Henderson and T. F. Koetzle, *Inorg. Chem.*, 1982, **21**, 2556.
63 H. E. Selnau and J. S. Merola, *Organometallics*, 1993, **12**, 1583.
64 (*a*) J. A. Gagliardi, R. G. Teller, P. A. Vella and J. M. Williams, *Cryst. Struct. Commun.*, 1982, **11**, 861; (*b*) A. J. Schultz, J. M. Williams, R. B. Calvert, J. R. Shapley and G. D. Stucky, *Inorg. Chem.*, 1979, **18**, 319; (*c*) G. D. Gusev, D. Nietlispach, I. L. Eremenko and H. Berke, *Inorg. Chem.*, 1993, **32**, 3268; (*d*) S. Krogsrud, L. Toniolo, U. Croatto and J. A. Ibers, *J. Am. Chem. Soc.*, 1977, **99**, 5277; (*e*) R. A. Paciello, P. Kiprof, E. Herdtweck and W. A. Herrmann, *Inorg. Chem.*, 1989, **28**, 2890; (*f*) T. Yoshida, T. Adachi, T. Ueda, T. Tanaka and F. Goto, *J. Chem. Soc., Chem. Commun.*, 1990, 342; (*g*) R. D. Wilson, T. F. Koetzle, D. W. Hart, A. Kvick, D. L. Tipton and R. Bau, *J. Am. Chem. Soc.*, 1977, **99**, 1775; (*h*) D. W. Hart, R. Bau and T. F. Koetzle, *J. Am. Chem. Soc.*, 1977, **99**, 7557; (*i*) T. J. Johnson, A. Albinati, T. F. Koetzle, J. Ricci, O. Eisenstein, J. C. Huffmann and K. G. Caulton, *Inorg. Chem.*, 1994, **33**, 4966.
65 L. M. Epstein, E. S. Shubina, E. V. Bakhmutova, L. N. Saitkulova, V. I. Bakhmutov, A. L. Chistyakov and I. V. Stankevich, *Inorg. Chem.*, 1998, **37**, 3013.
66 I. Alkorta, J. Elguero and C. Foces-Foces, *Chem. Commun.*, 1996, 1633.
67 (*a*) S. J. La Placa, W. C. Hamilton, J. A. Ibers and A. Davison, *Inorg. Chem.*, 1969, **8**, 1928; (*b*) E. McNeill and F. R. Scholer, *J. Am. Chem. Soc.*, 1977, **99**, 6243.
68 S. A. Jackson, O. Eisenstein, M. D. Martin, A. C. Albeniz and R. H. Crabtree, *Organometallics*, 1991, **10**, 3061; E. Folga and T. Ziegler, *J. Am. Chem. Soc.*, 1993, **115**, 5169.
69 G. A. Luistra, U. Rief and M. H. Prosenc, *Organometallics*, 1995, **14**, 1551.
70 J. J. Novoa and M.-H. Whangbo, *J. Chem. Phys.*, 1991, **94**, 4835.

Changing cage structures through inter-ligand repulsions

Alasdair Graham, Stephanie Meier, Simon Parsons and Richard E. P. Winpenny*

Department of Chemistry, The University of Edinburgh, West Mains Road, Edinburgh, UK EH9 3JJ. E-mail: repw01@holyrood.ed.ac.uk

Received (in Cambridge, UK) 18th January 2000, Accepted 29th March 2000
Published on the Web 25th April 2000

The synthesis and crystal structure of decanuclear Co and nonanuclear Ni cages are reported: the cages feature carboxylate and pyridonate ligands and demonstrate that inter-ligand repulsions can lead to novel structures.

Considerable progress has been made in the rational design of supramolecular systems.[1] However, there is little element of design in the synthesis of large polynuclear cages. At present the best we can do is take note of similarities between structures, with the hope that the recognition of trends will lead to targeted synthesis in the future. A family of cages exists which are based on tricapped-trigonal prisms (ttps); such cages are known for the 3d metals chromium,[2] iron,[3] cobalt[4,5] and nickel.[5] As this polyhedron seems so favoured, it appeared the ideal candidate for examining whether the core could be disrupted by using ligands which are sterically demanding thus creating unusual cages. We have reported reactions with pivalate (trimethylacetate) which lead to nickel cages based on tetraicosahedral cores,[5] and here we report further studies which indicate that ligands which are either bigger, such as triphenylacetate, or where there are Coulombic inter-ligand repulsions, such as betaine ($O_2CCH_2NMe_3$), can cause further disruption. We feel this is a general method for synthesising novel cage structures.

Reaction of hydrated cobalt chloride (2.1 mmol) with $Na(O_2CCPh_3)$ (2.1 mmol) and Na(mhp) (4.2 mmol) (mhp = 6-methyl-2-pyridonate) in MeOH (50 ml) at room temperature for one day, followed by evaporation to dryness generates a purple paste. This was then extracted with ethyl acetate (10 ml), and the resulting purple solution allowed to stand at room temperature. Over four months the solution required repeated filtration before small red blocks of $[Co_{10}(OH)_6(mhp)_6(O_2CCPh_3)_6(Hmhp)_3(HCO_3)_3]$ **1** formed in *ca.* 4% yield.† X-Ray analysis‡ reveals a centred ttp which lies on a crystallographic C_3 axis (Fig. 1), however, the capping metal atoms are found on the edges of the prism rather than the faces, as in all previous ttp based structures.

At the centre of the cage is a Co(III) site [Co(2)], with all remaining cobalt atoms present in the +2 oxidation state. Both charge balance, and bond length considerations support this view. This site lies on crystallographic three- and two-fold axes, and the metal is surrounded by six μ_3-hydroxides which each bridge to one cobalt at a vertex of the prism, and one capping the edge. The cobalt sites capping the edges of the prism [Co(3) and symmetry equivalents (s.e.)] also lie on the crystallographic two-fold axes, while the cobalt sites [Co(1) and s.e.] at the vertices of the prism are in general positions. Triphenylacetate ligands bridge in a 1,3-fashion between vertex- and edge-capping cobalts, and the mhp ligands chelate to vertex-cobalt sites with the O atom forming a μ_2-bridge to a neighbouring vertex cobalt. Thus the upper- and lower-trigonal faces of the prism are covered by pyridonate ligands, while the sides of the prism have triphenylacetate groups attached.

This latter feature creates another oddity in the structure. The triphenylacetate groups do not pack sufficiently well to cover the surface of the cage, and two coordination sites on each face of the prism are left vacant. These are occupied by disordered Hmhp and HCO_3^- groups. While the assignment of a coordinated Hmhp fragment is uncontroversial, the assignment as coordinated hydrogencarbonate was only arrived at after careful consideration of the diffraction data. This indicates the presence of a trigonal fragment, and charge balance requires a monoanion in half these sites. Nitrate was not present in the reaction at any stage therefore it appears that atmospheric CO_2 has been incorporated into the structure. The requirement for formation of hydrogencarbonate may explain the long crystallisation times and low yield of this reaction. Preliminary results indicate formation of an equivalent cage with 6-chloro-2-pyridonate (chp). While refinement of this structure is incomplete owing to severe disorder problems involving lattice solvent, it is clear that the metal atoms form a tricapped trigonal prism with the same topology as **1**.

Reaction of CO_2 is also involved in the chemistry which leads to the cage $[Ni_9(CO_3)(OH)_6(chp)_3(Hchp)_3(O_2CCH_2NMe_3)_9Cl]^{6+}$ **2**. This is formed from the reaction of hydrated nickel chloride (1 mmol), Na(chp) (1 mmol) and $O_2CCH_2NMe_3$ (1 mmol) in MeOH (20 ml) followed by evaporation to dryness, and extraction of the green powder with EtOAc. Crystallisation takes a period of three months, whereupon green plates are found in 6% yield.† X-Ray analysis‡ shows the formation of the nonanuclear cage **2**, with a complicated set of anions including four $[Ni(chp)_3]^-$, a half-weight chloride and an anion consisting of chp hydrogen-bonded to Hchp.

The structure of **2** (Fig. 2), which lies on a crystallographic threefold axis, is dominated by two features. Firstly, the central carbonate ion which is μ_6-bridging, leading to a planar hexagon of Ni centres [Ni(1), Ni(2) and s.e.]. Secondly, the preference of the tertiary ammonium groups of the nine betaine ligands to lie as far apart as possible also supports a very open structure. Three of the betaines bridge alternate Ni···Ni vectors of the

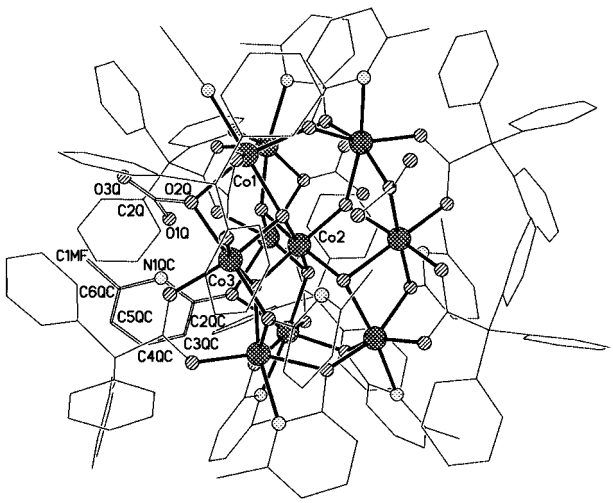

Fig. 1 The structure of **1** in the crystal, viewed perpendicular to the three-fold axis which passes through Co(2). One disordered hydrogencarbonate/Hmhp fragment is shown with open bonds. Selected bond lengths (Å): Co(1)–O(2P) 2.025, Co(1)–O(1A) 2.036, Co(1)–O(2P)′ 2.103, Co(1)–O(1V) 2.128, Co(1)–O(2Q) 2.183, Co(1)–N(1P)′ 2.220, Co(2)–O(1V) 1.898, Co(3)–O(2A) 2.050, Co(3)–O(1V) 2.102, Co(3)–O(2Q) 2.176 Å. Av. esd. 0.008 Å. (Co, cross-hatched; O, diagonal-shaded; N, speckled; C, black lines; H, not shown for clarity).

DOI: 10.1039/b000385i

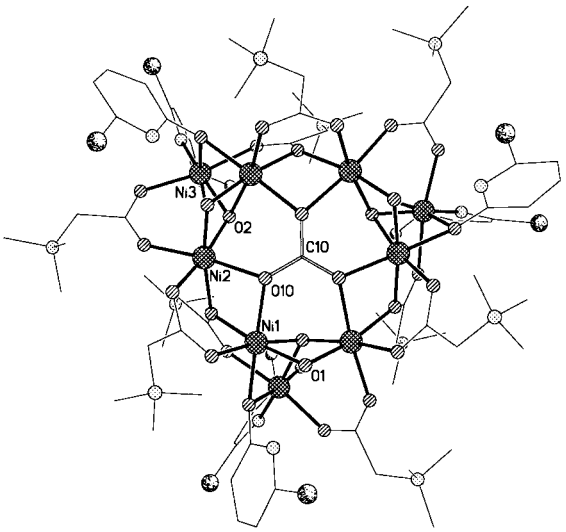

Fig. 2 The structure of hexacation **2** in the crystal, viewed down the threefold axis. The carbonate ion is shown with open bonds. Selected bond lengths: Ni(1)–O(1A) 2.010, Ni(1)–O(2)′ 2.017, Ni(1)–O(1) 2.053, Ni(1)–O(10) 2.057, Ni(1)–O(2B)′ 2.073, Ni(1)–O(21)′ 2.073, Ni(2)–O(2) 1.987, Ni(2)–O(1C) 2.005, Ni(2)–O(2A) 2.022, Ni(2)–O(10) 2.076, Ni(2)–O(1)″ 2.077, Ni(2)–O(2B)′ 2.104, Ni(3)–O(22) 2.000, Ni(3)–O(2) 2.026, Ni(3)–O(2C) 2.030, Ni(3)–O(21) 2.085, Ni(3)–O(1B) 2.097, Ni(3)–N(12) 2.232, Ni(4)–N(13) 2.072, Ni(4)–O(23) 2.118 Å. Av. esd. 0.006 Å. (Ni, cross-hatched; O, diagonal shaded; N, speckled; Cl, heavy random dots; C black lines; H, not shown for clarity).

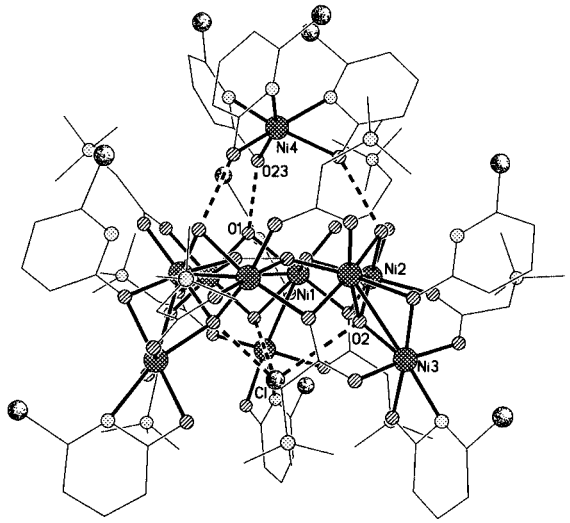

Fig. 3 The H-bonding between **2**, an $[Ni(chp)_3]^-$ unit and a chloride (shading as Fig. 2).

hexagon in a 1,3-fashion. Three further betaines attach three additional Ni atoms below the hexagon (Figs. 2 and 3), while the final three betaines bridge in a 1,1,3-manner, using one O-donor as a μ_2-bridge between Ni atoms within the hexagon, and the second O-donor to bind to one of the Ni atoms below the hexagon.

There are also six hydroxide anions in the cage. Three are μ_3-bridging [O(2) and s.e.], and are also involved in attachment of the three Ni atoms below the hexagonal plane. These three μ_3-OH groups are arranged so that the H atoms point towards the trigonal axis of the cage, and a chloride anion (Cl in Fig. 3) is attached at this point through three H-bonds (O···Cl 3.17 Å). The remaining three OH groups [O(1) and s.e.] are μ_2-bridging and lie above the hexagon, with the H atoms now involved in an interaction with a $[Ni(chp)_3]^-$ anion (Fig. 3). The three chp ligands chelate to the Ni atoms above the hexagon, while the three Hchp ligands act as μ_2-bridges through the O-donors, while forming H-bonds through the protonated N atom (O···N 2.63 Å). We have seen $[Ni(chp)_3]^-$ act as a 'tridentate' H bond acceptor in previous structures.[5]

As in **1**, one fragment, in this case carbonate, must have arisen from reaction of atmospheric CO_2 with the complicated metal–ligand 'soup' present during crystallisation. This, along with the low yields and long crystallisation times suggests that as syntheses these reactions are extremely poor. Conceptually something interesting is happening. By preventing formation of a strongly preferred structure—the ttp cage—we are inevitably going to lower yields and slow reaction times, but this process has also led to activation of small molecules, and, in the case of **2**, incorporation of a templating carbonate ligand which imposes structure on the metal array coordinated to it. This metal array in turn imposes a specific orientation on the zwitterionic betaine ligands, and probably brings them into a proximity they would rather avoid.

We thank the EPSRC for funding for a diffractometer and for a studentship (for A. G.), and the EU for an Erasmus Scholarship (for S. M.).

Notes and references

† Satisfactory elemental analysis obtained.

‡ *Crystal data*: for $C_{177}H_{156}Co_{10}N_9O_{36}\cdot 2H_2O\cdot CH_4O$, **1**·$2H_2O$·$CH_4O$: rhombohedral, space group $R\bar{3}c$, a = 19.054(3), c = 81.85(2) Å, V = 25737(7) Å^3, M = 3642.5, Z = 6 (the molecule lies on a threefold axis), T = 220.0(2) K, $R1$ = 0.0715.

For $C_{193.5}H_{240.5}Cl_{22.5}N_{30}Ni_{13}O_{65}$ **2**·4$[Ni(C_5H_3ClNO)_3]$·0.5Cl. 1.5$(C_5H_3ClNO\cdots C_5H_4ClNO)$·8.5 $C_5H_{10}O_2$: rhombohedral, space group $R\bar{3}$, a = 30.603(2), c = 46.202(5) Å, V = 37473(5) Å^3, M = 5587.5, Z = 6 (the molecule lies on a threefold axis), T = 220.0(2) K, $R1$ = 0.0794.

Data collection, structure solution and refinement for both structures were performed as detailed in ref. 4 using programs SHELXS-97,[6] DIRDIF,[7] SHELXTL-PC[8] and PLATON.[9] Full details have been deposited and will be published later. CCDC 182/1588. See http://www.rsc.org/suppdata/cc/b0/b000385i/ for crystallographic files in .cif format.

1 R. W. Saalfrank and B. Demleitner, in *Transition Metals in Supramolecular Chemistry*, (ed. J. P. Sauvage), *Perspectives in Supramolecular Chemistry Vol. 5*, Wiley, Weinheim, 1999, p. 1; D. L. Caulder and K. N. Raymond, *J. Chem. Soc., Dalton Trans.*, 1999, 1185; P. J. Stang and B. Olenyuk, *Acc. Chem. Res.*, 1997, **30**, 502; M. Fujita, *Chem. Soc. Rev.*, 1998, **27**, 417; C. J. Jones, *Chem. Soc. Rev.*, 1998, **27**, 289.
2 A. S. Batsanov, G. A. Timko, Y. T. Struchkov, N. V. Gérbéléu and K. M. Indrichan, *Koord. Khim.*, 1991, **17**, 662.
3 S. M. Gorun, G. C. Papaefthymiou, R. B. Frankel and S. J. Lippard, *J. Am. Chem. Soc.*, 1987, **109**, 3337.
4 W. Clegg, C. D. Garner and M. H. Al-Samman, *Inorg. Chem.*, 1983, **22**, 1534.
5 C. Benelli, A. J. Blake, E. K. Brechin, S. J. Coles, A. Graham, S. G. Harris, S. Meier, A. Parkin, S. Parsons, A. M. Seddon and R. E. P. Winpenny, *Chem. Eur. J.*, 2000, **6**, 883.
6 G. M. Sheldrick, University of Göttingen, 1997.
7 P. T. Beurskens, G. Beurskens, W. P. Bosman, R. de Gelder, S. Garcia-Granda, R. O. Gould, R. Israel and J. M. M. Smits, DIRDIF-96 program system, University Crystallography Laboratory, University of Nijmegen, The Netherlands 1996.
8 SHELXTL-PC, Bruker AXS, Madison, WI, 1995.
9 A. L. Spek, PLATON, Utrecht University, The Netherlands, 1997.

ChemComm

A combined intramolecular–intermolecular one-pot glycosylation approach for the synthesis of a branched trisaccharide

Serafín Valverde,* Mercedes García, Ana M. Gómez and J. Cristóbal López

Instituto de Química Orgánica General (CSIC), Juan de la Cierva 3, 28006 Madrid, Spain.
E-mail: iqov105@iqog.csic.es

Received (in Cambridge, UK) 24th January 2000, Accepted 29th March 2000
Published on the Web 20th April 2000

Intramolecular and intermolecular glycosidic couplings have been combined in a one-pot protocol for the synthesis of a branched trimannan.

In the last few years strategies for stereocontrol in saccharide synthesis[1,2] based on intramolecular glycosidic couplings have been described,[3–15] and the rapid assembly of oligosaccharides has been addressed through a new chemoselective glycosylation strategy, the one-pot glycosylation,[16–20] which is based on reactivity differences between glycosyl donors.[21–23] Our group[8–10] has been interested in the development of an intramolecular approach for saccharide synthesis (*e.g.* **I→II**, Scheme 1), in which medium rings[8–15] rather than five-membered intermediates[3–7] are formed upon glycosidation. Here, we disclose some preliminary results of the extension of this approach for the synthesis of branched oligosaccharides by intermolecular glycosylation of an external glycosyl donor (*e.g.* **III**) onto the macrocyclic disaccharide (*e.g.* **II→IV**, Scheme 1). More interestingly, the sequence **I→IV** has also been carried out in one-pot operations, and applied to the preparation of the biologically important methyl 3,6-di-*O*-(α-D-mannopyranosyl)-α-D-mannopyranose **9**[24] (Scheme 2).

Phenyl thioglycoside, **1**, was readily transformed into the phthaloyl derivative **2**, and its carboxylic acid function activated on treatment with $SOCl_2$ to furnish **3**. Dialkylstannilen mediated coupling[25,26] of acid chloride **3** with diol **4** gave mixed diester **5** which upon removal of the benzylidene ring led to triol **6**. Glycosylation of **6** (CH_2Cl_2, NIS, TfOAg, 0 °C) led to disaccharide **7**.† Intermolecular glycosylation of glycosyl donor **1** with **7** (CH_2Cl_2, NIS, TfOAg, −20 °C) proceeded regioselectively at *O*-3‡ to give branched trimannose derivative **8**§ (55% yield),¶ which upon deprotection and re-acetylation afforded methyl 3,6-di-*O*-(α-D-mannopyranosyl)-α-D-mannopyranose derivative, **9**.§ A one-pot sequential glycosylation strategy was next examined in which cycloglycosylation of **6** (CH_2Cl_2, TfOAg 0.3 equiv., 0.018 M, −13 °C, 20 min) was followed by addition of **1** (1.1 equiv, −27 °C, 10 min) resulting in the formation of **8** (39% yield) [Scheme 3(a)]. Reaction of premixed **1** and **6** at lower temperature (CH_2Cl_2, TfOAg 0.3 equiv., 0.014 M, −40 °C, 40 min, then −30 °C, 40 min) resulted in the isolation of pseudotrisaccharide **10** (19%) along with unreacted **6** (30%) [(Scheme 3(b)], thus showing that intermolecular glycosylation had taken place prior to the intramolecular coupling.‖ On the hypothesis that the latter result could be a consequence of the difference in reactivities between donors **6** and **1**, owing to the influence of the electron withdrawing ester at *O*-6 in compound **6** when compared with the OTBDPS substituent at *O*-6 in **1**, as recently reported by Ley and coworkers in mannose systems,[22] we decided to examine the one-pot glycosylation of **6** and **11**. Accordingly, treatment of compounds **6** and **11** with TfOAg (CH_2Cl_2, 0.03 M, TfOAg, −8 °C, 10 min) resulted in the formation of a mixture of saccharides from which the branched saccharide **12** (30% yield) was the major observed isomer [Scheme 3(b)].** The structure for trisaccharide **12** was assigned by correlation with compound **13**§ which had been prepared from trimannan **8** [Scheme 3(c)].

In our opinion, several aspects of the synthetic scheme deserve further comment: (i) tethered cyclo-glycosylation of triol **6** takes place with complete regio- and stereo-control at *O*-6 to afford disaccharide **7**; (ii) intermolecular glycosylation of donor **1** and diol **7** occurs regioselectively at *O*-3 to yield trisaccharide **8**. The regio- and stereo-selectivies in the glycosyl couplings observed in this work (i, ii) are similar to those reported by Kaur and Hindsgaul in their relevant synthesis of a related trimannan by classical non-tethered methods with minimal hydroxy group protection.[24]

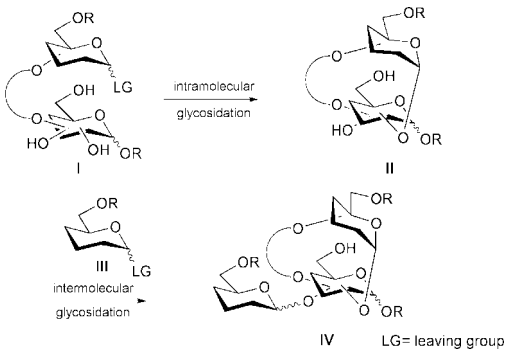

Scheme 1

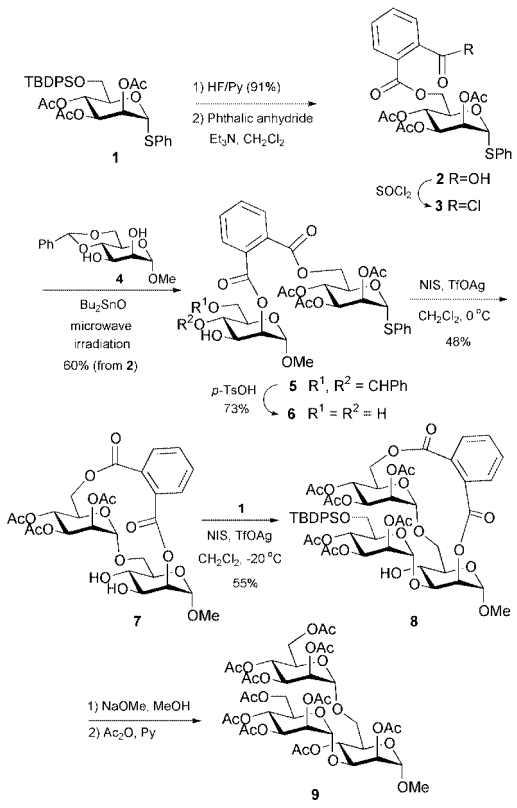

Scheme 2

DOI: 10.1039/b000771o

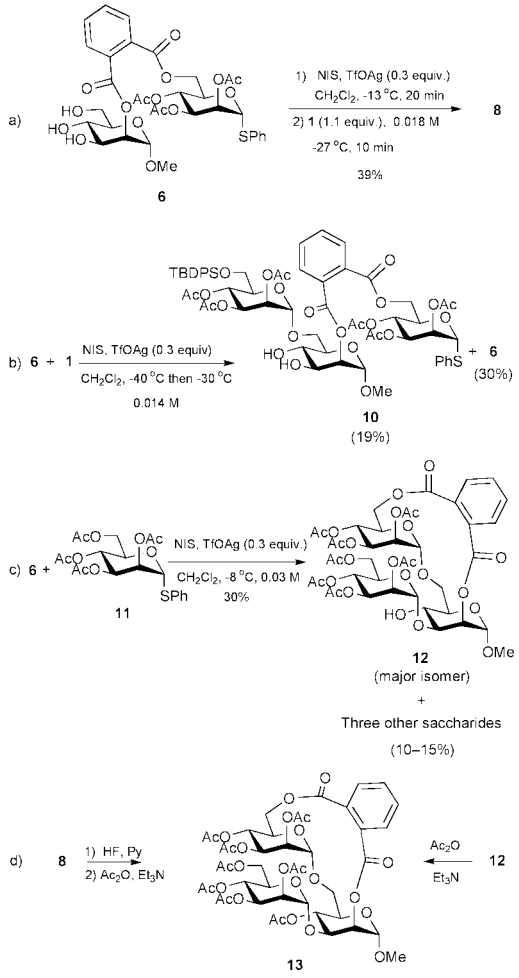

Scheme 3

Another interesting aspect of our results, with implications in the success of the synthetic scheme, is the striking difference in behavior between glycosyl donors **1** and **11**, which is illustrated by the contrast between the results in Scheme 3(b) and 3(c). Thus, while one-pot glycosylation of **6** and **1** [Scheme 3(b)] resulted in the formation of pseudotrisaccharide **10** (with the intermolecular glycosylation taking place prior to the tethered cyclo-glycosylation), the one-pot glycosylation of **6** and **11** [Scheme 3(c)] yielded trisaccharide **12**, as the major isomer formed,** where the cyclo-glycosylation had preceded the intermolecular glycosyl coupling. The tuning of donor reactivity, by changes in the protecting group at *O*-6, in mannopyranosyl donors, **1** and **11**, is thus responsible for this behavior,[22] and, in our opinion, when coupled to further tuning between intra- and inter-molecular glycosidic coupling could open a new avenue for the preparation of branched saccharides and small saccharide libraries.

The procedures outlined here, although not yet optimized, serve to illustrate a novel concept for one-pot glycosylation which relies in the kinetic acceleration of an intramolecular *versus* an intermolecular glycosidic coupling rather than in large disparities between the reactivities of different glycosyl donors. The optimization of this protocol by changes in the concentration and/or nature of the glycosyl donors is currently under study.

This research was supported with funds from the Dirección General de Enseñanza Superior (grants: PB96-0822 and PB97-1244). M. G. thanks the Ministerio de Educación y Cultura for a predoctoral scholarship.

Notes and references

† A minor amount of the corresponding α-1,3 derivative was also isolated 3–5%.

‡ When the reaction was carried out at 0 °C in the presence of 1.7 equiv. of glycosyl donor **1**, a tetrasaccharide resulting from the glycosylation of **1** at positions *O*-3 and *O*-4 in **8** was the only isolated compound (68%).

§ *Selected data*: for **8**: $[\alpha]_D$ −5.7 (*c* 0.5, $CHCl_3$); for **9**: $[\alpha]_D$ +17.6 (*c* 1, $CHCl_3$), API-ES positive (M^+Na^+): *m*/*z* 961.2; for **13**: $[\alpha]_D$ −35.5 (*c* 0.9, $CHCl_3$), API-ES positive (M^+Na^+): *m*/*z* 1007.5.

¶ Hydrolysis of the anomeric thiophenyl group was also observed.

‖ Other attempts to carry out the one-pot glycosylation with premixed **1** and **6** (*e.g.* CH_2Cl_2, TfOAg 0.3 equiv., 0.03 M, −13 °C, 20 min) gave complex reaction mixtures.

** Three other saccharides (10–15%) were also present in the reaction mixture, possibly resulting from the glycosidic coupling of **11** with hydrolyzed **6**.

1 H. Paulsen, *Angew. Chem., Int. Ed. Engl.*, 1990, **29**, 823; H. Kunz, *Angew. Chem., Int. Ed. Eng.*, 1987, **26**, 294.
2 Reviews: K. Toshima and K. Tatsuta, *Chem. Rev.*, 1993, **93**, 1503; G.-J. Boons, *Tetrahedron*, 1996, **52**, 1095; S. J. Danishefsky and M. T. Bilodeau, *Angew. Chem., Int. Ed. Engl.*, 1996, **35**, 1380.
3 F. Barresi and O. Hindsgaul, *J. Am. Chem. Soc.*, 1991, **113**, 9376; F. Barresi and O. Hindsgaul, *Can. J. Chem.*, 1994, **72**, 1447.
4 G. Kim and G. Stork, *J. Am. Chem. Soc.*, 1992, **114**, 1087.
5 M. Bols, *J. Chem. Soc., Chem. Commun.*, 1992, 913; M. Bols, *Acta Chem. Scand.*, 1996, **50**, 931.
6 Y. Ito and T. Ogawa, *Angew. Chem., Int. Ed. Engl.*, 1994, **33**, 1765; Y. Ito and T. Ogawa, *J. Am. Chem. Soc.*, 1997, **119**, 5562.
7 C. Krog-Jensen and S. Oscarson, *J. Org. Chem.*, 1998, **63**, 1780.
8 S. Valverde, A. M. Gómez, A. Hernández, B. Herradón and J. C. López, *J. Chem. Soc., Chem. Commun.*, 1995, 2005.
9 S. Valverde, A. M. Gómez, J. C. López and B. Herradón, *Tetrahedron Lett.*, 1996, **37**, 1105.
10 S. Valverde, M. García, A. M. Gómez and J. C. López, *Synlett*, 2000, 22.
11 T. Ziegler and R. Lau, *Tetrahedron Lett.*, 1995, **36**, 1417; G. Lemanski and T. Ziegler, *Tetrahedron*, 2000, **56**, 563.
12 H. Yamada, K. Imamura and T. Takahashi, *Tetrahedron Lett.*, 1997, **38**, 391.
13 M. Müller, U. Huchel, A. Geyer and R. R. Schmidt, *J. Org. Chem.*, 1999, **64**, 6190.
14 R. J. Tennant-Eyles, B. G. Davis and A. J. Fairbanks, *Chem. Commun.*, 1999, 1037
15 M. Wakao, K. Fukase and S. Kusumoto, *Synlett* , 1999, 1911.
16 S. Raghavan and D. Kahne, *J. Am. Chem. Soc.*, 1993, **115**, 1580.
17 H. Yamada, T. Harada and T. Takahashi, *J. Am. Chem. Soc.*, 1994, **116**, 7919; H. Yamada, T. Harada, H. Miyazaki and T. Takahashi, *Tetrahedron Lett.*, 1994, **35**, 3979; H. Yamada, T. Kato and T. Takahashi, *Tetrahedron Lett.*, 1999, **40**, 1581.
18 H. K. Chenault and A. Castro, *Tetrahedron Lett.*, 1994, **35**, 9145.
19 S. V. Ley and H. W. M. Priepke, *Angew. Chem., Int. Ed. Engl.*, 1994, **33**, 2292; P. Grice, S. V. Ley, J. Pietruszka, H. W. M. Priepke and E. P. E. Walther, *Synlett*, 1995, 781; P. Grice, S. V. Ley, J. Pietruszka, H. M. I. Osborn, H. W. M. Priepke and S. L. Warriner, *Chem. Eur. J.*, 1997, **3**, 431; M.-K. Cheung, N. L. Douglas, B. Hinzen, S. V. Ley and X. Pannecoucke, *Synlett*, 1997, 257; L. Green, B. Hinzen, S. J. Ince, P. Langer, S. V. Ley and S. L. Warriner, *Synlett*, 1998, 440.
20 G.-J. Boons and T. Zhu, *Synlett*, 1997, 809.
21 D. R. Mootoo, P. Konradsson and B. Fraser-Reid, *J. Am. Chem. Soc.*, 1988, **110**, 5583; B. Fraser-Reid, Z. Wu, C. W. Andrews, E. Skowronski and J. P. Bowen, *J. Am. Chem. Soc.*, 1991, **113**, 1434; B. Fraser-Reid, U. E. Udodong, Z. Wu, H. Ottosson, J. R. Merritt, C. S. Rao and C. Roberts, *Synlett*, 1992, 927.
22 N. L. Douglas, S. V. Ley, U. Lücking and S. L. Warriner, *J. Chem. Soc., Perkin Trans. 1*, 1998, 51.
23 Z Zhang, I. R. Ollmann, X.-S. Ye, R. Wischnat, T. Baasov and C.-H. Wong, *J. Am. Chem. Soc.*, 1999, **121**, 734.
24 K. J. Kaur and O. Hindsgaul, *Glycoconjugate J.*, 1991, **8**, 90; K. J. Kaur, G. Alton and O. Hindsgaul, *Carbohydr. Res.*, 1991, **210**, 145.
25 S. David and S. Hanessian, *Tetrahedron*, 1985, **41**, 643; T. B. Grindley, in *Synthetic Oligosaccharides: Indispensable Probes for the Life Sciences*, ed. P. Kovac, ACS, Washington DC, 1994, ch. 4, p. 51.
26 A. Morcuende, S. Valverde and B. Herradón, *Synlett*, 1994, 89; B. Herradón, A. Morcuende and S. Valverde, *Synlett*, 1995, 455.

Effects of monodentate oxazoline ligands in Ni/Al-catalyzed regioselective cyclotrimerization of enones and alkynes†

Shin-ichi Ikeda,* Hirokazu Kondo and Naoyoshi Mori

Faculty of Pharmaceutical Sciences, Nagoya City University, Tanabe-dori, Mizuho-ku, Nagoya 467-8603, Japan. E-mail: ikeshin@phar.nagoya-cu.ac.jp

Received (in Cambridge, UK) 10th February 2000, Accepted 3rd April 2000
Published on the Web 20th April 2000

A nickel and aluminium system including monodentate oxazoline ligands catalyzed the regioselective cyclotrimerization of enones and alkynes.

Since the pioneering work by Reppe,[1] the cyclotrimerization of unsaturated hydrocarbons using various transition-metal catalysts has represented a new method for preparing six-membered cyclic compounds.[2] In particular, intramolecular reactions have been used as an efficient synthetic approach.[3] In contrast, two- or three-component intermolecular cyclotrimerization has not yet been shown to be useful, since it is more difficult to control the chemo-, regio-, and stereo-selectivity. We recently reported a new cyclotrimerization of enones **1** and alkynes **2** by the synergistic effects of nickel and aluminium catalysts (L = PPh_3 in Scheme 1).[4] In this reaction, however, regioselection was dependent on the nature of **2** used (*vide infra*). We report here, a more efficient catalytic system for regioselective cyclotrimerization of **1** and **2**.

We investigated the effects of some ligands (L) on regioselection in the cyclotrimerization of 2-cyclopenten-1-one **1a** with (trimethylsilyl)acetylene **2a** by the $Ni(acac)_2$/L/Me_3Al/PhOH catalytic system (Table 1).‡ The cyclotrimerization

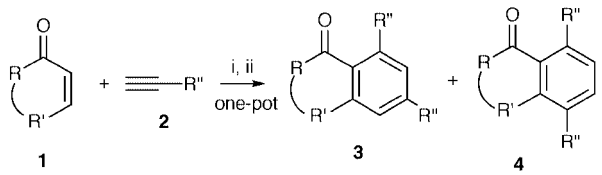

1: R-R' = $-(CH_2)_2-$
2: R" = TMS
3aa, **4aa**: R-R' = $-(CH_2)_2-$, R" = TMS
3ab, **4ab**: R-R' = $-(CH_2)_2-$, R" = Bu^t
3ac, **4ac**: R-R' = $-(CH_2)_2-$, R" = TBDMSO$(CH_2)_2$
3ba, **4ba**: R-R' = $-(CH_2)_3-$, R" = TMS
3bd, **4bd**: R-R' = $-(CH_2)_3-$, R" = Bu
1b: R-R' = $-(CH_2)_3-$
2b: R" = Bu^t
2c: R" = TBDMSO$(CH_2)_2$
2d: R" = Bu
(TBDMS = Bu^tMe_2Si)

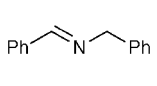

5

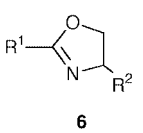

6
6a: R^1 = R^2 = Ph
6b: R^1 = Me, R^2 = Ph
6c: R^1 = Ph, R^2 = Pr^i
6d: R^1 = Ph, R^2 = Bn
6e: R^1 = Ph, R^2 = Me
6f: R^1 = Ph, R^2 = H

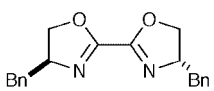

7

Scheme 1 *Reagents and conditions*: i, $Ni(acac)_2$ (10 mol%), L (20 mol%), Me_3Al (80 mol%), PnOH (200 mol%), THF, room temp.; ii, DBU, air, overnight.

† Electronic supplementary information (ESI) available: experimental and characterization data. See http://www.rsc.org/suppdata/cc/b0/b001151g/

adducts (regioisomeric mixture) obtained were treated with DBU in air to convert them to the corresponding aromatic compounds **3** and/or **4**, owing to the ease of regiochemical analysis by ^1H NMR spectroscopy. The reaction in the presence of PPh_3 or $P(C_6H_4Me\text{-}o)_3$ gave **4aa** as the sole product (runs 1 and 2), while the addition of other organophosphorus ligands or $AsPh_3$ failed (runs 3–6). In sharp contrast, the reaction using pyridine or **5** led to the selective synthesis of **3aa** (runs 7 and 8). Monodentate oxazoline ligands **6** strongly affected the regioselective cycloaddition (runs 9–14).[5,6] Most strikingly, when the reaction was carried out in the presence of **6d**–**f**, **3aa** was obtained in 95–96% selectivity (runs 12–14). Thus, ligands **6** in place of triarylphosphines caused *switching* of the regioselectivity in the cyclotrimerization. When a bidentate bis-oxazoline **7** (10 mol%) was used in the reaction,[7] the yield of **3aa** was low, even after 24 h (run 15).

The results of the catalytic cyclotrimerization of a variety of enones **1** and alkynes **2** are summarized in Table 2. In our initial efforts to achieve the regioselective cyclotrimerization of **1** and **2** using a $Ni(acac)_2$/PPh_3/Me_3Al/PhOH catalytic system, **2b** was reacted with **1a** to selectively give **4ab** (entry 1).[4] However, when the reaction was carried out in the presence of a Ni/Al catalytic system using **6e**, **3ab** was obtained predominantly (entry 2). A similar tendency was found in the reactions of **2a** with **1b** (entry 5 *vs*. 6). The product ratio of **8** and **9** derived from the reaction of **1c** with **2a** also depended on the nature of the employed ligands (L) (Scheme 2).[8] On the other hand, the reactions of alkyl-substituted alkynes such as **2c** and **2d** with **1** using **6e** gave a higher regioselection of **3** than those using PPh_3 (entries 3 *vs*. 4 and 7 *vs*. 8).

In summary, we have clarified the effects of monodentate oxazolines **6**, which have scarcely been used as ligands in catalytic reactions, in the Ni/Al-catalyzed cyclotrimerization of

Table 1 Cyclotrimerization of **1a** and **2a** in the presence of the $Ni(acac)_2$/L/Me_3Al/PhOH catalytic system[a]

Run	L	Time/h	Yield[b] (%) (**3aa** + **4aa**)	Ratio[c] (**3aa**:**4aa**)
1[d]	PPh_3	2	33	0:100
2	$P(C_6H_4Me\text{-}o)_3$	2	49	0:100
3	PBu_3	24	Trace	—
4	$P(OPh)_3$	24	Trace	—
5	dppe[e]	24	No reaction	—
6	$AsPh_3$	24	Trace	—
7	Pyridine	24	6	72:28
8	**5**	24	12	80:20
9	**6a**	2	61	86:14
10	**6b**	2	60	72::8
11	**6c**	2	61	85:15
12	**6d**	2	59	95:5
13	**6e**	2	69	96:4
14	**6f**	2	59	96:3
15	**7**	24	23	97:3

[a] Reaction conditions as in Scheme 1. [b] Yield after purification by silica gel chromatography. [c] Determined by ^1H NMR. [d] See ref. 4. [e] 1,2-Bis(diphenylphosphino)ethane.

DOI: 10.1039/b001151g

Table 2 Cyclotrimerization of **1** and **2** in the presence of the $Ni(acac)_2$/L /Me_3Al/PhOH catalytic system (L = PPh_3 *vs.* **6e**)[a]

Entry	1	2	L	Product(s) major, (minor)	Yield[b] (%) (**3** + **4**)	Ratio[c] (**3**:**4**)
1[d,e]	**1a**	**2b**	PPh_3	**4ab** (**3ab**)	45	11:89
2[e]			**6e**	**3ab**	67	100:0
3[d]	**1a**	**2c**	PPh_3	**3ac** (**4ac**)	81	92:8
4			**6e**	**3ac**	87	100:0
5[f]	**1b**	**2a**	PPh_3	**4ba** (**3ba**)	29	17:83
6			**6e**	**3ba**	78	100:0
7[d,g]	**1b**	**2d**	PPh_3	**3bd** (**4bd**)	83	92:8
8[g]			**6e**	**3bd**	81	100:0

[a] Reaction conditions as in Scheme 1. Unless stated otherwise, the cycloadditions were performed with stirring for 2 h. [b] Yield after purification by silica gel chromatography. [c] Determined by ^1H NMR. [d] See ref. 4. [e] The aromatization was carried out with 0.2 M NaOH in MeOH. [f] Reaction time: 24 h. [g] Reagents: **1**:**2**:$Ni(acac)_2$:L:Me_3Al:PhOH = 1:2:0.05:0.1:0.4:4:1.

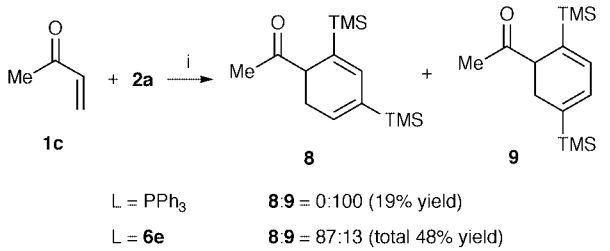

Scheme 2 *Reagents and conditions*: i, **1c** (1 equiv.), **2a** (2 equiv.) $Ni(acac)_2$ (10 mol%), L (20 mol%), Me_3Al (80 mol%), PnOH (200 mol%), THF, room temp., 24 h.

enones **1** and alkynes **2**. The reaction using **6** resulted in the selective formation of **3**, independent on the alkynes used.

This work was supported by a Grants-in-Aid for Scientific Research (No. 11672112) from Japan Society for the Promotion of Science.

Notes and references

‡ *Typical experimental procedure* (entry 2 in Table 2): to a solution of $Ni(acac)_2$ (27 mg, 0.1 mmol) and **6e** (0.1 mmol) in THF (4 mL) was added Me_3Al in 1.0 M hexane solution (0.8 mL) at 0 °C under N_2. After stirring for 5 min, PhOH (190 mg, 2.0 mmol) was added, and the mixture was stirred for 5 min. To the resulting dark red solution were added **1a** (1.0 mmol) and **2b** (2.0 mmol) at 0 °C. After the addition was completed, the whole mixture was stirred at room temperature for 2 h. DBU (350 mg, 2.3 mmol) was added to this reaction mixture in air, and this was again stirred at room temperature overnight. Aqueous HCl (0.2 M, 30 mL) was added, and stirring was continued for 10 min. The aqueous layer was extracted with diethyl ether. The combined organic layer was washed with $NaHCO_3$ and then with brine, dried over $MgSO_4$ for 30 min, filtered, and concentrated *in vacuo*. The residue was purified by column chromatography on silica gel (hexane–AcOEt, 14:1) to yield **3ab** (67%) as the sole product as a colorless oil; δ_H(400 MHz, $CDCl_3$, Me_4Si) 1.36 (s, 9 H, CH_3), 1.47 (s, 9 H, CH_3), 2.66 (t, *J* 6.1 Hz, 2 H, CH_2), 3.07 (t, *J* 6.1 Hz, 2 H, CH_2), 7.29 (s, 1 H, =CH), 7.40 (s, 1 H, =CH); δ_C(100 MHz, $CDCl_3$, Me_4Si) 25.85, 29.75, 31.12, 35.37, 35.95, 37.54 (CH_3, CH_2 and C), 121.20, 122.26, 132.30, 151.41, 157.81, 158.80 (Ar), 206.07 (CO); IR(neat) 1705 (ν_{CO}) cm^{-1}; GC–MS (EI, 70 eV) *m/z* (rel int, %) 244 (M^+, 55), 229 (100). Anal. Calc. for $C_{17}H_{24}O$: C, 83.55; H, 9.90. Found: C, 83.51; H, 9.99%.

1 W. Reppe and W. J. Schweckendiek, *Justus Liebigs Ann. Chem.*, 1948, **560**, 104.
2 N. E. Schore, in *Comprehensive Organic Synthesis*, ed. B. M. Trost and I. Fleming, Pergamon, Oxford, 1991, vol. 5, ch. 9.4, p. 1129; D. B. Grotjahn, in *Comprehensive Organometallic Chemistry II*, ed. L. S. Hegedus, Pergamon, Oxford, 1995, vol. 12, ch. 7.4; N. E. Schore, *Chem. Rev.*, 1988, **88**, 1081.
3 K. P. C. Vollhardt, *Angew. Chem., Int. Ed. Engl.*, 1984, **23**, 539; M. Lautens, W. Klute and W. Tam, *Chem. Rev.*, 1996, **96**, 49.
4 S. Ikeda, N. Mori and Y. Sato, *J. Am. Chem. Soc.*, 1997, **119**, 4779; N. Mori, S. Ikeda and Y. Sato, *J. Am. Chem. Soc.*, 1999, **121**, 2722.
5 D. J. Ager, I. Prakash and D. R. Schaad, *Chem. Rev.*, 1996, **96**, 835; K. Kamata, I. Agata and A. I. Meyers, *J. Org. Chem.*, 1998, **63**, 3113.
6 For the efficiency of mono-oxazoline ligands in a catalytic asymmetric multiple-component domino coupling, see: S. Ikeda, D.-M. Cui and Y. Sato, *J. Am. Chem. Soc.*, 1999, **121**, 4712.
7 A. Pfaltz, *Acc. Chem. Res.*, 1993, **26**, 339.
8 Attempted conversion of a mixture of **8** and **9** to the corresponding aromatic compounds by treatment with base (DBU or NaOH/MeOH) failed.

A mixed-metal $Cu^{II}_2Ni^{II}_2$ complex derived from a phenol-based heterotetranucleating macrocyclic ligand

Masami Yonemura,[a] Hisashi Ōkawa,*[a] Masaaki Ohba,[a] David E. Fenton[b] and Laurence K. Thompson[c]

[a] *Department of Chemistry, Faculty of Science, Kyushu University, Hakozaki, Higashiku, Fukuoka 812-8581, Japan. E-mail: okawascc@mbox.nc.kyushu-u.ac.jp*
[b] *Department of Chemistry, The University of Sheffield, Sheffield, UK S3 7HF*
[c] *Department of Chemistry, Memorial University of Newfoundland, St. John's, Newfoundland A1B 3X7, Canada*

Received (in Cambridge, UK) 17th January 2000, Accepted 3rd April 2000
Published on the Web 25th April 2000

A new phenol-based tetranucleating macrocycle, having two $N(amine)_2O_2$ and two $N(imine)_2O_2$ metal-binding sites in the macrocyclic framework, forms a $Cu^{II}_2Ni^{II}_2$ complex of a defective double-cubane structure.

Heteronuclear metal complexes are of current interest for their physicochemical properties and functions arising from an interplay of dissimilar metal ions in close proximity. In order to provide discrete heterodinuclear metal complexes, phenol-based dinucleating macrocyclic ligands containing two different metal-binding sites have been developed.[1] In contrast, less attention has been paid to multinucleating ligands that can provide mixed-metal complexes with higher nuclearities, though phenol-based macrocyclic ligands having four $N(amine)_2O_2$ or four $N(imine)_2O_2$ metal-binding sites have been reported.[2] We report here, a mixed-metal $Cu^{II}_2Ni^{II}_2$ complex derived from a phenol-based heteronucleating macrocycle R^{4-} that has two $N(amine)_2O_2$ and two $N(imine)_2O_2$ metal-binding sites (Fig. 1).

The macrocycle was obtained as a by-product in the cyclization of *N*,*N*′-dimethyl-*N*,*N*′-ethylenebis(2-aminomethyl-4-bromo-6-formylphenolato)copper(II)[3] ([Cu(L′)]) with ethylenediamine (Scheme 1). A solution of ethylenediamine (0.06 g, 1 mmol) in methanol (5 cm^3) was added dropwise to a hot solution of [Cu(L′)] (0.58 g, 1 mmol) in *N*,*N*-dimethylformamide (40 cm^3), and the mixture was stirred under reflux for 1 h to give a brown precipitate. This was shown to be a mixture of [Cu(L)] and $[Cu_2(R)]$ using FAB mass spectrometry; multiple signals centered at *m/z* 600 and 1200 are assigned to $\{Cu(L)\}^+$ and $\{Cu_2(R)\}^+$, respectively. The separation of the two products by fractional crystallization was difficult owing to the very low solubility of the two complexes in common solvents. The mixture of the complexes (0.20 g) was treated with $NiCl_2{\cdot}6H_2O$ (0.08 g) in methanol to form a $Cu^{II}Ni^{II}$ complex, $[CuNi(L)Cl_2]{\cdot}0.5H_2O$,[4] as dark green microcrystals (0.06 g). The solution remaining after removal of the CuNi complex was diffused with diethyl ether to obtain brown crystals, which were shown to be a mixed-metal tetranuclear $Cu^{II}_2Ni^{II}_2$ complex, $[Cu_2Ni_2(R)(Cl)_2]Cl_2{\cdot}H_2O$ (0.12 g).[5] FAB mass spectrometry showed signals centered at *m/z* 1422 and 1387 which are assigned to $\{Cu_2Ni_2(R)Cl_3\}^+$ and $\{Cu_2Ni_2(R)Cl_2\}^{2+}$, respectively.

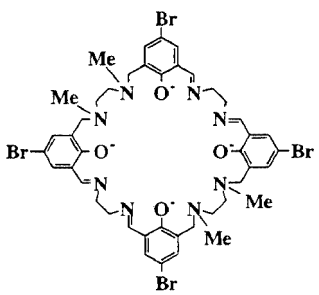

Fig. 1 Chemical structure of R^{4-}.

The structure of the $Cu^{II}_2Ni^{II}_2$ complex was determined by single-crystal X-ray crystallography[6] and an ORTEP view is shown in Fig. 2(a). The asymmetric unit consists of one half of the macrocycle $(R)^{4-}$, one Cu^{II} ion, one Ni^{II} ion and two chloride ions; the remaining two chloride ions and one water molecule are captured in the crystal lattice. Each Cu^{II} resides in an $N(imine)_2O_2$ site and each Ni^{II} resides in an $N(amine)_2O_2$ site. Thus, the Cu migrates from an aminic site to an iminic site in the cyclization process as previously observed in the conversion of [Cu(L′)] into [Cu(L)] and analogues.[7,8] The Cu adopts a square-pyramidal geometry with a chloride ion at the axial site. The Cu–Cl bond distance [2.563(4) Å] is elongated relative to the in-plane bond distances (1.93–1.98 Å) owing to the Jahn–Teller effect. The Ni in the $N(amine)_2O_2$ site has a near

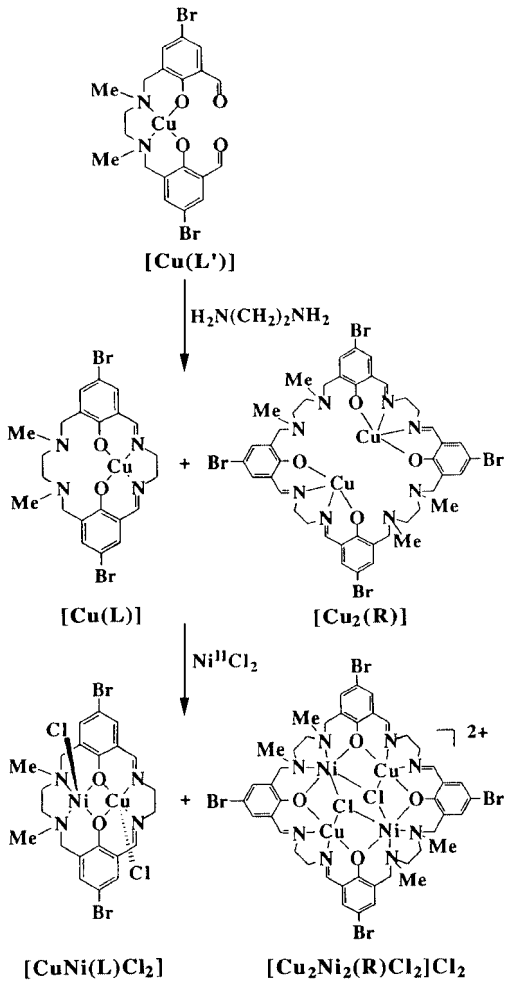

Scheme 1 Synthetic scheme for hetero-dinucleating and -tetranucleating macrocyclic complexes.

DOI: 10.1039/b000516i

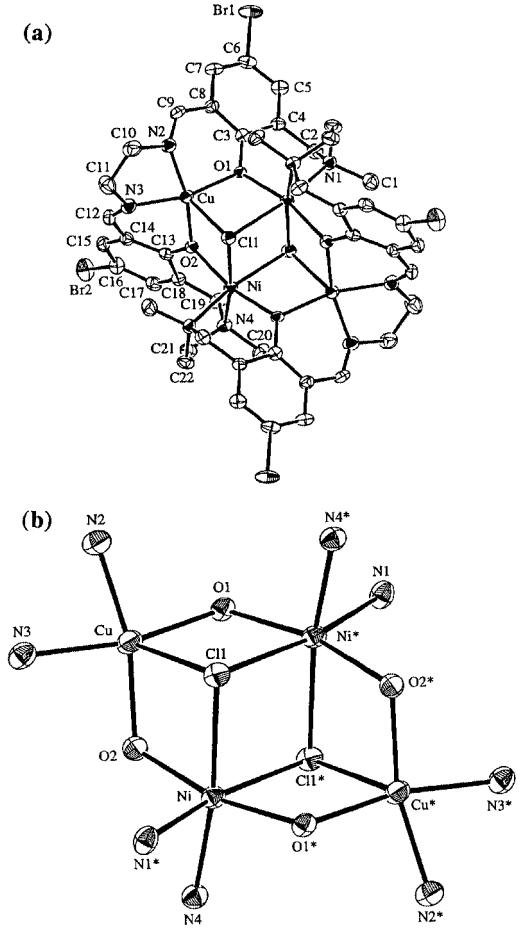

Fig. 2 (a) An ORTEP view of $[Cu_2Ni_2(R)Cl_2]Cl_2{\cdot}H_2O$ and (b) its core structure. Selected bond distances (Å) and angles (°): Cu–O(1) 1.972, Cu–O(2) 1.978(9), Cu–(2) 1.93(1), Cu–N(3) 1.93(1), Cu–Cl(1) 2.563(4), Ni(1)–O(1)* 2.068(9), Ni–O(2) 2.078(9), Ni–N(1)* 2.09(1), Ni–N(4) 2.08(1), Ni–Cl(1) 2.451(4), Ni–Cl(1)* 2.471(4), Cu··Ni 3.375(3), Cu··Ni* 3.366(3), Ni··Ni* 3.543(4); Cu–O(1)–Ni* 112.8(4), Cu–O(2)–Ni 112.6(5), Ni–Cl(1)–Ni* 92.0(1), Cl(1)–Cu–O(1) 81.1(3), Cl(1)–Cu–O(2) 80.6(3), Cl(1)–Ni–O(2) 81.5(3), Cl(1)–Ni–Cl(1)* 88.0(1), Cl(1)–Ni*–O(1) 81.6(3).

octahedral geometry together with two chloride ions [Cl(1) and Cl(1)*] in *cis* positions. The Cl(1) [Cl(1)*] is involved in a μ_3-bridge to Cu, Ni and Ni* (Cu*, Ni and Ni*), forming a defective double-cubane structure [Fig. 2(b)]. The Cu··Ni, Cu··Ni* and Ni··Ni* separations are 3.375(3), 3.366(3) and 3.543(3) Å, respectively. The asymmetric nitrogens N(1) and N(4) [N(1)* and N(4)*] have *R* and *S* configurations, respectively.

The electronic spectrum of the $Cu^{II}_2Ni^{II}_2$ complex in dmso shows an intense band at 354 nm (ε = 14000 M^{-1} cm^{-1} per molecule), a discernible shoulder near 440 nm and a weak band at 747 nm (ε = 380 M^{-1} cm^{-1}). The former intense band is assigned to the π–π* transition associated with the azomethine linkage[9] and the latter weak band to a d–d band due to Cu^{II}. A shoulder near 440 nm can be assigned to a charge-transfer band from Cl^- to Cu^{II}.[8] The d–d transition bands arising from Ni^{II} are not resolved.

The $Cu^{II}_2Ni^{II}_2$ complex has a magnetic moment of 4.94 μ_B (per Cu_2Ni_2) at room temperature, and the moment decreased with decreasing temperature to a plateau value of 3.3 μ_B around 30 K before sharply decreasing below 10 K. Evidently antiferromagnetic spin-exchange interaction operates within the tetanuclear core. Detailed magnetic analyses are under way.

A related macrocycle having four $N(amine)_2O_2$ metal-binding sites forms homotetranuclear Ni^{II} complexes of a rectangular or a non-symmetric core structure.[2] Mixed-metal trinuclear $Cu^{II}_2M^{II}$ (M = Zn or Mg) complexes have also been obtained which consist of a dinuclear $Cu^{II}M^{II}$ core and an isolated Cu^{II} center. The present macrocycle possessing alternating dissimilar $N(amine)_2O_2$ and $N(imine)_2O_2$ sites is a promising ligand for providing mixed-metal complexes of the $M^a_2M^b_2$ type; detailed studies for $Cu^{II}_2M^{II}_2$ complexes (M = Mn, Co, *etc*.) will be shortly reported.

This work was supported by a Grants-in-Aid for Scientific Research (No. 09440231) and an International Scientific Research Program (No. 09044093) from the Ministry of Education, Science and Culture, Japan. Thanks are also due to The Daiwa Anglo–Japanese Foundation and The British Council for support.

Notes and references

1 H. Ōkawa and H. Furutachi, *Coord. Chem. Rev.*, 1998, **174**, 51.
2 K. K. Nanda, K. Venkatsubramanian, D. Majumdar and K. Nag, *Inorg. Chem.*, 1994, **33**, 1581; K. K. Nanda, S. Mohanta, U. Florke, S. K. Dutta and K. Nag, *J. Chem. Soc., Dalton Trans.*, 1995, 3831; S. Mohanta, K. K. Nanda, R. Werner, W. Haase, A. K. Mukherjee, S. K. Dutta and K. Nag, *Inorg. Chem.*, 1997, **36**, 4656 and references therein .
3 M. Yonemura, Y. Matsumura, M. Ohba, H. Okawa and D. E. Fenton, *Chem. Lett.*, 1996, 601.
4 Anal. Found: C, 35.63; H, 3.32; N, 7.48; Cu, 9.12; Ni, 7.64. Calc. for $C_{22}H_{25}Br_2Cl_2CuN_4NiO_{2.5}$: C, 35.79; H, 3.41; N, 7.59; Cu, 8.61; Ni, 7.95%. FAB mass: *m/z* 694 for $\{NiCu(L)Cl\}^+$.
5 Anal. Found: C, 35.84; H, 3.39; N, 7.53; Cu, 8.72; Ni, 6.54%. Calc. for $C_{44}H_{50}Br_4Cl_4Cu_2N_8Ni_2O_5$: C, 35.79; H, 3.41; N, 7.59; Cu, 8.64; Ni, 7.95%.
6 *Crystal data*: $C_{44}H_{50}Br_4Cl_4Cu_2N_8Ni_2O_5$; *M* = 738.42, triclinic, space group $P\bar{1}$, *a* = 11.592(4), *b* = 12.132(3), *c* = 11.024(3) Å, α = 114.66(2), β = 101.92(3), γ = 85.74(2)°, *V* = 11378.3(7) $Å^3$, *Z* = 1, D_c = 1.779 g cm^{-3}, μ(Mo-Kα) = 45.85 cm^{-1} and *T* = 296 K.
CCDC 182/1592. See http://www.rsc.org/suppdata/cc/b0/b000516i/ for crystallographic files in .cif format.
7 M. Yonemura, Y. Matsumura, H. Furutachi, M. Ohba and H. Ōkawa, *Inorg. Chem.*, 1997, **36**, 2711.
8 M. Yonemura, M. Ohba, K. Takahashi, H. Ōkawa and D. E. Fenton, *Inorg. Chim. Acta*, 1998, **283**, 72.
9 B. Bosnich, *J. Am. Chem. Soc.*, 1968, **90**, 627.

ChemComm

Toward high nuclearity ruthenium complexes: creating new binding sites in metal complexes

K. Olof Johansson, John A. Lotoski, Christine C. Tong and Garry S. Hanan*

Department of Chemistry, University of Waterloo, ON, Canada N2L 3G1. E-mail: ghanan@uwaterloo.ca

Received (in Columbia, MO, USA) 20th December 1999, Accepted 31st March 2000
Published on the Web 20th April 2000

The nickel-catalyzed coupling of a ruthenium *ortho*-chloroimine complex creates a new vacant bidentate binding site suitable for generating higher nuclearity ruthenium complexes.

Current interest in ruthenium dendrimers stems from their light-harvesting properties.[1] Enhanced ruthenium content is vital to ascertain an increased probability of light absorption, however, there are inherent difficulties in synthesizing large metallodendrimers.[2] One synthetically powerfully approach (complexes-as-metals/complexes-as-ligands) calls for an iterative protection/deprotection sequence, which consumes both time and material.[3] Another drawback to most systems is the slow increase in metal ion content, which necessitates several more steps to obtain dendrimers with high (>20) metal ion content.[2a,b] In this work, we propose to create new binding sites in metal complexes in order to rapidly increase ion content in metallodendrimers. Previous work has demonstrated that ruthenium complexes containing anionic ligands may be homocoupled,[4] however, new chelating sites have never been created and utilized for further metal complexation.

In our synthetic approach, a ligand (Fig. 1, **a**) containing a bidentate binding site and an *ortho*-chloroimine site forms a ruthenium complex by selectively complexing a metal ion with octahedral coordination geometry in the free bidentate site of the ligand (Fig. 1, **b**). The *ortho*-chloroimine site in **b** is then coupled to create a new bidentate binding site (Fig. 1, **c**), which may in turn bind to another metal ion (Fig. 1, **d**), form a 'complex-metal' [Fig. 1, **e**; *cf.*, $Ru(bpy)_2Cl_2$], or give a closed dendrimer (Fig. 1, **f**). Repeating the steps that lead to **b** and **c** on the 'complex-metal' **e** will afford a new 'complex-ligand', capable of forming large metallodendrimers. The total metal ion content will grow more rapidly than with current approaches.[3] Although many stereoisomers may exist, the differences in their electrochemical and spectroscopic properties are not expected to be great.[5]

Our first goal was to outline the conditions for the nickel-catalyzed coupling reaction. Allowing 4-chloro-2,2′-bipyridine (Clbpy) to react with $Ru(bpy)_2Cl_2{\cdot}2H_2O$ gave monometallic complex **1a** in 92% yield.† Mixing 2 equivalents of **1a** in DMF with an *in situ* generated nickel catalyst[6] gave dimetallic complex **2a** in 57% yield,† in which the newly formed 2,2′:4′,4″:2″,2‴-quaterpyridine (qpy) ligand bridges two metal centres.[7]

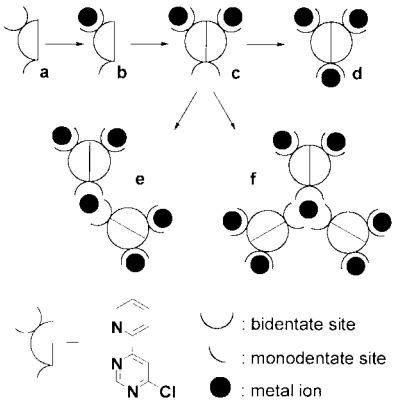

Fig. 1 Ligand **a** [*e.g.* 4-chloro-6-(2′-pyridyl)pyrimidine] contains a bidentate and a monodentate binding site, and reacts with a metal ion to give complex **b**. Homocoupling complex **b** creates a new bidentate binding site in **c**, which may then form a trinuclear complex **d**, a 'complex-metal' **e** (*cf.*, $Ru(bpy)_2Cl_2$), or a closed dendrimer **f**.

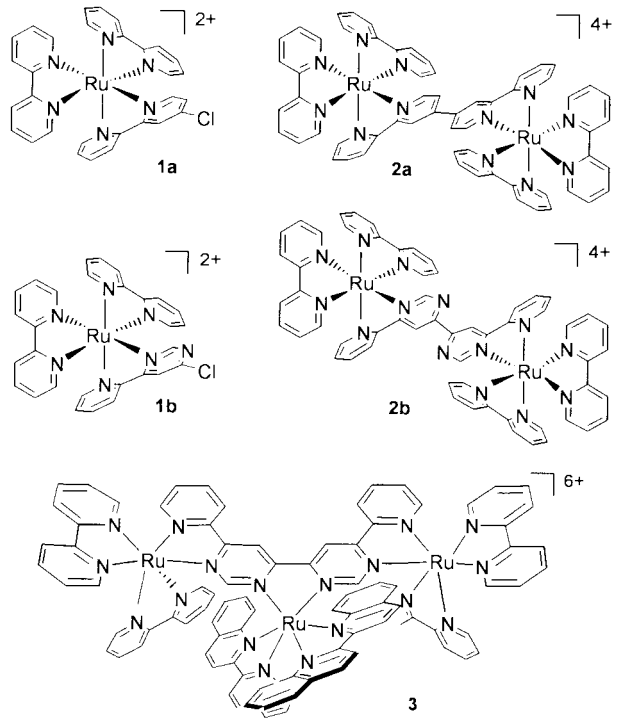

The absorption spectra (acetonitrile solution) of **1a** and **2a** are dominated by ligand-centred (LC) transitions in the UV region and metal-to-ligand charge-transfer (CT) transitions in the visible region.‡ A small red shift is noted in the metal-to-ligand CT band in **2a** (465 nm) compared to **1a** (448 nm) owing to the greater extent of electron delocalization in the qpy bridging (BL) compared to bpy. However, little electronic interaction between the metal centres is revealed by cyclic voltammetry (acetonitrile solution *vs.* SCE). Two chemically reversible coincidental one-electron oxidations are centred at +1.24 V. A reversible one-electron reduction at −1.12 V is followed by three further reductions at −1.42, −1.56 and −1.65 V.

With the proper reaction conditions now available, our next target ligand was 4-chloro-6-(2′-pyridyl)pyrimidine (ClPpy), as metal complexation is favoured at the bidentate pyridylpyrimidine site rather than the *ortho*-chloropyrimidine site. Thus, ClPpy was allowed to react with $Ru(bpy)_2Cl_2{\cdot}2H_2O$ in ethanol–water to afford red monometallic complex **1b** in 79% yield.† It is important to note that no protection/deprotection sequence was required; the bidentate pyridylpyrimidine moiety is a better binding site than the monodentate, sterically encumbered *ortho*-chloropyrimidine site.

DOI: 10.1039/a910257o

In complex **1b**, the Ru-to-BL CT band (480 nm) is lower in energy than the Ru-to-bpy CT band (433 nm), as expected based on earlier work with pyridylpyrimidines.[8] The higher energy UV region is dominated by LC π–π* transitions.[9] The first one-electron reduction is ascribed to the pyridylpyrimidine ligand (−0.92 V) and is followed by coincidental reductions of the two bpy units (−1.52 V).[8] The metal-based oxidation (+1.38 V) is at a slightly higher potential than that of $Ru(bpy)_3$ (+1.26 V), which is consistent with stabilized metal d_π orbitals owing to the presence of the electron deficient pyridylpyrimidine BL.

The addition of **1b** to the Ni-catalyst in DMF[6] gave the purple binuclear complex **2b** in 80% yield.†‡§ Thus, the sterically hindered *ortho*-chloropyrimidine site in **1b** has undergone C–C coupling to give a bidentate diimine site. The Ru-to-BL CT band undergoes a red shift to 554 nm as well as a slight blue shift to 431 nm for the Ru-to-bpy CT band. The latter is expected owing to the stabilization of the metal orbital due to better π-backbonding with the extended BL. The former usually occurs only on binucleation of the same heterocycle.[8] In this case, the electronic conjugation between the two heterocycles is enhanced owing to the *trans*-conformation of the pyridimine nitrogen lone pairs (N_{1p}), which minimize N_{1p}–N_{1p} and C–H···C–H repulsion, leading to a co-planar arrangement.[10]

The first two reductions (−0.57 and −0.99 V) are ascribed to the BL as the reduction of the bridging qpy in **2a** occurs at −1.12 V. Subsequent reductions at bpy (−1.49 and −1.78 V) are in accord with reductions of bpy in diruthenium complexes of diazine heterocycles.[11] The metal-centred oxidations occur at +1.42 V, with an anodic and cathodic separation of 120 mV, indicative of metal–metal interaction rather than irreversibility.[12]

The effectiveness of our approach was confirmed by the reaction of $Ru(biq)_2Cl_2$ (biq = 2,2′-biquinoline) with **2b**, which gave the green trinuclear complex **3** in 55% yield.† The effect of binding the $Ru(biq)_2$ unit into the central chelating site was threefold: it introduced biq LC bands at 271, 360 and 380 nm, a Ru-to-biq CT band at 567 nm and caused a red shift in the Ru-to-BL CT out to 616 nm. These effects are similar to those reported for the polynucleation of Ru(II)(2,3-dipyridylpyrazine)$_3$ with three $Ru(biq)_2$ units.[13] The oxidation potential is as expected for a linear trimetallic system; the external Ru centres oxidize first (+1.58 V), followed by the central Ru centre. However, the latter oxidation occurs outside of the solvent potential window (> +2.00 V) owing to the proximity of two Ru(III) ions and the stabilization of the metal d_π orbital by enhanced back-donation to biq.

The first reduction (+0.04 V) is ascribed to the bridging ligand and is induced by the electron-accepting $Ru(biq)_2$ unit. The next BL reduction (−0.38 V) occurs at a more positive value than the first reduction potential of **2b**. The next two one-electron reductions (−0.83 and −1.20 V) occur on the $Ru(biq)_2$ unit as biq has a lower reduction potential than bpy.[9] The next two waves are two simultaneous one-electron reductions of the external bpy units at −1.50 and −1.80 V. They are fully reversible and follow what one would expect in a heteroligand complex.[9]

Interestingly, the separation between the first and second reduction potential of the bridging ligand in both **2b** and **3** is approximately the same. This suggests that the delocalized BL orbital stays approximately the same 'size' in both **2b** and **3**. Electron delocalisation appears to be as complete with or without a metal ion, restricting rotation about the pyrimidine–pyrimidine C–C bond.

In conclusion, we have introduced a powerful new method for creating new binding sites for metal ions in polynuclear complexes. This methodology is extendable to other types of binding sites and metal ions. We are currently investigating the formation of dendrimeric complexes by using **2b** and analogues as 'complex-ligands' as well as the photophysical properties of these complexes.

We thank the Natural Sciences and Engineering Research Council (Canada), the Research Corporation (Tucson, Arizona), and the University of Waterloo for financial support.

Notes and references

† All new complexes were isolated as their PF_6 salts, recrystallized from acetonitrile–toluene, and characterized by ^1H and ^{13}C NMR, MS, IR, UV-VIS and electrochemistry. Yields are unoptimized.

‡ λ_{max}/nm(MeCN) (ε/L mol^{-1} cm^{-1}); **1a**: 245 (21 500), 287 (61 400), 448 (11 000); **2a**, 244 (45 100), 285 (68 300), 465 (19 100); **1b**: 245 (25 900), 282 (56 100), 433 (11 400), 480 (8300); **2b**: 247 (57 000), 285 (122 000), 431 (24 700), 554 (31 700); **3**: 271 (99 000), 283 (104 000), 358 (37 400), 382 (31 000), 435 (27 000), 567 (20 000), 616 (19 000).

§ To $NiBr_2(PPh_3)_2$ (25 mg, 3.4×10^{-5} mol), Zn-dust (10 mg, 1.5×10^{-4} mol) and NEt_4I (29 mg, 1.1×10^{-4} mmol) was added DMF (3.4 mL).[6] The mixture was stirred under nitrogen at 50 °C for 1 h before adding **1b** (100 mg, 1.1×10^{-4} mol). After 1 h, the mixture was cooled to room temp. and and KPF_6 (0.1 g, 5.4×10^{-4} mol) in water (10 mL) added. The mixture was filtered and the remaining solid was recrystallized twice from acetonitrile–toluene giving **2b** as a purple solid (78 mg, 79%).

1 V. Balzani and F. Scandola, *Supramolecular Photochemistry*, Ellis Horwood, 1991; V. Balzani, *Tetrahedron*, 1992, **48**, 10 443; V. Balzani, *New Sci.*, 1994, Nov. 12, 31.

2 (*a*) M. A. Hearshaw and J. R. Moss, *Chem. Commun.*, 1999, 1; (*b*) G. R. Newkome, E. He and C. N. Moorefield, *Chem. Rev.*, 1999, **99**, 1689; (*c*) E. C. Constable, P. Harverson and M. Oberholzer, *Chem. Commun.*, 1996, 1821.

3 S. Campagna, G. Denti, S. Serroni, A. Juris, M. Venturi, V. Ricevuto and V. Balzani, *Chem. Eur. J.*, 1995, **1**, 211.

4 M. Beley, J.-P. Collin, R. Louis, B. Metz and J.-P. Sauvage, *J. Am. Chem. Soc.*, 1991, **113**, 8521; E. C. Constable, A. M. W. Cargill Thompson and S. Greulich, *J. Chem. Soc., Chem. Commun.*, 1993, 1444; S. Fanni, C. Di Pietro, S. Serroni, S. Campagna and J. G. Vos, *Inorg. Chem. Commun.*, 2000, **3**, 42.

5 R. Hage, A. H. J. Dijkhuis, J. G. Haasnoot, R. Prins, J. Reedijk, B. E. Buchanan and J. G. Vos, *Inorg. Chem.*, 1988, **27**, 2185.

6 M. Iyoda, H. Otsuka, K. Sato, N. Nisato and M. Oda, *Bull. Chem. Soc. Jpn.*, 1990, **63**, 80.

7 Complex **2a** was previously synthesized by the reaction of qpy with 2 equiv. of $Ru(bpy)_2Cl_2$; A. J. Downard, G. E. Honey, L. F. Phillips and P. J. Steel, *Inorg. Chem.*, 1991, **30**, 2259.

8 G. S. Hanan, C. R. Arana, J.-M. Lehn and D. Fenske, *Angew. Chem., Int. Ed. Engl.*, 1995, 1122; G. S. Hanan, C. R. Arana, J.-M. Lehn, G. Baum and D. Fenske, *Chem. Eur. J.*, 1996, 1292; I. G. Phillips and P. J. Steel, *Inorg. Chim. Acta*, 1996, **244**, 3; I. G. Phillips and P. J. Steel, *Aust. J. Chem.*, 1998, **51**, 371.

9 A. Juris, V. Balzani, F. Barigelletti, S. Campagna, P. Belser and A. Von Zelewsky, *Coord. Chem. Rev.*, 1988, **84**, 85.

10 G. S. Hanan, J.-M. Lehn, N. Kyritsakas and J. Fischer, *J. Chem. Soc., Chem. Commun.*, 1995, 765.

11 S. D. Ernst and W. Kaim, *Inorg. Chem.*, 1989, **28**, 1520.

12 B. R. Serr, K. A. Andersen, C. M. Elliott and O. P. Anderson, *Inorg. Chem.*, 1988, **27**, 4499.

13 G. Denti, S. Campagna, L. Sabatino, S. Serroni, M. Ciano and V. Balzani, *Inorg. Chem.*, 1990, **29**, 4750.

ChemComm

Singlet oxygenation of 4-(4-*tert*-butyl-3,3-dimethyl-2,3-dihydrofuran-5-yl)-2-pyridone: non-stereospecific 1,4-addition of singlet oxygen to a 1,3-diene system and thermal rearrangement of the resulting 1,4-endoperoxides to stable 1,2-dioxetanes

Masakatsu Matsumoto,* Shigeru Nasu, Manabu Takeda, Hiroyuki Murakami and Nobuko Watanabe

Department of Materials Science, Kanagawa University, Tsuchiya, Hiratsuka, Kanagawa 259-1205, Japan. E-mail: matsumo@info.kanagawa-u.ac.jp

Received (in Cambridge, UK) 3rd February 2000, Accepted 30th March 2000
Published on the Web 20th April 2000

Singlet oxygen adds easily to a 1,3-diene 1, whose *E–Z* double bond isomerization can not take place, to give a mixture of stereoisomeric 1,4-endoperoxides 2 which rearranges into a thermally stable 1,2-dioxetane 5 selectively on heating in benzene.

Diels–Alder addition of singlet oxygen to certain 1,3-dienes has been reported to give 1,4-endoperoxides with lack of stereospecificity, for which two mechanisms have been proposed. The first is a mechanism where *E–Z* double bond isomerization of 1,3-diene proceeds under the reaction conditions and is followed by a concerted Diels–Alder addition of singlet oxygen.[1] The second is a stepwise addition of singlet oxygen, including participation of zwitterions, which causes isomerization of the initial 1,3-diene unit prior to the intramolecular cyclization.[2] Although these two are crucially different from each other (concerted or stepwise process), both mechanisms include, in common, isomerization of the initial double bond in the substrate followed by cyclization giving the endoperoxide. However, there formally remain other pathway(s) for Diels–Alder addition of singlet oxygen leading to a mixture of stereoisomeric endoperoxides without any isomerization of the initial double bond in a substrate; especially for the stepwise mechanism, if the intramolecular attack of a peroxidic intermediate such as peroxirane and zwitterion occurs onto both π-faces of the remaining double bond, the Diels–Alder addition would give a mixture of stereoisomeric endoperoxides (the third mechanism). We report here an example of non-stereospecific 1,4-addition of singlet oxygen for which the third mechanism would be the most advantageous. In addition, we report a unique rearrangement of the resulting 1,4-endoperoxides which occurs simply on heating without any catalyst to yield thermally stable 1,2-dioxetanes exclusively.

In the course of our investigation on the design of highly efficient chemiluminescent substrates, we attempted to examine the singlet oxygenation of *N*-benzyl-4-(4-*tert*-butyl-3,3-dimethyl-2,3-dihydrofuran-5-yl)-2-pyridone **1a**. When a pyridone **1a** (100 mg) was irradiated together with a catalytic amount of tetraphenylporphin (TPP) in dichloromethane (5 mL) with a 940 W Na-lamp at −78 °C, singlet oxygenation proceeded smoothly (1 h) to give a 65 : 35 mixture of stereoisomeric 1,4-endoperoxides **2a** exclusively (Scheme 1).† The mixture was separated into *cis*-**2a** (major isomer, colorless granules, mp 127.0–128.0 °C) and *trans*-**2a** (minor isomer, colorless oil) by silica gel chromatography. These two endoperoxides were characterized by ^{1}H and ^{13}C NMR, ^{1}H–^{1}H COSY, ^{13}C–^{1}H COSY, NOE, IR and mass spectral analysis.‡ It should be noted that little isomerization between *cis*- and *trans*-**2a** was observed under the reaction conditions and even at higher temperature. The parent pyridone **1b** and *N*-methyl analog **1c** were similarly oxygenated to give the corresponding mixture of isomeric endoperoxides **2b** and **2c**, respectively, though these mixtures could not be separated into pure isomers. These results provide the first example wherein singlet oxygenation of a 1,3-diene gives a mixture of stereoisomeric 1,4-endoperoxides though neither of the carbon–carbon double bonds of the diene system can undergo *E–Z* isomerization.

The rather simple 1,3-diene, (*E,E*)-hexa-2,4-diene (*E,E*-**3**) undergoes stereospecific 1,4-addition of singlet oxygen to give a *cis*-endoperoxide (*cis*-**4**), whereas singlet oxygenation of (*E,Z*)-hexa-2,4-diene (*E,Z*-**3**) affords a mixture of *cis*-**4** (main product) and its *trans*-isomer (*trans*-**4**).[1,2] Gollnick has suggested that the (*E,Z*)-diene isomerizes to the (*E,E*)-isomer prior to the concerted 1,4-addition of singlet oxygen as shown in Scheme 2,[1] and his suggestion has very recently been supported by Motoyoshiya *et al.* who have observed a similar phenomenon for the sensitized photooxygenation of 1-arylpenta-1,3-dienes.[3] On the other hand, O'Shea and Foote have suggested that the non-stereospecific endoperoxide formation from *E,Z*-**3** is most likely rationalized by the formation of a zwitterion which causes the isomerization leading to the *cis*-endoperoxide (*cis*-**4**) as shown in Scheme 3.[2] However, neither mechanism would apply to the present oxygenation of **1** giving **2** without any revision, since no *E-Z* double bond isomerization and only s-*cis*–s-*trans* isomerization can occur for the furanylpyridones **1**.

The concerted Diels–Alder reaction of singlet oxygen with **1** would give only *cis*-**2** so that this mechanism should be ruled out for the reaction giving *trans*-**2**, though *trans*-**2** could be formally produced by an antarafacial attack of singlet oxygen. Thus, a stepwise mechanism should be considered to rationalize

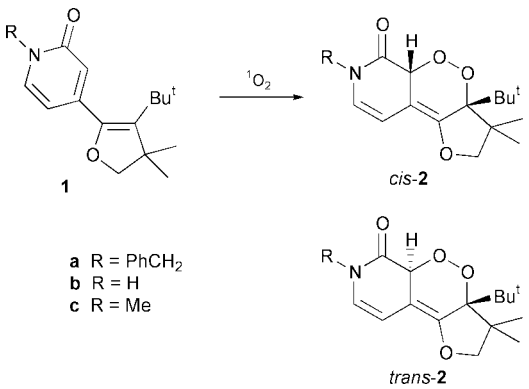

Scheme 1

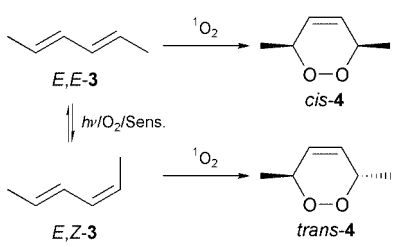

Scheme 2

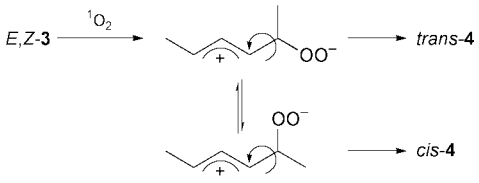

Scheme 3

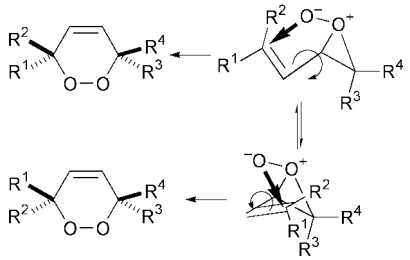

Scheme 4

the present non-stereospecific 1,4-addition of singlet oxygen. Since no *E*–*Z* isomerization of the double bond in pyridone and dihydrofuran rings can occur for **1**, the isomerization of an intermediary zwitterion as in Scheme 3 can not proceed. The most likely explanation is that the initially formed peroxirane or zwitterion attacks the remaining double bond of the starting 1,3-diene from both π-faces. This process should be operable when two ethylene units of the 1,3-diene lie far from apart in the same plane as illustrated in Scheme 4 in which a peroxirane intermediate is adopted for convenience. Such structure of a 1,3-diene system is most likely feasible for **1** because of steric repulsion between the pyridone ring and a *tert*-butyl group in the dihydrofuran ring.§ Although singlet oxygen attacks possibly in the first step to a double bond of the pyridone and/or the double bond of dihydrofuran for **1**, the initial addition of singlet oxygen to the former may be more likely since the addition to the latter may lead more or less to a dioxetane as in the case of 4-*tert*-butyl-3,3-dimethyl-2,3-dihydrofurans bearing an aryl[4] or a styryl group[5] at the 5-position.

Although endoperoxides *cis* and *trans*-**2a** were not isomerized to each other, both endoperoxides changed gradually into a dioxetane **5a** even at room temperature. On heating in hot benzene, **2a** was transformed selectively into **5a** (colorless needles, mp 114.0–115.0 °C)¶ which was stable enough for handling at room temperature though it decomposed into a ketoester **6a** in hot toluene (Scheme 5). It should be noted that the thermolysis of **5a** (90 °C, toluene) gave light (λ_{max} = 411 nm) whose spectrum was in good agreement with the fluorescence spectrum of **6a**. Both reaction rates for isomerization of endoperoxide **2a** to 1,2-dioxetane **5a** and for decomposition of dioxetane **5a** to ketoester **6a** followed first-order kinetics. Thus, these reaction rates were measured in toluene-d_8 at various temperatures by ^{1}H NMR spectroscopy, and their activation

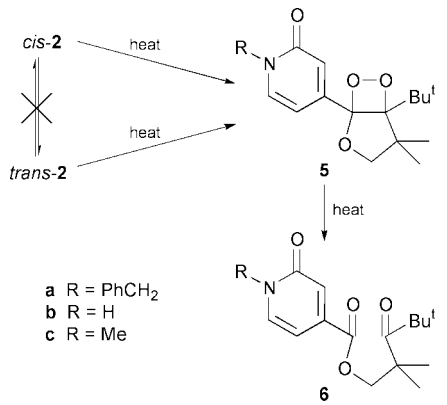

Scheme 5

Table 1 Thermal rearrangement of 1,4-endoperoxides **2a** to 1,2-dioxetanes **5a** and thermal decomposition of **5a** to ketoesters **6a**[ab]

Peroxide	$\Delta H^{\ddagger}$/kcal mol^{-1}	$\Delta S^{\ddagger}$/cal K^{-1} mol^{-1}	$\Delta G^{\ddagger}$/kcal mol^{-1}	$t_{1/2}$ (25 °C)/yr
cis-**2a**	29.8	13.9	25.7	0.07
trans-**2a**	29.1	11.9	25.5	0.05
5a	26.2	−9.5	29.1	19.6

[a] Rearrangement of **2a** to **5a** was carried out in toluene-d_8 at 40–60 °C, whereas decomposition of **5a** to **6a** was performed in toluene-d_8 at 90–110 °C. [b] For all the Arrhenius plots, $r > 0.999$.

parameters were estimated from Arrhenius plots as summarized in Table 1, which shows that dioxetanes **5a** are far more stable than endoperoxides **2a**. The other endoperoxides **2b** and **2c** rearranged thermally also into the corresponding dioxetanes **5b** and **5c**, whose thermolysis gave ketoesters **6b** and **6c**, respectively. Free energies of activation ($\Delta G^{\ddagger}$/kcal mol^{-1}) for these peroxides were also estimated as follows; **2b**: 24.3–24.4, **2c**: 24.4–24.7, **5b**: 27.1 and **5c**: 28.4.

Various 1,4-endoperoxides have been known to undergo acid-catalyzed decomposition to carbonyl fragments, presumably through 1,2-dioxetanes, whose spectroscopic identification and/or isolation has not been achieved in most cases. Schaap *et al*. have reported a successful spectroscopic identification of a dioxetane formed by the rearrangement of endoperoxide, and suggested that the relatively unstable dioxetane as a chemiluminescent substrate can be 'stored' as a precursor endoperoxide and generated when needed.[6] In contrast, the present dioxetanes **5** are far more stable than endoperoxides **2** so that they can be stored as such rather than be regarded as precursors.

Notes and references

† Similar singlet oxygenation of **1a** at 0 °C gave a 57 : 43 mixture of *cis* and *trans* isomers of **2a**.

‡ *Selected data*: for *cis*-**2a**: δ_H(500 MHz, $CDCl_3$) 1.11 (s, 3H), 1.15 (s, 9H), 1.25 (s, 3H), 3.81 (d, *J* 8.2 Hz, 1H), 4.41 (d, *J* 15.1 Hz, 1H), 4.45 (d, *J* 8.2 Hz, 1H), 4.82 (d, *J* 15.1 Hz, 1H), 5.13 (d, *J* 2.3 Hz, 1H), 5.59 (d, *J* 5.7 Hz, 1H), 6.95 (dd, *J* 5.7 and 2.3 Hz, 1H), 7.16–7.20 (m, 2H), 7.28–7.38 (m, 3H); δ_C(125 Hz, $CDCl_3$) 18.1, 24.9, 26.4, 36.5, 45.3, 47.0, 78.1, 80.6, 82.6, 106.0, 113.1, 128.1, 128.2, 129.0, 134.9, 135.1, 138.3, 167.4; MS (*m*/*z*, %) 369 (M^+, 46), 325 (4), 313 (9), 285 (12), 284 (16), 230 (33), 212 (60), 91 (100).

For *trans*-**2a**: δ_H(500 MHz, $CDCl_3$) 1.11 (s, 3H), 1.12 (s, 9H), 1.28 (s, 3H), 3.79 (d, *J* 8.2 Hz, 1H), 4.31 (d, *J* 15.4 Hz, 1H), 4.49 (d, *J* 8.2 Hz, 1H), 5.06 (d, *J* 15.4 Hz, 1H), 5.23 (d, *J* 2.3 Hz, 1H), 5.61 (d, *J* 5.5 Hz, 1H), 6.93 (dd, *J* 5.5, 2.3 Hz, 1H), 7.19–7.23 (m, 2H), 7.30–7.39 (m, 3H); δ_C(125 Hz, $CDCl_3$) 18.0, 24.8, 26.7, 36.3, 45.3, 46.9, 78.8, 80.7, 83.2, 105.7, 113.4, 128.0, 128.3, 129.1, 134.5, 135.2, 138.2, 167.0; MS (*m*/*z*, %) 369 (M^+, 47), 313 (10), 285 (13), 284 (17), 230 (35), 212 (63), 91 (100).

§ An MM2 calculation suggested that the torsion angle between the pyridone ring and the dihydrofuran ring in **1a** was 73.4° at the most stable conformation.

¶ *Selected data* for **5a**: δ_H(500 MHz, $CDCl_3$) 1.08 (s, 9H), 1.13 and 1.31 (2 s, 6H), 3.80 (d, *J* 8.3 Hz, 1H), 4.54 (d, *J* 8.3 Hz, 1H), 5.09 (d, *J* 14.4 Hz, 1H), 5.20 (d, *J* 14.4 Hz, 1H), 6.32 (dd, *J* 7.4, 1.8 Hz, 1H), 6.94 (d, *J* 1.8 Hz, 1H), 7.23–7.38 (m, 6H); δ_C(125 Hz, $CDCl_3$) 18.2, 24.9, 27.0, 36.7, 45.5, 51.8, 80.7, 105.3, 105.7, 114.7, 121.4, 128.1, 128.1, 129.0, 135.9, 136.7, 147.8, 161.9; MS (*m*/*z*, %) 369 (M^+, 51), 337 ($M^+ - O_2$, 2), 313 (11), 230 (39), 212 (71), 185 (15), 91 (100).

1 K. Gollnick and A. Griesbeck, *Tetrahedron Lett.*, 1983, **24**, 3303.
2 K. E. O'Shea and C. S. Foote, *J. Am. Chem. Soc.*, 1988, **110**, 7167.
3 J. Motoyoshiya, Y. Okuda, I. Matsuoka, S. Hayashi, Y. Takaguchi and H. Aoyama, *J. Org. Chem.*, 1999, **64**, 493.
4 M. Matsumoto, H. Murakami and N. Watanabe, *Chem. Commun.*, 1998, 2319.
5 M. Matsumoto, T. Ishihara, N. Watanabe and T. Hiroshima, *Tetrahedron Lett.*, 1999, **40**, 4571.
6 A. P. Schaap, P. A. Burns and K. A. Zaklika, *J. Am. Chem. Soc.*, 1977, **99**, 1270.

ChemComm

A new approach for the synthesis of conjugated/non-conjugated poly(phenylene vinylene)–polyacrylamide copolymers

Ruifeng Zhang,* Guoqiang Zhang and Jiacong Shen

Key Lab of Supramolecular Structure and Spectroscopy, Department of Chemistry, Jilin University, Changchun 130023, P.R. China. E-mail: zhangrf@yahoo.com

Received (in Cambridge, UK) 2nd February 2000, Accepted 13th March 2000
Published on the Web 26th April 2000

A new type of poly(phenylene vinylene)–polyacrylamide copolymer has been synthesized by a modified sulfonium precursor route; the obtained copolymer is composed of hydrophobic PPV conjugated blocks and hydrophilic polyacrylamide segments; these two parts show strong phase separation and produce a multiphase structure in the solid state.

Some of the most promising candidates for the active layer in organic light-emitting diodes (LEDs) are polymers derived from poly(phenylene vinylene) (PPV).[1–5] Fully conjugated PPV derivatives often show low luminescent efficiencies owing to non-radiative decay resulting from the movement of excitons to quenching centers.[6,7] Exciton confinement can be achieved by preparing a polymer with low HOMO–LUMO gap energy blocks in between high ones. Therefore, attention has been paid to synthesizing conjugated/non-conjugated PPV derivatives. One way to realize this structure is to interrupt the conjugation of the polymer at short intervals with non-conjugated segments by sample modification during PPV synthesis.[8,9] Another way to obtain a polymer with well defined fluorescent units makes use of a Wittig condensation of an arylene bisphosphonium salt with a spacer containing bis(benzaldehyde).[10–12]

Recently, we found a new method for the synthesis of such copolymers. Our method originated from investigating the mechanism in the sulfonium precursor route (SPR) to PPV derivatives established by Wessling and Zimmerman.[13,14] We observed what happened when water-soluble monomer acrylamide (Am) was added in the polymerization of bis(sulfonium) compound **1** in an aqueous system, and found that copolymerization occurred in which the *p*-quinodimethane intermediate **2** might act as both monomer and free radical initiator. Scheme 1 outlines the process of the formation of PPV/polyacrylamide copolymers. Obviously, this copolymerization strongly supports a free radical mechanism for SPR. In fact, the copolymerization proceeds so well that the color of the product can be tuned by the feed ratio of two monomers. In other words, the conjugated length of the PPV blocks is shortened by the incorporation of polyacrylamide (PAm) segments in between. Furthermore, this kind of copolymerization also offers an opportunity to prepare amphiphilic polymers which may be very useful for self-assembly into ultrathin films and nanocomposites.

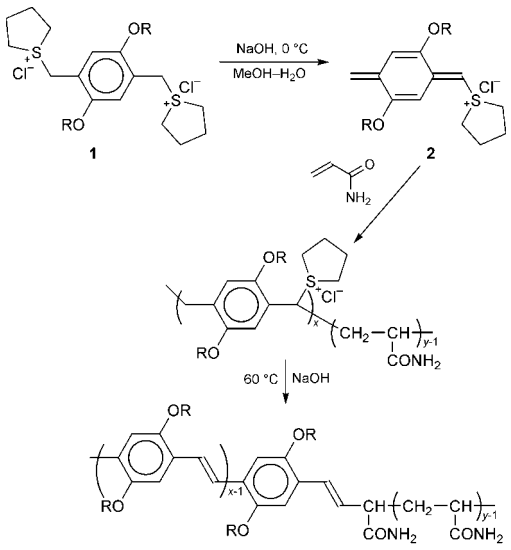

Scheme 1

The copolymers were synthesized through the following procedure: under vigorous stirring and nitrogen atmosphere, a solution of bis(sulfonium) salt **1** (1.04 g, 2 mmol) in MeOH (10 ml) was added dropwise to a solution of acrylamide and NaOH (0.08 g, 2 mmol) in 25 ml of water. The temperature was kept at 0 °C for 1 h. Then additional aqueous NaOH (0.5 M, 10 ml) was added, and the reaction mixture was heated to 60 °C for another hour. An orange precipitate was obtained and filtered off. After washing well with water and MeOH, the product was dried *in vacuo*. When the amount of acrylamide exceeded 20 g the produced copolymer was water-soluble. The polymer was purified by dialyzing against water for three days (3×1000 ml) to remove unreacted monomers and some acrylamide homopolymer (polymers with molecular weight of less than 12 000 were removed). The final solution was poured into a large amount of MeOH, and a pale yellow polymer was obtained and washed with refluxing MeOH and then dried *in vacuo*. Except for the water-soluble copolymer, the other polymers show poor solubility in solvents such as THF and DMF, probably owing to hydrogen bonding between amide groups. However, they are partially soluble in $CHCl_3$, which allows the photoluminescence (PL) spectra to be obtained. Such a low solubility, however, is not sufficient for GPC measurements. Therefore we focused our attention on the viscosity of the water-soluble copolymer at various concentrations and the GPC result obtained in aqueous solution. The composition of the copolymers were calculated according to the amount of nitrogen obtained by elemental analysis.

Table 1 summarizes the results of copolymerizations for different concentrations of acrylamide. With an increase in the amount of acrylamide in the reaction system, the weight percentage of PAm segments in the copolymers increase, while the product changes from red to pale yellow, and the PL peak shifts from 550 nm (yellow) to 509 nm (green). All these data showed that the conjugation length of the PPV block became shorter as more Am units were inserted into the polymer chain. However, even when a large excess of acrylamide was added to the reaction system, we failed to produce a copolymer with sufficiently short conjugated lengths of PPV blocks to produce blue luminescence. It seems that the present copolymerization is quite different from those in traditional free radical copolymerizations for vinyl monomers. The *p*-quinodimethane intermediate **2** shows a strong tendency to undergo homopolymerization even under very dilute concentrations and in the presence of a large excess of Am. The FTIR spectra of all the prepared copolymers support the structure of copolymer suggested. Peaks characteristic of PPV blocks such as at 1203 cm^{-1} (C–O stretching), 2961 cm^{-1} (C–H stretching of CH_3) and 970 cm^{-1} (C–H bending of *trans* vinylene) can be clearly

DOI: 10.1039/b000926l

Table 1 Results of copolymerizations using various amounts of acrylamide

Sample	Acrylamide/g	Weight of polymer obtained/g	Colour	PAm segemnt (wt%)	Solubility (in $CHCl_3$)	λ_{max} (PL) ($CHCl_3$)/nm
1	0	0.76	Red	0	Soluble	550 (λ_{ex} = 420 nm)
2	5	1.05	Red–orange	38	Slightly soluble	542 (λ_{ex} = 420 nm)
3	10	1.58	Orange	47	Slightly soluble	536 (λ_{ex} = 420 nm)
4	15	2.46	Yellow	64	Slightly soluble	524 (λ_{ex} = 420 nm)
5	20	3.85	Pale yellow	82	Water-soluble	509 (H_2O) (λ_{ex} = 400 nm)

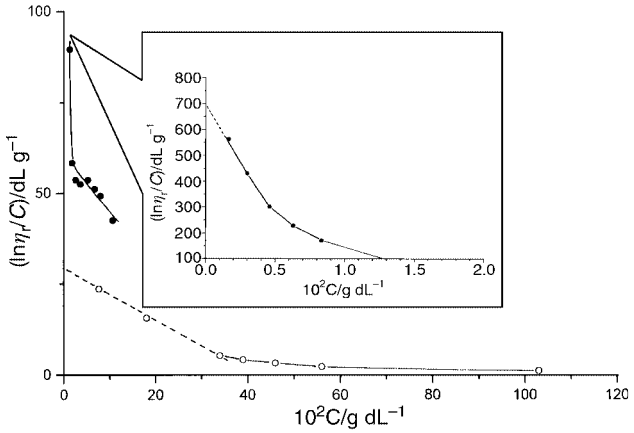

Fig. 1 The dependence of $\ln\eta_r/C$ on the concentration of polyacrylamide (○) or copolymer (●) in water at 30 °C.

observed. Signals from PAm segments including at 3400 cm^{-1} (wide band, N–H stretching of amide) and 1669 cm^{-1} (C=O stretching of amide) also appear in the spectra.

Fig. 1 shows the viscosity of the water-soluble copolymer and pure PAm measured at different concentrations in water at 30 °C; η_r is the relative viscosity using water as a reference. The insert is an enlarged plot for the copolymer at very low concentration. For both polymers, the value of $\ln\eta_r/C$ increases sharply as the concentration of polymer approaches zero. Obviously, the viscosity of the copolymer is higher than that of PAm at any concentration. By extrapolation of $\ln\eta_r/C$ to C = 0, it is seen that the intrinsic viscosity of the copolymer ($[\eta]$ = 700 dL g^{-1}) is 24 times as high as that of PAm ($[\eta]$ = 28 dL g^{-1}). According to the formula $[\eta] = KM_\eta^\alpha$ ($K = 6.31 \times 10^{-3}$, α = 0.80, T = 30 °C),[15] M_η of PAm is calculated as 3.46×10^4. Owing to the absence of a relationship between M_η and $[\eta]$, an exact value of M_η of the copolymer could not be obtained. We also studied M_w of the two polymers by GPC using sulfonated polystyrene as a standard in aqueous medium. The result showed that M_w of PAm and the copolymer were 4.12×10^4 and 9.67×10^4, respectively, with a PDI of 2.13 and 2.74, respectively. If we calculate the M_η of the copolymer using the relation KM_η^α, the result is 2×10^6, much higher than M_w of the copolymer measured by GPC. The above result confirmed that a high molecular weight copolymer was produced by copolymerization. The extraordinarily high viscosity of the copolymer may well be due to the presence of rod-like and alkyl chain-bearing PPV blocks which can aggregate with each other and form hydrophobic domains in aqueous medium. These domains are dispersed in solution and act as solid particles, or on the other hand, as physically cross-linking joints which link PAm segments to form a network and therefore considerably lower the mobility of the polymer solution. A multiphase structure in the solid state was revealed by TEM observation after hydrolysis of the copolymer in KOH solution and then treating with $BaCl_2$. Barium ions were introduced to increase the contrast of the two microphases in electron transmission. Fig. 2 is a TEM photograph of the Ba^{2+}-modified copolymer which can be denoted as poly[2,5-bis(heptyloxy)phenylene vinylene-*co*-Ba(acrylate)$_2$]. The light regions correspond to the hydrophobic domains occupied by PPV blocks, while the dark regions correspond to the hydrophilic phase mainly composed of poly[Ba(acrylate)$_2$] segments. The size of these domains is in the range of several nanometers. Since the conjugated and non-conjugated blocks are randomly arranged in the copolymer the formed multiphase structure is disordered. The above two results indicate that the copolymer has a rod/coil structure in which the two different units are not statistically distributed along the main chain.

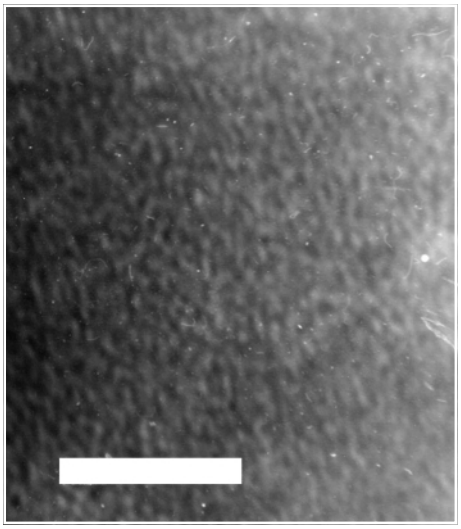

Fig. 2 TEM image of poly[2,5-bis(heptyloxy)phenylene vinylene-*co*-Ba(acrylate)$_2$]. The white bar corresponds to 20 nm.

This work was supported by National Science Foundation in China.

Notes and references

1 J. H. Burroughes, D. D. C. Bradley, A. R. Brown, R. N. Marks, K. MacKay, R. H. Friend, P. L. Burn and A. B. Holmes, *Nature*, 1990, **347**, 539.
2 D. Braun and A. J. Heeger, *J. Appl. Phys. Lett.*, 1991, **58**, 1982.
3 G. Gustafsson, Y. Cao, G. M. Treacy, F. Klavetter, N. Colaneri and A. J. Heeger, *Nature*, 1992, **357**, 477.
4 P. L. Burn, A. B. Holmes, A. Kraft, D. D. C. Bradley, A. R. Brown and R. H. Friend, *J. Chem. Soc., Chem. Commun.*, 1992, 32.
5 A. R. Brown, D. D. C. Bradley, P. L. Burn, J. H. Burroughes, R. H. Friend, N. C. Greenham, A. B. Holmes and A. Kraft, *Appl. Phys. Lett.*,1992, **61**, 2793.
6 H. Kuzmany, M. Mehring and S. Roth, *Springer Ser. Solid-State Sci.*, 1992, **107**, 304.
7 A. R. Brown, N. C. Greenham, J. H. Burroughes, D. D. C. Bradley, R. H. Friend, P. L. Burn, A. B. Holmes and A. Kraft, *Chem. Phys. Lett.*, 1992, **200**, 46.
8 P. L. Burn, A. B. Holmes, A. Kraft, D. D. C. Bradley, A. R. Brown, R. H. Friend and R. W. Gymer, *Nature*, 1992, **356**, 47.
9 P. L. Burn, A. Kraft, D. R. Baigent, D. D. C. Bradley, A. R. Brown, R. H. Friend, R. W. Gymer, A. B. Holmes and R. W. Jackson, *J. Am. Chem. Soc.*, 1993, **115**, 10117.
10 I. Sokolik, Z. Yang, F. E. Karasz and D. C. Morton, *J. Appl. Phys.*, 1993, **74**, 3584.
11 Z. Yang, I. Sokolik and F. E. Karasz, *Macromolecules*, 1993, **26**, 1188.
12 T. Zyung, D.-H. Hwang, I.-N. Kang, H.-K. Shim, W.-Y. Hwang and J.-J. Kim, *Chem. Mater.*, 1995, **7**, 1499.
13 R. A. Wessling and R. G. Zimmerman (Dow Chemical), *US Pat.*, US-B 3401152, 1968 [*Chem. Abstr.*, 1968, **69**, 87735q].
14 R. A. Wessling, *J. Polym. Sci. Polym. Symp.*, 1985, **72**, 55.
15 J. Brandrup and E. H. Immergut, *Polymer Handbook*, Wiley, New York, 2nd edn. 1975, ch. 4.

ChemComm

1,1-Dimethylhydrazidogallane and a gallium hydrazide with two Ga_2N_2 rings bridged by two $NNMe_2$ ligands

Bing Luo and Wayne L. Gladfelter*

Department of Chemistry, University of Minnesota, 207 Pleasant St. SE, Minneapolis, MN, 55455, USA. E-mail: gladfelt@chem.umn.edu

Received (in Columbia, MO, USA) 25th January 2000, Accepted 24th March 2000
Published on the Web 28th April 2000

Volatile, thermally robust 1,1-dimethylhydrazidogallane, $[H_2GaN(H)NMe_2]_2$ 1 has been synthesized from the reaction of $H_3Ga(NMe_3)$ with H_2NNMe_2, whereas reaction of compound 1 with an excess of H_2NNMe_2 at elevated temperature afforded a gallium hydrazide derivative, $Ga_4[N(H)NMe_2]_8(NNMe_2)_2$ 2, which possessed a novel structure of two Ga_2N_2 rings bridged by $NNMe_2$ groups.

Gallium hydride derivatives with direct Ga–N bonds are attractive single-source precursors to gallium nitride. Two main advantages of these compounds over conventional precursors, such as trimethylgallium and triethylgallium, which are extensively used in MOCVD processes, are minimization of carbon contamination and reduction of deposition temperatures. We[1,2] and others[3,4] have reported that compounds with the above features, $(H_2GaNH_2)_3$ and $(H_2GaN_3)_n$, formed nanocrystalline GaN or GaN films at low temperatures. Related triazidogallium derivatives have also produced GaN nanoparticles.[5] Here, we report the syntheses and structures of a volatile, thermally robust dimeric 1,1-dimethylhydrazidogallane, $[H_2GaN(H)NMe_2]_2$ **1**, and a gallium hydrazide derivative with two Ga_2N_2 rings bridged by $NNMe_2$ groups, $Ga_4[N(H)NMe_2]_8(NNMe_2)_2$ **2**.

Hydrazine and 1,1-dimethylhydrazine have been used in conjunction with trialkyl-aluminum and -gallium compounds as alternative nitrogen sources replacing NH_3 for the preparation of AlN and GaN.[6–8] Several related group 13 hydrazide derivatives have been structurally characterized, including dimeric $[Me_2GaN(H)N(H)Ph]_2$,[9] $[Et_2GaN(H)NPh_2]_2$[10] and $[Me_2AlN(H)NMe_2]_2$,[11] a compound with a ladder-type structure, $Al_4[N(H)NMe_2]_6(NNMe_2)_4$,[12] and a compound with a Ga_4N_8 cage structure, $[MeGaN(H)NPh]_4$.[9]

Compound **1**[13] was obtained nearly quantitatively as a white crystalline solid after removal of the volatiles from the reaction of $H_3Ga(NMe_3)$ in excess H_2NNMe_2 at room temperature for 2 days (Scheme 1). Having an appreciable volatility (*ca.* 0.07 Torr) at room temperature, colorless crystals were obtained by sublimation at 55 °C under nitrogen (1 atm). Compound **1** melted at 62 °C and remained a stable liquid up to 90 °C. When heated at higher temperatures, compound **1** decomposed to gallium metal. These results suggested that compound **1** is potentially a clean precursor for deposition of gallium-containing films. The chemical ionization mass spectroscopic data of **1** were in good agreement with the formula of $[H_2GaN(H)NMe_2]_2$ ($[M + H]^+$, *m/z* 261.0, 100%). Two strong $\nu_{Ga–H}$ (KBr pellet) absorptions at 1897 and 1912 cm^{-1} and two $\nu_{N–H}$ absorptions at 3099 (broad) and 3145 (sharp) cm^{-1} were observed. Two singlets at δ 2.11 (sharp) and 2.35 (broad) in the ^1H NMR spectrum were assigned to N–H groups with the total integration of 2 H. The hydrides appeared as a broad resonance at δ 5.21. The presence of two N–H groups indicated the existence of a second isomer in solution. The ratio of the intensity of the δ 2.11 to the δ 2.35 resonances increased from 0.66 at 21 °C to 0.77 at 50 °C.

The molecular structure of **1**[14] (Fig. 1) was dimeric with a planar Ga_2N_2 core and a *trans* arrangement of the NMe_2 substituents. Along the *z* axis intermolecular hydrogen bonds were found between N(1) and N(2) of the neighboring molecule [N(1)···N(2) 3.238(7) Å, N(1)–H(1N)···N(2) 167(5)°]. The atoms N(3) and N(4) were not involved in hydrogen bonding. The hydrides were located on the difference Fourier map, and the only restraint applied in their refinement was to set similar the Ga–H bond lengths to the corresponding gallium atoms.

As also shown in Scheme 1, compound **2**[13] was obtained by refluxing the solution of compound **1** in H_2NNMe_2 for 4 days, followed by removal of volatiles and recrystallization from hexanes (63% yield based on gallium). The ^1H NMR spectrum of compound **2** was consistent with the solid state strtucture[14] (Fig. 2); the two unusual downfield shifts (δ 5.11 and 5.57) were assigned to two N–H bonds involved in hydrogen bonding (*vide infra*).

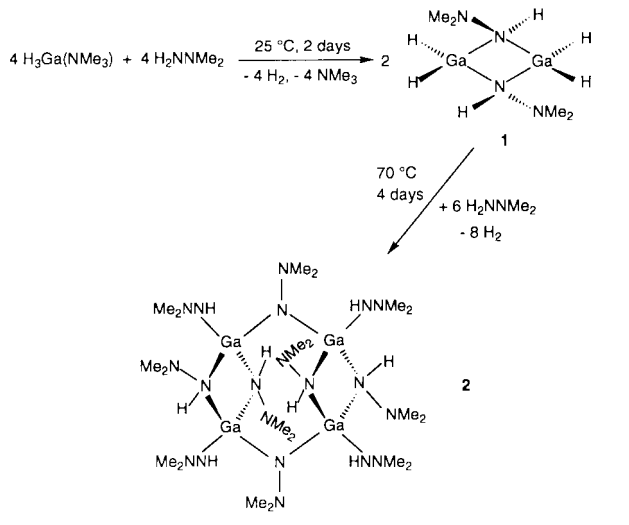

Scheme 1

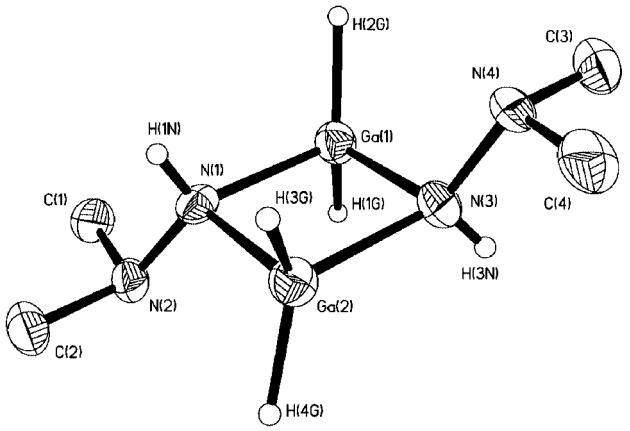

Fig. 1 Structure of **1** showing 50% thermal ellipsoids. Hydrogen atoms in the methyl groups are omitted for clarity. Selected bond distances (Å) and angles (°): Ga(1)–N(1) 1.991(5), Ga(1)–N(3) 2.017(5), Ga(1)–H(1G) 1.51(3), Ga(2)–N(1) 1.997(5), Ga(2)–N(3) 2.024(6), N(1)–N(2) 1.454(7), N(3)–N(4) 1.449(7); N(1)–Ga(1)–N(3) 87.3(2), N(1)–Ga(2)–N(3) 86.9(2), Ga(1)–N(1)–Ga(2) 93.6(2), Ga(1)–N(3)–Ga(2) 92.1(2).

DOI: 10.1039/b001010n

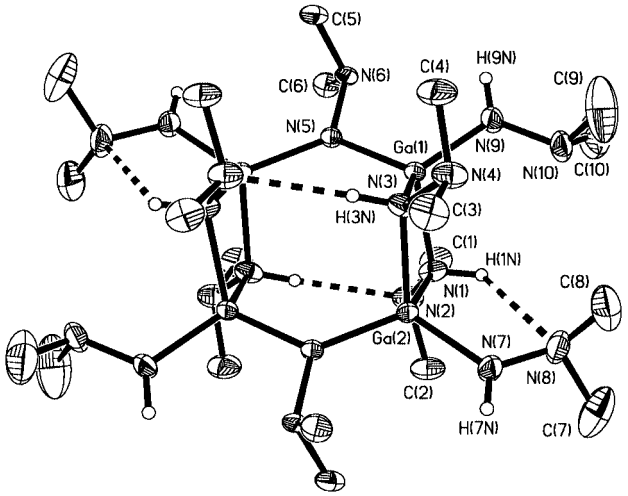

Fig. 2 Structure of **2** showing 30% thermal ellipsoids. Hydrogen atoms in the methyl groups are omitted for clarity. Selected bond distances (Å) and angles (°): Ga(1)–N(1) 1.989(3), Ga(1)–N(3) 2.029(3), Ga(1)–N(5) 1.847(3), Ga(1)–N(9) 1.833(3), Ga(2)–N(1) 1.990(3), Ga(2)–N(3) 2.034(3), Ga(2)–N(5A) 1.860(3), Ga(2)–N(7) 1.851(3), N(1)–N(2) 1.402(4), N(3)–N(4) 1.427(4), N(5)–N(6) 1.461(3), N(7)–N(8) 1.403(4), N(9)–N(10) 1.409(4); N(1)–Ga(1)–N(3) 84.30(11), N(1)–Ga(2)–N(3) 84.13(11), Ga(1)–N(1)–Ga(2) 96.53(12), Ga(1)–N(3)–Ga(2) 93.94(12), Ga(1)–N(5)–Ga(2A) 129.76(14), N(6)–N(5)–Ga(1) 108.5(2), N(6)–N(5)–Ga(2A) 121.7(2).

An inversion center correlated the two halves of the molecule **2**, which were connected by bridging $NNMe_2$ ligands and an intramolecular hydrogen bond between N(3) and N(2A). The distance N(3)···N(2A) was 3.214(5) Å and the angle N(3)–H(3N)···N(2A) was 174.8°. An additional intramolecular hydrogen bond was found between N(1) and N(8) [3.175(5) Å, 120.1°]. Each Ga_2N_2 ring adopted a sightly twisted shape with the gallium ends bending toward and the nitrogen ends away from the inversion center. The torsion angle N(3)–Ga(2)–N(1)–Ga(1) was 8.0(2)°. The four gallium atoms [Ga(1), Ga(2), Ga(1A) and Ga(2A)] and the two bridging nitrogen atoms [N(5) and N(5A)] were essentially on the same plane. The atom N(5) adopted a trigonal planar geometry with the sum of the angles being 360.0°. This suggested delocalization of the lone pair electrons of the nitrogen to the two adjacent gallium atoms, however, the bond lengths N(5)–Ga(1) [1.847(3) Å] and N(5)–Ga(2A) [1.860(3) Å] were not unusual for covalent Ga–N bonds.[15] With the exception of N(5)–N(6) [1.461(3) Å], the N–N bond lengths ranged from 1.402(4) to 1.427(4) Å, shorter than those in compound **1** [1.449(7) and 1.454(7) Å], $[Et_2GaN(H)NPh_2]_2$ [1.457(8) and 1.446(8) Å] and $[MeGaN(H)NPh]_4$ [1.489(3) Å].

This work is supported by a grant from the National Science Foundation (CHE-9616501). We also thank Drs Victor G. Young, Jr. and Maren Pink for their assistance in the X-ray diffraction experiments.

Notes and references

1 J.-W. Hwang, J. P. Campbell, J. Kozubowski, S. A. Hanson, J. F. Evans and W. L. Gladfelter, *Chem. Mater.*, 1995, **7**, 517.
2 J. A. Jegier, S. Mckernan and W. L. Gladfelter, *Inorg. Chem.*, 1999, **38**, 2726.
3 J. McMurran, D. Dai, K. Balasubramanian, C. Steffek, J. Kouvetakis and J. L. Hubbard, *Inorg. Chem.*, 1998, **37**, 6638.
4 J. McMurran, J. Kouvetakis and D. J. Smith, *Appl. Phys. Lett.*, 1999, **74**, 883.
5 A. C. Frank, F. Stowasser, H. Sussek, H. Pritzkow, C. R. Miskys, O. Ambacher, M. Giersig and R. A. Fischer, *J. Am. Chem. Soc.*, 1998, **120**, 3512.
6 D. K. Gaskill, N. Bottaka and M. C. Lin, *J. Cryst. Growth*, 1986, **77**, 418.
7 R. T. Lee and G. B. Stringfellow, *J. Electron. Mater.*, 1999, **28**, 963.
8 V. Lakhotia, D. A. Neumayer, A. H. Cowley, R. A. Jones and J. G. Ekerdt, *Chem. Mater.*, 1995, **7**, 546.
9 D. W. Peters, M. P. Power, E. D. Bourret and J. Arnold, *Chem. Commun.*, 1998, 753.
10 D. A. Neumayer, A. H. Cowley, A. Decken, R. A. Jones, W. Lakhotia and J. G. Ekerdt, *Inorg. Chem.*, 1995, **34**, 4698.
11 Y. Kim, J. H. Kim, J. E. Park, H. Song and J. T. Park, *J. Organomet. Chem.*, 1997, **545**–**546**, 99.
12 J. S. Silverman, C. D. Abernethy, R. A. Jones and A. H. Cowley, *Chem. Commun.*, 1999, 1645.
13 Compound **1**: MS (CI, %): *m/z* 261.0 ($[M + H]^+$, 100), 188.0 ($[HGa[N(H)NMe_2]_2]^+$, 6), 131.0 ($[0.5M + H]^+$, 13), 74.1 ($[GaH_x]^+$, 23), δ_H(300 MHz, C_6D_6, 25 °C): 2.02 (12H, s, NMe_2), 2.11 (s) and 2.35 (br s) (total 2H, integration ratio: δ 2.35/δ 2.11 = 1.5, NH), 5.21 (2H, br s, GaH). Anal. Calc. for $C_4H_{18}N_4Ga_2$: C, 18.36; H, 6.93; N, 21.41. Found: C, 17.19; H, 6.67; N, 20.13%.

Compound **2**: decomp. at 130 °C without melting. δ_H(300 MHz, C_6D_6, 25 °C): δ 2.23 (4H, s, NH), 2.56 (12H, s, NMe_2), 2.61 (12H, s, NMe_2), 2.65 (12H, s, NMe_2), 2.67 (24H, s, NMe_2), 5.11 (2H, s, NH) and 5.57 (2H, s, NH). IR: ν_{NH}, 3054, 3087 and 3228 cm^{-1}.
14 *Crystal data*: for $C_4H_{18}Ga_2N_4$ **1**: M = 261.66, monoclinic, space group *Cc* (no. 9), a = 6.8583(5), b = 19.607(2), c = 8.0977(6) Å, β = 95.323(2)°, V = 1084.2(2) Å^3, T = 173 (2) K, Z = 4, μ(Mo-Kα) = 4.920 mm^{-1}, 3964 reflections collected, 1718 unique (R_{int} = 0.0378) which were used in all calculations, R_1 = 0.0294 and wR_2 = 0.0612 for 1554 reflections with $I > 2\sigma(I)$. A single crystal of compound **1** was mounted in inert oil and transferred to a cold N_2 gas stream of the diffractometer. The structure was solved using direct methods and refined by full-matrix least squares on F^2.

For $C_{20}H_{68}Ga_4N_{20}$ **2**: M = 867.82, monoclinic, space group $P2_1/c$ (no. 14), a = 9.8972(7), b = 22.489(2), c = 10.0230(7) Å, β = 112.824(1)°, V = 2056.2(3) Å^3, T = 173(2) K, Z = 2, μ(Mo-Kα) = 2.632 mm^{-1}, 12953 reflections collected, 4622 unique (R_{int} = 0.0372), R_1 = 0.0384 and wR_2 = 0.0887 for 3239 reflections with $I > 2\sigma(I)$. A single crystal of compound **2** was mounted in inert oil and transferred to a cold N_2 gas stream of the diffractometer. The structure was solved using direct methods and refined by full-matrix least squares on F^2. CCDC 182/1591. See http:/www.rsc.org/suppdata/cc/b0/b001010n/ for crystallographic files in .cif format.
15 P. J. Brothers and P. P. Power, *Adv. Organomet. Chem.*, 1996, **39**, 1.

New manganese β-polynitroporphyrins as particularly efficient catalysts for biomimetic hydroxylation of aromatic compounds with H_2O_2

Jean-François Bartoli, Virginie Mouries-Mansuy, Karine Le Barch-Ozette, Magali Palacio, Pierrette Battioni and Daniel Mansuy*

UMR 8601, Université Paris V, 45 Rue des Saints-Pères, 75270 Paris Cedex 06, France.
E-mail: Daniel.Mansuy@biomedicale.univ-paris5.fr

Received (in Basel, Switzerland) 6th March 2000, Accepted 7th April 2000
Published on the Web 27th April 2000

A series of Mn porphyrins bearing one to eight β-nitro substituents were synthesized in high yield in three steps by using a new general method for selective nitration of a Zn(*meso*-tetraarylporphyrin); this Mn porphyrin series exhibits a remarkably wide span of Mn(III)/Mn(II) redox potentials from −290 to + 1150 mV (*vs.* SCE), and the Mn porphyrins bearing one to five β-nitro groups are particularly good catalysts for hydroxylation of aromatic compounds with H_2O_2, with yields up to 98, 83, 80 and 12%, respectively for anisole, naphthalene, acetanilide and ethylbenzene.

Cytochrome P450-dependent monooxygenases very efficiently catalyze the epoxidation of alkenes, the hydroxylation of alkanes and of aromatic rings, as well as N- or S-oxidations by O_2 or oxygen atom donors.[1] Three successive generations of Fe(III) and Mn(III) porphyrins have been developed during the last fifteen years as catalysts mimicking cytochrome P450 chemistry.[2] Several systems based on such Fe(III) or Mn(III) porphyrins were found to be very efficient for alkene epoxidation with quantitative yields and high turnover numbers, and for alkane hydroxylation with satisfactory yields.[2] Reproducing the P450-dependent selective hydroxylation of aromatic rings appears to be more difficult, presumably because of the very easy further oxidation of the expected phenol products in the medium. In fact, systems using strong oxidants such as PhIO that directly react by themselves with phenols generally led to low hydroxylation yields.[3] The best reported aromatic hydroxylation yields with these systems have been obtained with H_2O_2, a milder oxidizing agent.[3c,d,f] However, even these H_2O_2-dependent systems only led to hydroxylation yields of between 10 and 60% for the most reactive aromatic molecules. Some of the best reported yields were obtained with H_2O_2 in the presence of Mn(III) porphyrins bearing several electron-withdrawing substituents.[3d]

Based on these data, it appeared to us that it would be interesting to compare the abilities of Mn-porphyrins bearing one to eight β-nitro substituents as catalysts for aromatic hydroxylation with H_2O_2. We have recently reported[4] the synthesis of a Mn β-heptanitroporphyrin and showed that the redox potential of this Mn-porphyrin is more than 1 V higher than that of Mn(TDCPP).[5] Much more recently, we have succeeded in finding a new general method for selective nitration of Zn(TDCPP) which affords a full series of Zn porphyrins bearing one through to eight β-nitro groups in high yield. Here we report that some of the corresponding Mn complexes are particularly good catalysts for the hydroxylation of aromatic compounds with H_2O_2.

Scheme 1 shows the procedure used for preparing the eight Mn-porphyrins, Mn(TDCPN$_x$P) with ($1 \leqslant x \leqslant 8$), from Zn(TDCPP). Titration of Zn(TDCPP) with increasing amounts of HNO_3–CF_3SO_3H–$(CF_3SO_2)_2O$ selectively afforded the eight compounds of the Zn(TDCPN$_x$P) series with yields between 50 and 95%. All compounds of the Zn(TDCPN$_x$P) and TDCPN$_x$PH$_2$ series were fully characterized by elemental analysis and UV–VIS, ^{1}H NMR spectroscopy and mass spectrometry. Their detailed synthesis and characteristics will be published elsewhere.

Preparation of the corresponding Mn complexes was performed by reaction of $Mn(OAc)_2$ with the free bases TDCPN$_x$PH$_2$. Insertion of Mn(II) was increasingly easier as the number of NO_2 substituents increased. For instance, insertion of Mn(II) in TDCPPH$_2$ required several hours reaction at 153 °C in DMF, whereas insertion in TDCPN$_5$PH$_2$ was complete within a few minutes at 20 °C in $CHCl_3$–CH_3OH (80:20). After purification by column chromatography and treatment with gaseous HCl in aerobic CH_2Cl_2, the Mn-porphyrin complexes bearing between one and four β-nitro groups exhibited UV-VIS spectra characteristic of Mn(III)Cl porphyrins with a red-shifted Soret peak around 490 nm (482, 487, 493 and 498 nm for x = 1, 2, 3 and 4, respectively) and a smaller peak around 400 nm. Their mass spectra (MALDI) showed molecular peaks appearing as isotopic clusters identical to those simulated for Mn(TDCPN$_x$P)Cl, and major peaks corresponding to Mn(TDCPN$_x$P). Above x = 4, the Mn(TDCPN$_x$P) compounds mainly exist as Mn(II) complexes. For x = 5, even treatment with HCl in aerobic CH_2Cl_2 led to a mixture of Mn(II) (TDCPN$_5$P) and Mn(III) (TDCPN$_5$P)Cl. For x = 6, 7 and 8, it was only possible to isolate the Mn(II) (TDCPN$_x$P) complexes, which showed a single Soret peak at 466, 467 and 468 nm, respectively, and molecular peaks by mass spectrometry (MALDI) corresponding to Mn(TDCPN$_x$P). The existence of these electron-poor Mn porphyrins as Mn(II) complexes is not surprising; similar behavior was previously reported for β-polyhalogenated Mn-porphyrins[6] and for Mn(TDCPN$_7$P) itself.[4] This is also easily explained if one considers the high redox potentials (*vs.* SCE) found for the Mn(III)/Mn(II) couple which vary from +750 mV for x = 5 to + 1150 mV for x = 8. In fact, the Mn(TDCPN$_x$P) series with x = 1–8 exhibits a remarkably wide span of Mn(III)/Mn(II) redox potentials that range from −290 to +1150 mV (*vs.* SCE in 0.1 M NBu_4PF_6–CH_2Cl_2). The oxidation states of the Mn complexes were clearly established on the basis of their UV-VIS and EPR spectra and of their electrochemical properties.

The ability of these Mn-porphyrin complexes to act as catalysts for the hydroxylation of aromatic compounds with H_2O_2 was studied in the presence of a cocatalyst, ammonium

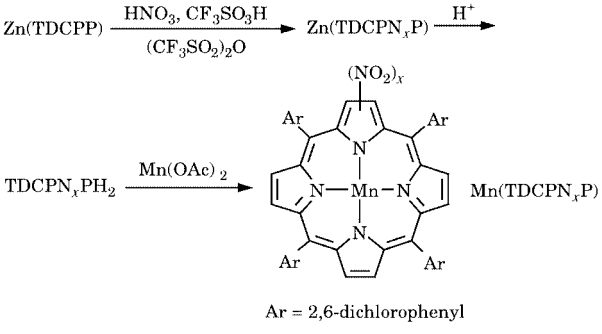

Scheme 1

DOI: 10.1039/b001776k

Table 1 Hydroxylation of aromatic compounds with H_2O_2 in the presence of Mn β-polynitroporphyrins and ammonium mandelate[a]

Substrate	Anisole			Naphthalene			Ethylbenzene					
Products	*p*-OH	*o*-OH	Total yield (%)	α-OH	β-OH	Total yield (%)	PhCHOH-CH_3	$PhCOCH_3$	*p*-OH	*o*-OH	*p*-OH + *o*-OH	arom./ benz. (%)
Mn(TDCPP)Cl	67	6	73	62	5	67	20	22	< 1	< 1	< 2	< 5
Mn(TDCPNP)Cl	90	7	97	72	7	79	23	15	2	1	3	8
Mn(TDCPN_2P)Cl	88	8	96	75	8	83	27	15	2	1	3	7
Mn(TDCPN_3P)Cl	88	10	98	61	8	69	21	14	6	3	9	26
Mn(TDCPN_4P)Cl	71	8	79	43	6	49	26	15	8	4	12	29
Mn(TDCPN_5P)	32	5	37	39	5	44	22	5	6	4	10	37
Mn(TDCPN_6P)	7	1	8	20	3	23	7	12	< 1	< 1	< 2	
Mn(TDCPN_7P)	5	< 1	5	18	3	21	4	24	< 1	< 1	< 2	
Mn(TDCPN_8P)	< 1	< 1	< 2	1	< 1	1	1	5	< 1	< 1	< 2	

[a] *Conditions*: Mn-porphyrin : H_2O_2 : cocatalyst ratio = 1 : 50 : 20, [Mn-porphyrin] = 2 mM in CH_2Cl_2–CH_3CN (1 : 1), 2 h at 20 °C in the presence of substrate in excess; substrate/catalyst = 3000, 1600 and 500 for anisole, ethylbenzene and naphthalene, respectively. Yields (%) are based on H_2O_2; *p*-OH and *o*-OH represent *para*- and *ortho*-hydroxylated products; arom./benz. is the ratio (%) between aromatic hydroxylation and benzylic oxidation products derived from ethylbenzene.

acetate, that was previously described to give good results for the Mn porphyrin-catalyzed transfer of an oxygen atom of H_2O_2 to various hydrocarbon substrates.[7] Thus, Mn(TDCPP)Cl catalyzed the hydroxylation of anisole to *para*- and *ortho*-hydroxyanisole with 60 and 4% yields based on starting H_2O_2 when anisole was used in large excess relative to H_2O_2. From various ammonium carboxylates that have been tested as necessary cocatalysts for that reaction, ammonium mandelate gave the best hydroxylation yields. The latter cocatalyst was thus used in our comparison of the various Mn-porphyrins (Table 1). Interestingly, Mn(TDCPN_1P)Cl led to markedly higher yields of anisole hydroxylation with an almost quantitative use of H_2O_2 for formation of 90% and 7% *para*- and *ortho*-hydroxyanisole respectively. Mn(TDCPN_2P)Cl and Mn(TDCPN_3P)Cl also gave very high total yields based on H_2O_2 and were recovered unchanged at the end of the reaction (*ca.* 50 turnovers under the used conditions). With more β-nitro substituents, the hydroxylation yields greatly decreased from 79% with Mn(TDCPN_4P)Cl to < 2% with Mn(TDCPN_8P). Similar results were observed for hydroxylation of naphthalene, the best total yield of formation of α- and β-naphthols being maximum (83%) for Mn(TDCPN_2P)Cl (Table 1). Interestingly, the regioselectivity slightly changed upon increasing the number of β-nitro substituents [α : β ratio from 12 with Mn(TDCPP)Cl to *ca.* 6 for Mn(TDCPN_7P)]. The most spectacular results were observed in the case of ethylbenzene. Its Mn(TDCPP)Cl catalyzed oxidation with H_2O_2 exclusively led to products arising from hydroxylation of its very reactive benzylic position, 1-phenylethanol and acetophenone. Upon introduction of an increasing number of β-NO_2 substituents on the catalyst, *para*- and *ortho*-hydroxyethylbenzene were formed in significant amounts and the aromatic hydroxylation yield increased up to 12% for $x = 4$; then it markedly decreased for $x > 5$. Thus, the aromatic hydroxylation/benzylic hydroxylation ratio reaches maximum values *ca.* 30% for $x = 3$–5.

The above results illustrate the particular efficiency of Mn-porphyrins bearing between one and four β-nitro substituents for hydroxylation of aromatic molecules with H_2O_2 in the presence of an NH_4CO_2R cocatalyst. By a proper choice of the Mn catalyst it is possible to hydroxylate anisole and naphthalene, used in excess relative to H_2O_2, with yields (based on H_2O_2) up to 98 and 83%, respectively. Even ethylbenzene, that has a very reactive benzylic position, was hydroxylated at its aromatic ring with yields up to 12%. Another aromatic compound bearing an electron-donating substituent, acetanilide, was hydroxylated with the Mn(TDCPN_2P)Cl–H_2O_2–ammonium mandelate system, affording *p*-hydroxyacetanilide in 80% yield. Benzene itself or aromatic compounds bearing electron-withdrawing substituents were much poorer substrates, and lead to phenol yields < 5%.

The origin of the particular efficiency of Mn(TDCPN_xP)Cl catalysts, with $x = 1$–4, for hydroxylation of electron-rich aromatic compounds with H_2O_2, and of the changes observed in the regioselectivity of these hydroxylations as a function of x (Table 1) is currently under investigation. It is likely that the lower activities of Mn catalysts with $x = 5$–8 are due to their pronounced tendency to exist in the Mn(II) state.

Notes and references

1 *Cytochrome P450: Structure, Mechanism and Biochemistry*, ed. P. Ortiz de Montellano, Plenum Press, New York, 1995.

2 For general reviews, see: B. Meunier, *Chem. Rev.*, 1992, **92**, 1411; D. Mansuy, *Coord. Chem. Rev.*, 1993, **125**, 129; R. A. Sheldon, *Metalloporphyrins in Catalytic Oxidations*, M. Dekker, New York, 1994; J. T. Groves and Y. Z. Han, in *Cytochrome P450: Structure, Mechanism and Biochemistry*, ed. P. Ortiz de Montellano, Plenum Press, New York, 1995, p. 3; D. Dolphin, T. G. Traylor and L. Xie, *Acc. Chem. Res.*, 1998, **31**, 155.

3 (*a*) C. K. Chang and F. Ebina, *J. Chem. Soc., Chem. Commun.*, 1981, 778; (*b*) J. R. Lindsay-Smith and P. R. Sleath, *J. Chem. Soc., Perkin Trans. 2*, 1982, 1009; (*c*) S. Tsuchiya and M. Seno, *Chem. Lett.*, 1989, 236; (*d*) M. N. Carrier, C. Scheer, P. Gouvine, J. F. Bartoli, P. Battioni and D. Mansuy, *Tetrahedron Lett.*, 1990, **31**, 6645; (*e*) K. Ikida, M. Nango, K. Okada, S. Matsumoto, M. Matsuura, K. Yamashita, K. Tsuda, Y. Kuruno and Y. Kimura, *Chem. Lett.*, 1994, 1307; (*f*) see also, as a recent review: B. Meunier, A. Robert, G. Pratviel and J. Bernadou, in *The Porphyrin Handbook*, ed. K. M. Kadish, K. M. Smith and R. Guilard, Academic Press, New York, 2000, vol. 31, 119.

4 K. Ozette, P. Battioni, P. Leduc, J. F. Bartoli and D. Mansuy, *Inorg. Chim. Acta*, 1998, **272**, 4.

5 TDCPP and TDCPN_xP represent *meso*-tetra(2,6-dichlorophenyl)porphyrin dianion and TDCPP bearing x β-NO_2 substituents ($1 \leqslant x \leqslant 8$) respectively.

6 P. Hoffmann, A. Robert and B. Meunier, *Bull. Soc. Chim. Fr.*, 1992, **129**, 85.

7 A. Thellend, P. Battioni and D. Mansuy, *J. Chem. Soc., Chem. Commun.*, 1994, 1035.

Vapor phase Beckmann rearrangement of cyclohexanone oxime over a novel tantalum pillared-ilerite

Younghee Ko,[a] Myung Hun Kim,[a] Sun Jin Kim,[a] Gon Seo,[b] Mi-Young Kim[b] and Young Sun Uh*[a]

[a] *Materials Chemistry Research Center, Korea Institute of Science and Technology, PO Box 131, Cheongryang, Seoul 130-650, Korea. E-mail: uhyoung@kistmail.kist.re.kr*

[b] *Department of Chemical Technology, Chonnam National University, Kwangju 500-757, Korea*

Received (in Cambridge, UK) 22nd February 2000, Accepted 4th April 2000
Published on the Web 27th April 2000

The vapor phase Beckmann rearrangement of cyclohexanone oxime has been studied using a novel tantalum pillared-ilerite as catalyst: the cyclohexanone oxime conversion rate reaches 97.1% and the selectivity for ε-caprolactam is up to 89.1% at 350 °C.

Sulfuric acid as a catalyst plays an essential role in the industrial mass production of ε-caprolactam, a raw material for nylon-6. However, it poses significant environmental and operational problems such as generating undesirable salt and causing equipment corrosion. To overcome these problems, a number of heterogeneous catalysts for the vapor phase Beckmann rearrangement of cyclohexanone oxime have been proposed. Among typical heterogeneous catalysts for this reaction include solid acid catalysts such as boric acid, silica–alumina, zeolites like Y, ZSM-5, TS-1, B-ZSM-5 and tantalum oxide on silica.[1–4] Highly siliceous ZSM-5 and ZSM-5 modified with boron showed high activity and selectivity in the Beckmann rearrangement reaction.[5] However, the catalysts gradually deactivated with time. Solid acid catalysts of high activity with long catalytic lifetime are still under investigation.

Various types of hydroxy groups in amorphous silica or zeolites have been investigated as catalytically active sites for the Beckmann rearrangement reaction. A majority of researchers found that neutral or weakly acidic hydroxy groups present on the external surface of zeolites are effective for the Beckmann rearrangement reaction, whereas Brönsted acid sites of zeolites accelerate the formation of by-products.[6,7] This is suggestive that an efficient solid acid catalyst for the rearrangement reaction can be obtained if the catalyst is designed to include not only a controlled acidity but also a sufficient number of hydroxy groups.

In our study, an efficient solid acid catalyst for the vapor phase Beckmann rearrangement reaction is designed using layered silicates. A small amount of metal was intercalated between the silicate layers by the usual pillaring process to generate moderate acidity as a mixed oxide and to increase the thermal stability of the layered silicate for use in catalysis. Layered silicates, such as kanemite ($NaHSi_2O_5{\cdot}3H_2O$), magadiite ($Na_2Si_{14}O_{29}{\cdot}11H_2O$), kenyaite ($K_2Si_{20}O_4{\cdot}11H_2O$), makatite ($Na_2Si_4O_9{\cdot}5H_2O$) and ilerite ($Na_2Si_8O_{17}{\cdot}xH_2O$) are composed of tetrahedral silicate sheets only and the each silicate sheet is terminated by hydroxy groups.[8] Layered silicates, therefore, possess abundant hydroxy groups oriented in a crystallographically regular manner, and have a great potential to act as new catalysts for the vapor phase Beckmann rearrangement reaction.

Here, the synthesis, characterization and catalytic application to the Beckmann rearrangement reaction of layered silicate catalysts pillared with tantalum oxide is presented.

Na-ilerite ($Na_2Si_8O_{17}{\cdot}xH_2O$) was synthesized hydrothermally at 100 °C for two weeks from a suspension of Ludox-HS 40 and NaOH solution with a molar ratio of $SiO_2:NaOH:H_2O = 1:0.5:7$.[9] H-ilerite was prepared by acid titration of Na-ilerite. A suspension of Na-ilerite in water was titrated with 0.1 M HCl to a final pH of 2.0 and allowed to stand with stirring for an additional 24 h. The H-ilerite was recovered by filtering off, washing, and was dried at 40 °C. The sodium content of the sample was 0.11 wt% as determined by atomic absorption spectroscopy. Octylamine intercalation was performed to increase the interlayer spacing of ilerite by allowing H-ilerite to react with an excess of octylamine at room temperature.

The pillar precusor for tantalum oxide pillaring was prepared by the hydrolysis of tantalum pentaethoxide.[10] A small amount of octylamine was added to the solution to increase the degree of hydrolysis of tantalum pentaethoxide. The molar ratio of $Ta(OC_2H_5)_5:H_2O$:octylamine was adjusted to 1:12:0.3. The pillar precusor can be represented as $Ta_xO_y(OR)_z$. For comparison, silicon pillared-ilerite was prepared according to the procedure in the literature.[9] The pillar precusor for silicon oxide pillaring was prepared by mixing octylamine and TEOS in the molar ratio of 2:5. The pillar precusor solution was added dropwise to the octylamine-ilerite gel with continuous stirring. The final suspension was allowed to stand for three days with stirring at room temperature. The resultant product was washed with ethanol, filtered off and dried at 100 °C. Samples were calcined at 700 °C for 1 h to eliminate residual organic molecules. The tantalum content of tantalum pillared-ilerite samples, as determined by inductively coupled plasma (ICP) spectroscopy, ranged from 3.8 to 5 wt%.

The as-synthesized metal pillared-ilerites have basal spacings of 27.2 Å (Ta) and 29.4 Å (Si) much larger than those of Na- and H-ilerites, (11.1 and 7.4 Å, respectively).[9] Although the basal spacings gradually decreased with increase in calcination temperature, the structures of the metal pillared-ilerites were preserved even after calcination at 700 °C (Fig. 1). Broad peaks in the XRD powder diffraction patterns indicate that poorly ordered structures are formed in metal pillared-ilerites. The N_2 adsorption–desorption isotherm of tantalum pillared-ilerite after complete elimination of organic molecules showed type IV behavior according to the BDDT classification. At high relative pressure ($P/P_o > 0.6$), hysteresis is observed owing to capillary condensation in mesopores, caused by pillaring of the layered silicates.

The BET surface areas of samples calcined at 700 °C are 395 $m^2\ g^{-1}$ for tantalum pillared-ilerite and 358 $m^2\ g^{-1}$ for silicon pillared-ilerite, much larger than those of the H- and Na-ilerites, (20 and 40 $m^2\ g^{-1}$, respectively).

The acidic properties of the tantalum pillared-ilerite was studied to identify the inherent acidity caused by incorporation of tantalum oxide between the layers of ilerite. In addition, the acidic properties of silicon pillared-ilerite was investigated to compare inherent acidities caused by incorporation of Ta or Si between the layers of ilerite. Acidities were determined by carrying out NH_3-TPD experiments. The TPD profile of the tantalum pillared-ilerite exhibits a broad desorption peak with a maximum at 220 °C. On the other hand, the silicon pillared-ilerite shows no desorption peak. This implies that tantalum pillared-ilerite contains a large number of acid sites of moderate acidity, whereas silicon pillared-ilerite shows no acidity.

The Beckmann rearrangement of cyclohexanone oxime was conducted using a continuous flow reactor under atmospheric

Table 1 Vapor phase Beckmann rearrangement of cyclohexanone oxime over various metal pillared-ilerites[a]

Catalyst	*t*/h	Conv. (%)	Selectivity (%)			
				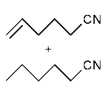	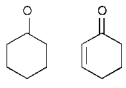	
Ta-Ilerite	2	97.1	89.1	5.9	3.0	2.0
	8	96.9	85.7	9.3	3.1	1.8
Si-Ilerite	2	70.4	80.6	2.4	11.2	5.1
	8	30.5	54.2	7.8	26.3	11.7
Silicalite-1[b]	2	92.6	93.0	3.8	2.0	1.2
	8	89.1	89.8	5.1	3.7	1.4

[a] *Conditions*: T = 350 °C, P = 1 atm, WHSV = 0.5 h^{-1}, cyclohexanone oxime:EtOH:He = 1:9:10, Time on stream = 8 h. [b] Silicalite-1 was synthesized at 150 °C for 5 days using the mol ratio 0.1 TPABr:0.2 NaOH:1.0 SiO_2:35 H_2O.

pressure. Cyclohexanone oxime was dissolved in ethanol and injected with syringe pump at a WHSV of 0.5 h^{-1} under He flow with reaction carried out at 350 °C. The product was analyzed by GC using an SE-54 column.

The results of the rearrangement reaction over tantalum pillared-ilerite are shown in Table 1. The catalytic activity of tantalum pillared-ilerite was compared to Silicalite-1 (pure silica ZSM-5), which is known as the most selective catalyst for the vapor phase Beckmann rearrangement of oxime to lactam (Table 1). The tantalum pillared-ilerite showed a higher conversion of oxime than silicalite-1 while the selectivity for lactam over tantalum pillared-ilerite was slightly lower than that over silicalite-1. Also, the data was compared with that of silicon pillared-ilerite to investigate the effect of the metal as a pillar. For the tantalum pillared-ilerite catalyst, the cyclohexanone oxime conversion rate reaches 97.1% and the selectivity for ε-caprolactam is 89.1% at 350 °C. Tantalum pillared-ilerite catalyst is superior to the silicon pillared-ilerite in terms of both conversion and selectivity. Silicon pillared-ilerite shows quite high conversion and selectivity initially owing to inherent hydroxy groups from its layered features. However, it is rapidly deactivated within 8 h, which may be explained by the fact that it does not possess the moderate acidity required to catalyze the rearrangement reaction (ammonia TPD).

Although the exact role of the metal is not yet fully understood, it can be speculated that acidity of hydroxy groups in the metal pillared-ilerite is controlled by the metal used as pillar. The acid strength of the assumed species –Ta–O–Si–OH generated by the pillaring process is adequate enough to catalyze the rearrangement reaction.

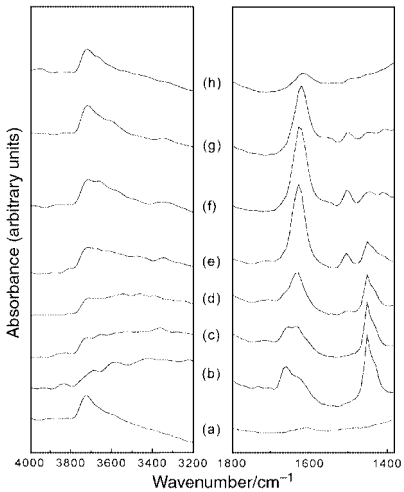

Fig. 1 FTIR spectra of tantalum pillared-ilerite measured at different temperatures (a) before and (b–h) after adsorption of cyclohexanone oxime [(a) 25, (b) 70, (c) 100, (d) 140, (e) 200, (f) 300, (g) 400 and (h) 550 °C]. These data were recorded on FTS-175 BIO-RAD FT-IR spectrometer.

FTIR spectra were measured for metal pillared-ilerite samples to elucidate the reaction pathway in detail. FTIR experiments were conducted using an *in situ* IR cell (Graseby, specac). Metal pillared-ilerite pellets were preheated at 550 °C under vacuum for 1 h. After the samples were cooled to room temperature, FTIR spectra were recorded [Fig. 1(a)]. One drop of a 1% ethanol solution of cyclohexanone oxime was added to the pellet held in the *in situ* cell under He gas flow. After the evacuation of physically adsorbed oxime at room temperature for 1 h, FTIR spectra were recorded at increments of 20 °C min^{-1} [(Fig. 1(b)–(h)].

The IR spectrum of tantalum pillared-ilerite [Fig. 1(a)] shows absorption bands of hydroxy groups[11] at *ca*. 3700 cm^{-1}. However, these bands disappeared upon adsorption of cyclohexanone oxime and new bands appeared at 1450 and 1663 cm^{-1} due to characteristic vibrations[12] of CH_2 and C=N groups of cyclohexanone oxime, respectively. This indicates strong interaction between the hydroxy groups of the catalyst and the reactant. For the temperatures above 100 °C, the characteristic vibration modes[12] of C=O and N–H of ε-caprolactam at 1635 and 1505 cm^{-1} were detected. However, with a stepwise rise of evacuation temperature, the C=O and N–H absorptions of ε-caprolactam were weakened around 400 °C and completely disappeared at 500 °C. The desorption temperature of the produced ε-caprolactam is shifted to a higher value than that observed in the catalytic reaction and might be due to the fast temperature increase rate in the FTIR experiment. IR spectra of silicon pillared-ilerite taken at different temperatures were similar to those of tantalum pillared-ilerite. However, the intensities of bands at 1635 and 1505 cm^{-1} due to the characteristic vibrations of C=O and N–H groups of ε-caprolactam were lower than those on tantalum pillared-ilerite, which implies that silicon pillared-ilerite has a low catalytic activity.

From the FTIR data, it is seen that the rearrangement to ε-caprolactam from cyclohexanone oxime over the tantalum pillared-ilerite takes place around 100 °C, while the desorption of the produced ε-caprolactam occurs at a higher temperature (> 350 °C). Also this data strongly suggests that the hydroxy groups are active sites as reported for other zeolite catalysts.[6,7]

In conclusion, we report the synthesis and characterization of a novel tantalum pillared-ilerite that is shown to be a new advantageous catalyst for the vapor phase Beckmann rearrangement of cyclohexanone oxime. The excellent catalytic performance of tantalum pillared-ilerite for the Beckmann rearrangement reaction is ascribed to a large number of well dispersed hydroxy groups over the interlayer surface of tantalum pillared-ilerite and their relatively weak acidity.

This work was supported by the Korea Institute of Science and Technology under contract 2E15210 and Brain Pool Program of the Korean Government.

Notes and references

1 S. Sato, S. Hasebe, H. Sakurai, K. Urabe and Y. Izumi, *Appl. Catal.*, 1987, **29**, 107.
2 A. Aucejo, M. C. Burgent, A. Corma and V. Fornes, *Appl. Catal.*, 1986, **22**, 187.
3 A. Corma, H. Garcia and J. Primo, *Zeolites*, 1991, **11**, 593.
4 T. Ushikubo and K. Wada, *J. Catal.*, 1994, **148**, 138.
5 J. Röseler, G. Heitmann and W. F. Hölderich, *Stud. Surf. Sci. Catal.*, 1997, **105**, 1173.
6 H. Sato, K. Hirose, M. Kitamura and Y. Nakamura, *Stud. Surf. Sci. Catal.*, 1989, **49**, 1213.
7 G. P. Heitmann, G. Dahlhoff and W. F. Hölderich, *J. Catal.*, 1999, **186**, 12.
8 Y. Ko, S. J. Kim, M. H. Kim, J. H. Park, J. B. Parise and Y. S. Uh, *Microporous Mesoporous Mater.*, 1999, **30**, 213.
9 K. Kosuge and A. Tsunashima, *J. Chem. Soc., Chem. Commun.*, 1995, 2427.
10 G. Guiu, A. Gil, M. Montes and P. Grange, *J. Catal.*, 1997, **168**, 450.
11 G. L. Woolery, L. B. Alemany, R. M. Dessau and A. W. Chester, *Zeolites*, 1986, **6**, 14.
12 H. Sato, K. Hirose and Y. Nakamura, *Chem. Lett.*, 1993, 1987.

ChemComm

Dipolar H_2 activation by H_2O

Elisabeth Leere Øiestad and Einar Uggerud*

Department of Chemistry, University of Oslo, PO Box 1033 Blindern, N-0315 Oslo, Norway. E-mail: einar.uggerud@kjemi.uio.no

Received (in Cambridge, UK) 10th February 2000, Accepted 5th April 2000
Published on the Web 28th April 2000

When a water molecule can act as a proton acceptor during the critical H–H bond heterolytic dissociation step of formaldehyde hydrogenation, the barrier drops—an observation which links dihydrogen activation chemistry to hydride transfer at a detailed molecular level.

The hardness of the H–H molecule is an obstacle to hydrogenation reactions, and consequently they usually require a catalyst, often in the form of a transition metal, in order to proceed. The reverse reaction type, H_2 eliminations, has been the subject of many gas phase studies. For example, detailed experimental and theoretical work has shown that loss of H_2 from protonated molecules of the type CH_3XH^+ (X = NH_2, OH, F, SH) take place *via* non-symmetrical 1,2-elimination mechanisms [Scheme 1(a)].[1–3] The resulting tight transition structures for these and similar H_2 eliminations give rise to substantial potential energy barriers. The dipolar nature of the emerging H_2 molecule during passage of the transition state has been noted.[4]

Very interestingly, it appears that intermolecular hydride transfer[5] is related to these hydrogenations/dehydrogenations. A special hydride transfer mechanism is found in superacid systems, particularly in the gas phase, where proton transfer may initiate H_2 elimination: $AH^+ + CH_3X \rightarrow CH_2X^+ + H_2 + A$. This reaction type has been reviewed in the context of chemical ionization mass spectrometry.[6] A reasonable transition structure for such a reaction is illustrated in Scheme 1(b). Although mechanisms of both unimolecular H_2 eliminations and hydride abstractions are reletively well known, the idea behind the present paper is to see how they are linked together at a detailed molecular level. We pursue this idea further by specifically asking if a third molecule, A, may change the reactivity in H_2 additions/eliminations.

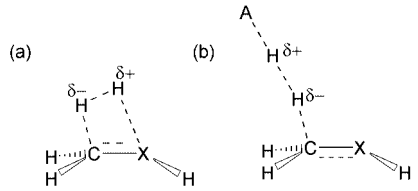

Scheme 1

In order to do this we decided to perform quantum chemical calculations on a prototype system, hydrogenation of formaldehyde, using the methods MP2/6-31G(d,p)[7,8] and G2[9] with help of the program package GAUSSIAN 98.[10] Only the G2 values will be displayed in the following discussion.

According to our calculations hydrogenation of formaldehyde to give methanol [eqn. (1)]

$$CH_2O + H_2 \rightarrow CH_3OH \qquad (1)$$

is exoergic by $\Delta E = -78$ kJ mol^{-1} and has $\Delta G^o = -52$ kJ mol^{-1} which is in acceptable agreement with the experimentally known[11] exothermicity (at room temperature) of $\Delta H^o = -93$ kJ mol^{-1}. The reaction has a critical energy of $E_o = 301$ kJ mol^{-1} (Fig. 1, upper reaction path *via* the transition structure **TSa**).

Upon protonation [eqn. (2)],

$$CH_2OH^+ + H_2 \rightarrow CH_3OH_2^+ \qquad (2)$$

the critical energy is reduced to $E_0 = 122$ kJ mol^{-1} (Fig. 1, middle path *via* the transition structure **TSb**), which still is quite unfavourable for a direct gas phase reaction, but significantly below that of reaction (1). At the same time, as the result of the higher proton affinity of methanol, the overall reaction becomes somewhat more exoergic, with $\Delta E^o = -145$ kJ mol^{-1} and $\Delta G^o = -94$ kJ mol^{-1}. The corresponding experimental value[11] is $\Delta H^o = -142$ kJ mol^{-1}.

Upon providing the proton *inter*- rather than *intra*-molecularily a further, and substantial, drop in the critical energy is observed. The termolecular gas phase reaction [eqn. (3)]

$$CH_2O + H_2\ (+ H_3O^+) \rightarrow CH_3OH\ (+ H_3O^+) \qquad (3)$$

has barriers (corresponding to **TSc** and **TSd**) for which the potential energies are below that of the reactants (these values are $E_0 = -36$, -34 kJ mol^{-1}, respectively). Water is seen to promote reaction strongly through either of these closely parallel mechanisms. In the first step a proton is donated from the hydronium ion **3** to the oxygen of formaldehyde. Protonated formaldehyde may then form one of the two complexes **6a** (a C–H···O complex) or **6b** (a O–H···O complex) with the water

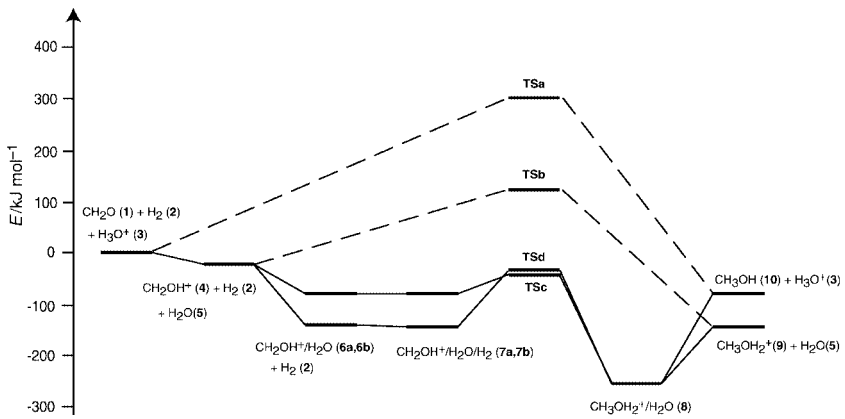

Fig. 1 Schematic potential energy diagram (G2) for the various routes for hydrogenation of formaldehyde. Potential energies are given in kJ mol^{-1}.

DOI: 10.1039/b001209m

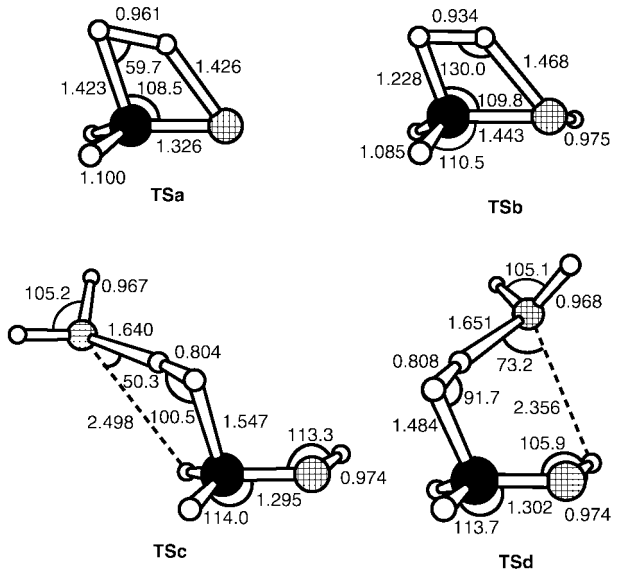

Fig. 2 Structures of the found transition structures (MP2/6-31G(d,p)) of the reactions studied. Black filled circles represent carbon, white open circles are hydrogen, while the patterned circles are oxygen. Bond lengths are given in Å and angles are in degrees. The connection between the transition structures and the minima indicated in Fig. 1 was verified through explicit calculation of minimum energy paths (intrinsic reaction coordinate).

molecule. In the next step of the parallel mechanisms, H_2 is associated with the corresponding complex (**6a** or **6b**). These new complexes are **7a** and **7b**, respectively. In the key step (*via* **TSc** or **TSd**) of the two parallel mechanisms, the H_2 molecule is split in a heterolytic process: the hydride ends up at the carbon and the proton ends up on water. All along the reaction the water is docked to the organic part through a hydrogen bond. The final products are obtained by breaking the hydrogen bonded complex **8**.

The transition structures **TSc** and **TSd**, are characterized by being cyclic. In contrast to **TSb** which has a tight four-membered ring, **TSc** and **TSd** form loose six-membered rings. While the H–H bond of **TSa** is 0.934 Å, it is only 0.804 Å in **TSc** and 0.808 Å in **TSd**, demonstrating that the latter transition structures are earlier along the reaction coordinate. These values should be compared to the MP2/6-31G(d,p) value of 0.734 Å for an intact H_2 molecule.

As indicated above, reaction (3), can be regarded from another perspective. When read from right to left (Fig. 1) **TSc** and **TSd** are the possible transition structures for the weakly endoergic hydride abstraction of methanol by H_3O^+.

We are not sure that the findings presented here may be of immediate practical use; a termolecular reaction through **TSc** or **TSd** is certainly difficult to achieve in the gas phase. This is illustrated by the fact that the free energies of these transition structures are +24 and +28 kJ mol^{-1}, respectively, compared to that of the reactants (**1** + **2** + **3**). In a strongly acidic water solution, in a suitable supercritical phase, or on an acidic surface (*e.g.* in a zeolite) the molecules are solvated, approximately corresponding to the situation in the complexes **7a** and **7b**. Despite this, the results presented here give an optimistic perspective on a non-transition metal hydrogenation catalysis chemistry.

We are aware of previous studies that illustrate the mediating effect of a water molecule in similar situations. As a good example we would mention that McKee *et al.*[12] showed that a water molecule slightly lowers the activation energy for the concerted dihydrogen exchange reaction (4).

$$CH_2O + CH_3OH \rightarrow CH_3OH + CH_2O \qquad (4)$$

In this reaction the two hydrogens are transferred through a one step cyclic relay type mechanism, which has several common features with reaction (3) above.

In summary we have shown (a) that protonation of formaldehyde lowers the energy barrier for hydrogenation, and (b) the barrier is further lowered upon inclusion of a water molecule.

These calculations were made possible thanks to support through the NFR (The Norwegian Research Council) Programme for Supercomputing.

Notes and references

1 J. R. Gilbert, P. A. M. van Koppen, W. T. Huntress and M. T. Bowers, *Chem. Phys. Lett.*, 1981, **82**, 455.
2 R. H. Nobes and L. Radom, *Chem. Phys.*, 1983, **74**, 163.
3 E. L. Øiestad, M. L. Øiestad, H. Skaane, K. Ruud, T. Helgaker, E. Uggerud and T. Vulpius, *Eur. Mass Spectrom.*, 1995, **1**, 121.
4 E. Uggerud, *Mass Spectrom. Rev.*, 1999, **18**, 285.
5 C. I. F. Watt, *Adv. Phys. Org. Chem.*, 1988, **24**, 57.
6 A. G. Harrison, *Chemical Ionization Mass Spectrometry*, CRC, Boca Raton, FL, 1992.
7 C. Möller and M. S. Plesset, *Phys. Rev.*, 1934, **46**, 618.
8 M. J. Frisch, J. A. Pople and J. S. Binkley, *J. Chem. Phys.*, 1984, **80**, 3265.
9 L. A. Curtiss, K. Raghavachari, G. W. Trucks and J. A. Pople, *J. Chem. Phys.*, 1991, **94**, 7221.
10 M. J. Frisch, G. W. Trucks, H. B. Schlegel, G. E. Scuseria, M. A. Robb, J. R. Cheeseman, V. G. Zakrzewski, J. A. Mongomery, R. E. Stratmann, J. C. Burant, S. Dapprich, J. M. Millam, A. D. Daniels, K. N. Kudin, M. C. Strain, O. Farkas, J. Tomasi, V. Barone, M. Cossi, R. Cammi, B. Mennucci, C. Pomelli, C. Adamo, S. Clifford, J. Ochterski, G. A. Petersson, P. Y. Ayala, Q. Cui, K. Morokuma, D. K. Malick, A. D. Rabuck, K. Raghavachari, J. B. Foresman, J. Cioslowski, J. V. Ortiz, A. G. Baboul, B. B. Stefanov, G. Liu, A. Liashenko, P. Piskorz, I. Komaromi, R. Gomperts, R. L. Martin, D. J. Fox, T. Keith, M. A. Al-Laham, C. Y. Peng, A. Nanayakkara, C. Gonzalez, M. Challacombe, P. M. W. Gill, B. G. Johnson, W. Chen, M. W. Wong, J. L. Andres, A. Gonzales, M. Head-Gordon, E. S. Replogle and J. A. Pople, GAUSSIAN 98, Pittsburgh, PA, 1998.
11 S. G. Lias, J. E. Bartmess, J. F. Liebman, J. H. Holmes, R. D. Levin and W. G. Mallard, *J. Phys. Chem. Ref. Data*, 1988, **17**, 1.
12 M. L. McKee, P. B. Shevlin and H. S. Rzepa, *J. Am. Chem. Soc.*, 1986, **108**, 5793.

A new highly selective calix[4]crown-6 fluorescent caesium probe

Hai-Feng Ji, Reza Dabestani,* Gilbert M. Brown and Richard A. Sachleben

Chemical and Analytical Sciences Division, Oak Ridge National Laboratory, PO Box 2008, MS-6100, Oak Ridge, TN 37831-6100, USA. E-mail: dabestanir@ornl.gov

Received (in Columbia, MO, USA) 1st November 1999, Accepted 30th March 2000

We have synthesized 1,3-alternate di-deoxygenated calix[4](9-cyano-10-anthrylmethyl)benzocrown-6, 1 and 1,3-alternate calix[4](9-cyano-10-anthrylmethyl)benzocrown-6, 2 as the second generation of caesium selective fluorescent probes; probe 1 shows 54-fold fluorescence enhancement upon caesium complexation while 2 exhibits only 8-fold enhancement; the selectivity ratios for 1 to complex caesium ion over potassium and rubidium (K_{Cs}/K_K and K_{Cs}/K_{Rb}) are *ca.* 10 fold higher than those of 2 for the same ions; the observed selectivity ratios are consistent with data reported for other 1,3-alternate calix[4]crown-6 derivatives.

Calix[4]crown-6 ethers in the 1,3-alternate conformation bind caesium with remarkable strength and selectivity.[1] Consequently, significant effort has been directed towards their use in the sensing, monitoring and remediation of ^{137}Cs, a fission product present in the wastes generated during the reprocessing of irradiated nuclear fuels.[2] The need for sensitive caesium sensors has led to the study of calix[4]crown-6 ethers as fluorescent caesium probes, and we have shown that 1,3-alternate calix[4]-bis-*o*-benzocrown-6[3a] ethers bearing cyanoanthracene fluorophores exhibit 8–12 fold fluorescence enhancement in the presence of caesium ion. The K_{Cs}/K_K and K_{Cs}/K_{Rb} ratios of 13[3b] and 1.3,[3b] respectively, indicate that the observed selectivities are consistent with data reported for other 1,3-alternate calix[4]crown-6 derivatives using UV absorption and potentiometric measurements.[4]

Recently, it was reported[5] that 1,3-alternate di-deoxygenated calix[4]crown-6 ethers exhibit enhanced selectivity for caesium over potassium and rubidium compared with their 1,3-alternate dialkoxy calix[4]crown-6 derivatives. Here, we have taken advantage of this higher caesium to potassium selectivity to synthesize a new caesium selective probe **1**. Our results suggest that **1** exhibits not only enhanced selectivity towards caesium, but also shows a fluorescence turn-on response significantly higher than any previously reported caesium sensor.

The 1,3-alternate di-deoxygenated calix[4](9-cyano-10-anthrylmethyl)-benzocrown-6, **1** was synthesized from di-dehydroxylated calix[4]arene and 1,2-bis(5-iodo-3-oxa-1-pentyloxy)-4-(10-cyano-9-anthrylmethyl)benzene[3b] by a standard procedure reported earlier.[6] The fluorescence of the 9-cyanoanthracene is quenched by the benzo moiety owing to a photoinduced electron transfer (PET) process.[7] It has been shown that binding the oxygen lone pair electrons (on the benzo moiety) by metal ion complexation partially suppresses the PET process, causing the fluorescence of the cyanoanthracene to increase.[3a,7]

The emission behavior of **1** (1×10^{-6} M) in CH_2Cl_2–MeOH (1 : 1) in the presence of five different alkali metal cations is shown in Fig. 1. The data indicates that probe **1** exhibits a significant emission enhancement upon caesium complexation (*ca.* 20-fold increase compared to uncomplexed probe) at a concentration as low as 2×10^{-7} M where no other alkali metal ion shows any response (except for Rb^+ that shows *ca.* 2-fold emission enhancement at the same concentration, Fig. 1). The fluorescence quantum yields of **1** for various alkali metal cations shown in Table 1 were determined relative to 9,10-diphenylanthracene in MeOH, Φ_f = 0.94.[8] The fluorescence quantum yield of **1** is enhanced 54 times (relative to free ligand, Table 1) when fully complexed with caesium at *ca.* 2×10^{-5} M concentration of caesium ion. This is the most dramatic emission response upon caesium ion complexation of any caesium optical sensors reported to date. In comparison, the fluorescence of **2**, 1,3-alternate calix[4](9-cyano-10-anthrylme-

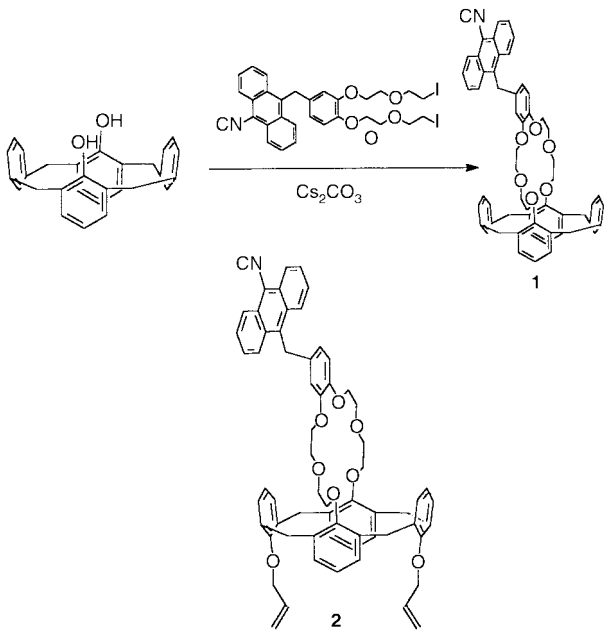

Scheme 1 The structures of **1** and **2**.

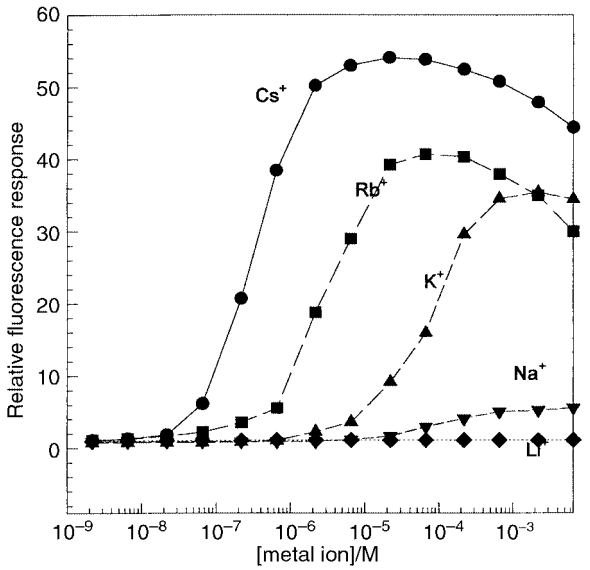

Fig. 1 Changes in the emission intensity of **1** (1×10^{-6} M) in CH_2Cl_2–MeOH (1 : 1) upon addition of alkali metal ions (as acetate salts), λ_{ex} = 376 nm. Each data point represents the integrated total area under the emission curve (λ_{em} = 400–600 nm).

DOI: 10.1039/a908720f

Table 1 Maximum fluorescence quantum yields and the complexation constants for both **1** and **2** in the presence of different alkali metal ions[a]

	Free	Li^+	Na^+	K^+	Rb^+	Cs^+
Φ_{em-max} of **1**	0.012	0.014	0.068	0.405	0.491	0.625
Φ_{em-max} of **2**	0.010	0.010	0.036	0.044	0.061	0.082
log (*K*) of **1**	—	—	—	4.06	5.48	6.60
log (*K*) of **2**	—	—	2.60	5.50	6.96	7.08

[a] [**1**], [**2**] = 1×10^{-6} M in CH_2Cl_2–MeOH (1:1, v/v). Metal ion concentrations: $[Cs^+] = 2 \times 10^{-5}$ M, $[Rb^+] = 4 \times 10^{-5}$ M, $[K^+] = 1 \times 10^{-3}$ M, $[Na^+] = 1 \times 10^{-2}$ M, $[Li^+] = 0.1$ M.

thyl)benzocrown-6, with the same fluorophore but based on a slightly different calix[4]arene platform, showed only 8.2-fold enhancement when fully complexed with caesium (Table 1). The dramatic fluorescence increase of **1** compared to **2** could be attributed to changes in the binding cavity of **1** (*vida supra*). Although Rb^+ and K^+ complexation cause the fluorescence of **1** to increase (42.6- and 35.2-fold, respectively), their maximum responses occur at higher concentrations (6×10^{-5} M and 2×10^{-3} M, respectively), indicating that their association constants with **1** are much weaker than that of caesium. Na^+ and Li^+ ions show little effect on the fluorescence of **1**, suggesting a weak interaction (complexation) between these ions and **1**.

The 1:1 complexation constant can be calculated from the emission intensity and concentration of metal ion, [M], profile shown in Fig. 1 according to eqn. (1)[7]

$$\frac{I - I_0}{I_\infty - I_0} = K([\mathrm{M}]_t - [\mathrm{L}]_t(\frac{I - I_0}{I_\infty - I_0})) \quad (1)$$

where I is the emission response of the probe at certain metal ion concentration, I_0 is the emission response of the probe in the absence of metal ions, I_∞ is the emission response when no further changes occur upon addition of the metal ion, $[L]_t$ is the total concentration of probe molecule (**1** or **2**) and $[M]_t$ represents the total metal ion concentration. The complexation constants K reported in Table 1 were calculated using a non-linear curve-fitting method[9] to fit the observed experimental emission data.

The complexation constant of **1** with caesium (4.0×10^6 M^{-1}) is about one-third of the value obtained for **2** (1.2×10^7 M^{-1}). On the other hand, the emission enhancement for **1** is about 7 times higher than that of **2**. The more sensitive response of **1** to caesium complexation suggests a stronger interaction between the caesium cation and the ether oxygens of the benzo group in **1**. This in turn results in a greater charge dispersion onto the oxygen of the crowns and subsequently stronger interaction between caesium and the benzo moiety. Experimental support substantiating the above argument has been provided by X-ray crystallography data.[10] Crystallographic results for a closely related series of compounds show that the average Cs–O (benzo oxygen) distance of an analog to **1** is 0.15 Å shorter than the average bond length in an analog to **2**.[10]

The complexation constants of **1** with Rb^+ (3.0×10^5 M^{-1}) and K^+ (1.2×10^4 M^{-1}) are significantly lower than those of **2** (Rb^+: 9.1×10^6 M^{-1}, K^+: 3.2×10^5 M^{-1}), resulting in the selectivity ratios of $K_{Cs}/K_{Rb} = 13.2$ and $K_{Cs}/K_K = 347$. These selectivities are *ca.* 10-fold higher than those calculated for **2** ($K_{Cs}/K_{Rb} = 1.3$ and $K_{Cs}/K_K = 38$) and other 1,3-alternate calix[4]benzocrown-6 derivatives reported previously.[3,4] Such observation clearly highlights the remarkable sensitivity of **1** as a caesium selective sensor for low Cs^+ concentrations.

We also measured the change in emission behavior of **1** with caesium in MeOH and observed only a 6.5-fold enhancement. In addition, the complexation constants of **1** with caesium and potassium were much smaller in MeOH than in CH_2Cl_2–MeOH (1:1) (8.6×10^5 M^{-1} and 3.0×10^3 M^{-1}, respectively). This could indicate that PET quenching is more efficient in the more polar MeOH environment because polarity can affect the energetics of the receptor (crown moiety) relative to that of fluorophore (to enhance PET effect) and/or MeOH can complex with the receptor competing with caesium for binding.[11] The effect of solvent polarity on the emission behavior of **1** and previously reported probes will be published later.[3b]

In conclusion, the new di-deoxygenated calix[4]arene derived fluorescence sensor **1** shows a significantly greater emission response (fluorescence turn on) to caesium compared to **2** and the other previously reported probes and holds promise for the development of a highly selective caesium detection and monitoring system.

This research was funded by the Environmental Management Science Program, Office of Environmental Management, U.S. Department of Energy and in part by an appointment sponsored by the Oak Ridge National Laboratory Postdoctoral Research Associates Program administered jointly by the Oak Ridge Institute for Science and Education and Oak Ridge National Laboratory. Oak Ridge National Laboratory is operated by Lockheed Martin Energy Research Corporation for the U.S. Department of Energy under contract number DE-AC05-96OR22464. We thank J. C. Bryan for helpful discussions.

Notes and references

1 Z. Asfari, S. Wenger and J. Vicens, *J. Inclusion Phenom. Mol. Recog. Chem.*, 1994, **19**, 137; T. J. Haverlock, P. V. Bonnesen, R. A. Sachleben and B. A. Moyer, *Radiochim. Acta*, 1997, **76**, 103; C. Hill, J.-F. Dozol, V. Lamare, H. Rouquette, S. Eymard, B. Tournois, J. Vicens, Z. Asfari and C. Bressot, *J. Inclusion Phenom. Mol. Recog. Chem.*, 1994, **19**, 399.

2 C. Bocchi, M. Careri, A. Casnati and G. Mori, *Anal. Chem.*, 1995, **67**, 4234; H. Zeng and B. Dureault, *Talanta*, 1998, **46**, 1485; J. S. Kim, A. Ohki, R. Ueki, T. Ishizuka, T. Shimotashiro and S. Maeda, *Talanta*, 1999, **48**, 705; C. Perez-Jimenez, L. Escriche and J. Casabo, *Anal. Chim. Acta*, 1998, **371**, 155; R. J. W. Lugtenberg, Z. Brzozka, A. Casnati, R. Ungaro, J. F. J. Engbersen and D. N. Reinhoudt, *Anal. Chim. Acta*, 1995, **310**, 263.

3 (*a*) H.-F. Ji, G. B. Brown and R. Dabestani, *Chem. Commun.*, 1999, 609; (*b*) H.-F. Ji, R. Dabestani and G. B. Brown, manuscript in preparation.

4 A. Casnati, A. Pochini, R. Ungaro, F. Ugozzoli, F. Arnaud, S. Fanni, M.-J. Schwing, R. J. M. Egberink, F. de Jong and D. N. Reinhoudt, *J. Am. Chem. Soc.*, 1995, **117**, 2767; F. Arnard-Neu, Z. Asfari, B. Souley and J. Vicens, *New J. Chem.*, 1996, **20**, 453.

5 R. A. Sachleben, A. Urvoas, J. C. Bryan, T. J. Haverlock, B. P. Hay and B. A. Moyer, *Chem. Commun.*, 1999, 1751.

6 Z. Asfari, C. Bressot, J. Vicens, C. Hill, J.-F. Rozol, H. Rouquette, S. Eymard, V. Lamare and B. Tourmois, *Anal. Chem.*, 1995, **67**, 3133.

7 A. P. de Silva and K. R. A. S. Sandanayake, *J. Chem. Soc., Chem. Commun.*, 1989, 1183.

8 A. Maciejewski and R. P. Steer, *J. Photochem.*, 1986, **35**, 59.

9 H.-F. Ji, R. Dabestani, G. M. Brown and R. L. Hettich, *Photochem. Photobiol.*, 1999, **69**, 513.

10 J. C. Bryan, unpublished results.

11 We thank the reviewers for bringing this point to our attention.

ChemComm

Non-ionic surfactant assembly of wormhole silica molecular sieves from water soluble silicates

Seong-Su Kim, Thomas R. Pauly and Thomas J. Pinnavaia*

Department of Chemistry, Michigan State University, East Lansing, Michigan 48824, USA

Received (in Columbia, MO, USA) 18th January 2000, Accepted 23rd March 2000
Published on the Web 28th April 2000

Thermally stable mesoporous silica molecular sieves with wormhole framework structures, previously obtainable only from silicon alkoxides, have been prepared from low cost soluble silicate precursors in the presence of non-ionic surfactants as structure directors.

Mesoporous molecular sieve silicas with wormhole framework structures (*e.g.* MSU-X,[1,2] and HMS[3]) are generally more active heterogeneous catalysts in comparison to their ordered hexagonal analogs (*e.g.* MCM-41,[4] SBA-3[5] and SBA-15[6]). The enhanced reactivity has been attributed, in part, to a pore network that is connected in three dimensions, allowing the guest molecules to more readily access reactive centers that have been designed into the framework surfaces.[7–10] All of the wormhole framework structures reported to date have been prepared through supramolecular S^oI^o[3] and N^oI^o[1,2] assembly pathways wherein I^o is an electrically neutral silica precursor (typically, tetraethylorthosilicate, TEOS), S^o is a neutral amine surfactant, and N^o is a neutral di- or tri-block surfactant containing polar polyethylene oxide (PEO) segments. One disadvantage of these pathways, as with other assembly pathways based on TEOS, is the high cost of the hydrolyzable silicon alkoxide precursor. Greater use of wormhole framework structures as heterogeneous catalysts may be anticipated if a more efficient approach to either S^oI^o or N^oI^o assemblies could be devised based on the use of low cost soluble silicate precursors, without sacrificing the intrinsically desirable processing advantages of these pathways (*e.g.* facile removal and recycling of the surfactant).

Recently, Guth and coworkers reported the preparation of disordered silica mesostructures by precipitation from sodium silicate solutions over a broad range of pH in the presence of Triton-X 100, an N^o surfactant.[11] The retention of a mesostructure was observed up to a calcination temperature of 480 °C, but the complete removal of the surfactant at 600 °C led either to the extensive restructuring of the silica framework, as indicated by the loss of mesoporosity or the formation of a completely amorphous material. In contrast, MSU-X mesostructures are structurally stable to calcination temperatures in excess of 800 °C. The present work demonstrates that mesoporous molecular sieve silicas equivalent in structure and thermal stability to MSU-X silicas (denoted MSU-X′) can in fact be prepared from soluble silicate precursors under the appropriate assembly conditions.

Our approach, like that of Guth and coworkers, uses a sodium silicate as the silica source and an N^o surfactant as the structure director, but our methodology results in thermally stable wormhole structures. In a typical synthesis the surfactant and an amount of acid equivalent to the hydroxide content of the sodium silicate solution (*e.g.* 27% SiO_2, 14% NaOH, Aldrich) are first mixed at ambient temperature and then added to the sodium silicate solution to form reactive silica in the presence of the surfactant. This allows the assembly of the framework structure at near-neutral pH and avoids the need for readjusting the pH once the reactive silica has been formed. The assembly process is carried out at a molar ratio SiO_2/surfactant in the range 13–7.0 and at a temperature in the range 25–60 °C for a period of 10–20 h. The surfactant is then removed from the washed and air-dried products either by solvent extraction with hot ethanol or by calcination in air at 600 °C.

Fig. 1 illustrates the powder X-ray diffraction patterns of as-synthesized and calcined MSU-X′ silicas prepared at three different temperatures using Brij 56 [$C_{16}H_{33}(EO)_{10}H$] as the structure-directing surfactant. Each product exhibits an intense reflection at low 2θ corresponding to a pore–pore correlation distance of *ca.* 63 Å with a broad shoulder in the 2θ range 2–3. These patterns are typical of disordered wormhole-like pore structures and are similar to those of MSU-X silicas assembled from the same surfactant, but with TEOS as the silica precursor. After calcination at 600 °C, the intensities of the pore–pore correlation peaks are substantially greater than the as-synthesized samples due to the removal of the contrast-matching surfactant. This result is consistent with the retention of the framework pore structure upon complete removal of the surfactant from the framework.

Further evidence for the wormhole framework pore structure of MSU-X′ silicas is provided by the typical transmission electron micrograph (TEM) image shown in Fig. 2. This micrograph clearly exhibits disordered wormhole-like pores similar to MSU-X materials. Fig. 3 illustrates the N_2 adsorption–desorption isotherms and Horvath–Kawazoe pore size distributions (inset) for the calcined MSU-X′ products assembled at 25, 45 and 60 °C. The sample assembled at 25 °C exhibits the smallest pore size (32 Å) in the series, and the largest HK pore diameter (50 Å) is observed for the 60 °C sample. The increase in framework pore size with increasing assembly temperature is a characteristic feature of an N^oI^o assembly pathway.[2] The desorption hysteresis observed for the product prepared at 60 °C is indicative of the necking of the interconnected wormhole pore structure. In addition, the pore

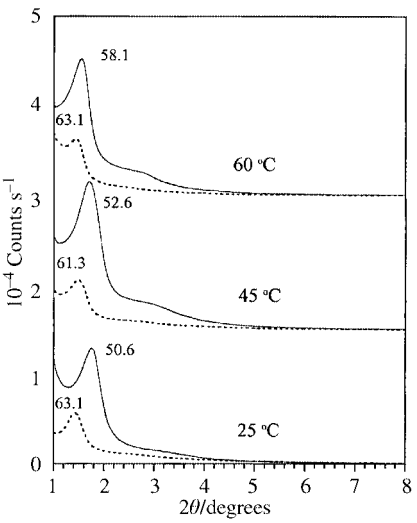

Fig. 1 XRD patterns of MSU-X′ silica molecular sieves formed from sodium silicate and Brij 56 under neutral pH conditions at 25, 45 and 60 °C, respectively. Dashed and solid curves are for the as-synthesized and calcined products, respectively. The numbers adjacent to each diffraction peak are the pore–pore correlation distances in angstrom (Å) units.

DOI: 10.1039/b001012j

Table 1 Physicochemical properties of mesoporous silica (MSU-X′) prepared using sodium silicate and non-ionic surfactants

Surfactant	Synthesis temperature/°C	Pore–pore distance/Å		BET surface area/m² g⁻¹	Pore size/Å	Wall thickness[b]/Å	Pore volume/cm³ g⁻¹
		As-synth.	Calcined[a]				
Brij 56	25	63.1	50.6	602	32	25	0.36
Brij 56	45	61.3	52.6	769	37	16	0.57
Brij 56	60	63.1	58.1	849	50	8	0.90
Brij 35	60	59.7	52.5	853	33	20	0.65
Brij 58	60	66.9	58.1	821	43	15	0.80
Brij 78	60	69.0	61.4	851	48	13	0.83
Tergital (15-S-15)	60	59.7	53.2	979	40	13	0.86
Tween 20	60	58.9	52.9	883	42	11	0.84
Tween 40	60	65.9	58.9	753	49	10	0.80
Tween 60	60	66.9	58.9	773	48	11	0.75
Tween 80	60	71.2	65.0	867	51	14	0.89

[a] Calcined at 600 °C for 4 h in air. [b] The wall thickness was calculated by subtracting the HK pore diameter from the correlation distance.

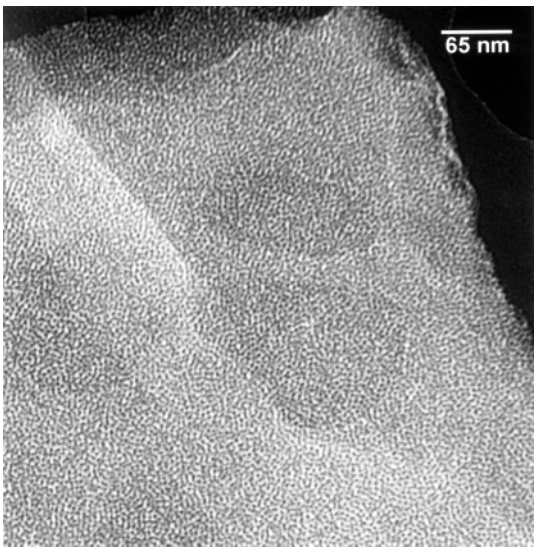

Fig. 2 TEM image of wormhole pore structure of the calcined MSU-X′ sample prepared from sodium silicate and Brij 56 under neutral pH conditions at 60 °C.

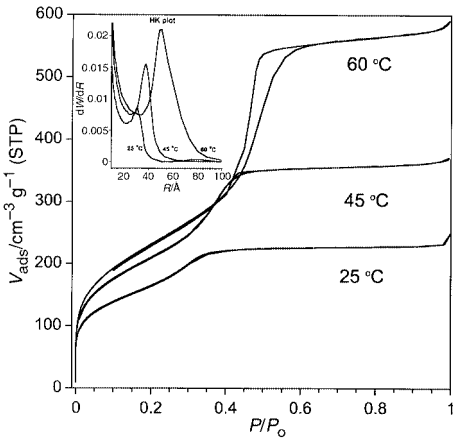

Fig. 3 N_2 adsorption–desorption isotherms for the calcined MSU-X′ silica molecular sieves formed from sodium silicate and Brij 56 under neutral pH conditions at 25, 45 and 60 °C, respectively. The insert provides the Horvath–Kawazoe pore size distributions.

wall thickness, as obtained from the difference between the pore–pore correlation distance and the HK pore size, decreases with increasing assembly temperature (Table 1). This latter behavior, which is related to the increase in the hydrophobic character of the PEO block as the surfactant approaches the cloud point, also is a characteristic feature of N^oI^o assembly.[2] Because Na^+ ions are present in the assembly process, there may also be an electrostatic contribution to framework formation through complexation of Na^+ by the N^o surfactant. However, electrostatically controlled $[N^oM^+]I^o$ assembly processes tend to form ordered hexagonal or cubic framework structures, not wormhole frameworks.[12]

Wormhole silica molecular sieves can also be assembled from water-soluble silicate precursors using N^o surfactants other than Brij 56. Table 1 summarizes the textural properties of wormhole silica assembled from sodium silicate and other Brij surfactants, a Tergitol $[C_{11–15}H_{23–31}(EO)_{15}H]$ surfactant, and several alkyl-PEO/furan Tween X surfactants (X = 20, 40, 60 and 80). Table 1 shows that each of these surfactants form mesostructures with 33–51 Å pore sizes, and surface areas and pore volumes comparable to MSU-X silicas prepared from TEOS. TEM analysis of each product conformed the wormhole pore structure.

The successful assembly of thermally stable mesoporous silica molecular sieve silicas with wormhole frameworks from soluble silicate precursors suggests that it may be possible to substitute soluble silicate precursors for the assembly of many other silica mesostructures that heretofore have been assembled exclusively from silicon alkoxide precursors. Future studies will focus on the assembly of other members of the MSU family of mesostructures, as well as SBA mesostructures obtained through an electrostatic $N^o(H^+X^-)I^+$ assembly pathway.[6]

The support of this research by NSF-CRG grant CHE-9903706 is gratefully acknowledged.

Notes and references

1 S. A. Bagshaw, E. Prouzet and T. J. Pinnavaia, *Science*, 1995, **269**, 1242; S. A. Bagshaw and T. J. Pinnavaia, *Angew. Chem., Int. Ed. Engl.*, 1996, **35**, 1102.

2 E. Prouzet and T. J. Pinnavaia, *Angew. Chem., Int. Ed. Engl.*, 1997, **36**, 516.

3 P. T. Tanev and T. J. Pinnavaia, *Science*, 1995, **267**, 865.

4 J. S. Beck, J. C. Vartuli, W. J. Roth, M. E. Leonowicz, C. T. Kresge, K. D. Schmitt, C. T.-W. Chu, D. H. Olson, E. W. Sheppard, B. McCullen, J. B. Higgins and J. L. Schlenker, *J. Am. Chem. Soc.*, 1992, **114**, 10 834.

5 Q. Huo, D. I. Margolese, U. Ciesla, P. Feng, T. E. Gier, P. Sieger, R. Leon, P. M. Petroff, F. Schüth and G. D. Stucky, *Nature*, 1994, **368**, 317.

6 D. Zhao, Q. Huo, J. Feng, B. F. Chmelka and G. D. Stucky, *J. Am. Chem. Soc.*, 1998, **120**, 6024.

7 W. Zhang and T. J. Pinnavaia, *Stud. Surf. Sci. Catal.*, 1998, **117**, 23.

8 J. S. Reddy, I. Moudrakovski and A. Sayari, *J. Chem. Soc., Chem. Commun.*, 1994, 1059; J. S. Reddy and A. Sayari, *J. Chem. Soc., Chem. Commun.*, 1995, 2231; A. Sayari, *Chem. Mater.*, 1996, **8**, 1840.

9 R. Mokaya and W. Jones, *J. Catal.*, 1997, **172**, 211.

10 K. R. Kloetstra, H. van Bekkum and J. C. Jansen, *Chem. Commun.*, 1997, 228.

11 L. Sierra, B. Lopez, J. Gil and J.-L. Guth, *Adv. Mater.*, 1999, **11**, 307; L. Sierra and J.-L. Guth, *Microporous Mesoporous Mater.*, 1999, **27**, 243.

12 W. Z. Zhang, B. Glomski, T. R. Pauly and T. J. Pinnavaia, *Chem. Commun.*, 1999, 1803.

ChemComm

Practical method to recycle a chiral (salen)Mn epoxidation catalyst by using an ionic liquid

Choong Eui Song* and Eun Joo Roh

Life Sciences Division, Korea Institute of Science and Technology, PO Box 131, Cheongryang, Seoul, 130-650, Korea. E-mail: s1673@kistmail.kist.re.kr

Received (in Cambridge, UK) 18th February 2000, Accepted 11th April 2000
Published on the Web 28th April 2000

A practical recycling procedure for Jacobsen's chiral (salen)Mn^{III} epoxidation catalyst involving the use of the air- and moisture-stable ionic liquid [bmim][PF_6] has been developed.

Development of practical immobilisation methods[1] for chiral homogeneous catalysts is highly desirable, since immobilised chiral catalysts offer several practical advantages over soluble catalysts such as facilitation of catalyst separation from reagents and products, simplification of methods for catalyst recycling, and the possible adaptation of the immobilised catalyst for continuous flow processes. To this end, some homogeneous chiral catalysts have been immobilised either by anchoring the catalyst on a solid support[1a] or by use of a two-phase system.[1b] All of these approaches are interesting but usually require additional modifications of the catalyst. Moreover, such approaches frequently lead to partial loss of activity and/or enantioselectivity.

For Jacobsen's chiral (salen)Mn^{III} epoxidation catalyst,[2] [*N*,*N*′-bis(3,5-di-*tert*-butylsalicylidene)-1,2-cyclohexanediamine]manganese(III)] chloride **1**, several attempts to immobilise this catalyst have been made.[3–6] However, no successful immobilisation procedure has, as yet, been reported. Attempts to immobilise Jacobsen's catalyst up to now consisted of covalent attachment of the complex to insoluble solid supports,[3] steric occlusion in nano-sized cages of zeolites,[4] physical entrapment in a polydimethylsiloxane membrane,[5] and use of a fluorous biphasic system (FBS).[6]

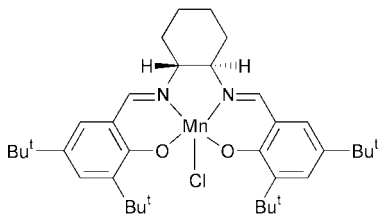

(*R*,*R*)-**1**

Recently, a new approach has been adopted for catalyst separation and recycling in a few types of catalytic reaction involving the use of ionic liquids,[7] *i.e.* a salt mixture with a melting point below ambient. Air and moisture-stable room temperature ionic liquids consisting of 1,3-dialkylimidazolium cations and their counter anions, in particular, have attracted growing interest in the last few years.[8] In these solvents, catalysts having polar or ionic character can be immobilised and thus the ionic solutions containing the catalyst can be easily separated from reagents and products. Recent applications include Friedel–Crafts reactions,[8a] Diels–Alder reactions,[8b] alkylations,[8c] olefin dimerisation and oligomerisation,[8d] hydrogenation,[8e] Heck reaction,[8f] hydroformylation[8g] and palladium catalysed allylation reactions.[8h]

Herein, we report a practical recycling procedure of Jacobsen's catalyst (*R*,*R*)-**1** involving the use of the air- and moisture-stable ionic liquid, [bmim][PF_6] **2** ([bmim]$^+$ = 1-butyl-3-methylimidazolium cation). The ionic liquid **2** is conveniently prepared,[9] and an excellent solvent for many organic compounds, but is immiscible with saturated hydrocarbon solvents, dialkyl ethers and water. Taking into account the conditions of asymmetric epoxidation (involving the use of aqueous NaOCl) and the unique solvating properties of **2**, it was selected as a solvent for our experiments among many other ionic liquids (*cf.* the BF_4^- or triflate salts which are soluble in water).

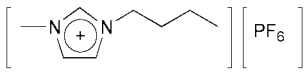

[bmim][PF_6] **2**

Asymmetric epoxidations† were carried out in the presence of 4 mol% of (*R*,*R*)-**1** with 2,2-dimethylchromene, 6-cyano-2,2-dimethylchromene, indene, *cis*-β-methylstyrene, and 1-phenylcyclohexene as substrates in [bmim][PF_6]–CH_2Cl_2 (1 : 4, v/v) using NaOCl as the oxidant at 0 °C. Since the ionic liquid **2** solidifies at the reaction temperature (0 °C), the co-solvent system was used. Both the catalyst (*R*,*R*)-**1** and the ionic liquid **2** are soluble in CH_2Cl_2. The results obtained are shown in Table 1.

As shown in Table 1, conversion of alkenes to epoxides and enantioselectivity were satisfactory and comparable to those[10] obtained without an ionic liquid. In particular, the epoxidation of 2,2-dimethylchromene and 6-cyano-2,2-dimethylchromene in [bmim][PF_6]-CH_2Cl_2 afforded the corresponding chromene oxides in very high ee (96 and 94%, entries 1 and 2). Moreover, the reaction in the presence of the ionic liquid **2** proceeded faster than without an ionic liquid. For example, the epoxidation of 2,2-dimethylchromene in the presence of **2** was complete in 2 h (entry 1) whereas in a control experiment, the same reaction without **2** required 6 h to achieve a comparable degree of conversion. Furthermore, both the catalyst (*R*,*R*)-**1** and the ionic liquid could be easily recovered after reaction. The recovery procedure was as follows: the organic phase of the reaction

Table 1 Asymmetric epoxidation of alkenes in ionic liquid **2**[a]

Entry	Substrate	*t*/h	Yield[b] (%)	% ee[c]	Confign.[c]
1	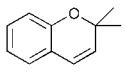	2	86	96	(3*R*,4*R*)
2	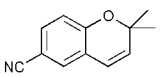	4	72	94	(3*R*,4*R*)
3		4	72	84	(1*R*,2*S*)
4		3	72 (3.7 : 1)[d]	86	(1*R*,2*S*)
5	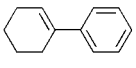	4	77	84	(*S*,*S*)

[a] See footnote.† [b] Isolated yield. [c] Determined by chiral GC or chiral HPLC: see footnote† and ref. 11. [d] *Cis* : *trans* selectivity.

DOI: 10.1039/b001403f

Table 2 Recovery and reuse of the ionic liquid phase containing (*R*,*R*)-**1**[a]

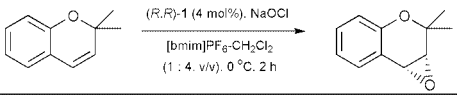

Run	1	2	3	4	5
Yield (%)[b]	86	73	73	60	53
% ee[c]	96	90	90	89	88

[a] See footnote†. [b] Isolated yield. [c] Determined by chiral HPLC.

mixture was washed with water and concentrated. After extraction of the product with hexane, the brown oily ionic liquid which contains the catalyst, was recovered, which could be reused for further catalytic reactions. The above procedure was repeated five times and results obtained are shown in Table 2. However, the enantioselectivity and the activity of the recovered catalyst decreased slightly upon successive use possibly due to minor degradation of the salen catalyst (*R*,*R*)-**1** under the oxidation conditions.

In summary, we have developed a practical recycling procedure for Jacobsen's chiral (salen)Mn^{III} catalyst **1** by use of ionic liquid **2**. Our results showed that the catalyst (*R*,*R*)-**1** in a reaction medium containing ionic liquid **2** exhibited comparable enantioselectivity (96% ee for 2,2-dimethylchromene) in asymmetric epoxidation of alkenes as those obtained without ionic liquid and, moreover, showed an increase in activity. At the end of reaction the immobilised catalyst in ionic liquid **2** could be easily recycled. In conclusion, the immobilisation method of **1** by using an ionic liquid provides not only simple recycling of catalyst, but also the additional advantage of use of the catalyst without any modification of its structure. A detailed study concerning the optimisation of this process and extension of this methodology to recycle other homogeneous chiral catalysts are currently in progress.

This research was supported by a grant from Korea Institute of Science and Technology.

Notes and references

† *Representative procedure* for asymmetric epoxidation using an ionic liquid: the pH of a solution of commercial household bleach (Clorox®) was buffered to pH = 11.3 with 0.05 M Na_2HPO_4 and 1 M NaOH (a few drops) and then cooled to 0 °C. To 110 mL of this solution was added a precooled solution (0 °C) of 2,2-dimethylchromene (5.0 g, 31.3 mmol) and the catalyst (*R*,*R*)-**1** (0.79 g, 1.25 mmol) in CH_2Cl_2 (30 mL) and [bmim][PF_6] (7.5 mL). The two-phase system was stirred at 0 °C and the progress of reaction was monitored by TLC. After 2 h, the organic phase was separated and washed twice with water. The volatiles were concentrated *in vacuo* and the residue was stirred with hexane. After concentration of the upper hexane phase *in vacuo*, the residue was purified by column chromatography on silica gel (deactivated with 1% NEt_3 solution in ethyl acetate–hexane) with ethyl acetate–hexane (1 : 10) as eluent, to afford 4.74 g (86% yield) of the epoxide with 96% ee. The brown oily ionic liquid phase (the lower phase) containing the catalyst was reused.

Ee values of products were determined by chiral HPLC or chiral GC: for 3,4-epoxy-2,2-dimethylchroman: Daicel Chiralpak AD, propan-2-ol–hexane (5/95), 0.8 mL min^{-1}; 9.30 min (3*R*,4*R*), 10.63 min (3*S*,4*S*). For 3,4-epoxy-6-cyano-2,2-dimethylchroman: Daicel Chiralcel OJ, propan-2-ol–hexane (30/70), 1 mL min^{-1}; 13.95 min (3*R*,4*R*), 26.88 min (3*S*,4*S*). For other epoxides: see ref. 11.

1 (*a*) B. Pugin and H.-U. Blaser, *Catalyst Immobilization: Solid Supports*, in *Comprehensive Asymmetric Catalysis III*, ed. E. N. Jacobsen, A. Pfaltz and H. Yamamoto, Springer-Verlag, Berlin–Heidelberg–New York, 1999, p. 1367; (*b*) G. Oehme, *Catalyst Immobilization: Two-Phase Systems*, in *Comprehensive Asymmetric Catalysis III*, ed. E. N. Jacobsen, A. Pfaltz and H. Yamamoto, Springer-Verlag, Berlin–Heidelberg–New York, 1999, p. 1378.

2 E. N. Jacobsen and M. H. Wu, *Epoxidation of Alkenes Other than Allylic Alcohols*, in *Comprehensive Asymmetric Catalysis II*, ed. E. N. Jacobsen, A. Pfaltz and H. Yamamoto, Springer-Verlag, Berlin–Heidelberg–New York, 1999, p. 649.

3 Recent papers: L. Canali, E. Cowan, H. Deleuze, C. L. Gibson and D. C. Sherrington, *Chem. Commun.*, 1998, 2561; M. D. Angelino and P. E. Laibinis, *Macromolecules*, 1998, **31**, 7581; G.-J. Kim and J.-H. Shin, *Tetrahedron Lett.*, 1999, **40**, 6827; D. Pini, A. Mandoli, S. Orlandi and P. Salvadori, *Tetrahedron: Asymmetry*, 1999, **10**, 3883; C. E. Song, E. J. Roh, B. M. Yu, D. Y. Chi, S. C. Kim and K.-J. Lee, *Chem. Commun.*, 2000, 615.

4 M. J. Sabater, A. Corma, A. Domenech, V. Fornes and H. Garcia, *Chem. Commun.*, 1997, 1285; S. B. Ogunwumi and T. Bein, *Chem. Commun.*, 1997, 901.

5 I. F. J. Vankelecom, D. Tas, R. F. Parton, V. Van de Vyver and P. A. Jacobs, *Angew. Chem., Int. Ed. Engl.*, 1996, **35**, 1346; K. B. M. Janssen, I. Laquiere, W. Dehaen, R. F. Parton, I. F. J. Vankelecom and P. A. Jacobs, *Tetrahedron: Asymmetry*, 1997, **8**, 3481.

6 G. Pozzi, F. Cinato, F. Montanari and S. Quici, *Chem. Commun.*, 1998, 877.

7 Review: T. Welton, *Chem. Rev*., 1999, **99**, 2071.

8 Catalytic reactions: (*a*) A. Stark, B. L. MacLean and R. D. Singer, *J. Chem. Soc., Dalton Trans.*, 1999, 63; (*b*) T. Fischer, A. Sethi, T. Welton and J. Woolf, *Tetrahedron Lett.*, 1999, **40**, 793; (*c*) M. J. Earle, P. B. McCormac and K. R. Seddon, *Chem. Commun.*, 1998, 2245; (*d*) B. Ellis, W. Keim and P. Wasserscheid, *Chem. Commun.*, 1999, 337; (*e*) A. L. Monteiro, F. K. Zinn, R. F. de Souza and J. Dupont, *Tetrahedron: Asymmetry*, 1997, **8**, 177; (*f*) W. A. Herrmann and V. P. W. Bohm, *J. Organomet. Chem.*, 1999, **572**, 141; (*g*) W. Keim, D. Vogt, H. Waffenschmidt and P. Wasserscheid, *J. Catal.*, 1999, **186**, 481; (*h*) W. Chen, L. Xu, C. Chatterton and J. Xiao, *Chem. Commun.*, 1999, 1247.

9 P. A. Z. Suarez, J. E. L. Dullius, S. Einloft, R. F. de Souza and J. Dupont, *Polyhedron*, 1996, **15**, 1217; J. Fuller, R. T. Carlin, H. C. De Long and D. Harworth, *J. Chem. Soc., Chem. Commun.*, 1994, 299.

10 N. H. Lee, A. R. Muci and E. N. Jacobsen, *Tetrahedron Lett.*, 1991, **32**, 5055.

11 Determination of enantiomeric excess: for indene oxide: M. Palucki, G. J. McCormick and E. N. Jacobsen, *Tetrahedron Lett.*, 1995, **36**, 5457; for *cis*-β-methylstyrene oxide: W. Zhang and E. N. Jacobsen, *J. Org. Chem.*, 1991, **56**, 2296; for 1-phenylcyclohexene oxide: B. Brandes and E. N. Jacobsen, *J. Org. Chem.*, 1994, **59**, 4378.

ChemComm

Fluorous soluble polymer catalysts for the fluorous biphase hydroformylation of olefins

Weiping Chen, Lijin Xu and Jianliang Xiao*

Leverhulme Centre for Innovative Catalysis, Department of Chemistry, University of Liverpool, Liverpool, UK L69 7ZD. E-mail: j.xiao@liv.ac.uk

Received (in Cambridge, UK) 20th January 2000, Accepted 5th April 2000
Published on the Web 28th April 2000

Fluorous soluble polymer ligands have been prepared and shown to be active and selective catalysts when combined with rhodium for the fluorous biphase hydroformylation of various olefins.

One of the most interesting recent developments in homogeneous catalysis is the concept and application of fluorous biphase catalysis (FBC).[1] The principle of FBC is based on the limited miscibility of common organic solvents with perfluorinated compounds. A very attractive aspect of FBC is that it provides, by means of phase separation, an elegant solution to the catalyst/product separation problem associated with homogeneous catalysis. Undoubtedly, successful application of FBC depends on rational design of catalysts that show high affinities to the fluorous phase. Until now, all the fluorous soluble metal catalysts have been based on molecular metal complexes containing conventional ligands modified with fluorinated groups.[2,3] The best known such catalysts are perhaps rhodium trialkylphosphine complexes appended with fluorous ponytails such as $[RhH(CO)\{P(CH_2CH_2C_6F_{13})_3\}_3]$. The applicability of these complexes has been convincingly demonstrated by Horváth and Gladysz in the fluorous biphase hydroformylation,[4] hydrogenation[5] and hydroboration[6] of olefins. As with their nonfluorinated counterparts, however, the rhodium fluoroalkylphosphine catalysts exhibit lower activity in the reactions studied in comparison with complexes containing arylphosphine ligands. Fluorinated, low molecular weight arylphosphines are less useful in FBC, on the other hand, owing to their solubility in common organic solvents such as toluene and hexane.[2,7] Herein we describe fluorous soluble fluoropolymer-supported arylphosphine ligands as an alternative to fluorous soluble low molecular weight ligands for FBC and the application of the new ligands in fluorous biphase hydroformylation of higher and functionalised olefins. We anticipated that by incorporating an arylphosphine into a fluoropolymer the solubility of the former in normal solvents would be minimised. A fluorous soluble copolymer has recently been reported by Bergbreiter and Franchina.[8]

Hydroformylation of higher olefins has been addressed in a number of publications.[9] The focal point is to search for more active and selective rhodium catalysts in conjunction with easy catalyst separation and reuse. The difficulty in catalyst separation encountered in the hydroformylation of higher olefins lies in the thermolability of conventional rhodium phosphine catalysts, high boiling points of the aldehyde product, and limited solubility of higher olefins in water, which could otherwise be employed to immobilise aqueous soluble catalysts. Polymer-supported rhodium catalysts including those that are water soluble have been investigated for the hydroformylation of olefins.[10–13] These catalysts, while potentially having the advantages of both homogeneous and heterogeneous catalysts, often display low catalytic activities.

The poly(fluoroacrylate-*co*-styryldiphenylphosphine) ligands **1** and **2** were prepared by free radical copolymerisation of 1*H*,1*H*,2*H*,2*H*-perfluorodecylacrylate with styryldiphenylphosphine at 65 °C in the presence of AIBN in α,α,α-trifluorotoluene (Scheme 1).[14] For the fluoropolymer **1**, an acrylate to styryldiphenylphosphine molar ratio of 5:1 was used. For **2**, the ratio was 9:1. After removing the solvent, the resultant solid was washed with hot toluene, affording the polymers as white powders in >90% yields. As expected, the polymers are not soluble in normal organic solvents such as toluene, acetone or alcohols but highly soluble in fluorinated solvents such as α,α,α-trifluorotoluene and perfluoromethylcyclohexane. The IR spectrum of both polymers showed the disappearance of the absorption due to C=C stretching, in line with the lack of resonances from olefinic protons in ^{1}H NMR spectra. The C=O absorption appeared at 1738 cm^{-1} for **1** and 1740 cm^{-1} for **2** in the IR spectra. The ^{31}P NMR spectrum of each polymer in α,α,α-trifluorotoluene ($CDCl_3$ external lock) displayed a relatively sharp singlet at δ *ca.* −6.2. The phosphorus content of the polymers was estimated to be 1.2% for **1** and 0.8% for **2** by ^{31}P NMR spectroscopy using bis(diphenylphosphino)methane as an internal standard. These values are close to the values of 1.1 and 0.6% calculated on the basis of the monomer ratios, and are consistent with the high yields of polymer synthesis.

To demonstrate the feasibility of phase separation when using the two polymers as ligands in catalysis, $[Rh(CO)_2(acac)]$ was added to a mixture of hexane (2 mL), toluene (1 mL) and perfluoromethylcyclohexane (2 mL) containing 100 mg of **1** (P/Rh = 6). The fluorous phase attained a yellow colour immediately, while the organic phase remained colourless and phase-separated from the perfluoro solvent at ambient temperature. Upon heating the solvent mixture to *ca.* 50 °C, a single homogeneous yellow phase formed and on cooling, the coloured fluorous phase separated quickly from the colourless organic phase. However, in the absence of hexane, the phase boundary remained even at reflux.

The catalytic performance of the fluoropolymer ligands **1** and **2** was tested in the fluorous biphase hydroformylation of alk-1-enes, styrene and *n*-butyl acrylate. The reaction was conducted in a batch reactor in a hexane–toluene–perfluoromethylcyclohexane (40:20:40, v/v) solvent mixture (10 mL). The catalyst was formed *in situ* by adding $[Rh(CO)_2(acac)]$ (5 μmol, P/Rh = 6) to the polymer-containing solvent mixture followed by introduction of syngas (30 bar, CO–H_2 = 1:1). Table 1 summarises the results obtained. The salient features of the results are (i) the activity of the fluorous soluble polymer catalysts are significantly higher than those reported for solid polymer- and aqueous soluble polymer-supported rhodium catalysts.[10–13] For example, the average turnover frequency

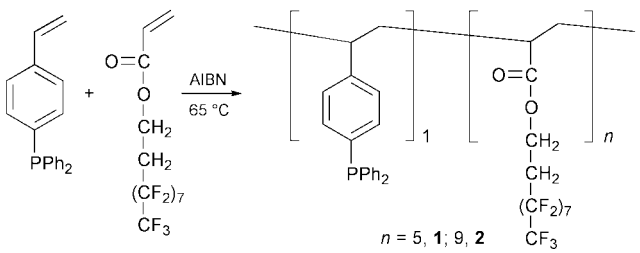

Scheme 1 Preparation of fluorocopolymer-supported arylphosphines.

DOI: 10.1039/b000574f

Table 1 Fluorous biphase hydroformylation of olefins by soluble polymer catalysts[a]

Olefin	Polymer	Olefin/Rh	Conversion (%)	Selectivity[b] (%)	L/B[c]
Dec-1-ene	**1**	2120	97	99	4.8/1
	2	2120	90	99	5.9/1
Hexadec-1-ene	**1**	2100	78	98	4.8/1
	2	2100	59	99	5.0/1
Styrene	**1**	3500	85	> 99	1/6.2
	2	3500	80	> 99	1/5.4
n-Butyl acrylate	**1**	2800	100	> 99	B[d]
	2	2800	100	> 99	B[d]

[a] *Reaction conditions*: 5 μmol $[Rh(CO)_2(acac)]$ (P/Rh = 6), 30 bar $CO–H_2$ (1 : 1), 100 °C for dec-1-ene and hexadec-1-ene, 80 °C for styrene and *n*-butyl acrylate, hexane–toluene–perfluoromethylcyclohexane = 4 : 2 : 4 (mL), 15 h reaction time. The products were analysed by ^1H NMR and the conversion and selectivity confirmed by GC. [b] To aldehyde, olefin isomerisation accounts for the product balance. [c] Linear to branched aldehyde ratio, determined by ^1H NMR. [d] The branched product was a 1 : 1 mixture of enol and aldehyde, the linear aldehyde was < 1%.

(TOF) for the fluorous biphase hydroformylation of dec-1-ene is 136 mol aldehyde h^{-1} per mol of rhodium catalyst with an aldehyde selectivity of 99%. In comparison, a rhodium catalyst supported on the water soluble polymer poly(enolate-*co*-vinyl alcohol-*co*-vinyl acetate) gave a TOF of 56 (100 °C, 41 bar) with an aldehyde selectivity < 70% in the aqueous hydroformylation of oct-1-ene.[13] As might be expected, ligand **1**, which has a higher phosphine loading, gave higher turnovers. (ii) As with solid polymer-supported catalysts,[10] the linear/branched (L/B) ratio is markedly higher than achievable with similar P/Rh ratios when using homogeneous rhodium phosphine catalysts, *e.g.* $[RhH(CO)(PPh_3)_3]$, which yielded a L/B ratio of 2.9 only in the presence of an excess of PPh_3 (P/Rh = 19) in the hydroformylation of pent-1-ene in benzene (100 °C, 27 bar).[15] (iii) Smaller olefins appear to give higher turnovers, probably owing to better miscibility of the olefins with the fluorous phase. In fact, when hex-1-ene was hydroformylated under conditions identical to those for dec-1-ene, a conversion of 70% with an aldehyde selectivity of 98% and a L/B ratio of 4.4 was obtained in 1 h reaction time, corresponding to a remarkable TOF of 1454. Again, a low olefin isomerisation selectivity of 1.7% was observed.

The activity and stability of the soluble fluoropolymer catalysts may also be judged by the hydroformylation of hex-1-ene when the olefin/Rh ratio was increased to 200 000. At 100 °C and 50 bar syngas with polymer **1** as the supporting ligand, the catalyst afforded a turnover number (TON, mole of aldehyde per mol of rhodium) of *ca.* 140 000 with a 98% selectivity to aldehyde (L/B = 4.4; 2% isomerisation) for 58 h reaction time. We also examined the recyclability of the fluoropolymer catalysts taking the reaction of hex-1-ene as a model example. The other substrates and related products should be easier to separate under the fluorous biphase conditions as they are less miscible with the perfluoro solvent. At 100 °C and 50 bar with olefin/Rh = 48 000, three consecutive hydroformylation reactions were run, giving a combined TON of 70 000 and an average aldehyde selectivity of 99%. A 1 ppm loss of rhodium accompanied with a 6% decrease in conversion in each recycle experiment was measured. This loss in rhodium and in catalyst activity appears to be largely due to the finite miscibility of the substrate/product with the perfluorinated solvent. At the end of the third run, all the perfluoromethylcyclohexane had leached to the product phase, thus making the polymer catalyst partially soluble in the product. By optimising the operating conditions, *e.g.* by varying the organic solvent, the problem of rhodium leaching can be minimised.

In conclusion, we have introduced a fluorous soluble polymer ligand for FBC and shown the arylphosphine-containing ligand, when combined with rhodium, to be highly active and selective in the fluorous biphase hydroformylation of various olefins. Given the easy availability of various vinyl monomers that can be used for fluoropolymer synthesis and the variability in FBC conditions, better performing soluble polymer catalysts coupled with efficient phase separation could be envisioned not only for FBC but also for fluorous combinatorial chemistry.

We are indebted to the EPSRC and the University of Liverpool Graduates Association (Hong Kong) for postdoctoral research fellowships (W. C. and L. X.).

Notes and references

1 I. T. Horváth and J. Rábai, *Science*, 1994, **266**, 72.
2 I. T. Horváth, *Acc. Chem. Res.*, 1998, **31**, 641.
3 E. de Wolf, G. van Koten and B. J. Deelman, *Chem. Soc. Rev.*, 1999, **28**, 37.
4 I. T. Horváth, G. Kiss, R. A. Cook, J. E. Bond, P. A. Stevens, J. Rábai and E. J. Mozeleski, *J. Am. Chem. Soc.*, 1998, **120**, 3133.
5 D. Rutherford, J. J. J. Juliette, C. Rocaboy, I. T. Horváth and J. A. Gladysz, *Catal. Today*, 1998, **42**, 381.
6 J. J. J. Juliette, D. Rutherford, I. T. Horváth and J. A. Gladysz, *J. Am. Chem. Soc.*, 1999, **121**, 2696.
7 D. Sinou, G. Pozzi, E. G. Hope and A. M. Stuart, *Tetrahedron Lett.*, 1999, **40**, 849.
8 D. E. Bergbreiter and J. G. Franchina, *Chem. Commun.*, 1997, 1531.
9 M. Beller, B. Cornils, C. D. Frohning and C. W. Kohlpaintner, *J. Mol. Catal.*, 1995, **104**, 17 and references therein.
10 F. R. Hartley, *Supported Metal Complexes. A New Generation of Catalysts*, Reidel, Dordrecht, 1985.
11 T. Malmström, C. Andersson and J. Hjortkjaer, *J. Mol. Catal.*, 1999, **139**, 139.
12 A. N. Ajjou and H. Alper, *J. Am. Chem. Soc.*, 1998, **120**, 1466.
13 J. Chen and H. Alper, *J. Am. Chem. Soc.*, 1997, **119**, 893.
14 D. C. Sherrington, *Chem. Commun.*, 1998, 2275 and references therein.
15 C. U. Pittman, Jr. and R. M. Hanes, *J. Am. Chem. Soc.*, 1976, **98**, 5402.

Configurationally stable metal-centered chirality: stereospecific and regioselective rhodaacylation of alkynes controlled by the third generation of the [Cp′-P]H ligand

Yasutaka Kataoka,* Yoko Iwato, Atsushi Shibahara, Tsuneaki Yamagata and Kazuhide Tani*

Department of Chemistry, Graduate School of Engineering Science, Osaka University, Toyonaka, Osaka 560-8531, Japan. E-mail: tani@chem.es.osaka-u.ac.jp

Received (in Cambridge, UK) 3rd March 2000, Accepted 7th April 2000

The rhodium cationic complex [[η⁵:η¹-{3-(NIM)Ind-P}$_{n=2}$]Rh(CO)Me]BF_4 (1) reacts with 1-phenylpropyne regioselectively and stereospecifically to afford the alkenyl complex [[η⁵:η¹-{3-(NIM)Ind-P}$_{n=2}$]Rh{η²-O=C(CH_3)-C(CH_3)=CPh}]BF_4 (2).

The design and synthesis of novel chiral transition-metal complexes having a stereogenic metal center provide an elegant and powerful method for stoichiometric or catalytic asymmetric transformations.[1–5] Nonetheless, chemistry using metal-centered chirality is much less developed than that using chiral auxiliaries or ligands.[6] In order to accomplish asymmetric reactions using metal-centered chirality, easy and convenient methods for the preparation of optically active complexes which are configurationally stable at the metal center should be supplied. Recently we have found that the third generation of

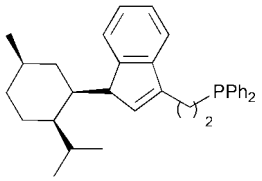

[{3-(NIM)Ind-P}$_{n=2}$] H

the [Cp′-P]H ligand, [{3-(NIM)Ind-P}$_{n=2}$]H was effective for controlling the central metal chirality in the oxidative addition of alkyl halide to the Rh carbonyl complex, compared to the first and the second generation of the [Cp′-P]H ligand.[7,8] Thus, oxidative addition using metal complexes with the third generation of the Cp′-P ligand could become a new preparation of an optically active complex having a metal-centered chirality. In order to use the chiral complex as an asymmetric catalyst, racemization or epimerization at the metal center must be prevented. Herein we show that the metal-centered chirality controlled by the {3-(NIM)Ind-P}$_{n=2}$ ligand[9] is configurationally stable, which causes the stereospecific and regioselective addition of alkynes to its cationic Rh complex.

The cationic rhodium complex, [[η⁵:η¹-{3-(NIM)Ind-P}$_{n=2}$]Rh(CO)Me]BF_4 (**1**), which was readily prepared from [η⁵:η¹-{3-(NIM)Ind-P}$_{n=2}$]RhI(COMe) and $AgBF_4$,[8] is a mixture of two diastereomers (major : minor = 96 : 4, 92% de).† Reaction of complex **1** with 1-phenylpropyne in CH_2Cl_2 at room temperature for 48 h afforded the alkenyl complex **2** in 79% isolated yield (Scheme 1).‡ From the ^1H or ^{31}P NMR of the reaction mixture, **2** was found to contain only two isomers (major : minor = 96 : 4). The structure of **2**-major was confirmed by the usual spectroscopic methods as well as X-ray crystallography (Fig. 1).§ The stereochemistry around the Rh is *S*, and the planar chirality is *R*. Complex **2** was produced through migratory insertion of CO into the Rh–Me bond in **1**[10] and the subsequent rhodaacylation of the alkyne,[11] followed by intramolecular coordination of the acyl oxygen to the Rh. Since four isomers from each diastereomer of **1**, based on the difference in the metal-centered chirality and the regiochemistry of the olefin, are possible, this transformation totally has the potential for the formation of the eight isomers. The results, however, indicated that only one isomer was produced from each diastereomer of **1**; the isomer ratio of **2** was the same as that of the starting complex **1**.† Thus, the metal-centered chirality did

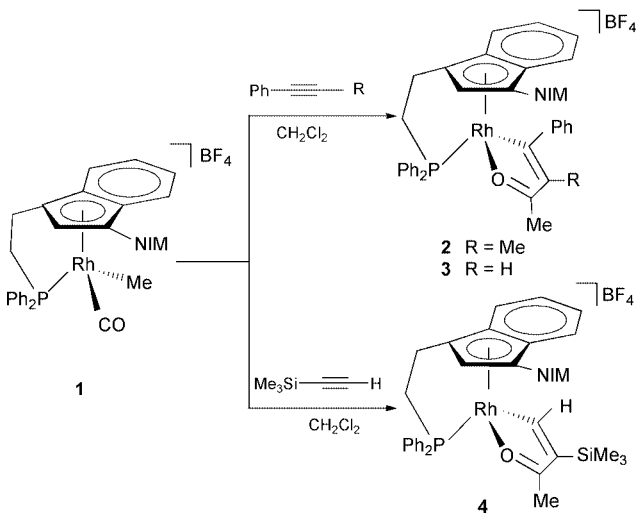

Scheme 1

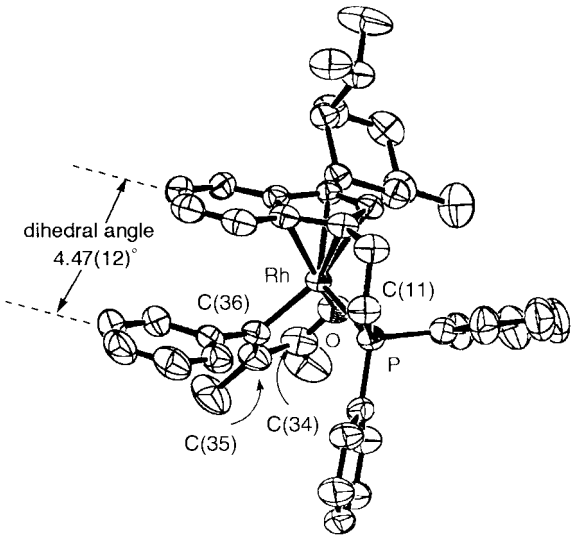

Fig. 1 ORTEP drawing of the X-ray crystal structure of the cationic part of **2**-major. Selected bond lengths (Å) and angles (°): Rh–O 2.0719(15), Rh–P 2.2690(6), Rh–C(36) 2.023(2), C(36)–C(35) 1.362(3), C(34)–C(35) 1.428(4), O–C(34) 1,258(3); Rh–O–C(34) 114.79(17), Rh–C(36)–C(35) 115.13(19), Rh–P–C(11) 105.86(12), O–C(34)–C(35) 118.5(2), C(36)–Rh–O 77.98(8), C(34)–C(35)–C(36) 113.5(2). The shortest interatomic distance between the indenyl group and the phenyl ring is 3.278(4) Å.

DOI: 10.1039/b001735n

not racemize or epimerize throughout these transformations and the regiochemistry of the olefinic part was completely controlled.

The mixed ligand complex containing both an indenyl and a tertiary phosphine ligand which are not connected by a spacer, $[Rh(\eta^5\text{-}C_9H_7)(PPh_3)(CO)Me]BF_4$, did not react with 1-phenylpropyne at room temperature. Although the cationic complex having the second generation Cp′-P ligand, $[[\eta^5:\eta^1\text{-}(Ind\text{-}P)_{n=2}]Rh(CO)Me]BF_4$, with 46% de (major : minor = 73 : 27) also reacted with 1-phenylpropyne under the same conditions, the corresponding alkenyl complexes comprised four diastereomers (69 : 24 : 5 : 1).† The third generation of the [Cp′-P]H ligand was much more effective for controlling the stereochemistry in this rhodaacylation.

Reaction of **1** (92% de) with phenyl acetylene in CH_2Cl_2 at room temperature for 12 h gave the corresponding alkenyl complex **3** with 92% de (Scheme 1).† The diastereomer excess of **3** was also almost the same as that of **1**. This reaction also proceeded stereospecifically. ^{1}H NMR of **3** showed a doublet with a small coupling constant (J = 1.4 Hz) at δ 6.21 for the olefinic proton and the HMQC spectrum showed that the proton was correlated to the β-olefinic carbon from Rh. Reaction of complex **1** (92% de) with trimethylsilylacetylene under the same conditions afforded the alkenyl complex **4** with 91% de (Scheme 1).†¶ This reaction also proceeded stereospecifically, but the opposite regioisomer to the product of the reaction with phenylacetylene was obtained. The structure of **4**-major was confirmed by the usual spectroscopic methods as well as X-ray crystallography. ^{1}H NMR revealed a doublet of doublets at δ 9.06 (J = 11.8 and 1.6 Hz) for the olefinic proton originating from the terminal acetylenic hydrogen. When trimethylsilylacetylene was used, the bulkier indenyl Rh moiety would attack the less hindered acetylenic terminal carbon selectively in the rhodaacylation process. In contrast, in the rhodaacylation of 1-phenylpropyne or phenylacetylene, the Rh–carbon bond was formed at the more hindered site.[12]

We are currently investigating application of the reaction to the stereoselective synthesis of general substituted olefins using a catalytic amount of a rhodium complex containing the Cp′-P ligand. This work was supported by a Grant-in-Aid for Scientific Research from the Ministry of Education, Science, Sports, and Culture of Japan, and General Sekiyu Research & Development Encouragement & Assistance Foundation.

Notes and references

† The isomer ratio was determined by ^{31}P NMR of the crude product obtained after removal of the solvents from the reaction mixture.

‡ *Preparation* of **2**: to a solution of **1** (20 mg, 0.028 mmol, 92% de) in CH_2Cl_2 (5 mL) was added 1-phenylpropyne (4 μL, 0.032 mmol) at room temperature. The reaction mixture was stirred for 48 h and then the solvent was removed *in vacuo* to give orange powders, which contained a diastereomeric mixture of **2**. The ratio was determined by ^{31}P NMR (major : minor = 94 : 6, 92% de). After washing with Et_2O (10 mL) and hexane (2 × 10 mL), recrystallization of the crude product from CH_2Cl_2 and Et_2O afforded **2** (18 mg, 0.022 mmol, 79%, major : minor = 94 : 6, 92% de) as analytically pure orange powders, mp 118–122 °C (dec.). δ_H ($CDCl_3$, major) 0.37 (d, J = 6.3 Hz, 3 H), 0.86 (d, J = 6.6 Hz, 3 H), 1.15 (d, J = 6.0 Hz, 3 H), 1.42 (d, J = 1.6 Hz, 3 H), 1.48–1.89 (m, 6 H), 1.92–2.10 (m, 2 H), 2.38 (d, J = 2.2 Hz, 3 H), 2.30–2.53 (m, 2 H), 2.69–2.98 (m, 2 H), 3.82–3.99 (m, 1 H), 4.05–4.23 (m, 1 H), 5.39 (s, 1 H), 6.15 (dd, J = 8.2, 1.1 Hz, 2 H), 6.29–6.38 (m, 1 H), 6.40–6.48 (m, 1 H), 6.83–6.93 (m, 1 H), 6.99–7.09 (m, 1 H), 7.16–7.41 (m, 8 H), 7.46–7.61 (m, 3 H) and 7.87–7.99 (m, 2 H). ^{31}P{^{1}H} NMR ($CDCl_3$) δ 55.1 (d, $J_{P–Rh}$ = 179 Hz, major) and 62.0 (d, $J_{P–Rh}$ = 181 Hz, minor). ^{13}C{^{1}H} NMR ($CDCl_3$) δ 232.2 (dd, J = 26, 12 Hz, *C*=C(Ph), major). IR (KBr, Nujol, cm^{-1}) 1544, 1261, 1058, 727, 694 and 522. MS (FAB) *m/z* 727 ($M^+ - BF_4$, cationic part of **2**). Anal. Found: C, 64.92; H, 6.10%. Calcd. for $C_{44}H_{49}BF_4OPRh$: C, 64.88; H, 6.06%.

§ *Crystal data* for $C_{44}H_{49}BF_4OPRh$ **2**-major: M = 814.52, triclinic, a = 10.0645(14), b = 10.9349(13), c = 9.9598(13) Å, α = 108.124(9), β = 106.426(10), γ = 84.967(11)°, U = 999.2(2) Å^3, T = 296 K, space group $P\bar{1}$ (No. 1), Z = 1, μ(Mo-Kα) = 0.519 mm^{-1}, 18387 reflections measured, 17568 unique (R_{int} = 0.0099) which were used in all calculations. $R1$(all) = 0.0416, $R1$(obsd) = 0.0316 (> 2σ(I)), $wR2$(all) = 0.0875, $wR2$(obsd) = 0.0826 (> 2σ(I)). CCDC 182/1600. See http://www.rsc.org/suppdata/cc/b0/b001735n/ for crystallographic files in .cif format.

¶ Spectroscopic data for **4**: mp 155–157 °C (dec.). δ_H ($CDCl_3$, major) 0.29 (d, J = 0.8 Hz, 9 H), 0.49 (d, J = 6.3 Hz, 3 H), 0.89 (d, J = 6.9 Hz, 3 H), 1.02–1.21 (m, 1 H), 1.11 (d, J = 6.0 Hz, 3 H), 1.51–1.73 (m, 2 H), 1.64–1.89 (m, 3 H), 1.93–2.23 (m, 3 H), 2.28 (s, 3 H), 2.37–2.65 (m, 1 H), 2.98–3.28 (m, 2 H), 3.45–3.68 (m, 1 H), 3.86–4.06 (m, 1 H), 5.58 (s, 1 H), 7.01–7.15 (m, 3 H), 7.31–7.42 (m, 4 H), 7.48–7.65 (m, 4 H), 7.67–7.78 (m, 3 H) and 9.06 (dd, J = 11.8, 1.6 Hz, 1 H). ^{31}P{^{1}H} NMR ($CDCl_3$) δ 63.7 (d, $J_{P–Rh}$ = 184 Hz, major) and 64.0 (d, $J_{P–Rh}$ = 179 Hz, minor). ^{13}C{^{1}H} NMR ($CDCl_3$): δ 232.8 (dd, J = 28, 15 Hz, *C*(H)=CSi(CH$_3$)$_3$, major). IR (KBr, Nujol, cm^{-1}) 3098, 3060, 1526, 1309, 1251, 1063, 845, 755, 709, 694 and 521. MS (FAB) *m/z* 709 ($M^+ - BF_4$, cationic part of **4**). Anal. Found: C, 60.45; H, 6.54%. Calcd. for $C_{40}H_{51}BF_4OPRhSi$: C, 60.31; H, 6.45%.

1 For a review of optically active organometallic compounds having a metal-centered chirality, see: H. Brunner, *Angew. Chem., Int. Ed.*, 1999, **38**, 1194.

2 For example from the Davies lab, see: S. G. Davies, *Aldrichim. Acta*, 1990, **23**, 31 and references cited therein.

3 For example from the Faller lab, see: J. W. Faller, J. T. Nguyen and M. R. Mazzieri, *Appl. Organomet. Chem.*, 1995, **9**, 291 and references cited therein.

4 For an example from the Gladysz lab, see: J. A. Gladysz and B. J. Boone, *Angew. Chem., Int. Ed. Engl.*, 1997, **36**, 550 and references cited therein.

5 B. Therrien and T. R. Ward, *Angew. Chem., Int. Ed.*, 1999, **38**, 405; D. Carmona, C. Vega, F. J. Lahoz, S. Elipe, L. A. Oro, M. P. Lamata, F. Viguri, R. García-Correas, C. Cativiela and M. P. López-Ram de Víu, *Organometallics*, 1999, **18**, 3364 and references cited therein; C. Slugovc, W. Simanko, K. Mereiter, R. Schmid and K. Kirchner, *Organometallics*, 1999, **18**, 3865.

6 *Catalytic Asymmetric Synthesis*, ed. I. Ojima, VCH, New York, 1993; R. Noyori, *Asymmetric Catalysis in Organic Synthesis*, Wiley, New York, 1994; S.-P. Jacqueline, *Chiral Auxiliaries and Ligands in Asymmetric Synthesis*, Wiley, New York, 1995.

7 Y. Saito, T. Yamagata, Y. Kataoka and K. Tani, The 41st Symposium on Organometallic Chemistry, Japan, 1994, abst. PA.109; Y. Kataoka, Y. Saito, K. Nagata, K. Kitamura, A. Shibahara and K. Tani, *Chem. Lett.*, 1995, 833; Y. Kataoka, Y. Saito, A. Shibahara and K. Tani, *Chem. Lett.*, 1997, 621; Y. Kataoka, A. Shibahara, T. Yamagata and K. Tani, *Organometallics*, 1998, **17**, 4338.

8 Y. Kataoka, Y. Iwato, T. Yamagata and K. Tani, *Organometallics*, 1999, **18**, 5423.

9 {3-(NIM)Ind-P}$_{n=2}$ is the anion of the [{3-(NIM)Ind-P}$_{n=2}$]H ligand.

10 K. J. Carvell, *Coord. Chem. Rev.*, 1996, **155**, 209 and references cited therein.

11 T. Mise, P. Hong and H. Yamazaki, *Chem. Lett.*, 1982, 401; P. Hong, T. Mise and H. Yamazaki, *J. Organomet. Chem.*, 1987, **334**, 129; I. Ojima, J. Zhu, E. S. Vidal and D. F. Kass, *J. Am. Chem. Soc.*, 1998, **120**, 6690.

12 Although DeShong *et al.* reported that regiochemistry in the insertion of an unsymmetrical alkyne into the Mn–carbon bond was controlled by the electronic character of the substituents of the alkyne,[13] we think that one of the reasons for the regioselectivity in the reaction of arylacetylenes could be the π–π stacking between the phenyl ring and the indenyl benzene ring. The presence of the π–π stacking could be also supported by the X-ray crystallographic analysis of **2**-major (Fig. 1).

13 P. DeShong, D. R. Sidler, P. J. Rybczynski, G. A. Slough and A. L. Rheingold, *J. Am. Chem. Soc.*, 1988, **110**, 2575.

ChemComm

Effect of substitution on the curvature and bowl-to-bowl inversion barrier of bucky-bowls. Study of mono-substituted corannulenes ($C_{19}XH_{10}$, X = B^-, N^+, P^+ and Si)

G. Narahari Sastry,*[a] H. Surya Prakash Rao,[a] Pawel Bednarek[b] and U. Deva Priyakumar[a]

[a] *Department of Chemistry, Pondicherry University, Pondicherry-605014, India. E-mail: sastry@pu.pon.nic.in*
[b] *Institute of Physical Chemistry, University of Fribourg, CH-1700, Fribourg, Switzerland*

Received (in Cambridge, UK) 1st February 2000, Accepted 5th April 2000
Published on the Web 28th April 2000

***Ab initio* MO and DFT calculations predict that replacement of a single carbon by an isoelectronic species on the corannulene skeleton can effectively arrest the bowl shape or flatten it and the bowl rigidity, curvature and relative stabilties of the positional isomers are solely controlled by the size of the substituent and site of substitution.**

Corannulene, $C_{20}H_{10}$, which forms the 'polar cap' of the buckminister-fullerene is the simplest bucky-bowl, where the warping of sp^2-carbon surface enforces the molecule to adopt a bowl-like geometry. The curvature in bucky-bowls results in two distinct surfaces, convex and concave, and alters the properties such as dipole moment, ionization potential, metal binding *etc*.[1] Despite the substantial curvature present in corannulene, it is highly fluxional and the bowl-to-bowl inversion is rapid,[2,3] the resulting non-rigidity of its bowl structure is in contrast to that of fullerenes. Our interest lies in finding out simpler modifications that are required to effectively 'lock' the bowl geometry of corannulene. Previous studies indicate that locking the bowl structure requires the addition of one more fused five-membered ring.[4] Construction of a cyclophane bridge seems to be another strategy to lock the bowl structure.[5] Substitution on corannulene is not expected to have any significant effect on the rigidity or inversion barrier.[1b] It occurred to us that the simplest of the strategies might be to look at the replacement of skeletal carbon atoms on the corannulene by an electronically equivalent heteroatom substituent, such as X = B^-, N^+, P^+ or Si. Accordingly, as a first step mono-substitutions have been placed at three unique positions of corannulene namely at hub (**1**), rim-quat (**2**) and rim (**3**).

The geometries of all the structures of substituted corannulenes depicted in Scheme 1 are optimized at *ab initio* Hartree–Fock level using 3-21G basis set using the GAUSSIAN 94 program package.[6] Frequency calculations confirm that all the bowl structures are minima and planar structures are transition states corresponding to bowl-to-bowl inversion.† The effects of inclusion of electron correlation and improving the basis set quality on energetics are estimated by performing single point calculations using the B3LYP procedure with the 6-31G* basis set.

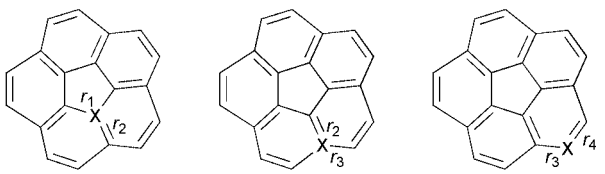

1 (hub) **2** (rim-quat) **3** (rim)

	a	b	c	d
X	B^-	N^+	P^+	Si

Scheme 1

The relative energies of the positional isomers in their minimum energy conformation as well as the TS for bowl-to-bowl inversions are given in Table 1. The reference structure is taken as the hub (**1**) substituted minimum energy isomer, which in general has a non-planar bowl-like geometry. A strong preference is shown to occupy the rim position (**3**) followed by rim-quat (**2**) and hub (**1**) positions for substituents, where X = B^-, P^+, or Si. In contrast, a complete reversal of the relative stabilities of positional isomers is seen for X = N^+, which results in the following increasing order of stability, **3b** < **2b** < **1b**. The thermodynamics of the positional isomers seems to be solely controlled by the size of the substituent. In this context, the C–X bond length is taken to gauge the size of X, as C–B, C–P and C–Si bonds are longer and C–N is shorter than the C–C bond, B^-, P^+ and Si are classified as larger substituents and N^+ as a smaller substituent. Accordingly, larger heteroatom substituents when compared to C prefer to occupy the rim position and smaller ones prefer the hub position, and this preference seem to be independent of the charge present on the system, as well as the electronegativity of the substituent. The relative stabilities of these positional isomers may be directly traced to the angular strain caused by the substituent, *i.e.* a larger atom at hub position will bring in more strain in the corannulene skeleton where as it relieves the strain at the terminal position. Accordingly, larger atoms prefer to be substituted at the rim (**3**) position, while the smaller at the hub (**1**) position. The curvature of the minimum energy bowl structures and the alteration of C–X bond lengths when going from the bowl structure to the transition state, which are key geometric changes, are depicted

Table 1 Relative energies (kcal mol^{-1}) of the various structures. Total energies are given in E_h and the frequencies in cm^{-1}

	HF/3-31G			B3LYP/6-31G*[a]	
	Bowl	Planar-TS	Imaginary frequency	Bowl	Planar-TS
1a	0.0 (−745.80417)	22.80	140.0i	0.0 (−754.91705)	22.03
2a	−20.15	−11.86	107.2i	−18.26	−11.42
3a	−17.34	−12.03	95.1i	−20.36	−16.08
1b	0.0 (−775.21444)	3.30	83.2i	0.0 (−784.58523)	4.36
2b	15.43	25.89	116.1i	16.12	26.20
3b	13.81	26.79	124.0i	13.17	24.82
1c	0.0 (−1059.97337)	88.32	184.2i	0.0 (−1071.10510)	67.57
2c	−14.83	−6.00	102.6i	−14.44	−4.66
3c[b]	−21.04	−12.66	127.9i, 69.1i	−19.18	−14.70
1d	0.0 (−1008.55907)	90.22	188.9i	0.0 (−1019.43484)	74.33
2d	−45.14	−39.56	93.4i	−39.33	−33.55
3d	−54.04	−53.20	57.3i	−52.12	−51.41

[a] Single point calculations at HF optimized geometries. [b] **3c** shows two imaginary frequencies of which the first represents the bowl-to-bowl inversion.

DOI: 10.1039/b000893l

Table 2 The pyramidalization angle ϕ (°) and the changes in C–X bond lengths (r_n/Å) going from the bowl structure to the transition state at the HF/ 3-21G level

	$\phi^{a,b}$			**1**[c]		**2**[c]		**3**[c]	
	1	**2**	**3**	r_1	r_2	r_2	r_3	r_3	r_4
a	13.5	9.3	4.0	1.513 → 1.468	1.457 → 1.420	1.469 → 1.446	1.579 → 1.604	1.581 → 1.604	1.513 → 1.527
b	2.5	3.5	7.2	1.376 → 1.363	1.331 → 1.323	1.313 → 1.296	1.418 → 1.433	1.396 → 1.408	1.343 → 1.361
c	78.0	2.7	3.0	1.815 → 1.641	1.812 → 1.606	1.707 → 1.658	1.821 → 1.824	1.859 → 1.799	1.860 → 1.742
d	78.1	6.6	1.5	1.852 → 1.692	1.816 → 1.645	1.716 → 1.734	1.882 → 1.858	1.860 → 1.868	1.778 → 1.784

[a] The angle ϕ which is a measure of pyramidalization is defined as $\phi = 360 - (\theta_1 + \theta_2 + \theta_3)$ where θ_1, θ_2 and θ_3 are the bond angles around the unique hub atom, which is X in **1** and C closest to X in **2** and **3**. [b] $\phi = 6.4$ for corannulene. [c] Unsubstituted corannulene shows: $r_1 = 1.415 \rightarrow 1.393$, $r_2 = 1.359 \rightarrow 1343$, $r_3 = 1.449 \rightarrow 1.467$, $r_4 = 1.368 \rightarrow 1.383$.

in Table 2. The curvature especially of hub substituted isomers, depends on the pyramidalization tendency of the substituent. Thus, second row substituents (P^+ and Si) gives deeper and more rigid bowls compared to their first row analogs (B^- and N^+). This reflects the fact that the structures with higher barriers show greater changes in C–X bond lengths and *vice versa*. The values of ϕ ranging from 1.5 to 78.1° indicate a broad spectrum of variations in the curvatures of the bowl isomers considered in the present study.

The most interesting finding is the effect of substitution on bowl-to-bowl inversion barriers. A clear qualitative difference between the substituents with larger atomic size than carbon and those with smaller atomic size is noted. Thus, when X = B^-, P^+ or Si, the inversion barrier is very high for **1** and decreases while going to rim-quat (**2**) and rim (**3**) substituted ones. In sharp contrast N^+ substituted at hub (**1**) position, **1b**, substantially reduces the bowl-to-bowl inversion barrier while the rim (**3**) substituted isomer, **3b**, doubles the inversion barrier compared to that of the pristine corannulene molecule. Thus, mono-substitution with larger substituents at hub (**1**) positions rigidifies the bowl, while at rim (**3**) position makes it more fluxional and flatter compared to the parent corannulene. The substitution by smaller substituents has exactly the opposite effect with regards to bowl-to-bowl inversion. The inversion barrier for all the rim-quat substituted (**2**) positional isomers, seems to be less sensitive to the nature of substituent and in all cases the barrier is of similar magnitude to that of corannulene.

Interestingly, the isomer with largest inversion barrier is found to be the least stable and possesses the highest ϕ indicating the maximum curvature. This highlights the interconnectivity of the curvature, stability and inversion barriers in this series of isomers. Therefore, effectively the size and site of substitution decides the curvature, stability and bowl-to-bowl inversion barriers. Thus, Si, the largest substituent considered, when substituted at hub (**1**) position gives the most rigid bowl and leads to an increase in the inversion barrier by almost seven-fold compared to that of unsubstituted corannulene! In contrast, **3d**, the rim (**3**) substituted Si isomer yields the least curved surface with an insignificant inversion barrier. The magnitude of the imaginary frequency seems to give a good measure of the inversion barrier, thus the highest value of 188.9i cm^{-1} and lowest of 53.2i cm^{-1} correspond to the structures with highest (**1d**) and lowest (**3d**) bowl-to-bowl inversion barriers, respectively.

The stabilities of the mono-substituted corannulenes are estimated using the isodesmic equation eqn. (1), in which the most stable isomer is considered in each case (**2a**, **1b**, **3c** and **3d**). C_5XH_6 and C_6H_6 represent the mono- and un-substituted benzene ring respectively in eqn. (1). The results indicate that, except for **1c** (P^+) and **1d** (Si), in all other isomers the replacement of a C by the isoelectronic X is more feasible (thermodynamically) in corannulene than in benzene.‡

$$C_{20}H_{10} + C_5XH_6 \longrightarrow C_{19}XH_{10} + C_6H_6 \quad (1)$$

X	a(2)	b(1)	c(3)	d(3)
ΔE/kcal mol^{-1}	−31.6	−19.8	−30.1	−21.6

The present study indicates that in mono-substituted corannulenes, the relative stabilities of positional isomers, curvature and bowl-to-bowl inversion barriers are interconnected and all of which seem to be mainly controlled by the size of the substituent. Rational synthetic design of fullerenes in a stepwise manner is severely hampered owing to the enormous strain energy build-up in the skeleton which is chiefly attributed to high incremental jumps in the strain as the curvature increases.[7] A rigid bowl with a substantial built-in strain might be a better precursor for further building-up of the cage structure, compared to a flat or flexible bowl. In this regard, P^+ or Si substituted corannulenes at **1** position promise to be good rigid frameworks for further fusing of five/six-membered rings *en route* to hetero-fullerene cages.

We thank UGC, New Delhi and AICTE for financial assistance.

Notes and references

† The planar isomer **3c** gives two imaginary frequencies in the force calculation. That with higher magnitude corresponds to bowl-to-bowl inversion, while the other much lower frequencies (69.1i cm^{-1}) can be ignored and the planar structure can be considered as a TS for all practical purposes.

‡ The energetics given are at HF/3-21G level.

1 (*a*) R. Faust, *Angew. Chem., Int. Ed. Engl.*, 1995, **34**, 1429; (*b*) P. W. Rabideau and A. Sygula, *Acc. Chem. Res.*, 1996, **29**, 235; (*c*) G. Mehta and H. S. P. Rao, in *Advances in Strain in Organic Chemistry*, ed. B. Halton, JAI Press, London, 1997, vol. 6, pp. 139–187.
2 L. T. Scott, M. M. Hashemi and M. S. Bratcher, *J. Am. Chem. Soc.*, 1992, **114**, 1920.
3 P. U. Biedermann, S. Pogodin and I. Agranat, *J. Org. Chem.*, 1999, **64**, 3655.
4 A. H. Abdourazak, A. Sygula and P. W. Rabideau, *J. Am. Chem. Soc.*, 1993, **115**, 3010.
5 T. J. Seiders, K. K. Baldridge and J. S. Seigel, *J. Am. Chem. Soc.*, 1996, **118**, 2734.
6 GAUSSIAN 94: M. J. Frisch, G. W. Trucks, H. B. Schlegel, P. M. W. Gill, B. G. Johnson, M. A. Robb, J. R. Cheeseman, T. Keith, G. A. Patersson, J. A. Montgomary, K. Raghavachari, M. A. Al-Laham, V. G. Zakrzewski, J. V. Ortiz, J. B. Foresman, J. Cioslowski, B. B. Stefanov, A. Nanayakkara, M. Challacombe, C. Y. Peng, P. Y. Ayala, W. Chen, M. W. Wong, J. L. Andres, E. S. Replogle, R. Gomperts, R. L. Martin, D. J. Fox, J. S. Binkley, D. J. Defrees, J. Baker, J. J. P. Stewart, M. Head-Gordon, C. Gonzalez and J. A. Pople, Gaussian 94, Gaussian, Inc: Pittsburgh, PA, 1995.
7 (*a*) G. N. Sastry, E. D. Jemmis, G. Mehta and S. R. Shah, *J. Chem. Soc., Perkin Trans. 2*, 1993, 1867; (*b*) E. D. Jemmis, G. N. Sastry and G. Mehta, *J. Chem. Soc., Perkin Trans. 2*, 1994, 437.

ChemComm

[3]Rotaxanes employing multiple 1,2-bis(pyridinium) ethane binding sites and dibenzo-24-crown-8 ethers†

Stephen J. Loeb* and James A. Wisner

School of Physical Sciences, Chemistry & Biochemistry, University of Windsor, Windsor, Ontario, Canada N9B 3P4. E-mail: loeb@uwindsor.ca

Received (in Columbia, MO, USA) 17th January 2000, Accepted 31st March 2000
Published on the Web 28th April 2000

Two binding sites of the 1,2-bis(pyridinium)ethane type are built into an extended axle on to which two molecules of dibenzo-24-crown ether (DB24C8) can thread to produce the first examples of [3]rotaxanes employing this templating motif.

[2]Pseudorotaxanes are commonly used as precursors for the formation of permanently interlocked [2]rotaxanes by addition of 'stopper' components which are bulky enough to prevent unthreading.[1,2] We have recently demonstrated that various 1,2-bis(pyridinium)ethane dications will thread through the 24-membered crown ethers 24C8, B24C8 and DB24C8 to produce a new series of [2]pseudorotaxanes **1a**–**e**.[3]

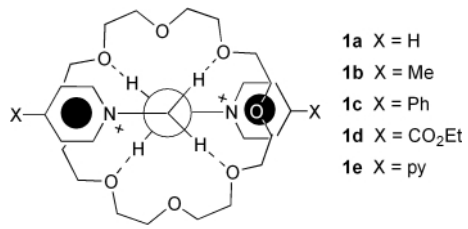

For a 1,2-bis(4,4′-bipyridinium)ethane **1e**, (X = py) axle and a DB24C8 wheel, we have shown that the [2]pseudorotaxane is easily converted to a permanently interlocked [2]rotaxane.[4] This was achieved either by alkylation at the terminal pyridine nitrogen atoms with bulky *tert*-butylbenzyl groups, **2**, or stoppering with appropriately large organopalladium fragments, **3**.

Herein, we describe the synthesis of both symmetrical and unsymmetrical [3]rotaxanes by employing extended axles containing two binding sites for a dibenzo-24-crown-8 ether molecule. Although the rotaxanes presented here are saturated and therefore display no translational isomerism, such higher order [*n*]rotaxanes ($n > 2$) are not nearly as prevalent as simpler [2]rotaxanes.[5] The study of these multiple-sited systems is important for the future development of molecular devices such as those based on Stoddart's notion of a molecular shuttle.[6,7]

The key synthetic intermediate in this work is **4b**, which can be used to alkylate a pyridine derivative to create a second

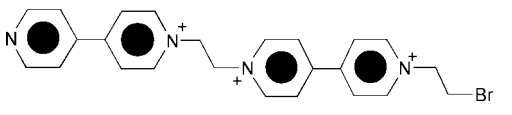

4a X = Br
4b X = BF_4

bis(pyridinium)ethane binding site.[8] We reacted **4b** with 4-*tert*-butylpyridine, to produce **5** (Scheme 1), since the Bu^t group can act directly as a stopper and with 4,4-bipyridine, to yield **6** (Scheme 2), as this provides a terminal pyridine moiety. Subsequent monoalkylation of **5** and dialkylation of **6** with *tert*-butylbenzyl bromide yields the dumbbell shaped axles **7** and **8**.

† Dedicated to Professor Christopher J. Willis on the occasions of his retirement and 66th birthday.

The [3]rotaxanes **9** and **10** were prepared by mixing **5** and **6**, respectively, with four equivalents of DB24C8 in MeCN solution followed by a two-fold excess of the required equivalents of *tert*-butylbenzyl bromide.‡

Non-covalent interactions between axle and wheel are evident from significant chemical shift differences in the solution (CD_3CN) ^{1}H NMR spectra of **9** and **10** when compared to **7**, **8** and free DB24C8. A network of *sixteen* C–H···O hydrogen bonds from axle protons to crown ether O-atoms is evident in both **9** and **10** from the significant *downfield* shifts for all α^+-pyridinium (0.30–0.36 ppm) and $^+NCH_2$ protons (0.21–0.42 ppm). In addition, π-stacking between the electron-rich catechol and electron-poor pyridinium rings is indicated for both rotaxanes by *upfield* shifts observed for the β-pyridinium protons (0.25–0.56 ppm) and crown aromatic protons (0.17–0.42 ppm). Also, since the *tert*-butylpyridinium stopper for the asymmetric [3]rotaxane **9**, is one aromatic ring closer to the center of the molecule, we also observe a C–H···π interaction between the *tert*-butylpyridinium methyl protons and the crown aromatic group ($\Delta\delta = -0.24$ ppm). Unfortunately, the different environments of the DB24C8 catechol rings could not be distinguished by low temperature ^{1}H NMR spectroscopy owing to the facile nature of the interconversion process.

An X-ray crystal structure determination§ of **10** verified the nature of the interactions observed in solution (Fig. 1). The two DB24C8 rings are threaded on to the centrosymmetric tris(bi-

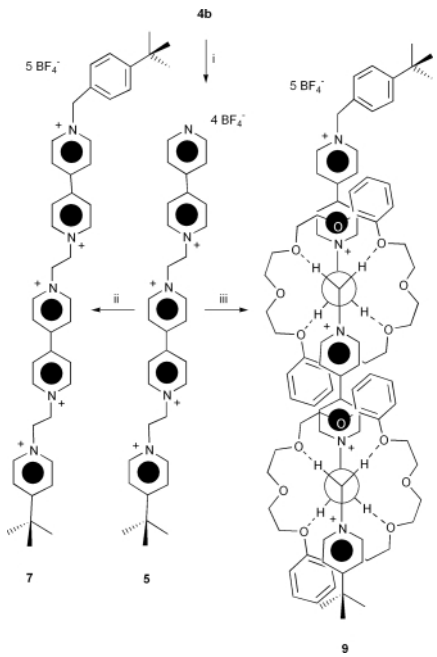

Scheme 1 *Reagents and conditions*: i, 4-*tert*-butylpyridine, MeCN, 60 °C, 3 days, $NaBF_4$(aq), 45%; ii, 4-*tert*-butylbenzyl bromide, MeCN, 60 °C, 3 days, $NaBF_4$(aq), 25%; iii, 4-*tert*-butylbenzyl bromide, DB24C8, MeCN, room temp., 2 days, SiO_2 [MeOH–$MeNO_2$–2.0 M NH_4Cl(aq), 3 : 1 : 1], R_f = 0.47, $NaBF_4$(aq), 18%.

DOI: 10.1039/b001018i

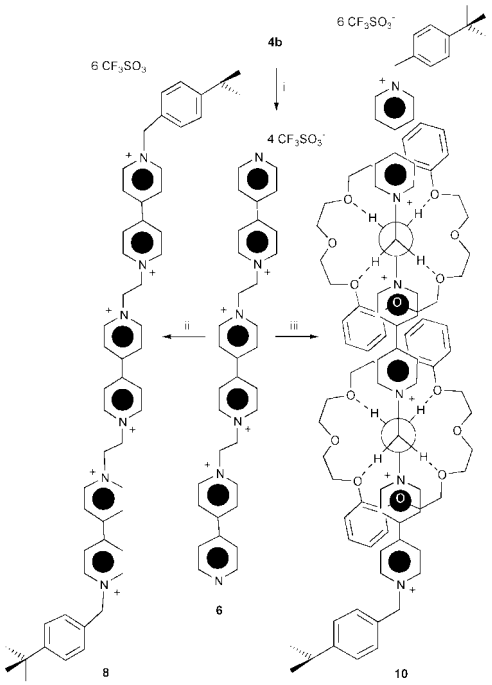

Scheme 2 *Reagents and conditions*: i, 4,4′-bipyridine, $MeNO_2$, 60 °C, 3 days, $NaCF_3SO_3$(aq), 18%; ii, 4-*tert*-butylbenzyl bromide, $MeNO_2$, 60 °C, 24 h, $NaCF_3SO_3$(aq), 22%; iii, 4-*tert*-butylbenzyl bromide, DB24C8, MeCN, room temp., 2 days, SiO_2 [MeOH–$MeNO_2$–2.0 M NH_4Cl(aq), 3 : 1 : 1], R_f = 0.44, $NaCF_3SO_3$(aq), 15%.

pyridinium) axle such that the S-shaped crown ether rings stack stepwise over the three sets of bipyridinium rings. A unique feature of this particular [3]rotaxane design is that the central bipyridinium ring is sandwiched between two aromatic rings from separate crown ether wheels. This has the potential to allow direct communication between the two binding sites through the wheel–axle–wheel overlap. The centrosymmetric [3]rotaxane **10** shows $N^+\cdots O$ interactions ranging from 3.51 to 3.65 Å and *sixteen* C–H···O hydrogen bonds with CH···O distances in the range 2.26–2.77 Å. The orange–red colour of the solid material and the UV absorption data in MeCN solution are consistent with charge transfer interactions between the electron-rich rings of the crown ether and the electron-poor rings of the bipyridinium fragments.

It is clear that the 1,2-bis(pyridinium)ethane/24-crown-8 ether templating motif can be extended to multiply interlocked molecules as demonstrated herein by the synthesis of symmetrical and unsymmetrical [3]rotaxanes.

We thank the Natural Sciences and Engineering Council of Canada for financial support of this research and J. A. W. thanks the Ontario Graduate Scholarship program for funding.

Notes and references

‡ All new compounds were successfully characterized by ^{1}H NMR spectroscopy (500 MHz, 298 K) and LSI-MS or ESI-MS. NOESY experiments were used make individual ^{1}H NMR assignments.

Selected data: for **9**: $\delta_H(CD_3CN)$: 9.30 (m, 6H), 8.95 (m, 4H), 8.13 (d, 2H, *J* 6.72 Hz), 8.08 (d, 2H, *J* 6.76), 7.95 (m, 4H), 7.75 (d, 2H, *J* 6.85 Hz), 7.59 (d, 2H, *J* 8.44 Hz), 7.48 (d, 2H), 6.74 (m, 8H), 6.68 (m, 4H), 6.51 (m, 4H), 5.82 (s, 2H), 5.61 (m, 6H), 5.45 (m, 2H), 4.04 (m, 48H), 1.34 (s, 9H), 1.18 (s, 9H). UV/VIS (MeCN, CT band): λ_{max} = 406 nm. ESI-MS: *m*/*z* 1894.8 ([M − BF_4]$^+$). For **10**: $\delta_H(CD_3CN)$: 9.33 (d, 4H, *J* 6.84 Hz), 9.30 (d, 4H, *J* 6.84 Hz), 8.95 (d, 4H, *J* 6.84), 8.14 (d, 4H), 8.10 (d, 8H), 7.60 (d, 4H, *J* 7.81 Hz), 7.49 (d, 4H), 6.68 (m, 8H), 6.49 (m, 8H), 5.81 (s, 4H), 5.48 (s, 8H), 4.07 (m, 48H), 1.34 (s, 18H). UV/VIS (MeCN, CT band): λ_{max} = 399 nm. ESI-MS: *m*/*z* 2459.4 ([M − OTf]$^+$).

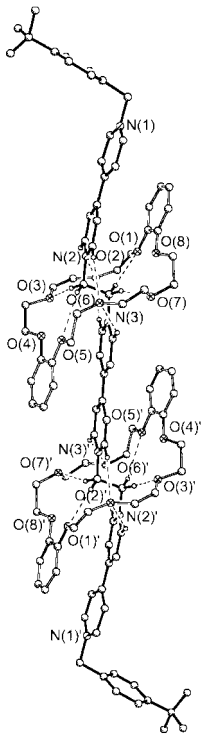

Fig. 1 A ball-and-stick representation of the X-ray crystal structure of the [3]rotaxane **8** showing the basic numbering scheme. $N(2)^+\cdots O$ distances (Å); O(1) 3.65, O(8) 3.61. $N(3)^+\cdots O$ distances (Å) ; O(4) 3.53, O(5) 3.51. C–H···O distances (Å) and angles (°): H(19A)···O(6) 2.52, C(19)–H(19A)···O(6) 149.8; H(20A)···O(2) 2.57, C(20)–H(20A)···O(2) 142.4; H(22A)···O(5) 2.77, C(22)–H(22A)···O(5) 140.9; H(22B)···O(3) 2.35, C(22)–H(22B)···O(3) 169.2; H(23A)···O(7) 2.26, C(23)–H(23A)···O(7) 162.0; H(23B)···O(1) 2.45, C(23)–H(23B)···O(1) 152.6; H(24A)···O(6) 2.53, C(24)–H(24A)···O(6) 140.8; H(28A)···O(2) 2.48, C(28)–H(28A)···O(2) 154.7.

§ *Crystal data* for **10**: $C_{110}H_{126}F_{18}N_6O_{34}S_6$, *M* = 2610.53, monoclinic, space group $P2_1/n$, *a* = 16.892(4), *b* = 14.926(7), *c* = 25.494(13) Å, β = 107.94(2)°, *U* = 6115(4) Å^3, *T* = 293(2) K, *Z* = 2, μ = 0.219 mm^{-1}, 8401 independent reflections (R_{int} = 0.0583), *R*1 = 0.1368, *wR*2 = 0.3516 ($I > 2\sigma I$), *R*1 = 0.2204, *wR*2 = 0.3959 (all data), Goodness of fit (F^2) = 1.212. Data were collected on a Siemens SMART CCD instrument and solutions performed using the SHELXTL 5.03 Program Library for Structure and Solution and Molecular Graphics, Siemens Analytical Instrument Division, Madison, WI, USA, 1997. CCDC 182/1593. See http://www.rsc.org/suppdata/cc/b0/b001018i/ for crystallographic files in .cif format.

1 D. B. Amabilino and J. F. Stoddart, *Chem. Rev.*, 1995, **95**, 2725 and references therein; D. Philp and J. F. Stoddart, *Angew. Chem.*, 1996, **108**, 1242; *Angew. Chem., Int. Ed. Engl.*, 1996, **35**, 1154 and references therein.
2 P. R. Ashton, P. T. Glink, J. F. Stoddart, P. A. Tasker, A. J. P. White and D. J. Williams, *Chem. Eur. J.*, 1996, **2**, 729.
3 S. J. Loeb and J. A. Wisner, *Angew. Chem.*, 1998, **110**, 3010; *Angew. Chem., Int. Ed.*, 1998, **37**, 2838.
4 S. J. Loeb and J. A. Wisner, *Chem. Commun.*, 1998, 2757.
5 R. Schmieder, G. Hübner, C. Seel and F. Vögtle, *Angew. Chem.*, 1999, **111**, 3741; *Angew. Chem., Int. Ed.*, 1999, **38**, 3528 and references therein.
6 M.-V. Martínez-Díaz, N. Spencer and J. F. Stoddart, *Angew. Chem.*, 1997, **109**, 1991; *Angew. Chem., Int. Ed. Engl.*, 1997, **36**, 1904 and references therein.
7 P.-L. Anelli, M. Asakawa, P. R. Ashton, R. A. Bissell, G. Clavier, R. Górski, A. E. Kaifer, S. J. Langford, G. Mattersteig, S. Menzer, D. Philp, A. M. Z. Slawin, N. Spencer, J. F. Stoddart, M. S. Tolley and D. J. Williams, *Chem. Eur. J.*, 1997, **3**, 1113 and references therein.
8 J. McGeachie and L. A. Summers, *Z. Naturforsch., Teil B*, 1986, **41**, 1255.

ChemComm

Axially coordinated porphyrins as new rotaxane stoppers

Kelly Chichak, M. Catherine Walsh and Neil R. Branda*

Department of Chemistry, University of Alberta, Edmonton, AB, Canada T6G 2G2. E-mail: neil.branda@ualberta.ca

Received (in Columbia, MO, USA) 14th February 2000, Accepted 24th March 2000

Coordination to the axial position of the metalloporphyrin Ru(TTP)(CO) is an effective means to end-cap the 1,2-bis(4,4′-dipyridinium)ethane dication·dibenzo[24]-crown-8 [2]pseudo-rotaxane and generate the stable porphyrinic [2]rotaxane 4.

In order for rotaxanes to be used effectively as architectures when building nanoscale machines and new materials, the macrocyclic wheel, once threaded onto the molecular axle, must be held there to prevent the components from disassembling.[1] This task is typically carried out by covalently fastening bulky stoppers onto the two ends of the axle. Using this strategy, pseudo-rotaxanes are transformed into permanently interlocked rotaxanes.[2] An alternative approach (slippage), which is a thermodynamically driven self-assembly process, involves the threading of a presynthesized axle through the macrocyclic wheel under the influence of appropriate heating.[3] However, the harsh reaction conditions that tend to accompany the first strategy may not be conducive for synthesizing rotaxanes containing highly sensitive molecular components. The slippage strategy is also limiting in that rotaxanes can only be prepared from axles small enough to allow for the wheel to pass over them. A recently reported solution to these problems utilizes the dynamic nature of the imine bond to end-cap pseudo-rotaxanes under thermodynamic control.[4] An alternative to using reversible carbon–heteroatom bond formation is to exploit metal-directed self-assembly synthesis, which again has the advantage of being thermodynamically driven but is accomplished more rapidly and under milder conditions. Despite its being introduced almost two decades ago, there are few examples that utilize this approach to generate interlocking structures.[5]

The growing interest in rotaxanes containing chromophores as stoppers[6] prompted us to develop mild porphyrin-based end-capping methods. Porphyrins are particularly attractive stoppers not only because of their bulkiness, but also because of their rich electro- and photo-physical properties, which have played important roles in synthetic electron and energy transfer systems.[6] In this study, we continue to use axial coordination to the central metal of Ru(TTP)(CO)† as a means to self-assemble porphyrin arrays in light of our recent success in rapidly generating thermodynamically controlled multicomponent arrays.[7] What we sought was a pseudo-rotaxane displaying divergent Lewis-basic sites appropriately distanced from the threaded wheel so as not to interfere with the self-assembly process. The 1,2-bis(4,4′-dipyridinium)ethane dication·dibenzo[24]crown-8 [2]pseudo-rotaxane **3** recently spot-lighted by Loeb and Wisner[5] provided the suitable model rotaxane for our purpose (Scheme 1).

Dissolving equimolar amounts of **1** and **2** in a 1 : 1 mixture of $CDCl_3$ and CD_3NO_2‡ immediately generated [2]pseudo-rotaxane **3** as apparent by ^{1}H NMR spectroscopy. A comparison of the integrals of the signals for free and bound **1** and **2**, both of which were clearly separated in the ^{1}H NMR spectrum, allows for facile determination of the association constant (K_a) in the slow-exchange threading process. This value was measured to be in the range of 3000–10000 M^{-1} in the mixed-solvent system (1–3 mM solutions). We prefer to report K_a as being within a range because we found that the extent of threading was sensitive to the concentration of **1** and **2** in the sample, with the magnitude of the association constant increasing as the concentration of both components are raised.§ We attribute this unexpected concentration dependency to the trace amount of residual water in the solvents. Because the solvent shells surrounding all species (**1**–**3**) certainly can include water, it is reasonable to assume that the concentration of free and bound water would change throughout the complexation reaction at the low water concentrations found in these solutions. The result is that water cannot be eliminated from the thermodynamic equilibrium equation and will thus have a great effect on the ability to form the [2]pseudo-rotaxane **3**. In this way, the slightly hydrous nature of the solvents used affects the precision of our measurements. Our support for this suggestion comes in the observed lowering of K_a for solutions at any concentration when additional water was added to the sample. The association constants leveled out to 800–1000 M^{-1} when enough water (200–300 equivalents) was added so that its concentration remains unchanged during the threading process. Despite this, the strength of the interactions holding the interlocked components together compensates for the presence of such a competitive solvent like water.

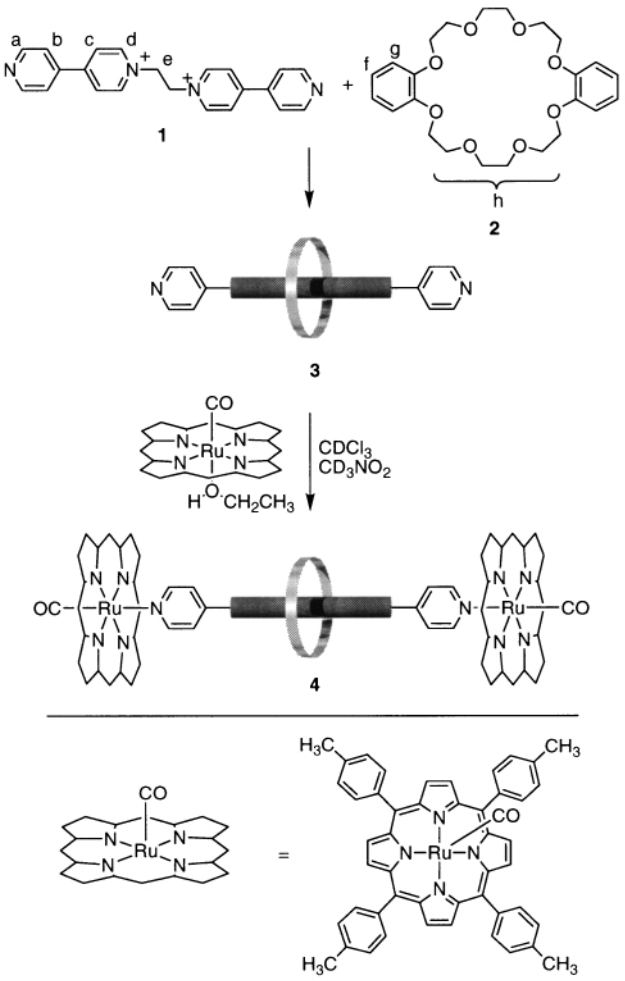

Scheme 1 PF_6^- counter ion.

DOI: 10.1039/b001259i

^{1}H NMR analysis of **3** also revealed the C–H···O hydrogen bonds and π–π stacking interactions responsible for driving the threading process.[5] When 2 mol equivalents of Ru(TTP)(CO)(EtOH) are added directly to the NMR sample, signals for the hydrogen atoms of both **1** and **2** shift significantly upfield, as would be expected for protons that reside within the additive shielding cones of the porphyrin stoppers.¶ The hydrogen atoms immediately adjacent to the coordinating nitrogen are closest to the end-caps (2.7 Å average nitrogen-to-porphyrin distance) and are the most affected by the anisotropic effect (Table 1). The shielding is minimally felt by the methylene (CH_2) protons of the dication axle which are as far as 10.2 Å from the stoppers, although it is still significant ($\Delta\delta$ = 0.72 ppm). All protons on the crown ether are also shielded, the most effected being those on the phenyl ring which are 3.0 and 5.1 Å from the mean centre of the porphyrin planes.

Table 1 Selected ^{1}H NMR data (500 MHz) of **4** in $CDCl_3$–CD_3NO_2 (1:1)

Axle fragment					Wheel fragment			
	H(a)[a]	H(b)	H(c)	H(d)	H(e)	H(f)	H(g)	H(h)
δ	1.65	5.36	6.91	8.60	5.01	5.33	5.94	3.67–3.59
$\Delta\delta$[b]/ppm	−7.18	−2.14	−1.17	−0.72	−0.72	−1.37	−0.76	−0.48

[a] Atom numbering scheme refers to Scheme 1. [b] Refers to upfield shifts of the protons relative to those in the spectrum of [2]pseudo-rotaxane **3**.

Addition of an excess of a competitive Lewis basic solvent such as pyridine to solutions of **4** resulted in the quantitative displacement of the stoppers as Ru(TTP)(CO)(py) and the regeneration of the dynamic mixture of pseudo-rotaxane **3** and the non-threaded wheel and axle. This study reveals the dynamic nature of the end-capping process.

Crystals of [2]rotaxane **4** suitable for structure determination were obtained by treating acetone solutions of **1** with excess **2**, end-capping the quantitatively formed [2]pseudo-rotaxane **3** with 2 mol equivalents of Ru(TTP)(CO)(EtOH), followed by slow evaporation. The crystal structure‖ (Fig. 1) is consistent with the binding interactions observed in the ^{1}H NMR spectrum. All methylene protons of **1** are within hydrogen bond distances to the oxygen atoms of the crown ether (average C···O distance = 3.54 Å). Also, the phenyl rings of the crown ether wheel are lying parallel to the heterocycles of the axle within π–π stacking range (mean Ar–Ar distance = 3.4 Å). The crystal structure shows that the distance between the porphyrin walls [Ru(1)···Ru(2) 21.692(3) Å] is just enough to accommodate the entire crown ether fragment without sacrificing any of the favourable π–π stacking interactions between the wheel and the axle.

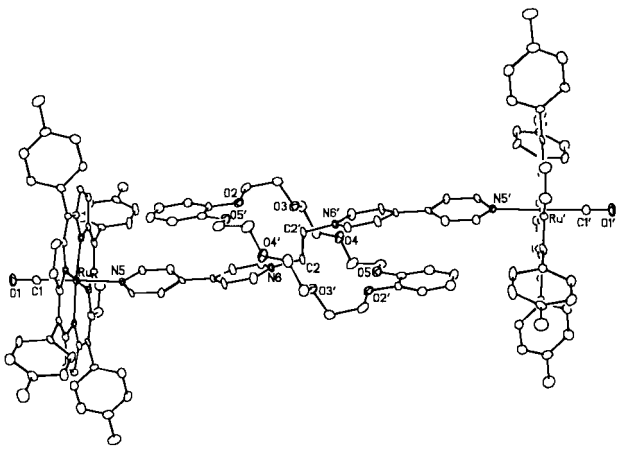

Fig. 1 Molecular structure of [2]rotaxane **4** in the crystal. The thermal ellipsoids are drawn at the 20% probability level.

We have shown that axial coordination is an effective self-assembly method to convert dynamic [2]pseudo-rotaxanes into stable interlocked [2]rotaxanes. The stoppers can be removed under mild conditions by treating **4** with the appropriate solvent. This end-capping strategy will be useful when removable stoppers are desired. Photochemical studies are underway in order to evaluate the influence the porphyrins have on the charge transfer process that has already been observed in the [2]pseudo-rotaxane.[5]

This work was supported by the Natural Sciences and Engineering Research Council of Canada and the University of Alberta and by the University of Alberta.

Notes and references

† TTP = 5,10,15,20-tetratolylporphyrinato dianion.

‡ Although the [2]pseudo-rotaxane is soluble in single-solvent systems such as nitromethane and acetonitrile, the poor solubility of Ru(TTP)(CO)(EtOH) in nitromethane alone eliminated the possibility of using this solvent. Acetonitrile was avoided as its nitrogen atom effectively competes as a Lewis base with those on **1** for coordinating to the transition metal. Once formed, however, the [2]rotaxane **4** is freely soluble in organic solvents alone such as $CHCl_3$ and CH_2Cl_2.

§ Representative K_a values were measured to be 4161 M^{-1} (1.2 mM solution), 4647 M^{-1} (2.2 mM solution) and 9356 M^{-1} (3.3 mM solution).

¶ Rotaxane **4** was also characterized by IR and ES-MS.

‖ *Crystal data* for **4**: $C_{166.5}H_{169}F_{12}N_{12}O_{17.5}P_2Ru_2$, M = 3110.22, monoclinic, space group $P2_1/n$ (a non-standard setting of $P2_1/c$ (no. 14)], a = 11.655(2), b = 30.385(5), c = 24.340(4) Å, β = 103.745(3)°, V = 8373(2) Å^3, T = −80 °C, Z = 2, μ = 0.276 mm^{-1}, number of reflections = 41325; number of independent reflections = 17184, $R_1(F)$ = 0.0877 [for 4929 data with $F^2 \geqslant 2\sigma(F^2)$], wR_2 (F^2) = 0.2673 (all data).

CCDC 182/1594. See http://www.rsc.org/suppdata/cc/b0/b001259i/ for crystallographic files in .cif format.

1 L. Flamigni, N. Armaroli, F. Barigelletti, J.-C. Chambron, J.-P. Sauvage and N. Solladie, *New J. Chem.*, 1999, **23**, 1151 and references therein.

2 Previously employed stoppers include: phosphines, S. J. Rowan and J. F. Stoddart, *J. Am. Chem. Soc.*, 2000, **122**, 164; calixarenes, C. Fischer, M. Nieger, O. Mogck, V. Bohmer, R. Ungaro and F. Vogtle, *Eur. J. Org. Chem.*, 1998, 155; fullerenes, N. Armaroli, F. Diederich, C. O. Dietrich-Buchecker, L. Flamigni, G. Marconi, J.-F. Nierengarten and J.-P. Sauvage, *Chem. Eur. J.*, 1998, **4**, 406; ferrocene, A. C. Benniston, A. Harriman and V. M. Lynch, *J. Am. Chem. Soc.*, 1995, **117**, 5275; saccharides, C. Kauffmann, W. M. Muller, F. Vogtle, S. Weinman, S. Abramson and B. Fuchs, *Synthesis*, 1999, 849; T. Schmidt, R. Schmieder, W. M. Muller, B. Kiupel and F. Vogtle, *Eur. J. Org. Chem.*, 1998, 2003; dendrimers, D, B. Amabilino, P. R. Ashton, V. Balzani, C. L. Brown, A. Credi, J. M. J. Frechet, J. W. Leon, F. M. Raymo, N. Spencer, J. F. Stoddart and M. Venturi, *J. Am. Chem. Soc.*, 1996, **118**, 12 012; trityl, C. Heim, A. Affeld, M. Nieger and F. Vogtle, *Helv. Chim. Acta.*, 1999, **82**, 746.

3 F. M. Raymo, K. N. Houk and J. F. Stoddart, *J. Am. Chem. Soc.*, 1998, **120**, 9318.

4 S. J. Rowan and J. F. Stoddart, *Org. Lett.*, 1999, **1**, 1913; S. J. Cantrill, S. J. Rowan and J. F. Stoddart, *Org. Lett.*, 1999, **1**, 1363.

5 For examples of using coordination chemistry to interlock rotaxanes, see: S. J. Loeb and J. A. Wisner, *Chem. Commun.*, 1998, 2757; S. J. Loeb and J. A. Wisner, *Angew. Chem., Int. Ed.*, 1998, **37**, 2838; D. J. Cárdenas, P. Gaviña and J.-P. Sauvage, *Chem. Commun.*, 1996, 1915; A. P. Lyon and D. H. Macartney, *Inorg. Chem.*, 1997, **36**, 729 and references therein. For examples to interlock catenanes, see: M. Fujita, *Acc. Chem. Res.*, 1999, **32**, 53; A. C. Try, M. M. Harding, D. G. Hamiltion and J. K. M. Sanders, *Chem. Commun.*, 1998, 723. For examples to link rotaxanes into oligomers and necklaces, see: S.-G. Roh, K.-M. Park, G.-J. Park, S. Sakamoto, K. Yamaguchi and K. Kim, *Angew. Chem., Int. Ed.*, 1999, **38**, 638; D. Whang, K.-M. Park, J. Heo, P. Ashton and K. Kim, *J. Am. Chem. Soc.*, 1998, **120**, 4899.

6 N. Solladie, J.-C. Chambron and J.-P. Sauvage, *J. Am. Chem. Soc.*, 1999, **121**, 3684; M.-J. Blanco, M. C. Jimenez, J.-C. Chambron, V. Heitz, M. Linke and J.-P. Sauvage, *Chem. Soc. Rev.*, 1999, **28**, 293; F. Vogtle, F. Ahuis, S. Baumann and J. L. Sessler, *Liebigs Ann. Rec.*, 1996, 921; R. Ishin and A. E. Kaifer, *J. Am. Chem. Soc.*, 1991, **113**, 8188.

7 K. Chichak and N. R. Branda, *Chem. Commun.*, 1999, 593.

Cooperative hydrogen bonding and yttrium(III) complexation in the assembly of molecular capsules

Michaele J. Hardie,[a] Julian A. Johnson,[b] Colin L. Raston*[a] and Helen R. Webb[a]

[a] *Department of Chemistry, Monash University, Clayton, Melbourne, Victoria 3800, Australia*
[b] *CSIRO Minerals, PO Box 90, Bentley, WA, 6982, Australia*

Received (in Columbia, MO, USA) 20th December 1999, Accepted 24th March 2000

A combination of hydrogen bonding and metal coordination leads to the formation of the new solid state molecular capsule [{18-crown-6}⊂{($Y(H_2O)_7^{3+}$)$_{1.33}$(*p*-sulfonatocalix[4]arene^{4-})}$_2$] at pH between 1.0 and 4.0.

Certain rigid, non-planar molecules with curved or bowl shaped micro-environments have the extraordinary ability to assemble into capsules or cage molecules or ions.[1–12] These species may form nano-structures of relevance to materials and biological science, and their encapsulation of guest molecules has implications for drug delivery and catalysis.[13] The hydrophobic, bowl shaped motif of calixarenes and related resorcinarenes make them inherently versatile building blocks for the construction of ionic or molecular capsules. They afford capsules based on the assembly of two[4] or six[3] sub-units or supramolecular tectons in which the assembly is primarily driven by the interplay of hydrogen bonding between the subunits. This may involve additional hydrogen bonding associations with solvent molecules. Capsules derived from aqueous media usually rely on metal ion complexation to drive the assembly process.[10,11] An exception is the ionic capsule [{Na^+⊂(18-crown-6)$(OH_2)_2$}⊂{*p*-sulfonatocalix[4]arene^{4-})$_2$} + nH^+]$^{(7+n)-}$, which incorporates both hydrogen bonding and metal complexation.[12]

Herein, we report the use of a combinatorial approach for the synthesis of a complex based on molecular capsules, [{18-crown-6}⊂{($Y(H_2O)_7^{3+}$)$_{1.33}$(*p*-sulfonatocalix[4]arene^{4-})}$_2$] **1**.† Combinatorial chemistry has thus far been of limited application in supramolecular chemistry.[14] The supramolecular combinatorial library used contains all the interacting synthons including the degree of protonation of the calixarene (achieved by varying pH) and the relative ratios of the synthons, with crystallisation indicative of capsule formation. Its noteworthy that Atwood *et al.* have established a rich supramolecular chemistry of *p*-sulfonatocalix[4]arene and the lanthanides in the absence of crown ethers.[15,16]

Complex **1** crystallises from an aqueous solution of sodium *p*-sulfonatocalix[4]arene, 18-crown-6, yttrium(III) chloride, and hydrochloric acid as the tetrahydrate at a pH between 1.0 and 4.0 (Scheme 1). The highest optimised yield of 68% was for a pH close to 2.0 with the pH varied by 0.25 pH units. Above pH 4.0 and below pH 1.0 no complex precipitated from solution. Interestingly using perchloric acid resulted in oxidation of the calixarene and formation of crystalline $Y_2(SO_4)_3(H_2O)_8$ at pH < 2.0,‡ isostructural with other known $Ln_2(SO_4)_3(H_2O)_8$ complexes.[17] Complex **1** was characterised by electron microprobe analysis, which indicated a Y:S ratio of *ca.* 1:3, as well as microanalysis, IR spectroscopy and single crystal X-ray crystallography.§ The IR spectrum displayed a shift in the sulfonate absorptions from 1186 and 1048 cm^{-1} (for the sodium salt) to 1166 and 1041 cm^{-1}, which is indicative of metal coordination through oxygen centres.[18] Similar reactions were tried using other lanthanoid salts, and an isostructural Eu^{3+} complex has also been obtained at an optimal pH 2.5.¶

Complex **1** crystallises in the space group $P2_1/n$ with the capsule residing over a centre of inversion. The unit cell also contains eight solvent water molecules disordered over several

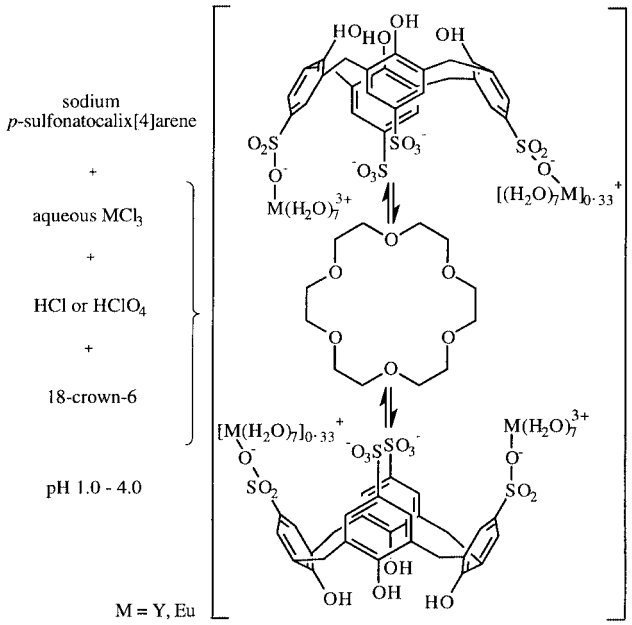

Scheme 1

positions. Results are shown in Fig. 1. Yttrium cations coordinate to the 1,3-sulfonate groups of the calixarene with two calixarene sub-units encapsulating an 18-crown-6 molecule, and indeed the crown ether may be the primary building component around which the capsule is formed. Surprisingly the 18-crown-6 is devoid of Na^+, and also Y^{3+}, but this ion is not well suited to interact with this crown ether.[19] The absence of Na^+ is in direct contrast to the ionic capsule [{Na^+⊂(18-crown-6)$(OH_2)_2$}⊂{(*p*-sulfonatocalix[4]arene^{4-})$_2$} + nH^+]$^{(7+n)-}$ and the related perched 'Ferris wheel' structure [{La^{3+}⊂(18-crown-6)$(OH_2)_3$}∩{(*p*-sulfonatocalix[4]arene^{4-} + 2H^+)}]$^+$.[20]

There are two types of Y metal, one of which is partially occupied and disordered, and both coordinate to seven water molecules [Y(1)–O 2.324(4)–2.405(4) Å, Y(2)–O 2.31(2)–2.38(2) Å], and one sulfonato group of the calixarene [Y(1)–O 2.308(4) Å, Y(2)–O 2.30(2) Å]. This is unexceptional for Y^{3+}.[21] Both are involved in RSO–Y–HOH···OSR hydrogen bonding leading to the dimerisation of calixarene sub-units in two distinct modes, shown schematically in Fig. 1(a). The first mode, of the ordered Y(1), involves a head-to-head dimerisation of the calixarenes [Fig. 1(a)(i)] to form the capsule, with YO···OS separations of 2.71–2.80 Å. This is undoubtedly facilitated by the encapsulation of the crown ether macrocycle (as discussed later). The second mode forms an S-type motif and involves the partially occupied Y(2)$(H_2O)_7$, [Fig. 1(a)(ii)]. This moiety is disordered over two adjacent sites by symmetry and each site has an occupancy of 1/3, determined by microprobe analysis, analysis of anisotropic displacement parameters and charge balance considerations. The YO···OS separations are 2.70 and 2.76 Å. The combination of the two modes of RSO–Y–HOH···OSR hydrogen bonding leads to a linear chain of

DOI: 10.1039/a910256f

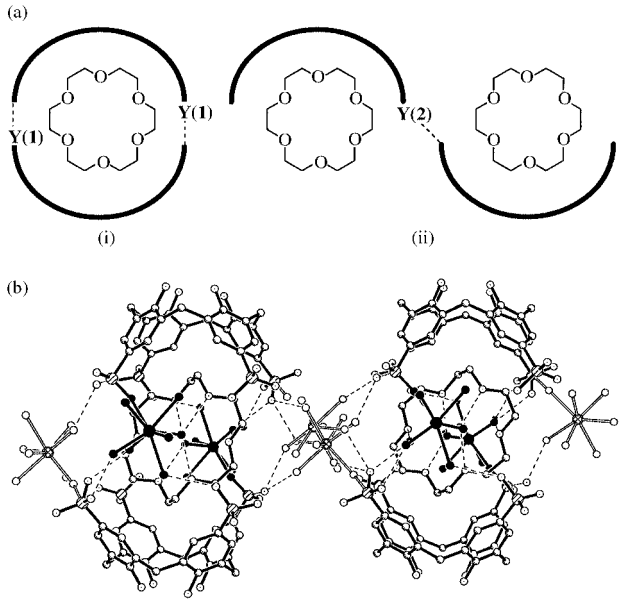

Fig. 1 (a) Schematic diagram of RSO–Y–HOH···OSR hydrogen bonding modes in $[(18\text{-crown-}6)_{0.5}(Y(H_2O)_7)_{1.33}(p\text{-sulfonatocalix[4]arene})]\cdot 4H_2O$ **1**, (i) head-to-head dimerisation of calixarenes around an 18-crown-6 molecule, (ii) S-type motif; (b) section of the crystal structure of **1** showing the linear chian of capsules,¶ $Y(1)(H_2O)_7$ is shown in black, while $Y(2)(H_2O)_7$ which is disordered with 1/3 occupancy is white. Hydrogen atoms have been removed for clarity and implied hydrogen-bonding interactions are represented by dashed lines. An isostructural complex can be formed with Eu.

capsules, a section of which is shown in Fig. 1(b). It is noteworthy that the sulfonatophenol group involved in Y(2) coordination has the largest tilt angle from the calixarene phenolic O_4 plane of 126.3° *cf.* 119.3, 115.6 and 124.5° for the other phenols.

The crown ether is at the core of the capsule. Hydrogen bonding occurs through each oxygen centre to water molecules coordinated to Y(1) at O···O separations of 2.77, 2.76 and 2.80 Å [Fig. 1(b)]. Driven primarily by this hydrogen bonding, but also by the complementarity of curvature of the calixarene cavity with the curvature of the crown ether (which optimises van der Waals interactions) the crown ether is held in the hydrophobic interior of the capsule. It is significantly distorted from its usual 'crown' shape due to exo-crown ether cavity hydrogen bonding, and hydrophobic interplay with the calixarenes.

In conclusion, using a combinatorial approach we have gained access to a novel multi-component capsule containing either Y^{3+} or Eu^{3+}. The same conditions for the formation of the capsule for solutions containing La^{3+} affords a perched structure involving one calixarene, one crown ether and a metal centre.[20] Other structural types are likely to be obtained from subtle changes in metal ion size and pH. We note that in the absence of crown ether, Ln^{3+} (Ln = Yb, Eu) can form complexes with *p*-sulfonatocalix[4]arene with the metal centre also bound to one sulfonato group, but ionic capsules do not form.[16] Clearly the presence of the crown ether is important for the formation of the capsule. However, other molecules with complementary size and curvature, which are also capable of hydrogen bonding, may also result in the formation of capsules.

We are grateful to the Australian Research Council for support of this work.

Notes and references

† *Synthesis* of **1**: $YCl_3\cdot 6H_2O$ (4.4 mg, 14.5 μmol), 18-crown-6 (5 mg, 18.9 μmol) and tetrasodium *p*-sulfonatocalix[4]arene (6 mg, 7.25 μmol) were dissolved in water (700 μL) and the pH adjusted to 2.0 using concentrated HCl. Colourless crystals of **1** grew overnight (6.1 mg, 68%). The crystals were sensitive to solvent loss. Electron microprobe results indicate that sulfur is *ca.* three times more abundant than yttrium (microanalysis: C, 32.0; S, 10.44%).

‡ $Y_2(SO_4)_3(H_2O)_8$ unit cell parameters: monoclinic, space group *C*2/*c*. a = 13.474(2), b = 6.688(1), c = 18.237(2) Å, β = 102.02(1)°.

§ *X-Ray Crystallography*: a crystal of dimensions 0.25 × 0.13 × 0.10 mm was grown from aqueous perchloric acid. Data were collected at 123(1) K on an Enraf-Nonius KappaCCD diffractometer with Mo-Kα radiation. The structure was solved by a combination of Patterson map and partial structure expansion (SHELXS-97) and refined using full-matrix least squares on F^2(SHELXL-97). All non-hydrogen atoms were refined anisotropically. All C–H and calixarene O–H hydrogens were fixed at geometrically calculated positions. *Crystal data* for $[(18\text{-crown-}6)_{0.5}(Y(H_2O)_7)_{1.33}(p\text{-sulfonatocalix[4]arene})]\cdot 4H_2O$ **1**: $C_{34}H_{58.67}O_{32.33}S_4Y_{1.33}$: M_r = 1231.59; monoclinic, space group $P2_1/n$; a = 12.0226(2), b = 28.2424(7), c = 15.1695(4) Å, β = 97.512(1)°; Z = 4; U = 5106.6(2) Å^3; μ = 1.776 mm^{-1} (no correction); 67206 data collected, 13671 unique (R_{int} = 0.101); number of parameters = 738, final GOF = 1.062, R_1 = 0.0851 [on 8255 observed data with $I > 2\sigma(I)$], wR_2 = 0.2559, (all data).

CCDC 182/1599. See http://www.rsc.org/suppdata/cc/a9/a910256f/ for crystallographic files in .cif format.

¶ Unit cell parameters for the isostructural complex $[(18\text{-crown-}6)_{0.5}(Eu(H_2O)_7)_{1.33}(p\text{-sulfonatocalix[4]arene})]\cdot 4H_2O$: monoclinic, space group $P2_1/n$, a = 11.9930(4), b = 28.4063(15), c = 15.0737(7) Å, β = 96.890(3)°.

1 J. Kang and J. Rebek, *Nature*, 1997, **385**, 50.
2 T. Heinz, D. M. Rudkevich and J. Rebek, *Nature*, 1998, **394**, 764; J. Kang, J. Santamaria, G. Hilmersson and J. Rebek, *J. Am. Chem. Soc.*, 1998, **120**, 7389; T. Szabo, G. Hilmersson and J. Rebek, *J. Am. Chem. Soc.*, 1998, **120**, 6193; Y. Tokunaga, D. M. Rudkevich, S. Goran and J. Rebek, *Chem. Eur. J.*, 1998, **4**, 1449; K. R. Castellano, D. M. Rudkevich and J. Rebek, *J. Am. Chem. Soc.*, 1996, **118**, 10 002.
3 L. R. MacGillivray and J. L. Atwood, *Nature*, 1997, **389**, 469.
4 K. N. Rose, L. J. Barbour, G. W. Orr and J. L. Atwood, *Chem. Commun.*, 1998, 407.
5 O. Mogek, M. Pons, V. Bohmer and W. Vogt, *J. Am. Chem. Soc.*, 1997, **119**, 5706.
6 R. G. Chapman and J. C. Sherman, *J. Am. Chem. Soc.*, 1995, **117**, 9081.
7 K. Nakamura, C. Sheu, A. E. Keating, K. N. Houk, J. C. Sherman, R. G. Chapman and W. L. Jorgensen, *J. Am. Chem. Soc.*, 1997, **119**, 4321.
8 K. Murayama and K. Aoki, *Chem. Commun.*, 1998, 607.
9 J. de Mendoza, *Chem. Eur. J.*, 1998, **4**, 1373 and references therein.
10 M. Fujita, D. Oguro, M. Miyazawa, H. Oka, K. Yamaguchi and K. Ogura, *Nature*, 1995, **378**, 469; T. Kusukawa and M. Fujita, *Angew. Chem., Int. Ed.*, 1998, **37**, 3142; T. Ibukuro, T. Kusukawa and M. Fujita, *J. Am. Chem. Soc.*, 1998, **129**, 8561; N. Takeda, K. Umemoto, K. Yamaguchi and M. Fujita, *Nature*, 1999, **398**, 794; B. Olenyuk, J. A. Whiteford, A. Fechtenkötter and P. J. Stang, *Nature*, 1999, **398**, 796 and references therein.
11 T. N. Parac, D. L. Caulder and K. N. Raymond, *J. Am. Chem. Soc.*, 1998, **120**, 8003; C. Bruckner, R. E. Powers and K. Raymond, *Angew. Chem., Int. Ed.*, 1998, **37**, 1837; D. L. Caulder, R. E. Powers, T. N. Parac and K. Raymond, *Angew. Chem., Int. Ed.*, 1998, **37**, 1840 and references therein.
12 A. Drljaca, M. J. Hardie, C. L. Raston and L. Spiccia, *Chem. Eur. J.*, 1999, **5**, 1828.
13 T. Douglas and M. Young, *Nature*, 1998, **393**, 152; G. D. Stucky and J. E. MacDouglas, *Science*, 1990, **247**, 669; K. Park, *Controlled Drug Delivery: Challenges and Strategies*, American Chemical Society, Washington DC, 1997 and references therein.
14 M. C. Calama, R. Hulst, R. Fokkens, N. M. M. Nibbering, P. Timmerman and D. N. Reinhoudt, *Chem. Commun.*, 1998, 1021.
15 J. L. Atwood and S. Bott, *Calixarenes: A Versatile Class of Macrocyclic Compounds*, ed. J. Vicens and V. Bohmer, Kluwer Academic Publishers, Boston, MA, 1991.
16 J. L. Atwood, G. W. Orr, N. Means, F. Hamada, H. Zhang, S. Bott and K. Robinson, *Inorg. Chem.*, 1992, **31**, 603; J. L. Atwood, G. W. Orr and K. D. Robinson, *Supramol. Chem.*, 1994, **3**, 89; G. W. Orr, L. J. Barbour and J. L. Atwood, *Science*, 1999, **285**, 1049.
17 E. G. Sherry, *J. Solid State Chem.*, 1976, **19**, 271; L. Hiltunen and L. Niinistö, *Cryst. Struct. Commun.*, 1976, **5**, 561.
18 L. J. Bellamy, *The Infrared Spectra of Complex Molecules: Advances in Infrared Group Frequencies*, Chapman and Hall, London, 1980, vol. 2.
19 R. Rogers and C. Bauer, in *Comprehensive Supramolecular Chemistry*, ed. J. L. Atwood, J. Davies, D. Macninol and F. Vogtle, Pergamon, New York, 1996, vol. 1, p. 315.
20 A. Drljaca, M. J. Hardie, J. A. Johnson, C. L. Raston and H. R. Webb, *Chem. Commun.*, 1999, 1135.
21 See, for example: M. Bukowska-Strzyzewska and A. Tosik, *Acta Crystallogr., Sect. B*, 1982, **38**, 950.

ChemComm

Nematic silsesquioxanes—towards nanocrystals dispersed in a nematic liquid crystal matrix

Ralf Elsäßer,[a] Georg H. Mehl,*[a] John W. Goodby[a] and Demetri J. Photinos[b]

[a] *Department of Chemistry, Hull University, Hull, UK HU6 7RX. E-mail: G.H.Mehl@chem.hull.ac.uk*
[b] *Department of Physics, University of Patras, Patras, Greece*

Received (in Oxford, UK) 10th March 2000, Accepted 4th April 2000

The reaction of suitable organic groups in combination with well defined inorganic silsequioxane cores leads to covalently bound organic–inorganic hybrid materials, which exhibit nematic and smectic C phase behaiour close to room temperature.

Much attention has been paid to the investigation of nanoscopic organic–inorganic hybrids which are amorphous, crystalline or which exhibit bicontinuos, columnar or lamellar morphologies.[1–4] This makes the investigation of systems where a covalently attached inorganic core is dispersed homogeneously in a nematic matrix a fascinating proposition.

Our approach is based on molecular designed LC materials where it has been established that the linkage of polyphilic groups to nematogenic molecules leads to layered structures.[5,6] This requires a systematic approach to arrive at the targeted nematic materials based on crystalline silsesquioxane cores **A**, shown in Fig. 1 as a model system for a monodisperse inorganic crystal of defined stereochemistry. The linkage of the liquid-crystalline rod-shaped mesogenic moieties to the inorganic cores is effected by spacers consisting of organic methylene groups bonded *via* 1,1,3,3-tetramethyldisiloxane groups to the core. Eight mesogenic groups are appended from the cuboid core leading to a molecular structure, where in the LC phase the nematic director field is responsible for the deformation of the spatially isotropic molecules to assemble into the nematic phase structure.

In order to assure the formation of liquid-crystalline phases above ambient temperature aromatic core structures of the mesogenic units were selected containing three and four aromatic rings, linked by C–C single bonds or ester groups shown in Scheme 1. In order to assure a suitable stability range of the liquid-crystalline phase terminal alkyl chains of eight or eleven methylene groups were selected. The lateral attachment of the mesogens to the central core was chosen to favour side-on interactions of the mesogens following an established concept.[7] A spacer of five methylene groups and a siloxane unit was used to obtain a suitable degree of decoupling of the rigid aromatic mesogens and the silsesquioxane crystalline core.

The synthesis of the functionalised monomer **5** is shown in Scheme 1. Alkylation of 2,4-dihydroxymethylbenzoate **1** with 1-bromooctane in the *p*-position of the aromatic ring and subsequently with 5-bromopent-1-ene in the *o*-position followed by removal of the protective methyl group leads to the intermediate **2**. Compound **4** containing four aromatic rings was obtained by esterification of **2** with **3**, the product of the esterification of octyloxybenzoic acid with one of the phenol groups of 4,4′-biphenol. The attachment of a 1,1,3,3-tetramethyldisiloxane group **B** to **4** in a hydrosilylation reaction using Karstedt's catalyst leads to the functionalised monomer **5**.

The structurally related mesogen **6** containing only three aromatic rings was synthesised as published earlier and hydrosilylated as described for **4** leading to the material **7**.[2]

In order to assess whether the phase behaviour is determined by microphase separation or by the size of the relatively bulky methyl groups of the siloxane units, **4** was reacted with 1,1,3,3,3-pentamethyldisiloxane **C** leading to material **8**, an anologue to compound **5**. The reaction of **6** with **C** in a similar manner yields compound **9**, structurally similar to material **6**.

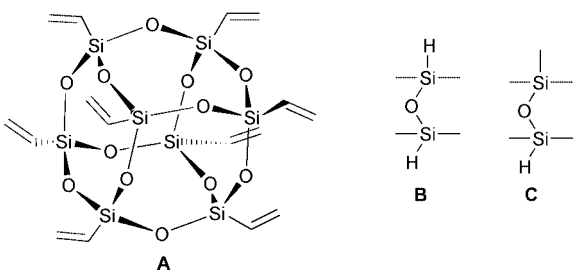

Fig. 1 Structures of the siloxane and silsequioxane cores.

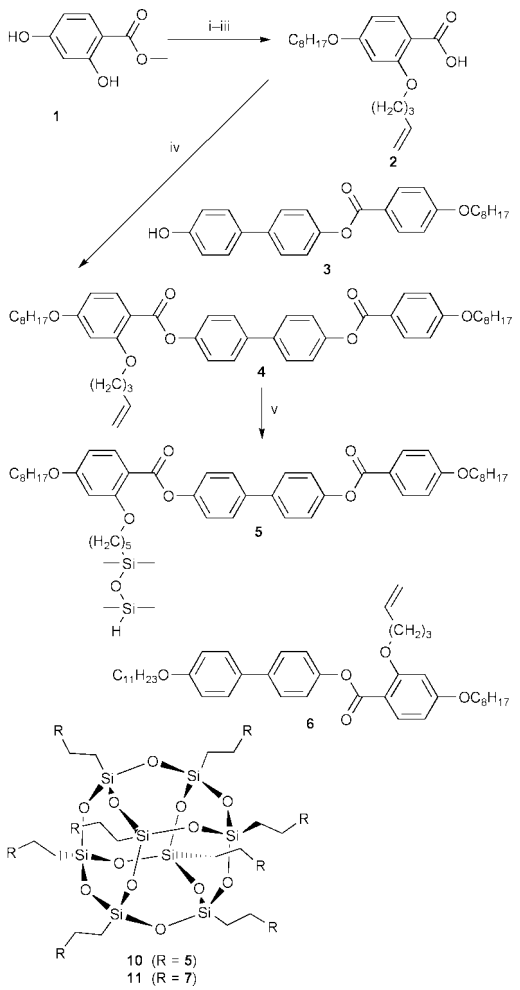

Scheme 1 *Reagents and conditions*: i, K_2CO_3, KI, butanone, 1-bromooctane; ii, K_2CO_3, KI, butanone, 5-bromopent-1-ene; iii, NaOH–MeOH, HCl–H_2O; iv, DCC–DMAP, **3**; v, 1,1,3,3-tetramethyldisiloxane, Karstedt's catalyst.

DOI: 10.1039/b001951h

Table 1 Transition temperatures as determined by DSC

Compound	Structure	Phase transitions/°C
4	**4**	cr 99.4 N 173.2 Iso
5	**4-B**	cr 67.1 [SmC 51.3] N 123.8 Iso
6	**6**	cr 53.8 N 72.7 Iso
7	**6-B**	cr 18.0 N 39.1 Iso
8	**4-C**	cr 76.6 [SmC 58.2] N 122.0 Iso
9	**6-C**	cr 24.8 N 39.5 Iso
10	[**4-B**]$_8$-**A**	cr 59.5 [SmX 33.1] SmC 111.3 N 145.8 Iso
11	[**6-B**]$_8$-**A**	T_g −19.3 SmX 37.6 N 50.5 Iso

The organic–inorganic hybrid materials containing a central silsesquioxane core were obtained by reacting octavinylsilsesquioxane **A** with **5** in a hydrosilylation reaction leading to material **10**. The bond formation could be monitored by the occurrence of the signals for the ethylene bridge in the ^{1}H NMR spectrum and unambiguously in this context by the appearance of peaks at δ 4.1 and 9.8 in the ^{13}C NMR spectra. The fusion of the inorganic core **C** in a similar manner with the functionalised mesogenic side-chain **7** containing three aromatic rings resulted in compound **11**. The materials were purified by column chromatography, indicating that the incorporation of siloxane groups in the spacer alters the solubility of these materials, when compared to related structures.[8,9] The eluent for material **11** was dichloromethane–hexane with the mixture gradient changed from 1 : 1 to 4 : 1 during the elution.

The transition temperatures of the liquid-crystalline materials **4**–**11** are listed in Table 1. All of these materials exhibit a nematic phase as the highest stable liquid-crystalline phase, characterised by a typical *schlieren* texture when observed using optical polarising microscopy.

For the four-ring system **4** the side-on attachment of the microphase seperating tetramethylsiloxane group leads to a marked decrease of the isotropisation temperature from 173.2 °C for **4** to 123.8 °C for compound **5**, a fall of 49.4 °C.

For the three-ring system **6** with an isotropisation temperature of 72.7 °C fusion to be tetramethylsiloxane group, leading to compound **7**, results in a decrease of the clearing temperature to 39.1 °C, a fall of 33.6 °C.

This modification of the mesogenic moieties by siloxane groups is additionally accompanied by a strong fall in the melting temperatures to 67.1 °C for **5** (99.4 °C for **4**) and to 18.0 °C for **7** (53.8 °C for **6**) when compared to the starting materials. An interesting feature is the occurrence of a low temperature smectic C phase characterised by broken focal conics and a *schlieren* texture for material **5**, a feature very unusual in rod shaped materials with a lateral side-chain.[10–12]

The structurally related materials containing a pentamethyldisiloxane endgroup, **8** and **9**, have similar isotropisation temperatures as observed for **5** and **7** containing tetramethyldisolaxane groups, indicating that the liquid-crystal phase behaviour is governed mainly by microphase separation of the organic and siloxane groups. The increase in the melting points for **8** (76.6 °C *cf.* 67.1 °C for **5**) and **9** (24.8 °C *cf.* 18 °C for **7**) can be attributed to the more bulky siloxane groups, leading to more stable crystalline phases.

The material **10** containing an inorganic core has an isotropisation temperature of 145.8 °C, a rise by 22 °C compared to the monomer **5**, indicating that the incorporation of a suitably functionalised inorganic core can promote the stability of the mesomorpic state. The increase of the stability range of the smectic C phase by 60 °C to 111.3 °C observable for material **10** is remarkable. This is accompanied by a fall of the crystallisation temperature to 59.5 °C of this structure. Additionally a monotropic highly ordered LC phase of undetermined structure was observed below 33.1 °C.

A special feature of the cuboid material **11**, where the inorganic core is decorated with eight mesogens containing three aromatic is the absence of a crystalline state, only a low glass transition temperature of −19.3 °C could be observed. The material clears from the nematic phase to the isotropic state at 50.5 °C and shows an underlying smectic phase (smectic X) at 37.6 °C, confirming thus the versatility of the selected systematic approach, geared towards low temperature organic–inorganic anisotropic fluids incorporating nanocrystalline cores.

We acknowledge the EC for funding in the framework of the TMR network 'Molecular Design of Functional Liquid Crystals' and thank the members of the network for the many helpful discussions.

Notes and references

1 C. T. Kresge, M. E. Leonwicz, W. J. Roth, J. C. Vartuli and J. S. Beck, *Nature*, 1992 **359**, 710; G. S. Attard, J. C. Glyde and C. G. Göltner, *Nature*, 1995, **378**, 366.
2 C. G. Göltner, *Angew. Chem., Int. Ed.*, 1999, **38**, 3155; K. C. McGrath, D. M. Dabbs, N. Yao, I. A. Aksay and S. M. Gruner, *Science*, 1997, **277**, 552.
3 S. A . Miller, E. Kim, D. H. Gray and G. L. Gin, *Angew. Chem., Int. Ed.*, 1999, **38**, 3022.
4 A. Sellinger, P. M. Weiss, A. Nguyen, Y. Lu, R. A. Assink, W. Gong and C. F. Brinker, *Nature*, 1998, **394**, 256.
5 C. Tschierske, *J. Mater. Chem.*, 1998, **8**, 1485.
6 M. Ibn-Elhaj, H. J. Coles, D. Gouillon and A. Skoulios, *J. Phys. (Paris) II*, 1993, **3**, 1807; T. Chuard, R. Deschenaux, A. Hirsch and H. Schönberger, *Chem. Commun.*, 1999, 2103.
7 F. Hessel and H. Finkelmann, *Polym. Bull.*, 1985, **3751**, 14.
8 G. W. Gray, J. S. Hill and D. Lacey, *Mol. Cryst. Liq. Cryst.*, 1991, **197**, 43.
9 G. H. Mehl and J. W. Goodby, *Chem. Ber.*, 1996, **129**, 521; G. H. Mehl and J. W. Goodby, *Angew. Chem., Int. Ed, Engl.*, 1996, **35**, 2641.
10 G. H. Mehl and J. W. Goodby, *Chem. Commun.*, 1999, 13.
11 W. Weissflog, J. Risse, D. Lose, S. Diele and G. Pelzl, *Int. Liq. Cryst. Conf., Strasbourg, France*, P4-58, 1998; W. Weissflog, personal communication.
12 S. Lecommandoux, M. F. Archard and F. Hardouin, *Liq. Cryst.*, 1998, **25**, 85 and references therein.

Dendrimers as fluorescent sensors with signal amplification

Vincenzo Balzani,*[a] Paola Ceroni,[a] Sven Gestermann,[b] Christopher Kauffmann,[b] Marius Gorka[b] and Fritz Vögtle*[b]

[a] *Dipartimento di Chimica "G. Ciamician" Università di Bologna, via Selmi 2, I-40126 Bologna, Italy. E-mail: vbalzani@ciam.unibo.it*

[b] *Kekulé-Institut für Organische Chemie und Biochemie der Universität Bonn, Gerhard-Domagk Strasse 1, D-53121 Bonn, Germany*

Received (in Cambridge, UK) 15th March 2000, Accepted 7th April 2000

In a fourth generation poly(propylene amine) dendrimer decorated with 32 dansyl units at the periphery and containing 30 aliphatic amine units in the interior, the strong fluorescence of all the dansyl units is quenched when a Co^{2+} ion is incorporated into the dendrimer.

In the last few years there has been a great development in the field of fluorescent chemosensors.[1] These compounds are usually made of a fluorescent unit connected with a receptor. Recognition of a substrate by the receptor affects the fluorescent properties of the fluorophore. For example [Fig. 1(a)], coordination of a metal ion to the receptor can cause quenching of the excited state of the fluorophore by energy or electron transfer, thereby switching off the fluorescent signal. In order to achieve sensory signal amplification, we have designed and synthesized compounds in which one transition metal ion is able to quench the excited state of a great number of fluorophores [Fig. 1(b)].

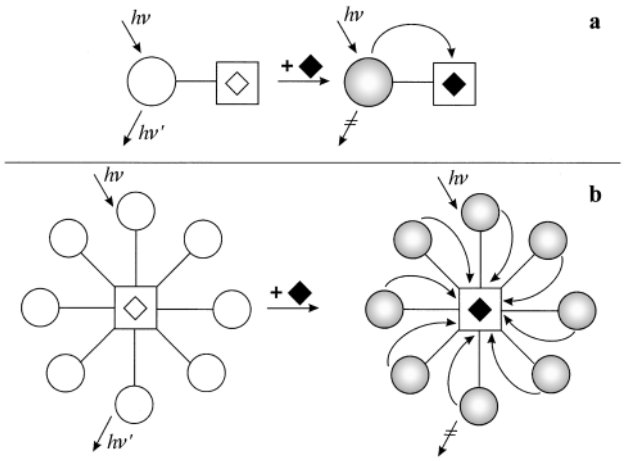

Fig. 1 Schematic representation of (a) a conventional fluorescent sensor and (b) a fluorescent sensor with signal amplification. The curved arrows indicate a quenching process. For more details, see text.

The described system belongs to the family of dendrimers, which are well defined macromolecules exhibiting tree-like structures.[2] By suitable design and synthetic strategies, it is possible to incorporate in a dendritic structure components exhibiting specific properties whose integration can lead to useful functions.[3] Continuing our investigations in the field of photoactive dendrimers,[4] we have prepared compounds that incorporate both receptor and fluorophore units, and we have shown that they can give rise to a strong signal amplification compared to fluorescence sensors carrying only one fluorescent unit (Fig. 1).

Because of its strong fluorescence, the dansyl group is often used as a fluorophore for sensory purposes.[5] When the dansyl unit is linked to a polyamine receptor,[6] coordination of a suitable metal ion by the receptor causes the quenching of the dansyl fluorescence. We have appended fluorescent dansyl units at the periphery of poly(propylene amine) dendrimers[7] which are able to coordinate metal ions by the aliphatic amine units contained in the interior of the structure. The formula of the fourth generation dendrimer **4D**, which contains 32 dansyl units at the periphery and 30 aliphatic amine units in the interior, is shown in Fig. 2.

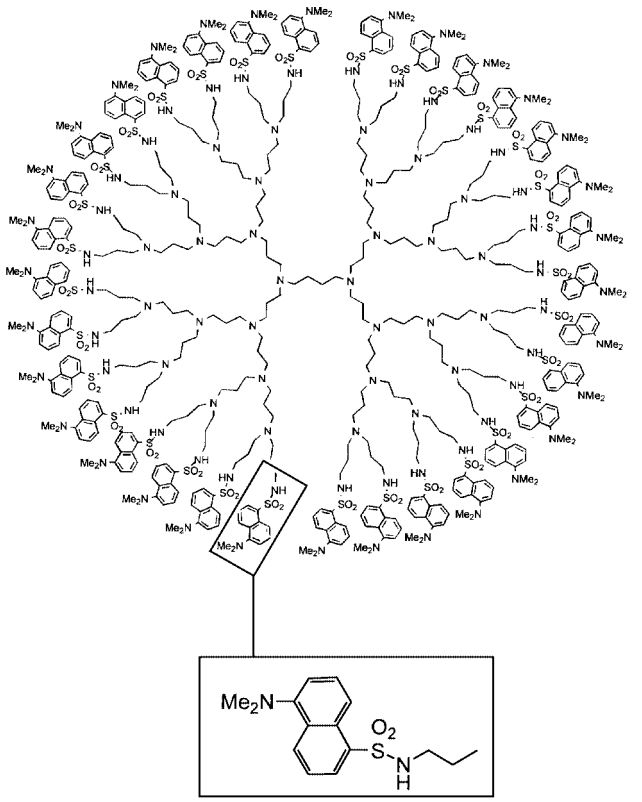

Fig. 2 Structure formula of the **4D** fourth-generation poly(propylene amine) dendrimer decorated with 32 dansyl units.

In acetonitrile–dichloromethane (5:1 v/v) solution, dendrimer **4D** exhibits intense absorption bands in the near UV spectral region (λ_{max} = 253 and 339 nm, ε_{max} = 357 000 and 113 000 M^{-1} cm^{-1}, respectively) and a strong fluorescence band in the visible region (λ_{max} = 514 nm, Φ = 0.25, τ = 13 ns).† Addition of Co^{2+} (up to 1.0×10^{-4} M, as $Co(NO_3)_2 \cdot 6H_2O$) to a 4.6×10^{-6} M solution of **4D** caused a strong quenching on the fluorescence intensity of the dansyl units appended at the periphery of the dendrimer, without affecting the absorption spectrum.

The observed quenching cannot be attributed to a dynamic process,‡ but it must originate from coordination of metal ions by the aliphatic amine groups which are present in the interior part of the dendrimer.[8] The **4D** dendrimer, in fact, can be considered as a polydentate ligand. In view of its size and of the 30 amine units, it can be expected that each dendrimer

DOI: 10.1039/b002116o

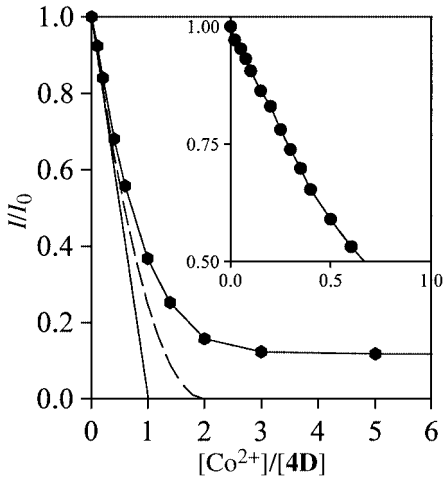

Fig. 3 Effect of addition of Co^{2+} ions on the fluorescence intensity of the **4D** dendrimer. The concentration of **4D** is 4.6×10^{-6} M. Inset shows the results of a detailed investigation at low Co^{2+} concentration.

coordinates several metal ions, giving rise to a complex titration curve (Fig. 3). The inset of Fig. 3 shows that for low Co^{2+} concentrations ($[Co^{2+}]/[\mathbf{4D}] \leqslant 0.3$) the fluorescence intensity decreases linearly with increasing $[Co^{2+}]$. More specifically, in this concentration range each Co^{2+} equivalent quenches 32 dansyl units, a number that corresponds to the dansyl units contained in each dendrimer. This means that at *low* metal ion concentration, 1 : 1 metal ion–dendrimer species are formed in which the dansyl fluorescence is completely quenched.§ Apparently, upon coordination of a metal ion the dendrimer shrinks around the metal, thereby allowing all the 32 dansyl units to be quenched when they are excited.

The titration curve (Fig. 3) is no longer linear on increasing Co^{2+} concentration further, which shows that species containing more than one metal ion per dendrimer are formed. The dashed curve in Fig. 3 corresponds to the behaviour expected if two metal ions can independently enter the dendrimer; the lack of fitting to this titration curve suggests that species containing more than two metal ions are also formed. Finally, it can be noted that the luminescence intensity does not fall to zero. Perhaps, since the metal ion is added as $Co(NO_3)_2 \cdot 6H_2O$, at very high Co^{2+} concentrations water molecules and/or counter ions may occupy part of the coordination sphere or even prevent complete dendrimer–Co^{2+} association. We have also found that, at high Co^{2+} concentrations, the titration curve is somewhat different when the metal ion is added as a chloride salt.

A most important property of a fluorescent sensor is, of course, sensitivity. By using dendrimer **4D** it is possible to amplify the sensitivity of a monodansyl compound by 32 times. The detection limit of Co^{2+} depends on the concentration used. Our results indicate that with a **4D** concentration of 4.6×10^{-6} M, a Co^{2+} concentration of 4.6×10^{-7} M causes a decrease in the fluorescence intensity of 5%. A signal amplification effect has already been obtained with polymeric chains of sensors.[9] Because of their well defined and fully programmable structures, dendrimers are more promising species for this kind of application.[10] Of course, several other requirements (*e.g.*, selectivity) are needed for useful sensory application.

This work has been supported by MURST (Supramolecular Devices Project), University of Bologna (Funds for Selected Topics), and CNR (Sensori Fluorescenti Supramolecolari).

Notes and references

† The equipment used has been described elsewhere.[4]

‡ Since the lifetime of the fluorescent excited state of the dansyl unit is 13 ns, the metal ion concentration is too low to cause sizeable effects even in the case of a diffusion controlled quenching process.

§ The straight line shown in the inset of Fig. 3 extrapolates to $I/I_0 = 0$ at $[Co^{2+}]/[\mathbf{4D}] = 1$, which confirms that at *low* metal ion concentration 1 : 1 metal ion/dendrimer species are formed in which the dansyl fluorescence is completely quenched.

1 R. A. Bissell, A. P. de Silva, H. Q. N. Gunaratne, P. L. M. Lynch, G. E. M. Maguire, G. P. McCoy and K. R. A. S. Sandanayake, *Top. Curr. Chem.*, 1993, **168**, 223; A. P. de Silva, H. Q. N. Gunaratne, T. Gunnlaugsson, A. J. M. Huxley, G. P. McCoy, J. T. Rademacher and T. E. Rice, *Chem. Rev.*, 1997, **97**, 1515; M. D. Ward, *Chem. Ind.*, 1997, 640; *Chemosensors of Ion and Molecule Recognition*, ed. J. P. Desvergne and A. W. Czarnik, Kluwer, Dordrecht, 1997; P. D. Beer, *Acc. Chem. Res.*, 1998, **31**, 71; L. Fabbrizzi, M. Licchelli and P. Pallavicini, *Acc. Chem. Res.*, 1999, **32**, 846.

2 D. A. Tomalia and H. D. Durst, *Top. Curr. Chem.*, 1993, **165**, 193; N. Ardoin and D. Astruc, *Bull. Soc. Chim. Fr.*, 1995, **132**, 875; E. C. Constable, *Chem. Commun.*, 1997, 1073; G. R. Newkome, C. Moorefield and F. Vögtle, *Dendritic Molecules: Concepts, Syntheses, Perspectives*, VCH, Weinheim, 1996; J.-P. Majoral and A.-M. Caminade, *Top. Curr. Chem.*, 1998, **197**, 79; A. W. Bosman, H. M. Janssen and E. W. Meijer, *Chem. Rev.*, 1999, **99**, 1665; G. R. Newkome, E. He and C. Moorefield, *Chem. Rev.*, 1999, **99**, 1689.

3 See, for example: J. F. G. A. Jansen, E. M. M. de Brabander-van der Berg and E. W. Meijer, *Science*, 1994, **266**, 1226; J. F. G. A. Jansen and E. W. Meijer, *J. Am. Chem. Soc.*, 1995, **117**, 4417; C. Devadoss, P. Bharathi and J. S. Moore, *Angew. Chem., Int. Ed. Engl.*, 1997, **36**, 1633; V. Balzani, S. Campagna, G. Denti, A. Juris, S. Serroni and M. Venturi, *Acc. Chem. Res.*, 1998, **31**, 26; T. Sato, D.-L. Jiang and T. Aida, *J. Am. Chem. Soc.*, 1999, **121**, 10 658; S. L. Gilat, A. Andronov and J. M. J. Fréchet, *Angew. Chem., Int. Ed.*, 1999, **38**, 1422; G. E. Oesterom, R. J. van Haaren, J. N. H. Reek, P. C. J. Kramer and P. W. N. M. van Leeuwen, *Chem. Commun.*, 1999, 1119.

4 J. Issberner, F. Vögtle, L. De Cola and V. Balzani, *Chem. Eur. J.*, 1997, **3**, 706; A. Archut, F. Vögtle, L. De Cola, G. C. Azzellini, V. Balzani, P. S. Ramanujam and R. H. Berg, *Chem. Eur. J.*, 1998, **4**, 699; A. Archut, G. C. Azzellini, V. Balzani, L. De Cola and F. Vögtle, *J. Am. Chem. Soc.*, 1998, **120**, 12 187; M. Plevoets, F. Vögtle, L. De Cola and V. Balzani, *New J. Chem.*, 1999, **23**, 63; F. Vögtle, M. Plevoets, M. Nieger, G. C. Azzellini, A. Credi, L. De Cola, V. De Marchis, M. Venturi and V. Balzani, *J. Am. Chem. Soc.*, 1999, **121**, 6290.

5 H. F. M. Nelissen, F. Venema, R. M. Uittenbogaard, M. C. Feiters and R. J. M. Nolte, *J. Chem. Soc., Perkin Trans. 2*, 1997, 2045; H. Ikeda, M. Nakamura, N. Ise, N. Oguma, A. Nakamura, T. Ikeda, F. Toda and A. Ueno, *J. Am. Chem. Soc.*, 1996, **118**, 980; T. Ikunaga, H. Ikeda and A. Ueno, *Chem. Eur. J.*, 1999, **5**, 2698.

6 M. Schuster and M. Sandor, *Fresenius Z. Anal. Chem.*, 1996, **356**, 326; G. De Santis, L. Fabbrizzi, M. Licchelli, N. Sardone and A. H. Velders, *Chem. Eur. J.*, 1996, **2**, 1243; L. Prodi, F. Bolletta, M. Montalti and N. Zaccheroni, *Chem. Eur. J.*, 1999, **5**, 445.

7 F. Vögtle, S. Gestermann, C. Kauffmann, P. Ceroni, V. Vicinelli, L. De Cola and V. Balzani, *J. Am. Chem. Soc.*, 1999, **121**, 12 161.

8 For copper ion complexation by poly(amidoamine) dendrimers, see: M. Zhao, L. Sun and R. M. Crooks, *J. Am. Chem. Soc.*, 1998, **120**, 4877; M. Zhao and R. M. Crooks, *Angew. Chem., Int. Ed.*, 1999, **38**, 364; L. Balogh and D. A. Tomalia, *J. Am. Chem. Soc.*, 1998, **120**, 7355.

9 T. M. Swager, *Acc. Chem. Res.*, 1998, **31**, 201.

10 For a 'dendrimer effect' in the NMR anion sensing by dendrimers containing peripheral cationic units, see: C. Valerio, E. Alonso, J. Ruiz, J.-C. Blais and D. Astruc, *Angew. Chem., Int. Ed.*, 1999, **38**, 1747.

Effective alkene epoxidation with dilute hydrogen peroxide on amorphous silica-supported titanium catalysts

M. C. Capel-Sanchez,[a] J. M. Campos-Martin,[a] J. L. G. Fierro,*[a] M. P. de Frutos[b] and A. Padilla Polo[b]

[a] *Instituto de Catálisis y Petroleoquímica, CSIC, Cantoblanco, 28049 Madrid, Spain. E. mail: jlgfierro@icp.csic.es*
[b] *Centro de Investigacion y Desarrollo REPSOL-YPF, Embajadores 183, 28045 Madrid, Spain*

Received (in Cambridge, UK) 2nd February 2000, Accepted 5th April 2000

The use of amorphous silica-supported titanium catalysts in which the titanium ions display a chemical environment similar to that of Ti-substituted zeolites, afforded excellent activity in the epoxidation of terminal linear and bulky alkenes with dilute solutions of hydrogen peroxide.

Despite numerous reports in the literature, the epoxidation of terminal alkenes remains a challenge in petrochemistry. Many different methods have been developed for the preparation of epoxides. However, in recent years maximum interest has focused on titanium-substituted zeolites in the framework, including TS-1,[1] Ti-β[2] and Ti-incorporated mesoporous silica,[3] which are claimed to be good catalysts for epoxidation with hydrogen peroxide. Although in the presence of methanol as a solvent all these catalysts display high activity and selectivity levels towards epoxide, they have poor mechanical strength and low thermal stability. Non-zeolitic TiO_2–SiO_2-supported catalysts are effective in the epoxidation of alkenes with organic hydroperoxides,[4,5] but it is generally believed that they are not effective in the epoxidation of alkenes with hydrogen peroxide. Nevertheless, titanium silica-supported catalysts have been reported to be active to the epoxidation of alkenes with hydrogen peroxide, but with low selectivity towards epoxide.[6]

Here we report a very simple route for the preparation of TiO_2/SiO_2 catalysts with highly dispersed titanium atoms. These catalysts are relatively inexpensive, easy to synthesise and regenerate, and at the same time show high conversion rates without the requirement of methanol as a solvent. Hitherto, these materials have not been used as catalysts in the epoxidation of alkenes (oct-1-ene, cyclohexene and norbornene) with hydrogen peroxide solutions.

The catalysts were prepared in the following manner:[7] 0.75 g of titanium isopropoxide was dispersed in the solvent (either *n*-decane, toluene or cyclohexanol to produce catalysts C3, C2 and C1, respectively) (150 ml). The solution was heated to 423 K (the boiling point of toluene solution) under stirring and then 5 g of silica (Grace Davison G-952, surface area: 310 $m^2\ g^{-1}$, pore volume: 1.5 ml g^{-1}) was added to the solution, which was stirred at 423 K for 2 h. The solid obtained was filtered off and washed twice with 150 ml of hot solvent and subsequently dried at 383 K and calcined at 773 K for 5 h. As reference catalysts, a titanium-supported silica (TiF/SiO_2), as described by Jorda *et al.*,[6] and a titanium silicalite (TS-1), as reported by Taramaso *et al.*,[1] were prepared.

The total amount of titanium introduced into the synthesis solution was incorporated to catalysts TiF/SiO_2, C2 and C3 (Table 1). However, when cyclohexanol was employed as the solvent (C1), only part of the titanium was incorporated into the catalyst. For TS-1, the degree of titanium incorporation was similar to that reported in the literature. The structural FTIR spectra of the catalysts diluted in KBr were inconclusive because the silica support displayed a broad peak at 960 cm^{-1}, which overshadowed the Ti–O–Si vibration mode (960 cm^{-1}).[8]

The DRS UV–VIS spectra (Fig. 1) of catalysts C1, C2, C3 and TiF/SiO_2 were clearly different from that of the TS-1 sample. The spectrum of the latter showed a single peak at 210 nm, which can be taken as a clear indication of isolated Ti(IV) in tetrahedrally coordinated sites. The slight shift in band position and the increase in bandwidth point to a distorted tetrahedral environment of the titanium. The broad adsorption band of the silica-supported samples shifted to high wavelength values; this can be explained in terms of: (i), the presence of titanium atoms in octahedral coordination (values between 290 and 333 nm),[9] as observed in catalysts C2 and C3, and as a small component in TiF/SiO_2; (ii) the hydrophilic nature of the silica surface, which favours the presence of hydrated titanium in tetrahedral coordination (232 nm),[9] as already seen for catalyst C1 and the major proportion of TiF/SiO_2. However, the absence of a band at 370–410 nm rules out the presence of free TiO_2 in all the catalysts.[9]

Table 1 Characteristics of the catalysts

Catalyst	Synthesis	Titanium content (%) (XPS)	XPS ratio (460 eV/ 458.5 eV)
C1	Cyclohexanol	0.8	2.1
C2	Toluene	2.6	0.5
C3	*n*-Decane	2.6	0.1
TS-1[1]		1.7	2.5
TiF/SiO_2[6]		1.1	—[a]

[a] Not determined owing to the presence of fluorinated species.

High resolution photoelectron spectra of Ti 2p core-levels of the *in situ* outgassed samples (Fig. 2) displayed the characteristics Ti $2p_{1/2}$/Ti $2p_{3/2}$ doublet. Although chemical information can be derived from each component, discussion should be based on the most intense Ti $2p_{3/2}$ component. Curve fitting of

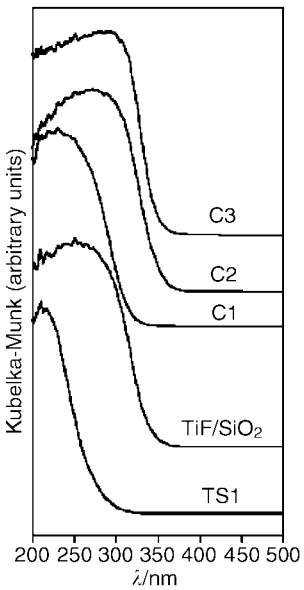

Fig. 1 DRS UV–VIS spectra of solids in ambient conditions recorded with a Shimadzu UV-2100 spectrometer.

DOI: 10.1039/b000929f

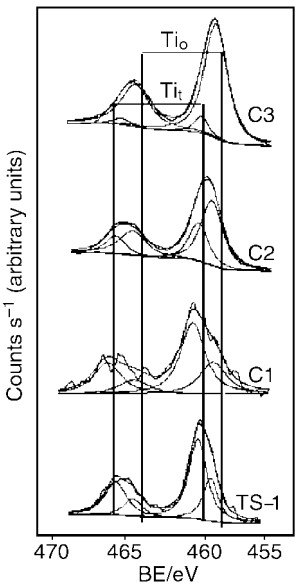

Fig. 2 Ti 2p core-level spectra of outgassed samples *in situ* at 473 K acquired with a VG Escalab 200R spectrometer.

the Ti $2p_{3/2}$ core level to two components shows the highest binding energy component (460.0 eV) can be attributed to titanium in tetrahedral coordination,[10] while the lowest binding energy component (458.5 eV) is usually assigned to titanium in octahedral coordination[10] or in interaction with surface hydroxy groups. Catalyst C3 shows a large part of the titanium in octahedral coordination (Table 1). For catalyst C2, the proportion of titanium in tetrahedral sites is higher than in C3, but most of the titanium still remains in octahedral coordination (Table 1). Catalysts C1 and TS-1 exhibit a titanium peak in tetrahedral coordination that is clearly more intense than the lowest binding energy component. This indicates that titanium ions are in a very similar environment in catalysts C1 and TS-1, although the synthesis route of silica-supported titanium catalyst (C1) is considerably easier than that for the Ti-silicalite sample. Both DRS UV–VIS and XPS spectroscopic techniques pointed to the necessity of carefully controlling the incorporation of titanium into silica (preparation of C1 in cyclohexanol) to obtain titanium in tetrahedral coordination. This is due to the fact that cyclohexanol interacts strongly with the titanium precursor which favours the formation of isolated titanium species, and also that only a fraction of the titanium added is incorporated as a consequence of the equilibrium of adsorption.

These catalysts were tested in the epoxidation of alkenes with dilute aqueous hydrogen peroxide solutions. Epoxidation was performed under ambient pressure in a round-bottomed flask equipped with a condenser and magnetic stirrer. The reaction procedure was as follows: 0.2 mol of alkene, 11 g of *tert*-butyl alcohol and 1 g of catalyst were stirred and heated to the reaction temperature (353 K). Then, 4 g of a dilute solution of hydrogen peroxide (6 wt% in 1-phenylethanol) was added dropwise under stirring over 2 h. Aliquots were taken at regular intervals. H_2O_2 consumption was evaluated by iodometric titration, and organic compounds were analysed by GC to determine their selectivity. The results are summarised in Table 2. The reference catalyst TS-1 showed low selectivity values towards epoxide, which is consistent with the requirement of the presence of methanol to obtain high selectivity values.[11] The method for preparing silica-supported titanium had a strong effect on performance for the epoxidation of oct-1-ene. The TiF/SiO_2 catalyst showed similar conversion and selectivity values to those reported in previous work,[6] but lower than those of TS-1. Catalysts C3 and C2 showed very low selectivity towards epoxide, in agreement with the high proportion of octahedrally coordinated titanium, as revealed by DRS UV–VIS and XPS spectroscopic techniques. Nevertheless, catalyst C1 had very high (95%) selectivity values towards epoxide, related to the high proportion of titanium in tetrahedral coordination as revealed by the DRS UV–VIS technique, and specifically by XPS spectroscopy. Finally, catalyst C1 also displayed very good performance in the epoxidation of bulky alkenes with hydrogen peroxide. In cyclohexene and norbornene, 91 and 98% selectivity towards epoxide, respectively, were reached. Used catalyst C1 was analysed and the Ti content found to be the same as in the fresh sample, thus excluding leaching.

Table 2 Data for alkene epoxidation with hydrogen peroxide after 1 h of reaction (T = 353 K)

Catalyst	Alkene	Conversion of H_2O_2 (%)	Selectivity to epoxide[a] (%)
TS-1	Oct-1-ene	96	70
TiF/SiO_2	Oct-1-ene	75	65
C3	Oct-1-ene	96	32
C2	Oct-1-ene	97	56
C1	Oct-1-ene	97	95
C1	Cyclohexene	98	91
C1	Norbornene	98	98

[a] Selectivity to epoxide = mol of epoxide formed/mol of H_2O_2 consumed.

In short, using a very simple route, we have prepared titanium-supported amorphous silica catalysts in which the chemical environment of titanium atoms is very similar to Ti-substituted zeolites. The use of cyclohexanol is pivotal to the production of very active and selective catalysts in the reaction of alkene epoxidation with hydrogen peroxide. These catalysts also display excellent performance with linear as well as larger or bulky alkenes.

Notes and references

1 M. Taramaso, G. Perego and B. Notari, *US Pat.*, 4410501, 1983.
2 P. J. Saxton, W. Chester, J. G. Zajacek, G. L. Crocco and K. S. Wijesekera, *US Pat.*, 5621122, 1997.
3 J. S. Reddy, A. Dicko and A. Sayari, *Chem. Ind.*, 1997, **69**, 405.
4 H. P. Wulff, *US Pat.*, 3923843, 1975; M. Tamura, K. Yamauchi and K. Uchida, *Eur. Pat.*, 734764, 1996.
5 J. M. Fraile, J. I. Garcia, J. A. Mayoral, L. C. De Menorval and F. Rachdi, *J. Chem. Soc., Chem. Commun.*, 1995, 539.
6 E. Jorda, A. Tuel, R. Teissier and J. Kerneval, *J. Chem. Soc., Chem. Commun.*, 1995, 1775.
7 J. M. Campos-Martin and M. P. de Frutos, WO9948884, 1999.
8 E. Astorino, J. B. Peri, R. J. Willey and G. Busca, *J. Catal.*, 1995, **157**, 482.
9 F. Geobaldo, S. Bordiga, A. Zecchina, E. Giamello, G. Leofanti and G. Petrini, *Catal. Lett.*, 1992, **16**, 109.
10 T. Blasco, M. A. Camblor, J. L. G. Fierro and J. Perez-Pariente, *Microporous Mater.*, 1994, **3**, 259.
11 M. G. Clerici, G. Bellussi and U. Romano, *J. Catal.*, 1991, **129**, 159.

ChemComm

Structural studies of supramolecular β-cyclodextrin complexes with butyrophenone and valerophenone: an explanation for photochemical reaction modification†‡

Tom J. Brett and John J. Stezowski*

Department of Chemistry, University of Nebraska-Lincoln, Lincoln, Nebraska 68588-0304, USA.
E-mail: jstezowski1@unl.edu
Center for Materials Research and Analysis, University of Nebraska-Lincoln, Lincoln, Nebraska 68588-0113, USA

Received (in Columbia, MO, USA) 31st March 2000, Accepted 5th April 2000

X-Ray crystallographic studies of β-cyclodextrin (β-CD) inclusion complexes with butyrophenone and valerophenone characterize these complexes as 2:2 β-CD/guest systems with the alkyl chains of the included guest molecules conformationally restricted; the structures explain the reported observation of the modification of the Norrish type II photoreaction for the included aryl alkyl ketones in crystalline β-CD complexes.

The use of controlling media to modify the outcome of photochemical reactions has been an active area of research since the late 1970s.[1] Understanding how the controlling media changes the outcome of a reaction is important for designing future experiments in which a specific outcome is desired. X-Ray crystallography represents a powerful tool for observing these influences at a molecular level.

β-Cyclodextin (β-CD), a cyclic oligomer composed of seven D-glucose units, is an example of one such host system in which the outcome of photochemical reactions, *e.g.* the photoreaction of aryl alkyl ketones, can be modified.[2] This Norrish Type II photochemical process involves photoexcitation of the carbonyl group and has been rigorously examined for aryl alkyl ketones.[3–5] They undergo γ-hydrogen abstraction exclusively from the $(n\pi^*)^3$ state yielding a triplet 1,4-diradical as the primary intermediate (Scheme 1). Once the 1,4-diradical is formed, intersystem crossing produces the singlet diradical which then reacts *via* one of two pathways. Overlap of radical orbitals leads to cyclization (C), producing cyclobutanols. The elimination pathway (E) involves cleavage of the central 2,3 σ bond producing acetophenone and alkenes.

The use of β-CD as a controlling media for modifying the outcome of the Norrish Type II photoreaction of aryl alkyl ketones in the solid state has been reported.[6] In these studies, crystalline powder samples of β-CD complexes with various aryl alkyl ketones were prepared and their photochemical reactions analyzed. The general observation was that inclusion in β-CD lead to an increase in cyclization products (as compared to solution phase studies), and this trend became more pronounced as the alkyl chain became longer. In an effort to determine how the β-CD environment influences the outcome of the photoreaction of the included aryl alkyl ketones,[7] crystallographic studies were pursued. This report presents the structures of the β-CD/butyrophenone inclusion complex and the β-CD/valerophenone inclusion complex.

The two crystal structures are very similar.[8] Both are composed of face-to-face β-CD dimers containing two included aryl alkyl ketone molecules with the β-CD dimers packing in a channel[9] (Fig. 1). The guest molecules are packed with their phenyl rings face-to-face located in the center of the β-CD dimer. This leaves the alkyl chains of the ketones extending to the primary hydroxy ends of the β-CD dimer.

Examination of the structures reveals the influence the β-CD dimer environment has on the observed reaction outcomes. Although defined conformations for the included guest molecules could not be unequivocally obtained because of disorder,

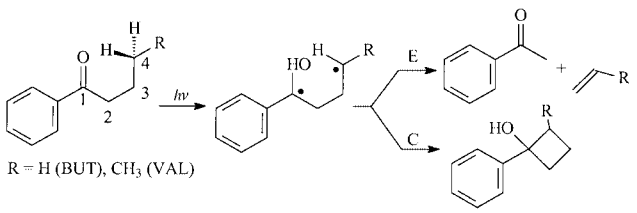

Scheme 1 Reaction scheme of the Norrish Type II reaction for butyrophenone (BUT) and valerophenone (VAL). Atom numbering shown pertains to text discussion.

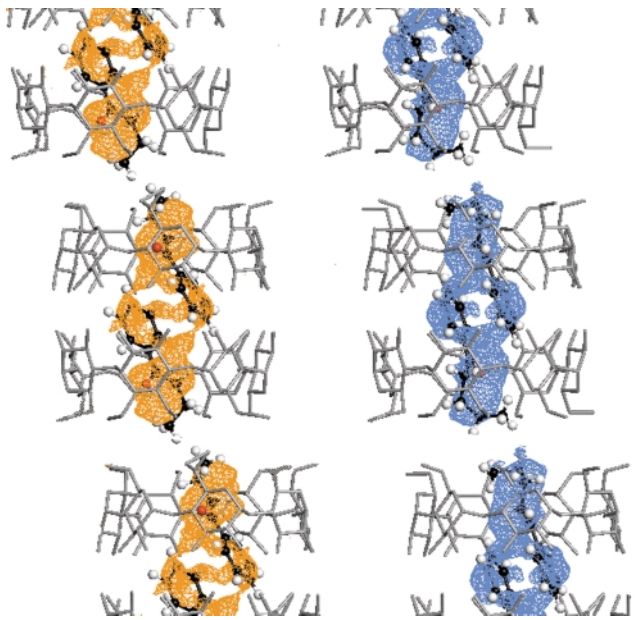

Fig. 1 Structures of the β-CD/butyrophenone (left) and β-CD/valerophenone (right) inclusion complexes. β-CD is shown as gray sticks while the guest molecules are shown in ball and stick with coloring as follows: red = oxygen; white = hydrogen; black = carbon. The difference electron density ($F_o - F_c$) the disordered guest molecules were fit to is shown in orange (β-CD/butyrophenone) and blue (β-CD/valerophenone).

† Electronic supplementary information (ESI) available: full experimental details. See http://www.rsc.org/suppdata/cc/b0/b00282m/

‡ Chemical Insight from Crystallographic Disorder–Structural Studies of Supramolecular Photochemical Systems, Part 4; Part 3, T. J. Brett, J. M. Alexander and J. J. Stezowski, *J. Chem. Soc., Perkin Trans. 2*, 2000, in press.

DOI: 10.1039/b002828m

the interpretation of this disorder does reveal some relevant conformational restrictions. With the molecules included in the β-CD dimer with the phenyl rings packing face-to-face in the center, the alkyl chains must take on a cisoid conformation about the 2,3-bond. This helps bring a γ-hydrogen into close proximity with the carbonyl oxygen, as would be required for its abstraction.[10]

Once a γ-hydrogen is abstracted, the resultant 1,4-diradical is most surely conformationaly restricted by the β-CD dimer environment. It is well established that efficient cleavage requires a 1,4-diradical conformation in which the radical p orbitals can overlap significantly with the central σ bond being cleaved. If this does not happen, cyclization occurs from a conformation involving minimal orbital overlap.[11,12] Given these requirements, cyclization can only occur from a cisoid conformation of the 1,4-diradical while elimination can occur from either cisoid or transoid forms. With the phenyl rings of the molecules packed tightly in the center of the β-CD dimer, any such rotation must occur at the alkyl chain end of the molecule. Given the boundaries imposed by the β-CD dimer, the alkyl chains are not be able to undergo free rotations to transoid geometries.

The fashion in which the β-CD dimers pack also plays a role in the reaction modification. The observed channel type packing brings the alkyl chains of included molecules in adjacent β-CD dimer cavities within close proximity. Extension of the alkyl chain by one methyl group, *i.e.* going from butyrophenone to valerophenone, effectively stuffs the channel more tightly, limiting the allowed motion of the alkyl chain even more. This hindered motion accounts for the observed increase in cyclization products with increasing alkyl chain length.

The β-CD complexes with butyrophenone and valerophenone can be considered as 'reaction nanotubes' much akin to the β-CD/coumarin complex.[13] The mode of inclusion of the guest molecules produces conformational restrictions for the alkyl chains imposed by the surrounding β-CD dimer walls and intratube packing. Said restrictions produce cisoid conformations about the central 2,3-bond which will allow for the γ-hydrogen abstraction. The 1,4-diradical produced is also conformationally hindered in this manner and additionally restricted because of interactions between molecules in adjacent dimer cavities in the channel. This effect becomes more pronounced as the alkyl chain length is increased and is a contributing factor in the observed increase in cyclization products with increasing alkyl chain length. Further studies of inclusion complexes with aryl alkyl ketones possessing longer alkyl chains (*e.g.* hexanophenone, heptanophenone and ocatanophenone) will shed more light on this affect and are in progress.

Partial funding for this work was provided by the NSF (CHE-9812146). We thank Cerestar USA, Inc. (Hammond, IN) for samples of β-CD.

Notes and references

1 V. Ramamurthy, in *Photoprocesses of Host–Guest Complexes in the Solid State*, ed. V. Ramamurthy, VCH, New York, 1991.
2 V. Ramamurthy, *Tetrahedron*, 1986, **42**, 5753.
3 P. J. Wagner, *Acc. Chem. Res.*, 1971, **4**, 168.
4 N. J. Turro, J. C. Dalton, K. Dawes, G. Farrington, R. Hautala, D. Morton, M. Niemczyk and N. Shore, *Acc. Chem. Res.*, 1971, **5**, 92.
5 J. C. Scaiano, *Acc. Chem. Res.*, 1982, **15**, 252.
6 G. D. Reddy, B. Jayasree and V. Ramamurthy, *J. Org. Chem.*, 1987, **52**, 3107.
7 Since the study in ref. 6 was conducted on powder crystalline samples, it was necessary to verify that the elimination and cyclization processes occurred in our crystals. This was done as follows: photolyzed inclusion complex crystals were dissolved in water and the included compounds (unreacted ketones and photoproducts) were extracted with CH_2Cl_2. Analysis of the extraction mixtures by GC–MS and TLC revealed three components: the unreacted ketones, a cyclobutanol (C product) and acetophenone (E product). Full details are available as ESI.†
8 For both complexes, the methods of X-ray diffraction data collection and structure determination and refinement were similar and will be summarized here. Full details are available in the .cif file. Data were collected at room temperature on crystals sealed in glass capillaries using an automated Siemens P4 diffractometer with a sealed tube Mo target source. For the β-CD/butyrophenone complex, 6708 unique reflections (R_{int} = 0.0306) were collected to $2\theta_{max}$ = 50°. For the β-CD/valerophenone complex, 11163 unique reflections (R_{int} = 0.0241) were collected to $2\theta_{max}$ = 60°. For both structures, the phase problem was solved by molecular replacement of the β-CD coordinates from the isomorphous β-CD/coumarin complex (ref. 13). Difference electron density maps revealed the guest molecules were very disordered in both cases. The disorder was interpreted as phenyl ring face-to-face packing of the guest molecules with identically packing pairs distributed over multiple sites. Least-squares refinement on F^2 was carried out using SHELXL97 (G. M. Sheldrick, SHELXL97. Program for the Refinement of Crystal Structures. University of Göttingen, Germany, 1997). *Crystal data*: for $C_{42}H_{70}O_{35}{\cdot}C_{10}H_{12}O{\cdot}11.5H_2O$, M_r = 1490.36, monoclinic, space group *C*2 (no. 5), a = 19.352(2), b = 24.599(2), c = 15.916(2) Å, β = 109.378(7)°, Z = 4, D_c = 1.385 g cm^{-3}, crystal size 0.7 × 0.5 × 0.4 mm. Final refinement details: 923 parameters, R_1 = 0.0668, wR_2 = 0.1748 and GOF = 1.052 for 5202 reflections with $F_o > 4\sigma(F_o)$. For $C_{42}H_{70}O_{35}{\cdot}C_{11}H_{14}O{\cdot}11H_2O$, M_r = 1495.38, monoclinic, space group *C*2 (no. 5), a = 19.339(2), b = 25.581(1), c = 16.010(2) Å, β = 109.080(7)°, Z = 4, D_c = 1.327 g cm^{-3}, crystal size 0.6 × 0.4 × 0.4 mm. Final refinement details: 907 parameters, R_1 = 0.0915, wR_2 = 0.2504 and GOF = 1.020 for 6425 reflections with $F_o > 4\sigma(F_o)$. CCDC 182/1595. See http://www.rsc.org/suppdata/cc/b0/b002828m/ for crystallographic files in .cif format.
9 D. Mentzafos, I. M. Mavridis, G. LeBas and G. Tsoucaris, *Acta Crystallogr., Sect. B*, 1991, **47**, 746.
10 See: H. Immels and J. R. Scheffer, *Tetrahedron*, 1999, **55**, 885 and references therein.
11 F. D. Lewis and D. Hillard, *J. Am. Chem. Soc.*, 1972, **94**, 3852.
12 P. J. Wagner, P. A. Kelso, A. E. Kemppainen, J. M. McGrath, H. N. Schott and R. G. Zepp, *J. Am. Chem. Soc.*, 1972, **94**, 7506.
13 T. J. Brett, J. M. Alexander, J. L. Clark, C. R. Ross, II, G. S. Harbison and J. J. Stezowski, *Chem. Commun.*, 1999, 1275.

ChemComm

Characterization of a well resolved supramolecular ice-like $(H_2O)_{10}$ cluster in the solid state†

Leonard J. Barbour, G. William Orr and Jerry L. Atwood*

Department of Chemistry, University of Missouri-Columbia, Columbia, Missouri 65211, USA.
E-mail: atwoodj@missouri.edu

Received (in Cambridge, UK) 7th March 2000, Accepted 30th March 2000

The conformation of a previously observed ice-like water cluster in the solid state proves to be robust to geometric changes in its surroundings and the hydrogen bonded arrangement is finally revealed in detail.

Water clusters can play an important role in the stabilization of supramolecular systems both in solution and in the solid state and there is clearly a need for a better understanding of how such aggregates influence the overall structure of their surroundings.[1–5] In this context, we recently characterized a solid-state structure of a $[Cu_2(H_2O)_4L_4]\cdot nH_2O$ complex **1** (Scheme 1) featuring an $(H_2O)_{10}$ cluster with an ice I_c-like arrangement of the water molecules.[6] At the time, owing to inherently poor crystal quality and the lack of low temperature X-ray data collection capability, the structure was only modestly resolved and several important points remained to be addressed. First, although the positions of the water molecules constituting the decameric cluster were determined unequivocally, the water hydrogen atoms were never located. While an ordered arrangement of these hydrogen atoms was inferred from the discontinuous nature of the cluster (in contrast to the disordered hydrogen arrangement in the continuous ice lattice[7]), we were not able to verify this conjecture experimentally. Second, disorder of the contents of the macrocyclic cage, coupled with poor resolution, precluded us from determining the composition of the interior of the cage with sufficient certainty. Third, it was not known to what extent the geometry of the water cluster would be affected by relatively small changes in the overall geometry of the system (*e.g.* substitution of Cu by Ni or Co). We now present a new, well resolved low-temperature crystal structure that addresses all of the above issues satisfactorily.

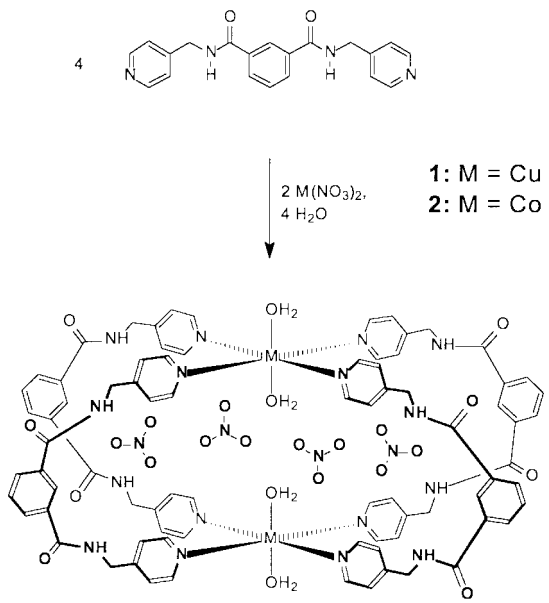

Scheme 1

Since the metal ion of the Cu^{2+} complex exhibits Jahn–Teller distortion along the M···M vector that also passes through the center of the water cluster, we decided to introduce a slight geometric change to the system by substituting cobalt for copper. Crystals of **2** were grown as previously described[6] and the sngle crystal X-ray structure‡ is discussed below. While the cage complex in **2** is remarkably similar to that of **1**, the extended structures of the two systems are slightly different as evidenced by the unit cell information given in Table 1.

Both structures consist of linear arrays of the dinuclear cage complex (aligned parallel to the M···M axis) with the water cluster effectively acting as an exo-bidentate bridging ligand. Each of these arrays is surrounded by four identical arrays that are offset by half a structural unit along the M···M vector. This staggered arrangement of the globular cage molecules results in the formation of relatively large voids which are occupied by the decameric water clusters.

Fig. 1 shows selected portions of the two structures overlaid in order to illustrate the major differences between them. In the structure of **1**, successive cages are related to one another by $\bar{4}$ site symmetry and, accordingly, the orientation of the ligand amide groups alternates from one cage to the next within each strand. However, successive cages in **2** are related to one another by a simple unit cell translation and all the ligand arms therefore have the same orientation within a linear strand. Note that the cage complexes of **1** and **2** shown at bottom are almost identical in geometry with their M···M distances differing by only 0.441 Å [Cu···Cu 9.582(7) Å, Co···Co 9.141(4) Å].

Fig. 2 shows the arrangement of the water cluster in **2**. The distance across the decamer from O(1W) to O(4W) is 6.287(4) Å (*cf.* 6.35 Å in ice I_c)[7] while the corresponding distance in **1** is 5.65 Å [average of two unique distances: 5.779(7) and 5.512(7) Å]. This difference of about 0.6 Å in the length of the water cluster along the M···M vector is attributed to the longer M–O coordination bond in the Cu complex (average Cu–O 2.33 Å, average Co–O 2.10 Å). This clearly demonstrates that the flexibility of its internal hydrogen bonds allows the cluster to adjust its geometry in response to small changes in its environment and that the overall ice-like conformation is quite robust to such changes. All of the water hydrogen atoms were

Table 1 Unit cell parameters for $[M_2L_4(H_2O)_4](NO_3)_4\cdot 16H_2O$

	1	**2**
M	Cu^{2+}	Co^{2+}
T/°C	20	−100
Crystal system	Tetragonal	Monoclinic
Space group	$I4_1/a$	$C2/c$
Unit cell dimensions		
a/Å	21.9265(8)	21.886(1)
b/Å	21.9265(8)	19.623(1)
c/Å	39.754(2)	22.170(1)
β/°	—	90.886(1)

† Electronic supplementary information (ESI) available: thermal ellipsoid plots and labeling schemes for **2**. See http://www.rsc.org/suppdata/cc/b0/b001862g/

DOI: 10.1039/b001862g

located in difference electron density maps and the hydrogen bonded arrangement is indeed as inferred in our report of the structure of complex **1** (see .cif file for distances and angles relating to hydrogen bonds). The water cluster is situated on a two-fold rotation axis passing through O(1W) and O(4W) and only half of the remaining water molecules are crystallographically unique. O(1W) donates hydrogen bonds to O(9W) which in turn donates to O(8W) and O(10W). Similarly, O(4W) donates to O(7W) which also donates to O(8W) and O(10W). O(8W) and O(10W) each donates a hydrogen bond to a nitrate oxygen atom as well as to an amide oxygen atom from a cage complex of a neighboring strand. With the exception of O(7W) and O(9W), all water hydrogen atoms participate in the formation of four relatively strong hydrogen bonds. The closest non-covalent approach of any atoms to O(7W) and O(9W) are by the amide nitrogen atoms N(8B) and N(8A) of neighboring strands at distances of 3.549(4) and 3.357(4) Å, respectively. These distances are too long to be considered appreciably strong hydrogen bonds and are due to steric effects that inhibit a closer approach.

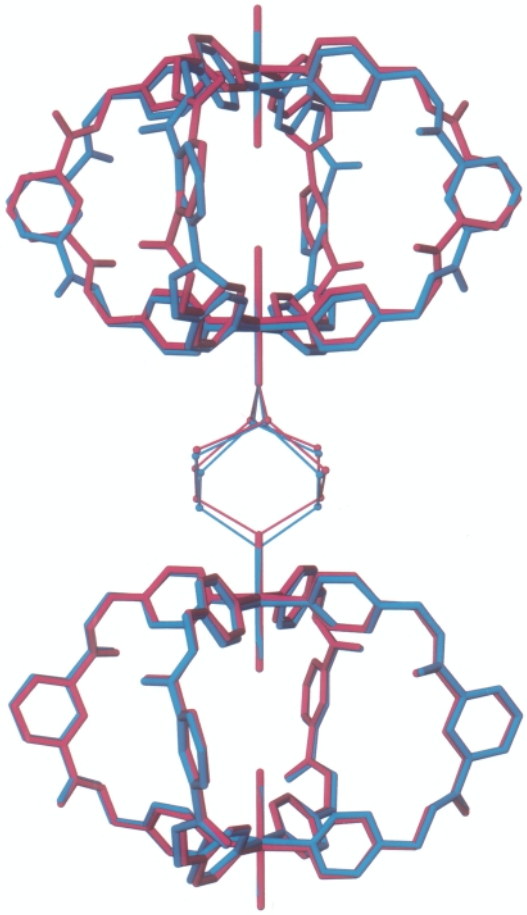

Fig. 1 Overlay of structures **1** (red) and **2** (blue) showing two cage complexes linked by an $(H_2O)_{10}$ water cluster.

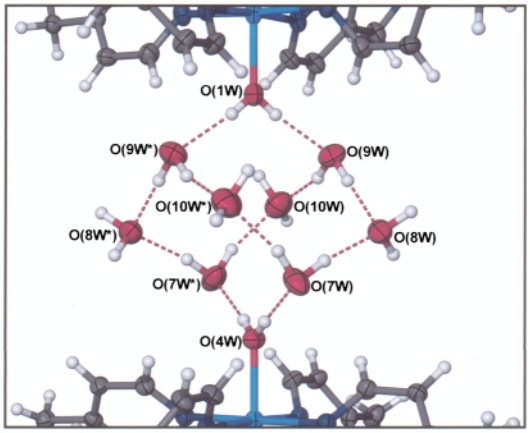

Fig. 2 Thermal ellipsoid (50% probability) plot of the water cluster in **2**. Asterisks within atom labels denote symmetry equivalent atoms.

The structure of **1** had not been determined with sufficiently high resolution to reveal with certainty the contents of the cage complex. Although **1** was modeled with six water molecules in the cage, it was thought that at least another two water molecules resided within the arms of the ligand. However, the low-temperature structural determination of **2** shows unequivocally that the interior of the cage complex does indeed consist of four nitrate anions and six water molecules. Two of the latter are coordinated to the metal cations and form hydrogen bonded contacts with the remaining four water molecules which, in turn, hydrogen bond to the nitrate oxygen atoms and this intricate hydrogen bonded arrangement imparts a high degree of rigidity to the cage interior.

We are grateful for funding from the National Science Foundation.

Notes and references

‡ *Crystal data* for **2**: $C_{80}H_{104}Co_2N_{20}O_{36}$: M = 2039.69, dark blue prismatic crystal, 0.30 × 0.30 × 0.20 mm, monoclinic space group $C2/c$ (no. 15), a = 21.8855(11), b = 19.6232(10), c = 22.1697(11) Å, β = 90.886(1), Z = 4, V = 9519.9(8) Å^3, D_c = 1.423 g cm^{-3}, Bruker SMART CCD diffractometer, Mo-Kα radiation, λ = 0.7107 Å, T = −100 °C, $2\theta_{max}$ = 54.3°, 29439 reflections collected, 10498 unique (R_{int} = 0.0330). The structure was solved and refined using the programs SHELXS-97 and SHELXL-97 respectively.[8] The program X-Seed[9] was used as an interface for the SHELX programs, and to prepare the figures. Final GOF = 1.071, $R1$ = 0.0673, $wR2$ = 0.1857, R indices based on 7050 reflections with $I > 2\sigma(I)$ (refinement on F^2), 691 parameters, L_p and absorption corrections applied, μ = 0.444 mm^{-1}. All non-hydrogen atoms were refined anisotropically with the exception of those belonging to the minor component of a disordered nitrate anion. Hydrogen atoms on the ligand were placed using standard geometric models and with thermal parameters riding on those of their parent atoms. Water hydrogen atoms were located in difference electron density maps and refined with nominal geometric restraints. CCDC 182/1590. See http://www.rsc.org/suppdata/cc/b0/b001862g/ for crystallograpic files in .cif format.

1 R. E. Dehl and C. A. Hoeve, *J. Chem. Phys.*, 1969, **50**, 3245.
2 C. Migchelsen, H. J. C. Berendsen and A. Rupprecht, *J. Mol. Biol.*, 1968, **37**, 235.
3 F. Steckel and S. Szapiro, *Trans. Faraday Soc.*, 1963, **59**, 331.
4 S. D. Colson and T. H. Dunning, *Science*, 1994, **265**, 43.
5 K. Liu, J. D. Cruzan and R. J. Saykally, *Science*, 1996, **271**, 929.
6 L. J. Barbour, G. W. Orr and J. L. Atwood, *Nature*, 1998, **393**, 671.
7 H. König, *Z. Kristallogr.*, 1944, **105**, 279.
8 G. M. Sheldrick, SHELX-97: Structure solution and refinement programs, University of Göttingen, 1997.
9 L. J. Barbour, X-Seed: Graphical interface to SHELX-97 and POV-Ray, 1999 (http://www.lbarbour.com/xseed).

Formation of giant vesicles from diacylmannosylerythritols, and their binding to concanavalin A†

Dai Kitamoto,*[a] Sangita Ghosh,[b] Guy Ourisson[b] and Yoichi Nakatani*[b]

[a] *National Institute of Materials and Chemical Research, 1-1 Higashi, Tsukuba, Ibaraki 305-8565, Japan. E-mail: kitamoto@nimc.go.jp*

[b] *Laboratoire de Chimie Organique des Substances Naturelles, Associé au CNRS, Centre de Neurochimie, Université Louis Pasteur, 5 rue Blaise Pascal, F-67084 Strasbourg, France. E-mail: nakatani@chimie.u-strasbg.fr*

Received (in Liverpool, UK) 3rd February 2000, Accepted 11th April 2000

The structures of diacylmannosylerythritols, MEL-A, -B and -C, are determined; these microbial glycolipid biosurfactants efficiently self-assemble in water to form giant vesicles, which show excellent binding affinity towards the mannose-binding protein, concanavalin A.

The 'diacyl-mannosylerythritol' lipids (MELs) are very promising 'biosurfactants',[1] owing to their attractive properties (*e.g.* easy production conditions, low toxicity, biodegradability, biological activity) compared to most synthetic surfactants. MELs are abundantly produced by the yeast strain *Candida antarctica* T-34,[2a] and mainly consist of three components: MEL-A, -B and -C.[2b] These yeast glycolipids show not only excellent surface-activity[2c] but also remarkable cell differentiation and growth inhibition activities against human leukemia[2d] and mouse melanoma cells.[2e] On the other hand, glycolipids have received much attention as leading materials for drug-carrying microcapsules and artificial cells,[3] owing to their stabilizing effect on liposomes.[4] Finally, glycolipids also carry out vital functions in biomembranes, *e.g.* cell recognition, histocompatibility, antigenicity, and are of particular interest in studying surface recognition processes.[4c,5]

Here we report the complete structural characterization of the MEL glycolipids (MEL-A, -B and -C). We also describe, for the first time the spontaneous formation of giant vesicles from each of these glycolipids; finally, we show that these giant vesicles show an excellent binding affinity towards a mannose-binding protein, concanavalin A (Con A).

The three MELs consist of 4-*O*-[β-D-mannopyranosyl] *meso*-erythritol, esterified by two medium-chain fatty acids (C_8 to C_{12}) and one or two acetic acids; the individual esterified positions, however, remained to be determined precisely.[2b] Further structural characterization of the MELs was thus carried out. The mixture of MELs was obtained as reported previously,[2a] and purified by silica-gel column chromatography with modifications of the elution conditions.

The esterified positions of the individual acetyl and acyl groups on the mannosyl back-bone were determined by ^{1}H and ^{13}C 2D NMR ($CDCl_3$, 500 MHz) (Fig. 1). HMBC (heteronuclear multiple bond connectivity) long-range correlations ($^3J_{C-H}$) between the carbonyl carbons of the acyl groups and H-2′ and H-3′ of mannose were clearly observed on all the MELs,‡ indicating that the fatty acids are linked to the hydroxy groups at C-2′ and C-3′ of mannose. $^3J_{C-H}$ correlations between the acetyl carbons (δ_{CO} 169.6 and 170.9) and the mannose protons ($\delta_{H\text{-}4'}$ 5.24 and $\delta_{H\text{-}6'}$ 4.23), respectively, were observed exclusively on MEL-A, which was thus shown to be 4-*O*-[(4′,6′-di-*O*-acetyl-2′,3′-di-*O*-alkanoyl)-β-D-mannopyranosyl] *meso*-erythritol. On the other hand, a $^3J_{C-H}$ correlation between the acetyl carbon (δ_{CO} 171.8) and H-6′ (δ 4.44) was observed with MEL-B, while a correlation between the acetyl carbon (δ_{CO} 170.1) and H-4′ (δ 5.16) was observed only with MEL-C. From these results, MEL-B and -C were shown to be 4-*O*-[(6′-*O*-acetyl-2′,3′-di-*O*-alkanoyl)-β-D-mannopyranosyl] *meso*-erythritol and 4-*O*-[(4′-*O*-acetyl-2′,3′-di-*O*-alkanoyl)-β-D-mannopyranosyl] *meso*-erythritol, respectively. It was also confirmed that none of the three hydroxy groups in the erythritol moiety is esterified in any of the MELs.

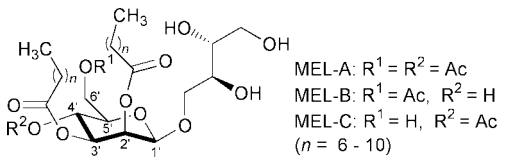

Fig. 1 Structure of diacylmannosylerythritols.

Membrane-forming properties of these MELs were then examined by phase contrast microscopy. All the MELs, when dispersed in water (pH 7.0) at 25 °C, spontaneously formed giant vesicles.§ Unilamellar vesicles of diameter larger than 10 μm were observed, beside multilamellar structures and tubules. Vesicle formation was confirmed by fluorescence microscopy, after addition of the lipophilic fluorescent probe Nile Red to the pre-formed vesicles (5 mol% to MEL) (Fig. 2). Some synthetic and natural glycolipids bearing a disaccharide or larger hydrophilic head group have been reported to form by themselves vesicular systems;[3] however, with the only exception of rhamnolipids,[3e] microbial glycolipids do not appear to have been reported to do the same.

Formation of giant vesicles should lead to surfaces covered by the multiantennary mannopyranoside residues, which could act as high affinity receptors for mannose-binding proteins. We therefore investigated the interaction between these giant vesicles and concavalin A. Succinyl Con A,[6] labeled with a fluorescence probe (FITC), was dissolved in a phosphate buffer

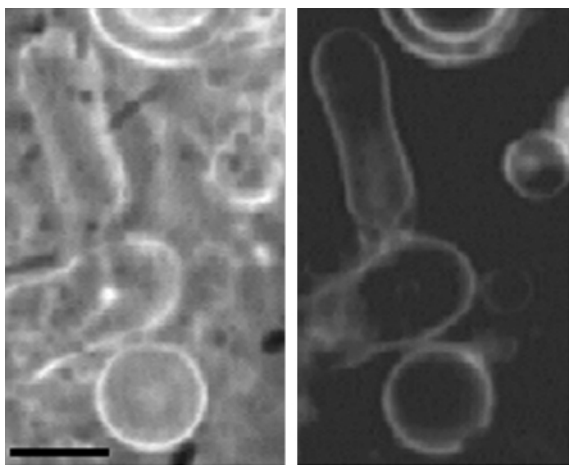

Fig. 2 Phase contrast (left) and fluorescence (right) microscope images of MEL-C giant vesicles stained with Nile Red. The bar represents 10 μm.

† Electronic supplementary information (ESI): preparation, optical microscopy details and NMR data for MELs. See http://www.rsc.org/suppdata/cc/b0/b000968g/

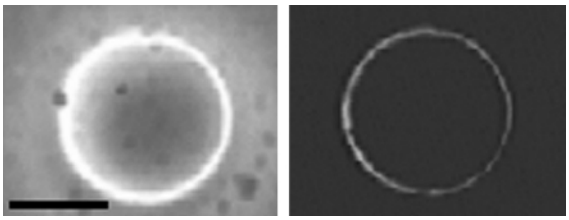

Fig. 3 Phase contrast (left) and fluorescence (right) microscope images of MEL-B giant vesicles coated with FITC-labeled concanavalin A. The bar represents 10 μm.

(pH 7.0) and added to the pre-formed vesicles, and were observed under fluorescence microscope. With MEL-B and -C vesicles, a clear fluorescent ring was observed around the outer edge of the vesicle. This clearly indicates the recognition by the fluorescence labeled Con A of the mannose residues of the glycolipid head-groups that are located on the vesicular surface (Fig. 3). The coating, as judged by the abundance of fluorescent vesicles, appeared to be efficient on the giant vesicles of MEL-B and -C; however, no clear coating was observed on those made of MEL-A.

Interactions of Con A with disk-like assemblies[4c] or small vesicles[5] of synthetic glycolipids have been previously reported. However, these small lipidic assemblies showed a tendency to aggregate and precipitate when treated with Con A, presumably due to interactions of one ConA molecule with several lipidic systems.[5,7] In the case of giant vesicles of MEL-B and -C, coating of the outer surface was not accompanied by aggregation and precipitation : the giant vesicles presumably provide a very large surface relative to the molecular size of Con A, which probably impedes the binding of the lectin to more than one vesicle at the same time, and thus aggregation does not occur.

In addition, most of the carbohydrate–receptor interactions observed are weak,[8] and in order to compensate for this low binding affinity, different strategies based on multivalent interactions have been designed, including carbohydrate clusters, glycopolymers and glycodendrimers.[5c,9] Our work describes yet another way of enhancing the interaction between a receptor (Con A) and a carbohydrate moiety (mannose), which is based on the spontaneous self-assembly of the glycolipids onto vesicles, thereby generating a multivalent surface. It should be noted that only the giant vesicles prepared from MEL-B and -C, both of which carry a free OH at C-4′ or C-6′, bind efficiently with Con A. There must therefore be a specific mode of binding, like multivalent interactions, on the vesicular surface, because Con A mainly recognizes and binds to the hydroxy groups at C-3′, C-4′ and C-6′ in D-mannose or D-glucose.[10]

We thank Dr R. Graf for NMR experiments, and Drs K. Haraya and H. Yanagishita, National Institute of Materials and Chemical Research, Japan, for helpful discussions.

Notes and references

‡ The following correlations ($^3J_{C-H}$) were observed between the carbonyl carbon of acyl groups and mannose protons: MEL-A, (δ_{CO} 173.8 and $\delta_{H\text{-}2'}$ 5.51) and (δ_{CO} 172.9 and $\delta_{H\text{-}3'}$ 5.06); MEL-B, (δ_{CO} 173.8 and $\delta_{H\text{-}2'}$ 5.49) and (δ_{CO} 173.7 and $\delta_{H\text{-}3'}$ 4.91); MEL-C, (δ_{CO} 173.6 and $\delta_{H\text{-}2'}$ 5.50) and (δ_{CO} 172.8 and $\delta_{H\text{-}3'}$ 5.09).

§ A typical procedure was as follows: MEL (10 mg) was dissolved in 1 mL of a 2:1 mixture of chloroform and methanol. An aliquot (5–10 μL) of the solution was dropped on a glass microscope slide with a well of 15 mm diameter. After 10 min drying (argon flow), 0.5 mL of water or a buffer (137 mM NaCl, 2.7 mM KCl, 4.3 mM Na_2HPO_4, 1.4 mM KH_2PO_4, pH 6.98) was added to the film, and the slide was incubated for 30 min at 25 °C to allow lipid hydration. Optical (phase contrast) and fluorescence microscopies were carried out according to the procedures described in ref. 11.

This showed unilamellar and multilamellar vesicles (diameter > 10 μm) as well as tubules. This was confirmed by the fluorescence observed after addition of Nile Red (5 mol%/MEL) to the pre-formed vesicle suspension.

The vesicles observed retained their structures at room temperature for at least 2 days.

1 J. D. Desai and I. M. Banat, *Microbiol. Mol. Biol. Rev.*, 1997, **61**, 47; S.-C. Lin, *J. Chem. Tech. Biotechnol.*, 1996, **66**, 109; I. M. Banat, *Acta Biotechnol.*, 1995, **15**, 251.

2 (*a*) D. Kitamoto, H. Yangishita, K. Haraya and H. K. Kitamoto, *Biotechnol. Lett.*, 1998, **20**, 813; (*b*) D. Kitamoto, S. Akiba, T. Hioki and T. Tabuchi, *Agric. Biol. Chem.*, 1990, **54**, 31; (*c*) D. Kitamoto, H. Yanagishita, T. Shinbo, T. Nakane, T. Nakahara and C. Kamisawa, *J. Biotechnol.*, 1993, **29**, 91; (*d*) H. Isoda, H. Shinmoto, D. Kitamoto, M. Matsumura and T. Nakahara, *Lipids*, 1997, **32**, 263; (*e*) X. Zhao, Y. Wakamatsu, M. Shibahara, N. Nomura, C. Geltinger, T. Nakahara, T. Murata and K. K. Yokoyama, *Cancer Res.*, 1999, **59**, 482.

3 (*a*) T. Endo, K. Inoue and S. Nojima, *J. Biochem.*, 1983, **93**, 1; (*b*) B. Maggio, J. Albert and R. K. Yu, *Biochim. Biophys. Acta*, 1988, **945**, 145; (*c*) Y. Ishigami and H. Machida, *J. Am. Oil Chem. Soc.*, 1989, **66**, 599; (*d*) C. Guedj, B. Pucci, L. Zarif, C. Coulomb, J. G. Riess and A. A. Pavia, *Chem. Phys. Lipids*, 1994, **72**, 153; (*e*) Y. Ishigami, Y. Gama, H. Nagahora, M. Yamaguchi, H. Nakahara and T. Kamata, *Chem. Lett.*, 1987, 763.

4 (*a*) T. M. Allen, C. Hansen and J. Rutledge, *Biochim. Biophys. Acta*, 1989, **981**, 27; (*b*) S. K. Huang, K.-D. Lee, K. Hong, D. S. Friend and D. Papahadjopoulos, *Cancer Res.*, 1992, **52**, 5135; (*c*) S. Takeoka, K. Sou, T. Ohgushi and E. Tsuchida, *Supramol. Sci.*, 1998, **5**, 159.

5 (*a*) W. Curatolo, *Biochim. Biophys. Acta*, 1987, **906**, 111; (b) A. Varki, *Glycobiology*, 1993, **3**, 97; (c) R. Roy, *Trends Glycosci. Glycotechnol.*, 1996, **8**, 79.

6 G. R. Gunther, *Proc. Natl, Acad. Sci. USA*, 1973, **70**, 1012.

7 T. Suzuki, K. Inoue, S. Nojima and H. Wiegant, *J. Biochem.*, 1983, **94**, 373; R. Sundler, *FEBS Lett.*, 1982, **141**, 11; H. Bader, H. Ringsdorf and J. Skura, *Angew. Chem., Int. Ed. Engl.*, 1981, **20**, 91.

8 E. J. Toone, *Curr. Opin. Struc. Biol.*, 1994, **4**, 719; D. A. Mann, M. Kanai, D. J. Maly and L. L. Kiessling, *J. Am. Chem. Soc.*, 1998, **120**, 10 575.

9 K. Ozaki, R. T. Lee, Y. C. Lee and T. Kawasaki, *Glycoconjugate J.*, 1995, **12**, 268; A. Kichler and F. Schuber, *Glycoconjugate J.*, 1995, **12**, 275; R. Roy and J.-M. Kim, *Angew. Chem., Int. Ed.*, 1999, **38**, 369.

10 J. H. Naismith and R. A. Field, *J. Biol. Chem.*, 1996, **271**, 972.

11 F. M. Menger and S. J. Lee, *Langmuir*, 1995, **11**, 3685; F. M. Menger, S. J. Lee and J. S. Keiper, *Langmuir*, 1996, **12**, 4479; T. Ueda, S. J. Lee, Y. Nakatani, G. Ourisson and J. Sunamoto, *Chem. Lett.*, 1998, 417.

Intramolecular 1,3-dipolar cycloadditions of 2-substituted norbornadiene-tethered nitrones

Geoffrey K. Tranmer, Peter Keech and William Tam*

Guelph-Waterloo Centre for Graduate Work in Chemistry and Biochemistry, Department of Chemistry and Biochemistry, University of Guelph, Guelph, Ontario, Canada N1G 2W1. E-mail: tam@chembio.uoguelph.ca

Received (in Corvallis, OR, USA) 24th February 2000, Accepted 31st March 2000

Efficient routes for the synthesis of norbornadiene-tethered nitrones have been developed and their intramolecular 1,3-dipolar cycloadditions were found to be highly regio- and stereo-selective.

Intramolecular cycloadditions with high regio- and stereo-control are important tools for the efficient assembly of complex molecular structures. We have recently initiated a program on the study of various types of intramolecular cycloadditions of substituted norbornadienes.[1] Our long-term goal is to develop an efficient route for the construction of angular fused tricyclic frameworks and spirocyclic frameworks with high regio- and stereo-control. 1,3-Dipolar cycloadditions offer a convenient one-step route for the construction of a variety of complex five-membered heterocycles.[2,3] Here we report our initial result on the intramolecular 1,3-dipolar cycloadditions of 2-substituted norbornadiene-tethered nitrones (Scheme 1).

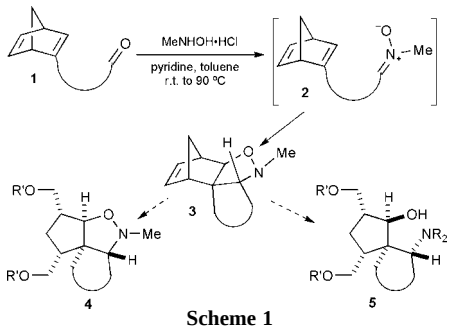

Scheme 1

Three different types of regioisomers could be formed from the intramolecular 1,3-dipolar cycloaddition of the norbornadiene-tethered nitrone **2** (Scheme 2). Cycloaddition on the C_2–C_3 double bond would give cycloadducts **6**–**9**; cycloaddition on the C_5–C_6 double bond would give **10** or **11**, and a [3 + 2 + 2] cycloaddition with both of the double bonds would give cycloadducts **12** or **13**. Other than regiochemistry problems, different stereoisomers are also possible. Thus, a total of eight possible cycloadducts (**6**–**13**) could be formed in the cycloaddition of norbornadiene-tethered nitrone **2**.

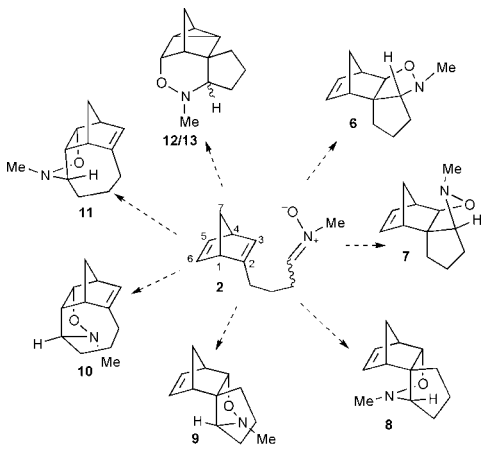

Scheme 2 Possible cycloadducts

Efficient routes to the synthesis of norbornadiene-tethered aldehydes **19**, **20**, **27**–**29** and **32** were developed (Scheme 3) and these aldehydes served as precursors of the required nitrones for the cycloadditions. Deprotonation of norbornadiene **14** with Schlosser's base (Bu^tOK/Bu^nLi)[4] in THF at −78 °C, followed by addition of the resulting norbornadienyl anion to an excess of 1,4-dibromobutane or 1,5-dibromopentane provided the norbornadiene-tethered bromide **15** and **16**.[1] Conversion of these bromides to the corresponding alcohols followed by Swern oxidation provided the required aldehydes **19** and **20**. Norbornadiene-tethered aldehydes with an oxygen atom within the tether were prepared using a similar protocol. Trapping the norbornadienyl anion with paraformaldehyde, ethylene oxide and 3-bromopropan-1-ol provided norbornadiene-tethered alcohols **21**–**23**. A two-carbon homologation to the alcohols **24**–**26** was achieved by a two-step sequence[5] and Swern oxidation provided the required aldehydes **27**–**29**. An ester functionality

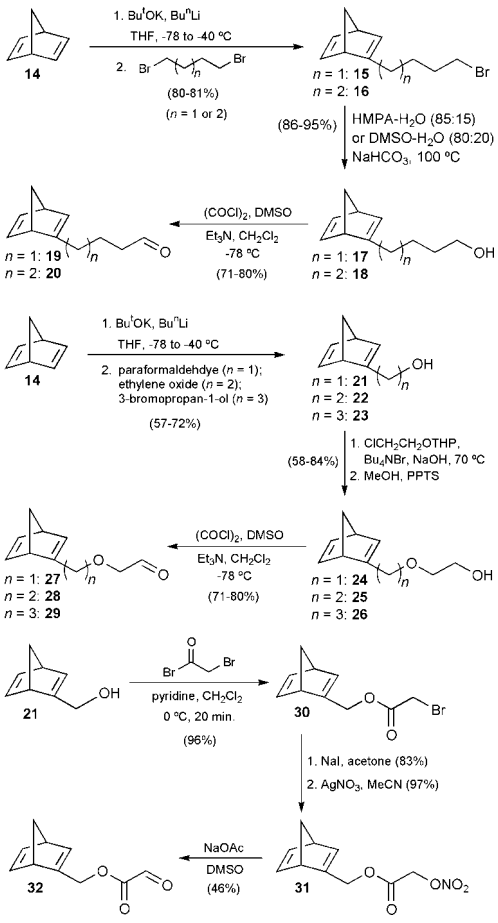

Scheme 3

DOI: 10.1039/b001543l

Table 1 1,3-Dipolar cycloaddition of norbornadiene-tethered nitrones

Entry	Starting aldehyde	Cycloadduct[a,b]	Yield[d](%)
1	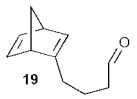 **19**	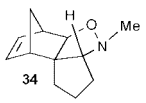 **34**	51
2	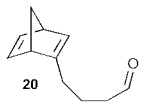 **20**	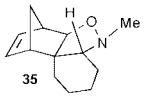 **35**	19
3	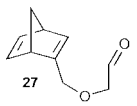 **27**	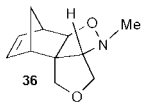 **36**	71
4	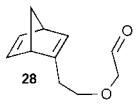 **28**	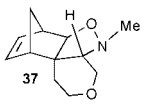 **37**	60
5	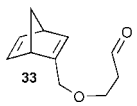 **33**	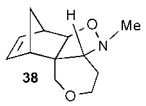 **38**	47
6	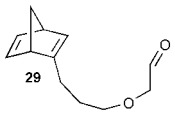 **29**	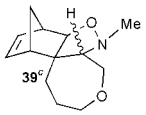 **39**[c]	52
7	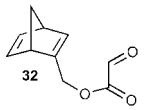 **32**	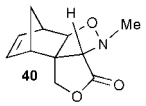 **40**	43

[a] *Reaction conditions*: MeNHOH·HCl (1.2–2 eq.), pyridine (3–5 eq.), 4 Å molecular sieves, toluene, r.t., 12–24 h then 60 to 90 °C 12–48 h. [b] Except in entry 6, the cycloadducts shown were the only regio- and stereo-isomers isolated in the cycloadditions. [c] An inseparable mixture of three isomers was obtained. [d] Isolated yields after column chromatography.

within the tether was prepared from alcohol **21**. Reaction of **21** with bromoacetyl bromide gave the a-bromo ester **30** which was converted to the nitrate ester **31** in two steps.[6,7] Treatment of the nitrate ester **31** with sodium acetate in DMSO provided the required aldehyde **32**.[6,7]

Addition of *N*-methylhydroxylamine to a solution containing aldehyde **19**, pyridine and 4 Å molecular sieves in toluene at room temperature lead to the formation of the corresponding norbornadiene-tethered nitrone which underwent spontaneous intramolecular 1,3-dipolar cycloaddition at 80 ºC to provide a single cycloadduct **34** in 51% isolated yield (Table 1, entry 1). Very little reaction was observed at a lower temperature and prolonged heating led to decomposition of the cycloadduct. Although as many as eight different cycloadducts could be formed in the reaction, only cycloadduct **34** was isolated. With one more carbon in the tether (entry 2), the only cycloadduct isolated was **35** but the yield was only 19%. For aldehydes with an oxygen atom within the tether (entries 3–5), the yields of the cycloadditions were generally much better than the all-carbon tethered substrates. Aldehyde **27** provided the 5-membered ring cycloadduct **36** in 71% yield while aldehydes **28** and **33** gave the corresponding 6-membered ring cycloadducts **37** and **38** in 60 and 47% yield. In all these reactions, cycloadducts **36**–**38** were the only cycloadducts isolated. Formation of a 7-membered ring cycloadduct **39** was also possible starting from aldehyde **29** (entry 6). In this case, 54% of an inseparable mixture of three isomers was obtained. Although some literature examples have shown that as the tether length increases, an alternative regioisomer (with oxygen attached to C_2 and carbon attached to C_3) could be formed as the major regioisomer,[8] we are certain that the two major isomers in this mixture have the same regiochemistry as in other cases (with oxygen attached to C_3 and carbon attached to C_2), since ^{1}H NMR showed that both of these two isomers have two vinylic protons and one proton next to an oxygen (regioisomers with oxygen attached to C_2 and carbon attached to C_3 will not have such a proton peak since the oxygen is attached to a quaternary carbon center). However, we are not certain about the regiochemistry of the third minor isomer in the mixture. Cycloaddition of the substrate with an ester functionality within the tether (entry 7) gave a single cycloadduct **40** in 43% yield. As we noticed that most of the cycloadducts were thermally unstable and they decomposed on prolonged heating, we attempted the reactions at a lower temperature with the use of Lewis acid catalysts. Unfortunately the isolated yields were even lower than the thermal reactions. The regio- and stereo-chemistry of the cycloadducts were confirmed by NMR experiments (HCOSY, HSQC and NOESY experiments). These assignments were also supported by X-ray crystallography.[9]

Several factors could control the regio- and stereo-selectivity of the cycloadditions. Those factors include: the *E/Z* ratio of the nitrones generated from the corresponding aldehydes, the distance and the flexibility of the tether to reach the double bonds, the *exo/endo* selectivity of the double bond (C_2–C_3) in the norbornadiene in the cycloadditions, and the strain and the stability of the cycloadducts formed. At this stage, we are not sure the reasons for the formation of single cycloadducts in the cycloadditions. Either the *E/Z* selectivity of the formation of nitrones was very high and the cycloadditions were highly regio- and stereo-selective, or other cycloadducts were formed but were too unstable and decomposed under the reaction conditions. The cycloadditions can also be reversible and thus giving rise to the most stable cycloadducts. Nevertheless, although up to eight possible cycloadducts could be formed in the cycloadditions, we were able to generate and to isolate single regio- and stereo-isomers in the cycloadditions.

In conclusion, we have demonstrated the first examples of the intramolecular 1,3-dipolar cycloadditions of norbornadiene-tethered nitrones. Single regio- and stereo-isomers were obtained in moderate to good yields. Further investigation on the effect of a substitutent at C_3 on the norbornadiene in the cycloaddition (*e.g.* electron-withdrawing groups on the norbornadiene may activate the alkene component in the cycloaddition and thus a lower reaction temperature may be possible), as well as subsequent cleavage reactions of the cycloadducts (Scheme 1) for the construction of angular-fused tricyclic and spirocyclic frameworks, are ongoing in our laboratory.

We thank the Natural Science and Engineering Research Council (NSERC) of Canada and the University of Guelph for the generous financial support of our program. G. K. T. thanks the Ontario government for a Ontario Graduate Scholarship (OGS). Dr Alan Lough (University of Toronto) is thanked for X-ray structure determination and Ms Valerie Robinson from our department is thanked for NMR experiments.

Notes and references

1 C. Yip, S. Handerson, R. Jordan and W. Tam, *Org. Lett.*, 1999, **1**, 791.
2 A. Padwa, *1,3-Dipolar Cycloaddition Chemistry*, John Wiley & Sons, New York, 1984, vols. 1 and 2; K. V. Gothelf and K. A. Jørgensen, *Chem. Rev.*, 1998, **98**, 863 and references therein.
3 P. A. Wade, in *Comprehensive Organic Synthesis*, ed. B. M. Trost, I. Fleming and L. A. Paquette, Pergamon, Oxford, 1991, vol. 4, pp. 1113–1124.
4 M. Stäble, R. Lehmann, J. Kramař and M. Schlosser, *Chimia*, 1985, **39**, 229; H. D. Verkruijsse and L. Brandsma, *Recl. Trav. Chim. Pays-Bas*, 1986, **105**, 66.
5 I. Heinze, K. Knoll, R. Mòller and W. Eberbach, *Chem. Ber.*, 1989, **122**, 2147.
6 M. J. Melnick and S. M. Weinreb, *J. Org. Chem.*, 1988, **53**, 850.
7 R. Annunziata, M. Cinquini, F. Cozzi and L. Raimondi, *J. Org. Chem.*, 1990, **55**, 1901.
8 W. Oppolzer, S. Siles, R. L. Snowden, B. H. Bakker and M. Petrzilka, *Tetrahedron*, 1985, **41**, 3497.
9 Recrystallization of cycloadduct **40** in 20% EtOAc–hexanes provided suitable crystals for X-ray analysis. Details of the X-ray analysis will be submitted for publication in *Acta Crystallogr., Sect. C.*

ChemComm

Synthesis and molecular structure of the unsymmetrically substituted magnesium alkyl Mg(Bu^n){CH[SPh][SiPh$_2$(CH$_2$NC$_5$H$_{10}$)]}

Carsten Strohmann,* Bors C. Abele, Daniel Schildbach and Katja Strohfeldt

Institut für Anorganische Chemie, Universität Würzburg, Am Hubland, 97074 Würzburg, Germany. E-mail: c.strohmann@mail.uni-wuerzburg.de

Received (in Basel, Switzerland) 12th January 2000, Accepted 10th April 2000

The unsymmetrically substituted magnesium alkyl Mg(Bu^n){CH[SPh][SiPh$_2$(CH$_2$NC$_5$H$_{10}$)]} (NC$_5$H$_{10}$ = 1-piperidyl) with a stereogenic metalated carbon atom is obtained by deprotonation of an (aminomethyl)[(phenylthio)methyl]silane with MgBu^{n}Bu^s and examined by single crystal X-ray diffraction analysis and theoretical methods.

In selective transformations, enantiomerically enriched metal alkyls can work as chiral alkyl-transfer reagents. Moreover, they are valuable tools for studies on the stereochemical course of transmetalation and protonation reactions. Stereogenic metalated carbon centres are usually generated by deprotonation using alkyllithium reagents, giving the corresponding enantiomerically enriched lithium alkyls. These molecules have been investigated intensively.[1] Despite the huge synthetic potential of magnesium alkyls, only one example of an enantiomerically enriched magnesium alkyl is described in the literature.[2]

In a few reported cases, organomagnesium compounds have been used to abstract aryl protons (*e.g.* as part of crown ether systems[3]) and to deprotonate C–H-acidic molecules, such as cyclopentadiene or fluorene.[4,5,6] To turn the nucleophilic magnesium reagent into a deprotonating agent, the metal must be fixed next to the reactive centre by coordinating donor groups. (Aminomethyl)silanes, such as **1a** and **1b**, which are established in our workgroup,[7] intramolecularly provide a coordinating amino group. These (aminomethyl)silanes can be deprotonated easily by *tert*-butyllithium in non-polar solvents leading to (aminomethyl)(lithiomethyl)silanes that form definite aggregates in the solid state.[8]

Here we report the formation and molecular structure of the unsymmetrically substituted magnesium alkyls *rac*-**2a** and *rac*-**2b** with metalated stereogenic centres. *Rac*-**2a**,**b** were generated by deprotonation reaction with the purchasable MgBu^{n}Bu^s in *n*-pentane/*n*-heptane (6:1) in racemic form.

The synthesis of *rac*-**2a**,**b**† was carried out in *n*-pentane, kinetically controlled at low temperatures (−78 °C), by treating **1a**,**b** with 1 equiv. of MgBu^{n}Bu^s (solution in *n*-heptane). To our surprise, all attempts of building up the symmetrically substituted bis{[(aminomethyl)diphenylsilyl]methyl}magnesium compounds *rac*-**3a**,**b** by treating **1a**,**b** with only 0.5 equiv. of MgBu^{n}Bu^s failed. In all of these experiments, *rac*-**2a**,**b** was obtained in *ca.* 50% yield, while half the starting material remained unreacted. Even when the reaction mixture was heated to reflux temperature, only mono substitution occured. Furthermore, neither a *sec*-butyl-substituted product, nor a mixture of *sec*-butyl- and *n*-butyl-substituted products were observed. In all reactions, exclusively the MgBu^n fragment was transferred to the (aminomethyl)silanes **1a**,**b** (Scheme 1).

Earlier results in reactions of organolithium reagents indicated that there is a significant solvent effect on the reactivity of such polar metal–carbon bonds.[7] No detectable amounts of *rac*-**2a**,**b** were obtained, when the reaction of **1a**,**b** with MgBu^{n}Bu^s was carried out in THF. This can be explained by the fact that vacant coordination sites, which are essential for the precoordination of the metal by the aminomethyl ligand, are then occupied by solvent molecules. The importance of this

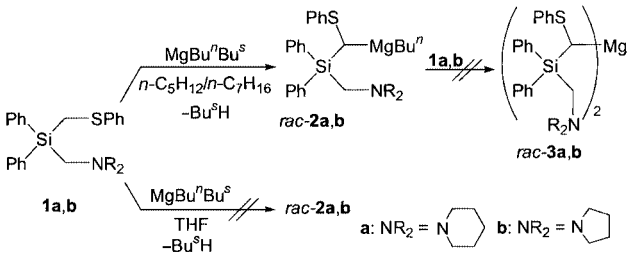

Scheme 1

intramolecular activation is revealed by the result that dimethylbis[(phenylthio)methyl]silane (**4**) is not metalated by MgBu^{n}Bu^s under the same conditions (Scheme 2).

To the best of our knowledge, the only magnesium alkyls containing a sulfur–carbon–magnesium unit, (PhSCH$_2$)$_2$Mg(thf)$_3$ (**5**) and (MeSCH$_2$)$_2$Mg(thf)$_3$ (**6**), were obtained by transmetalation and crystallographically examined by Steinborn and coworkers.[9] In the monomeric molecular structures of **5** and **6**, the magnesium atom is coordinated by three THF molecules. The crystal data of *rac*-**2a**,‡ together with that of **5** and **6**, is important for examining the role of the sulfur atom with respect to aggregation and reactivity.

Compound *rac*-**2a** crystallised from *n*-pentane/*n*-heptane in the triclinic crystal system, space group $P\bar{1}$. We detected two symmetry independent dimers of *rac*-**2a** in the asymmetric unit (molecule A and B) that are different in the conformation of the *n*-butyl groups and the phenyl substituents (Fig. 1). The central six-membered ring of two carbon, two magnesium and two sulfur atoms is built up by the intermolecular S–Mg coordination, that leads to an S(1)–Mg(1) distance of 275.5(1) pm. The Mg(1)–C(1) bond, which is 223.2(3) pm long, is part of another five-membered ring, due to the intramolecular coordination of the aminomethyl substituent [N(1)–Mg(1) 221.4(2) pm]. In the crystal, the metal is surrounded by four different substituents, which makes *rac*-**2a** a magnesium alkyl with a stereogenic magnesium centre. The S(1)–C(1) distances of **5** [177.7(6) pm] and *rac*-**2a** [178.1(3) pm] are nearly identical. This is not true for the S(1)–C(2) distance, which is 176.6(5) pm for **5** and 179.4(3) pm for *rac*-**2a**, as a result of the S → Mg coordination for *rac*-**2a**. The second dimer (molecule B) of *rac*-**2a** may be described in the same way and will, therefore, not be discussed. The crystal data of both molecules A and B can be found in Table 1.

Despite the intensive theoretical studies on organolithium compounds, the corresponding magnesium alkyls have not been investigated to this extent.[10] Sulfur substituents at metalated carbon atoms can increase the stability of the configuration at this centre.[11] For α-lithiated organosulfanes the rotation around

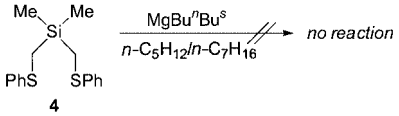

Scheme 2

DOI: 10.1039/b000494o

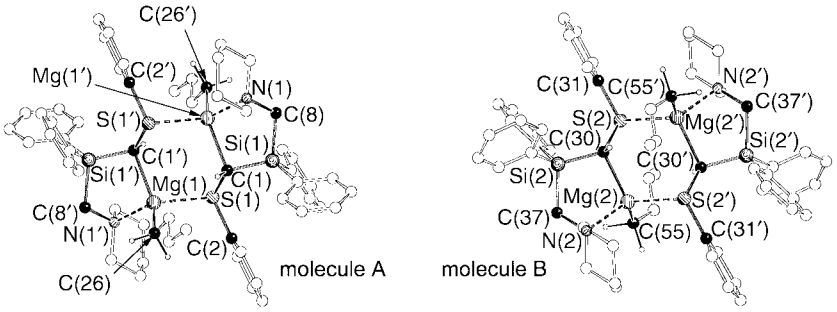

Fig. 1 Molecular structure and numbering scheme of the two crystallographically independent dimers A and B of *rac*-**2a** in the crystal.

Table 1 Selected bond lengths (pm) and angles (°) of the two molecules A and B of *rac*-**2a**, compared with the B3LYP/6-31+G(d)-optimized structure **7**

Molecule A/molecule B	Molecular structure	B3LYP [6-31 + G(d)]
S(1)–C(1)/S(2)–C(30)	178.1(3)/176.8(3)	180.4
S(1)–C(2)/S(2)–C(31)	179.4(3)/178.5(3)	184.4
Mg(1)–S(1)/Mg(2)–S(2)	257.4(1)/257.8(1)	262.0
Mg(1)–C(1)′/Mg(2)–C(30)	223.3(3)/224.7(3)	224.3
Mg(1)–N(1)′/Mg(2)–N(2)	221.4(2)/219.4(3)	223.5
C(1)′–Mg(1)–C(26)/C(30)–Mg(2)–C(55)	129.2(1)/129.2(2)	133.0
N(1)′–Mg(1)–S(1)/N(2)–Mg(2)–S(2)′	115.5(1)/114.8(1)	112.4

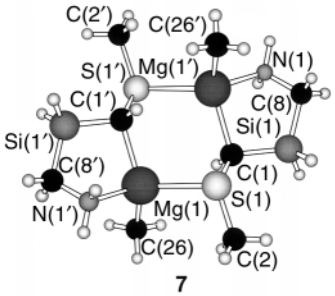

Fig. 2 B3LYP/6-31 + G(d)-optimized structure of a model system for *ab initio* studies on *rac*-**2a** (numbering scheme adopted from Fig. 1).

the C–S bond is the rate-determining step of the racemisation process. We tried to reproduce the molecular structure of *rac*-**2a** by applying density functional calculations [at the B3LYP/6-31+G(d) level] to the model system **7** (Fig. 2).[12]

Structural features, such as the shortened C–S_{alkyl} distance and the longer C–S_{aryl} bond, as well as the antiperiplanar conformation of the C–S–C–Mg unit, could be reproduced by our density functional calculations. Further studies on model systems of sulfur-substituted organomagnesium and organolithium compounds are currently in progress.

In order to build up enantiomerically enriched magnesium alkyls, which have a stereogenic carbon centre, systems of defined aggregation are necessary. The facile generation of unsymmetrically substituted dialkylmagnesium compounds like *rac*-**2a**,**b** opens up a new route to enantiomerically enriched (magnesiomethyl)silanes by using optically active aminomethyl substituents as chiral auxillaries. This has already been successfully demonstrated in the case of enantiomerically enriched (lithiomethyl)silanes.[7,13]

We gratefully acknowledge the Deutsche Forschungsgemeinschaft (DFG), the Sonderforschungsbereich (SFB) 347, and the Fonds der Chemischen Industrie (FCI) for financial support. B. C. A., D. S. and K. S. thank the FCI for the grant of three scholarships.

Notes and references

† *Synthesis of rac*-**2a**,**b**: a colourless solution of 0.50 mmol **1a**,**b** in *n*-pentane (3 ml) was cooled to −78 °C. 0.50 ml (0.50 mmol) of $MgBu^nBu^s$ (1.0 M in *n*-heptane) was added and the reaction mixture was allowed to warm to room temperature. After 6 to 72 h, single crystals of *rac*-**2a**,**b** could be isolated that were suitable for single crystal X-ray structural studies. *Spectroscopic data* for *rac*-**2a**: δ_H(200.1 MHz, C_6D_6) 0.50–2.20 [m, 18 H, SiC(SPh)*H*Mg, NCCCH_2C, NCCH_2C, SiCH_2N, MgCH_2CH_2CH_2CH_3], 2.40–3.10 (m, 4 H, NCH_2C), 6.80–7.50, 7.80–8.10 [m, 15 H, Si(C_6H_5)$_2$, S(C_6H_5)]; δ_C(50.3 MHz, C_6D_6): 0.1 [SiC(SPh)HMg], 8.3 (MgCH_2C), 13.9 (CCH_2CH$_3$), 14.8 (CH_3), 17.4 (MgCCH_2C), 22.3 (NCCCH_2C), 25.1 (NCCH_2C), 40.4 (SiCH_2N), 59.8 (NCH_2C), 127.1 (C-*p*), 128.2 [C-*p* (S*Ph*)], 128.3 (C-*m*), 129.3 [C-*m* (S*Ph*)], 135.4 [C-*o* (S*Ph*)], 136.5 (C-*i*), 139.8 (C-*o*), 142.3 [C-*i* (S*Ph*)]; δ_{Si}(39.8 MHz, C_6D_6) −7.2. *Spectroscopic data* for *rac*-**2b**: δ_H(300.1 MHz, C_6D_6) 0.06–2.20 [s, 1 H, SiC(SPh)*H*Mg], 0.35–0.55 (m, 2 H, MgCH_2C), 0.80–3.40 (m, 17 H, NCCH_2C, NCH_2C, SiCH_2N, MgCH$_2$CH_2CH_2CH_3), 6.65–8.20 [m, 15 H, Si(C_6H_5)$_2$, S(C_6H_5)]; δ_C(75.5 MHz, C_6D_6) 0.4 [SiC(SPh)HMg], 8.0 (MgCH_2C], 14.9 (CH_3), 22.4, 23.1 (CH_2), 33.0, 34.4 (NCCH_2C), 47.6 (SiCH_2N), 57.4, 61.9 (NCH_2C), 125.8 (C-*p*), 126.1 [C-*p* (S*Ph*)], 128.6 (C-*m*), 129.0 [C-*m* (S*Ph*)], 130.0 [C-*o* (S*Ph*)], 135.3 (C-*i*), 135.8 (C-*o*), 140.7 [C-*i* (S*Ph*)]; δ_{Si}(59.6 MHz, C_6D_6) −12.4.

‡ *Crystal data* for *rac*-**2a** (colourless crystals from *n*-pentane/*n*-heptane, 0.40 × 0.40 × 0.20 mm^3): $C_{29}H_{37}MgNSSi$, M = 464.06, triclinic, space group $P\bar{1}$, a = 12.053(3), b = 13.678(3), c = 18.810(4) Å, α = 89.84(2), β = 81.13(2), γ = 68.37(2)°, V = 2843.5(11) Å^3, Z = 4, D_c = 1.131 Mg m^{-3}, Type of radiation: Mo-Kα, λ = 0.71073 Å, μ = 0.195 mm^{-1}. Measurements: Stoe IPDS diffractometer, T = 293 K. The structure was solved using direct and Fourier methods. 22 940 reflections measured with θ in the range 1.89–24°, 8437 unique reflections; 6024 with $I > 2\sigma(I)$; refinement by full-matrix least-squares methods (based on F_o^2, SHELXL-93); anisotropic thermal parameters for all non-H atoms in the final cycles; the H atoms were refined on a riding model in their ideal geometric positions, except H(1), H(26a), H(26b), H(30), H(55a), H(55b), which were refined isotropic; R = 0.0493 [$I > 2\sigma(I)$], wR_2 = 0.1519 (all data). SHELXS-86 and SHELXL-93 computer programs were used. CCDC 182/1598. See http://www.rsc.org/suppdata/cc/b0/b000494o/ for crystallographic files in .cif format.

1 D. Hoppe and T. Hense, *Angew. Chem., Int. Ed. Engl.*, 1997, **36**, 2282.
2 R. W. Hoffmann and P. G. Nell, *Angew. Chem., Int. Ed.*, 1999, **38**, 338.
3 P. R. Markies, T. Nomoto, O. S. Akkerman, F. Bickelhaupt, W. J. J. Smeet and A. L. Spek, *Angew. Chem., Int. Ed. Engl.*, 1988, **27**, 1084; P. R. Markies, T. Nomoto, G. S. Schat, O. S. Akkerman and F. Bickelhaupt, *Organometallics*, 1991, **10**, 3826.
4 A. W. Duff, P. B. Hitchcock, M. F. Lappert, R. G. Taylor and J. A. Segal, *J. Organomet. Chem.*, 1985, **293**, 271; H. Viebrock, D. Abeln and E. Weiss, *Z. Naturforsch., Teil B*, 1994, **49**, 89.
5 M. J. Henderson, R. I. Papasergio, C. L. Raston, A. H. White and M. F. Lappert, *J. Chem. Soc., Chem. Commun.*, 1986, 672.
6 J. J. Eisch and R. Sanchez, *J. Organomet. Chem.*, 1985, **296**, C27.
7 B. C. Abele, *Dissertation*, University of Saarbrücken, Germany, 1997.
8 B. C. Abele and C. Strohmann, in *Organosilicon Chemistry III*, ed. N. Auner and J. Weis, Wiley-VCH, Weinheim, 1998, pp. 206–210.
9 D. Steinborn, T. Rüffer, C. Bruhn and F. W. Heinemann, *Polyhedron*, 1998, **17**, 3275; T. Rüffer, C. Bruhn, F. W. Heinemann and D. Steinborn, *5th International Conference of Inorganic Chemistry*, Brighton, England, 1999, Poster 45.
10 P. R. Markies, O. S. Akkerman, F. Bickelhaupt, W. J. J. Smeets and A. L. Spek, *Adv. Organomet. Chem.*, 1991, **32**, 152.
11 R. K. Dress, T. Rölle and R. W. Hoffmann, *Chem. Ber.*, 1995, **128**, 673.
12 Gaussian 98, Revision A.7, Gaussian, Inc., Pittsburgh PA, 1998.
13 T. H. Chan and D. Wang, *Chem. Rev.*, 1992, **92**, 995.

ChemComm

Optimization of enantiocontrol in *cis*-selective cyclopropanation reactions catalyzed by dirhodium(II) tetrakis[alkyl 2-oxaazetidine-4(*S*)-carboxylates]

Michael P. Doyle,* Simon B. Davies and Wenhao Hu

Department of Chemistry, University of Arizona, Tucson, Arizona, 85721, USA. E-mail: mdoyle@u.arizona.edu

Received (in Corvallis, OR, USA) 18th February 2000, Accepted 7th April 2000

Both intermolecular and macrocyclic intramolecular cyclopropanation reactions occur with greater selectivity for the *cis*-(*Z*)-diastereoisomer than for the *trans*-(*E*)-diastereomer in reactions catalyzed by chiral dirhodium(II) azetidinonecarboxylates; the influence of the catalyst's ester alkyl group on enantiocontrol is substantial but appears to be delicately balanced by steric factors.

Chiral dirhodium(II) carboxamidate catalysts having the general structural framework of **1** have been widely employed to achieve high diastereoselectivity and enantiocontrol in a wide variety of catalytic metal carbene transformations.[1–3] The

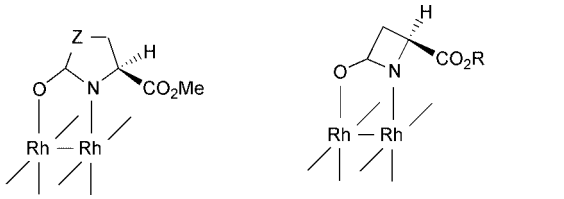

1a Z = CH_2: Rh_2(5*S*-MEPY)$_4$
1b Z = O: Rh_2(4*S*-MEOX)$_4$
1c Z = $NCOCH_2CH_2Ph$: Rh_2(5*S*-MPPIM)$_4$

2a R = Bu^i: Rh_2(4*S*-IBAZ)$_4$
2b R = Bn: Rh_2(4*S*-BNAZ)$_4$
2c R = Me: Rh_2(4*S*-MEAZ)$_4$
2d R = CH_2CMe_3: Rh_2(4*S*-NEPAZ)$_4$
2e R = *c*-C_6H_{11}: Rh_2(4*S*-CHAZ)$_4$

methyl ester has been commonly employed because early investigations showed no significant difference in enantiocontrol with ester variation from methyl to octadecyl and from isopropyl to neopentyl.[4–6] However, we recently reported the preparation of two chiral azetidinone-4-carboxylate-ligated dirhodium(II) catalysts, Rh_2(4*S*-IBAZ)$_4$ **2a** and Rh_2(4*S*-BNAZ)$_4$ **2b**, whose ester alkyl group seemed to have a significant influence on enantiocontrol in cyclopropanation[7] and insertion[8] transformations. We now report, from results obtained with a broad selection of these catalysts, that the size of the ester alkyl group has a modest influence on diastereoselectivity but has a substantial, but irregular, effect on enantiocontrol in addition reactions.

The catalytic reaction of ethyl diazoacetate (EDA) with styrene is the classic transformation with which stereoselectivity for cyclopropanation is measured and catalyst effectiveness is determined.[1,9] Products are *cis*- and *trans*-2-phenylcyclopropanecarboxylate esters **3** and **4**.

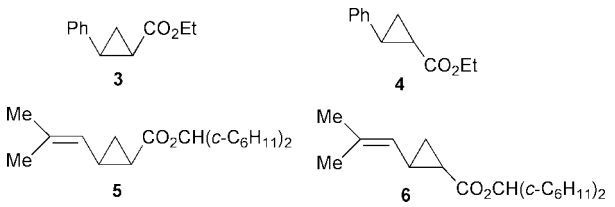

3 **4** **5** **6**

Chiral copper, ruthenium and cobalt catalysts show a marked preference for the *trans* isomer **4**, and this is also true for application of the dirhodium carboxamidate catalyst **1a**.[1,9] An exception is the Ru–salen catalyst recently reported by Katsuki and co-workers.[10] However, the use of chiral azetidinone catalysts **2** provides a distinct preference for the thermodynamically less stable **3** (Table 1), and enantiocontrol for the favored isomer is quite respectable. With 4-methylpenta-l,3-diene and dicyclohexylmethyl diazoacetate (DCDA)[11] these same catalysts show exclusive regioselection for addition to the less-substituted double bond (**5** + **6**), comparable diastereocontrol to that obtained with styrene/EDA, and exceptional enantiocontrol in the formation of **5**. The absolute configuration for the major isomer of **3** (and **5**) is (1*S*, 2*R*); that for **4** (and **6**) is (1*S*, 2*S*).

Table 1 Stereocontrol in intermolecular asymmetric cyclopropanation reactions catalyzed by **2**[a]

Catalyst	Isolated yield (%)[b]	**3**:**5**(**5**:**6**)	Ee(%) **3**(**5**)	Ee(%) **4**(**6**)
$PhCH{=}CH_2$ + EDA:[c]				
Rh_2(4*S*-IBAZ)$_4$ **2a**	62	69:31	76	52
Rh_2(4*S*-BNAZ)$_4$ **2b**	74	58:42	60	32
Rh_2(4*S*-MEAZ)$_4$ **2c**	65	55:45	58	32
Rh_2(4*S*-NEPAZ)$_4$ **2d**	69	66:34	67	34
Rh_2(4*S*-CHAZ)$_4$ **2e**	68	64:36	70	50
$Me_2C{=}CHCH{=}CH_2$ + DCDA:[d]				
Rh_2(4*S*-IBAZ)$_4$ **2a**[e]	81	54:46	>98	66
Rh_2(4*S*-BNAZ)$_4$ **2b**	89	42:58	>98	70
Rh_2(4*S*-MEAZ)$_4$ **2c**	86	43:57	91	63
Rh_2(4*S*-NEPAZ)$_4$ **2d**	91	49:51	>98	70
Rh_2(4*S*-CHAZ)$_4$ **2e**	80	53:47	83	60

[a] Reactions were performed in refluxing CH_2Cl_2 using 1.0 mol% catalyst. [b] Yield of **3** + **4** (or **5** + **6**) after chromatography. [c] [Styrene]/[EDA] = 10; % ee values obtained by GC on a 30 m Chiraldex B-DM column with *cis*-isomers eluting before *trans*-isomers. [d] [Diene]/[DCDA] = 4; % ee values obtained from the methyl esters following saponification and resterification with analysis on a 30 m Chiraldex G-TA column. [e] Data from ref. 7.

As can be seen from the data in Table 1, diastereoselectivity and enantioselectivity are responsive to the ester alkyl group of the catalyst ligand. Larger alkyl groups favor the *cis*-cyclopropanecarboxylate isomer more than do the smaller ones (**2b** and **2c**). In addition to suggesting the potential of **2** for predominant formation of highly enantioenriched *cis*-substituted cyclopropanecarboxylates, however, the data in Table 1 also allow us to correct data previously reported for Rh_2(4*S*-BNAZ)$_4$[7] which showed considerably lower enantioselectivities from those reported in Table 1.

Catalysts **1** have been shown to be particularly suitable for high enantiocontrol in intramolecular cyclopropanation reactions of allylic diazoacetates, providing the cyclized products in high yields and with ee values >94%.[1,3,12] With allyl diazoacetate **7**, for example, use of Rh_2(5*S*-MEPY)$_4$ **1a** gives the corresponding bicyclic lactone **8** in good yield and with 95% ee. In contrast, chiral azetidinones **2** do not have such high enantiocontrol in reactions with **7** (Table 2), but they do show a remarkable variation in % ee as a function of the ester alkyl group on the catalyst.

DOI: 10.1039/b001464h

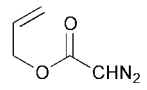

7

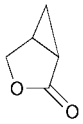

8

Table 2 Enantiocontrol in intramolecular asymmetric cyclopropanation reaction of allyl diazoacetate by **2**[a]

Catalyst	Isolated yield of **8** (%)[b]	Ee (%) of **8**[c]
Rh_2(4S-IBAZ)$_4$ **2a**	74	80
Rh_2(4S-BNAZ)$_4$ **2b**	70	56
Rh_2(4S-MEAZ)$_4$ **2c**	77	76
Rh_2(4S-NEPAZ)$_4$ **2d**	63	58
Rh_2(4S-CHAZ)$_4$ **2e**	90	68

[a] Reactions were performed in refluxing CH_2Cl_2 using 1.0 mol% catalyst. [b] Yield of **8** after chromatography. [c] Determined by GC on a 30 m Chiraldex G-PN column at 100 °C; the major isomer elutes first.

Macrocyclization in cyclopropanation reactions has recently been demonstrated to be a general transformation,[13] although less suitable for enantiocontrolled syntheses with catalysts **1** than with chiral copper(I) bis-oxazoline complexes.[14] In the limit, as the attachment of the carbon–carbon double bond to the diazoacetate becomes increasingly longer, enantioselectivity is expected to approach that obtained in the intermolecular transformation. To further evaluate the macrocyclization process, methallyl diazoacetate **9** was treated with each catalyst in the series of chiral dirhodium(II) azetidinones **2**. The (*Z*)- and (*E*)-cyclopropane products **10** were formed in high yield, and

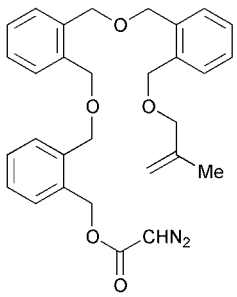

9

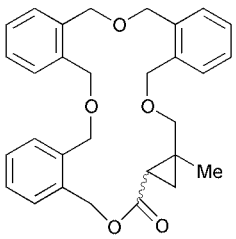

10

% ee values for (*Z*)-**10** reached moderately high levels (Table 3). For comparison, intramolecular cyclopropanation of methallyl diazoacetate using Rh_2(4S-IBAZ)$_4$ formed the corresponding bicyclo[3.1.0]-derivative in 28% ee, which is consistent with our original hypothesis regarding enantiocontrol in macrocyclic cyclopropanation reactions.

Table 3 Stereocontrol in intramolecular asymmetric cyclopropanation reactions of **9** catalyzed by **2**[a]

Catalyst	Isolated yield of **10** (%)[b]	(*Z*)-**10**:(*E*)-**10**	Ee (%) of (*Z*)-**10**[c]
Rh_2(4S-IBAZ)$_4$ **2a**	64	78:22	69
Rh_2(4S-BNAZ)$_4$ **2b**	74	82:18	53
Rh_2(4S-MEAZ)$_4$ **2c**	78	78:22	56
Rh_2(4S-NEPAZ)$_4$ **2d**	64	82:18	62
Rh_2(4S-CHAZ)$_4$ **2e**	67	83:17	63

[a] Reactions were performed in refluxing CH_2Cl_2 using 1.0 mol% catalyst. [b] Yield of **10** following chromatography. [c] Determined following hydrogenolysis of **10** that converted (*Z*)-**10** to its bicyclo[3.1.0]-derivative with analysis performed by GC on a Chiraldex G-TA column.

The overall effectiveness of Rh_2(4S-IBAZ)$_4$ for the catalytic asymmetric cyclopropanation reactions reported here does not follow size considerations of the ligand's ester alkyl group. The isobutyl group is neither the largest nor the smallest alkyl group in the series. Yet in spite of differences exceeding 20% in enantiomeric excess, this catalyst consistently gives the highest level of enantiocontrol.

We are grateful to the National Science Foundation and to the National Institutes of Health (GM-46503) for their support of this research.

Notes and references

1 M. P. Doyle, M. A. McKervey and T. Ye, *Modern Catalytic Methods for Organic Synthesis with Diazo Compounds*, Wiley, New York, 1998, ch. 2–5.
2 M. P. Doyle and M. A. McKervey, *Chem. Commun.*, 1997, 983.
3 M. P. Doyle and D. C. Forbes, *Chem. Rev.*, 1998, **98**, 911.
4 M. P. Doyle, in *Selectivity in Catalysis*, ed. M. E. Davis and S. L. Suib, ACS Symp. Series 517, American Chemical Society, Washington, D.C., 1993, pp. 40–57.
5 M. P. Doyle, A. van Oeveren, L. J. Westrum, M. N. Protopopova and T. W. Clayton, Jr., *J. Am. Chem. Soc.*, 1991, **113**, 8982.
6 M. P. Doyle, M. Y. Eismont, D. E. Bergbreiter and H. N. Gray, *J. Org. Chem.*, 1992, **57**, 6103.
7 M. P. Doyle, Q.-L. Zhou, S. H. Simonsen and V. Lynch, *Synlett.*, 1996, 697.
8 R. T. Buck, M. P. Doyle, M. J. Drysdale, L. Ferris, D. C. Forbes, D. Haigh, C. J. Moody, N. D. Pearson and Q.-L. Zhou, *Tetrahedron Lett.*, 1996, **37**, 7631.
9 M. P. Doyle and M. N. Protopopova, *Tetrahedron*, 1998, **54**, 7919.
10 T. Uchida, R. Irie and T. Katsuki, *Synlett.*, 1999, 1163.
11 R. E. Lowenthal and S. Masamune, *Tetrahedron Lett.*, 1991, **32**, 7373.
12 M. P. Doyle, C. S. Peterson, Q.-L. Zhou and H. Nishiyama, *Chem. Commun.*, 1997, 211.
13 M. P. Doyle, C. S. Peterson, M. N. Protopova, A. B. Marnett, D. L. Parker, Jr., D. G. Ene and V. Lynch, *J. Am. Chem. Soc.*, 1997, **119**, 8826.
14 M. P. Doyle, C. S. Peterson and D. L. Parker, Jr., *Angew. Chem., Int. Ed. Engl.*, 1996, **35**, 1334.

Preparation of a zeolite X-encapsulated copper(II) chloride complex and its catalysis for liquid-phase oxygenation of enamines in the presence of molecular oxygen

Kohki Ebitani, Kohji Nagashima, Tomoo Mizugaki and Kiyotomi Kaneda*

Department of Chemical Science and Engineering, Graduate School of Engineering Science, Osaka University, 1-3 Machikaneyama, Toyonaka, Osaka 560-8531, Japan. E-mail: kaneda@cheng.es.osaka-u.ac.jp

Received (in Cambridge, UK) 24th February 2000, Accepted 11th April 2000

Copper(II) chloride complexes were readily prepared within pores of zeolite X with the modified zeolite found to act as a heterogeneous catalyst for the oxygenation of a variety of enamines in the presence of molecular oxygen without leaching of the active copper species.

Highly selective transformation of organic compounds catalysed by solid materials can contribute to the strong demand of environmental concerns in chemical processes because of the following advantages: (i) simple work-up procedures, (ii) reusable catalysts, and (iii) high thermal stabilities.[1–3] Use of metal catalysts in a liquid phase, however, sometimes leads to leaching of the active species from the solid surface into solution[4] which causes a serious loss of activity and contamination of the products. Here, we describe the synthesis of a Cu(II) chloride complex catalyst within the pores of zeolite X for the selective oxygenation of enamines in the presence of molecular oxygen (Scheme 1). This catalyst can be reused without leaching of the Cu species and retains its high catalytic activity and selectivity for the above oxygenation.

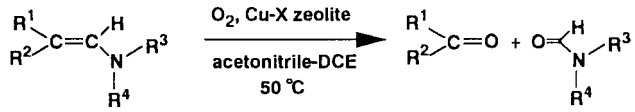

Scheme 1

Copper ion-exchanged X zeolite (Cu–X) was prepared by a treatment of Na–X zeolite, $Na_{86}(Al_{86}Si_{106}O_{384})\cdot 264H_2O$ (Si/Al = 1.23, Wako Co. Ltd.), with a 0.01 M aqueous solution of $Cu(NO_3)_2\cdot 3H_2O$. The powder was washed with deionized water, followed by drying and calcination at 300 °C to give a sky-blue Cu–X sample. The Cu content in this sample was 12.0 wt%, which corresponds to 83% ion exchange degree of Na^+. Retention of the crystal structure of the X zeolite was confirmed by XRD. *In situ* EPR, UV–VIS and Cu K-edge XANES spectra for the Cu–X sample indicated dispersed divalent Cu^{2+} with a centrosymmetric coordination environment, *i.e.* octahedral. Curve-fitting analysis of the Fourier-transformed copper EXAFS showed that the Cu^{2+} cations displayed Jahn–Teller distorted CuO_6 octahedra[5] with four short Cu–O distances (1.91 Å) and two long Cu–O distances (2.28 Å). The Cu–O distance of 1.91 Å is slightly shorter than the value of 1.97 Å found in Cu–Y zeolites.[6] A lack of a peak at *ca.* 3 Å in the Fourier transform of the Cu K-edge EXAFS indicated selective formation of monomeric Cu^{2+} species. A coordination sphere of the CuO_6 octahedra within the zeolite pores is proposed as shown in Fig. 1(a) where the Cu^{2+} ion is reasonably located in a vicinity of the exchangeable site II, just outside the sodalite cage in a large pore with 7.4 Å diameter.[7]

Cu–X (0.50 g) was further treated with 1,2-dichloroethane (DCE, 10 mL) at 50 °C for 1 h, followed by drying to afford an emerald greenish powder, Cu(Cl)–X. The presence of Cu–Cl bonds was confirmed by XPS measurements and elemental analysis; the atomic ratio of Cu to Cl was 1:1.8. EXAFS analysis of Cu(Cl)–X also revealed a Jahn–Teller distorted Cu^{2+}

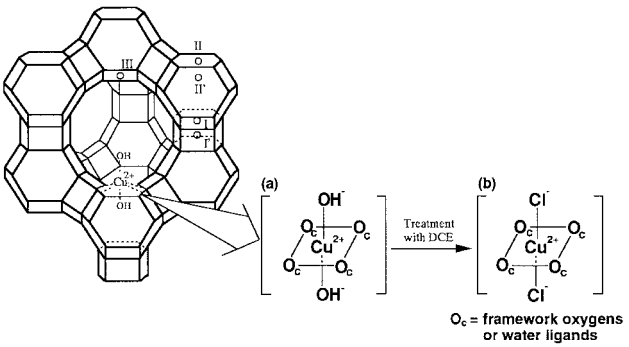

Fig. 1 Proposed schematic structure of Cu^{2+} octahedral species within the framework structure of zeolite X. (a) CuO_6 octahedral species, (b) CuO_4Cl_2 octahedral species. The octahedral CuO_4X_2 species is coordinated to oxygens of zeolite framework and H_2O ligands. The positions of exchangeable cations are indicated by Roman letters.

octahedron with four Cu–O bonds (1.92 Å) and two Cu–Cl bonds (2.29 Å). The Cu–Cl distance of 2.29 Å is consistent with a Cu–Cl bond length of 2.30 Å in $CuCl_2$ and a proposed structure of the monomeric Cu^{2+} chloride complex is shown in Fig. 1(b). To our knowledge, this is the *first* example of the synthesis of a copper(II) chloride species within a pore of zeolite X. It has been stated that Cu chloride complexes can not be formed within the pores of zeolite X by a simple exchange reaction of Na–X with $CuCl_2$ solution because of destruction of the faujasite structure of zeolite X.[8] In zeolite Y, adoption of burdensome methods such as chemical vapor deposition[6] or a solid-state ion-exchange[8] can afford monovalent copper chloride species. The chlorine in Cu(Cl)–X originates from a DCE molecule during the treatment of Cu–X with DCE. The fact is supported by the formation of dibenzyl ether upon treatment of Cu–X with benzyl chloride in place of DCE.[9]

We have already reported that copper chloride compounds are effective homogeneous catalysts for the oxidative cleavage of carbon double bonds of enamines in the presence of molecular oxygen.[10] To explore the potential catalytic abilities of the Cu(II) chloride complexes within the zeolite X,[11] oxygenation of enamines using Cu–X was performed.† Typical results for the oxygenation of enamines with Cu–X in acetonitrile–DCE are summarized in Table 1.‡ The carbon double bonds of many enamines were smoothly cleaved to give the corresponding amides and ketones (entries 1, 2 and 4–8). For a bulky enamine such as 1-(4-morpholino)-2,2-diphenylethene, the oxygenation rate with Cu–X was slower than that of a homogeneous $CuCl_2$ catalyst (entry 9 *vs.* 10). This different activity between the heterogeneous Cu–X and the homogeneous $CuCl_2$ catalyst might be ascribed to a shape-selective effect of Cu^{2+} species within the three-dimensional zeolite pores. The Cu–X catalyst was also active for the oxygenation of 2,3-dimethylindole (entry 11).§

The Cu–X catalyst could be easily separated from the reaction mixture and reused without an appreciable loss of its

DOI: 10.1039/b001515f

Table 1 The oxidative cleavage of enamines catalysed by Cu–X zeolite in the presence of molecular oxygen[a]

Entry	Substrate	*t*/h	Conv. (%)	Yield of products (%)[b]	
				Amide	Ketone
1	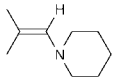	5	100	97	*c*
2	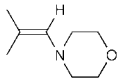	5	100	93 (fresh)	*c*
		5	98	90 (reuse-1)	*c*
		5	99	90 (reuse-2)	*c*
		5	98	90 (reuse-3)	*c*
3[d]		1	100	80	*c*
4	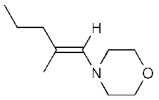	6	100	83	80
5	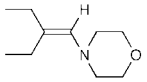	5	100	90	82
6	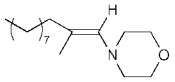	5	100	96	97
7	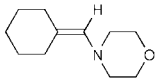	5	100	76	73
8	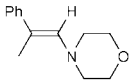	5	100	70	84
9	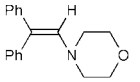	24	91	61	66
10[d]		1	100	95	87
11	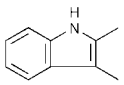	3	100	84[e]	

[a] Substrate (2 mmol); Cu–X (0.10 g, 0.19 mmol-Cu); solvent (8 mL; acetonitrile–DCE, 7:1); temperature = 50 °C; O_2 atmosphere. [b] Yields based on enamine. [c] Acetone formed, however, the yields were not determined. [d] Homogeneous oxidation using $CuCl_2$ (0.19 mmol). [e] *N*-(2-Acetylphenyl)acetamide isolated by column chromatography on silica gel.

activity for the oxygenation; the first, second and third runs of the reused catalyst for 1-(4-morpholino)-2-methylpropene gave *N*-formylmorpholine in >90% yield. The loss of Cu content in the spent Cu–X catalyst after several reuse experiments was <1%; the Cu content in the catalyst did not change even after the third reuse. ICP analysis of copper in the liquid phase after oxygenation showed that leached copper from the catalyst was <1% in the spent Cu–X catalyst.¶ The fact that the active copper complex does not leach from the zeolite X during the oxygenation and recycling procedures, indicates a reusable heterogeneous catalyst for the liquid-phase oxidation.

We presume that the oxygenation catalysed by the Cu(Cl)–X catalyst might involve one-electron transfer from the enamine to molecular oxygen in a ternary Cu^{2+} complex bonded to enamine and O_2, followed by the formation of Cu^{2+} and a dioxetane intermediate.[10] Strong binding of the Cu chloride complexes on the zeolite is due to the location of the divalent Cu ions within large supercages, bound to oxygens of the zeolite framework [Fig. 1(b)].[12] During the oxygenation, facile coordination of enamine and O_2 to the active Cu center can occur since some ligands such as H_2O on the Cu active species are labile.

In conclusion, monomeric copper(II) chloride species within the pore of zeolite X can be synthesized by a novel and convenient method, and are found to be effective catalysts for the cleavage of enamine double bonds in the presence of molecular oxygen. This zeolite X-encapsulated copper chloride complex is a unique instance of a heterogeneous and reusable catalyst which does not undergo leaching of the active species.

This work is supported by the Grant-in-Aid for Scientific Research from the Ministry of Education, Science, Sports and Culture of Japan (11450307). X-Ray absorption experiments were carried out under the approval of Japan Synchrotron Radiation Research Institute (JASRI) (proposal no. 1999A0083). We thank Professor Tsunehiro Tanaka at Kyoto University for providing his program for analysis of EXAFS. We are also grateful to Dept. Chem. Sci. Eng., Fac. Eng. Sci., Osaka Univ., for scientific support *via* 'Gas-Hydrate Analyzing System (GHAS)'.

Notes and references

† The order of the catalytic activity of various copper catalysts for the oxygenation of 1-(4-morpholino)-2-methylpropene is: Cu–X(93) > Cu–Y(82) > Cu-mordenite(76) > Cu/Al_2O_3(72) > Cu/SiO_2 (38), where values in parentheses are yields of *N*-formylmorpholine.

‡ We confirmed that the catalysis of Cu–X in the mixed solvent corresponded to that of Cu(Cl)–X. Cu(Cl)–X itself effectively oxygenated the enamine in acetonitrile alone (yield: 70%). Solvents having high dielectronic constants such as acetonitrile, DMF and ethanol were effective co-solvents for DCE, as similarly observed in the homogeneous catalyst system using $CuCl_2$.[10]

§ Interestingly, this heterogeneous catalyst showed higher activity than $CuCl_2$ for 2,3-dimethylindole,[13] however, the oxidation of 3-methylindole resulted in a low yield (34% after 24 h).

¶ When the filtrate at 50% enamine conversion was allowed to react further at 50 °C under an oxygen atmosphere, oxygenation did not occur.

1 P. T. Anastas and J. C. Warner, *Green Chemistry; Theory and Practice*, Oxford University Press, Oxford, 1998; J. H. Clark, *Green Chem.*, 1999, **1**, 1.
2 K. Yamaguchi, K. Ebitani, T. Yoshida, H. Yoshida and K. Kaneda, *J. Am. Chem. Soc.*, 1999, **121**, 4526; T. Matsushita, K. Ebitani and K. Kaneda, *Chem. Commun.*, 1999, 265; K. Yamaguchi, K. Ebitani and K. Kaneda, *J. Org. Chem.*, 1999, **64**, 2966; K. Yamaguchi, T. Mizugaki, K. Ebitani and K. Kaneda, *New. J. Chem.*, 1999, **23**, 799.
3 R. Sreekmar, R. Padmakumar and P. Rugmini, *Tetrahedron Lett.*, 1998, **39**, 2695; J.-I. Tateiwa, E. Hayama, T. Nishimura and S. Uemura, *J. Chem. Soc., Perkin Trans. 1*, 1997, 1923; P. Laszlo, *Acc. Chem. Res.*, 1986, **19**, 121.
4 R. A. Sheldon, M. Wallau, I. W. C. E. Arends and U. Shuchardt, *Acc. Chem. Res.*, 1998, **31**, 485.
5 M. Kökerling, G. Geismar, G.Henkel and H.-F. Nolting, *J. Chem. Soc., Faraday Trans.*, 1997, **93**, 481.
6 C. Lamberti, G. Spoto, D. Scarano, C. Pazé, M. Salvalaggio, S. Bordiga, Z. Zecchina, G. Turnes Palomino and F. D'Acapito, *Chem. Phys. Lett.*, 1997, **269**, 500.
7 *Catalysis and Zeolites: Fundamentals and Applications*, ed. J. Weitkamp and L. Puppe, Springer-Verlag, Berlin–Heidelberg, 1999; Y.-H. Yeom, S.-B. Jang, Y. Kim, S.-H. Song and K. Seff, *J. Phys. Chem. B*, 1997, **101**, 6914.
8 S. T. King, *Catal. Today*, 1997, **33**, 173.
9 T. Shirafuji, Y. Yamamoto and H. Nozaki, *Bull. Chem. Soc. Jpn.*, 1971, **44**, 1994.
10 *Homogeneous catalytic oxygenation of enamines*, K. Kaneda, T. Ito, N. Kii, K. Jitsukawa and S. Teranishi, *J. Mol. Catal.*, 1982, **15**, 349; T. Ito, K. Kaneda, I. Watanabe, S. Ikeda and S. Teranishi, *Chem. Lett.*, 1976, 227.
11 *Heterogeneous oxygenation of enamines using stoichiometric reagents*, H. Benhaliliba, A. Derdour, J.-P. Bazureau, F. Texier-Boullet and J. Hamelin, *Tetrahedron Lett.*, 1998, **39**, 541; R. Sreekumar and R. Padmakumar, *Tetrahedron Lett.*, 1997, **38**, 5143; C. E. Harris, W. Chrisman, S. A. Bickford, L. Y. Lee, A. E. Torreblanca and B. Singaram, *Tetrahedron Lett.*, 1997, **38**, 981.
12 K. Matar and D. Goldfarb, *J. Phys. Chem.*, 1992, **96**, 3100.
13 J. Tsuji, H. Kezuka, H. Takayanagi and K. Yamamoto, *Bull. Chem. Soc. Jpn.*, 1981, **54**, 2369; E. Balogh-Hergovich and G. Speier, *J. Chem. Soc., Perkin Trans. 1*, 1986, 2305.

Amidoalane, amidogallane and amidoindane, H_2MNH_2 (M = Al, Ga or In): a matrix study of three prototypal molecules with the potential for M–N multiple bonding

Hans-Jörg Himmel,* Anthony J. Downs and Tim M. Greene

Inorganic Chemistry Laboratory, University of Oxford, South Parks Road, Oxford, UK OX1 3QR. E-mail: tony.downs@chem.ox.ac.uk

Received (in Basel, Switzerland) 29th February 2000, Accepted 7th April 2000

Photolysis of Al, Ga or In atoms (M) isolated in NH_3-doped Ar matrices gives first the divalent amido derivative $HMNH_2$ (λ = 436 nm) and then the univalent and trivalent amido derivatives MNH_2 and H_2MNH_2 (λ = 200–800 nm); the measured and calculated properties of H_2MNH_2 are outlined.

Amido derivatives of group 13 metals are potentially relevant to the fabrication and properties of the III–V semiconductor materials AlN, GaN and InN.[1] Such compounds are normally oligomeric or polymeric, with a coordination number of four or greater at M; only with the introduction of bulky substituents at M and N can monomeric compounds with tri-coordinated M atoms be sustained under normal conditions.[2] The properties of these monomeric amido derivatives have attracted considerable theoretical attention, mainly in relation to the potential for M–N multiple bonding.[2,3]

Matrix isolation offers a highly instructive method of reconnaissance and characterisation for simple, previously unknown hydride derivatives of the main group metals.[4–6] Hence, for example, photoexcitation of metal atoms contained in solid Ar matrices doped with NH_3 has been shown previously to result in insertion of the metal into an N–H bond of NH_3 with the formation of the species $HMNH_2$ (M = Al[7]) and MNH_2 (M = Li[8] or Al[7]). Here we report specifically on the formation of the simple monomeric compounds H_2MNH_2 (M = Al, Ga or In) as products of the reactions set in train by photolysis of NH_3-doped Ar matrices containing the relevant M atoms.[9] The molecules have been identified by their IR spectra, with the conclusions being underpinned (i) by the observed effects of exchanging $^{14}NH_3$ for $^{14}ND_3$ or $^{15}NH_3$, and of the isotopes ^{69}Ga and ^{71}Ga present in natural Ga; (ii) by parallels with the spectra of related hydrido and amido derivatives, *e.g.* MH_3,[4] H_2MCl,[5,10] and $AlNH_2$[7] (M = Al, Ga or In); and (iii) by comparisons with the IR spectra forecast by density functional theory (DFT) calculations.[11] In the following account we will concentrate on the formation and characterisation of H_2GaNH_2; the aluminium and indium analogues follow a very similar pattern, with the results summarized in Table 1.

An Ar matrix containing *ca.* 0.2% Ga atoms and up to 2% NH_3 gave an IR spectrum including, in addition to the absorptions characteristic of NH_3 and $[NH_3]_n$,[12] a new absorption at 1104.2 cm^{-1} attributable to an adduct $Ga{\cdot}NH_3$ **1**. There was also associated with this product a visible absorption centered at 440 nm. Irradiation of the matrix with radiation having λ = 436 nm for 5 min resulted in the decay of the spectroscopic features due to **1** and the appearance of new IR bands at 1721.8, 1528.7, 746.2, 668.5/667.4 494.1 and 210.9 cm^{-1} attributable on the strength of their constant relative intensities to a second product **2**. All the criteria (i)–(iii) indicate that **2** is the gallium(II) amide $HGaNH_2$, showing clear spectroscopic analogies with GaH_2[4] and CH_3GaH.[6]

Photolysis for a further 30 min, but with broad-band UV–VIS light (200 < λ < 800 nm) led to the decay of the bands due to

Table 1 Structures (distances in Å, angles in degrees), rotational barriers ΔE (kJ mol^{-1}), wavenumbers [cm^{-1}, intensities (km mol^{-1}) are given in parentheses] and M–N force constants *f*(MN) (N m^{-1}) for H_2MNH_2 molecules (M = Al, Ga and In)

Parameter		H_2AlNH_2		H_2GaNH_2		H_2InNH_2	
M–N		1.7790		1.8211		1.9703	
M–H		1.5811		1.5621		1.7252	
N–H		1.0100		1.0086		1.0169	
H–M–H		124.4		126.7		126.9	
H–N–H		110.0		111.7		110.3	
ΔE		50.6		65.7		51.5	
Description of vibrational mode	Assignment	Obs.	Calc.	Obs.	Calc.	Obs.	Calc.
ν_{sym}(N–H)	ν_1 (a_1)	3499.7	3572.0 (11)	3413.4	3581.9 (9)	—[a]	3517.1 (10)
ν_{sym}(M–H)	ν_2 (a_1)	1891.0	1959.3 (81)	1970.8—[c]	1995.9 (64)	—[a]	1770.2 (68)
δ(NH_2)	ν_3 (a_1)	1541.6	1631.2 (49)	1530.4	1621.6 (30)	1506.6	1579.4 (23)
ν(M–N)	ν_4 (a_1)	818.7	830.1 (192)	706.2/704.1	689.0 (124)	616.3	575.8 (153)
δ(MH_2)	ν_5 (a_1)	755.0	754.6 (86)	779.6	740.3 (40)	—[a]	634.2 (84)
Twist	ν_6 (a_2)	—[b]	499.9 (0)	—[b]	545.8 (0)	—[b]	480.8 (0)
$\rho_{out\text{-}of\text{-}plane}$($MH_2$)	ν_7 (b_1)	608.7	608.4 (150)	567.7	607.9 (43)	—[a]	535.2 (95)
$\rho_{out\text{-}of\text{-}plane}$($NH_2$)	ν_8 (b_1)	518.3	483.0 (309)	304.9	337.3 (280)	—[a]	177.6 (237)
ν_{asym}(N–H)	ν_9 (b_2)	—[a]	3655.8 (11)	3510.7	3681.7 (13)	—[a]	3621.9 (18)
ν_{asym}(M–H)	ν_{10} (b_2)	1899.3	1964.2 (288)	1970.8—[c]	1998.6 (245)	1805.9	1756.9 (272)
$\delta_{in\text{-}plane}$(NH_2)	ν_{11} (b_2)	769.8	767.6 (151)	782.8	789.8 (110)	733.3	696.3 (126)
$\delta_{in\text{-}plane}$(MH_2)	ν_{12} (b_2)	—[a]	433.5 (22)	—[a]	441.8 (26)	—[a]	368.5 (33)
f(MN)		407.5		384.9		315.3	

[a] Not observed. [b] IR silent. [c] Both modes contained within a single broad absorption.

DOI: 10.1039/b001652g

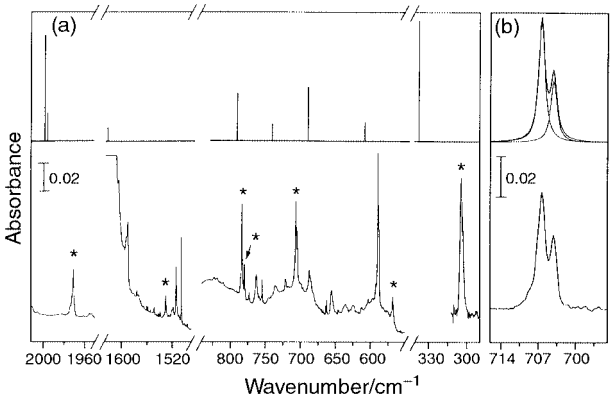

Fig. 1 (a) Bottom: IR spectrum of an Ar matrix containing Ga and NH_3 following photolysis first at λ = 436 nm and then at λ = 200–800 nm; top: calculated IR absorptions for H_2GaNH_2. (b) Bottom: IR spectrum of H_2GaNH_2 in the region around 700 cm^{-1}; top: curve fit with two Lorentzian-type functions with an intensity ratio reflecting the proportions $^{69}Ga/^{71}Ga$ = 60.1 : 39.9 in naturally occurring Ga.

2 with the simultaneous appearance and growth of a new family of bands having a common origin in a third product **3**. Occurring at 3471.6, 1505.9, 589.3/587.9 and 314.5 cm^{-1}, these could be identified with the gallium(I) amide $GaNH_2$, a conclusion supported by the criteria (i)–(iii) and by analogy with the IR spectrum reported for $AlNH_2$.[7] Extending the period of photolysis resulted in the continued accumulation of **3** at the expense of **2**. Additionally, another group of bands, also with constant relative intensities and therefore associated with a fourth distinct product **4**, was observed to develop (see Fig. 1). The members of this group were located at 3510.7, 3413.4, 1970.8, 1530.4, 782.8, 779.6, 706.2/704.1, 567.7 and 304.9 cm^{-1}, those at 1970.8, 782.8, 706.2/704.1 and 304.9 cm^{-1} being the most prominent. Diagnostic aspects are (i) the strong absorption at 1970.8 cm^{-1} occurring in the region characteristic of ν(Ga–H) vibrations of terminal Ga(III)–H bonds (*cf.* GaH_3 1923.2 cm^{-1} [4] and H_2GaCl 1964.6–1978.1 cm^{-1} [9]); (ii) the absorptions at 3510.7, 3413.4 and 1530.4 cm^{-1} implying the presence of an NH_2 group; and (iii) the doublet pattern at 706.2/704.1 cm^{-1} attributable to $^{69}Ga/^{71}Ga$ splitting arising from the motion of a single Ga atom (see Fig. 1). The criteria (i)–(iii) leave little doubt that **4** is monomeric amidogallane, H_2GaNH_2, more familiar as a trimer which is stable at temperatures up to nearly 150 °C.[13] Out of the 11 IR-active modes ($5a_1 + 2b_1 + 4b_2$) expected for planar H_2GaNH_2 with C_{2v} symmetry, all but one have been satisfactorily located in the spectrum measured for **4**, the only absentee being ν_{12} (b_2) which is expected to lie near 420 cm^{-1} but is probably obscured by extraneous absorptions. In other respects the calculations anticipate remarkably closely the observed wavenumbers, relative intensities, and isotopic shifts to provide a convincing basis for the assignments entered in Table 1. For example, the observed $^{69}Ga/^{71}Ga$ splitting of 2.1 cm^{-1} displayed by the absorption near 705 cm^{-1} matches admirably the calculated value of 1.9 cm^{-1} for the ν(Ga–N) mode, ν_5 (a_1).

The amides H_2AlNH_2 and H_2InNH_2 have each been formed and characterised in analogous experiments involving Al and In atoms, respectively. With the indium compound, formed only in low concentrations, no more than four weak IR absorptions could be clearly associated, although the wavenumbers and isotopic shifts, allied to the circumstances, vouch for its identity. Nine of the IR-active fundamentals of H_2AlNH_2 were located with confidence. Two of the most prominent bands, at 1899.3 and 1891.0 cm^{-1}, tally with features reported in earlier matrix studies[7] of the reactions between laser-ablated Al atoms and NH_3 and assigned somewhat tentatively not to H_2AlNH_2 but to the quasi-linear, high-energy HAlNH molecule. Experiments with all three metals and involving different concentrations of NH_3 or mixtures of NH_3 and H_2 make it clear that H_2MNH_2 is formed from $HMNH_2$ or MNH_2 by the addition of H atoms generated by the photodecomposition of $HMNH_2$ (or MH_2 when H_2 is present[4]).

Calculated and observed properties of H_2AlNH_2, H_2GaNH_2 and H_2InNH_2 are listed in Table 1. In each case, the global minimum is calculated to correspond to a planar ethene-like geometry, although, as noted elsewhere,[2] a planar M–NH_2 geometry is not necessarily a sign of strong π bonding. The calculated M–N distances are indeed short, near or below the lower limits for the observed distances in tri-coordinated amido derivatives of these elements (1.78, 1.818 and 2.049 Å for M = Al, Ga and In, respectively);[2] with respect to related species the order is $M{\cdot}NH_3 > H_3M{\cdot}NH_3 > MNH_2 > MN > HMNH_2 \geqslant H_2MNH_2 > HMNH'$. The M–N stretching force constants, based where possible on the measured spectra, vary in the orders (i) $H_2MNH_2 \geqslant HMNH_2 \geqslant MNH_2 \gg H_3M{\cdot}NH_3 \gg M{\cdot}NH_3$, and (ii) M = B $\gg$ Al $\geqslant$ Ga > In for H_2MNH_2. Calculation of the energy of the transition state in which the H_2M and NH_2 planes are orthogonal gives an estimate of the barrier to rotation about the M–N bond, ΔE, in H_2MNH_2. The results included in Table 1 are consistent with those reported elsewhere,[2] with ΔE = 161.9, 50.6, 65.7 and 51.5 kJ mol^{-1} for M = B, Al, Ga and In, respectively. Gallium may then be seen once again to be out of line with its neighbours and to show a modest return to the behaviour of boron,[1] but the barriers support the general view that, with the exception of M = B, the primary influence on the M–N bonding is not the π interaction but the polarity of the unit.

We thank (i) the EPSRC for support of this research and the award of an Advanced Fellowship to T. M. G., and (ii) the Deutsche Forschungsgemeinschaft for the award of a post-doctoral grant to H.-J. H.

Notes and references

1 See, for example: *Chemistry of Aluminium, Gallium, Indium and Thallium*, ed. A. J. Downs, Blackie, Glasgow, UK, 1993; *Properties of Group III Nitrides*, ed. J. H. Edgar, EMIS, London, 1994.
2 K. Knabel, I. Krossing, H. Nöth, H. Schwenk-Kirchner, M. Schmidt-Amelunxen and T. Seifert, *Eur. J. Inorg. Chem.*, 1998, 1095; P. P. Power, *Chem. Rev.*, 1999, **99**, 3463.
3 See: R. D. Davy and K. L. Jaffrey, *J. Phys. Chem.*, 1994, **98**, 8930; T. P. Hamilton and A. W. Shaikh, *Inorg. Chem.*, 1987, **36**, 754.
4 P. Pullumbi, C. Mijoule, L. Manceron and Y. Bouteiller, *Chem. Phys.*, 1994, **185**, 13, 25.
5 H.-J. Himmel, A. J. Downs and T. M. Greene, *J. Am. Chem. Soc.*, 2000, **122**, 922.
6 H.-J. Himmel, A. J. Downs, T. M. Greene and L. Andrews, *Chem. Commun.*, 1999, 2243; *Organometallics*, 2000, **19**, 1060.
7 D. V. Lanzisera and L. Andrews, *J. Phys. Chem. A*, 1997, **101**, 5082.
8 P. F. Meier, R. H. Hauge and J. L. Margrave, *J. Am. Chem. Soc.*, 1978, **100**, 2108.
9 Full experimental details may be found in ref. 5.
10 R. Köppe and H. Schnöckel, *J. Chem. Soc., Dalton Trans.*, 1992, 3393.
11 DFT calculations employed GAUSSIAN 98 [B3LYP hybrid method, 6-311G* basis set for Al and Ga, LANL2DZ basis set with additional d-polarisation function (exponent 0.5) for In]. No scaling factor was used in computing the vibrational frequencies. GAUSSIAN 98, Revision A.3: M. J. Frisch, G. W. Trucks, H. B. Schlegel, G. E. Scuseria, M. A. Robb, J. R. Cheeseman, V. G. Zakrzewski, J. A. Mongomery, R. E. Stratmann, J. C. Burant, S. Dapprich, J. M. Millam, A. D. Daniels, K. N. Kudin, M. C. Strain, O. Farkas, J. Tomasi, V. Barone, M. Cossi, R. Cammi, B. Mennucci, C. Pomelli, C. Adamo, S. Clifford, J. Ochterski, G. A. Petersson, P. Y. Ayala, Q. Cui, K. Morokuma, D. K. Malick, A. D. Rabuck, K. Raghavachari, J. B. Foresman, J. Cioslowski, J. V. Ortiz, A. G. Baboul, B. B. Stefanov, G. Liu, A. Liashenko, P. Piskorz, I. Momaromi, R. Gomperts, R. L. Martin, D. J. Fox, T. Keith, M. A. Al-Laham, C. Y. Peng, A.Nanayakkara, C. Gonzalez, M. Challacombe, P. M. W. Gill, B. G. Johnson, W. Chen, M. W. Wong, J. L. Andres, A. Gonzales, M. Head-Gordon, E. S. Replogle and J. A. Pople, *Gaussian Inc., Pittsburgh PA*, 1998.
12 L. Abouaf-Marguin, M. E. Jacox and D. E. Milligan, *J. Mol. Spectrosc.*, 1977, **67**, 34.
13 J. P. Campbell, J.-W. Hwang, V. G. Young, Jr., R. B. Von Dreele, C. J. Cramer and W. L. Gladfelter, *J. Am. Chem. Soc.*, 1998, **120**, 521.

ChemComm

Palladium catalysed synthesis of pyrroles from enamines

Ronald Grigg* and Vladimir Savic

Molecular Innovation, Diversity and Automated Synthesis (MIDAS) Centre, School of Chemistry, Leeds University, Leeds, UK LS2 9JT. E-mail: r.grigg@chem.leeds.ac.uk

Received (in Cambridge, UK) 20th March 2000, Accepted 14th April 2000

Substituted pyrroles are formed in moderate to good yields by the Pd-catalysed cyclisation of enamines containing β-vinyl bromide functionalities.

Pyrrole and its derivatives feature widely in natural products, drugs, polymers and dyes.[1,2] As a result many efficient synthetic procedures for their preparation have been developed.[3] The synthetic methodology for the preparation of pyrrole and its derivatives can be classified in terms of the number and location of the bonds formed in the reaction.[3a] We are particularly interested in the ***Ic*** approach (Scheme 1) since this approach although frequently used in the synthesis of indoles,[3a,b,4] is quite rare for pyrrole synthesis. It was expected that easily accessible enamines of type **1** would provide access to the desired synthetic procedure ***Ic*** (Scheme 1).

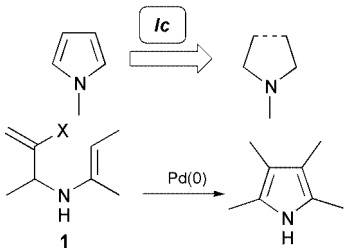

Scheme 1

The results of an initial experiment are shown in Scheme 2. The enamine **2** was prepared in 84% yield by reacting amine **3** and alkyne **4** in DMF at room temperature. The cyclisation step (DMF, 85 °C, oil bath temperature) in the presence of $Pd(OAc)_2$ (10 mol%)/PPh_3 (20 mol%) and K_2CO_3 (2 equiv.) as a base afforded the expected pyrrole **5** but in only 24% yield.

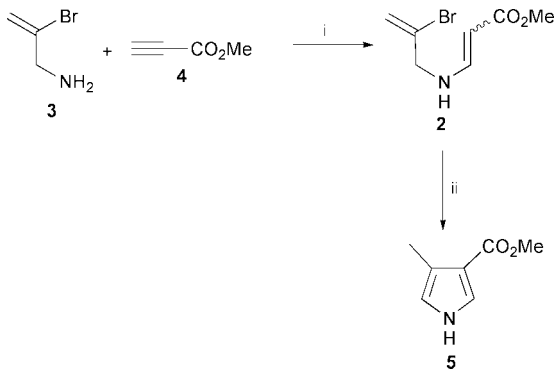

Scheme 2 *Reagents and conditions*: i, DMF, room temp., 84%; ii, $Pd(OAc)_2$, PPh_3, K_2CO_3, DMF, 85 °C, 24%.

Assuming that the low yield of **5** could be caused by instability of the pyrrole product, several other enamines (Table 1) were prepared using similar synthetic procedures in order to further investigate the cyclisation reaction. With bis-substituted alkynes (Table 1, entries c, d and h) the reactions were performed in DMF at 60–65 °C (oil-bath temperature) or in boiling ethanol[5] (Table 1, entry e) producing the required enamines in good yield. Monosubstituted alkynes (Table 1, entries a, f and g) afforded the enamines at room temperature. Enamine **8b** was prepared by addition of propenylamine to the allene in DMF at room temperature. Most of the enamines comprised mixtures of *Z*- and *E*-isomers and these mixtures were used for the cyclisation reactions without attempts to separate the stereoisomers.

With **8a**–**h** in hand their conversion to the corresponding pyrroles was investigated. The reactions were performed in DMF at 85 °C in the presence of $Pd(OAc)_2/PPh_3$ and K_2CO_3 as already explained affording **9a**–**h** in moderate to good yields. The reaction tolerates a range of functional groups and reaction times are in most cases between 1 and 3 h.

Mechanistically the cyclisation step can be rationalised in several ways. It is possible that Pd(II) acts as a Lewis acid by coordinating either the enamine double bond or the electron withdrawing group (CO_2Me, $SO_2C_6H_4Me$-*p*) lowering the pK_a of the N–H group. This would facilitate the formation of the corresponding anion leading to cyclisation *via* nucleophilic attack on the vinyl bromide moiety. Interestingly we observed that for enamine **10**, where the pK_a of the N–H group is sufficiently low to allow deprotonation by K_2CO_3, the Pd-catalyst is not required (Scheme 3). The expected product **11** was formed by heating **10** in DMF (85 °C) in the presence of only K_2CO_3. The reaction with other enamines used in this study without the Pd-catalyst but in the presence of K_2CO_3 resulted in recovery of the starting materials. ^{1}H NMR spectroscopy of the crude reaction mixtures indicated the presence of a small amount of product only in the case of enamine **8e** after a significantly longer reaction time than for reaction performed in the presence of Pd-catalyst (6 *cf.* 1 h).

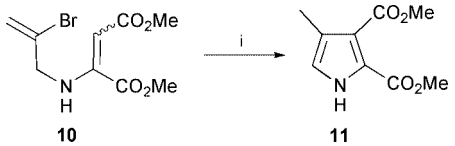

Scheme 3 *Reagents and conditions*: i, K_2CO_3, DMF, 85 °C, 53%.

Another mechanistic rationalisation of the reaction is shown in Scheme 4. This involves the oxidative addition of Pd(0) into the C–Br bond followed by coordination to the enamine double bond to form **12**. Formation of the anion **13** and nucleophilic substitution of bromide at the Pd[7] leads to palladacycles **14**

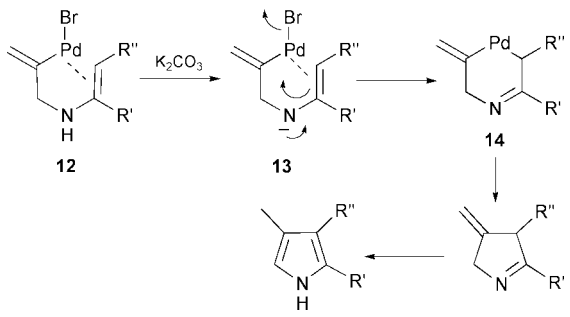

Scheme 4

DOI: 10.1039/b002211j

Table 1

Entry	Amine	Alkyne/allene **7**	Enamine **8** (yield)	Pyrrole **9** (yield)
a	**3**	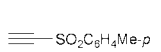	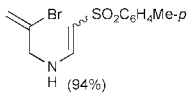 (94%)	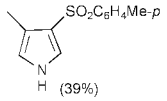 (39%)
b	**3**	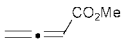	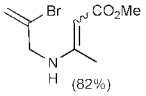 (82%)	 (41%)
c	**3**	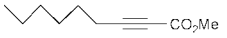	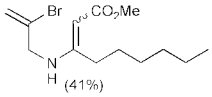 (41%)	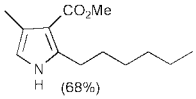 (68%)
d	**3**		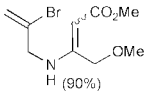 (90%)	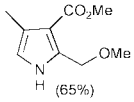 (65%)
e	**3**	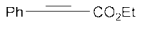	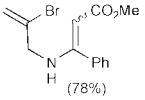 (78%)	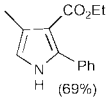 (69%)
f	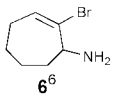 **6**[6]		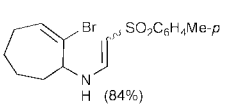 (84%)	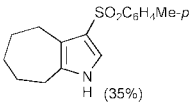 (35%)
g	**6**		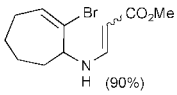 (90%)	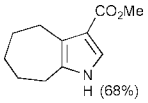 (68%)
h	**6**		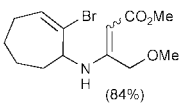 (84%)	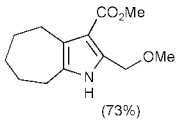 (73%)

which after reductive elimination and isomerisation produces the pyrroles.

Nucleophilic substitution at Pd(II) followed by reductive elimination is a process well known in the literature[7] and in the current reactions more likely than disfavoured 5-*endo* cyclisation. Some related synthesis of pyrrolidine[8] and pyrroline[9] derivatives that involve nucleophilic substitution at Pd(II) are known.

The same approach was applied for the synthesis of **15**, a potentially important pyrrole for the preparation of compounds with anti-inflammatory activity[10] (Scheme 5). Performing the cyclisation reaction in the presence of a Pd-catalyst afforded the desired pyrrole in 94% yield. In this case the anion is formed by deprotonation at the methylene group adjacent to the ester functionality.

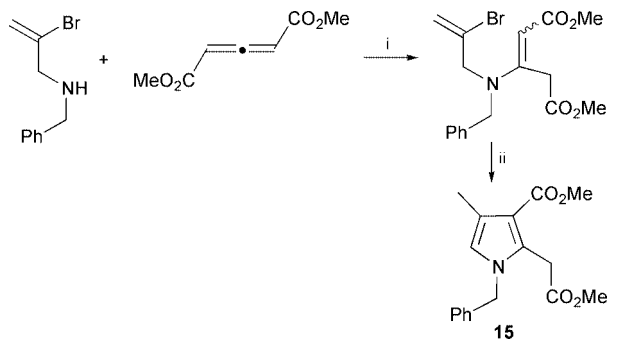

Scheme 5 *Reagents and conditions*: i, DMF, room temp., 86%; ii, $Pd(OAc)_2$, PPh_3, K_2CO_3, DMF, 85 °C, 94%.

In conclusion, we report a novel synthetic route for the preparation of substituted pyrroles. The two step procedure involving enamine formation followed by Pd-catalysed cyclisation produces pyrroles in good yields.

We thank the EPSRC and Leeds University for support.

Notes and references

1 *Comprehensive Heterocyclic Chemistry*, ed. A. Katritzky and C. W. Rees, Pergamon Press, Oxford, 1984, vol. 4, pp. 1–531; *Comprehensive Heterocyclic Chemistry*, ed. A. Katritzky, C. W. Rees and E. F. V. Scriven, Pergamon Press, Oxford, 1996, vol. 2, pp. 1–257.

2 G. Grible, in *Comprehensive Heterocyclic Chemistry*, ed. A. Katritzky, C. W. Rees and E. F. V. Scriven, Pergamon Press, Oxford, 1996, vol. 2, pp. 207–257.

3 (*a*) R. J. Sundberg, in *Comprehensive Heterocyclic Chemistry*, ed. A. Katritzky, C. W. Rees and E. F. V. Scriven, Pergamon Press, Oxford, 1996, vol. 2, pp. 119–206; (*b*) T. L. Gilchrist, *J. Chem. Soc., Perkin Trans. 1*, 1999, 2849.

4 M. Mori, K. Chiba and Y. Ban, *Tetrahedron Lett.*, 1977, 1037; C. Chen, D. R. Lieberman, R. D. Larsen, T. R. Verhoven and P. J. Reider, *J. Org. Chem.*, 1997, **62**, 2676; L. Hegedus, T. A. Mulhern and A. Mori, *J. Org. Chem.*, 1985, **50**, 4282.

5 J. S. McManis and B. Ganem, *J. Org. Chem.*, 1980, **45**, 2041; H. Yamamoto and K. Maruoka, *J. Am. Chem. Soc.*, 1981, **103**, 6133.

6 S. R. Sandler, *J. Org. Chem.*, 1967, **32**, 3876; M. Banwel and C. Cowden, *Aust. J. Chem.*, 1994, **47**, 2235.

7 I. Coudanne and G. Balme, *Synlett*, 1998, 998; G. Balme, D. Bouyssi, R. Faure, J. Gore and B. Vanhemelryck, *Tetrahedron*, 1992, **48**, 3891; G. Balme and D. Bouyssi, *Tetrahedron*, 1994, **50**, 403; P. Vittoz, D. Bouyssi, C. Traversa, J. Gore and G. Balme, *Tetrahedron Lett.*, 1994, 1871.

8 B. Clique, N. Monteiro and G. Balme, *Tetrahedron Lett.*, 1999, 1301.

9 R. Larock, M. J. Doty and X. Han, *Tetrahedron Lett.*, 1998, 5143.

10 M. N. Chang, T. Biftu, D. A. Boulton, P. E. Finke and M. L. Hamond, *Eur. J. Med. Chem. Chim. Ther.*, 1986, 363; H. Carpio, E. Galeazzi, R. Greenhouse, A. Guzman, E. Velarde, Y. Antonio, F. Franco, A. Leon, V. Perez, R. Salas, D. Valdes, J. Ackrell, D. Cho, P. Gallegra, O. Halpern, R. Koehler, M. L. Maddox, J. M. Muchowski, A. Prince, D. Tegg, T. C. Thurber, A. R. VanHorn and D. Wren, *Can. J. Chem.*, 1982, **60**, 2295.

ChemComm

Completion of a catalytic cycle of zirconium-catalyzed alkylation of silanes by addition of organic halides

Yasuyuki Ura, Ryuichiro Hara and Tamotsu Takahashi*

Catalysis Research Center and Graduate School of Pharmaceutical Sciences, Hokkaido University; and CREST, Science and Technology Corporation (JST) Sapporo 060-0811, Japan. E-mail: tamotsu@cat.hokudai.ac.jp

Received (in Cambridge, UK) 28th March 2000, Accepted 11th April 2000

A catalytic cycle in zirconium-catalyzed alkylation of silanes with secondary Grignard reagents was completed by addition of organic halides which were not incorporated in the products.

We have found and reported catalytic cycles containing a Zr(II) species and zirconacycles in carbon–carbon bond formation by the reaction of olefins and/or acetylenes with Grignard reagents.[1–5] One principle of the Zr(II)-mediated or -catalyzed reactions is the use of facile interchange of its oxidation states, II and IV. The zirconium(II) species is known to be of good π-electron accepting ability and oxidatively couples two unsaturated organic molecules. During the coupling reaction, the Zr(II) species is converted into Zr(IV). On these bases, zirconium(II)-catalyzed reactions have been developed involving olefins[1–4] and, in some cases, acetylenes.[5] We also reported not only unsaturated substrates but also dihydrogen[2] or silanes[3] as partners of unsaturated compounds such as olefins. During our investigations of zirconium-mediated alkylation reactions of silanes, we found that addition of organic halides led to a catalytic cycle in which the organic halides were not incorporated in the products. Herein, we report a novel type of catalytic cycle in alkylation of silanes with secondary Grignard reagents using zirconium.

It is well known that when H_2SiPh_2 is treated with Pr^nMgBr in THF at room temperature, a nearly quantitative yield of $Pr^nSi(H)Ph_2$ **1** is obtained [eqn. (1)].[6] It is interesting that

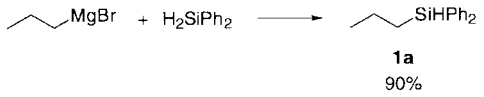

(1)

H_2SiPh_2 does not react at all with the more sterically hindered Pr^iMgBr under the same conditions [eqn. (2)].

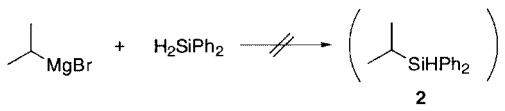

(2)

However, we found that when a stoichiometric amount of $(C_5H_5)_2ZrCl_2$ was added in the presence of a two-fold amount of Pr^iMgBr, the reaction of H_2SiPh_2 with Pr^iMgBr proceeded to give **1a**, instead of the expected product $Pr^iSi(H)Ph_2$ **2** [eqn. (3)]. A stoichiometric amount of $(C_5H_5)_2ZrCl_2$ is required

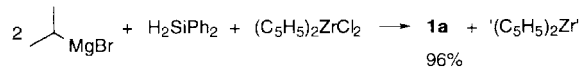

(3)

since the outcome of the reaction is explained by the total conversion to **1a**, '$(C_5H_5)_2Zr$,' *n*-C_3H_8 and 2 equiv. of MgX_2. Since the Pr^i group was changed to an Pr^n group in the product, it is reasonable to consider that the Pr^i group is converted into propene on zirconium and then reacts with silane to afford $Pr^nSi(H)Ph_2$ and the Zr(II) species.

In order to extend this stoichiometric reaction to a catalytic reaction, oxidation of the built-up Zr(II) species was investigated. We found that certain organic halides were suitable for oxidation of the '$(C_5H_5)_2Zr$' species *via* oxidative addition[7–9] and tolerate the reaction conditions.

Under catalytic conditions, typically 10 mol% of $(C_5H_5)_2ZrCl_2$ and 1 equiv. of an organic halide were employed [eqn. (4)]. The results of a comparison study using various

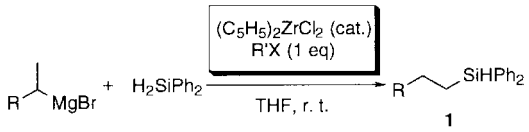

(4)

organic halides as additives are shown in Table 1 As a control experiment, when no organic halide was added, the reaction gave only 22% yield of Pr^nSiHPh_2 **1a**. When 1 equiv. of bromo- or iodo-propane was added, the desired product was obtained in 67 and 91% yield, respectively. This remarkable improvement clearly showed that a catalytic cycle was achieved. The best result of 99% yield was obtained when 1,3-dibromopropane was used as the additive. Though bromobenzene, bromopropane and iodopropane showed fairly good performances, iodobenzene showed a very poor effect on this reaction, which may be due to the readily occurring deiodination.[9] 1,3-Dibromopropane was the best choice by far as additive and the reaction proceeded with as little as 2 mol% of the catalyst. In the absence of $(C_5H_5)_2ZrCl_2$ **1a** was not formed.

Similarly, when H_2SiPh_2 was treated under the same conditions with 2 equiv. of Bu^sMgCl, Bu^nSiHPh_2 **1b** was obtained in 89% yield. In spite of our attempts, tertiary Grignard reagents such as Bu^tMgCl or secondary Grignard reagents such as cyclohexylmagnesium bromide did not successfully promote this reaction owing, probably, to the instability of the corresponding disubstituted-olefin zirconium complexes.

To understand the role and the superiority of 1,3-dibromopropane, 2-benzyl-1,3-dibromopropane **3** was used as an

Table 1 Reactions of Pr^iMgBr with H_2SiPh_2 in the presence of a catalytic amount of $(C_5H_5)_2ZrCl_2$ and various organic halides[a,b]

Entry	R′X	Cp_2ZrCl_2/ eq	Time/h	Yield (%)[c]
1	—	0.1	24	22
2	1-Bromopropane	0.1	6	67
3	1-Iodopropane	0.1	6	91
4	1,3-Dibromopropane	0.1	3	99
5	1,3-Dibromopropane	0.02	24	93
6	1,3-Dibromopropane	0.01	18	41
7	1,3-Diiodopropane	0.1	3	3
8	Bromobenzene	0.1	6	78
9	Iodobenzene	0.1	1	2[d]
10	2-Bromopropene	0.1	24	73

[a] R = Me, corresponding to eqn. (4). [b] Typical reaction conditions: H_2SiPh_2 (0.5 mmol), $(C_5H_5)_2ZrCl_2$ (as indicated), Pr^iMgBr (1.5 mmol), R′X (0.5 mmol); room temp. [c] Yields were determined by GC. [d] PhI was consumed in 1 h and further reaction did not proceed.

DOI: 10.1039/b002516j

oxidation reagent and the catalytic reaction was carried out [eqn. (5)]. A mixture of three products, benzylcyclopropane **4**

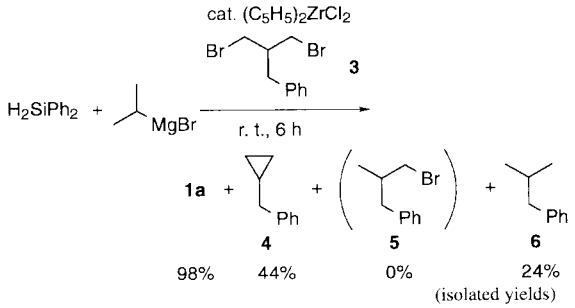

(5)

and reduction products **5** and **6** were obtained with **5** observed at an early stage. After completion of the reaction, two products, **4** and **6** were obtained in 44 and 24% yields, respectively. The formation of the major product **4** is explained by an oxidative addition of one carbon–bromine bond of **3** to the zirconium(II) species, followed by nucleophilic ring closure forming a cyclopropane ring and $(C_5H_5)_2ZrBr_2$.

On the basis of these observations, the mechanism of Scheme 1 is proposed. Zirconium–olefin complex **7** is formed and reacts with H_2SiPh_2 (**7** → **8**). Reductive elimination of the silylated compound gives Pr^nSiHPh_2 **1**. The so-formed '$(C_5H_5)_2Zr$' reacts with an alkyl bromide (RX) to give **9**,[7] followed by ligand exchange with Pr^iMgBr and β-hydride elimination to regenerate $(C_5H_5)_2Zr(C_3H_6)$ **7**. Alternatively, oxidation of '$(C_5H_5)_2Zr$' with alkyl bromides might afford $(C_5H_5)_2ZrX_2$ which is also converted into **7** by the reaction with Pr^iMgBr. An alkyl bromide plays an important role in reoxidizing the zirconium(II) species to zirconium(IV). In its absence, regeneration of the catalyst does not occur and '$(C_5H_5)_2Zr$' reacts with H_2SiPh_2 leading to the μ-hydride bridged dimer **10**.[3a]

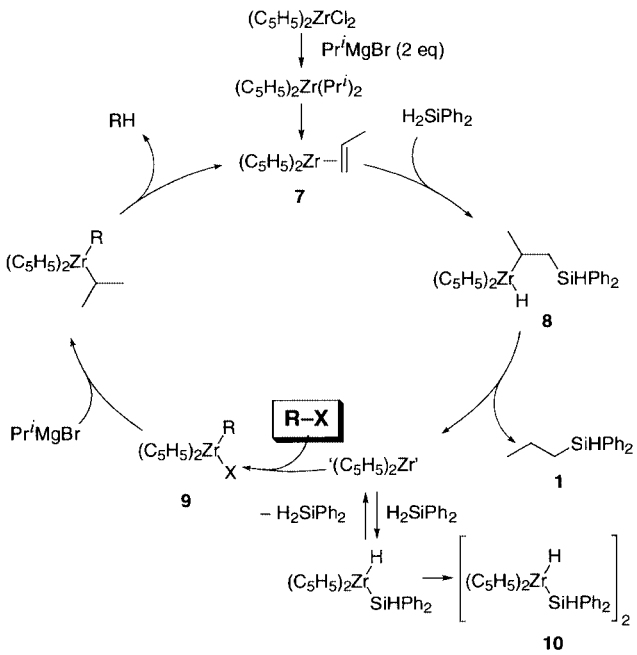

Scheme 1

One-pot reaction of H_3SiPh with 3 Pr^iMgBr without a catalyst for 1 h followed by the addition of 10 mol% of $(C_5H_5)_2ZrCl_2$ and 1,3-dibromopropane selectively afforded $HSi(Pr^i)(Pr^n)Ph$ **11** in 66% yield [eqn. (6)]. An Pr^i group was

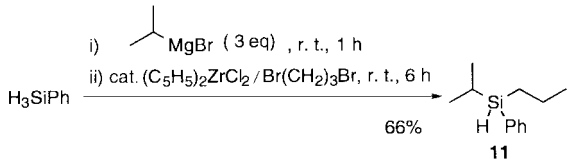

(6)

incorporated directly from the Grignard reagent in the absence of the catalyst, and an Pr^n group was incorporated after the addition of the zirconium catalyst with 1,3-dibromopropane.

We conclude that a zirconium(II) species is efficiently oxidized by organic halides, which assists regeneration of the active catalyst. We believe this is the first example of a zirconium(II)-catalyzed reaction in which an oxidant is explicitly added to complete the catalytic cycle. Further studies to clarify the mechanism are in progress.

Notes and references

1 T. Takahashi, T. Seki, Y. Nitto, M. Saburi, C. J. Rousset and E. Negishi, *J. Am. Chem. Soc.*, 1991, **113**, 6266.

2 T. Takahashi, N. Suzuki, M. Kageyama, Y. Nitto, M. Saburi and E. Negishi, *Chem. Lett.*, 1991, 1579.

3 (*a*) T. Takahashi, M. Hasegawa, N. Suzuki, M. Saburi, C. J. Rousset and E. Negishi, *J. Am. Chem. Soc.*, 1991, **113**, 8564; (*b*) J. Y. Corey and X.-H. Zhu, *Organometallics*, 1992, **11**, 672; (*c*) M. R. Kesti and R. M. Waymouth, *Organometallics*, 1992, **11**, 1095.

4 N. Suzuki, D. Y. Kondakov and T. Takahashi, *J. Am. Chem. Soc.*, 1993, **115**, 8485.

5 K. Kasai, Y. Liu, R. Hara and T. Takahashi, *Chem. Commun.*, 1998, 1989.

6 I. Fleming, *Organic Silicon Chemistry* in *Comprehensive Organic Chemistry*, ed. D. Barton and W. D. Ollis, Pergamon, Oxford, 1979, vol. 3, p. 541; R. N. Meals, *J. Am. Chem. Soc.*, 1946, **68**, 1880; W. H. Nebergall, *J. Am. Chem. Soc.*, 1950, **72**, 4702.

7 G. M. Williams, K. I. Gell and J. Schwartz, *J. Am. Chem. Soc.*, 1980, **102**, 3660.

8 T. Takahashi, M. Kotora, R. Fischer, Y. Nishihara and K. Nakajima, *J. Am. Chem. Soc.*, 1995, **117**, 11039.

9 R. Hara, W.-H. Sun, Y. Nishihara and T. Takahashi, *Chem. Lett.*, 1997, 1251.

Unusual solvatochromism in phosphonylated polythiophenes. Poly[3-(11-diethylphosphorylundecyl)thiophene]†‡§

Janusz Kowalik and Laren M. Tolbert

School of Chemistry and Biochemistry, Georgia Institute of Technology, Atlanta, GA 30332-0400, USA. E-mail: janusz.kowalik@chemistry.gatech.edu

Received (in Corvallis, OR, USA) 25th February 2000, Accepted 6th April 2000

Highly stereoregular poly[3-(11-diethylphosphorylundecyl)thiophene] 2 is soluble in both aprotic and protic solvents, yet displays a remarkable solvatochromism involving a hydrogen bond network with the phosphonate moiety.

Since their discovery and synthesis two decades ago, polythiophenes (pT) have progressed swiftly to applications.[1] A promising area for conducting polymers includes development of sensors by using macromolecules with specific receptor groups.[1b,2] The search for functional groups influencing the properties of pTs as well as allowing the design of multidimensional, supramolecular systems for truly molecular applications is well underway. Among the most important properties of polythiophenes are thermochromism and solvatochromism. The origin of both phenomena is the optical response to a conformon formation, twists in which the planarity of the backbone has been disrupted. Both features are believed to be single chain phenomena, that is, the coexistence of two separate phases in different ratios during the process is responsible for the chromic behavior.[3] Given the diverse conformational chemistry produced in nature by organophosphorus moieties, the use of a phosphonate group in the polythiophene structure provides an attractive approach to developing higher orders of organization (supramolecular systems). Here, we offer the first example of a polythiophene containing the dialkylphosphonate functionality.[4] The polymer belongs to a limited group of polythiophenes soluble in both protic and aprotic solvents, yet exhibits remarkably divergent behavior in the two solvents. Polymer **2** was synthesized in a stereocontrolled process involving nickel-mediated Negishi-type condensation of **1**[5a] obtained in a series of reactions illustrated in Scheme 1.

The resulting polymer was *ca.* 90% stereoregular, with a predominantly head-to-tail (HT–HT) connectivity.[5a,6] The

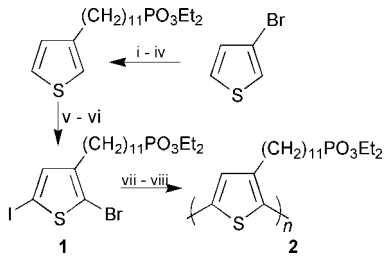

Scheme 1 *Reagents and conditions*: i, $BrMg(CH_2)_{11}OMOM$, $Ni(dppe)Cl_2$, Et_2O, r.t. → reflux, 2 h, 70%; ii, HCl(aq)/MeOH, reflux, 6 h, 100%; iii, MsCl, Py, CH_2Cl_2, 0–5 °C, 5 h, 85%; iv, $NaPO_3Et_2$, THF, reflux, 30 h, 89%; v, NBS, DMF, r.t., 3 h, 88%; vi, I_2, HgO, PhH, 12 h, 80%; vii, Zn*,[5a] THF; viii, $Ni(dppe)Cl_2$, THF, r.t., 3 d.

† Dedicated to Professor Przemysław Mastalerz on the occasion of his 75th birthday.

‡ First presented in part at *The Fifth Chemical Congress of North America*, Cancun, Quintana Roo, Mexico, November 11–15, 1997, p. 123.

§ Electronic supplementary information (ESI) available: solutions of **2** in CH_2Cl_2 (left) and MeOH (right). See http: www.rsc.org/suppdata/cc/b0/b001621g/

polymer displayed a high degree of conjugation in the solid state, as indicated by the presence of a vibrational structure in the UV–VIS spectrum and a λ_{max} value at 558 nm with a shoulder at 606 nm.[5] In aprotic solvents (THF, $CHCl_3$) the absorption spectrum became featureless and the absorption maximum shifted to 440 nm ($\Delta\lambda_{max}$ = 118 nm). Remarkably, in protic solvents (ethanol, methanol) the shape of the absorption spectrum remained similar to that in the solid state with only a small higher-energy shift in the absorption maxima, Fig.1(*a*) and (*b*).

The solvatochromic properties of **2** were observed in a mixed CH_2Cl_2–MeOH system, with the results shown in Fig. 1. Increasing the concentration of the CH_2Cl_2 caused a reduction in the intensity of the absorption in the 550–650 nm region, with concomitant increase in the higher energy region with a maximum at *ca.* 440 nm. The presence of a pseudo-isosbestic point[7] suggested two separate species (conformons) existing in equilibrium at ratios which depended on the concentration of the protic and aprotic solvents. Interestingly, the vibrational structure of the absorption is maintained at 10% CH_2Cl_2 in MeOH, which suggests the extended conjugation within the polyaromatic backbone was rapidly lost beyond that point, owing to the enhanced freedom of rotation. There are at least three possible self-organization mechanisms to be considered: self-assembly *via* alkyl chain association, phosphoryl group dipole–dipole interaction and hydrogen bonding. Owing to exceptionally good vibrational characteristics and the sensitivity of the phosphonate moiety to its microenvironment, IR spectroscopy has long been an attractive technique in studying its hydrogen bond interactions. The highly polarized P=O bond in organophosphorus compounds is an excellent hydrogen bond acceptor, yielding complexes ranging from weak (<1 kcal mol^{-1})[8] to strong (>10 kcal mol^{-1})[9] as a function of the hydrogen bond donor. Fig. 2 illustrates the dependence of the wavenumber shift of the ν(P=O) vibration on the solvent used.

As expected by analogy with adsorption of phosphonates on transition metal surfaces,[10] the major interaction with the hydrogen donor involves bonding *via* the lone pair orbitals of

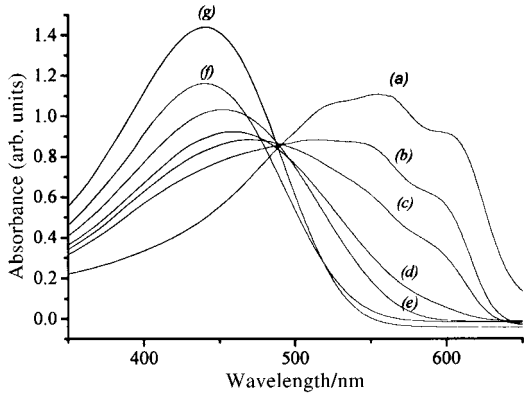

Fig. 1 Absorption spectra and solvatochromism of **2**: (*a*) solid film and (*b*)–(*g*) 10^{-4} M solutions in CH_2Cl_2–MeOH, v/v = *(b)* 0:10, (*c*) 1:9, (*d*) 2:8, (*e*) 3:7, (*f*) 8:2, (*g*) 10:0.

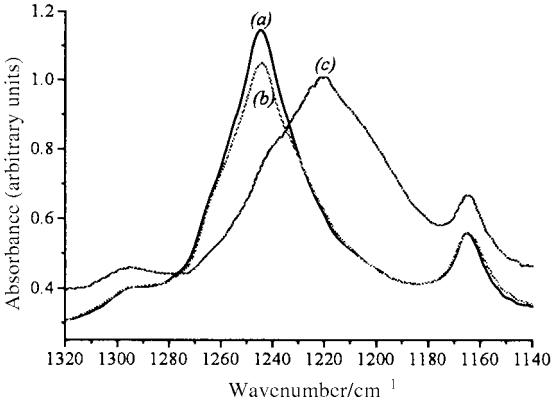

Fig. 2 IR spectra of **2** (P=O vibration): (*a*) solid film, (*b*) solid film saturated with CCl_4, (*c*) solid film saturated with MeOH.

the P=O oxygen atom. This leads to a weakening of the P=O bond and to a lowering of the corresponding mode frequency. In the gas phase, where the molecule is considered free, this peak has a maximum at 1276 cm^{-1}.[8] In our solid polymer film and the sample saturated with CCl_4 the P=O stretch appears at 1244 cm^{-1}. In the absence of a hydrogen donor it is likely that a dipole–dipole interaction between the phosphonate groups leads to aggregation[8,10a,11] and is responsible for the shift. Saturation of the polymer film with methanol leads to a shift of the P=O vibration to 1216 cm^{-1}. This absorption displays a shoulder at 1208 cm^{-1}. We suggest that the presence of two vibrational modes relates to the presence of two modes of interaction of the phosphoryl oxygen atom with the hydrogen bond donor, the 1208 cm^{-1} peak corresponding to interaction of the P=O group using both lone electron pairs.[8] The frequency shift of 28 cm^{-1} is considered indicative of a strong hydrogen-bonding interaction.[12] Hydrogen bond interactions were tested by NMR spectroscopy. ^{1}H NMR spectra for solutions of the polymer **2** in THF-d_8 and CD_3OD are shown in Fig. 3(*a*) and (*b*).

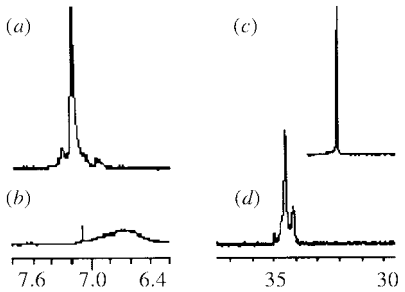

Fig. 3 ^{1}H NMR spectra of **2** (aromatic region) in: (*a*) THF-d_8, (*b*) CD_3OD (δ relative to TMS). ^{31}P NMR spectra of **2** in: (*c*) THF-d_8, (*d*) CD_3OD (δ relative to 85% H_3PO_4 (external)).

While the aromatic proton resonance of **2** in deuterated THF solution appeared as a sharp singlet at δ 7.08 (fast spin–spin relaxation), the corresponding resonance in CD_3OD solution showed line broadening characteristic of a spectrum of a highly associated species. The breadth of the aromatic proton signal in the range δ 6.3–7.1 could also arise from paramagnetic line broadening,[13] which is related to the observed extension of the effective conjugation in the polyheterocyclic chain. This is in agreement with the results of the UV–VIS spectroscopy. Fig. 3(*c*) and (*d*) illustrate ^{31}P NMR spectra of **2** in THF-d_8 and CD_3OD. The observed chemical shifts of δ *ca.* 32–34 (*vs.* 85% H_3PO_4, external) are consistent with the dialkyl phosphonate moiety.[14] A sharp, narrow signal at δ 32.11 due to an averaged species appeared in the THF-d_8 solution, whereas in CD_3OD solution broader, multiple resonances were observed in the range δ 34.97–34.12 ppm, with the most intense feature at δ 34.48. In contrast to the THF solution, for which delocalization of rapid spin diffusion resulted in a single averaged ^{31}P resonance, in CD_3OD solution the protonated segments of solvated phosphonate remained distinct on the NMR time scale giving rise to a multiplet of signals. The downfield shift of the resonance peak in methanol solution, $\Delta\delta$ = 2.4 ppm, is most likely a result of the deshielding effect due to hydrogen-bonding interactions. For interactions of diethyl 4-vinylphenylphosphonate with 1,1,1,3,3,3-hexafluoroisopropyl alcohol the $\Delta\delta$ value at 0.7 ppm corresponds to an enthalpy of hydrogen bond formation of $-\Delta H$ = 8.6 kcal mol^{-1}.[12b] Our considerably larger value of $\Delta\delta$ seems to indicate cooperative interaction of several factors, leading to a very efficient self-organization of **2** in a protic solvent.

In summary, we describe the first synthesis of a polythiophene containing a phosphonate function. The energy gap difference of *ca.* 0.4 eV between the polymer dissolved in a protic *vs.* aprotic solvent results in a remarkable solvatochromic effect. We suggest that a combination of London forces, dipole–dipole interactions and a hydrogen-bond network involving a protic solvent and the phosphonate moiety cooperate in stabilizing an extended conjugated form of the polymer.

Support of this research from the US Department of Energy is gratefully acknowledged. We thank Dr Tomasz Wąsowicz for the EPR spectra and Dr David M. Collard for valuable discussions.

Notes and references

1 (*a*) *Handbook of Conducting Polymers*, ed. T. A. Skotheim, R. L. Elsenbaumer and J. R. Reynolds, Marcel Dekker Inc., New York, NY, 2nd edn., 1998, pp. 823–1073; (*b*) *Polythiophenes–Electrically Conductive Polymers*, ed. G. Schopf and G. Koßmehl, Springer-Verlag, New York, 1997, pp. 113–123.

2 G. Bidan, M. Billon, T. Livache, G. Mathis, A. Roget and L. M. Torres-Rodrigues, *Synth. Met.*, 1999, **102**, 1363; P. N. Bartlett and Y. Astier, *Chem. Commun.*, 2000, 105.

3 S. D. D. V. Rughooputh, S. Hotta, A. J. Heeger and F. Wudl, *J. Polym. Sci. Polym. Phys. Ed.*, 1987, **25**, 1071; D. J. Sandman, *TRIPS*, 1994, **2**, 44; O. Inganäs, *TRIPS*, 1994, **2**, 189; K. Faïd, M. Fréchette, M. Ranger, L. Mazerolle, I. Lévesque and M. Leclerc, *Chem. Mater.*, 1995, **7**, 1390; R. D. McCullough, P. C. Ewbank and R. S. Loewe, *J. Am. Chem. Soc.*, 1997, **119**, 633, for a review on chromism in polythiophenes discussing possible mechanism and driving force, see: ref. 1(*a*) pp. 695–706..

4 J. Kowalik and L. M. Tolbert, *The Fifth Chemical Congress of North America*, Cancun, Quintana Roo, Mexico, November 11–15, 1997, p. 123. Subsequent to this report, another synthesis of phosphonic acid modified polyalkylbithiophene has appeared: K. Heuze and R. D. McCullough, *Abstracts of Papers of the American Chemical Society*, 1999, vol. 218, p. 219.

5 (*a*) 'Rieke zinc' (Zn*) was used in the preparation of organozinc derivatives and subsequent polymerization reactions; T.-A. Chen, X. Wu and R. Rieke, *J. Am. Chem. Soc.*, 1995, **117**, 233; (*b*) T. Kaniowski, W. Łużny, S. Nizioł, J. Sanetra and M. Trznadel, *Synth. Met.*, 1998, **92**, 7; (*c*) J. Mardalen, E. J. Samuelsen and A. O. Pedersen, *Synth. Met.*, 1993, **55**, 378; (*d*) D. Fichou, G. Horowitz, B. Xu and F. Garnier, *Synth. Met.*, 1992, **48**, 167.

6 Based upon ^{1}H NMR evidence: major aromatic resonance at δ 6.95 and the relative ratio of α-methylene resonances at δ 2.77 (HT) and δ 2.53 (HH); *cf.* M. Sato and H. Morii, *Macromolecules*,1991, **24**, 1196.

7 The presence of an isosbestic point is, strictly speaking, a consequence of Beer's law. For this system, in which the solvent changes occur as well as solute concentration changes, strict adherence to isosbestic behavior is not expected.

8 L. Bertilsson, I. Enquist and B. Liedberg, *J. Phys. Chem. B*, 1997, **101**, 6021.

9 D. Hadži and N. Kobilarov, *J. Chem. Soc. A*, 1966, 439.

10 (*a*) M. A. Henderson and J. M. White, *J. Am. Chem. Soc.*, 1988, **110**, 6939; (*b*) R. I. Hedge, C. M. Greenlief and J. M. White, *J. Phys. Chem.*, 1985, **89**, 2886.

11 A. J. Barnes, S. Lomax and B. J. Van Der Veken, *J. Mol. Struct.*, 1983, **99**, 137.

12 (*a*) J. Sun and I. Cabasso, *J. Polym. Sci., Polym. Chem. Ed.*, 1989, **27**, 3985; (*b*) H. Zhuang, E. Pearce and T. K. Kwei, *Macromolecules*, 1994, **27**, 6398.

13 For the methanol solution of **2** a weak EPR signal was observed at 298 K, which increased in intensity at 77 K. The signal was a single line with g_{iso} = 2.0040 and ΔH_{pp} = 4 G at 77 K. No signal was detected in the THF solution under similar conditions. J. Kowalik, T. Wąsowicz and L. M. Tolbert, manuscript in preparation.

14 *Phosphorus-31 NMR: Principles and Applications*, ed. D. G. Gorenstein, Academic Press Inc., New York, NY, 1984, p. 568.

ChemComm

Synthesis, crystal and molecular structures of the novel, structurally different, cage compounds $P_6C_4Bu^t_4SiI_2$ and $P_6C_4Bu^t_4GeI_2$, resulting from *intra*-molecular coupling of two 1,2,4-triphospholyl rings

Anthony G. Avent, F. Geoffrey N. Cloke,* Matthew D. Francis, Peter B. Hitchcock and John F. Nixon*

School of Chemistry, Physics and Environmental Science, University of Sussex, Sussex, Brighton, UK BN1 9QJ. E-mail: j.nixon@sussex.ac.uk

Received (in Cambridge, UK) 29th February 2000, Accepted 12th April 2000

Treatment of EI_4 (E = Si or Ge) with 2 equivalents of $K[P_3C_2Bu^t_2]$ affords the novel cage compounds $P_6C_4Bu^t_4SiI_2$ and $P_6C_4Bu^t_4GeI_2$ respectively, whose molecular structures, determined spectroscopically and by single crystal X-ray diffraction studies, are different both in solution and in the solid state.

Phosphorus substituted analogues of the aromatic cyclopentadienyl anion, $C_nR_nP_{5-n}$ (n = 0–4), are of considerable current interest.[1] In particular, the 3,5-di-*tert*-butyl-1,2,4-triphospholyl anion, $P_3C_2Bu^t_2{}^-$ **1**, has been used in the preparation of a range of transition metal complexes[2–7] in which a variety of bonding modes have been observed such as in $[M(\eta^5\text{-}P_3C_2Bu^t_2)_2]$ (M = Fe or Ru), $[M(\eta^5\text{-}P_3C_2Bu^t_2)(\eta^5\text{-}C_5Me_5)\{W(CO)_5\}]$ (M = Fe or Ru) and *trans*-$[M(\eta^1\text{-}P_3C_2Bu^t_2)_2(PEt_3)_2]$ (M = Pt or Pd).

In contrast however, examples of main group element compounds derived from **1** are comparatively rare and to date are restricted to a handful of examples, namely $[In(\eta^5\text{-}P_3C_2Bu^t_2)]$, $P_3C_2Bu^t_2CH(SiMe_3)_2$, $[Tl(\eta^5\text{-}P_3C_2Bu^t_2)]$, $[M(\eta^5\text{-}P_3C_2Bu^t_2)_2]$ and $[M(\eta^5\text{-}P_3C_2Bu^t_2)(\eta^5\text{-}C_5Me_5)]$ (M = Sn or Pb).[8–11] We therefore decided to examine the reaction of **1** (in the form of its recently synthesised potassium salt),[9] with silicon and germanium tetraiodides.

Surprisingly, although the resulting products both have the anticipated formulae $P_6C_4Bu^t_4EI_2$ (E = Ge **2**, E = Si **3**) in which two iodides may have been expected to have been replaced by $\eta^1\text{-}P_3C_2Bu^t_2$ ligands, they actually contain two different novel $P_6C_4Bu^t_4$ cages which arise from different *intra*-molecular coupling reactions of the adjacent 1,2,4-triphospholyl rings.

Thus, treatment of 2 equivalents of **1** with EI_4 (E = Si or Ge) led to the moisture sensitive compounds **2** (E = Ge) and **3** (E = Si), respectively (Scheme 1), which were recrystallised from diethyl ether (**3**, orange crystals, mp 190 °C; yield 55%) or hot heptane (**2**, red crystals, mp 275 °C; yield 52%). Both compounds exhibited the expected parent ions in their mass spectra (*m/z* 789 for **2**; 744 for **3**), however the solution $^{31}P\{^1H\}$ and ^1H NMR spectroscopic data are only consistent with the proposed cage structures, which were subsequently confirmed by single crystal X-ray diffraction studies (*vide infra*).

The ^1H NMR spectrum of **2** shows only two singlets for the two different types of Bu^t groups, while the $^{31}P\{1H\}$ NMR spectrum, which has been fully analysed and successfully simulated as an AA′MM′XX′ spin system,† confirms the symmetric structure and as expected contains no resonances involving unsaturated phosphorus atoms. The formation of the cage compound **2** clearly results from the anticipated bis-$(\eta^1\text{-}P_3C_2Bu^t_2)$–$GeI_2$ intermediate **4** which then rapidly undergoes two further intramolecular [2 + 2] cycloaddition reactions generating four new P–C bonds.

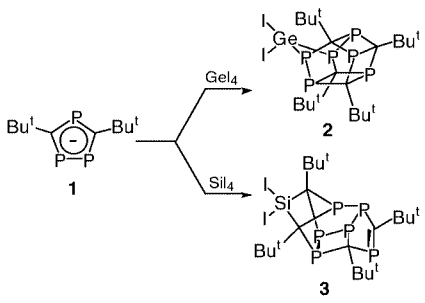

Scheme 1

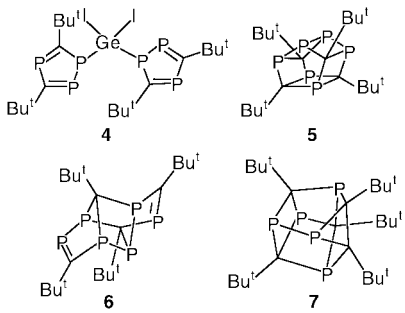

The molecular structure of **2**‡ which is shown in Fig. 1, shows some similar features to the recently reported hexaphosphaprismane $P_6C_4Bu^t_4$ **5** synthesised by Regitz and coworkers[12] *via* an unusual light-induced valence isomerisation reaction of **6**, but is different from the $P_5C_5Bu^t_5$ cage structure **7** constructed by oxidative coupling of $P_3C_2Bu^t_2$ and $P_2C_3Bu^t_3$ ring anions.[13] Presumably the steric effect of the large iodide ligands attached to Ge in the presumed intermediate **4** facilitates the ring coupling reaction leading to **2**.

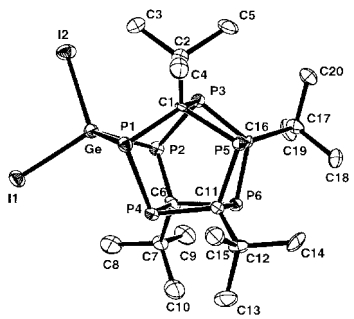

Fig. 1

The molecular structure of **3**, determined by a single crystal X-ray diffraction study,‡ which is shown in Fig. 2, unexpectedly shows that the Si is attached to two *carbon* atoms within the cage, resulting in a much more asymmetric structure than observed for **2** involving a P=C double bond between P(6) and C(4) and a five-atom phosphorus network P(1)–P(2)–P(3)–P(4)–P(5). In accord with the above structure, the 1H NMR spectrum exhibits four distinct resonances for the non-equivalent Bu^t groups, while $^{31}P\{1H\}$ NMR spectrum of **3** consists of

DOI: 10.1039/b001632m

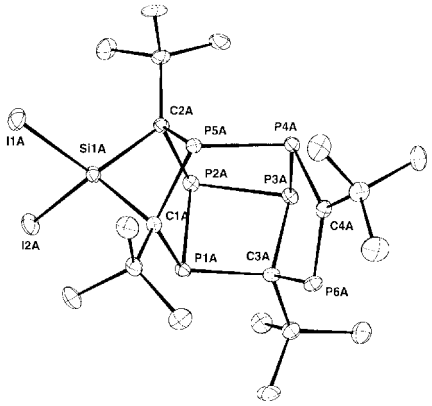

Fig. 2

six distinct resonances exhibiting several $^1J_{(PP)}$ couplings in the range 110–300 Hz. The lowest field signal (δ 357.0) which is in the region typical of P=C bonds and involves only small couplings clearly corresponds to P(6). The two highest field resonances (δ = −19.1 and −24.4) which exhibit a single large coupling, can readily be assigned to P(5) and P(1), respectively. The remaining resonances at δ 124.1, 78.4 and 24.6 can be attributed to P(2), P(3) and P(4), respectively.

The mechanism of formation of **3** is currently unknown but it seems likely that the first step involves Si–P bond formation. Attempts to form the novel silylene or germylene species $P_6C_4Bu^t{}_4E$: (E = Si, **8** , E = Ge, **9**) by treatment of **2** and **3** with sodium napthalenide in THF, led in each case to regeneration of the $P_3C_2Bu^t{}_2$ ring anion **1**.

The EPSRC is gratefully acknowledged for financial support of this work.

Notes and references

† *Spectroscopic data*: for **2**: NMR (C_6D_6, 298 K): δ_H(300 MHz) 1.33 (s, 18H, Bu^t), 1.03 (s, 18H, But). δ_p(121.68 MHz) 37.23 (m, P(1), ^2JP(1)P(2)) −40.42, ^1J(P(1)P(4)) +294.99, ^2J(P(1)P(5)) +9.93, ^2J(P(1)P(3)) −10.73, ^3J(P(1)P(6)) +2.12 Hz) 145.91 (m, P(4), ^3JP(4)P(3)) +0.30, ^2JP(4)P(6)) +18.92 Hz), 217.34 (m, P(5), ^2J(P(5)P(6)) +6.16, ^2J(P(5)P(4)) −10.06 Hz). Microanalysis: Found: C, 31.5; H, 4.4. Calc.: C, 30.5; H, 4.6%.

For **3**: NMR (C_6D_6, 298 K): δ_H(300 MHz) 1.30 (s, 9H, Bu^t), 1.33 (s, 9H, Bu^t), 1.40 (s, 9H, Bu^t), 1.44 (s, 9H, Bu^t). δ_p(121.68 MHz) 357.0 (m, P(6), ^2JP(6)P(4)) 19 Hz, ^2J(P(6)P(1)) = 20, ^3J(P(6)P(2)) 19, ^3JP(6)P(5)) 11 Hz), 124.1 (m, P(2), ^1JP(2)P(3)) 291, ^1J(P(2)P(1)) 303, ^3J(P(2)P(5)) 11, ^2J(P(2)P(4)) = 11, ^3J(P(2)P(6)) 19 Hz), 88.4 (ddd, P(3), ^1J(P(3)P(2)) 291, ^1JP(3)P(4)) 150, ^2JP(3)P(1)) 12 Hz), 24.6 (m, P(4), ^2JP(4)P(6)) 19, ^1JP(4)P(3)) 150, ^3JP(4)P(1)) 8, ^2JP(4)P(2)) 11, ^1JP(4)P(5)) 110 Hz), −19.1 (dqt, P(5), ^2JP(6)P(5)) ^2JP(5)P(2)) 11, ^3JP(5)P(1)) 11 Hz, ^1JP(5)P(4)) 110 Hz), −24.4 (m, P(1), ^2JP(1)P(3)) 12, ^2JP(1)P(6)) 20, ^3JP(1)P(4)) 8, ^3JP(1)P(5)) 11, ^1JP(1)P(2)) 303 Hz). Microanalysis. Found: C, 33.1; H, 5.2. Calc.: C, 32.3, H, 4.9%.

‡ *Crystal data*: for **2**: $C_{20}H_{36}P_6GeI_2$, M = 788.70, monoclinic, space group $P2_1/n$ (no. 14), a = 11.8196(12), b = 17.491(3), c = 13.850(3) Å, β = 95.009(14)°, V = 2852.4(8) Å^3; T = 173(2) K, Z = 4, μ = 3.58 mm^{-1}, λ = 0.71073 Å, 5261 reflections collected, 5021 independent (R_{int} = 0.0458), R_1 = 0.046, wR_2 = 0.089 for $I > 2\sigma I$, R_1 = 0.090, wR_2 = 0.108 for all data.

For **3**: $C_{20}H_{36}P_6SiI_2$: M = 744.2, monoclinic, space group $P2_1$ (no. 4), a = 11.827(4), b = 15.837(9), c = 15.626(5) Å, β = 94.87(3)°, V = 2916(2) Å^3; T = 173(2) K, Z = 4, μ = 2.54 mm^{-1}, λ = 0.71073 Å, 9137 reflections collected, 8776 independent (R_{int} = 0.020), R_1 = 0.033, $wR2$ = 0.065 for $I > 2\sigma I$, R_1 = 0.042, wR_2 = 0.070 for all data.

The G. M. Sheldrick, SHELX-97 suite of programs for crystal structure analysis, University of Gottingen, Gottingen, Germany, 1997, were used to elucidate both structures.

CCDC 182/1601. See http://www.rsc.org/suppdata/cc/b0/b001632m/ for crystallographic files in .cif format.

1 K. B. Dillon, F. Mathey and J. F. Nixon, *Phosphorus: The Carbon Copy. From Organophosphorus to Phosphaorganic Chemistry*, John Wiley and Sons, Chichester, UK, 1998, pp. 1–366 and references therein.
2 R. Bartsch, P. B. Hitchcock and J. F. Nixon, *J. Chem. Soc., Chem. Commun.*, 1987, 1946.
3 P. B. Hitchcock, R. M. Matos and J. F. Nixon, *J. Organomet. Chem.*, 1995, **490**, 155.
4 R. Bartsch, P. B. Hitchcock and J. F. Nixon, *J. Organomet. Chem.*, 1988, **340**, C37.
5 R. Bartsch, A. Gelessus, P. B. Hitchcock and J. F. Nixon, *Phosphorus, Sulfur, Silicon, Relat. Elem.*, 1993, **77**, 276.
6 R. Bartsch, D. Carmichael, P. B. Hitchcock, M. F. Meidine, J. F. Nixon and G. J. D. Sillett, *J. Chem. Soc., Chem. Commun.*, 1988, 1615.
7 P. B. Hitchcock, J. F. Nixon and G. J. D. Sillett, *Nouv. J. Chimie.*, 1989, **13**, 353.
8 J. J. Durkin, M. D. Francis, P. B. Hitchcock, C. Jones and J. F. Nixon, *J. Chem. Soc., Dalton Trans.*, 1999, 4057.
9 C. S. J. Callaghan, G. K. B. Clentsmith, F. G. N. Cloke, P. B. Hitchcock, J. F. Nixon and D. M. Vickers, *Organometallics*, 1999, 18, 793.
10 V. Caliman, P. B. Hitchcock and J. F. Nixon, *J. Chem. Soc., Chem. Commun.*, 1995, 1661.
11 J. F. Nixon and G. J. D. Sillett, unpublished work.
12 A. Mack and M. Regitz, in *Carbocyclic and Heterocyclic Cage Compounds and their Building Blocks*, ed. K. K. Laali, AI Press, Stamford, CT, USA, 1999, p. 199; B. Breit, Ph.D Thesis, University of Kaiserslautern, 1992; B. Breit, U. Bergstrasser, G. Maas and M. Regitz, *Angew. Chem., Int. Ed. Engl.*, 1992, **31**, 1055; B. Breit and M. Regitz, *Chem. Ber.*, 1996, **129**, 489.
13 R. Bartsch, P. B. Hitchcock and J. F. Nixon, *J. Organomet. Chem.*, 1989, **375**, C31.

ChemComm

pH-dependent reversible polymers formed from cyclic sugar- and aromatic boronic acid-based bolaamphiphiles

Ikuo Nakazawa,[a] Sakae Suda,[a] Mitsutoshi Masuda,[b] Michihiko Asai[b] and Toshimi Shimizu*[b]

[a] *Joint Research Center for Precision Polymerization, Japan Chemical Innovation Institute, NIMC, 1-1 Higashi, Tsukuba, Ibaraki 305-8565, Japan*

[b] *National Institute of Materials and Chemical Research, 1-1 Higashi, Tsukuba, Ibaraki 305-8565, Japan. E-mail: tshmz@home.nimc.go.jp*

Received (in Columbia, MO, USA) 18th January 2000, Accepted 27th March 2000

Glucuronamide-based bolaamphiphiles are found to form a reversible, linear polymolecular array, *via* a boronate ester linkage attached to the 1,2-positions of the pyranose or furanose ring, upon complexation with an aromatic boronic acid-based homologue in aqueous solutions.

Aromatic boronic acids form complexes with *cis* diol-type hydroxy groups of carbohydrates *via* ester-linkage formation.[1–3] In particular, Shinkai *et al*. have intensively developed new aspects on aqueous sugar sensing by employing aromatic boronic acids.[4] Even though there have been some arguments about the boronate structure in aqueous solutions,[5–7] the complexes should contain a furanose form of the glucose moiety.[8] Norrild and Eggert have confirmed by ^{1}H and ^{13}C NMR spectroscopy that monoboronic acids bind preferentially to the 1,2-position and secondly to the 3,5,6-position of α-D-glucofuranose in aqueous solutions.[3] We have so far investigated the self-assembling properties of 1-glucosamide (**1**)[9] and 2-glucosamide bolaamphiphiles (**2**)[10] in water. Although the former derivative **1** possesses free C-3, C-4 and C-6 hydroxy groups, it cannot convert into the furanose form. On the contrary, the latter homologue **2** possessing the same free hydroxy groups can rearrange to the furanose resulting in free C-3, C-5 and C-6 hydroxy groups. In line with this molecular design, we have newly synthesized a glucuronamide-based bolaamphiphile (**3**)† possessing free 1,2-diols available for ester formation with a boronic acid. Comparison of the complex formation between these three sugar-based bolaamphiphiles (**1**, **2** or **3**) and an aromatic boronic acid-based homologue **4**,† should provide further insight into the complex structures. Mikami and Shinkai are the first to prepare main-chain sugar-containing polymers *via* self-condensation with diboronic acid under nonaqueous conditions.[11] Advantageously, we are also able to solve a problem concerning the sequential head-to-tail irregularity of the cyclic sugar-containing polymer. Here we describe the pH-dependent, reversible polymolecular boronate complexation between glucuronamide- **3** and boronic acid-based bolaamphiphiles **4** in aqueous solutions.

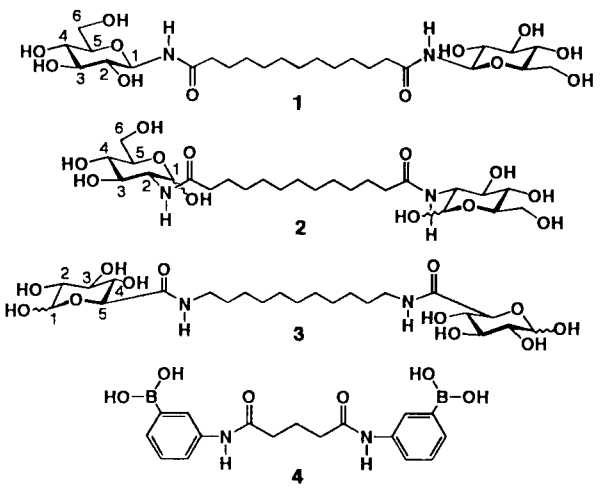

The glucuronamide bolaamphiphile **3** was efficiently synthesized in 4 steps from commercially available glucuronic acid, in a similar manner to that reported by Falkowski *et al.*[12] The related derivatives, 1-glucosamide (**1**) and 2-glucosamide bolaamphiphiles **2** were prepared according to a published procedure.[10,13] The boronic acid-appended bolaamphiphile **4** was also synthesized in the same manner as described by Kimura *et al.*[14]

^{1}H NMR spectroscopy of **3** in DMSO-d_6 containing a trace amount of D_2O clearly displayed two sets of well-defined signals for the H-1 (δ 4.32 and 4.93), H-5 (δ 3.51 and 3.93) and hydroxy OH-1 protons (δ 6.52 and 6.82). The presence of these two sets of signals with an average integral ratio of 56 : 44 implies that the bolaamphiphile **3** exists as a mixture of α-(56%) and β-anomers (44%) in the solution. ^{1}H NMR spectra of **4** were measured in the weak acidic (pD = 3) and alkaline aqueous solutions (pD = 10–12). The aromatic proton regions of the obtained spectra displayed entirely different spectral patterns under each condition, suggesting that the sp^2-hybridized boron atom can convert completely into the sp^3 mode at pH values above 10.

In order to confirm the linear complex formation between the cyclic sugar- and boronic acid-based bolaamphiphiles, we employed ^{11}B NMR spectroscopy‡ since it is very sensitive to the spin state of the boron atom. Therefore, we can easily differentiate the neutral sp^2, anion sp^3 and coordinated sp^3 states of the aromatic boronic acid moiety in the bolaamphiphile. Actually, ^{11}B NMR spectra of the boronic acid bolaamphiphile **4** (0.1 M) displayed distinct chemical shifts for the boron atom under weak acidic and alkaline conditions [δ 11 and −16, respectively, Figs. 1(*a*) and 1(*b*)]. The addition of equimolar 1-glucosamide bolaamphiphile **1** induced no spectral change in the ^{11}B NMR of **4** [Fig. 1(*c*)]. Thus, the potent C-4 and C-6 hydroxy groups of **1** in the pyranose form proved inactive for the ester linkage formation, resulting in no polymer formation. In contrast to this spectral feature, two separate ^{11}B NMR signals (δ −11 and −16), with an integral ratio of 1 : 2, appeared for **4** coexisting with equimolar 2-glucosamide bolaamphiphile **2** [Fig. 1(*d*)]. The minor signal in intensity (*ca.* 33%) is compatible with the presence of a covalently attached sp^3-type boronic moiety. Considering no possibility of the pyranose form existing, this finding implies that either of the C-3, C-5 and C-6 hydroxy groups of the glucofuranose can participate in binding. For a linear non-strained polymolecular complex with **4** the 3,5,6-binding mode could be the more probable compared to the binding of monoboronic acids [Fig. 2(*a*)].[3] On the other hand, the glucuronamide derivative **3** with the free C-1 and C-2 hydroxy groups was found to produce covalently attached sp^3 hybridization, giving a polymolecular complex (*ca.* 70%) equilibrated with a small amount of free anions [*ca.* 30%, Fig. 1(*e*)]. Whether the complex structure is a pyranose or a furanose form cannot be concluded at present from any other NMR

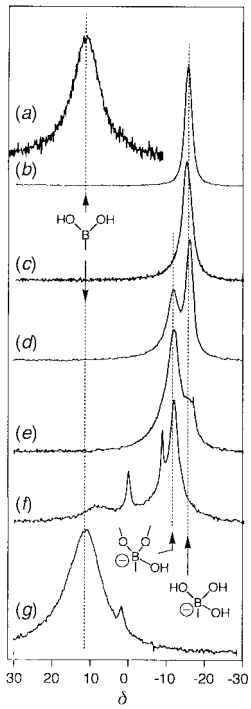

Fig. 1 ^{11}B NMR spectral change of the bolaamphiphiles **1**, **2** or **3** upon complexation with **4** (0.1 M, at 25 °C in D_2O/methanol-d_4 (6:4, *v/v*)). (*a*) **4** under weak acidic aqueous condition (pD = 3.0); (*b*) **4** under alkaline aqueous condition (pD = 12.7); a 1:1 mixture of (*c*) **1** and **4** (pD = 10.7); (*d*) **2** and **4** (pD = 10.3); (*e*) **3** and **4** (pD = 10.9); (*f*) **3** and **4** (pD = 6.4); (*g*) **3** and **4** (pD = 3.0).

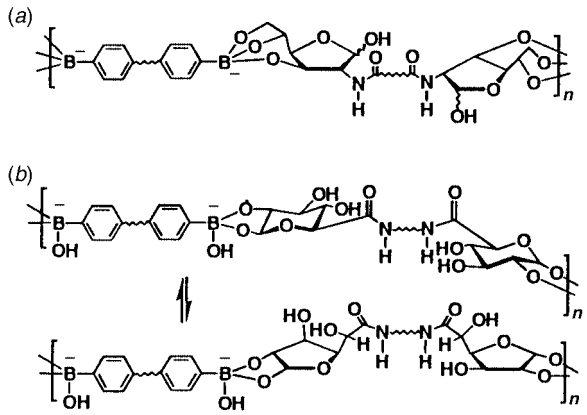

Fig. 2 Possible structures of the polymer main chains formed from (*a*) the mixture of **2** and **4**; (*b*) the mixture of **3** and **4**.

measurements including ^{13}C NMR [Fig. 2(*b*)]. Detailed structural analysis remains to be further investigated using single-head single-chain amphiphile models of **1**–**4**. It is well known that multiangle laser light scattering (MALLS)‡ detector measures, from the intensity of the scattering, the molar mass of biopolymers in solutions.[15] Especially, MALLS can provide a highly sensitive and useful method for the characterization of polysaccharides and protein oligomers. The weight-averaged molecular weight (M_w) for the present aqueous **3**·**4** polymer was evaulated by MALLS to be 2.04×10^6 g mol^{-1} at pD 10.8.

Dissociation of the boronate polymer complexes into each component **3** and **4** was investigated by neutralizing the solution with dilute hydrochloric acid. At neutral pH range (pD = 6.4), the ^{11}B NMR spectrum of the polymer indicated that a main signal (*ca.* 48%) attributable to the boronate complex still apears at δ −11 in addition to three minor signals at δ −8 (*ca.* 24%), 1 (*ca.* 13%) and 9 (*ca.* 15%), [Fig. 1(*f*)]. Complete dissociation of the polymer was achieved under weak acidic aqueous conditions (pD = 3). Namely, the decrease in the pH value of the aqueous solution from 11 to 3 resulted in a down-field shift of the main signal from δ −11 to 11 [Fig. 1(*g*)]. Thus, a reversible polymer formation and dissociation was realized depending on the pH conditions of the aqueous solutions. The monomers are connected to each other through identical cyclic sugar–boronate ester linkages, unike Mikami and Shinkai's cyclic sugar-containing polymer,[11] in a one-dimensional poly-molecular array. This kind of polymer system can be realized using both cyclic sugar- and boronic acid-based bola-form derivatives. In addition, the notably different features of **1** and **2** upon complexation with **4** gave unequivocal evidence for the participation of the furanose form of **2**.

Notes and references

† *Selected data* for **3**: yield 28%, mp 198–200 °C (decomp.), FAB mass (in glycerol) *m*/*z* 553 (M^+). ^{1}H NMR (in DMSO-d_6 plus one drop of D_2O at 25 °C) δ 1.24 (s, 16H, $CH_2(CH_2)_8CH_2$), 1.38 (dd, 4H, $CH_2(CH_2)_8CH_2$), 3.05 (m, 4H, CH_2CH_2NHCO), 2.90–3.45 (m, 8H, H-2, H-3, H-4), 3.51 (d, 0.96H, H-5(β)), 3.93 (d, 1.04H, 2H, H-5(α)), 4.32 (d, 0.88H, H-1(β)), 4.94 (d, 1.12H, H-1(α)), 6.52 (d, 2H, OH-1(β)), 6.82 (d, 2H, OH-1(α)) and 7.91 (dd, 2H, CH_2NHCO-). Anal. Calcd. for $C_{24}H_{44}O_{12}N_2$: C, 52.16; H, 8.03; N, 5.07. Found: C, 51.96; H, 8.07; N 4.83%. For **4**: yield 36%, mp 210 °C, ^{1}H NMR (in DMSO-d_6 at 25 °C) δ 1.98 (m, 2H, $CH_2CH_2CH_2$), 2.37 (t, 4H, CH_2CH_2CONH), 7.24, 7.46, 7.72, 7.85 (s, d, d, t, 8H, Ar-H), 7.97 (s, 4H, $B(OH)_2$) and 9.84 (s, 2H, CH_2CONH). Anal. Calcd. for $C_{17}H_{20}O_6N_2B_2$: C, 55.19; H, 5.45; N, 7.57. Found: C, 55.02; H, 5.48; N 7.36%.

‡ ^{1}H and ^{11}B NMR spectra were collected with a JEOL 600 Fourier transform spectrometer operating at 600.05 and 192.45 MHz, respectively. All solutions were prepared in a mixture of D_2O and methanol-d_4 (6:4 *v/v*) with the spectrometer locked onto D_2O. Each pH value of the solutions was adjusted with NaOD aqueous solutions.^{11}B NMR chemical shifts were measured relative to external $NaBF_4$. MALLS was measured using a Wyatt DAWN DSP, coupled with refractive index detectors operated in a microbatch mode.

1 Y. Nagai, K. Kobayashi, H. Toi and Y.Aoyama, *Bull. Chem. Soc. Jpn.*, 1993, **66**, 2965.
2 T. J. James, K. R. A. S. Sandanayake and S. Shinkai, *Angew. Chem., Int. Ed. Engl.*, 1996, **35**, 1910 and references cited therein.
3 J. C. Norild and H. Eggert, *J. Am. Chem. Soc.*, 1995, **117**, 1479 and references cited therein.
4 S. Shinkai, in *Chemosensors of Ion and Molecule Recognition*, Kluwer Academic Publishers, The Netherlands, 1997, p. 37.
5 E. J.Bourne, I. R. Mckinley and H. Weigel, *Carbohydr. Res.*, 1972, **25**, 516.
6 P. J. Wood and I. R. Siddiqui, *Carbohydr. Res.*, 1974, **36**, 247.
7 T. D. James, T. Harada and S. Shinkai, *J. Chem. Soc., Chem. Commun.*, 1993, 857; T. D. James, K. R. A. S. Sandanayake and S. Shinkai, *J. Chem. Soc., Chem. Commun.*, 1994, 477.
8 H. Eggert, J. Frederiksen, C. Morin and J. C. Norrild, *J. Org. Chem.*, 1999, **64**, 3846; M. Bielecki, H. Eggert and J. C. Norrild, *J. Chem. Soc., Perkin Trans. 2*, 1999, 449.
9 T. Shimizu and M. Masuda, *J. Am. Chem. Soc.*, 1997, **119**, 2812; M. Masuda, T. Hanada, K. Yase and T. Shimizu, *Macromolecules*, 1998, **31**, 9403.
10 I. Nakazawa, M. Masuda, Y. Okada, T. Hanada, K. Yase, M. Asai and T. Shimizu, *Langmuir*, 1999, **15**, 4757.
11 M. Mikami and S. Shinkai, *J. Chem. Soc., Chem. Commun.*, 1995, 153; M. Mikami and S. Shinkai, *Chem. Lett.*, 1995, 603.
12 L. Falkowski, B. Stefanska, E. Bylec and P. Kolodzeijczyk, *Pol. J. Chem.*, 1980, **54**, 599.
13 M. Masuda and T. Shimizu, *J. Carbohydr. Chem.*, 1998, **17**, 405.
14 T. Kimura, T. Yamashita, K. Koumoto and S. Shinkai, *Tetrahedron Lett.*, 1999, **40**, 6631.
15 For example: P. Wyatt, *J. Anal. Chim. Acta*, 1993, **272**, 1; R. Mendichi, G. Giammona, G. Cavallaro and A. G. Schieroni, *Polymer*, 1999, **40**, 7109.

ChemComm

(η⁶-Arene)ruthenium oxomolybdenum and oxotungsten clusters. Stereochemical non-rigidity of [{Ru(η⁶-*p*-MeC$_6$H$_4$Pr^i)}$_4$Mo$_4$O$_{16}$] and crystal structure of [{Ru(η⁶-*p*-MeC$_6$H$_4$Pr^i)}$_4$W$_2$O$_{10}$]

Vincent Artero, Anna Proust,* Patrick Herson, René Thouvenot and Pierre Gouzerh*

Laboratoire de Chimie Inorganique et Matériaux Moléculaires, Unité CNRS 7071, Case 42, Université Pierre et Marie Curie, 4 Place Jussieu, 75252 Paris Cedex 05, France. E-mail: proust@ccr.jussieu.fr and pg@ccr.jussieu.fr

Received (in Basel, Switzerland) 21st January 2000, Accepted 7th April 2000

According to a multinuclear NMR study, the cluster [{Ru(η⁶-*p*-MeC$_6$H$_4$Pr^i)}$_4$Mo$_4$O$_{16}$] exists as two isomers, the windmill-like form and the triple-cubane form, which are in equilibrium in solution, while the tungsten analogue, which has been obtained together with the double-cubane type cluster [{Ru(η⁶-*p*-MeC$_6$H$_4$Pr^i)}$_4$W$_2$O$_{10}$] by reaction of [{Ru(η⁶-*p*-MeC$_6$H$_4$Pr^i)Cl$_2$}$_2$] with (NBu$^n_4$)$_2$[WO$_4$] in acetonitrile, only displays the windmill-like structure.

Organometallic derivatives of polyoxometalates now form a full class of compounds.[1] We have recently reported a series of integrated organometallic oxo(alkoxo)molybdenum clusters containing *fac*-{M(CO)$_3$}$^+$ (M = Mn or Re) units.[2] The apparent structural relationships between these clusters and those of previously reported polyoxo(alkoxo)molybdates underscore the electronic connection between d^6-*fac*-{ML$_3$} (M = Mn or Re) and d^0-*fac*-{MoO$_3$} or d^0-*fac*-{MoO$_2$(OR)}$^+$ units. Then we turned towards the reactivity of [{(η⁶-arene)RuCl$_2$}$_2$] with oxometalates in order to extend the concept of topological equivalent units.

The cluster [{Ru(η⁶-*p*-MeC$_6$H$_4$Pr^i)}$_4$W$_4$O$_{16}$] **2**, whose molybdenum analogue [{Ru(η⁶-*p*-MeC$_6$H$_4$Pr^i)}$_4$Mo$_4$O$_{16}$] **1** was recently reported by Süss-Fink *et al.*,[3,4] has been obtained by reacting [{(η⁶-*p*-MeC$_6$H$_4$Pr^i)RuCl$_2$}$_2$] with (NBu$^n_4$)$_2$[WO$_4$] in acetonitrile.† In the solid state, **2** is isostructural with **1** and displays the so-called windmill-like structure,[3,4] *i.e.* it consists of a [W$_4$O$_{16}$]$^{8-}$ cubic core capped by four {Ru(η⁶-*p*-MeC$_6$H$_4$Pr^i)}$^{2+}$ groups each bound to a triply bridging and two terminal oxo ligands.‡ The only previous example of a polyoxoanion-supported organometallic complex based on [W$_4$O$_{16}$]$^{8-}$ is [{Ir(cod)}$_6$W$_4$O$_{16}$].[5] The ^{1}H, ^{183}W and ^{17}O NMR spectra indicate that **2** exists in a single form in chloroform. Moreover, the ^{17}O NMR spectrum of **2** is fully consistent with the windmill-like structure. Indeed, it displays four signals in approximate relative intensities 1:1:1:1 assigned to terminal (O$_t$), doubly bridging (there are two sets of four μ$_2$-O ligands) and quadruply bridging (μ$_4$-O) oxo ligands, in the order of increasing shielding (Fig. 1). On the other hand, a different pattern has been reported for the ^{17}O NMR spectrum of **1** in CD$_2$Cl$_2$,[4] and this prompted us to reinvestigate the behaviour of **1**.

During the course of this study, **1** and **1**·C$_6$H$_5$Me have been characterized by X-ray diffraction in addition to **1**·2C$_6$H$_5$Me that was described by Süss-Fink *et al.*[3,4] In the three compounds **1** displays the windmill-like geometry. The ^{1}H NMR spectra of the three compounds in solution are similar apart from the signals due to toluene. However the ^{1}H, ^{17}O and ^{95}Mo NMR spectra are dependent on the solvent and indicate the presence of two distinct species. Indeed two signals (^{95}Mo) or two sets of signals (^{1}H and ^{17}O) are observed with nearly equal intensities in chloroform but quite different intensities in dichloromethane. The change in solution was shown to be reversible. The major set of ^{17}O resonances in CH$_2$Cl$_2$ is consistent with the triple-cubane structure **1b** (Fig. 1). Indeed, it is composed of three signals in relative intensities 2:1:1, assigned to O$_t$, μ$_3$-O and μ$_4$-O, respectively, in the order of increasing shielding. This assignment, which is at variance with that of Süss-Fink *et al.*,[4] is further supported by the comparison with the ^{17}O NMR spectrum of the triple-cubane cluster [(Cp*Rh)$_4$Mo$_4$O$_{16}$].[6] The minor set of signals in CH$_2$Cl$_2$ is consistent with the windmill-like structure **1a**. It follows from this multinuclear NMR study that **1** predominantly exists in the triple-cubane form **1b** in dichloromethane. Considering the significant change in the equilibrium constant on going from dichloromethane to chloroform, the energy difference between the two forms of **1** should be low. This stereochemical change, which is slow on the NMR time scales, does not depend on the residual water content and could involve a concerted motion of two {Ru(η⁶-*p*-MeC$_6$H$_4$Pr^i)}$^{2+}$ groups (Fig. 1). There are only a few precedents for the mobility of organometallic cations on polyoxometalates.[7] In addition to the equilibrium between **1a** and **1b**, there is a faster dynamic process which exchanges the μ$_2$-O oxo ligands in **1a**.

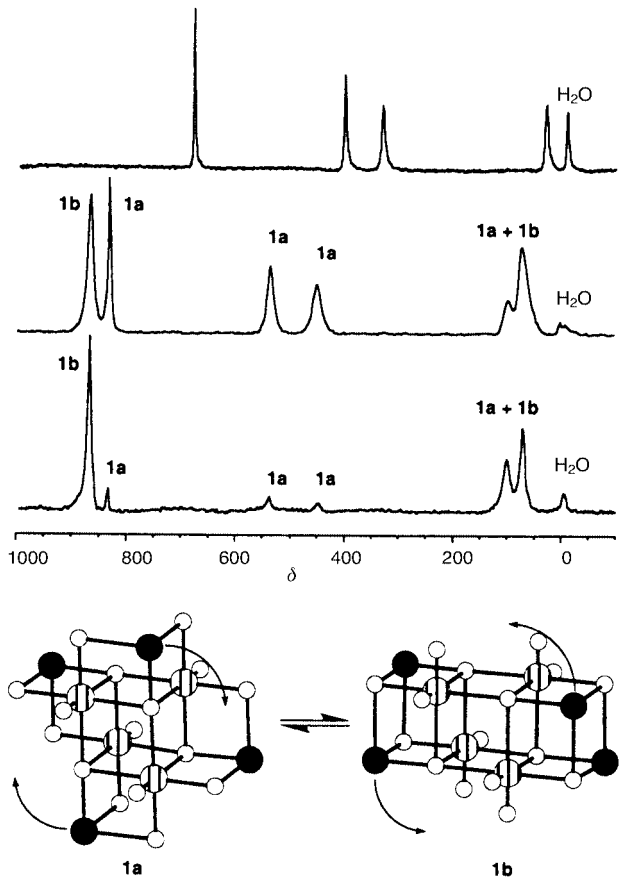

Fig. 1 Unlocked 40.7 MHz ^{17}O NMR spectra of enriched samples of **2** (top, CHCl$_3$, 333 K) and **1** (middle, CHCl$_3$, 297 K; bottom, CH$_2$Cl$_2$, 293 K) and postulated mechanism for the interconversion between the windmill-like form **1a** and the triple-cubane form **1b** (Mo atoms are shown as hatched spheres and Ru atoms as black spheres; *p*-cymene ligands have been omitted for clarity).

DOI: 10.1039/b000782j

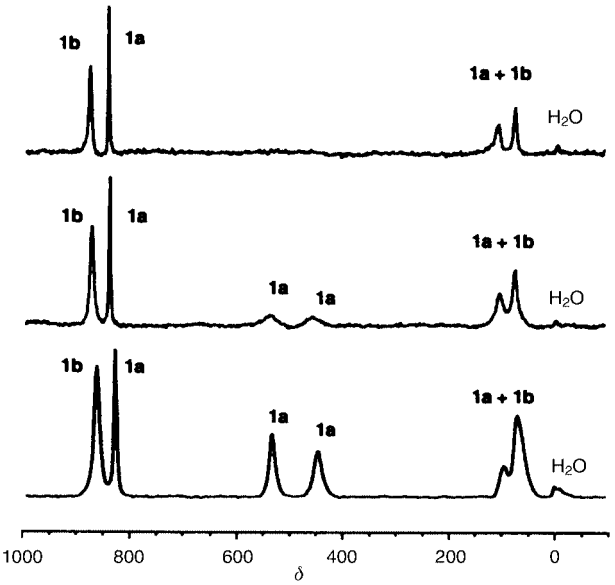

Fig. 2 Unlocked 40.7 MHz ^{17}O NMR spectra of enriched samples of **1** in $CHCl_3$ at 333 K (top), 313 K (middle) and 297 K (bottom).

Indeed the signals for the two types of μ_2-O ligands broaden as the temperature is raised and are hardly observed above 313 K (Fig. 2). The most likely mechanism to explain this phenomenon is a concerted motion of the four organometallic units along the diagonals of the faces of the central cubic core.

Another cluster, $[\{Ru(\eta^6\text{-}p\text{-}MeC_6H_4Pr^i)\}_4W_2O_{10}]\cdot 3H_2O$ (**3**·$3H_2O$), was obtained as a by-product in the preparation of **2**. An X-ray structure analysis‡ revealed that **3** displays a double-cubane framework consisting of two fused $[\{Ru(\eta^6\text{-}p\text{-}MeC_6H_4Pr^i)\}_2W_2O_8]$ cubes (Fig. 3). Discrete mono-cubane,[2,8] triple-cubane[6,9] and quadruple-cubane[9] clusters have been reported. To the best of our knowledge, **3** provides the first example of a discrete double-cubane cluster. The mono-cubane clusters $[\{Ru(\eta^6\text{-}p\text{-}MeC_6H_4Pr^i)\}_2W_2O_{10}]$ (M = Mo or W) are not expected to be stable because the environments of the two M atoms would violate the Lipscomb rule.[10] Thus such units, once formed, should undergo condensation processes.

We are currently investigating the influence of the arene on the equilibium between the two forms of **1** and we are exploring the potential of these and related species in catalytic reactions.

Notes and references

† *Synthesis* of **2** and **3**. A solution of $[\{(\eta^6\text{-}p\text{-}MeC_6H_4Pr^i)RuCl_2\}_2]$ (306 mg, 0.5 mmol) and $(NBu^n_4)_2[WO_4]$ (733 mg, 1 mmol) in MeCN (15 mL) was stirred at room temperature for 5 h upon which a yellow precipitate of **2** formed. It was filtered and washed with 3 mL MeCN (215 mg, 51%). ^1H NMR (300.13 MHz, $CDCl_3$): δ 1.34_5 (d, J 6.9 Hz, 3H), 1.35 (d, J 6.9 Hz, 3H), 2.41 (s, 3 H), 3.05 (heptet, J 6.9 Hz, 1H), 5.34 (d, J 5.7 Hz, 1H), 5.56 (d, J 5.8 Hz, 1H), 5.64 (d, J 5.7 Hz, 1H), 5.75 (d, J 5.8 Hz, 1H); ^{17}O NMR (40.7 MHz, $CHCl_3$, 333 K): δ 27 (4O), 329 (4O), 399 (4O), 676 (4O); ^{183}W NMR (20.8 MHz, $CDCl_3$): δ 351; IR (KBr pellet, $\bar{\nu}$/cm^{-1}): 935s(W=O), 878w, 803s, 750s, 644w(W–O), 608m, 492m; Anal.: C, 24.29; H, 2.91; Ru, 19.23; W. 37.35. $C_{40}H_{56}O_{16}Ru_4W_4$ requires C, 24.86; H, 2.92; Ru, 20.92; W, 38.05%.

Slow evaporation of the filtrate at 25–30 °C afforded red sticky crystals of **3**·$3H_2O$ (40 mg, 10%); ^1H NMR (300.13 MHz, $CDCl_3$): δ 1.39 (d, J 6.8 Hz, 6H), 2.29 (s, 3 H), 3.07 (heptet, J 6.8 Hz, 1H), 5.29 (d, J 5.9 Hz, 2H), 5.34 (d, J 5.9 Hz, 2H); IR (KBr pellet, $\bar{\nu}$/cm^{-1}): 916s, 897s (W=O), 652m, 624(sh), 607s, 574m, 512m (W–O); Anal.: C, 31.59; H, 4.19; Ru, 25.13; W, 23.79. $C_{40}H_{62}O_{13}Ru_4W_2$ requires C, 31.55; H, 4.07; Ru, 26.55; W 24.14%.

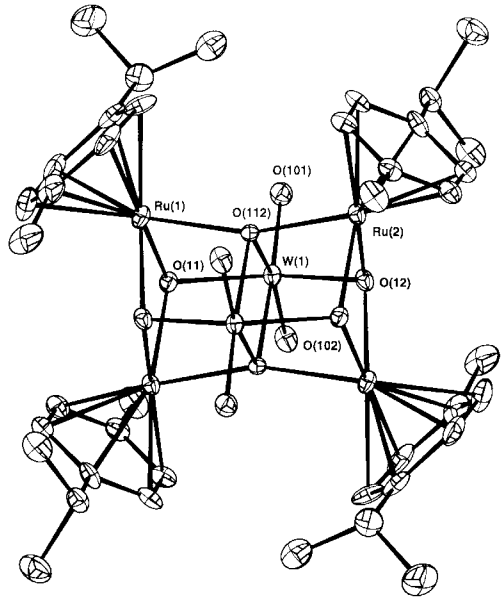

Fig. 3 Molecular structure of $[\{Ru(\eta^6\text{-}p\text{-}MeC_6H_4Pr^i)\}_4W_2O_{10}]$ in **3**·$3H_2O$. Selected bond lengths (Å): W(1)–O(11) 1.947(7), W(1)–O(12) 1.932(8), W(1)–O(101) 1.731(9), W(1)–O(102) 1.748(9), W(1)–O(112) 2.180(7), W(1)–O(112)′ 2.268(7), Ru(1)–O(11) 2.104(8), Ru(1)–O(12)′ 2.089(9), Ru(1)–O(112) 2,084(7), Ru(2)–O(11)′ 2.114(8), Ru(2)–O(12) 2.085(8), Ru(2)–O(112) 2.095(7). Primed atoms are generated by the crystallographic inversion centre. Carbon atom labels have been omitted for clarity.

‡ *Crystal data*: for **2**·C_6H_5Me: M = 2116.83, a = 15.031(5), b = 15.303(5), c = 15.334(6) Å, α = 72.85(3), β = 73.09(3), γ = 64.30(3)°, U = 2982(2) Å^3, T = 298 K, space group $P\bar{1}$, Z = 2. Single crystals of **2**·C_6H_5Me were obtained from a CH_2Cl_2 solution of **2** layered by toluene; they decayed during data collection so that accurate structural parameters could not be obtained owing to an insufficient number of observed data.

For **3**·$3H_2O$: M = 1522.90, a = 13.857(7), b = 13.898(8), c = 14.232(6) Å, α = 114.01(4), β = 91.01(4), γ = 112.79(4)°, U = 2257(3) Å^3, T = 298 K, space group $P1$, Z = 2, μ(Mo–Kα) = 2.24 cm^{-1}, 8300 reflections measured, 7942 unique (R_{int} = 8.3%). Structure solution (direct methods) and refinement (full matrix least squares on F^2) based on 5326 refgictions with $I > 3\sigma(I)$ converged at a conventional R of 0.056.

CCDC 182/1597. See http://www.rsc.org/suppdata/cc/b0/b000782j/ for crystallographic files in .cif format.

1 P. Gouzerh and A. Proust, *Chem. Rev.*, 1998, **98**, 77.
2 R. Villanneau, R. Delmont, A. Proust and P. Gouzerh, *Chem. Eur. J.*, 2000, **6**, 1184.
3 G. Süss-Fink, L. Plasseraud, V. Ferrand and H. Stoeckli-Evans, *Chem. Commun.*, 1997, 1657.
4 G. Süss-Fink, L. Plasseraud, V. Ferrand, S. Stanislas, A. Neels, H. Stoeckli-Evans, M. Henry, G. Laurenczy and R. Roulet, *Polyhedron*, 1998, **17**, 2817.
5 Y. Hayashi, F. Müller, Y. Lin, S. M. Miller, O. P. Anderson and R. G. Finke, *J. Am. Chem. Soc.*, 1997, **119**, 11 401.
6 Y. Hayashi, K. Toriumi and K. Isobe, *J. Am. Chem. Soc.*, 1988, **110**, 3666.
7 C. J. Besecker, V. W. Day, W. G. Klemperer and M. R. Thompson, *J. Am. Chem. Soc.*, 1984, **106**, 4125; M. Abe, K. Isobe, K. Kida and A. Yagasaki, *Inorg. Chem.*, 1996, **35**, 5114; T. Nagata, M. Pohl, H. Weiner and R. G. Finke, *Inorg. Chem.*, 1997, **36**, 1366.
8 K. Isobe and A. Yagasaki, *Acc. Chem. Res.*, 1993, **26**, 524; U. Koelle, *Chem. Rev.*, 1998, **98**, 1313; C. D. Abernethy, F. Bottomley, R. W. Day, A. Decken, D. A. Summers and R. C. Thompson, *Organometallics*, 1999, **18**, 870.
9 Y. Do, X.-Z. You, C. Zhang, Y. Ozawa and K. Isobe, *J. Am. Chem. Soc.*, 1991, **113**, 5892.
10 W. N. Lipscomb, *Inorg. Chem.*, 1965, **4**, 132.

Typeset and printed by Black Bear Press Limited, Cambridge, England

ChemComm
FEATURE ARTICLE

Chiral autocatalysis: where stereochemistry meets the origin of life

Martín Avalos, Reyes Babiano, Pedro Cintas, José L. Jiménez and Juan C. Palacios

Departamento de Química Orgánica, Facultad de Ciencias, Universidad de Extremadura, E-06071 Badajoz, Spain. E-mail: pecintas@unex.es

Received (in Cambridge, UK) 18th October 1999, Accepted 7th December 1999
Published on the Web 10th April 2000

This article summarizes a series of recent and simple experiments to produce optically active substances from achiral precursors. These symmetry-breaking processes include either autocatalytic crystallization or asymmetric autocatalysis, and provide new insights into the origin of biomolecular homochirality. In addition, support from an extraterrestrial origin of chiral molecules has also come from recent findings.

Introduction

The question of the origin of life on Earth is invariably linked to the origin of enantiomerically pure compounds, even if there are no definitive arguments embracing both premises.[1] Ever since Pasteur's time, scientists have been fascinated with trying to understand the origin and amplification of chirality. A preliminary argument is that perhaps life needed no external influence beyond chance to choose its handedness. However, many scientists believe chirality of one or another form was inevitable because homochirality would have been a pre-condition for life. Racemic molecules would have been too inefficient for achieving biological processes such as self-replication, protein synthesis, regulation, and ultimately gene expression. Likewise, polymerization reactions affording long-chain stereoregular polymers (*e.g.* all-L-polypeptides or all-D-oligosaccharides) will not proceed in racemic solution since addition of a wrong monomer tends to stop the process.[2]

In principle, a biochemistry made up of D-amino acids or L-sugars should be just as efficient as L-amino acids or D-sugars found in our terrestrial life. An argument that reinforces this hypothesis is the fact that alternatives to ribose or deoxyribose can be synthesized and tried out as the sugar components of nucleic acids or new bases can be substituted for those nature uses. Evolution has selected the best available solution and not necessarily the best possible solution.[3] Nevertheless, even though the initial molecules are achiral, the handedness of the building blocks or the appropriate helicity of the oligomers had to be determined at an early stage. In fact only a small enantiomeric excess (ee) is required because such a value could be amplified by a series of mechanisms related to the concept of nonlinear stereochemistry.[4] Thus, a partially resolved chiral catalyst or auxiliary could give a stereoselection higher than its own ee. The phenomenon may be ascribed to diastereomeric interactions in solution, but there are also profound kinetic implications involved,[5] including the possibility that the diastereomeric catalysts have very different reaction rates.[6] Unfortunately, most nonlinear effects have been observed with organometallic reagents and in organic solvents. It is unlikely that these reaction conditions could be found in the prebiotic scene. Anyway, as we shall see later these unusual mechanisms involving cooperativity among the molecules do provide food for thought.

Martín Avalos, Reyes Babiano, Pedro Cintas, José L. Jiménez and Juan C. Palacios received their graduate degrees in chemistry and their PhD degrees from the University of Extremadura (UEX), where they are Professors of Organic Chemistry. Together with a group of talented and enthusiastic collaborators, they are investigating diverse areas of organic chemistry with a focus on stereochemistry. Their current research interests include the development of asymmetric reactions, conformational analysis, solvent-free reactions and the use of nonconventional techniques to accomplish organic transformations under milder conditions.

Cosmic chirality

Before we go any further, a few comments about the inherent handedness of matter are unavoidable. There are four forces in nature: electromagnetic, strong, gravitational and weak interactions, but only the latter is chiral. In other words, it can distinguish between right- and left-handedness in the spin polarization of elementary particles. Parity violation in the weak interactions was discovered in the late fifties as the radioactive decays of polarized ^{60}Co nuclei release more left-handed spinning electrons than right-handed spinning ones. Likewise, as far as we know there are no right-handed neutrinos: they are always left-handed.[7] The direct implication of these interactions is that there is a parity-violating energy difference between two enantiomers. Unfortunately, this energy shift is too small ($\sim 10^{-18}$ eV) to be measured with our current instruments, but theoretical calculations do confirm that the natural L-amino acids L-alanine, L-valine, L-serine and L-aspartate are more stable than their D-enantiomers by 10^{-17} kT, and D-glyceraldehyde was likewise found to be more stable than its unnatural counterpart by about 10^{-17} kT.[8] Although amplification mechanisms by factors of about 10^{17} could be suggested to explain the observed homochirality of molecules,[9] alternative hypotheses appear to be more plausible.

If the foundations of life are chiral cosmic forces operating at their origin, the finding of extraterrestrial chirality would provide a reasonable argument. In fact, we have learnt that circularly polarized light (CPL) or vortices may cause symmetry breaking, but even falsely chiral influences such as magnetic or gravitational fields, under kinetic conditions, might be sufficient.[10] The search for homochiral substances in the well-known Murchison meteorite reveals that L-enantiomers predominate slightly over D-enantiomers.[11] In particular, Cronin and Pizzarello have concentrated on branched α-amino acids,[11a] which are not present in terrestrial proteins, in order to exclude any sort of contamination from living systems. Although no appreciable ees were found for α-aminobutyric acid or norvaline, other ramified amino acids gave ees up to 10% (Scheme 1).

In an irony of fate, astronomers from the Anglo-Australian Laboratory reported that they had discovered high levels of CPL

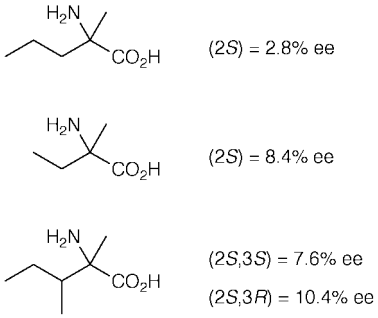

Scheme 1 Enantiomeric excesses of α-ramified amino acids of extraterrestrial origin found in the Murchison meteorite.

(as much as 17%) in the constellation Orion.[12] Such radiation might have induced asymmetry in interstellar organic molecules, which could be delivered to the primitive Earth by comets or meteorites, a necessary surmise if one assumes that the distance from the solar system to the center of the nebula is estimated at about 1500 light-years!

One objection to this exciting work is that the authors observed only CPL in the infrared region, whereas UV light is required to deracemize chiral molecules. However, computations showed that circularly polarized ultraviolet light should also be present.[12,13]

Crystallization–induced resolution and autocatalysis

It would be interesting to devise a chemical system capable of producing a slight enantiomeric imbalance comparable with the levels of ees found in meteorites or achieved by CPL photolysis,[10a] which may be as low as 0.1%, but larger than those predicted by parity violation.

We must first overcome a common misconception taught at the freshman or even sophomore level: the assumption that racemates are made of *exactly equal* amounts of enantiomers. This belief goes against the logic of statistics, and in fact for n molecules in a racemate, the dominant component will have $(n/2) + n^{1/2}$ molecules.[14] As n becomes very large the ratio of the two enantiomers becomes very close to one. This does mean that the simple diffusional distance from 50:50 will result in a macroscopic observation (for instance through the examination of $[\alpha]_D$ values) of an optically inactive mixture.

Crystal growth is a good scenario that takes advantage of the statistical fluctuations in a system where crystallization of, let us say, a left-handed crystal acts as a seed and causes other crystals nearby to be left-handed also. This chiral primary nucleation is the origin of the known spontaneous resolutions, which will occur only if the racemate is a conglomerate in the solid state.[15]

An unusual enantiomeric resolution by recrystallization of a racemate has been recently disclosed by Japanese authors.[16] Compounds susceptible to this preferential enrichment were a series of racemic sulfonium sulfonates, and the flow diagram of Scheme 2 highlights its particular features. Thus, repeated recrystallization of the racemate results in an alternating enrichment of the two enantiomers in the mother liquors (up to 100% ee!) and at the same time when crystals with low ee are recrystallized, the deposited crystals have invariably the opposite handedness.

As might be expected, the authors were able to identify by X-ray diffraction analysis the presence of a racemic conglomerate composed of a regular packing of the *R* and *S* enantiomers in the crystal lattice, whereas compounds existing as disordered mixed crystals in which sites are occupied by the *R* and *S* enantiomers cannot be resolved.

Spontaneous resolution in fluid systems (*e.g.* liquid crystals) is rather unusual due to thermal fluctuations and molecular

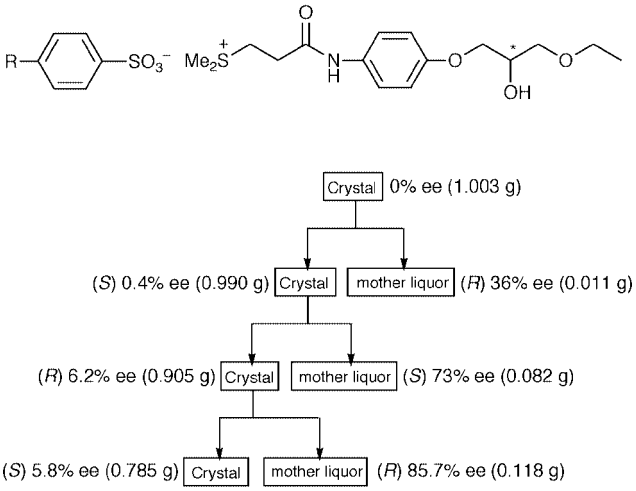

Scheme 2 Preferential enrichment by recrystallization.

diffusion. Nevertheless, Mikami and his associates have described a spontaneous enantiomeric resolution in a fluid smectic phase of a racemate.[17] Similarly, a racemic liquid crystalline substance may be resolved on a crystalline graphite surface.[18]

Autocatalytic secondary nucleation

Chiral amplification by spontaneous nucleation may in practice be ineffective. Thus, sodium chlorate, which is an achiral molecule, may form left- and right-handed crystals by crystallization from a supersaturated solution. A statistically equal number of (+)- and (–)-$NaClO_3$ crystals are obtained from an unstirred solution, but if the solution is rapidly stirred, a large excess of either left- or right-handed crystals results.[19] It should be noted that the direction of stirring had no effect on the handedness of the crystals. The experiment was reproducible and could even be videotaped by McBride and Carter,[20] who noted that the process began with a single crystal and massive crystallization took place when the single crystal first contacted the stir bar. The overall process is called *secondary nucleation*, which involves the formation of new crystals by breaking up the dendritic structures that are constructed on the parent growing crystal. Presumably, stirring contributes to spread these secondary nuclei around the solution. Remarkably, the process is a chiral autocatalysis because the crystal nuclei generated have the same handedness as the mother crystal (compare with *primary nucleation* operating in the spontaneous resolutions mentioned above). In other words, all of the microcrystals were homochiral to the parent crystal. Both the stirring rate and the size of the nucleating crystal are critical parameters on the distribution of enantiomeric excess.[21]

The mechanism of secondary nucleation is not fully understood, even though a theory has been recently proposed.[22] Be that as it may, the phenomenon is thought-provoking, as natural crystals might have experienced this chiral nucleation under geological conditions.

Spontaneous resolution through stirring can be observed not only in solution but also in crystallization of a melt. When a large number of 0.20 g samples of 1,1′-binaphthyl are heated at 180 °C and the melt is then cooled from 180 to 150 °C and allowed to crystallize (mp is 158 °C) without any intervention, a statistically equal number of (*R*)-(−)- and (*S*)-(+)-crystals (*i.e.* a Gaussian-like distribution of optical activity centered around zero) are formed.[23] Alternatively, crystallization carried out with *constant stirring* gives rise to large ees (averaging 80%) in almost every crystallization,[24] though *R* or *S* enantiomers were randomly created (Scheme 3). Apparently, stirring suppresses the slow process of primary nucleation, thereby favoring the formation of secondary crystals with the same homochirality. In

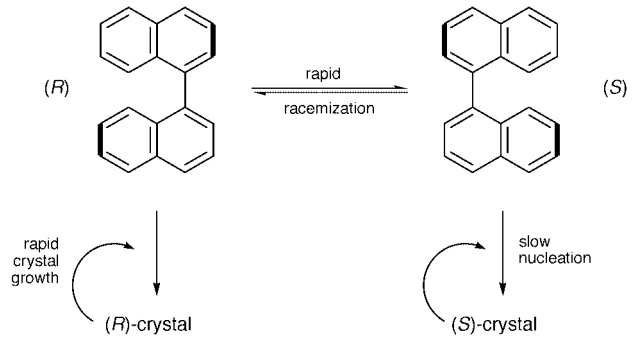

Scheme 3 Chirally autocatalytic spontaneous resolution.

addition, owing to stirring, the heat released will increase the temperature slightly, a factor that will also decrease the primary nucleation rate.

The authors have likewise studied the effect of seeding 1,1′-binaphthyl melts with (*R*)-(+)- or (*S*)-(−)-1,1′-bi-2-naphthol. Thus, a racemic sample of 1,1′-binaphthyl was cooled from 180 to 150 °C and a small amount of (*R*)-(+)- or (*S*)-(−)-1,1′-bi-2-naphthol was added, and the melt was stirred until all of it crystallized. There was a strong chiral influence of the added seed since (*R*)-(−)-1,1′-binaphthyl is isomorphous with (*R*)-(+)-1,1′-bi-2-naphthol. All of the samples seeded with (*R*)-(+)-1,1′-bi-2-naphthol presented a high value of optical rotation and close to 100% ee. Similarly, high ees were obtained for the samples seeded with (*S*)-(−)-1,1′-bi-2-naphthol.

Autocatalytic asymmetric reactions

In the early fifties Frank proposed a mathematical model of chiral autocatalysis in which each enantiomer catalyzes its own formation and suppresses the production of the opposite enantiomer.[25] Owing to statistical fluctuations, a very small ee in an early stage can be amplified as the reaction proceeds (Scheme 4).

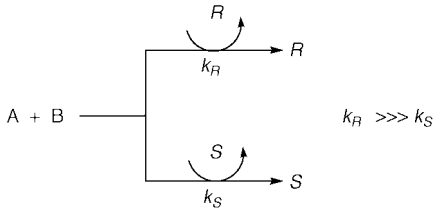

Scheme 4 Frank's hypothesis for chiral autocatalysis.

Autocatalysis implies the growth of the amount of catalyst, thereby modifying the initial *R/S* enantiomeric ratio. However, it can easily be demonstrated that an iterative autocatalytic process starting from a chiral catalyst with 100% ee and assuming a very high kinetic ratio k_R/k_S will inevitably end up with a lower ee unless nonclassical mechanisms such as a mutual inhibition of enantiomers are present.[4a] Furthermore, the use of catalysts of low optical purity may result in unpractical ees. Anyhow, a group of Japanese researchers led by Kenso Soai have found remarkable autocatalytic systems in the addition reactions of dialkylzincs to aromatic aldehydes.[26] Thus, a pyridyl alcohol of (*R*)-configuration with 86% ee catalyzes its own formation, although with a rather modest enantioselection (35% ee after subtracting the contribution of the catalyst, Scheme 5).

Better results were obtained by treating pyrimidine-5-carbaldehyde with diisopropylzinc in the presence of a pyrimidine alcohol with 2% ee, which gave the same chiral alcohol with up to 88% ee.[26d] In an extension of the latter autocatalysis, Soai *et al.* have recently reported that α-amino acids (*e.g.* leucine or valine) with 1–2% ee can serve as chiral initiators for the same addition reaction (Scheme 6). The configuration of the product

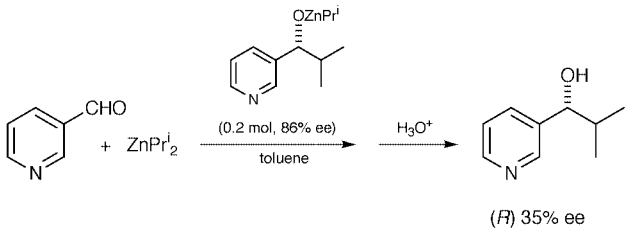

Scheme 5 Asymmetric autocatalysis in the reaction of pyridyl aldehydes with organozinc reagents.

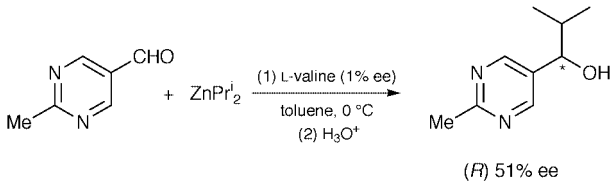

Scheme 6 Chiral autocatalysis promoted by nonracemic initiators.

is dependent on the configuration of chiral initiators. For example, L-leucine with 2% ee gives rise to an alcohol highly enriched in the *R* enantiomer, whereas addition of D-leucine causes the formation of the *S* alcohol in high ee.[27]

Improved results could be obtained with other chiral initiators such as (*R*)- or (*S*)-methyl mandelate and (*R*)- or (*S*)-butan-2-ol, even with 0.1% ee. The importance of this work lies in the fact that these initiators can be resolved by the action of CPL, thereby establishing a link between the influence of an external chiral force and autocatalysis. As mentioned, a process involving organometallic species in toluene is far from prebiotic conditions. Likewise, it would also be interesting if the same results could be obtained by irradiating with CPL the autocatalytic reaction in the presence of racemic initiators. In fact, this experiment will be attempted by these authors.[28]

An almost perfect asymmetric autocatalysis, in terms of enantioselectivity (> 99.5% ee), has been achieved in the addition of diisopropylzinc to 2-alkynylpyrimidine-5-carbaldehydes, albeit the autocatalytic alcohol had to be used with > 99.5% ee (Scheme 7).[29] The enantioselectivity was also

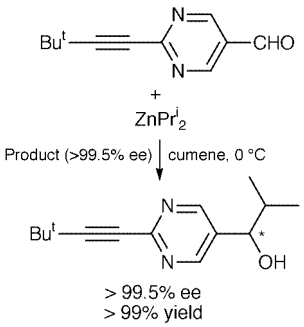

Scheme 7 Chiral self-replication of pyrimidyl alkanols.

dependent on both structural factors and reaction conditions. A rapid screening of 2-alkynylpyrimidyl alkanols revealed that a moderate electron-withdrawing alkynyl group along with a suitable bulkiness of the entire alkyne moiety are required. Accordingly, 1-(2-*tert*-butylethynyl-5-pyrimidyl)-2-methylpropan-1-ol was found to be an excellent autocatalyst. On the other hand, small differences in enantioselectivity were found when cumene was used instead of toluene, or better yet when a cumene solution of the organozinc reagent was used. It should be noted that either (*R*)- or (*S*)-pyrimidyl alkanols gave asymmetric autocatalysis with > 99.5% ee and in almost quantitative yields. If the reaction is performed consecutively with the product of one run serving as the autocatalytic reagent for the next entry, large multiplicative factors (10^3–10^7) are observed after a few rounds. An additional importance of these

chiral 5-pyrimidyl alkanols, which are obtained as single products, is their easy conversion into other important building blocks such as nonracemic α-hydroxycarboxylic acids.

Besides asymmetric autocatalysis, a related process called *asymmetric autoinduction* may also amplify a small ee.[4] From a conceptual viewpoint, however, the term autoinduction implies a certain degree of interaction between the product and a chiral autocatalyst, which may be different or the same substance. There must be cooperativity between the two components through diastereomeric interactions, which anticipates any type of nonlinear effect. An enantioselective autoinduction has also been reported by Soai and his group in the addition of diisopropylzinc to aromatic dialdehydes.[30] The catalyst is a chiral titanium complex derived from $Ti(OPr^i)_4$ with the chiral diol (Scheme 8). This catalyst is different from

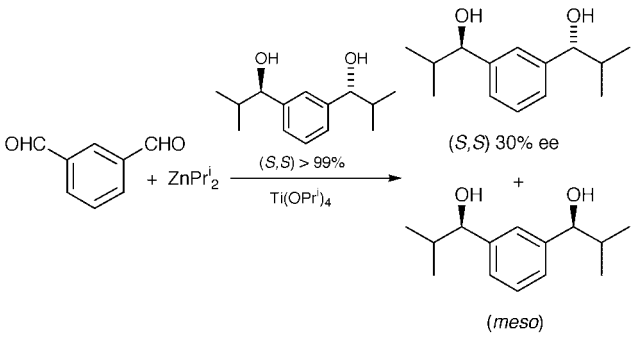

Scheme 8 Autoinductive addition of organometallic reagents to aromatic aldehydes.

the chiral zinc alkoxide which should be the actual intermediate, and this consideration justifies the term autoinduction rather than autocatalysis. Unfortunately, the product is obtained in only 30% ee along with a large amount of *meso* diol, starting from a catalytic diol with > 99% ee.

One of the most salient examples of chiral autoinduction has been reported by Danda *et al*. in the addition of HCN to aromatic aldehydes in the presence of small amounts of cyclopeptides.[31] The authors suggested that the catalyst arose from an *in situ* combination of the cyclic dipeptide with the resulting cyanohydrin. This hypothesis could be confirmed by adding a small amount of (*S*)-cyanohydrin with high ee to the cyclic dipeptide, either enantiopure or of low ee, at the beginning of the reaction (Scheme 9). Thus, catalyst with 2% ee

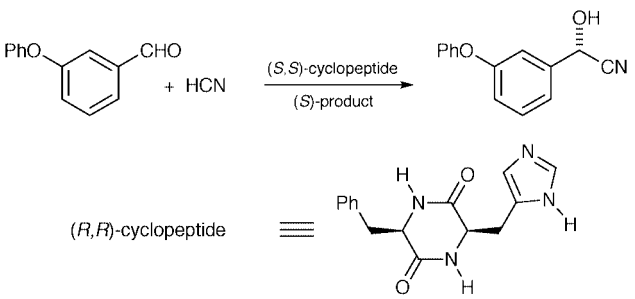

Scheme 9 Cyclopeptide-mediated asymmetric autoinduction.

gave product in 43% yield and 82% ee. Nevertheless, a catalyst prepared from the cyclic dipeptide in 67% ee plus (*S*)-cyanohydrin in 92% ee gave product in 89% yield and 96% ee, which is higher than the ee of both components of the catalyst. This does mean that the enantiomeric purity of cyanohydrin constitutes a key stereocontrolling factor on the catalytic cycle.

A very interesting autocatalytic reaction involving the formation of chiral coordination compounds in an aqueous environnement has been devised by Asakura and his associates.[32] The chiral octahedral cobalt complex *cis*-$[CoBr(NH_3)(en)_2]Br_2$ can be prepared by reaction of a diaquacobalt(II) complex, $[Co(H_2O)_2\{(OH)_2Co(en)_2\}_2](SO_4)_2$, with ammonium bromide in water. Despite the fact that all the reactants are optically inactive, when the reaction is stirred at room temperature for 1 min or at 50 °C for 5 min, crystalline optically active complexes are obtained in almost all runs. The ee, however, fluctuates randomly (Scheme 10).

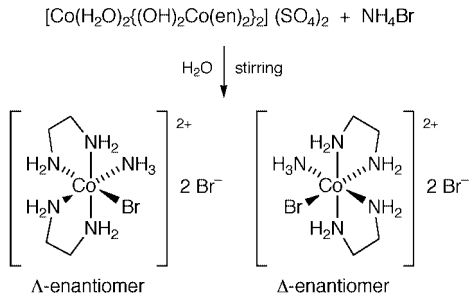

Scheme 10 Autocatalytic nucleation of enantiomeric crystals of coordination compounds.

The chiral complex crystallizes as a conglomerate in which each crystal consists of either Λ- or Δ-enantiomers. In a stirring system, a crystal of a particular enantiomer can be self-replicated through secondary nucleation, thereby catalyzing its own formation. Again, the ee of the product was largely dependent on the stirring rate. In addition, when the stirred reactions were carried out in the presence of a tiny amount of crystals of one enantiomer, that enantiomer was preferentially produced. If an enantiomer is added in dissolution, such a preference is not observed. This does mean that an autocatalytic reaction operating *via* secondary nucleation *requires the presence of crystals* to induce symmetry breaking.

Prospects: symmetry breaking and evolution

If an aspect of chiral amplification dominates molecular evolution, it must surely be the formation of macromolecules, since enzymes, nucleic acids, and other biopolymers have acquired a definite handedness. More than four decades ago, Wald suggested that the regular secondary structure of peptides would have resulted from the helical sense preferred by the major enantiomeric amino acid whose handedness also permitted its own selection and growth.[33] Shortly afterwards, this hypothesis was verified on polypeptides derived from nearly an equal population of enantiomeric amino acids and on regularly isotactic vinyl polymers prepared by Ziegler–Natta polymerization.[21b,34]

Detailed studies and an in-depth interpretation of this so-called 'Majority Rule', which arises from the excess energy of the opposite helicity, has been recently carried out by Green, Selinger and their co-workers.[35,36] Thus, chiroptical measurements reveal that a polymer made of 98.4% achiral units and 1.6% chiral units, with an ee of only 2.8% among these chiral monomers, has the same optical activity as a polymer of just the chiral units with the same ee. Notably, the theory allows prediction of the helical sense ratio for any ee and, within certain limits, it is also possible to reduce the chiral component without affecting the optical purity.[36b,e,f] In the latter case, the circular dichroism (CD) spectrum does not show any variation until the composition of monomers reaches 99.2% achiral and 0.8% chiral.[36a] It seems that cooperative interactions in helical systems may lead to an important chiral amplification.[37]

Homochiral crystals of helical coordination polymers from achiral components have been obtained by Aoyama and his

group by treating an achiral pyrimidine derivative with cadmium nitrate in aqueous ethanol.[38] The achiral precursor itself, orthogonal 9-(5-pyrimidyl)anthracene, forms achiral $P2_1/n$ crystals with $Cd(NO_3)_2$ in methanol and without forming helical chains. However, the slow cooling (~ 6 h) of a hot (80 °C) ethanol–water solution of this compound and $Cd(NO_3)_2$ to room temperature afforded an adduct which crystallizes in chiral space group $P2_1$. The metal ion is hexacoordinated with two pyrimidine ligands, two nitrate ions, ethanol and water. The crystal structure contains an alternate arrangement of pyrimidine–metal helical layers and anthracene layers. The chirality results from a twist of the two pyrimidine rings and the overall helicity of the pyrimidine–metal array is maintained in the crystal by interstrand hydrogen bonding between the nitrate anions and water.

That the crystallization is homochiral is evidenced by the fact that all the crystals isolated from one crystallization show the same CD sign and hence the same helicity. Remarkably, chirality of this helical coordination polymer can be controlled by seeding. Thus, an achiral adduct can be converted into *P* or *M* helices at will, when the former is coground with a small amount of *P* or *M* adducts, respectively, and then exposed to vapors of ethanol.

In principle, the formation of chiral crystals from achiral building blocks is not surprising since achiral molecules can crystallize in chiral space groups.[15,39] However, these substances are obtained either as an in-crystal racemate or as a mixture of self-resolved enantiomeric chiral crystals.[40] The work by Aoyama and coworkers provides evidence for homochiral crystallization, by which achiral molecules afford spontaneously crystals with the same chirality, which can also be related to the concept of secondary nucleation mentioned above.

As long as a polymer can replicate, perhaps to perform a biological function, it could serve as the seed molecule. Its autocatalytic 'nucleation' would continue in an enantiomerically pure fashion. Thus, the number of copies of the selected homochiral polymer will become greater and greater while the number of competing stereoisomers will become fewer and fewer. The slight enantiomeric imbalance would have provided the driving force for such a selection, regardless of the appropriateness of structures or shapes.[3] Recent works by Eschenmoser *et al*. reinforce the idea that the choices of Nature were a question of availability. Pyranosyl-RNA has been found to be not only a stronger pairing system than furanosyl-RNA (and DNA as well), but also such a pairing is more selective and Watson–Crick purine–pyrimidine pairing in strictly antiparallel orientation was obtained.[41] Base sequences of pyranosyl-RNA can be copied with high regioselectivity and chiroselectivity. In general, the copying proceeds slower when one of the D-ribopyranosyl units of a homochiral tetramer-2′,3′-cyclophosphate is replaced by the corresponding L-unit.

Nevertheless, a general problem associated with the stereocontrol of self-assembly is the fact that the large number of random sequences from a mixture of right- and left-handed libraries will hinder the formation of regular cycles with specific-ordered sequences. At the molecular level effective self-replication may adopt the form of a hypercycle,[42] a type of nonlinear autocatalysis in which cross-catalysis superposes onto autocatalytic replication. These processes would have played a key role in the transition from inanimate to living systems, and hypercyclic peptide networks have been studied in detail. Thus, Reza Ghadiri and his associates have recently described two peptide autocatalysts that not only accelerate their own formation but also behave as cross-catalysts, each speeding up the production of the other more efficiently than its own duplication.[43]

At a discrete molecular level, only a few autocatalytic chemical systems contain vestiges of hypercylic organization.[44] Still, chiral hypercycles need to be disclosed and understood, but the above-mentioned transformations by Soai *et al*. constitute a good toehold for promising developments.

Conclusions

The ultimate origin of asymmetry in the universe is an unanswered question. During the last decade, however, a series of rather simple experiments have demonstrated the feasibility of producing optically active compounds from achiral materials. Crystallization processes, not involving spontaneous resolutions, and a few asymmetric reactions have established a direct linkage with the inherent handedness of prebiotic molecules and the biopolymers thereof. While we have seen the triumph of reductionism in explaining life in molecular terms, with stunning revelations of self-replication and regulation, still the large gap between molecular chirality and molecular evolution has become painfully clear. As noted by Avetisov and Goldanskii,[1d] this emerges from the lack of knowledge about the interrelations between the asymmetry of chemical processes involving simple organics and the chiral specificity of biological polymers. Accordingly, only a few assertions can be formulated about the role of symmetry breaking at the chemical stage of evolution, even though homochirality was forced by the initiation of enantiospecific functions in living systems. In any event, other recent studies, especially concerning oligonucleotide systems, suggest mirror symmetry breaking before replication.[39] This also supports the idea of autocatalytic processes capable of propagating the homochirality from an initial statistical mixture of chiral molecules. The interesting findings of enantiomeric excesses in extraterrestrial samples do not answer definitely the question of the generation of asymmetry, nor do they conflict with the statistical arguments.[14]

There will come a time, perhaps ten years from now, perhaps sooner, when we would not be able to discuss evolution at any finer level of detail without claiming the origin of enantiomeric homogeneity. That's what life is all about.

Acknowledgments

One of us (P. C.) thanks a group of talented colleagues: K. Asakura, D. G. Blackmond, A. Eschenmoser, H. B. Kagan, J. V. Selinger, J. Siegel, K. Soai and R. Tamura, for kindly providing copies and preprints of their contributions, and for helpful discussions. The Ministry of Education and Culture (PB95-0259) and the Junta de Extremadura-Fondo Social Europeo (IPR98-C040) supported this work.

Notes and references

1 (*a*) S. F. Mason, *Molecular Optical Activity and the Chiral Discriminations*, Cambridge University Press, Cambridge, 1982; (*b*) R. Janoschek, in *Chirality: From the Weak Boson to the α-Helix*, ed. R. Janoschek, Springer, New York, 1991, pp. 18–33; (*c*) W. A. Bonner, *Origins Life Evol. Biosphere*, 1994, **24**, 63; (*d*) V. Avetisov and V. Goldanskii, *Proc. Natl. Acad. Sci. U.S.A.*, 1996, **93**, 11435.

2 G. F. Joyce, G. M. Visser, C. A. A. van Boeckel, J. H. van Boom, L. E. Orgel and J. van Westresen, *Nature*, 1984, **310**, 602.

3 W. R. Loewenstein, *The Touchstone of Life: Molecular Information, Cell Communication, and the Foundations of Life*, Oxford University Press, Oxford, 1999.

4 For recent reviews: (*a*) C. Girard and H. B. Kagan, *Angew. Chem., Int. Ed.*, 1998, **37**, 2922; (*b*) M. Avalos, R. Babiano, P. Cintas, J. L. Jiménez and J. C. Palacios, *Tetrahedron: Asymmetry*, 1997, **8**, 2997.

5 (*a*) D. G. Blackmond, *J. Am. Chem. Soc.*, 1997, **119**, 12934; (*b*) D. G. Blackmond, *J. Am. Chem. Soc.*, 1998, **120**, 13349.

6 D. G. Blackmond, T. Rosner, T. Neugebauer and M. T. Reetz, *Angew. Chem., Int. Ed.*, 1999, **38**, 2196.

7 M. Gardner, *The New Ambidextrous Universe*, Freeman, New York, 1990, pp. 211–230.

8 A. J. MacDermott, in *Physical Origin of Homochirality in Life*, ed. D. B. Cline, American Institute of Physics, Woodbury, NY, 1996, pp. 241–254.

9 D. K. Kondepudi, *BioSystems*, 1987, **20**, 75.
10 (*a*) M. Avalos, R. Babiano, P. Cintas, J. L. Jiménez, J. C. Palacios and L. D. Barron, *Chem. Rev.*, 1998, **98**, 2391; (*b*) L. M. Pismen, *Vortices in Nonlinear Fields*, Clarendon Press, Oxford, 1998.
11 (*a*) J. R. Cronin and S. Pizzarello, *Science*, 1997, **275**, 951; (*b*) M. H. Engel and S. A. Macko, *Nature*, 1997, **389**, 265; (*c*) S. Pizzarello and J. R. Cronin, *Nature*, 1998, **394**, 236.
12 J. Bailey, A. Chrysostomou, J. H. Hough, T. M. Gledhill, A. McCall, S. Clark, F. Ménard and M. Tamura, *Science*, 1998, **281**, 672.
13 E. Rubenstein, W. A. Bonner and G. S. Brown, *Science*, 1999, **283**, 1415.
14 J. S. Siegel, *Chirality*, 1998, **10**, 24.
15 (*a*) E. L. Eliel and S. H. Wilen, *Stereochemistry of Organic Compounds*, Wiley, Chichester, 1994, pp. 298–304; (*b*) M. Sakamoto, *Chem. Eur. J.*, 1997, **3**, 684; (*c*) I. Kuzmenko, I. Weissbuch, E. Gurovich, L. Leiserowitz and M. Lahav, *Chirality*, 1998, **10**, 415; (*d*) H. Koshima, S. Honke and J. Fujita, *J. Org. Chem.*, 1999, **64**, 3916; (*e*) M. Lahav and L. Leiserowitz, *Angew. Chem., Int. Ed.*, 1999, **38**, 2533.
16 (*a*) R. Tamura, H. Takahashi, K. Hirotsu, Y. Nakajima, T. Ushio and F. Toma, *Angew. Chem., Int. Ed.*, 1998, **37**, 2876; (*b*) H. Takahashi, R. Tamura, T. Ushio, Y. Nakajima and K. Hirotsu, *Chirality*, 1998, **10**, 705.
17 Y. Takahashi, H. Takezoe, Y. Suzuki, I. Kobayashi, T. Yajima, M. Terada and K. Mikami, *Angew. Chem., Int. Ed.*, 1999, **38**, 2354.
18 F. Stevens, D. J. Dyer and D. M. Walba, *Angew. Chem., Int. Ed. Engl.*, 1996, **35**, 900.
19 D. K. Kondepudi, R. J. Kaufman and N. Singh, *Science*, 1990, **250**, 975.
20 J. M. McBride and R. L. Carter, *Angew. Chem., Int. Ed. Engl.*, 1991, **30**, 293.
21 (*a*) D. K. Kondepudi, K. L. Bullock, J. A. Digits and P. D. Yarborough, *J. Am. Chem. Soc.*, 1995, **117**, 401; (*b*) for an excellent review: K. Asakura, K. Kobayashi, Y. Mizusawa, T. Ozawa, T. Miura, A. Tanaka, Y. Kushibe and S. Osanai, *Recent Res. Dev. Pure Appl. Chem.*, 1997, **1**, 123.
22 R.-Y. Qian and G. D. Botsaris, *Chem. Eng. Sci.*, 1997, **52**, 3429.
23 R. E. Pincock, R. R. Perkins, A. S. Ma and K. R. Wilson, *Science*, 1971, **174**, 1018.
24 D. K. Kondepudi, J. Laudadio and K. Asakura, *J. Am. Chem. Soc.*, 1999, **121**, 1448.
25 F. C. Frank, *Biochim. Biophys. Acta*, 1953, **11**, 459.
26 (*a*) K. Soai, T. Hayase and K. Takai, *Tetrahedron: Asymmetry*, 1995, **6**, 637; (*b*) T. Shibata, K. Choji, T. Hayase, Y. Aizu and K. Soai, *Chem. Commun.*, 1996, 751 and 1235; (*c*) T. Shibata, T. Hayase, J. Imamoto and K. Soai, *Tetrahedron: Asymmetry*, 1997, **8**, 1717; (*d*) K. Soai, T. Shibata, H. Marioka and K. Choji, *Nature*, 1995, **378**, 767.
27 T. Shibata, J. Yamamoto, N. Matsumoto, S. Yonekubo, S. Osanai and K. Soai, *J. Am. Chem. Soc.*, 1998, **120**, 12157.
28 K. Soai, personal communication (to P. C.)
29 T. Shibata, S. Yonekubo and K. Soai, *Angew. Chem., Int. Ed.*, 1999, **38**, 659.
30 K. Soai, Y. Inoue, T. Takahashi and T. Shibata, *Tetrahedron*, 1996, **52**, 13 355.
31 H. Danda, H. Nishikawa and K. Otaka, *J. Org. Chem.*, 1991, **56**, 6740.
32 (*a*) K. Asakura, K. Kobayashi, Y. Mizusawa, T. Ozawa, S. Osanai and S. Yoshikawa, *Physica D*, 1995, **84**, 72; (*b*) K. Asakura, D. K. Kondepudi and R. Martin, *Chirality*, 1998, **10**, 343.
33 J. Wald, *Ann. N.Y. Acad. Sci.*, 1957, **69**, 353.
34 E. L. Eliel and S. H. Wilen, *Stereochemistry of Organic Compounds*, Wiley, Chichester, 1994, pp. 1067–1071.
35 M. M. Green and J. V. Selinger, *Science*, 1998, **282**, 880.
36 (*a*) S. K. Jha, K.-S. Cheon, M. M. Green and J. V. Selinger, *J. Am. Chem. Soc.*, 1999, **121**, 1665; (*b*) J. V. Selinger and R. L. B. Selinger, *Macromolecules*, 1998, **31**, 2488; (*c*) H. Gu, Y. Nakamura, T. Sato, A. Teramoto, M. M. Green, S. K. Jha, C. Andreola and M. P. Reidy, *Macromolecules*, 1998, **31**, 6362; (*d*) J. V. Selinger and J. M. Schnur, *Biophys. J.*, 1997, **73**, 966; (*e*) J. V. Selinger and R. L. B. Selinger, *Phys. Rev. E*, 1997, **55**, 1728; (*f*) J. V. Selinger and R. L. B. Selinger, *Phys. Rev. Lett.*, 1996, **76**, 58.
37 For a review: M. M. Green, J. W. Park, T. Sato, A. Teramoto, S. Lifson, R. L. B. Selinger and J. V. Selinger, *Angew. Chem., Int. Ed.*, 1999, **38**, 3138.
38 T. Ezuhara, K. Endo and Y. Aoyama, *J. Am. Chem. Soc.*, 1999, **121**, 3279.
39 I.-H. Suh, K. H. Park, W. P. Jensen and D. E. Lewis, *J. Chem. Educ.*, 1997, **74**, 800.
40 A particular case of spontaneous resolution involves achiral compounds having chiral conformations, which may be 'frozen' in the solid state or in solution at low temperature. Thus, enantiomeric crystals of an *N*-methylbenzamide, which correspond to a stable *anti* conformer, could be distinguished morphologically as in Pasteur's experiments. Moreover, slow crystallization may lead to homochiral crystals. All four molecules in the unit cell of the chiral crystal have the same chirality. See for instance: I. Azumaya, I. Okamoto, S. Nakayama, A. Tanatani, K. Yamaguchi, K. Shudo and H. Kagechika, *Tetrahedron*, 1999, **55**, 11 237.
41 (*a*) M. Bolli, R. Micura and A. Eschenmoser, *Chem. Biol.*, 1997, **4**, 309; (*b*) see also: M. Beier, F. Reck, T. Wagner, R. Krishnamurthy and A. Eschenmoser, *Science*, 1999, **283**, 699.
42 U. Müller-Herold, *J. Theor. Biol.*, 1983, **102**, 569.
43 D. H. Lee, K. Severin, Y. Yokobayashi and M. Reza Ghadiri, *Nature*, 1997, **390**, 591.
44 (*a*) J.-I. Hong, Q. Feng, V. Rotello and J. Rebek Jr., *Science*, 1992, **255**, 848; (*b*) T. Achilles and G. von Kiedrowski, *Angew. Chem., Int. Ed. Engl.*, 1993, **32**, 1198.

A new synthesis of [2,3]naphthoporphyrins

Satoshi Ito,[a] Naoyuki Ochi,[a] Hidemitsu Uno,[b] Takashi Murashima[a] and Noboru Ono*[a]

[a] *Department of Chemistry, Faculty of Science, Ehime University, Matsuyama 790-8577, Japan. E-mail: ononbr@dpc.ehime-u.ac.jp*

[b] *Advanced Instrumentation Center for Chemical Analysis, Ehime University, Matsuyama 790-8577, Japan*

Received (in Cambridge, UK) 20th March 2000, Accepted 14th April 2000

A new synthesis of [2,3]naphthoporphyrins using 4,9-ethano-*2H*-benz[*f*]isoindole as a synthon of *2H*-benz[*f*]-isoindole is described; soluble precursors of [2,3]naphthoporphyrins are converted into insoluble [2,3]naphthoporphyrins by simply heating at 290 °C.

Highly conjugated porphyrins have attracted attention as conducting materials, near-IR dyes, nonlinear optical materials,[1] or photosensitizers for photodynamic therapy (PDT) of cancer tissues on *in vivo* studies.[2] We and Lash *et al*. have reported syntheses of various highly conjugated porphyrins using pyrroles fused with polycyclic aromatic rings.[3] The requisite pyrroles are prepared by the reaction of polycyclic aromatic nitro compounds with ethyl isocyanoacetate. However, this method has a severe limitation. The reaction of nitrobenzene and nitronaphthalene with ethyl isocyanoacetate does not give the desired isoindole[4] and benz[*f*]isoindole.[5] In general, such isoindole derivatives are very difficult to prepare owing to their instability. In addition, highly conjugated porphyrins and their metal complexes are very difficult to purify, since they are insoluble in most organic solvents.[6] We have reported a simple solution of these problems using 4,7-dihydro-4,7-ethano-*2H*-isoindole as a synthon of isoindole for benzoporphyrin synthesis.[7,8] Thus, heating porphyrins fused with bicyclo[2.2.2]octadiene rings at 200–230 °C results in clean formation of benzoporphyrins *via* retro Diels–Alder reaction; the products are pure and do not require further purification. Here, we report a new synthesis of [2,3]naphthoporphyrins using a similar strategy, in which 4,9-ethano-*2H*-benz[*f*]isoindole is used as a synthon of *2H*-benz[*f*]isoindole.

The synthesis of 4,9-dihydro-4,9-ethano-*2H*-benz[*f*]isoindole **6** is summarized in Scheme 1.† 1,4-Dihydro-1,4-ethanonaphthalene **1** was converted into sulfide **2** by reaction with PhSCl. Oxidation of **2** with *m*-CPBA followed by treatment with DBU gave α,β-unsaturated sulfone **4**. The pyrrole **5** was prepared in good yield by treatment of **4** with ethyl isocyanoacetate in the presence of 2.0 equivalents of Bu^{t}OK.[9] Deethoxycarbonylation upon heating **5** with KOH in ethylene glycol at 165 °C gave 4,9-dihydro-4,9-ethano-*2H*-benz[*f*]-isoindole **6** in 83% yield.

Porphyrin **7a** was prepared from pyrrole **5** by reduction with $LiAlH_4$ at 0 °C followed by subsequent tetramerization and oxidation. Various metals can be introduced into **7a** by the usual method using metal acetates. Porphyrins **7a**,**b** were purified by column chromatography (alumina, $CHCl_3$) followed by washing the resulting powder with MeOH–H_2O (*ca.* 1:1). Porphyrins **7a**,**b** were converted into pure tetranaphtho[2,3-*b*;2′,3′-*g*;2″,3″-*l*;2‴,3‴-*q*]porphyrins **8a**,**b** in 100% yield by heating at 290 °C under vacuum (10 mm Hg) for 10 min. Thus, porphyrins **7a**,**b** can be regarded as soluble equivalents of the corresponding tetra[2,3]naphthoporphyrins **8a**,**b**. The reaction of **6** with benzaldehydes in the presence of $BF_3{\cdot}OEt_2$ followed by oxidation and metallation gave *meso*-tetraarylated porphyrin zinc complexes **9a**,**b**. They were also converted into the corresponding *meso*-tetraarylnaphtho[2,3-*b*;2′,3′-*g*;2″,3″-*l*;2‴,3‴-*q*]porphyrin zinc complexes **10a**,**b** in 100% yield by heating at 290 °C *in vacuo* for 10 min (Scheme 2).

Mono[2,3-*b*]naphthoporphyrin **13** was also prepared in 100% yield by heating porphyrin **12** at 290 °C (Scheme 3).† Porphyrin **12** was prepared by the well established 3 + 1 approach consisting of the reaction of tripyrrane **11** with 3,4-diethylpyrrole-2,5-dicarbaldehyde followed by oxidation.[10] The requisite **11** was prepared by the reaction of **6** with 2.0 equivalents of *tert*-butyl 5-acetoxymethyl-4-butyl-3-methyl-1*H*-pyrrole-2-carboxylate in Pr^{i}OH–AcOH.

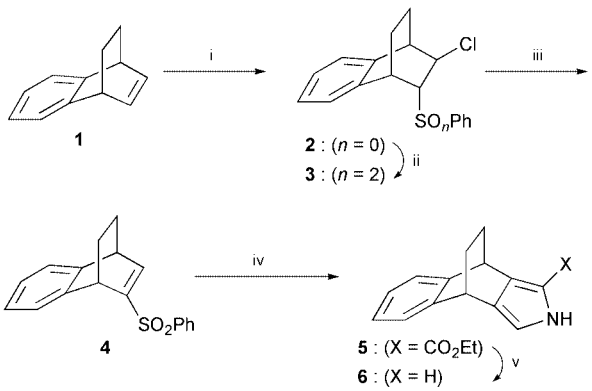

Scheme 1 *Reagents and conditions*: i, PhSCl, CH_2Cl_2, −78 °C, 1 h, 99%; ii, *m*-CPBA, $CHCl_3$, room temp., 2 h, 99%; iii, DBU, THF, 0 °C, 30 min, 99%; iv, ethyl isocyanoacetate, Bu^{t}OK, THF, 0 °C, 3 h, 91%; v, KOH, $HO(CH_2)_2OH$, 165 °C, 1.5 h, 83%.

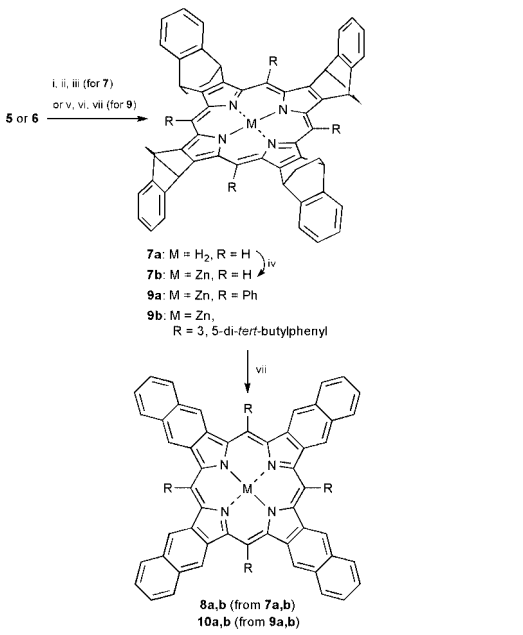

Scheme 2 *Reagents and conditions*: i, $LiAlH_4$, THF, 0 °C, 1 h; ii, *p*-TsOH, $CHCl_3$, room temp., 15 h; iii, *p*-chloranil, room temp., 24 h, 20% (three steps from **5**); iv, Zn(OAc), $CHCl_3$–MeOH (9:1), room temp., 30 min, 95%; v, ArCHO, $BF_3{\cdot}OEt_2$, $CHCl_3$, room temp., 4 h; vi, *p*-chloranil, room temp., 4 h; vii, $Zn(OAc)_2$, $CHCl_3$–MeOH (9:1), room temp., 30 min (**9a** = 39%; **9b** = 16%, for three steps from **6**); viii, 290 °C, 10 min, 100%.

DOI: 10.1039/b002213f

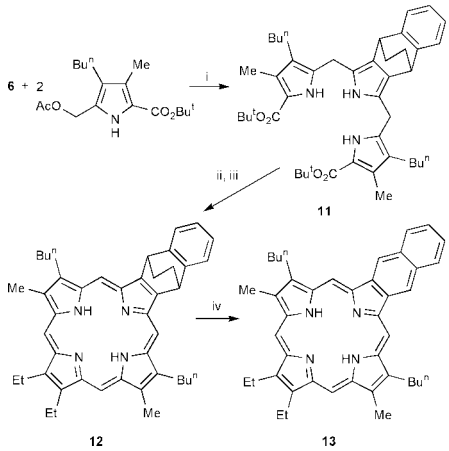

Scheme 3 *Reagents and conditions*: i, AcOH–Pr^{i}OH (1 : 1), reflux, 17 h; ii, 3,4-diethylpyrrole-2,5-carbaldehyde, TFA, room temp., 2 h; iii, Et_3N, DDQ, $CHCl_3$, room temp., 1 h, 18% for three steps; iv, 290 °C, 100%.

Table 1 Selected UV–VIS data for [2,3]naphthoporphyrins and their precursors

Porphyrin	λ_{max} ($CHCl_3$)/nm ($\log_{10}\varepsilon$)
7a	392 (5.20), 495 (4.14), 527 (3.66), 563 (3.69), 615 (3.12)
8a[a]	359 (0.34), 419 (0.50), 464 (1.00), 697 (0.13), 773 (0.87)
9a	349 (3.29), 426 (5.43), 549 (4.17)
10a	487 (4.96), 662 (3.73), 723 (4.87)
12	399 (5.17), 497 (4.12), 531 (3.86), 566 (3.73), 619 (3.49)
13	419 (5.34), 519 (3.92), 551 (4.53), 587 (3.75), 643 (4.34)

[a] In 5% TFA–$CHCl_3$; here relative intensities are given in parentheses.

Absorption spectrum data of [2,3]naphthoporphyrins and their precursors are summarized in Table 1. As porphyrin **8a** was insoluble in most solvents, its absorption spectrum was measured in 5% TFA-$CHCl_3$. The Soret and Q bands of the dication **8a** were observed at 464, 697 and 773 nm, respectively. The absorbance at 773 nm is unusually intense (0.87 × that of Soret band), showing behaviour reminiscent of phthalocyanines. *meso*-Tetraphenyltetra[2,3]napthoporphyrin **10a** was moderately soluble in organic solvents such as CH_2Cl_2 or $CHCl_3$. The Soret band of **10a** was rather weak compared to that of other porphyrins, owing to steric hindrance between *meso*-Ph and fused [2,3]naphthalene rings. By contrast, the intensity of the absorption at 723 nm is very strong ($\log_{10}\varepsilon$ = 4.87), this value is considerably larger than that of known π-extended *meso*-tetraphenylporphyrins.[3] The UV–VIS spectrum of **13** is rhodo-type (Q band: III > I > IV > II) which is typical for monobenzoporphyrins.[7]

In conclusion, we have succeeded in developing a new strategy for the preparation of [2,3]naphthoporphyrins using 4,9-ethano-2*H*-benz[*f*]isoindole as a synthetic equivalent of 2*H*-benz[*f*]isoindole. This strategy may extend to the synthesis of other π-extended molecules such as polypyrroles or pyrrole oligomers, which are fused with naphthalene rings.

The work was partly supported by Grants-in Aid for Scientific Research from the Ministry of Education, Science, Sports and Culture of Japan. We are also grateful to Dr Y. Takahashi (JEOL) for recording the FAB mass spectra of porphyrins (**8a** and **10a**).

Notes and references

† New compounds gave satisfactory elementary analyses. *Selected data*: for **5**: white plates, mp 144–145 °C, ^{1}H NMR ($CDCl_3$, *J*/Hz) δ 1.39 (3H, t, *J* 7.08), 1.58–1.80 (4H, m), 4.28 (1H, m), 4.33 (2H, q, *J* 7.33, 14.16), 4.79 (1H, m), 6.66 (1H, d, *J* 2.44), 7.04–7.13 (2H, m), 7.16–7.32 (2H, m), 8.41 (1H, br s); *m/z* 267 (M^+, 9), 239 (95), 193 (100). For **6**: white needles, mp 182–183 °C, ^{1}H NMR ($CDCl_3$) δ 1.65–1.83 (4H, m), 4.26 (2H, m), 6.53 (2H, d, *J* 2.44), 7.03–7.07 (2H, m), 7.18–7.22 (2H, m), 7.53 (1H, br s); *m/z* (EI) 195 (M^+, 14), 167 (100). For **7a** (a mixture of four isomers): ^{1}H NMR ($CDCl_3$) δ −4.66 (2H, br s), 2.15–2.52 (16H, m), 6.18 (8H, m), 7.25 (8H, m), 7.80 (8H, m), 10.52 (4H, m); *m/z* (FAB) 823 (M^+ + 1). Calc. for $C_{60}H_{46}N_4{\cdot}0.5H_2O$: C, 86.61; H, 5.69; N, 6.73. Found: C, 86.49; H, 5.71; N, 6.53%. For **8a**: *m/z* (FAB) not assigned. Calc. for $C_{52}H_{30}N_4{\cdot}H_2O$: C, 85.69; H, 4.43; N, 7.69. Found: C, 85.92; H, 4.31; N, 7.62%. For **9a** (a mixture of four isomers): ^{1}H NMR ($CDCl_3$) δ 1.0–2.2 (16H, m), 3.77 (8H, m), 6.9–7.2 (16H, m), 7.9–8.6 (20H, m); *m/z* (FAB) 1189 (M^+). Calc. for $C_{84}H_{60}N_4{\cdot}3.5H_2O$: C, 80.47; H, 5.39; N, 4.47. Found: C, 80.44; H, 5.35; N, 4.21%. For **10a**: ^{1}H NMR ($CDCl_3$) δ 7.48 (8H, m), 7.67 (8H, s), 7.69 (8H, m), 7.98 (8H, m), 8.11 (4H, m), 8.39 (8H, m); *m/z* (FAB) 1076 (M^+). Calc. for $C_{76}H_{44}N_4{\cdot}2.5H_2O$: C, 81.24; H, 4.40; N, 4.99. Found: C, 81.53; H, 4.58; N, 4.84%. For **12**: ^{1}H NMR ($CDCl_3$) δ −3.95 (2H, br s), 1.15 (6H, t, *J* 7.33), 1.81 (4H, m), 1.92 (6H, t, *J* 7.33), 2.21 (2H, m), 2.28–2.39 (4H, m), 2.31 (2H, m), 3.63 (6H, s), 4.09–4.14 (8H, m), 6.07 (2H, m), 7.25 (2H, m), 7.78 (2H, m), 10.11 (2H, s), 10.23 (2H, s); *m/z* (FAB) 635 (M^+ + 1). Calc. for $C_{44}H_{50}N_4{\cdot}CH_3OH$: C, 81.04; H, 8.16; N, 8.40. Found: C, 81.38; H, 8.18; N, 8.11%. For **13**: ^{1}H NMR ($CDCl_3$) δ −3.52 (2H, br s), 1.14 (6H, t, *J* 7.32), 1.78 (4H, m), 1.89 (6H, t, *J* 7.32), 2.29 (4H, m), 3.63 (6H, m), 3.93–4.12 (8H, m), 7.80 (2H, m), 8.51 (2H, m), 9.56 (2H, s), 9.96 (2H, s), 10.18 (2H, s); *m/z* (FAB) 607 (M^+ + 1). Calc. for $C_{42}H_{46}N_4{\cdot}0.5H_2O$: C, 81.91; H, 7.69; N, 9.10. Found: C, 81.78; H, 7.64; N, 8.78%.

1 S. A. Vinogradov and D. F. Wilson, *J. Chem. Soc., Perkin Trans. 2*, 1995, 103; P. Chen, A. S. Dvornikov, M. Nakashima, J. F. Roach, D. M. Alabran and P. M. Rentzepis, *J. Phys. Chem.*, 1996, **100**, 17 507.
2 R. Bonnett, *Chem. Soc. Rev.*, 1995, **24**, 19 and references therein.
3 N. Ono, H. Hironaga, K. Ono, S. Kaneko, T. Murashima, T. Ueda, C. Tsukamura and T. Ogawa, *J. Chem. Soc., Perkin Trans. 1*, 1996, 417; T. D. Lash, P. Chandrasekar, A. T. Osuma, S. T. Chaney and J. D. Spence, *J. Org. Chem.*, 1998, **63**, 8455.
4 R. Bonnett and S. A. North, *Adv. Heterocycl. Chem.*, 1981, **29**, 341.
5 J. E. Shields and J. Bornstein, *Chem. Ind. (London)*, 1967, 1404; W. Rettig and J. Wirz, *Helv. Chim. Acta*, 1976, **59**, 1054; D. E. Remy and F. H. Bissett, *J. Org. Chem.*, 1978, **43**, 4469.
6 M. Rein and M. Hanack, *Chem. Ber.*, 1988, **121**, 1601; A. M. Vorotnikov, V. N. Kopranenkov and E. A. Lukyanets, *J. Gen. Chem., USSR*, 1991, **61**, 1128; N. Kobayashi, W. A. Nevin, S. Mizunuma, H. Awaji and M. Yamaguchi, *Chem. Phys. Lett.*, 1993, **205**, 51; A. C. Tome, P. S. S. Lacerda, M. G. P. M. S. Neves and J. A. S. Cavaleiro, *Chem. Commun.*, 1997, 1199.
7 S. Ito, N. Ochi, T. Murashima, H. Uno and N. Ono, *Heterocycles*, 2000, **52**, 399 and references therein.
8 S. Ito, T. Murashima and N. Ono, *J. Chem. Soc., Perkin Trans. 1*, 1997, 3161.
9 Pyrrole synthesis from α,β-unsaturated sulfones; Y. Abel and F.-P. Montforts, *Tetrahedron Lett.*, 1997, **38**, 1745.
10 T. D. Lash, *Chem. Eur. J.*, 1996, **2**, 1197 and references therein.

1:1 Complex of guanine quartet with alkali metal cations detected by electrospray ionization mass spectrometry

Kazuaki Fukushima and Hideo Iwahashi*

Wakayama Medical College, 811-1 Kimiidera, Wakayama 641-8509 Japan. E-mail: chem1@wakayama-med.ac.jp

Received (in Cambridge, UK) 20th March 2000, Accepted 17th April 2000
Published on the Web 9th May 2000

Selective 1:1 complex formation of a square quartet of 9-ethylguanine with small alkali metal cations (Li^+, Na^+) was detected by electrospray mass spectrometry

The guanine base is unique as a pair of hydrogen-donating groups (NH and NH_2) and a pair of hydrogen-accepting groups (C=O and N) are arranged on adjacent edges of the molecule [Fig. 1(a)]. Thus, a guanine base can form a self-complementary, hydrogen-bonded square quartet [Fig. 1(b)], which has been widely found in gels of guanosine derivatives **1**[1,2] and in parallel[3] and antiparallel[4] quadruple strands of guanine-rich oligonucleotides such as telomeric DNA.

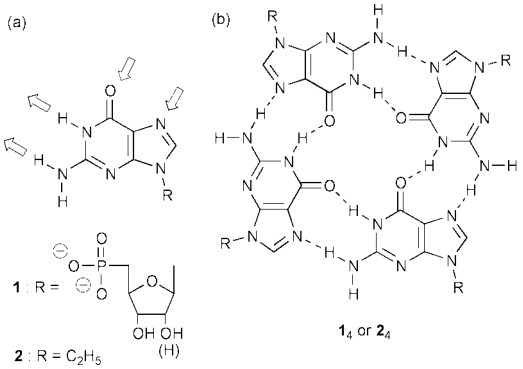

Fig. 1 (a) Guanosine-5′-monophosphate **1** and 9-ethylguanine **2**, (b) guanine quartet ($\mathbf{1}_4$ and $\mathbf{2}_4$).

Pinnavaia *et al.* and Laszlo and coworkers have independently reported that the aggregate of guanosine-5′-monophosphate (5′-GMP) in the presence of K^+ is a 2:1 complex (a sandwich complex) composed of two stacked $\mathbf{1}_4$ and one K^+ ion [Fig. 2(a)].[5] In order to stabilize the sandwich structure, chelation of cations with phosphate groups is essential,[5b,c] although stacking interactions between guanine bases and ion–dipole interaction between K^+ and carbonyl groups may also be important. In contrast to 5′-GMP, 9-alkylguanines do not have the ability to show such chelation. In this work, we have detected a 1:1 complex of guanine quartets with alkali metal cations by electrospray ionization mass spectrometry (ESI-MS)[6] in the system of 9-ethylguanine **2**.†

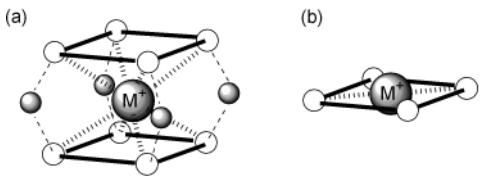

Fig. 2 Schematic representations of (a) a 2:1 complex (a sandwich complex) and (b) a 1:1 complex of a guanine quartet with alkali metal cations: ○, guanine base; (⋯⋯), interaction between alkali metal cation (M^+) and carbonyl group; (—), hydrogen bonding between guanine bases; (-----), chelation of alkali metal cation (◍) with phosphate groups.

The ESI-MS spectrum of **2** [Fig. 3(a)] shows prominent peaks at *m/z* 202, 381 and 739, corresponding to $[\mathbf{2} + Na]^+$, $[\mathbf{2}_2 + Na]^+$ and $[\mathbf{2}_4 + Na]^+$ in the presence of 0.1 mM $NaClO_4$. Other $[\mathbf{2}_n + Na]^+$ ($n = 3$ and $n \geqslant 5$) complexes were scarcely observed under these conditions. When the concentration of Na^+ was reduced to 0.01 mM [Fig. 3(b)], only the $[\mathbf{2}_4 + Na]^+$ ion was observed. The above results indicate that the 1:1 complex of the guanine quartet ($\mathbf{2}_4$) with sodium cation, $[\mathbf{2}_4 + Na]^+$, is remarkably stable.

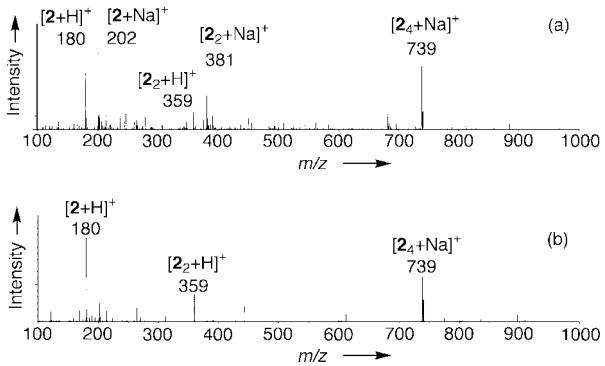

Fig. 3 ESI-MS spectra of 9-ethylguanine **2**: in the presence of (a) 0.1 mM and (b) 0.01 mM $NaClO_4$.

Similarly, **2** also gave the corresponding $[\mathbf{2}_4 + M]^+$ along with $[\mathbf{2} + M]^+$ and $[\mathbf{2}_2 + M]^+$ in the presence of 0.1 mM of other alkali metal cations (Li^+, K^+, Rb^+ and Cs^+) (Fig. 4). The peak intensity ratios of $[\mathbf{2}_4 + M]^+/[\mathbf{2} + M]^+$ for Li^+ and Na^+ (Li^+, 0.69 and Na^+, 0.80) are considerably higher than those of the other alkali

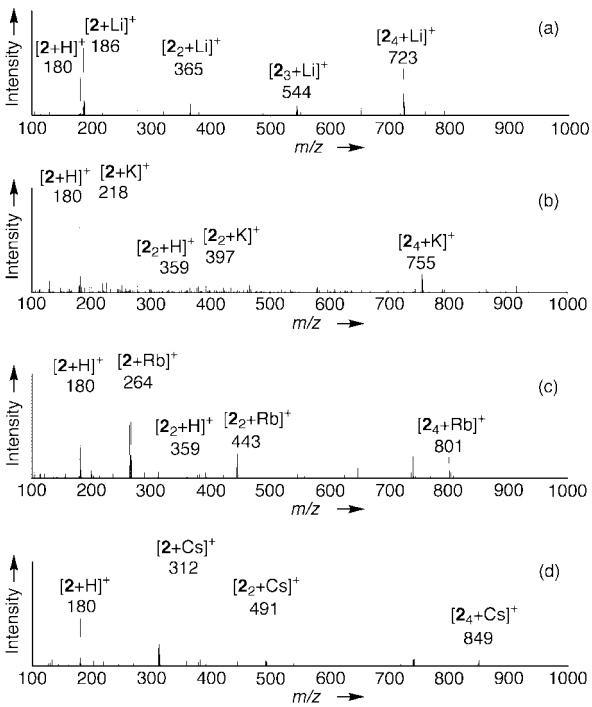

Fig. 4 ESI-MS spectra of 9-ethylguanine **2** in the presence of 0.1 mM $MClO_4$: (a) M = Li, (b) M = K, (c) M = Rb and (d) M = Cs.

DOI: 10.1039/b002235g

metals (K^+, 0.20; Rb^+, 0.20; and Cs^+, 0.16), suggesting that Li^+ as well as Na^+ form a stable $[\mathbf{2}_4 + M]^+$ complex. To confirm this tendency, ESI-MS measurements were performed in the presence of a pair of cations both 0.1 mM (Na^+–Li^+, Li^+–K^+, K^+–Rb^+, or Rb^+–Cs^+). The relative peak intensities of $[\mathbf{2}_4 + M]^+$ increased as $Na^+ > Li^+ > K^+ \gg Rb^+, Cs^+$.

NMR studies of 2:1 complexes $[(\mathbf{1}_4)_2 + M]^+$ showed that the stability increases in the order $K^+ > Na^+, Rb^+ \gg Li^+, Cs^+$.[5a] The K^+-selectivity in the 2:1 complex shows that size of the cavity between two 5′-GMP quartets ($\mathbf{1}_4$) is appropriate to accommodate K^+ [Fig. 2(a)].[5c] On the other hand, our results indicate that Li^+ and Na^+ bind with $\mathbf{2}_4$ more strongly than does K^+.[7] The selectivity for Na^+ and Li^+ is possibly explained by a correspondence between the size of M^+ and that of the central cavity of $\mathbf{2}_4$. Average distances from the center of $\mathbf{2}_4$ to carbonyl oxygens are estimated to be 2.41 Å by molecular orbital calculation,[8,9] close to the experimentally observed Na–O distance (2.34 ± 0.02 Å) by X-ray analysis.[4c] Accordingly, Na^+ can fit exactly in the central cavity of $\mathbf{2}_4$. Li^+ (Li–O, 2.04–2.24 Å[10]) may also be located inside the cavity. On the other hand, K^+, Rb^+ and Cs^+ (K–O, 2.75–2.81 Å;[11] Rb–O, 2.88–2.93 Å;[11] and Cs–O, 3.06–3.18 Å[12]) are too large to fit in the central cavity of $\mathbf{2}_4$ and would be located out-of-plane.

In conclusion, we have observed 1:1 complexes of $\mathbf{2}_4$ with alkali metal cations in the systems of 9-ethylguanine **2** using ESI–MS. The sodium complex $[\mathbf{2}_4 + Na]^+$ was the most stable, in contrast to the K^+-selective 2:1 complex of $\mathbf{1}_4$. The differences in the composition and in the cation selectivity between $[(\mathbf{1}_4)_2 + M]^+$ and $[\mathbf{2}_4 + M]^+$ may be ascribed to the difference in stacking ability of $\mathbf{1}_4$ and $\mathbf{2}_4$. For $\mathbf{2}_4$, the absence of phosphate groups may significantly reduce the stacking interaction in comparison with $\mathbf{1}_4$. Therefore, the stability of $[\mathbf{2}_4 + M]^+$ depends on the size of M^+ which is located in the central cavity of $\mathbf{2}_4$.

Notes and references

† *General procedure*. 9-ethylguanine **2** was purchased from Sigma and purified by reverse phase HPLC. The column (150 mm × 4.6 mm i.d.) packed with TSKgel ODS-120T (5 μm particle size) (Tosoh) was used in the LC-MS system. The solvents used in the LC-MS system were MeOH–H_2O (1:9, v/v) containing $MClO_4$ (M = Li, Na, K, Rb or Cs). 100 μl of 1.0 mM of an aqueous solution of **2** was applied to the HPLC. The flow rate was 1.0 ml min^{-1}. Mass spectra of the 9-ethylguanine fraction were obtained by introducing the effluent into the ESI-MS apparatus, a Hitachi M–1200HS mass spectrometer, just before the peak was eluted. The flow-rate of the pump was kept at 50 μl min^{-1} while the effluent was introduced into the ESI-MS apparatus.

1 W. Guschlbauer, J. F. Chantot and D. Thiele, *J. Biomol. Struct. Dyn.*, 1990, **8**, 491.
2 M. Gellert, M. N. Lipsett and D. R. Davies, *Proc. Natl. Acad. Sci. USA*, 1962, **48**, 2013.
3 D. Sen and W. Gilbert, *Nature*, 1988, **334**, 364; F. Aboul-ela, A. I. H. Murchie and D. M. J. Lilley, *Nature*, 1992, **360**, 280; G. Laughlan, A. I. H. Murchie, D. G. Norman, M. H. Moore, P. C. E. Moody, D. M. J. Lilley and B. Luisi, *Science*, 1994, **265**, 520.
4 (*a*) W. I. Sundquist and A. Klug, *Nature*, 1989, **342**, 825; (*b*) F. W. Smith and J. Feigon, *Nature*, 1992, **356**, 164; (*c*) C. Kang, X. Zhang, R. Ratliff, R. Moyzis and A. Rich, *Nature*, 1992, **356**, 126.
5 (*a*) T. J. Pinnavaia, C. L. Marshall, C. M. Mettler, C. L. Fisk. H. T. Miles and E. D. Becker, *J. Am. Chem. Soc.*, 1978, **100**, 3625; (*b*) E. Bouhoutsos-Brown, C. L. Marshall and T. J. Pinnavaia, *J. Am. Chem. Soc.*, 1982, **104**, 6576; (*c*) C. Detellier and P. Laszlo, *J. Am. Chem. Soc.*, 1980, **102**, 1135.
6 ESI-MS has been successfully applied to detection of weakly associated complexes: M. Yamashita and J. B. Fenn, *J. Phys. Chem.*, 1984, **88**, 4451; M. Yamashita and J. B. Fenn, *J. Phys. Chem.*, 1984, **88**, 4671; C. M. Whitehouse, R. N. Dreyer, M. Yamashita and J. B. Fenn, *Anal. Chem.*, 1985, **57**, 675; J. B. Fenn, M. Mann, C. K. Meng, S. F. Wong and C. M. Whitehouse, *Science*, 1989, **246**, 64.
7 Successful assessment of correlation of solution and gas phase complexation of macrocyclic compounds with alkali metal cations by ESI-MS has been reported: K. Wang and G. W. Gokel, *J. Org. Chem.*, 1996, **61**, 4693; E. Leize, A. Jaffrezic and A. V. Dorsselaer, *J. Mass Spectrom.*, 1996, **31**, 537.
8 Density functional calculations (pBP/DN**) were carried out using SPARTAN 5.0, Wavefunction Inc., Irvine, CA.
9 A. D. Becke, *Phys. Rev. A*, 1988, **38**, 3098; J. P. Perdew, *Phys. Rev. B*, 1986, **33**, 8822.
10 I. L. Karle, *J. Am. Chem. Soc.*, 1974, **96**, 4000.
11 T. Sakamaki, Y. Iitaka and Y. Nawata, *Acta Crystallogr., Sect. B*, 1976, **32**, 768; Y. Iitaka, T. Sakamaki and Y. Nawata, *Chem. Lett.*, 1972, 1225.
12 T. Sakamaki, Y. Iitaka and Y. Nawata, *Acta Crystallogr., Sect. B*, 1977, **33**, 52.

ChemComm

Unexpected and then rational synthesis of a new class of anionic phosphino–oxazoline ligands; structure and catalytic properties of a ruthenium complex†

Pierre Braunstein,*[a] Frédéric Naud,[a] Claudia Graiff[b] and Antonio Tiripicchio[b]

[a] *Laboratoire de Chimie de Coordination (UMR 7513 CNRS), Université Louis Pasteur, 4, rue Blaise Pascal, F-67070 Strasbourg Cedex, France. E-mail: braunst@chimie.u-strasbg.fr*

[b] *Dipartimento di Chimica Generale ed Inorganica, Chimica Analitica, Chimica Fisica, Università di Parma, Centro di Studio per la Strutturistica Diffrattometrica del CNR, Parco Area delle Scineze 17A, I-43100 Parma, Italy*

Received (in Basel, Switzerland) 29th March 2000, Accepted 11th April 2000
Published on the Web 9th May 2000

A new class of anionic, hybrid chelating ligands is reported which contain a phosphine moiety covalently linked to an oxazoline of which the nitrogen atom formally carries a partly delocalized negative charge; the first metal complex, a ruthenium derivative, has been characterized by X-ray diffraction and shown to be active in catalytic transfer hydrogenation.

The numerous synthetic pathways to oxazolines make them versatile synthons for ligand design[1] and their availability in enantiomeric pure forms accounts for the increasing use over the last 10 years of oxazoline-based ligands for asymmetric reactions catalyzed by transition metal complexes.[2] We have recently investigated the synthesis of Pd and Ru complexes with the neutral *P,N*-type ligand (oxazolinylmethyl)diphenylphosphine **I** (abreviated PCH_2ox^{Me2}) and studied their catalytic properties for ethylene/CO copolymerization and asymmetric transfer hydrogenation of ketones, respectively.[3]

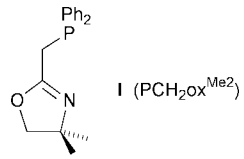

I (PCH_2ox^{Me2})

We then felt it would be of interest to isolate Ru hydrido complexes of potential catalytic relevance but reactions of $[Ru(H)Cl(PPh_3)_3]$ or $[Ru(H)(OAc)(PPh_3)_3]$ with **I** were not selective and although hydrido species were observed by ^1H NMR spectroscopy, no pure complexes could be isolated. We then reacted $[Ru(OAc)(PCH_2ox^{Me2})_2]Cl$ **1**,† prepared from $[RuCl_2(PCH_2ox^{Me2})_2]$[3b] and Tl(OAc), with CsF in acetone in order to prepare a monofluoride derivative that could be subsequently cleanly transformed into a hydride complex.[4] The $^{31}P\{^1H\}$ NMR spectrum of the only product formed, **2**, exhibited an AB spin system at δ 46.8 and 58.3 with ^2J(PP) 35.8 Hz which, surprinsingly, showed no coupling with a ^{19}F nucleus. The reaction of $[RuCl_2(PCH_2ox^{Me2})_2]$ itself with CsF was found to be less selective and not further investigated. An X-ray diffraction study‡ established the ligand arrangement in **2** and the fact that one of the *P,N*-ligands had unexpectedly been deprotonated. The crystals contain two crystallographically independent, but almost identical, molecules (A and B). A view of the structure of one of them (A) is shown in Fig. 1. Both ligands (excepting for the substituents) are roughly planar, but in the deprotonated one the N(1)C(14)C(13)P(1) moiety is practically planar. The two Ru–N bond distances in the octahedral complexes differ remarkably and the shorter, 2.102(3) Å in (A) and 2.111(3) Å in (B), involves the N(1) atom bearing the partial negative charge. Whereas the double bond is mainly localized on the C–N bond in the PCH_2ox^{Me2} ligand [bond distance 1.281(4) Å in both A and B], electronic delocalization occurs within the N(1)C(14)C(13)P(1) moiety of $PCHox^{Me2}$, as indicated by the values of the C–C [1.370(5) Å in (A) and 1.371(5) Å in (B)], C–N [1.328(4) Å in (A) and 1.317(4) Å in (B)] and P–C [1.753(3) Å in (A) and 1.754(4) Å in (B)] bond distances. Consistently, the IR spectrum of **2** contains two bands at 1618 and 1535 cm^{-1} assigned to the C=N and C⋯N vibrations of PCH_2ox^{Me2} and $PCHox^{Me2}$, respectively. In the ^1H NMR spectrum, each proton in PCH_2ox^{Me2} and $PCHox^{Me2}$ appears as a single resonance in agreement with the lack of any symmetry element in the molecule.

The selective synthesis of **2** was unexpected and found to depend on the nature of the cation associated with the fluoride anion. Thus, reaction of **1** with LiF only afforded a low yield of **2**. A more rational and general access to the anionic chelate in **2** consisted in the reaction of **1** with Bu^tOK in THF and selective deprotonation of only one PCH_2 group was observed [eqn. (1)].

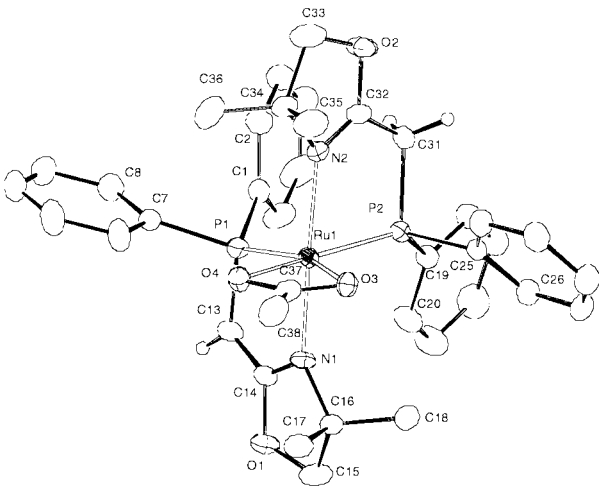

Fig. 1 View of the molecular structure of one (A) of the two crystallographic independent (A and B) molecules $[Ru(OAc)(PCHox^{Me2})(PCH_2ox^{Me2})]$ **3** together with the atomic numbering system. Selected bond distances (Å) and angles (°) in molecule A (values in square brackets refer to molecule B): Ru–P(1) 2.278(2) [2.270(1)], Ru–P(2) 2.226(1) [2.231(1)], Ru–N(1) 2.102(3) [2.111(3)], Ru–N(2) 2.166(3) [2.150(3)], Ru–O(3) 2.236(2) [2.228(2)], Ru–O(4) 2.209(2) [2.222(2)], P(1)–C(13) 1.753(3) [1.754(4)], C(13)–C(14) 1.370(5) [1.371(5)], C(14)–N(1) 1.328(4) [1.317(4)], C(16)–N(1) 1.495(4) [1.479(4)], P(2)–C(31) 1.857(4) [1.851(4)], C(31)–C(32) 1.474(5) [1.481(5)], C(32)–N(2) 1.281(4) [1.281(4)], C(34)–N(2) 1.515(4) [1.499(4)]; Ru–N(1)–C(14) 116.8(2) [116.5(2)], N(1)–C(14)–C(13) 126.3(3) [126.4(3)], C(14)–C(13)–P(1) 111.9(3) [111.7(3)], Ru–N(2)–C(32) 119.8(2) [119.6(2)], N(2)–C(32)–C(31) 124.8(3) [124.7(3)], C(32)–C(31)–P(2) 105.9(2) [106.7(3)].

† Electronic supplementary information (ESI) available: synthesis and spectral characterisation of **1**–**3**, See http://www.rsc.org/suppdata/cc/b0/b002515l/

DOI: 10.1039/b002515l

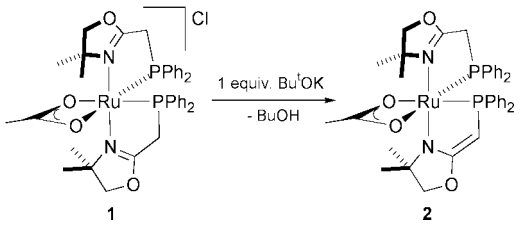

1 2 (1)

Anionic ligands incorporating an oxazoline ring are few compared to their neutral analogs and they belong to two main families. In class **A**, the anionic charge is carried by an exocyclic atom (C^-,[5] O^-,[6] S^- [7]) and the nitrogen atom of the oxazoline formally remains a neutral donor.

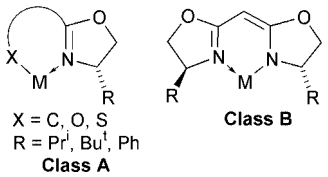

Some of their complexes are catalysts for, *e.g.* ethylene polymerization,[6a] sulfide oxidation,[8] alkyl- and phenyl-zincation of aldehydes[6b,c] and conjugate addition to enones.[7] In the second class of ligands, **B**, the anionic charge is partly localized on the nitrogen atom of the oxazoline but only one representative is known which has led to efficient Ti,[9] Cu,[10] Zn[11] or Mg[12] catalysts for several asymmetric reactions, *e.g.* reduction of ketones,[9b] cyclopropanation of olefins,[10] allylzincation,[11] and hydrocyanation of aldehydes.[12] Although there are two reported X-ray crystal structures of Cu[13] and Rh complexes,[14] the precatalysts were usually prepared *in situ* and not isolated (Zn, Mg, Ti).

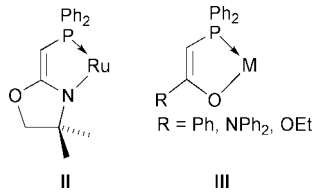

The new ligand system in **II** provides an interesting extension to *anionic* four-electron donor phosphino enolate ligands of type **III** currently much investigated. These and related phosphorus/oxygen chelates confer special reactivity to their complexes, as found, *e.g.* in reactions with various organic or inorganic electrophiles[15] or in the highly selective convertion of ethylene into linear α-olefins.[16] The anionic ligand $PCHox^{Me2}$ found in **2** is therefore the first representative of a new class of hybrid ligands which combine some of the aspects of systems **B** and **III** and its chemistry therefore offers considerable potential. Preliminary catalytic studies with complex **2** have been performed for the transfer hydrogenation of aryl alkyl and dialkyl ketones by propan-2-ol, a reaction of current interest.[17] Under standard conditions ([Ru]/[ketone]/[PrⁱONa] = 1:200:5, [ketone] = 0.1 M, T = 82 °C), **2** exhibits very high to high activity for hydrogenation of acetophenone (98% yield in 5 min) and cyclohexylmethyl ketone (91% in 5 h) respectively.§

Access to complexes containing this new anionic *P,N*-ligand can be generalized, as shown with Pd since reaction of [Pd(dmba)Cl(PCH_2ox)] with BuᵗOK in THF afforded [Pd(dmba)(PCHox)] **3** in 84% yield.

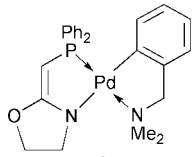

3

Notes and references

‡ *Crystal data* for **2**: $C_{38}H_{42}N_2O_4P_2Ru$, M = 753.75 monoclinic, space group $P2_1/c$, graphite monochromated Mo-Kα radiation, λ = 0.71073 Å, μ = 0.569 mm^{-1}, a = 18.256(4), b = 20.590(5), c = 20.454(5) Å, β = 111.28(6)°, V = 7164(3) $Å^3$, Z = 8, D_c = 1.398 g cm^{-3}. Philips PW 1100 diffractometer, θ–2θ scan technique, room temperature. 20871 Unique reflections measured ($3 < \theta < 30°$) and used in the refinement. All hydrogen atoms placed at their geometrically calculated positions and refined riding on their parent atoms, excepting those bonded to C(31) and C(13), which were localized in the final ΔF map and refined isotropically, wR_2 0.0876 and R_1 [for 8473 reflections with $I > 2\sigma(I)$] 0.0369. All calculations were carried out on the DIGITAL Alpha Station 255 computers of the "Centro di Studio per la Strutturistica Diffrattometrica " del CNR, Parma, using the SHELX-97 systems of crystallographic computer programs.[18] CCDC 182/1603. See http://wwww.rsc.org/suppdata/cc/b0/b002515l/ for crystallographic files in .cif format.

§ *Catalytic transfer hydrogenation*: Typical procedure for the catalytic transfer hydrogenation of acetophenone: **2** (0.0052 g, 0.0068 mmol) was dissolved in 13 mL PrⁱOH in a 50 mL two-neck round bottom flask fitted with a reflux condenser. Acetophenone (0.158 mL, 1.36 mmol) was added and the yellow solution was brought to reflux. The solution was stirred for 10 min and 0.36 mL (0.034 mmol) of a solution of PrⁱONa in PrⁱOH (0.1 M) was added. The volume of PrⁱOH was adjusted so that all catalytic runs were performed with an initial concentration in acetophenone of 0.1 M. The addition of PrⁱONa was considered as the starting time of the reaction. Conversion was determined by gas chromatography using a Lipodex A 25 m × 0.25 mm column.

1 T. G. Gant and A. I. Meyers, *Tetrahedron*, 1994, **50**, 2297.
2 C. Bolm, *Angew. Chem., Int. Ed. Engl.*, 1991, **30**, 542; A. K. Ghosh, P. Mathivanan and J. Cappiello, *Tetrahedron: Asymmetry*, 1998, **9**, 1; A. Pfaltz, *Synlett*, 1999, **51**, 835.
3 (*a*) P. Braunstein, M. D. Fryzuk, M. Le Dall, F. Naud, S. J. Rettig and F. Speiser, *J. Chem. Soc., Dalton Trans.*, 2000, 1067; (*b*) P. Braunstein, C. Graiff, F. Naud, A. Pfaltz and A. Tiripicchio, manuscript in preparation.
4 D. Huang and K. G. Caulton, *J. Am. Chem. Soc.*, 1997, **119**, 3185.
5 S. E. Denmark, R. A. Stavenger, A.-M. Faucher and J. P. Edwards, *J. Org. Chem.*, 1997, **62**, 3375; Y. Motoyama, Y. Mikami, H. Kawakami, K. Aoki and H. Nishiyama, *Organometallics*, 1999, **18**, 3584.
6 (*a*) P. G. Cozzi, E. Gallo, C. Floriani, A. Chiesi-Villa and C. Rizzoli, *Organometallics*, 1995, **14**, 4994; (*b*) C. Bolm, K. Muñiz-Fernández, A. Seger, G. Raabe and K. Günther, *J. Org. Chem.*, 1998, **63**, 7860; (*c*) C. Bolm and K. Muñiz, *Chem. Commun.*, 1999, 1295; (*d*) C. J. Fahrni and A. Pfaltz, *Helv. Chim. Acta*, 1998, **81**, 491.
7 Q.-L. Zhou and A. Pfaltz, *Tetrahedron*, 1994, **50**, 4467.
8 C. Bolm, T. K. K. Luong and K. Harms, *Chem. Ber.*, 1997, **130**, 887.
9 (*a*) R. P. Singh, *Synth. React. Inorg. Met.-Org. Chem.*, 1997, **27**, 155; (*b*) M. Bandini, P. G. Cozzi, L. Negro and A. Umani-Ronchi, *Chem. Commun.*, 1999, 39.
10 R. E. Lowenthal, A. Abiko and S. Masamune, *Tetrahedron Lett.*, 1990, **31**, 6005; D. A. Evans, K. A. Woerpel, M. M. Hinman and M. M. Faul, *J. Am. Chem. Soc.*, 1991, **113**, 726.
11 M. Nakamura, A. Hirai and E. Nakamura, *J. Am. Chem. Soc.*, 1996, **118**, 8489.
12 E. J. Corey and Z. Wang, *Tetrahedron Lett.*, 1993, **34**, 4001.
13 J. Hall, J.-M. Lehn, A. DeCian and J. Fischer, *Helv. Chim. Acta*, 1991, **74**, 1.
14 J. M. Brown, P. J. Guiry, D. W. Price, M. B. Hursthouse and S. Karalulov, *Tetrahedron: Asymmetry*, 1994, **5**, 561.
15 P. Braunstein, D. Matt and D. Nobel, *J. Am. Chem. Soc.*, 1988, **110**, 3207; J. Andrieu, P. Braunstein, M. Drillon, Y. Dusausoy, F. Ingold, P. Rabu, A. Tiripicchio and F. Ugozzoli, *Inorg. Chem.*, 1996, **35**, 5986.
16 W. Keim, *Angew. Chem., Int. Ed. Engl.*, 1990, **29**, 235; U. Klabunde, T. H. Tulip, D. C. Roe and S. D. Ittel, *J. Organomet. Chem.*, 1987, **334**, 141; P. Braunstein, Y. Chauvin, S. Mercier, L. Saussine, A. DeCian and J. Fischer, *J. Chem. Soc., Chem. Commun.*, 1994, 2203.
17 R. Noyori and S. Hashiguchi, *Acc. Chem. Res.*, 1997, **30**, 97; M. J. Palmer and M. Willis, *Tetrahedron: Asymmetry*, 1999, **10**, 2045.
18 G. M. Sheldrick, SHELXL-97 Program for the solution and refinement of crystal structures, University of Göttingen, Göttingen, Germany, 1997.

ChemComm

A new template for the synthesis of triphosphorus macrocycles

Andrew J. Price and Peter G. Edwards*

Department of Chemistry, Cardiff University, P.O. Box 912, Cardiff, UK CF10 3TB.
Email: edwardspg@cardiff.ac.uk

Received (in Cambridge, UK) 17th March 2000, Accepted 10th April 2000
Published on the Web 9th May 2000

A new template synthesis of triphosphorus macrocycles has been developed based upon the intramolecular hydrophosphination of allylphosphine coordinated to the (η^5-cyclopentadienyl)iron(II) cation; the resulting tri-secondary macrocycle 1,5,9-triphosphacyclododecane is readily alkylated with ethene to give (η^3-1,5,9-[12]aneP_3Et_3)Fe(η^5-Cp)$^+$ which is in turn liberated as the free ligand stereospecifically as the *syn–syn* isomer; related reactions with phenyl(allyl)phosphine lead directly to the triphenyl macrocycle (1,5,9-[12]aneP_3Ph_3) which is also liberated stereospecifically.

The first examples of C_3 symmetrical triphosphamacrocycles were those based upon the 1,5,9-[12]aneP_3 core prepared by a stereoselective metal template assisted synthesis using a $Mo(CO)_3$ template.[1,2] Early results confirm that they support relatively very stable facially capped complexes for a range of transition metals,[3] they may also impose unusual structural distortions on metal centres (*e.g.* for metals that prefer square planar geometries).[4] These observations highlight distinct differences in comparison to the behaviour of analogous nitrogen or sulfur ligands or of related tripodal phosphines. In view of their influences on structure and reactivity and their ability to stabilise low oxidation states, the study of their complexes is of substantial interest.

The current and only route to this class of ligands, by radical initiated hydrophosphination, does however have significant preparative limitations. The tris-allylphosphine precursor complexes required for this route are very sensitive to oxygen, moisture and large scale reactions require fastidious care in order to be reproducible. Of greater significance is that this method is currently limited to a minimum ring size of twelve atoms. We have previously commented upon the inability of the $Mo(CO)_3$ template, and its smaller chromium analogue, to support the cyclisation of vinyl phosphines in attempts to achieve smaller ring sizes.[5] These templates lack any possible steric control over the *trans*-coordinated precursor phosphines precluding any freedom to force the ring closure of vinyl phosphines by compression of the non-bonded P–P distances. In order to address these problems and to develop a more reliable synthetic route to tri-phosphines of this nature, we have undertaken a study of alternative methods. For these reasons we have chosen to investigate the [(η^5-Cp)Fe(η^6-arene)]$^+$ class of complexes which readily form tris-phosphine adducts[6] including those of acyclic triphosphines (linear[6b] and tripodal[6c]) and of primary phosphines,[6d] all of which are of course restricted to *facial* coordination by the η^5-Cp group. This approach has led us to an entirely new template method for the stereoselective synthesis of 1,5,9-[12]aneP_3R_3 triphosphorus macrocycles; preliminary results of which are presented herein.

The photolytically activated substitution of the aryl ligand in [(η^5-C_5H_5)Fe(η^6-C_6H_6)]$^+$ (**1**) in the presence of allylphosphine gives the tris-primary phosphine complex [(η^5-C_5H_5)Fe($H_2PC_3H_5$)$_3$]$^+$ **2**, as the hexafluorophosphate salt, in quantitative yield (Scheme 1). In the IR spectrum, a peak due to ν_{P-H} is observed (2318 cm^{-1}). The microcrystalline solid is indefinitely air-stable, although in CH_2Cl_2 solution the complex decomposes over several days to give a green, NMR silent and presumably paramagnetic species of undetermined composition. Complex **2** is readily soluble in most polar solvents, such as THF and CH_2Cl_2, but insoluble in hydrocarbons and other non-polar solvents. The ^{31}P {^{1}H} NMR and ^{31}P NMR spectra consist of a singlet and triplet, respectively (δ −9.0, $^1J_{P-H}$ 328 Hz), consistent with magnetically equivalent coordinated allylphosphine ligands (*cf.* for free allylphosphine, δ−134.4, $^1J_{P-H}$ 195 Hz).

Cyclotrimerisation of **2** has been attempted in tetrahydrofuran (THF), chlorobenzene and anisole, using AIBN [azobis(isobutyronitrile)] as radical initiator (*ca.* 1–2% mol equivalents). In THF, both the cyclisation intermediates and final macrocyclic product slowly precipitate during the reaction which remains incomplete as a result, unless performed in dilute solution. Attempts to separate and characterise these intermediates have not been successful.

In chlorobenzene the cyclisation is more efficient, forming [(η^5-C_5H_5)Fe(η^3-1,5,9-[12]aneP_3H_3)]$^+$[PF_6]$^-$ **3**, in moderate yield. Complex **3** has a band due to the P–H stretch in its IR spectrum (ν_{P-H} 2303 cm^{-1}) and a doublet in the ^{31}P NMR spectrum (δ 12.7, $^1J_{P-H}$ 336 Hz) assigned to phosphorus atoms in the coordinated macrocycle. This increase in chemical shift ($\Delta\delta$ 21.8 ppm) and coupling constant is similar to that observed in the analogous Mo(0) complexes, ($H_2PC_3H_5$)$_3$Mo(CO)$_3$ and (η^3-1,5,9-[12]aneP_3H_3)Mo(CO)$_3$, ($\Delta\delta$ 27.0 ppm, for the latter $^1J_{P-H}$ 318 Hz).

Hydrophosphination of ethene by **3** gives the tris-ethylated macrocyclic complex [(η^5-C_5H_5)Fe(η^3-1,5,9-[12]aneP_3Et_3)]$^+$[PF_6]$^-$ **4** which is characterised by a singlet in the ^{31}P

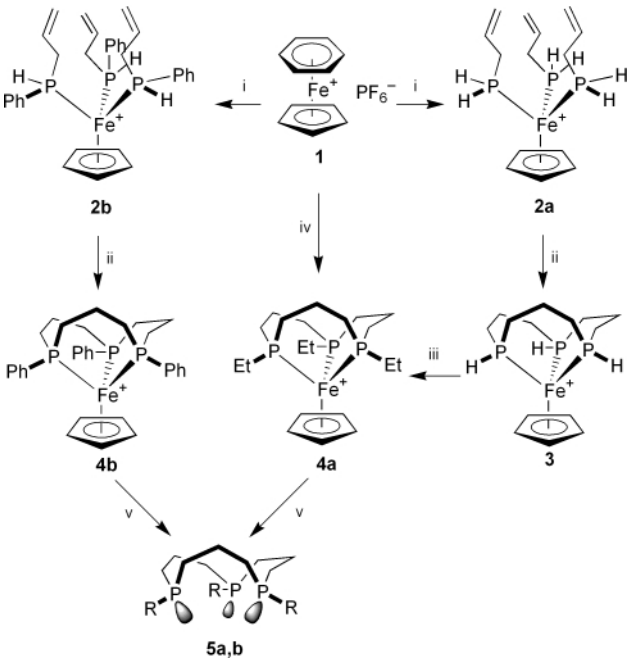

Scheme 1 *Reagents and conditions*: i > 3 allylphosphine for **2a** or > 3 phenyl(allyl)phosphine for **2b**, CH_2Cl_2, $h\nu$ (> 400 nm); ii, chlorobenzene, AIBN (2 mol%), 90 °C; iii, ethene (2 atm), chlorobenzene, AIBN (2 mol%); iv, [12]aneP_3Et_3, CH_2Cl_2, $h\nu$ (> 400 nm); v, Na/NH_3(l); **5a**, R = Et; **5b**, R = Ph.

DOI: 10.1039/b002174l

{^{1}H} NMR spectrum (δ 38.1) and the absence of a band due to ν_{P-H} in its IR spectrum. The identity of **4** is further supported by its preparation in THF directly from the template precursor complex **1** by addition of free 1,5,9-[12]aneP_3Et_3 obtained by our previously reported route.[2] The products obtained by either method have identical spectroscopic, analytical and physical properties. This independent confirmation of the nature of **4**, in turn confirms the characterisation of **3** as the secondary phosphine macrocycle complex. Both **3** and **4** are air stable for extended periods in both solution and the solid state.

The reaction of $[(\eta^5\text{-}C_5H_5)Fe(\eta^6\text{-}C_6H_6)]^+$ with phenyl-(allyl)phosphine in a manner similar to that for the formation of **2a**, leads to the tri-secondary phosphine complex, **2b**, in excellent yield (99%). Complex **2b** is characterised by its ^{31}P{^{1}H} NMR spectrum which has two multiplets from the presence of both diastereomers and enantiomers arising from the three chiral phosphines in **2b** (δ 55.8). The radical induced cyclisation of the coordinated secondary phosphines in **2b** proceeds to the tri-tertiary phosphine macrocycle complex, **4b**. Intermediates which do not readily cyclise are also observed after extended reaction times; these are readily separated from **4b** upon work up. The resistance of these intermediates to cyclisation is presumably dependant upon the relative chirality at adjacent phosphines. Although we have recently reported the synthesis of the triphenyl macrocycle, **5b**,[7] this is the first example of the cyclotrimerisation of a secondary phosphine to a tri-tertiary triphosphorus macrocycle and may offer direct routes to tri-tertiary phosphines which might otherwise be difficult to obtain.

The macrocycle complexes, **4a** and **4b**, are digested by sodium in liquid ammonia resulting in the high yield liberation of the free macrocyclic ligands **5a** and **5b** stereoselectively as the *syn–syn* isomers. The identities and stereochemistries of both the triphosphines **5a** and **5b**, are confirmed by singlets in their ^{31}P {^{1}H} NMR spectra (δ −31.7 and −34.6, respectively); their spectra are identical to those previously reported.[2,7] In all cases analytical, conductivity, ^{1}H and ^{13}C{^{1}H} NMR data are consistent with the formulations.[8]. In addition to the ^{31}P NMR data discussed above, a resonance due to PF_6^- is also observed in each case (δ −144.0, $^1J_{P-F}$ 711 Hz).

This new route to the coordinated secondary phosphine ligands, the facile alkylation of the secondary phosphine macrocycle complex **3** to the corresponding tertiary phosphines and the successful and stereospecific liberation of the free ligands offers an alternative preparation based upon a more readily accessible template than the sole current literature route and *via* relatively air-stable precursor and intermediate complexes. We are currently investigating the influences of variations in substituents on the Cp ring upon the course of the macrocyclisation reactions. We are also investigating the application of this method to the cyclisation of alternative phosphine precursors in order to achieve both different ring sizes as well as different 'backbone' bridging functions; preliminary results are encouraging.

We thank the EPSRC for a studentship (A. J. P.).

Notes and references

1 B. N. Diel, P. F. Brandt, R. C. Haltiwanger and A. D. Norman, *J. Am. Chem. Soc.*, 1982, **104**, 4700; B. N. Diel, P. F. Brandt, R. C. Haltiwanger, M. L. J. Hackney and A. D. Norman, *Inorg. Chem.*, 1989, **28**, 2811.

2 P. G. Edwards, J. S. Fleming and S. S. Liyanage, *Inorg. Chem.*, 1996, **35**, 4563.

3 P. G. Edwards, J. S. Fleming, S. J. Coles and M. B. Hursthouse, *J. Chem. Soc., Dalton Trans.*, 1997, 3201.

4 P. G. Edwards, F. Ingold, S. J. Coles and M. B. Hursthouse, *Chem. Commun.*, 1998, 45.

5 P. G. Edwards, J. S. Fleming, S. S. Liyanage, S. J. Coles and M. B. Hursthouse, *J. Chem. Soc., Dalton Trans.*, 1996, 1801.

6 (*a*) H. Schumann, L. Eguren and J. W. Ziller, *J. Organomet. Chem.*, 1991, **408**, 361; (*b*) D. Catheline and D. Astruc, *Organometallics*, 1984, **3**, 1094; (*c*) G. T. Crisp, G. Salem and S. B. Wild, *Organometallics*, 1989, **8**, 2360; (*d*) D. C. R. Hockless, Y. B. Kang, M. A. McDonald, M. Pabel, A. C. Willis and S. B. Wild, *Organometallics*, 1996, **15**, 1301; (*e*) **4b**: R. B. King, P. N. Kapoor and R. N. Kapoor, *Inorg. Chem.*, 1971, **10**, 1841; (*f*) S. G. Davies, H. Felkin and D. Watts, *J. Chem. Soc., Chem. Commun.*, 1980, 159; (*g*) **4c**: R. B. King, L. W. Houk and K. H. Pannell, *Inorg. Chem.*, 1969, **8**, 1042; (*h*) J. D. Goodrich and J. P. Selegue, *Organometallics*, 1989, **8**, 2360.

7 D. J. Jones, P. G. Edwards and R. P. Tooze, *J. Chem. Soc., Dalton Trans.*, 1999, 1045.

8 *Selected data*: for **2a**: yield: 99%. Anal. Found (calc.): C, 34.5 (34.4); H, 5.3 (5.4)%. MS(ES), *m/z* 343 (100%, $[M-PF_6]^+$). IR (KBr disc): ν(P–H), 2319.4 cm^{-1}. Λ_M = 25 Ω cm^2 mol^{-1}. ^{31}P NMR: δ −9.1 (t, $^1J_{P-H}$ = 328 Hz, cation), −145.0 (septet, $^1J_{P-F}$ 711 Hz, anion). ^{1}H NMR, δ 2.54 (m, $H_2PCH_2CHCH_2$), 4.12, 5.00 (d m, $^1J_{P-H}$ 328 Hz, $H_2PCH_2CHCH_2$), 4.55 (q, $^3J_{P-H}$ 2 Hz, Cp-H); 5.20 (m, $H_2PCH_2CHCH_2$), 5.82 (m, $H_2PCH_2CHCH_2$). ^{13}C{^{1}H} NMR: δ 28.2 (d, $^1J_{P-C}$ = 40 Hz, $H_2PCH_2CHCH_2$), 80.1 (s, Cp), 119.7 (s, $H_2PCH_2CHCH_2$), 133.9 (s, $H_2PCH_2CHCH_2$). For **2b**: yield: 95%. Anal. Found (calc.): C, 53.6 (53.7); H, 5.3 (5.4)%; Λ_M = 39 Ω cm^2 mol^{-1}. IR (KBr disc): δ(P–H), 2303 cm^{-1}. MS(ES), *m/z* 571(100%) $[(\eta^5\text{-}C_5H_5)Fe(PhPHC_3H_5)_3]^+$. ^{31}P{^{1}H} NMR ($CDCl_3$, 36.23 MHz), δ 56.5 (m); 60.2 (m). ^{1}H NMR: δ 4.30 (q), 4.55 (s), 4.69 (s), 4.78 (br m), 4.93 (s), 5.08 (br m), 5.24 (br m), 5.35 (br m), 5.52 (br m), 5.76 (br m), (15H, allyl groups). For **3**: yield: 40%. Anal. Found (calc.): C, 33.5 (34.4); H, 4.8 (5.4)%. MS(ES), *m/z* 343 (100%, $[M-PF_6]^+$). IR (KBr disc): δ(P–H), 2302.6 cm^{-1}. Λ_M = 32 Ω cm^2 mol^{-1}. ^{31}P NMR: δ 12.7 (d, $^1J_{P-H}$ 336 Hz, cation), −145 (septet, $^1J_{P-F}$ = 711 Hz, anion). For **4a**. Yield: 95%. Anal. Found (calc): C, 47.0 (46.7); H, 7.6 (7.4)%. MS(ES), *m/z* 427 (100 %, $[M-PF_6]^+$). Λ_M = 40 Ω cm^2 mol^{-1}. ^{31}P NMR: δ 38.1 (s, cation), −145 (septet, $^1J_{P-F}$ = 711 Hz, anion). ^{1}H NMR: δ 1.28 (br m, PCH_2CH_3), 1.61 (br m, PCH_2CH_3 and $PCH_2CH_3CH_2P$); 1.87 (br m, $PCH_2CH_2CH_2P$), 4.26 (q, $^3J_{P-H}$ 2 Hz, Cp-H). For **4b**: yield: 30%. Anal. found (calc.): C, 53.6 (53.6); H, 5.4 (5.3)%. MS (ES), *m/z* 571 (100%, $[M-PF_6]^+$).^{31}P{^{1}H} NMR: δ 35.0 (s). ^{1}H NMR: δ 1.97, 2.10, 2.20, 2.33, 2.46, 2.60 (all br m, PCH_2 CH_2 CH_2P), 3.99 (q, $^3J_{P-H}$ 2 Hz, Cp-H), 7.19 (s, phenyl-H), 7.46 (m, phenyl-H), 7.56 (br m, phenyl-H), 7.66 (br m, phenyl-H).

A continuous and clean one-step synthesis of nano-particulate $Ce_{1-x}Zr_xO_2$ solid solutions in near-critical water

Albertina Cabanas,[a] Jawwad A. Darr,[a] Edward Lester[b] and Martyn Poliakoff*[a]

[a] *School of Chemistry, The University of Nottingham, University Park, Nottingham, UK NG7 2RD. E-mail: Martyn.Poliakoff@nottingham.ac.uk*

[b] *School of Chemical, Environmental and Mining Engineering, The University of Nottingham, University Park, Nottingham, UK NG7 2RD*

Received (in Oxford, UK) 16th February 2000, Accepted 10th April 2000
Published on the Web 9th May 2000

Gram-scale quantities of microcrystalline powdered CeO_2–ZrO_2 solid solutions can be produced continuously in a near-critical water flow reactor at *ca.* 300 °C and 25 MPa; rapid hydrothermal co-precipitation leads to nano-particulate $Ce_{1-x}Zr_xO_2$ (x = 0 to 1), the composition of which is merely determined by the initial concentrations of Ce^{4+} and Zr^{4+} ions in the starting solution.

The synthesis of ceria-containing materials has long been of considerable scientific interest for applications as diverse as UV absorbers and solid oxide fuel cells.[1] Mixed CeO_2–ZrO_2 systems show improved oxygen storage capacity and greater thermal stability compared to CeO_2 itself,[2–4] which is particularly important for three-way exhaust catalysts. $Ce_{1-x}Zr_xO_2$ is prepared conventionally using various methods including high temperature solid-state reactions,[5] use of micro-emulsions,[6] high energy ball milling,[7,8] the sol–gel method,[9,10] and ageing of solutions.[11] However, many of these techniques are quite time consuming (involving multi-step syntheses or ageing), energy intensive and/or environmentally unfriendly. When extremely small particle sizes are needed, the complexity (and sometimes the cost) of manufacture increases further.

Arai and coworkers[12,13] have recently shown that particulate CeO_2 and ZrO_2 can be made continuously by decomposition of the corresponding metal nitrates in super-critical water, scH_2O. The reaction is believed to proceed *via hydrolysis* to the hydroxides, followed by *dehydration* to the oxides. Here, we show for the first time that the *mixed oxide* $Ce_{1-x}Zr_xO_2$ can be obtained continuously by hydrolysis of mixtures of $[NH_4]_2[Ce(NO_3)_6]$ (CAN) and $[Zr(ac)_4]$† in near-critical water, ncH_2O, in the appropriate ratios. The reactor shown in Fig. 1 gave single phase $Ce_{1-x}Zr_xO_2$ at rates close to 10 g h^{-1}. The high diffusivity of the reactants and the fast dehydration reaction in ncH_2O and scH_2O result in very high hydrolysis and dehydration reaction rates. Thus, residence times at the mixing point of only a few seconds were sufficient. In most cases, decomposition of the metal precursors appeared to be virtually complete. The composition in $Ce_{1-x}Zr_xO_2$ mixed oxides could be *changed* from x = 0.2 to 0.9 merely by *varying* the Ce : Zr ratios in the metal feed solution. Pure CeO_2 and ZrO_2 oxides could also be synthesised by using just one of the precursors.‡

The samples of $Ce_{1-x}Zr_xO_2$ were characterised by powder X-ray diffraction (PXD), Raman spectroscopy, BET surface area measurements and, in selected cases, TEM. The PXD patterns of the materials indicated the formation of CeO_2–ZrO_2 solid solutions (Fig. 2). The individual solid phases were identified by combining PXD and Raman data. A crude estimate of the apparent particle size was obtained by application of the Scherrer equation to the PXD line-widths (Fig. 3). For selected cases, the particle size was also investigated by TEM. For the 1 : 1 mixture (*i.e.* $Ce_{0.5}Zr_{0.5}O_2$), the TEM image showed particles with well-defined edges, well dispersed, between 3 and 5 nm in size, values which agree with the estimates from the Scherrer equation (4.6 nm). Diffraction rings (TEM) confirmed

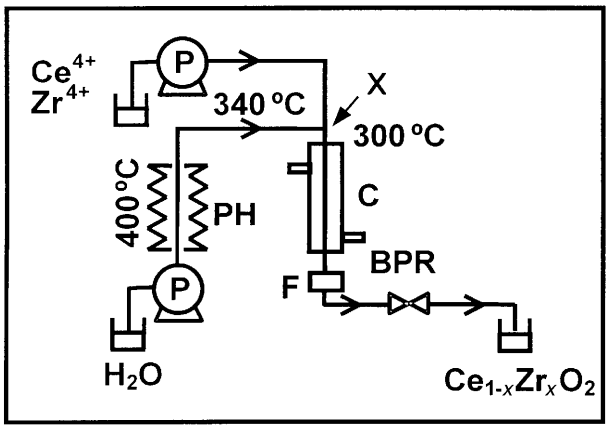

Fig. 1 Diagram of the flow reactor for the synthesis of metal oxide powders and solid solutions in ncH_2O. A solution of Ce^{4+} and Zr^{4+} salts at room temperature is mixed with a stream of H_2O heated up to 400 °C by the preheater (PH). The mixture is cooled immediately after the mixing point (X) by a water cooling (C) and is then passed through the filter (F) (to remove any large aggregates) and the back-pressure regulator (BPR). Particles are then collected as a suspension. P denotes pumps.

the crystallinity of the materials obtained. For pure ZrO_2, TEM showed a fluffy 'cloud-like' image with nano-particles of *ca.* 5 nm (5.6 nm by PXD). All materials have medium to high surface areas as measured by BET, S_{BET} (Fig. 3). It is also clear from Fig. 3 that there is a correlation between S_{BET} values and the apparent particle size. S_{BET} values for the samples appear to reach a maximum for the oxides with higher zirconium content (181, 184 and 183 m^2 g^{-1} for the 1 : 4 and 1 : 9 Ce–Zr materials and pure ZrO_2, respectively).

CeO_2 and $Ce_{1-x}Zr_xO_2$ (x = 0–0.5) showed cubic fluorite PXD patterns. Increasing Zr content in the solid solutions resulted in a decrease in the lattice parameter, owing to the incorporation of smaller Zr^{4+} ions into the fluorite (mainly

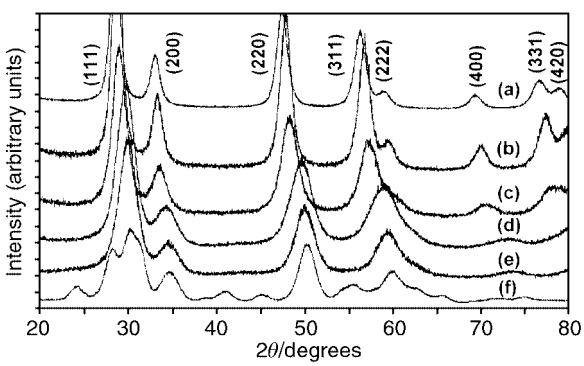

Fig. 2 Powder X-ray diffraction (PXD) patterns for $Ce_{1-x}Zr_xO_2$ materials prepared in the near-critical water flow reactor: (a) x = 0 (pure CeO_2), (b) x = 0.2, (c) x = 0.5, (d) x = 0.8, (e) x = 0.9, (f) x = 1 (pure ZrO_2).

DOI: 10.1039/b001424i

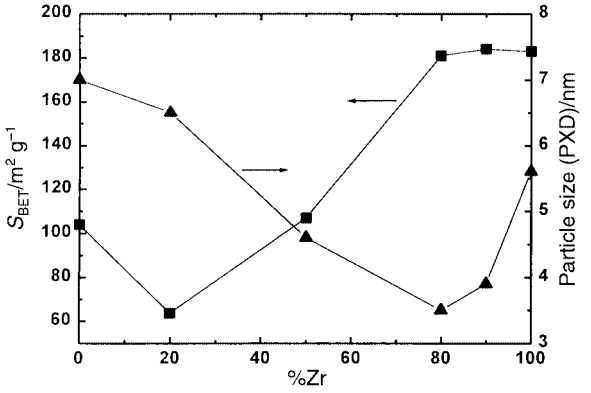

Fig. 3 S_{BET} area measurements (■) and estimated particle sizes by PXD (▲) of the materials *vs.* zirconium content (%Zr).

Ce^{4+}) lattice. For the samples of Ce : Zr ratios 1 : 4 and 1 : 9, a tetragonal phase was assigned.§ For pure ZrO_2, PXD and Raman data revealed a mixture of monoclinic and tetragonal phases. Considering the relative intensities of the most intense reflection in the PXD of both phases, the ratio of monoclinic to tetragonal phases was estimated to be 40 : 60.

The precise phase assignment is slightly different from that reported in the literature.[3,14] One possible explanation is that the Zr content in the solid solutions is lower than the expected. However, this would not explain why our samples of pure ZrO_2 contained a mixture of monoclinic and tetragonal phases rather than the monoclinic (thermodynamically stable) phase reported in the literature.[14] Therefore is likely that the differences are due to the small particle sizes of the materials produced. Fornasiero *et al*.[3] have reported that below a critical crystalline size, the tetragonal phase is favoured over the monoclinic and, with extremely small particles, the cubic phase is favoured over the tetragonal, which is consistent with our phase assignment. As discussed before, the extremely small particle sizes may be as a result of the rapid precipitation and relatively low synthesis temperature. All samples were studied by TGA. In each case, there was a weight loss (2–12%) at ⩽100 °C, presumably due to adsorbed water. Some samples showed smaller weight losses (4–7%) around 250 and 310 °C; IR spectra suggest that theses losses may be associated with residual nitrate and acetate.

In conclusion, we have reported a new and extremely rapid one-step synthesis of ceria–zirconia solid solutions (at the concentrations and flow rates employed in the experiments, between *ca.* 8 and 11 g h^{-1}, depending on the composition of $Ce_{1-x}Zr_xO_2$, can be produced continuously). The chemistry is simple and clean. The reaction does not require the addition of organic solvents, modifiers (to control pH) or prolonged reaction times. The temperatures are low (300 °C) compared to those used in conventional techniques. Most importantly, the composition of $Ce_{1-x}Zr_xO_2$ can be tuned simply by varying the amounts of precursors in the starting solution. The products are completely homogenous. The particles are highly crystalline (TEM) despite the relatively low temperatures of formation, and the primary particle sizes are extremely small imparting relatively high surface areas of up to *ca.* 180 $m^2\ g^{-1}$ for the materials. Currently we are exploring the potential of our technique for synthesising other solid solutions.

We gratefully acknowledge the financial support of the EPSRC: Clean Technology Fellowship (M. P.), Grant No. GR/K76023 (J. A. D.) and ICI (A. C.). We thank Dr M. G. Barker and his group, Dr A.A. Galkin, Dr D. A. Graham, Dr. P. A. Hamley, S. J. Barlow and M. Guyler for their assistance and discussions.

Notes and references

† Zirconium acetate/dilute acetic acid solution with a 15% Zr content as supplied by Aldrich.

‡ **CAUTION:** this experiment involves high pressure and temperature and requires appropriate apparatus.

The total concentration of the metal solution (Ce + Zr) was kept constant and equal to 0.21 M. The flow rates of the metal salt and water streams were 5.0 and 10.0 mL min^{-1}, respectively. Pressure was kept constant at 25 ± 1 MPa and the H_2O inlet temperature was *ca.* 360 °C. At the mixing point, the temperature was close to 300 °C. The resulting coloured suspensions of metal oxides were separated from the clear aqueous phase by decantation, and the solids were dried at 100 °C after washing with water.

§ Although the characteristic tetragonal splittings of the reflections (200), (220), (311) and (400) in the fluorite structure (Fig. 2) were not visible owing to the broadness of the PXD peaks, the appearance of bands at 625, 460 and 315 cm^{-1} in the Raman spectra of the fresh materials (not illustrated) suggests a tetragonal phase.[8]

1 T. Masui, K. Fujiwara, K. Machida and G. Adachi, *Chem. Mater.*, 1997, **9**, 2197.
2 A. Trovarelli, *Catal. Rev.*, 1996, **38**, 439.
3 P. Fornasiero, G. Balducci, R. DiMonte, J. Kaspar, V. Sergo, G. Gubitosa, A. Ferrero and M. Graziani, *J. Catal.*, 1996, **164**, 173.
4 G. Vlaic, R. DiMonte, P. Fornasiero, E. Fonda, J. Kaspar and M. Graziani, *Stud. Surf. Sci. Catal.*, 1998, **116**, 185.
5 M. Yashima, K. Morimoto, N. Ishizawa and M. Yoshimura, *J. Am. Ceram. Soc.*, 1993, **76**, 1745.
6 T. Masui, K. Fujiwara, Y. Peng, T. Sakata, K. Machida, H. Mori and G. Adachi, *J. Alloys Compd.*, 1998, **269**, 116.
7 C. de Leitenberg, A. Trovarelli, F. Zamar, G. Maschio, G. Dolcetti and J. Llorca, *J. Chem. Soc., Chem. Commun.*, 1995, 2181.
8 A. Trovarelli, F. Zamar, J. Llorca, C. de Leitenburg, G. Dolcetti and J. T. Kiss, *J. Catal.*, 1997, **169**, 490.
9 T. Settu and R. Gobinathan, *Bull. Chem. Soc. Jpn.*, 1994, **67**, 1999.
10 T. Masui, Y. Peng, K. Machida and G. Adachi, *Chem. Mater.*, 1998, **10**, 4005 and references therein.
11 B. Djurcic, D. McGarry and S. Pickering, *J. Mater. Sci. Lett.*, 1993, **12**, 1320.
12 T. Adschiri, K. Kanazawa and K. Arai, *J. Am. Ceram. Soc.*, 1992, **75**, 1019.
13 Y. Hakuta, S. Onai, S. Terayama, T. Adschiri and K. Arai, *J. Mater. Sci. Lett.*, 1998, **17**, 1211.
14 M. Yashima, K. Morimoto, N. Ishizawa and M. Yoshimura, *J. Am. Ceram. Soc.*, 1993, **76**, 2865.

Molecular selective adsorption of nonylphenol in aqueous solution by organo-functionalized mesoporous silica

Kei Inumaru,* Junichi Kiyoto and Shoji Yamanaka

Department of Applied Chemistry, Faculty of Engineering, Hiroshima University, 1-4-1, Kagamiyama, Higashi-Hiroshima 739-8527, Japan. E-mail: inumaru@hiroshima-u.ac.jp

Received (in Cambridge, UK) 22nd March 2000, Accepted 17th April 2000
Published on the Web 9th May 2000

Octylsilane-grafted hexagonal mesoporous silica removed low-concentrated nonylphenol, an endocrine disrupter, in water with high efficiency comparable to that of activated carbon, while the adsorbent showed no detectable uptake of phenol.

Mesoporous materials such as MCM-41[1] and FSM-16[2] have been extensively studied as catalyst supports and adsorbents. They have advantages for the adsorption of large molecules because of their large pore size and high surface areas. It has been reported that an as-synthesised surfactant–silica mesophase effectively absorbs 4-chlorophenol into its confined 'micelles' from aqueous solution.[3] Functionalization of the inner wall by grafting organic or organometallic groups is a promising strategy in designing the nature of pore spaces at the molecular levels.[4–8] Considering that grafted alkyl groups provide hydrophobic regions confined within the ionic surface of the inorganic phase, it is expected that control of the hydrophobicity would improve the performance of the absorbent for organic moelcules having both hydrophilic hydrophobic regions.

Alkylphenolic chemicals such as nonylphenol, which are biodegradaion products of alkylphenol polyethoxylate resin, have been found to be the major oestrogenic contaminants to induce feminising effects in fish.[9–11] The minimum effective concentration of nonylphenol was estimated *in vitro* to be in the range of 10 nM–10 μM (2.2–2200 ppb).[11] For the removal of a pollutant by adsorption with such a low concentration in sewage disposal plants, the adsorbent should have a very high molecular selectivity, otherwise many coexisting compounds with higher concentrations would saturate the capacity of the adsorbent.

Here we report that the grafting of alkylsilanes with intermediate chain lengths provides mesoporous silica with a high molecular selectivity. Octylsilane-grafted mesoporous silica effectively removed nonylphenol from water, while it showed no detectable adsorption of phenol. The capacity of the adsorbent for nonylphenol was comparable to that of an activated carbon which is currently used in sewage disposal plants and water purification plants.

Hexagonal mesoporous silica (MPS) was prepared by the following procedure: 0.011 mol of octadecyltrimethylammonium chloride was dissolved in 25 ml hydrochrolic acid (12.5 wt%) at 328 K. Then 0.011 mol of tetraethoxysilane was added with stirring to immediately give a white precipitate. After filtration, the obtained mesophase was dehydrated at 473 K for 2 h and then calcined at 813 K in air for 6 h to obtain MPS. For synthesis of alkylsilane-grafted MPS, 0.32 g of the MPS was refluxed in fresh distilled toluene with 9.6×10^{-3} mol of *n*-octyltriethoxysilane or *n*-dodecyltriethoxysilane for 48 h. Prior to the silylation, MPS was dried at 473 K for 2 h *in vacuo*. After the silylation, the samples were washed with distilled toluene and then with anhydrous methanol. During these procedures, the materials were treated in a glove-box filled with dry Ar (H_2O was monitored to be < 1 ppm). In typical adsorption experiments, 1 mg of the adsorbent was added to 10 g of an aqueous solution of nonylphenol (2100 ppb). After the adsorption with stirring for a given time, the supernatant solution was separated by centrifugation and the residual nonylphenol was analysed with an ultraviolet (UV) spectrometer at 278 nm. Blank experiments confirmed that the adsorption of nonylphenol on the flask wall was low ($< 10\%$). The data were corrected using the results of the blank tests. Adsorption of phenol in water (2000 ppb) was also measured in the same way. For comparison, an activated carbon (Calgon F-400, surface area *ca.* 1000 $m^2\ g^{-1}$) was used.

Fig. 1 shows the N_2 adsorption isotherm for the samples synthesised in this study. The pristine MPS showed a curve with no hysteresis, which is typical for materials having cylindrical regulated pores like MCM-41. For the octylsilane-grafted MPS (C_8-MPS), the amounts of N_2 adsorption at relative pressures above 0.4 were *ca.* one third of that for MPS and the isotherm showed no hysteresis. The dodecylsilane-grafted MPS (C_{12}-MPS) gave a similar curve. This demonstrates that the alkylsilanes were grafted successfully onto the inner walls of the mesopores. Since the lengths of grafted alkylchains are shorter than the template used for the synthesis of MPS, it is expected that there are spaces at the centre of the pores. An α_s plot[12] on the basis of the N_2 isotherms of C_8-MPS (not shown) gave a shape similar to that of MPS, where the condensation of nitrogen was observed at lower α_s (*ca.* 0.6) for C_8-MPS than for MPS (α_s = *ca.* 0.8). These results demonstrated that the pores are narrower than the original ones. These spaces however, can still provide pathways for effective molecular diffusion. The inset in Fig. 1 shows the powder X-ray diffraction (XRD) pattern of C_8-MPS. This pattern shows that the mesostructure of silica (d_{100} = 35 Å) was maintained after grafting with the *n*-alkylsilane. Thermogravimetry and differential thermal analysis (TG-DTA) of C_8 and C_{12}-MPS gave exothermic weight losses due to the decomposition of alkyl groups at *ca.* 493–573 K (not shown). The molar ratios of the alkyl group to Si were

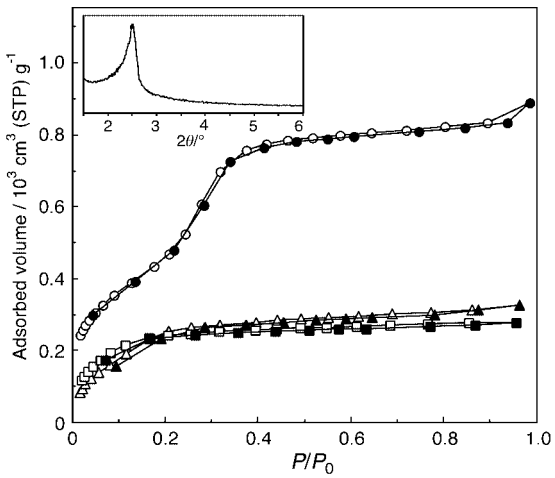

Fig. 1 N_2 adsorption isotherms of non-treated and *n*-alkylsilane-grafted mesoporous silica. Filled and open symbols represent adsorption and desorption branches, respectively. Circles, squares and triangles correspond to MPS, C_8-MPS and C_{12}-MPS, respectively. The inset shows the powder X-ray diffraction pattern of C_8-MPS.

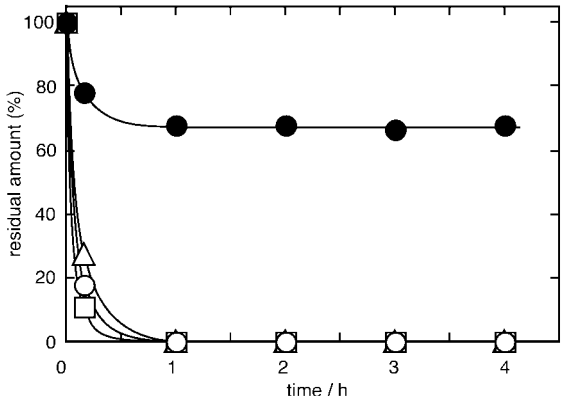

Fig. 2 Time courses of concentration of nonylphenol in water. 1 mg of adsorbent was used for 10 g of solution with an initial concentration of nonylphenol of 2100 ppb. Filled circles, open circles, open squares and open triangles correspond to MPS, C_8-MPS, C_{12}-MPS and activated carbon, respectively.

calculated from the TG data to be *ca.* 0.18 and 0.14 for C_8-MPS and C_{12}-MPS, respectively. These values are much smaller than the ratio of surfactant to Si for the as-synthesised mesophase (0.23), indicating that the materials have adequate space for molecular adsorption between the grafted alkyl groups in the mesopores.

Fig. 2 shows the time course of the concentration of nonylphenol during the adsorption. For the pristine MPS, *ca.* 30% of nonylphenol was removed. On the other hand, C_8-MPS removed nonylphenol totally within 1 h, showing that the grafting of alkyl groups is very effective in improving the performance of MPS. C_{12}-MPS and activated carbon also completely adsorbed nonylphenol within 1 h under the same conditions. A comparison between the alkyl-grafted MPSs and the activated carbon was carried out under much more severe conditions: 2 mg of the adsorbents were used for 200 g of the solution (1700–2100 ppb). The amounts of nonylphenol adsorbed at equilibrium are listed in Table 1. It was found that C_8-MPS showed a superior performance to the activated carbon. In addition, C_8-MPS was highly superior to C_{12}-MPS, while the differences of their surface areas and pore volumes were small. This indicates that the hydrophobicity of the dodecyl group is too strong while the moderate hydrophobicity of the octyl group is suitable for the effective adsorption of nonylphenol.

Table 1 Amounts of nonylphenol adsorbed on various adsorbents

Adsorbent	Concentration of nonylphenol/ppb	Amount of adsorbed nonylphenol/mol g^{-1}
C_8-MPS	6.2×10^2	6.5×10^{-4}
C_{12}-MPS	9.8×10^2	2.3×10^{-4}
MPS	1.3×10^3	9×10^{-5}
Activated carbon	6.2×10^2	5.3×10^{-4}

For comparison, adsorption of phenol in water (2000 ppb) was examined. 1 mg of absorbents were used for 10 g of solution. The activated carbon adsorbed 95% of phenol while MPS showed an uptake of 6%. On the other hand, C_8-MPS showed no detectable adsorption of phenol, while nonylphenol (2100 ppb) was completely removed under the same conditions. C_{12}-MPS gave the same results as C_8-MPS. Clearly, the grafting of alkyl group on the mesoporous silica provides a high molecular selectivity of nonylphenol against phenol.

In conclusion, MPS was made more hydorphobic by grafting alkyl chains on the inner surface of the mesopores and the resulting materials showed a high adsorption capacity for nonylphenol, an endocrine disrupter, comparable to that of activated carbon. The C_8-MPS adsorbent showed high molecular selectivity, distinguishing the hydrophobicity of molecules. These results indicate that the introduction of tuned hydrophobic regions in inorganic nanospaces is an effective strategy to design molecular selective adsorbents.

Notes and references

1 C. T. Kresge, M. E. Leonowicz, W. J. Roth, J. C. Vartuli and J. S. Beck, *Nature*, 1992, **359**, 710; J. S. Beck, J. C. Vartuli, W. J. Roth, M. E. Leonowicz, C. T. Kresge, K. D. Schmitt, C. T.-W. Chu, D. H. Olson, E. W. Sheppard, S. B. McCullen, J. B. Higgins and J. L. Schlenker, *J. Am. Chem. Soc.*, 1992, **114**, 10 834.
2 T. Yanagisawa, T. Shimizu, K. Kuroda and C. Kato, *Bull. Chem. Soc. Jpn.*, 1990, **63**, 988; S. Inagaki, A. Koiwai, N. Suzuki, Y. Fukushima and K. Kuroda, *Bull. Chem. Soc. Jpn.*, 1996, **69**, 1449.
3 R. Denoyel and E. S. Rey, *Langmuir*, 1998, **14**, 7321.
4 C. E. Fowler, S. L. Burkett and S. Mann, *Chem. Commun.*, 1997, 1769.
5 J. F. Díaz, K. J. Balkus Jr., F. Bedioui, V. Kurshev and L. Kevan, *Chem. Mater.*, 1997, **9**, 61.
6 X. Feng, G. E. Fryxell, L.-Q. Wang, A. Y. Kim, J. Liu and K. M. Kemner, *Science*, 1997, **276**, 923.
7 R. Richer and L. Mercier, *Chem. Commun.*, 1998, 1775.
8 K. A. Koyano, T. Tatsumi, Y. Tanaka and S. Nakata, *J. Phys. Chem. B.*, 1997, **101**, 9436.
9 P. Preziosi, *Pure Appl. Chem.*, 1998, **70**, 1617 and references therein.
10 C. R. Tyler and E. J. Routledge, *Pure Appl. Chem.*, 1998, **70**, 1795.
11 S. Müller and C. Schlatter, *Pure Appl. Chem.*, 1998, **70**, 1847 and references therein.
12 F. Rouquerol, J. Rouquerol and K. Sing, *Adsorption by Powders and Porous Solids*, Academic Press, London, 1999, p. 288.

ChemComm

Rotaxane-encapsulated cyanine dyes: enhanced fluorescence efficiency and photostability

Jonathan E. H. Buston, James R. Young and Harry L. Anderson*

Department of Chemistry, University of Oxford, Dyson Perrins Laboratory, South Parks Road, Oxford, UK OX1 3QY. E-mail: harry.anderson@chem.ox.ac.uk

Received (in Liverpool, UK) 6th March 2000, Accepted 17th April 2000
Published on the Web 9th May 2000

Two isomers of a cyanine dye α-cyclodextrin rotaxane have been synthesised in aqueous solution, and structurally characterised by 2D NMR spectroscopy; they exhibit enhanced fluorescence and photostability, compared with the free dye.

Cyanine dyes are used as photographic sensitisers, laser dyes and biological fluorescence probes, and in optical data recording.[1,2] Their main limitation is low photochemical stability.[3] Here we report the first synthesis of a cyanine dye rotaxane, in which the chromophore is locked inside the cavity of a cyclodextrin.[4] Two diastereomers of the rotaxane have been isolated; one of these isomers exhibits substantially enhanced fluorescence quantum yield and photostability, in oxygen-saturated dioxane, relative to the unencapsulated dye.

Many dyes form inclusion complexes with cyclodextrins in aqueous solution, due to hydrophobic binding. These complexes often exhibit enhanced fluorescence[5] and photostability,[5g,6] but they can only be studied in water, in the presence of excess cyclodextrin, because they readily dissociate; the equilibrium constants are typically 10^2–10^3 M^{-1} in water, and much lower in other solvents. Rotaxane-encapsulated dyes[7] are similar to inclusion complexes except that they cannot dissociate, because the ends of the dye are too bulky to pass through the macrocycle, so they can be studied in a wide range of solvents.

Our strategy for preparing these rotaxanes is to synthesise a dumbbell-shaped dye in water, in the presence of a macrocycle; hydrophobic binding between the dye-precursors and the macrocycle results in rotaxane formation.[7] Cyanine dyes are not usually synthesised in aqueous solution, but we have found that reaction of 3-(9-julolidinyl)prop-2-en-1-al[8] **1** with *N*-(1-adamantyl)-4-methylpyridinium chloride[9] **2** and α-cyclodextrin in aqueous sodium hydroxide gives cyanine dye rotaxanes **3a** and **3b** as well as the free dye **4** (Scheme 1).† α-Cyclodextrin is cone-shaped; it has a narrow 6-rim (with primary OH groups) and a wide 2,3-rim (with secondary OH groups). So there are two possible orientations of the cyclodextrin unit, giving rise to the two stereoisomers **3a** and **3b**. The yield of **3a** and **3b** is low (6%, based on re-isolated aldehyde **1**), which is not surprising since the reaction involves dehydration in aqueous solution. ^{1}H NMR showed that this product was a 1:2 mixture of two stereoisomers **3a** and **3b**, which were separated by reverse phase chromatography. There is only one previous report of the separation of rotaxane stereoisomers of this type.[10]

The two pure cyanine dye rotaxanes **3a** and **3b** were both thoroughly authenticated by ^{1}H and ^{13}C NMR spectroscopy, and mass spectrometry, and their ^{1}H NMR spectra were fully assigned using 2D techniques. The vicinal ^{1}H–^{1}H coupling constants across each alkene unit in **3a** and **3b** (H_E–H_F and H_G–H_H) are in the range 15.1–15.4 Hz, proving that both isomers have the *trans–trans* geometry. NOESY experiments confirmed that the isomers have different orientations of the cyclodextrin unit. In rotaxane **3a**, NOEs were observed from H3 of the cyclodextrin (the wide rim) to both the aromatic and benzylic julolidine signals (H_C and H_D), and from H5 (near the narrow rim) to H_I at the other end of the dye. The opposite pattern of NOEs was observed in **3b**: from H3 to H_I and H_J; from H5 to H_D and from H6 to H_C. These NOE measurements not only elucidate the isomerism in **3a** and **3b**, but also show that the cyclodextrin is sitting round the reactive polymethine region in both rotaxanes. In both cases the NOEs are not consistent with a single static position of the cyclodextrin, showing that each isomer is dynamic in solution.

Encapsulation results in a bathochromic shift in the electronic absorption and emission spectra of both rotaxanes (for **3a**, **3b** and **4** in water λ_{max}(abs.) = 525, 535 and 477 nm; λ_{max}(em.) = 710, 718 and 678 nm respectively). The relative fluorescence quantum yields[11] of these three compounds in water, and a range of other solvents, are listed in Table 1. In water, the fluorescence quantum yields of both of the rotaxanes are lower than that of the free dye,[12] whereas in other solvents, especially dioxane, rotaxane **3b** is spectacularly more fluorescent. The fluorescence behaviour of the two isomers **3a** and **3b** are surprisingly different, with **3a** behaving more like the free dye **4**.

The higher fluorescence efficiency of **3b** in dioxane is not consistent with several common explanations for enhanced

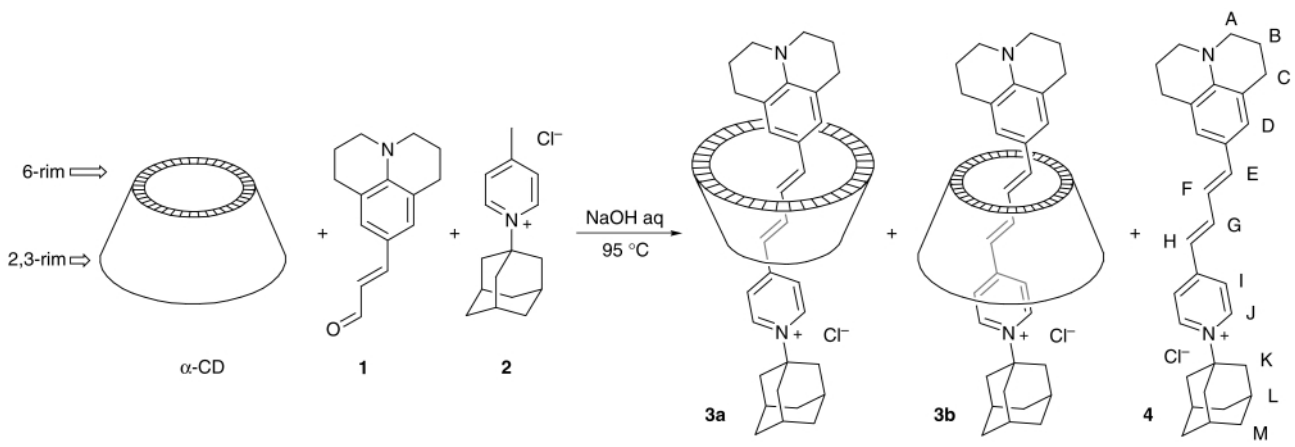

Scheme 1

DOI: 10.1039/b001812k

Table 1 Relative fluorescence quantum yields of rotaxanes **3a** and **3b**, and free dye **4** in a range of solvents[11]

Solvent	ϕ_f **3a**	ϕ_f **3b**	ϕ_f **4**
H_2O	0.71	0.71	1.0
MeCN	1.6	4.8	2.0
Me_2CO	2.6	11	2.0
Me_2SO	4.8	9.1	4.3
MeOH	2.5	4.0	2.1
EtOH	4.8	10	4.4
Pr^iOH	6.8	21	10
THF	16	46	18
Dioxane	81	124	22

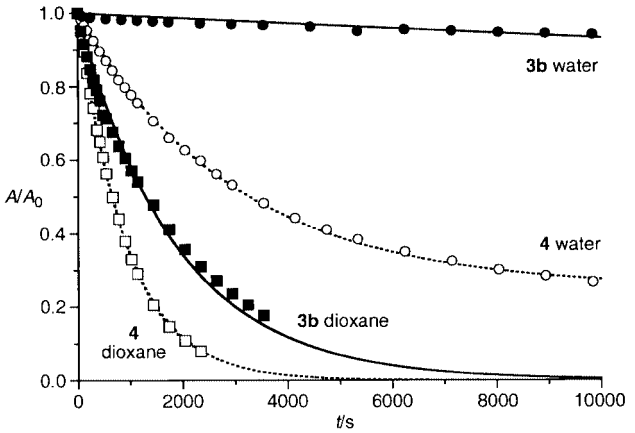

Fig. 1 Photo-bleaching curves for rotaxane **3b** in water, free dye **4** in water, **3b** in dioxane and **4** in dioxane, fitted to first-order decay curves with rate constants of 7.1×10^{-6}, 3.3×10^{-4}, 5.4×10^{-4} and 1.1×10^{-3} s^{-1}, respectively. Photolyses were carried out in 10 mm quartz cuvettes and O_2-saturated solvents with light from a tungsten filament bulb, using a 35 mm slide projector; A is the absorbance at time t and A_0 is the initial absorbance.

fluorescence in aqueous cyclodextrin–dye inclusion complexes, such as the exclusion of water from the dye surface and the changes in polarity around the dye when it enters the cyclodextrin.[5b,e,f] Here the fluorescence is enhanced in a range of non-aqueous solvents, and especially in dioxane which has a similar polarity to the cyclodextrin cavity. Cyclodextrin-encapsulation has been viewed as a way of reducing the quenching effect of an aqueous environment, whereas here encapsulation dramatically increases the fluorescence efficiency in a solvent in which the dye is already highly fluorescent. The enhanced fluorescence of **3a** and **3b**, compared to **4**, in dioxane is probably due to the reduced flexibility of the encapsulated chromophore.[5i] The possibility that this fluorescence enhancement is due to reduced aggregation[5c,d,i] can be discounted since **4** shows no sign of aggregation under these conditions.

The photostability of rotaxane **3b** was compared with that of the free dye **4**, in both water and dioxane, by monitoring the decrease in absorbance during irradiation of oxygen-saturated solutions with visible white light.[3c,6] Pseudo first order photo-bleaching curves were obtained in all cases, as shown in Fig. 1 (see caption for rate constants). The rotaxane **3b** exhibits higher photostability in both solvents (40-fold in water and 2-fold in dioxane, compared to the free dye **4**), and both compounds fade much faster in dioxane than in water. The mechanism of photo-bleaching has not yet been elucidated, but whatever process is involved, the faster bleaching in dioxane is probably related to the stronger fluorescence in this solvent, since a lower rate of quenching allows excited states to undergo more photo-chemistry. Matsuzawa *et al.*[6a] have shown that inclusion of cyanine dyes in β-cyclodextrin can enhance the photostability both by reducing the rate of singlet oxygen formation and by reducing the rate of reaction between singlet oxygen and the dye; both these factors may be involved here. It is remarkable that, in dioxane, **3b** exhibits a 5-fold fluorescence enhancement simultaneously with a 2-fold photostability enhancement.

The discovery that cyclodextrin encapsulation can increase the fluorescence and photostability of dyes under solvent conditions which already favour fluorescence indicates that this may be a valuable way of improving the stability and brightness of luminescent and electro-luminescent materials.

We are grateful to Dr T. D. W. Claridge for valuable assistance with NOE spectroscopy, and to Dr P. Gaffney for advice on reverse phase chromatography. This work was supported by the EPSRC.

Notes and references

† *Experimental:* 3-(9-Julolidinyl)prop-2-en-1-al **1** (1.0 mmol, 0.22 g), *N*-(1-adamantyl)-4-methylpyridinium chloride **2** (1.0 mmol, 0.26 g), α-cyclodextrin (4 mmol, 3.9 g) and aqueous NaOH (0.1 M, 20 ml) were stirred under N_2 at 95 °C for 24 h. The mixture was extracted with CH_2Cl_2, from which unreacted **1** (0.15 g, 67%) was recovered, together with **4** (14 mg, 2.9%). The aqueous phase was chromatographed (Sephadex CM25, eluting with NH_4HCO_3 aq) and lyophilized to yield 29 mg (6% based on re-isolated **1**) of a mixture of **3a** and **3b**. These isomers were separated by reverse-phase C18 silica chromatography, eluting with Pr^iOH–H_2O–0.01 M NH_4HCO_3 1:3:1, to give, in order of elution, rotaxanes **3a** and **3b**. Each fraction was anion-exchanged to the chloride and dried to give a purple powder.

1 H. Zollinger, *Color Chemistry*, VCH, Weinheim, 2nd edn., 1991; Z. Zhu, *Dyes Pigm.*, 1995, **27**, 77.
2 A. Hassner, D. Birnbaum and L. M. Loew, *J. Org. Chem.*, 1984, **49**, 2546; E. Fluhler, V. G. Burnham and L. M. Loew, *Biochemistry*, 1985, **24**, 5749.
3 (*a*) P. Chen, S. Sun, Y. Hu, Z. Qian and D. Zheng, *Dyes Pigm.*, 1999, **41**, 227; (*b*) G. W. Byers, S. Gross and P. M. Henrichs, *Photochem. Photobiol.*, 1976, **23**, 37; (*c*) S. Lepaja, H. Strub and D.-J. Lougnot, *Z. Naturforsch, Teil A*, 1983, **38**, 56.
4 Cyclodextrin-based rotaxanes have been reviewed recently: S. A. Nepogodiev and J. F. Stoddart, *Chem. Rev.*, 1998, **98**, 1959.
5 (*a*) F. Cramer, W. Saenger and H.-Ch. Spatz, *J. Am. Chem. Soc.*, 1967, **89**, 14; (*b*) M. Hoshino, M. Imamura, K. Ikehara and Y. Hama, *J. Phys. Chem.*, 1981, **85**, 1820; (*c*) I. Willner, N. S. Dixit and R. A. Mackay, *J. Chem. Soc., Perkin Trans. 2*, 1984, 455; (*d*) I. R. Politzer, K. T. Crago, T. Hampton, J. Joseph, J. H. Boyer and M. Shah, *Chem. Phys. Lett.*, 1989, **159**, 258; (*e*) W. R. Bergmark, A. Davis, C. York, A. Macintosh and G. Jones, II, *J. Phys. Chem.*, 1990, **94**, 5020; (*f*) S. Das, K. G. Thomas, M. V. George and P. V. Kamat, *J. Chem. Soc., Faraday Trans.*, 1992, **88**, 3419; (*g*) O.-K. Kim, L.-S. Choi, H.-Y. Zhang, X.-H. He and Y.-H. Shih, *J. Am. Chem. Soc.*, 1996, **118**, 12 220; (*h*) W. L. Hinze, F. Dai, R. P. Frankewich, K. N. Thimmaiah and J. Szejtli, in *Comprehensive Supramolecular Chemistry*, ed. J. Szejtli and T. Osa, Elsevier, Oxford, 1996, vol. 3, ch. 20; (*i*) C. Lee, Y. W. Sung and J. W. Park, *J. Phys. Chem. B*, 1999, **103**, 893.
6 (*a*) Y. Matsuzawa, S. Tamura, N. Matsuzawa and M. Ata, *J. Chem. Soc., Faraday Trans.*, 1994, **90**, 3517; (*b*) R. Guether and M. V. Reddington, *Tetrahedron Lett.*, 1997, **38**, 6167; (*c*) T. V. S. Rao, J. B. Huff and C. Bieniarz, *Tetrahedron*, 1998, **54**, 10 627.
7 S. Anderson, T. D. W. Claridge and H. L. Anderson, *Angew. Chem., Int. Ed. Engl.*, 1997, **36**, 1310; S. Anderson, W. Clegg and H. L. Anderson, *Chem. Commun.*, 1998, 2379 and 2773; M. R. Craig, T. D. W. Claridge, M. G. Hutchings and H. L. Anderson, *Chem. Commun.*, 1999, 1537.
8 A. C. Friedli, E. Yang and S. R. Marder, *Tetrahedron*, 1997, **53**, 2717.
9 V. A. Sokolenko and N. M. Svirskaya, *Chem. Heterocycl. Compds. (Engl. Transl.)*, 1987, **23**, 675.
10 R. Isnin and A. E. Kaifer, *J. Am. Chem. Soc.*, 1991, **113**, 8188; *Pure Appl. Chem.*, 1993, **65**, 495.
11 The absolute fluorescence yield of **4** in air-saturated water was measured as 0.00040 using rhodamine 6G in air-saturated ethanol as a standard (ϕ_f = 0.88; J. Olmsted, III, *J. Phys. Chem.*, 1979, **83**, 2581).
12 Although cyclodextrin-dye inclusion complexes generally exhibit enhanced fluorescence in aqueous solution, examples of fluorescence quenching have also been reported;[5d,e] B. Sarkar, U. Das, S. Bhattacharyya and S. K. Bose, *Bull. Chem. Soc. Jpn.*, 1995, **68**, 1807.

Preparation of aqueous solutions of hypovalent germanium; reactions involving germanium-(II) and -(III)

Olga A. Babich,* Manik C. Ghosh† and Edwin S. Gould*

Department of Chemistry, Kent State University, Kent, Ohio 44242, USA. E-mail: obabich@kent.edu

Received (in Irvine, CA, USA) 11th January 2000, Accepted 5th April 2000
Published on the Web 9th May 2000

Solutions 0.2–0.4 mol dm^{-1} in Ge^{II} and 6 mol dm^{-1} in HCl, generated by reaction of Ge^{IV} with H_3PO_2, are stable for more than three weeks and can be diluted 200-fold with dilute HCl to give $GeCl_4^{2-}$ preparations that may be handled by conventional techniques; kinetic profiles for the reduction of Fe^{III} by Ge^{II}, as catalyzed by Cu^{II} in this medium, implicate, for the first time, the odd-electron intermediate Ge^{III}, which is formed from Cu^{II} and Ge^{II} (k = 30 M^{-1} s^{-1} in 0.50 M HCl) and is consumed by reaction with Fe^{III} (k = 6 × 10^2 M^{-1} s^{-1}).

Only a few accounts decribing the preparation and reactions of germanium(II) species in aqueous solution are at hand,[1–4] and no systematic redox studies of this unusual donor have yet appeared. This oxidation state ($E^o_{IV,II}$ = −0.22 V at pH 0) is described as unstable in aqueous media in the absence of halide.[5]

We here report the prepartion of aqueous germanium(II) solutions which may be handled using conventional techniques. These have been used to compare the rates at which Ge(II) reacts with several oxidants in chloride media.

In a modification of the procedure of Jolly and Latimer,[1] all operations were carried out under high purity (99.99%) argon. 1.0 g of GeO_2 was dissolved in 5 ml of conc. NaOH, then reprecipitated and redissolved by adding 20 ml of 6 M HCl. The resulting Ge^{IV} solution was reduced with 7.5 ml of 50% H_3PO_2 at 100 °C for 5–6 h [eqn. (1)].

$$Ge^{IV} + H_2O + H_3PO_2 \rightarrow H_3PO_3 + Ge^{II} + 2H^+ \quad (1)$$

Germanium(II) hydroxide was precipitated from the cooled solution by addition of conc. NH_3, washed twice with 1 M HCl, then dissolved in 6 M HCl. Alternatively, crystalline $GeCl_2$ may separate slowly from the reduced solution and can be dissolved directly in 6 M HCl. Solutions 0.2–0.4 M in Ge(II) in 6 M HCl were unchanged after several weeks, but diluted solutions ([Ge^{II}] = 10^{-3} M, [Cl^-] = 0.08 M, [H^+] = 0.3 M) decomposed slowly ($t_{½}$ = 60 min). Germanium(II) hydroxide is not appreciably soluble in 4 M $HClO_4$. In analogy with the behavior of Sn(II),[6] Ge(II) may be taken to exist predominantly as $GeCl_4^{2-}$ at Cl^- concentrations > 0.3 M.

† Present address: Department of Chemistry, BITS, Pilani, Rajasthan 333031, India.

Solutions of Ge(II) rapidly reduce I_3^-, $IrCl_6^{2-}$, and the quinoxalinium cation, QH^+,[7] first to its radical, $QH^\bullet$, and thence to its dihydro derivative, QH_2:

$$Ge^{II} + I_3^- \rightarrow Ge^{IV} + 3I^- \quad k_{24\,°C}\ M^{-1}\ s^{-1} > 5 \times 10^6\ (0.5\ M\ Cl^-) \quad (2)$$

$$Ge^{II} + 2IrCl_6^{2-} \rightarrow Ge^{IV} + 2IrCl_6^{3-} \quad 2 \times 10^4\ (0.2\ M\ Cl^-) \quad (3)$$

$$Ge^{II} + 2QH^+ \rightarrow Ge^{IV} + 2QH^\bullet \quad 1.3 \times 10^2\ (1.0\ M\ Cl^-) \quad (4)$$

$$Ge^{II} + 2QH^\bullet \xrightarrow{2H^+} Ge^{IV} + 2QH_2 \quad 3 \times 10\ (1.0\ M\ Cl^-) \quad (5)$$

The very slow reduction of Fe(III) by Ge(II) is catalyzed markedly by Cu(II), even at the 10^{-7} M level. With [Cl^-] < 0.2 M, rates are proportional to [Ge^{II}] and [Cu^{II}] but are *independent* of [Fe^{III}], pointing to a slow formation of one or more active intermediates, the faster reactions of which are kinetically silent. At higher [Cl^-] and [Ge^{II}], the linear profiles become curved, most perceptibly near the end of the conversions, indicating that the initial catalytic act and the loss of Fe^{III} proceed at more nearly equal rates. Such patterns strongly support the sequence (6)–(8)

$$Ge^{II} + Cu^{II} \rightarrow Ge^{III} + Cu^{I} \quad k_6 \quad (6)$$

$$Fe^{III} + Ge^{III} \rightarrow Ge^{IV} + Fe^{II} \quad k_7 \quad (7)$$

$$Fe^{III} + Cu^{I} \rightarrow Fe^{II} + Cu^{II} \quad k_8 \quad (8)$$

Expression of this sequence as a trio of differential equations, and numerical integration using the program KINSIM[8] led, after slight adjustment for the slow unimolecular loss of Ge^{II} (k = 2 × 10^{-4} s^{-1}) to bimolecular rate constants k_6 and k_7 listed in Table 1. Values for k_8 (the Cu^I–Fe^{III} reaction) have been shown by Orth and Liddell[9] to vary with both [H^+] and [Cl^-] and have been taken from the report of these workers. A curved calculated in this manner is compared to a representative profile in Fig. 1. The constants k_6 and k_7, pertaining to the formation and oxidation of Ge^{III}, appear to be the first reported kinetic parameters associated with this odd-electron state. Within the ranges examined, the rate of formation of Ge^{III}, but not its oxidation, is proportional to [Cl^-]; neither rate is acid-dependent.

At [Cl^-] = 0.8–1.0 M and [Ge^{II}] > 3 × 10^{-3} M, decay curves become exponential, and the unimolecular loss of Ge^{II} is negligible. Combinations of parameters k_7, k_6 and k_8 (the latter two adjusted for [Cl^-]-dependence)[9] fit the observed curves

Table 1 Representative kinetic data for the oxidation of germanium(II) by iron(III) as catalyzed by copper(II)[a]

[H^+]/M	[Cl^-]/M	10^4[Ge^{II}]/M	10^6[Cu^{II}]/M	k_6/M^{-1} s^{-1}	10^{-2} k_7/M^{-1} s^{-1}	10^{-5} k_8[b]/M^{-1} s^{-1}
0.40	0.50	5.4	5.0	31	6.5	5.4
0.40	0.50	10.0	5.0	34	7.0	5.4
0.40	0.50	10.0	10.0	34	7.0	5.4
1.0	0.20	6.6	5.0	9.8	6.0	1.25
1.0	0.20	10.0	5.0	10.3	5.5	1.25
1.0	0.40	10.0	5.0	23	5.4	2.1

[a] Reactions were carried out under argon at 24 °C and at ionic strength 1.0 M (Cl^-, ClO_4^-). $[Fe^{III}]_{initial}$ = 1.0 × 10^{-4} M throughout. Kinetic parameters k_6 and k_7 were obtained from the best fit of integrated forms of the sequence (6)–(8) to experimental curves (see text and ref. 8). [b] Values of k_8 were obtained from data of Orth and Liddell (ref. 9).

DOI: 10.1039/b000401o

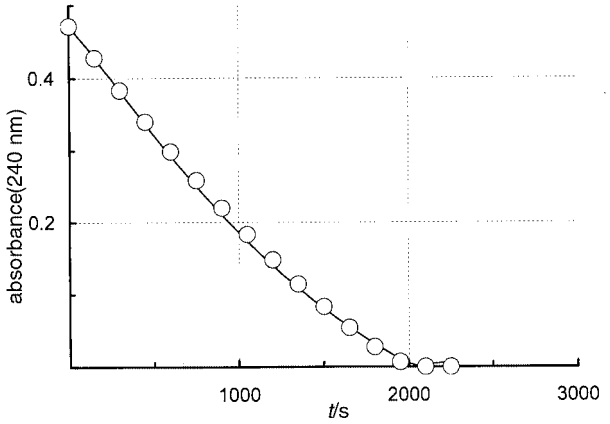

Fig. 1 Kinetic profile at 240 nm for the reduction of Fe(III) (1.0×10^{-4} M) by Ge(II) (6.6×10^{-4} M), as catalyzed by Cu(II) (5×10^{-6} M) in 0.20 M Cl^- at 24 °C; $[H^+]$ = 1.0 M. The solid line represents the experimental curve whereas the circles denote absorbances calculated from numerical integration of differential equations based on reaction sequence (6)–(8), taking k_6 as 9.8 M^{-1} s^{-1}, k_7 as 6×10^2 M^{-1} s^{-1}, and k_8 = 1.25×10^5 M^{-1} s^{-1} (ref. 9). The extinction coefficient used for Fe(III) is 4.7×10^3 M^{-1} cm^{-1}, and other species were considered to be negligibly absorbent. Optical path length = 1.00 cm.

only if an additional term (0.66 M^{-1} s^{-1}), pertaining to the uncatalyzed Ge^{II}–Fe^{III} reaction, is included in the treatment. This non-complementary redox change very probably passes through Ge^{III} as well. As expected, the initial step is much slower than the Fe(III)–Ge(III) reaction ($k_7 = 6 \times 10^2$ M^{-1} s^{-1}). In analogy to the In(I,III) system,[10] the odd-electron s^1 intermediate should be much more strongly reducing than the parent s^2 cation.

We are grateful to the National Science Foundation for the support of this work; to Dr Shawn Swavey and Dr Ksenija Namjesnik-Dejanovic for help in experimental procedures, and to Mrs Arla McPherson for technical assistance.

References

1 W. L. Jolly and W. M. Latimer, *J. Am. Chem. Soc.*, 1952, **74**, 5751.
2 L. S. Foster, *Inorg. Synth.*, 1950, **3**, 63.
3 H. P. Mayer and S. Rapsomanikis, *Appl. Organomet. Chem.*, 1992, **6**, 173.
4 K. Pan, J.-S. Chen and T.-S. Huang, *J. Chin. Chem. Soc. (Taipei)*, 1975, **22**, 171.
5 A. J. Bard, R. Parsons and J. Jordan, *Standard Potentials in Aqueous Solution*, Marcel Dekker, New York, 1985, p. 212.
6 A. E. Martell and R. M. Smith, *Critical Stability Constants*, Plenum, New York, 1976, vol. 4, p. 109.
7 C.-R. Chang, S. J. Paton, E. Gelerinter and E. S. Gould, *Inorg. Chem.*, 1979, **18**, 1294.
8 B. A. Barshop, R. F. Wrenn and C. Frieden, *Anal. Biochem.*, 1983, **130**, 134; S. K. Chandra, P. C. Paul and E. S. Gould, *Inorg. Chem.*, 1997, **36**, 4688.
9 R. J. Orth and K. C. Liddell, *Ind. Eng. Chem. Res.*, 1990, **29**, 1178.
10 A. M. Al-Ajlouni and E. S. Gould, *Res. Chem. Intermed.*, 1998, **24**, 653.

Chemical modification of chitosan: preparation of chitosan–sialic acid branched polysaccharide hybrids

Hitoshi Sashiwa,[a] Yutaka Makimura,[a] Yoshihiro Shigemasa[b] and René Roy*[a]

[a] *Department of Chemistry, University of Ottawa, Ottawa, Ontario K1N 6N5, Canada. E-mail: rroy@science.uottowa.ca*
[b] *Faculty of Engineering, Tottori University, Tottori, 680-8552, Japan*

Received (in Corvallis, OR, USA) 6th March 2000, Accepted 11th April 2000
Published on the Web 9th May 2000

Water soluble hybrids of chitosan and sialic acid were prepared in good yields *via* reductive *N*-alkylation of *p*-formylphenyl α-sialoside 2 onto chitosan amine functionalities.

Chitosan **1** is a polysaccharide mainly composed of the β(1-4)-2-amino-2-deoxy-D-glucopyranose (D-glucosamine) repeating unit and includes a small amount (< 20%) of *N*-acetyl-D-glucosamine (GlcNAc) residues. At present, several interesting biological properties have been reported for chitosan alone, such as wound healing,[1] immunological activity,[2] and antibacterial effects.[3] Moreover, chitosan itself is non-toxic. Therefore, chitosan is an appealing bioactive polymer for further development. Additionally, sialic acid-containing polymers[4] have been shown to be potent inhibitors of hemagglutinination of human erythrocytes by *influenza* viruses.[4–6] *N*-Acetylneuraminic acid (Neu5Ac) is the most ubiquitous member of the sialic acid family of derivatives present on mammalian cell surface glycolipids and glycoproteins and is the key epitope recognized as being essential for a number of pathogenic infections.[7] We are now investigating the preparation and biological properties of sialic acid-bound chitosan (chitosan–sialic acid hybrid) as a new family of sialic acid-containing polymers. A noteworthy point is the effect of chitosan as a backbone polymer for investigating the biological properties of sialic acid, especially against infection by the *influenza* virus and for its immunological activity. We report herein the first preparation and chemical aspects of chitosan–sialic acid hybrids.

Reductive *N*-alkylation[8,9] of chitosan with aldehydes is a very convenient method for its chemical modification. Therefore, we attempted the direct reductive *N*-alkylation of chitosan with *p*-formylphenyl α-sialoside **2**.[10] Scheme 1 shows the preparation of the chitosan–sialic acid hybrid **3**† by reductive *N*-alkylation using sodium cyanoborohydride ($NaCNBH_3$). The degree of substitution (DS) of Neu5Ac can be controlled by increasing the amount of aldehyde **2** in the reaction mixture (Table 1). The reactivity level of **2** to chitosan was found to vary in the range 25–48%, which was caused by the simultaneous reduction of some of the aldehyde groups of **2** under the acidic reaction conditions. Water soluble material was obtained only at high DS (DS = 0.53) due to the high level of charged carboxyl groups.

Hybrids **3** of low DS were insoluble in neutral water and thus would not be useful for biological evaluation. To improve the solubility, the remaining amino groups of the hybrids were transformed by succinylation with succinic anhydride (AcOH, H_2O, MeOH, room. temp., 1 day, neutralized with aq. NaOH then dialyzed and lyophilized) to give hybrids **4** in 90–100% yields. Under these mild aqueous conditions and basic workup, no lactones or cyclic imides were formed.[9] The chemical structures of the succinylated hybrids **4** are summarized in Table 2. Despite using a large excess of succinic anhydride, some unreactive amino groups (DS = 0.07–0.17) still remained. Complete succinylation was difficult owing to increasing steric hindrance of the polymer. High field ^1H NMR spectra also indicated that no succinylation had occurred at the *N*-glycosylation sites (δ H-1 of GclN-Neu5Ac). All succinylated products **4** were soluble in water. The protein binding properties of the novel sialylated polysaccharides were initially evaluated with wheat germ agglutinin (WGA: *Triticum vulgaris*) which is a plant lectin specific toward GlcNAc and Neu5Ac residues. Strong immunodiffusion bands were observed for water soluble hybrids **3** and **4** when compared to a negative control (*N*-succinylated chitosan), thus demonstrating the specificity of the binding of the Neu5Ac epitope in the hybrid to WGA lectin. The

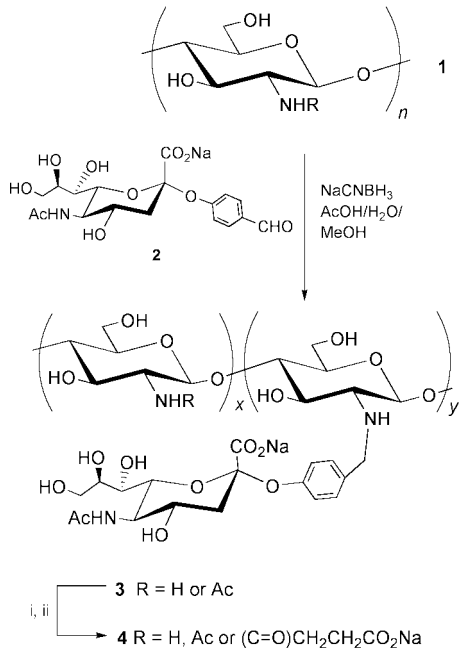

Scheme 1 *Reagents and conditions*: (i) succinic anhydride (0.2 g, 2 mmol), AcOH (50 mg, 0.83 mmol), H_2O (8 mL), MeOH (32 mL); (ii) 1% aq. NaOH (20 mL), room temp., 2 h.

Table 1 Preparation of conjugates **3** with aldehyde **2**

Entry	**2** (equiv.)	DS[a]	Yield[b] (%)	Solubility in H_2O	MW[c]
1	0.2	0.06	100	No	27000
2	0.4	0.10	77	No	29000
3	0.6	0.29	76	No	39000
4	0.9	0.44	74	No	48000
5	1.2	0.53	84	Yes	53000

[a] DS was determined from the peak area of phenyl protons (δ 7.0–7.4) and H-2 of GlcN and *N*-alkylated GlcN residues (δ 3.2: 0.96 H). [b] Yield determined by weight recovery and accounting for changes in FW according to the substitution level determined by NMR spectroscopy. [c] MW calculated on the basis of the original chitosan MW of 23 061 (DP = 140) and accounting for FW changes based on NMR data (values rounded to the nearest thousand).

DOI: 10.1039/b001861i

Table 2 Chemical structures and binding assay of chitosan–Neu5Ac derivatives to WGA lectin

Compd.	Functional group (DS) –Sugar	–Suc	$–NH_2$	–NHAc	MW	Binding to lectin[a]
4	0.10	0.79	0.07	0.04	40000	++
4	0.29	0.53	0.14	0.04	47000	++
4	0.53	0.26	0.17	0.04	59000	++
3	0.53	0	0.43	0.04	53000	++
—[b]	0	0.50	0.46	0.04	30000	±

[a] ++, strong band; ±, very faint band. [b] *N*-succinylated chitosan.

very faint band shown in *N*-succinylated chitosan could be due to the small amount of GlcNAc residues already present in the initial polymer chain (DS = 96% GlcN; 4% GlcNAc).

In conclusion, water soluble and lectin binding chitosan–sialic acid hybrids have been successfully prepared. Further biological evaluation of these promising compounds will be investigated.

We are indebted to Nippon Gaishi Co., Japan for generously supplying sialic acid.

Notes and references

† *Materials and methods:* chitosan **1** [DS = 96% GlcN, 4% GlcNAc, DP = 140; molecular weight (MW) 23061] was used in this study. The degree of polymerization (DP) of the initial chitosan **1** was determined by GPC using pullulan as standard. The DS of the hybrids was determined by ^{1}H NMR spectroscopy (Bruker 500 MHz AMX). The remaining unmodified primary amino groups of the hybrids were quantitated by colorimetric determination using ninhydrin at 570 nm.

Typical procedure for the preparation of hybrid **3**: Chitosan (50 mg, 0.24 mmol NH_2) was dissolved in H_2O (8 mL) and MeOH (32 mL) containing AcOH (50 mg, 0.83 mmol). Various amounts of **2** (Table 1) were added to the solution which was stirred at room temperature. After 1 h, $NaCNBH_3$ (100 mg, 1.6 mmol) was added and after 1 day, the reaction mixture was quenched by precipitation with 5% aq. NaOH (2 mL, 2.5 mmol) and acetone (80 mL). The precipitate was collected by filtration, dispersed with H_2O containing NaOH (100 mg), dialyzed and lyophilized.

Selected data for **3** (DS = 0.53)**:** ^{1}H NMR (0.2 M DCl in D_2O) δ 1.88 (t, 0.53 H, $J_{3ax–4eq}$ 12.1 Hz, H-3_{ax} of NeuNAc), 2.06 (m, 1.71 H, NHAc of Neu5Ac and GlcNAc in chitosan), 2.32 (dd, 0.53 H, $J_{3eq–4eq}$ = 5.0 Hz, H-3_{eq} of Neu5Ac), 3.20 (br, 0.96 H, H-2 of GlcN and *N*-alkylated GlcN), 3.55–4.10 (m, H-4,5,6,7,8,9 of Neu5Ac, H-2 of GlcNAc, H-3,4,5,6 of GlcN and GlcNAc), 6.97 (d, 1.06 H, J = 7.44 Hz, H-3 and H-5 of –OPh), 7.27 (d, 1.06 H, *J* 7.44 Hz, H-2 and H-6 of –OPh); ^{13}C NMR δ 25.0 (NAc), 41.7 (C-3 of Neu5Ac), 53.3 (CH_2Ph), 55.0 (C-5 of Neu5Ac), 58.8 (C-2 of GlcN), 63.0 (C-6 of GlcN), 66.1 (C-9 of Neu5Ac), 69.5 (C-4 of Neu5Ac), 71.2 (C-7 of Neu5Ac), 73.2 (C-8 of Neu5Ac), 73.4 (C-6 of Neu5Ac), 77.7 (C-3 and C-5 of GlcN), 79.4 (C-4 of GlcN), 98.1 (C-2 of Neu5Ac), 100.4 (C-1 of GlcN), 119.0 (C-2 and C-6 of Ph), 125.0 (C-4 of Ph), 135.0 (C-3 and C-5 of Ph), 159.8 (C-1 of Ph), 175.9 (NHCO), 177.9 (CO_2H of Neu5Ac).

Succinylation of hybrid was performed as described previously.[9]

Agar gel diffusion experiments were performed in 1% agarose (BDH) containing 2% poly(ethylene glycol) (MW = 8000, Sigma) in phosphate-buffered saline (PBS) according to the method of Ouchterlony and Nilsson.[11] The concentration of conjugate **3** was 1 mg mL^{-1} in PBS, and that of WGA lectin was 2 mg mL^{-1}. The precipitation bands were allowed to form overnight at 4 °C in a humid chamber.

1 S. Minami, Y. Okamoto, A. Matsuhashi, H. Sashiwa, H. Saimoto, Y. Shigemasa, T. Tanigawa, T. Tanaka and S. Tokura, in *Advances in Chitin and Chitosan*, ed. C. J. Brine, P. A. Sandford and J. P. Zikakis, Elsevier, London, 1992, p. 61.

2 K. Nishimura, S. Nishimura, N. Nishi, I. Saiki, S. Tokura and I. Azuma, *Vaccine*, 1984, **2**, 93.

3 T. Tanigawa, Y. Tanaka, H. Sashiwa, H. Saimoto and Y. Shigemasa, in *Advances in Chitin and Chitosan*, ed. C. J. Brine, P. A. Sandford and J. P. Zikakis, Elsevier, London, 1992, p. 206.

4 R. Roy, C. A. Laferrière, A. Gamian, M. Chomik and H. J. Jennings, *J. Carbohydr. Chem.*, 1987, **6**, 161; R. Roy and C. A. Laferrière, *Carbohydr. Res.*, 1988, **177**, C1; A. Gamian, M. Chomik, C. A. Laferriere and R. Roy, *Can. J. Microbiol.*, 1991, **37**, 233; R. Roy, F. O. Andersson, G. Harm, S. Kelm and R. Schauer, *Angew. Chem., Int. Ed. Engl.*, 1992, **31**, 1478.

5 N. E. Byramova, M. N. Mochalova, J. M. Belyanchikov, M. N. Matrosovich and N. V. Bovin, *J. Carbohydr. Chem.*, 1991, **10**, 691.

6 G. B. Sigal, M. Mammen, G. Dahmann and G. M. Whitesides, *J. Am. Chem. Soc.*, 1996, **118**, 3789 and references therein.

7 K. A. Karlsson, *Curr. Opin. Struct. Biol.*, 1995, **5**, 622.

8 R. A. A. Muzzarelli, F. Tanfani, M. Emanuell and S. Mariotti, *Carbohydr. Res.*, 1982, **107**, 199; R. A. A. Muzzarelli, F. Tanfani, S. Mariotti and M. Emanuell, *Carbohydr. Polym.*, 1982, **2**, 145.

9 H. Sashiwa and Y. Shigemasa, *Carbohydr. Polym.*, 1999, **39**, 127.

10 R. Roy, D. F. Tropper, A. Romanowska, M. Letellier, L. Cousineau, S. J. Meunier and J. Boratynski, *Glycoconjugate J.*, 1991, **8**, 75.

11 O. Ouchterlony and L. A. Nilsson, in *Handbook of Experimental Immunology*, ed. D. M. Weir, Blackwell Scientific Publications, Oxford, 1978, ch. 19.

ChemComm

The structure of the decamethylborocenium cation: the most tightly-squeezed metallocene?

Andreas Voigt, Silvia Filipponi, Charles L. B. Macdonald, John D. Gorden and Alan H. Cowley*

Department of Chemistry and Biochemistry, The University of Texas at Austin, Austin, Texas 78712, USA. E-mail: cowley@mail.utexas.edu

Received (in Columbia, MO, USA) 9th February 2000, Accepted 5th April 2000
Published on the Web 10th May 2000

X-Ray crystallographic analysis along with DFT calculations on the decamethylborocenium cation provide definitive structural and electronic information about this most tightly-squeezed main group metallocene—the first to adopt the elusive σ/π geometry in the solid state.

The unusual structure of beryllocene, $Be(Cp)_2$ **1**, has attracted the attention of chemists for several years.[1] In both the solid and vapour states **1** adopts a 'slip-sandwich' structure in which the parallel Cp rings are attached to beryllium in an $\eta^1(\pi)/\eta^5$ fashion.[2] In solution **1** is fluxional owing to rapid changes in ring hapticities.[3] The observed structure contrasts with the $\eta^1(\sigma)/\eta^5$ structure predicted on the basis of numerous theoretical calculations.[3,4]

The borocenium cation $[B(Cp)_2]^+$, which is isoelectronic with **1**, is not known and unlikely to be stable at ambient temperature. Although the decamethylborocenium cation $[B(Cp^*)_2]^+$ **2** has been characterized by ^1H and ^{11}B NMR spectroscopy,[5] such data cannot be used to distinguish between $\eta^1(\pi)/\eta^5$ and $\eta^1(\sigma)/\eta^5$ structures. It was therefore necessary to perform an X-ray analysis of a suitable salt of **2**.

It was found that a variety of salts of **2** can be generated by treatment of $(Cp^*)_2BCl$[5] with *e.g.* $LiB(C_6F_5)_4$, $Ga(C_6F_5)_3$, $GaCl_3$ or $AlCl_3$. However, from the standpoint of single crystal growth, the best reaction was that between equimolar quantities of $(Cp^*)_2BCl$ and $AlCl_3$ in CH_2Cl_2–C_6D_6 solution which afforded an 86% yield of **2**$[AlCl_4]$ [mp *ca.* 60 °C (decomp.)].[6] The solid state structure of **2**$[AlCl_4]$ consists of an array of two independent cations and anions.† There are no unusually short interionic contacts and the metrical parameters for the independent cations are very similar and hence only one set of data is discussed here. The decamethylborocenium cation **2** (Fig. 1) features one η^5-bonded and one $\eta^1(\sigma)$-bonded Cp* substituent, both of which feature, within experimental error, planar C_5 rings. Such an arrangement for a main group metallocene has been predicted (*vide supra*) but never observed experimentally in the solid state. The boron–carbon distance for the η^1-bonded Cp* ring, B(1)–C(1) [1.582(6) Å] is considerably longer than the boron–η^5-Cp* ring centroid distance [1.269(5) Å] and the C(1)–B(1)–Cp* ring centroid arrangement is nearly lienar [177.9(5)°]. In contrast to beryllocene, which has an η^1/η^5 parallel-ring structure in the solid state,[7] the Cp* rings of **2** are non-parallel as indicated, for example, by the 114.4(5)° tilt angle between the B(1)–C(1) bond and the least squares plane of the η^1-Cp* ring. A further differentiating feature is that the η^1-attached ring of **2** exhibits a typical localized structure with average C_α–C_β and C_β–C_β bond distances of 1.339(5) and 1.476(6) Å, respectively.

The structure of **2** also contrasts with that of the isovalent decamethylaluminocenium cation, which adopts a staggered bis(η^5-Cp*) ferrocene-like geometry.[8] To provide insight into the reason(s) for this structural difference, DFT calculations were performed on $[B(Cp^*)_2]^+$, $[B(Cp)_2]^+$ and $[Al(Cp)_2]^+$. Geometry optimization of **2** at the BP86/A level of theory[9] provides excellent agreement with the experimental structure. Thus, the global minimum is the observed η^1/η^5 structure with B(1)–C(1) and B(1)–η^5-Cp* ring centroid distances of 1.593 and 1.291 Å, respectively, a C(1)–B(1)–Cp* ring centroid angle of 179°, and an η^1-Cp* ring tilt angle of 123°. Moreover, calculation of the ^{11}B chemical shift for this structure using the GIAO method[10] (δ −43.1) is in excellent agreement with the experimental value (δ −41.5).[5,6] The staggered bis-η^5 (D_{5d}) structure of **2** is computed to be 48.95 kcal mol^{-1} higher in energy than the η^5/η^1 structure, thus confirming that the observed geometry is not caused by crystal packing forces. Examination of space-filling models reveals the existence of pronounced steric congestion in $[(\eta^5\text{-}Cp^*)_2B]^+$ which is relieved somewhat in proceeding to the η^1/η^5 structure. However, traditional steric effects are not responsible for the observed geometry of **2** since DFT calculations on the unsubstituted borocenium cation, $[(Cp)_2B]^+$ reveal that the ground state geometry is also η^1/η^5 and remarkably similar to that of **2**. More importantly, the difference in energy between the η^1/η^5 and bis-η^5 structures is essentially the same for both the Cp*- and Cp-substituted cations (45.39 kcal mol^{-1} for the latter). Surprisingly, the D_{5d} $[(Cp)_2B]^+$ structure is not even a true minimum (N_{imag} = 4) on the potential energy surface (PES). Conversely, no η^1/η^5 minimum is found for $[(Cp)_2Al]^+$; geometry optimization on the C_s symmetry PES proceeds smoothly to the D_{5h} bis-η^5 structure instead. The difference in bonding modes is attributable to the higher electronegativity of boron and greater strength (and lower ionicity) of B–C *vs.* Al–C bonding. The smaller size and greater effective nuclear charge of boron is also important, expecially in comparison to Cp_2Be,

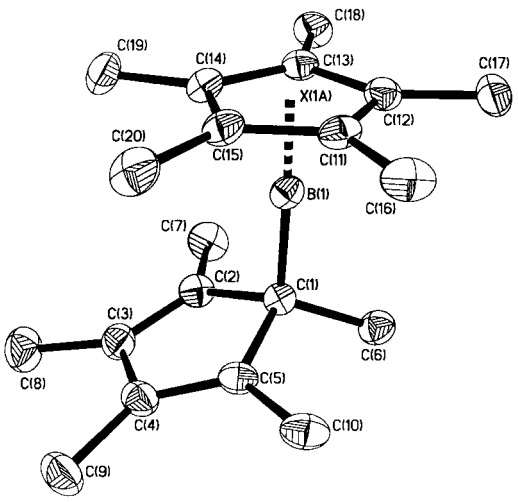

Fig. 1 ORTEP drawing of $[B(\eta^5\text{-}C_5Me_5)(\eta^1\text{-}C_5Me_5)]^+$ **2**. There are two independent cations: the bond distances (Å) and bond angles (°) for the second cation are shown in square brackets: B(1)–C(1) 1.583(5) [1.586(5)], B(1)–X(1A) (ring centroid) 1.290(5) [1.282(5)], B(1)–C(11) 1.782(6) [1.770(5)], B(1)–C(12) 1.775(5) [1.769(5)], B(1)–C(13) 1.782(5) [1.753(5)], B(1)–C(14) 1.757(5) [1.774(5)], B(1)–C(15) 1.757(5) [1.756(5)], C(1)–C(2) 1.515(5) [1.520(5)], C(2)–C(3) 1.343(5) [1.348(6)], C(3)–C(4) 1.473(6) [1.465(6)], C(4)–C(5) 1.340(5) [1.339(6)], C(1)–C(5) 1.523(5) [1.521(5)], C(1)–B(1)–X(1A) 177.9(5) [177.2(5)], B(1)–C(1)-least-squares-plane of (η^1-Cp*) 114.4(5) [112.4(5)], B(1)–C(1)–C(6) 112.4(3) [112.9(3)].

DOI: 10.1039/b001271h

because the putative D_{5d} structure is rendered much less stable owing to the increased repulsion between the π-clouds on the Cp ligands. Adoption of the $\eta^1(\pi)/\eta^5$ 'slipped-sandwich' structure by Cp_2Be relieves this strain sufficiently, but the closer ligand proximity in $[(Cp)_2B]^+$ mandates the non-parallel, π-localized $\eta^1(\sigma)/\eta^5$ alternative. In effect, the change from Be to B^+ results in a much steeper PES which more clearly favours the $\eta^1(\sigma)/\eta^5$ structure.

In conclusion, we have elucidated the structure of, and bonding in, the first authentic example of an $\eta^1(\sigma)/\eta^5$ metallocene. Because of the small size, combined with the high effective nuclear charge of the cationic boron(III) centre, we do not anticipate the isolation of a more tightly squeezed metallocene. Investigations of the reactivity of salts of **2** are currently underway.

We are grateful to the National Science Foundation and the Robert A. Welch Foundation for financial support.

Notes and references

† *Crystal data* for **2**[$AlCl_4$]: $C_{40}H_{60}Al_2B_2Cl_8$, M = 900.06 (two independent cation and anion pairs per asymmetric unit), colourless blocks, monoclinic, space group $P2_1/n$, a = 7.133(3), b = 13.611(3), c = 20.493(4) Å, β = 90.30(3)°, V = 4779(2) Å^3, Z = 4, D_c = 1.251 g cm^{-3}, μ(Mo-Kα) = 0.535 mm^{-1}. A suitable single crystal of **2**[$AlCl_4$] was covered with mineral oil and mounted on a Nonius Kappa CCD diffractometer at 153 K. A total of 19 718 reflections were collected in the range 5.96 < 2θ < 54.98° using Mo-Kα radiation (λ = 0.71073 Å). Of these, 10 898 were considered observed [$I > 2.0\sigma(I)$] and were used to solve (direct methods) and refine (full-matrix least squares on F^2) the structure of **2**[$AlCl_4$]; R_w = 0.2069, R = 0.0713. CCDC 182/1606. See http://www.rsc.org/suppdata/cc/b0/b001271h/ for crystallographic data in .cif format.

1 For a recent review, see: P. Jutzi and N. Burford, *Chem. Rev.*, 1999, **99**, 969.
2 Cp^*_2Zn adopts a similar parallel-ring structure in the gas phase: R. Blom, A. Haaland and J. Weidlein, *J. Chem. Soc., Chem. Commun.*, 1985, 266.
3 P. Margl, K. Schwartz and P. E. Blöchl, *J. Am. Chem. Soc.*, 1994, **116**, 11 177.
4 See, for example: L. W. Mire, S. D. Wheeler, E. Wagenseller and D. S. Marynick, *Inorg. Chem.*, 1998, **37**, 3099 and references therein; J. K. Beatty and K. W. Nugent, *Inorg. Chim. Acta*, 1992, **198**–**200**, 309.
5 P. Jutzi and A. Seufert, *J. Organomet. Chem.*, 1978, **161**, 5.
6 ^{1}H NMR (300.00 MHz, 295 K, C_6D_6): δ 1.65 (s, 15H, η^5-Cp* CH_3), 1.49 (s, 3H, η^1-Cp* *ipso*-CH_3), 1.63 (s, 6H, η^1-Cp* α-CH_3), 1.69 (s, 6H, η^1-β-CH_3). ^{13}C{^{1}H} NMR (75.48 MHz, 295 K, C_6D_6): δ9.13 (η^5-CH_3), 112.93 (η^5-Cp* ring C), 15.48 (η^1-Cp* *ipso*-CH_3), 51.79 (η^1-Cp* *ipso* ring C), 10.63 (η^1-Cp* α-CH_3), 136.36 (η^1-Cp* α-ring C), 12.17 (η^1-Cp* β-CH_3), 138.10 (η^1-Cp* β-ring C). ^{11}B NMR (96.28 MHz, 295 K, C_6D_6): δ −41.5 (s). ^{27}Al NMR (78.21 MHz, C_6D_6): δ 100 (s).
7 K. W. Nugent, J. K. Beattie, T. W. Hambley and R. S. Snow, *Aust. J. Chem.*, 1984, **37**, 1601.
8 C. Dohmeier, H. Schnöckel, C. Robl, U. Schneider and R. Ahlrichs, *Angew. Chem., Int. Ed. Engl.*, 1993, **32**, 1655.
9 A. D. Becke, *Phys. Rev.*, 1988, **38**, 3098; J. P. Perdew, *Phys. Rev.*, 1986, **33**, 8822. All DFT calculations were performed using the Gaussian 94 (Revision B2) suite of programs. All-electron basis sets were used for C, H (6-31G(d)) and the group 13 elements (6-31 + G(d)).
10 R. Ditchfield, *Mol. Phys.*, 1974, **27**, 789; K. Wolinski, J. F. Hinton and P. Pulay, *J. Am. Chem. Soc.*, 1990, **122**, 8251.

Programmed assembly of expanded rigid-rod β-barrels by supramolecular preorganization

Bodo Baumeister[ab] and Stefan Matile*[ab]

[a] *Department of Organic Chemistry, University of Geneva, CH-1211 Geneva 4, Switzerland*
[b] *Department of Chemistry, Georgetown University Washington, DC 20057-1227, USA.*
E-mail: stefan.matile@chiorg.unige.ch

Received (in Cambridge, UK) 15th March 2000, Accepted 26th April 2000

A simple strategy for (a) expansion and (b) variation of the internal chemical nature of rigid-rod β-barrels is reported, and the importance of supramolecular preorganization for their programmed assembly is discussed.

In nature, barrel-like folds[1] serve to recognize antigens[2] and secondary metabolites,[3,4] to mediate transport across biomembranes,[5] to catalyze enolate chemistry,[2,6] and to let jellyfish fluoresce.[7] In view of this functional diversity in nature, it is surprising to note that the design of artificial barrels has attracted little scientific attention. According to Fujita and coworkers, the assembly of nanotubes[8–11] with precisely defined length but flexible diameter in isotropic media, *i.e.* 'nanobarrels', was achieved last year for the first time.[12,13]† More recently, we have used the unique properties of rigid-rod molecules to create tetrameric barrel **1** in detergent-free water by programmed assembly of the complementary tripeptide-rods **2** and **3** (Scheme 1).[14] Rigid-rod β-barrel **1** is characterized by a length of 3.4 nm and an internal diameter of *ca.* 0.8 nm.[14] Constructive electrostatic interactions between lysine and glutamate residues account for the hydrophilicity of the barrel surface, while leucine residues produce a hydrophobic interior that can accommodate planarized β-carotene.[14] Several design strategies for further expansion of rigid-rod β-barrels are conceivable.[15] Here we report programmed assembly of the hexameric rigid-rod β-barrel **4** in detergent-free water. In this case, barrel expansion was accomplished by partial replacement of the internal leucine residues in tetramer **1** by the more bulky tryptophan residues in hexamer **4** (Fig. 1). We further provide experimental support that supramolecular preorganization may play an important general role in the programmed assembly of rigid-rod β-barrels in water (Scheme 1).

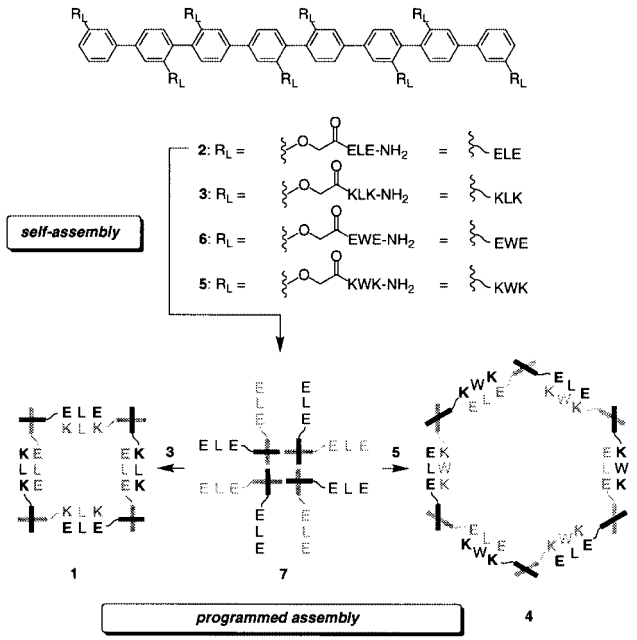

Scheme 1 Programmed assembly of rigid-rod β-barrels **1** and **4** by supramolecular preorganization with pinwheel **7** in water, pH 6.4. One-letter abbreviations for amino acids are used (E: glutamate, K: lysine, W: tryptophan, L: leucine). All supramolecules are displayed schematically in axial view with the benzene rings as bold lines. The first 'layer' of arene-tripeptides is in black, the second in grey, and the following six not shown for clarity. Amino acids with residues located at the outer barrel surface are in bold, those at the inner surface not.

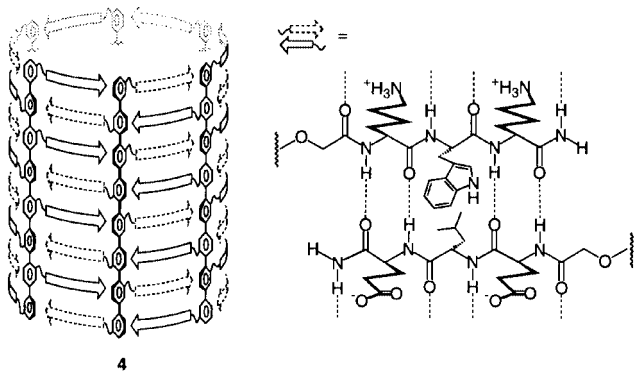

Fig. 1 Structure of hexameric rigid-rod β-barrel **4**. Amino acid residues located at the outer barrel surface are in bold, those at the inner surface not.

For programmed assembly of expanded rigid-rod β-barrels, we synthesized and characterized the complementary KWK-rod **5** and EWE-rod **6** following the experimental procedure for ELE-rod **2** and KLK-rod **3** that has been published in detail.[14] Size exclusion chromatogram (SEC) and circular dichroism (CD) spectrum of KWK-rod **5** in detergent-free water, pH 6.4, supported the previous observation with KLK-rod **3**[14] that cationic tripeptide-rods are monomeric under these conditions (Fig. 2, dashed line). Increasing amounts of ELE rod **2** converted the CD spectrum of KWK-rod **5** into that typical for rigid-rod β-barrels,[13–15] *i.e.* **4** (Fig. 2, continuous line). Namely, low energy negative (341 nm, $\Delta\varepsilon$ −5.8) and positive (294 nm, $\Delta\varepsilon$ +2.0) CD Cotton effects (CEs) centered around the octa(*p*-phenylene) ^{1}L transitions (319 nm, ε 28.6 mM^{-1} cm^{-1}) are followed by weaker negative and 'positive' CD CEs (253 nm, $\Delta\varepsilon$ −4.0; 242 nm, $\Delta\varepsilon$ −0.5) and two strong high energy CD CEs (232 nm, $\Delta\varepsilon$ −12.5; 216 nm, $\Delta\varepsilon$ +8.8; not shown). The circular dichroic absorption at 341 nm increased with decreasing mole fraction x = [**5**]/([**5**] + [**2**]) until a maximal $\Delta\varepsilon$ of −5.8 was reached at x = 0.5 [Fig. 2, inset (a)]. This corroborated the expected 1 : 1 stoichiometry of rigid-rod β-barrel **4**. An identical CD spectrum at x = 0.5 was obtained by addition of KWK-rod **5** to ELE-rod **2** [Fig. 2, inset (b)]. The nonlinear mixing curve suggested that β-barrel formation is inhibited at $x < 0.33$ [Fig. 2, inset (b)]. Addition of ELE-rods **2** to preformed barrel **4** (x = 0.5) did not, however, cause barrel deconstruction at $x < 0.33$ [Fig. 2, inset (c)].

In water, ELE-rods **2** self-assemble into the tetrameric pinwheel **7** (Scheme 1).[16] These supramolecules are composed

DOI: 10.1039/b002113j

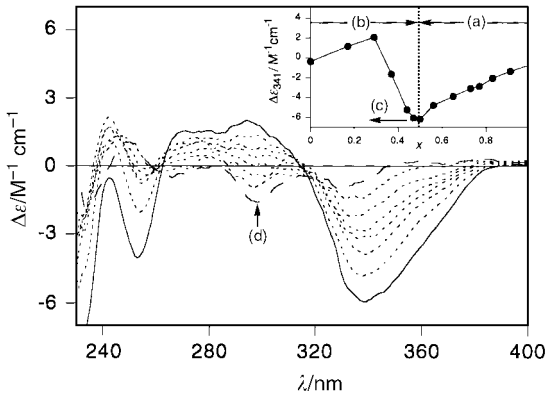

Fig. 2 Circular dichroism spectra of KWK-rod **5** (----) in the presence of increasing (····) and equimolar amounts of ELE-rod **2** (—). Inset: mixing curve for β-barrel **4**; x = [**5**]/([**5**] + [**2**]). (a) Addition of ELE-rod **2** (= pinwheel **7**) to KWK-rod **5** (identical with the displayed curves). (b) Addition of KWK-rod **5** to ELE-rod **2** (= pinwheel **7**). (c) Addition of ELE-rod **2** (= pinwheel **7**) to KWK-rod **5** (= barrel **4**) did not significantly change the initial CD spectrum (—). (d) The Cotton effect at 298 nm ($\Delta\varepsilon$ −1.1) was not observed in other peptide-rods[13–15] and is expected to originate from the L_a transition of the indoles in KWK-rod **5**. All experiments were performed in phosphate buffer (10 mM) at pH 6.4 with oligo(*p*-phenylene) concentrations around 10 μM, using a JASCO-710 spectropolarimeter. $\Delta\varepsilon$ values refer to the respective total octa(*p*-phenylene) concentration.

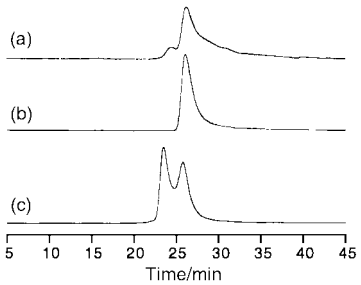

Fig. 3 Size exclusion chromatograms of (a) EWE-rod **6**, (b) ELE-rod **2** (= pinwheel **7**) and (c) β-barrel **4** (x = 1.0) with subsequently added ELE-rod **2** (= pinwheel **7**, final concentrations: [**2**]/[**5**] = 1.5/1.0). Chromatogram (b) displays new experiments that qualitatively reproduce previously reported data.[16] All experiments were performed in phosphate buffer (10 mM) at pH 6.4 with oligo(*p*-phenylene) concentrations around 10 μM, using a Superdex® 75 HR 10/30 prepacked column from Pharmacia Biotech (MW 70 000–3000, 1 mL buffer min^{-1}) coupled with a Jasco PU-980 pump and a Jasco UV-970 UV–VIS detector.

of a core of (presumably) edge-to-face π,π-stacked oligo(*p*-phenylene)s that is surrounded by anionic peptide strands in random-coil conformation.[16] The sharp peak of pinwheel **7** at R_t = 25.8 min [Fig. 3(b)] was used as a reliable internal standard for the determination of the molecular weight of barrels **4** by SEC [Fig. 3(c)]. Comparison of oligo(*p*-phenylene) and tryptophan absorption maxima at 319 nm and 282 nm,[17] respectively, confirmed that only the peak at R_t = 23.5 min [Fig. 3(c)] contained KWK-rod **5**. Rigid-rod β-barrel **4** is thus a hexamer under these conditions.

Programmed assembly of rigid-rod β-barrels using EWE-rod **6** instead of ELE-rod **2** was unsuccessful. Mixing of EWE-rod **6** with KWK-rod **5** resulted in immediate precipitation, and mixing with KLK-rod **3** did not result in clearly detectable supramolecular organization. The latter finding was of interest, because this non-forming barrel (composed of EWE-rods **6** and KLK-rods **3**) is the structural isomer of hexamer **4** (composed of ELE-rods **2** and KWK-rods **5**). This counter-intuitive result thus suggested that the (presumably) perpendicularly zigzagged preorientation of the lateral tripeptide strands of **2** in pinwheel **7** may significantly support the programmed assembly of rigid-rod β-barrels in water (Scheme 1). We further noted that the apparently reduced supramolecular preorganization in self-assembled EWE-rods **6** [Fig. 3(a) *cf.* ELE-rods **2** in Fig. 3(b)] and the capacity of pinwheel **7** to bind two KWK-rods **5** without significant suprastructural transformation [Fig. 2, inset (b), x = 0.33] are consistent with this view.

In summary, we have described the design and synthesis of expanded rigid-rod β-barrel **4** and obtained experimental support for the importance of supramolecular preorganization for programmed barrel assembly in detergent-free water. Compared to tetramer **1**,[14] hexamer **4** is of particular interest with regard to its enlarged hydrophobic interior (d > 2.0 nm in molecular models) and tryptophan residues at the inner barrel surface. We are currently interested in the influence of these 24 intratoroidal indoles in hexamer **4** on encapsulated chromophores of biological relevance.[3,4,7,18]

This work was supported by the Swiss NSF (21-57059.99), the NIH (GM56147), and Suntory Institute for Bioorganic Research (SUNBOR Grant). Warm thanks to A. Pinto and J.-P. Saulnier, the group of Professor Gülaçar and Dr H. Eder for NMR, MS and elemental analyses, respectively.

Notes and references

† Interestingly, the design of artificial barrels in liquid crystalline media is much more developed because of their possible function as ion channels. See, *e.g.* S. Otto, M. Osifchin and S. L. Regen, *J. Am. Chem. Soc.*, 1999, **121**, 7276; 10 440.

1 J. S. Richardson, *Nature*, 1977, **268**, 495.
2 C. F. Barbas III, A. Heine, G. Zhong, T. Hoffmann, S. Gramatikova, R. Björnestedt, B. List, J. Anderson, E. A. Stura, I. A. Wilson and R. A. Lerner, *Science*, 1997, **278**, 2085.
3 D. R. Flower, *Biochem. J.*, 1996, **318**, 1.
4 G. Beste, F. S. Schmidt, T. Stibora and A. Skerra, *Proc. Natl. Acad. Sci. USA*, 1999, **96**, 1898.
5 L.-Q. Gu, O. Braha, S. Conlan, S. Cheley and H. Bayley, *Nature*, 1999, **398**, 686.
6 P. C. Babbitt and J. A. Gerlt, *J. Biol. Chem.*, 1997, **272**, 30 591.
7 M. Ormö, A. B. Cubitt, K. Kallio, L. A. Gross, R. Y. Tsien and S. J. Remington, *Science*, 1996, **273**, 1392.
8 M. R. Ghadiri, J. R. Granja and L. K. Buehler, *Nature*, 1994, **369**, 301.
9 D. Venkataraman, S. Lee, J. Zhang and J. S. Moore, *Nature*, 1994, **271**, 591.
10 A. Harada, J. Li and M. Kamachi, *Nature*, 1993, **289**, 516.
11 D. Ranganathan, C. Lakshimi and I. L. Karle, *J. Am. Chem. Soc.*, 1999, **121**, 6103.
12 M. Aoyagi, K. Biradha and M. Fujita, *J. Am. Chem. Soc.*, 1999, **121**, 7457.
13 N. Sakai, N. Majumdar and S. Matile, *J. Am. Chem. Soc.*, 1999, **121**, 4294.
14 B. Baumeister and S. Matile, *Chem. Eur. J.*, 2000, **6**, 1739.
15 B. Baumeister, N. Sakai and S. Matile, *Angew. Chem., Int. Ed.*, in press.
16 B. Baumeister, A. C. de Dios and S. Matile, *Tetrahedron Lett.*, 1999, **40**, 4623.
17 R. W. Woody, in *Circular Dichroism—Principles and Applications*, ed. K. Nakanishi, N. Berova and R. W. Woody, VCH, Weinheim, Germany, 1994, pp. 473–496.
18 H. Houjou, Y. Inoue and M. Sakurai, *J. Am. Chem. Soc.*, 1998, **120**, 4459.

ChemComm

1,2-Phenylene diisocyanide for metallotriangles

Pablo Espinet,*[a] Katerina Soulantica,[a] Jonathan P. H. Charmant[b] and A. Guy Orpen[b]

[a] *Departamento de Química Inorgánica, Facultad de Ciencias, Universidad de Valladolid, E-47005 Valladolid, Spain. E-mail: espinet@qi.uva.es*

[b] *School of Chemistry, University of Bristol, Bristol, UK BS8 1TS*

Received (in Basel, Switzerland) 4th February 2000, Accepted 20th April 2000

A strain free platinotriangle has been produced using 1,2-phenylene diisocyanide as the ligand determining 60° angles at the vertices, and *trans*-Pt(C_6F_5)$_2$ as the linear link building the sides.

Compared to the number of metallosquares and metallorectangles reported, where the metal occupies either the vertices of the polygon (affording two *cis* coordination positions at 90°), the sides (affording two *trans* coordination positions at 180°), or both, reports on metallotriangles are surprisingly scarce.[1] Moreover, the majority of metallotriangles reported are of class **I**, with metal fragments offering two *cis* coordination positions

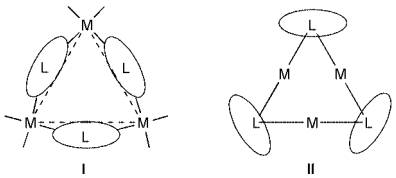

I II

at 90° occupying the vertices of a distorted equilateral triangle.[2] Curiously there are fewer of the apparently more favorable type **II** structure, where ligands imposing hexagonally based bonds at 60° should yield strain free triangles.

A well known family of triangles based on **II**, is that of [M(μ-pz)]$_3$ (pz = pyrazole or substituted pyrazole; M = Au, Ag) compounds **1**, even though the bonding angle determined by the

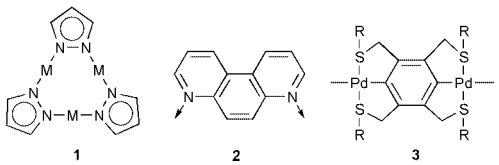

1 2 3

two pz nitrogens in a pentagonal ring is too open (*ca.* 72°).[3] Such triangles have been used to make hexagonal columnar liquid crystals.[4] Some years ago a number of complexes with iminoacyl, [M(CER$_n$=NR′)]$_3$ (M = Au, Ag; ER$_n$ = OR, NR$_2$),[5] or with 2-pyridyl, [Au(C_5H_4N)]$_3$,[6] as bridging groups were reported. These make triangles of the same small size as pyrazolate, and determine M···M distances of 3.3–3.5 Å. For trimeric mercury derivatives with *o*-phenylene, *o*-perfluorophenylene, or 1,2-$C_2B_{10}H_{10}$ at the corners these distances are 3.5–3.7 Å.[7] Only very recently a larger triangle has been reported, in which 4,7-phenanthroline **2** occupies the corners and the dipalladium fragment **3** makes the sides of the triangle.[8]

Isocyanides are known to bind strongly to many different transition metals. Diisocyanides have been used in the building of coordination polymers, and mixed donors 1,3- and 1,4-cyanoisocyanoarenes have afforded interesting mixed Pd–Cu polymers.[9] So far the only discrete metallapolygon reported involves 1,4-phenylene diisocyanide, making part of a very large tetragold rectangular ring.[10] On the other hand, Takahashi and coworkers have reported the metallosquare [Pd(PEt_3)$_2${μ-C_6H_4(C≡C)$_2$}]$_4$, with *o*-diethynylbenzene at the corners. Although the 60° angles determined by the two ethynyl groups are ideal for an equilateral triangle, steric repulsion of the PEt_3 ligands forces a strained square instead.[11]

1,2-Phenylene diisocyanide **4** is a neutral ligand geometrically equivalent to the dianionic *o*-diethynylbenzene used by Takahashi and coworkers.[12] We have tested its ability to make metallotriangles by reacting it with *trans*-[Pt(C_6F_5)$_2$($AsPh_3$)$_2$] **5**.[13] The pentafluorophenyl derivative **5** was chosen because it is quite inert towards isomerization, keeping its *trans* arrangement in substitution reactions. The reaction takes place very easily in CH_2Cl_2 at room temp., leading to the formation of [Pt(C_6F_5)$_2${μ-C_6H_4(NC)$_2$}]$_3$ **6** in high yield (Scheme 1).†

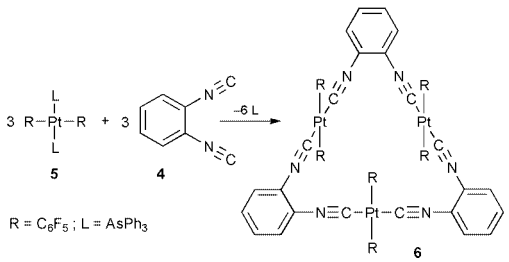

Scheme 1

The molecular structure of **6** is shown in Fig. 1.‡ There is a Pt atom at the center of each side of an equilateral triangle determined by the centers of the aryl rings of the diisocyanide ligands. The non-bonding Pt···Pt distances are *ca.* 5.65 Å. The coordination around the Pt atoms is square planar, with two *trans* isonitriles and two *trans* C_6F_5 groups. It is noteworthy that the metal atom is bonded only to C-donor ligands. The C_6F_5 groups are situated perpendicular to the planar triangle and their planes are more or less coplanar for each Pt(C_6F_5)$_2$ fragment. This can be better seen in Fig. 2, a space filling representation

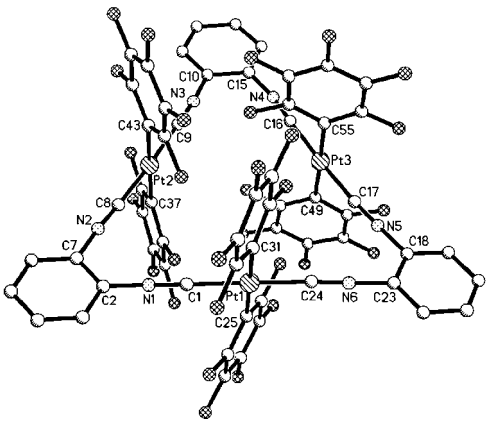

Fig. 1 Molecular structure of **6**. Phenylene hydrogens have been omitted for clarity. Selected distances (Å) and angles (°): Pt(1)–C(1) 1.918(10), Pt(1)–C(24) 1.925(10), Pt(1)–C(25) 2.057(9), Pt(1)–C(31) 2.076(10), C(1)–N(1) 1.170(11), C(2)–N(1) 1.402(11), C(2)–C(7) 1.380(12), C(1)–Pt(1)–C(24) 179.3(4), C(1)–Pt(1)–C(25) 90.9(4), C(1)–Pt(1)–C(31) 88.6(4), C(24)–Pt(1)–C(25) 89.4(4), C(24)–Pt(1)–C(31) 91.0(4), C(25)–Pt(1)–C(31) 178.6(4), Pt(1)–C(1)–N(1) 176.5(8), C(7)–C(2)–N(1) 121.6(8), C(1)–N(1)–C(2) 178.6(9).

DOI: 10.1039/b001027h

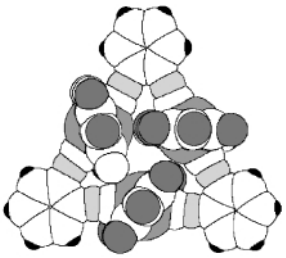

Fig. 2 Space filling structure of **6** viewed perpendicular to the plane of the triangle, showing the orientation of the C_6F_5 rings.

viewed perpendicular to the plane containing the triangle, where the C_6F_5 groups above and below this plane are eclipsing each other almost perfectly. The usual arrangement found for aryl ligands in square planar complexes has the aryl plane perpendicular to the metal coordination plane (torsion angle 90°).[14] In the triangle, this would cause them to clash in the center of the triangle. This is relieved by twisting the pentafluorophenyls about the Pt–C_6F_5 bond (we define twist as 0° for the perpendicular arrangement, thus torsion angle + twist angle = 90°). The average torsion angle around the Pt–C_{ipso} bonds is 54°. The maximum torsion is for C(24)–Pt(1)–C(31)–C_{ortho} = 63°, and the minimum is for C(9)–Pt(2)–C(37)–C_{ortho} = 46°. In addition there is some variation in the torsion angle along the Pt···C_{ipso} (phenylene) vectors. These angles give an idea of how orthogonal are the Pt–C_{ipso} (pentafluorophenyl) bonds to the 'plane' of the triangle. They vary between 103.0° [for C(31)–Pt(1)–C(23)–C(18)] and 77.4° for C(55)–Pt(3)–C(18)–C(23), and their average is close to 90°. van der Waals distances of the order 3.1–3.3 Å are found between the internal F_m or F_o of each ring and the closest carbons of another ring (C_m or C_p for F_m; C_o or C_{ipso} for F_o).[15]

In the C_{3h} symmetry found in the solid state structure, the F atoms inside and outside the triangle, as well as the four H atoms in each phenylene ring, should be diastereotopic (5 F signals and 4 H signals are expected). However only one signal is observed for each type of fluorine (F_o, F_m or F_p) in the ^{19}F NMR spectrum, and the hydrogens display an AA′XX′ pattern. This reveals fast rotation or tilting of the C_6F_5 groups.

A further structural feature worth commenting upon is the Pt–C_6F_5 distances: they range from 2.051 to 2.076 Å (average 2.061 Å), similar to other Pt–C_6F_5 distances and not particularly long. This suggests that the π back donation, which is sometimes invoked as a further source of stability for M–C_6F_5 compared to M–C_6H_5,[16] either is not very important in this case, or is not very much affected by the tilting.

The structural type found for **6** interesting for further elaboration. Both the diisocyanide and the R groups on the Pt can be easily modified to introduce other characteristics. For instance, *p*-substituted fluorinated rings have been used to produce metallomesogens.[17] We are currently pursuing these ideas.

We gratefully acknowledge financial support by the Spanish Dirección General de Enseñanza Superior e Investigación Científica (Project MAT99-0971). K. S. thanks the Spanish Ministerio de Educación y Cultura (SB95-BOZ67791015).

Notes and references

† To a stirred solution of *trans*-[Pt(C_6F_5)$_2$($AsPh_3$)$_2$] (156.6 mg, 0.137 mmol) in 40 mL of CH_2Cl_2 was added 1,2-phenylene diisocyanide (17.5 mg, 0.137 mmol) dissolved in 10 mL of CH_2Cl_2. After stirring for 2 h *n*-hexane (20 mL) was added. Upon evaporation, **6** separated as a white solid, which was filtered off, thoroughly washed with *n*-hexane, and dried. Yield: 71 mg (79%). IR: ν(C≡N) 2189 cm^{-1}. δ_H[$(CD_3)_2CO$, room temp., 300 MHz]: 7.83 (m, 6H) and 7.98 (m, 6H), AA′XX′ spin system. δ_F[$(CD_3)_2CO$, ref. $CFCl_3$, room temp., 282 MHz]: −114.3 (m, 12F_o, $^3J_{FPt}$ 284.8 Hz), −161.7 (t, 6F_p, $^3J_{FF}$ 19.9 Hz), −164.1 (m, 12F_m). Crystals for X-ray diffraction were obtained by slow diffusion from THF/hexane.

‡ *Crystal data* for [Pt{μ-$C_6H_4(NC)_2$}]$_3$·2THF (**6**·2THF): M = 2116.23, triclinic, space group $P\bar{1}$ (no. 2), a = 11.732(2), b = 11.907(2), c = 26.506(3) Å, α = 78.77(1), β = 83.180(1), γ = 65.11(1)°, U = 3291.5(8) Å^3, T = 163(2) K, Z = 2, μ = 6.5 mm^{-1}, 30636 reflections measured, 14436 unique (R_{int} = 0.085), wR_2 = 0.111 (for all 14436 data), R_1 = 0.053 [for 8872 data with $I > 2\sigma(I)$].

CCDC 182/1612. See http://www.rsc.org/suppdata/cc/b0/b001027h/ for crystallographic files in .cif format.

1 For reviews see: B. Olenyuk, A. Fechtenkötter and P. J. Stang, *J. Chem. Soc., Dalton Trans.*, 1998, 1707; M. Fujita, *Chem. Soc, Rev.*, 1998, 417; J. A. R. Navarro and B. Lippert, *Coord. Chem. Rev.*, 1999, **185**–**186**, 653.

2 For recent and leading examples, see: R.-D. Schnebeck, E. Freisinger, F. Glahé and B. Lippert, *J. Am. Chem. Soc.*, 2000, **122**, 1381; G. Baum, E. C. Constable, D. Fenske, C. E. Housecroft and T. Kulke, *Chem. Commun.*, 1999, 195; S.-W. Lai, M. C.-W. Chan, S.-M. Peng and C.-M. Che, *Angew. Chem., Int. Ed.*, 1999, **38**, 669; T. Habereder, M. Warchhold, H. Nöth and K. Severin, *Angew. Chem., Int. Ed.*, 1999, **38**, 3225; R.-D. Schnebeck, L. Randaccio, E. Zangrando and B. Lippert, *Angew. Chem., Int. Ed. Engl.*, 1998, **37**, 119; P. N. Baxter, J.-M. Lehn and K. Rissanen, *Chem. Commun.*, 1997, 1323; S. Rüttimann, G. Bernardelli and A. F. Williams, *Angew. Chem., Int. Ed. Engl.*, 1993, **32**, 392.

3 H. H. Murray, R. G. Raptis and J. P. Fackler, Jr., *Inorg. Chem.*, 1988, **27**, 26; R. G. Raptis and J. P. Fackler, Jr., *Inorg. Chem.*, 1990, **297**, 5003; F. Bonati, G. Minghetti and G. Banditelli, *J. Chem. Soc., Chem. Commun.*, 1974, 88; B. Bovio, F. Bonati and G. Banditelli, *Inorg. Chim. Acta*, 1984, **87**, 25.

4 J. Barberá, A. Elduque, R. Giménez, L. A. Oro and J. L. Serrano, *Angew. Chem., Int. Ed. Engl.*, 1996, **35**, 2832; J. Barberá, A. Elduque, R. Giménez, F. J. Lahoz, J. A. López, L. A. Oro and J. L. Serrano, *Inorg. Chem.*, 1998, **37**, 2960; S. J. Kim, S. H. Kang, K.-M. Park, H. Kim, W.-C. Zin, M.-G. Choi and K. Kim, *Chem. Mater.*, 1998, **10**, 1889.

5 A. Tiripicchio, M. Tiripicchio-Camellini and G. Minghetti, *J. Organomet. Chem.*, 1979, **171**, 399; F. Bonati and G. Minghetti, *Angew. Chem., Int. Ed. Engl.*, 1972, **11**, 429; G. Minghetti, F. Bonati and M. Massobrio, *Inorg. Chem.*, 1975, **143**, 1974; G. Minghetti and F. Bonati, *Inorg. Chem.*, 1974, **13**, 1600; J. E. Parks and A. L. Balch, *J. Organomet. Chem.*, 1974, **71**, 453; W. P. Felhammer and W. Finck, *J. Organomet. Chem.*, 1991, **414**, 261.

6 L. G. Vaughan, *J. Am. Chem. Soc.*, 1970, **92**, 730.

7 D. S. Brown, A. G. Massey and D. A. Wickens, *Acta Crystollogr., Sect. B*, 1978, **34**, 1695; D. S. Brown, A. G. Massey and D. A. Wickens, *Inorg. Chim. Acta*, 1980, **44**, L193; M. C. Ball, D. S. Brown, A. G. Massey and D. A. Wickens, *J. Organomet. Chem.*, 1981, **206**, 265; X. Yang, Z. Zheng, C. B. Knobler and M. F. Hawthorne, *J. Am. Chem. Soc.*, 1993, **115**, 4904.

8 J. R. Hall, S. J. Loeb, G. K. H. Shimizu and G. P. A. Yap, *Angew. Chem., Int. Ed.*, 1998, **37**, 121.

9 A. Mayr and L.-F. Mao, *Inorg. Chem.*, 1998, **37**, 5776 and references therein.

10 M. J. Irvin, L. M. Rendina, J. J. Vittal and R. J. Puddephatt, *Chem. Commun.*, 1996, 1281.

11 K. Onitsuka, S. Yamamoto and S. Takahashi, *Angew. Chem., Int. Ed.*, 1999, **38**, 174.

12 Y. Ito, A. Ohnishi, H. Ohsaki and M. Murakami, *Synthesis*, 1988, 714.

13 R. Usón, J. Forniés and P. Espinet, *J. Organomet. Chem.*, 1976, **116**, 353.

14 See, for example, structures reported in: *Comprehensive Organometallic Chemistry*, ed. G. Wilkinson, F. G. A. Stone and E. W. Abel, Pergamon Press, Oxford, 1982, vol 6, p. 471 and references therein; *Comprehensive Organometallic Chemistry II*, ed. E. W. Abel, G. Wilkinson and F. G. A. Stone, Pergamon Press, Oxford, 1995, vol 8, p. 431 and references therein.

15 $R(C)_{vdW}$ = 1.85 Å; $R(F)_{vdW}$ = 1.35 Å: J. Emsley, *The Elements*, Oxford University Press, Oxford, 2nd edn., 1991.

16 Ref. 15, p. 540 and references therein.

17 P. Espinet, *Gold Bull.*, 1999, **32**, 127.

Adduct removal from methanofullerenes *via* reductive electrochemistry

Marcel W. J. Beulen,[a] Luis Echegoyen,*[a] José A. Rivera,[b] M. Ángeles Herranz,[c] Ángel Martín-Domenech[c] and Nazario Martín*[c]

[a] *Department of Chemistry and Center for Supramolecular Science, University of Miami, Coral Gables, Florida 33124, USA*
[b] *Department of Chemistry, Pontifical Catholic University of Puerto Rico, Ponce, Puerto Rico 00731, USA*
[c] *Departamento de Química Orgánica, Facultad de Ciencias Químicas, Universidad Complutense, E-28040 Madrid, Spain. E-mail: nazmar@eucmax.sim.ucm.es*

Received (in Liverpool, UK) 18th February 2000, Accepted 17th April 2000
Published on the Web 15th May 2000

Electrochemical reduction of different spiromethanofullerenes leads to adduct removal, opening the way to new protecting–deprotecting groups in fullerene chemistry.

The Bingel reaction has been used as a synthetic tool for the addition of di(alkoxycarbonyl)methano bridges to fullerenes for several years.[1] The resulting Bingel adducts are relatively stable thermally[2] and under a variety of chemical environments. However, Diederich and Echegoyen recently reported the retro-Bingel reaction, an electrochemical reduction reaction which efficiently removes the cyclopropane ring adduct, resulting in the formation of the parent C_{60}.[3] This electrochemical reduction reaction has also been employed successfully on other fullerene systems.[4,5] Before the work reported here, to our knowledge the only fullerene adducts that were removable *via* electrochemical reduction were the Bingel adducts.

Fullerenes substituted with electron-donating and electron-accepting addends have been studied extensively, mainly within the context of developing optically and electronically active systems for potential applications.[6] Previously, Wudl and coworkers described the electrochemical properties of the methanofullerenes **1** and **2**, which bear quinone type addends (Fig. 1).[7] These compounds exhibit irreversible electrochemistry, presumably resulting from the cleavage of one of the cyclopropane bonds connecting the addend to C_{60} upon reduction.[8] These observations, coupled with those of the retro-Bingel reaction, motivated the work reported here, to observe the behavior of compounds **1**–**4** under controlled potential electrolysis (CPE) for potential adduct removal. Compound **3** is similar to the Bingel adduct owing to the presence of the two carbonyls α to the methano bridge carbon. **4** is structurally and electronically very different from the others, and was used mainly for comparison.

The synthesis of the spiromethanofullerenes **1** and **2** was carried out according to the method previously reported in the literature.[9] Compound **3** was synthesized in two steps from indan-1,3-dione which was transformed into 2-diazoindan-1,3-dione by reaction with tosyl azide under basic conditions. Further reaction of 2-diazoindan-1,3-dione with C_{60} in ODCB (*o*-dichlorobenzene) at 120 °C for 4 h afforded spiromethanofullerene **3**[10] in 33% yield (62% based on consumed C_{60}). Compound **3** showed the presence of the carbonyl groups as a single signal at δ 191.7 in the ^{13}C NMR spectrum, which shows the presence of 17 signals, suggesting a C_{2v} symmetry. Spiromethanofullerene **4** was obtained from diphenylcyclopropenone in two steps, by formation of the tosylhydrazone and further *in situ* generation of the intermediate diazo compound under basic conditions,[11] which reacted with C_{60} by heating in ODCB to lead to **4** in 20% yield (46% based on consumed C_{60}). Spiromethanofullerene **4** shows a characteristic signal in the FTIR spectrum at 1712 cm^{-1} due to the cyclopropene double bond.

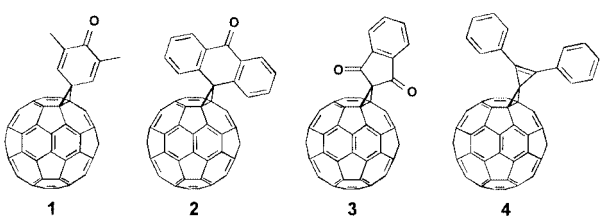

Fig. 1 Novel spiromethanofullerenes for reductive electrochemistry.

The electrochemistry of **1**–**4** in dichloromethane was studied by cyclic voltammetry (CV) and Osteryoung square wave voltammetry (OSWV) (Fig. 2 and Table 1).[12,13] The methanofullerenes **1** and **2** both exhibit, besides several reversible electrochemical processes, an irreversible electrochemical reduction wave between the first and third reductions. Compound **3** undergoes a two-electron reduction, followed by two one-

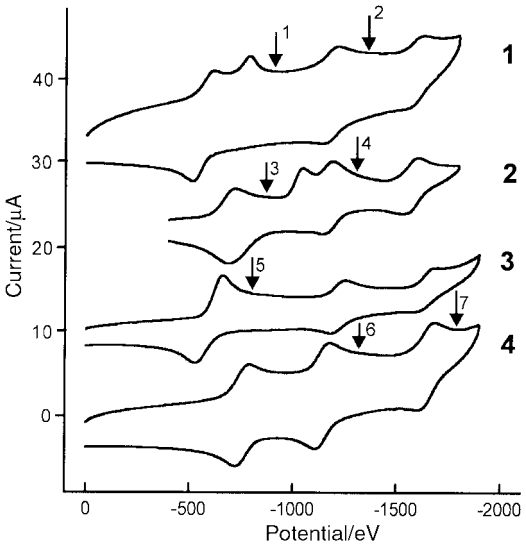

Fig. 2 Cyclic voltammograms of the methanofullerenes **1**–**4**.

Table 1 Redox potentials of **1**–**4** *vs.* ferrocene in dichloromethane[a]

	E_1/mV	E_2/mV	E_3/mV	E_4/mV
3	−859	−1119[b]	−1522	−1926
4	−1038	−1383[b]	−1492	−1893
5	−971[c]	−1598	−2015	
6	−1035	−1426	−1929	

[a] Electrochemical measurements were performed using a BAS 100W Electrochemical Analyzer (Bioanalytical system), GC working electrode, a Ag wire pseudo-reference electrode and a Pt-mesh counter electrode, NBu_4PF_6 was used as supporting electrolyte. [b] Electrochemically irreversible. [c] Two-electron process.

DOI: 10.1039/b001428l

electron reductions. By contrast, the reference methanofullerene **4**, which bears no electron accepting addends, has three reversible redox waves.

Typically 2–5 mg of each compound were subjected to CPE. CPE of **1** was performed at a potential *ca.* 100–150 mV more cathodic than the second, irreversible, reduction wave (Fig. 2, arrow 1). This electrolysis consumed *ca.* 3.9 electrons molecule^{-1} and induced clear changes in the CV and OSWV, indicating that a chemical reaction had taken place. Subsequent reoxidation at 0 V and purification of the product mixture by column chromatography (eluent toluene) yielded fullerene products in *ca.* 60% yield. Analysis of this mixture by HPLC, UV–VIS spectroscopy and MALDI-TOF spectrometry showed the complete disappearance of the starting material, but no C_{60} was isolated. Unfortunately, the structure of the products could not be assigned.[14]

CPE of methanofullerene **2** was initially performed after the first reduction wave in order to completely dissolve methanofullerene **2** in CH_2Cl_2 (arrow 3, Fig. 2; 1.0 electron molecule^{-1}). No changes in the CV or OSWV were observed after electrolysis. Subsequent electrolysis after the third reduction wave (arrow 4, Fig. 2) consumed *ca.* 3.7 electrons molecule^{-1}. At that point the cyclic voltammogram had completely changed. This voltammogram exhibited three reversible electrochemical waves. After reoxidation and purification, analysis of the reaction mixture by HPLC and UV–VIS clearly proved the formation of C_{60} in a 65% yield. Thus electrolysis leads to the clean and efficient removal of the spiroanthraquinone adduct.

Electrolysis of methanofullerene **3** was performed after the first, two-electron, reduction (arrow 5, Fig. 2; 2.3 electrons molecule^{-1}). CV and OSWV clearly showed that chemical processes accompanied the electrochemical reductions.

Reoxidation, purification and subsequent analysis showed the formation of the parent C_{60} in a 58% yield.[15]

CPE of methanofullerene **4** after the second reduction (arrow 6, Fig. 2) consumed 2.0 electrons molecule^{-1} and is fully reversible: no changes in the cyclic or OSWV voltammogram were observed. Electrolysis after the third reduction wave (arrow 7, Fig. 2; 7.3 electrons molecule^{-1}) leads to passivation of the working electrode and to the formation of insoluble and intractable products.

In conclusion, the electrochemical measurements described above show that for all 'quinone' type methanofullerenes **1**–**3**, a chemical reaction occurs after reduction. This reaction leads to the parent C_{60} for compounds **2** and **3**, in a 'retro-Bingel' like reaction. Thus the range of fullerene adducts that can be removed *via* electrochemical reduction is here extended beyond the Bingel adducts.

Financial support for this work from the National Science Foundation through grant CHE-9816503, the Netherlands Organization for Scientific Research (NWO, talent stipendium, M. B.) and the DGESIC of Spain (PB98-0818) is greatly appreciated. We also acknowledge the Fullbright Foundation (Project 99125) for financial support.

Notes and references

1 C. Bingel, *Chem. Ber.*, 1993, **126**, 1957.
2 For a hint that the Bingel-addend may be removed at very high temperatures, see: A. Hirsch, I. Lamparth, T. Grösser and H. R. Karfunkel, *J. Am. Chem. Soc.*, 1994, **116**, 9385.
3 R. Kessinger, J. Crassous, A. Herrmann, M. Rüttimann, L. Echegoyen and F. Diederich, *Angew. Chem., Int. Ed.*, 1998, **37**, 1919.
4 C. Boudon, J.-P. Gisselbrecht, M. Gross, A. Herrmann, M. Rüttimann, J. Crassous, F. Cardullo, L. Echegoyen and F. Diederich, *J. Am. Chem. Soc.*, 1998, **120**, 7860; J. Crassous, J. Rivera, N. S. Fender, L. Shu, L. Echegoyen, C. Thilgen, A. Herrmann and F. Diederich, *Angew. Chem., Int. Ed.*, 1999, **38**, 1613.
5 Another example of the electrochemical 'instability' of fullerenes is the conversion of the monoanion of 1,2-methano[60]fullerene-61,61-dinitrile to C_{60} under CV conditions: M. Keshavarz-K., B. Knight, R. C. Haddon and F. Wudl, *Tetrahedron*, 1996, **52**, 5149.
6 N. Martín, L. Sánchez, B. Illescas and I. Pérez, *Chem. Rev.*, 1998, **98**, 2527.
7 M. Eiermann, R. C. Haddon, B. Knight, Q. Chan Li, M. Maggini, N. Martín, T. Ohno, M. Prato, T. Suzuki and F. Wudl, *Angew. Chem., Int. Ed. Engl.*, 1995, **34**, 1591.
8 B. Knight, N. Martín, T. Ohno, E. Ortí, C. Rovira, J. Veciana, J. Vidal-Gancedo, P. Viruela, R. Viruela and F. Wudl, *J. Am. Chem. Soc.*, 1997, **109**, 9871.
9 T. Ohno, N. Martín, B. Knight, F. Wudl, T. Suzuki and H. Yu, *J. Org. Chem.*, 1996, **61**, 1306.
10 *Selected spectroscopic data* for **3**: FTIR (KBr) 1712, 1515, 1345, 1265, 1232, 739, 529 cm^{-1}; ^{1}H NMR ($CDCl_3$, 300 MHz) δ 8.22 (2H, m), 8.02 (2H, m); ^{13}C NMR [$CDCl_3$–CS_2 (1:1), 75 MHz] δ 191.7 (CO), 144.9, 144.8, 144.6, 144.4, 143.7, 143.4, 142.9, 142.0, 141.5, 141.4, 141.3, 140.8, 135.7, 123.2, 77.1, 76.3; UV–VIS (CH_2Cl_2) λ_{max}(log ε) 290 (4.70), 338 (4.64), 432 (3.34), 510 (3.12) nm; MS (FAB$^-$) *m/z*: 864 (M^+, 55), 720 (C_{60}, 80). **4**: FTIR (KBr) 1712, 1461, 1154, 761, 720, 702, 691, 546 cm^{-1}; ^{1}H NMR [$CDCl_3$–CS_2 (3:1), 300 MHz] δ 7.65–7.63 (4H, m, ArH), 7.45–7.41 (6H, m, ArH); UV–VIS (CH_2Cl_2) λ_{max}(log ε) 290 (4.73), 336 (4.58), 438 (3.70), 702 (3.03) nm.
11 J. C. Hummelen, B. W. Knight, F. Le Peq and F. Wudl, *J. Org. Chem.*, 1995, **60**, 532.
12 For a review on the electrochemistry of fullerenes see: L. Echegoyen and L. E. Echegoyen, *Acc. Chem. Res.*, 1998, **31**, 593.
13 M. Diekers, A. Hirsch, S. Pyo, J. Rivera and L. Echegoyen, *Eur. J. Org. Chem.*, 1998, 1111.
14 HPLC measurements indicated that the polarity of the products is in the range of that for the parent C_{60}, rather than around that of the starting methanofullerene **1**. UV–VIS spectroscopy measurements showed a broad band around 450 nm. Furthermore, the main peak in the MALDI-TOF mass-spectrum of the reaction mixture is at *m/z* 890. A separate electrolysis experiment performed after the third reduction potential of methanofullerene **1** (Fig. 2, arrow 2; 4.3 electrons molecule^{-1}), leads to a similar result: yield = 65%, main peak in the MALDI-TOF is at *m/z* 890.
15 Besides the retro-Bingel product C_{60}, 22% of starting material, methanofullerene **3** was also isolated.

Persistent carbenes containing acetylenes: 4,5-dialkynylimidazol-2-ylidene

Rüdiger Faust*[a] and Bernd Göbelt[bc]

[a] *Christopher-Ingold-Laboratories, Department of Chemistry, University College London, 20 Gordon Street, London, UK WC1H 0AJ. E-mail: r.faust@ucl.ac.uk*

[b] *Pharmazeutisch-Chemisches Institut, Ruprecht-Karls-Universität Heidelberg, Im Neuenheimer Feld 364, D-69120 Heidelberg, Germany*

[c] *Department of Chemistry, Carnegie Mellon University, 4400 Fifth Avenue, Pittsburgh, PA 15213, USA*

Received (in Liverpool, UK) 23rd February 2000, Accepted 20th April 2000
Published on the Web 15th May 2000

A nucleophilic imidazole carbene featuring acetylene substituents in the 4- and 5-positions is prepared in three steps from dialkynyl diimines and is characterised by low temperature NMR spectroscopy and trapping reactions with MeI, CS_2 and $HgCl_2$.

The remarkable renaissance of nucleophilic carbenes, triggered by the isolation of the first crystalline imidazol-2-ylidene by Arduengo *et al.*,[1] is witnessed by recent syntheses of a variety of derivatives of this class of compounds[2] and has culminated in the development of imidazol-2-ylidenes as versatile ligands in transition metal complexes for use in catalysis applications.[3] In the course of these investigations it emerged that the variation of the 4,5-imidazole substituents can have striking effects on the stability of the corresponding carbenes. For example, the notion that a CC double bond between these positions is a crucial prerequisite for the generation of isolable carbenes could not be maintained after the preparation of a stable imidazolidine carbene.[4] Furthermore, a 4,5-dichloroimidazol-2-ylidene proved to be the first heterocyclic carbene stable to the air,[5] and an analogous 4,5-bistrifluoromethyl derivative could even be subjected to bulb-to-bulb distillations.[6]

We were intrigued by the challenge to introduce seemingly carbene-incompatible alkynyl groups into the 4,5-positions of imidazol-2-ylidenes as in **1** (Fig. 1), and are driven by the prospect to use the acetylene substituents as delocalising linkages able to connect several carbene sites within one molecular framework (**2**). Monomolecular multi-carbene arrays like **2** are deemed to be of particular interest with respect to metal coordination and to the exploitation of synergistic metal cooperativity. We report here the synthesis of a 4,5-dialkynyl imidazol-2-ylidene as the first representative of this class of compounds.

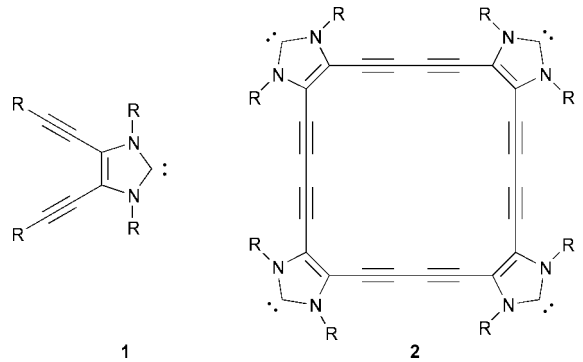

Fig. 1

We have recently reported two complementary pathways to dialkynyldiimines such as **3** (Scheme 1) from oxalyl chloride and bisimidoyl chlorides, respectively.[7,8] These building blocks were deemed to be convenient starting materials for the rapid assembly of the 4,5-diacetylenyl imidazole core, since ring closure to the corresponding imidazole-2-thiones can be

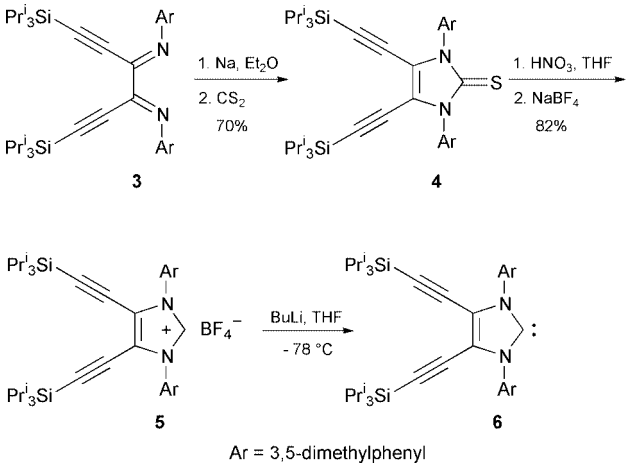

Scheme 1

effected by quenching diimine dianions with CS_2.[9] Imidazole-2-thiones in turn are precursors to Arduengo-type carbenes which can be obtained either directly by alkali metal reduction of the thiones[10] or *via* deprotonation of an intermediate imidazolium salt derived from them.[1] Hence, stirring **3** together with sodium in dry diethyl ether at room temperature furnished an initially deep blue solution which slowly turned orange-red to indicate the formation of the dianion of **3**. Treatment of this solution with CS_2 led to the imidazole-2-thione **4** in 70% yield. Attempts to isolate an acetylenic carbene directly from **4** by a potassium-mediated reductive desulfurisation were unsuccessful and led only to the decomposition of the starting material. We therefore prepared the dialkynyl imidazolium salt **5** by oxidative desulfurisation of **4** with dilute nitric acid in THF followed by anion exchange with sodium tetrafluoroborate. Gratifyingly, deprotonation of **5** could be effected with BuLi in THF at −78 °C and resulted in a yellow-coloured solution of 4,5-dialkynyl imidazol-2-ylidene **6**. Interestingly, carbene **6** could only be generated from **5** using BuLi or LDA in THF. With potassium *tert*-butanolate, sodium or potassium hydride in either THF or DMSO on the other hand, only decomposition products were observed even at temperatures as low as −100 °C.

The acetylenic carbene **6** was clearly identified in the low temperature ^{13}C NMR spectrum (90.56 MHz, THF with external D_2O-lock, −78 °C) featuring a diagnostic signal for the ylidene carbon at 214.3 ppm.[11] However, and in contrast to many non-acetylenic imidazol-2-ylidenes, we were unable to isolate **6** in neat or in crystalline form. THF solutions of **6** could be kept at −78 °C for several hours without change, but allowing the solutions to gradually warm to −40 °C led to brown, unidentified decomposition products. Apparently, a 4,5-diacetylene substitution appears to have a detrimental effect on the thermal stability of the imidazol-2-ylidene. While this finding is somewhat unexpected in light of the remarkable persistence of 4,5-dichloroimidazol-2-ylidene[5] and the elec-

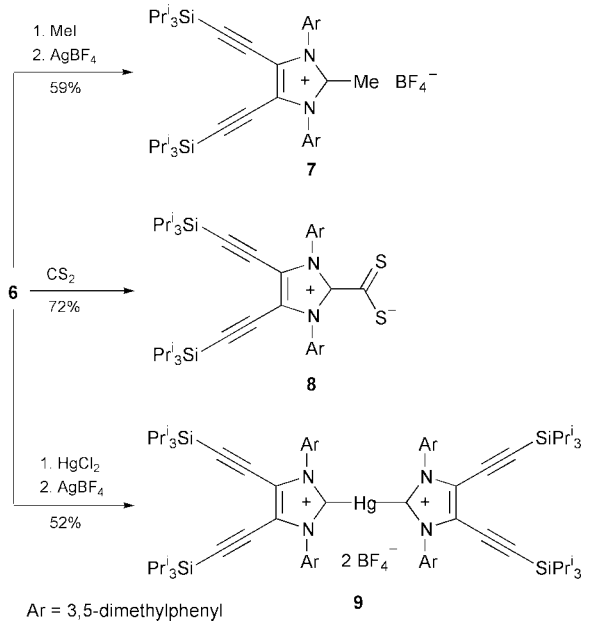

Scheme 2

tron-withdrawing properties of alkynyl substituents, it should be noted that nucleophilic carbenes are known to react with activated acetylenes[12] and that **6** therefore may be susceptible to intermolecular cycloaddition reactions.

The reactivity of **6** even at low temperature prompted us to further establish its identity by trapping reactions with various electrophiles (Scheme 2). Hence, treatment of a solution of **6** in THF with methyl iodide furnished, after anion exchange, the corresponding 2-methylimidazolium ion **7** in 58% yield. Similarly, the zwitterionic imidazolium dithiocarboxylate **8** could be obtained from the reaction of **6** with CS_2. Lastly, a further indirect proof of the intermediacy of carbene **6** was assembled by performing one of Wanzlick's original experiments,[13,14] namely the reaction of **6** with mercury dichloride. The reaction furnished, after anion exchange, the diimidazol-2-yl-mercurium salt **9** as a colourless solid. All adducts of **6** are fully characterised by spectroscopic data and elemental analyses. In addition, a qualitative X-ray diffraction study performed on crystals of **9** confirmed the presence of a bridging mercury atom between two imidazole ring structures. Unfortunately, severe disorder in the crystals caused by the anions and the floppy triisopropylsilyl groups prevented a refinement of the observed data below an *R*-value of 15%.

This work has demonstrated the feasibility of introducing alkynyl groups into the structural framework of nucleophilic carbenes and has therefore opened the way for the exploration of the metal coordination behaviour of these species and for the assembly of acetylene-linked, multinuclear metal-carbene complexes. Developments along those lines are currently underway.

We acknowledge the generous support from Professor Dr R. Neidlein, Pharmazeutisch-Chemisches Institut of the University of Heidelberg, Germany and from the Fonds der chemischen Industrie, Germany.

Notes and references

1 A. J. Arduengo, III, R. L. Harlow and M. Kline, *J. Am. Chem. Soc.*, 1991, **113**, 361.
2 D. Bourisson, O. Guerret, F. P. Gabbai and G. Bertrand, *Chem. Rev.*, 2000, **100**, 39.
3 T. Weskamp, W. C. Schattenmann, M. Spiegler and W. A. Herrmann, *Angew. Chem., Int. Ed.*, 1998, **37**, 2490.
4 A. J. Arduengo, III, J. R. Goehrlich and W. J. Marshall, *J. Am. Chem. Soc.*, 1995, **117**, 11 027.
5 A. J. Arduengo, III, F. Davidson, H. V. R. Dias, J. R. Goerlich, D. Khasnis, W. J. Marshall and T. K. Prakasha, *J. Am. Chem. Soc.*, 1997, **119**, 12 742.
6 A. J. Arduengo, III, *Acc. Chem. Res.*, 1999, **32**, 913.
7 R. Faust and B. Göbelt, *Tetrahedron Lett.*, 1997, **38**, 8017.
8 R. Faust, B. Göbelt and C. Weber, *Synlett*, 1998, 64.
9 M. Zettlitzer, H. tom Dieck, E. T. K. Haupt and L. Stamp, *Chem. Ber.*, 1986, **119**, 1868.
10 N. Kuhn and T. Kratz, *Synthesis*, 1993, 561.
11 A coordination of the carbene to lithium ions can not be ruled out. See: R. W. Alder, M. E. Blake, C. Bortolotti, C. Bufali, C. P. Butts, E. Linehan, J. M. Oliva, A. G. Orpen and M. J. Quayle, *Chem. Commun.*, 1999, 241.
12 D. Enders, K. Breuer, J. Runsink and J. H. Teles, *Liebigs Ann. Chem.*, 1996, 2019.
13 H.-J. Schönherr and H.-W. Wanzlick, *Liebigs Ann. Chem.*, 1970, **731**, 176.
14 For some recent developments pertaining to Wanzlick's original work see: Y. Liu and D. M. Lemal, *Tetrahedron Lett.*, 2000, **41**, 599.

A dinuclear iron(III) complex with a bridging urea anion: implications for the urease mechanism†

Sergey V. Kryatov,[a] Alexander Y. Nazarenko,[b] Paul D. Robinson[c] and Elena V. Rybak-Akimova*[a]

[a] *Department of Chemistry, Tufts University, Medford, Massachusetts 02155, USA. E-mail: erybakak@emerald.tufts.edu*
[b] *Department of Chemistry and Biochemistry, Southern Illinois University, Carbondale, Illinois 62901, USA*
[c] *Department of Geology, Southern Illinois University, Carbondale, Illinois 62901, USA*

Received (in Irvine, CA, USA) 5th January 2000, Accepted 18th April 2000

A novel complex $[Fe^{III}_2(\mu\text{-}O)\{\mu\text{-}OC(NH_2)NH\}(tpa)_2](ClO_4)_3$ [tpa = tris(2-pyridylmethyl)amine] has been synthesized and fully characterized; its formation from urea and the $[Fe^{III}_2(\mu\text{-}O)(tpa)_2(OH)(H_2O)]^{3+}$ precursor in aqueous acetonitrile is a reversible multistep process.

Dinuclear metallohydrolases have been recognized as a wide class of enzymes which utilize two metal cations (Zn, Mg, Mn, Fe, Co, Ni) for the activation of different organic substrates for hydrolysis.[1] Urease, which catalyses urea hydrolysis, is probably the best known enzyme in this class. Ureases isolated from various species of plants, fungi and bacteria have invariably contained two Ni^{II} ions in their active site.[1,2] However, relevant substrates such as ethylurethane can be hydrolyzed by enzymes utilizing other metals. A urethanase with four Fe^{III} ions per molecule has been reported.[3]

The mechanism of urease action remains under debate. Initially it was proposed that urea binds monodentately to one Ni^{II} ion and is attacked by a hydroxide which is attached to the second Ni^{II} ion.[1,2,4] A new proposal for the urease mechanism suggests that both urea and hydroxide initially form bidentate bridges between the Ni^{II} atoms.[5] Two model nickel compounds with bridging urea anions have been recently characterized.[6] Here, we report the first dinuclear iron complex with bridging ureate having distinct metal sites.

Our approach was based on the rich chemistry of diiron oxo-bridged complexes with tris(2-pyridylmethyl)amine (tpa).[7] The $[Fe^{III}_2(\mu\text{-}O)(tpa)_2(OH)(H_2O)]^{3+}$ precursor **1** reacts with various ligands HL to form $[Fe^{III}_2(\mu\text{-}O)(\mu\text{-}L)(tpa)_2]^{n+}$ complexes.[7c,d,8] Compound **1** can also activate acetonitrile for hydrolysis.[7c,d]

The complex $[Fe_2(\mu\text{-}O)\{\mu\text{-}OC(NH_2)NH\}(tpa)_2]^{3+}$ **2** can be prepared either from **1** and urea in MeCN solution or directly from $Fe(ClO_4)_3$, tpa, urea and Et_3N in MeOH.‡ The spectral characteristics of **2** obtained by either method are identical.† The UV–VIS and ^1H NMR spectra of **2** are similar to those of relevant acetamidate and acetate bridging complexes, $[Fe^{III}_2(\mu\text{-}O)\{\mu\text{-}OC(Me)NH\}(tpa)_2]^{3+}$ and $[Fe^{III}_2(\mu\text{-}O)(\mu\text{-}MeCO_2)(tpa)_2]^{3+}$.[7] A detailed mass spectrometric study allowed the unambiguous assignment of **2** as a ureate complex. The peak with *m/z* 965 {corresponding to $[\mathbf{2}(ClO_4)_2]^+$} is the most prominent in both the $ESMS^+$ and FAB^+ spectra. The peak is shifted to *m/z* 967 in the spectra of the sample of $\mathbf{2}(ClO_4)_3$ prepared from urea-$^{15}N_2$. Satellite peak intensities and exact mass determinations confirm the compositions of the *m/z* 965 and 967 ions as $[\mathbf{2}(ClO_4)_2]^+$ and $[(\mathbf{2}\text{-}^{15}N_2)(ClO_4)_2]^+$, respectively.

Two different solvated complexes, $\mathbf{2}(ClO_4)_3\cdot 2H_2O$ and $\mathbf{2}(ClO_4)_3\cdot 0.75CO(NH_2)_2\cdot 0.25H_2O$, were crystallized and characterized by X-ray diffraction. The molecular dimensions of the complex dinuclear cation **2** in both are very similar (Fig. 1). Bond distances and angles in the asymmetric (tpa)Fe–O–Fe(tpa) unit of **2** are close to those in the relevant carboxylate bridged $[Fe_2(\mu\text{-}O)(\mu\text{-}RCO_2)(tpa)_2]^{3+}$ complexes [α(Fe–O–Fe) = 130(1)°],[7] which is in agreement with the isoelectronic nature and similar sizes of the delocalized carboxylate ($-CO_2^-$) and amidate groups ($-CONH^-$). The structural parameters of the planar ureate anion in **2** [*d*(C–O) = 1.238(12), *d*(C–NH) = 1.311(13), *d*(C–NH_2) = 1.439(15) Å] are close to those found in the $[Ni^{II}_4\{\mu_3\text{-}OC(NH)NH_2\}(L)_2]^{4+}$ complex [*d*(C–O) = 1.254, *d*(C–NH) = 1.311, *d*(C–NH_2) = 1.427 Å][6b] and those calculated by an *ab initio* method for $OC(NH_2)NH^-$ [*d*(C–O) = 1.260, *d*(C–NH) = 1.324, *d*(C–NH_2) = 1.488 Å].[9] The bent (tpa)Fe–O–Fe(tpa) core has two non-equivalent vacant positions at the potentially hexacoordinate Fe^{III} atoms, one with a tertiary aliphatic N atom and the other with a pyridine N atom as *trans* donors. The ureate anion in **2** coordinates with its oxygen atom *trans* to the pyridine N atom, which apparently allows for a stronger π-interaction along the O_{ureate}–Fe–N_{pyr} axis *versus* the possible N_{ureate}–Fe–N_{pyr} alignment.[10]

The equilibrium and kinetics of formation of **2** from the precursor **1** and urea were studied in aqueous acetonitrile (0.05–1.3 M H_2O) at 25 °C. In the presence of excess urea, **2** is stable in these solutions for weeks.

Spectrophotometric titrations gave the equilibrium constant $K = 650 \pm 100$ M for reaction (1) confirming the release of two molecules of water.

$$\mathbf{1} + CO(NH_2)_2 \rightleftarrows \mathbf{2} + 2H_2O \qquad (1)$$

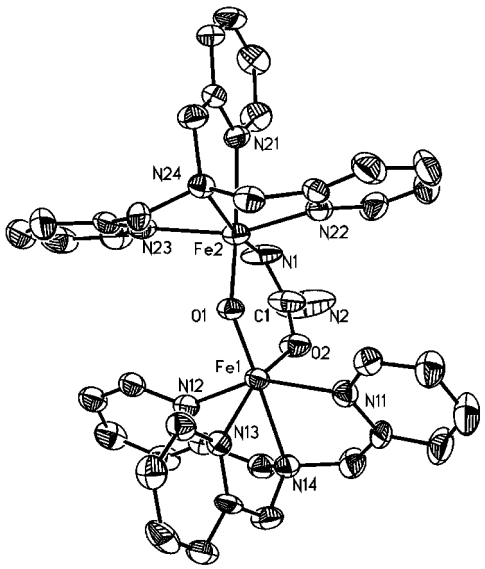

Fig. 1 Molecular structure of the complex cation in $\mathbf{2}(ClO_4)_3\cdot 0.75CO(NH_2)_2\cdot 0.25H_2O$. Selected distances (Å) and angles (°): Fe1–O1 1.791(5), Fe1–O2 2.001(6), Fe2–O1 1.812(5), Fe2–N1 1.984(8); Fe1–O1–Fe2 129.9(3), O2–C1–N1 125.1(11), O2–C1–N2 115.2(11), N1–C1–N2 119.7(11).

† Electronic supplementary information (ESI) available: selected data for **2** kinetic data and rotatable 3-D crystal structure diagram in CHIME format. See http://www.rsc.org/suppdata/cc/b0/b000286k/

DOI: 10.1039/b000286k

The kinetics of reaction (1) were studied by a stopped-flow technique under concentration conditions, which made the formation of **2** almost irreversible (yield > 96%). The excess of urea (8–60 fold) and water (> 100 fold) also provided pseudo-first order conditions. Two distinct steps are observed in reaction (1). In the first step, there is a nearly instantaneous (within the mixing time of the stopped-flow instrument, 1–2 ms) change in the optical spectrum when the solutions of **1** and urea are mixed. The dependence of this initial absorbance change on $[H_2O]$ and $[CO(NH_2)_2]$ corresponds to the formation of intermediate **1a** in a preequilibrium with $K_1 = 9 \pm 3$ (Scheme 1). It has been shown that the O-bonded urea is usually the first kinetic product of complex formation.[11] Thus, **1a** is most likely the $[Fe_2(\mu\text{-}O)(tpa)_2(OH)\{\eta_1\text{-}OC(NH_2)_2\}]^{3+}$ complex.

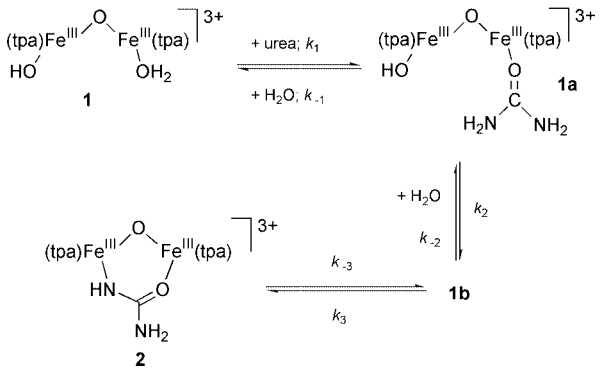

Scheme 1

The following step is observed as a nearly single exponential change of optical absorbance with the rate constant k_{obs} (0.1–1.8 s^{-1} under our experimental conditions) and corresponds to the formation of **2** from the preequilibrium mixture of **1** and **1a**. The process is accelerated by urea and decelerated by water. The simplest model that can account for the concentration dependences is shown in Scheme 1 and eqn. (2) (see also ESI).†

$$k_{obs} = \frac{k_2(k_3/k_{-2})}{(k_3/k_{-2})+[H_2O]} \cdot \frac{K_1[CO(NH_2)_2]}{K_1[CO(NH_2)_2]+[H_2O]} \qquad (2)$$

Optimization of this model by non-linear least squares methods gave the parameters $K_1 = k_1/k_{-1} = 8.9$, $k_2 = 2.6\ s^{-1}$ and $k_3/k_{-2} = 0.185$ M. Combination of the kinetic data with the equilibrium constant $K = 650$ M for the overall process (1) gave $k_{-3} = 6.6 \times 10^{-3}\ s^{-1}$ (Scheme 1).

The results of this study help us to understand the potential advantages and drawbacks of the new bidentate mechanism of urease activity[5] when compared to the previously accepted monodentate mechanism.[2,4] It is believed that the hydrolytic stability of the urea molecule is due to high resonance stabilization energy, which may be reduced on coordination to metal ion(s).[2,12] Bidentate N,O-coordination of urea leads to partial loss of resonance as witnessed by a significant elongation of the C–NH_2 bond in the μ-$OC(NH_2)NH^-$ ligand of **2** [d(C–NH_2) = 1.44 Å] *versus* uncoordinated urea [d(C–NH_2) = 1.34 Å].[13] In the neutral μ-$OC(NH_2)NH_2$ ligand both C–NH_2 bonds are elongated [$d(C–NH_2)_{endo}$ = 1.42, $d(C–NH_2)_{exo}$ = 1.37 Å] as was found in a Co^{II} complex.[14] In contrast, monodentate coordination of urea (typically *via* the O atom) is known to preserve its metric parameters [d(C–NH_2) = 1.34(1) Å].[15] Thus, the loss of resonance stabilization on bidentate N,O-coordination might be a key factor in urea activation by two metal ions in urease.

The protonation state of the bridging urea ligand is another important issue which was overlooked in the bidentate mechanism of urease action.[5] In the monodentate mechanism it did not arise,[2,4] because monodentate O-coordinated urea in model complexes has almost the same high pK_a as the free ligand (13 *cf.* 13.5).[16] However, N-coordination (which can be achieved in kinetically inert model complexes) is known to change the acidity of urea protons dramatically, down to pK_a = 3(1) in aqueous solution.[16] Quantitative formation of ureate complex **2** in the Et_3N/Et_3NH^+ buffer in MeOH confirms the enhanced acidity of urea on bidentate N,O-coordination. Because of the lower polarizing power of the Ni^{II} ions, a μ-$OC(NH_2)NH_2$ ligand coordinated to them will probably be less acidic than that coordinated to Fe^{III}. However, formation of a bridging urea anion still should be considered in urease under its optimal pH 4–8.[4] Relatively slow formation of the bidentate ureate and its hydrolytic stability as seen in complex **2** suggest that μ-$OC(NH_2)NH^-$ is unlikely to be the actual activated form of urea in the enzyme. An alternative possibility is that urease modulates the pK_a of the μ-$OC(NH_2)NH_2$ ligand to avoid its premature deprotonation.

Notes and references

‡ Precursor **1**$(ClO_4)_3$ was prepared by a published procedure.[7d]

Synthesis of **2**: urea (0.03 g, 0.5 mmol), tpa (0.29 g, 1 mmol) and Et_3N (0.152 g, 1.5 mmol) were dissolved in 40 ml of MeOH and added to a solution of $Fe(ClO_4)_3{\cdot}9H_2O$ (0.516 g, 1 mmol) in 10 ml of MeOH. Compound **2**$(ClO_4)_3{\cdot}H_2O$ crystallized as a brown solid from the resulting yellow solution on standing overnight in a refrigerator. Elemental analysis: calc. for $C_{37}H_{43}Cl_3Fe_2N_{10}O_{16}$: C, 40.33; H, 3.93; N, 12.71; Fe, 10.14. Found: C, 40.27; H, 3.55; N, 12.46; Fe, 10.37%. Single crystals of **2**$(ClO_4)_3{\cdot}2H_2O$ formed on recrystallization from MeCN. When the recrystallization was carried out in the presence of an added excess of urea, single crystals of **2**$(ClO_4)_3{\cdot}0.75CO(NH_2)_2{\cdot}0.25H_2O$ were obtained.

Crystal data for **2** $(ClO_4)_3{\cdot}2H_2O$: $C_{37}H_{43}Cl_3Fe_2N_{10}O_{16}$, M_w = 1101.86, monoclinic, space group $P2_1/c$, a = 12.178(3), b = 10.329(5), c = 39.179(10) Å, β = 94.65(2)°, V = 4912(3) Å^3, Z = 4, μ(Mo-Kα) = 0.829, T = 293(2) K, 5489 reflections measured, $R1[I > 2\sigma(I)]$ = 0.070, $wR2$ = 0.28 for all reflections. For **2**$(ClO_4)_3{\cdot}0.75CO(NH_2)_2{\cdot}0.25H_2O$: $C_{37.5}H_{42.5}Cl_3Fe_2N_{11.5}O_{15}$, M_w = 1115.38, monoclinic space group $P2_1/c$, a = 12.1610(15), b = 10.4451(17), c = 38.758(10) Å, β = 97.137(16)°, V = 4885.1(16) Å^3, Z = 4, μ(Mo-Kα) = 0.834, T = 293(2) K, 6383 reflections measured, $R1[I > 2\sigma(I)]$ = 0.067, $wR2$ = 0.206 for all reflections. CCDC 182/1607. See http://www.rsc.org/suppdata/cc/b0/b000286k/ for crystallographic files in .cif format.

1 D. E. Wilcox, *Chem. Rev.*, 1996, **96**, 2435; N. Sträter, W. N. Lipscomb, T. Klabunde and B. Krebs, *Angew. Chem., Int. Ed. Engl.*, 1996, **35**, 2024.
2 P. A. Karplus, M. A. Pearson and R. P. Hausinger, *Acc. Chem. Res.*, 1997, **30**, 330.
3 C.-J. Zhao and K. Kobashi, *Biol. Pharm. Bull.*, 1994, **17**, 773.
4 N. E. Dixon, P. W. Riddles, C. Gazzola, R. L. Blakely and B. Zerner, *Can. J. Biochem.*, 1980, **58**, 1335.
5 S. Benini, W. R. Rypniewski, K. S. Wilson, S. Miletti, S. Ciurli and S. Mangani, *Structure*, 1999, **7**, 205; S. Ciurli, S. Benini, W. R. Rypniewski, K. S. Wilson, S. Miletti and S. Mangani, *Coord. Chem. Rev.*, 1999, **190**–**192**, 331.
6 (*a*) F. Meyer and H. Pritzkow, *Chem. Commun.*, 1998, 1555; (*b*) F. Meyer, M. Konrad and E. Kaifer, *Eur. J. Inorg. Chem.*, 1999, 1851.
7 (*a*) R. E. Norman, S. Yan, L. Que, Jr., G. Backes, J. Ling, J. Sanders-Loehr, J. H. Zhang and C. J. O'Connor, *J. Am. Chem. Soc.*, 1990, **112**, 1554; (*b*) R. E. Norman, R. C. Holz, S. Ménage, C. J. O'Connor, J. H. Zhang and L. Que, Jr., *Inorg. Chem.*, 1990, **29**, 4629; (*c*) E. C. Wilkinson, Y. Dong and L. Que, Jr., *J. Am. Chem. Soc.*, 1994, **116**, 8394; (*d*) A. Hazell, K. B. Jensen, C. J. McKenzie and H. Toftlund, *Inorg. Chem.*, 1994, **33**, 3127.
8 S. V. Kryatov and E. V. Rybak-Akimova, *J. Chem. Soc., Dalton. Trans.*, 1999, 3335.
9 S. Ma, F. Wang and R. G. Cooks, *J. Mass. Spectrom.*, 1998, **33**, 943.
10 H. Sigel, *Inorg. Chem.*, 1980, **19**, 1411.
11 A. A. Watson and D. P. Fairlie, *Inorg. Chem.*, 1995, **34**, 3087; N. V. Kaminskaia and N. M. Kostić, *Inorg. Chem.*, 1997, **36**, 5917.
12 P. Maslak, J. J. Sczepanski and M. Parvez, *J. Am. Chem. Soc.*, 1991, **113**, 1062.
13 T. Theophanides and P. D. Harvey, *Coord. Chem. Rev.*, 1987, **76**, 237.
14 P. S. Gentile, J. White and S. Haddad, *Inorg. Chim. Acta*, 1974, **8**, 97.
15 M. Konrad, F. Meyer, A. Jacobi,, P. Kircher, P. Rutsch and L. Zsolnai, *Inorg. Chem.*, 1999, **38**, 4559 and references thererin.
16 T. C. Woon, W. A. Wickramasinghe and D. P. Fairlie, *Inorg. Chem.*, 1993, **32**, 2190.

A heptacyclic polyprenoid hydrocarbon in sediments: a clue to unprecedented biological lipids†

Emmanuelle Grosjean,[a] Jacques Poinsot,[a] Armelle Charrié-Duhaut,[a] Stéphanie Tabuteau,[a] Pierre Adam,[a] Jean Trendel,[a] Philippe Schaeffer,[a] Jacques Connan,[b] Daniel Dessort[b] and Pierre Albrecht*[a]

[a] *Institut de Chimie, UMR 7509 du CNRS, Université Louis Pasteur, 1 rue Blaise Pascal, Strasbourg, 67000 France. E-mail: albrecht@chimie.u-strasbg.fr*

[b] *Centre de Recherche, Elf Exploration-Production, Avenue Larribau, 64000 Pau, France*

Received (in Liverpool, UK) 2nd March 2000, Accepted 17th April 2000
Published on the Web 15th May 2000

A novel heptacyclic C_{37} alkane presenting a regular polyprenoid structure has been isolated from a biodegraded bituminous rock and identified by NMR; this hydrocarbon is the most highly cyclized polyprenoid alkane ever completely identified; the absence of specific methyl groups give clues to unprecedented biological precursor lipids resulting from the extensive cyclization of regular octaprenoids.

Polycyclic hydrocarbons of high molecular weight (> C_{30}) with a regular polyprenic skeleton identified in sediments and petroleum were for a long time restricted to tricyclopolyprenanes.[1] Recently, the structures and the occurrence of highly cyclized compounds based on regular polyprenoid skeletons could be established in various sediments; they were essentially identified as monoaromatic hydrocarbons[2,3] and sulfides.[4] Their regular polyprenoid structure strongly suggests that the biological precursors from which these molecular fossils originate, most likely derive from proton-induced enzymatic cyclization of all-*trans* regular isoprenoids. Biological precursors have not been observed until now in living organisms and so these molecular fossils would appear to belong to a new class of biolipids whose origin and function remain unclear. More recently, investigation of the saturated hydrocarbon fraction of sediments from various origins revealed the occurrence of new sedimentary polycyclic alkanes (four to seven rings) which were suggested to have a complete regular polyprenoid structure according to mass spectral data.[2,5] We report here on the first unambiguous identification of a heptacyclic alkane **1**, which is related to this new series of saturated hydrocarbons.

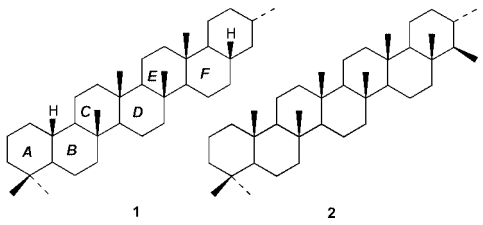

1 **2**

The studied sample was collected from a quarry (Maestu, Spain) which consisted of a calcareous reservoir rock of Campanian age impregnated by a heavy, partially biodegraded, petroleum.[5a] The crushed rock sample was extensively extracted with $CHCl_3$–CH_3OH (1/1, v:v) and the resulting extract chromatographed (SiO_2 / hexane) yielding the saturated hydrocarbon fraction. The major part of the low molecular weight constituents of the alkane fraction was removed by precipitating successively the heavy saturated hydrocarbons, including the polycyclic polyprenoid hydrocarbons, with acetone. Consecutive reverse-phase HPLC fractionation performed on the precipitated fraction led to the isolation of *ca.* 1 mg of the heptacyclic compound **1** with a purity of 91% (GC).

The EIMS spectrum of product **1**‡ exhibits a molecular ion at *m/z* 506 corresponding to the formula $C_{37}H_{62}$. Two characteristic fragmentation patterns composed of two sets of major fragments regularly shifted by 68 Da (one isoprene unit) were observed (*m/z* 177, 245, 313 and *m/z* 135, 203, 271) and were consistent with a polycyclic polyterpenoid structure.

1D- and 2D-NMR studies including homonuclear (^{1}H–^{1}H, COSY and NOESY) and heteronuclear (^{1}H–^{13}C, HMQC and HMBC) correlation experiments allowed us to assign the signals of all the protons and all the carbon atoms (ESI)† and to establish unequivocally the structure of the isolated compound.

The ^{13}C NMR spectrum of **1** shows 37 resonances, resolved into 7 methyl, 16 methylene, 9 methine and 5 quaternary carbon signals (as deduced from DEPT spectra and ^{1}H–^{13}C correlation experiments). The ^{1}H NMR spectrum also reveals 7 methyl signals, including 6 singlets and one doublet. A part of the carbon skeleton [Fig. 1(b)] could be established using ^{1}H–^{13}C long-range ($^{2,3}J$) couplings, the most intense of which are observed from the methyl groups. Two of the methyls exhibit remote connections ($^{2,3}J$) to each other as well as to the same quaternary, methine and methylene carbons, which implies that they must be geminal. The sector formed by these geminal methyl groups (*i.e.* atoms 26, 30, 32 and 32′) appears to be isolated from the rest of the molecule. Indeed, C-26 does not show remote connections with any remaining methyl groups, thus suggesting the absence of the Me-28′ at C-27. The nuclear Overhauser effects (NOE) observed between H-27 and protons of both 32′- and 24′-methyl groups [Fig. 1(a)] confirm the presence of a hydrogen atom at C-27 instead of a methyl group.

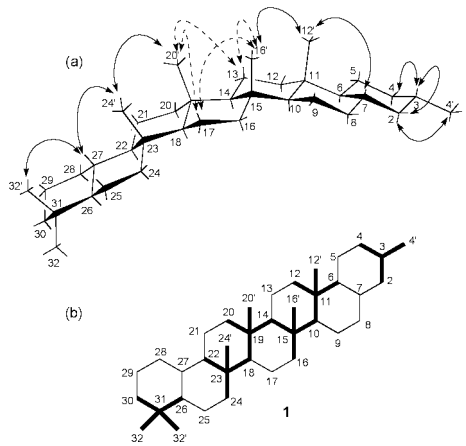

Fig. 1 (a) Spatial representation of **1** showing the most important NOEs observed. (b) Carbon sequence (bold) established from inverse long-range ^{1}H–^{13}C correlation experiment. Numbering is based on that of an acyclic octaprenol. The absolute configuration of compound **1** is not known and has been chosen arbitrarily.

† Electronic supplementary information (ESI) available: ^{13}C and ^{1}H NMR data for hydrocarbon **1**. See http://www.rsc.org.suppdata/cc/b0/b001804j/

The central part of the molecule is constituted by the 12′, 16′, 20′ and 24′ methyl groups which are linked two by two to each other through one remote connection (^3J) with a methine (C-10, C-14 and C-18).

The remote connections of the last methyl group 4′ with the methylene (C-2 and C-4) and the methine (C-3) carbons confirm the position of substitution for this ring. This sequence Me-4′, C-2, C-3, C-4 also forms an isolated sector as demonstrated by the ^{1}H–^{13}C long-distance correlation experiment. However, linkage of this sector to the main structure, as well as final assignment of all remaining ^{1}H and ^{13}C chemical shifts was made possible through the COSY and NOESY experiments. Thus, the NOE observed between the proton H-7 and the protons of the 12′-methyl group demonstrates the lack of a methyl group (replaced by a H atom) on the ring junction at C-7. The ^{1}H–^{1}H COSY connectivities between H-7 and the protons of the methylene carbon C-2 confirm the sequence Me-4′, C-2, C-3, C-4 on the skeleton.

Stereochemical assignments can be made from the NOESY data: the NOEs observed between Me-32′/H-27, H-27/Me-24′, Me-24′/Me-20′, Me-16′/Me-12′, Me-12′/H-7 afford evidence that Me-32′, H-27, Me-24′, Me-20′ on one hand and Me-16′, Me-12′, H-7 on the other hand are on the same side of the molecule. Moreover, as no correlation between protons 7, 12′, 16′, 20′, 24′, 27 and protons 6, 10, 14, 18, 22, 26 could be detected on the NOESY spectrum, all the ring junctions are likely to be *trans* along the whole structure. As a result of all the NOEs reported in Fig. 1(a), both sectors comprising, respectively, Me-32′, H-27, Me-24′, Me-20′ and Me-16′, Me-12′, H-7, H-3 present *trans–transoid–trans* stereochemistries. Unfortunately, the determination of the global relative stereochemistry is hindered by the superposition of ^{1}H and ^{13}C chemical shifts of Me-16′ and Me-20′, as well as those of methylene groups C-13 and C-17. Thus, NOEs are indeed observed between the group of overlapping axial protons from methylene groups C-13 and/or C-17 and the overlapping methyl groups C-20′/C-16′ [indicated by dashed arrows on Fig. 1(a)] but individual interactions cannot be distinguished. This feature is not surprising in the case of highly symmetrical polycyclized regular polyprenoids since methyls 16′ and 20′, as well as methylenes 13 and 17, located in the 'middle' of the structure (*i.e.* far from demethylated positions which induce dissymmetry) have almost identical environments. The uncertainty concerning the global relative stereochemistry which arose from the interpretation of the NOESY spectrum could, however, be cleared by interpreting the chemical shift values. A *trans–transoid–trans* stereochemistry along the whole structure of compound **1** is indeed strongly supported by the underscoring of γ-*gauche* effects reflected by the chemical shifts of ^{1}H and ^{13}C proton and carbon signals.[6] In particular, the resonances of axial methylene protons Hβ-13 and Hβ-17 appear at high field (δ_H 1.35) and those of their related carbons at very low field (δ_C 17.4). This is concordant with triple γ-*gauche* interactions with the methyl groups. Furthermore, the strong deshielding of the methine carbon C-14 (δ_C 61.7), as well as the shielding of the corresponding proton (δ_H 0.73) can be taken as firm evidence for an absence of γ-*gauche* effects and thereby confirm the global relative stereochemistry with all the ring-junction axial methyl groups on the same side of the molecule. An equatorial position can reasonably be envisaged for methyl 4′ given the NOE between protons of Me-4′ and the axial proton located on C-2 and those between H-3 and H-4β, H-3 and H-2β.

From its structure, it appears that the new hydrocarbon **1**, which represents the most highly cyclized polyprenoid alkane ever identified, is likely to result from the diagenetic transformation of polycyclic polyprenoid precursors formed by proton induced cyclization of regular all-*trans* octaprenoids.[2] Indeed, the isolated compound definitely corresponds to a demethylated counterpart of a complete polycyclic octaprenoid hydrocarbon such as **2**. Until now, only one example of a polycyclic biological lipid **3** with more than four rings has been

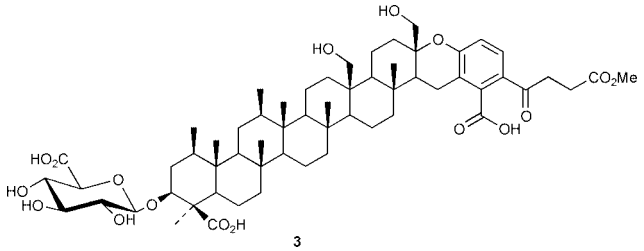

3

identified in a living organism (bacterium *Streptomyces argenteolus*).[7] This bacterium can probably not account solely for the large sedimentary record of highly cyclized polyprenoid structures.[2,4,5] Therefore, the biological organisms able to biosynthesize the precursors of **1** still remain to be discovered. A wider survey of the occurrence of these new polyprenoid hydrocarbons in sediments could eventually pin-point the type of actual natural environments likely to contain their source-organism(s) and orient further research for their discovery.

Some structural features of the unknown biological precursors can, however, already be inferred from the structure of the molecular fossil **1**. Thus, the absence of three methyl groups compared to a complete octaprenoid hydrocarbon suggests either that these methyl groups were absent within the biological precursor or, that these positions were functionalized (*e.g.* **3**) and susceptible to various diagenetic processes (*e.g.* by decarboxylation). It can, however, not be excluded, that functionalization of methyl groups on the precursor polyprenoid was induced by microbial oxidation processes occurring at the earliest stages of diagenesis.[8]

We thank the Centre National de la Recherche Scientifique and Elf Exploration Production for doctoral fellowships (A. C.-D., and E. G.) and financial support; the ECODEV-CNRS program for financial support; E. Mastio-Motsch and P. Wehrung, Université Louis Pasteur, Strasbourg, for mass spectral analysis; R. Graff, Université Louis Pasteur, Strasbourg, for NMR measurements.

Notes and references

‡ *MS data* (Finnigan MAT TSQ 700) EI (70 eV), *m/z* (rel. int.) for **1**: 506([M$^+$] $C_{37}H_{62}$, 59%), 491(14), 313(36), 271(7), 259(3), 245(36), 231(15), 217(4), 203(100), 190(8), 177(16), 163(22), 149(23), 135(33), 121(32), 109(57), 95(71), 81(59), 69(31), 55(28).

1 D. Heissler, R. Ocampo, P. Albrecht, J. J. Riehl and G. Ourisson, *J. Chem. Soc., Chem. Commun.*, 1984, 496; B. R. T. Simoneit, R. N. Leif, F. R. Aquino Neto, D. A. Azevedo, A. C. Pinto and P. Albrecht, *Naturwissenschaften*, 1990, **77**, 380; S. M. B. De Grande, F. R. Aquino Neto and M. R. Mello, *Org. Geochem.*, 1993, **20**, 1039.

2 P. Schaeffer, J. Poinsot, V. Hauke, P. Adam, P. Wehrung, J.M. Trendel, P. Albrecht, D. Dessort and J. Connan, *Angew. Chem., Int. Ed. Engl.*, 1994, **33**, 1166.

3 E. J. Corey, G. J. Luo and L. U. S. Z. Lin, *Angew. Chem., Int. Ed.* , 1998, **37**, 1126.

4 J. Poinsot, P. Schneckenburger, P. Adam, P. Schaeffer, J. M. Trendel, A. Riva and P. Albrecht, *Chem. Commun.*, 1997, 2191; J. Poinsot, P. Schneckenburger, P. Adam, P. Schaeffer, J. M. Trendel, A. Riva and P. Albrecht, *Geochim. Cosmochim. Acta*, 1998, **62**, 805.

5 (*a*) C. Dorronsoro, M. R. Garcia and J. O. Grimalt, *Fuel*, 1994, **73**, 83; (*b*) C. L. Riediger, P. W. Brooks, M. G. Fowler and L. R. Snowdon, in *Organic Geochemistry*, ed. K. Øygard, Falch Hurtigtrykk, Kalbakken, 1993, p. 302; (*c*) M. Li , C. L. Riediger, M. G. Fowler, L. R. Snowdon and T. A. Abrajano Jr, *Org. Geochem.*, 1996, **25**, 199.

6 H. Beierbeck, J. K. Saunders and J. W. ApSimon, *Can. J. Chem.*, 1977, **55**, 2813; P. E. Hammann, H. Kluge and G. G. Habermehl, *Magn. Reson. Chem.*, 1991, **29**, 133; R. J. Abraham, M. Edgar, L. Griffith and R. L. Powell, *J. Chem. Soc., Chem. Commun.*, 1993, 1544.

7 Y. Saitoh, Y. Ikuina, T. Yasuzama, S. Kakita, S. Nakanishi, M. Yoshida and H. Sano, *Tennen Yuki Kagobutsu Toronkai Koen Yoshishu, 33rd*, 1991, p. 707. A symposium report.

8 J. M. Trendel, R. Graff, P. Albrecht and A. Riva, *Tetrahedron Lett.*, 1991, **32**, 2959.

The synthesis of kermesic acid by acetylation-aided tautomerism of 6-chloro-2,5,8-trihydroxynaphtho-1,4-quinone

Steve J. Bingham and John H. P. Tyman*

Department of Chemistry, Brunel University, Uxbridge, Middlesex, UK UB8 3PH. E-mail: john.tyman@brunel.ac.uk
Laboratories of European Colour plc, Nathan Way, London, UK SE18

Received (in Cambridge, UK) 14th March 2000, Accepted 20th April 2000

6-Chloro-2,5,8-trihydroxynaphtho-1,4-quinone does not undergo cycloaddition reactions but the 1,2-diacetate, 2-chloro-5,6-diacetoxy-8-hydroxynaphtho-1,4-quinone, formed by acetylation-aided tautomerism added (*E*)- and (*Z*)-3-alkoxycarbonyl-2,4-bis(trimethylsiyloxy)penta-1,3-diene to afford kermesic acid after hydrolysis.

Kermesic acid **1a**, the red colourant component of kermes, a dyestuff of great antiquity and probably the earliest of which

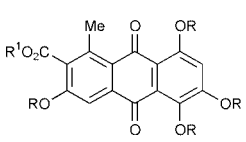

1a R = R^1 = H
b R = H; R^1 = Me
c R = R^1 = Me

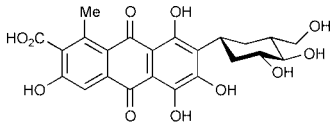

2

there is a record,[1] is also the aglycone of carminic acid[2] **2**, the colourant principle of cochineal.

Although carminic acid historically, through its brilliant range of red hues, superseded kermesic acid, dyeing with kermes is still active.[3] Nevertheless, the natural source of kermesic acid, for example from the wingless insect *Kermes illicis* which infects the kermes oak, is not abundant, and it was of interest to devise a synthetic approach that could provide an intermediate from which, by different strategies, either kermesic or carminic acid could be obtained. It was desirable to avoid penultimate tricyclic intermediates having an halogeno group requiring difficult hydrolysis[4,5] to the required hydroxy group and in another method[6] the simultaneous formation of isokermesic acid. Therefore, effort was focused on the preparation of 2-halogeno-5,6,8-trihydroxynaphtho-1,4-quinone **3**,

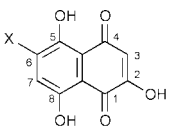

3 (form 1)

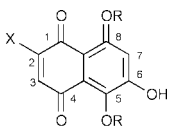

3 (form 2)

(form 2) which, as with naphthazarins generally, could be expected to exist as the 6-halogeno-2,5,8-trihydroxynaphtho-1,4-quinone tautomer **3** (form 1) where the halogeno atom is required to aid subsequent cycloaddition.

The starting point of the synthesis (Scheme 1) was 3-bromo-2-hydroxy-5-methoxyacetophenone[7] **4** (X = Br), and its chloro-analogue **4** (X = Cl), prepared in 80% yield by selective chlorination of 2-hydroxy-5-methoxyacetophenone with *N*-chlorosuccinimide (NCS) in acetic acid containing $Mg(OAc)_2$. Methylation of **4** with DMS in acetone containing K_2CO_3 afforded **5** (X = Br) 82% and **5** (X = Cl) 81%. Reaction of each with dimethyl carbonate in methanolic sodium methoxide gave the β-ketoesters **6** (X = Br, Cl), both in quantitative yield which by treatment with oxalyl chloride in nitromethane containing anhydrous aluminium chloride, a process used to prepare

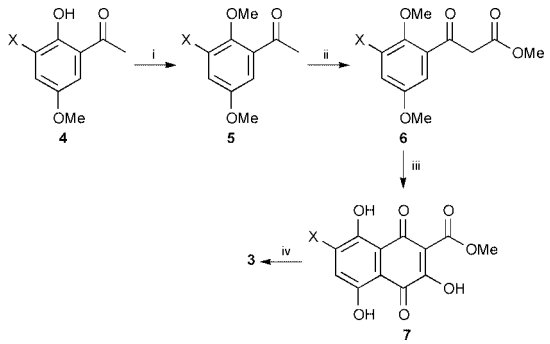

4 **5** **6** **7**

Scheme 1 *Reagents and conditions*: **4** (X = Cl) from **4** (X = H), NCS, HOAc, $Mg(OAc)_2$ r.t., 24 h: i, DMS, Me_2CO, K_2CO_3, heat, 24 h; ii, NaOMe, MeOH, $(MeO)_2CO$, hear; iii, $(COCl)_2$, $MeNO_2$, $AlCl_3$, 0 to 80 °C, 3 h; iv, 10% conc. HCl–HOAc, 100 °C, 5 h.

unhalogenated naphthoquinones,[8] afforded the two 3-carbonylmethoxy-6-halogeno-2,5,8-trihydroxynaphth-1,4-quinones **7** (X = Br) 48% and **7** (X = Cl) 56% together with some partially demethylated quinones. Hydrolysis of the trihydroxyquinone esters with either aqueous sodium hydroxide followed by acidification, or with hot acetic acid containing hydrochloric acid (the preferred method) then gave the parent compounds **3** (X = Br) 69% and **3** (X = Cl) 53%.

Under a variety of conditions **3** (X = Cl) failed to undergo Diels–Alder cycloaddition with the dienes (*E*)- and (*Z*)-3-methoxycarbonyl-2,4-bis(trimethylsilyloxy)penta-1,3-diene[2] **8a**. This was attributed primarily to the intramolecular hydrogen bonding[9] of the 2-OH group thus inhibiting the normal tautomerism of the naphthazarin system and locking the structure in form 1. Further support for this exclusive structure was provided by an X-ray structure determination (Fig. 1)† and that, under mild conditions, **3** (X = Cl) readily underwent: (a) Michael addition at the 3-position and (b) selective O-methylation in 77% yield at the 2-OH with BF_3·MeOH which then removed the impediment to tautomerism and was expected to assist cycloaddition.

Acetylation of **3** (X = Cl) in dichloromethane with pyridine–acetic anhydride afforded the triacetoxy-compound in 91% yield as a 2:1 mixture (confirmed by NMR) of 6-chloro-2,5,8-triacetoxynaphtho-1,4-quinone and 2-chloro-5,6,8-triacetoxynaphtho-1,4-quinone. However, upon heating **3** (X = Cl) in acetic anhydride alone at 100 °C the 2-chloro-5,6-diacetoxy

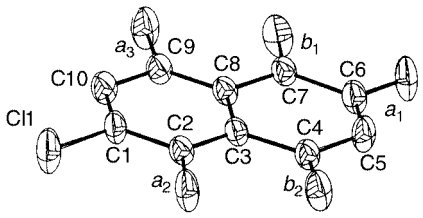

Fig. 1 X-Ray crystal structure of 6-chloro-2,5,8-trihydroxynaphtho-1,4-quinone; C–OH: a_1, a_2, a_3 = 1.33, 1.34, 1.35 Å; C=O: b_1, b_2 = 1.22, 1.24 Å.

DOI: 10.1039/b002591g

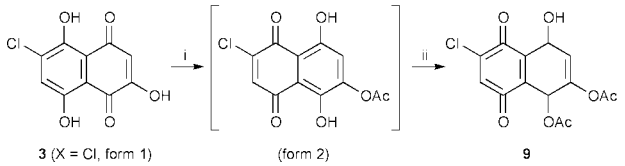

Scheme 2 *Reagents and conditions*: i, ii, Ac_2O, 100 °C, 3 h; vac. to dryness.

compound **9** resulted quantitatively. It is believed (Scheme 2) that acetylation of the 2-OH occurs first allowing tautomerism to form 2 to take place and is then followed by acetylation at the 5-position which locks the structure as form 2. It is conjectural that since hydrogen-bonded OH groups are more difficult to acetylate, migration of the 6-acetyl group to the 5-position may possibly occur enabling the more susceptible 6-OH group to then react. This tentative notion may explain the non-acetylation of the hydrogen-bonded 8-OH although we have no distinct evidence to support this pathway. X-Ray crystallography provided confirmation of the structure of the 5,6-diacetoxy compounds (Fig. 2).†

The diacetyl compound **9** readily underwent cycloaddition with (*E*)- and (*Z*)-3-methoxycarbonyl-2,4-bis(trimethylsilyloxy)penta-1,3-diene **8a** followed by aromatisation in boiling toluene to afford **10**, methyl 5,6-diacetoxy-3,8-dihydroxy-1-methylanthra-9,10-quinone-2-carboxylate in 87% yield after column chromatography, with definitive proof of structure being provided by an X-ray study (Fig. 3).† The isopropyl analogue **8b** reacted similarly in 64% yield.

2-Chloro-6-methoxy-5,8-dihydroxynaphtho-1,4-quinone **11**, in which normal naphthazarin tautomerism is able to operate, although the structure is not locked as with the diacetate, also underwent cycloaddition with the diene **8a** in boiling toluene to afford after work-up, methyl 6-methoxy-3,5,8-trihydroxy-1-methylanthra-9,10-quinone-2-carboxylate **12** in 42% yield. Possibly both forms 1 and 2 are present owing to the fact that there is no locking of the structure in this compound. Hydrolysis of **10** in 1% methanolic sodium carbonate followed by acidification gave methyl kermesate **1b** quantitatively and thence by refluxing in acetic acid containing hydrochloric acid, kermesic acid **1a** was obtained (Scheme 3). Methylation of

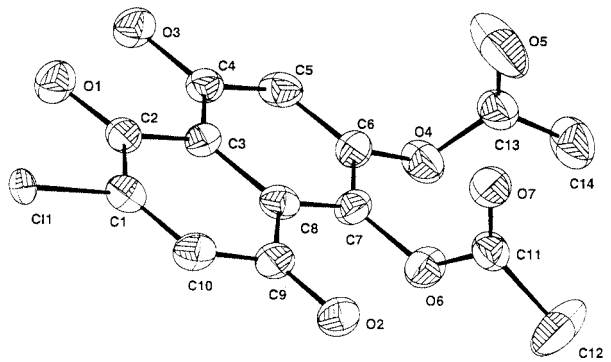

Fig. 2 X-Ray crystal structure of 2-chloro-5,6-diacetoxy-8-hydroxynaphtho-1,4-quinone.

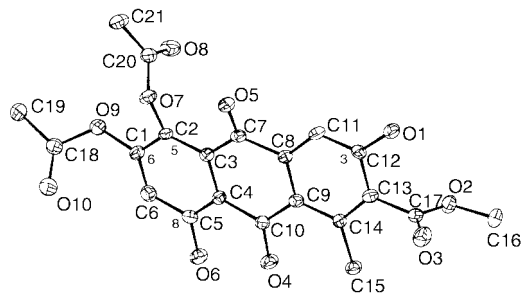

Fig. 3 X-Ray crystal structure of methyl 5,6-diacetoxy-3,8-dihydroxy-1-methylanthra-9,10-quinone-2-carboxylate.

methyl kermesate **1b** with DMS in acetone solution containing potassium carbonate gave methyl 3,5,6,8-tetramethoxy-1-methylanthra-9,10-quinone-2-carboxylate **1c**, which was identical with an authentic sample[4] kindly made available by Paul Brassard. Correct spectroscopic, elemental analysis and mass spectral data were obtained for all compounds.

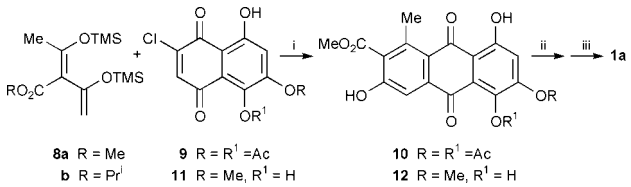

Scheme 3 *Reagents and conditions*: i, **9**, toluene, **8**, heat, 24 h; col chrom. SiO_2, ii, MeOH, 1% Na_2CO_3; iii, HOAc–HCl, heat; iv, **1b**, DMS, Me_2CO, K_2CO_3, heat **11** from **3** with BF_3·MeOH; toluene, **8**, heat; col. chrom. SiO_2.

Finally, it is believed that **3** (X = Cl) also has the potential utility to facilitate efficient access to carminic acid and work is continuing in this approach.[10]

Financial support is acknowledged from the SPUR initiative (DTI) and Mr G. Marshall (European Colour) is thanked for critical comments. We thank Professor S. Roberts (Exeter University) for facilitating and Professor M. Hursthouse (University of Wales, Cardiff) for effecting X-ray structure determinations.

Notes and references

† *Crystal data*: **3**: $C_{20}H_{10}Cl_2O_{10}$, *M* 479.16, triclinic, space group $P\bar{1}$, a = 6.756(4), b = 9.329(7), c = 11.536(9) Å, V = 676.4(8) Å^3, Z = 3, μ = 0.425 mm^{-1}; 1913 independent reflections (R_{int} = 0.0484), R indices (all data): R_1 = 0.0894, wR_2 = 0.1282.

9: $C_{14}H_9ClO_7$, *M* 324.66, monoclinic, space group *C*2/*c*, a = 16.0510(8), b = 5.5590(8), c = 30.980(8) Å, V = 2743.7(9) Å^3, Z = 8, μ = 0.313 mm^{-1}, 1926 independent reflections: (R_{int} = 0.0742), R indices (all data): R_1 = 0.1202, wR_2 = 0.2532.

10: $C_{21}H_{16}O_{10}$, *M* = 428.34, triclinic, space group $P\bar{1}$, a = 8.295(4), b = 8.8970(10), c = 12.799(8) Å, V = 922.0(7) Å^3, Z = 2, μ = 0.125 mm^{-1}, 2459 independent reflections (R_{int} = 0.0518), R indices (all data): R_1 = 0.0836, wR_2 = 0.1125.

CCDC 182/1611.

1 R. H. Thomson, *Naturally Occurring Quinones*, Academic Press, London, New York, 1971, p. 458.
2 P. Allevi, M. Anastasia, S. J. Bingham, P. Ciuffreda, A. Fiecchi, G. Cighetti, M. Muir, A. Scala and J. H. P. Tyman, *J. Chem. Soc., Perkin Trans. 1*, 1998, 575; J. H. P. Tyman, *Synthetic and Natural Phenols*, Elsevier, Amsterdam, 1996, p. 623.
3 A. Verhecken, *J. Soc. Dyers Col.*, 1989, **105**, 389.
4 G. Roberge and P. Brassard, *J. Chem. Soc., Perkin Trans. 1*, 1978, 1041.
5 D. W. Cameron, D. J. Deutscher, G. I. Feutrill and P. G. Griffiths, *Aust. J. Chem.*, 1981, **34**, 2401.
6 S. J. Bingham and J. H. P. Tyman, *J. Chem. Soc., Perkin Trans. 1*, 1997, 3637; K. Venkataraman and A. V. Rama Rao, in *Some Recent Developments in the Chemistry of Natural Products*, Prentice Hall of India, New Delhi, 1972.
7 C. T. Chang, M. F. Young and F. C. Chen, *Formosan Sci.*, 1962, **16**, 29.
8 G. Sartori, F. Bigi, G. Canali, R. Maggi, G. Casnati and X. Tao, *J. Org. Chem.*, 1993, **58**, 840.
9 The 2-, 5- and 8-OH groups in **3** (form 1) are hydrogen bonded, as seen in the ^{1}H NMR spectrum, with δ (DMSO-d_6) at 12.75 (br, s), 11.70, 13.35 ppm, respectively, *cf.* δ ($CDCl_3$) (Sadtler 19857) 10.34 for lawsone (2-hydroxynaphtho-1,4-quinone) and δ (Me_2CO) (Sadtler 3230) 8.35 for 2-naphthol. No NMR data for the 2-OH are given in ref. 8. In F. Farina, R. Martinez-Utrilla and M. C. Paredes, *Synthesis*, 1981, 300, the authors do not list the 2-OH group in data for 2-hydroxy-5,8-dimethoxynaphtho-1,4-quinone).
10 For this **3** (form 1) appears to be an ideal candidate from initial work on Michael addition and enamine reactions. Chemical approaches to using kermesic acid itself as an intermediate to carminic acid have not so far been successful although this or xanthokermesic acid are the likely biosynthetic precursors.

Theoretical investigation of the pathway for reductive cleavage of dinitrogen by a vanadium diamidoamine complex

Vanessa M. E. Bates,[a] Guy K. B. Clentsmith,[a] F. Geoffrey N. Cloke,[a] Jennifer C. Green*[b] and Huw D. Ll. Jenkin[b]

[a] *The Chemistry Laboratory, School of Chemistry, Physics and Environmental Science, University of Sussex, Brighton, UK BN1 9QJ*

[b] *Inorganic Chemistry Laboratory, University of Oxford, South Parks Road, Oxford, UK OX1 3QR. E-mail: jennifer.green@chem.ox.ac.uk*

Received (in Cambridge, UK) 30th March 2000, Accepted 19th April 2000

Density functional calculations show that $[HN(CH_2CH_2NH)_2V]$ will bind N_2 in a sideways fashion; further reaction with another molecule of $[HN(CH_2CH_2NH)_2V]$ leads to reductive cleavage of the N_2 moiety to form a bridged nitrido dimer, $[HN(CH_2CH_2NH)_2V(\mu\text{-}N)]_2$; this study provides a model for the formation of $[RN(CH_2CH_2NR)_2V(\mu\text{-}N)]_2$ (R = $SiMe_3$) by reduction of $[RN(CH_2CH_2NR)_2V(\mu\text{-}Cl)]_2$ under an N_2 atmosphere.

Examples of well-defined molecular systems which completely reductively cleave the dinitrogen molecule are extremely rare. The original case is the neutral Mo(III)–tris(anilide) complex of Laplaza and Cummins which yields a Mo(VI) terminal nitride upon reaction with N_2;[1] a comprehensive study has demonstrated that the mechanism of formation of the latter involves formation of a binuclear complex containing a linear μ-dinitrogen ligand which subsequently cleaves symmetrically *via* a transition state in which the μ-dinitrogen ligand is bound in a zigzag fashion.[2] Subsequently Floriani and coworkers reported an anionic Nb(III)–calixarene dinitrogen complex which affords an anionic nitrido-bridged dimer on further reduction.[3] The very recent report that reduction of the V(III) complex $[V(N\{N''\}_2)Cl]_2$, where $N\{N''\}_2$ = $(Me_3Si)N\{CH_2CH_2N(SiMe_3)\}_2$, under a dinitrogen atmosphere completely cleaves the N≡N bond to afford the doubly nitrido-bridged V(V)–V(V) dimer $[V(N\{N''\}_2)(\mu\text{-}N)]_2$,[4] has prompted us to investigate a possible pathway for this unusual reaction using density functional methods.[5]

Use of a mixture of $^{14}N_2$ and $^{15}N_2$ shows that both nitrido bridging atoms in the dimer molecule originate from the same dinitrogen molecule. If the reduction is carried out under argon and N_2 is subsequently introduced the nitrido-bridged dimer is not isolated. On the assumption that reaction of $[V(N\{N''\}_2)Cl]_2$ with potassium graphite in toluene results in the V(II) species $[V(N\{N''\}_2)]$, a possible route is given by eqn. (1). The V(II) species first binds dinitrogen and then reacts with a further V(II) species to give the product.

$$[V(N(N'')_2)(\mu\text{-}Cl)]_2 \xrightarrow{KC_8} 2[V(N(N'')_2)] \xrightarrow{N_2} [V(N(N'')_2)](N_2) + [V(N(N'')_2)] \rightarrow [V(N(N'')_2)(\mu\text{-}N)]_2 \quad (1)$$

We first tested whether theoretical calculations produced a good model of $[V(N\{N''\}_2)(\mu\text{-}N)]_2$, and whether the structural features could be reproduced with the $SiMe_3$ groups being replaced by SiH_3 and by H. Geometry optimization of these three dimers, **1a**, **1b** and **1c** reproduced the trigonal bipyramidal coordination found for $[V(N\{N''\}_2)(\mu\text{-}N)]_2$, and gave the V–N distances listed in Table 1. Frequency calculations showed **1a** to be a local minimum. Good agreement with the experimental distances (Table 1) was found for **1c**, and the only significant change on substitution was the magnitude of the long V–N (amino) distance which was calculated to be reduced by 0.3 Å on replacing $SiMe_3$ by the smaller H atom. We thus felt justified in modeling possible intermediates with the simpler $[HN(CH_2CH_2NH)_2]$ ligand (denoted L).

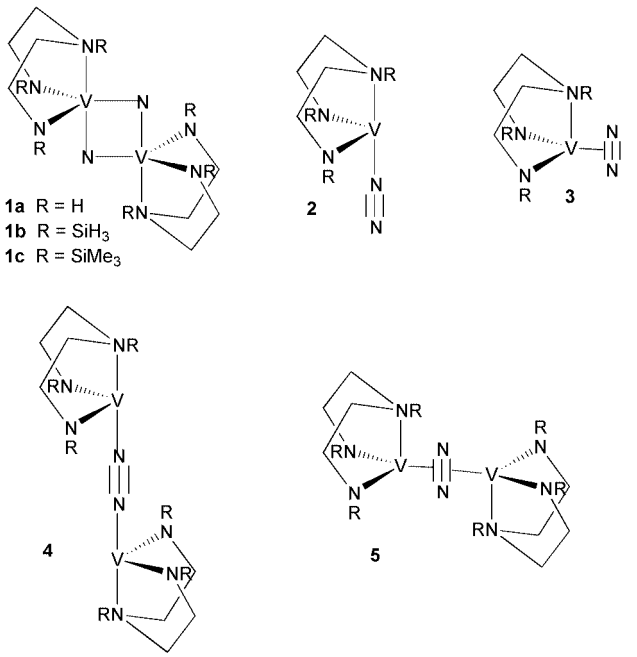

A search for stable $[LV(N_2)]$ intermediates yielded two promising candidates, **2** and **3**. Structure **2** had the N_2 moiety bound in an end on fashion in the axial site of a trigonal bipyramid and the quartet spin state was found to be lower in energy than a doublet for this intermediate. In **3** the N_2 was bound sideways in an equatorial site and in this case a doublet spin state was lower in energy. V–N and N–N distances for **2** and **3** are listed in Table 2 together with the energy of the various spin states relative to [LV] and N_2. Frequency calculations showed both **2** and **3** to be local minima. It should be noted that both $[LVN_2]$ intermediates show substantial binding energies for the N_2 molecule and also that **3** is predicted to be marginally more stable than **2** and to have a longer N–N

Table 1 Calculated and experimental V–N distances (Å) for $[V\{RN(CH_2CH_2NR)\}N]_2$ (R = H, SiH_3 or $SiMe_3$)

	H (calc.)	SiH_3 (calc.)	$SiMe_3$ (calc.)	$SiMe_3$ (exptl.)
V1–N1	1.88	1.86	1.86	1.862, 1.912
V1–N2	1.68	1.67	1.67	1.713, 1.769
V1–N3	2.34	2.48	2.64	2.539
V1–N4	1.87	1.87	1.87	1.877
V1–N5	1.87	1.87	1.87	1.897

DOI: 10.1039/b002534h

Table 2 Calculated V–N and N–N distances (Å) and energies (eV) relative to LV and N2 for **1a**, **2**, **3**, **4** and **5**

	1a (*S* = 0)	**2** (*S* = 3/2)	**2** (*S* = 1/2)	**3** (*S* = 3/2)	**3** (*S* = 1/2)	**4** (*S* = 1)	**5** (*S* = 1)
V–N	1.88, 1.68	1.92	1.85	2.10, 2.12	1.95, 1.90	1.72	1.93, 1.81
N–N	2.49	1.13	1.15	1.16	1.20	1.23	1.41
Energy	−7.09	−2.94	−2.47	−2.49	−2.99	−4.75	−5.04

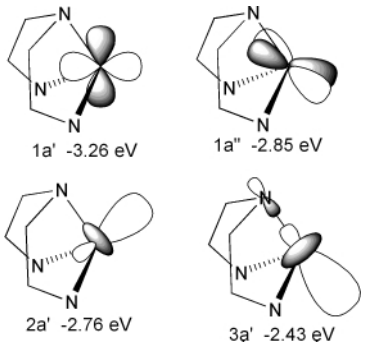

Fig. 1 Frontier orbital*S* of the [HN(CH_2CH_2NH)$_2$V] (LV) fragment.

distance. As the N_2 unit in **3** lies close to the substituent on the amino N we were concerned that this binding mode might be sterically hindered. However, geometry optimization of the fully trimethylsilylated analogue resulted in a similar structure with the N_2 only slightly displaced away from the amino substituent. The V–N (amino) distance was also lengthened by 0.061 Å.

Attachment of a second [LV] unit to **2** yielded the minimum energy structure **4** which had a triplet as the lowest spin state. The N–N bond was lengthened further (Table 2).

Attachment of a further [LV] fragment to **3** and geometry optimization of a triplet state led to **5**. This was more stable than **4** and had a considerably stretched N–N distance of 1.41 Å (Table 2) indicative of a bond order of 2 between the N atoms. The two half filled orbitals of **5** lay very close in energy and were of a_u and b_u symmetry. This closeness in energy led to problems with SCF convergence for geometry optimization of the singlet state. However, when the configuration was fixed with both electrons occupying the b_u orbital, the molecule optimized to a structure in which the N–N bond was broken and which was indistinguishable from **1a**.

Inspection of the frontier orbitals (Fig. 1) of the [LV] fragment neatly explains the two different coordination modes and sites for the N_2 molecule in **2** and **3**. The 2a′ and 3a′ orbitals are those that form σ bonds in a trigonal bipyramidal geometry, 2a′ providing equatorial coordination and the higher lying 3a′ axial coordination. In **2**, with the quartet ground state, the end on axially coordinated [LV(N_2)] intermediate, 3a′ is the acceptor orbital and 1a′ and 1a″ back donate in a π fashion to the antibonding π_g orbitals of the nitrogen molecule. Both of the back-donation MOs are singly occupied. The third unpaired electron occupies the 2a′ orbital. In **3**, the doublet ground state, the side-on bound [LV(N_2)] intermediate, the 2a′ orbital accepts electron density from the bonding π_u orbital and back donates in a π fashion from the 1a′ orbital (doubly occupied) and in δ fashion from the 1a″ orbital (singly occupied). The 3a′ orbital is unoccupied. Thus in **3,** more electrons are involved in back-donation to the N_2 unit. This results in a longer N–N distance.

In **4** additional back donation ensues from the π type orbitals, which are doubly occupied, and further lengthening of the N–N bond results. However, two unpaired electrons still occupy non-bonding orbitals of 2a′ origin.

The a_u and b_u half-occupied orbitals of **5** are shown in Fig. 2. The b_u orbital has N–N σ_u character and its partial occupancy results in further lengthening of the N–N bond. When it is

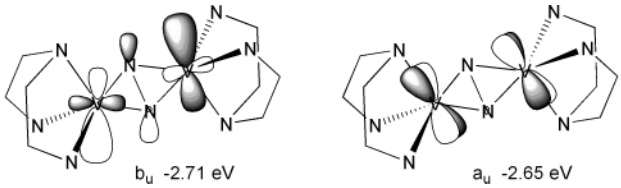

Fig. 2 Representation*S* of the b_u and a_u half-occupied orbital*S* of **5**.

doubly occupied, in the singlet state, all three N–N antibonding orbitals are receiving maximum input from the electron-rich vanadium centres and rupture of the N–N bond is achieved.

In essence, cleavage of the N_2 unit requires not only donation into its π_g orbitals but also into the antibonding σ_u orbital. This can only be sensibly achieved by sideways bonding of the N_2 unit where the acceptor function of the metal fragment is spatially separated from the interaction with the σ_u N_2 orbital. There are parallels between the N_2 cleavage discussed here and the relative stabilities of (μ-η^2:η^2-peroxo)dicopper(II) and bis(μ-oxo)dicopper(III) complexes, where donation into the σ_u* orbitals of O_2 is a key step in breaking the O–O bond.[11,12]

In conclusion a promising pathway for N_2 cleavage by [V(N{N″}$_2$)] to give [V(N{N″}$_2$)(μ-N)]$_2$, is side-on binding of N_2 by [V(N{N″}$_2$)] followed by association of a further molecule of [V(N{N″}$_2$)]. In a singlet state the N–N bond in the resultant sideways dinitrogen-bridged dimer will break and the nitrido bridged dimer is formed.

We thank EPSRC (ROPA) for support. Results were obtained using the resources of the Oxford Supercomputing Centre.

Notes and references

1 C. E. Laplaza and C. C. Cummins, *Science*, 1995, **268**, 861.
2 C. E. Laplaza, M. J. A. Johnson, J. C.Peters, A. L. Odom, E. Kim, C. C. Cummins, G. N. George and I. J. Pickering, *J. Am. Chem. Soc.*, 1996, **118**, 8623.
3 A. Zanotti-Gerosa, E. Solari, L. Giannini, C. Floriani, A. Chiesi-Villa and C. Rizzoli, *J. Am. Chem. Soc.*, 1998, **120**, 437.
4 G. K. B. Clentsmith, V. M. E. Bates, P. B. Hitchcock and F. G. N. Cloke, *J. Am. Chem. Soc.*, 1999, **121**, 10444.
5 All calculations were performed using density functional methods of the Amsterdam Density Functional package (Version ADF99).[6] The basis set used triple-ζ accuracy sets of Slater type orbitals, with relativistic corrections, with a single polarisation functional added to the main group atoms. The cores of the atoms were frozen [C (1s), Rh (3d), Ir (4d)]. The GGA (Non-local) method was used, using Vosko, Wilk and Nusair's local exchange correlation[7] with non-local-exchange corrections by Becke[8] and non-local correlation corrections by Perdew.[9,10] Structures were idealized to C_{2h} or C_s symmetry.
6 E. J. Baerends, A. Berces, C. Bo, P. M. Boerringter, L. Cavallo, L. Deng, R. M. Dickson, D. E. Ellis, L. Fan, T. H. Fischer, C. Fonseca Guerra, S. J. van Gisbergen, J. A. Groeneveld, O. V. Gritsenko, F. E. Harris, P. van den Hoek, H. Jacobsen, G. van Kessel, F. Kootstra, E. van Lenthe, V. P. Osinga, P. H. T. Philipsen, D. Post, C. C. Pye, W. Ravenek, P. Ros, P. R. T. Schipper, G. Schreckenbach, J. G. Snijiders, M. Sola, D. Swerhone, G. te Velde, P. Vernooijis, L. Versluis, O. Visser, E. van Wezenbeek, G. Wiesenekker, S. K. Wolff, T. K. Woo and T. Ziegler, *ADF Program System Release 1999*, 1999.02, Amsterdam.
7 S. H. Vosko, L. Wilk and M. Nusair, *Can. J. Phys.*, 1980, **58**, 1200.
8 A. D. Becke, *Phys. Rev. A*, 1988, **38**, 2398.
9 J. P. Perdew, *Phys. Rev. B*, 1986, **33**, 8822.
10 J. P. Perdew, *Phys. Rev. B*, 1986, **34**, 7046.
11 P. L. Holland and W. B. Tolman, *Coord. Chem. Rev.*, 1999, **190–192**, 855.
12 X.-Y. Liu, A. A. Palacios, J. J. Novoa and S. Alvarez, *Inorg. Chem.*, 1998, **37**, 1202.

Synthesis and structural characterization of adaptable shape-persistent building blocks

Charles Degenhardt III, David Brian Shortell, Richard D. Adams and Ken D. Shimizu*

Department of Chemistry and Biochemistry, University of South Carolina, Columbia, SC 29208 USA. E-mail: shimizu@mail.chem.sc.edu

Received (in Columbia, MO, USA) 8th March 2000, Accepted 5th April 2000

The rigid *syn*- and *anti*-atropisomers of diacids 1 and 2 were synthesized and assigned by symmetry-based methods and X-ray crystallography.

Rigid difunctional molecules are key components in synthetic molecular receptors and shape-persistent molecular polymers.[1,2] Reported herein are the syntheses and structures of two new diacid building blocks **1** and **2**. Both maintain highly rigid

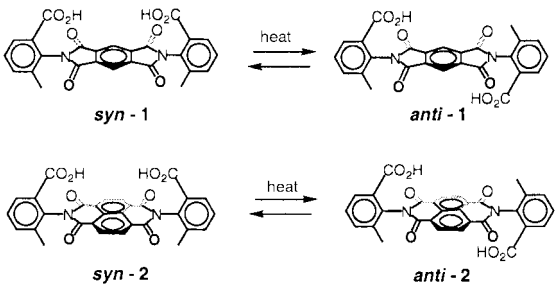

and coherent conformations due to aromatic components and restricted rotation about two linking N_{imide}–C_{aryl} bonds.[3] The resulting *syn*- and *anti*-atropisomers are stable at room temperature but interconvert on heating.

Diacids **1** and **2** were synthesized in high yields by condensation of the corresponding arylamine and aromatic dianhydrides (Scheme 1).[4] In each case, the presence of restricted rotation was immediately evident by the isolation of two spectroscopically similar molecules that interconverted on heating. The stable atropisomers were readily separated by flash chromatography and could be derivatized without isomerization. To further demonstrate their stability, the individual *syn*- and *anti*-isomers of diamides **3** and **4** were synthesized from the corresponding isomers of diacids **1** and **2**.

The rotational barrier of the C_{aryl}–N_{imide} bonds was measured in diamides **3** and **4**. Rotational barriers of $\Delta G^{\ddagger}$ = 29.4 kcal mol^{-1} ($t_{1/2}$ = 35 h at 77 °C) for **3** and $\Delta G^{\ddagger}$ = 34.0 kcal mol^{-1}

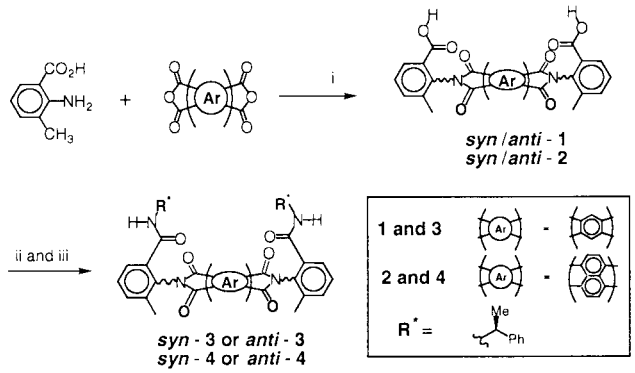

Scheme 1 *Reagents and conditions*: i, DMF, reflux, 8 h, (80% yield) or neat, *in vacuo*, 150 °C, 12 h, (95% yield); ii, oxalyl chloride, cat. DMF, CH_2Cl_2, reflux 2 h; iii, (*S*)-α-methylbenzylamine, triethylamine, CH_2Cl_2, 1 h, (70–80% yield for steps ii and iii).

($t_{1/2}$ = 4.1 h at 152 °C) for **4** were determined from the equilibration rates in DMSO. The higher rotational barrier of naphthalene diimide **4** appears to be due to increased steric effects in the six-membered cyclic imides. Molecular modeling calculations correctly predicted the magnitude and ordering of this trend.[5]

For diacids **1** and **2**, 1D and NOE NMR experiments could not lead to assignment of the atropisomers owing to their high symmetries. Instead, symmetry-based characterization methods were applied which efficiently identified the *syn*- and *anti*-isomers without the necessity of X-ray crystallography.[6] Derivatization of the diacids with a chiral auxiliary reduced the symmetry of the corresponding isomers in a predictable manner that yielded characteristic ^{1}H NMR spectra. This was achieved experimentally by reaction of the individual *syn*- and *anti*-isomers of the diacid chlorides of **1** and **2** with (*S*)-α-methylbenzylamine to yield the *syn*- and *anti*-isomers of diamides **3** and **4**. The chiral auxiliary accentuates the differences in symmetry of the *syn*- and *anti*-isomers and allowed assignment based on the chemical equivalence or inequivalence of the protons of the diimide spacer. For example, the two protons of the benzene diimide spacer in **3** are chemically equivalent in the *syn*-isomer and inequivalent in the *anti*-isomer (Fig. 1). A similar analysis of diamide **4** predicts that adjacent protons in *anti*-**4** and diagonal protons in *syn*-**4** are chemically equivalent. The corresponding ^{1}H NMR spectra of *anti*- and *syn*-**4** exhibited two singlets and two doublets, respectively.

Corroboration for the symmetry-based assignments was provided by polarity-based arguments and an X-ray crystal

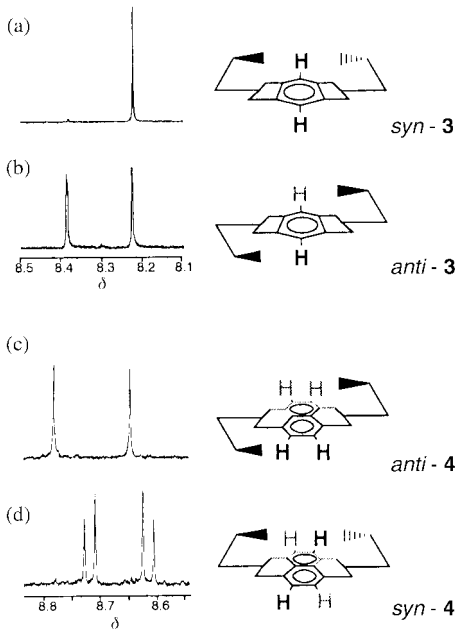

Fig. 1 Proton NMR spectra (DMSO-d_6, 400 MHz) of chiral diamides **3** and **4** and schematic representations showing the symmetry present in each rotamer; (a) *syn*-**3**, (b) *anti*-**3**, (c) *anti*-**4**, (d) *syn*-**4**.

DOI: 10.1039/b002085k

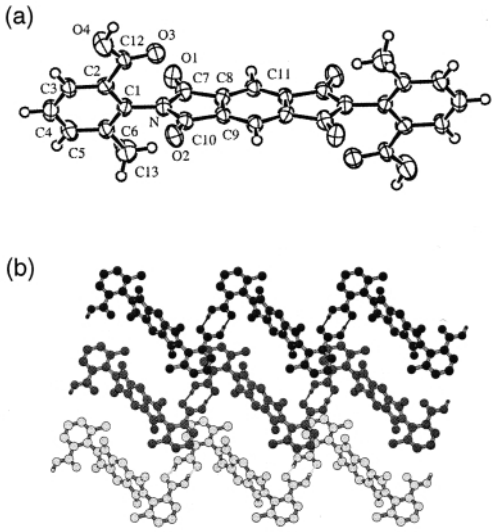

Fig. 2 (a) X-Ray structure of *anti*-**1** and (b) extended hydrogen-bonded ribbon structure of **1**. Solvent molecules and non-carboxylic acid hydrogens have been omitted for viewing clarity.

structure of *anti*-**1**. Initially, the atropisomers were tentatively identified based on polarity as measured by thin layer chromatography on silica gel. The *anti*-conformer was expected to be the less polar (higher R_f) owing to its inversion symmetry.[7] For all of the *N*,*N*′-diarylimide atropisomers examined thus far, the symmetry- and polarity-based assignments have been in agreement. In the case of diacid **1**, further evidence for the correct assignment was provided by an X-ray crystal structure [Fig. 2(a)] of the *anti*-isomer, which was crystallized from $MeCO_2H$–CH_2Cl_2.† The *anti*-configuration was immediately evident from the inversion symmetry of the space group ($P\bar{1}$) coupled with the small unit cell that contained approximately half of the atoms in diacid-**1**.

The structure also revealed interesting information about the molecular and extended structures. The positions of the non-hydrogen atoms of *anti*-**1** were well defined and revealed a structure with the *N*-aryl rings rotated 73° out of the plane of the diimide spacer. In the extended structure [Fig. 2(b)] *anti*-diacid **1** forms a hydrogen-bonded ribbon polymer with channels along the *a*-axis filled with disordered acetic acid dimers which was the source of the relatively high *R*-value for the structure.

This work was supported by grants from the NSF (DMR-9807470) and the Research Corporation (RI0081).

Notes and references

† *Crystal data for anti*-**2**: $C_{26}H_{16}N_2O_8{\cdot}2CH_3CO_2H$, M = 578.49, triclinic, space group $P\bar{1}$, a = 8.403(2), b = 11.995(3), c = 7.7872(2) Å, α = 98.41(2), β = 95.41(2), γ = 109.72(2)°, U = 722.5(4) A^3, T = 293 K, Z = 1, μ(Mo-Kα) = 0.106 mm^{-1}, 1444 observed reflections, R = 0.105, R_w = 0.176. The high R-factor is a consequence of disorder in the cocrystallized acetic acid molecules.

CCDC 182/1605. See http://www.rsc.org/suppdata/cc/b0/b002085k/ for crystallographic files in .cif format.

1 J.-M. Lehn, *Supramolecular Chemistry: Concepts and Perspectives*, VCH, New York, 1995; F. Vögtle, *Supramolecular Chemistry*, John Wiley and Son, 1993.

2 J. S. Moore, *Acc. Chem. Res.*, 1997, **30**, 402; S. Hoger, *J. Polym. Sci. Polym. Chem.*, 1999, **37**, 2685; A. J. Berresheim, M. Muller and K. Mullen, *Chem. Rev.*, 1999, **99**, 1747.

3 K. D. Shimizu, T. M. Dewey and J. Rebek Jr., *J. Am. Chem. Soc.*, 1994, **116**, 5145; J. Rebek Jr., *Angew. Chem., Int. Ed. Engl.*, 1990, **29**, 245.

4 All new compounds reported here were fully characterized on the basis of their spectral (UV, IR, ^{1}H and ^{13}C NMR, MS). Selected data for *anti*-**1**: IR (KBr) 3425, 2976, 1781, 1686 cm^{-1}; ^{1}H NMR (400 MHz, DMSO-d_6) δ 8.49 (s, 2H), 7.94 (dd, J 6.6, 1.2 Hz, 2H), 7.70 (d, J 7.1 Hz, 2H), 7.58 (t, J 7.7 Hz, 2H), 2.26 (s, 6H). ^{13}C NMR (100 MHz, DMSO-d_6) δ 165.78, 165.15, 138.54, 137.14, 134.77, 129.86, 129.49, 128.95, 128.8, 118.46, 17.35; HRMS (FAB, NBA) calc. for $C_{26}H_{16}N_2O_8$ (M + H) *m/z* 485.0985, obs. 485.0976. Anal. Calc. for $C_{26}H_{16}N_2O_8{\cdot}H_2O$: C, 60.00; H, 3.87; N, 5.38. Found: C, 60.14; H, 3.64; N, 5.39%. For *syn*-**1**: IR (KBr) 3425, 1780, 1729, 1690 cm^{-1}; ^{1}H NMR (400 MHz, DMSO-d_6) δ 8.53 (s, 2H), 7.94 (dd, J 5.5, 1.5 Hz, 2H), 7.71 (d, J 7.5 Hz, 2H), 7.59 (t, J 7.7 Hz, 2H), 2.25 (s, 6H). ^{13}C NMR (100 MHz, DMSO-d_6) δ 165.77, 165.12, 138.37, 137.09, 134.78, 129.83, 129.55, 129.04, 128.88, 118.65, 17.26; HRMS (FAB, NBA) calc. for $C_{26}H_{16}N_2O_8$ (M + H) *m/z* 485.0985, obs. 485.0995. Anal.Calc. for $C_{26}H_{16}N_2O_8$: C, 64.47; H, 3.33; N, 5.78. Found: C, 64.21; H, 3.55; N, 5.85%. For *syn*-**2**: IR (KBr) 3200, 1715, 1664, 1582 cm^{-1}; ^{1}H NMR (400 MHz, DMSO-d_6) δ 12.91 (br s, 2H), 8.77 (s, 4H), 7.98 (d, J 6.8 Hz, 2H), 7.70 (d, J 6.9 Hz, 2H), 7.55 (t, J 6.7 Hz, 2H), 2.21 (s, 6H). ^{13}C NMR (100 MHz, DMSO-d_6) δ 167.49, 164.02, 139.37, 136.52, 136.10, 132.53, 130.92, 130.50, 129.94, 128.62, 128.27, 18.90; HRMS (FAB, NBA) calc. for $C_{30}H_{18}N_2O_8$ (M + H) *m/z* 535.1141, obs. 535.1147. For *anti*-**2**: IR (KBr) 3199, 1713, 1676, 1580 cm^{-1}; ^{1}H NMR (400 MHz, DMSO-d_6) δ 12.42 (br s, 2H), 8.79 (s, 4H), 7.98 (d, J 7.5 Hz, 2H), 7.71 (d, J 7.2 Hz, 2H), 7.56 (t, J 7.6 Hz, 2H), 2.21 (s, 6H). ^{13}C NMR (100 MHz, DMSO-d_6) δ 165.68, 162.21, 137.41, 134.77, 134.26, 130.95, 129.25, 128.81, 128.21, 126.76, 126.37, 17.06; HRMS (FAB, NBA) calc. for $C_{30}H_{18}N_2O_8$ (M + H) *m/z* 535.1141, obs. 535.1144.

5 The barriers of rotation were calculated using MM2 as implemented in MacroModel v5.5 (F. Mohamadi, N. G. J. Richards, W. C. Cuida, R. Liskamp, M. Lipton, C. Caufield, G. Chang, T. Hendrickson and W. C. Still, *J. Comput. Chem.*, 1990, **11**, 440). The rotational barrier varied greatly with the step angle of the dihedral driver. Accurate values were attained only for small step angles of < 1°. Larger step angles would jump over the barrier and predict considerably smaller rotational barriers.

6 E. L. Eliel and S. H. Wilen, *Stereochemistry of Organic Compounds*, John Wiley & Sons, New York, 1994, pp. 669–670.

7 G. M. Sanders, M. Van Dijk, B. M. Machiels and A. van Veldhuizen, *J. Org. Chem.*, 1991, **56**, 1301.

ChemComm

Novel hepta-coordinated molybdenum(II) and tungsten(II) carbene complexes by oxidative decarbonylation of Mo(0) and W(0) carbene complexes

Monika Jaeger, Rüdiger Stumpf, Carsten Troll and Helmut Fischer*

Fachbereich Chemie, Universität Konstanz, Fach M727, D-78457 Konstanz, Germany.
E-mail: hfischer@dg6.chemie.uni-konstanz.de

Received (in Basel, Switzerland) 16th March 2000, Accepted 17th April 2000

***C,O*-Chelated tetracarbonyl[*o*-methoxyphenyl(methoxy)-carbene] complexes of molybdenum(0) and tungsten(0) react with tin tetrahalides SnX_4 (X = Cl, Br, I) by oxidative decarbonylation and incorporation of two halides to form novel chelated hepta-coordinated Fischer-type tricarbonyl-(bishalogeno)carbene molybdenum(II) and tungsten(II) complexes**

Heteroatom-stabilized Fischer-type transition-metal carbene complexes are important stoichiometric or catalytic reagents for the transformation of organic substrates and for the synthesis of organometallic compounds.[1] For instance, the carbene complexes $[(CO)_5M{=}C(OR)R']$ (M = Cr, Mo, W; R = Me, Et; R′ = alkyl, aryl, ...) react with boron trihalides BX_3 by abstraction of OR^- and substitution of a halide ion for a CO ligand to give carbyne complexes, *trans*-$[X(CO)_4M{\equiv}CR']$ (Scheme 1).[2] Apart from boron trihalides, other Lewis acids such as aluminium or gallium trihalides[3,4] or ethyl aluminium dichloride[4] have also been employed in the synthesis of carbyne complexes.[5]

We now observed that the reactions of chelated alkoxy-carbene complexes of molybdenum and tungsten with the Lewis acids SnX_4 deviate from this carbene → carbyne transformation pattern and report (i) on the facile oxidation of the central metal in these complexes and (ii) on the formation of novel hepta-coordinated group 6 metal(II) carbene complexes.

Addition of a solution of $SnCl_4$ to the *C,O* carbene chelate complex **1a**[6] in CH_2Cl_2 led to an immediate gas evolution. The originally brown solution turned red and a white precipitate formed. From the position and the intensity ratio of the ν(CO) absorptions (2049s and 1974vs cm^{-1}) in the IR spectrum† of the reaction solution it followed that very likely a carbyne complex[7] had not been formed. The conclusion was confirmed by the ^{1}H NMR spectrum of the new complex (Scheme 2, **2a**). The spectrum exhibited, in addition to signals for four aromatic protons, two singlets at δ 4.49 and 4.94 (ratio 4 : 3 : 3) indicating that both MeO groups of **1a** were still present in the new complex. The mass spectrum indicated that two chloride atoms had been incorporated into the complex.

Finally, from pentane–CH_2Cl_2, crystals suitable for an X-ray analysis were grown.‡ The structure of **2a** is shown in Fig. 1. The metal is hepta-coordinated and the complex is C_s-symmetric. The mirror plane formed by the *C,O*-chelating carbene ligand, the tungsten atom and one CO ligand bisects the Cl–W–Cl angle and one OC–W–CO angle.

Obviously, $SnCl_4$ had not induced the abstraction of the methoxide substituent from the carbene carbon atom to give a tungsten(0) carbyne complex but rather acted as an oxidizing agent to give a tungsten(II) carbene complex.

The conversion of **1a** into **2a** is quantitative as could be shown by following the reaction of **1a** with $SnCl_4$ in $CDCl_3$ by

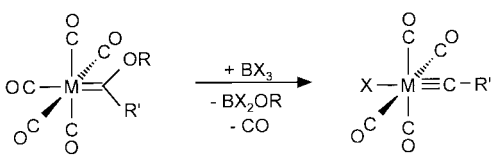

Scheme 1

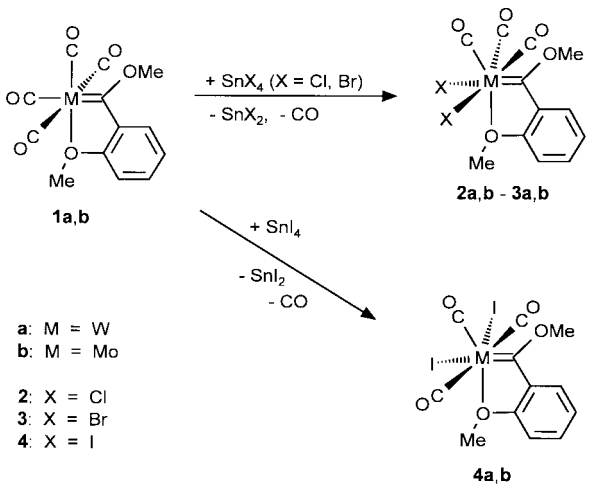

Scheme 2

^{1}H NMR spectroscopy. Analogously to $SnCl_4$, treatment of **1a** with $SbCl_5$ or $TiCl_4$ also afforded complex **2a**. In contrast, when $AlCl_3$ was added to a solution of **1a** only rapid decomposition of the complex was observed.

The related tungsten(II) dibromo carbene chelate complex **3a** and the corresponding molybdenum(II) complexes **2b** and **3b** (Scheme 2) were obtained by reaction of **1a** with $SnBr_4$ and of **1b**[5] with $SnCl_4$ and $SnBr_4$, respectively. The IR spectra of the resulting complexes were similar to that of **2a** indicating a similar structure.

In contrast, the diiodo carbene chelate complex **4a** (Scheme 2), formed when **1a** was treated with SnI_4, exhibited three rather than two ν(CO) absorptions and three CO resonances in the ^{13}C NMR spectrum, as compared to two for **2a**,**b** and **3a**,**b**. These observations indicated that the structure of **4a**,**b** deviates from

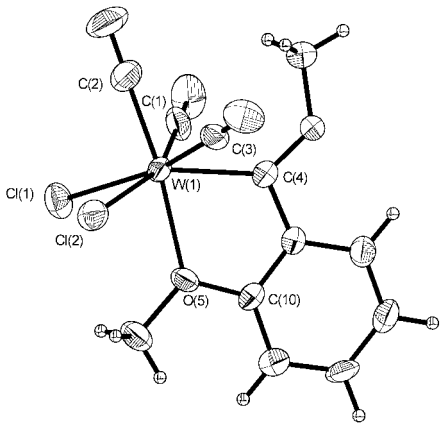

Fig. 1 Molecular structure of **2a**. Selected bond distances (Å) and angles (°): W(1)–C(1) 2.483(2), W(1)–Cl(2) 2.480(2), W(1)–C(1) 2.008(8), W(1)–C(2) 1.983(8), W(1)–C(4) 2.133(8), W(1)–O(5) 2.261(5); Cl(1)–W(1)–Cl(2) 85.1(1), Cl(1)–W(1)–C(4) 130.1(2), Cl(2)–W(1)–C(4) 131.5(2), Cl(1)–W(1)–C(1) 77.1(2), Cl(2)–W(1)–C(3) 78.8(2), C(1)–W(1)–C(3) 115.7(3), C(4)–W(1)–O(5) 73.6(2), W(1)–O(5)–C(10) 117.8(4).

DOI: 10.1039/b002228o

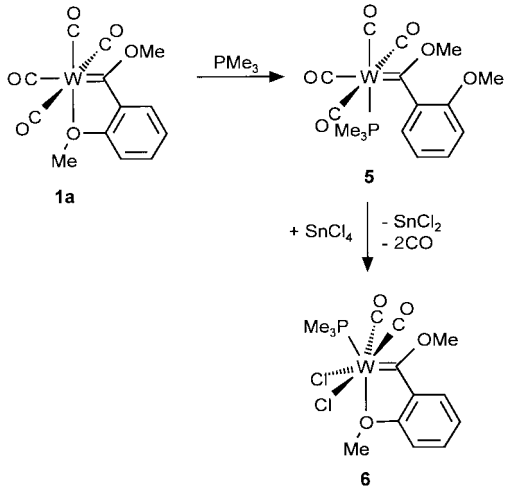

Scheme 3

that of **2a**. Presumably, the structure of **4a** is derived from that of **2a** by a mutual halide/CO exchange of two ligands outside the mirror-plane. The reaction of the molybdenum complex also proceeded rapidly, however, the resulting compound **4b** turned out to be very labile and could not be isolated. Its formation could only be established by IR spectroscopy.

Deviating from the tungsten and molybdenum complexes **1a**,**b** the corresponding chromium complex did not react with $SnCl_4$. Within several hours in solution in the presence of $SnCl_4$, as well as in its absence, only a slow decomposition of the carbene complex and formation of $[Cr(CO)_6]$ was observed.

From these observations it was concluded that an energetically high-lying HOMO at the metal is required for the oxidative decarbonylation of **1a**,**b** by SnX_4. The assumption is supported by the absence of a reaction between $SnCl_4$ and the non-chelated *o*-anisylcarbene(pentacarbonyl) complex $[(CO)_5W{=}C(OMe)C_6H_4OMe\text{-}o]$. After several hours at room temperature in CH_2Cl_2 only small amounts of **2a** could be detected, presumably formed *via* CO elimination to form **1a** which then rapidly reacts with $SnCl_4$. In contrast, the reaction of the phenylcarbene complex $[(CO)_5W{=}C(OMe)Ph]$ with excess $SnCl_4$ afforded among other compounds a carbyne complex.

However, chelation of the carbene ligand is not a prerequisite for the oxidative decarbonylation as is shown by the reaction of **1a** with PMe_3. Ring-opening of the metallacycle in **1a** by PMe_3 afforded the *cis*-carbene(tetracarbonyl)phosphine complex **5** which subsequently was transformed by $SnCl_4$ into the chelated tungsten(II) carbene complex **6** (Scheme 3).

Tungsten(II) complexes of the type $(CO)_3(L)_2(X)_2W$ have been shown to catalyze the ring-opening polymerization of norbornene.[8] Likewise, complexes **2**–**4** are active ROMP catalysts for norbornene even at room temperature. The highest catalytic activity was observed with the molybdenum complex **2b** which even at room temperature readily induces without a cocatalyst (i) the ring-opening polymerization of norbornene and norbornadiene and (albeit slowly) of cyclopentene, (ii) the polymerization of phenylacetylene, and (iii) the isomerization of pent-1-ene into pent-2-ene.

Hepta-coordinated Fischer-type Mo(II) and W(II) carbene complexes are exceedingly rare. Usually, Fischer-type carbene complexes react with oxidizing agents by oxidative decomplexation of the *carbene* ligand.[1a] Until now, the oxidative decarbonylation of group 6 carbonyl–carbene complexes has only been observed in the reactions of Br_2 with some Lappert-type carbene complexes in which the electron density at the central metal is increased by cyclic strongly electron-donating bisaminocarbene ligands $=C[N(R)–CH_2–]_2$.[9] Our results indicate that Fischer-type Mo(II) and W(II) carbene complexes are readily accessible by oxidation of Mo(0) and W(0) carbene complexes as soon as their oxidation potential is reduced by substitution of a suitable strong donor for a CO ligand.

Financial support of this work by the Fonds der Chemischen Industrie is gratefully acknowledged.

Notes and references

† *Selected spectroscopic data*: IR (CH_2Cl_2): ν(CO): 2049s, 1974vs (**2a**), 2056, 1989vs (**2b**), 2048s, 1973vs (**3a**), 2052s, 1986vs (**3b**), 2040vs, 1975s, 1922m (**4a**), 2046vs, 1985s, 1936 cm^{-1} (**4b**); ^1H NMR ($CDCl_3$, room temp., rel. TMS): δ(OMe) 4.49, 4.95 (**2a**), 4.53, 4.85 (**2b**), 4.51 (86%), 4.74 (14%), 5.06 (**3a**), 4.55, 4.96 (**3b**), 4.60, 5.16 (**4a**); ^{13}C NMR ($CDCl_3$, room temp., rel. TMS): $\delta(C_{Carbene})$ 285.2 (**2a**), 295.6 (**2b**), 282.5 (**3a**), 293.2 (**3b**), 293.2 (**4a**); δ(CO) 210.8, 214.6 (**2a**), 216.3, 220.4 (**2b**), 208.1, 213.3 (**3a**), 214.0, 219.8 (**3b**), 211.4, 213.7, 231.3 (**4a**).

‡ *Crystal data* for **2a** (from pentane–CH_2Cl_2, 1:1): $C_{12}H_{10}Cl_2O_5W{\cdot}CH_2Cl_2$, M = 573.9, monoclinic, space group $P2_1/c$, a = 9.567(6), b = 11.994(6), c = 15.986(5) Å, β = 100.57(4)°, V = 1803.3(15) Å^3, T = 246 K, Z = 4, μ(Mo-Kα) = 0.71073 Å. 3949 Unique reflections were collected of which 2782 were observed with $F > 4.0\sigma(F)$ (ω-scan). $R(R_w)$ = 0.035 (0.037) (observed data). The structure was solved by Patterson methods using the SHELXTL PLUS (VMS) program package.

CCDC 182/1608. See http://www.rsc.org/suppdata/cc/b0/b002228o/ for crystallographic files in .cif format.

1 Selected reviews: (*a*) *Transition Metal Carbene Complexes*, ed. K. H. Dötz, H. Fischer, P. Hoffmann, F. R. Kreissl, U. Schubert and K. Weiss, VCH, Weinheim, 1983; (*b*) K. H. Dötz, *Angew. Chem.*, 1984, **96**, 573; *Angew. Chem., Int. Ed. Engl.*, 1984, **23**, 587; (*c*) L. S. Hegedus, in *Comprehensive Organometallic Chemistry II*, ed. F. W. Abel, F. G. A. Stone and G. Wilkinson, Pergamon, Oxford, 1995, vol. 12, p. 549; (*d*) W. D. Wulff, in *Comprehensive Organometallic Chemistry II*, ed. F. W. Abel, F. G. A. Stone and G. Wilkinson, Pergamon, Oxford, 1995, vol. 12, p. 469.

2 E. O. Fischer, G. Kreis, C. G. Kreiter, J. Müller, G. Huttner and M. Lorenz, *Angew. Chem.*, 1973, **85**, 618; *Angew. Chem., Int. Ed. Engl.*, 1973, **12**, 564.

3 E. O. Fischer, H. Hollfelder, P. Friedrich, F. R. Kreißl and G. Huttner, *Angew. Chem.*, 1977, **89**, 416; *Angew. Chem., Int. Ed. Engl.*, 1977, **16**, 401.

4 E. O. Fischer, S. Walz and W. R. Wagner, *J. Organomet. Chem.*, 1977, **134**, C37.

5 For a review on carbyne complex chemistry, see: *Carbyne Complexes*, ed. H. Fischer, P. Hoffmann, F. R. Kreissl, R. R. Schrock, U. Schubert and K. Weiss, VCH, Weinheim, 1988.

6 K. H. Dötz, H. G. Erben, W. Staudacher and K. Harms, *J. Organomet. Chem.*, 1988, **355**, 177.

7 For IR-data on *mer*-$X(CO)_3LW{\equiv}CR$ complexes, see (*a*) E. O. Fischer and K. Richter, *Chem. Ber.*, 1976, **109**, 2547; (*b*) E. O. Fischer, A. Ruhs and F. R. Kreißl, *Chem. Ber.*, 1977, **110**, 805.

8 L. Bencze and A. Kraut-Vass, *J. Mol. Catal.*, 1984, **28**, 369.

9 M. F. Lappert and P. L. Pye, *J. Chem. Soc., Dalton Trans.*, 1977, 1283.

Palladium catalysed cyclisation-Barbier-type allylation cascades

Usman Anwar, Ronald Grigg* and Visuvanathar Sridharan

Molecular Innovation, Diversity and Automated Synthesis (MIDAS) Centre, School of Chemistry, Leeds University, Leeds, UK LS2 9JT. E-mail: r.grigg@chem.leeds.ac.uk

Received (in Cambridge, UK) 5th April 2000, Accepted 18th April 2000

Pd(0) catalysed termolecular queuing processes involving cyclisation of aryl halides onto proximate alkynes, allene (1 bar) insertion, transmetallation of the resulting π-allylpalladium(II) species with indium and addition to an aldehyde affords heterocyclic and carbocyclic dienes.

Our ongoing development of palladium catalysed polycomponent cyclisation-queuing processes has provided powerful methodology for the construction of carbocyclic and heterocyclic rings with accompanying substantial increases in molecular complexity.[1]

Recently we reported the palladium–indium mediated Barbier-type allylation of aldehydes with allenes[2] and identified four synthetic variants of this Pd–In mediated reaction depending on whether the Pd or In step was *intra*- or *inter*-molecular.

We now describe the incorporation of this reaction into a palladium catalysed cyclisation-termolecular queuing cascade. This cascade involves palladium catalysed cyclisation of an aryl iodide moiety onto proximate alkynes followed by allene insertion.[3] The resulting π-allylpalladium(II) species then undergoes transmetallation with indium metal generating an allylindium species which subsequently adds to the aldehyde component, affording heterocyclic and carbocyclic dienes (Scheme 1). Marshall and Grant have described transmetallation of allenylpalladium(II) species (sp^2-C–Pd) with indium salts[4] and very recently a report of the transmetallation of conventionally generated π-allylpalladium(II) species with In(I) and In(III) halides has appeared.[5]

Reaction (DMF, 84 °C, 8–16 h, Schlenk tube) of alkynes **1a**–**c** (1.0 mmol) with allene (1 bar), aldehydes (1.0 mmol) and indium powder (1.6 mmol) in the presence of a catalytic system comprising 10 mol% $Pd(OAc)_2$ and 20 mol% tris(2-furyl)-phosphine afforded the expected six- and seven-membered

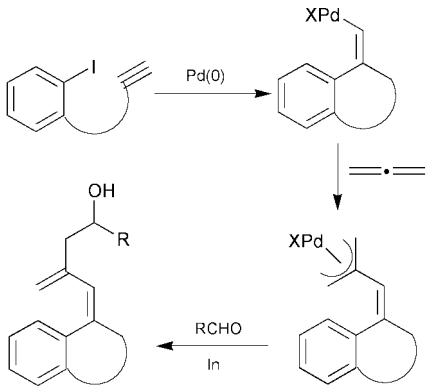

Scheme 1

Table 1

Alkyne	Aldehyde	Product	Yield(%)[a]	Alkyne	Aldehyde	Product	Yield(%)[a]
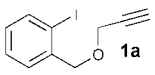 **1a**	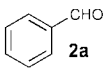 **2a**	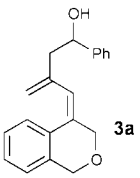 **3a**	52	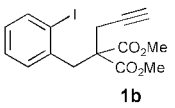 **1b**	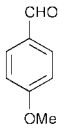 **2e**	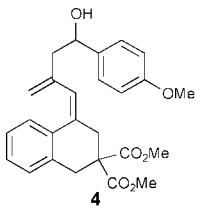 **4**	54
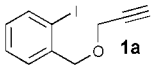 **1a**	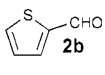 **2b**	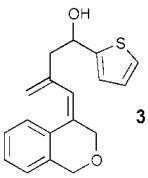 **3b**	51	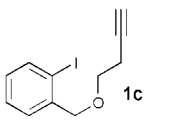 **1c**	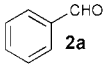 **2a**	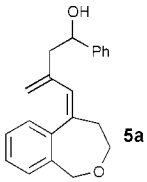 **5a**	46
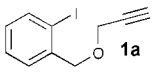 **1a**	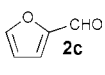 **2c**	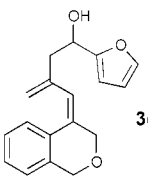 **3c**	50	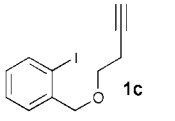 **1c**	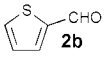 **2b**	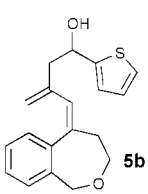 **5b**	53
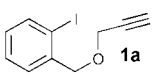 **1a**	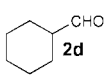 **2d**	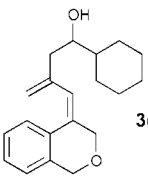 **3d**	46	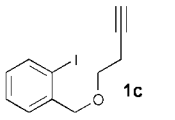 **1c**	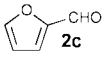 **2c**	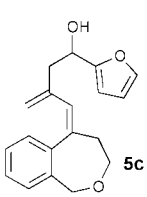 **5c**	53

[a]Isolated yield.

DOI: 10.1039/b002713h

Table 2

Alkyne	Aldehyde	Product	Yield(%)
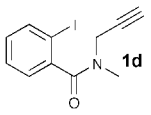 **1d**	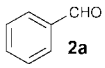 **2a**	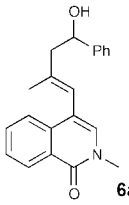 **6a**	43
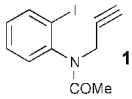 **1e**	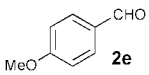 **2e**	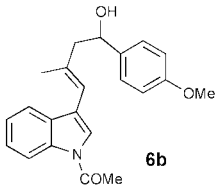 **6b**	43

carbo- and hetero-cyclic products with aromatic, hetero-aromatic and aliphatic aldehydes. Products of alkene isomerisation were not detected under these conditions (Table 1).

We next turned our attention to alkynes **1d** and **1e** (Table 2). When these compounds were subjected to the same reaction conditions as **1a**–**c** the expected cascade ensued but the resulting products, **6a** and **6b**, were the isomeric conjugated dienes.

A possible mechanism, which explains the formation of **6a** and **6b**, is shown in Scheme 2. The driving force for the proposed 1,5-H shift is the developing aromaticity in the rearrangement transition state. This latter factor is absent in **3a**–**d**, **4** and **5a**–**c**.

These reactions further emphasise the versatility of the palladium–indium cascade process. There is clearly considerable scope for variation of the carbonyl and allene components and further developments are in hand.

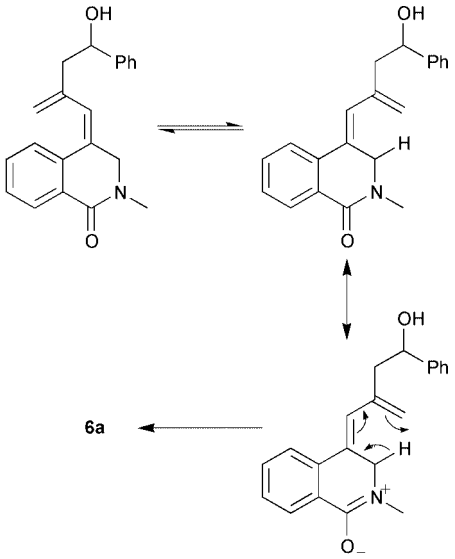

Scheme 2

We thank the EPRSC and Leeds University for support.

Notes and references

1 R. Grigg and V. Sridharan, *J. Organomet. Chem.*, 1999, **576**, 65.
2 U. Anwar, R. Grigg, M. Rasparini, V. Savic and V. Sridharan, *Chem. Commun.*, 2000, 645.
3 R. Grigg and V. Savic, *Tetrahedron Lett.*, 1996, **37**, 6565.
4 J. A. Marshall and C. M. Grant, *J. Org. Chem.*, 1999, **64**, 8214.
5 S. Araki, T. Kamei, T. Hirashita, H. Yamamura and M. Kawai, *Org. Lett.*, 2000, **2**, 847.

ChemComm

Deliberate combination of coordination polymers and hydrogen bonds in a supramolecular design strategy for inorganic/organic hybrid networks

Christer B. Aakeröy, Alicia M. Beatty, Destin S. Leinen and Keith R. Lorimer

Department of Chemistry, Kansas State University, Manhattan, KS, USA. E-mail: aakeroy@ksu.edu

Received (in Columbia, MO, USA) 1st February 2000, Accepted 20th April 2000

Two crystal structures containing infinite CuI chains connected into 2-D layers by non-covalent interactions demonstrate how coordinate covalent bonds and hydrogen bonds can be combined in the design of new inorganic/organic hybrid materials.

Crystal engineering of inorganic/organic hybrid materials is typically based on a modular approach, where discrete building blocks are linked into larger networks.[1] The construction of these metal-containing networks has, so far, been achieved using two different design philosophies: adjacent transition-metal complexes are linked either through (i) coordinate covalent bonds[2] or (ii) weaker intermolecular forces (*e.g.* hydrogen bonds, aryl–aryl interactions, *etc.*).[3] Both methods have enjoyed considerable success, but there have been few *planned* attempts at using a combination of these approaches to build lamellar or 3-D architectures. Here we present two crystal structures based on copper(I) iodide and an auxiliary hydrogen-bonding ligand that demonstrate how the two philosophies can be forged into a supramolecular tool that has not yet been employed in a systematic manner.

One of the main challenges in crystal engineering is to control the assembly and solid state structures in three dimensions. This task is complicated by the fact that ionic/molecular building blocks are capable of adopting a vast number of orientations in the crystal, thus making predictions of the resulting structure very difficult. Coordination polymers, however, are typically very robust and the topology of such networks can often be predicted with the aid of well known principles of coordination chemistry.[4] Thus, by using an infinite coordination polymer with known topology instead of a discrete complex as a synthetic module, the resulting assembly process will have fewer degrees of freedom, which facilitates intermolecular synthesis. Why then use anything but coordination polymers in the design of hybrid materials? Weaker intermolecular forces can impart properties to solids that sometimes offer advantages over 'pure' coordination polymers. Materials held together by hydrogen bonds tend to be more readily soluble, which is desirable for reasons ranging from ease of synthetic modification and manipulation to crystal growth and structural characterization.[5] In addition, unlike the more rigid frameworks of coordination polymers, a network generated through hydrogen bonds[6] can 'flex' to accommodate changes in its environment, and may therefore lend itself to host–guest applications that are less accessible in a rigid framework.[7]

Copper(I) complexes with monodentate ligands, $(CuXL)_\infty$ (where L is a pyridine derivative and X is a halide), are known to form robust halogen-bridged 1-D step, stair or chain structures,[8] and several 2-D coordination polymers based on 'pre-formed' 1-D copper(I) iodide chains and cross-linking bidentate ligands have recently been reported.[9–11]

In order to change network strength and flexibility without making significant changes to the *topology* of the structure, we have replaced the bidentate bridging ligand (*e.g.* pyrazine or 4,4′-bipyridine) with a supramolecular linker capable of simultaneous metal coordination and self-complementary hydrogen bonding. To this end, we report the syntheses† and crystal structures‡ of $[CuI(3\text{-pyridinealdoxime})]_\infty$ **1** and $[CuI(\text{isonicotinamide})]_\infty$ **2**.

The crystal structure of **1** contains 3-pyridinealdoxime ligands coordinated to a polymeric 'staircase' of CuI. Each tetrahedral Cu(I) ion is coordinated to three μ_3-I ligands to generate an infinite 1-D motif. The 3-pyridinealdoxime ligand is attached to each Cu(I) ion through the pyridine nitrogen atom [Cu(1)–N(1) 2.059(3) Å], to complete the coordination sphere. The oxime ligands are staggered ($N_{py}\cdots N_{py}$ internuclear distance *ca.* 4.1 Å) along the polymeric CuI chain and protrude outward. Adjacent oxime moieties are connected *via* O–H···N hydrogen bonds [O(7)···N(7), 2.841(3) Å], in a catemer-like fashion, to propagate the 1-D polymeric chains into an infinite 2-D sheet (Fig. 1). The sheets are non-interpenetrating resulting in a lamellar structure. There are no short contacts or noteworthy aryl–aryl interactions between adjacent chains, or between neighboring sheets.

The crystal structure of **2** is very similar to **1** and also contains infinite polymeric Cu(I) chains. The isonicotinamide ligand occupies the fourth coordination site of the Cu(I) center by coordination through the pyridine nitrogen atom [Cu(1)–N(1) 2.02(2) Å].

Adjacent isonicotinamide molecules form two self-complementary N–H···O hydrogen bonds [N(8)···O(9) 2.87(3) Å] to yield a head-to-head amide–amide dimer. Through this intermolecular interaction, the carboxamide functionalities act as linear, bridging linkers between CuI 'staircases' to generate two-dimensional infinite sheets almost identical to those displayed by **1**, Fig. 2.

The structures of **1** and **2** are very similar to copper(I) iodide architectures where copper–halide staircases are interconnected through covalent bonds by bridging bidentate ligands.[10] In general, these staircases are normally aligned parallel to each other along the short axis of the unit cell. The length of this axis (which also corresponds to the Cu···Cu separation within a staircase) is *ca.* 4.1–4.4 Å for CuI,[9,10] 3.95–3.98 Å for CuBr, and 3.75–3.78 Å for CuCl containing motifs. The precise orientation and separation of neighbouring ribbons is determined by the specific geometry of the ligand(s). Variations in

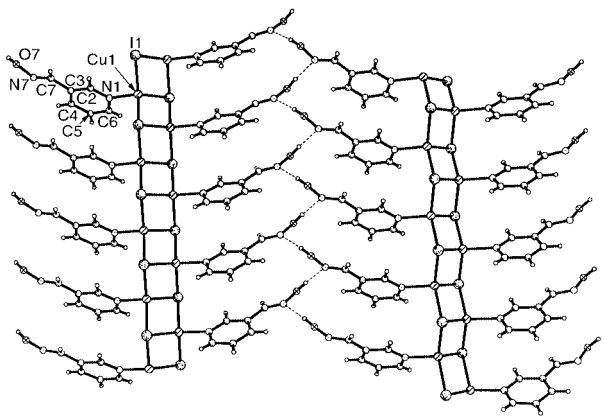

Fig. 1 Infinite 2-D sheets of $[CuI(3\text{-pyridinealdoxime})]_\infty$ **1**. Adjacent oxime moieties bridge polymeric 'staircases' of CuI *via* catemeric hydrogen bonds.

DOI: 10.1039/b001001o

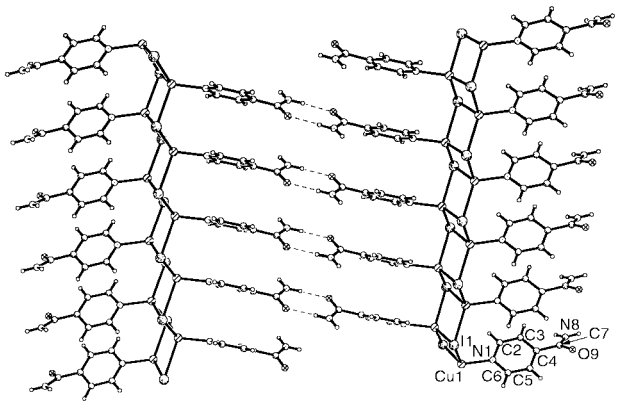

Fig. 2 Infinite 2-D sheets of $[CuI(isonicotinamide)]_\infty$ **2**. Head-to-head amide–amide interactions between isonicotinamide ligands cross-link CuI 'staircases'.

the size and substituent position(s) of the ligand also lead to modifications of the resulting layer (*e.g.* planar *vs.* undulating).

Although the chemical properties of the hydrogen-bonding moieties on the two pyridine-based ligands in **1** and **2** are different, their structural influence is very similar: network topologies and unit cell dimensions are nearly identical.[12] This, of course, is a benefit of using 1-D polymeric chains as building blocks; they are structurally reliable and therefore reduce the task of prediction and control to a much simpler problem. By extending this combined coordination polymer/hydrogen-bond design strategy, one can envisage using a 'pre-formed' 2-D coordination polymer in combination with suitable organic hydrogen-bonding linkers to obtain custom-built porous solids for host–guest applications, *e.g.* separation and catalysis. Further development and applications of this design principle are currently underway in our laboratories.

We acknowledge financial support from Kansas State University and DuPont.

Notes and references

† All starting materials were purchased from Aldrich and used as received. Melting points were determined on a Fisher–Johns melting point apparatus and are uncorrected. In both cases, yields were *ca.* 70–75%.

$[CuI(3\text{-pyridinealdoxime})]_\infty$, **1**: 3-pyridinealdoxime (0.10 g, 0.82 mmol) in the minimum amount of diethyl ether was layered on top of CuI (0.16 g, 0.84 mmol) in acetonitrile. The layered solution was covered and allowed to stand in ambient air. After 1–2 days, yellow rods of **1** were obtained. Mp > 210 °C (decomp.).

$[CuI(isonicotinamide)]_\infty$, **2**: acetonitrile was carefully layered over a solution of isonicotinamide in THF. A saturated solution of CuI in acetonitrile was then added dropwise to the acetonitrile layer. The layered solution was allowed to stand in ambient air. Slow diffusion produced yellow rods of **2** in 1–2 days. Mp > 270 °C (decomp.).

‡ *X-Ray crystallography*: crystalline samples of **1** and **2** were placed in inert oil, mounted on a glass pin, and transferred to the cold gas stream of the diffractometer. Crystal data were collected and integrated using a Bruker SMART 1000 system with graphite monochromated Mo-Kα (λ = 0.71073 Å) radiation at 173 K. The structures were solved using heavy-atom methods using SHELXS-97 and refined using SHELXL-97 (G. M. Sheldrick, University of Göttingen). Non-hydrogen atoms were found by successive full matrix least squares refinement on F^2 and refined with anisotropic thermal parameters. Hydrogen atoms for **1** were located on the difference map, and those for **2** were placed at calculated positions. All hydrogen atoms were then refined using a riding model with fixed thermal parameters [U_{ij} = 1.2 U_{ij}(eq) for the atom to which they are bonded] for subsequent refinements.

Crystal data: for **1**: $C_6H_6N_2OCuI$, M = 312.57, monoclinic, space group $P2_1/c$, a = 13.544(1), b = 4.1098(4), c = 15.094(1) Å, β = 105.583(2)°, U = 809.3(1) Å^3, Z = 4, D_c = 2.565 g cm^{-3}, T = 173(2) K, μ(Mo-Kα) = 6.452 mm^{-1}, wR_2 = 0.0665 (1859 reflections collected, 1752 unique), R = 0.0253 [$I > 2\sigma(I)$].

For **2**: $C_6H_6N_2OCuI$, M = 312.57, monoclinic, space group $P2_1/c$, a = 13.459(2), b = 4.0960(6), c = 16.649(3) Å, β = 109.617(3)°, U = 864.6(2) Å^3, Z = 4, D_c = 2.401 g cm^{-3}, T = 173(2) K, μ(Mo-Kα) = 6.040 mm^{-1}, wR_2 = 0.3177 (1997 reflections collected, 1768 unique), R = 0.0868 [$I > 2\sigma(I)$].

CCDC 182/1617. See http://www.rsc.org/suppdata/cc/b0/b001001o/ for crystallographic files in .cif format.

1 B. F. Abrahams, S. R. Batten, H. Hamit, B. F. Hoskins and R. Robson, *Angew. Chem., Int. Ed. Engl.*, 1996, **35**, 1690; *Crystal engineering: From molecules and crystals to materials*, A NATO Advanced Study Institute and a Euroconference, ed. D. Braga, F. Grepioni and A. G. Orpen, Erice, Italy, 1999, p. 58.

2 Z. Wang, R.-G. Xioing, B. M. Foxman, S. R. Wilson and W. Lin, *Inorg. Chem.*, 1999, **38**, 1523; G. K. H. Shimizu, G. D. Enright, C. I. Ratcliffe, J. A. Ripmeester and D. D. M. Wayner, *Angew. Chem., Int. Ed.*, 1998, **37**, 1407; K. Biradha, C. Seward and M. J. Zaworotko, *Angew. Chem., Int. Ed.*, 1999, **38**, 492; K. A. Hirsch, S. R. Wilson and J. S. Moore, *Chem. Commun.*, 1998, 13; S. W. Keller, *Angew. Chem., Int. Ed. Engl.*, 1997, **36**, 247.

3 C. B. Aakeröy, A. M. Beatty and D. S. Leinen, *Angew. Chem., Int. Ed.*, 1999, **38**, 1815; C. B. Aakeröy, A. M. Beatty and D. S. Leinen, *J. Am. Chem. Soc.*, 1998, **120**, 7383; C. B. Aakeröy and A. M. Beatty, *Chem. Commun.*, 1998, 1067; A. S. Batasanov, P. Hubberstey, C. E. Russel and P. H. Walton, *J. Chem. Soc., Dalton Trans.*, 1997, 2667; C.-W. Chan, D. M. P. Mingos and D. J. Williams, *J. Chem. Soc., Dalton Trans.*, 1995, 2469; M. Munkata, L. P. Wu, M. Yamamoto, T. Kuroda-Sowa and M. Maekawa, *J. Am. Chem. Soc.*, 1996, **118**, 3117; J. C. M. Rivas and L. Brammer, *New J. Chem.*, 1998, **22**, 1315; M. Scudder and I. Dance, *J. Chem. Soc., Dalton Trans.*, 1998, 3167.

4 O. M. Yaghi and H. Li, *J. Am. Chem. Soc.*, 1996, **118**, 295; M. Fujita, Y.-J. Kwon, S. Osamu, K. Yamaguchi and K. Ogura, *J. Am. Chem. Soc.*, 1995, **117**, 7287; C. Janiak, *Angew. Chem., Int. Ed. Engl.*, 1997, **36**, 1431.

5 M. M. Chowdhry, D. M. P. Mingos, A. J. P. White and D. J. Williams, *Chem. Commun.*, 1996, 899; Z.-N. Chen, H.-X. Zhang, K. B. Yu, K. C. Zheng, H. Cai and B.-S. Kang, *J. Chem. Soc., Dalton Trans.*, 1998, 1133; L. Carlucci, G. Ciani, D. M. Proserpio and A. Sironi, *J. Chem. Soc., Dalton Trans.*, 1997, 1801; C. B. Aakeröy and A. M. Beatty, *Cryst. Eng.*, 1998, **1**, 39.

6 V. A. Russell and M. D. Ward, *Chem. Mater.*, 1996, **8**, 1654; C. B. Aakeröy, *Acta Crystallogr., Sect. B*, 1997, **53**, 569; S. Subramanian and M. Zaworotko, *Coord. Chem. Rev.*, 1994, **137**, 357.

7 P. Brunet, M. Simard and J. D. Wuest, *J. Am. Chem. Soc.*, 1997, **119**, 2737.

8 Cu(I)X complexes are also capable of forming cube-like clusters and other discrete species, see: F. A. Cotton and G. Wilkinson, *Advanced Inorganic Chemistry*, Wiley, New York, 5th edn., 1998.

9 S. Kawata, S. Kitagawa, H. Kumagai, S. Iwabuchi and M. Katada, *Inorg. Chim. Acta*, 1998, **267**, 143.

10 A. J. Blake, N. R. Brooks, N. R. Champness, P. A. Cooke, M. Crew, A. M. Deveson, L. R. Hanton, P. Hubberstey, D. Fenske and M. Schröder, *Cryst. Eng.*, 1999, **2**(2/3), 181.

11 B. Rossenbeck and W. S. Sheldrick, *Z. Naturforsch., Teil B*, 1999, **54**, 1510.

12 The same type of lamellar structure with Cu(I)X ribbons connected into sheets is also present in $[Cu(I)Cl(isonicotinic\ acid)]_\infty$; M. A. S. Goher and T. C. W. Mak, *Inorg. Chim. Acta*, 1985, **101**, L27.

ChemComm

Facile dynamical intramolecular exchange of a phosphine ligand between two different metal atoms†

Richard D. Adams,* Burjor Captain, Wei Fu and Perry J. Pellechia

Department of Chemistry and Biochemistry, University of South Carolina, Columbia, SC 29208, USA. E-mail: Adams@mail.chem.sc.edu

Received (in Irvine, CA, USA) 8th February 2000, Accepted 5th April 2000

The cluster complex $PtRu_5(CO)_{15}(PMe_2Ph)(\mu_6\text{-}C)$ has been shown to exhibit facile intramolecular exchange of the phosphine ligand between a platinum and ruthenium atom that is rapid on the NMR timescale at 160 °C.

The ability of polynuclear metal complexes to rearrange their ligand frameworks is central to understanding their reactivity.[1] Today, there are many examples of dynamical exchange of ligands between metal atoms in polynuclear metal complexes.[1,2] CO, CNR and NO ligands are the most common examples of ligands that undergo these exchange processes intramolecularly. Although there is evidence that phosphine ligands may change sites between metal atoms in polynuclear metal complexes,[3] there has heretofore been only one demonstrated example of the *intramolecular* exchange of phosphine ligand between two metal atoms that is rapid on the NMR timescale.[4] Here, we report the first example of facile intramolecular exchange of a phosphine ligand between two different metal atoms in a heteronuclear metal cluster complex.

Reaction of the complex $PtRu_5(CO)_{16}(\mu_6\text{-}C)$ **1**[5] with PMe_2Ph at 25 °C has yielded two new complexes, $PtRu_5(CO)_{15}(PMe_2Ph)(\mu_6\text{-}C)$ **2** (36% yield) and $PtRu_5(CO)_{14}(PMe_2Ph)_2(\mu_6\text{-}C)$ **3** (45% yield).‡ Compounds **2** and **3** were characterized by a combination of IR,§ NMR§ and single-crystal X-ray diffraction analyses.¶ The molecular structures of **2** and **3** are shown in Figs. 1 and 2, respectively. Both compounds are structurally similar to that of **1** and consist of an octahedral cluster containing one platinum and five ruthenium atoms and a single carbon atom in the center. The PMe_2Ph ligand is terminally coordinated to the platinum atom in **2**, while in compound **3** the two PMe_2Ph ligands are both coordinated to ruthenium atoms on opposite sides of the cluster. In both compounds there is a bridging carbonyl ligand between the platinum atom and one of the ruthenium atoms.

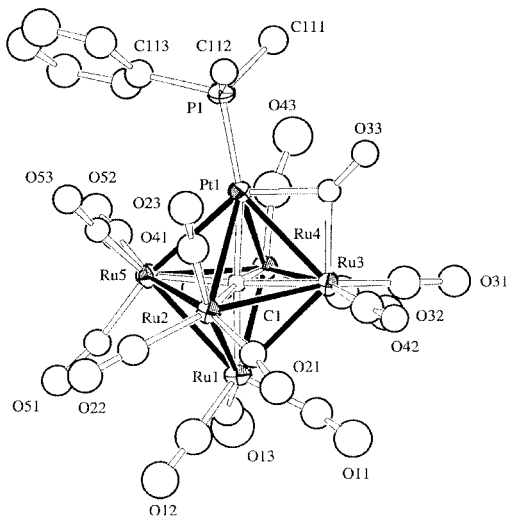

Fig. 1 An ORTEP diagram of the molecular structure of $PtRu_5(CO)_{15}(PMe_2Ph)(\mu_6\text{-}C)$, **2** showing 40% probability thermal ellipsoids. Selected bond distances (Å) and angles (°): Pt(1)–P(1) 2.26(1), Pt(2)–P(2) 2.27(1); Ru(3)–Pt(1)–P(1) 144.5(3), Ru(5)–Pt(1)–P(1) 123.5(3), Ru(10)–Pt(2)–P(2) 145.4(4), Ru(8)–Pt(2)–P(2) 123.6(3).

† Electronic supplementary information (ESI) available: experimental section. See http://www.rsc.org/suppdata/cc/b0/b001080o/

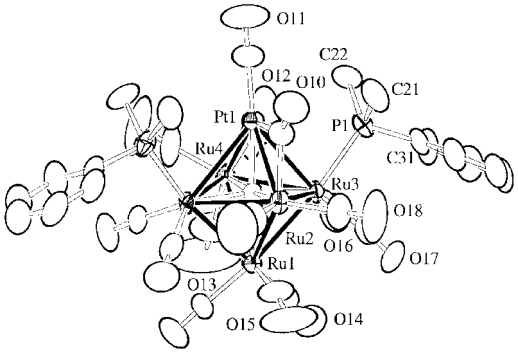

Fig. 2 An ORTEP diagram of the molecular structure of $PtRu_5(CO)_{14}(PMe_2Ph)_2(\mu_6\text{-}C)$ **3** showing 40% probability thermal ellipsoids. Selected bond distances (Å) and angles (°): Ru(3)–P(1) 2.344(2); Pt(1)–Ru(3)–P(1) 81.60(6).

The ^{31}P NMR spectrum of **2** indicates that it exists in solution as a mixture of two isomers in a 7:3 ratio at 25 °C. The resonance of the major isomer, δ −10.52, shows large coupling ($^1J_{PtP}$ 6084 Hz) to the platinum atom indicating that the P and Pt atoms are mutually bonded. By contrast, a small coupling ($^2J_{PtP}$ 115 Hz) to the ^{195}Pt in the phosphorus resonance of the minor isomer, δ 9.51, indicates that the phosphorus atom is coordinated to one of the neighboring ruthenium atoms. This is supported by the ^{31}P NMR spectrum of compound **3** which shows that **3** exists as a mixture of three isomers in solution. One isomer (40% abundance) shows only a single phosphorus resonance with a small ^{195}Pt–^{31}P coupling of 139 Hz. This is assigned to the isomer as found in the solid state that has equivalent phosphine ligands on separate ruthenium atoms. The major isomer (50% abundance) and the minor isomer (10% abundance) both show two phosphorus resonances. For both isomers there is one resonance with large ^{195}Pt –^{31}P coupling, $^1J_{PtP}$ 5999 Hz (major) and $^1J_{PtP}$ 6111 Hz (minor), and one resonance with small coupling, ^{195}Pt–^{31}P, $^2J_{PtP}$ 63 Hz for the major isomer (in the minor isomer the ^{195}Pt–^{31}P coupling was too small to measure). It is proposed that one PMe_2Ph ligand is coordinated to the platinum atom and one PMe_2Ph ligand is coordinated to a ruthenium atom in these two isomers.

^1H NMR spectra of the methyl resonances of **2** at various temperatures are shown in Fig. 3.‖ At 25 °C, two resonances are observed: δ 1.78 (d, 6H, CH_3, $^2J_{PH}$ 10, $^3J_{PH}$ = 53 Hz) (major isomer) and δ 1.98 (d, 6H, CH_3, $^2J_{PH}$ 10 Hz) (minor isomer). The major isomer shows significant ^{195}Pt–^1H coupling. No ^{195}Pt–^1H coupling was observed for the minor isomer. This is consistent with our interpretation of the ^{31}P NMR spectra of **2**. It was observed that the resonances of both isomers broaden and coalesce, reversibly, as the temperature is raised, and most importantly, ^{195}Pt satellites are observed on the resonances in

DOI: 10.1039/b001080o

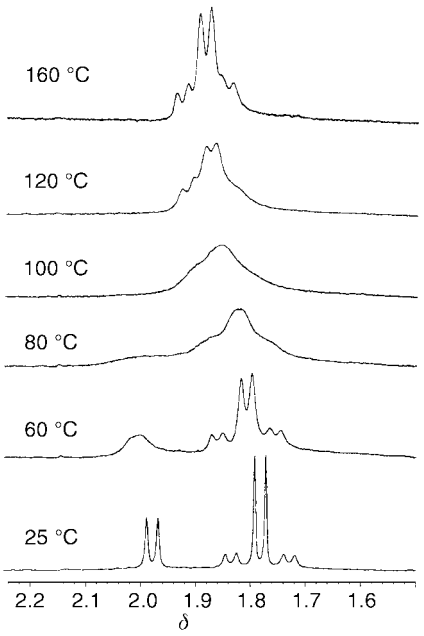

Fig. 3 ^{1}H NMR spectra of compound **2** at various temperatures in 1,2-$C_6D_4Cl_2$ solvent.

the averaged spectrum at 160 °C. The ^{195}Pt–^{1}H coupling of 41 Hz observed at 160 °C is a weighted average of the ^{195}Pt–^{1}H coupling of the two isomers.** These spectra confirm the existence of a dynamical isomerization process by which the phosphine ligand interchanges coordination sites between the platinum atom and one of the ruthenium atoms in **2**, and the observation of the ^{195}Pt–H coupling in the averaged spectra confirms that the process is intramolecular.[6] The exchange broadened spectra were simulated by line shape calculations‖ that have provided exchange rates and in turn activation parameters for the process, $\Delta H^{\ddagger}$ = 15.1(3) kcal mol^{-1} and $\Delta S^{\ddagger}$ = −7.7(9) cal K^{-1} mol^{-1} for the transformation of the major isomer to the minor isomer, and $\Delta H^{\ddagger}$ = 14.5(3) kcal mol^{-1} and $\Delta S^{\ddagger}$ = −11.4(9) cal K^{-1} mol^{-1} for the transformation of the minor isomer to the major isomer.**

A mechanism to explain these observations is shown in Fig. 4. The structure of the major isomer is represented in diagram **2a**. The proposed structure of the minor isomer is represented in diagram **2b**. The dynamical isomerization between **2a** and **2b** can be explained by a shift of the phosphine ligand from the platinum atom to one of the neighboring ruthenium atoms. It is proposed that the phosphine ligand is shifted to the ruthenium atom positioned opposite to that containing the bridging carbonyl ligand. The process may be initiated by a series of CO ligand shifts that traverse the intermediate **A**. To form **A** from **2a**, the bridging CO ligand is shifted to a terminal position on the platinum atom and two terminal CO ligands on ruthenium atoms are shifted to bridging positions across two adjacent Ru–Ru bonds. The structure of **A** is analogous to that of the compound $PtRu_5(CO)_{14}(PPh_2CH_2CH_2PPh_2)(\mu_6\text{-}C)$ **4** recently reported by Lee and Shapley in which both phosphorus atoms of the chelating ligand are coordinated to the platinum atom.[7] The exchange process is completed by a shift of the phosphine ligand from the platinum atom to the ruthenium atom. The bridging CO ligands are shifted to terminal positions as indicated by the arrows in **A** and a terminal CO ligand is moved into a bridging position across the same Pt–Ru bond that contained the bridging CO ligand in **2a**.

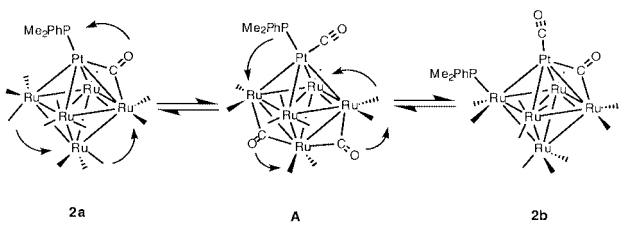

Fig. 4 A proposed mechanism for the isomerization of two isomers of compound **2** by intramolecular shifts of the phosphine and carbonyl ligands between the metal atoms. The carbon atom in the center of the cluster is omitted for clarity.

This research was supported by the Division of Chemical Sciences of the Office of Basic Energy Sciences of the U. S. Dept. of Energy.

Notes and references

‡ A 12.6 mg amount of **1** (0.011 mmol) was allowed to react with 1.2 μL of PMe_2Ph (0.014 mmol) in 15 mL of CH_2Cl_2 at 25 °C for 30 min. Separation by TLC in air using hexane solvent yielded 3.9 mg of **2** (36% yield) and 5.2 mg of **3** (45% yield).

§ *Spectral data*: for **2**: IR ν_{CO}/cm^{-1} (CH_2Cl_2): 2085m, 2066 (sh), 2054vs, 2037vs, 1995 (sh), 1852w, br. ^{1}H NMR (in 1,2-dichlorobenzene-d_4): major isomer **2a**: minor isomer **2b** = 7:3 at 25 °C. For **2a**: δ 1.78 (d, 6H, CH_3, $^2J_{PH}$ 10, $^3J_{PtH}$ 53 Hz); ^{31}P{^{1}H} NMR (in 1,2-dichlorobenzene-d_4): δ −10.52 ($^1J_{PtP}$ 6084 Hz). For **2b**: ^{1}H NMR (in 1,2-dichlorobenzene-d_4): δ 1.98 (d, 6H, CH_3, $^2J_{PH}$ 10 Hz); ^{31}P{^{1}H} NMR (in 1,2-dichlorobenzene-d_4): δ 9.51 ($^2J_{PtP}$ 115 Hz). For **3**: IR ν_{CO}/cm^{-1} (in CH_2Cl_2): 2069m, 2021vs, 1968 (sh), 1811w, br. ^{1}H NMR (in 1,2-dichlorobenzene-d_4): 50% isomer: δ 1.85 (d, 6H, CH_3, $^2J_{PH}$ 9.8, $^3J_{PtH}$ 51.0 Hz), 1.51 (d, 6H, CH_3, $^2J_{PH}$ 10.8 Hz). 40% isomer: δ 1.94 (d, 6H, CH_3, $^2J_{PH}$ 9.5 Hz). 10% isomer: δ 1.75–2.04, J_{PtH} and J_{PH} were obscured in this region. ^{31}P{^{1}H} NMR (in 1,2-dichlorobenzene-d_4): 50% isomer: δ −13.45 (d, $^1J_{PPt}$ 5999, J_{PP} 8 Hz), 9.62 (d, J_{PtP} 63, J_{PP} 8 Hz). 40% isomer: δ 4.35 (s, $^2J_{PPt}$ 139 Hz). 10% isomer: δ −11.80 (d, $^1J_{PtP}$ 6111, J_{PP} 7 Hz), −1.11 (d, J_{PP} 7 Hz).

¶ *Crystal data*: for **2**: $PtRu_5PO_{15}C_{24}H_{11}$, M_r = 1270.76, orthorhombic, space group $Pna2_1$, a = 44.897(5), b = 14.590(2), c = 10.208(2) Å, V = 6687(2) Å^3, T = 20 °C, μ = 6.47 mm^{-1}, R_1 = 0.050, R_2 = 0.080. Two structurally similar independent molecules in the asymmetric crystal unit; anisotropic refinement on Pt, Ru and P only.

For **3**: $PtRu_5P_2O_{14}C_{37}H_{28}$, M_r = 1459.01, monoclinic, space group $P2_1/m$, a = 9.407(1), b = 25.955(7), c = 9.980(1) Å, β = 113.41(1)°, V = 2236.0(7) Å^3, T = 20 °C, μ = 4.88 mm^{-1}, R_1 = 0.034, R_2 = 0.046. Compound **2** has mirror symmetry in the solid state; anisotropic refinement of all non-hydrogen atoms.

CCDC 182/1610. See http://www.rsc.org/suppdata/cc/b0/b001080o/ for crystallographic files in .cif format.

‖ Lineshape simulations of spectra in the exchange broadened region were preformed by using the program EXCHANGE written by R. E. D. McClung, Dept. of Chemistry, University of Alberta, Edmonton, Alberta, Canada. Variable temperature ^{1}H NMR spectra of compound **3** show that it is also undergoing dynamical processes indicative of rapid phosphine ligand exchanges.

** A plot of the temperature dependence of the equilibrium, minor isomer to major isomer, provided the thermodynamic parameters $\Delta H°$ = 0.58(8) kcal mol^{-1} and $\Delta S°$ = 3.7(3) cal K^{-1} mol^{-1}. From these parameters the ratio of the major isomer/minor isomer is calculated to be 3.3:1 at 160 °C. From this ratio, the weighted average of the ^{195}Pt–^{31}P coupling constant is calculated to be 40.7 Hz.

1 B. F. G. Johnson and R. E. Benfield, in *Transition Metal Clusters*, B. F. G. Johnson, John Wiley, Chichester, 1980, ch. 7; E. L. Muetterties and E. Band, *Chem. Rev.*, 1978, **78**, 639.
2 R. D. Adams and F. A. Cotton, in *Dynamic Nuclear Magnetic Resonance Spectroscopy*, ed. L. Jackman and F. A. Cotton, Academic Press, New York, 1975, ch. 12; L. J. Farrugia and A. G. Orpen, in *Metal Clusters in Chemistry*, ed. P. Braunstein, L. A. Oro and P. R. Raithby, Wiley-VCH, Weinheim, 1999, ch. 3.4.
3 G. Bondietti, G. Laurenczy, R. Ros and R. Roulet, *Helv. Chim. Acta*, 1994, **77**, 1869; G. Laurenczy, G. Bondietti, A. Merbach, B. Moullet and R. Roulet, *Helv. Chim. Acta*, 1994, **77**, 547; S. Bouherour, P. Braunstein, J. Rosé and L. Toupet, *Organometallics*, 1999, **18**, 4908; P. Braunstein, J. Rosé, D. Toussaint, S. Jääskeläinen, M. Ahlgren, T. A. Pakkanen, J. Pursiainen, L. Toupet and D. Grandjean, *Organometallics*, 1994, **13**, 2472.
4 A. M. Bradford, G. Douglas, L. Manojlovic'-Muir, K. W. Muir and R. J. Puddephatt, *Organometallics*, 1990, **9**, 409.
5 R. D. Adams and W. Wu, *J. Cluster Sci.*, 1991, **2**, 271.
6 J. P. Jesson and E. L. Muetterties, in *Dynamic Nuclear Magnetic Resonance Spectroscopy*, ed. L. Jackman and F. A. Cotton, Academic Press, New York, 1975, ch. 8.
7 K. Lee and J. R. Shapley, *Organometallics*, 1998, **17**, 3020.

ChemComm

Proquinoid acceptors as building blocks for the design of efficient π-conjugated fluorophores with high electron affinity

Jean-Manuel Raimundo, Philippe Blanchard, Hugues Brisset, Said Akoudad and Jean Roncali*

Ingénierie Moléculaire et Matériaux Organiques, CNRS UMR 6501, Université d'Angers, 2 Bd Lavoisier, 49045 Angers Cedex, France. E-mail: jean.roncali@univ-angers.fr

Received (in Cambridge, UK) 24th March 2000, Accepted 17th April 2000

The association of aromatic electron donor groups with proquinoid acceptors leads to π-conjugated fluorophores combining tunable emission wavelength at constant geometry, high fluorescence efficiency and high electron affinity.

Conjugated fluorophores usable as active materials for light emitting diodes (LEDs) should ideally combine high emission quantum yields, tunable emission spectra and high electron affinity in order to allow electron injection from stable metal cathodes.[1]

The difficulty of meeting these various prerequisites with a single compound has given rise to specific synthetic approaches. Thus, control of the emission wavelength has been realized by adjusting the conjugation length of the fluorophore,[1,2] while increases in electron affinity have been achieved by incorporation of electron deficient groups, such as *e.g.* cyano or oxadiazole, in the π-conjugated system.[1,3]

It has been shown that the association of five-membered heterocycles with electron-deficient systems such as thienopyrazine or benzo[*c*]thiadiazole (BTD) which have a strong propensity to impose a quinoid geometry on the ground state of the conjugated system, leads to polymers with small intrinsic band gaps.[4] As part of our continuing interest in band gap engineering,[5] we have synthesized a new series of tricyclic π-conjugated systems **1**–**4** based on this approach. Besides their

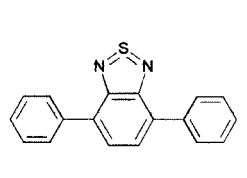

1

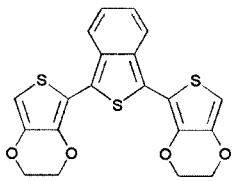

2

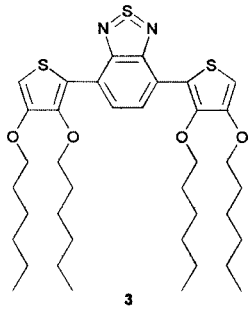

3

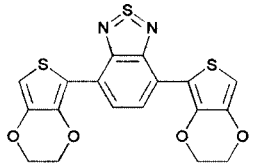

4

use as precursors for low band gap polymers,[6] these compounds exhibit original electronic and optical properties which make them potentially interesting for the design of photoluminescent materials for LEDs.

Compounds **1**, **3** and **4** were synthesized from 4,7-dibromo-2,1,3-benzothiadiazole.[7] Compound **1** was obtained by Suzuki coupling with phenyl boronic acid and compounds **3** and **4** were prepared by Stille coupling with the tributylstannyl derivatives of 3,4-dihexyloxythiophene[8] and 3,4-ethylenedioxythiophene, respectively (Scheme 1). Compound **2** was prepared using a procedure already described for the synthesis of 2,5-dithienylbenzo[*c*]thiophene.[9] Reaction of phthaloyl chloride with 2-mercaptopyridine led to 1,2-bis[*S*-(2-pyridyl)]benzenedithioate **6** which was then reacted with 3,4-ethylenedioxy-2-thienylmagnesium bromide to give diketone **5**. Compound **2** was then obtained by ring closure with the Lawesson reagent (L.R.). Compounds **1**–**4** have been characterized by ^{1}H and ^{13}C NMR spectroscopy, mass spectrometry and elemental analysis.†

Table 1 lists the cyclic voltammetric (CV) and optical data for compounds **1**–**4**. Literature data for terphenyls (**3P**) and terthienyl (**3T**) have been included for comparison. Compounds **1**–**4** are reversibly reduced to their anion radicals and irreversibly oxidized owing to electropolymerisation. The values of the absorption maximum (λ_{max}) and HOMO–LUMO gap, ΔE (estimated from the absorption edge), for **3P** and **1** show that replacement of the median phenyl ring by the BTD group produces a 100 nm red shift of λ_{max} and a 1.10 eV decrease in ΔE. Comparison of the anodic peak potentials (E_{pa}) for **3P** and **1** shows that the BTD group scarcely affects the oxidation

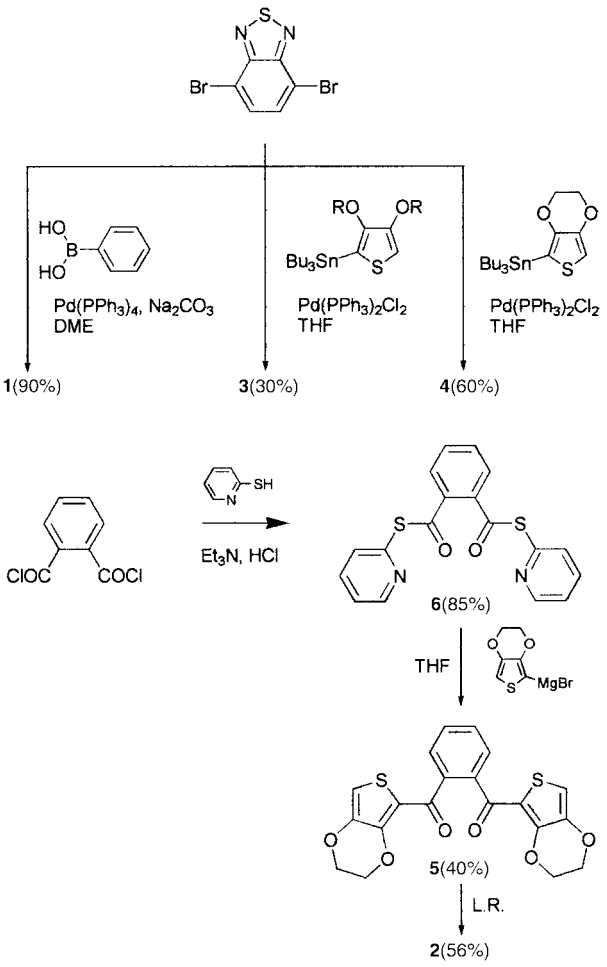

Scheme 1

DOI: 10.1039/b002369h

Table 1 CV[a] and optical[b] data for compounds **1**–**4**

Compd.	E_{pa}/V	E_{pr}/V	λ_{max}/nm	ΔE/eV	λ_{em}/nm	ϕ_f
3P	1.80[c]	−2.70[c,d]	279[e]	3.97	339[e]	0.93[e]
1	1.82	−1.36	380	2.87	490	0.80
3T	1.10	−2.00[f]	350	3.05	430	0.066[g]
2	0.56	−1.80	450	2.33	613	0.92
3	1.06	−1.28	456	2.29	542	0.73
4	0.92	−1.40	481	2.19	630	0.75

[a] In 0.1 M NBu_4PF_6–MeCN, ref. SCE, 100 mV s^{-1}. [b] In CH_2Cl_2. [c] *vs.* Ag/AgCl (ref. 11). [d] In NBu_4Br–DMA (ref. 11). [e] In cyclohexane (ref. 12). [f] In NBu_4–DMF (ref. 13). [g] In dioxane (ref. 14).

potential but produces a positive shift of the reduction peak potential (E_{pr}) by more than 1.30 V, indicating a considerable increase in electron affinity.

As expected, thiophene-based compounds exhibit smaller ΔE values than **1** owing to the lower resonance energy of thiophene and the electron releasing effect of the alkoxy groups.[5]

Comparison of the optical data for **3T** and **2** shows that the combined effects of replacement of the median thiophene by benzo[*c*]thiophene and electron-releasing ethylenedioxy substituents produce a *ca.* 100 nm red shift of λ_{max} associated with a 0.70 eV decrease in ΔE. On the other hand, the 0.54 V decrease in E_{pa} and the 0.20 V positive shift of E_{pr}, indicated by the CV data, show that the gap reduction is essentially related to raising of the HOMO level.

Further replacement of the benzo[*c*]thiophene in **2** by the BTD group (**3** and **4**) produces a 6–31 nm red shift of λ_{max} and a small decrease in ΔE. However, the 0.40–0.50 V parallel positive shift of both E_{pa} and E_{pr} shows that the BTD group induces major changes in the HOMO and LUMO levels, with again a large enhancement of electron affinity. The small decrease in ΔE from **3** to **4** and the slight negative shift of E_{pa} reflects the stronger electron-donating effect of the ethylenedioxy bridge compared to dialkoxy chains.[8]

The fluorescence properties of compounds **1**–**4** have been analyzed in CH_2Cl_2 and the emission quantum yields (ϕ_f) have been determined against anthracene in 95% EtOH for **1**, and perylene in 95% EtOH for **2**–**4**. Introduction of BTD in the **3P** system produces a 150 nm red shift of the emission maximum (λ_{em}) and a 50 nm increase in the Stokes shift. Whereas the effect of BTD on ϕ_f is difficult to evaluate due to the different experimental conditions, the measured value of 0.80 for **1** shows that ϕ_f remains high.

Comparison of the data for **3T** and **2**–**4** reveals a large red shift of λ_{em} (up to 200 nm for **4**) and a 70–80 nm increase in the Stokes shift for **2** and **4**. Furthermore, the three compounds exhibit a considerable increase in ϕ_f which reaches a value as high as 0.92 for **2**. The significant increase in ϕ_f compared to the analog of **2** based on unsubstituted thiophene (ϕ_f = 0.67),[10] underlines the strong effect of the ethylenedioxy substituents on the fluorescence efficiency.

To summarize, we have shown that the insertion of proquinoid acceptor groups in short-chain π-conjugated oligomers leads to fluorophores with a unique combination of enhanced electron affinity, high fluorescence efficiency and ready control of the emission wavelength at constant chain length. In addition to the intrinsic interest of these compounds as a new class of efficient fluorophores, the above synthetic strategy could open interesting perspectives for the design of active molecular or polymeric materials for LEDs.

Notes and references

† **1**: yellow powder, mp 127–129 °C. $\delta_H(CDCl_3)$: 7.97 (dd, 4H, ^3J 8.39, ^4J 1.17 Hz), 7.80 (s, 2H), 7.56 (t, 4H, ^3J 7.51 Hz), 7.47 (t, 2H, ^3J 7.42 Hz). $\delta_C(CDCl_3)$: 154.1, 137.4, 133.3, 129.3, 128.6, 128.4, 128.1. Anal: found (calc.): C, 74.99 (74.98); H, 4.35 (4.20); N, 9.51 (9.72); S, 11.10 (11.15)%.

2: brown solid, mp 146–148 °C. $\delta_H(CDCl_3)$: 7.96 (m, 2H), 7.13 (m, 2H), 6.42 (s, 2H), 4.32 (m, 4H), 4.27 (m, 4H). MS: *m/z* (%) 414 (M^+; 100), 317 (60). HRMS: calc. 414.0058, found 414.0054. Anal: found (calc.): C, 57.58 (56.95); H, 3.49 (3.40); O, 16.02 (15.44); S, 22.96 (23.21)%.

3: orange solid, mp 79–80 °C. $\delta_H(CDCl_3)$: 8.39 (s, 2H), 6.37 (s, 2H), 4.10 (t, 4H, ^3J 6.60 Hz), 4.02 (t, 4H, ^3J 6.60 Hz), 1.82 (m, 4H), 1.70 (m, 4H), 1.50 (m, 4H), 1.36 (m, 12H), 1.24 (m, 8H), 0.92 (m, 6H), 0.84 (m, 6H). $\delta_C(CDCl_3)$: 152.8, 150.3, 144.9, 127.6, 124.5, 120.6, 98.2, 72.9, 70.0, 31.5, 30.1, 29.1, 25.8, 25.6, 22.6, 22.5, 14.1, 14.0. MS: *m/z* (%) 700 (M^+; 100), 615 (20), 531 (20). HRMS: calc. 700.3402, found 700.3412.

4: brown solid, mp 314 °C. $\delta_H(CDCl_3)$: 8.4 (1s, 2H), 6.55 (s, 2H), 4.44 (t, 4H), 4.31 (t, 4H). $\delta_C(CDCl_3)$: 152.3, 141.6, 140.2, 126.6, 123.6, 113.7, 101.9, 64.9, 64.3. Anal: found (calc.): C, 51.77 (51.91); H, 3.04 (2.90); N, 6.62 (6.73); O, 15.28 (15.37); S, 23.29 (23.09)%.

1 A. Kraft, A. C. Grimsdale and A. B. Holmes, *Angew. Chem., Int. Ed.*, 1998, **37**, 402.
2 B. S. Kang, M.-L. Seo, Y. S. Jun, C. K. Lee and S. C. Shin, *Chem. Commun.*, 1996, 1167; R. Gomez, J. L. Segura and N. Martin, *Chem. Commun.*, 1999, 619.
3 N. C. Greeham, S. C. Moratti, D. C. C. Bradley, R. H. Friend and A. B. Holmes, *Nature*, 1993, **365**, 628; X.-C. Li, A. B. Holmes, A. Kraft, S. C. Moratti, G. W. Spencer, F. Cacialli, J. Grüner and R. H. Friend, *J. Chem. Soc., Chem. Commun.*, 1995, 2211; W.-L. Yu, H. Meng, J. Pei, Y.-H. Lai, S.-J. Chua and W. Huang, *Chem. Commun.*, 1998, 1957; U. Mitschke, E. Mena Osteritz, T. Debaerdemaeker, M. Sokolowski and P. Bäuerle, *Chem. Eur. J.*, 1998, **4**, 2211.
4 S. Kitamura, S. Tanaka and Y. Yamashita, *Chem. Mater.*, 1996, **8**, 570; S. Akoudad and J. Roncali, *Chem. Commun.*, 1998, 2081.
5 J. Roncali, *Chem. Rev.*, 1997, **97**, 173.
6 J.-M. Raimundo, P. Blanchard, S. Akoudad and J. Roncali, unpublished work.
7 K. Pilgram, M. Zupan and R. Skiles, *J. Heterocycl. Chem.*, 1970, **7**, 629.
8 S. Akoudad, P. Frère, N. Mercier and J. Roncali, *J. Org. Chem.*, 1999, **64**, 4267.
9 D. Vangeneugden, R. Kiebooms, P. Adriaensens, D. Vanderzande, J. Gelan, J. Desmet and G. Huyberechts, *Acta Polym.*, 1998, **49**, 687.
10 P. Bäuerle, G. Götz, P. Emerle and H. Port, *Adv. Mater.*, 1992, **9**, 564.
11 K. Meerholtz and J. Heinze, *Electrochim. Acta*, 1996, **41**, 1839.
12 H. Du, R. A. Fuh, J. Li, A. Corkan and J. S. Lindsey, *Photochem. Photobiol.*, 1998, **68**, 141.
13 D. Jones, M. Guerra, L. Favaretto, A. Modelli, M. Fabrizio and G. Distefano, *J. Phys. Chem.*, 1990, **94**, 5761.
14 R. S. Becker, J. Seixas de Melo, A. L. Maçanita and F. Elisei, *Pure Appl. Chem.*, 1995, **67**, 9.

ChemComm

Colloid-catalysed arene hydrogenation in aqueous/supercritical fluid biphasic media†

R. Jason Bonilla,[a] Brian R. James[b] and Philip G. Jessop*[a]

[a] *Department of Chemistry, University of California, Davis, CA, USA 95616. E-mail: jessop@chem.ucdavis.edu*
[b] *Department of Chemistry, University of British Columbia, 2036 Main Mall, Vancouver, B.C., Canada V6T 1Z1*

Received (in Bloomington, IN, USA) 3rd September 1999, Revised manuscript received 15th December 1999, Accepted 15th March 2000

Hydrogenation of arenes, including the lignin model compound 2-methoxy-4-propylphenol, has been effected using a Rh colloid in biphasic aqueous/supercritical ethane reaction media; this is the first successful example of an unsupported colloid-catalysed hydrogenation of a substrate in a supercritical fluid; the same reaction does not proceed in aqueous/supercritical carbon dioxide or ionic liquid/supercritical fluid media.

Catalysis performed in aqueous/organic biphasic media, with the catalyst in the aqueous phase and hydrophobic substrates and products in the organic phase, is appealing for industry because the products can be separated cleanly and easily from the catalyst with negligible loss of catalyst.[1] However, given the ability of water to retain high levels of organic solvent residues, the disposal of the aqueous phase can be problematic. A more environmentally benign alternative is to use aqueous/supercritical fluid (SCF) biphasic media for catalysis. In such a scheme the catalyst resides in the aqueous phase and the non-polar SCF phase dissolves and transports the substrates, reagent gases (if any) and products. The advantages of using SCFs such as carbon dioxide ($scCO_2$) or ethane (scC_2H_6) over liquid organic solvents include lower environmental impact, enhanced diffusion rates of H_2, ease of recycling, and facile removal of the SCF solvent from the product and from the aqueous phase.[2] Aqueous/SCF biphasic media have been found to be effective for several types of catalysts, including enzymes,[3] antibodies,[4] and water-soluble homogeneous catalysts.[5,6] We now report the use of aqueous/SCF biphasic media for arene hydrogenation with a colloidal catalyst.

Hydrogenation of arenes, an important chemical process in the synthesis of fine chemicals,[7] can be catalysed by Raney nickel, supported palladium or nickel catalysts, homogeneous catalysts or colloidal catalysts. Many of the "homogeneous" catalysts that have been reported for arene hydrogenation are in fact catalytically active colloidal metal particles.[8] Such particles are known to be quite active and are usually prepared *in situ* in biphasic aqueous/organic reaction media.[9] Hydrogenations with this type of catalyst can be achieved at room temperature and low hydrogen pressure.[10,11]

Colloid-catalysed reactions in SCFs or aqueous/SCF biphasic media have not been much studied in the past. Zemanian *et al.* reported minimal conversion (0.25–1%) in the hydrogenation of naphthalene to tetralin using a colloidal $CoMoO_3$ catalyst in reverse micelles in supercritical butane at 135–155 °C.[12] In our laboratory we have tested the hydrogenation of a series of arenes in a biphasic, aqueous/SCF using Rh colloids generated *in situ* from the complex $[RhCl(cod)]_2$.

The first tests in this series were of the hydrogenation of 2-methoxy-4-propylphenol. This compound was selected because results published earlier[13] showed it to be particularly difficult to hydrogenate and because it is a model for the phenolic groups in lignin; the hydrogenation of the aromatic rings in lignin has been proposed as a method of preventing the yellowing of mechanical pulps.[13,14] The reactions were performed in 1.5 mL aqueous buffer and 29.5 mL of supercritical fluid, with the catalyst precursor, surfactant (tetrabutylammonium hydrogen sulfate, THS) and arene typically in a Rh : THS : arene ratio of 1 : 3 : 50.

The hydrogenation did not proceed in aqueous/$scCO_2$ biphasic media (Table 1); the likely reason being the low pH due to the dissolution of CO_2 in the aqueous phase (see ESI†). Rh colloidal catalysts are particularly sensitive to pH, with optimum activity at pH 7.4–7.6.[10] In order to bypass the pH problem, attempts were made to use a non-aqueous polar solvent in place of the water.‡ For example, the ionic liquid $[bmim]BF_4$ (bmim = 1-butyl-3-methylimidazolium cation) is insoluble[15] in $scCO_2$ and therefore is an appropriate substitute. Unfortunately, the colloidal catalyst in the present experiments was not active for hydrogenation in $[bmim]BF_4/scCO_2$, $[bmim]BF_4/scC_2H_6$, or $[bmim]BF_4$/pentane mixtures. The catalyst may have been inactivated by the ionic liquid itself or by trace chloride ions[16] remaining from the preparation of the ionic liquid.

In an aqueous/supercritical ethane (scC_2H_6) biphasic medium, excellent results were obtained (Scheme 1 and Table 1). At a substrate : Rh ratio of 10 : 1, complete conversion was obtained, while at 50 : 1, the reaction was 88% complete (Table 1). This is the first successful example of the use of an aqueous-phase colloidal catalyst for the hydrogenation of a substrate in a supercritical phase. Hydrogenations using liquid C_2H_6 as the non-polar phase were also achieved. In all cases, the major

Table 1 Reaction conditions for the hydrogenation of 2-methoxy-4-propylphenol[a]

Non-polar Phase	S/Rh[b]	Surfactant	Buffer pH	P_{total}/bar	*t*/h	Conv. (%)
At room temp. and 4 bar H_2						
liq. C_5H_{12}	10	THS	7.5	4	46	100
liq. C_2H_6	10	THS	7.5	49	64	100
liq. CO_2	50	THS	7.5	74	66	0
At 36 °C and 10 bar H_2						
liq. C_5H_{12}	50	THS	7.5	10	72	100
scC_2H_6	10	THS	7.5	240	72	100
scC_2H_6	50	THS	7.5	240	72	88
scC_2H_6	50	AOT[c]	7.5	240	96	4
$scCO_2$	10	None	None	240	78	0
$scCO_2$	50	THS	7.5	210	50	0
$scCO_2$	50	THS	11.2[d]	210	60	8
$scCO_2$	50	THS	7.2[e]	220	72	0

[a] The catalyst precursor $[RhCl(1,5\text{-cod})]_2$ was used for all reactions. The buffer is 0.1 M Na_3PO_4, 0.05 M citric acid, and 0.2 M boric acid except where noted. The buffer pH refers to the pH at room pressure. [b] Substrate / rhodium mole ratio. [c] 1 M AOT, conversion determined by GC. [d] 0.5 M Na_3PO_4, 0.05 M citric acid and 0.2 M boric acid. [e] 1 M MOPS solution.

† Electronic supplementary information (ESI) available: experimental details, description of the effect of changing the buffer, plot of pH of aqueous buffers under 10 atm H_2 and varying pressures of CO_2. See http://www.rsc.org/suppdata/cc/a9/a907193h/

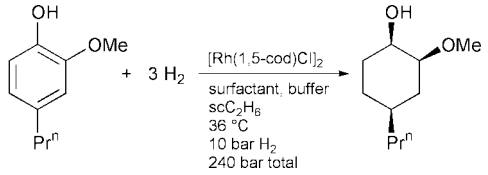

Scheme 1

product was *cis*-2-methoxy-*cis*-4-propylcyclohexanol. The minor product, which had been observed in small amounts in earlier studies, was *cis*-2-methoxy-*trans*-4-propylcyclohexanol. The ratio of products was 8 : 1 in all runs, regardless of whether scC_2H_6 or an organic liquid was used. This high selectivity indicates that the hydrogenation of the arene ring takes place without the partially-hydrogenated substrate dissociating from the catalyst.[14]

Switching the surfactant from THS (0.04 M) to AOT (dioctylsulfosuccinate, sodium salt, 1 M), which has been used previously for the preparation of aqueous/scC_2H_6 emulsions,[17–20] resulted in a dramatic drop in the catalytic activity.§

The extension of the method to the hydrogenation of simpler arenes was also explored (Table 2). In these experiments, an even higher substrate : Rh ratio of 100 : 1 was used. Conversions were high in all cases. The hydrogenation of 4-phenylbutanone was essentially complete and highly selective for hydrogenation at the arene ring only. *p*-Xylene was primarily converted to *cis*-1,4-dimethylcyclohexane, although it is interesting that the selectivity for hydrogenation on a single face was greater for 2-methoxy-4-propylphenol than xylene. One could speculate that the hydroxy and methoxy groups help anchor the substrate to the metal surface.

Catalytic activity in this system may be related to the solubility of the substrates. The range of arenes tested encompasses hydrophilic and hydrophobic arenes. Phenol, which is very soluble in water and essentially insoluble in alkanes, was completely hydrogenated. It is tempting to conclude that solubility in water is a requirement for efficient hydrogenation by this method, but the conversion of *p*-xylene, which is far more soluble in alkanes than it is in water, was still fair. Unfortunately, the literature does not contain solubility data for these arenes in scC_2H_6, but the solubility is expected to be similar to that in $scCO_2$. Xylene[21] and anisole[22] are completely miscible with $scCO_2$ but benzyl alcohol[23] and phenol[24] have limited solubilities of 1–2 mol% at 36–40 °C and elevated pressures (above 140 bar). Despite this wide range of solubilities, the extent of hydrogenation was satisfactory for all substrates.

Table 2 The hydrogenation of other arenes in H_2O/scC_2H_6[a]

Substrate	TON	Products (%)
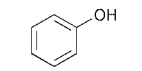	100	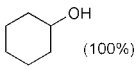 (100%)
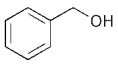	110[b]	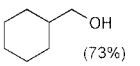 (73%)
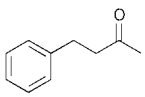	99	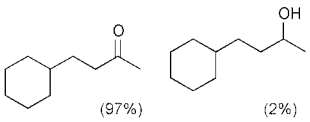 (97%) (2%)
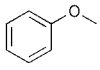	77	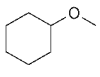 (77%)
	79	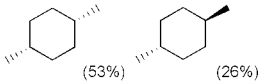 (53%) (26%)
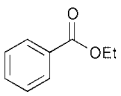	96	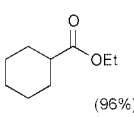 (96%)

[a] Conditions: 36 °C, 62 h, 31 mL vessel, 240 bar total pressure (10 bar H_2, balance ethane), 9.5 μmol $[RhCl(1,5\text{-cod})]_2$, 76 μmol THS, and 1.9 mmol arene (arene : Rh ratio of 100 : 1) were used for all reactions. The buffer is 0.1 M Na_3PO_4, 0.05 M citric acid and 0.2 M boric acid (buffer volume 1.7 mL, pH at atmospheric pressure 7.5). TON = turnover number = mol product per mol Rh. [b] Arene : Rh ratio of 150 : 1.

In conclusion, arene hydrogenation is catalysed by Rh colloids with high conversion in an aqueous/scC_2H_6 biphasic medium. The same reaction in aqueous/$scCO_2$ biphasic medium does not proceed, probably due to pH problems which could not be alleviated by the use of buffers. These results are new examples of transition-metal catalysed reactions in aqueous/SCF biphasic solvent mixtures.

We acknowledge experimental assistance from Miss Denise Nakawatase and Mr Christopher Ablan, valuable discussions with Dr Joan Brennecke (University of Notre Dame), and funding from the University of California.

Notes and references

‡ This is complicated by the fact that most polar organic solvents are quite soluble in $scCO_2$. For example, using a methanol or methoxyethanol solution of the Rh catalyst precursor gave no conversion, presumably because the organic solvent entirely dissolved in the supercritical phase.
§ The effect of applying shear to create an emulsion was not tested.

1 *Aqueous-Phase Organometallic Catalysis*, ed. B. Cornils and W. A. Herrmann, Wiley-VCH, Weinheim, 1998.
2 *Chemical Synthesis using Supercritical Fluids*, ed. P. G. Jessop and W. Leitner, Wiley-VCH, Weinheim, 1999.
3 O. Aaltonen, in *Chemical Synthesis using Supercritical Fluids*, ed. P. G. Jessop and W. Leitner, Wiley-VCH, Weinheim, 1999.
4 P. Fong, J. Hasserodt and P. G. Jessop, in preparation.
5 B. M. Bhanage, Y. Ikushima, M. Shirai and M. Arai, *Chem. Commun.*, 1999, 1277.
6 B. M. Bhanage, Y. Ikushima, M. Shirai and M. Arai, *Tetrahedron Lett.*, 1999, **40**, 6427.
7 R. J. Farrauto and C. H. Bartholomew, *Fundamentals of Industrial Catalytic Processes*, Blackie Academic & Professional, London, 1997.
8 K. S. Weddle, J. D. Aiken III and R. G. Finke, *J. Am. Chem. Soc.*, 1998, **120**, 5653.
9 S. Yang and L. M. Stock, *Energy Fuels*, 1998, **12**, 644.
10 K. R. Januszkiewicz and H. Alper, *Organometallics*, 1983, **2**, 1055.
11 J. Schulz, A. Roucoux and H. Patin, *Chem. Commun.*, 1999, 535.
12 T. S. Zemanian, R. M. Bean, J. L. Fulton, J. C. Linehan and R. D. Smith, *Proceedings 2nd International Symposium on Supercritical Fluids, Boston, Massachusetts*, 1991, pp. 193–195.
13 T. Q. Hu, B. R. James and C. L. Lee, *J. Pulp Paper Sci.*, 1997, **23**, J153.
14 T. Q. Hu, B. R. James, S. J. Rettig and C.-L. Lee, *Can. J. Chem.*, 1997, **75**, 1234.
15 L. A. Blanchard, D. Hancu, E. J. Beckman and J. F. Brennecke, *Nature*, 1999, **399**, 28–29.
16 P. J. Dyson, D. J. Ellis, D. G. Parker and T. Welton, *Chem. Commun.*, 1999, 25.
17 J. Eastoe, B. H. Robinson, A. J. W. G. Visser and D. C. Steytler, *J. Chem. Soc., Faraday Trans.*, 1991, **87**, 1899.
18 Y. Ikushima, N. Saito and M. Arai, *J. Colloid Interface Sci.*, 1997, **186**, 254.
19 Z. Shervani and Y. Ikushima, *J. Supercrit. Fluids*, 1998, **13**, 375.
20 K. P. Johnston, G. B. Jacobsen, C. T. Lee, C. Meredith, S. R. P. Da Rocha, M. Z. Yates, J. DeGrazia and T. W. Randolph, in *Chemical Synthesis using Supercritical Fluids*, ed. P. G. Jessop and W. Leitner, Wiley-VCH, Weinheim, 1999.
21 R. S. Mohamed and G. D. Holder, *Fluid Phase Equilib.*, 1987, **32**, 295.
22 S.-D. Park, C.-H. Kim and C.-S. Choi, *J. Chem. Eng. Data*, 1991, **36**, 80.
23 D. Walther and G. Maurer, *J. Chem. Eng. Data*, 1993, **38**, 247.
24 R. A. Van Leer and M. E. Paulaitis, *J. Chem. Eng. Data*, 1980, **25**, 257.

A new open-framework fluorinated gallium phosphate with large 18-ring channels (MIL-31)

Capucine Sassoye,[a] Thierry Loiseau,[a] Francis Taulelle[b] and Gérard Férey*[a]

[a] *Institut Lavoisier, UMR CNRS 8637, Université de Versailles St Quentin, 45, Avenue des Etats-Unis, Versailles cedex, 78035 France. E-mail: ferey@chimie.uvsq.fr*

[b] *Laboratoire de RMN et Chimie du Solide, UMR Brüker-CNRS-ULP 7510, Institut Le Bel, Université Louis Pasteur, 4, rue Blaise Pascal, 67070 Strasbourg, France*

Received (in Oxford, UK) 9th March 2000, Accepted 26th April 2000

A new open-framework fluorinated gallium phosphate (MIL-31) containing the $Ga_9(PO_4)_9(H_2O)(OH)(OH,F)_4^{5-}$ anion was hydrothermally synthesized by using long alkyl chain diamines (C_9 and C_{10}) as structure-directing agents; its crystal structure is built up from hexameric units and exhibits large one-dimensional hexagonal channels delimited by 18-rings.

The search for new large pore materials has received much attention because of their potential applications in catalysis, ion exchange or molecular sieving. Historically, most of the porous solids are zeolite aluminosilicates and metal phosphates. Since the discovery of $AlPO_4$-*n*[1] in 1982, the syntheses of a large diversity of new open-framework structures[2] have been reported, many incorporating other elements such as B, Be, Ga, In, Sn, Sb or transition metals as well as oxyfluorides, sulfides, phosphonates, carboxylates, *etc*. Phosphate-based three-dimensional architectures contain pores larger than those usually observed in aluminosilicates. Whereas the pore size limit encountered in silicates corresponds to 14-membered rings (UTD-1[3]), some phosphates are characterized by extra large pore open-frameworks with 16-ring (Ga-ULM-5,[4] Ga-ULM-16,[5] Fe-ULM-15[6]), 18-ring (Al-VPI-5[7]), 20-ring (Al-JDF-20,[8] Ga-cloverite,[9] FePO,[10] GaPO[11]) and very recently 24-ring channels (Ni-VSB-1,[12] Zn-ND-1[13]). We now report here a new fluorinated gallium phosphate exhibiting a three-dimensional open-framework with 18-ring channels.

The MIL-31 compounds were synthezised under mild hydrothermal conditions by using either 1,9-diaminonane (DAN) or 1,10-diaminodecane (DAD) as structure-directing agents. There were prepared (180 °C, 3 days, autogenous pressure) from a mixture of gallium oxyhydroxide [GaO(OH), prepared from the reaction of gallium metal (4N, Rhône-Poulenc) with water at 200 °C for 24 h), phosphoric acid (H_3PO_4, 85%, Prolabo), hydrofluoric acid (HF, 48%, Prolabo), tripropylamine [NPr^n_3 (TPA), 98% Aldrich], 1,9-diaminononane [$H_2N(CH_2)_9NH_2$, 98% Aldrich] or 1,10-diaminodecane [$H_2N(CH_2)_{10}NH_2$, 97% Aldrich] and deionized water. Typically, the molar ratio was 1 Ga (0.356 g) : 1 P (0.16 ml) : 0.5 F (0.06 ml) : 80 H_2O (5 ml) : 0.4 TPA (0.25 ml) : 0.25 DAN (0.137 g) or 0.25 DAD (0.149 g). TPA was added in order to fix the reaction pH to between 3 and 4. Without TPA, only dense quartz-type $GaPO_4$ is formed. The resulting white thin needle-like crystals were filtered off, washed with water and dried at room temperature. The XRD patterns of both powdered samples were new and identical. With DAN, the compound was obtained with a yield of 90% together with a small amount of unreacted GaO(OH) whereas the yield is lower (70%) using DAD. However, only single crystals of the phase using DAD were suitable for X-ray structure determination† after hydrothermal treatment for one month. With DAN, the crystals were too small (even after a long reaction time). Only cell parameters can be extracted by using a conventional X-ray source diffractometer.‡

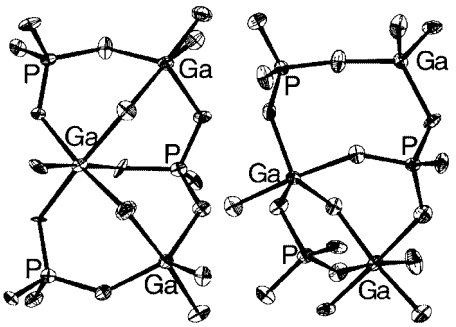

Fig. 1 Hexameric building units of MIL-31: $Ga_3(PO_4)_3(OH,F)_2$ of type I (left) and $Ga_3(PO_4)_3(OH)(H_2O)$ or type II (right).

The structure of MIL-31 consists of the connection of three crystallographically distinct building units (BU) composed of three phosphate groups and three gallium polyhedra (Fig. 1). Two of them are identical to that already observed in the ULM-*n* series[13] (denoted type I) built up from three PO_4 tetrahedra corner-sharing with one $GaO_4(OH,F)_2$ octahedron and two $GaO_4(OH,F)$ trigonal bipyramids. Within these hexameric units, the octahedron is in a central position and linked to the two $GaO_4(OH,F)$ trigonal bipyramids by corner-sharing *via* fluorine or hydroxy groups. These hexameric blocks are connected to each other whilst conserving strict Ga–P alternation in order to generate a sheet of composition $[Ga_6(PO_4)_6(OH,F)_4]$ in the *ab* plane (Fig. 2). In this layer, two adjacent units have opposite orientation, as already encountered in the 3D framework of ULM-16[5] or the 2D solid ULM-8.[14]

These hexameric-based layers are connected through a second type of BU (type II) with Ga_3P_3 stoichiometry. In this entity, the three phosphate groups share corners with three gallium polyhedra which exhibit three different coordinations:

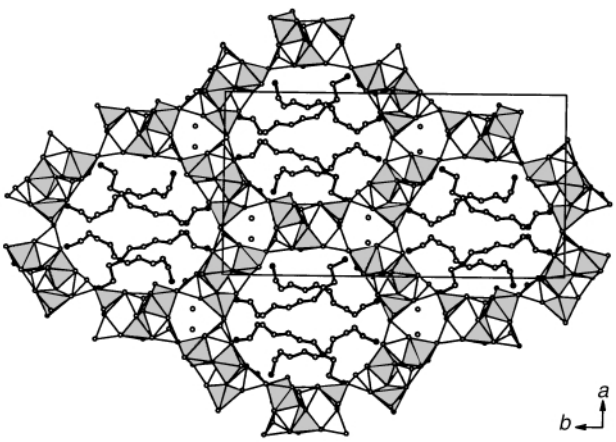

Fig. 2 View of the structure of MIL-31 along the 18-ring channels (along the *c* axis).

DOI: 10.1039/b001948h

GaO_4 tetrahedra, $GaO_4(OH)$ trigonal bipyramids and $GaO_4(OH)(H_2O)$ octahedra. The gallium bipyramidal unit is in the central position and has one common hydroxy group with the gallium octahedral unit. This BU is derived from TO_4-based 4-ring units (T = tetrahedral Ga or P species) forming infinite double-crankshaft chains as found in ULM-16.[5] In MIL-31, additional $GaO_4(OH)(H_2O)$ and PO_4 groups are connected to the 4-ring unit. This induces a change of the coordination of one of the GaO_4 tetrahedra to give a $GaO_4(OH)$ bipyramid. All the vertices of the gallium polyhedra are shared with the PO_4 polyhedra, except the terminal water molecule attached to the $GaO_4(OH)(H_2O)$ octahedron [Ga–OH_2 2.115(7) Å] pointing towards the channel centre. Such a situation was previously observed for the aluminophosphate VPI-5[15] in which one of the aluminium sites has an octahedral surrounding. This aluminium atom is at the center of the Al_3P_3 hexameric unit and is coordinated to four PO_4 groups and to two terminal water molecules.

Fluorine chemical analysis gave three fluorine atoms per $Ga_9(PO_4)_9$ unit which implies a statistical OH/F occupancy for the five observed Ga–X–Ga (X = OH or F) bridging positions. The ^{19}F NMR spectrum indicates only one signal at δ −93.8 (ref. $CFCl_3$) characteristic of bridging fluorine, but the spectral resolution precludes any assignment. However, in BU II the Ga–X distance (< Ga–X > = 1.93 Å) is smaller than in BU I (< Ga–X > = 2.00 Å). As only one peak is visible by ^{19}F NMR spectroscopy and given the measured fluorine content in the material, we can assume that the bridging site in BU II is only occupied by a hydroxy group and the fluorine would thus be located on the other bridging sites of the BU I.

The connection of these different building units generates a three-dimensional framework $[Ga_9(PO_4)_9(OH,F)_4(OH)(H_2O)]^{5-}$ composed of large hexagonal-shaped tunnels with 18- and 6-membered rings running along the *c* axis (Fig. 2). Two diprotonated diamines are inserted within the larger channels whereas two water molecules are trapped in the 6-ring channels. Each terminal ammonium group of the organic template interacts with anions of the framework *via* hydrogen bonds, with distances in the range 2.8–3.1 Å. These interactions occur between fluorine or hydroxy anions and one of the terminal ammonium groups of the template as already found in other phases of the ULM-*n* series.[14] The water molecules in the 6-ring channels interact with the ammonium groups *via* hydrogen bonding.

Besides the four positive charges from the organic molecules, an additional positive charge is required for the electroneutrality of the structure and might come from one H_3O^+ residing within the pore system. The pore opening diameter is *ca.* 12 Å but the presence of the terminal water of the gallium octahedron reduces thus to 10 Å along the *b* axis. The framework density calculated from the number of cations per 1000 Å^3 is 12.6 for MIL-*n* and is comparable to that found in the faujasite[16] structure (12.7) but lower than that observed in VPI-5 (14.2) which is also of 18-ring based topology.

The thermal behaviour of the DAN phase was characterized by X-ray diffraction and thermogravimetric analyses. The TG curve (Fig. 3) shows three major events. The first step (30–150 °C) is related to the removal of water (exptl: 4.30%; calc: 1.84%). The difference between the values would be due to the departure of five water molecules (calc: 4.50%) per $Ga_9(PO_4)_9$ unit, two found in the crystal structure analysis and three corresponding to adsorbed water. The second event (300–500 °C) can be assigned to the departure of the alkyldiamine and the observed experimental weight loss shows that the organic template is partly removed from the framework (exptl: 10.51%; calc: 16.51%). Above 600 °C, the weight loss is continuous and corresponds to 6.61% at 1000 °C. The XRD diagrams show clearly that the resulting structure is collapsed and transforms into dense $GaPO_4$ (high cristobalite). The weight loss can be assigned by assuming the removal of hydroxy groups and fluorine (exptl: 6.61%; calc: 4.67%) and additional organic template.

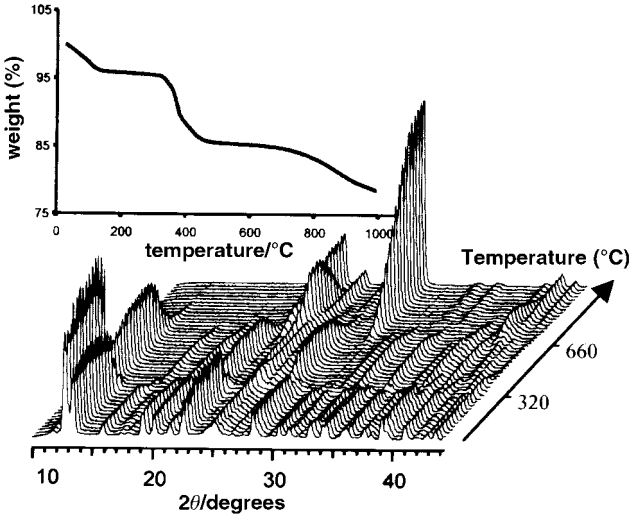

Fig. 3 Evolution of X-ray diffraction powder patterns as a function of temperature (30–1000 °C under air) and TG curve of MIL-31 (2 °C min^{-1} under N_2).

Notes and references

† *Crystal data* for MIL-31(DAD): $Ga_9(PO_4)_9F_3(OH)_2(H_2O)\cdot N_4C_{20}H_{52}\cdot 2H_2O$, M = 1975.93, orthorhombic, space group $Pca2_1$, μ = 4.549 mm^{-1}, $R1$ = 0.0624, $wR2$ = 0.1066 [for 8228 reflections with $I > 2\sigma(I)$], a = 17.4941(1), b = 32.3930(4), c = 10.0749(2) Å, V = 5709.3(1) Å^3, T = 293(2) K, Z = 4, 38201 reflections measured/13247 independent (R_{int} = 0.1030). Data collection was performed on a SMART three-circle diffractometer equipped with a CCD area detector (Mo-Kα radiation). The alkyldiamine molecules were refined with geometrical restraints. All atoms except for carbon and nitrogen were refined anisotropically. CCDC 182/1616. See http://www.rsc.org/suppdata/cc/b0/b001948h/ for crystallographic files in .cif format.

‡ *Crystal data* for MIL-31(DAN): orthorhombic, a = 17.4442(3), b = 32.1242(4), c = 10.1037(2) Å, V = 5661.921(2) Å^3. Elemental analysis: calc. for $Ga_9P_9O_{41}F_3N_4C_{18}H_{56}$: P, 14.33; F, 2.62; N, 2.87; C, 11.09. Found: P, 12.35; F, 2.54; N, 2.63; C, 9.78%.

1 S. T. Wilson, B. M. Lok, C. A. Messina, T. R. Cannan and E. M. Flanigen, *J. Am. Chem. Soc.*, 1982, **102**, 1146.
2 A. K. Cheetham, G. Férey and T. Loiseau, *Angew. Chem., Int. Ed.*, 1999, **38**, 3268.
3 C. C. Freyhardt, M. Tsapatsis, R. F. Lobo, K. J. Balkus and M. E. Davis, *Nature*, 1996, **381**, 295.
4 T. Loiseau and G. Férey, *J. Solid State Chem.*, 1994, **111**, 403.
5 T. Loiseau and G. Férey, *J. Mater. Chem.*, 1996, **6**, 1073.
6 M. Cavellec, J. M. Grenèche, D. Riou and G. Férey, *Microporous Mater.*, 1997, **8**, 103.
7 M. E. Davis, C. Saldarriaga, C. Montes, J. Garces and C. Crowder, *Nature*, 1988, **331**, 698.
8 Q. Huo, R. Xu, S. Li, Z. Ma, J. M. Thomas, R. H. Jones and A. M. Chippindale, *J. Chem. Soc., Chem. Commun.*, 1992, 875.
9 M. Estermann, L. B. McCusker, C. Baerlocher, A. Merrouche and H. Kessler, *Nature*, 1991, **352**, 320.
10 K.-H. Lii and Y.-F. Huang, *Chem. Commun.*, 1997, 839.
11 A. M. Chippindale, K. J. Peacock and A. R. Cowley, *J. Solid State Chem.*, 1999, **145**, 379.
12 N. Guillou, Q. Gao, M. Nogues, R. E. Morris, M. Hervieu, G. Férey and A. K. Cheetham, *C. R. Acad. Sci. Paris, Sér. IIc*, 1999, **2**, 387.
13 G.-Y. Yang and S. C. Sevov, *J. Am. Chem. Soc.*, 1999, **121**, 8389.
14 G. Férey, *J. Fluorine Chem.*, 1995, **72**, 187; G. Férey, *C. R. Acad. Sci., Paris, Sér. IIc*, 1998, **1**, 1.
15 F. Serpaggi, T. Loiseau, D. Riou, G. Férey and M. W. Hosseini, *Eur. J. Solid State Inorg. Chem.*, 1994, **31**, 595.
16 L. B. McCusker, C. Baerlocher, E. Jahn and M. Bülow, *Zeolites*, 1991, **11**, 308; G. Cheetham and M. M. Harding, *Zeolites*, 1996, **16**, 245.
17 W. M. Meier, D. H. Olson and Ch. Baerlocher, *Atlas of Zeolite Structure Types*, Elsevier, 4th edn., 1996.

ChemComm

Di- and oligo-nuclear nickel complexes with oxalic amidinato bridging ligands: syntheses, structures and catalytic reactions†

Thomas Döhler, Helmar Görls and Dirk Walther*

Institut für Anorganische und Analytische Chemie der Friedrich-Schiller-Universität, D-07743 Jena, Germany. E-mail: cdw@rz.uni-jena.de

Received (in Basel, Switzerland) 21st January 2000, Accepted 26th April 2000

A new family of di-, tri- and tetra-nuclear Ni(II) complexes containing oxalic amidinates as bridging ligands is described in which both peripheral Ni centres are catalytically active in the oligomerization or polymerization of ethylene or in the selective cross coupling of Ar–X with Ar′–MgX.

Di- or oligo-nuclear metal complexes of late d metals connected *via* the conjugated π-system of oxalic amidinato ligands ('oxam') are attractive candidates for catalytic reactions, because the ligands are easily accessible and their steric and electronic properties can be easily modified. Furthermore, systems with different metals in peripheral positions enable catalysts to be designed in which either one or two metals are catalytically active. In addition, the metal coordinated at the opposite side of an active metal centre may be used for fine tuning the catalytic activity.

Since oxalic amidinato ligands tend to form ill-defined polymers with metal salts[1,2] their coordination chemistry is very limited.[3–6] Neither dinuclear d^8 metal complexes nor tri- or oligo-metallic complexes are known. Furthermore, catalytic C–C-linking reactions are also unknown.

Surprisingly, the Ni(II) complexes **1**–**4** (Scheme 1, $m = 0$) are obtained by reacting $Ni(acac)_2$ in toluene or THF with a variety of oxalamidines. Recrystallisation from toluene resulted in red–brown diamagnetic crystalline complexes in 35–60% yields. According to ^{1}H NMR spectroscopy on **1**–**5** the ratio of acac to oxalic amidine ligand was 2:1 supporting dimeric structures (Scheme 1).‡

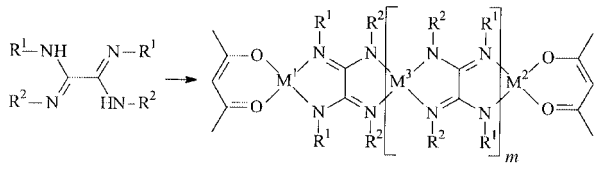

1 $m = 0$, R^1, R^2 = phenyl, M^1, M^2 = Ni
2 $m = 0$, R^1, R^2 = tolyl, M^1, M^2 = Ni
3 $m = 0$, R^1, R^2 = mesityl, M^1, M^2 = Ni
4 $m = 0$, R^1 = tolyl, R^2 = mesityl, M^1, M^2 = Ni
5 $m = 0$, R^1, R^2 = mesityl, M^1 = Ni, M^2 = Zn
6 $m = 1$, R^1, R^2 = mesityl, M^1, M^2 = Ni, M^3 = Zn

Scheme 1

The solid state structure of the key complex **4** was determined by X-ray diffraction and Fig. 1 displays its molecular structure.§

As expected, the oxalamidinate acts as bridging ligand connecting two (acac)Ni(II) fragments with both metal centres essentially planar. Although **4**, containing different N-substituents, may exist as two isomers, to our surprise only one isomer was observed, in which both metal centres have different coordination environments: one metal is surrounded by two mesityl–N groups, the other by two *p*-tolyl–N groups. The aromatic substituents are oriented to the ligand plane at an angle of 90°. The ^{1}H NMR spectrum confirms the presence of only one isomer in solution. Complexes **1**–**5** can be considered as the first members of a series of oxalamidinato complexes of general composition $L_nM^1(oxam)[M^3(oxam)]_mM^2L_n$ ($m = 0$).

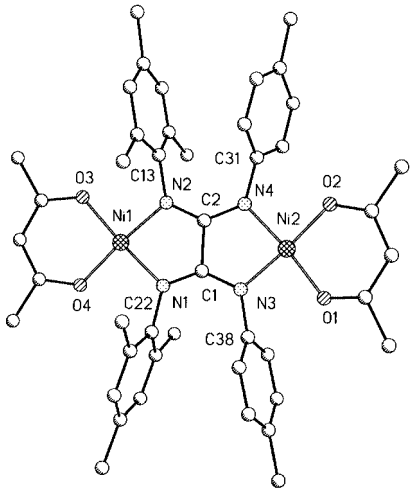

Fig. 1 Molecular structure of **4**. Selected bond distances (Å) and bond angles (°): Ni1–N1 1.880(8), Ni2–N2 1.886(8), Ni1–O3 1.841(7), Ni1–O4 1.843(7), Ni2–N3 1.879(8), Ni2–N4 1.902(8), Ni2–O1 1.845(7), Ni2–O2 1.854(7), C1–C2 1.518(13), N1–C1 1.304(12), N2–C2 1.311(12), N3–C1 1.316(13), N4–C2 1.334(12); O4–Ni1–N1 90.3(3), O3–Ni1–N2 90.9(3), N2–Ni1–N1 83.9(3), O3–Ni1–O4 94.8(3), O1–Ni2–N3 89.7(3), O2–Ni2–N4 91.4(3), N3–Ni2–N4 84.5(4), O1–Ni2–O2 94.4(3).

The trimetallic complex [(acac)Ni(oxam)Zn(oxam)Ni(acac)] **6** is the first example of the next generation of this series (m = 1, M^1, M^2 = Ni; M^3 = Zn, oxam = tetramesityloxalamidine) which was prepared by reacting of 2 equiv. of oxam with $ZnEt_2$ in toluene , followed by addition of 2 equiv. of $Ni(acac)_2$ in good yields.

The Ni_2Zn_2 complex **7** is the first example of a tetrametallic complex of the above-mentioned range prepared from 2 equiv. of $ZnEt_2$ and 3 equiv. of bis(mesityl)bis(*p*-tolyl)oxalamidine in THF, followed by reaction with 2 equiv. of $Ni(acac)_2$. Red crystalline complex **7** was isolated upon recrystallisation of the product from toluene. Elemental analyses, mass spectra, and the ^{1}H NMR spectrum confirm its composition. Its X-ray structure (Fig. 2) shows that both peripheral Ni centres have the same planar environment as in **4**, while the two central Zn atoms are tetrahedrally coordinated.

Table 1 shows that all the complexes are catalytically active towards ethylene when activated with MAO or Et_3Al. In contrast to the well established Ni catalysts for the SHOP process,[7] in which negatively charged P–O ligands support the oligomerization of ethylene, we observed both oligomerization and polymerization of ethylene (Table 1).

A comparison of **2** (runs 1 and 2 in Table 1) and **3** (runs 5 and 6 in Table 1) clearly shows that the *p*-tolyl groups in **2** promote the oligomerization of ethylene; however, substitution by

† Electronic supplementary information (ESI) available: general procedures and full spectroscopic characterisation of complexes **1**–**7**. See http://www.rsc.org/suppdata/cc/b0/b000791i/

Table 1 Catalytic reactions of **1**–**7** with ethylene in the presence of MAO or Et_3Al[a]

Run	Precat.	Cocatalyst	C_4/C_6 (%)	Polymer (%)	Polymer selectivity (%)	M_w	M_n	$D = M_w/M_n$
1	**2**	MAO (300)	33	—	—	—	—	—
2	**3**	MAO (2)	—	4	100	357000	244000	1.46
3	**3**	MAO (6)	—	24	100	673000	451000	1.49
4	**3**	MAO (20)	2	42	95	491000	185000	2.66
5	**3**	MAO (300)	9	74	89	157000	88000	1.78
6	**3**	MAO (1000)	6.5	54	89	75000	30000	2.49
7	**3**	$AlEt_3$ (300)	—	62	92	246000	165000	1.49
8	**4**	MAO (300)	16	16	50	237000	117000	2.02
9	**6**	MAO (300)	7	82	92	189200	132700	1.43
10	**7**	MAO (300)	24	2	—	—	—	—
11	$Ni(acac)_2$	MAO (300)	38	—	—	—	—	—

[a] *General conditions:* 0.031 mmol catalyst, 10 bar ethylene, 20 ml toluene, 16 h reaction time, room temperature; run 9: most of the polymer was insoluble, only the molecular weight of the soluble fraction was determined.

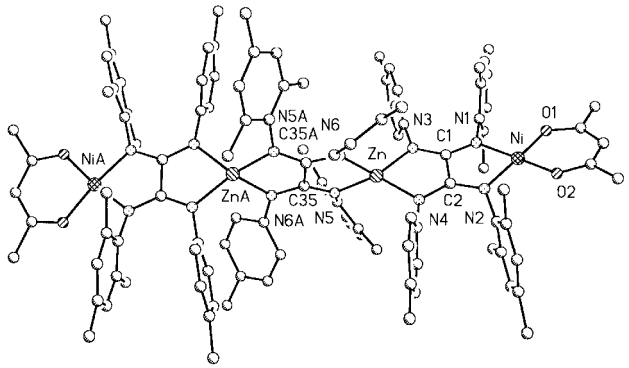

Fig. 2 Molecular structure of **7.** Selected bond distances (Å) and angles (°): Ni–O1 1.840(4), Ni–O2 1.864(4), Ni–N1 1.897(4), Ni–N2 1.885(4), Zn–N3 2.002(4), Zn–N4 2.007(4), Zn–N5 1.996(5), Zn–N6 2.000(5), C1–N1 1.309(6), C1–N3 1.334(7), C2–N2 1.312(7), C2–N4 1.344(7), C1–C2 1.524(8), C35–N5 1.343(7), C35–N6A 1.338(7), C35–C35A 1.518(12), dihedral angle between planes (Ni–O1–O2)/(Ni–N1–N2) 6.9(2), (Zn–N2–N4)/(Zn–N5–N6) 100.8(2). Symmetry transformations used to generated equivalent atoms: A $-x + 3/2, y, -z + 1$.

mesityl groups (in **3**) results in the formation of a selective polymerization catalyst. In contrast to recently described 1.2-diimine or salicylaldiminato complexes of d^8 metals, where very bulky substituents have to be used for selective polymerization,[8–11] in the oxalic amidinato complexes only two additional *ortho*-methyl groups are necessary to switch the reaction from oligomerization to polymerization of ethylene. Since both oligomerization and the polymerization of ethylene occur using **4** as catalyst which contains two different coordination spheres, we can conclude that *both* metals are catalytically active (runs 3 and 4 in Table 1). If the reaction with **3** was carried out heating the reaction mixture from room temperature to 69 °C within 10 min (50 bar ethylene) then 3.7 g of polyethylene was produced giving a TOF of 102 000 h^{-1}.

The catalytic reaction of **6**/MAO with ethylene shows that the Zn moiety in the middle of **6** increases the selectivity towards polymerization compared with **3** (Table 1, runs 5 and 9). This demonstrates the possibility for fine tuning the catalytic activity by using different metals. The tetranuclear complex **7**, however, is a dimerization catalyst when activated with MAO. The complexes can also be used as catalysts in other C–C coupling reactions such as the polymerization of styrene (*e.g.*: **3**/300 equiv. MAO/4000 equiv. styrene yielded 94% polystyrene) or cross coupling, *e.g.* of mesitylmagnesium bromide (500 equiv.) with *p*-tolyl bromide (500 equiv.) to give mesityl–4-tolyl in 99% selectivity and an overall yield of 95% when **4** in THF at ambient temperature was used.

In conclusion, we have shown that di-, tri- and tetra-nuclear complexes of late d metals with oxalamidinates can easily be prepared and used in a number of catalytic C–C-linking reactions. Both peripheral Ni centres are catalytically active in these complexes.

This work was supported by Deutsche Forschungsgemeinschaft und Volkswagenstiftung.

Notes and references

‡ Satisfactory microanalysis have been obtained. *Selected spectroscopic data*: for **4**: $C_{44}H_{50}N_4O_4Ni_2$: MS (EI): *m/z* 816 (42%, $M + 2^+$); δ_H(toluene-d_8, 25 °C): 0.89, 0.94 (CH_3-acac, 2× s, 12H), 1.89, 1.9 (*p*-CH_3, 2× s, 12H), 2.68 (*o*-CH_3-mes, s, 12H), 4.62, 4.68 (CH-acac, 2× s, 2H), 6.25 (CH-mes, s, 4H), 6.37, 6.71 (CH-tol, AA′BB′, 8H).

For **7**: $C_{112}H_{122}N_{12}Ni_2O_4Zn_2$: δ_H(THF-d_8, 25 °C): 1.01, 1.04, 1.29, 1.39, 1.48, 1.64, 1.83, 1.88, 1.90, 1.99, 2.03, 2.08, 2.12, 2.20, 2.25, 2.30, 2.34, 2.48 (CH_3, 72H), 4.97, 5.00 (CH-acac, 2H), 5.75, 5.79, 5.89, 5.93, 6.02–6.29 (m, CH-aryl, 23H), 6.44, 6.48, 6.56, 6.61, 6.65 (m, CH-aryl, 6H), 7.08–7.2 (m, CH-aryl, 7H).

§ *Crystal data* for **4**:[12] $C_{44}H_{50}N_4Ni_2O_4$, M_r = 816.30, brown prism, size 0.40 × 0.35 × 0.10 mm, monoclinic, space group $P2_1/n$, a = 12.696(2), b = 8.873(1), c = 36.989(4) Å, β = 98.278(6)°, V = 4123.5(9) Å^3, T = −90 °C, Z = 4, D_c = 1.315 g cm^{-3}, μ(Mo-Kα) = 9.59 cm^{-1}, F(000) = 1720, 4609 reflections with h(−13/13), k(0/9), l(−41/40), measured in the range $2.81 \leqslant \theta \leqslant 23.27°$, completeness θ max = 98.7%, 3331 independent reflections, R_{int} = 0.089, 2607 reflections with $F_o > 4\sigma(F_o)$, 487 parameters, 0 restraints, $R1_{obs}$ = 0.080, wR^2_{obs} = 0.231, $R1_{all}$ = 0.108, wR^2_{all} = 0.271, GOF = 1.074, largest difference peak and hole: 0.385, −0.563 e Å^{-3}.

For **7**:[12] $C_{112}H_{122}N_{12}Ni_2O_4Zn_2$, M_r = 1948.38, red prism, size 0.32 × 0.28 × 0.20 mm, monoclinic, space group $I2/a$, a = 22.2023(8), b = 21.6541(6), c = 25.343(1) Å, β = 105.960(2)°, V = 11714.5(7) Å^3, T = −90 °C, Z = 4, D_c = 1.125 g cm^{-3}, μ(Mo-Kα) = 7.71 cm^{-1}, F(000) = 4176, 22567 reflections for h(−27/27), k(−26/27), l(−31/31), measured in the range $3.01° \leqslant \theta \leqslant 26.42°$, completeness θ max = 98.9%, 11922 independent reflections, R_{int} = 0.091, 6125 reflections with $F_o > 4\sigma(F_o)$, 615 parameters, 0 restraints, $R1_{obs}$ = 0.086, wR^2_{obs} = 0.217, $R1_{all}$ = 0.175, wR^2_{all} = 0.261, GOF = 1.010, largest difference peak and hole: 0.927, −0.451 e Å^{-3}.

CCDC 182/1615. See http://www.rsc.org/suppdata/cc/b0/b000791i/ for crystallographic files in .cif format.

1 W. E. Hofman, *Proc. Indiana Acad. Sci.*, 1969, **79**, 129; (*Chem. Abstr.*, 1970, **73**, 126513r).
2 E. Papavil, *Anal. Stiint. Univ. Jasi, Sect. 1*, 1964, **10c**, 115; (*Chem. Abstr.*, 1965, **63**, 14351h).
3 M. Döring, H. Görls and R. Beckert, *Z. Anorg. Allg. Chem.*, 1994, **620**, 551.
4 P. Feeling, M. Döring, F. Knoch, R. Beckert and H. Görls, *Chem. Ber.*, 1995, **128**, 405.
5 R. Beckert, S. Vorwerk, D. Lindauer and M. Döring, *Z. Naturforsch., Teil B*, 1993, **48**, 1186.
6 M. Pasquali, C. Floriani, A. Chiesi-Villa and C. Guastini, *J. Am. Chem. Soc.*, 1979, **101**, 4740.
7 W. Keim, F. H. Kowaldt, R. Goddard and C. Krüger, *Angew. Chem., Int. Ed. Engl.*, 1978, **17**, 466.
8 L. K. Johnson, C. M. Kilian and M. Brookhart, *J. Am. Chem. Soc.*, 1995 **117**, 6414.
9 S. Mecking, L. K. Johnson and M. Brookhart, *J. Am. Chem. Soc.*, 1996, **118**, 267.
10 G. J. P. Britovsek, V. C. Gibson and D. F. Wass, *Angew. Chem.*, 1999, **111**, 448; *Angew. Chem., Int. Ed.*, 1999, **38**, 428 and references therein.
11 C. Wang, S. Friedrich, T. R. Younkin, R. T. Li, R. H. Grubbs, D. A. Bansleben and M. W. Day, *Organometallics*, 1998, **17**, 3149.

New FeS clusters with NO: associative formation of $[Fe_5S_4(NO)_8]^-$ and $[Fe_7S_6(NO)_{10}]^-$, and larger clusters†

Mark Lewin, Keith Fisher and Ian Dance*

School of Chemistry, University of New South Wales, Sydney 2052, Australia. E-mail: I.Dance@unsw.edu.au

Received (in Cambridge) 3rd March 2000, Accepted 20th April 2000

Solutions of $[Fe_2S_2(NO)_4]^{2-}$ or $[Fe_4S_3(NO)_7]^-$ undergo facile aggregation to new clusters $[Fe_5S_4(NO)_8]^-$ and $[Fe_7S_6(NO)_{10}]^-$, but do not form the known species $[Fe_4S_4(NO)_4]^z$ and $[Fe_6S_6(NO)_6]^{2-}$; reactivities and reactions in solution and gas phases were monitored by electrospray Fourier transform ion cyclotron resonance mass spectrometry, and the probable structures of $[Fe_5S_4(NO)_8]^-$ and $[Fe_7S_6(NO)_{10}]^-$ were determined by density functional calculations.

In 1858 Roussin reported salts of $[Fe_2S_2(NO)_4]^{2-}$ **1** and $[Fe_4S_3(NO)_7]^-$ **2**.[1] Since then there have been numerous publications on derivatives of **1** and **2**,[2–6] but $[Fe_4S_4(NO)_4]^z$ (z = 0, −1) **3**[7–9] and $[Fe_6S_6(NO)_6]^{2-}$, **4**[10] are the only other

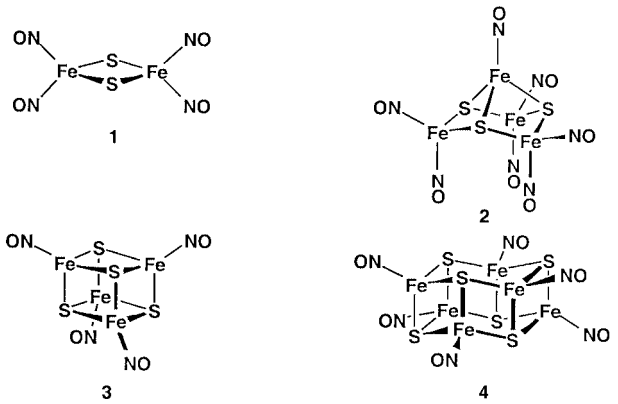

known iron sulfide clusters containing only NO ligands. We report here the formation of $[Fe_5S_4(NO)_8]^-$ and $[Fe_7S_6(NO)_{10}]^-$ by a facile aggregation process, which also yields other larger clusters.

Negative ion electrospray mass spectrometry (ESMS) of a solution of $Na_2[Fe_2S_2(NO)_4]$ in methanol immediately after preparation shows $[Fe_2S_2(NO)_4H]^-$, which rapidly (*ca.* 15 min at 10^{-4} M concentration, 25 °C) converts to a species of *m/z* 647.† By accurate mass analysis of the isotopomer pattern, and collision induced dissociation of NO, this species was confirmed as $[Fe_5S_4(NO)_8]^-$. Subsequently (40 min), $[Fe_5S_4(NO)_8]^-$ in this methanol solution converts to a mixture of $[Fe_4S_3(NO)_7]^-$ and a new species with *m/z* 883, which is confirmed to be $[Fe_7S_6(NO)_{10}]^-$. A solution of $Na_2[Fe_2S_2(NO)_4]$ in acetonitrile also shows the formation of $[Fe_4S_3(NO)_7]^-$ and $[Fe_5S_4(NO)_8]^-$, and eventually $[Fe_7S_6(NO)_{10}]^-$, together with transitory low intensity species at *m/z* 412, 478, only during the early stages.† Solutions of $Na[Fe_4S_3(NO)_7]$ in methanol also show the formation of $[Fe_5S_4(NO)_8]^-$ and $[Fe_7S_6(NO)_{10}]^-$, although generated more slowly (7 to 14 d at 10^{-4} M and 25 °C).

These spectra are significant also for the species that are absent. There is no evidence of $[Fe_4S_4(NO)_4]^{z-}$ or $[Fe_6S_6(NO)_6]^{z-}$ (z = 1 or 2) in any of the numerous spectra recorded.† Apart from the strong peaks for $[Fe_4S_3(NO)_7]^-$, $[Fe_5S_4(NO)_8]^-$ and $[Fe_7S_6(NO)_{10}]^-$ the spectra are devoid of peaks in the mass range 500–900. Additional high mass peaks above *m/z* 900 have been observed, but not identified unambiguously.

With ESMS there is a fundamental question whether the observed species exist in the electrosprayed solution or are artefacts of the energetic ES desolvation process. The dependence of the spectra on the history of the solutions is strong evidence for the transformations in solution. Further, we have adjusted the ES capillary potential to effect controlled fragmentation, which involves only NO dissociation and occurs well above the threshold capillary voltage for observation of $[Fe_5S_4(NO)_8]^-$ and $[Fe_7S_6(NO)_{10}]^-$.† It is significant that induced fragmentation does not disrupt the FeS cores. The stability and coordinative saturation of $[Fe_5S_4(NO)_8]^-$ and $[Fe_7S_6(NO)_{10}]^-$ are demonstrated by their inertness to reactive $NO_{2\,(g)}$ in the FTICR cell. After controlled partial dissociation of NO from $[Fe_5S_4(NO)_8]^-$ or $[Fe_7S_6(NO)_{10}]^-$ they do react with NO_2, by oxygen addition.

We have not yet been able to crystallise the new species, but have investigated their structures by validated density functional calculations,[11] evaluating the minimised energies of postulated structures. For $[Fe_5S_4(NO)_8]^-$ eight structure types were investigated, and Fig. 1 shows the best structure found, **548A**, which is a flattened FeS_4 tetrahedron with four edge-bridging $Fe(NO)_2$, and a spin doublet ground state (HOMO–LUMO gap of 1.1 eV). This is 22 kcal mol^{-1} more stable than the next best structure, **548B** (Fig. 1). For $[Fe_7S_6(NO)_{10}]^-$, 29 postulated structures were investigated. The most probable structure, **7610A** (Fig. 2), contains two of the Fe_4S_3 cores fused at one Fe: structures **7610B** and **7610E** are configurational isomers with Fe_4S_3 cores linked by Fe–S bonds; **7610C** also contains the Fe_4S_3 core; while **7610D** is $[Fe_2S_2(NO)_4]$ linked to **548A**. These four isomers are not strongly differentiated in total energy (see Fig. 2). One of the isomers for $[Fe_7S_6(NO)_{10}]^-$ is **5**,

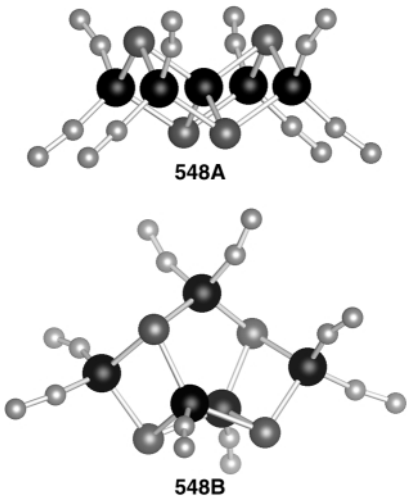

Fig. 1 The optimised structures of isomers **548A** (symmetry D_{2d}) and **548B** (symmetry C_2) of $[Fe_5S_4(NO)_8]^-$: Fe black; S grey, intermediate size; N, O small. The energy of **548B** relative to **548A** is +22 kcal mol^{-1}.

† Electronic supplementary information (ESI): representative spectra and further experimental details. See http://www.rsc.org/suppdata/cc/b0/b001738h/

DOI: 10.1039/b001738h

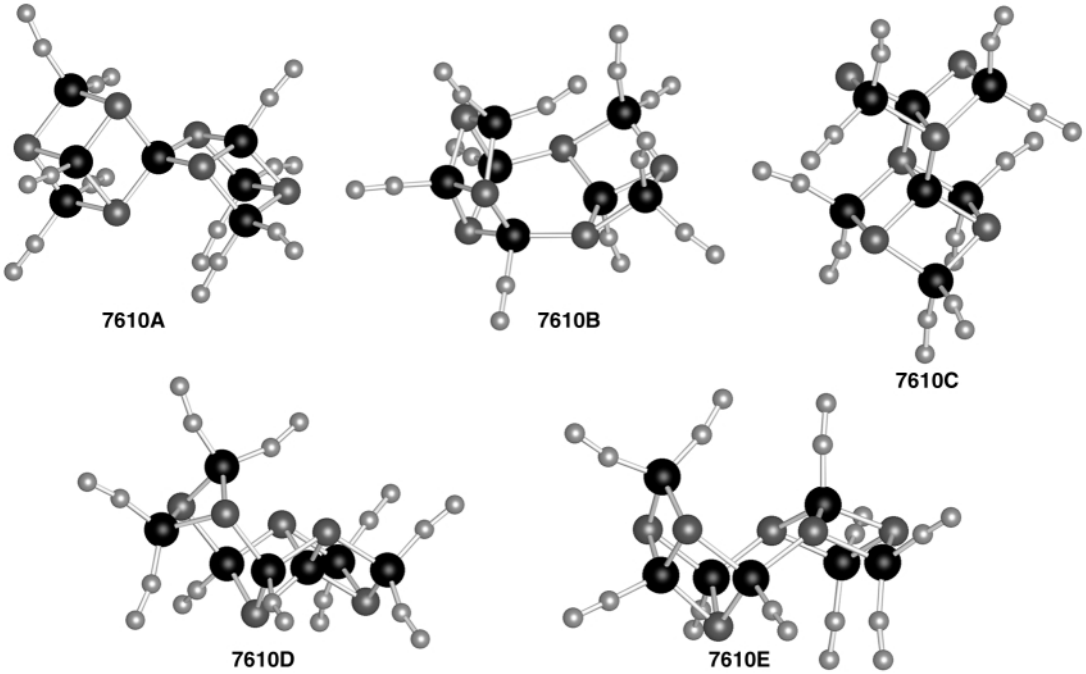

Fig. 2 The optimised structures of the five best isomers of $[Fe_7S_6(NO)_{10}]^-$: Fe black; S grey, intermediate size; N, O small. The symmetries and relative energies (kcal mol^{-1}) are: **7610A**, C_2, 0; **7610B**, C_s, +15; **7610C**, C_s, +18; **7610D**, C_s, +19; **7610E**, C_s, +22.

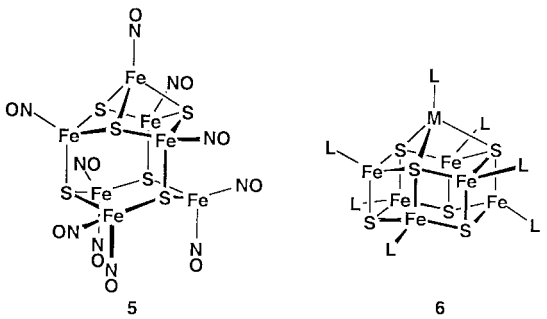

5

6

which is a logical extension of **2**, and is related to the established metal sulfide cluster type **6**,[12] but **5** is 38 kcal mol^{-1} less stable than **7610A**. We believe that our geometry searches have canvassed all reasonable possibilities.

The comparatively fast formation of $[Fe_5S_4(NO)_8]^-$ and $[Fe_7S_6(NO)_{10}]^-$ suggests facile mechanisms, with uncomplicated connectivity changes between the precursors and the proposed structures. The general absence of observable intermediates during the formation of $[Fe_5S_4(NO)_8]^-$ and $[Fe_7S_6(NO)_{10}]^-$ indicates that the mechanisms are associative. We can propose a facile mechanism for the assembly of **548A** from three $[Fe_2S_2(NO)_4]$, involving the breaking of only three Fe–S bonds and dissociation of two Fe–NO, with reformation of five Fe–S bonds [stoichiometry eqn. (1)]. For the assembly of **7610A** from $[Fe_5S_4(NO)_8]^-$ in solution according to eqn. (2) we can propose a mechanism involving the breaking of a total of only eight Fe–S bonds in concert with transfer of two NO ligands, and reformation of eight Fe–S bonds.

$$3\,[Fe_2S_2(NO)_4] \rightarrow [Fe_5S_4(NO)_8] + [FeS_2(NO)_2] + 2\,NO \quad (1)$$

$$3\,[Fe_5S_4(NO)_8] \rightarrow [Fe_7S_6(NO)_{10}] + 2\,[Fe_4S_3(NO)_7] \quad (2)$$

An important feature of the reactions observed is that they occur at ambient temperature and low concentration. This is associative cluster formation which is thermodynamically favourable and kinetically facile. In contrast, the formation of **4** (and its precursors) required extended reactions at elevated temperatures.[10] The difference is in the degree of NO dissociation: the Fe–S–NO clusters easily formed by association in solution retain $Fe(NO)_2$ groups, while other established Fe–S cluster cores have at most one terminal ligand per Fe.

The facility of the associative formation of Fe–S aggregates described here could be relevant to the biosynthesis of Fe–S cofactors.[13–15]

The resources used in this research were provided by the Australian Research Council and the University of NSW.

Notes and references

1 F. Z. Roussin, *Ann. Chim. Phys.*, 1858, **52**, 285.
2 A. R. Butler, C. Glidewell, J. Hyde and R. N. McGinnis, *Polyhedron*, 1983, **2**, 1399.
3 A. R. Butler, C. Glidewell and M.-H. Li, *Adv. Inorg. Chem.*, 1988, **32**, 335.
4 A. R. Butler, C. Glidewell and S. M. Glidewell, *Polyhedron*, 1990, **9**, 2399.
5 S. D'Addario, F. Demartin, L. Grossi, M. C. Iapalucci, F. Laschi, G. Longoni and P. Zanello, *Inorg. Chem.*, 1993, **32**, 1153.
6 P. C. Ford, J. Bourassa, K. Miranda, B. Lee, I. Lorkovic, S. Boggs, S. Kudo and L. Laverman, *Coord. Chem. Rev.*, 1998, **171**, 185.
7 R. S. Gall, C. T. W. Chu and L. F. Dahl, *J. Am. Chem. Soc.*, 1974, **96**, 4019.
8 C. T. W. Chu, F. Y. Lo and L. F. Dahl, *J. Am. Chem. Soc.*, 1982, **104**, 3409.
9 C. T. W. Chu, R. S. Gall and L. F. Dahl, *J. Am. Chem. Soc.*, 1982, **104**, 737.
10 M. J. Scott and R. H. Holm, *Angew. Chem., Int. Ed. Engl.*, 1993, **32**, 564.
11 Program DMol (www.msi.com) double numerical basis sets with polarisation functions, functional blyp, restricted and unrestricted spin. This methodology was validated by comparison of the optimised and crystallographically observed structures of $[Fe_2S_2(NO)_4]^{2-}$ and $[Fe_4S_3(NO)_7]^-$: the discrepancies were 0.04 Å for all Fe–S and Fe–N bonds and $< 3°$ for all angles.
12 I. Noda, B. S. Snyder and R. H. Holm, *Inorg. Chem.*, 1986, **25**, 3851.
13 B. K. Burgess, *ACS Symp. Ser.*, 1993, **535**, 145.
14 P. W. Ludden, V. K. Shah, G. P. Roberts, M. Homer, R. Allen, T. Paustian, J. Roll, R. Chatterjee, M. Madden and J. Allen, *ACS Symp. Ser.*, 1993, **535**, 196.
15 A. Müller and E. Krahn, *Angew. Chem., Int. Ed. Engl.*, 1995, **34**, 1071.

Engineering the surface chemical properties of semiconductor nanoparticles: surfactant-encapsulated CdTe-clusters

Dirk G. Kurth,* Pit Lehmann and Constanze Lesser

Max-Planck-Institute of Colloids and Interfaces, D-14424 Potsdam, Germany. E-mail: kurth@mpikg-golm.mpg.de

Received (in Cambridge, UK) 25th February 2000, Accepted 26th April 2000

Self-assembly of CdTe-nanoparticles and alkylammonium surfactants gives stable, hydrophobic surfactant-encapsulated CdTe-clusters that can be isolated as solid materials which dissolve in common organic solvents, spread at the air–water interface, and show enhanced photochemical stability.

Nanoparticles of semiconductors are at the focus of materials research owing to the novel electronic, catalytic and optical properties of these materials. The unusual properties can be attributed to two main factors: the high surface area to volume ratio and the spatial confinement of electronic states. The confinement results in discrete transitions with highly polarizable excited states that are tunable with particle size.[1]

The synthesis, purification and isolation of stable, discrete nanoparticles preferentially with a narrow size distribution and tailored surface chemical properties represents a considerable challenge because the large surface energy promotes aggregation to minimize the surface area. A successful synthesis should, therefore, result in monodisperse nanoparticles with robust surface passivation. Essentially, there are three methods to achieve these goals with varying success.[2] A common approach relies on decomposition of organometallic precursors, where surface passivation is achieved by coordination of solvent molecules, such as alkylphosphine oxides, to the cluster surface *in situ*.[3] In a second method, particle growth is restricted in confined media, such as polymer micelles.[4] Finally, nanoparticles can be synthesized *via* colloid chemistry where the particles are capped by suitable stabilizing molecules, such as thiocarboxylic acids.[5]

Following our recent work on encapsulated polyoxometalate clusters,[6] we present here, the synthesis and isolation of stable surfactant encapsulated CdTe-clusters (SECs). This self-assembly strategy relies on an ion exchange process of the cluster counter ions with surfactants. This approach has been applied to a variety of particles,[7] including gold colloids,[8] metal[9] and metal oxide clusters.[10] The advantage of our approach is that the preparation of the parent CdTe-clusters rests on well established experimental procedures.[11] The synthesis of CdTe-SECs is achieved in a second independent step by treating aqueous CdTe-solutions with the surfactant dimethyldioctadecylammonium bromide (DODABr). Encapsulation of the CdTe-clusters with surfactants results in hydrophobic SECs, which are readily isolated as solid powder. These semiconductor clusters possess many interesting properties and are, therefore, of considerable technological interest.[12]

The CdTe-clusters were synthesized by treating a demineralized aqueous solution containing thioglycolic acid and $Cd(ClO_4)_2 \cdot 6H_2O$ (0.013 M) at pH 11 with NaHTe in an inert gas atmosphere,[5,11] leading to particles of diameter *ca*. 4 nm.[13] A 4.5 ml aliquot of this solution was diluted to 100 ml with water and the pH was adjusted to 6 by addition of HCl. 50 mg of DODABr was then added and the resulting CdTe-SEC was extracted with chloroform. Quantitative transfer of the CdTe-clusters into the organic phase was observed by visual inspection after 20 min: the chloroform phase turned yellow–brown, while the aqueous phase became colourless. The organic phase was separated, dried and evaporated to yield the CdTe-SEC material as a brown–yellow solid, which readily dissolved in common organic solvents. The solubility properties imply that the surfactant molecules form a closed, hydrophobic shell around the CdTe-core with the positive head groups of the surfactant molecules binding to the surface carboxylates.

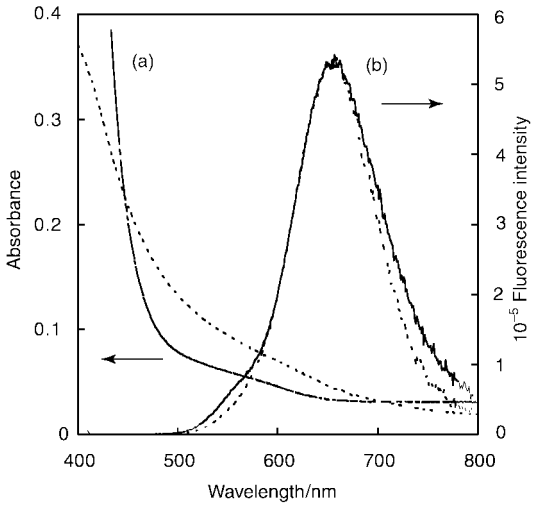

Fig. 1 UV–VIS spectra (a) and fluorescence spectra (b) of CdTe-clusters (——) and CdTe-SECs (- - - -). The fluorescence spectra are normalized for better comparison (excitation wavelength 400 nm). The spectra of the CdTe-clusters and the CdTe-SECs are nearly identical, indicating the structural integrity of the CdTe-clusters within the surfactant encapsulated clusters.

UV–VIS and fluorescence spectroscopy demonstrate that the CdTe-clusters maintain their structural integrity upon encapsulation. The absorbance spectra of the parent CdTe-clusters and the CdTe-SECs are fairly similar (Fig. 1) with both samples showing characteristic shoulders at *ca*. 400 and 600 nm. The fluorescence spectra have similar band positions and widths, indicating that the particle size distributions of the two samples are similar. It is interesting that the apparent fluorescence intensity for the CdTe-SECs is larger by almost a factor of two. These observations demonstrate how sensitive the photophysical properties of the CdTe-nanoparticles are to surface derivatization and local field effects.[14]

A comparison of the long-term development of the fluorescence intensity is shown in Fig. 2. The parent CdTe-clusters show a decay of the fluorescence intensity by an order of magnitude within 4 h. Also shown is the UV–VIS absorbance as a function of time. A decrease in absorbance indicates a loss of material from within the probe beam volume. Although the use of thioglycolic acid for adjusting the pH of the aqueous solution extends the photochemical stability of the CdTe-clusters, the particles are completely decomposed after seven days with the fluorescence intensity and the absorbance falling close to zero. Because CdTe-solutions stored in the dark are stable over extended periods of time, we conclude that a light induced reaction occurs, which eventually results in precipitation of the CdTe-clusters. In contrast, the CdTe-SECs show a steady fluorescence intensity under the same experimental conditions (Fig. 2).† Even after seven days of illumination, the CdTe-SECs maintain most of their initial fluorescence. Clearly, the

DOI: 10.1039/b001563f

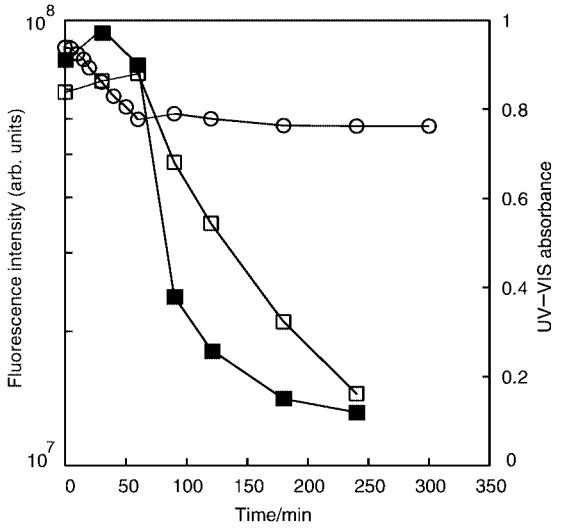

Fig. 2 Fluorescence intensity of CdTe-clusters (□) and CdTe-SECs (○) as a function of time. The CdTe-SECs show a nearly constant fluorescence intensity under irradiation at the excitation wavelength (400 nm). By contrast, the fluorescence intensity of parent CdTe-clusters decays under identical conditions. Also shown is the UV–VIS absorbance at 400 nm of the CdTe-clusters (■). The diminution with time corresponds to a loss of material within the probe beam volume (precipitation) which causes the decrease of fluorescence intensity.

surfactant shell effectively protects the CdTe-core from photo-induced decomposition and precipitation.

The hydrophobic nature of the CdTe-SECs is shown by the fact that they form stable Langmuir monolayers at the air–water interface‡ and Fig. 3 shows a representative compression isotherm which are very reproducible. The area per SEC cannot be obtained from the isotherm because the molecular mass of the CdTe-SECs is, as yet, not known. The isotherm does not show well defined phase transitions, but only a slight shoulder at 20 mN m^{-1} while the collapse pressure is *ca*. 42 mN m^{-1}. Upon expansion a slight hysteresis is visible. The collapse pressure is relatively high, which indicates a good stability of the monolayer. This behavior is similar to that of structurally related surfactant encapsulated polyoxometalate clusters.[6]

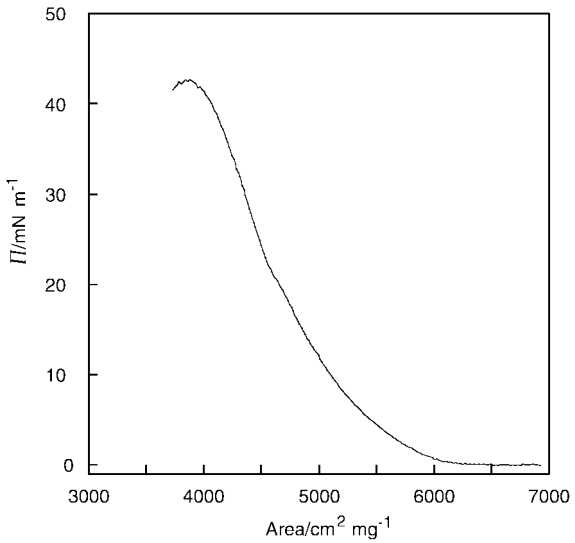

Fig. 3 Representative compression isotherm of a CdTe-SEC at the air–water interface. The Langmuir monolayers are quite stable as indicated by the high collapse pressure of *ca*. 42 mN m^{-1}.

In summary, we have presented a facile non-covalent strategy to tailor the surface chemical properties of semiconductor nanoparticles, including solubility and surface activity. The nanoparticles have been synthesized according to an established experimental procedure. Self-assembly of the charged clusters and dialkylammonium surfactants results in encapsulation and formation of discrete, hydrophobically encapsulated CdTe-clusters. Encapsulation enhances the fluorescence intensity and photochemical stability of the CdTe-nanoparticles.

The study was supported by the Max-Planck Society. Helmuth Möhwald and Stefan Kirstein are acknowledged for valuable discussions.

Notes and references

† Samples were directly irradiated at an excitation wavelength of 400 nm in the spectrometer (Spex Fluorolog 1680 Double Spectrometer) with fully opened slits with fluorescence intensity recorded periodically. UV–VIS spectra were recorded with a Varian Cary 50 Spectrophotometer. After 4 h the samples where removed from the spectrophotometer and stored under daylight. CdTe-SECs were dissolved in chloroform while the CdTe-clusters were investigated in aqueous solution.

‡ Langmuir isotherms were measured with a Lauda film balance (Lauda GmbH&Co KG, Königshofen, Germany) at 20 °C. 2.69 mg of the solid CdTe-SEC were dissolved in 2 ml chloroform and 100 μL of the solution were spread on Milli-Q water (resistance > 18.2 MΩ cm).

1 A. P. Alivisatos, *Science*, 1996, **271**, 933.
2 M. Green and P. O'Brien, *Chem. Commun.*, 1999, 2235.
3 C. B. Murray, D. J. Norris and M. G. Bawendi, *J. Am. Chem. Soc.*, 1993, **115**, 8706.
4 S. Förster and M. Antonietti, *Adv. Mater.*, 1998, **10**, 195.
5 A. L. Rogach, L. Katsikas, A. Kornowski, S. Dangsheng, A. Eychmüller and H. Weller, *Ber. Bunsenges. Phys. Chem.*, 1996, **100**, 1772.
6 D. G. Kurth, P. Lehmann, D. Volkmer, H. Cölfen, M. J. Koop, A. Müller and A. Du Chesne, *Chem. Eur. J.*, 2000, **6**, 385; D. Volkmer, A. Du Chesne, D. G. Kurth, H. Schnablegger, P. Lehmann, M. J. Koop and A. Müller, *J. Am. Chem. Soc.*, 2000, **122**, 1995.
7 J. H. Fendler and F. C. Meldrum, *Adv. Mater.*, 1995, **7**, 607.
8 G. Schmid, *Chem. Rev.*, 1992, **92**, 1709; M. Brust, J. Fink, D. Bethell, D. J. Schiffrin and C. Kiely, *Chem. Commun.*, 1995, 1655; M. J. Hostetler and R. W. Murray, *Curr. Opin. Colloid Interface Sci.*, 1997, **2**, 42.
9 M. T. Reetz, M. Winter and B. Tesche, *Chem. Commun.*, 1997, 147; M. T. Reetz, W. Helbig, S. A. Quaiser, U. Stimming, N. Breuer and R. Vogel, *Science*, 1995, **267**, 367; G. Schön and U. Schön, *Colloid Polym. Sci.*, 1995, **273**, 101; G. Schön and U. Schön, *Colloid Polym. Sci.*, 1995, **273**, 202.
10 L. Shen, P. E. Laibinis and T. A. Hatton, *Langmuir*, 1999, **15**, 447.
11 M. Gao, S. Kirstein, H. Möhwald, A. L. Rogach, A. Kornowski, A. Eychmüller and H. Weller, *J. Phys. Chem. B*, 1998, **102**, 8360.
12 M. Gao, B. Richter and S. Kirstein, *Synth. Met.*, 102, **1–3**, 1213; M. Gao, B. Richter and S. Kirstein, *Adv. Mater.*, 1997, **9**, 802.
13 C. Lesser, M. Gao and S. Kirstein, *Mater. Sci. Eng., C*, 1999, **8–9**, 159; M. Gao, C. Lesser, S. Kirstein, H. Möhwald, A. L. Rogach and H. Weller, *J. Appl. Phys.*, 2000, **87**, 2297.
14 Y. Wang, *J. Phys. Chem.*, 1991, **95**, 1119.

ChemComm

Unprecedented C-6 functionalisation of 3-picoline induced by a methyl to C-6 lithium shift

Julien Mathieu, Philippe Gros and Yves Fort*

Synthèse Organique et Réactivité, UMR CNRS-UHP 7565, Faculté des Sciences, Université Henri Poincaré-Nancy I, BP 239, 54506, Vandoeuvre-Les-Nancy, France. E-mail: yves.fort@sor.uhp-nancy.fr

Received (in Liverpool, UK) 28th February 2000, Accepted 13th April 2000

BuLi–$Me_2N(CH_2)_2OLi$ (BuLi–LiDMAE) promoted the clean C-6 functionalisation of 3-picoline *via* a methyl to C-6 lithium shift.

The selective lithiation-functionalisation of 3-picoline **1** remains a synthetic challenge since the potential electrophilicity of the azomethine bond towards alkyllithium reagents as well as a competitivity between acidic protons of the methyl group and those of the heteroaromatic ring must be considered. In fact, a survey of the literature revealed that major studies concern the abstraction of side-chain protons[1] while the selective lithiation of the pyridinic ring has been performed only *via* halogen–metal exchange on the corresponding brominated derivatives.[2] To our knowledge, direct lithiation of the cheap and easily available parent **1** has not yet been described.

Recently, we have reported the usefulness of BuLi–$Me_2N(CH_2)_2OLi$ (denoted BuLi–LiDMAE) for the metallation of pyridine derivatives in apolar solvents. This new reagent prevented the classical nucleophilic addition of BuLi while promoting the regioselective lithiation at C-α of the pyridinic ring.[3] Herein, we describe our investigations on the selective metallation of 3-picoline **1** with BuLi–LiDMAE and its efficiency for the synthesis of 2-substituted-5-methylpyridines.

All our initial attempts to metallate the pyridinic ring of **1** with classical lithium reagents failed (Scheme 1). Reaction with LDA affected exclusively the methyl group[1] giving **2** while BuLi or BuLi–TMEDA led to complex mixtures containing the nucleophilic addition product **3**.

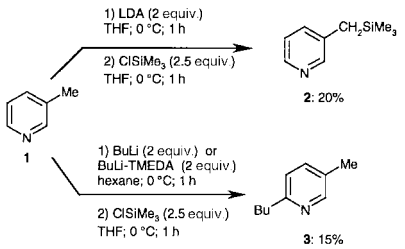

Scheme 1

In contrast, when **1** was treated with BuLi–LiDMAE (3 equiv.),[4] after subsequent quenching with $ClSiMe_3$, neither silylation of the methyl group nor addition products were detected. Moreover, exclusive C-6 silylation of the pyridinic ring occurred and **4a** was isolated in 90% yield. The versatility of this unprecedented reaction was further nicely illustrated by condensation of representative electrophiles[5] (Table 1).†

As shown, clean C-6 functionalisation was observed and products **4b**–**h** were isolated in good to very good yields. Note that the derivatives **4g**–**j** are of particular interest as potentially reactive precursors for further chemical modifications.

Our attention then focused on the interpretation of the obtained regioselectivity. At first we felt that owing to the known higher acidity of side-chain protons,[6] lithiation at the methyl group could be considered as the initial step of the reaction pathway. Thus, we attempted the metallation of

Table 1 Preparation of 2,5-disubstituted pyridines[a]

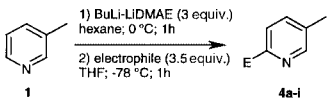

Electrophile	Product E		Yield (%)[b]
Me_3SiCl	Me_3Si	**4a**	91
DCl/D_2O	D	**4b**	100[c]
MeSSMe	MeS	**4c**	90
Me_2NCOPh	PhCO	**4d**	60
Bu^tCHO	Bu^tCHOH	**4e**	75
MeCOEt	Me(Et)COH	**4f**	50
$ClSnBu_3$	Bu_3Sn	**4g**	50[d]
C_2Cl_6	Cl	**4h**	70
CBr_4	Br	**4i**	65
I_2	I	**4j**	68

[a] Reactions performed using 4 mmol of **1**. [b] Isolated yields after purification. [c] Deuterium content determined by ^1H NMR. [d] Loss of material upon chromatographic purification (^1H NMR yield was 95%).

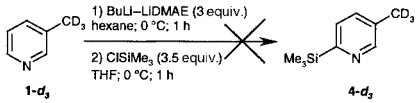

Scheme 2

3-(methyl-d_3)pyridine **1**-d_3 with BuLi–LiDMAE. Deuterium was here expected to act as a carbon protecting group preventing methyl proton abstraction owing to a kinetic isotope effect (KIE).[7] As shown in Scheme 2, no silylated product **4**-d_3 was detected.

This strong KIE clearly indicated that the availability of methyl protons was critical to ensure functionalisation of the pyridinic ring. An eventual direct metallation at C-6 was thus excluded and the reaction pathway probably involves a fast lithium migration from the side chain to the 6 position. According to our previous observations,[3] this unusual shift is assumed to be favoured by a strong complexation of BuLi–LiDMAE aggregates in the neighbourhood of the pyridine nitrogen atom. Subsequent electrophilic quenching followed by

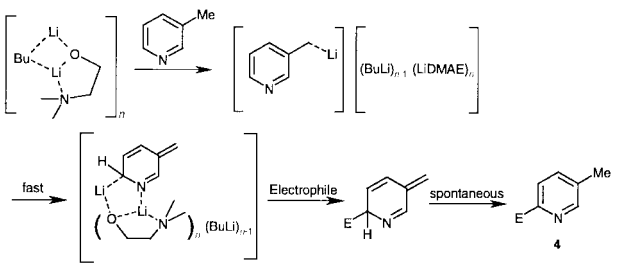

Scheme 3

DOI: 10.1039/b001690j

spontaneous aromatisation[8] would then afford product **4** (Scheme 3).

In summary, we have shown that BuLi–LiDMAE promoted the unprecedented regioselective C-6 functionalisation of 3-picoline. This efficient method was found to be a direct and simple route to functional picolinic derivatives which constitute the key structure of many biologically active compounds.

Notes and references

† All compounds gave satisfactory spectral data (^{1}H, ^{13}C NMR) and new compounds gave satisfactory elemental analyses. The preparation of **4a** is given as a typical procedure. To a solution of 2-dimethylaminoethanol (1.07 g; 12 mmol) in hexane (5 mL) cooled at 0 °C, was added dropwise BuLi (24 mmol; 15 mL of a 1.6 M solution in hexanes). After 15 min, a solution of 3-picoline (0.37 g; 4 mmol) in hexane (5 mL) was added dropwise and the orange solution stirred for 1 h at 0 °C. After cooling at −78 °C, a solution of TMSCl (1.55 g, 14 mmol) in THF (25 mL) was added dropwise. The reaction mixture was maintained at −78 °C for 1 h and then allowed to warm to room temperature. Hydrolysis at 0 °C with water (15 mL) was followed by extraction with diethyl ether (20 mL) and drying over $MgSO_4$. After evaporation of solvents, the crude product was purified by flash-chromatography using hexane–AcOEt (85:15) as eluent. **4a** was obtained as an oil (0.59 g, 90%). δ_H($CDCl_3$, TMS), 0.32 (s, 9H), 2.31 (s, 3H); 7.41 (s, 1H), 7.42 (s, 1H), 8.62 (s, 1H). δ_C($CDCl_3$, TMS), −1.3, 18.95, 128.7, 132.7, 135.0, 151.2, 164.8. *m/z* (EI): 165 (M^+, 59%), 164 (54%), 150 (100%), 93 (18%), 73 (36%), 65 (47%).

1 M. L. Davis, B. J. Wakefield and J. A Wadell, *Tetrahedron*, 1992, **5**, 939; W. M. Stalick and J. H. Murray, *Org. Prep. Proced. Int.*, 1994, **26**, 677.

2 F. Effenberger, A. Krebs and P. Willrett, *Chem. Ber.*, 1992, **125**, 1131; G. A. Kraus and J. Malpert, *Synlett*, 1997, **1**, 107; G. Hanan, U. Schubert, D. Volkmer, E. Rivière, J.-M. Lehn, N. Kyritsakas and J. Fisher, *Can. J. Chem.*, 1997, **75**, 169.

3 Ph. Gros, Y. Fort and P. Caubère, *J. Chem. Soc., Perkin Trans. 1*, 1997, **20**, 3071; Ph. Gros, Y. Fort and P. Caubère, *J. Chem. Soc., Perkin Trans. 1*, 1997, **24**, 3597; Ph. Gros, C. Ben Younès-Millot and Y. Fort, *Tetrahedron Lett.*, 2000, **41**, 303; S. Choppin, Ph. Gros and Y. Fort, *Org. Lett.*, 2000, in press.

4 The reaction with 2 equiv. of BuLi–LiDMAE led also to clean C-6 substitution but in lower yield (76%).

5 Condensation with epoxides (styrene oxide and propylene oxide) was also attempted but was found to be unsuccessful and 3-picoline was recovered quantitatively in both cases.

6 R. Fraser, T. Mansour and S. Savard, *J. Org. Chem.*, 1985, **50**, 3232.

7 Examples using KIE to control the regioselectivity of lithiations have been reported. See, for example: M. Kopach and A. I. Meyers, *J. Org. Chem.*, 1996, **61**, 6764; J. Clayden, J. Pink, N. Westlund and F. Wilson, *Tetrahedron Lett.*, 1998, **39**, 303.

8 Despite all our efforts we were unable to isolate the hydro intermediate.

ChemComm

Amplified microgravimetric gene sensor using Au nanoparticle modified oligonucleotides

Xi Chun Zhou,*[a] Sean J. O'Shea[a] and Sam Fong Yau Li*[b]

[a] *Institute of Materials Research and Engineering, 3 Research Link, Singapore 117602. E-mail: xc-zhou@imre.org.sg*
[b] *Institute of Materials Research and Engineering and Department of Chemistry, National University of Singapore, Singapore 119260*

Received (in Cambridge, UK) 3rd March 2000, Accepted 26th April 2000

A novel microgravimetric gene sensing system has been developed using an oligonucleotide anchored on the gold electrode of a quartz crystal microbalance and an Au nanoparticle modified oligonucleotide, both of which formed a sandwich-type ternary complex with the target DNA to give an amplified frequency response.

The microgravimetric quartz crystal microbalance (QCM) is a promising candidate for biosensor applications, and its potential for the detection of DNA hybridization has been demonstrated recently.[1–6] Although the QCM has a high inherent sensitivity (capable of measuring sub-nanogram levels of mass changes), methods for improving the detection limit of this device are being sought to enable wide application of the technique for DNA hybridization detection. A detection limit of *ca*. 10^{-18} M, which corresponds to *ca*. 10^{-12} g (depending on the number of DNA base pairs) of target DNA is required for many applications. The sensitivity can in some cases be improved by using QCM crystals of higher frequencies[7] or by amplification of the nucleic acids to increase the concentration of the analyte DNA by polymerase chain reaction (PCR).[8] These two methods, however, have practical limitations, particularly in the development of automated biosensor systems for genetic detection: QCM devices of higher frequencies (> *ca*. 10 MHz) are often difficult to operate in liquids because of frequency stability problems, while use of PCR can be laborious and time consuming and requires a number of manipulations. Amplifications of QCM gene sensors by adsorption of an anti-ds-DNA antibody to the formed ds-DNA complex[9] or using dendritic nucleic acid as sensing probes[10] have been reported, but the sensitivities are not good enough.

Here we describe a novel microgravimetric technique for gene detection in which a sandwich-type ternary complex consisting of an oligodeoxynucleotide (ODN) immobilized on a QCM electrode, the target DNA and a Au nanoparticle modified oligonucleotide is formed to give an amplified frequency signal (Scheme 1). Because the mass of each nanoparticle is relatively large in comparison to the masses of the binding pair members themselves, the mass coupling of the nanoparticles to the oscillator surface effectively amplifies the mass increase. As a result, this method provides an amplified frequency shift and substantially extends the limits of sensitivity of the QCM detection system.

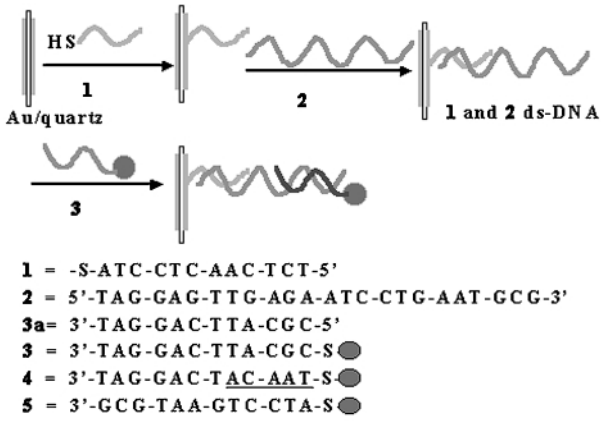

Scheme 1 Schematic illustration of the sensing and amplified system based on the formation of a complementary sandwich-type complex.

All ODNs used in this study were prepared on a fully automated DNA synthesizer (GENSET CA). The 12-mer oligonucleotide **1**, which includes a hexanethiol residue linked to the 3′-terminus, has a sequence that is complementary to part of the target DNA **2**. Oligonucleotide **1** was immobilized *via* self-assembly on a cleaned Au electrode of the QCM (AT-cut, 10 MHz, ICM Co., 0.204 cm^{-2} area Au electrode; the detection limit of the QCM instrument in liquid = 1 Hz) from a 10 μg mL^{-1} solution of **1** (0.05 M HEPES buffer, pH 7.5) for 1 h. The immobilized amount of the probe was estimated to be 7.4 ± 1 pmol cm^{-2} from the frequency change of 6 Hz (in air), which corresponds to *ca*. 11% coverage of single strand nucleotide (area per molecule *ca*. 2.2 nm^2) on the electrode.

Gold nanoparticle modified ODN probes **3**, **4** and **5** were synthesized by derivatizing 1 mL of aqueous 13 nm diameter Au nanoparticle solution (≅17 nM)[11] with 10.5 μg of (alkanethiol) oligonucleotide. After standing for 16 h, the solution was adjusted to buffer conditions (0.1 M NaCl, 0.05 M HEPES buffer, pH 7.5) and allowed to stand for 40 h, followed by centrifugation to remove excess reagents. After removal of the supernatant, the red oily precipitate was washed twice with 0.5 mL of 0.1 M NaCl, 0.05 M HEPES buffer solution, recentrifuged, and redispersed in 0.5 mL of 0.05 M HEPES buffer (containing 0.1 M NaCl, 0.01% azide) as stock solution.

The **1**-functionalized QCM was reacted with target DNA **2** at different concentrations to form **1** and **2** ds-DNA complex. The frequency decrease resulting from the interaction of the **1**-functionalized crystal with **2** is enhanced as the bulk concentration of **2** increases. This is consistent with the increased surface coverage of the sensing interface by **2**. At a bulk concentration of **2** corresponding to 3.2×10^{-8} M, the crystal frequency decreases by 12 Hz and levels off to a constant value after 300 s exposure. Interaction of the monolayer-functionalized crystal with higher concentrations of **2** does not increase the crystal frequency change. This implies that the **1**-monolayer interface is saturated as a result of the formation of the ds-DNA complex. At a bulk concentration of **2** corresponding to 1.7×10^{-9} M, a frequency change of only 3 Hz is observed after 300 s exposure. This seems to be the sensitivity limit according to the IUPAC 3:1 signal to noise guideline.

Fig. 1 illustrates the amplification of the sensing signal by interaction of the resultant **1** and **2** ds-DNA interface (formed by interaction of the **1**-functionalized crystal with **2** at 1.7×10^{-9} M) with the Au nanoparticle modified oligonucleotide **3**. The resulting frequency decrease is enhanced as the bulk concentration of **3** increases, up to 1.3×10^{-7} M where the largest frequency decrease Δf = 67 Hz is observed [Fig. 1(*a*), (*b*) and (*c*)]. Interaction of the **1** and **2** ds-DNA with oligonucleotide **3a** at 3.5×10^{-7} M which is not modified with

DOI: 10.1039/b001737j

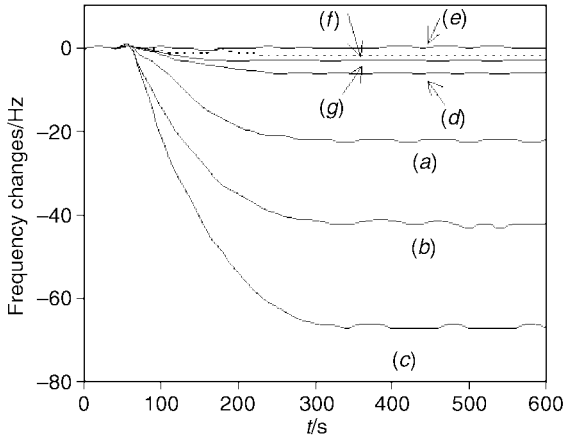

Fig. 1 Response of the **1** and **2** ds-DNA functionalized QCM upon addition of (*a*) Au nanoparticle labeled DNA probe **3,** 2.2×10^{-8} M; (*b*) probe **3,** 6.7×10^{-8} M; (*c*) probe **3,** 1.3×10^{-7} M; (*d*) **3a,** 3.5×10^{-7} M; (*e*) pure Au nanoparticle solution; (*f*) probe **5**, 7.6×10^{-8} M and (*g*) probe **4**, 6.7×10^{-8} M.

Au nanoparticles results in low frequency changes, $\Delta f = -(6 \pm 1)$ Hz, [Fig. 1(*d*)]. Increasing the oligonucleotide **3a** concentration further does not change the frequency further. The frequency change of $\Delta f = -(6 \pm 1)$ Hz at saturated adsorption for oligonucleotide **3a** is consistent with the estimated 100% hybridization of the **1** and **2** ds-DNA interface. The similar time dependency of the frequency changes (*i.e*. the attainment of steady-state signals within 300 s) observed for Au nanoparticle modified oligonucleotide **3** as compared with conventional oligonucleotide **3a** indicates that the Au nanoparticle does not compromise the hybridization kinetics. Control experiments reveal that the **1** and **2** ds-DNA interface is unaffected upon interaction with pure Au nanoparticle solution, $\Delta f = -(1 \pm 1)$ Hz, [Fig. 1(*e*)]. Furthermore, treatment of the **1** and **2** ds-DNA interface with Au nanoparticle modified oligonucleotide **5** at 7.6×10^{-8} M, does not yield any significant change in the frequency response, $\Delta f = -(2 \pm 1)$ Hz, [Fig. 1(*f*)].

Note that the oligonucleotide **5** is essentially complementary to **3**. Thus, the lack of frequency change upon interaction of the **1** and **2** ds-DNA interface with **5** indicates that non-specific oligonucleotide binding is negligible on the interface. The specificity of the sensing interface with oligonucleotide mutants was also investigated. Fig. 1(*g*) shows the interaction of the **1** and **2** ds-DNA with the Au nanoparticle labeled 12-mer oligonucleotide **4** (6.7×10^{-8} M), which has a five-base mutation in the base order compared to **2**. No detectable frequency decrease is observed, indicating that the removal of the five-base pair recognition between the sensing interface and **5** is sufficient to eliminate significant binding interactions. Note that with a fully Au nanoparticle labeled complementary oligonucleotide **3**, a frequency change of −67 Hz was observed at this bulk concentration. Therefore, the oligonucleotides modified with Au nanoparticles still preserve the specificity as that observed on QCM gene sensors with normal oligonucleotide probes.[9,10]

The results show that Au nanoparticle modified oligonucleotides can be applied to detect target DNA at sub-nanomolar concentration. The frequency changes after treatment with different concentrations of the analyte **2** followed by the Au nanoparticle modified DNA probe **3** were investigated. When the concentration of analyte **2** $> 5 \times 10^{-9}$ M, a constant frequency change was observed, implying saturation of the sensing surface. When the analyte **2** is in the concentration range of 3.2×10^{-11} M to 5×10^{-9} M, the frequency changes show a linear behavior. The crystal frequency changes from $\Delta f = -3$ Hz at 3.2×10^{-11} M of **2** to $\Delta f = -160$ Hz at 5×10^{-9} M. The linear regression line was $\Delta f(\text{Hz}) = 0.33C + 3.1$ (with C in units of 10^{-11} M) with $R^2 = 0.98$. A detection limit of *ca*. 3.2×10^{-11} M of the target DNA **2** has been estimated from the response of the QCM signal according to the IUPAC 3 : 1 signal to noise guideline. The significant sensitivity enhancement achieved with the Au nanoparticle modified oligonucleotides compared to the conventional detection system (detection limit of 1.7×10^{-9} M) is attributed to the high density of the Au nanoparticles which are capped to the DNA probes.

In conclusion, we have demonstrated a novel approach for highly sensitive detection of DNA using Au nanoparticle modified oligonucleotides as amplifying probes. The sensing process also showed specificity. This method exhibits extraordinary sensitivity and provides a simple means for rapid detection of a target oligonucleotide at sub-nanomolar concentration. Although the reported sensitivity is impressive, the sensitivity of the system may be further enhanced by using oligonucleotides modified with much smaller Au nanoparticles.

Notes and references

1 S. Yamaguchi, T. Shimomura, T. Tatsuma and N. Oyama, *Anal. Chem.*, 1993, **65**, 1925.
2 H. Su, K. M. R. Kallury, M. Thompson and A. Roach, *Anal. Chem.*, 1994, **66**, 769.
3 J. Wang, P. E. Nielsen, M. Jiang, X. H. Cai, J. R. Fernandes, D. H. Grant, M. Ozsoz, A. Beglieter and M. Mowat, *Anal. Chem.*, 1997, **69**, 5200.
4 R. C. Ebersole and M. D. Ward, *J. Am. Chem. Soc.*, 1988, **110**, 8623.
5 Y. Okahata, M. Kawase, K. Niikura, F. Ohtake, H. Furusawa and Y. Ebara, *Anal. Chem.*, 1998, **70**, 1288.
6 K. Niikura, H. Matsuno, H. Ohatake, H. Furasama and Y. Ebara, *J. Am. Chem. Soc.*, 1998, **120**, 8537.
7 K. Bizet, C. Gabrielli, H. Perrot and J. Therasse, *Proceedings of The Fourth World Congress on Biosensors*, Bangkok, Thailand, 29–31 May 1996. Elsevier Advanced Technology, Oxford, UK, 1996.
8 H. A. Erlich, D. Gelfand and J. J. Sminsky, *Science*, 1991, **252**, 1643.
9 A. Bardea, A. Dagan, I. Ben-Dov, B. Amit and I. Willner, *Chem. Commun.*, 1998, 839.
10 J. Wang and M. Jiang, *J. Am. Chem. Soc.*, 1998, **120**, 8281.
11 J. J. Storhoff, R. Elghanian, R. C. Mucic, C. A. Mirkin and R. L. Letsinger, *J. Am. Chem. Soc.*, 1998, **120**, 1959.

ChemComm

The synthesis and properties of surfactant aza macrocycles†

Andrew D. Pidwell,[a] Simon R. Collinson,[a] Simon J. Coles,[b] Michael B. Hursthouse,[b] Martin Schröder*[c] and Duncan W. Bruce*[a]

[a] *School of Chemistry, University of Exeter, Stocker Road, Exeter, UK EX4 4QD. E-mail: d.bruce@exeter.ac.uk*
[b] *Department of Chemistry, University of Southampton, Highfield, Southampton, UK SO17 1BJ*
[c] *Department of Chemistry, University of Nottingham, University Park, Nottingham, UK NG7 2RD*

Received (in Cambridge, UK) 24th January 2000, Accepted 27th April 2000

Surfactant derivatives of [9]aneN$_3$ and [12]aneN$_3$ are prepared; micelles are formed at low concentrations in water while at higher concentrations lyotropic hexagonal, cubic and lamellar phases are characterised.

The study of surfactant materials is very well established,[1] the materials being used on a vast scale worldwide and in a number of settings such as soaps, detergents and emulsifiers. Surfactants are also important in a number of other areas, for example in cell membranes[2] and in the preparation of mesoporous silicates.[3] Similarly, the study of macrocyclic materials is also a mature area of investigation, especially in the development of sensors for selective cation and anion binding, host–guest chemistry and in supramolecular chemistry.[4]

We have become interested in the synthesis and properties of liquid-crystalline macrocycles with a view to establishing and understanding their structure/property relationships and to combine the substrate binding ability of macrocycles with their known properties as liquid crystals.[5] Previously, Neve has studied difunctionalised derivatives of [18]aneN$_2$S$_4$ which were treated with AgOTf and AgPF$_6$ to give the corresponding Ag^{I} complexes.[6] In the anhydrous state, these complexes showed a viscous, birefringent mesophase which was investigated by X-ray scattering which implied an undulating, bilayer mesophase in which the metal-containing cations describe a 'U'-shaped motif. The same materials were also found to show lyotropic mesomorphism in acetonitrile at concentrations between 15 and 35 wt% complex, giving a lamellar ripple phase (*i.e.* again, a modulated phase). Later, Fallis[7] reported a related system in which [9]aneN$_3$ was functionalised with a long-chain secondary alcohol and then complexed to Ni(II) and Cu(II) centres. In this case, the neutral macrocycle was poorly soluble in water and surfactant properties were reported only for the cationic complexes. As part of our own work in this area,[5] we have begun to investigate surfactant derivatives of simple, uncomplexed aza macrocycles and report herein the synthesis of new surfactants derived from [9]aneN$_3$ and [12]aneN$_3$.

A general model for a surfactant consists of a polar head group bound to a non-polar chain and so initially we confined ourselves to systems bearing one alkyl chain. We argued that the simplest way of accessing such systems was *via* orthoamide protection of the triazamacrocycles (Fig. 1). These are obtained after a multistep synthesis for the [9]aneN$_3$ derivative[8] (**1**) or after a one-step synthesis for the [12]aneN$_3$ derivative (**2**).[9] Once obtained, these orthoamides can be reacted with, for example, a haloalkane which opens up the orthoamide to give a cationic, *N*-alkylated macrocycle with two nitrogens still protected by a bridgehead carbon.[10] Our initial attempts focused on functionalisation using a C_{12} chain which ought to be sufficiently long to give rise to surfactant behaviour. However, following reaction of 1-bromododecane with the orthoamide of [12]aneN$_3$ in acetonitrile, we were unable to recover a pure, alkylated macrocycle. This is most likely due to quaternisation at nitrogen followed by Hoffmann elimination to give ring-opened products.

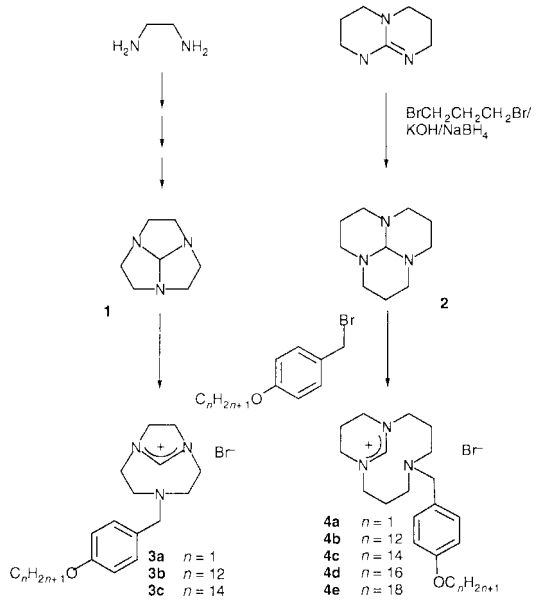

Fig. 1 Synthesis of the surfactant derivatives of [9]aneN$_3$ and [12]aneN$_3$.

However, we were more successful using 4-alkoxybenzyl bromides which reacted smoothly with the orthoamide derivatives of [9]aneN$_3$ and [12]aneN$_3$ to give the desired products (**3** and **4**) which were isolated in near quantitative yields (Fig. 1).[11] For the methoxy derivative of [12]aneN$_3$ (**4a**) we were able to obtain single crystals, and the molecular structure resulting from the X-ray diffraction study‡ is shown in Fig. 2. The structure confirms the substitution at the macrocyclic core with the bridgehead still in place, forming a 6-membered ring within the macrocycle in an envelope conformation, with the two N–C bonds [N(2)–C(4) and N(3)–C(4)] being virtually identical in length [1.308(3) and 1.312(3) Å respectively]. The conformation of the flexible [12]aneN$_3$ ring is distorted considerably by the formation of the bridgehead, shown by a comparison of the torsion angles in the bridge ring [C(3)–N(2)–C(5)–C(6) and C(6)–C(7)–N(3)–C(8) = 172.0(2) and 174.9(3)° respectively] with those in the conformationally more flexible region of the macrocycle [C(9)–C(10)–N(1)–C(1) and C(2)–C(1)–N(1)–C(10) = 152.0(2) and 143.5(2)° respectively]. An additional indicator of the strain induced in the macrocycle by the formation of a 6-membered ring is the observed shortening of the non-bonded N···N distance about the bridge [N(1)–N(2), N(1)–N(3) and N(2)–N(3) = 3.11(3), 3.10(3) and 2.33(4)° respectively]. Further, the structure reveals that the bromide counter anion is reasonably close to the head group, the average N–Br distance being 4.3(3) Å.

Thus far, we have synthesised three derivatives of [9]aneN$_3$, **3a**–**c**, and five derivatives of [12]aneN$_3$, **4a**–**e** (Fig. 1) and evaluation of their critical micelle concentration in water was undertaken using an automated tensiometer. The trend in cmc

† Electronic supplementary information (ESI) available: Fig, S1. See http://www.rsc.org/suppdata/cc/b0/b003368p/

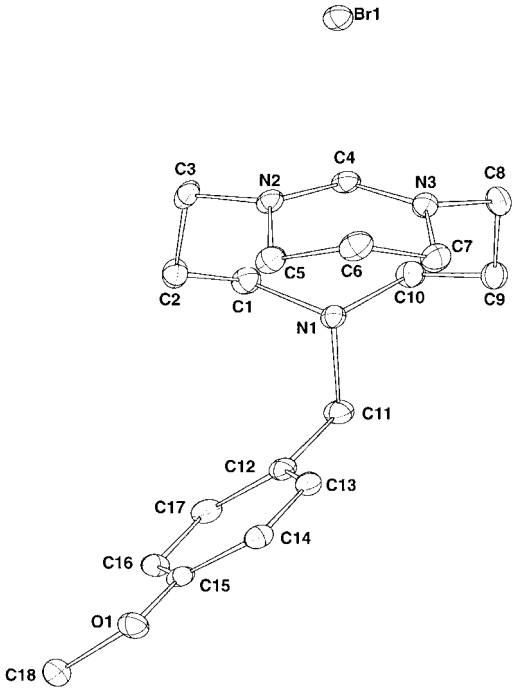

Fig. 2 Molecular structure of compound **4a**.

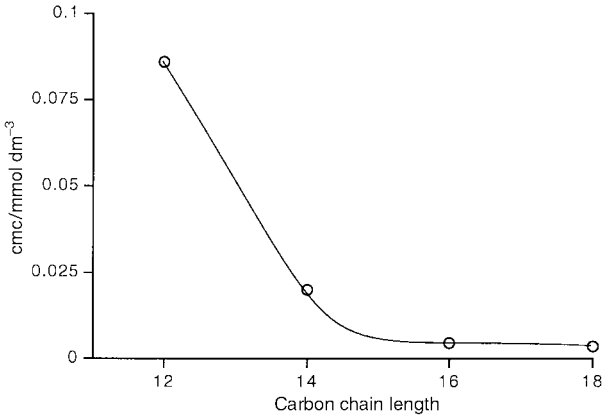

Fig. 3 Plot of cmc *vs* chain length for compounds **4**.

values for the [12]aneN$_3$ derivatives is shown in Fig. 3 and reveals the expected decrease in cmc with increasing chain length on account of the increasing hydrophobicity of the chain. While it is perhaps surprising that the cmc of the two longest-chain derivatives are very similar, we have repeated these measurements and found them to be reproducible. We did not attempt to measure the cmc of **3a** and **4a** which were synthesised for the purpose of single crystal structural analysis.

Absolute and relative values of the cmc for these materials deserve some comment. In general, the cmc values for simple monocationic surfactants are of the order of 10^{-3} mol dm^{-3} while those of neutral surfactants are up to two orders of magnitude lower.[12] The reason for this difference is accounted for by the greater dirving force required to push together head groups of like charge. However, the cmc is also affected by the hydrophobicity of the headgroup and as, in these examples, this contains not only the macrocyclic ring but a benzyl group, too, then the fact that the cmc values are $< 10^{-4}$ mol dm^{-3} is not entirely unexpected. For such an argument to hold, we would predict that the cmc values for the [9]aneN$_3$ derivatives would be higher for the [12]aneN$_3$ derivatives since the head group in this system is smaller, less hydrophobic and more charge-dense. This prediction appeared to be borne out by initial experiments which indicated that the cmc value of surfactant **3b** was approximately three times higher than that of **4b**. Similar arguments had been advanced by Fallis *et al.* to explain lower-than-expected cmc values in their cationic surfactant complexes.[7] However, subsequently we found that the [9]aneN$_3$ derivatives were unstable in water and NMR studies in D_2O implied that between 5–10% decomposed over 24 h. The nature of the decomposition was not clear, but we suspect that the instability of compounds **3** was due to the greater ring strain present when compared to **4**. Thus, we cannot say anything conclusive about the relative cmc values of **3** and **4**.

We have studied the properties of one of the surfactants in more concentrated solution to see whether lyotropic liquid crystal phases can be observed. Using the Lawrence penetration method,[13] we studied **4b** and found that at temperatures of 40 °C a normal hexagonal (H_1) phase was observed, while at 50 °C, a bicontinuous cubic (V_1) phase was also observed (Fig. S1a†). At much higher temperatures, a lamellar (L_α) phase was observed (Fig. S1b†). Thus, we have the possibility of organising and tuning the behaviour of these macrocyclic materials in a predetermined fashion.

The present study has shown that rather simple, functionalised triazamacrocycles can lead to materials which aggregate on a local (micelle) or extended (mesophase) scale. These bridgehead-protected materials will not complex to metal cations and so we are now investigating free-base derivatives with respect to both solution behaviour and to metal complexation chemistry. Details of these studies will be reported in due course.

We thank the EPSRC, Leverhulme Trust and the Royal Society for financial support.

Notes and references

‡ *Crystal data* for **4a**. Empirical formula: $C_{18}H_{28}BrN_3O$; formula weight: 382.34; crystal system: orthorhombic; space group: *Pbca*; Final *R* indices [$F^2 > 2\sigma(F^2)$]: *R*1 = 0.0410, *wR*2 = 0.1123; unit cell dimensions: a = 13.352(3), b = 14.822(3), c = 18.105(4) Å; $\alpha = \beta = \gamma = 90°$; V 3583.0(13) Å^3; 150(2) K; Z = 8; μ = 2.303 mm^{-1}; reflections collected: 24587; independent reflections: 4107 [R_{int} = 0.0807]; *R* indices (all data): *R*1 = 0.0601, *wR*2 = 0.1283. Absorption corrections applied using SORTAV;[14] solution obtained *via* direct methods and refined[15] by full-matrix least-squares on F^2, with hydrogens included in idealised positions. CCDC 182/1619. See http://www.rsc.org/suppdata/cc/b0/b003368p/ for crystallographic files in .cif format.

1 R. G. Laughlin, *The Aqueous Phase Behaviour of Surfactants*, Academic Press, London, 1994.
2 J. M. Seddon, *Biochim. Biophys. Acta*, 1990, **1031**, 1.
3 M. Raimondi and J. M. Seddon, *Liq. Cryst.*, 1999, **26**, 305.
4 L. F. Lindoy, *The Chemistry of Macrocyclic Ligand Complexes*, 1989, Cambridge University Press, Cambridge; F. Vögtle, *Supramolecular Chemistry*, 1991, Wiley, Chichester.
5 A. J. Blake, B. W. Bruce, I. A. Fallis, S. Parsons and M. Schröder, *J. Chem. Soc., Chem. Commun.*, 1994, 2471; A. J. Blake, D. W. Bruce, I. A. Fallis, S. Parsons, H. Richtzenhain, S. A. Ross and M. Schröder, *Proc. R. Soc. London, A: Math. Phys. Sci.*, 1996, **354**, 395; N. R. Champness, D. W. Bruce and M. Schröder, *New J. Chem.*, 1999, **23**, 671.
6 F. Neve, M. Ghedini, G. de Munno and A.-M. Levelut, *Chem. Mater.*, 1995, **7**, 688.
7 I. A. Fallis, P. C. Griffiths, D. E. Hibbs, M. B. Hursthouse and A. L. Winnington, *Chem. Commun.*, 1998, 665.
8 T. J. Atkins, J. E. Richmann and W. F. Oettle, *Org. Synth.*, 1978, **58**, 86; T. J. Atkins, *J. Am. Chem. Soc.*, 1980, **102**, 6364.
9 D. H. Kim, M. Wilson and J. Hesteltine, *Synth. Commun.*, 1994, **24**, 3109.
10 R. W. Alder, R. W. Mowlam, D. J. Vachon and G. R. Weisman, *J. Chem. Soc., Chem. Commun.*, 1992, 507; A. J. Blake, I. A. Fallis, R. O. Gould, S. Parsons, S. A. Ross and M. Schröder, *J. Chem. Soc., Dalton Trans.*, 1996, 4379.
11 All new compounds were characterised by elemental analysis and ^{1}H and ^{13}C NMR spectroscopy.
12 C. Fairhurst, S. Fuller, J. Gray, M. C. Holmes and G. J. T. Tiddy, in *Handbook of Liquid Crystals*, eds. D. Demus, J. Goodby, G. W. Gray, H.-W. Spiess and V. Vill, Wiley-VCH, Weinheim, 1998, vol. 3, ch. VII.
13 A. S. C. Lawrence, *Liquid Crystals 2*, ed. G. H. Brown, Gordon and Breach, London, 1969, part 1, p. 1.
14 R. H. Blessing, *Acta Crystallogr., Sect. A*, 1995, **51**, 33; R. H. Blessing, *J. Appl. Crystallogr.*, 1997, **30**, 421.
15 G. M. Sheldrick, SHELXL-97. Program for refinement of crystal structures. University of Göttingen, 1997.

Preparation of mordenite membranes on α-alumina tubular supports for pervaporation of water–isopropyl alcohol mixtures

X. Lin, E. Kikuchi and M. Matsukata*

Department of Applied Chemistry, Waseda University, 3-4-1 Okubo, Shinjuku, Tokyo 169-8555, Japan. E-mail: mmatsu@mn.waseda.ac.jp

Received (in Cambridge, UK) 15th December 1999, Accepted 20th April 2000

Mordenite membranes prepared on α-alumina tubular supports by *in situ* hydrothermal synthesis using organic template-free media showed high water permselectivity for pervaporation of water–isopropyl alcohol mixtures.

Zeolite membranes have been widely studied in recent years because of their great potential applications in separations, membrane reactors and sensors. A continuous zeolite layer can be grown on various supports, including α-alumina and stainless steel generally by *in situ* hydrothermal synthesis. Different types of zeolites such as MFI, zeolite A, zeolite Y, mordenite and ferrierite have been synthesized on flat and tubular supports. Research has so far mainly focused on MFI (silicalite and ZSM-5) membranes for gas separation because their pore sizes, which are close to the sizes of gas molecules, allow separation of molecules based on their size. In addition, MFI crystals are easily grown on a support with structure-directing agents (SDAs). Some MFI membranes showing good separation of hydrocarbon isomers such as *n*-butane–isobutane have been reported by several groups.[1–3]

With respect to pervaporation separation, not only the pore sizes of zeolites, but also their surface properties (hydrophobicity and hydrophilicity) play an important role. Hydrophobic MFI membranes exhibit preferential alcohol permeation for pervaporation of a water–alcohol mixture although the molecular size of water is smaller than that of the alcohol.[4] In contrast, water permeated much faster than alcohols through hydrophilic zeolite A and Y membranes.[5,6] Since mordenite zeolite with large channels of 0.67 × 0.7 nm and small channels of 0.26 × 0.56 nm is hydrophilic, mordenite membranes would be selective for permeating water against alcohols.

In 1990, Suzuki *et al.*[7] first claimed the synthesis of a zeolite membrane (mordenite) onto a porous silica–alumina plate using an *in situ* hydrothermal synthesis method. Their membrane, synthesized at 160 °C for 2 days, exhibited Knudsen-diffusion behavior. Matsukata and coworkers[8] applied the vapor-phase transport method to obtain a mordenite membrane on a porous α-alumina disk. Their membranes showed a good separation factor of 160 for pervaporation of a benzene–*p*-xylene mixture. Very recently, Santamaría and coworkers[9,10] synthesized mordenite membranes onto a tubular support by *in situ* hydrothermal synthesis using TEAOH and reported the formation of composite mordenite/ZSM-5/chabazite membranes. They studied the separation of a water–n-propanol mixture through their composite membranes by a sweep gas method. Permeance ratios as high as 70 to 140 for water and *n*-propanol were achieved through their membranes. To our knowledge, the synthesis of mordenite membranes under SDA-free conditions on tubular supports has not been reported. Here we report the synthesis of a mordenite membrane onto a tubular support for pervaporation of a water–isopropyl alcohol mixture.

Mordenite membranes were synthesized on porous 6 cm long α-alumina tubes (NGK, Ltd.) with 0.1 μm diameter pores by *in situ* hydrothermal synthesis. The parent aluminosilicate gel was prepared as follows. An appropriate amount of alumina sulfate (Wako Pure Chem. Ind. Co. Ltd.) was added to a NaOH solution and stirred at room temperature until it dissolved. Colloidal silica containing 30–31 wt% of SiO_2 and 0.6 wt% of Na_2O ST-S, Nissan Chem. Ind. Ltd.) was then added to this solution and stirred vigorously for 1 h to give a gel of molar composition $0.38Na_2O:SiO_2:0.025Al_2O_3:40H_2O$.[7] The tubular support was washed, coated with a water slurry of seed crystals of zeolite mordenite (HSZ600, 70A, Tosoh Co.), SiO_2/Al_2O_3 ratio = 10.2), and then dried at 100 °C for 15 min. The support was then vertically immersed in the gel. Crystallization was carried out at 180 °C for a given period. After the crystallization, the sample was removed, washed carefully with distilled water, and then dried at 100 °C.

The membranes obtained were characterized by X-ray diffraction (XRD) with Cu-Kα radiation (Rigaku RINT2000). Fig. 1 shows the XRD patterns for the products crystallized at 180 °C for 8 and 24 h together with that for the seed powder. These XRD patterns were consistent with the mordenite structure. The XRD patterns of the membranes crystallized for different periods of crystallization showed that the (150) reflection intensity at 22.24°, became dominant with increasing crystallization time. Thus, mordenite crystals appear to grow randomly in the early stages of crystallization, and further crystal growth occurred mainly with the (150) face parallel to the support surface. Mordenite crystals were also grown on an unseeded support and gave almost the same XRD pattern as those on the seeded supports.

The morphology of the mordenite membranes was studied by scanning electron microscopy (SEM) (Hitachi S2150) and Fig. 2 shows SEM images for the surface and cross section of the mordenite membrane crystallized at 180 °C for 24 h. A continuous, intergrown layer fully covers the surface of support. The crystal sizes are *ca.* 6–7 μm, and the thickness of crystal

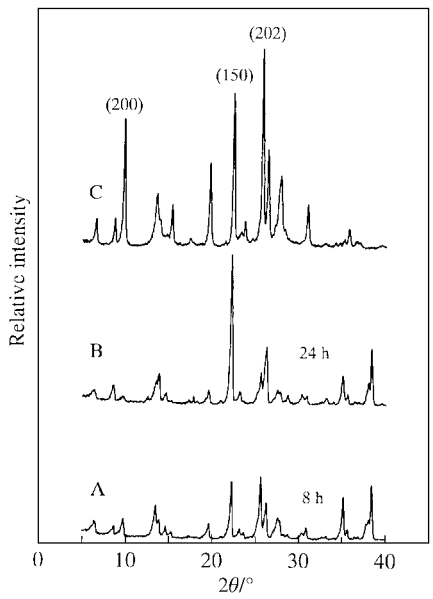

Fig. 1 XRD patterns for mordenite membranes crystallized at 180 °C for (A) 8 and (B) 24 h, and (C) mordenite seed powder.

DOI: 10.1039/a909867d

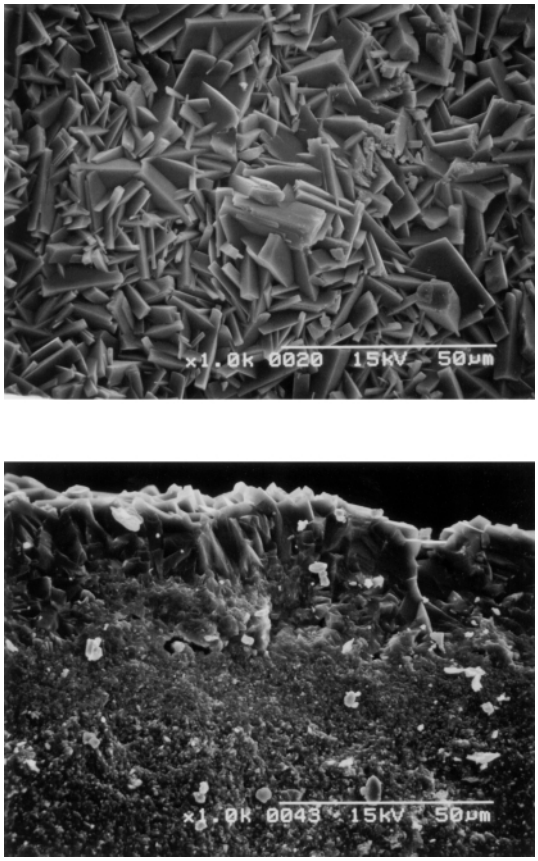

Fig. 2 SEM images for the surface and cross section of the mordenite membrane synthesized at 180 °C for 24 h.

layer is *ca.* 35 μm. The SiO_2/Al_2O_3 ratio of the mordenite zeolites determined by EDAX was *ca.* 12. In addition, the mordenite crystals have a rectangular form.

The pervaporation (PV) tests for water–isopropyl alcohol, and water–n-propanol mixtures were carried out at 75 °C using the pervaporation experimental apparatus described elsewhere.[8] The effective membrane area was *ca.* 15 cm^2 and the permeation side was kept under vacuum. The flux was calculated by weighing the condensed permeate. The separation factor was determined as $\alpha_{A/B} = (Y_A/Y_B)/X_A/X_B)$, where X_A, X_B, Y_A and Y_B denote the mass fractions of components A and B in the feed and permeate sides. The pervaporation results through the mordenite membranes crystallized at 180 °C for 24 h are listed in Table 1 and clearly show that water preferentially permeated through the mordenite membranes. The membrane synthesized on the seeded support exhibited a very high separation factor of 3360 for the water–isopropyl alcohol mixture compared with that of the unseeded support (192). We propose that the seed crystals increased the density of mordenite crystals on the support, resulting in a pinhole-free structure in contrast to the membrane formed on the unseeded support.

Table 1 Pervaporation results through mordenite membranes

Membrane[a]	Feed solution (A/B) (wt% of A)	Separation factor (A/B)[b]	Flux/ kg m^{-2}
M1	Water–n-propanol (10)	1782	0.2
M2	Water–isopropyl alcohol (10)	3360	0.1
M3[c]	Water–isopropyl alcohol (10)	192	0.2

[a] Membranes were crystallized at 180 °C for 24 h; [b] PV carried out at 75 °C. [c] Prepared without seeds.

Mordenite is formed for Si/Al ratios of *ca.* 5–6, higher than those for LTA (Si/Al = 1) and Y (Si/Al ratio = *ca.* 2.5). Thus, in comparison with LTA and Y, mordenite has potential application in acidic solutions under which esterification can occur. In addition, it is known that the effective pore size of mordenite can be precisely controlled in the range of *ca.* 0.3–0.6 nm by ion exchange, possibly leading to a wide variety of applications such as hydrocarbon separation and use as membrane reactors.

Notes and references

1 W. J. Bakker, F. Kapteijn, J. Poppe and J. A. Moulijn, *J. Membr. Sci.*, 1996, **117**, 57.
2 Z. A. P. Vroon, K. Keizer, M. J. Gilde, H. Verweij and A. J. Burggraaf, *J. Membr. Sci.*, 1996, **113**, 293.
3 X. Lin, J. L. Falconer and R. D. Noble, *Chem. Mater.*, 1998, **10**, 3716.
4 T. Sano, H. Yanagishita, Y. Kiyozumi, F. Mizukami and K. Haraya, *J. Membr. Sci.*, 1994, **95**, 221.
5 H. Kita, K. Horii, Y. Ohtoshi and K. Okamoto, *J. Mater. Sci. Lett.*, 1995, **14**, 206.
6 H. Kita, T. Inoue, H. Asamura, K. Tanaka and K. Okamoto, *Chem. Commun.*, 1997, 45.
7 K. Suzuki, Y. Kiyozumi, T. Sekine, K. Obata, Y. Shindo and S. Shin, *Chem. Express*, 1990, **5**, 793.
8 N. Nishiyama, K. Ueyama and M. Matsukata, *Microporous Mater.*, 1996, **7**, 299.
9 M. A. Salomón, J. Coronas, M. Menéndez and J. Santamaría, *Chem. Commun.*, 1998, 125.
10 E. Piera, M. A. Salomón, J. Coronas, M. Menéndez and J. Santamaría, *J. Membr. Sci.*, 1998, **149**, 99.

ChemComm

Electrophilic fluorination at saturated sites

Richard D. Chambers,*[a] Mandy Parsons,[a] Graham Sandford*[a] and Roy Bowden[b]

[a] *Department of Chemistry, University of Durham, South Road, Durham, UK DH1 3LE. E-mail: graham.sandford@durham.ac.uk*

[b] *F2 Chemicals Ltd., Lea Lane, Lea Town, Preston, UK PR4 0RZ*

Received (in Liverpool, UK) 23rd February 2000, Accepted 20th April 2000

Transformation of carbon–hydrogen bonds to carbon–fluorine bonds at saturated secondary and tertiary carbon sites by electrophilic aliphatic substitution processes is possible using either elemental fluorine or fluorinating reagents of the N–F class.

The development of effective methodology for the selective introduction of fluorine atoms into organic molecules has received much attention recently because of the significant effects on the physical, chemical and biological properties that incorporation of one or several fluorine atoms into a substrate can impart.[1] These sometimes unique effects are especially important in the life-science industries and there are now many pharmaceuticals and plant-protection agents that are commercially available which owe their biological activity to the presence of fluorine in their structures.

Synthetic procedures for the selective transformation of carbon–hydrogen bonds to carbon–fluorine bonds offer, in principle, efficient, direct processes for introducing fluorine atoms into organic molecules. In this context, during the last few years we, and others,[2] have been able to demonstrate that elemental fluorine is a viable reagent for selective introduction of fluorine into organic compounds, including aromatic systems[3] and a wide range of carbon sites that are nucleophilic, *e.g.* dicarbonyl compounds,[4] diesters,[5] *etc.* Fluorination of unactivated sp^3 hybridised carbon–hydrogen sites offers significant opportunities for the incorporation of fluorine into an even wider range of hydrocarbon derivatives. However, selective direct fluorination at saturated carbon sites is largely limited to the work of Rozen and co-workers[6] who demonstrated that tertiary C–H sites could be fluorinated using elemental fluorine in a reaction medium of $CHCl_3/CFCl_3$ at −78 °C. These reaction conditions are clearly limiting, especially for scale-up, and therefore we have explored other systems.

We have now established that acetonitrile as a solvent is highly beneficial over a variety of other media that we have investigated. Reactions are conveniently carried out by passing fluorine gas, diluted to a 10% solution (*v/v*) in nitrogen, through a mixture consisting of the substrate and acetonitrile, cooled to 0 °C, and efficient, selective fluorination of a variety of systems has now been achieved this way (see Table 1). Both secondary C–H (**1a** to **2a**) and tertiary C–H sites (*e.g.* **1b** to **2b**) were transformed to C–F bonds using these convenient reaction conditions. Fluorination of cyclohexane **1a**, *trans*-decalin **1b** and norbornane **1c** gave a single mono-fluorinated isomer in each case whereas fluorination of decane **1d** led to a mixture of four mono-fluorinated positional isomers **2f** in similar amounts, indicating that fluorine substitution had occurred at all possible secondary sites of the alkyl chain. In contrast, fluorination of ester **1e** gave a mixture consisting of four mono-fluorinated isomers in a ratio of 5.8:3.9:3.2:1 which were identified by NMR studies to be the 6-, 5-, 4- and 3-fluoroheptanoate derivatives respectively. Therefore, fluorination occurs preferentially at secondary sites that are furthest removed from the electron withdrawing ester group. In all cases the yields quoted are based upon analysis of the crude product obtained after separation from the acetonitrile reaction medium (*i.e.* after washing with water and extraction into dichloromethane). All reactions were clean, in that no tar formation was observed. Additional products contained in the crude product were present in very low concentration and too minor to be identified. Inevitably handling losses on the scale used (*ca.* 5 g of starting material) are relatively high, especially in the cases of very volatile substrates, but would obviously be reduced by an increase in scale.

Table 1 Selective fluorination of saturated systems

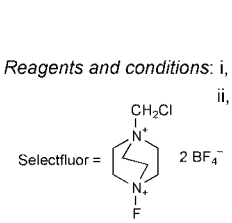

Substrate	Conditions	Product(s)	Yield (Conv.%)
 **1a**	i	 **2a**	63 (53)
1a	ii	**2a**	22 (100)
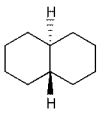 **1b**	i	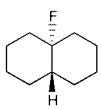 **2b**	54 (68)
1b	ii	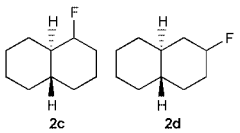 **2c** **2d**	23 (81)
 **1c**	i	 *exo* : *endo* = 5 : 1 **2e**	41 (60)
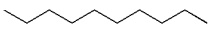 **1d**	i	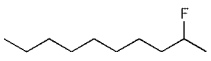 and 3-, 4- and 5-fluorodecane **2f** (2.6 : 1.2 : 1.1 : 1.0)	63 (61)
1d	ii	**2f** (2.4 : 1.3 : 1.1 : 1.0)	58 (84)
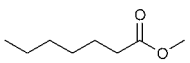 **1e**	i	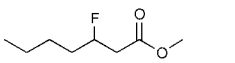 and methyl 4-, 5- and 6-fluoroheptanoate **2g** (5.9 : 3.9 : 3.2 : 1.0)	49 (42)
1e	ii	**2g** (3.7 : 1.3 : 1.3 : 1.0)	48 (57)

The question of the mechanism of direct fluorination processes arises and the obvious difficulty of distinguishing between electrophilic and radical substitution presents a

DOI: 10.1039/b001624l

problem. Consequently, we have explored corresponding reactions between these hydrocarbon systems and Selectfluor™ (available from Air Products), an easily handled, commercially available fluorinating reagent of the N–F class.[7,8] Selectfluor™ and structurally related N–F reagents have themselves been characterised as electrophilic reagents in mechanistic studies by Wong[9] and Differding[10,11] because no evidence of radical intermediates or products arising from one-electron transfer processes were obtained in radical-clock experiments.

Fluorinations of **1** were achieved by heating a mixture consisting of the substrate, Selectfluor™ and acetonitrile at reflux temperature and, for most of the systems that we have investigated, nearly parallel results to those observed using fluorine were obtained. For example, fluorination of decane **1d** using Selectfluor™ led to a similar product distribution to that obtained when fluorine was used. In the case of decalin, however, fluorine gave products arising from substitution at the tertiary site whereas, in contrast, Selectfluor™ gave fluorine substitution exclusively at the CH_2 sites. We attribute this difference simply to the greater steric requirements of the Selectfluor™ reagent. Therefore, the general similarity in product distribution obtained upon fluorination of saturated systems with both fluorine or Selectfluor™, suggests that these transformations of C–H bonds to C–F bonds may be considered to proceed *via* relatively uncommon aliphatic electrophilic substitution reactions at saturated sites (S_E2) involving 3 centre–2 electron bond transition states[12] (see Scheme 1). Addition of nitrobenzene, a free-radical scavenger, to the direct fluorination reaction medium does not affect product distribution or yield, further supporting an electrophilic process.

In the light of the intense interest in electrophilic N–F reagents[8,13] it is surprising that substitution at saturated sites has been so little developed because the examples shown in Table 1 demonstrate that it is a quite general process. However, Zupan[14] and co-workers have reported unusual fluorinations of methyl groups in tertiary alcohol systems but a mechanism is not advanced for the process.

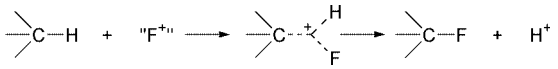

Scheme 1

In summary, we are confident in describing the reactions of elemental fluorine, shown here, as electrophilic rather than fluorine atom processes. Indeed, the electrophilic fluorination of saturated sites shown here, using either fluorine or N–F fluorinating reagents, are surprisingly efficient, convenient processes.

We thank F2 Chemicals (Studentship to M. P.) for funding and the Royal Society (University Research Fellowship to G. S.).

Notes and references

1 *Organofluorine Chemistry. Principles and Commercial Applications*, ed. R. E. Banks, B. E. Smart and J. C. Tatlow, Plenum, New York, 1994.
2 J. Hutchinson and G. Sandford, *Top. Curr. Chem.*, 1997, **193**, 1.
3 R. D. Chambers, C. J. Skinner, J. Huchinson and J. Thomson, *J. Chem. Soc., Perkin Trans. 1*, 1996, 605.
4 R. D. Chambers, M. P. Greenhall and J. Hutchinson, *Tetrahedron*, 1996, **52**, 1.
5 R. D. Chambers, J. Hutchinson and J. Thomson, *J. Fluorine Chem.*, 1996, **78**, 165.
6 S. Rozen, *Acc. Chem. Res.*, 1988, **21**, 307.
7 R. E. Banks, S. N. Mohialdin-Khaffaf, G. S. Lal, I. Sharif and R. G. Syvret, *J. Chem. Soc., Chem. Commun.*, 1992, 595.
8 G. S. Lal, G. P. Pez and R. G. Syvret, *Chem. Rev.*, 1996, **96**, 1737.
9 S. P. Vincent, M. D. Burkhart, C. Y. Tsai, Z. Zhang and C. H. Wong, *J. Org. Chem.*, 1999, **64**, 5264.
10 E. Differding and G. M. Ruegg, *Tetrahedron Lett.*, 1991, **32**, 3815.
11 E. Differding and M. Wehrli, *Tetrahedron Lett.*, 1991, **32**, 3819.
12 G. A. Olah, G. K. S. Prakash, R. E. Williams, L. D. Field and K. Wade, *Hypercarbon Chemistry*, Wiley-Interscience, New York, 1987.
13 S. D. Taylor, C. C. Kotaris and G. Hum, *Tetrahedron*, 1999, **55**, 12431.
14 S. Stavber and M. Zupan, *J. Chem. Soc., Chem. Commun.*, 1994, 149.

ChemComm

Biarylphosphonites: a class of monodentate phosphorus(III) ligands that outperform their chelating analogues in asymmetric hydrogenation catalysis

Carmen Claver,[b] Elena Fernandez,[b] Amy Gillon,[a] Katie Heslop,[a] David J. Hyett,[a] Aina Martorell,[a] A. Guy Orpen*[a] and Paul G. Pringle*[a]

[a] *School of Chemistry, University of Bristol, Cantock's Close, Bristol, UK BS8 1TS. E-mail: paul.pringle@bristol.ac.uk*

[b] *Universitat Rovira i Virgili, Department de Química Fisica Inorgànica, Plaça Imperial Tàrraco, 1, Tarragona, Spain*

Received (in Cambridge, UK) 29th February 2000, Accepted 17th April 2000

Rhodium(I) complexes of monodentate phosphonites derived from 2,2′-binaphthol and 9,9′-biphenanthrol are compared with diphosphonite chelate analogues as catalysts for asymmetric hydrogenation; the high ee's (up to 92%) obtained with the monodentate systems and the observation that they are sometimes superior to the chelate analogues are discussed.

The enantioselective hydrogenation of prochiral alkenes is perhaps the most important application of asymmetric catalysis with synthetic catalysts and is decidedly the most studied and best understood. In 1972 Kagan *et al.*[1] were the first to show that a diphosphine was more efficient as an ancillary ligand for asymmetric hydrogenation than corresponding monophosphines. Since then, it has been found[2] that complexes of bidentate ligands consistently give higher asymmetric inductions in hydrogenation. This has been rationalised in terms of the chirality of the phosphorus substituents whose retention is enforced by the chelate ring. We report here, hydrogenation catalysis that challenges this received wisdom in that monodentate phosphonite species show, in some cases, higher enantioselectivity than the analogous bidentate phosphonites.

The resolved monodentate biarylphosphonites **1a–c** and **2a–c** and the related diphosphonites **3** and **4** are afforded by the routes shown in Scheme 1. The corresponding rhodium(I)–monophosphonite complexes **5a–f** and rhodium(I)–diphosphonite complexes **6a**,**b** have been isolated and characterised by a combination of elemental analysis, ^{31}P, ^{1}H and ^{13}C NMR spectroscopy; the monophosphonite **2b** has been previously reported[3] and while this work was in progress[4] Reetz *et al.*,[5] reported the preparation of **3**.

The results for the asymmetric hydrogenation of methyl-2-acetamido acrylate [eqn. (1)] catalysed by our rhodium

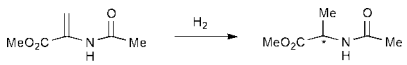

(1)

phosphonite complexes are given in Table 1. The monophosphonite complexes give remarkably high enantioselectivities, up to 92% ee with **5c** (entry 3). Furthermore the monophosphonite complexes **5e** and **5f**, derived from biphenanthrol are much more selective than the corresponding diphosphonite **6b**.

The results for the asymmetric hydrogenation of methyl-2-acetamido cinnamate [eqn. (2)] are also given in Table 1. For

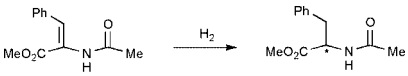

(2)

this reaction, the diphosphonite complexes **6a** and **6b** both give poor (< 20% ee) enantioselectivities (entries 15 and 16) and in several cases (see entries 9, 10, 13 and 14) the monophosphonite analogues give superior enantioselectivities (ee up to 80%).

The phosphonite ligands reported here are therefore an apparent exception to the rule in enantioselective hydrogenation that catalysts based on bidentate phosphorus(III) ligands are

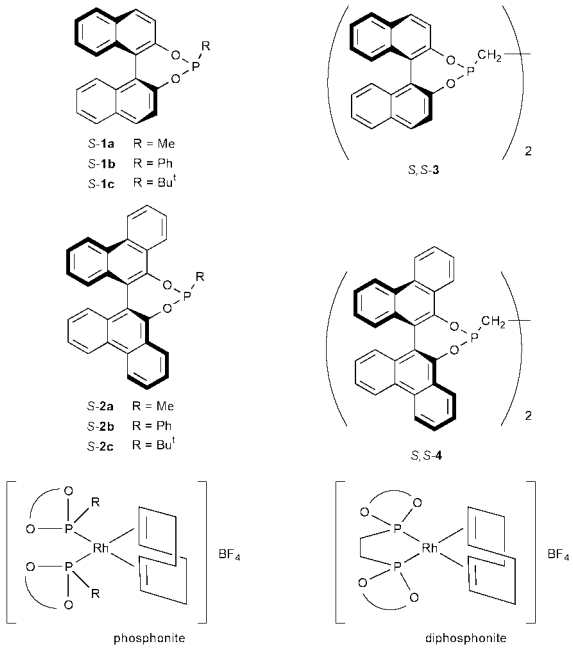

superior to their monodentate analogues. This dogma is based on the idea that the conformational control in metallochelates provides efficient stereocontrol that is not possible with monodentate ligands because of a low energy barrier to M–P bond rotation in the latter case. The most effective monophosphine for asymmetric hydrogenation to date (up to 90% ee) is PMePh(C_6H_4OMe-2);[6] however this ligand may form a hemilabile chelate *via* coordination of the *o*-methoxy group and moreover the bidentate analogue (dipamp) gives a much more enantioselective hydrogenation catalyst.[7]

The solution ^{31}P NMR behaviour of the rhodium complexes **5b** and **5e** was unexceptional. In each case a single sharp doublet was observed at +25 °C which remained essentially unaltered down to −90 °C. This is consistent with rapid M–P bond rotation and/or the presence of predominantly one rotamer.

We have been unable to obtain crystals of salts of the rhodium(I) complexes suitable for X-ray crystallography but the crystal structures of [$PtCl_2$(*R*-**2b**)$_2$] *R*,*R*-**7** (an analogue of the enantiomer of **5e**) and [$PtCl_2$(*S*,*S*-**4**)$_2$] *S*,*S*-**8** (an analogue of **6b**)

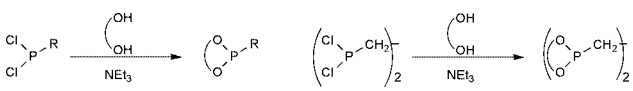

Scheme 1

DOI: 10.1039/b001638l

Table 1 Asymmetric hydrogenations of methyl-2-acetamido acrylate and cinnamate[a]

	Acrylate				Cinnamate		
Entry	Catalyst	Conv.	%ee	Entry	Catalyst	Conv.	%ee
1	**5a**	76	78(*R*)	9	**5a**	100	80(*R*)
2	**5b**	100	73(*R*)	10	**5b**	100	63(*R*)
3	**5c**	73	92(*R*)	11	**5c**	100	10(*R*)
4	**5d**	100	29(*R*)	12	**5d**	97	14(*S*)
5	**5e**	100	78(*R*)	13	**5e**	100	59(*S*)
6	**5f**	30	70(*R*)	14	**5f**	100	49(*R*)
7	**6a**	100	90(*R*)[b]	15[c]	**6a**	81	19(*R*)
8	**6b**	99	23(*R*)	16	**6b**	100	14(*R*)

[a] Reaction conditions: methyl-2-acetamido acrylate or cinnamate (3.5 mmol), catalyst (0.0073 mmol) and CH_2Cl_2 (7.5 cm^3) were placed in a stainless steel autoclave, which was then pressurised to 1.5 atm with hydrogen and the reaction mixture was stirred at 25 °C for 3 h (acrylate) or 20 h (cinnamate). Conversions and ee's were determined by GC using a Hewlett-Packard 5800 A with a L-Chirasil-Val column. [b] This ee agrees with the literature report[5] but we unambiguously assign the opposite configuration to the major enantiomer.[c] In MeOH.

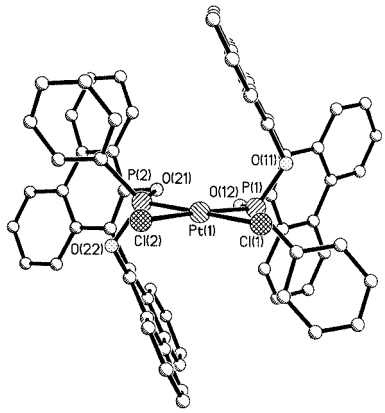

Fig. 1 Molecular structure of *S*,*S*-**7**. Important bond lengths (Å) and angles (°) include: Pt(1)–P(1) 2.201(2), Pt(1)–P(2) 2.199(2), Pt(1)–Cl(1) 2.346(2), Pt(1)–Cl(2) 2.344(2); P(1)–Pt(1)–P(2) 100.84(8). Hydrogen atoms have been omitted for clarity.

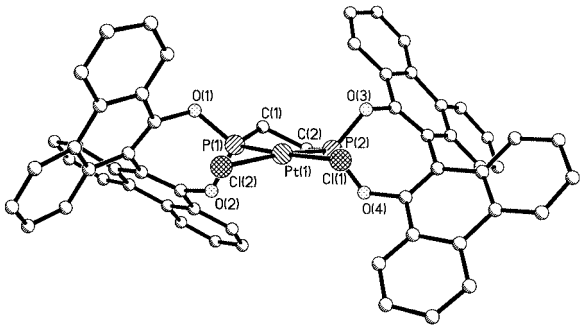

Fig. 2 Molecular structure of *S*,*S*-**8**. Important bond lengths (Å) and angles (°) include: Pt(1)–P(1) 2.189(2), Pt(1)–P(2) 2.183(3), Pt(1)–Cl(1) 2.351(2), Pt(1)–Cl(2) 2.337(3); P(1)–Pt(1)–P(2) 85.93(9). Hydrogen atoms have been omitted for clarity.

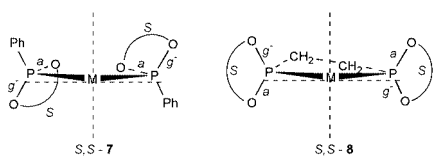

Scheme 2

as solvates† have been obtained. The structures of the *mirror image* of *R*,*R*-**7,** *i.e*. *S*,*S*-**7** (for ease of comparison) and *S*,*S*-**8** are shown in Figs. 1 and 2. In both cases the conformation about the P–O bonds is of note. In *S*,*S*-**7**, both P(1) and P(2) show *a* and g^- Pt–P–O–C conformations [*i.e*. *anti* (*a*, Pt–P–O–C torsion angle *ca*. 180°) and *gauche* negative (g^-, Pt–P–O–C torsion angle *ca*. −80°)] at the P–O bonds as counted clockwise from the P–C bond, viewed down the M–P bond, see Scheme 2. Identical behaviour is observed for *S*,*S*-**8** and a range of > 20 phosphonites and phosphites in which the phosphorus is incorporated in a seven-membered POC_4O ring containing a biaryl unit.[8] The implication of this observation is that the absolute stereochemistry of the biaryl unit controls the conformations of the P–O bonds at the phosphorus in such species (enforcing ag^- conformations for *S* and g^+a for *R* biaryls).

The *anti* arm of the phosphonites in **7** and **8** has the attached phenanthryl group far from the metal and the *gauche* arm phenanthryl closer to it. This arrangement provides a highly asymmetric ligand profile. Models suggest that as a result, rotation about the M–P bond in **7** is not possible and that the observed conformation (with the two *anti* arm oxygens essentially in the coordination plane, see Fig. 1 and Scheme 2) is the only likely rotamer. Similar conclusions seem likely to hold for other cases where the carbon substituent is significantly more bulky than the *anti* arm of the phosphonite (and less bulky than the *gauche* arm). Quadrant diagrams for *S*,*S*-**7** and *S*,*S*-**8** based on this analysis are shown in Scheme 2. It is notable that in the chelate species, **8**, the quadrant occupied by the *gauche* arm of the phosphonite is altered as compared with **7**. Hence, in this instance, it seems the primary effect of chelation is to *change* the preferred rotamer rather than to stop rotation about the M–P bond. Furthermore the rotamer favoured in the chelate form (as in **8** or **6b**) has the *gauche* arm phenanthryl group essentially face-on to the coordination plane whereas the rotamer favoured in the monodentate case (as in **7** or **5e**) has the *gauche* arm phenanthryl edge-on (see Figs. 1 and 2). The implication of the higher ee's observed for **5e** as compared with **6b** is that the edge-on phenanthryl in the former causes greater asymmetric induction.

In conclusion, the asymmetric ligand profile caused by the biaryl backbone in these phosphonites has three consequences: (i) rotation about the M–P bond in monodentate phosphonites is prevented; (ii) a different rotamer from that in the chelate analogues is favoured; (iii) the favoured rotamer causes more effective chiral induction in the hydogenation catalyses. The results presented here challenge the view that chelating ligands are essential for high stereocontrol and open the possibility that chiral monodentate phosphorus ligands may be designed that can equal or better their bidentate analogues for hydrogenation.

Notes and references

† *Crystal data*: *R*,*R*-**7**·thf·0.76$CHCl_3$): $C_{72.76}H_{50.76}Cl_{4.27}O_5P_2Pt$, M = 1413.38, orthorhombic, space group $P2_12_12_1$ (no. 19), a = 13.3036(19), b = 19.602(4), c = 23.287(4) Å, U = 6072.9(18) $Å^3$, Z = 4, μ = 2.605 mm^{-1}, T = 173 K, 10674 unique data, $R1$ = 0.0445. *S*,*S*-**8**·3thf·2$CHCl_3$: $C_{72}H_{50}Cl_8O_7P_2Pt$, M = 1555.65, orthorhombic, space group $P2_12_12_1$ (no. 19), a = 14.8155(16), b = 19.132(3), c = 23.690(2) Å, U = 6714.8(14) $Å^3$, Z = 4, μ = 2.510 mm^{-1}, T = 173 K, 10534 unique data, R1 = 0.0498. CCDC 182/1604. See http://www.rsc.org/suppdata/cc/b0/b001638i/ for crystallographic files in .cif format.

1 H. B. Kagan and T. P. Dang, *J. Am. Chem. Soc*., 1972, **94**, 6429.
2 P. A. Chaloner, M. A. Esteruelas, F. Joó and L. A. Oro, *Homogeneous Hydrogenation*, Kluwer, London, 1994.
3 K. Tani, P. Yamagada and K. Nagada, *Acta Crystallogr., Sect. C*, 1994, **50**, 1274.
4 A. Martorell, E. Fernandez, C. Claver and P. G. Pringle, *The XVIIIth International Conference on Organometallic Chemistry*, Munich, 1998, Book of Abstracts, B168.
5 M. T. Reetz, A. Gosberg, R. Goddard and S.-H. Kyung, *Chem. Commun.*, 1998, 2077.
6 W. S. Knowles, M. J. Sabacky and B. D. Vineyard, *J. Chem. Soc., Chem. Commun.*, 1972, 10.
7 B. D. Vineyard, W. S. Knowles, M. J. Sabacky, G. L. Bachman and D. J. Weinkauff, *J. Am. Chem. Soc.*, 1977, **99**, 5946.
8 A. G. Orpen and K. Heslop, unpublished work.

Redox-active heterobinuclear triazenide-bridged complexes; ancillary ligand control of electron distribution in a three-electron metal–metal bond

Neil G. Connelly,*[a] Owen D. Hayward,[a] Phimphaka Klangsinsirikul,[a] A. Guy Orpen*[a] and Philip H. Rieger*[b]

[a] *School of Chemistry, University of Bristol, Bristol, UK BS8 1TS. E-mail: Neil.Connelly@bristol.ac.uk*
[b] *Department of Chemistry, Brown University, Rhode Island, RI 02912, USA*

Received (in Basel, Switzerland) 3rd March 2000, Accepted 14th April 2000

Neutral heterobinuclear triazenide-bridged complexes are oxidised to paramagnetic monocations; the electron distribution in the σ* metal–metal orbital of rhodium–iridium complexes may be controlled by the ancillary ligands at the two metals.

Systematic carbonyl substitution reactions[1–3] of the redox-active $[Rh_2]^{2+}$ complex $[Rh(CO)_2(\mu\text{-RNNNR})_2Rh(CO)_2]$ (R = C_6H_4Me-*p* throughout) have led to the stabilisation of the core oxidation levels $[Rh_2]^{3+}$ {*e.g.* in $[Rh(CO)(PPh_3)(\mu\text{-RNNNR})_2Rh(CO)(PPh_3)]^+$}[1] and $[Rh_2]^{4+}$ {*e.g.* in $[RhCl(CO)(PPh_3)(\mu\text{-RNNNR})_2Rh(bipy)]^+$ (bipy = 2,2′-bipyridine)}.[2] Moreover, detailed structural and EPR spectroscopic studies have shown the SOMO of the $[Rh_2]^{3+}$ complexes to be σ* with respect to the Rh–Rh bond.[4] We now describe the synthesis, characterisation and redox properties of novel *hetero*binuclear triazenide-bridged analogues, with RhM (M = Ir or Pd) cores, and show how the electron distribution in the Rh–Ir bond of paramagnetic $[RhIr]^{3+}$ complexes is remarkably dependent on the ancillary ligands at the two linked metals.

Mixing CH_2Cl_2 solutions of the neutral triazene complexes $[RhCl(CO)_2\{N(H)RNNR\}]$ [ν(CO) 2095 and 2025 cm^{-1}] and $[IrCl(\eta^4\text{-cod})\{N(H)RNNR\}]$ (formed from the triazene and $[\{Rh(\mu\text{-Cl})(CO)_2\}_2]$ or $[\{Ir(\mu\text{-Cl})(\eta^4\text{-cod})\}_2]$, respectively) resulted in ligand exchange to give a mixture of $[IrCl(CO)_2\{N(H)RNNR\}]$ [ν(CO) 2082 and 2004 cm^{-1}][5] and $[RhCl(\eta^4\text{-cod})\{N(H)RNNR\}]$. Subsequent addition of NEt_3 to the mixture then gave a dark red solution containing $[Rh(\eta^4\text{-cod})(\mu\text{-RNNNR})_2Ir(CO)_2]$ **1** which was separated (from the homobinuclear dimer $[Ir(CO)_2(\mu\text{-RNNNR})_2Ir(CO)_2]$[5]) by column chromatography (Table 1).† A comparison of the IR carbonyl spectrum of **1** with those of $[M(\eta^4\text{-cod})(\mu\text{-RNNNR})_2M(CO)_2]$ [M = Rh, ν(CO) 2064vs and 2002s; M = Ir, ν(CO) 2049vs and 1986s cm^{-1}] suggested the presence of an $Ir(CO)_2$ unit {rather than $Rh(CO)_2$}, supported by the observation of two doublet ^{13}C resonances at δ 31.2 and 31.0 [$J(^{103}Rh^{13}C)$ 15 Hz], for the pairs of inequivalent rhodium-bound alkenic carbons of the cod ligand and confirmed by the X-ray crystal structure (Fig. 1).‡

Passing CO gas through a CH_2Cl_2 solution of **1** yielded $[Rh(CO)_2(\mu\text{-RNNNR})_2Ir(CO)_2]$ **2** which reacted with P-donor ligands to give the heterobinuclear complexes $[Rh(CO)(PPh_3)(\mu\text{-RNNNR})_2Ir(CO)_2]$ **3** and $[Rh(CO)L(\mu\text{-RNNNR})_2Ir(CO)L]$ [L = PPh_3 **4** or $P(OMe)_3$ **5**]. A comparison of the ^{31}P NMR spectra of **3** {δ 38.9 [d $J(^{103}Rh^{31}P)$ 151 Hz]} and **4** {δ 39.2 [d, $J(^{103}Rh^{31}P)$ 154 Hz], 14.3, s} confirms sequential phosphine substitution at Rh and then Ir. The preference for the $Ir(CO)_2$ isomers of **1** and **3** and the lower ν(CO) wavenumbers for $Ir(CO)_2$ than for $Rh(CO)_2$ in $[Rh(\eta^4\text{-cod})(\mu\text{-RNNNR})_2M(CO)_2]$ are consistent with the Ir centre being somewhat more electron rich than the Rh centre in cases such as **2**, *i.e.* Ir orbital energies are slightly higher than Rh, other things, such as ancillary ligands, being equal.

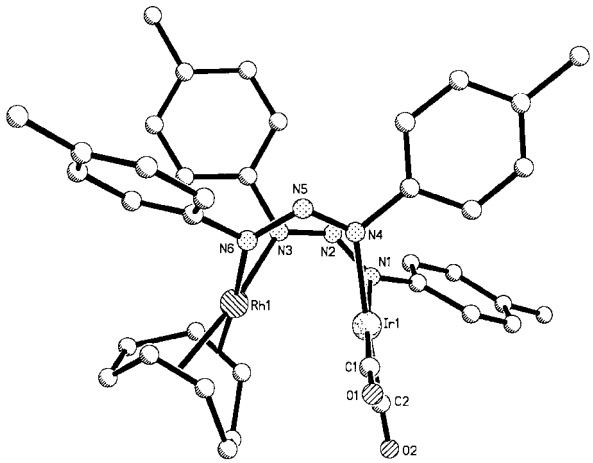

Fig. 1 Structure of **1** (H atoms omitted for clarity); Rh–Ir 2.8462(8) Å.

Table 1 IR and electrochemical data for $[RhL_m(\mu\text{-RNNNR})_2M'L'_n]^z$

Complex	L_m	$M'L'_n$	z	Yield (%)	Colour	ν(CO)/cm^{-1} (in CH_2Cl_2)	$E°'$/V[a]
1	η^4-cod	$Ir(CO)_2$	0	46	Dark red	2052vs, 1984s	0.53, 1.39
1^{+}[b]	η^4-cod	$Ir(CO)_2$	1	90	Dark brown	2089vs, 2040s	—
2	$(CO)_2$	$Ir(CO)_2$	0	82	Red–purple	2084vs, 2052m, 2019m, 1995w	0.76, 1.40(I)
3	$(CO)(PPh_3)$	$Ir(CO)_2$	0	81	Dark red	2049vs, 1987sh	0.43, 1.35(I)
4	$(CO)(PPh_3)$	$Ir(CO)(PPh_3)$	0	51	Dark red	1974s, 1953vs	0.07, 1.27
4^{+}[b]	$(CO)(PPh_3)$	$Ir(CO)(PPh_3)$	1	92	Dark orange	2043s, 2011vs	—
5	$(CO)\{P(OMe)_3\}$	$Ir(CO)\{P(OMe)_3\}$	0	65	Red–purple	1992s, 1970vs	0.08, 1.09(I)
6	$(CO)_2$	$Pd(\eta^3\text{-allyl})$	0	39	Orange	2071vs, 2009s	0.97
7	$(CO)_2$	$PdCl(PPh_3)$	0	50	Orange–red	2075vs, 2012s	1.09, −1.31(I)[c]
8	(CO)(NCMe)	$PdCl(PPh_3)$	0	61	Brown	1983s	0.67, 1.41(I), −1.54(I)[c]

[a] In CH_2Cl_2, at a platinum electrode, with 0.1 mol dm^{-3} $[NBu_4][PF_6]$ as supporting electrolyte. For an irreversible (I) process, the oxidation peak potential, $(E_p)_{ox}$, is given at a scan rate of 200 mV s^{-1}. All potentials are relative to the saturated calomel electrode. Under the experimental conditions, $E°'$ for the one-electron oxidation of $[Fe(\eta\text{-}C_5H_5)_2]$ is 0.47 V. [b] Isolated as the $[PF_6]^-$ salt. [c] Irreversible reduction process; $(E_p)_{red}$ at a scan rate of 200 mV s^{-1}.

DOI: 10.1039/b001764g

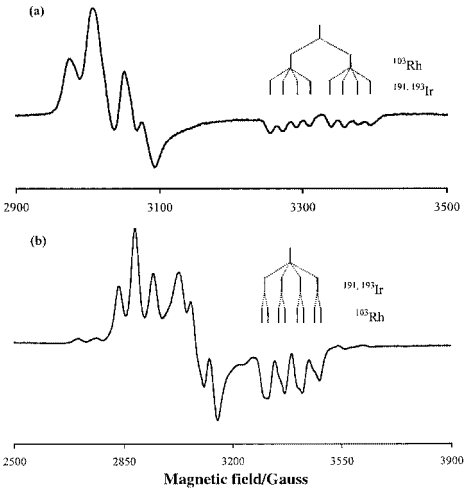

Fig. 2 EPR spectra of (a) $\mathbf{1}^+$ and (b) $\mathbf{4}^+$ at 100 K in CH_2Cl_2–thf (1:2).

Table 2 EPR spectroscopic data[a] for $[RhL_m(\mu\text{-RNNNR})_2IrL'_n]^+$

Ion	L_m	L'_n	$g_{\text{high field}}$	$A(^{103}Rh)$	$A(^{191,193}Ir)$
$\mathbf{1}^+$	η⁴-cod	$(CO)_2$	2.0246(1)	82.6(2)	17.2(1)
$\mathbf{3}^+$	$(CO)(PPh_3)$	$(CO)_2$	2.0017(1)	95.9(2)	22.3(2)
$\mathbf{4}^+$	$(CO)(PPh_3)$	$(CO)(PPh_3)$	1.9827(1)	16.6(2)	51.6(3)
$\mathbf{5}^+$	$(CO)\{P(OMe)_3\}$	$(CO)\{P(OMe)_3\}$	1.9882(4)	19.4(9)	57.4(6)

[a] High field feature only; A in 10^{-4} cm^{-1}.

Cyclic voltammetry in CH_2Cl_2 shows that **1**–**5** undergo two one-electron oxidation processes (Table 1) the first of which is fully reversible in all cases (the second is also reversible for **1** and **4**). Treatment of the neutral complexes **1** and **4** with $AgPF_6$ and $[Fe(\eta\text{-}C_5H_5)_2][PF_6]$ respectively gave near quantitative yields of the paramagnetic $[RhIr]^{3+}$-containing cations $\mathbf{1}^+$ and $\mathbf{4}^+$ (as their $[PF_6]^-$ salts). X-Ray structural studies on the redox-related pair **4** and $\mathbf{4}^+$ show a shortening of the Rh–Ir distance on oxidation, from 2.945(2) to 2.7131(9) Å, consistent with removal of an electron from a σ* metal–metal orbital derived from the interaction of d_{z^2} orbitals, and the formation of a three-electron metal–metal bond. A similar structural difference was observed with the homobinuclear redox pair $[Rh(CO)(PPh_3)(\mu\text{-}RNNNR)_2Rh(CO)(PPh_3)]^z$ (z = 0 and 1).[4]

Cations $\mathbf{1}^+$ and $\mathbf{4}^+$, and also $\mathbf{3}^+$ and $\mathbf{5}^+$ (generated *in situ* by treatment of **3** and **5** with $[Fe(\eta\text{-}C_5H_4COMe)(\eta\text{-}C_5H_5)][PF_6]$ and $[Fe(\eta^5\text{-}C_5H_5)_2][PF_6]$, respectively) show well resolved EPR spectra in CH_2Cl_2–thf (1:2); those of $\mathbf{1}^+$ and $\mathbf{4}^+$ at 100 K are shown in Fig. 2. The spectra show hyperfine coupling to ^{103}Rh (I = 1/2) and to ^{191,193}Ir (I = 3/2), but are complicated by Ir quadrupole coupling.[6] The high-field g-feature is generally well resolved; the corresponding parameters are given in Table 2. These parameters clearly indicate that the distribution of unpaired electron density in the three-electron Rh–Ir bond is strongly dependent on the nature of the terminal ligands at each metal. Thus, Rh makes the major contribution to the SOMO of $\mathbf{1}^+$ and $\mathbf{3}^+$, whereas Ir makes the major contribution in $\mathbf{4}^+$ and $\mathbf{5}^+$.

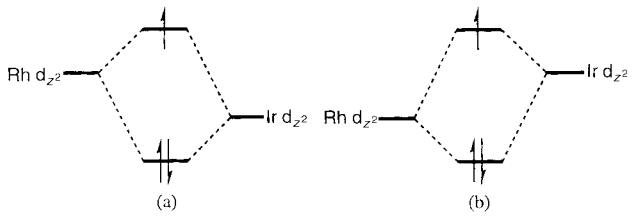

Scheme 1 Schematic orbital interactions in the three-electron metal–metal bond of species such as (a) $\mathbf{1}^+$ and (b) $\mathbf{4}^+$ in which the ancillary ligand sets are asymmetric and symmetric, respectively.

In a first-order semi-quantitative analysis the spin density is *ca.* 75% on Ir in the species $\mathbf{4}^+$ and $\mathbf{5}^+$ in which the ancillary ligand sets at Ir and Rh are the same. When the iridium centre carries more electron withdrawing ligands (as in $\mathbf{1}^+$ and $\mathbf{3}^+$) *ca.* 80% of the spin density is located at the rhodium centre. This is consistent with the carbonyl ligands of the $Ir(CO)_2$ unit reducing the Ir d_{z^2} energy below that of the Rh d_{z^2} (*i.e.* the reverse of their order in $\mathbf{1}^+$ and $\mathbf{3}^+$, for example) leading to an inversion of the dominant contributions to the SOMO (Scheme 1). We therefore conclude that asymmetry of the ancillary ligand set can overturn the inherent metal orbital energy difference (as noted above) and reverse spin localisation in these species.

The preparative route to complexes **1**–**5** can also be applied to the synthesis of redox-active rhodium–palladium complexes $[Rh(CO)_2(\mu\text{-}RNNNR)_2PdL_n]$ [L_n = η³-allyl **6**, L_n = $Cl(PPh_3)$ **7**], *i.e.* by reacting $[RhCl(CO)_2\{N(H)RNNR\}]$ with $[PdCl(\eta^3\text{-allyl})\{N(H)RNNR\}]$ and $[PdCl_2(PPh_3)\{N(H)RNNR\}]$, respectively (again prepared *in situ* from the triazene and the corresponding halide-bridge dimer). Subsequent treatment of **7** with $ONMe_3$ in MeCN gave the highly asymmetric complex $[Rh(CO)(NCMe)(\mu\text{-}RNNNR)_2PdCl(PPh_3)]$ **8** in which four different terminal ligands are selectively distributed between the two different metals.

In summary, the new preparative route described leads to novel redox-active heterobinuclear species which are oxidised to paramagnetic complexes in which the distribution of unpaired electron density in a metal–metal bond can be tuned by systematic ligand variation.

We thank the Royal Thai Government and the EPSRC for Studentships (to P. K. and O. D. H., respectively).

Notes and references

† All new complexes had satisfactory elemental analyses (C, H and N).

‡ X-Ray data were collected on a Siemens SMART diffractometer at 173 K for $\theta < 27.5°$ with λ = 0.71073 Å. The structures were solved by direct methods and refined by least-squares against all F^2 values corrected for absorption.

Crystal data: $[Rh(\eta^4\text{-cod})(\mu\text{-}RNNNR)_2Ir(CO)_2]\cdot 0.14CH_2Cl_2$, $\mathbf{1}\cdot 0.14CH_2Cl_2$ (from CH_2Cl_2–propan-2-ol): $C_{38.14}H_{40.28}Cl_{0.28}IrN_6O_2Rh$, M = 919.76, monoclinic, space group $P2_1/c$ (no. 14), a = 15.052(4), b = 13.982(2), c = 17.202(3) Å, β = 98.426(14)°, V = 3581.3(12) Å³, Z = 4, μ = 4.24 mm^{-1}, $R1$ = 0.0470.

$[Rh(CO)(PPh_3)(\mu\text{-}RNNNR)_2Ir(CO)(PPh_3)]\cdot 3CH_2Cl_2$, $\mathbf{4}\cdot 3CH_2Cl_2$ (from CH_2Cl_2–propan-2-ol): $C_{69}H_{62}Cl_6IrN_6O_2P_2Rh$, M = 1577.00, triclinic, space group $P\bar{1}$ (no. 2), a = 12.9339(5), b = 15.1205(8), c = 18.3009(15) Å, α = 83.50(4), β = 71.74(3), γ = 88.57(4)°, V = 3376.7(4) Å³, Z = 2, μ = 2.546 mm^{-1}, $R1$ = 0.0299.

$[Rh(CO)(PPh_3)(\mu\text{-}RNNNR)_2Ir(CO)(PPh_3)][PF_6]\cdot 1.5CH_2Cl_2$, $\mathbf{4}^+[PF_6]^-\cdot 1.5CH_2Cl_2$ (from CH_2Cl_2–*n*-hexane): $C_{67.5}H_{60}Cl_3F_6IrN_6O_2P_3Rh$, M = 1595.58, triclinic, space group $P\bar{1}$ (no. 2), a = 12.967(3), b = 13.714(2), c = 19.830(3) Å, α = 97.712(12), β = 98.499(19), γ = 90.430(12)°, V = 3454.7(11) Å³, Z = 2, μ = 2.412 mm^{-1}, $R1$ = 0.0640.

CCDC 182/1602. See http://www.rsc.org/suppdata/cc/b0/b001764g/ for crystallographic files in .cif format.

1 N. G. Connelly, G. Garcia, M. Gilbert and J. S. Stirling, *J. Chem. Soc., Dalton Trans.*, 1987, 1403.
2 T. Brauns, C. Carriedo, J. S. Cockayne, N. G. Connelly, G. Garcia Herbosa and A. G. Orpen, *J. Chem. Soc., Dalton Trans.*, 1989, 2049.
3 N. G. Connelly, T. Einig, G. Garcia Herbosa, P. M. Hopkins, C. Mealli, A. G. Orpen, G. M. Rosair and F. Viguri, *J. Chem. Soc., Dalton Trans.*, 1994, 2025; N. G. Connelly, P. M. Hopkins, A. G. Orpen, G. M. Rosair and F. Viguri, *J. Chem. Soc., Dalton Trans.*, 1992, 2907; M. Bardaji, N. C. Brown, A. Christofides and N. G. Connelly, *J. Organomet. Chem.*, 1994, **474**, 24.
4 D. C. Boyd, N. G. Connelly, G. Garcia Herbosa, M. G. Hill, K. R. Mann, C. Mealli, A. G. Orpen, K. E. Richardson and P. H. Rieger, *Inorg. Chem.*, 1994, **33**, 960.
5 N. G. Connelly and G. Garcia, *J. Chem. Soc., Dalton Trans.*, 1987, 2737.
6 J. A. DeGray, P. H. Rieger, N. G. Connelly and G. Garcia Herbosa, *J. Magn. Reson.*, 1990, **88**, 376.

ChemComm

The arched four-rung ladder structure of the unsolvated dilithium salt of *N,N′*-bis(trimethylsilyl)-2-aminobenzylamine, and its structural deformation on THF complexation

Régis M. Gauvin,[a] Nathalie Kyritsakas,[b] Jean Fischer[b] and Jacky Kress*[a]

[a] *Laboratoire de Chimie des Métaux de Transition et de Catalyse, UMR 7513, Université Louis Pasteur, Institut Le Bel, 4 rue Blaise Pascal, 67070 Strasbourg Cedex, France. E-mail: jkress@chimie.u-strasbg.fr*

[b] *Laboratoire de Cristallochimie et de Chimie Structurale, UMR 7513, Université Louis Pasteur, Institut Le Bel, 4 rue Blaise Pascal, 67070 Strasbourg Cedex, France*

Received (in Basel, Switzerland) 9th March 2000, Accepted 2nd May 2000

The X-ray crystal structures of 2-Li($SiMe_3$)$NC_6H_4CH_2N(SiMe_3)$Li 1 and 2-Li($SiMe_3$)$NC_6H_4CH_2N(SiMe_3)$Li·THF 2 show that both compounds exist in the solid state as discrete dimers that display an analogous four-rung ladder core, allowing us to analyse the effect of THF coordination.

The aggregation of lithium amides *via* so-called ring-laddering processes is now well documented, and a wide variety of architectures has been described in the literature.[1] In the absence of coordinating Lewis bases, these compounds generally adopt polymeric infinite ladder structure, but examples of shorter arrangements have been reported. On exposure to solvating ligands, these structures are often broken down to smaller entities which can however still be assembled into oligomeric ladders of limited length if only partial solvation has taken place.[1] Here, we present the first structural characterization of a heteroditopic dilithium diamide, both in its unsolvated and THF monoadduct forms. The unsolvated compound 2-Li($SiMe_3$)$NC_6H_4CH_2N(SiMe_3)$Li **1** is dimeric and exhibits an arched four-rung ladder structure which had not been observed previously for an uncomplexed amidolithium compound. Coordination of THF to give 2-Li($SiMe_3$)$NC_6H_4CH_2N(SiMe_3)$Li·THF **2** changes the structural parameters of this edifice, but alters neither its dimeric nature nor its conformation, providing the opportunity to analyse the fundamental bond modifications upon lithium complexation in such ladder frameworks.

Compound **1**† was obtained as colourless crystals through double deprotonation of the diamine 2-NH($SiMe_3$)$C_6H_4CH_2NH(SiMe_3)$[2] by Bu^nLi in pentane, followed by concentrating the reaction mixture under reduced pressure and cooling the resulting solution to −20 °C. Its high solubility in hydrocarbons restricted the isolated yield to 58%. Its molecular structure was established by X-ray diffraction analysis‡ (Fig. 1). The three fused $(NLi)_2$ rings that build the four-rung ladder are strictly planar and significantly twisted with respect to each other, as shown by the average value of the two N–Li–N–Li edge dihedral angles (51.1°). The chelating 2-benzyl linkages bridge the nitrogen atoms along each edge and are located on the same face of the ladder, which imposes the arch-like folding, the nearly parallel orientation of the two aromatic rings (which is not the result of π-stacking, the two ring planes being staggered and distant by *ca.* 4 Å), and the cisoid configuration of the four $SiMe_3$ substituents.

The four-coordinate anilinic nitrogens are located in the outer rungs, while the five-coordinate benzylic nitrogens occupy the inner positions, leading to a 'head-to-tail' arrangement. Although the molecule shows only approximate and not crystallographic C_2 symmetry, the discussion of its dimensional parameters can be restricted to one half of the dimer.

Interestingly, the two outer lithium atoms are only two-coordinate with respect to nitrogen ligation and hence highly electron-deficient, which results in short outer rungs [Li(1)–N(4) 1.964(4) Å] and close contacts with carbons of the neighbouring aromatic rings [Li(1)–C(5) 2.350(5) Å, Li(1)–C(10) 2.627(5) Å]. These relatively strong lithium–carbon interactions are certainly at the origin of the limited length of this unsolvated ladder (together with the steric hindrance of the $SiMe_3$ substituents at the ladder ends), and of its folding down into an arch. On the other hand, the inner lithium atoms are three-coordinate with respect to nitrogen ligation and pyramidal. Although less unsaturated, they interact similarly with the benzylic carbons [Li(2)–C(4) 2.484(4) Å], tying the 2-benzyl framework even closer to the $(NLi)_4$ core, accounting further for the severely folded structure of the ladder [Li(1)–N(1)–Li(2) 106.00(2)°, N(1)–Li(2)–N(2) 108.8(2)°], and leading to inner Li–N edges that are relatively shorter than the inner rungs [Li(2)–N(1) 2.025(4) Å, Li(4)–N(1) 2.113(4) Å]. ^1H NMR spectra† suggest that this dimeric structure is maintained in benzene solution, and show that the molecule is fluxional.

It should be pointed out that lithium amides exhibiting a four-rung ladder structure have been described previously, but are either solvated at the terminal lithium centers[3] (as **2**, *vide infra*) or folded into stairs.[4] Both of these characteristics are found together in a few compounds.[5] The example of unsolvated dimeric $[Li(Dipp)NCH_2CH_2N(Dipp)Li]_2$[4] (Dipp = 2,6-diisopropylphenyl) is of particular interest owing to its close analogy with **1**. It similarly contains strong lithium–carbon interactions, but exists as a stepped four-rung ladder.[4] We presume this different geometry arises from the fact that the Li–C inter-

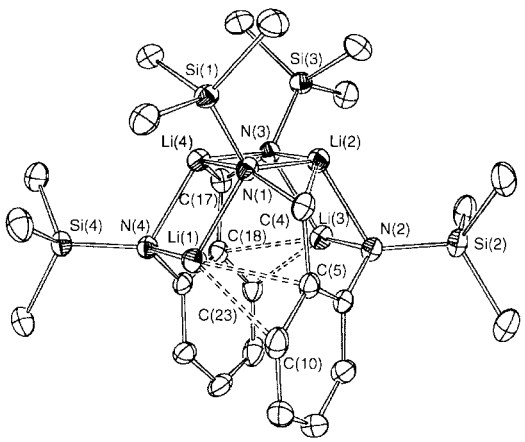

Fig. 1 Molecular structure of **1** showing the atom numbering scheme. The H atoms have been omitted for clarity. Selected interatomic distances (Å) and angles (°): Li(1)–N(1) 2.038(4), Li(2)–N(1) 2.025(4), Li(2)–N(2) 2.035(4), Li(1)–N(4) 1.964(4), Li(4)–N(1) 2.113(4), Li(1)–C(5) 2.350(5), Li(1)–C(10) 2.627(5), Li(2)–C(4) 2.484(4), Li(1)–Li(4) 2.427(5), Li(2)–Li(4) 2.389(6); Li(1)–N(1)–Li(4) 71.52(2), Li(2)–N(1)–Li(4) 70.47(2), Li(1)–N(1)–Li(2) 106.00(2), Li(1)–N(4)–Li(4) 74.99(2), N(1)–Li(1)–N(4) 109.2(2), N(1)–Li(2)–N(2) 108.8(2), N(1)–Li(4)–N(3) 108.4(2), N(1)–Li(4)–N(4) 104.1(2), N(3)–Li(4)–N(4) 110.9(2).

DOI: 10.1039/b002004o

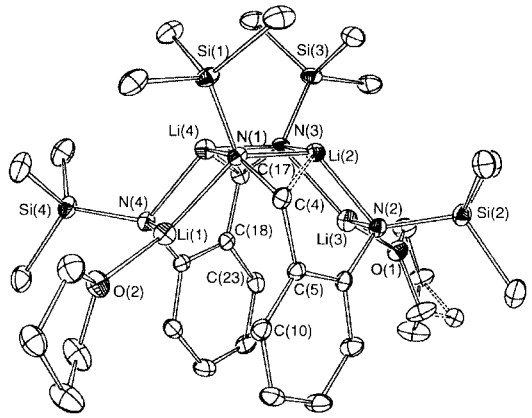

Fig. 2 Molecular structure of **2** showing the atom numbering scheme. The H atoms have been removed for clarity. Selected interatomic distances (Å) and angles (°): Li(1)–N(1) 2.116(6), Li(2)–N(1) 2.051(5), Li(2)–N(2) 1.974(6), Li(1)–N(4) 2.030(5), Li(4)–N(1) 2.063(5), Li(1)–O(2) 1.979(5), Li(1)–C(5) 2.762(6), Li(1)–C(10) 2.906(5), Li(2)–C(4) 2.546(5), Li(1)–Li(4) 2.467(7), Li(2)–Li(4) 2.318(7); Li(1)–N(1)–Li(4) 72.3(2), Li(2)–N(1)–Li(4) 68.6(2), Li(1)–N(1)–Li(2) 116.7(2), Li(1)–N(4)–Li(4) 75.9(2), N(1)–Li(1)–N(4) 103.8(2), N(1)–Li(2)–N(2) 114.3(2), N(1)–Li(4)–N(3) 110.8(2), N(1)–Li(4)–N(4) 107.7(2), N(3)–Li(4)–N(4) 113.9(2).

actions in this latter compound do not involve the edge-hugging chelating bridges as in **1**, but the other nitrogen substituent of the secondary amides (Dipp in that case).

Compound **2**† was obtained serendipitously by the reaction of **1** with 0.5 equiv. $ZrCl_4(THF)_2$ in toluene.[6] A single-crystal X-ray structure determination‡ showed that its molecular structure is in all respects similar to that of **1**, and the same numbering scheme was thus used for the sake of clarity (Fig. 2). Coordination of THF occurs at the outer lithium atoms which become three-coordinate, but the four-rung ladder core of **1** is not broken down in **2** and its peculiar geometry is furthermore retained. However, the $(NLi)_4$ arch is significantly flattened, as shown by the increased distance between the two outer rungs [from 3.653 Å in **1** to 4.337 Å in **2** for Li(1)–N(2) for instance], the more obtuse edge angles Li(1)–N(1)–Li(2) and N(1)–Li(2)–N(2) (+10.7 and +5.5°, respectively), and the less pyramidal inner lithium atoms, whose average summed angles vary from 323.3° in **1** to 333.6° in **2**. Moreover, the ladder framework is more severely twisted in **2**, the N–Li–N–Li edge dihedral angles increasing to 67° (average value), and, most importantly, the 2-benzyl aromatic rings are considerably withdrawn from the outer lithium atoms [Li(1)–C(5) 2.762 Å, Li(1)–C(10) 2.906 Å]. Undoubtedly, the outer lithium atoms have become less electron deficient on complexation by THF, and the above structural modifications are the consequence of subsequent weakening of their interactions with the aromatic ring of the 2-benzyl bridges.

The Li–N bond distances within the ladder core are also modified accordingly, both edges and rungs involving the outer lithiums being lengthened by an average value of 0.078 Å. The electrons of the four nitrogen atoms become thereby more available for the inner lithium atoms, leading to the strengthening of the corresponding Li–N bonds and to their average shortening by *ca.* 0.045 Å, with the notable exception of the two inner edges Li(2)–N(1) and Li(4)–N(3). These indeed are slightly longer in **2** than in **1**, [+0.026 Å for Li(2)–N(1) for instance], as are the lithium–carbon distances between the inner lithium atoms and the benzylic carbons [+0.062 Å for Li(2)–C(4)]. THF complexation of the outer lithium atoms hence also results in higher electron density on the inner ones. This weakens the lithium–methylene interactions that squeezed the inner Li–N edges in **1**, to such an extent that also these latter bonds are lengthened in **2**.

We dedicate this paper to the memory of Professor John A. Osborn. We thank the CNRS and the Ministère de l'Education Nationale, de la Recherche et de la Technologie for funding this work.

Notes and references

† **1**: satisfactory C, H, N analysis; δ_H(25 °C, 300 MHz, C_6D_6): 6.94 (dt, 1H, C^5H), 6.84 (dd, 1H, C^3H), 6.58 (dt, 1H, C^4H), 6.27 (d, br, 1H, C^6H), 4.39 and 3.68 (d, ^2J 10.3 Hz, br, 1H, ArC*H*H′ and ArCH*H*′), 0.22 (s, 9H, ArNSi*Me*$_3$), 0.05 (s, 9H, CH_2NSi*Me*$_3$); δ_C(25 °C, 75 MHz, C_6D_6): 157.26 (C^2), 136.53 (C^1), 131.60, 129.62, 125.83 and 119.11 (C^3, C^4, C^5 and C^6), 48.78 (CH_2), 2.96 and 0.60 (ArNSi*Me*$_3$ and CH_2NSi*Me*$_3$). **2**: δ_H(25 °C, 300 MHz, C_6D_6); 7.04 (m, 2H, C^3H or C^6H and C^4H or C^5H), 6.70 (m, br, 1H, C^3H or C^6H), 6.59 (t, 1H, C^4H or C^5H), 4.10 (s, br, 2H, ArC*H*$_2$) 3.37 (m, 4H, OCH_2), 1.21 (m, 4H, OCH_2CH_2), 0.26 (s, br, 18H, ArNSi*Me*$_3$ and CH_2NSi*Me*$_3$).

‡ *Crystal data* for $C_{26}H_{48}N_4Li_4Si_4$ **1**: M = 556.81, monoclinic, space group $P2_1/n$, a = 9.7590(2), b = 21.3540(4), c = 16.7940(6) Å, β = 98.073(5)°, U = 3465.1(3) Å^3, Z = 4, D_c = 1.07 g cm^{-3}, μ = 0.186 mm^{-1} (Mo-Kα, λ = 0.71073 Å), T = 173 K, 25648 data measured, 4455 data with $I > 3\sigma(I)$, R = 0.038, R_w = 0.058.

For $C_{34}H_{64}Li_4N_4O_2Si_4$ **2**: M = 701.02, monoclinic, space group $P2_1/c$, a = 19.9167(9), b = 9.8818(2), c = 22.1151(9) Å, β = 99.750(2)°, U = 4289.7(5) Å^3, Z = 4, D_c = 1.09 g cm^{-3}, μ = 0.170 mm^{-1} (Mo-Kα, λ = 0.71073 Å), T = 173 K, 29787 data measured, 4972 data with $I > 3\sigma(I)$, R = 0.043, R_w = 0.064. One β carbon atom of one THF molecule occupies two distinct positions (Fig. 2).

The structures were solved using direct methods and refined by full-matrix least squares on F.

CCDC 182/1609. See http://www.rsc.org/suppdata/cc/b0/b002004o/ for crystallographic files in .cif format.

1 K. Gregory, P. von Ragué Schleyer and R. Snaith, *Adv. Inorg. Chem.*, 1991, **37**, 47; R. E. Mulvey, *Chem. Soc. Rev.*, 1991, **20**, 167; R. E. Mulvey, *Chem. Soc. Rev.*, 1998, **27**, 339 and references therein; W. Clegg, S. T. Liddle, R. E. Mulvey and A. Robertson, *Chem. Commun.*, 1999, 511; W. Clegg, S. T. Liddle, R. E. Mulvey and A. Robertson, *Chem. Commun.*, 2000, 223.

2 Y.-M. Jeon, J. Heo, W. M. Lee, T. Chang and K. Kim, *Organometallics*, 1999, **18**, 4107.

3 M. G. Gardiner and C. L. Raston, *Inorg. Chem.*, 1996, **35**, 4162; W. Clegg, K. W. Henderson, L. Horsburgh, F. M. MacKenzie and R. E. Mulvey, *Chem. Eur. J.*, 1998, **4**, 53; G. Boche, I. Langlotz, M. Marsch, K. Harms and N. E. S. Nudelman, *Angew. Chem., Int. Ed. Engl.*, 1992, **31**, 1205; D. R. Armstrong, J. E. Davies, R. P. Davies, P. R. Raithby, R. Snaith and A. E. H. Wheatley, *New J. Chem.*, 1999, 35.

4 H. Chen, R. A. Bartlett, H. V. R. Dias, M. M. Olmstead and P. P. Power, *Inorg. Chem.*, 1991, **30**, 2487.

5 D. R. Armstrong, D. Barr, W. Clegg, R. E. Mulvey, D. Reed, R. Snaith and K. Wade, *J. Chem. Soc., Chem. Commun.*, 1986, 869; D. R. Armstrong, D. Barr, W. Clegg, S. M. Hodgson, R. E. Mulvey, D. Reed, R. Snaith and D. S. Wright, *J. Am. Chem. Soc.*, 1989, **111**, 4719; M. G. Gardiner and C. L. Raston, *Inorg. Chem.*, 1996, **35**, 4047.

6 Adding an excess of THF to **1** or **2** leads to the monomeric tetra-THF adduct.

ChemComm

Chemo- and regio-selective synthesis of functionalized 3(2*H*)-furanones by the first cyclization reactions of 1,3-bis(trimethylsiloxy)buta-1,3-dienes with α-chlorocarboxylic acid chlorides

Peter Langer* and Thilo Krummel

Institut für Organische Chemie der Georg-August-Universität Göttingen, Tammannstr. 2, 37077 Göttingen, Germany. E-mail: planger@gwdg.de

Received (in Cambridge, UK) 24th February 2000, Accepted 20th April 2000

Reaction of 1,3-bis(trimethylsiloxy)buta-1,3-dienes with α-chlorocarboxylic acid chlorides resulted in chemo- and regio-selective formation of 6-chloro-3,5-dioxoesters which were regioselectively converted into functionalized 3(2*H*)-furanones.

Domino and consecutive reactions are of great interest in organic chemistry since they enable the rapid assembly of complex products in a one-pot process.[1] Surprisingly, despite the simplicity of the idea, only few domino and consecutive reactions of 1,3-dianions[2] with 1,2-dielectrophiles have been reported so far.[3] Several drawbacks are possible for these reactions: on the one hand, dianions are highly reactive compounds which can react both as a nucleophile and a base; on the other hand, 1,2-dielectrophiles often represent rather labile compounds. Therefore, previous attention in dianion chemistry has been mainly focused on reactions with monofunctional electrophiles after which the resultant monoanion is simply quenched with water following the initial reaction. We have recently reported the first domino reactions of 1,3-dianion synthons with oxalic acid dielectrophiles to give γ-alkylidene-butenolides.[4,5] Herein, to the best of our knowledge, we report the first cyclization reactions of 1,3-dianion synthons with α-chlorocarboxylic acid chlorides. These reactions provide a convenient, chemo- and regio-selective access to a variety of functionalized 3(2*H*)-furanones. A large number of natural products and pharmacologically important compounds belong to the group of 3(2*H*)-furanones: prominent examples include polyketides from *siphonaria pectinata*,[6a] the antitumor active trachyspic acid,[6b] antiallergic 4,5-dihydro-4-oxo-2-amino-3-furancarboxylic acids,[6c] the mutagenic furaneols,[6d] pseurotin A,[6e] the antitumor active sesquiterpenes eremantholide A-C,[6f] lychnophorolide A,[6g] ciliarin,[6h] and the recently reported metabolite longianone.[6i,j]

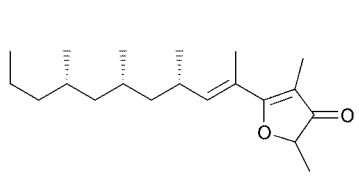

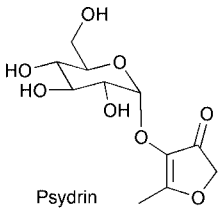

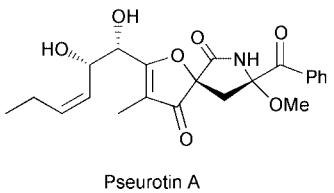

A variety of products are, in principle, possible in the reaction of 1,3-dicarbonyl dianions with α-chloroacetic acid derivatives. Both the initial attack of the dianion onto the dielectrophile and the subsequent cyclization can proceed with different chemo- and regio-selectivities. Reaction of the disodium salt of acetylacetone **1a** with the sodium salt of chloroacetic acid **2a** was reported to give 4,6-dioxoheptanoic acid **3** by attack of the terminal carbon of the dianion onto the carbon attached to the chlorine atom.[7] Unfortunately, our first attempts to induce a chemoselective attack of 1,3-dicarbonyl dianions onto the carbonyl group of chloroacetic acid derivatives in order to prepare the ester **5a** were unsuccessful: reaction of the dianion of ethyl acetoacetate **1b** with ethyl chloroacetate **2b**, *N*-methyl-*N*-methoxy-chloroacetic acid amide **2c** or chloroacetyl chloride **2d** resulted in formation of complex mixtures only (Scheme 1).

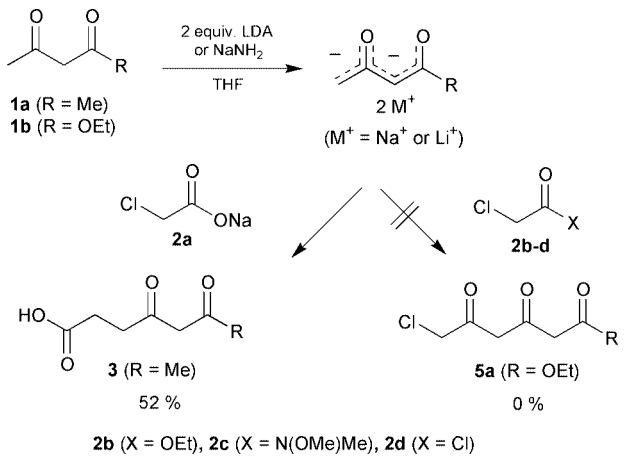

Scheme 1

In order to overcome these problems, we decided to study the Lewis-acid catalyzed reaction of 1,3-bis-(trimethylsiloxy)buta-1,3-dienes, synthons of 1,3-dicarbonyl dianions,[8] with chloroacetyl chloride **2d**. Our initial attempts to realize this concept were unsuccessful. Reaction of **2d** with the diene **4a** in the presence of stoichiometric amounts of $BF_3{\cdot}OEt_2$ or $TiCl_4$ resulted in formation of complex mixtures. Much to our satisfaction, the use of catalytic amounts of TMSOTf resulted in chemo- and regio-selective formation of the desired 6-chloro-3,5-dioxoester **5a** (Scheme 2).† Optimal yields (up to 71%) were obtained when the reaction was started at −78 °C and slowly warmed to ambient during 12 h. Treatment of **5a** with base resulted in regioselective cyclization[9] *via* the oxygen atom

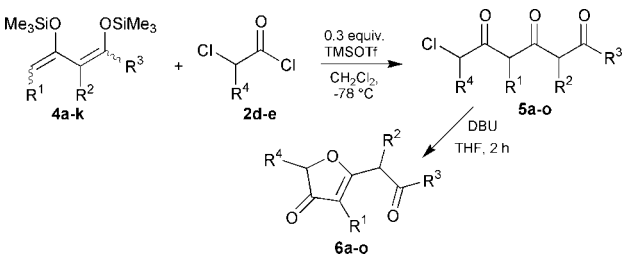

Scheme 2

DOI: 10.1039/b001529f

to give the 3(2*H*)-furanone **6a**.† The use of KOBu^t resulted in the formation of a complex mixture from which **6a** could be isolated in only 23% yield. Eventually, we found that optimal yields (up to 91%) were obtained when 2 equivalents of DBU were used as the base. It is noteworthy that isolation of **5a** was not necessary: the crude product of **5a** could be directly transformed into **6a** which was isolated in 65% overall yield (from **4a**).

In order to study the preparative scope of the new methodology for the synthesis of 3(2*H*)-furanones the substituents of the 1,3-bis(trimethylsiloxy)-1,3-dienes were systematically varied (Table 1). Reaction of chloroacetyl chloride **2d** with the diene derived from methyl acetoacetate and subsequent cyclization afforded the 3(2*H*)-furanone **6b** in 70% overall yield. Reaction of **2d** with 1,3-bis(trimethylsiloxy)-1,3-dienes **4c**–**g**, containing methyl, ethyl, butyl, benzyl, and allyl groups, respectively at the terminal carbon atom, afforded the 4-alkyl-3(2*H*)-furanones **6c**–**g** in good yields and with very good chemo- and regio-selectivities.

Table 1

6	R^1	R^2	R^3	R^4	Yield[a] (%)
a	H	H	OEt	H	65
b	H	H	OMe	H	70
c	Me	H	OMe	H	54
d	Et	H	OEt	H	53
e	Bu	H	OEt	H	40
f	Bn	H	OEt	H	38
g	Allyl	H	OEt	H	54
h	OMe	H	OMe	H	56
i	H	Me	OEt	H	54
j	H	Et	OEt	H	50
k	$CH_2CH_2CH_2$		OEt	H	34
l	H	H	OEt	Me	56
m	Me	H	OMe	Me	40
n	Et	H	OEt	Me	32
o	$CH_2CH_2CH_2$		OEt	Me	26

[a] Isolated yields of **6a**–**o** over two steps from **4a**–**k** and **2d**–**e**.

A variety of naturally occuring 3(2*H*)-furanones contain an oxygen atom at carbon C-4.[10] The synthesis of 3(2*H*)-furanone **6h**, containing a methoxy group at carbon C-4, was therefore of special interest. Dianions cannot be used for the synthesis of **6h** since, besides the severe selectivity problems discussed above, dianions of methyl 4-methoxyacetoacetate and related substrates cannot be generated. This is presumably due to the fact that the dianion is destabilized by lone pair–lone pair interactions and by the π-donor effect of the oxygen atom.[11] Much to our satisfaction, reaction of **2d** with 4-methoxy-1,3-bis(trimethylsiloxy)-1,3-diene **4h**[12] afforded the 4-methoxy-3(2*H*)-furanone **6h** in good yield and with very good chemo- and regio-selectivity. Starting with the 1,3-bis(trimethylsiloxy)-1,3-dienes **4i**–**j**, which are substituted at the central carbon atoms, the 3(2*H*)-furanones **6i**,**j** were isolated in good yields. Reaction of **2d** with the cyclic diene **4k**, which is derived from ethyl cyclohexanone-2-carboxylate, afforded the interesting bicyclic 3(2*H*)-furanone **6k** in good yield.

Variation of the substituents of the dielectrophile was then studied. Reaction of diene **4a** with 2-chloropropionyl chloride **2e** afforded the 6-chloro-3,5-dioxoester **5l** which was transformed into the 2-methyl-3(2*H*)-furanone **6l**. Reaction of 2-chloropropionyl chloride with the methyl- and ethyl-substituted dienes **4b** and **4c** afforded the 2-methyl-3(2*H*)-furanones **6m** and **6n** in good yields and with very good chemo- and regioselectivities, respectively. Reaction of **2e** with the diene derived from ethyl cyclohexanone-2-carboxylate afforded the bicyclic 2-methyl-3(2*H*)-furanone **6o** as a 1:1 mixture of diastereomers.

In conclusion, we have developed a new approach for the synthesis of a wide range of functionalized 3(2*H*)-furanones which are of pharmacological relevance and of interest for the synthesis of natural products.

P. L. thanks Professor A. de Meijere for his support. Financial support from the Fonds der Chemischen Industrie e. V. (Liebig-scholarship and funds for P. L.) is gratefully acknowledged.

Notes and references

† *General procedure* for the preparation of **6a**–**o**: to a CH_2Cl_2 solution (70 ml) of **2d** (5.5 mmol, 0.62 g) and of **4a** (5.5 mmol, 1.5 g) was added TMSOTf (1.65 mmol, 0.35 g) at −78 °C. The temperature of the reaction mixture was allowed to rise to 20 °C during 12 h. After stirring for 2 h at 20 °C a saturated solution of $NaHCO_3$ was added, the organic layer was separated and the aqueous layer was repeatedly extracted with diethyl ether. The combined organic extracts were dried ($MgSO_4$), filtered and the solvent of the filtrate was removed *in vacuo*. The residue was purified by column chromatography [silica gel, ether–petroleum (bp 40–70 °C)] to give **5a** as a colourless oil (805 mg, 71%). To a THF solution (5 ml) of **5a** (0.64 mmol, 122 mg) was added DBU (1.28 mmol, 195 mg). After stirring for 2.5 h, glacial acetic acid (0.4 ml) was added. The solvent was removed *in vacuo* and the residue was purified by chromatography to give **6a** as a colourless oil (100 mg, 91%): δ_H($CDCl_3$, 250 MHz): 1.22 (t, 8 Hz, 3 H, CH_3), 3.55 (s, 2 H, CH_2), 4.18 (q, 8 Hz, 2 H, OCH_2CH_3), 4.48 (s, 2 H, OCH_2), 5.66 (s, 1 H, CH). δ_C($CDCl_3$, 62.5 MHz): 13.79, 36.46, 61.57, 75.10, 106.13, 166.39, 185.95, 202.15. MS (70 eV) *m*/*z* 170 (M^+, 20). Anal. Calc. for $C_8H_{10}O_4$: C, 56.47; H, 5.92. Found: C, 56.35; H, 6.08%. All new compounds gave satisfactory spectroscopic and analytical and/or high resolution mass data.

1 L. F. Tietze and U. Beifuss, *Angew. Chem.*, 1993, **105**, 137; *Angew. Chem., Int. Ed. Engl.*, 1993, **32**, 131.

2 For reviews of dianions, see: A. Maercker, *Methoden Org. Chem.* (*Houben-Weyl*) 4. Aufl., Bd. E19d, 1993, 448; C. M. Thompson and D. Green, *Tetrahedron*, 1991, **47**, 4223; for 1,3-dicarbonyl dianions, see: L. Weiler, *J. Am. Chem. Soc.*, 1970, **92**, 6702; D. Seebach and V. Ehrig, *Angew. Chem.*, 1974, **86**, 446; *Angew. Chem., Int. Ed. Engl.*, 1974, **13**, 401.

3 K. G. Bilyard, P. J. Garratt, R. Hunter and E. Lete, *J. Org. Chem.*, 1982, **47**, 4731; R. B. Bates, B. Gordon, T. K. Highsmith and J. J. White, *J. Org. Chem.*, 1984, **49**, 2981; K. Tanaka, H. Horiuchi and H. Yoda, *J. Org. Chem.*, 1989, **54**, 63; A. Maercker and A. Groos, *Angew. Chem.*, 1996, **108**, 216; *Angew. Chem., Int. Ed. Engl.*, 1996, **35**, 210.

4 P. Langer and M. Stoll, *Angew. Chem.*, 1999, **111**, 1919; *Angew. Chem., Int. Ed.*, 1999, **38**, 1803; P. Langer, T. Schneider and M. Stoll, *Chem. Eur. J.*, 2000, in press.

5 For other cyclization and domino reactions of dianion synthons from our laboratory, see: P. Langer and M. Döring, *Synlett*, 1998, 396; P. Langer and M. Döring, *Synlett*, 1998, 399; P. Langer, J. Wuckelt, M. Döring and R. Beckert, *Eur. J. Org. Chem.*, 1998, 1467; P. Langer, M. Döring and D. Seyferth, *Synlett*, 1999, 135; P. Langer and M. Döring, *Chem. Commun.*, 1999, 2439; P. Langer, J. Wuckelt, M. Döring and H. Görls, *J. Org. Chem.*, in press; P. Langer, I. Freifeld and E. Holtz, *Synlett*, 2000, 501; P. Langer and T. Schneider, *Synlett*, 2000, 497; P. Langer and I. Karimé, *Synlett*, in press; P. Langer and B. Kracke, *Tetrahedron Lett.*, in press; P. Langer and E. Holtz, *Angew. Chem.*, in press.

6 (*a*) M. C. Paul, E. Zubia, M. J. Ortega and J. Salvá, *Tetrahedron*, 1997, **53**, 2303; (*b*) H. Shiozawa, M. Takahashi, T. Takatsu, T. Kinoshita, K. Tanzawa, T. Hosoya, K. Furuya and S. Takahashi, *J. Antibiot.*, 1995, **48**, 357; (*c*) R. A. Mack, W. I. Zazulak, L. A. Radov, J. E. Baer, J. D. Stewart, P. H. Elzer, C. R. Kinsolving and V. St. Georgiev, *J. Med. Chem.*, 1988, **31**, 1910; (*d*) G. Comte, D. P. Allais, A. J. Chulia, J. Vercauteren and C. Bosso, *Tetrahedron Lett.*, 1996, 2955; (*e*) X. Shao, M. Dolder and C. Tamm, *Helv. Chim. Acta*, 1990, **73**, 483; (*f*) K.-I. Takao, H. Ochiai, K.-I. Yoshida, T. Hashizuka, H. Koshimura, K.-I. Tadano and S. Ogawa, *J. Org. Chem.*, 1995, **60**, 8179; (*g*) P. W. Le Quesne, M. D. Menachery, M. P. Pastore, C. J. Kelley, T. F. Brennan, K. D. Onan, R. F. Raffauf and C. M. Weeks, *J. Org. Chem.*, 1982, **47**, 1519; (*h*) P. K. Chowdhury, R. P. Sharma, G. Thyagarajan, W. Herz and S. V. Govindan, *J. Org. Chem.*, 1980, **45**, 4993; (*i*) R. J. M. Goss, J. Fuchser and D. O'Hagan, *Chem. Commun.*, 1999, 2255; (*j*) P. G. Steel, *Chem. Commun.*, 1999, 2257.

7 R. O. Pendarvis and K. G. Hampton, *J. Org. Chem.*, 1974, **39**, 2289.

8 T.-H. Chan and P. Brownbridge, *J. Am. Chem. Soc.*, 1980, **102**, 3534; G. A. Molander and K. O. Cameron, *J. Am. Chem. Soc.*, 1993, **115**, 830.

9 M. Yamaguchi and K. Shibato, *Tetrahedron*, 1988, **44**, 4767.

10 A. Nahrstedt, J. Rockenbach and V. Wray, *Phytochemistry*, 1995, **39**, 375; F. Mayerl, R. Näf and A. F. Tomas, *Phytochemistry*, 1989, **28**, 631.

11 For an account of the regioselectivity of deprotonations of α-alkoxy and α-acyloxy ketones, see: L. A. Paquette, S. V. O'Neil, N. Guillo, Q. Zeng and D. G. Young, *Synlett*, 1999, 1857.

12 B. Simoneau and P. Brassard, *Tetrahedron*, 1986, **14**, 3767.

A diphthalocyanino-dehydro[12]annulene

Michael J. Cook* and Martin J. Heeney

School of Chemical Sciences, University of East Anglia, Norwich, UK NR4 7TJ. E-mail: m.cook@uea.ac.uk

Received (in Cambridge, UK) 6th March 2000, Accepted 11th April 2000

A diphthalocyanino-dehydro[12]annulene, synthesised by oxidative coupling of a dialkynylphthalocyanine, has been characterised by mass spectrometry and UV–VIS spectroscopy and shown to undergo thermal oligomerisation.

Phthalocyanines (Pcs) are important functional materials, their 18π electron system providing the basis for their characteristic photophysical, optoelectronic and conductiometric properties.[1] More complex structures such as covalently linked binuclear Pc structures are attracting attention because of interesting effects arising from the further extension of the π conjugation.[2] Formally planar structures in which two Pc cores share a common benzene ring have been characterised satisfactorily[3] and applications of palladium coupling reactions have provided access to alkynyl Pcs[4–6] of which some monoalkynyl derivatives[6] have been coupled to give both ethynyl and butadiynyl linked Pcs. These coupling methods are here applied to the synthesis of the first example of a diphthalocyanino-dehydroannulene **1** which is highly substituted to promote solubility in organic solvents. A report that annulenes are polymerisable at a diyne unit[7] indicates that phthalocyanino-dehydroannulenes could act as useful precursors for the synthesis of novel phthalocyanine network polymers. Preliminary studies of the thermolysis of **1** are described.

The synthesis of **1** is summarised in Scheme 1. The principal features are that the dehydroannulene ring is constructed in the last stage, requiring a non-uniformly substituted Pc as precursor. The latter is the dibromo derivative **2**,† obtained by a conventional mixed condensation of 3,6-didecylphthalonitrile[8] and 3,6-dibutoxy-4,5-dibromophthalonitrile[9] (ratio 6 : 1). Stille coupling,[10] converted **2** into **3**.† The conversion of **3** into **1** was achieved by copper(II) acetate mediated oxidative coupling in dry THF–pyridine–methanol (1 : 1 : 0.25). The reaction was investigated under various conditions, its progress monitored by visible region spectroscopy. Fig. 1 (top) shows the spectrum of **3**, line (a), with the visible region (Q-band) absorptions at 698 and 729 nm. The spectrum of the reaction mixture after 20 min at 50 °C under an argon atmosphere shows a broadened spectrum, line (b), with prominent peaks at λ_{max} 701 and 756 nm. After further time, there is a gradual appearance of a new peak at 822 nm, whose intensity maximises after 48 h. This same absorption band envelope was also obtained in a separate coupling reaction of **3** (39 mg) after 8 h at 80 °C, Fig. 1 (top), line (c). The crude reaction products were filtered through silica (eluent: light petroleum (bp 40–60 °C)–THF, 9 : 1) to remove copper salts and polymeric material. MALDI-TOF MS of the filtrate gave a base peak corresponding to **1** with smaller peaks attributable to a cyclic trimer and cyclic tetramer. Size exclusion chromatography failed to separate the mixture. However, purification by repeated column chromatography over silica (eluent: light petroleum (bp 40–60 °C)–THF, 19 : 1) afforded **1** as the major fraction (9.5 mg); MALDI-TOF showed an isotopic cluster at *m*/*z* 3206 corresponding to a singularly charged molecular ion. Scanning to higher mass gave no indication of higher molecular weight species. The high resolution FT-ICR MS of **1** using electrospray ionisation in THF confirmed the structure. The base signal corresponds to the doubly charged M^{2+} ion at *m*/*z* 1601.1211 (requires 1601.1235),

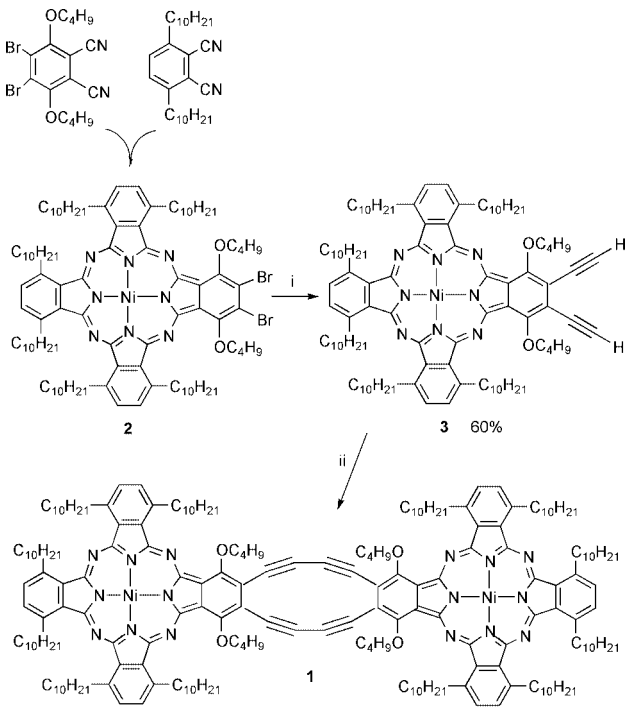

Scheme 1 *Reagents and conditions*: i, $Bu_3SnC{\equiv}CH$, $Pd(PPh_3)_2Cl_2$/$Pd(PPh_3)_4$; ii, $Cu(OAc)_2$, THF–pyridine–MeOH.

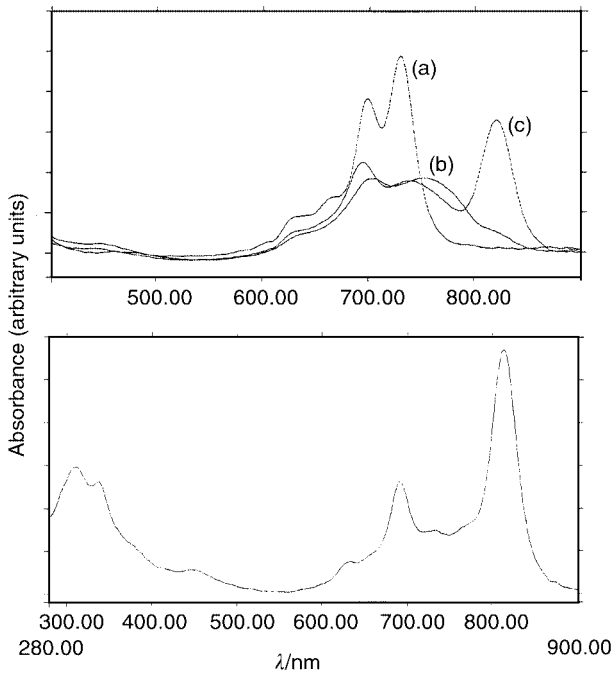

Fig. 1 UV–VIS spectra: (top) line (a), compound **3** as a solution in toluene; line (b), spectrum (toluene) of oxidative cross-coupling product from **3** after 20 min at 50 °C; line (c), the oxidative cross-coupling product from **3** after 8 h at 80 °C. (Bottom) spectrum of **1** as a solution in cyclohexane, showing the split Q-band. There is also evidence of splitting of the Soret band in the UV region.

DOI: 10.1039/b001783n

isotopic distribution showing a mass difference between each peak of 0.5 u. Signals are also present for M^+ at *m*/*z ca*. 3206 (poorly resolved) and M^{3+}, *m*/*z* 1067.4227 (requires 1067.4157). The spectrum also indicates the presence of aggregated structures. A peak cluster at *m*/*z ca*. 2138 corresponds to a triply charged two molecule aggregate of **1** and a very weak peak at *m*/*z ca*. 2400 corresponds to a quadruply charged trimeric aggregate.

Aggregation is also apparent from the ^{1}H NMR spectrum. Thus unlike the spectra of **2** and **3**, the spectrum of **1** (4.5 mg per 0.5 ml benzene-d_6) shows broadening of the signals for the aromatic protons, and the $-OCH_2$ and benzylic protons. Addition of pyridine-d_5 failed to inhibit aggregation at this concentration. Aggregation of **1** implies the possibility that π–π interactions lead to a supramolecular structure involving Pc units stacking to encapsulate a π electron rich channel formed by the dihydroannulene units. At higher dilution, (*ca*. 0.9 mg per 0.5 ml benzene-d_6), and at 40 °C the ^{1}H NMR spectrum is better resolved. Apart from aliphatic protons, there are overlapping signals for the aromatic protons, an 8 proton triplet at δ 4.91 (OCH_2 protons), a multiplet for 8 benzylic protons at δ 4.76 and a 16 proton multiplet for the remaining benzylic protons at δ 4.62.

The Q-band absorption for **1** is split, λ_{max} 822 and 691 nm, Fig. 1 (bottom). This is expected for metallated macrocycles of lower symmetry than D_{4h}[11] and is indeed observed for compounds **2** and **3.** However, the splitting is much more significant for compound **1**. A sample of **1** was heated on a hotstage and analysed by visible region spectroscopy. After heating for 5 min at 220 °C, the solution phase spectrum of the material shows reduction in absorbance of the two main components of the Q-band and growth of a broad band between them. Continued heating gives a sample whose spectrum shows an irreversible disappearance of the original bands and a featureless band envelope in the region 680–820 nm. The MALDI-TOF spectrum of the product shows broadened high molecular mass clusters corresponding to multiples of *m*/*z* 3206, the highest centered at *m*/*z ca*. 19200. This provides a clear indication that oligomerisation has occurred. The potential for developing large and potentially well organised phthalocyanine networks from these and related materials is under investigation.

We thank EPSRC for a studentship (M. J. H.), the EPSRC Mass Spectrometry Service at Swansea for FAB mass spectra, Ms V. Boote at University of Manchester for running MALDI-TOF mass spectra, and Dr Helen Cooper at Warwick University for providing FT-ICR mass spectra.

Notes and references

† Compound **2**: found C 70.40, H 8.90, N 6.30. $C_{100}H_{150}N_8O_2Br_2Ni$ requires C 70.04, H 8.82, N 6.53%. ^{1}H NMR (300 MHz, C_6D_6): δ 7.82 (s, 4H), 7.81 (s, 2H), 4.75 (t, 4H, *J* 7.5 Hz), 4.66–4.57 (3 overlapping t, 12H), 2.34–2.17 (m, 16H), 1.92–1.11 (m, 88H), 0.95 (t, 6H, *J* 7.4 Hz), 0.87–0.80 (m, 18H); UV–VIS (3.68×10^{-6} M in toluene, log ε) l 716 (5.10), 698 (5.03), 636 (4.39) nm; MS (FAB): isotopic cluster at *m*/*z* 1716 $[M + H]^+$; requires 1715.84.

Compound **3**: found C 76.99, H 9.56, N 6.98. $C_{104}H_{152}N_8O_2Ni{\cdot}CH_3OH$ requires C 77.03, H 9.60, N 6.84%. ^{1}H NMR (270 MHz, C_6D_6): δ 7.81–7.78 (m, 6H), 4.83–4.76 (m, 8H), 4.61–4.56 (m, 8H), 3.53 (s, 2H), 2.33–2.21 (m, 16H), 1.93–1.11 (m, 88H), 0.96 (t, 6H, *J* = 7.4 Hz), 0.92–0.81 (m, 18H).UV–VIS (2.51×10^{-6} M in toluene, log ε) l 729 (4.99), 698 (4.88), 666 (4.44), 628 (4.23) nm; MS (FAB): isotopic cluster at *m*/*z* 1606 $[M + H]^+$, requires 1605.1.

1 See, for example: N. B. McKeown, *Phthalocyanine Materials: Synthesis, Structure and Function*, Cambridge University Press, Cambridge, 1998.
2 G. de la Torre, P. Vázquez, F. Agulló-López and T. Torres, *J. Mater. Chem.*, 1998, **8**, 1671.
3 D. Delièvre, O. Damette and J. Simon, *J. Chem. Soc., Chem. Commun.*, 1993, 939; N. Kobayashi, H. Lam, W.A. Nevin, P. Janda, C. C. Leznoff, T. Koyama, A. Monden and H. Shirai, *J. Am. Chem. Soc.*, 1994, **116**, 879; N. Kobayashi, Y. Higashi and T. Osa, *J. Chem. Soc., Chem. Commun.*, 1994, 1785; G. de la Torre, M. V. Martínez-Díaz, P. Ashton and T. Torres, *J. Org. Chem.*, 1998, **63**, 8888; G. de la Torre, M. V. Martínez-Díaz and T. Torres, *J. Porphyrins Phthalocyanines*, 1999, **3**, 560.
4 D. S. Terekhov, K. J. M. Nolan, C. R. McArthur and C. C. Leznoff, *J. Org. Chem.*, 1996, **61**, 3034; H. Isago, D. S. Terekhov and C. C. Leznoff, *J. Porphyrins Phthalocyanines*, 1997, **1**, 135; C. C. Leznoff, Z. Li, H. Isago, A. M. D'Ascanio and D. S. Terekhov, *J. Porphyrins Phthalocyanines*, 1999, **3**, 406.
5 H. Ali and J. E. van Lier, *Tetrahedron Lett.*, 1997, **38**, 1157.
6 E. M. Maya, P. Vázquez and T. Torres, *Chem. Commun.*, 1997, 1175; E. M. Maya and T. Torres, *Chem. Eur. J.*, 1999, **5**, 2004.
7 Q. Zhou, P. Carroll and T. Swager, *J. Org. Chem.*, 1994, **59**, 1294; K. P. Baldwin, A. J. Matzger, D. A. Scheiman, C. A. Tessier, K. P. C. Vollhardt and W. J. Youngs, *Synlett.*, 1995, 1215.
8 N. B. McKeown, I. Chambrier and M. J. Cook, *J. Chem. Soc., Perkin Trans. 1*, 1990, 1169.
9 M. J. Heeney, PhD thesis, University of East Anglia, Norwich, UK, 1999.
10 D. E. Rudisill and J. K. Stille, *J. Org. Chem.*, 1989, **54**, 5856.
11 N. Kobayashi and H. Konami, *Phthalocyanines: Properties and Applications*, ed. C. C. Leznoff and A. B. P. Lever, VCH, 1996, vol. 4, pp. 343–404.

A spontaneously resolved chiral molecular box: a cyclic tetranuclear Zn^{II} complex with DPTZ (DPTZ = 3,6-di-2-pyridyl-1,2,4,5-tetrazine)

Xian-He Bu,*[abc] Hiromasa Morishita,[d] Kentaro Tanaka,[a] Kumar Biradha,[b] Sanae Furusho[e] and Mitsuhiko Shionoya*[a]

[a] *Department of Chemistry, School of Science, the University of Tokyo, Hongo, Bunkyo-ku, Tokyo 113-0033, Japan. E-mail: shionoya@chem.s.u-tokyo.ac.jp*
[b] *Institute for Molecular Science, Myodaiji, Okazaki 444-8585, Japan*
[c] *Department of Chemistry, Nankai University, Tianjin 300071, P.R. China*
[d] *The Graduate University for Advanced Studies, Myodaiji, Okazaki 444-8585, Japan*
[e] *Jasco International Co Ltd., Myojin, Hachioji, Tokyo 192-0046, Japan*

Received (in Columbia, MO, USA) 9th December 1999, Accepted 21st March 2000

A quantitative synthesis of a novel cyclic tetranuclear Zn^{II} complex with 3,6-di-2-pyridyl-1,2,4,5-tetrazine (DPTZ), which was spontaneously resolved as chiral crystals, has been developed.

The rational design of discrete self-assembling systems is one of the most challenging tasks in the exploitation of supramolecular synthons. In particular, the metal-assisted assembly of cyclic molecular arrays plays an integral part in the development of inclusion chemistry as well as 'engineering up' molecular architectures. To date, the groups of Fujita,[1] Stang,[2] and others[3] have been exploiting the coordination-based syntheses of molecular squares or rectangles with right angles at their corners, which are one of the simplest members of the polygon family. The creation of a new class of artificial *chiral* supramolecular species *via* spontaneous self-assembly has been one key to further development of this rapidly expanding field. Stang and coworkers have explored the syntheses of chiral Pt^{II}_4 or Pd^{II}_4 molecular squares by using either chiral chelating ligands or C_{2h}-symmetrical bridging ligands.[4] As described previously, there are several ways of creating chiral supramolecular architectures, of which use of an inherently chiral octahedral metal complex has been recognized as a promising strategy. Unlike the square-planar Pt^{II} or Pd^{II} complexes, octahedral metal complexes are inherently chiral[5] and therefore no chiral auxiliary ligands are required. Recently, Wang and coworkers have reported a Co^{II} molecular square complex that exhibits a chiral molecular structure in the solid state,[6] where no chiral auxiliary ligands were employed, and the individual single crystal was found to consist of one enantiomer only. However, the reaction yield was low and the solution behavior of the molecular square remains unsolved.

We report herein a *quantitative* preparation of a novel cyclic tetranuclear Zn^{II} complex that was *spontaneously resolved* as *chiral* crystals. The bridging ligand used in this study is 3,6-di-2-pyridyl-1,2,4,5-tetrazine (DPTZ). Although the two pyridyl groups of DPTZ can rotate around the C–C bonds between the pyridine rings and tetrazine ring, upon coordinating to metal ions the three aromatic rings can become almost coplanar to bridge two metal centers. We therefore anticipated that DPTZ would serve as a rigid multitopic spacer ligand and that a thermodynamically stable yet kinetically labile chiral assembly could be formed by the use of the Zn^{II} ion which is inherently chiral in an octahedral coordination geometry.[7]

The reaction of $Zn^{II}(ClO_4)_2{\cdot}6H_2O$ with an equimolar amount of DPTZ in chloroform–acetonitrile at ambient temperature produced orange prisms of $[Zn^{II}_4(DPTZ)_4(H_2O)_4(CH_3CN)_4](ClO_4)_8{\cdot}2CHCl_3{\cdot}4CH_3CN$ **1**, in 90% yield (Scheme 1). The structure of **1** was determined by a single-crystal X-ray diffraction analysis with a Siemens CCD X-ray diffractometer. Complex **1** crystallizes in the chiral space group $C222_1$.[8] As shown in Fig. 1, complex **1** has a crystallographically imposed

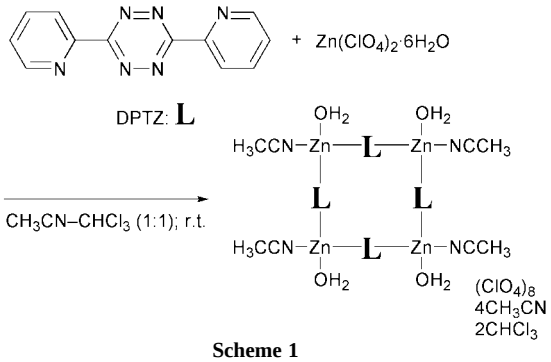

Scheme 1

D_2 symmetry with half of the molecule being in the asymmetric unit. As a consequence of the D_2symmetry, the four Zn^{II} centers have identical chirality, *i.e.* either all Δ or all Λ optical geometry. The Flack parameter was nearly zero, indicating *each* individual crystal of **1** consists of *a single* enantiomer.[9] Indeed, all four Zn^{II} centers of the single crystal used in this analysis have Λ geometry and therefore complex **1** is a chiral molecular box in the solid state.

Space-filling diagrams of the molecular box **1** are shown in Fig. 2. Each Zn^{II} ion of complex **1** has a typical octahedral coordination geometry with two DPTZ ligands bridging the other two Zn^{II} centers. The other two coordination sites of the Zn^{II} ion are occupied by one acetonitrile and one water molecule. It is noteworthy that there should be many possible structures in the four Zn^{II} centers if the acetonitrile and water molecules occupy their positions randomly. However, all the

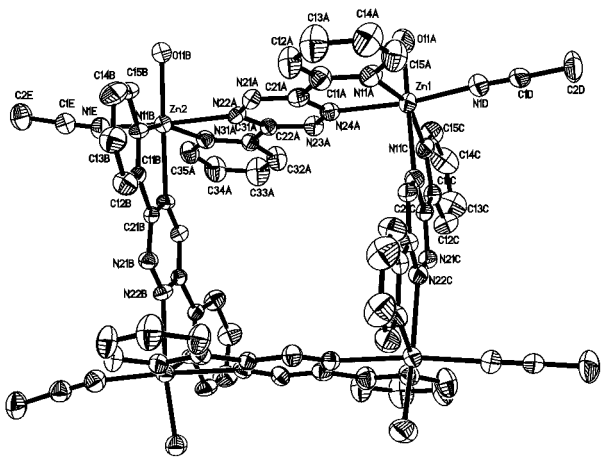

Fig. 1 ORTEP view of the molecular structure of **1** with 50% thermal ellipsoids and labeling scheme. Perchlorate anions and solvent molecules are omitted for clarity.

DOI: 10.1039/a909742b

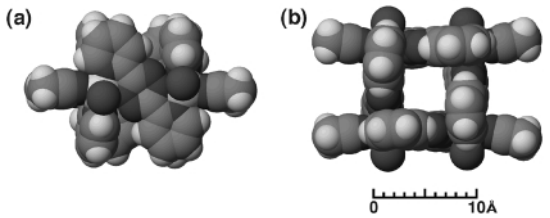

Fig. 2 Space-filling diagrams showing (a) a side-view and (b) a top-view of the box cavity of complex **1**.

four acetonitrile and four water molecules coordinate to Zn^{II} in a highly symmetrical manner, and the formation of a single diastereomer was observed. The $Zn^{II}\cdots Zn^{II}$ distances along the corners of the box are *ca.* 7.2 Å. The dimensions of the box cavity are estimated to be *ca.* 4 Å × 4 Å [Fig. 2(b)]. It is of interest that one perchlorate ion and two chloroform molecules are encapsulated within the box cavity of **1**, where the two chloroform molecules interpose the perchlorate ion like two caps to close the box. Such guest molecules may facilitate the cyclization and therefore stabilize the resulting cyclic box structure.

The ^{1}H NMR spectrum of **1** in CD_3CN showed one set of proton signals for the pyridine parts of DPTZ,[10] suggesting that the DPTZs are bridging ligands and are coordinated symmetrically between two Zn^{II} centers. The discrete tetrameric structure of **1** in acetonitrile was confirmed by ESI-TOF mass spectroscopy. The isotopically resolved ESI-TOF mass spectrum of this assembly is shown in Fig. 3. The signals of Zn^{II} tetrameric species for **1** are centered at *m/z* 2166.6, 1954.6, 1900.6 and 1664.6, which correspond to the +1 charged cationic species [Fig. 3(a)].[11] For example, the enlarged plot of the signal for *m/z* 1954.6 $[Zn^{II}_4(DPTZ)_4(H_2O)_3(CH_3CN)_2(OH)(ClO_4)_6]^+$ gave excellent agreement between the experimental and theoretical isotopic distributions, indicating the tetrameric character of **1** [Fig. 3(b) and 3(c)]. These results establish that the cyclic Zn^{II} tetramer is stable in solution.

A solution of complex **1** in acetonitrile exhibited an essentially zero optical rotation, indicating that the bulk of the crystals is a racemate. Although the single-crystal X-ray diffraction analysis demonstrated that each individual crystal of **1** consists of one enantiomer only, the question of whether the single enantiomer of **1** undergoes racemization in solution still remains unsolved because the individual chiral crystals of **1** are too small to allow any meaningful kinetic study and circular dichroism measurement. Attempts for preferential crystallization of either enantiomer Δ or Λ through seeding of the racemic supersaturated solution with a seed of one crystal were unsuccessful.

The present molecular box **1** is the first example of spontaneous resolution of a quantitatively self-assembled Zn^{II} molecular box.

This work was supported by Grant-in-Aids for Scientific Research on Priority Areas (No. 11136255 'Metal-assembled Complexes' and No. 706 'Dynamic Control of Stereochemistry') to M. S. from the Ministry of Education, Science, Sports, and Culture, Japan. Financial support by National Natural Science Foundation of China (No. 29771022 for X.-H. B.) is also greatly appreciated.

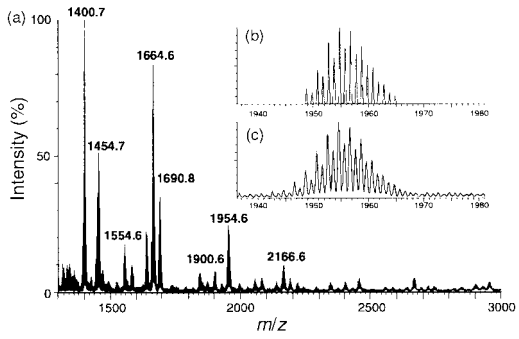

Fig. 3 ESI-TOF mass spectrum of complex **1** in acetonitrile: (a) *m/z* 1300 –3000, (b) theoretical isotopic distribution at *m/z* 1954.6, and (c) experimental isotopic distribution at *m/z* 1954.6.

Notes and references

1 M. Fujita, J. Yazaki and K. Ogura, *J. Am. Chem. Soc.*, 1990, **112**, 5645; M. Fujita, S. Nagao, M. Iida, K. Okada and K. Ogura, *J. Am. Chem. Soc.*, 1993, **115**, 1574; M. Fujita, O. Sasaki, T. Mitsuhashi, T. Fujita, J. Yazaki, K. Yamaguchi and K. Ogura, *Chem. Commun.*, 1996, 1535.

2 P. J. Stang and V. Zhdankin, *J. Am. Chem. Soc.*, 1993, **115**, 9808; P. J. Stang and D. H. Cao, *J. Am. Chem. Soc.*, 1994, **116**, 4981; P. J. Stang, D. H. Cao, S. Saito and A. M. Arif, *J. Am. Chem. Soc.*, 1995, **117**, 6273; P. J. Stang and K. Chen, *J. Am. Chem. Soc.*, 1995, **117**, 1667; J. Mana, J. A. Whiteford and P. J. Stang, *J. Am. Chem. Soc.*, 1996, **118**, 8731; J. A. Whiteford, E. M. Rachlin and P. J. Stang, *Angew. Chem., Int. Ed. Engl.*, 1996, **35**, 2524; J. Fan, J. A. White, B. Olenyuk, M. D. Levin, P. J. Stang and E. B. Fleischer, *J. Am. Chem. Soc.*, 1999, **121**, 2741.

3 C. A. Hunter, *Angew. Chem., Int. Ed. Engl.*, 1995, **34**, 1079; R. V. Slone, D. I. Yoon, R. M. Calhoun and J. T. Hupp, *J. Am. Chem. Soc.*, 1995, **117**, 11 813; P. Losier and M. J. Zaworotko, *Angew. Chem., Int. Ed. Engl.*, 1996, **35**, 2779; M. J. Irwin, J. J. Vittal, G. P. Yap and R. J. Puddephatt, *J. Am. Chem. Soc.*, 1996, **118**, 13 101; M. J. Irwin, L. M. Rendina, J. J. Vittal and R. J. Puddephatt, *Chem. Commun.*, 1996, 1281; W. H. Leung, J. K. Cheng, T. S. M. Hun, C. M. Che, W. T. Wong and K. K. Cheung, *Organometallics*, 1996, **15**, 1497; H. Rauter, I. Mutikainen, M. Blomberg, C. J. Lock, P. Amo-Ochoa, E. Freisinger, L. Randaccio, E. Zangrando, E. Chiarparin and B. Lippert, *Angew. Chem., Int. Ed. Engl.*, 1997, **36**, 1296; G. S. Hanan, D. Volkmer, U. S. Schubert, J.-M. Lehn, G. Bauum and D. Fenske, *Angew Chem., Int. Ed. Engl.*, 1997, **36**, 1842; J. Li, H. Zeng, J. Chen, Q. Wang and X. Wu, *Chem. Commun.*, 1997, 1213; C. J. Duan, Z. M. Liu, X. Z. You and T. C. W. Mak, *Chem. Commun.*, 1997, 381; J. W. Canary and B. C. Gibb, *Prog. Inorg. Chem.*, 1997, **45**, 1; R. V. Slone, K. D. Benkstein, S. Belanger, J. T. Hupp, H. A. Guzei and A. L. Rheingold, *Coord. Chem. Rev.*, 1998, **171**, 221.

4 B. Olenyuk, J. A. Whiteford and P. J. Stang, *J. Am. Chem. Soc.*, 1996, **118**, 8221; P. J. Stang and B. Olenyuk, *Acc. Chem. Res.*, 1997, **30**, 502; P. J. Stang, B. Olenyuk, D. C. Muddiman and R. D. Smith, *Organometallics*, 1997, **16**, 3094; B. Olenyuk, P. Fechtenkotter and P. J. Stang, *J. Chem. Soc., Dalton Trans.*, 1998, 1707.

5 F. A. Cotton and G. Wilkinson, *Advanced Inorganic Chemistry*, John Wiley & Sons, New York, 1988.

6 Y. Zhang, S. Wang, G. D. Enright and S. R. Breeze, *J. Am. Chem. Soc.*, 1998, **120**, 9398.

7 Very recently, a synthesis and structure of a cyclic tetranuclear Ni(II) complex with DPTZ and its magnetic properties have been developed independently. See: C. S. Campos-Fernandez, R. Clerac and K. R. Dunbar, *Angew. Chem., Int. Ed.*, 1999, **38**, 3477.

8 *Crystal data* for complex **1**: $C_{66}H_{66}Cl_{14}Zn_4N_{32}O_{36}$, M_w = 2641.28, orthorhombic, space group $C222_1$, a = 13.6982(17), b = 30.091(4), c = 25.195(3) Å, V = 10 385 (2) Å^3, Z = 4, μ = 13.68 cm^{-1}, D_c = 1.689 g cm^{-3}, $F(000)$ = 5304. Data were collected over the 2θ range 3.18–57.56° at 193(2) K on a Siemens CCD X-ray diffractometer with Mo-Kα radiation (λ = 0.71073 Å). A total of 15576 reflection data were collected, of which 10552 (R_{int} = 0.0327) were independent. Convergence to the final R values of R_1 = 0.0505, wR_2 = 0.1129 [$I > 2\sigma(I)$] and R_1 = 0.0886, wR_2 = 0.1239 (all data) for **1** was achieved by using 10 552 unique reflections and 687 parameters (on F^2), with S = 0.941 and maximum residual peak of 0.563 e Å^{-3}.

CCDC 182/1596. See http://www.rsc.org/suppdata/cc/a9/a909742b/ for crystallographic files in .cif format.

9 H. D. Flack, *Acta Crystallogr., Sect. A*, 1983, **39**, 876.

10 ^{1}H NMR [500 MHz, CD_3CN, external TMS–CD_3CN]: for **1**; δ 8.14 (d, J 7.5 Hz, 8H, 3,3′-H), 8.33 (ddd, J 1.0, 5.0, 8.0 Hz, 8H, 5,5′-H), 8.54 (ddd, J 1.5, 7.8, 7.8 Hz, 8H, 4,4′-H), 9.26 (d, J 4.5 Hz, 8H, 6,6′-H); for DPTZ: δ 7.66 (ddd, J 1.3, 4.8, 7.7 Hz, 2H, 5,5′-H), 8.09 (ddd, J 1.7, 7.8, 7.8 Hz, 2H, 4,4′-H), 8.65 (ddd, J 1.1, 1.1, 7.9 Hz, 2H, 3,3′-H), 8.94 (ddd, J 0.9, 1.6, 4.6 Hz, 2H, 6,6′-H).

11 *MS* (*ESI-TOF*) *data* for **1** (CH_3CN): *m/z* 2166.6 $[M - (H_2O)_6 + H^+]^+$, 1954.6 $[M - (CH_3CN)_2 - (ClO_4)_2 - H^+]^+$, 1900.6 $[M - (CH_3CN)_2 - (H_2O)_3 - (ClO_4)_2 - H^+]^+$, 1690.8 $[M - Zn^{II} - (CH_3CN)_2 - (ClO_4)_4 - H^+]^+$, 1664.6 $[M - L - (CH_3CN)_2 - (H_2O)_3 - (ClO_4)_2 - H^+]^+$, 1554.6 $[M - L - Zn^{II} - (CH_3CN)_2 - (ClO_4)_3]^+$, 1454.7 $[M - L - Zn^{II} - (CH_3CN)_2 - (ClO_4)_4 - H^+]^+$, 1400.7 $[M - L - Zn^{II} - (CH_3CN)_2 - (H_2O)_3 - (ClO_4)_4 - H^+]^+$, 1136.9 $[M - L - Zn^{II}_2 - (CH_3CN)_2 - (H_2O)_3 - (ClO_4)_6 - H^+]^+$, 900.8 $[M - L_2 - Zn^{II}_2 - (CH_3CN)_2 - (H_2O)_3 - (ClO_4)_6 - H^+]^+$, 635.0 $[M - L_2 - Zn^{II}_3 - (CH_3CN)_4 - (H_2O)_4 - (ClO_4)_7]^+$, 439.9 $[M - L_3 - Zn^{II}_3 - (CH_3CN)_3 - (H_2O)_4 - (ClO_4)_7]^+$, where M = $[L_4Zn^{II}_4(H_2O)_4(CH_3CN)_4](ClO_4)_8$ and L = DPTZ.

ChemComm

Novel structural determination of a bilayer network formed by a tripodal lipophilic amide in the presence of anions

Andrew Danby,[a] Larry Seib,[a] Nathaniel W. Alcock[b] and Kristin Bowman-James*[a]

[a] *Department of Chemistry, University of Kansas, Lawrence, Kansas 66045, USA. E-mail: kbowman-james@ukans.edu*

[b] *Department of Chemistry, University of Warwick, Coventry, UK CV4 7AL*

Received (in Columbia, MO, USA) 15th November 1999, Accepted 31st December 1999

The crystal structure of a protonated tripodal lipophilic amide, *N*-{2-[bis(2-octanoylaminoethyl)amino]ethyl}octanamide, identified an elegantly architected bilayer hydrogen bonded structure consisting of ladder-like cascades of the amide, with the rungs comprised of the lipophilic tails pointing inward and the poles made up of polar quaternary ammonium heads lining channels filled with nitrate ions.

In our investigation of the anion binding capabilities of a series of lipophilic amide receptors of varying chain length, we recently isolated the nitrate salt of a protonated triamide **1** with

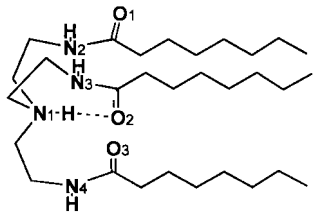

1

three seven-carbon alkyl chains. The unanticipated structure shows a novel and elegant bilayer structure comprised of ladder-like cascades of the amide, with the rungs consisting of the lipophilic tails pointing inward and the polar heads lining channels filled with nitrate ions. Because of the high thermal motion usually exhibited by such chains, crystallographic determinations are limited. This most unusual structure thus provides solid state insights into the forces holding such frameworks together.

Anion complexation is a swiftly emerging field of chemistry with relevance to biology, the environment, and industry.[1] Of the oxo-anions, nitrate is important because of its prevalence in soil and groundwater as well as at nuclear waste facilities. Our interest in nitrate binding began several years ago with the isolation and structural characterization of the nitrate salt of an inclusion complex of nitrate with a polyammonium macromonocycle,[2] and more recently with a *di*nitrate inclusion complex within a tripodal bicyclic aza cryptand.[3] Drawbacks associated with polyammonium receptors, however, are their binding dependency on pH as well as high water solubilities, which limit their effectiveness in many applications. In this regard, receptors soluble in organic phases and capable of binding over a range of pH are desirable. Hence we, along with a number of other researchers, have begun to explore hosts containing amide functionalities, a logical choice considering that Nature employs such moieties in the biological binding and transport of anions.[4]

In our study of lipophilic receptors we have synthesized and characterized a series of tripodal amides with hydrocarbon tails based on the triamine building block, tren. In earlier work, Reinhoudt and coworkers examined related tren-based systems, and were successful in identifying several excellent neutral receptors for phosphate.[5] Only one hydrocarbon chain (with six carbons) was included in that study,which focussed on aromatic 'tails'. Potvin and Jairam also have employed similar types of ligands, but primarily for binding metal ions and especially as models for zinc enzymes.[6] Crystallographic characterization of such receptors with lipophilic tails tends to be very limited because of the floppy nature of the hydrocarbon chains, which generally results in poor crystallinity and in large thermal motion and very high *R* factors.[7] By contrast, the structure reported herein was 'well behaved', and, as such, provides a significant addition to the structural database of bilayers.

Synthesis of the tripodal amide receptor from tren and octanoic acid was found to proceed in high yield using triphenyl phosphite as a coupling agent.[8]† To purify the resulting triamide, the crude product was dissolved in DMSO and acidified with nitric acid to pH 1. The crystalline product, when recrystallized from a DMSO–water mixture, gave crystals suitable for X-ray diffraction.

The crystal structure shows the crystals to be the mononitrate salt of the amide, singly protonated at the apical nitrogen.‡ While it was initially disappointing to us that the nitrate was not encapsulated within the tren unit, the reason is apparent: one of the amide carbonyl oxygen atoms points into the cavity to hydrogen bond with the *endo*-oriented proton of the apical amine [O(2)···N(1) 2.74(1) Å], effectively 'closing' the cavity. The receptor packs in beautifully patterned three-dimensional arrays reminiscent of bilayer structures, with the hydrophilic tren 'heads' lining open channels for the nitrates [Fig. 1(a) and (b)]. The bilayer is held together by hydrogen bonding between pairs of cations, O(1)···N(3′) 2.816(9) and O(3)···N(2″) 2.800(9) Å, in adjacent unit cells. The distance between apical nitrogens through the bilayer is 25.3 Å, while the distance between apical nitrogens across the bilayer is 6.2 Å. The torsion angles in **1** indicate that the carbon chains are highly ordered. Within the polar head of the tripod, the $N_{apical}CCN_{amide}$ angles approximate the *gauche* conformation, while the hydrocarbon portion of the tail exhibits a consistent array of *trans* angles. One exception to this pattern occurs on the chain in which the amide oxygen points inward, to hydrogen bond with the apical nitrogen of the tren unit. In the latter case both the CCN(3)C(O) [−73.1(6)°] and N(3)CC(O)C angles [132.3(5)°] differ significantly from their $CN_{amide}C(O)C$ [−124.3(5) and −139.1(5)°] and $N_{amide}C(O)CC$ [176.6(5) and 177.1(6)°] counterparts on adjacent tails.

The closest nitrate–nitrate approach along the channels is 5.75 Å between nitrogen centers. Only the two disordered oxygen atoms on the nitrate are within strong hydrogen bonding range of one of the amide nitrogens, O(6)···N(4) 2.98(2) and O(7)···N(4) 2.96(3) Å. One of the two ordered oxygens, O(5) of the nitrate, lies within a 3.5 Å distance of both N(3) and N(4).

In conclusion, while **1** is not a selective receptor for nitrate, having rather similar K_{as} values for a series of ions,[9] this is one of the few crystallographically confirmed bilayer structures. A structure of 1,2-dilauroyl-DL-phosphatidylethanolamine with two chains forming the bilayer, in which the unweighted *R* factor was extremely high (0.28), would appear to be the only crystal structure closely related to **1**.[7] Thus the structure of the

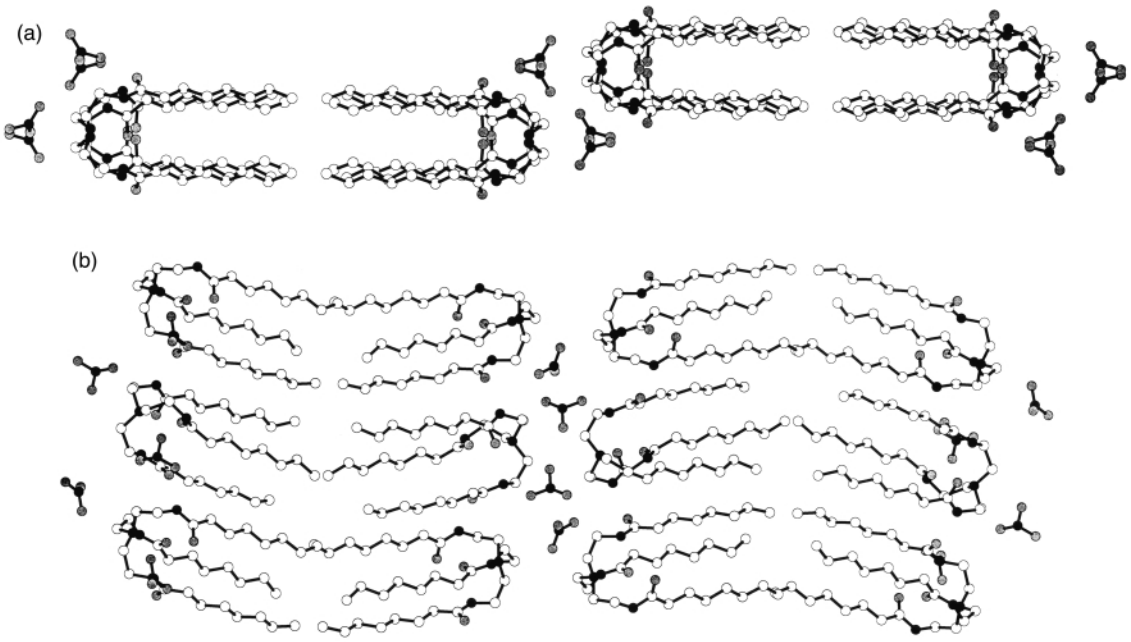

Fig. 1 (a) View of the *ab* plane (*b* along the horizontal axis) looking down *c*. (b) View of the *ac* plane (*b* along the horizontal axis) looking down *a*.

nitrate complex of **1** with its three-chain bilayer formation provides rare evidence of the elegant architectural pattern that is undoubtedly inherent in these systems in their biological habitats.

This research was supported by a grant from the Department of Energy DE-FG07-96ER62307. We are grateful for helpful discussions with Professor Nathaniel W. Alcock.

Notes and references

† *Spectroscopic data*: ^{1}H NMR (300 MHz, $CDCl_3$, TMS) δ 7.65 (t, 3H, NH), 3.63 (m, 6H, NCH_2), 3.47 (t, 6H. CH_2NH), 2.25 (t, 6H, COCH_2CH$_2$), 1.59 (t, 6H, COCH$_2$CH_2), 1.28 [m, 12H, (CH_2)$_2$CH$_3$], 0.88 (t, 9H, CH_3); Anal. Calc. for $C_{30}H_{61}N_5O_6$: C, 61.30; H, 10.46; N, 11.91. Found: C, 61.67; H, 10.16; N, 11.91%.

‡ *Crystal data*: $C_{30}H_{61}N_5O_6$, M_w = 587.84, orthorhombic, space group *Pccn* (no. 56), a = 8.383(3), b = 58.887(5), c = 14.673(3) Å, V = 7244(2) Å^3, D_c = 1.08 g cm^{-3}, Z = 8. Single crystal X-ray structure analysis was carried out on a crystal of dimensions 0.40 × 0.40 × 0.50 mm using a Rigaku AFC5R diffractometer with graphite-monochromated Cu-Kα (λ = 1.54178 Å) radiation at 23 °C. Data collection to $2\theta_{max}$ of 120.2° gave 6558 unique reflections. The structure was solved according to previously reported methods.[2] All of the hydrogen atoms were placed in calculated positions and were included in subsequent calculations but not refined. Refinement included 379 parameters on 2646 reflections for which $I > 3.00\sigma(I)$, to give R = 0.063, R_w = 0.063 and GOF = 3.17. As is common in nitrate structures, the nitrate exhibited disorder (four oxygen peaks, two given 50% occupancy). CCDC 182/1570. See http://www.rsc.org/suppdata/cc/a9/a909341i/ for crystallographic files in .cif format.

1 Some treatises on anion recognition are: *Supramolecular Chemistry of Anions*, ed. A. Bianchi, K. Bowman-James and E. García-España, Wiley–VCH, New York, 1997; H. E. Ktaz, in *Inclusion Compounds*, ed. J. L. Atwood, J. E. D. Davies and D. D. MacNichol, Oxford University Press, Oxford, 1991, p. 391; B. Dietrich, J. Guilhem, J.-M. Lehn, C. Pascard and E. Sonveaux, *Helv. Chim. Acta*, 1984, **67**, 91; B. Dietrich, *Pure Appl. Chem.*, 1993, **65**, 1457; R. M. Izatt, K. Pawlak, J. L. Bradshaw and R. L. Bruening, *Chem. Rev.*, 1991, **91**, 1721; F. Vögtle, H. Sieger and W. M. Müller, *Top. Curr. Chem.*, 1981, **98**, 107; E. Kimura, *Top. Curr. Chem.*, 1985, **128**, 113; J. L. Sessler, M. Cyr, H. Furuta, V. Kral, T. Mody, T. Morishma, M. Shionaya and S. Weghorn, *Pure Appl. Chem.*, 1993, **65**, 393; P. D. Beer and D. K. Smith, *Prog. Inorg. Chem.*, 1997, **46**, 1.
2 G. Papoyan, K. Gu, J. Wiórkiewicz-Kuczera, K. Kuczera and K. Bowman-James, *J. Am. Chem. Soc.*, 1996, **118**, 1354.
3 S. Mason, T. Clifford, L. Seib, K. Kuczera and K. Bowman-James, *J. Am. Chem. Soc.*, 1998, **120**, 8988.
4 F. A. Quiocho and H. Luecke, *Nature*, 1990, **347**, 402; M. P. Anderson, R. J. Gregory, S. Thompson, D. W. Souza, S. Paul, R. C. Mulligan, A. E. Smith and M. J. Welsh, *Science*, 1991, **253**, 202; M. K. Mansoura, S. S. Smirth, A. D. Choi, N. W. Richards, T. V. Strong, M. L. Drumm, F. S. Collins and D. C. Dawson, *Biophys. J.*, 1998, **74**, 1320.
5 S. Valiyaveettil, J. F. J. Engbersen, W. Verboom and D. N. Reinhoudt, *Angew. Chem., Int. Ed. Engl.*, 1993, **32**, 900.
6 R. Jairam and P. G. Potvin, *J. Org. Chem.*, 1992, **57**, 4136.
7 P. B. Hitchcock, R. Mason, K. M. Thomas and G. G. Shipley, *Proc. Natl. Acad. Sci., USA*, 1974, **71**, 3036; P. B. Hitchcock, R. Mason, K. M. Thomas and G. G. Shipley, *J. Chem. Soc., Chem. Commun.*, 1974, 539.
8 Y. V. Mitin and O. V. Glinskaya, *Tetrahedron Lett.*, 1969, 5267.
9 A. Danby and K. Bowman-James, unpublished results.

ChemComm

Synthesis of *O*-alkylhydroxylamines by electrophilic amination of alkoxides

Oliver F. Foot and David W. Knight*

Chemistry Department, Cardiff University, PO Box 912, Cardiff, UK CF10 3TB. E-mail: knightdw@cf.ac.uk

Received (in Liverpool, UK) 21st March 2000, Accepted 27th April 2000

The 3-trichloromethyloxaziridine 7 reacts smoothly with lithium alkoxides, derived from a representative range of alcohols, transferring an NHBoc function to the oxygen to provide good to excellent yields of *N*-Boc-*O*-alkylhydroxylamines 8–16 by this new *O*-amination protocol.

In pursuance of our studies of various electrophile-driven 5-*endo* cyclisation processes,[1] we required access to the hydroxylamines represented by structures **2** and **6** and sought to obtain these by a Mitsunobu displacement[2] using the corresponding and readily available alcohols **1** and **5**, as this seemed the best of a relatively limited number of options.[3] Unfortunately, both approaches suffered from serious drawbacks. For the allylic alcohol **1**, the Mitsunobu method using *N*-hydroxyphthalimide,[4] under standard conditions delivered good yields of the required substrate **2a**; in contrast, when *N*-(4-toluenesulfonyl)hydroxylamine (TsNHOH)[5] was used as the nucleophile, yields were very poor (Scheme 1). However, when

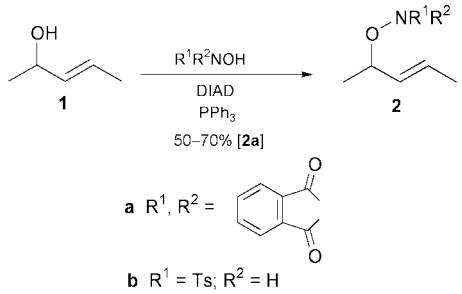

Scheme 1

applied to unsymmetrical substrates, both the S_N2 and S_N2' pathways were followed (Fig. 1) to give both possible products

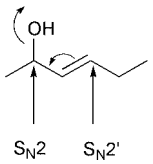

Fig. 1

(*i.e.* hydroxylamines **3** and **4**). For propargylic alcohols **5**,

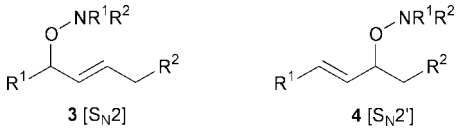

Mitsunobu displacement with either nucleophile (R^1R^2NOH) gave very variable, precursor dependent yields of the required products **6** (Scheme 2). Despite these problems, and the additional necessity of converting the phthalimides (*e.g.* **2a**, **6a**), into the corresponding *N*-tosylates (*e.g.* **2b**, **6b**)we were able to access the latter substrates in sufficient quantities to demonstrate that the projected 5-*endo*-trig and 5-*endo*-dig cyclisations generally work extremely well to provide a new entry into

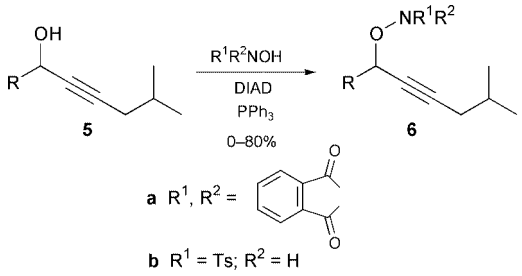

Scheme 2

isoxazolidines and isoxazolines, respectively.[6] We were therefore prompted to find an alternative and more efficient approach to these classes of compounds (**2**–**4** and **6**), both for this reason and also because approaches to hydroxylamines in general are somewhat lacking.[7] We were attracted by recent reports from the Vidal–Collet group[8] that various electron-deficient oxaziridines could behave as positive nitrogen sources ($^+$NHBoc), rather than as the more familiar positive oxygen sources ($^+$OH), popularized by the work of Davis and his colleagues.[9] However, while such species were reported to react efficiently with various amines and enolates and both sulfur and phosphorus nucleophiles, there was no report of similar reactions with alcohols or the derived alkoxides.[8] Such a transformation has been achieved using chloramine, but only with a large excess of alkoxide and in relatively poor yields,[10] and it was not until a very recent report that 3,3′-di-*tert*-butyloxaziridine reacts with a range of potassium alkoxides in DMPU and in the presence of 18-crown-6 to provide *O*-alkylhydroxylamines in 10–86% yields that such a process had synthetic value.[11] We report herein, that the highly electron deficient oxaziridine **7** reacts

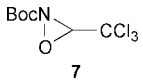

smoothly with lithium alkoxides using very practical conditions, despite our fears that it would simply act as a proton source for these basic species.

Oxaziridine **7** was prepared as previously described[8] starting from *tert*-butyl carbazate, diazotization of which provided *tert*-butyl azide. This potentially dangerous material was not isolated but only handled in solution and was immediately treated with triphenylphosphine in wet ether to give the imine Ph_3P=NBoc; subsequent aza-Wittig reaction with chloral and oxone® oxidation gave the oxaziridine **7**, as previously reported.[8] The compound was purified by column chromatography[8] and, in our hands, was sufficiently stable for use for *ca.* two months if stored below 0 °C, after which repurification was necessary. We were delighted to find that generation of the lithium alkoxide of benzyl alcohol using lithium hexamethyldisilazide (LHMDS) in tetrahydrofuran at −78 °C followed by the addition of oxaziridine **7** and slow warming to ambient temperature delivered an essentially quantitative yield of the *O*-benzyl-*N*-Boc-hydroxylamine **8** after a simple aqueous work-up.[8] Using the same method, we tested its viability with a range of other alcohols of varying structure and the results are collected in Table 1. A primary saturated alcohol, phenethanol,

DOI: 10.1039/b002388o

Table 1

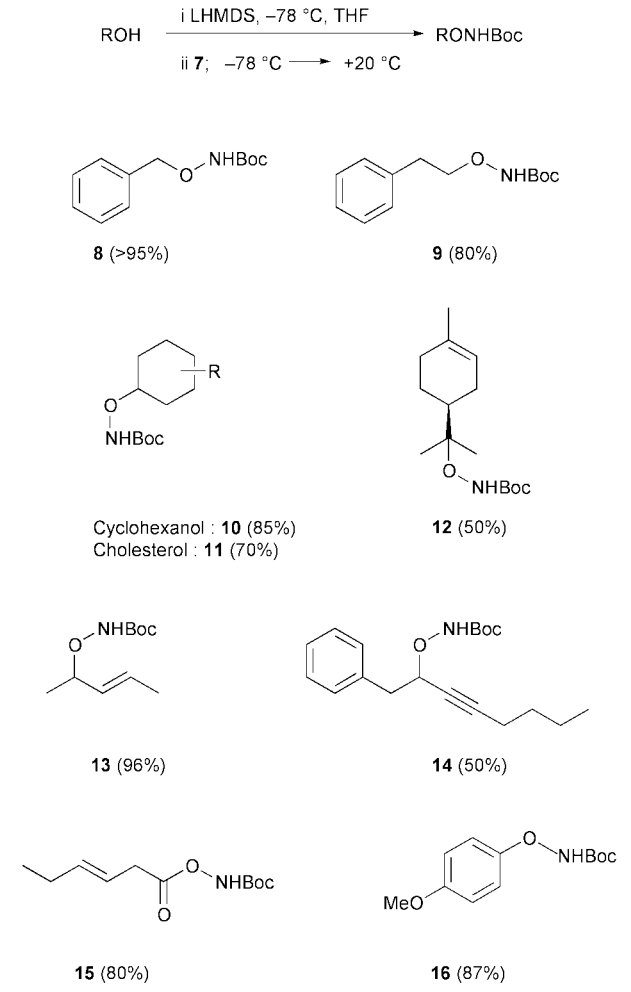

reacted slightly less efficiently giving the hydroxylamine derivative **9** in 80% yield. Two secondary alcohols, cyclohexanol and cholesterol, similarly gave the hydroxylamines **10** and **11** in 85 and 70% yields, respectively. Even the tertiary alcohol group in α-terpineol reacted reasonably efficiently to give the derivative **12** in 50% yield. This contrasts with the use of 3,3′-di-*tert*-butyloxaziridine,[11] which delivered only a 10% yield from a similar tertiary alcohol. However, it should be noted that this latter method leads directly to *O*-alkylhydroxylamines as the free bases, which could be useful in some contexts. Returning to our original substrates, we were glad to find that yields were again viable, the allylic alcohol derivative **13** being isolated in almost quantitative yield while the relatively sensitive propargylic derivative **14** was isolated in 50% yield, with the material balance being largely unreacted alcohol. Hence, it appears that the present method is especially efficient when applied to benzylic or allylic alcohols. Other oxygen-based nucleophiles also react successfully. Thus, under the same conditions, (*E*)-hex-3-enoic acid was converted into the *O*-acylhydroxylamine **15** and 4-methoxyphenol into the *O*-arylhydroxylamine **16**, both in excellent yields. In general, all of the foregoing derivatives appeared rather sensitive to chromatography over silica gel; Grade II alumina was more suitable but its use still often resulted in losses of some 10–20%[12] deprotection to give the corresponding *O*-alkylhydroxylamines (*i.e.* **2**, **6**; $R^1 = R^2 = H$) has ample literature precedent,[13] which we have confirmed during the present work, during which we have also been able to exchange the *N*-protecting group from Boc to TS (*e.g.* **13** → **2b**) in an efficient manner.

The ease with which alkoxides in general can be formed led us to briefly investigate some alternative protocols, using benzyl alcohol **17** as a test substrate. As outlined in Scheme 3, generation of the sodium alkoxide using sodium hydride in

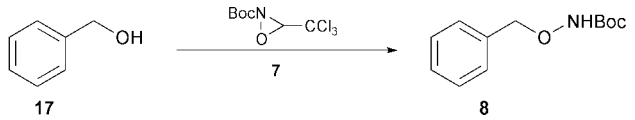

Scheme 3 *Reagents and conditions*: NaH, Et_2O, 20 °C, > 95% yield *or* BuLi, THF, −78 °C for 1 h then warming to 20 °C, > 90% yield.

diethyl ether at ambient temperature followed by addition of the oxaziridine **7** again gave an excellent yield of the hydroxylamine **8** as did the use of butyllithium as base. Finally, we have succeeded in preparing suitable substrates for the 5-*endo*-dig cyclisations by a very direct, 'one-pot' method (Scheme 4). Thus, condensation of hex-1-yne **18**, after deprotonation using butyllithium, with phenylacetaldehyde, addition of the oxaziridine **7** to the resulting alkoxide and warming to ambient temperature gave a 55% yield of the desired hydroxylamine **19**. These results suggest that there could well be a number of (substrate-dependent) modifications which could usefully be applied to this type of chemistry. Further studies along these lines are underway, along with work on the 5-*endo* cyclisations, which is now viable in the light of the foregoing results.

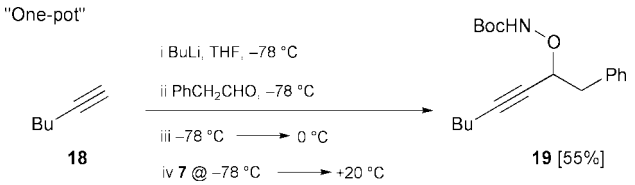

Scheme 4

We are very grateful for some helpful referees comments and to the EPSRC mass Spectrometry Centre (University College, Swansea) for the provision of mass spectral data and to the EPSRC for financial support.

Notes and references

1 A. D. Jones and D. W. Knight, *Chem. Commun.*, 1996, 915; S. P. Bew and D. W. Knight, *Chem. Commun.*, 1996, 1007; A. D. Jones, D. W. Knight, A. L. Redfern and J. Gilmore, *Tetrahedron Lett.*, 1999, **40**, 3267; S. B. Bedford, K. E. Bell, F. Bennett, C. J. Hayes, D. W. Knight and D. E. Shaw, *J. Chem. Soc., Perkin Trans. 1*, 1999, 2143.
2 O. Mitsunobu, *Synthesis*, 1981, 1; O. Mitsunobu, *Comp. Org. Synth*, 1991, **6**, 1; O. Mitsunobu, *Comp. Org. Synth*, 1991, **6**, 65; D. L. Hughes, *Org. React.*, 1992, **42**, 335; D. L. Hughes, *Org. Prep. Proced. Int.*, 1996, **28**, 127.
3 E. Breuer, H. G. Aurich and A. Nielsen, *Nitrones, Nitronates and Nitroxides*, ed. S. Patai and Z. Rappoport, John Wiley and Sons, Chichester, 1989.
4 E. Grochowski and J. Jurczak, *Synthesis*, 1976, 682. We found that ethyl acetate was a superior solvent for this reaction; see: H. Iwagami, M. Yatagi, M. Nakazawa, H. Orita, Y. Honda, T. Ohnuki and T. Yukawa, *Bull. Chem. Soc. Jpn.*, 1991, **64**, 175.
5 M. Fujimoto and M. Sakai, *Chem. Pharm. Bull.*, 1965, **13**, 248.
6 O. F. Foot and D.W. Knight, in preparation.
7 For recent notable contributions, see: S. D. Bull, S. G. Davies, S. Jones, J. V. A. Ouzman, A. J. Price and D. J. Watkin, *Chem. Commun.*, 1999, 2079; Y.-M. Lin and M. J. Miller, *J. Org. Chem.*, 1999, **64**, 7451.
8 J. Vidal, S. Damestoy, L. Guy, J.-C. Hannachi, A. Aubry and A. Collet, *Chem. Eur. J.*, 1997, **3**, 1691; J. Vidal, J.-C. Hannachi, G. Hourdin, J.-C. Mulatier and A. Collet, *Tetrahedron Lett.*, 1998, **39**, 8845 and references cited therein.
9 F. A. Davis and A. C. Sheppard, *Tetrahedron*, 1989, **45**, 5703; F. A. Davis and B.-C Chen, *Chem. Rev.*, 1992, **92**, 912.
10 W. Theilacker and K. Ebke, *Angew. Chem.*, 1956, **68**, 303. For a review of electrophilic amination in general, see: S. Andreae and E. Schmitz, *Synthesis*, 1991, 327.
11 I. C. Choong and J. A. Ellman, *J. Org. Chem.*, 1999, **64**, 6528.
12 Satisfactory spectroscopic and analytic data have been obtained for all compounds reported herein.
13 For examples of Boc hydrolysis in such hydroxylamine derivates, see, for example, L. A. Carpino, C. A. Giza and B. A. Carpino, *J. Am. Chem. Soc.*, 1959, **81**, 955; T. Sheradsky, G. Salemnick and Z. Nir, *Tetrahedron*, 1972, **28**, 3833; C. Baloli, P. D. Buttero, E. Licandro and S. Mairona, *Synthesis*, 1988, 344.

N=N bond cleavage of azobenzene through Pt/TiO_2 photocatalytic reduction

Hiroaki Tada,*[a] Masanobu Kubo,[b] Yoichi Inubushi[c] and Seishiro Ito[b]

[a] *Environmental Science Research Institute, Kinki University, 3-4-1, Kowakae, Higashi-Osaka, 577-8502, Japan. E-mail: h-tada@apsrv.apch.kindai.ac.jp*

[b] *Department of Applied Chemistry, Faculty of Science and Engineering, Kinki University, 3-4-1, Kowakae, Higashi-Osaka, 577-8502, Japan*

[c] *Fuji Pigment Co. Ltd., 2-23-2, Obana, Kawanishi, Hyogo 606-0015, Japan*

Received (in Cambridge, UK) 7th February 2000, Accepted 27th April 2000

TiO_2 photocatalytic 2e$^-$-reduction of azobenzene to hydrazobenzene is found to occur at λ_{ex} > 300 nm while loading of nanometer-sized Pt particles on TiO_2 induces N=N bond cleavage *via* 4e$^-$-reduction; only photoisomerization occurs in the absence of TiO_2.

From the viewpoint of "green chemistry", it is important to develop new processes for synthesizing useful compounds or detoxifying harmful compounds utilizing solar energy. Heterogeneous photocatalytic oxidations derived from valence band holes (h^+_{vb}) are attracting a great deal of attention for application to environmental problems.[1,2] Much less interest has been shown in reductive photochemistry despite the fact that conduction band electrons (e^-_{cb}) have a potential to induce highly selective reduction because of their mild reducing power.[3–6] Most of the azo dyes used widely in textile industries are carcinogenic and resistant to bacterial degradation, thus requiring effective wastewater treatment. The groups of Kiwi[7] and Oliveira-Campos[8] have recently reported photocatalytic oxidation of azo dyes using TiO_2 and Fe_2O_3. On the other hand, to our knowledge, the present work is the first study on heterogeneous photocatalytic reduction of azo dyes. Particular emphasis is placed on the loading effect of Pt nanoparticles on a TiO_2-photocatalyst.

Anatase TiO_2 particles (average diameter = 180 nm, BET surface area = 9.0 $m^2\ g^{-1}$) were supplied from Tayca Co. (JA-1) and 0.1 wt% Pt was deposited on them by photodeposition (Pt/TiO_2).[9] The particles (20 mg) were suspended in a 1.0 × 10^{-4} M solution [50 mL, solvent H_2O–EtOH (9/1 v/v)] of azobenzene (AB, > 95%, Tokyo Kasei Co.) in a double-jacketed cell. After the suspension had been purged with N_2 for 15 min, irradiation (λ_{ex} > 300 nm) was carried out with a 400 W high-pressure mercury arc (H-400P, Toshiba); the light intensity integrated from 320 to 400 nm ($I_{320–400}$) was measured as 3.4 mW cm^{-2}. N_2 bubbling and magnetic stirring of the suspension were continued throughout the irradiation while the reaction temperature was maintained at 31 ± 1 °C by circulating thermostatted water around the cell through the outer jacket. Product analysis was performed by both UV–VIS spectroscopy and high performance liquid chromatography [HPLC measurement conditions: column = Fluofix INW425 4.6 × 250 mm (NEOS); mobile phase H_2O–MeOH (1/1 v/v); flow rate = 3 mL min^{-1}; λ = 230 nm].

High-resolution transmission electron micrograph (HRTEM) images of Pt/TiO_2 demonstrated that Pt particles of diameter 2–5 nm are dispersed on the surface of TiO_2. The degree of adsorption of AB increased with loading of Pt (4.3 × 10^{-7} mol g^{-1} for TiO_2 and 2.6 × 10^{-6} mol g^{-1} for Pt/TiO_2 at an equilibrium concentration of 4.0 × 10^{-5} M), whereas the degree of adsorption of EtOH was essentially invariant with Pt loading. This finding indicates that AB and EtOH preferentially adsorb on Pt and TiO_2 surfaces of Pt/TiO_2, respectively. The interaction between AB and Pt would involve both σ-bonding [π orbital (AB) → d orbital (Pt)] and π-backbonding [d orbitals (Pt) → π* orbital (AB)]. Aliphatic alcohols are known to adsorb strongly on the surface of TiO_2.[10]

The electronic absorption spectrum of AB showed two absorption bands at 423 and 321 nm assignable to the n→π* and π→π* transitions, respectively, for the *trans* isomer. The absorptivity of the π→π* band for the *trans* isomer is 3.3 times that for the *cis* isomer.[11] The visible absorption at λ > 400 nm vanishes when the N=N bond of AB is broken. Accordingly, the n→π* band is a good indication of the presence of the N=N bond. Without either TiO_2 (or Pt/TiO_2) or irradiation, the intensity of the n→π* band was almost invariant, while that of the π→π* band significantly decreased. This fact suggests that only *trans–cis* isomerization occurs under these conditions.[12] Also, Pt loading on TiO_2 increased the rate of isomerization in the dark. This is probably due to the decrease in the energy barrier for molecular rotation around the N=N bond with adsorption of AB on Pt surfaces. No products other than AB were detected from the irradiated solution by HPLC, which supports the above conclusion.

Fig. 1 shows the variation of the concentrations of AB and products in the presence of TiO_2 as a function of irradiation time (t). AB is slowly reduced to hydrazobenzene (HAB) with a selectivity of 97% at 0 < t < 3 h. Since the turnover frequency is calculated to be *ca*. 3 at t = 3 h, this reaction can be regarded as photocatalytic. In the absorption spectra, the n→π* band gradually weakened concurrently with a rapid decrease in the π→π* band intensity. Providing direct evidence for cleavage of the N=N bond.

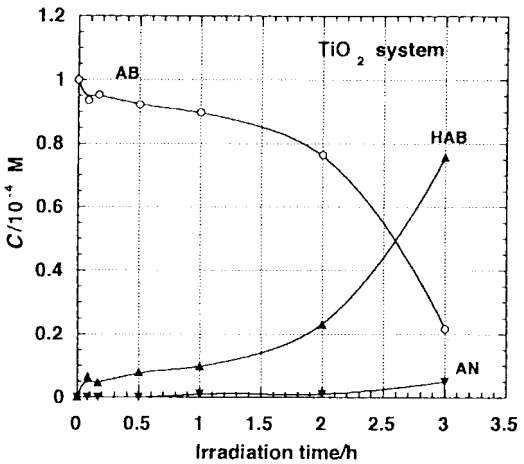

Fig. 1 TiO_2 photocatalytic reduction of AB at 31 ± 1 °C: initial pH = 6.4; TiO_2 20 mg/50 mL.

Fig. 2 shows time profiles of the concentrations of AB and products with irradiation in the presence of Pt/TiO_2. The rate of reduction of AB to HAB markedly increases with loading of Pt [conversion *ca*. 100%, selectivity (HAB) = 91% at t = 1 h]. Noticeably, further reduction of HAB to aniline (AN) occurs [selectivity(AN) = 19.2% at t = 3 h]. In the absorption spectra, the n→π* band of AB completely disappeared at t = 1 h and new absorption bands appeared at 280 and 230 nm at 3 h that are in accordance with the positions for the n→π* and π→π*

DOI: 10.1039/b001062f

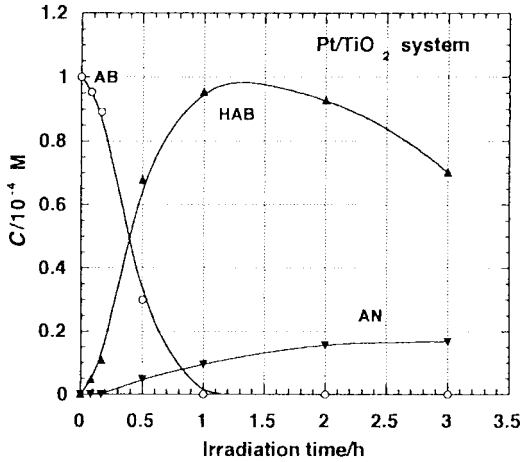

Fig. 2 Pt/TiO_2 photocatalytic reduction of AB at 31 ± 1 °C: initial pH = 6.5; Pt(0.10 wt%)/TiO_2.

bands, respectively, of AN. These facts are consistent with the results of Fig. 2. The pH of the Pt/TiO_2 system decreased from 6.5 (t = 0) to 5.6 (t = 1 h), while the corresponding change was very small for the unmodified TiO_2 system (Δ pH = 0.2). Product analysis by gas chromatography confirmed generation of MeCHO and CO_2 in each system. Evidently, EtOH acts as a reductant in the present photocatalytic reaction.[13] It has been established that EtOH exerts a current doubling effect in TiO_2 photocatalysis,[14] which would also be responsible for the reduction to proceed.

The results above clarified the two effects of Pt loading; one is to increase the rate of 2e$^-$-reduction (AB→HAB) and the other is to enable 4e$^-$-reduction (AB→AN). Pt loading enhances both the adsorption of AB (adsorption effect)[4] and the charge separation of $e^-_{cb}\cdots h^+_{vb}$ pairs (charge separation effect).[15] In addition, selective adsorption of the reactant (AB) on reduction sites (Pt) and the reductant (EtOH) on oxidation sites (TiO_2) is observed (reasonable delivery effect).[16] The remarkable increase in the reduction rate can be explained in terms of these effects. Also, inspection of Fig. 1 and comparison with Fig. 2 suggests that Pt loading leads to the absence of an induction period. Further the surface multi-electron transfer is thought to be assisted by an electron-pool effect of Pt with a large work function.

In conclusion, the 2e$^-$-reduction of AB to HAB proceeds selectively by using TiO_2 as a photocatalyst, whereas only photoisomerization occurs in the absence of TiO_2. Loading of Pt on TiO_2 not only accelerates the reduction but also enables the 4e$^-$-reduction of AB to AN. Our work thus represents a novel method for treating wastewater containing azo dyes *via* reductive cleavage of the N=N bonds.

We express sincere gratitude to Professor Masakuni Yoshihara (Kinki University) for permission to use HPLC and to Dr Tomoki Akita (Osaka National Research Institute) for the HRTEM measurements.

Notes and references

1 *Photocatalytic Purification and Treatment of Water and Air*, ed. F. D. Ollis and H. Al-Ekabi, Elsevier Science, Amsterdam, 1977.
2 A. Mills and S. Le Hunte, *J. Photochem. Photobiol. A*, 1997, **108**, 1.
3 J. L. Ferry and W. H. Glaze, *Langmuir*, 1998, **14**, 3551.
4 H. Tada, K. Teranishi, Y. Inubushi and S. Ito, *Chem. Commun.*, 1998, 2345.
5 W. Choi and M. R. Hoffmann, *J. Phys. Chem.*, 1996, **100**, 2161.
6 P. Piccinini, C. Minero, M. Vincenti and E. Pelizzetti, *J. Chem. Soc., Faraday Trans.*, 1997, **93**, 1863.
7 J. Bandara, J. A. Mielczarski and J. Kiwi, *Langmuir*, 1999, **15**, 7680.
8 M. S. Goncalves, A. M. F. Oliveira-Campos, E. M. M. S. Pinto, P. M. S. Plasencia and M. J. R. P. Queiroz, *Chemosphere*, 1999, **39**, 781.
9 TiO_2 particles (10 g) were dispersed in a 5.52×10^{-4} M aqueous solution (245 mL) of $H_2PtCl_6{\cdot}6H_2O$, and then 5 mL of MeOH was added as a reducing agent. After the suspension had been allowed to stand overnight with stirring in the dark, it was irradiated with UV-light (λ_{ex} > 300 nm) for 1 h under an N_2 atmosphere.
10 R. I. Bickley, *Heterogeneous Photocatalysis*, ed. M. Schiavello, John Wiley & Sons, Chichester, 1997, pp. 87–107.
11 J. Griffiths, *Chem. Soc. Rev.*, 1972, **1**, 48.
12 G. S. Hartley, *Nature*, 1937, **140**, 281.
13 H. Tada, K. Teranishi and S. Ito, *Langmuir*, 1999, **15**, 7084.
14 S. R. Morrison and T. Freund, *Electrochim. Acta*, 1968, **13**, 1968.
15 P. Pichat and J.-M. Herrmann, *Photocatalysis Fundamentals and Applications*, ed. N. Serpone and E. Pelizzetti, John Wiley & Sons, New York, 1989, pp. 217–250.
16 H. Tada, K. Teranishi, Y. Inubushi and S. Ito, *Langmuir*, 2000, **16**, 3304.

A convenient synthesis of benz-1,2-oxazine derivatives

Sukhen Chandra Ghosh and Asish De*

Department of Organic Chemistry, Indian Association for the Cultivation of Science, Jadavpur Calcutta-700032, India. E-mail: ocad@mahendra.iacs.res.in

Received (in Cambridge, UK) 29th March 2000, Accepted 27th April 2000

An expedient synthesis of benz-1,2-oxazine derivatives involving nitrene insertion on a methoxy group is described.

Our findings[1,2] in the course of synthesis of novel photoconducting materials consisting of electron donor and acceptor molecules linked by polymethylene spacers induced us to synthesize the linear tricyclic system **1**, which is expected to be

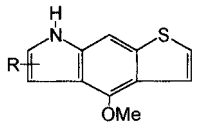

1

a good electron donor. This system can be conveniently accessed by annelation of a pyrrole ring to the 4-methoxy-1-benzothiophene core, through insertion of vinyl nitrene, incipiently liberated by thermolysis of the corresponding vinyl azide. We have previously used this methodology developed by Rees and coworkers[3] in the synthesis of angular thienoindoles.[4]

The vinyl azide **2** obtained from 4-methoxy-1-benzothiophene-5-carbaldehyde and methyl azido acetate, afforded upon heating for 2.5 h in xylene, a mixture of two compounds, separable by careful chromatography over silica gel. The desired 2-methoxycarbonylthieno[3,2-*f*]indole **1** (R = 2-CO_2Me) was eluted with light petroleum (bp 60–80 °C)–ethyl

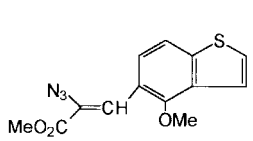

2

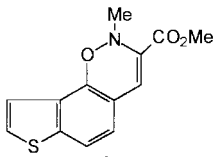

3

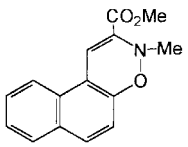

4

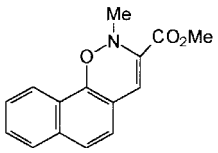

5

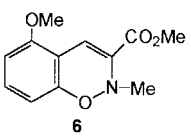

6

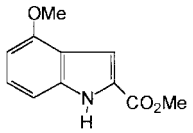

7

acetate (23 : 2) while the second compound, eluted with ethyl acetate–light petroleum (bp 60–80 °C) (1 : 9) was found to be 2-methyl-3-methoxycarbonylthieno[2,3-*h*]benz-1,2-oxazine **3** the structure of which was confirmed from elemental analysis and spectral data.†

Thermolysis of vinyl azides derived from 2-methoxy-1-naphthaldehyde, 1-methoxy-2-naphthaldehyde and 2,6-dimethoxybenzaldehyde afforded the corresponding condensed 1,2-oxazines **4**, **5** and **6**, respectively,† showing the general applicability of this methodology. However, the vinyl azide derived from 2-methoxybenzaldehyde afforded 2-carbomethoxy-4-methoxyindole **7**† as the exclusive product.

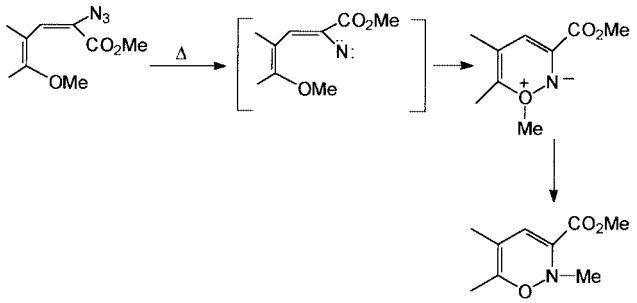

Scheme 1

Insertion of nitrene on to the adjacent methoxy group followed by rearrangement plausibly leads to benz-1,2-oxazine (Scheme 1).

The methyl migration most likely involves a radical pathway since a concerted pathway appears unlikely.[5]

In summary, a simple method is reported which accesses benzo-1,2-oxazines, little reported in the literature, presumably owing to the absence of expedient synthetic routes.[6] Further work is in progress to establish the general nature and mechanism of this reaction by thermolysis of vinyl azides derived from other *o*-methoxyarylaldehydes.

We thank Professor Charles W. Rees for helpful discussion. S. C. G. thanks the Council of Scientific and Industrial Research (New Delhi) for a Senior Research Fellowship.

Notes and references

† *Selected data*: for compound **1**: yield 55%, mp 170–172 °C; δ_H(300 MHz, $CDCl_3$) 8.73 (br s, 1H, NH), 7.56 (s, 1H, Ar), 7.51 (s, 1H, Ar), 7.49–7.47 (d, 1H, *J* 5.7 Hz, Ar), 7.18–7.16 (d, 1H, *J* 5.7 Hz, Ar), 4.28 (s, 3H, CO_2CH_3), 3.96 (s, 3H, OCH_3); δ_C(300 MHz, $CDCl_3$) 53.76 (OCH_3), 62.14 (CO_2*Me*), 106.64 (CH), 118.03 (C), 120.06 (CH), 122.52 (CH), 125.90 (C), 127.11 (C), 127.37 (CH), 138.18 (C), 143.23 (C), 152.73 (C), 165.76 (C). Anal. Calc. for $C_{13}H_{10}O_3NS$: C, 59.77; H, 4.21; N, 5.36. Found: C, 59.81; H, 4.15; N, 5.26%.

For compound **3**: yield 45%, δ_H(300 MHz, $CDCl_3$) 7.69–7.66 (d, 1H, *J* 8.7 Hz, Ar), 7.51–7.49 (d, 1H, *J* 5.7 Hz, Ar), 7.49–7.47 (d, 1H, *J* 5.7 Hz, Ar), 5.22 (s, 1H), 4.08 (s, 3H, CO_2CH_3), 3.83 (s, 3H, NCH_3); δ_C(300 MHz, $CDCl_3$) 37.52 (CH), 52.01 (NMe), 60.99 (CO_2*Me*), 98.48 (CH), 116.04 (C), 118.86 (CH), 120.31 (CH), 122.8 (C), 124.65 (CH), 132.84 (C), 140.09 (C), 148.71 (C), 162.09 (C). Anal. Calc. for $C_{13}H_{10}O_3NS$: C, 59.77; H, 4.21; N, 5.35. Found: C, 59.50; H, 4.20; N, 5.40%.

For compound **4**: yield 77%, mp 52–54 °C; δ_H(300 MHz, $CDCl_3$) 7.90–7.88 (d, 1H, *J* 8.4 Hz, Ar), 7.83–7.81 (d, 1H, *J* 5.7 Hz, Ar), 7.80–7.78 (d, 1H, *J* 4.8 Hz, Ar), 7.51–7.46 (m, 1H, Ar), 7.39–7.34 (m, 1H, Ar), 7.31–7.28 (d, 1H, *J* 8.7 Hz, Ar), 6.84 (s, 1H), 3.99 (s, 3H, CO_2CH_3), 3.85 (s, 3H, NCH_3); δ_C(300 MHz, $CDCl_3$) 52.46 (NMe), 56.65 (CO_2*Me*), 103.00 (CH) 113.4 (CH), 123.81 (CH), 124.77 (CH), 126.51 (CH), 128.21 (CH), 129.39 (CH), 112.82 (C), 117.72 (C), 129.10 (C), 133.60 (C), 153.99 (C), 165.83 (C). Anal. Calc. for $C_{15}H_{13}O_3N$: C, 70.57; H, 5.13; N, 5.48. Found: C, 70.50; H, 5.20; N, 5.00%.

For compound **5**: yield 74%, mp 76–78 °C; δ_H(300 MHz, $CDCl_3$) 8.11–8.07 (m, 1H, Ar), 7.88–7.85 (m, 1H, Ar), 7.70–7.67 (d, 1H, *J* 8.7 Hz,

DOI: 10.1039/b002509g

Ar), 7.59–7.53 (m, 2H, Ar), 7.52–7.49 (d, 1H, *J* 8.4 Hz, Ar), 5.37 (s, 1H), 4.04 (s, 3H, CO_2CH_3), 3.86 (s, 3H, NCH_3); δ_C(300 MHz, $CDCl_3$) 37.44 (CH), 53.82 (NMe), 62.98 (CO_2*Me*), 115.90 (C), 119.14 (C), 122.40 (CH), 125.00 (CH), 125.35 (CH), 126.7 (CH), 127.18 (CH), 127.40 (C), 128.33 (CH), 135.35 (C), 153.98 (C), 165.62 (C). Anal. Calc. for $C_{15}H_{13}O_3N$: C, 70.57; H, 5.13; N, 5.48. Found: C, 70.50, H 5.21, N, 5.35%.

For compound **6**: yield 45%, mp 90–94 °C; δ_H(300 MHz, $CDCl_3$) 7.35–7.26 (dd, 1H, *J* 8.49 Hz, Ar), 6.60–6.57 (d, 2H, *J* 8.4 Hz, Ar), 5.38 (s, 1H), 3.86 (s, 6H, CO_2CH_3, OCH_3), 3.80 (s, 3H, NCH_3); δ_C(300 MHz, $CDCl_3$) 31.98 (CH), 53.48 (NCH_3), 56.09 (CO_2*Me*, OCH_3), 104.06 (CH), 115.99 (C), 128 (C) 130.85 (2 CH), 132.4 (C), 166.45 (C), 157.65 (C). Anal. Calc. for $C_{12}H_{13}O_4N$: C, 61.27; H, 5.56; N 5.95. Found: C, 61.07; H, 5.90; N 5.89%.

For compound **7**: yield 90%, mp 135–136 °C; δ_H(300 MHz, $CDCl_3$) 9.12 (br s, 1H, NH), 7.34 (s, 1H, Ar), 7.25–7.20 (m, 1H, Ar), 7.02–7.00 (d, 1H, *J* 8.1 Hz, Ar), 6.51–6.48 (d, 1H, *J* 7.8 Hz, Ar), 3.94 (s, 3H, CO_2CH_3), 3.91 (s, 3H, OCH_3); δ_C(300 MHz, $CDCl_3$) 51.88 (OMe), 55.25 (CO_2*Me*), 99.66 (CH), 104.75 (CH), 106.43 (CH), 118.88 (C), 125.69 (C), 138.21 (C), 154.53 (C), 162.43 (C). Anal. Calc. for $C_{11}H_{10}O_3N$: C, 64.69; H, 4.93; N, 6.85. Found: C, 64.70; H 4.90; N, 6.90%.

1 M. Maiti, S. Sinha, C. Deb, A. De and T. Ganguly, *J. Lumin.*, 1999, **82**, 259.
2 C. Deb, A. De, M. Maiti and T. Ganguly, Paper presented in *The XVIIIth European Colloquium on Heterocyclic Chemistry*, 4–7 October, 1998, Rouen, France.
3 L. Henn, D. M. B. Hickey, C. J. Moody and C. W. Rees, *J. Chem. Soc., Perkin Trans. 1*, 1984, 2189.
4 S. Datta and A. De, *J. Chem. Soc., Perkin Trans. 1*, 1989, 603; S. S. Samanta, S. C. Ghosh and A. De, *J. Chem. Soc., Perkin Trans. 1*, 1997, 3673.
5 We thank one of the referees for pointing out such a possibility.
6 M. Sainsbury, in *Comprehensive Heterocyclic Chemistry*, ed. A. J. Boulton and A. Mckillop, Pergamon Press, Oxford, 1984, vol. 8, p. 995.

First gold complex-catalysed selective hydrosilylation of organic compounds†

Hajime Ito,[a] Tatsuki Yajima,[b] Jun-ichi Tateiwa[b] and Akira Hosomi*[b]

[a] *Institute for Molecular Science, Research Center for Molecular Materials, Myodaiji, Okazaki, 444-8585, Japan*
[b] *Department of Chemistry and Graduate School of Pure Applied Sciences, University of Tsukuba, Tsukuba, Ibaraki 305-8571, Japan. E-mail: hosomi@chem.tsukuba.ac.jp*

Received (in Cambridge, UK) 3rd March 2000, Accepted 20th April 2000

The first examples of the hydrosilylation of organic compounds such as aldehydes and an aldimine using a catalytic amount of a gold complex, which accomplished versatile regio- and chemo-selective reduction of carbonyl compounds, are described.

The exploration of catalytic reactions using soluble gold complexes has been a challenging area in organic synthesis.[1,2] The design of synthetic reactions using gold complex catalysts is still considered to be a difficult subject, though some successful systems have been reported. A considerable number of transition metal complexes have been employed as catalysts for the hydrosilylation of organic compounds.[3] However, to our knowledge, no examples of hydrosilylation catalyzed by gold complexes have been reported. Recently, we found a highly reactive catalysis by a gold complex for the dehydrogenative dimerization of a hydrostannane, offering new clues to the further development of gold complex-catalyzed reactions.[4] Here we describe the first example of the hydrosilylation of organic compounds using a gold complex as a catalyst. These results reveal the novel reactivity of the gold complex as well as its versatile selectivity in the reduction of organic compounds.

We first examined the hydrosilylation of benzaldehyde **1a** using a catalytic amount of chloro(triphenylphosphine)gold(I) alone [eqn. (1), Table 1, entry 1].[5] After the addition of

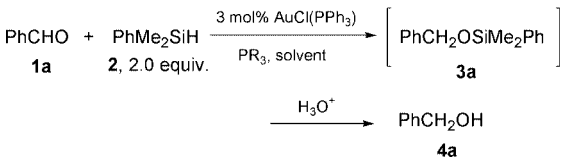

(1)

dimethylphenylsilane **2** (2.0 mmol), the colorless mixture of chloro(triphenylphosphine)gold(I) (0.03 mmol), benzaldehyde **1a** (1.0 mmol) and dry DMF (1.0 ml) changed to a deep-purple solution and precipitation of metallic gold was observed within 10 min at 70 °C.[6] No silylated product was found under these conditions. We next examined a combination of chloro(triphenylphosphine)gold(I) and triphenylphosphine as catalyst, which gave good results in our previous study of gold catalysis; however, here it gave a similar disappointing result (entry 2).[4] Use of tributylphosphine, which is more basic and is strongly coordinating, as an additive ligand to chloro(triphenylphosphine)gold(I) provided remarkable catalytic activity for the hydrosilylation of **1a** (entry 3). Compound **2** (2.0 mmol) was added to a mixture of chloro(triphenylphosphine)gold(I) (0.03 mmol), tributylphosphine (0.20 mmol), **1a** (1.0 mmol) and DMF (1.0 ml) under nitrogen. After stirring for 1.5 h at 70 °C, the quantitative formation of the corresponding silyl ether **3a**, the hydrosilylation product of **1a** and **2**, was observed by ^{1}H NMR spectroscopy, and alcohol **4a** was isolated in 90% yield after acidic hydrolysis.[7,8] In sharp contrast to the previous two

† Studies on Organosilicon Chemistry: no. 152. For no. 151, see K. Miura, K. Tamaki, T. Nakagawa and A. Hosomi, *Angew. Chem., Int. Ed.*, 2000, in press.

Table 1 Gold complex-catalyzed hydrosilylation of benzaldehyde **1a** under various conditions

Entry[a]	Additive/equiv.	Solvent	Conditions	Yield[b] of **4a** (%)
1	—	DMF	70 °C, 1.5 h	0
2	PPh_3, 0.2	DMF	70 °C, 1.5 h	0
3	PBu_3, 0.2	DMF	70 °C, 1.5 h	90
4	PBu_3, 0.2	Toluene	70 °C, 11 h	65
5	PBu_3, 0.2	THF	70 °C, 3.0 h	92
6	PBu_3, 0.2	MeCN	70 °C, 5.0 h	77

[a] To a solution of benzaldehyde **1a** (1.0 mmol), AuCl(PPh_3) (3 mol%, 0.03 mmol), and phosphine (0–20 mol%, 0–0.20 mmol) in dry DMF (1.0 ml) was added dimethylphenylsilane **2** (2.0 equiv., 2.0 mmol) under nitrogen. [b] Isolated yield after hydrolysis.

systems, the reaction mixture was colorless and a precipitate of metallic gold was not observed. Although this catalytic system was compatible with other solvents, DMF was found to be optimal (entries 4–6).[9] The generality of this gold complex-catalysed hydrosilylation was successfully demonstrated by reaction with various aldehydes [eqn. (2), Table 2]. In

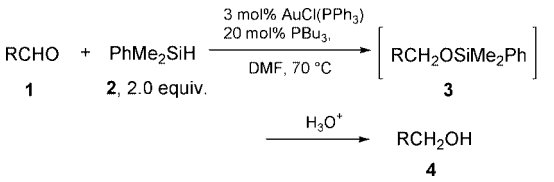

(2)

particular, cinnamaldehyde, which contains a conjugated double bond, was converted to the 1,2-addition product with high selectivity, and the corresponding allyl alcohol **4c** was exclusively obtained in 94% yield after hydrolysis (entry 2).[3,10] When this catalytic system was applied to the reduction of ketone **1f**, no reduced product was obtained (entry 5). The versatile chemoselectivity of the catalyst was clearly shown by the selective reduction of the aldehyde **1b** irrespective of the presence of ketone **1f** under modified conditions [eqn. (3)].[3,10]

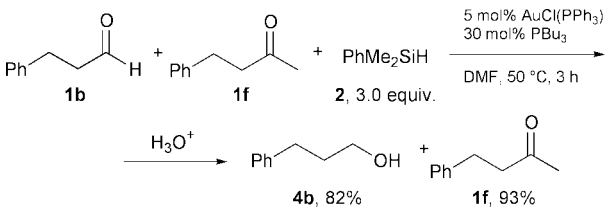

(3)

Reduction of an aldimine was also carried out with hydrosilane in the presence of the gold catalyst [eqn. (4)].

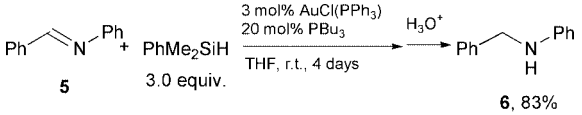

(4)

DOI: 10.1039/b001743o

Table 2 Gold complex-catalyzed hydrosilylation of various carbonyl compounds

Entry[a]	Carbonyl compounds **1**	Conditions	Yield[b] of **4** (%)
1	3-Phenylpropanal **1b**	70 °C, 1.5 h	**4b**, 93
2	Cinnamaldehyde **1c**	70 °C, 5.0 h	**4c**, 94[c]
3	Decanal **1d**	70 °C, 1.5 h	**4d**, 51
4	Cyclohexanecarboxaldehyde **1e**	70 °C, 11 h	**4e**, 78
5	4-Phenylbutanone **1f**	70 °C, 15 h	**4f**, 0[d]

[a] To a solution of carbonyl compound **1** (1.0 mmol), $AuCl(PPh_3)$ (3 mol%, 0.03 mmol) and tributylphosphine (20 mol%, 0.20 mmol) in dry DMF (1.0 ml) was added dimethylphenylsilane **2** (2.0 equiv., 2.0 mmol) under nitrogen. [b] Isolated yield after hydrolysis. [c] Only a 1,2-reduced product was detected. [d] The starting material was recovered in good yield (**1f**, 93%).

Although it took four days for the reaction to be complete, the corresponding reduced product **6** of aldimine **5** was obtained in good yield (83%).

The effect of the amount of the additional ligand on the reactivity is shown in Fig. 1. Monitoring of the reaction by ^{1}H NMR spectroscopy showed that the hydrosilylation product was formed continuously at 50 °C in the presence of 3 mol% of chloro(triphenylphosphine)gold(I) and 20 mol% of tributylphosphine with the reaction almost complete after 600 min (experiment **A**) during which the reaction mixture was colorless and transparent throughout. In experiment **B**, which was carried out with a lower amount of tributylphosphine (10 mol%) than in experiment **A**, considerable rate retardation was observed as the reaction time approached 400 min, though the initial reaction rate in experiment **B** was slightly higher than that of **A** within 200 min. A deep-purple coloration was observed immediately after adding the hydrosilane to reaction mixture and the slow precipitation of gold(0) was observed in experiment **B**. These results indicate that the role of the excess tributylphosphine is the prevention of catalyst decomposition rather than increasing the reaction rate.

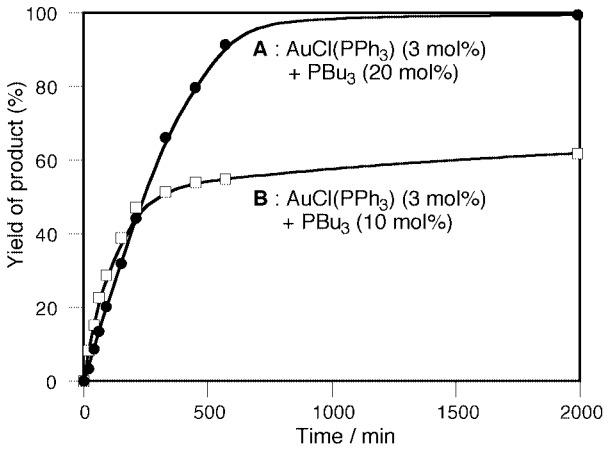

Fig. 1 Product formation *vs.* time for reactions carried out with benzaldehyde **1a** (1.0 mmol), dimethylphenylsilane **2** (2.0 mmol), 3 mol% of chloro(triphenylphosphine)gold(I) (0.03 mmol) and 20 mol% of tributylphosphine (0.2 mmol) (experiment **A**, ●) or 10 mol% of tributylphosphine (0.1 mmol) (experiment **B**, □) in DMF (1.0 ml) at 50 °C. Yields determined by ^{1}H NMR spectroscopy.

Although the active species of this catalyst is still unclear at this stage, we propose that colorless monomeric gold complexes stabilized by the excess tributylphosphines play an important role in this reaction and that the predominant deactivation process is the formation of gold clusters and metallic gold(0) upon reduction of gold(I).

In conclusion, we have described the unprecedented hydrosilylation of organic compounds by a gold complex catalyst with high chemoselectivity. The deactivation of the gold catalyst was suppressed in the presence of an additional ligand (tributylphosphine). These results provide an important principle for the design of gold complex-catalyzed systems.

This work was partly supported by Grants-in-Aid for Scientific Research and Grants-in-Aid for Scientific Research on Priority Areas (No. 706: Dynamic Control of Stereochemistry) from the Ministry of Education, Japan, Pfizer Inc., and Hitachi Chemical Co., Ltd. We thank Dow Corning Toray Silicone Co., Ltd., Chisso Co., Ltd., and Shin-Etsu Chemical Co., Ltd. for a gift of organosilicon compounds.

Notes and references

1 Y. Ito, M. Sawamura and T. Hayashi, *J. Am. Chem. Soc.*, 1986, **108**, 6405; Y. Fukuda and K. Utimoto, *J. Org. Chem.*, 1991, **56**, 3729; S. Komiya, T. Sone, Y. Usui, M. Hirano and A. Fukuoka, *Gold Bull.*, 1996, **29**, 131; Q. Xu, Y. Imamura, M. Fujiwara and Y. Souma, *J. Org. Chem.*, 1997, **62**, 1594; J. H. Teles, S. Brode and M. Chabanas, *Angew. Chem., Int. Ed.*, 1998, **37**, 1415.

2 For heterogeneous gold catalysts, see: J. E. Bailie and G. J. Hutchings, *Chem. Commun.*, 1999, 2151 and references therein.

3 *Comprehensive Handbook on Hydrosilylation*, ed. B. Marciniec, Pergamon Press, New York, 1992; M. Hudlicky, *Reductions in Organic Chemistry*, American Chemical Society, Washington DC, 2nd edn., 1996; M. A. Brook, *Silicon in Organic, Organometallic, and Polymer Chemistry*, Wiley, New York, 2000.

4 H. Ito, T. Yajima, J. Tateiwa and A. Hosomi, *Tetrahedron Lett.*, 1999, **40**, 7807.

5 C. A. McAuliffe, R. V. Parish and P. D. Randall, *J. Chem. Soc., Dalton Trans.*, 1979, 1730.

6 It was reported that the reduction of a gold(I) complex with a hydride reagent gave metallic gold(0) and deeply colored gold clusters: K. P. Hall and D. M. P. Mingos, *Prog. Inorg. Chem.*, 1984, **32**, 237; G. Schmid, R. Pfeil, R. Boese, F. Bandermann, S. Meyer, G. H. M. Calis and J. W. A. van der Velden, *Chem. Ber.*, 1981, **114**, 3634.

7 When the isolation of the products was carried out by column chromatography (SiO_2) without acidic workup both **3a** (30%) and **4a** (58%) were obtained.

8 In the absence of a gold complex and tributylphosphine or in the presence of tributylphosphine alone as catalyst, no reaction was observed under the same conditions. See also ref. 3.

9 Although other hydrosilanes were also tested, use of phenyldimethylsilane **2** gave good results in most cases.

10 R. C. Larock, *Comprehensive Organic Transformations*, Wiley, New York, 2nd edn., 1999, pp. 1089–1096.

ChemComm

Poly(ethylene glycol)-linked dimers of D-*myo*-inositol 1,4,5-trisphosphate

Andrew M. Riley and Barry V. L. Potter*

Wolfson Laboratory of Medicinal Chemistry, Department of Pharmacy and Pharmacology, University of Bath, Claverton Down, Bath, UK BA2 7AY. E-mail: b.v.l.potter@bath.ac.uk

Received (in Cambridge, UK) 23rd March 2000, Accepted 27th April 2000

The first poly(ethylene glycol)-linked dimers of D-*myo*-inositol 1,4,5-trisphosphate have been synthesised as probes for multi-subunit binding proteins of this ubiquitous second messenger.

D-*myo*-inositol 1,4,5-trisphosphate [Ins(1,4,5)P_3] acts as an intracellular second messenger in almost all mammalian cells by evoking the release of Ca^{2+} ions from intracellular stores through Ins(1,4,5)P_3-gated ion channels[1] [Ins(1,4,5)P_3 receptors, IP_3Rs] located in the endoplasmic reticulum. IP_3Rs are tetramers, composed of four subunits, each with a single Ins(1,4,5)P_3 binding site, surrounding the central ion channel. This suggests the possibility of designing multivalent ligands for IP_3Rs, in which two or more copies of the natural ligand connected by a linker may be able to access multiple binding sites simultaneously, potentially giving enhanced potency, selectivity or other novel effects. To this end, a synthesis of bivalent and tetravalent analogues has been reported in which two or four molecules of a synthetic carbohydrate-based Ins(1,4,5)P_3 mimic were directly attached to a small hydrophobic hub.[2] As the IP_3R is large (12 nm width, estimated from electron microscopy[3]) and the locations of the Ins(1,4,5)P_3 binding sites are unknown, a more promising and versatile approach may be to use bivalent ligands with hydrophilic polymeric linkers in a realistic range of lengths. This strategy has been successfully employed, using very simple chemistry, to identify super-potent dimeric ligands for tetrameric cyclic nucleotide gated (CNG) channels of photoreceptor and olfactory neurones by using a series of dimers of the 8-thio derivative of the natural ligand (cGMP) linked by PEG chains.[4] These PEG-linked dimers of cGMP also showed partial agonist properties at photoreceptor CNG channels, and some were membrane-permeant.

Application of this approach to Ins(1,4,5)P_3 is, however, synthetically much more difficult. Nevertheless, studies have shown that bulky groups may be attached to the axial 2-oxygen atom of Ins(1,4,5)P_3 with minimal reduction in affinity for the IP_3R,[5] suggesting that at the Ins(1,4,5)P_3 binding sites of the IP_3R this area may be open to solvent. We therefore chose to synthesise Ins(1,4,5)P_3 dimers linked *via* the 2-position (Fig. 1). The synthetic strategy was first explored using a short PEG linker derived from hexa(ethylene glycol) (estimated[4] r.m.s. length 1.5 nm), and then three larger dimers were synthesised from PEGs with average molecular weights 1450, 3350 and 8000 (estimated rms lengths 3, 5 and 8 nm, respectively).

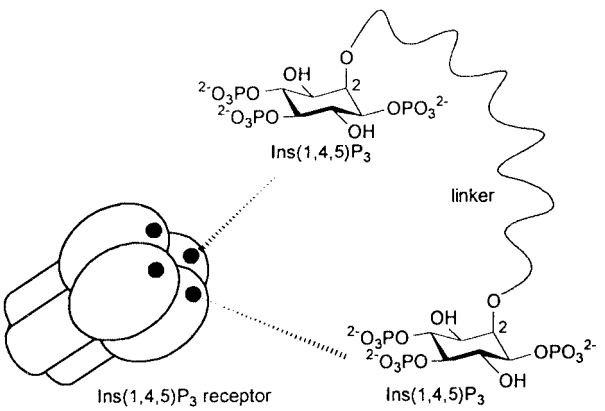

Fig. 1 Ins(1,4,5)P_3 dimers could target multiple receptor binding sites.

The synthesis begins with diol **1**[6] (Scheme 1). Stannylene-mediated regioselective alkylation of the equatorial 1-OH group with *p*-methoxybenzyl chloride in the presence of CsF gave the alcohol **2** in 80% yield. Alkylation of **2** with bromoacetonitrile and sodium hydride in acetonitrile at reduced temperatures[7] then gave the 2-*O*-cyanomethyl derivative **3** {mp 120–121 °C, $[\alpha]_D^{18}$ +56 (*c* 1, $CHCl_3$)} in 83% yield. The nitrile was smoothly reduced with LAH in THF to the primary amine, which was not isolated but temporarily protected as the trifluoroacetamide by reaction with ethyl trifluoroacetate in THF at room temperature.[8] Finally, the acid-labile butanediacetal (BDA) and PMB protecting groups were cleaved using TFA, exposing the hydroxy groups at positions 1, 4 and 5. The trifluoroacetyl protection was not affected under these conditions, and the triol **4** {mp 130–131 °C, $[\alpha]_D^{18}$ +3 (*c* 1, $CHCl_3$)} was obtained in 77% overall yield from **3**. Phosphitylation using bis(benzyloxy)(*N*,*N*-diisopropylamino)phosphine and 1*H*-tetrazole followed by *in situ* oxidation with MCPBA gave crystalline **5** {mp 85–87 °C, $[\alpha]_D^{20}$ −6 (*c* 1, $CHCl_3$)}.

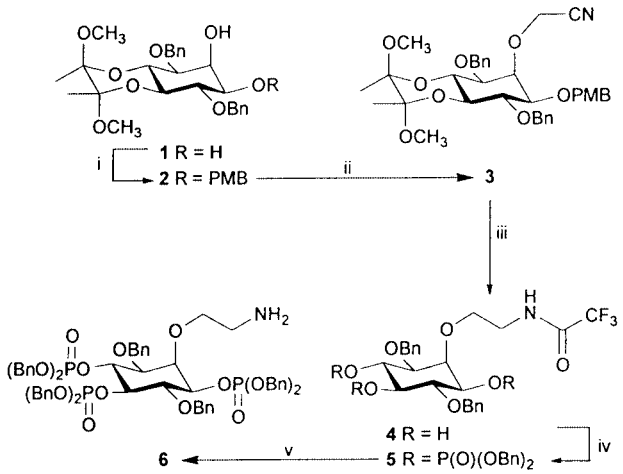

Scheme 1 *Reagents and conditions*: i, (a) Bu_2SnO, MeOH, 4 Å sieves, Soxhlet, reflux, 16 h; (b) PMBCl, CsF, DMF, 50 °C, 5 h, 84%; ii, NaH, $BrCH_2CN$, CH_3CN, −20 to −40 °C 5 h then room temp., 16 h, 83%; iii, (a) LAH, THF, room temp, 1 h, (b) ethyl trifluoroacetate, THF, room temp., 1 h, (c) TFA–CH_2Cl_2–H_2O (19:20:1), room temp., 30 min, 77% from **3**; iv, $(BnO)_2PNPr^i_2$, 1 *H*-tetrazole, CH_2Cl_2, room temp., 1 h, then MCPBA, −78 °C to room temp., 30 min (96%); v, LiOH·H_2O (10 equiv.) in THF–MeOH–H_2O (2:2:1), room temp., 1 h, 91%. Bn = benzyl, PMB = *p*-methoxybenzyl.

It was now necessary to expose the primary amine by selective removal of the trifluoroacetyl group. Treatment of **5** with methanolic ammonia or K_2CO_3 in aqueous methanol was only partially successful; long reaction times were required, leading to the formation of various polar products, presumably from partial cleavage of benzylphosphate esters. However, it was found that the trifluoroacetyl group could cleanly be removed by treatment with LiOH in THF–MeOH–H_2O[9] for 1 h.

DOI: 10.1039/b002312o

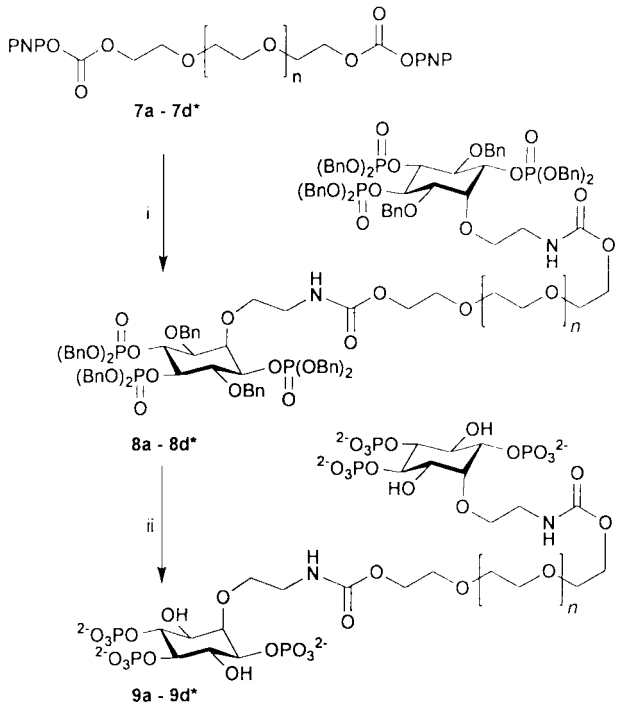

Scheme 2 *Reagents and conditions*: i, **6** (3–4 equiv.), DMF, room temp., 24 h, 31–58%; ii, Pd–C, H_2, 50 psi, room temp., 24 h, 52–65%. Bn = benzyl, PNP = *p*-nitrophenyl. ***a**, n = 4; **b**, $n \approx 30$; **c**, $n \approx 75$; **d**, $n \approx 180$.

Within this time there was little effect on the benzylphosphate groups. The amine **6** was found to be unstable, and was therefore freshly prepared for each cross-linking reaction and used immediately.

Cross-linking of two molecules of **6** was first attempted using the bis(*p*-nitrophenylcarbonate) derivative† **7a** of hexa(ethylene glycol) (Scheme 2). Reaction of **7a** with 3 equivalents of **6** in DMF gave the protected PEG-linked dimer **8a**, which was isolated in moderate yield (58% based on **7a**) yield after purification by flash chromatography on silica gel. The ^{1}H NMR spectrum of **8a** confirmed that it was a dimer‡ and the ^{31}P NMR spectrum showed three signals, each corresponding to two equivalent phosphorus atoms in **8a**. Removal of all sixteen benzyl groups from **8a** was easily achieved by hydrogenation over Pd–C. Purification by ion-exchange chromatography on Q-Sepharose Fast Flow resin, eluting with a gradient of triethylammonium hydrogencarbonate buffer gave **9a** as the triethylammonium salt, which eluted between 0.7 and 0.9 mol dm^{-3} buffer. The structure of **9a** was confirmed by ^{1}H and ^{31}P NMR spectroscopy, and by negative ion FAB mass spectrometry§ before accurate quantification by total phosphate assay.[10] The larger protected dimers **8b**, **8c** and **8d** were then synthesised by reaction of **6** with bis(*p*-nitrophenylcarbonate)-PEGs **7b**, **7c** and **7d** under the conditions established for **7a**. In each case, the product was purified by flash chromatography and its dimeric structure was confirmed by ^{1}H NMR spectroscopy before deprotection as for **8a**. Finally, purification of each dimer by ion exchange chromatography as for **9a** gave **9b**, **9c** and **9d** as their triethylammonium salts, which were all freely soluble in water.

Thus we have demonstrated, for the first time, a viable synthetic route to high molecular weight bivalent ligands as potential pharmacological tools to probe the IP_3R. Other proteins are known to have multiple binding sites[11] for Ins(1,4,5)P_3 or phosphatidylinositol 4,5-bisphosphate and the Ins(1,4,5)P_3 dimers could also be used to investigate these. A particularly attractive application might be to use Ins(1,4,5)P_3 metabolising enzymes to convert Ins(1,4,5)P_3 dimers into dimers of other inositol phosphates, which may have their own intracellular targets proteins.

We thank the Wellcome Trust for Programme Grant support (045491) and Drs S. W. Garrett and I. S. Blagborough for valuable advice.

Notes and references

† **7a**: this was synthesised by reaction of hexa(ethylene glycol) with 6 equivalents of bis(*p*-nitrophenyl) carbonate in DMF in the presence of diisopropylethylamine, and was purified by flash chromatography on silica gel before use. **7b** and **7d** were synthesised in a similar way from PEGs with average molecular weights of 1450 and 8000, respectively. The bis(*p*-nitrophenyl carbonate)-PEG **7c**, derived from a PEG of average molecular weight 3350, is commercially available (Sigma).

‡ *Selected data* for **8a**–**8d**: **8a** δ_H($CDCl_3$, 400 MHz) 3.24–3.30 (4H, m, OCH_2CH_2N), 3.38 (2H, dd, *J* 10.0, 2.1 Hz, 3-H), 3.50 (4H, s, OCH_2CH_2N), 3.55–3.58 (16H, m, 8 × PEG CH_2), 3.66–3.70 (4H, m, 2 × PEG CH_2), 4.00 (2H, dd, *J* 9.7, 9.4 Hz, 6-H), 4.04 (2H, br s, 2-H), 4.10–4.16 (4H, m, 2 × PEG CH_2), 4.18 (2H, ddd, *J* 9.7, 7.3, 2.3 Hz, 1-H), 4.48 (2H, ddd, *J* 9.4, 9.4, 9.1 Hz, 5-H), 4.47, 4.57 (4H, AB_q, J_{AB} 11.7 Hz, OCH_2Ph), 4.62–4.68 (2H, 0.5 of AB_q with $^3J_{HP}$ coupling, J_{AB} 11.7, J_{HP} 8.5 Hz, $POCH_2Ph$), 4.74–5.07 (28H, m, 4-H and 6.5 AB systems of OCH_2Ph), 5.60 (2H, br t, *J* 5.3 Hz, NH), 6.96–6.98 (4H, m, Ph), 7.08–7.36 (76H, Ph); protected dimers **8b**–**8d** had similar ^{1}H NMR spectra to **8a**, except; **8b**: δ 3.55–3.70 (approx. 130H, m, CH_2 of PEG), **8c**: δ 3.55–3.70 (approx. 300H, m, CH_2 of PEG); **8d**: δ 3.55–3.70 (approx. 700H, m, CH_2 of PEG).

§ *Selected data* for **9a**–**d**: **9a**: δ_H(CD_3OD, 400 MHz) δ *ca.* 3.3 [4H, m (buried), OCH_2CH_2N], 3.61–3.70 (22H, m, 3-H and 10 × PEG CH_2), 3.77–3.85 (2H, m, $OCHHCH_2N$), 3.92–4.00 (6H, m, 5-H, 6-H and $OCHHCH_2N$), 4.01–4.06 (4H, m, 1-H and 2-H), 4.14–4.20 (4H, m, 2 × CH_2 of PEG), 4.32 (2H, ddd, *J* 9.4, 8.9, 8.6 Hz, 4-H); δ_P(CD_3OD, 162 MHz) 2.06 (2 P), 3.19 (2 P) and 3.66 (2 P); MS *m/z* (−ve ion FAB, relative intensity); 1281 (90%), 1259 [M^-, 80%], 97 [$H_2PO_4^-$, 100%]; Accurate mass FAB^-: calc. for $C_{30}H_{61}N_2O_{39}P_6^-$, 1259.127; found 1259.122. Dimers **9b**–**d** had similar ^{1}H NMR spectra to that of **9a**, except for the increasing integral of the signal at δ *ca.* 3.60–3.70 corresponding to CH_2 of PEG. Their ^{31}P NMR spectra were also similar to that of **9a**.

1 M. J. Berridge, *Nature (London)*, 1993, **361**, 315. For recent reviews, see: R. A. Wilcox, W. U. Primrose, S. R. Nahorski and R. A. J. Challiss, *Trends Pharmacol. Sci.*, 1998, **19**, 467; C. W. Taylor, *Biochim. Biophys. Acta*, 1998, **1436**, 19.
2 M. de Kort, A. R. P. M. Valentijn, G. A. van der Marel and J. H. van Boom, *Tetrahedron Lett.*, 1997, **38**, 7629.
3 E. Katayama, H. Funahashi, T. Michikawa, T. Shiraishi, T. Ikemoto, M. Iino, K. Hirosawa and K. Mikoshiba, *EMBO J.*, 1996, **15**, 4844.
4 R. H. Kramer and J. W. Karpen, *Nature (London)*, 1998, **395**, 710.
5 M. Hirata, F. Yanaga, T. Koga, T. Ogasawara, Y. Watanabe and S. Ozaki, *J. Biol. Chem.*, 1990, **265**, 8404; B. V. L. Potter and D. Lampe, *Angew. Chem., Int. Ed. Engl.*, 1995, **34**, 1933.
6 A. M. Riley and B. V. L. Potter, *Tetrahedron Lett.*, 1999, **40**, 2213.
7 C. Malet and O. Hindsgaul, *J. Org. Chem.*, 1996, **61**, 4649.
8 D. Xu, K. Prasad, O. Repic and T. J. Blacklock, *Tetrahedron Lett.*, 1995, **36**, 7357.
9 R. Baker and J. L. Castro, *J. Chem. Soc., Perkin Trans. 1*, 1990, 47.
10 B. N. Ames and D. T. Dubin, *J. Biol. Chem.*, 1960, **235**, 769.
11 See for example: C. B. Baron, D. R. Tolan, K. H. Choi and R. F. Coburn, *Biochem. J.*, 1999, **341**, 805; M. J. Bottomley, P. Lo Surdo and P. C. Driscoll, *Curr. Biol.*, 1999, **9**, R301.

ChemComm

Passerini multicomponent reaction of protected α-aminoaldehydes as a tool for combinatorial synthesis of enzyme inhibitors

Luca Banfi,* Giuseppe Guanti* and Renata Riva

Università di Genova, Dipartimento di Chimica e Chimica Industriale, and C.N.R., CSCCCA, via Dodecaneso 31, I-16146 Genova, Italy. E-mail: banriv@chimica.unige.it, guanti@chimica.unige.it

Received (in Liverpool, UK) 10th March 2000, Accepted 20th April 2000

Three-component Passerini condensation of *N*-Boc-α-aminoaldehydes with various isocyanides and carboxylic acids leads, after Boc-deprotection/transacylation, to complex peptide-like structures containing an α-hydroxy-β-aminoacid unit or, after oxidation, an α-oxo-β-aminoacid unit.

Isocyanide employing multicomponent reactions have emerged as very powerful tools for the combinatorial synthesis of various pharmacologically important derivatives.[1] Of the two classical reactions belonging to this family, the Ugi condensation has been more widely studied and used in the generation of chemical libraries. On the other hand, the Passerini reaction, although older, has been employed less in combinatorial chemistry.[2] The reasons for this lower success are associated with the fact that a four-component condensation (Ugi) introduces a higher degree of diversity than a three-component one (Passerini). Moreover, the two amide bonds that link the components in Ugi adducts are more suitable for the synthesis of peptidomimetics, than the combination of one ester and one amide bond produced in the Passerini reaction. Finally, intramolecular variants declass the Passerini process to a two-component reaction, making it less suited for combinatorial chemistry.

In this work we show that, when protected α-aminoaldehydes are employed in Passerini condensation, a simple rearrangement of the reaction products allows an easy combinatorial entry to peptide-like structures, making this old methodology more valuable, particularly in the field of peptidomimetics and enzyme inhibitors.

The general strategy is depicted in Scheme 1 and involves condensation of *N*-Boc protected α-aminoaldehydes **1** with various isocyanides and various carboxylic acids, followed by one-pot Boc deprotection and acyl migration. This two step protocol gives rise to complex peptide-like substances **3** possessing a central α-hydroxy-β-aminoacid unit. This type of monomer has been widely used in the synthesis of enzyme inhibitors.[3] Moreover, a simple oxidation will produce oligopeptides **4** containing an α-oxo-β-aminoacid unit, which is an even more attractive structure, thanks to its similarity with protease transition state.[4]

Only two examples of Passerini reactions involving protected α-aminoaldehydes have been reported previously.[5] In one case, however,[5a] the carboxylic component was not retained during course of the synthesis; in the other case the yields were low and no further manipulation of the condensation adduct was attempted.[5b]

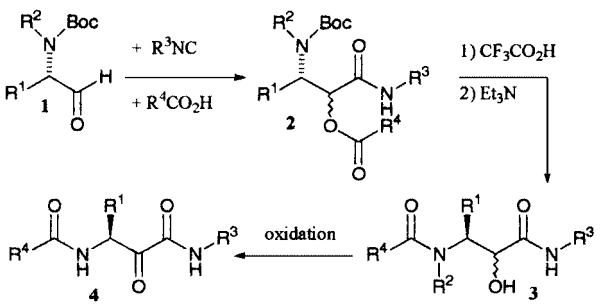

Scheme 1

The L-*N*-Boc protected α-aminoaldehydes employed in this work are all known[4c,6] and have been prepared either through $LiAlH_4$ reduction of Weinreb hydroxamates,[6b] or by Swern oxidation of the corresponding *N*-Boc aminoalcohols,[6d,e] in turn prepared by $BH_3{\cdot}Me_2S$ reduction of the *N*-Boc aminoacids.[6a] The latter are all commercially available compounds except for *O*-methyl-*N*-Boc-serine, which was prepared as previously described.[7]

Table 1 reports the results obtained in this two-step protocol for various combination of six *N*-Boc-α-aminoaldehydes, six isocyanides and ten carboxylic acids (including also protected aminoacids). In particular, isocyanides and carboxylic acids were chosen in order to check the effect of various kinds of side chains with different steric and electronic requirements. All isocyanides and carboxylic acids were commercially available, apart from benzyl 3-isocyanopropionate, which was prepared in two steps (1, BnOH, DCC, DMAP, 70%; 2, diphosgene, *N*-methylmorpholine, CH_2Cl_2, −15 °C, 67%) from known *N*-formyl-β-alanine.[8]

Although we did not perform all the 360 possible combinations, we think that the 20 examples shown represent a good 'statistical sample', which gives an idea of the generality of the presented methodology. In all cases, even when the reaction involved bulky substrates (*e.g.* entry 18), the yields of the Passerini condensation were satisfactory. Surprisingly, notwithstanding the wide variety of substrates employed, the stereoselectivity was at nearly the same level in all cases, being *ca.* 2:1. In view of combinatorial applications, the modest diastereoselection is not necessarily a drawback. Moreover, if the final targets are α-oxoamides **4**, diastereoselection at this level is unimportant.

When enantiomerically pure carboxylic acids were employed (entries 10–12, 14 and 15), only two diastereoisomers were detected by NMR spectroscopy, indicating that the starting α-aminoaldehydes do not undergo significant racemization under the reaction conditions. For entries 14 and 15 the diastereoisomeric mixtures were also checked by HPLC, which showed only 2–5% of isomers deriving from aldehyde racemization. This percentage was shown to depend on the method of preparation of the α-aminoaldehyde, the reduction–oxidation protocol turning out better from this point of view.

In most cases, treatment of the Passerini adducts **2** with CF_3CO_2H led to both Boc cleavage and *in situ* transacylation to give directly the oligopeptides **3**. However under these conditions, the acyl migration was not always complete and in some cases (entries 16–18) it did not take place at all. Thus the procedure of choice involves brief treatment with Et_3N in CH_2Cl_2 after CF_3CO_2H removal. For adducts deriving from Boc-protected aminoacids as the acid component (entries 12, 14 and 15) this procedure cleaved both Boc groups producing the expected transacylated compounds, whose identity was further confirmed by acylation with various reagents of the free amino group.

The overall yields of the sequence leading to **3** from **1** were in all cases > 50% and often > 70%.

DOI: 10.1039/b002027n

Table 1 Synthesis of oligopeptides **3** *via* Passerini condensation of *N*-Boc-α-aminoaldehydes followed by deprotection/transacylation[a]

Entry	R^1	R^2	R^3	R^4CO_2H	Yield of **2**[a] (%)	Dr of **2**[b]	Yield **2** → **3**[c] (%)	Overall yield of **3** (%)
1	$PhCH_2$	H	Bn	$PhCH_2CO_2H$	81	67:33	81	77
2	$PhCH_2$	H	Bn	$PhCO_2H$	67	62:38	96	64
3	$PhCH_2$	H	Bu^t	Pr^nCO_2H	82	71:29	86	71
4	$PhCH_2$	H	MeO_2CCH_2	$PhCH_2CO_2H$	91	64:36	99	90
5	$PhCH_2$	H	MeO_2CCH_2	Bu^sCO_2H	73	63:37[d]	68	50
6	Me	H	Bn	Pr^nCO_2H	85	65:35	94	80
7	Me	H	*c*-C_6H_{11}	*p*-Toluic acid	80	67:33	77	62
8	Me	H	MeO_2CCH_2	$PhCH_2CO_2H$	71	63:37	84	60
9	Et	H	Bu^t	$PhCH_2CO_2H$	83	69:31	89	74
10	Et	H	Bu^n	L-(Z)-Leu	65	61:39	91	59
11	Et	H	$BnO_2CCH_2CH_2$	L-(Z)-Leu	69	66:34	92	64
12	Et	H	MeO_2CCH_2	L-(Boc)-Leu	59	66:34	83	49
13	Pr^i	H	MeO_2CCH_2	(Z)-Gly	77	60:40	75	58
14	Pr^i	H	MeO_2CCH_2	L-(Boc)-Phe	95	52:48	75	71
15	Pr^i	H	MeO_2CCH_2	D-(Boc)-Phe	89	63:37	77	72
16	$-(CH_2)_3-$		*c*-C_6H_{11}	$PhCH_2CO_2H$	85	69:31	99	85
17	$-(CH_2)_3-$		Bn	Pr^n	93	62:38	80	65
18	$-(CH_2)_3-$		Bu^t	$PhCH_2CO_2H$	94	65:35	97	91
19	$MeOCH_2$	H	Bn	Pr^n	95	57:43	98	93
20	$MeOCH_2$	H	*c*-C_6H_{11}	$PhCH_2CO_2H$	95	61:59	82	78

[a] Transformation of **1** into **2** was carried out in CH_2Cl_2 at r.t. for 20–40 h, using 1.1 equiv. each of isocyanide and carboxylic acid. Isolated yields (after chromatography) reported. [b] Diastereoisomeric ratio, determined by ^1H NMR spectroscopy and/or HPLC. Relative configuration not determined. [c] Transformation of **2** into **3** was performed by: 1, CF_3CO_2H–CH_2Cl_2 (1:3 v/v), r.t., 1 h; 2, (after evaporation of CF_3CO_2H): Et_3N–CH_2Cl_2 (1:3 v/v), 1 h. Isolated yields are reported. [d] The ratio of the diastereoisomeric couples differentiated by the relative configuration between CH–N and CH–O is given.

It is worth noting that purification of Passerini adducts **2** could be performed quite simply by fast chromatography of the crude reaction solution on silica gel or alumina. The isocyanides (in excess) in all cases elute much faster than **2**, while the carboxylic acids, especially when alumina is used, remain adsorbed on the column. On the other hand the adducts **3** are usually pure enough to be used as such for further reactions (the only significant by-product being $Et_3NH^+CF_3CO_2^-$ which can be removed by extraction with H_2O). Thus several parallel preparations of compounds **3** can be run and processed in two days by a single operator even without the aid of automatic synthesizers.

Compounds **3** obtained as described in entries 10 and 11 of Table 1 were converted in high yields (NaOClO, KBr, cat. TEMPO$^{\cdot}$, 91 and 80%)[4c] into the corresponding α-ketoamides **4** (R^1 = Et, R^2 = H, R^4CO = (Z)-L-leucyl, R^3 = Bu^n or $CH_2CH_2CO_2Bn$), which are very similar to recently discovered potent calpain inhibitors (where R^3 = Et or Pr^n).[4a,c] This straightforward three-step synthesis of complex peptidomimetics is a clear example of the potentiality of this reported methodology. Accepting a wide variety of substrates, it appears ideally suited for the combinatorial synthesis of oligopeptides containing an α-hydroxy-β-aminoacid or α-oxo-β-aminoacid unit, which are of paramount interest as enzyme inhibitors.

We thank Dr Emiliano Calcagno for his important contribution to this work and CNR, University of Genova, and MURST (COFIN 98) for financial support.

Notes and references

1 R. W. Armstrong, A. P. Combs, P. A. Tempest, D. A. Brown and T. A. Keating, *Acc. Chem. Res.*, 1996, **29**, 123.
2 M. Passerini, *Gazz. Chim. Ital.*, 1921, **51**, 126; M. Passerini, *Gazz. Chim. Ital.*, 1921, **51**, 181.
3 Selected examples: (*a*) B. E. Evans, K. E. Rittle, M. G. Bock, C. D. Bennett, R. M. DiPardo, J. Boger, M. Poe, E. H. Ulm, B. I. LaMont, E. H. Blaine, G. M. Fanelli, I. I. Stabilito and D. F. Veber, *J. Med. Chem.*, 1985, **28**, 1756; (*b*) T. Mimoto, J. Imai, S. Tanaka, N. Hattori, S. Kisanuki, K. Akaji and Y. Kiso, *Chem. Pharm. Bull.*, 1991, **39**, 3088.
4 Selected examples: (*a*) Z. Li, A.-C. Ortega-Vilain, G. S. Patil, D.-L. Chu, J. E. Foreman, D. D. Eveleth and J. C. Powers, *J. Med. Chem.*, 1996, **39**, 4089; (*b*) J. Cacciola, R. S. Alexander, J. M. Fevig and P. F. W. Stouten, *Tetrahedron Lett.*, 1997, **38**, 5741; (*c*) S. L. Harbeson, S. M. Abelleira, A. Akiyama, R. Barrett III, R. M. Carroll, J. A. Straub, J. N. Tkacz, C. Wu and G. F. Musso, *J. Med. Chem.*, 1994, **37**, 2918.
5 (*a*) U. Schmidt and S. Weinbrenner, *J. Chem. Soc., Chem. Commun.*, 1994, 1003; (*b*) T. Ziegler, H.-F. Kaisers, R. Schlömer and C. Koch, *Tetrahedron*, 1999, **55**, 8397.
6 (*a*) J. Jurczak and A. Golebiowski, *Chem. Rev.*, 1989, **89**, 149; (*b*) O. P. Goel, U. Krolls, M. Stier and S. Kesten, *Org. Synth.*, 1988, **67**, 69; (*c*) J. A. Sowinski and P. L. Togood, *J. Org. Chem.*, 1996, **61**, 7671; (*d*) L. F. Tietze and O. Burkhardt, *Synthesis*, 1994, 1331; (*e*) R. P. Beckett, S. G. Davies and A. A. Mortlock, *Tetrahedron: Asymm.*, 1992, **3**, 123.
7 F. M. F. Chen and N. L. Benoiton, *J. Org. Chem.*, 1979, **44**, 2299.
8 C. Zhang, E. J. Moran, T. F. Woiwode, K. M. Short and A. M. M. Mjalli, *Tetrahedron Lett.*, 1996, **37**, 751.

Trifluoromethylthiodediazoniation: a simple, efficient route to trifluoromethyl aryl sulfides

Dave J. Adams, Andrew Goddard, James H. Clark* and Duncan J. Macquarrie

Clean Technology Centre, Chemistry Department, University of York, Heslington, York, UK YO10 5DD. E-mail: jhc1@york.ac.uk

Received (in Liverpool, UK) 15th February 2000, Accepted 28th April 2000

Copper(I) trifluoromethanethiolate reacts with a range of diazonium salts containing electron-withdrawing groups to give the corresponding trifluoromethyl aryl sulfides in high yield; it is also possible to carry out the diazotisation and trifluoromethylthiolation in one pot directly from the anilines.

Incorporation of a SCF_3 group into an aromatic molecule is of interest to the pharmaceutical and agrochemical industries, where the high lipophilicity and high electron-withdrawing ability of the group have important implications.[1] Current industrial methods for the formation of trifluoromethyl aryl sulfides generally involve multi-step processes which requires harsh conditions, restricting the nature of the other substituents on the ring as well as being environmentally damaging.[2] A simple, direct method for the formation of these compounds is thus highly desirable. One pot methods for preparing trifluoromethyl aryl sulfides have been reported but these are based on preformed thioaryl units (ArSCl and ArSCN) and require excess quantities of both of the expensive reagents CF_3SiMe_3 and Bu_4NF.[3] The Sandmeyer reaction is a well known method for the formation of chloro-, bromo- and cyanoarenes *via* reaction of the diazonium salts with copper(I) chloride, bromide or cyanide respectively.[4] However, despite copper(I) trifluoromethanethiolate ($CuSCF_3$) being used for the formation of trifluoromethyl aryl sulfides *via* reaction with iodobenzenes at high temperature[5] there are no reports of its reaction with diazonium salts. We have found that it is possible to form trifluoromethyl aryl sulfides from the corresponding diazonium tetrafluoroborates or directly in one pot from the anilines simply by reacting with $CuSCF_3$.

Addition of a solution of 2-nitrobenzenediazonium tetrafluoroborate **1a**[6] to an acetonitrile solution of $CuSCF_3$ at 50 °C[7] leads to rapid evolution of gas with concurrent formation of a deep yellow colour[8] ^{1}H NMR, ^{19}F NMR and GC of the solution all show that the major aromatic product is the 2-nitrophenyl trifluoromethylsulfide **2a**. Phenol, biphenyl or azo compounds, which are often observed as byproducts in diazonium reactions, were not formed in this system[9] although a small amount of nitrobenzene was detected.[10] At room temperature, the reaction is slower, but leads to a very similar product distribution. Other diazonium salts (Fig. 1) containing electron-withdrawing groups react similarily (Table 1). Halo, nitro and cyano groups

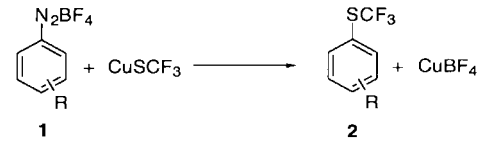

Fig. 1 Conversion of aryl diazonium tetrafluoroborates to trifluoromethyl aryl sulfides.

Table 1 Yields of $ArSCF_3$ from two-stage dediazoniations

Diazonium salt	Yield of $ArSCF_3$[a] (%)	Diazonium salt	Yield of $ArSCF_3$[a] (%)
1a	89 (83)	**1g**	60
1b	97	**1h**	95 (67)
1c	98 (76)	**1i**	91
1d	95	**1j**	17
1e	98	**1k**	7
1f	92	**1l**	3

[a] Yields calculated on the basis of GC area, unoptimised isolated yields in parentheses.

all survived the reaction. Steric factors do not appear to have an important effect: 2-, 3- and 4-nitrobenzenediazonium tetrafluoroborates all reacted immediately under the same conditions to give very similar product yields and impurity profiles, whereas it can be difficult to synthesise *ortho*-substituted derivatives by traditional means.[11]

Unfortunately, when electron-donating groups are present, the product yields are generally low (Table 1). This is due to a lack of reaction selectivity, thus while 2-diazobiphenyl tetrafluoroborate completely reacts the major product is the amide (Fig. 2). Such reactions have been reported to occur *via* reaction of a diazonium salt with acetonitrile.[12] In benzonitrile, no reaction of this substrate with $CuSCF_3$ was observed, with the only detected product being 2-hydroxybiphenyl. This was also the major product when the reaction was carried out in acetone. Methylbenzenediazonium tetrafluoroborates reacted similarily.

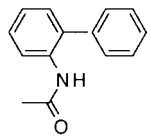

Fig. 2 Product from the reaction of 2-diazobiphenyl tetrafluoroborate with $CuSCF_3$.

In an effort to avoid the isolation of the diazonium intermediate, we investigated other diazotisation methods. Because $CuSCF_3$ reacts with acids to give $HSCF_3$, a non-protic system was required. Although, classically, diazotisation is achieved using sodium nitrite and a mineral acid, alternative methods do exist.[13] Doyle *et al.* have decribed the conversion of aryl amines to the corresponding halides in one-pot using *tert*-butyl nitrite and a copper(II) halide.[14] We have found that it is possible to effect a similar one-pot conversion of an aryl amine to a trifluoromethyl aryl sulfide (Fig. 3). Hence, when *tert*-butyl nitrite in acetonitrile was added to a pre-heated solution of 2-nitroaniline and $CuSCF_3$ in acetonitrile at 50 °C, the solution

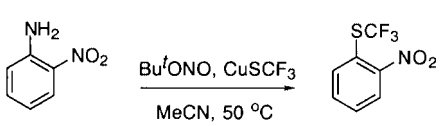

Fig. 3 One-pot synthesis of trifluoromethyl aryl sulfides from anilines.

DOI: 10.1039/b002560g

gradually became black. The formation of 2-nitrotrifluoromethylphenyl sulfide (29%) was detected, along with nitrobenzene (34%) and 2-nitrophenol (2%). It occurred to us that while it is not possible to use a Brønsted acid to improve the reaction, a Lewis acid may be beneficial. Repeating the one-pot reaction of 2-nitroaniline in the presence of BF_3 improved the selectivity to the 2-nitrotrifluoromethylphenyl sulfide to 45%. This method proved to be even more successful with 3-nitroaniline (72%) and 4-nitroaniline (66%), and moderately successful with other activated substrates and aniline itself (Table 2).[15] Substrates containing electron donating groups gave no appreciable yield of the desired trifluoromethyl aryl sulfide.

Table 2 Yields of $ArSCF_3$ from one-pot reactions of anilines

Aniline	GC yield of $ArSCF_3$ (%)
Aniline	42
2-Nitroaniline	45
3-Nitroaniline	72
4-Nitroaniline	66
3-Trifluoromethylaniline	46
3-Chloroaniline	18

In conclusion, we have demonstrated a new approach to trifluoromethyl aryl sulfides which is applicable to a wide range of substrates. This has advantages over current methodologies—the yields and product purity are high after a very simple work up procedure; the route is shorter than the traditional multi-step methods; and a wider range of functional groups is accessible owing to the mild conditions utilised. Unfortunately, this methodology is apparently restricted to substrates which are not electron-rich. It is also possible to form trifluoromethyl aryl sulfides in one pot directly from the anilines in a clean, safe and efficient direct route to these important compounds.

We gratefully acknowledge the support of the EPSRC (ROPA grant), the EPSRC/RAEng (Clean Technology Fellowship to J. H. C.) and the Royal Society (University Research Fellowship to D. J. M.). We would also like to thank Alec Taylor for helpful discussions.

Notes and references

1 R. Filler, in *Organofluorine Chemical and their Industrial Applications*, ed. R. E. Banks, Ellis Horwood Ltd, Chichester, 1979; B. E. Smart, in *Organofluorine Chemistry. Principles and Commercial Applications*, ed. R. E. Banks, B. E. Smart and C. Tatlow, Plenum Press, New York, 1994; R. M. DeMarinis and W. M. Bryan, *J. Org. Chem.*, 1977, **42**, 2024.
2 M. A. McClinton and D. A. McClinton, *Tetrahedron*, 1992, **37**, 6555; J. F. Harris, *J. Org. Chem.*, 1967, **32**, 2063; J. H. Clark, D. Wails and T. W. Bastock, *Aromatic Fluorination*, CRC Press, New York, 1997.
3 T. Billard and B. R. Langlois, *Tetrahedron Lett.*, 1996, **37**, 6865; T. Billard, S. Large and B. R. Langlois, *Tetrahedron Lett.*, 1997, **38**, 65.
4 A. F. Hegarty, in *The Chemistry of the Diazonium and Diazo Groups*, ed. S. Patai, J. Wiley and Sons, Bristol, 1978.
5 L. M. Yagupolskii, N. V. Kondratenko and V. P. Sabur, *Synthesis*, 1975, 721; D. C. Remy, K. E. Rittle, C. A. Hunt and M. B. Freedman, *J. Org. Chem.*, 1976, **41**, 1644.
6 Diazonium salts were prepared *via* the method described in A. Roe, *Org. React.*, 1949, **5**, 193.
7 J. H. Clark, C. W. Jones, A. P. Kybett, M. A. McClinton, J. M. Miller, D. Bishop and R. J. Blade, *J. Fluorine Chem.*, 1990, **48**, 249.
8 In a typical reaction, to a solution of $CuSCF_3$ (0.165 g, 1.0 mmol) in acetonitrile (3 ml) was added **1a** (0.237 g, 1.0 mmol) in acetonitrile (2 ml) at 50 °C with stirring. Rapid evolution of gas was observed and the solution became deep yellow. After stirring for 30 min, the solution was diluted with diethyl ether (200 ml) and filtered through Celite. The solvent was then removed to give **2a** (0.1883 g, 83%). *Selected analytical data*: 2-nitrophenyl trifluoromethyl sulfide **2a** δ_F(254 MHz, CD_3CN) −41.3 (s); δ_H(270 MHz, CD_3CN) 7.66–7.82 (m), 7.90 (m), 8.12 (m); *m*/*z* 223 (M^+); Anal. Calc. for $C_7H_4SF_3NO_2$ *m*/*z* 222.991485; Found *m*/*z* 222.991794; ν_{max}/cm^{-1} 1570s (C–NO_2), 1345s (C–NO_2), 1103s (C–F), 777m (C–S).
9 H. Ku and J. R. Barrio, *J. Org. Chem.*, 1981, **46**, 5239.
10 H. H. Hodgson and A. P. Mahaderon, *J. Chem. Soc.*, 1947, 173.
11 O. Schere, *Angew. Chem.*, 1939, **52**, 457.
12 W. E. Hanby and W. A Waters, *J. Chem. Soc.*, 1939, 1792.
13 L. Friedman and J. F. Chelbowski, *J. Org. Chem.*, 1968, **33**, 1636.
14 M. P. Doyle, B. Siegfried and J. F Dellona, *J. Org. Chem.*, 1977, **42**, 2426.
15 In a typical reaction to a preheated solution of 2-nitroaniline (0.0553 g, 0.4 mmol) and $CuSCF_3$ (0.0825 g, 0.5 mmol) in acetonitrile at 50 °C is added BF_3 etherate (0.4 mmol BF_3), followed by *tert*-butyl nitrite in acetonitrile. Evolution of a gas was observed and a darkening in the colour of the reaction mixture. Samples for GC, GC–MS and NMR analysis were first added to saturated calcium carbonate solution and then extracted with diethyl ether.

Typeset and printed by Black Bear Press Limited, Cambridge, England

ChemComm
FEATURE ARTICLE

Asymmetric functionalisation of tricarbonylchromium(0) complexes of arenes by non-racemic chiral bases

Susan E. Gibson (née Thomas)* and Ellian G. Reddington

Department of Chemistry, King's College London, Strand, London, UK WC2R 2LS. E-mail: susan.gibson@kcl.ac.uk

Received (in Cambridge, UK) 15th November 1999, Accepted 22nd February 2000
Published on the Web 29th March 2000

Non-racemic chiral bases have been proven to be of significant use in the synthesis of a wide range of enantiomerically enriched *organic* molecules. Their use in the synthesis of *organometallic* reagents and catalysts, however, is still in its infancy. This article reviews one of the first areas of organometallic chemistry to be examined in this context, *i.e.* asymmetric functionalisation of tricarbonylchromium(0) complexes of arenes using non-racemic chiral bases.

Introduction

The use of chiral lithium amide bases[1] and alkyllithiums in conjunction with chiral ligands[2] to desymmetrise organic molecules began in earnest in the late 1980s and early 1990s. In view of the excitement generated by the pioneering studies in this area, it was clear that this approach to the synthesis of non-racemic chiral molecules would have applications in organometallic chemistry and, in particular, the study of organometallic complexes used in organic synthesis. Tricarbonylchromium(0) complexes of aromatic compounds have received much attention as building blocks for organic synthesis, partly because of the intriguing changes in reactivity that occur on complexation of an aromatic compound to the tricarbonylchromium(0) unit, and partly because of the inherent stereochemical properties of complexes of polysubstituted arenes. Two major changes that occur when an arene ring is complexed to a tricarbonylchromium(0) unit are: (i) an increase in the acidity of the hydrogens attached to the aromatic ring,[3] and (ii) an increase in the acidity of any benzylic hydrogens associated with the arene.[4] Thus, it is not too surprising that some of the first attempts to exploit chiral bases in organometallic chemistry focused on the introduction of chirality into tricarbonylchromium(0) complexes of arenes. This article reviews progress to date on the application of chiral bases to aromatic functionalisation and benzylic functionalisation of tricarbonylchromium(0) complexes of arenes.

Sue Gibson did her first degree in Cambridge and her D. Phil. in Oxford under the supervision of Professor Steve Davies. She was then awarded a Royal Society European Fellowship to study at the ETH, Zürich with Professor Albert Eschenmoser. In 1985, she returned to the UK to a lectureship in organic chemistry at the University of Warwick, in 1990 she was appointed to a lectureship at Imperial College, London, and last year, she took up the Daniell Chair of Chemistry at King's College London. Her research interests revolve around the application of transition metals in organic synthesis. Current projects include the immobilisation of transition metal catalysts on solid supports, the biological and catalytic applications of conformationally constrained amino acids, and the application of chiral base chemistry and tricarbonylchromium(0) complexes of arenes to natural product synthesis and catalyst design.

Ellie Reddington attended school in North America, Asia and Europe. In 1996, she received her B.Sc. Hons. in Chemistry from Imperial College, London. She then started her Ph.D. on 'Chiral base-mediated asymmetric functionalisation of organometallic complexes' under the supervision of Sue Gibson. In 1999, she moved to King's College London with Professor Gibson where she completed her Ph.D.

Aromatic functionalisation

Aromatic functionalisation of tricarbonylchromium(0) complexes of arenes using a chiral amide base or an alkyllithium/chiral ligand combination was first reported in 1994. Indeed, there was a flurry of publications in this year from three groups, all of whom had identified and realised the potential of chiral bases in this area. Although the overall goal was the same, *i.e.* selective functionalisation of one of the *ortho* positions of a monofunctionalised arene complex, the methods of achieving this goal differed. Each group obtained success with a different directing group and a different chiral base or alkyllithium/chiral ligand combination. The introduction of a trimethylsilyl substituent was examined by each group and the result obtained was either typical or optimal. The Simpkins group successfully desymmetrised the tricarbonylchromium(0) complex of anisole **1** ([Cr] = tricarbonylchromium(0)) using chiral base (*R,R*)-**2** to give the planar chiral complex **3** in very good yield and enantiomeric excess,[5] the Kündig group successfully desymmetrised the prochiral carbamate complex **4** using chiral base **5** to give the trimethylsilyl derivative **6**,[6] and the Uemura group successfully desymmetrised the Boc-protected amine complex **7** using diamine **8** in conjunction with Bu^{t}Li to yield **9** (Scheme 1).[7] These results, and the many others described in these papers, demonstrated for the first time that planar chirality in (arene)tricarbonylchromium(0) complexes could be created using chiral bases. In parallel, the Schmalz group had been considering the possibility of using enantioselective *ortho*-deprotonation/silylation of 1,2-dimethoxyarene complexes in connection with their work on the synthesis of calamenen, pseudopterosin and helioporin. They discovered they were able to desymmetrise the disubstituted complex **10** using (*S,S*)-**2** to give the trisubstituted planar chiral complex **11** in excellent yield and enantiomeric excess.[8]

In the course of the studies described above, a problem was encountered with arguably one of the most synthetically useful classes of (arene)tricarbonylchromium(0) complexes, *i.e.* benzaldehyde acetal complexes; benzylic deprotonation often competed effectively with *ortho*-lithiation. This problem was addressed by the Green group using organolithium reagents derived from (1*R*)-menthyl chloride and (1*R*)-8-phenylmenthyl chloride. Reaction of these two reagents with the acetal complex **12** followed by addition of chlorotrimethylsilane afforded enantiomers (*R*)-**13** and (*S*)-**13**, respectively, in acceptable yield

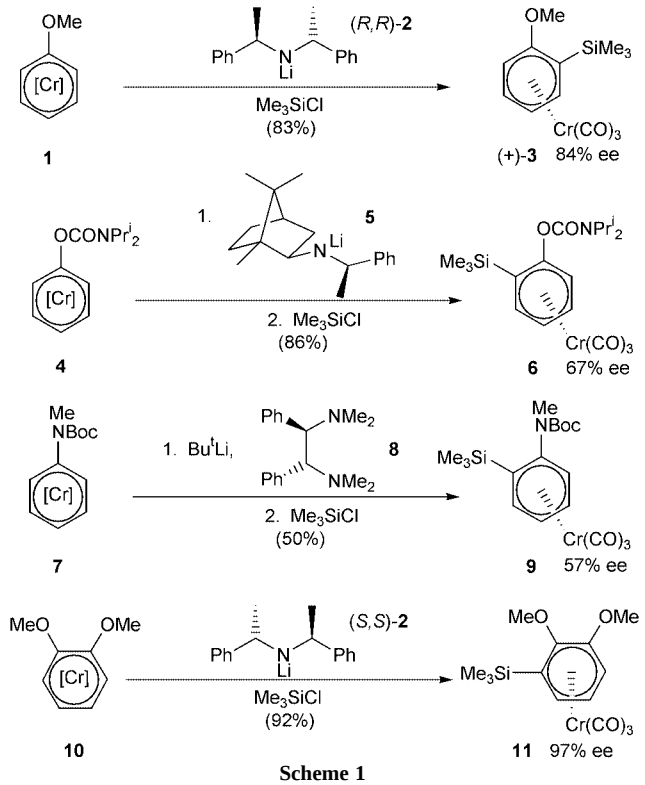

Scheme 1

and enantiomeric excess (Scheme 2).[9] A solution to the enantioselective functionalisation of (benzaldehyde)tricarbonylchromium(0) itself was provided by the Alexakis group,

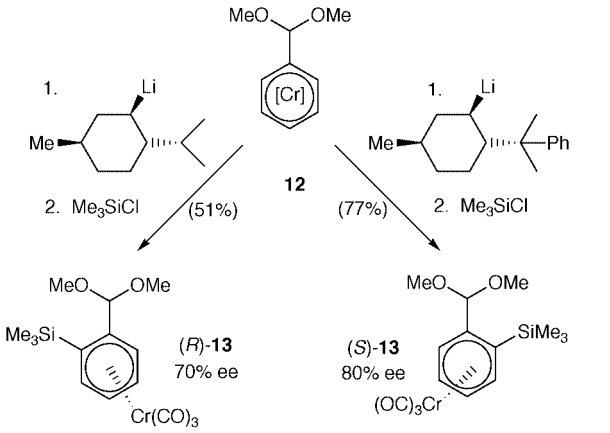

Scheme 2

which although strictly outside the scope of this review is nevertheless of interest in this context. In a typical example of their approach, reaction of complex **14** with **15** gave an amino alcoholate with an appended tertiary amine; subsequent addition of *n*-butyllithium followed by chlorotrimethylsilane gave complex **16** in notable enantiomeric excess (Scheme 3).[10]

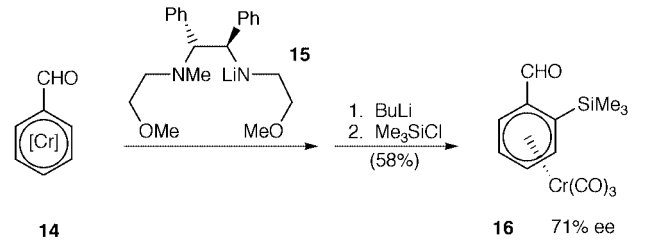

Scheme 3

Recently, the reaction of complex **4** with lithium amide **5** has been used to initiate an anionic *ortho*-Fries rearrangement. Warming the anion generated to −20 °C and stirring for 12 h induced the rearrangement; after quenching, product **17** was isolated and shown to be enantiomerically enriched (Scheme 4).[11]

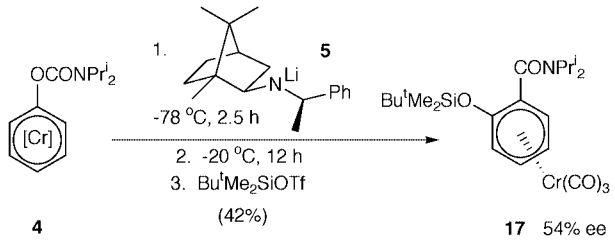

Scheme 4

The chiral base approach to enantiomerically enriched (arene)tricarbonylchromium(0) complexes is starting to be applied in the synthetic arena. Thus complex **3**, made using the Simpkins method, has been used at the start of two synthetic studies. Kündig used a nucleophilic addition to (+)-**3** followed by an electrophilic quench and *in situ* hydrolysis to form the substituted cyclohexenone **18**. A subsequent Pauson–Khand reaction gave diastereomerically pure tricycle **19** in enantiomeric excess equal to that of (+)-**3** (Scheme 5).[12] Elaboration of

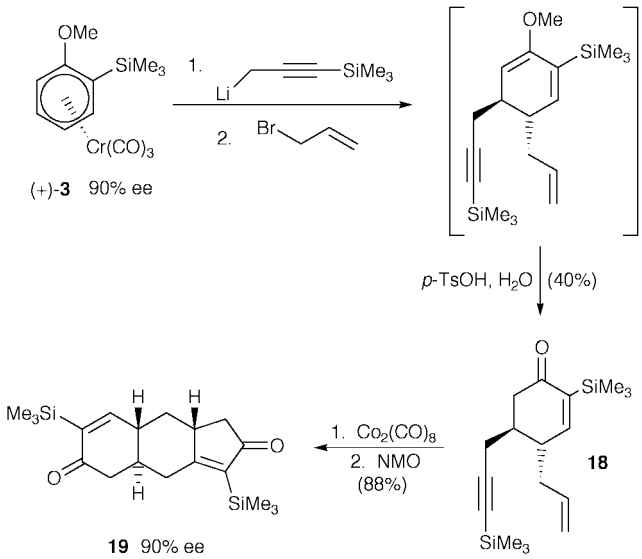

Scheme 5

(−)-**3** by the Schmalz group followed by nucleophilic addition and work-up gave substituted cyclohexenone **20**.[13] This was subsequently converted into (+)-ptilocaulin nitrate, an antimicrobial and cytotoxic metabolite of a Caribbean sponge (Scheme 6).[14] In both of these studies, the stereochemical information introduced using the chiral base is relayed first of all across the complexed arene ring to the chiral centre constructed on addition of the nucleophile. The stereochemistry of this chiral centre subsequently controls the formation of the remaining chiral centres in the product.

Benzylic functionalisation

Ethers: simple functionalisation

In 1996, we decided to examine the possibility of using chiral base methodology to asymmetrically functionalise the benzylic position of (arene)tricarbonylchromium(0) complexes. We selected the tricarbonylchromium(0) complex of benzyl methyl ether **21** as our test substrate as: (i) it was readily available and (ii) it had been demonstrated previously that it could be alkylated in good yield using *n*-butyllithium followed by quenching with a range of alkylating reagents.[15] That said, we

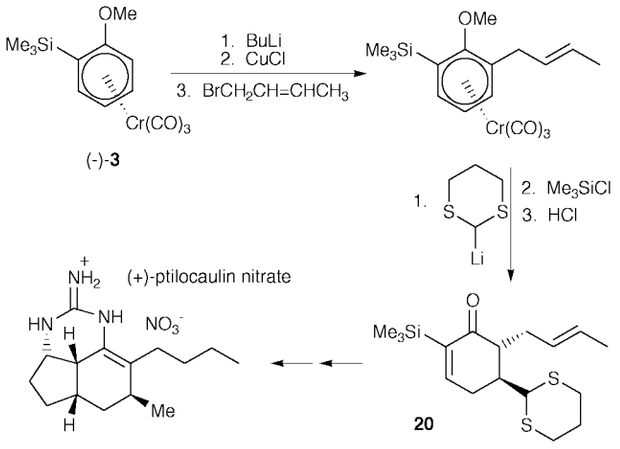

Scheme 6

were somewhat concerned that the high degree of conformational flexibility of complex **21**, compared to other substrates that had been successfully desymmetrised by chiral base technology, would render discrimination between its two benzylic sites difficult.

In an initial exploratory experiment, the well-established chiral base (*R*,*R*)-**2** was used to deprotonate **21** and diphenyl disulfide was used to quench the reaction. Workup provided the novel complex (+)-**22** in 52% yield. Complex **22** proved easy to analyse by chiral HPLC and its ee was found to be a moderate 22% (Scheme 7). In view of our reservations about the

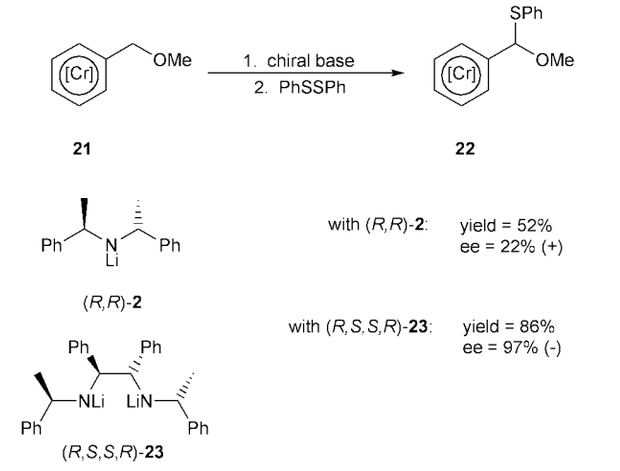

Scheme 7

conformational flexibility of **21**, we were highly encouraged by this seemingly modest result and decided to undertake further experiments with different bases. The next base used was the C_2-symmetric vicinal diamide **23**. A straightforward two-step synthesis of this base had been reported in 1994,[16] but its potential as a chiral base had not been explored in any detail. Using this base, the reaction of complex **21** to give the α-phenylsulfenyl derivative (−)-**22** proceeded in 86% yield and, to our delight, the ee of the product was found to be 97% (Scheme 7).[17]

In order to glean information about the absolute stereochemistry of the products of this highly enantioselective system, the reaction between ether complex **21** and chiral base (*R*,*S*,*S*,*R*)-**23** was next quenched with iodomethane. This gave the α-methylbenzyl methyl ether complex **24** in 96% yield and 97% ee (Scheme 8). Comparison of the $[\alpha]_D$ of this material with literature data[18] revealed that the absolute configuration of **24** was *R*.

In parallel to our benzylic deprotonation studies on the acyclic ether **21**, the Simpkins group had been examining the effect of chiral bases on the cyclic ether complex **25**.[19] In a

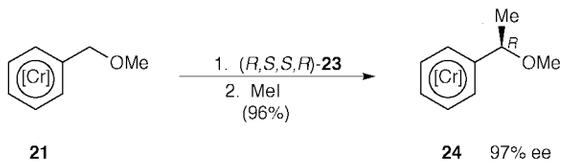

Scheme 8

typical example from their work, (1,3-dihydroisobenzofuran)-tricarbonylchromium(0) **25** was treated with the monoamide base (*R*,*R*)-**2** in the presence of chlorotrimethylsilane. The product of benzylic functionalisation **26** was isolated in 82% yield and 76% ee (Scheme 9). Thus, in this case, in contrast to

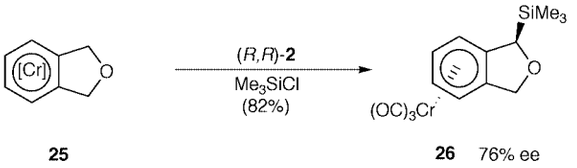

Scheme 9

the acyclic ether case, the well-established monoamide base (*R*,*R*)-**2** led to good enantioselectivity. The absolute configuration of **26** was assigned by analogy with the product of methylation, the stereochemistry of which was rigorously determined by chemical correlation.

A little later, the reactions of the cyclic ether complex **25** with monoamide base (*R*,*R*)-**2** and the diamide base (*R*,*S*,*S*,*R*)-**23** followed by a benzophenone quench were reported by Simpkins.[20] Interestingly, switching from the monoamide base to the diamide base raised the enantioselectivity of this reaction from 75% to 99% (Scheme 10). Moreover, the absolute configuration

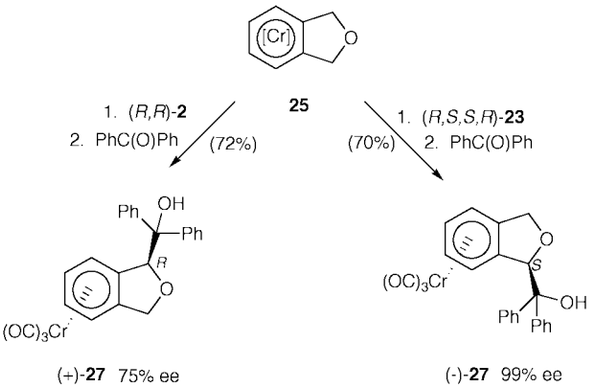

Scheme 10

of the product **27** changed from *R* to *S* with the change of base, an observation reminiscent of the change from (+) to (−) observed with acyclic ether complex **21** in the production of sulfur derivative **22**.

Ethers: further elaboration

As a result of the studies described above, it was clear that asymmetric functionalisation of the benzylic position of ether complexes using the diamide base (*R*,*S*,*S*,*R*)-**23** was a high-yielding and highly enantioselective reaction. At this point, we decided to examine whether or not the reactivity discovered could be used as a basis for further elaboration of ether complexes and the generation of enantiomerically enriched products.

Synthesis of tertiary ethers. The synthesis of enantiomerically enriched tertiary alcohols is more challenging than their secondary counterparts, which are now readily available by a

variety of reliable and versatile routes. In 1996, Hoppe and Dewing reported that enantiomerically enriched secondary alcohols **28**, derived from racemic mixtures by enzymatic hydrolysis, could be converted into enantiomerically enriched tertiary alcohols *via* deprotonation/electrophilic quench sequences on carbamate derivatives **29** (Scheme 11).[21] Some of

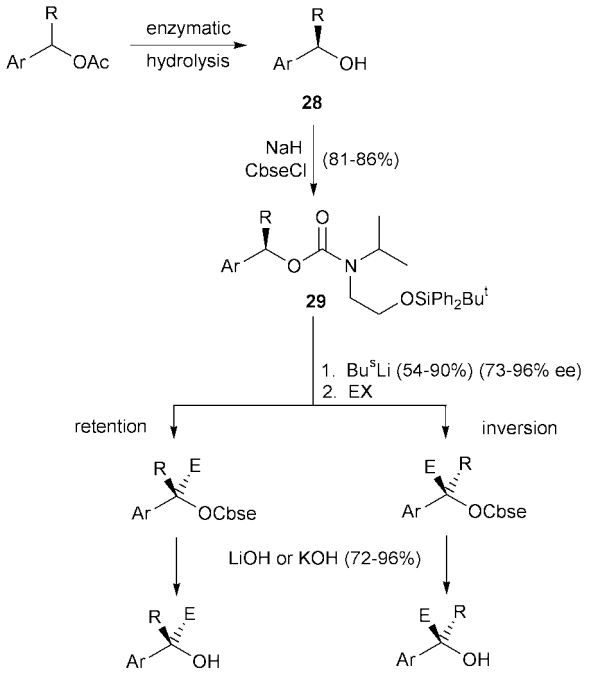

Scheme 11

the electrophilic quenches proceeded with retention of configuration, others with inversion. We thus decided to probe whether or not optically active complexes of secondary benzyl ethers. such as **24**, could be converted into optically active complexes of tertiary benzyl ethers by a deprotonation/electrophilic quench protocol. If so, it would be of interest to determine whether the reaction proceeded with retention or inversion of configuration.

Complex **24** (98.5% ee and *R* configuration) was deprotonated with *tert*-butyllithium in THF at −78 °C, and, after 90 min at this temperature, the anion was quenched with deuteriomethanol. Work-up gave a 90% yield of complex D-**24** (91% D incorporation) which HPLC analysis revealed had an ee of 98.5% and was also of *R* configuration (Scheme 12). Thus the

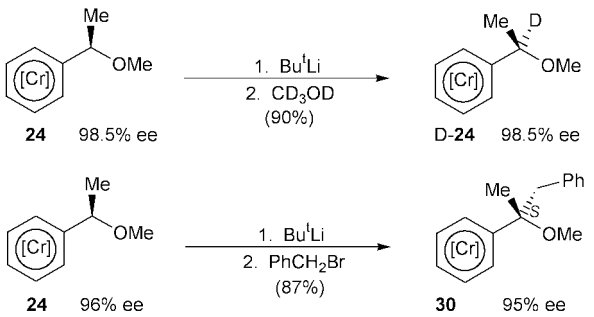

Scheme 12

deprotonation/quench sequence had clearly proceeded with overall retention of configuration, presumably *via* a configurationally stable anion.[22]

Having ascertained that the lithium anion of **24** is configurationally stable at −78 °C, our attention turned to synthetically more interesting electrophiles. Whilst deprotonation of (±)-**24** followed by quenching with iodomethane and chlorotrimethylsilane has been shown to proceed in yields of 93 and 53%, respectively, indicating that the formation of carbon–carbon and carbon–heteroatom bonds in this system is chemically feasible,[23] the stereochemical consequences and the synthetic scope of this type of process needed to be determined. We examined several systems varying both the benzylic substituent on the secondary ether and the electrophile used in the quench. In a typical example, complex **24** was deprotonated and quenched with benzyl bromide. Work-up led to the isolation of the novel complex **30** of essentially the same enantiomeric purity as its precursor in 87% yield (Scheme 12). An X-ray crystallographic analysis of this product revealed that its absolute configuration was *S*. Thus the deprotonation/benzylation of **24** proceeds with overall retention of configuration. This may be rationalised as follows: abstraction of the benzylic proton of **24** from a conformation that places it antiperiplanar to the tricarbonylchromium(0) unit gives the chromium-centred and configurationally-locked anion **31** (Scheme 13). The

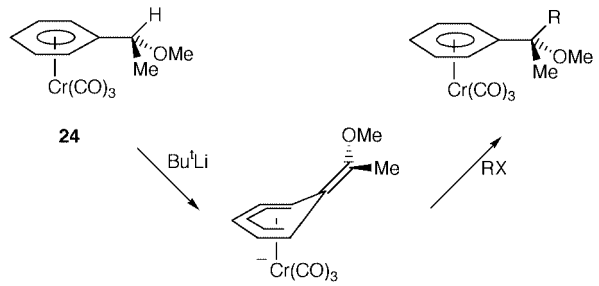

Scheme 13

incoming electrophile then approaches the sterically less-hindered *exo*-face of the intermediate to give the observed product under excellent stereochemical control.

[2,3]-Wittig rearrangement. Our attention turned next to stereochemical control of the [2,3]-Wittig rearrangement. This is a useful carbon–carbon bond-forming reaction[24] and, as such, asymmetric versions of it are a desirable goal.[25] Research in recent years has produced several approaches, the greatest success being achieved using chiral auxiliaries.[26] Enantioselective versions of the [2,3]-Wittig rearrangement involving an achiral substrate and a chiral non-racemic base are synthetically more attractive, but this approach has been much less successful. The best result to date for a *cyclic* system is the conversion of the 13-membered ether **32** into the 10-membered alcohol **33** in 69% ee and 82% yield using (*S*,*S*)-**2** (Scheme 14).

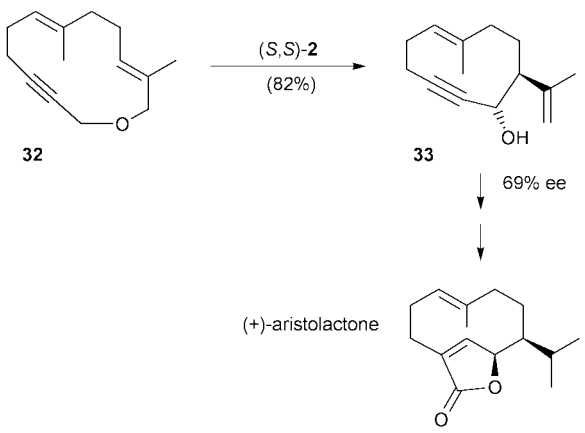

Scheme 14

This success was attributed to special conformational effects as the same base gave a poorer result with a 17-membered homologue, and racemic products when applied to acyclic α-(allyloxy)acetic acids and amides.[27] Typical results to date for

linear systems are exemplified by reactions carried out using a norpseudoephedrine/BuLi combination.[28] Thus Wittig rearrangement of dialkyne **34**, under the influence of **35**, produced alcohol **36** in moderate yield and ee, whilst rearrangement of unsaturated ether **37** gave a moderate yield of a diastereomeric mixture of alcohols each of poor optical purity (Scheme 15).

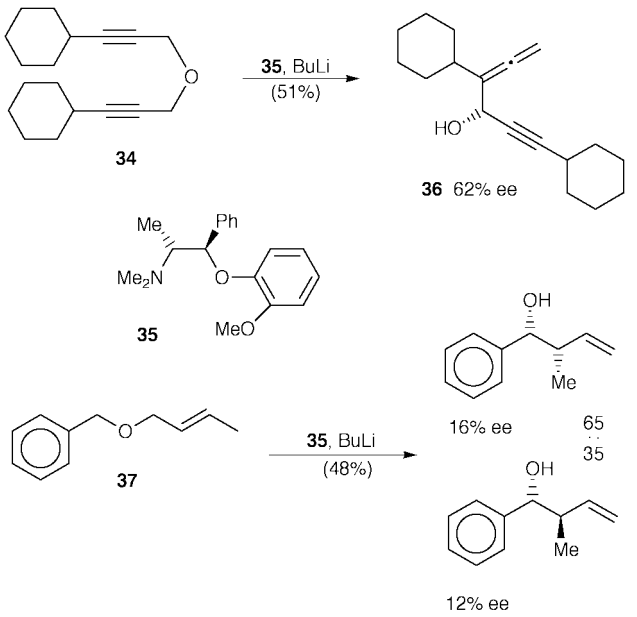

Scheme 15

In view of the high enantioselectivities and yields obtained for the asymmetric functionalisation of tricarbonylchromium(0) complexes of alkyl benzyl ethers, and earlier reports that tricarbonylchromium(0) complexes of allyl benzyl ethers undergo [2,3]-Wittig rearrangements,[29] we decided that it would be of interest to determine whether or not such Wittig rearrangements could be performed under good enantiomeric control using non-racemic chiral bases.

The first reaction to be examined was that of parent allyl benzyl ether complex **38** with diamide base (*R,S,S,R*)-**23**. This was found to proceed in good yield (80%) and excellent ee (96%) (Scheme 16).[30] In order to determine the absolute

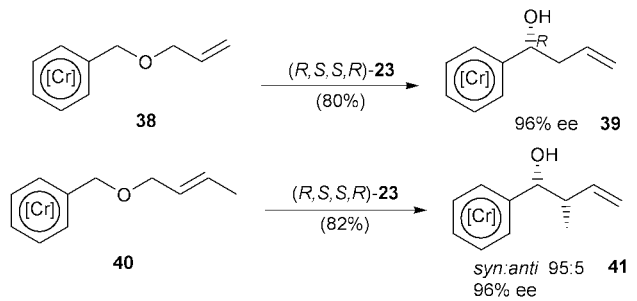

Scheme 16

configuration of the product **39**, the tricarbonylchromium(0) unit was removed by photolysis and the $[\alpha]_D$ of the resulting alcohol compared with literature values.[31] This revealed that the absolute configuration of **39** was *R*, a result consistent with the sense of asymmetric induction observed for the functionalisation of complex **21** with external electrophiles.

A series of rearrangements were examined in order to determine the effect of substituents on chemical yields and enantioselectivities. In the first series of experiments, substituent patterns were chosen which would lead to products containing just one chiral centre. These experiments gave products of very good optical purity (84–94%), but the chemical yields ranged from good to poor (82–25%). Next the rearrangement of complex **40** was examined, as this gives rise to two chiral centres, raising the issue of diastereoselectivity. Pleasingly, the but-2-enyl complex **40** rearranged smoothly to give a good yield (82%) of alcohol **41** (Scheme 16). The diastereomeric ratio of the product complex was found to be 95 : 5 and the relative stereochemistry of the major isomer was identified as *syn* by comparison of its spectroscopic data and the data of its decomplexation product with literature values obtained from a racemic sample. HPLC analysis of **41** revealed that its ee was 96%. Thus the yield, diastereoselectivity and enantioselectivity observed for the rearrangement of **40** to **41** under the influence of base (*R,S,S,R*)-**23** compare well with the rearrangement of the non-complexed material **37** under the influence of the norpseudoephedrine/BuLi combination.

Thioethers

The configurational instability of α-sulfur substituted alkyllithium compounds **42**[32] and benzyllithium compounds **43**[33] is

well documented and attempts to use these species in asymmetric synthesis have met with little success to date. Indeed, the first examples of enantiomerically enriched α-sulfur substituted alkyllithium compounds, whose chirality is determined solely by the stereogenic carbon centre, were prepared only quite recently. Thus, generation of α-sulfur substituted alkyllithiums by deprotonation of **44** with Bu^{s}Li/(−)-sparteine and subsequent quenching with carbon dioxide or chlorotrimethylsilane gave products in 77–95% yield and 40–60% ee (Scheme 17).[32]

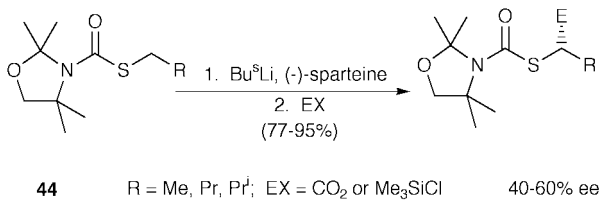

Scheme 17

In view of (i) the recognised instability of α-sulfur substituted lithium compounds, and (ii) the emerging potential of chiral sulfides as ligands in asymmetric synthesis,[34] we wanted to determine whether or not anions of tricarbonylchromium(0) complexes of alkyl/aryl benzyl sulfides would be sufficiently configurationally stable to undergo bond-forming reactions and produce enantiomerically enriched products.

A series of thioether complexes was easily and efficiently prepared by reacting (benzyl alcohol)tricarbonylchromium(0) with a range of thiols in the presence of tetrafluoroboric acid.[15] After some experimentation, it emerged that enantioselectivity was a function of the thioether substituent and that methyl and benzyl substituents gave the best results. In a typical experiment, thioether complex **45** was reacted with (*R,S,S,R*)-**23** and quenched with benzyl bromide to give the benzylic substitution product **46** in 91% yield and 88% ee (Scheme 18).[35] In order to determine the absolute stereochemistry of the chiral sulfides generated by this new approach, we subjected the silyl substituted complex **47** (Scheme 18) to X-ray crystallographic analysis. To our surprise, this revealed that **47** was the opposite enantiomer to the one we had predicted based on the results obtained with the analogous ether complexes.

In order to probe this change in stereochemical outcome further, the ether complex **48** (97% ee) was reacted with benzyl

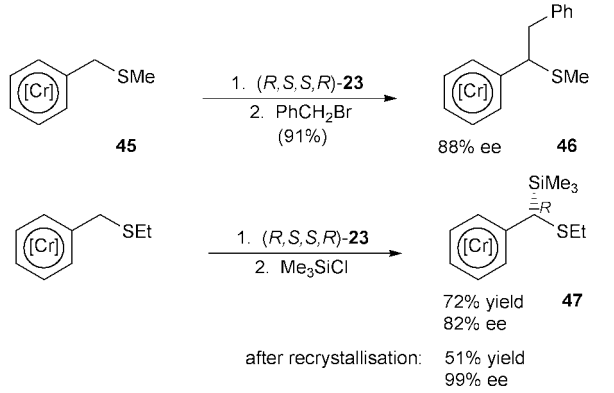

Scheme 18

thiol in the presence of acid. Work-up gave a thioether complex in 65% yield and HPLC analysis of this material revealed that it was the opposite enantiomer to that obtained by the deprotonation/quench route (Scheme 19). As acid catalysed substitutions

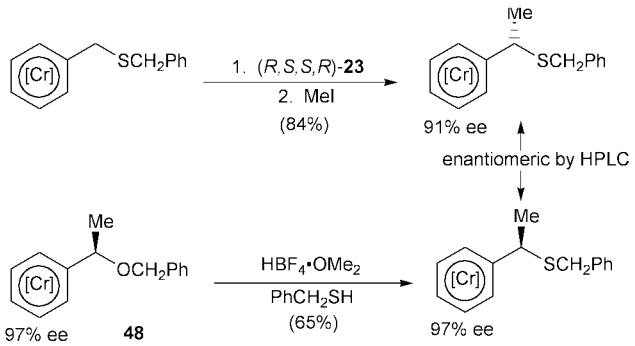

Scheme 19

of this type are known to proceed with retention of configuration,[36] this result is stereochemically consistent with the X-ray crystallographic analysis of **47**. It thus appears that deprotonation of tricarbonylchromium(0) complexes of benzyl sulfides with the chiral base (*R*,*S*,*S*,*R*)-**23** proceeds in the opposite stereochemical sense to deprotonation of the corresponding ethers.

The Simpkins group also examined the effect of chiral bases on tricarbonylchromium(0) complexes of thioethers, but their focus was on the cyclic system **49**. Initially, **49** was reacted with the monoamide base (*R*,*R*)-**2** and subjected to a range of quenches, but these reactions gave products of very low ee (*ca.* 5%) (Scheme 20).[19] On re-examining the system with the

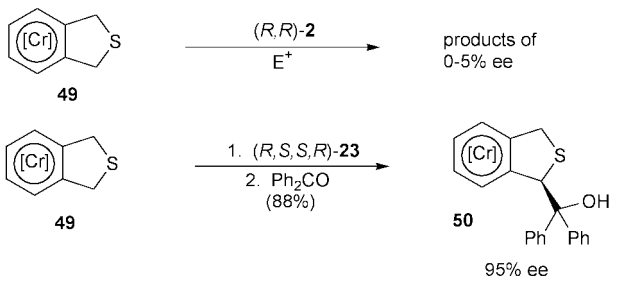

Scheme 20

diamide base (*R*,*S*,*S*,*R*)-**23**, however, they were able to generate products in excellent yield and ee.[37] Addition of benzophenone to **49** using (*R*,*S*,*S*,*R*)-**23**, for example, generated **50** in 88% yield and 95% ee (Scheme 20). Interestingly, comparison of **50** with (−)-**27** obtained from the cyclic ether **25** indicates that the change in stereochemistry observed in the acyclic systems is not repeated here. This may be a function of the increased rigidity of the cyclic system.

In summary, diamide base (*R*,*S*,*S*,*R*)-**23** can be used to asymmetrically functionalise complexes of benzylic sulfides. Although the enantiomeric excesses observed in the acyclic system are slightly lower than those observed in the corresponding oxygen ether system, the relatively high selectivity compared to other α-sulfur substituted lithium systems suggests that the anion involved possesses unusually high stereochemical stability. This is attributed to the delocalisation of the negative charge onto chromium (and beyond onto the carbonyl ligands) which raises the energy barrier to rotation about the *ipso* carbon–benzylic carbon bond.

Amines

The efforts of our group and the Simpkins group to use chiral bases to asymmetrically functionalise tricarbonylchromium(0) complexes of benzylic amines, or their derivatives, have, to date, proved unsuccessful. Nevertheless, we have demonstrated that it is possible to access this important class of compounds using the reliable and robust ether chemistry.

Initial experiments were carried out using complex **24** of 99% ee. It was hoped that nucleophilic substitution of this complex using a nitrogen nucleophile would give us access to enantiomerically enriched amines. Literature precedent, however, was not encouraging: although substitution of α-oxygenated (arene)tricarbonylchromium(0) complexes with acid/nucleophile combinations *via* a chromium-stabilised carbocation intermediate **51** (Scheme 21) is well-established for carbon,

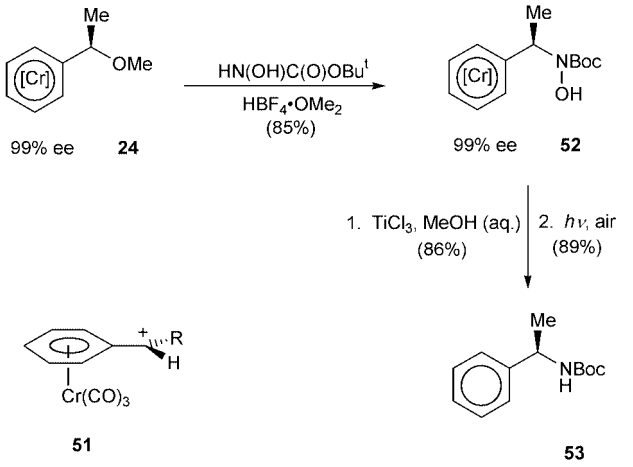

Scheme 21

hydrogen, and oxygen nucleophiles, the use of nitrogen nucleophiles is rare and inefficient. Thus, reactions of ammonia and primary and secondary amines with benzyl alcohol complexes in the presence of hexafluorophosphoric acid gives low yields of substitution products.[38] Indeed our initial reactions of complex **24** with a wide range of amines in the presence of tetrafluoroboric acid were disappointing, providing only very low levels of nitrogen incorporation and complex mixtures of products. In contrast, protonation of **24** at −40 °C with tetrafluoroboric acid followed by addition of commercially available *tert*-butyl-*N*-hydroxycarbamate gave the nitrogen substitution product **52** in 85% yield (Scheme 21). Moreover the ee of the novel complex **52** was measured by chiral HPLC and found to be 99%.[39]

The absolute configuration of the nitrogen substitution product **52** was determined by chemical correlation. Reduction of the nitrogen–oxygen bond using titanium trichloride in aqueous methanol proceeded smoothly. Subsequent oxidative removal of the tricarbonylchromium(0) unit gave carbamate **53** (Scheme 21), the optical rotation of which was essentially identical to a sample prepared from authentic (*R*)-α-methylbenzylamine. Thus the absolute configuration of **52** is *R* and the conversion of **24** to **52** proceeds with retention of configuration, presumably *via* a chromium stabilised carbocation **51**.

In order to probe the effect of increasing steric hindrance around the benzylic position on the nitrogen substitution reaction, complexes **54** and **55** bearing ethyl and *iso*-propyl groups, respectively, were prepared and reacted with *tert*-butyl-*N*-hydroxycarbamate. The reactions gave products **56** and **57** in moderate yield and 96 and 91% ee respectively (Scheme 22).

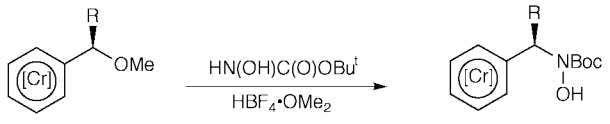

R	educt	ee (%)	product	ee (%)	yield (%)
Me	**24**	99	**52**	99	85
Et	**54**	96	**56**	96	53
i-Pr	**55**	98	**57**	91	43

Scheme 22

Thus, increasing steric hindrance on going from methyl to *iso*-propyl leads to notable yield reduction and a small but significant stereochemical leakage. These effects are attributed to a reduced rate of addition of the nitrogen nucleophile to the intermediate carbocation, the increased lifetime of which leads to byproducts and rotation about the *ipso* carbon–benzylic carbon bond.

Mechanistic probes

Several studies have been carried out in order to probe the mechanism of the highly selective reactions described above.

Addition of diamine after BuLi. In order to test whether the benzylic asymmetric functionalisations described in previous sections were due to asymmetric deprotonations or to asymmetric electrophilic quenches, we performed an experiment in which the substrate was deprotonated with the achiral base *n*-butyllithium and the chiral diamine was added afterwards.[40] Thus methyl ether complex **21** was treated with 1.1 equiv. of butylithium followed by 1.1 equiv. of diamine **58** (and 1 equiv. of lithium chloride). The reaction was subsequently quenched with 2 equiv. of diphenyl disulfide to give the expected product **22** in 79% yield (Scheme 23). The ee of **22** was measured and

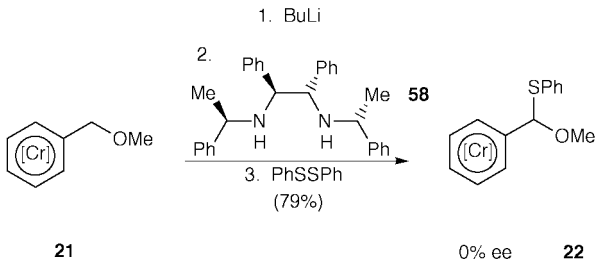

Scheme 23

found to be zero. Thus the racemic anion generated in this experiment did not undergo an asymmetric electrophilic quench under the control of the chiral diamine present in the reaction mixture. This result is consistent with the asymmetric control observed in the benzylic functionalisations originating in the deprotonation step rather than the quench step.

Effect of base structure. As diamide base (*R*,*S*,*S*,*R*)-**23** was only the second base we had examined in our initial studies on the functionalisation of oxygen ether **21**, we thought it prudent to screen other chiral bases to establish whether or not the high yields and ees obtained with (*R*,*S*,*S*,*R*)-**23** were unique to this structure. Amides **59**–**64** were used in the conversion of ether **21** to sulfur derivative **22** and found to give only moderate yields and enantioselectivities compared to (*R*,*S*,*S*,*R*)-**23**.[41] We also synthesised and tested bases **65** and **66** to probe whether all the features of (*R*,*S*,*S*,*R*)-**23** were essential to the high yields and

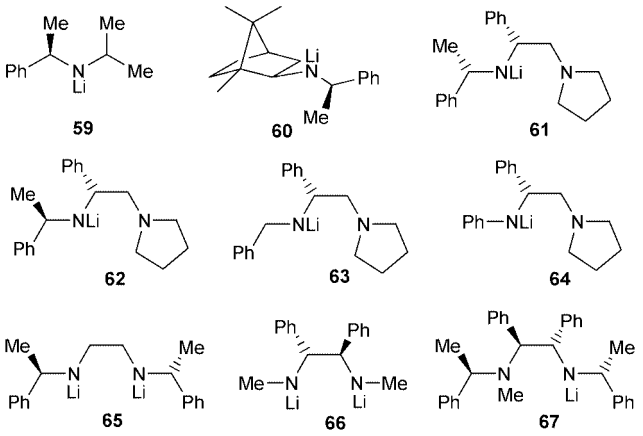

selectivities. These studies revealed that both the backbone and the side chain chirality were necessary for optimum results.[41] Finally, in order to ascertain whether the second lithium amide was necessary for success, base **67** was synthesised[42] and tested on substrate **21** (Scheme 24). This gave a good yield (80%) and

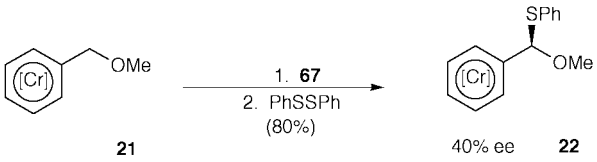

Scheme 24

moderate ee (40%) of the *R* enantiomer of **22**, a finding which was later used to explain results obtained by varying the equivalents of BuLi used in the reaction (*vide infra*).

Effect of BuLi stoichiometry. All the reactions described above were carried out using 2.2 equiv. of BuLi and 1.1 equiv. of diamine. In an effort to minimise the amount of BuLi required in these experiments, **21** was converted to **22** using 1.1 equiv. of BuLi and the effect on yield and ee determined. In order to determine the effect on ee of reducing the equivalents of BuLi used still further, reactions using 0.55 and 0.275 equiv. of BuLi were also performed (Scheme 25). Pleasingly, use of

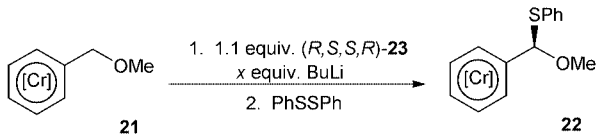

BuLi (equiv.) (*x*)	yield (%)	ee (%)	recovered substrate (%)
2.2	95	98	0
1.1	96	95	0
0.55	60	92	40
0.275	21	96	67

Scheme 25

1.1 equiv. of BuLi had negligible detrimental effect on yield and ee, producing **22** in 96% yield and 95% ee. It was interesting to note that although reduction of the equivalents of BuLi to 0.55 and 0.275 gave the expected drop in yield (60 and 21% respectively; an experimental error of ±5% in BuLi measurement accounts for the unreasonably high yield in the first case), the enantioselectivity of the reaction remained very high (92 and 96% respectively).

The results obtained by varying the equivalents of BuLi may be explained as follows. The dilithiated species (*R*,*S*,*S*,*R*)-**23** (or an aggregate thereof) is clearly a highly enantioselective

reagent. If we assume that the monolithiated species **68** is relatively unselective, a hypothesis supported to a degree by the low ee (40%) obtained with **67**, then it follows from the results obtained on reducing the number of BuLi equivalents that (i) there is a ready exchange of lithium cations between all the nitrogen sites in the system, and (ii) (*R*,*S*,*S*,*R*)-**23** is more reactive than **68** with respect to complex **21**. In conclusion, it

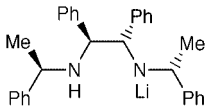

68

appears that all the deprotonation power of the BuLi is channelled through the highly selective diamide species rather than the relatively unselective monoamide species.

Conclusion

Studies carried out in the last five years have demonstrated that chiral bases provide an excellent entry into enantioenriched tricarbonylchromium(0) complexes of arenes. Moreover, the products of these studies are starting to be used in synthetic endeavours. It is anticipated that in the next few years, chiral bases will be used to generate a wide variety of enantioenriched organometallic complexes which will find uses both in synthesis and catalysis. Whilst the selectivities that can be achieved are impressive and useful, discovery of the origin of this selectivity in both the organometallic systems described here and the organic systems developed over the last fifteen years remains a significant challenge.

Acknowledgements

The authors wish to thank the past members of the Gibson group who initiated and developed asymmetric benzylic functionalisation: Mark H. Smith, P. Caroline V. Potter, Gary R. Jefferson and Domenico Albanese; our industrial and academic collaborators: E. Lucy M. Cowton, Michael J. Schneider, Peter Ham and Peter O'Brien; the following organisations for financial assistance: Associated Octel Company, Zeneca Pharmaceuticals, SmithKline Beecham, The Accademia Nazionale dei Lincei/The Royal Society and EPSRC, and Surojit Sur and Hasim Ibrahim for proof reading and helpful comments.

References

1 For reviews of this area, see: P. J. Cox and N. S. Simpkins, *Tetrahedron: Asymmetry*, 1991, **2**, 1; P. O'Brien, *J. Chem. Soc., Perkin Trans. 1*, 1998, 1439.
2 For reviews of this area, see: P. Beak, A. Basu, D. J. Gallagher, Y. S. Park and S. Thayumanavan, *Acc. Chem. Res.*, 1996, **29**, 552; D. Hoppe, *Angew. Chem., Int. Ed. Engl.*, 1997, **36**, 2282.
3 M. F. Semmelhack, in *Comprehensive Organometallic Chemistry II*, ed. E. W. Abel, F. G. A. Stone and G. Wilkinson, Pergamon, Oxford, 1995, vol. 12, p. 1017.
4 S. G. Davies and T. D. McCarthy, in *Comprehensive Organometallic Chemistry II*, ed. E. W. Abel, F. G. A. Stone and G. Wilkinson, Pergamon, Oxford, 1995, vol. 12, p. 1054.
5 D. A. Price, N. S. Simpkins, A. M. MacLeod and A. P. Watt, *J. Org. Chem.*, 1994, **59**, 1961; D. A. Price, N. S. Simpkins, A. M. MacLeod and A. P. Watt, *Tetrahedron Lett.*, 1994, **35**, 6159; R. A. Ewin, A. M. MacLeod, D. A. Price, N. S. Simpkins and A. P. Watt, *J. Chem. Soc., Perkin Trans. 1*, 1997, 401.
6 E. P. Kündig and A. Quattropani, *Tetrahedron Lett.*, 1994, **35**, 3497.
7 M. Uemura, Y. Hayashi and Y. Hayashi, *Tetrahedron: Asymmetry*, 1994, **5**, 1427.
8 H-G. Schmalz and K. Schellhaas, *Tetrahedron Lett.*, 1995, **36**, 5515.
9 M. J. Siwek and J. R. Green, *Chem. Commun.*, 1996, 2359.
10 A. Alexakis, T. Kanger, P. Mangeney, F. Rose-Munch, A. Perrotey and E. Rose, *Tetrahedron: Asymmetry*, 1995, **6**, 2135.
11 A. Quattropani, G. Bernardinelli and E. P Kündig, *Helv. Chim. Acta*, 1999, **82**, 90.
12 A. Quattropani, G. Anderson, G. Bernardinelli and E. P. Kündig, *J. Am. Chem. Soc.*, 1997, **119**, 4773.
13 H-G. Schmalz and K. Schellhaas, *Angew. Chem., Int. Ed. Engl.*, 1996, **35**, 2146.
14 K. Schellhaas, H-G. Schmalz and J. W. Bats, *Chem. Eur. J.*, 1998, **4**, 57.
15 J. Blagg, S. G. Davies, N. J. Holman, C. A. Laughton and B. E. Mobbs, *J. Chem. Soc., Perkin Trans. 1*, 1986, 1581.
16 K. Bambridge, M. J. Begley and N. S. Simpkins, *Tetrahedron Lett.*, 1994, **35**, 3391.
17 E. L. M. Cowton, S. E. Gibson (née Thomas), M. J. Schneider and M. H. Smith, *Chem. Commun.*, 1996, 839.
18 S. Top, G. Jaouen and M. J. McGlinchey, *J. Chem. Soc., Chem. Commun.*, 1980, 1110.
19 R. A. Ewin and N. S. Simpkins, *Synlett*, 1996, 317.
20 R. A. Ewin, A. M. MacLeod, D. A. Price, N. S. Simpkins and A. P. Watt, *J. Chem. Soc., Perkin Trans. 1*, 1997, 401.
21 C. Dewing and D. Hoppe, *Synthesis*, 1996, 149.
22 S. E. Gibson (née Thomas), P. C. V. Potter and M. H. Smith, *Chem. Commun.*, 1996, 2757.
23 J. Blagg, S. G. Davies, C. L. Goodfellow and K. H. Sutton, *J. Chem. Soc., Perkin Trans. 1* , 1987, 1805.
24 T. Nakai and K. Mikami, *Org. React.*, 1994, **46**, 105.
25 T. Nakai and K. Tomooka, *Pure Appl. Chem.*, 1997, **69**, 595.
26 For example, see: D. Enders and D. Backhaus, *Synlett*, 1995, 31; O. Takahashi, K. Mikami and T. Nakai, *Chem. Lett.*, 1987, 69.
27 J. A. Marshall and J. Lebreton, *J. Am. Chem. Soc.*, 1988, **110**, 2925.
28 S. Manabe, *Chem. Commun.*, 1997, 737.
29 M. Uemura, H. Nishimura and Y. Hayashi, *J. Organomet. Chem.*, 1989, **376**, C3; J. Brocard, M. Kahmoudi, L. Pelinski and L. Maciejewski, *Tetrahedron Lett.*, 1989, **30**, 2549; M. Uemura, H. Nishimura, T. Minami and Y. Hayashi, *J. Am. Chem. Soc.*, 1991, **113**, 5402; M. Mahmoudi, L. Pelinski, L. Maciejewski and J. Brocard, *J. Organomet. Chem.*, 1991, **405**, 93.
30 S. E. Gibson (née Thomas), P. Ham and G. R. Jefferson, *Chem. Commun.*, 1998, 123.
31 E. J. Corey and S. S. Kim, *Tetrahedron Lett.*, 1990, **31**, 3715.
32 B. Kaiser and D. Hoppe, *Angew. Chem., Int. Ed. Engl.*, 1995, **34**, 323 and references therein.
33 H. Ahlbrecht, J. Harbach, R. W. Hoffmann and T. Ruhland, *Liebigs Ann. Chem.*, 1995, 211 and references therein.
34 See for example: G. A. Cran, C. L. Gibson, S. Handa and A. R. Kennedy, *Tetrahedron: Asymmetry*, 1996, **7**, 2511.
35 S. E. Gibson (née Thomas), P. Ham, G. R. Jefferson and M. H. Smith, *J. Chem. Soc., Perkin Trans. 1*, 1997, 2161.
36 S. G. Davies and T. D. McCarthy, in *Comprehensive Organometallic Chemistry II*, ed. E. W. Abel, F. G. A. Stone and G. Wilkinson, Pergamon, Oxford, 1995, vol. 12, pp. 1049–51.
37 A. Ariffin, A. J. Blake, R. A. Ewin and N. S. Simpkins, *Tetrahedron: Asymmetry*, 1998, **9**, 2563.
38 S. Top, B. Caro and G. Jaouen, *Tetrahedron Lett.*, 1978, 787.
39 D. Albanese, S. E. Gibson (née Thomas) and E. Rahimian (now Reddington), *Chem. Commun.*, 1998, 2571.
40 S. E. Gibson (née Thomas) and E. Reddington, unpublished results.
41 S. E. Gibson (née Thomas) P. O'Brien and E. Rahimian (now Reddington), *J. Chem. Soc., Perkin Trans. 1*, 1999, 909.
42 A. Alexakis, T. Kanger, P. Mangeney, F. Rose-Munch, A. Perrotey and E. Rose, *Tetrahedron: Asymmetry*, 1995, **6**, 2135.

ChemComm

Electrodeposited nickel and gold nanoscale metal meshes with potentially interesting photonic properties

Lianbin Xu,[ab] Weilie L. Zhou,[b] Christoph Frommen,[b] Ray H. Baughman,[c] Anvar A. Zakhidov,[c] Leszek Malkinski,[b] Jian-Qing Wang[b] and John B. Wiley*[ab]

[a] *Department of Chemistry, University of New Orleans, New Orleans, LA 70148-2820, USA. E-mail: jwiley@uno.edu*
[b] *Advanced Materials Research Institute, University of New Orleans, New Orleans, LA 70148-2820, USA*
[c] *Honeywell Int., Corporate Technology, Morristown, NJ 07962-1021, USA*

Received (in Irvine, CA, USA) 11th January 2000, Accepted 14th April 2000
Published on the Web 22nd May 2000

Nickel and gold meshes having three-dimensional periodicity at optical wavelengths and nanoscale structural fidelity have been prepared by electrodeposition within close-packed silica sphere arrays.

There is major current interest in the fabrication of nanoporous metal arrays.[1–4] Routine access to such materials could impact a variety of areas including photonics, magnetics, catalysis, electrochemical applications and thermoelectrics. Recent reports have described the formation of 3-D metal meshes within colloidal silica or polymer membranes through the use of molten metal infiltration, nanoparticle infiltration and electroless methods.[4–6] Though metal electrodeposition methods have been effectively used for membranes with one-dimensional pore structures,[7] the extension of this technique to three-dimensional structures has not been reported. This electrochemical method has the major advantage of readily producing well defined metal meshes of materials melting at such high temperatures that melt infiltration is prohibited by template structural instability. Herein, we describe the use of this approach for the fabrication of nickel and gold arrays having three-dimensional periodicity at optical wavelengths.

Silica membranes (opal) were prepared by published methods.[8] Silica spheres with a diameter of *ca.* 300 nm diameter were initially prepared from tetraethylorthosilicate (TEOS). The spheres were then formed into close-packed lattices through a sedimentation process over several months. This precipitate was then sintered at 120 °C for two days and then 750 °C for 4 h, producing a robust opalescent piece that could be readily cut into smaller sections. Electrodes were formed from the opal (typically 7 × 10 × 1.5 mm) by first depositing *ca.* 0.5 μm thick copper films on one side of the piece by magnetron sputtering. A length of wire was attached to the copper backing with silver paste (Ted Pella, Inc.) and the copper/wire side of the electrode, as well as the edges, were sealed off with neoprene glue (Elmer's). For metal deposition, the electrodes were immersed into nickel or gold plating solutions (Technic, Inc.) with a platinum wire counter electrode. Electrodeposition was carried out by a constant current method over a 36 h period; a low current density (0.50 mA cm^{-2}) was used in an effort to achieve even deposition within the opal membrane. Low current densities such as that used here have been found to be effective in the growth of nanowires. After deposition, the opal was washed thoroughly with distilled water and the neoprene layer peeled off. To remove the silica matrix, the metal–opal pieces were soaked in a 2% HF solution for 24 h. This resulted in a dark opalescent metal membrane (*ca.* 100 μm thick). Scanning electron micrographs (SEM) were obtained on a JEOL JSM 5410 SEM. Magnetic measurements on the nickel mesh were performed on a Quantum Design MPMS-5S SQUID susceptometer. The mesh was fixed between two pieces of Kapton tape and placed in a commercially available soda straw. No correction for the diamagnetic contribution of the sample holder was taken into account because it was by at least three orders of magnitude smaller than the response generated from the Ni-mesh. The field dependence was studied at various temperatures (2, 10 and 300 K) in external fields up to ±5 T. The temperature dependence was measured in a zero-field cooled (zfc) and a field-cooled (fc) cycle at 1000 G.

This electrodeposition method produces well-defined metal meshes. Fig. 1(a) shows a cross-section of the closed-packed silica membrane (10 000× magnification). Stacking faults are present on (111) planes in the original opal, which will be replicated in the metal mesh. Electrodeposition fills the void space between the close-packed spheres. Fig. 1(b) shows a section of a nickel metal mesh (10 000×) after dissolution of the silica spheres. This image highlights the packing variation for these spheres. Different sections corresponding to (111), (100) and (110) orientations can be observed. Fig. 2(a) and (b) are views of predominately the (100) and the (110) planes, respectively. Fig. 2(c) is a higher magnification (50 000×) of the (100) plane. The square features are essentially cubes with concave sides that arise from filling the octahedral sites in the close-packed structure. Each cube is connected to eight other cubes through its vertices *via* tetrahedra [Fig. 2(d)]. The structure is akin to the fluorite structure (CaF_2) where the calcium ions, representing the cubes, are eight coordinate and the fluoride ions, representing the tetrahedra, are four coordinate. Based on the diameter of the closed-packed spheres of *ca.* 300 nm, one would predict minimum diameters of *ca.* 50, 70 and 120 nm for the interconnects, tetrahedra and cubes, respectively, as is observed. Since the metal mesh crystals are interpenetrating air- and metal-phase networks, they are

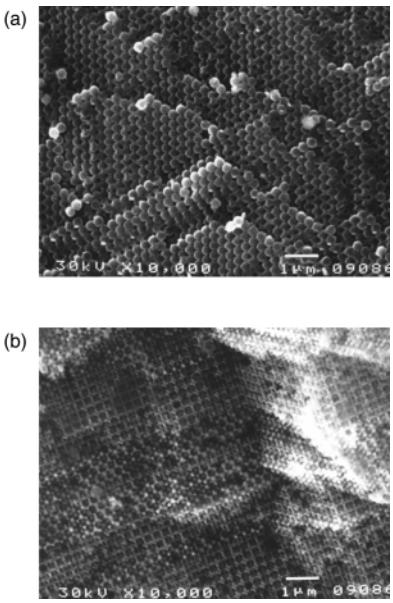

Fig. 1 (a) Scanning electron micrograph of a silica opal piece at 10 000× in the (111) plane. (b) Electrodeposited nickel mesh after dissolution of the opal membrane (10 000×).

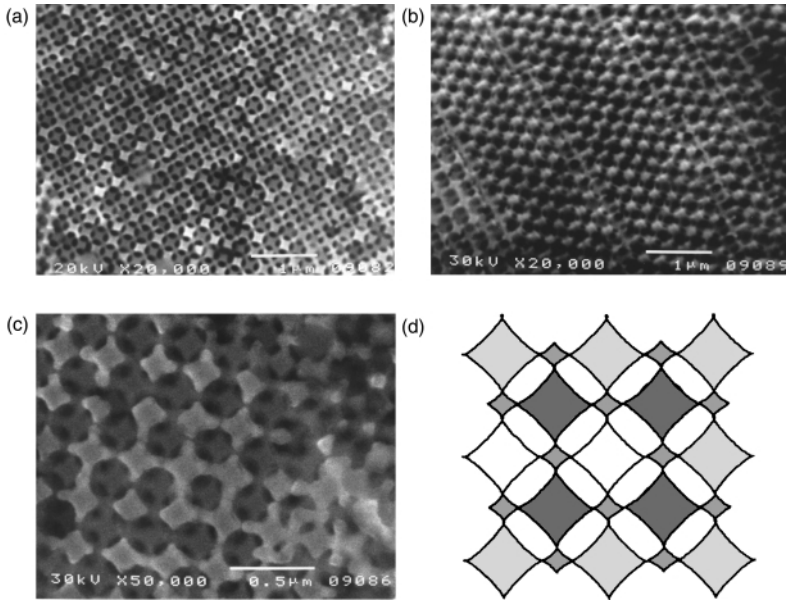

Fig. 2 SEM photographs of (a) nickel metal mesh along the 100 direction, (b) gold mesh predominately along the 110 direction, (c) 50 000× magnification of square nickel mesh and (d) illustration of square motif seen in (c) (the lighter regions are closer and the darker regions are progressively further away).

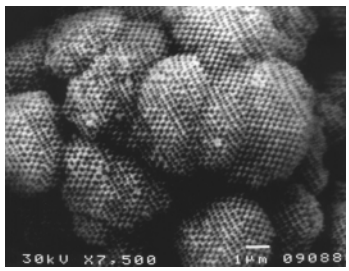

Fig. 3 SEM photograph showing the spherical morphology of the gold mesh (7500×).

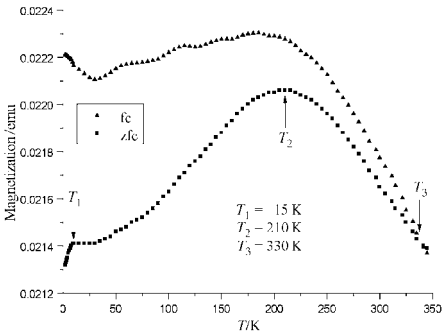

Fig. 4 Zero-field cooled (zfc), field-cooled (fc) cycle in an external field of 1000 G for the electrodeposited Ni-mesh after removal of the opal matrix.

metallo-dielectric photonic crystals, which are predicted to have an unusual metallicity bandgap.[1]

Interestingly, the extended nickel metal arrays maintain their structure after removal of the silica membrane, while the gold arrays appear to collapse in on themselves. Fig. 3 shows a low magnification image (7500×) of gold. Some areas of the mesh appear spherical in what look like 'florets'; localized structural features, however, are still quite apparent between the regions. Though this effect may simply be due to incomplete filling during electrodeposition, it is also possible that it may be associated with the greater malleability of gold relative to that of nickel. A possibly related effect has recently been described by Jiang *et al.*,[6] who reported curling of gold films made by the electroless method.

Magnetic measurements on the nickel mesh show size effects due to the nanometer dimensions of the components. The material exhibited a coercive field (H_c) of 500 G at 2 K that decreased slightly with increasing temperature (H_c = 300 G at 300 K). This value is much higher than that found in bulk nickel, which is on the order of a few tens of G. Such an enhancement in the coercivity is well known for other size-constrained magnetic systems.[9] The presently observed coercive field is about four times smaller than reported for 53 nm diameter electrodeposited Ni wires[10] (2000 G at T = 5 K), which is possibly due to the absence of a 'true' quantum confinement and/or structural disorder. The temperature dependence of the magnetization (Fig. 4) shows a sharp inflection at 15 K, a broad inflection at 210 K and a merging of the fc and zfc curves at 330 K. It is not clear at this point how these features relate to the combined superparamagnetic effects of the components in the metal meshes, interconnects, tetrahedra and cubes. Micromagnetics calculations may give some insight into the response of these arrays.

We gratefully acknowledge support from the Department of Defense (DARPA MDA972-97-1-0003 and DAA-96-J-036).

Notes and references

1 D. F. Sievenpiper, M. E. Sickmiller and E. Yablonovitch, *Phys. Rev. Lett.*, 1996, **76**, 2480; D. F. Sievenpiper, E. Yablonovitch, J. N. Winn, S. Fan, P. R. Villeneuve and J. D. Joannopoulos, *Phys. Rev. Lett.*, 1998, **80**, 2829.
2 M. P. Hogarth, J. Munk, A. K. Shukla and A. J. Hamnett, *Appl. Electrochem.*, 1994, **24**, 85.
3 J. Kleperis, G. Vaivars, A. Vitins, A. Lusis and A. Galkin, *NATO ASI Ser. 3* (New Promising Electrochemical Systems for Rechargeable Batteries), 1996, **6**, 285.
4 R. H. Baughman, A. A. Zakhidov, I. I. Khayrullin, I. A. Udod, C. Cui, G. U. Sumanasekera, L. Grigorian, P. C. Eklund, V. Browning and A. Ehrlich, *Proc. Intl. Conf. Thermoelectrics (ICT'98)*, Nagoya, Japan, 1998.
5 O. D. Velev, P. M. Tessier, A. M. Lenhoff and E. W. Kaler, *Nature*, 1999, **401**, 548.
6 P. Jiang, J. Cizeron, J. F. Bertone and V. L. Colvin, *J. Am. Chem. Soc.*, 1999, **121**, 7957.
7 C. R. Martin, *Chem. Mater.*, 1996, **8**, 1739 and references therein.
8 N. D. Deniskina, D. V. Kalinin and L. K. Kazantseva, *Gem Quality Opals: Synthetic and Natural Genesis*, Nauka, Novosibirsk, 1987 (in Russian); A. P. Philips, *J. Mater. Sci. Lett.*, 1987, **8**, 1371; P. J. Darragh, A. J. Gaskin and J. V. Sanders, *Sci. Am.*, 1976, **234**, 84.
9 B. D. Cullity, *Introduction to Magnetic Materials*, Addison-Wesley Publishing, Reading, MA, 1972, p. 383 and references therein.
10 J. Meier, B. Doudin and J.-Ph. Ansermet, *J. Appl. Phys.*, 1996, **79**, 6010.

On the competing hydrations of sulfur dioxide and sulfur trioxide in our atmosphere

Thomas Loerting,[a] Romano T. Kroemer[b] and Klaus R. Liedl*[a]

[a] *Institute of General, Inorganic and Theoretical Chemistry, University of Innsbruck, Innrain 52a, A-6020 Innsbruck, Austria. E-mail: klaus.liedl@uibk.ac.at*

[b] *Department of Chemistry, Queen Mary & Westfield College, University of London, Mile End Road, London, UK E1 4NS*

Received (in Cambridge, UK) 3rd April 2000, Accepted 2nd May 2000
Published on the Web 22nd May 2000

It is demonstrated that in our atmosphere sulfur trioxide (SO_3) is hydrated rather than the much more abundant sulfur dioxide (SO_2), *i.e.* atmospheric oxidation precedes hydration.

In our atmosphere sulfur dioxide is converted to sulfuric acid, a major component of acid rain, and sulfates, which increase Earth's reflectance by forming nuclei for cloud condensation. The pathway of this conversion is constituted of both an oxidative and hydration step. Whether SO_2 is first oxidized, as proposed by Stockwell and Calvert,[1] or first hydrated is still not fully clear. The direct oxidation of SO_2 by the hydroxyl radical proceeds either without[2] or with a very small energy barrier.[3] Also the activation barrier for oxidation of 'hydrated SO_2' ($HOSO_2^-$) by H_2O_2[4,5] or O_2[6] is rather low. Vincent, Hillier and Palmer conjectured that in fact SO_2 and not the hydrogensulfite anion ($HOSO_2^-$) is oxidized.[5] These low barriers indicate that both oxidations are fast. In order to investigate which of the two possible hydrations is fast or slow, we have performed direct dynamics calculations on reactions (1) and (2)

$$SO_2 + nH_2O \rightleftharpoons SO_2{\cdot}nH_2O \rightleftharpoons \{H_2SO_3{\cdot}(n-1)H_2O\} \quad (1)$$

$$SO_3 + nH_2O \rightleftharpoons SO_3{\cdot}nH_2O \rightleftharpoons H_2SO_4{\cdot}(n-1)H_2O \quad (2)$$

where the size of the involved water-cluster varies from $n = 1$ to 3. For reaction (2) both laboratory studies[7,8] and direct dynamics studies by us[9] on the atmospheric reaction rate constants showed that owing to hydration to sulfuric acid, the lifetime of SO_3 is comparable to that of SO_2 which undergoes oxidation by hydroxyl radicals. The good agreement in the obtained rates demonstrates the reliability of the theoretical methods, namely variational transition state theory corrected for microcanonical optimized multidimensional tunneling on the basis of a hybrid density functional theory potential energy surface [B3LYP/6-31+G(d)].[10,11] Because of the thermodynamic instability of 'sulfurous acid' (H_2SO_3) this species has never been isolated, and accordingly no experimental studies have been performed on reaction (1). This instability has been noted in the literature[12] and is here confirmed to amount to 6.8 kcal mol^{-1} in electronic energy at the CCSD(T)/aug-cc-pVDZ//MP2/aug-cc-pVDZ level of theory. Application of the theoretical approach to the unimolecular isomerization in reaction (1) leads to the reaction rates shown in Fig. 1. It becomes clear that the hydration of SO_3 is much faster than the hydration of SO_2 if more than one water molecule is allowed to participate for all temperatures prevailing in our atmosphere. Only in the case of very low water vapor pressures, under which conditions no complexes of $>1:1$ stoichiometry form, and at temperatures below 150 K the hydration of SO_2 is faster than the one of SO_3. However, 'faster' here in fact means 'less slow' as both conversions are unmeasurably slow under such conditions. In contrast to the facile and fast reactions in aqueous solution ($k = 3.4 \times 10^6$ s^{-1})[13] and the gas–liquid interface[14] the pure gas-phase process involving SO_2–water clusters[15] is very slow. As a consequence, the reaction path not involving hydration of SO_2, namely oxidation of SO_2 with subsequent hydration of SO_3, will be favored under atmospheric conditions. This arises mainly from the fact that the barrier for the SO_2 hydration decreases from 33 kcal mol^{-1} ($n = 1$) to 20 kcal mol^{-1} ($n = 2$) and 13 kcal mol^{-1} ($n = 3$), whereas the barrier for hydration of SO_3 decreases from 28 kcal mol^{-1} ($n = 1$) to 4 kcal mol^{-1} ($n = 3$, rotary)[9] according to the B3LYP/6-31+G(d) level of theory. At the CCSD(T)/aug-cc-pVDZ//MP2/aug-cc-pVDZ level of theory taking electron correlation more accurately into account, the barriers are different by at most 10%. In the literature at the G2[16] and QCISD(t) levels[12] the barriers are also found to be similar.

Additionally, the preassociation reaction forming the hydrogen bonded complex is more favorable for SO_3 than for SO_2, as indicated by a gain in electronic energy of 19.8 kcal mol^{-1} compared to 14.7 kcal mol^{-1} [CCSD(T)/aug-cc-pVDZ//MP2/aug-cc-pVDZ values for $n = 2$]. Therefore, the difference in the overall rate constant is increased by four orders of magnitude at 250 K in addition to the difference seen in Fig. 1. For a first order rate law for SO_2 or SO_3 this implies that the SO_2 pressure has to be 10 orders of magnitude higher than the SO_3 pressure at 250 K and as much as 20 orders of magnitude higher at 150 K for SO_2 hydration to become competitive. However, at an altitude of 30 km the steady state concentration of SO_3 of *ca.* 10^5 molecules cm^{-3} compared with that of SO_2 of *ca.* 10^{10} molecules cm^{-3} is only lower by 5 order of magnitude.[8] It is, therefore, safe to assume that the dominant mechanism converting S(IV) to S(VI) species if *first* the oxidation of SO_2 by OH$^{\cdot}$ and *second* the isomerization of a SO_3–H_2O cluster of a

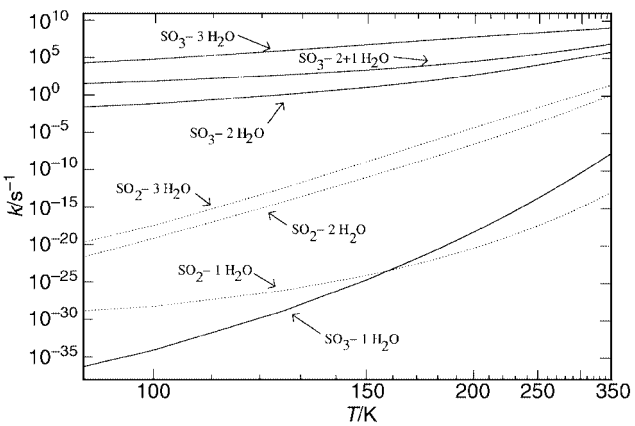

Fig. 1 Arrhenius plot of the hydration reactions of sulfur trioxide (——) and sulfur dioxide (·····) in the presence of up to three water molecules in the unimolecular complex. The meaning of n is explained in Fig. 2 for SO_2 and in our previous work for SO_3.[9]

DOI: 10.1039/b002602f

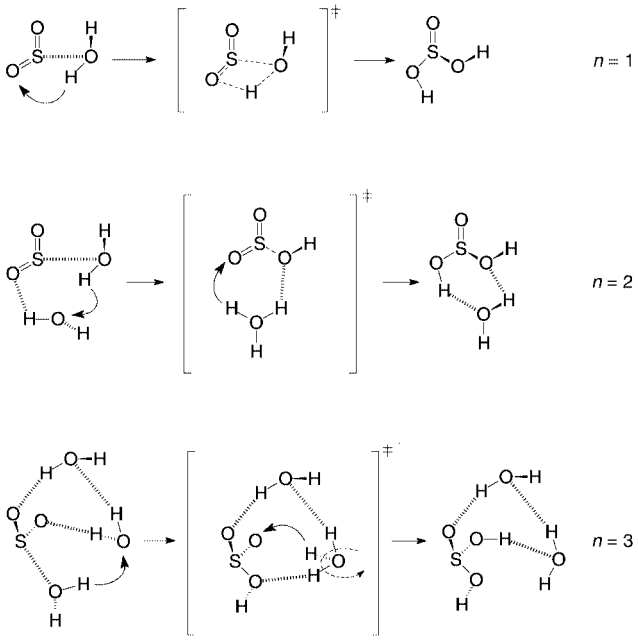

Fig. 2 Qualitative representation of the stationary points of the different unimolecular isomerization steps of the hydration of SO_2. Water addition concerted with a single proton transfer in the presence of a single water molecule (n = 1), hydration concerted with sequential water-mediated double proton transfer (n = 2), and hydration concerted with the sequence proton transfer–rotation of H_3O^+-proton transfer in the presence of a third stabilizing water molecule (n = 3).

stoichiometry of 1:2 or higher, since slow hydration of SO_2 is circumvented.

We are grateful to Markus Loferer for help in the initial stages of the work. Thomas Loerting acknowledges financial support of the Austrian Academy of Sciences. This work was supported by the Austrian Science Fund (grant number P14357-TPH).

Notes and references

1 W. R. Stockwell and J. G. Calvert, *Atmos. Environ.*, 1983, **17**, 2231.
2 P. H. Wine, R. J. Thompson, A. R. Ravishankara, D. H. Semmes, C. A. Gump, A. Tarabi and J. M. Nicovich, *J. Phys. Chem.*, 1984, **88**, 2094.
3 D. Fulle, H. F. Hamann and H. Hippler, *Phys. Chem. Chem. Phys.*, 1999, **1**, 2695.
4 J. V. McArdle and M. R. Hoffmann, *J. Phys. Chem.*, 1983, **87**, 5425.
5 M. A. Vincent, I. H. Hillier and I. J. Palmer, *Chem. Commun.*, 1997, 1725.
6 D. Majumdar, G.-S. Kim, K. S. Oh, J. Y. Lee, K. S. Kim, W. Y. Choi, S.-H. Lee, M.-H. Kang and B. J. Mhin, *J. Chem. Phys.*, 2000, **112**, 723.
7 E. R. Lovejoy, D. R. Hanson and L. G. Huey, *J. Phys. Chem.*, 1996, **100**, 19 911.
8 J. T. Jayne, U. Pöschl, Y.-m. Chen, D. Dai, L. T. Molina, D. R. Worsnop, C. E. Kolb and M. J. Molina, *J. Phys. Chem. A*, 1997, **101**, 10 000.
9 T. Loerting and K. R. Liedl, *Proc. Natl. Acad. Sci. USA*, 2000, **97**, accepted for publication.
10 GAUSSIAN 98. Revision A.7. M. J. Frisch, G. W. Trucks, H. B. Schlegel, G. E. Scuseria, M. A. Robb, J. R. Cheeseman, V. G. Zakrzewski, J. A. Montgomery, Jr., R. E. Stratmann, J. C. Burant, S. Dapprich, J. M. Millam, A. D. Daniels, K. N. Kudin, M. C. Strain, O. Farkas, J. Tomasi, V. Barone, M. Cossi, R. Cammi, B. Mennucci, C. Pomelli, C. Adamo, S. Clifford, J. Ochterski, G. A. Petersson, P. Y. Ayala, Q. Cui, K. Morokuma, D. K. Malick, A. D. Rabuck, K. Raghavachari, J. B. Foresman, J. Cioslowski, J. V. Ortiz, B. B. Stefanov, G. Liu, A. Liashenko, P. Piskorz, I. Komaromi, R. Gomperts, R. L. Martin, D. J. Fox, T. Keith, M. A. Al-Laham, C. Y. Peng, A. Nanayakkara, C. Gonzalez, M. Challacombe, P. M. W. Gill, B. Johnson, W. Chen, M. W. Wong, J. L. Andres, C. Gonzalez, M. Head-Gordon, E. S. Replogle and J. A. Pople, Gaussian, Inc., Pittsburgh PA, 1998.
11 Polyrate8.2. Y.-Y. Chuang, J. C. Corchado, P. L. Fast, J. Villá, E. L. Coitiño, W.-P. Hu, Y.-P. Liu, G. C. Lynch, K. A. Nguyen, C. F. Jackels, M. Z. Gu, I. Rossi, S. Clayton, V. S. Melissas, R. Steckler, B. C. Garrett, A. D. Isaacson and D. G. Truhlar, University of Minnesota, Minneapolis, 1999.
12 E. Bishenden and D. J. Donaldson, *J. Phys. Chem. A*, 1998, **102**, 4638.
13 M. Eigen, K. Kustin and G. Maass, *Z. Phys. Chem.*, 1961, **30**, 130.
14 J. T. Jayne, P. Davidovits, D. R. Worsnop, M. S. Zahniser and C. E. Kolb, *J. Phys. Chem.*, 1990, **94**, 6041.
15 Q. Zhong, S. M. Hurley and A. W. Castleman, Jr., *Int. J. Mass Spectrom. Ion Process.*, 1999, **185**–**187**, 905.
16 W.-K. Li and M. L. McKee, *J. Phys. Chem. A*, 1997, **101**, 9778.

Molybdenum polysulfide hollow microtubules grown at room temperature from solution

Pavel Afanasiev,* Christophe Geantet, Cecile Thomazeau and Bernadette Jouget

Institut de Recherches sur la Catalyse, 2 Avenue A. Einstein, 69626, Villeurbanne, Cédex, France.
E-mail: afanas@catalyse.univ-lyon1.fr

Received (in Oxford, UK) 16th February 2000, Accepted 27th April 2000
Published on the Web 23rd May 2000

Reaction of $(NH_4)_2MoS_4$ and $(NH_2OH)_2{\cdot}H_2SO_4$ under hydrothermal conditions led to the new compound $(NH_3OH)_{3.9}MoS_{4.8}$ I, which crystallises from acetone solution producing hollow tubules of nanoscopic size (50–500 nm diameter, 0.1–20 μm length); thermal decomposition of I led to the formation of highly dispersed tubular MoS_2.

The recent discovery of hollow graphite tubules of nanometer dimensions[1] has greatly stimulated the study of nanoscopic structures. Nanotubes are envisaged for potential applications in several areas such as catalysis, composite materials and nanowires, up to artificial muscles and intramolecular junctions.[2] Several types of nanotubes (and generally, hollow microtubules) have been synthesised. Arc discharge or high temperature treatment of molecular precursors have been applied to elaborate the nanotubes of simple materials such as C,[1] MoS_2[3] or BN.[4] Fullerene-like nanoparticles and nanotubules of the MS_2 sulfides (M = Mo, W) could be obtained using high temperature reactions of the corresponding oxides with H_2S, or by means of sonoelectrochemical syntheses.[5] Different types of nanoscopic tubules were obtained at low temperatures, using templating reactions with organic surfactants. This approach has led to hollow tubules of oxides such as SiO_2[6] or V_2O_5.[7] Tubular MoS_2 has been prepared by decomposition of $(NH_4)_2MoS_4$ within the pores of an alumina membrane, followed by dissolution of the templating oxide in aqueous NaOH.[8]

Here, we report on a new type of inorganic hollow tube, formed at low temperature without addition of template. A newly synthesised compound $(NH_3OH)_xMoS_y$, ($3 < x < 4$, $4 < y < 5$) prepared hydrothermally, led to tubules upon crystallization at room temperature.

The preparation technique was as follows. To a stainless steel vessel were added solutions of 2.8 g $(NH_4)_2MoS_4$ (ATM) in 100 ml of water and 8 g $(NH_2OH)_2{\cdot}H_2SO_4$ dissolved in 100 ml of water. An H_2S pressure of 20 bar was then applied to the reaction mixture and after 30 min at 493 K a brown powder was filtered off, washed with distilled water and dried in air. The product was then treated with acetone in a Soxhlet apparatus for 2 h. A dark red washing solution of **I** was obtained and a brown insoluble residual **II** (*ca.* 1 g) was collected from the filter. The acetone solution was cooled to room temperature and evaporated in a glass vessel in air. After evaporation of the acetone, 0.7 g of light brown powder **I** was obtained.

The solids were characterised by several physico-chemical techniques, including X-ray diffraction (XRD), FTIR spectroscopy and surface area measurements. High resolution transmission electron microscopy (HREM) combined with EDX analysis was performed on a JEOL 2010 microscope. EXAFS measurements were performed at the Laboratoire d'Utilisation du Rayonnement Electromagnétique (LURE), on the XAS2 spectrometer. Measurements were carried out in transmission mode at the Mo K edge in the range 19900–21000 eV at 8 K. The EXAFS data were treated with SEDEM[9] and FEFF[10] programs. X-Ray photoelectron spectra (XPS) were measured on a VG ESCALAB 200R spectrometer using Al-Kα radiation. Thermal decomposition of solids was studied using a mass-spectrometer Gas trace A instrument (FISONS Instruments).

Dispersed MoS_2 for catalytic applications is often obtained from the decomposition of ATM. To prepare dispersed MoS_2 in an aqueous medium, we studied the reactions of ATM in the presence of inorganic reducing agents, such as hydroxylamine and hydrazine.[11] If a solution of $(NH_2OH)_2{\cdot}H_2SO_4$ was added at room temperature to aqueous ATM, an MoS_3 suspension was formed according to reaction (1), due to the acidic pH of the reaction medium.

$$(NH_4)_2MoS_4 + 2\ H^+ \rightarrow MoS_3 + 2NH_4^+ + H_2S \qquad (1)$$

However, under the mild hydrothermal conditions used (20 bar H_2S, 493 K, 30 min), MoS_3 reacted further to give a dark brown solid **I** which was insoluble in water but partially soluble in acetone. According to chemical analysis, solid **I** had composition $(NH_3OH)_{3.9}MoS_{4.8}$, close to the idealised formula $(NH_3OH)_4MoS_5$.

The insoluble brown residual **II** had chemical composition $MoS_{7.88}$, close to the MoS_8 stoichiometry. The amounts of nitrogen and oxygen in solid **II** were $< 0.5\%$.

Scanning electron microscopy revealed that **I** consists mostly of hollow tubes of different diameters and lengths. The external diameter of tubules varied from 50 to 500 nm whereas the length was between 0.1 and 20 μm. Some irregular spherical agglomerates were also observed. Transmission electron microscopy (Fig. 1) showed that the tubes are hollow, with straight walls. Electron diffraction did not reveal any crystal ordering in the tubules or spherical agglomerates.

Solid **II** consisted of shapeless agglomerates and was XRD amorphous but was fairly homogeneous according to HREM

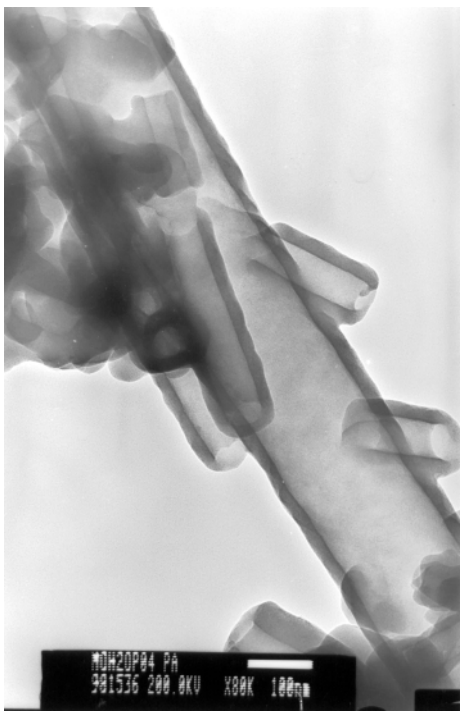

Fig. 1 Transmission electron micrograph of tubules of solid **I**.

DOI: 10.1039/b001406k

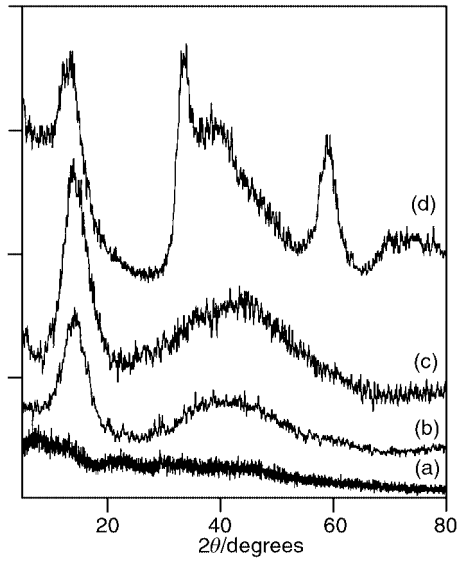

Fig. 2 Powder XRD patterns of (a) solid **I**, (b) solid **II**, (c) reference MoS_3 and (d) MoS_2 obtained from decomposition of **I** at 823 K.

and EDX studies. Formation of **II** has been observed under different reaction conditions. A solid of composition $MoS_{7.6}$ was obtained at 1 bar of H_2S and 373 K (in this case an acetone-soluble product was not formed). We suggest therefore that solid **II** is a distinct compound close to the MoS_8 composition.

The preparation of microtubules **I** was reproduced under various reaction conditions. For example, at 473 K and for a reaction time of 1 h, a solid of composition $(NH_3OH)_{3.4}MoS_{4.7}$ was obtained, in somewhat lower yield and with a decreased but still high number of tubules. Tubules **I** could be repeatedly redissolved in acetone and reprecipitated by slow evaporation, either at ambient conditions or at 313 K.

The role of hydroxylamine in the synthesis is, as yet, not clear but is certainly important, since without addition of hydroxylamine only poorly crystallised MoS_2 was obtained under the same reaction conditions. Our attempts to prepare single crystals of **I** suitable for structure determination, *via* crystallisation from alcohols or methylformamide were not successful.

The powder XRD pattern of **I** [Fig. 2(a)] showed only a broad peak, corresponding to an interplanar distance of *ca.* 1.08 nm. Solid **II** [Fig. 2(b)] was also XRD amorphous, with broad maxima close to those of the MoS_3 reference sample [Fig. 2(c)].

In the IR spectrum of **I**, intense absorptions at 499 and 350 cm^{-1} were observed, characteristic for Mo–S bonds.[12] The IR spectrum of **II** showed the same Mo–S features, and a broad peak at *ca.* 520 cm^{-1} attributed to S–S stretching vibrations. Comparison of the IR spectra suggests that **II** contains many S–S bonds whereas they are absent in **I**.

XPS binding energies were studied at the Mo 3d and S 2p levels (C 1s reference binding energy = 284.5 eV). The binding energies are estimated at an accuracy of *ca.* 0.2 eV. Single molybdenum species were observed in both **I** and **II**. The Mo $3d_{5/2}$ binding energies in **I** and **II** were 229.8 and 229.1, respectively, suggesting that in **I** the electron density on Mo is lower, than in **II**. The sulfur S 2p binding energies are 163.2 and 162.8 eV for **I** and **II**, at the positions of ionic (sulfoxide) sulfur[13] and terminal bidentate S_2^{2-} species, respectively.[14] Both changes of molybdenum and sulfur signals from **I** to **II** correspond to the removal of S–S bridges with simultaneous formation of terminal Mo–S species, in which sulfur is probably coordinated to nitrogen or oxygen.

Results of EXAFS studies of **I** and **II** are listed in Table 1 and compared to the literature data on Mo coordination in some reference compounds. For the EXAFS fit for **I** and **II**, the energy shift ΔE_0 was 4 eV for the Mo–S and 9 eV for the Mo–Mo shell. Debye–Waller factors for both shells were in the range *ca.* 2.10–5 nm^2. According to the EXAFS fitting results, molybdenum has approximately the same number (*N*) of S and Mo neighbours in **I** as in MoS_3, but a considerably longer Mo–Mo distance. By contrast, a short Mo–Mo distance was observed in **II**, but the number of S neighbours is significantly higher than in MoS_3, and even higher than that in $MoS_{4.7}$.[15]

Table 1 EXAFS fitting results of molybdenum coordination in **I** and **II** as well as for some reference sulfide compounds

Sample (state[a])	Mo–S	*N*(S)	Mo–Mo	*N*(Mo)	Ref.
I (am)	2.33	1.3	3.05	1.08	—
	2.49	3.8			
II (am)	2.40	4.1	2.75	0.92	—
	2.48	4.5			
MoS_3 (am)	2.43	6	2.75	1	15
$MoS_{4.7}$ (am)	2.44	7.33	2.78	1.33	15
MoS_3 (am)	2.44	5.5	2.75	1–2	16
$(NH_4)_2Mo_2S_{12}\cdot 2H_2O$ (cr)	2.38–2.5	8	2.82	1	17

[a] am = Amorphous, cr = crystalline.

Both **I** and **II** are chemically derived from MoS_3 (which itself possesses a poorly organized, probably chainlike structure). It can be suggested that **I** and **II** are formed by addition of sulfide ions or of zerovalent sulfur to the MoS_3 chains, giving, respectively, MoS_5^{2-} (solid **I**) or MoS_8 (solid **II**). Since **I** is soluble in acetone it is probably oligomeric with short chains, whereas **II** is insoluble in any solvent, which suggests a three-dimensional or chainlike structure. The reason why a tubular morphology is adopted by **I** is not yet understood and the reaction mechanism requires further clarification.

Heating compound **I** under an inert gas flow at 823 K leads to its decomposition with formation of pure MoS_2 [Fig. 2(d)]. Decomposition of **I** was monitored by mass spectrometry which established a multistep process with formation of water and ammonia at *ca.* 435 K, and water and nitrogen at 683 K. According to thermogravimetric analysis, the mass loss at 823 K was 64%, whereas the calculated value for $(NH_3OH)_4MoS_5$ decomposition to MoS_2 is 59%. The MoS_2 obtained from **I** showed a specific surface area of 65 $m^2\ g^{-1}$ with retention of the same tubular morphology as the precursor. The synthesis reported here provides therefore a route to large scale production of hollow microtubules of the technologically very important MoS_2.

Notes and references

1 S. Iijima, *Nature*, 1991, **354**, 56.
2 Z. Yao, H. W. Ch. Postma, L. Balents and C. Dekker, *Nature*, 1999, **402**, 273.
3 L. Margulis, G. Salitra, R. Tenne and M. Talianker, *Nature*, 1993, **365**, 113.
4 A. Loiseau, F. Willaime, N. Demoncy, G. Hug and H. Pascard, *Phys. Rev. Lett.*, 1996, **76**, 4737.
5 Y. Mastai, M. Homyonfer, A. Gedanken and G. Hodes, *Adv. Mater.*, 1999, **11**, 1010.
6 F. Miyaji, S. A. Davis, J. P. H. Charmant and S. Mann, *Chem. Mater.*, 1999, **11**, 3021.
7 M. E. Spahr, P. Bitterli, R. Nesper, M. Müller, F. Krumeich and H. U. Nissen, *Angew. Chem., Int. Ed.*, 1998, **37**, 1263.
8 C. M. Zelenski and P. K. Dorhout, *J. Am. Chem. Soc.*, 1998, **120**, 734.
9 D. Aberdam, *J. Synchrotron Radiat.*, 1998, **5**, 1287.
10 J. J. Rehr, S. I. Zabinsky and R. C. Albers, *Phys. Rev. Lett.*, 1992, **69**, 3397.
11 P. Afanasiev, G.-F. Xia, G. Berhault, B. Jouguet and M. Lacroix, *Chem. Mater.*, 1999, **11**, 3216.
12 Th. Weber, J. C. Muijers and J. W. Niemantsverdriet, *J. Phys. Chem.*, 1995, **99**, 9194.
13 B. J. Lindberg, K. Hamrin, G. Johansson, V. Gelius, A. Falhmann, C. Nordling and K. Siegbahn, *Phys. Scr.*, 1970, **1**, 286.
14 J. C. Muijers, Th. Weber, R. M. van Hardeveld, H. W. Zandbergen and J. W. Niemantsverdriet, *J. Catal.*, 1995, **157**, 698.
15 S. J. Hibble, D. A. Rice, D. M. Pickup and M. P. Beer, *Inorg. Chem.*, 1995, **34**, 5109.
16 S. P. Cramer, K. S. Liang, A. J. Jacobson, C. H. Chang and R. R. Chianelli, *Inorg. Chem.*, 1984, **23**, 1215.
17 A. Muller, W. O. Nolte and B. Krebs, *Inorg. Chem.*, 1980, **19**, 2835.

ChemComm

2D correlation IR spectroscopy of xylene isomerisation on H-MFI zeolite

F. Thibault-Starzyk,* Alexandre Vimont, Christian Fernandez and Jean-Pierre Gilson

Laboratoire Catalyse & Spectrochimie, CNRS - Institut des Sciences de la Matière et du Rayonnement, 6 Boulevard du Maréchal Juin, F-14050 Caen cedex, France. E-mail: fts@ismra.fr

Received (in Oxford, UK) 10th March 2000, Accepted 26th April 2000
Published on the Web 22nd May 2000

2D correlation IR spectroscopy (2D-COS) allows quantitative monitoring of xylene isomers in the pores of H-MFI zeolite under working conditions; coke bands invisible in the direct spectra are detected, indicating traces of coke localised on specific OH groups.

IR spectroscopy is nowadays used routinely for the study of the surface of working heterogeneous catalysts in catalytic reactors equipped with IR transparent windows. It has, for example, been applied to xylene isomerisation in zeolites.[1] The main difficulty resides in the complexity of the spectra, and in the choice of adequate bands for the characterisation and quantification of species of interest. Detection of trace compounds is often a problem because of the low signal to noise ratio obtained at high temperatures in the IR cell. New data treatment methods such as 2D correlation IR spectroscopy (2D-COS) have led to significant improvements in this area.[2,3] We report here, the application of 2D-COS to the *in situ* IR study of *o*-xylene isomerisation in H-MFI zeolite under working conditions. This led to an improvement in the quantitative monitoring of xylene isomers in the micropores of the solid and to the detection of traces of coke in the catalyst. A correlation was found between the degree of coke incorporation and the perturbation of specific hydroxy groups in the solid.

Experiments were performed in a microreactor-IR cell already described elsewhere,[4] in which the spectra of both the self supported wafer of the catalyst and the adsorbed species can be recorded during the reaction up to 725 K. A nitrogen gas stream was diverted to a saturator filled with *o*-xylene and maintained at a constant temperature (300 K) and the resulting mixture fed to the reactor/IR cell. The reaction conditions were: 473–573 K, 8 Torr *o*-xylene partial pressure, WHSV: 2.7 h^{-1}. The reaction products exiting the reactor were analysed by gas chromatography. The spectrometer was a Nicolet Magna 750, used at 2 cm^{-1} resolution (Happ-Genzel apodisation function).

The spectrum of the activated zeolite at 473 K shows in the ν(OH) stretching vibration region two intense bands at 3738 and 3602 cm^{-1}, assigned to the stretching vibrations of silanols and acidic bridged hydroxy groups, respectively. Upon *o*-xylene adsorption at this temperature, the intensities of both bands immediately decreased. Attenuation is moderate for the silanol band (10%), indicating only a weak interaction. By contrast, the intensity decrease of the acidic hydroxy band is much more substantial (70% reduction) and can be assigned to the formation of hydrogen bonds with the aromatic molecule. The perturbed OH leads to a broad band centred at 3200 cm^{-1}. At the same time, a complex group of bands appears between 1380 and 1600 cm^{-1}, assigned to vibrations of the adsorbed *o*-xylene. During the first few minutes of reaction, a new band appears at 1605 cm^{-1}, assigned to the ν_{8a} or ν_{8b} vibration of *m*-xylene (1610 cm^{-1} in the liquid phase). Although *p*-xylene should exhibit an intense and characteristic band (1515 cm^{-1} in the liquid phase), this is not observed on the surface, although *p*-xylene is present in the reaction products (GC analysis). This is probably related to its fast diffusion in the pore system preventing its building up and detection inside the catalyst pores under our reaction conditions (2 ± 0.2% conversion).

2D-IR spectroscopy was introduced by Noda *et al.*,[2] and was initially based on time resolved IR spectroscopy of a sinusoidal perturbation such as that produced by the mechanical strain of a vibrating polymer. Noda later proposed to generalise his method to non-sinusoidal perturbations such as irradiation or electrochemical perturbations,[3] leading to significant increases in sensitivity and resolution of complex band groups. Here, we consider the chemical reaction as the perturbation. We used 2D-COS analysis of a series of spectra recorded between 4 and 14 min reaction time in the *o*-xylene isomerisation reaction to resolve the aromatic vibration bands (Fig. 1).

2D-COS allows analysis of spectral changes with time. Spectra can be obtained either by a Fourier transform of the interferograms recorded at regular time intervals, or by a simple covariance analysis in the spectral series, by use of eqn. (1)

$$\mathrm{COV}\,(\nu_1,\nu_2) = \frac{1}{N}\sum_{i=1}^{i=N}[A_i(\nu_1) - \bar{A}(\nu_1)][A_i(\nu_2) - \bar{A}(\nu_2)]$$

$$r(\nu_1,\nu_2) = \frac{\mathrm{COV}\,(\nu_1,\nu_2)}{\sigma_{\nu 1},\sigma_{\nu 2}} \qquad (1)$$

where N is the total number of spectra recorded, $A_i(\nu_1)$ the absorbance at ν_1 for the ith spectrum, $\bar{A}(\nu_1)$ the absorbance at ν_1 for the reference spectrum and $r(\nu_1, \nu_2)$ the correlation coefficient between intensities at wavenumbers ν_1 and ν_2. The reference spectrum is generally the arithmetic mean spectrum but the first spectrum or the spectrum at steady-state can also be used. $\sigma_{\nu 1}$, $\sigma_{\nu 2}$ are the standard deviations at ν_1 and ν_2, respectively. A 2D display of the covariance or correlation between all frequencies in the spectrum gives information on the relationship existing between various bands, depending on their simultaneous or independent intensity variations. In the following, we elect to split the graphical display into two separate sets for positive and negative covariance, to identify bands varying in the same way (positive covariance, Fig. 2) or in opposite ways (negative covariance, not shown). During isomerisation, *o*-xylene is progressively replaced by *m*-xylene which accumulates in the pore system. A negative correlation

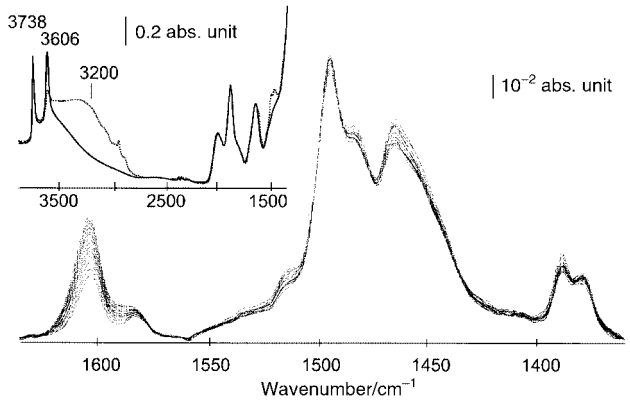

Fig. 1 Some spectra recorded between 4 and 14 min reaction time at 473 K. Inset: spectra of the clean catalyst (——) and of the catalyst under working conditions (····).

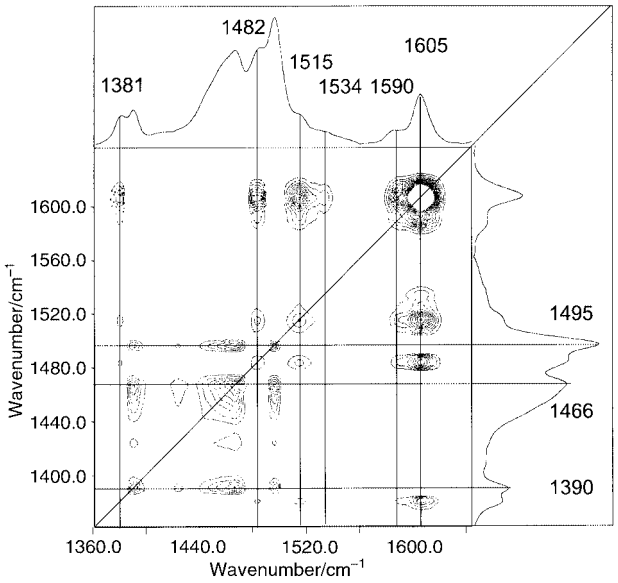

Fig. 2 2D positive covariance map obtained with 34 spectra recorded between 4 and 14 min reaction time at 473 K. The spectra shown on the axes are the mean spectra in the series.

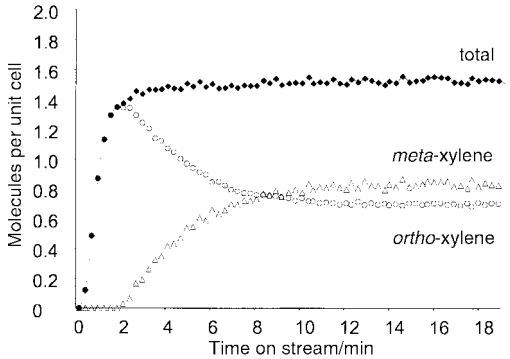

Fig. 3 Concentration of isomers in the pores at 473 K determined by IR using bands studied by 2D-COS.

should therefore appear between the *o*-xylene bands (whose intensities decrease) and the *m*-xylene bands (whose intensities increase). On the other hand, bands having contributions from *o*-xylene are autocorrelated, as are bands having contributions from *m*-xylene. Assignment of bands is thus considerably eased. Additionally, it was possible to detect very weak bands which are invisible in the normal 1D spectra. At 473 K, *m*-xylene bands occur at 1605, 1590, 1535, 1515, 1482 and 1381 cm^{-1}, and *o*-xylene bands are at 1495, 1466, 1458, 1423, 1412 and 1390 cm^{-1}. The regions exhibiting the most intense negative correlation were chosen for the *in situ* quantitative monitoring: 1605 cm^{-1} for *m*-xylene and 1466 cm^{-1} for *o*-xylene. Approximate extinction coefficients for these two bands were determined by adsorbing the two pure isomers on the catalyst at 400 K (highest temperature achievable without isomerisation) under the same conditions in the IR cell and in a thermogravimetric MacBain balance. The obtained values were ε_{1605} = 0.026 ± 0.004 cm μmol^{-1} and ε_{1466} = 0.029 ± 0.004 cm μmol^{-1}. The IR intensities of these two bands can be used to measure the concentrations of the isomers in the pore system and their change with time on stream (Fig. 3).

2D-COS is particularly powerful when applied to spectra recorded at higher temperature, with low signal to noise ratio, during the reaction at 573 K. When the steady state is reached after the initial adsorption step, no change is observable in the 1D spectra, but 2D-COS clearly shows a cross-peak in the region of aromatic vibrations at 1596 cm^{-1} (Fig. 4, left). A very weak band is found at this wavenumber in the 1D spectra, which is masked by overlapping xylene bands. The negative covariance map between the region of aromatic vibrations and ν(OH) bands (Fig. 4, right) indicates a link between the 1596 cm^{-1} band and a decrease of the intensity of two bands located at 3727 and 3656 cm^{-1} assigned to low frequency silanols and to extraframework AlOH groups, respectively.[5] By flushing the catalyst surface with pure helium at the reaction temperature, adsorbed xylenes are eliminated, and the corresponding bands disappear. A species, however, remains adsorbed on the surface, and is characterised by a band at 1596 cm^{-1}. Additionally ν(OH) bands are not completely recovered, and (very) weak negative bands appear in the difference spectrum at 3727 and 3656 cm^{-1}. These correspond to the perturbation of the low wavenumber silanols and of the extraframework AlOH groups detected in the course of the reaction by 2D-COS. We interpret this result in terms of traces of coke (bands around 1600 cm^{-1} are generally observed after coke formation on zeolites in hydrocarbon conversion reactions),[6,7] localised on these specific silanol and AlOH groups, but not on the acidic (bridged OH) sites. Coke is only present in trace amounts and the activity remains constant throughout the reaction. A slight increase in *para*-selectivity is however observed by GC analysis of the products. Unambiguous determination of the localisation of these OH groups in the microporous structure is currently in progress.

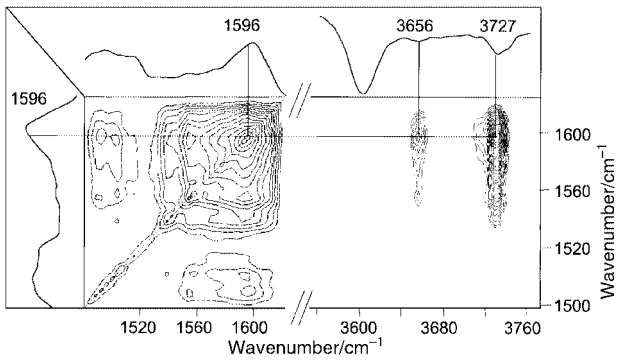

Fig. 4 Left: positive covariance analysis of the 1360–1650 cm^{-1} region during isomerisation at 573 K (188 spectra, 60 min). A large covariance peak centred at 1596 cm^{-1} was detected which could not be assigned to a xylene isomer. The weak signal to noise ratio in the direct spectra did not allow its observation without 2D-COS. Right: negative covariance analysis of the same series of spectra between the band at 1596 cm^{-1} and the ν(OH) region. Although adsorbed *m*-xylene led to the band at 1600 cm^{-1}, the maximum negative correlation was observed at 1596 cm^{-1}. It should be noted that the perturbation of the acidic sites [ν(OH) at 3600 cm^{-1}] was not linked to the perturbations described here. The spectra on the axes are not normal 1D spectra, but are mean spectra of the series which are displayed for clarity.

2D-COS treatment of the spectra is therefore a powerful new technique; it enables a much more detailed analysis of IR spectra, in particular for the monitoring of the working catalyst. Non-interfering bands can be chosen for the quantitative measurement of surface species under reaction conditions at 473K. At higher temperature (lower signal to noise ratio), traces of coke can be detected on H-MFI zeolite, linked to the perturbation of specific OH groups (not those of the acidic sites).

Notes and references

1 J. A. Lercher, G. Mirth and J. Cejka, *Zeolites*, 1996, **17**, 265.
2 I. Noda, A.E. Dowrey and C. Marcott, *Mikrochim. Acta (Wien)*, 1988, **1**, 101.
3 I. Noda, *Appl. Spectrosc.*, 1993, **47**, 1329.
4 J. F. Joly, N. Zanier-Szydlowski, S. Colin, F. Raatz, J. Saussey and J. C. Lavalley, *Catal. Today*, 1991, **9**, 31.
5 A. Maijanen, E. G. Derouane and J. B. Nagy, *Appl. Surf. Sci.*, 1994, **75**, 204.
6 A. Vimont, O. Marie, J. P. Gilson, J. Saussey, F. Thibault-Starzyk and J. C. Lavalley, *Stud. Surf. Sci. Catal.*, 1999, **126**, 147.
7 H. G. Karge, W. Niessen and H. Bludau, *Appl. Catal. A: General*, 1996, **146**, 339.

The development of an electropolymerisable unit for TTF-thiophene fused monomers

Peter J. Skabara,*† Donna M. Roberts, Igor M. Serebryakov and Cristina Pozo-Gonzalo

Materials Research Institute, Sheffield Hallam University, Sheffield, UK S1 1WB. E-mail: P.J.Skabara@shu.ac.uk

Received (in Oxford, UK) 10th March 2000, Accepted 27th April 2000
Published on the Web 22nd May 2000

A novel poly(terthiophene) species provides the first example of an annelated TTF-thiophene derivative which can be polymerised electrochemically.

In general, the electropolymerisation of a conducting polymer is of particular interest for the following reasons: (i) the process is relatively cheap and can be performed on a small scale; (ii) the 'clean' reaction proceeds in the absence of a catalyst or other chemical reagents; (iii) the electrochemistry of the polymer can be investigated almost immediately and (iv) the electronic bandgap of the polymer can be measured by cyclic voltammetry and is usually comparable to the optical bandgap measured by UV–VIS spectroscopy.

Although we have recently prepared polymer **1** using chemical coupling methods,[1] the electropolymerisation of thiophene units bearing fused **2**[2] or covalently attached[2,3] TTFs

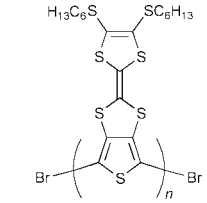

1

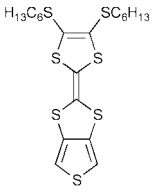

2

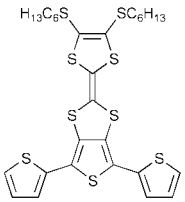

3

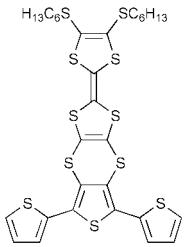

4

has so far eluded the field. The consensus of opinion points towards the fulvalene acting as a radical scavenger which, together with some degree of intramolecular coulombic repulsion between charged oxidised intermediates, renders the thiophene moiety inert to oxidative coupling reactions. The electrosynthesis of polythiophenes, linked to TTF units *via* saturated spacer groups, has been well established by the group of Roncali,[4] yet the successful electropolymerisation of conjugated TTF-thiophene monomers remains a challenge. In response to this, we have prepared compounds **3** and **4**, which are terthiophene analogues of **2**. The propensity towards electropolymerisation for these derivatives should be improved by the increased donor ability of the thiophene functionality (the oxidation potential of oligothiophenes decreases with an extension of the chain length).

The target compounds were prepared using standard phosphite-mediated cross-coupling reactions of 1,3-dithiole-2-chalcogenones (Scheme 1).[5] Thus, terthiophenes **5**[6] and **6**[7] were

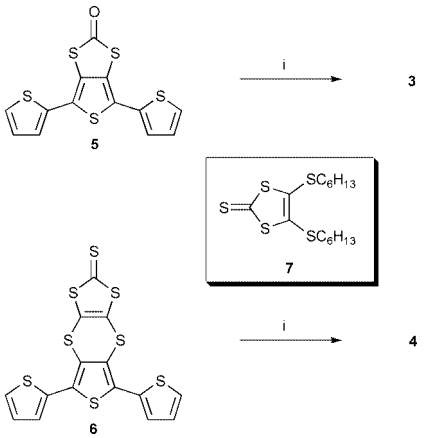

Scheme 1 *Reagents and conditions*: i, $P(OEt)_3$, **7**, 120 °C, 6 h.

reacted with dithiole **7**[8] in the presence of triethyl phosphite at 120 °C, to afford compounds **3** and **4** (30–40% yield in both cases).‡

The electrochemical behaviour of compounds **2**–**4** is summarised in Table 1.§ All three compounds show two sequential reversible oxidation waves corresponding to the formation of the TTF radical cation and dication, respectively. It is noteworthy that the oxidation values for the two terthiophene derivatives are almost identical, thereby indicating that any inductive effect due to the 1,4-dithiin ring is negligible. However, each oxidation of the TTF moiety in **2** is shifted to a more positive value by *ca.* 100 mV, compared to derivatives **3** and **4**. The electronic effect of the fused thiophene ring upon the TTF unit can be explained by a σ electron-withdrawing effect in **2**, which is reduced by a counter-active π-resonance effect of the two peripheral thiophene rings in **3** and **4**.

The high value for the irreversible oxidation of the thiophene ring in **2** (E_3 = +2.18 V)[9] is unfavourable for electropolymerisation, however, the corresponding oxidation processes for compounds **3** and **4** are reduced to +1.55 and +1.52 V, respectively. These values are relatively high for terthiophene derivatives in general and are probably due to an electron withdrawing effect of the TTF dication. For electropolymerisation experiments, repetitive scanning over the range 0.0 to +1.6 V was performed, using a Ag/AgCl reference electrode and a gold disk working electrode in a dichloromethane–hexane (2 : 1) solution containing tetrabutylammonium hexafluorophosphate (0.1 M) as the supporting electrolyte. As we have observed previously,[9] monomer **2** failed to polymerise; however, we were quite surprised to discover different electrochemical reactivities

Table 1 Cyclic voltammetric data for compounds **2**–**4**

Compound	$E_1^{\frac{1}{2}}$/V	$E_2^{\frac{1}{2}}$/V	E_3/V[a]
2	+0.74	+1.10	+2.18
3	+0.64	+1.02	+1.55
4	+0.64	+0.99	+1.52

[a] Irreversible peaks.

† New address: Department of Chemistry, University of Manchester.

DOI: 10.1039/b001943g

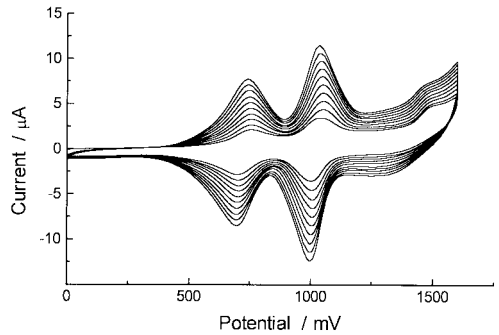

Fig. 1 Electropolymerisation of **4** in dichloromethane–hexane (2 : 1).

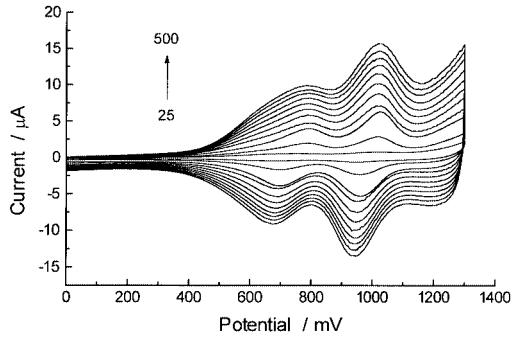

Fig. 2 Cyclic voltammograms of poly(**4**) in monomer-free acetonitrile solution at scan rates of 25, 50, 100, 150, 200, 250, 300, 350, 400, 450 and 500 mV s^{-1}.

for compounds **3** and **4**, despite the close similarity in redox potentials. Although, in the case of **3**, we observed the formation of a red film on the surface of the electrode, cyclic voltammetry clearly showed that this was not of polymeric nature. Conversely, reproducible films of poly(**4**) were obtained under identical conditions; a typical trace showing polymer growth over 10 cycles can be seen in Fig. 1. The proportionally higher increase in current between scans for $E_2^{\frac{1}{2}}$, compared to the first oxidation wave, has been seen previously in poly(bithiophenes) linked to TTF units *via* saturated spacer groups.[4c] This type of behaviour shows that the second oxidation of the TTF species develops independently of charge-transport through the film, which is not the case for $E_1^{\frac{1}{2}}$.

Fig. 2 features cyclic voltammograms of poly(**4**) at various scan rates (25–500 mV s^{-1}) in monomer-free acetonitrile solution. The relationship between the maximum peak current and the scan rate (100–500 mV s^{-1}) is linear with a high correlation coefficient ($r > 0.996$). This behaviour is typical of an electroactive polymer attached to an electrode surface and exemplifies the stability of poly(**4**) towards p-doping up to +1.3 V. At higher potentials the CV behaviour becomes ambiguous. Although the polymer does not appear to decompose or break down in the range −1.5 to +2.0 V, the CVs obtained within these limits are poorly defined and irreproducible.

Poly(**4**) was prepared on ITO glass and the electronic spectrum of the film was recorded. Two broad peaks are observed at λ_{max} = 459 and 833 nm (λ_{max} for compound **4** in dichloromethane is at 344 nm, Fig. 3). The latter peak indicates that the as-grown polymer remains in the oxidised state, however, since doped polythiophene and $TTF^{\bullet+}$ species absorb in this region, the identity of the oxidised species is uncertain. Rinsing the polymer film thoroughly with hydrazine had no effect on the electronic spectrum of poly(**4**), showing that the polymer is quite stable in the doped state. However, after repetitive cycling of the polymer film over the range −0.3 to 0.0 V for 2 h, we were able to obtain the electronic spectrum of the neutral polymer (Fig. 3). A broad band is observed (λ_{max} = 449 nm), extending to *ca.* 736 nm, which is typical behaviour for a

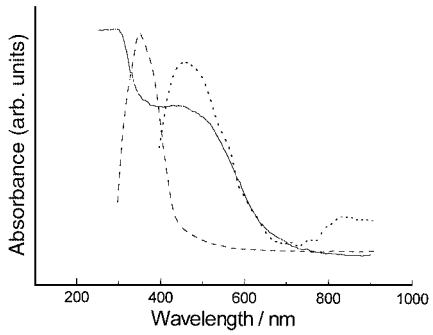

Fig. 3 Electronic absorption spectra of compound **4** in dichloromethane (- - - - -), oxidised poly(**4**) on ITO glass (·····) and neutral poly(**4**) on ITO glass (——).

polythiophene system. The absence of a second peak above 800 nm confirms the neutral state of poly(**4**) and the optical bandgap of the neutral polymer (1.69 eV) was found to be somewhat higher than the bandgap determined electrochemically (1.39 V).

In summary, we have presented a logical strategy towards the design of a polymerisable fused TTF-thiophene derivative. Beginning with a monomer unit **2** which has been acknowledged as being *a priori* for the formation of a regiospecific TTF-thiophene polymer,[10] we have highlighted the problems which arise from unfavourable interactions between the two redox units towards electropolymerisation. On one hand, the use of a terthiophene building-block is essential for a low oxidation value of the polymerisable moiety. Secondly, since **3** cannot be polymerised electrochemically, the incorporation of a fused 1,4-dithiin bridging unit in **4** presumably ensures a favourable spin density distribution in the radical trication for polymerisation to take place. We conclude that, in order to understand the nature of poly(**4**) at higher and lower potentials, a detailed spectroelectrochemical investigation would be extremely worthwhile.

We thank The Royal Society and NATO for a Postdoctoral Fellowship (to I. M. S.).

Notes and references

‡ Satisfactory elemental analysis, mass spectra and ^{1}H NMR spectra were obtained for all new compounds.

§ Data were obtained in dichloromethane *vs.* Ag/AgCl reference electrode, Au working electrode, Pt counter electrode at 20 °C using 0.1 M $NBu^n_4PF_6$ supporting electrolyte, 10^{-3} M substrate and 100 mV s^{-1} scan rate with *iR* compensation.

1 P. J. Skabara, D. M. Roberts, A. K. Ray, S. S. Umare, A. K. Hassan, A. V. Nabok and K. Müllen, manuscript in preparation.
2 P. J. Skabara, K. Müllen, M. R. Bryce, J. A. K. Howard and A. S. Batsanov, *J. Mater. Chem.*, 1998, **8**, 1719.
3 A. Charlton, A. E. Underhill, G. Williams, M. Kalaji, P. J. Murphy, K. M. Abdul Malik and M. B. Hursthouse, *J. Org. Chem.*, 1997, **62**, 3098.
4 For example, see: (*a*) C. Thobie-Gautier, A. Gorgues, M. Jubault and J. Roncali, *Macromolecules*, 1993, **26**, 4094; (*b*) L. Huchet, S. Akoudad, E. Levillain, J. Roncali, A. Emge and P. Bäuerle, *J. Phys. Chem. B*, 1998, **102**, 7776; (*c*) L. Huchet, S. Akoudad and J. Roncali, *Adv. Mater.*, 1998, **10**, 541; (*d*) J. Roncali, *J. Mater. Chem.*, 1999, **9**, 1875.
5 See, for example: N. Svenstrup and J. Becher, *Synthesis*, 1995, 215.
6 The synthesis of compound **5** directly from the trithiocarbonate derivative and mercury(II) acetate is inefficient (20% yield); an improved method for the preparation of **5** will be reported elsewhere.
7 P. J. Skabara, I. M. Serebryakov, D. M. Roberts, I. F. Perepichka, S. J. Coles and M. B. Hursthouse, *J. Org. Chem.*, 1999, **64**, 6418.
8 G. Saito, *Pure Appl. Chem.*, 1987, **59**, 999.
9 P. J. Skabara and K. Müllen, *Synth. Met.*, 1997, **84**, 345.
10 J. Roncali, *J. Mater. Chem.*, 1997, **7**, 2307.

ChemComm

Colloids as redox sensors: recognition of $H_2PO_4^-$ and HSO_4^- by amidoferrocenylalkylthiol–gold nanoparticles

Agnès Labande and Didier Astruc*

Groupe de Chimie Supramoléculaire des Métaux de Transition, LCOO, UMR CNRS N°5802, Université Bordeaux I, 351 Cours de la Libération, 33405 Talence Cédex, France. E-mail: d.astruc@lcoo.u-bordeaux.fr

Received (in Oxford, UK) 27th March 2000, Accepted 4th May 2000
Published on the Web 23rd May 2000

Gold colloids containing a mixture of alkylthiol and amidoferrocenylalkylthiol (AFAT) ligands are new redox sensors for $H_2PO_4^-$ and HSO_4^-.

A promising approach towards nanoscopic materials is the investigation of their supramolecular properties which may lead to new sensors, catalysts and nanoscale electronic devices.[1] Only a few molecular recognition studies have been reported with colloids, however.[3] We wished to combine the effect of the topology in alkylthiol–gold nanoparticles and the supramolecular properties of their redox-active termini for their use as exo-receptors.[4] In order to attain this goal, we have synthesized functional alkylthiol–gold nanoparticles containing a mixture of alkylthiol ligands and amidoferrocenylalkylthiol (AFAT) ligands (Fig. 1). We then monitored the titration of $NBu^n_4^+$ salts of $H_2PO_4^-$ and HSO_4^- by these nanoparticles using cyclic voltammetry (CV). These ligands have been introduced and studied by Creager on gold surfaces,[5] and ferrocenylalkylthiol colloids are known,[6] but the introduction of an amido group close to the ferrocene center now adds the supramolecular aspect to these colloids.

Recognition of anions is an important topic because a number of anions are found in biological systems.[7] In particular, Beer showed that amidoferrocenyl groups linked to endo-receptors are able to sense anions.[4a–c] We now find that the redox potential of the amidoferrocenyl group is sufficiently perturbed by the synergy between the hydrogen-bonding, electrostatic interaction and topology in alkylthiol–gold nanoparticles containing AFAT ligands (unlike in alkylamidoferrocene monomers) to recognize $H_2PO_4^-$ and HSO_4^-.

The AFAT-containg colloids were synthesized by ligand substitution using Brust's colloids, leaving the gold core unchanged.[2] We have applied this technique with a variable proportion of amidoferrocenylalkylthiol ligands of variable lengths (11 and 6 C atoms)[11] and verified using TEM that the core size is not modified upon ligand substitution. Indeed, the combination of elemental analysis, ^{1}H NMR spectroscopy and TEM leads, for instance, to an average number of 269 gold atoms per core of 2 nm diameter and 80–106 dodecanethiolate chains.[8] Table 1 shows the proportion of AFAT ligands (determined by ^{1}H NMR) which is introduced onto the nanoparticles as a function of the amount engaged in the ligand-substitution reactions. Saturation is reached for 38 AFAT ligands per particle. These thermally stable nanoparticles are unaffected by air and are soluble in CH_2Cl_2.

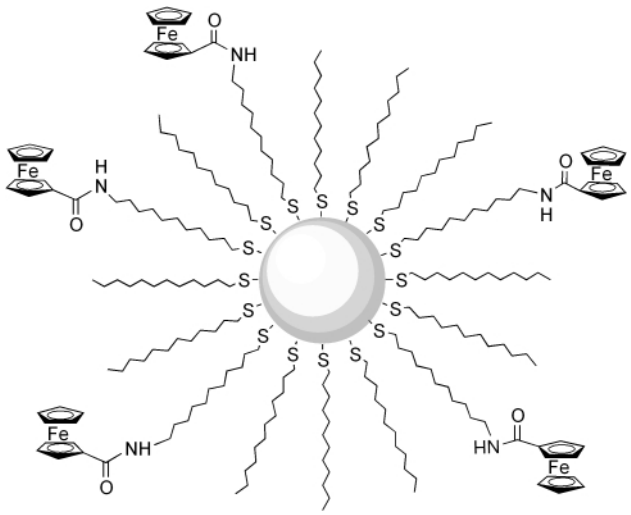

Fig. 1 Gold nanoparticles containing, on average, 29% of AFAT ligands (29-Fc).

The CVs of these colloids containing a variable amount of AFAT ligands always show a reversible ferrocene/ferrocenium wave (Pt, CH_2Cl_2, 0.1 M $[NBu^n_4][PF_6]$) at $E_{1/2}$ = 0.220 V *vs.* $FeCp_2^{0/+}$ in CH_2Cl_2[12] with some adsorption indicated by the E_{pa}–E_{pc} values (typically 20 mV) lower than the 58 mV value expected at 20 °C for classic monoelectronic waves. The observation of a single wave is due to the fact that all the redox centers of a particle appear identical and independent of the electrochemical time scale, indicating that the rotation of the particles and H-bonding formation and cleavage are faster than this time scale. Mediation of electron transfer among the ferrocenyl sites may also occur.[9] Addition of $[NBu^n_4][H_2PO_4]$ to a CH_2Cl_2 solution of these nanoparticles leads to the appearance of a new, cathodically shifted, wave the intensity of which increases at the expense of the initial wave. The replacement of the initial wave by the new one is complete after addition of 1 equivalent $[NBu^n_4][H_2PO_4]$ per AFAT branch (Fig. 2), indicating a 1:1 interaction between the anion and the amidoferrocenium group. It is remarkable that the potential shift upon addition of the anion is large ($\Delta E°$ = 220 mV) and constant whatever the proportion of AFAT ligand in the nanoparticles (from 7 to 38%) and its length (6 or 11 CH_2 units). This shift is much larger not only than that obtained for the alkylamidoferrocene monomer $FcCONHCH_2CH_2OPh$ (45 mV) but also for the tripod $PhC(CH_2CH_2CH_2NHCOFc)_3$ (110 mV), and is analogous to the value observed with a nona-branched amidoferrocene dendrimer.[9] Thus, it is probable that the channels defined between the parallel ligands create sufficient steric strain to provide a favorable particle effect comparable to

Table 1 Results of ligand-exchange reactions between AFAT– and dodecanethiol (DT)–gold nanoparticles

AFAT chain length	AFAT/DT ratio		AFAT/DT members in product[c]	%AFAT in product[d]
	Reaction[a]	Product[b]		
C_{11}	1:4	1:13	8/97	7
C_{11}	1:1	1:8	10/70	13
C_{11}	1.5:1	1:5	21/85	20
C_{11}	1.75:1	1:3.5	31/75	29
C_{11}	2:1	1:2.6	39/64	38
C_6	2:1	1:5.5	16/70	18

[a] Mole ratio of AFAT ligand to nanoparticle-bound DT ligands in ligand-exchange reactions. [b] Average mole ratio of AFAT/DT ligands in the nanoparticles. [c] Average numbers of AFAT/DT ligands in the particles. [d] Average percentage of AFAT ligands in the nanoparticles.

DOI: 10.1039/b002578j

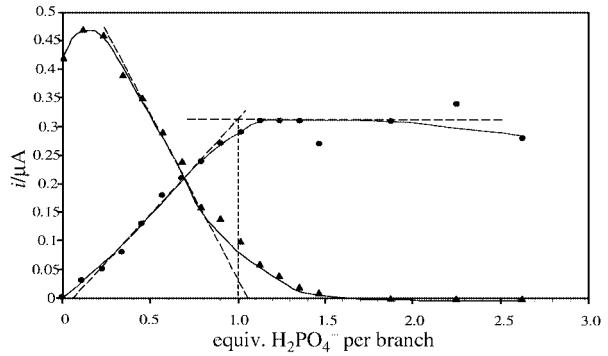

Fig. 2 Titration of the 20-Fc (AFAT) nanoparticles with $[NBu^n_4][H_2PO_4]$ monitored by CV. Decrease of the intensity of the initial ferrocene CV wave and increase of the intensity of the new wave *vs.* the number of equivalents of $[NBu^n_4][H_2PO_4]$ added per Fc (AFAT) branch; nanoparticles: 5×10^{-6} M in CH_2Cl_2; $[NBu^n_4][H_2PO_4]$: 10^{-2} M in CH_2Cl_2, $[NBu^n_4][PF_6]$: 0.1 M, 20 °C, reference electrodes: SCE and $FeCp_2$; auxiliary and working electrodes: Pt, scan rate: 200 mV s^{-1}. Plots of these intensities with particles containing various numbers of Fc (AFAT) branches (see text) gave analogous results: (▲) initial wave, (●) new wave.

the dendritic effect observed with metallodendrimers. This $\Delta E°$ value means that the apparent association constant $K_{(+)}$ between $H_2PO_4^-$ and the polyferrocenium form of the particle is 5350 ± 550 times larger than that, $K_{(0)}$, related to the neutral polyferrocene form (electrostatic effect).[10]

Gratifyingly, this technique also allows confirmation of the number of AFAT ligands in the particles determined by ^{1}H NMR, *viz*. 10–30% AFAT ligands on the particles (Table 2). It is also possible to titrate $[NBu^n_4][H_2PO_4]$ in the presence of both $[NBu^n_4][HSO_4]$ and NBu^n_4Cl (in addition to the electrolyte $[NBu^n_4][PF_6]$ in large excess), but the initial wave is now progressively shifted cathodically instead of being progressively replaced by another wave. This dramatic change of behavior may be understood in terms of a dynamic equilibrium among various anion complexes and by the fact that the kinetics of complexation can be different in the presence of a single anion or a mixture of anions.[11]

Finally, it is possible to titrate $[NBu^n_4][HSO_4]$ alone since the initial wave of those particles which have a low content of AFAT ligands (10–20%) is progressively shifted cathodically by addition of this anion up to 40 mV after addition of 1 equivalent of $[NBu^n_4][HSO_4]$, which again corresponds to a 1:1 interaction, with an apparent association constant $K_{(+)} = 480 \pm 120$ mol^{-1} L at a concentration of 10^{-2} M.[10] It is noteworthy that the $\Delta E°$ value is much smaller for HSO_4^- than for $H_2PO_4^-$, which shows the selectivity of the recognition by these nanoparticles. When the AFAT ligand content of the particles is larger (29–38% AFAT) or the chain shorter (C_6), this 1:1 interaction is no longer found, and equivalence points are reached with a lower quantity of added $[NBu^n_4][HSO_4]$. This distortion might best be accounted for by intramolecular amide–amide double hydrogen-bonding of two neighboring AFAT ligands at high AFAT ligand content. This effect is also more pronounced for HSO_4^- than for $H_2PO_4^-$. The moderate adsorption as monitored by the $E_a - E_p$ values along these titration studies changes slightly during the titration, but does not disturb the titrations. These particles do not recognize chloride, bromide and nitrate anions and thus there is a selectivity for the above oxo-anions. We are now continuing our research with other particles of similar and different types to extend the scope of the present reasults and investigate solvation and pH effects.

Table 2 Determination of the average number of AFAT ligands in the nanoparticles

	Total number of AFAT ligands			
		Titration by CV		
	H NMR	H_2PO_4	$H_2PO_4^{-a}$	HSO_4^-
7-Fc (C_{11})	8	8.3	—	—
13-Fc (C_{11})	10	9.5	9	10.25
20-Fc (C_{11})	21	22	19	18
29-Fc (C_{11})	31	29	25	17[b]
38-Fc (C_{11})	39	32	29.5	13[b]
18-Fc (C_6)	16	14	—	9[b]

[a] Titration carried out in the presence of excess $[NBu^n_4][HSO_4]$ (5×10^{-6} mol) and NBu^n_4Cl (2.5×10^{-6} mol). [b] Low value due to intramolecular H-bonding at high content of the AFAT ligand (see text).

In conclusion, these particles are used as exo-receptors which can sense $H_2PO_4^-$ and HSO_4^- owing to their hydrogen-bonding capacity with these oxo-anions, and excellent selectivity between the two oxo-anions has been found. They can be compared to dendrimers, but they show effects which are different, although the particles are as efficient as nona-amidoferrocene dendrimers to sense HPO_4^- (some of our polyamidoferrocene dendrimers[9b] do not recognize HPO_4^-). The particles also present a great advantage in that they are synthesized in one step whereas dendritic syntheses require a large number of steps.

We thank Michel Chambon for accurate TEM studies and the Institut Universitaire de France, the CNRS, the Université Bordeaux I and the Région Aquitaine (thesis grant to A. L.) for financial support. This paper is dedicated to the memory of John Osborn.

Notes and references

1 (*a*) J.-M. Lehn, *Supramolecular Chemistry: Concepts and Perspectives*, VCH, Weinheim, 1995; (*b*) A. Kumar, N. L. Arbott, E. Kim, A. Biebuyck and G. M. Whitesides, *Acc. Chem. Res.*, 1995, **28**, 219.
2 M. Brust, M. Walker, D. Bethell, D. J. Schiffrin and R. Whyman, *J. Chem. Soc., Chem. Commun.*, 1994, 801.
3 S. Sampath and O. Lev, *Adv. Mater.*, 1997, **9**, 410; J. Liu, R. Xu and A. E. Kaifer, *Langmuir*, 1998, **14**, 7337; D. Fitzmaurice, S. N. Rao, J. Preece, J. F. Stoddart, S. Wenger and N. Zaccheroni, *Angew. Chem., Int. Ed.*, 1999, **38**, 1147; W. S. Shenton, S. A. Davis and S. Mann, *Adv. Mater.*, 1999, **11**, 449; A. K. Boal and V. M. Rotello, *J. Am. Chem. Soc.*, 1999, **121**, 4914; A. K. Boal and V. M. Rotello, *J. Am. Chem. Soc.*, 2000, **122**, 734.
4 (*a*) For endo- and exo-receptors, see ref. 2(*a*), ch. 7; (*b*) for leading references on the recognition of anions, see ref. 1(*a*), ch. 2 and 3, ref. 7 and P. D. Beer, *Adv.. Inorg. Chem.*, 1992, **39**, 79; *Chem. Commun.*, 1996, 689; *Acc. Chem. Res.*, 1998, **31**, 71 (in particular for endo-receptors linked to amidometallocenes).
5 (*a*) K. Weber and S. E. Creager, *Anal. Chem.*, 1994, **66**, 3164; (*b*) K. Weber, L. Hockett and S. E. Creager, *J. Phys. Chem. B*, 1997, **101**, 8286.
6 R. S. Ingram, M. J. Hostetler and R. W. Murray, *J. Am. Chem. Soc.*, 1997, **119**, 9175; A. C. Templeton, W. P. Wuelfing and R. W. Murray, *Acc. Chem. Res.*, 2000, **33**, 27.
7 R. M. Izatt, K. Pawlak and J. S. Bradshaw, *Chem. Rev.*, 1995, **95**, 2529; S. Seel, *Top. Curr. Chem.*, 1995, **175**, 101; C. Seel and J. de Mendoza, in *Comprehensive Supramolecular Chemistry*, ed. J. L. Atwood, J. E. D. Davies, D. D. Mc Nichol and F. Vögtle, Elsevier, New York, 1996, vol. 2, ch. 17, pp. 519–552; J. L. Atwood, K. T. Holman and J. W. Steed, *Chem. Commun.*, 1996, 1401; T. J. James, S. Sandanayake and S. Shinkai, *Angew. Chem., Int. Ed. Engl.*, 1996, **35**, 1910.
8 D. V. Leff, P. C. Ohara, J. R. Heath and W. M. Gelbart, *J. Phys. Chem.*, 1995, **99**, 7036.
9 (*a*) C. Valério, J.-L. Fillaut, J. Ruiz, J. Guittard, J.-C. Blais and D. Astruc, *J. Am. Chem. Soc.*, 1997, **119**, 2588; (*b*) Valério, E. Alonso, J. Ruiz, J.-C. Blais and D. Astruc, *Angew. Chem., Int. Ed.*, 1999, **38**, 1747.
10 Seminal article: S. R. Miller, D. A. Gustowski, Z.-H. Chen, G. W. Gokel, L. Echegoyen and A. E. Kaifer, *Anal. Chem.*, 1988, **60**, 2021.
11 P. D. Beer, P.A. Gale and Z. Chen, *Adv. Phys. Org. Chem.*, 1998, **31**, 1.

The kinetic resolution of allylic alcohols by a non-enzymatic acylation catalyst; application to natural product synthesis†

Stéphane Bellemin-Laponnaz, Jennifer Tweddell, J. Craig Ruble, Frank M. Breitling and Gregory C. Fu*

Department of Chemistry, Massachusetts Institute of Technology, Cambridge, Massachusetts 02139 USA. E-mail: gcf@mit.edu

Received (in Corvallis, OR, USA) 7th March 2000, Accepted 24th April 2000
Published on the Web 22nd May 2000

A planar-chiral DMAP derivative is shown to serve as an effective catalyst for the kinetic resolution of allylic alcohols; to illustrate its practical utility, the catalyst is applied to the resolution of two alcohols that have been employed as intermediates in recent natural product total syntheses.

During the mid-1990s, Evans *et al.*[1] and Vedejs and Chen[2] reported the first stoichiometric chiral acylating agents that are effective for the kinetic resolution of alcohols [selectivity factor (*s*) > 10],[3] work that marked an important first step in the development of non-enzyme-based methods for enantioselective acylation.[4] Soon thereafter, the groups of Vedejs,[5] Oriyama,[6] Fuji,[7] Miller[8] and ourselves[9] described the first chiral non-enzymatic acylation *catalysts* that are effective for the kinetic resolution of alcohols. With regard to substrate scope, the generality that has been reported to date follows the order: arylalkylcarbinols[10] > cycloalkanols[11] > propargylic alcohols[12] > allylic alcohols.[13]

Our work on catalytic enantioselective acylation has focused on the application of planar-chiral DMAP derivative **1** to the kinetic resolution of arylalkylcarbinols and of propargylic alcohols.[9] In addition, we observed in a 1997 study that we could resolve two *allylic* alcohols with good selectivity.[9a,14] Herein, we report a systematic investigation of the kinetic resolution of allylic alcohols by catalyst **1** [eqn. (1)], establishing fairly broad substrate scope and applying the method to two alcohols that have served as key building blocks in recent natural product syntheses.

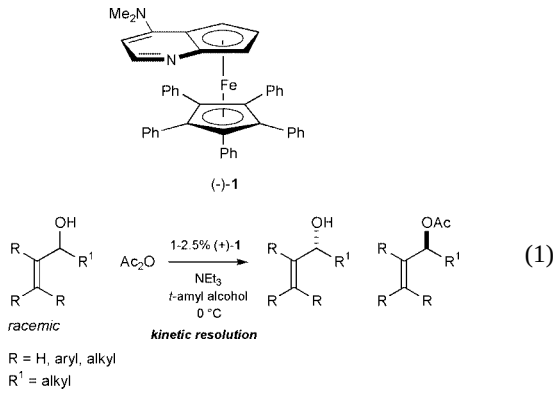

(1)

We have found that catalyst **1** can effect the kinetic resolution of most families of allylic alcohols with good selectivity [Table 1; 1.0–2.5% (+)-**1**, Ac_2O, NEt_3, *t*-amyl alcohol, 0 °C]. Allylic alcohols that do not possess a substituent either geminal or *cis* to the hydroxy-bearing group are usually resolved with modest selectivity (entry 1). A notable exception to this generalization occurs when there is a phenyl group in the *trans* position, in which case the selectivity factor increases dramatically (entry 2).

Allylic alcohols that possess a substituent geminal to the hydroxy-bearing group are usually resolved effectively by catalyst **1** (entries 3–8); again, the presence of a phenyl substituent in the *trans* position leads to substantially improved enantioselection (entry 9 *vs.* entries 3–8). Similarly, kinetic resolutions of allylic alcohols that possess a substituent *cis* to the hydroxy-bearing group generally proceed with good selectivity (entries 10–12). Furthermore, tetrasubstituted allylic alcohols are acylated with high stereoselection (entry 13).

Table 1 Kinetic resolutions of allylic alcohols catalyzed by (+)-**1** (Ac_2O, NEt_3, *t*-amyl alcohol, 0 °C)

Entry	Unreacted alcohol, major enantiomer	Selectivity factor[a] (ee of unreacted alcohol)
1	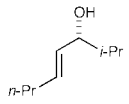	**5.4** 92% ee @ 75% conv.
2	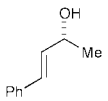	**64** 99% ee @ 54% conv.
3	R = *n*-pentyl	**4.7** 90% ee @ 77% conv.
4	R = *i*-Pr 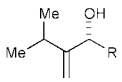	**10** 92% ee @ 63% conv.
5	R = Et 	**11** 93% ee @ 63% conv.
6	R = *i*-Pr	**17** 93% ee @ 58% conv.
7	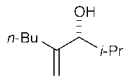	**25** 94% ee @ 55% conv.
8	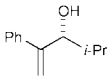	**14** 93% ee @ 59% conv.
9	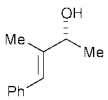	**80** 98% ee @ 53% conv.
10	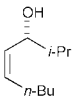	**5.3** 90% ee @73% conv.
11	R = *n*-pentyl 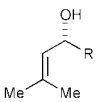	**12** 97% ee @ 66% conv.
12	R = *i*-Pr	**18** 97% ee @ 60% conv.
13	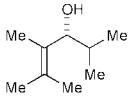	**29** 99% ee @ 59% conv.

[a]The selectivity factors are the average of two runs.

† Electronic supplementary information (ESI) available: full experimental details. See http://www.rsc.org/suppdata/cc/b0/b002041i/

In order to demonstrate the utility of this method, we have applied catalyst **1** to the kinetic resolution of two allylic alcohols that have served as key intermediates in recent natural product total syntheses. For example, Brenna *et al.* employed (−)-**2** in a 1997 synthesis of (−)-baclofen,[15] which is used as a muscle relaxant. We have determined that catalyst **1** effects the kinetic resolution of racemic **2** with a selectivity factor of 37 [eqn. (2)]. This reaction was run on a 2 g scale, exposed to air, thereby illustrating the practicality of the process. At the conclusion of the kinetic resolution, 96% of the catalyst was recovered.

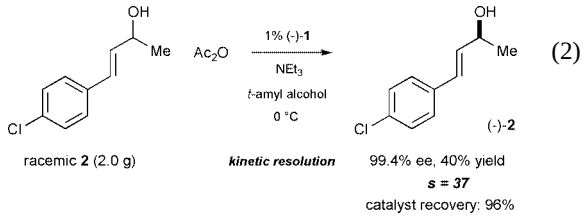

(2)

Aldol adduct (+)-**3** is a key intermediate in the recent Sinha–Lerner synthesis of epothilone A,[16] an exciting new potential anti-cancer drug.[17] Adduct (+)-**3** has itself been the focus of much attention, owing to the fact that it can be generated by an aldolase antibody through kinetic resolution of racemic **3** (96% ee at 60% conversion ⇒ $s \sim 17$).[16,18] We have determined that catalyst **1** can also effect the kinetic resolution of this compound, with a selectivity factor of 107 [eqn. (3); reaction run exposed to air on a 1.2 g scale; acetylated **3**: 52% yield, 91.8% ee].[19]

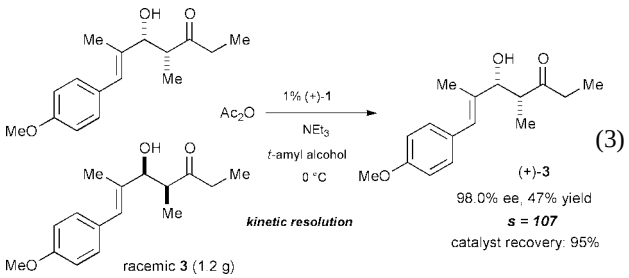

(3)

In conclusion, we have established that planar-chiral DMAP derivative **1** is the most versatile non-enzymatic acylation catalyst for the kinetic resolution of allylic alcohols that has been reported to date, furnishing good selectivity for most substrates. Furthermore, we have illustrated the usefulness of this method by applying it to the kinetic resolution of two alcohols that have served as intermediates in recent natural product total syntheses.

Support has been provided by Bristol-Myers Squibb, Merck, the Natural Sciences and Engineering Research Council of Canada (predoctoral fellowship to J. T.), the National Institutes of Health (National Institute of General Medical Sciences, R01-GM57034), Novartis, Pfizer, and Pharmacia & Upjohn.

This paper is dedicated to the memory of John A. Osborn.

Notes and references

1 D. A. Evans, J. C. Anderson and M. K. Taylor, *Tetrahedron Lett.*, 1993, **34**, 5563.
2 E. Vedejs and X. Chen, *J. Am. Chem. Soc.*, 1996, **118**, 1809.
3 Selectivity factor = [(rate of fast-reacting enantiomer)/(rate of slow-reacting enantiomer)]. For a review of kinetic resolution, see: H. B. Kagan and J. C. Fiaud, *Top. Stereochem.*, 1988, **18**, 249.
4 For a review of enantioselective acylations of alcohols by enzymes, see: K. Drauz and H. Waldmann, *Enzyme Catalysis in Organic Synthesis: A Comprehensive Handbook*, VCH, New York, 1995.
5 (*a*) E. Vedejs, O. Daugulis and S. T. Diver, *J. Org. Chem.*, 1996, **61**, 430; (*b*) E. Vedejs and O. Daugulis, *J. Am. Chem. Soc.*, 1999, **121**, 5813.
6 T. Oriyama, Y. Hori, K. Imai and R. Sasaki, *Tetrahedron Lett.*, 1996, **37**, 8543; T. Sano, K. Imai, K. Ohashi and T. Oriyama, *Chem. Lett.*, 1999, 265.
7 T. Kawabata, M. Nagato, K. Takasu and K. Fuji, *J. Am. Chem. Soc.*, 1997, **119**, 3169.
8 S. J. Miller, G. T. Copeland, N. Papaioannou, T. E. Horstmann and E. M. Ruel, *J. Am. Chem. Soc.*, 1998, **120**, 1629; G. T. Copeland, E. R. Jarvo and S. J. Miller, *J. Org. Chem.*, 1998, **63**, 6784; E. R. Jarvo, G. T. Copeland, N. Papaioannou, P. J. Bonitatebus, Jr. and S. J. Miller, *J. Am. Chem. Soc.*, 1999, **121**, 11 638.
9 (*a*) J. C. Ruble, H. A. Latham and G. C. Fu, *J. Am. Chem. Soc.*, 1997, **119**, 1492; (*b*) J. C. Ruble, J. Tweddell and G. C. Fu, *J. Org. Chem.*, 1998, **63**, 2794; (*c*) C. E. Garrett, M. M.-C. Lo and G. C. Fu, *J. Am. Chem. Soc.*, 1998, **120**, 7479; (*d*) B. Tao, J. C. Ruble, D. A. Hoic and G. C. Fu, *J. Am. Chem. Soc.*, 1999, **121**, 5091.
10 Fourteen examples with $s > 10$: refs. 5, 6 and 9(*a*)–(*c*).
11 Thirteen examples with $s > 10$: refs. 6–8.
12 Eight examples with $s > 10$: ref. 9(*d*).
13 Three examples with $s > 10$: refs. 5(*b*) and 9(*a*).
14 The most prominent non-enzymatic method for the kinetic resolution of allylic alcohols is the Sharpless asymmetric epoxidation: R. A. Johnson and K. B. Sharpless, in *Comprehensive Organic Synthesis*, ed. B. M. Trost, Pergamon, New York, 1991; vol. 7, ch. 3.2.
15 E. Brenna, N. Caraccia, C. Fuganti, D. Fuganti and P. Grasselli, *Tetrahedron: Asymmetry*, 1997, **8**, 3801.
16 S. C. Sinha, C. F. Barbas, III and R. A. Lerner, *Proc. Natl. Acad. Sci. USA*, 1998, **95**, 14603.
17 For example, see: S. Borman, *Chem. Eng. News*, Jan. 31, 2000, p. 7.
18 For commentaries, see: P. G. Schultz, *Proc. Natl. Acad. Sci. USA*, 1998, **95**, 14 590; S. Borman, *Chem. Eng. News*, Dec. 14, 1998, p. 15.
19 In the air, *t*-amyl alcohol (8.75 mL; distilled from CaH_2) and NEt_3 (0.36 mL, 2.6 mmol; EM Science, 98%) were added to a vial containing the alcohol (1.16 g, 4.42 mmol) and (+)-**1** (29.0 mg, 0.0439 mmol). The vial was closed with a Teflon-lined cap and sonicated to help dissolve the catalyst. The reaction mixture was cooled in an ice bath, and Ac_2O (0.25 mL, 2.6 mmol; Mallinckrodt, 99.8%) was added. After 42.5 h, the reaction was quenched with MeOH (0.25 mL). The mixture was passed through a silica gel column (20 → 100% EtOAc–hexanes, then 50% NEt_3–EtOAc) to separate the alcohol and the acetate from the catalyst [27.6 mg (95%) of pure catalyst was recovered]. The alcohol and the acetate were then separated by flash chromatography (10 → 25% EtOAc–hexanes), which afforded 0.70 g (52%) of acetate (HPLC analysis ⇒ 91.8% ee) and 0.55 g (47%) of alcohol (HPLC analysis ⇒ 98.0% ee). These ee values correspond to a selectivity factor (*s*) of 107 at 51.6% conversion.

ChemComm

Regioselectivity of the insertion of propene with achiral Pd(II) catalysts to highly isotactic poly[1-oxo-2-methylpropane-1,3-diyl]. Is the syndiotactic structure accessible?

Barbara Sesto and Giambattista Consiglio*

Eidgenössische Technische Hochschule, Laboratorium für Technische Chemie, ETH Zentrum, CH-8092 Zurich, Switzerland. E-mail: consiglio@tech.chem.ethz.ch

Received (in Liverpool, UK) 13th March 2000, Accepted 28th April 2000
Published on the Web 25th May 2000

Achiral cationic palladium catalysts, modified with 1,2-bis-(diarylphosphinomethyl)benzene ligands with different electronic properties, can efficiently produce poly(propene-*alt*-CO) with essentially complete regioregularity and high isotacticity, depending on the aryl substituent; the stereochemistry of the copolymers obtained is barely, if at all, influenced by the regiochemistry of the olefin insertion.

The alternating copolymerization of aliphatic olefins with carbon monoxide has attracted much attention in the last few years.[1–5] Useful catalytic systems in terms of productivity for this process are cationic palladium complexes of the type [(P–P)Pd$(S)_2$]$(X)_2$ [P–P is a chelate diphosphine ligand, typically

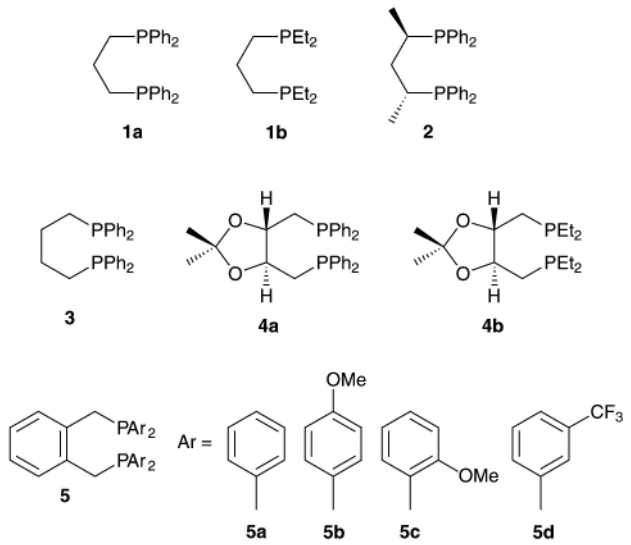

Fig. 1

1,3-bis(diphenylphosphino)propane **1a** (Fig. 1), S is a solvent molecule and X a weakly coordinating anion].[6]

When 1-olefins are used as the substrate, the microstructure of the produced copolymers depends on the characteristics of the regio- and stereo-chemistry of the step that corresponds to the migratory insertion of the olefin.[7] For the series of 1,3-propanediyl ligands tested so far in the copolymerization of aliphatic olefins, two factors have been identified as playing a role in the production of stereo- and regio-regular copolymers: chirality of the catalytic system, which brings about efficient enantioface discrimination and basicity of the ligand necessary to achieve regiospecificity during the insertion process.[8] The two selectivities seem to influence each other. Whereas the prototypical catalyst precursor **1a** leads to the production of stereoirregular poly(propene-*alt*-CO) (Scheme 1), which has a maximum head-to-tail (ht) diad content of *ca.* 60%,[9] the ht diad content for **2** can be as high as 90%[8] and is *ca.* 100% for **1b**[10] or for similar alkyl substituted ligands. At the same time a shift towards the preferential formation of *l*-sequences is observed.

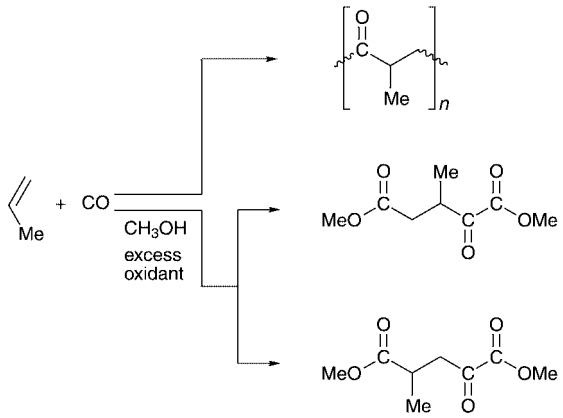

Scheme 1

The activity of ligand **3** was similar to that of ligand **1a**, but it showed somewhat better regioselectivity.[6,9]

Based on the above results, it was expected that **4a** would produce a substantially stereoregular material, which however is not the case.[9,11] Even **4b** did not seem to be very efficient from a stereochemical point of view, considering that the reported optical rotation of the produced copolymer is quite low.[12,13] The characteristics of these catalytic systems are clearly influenced to a considerable extent by the size of the coordination ring on the metal. We have continued our study, the aim of which is the identification of the factors involved in the regio- and stereo-chemical control of the insertion of the olefin substrate for this important carbonylation reaction, with the ultimate goal of achieving syndiotactic copolymerisation of aliphatic 1-olefins. We made the unexpected observation that electronic factors can substantially influence the regioselectivity and the enantioface discrimination of the efficient and largely regioregular copolymerization of propene with carbon monoxide caused by ligand **5a**.

Starting with ligands **5** (**5a** and **5c** have already been used for related copolymerization reactions[14,15]), the corresponding [(P–P)Pd$(H_2O)_2$]$(CF_3SO_3)_2$ derivatives **6** were synthesized[16] and used as catalyst precursors for the copolymerization of propene with carbon monoxide as well as for the triple carbonylation to dimethyl 3- and 4-methyl-2-oxopentanedioates (Table 1 and Scheme 1).[17] The catalytic activity of **5a** is about four times larger than that of **1a** under the same reaction conditions. Electron withdrawing and electron donating aryl substituents result in lower catalytic activity. The activity loss is larger for the latter substituents, particularly in conjunction with steric effects (**5b** and **5c**). Moreover, the results presented in Table 1 and in Fig. 2 reveal the good performance of the tested catalysts, especially of **5d**, with respect to regio- and stereo-chemistry. The concentration of the band associated to the isotactic pentad (82%) implies that the content of *l*-diads is $> 96\%$.[18]

The regioselectivity of the olefin insertion is inferred from the isomeric ratio of 3- to 4-methyl-2-oxopentanedioate

DOI: 10.1039/b002058n

Table 1 Copolymerization of propene with carbon monoxide using **6**[a]

Ligand	Reaction time/h	Productivity[b]/ g(g(Pd) h)$^{-1}$	Regioregularity[c] hh	ht	tt	Stereoregularity[d]	Regioselectivity[e]
5a	21.5	233	0.04	1.00	0.05	79	66/34
5b	142	11	0.06	1.00	0.11	54	34/66
5c	26.3	89	< 0.01	1.00	0.04	73	19/81
5d	5.6	126	< 0.01	1.00	0.02	82	~ 100/0

[a] *Reaction conditions*: 19 g of propene in 75 ml THF and 4.5 ml MeOH; 0.03 mmol catalyst precursor; 80 bar CO; 1.5 mmol 1,4-naphthoquinone; 44 °C. [b] Mean molecular masses were 5100, 9700, 4100 and 3500, respectively. [c] Relative intensity of signals centered at δ *ca.* 223, 219 and 214, respectively (Fig. 2). [d] Intensity (%) of the most intense band in the ht range of the CO signals in the ^{13}C NMR spectra (Fig. 2). [e] Isomeric ratio of 3- to 4-methyl-2-oxopentanedioate, both of which are formed under similar reaction conditions but in the presence of excess of 1,4-benzoquinone.

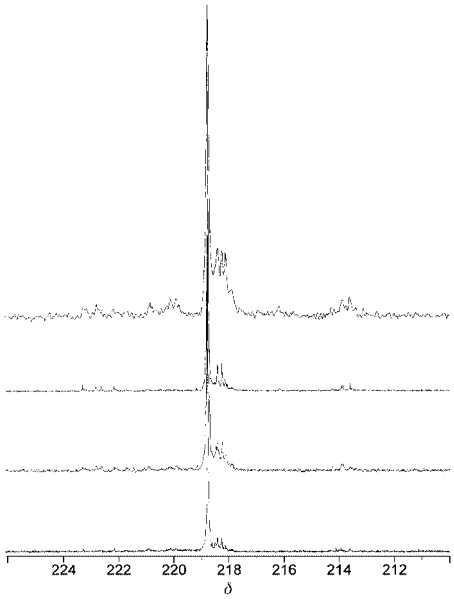

Fig. 2 ^{13}C NMR [125 MHz, $(CF_3)_2CDOD$] spectrum of the carbonyl region of poly(propene-*alt*-CO) prepared with catalysts **5** (from the bottom to the top: **5d**, **5b**, **5a** and **5c**).

(Scheme 1), which is affected by the tendency of propene to insert with primary or with secondary regiochemistry into a L_nPd–CO–OMe intermediate.[17] Catalysts **5c** and **5d** display an essentially reversed regioselectivity but, nevertheless both systems give poly(propene-*alt*-CO) with quite high regioregularity and a largely prevailing isotactic structure. Even though **5c** and **5d** are regioisomerically different, the position of the trifluoromethyl substituent in **5d** should have no influence on the electronic characteristics of the catalytic system.[19] Considering the achiral nature of the ligands,[20] it seems obvious that the enantioface discrimination during the copolymerization process is chain-end controlled. Chain-end control and secondary insertion result in the formation of syndiotactic copolymers during the related styrene copolymerization.[21] Therefore the reported results raise doubts about the accessibility of syndiotactic copolymerization of aliphatic 1-olefins with catalyst precursors containing diphosphines.

Notes and references

1 H.-K. Luo, Y. Kou, X.-W. Wang and D.-G. Li, *J. Mol. Catal. A: Chem.*, 2000, **151**, 91.
2 A. S. Abu-Surrah and B. Rieger, *Top. Catal.*, 1999, **7**, 165.
3 A. Sommazzi and F. Garbassi, *Prog. Polym. Sci.*, 1997, **22**, 1547.
4 E. Drent and P. H. M. Budzelaar, *Chem. Rev.*, 1996, **96**, 663.
5 A. Sen, *Acc. Chem. Res.*, 1993, **26**, 303.
6 E. Drent, J. A. M. van Broekhoven and M. J. Doyle, *J. Organomet. Chem.*, 1991, **417**, 235.
7 K. Nozaki and T. Hiyama, *J. Organomet. Chem.*, 1999, **576**, 248.
8 A. Batistini, G. Consiglio and U. W. Suter, *Angew. Chem., Int. Ed. Engl.*, 1992, **31**, 303.
9 F. Y. Xu, A. X. Zhao and J. C. W. Chien, *Makromol. Chem.*, 1993, **194**, 2579.
10 S. Bronco, G. Consiglio, R. Hutter, A. Batistini and U. W. Suter, *Macromolecules*, 1994, **27**, 4436.
11 Z. Jiang, S. E. Adams and A. Sen, *Macromolecules*, 1994, **27**, 2694.
12 K. Nozaki, M. Yasutomi, K. Nakamoto and T. Hiyama, *Polyhedron*, 1998, **17**, 1159.
13 P. K. Wong (Shell), *Eur. Pat.*, EP 0 384 517, priority date 20/02/1989.
14 W. Clegg, G. R. Eastham, M. R. J. Elsegood, R. P. Tooze, X. L. Wang and K. Whiston, *Chem. Commun.*, 1999, 1877.
15 E. Drent and A. W. van der Made (Shell), *World Pat.*, WO 00/09521, priority date 13/08/1998.
16 M. Sperrle, V. Gramlich and G. Consiglio, *Organometallics*, 1996, **15**, 5196.
17 M. Sperrle and G. Consiglio, *J. Organomet. Chem.*, 1996, **506**, 177.
18 S. Bronco and G. Consiglio, *Macromol. Chem. Phys.*, 1995, **197**, 355.
19 J. A. S. Howell, N. Fey, J. D. Lovatt, P. C. Yates, P. McArdle, D. Cunningham, E. Sadeh, H. E. Gottlieb, Z. Goldschmidt, M. B. Hursthouse and M. E. Light, *J. Chem. Soc., Dalton Trans.*, 1999, 3015.
20 M. Camalli, F. Caruso, S. Chaloupka, E. M. Leber, H. Rimml and L. M. Venanzi, *Helv. Chim. Acta*, 1990, **73**, 2263.
21 M. Barsacchi, G. Consiglio, L. Medici, G. Petrucci and U. W. Suter, *Angew. Chem., Int. Ed. Engl.*, 1991, **30**, 989.

Synthesis of sialyloligosaccharides using the *trans*-sialidase from *Trypanosoma cruzi*: novel branched and di-sialylated products from digalactoside acceptors

Suddham Singh,[a] Michaela Scigelova,[a] Marianne Lilja Hallberg,[a] Oliver W. Howarth,[a] Sergio Schenkman[b] and David H. G. Crout*[a]

[a] *Department of Chemistry, University of Warwick, Coventry, UK CV4 7AL. E-mail: msrky@csv.warwick.ac.uk*
[b] *Disciplina de Biologia Celular, Escola Paulista de Medicina, Rua Botucatú, 862-8A, 04023 São Paulo, Brazil*

Received (in Cambridge, UK) 22nd March 2000, Accepted 14th April 2000
Published on the Web 22nd May 2000

The *trans*-sialidase from *Trypanosoma cruzi* efficiently catalyses transfer of α-sialyl residues from *p*-nitrophenyl sialic acid (*p*-nitrophenyl *N*-acetylneuraminic acid) to acceptors containing β-galactose units.

The sialic acids are a class of C_9 monosaccharides comprising over thirty five variants.[1] The archetypal member is *N*-acetylneuraminic acid **1**. Colloquially this is referred to as

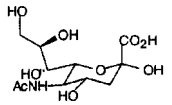

1

'sialic acid' unless another member of the family is indicated. Sialic acids are ubiquitous components of mammalian glycoproteins.[2] They are present in numerous other glycoconjugates[1] and are crucial determinants of their biological properties.[3]

Non-enzymatic syntheses of sialic acid-containing oligosaccharides[4] suffer from the drawbacks of a requirement for multiple protection–deprotection sequences and problems of control of configuration at the anomeric centre. In addition yields may be affected by side reactions involving 2,3-elimination. Accordingly, enzymatic methods have received much attention. Sialyl transferases catalyse sialylation regiospecifically and in high yield.[5] A major drawback to their use is that they require cytidine monophosphate *N*-acetylneuraminic acid (CMP-NeuAc) as sialyl donor. Although non-enzymatic syntheses of CMP-NeuAc have been reported[6] enzymatic methods have been preferred[7] and have been developed to permit multigram production[8] and *in situ* regeneration of the sialyl donor.[9]

Owing to the complexity of the donor and the limited availability of appropriate enzymes, sialylations with sialyl transferases have usually been limited to the preparation of sialylated oligosaccharides on the μmol scale. Sialyl transfers catalysed by sialidases has been demonstrated but proceed in extremely low yields ($< 15\%$).[10]

Against this background, the report of a novel retaining α-*trans*-sialidase in the parasite *Trypanosoma cruzi* was of particular interest.[11] Noteworthy was the finding that sialyl transfer was catalysed with much greater efficiency than hydrolysis.[12] The *trans*-sialidase required sialyl glycosides or oligosaccharides as sialyl donors. It was stated to be selective for transfer to β-galactosyl units; α-galactosides were reported not to be acceptors.[13]

The *trans*-sialidase has been shown to transfer sialyl residues α(2 → 3) on to galactose residues using sialyllactose,[14–17] 4-methylumbelliferyl α-sialoside[18–20] or *p*-nitrophenyl α-sialoside[13,21,22] as donors. However, the full synthetic potential of the enzyme has not been realised. The studies described above were carried out either on an analytical scale or, if preparatively, on a scale of < 10 μmol. We have now developed an approach that permits the synthesis of sialyl galactosides on a mmol or greater scale. The key to the improvement reported here is the use of the irreversible sialyl donor *p*-nitrophenyl α-sialoside **2** made readily available by improvement of a published synthesis[23] and the use of the recombinant form of the *T. cruzi trans*-sialidase referred to above, and which consists of the *N*-terminal catalytic domain. This fragment expresses the full catalytic activity of the wild-type enzyme.[24]

The effectiveness of the *trans*-sialidase is evident in the synthesis, on a mmol scale, of sialyllactose **3** and sialyl-*N*-acetyllactosamine **4** (Scheme 1). Yields of sialylated products are essentially quantitative; the data in Scheme 1 relate to pure, isolated products. It was noteworthy that hydrolysis of the sialyl donor **2** occurred to a significant extent only in the absence of acceptor.

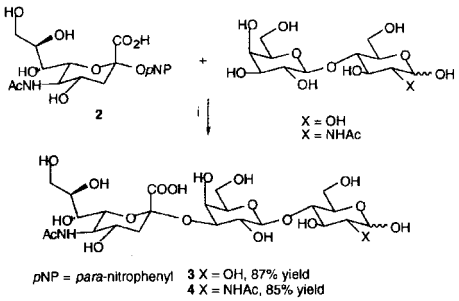

Scheme 1 *Reagent*: i, *trans*-Sialidase from *Trypanosoma cruzi*.

Because it had been reported that the *trans*-sialidase does not catalyse transfer to α-galactosides,[13] the acceptor behaviour of methyl α- and β-galactopyranosides **5** and **6**, respectively, was studied (Scheme 2). The β-anomer was an efficient acceptor giving the sialylgalactoside **7** in 81% yield. Surprisingly, the α-anomer was also sialylated to give glycoside **8** with moderate efficiency (54% yield). Clearly, a small aglycone in the α-anomeric position does not constitute a total barrier to *trans*-sialylation. However, it was considered that the presence of a bulky carbohydrate moiety in place of the much smaller methyl group in glycoside **5** would indeed create problems. Accordingly we studied the acceptor properties of disaccharide glycoside **9**. To our surprise, this was efficiently sialylated but the product was found to be the branched trisaccharide **10** (Scheme 3), formed in 89% yield. Thus the barrier to sialylation of α-galactosides is clearly expressed but the predeliction for sialylation of β-galactosides was not negated by substitution at C-6 in the acceptor.

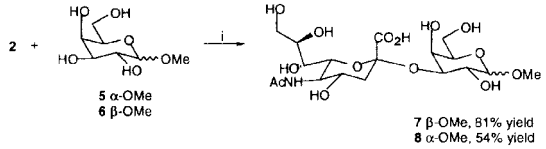

Scheme 2 *Reagent*: i, *trans*-Sialidase from *Trypanosoma cruzi*.

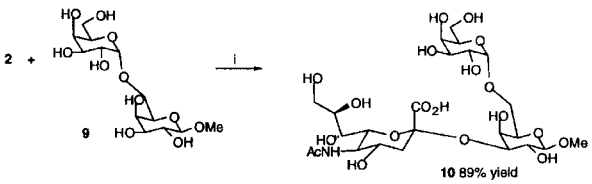

Scheme 3 *Reagent*: i, *trans*-Sialidase from *Trypanosoma cruzi*.

DOI: 10.1039/b002302g

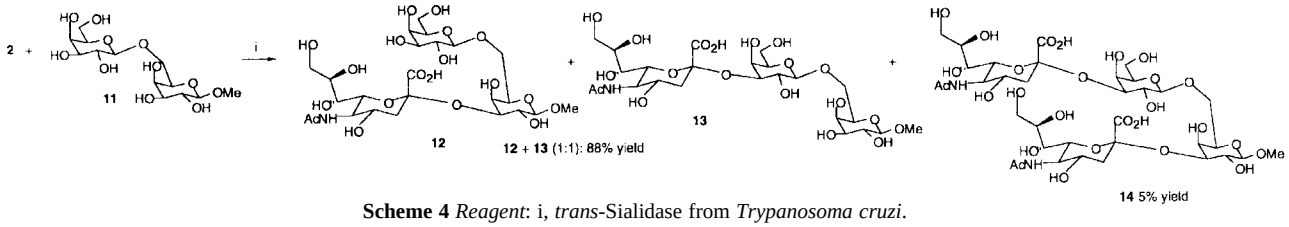

Scheme 4 *Reagent*: i, *trans*-Sialidase from *Trypanosoma cruzi*.

With β-D-Gal*p*-(1 → 6)-β-D-Gal*p*–OMe **11** as acceptor a mixture of three products was obtained (Scheme 4). The major component (88% isolated yield) proved to be a 1 : 1 mixture of the 3- and 3′-monosialylated products **12** and **13** which required HPLC separation. The third, minor product, formed in 5% isolated yield, proved to be the bis-sialylated product **14**. It was established that both of the monosialylated compounds **12** and **13** were converted quantitatively into the tetrasaccharide **14**. The selectivity for β-configured oligosaccharide acceptors and the specificity for α-(2 → 3) transfer were emphasised by the failure of sialyl transfer to α-D-Gal*p*-(1 → 3)-β-D-Gal*p*-(1 → 4)-D-GlcNAc*p*, α-D-Gal*p*-(1 → 3)-β-D-Gal*p*–OMe and α-D-Gal*p*-(1 → 3)-α-D-Gal*p*–OMe.

The studies reported here establish the *T. cruzi trans*-sialidase as a highly efficient catalyst for the sialylation of β-galactosides on a mmol scale. Moreover, they reveal the previously unsuspected ability of the enzyme to catalyse the formation of branched structures. We find that the enzyme is readily immobilised (Eupergit C) and retains its activity undiminished over at least nine catalytic cycles. Clearly, it should now be considered as a viable alternative to CMP-sialic acid-dependent sialyl transferases for α-2,3-sialylation of β-galactose-terminated oligosaccharides and with the added potential for sialylation of C-6-subsituted internal β-galactose units.

Besides its importance for the synthesis of sialyl oligosaccharides, the *T. cruzi trans*-sialidase provides a paradigm for the development, through mutagenesis, of glycosidases that would have high glycosyl transfer but low hydrolytic activity. The *T. cruzi* enzyme is homologous (*ca.* 70% identity for 640 amino acids) with the sialidase from *T. rangeli*, which lacks *trans*-sialidase activity. The latter enzyme has been crystallised. X-Ray structures have been determined at 2.2 Å resolution for the enzyme and at 2.9 Å resolution for the complex between the enzyme and 2,3-didehydro-2-deoxy-*N*-acetylneuraminic acid.[25] Homology modelling combined with mutagenesis studies have revealed several structural features that are crucial for the expression of *trans*-sialidase activity in the *T. cruzi* enzyme.[25,26] The acceptor studies reported here will also contribute to the elucidation of the *trans*-sialidase/sialidase mechanistic dichotomy.

Field and coworkers have also obtained evidence for the formation of branched sialyl galactosides (*cf.* Schemes 3 and 4).[27] We thank Professor Field for a useful exchange of information.

In a typical procedure, the *p*-nitrophenyl glycoside of sialic acid (0.1 g, 0.223 mmol) and *N*-acetyllactosamine (0.5 g, 1.31 mmol) in sodium acetate buffer (50 mM, pH 6.0, 7 cm^3) were incubated at 30 °C with recombinant *trans*-sialidase (1.38 U cm^{-3}, 0.225 cm^3) for 9 h. The reaction was stopped by filtration through a PTFE filter (0.45 μm pore size). The filtrate was applied to a Bio-Gel P-2 column which was eluted with water to give sialyl-*N*-acetyllactosaminelactose [α-Neu5Ac-(2 → 3)-β-D-Gal*p*-(1 → 4)-D-GlcNAc*p*] **4** (Scheme 2), 0.133 g (85%).

We thank Glaxo Wellcome for a gift of sialic acid and the BBSRC for financial support.

Notes and references

1 R. Schauer, S. Kelm, G. Reuter, P. Roggentin and L. Shaw, in *Biology of the Sialic Acids*, ed. A. Rosenberg, Plenum Press, New York, 1995, pp. 7–67.
2 S. Basu, M. Basu and S. S. Basu, in *Biology of the Sialic Acids*, ed. A. Rosenberg, Plenum Press, New York, 1995, pp. 69–94.
3 *Biology of the Sialic Acids*, ed. A. Rosenberg, Plenum Press, New York, 1995.
4 R. Hasegawa, in *Modern Methods in Carbohydrate Synthesis*, ed. S. H. Khan and R. A. O'Neill, Harwood Academic Publishers, Amsterdam, 1996, pp. 277–300 and references therein.
5 C. H. Wong and G. M. Whitesides, *Enzymes in Organic Synthesis*, Elsevier Science Ltd., Oxford, New York and Tokyo, 1994, pp. 269–270; U. Gambert and J. Thiem, *Top. Curr. Chem.*, 1997, **186**, 21.
6 E. S. Simon, S. Grabowski and G. M. Whitesides, *J. Org. Chem.*, 1990, **55**, 1834.
7 H. H. Higa and J. C. Paulson, *J. Biol. Chem.*, 1985, **260**, 8838; J. Thiem and W. Treder, *Angew. Chem., Int. Ed. Engl.*, 1986, **25**, 1096; D. H. van den Eijnden and W. van Dijk, *Hoppe-Seyler's Z. Physiol. Chem.*, 1972, **353**, 1817; J. Haverkamp, J.-M. Beau and R. Schauer, *Hoppe-Seyler's Z. Physiol. Chem.*, 1972, **360**, 159; E. L. Kean, *J. Biol. Chem.*, 1970, **9**, 239; C. Augé and C. Gautheron, *Tetrahedron Lett.*, 1988, **29**, 789.
8 J. Thiem and P. Stangier, *Liebigs Ann. Chem.*, 1990, 1101.
9 Y. Ichikawa, G.-J. Shen and C.-H. Wong, *J. Am. Chem. Soc.*, 1991, **113**, 4698; Y. Ichikawa, J. J.-C. Liu, G.-J. Shen and C.-H. Wong, *J. Am. Chem. Soc.*, 1991, **113**, 6300; G. F. Herrmann, Y. Ichikawa, C. Wandrey, F. C. A. Gaeta, J. C. Paulson and C.-H. Wong, *Tetrahedron Lett.*,1993, **34**, 1993.
10 J. Thiem and B. Sauerbrei, *Angew. Chem., Int. Ed. Engl.*, 1991, **30**, 1503; K. Ajisaka, H. Fujimoto and M. Isomura, *Carbohydr. Res.*, 1994, **259**, 103; Y. Makimura, H. Ishida, A. Kondo, A. Hasegawa and M. Kiso, *J. Carbohydr. Chem.*, 1998, **17**, 975.
11 J. O. Previato, A. F. B. Andrade, M. C. V. Pessolani and L. M. Previato, *Mol. Biochem. Parasitol.*, 1985, **16**, 85; B. Zingales, C. Carniol, R. M. de Lederkremer and W. Colli, *Mol. Biochem. Parasitol.*, 1987, **26**, 135; S. Schenkman, J. Man-Shiow, G. W. Hart and V. Nussenzweig, *Cell*, 1991, **65**, 1117.
12 A. J. Parodi, G. D. Pollevick, M. Mautner, A. Buschiazzo, D. O. Sanches and A. C. C. Frasch, *EMBO J.*, 1992, **11**, 1705; S. Schenkman, L. Pontes de Carvalho and V. Nussenzweig, *J. Exp. Med.*, 1992, **175**, 567.
13 P. Scudder, J. P. Doom, M. Chuenkova, I. D. Manger and M. E. A. Pereira, *J. Biol. Chem.*, 1993, **268**, 9886; A. Ferrero-García, S. E. Trombetta, D. O. Sánchez, A. Reglero, A. C. C. Frasch and A. J. Parodi, *Eur. J. Biochem.*, 1993, **213**, 765.
14 Y. Ito and J. C. Paulson, *J. Am. Chem. Soc.*, 1993, **115**, 7862.
15 P. R. Scudder, K. Shailubhai, K. L. Duffin, P. R. Streeter and G. S. Jacob, *Glycobiology*, 1994, **4**, 929.
16 A. Vetere and S. Paoletti, *FEBS Lett.*, 1996, **399**, 203.
17 A. Lubineau, K. Basset-Carpentier and C. Augé, *Carbohydr. Res.*, 1997, **300**, 161.
18 K. B. Lee and Y. C. Lee, *Anal. Biochem.*, 1994, **216**, 358.
19 A. Vetere, S. Ferro, M. Bosco, P. Cescutti and S. Paoletti, *Eur. J. Biochem.*, 1997, **247**, 4083.
20 N. Takahashi, K. B. Lee, H. Nakagawa, Y. Tsukamoto, Y. Kawamura, Y.-T. Li and Y. C. Lee, *Anal. Biochem.*, 1995, **230**, 333.
21 S.-I. Nishimura, K. B. Lee, K. Matsuoka and Y. C. Lee, *Biochem. Biophys. Res. Commun.*, 1994, **199**, 249.
22 M. A. Probert, M. J. Milton, R. Harris, S. Schenkman, J. M. Brown, S. W. Homans and R. A. Field, *Tetrahedron Lett.*, 1997, **38**, 5861.
23 J. Rothermel and H. Faillard, *Carbohydr. Res.*, 1990, **196**, 29; V. Eschengelder and R. Brossmer, *Carbohydr. Res.*, 1987, **162**, 294.
24 M. Ribeirão, V. L. Perreira-Chioccola, D. Eichinger, M. M. Rodrigues and S. Schenkman, *Glycobiology*, 1997, **7**, 1237.
25 A. Buschiazzo, G. A. Tavares, O. Campetella, S. Spinelli, M. L. Cremona, G. París, M. Fernanda Amaya, A. C. C. Frasch and P. M. Alzari, *EMBO J.*, 2000, **29**, 16.
26 M. L. Cremona, D. O. Sánchez, A. C. C. Frasch and O. Campetella, *Gene*, 1995, **160**, 123; L. E. Smith and D. Eichinger, *Glycobiology*, 1997, **7**, 445; M. L. Cremona, O. Campetella, D. O. Sánchez and A. C. C. Frasch, *Glycobiology*, 1999, **9**, 581; M. Chuenkova, M. Pereira and G. Taylor, *Biochem. Biophys. Res. Commun.*, 1999, **262**, 549.
27 J. A. Harrison, PhD thesis, St Andrews, 1998.

Supramolecular liquid crystals with columnar mesophases through self-assembly of carboxylic acids around a tribasic core

Arno Kraft,*[ab] Anja Reichert[b] and Ralf Kleppinger[c]

[a] *Department of Chemistry, Heriot-Watt University, Edinburgh, UK EH14 4AS. E-mail: a.kraft@hw.ac.uk*
[b] *Institut für Organische Chemie und Makromolekulare Chemie II, Heinrich-Heine-Universität Düsseldorf, Universitätsstr. 1, D-40225 Düsseldorf, Germany*
[c] *FOM Institute for Atomic and Molecular Physics, Kruislaan 407, NL-1098 SJ Amsterdam, The Netherlands. E-mail: kleppinger@amolf.nl*
Published on the Web 23rd May 2000

Received (in Liverpool, UK) 17th April 2000, Accepted 5th May 2000

The self-assembly of long chain alkoxy-substituted benzoic acids around tribasic core 1 provides a simple and flexible way to supramolecular liquid crystals with columnar mesophases.

During the last years several groups have developed a number of supramolecular approaches to the preparation of liquid crystals with columnar mesophases.[1] Disc-shaped mesogens can result, for example, from the association of a varying number of amphiphilic molecules whose incompatible polar and non-polar parts segregate on a microscopic scale. Microsegregation is seen as an important driving force in the formation of smectic, columnar and cubic phases; the type of liquid-crystalline phase depends on the curvature of the interface.[2] Typical examples for columnar systems are Lattermann's monoaryl esters of *cis*,*cis*-1,3,5-cyclohexanetriol,[3] Praefcke's inositol derivatives,[4] Tschierske's laterally substituted terphenyls,[2] and Percec's taper-shaped benzo-crown ethers.[5] The dimerisation of mesogenic benzamides,[6] of phenanthridinones,[7] the trimerisation of phthalhydrazides,[8] complexes of a 2,4,6-triarylamino-1,3,5-triazine with benzoic acids,[9] and complexes of certain pyridine derivatives with carboxylic acids[10,11] illustrate how the discotic unit can be made up of a defined number of components that are held together by hydrogen bonding. Non-covalent complexation between non-identical components has so far led to columnar phases in only a few exceptional cases.[9–11]

We have recently described that non-convalent complexes are readily obtained from carboxylic acids and trisimidazoline base **1**; these are held together by hydrogen bonds and salt bridges in non-polar solvents.[12] Two X-ray crystal structures indicated that such carboxylic acid complexes have an almost disc-like flat shape and therefore fulfill one of the structural requirements for discotic liquid crystals.[12a,13] Here, we report a new type of supramolecular liquid crystal based on the assembly of benzoic acids, which are substituted with a sufficient number of long alkoxy side chains, around a tribasic core **1**.

Long chain alkoxy-substituted benzoic acids **2a**–**d**[14] and tris(imidazoline) base **1**[12] were prepared as described in the literature. All compounds were used after extensive purification, which included gradient sublimation of **1** at 310 °C/ 10^{-4} mbar. Complexes **3a**–**d** were prepared by dissolution of the respective benzoic acid **2a**–**d** (3 equiv.) and base **1** (1 equiv.) in hot ethanol (*ca*. 80 mL per mmol of **1**). The hot solution was filtered and, if necessary, concentrated until the still warm solution became cloudy. The salts crystallised in analytically pure form upon standing at room temperature (Scheme 1). All complexes gave satisfactory ^{1}H NMR, ^{13}C NMR, IR and elemental analysis data.

As might be expected from multiple substitution with long-chain alkoxy groups, complexes **3a**–**c** showed high solubility in non-polar organic solvents, such as chloroform (solubility typically > 200 mg mL^{-1}), toluene, or even hexane, whereas polar solvents (DMSO, alcohols) were generally found to be non-solvents. The diagnostic downfield ^{1}H NMR chemical shifts for the NH signal ($\delta_H \approx 13$) as well as for the singlet assigned to the core's aromatic protons ($\delta_H \approx 10.1$ in $CDCl_3$ or C_6D_6) emphasised that the equilibrium between the salt and its ionic components lies on the side of the hydrogen-bonded 3:1 complex in non-polar solvents.[12] No evidence for dissociation was observed for any of the carboxylic acid complexes in chloroform solutions at concentrations > 10^{-5} M. It is therefore expected that dissociation is even more unfavourable in the condensed phase.

Although neither **1** nor benzoic acids **2** are mesogenic, differential scanning calorimetry (DSC) and polarising optical microscope (POM) experiments confirmed that complexes **3a**–**c** transform to birefringent, shearable liquid-crystalline mesophases at *ca*. 80 °C (Table 1). The clearing temperatures of the mesophases of all three complexes were above 200 °C. Crystal–mesophase melting transitions exhibited large enthalpic changes (138 J g^{-1} for **3c**), whereas enthalpies for the clearing transition from the mesophase to the isotropic liquid were much smaller (17 J g^{-1} for **3c**) albeit still considerably higher than for a typical smectic phase.

A very fine texture was observed during the first heating of complexes **3a**–**c**. Subsequent slow cooling (cooling rate ≤2 °C min^{-1}) from the isotropic melt led—after significant supercooling (*ca*. 15 °C for **3a**)—to the dendritic growth of homeotropic finger-like contours (Fig. 1) that are characteristic for columnar mesophase formation.[15] Further cooling to room temperature again produced a fine-structured texture, and even the previously homeotropic regions finally showed birefringence. The thermal stability of the mesophases was, however,

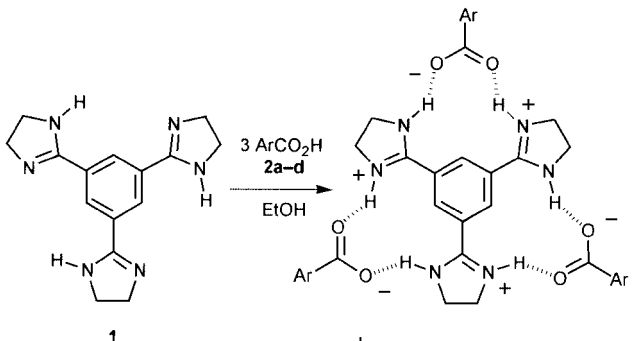

1

3	Ar-CO_2H
a	3,4,5-$(C_{12}H_{25}O)_3C_6H_2CO_2H$
b	3,4-$(C_{10}H_{21}O)_2C_6H_3CO_2H$
c	3,4-$(C_{12}H_{25}O)_2C_6H_3CO_2H$
d	4-$C_{12}H_{25}OC_6H_4CO_2H$

Scheme 1

DOI: 10.1039/b003091k

Table 1 Phase transition temperatures T and enthalpies ΔH of **3a–d** as determined by DSC[a]

	3a		**3b**		**3c**		**3d**	
	K–M	M–I	K–M	M–I	K–M	M–I	K–K	K–I
First heating/°C	63	214	79[b]	244	72	240	62	188
ΔH/J g^{-1}	53	9	111	19	138	17	34	36

[a] K: crystalline phase, M: mesophase, I: isotropic phase; heating and cooling rates 10 °C min^{-1}. [b] An additional endothermic transition with a peak at 71 °C can be detected if the crystallised sample was dried at < 60 °C prior to DSC measurements.

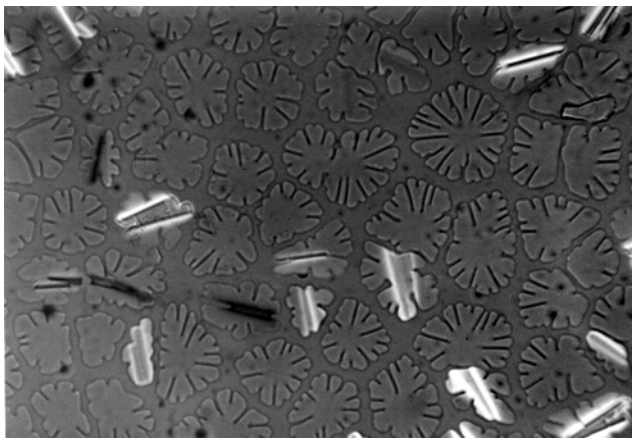

Fig. 1 Representative optical polarised micrograph showing the dendritic growth of homeotropic contours at 200 °C after slow cooling of complex **3b** from the isotropic melt (polarisers not completely crossed).

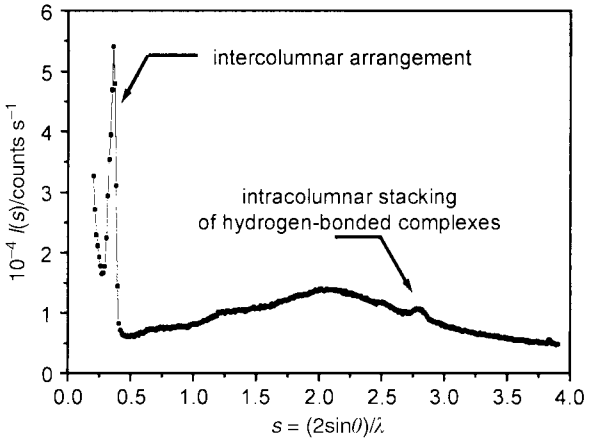

Fig. 2 Typical X-ray scattering diagram of hydrogen-bonded complex **3b** taken at 150 °C in the mesophase region.

somewhat limited. After prolonged annealing at 170 °C or heating at temperatures > 200 °C for more than a few minutes, extended domains evolved which lacked birefringence and were surrounded by brown shades indicating decomposition of the textures. Interestingly, the liquid-crystalline domains of the 3,4-disubstituted **3b–c** were found to be larger than those of the symmetrical complex **3a**, both during the first heating process and subsequent cooling. Although complex **3d** became malleable upon heating above 70 °C, a single dodecyloxy group per benzoic acid unit was evidently insufficient to stabilise a liquid-crystalline phase.

X-Ray scattering experiments confirmed the presence of liquid-crystalline mesophases in the high temperature regime of complexes **3a–c**. Fig. 2 shows a typical scattering pattern with a maximum at low angles, corresponding to Bragg spacings in the range of 3–4 nm, a broad maximum due to liquid-like arrangement of the terminal alkyl chains and a well defined maximum at wide angles, corresponding to a Bragg spacing of 0.36 nm. The value of the Bragg spacing associated with the scattering maximum at small angles clearly indicates that the scattering units are significantly larger compared to the dimensions of either the tribasic core or the benzoic acid derivatives. The Bragg spacing of 0.36 nm points towards a regular stacking of the aromatic components, a feature which is well known from structural studies on mesophases formed by covalently bonded discotic mesogens.[16] The presence of only a single maximum at low angles in the scattering pattern from non-oriented systems does not allow an assignment of the specific type of columnar arrangement; however, we obtained reasonable estimates for the macroscopic density by assuming hexagonally ordered columns of regularly stacked hydrogen-bonded complexes. Further studies on the morphology using X-ray scattering and AFM are in progress.

We thank Professor G. Wulff, to whom this paper is dedicated on the occasion of his 65th birthday, and the Deutsche Forschungsgemeinschaft for continuing support, Ms S. Johann for experimental help, and Professor W. Mormann (University of Siegen) for stimulating discussions.

Notes and references

1 For recent reviews on discotic liquid crystals see: S. Chandrasekhar, *Handbook of Liquid Crystals*, ed. D. Demus, J. W. Goodby, G. W. Gray, H. W. Spiess and V. Vill, Wiley-VCH, Weinheim, 1998, vol. 2B, p. 749; A. N. Cammidge and R. J. Bushby, *Handbook of Liquid Crystals*, ed. D. Demus, J. W. Goodby, G. W. Gray, H. W. Spiess and V. Vill, Wiley-VCH, Weinheim, 1998, vol. 2B, p. 693; and for a review on hydrogen-bonded LC systems: T. Kato, *Handbook of Liquid Crystals*, ed. D. Demus, J. W. Goodby, G. W. Gray, H. W. Spiess and V. Vill, Wiley-VCH, Weinheim, 1998, vol. 2B, p. 969.
2 C. Tschierske, *J. Mater. Chem.*, 1998, **8**, 1485.
3 G. Lattermann, *Liq. Cryst.*, 1987, **2**, 723.
4 K. Praefcke, P. Marquardt, B. Kohne, W. Stephan, A.-M. Levelut and E. Wachtel, *Mol. Cryst. Liq. Cryst.*, 1991, **203**, 149.
5 V. Percec, G. Johansson, D. Schlueter, J. C. Ronda and G. Ungar, *Macromol. Symp.*, 1996, **101**, 43.
6 U. Beginn and G. Lattermann, *Mol. Cryst. Liq. Cryst.*, 1994, **241**, 215.
7 R. Kleppinger, C. P. Lillya and C. Yang, *Angew. Chem., Int. Ed. Engl.*, 1995, **34**, 1637; R. Kleppinger, C. P. Lillya and C. Yang, *J. Am. Chem. Soc.*, 1997, **119**, 4097 and references therein.
8 M. Suárez, J.-M. Lehn, S. C. Zimmerman, A. Skoulios and B. Heinrich, *J. Am. Chem. Soc.*, 1998, **120**, 9526 and references therein.
9 D. Goldmann, R. Dietel, D. Janietz, C. Schmidt and J. H. Wendorff, *Liq. Cryst.*, 1998, **24**, 407.
10 H. Bernhardt, W. Weissflog and H. Kresse, *Chem. Lett.*, 1997, 151.
11 R. Deschenaux, F. Monnet, E. Serrano, F. Turpin and A.-M. Levelut, *Helv. Chim. Acta*, 1998, **81**, 2072.
12 (*a*) A. Kraft and R. Fröhlich, *Chem. Commun.*, 1998, 1085; (*b*) A. Kraft, F. Osterod, L. Peters and A. Reichert, *Polym. Mater. Sci. Eng.*, 1999, **80**, 18; (*c*) A. Kraft, *J. Chem. Soc., Perkin Trans. 1*, 1999, 705.
13 A. B. Holmes, S. C. Moratti, X.-C. Li, H. Sirringhaus, A. Kraft and M. M. Murray (Cambridge Display Technology Ltd.), *PCT Int. Pat. Appl.*, WO 99/12989, 1999 (*Chem. Abstr.*, 1999, **130**, 252238t).
14 H. Meier, E. Prass, G. Zerban and F. Kosteyn, *Z. Naturforsch., Teil B*, 1988, **43**, 889; A. R. A. Palmans, J. A. J. M. Vekemans, H. Fischer, R. A. Hikmet and E. W. Meijer, *Chem. Eur. J.*, 1997, **3**, 300; R. P. Tuffin, K. J. Toyne and J. W. Goodby, *J. Mater. Chem.*, 1996, **6**, 1271; F. D. Cukiernik, M. Ibn-Elhaj, Z. D. Chaia, J.-C. Marchon, A.-M. Giroud-Godquin, D. Guillon, A. Skoulios and P. Maldivi, *Chem. Mater.*, 1998, **10**, 83.
15 Y. Bouligand, *J. Phys. (Paris)*, 1980, **41**, 1307.
16 A. M. Levelut, *J. Phys. Lett. (Paris)*, 1979, **40**, L-81.

ChemComm

Radical carbon–carbon coupling reactions *via* organoboranes

Christine Cadot, Janine Cossy and Peter I. Dalko*

Laboratoire de Chimie Organique associé au CNRS, ESPCI, 10 rue Vauquelin, 75231 - Paris Cedex 05, France. E-mail: peter.dalko@espci.fr

Received (in Liverpool. UK) 7th March 2000, Accepted 26th April 2000
Published on the Web 22nd May 2000

Alkylboronic esters give rise to free-radical alkylation products in the presence of phenylcarbonyloxy(pyridine-2-thione) (Barton's ester) and a variety of Michael acceptors under irradiation.

The use of organoboranes in free-radical reactions[1–5] suffers from a notable limitation. The radicals generated from these compounds using, for example, molecular oxygen fail to add to certain good radical traps such as unsaturated esters, nitriles or sulfones.[1–3] The reason for this lack of reactivity is the unfavourable equilibrium in the postulated enol radical[2] required in the propagation step of the chain process. The design of a simple chain sequence, which eliminates the problem of the propagation step, is therefore of interest.

The boronate intermediates **2a**–**d** were prepared by hydroboration of olefin **1a** using borane–dimethylsulfide complex, followed by addition of NEt_3 and quenching of the aminoborane intermediate with alcohol or phenol derivatives (Scheme 1). The homolytic fragmentation of the boronates has been studied in the presence of phenylcarbonyloxy(pyridine-2-thione) (PTOC ester) **3**† (2 equiv.),[6] and irradiation at 0–5 °C, using a commercial halogen lamp (300 W).[7]‡ In all experiments, the reaction afforded the desired thiopyridyl derivatives **5a** and **5b** in a 6 : 1 *trans–cis* selectivity, independent of the ligand used. In addition, a variable amount of thiopyridyl dimer, characteristic of the Barton reaction, and benzoic acid arise from the decomposition of the postulated intermediate **4** (*vide infra*, Scheme 4) under the hydrolytic work-up.

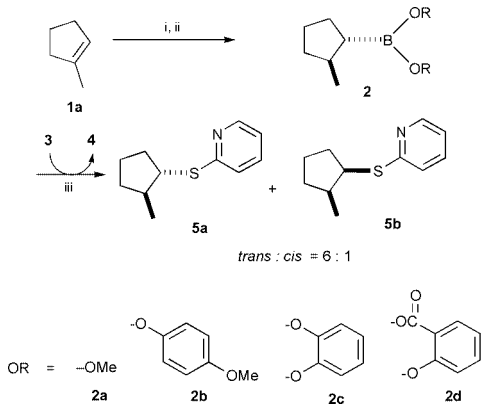

Scheme 1 *Reagents and conditions*: i, $BH_3{\cdot}Me_2S$ (1.25 equiv.), THF, 0–5 °C, 2 h; ii, NEt_3 (1.25 equiv.), 0–5 °C, then alcohol or phenol (1.25 equiv. per OH), room temp.; iii. **3** (2 equiv.), *hν*, CH_2Cl_2/PhH, 0–5 °C, 2 h. Yields (for three steps combined): **a**, 13%; **b**, 43%; **c**, 68%; **d**, 23%.

Among the tested derivatives, dimethyl boronate **2a** afforded poor yield of **5** (13% combined). Better yields were obtained using aryl boronates such as **2b** (43%). Similarly to oxygen initiated reactions, the best results were observed using the catechol derivative **2c** (68%).[5] Ligands substituted by electron withdrawing groups such as the salicylate **2d** afforded lower yields of **5** under the same conditions (23%).

The radical alkylation reaction was examined in the presence of the conventional Michael acceptors, **6a**–**e**, shown in Scheme 2. The catechol boronates were prepared, as before, by hydroboration of olefins **1a**–**d** followed by quenching with an equimolar amount of catechol and were not isolated. These intermediates were irradiated, respectively, in the presence of PTOC ester **3** (2 equiv.) and an excess of Michael acceptors **6a**–**c** (3–5 equiv.) (Scheme 2). The reaction afforded the adducts **7a**–**h** as inseparable mixtures of the diastereomers.§ In each reaction, a good selectivity, in favour of the *trans* isomer was observed and was determined after the cleavage of the thiopyridyl group (*vide infra*).¶ Likewise, β-pinene **1d** was hydroborated using either borane–dimethyl sulfide complex or thexylborane under standard conditions[10] followed by fragmentation and quenching of the corresponding aminoboranes with equimolar amounts of catechol. As before, the boronate was not isolated. Fragmentation in the presence of an excess (2 equiv.) of PTOC ester **3** and alkylation using methyl acrylate afforded the desired adduct **7i**.‖ The isolated yield of this transformation was considerably lower (30%) than that of the alkylation of secondary radicals. This difficulty in alkylation of primary radicals follows the earlier observed trends.[1–5]

Entry	Olefin	EWG	6	Yield (%)	7	*trans - cis* selectivity§
1	**1a**	CN	**6a**	54	**7a**	88 : 12
2	**1a**	$P(O)(OEt)_2$	**6b**	79	**7b**	99 : 5
3	**1a**	SO_2Ph	**6c**	70	**7c**	92 : 8
4	**1a**	CO_2Me	**6d**	55	**7d**	90 : 10
5	**1b**	CO_2Me	**6d**	82	**7e**	80 : 20
6	**1c**	CN	**6a**	91	**7f**	90 : 10
7	**1c**	COMe	**6e**	70	**7g**	93 : 7
8	**1c**	CO_2Me	**6d**	57	**7h**	95 : 5
9	**1d**	CO_2Me	**6d**	30	**7i**	——

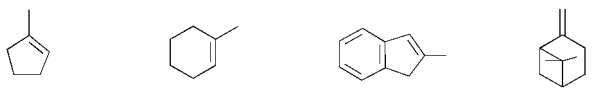

Scheme 2 *Reagents and conditions*: i, $BH_3{\cdot}Me_2S$ (1.25 equiv.), THF, 0–5 °C, 2 h; ii, NEt_3 (1.25 equiv.), 0–5 °C, then catechol (1.25 equiv.), room temp.; iii, **3** (2 equiv.), olefin **6a**–**e** (3–5 equiv.), CH_2Cl_2/PhH, *hν*, 0–5 °C, 2.5 h.

The relative stereochemistry of the carbon–carbon formation step was established after removing the thiopyridyl group. Although the α-keto thiopyridyl derivative **7g** (Scheme 3, entry 7) was reduced easily using samarium(II) iodide, other derivatives such as nitriles **7a** and **7f**, phosphonate **7b**, esters **7d**,**e** and **7h** and phenyl sulfone **7c** remained inert under these conditions. In these cases, the thiopyridyl esters were converted into the corresponding sulfones and were reduced using samarium iodide[11,12] in the presence or in the absence of HMPA as cosolvent (Scheme 3). Under these conditions the corresponding alkanes **8** were obtained upon quenching the organosamarium intermediates with water. The reaction conditions were not

DOI: 10.1039/b001903h

optimised for this reductive step and the low isolated yields observed for **8a**, **8d** and **8e** can be attributed to the volatility of the reduced products. In the examples discussed, this mild cleavage of the thiopyridyl group allowed unambiguous establishment of the stereoselectivity of the crucial carbon–carbon formation step (Scheme 3).

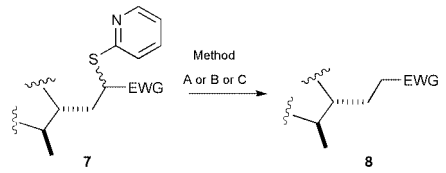

Entry	EWG	7	Method	Yield (%)	8
1	CN	**7a**	C	33	**8a**
2	$P(O)(OEt)_2$	**7b**	B	53	**8b**
3	SO_2Ph	**7c**	B	54	**8c**
4	CO_2Me	**7d**	C	21	**8d**
5	CO_2Me	**7e**	C	14	**8e**
6	CN	**7f**	C	46	**8f**
7	COMe	**7g**	A	51	**8g**
8	CO_2Me	**7h**	C	44	**8h**

Scheme 3 *Reagents and conditions*: method A: SmI_2 (3 equiv.), 0–5 °C, 20 min., then H_2O, room temp.; method B: i, MCPBA (3 equiv.), CH_2Cl_2, 0–5 °C, 3 h; ii, SmI_2 (3 equiv.), THF, 0–5 °C 20 min, then H_2O, room temp.; method C: i, MCPBA (3 equiv.), CH_2Cl_2, 0–5 °C, 3 h; ii, SmI_2 (3 equiv.), HMPA (15 equiv.), THF, 0–5 °C, 10 min, then H_2O, room temp.

In the postulated mechanism of the reaction (Scheme 4) the formed arylcarbonyloxyl radical **9** reacts with the boronic ester **2** resulting in selective fragmentation of the weak B–alkyl bond.** The use of the PTOC esters also offers a logical solution to the chain propagation problem, this being assured by the presence of the thiopyridyl group, and eliminating the necessity of formation of the enol radical form of the addition product.

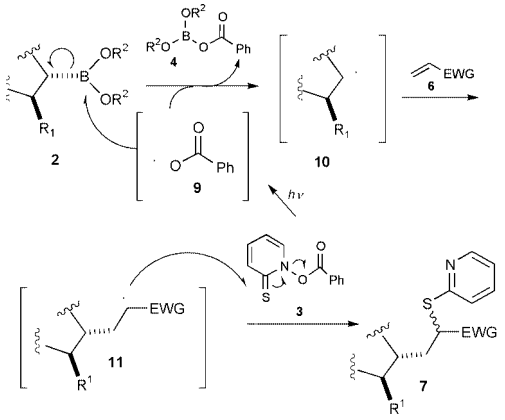

Scheme 4 Free-radical alkylation of alkylboronates **2** in the presence of phenylcarbonyloxy(pyridine-2-thione) **3** (Barton's ester) and olefin **6**.

In summary, a method, which combines the predictable and high degree of stereoselectivity of boron chemistry with a flexible method for radical carbon–carbon bond formation, is described.[4] In contrast to the previously developed methods,[1–3,5] the alkylation reaction can be extended to a seemingly unrestricted array of Michael acceptors. The reaction proceeds with addition of a thiopyridyl group in the α position of the radical trap. This function eventually can be selectively removed using SmI_2 after converting the thiopyridyl ether to the corresponding sulfone. Whilst organoboronates can be obtained in highly enantioenriched form using asymmetric hydroboration reactions,[13] this free-radical fragmentation/alkylation process may be of interest to develop new arrays of free-radical alkylation reactions in asymmetric synthesis. Beyond this, the synthetic value of the combination of boron and PTOC derivatives should also be contrasted with the generation of radicals by more conventional methods using organotin reagents.[14]

The CNRS, La Ville de Paris and the Fondation pour la Recherche Médicale (grant No: 40001838-01) are gratefully acknowledged for financial support.

Notes and references

† The commonly used PTOC esters (Barton esters) are anhydrides of carboxylic acids and the thiohydroxamic acid *N*-hydroxypyridine-2-thione.

‡ The primarily generated acyloxyl radicals may undergo radical decarboxylation reactions.[8] Decarboxylation of such aryl and vinylcarboxyl radicals is generally too slow to be useful for synthetic purposes. Such species may have lifetimes in the microsecond range.[9] This sluggish decarboxylation renders it possible to use them as valuable free-radical chain carriers in the discussed reaction.

§ The diastereoselectivity was measured by GC–MS on the reduced products **8**.

¶ Although NMR analyses showed the formation of the *trans* isomer as the major product, the presence of the two possible thiopyridyl diastereomers rendered it difficult at this stage to establish the precise stereoselectivity.

‖ A roughly 1 : 1 mixture of the two inseparable diastereomers was obtained, according to ^{13}C NMR spectroscopy (162.5 MHz).

** The aryl radical, formed by classical decarboxylation of **9** would lead to a similar chain reaction. No evidence, however, of formation of aryl boronates in the reaction was found.

1 A. Suzuki, A. Arase, H. Matsumoto, M. Itoh, H. C. Brown, M. M. Rogic and M. W. Rathke, *J. Am. Chem. Soc.*, 1967, **89**, 5708; H. C. Brown, M. M. Rogic, M. W. Rathke and G. W. Kabalka, *J. Am. Chem. Soc.*, 1967, **89**, 5709.

2 K. Nozaki, K. Oshima and K. Utimoto, *J. Am. Chem. Soc.*, 1987, **109**, 2547; K. Nozaki, K. Oshima and K. Utimoto, *Bull. Chem. Soc. Jpn.*, 1991, **64**, 403.

3 For a general review of this chemistry see: D. P. Curran, *Radical Addition Reaction*, in *Comprehensive Organic Chemistry*, ed. B. M. Trost and I. Fleming, Plenum Press, New York. 1991, vol. 4, p. 715; D. P. Curran, *Radical Cyclizations and Sequential Radical Reactions*, in *Comprehensive Organic Chemistry*, ed. B. M. Trost and I. Fleming, Plenum Press, New York. 1991, vol. 4, p. 779.

4 For related work on the use of organoboranes in radical chemistry, see: B. Giese and G. Kretzschmar, *Angew. Chem., Int. Ed. Engl.*, 1981, **20**, 965; B. Giese and G. Kretzschmar, *Chem. Ber.*, 1982, **115**, 2012; B. Giese and G. Kretzschmar, *Chem. Ber.*, 1983, **116**, 3267; B. Giese and G. Kretzschmar, *Chem. Ber.*, 1984, **117**, 3160; B. Giese and G. Kretzschmar, *Chem. Ber.*, 1984, **117**, 3175.

5 C. Ollivier and P. Renaud, *Chem. Eur. J.*, 1999, **5**, 1468; C. Ollivier, R. Chuard and P. Renaud, *Synlett*, 1999, 807; N. Kihara, C. Ollivier and P. Renaud, *Org. Lett.*, 1999, **1**, 1419.

6 E. A. Theodorakis and K. M. Wilcoxen, *Chem. Commun.* , 1996, 1927; D. H. R. Barton and A. J. Ferreira, *Tetrahedron*, 1996, **28**, 9347.

7 For the use of substituted thiopyridone derivatives as initiators in free radical chain reactions, see for example D. H. R. Barton and M. Ramesh, *J. Am. Chem. Soc.*, 1990, **112**, 891; D. H. R. Barton, P. I. Dalko and S. D. Géro, *Tetrahedron Lett.*, 1991, **36**, 4713.

8 D. H. R. Barton, D. Crich and W. B. Motherwell, *Tetrahedron*, 1985, **41**, 3901; A. L. J. Beckwith and B. P. Hay, *J. Am. Chem. Soc.*, 1989, **111**, 230.

9 B. M. Aveline, I. E. Kochevar and R. W. Redmond, *J. Org. Chem.*, 1995, **117**, 9699; C. Bohne, R. Boch and J. C. Scaiano, *J. Org. Chem.*, 1990, **55**, 5414; M. Newcomb, *Tetrahedron*, 1993, **49**, 1151 and references therein.

10 H. C. Brown, E. Negishi and J.-J. Katz, *J. Am. Chem. Soc.*, 1975, **97**, 2791.

11 I. E. Markó, F. Murphy and S. Dolan, *Tetrahedron Lett.*, 1996, **37**, 2089.

12 O. Jarreton, T. Skrydstrup, J.-F. Espinosa, J. Jiménez-Barbero and J.-M. Beau, *Chem. Eur. J.*, 1999, **5**, 430 and references therein.

13 H. C. Brown and B. Singaram, *J. Am. Chem. Soc.*, 1984, **106**, 1797; H. C. Brown, B. Singaram and T. E. Cole, *J. Am. Chem. Soc.*, 1985, **107**, 460; See also: K. Burgess, W. A. van der Donk and M. Ohlmeyer, *Tetrahedron: Asymmetry*, 1991, **2**, 613; J. M. Brown, D. I. Hulmes and T. P. Layzell, *J. Chem. Soc., Chem. Commun.*, 1993, 1673; A. Schnyder, L. Hintermann and A. Togni, *Angew. Chem., Int. Ed.*, 1998, **34**, 9043; U. P. Dhokte and H. C. Brown, *J. Org. Chem.*, 1997, **62**, 865.

14 P. A. Baguley and J. C. Walton, *Angew. Chem., Int. Ed.*, 1998, **37**, 3072.

ChemComm

The reaction of cyclohexyl isocyanide and dimethyl acetylenedicarboxylate with aldehydes: a novel synthesis of 2-aminofuran derivatives

Vijay Nair* and A. U. Vinod

Organic Chemistry Division, Regional Research Laboratory (CSIR), Trivandrum-695019, India.
E-mail: gvn@csrrltrd.ren.nic.in

Received (in Cambridge, UK) 1st March 2000, Accepted 20th April 2000
Published on the Web 22nd May 2000

The 1:1 intermediate generated by the additon of cyclohexyl isocyanide to dimethyl acetylenedicarboxylate is trapped by aldehydes to yield 2-aminofuran derivatives in good yields.

The addition of nucleophilic carbenes such as isocyanides to dimethyl acetylenedicarboxylate has been investigated in detail.[1–3] The initially formed 1:1 zwitterionic species undergo further reaction with DMAD and isocyanide in different molar proportions, ultimately leading to a variety of complex heterocyclic systems.[4–9] This highly reactive intermediate **1** can manifest carbanion or carbene character or even resemble a cyclopropenone imine (Fig. 1).

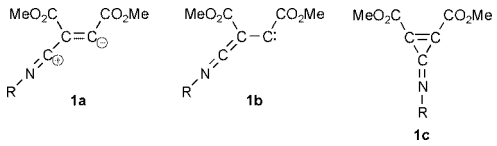

Fig. 1

In the context of our general interest in the synthesis of heterocyclic compounds by the reaction of dipolar species with carbonyl compounds,[10,11] we were intrigued by the possibility of trapping the zwitterionic intermediate† derived from isocyanides and DMAD with aldehydes. It is noteworthy that previous attempts to trap **1** with various olefinic dipolarophiles have failed.[6] The preliminary results of our investigations validating the usefulness of this process, leading to a novel aminofuran synthesis are presented here.

A mixture of 3-nitrobenzaldehyde and dimethyl acetylenedicarboxylate in dry benzene at 80 °C, when treated with cyclohexyl isocyanide afforded aminofuran **1a** in 69% yield (Scheme 1).‡

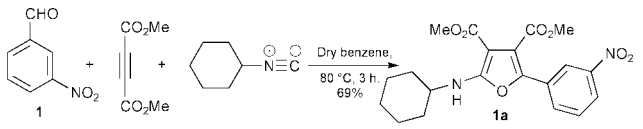

Scheme 1

In the ^{1}H NMR spectrum, the two carbomethoxy groups were observed at δ 3.79 and 3.94 as two singlets and the NH proton resonated at δ 6.70 supporting the IR absorption at 3367 cm^{-1}. The ^{13}C signals for the two ester carbonyls were seen at δ 165.20 and 164.62.

Similar results were obtained with a number of other aldehydes and results are summarised in Table 1.§

A mechanistic rationale for the formation of the aminofurans is presented in Scheme 2.

In conclusion, we have found that the one pot reaction of isocyanides and DMAD with aldehydes leads to a facile synthesis of aminofuran derivatives. It should be mentioned that recently aminofurans have been found to undergo facile Diels–Alder reactions leading to hexahydroindolinones;[12] they also serve as useful intermediates in the synthesis of aromatic as well as aliphatic molecules.[13] It is conceivable that the novel three component reaction described herein will be applicable to the synthesis of a variety of heterocycles; further studies are in progress.

A. U. V. thanks CSIR, New Delhi, for a research fellowship. Thanks are also due to Dr Mangalam S. Nair and Ms Soumini Mathew for recording high-resolution NMR spectra.

Table 1 Reaction of aldehydes with DMAD and cyclohexyl isocyanide

Entry	Aldehyde	*t*/h	Product	Yield(%)[a]
2		8	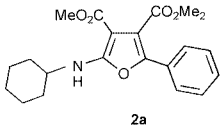 **2a**	61
3	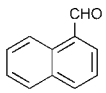	8	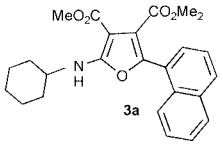 **3a**	54
4	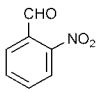	3	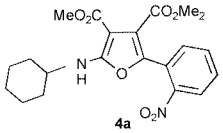 **4a**	68
5	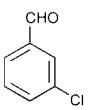	2	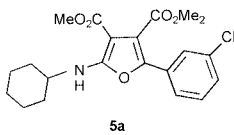 **5a**	61
6	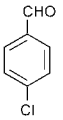	2.5	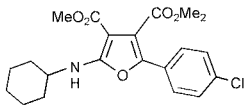 **6a**	67
7	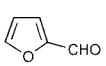	3	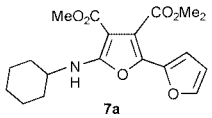 **7a**	68

[a]Isolated yield.

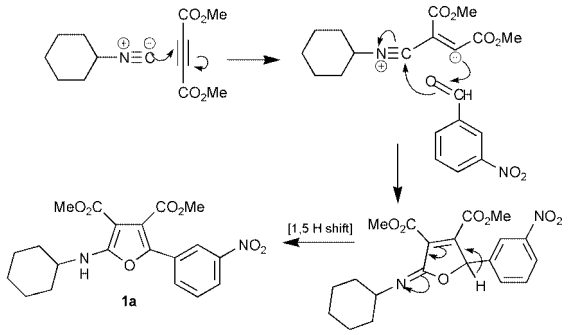

Scheme 2

Notes and references

† Earlier we reported on the addition of the zwitterion generated from triphenylphosphine and DMAD to quinones leading to novel γ-spirolactones.[14]

‡ *Experimental procedure and selected data* for **1a**: a mixture of 3-nitrobenzaldehyde **1** (0.200 g, 1.32 mmol) and DMAD (0.207 g 1.45 mmol) in dry benzene (15 ml) was purged with argon at 80 °C. Cyclohexyl isocyanide[15] (0.159 g, 1.45 mmol) was added to this mixture by syringe and refluxing was continued for a further 3 h. The solvent was then removed under vaccum and the residue on chromatographic separation on silica gel using hexane–ethyl acetate (85 : 15) gave aminofuran **1a** as a yellow solid (0.365 g, 69%); mp 122–123 °C (CH_2Cl_2–hexane) (Calc. for $C_{20}H_{22}N_2O_7$: C, 59.68; H, 5.51; N, 6.96. Found: C, 59.62; H; 5.47; N, 6.71%); ν_{max}/cm^{-1} 3367 (NH), 2943, 2849, 1726 (C=O), 1663 (C=O), 1620, 1532; δ_H(300 MHz, $CDCl_3$) 8.33 (s, 1H, ArH), 8.06 (d, 1H, *J* 8.05 Hz, ArH), 7.80 (d, 1H, *J* 7.71 Hz, ArH), 7.51 (t, 1H, ArH), 6.70 (d, 1H, *J* 7.80 Hz, NH), 3.94 (s, 3H, OMe), 3.79 (s, 3H, OMe), 3.79 (m, 1H, CH), 2.07–1.39 (m, 10H, 5 × CH_2); δ_C(75 MHz; $CDCl_3$) 165.20 (C=O), 164.62 (C=O), 161.51, 148.79, 138.32, 130.95, 129.75, 129.71, 121.73, 119.21, 116.34, 88.23, 52.84, 51.70, 51.34, 33.59, 25.53, 24.58.

§ All new compounds were fully characterised.

1 E. Winterfeldt, D. Schumann and H. J. Dillinger, *Chem. Ber.*, 1969, **102**, 1656.
2 T. R. Oakes, H. G. David and F. J. Nagel, *J. Am. Chem. Soc.*, 1969, **91**, 4761.
3 T. Takizawa, N. Obata, Y. Suzuki and T. Yanagida, *Tetrahedron Lett.*, 1969, 3407.
4 Y. Suzuki, N. Obata and T. Takizawa, *Tetrahedron Lett.*, 1970, 2667.
5 Y. Suzuki and Y. Iitaka, *Bull. Chem. Soc. Jpn.*, 1971, **44**, 56.
6 T. R. Oakes and T. J. Donovan, *J. Org. Chem.*, 1973, **38**, 1319.
7 H. J. Dillinger, G. Fengler, D. Schumann and E. Winterfeldt, *Tetrahedron*, 1974, **30**, 2553.
8 H. J. Dillinger, G. Fengler, D. Schumann and E. Winterfeldt, *Tetrahedron*, 1974, **30**, 2561.
9 F. Johnson, A. H. Gulbenkian and W. A. Nasutavicus, *Chem. Commun.*, 1970, 608.
10 V. Nair, K. C. Sheela, K. V. Radhakrishnan and N. P. Rath, *Tetrahedron Lett.*, 1998, **39**, 5627.
11 V. Nair, K. V. Radhakrishnan, K. C Sheela and N. P Rath, *Tetrahedron*, 1999, **55**, 14199.
12 A. Padwa, M. A. Brodney, K. Satake and C. S. Straub, *J. Org. Chem.*, 1999, **64**, 4617.
13 B. H. Lipschutz, *Chem. Rev.*, 1986, **86**, 795.
14 V. Nair, J. S. Nair, A. U. Vinod and N. P. Rath, *J. Chem. Soc., Perkin Trans. 1*, 1997, 3129.
15 For the preperation of cyclohexyl isocyanide, see I. Ugi, R. Meyr, M. Lipinski, F. Bodesheim and F. Rosendhal, in *Organic Syntheses*, ed. J. D. Roberts, John Wiley & Sons, New York, 1961, vol. 41, p. 13.

Singlet–triplet energy gap in a cyclophane-based organic diradical with parallel exchange coupling pathways†

Andrzej Rajca,* Suchada Rajca and Jirawat Wongsriratanakul

Department of Chemistry, University of Nebraska, Lincoln, NE 68588-0304, USA. E-mail: arajca1@unl.edu

Received (in Columbia, MO, USA) 9th February 2000, Accepted 20th April 2000
Published on the Web 23rd May 2000

The novel cyclophane diradical 1 possesses a singlet ground state with a singlet–triplet energy gap (ΔE_{ST}) of −0.20 and −0.24 kcal mol^{-1}, as measured with SQUID magnetometry and EPR spectroscopy, respectively. This large ΔE_{ST} may in part be associated with the two parallel 3,3′-biphenyl exchange coupling pathways (ECPs).

Elucidation of the structural factors affecting the singlet–triplet energy gap (ΔE_{ST}) in organic diradicals is of primary importance in the design of building blocks for molecular magnets and extended polyradicals.[1–5] The value of ΔE_{ST} may also be viewed as a measure of covalent bond strength in typical, singlet ground state, molecules.[6] Both the sign and magnitude of the ΔE_{ST} are predominantly determined by the through-bond exchange coupling.[1,2] As we wish to probe the dependence of $|\Delta E_{ST}|$ on the number of connecting exchange coupling pathways (ECPs) between the radicals,[7,8] we have designed a cyclophane-based diradical **1**, in which two 3,3′-biphenyl units correspond to two parallel ECPs.[2,8] A molecule with one ECP, an analogue of **1**, is diradical **2**.[9] (Diradical **1** may be related to the extended polycarbene proposed by Mataga in 1968 and **2** is a derivative of the well known Schlenk hydrocarbon.[10,11])

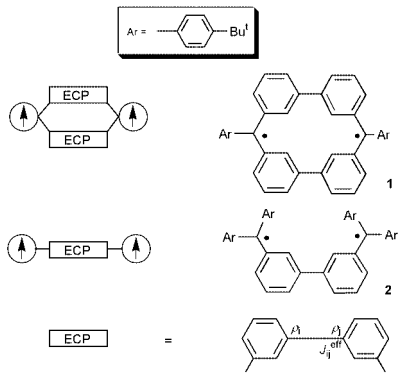

In the Heisenberg Hamiltonian model for a diradical ($H = -2J\boldsymbol{S}_1\cdot\boldsymbol{S}_2$, $S_1 = S_2 = ½$), $\Delta E_{ST} = 2J$. Here, J is the effective exchange interaction, which may be expressed in terms of the spin densities, ρ_i and ρ_j, and the effective exchange integral, J_{ij}^{eff}, between the connecting sites i and j,[12,13] giving

$$J = J_{ij}^{eff}\rho_i\rho_j, \quad \text{for the one-ECP system} \qquad (1)$$

$$J = 2J_{ij}^{eff}\rho_i\rho_j, \quad \text{for the two-ECP system} \qquad (2)$$

Therefore, $|\Delta E_{ST}|$ should be exactly doubled when the introduction of the second identical ECP does not affect the $J_{ij}^{eff}\rho_i\rho_j$ terms. The disjoint character of **1** and **2** is an important factor in minimizing the perturbation of ρ_i and ρ_j.[14] However, conformations of **1** and **2** will affect both $\rho_i\rho_j$ and J_{ij}^{eff}. Consequently, **1** should be viewed as an initial attempt to address the problem of multiple ECPs in diradicals. This novel approach to control exchange coupling should have implications for organic magnetism and weak covalent bonding.

Negishi coupling of compound **3** gave the macrocyclic diether **4**. Two stereoisomers of **4** were isolated in an overall yield of *ca*. 30% (Scheme 1).[15,16]† Both isomers possess qualitatively similar spectral data. FAB MS of **4** are dominated by the isotopic cluster ions corresponding to $(M - OCH_3)^+$, as expected for triarylmethyl ethers. ^{1}H and ^{13}C NMR spectra for **4** show the expected symmetry: all four benzene rings of the macrocycle are equivalent and the two 4-*tert*-butylbenzyl ether moieties are also equivalent.

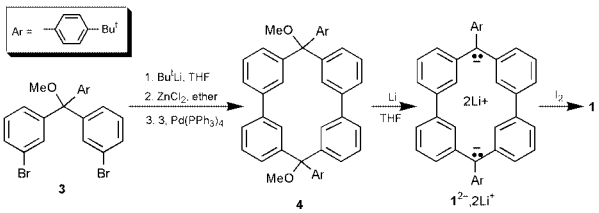

Scheme 1

Diradical **1** is generated from **4** using the previously developed carbanion methodology for polyarylmethyl radicals such as **2** (Scheme 1).[9,17] NMR spectra for carbodianion **1**$^{2-}$ as its lithium salt in tetrahydrofuran-d_8 (THF-d_8) at an ambient temperature show analogous molecular symmetry to that of **4**.[17] The EPR spectrum of **1** in frozen 2-methyltetrahydrofuran–tetrahydrofuran (2-MeTHF–THF) at 70 K shows a six-peak pattern in the $\Delta m_s = 1$ region, characteristic of a triplet ($S = 1$) state with the center peak assigned to $S = ½$ impurities (Fig. 1).[18] The presence of the $S = 1$ state is confirmed by a weak transition in the $\Delta m_s = 2$ region. For **1**, the zero field splitting parameters (zfs), $|D/hc| = 0.0081$ cm^{-1} and $|E/hc| \approx 8 \times 10^{-4}$ cm^{-1}, are somewhat larger than those for **2** ($|D/hc| \approx 0.005$ cm^{-1} and $|E/hc| \approx 0$ cm^{-1}). Because **1** is constrained to the '*syn*' conformation and **2** was previously established to possess the '*syn*' conformation,[9] this difference in $|D/hc|$ values

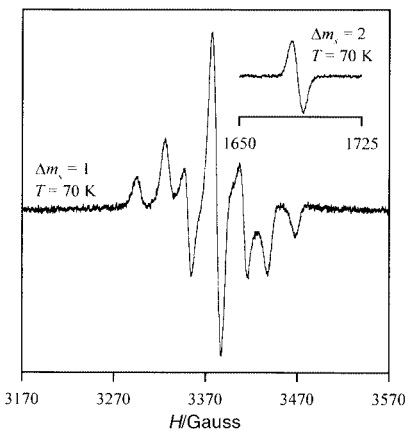

Fig. 1 EPR spectroscopy for diradical **1**, *ca*. 0.003 M in 2-MeTHF–THF (*ca*. 5/1).

† Electronic supplementary information (ESI) available: synthesis and characterisation data for **4**; minimum conformation for diradical **1**. See http://www.rsc.org/suppdata/cc/b0/b001273o/

DOI: 10.1039/b001273o

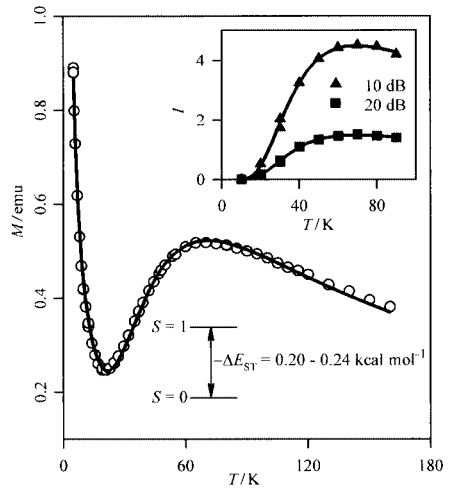

Fig. 2 Experimental determination of the singlet–triplet energy gap (ΔE_{ST}). Main plot: magnetization (M) by SQUID magnetometry. The solid line corresponds to a numerical fit with the following parameters (parameter dependence): $J/k = -61.4$ K (0.70), mol of diradical = 1.88×10^{-6} (0.69), mol of monoradical = 1.16×10^{-7} (0.05). Insert plot: EPR intensity (I) for the $\Delta m_s = 2$ signal *vs* temperature (T). The solid lines are two-parameter, $J/k = -55.5$ K and normalization constant, numerical fits with parameter dependence of 0.76. The EPR and SQUID data are obtained for **1** in 2-MeTHF/THF (*ca.* 5/1) and THF, respectively.

may arise from a significant delocalization of spin density into the proximate biphenyl moieties in **1**.[18,19] Furthermore, macrocyclic **1** is relatively persistent; more than half of the EPR signal intensity of **1** in 2-MeTHF–THF is left intact after 2 days at room temperature. However, attempts to isolate **1** as a solid were not successful.

At 4 K, the EPR spectrum for the $S = 1$ state becomes almost undetectable, suggesting that the observed $S = 1$ state is thermally populated. Measurement of the intensity (I) of the $\Delta m_s = 2$ signal *vs*. temperature (T) gives a curve with a maximum near $T = 70$ K. A numerical fit, based upon a simple two-center Heisenberg Hamiltonian ($H = -2J\boldsymbol{S}_1\cdot\boldsymbol{S}_2$), gives $J/k = -53 \pm 3$ K (Fig. 2).[2]

For 0.04 M **1** in THF, a plot of magnetization (M) *vs*. T in the range 5–100 K shows a broad maximum at $T_{max} \approx 60$ K and an upward turn at low temperatures, consistent with a singlet ground state of **1** and the presence of $S = \frac{1}{2}$ impurities.[20] A three-parameter fit to M *vs*. T gives $J/k = -60 \pm 2$ K (Fig. 2). At very low temperature, such as 3 K, M of a diradical with $J/k \approx -60$ K should be negligible. Numerical fits of M *vs*. magnetic field (H) data at 3 K to the Brillouin function with variable S and M at saturation (M_s) give $S = 0.5$, as expected for an $S = \frac{1}{2}$ impurity. M_s is within a few percent of the calculated value from the M *vs*. T fit.

Diradical **2** was reported to have J/k in the range -21 to -23 K.[9] Therefore, both **1** and **2** have singlet ($S = 0$) ground states and thermally populated $S = 1$ states; $\Delta E_{ST} = 2J$ for **1** (-0.20 to -0.24 kcal mol^{-1}) is about 2–3 times the value of $\Delta E_{ST} = 2J$ for **2** (-0.08 to -0.09 kcal mol^{-1}).

Previous work on derivatives of **2** indicated that the steric hindrance, causing out-of-plane twisting of the π-conjugated system, diminishes $|\Delta E_{ST}|$.[2,21] Possible conformations of **1** and **2** were obtained from MacroModel calculations.[22] The preference for the '*syn*' over the '*anti*' conformation in **2** (3 kcal mol^{-1}) is in agreement with the EPR data. The torsional angles indicate that the 3,3′-biphenyl moieties are significantly more twisted and bent in **1** (59–68°) *vs*. **2** (30°) (see ESI†); this implies that the J_{ij}^{eff} in **1** is smaller than in **2**. However, the torsional angles between the 3,3′-biphenyl and arylmethyl moieties in **1** and **2** are ~30 and 44°, respectively. This suggests that both ρ_i and ρ_j in **1** may be larger than in **2**. Therefore, it is reasonable to assume that the $J_{ij}^{eff}\rho_i\rho_j$ terms in eqns. (1) and (2) are comparable.[23]

In conclusion, the singlet–triplet energy gap in diradical **1**, with two parallel exchange coupling pathways, is more than doubled when compared to diradical **2**, with one exchange coupling pathway.

This research was supported by the National Science Foundation (CHE-9806954). The mass spectra were obtained at the Nebraska Center for Mass Spectrometry. The initial synthetic studies toward **4** were carried out by Chris Focke. We thank Professor Clark Stille of Columbia University for his help with parametrization of MacroModel for arylmethyl radicals.

Notes and references

1 D. A. Dougherty, *Acc. Chem. Res.*, 1991, **24**, 88; W. T. Borden, H. Iwamura and J. A. Berson, *Acc. Chem. Res.*, 1994, **27**, 109; J. S. Miller and A. Epstein, *Angew. Chem., Int. Ed. Engl.*, 1994, **33**, 385; J. A. Berson, *Acc. Chem. Res.*, 1997, **30**, 238; H. Iwamura, K. Inoue and N. Koga, *New J. Chem.*, 1998, 201; *Magnetic Properties of Organic Materials*, ed. P. M. Lahti, Marcel Dekker, New York, 1999.
2 A. Rajca, *Chem. Rev.*, 1994, **94**, 871.
3 A. Rajca, J. Wongsriratanakul, S. Rajca and R. Cerny, *Angew. Chem., Int. Ed.*, 1998, **37**, 1229.
4 H. Nishide, M. Miyasaka and E. Tsuchida, *Angew. Chem., Int. Ed.*, 1998, **37**, 2400.
5 A. Rajca, S. Rajca and J. Wongsriratanakul, *J. Am. Chem. Soc.*, 1999, **121**, 6308.
6 J. Michl, *Acc. Chem. Res*, 1990, **23**, 127.
7 For the effect of multiple pathways in electron transfer, see: J. N. Onuchcic, P. C. P. Andrade and D. N. Beratan, *J. Chem. Phys.*, 1991, **95**, 1131; D. N. Beratan, J. N. Onuchcic, J. R. Winkler and H. B. Gray, *Science*, 1992, **258**, 1740.
8 For different problems of multiple exchange coupling pathways, including spin coupling units and spin coupling paths, see: refs 1–3.
9 A. Rajca and S. Rajca, *J. Am. Chem. Soc.*, 1996, **118**, 8121.
10 W. Schlenk and M. Brauns, *Ber. Dtsch. Chem. Ges.*, 1915, **48**, 661; W. Schlenk and M. Brauns, *Ber. Dtsch. Chem. Ges.*, 1915, **48**, 716.
11 N. Mataga, *Theor. Chim. Acta*, 1968, **10**, 372.
12 H. McConnell, *J. Chem. Phys.*, 1963, **39**, 1910.
13 Y. Teki and K. Itoh, *Magnetic Properties of Organic Materials*, ed. P. M. Lahti, Marcel Dekker, New York, 1999, ch. 12.
14 W. T. Borden and E. R. Davidson, *J. Am. Chem. Soc.*, 1977, **99**, 4587.
15 E. Negishi, A. O. King and N. Okukado, *J. Org. Chem.*, 1977, **42**, 1821.
16 For analogous macrocycles, with 6,6′-connected 2,2′-bipyridines, see: S. Ogawa and S. Tsuchiya, *Chem. Lett.*, 1996, 709 and references therein.
17 The MeOH and MeOD quenches of the carbodianions, obtained from diether **4** and diradical **1**, give the corresponding hydrocarbons-h_2 and -d_2, respectively, according to MS, ^{1}H NMR, and IR analyses.
18 J. E. Wertz and J. R. Bolton, *Electron Spin Resonance*, Chapman and Hall, New York, 1986.
19 The spectral width of the $\Delta m_s = 1$ region, $2|D/hc|$, is a function of an 'average distance between the unpaired electrons' in the through-space magnetic dipolar model for zfs: *e.g.* ref. 18.
20 For the sample preparation techniques, see: A. Rajca, J. Wongsriratanakul and S. Rajca, *J. Am. Chem. Soc.*, 1997, **119**, 11674. Because only a small portion, with unknown weight of **1**, is measured, the spin concentration can not be estimated. Following the magnetization studies, the samples are kept at room temperature for 12+ months; the broad maximum in M *vs*. T is not detectable and paramagnetic susceptibility at 2 K (primarily from $S = 1/2$ impurities) is of the order of 10% or less of the original value. Subsequently, the identical sequence of measurements was repeated for the point-by-point background correction.
21 A. Rajca, S. Utamapanya and D. J. Smithhisler, *J. Org. Chem.*, 1993, **58**, 5650.
22 MacroModel 6.0 and 6.5, Columbia University. F. Mohamadi, N. G. J. Richards, W. C. Guida, R. Liskamp, M. Lipton, C. Caufield, G. Chang, T. Hendrickson and W. C. Still, *J. Comput. Chem.*, 1990, **11**, 440.
23 Single point DFT calculations on **1** and **2** at the UB3LYP/6-31G* level, which offers a reasonable trade-off between the accuracy and the computational feasibility, give $\Delta E_{ST} = 2(E_S - E_T) = -0.30$ and -0.03 kcal mol^{-1}, respectively. Values of $S(S + 1)$ are 2.05–2.06 and 1.04–1.05 for the triplets and the broken symmetry singlets, respectively. Also, the total spin densities at the sites i and j are -0.073 (for **1**) and -0.049 (for **2**). *Gaussian 98*, Gaussian, Inc., Pittsburgh, PA, 1998.

Self-assembly of freebase- and metallated-tetrapyridylporphyrins to modified gold surfaces

C. V. Krishnamohan Sharma, Grant A. Broker, Gregory J. Szulczewski* and Robin D. Rogers*

Department of Chemistry, The University of Alabama, Tuscaloosa, AL 35487, USA. E-mail: RDRogers@Bama.ua.edu

Received (in Columbia, MO, USA) 8th March 2000, Accepted 12th April 2000
Published on the Web 22nd May 2000

Freebase- and metallated-tetrapyridylporphyrins self-organize through multiple hydrogen bonding to carboxylic acid terminated self-assembled monolayers on gold surfaces, thereby producing surfaces with two additional functional sites, the porphyrin cavity and the terminal pyridyl groups.

Self-assembled monolayers (SAMs) with terminal functional groups can be used to construct organic surfaces with a variety of functional properties. SAMs derive their chemical selectivity from the outermost few angstroms of the film,[1] and in recent years, there have been many examples of self-assembly and self-organization to rationally synthesize novel functional materials.[2] We have recently demonstrated design strategies for solid-state supramolecular arrays containing both mixed-metallated and freebase porphyrins leading to multichromophoric arrays of defined rigidity, dimensionality, porosity, and selectivity.[3] Organization of porphyrinic chromophores on thin film organic surfaces through hydrogen bonds provides another powerful means for the design of novel systems with useful functional properties (*e.g.* magnetic materials, sensors, and artificial photosynthetic systems).[4] Recent strategies to prepare SAMs with porphyrinic chromophores have relied on either the modification of the porphyrin periphery with thiol side-chains,[5,6] or on the coordination of thiols terminating in N-donor heterocycles to metal ions[4,7] or P-ligands[8] already bonded in the porphyrin cavity. These approaches permit only a single attachment site, and in the case of the metallated-porphyrins, do not allow for the presence or use of the freebase porphyrin. In this communication, we report our strategies to link freebase and metallated porphyrinic chromophores to surface-confined monolayers of functionalized organomercaptans through multiple hydrogen bonds.

It is well known that carboxylic acid groups preferentially bind with pyridines, amines, and aminopyridines through O–H···N or N–H···O hydrogen bonding, either in solution[9] or in the solid state.[10] Recently, acid-terminated SAMs have been used to bind vapor phase bases, such as pyridine, pyrazine, and decylamine through hydrogen bonding, but these hydrogen-bonded bases partially desorb upon exposure to nitrogen gas.[11] It occurred to us that stable hydrogen-bonded supramolecular arrays on acid terminated surfaces can be generated with the aid of multifunctional organic ligands where multiple hydrogen bonds formed between the organic ligand and acidic surface substantially enhance the stabilization energy. For this purpose, we have considered freebase- and metallated-tetrapyridylporphyrins (TPyP) as potential building blocks.

We constructed carboxylic acid-terminated monolayers of 11-mercaptoundecanoic acid, $HS(CH_2)_{10}COOH$ (MUA), and 4-mercaptobenzoic acid, $HS(C_6H_4)COOH$, on gold surfaces for studying the hydrogen bonding properties of TPyP. SAMs were prepared by immersing thin gold films (*ca.* 100 nm thick deposited onto chromium primed Si(100) wafers) in *ca.* 1 mM methanolic solutions of the organomercaptans for 12–24 h. The acid-terminated monolayers obtained were thoroughly rinsed with ethanol and dried with argon before being immersed in *ca.* 0.1 mM chloroformic solutions of TPyP or ZnTPyP. After 1–12 h, the samples were removed and copiously rinsed with chloroform. The latter step is critical to yield reproducible results, since the chloroform rapidly evaporates when the sample is removed from solution. Also, it should be mentioned here that our attempts to generate acid-terminated SAMs hydrogen-bonded with porphyrins directly by dissolving both porphyrin and mercaptoacids together in methanol or chloroform did not yield reproducible thin films.

The presence of TPyP and ZnTPyP on carboxylic acid terminated SAMs was detected by X-ray photoelectron spectroscopy (XPS). The characteristic peaks for N and Zn identified the metallated-porphyrin along with O and S from the SAMs, as shown in Fig. 1. Analysis of the XPS data yielded a coverage of 0.04 monolayers of ZnTPyP, or approximately 6×10^{13} ZnTPyP molecules per cm^2. Several control experiments were conducted to verify the hydrogen bonding requirement to form the porphyrin monolayer. For example, XPS indicated that freebase or metallated TPyP does not adsorb to a methyl-terminated SAM $[HS(CH_2)_9CH_3]$ and tetraphenylporphyrin (*i.e.* no acceptor group available for hydrogen bonding) does not adsorb to a MUA/Au surface.

Low contact angle measurements of water on MUA/Au (28°) and MBA/Au (31°) are in accord with the hydrophilic nature imparted to the surfaces by the acid terminal groups. The contact angles were 6–10° higher when measured with the porphyrin-terminated groups (ZnTPyP/MUA/Au, 36°; ZnTPyP/MBA/Au, 37°; TPyP/MUA/Au, 38°; TPyP/MBA/Au, 37°), indicating the partial hydrophobic nature (caused by the large aromatic moieties) of these monolayers.

Ellipsometry was used to measure the thickness of TPyP on MUA/Au. In order to limit experimental errors in calculating the thickness of the organic layers on the gold surface, we have considered the average of three measurements at different points on each sample surface.[12] The thickness of the porphyrinic layer on MUA surfaces is calculated by subtracting the height of the acids MUA/Au (16.3 Å)[13] and the hydrogen bonding distance of carboxylic acid–pyridine (2.7 Å) from the total height above the gold surface Au/MUA/TPyP (27.9 Å). The thickness of the porphyrin layers is thus calculated to be *ca.* 10.2 Å.

The consistent thickness of about 10 ± 2 Å obtained for porphyrin layers on MUA/Au surfaces indicates the nature of the hydrogen bonding to TPyP. In principle, TPyP can hydrogen bond with the acidic moieties in three different ways, which involve hydrogen bonding of one, two, or possibly even four pyridyl groups, as shown in Fig. 2. The thickness of the porphyrins in these three different modes can be approximated

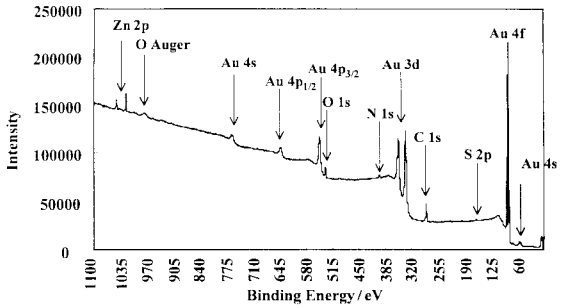

Fig. 1 XPS of ZnTPyP on MUA.

DOI: 10.1039/b002084m

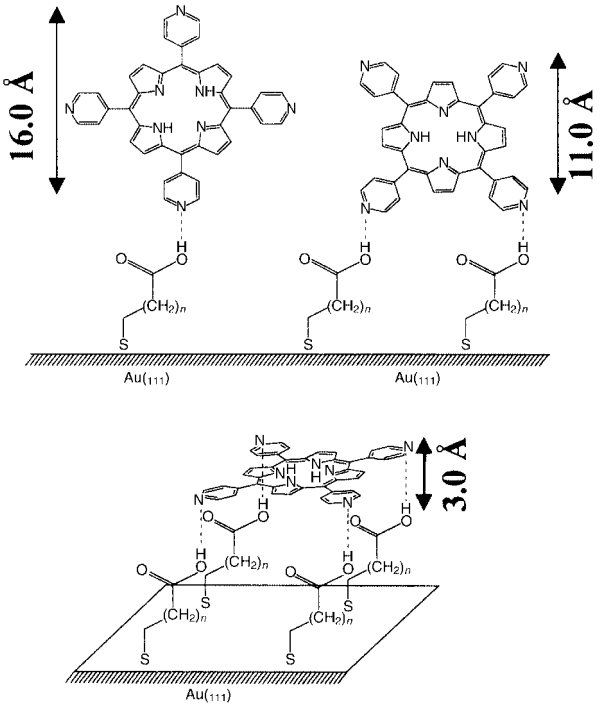

Fig. 2 Three possible orientations of TPyP on MUA.

as 16.0 Å (type-I), 10.8 Å (type-II), and 3.0 Å (type-III), if the O–H···N distance is taken into account. Within experimental uncertainty, the ellipsometry measurements correlate closely to the type-II hydrogen bonding, which is similar to that found in the solid state.

Further support for the model above comes from structural characterization of a cocrystal prepared by layering TPyP [0.5 mmol in TCE (1,1,2,2-tetrachloroethylene), 20.0 mL] with mercaptoacetic acid [2.0 mmol in MeOH, 10 mL]. Dimerization of the mercaptoacetic acid and inclusion of solvent led to the crystallization[14] of $[(S_2C_4H_{12}O_4)_2(TPyP)]\cdot 3TCE$. The crystal structure (Fig. 3) reveals the formation of linear 1D tapes with adjacent TPyP molecules bridged by hydrogen bonds to both ends of two mercaptoacetic acid dimers. These hydrogen bonded tapes are exactly analogous to the 1D tapes formed by coordination of HgX_2 to the external pyridyl moieties.[3]

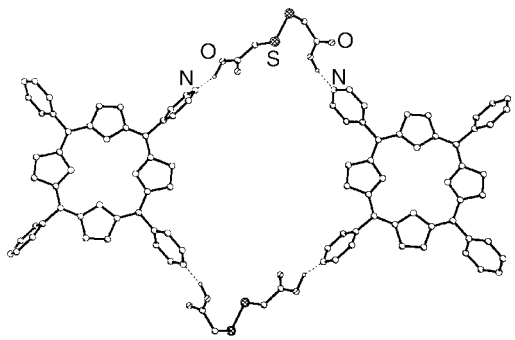

Fig. 3 A portion of the one dimensional molecular tape formed by hydrogen bonding in $[(S_2C_4H_{12}O_4)_2(TPyP)]\cdot 3TCE$. (The solvent has been omitted for clarity.)

The work presented here demonstrates a strategy to form stable hydrogen bonded arrays of both freebase- and metallated-porphyrins on acid-terminated gold surfaces for the design of functional materials. Some of the important implications of this include: (i) using multiple hydrogen bonds, the extended functional arrays are even stable enough to be seen in XPS studies. (ii) The optical properties of the surfaces can be fine-tuned by the organization of multiple porphyrinic chromophores in controlled metallation states and orientations at the interface. (iii) Use of the freebase porphyrin allows additional metal ion coordination *in situ* (as, for example, in applications involving metal ion sensors where the chromophoric response changes with metallation state). (iv) The pyridyl ligands of TPyP exposed on the surface (*i.e.* those not involved in the hydrogen bonding) serve as binding sites for systematically generating mixed multiple layers through additional hydrogen bonds.

This research is supported by the Division of Chemical Sciences, Office of Basic Energy Sciences, Office of Energy Research, U.S. Department of Energy (RDR, Grant No. DE-FG02-96ER14673). G. J. S would like to thank The University of Alabama for start-up funds. We would like to thank Dr Dehua Yang and Mr Brian Pyevick for making the XPS measurements. We would also like to thank Dr Robert M. Metzger for use of the contact angle goniometer and Materials for Information Technology Center on the UA campus for use of the spectroscopic ellipsometer.

Notes and references

1 A. Ulman, *An Introduction to Ultrathin Organic Films, from Langmuir–Blodgett to Self Assembly*, Academic Press, Boston, 1991.
2 J. H. Fendler, *Chem. Mater.*, 1996, **8**, 1616.
3 C. V. K. Sharma, G. A. Broker, J. G. Huddleston, J. W. Baldwin, R. M. Metzger and R. D. Rogers, *J. Am. Chem. Soc.*, 1999, **121**, 1137.
4 N. Kanayama, T. Kanbara and H. Kitano, *J. Phys. Chem. B*, 2000, **104**, 271.
5 J. E. Hutchison, T. A. Postlewaite and R. W. Murray, *Langmuir*, 1993, **9**, 3277.
6 J. Zak, H. Yuan, M. Ho, L. K. Woo and M. D. Porter, *Langmuir*, 1993, **9**, 2772.
7 D. A. Offord, S. B. Sachs, M. S. Ennis, T. A. Eberspacher, J. H. Griffin, C. E. D. Chidsey and J. P. Collman, *J. Am. Chem. Soc.*, 1998, **120**, 4478.
8 A. L. Bramblett, M. S. Boeckl, B. D. Ratner, T. Sasaki and J. W. Rogers, Jr., *Self-Assembly of Tetraphenylporphyrin Monolayers on Gold Substrates*, presented as a poster at the American Vacuum Society, Seattle, WA, October, 1999.
9 C. M. Paleos and D. Tsiourvas, *Angew. Chem., Int. Ed. Engl.*, 1995, **34**, 1696.
10 C. V. K. Sharma and M. J. Zaworotko, *Chem. Commun.*, 1996, 2655.
11 H. C. Yang, D. L. Dermody, C. Xu, A. J. Ricco and R. M. Crooks, *Langmuir*, 1996, **12**, 726.
12 We used the software provided by the manufacturer of the ellipsometer (R. J. Wollham, Inc.) in the data analysis.
13 Measured by ellipsometry.
14 *Crystal data*: $[(S_2C_4H_{12}O_4)_2(TPyP)]\cdot 3TCE$, M = 1486.61, triclinic, a = 7.0612(2), b = 15.4036(4), c = 16.4519(3) Å, α = 107.927(2), β = 100.605(1), γ = 100.569(1)°, U = 1617.40(7) Å^3, T = 173 K, space group $P\bar{1}$ (No. 2), Z = 1, μ(Mo-Kα) = 0.700 mm^{-1}, D_c = 1.526 Mg m^{-3}, 7252 reflections measured, $R1$ = 0.0642, $wR2$ = 0.1441 (for 3523 reflections with [$I > 2\sigma(I)$]); $R1$ = 0.0870, $wR2$ = 0.1691 [for all 4545 independent (R_{int} = 0.0305) reflections]. The structure was solved using direct methods and refined by full-matrix least-squares on F^2 using all data. CCDC 182/1614.

Dendritic amplification of DNA analysis by oligonucleotide-functionalized Au-nanoparticles

Fernando Patolsky, Koodali T. Ranjit, Amir Lichtenstein and Itamar Willner*

Institute of Chemistry, The Farkas Center for Light-Induced Processes, The Hebrew University of Jerusalem, Jerusalem, 91904, Israel. E-mail: willnea@vms.huji.ac.il

Received (in Cambridge, UK) 20th March 2000, Accepted 3rd May 2000
Published on the Web 25th May 2000

Dendritic amplification of DNA analysis is accomplished by the application of 5′- and 3′-terminated oligonucleotide-functionalized Au-colloids complementary to the analyte DNA.

The development of DNA sensors attracts recent research efforts directed to gene analysis, identification of genetic disorders, tissue matching, and forensic applications.[1,2] Photonic detection of DNA was accomplished by the use of fluorescence-labeled oligonucleotides,[3] the use of surface plasmon resonance, SPR,[4] and through the application of oligonucleotide-modified Au-nanoparticles which exhibit plasmon absorbance.[5,6] Electronic transduction of oligonucleotide–DNA recognition events, and the amplified transduction of DNA sensing, are major challenges in DNA-based bioelectronics.[7] Electrostatic attraction of transition metal complexes[8] or dyes[9] was used for the voltammetric probing of the formation of double-stranded assemblies. Amplified electronic transduction of DNA sensing events was accomplished by the application of enzyme labels that bind to the double-stranded (ds) assembly,[10] the use of protein labels,[11] or the use of branched oligonucleotides.[12] Other amplification routes of DNA sensing events included the application of enzymes that biocatalyze the precipitation of an insoluble product on the transducer,[13] or the use of liposomes that bind to the ds-DNA assembly.[14,15] Electrochemical[12–15] or microgravimetric, quartz-crystal-microbalance,[11,16] methods have been applied as electronic transduction signals for the sensing events. Here, we report on a novel method to amplify DNA sensing events by the application of oligonucleotide-functionalized Au-nanoparticles for the amplified sensing of DNA by a dendritic-type amplification route. Microgravimetric, quartz-crystal-microbalance (QCM) experiments are used to follow the amplified DNA-sensing processes.

Scheme 1(a) shows the method of the amplified sensing of a target DNA. A primer thiol-functionalized oligonucleotide **1** is assembled on the Au-electrode, and the target analyte DNA **2**, hybridizes with the sensing interface. The primary amplification of the sensing process is performed by the interaction of the surface with the **3**-functionalized Au-particles. The secondary, dendritic-type amplification is performed by the interaction of the resulting interface with the analyte sample **2** that is pretreated with the **1**-functionalized Au-nanoparticle. The mass associated with the Au-nanoparticles linked to the crystal in the primary hybridization step, and the dendritic structure formed in the secondary hybridization process, amplify the sensing of **2**. Note that the amplifying Au-nanoparticles that are used in the two modification steps have different modification layers, and are functionalized with the 3′-terminated and the 5′-terminated thiolated oligonucleotides, **3** and **1**, respectively. Both oligonucleotides, **3** and **1**, are complementary to the two ends of the analyte **2**. The **1**- and **3**-functionalized Au-nanoparticles were prepared according to the literature[6] by the reaction of citrate-stabilized Au-nanoparticles (12 ± 1 nm, 5 mL) with the thiolated oligonucleotides **1** or **3** for 20 h.

Fig. 1(A), curve (a), shows the frequency changes of the Au-quartz crystal (AT-cut, 9 MHz) functionalized with **1** (surface coverage 1.4×10^{-11} mol cm^{-2}) as a result of interaction with the analyte **2** (2×10^{-8} M). A frequency decrease of *ca*. 9 Hz is observed. Treatment of the resulting interface with the **3**-functionalized Au-nanoparticles results in an additional frequency change of *ca*. 60 Hz [Fig. 1(A), curve (b)], indicating that the binding of the Au-nanoparticles indeed amplified the primary sensing of **2**. The amplified sensing of **2** is specific and the interaction of the sensing interface with the non-complementary DNA **2a**, at a high concentration (5×10^{-6} M), does not yield any change in the crystal frequency (*ca*. −1 Hz) even after its interaction with the **3**-functionalized Au-nano-

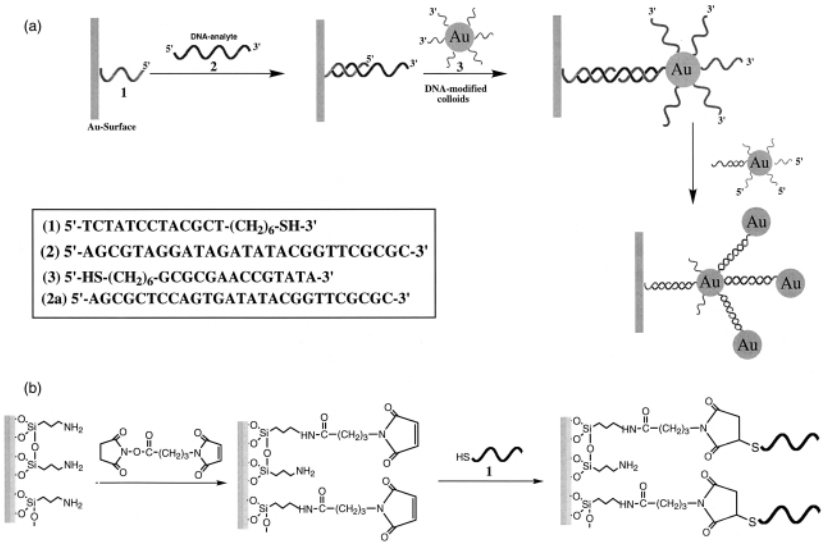

Scheme 1 (a) Dendritic amplified DNA-sensing using oligonucleotide-functionalized Au-nanoparticles. (b) Immobilization of the thiolated oligonucleotide **1** on a glass support.

DOI: 10.1039/b002221g

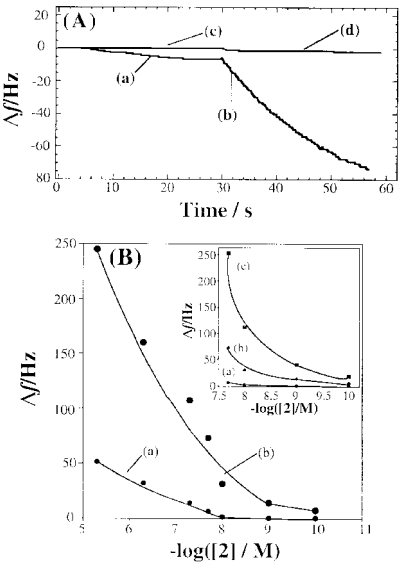

Fig. 1 (A) Time dependent frequency changes of a **1**-functionalized Au-quartz crystal upon interaction with: (a) the analyte DNA **2** (2×10^{-8} M). (b) After treatment of the double-stranded assembly of **1** and **2** with the **3**-functionalized Au-nanoparticles. (c) After treatment of the sensing interface with **2a** (5×10^{-6} M). (d) After treatment of the resulting surface with the **3**-functionalized Au-nanoparticles. All measurements were performed in $2 \times$ SSC buffer, pH = 7. (B) Frequency changes of the **1**-functionalized Au-quartz crystal upon the dendritic amplified sensing of different concentrations of the analyte DNA **2**: (a) upon the association of the analyte **2** with the sensing interface. (b) Upon the amplification of the primary double-stranded assembly of **1** and **2** with **3**-functionalized Au-nanoparticles. (c) Upon the dendritic amplification of the primary **1**–**2**–**3**–Au-nanoparticle array with the **2**–**1**–Au-nanoparticle probe. The Δf values reported in curves (a) and (b) were measured in solution ($2 \times$ SSC, pH = 7.0). The Δf values reported in curve (c) were measured in air. The double-stranded oligonucleotide–DNA assemblies in the first or second amplification steps were interacted for 25 min with the **3**-functionalized Au-nanoparticles or the **1**-functionalized Au-colloid. (SSC = 10 mM sodium citrate and 150 mM NaCl.)

particles [Fig. 1(A), curves (c) and (d), respectively]. The specificity of the sensing process is observed for at least three-base mismatches between the analyte and the probe monolayer interface. The crystal frequency changes resulting upon the primary amplified sensing of different concentrations of **2**, and those originated upon the secondary dendritic-type amplification, are shown in Fig. 1(B) and its inset, respectively. Note that the frequencies of the crystals resulting in the secondary amplification process are measured in air. The primary amplification path enables the sensing of the analyte **2** in the concentration range 2×10^{-8}–1×10^{-10} M, where no noticeable frequency changes can be observed as a result of the hybridization of **2** with the sensing interface itself. The secondary amplification step results in a dendritic type, non-linear amplified transduction of the initial sensing process [Fig. 1(B), inset]. For example, while the primary binding of the **3**-functionalized Au-nanoparticle to the sensing interface treated with 2×10^{-8}, 1×10^{-8}, 1×10^{-9} or 1×10^{-10} M of **2** results in frequency changes of −70, −40, −12 and −8 Hz, respectively, the secondary amplification process introduces a net decrease in the crystal frequencies corresponding to −250, −115, −45 and −20 Hz at these concentrations of **2**. The non-complementary DNA **2a** (1×10^{-6} M) does not show any frequency change of the crystal upon an attempt to follow the two-step amplification route. At a concentration of 2×10^{-8} M of the analyte **2**, the degree of amplification of the primary hybridization process by the two-step Au-nanoparticle array is *ca.* 30-fold within a probing time-frame of 50 min (Δf changes from 8 to 245 Hz). The dendritic-type amplification of the sensing of **2** by the two Au-nanoparticles probes is further supported by optical measurements (Fig. 2). The primer

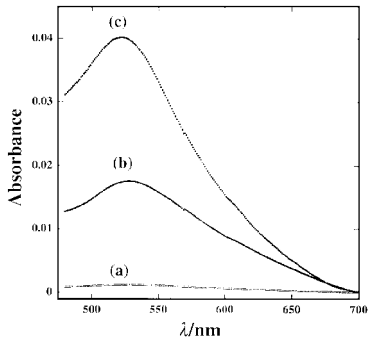

Fig. 2 Absorption spectra of a glass support: (a) after modification with **1** according to Scheme 1(B). (b) After interaction of the **1**-functionalized glass with **2** and then with the **3**-functionalized Au-nanoparticles. (c) After amplifying the primary **1**–**2**–**3**–Au-nanoparticle array with the **2**–**1**–Au-nanoparticle probe solution.

oligonucleotide **1** was immobilized on a glass support as shown in Scheme 1(B). Treatment of the **1**-functionalized glass with the analyte **2** and then with the **3**-functionalized Au-nanoparticles, results in the spectrum shown in Fig. 2, curve (b), consisting of the characteristic plasmon absorbance of Au-nanoparticles. Upon treatment of the sensing interface with the second amplification step, the Au-nanoparticle absorbance band is enhanced *ca*. 2.5-fold.

In conclusion, we have demonstrated the use of oligonucleotide-functionalized Au-nanoparticles as amplifying probes for microgravimetric QCM DNA-sensing. By the use of two different Au-nanoparticle probes consisting of oligonucleotide-functionalized Au-nanoparticles, complementary to the two ends of the analyte DNA, non-linear amplification of the sensing event was observed.

This research project is supported by the Israel–Japan Binational Program.

Notes and references

1 E. A. Winzeler, D. R. Richards, A. R. Conway, A. L. Goldstein, S. Kalman, M. J. McCullough, J. H. McCusker, D. A. Stevens, L. Wodicak, D. J. Lockhart and R. W. Davis, *Science*, 1998, **281**, 1194.
2 S. R. Mikkelsen, *Electroanalysis*, 1996, **8**, 15; M. S. Yang, M. E. McGovern and M. Thompson, *Anal. Chim. Acta*, 1997, **346**, 259.
3 A. C. Pease, D. Solas, E. J. Sullivan, M. T. Cronin, C. P. Holmes and S. P. A. Fodor, *Proc. Nat. Acad. Sci. USA*, 1994, **91**, 5022.
4 V. Jonsson, *Biotechniques*, 1991, **11**, 620; A. G. Frutos, L. M. Smith and R. M. Corn, *J. Am. Chem. Soc.*, 1998, **120**, 10 277.
5 R. Elghanian, J. J. Storhoff, R. C. Mucic, R. L. Letsinger and C. A. Mirkin, *Science*, 1997, **277**, 1078.
6 J. J. Storhoff, R. Elghanian, R. C. Mucic, C. A. Mirkin and R. L. Letsinger, *J. Am. Chem. Soc.*, 1998, **120**, 1959.
7 J. Wang, *Chem. Eur. J.*, 1999, **5**, 1681.
8 K. Hashimoto, K. Ito and Y. Ishimori, *Anal. Chem.*, 1994, **66**, 3830.
9 K. M. Millan, A. Saraullo and S. R. Mikkelsen, *Anal. Chem.*, 1994, **66**, 2943.
10 T. de Lumley-Woodyear, C. N. Campbell and A. Heller, *J. Am. Chem. Soc.*, 1996, **118**, 5504.
11 A. Bardea, A. Dagan, I. Ben-Dov, B. Amit and I. Willner, *Chem. Commun.*, 1998, 839; A. Bardea, F. Patolsky, A. Dagan and I. Willner, *Chem. Commun.*, 1999, 21.
12 J. Wang, M. Jiang, T. W. Nilsen and R. C. Getts, *J. Am. Chem. Soc.*, 1998, **120**, 8291.
13 F. Patolsky, E. Katz, A. Bardea and I. Willner, *Langmuir*, 1999, **15**, 3703.
14 F. Patolsky, A. Lichtenstein and I. Willner, *J. Am. Chem. Soc.*, 2000, **122**, 418.
15 F. Patolsky, A. Lichtenstein and I. Willner, *Angew. Chem., Int. Ed.*, 2000, **39**, 940.
16 For other QCM analyses of DNA, *cf.* Y. Okahata, M. Kawase, K. Niikura, F. Ohtake, H. Furusawa and Y. Ebara, *Anal. Chem.*, 1998, **70**, 1288; N. C. Fawcett, J. A. Evans, L. C. Chien and N. Flowers, *Anal. Lett.*, 1988, **21**, 1099.

Concise synthesis of indolizidines: total synthesis of (−)-coniceine

Michael D. Groaning and A. I. Meyers*

Department of Chemistry, Colorado State University, Ft. Collins, Colorado 80523-1872, USA.
E-mail: aimeyers@lamar.colostate.edu

Received (in Corvallis, OR, USA) 30th March 2000, Accepted 27th April 2000
Published on the Web 25th May 2000

The Ti-mediated allylsilane addition to bicyclic lactams occurs with high stereoselectivity and combined with a ring closure metathesis provides the title compounds in high ee.

Indolizidines represent an important class of biologically active compounds, including such alkaloids as slaframine, castanospermine (a potent glycosidase inhibitor) and a number of poisonous-frog alkaloids typified by pumiliotoxin B[1] (Fig. 1). Development of a general method to access these 1-azabicyclo-[4.3.0]nonanes would provide a useful tool in studying a host of derivatives.

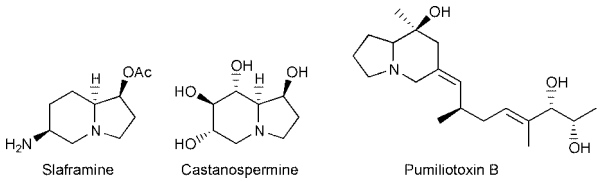

Fig. 1

The construction of optically pure heterocycles using the bicyclic lactam template has been of great interest in our group,[2] and over the years we have published[3] applications of the [4.3.0] bicyclic lactam to access a variety of alkaloids (*e.g.* 1-deoxy-6-epicastanospermine and coniceine), Fig. 2.

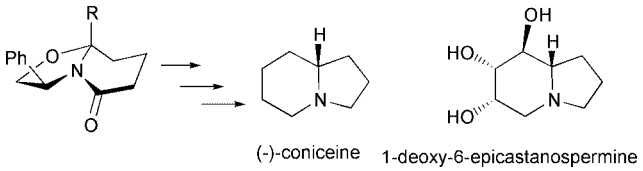

Fig. 2

We now report a general protocol utilizing bicyclic lactams **1a**–**d** for the construction of a variety of enantiomerically pure indolizidines (Scheme 1) including the naturally occurring parent ring system, (−)-coniceine **6a**.

The synthetic route to the 1-azabicyclic systems **6** began by the addition of allyltrimethylsilane to a dichloromethane solution of the enantiomerically pure bicyclic lactam and titanium tetrachloride to furnish the 5-substituted pyrrolidinone **2** with diastereomeric ratios ranging from 6:1 to 11:1. After the diastereomers in **2** were separated (silica gel column chromatography) the chiral auxiliary was removed by dissolving metal reduction using calcium metal (NH_3, −78 to −30 °C over 4 h) affording **3**. It is noteworthy that for compound **2d** containing two possible benzylic cleavage sites only the exocyclic *N*-benzyl bond was cleaved. Introduction of the *N*-allyl group to give **4** proceeded smoothly by addition of allyl bromide to the sodium salt of the pyrrolidinone. The bis-olefin **4** was subjected to a ring-closing metathesis (10 mol% **7** as catalyst, 25 °C, 1,2-dichloroethane) to afford the indolizidinones **5** in excellent yields.[4] Hydrogenation of the olefinic bond and reduction of the lactam carbonyl provided the target compounds **6a**–**d** in 32–51% overall yield. In the case where R = H, the reaction sequence provided a 49% overall yield of (−)-coniceine, which

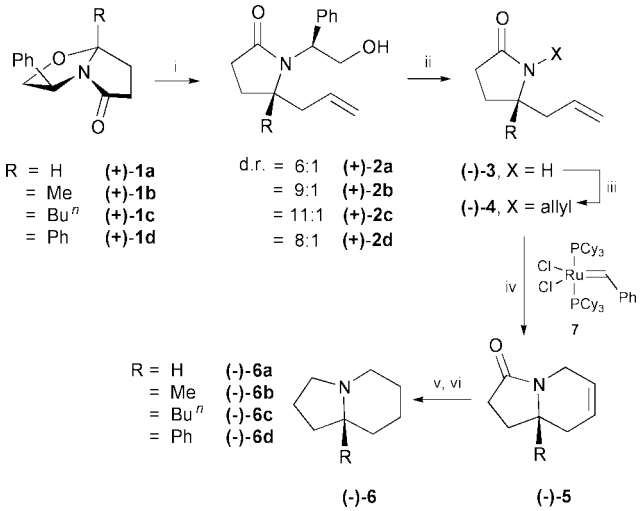

Scheme 1 *Reagents and conditions*: i, allyltrimethylsilane, $TiCl_4$, 68–79% 6:1–11:1 dr; ii, Ca/NH_3, 73–89%; iii, NaH/allylbromide, 81–92%; iv, cat. **7** (10 mol%), 89–93%; v, H_2, $Pd(OH)_2$, 92–96%; vi, $LiAlH_4$, 83–89%.

was identical with a sample previously reported from these laboratories.[3a]

To further illustrate the versatility of this methodology, the oxygenated derivatives of **6** were obtained by dihydroxylation of metathesis product **5b** providing the 3,4-dihydroxy indolizidinone **8** as a 4:1 mixture of diastereomers which were separable by column chromatography (Scheme 2). In order to simplify the purification and reduce water solubility of the diol **8**, it was protected as the acetonide **9** and reduced to the indolizidine **10** using lithium aluminium hydride. This route provides enantiomerically pure hydroxylated derivatives of 1-azabicyclo[4.3.0]nonanes.

In summary, a general method for the construction of a variety of optically pure indolizidines using the chiral non-racemic [3.3.0] bicyclic lactams **1a**–**d** in combination with ring-closing metathesis has been illustrated. The utility of this method is exemplified by the synthesis of (−)-coniceine with excellent stereocontrol and overall yield.[5]

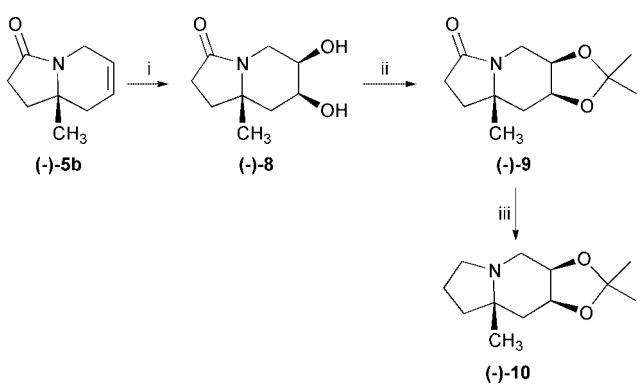

Scheme 2 *Reagents and conditions*: i, OsO_4/NMO, 73% 4:1 dr; ii, 2,2-dimethoxypropane, TsOH, 94%; iii, $LiAlH_4$, 89%.

DOI: 10.1039/b002621m

We are grateful to the National Institutes of Health for financial support. An ACS-Organic Division Graduate Fellowship to MDG (sponsored by Merck) is also warmly acknowledged.

Notes and references

1 For a review on indolizidines, see: J. P. Michael, *Nat. Prod. Rep.*, 1999, **16**, 675; for a review on slaframine and castanospermine, see: R. J. Molyneux and L. F. James, *Mycotoxins Phytoalexins*, 1991, 637; for a review on pumiliotoxins, see: A. S. Franklin and L. E. Overman, *Chem. Rev.*, 1996, **96**, 505.

2 G. P. Brengel and A. I. Meyers, *Chem. Commun.*, 1998, 1 and references therein.

3 (*a*) M. J. Munchhof and A. I. Meyers, *J. Org. Chem.*, 1995, **60**, 7084; (*b*) A. I. Meyers, C. J. Andres, J. E. Resek, C. C. Woodall, M. A. McLaughlin, P. H. Lee and D. A. Price, *Tetrahedron*, 1999, **55**, 8931.

4 For a review on olefin metathesis, see: R. H. Grubbs and S. Chang, *Tetrahedron* 1998, **54**, 4413; for a review on applications of the ring-closing metathesis reaction to the construction of a wide variety of nitrogen containing ring systems, see: U. K. Pandit, H. S. Overkleeft, B. C. Borer and H. Bieraugel, *Eur. J. Org. Chem.*, 1999, **5**, 959.

5 *Typical procedure*; the synthesis of **5c** from **1c**: A dichloromethane solution of the bicyclic lactam **1c** (1.4 g, 5.48 mmol) was cooled to −78 °C and $TiCl_4$ (9 ml of 1.0 M solution in dichloromethane, 1.6 equiv.) was slowly added *via* syringe followed by allyltrimethylsilane (1.3 mL, 1.5 equiv.). The solution was stirred under an argon atmosphere and allowed to warm to r.t. over a 4 h period. A solution of saturated NH_4Cl (50 mL) was added in one portion and the layers were separated. The aqueous layer was washed with dichloromethane (3 × 50 mL), the combined organic layers were dried over Na_2SO_4 and concentrated to an oil. ^1H NMR analysis of the crude material was used to analyze the diastereomeric ratio. Column chromatography (SiO_2, EtOAc) provided 1.25 g of **2c** (76%) as a colorless solid: mp 98 °C; $[\alpha]_D$ −177 (*c* 1.9, $CHCl_3$); δ_H (300 MHz, $CDCl_3$) 0.97 (t, *J* 7 Hz, 3H), 1.26–1.45 (m, 4H), 1.58–1.71 (m, 2H), 1.89–2.06 (m, 4H), 2.49 (t, *J* 9 Hz, 2H), 4.08–4.27 (m, 3H), 4.70–4.97 (m, 3H), 5.36 (dddd, *J* 17, 13, 10, 7 Hz, 1H), 7.24–7.43 (m, 5H); δ_C (75 MHz, $CDCl_3$) 14.0, 22.9, 25.5, 27.6, 30.4, 37.7, 44.7, 60. 3, 65.5, 68.2, 199.0, 127.2, 127.7, 128.2, 132.3, 139.1, 177.4; IR(film) ν/cm^{-1} 1658, 3351. Anal. Calc. for $C_{18}H_{27}NO_2$: C, 75.71; H, 9.03. Found: C, 75.44; H, 9.03%. A dichloroethane solution of the bis-olefin **4c** (200 mg, 0.9 mmol) was added to a solution of catalyst **7** (74 mg, 10 mol%). The purple solution slowly changed to brown. After 6 h the reaction was concentrated *in vacuo* to an oil and chromatographed (SiO_2, EtOAc) to provide **5c** (179 mg, 92%) as a colorless solid: mp 63 °C; $[\alpha]_D$ −58 (*c* 1.0, $CHCl_3$); δ_H (300 MHz, $CDCl_3$) 0.91 (t, *J* 7 Hz, 3H), 1.12–1.39 (m, 4H), 1.48–1.82 (m, 3H), 2.01–2.21 (m, 3H), 2.38–2.53 (m, 2H), 3.40 (d, *J* 9 Hz, 1H), 4.38 (d, *J* 9 Hz, 1H), 5.71 (m, 2H); δ_C (75 MHz, $CDCl_3$) 14.1, 23.1, 25.9, 27.8, 29.9, 30.3, 36.0, 38.4, 60.0, 122.8, 123.8, 173.5; IR(film) ν/cm^{-1} 1692.

Preparation of optically active *n*-butyl(methyl)phenyl-, *tert*-butyl(methyl)phenyl- and isopropyl(methyl)phenylsilanes from the corresponding silyl chlorides using 2,2′-dihydroxy-1,1′-binaphthyls as resolving agents

Paweł Jankowski,[a] Ernst Schaumann,*[b] Jerzy Wicha,*[a] Andrzej Zarecki,[a] Gunadi Adiwidjaja[c] and Monika Asztemborska[d]

[a] *Institute of Organic Chemistry, Polish Academy of Sciences, POB 58, 01-224 Warsaw 42, Poland*
[b] *Institute of Organic Chemistry, Technical University of Clausthal, 38678 Clausthal-Zellerfeld, Germany*
[c] *Institute of Mineralogy and Petrography, Grindelaee 48, D-20146 Hamburg, Germany*
[d] *Institute of Physical Chemistry, Polish Academy of Sciences, POB 58, 01-224 Warsaw 42, Poland*

Received (in Liverpool, UK) 18th February 2000, Accepted 3rd May 2000
Published on the Web 25th May 2000

Enantiomeric silanes 4a, 4b and 4c were obtained from the corresponding racemic silyl chlorides *via* diastereomeric derivatives with (*R*)-[1,1′]binaphthalenyl-2,2′-diol; the optical purity of silanes 4a and 4c was determined (> 98% ee) by HPLC using a chiral cyclodextrin-based column.

Increasing attention has been recently paid to the preparation and synthetic applications of organosilicon compounds with a stereogenic silicon atom.[1,2] Chiral tri(alkyl/aryl)silanes appear to be the most important reagents and synthetic intermediates in this field, owing to their facile reactions with carbon–carbon multiple bonds[3] and easy transformations into other organosilicon compounds, among others, to silyl halides. The pioneering work on tri(alkyl/aryl)silane stereochemistry has been conducted long ago using methyl(naphthyl)phenylsilane[4,5] which is crystalline and relatively easy to obtain in an optically pure form. Some other optically active silanes (non-crystalline in the majority of cases when the naphthyl group is not present) have been prepared only recently. Masuda and coworkers[6] have reported the preparation of several optically active tri(alkyl/aryl)silanes by asymmetric synthesis involving chiral auxiliaries. It has been shown that enzymatic methods have a considerable potential in synthesis of optically active organosilicon compounds.[7–9] Since racemic silane derivatives are readily available, a racemate resolution may provide a convenient and amenable to large-scale approach to a variety of optically active silanes. Along such lines, a method for the preparation of enantiomers of *tert*-butyl(methyl)phenylsilane **4a** (Scheme 1) from racemic *tert*-butyl(methyl)phenylsilyl chloride **2a**, based upon resolution of a particular racemic intermediate with enantiomeric 2-aminobutanols has been developed in our laboratories.[10] However, all our attempts to extend this method to other alkyl/arylsilanes failed. In the search for a more general procedure for racemic silane resolution we have chosen enantiomeric [1,1′]binaphthalenyl-2,2′-diols (BINOLs) as the resolving agents. These easily accessible crystalline compounds have found broad application as ligands and chiral recognition agents;[11,12] however, to the best of our knowledge, their use as resolving agents has not been reported. We present here a method for the preparation of enantiomeric silanes **4a–c** with use of BINOLs. We also report the first direct determination of optical purity of silanes by GC with a chiral column, which provides an important tool for further work with optically active silanes.

Treatment of the lithium derivative of (*R*)-BINOL **1** with racemic *tert*-butyl(methyl)phenylsilyl chloride[7] **2a** yielded diastereomeric derivatives **3a** quantitatively. This diastereomer mixture was separated on a silica gel column to give pure crystalline diastereomers **3a**(Si*R)* and **3a**(Si*S*) and some mixed fraction.† Complete separation of **3a**(Si*R*) and **3a**(Si*S*) was achieved using preparative HPLC‡ and their yields and some physical data are given in Table 1. The absolute configuration of the diastereomer **3a**(Si*R*) (more mobile on chromatography) follows from its single crystal X-ray analysis,§ and a plot of the X-ray structure of **3a**(Si*R*) is shown in Fig. 1. In a similar manner BINOL derivatives of *n*-butyl(phenyl)methylsilane **3b** and phenyl(isopropyl)methylsilane **3c** were prepared and their respective diastereomers were separated by chromatography. The yields and some physical properties of these compounds are given in Table 1. Neither of the diastereomers of **3b** or **3c** could be obtained in crystalline form.

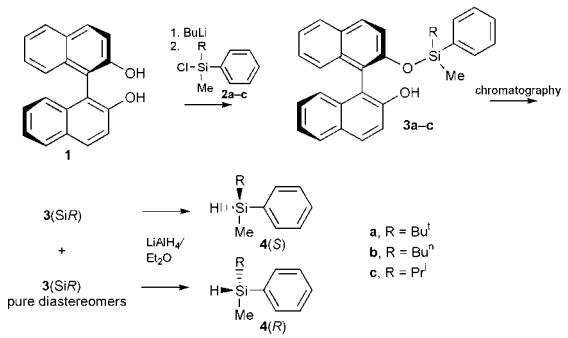

Scheme 1

Table 1 Preparation and some properties of 2′-alkyl(methyl)phenylsilanyloxy-[1,1′]binaphthalenyl-2-ols **3a–c** obtained from (*R*)-BINOL **1** and recemic alkyl(methyl)phenylsilyl chlorides **2a–c**

			More mobile isomer			Less mobile isomer		
R		Yield (%)	R_t/min	Mp/°C	Config.	R_t/min	Mp/°C	Config.
3a, Bu^t		95	19.73[a]	129–130	Si*R*	20.57[a]	133–134	Si*S*
3b, Bu^n		73	34.20[b]	—	Si*R*	39.92[b]	—	Si*S*
3c, Pr^i		84	16.15[a]	—	Si*R*	17.36[a]	—	Si*S*

[a] R_t refers to HPLC, analytical column,‡ eluent: 1% ethyl acetate in hexane. [b] Eluent: 0.5% ethyl acetate in hexane.

DOI: 10.1039/b001440k

Table 2 Preparation of optically active silanes by $LiAlH_4$ reduction of diastereomeric BINOL derivatives

	Si*R*			Si*S*		
R	Yield (%)	$[\alpha]_D(c)$	Ee (%)[a]	Yield (%)	$[\alpha]_D$ (*c*)‡	Ee (%)[a]
4a, Bu^t	78	−4.1(6.15)	> 98	83	+4.2(8.04)	> 98
4b, Bu^n	95	−6.2(6.50)	—	78	+6.5(7.10)	—
4c, Pr^i	82	−3.9(8.39)	98.7	80	+3.9(7.87)	98.2

[a] Determined by GC analysis using a chiral column (B-DM; ASTEC; 50 m × 0.32 mm; 100 kPa).

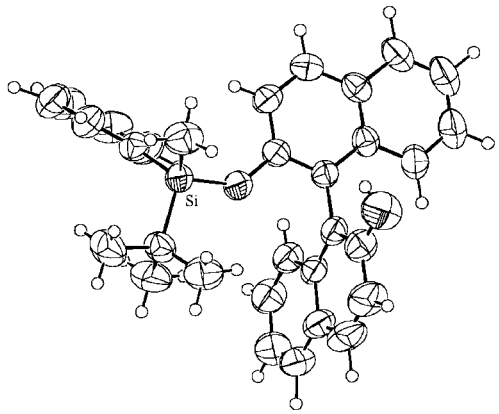

Fig. 1 X-Ray crystal structure of **3a**(Si*R*).

In order to generate optically active silane and to recover the BINOL, diastereomer **3a**(Si*R*) was reduced with $LiAlH_4$ in diethyl ether. Silane **4a**(*S*) was obtained in 83% yield, 95% ee. Specific rotation¶ and optical purity of this product (determined by GC analysis on a chiral column, *vide infra*) are presented in Table 2. Transformation of **3a**(Si*R*) into **4a**(*S*) indicates that $LiAlH_4$ reduction of the BINOL derivative occurred with retention of configuration around the Si atom, as expected by analogy to other O–Si derivatives.[13] Reduction of the more mobile diastereomer **3b**(Si*R*) afforded dextrorotatory silane **4b**(*S*).

Similarly, reduction of all other diastereomeric silyloxy derivatives afforded optically active silanes with yields and some properties compiled in Table 2. The optical purity of enantiomeric silanes **4c** was very high while the enantiomeric purity of **4b** could not be determined (*vide infra*). The absolute configuration of silanes **4b** and **4c** could not be determined by X-ray measurements. However, comparison with **4a** and some other silanes described[14] indicates an Si*S* configuration for the dextrorotatory enantiomers.

An attempt was made to use BINOL as a template for asymmetric synthesis of silanes. Treatment of *rac*-BINOL **1** (Scheme 2) with 2 mol equivalents of *n*-butyllithium followed by dichloro(methyl)phenylsilane (THF, −78 °C) gave an unstable intermediate which could not be isolated, presumably the [1,3,2]dioxasilepane derivative **6**. However, treatment of **6** *in situ* with 1 mol equivalent of *n*-butyllithium (THF, −78 °C) afforded **3b** as a mixture of diastereomers in a 1:1 ratio. Interestingly, stable [1,3,2]dioxasilepane derivatives with biphenyl frameworks have been prepared.[15]

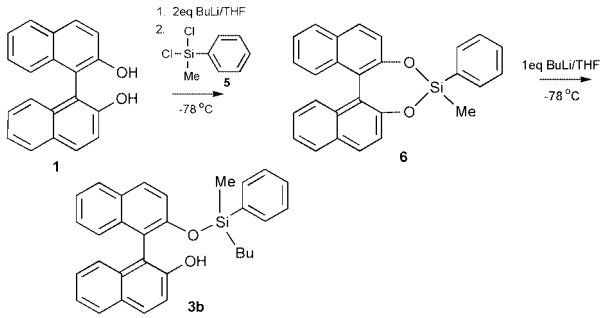

Scheme 2

Determining the optical purity of silanes **4a**–**c** was crucial for their intended use in asymmetric synthesis. An attempt was made to apply several analytical methods, including HPLC on chiral columns and NMR measurements in the presence of shift reagents. Eventually, it was found that GC analysis using a commercial cyclodextrin-based chiral column (B-DM; ASTEC; 50 m × 0.32 mm) provided base-line separation of enantiomers **4a** at 70 °C [R_t = 75.51 min, (*R*); R_t = 77.00 min (*S*)] and **4c** at 120 °C [R_t = 25.37 min (*S*); R_t = 26.95 min (*R*)]. Conversely, silane **4b** bearing an *n*-butyl group showed no enantiomer separation even for a much longer retention time. To the best of our knowledge, GC chiral column separation of **4a** and **4c** represents the first direct determination of enantiomeric purity of tri(alkyl/aryl)silanes.

In conclusion, a method for preparation silanes **4a**–**c** of high enantiomeric purity has been developed. It has been shown that the enantiomeric purity of virtually unpolar silanes may be determined by GC using a cyclodextrin-based chiral column.

Financial support from the State Committee of Scientific Researches, Poland and the Volkswagen Foundation, Germany, is gratefully acknowledged.

Notes and references

† Important ^1H NMR data of new compounds (200 MHz, $CDCl_3$, δ/ppm): **3a**(Si*S*): 5.10 (s, 1, OH); 0.40 (s, 3, SiMe); **3a**(Si*R*) 4.9 7 (s, 1, OH); 0.46 (s, 3, SiMe); **3b**(Si*S*): 5.07 (s, 1, OH), 0.26 (s, 3, SiMe); **3b**(Si*R*): 5.03 (s, 1, OH), 0.26 (s, 3, SiMe); **3c**(Si*S*): 5.03 (s, 1, OH), 0.20 (s, 3H, SiMe); **3c**(Si*R*): 4.94 (s, 1, OH), 0.31 (s, 3H, SiMe).

‡ Analytical HPLC was performed using a Nucleosil 50-5 column (250 × 4.6 mm), flow rate 1 ml min^{-1}, UV detector (254 nm); preparative HPLC was carried out using a Nucleosil 50-7 column (three units in sequence 250 × 20 mm).

§ *Crystal data* for $C_{31}H_{30}O_2Si$ **3a**(Si*R*): M = 462.64, orthorhombic, space group $P2_12_12_1$, a = 8.3530(10), b = 13.3170(10), c = 23.5330(10) Å, U = 2617.7(4) $Å^3$; T = 293 K, Z = 4, μ(Cu-Kα) = 1.54 mm^{-1}. The final $wR(F^2)$ was 0.1063.

CCDC 182/1624. See http://www.rsc.org/suppdata/cc/b0/b001440k/ for crystallographic files in .cif format.

¶ Specific rotations were measured with a Perkin-Elmer Model 141 polarimeter using an 8 cm^3 capacity cell (10 cm path length) for hexane solutions of distilled samples. Distillation of silanes was required to remove solvents and other volatile impurities.

1 T. H. Chan and D. Wang, *Chem. Rev.*, 1992, **92**, 995.
2 I. Fleming, A. Barbero and D. Walter, *Chem. Rev.*, 1997, **97**, 2063.
3 I. Ojima, in *The Chemistry of Organic Silicon Compounds*, ed. S. Patai and Z. Rappoport, John Wiley & Sons, Chichester, 1989, ch. 25.
4 L. H. Sommer, C. L. Frye, G. A. Parker and K. W. Michael, *J. Am. Chem. Soc.*, 1964, **86**, 3271.
5 R. J. P. Corriu, C. Guerin and J. J. E. Moreau, *Top. Stereochem.*, 1984, **15**, 43.
6 K. Kobayashi, T. Kato, M. Unno and S. Masuda, *Bull. Chem. Soc. Jpn.*, 1997, **70**, 1393.
7 R. Tacke, K. Fritsche, A. Tafel and F. Wuttke, *J. Organomet. Chem.*, 1990, **388**, 47.
8 A. Djerourou and L. Blanco, *Tetrahedron Lett.*, 1991, **32**, 6325.
9 S. Bienz, *Chimia*, 1997, **51**, 133.
10 P. Jankowski, E. Schaumann, J. Wicha, A. Zarecki and G. Adiwidjaja, *Tetrahedron: Asymmetry*, 1999, **10**, 519.
11 R. Noyori and H. Takaya, *Chim. Scr.*, 1985, **25**, 83.
12 L. Pu, *Chem. Rev.*, 1998, **98**, 2405.
13 R. J. P. Corriu and C. Guerin, *Tetrahedron*, 1981, **37**, 2467.
14 A. Holt, A. W. P. Jarvie and G. J. Jervis, *J. Chem. Soc., Perkin Trans. 2*, 1973, 114.
15 T. Takada, M. Arisawa, M. Gyoten, R. Hamada, H. Tohma and Y. Kita, *J. Org. Chem.*, 1998, **63**, 7698.

Molecular insight into the non-innocence of a silica-support: the structure of a platinum–silsesquioxane derivative

Elsje Alessandra Quadrelli, John E. Davies, Brian F. G. Johnson* and Neil Feeder

University Chemical Laboratories, University of Cambridge, Lensfield Road, Cambridge, UK CB2 1EW. E-mail: bfgj1@cam.ac.uk

Received (in Cambridge, UK) 4th February 2000, Accepted 27th April 2000
Published on the Web 25th May 2000

The cyclooctadiene ligand within the square planar Pt(II) complex [$PtCl_2(C_8H_{12})$] undergoes nucleophilic attack from a siloxo group of the thallated polyhedral silsesquioxane [(c-$C_5H_9)_7Si_7O_9(OSiMe_3)(OTl)_2$], to yield [($c$-$C_5H_9)_{14}Si_{14}O_{18}(OSiMe_3)_2O_4(\eta^4$-$C_8H_{12})PtTl_2$]; given the analogy between the silsesquioxane moiety and a silica surface, the presence of an SiO–C bond between the siloxo-cage and the Pt-bound olefinic ring is significant in the context of surface non-innocence in heterogeneous catalysis.

Metalla-derivatives of partially condensed silsesquioxanes (POSS) provide an appropriate manifold for gaining molecular insight into the nature of silica-supported heterogeneous catalysts.[1] Complexes of metallic POSS with centres are known to display close structural and chemical resemblance to their heterogeneous counterparts.[1] Here, we wish to report the structure of a highly novel mixed-metal silsesquioxane complex [[(c-$C_5H_9)_7Si_7O_9(OSiMe_3)O_2]_2(\eta^4$-$C_8H_{12})PtTl_2$] **2** that displays an unprecedented siloxo-metallacycle derived from the formal oxidative-addition of a Pt–OSi bond across a carbon–carbon double bond of a coordinated diolefin. Such interaction models a direct involvement of a 'non-innocent' silica surface into the activation of an unsaturated substrate. To date, no other molecular model for such 'support–catalytic center' interaction had been reported.

Upon addition of [$PtCl_2$(cod)] (cod = cycloocta-1,5-diene) to a benzene solution containing 2 equivalents of [(c-$C_5H_9)_7Si_7O_9(OSiMe_3)(OTl)_2$] **1**,[2] the mixed-metal compound **2** is formed in low yield (*ca.* 6%) (Scheme 1).† Compound **2** may also be isolated by fast addition of [$PtCl_2$(cod)] to an equimolar solution of **1**, followed by rapid work-up of the reaction mixture. Conversely, if [$PtCl_2$(cod)] is added slowly to an equimolar benzene solution of **1** and the mixture allowed to stand for 56 h, elimination of 2 equivalents of TlCl is observed and the metalla-silsesquioxane [(c-$C_5H_9)_7Si_7O_9(OSiMe_3)O_2Pt(\eta^4$-$C_8H_{12})$] **3** can be isolated in moderate yield (53%) (Scheme 1). Compound **2** has also been found to react with 1 equivalent of [$PtCl_2$(cod)] to give **3**.

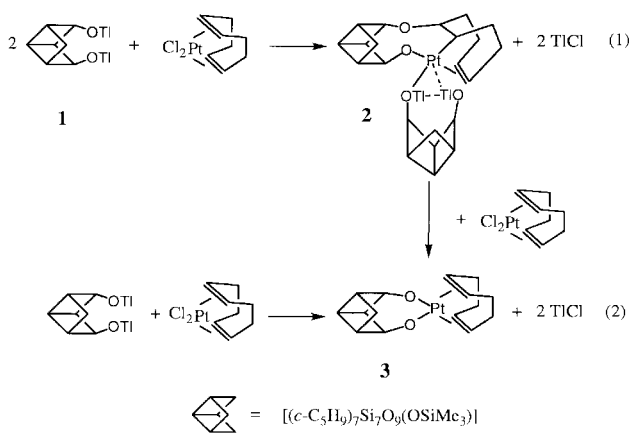

Scheme 1

Compound **2** was initially characterised by its ^{1}H NMR spectrum in C_6D_6 which clearly indicates that the Pt(cod) moiety is coordinated to the silsesquioxane cage. However, a complete elucidation of the structure based on the NMR data is hindered by the overlap of cyclopentyl and cyclooctadienyl resonances. The molecular structure of compound **2** was elucidated by single-crystal X-ray diffraction analysis (Fig. 1).‡

Compound **2** consists of two silsesquioxane moieties bridged by a trinuclear (C_8H_{12})$PtTl_2$ core. The metallic unit shows a Tl–Tl distance of 3.7382(13) Å and a Tl–Pt distance of 3.2393(15) Å. The central thallium atom [Tl(I)] forms an angle with its neighbours of 63°43′. The geometry at the platinum metal, excluding the thallium contact, is square planar with mean deviation from the plane of 0.1712 Å. The thallium atom sits above the plane, forming an angle with the perpendicular to the plane of 27°. The Pt(II) centre completes its coordination sphere with two Pt–O bonds [2.142(9) and 2.064(10) Å], one Pt–C σ-bond [2.05(3) and 2.16(4) Å, in the two disordered rings present in the solid state structure] and a Pt–C=C π bond [with Pt–C distances of 2.10(2) Å]. Such coordination results form the cyclooctadiene ring having undergone nucleophilic attack from a siloxo moiety. The structural disorder results from the SiO^- nucleophilic attack occurring at both possible sites of the C=C 1,2-double bond. The oxidative addition yields reaction both on Pt–C and a SiO–C bond [O–C 1.55(3) Å]. The C–C distances of 1.53(3) and 1.49(3) Å in the disordered structure show substantial lengthening with respect to the coordinated olefinic C=C bond [1.36(2) Å]. Both oxygen atoms involved in the Pt–O bonds are also involved in a Tl–O bond [2.514(11) and 2.681(11) Å]. This μ_2-siloxo-binding mode contributes one electron to the overall electron count for the platinum centre. The apparent electron deficiency at the Pt(II) centre may be taken to explain the presence of the thallium–platinum contact. Thallium(I)–platinum(II) bonds are known,[3] although in scarce

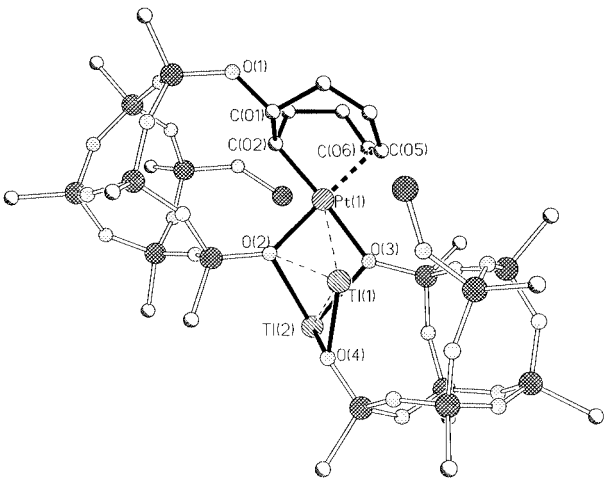

Fig. 1 Molecular structure of **2**. No H and only *ipso* carbons of cyclopentyl rings are shown for clarity. Only one of the two disordered cod rings is shown for clarity. See text for selected bond lengths and angles.

DOI: 10.1039/b000992j

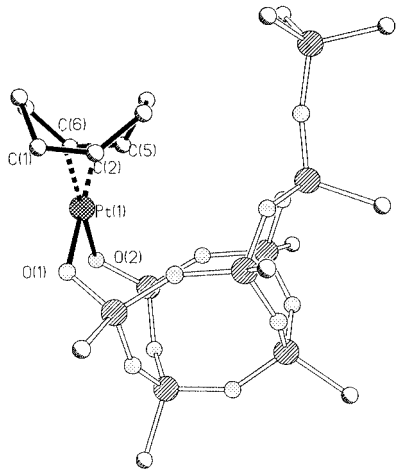

Fig. 2 Molecular structure of **3**. No H atoms and only *ipso* carbons of cyclopentyl rings are shown for clarity. Selected interatomic distances (Å) and angles (°) (CNT is the centroid of the coordinated double bond): Pt1–O1 1.987(5), Pt1–O2 1.990(5), Pt1–C1 2.16, Pt1–C2 2.139, Pt1–C5 2.143(7), Pt1–C6 2.131(7), Pt1–CNT1 2.015, Pt1–CNT2 2.021, C1–C2 1.376(10), C5–C6 1.387(11); O2–Pt1–O1 90.4(2), O1–Pt1–CNT1 90.3(3), CNT1–Pt1–CNT2 89.4(3).

number. They vary in length between 2.860 Å[3c] and 3.135 Å,[3b] making the presently reported one the longest to date. The bonding geometry encountered here is reminiscent of those previously reported, with the Tl–Pt vector approaching the prependicular of the square planar Pt(II) complex.[3b]

The most striking feature of compound **2** is the presence of a σ bond between the siloxane frame and the metal coordinated cyclooctenyl ligand. To our knowledge, this would appear to be the first derivative that displays activation of a metal ligand by the silsesquioxane frame. The only two previously reported platinasilsesquioxanes are [(*c*-C_5H_9)$_7$$Si_7O_9$(OSi$Me_3$)$O_2$Pt(dppe)][4] (dppe = diphenyldiphosphinoethane) and [(*c*-C_6H_{11})$_7$$Si_7O_9$($OSiMe_3$)$O_2$Pt(η^4-$C_8H_{12}$)].[1b] While no experimental details are available for the latter, the former has been fully characterised, and consists of a square planar Pt(dppe) complex of the dipodal silsesquioxane cage. The chemistry at the platinum centre can be described as resulting from the exchange of two chloride ions from the appropriate Pt(II) salt with a dipodal silsesquioxane frame, with no other variation in the remaining coordination sphere of the metal centre. This reaction, which is the most used synthetic strategy for obtaining metalla silsesquioxanes,[1c] has been applied successfully in this work and compound **3** obtained [see reaction (2) in Scheme 1].§ This has been characterised by analytical and spectroscopic techniques, and its molecular structure determined by a single crystal X-ray diffraction study (Fig. 2),‡ making it the first organometallic platina-silsesquioxane structurally characterised.

The structure of **3** is similar to the dppe derivative described above. The Pt(cod) moiety retains most of its structural characteristics upon grafting onto the silanol. The presence of two distinct ^{1}H NMR resonances for the olefinic protons confirms the asymmetry in the ring-coordination arising from the presence of the POSS cage. This complex is also related to the complex [(η^4-cod)Pt($OSiPh_3$)$_2$],[5] obtained from the reaction of [$PtCl_2$(cod)] with triphenylsilanol.

The structures of compounds **2** and **3** shed considerable light into the nature of silica-supported platinum-based catalysts. With compound (η^4-cod)Pt($OSiPh_3$)$_2$,[5] they are the only reported organometallic siloxo complexes of platinum(II), and therefore constitute the only available models for silica supported organoplatinum catalysts. Such heterogeneous systems are of interest, given their use as catalysts in the heterogeneous hydrogenolysis of hydrocarbons.[5] As with supported heterogeneous catalysts in general, the molecular structure of their active site is seldom known with precision. In such materials the activity is normally believed to reside at the metal centre, although the existence of a 'support-effect' in the solid state has been invoked.[6] Compound **3** shows no interaction of the 'silica-like' silsesquioxane frame with the coordinated unsaturated substrate. Such structural motif models a catalyst supported on an *inactive* silica surface, and modeled in POSS chemistry. In contrast, compound **2** exemplifies the opposite situation; the coordinated unsaturated bond establishes a direct bond with the 'silica-like' part of the metalla-POSS emphasising the possible non-innocence of a silica surface.

Financial support from the European Union (TMR grant to E. A. Q.) is gratefully acknowledged.

Notes and references

† *Synthesis* of **2**: solid [$PtCl_2$(cod)] (20 mg, 0.054 mmol) was added to a benzene solution (5 mL) of **1** prepared *in situ* from [(*c*-C_5H_9)$_7$$Si_7O_9$(OSi$Me_3$)$(OH)_2$] (100 mg, 0.106 mmol).[2] The immediate precipitation of a fine white powder ensued. After 5 h of stirring, the suspension was filtered off and the colorless supernatant was dried under vacuum. The residue was extracted with benzene (3 mL) and, by slow diffusion of MeCN in the solution, pale yellow needles were obtained and studied by X-ray diffraction. δ_H(C_6D_6): 4.35 (br m, 2H, CH=CH), 4.15 (m, 1H, C*H*CH=CH), 3.15 (br, 1H, CHOSi), 2.40 (m, 2H), 2.15 (m, 2H), 1.80–1.30 [br m, *c*-CH(CH_2)$_2$], 0.90 [br m, 7H, *c*-C*H*(CH_2)$_2$], 0.15 [m, 9H, Si(CH_2)$_3$].

‡ *Crystal data*: for **2**: $C_{84}H_{156}O_{24}PtSi_{16}Tl_2$, M = 2603.36, triclinic, space group $P\bar{1}$ a = 14.613(2), b = 19.703(2), c = 20.723(2) Å, α = 98.04(4), β = 101.92(4), γ = 92.99(3)°, U = 5760.3(11) Å^3, Z = 2, μ = 4.229 mm^{-1}, T = 180(2) K, 14691 independent reflections, final R index [I_o > 2σ(I_o)] = 0.0803, R' = 0.2040, GOF = 1.045.

For **3**: $C_{46}H_{84}O_{12}PtSi_8$, M = 1248.94, triclinic, space group $P\bar{1}$, a = 11.0900(4), b = 11.7050(4), c = 23.3350(9) Å, α = 75.9010(19), β = 80.6610(19), γ = 83.003(2)°, U = 2888.16(18) Å^3, Z = 2, μ = 2.649 mm^{-1}, T = 230(2) K, 10099 independent reflections, final R index [I_o > 2σ(I_o)] = 0.0530, R' = 0.1228, GOF = 1.010. CCDC 182/1618. See http://www.rsc.org/suppdata/cc/b0/b000992j/ for crystallographic files in .cif format.

§ *Synthesis* of **3**: a benzene solution (5 mL) of [$PtCl_2$(cod)] (45 mg, 0.120 mmol) was added dropwise to a benzene solution (10 mL) of **1** prepared as above from [(*c*-C_5H_9)$_7$$Si_7O_9$($OSiMe_3$)$(OH)_2$] (115 mg, 0.121 mmol). An immediate precipitation of a fine white powder ensued. After 48 h of stirring, the suspension was filtered off and the pale yellow supernatant was dried under vacuum. The residue was extracted with benzene (3 mL) and dried again leaving a white powder (32 mg, yield as **3**: 53%). By slow diffusion of MeCN in a benzene solution, pale yellow needles were obtained and studied by X-ray diffraction. *Elemental analysis* for $C_{46}H_{84}O_{12}PtSi_8$: found (calc.): C, 43.89 (44.24); H, 6.98 (6.78). δ_H(C_6D_6) 5.12 (m, 2H, CH_a=CH_b), 4.94 (m, 2H, CH_a=CH_b), 2.82 (br, 2H, CH_2 in cod), 2.64 (m, 2H, CH_2 in cod), 2.14 (m, 4H, CH_2 in cod), 1.76 (br, 7H, CH_2 in *c*-C_5H_9), 1.40 (br, 7H, CH_2 in *c*-C_5H_9), 0.98 (br m, 7H, CH in *c*-C_5H_9), 0.11 [m, 9H, Si(CH_3)$_3$].

1 (*a*) F. J. Feher, D. A. Newman and J. F. Walzer, *J. Am. Chem. Soc.*, 1989, **111**, 1741; (*b*) F. J. Feher, T. A. Budzichowski, R. L. Blanski, K. J. Weller and J. W. Ziller, *Organometallics*, 1991, **10**, 2526; (*c*) R. H. Baney, M. Itoh, A. Sakakibara and T. Suzuki, *Chem. Rev.*, 1995, **95**, 1409.
2 F. J. Feher, K. Rahimian, T. A. Budzichowski and J. W. Ziller, *Organometallics*, 1995, **14**, 3920.
3 (*a*) J. K. Nagle, A. L. Balch and M. M. Olmstead, *J. Am. Chem. Soc.*, 1990, **110**, 3191321; (*b*) I. Ara, J. R. Berenguer, J. Forníes, J. Gomez, E. Lalinde and R. I. Merino, *Inorg. Chem.*, 1997, **36**, 6461 and references therein; (*c*) L. Hao, J. J. Vittal and R. J. Puddephatt, *Organometallics*, 1996, **15**, 3115.
4 H. C. L. Abbenhuis, A. D. Burrows, H. Kooijman, M. Lutz, M. T. Palmer, R. A. van Santen and A. L. Spek, *Chem. Commun.*, 1998, 2627.
5 A. Fukuoka, A. Sato, Y. Mizuho, M. Hirano and S. Komiya, *Chem. Lett.*, 1994, 1641.
6 K. Foger, *Catalysis Science and Technology*, ed. M. Boudart, Springer–Verlag, Berlin, 1984, vol. 6, p. 227.

Synthesis and crystal structure of the first d–f heterodinuclear Dy(III)–Cu(II) cryptate

Qiu-Yun Chen,[ab] Qin-Hui Luo,[ab] Zhi-Lin Wang[ab] and Jiu-Tong Chen[b]

[a] *Coordination Chemistry Institute and State Key Laboratory of Coordination Chemistry, Nanjing University, Nanjing 210093, P.R. China. E-mail: qhluo@netra.nju.edu.cu*

[b] *FuZhou State Key Laboratory of Structural Chemtry, FuZhou, 350002, P.R. China*

Received (in Cambridge, UK) 21st December 1999, Accepted 3rd May 2000

The heterodinuclear cryptate [DyCuL(DMF)](ClO$_4$)$_2$·MeCN [where L denotes the deprotonated anionic cryptand obtained by condensation of tris(2-aminoethyl)amine with 2,6-diformyl-4-chlorophenol] has been obtained by a stepwise method; the presence of copper(II) and dysprosium(III) in the cavity of the cryptand was evidenced by X-ray structure analysis and ESMS spectroscopy.

Heterodinuclear complexes have received much attention owing to their electronic, electrochemical, and magnetic properties arising from the metal–metal interaction,[1] and mimicking of the active centers of some metalloenzymes, for example, copper–zinc superoxide dismutase,[2] cytochromic oxidase,[3] hydrogenase,[4] *etc*. Heterodinuclear complexes of dinucleating 'Robson-type' macrocycles[5] have been recognized for many years.[6] Most of these are two-dimensional macrocyclic complexes encapsulating transition metal ions. A few d–f heteronuclear macrocyclic complexes have been reported.[7] Since it was found that the Gd(III)–Cu(II) intramolecular interaction in the complexes is ferromagnetic,[8] interest has been aroused in the synthesis of d–f heteronuclear macrocyclic complexes in order to develop new functions. The cryptates have good thermodynamical stability and kinetic inertness toward metal dissociation. The first homodinuclear lanthanide cryptate was synthesized in 1999,[9] but up to date no examples of heteronuclear d–f cryptates have been described in the literature. Here, we report the first example of a d–f heteronuclear Dy(III)–Cu(II) complex of a Robson-type cryptand together with its crystal structure. The mononuclear dysprosium cryptate was synthesized by metal-templated reaction between 2,6-diformyl-4-chloro-phenol (dcp) and tris(2-aminoethyl)-amine (tren) in the presence of hydrated dysprosium nitrate in 3:2:1 mol ratio in absolute methanol. After refluxing for 3–4 h, the yellow mononuclear dysprosium cryptate was produced, which was used as a precursor to synthesize the heteronuclear complex. The yellow complex (117 mg, 0.1 mmol) was dissolved in methanol (20 cm^3) containing a small amount of DMF. The pH of the solution was *ca*. 6. After adding an excess of CaH_2 powder, the pH of the solution changed to 7–8. After filtering the solution, copper perchlorate (0.1 mmol) in methanol (5 cm^3) was added resulting in a green solution. After refluxing for *ca*. 2 h a red solid was produced. Slow diffusion of diethyl ether into an acetonitrile solution of the complex gave red prismatic crystals of [DyCuL(DMF)](ClO$_4$)$_2$·MeCN suitable for an X-ray study,†‡ where L is the deprotonated anionic cryptand obtained by condensation of tren with dcp (Scheme 1).

The ESMS spectra display intense peaks corresponding to the fragments [DyCu(L − 3Cl)(DMF)(MeCN)]$^{2+}$ (100), [DyCu(L − 3Cl)(DMF) + (Cl$^-$) + 2(MeOH)]$^+$ (42) and [DyCu(L − 3Cl)(DMF) + (Cl$^-$) + 2(MeOH) + (MeCN)]$^+$ (24%), confirming the presence of the Dy(III)–Cu(II) core in the cryptate. It is found that the chlorine atom of the phenyl rings can be lost under ESMS conditions, whereas the Dy(III)–Cu(II) macrobicycle remained intact and [DyCu(L − 3Cl)(DMF)(MeCN)]$^{2+}$ appears with 100% base peak intensity.

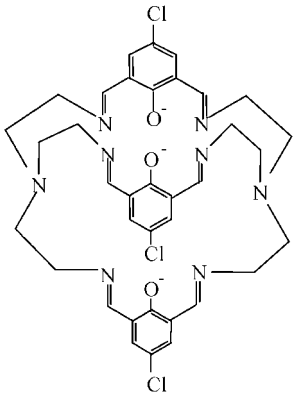

Scheme 1 Anionic cryptand L.

Structural analysis of this complex comfirmed the presence of the Dy(III)–Cu(II) unit in the cavity of the macrocycle. The crystals contain the cation [DyCuL(DMF)]$^{2+}$, two independent perchlorate anions and an acetonitrile molecule. Fig. 1 illustrates the structure of the cation.

The Dy(III) ion is located at one end of the cavity and is eight coodinated with the bridgehead nitrogen atom [N(1)], three imino-nitrogen atoms [N(2), N(3), N(4)], the three μ-phenolate oxygen atoms [O(1), O(2), O(3)] and the oxygen atom O(4) of DMF. The coordination polyhedron is best described as distorted dodecahedral. The Dy–N(imino) distances are in the range 2.443–2.509 Å, with Dy(III)–N(1) 2.617 Å, shorter than found in a Dy(III) mononuclear cryptate reported by Fenton and coworkers,[10] however the Dy(III)–O(phenolate) distances are longer than those reported in the literature.[10] The other end of the cavity is occupied by the Cu(II) ion. Three μ-phenolate oxygen and three imino-nitrogen atoms coodinate to Cu(II), forming a distorted octahedron. The Dy···Cu distance is

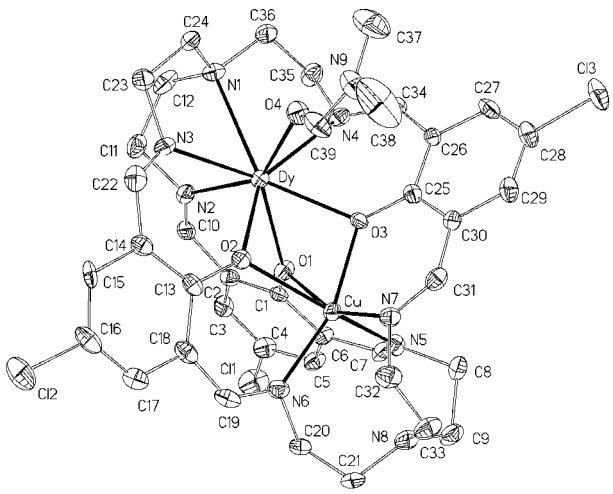

Fig. 1 Crystal structure of [DyCuL(DMF)]$^{2+}$.

DOI: 10.1039/a909926n

3.255 Å. The Dy(III)–O(1)–Cu(II), Dy(III)–O(2)–Cu(II) and Dy(III)–O(3)–Cu(II) angles are 92.1, 90.0 and 97.1°, respectively. The distance between the two bridgehead nitrogens, N(1)···N(8) 9.003 Å, is larger than that found for a mononuclear dysprosium(III) cryptate (8.361 Å)[10] or in a homobinuclear Lu(III) cryptate (8.65 Å),[9] and slightly shorter than that in $[Cd_2L]^{2+}$ (9.01 Å),[11] revealing that the cryptand (L) can expand or contract as appropriate to encapsulate one or two metal ions.

Previously we have described a mononuclear neodymium(III) cryptate of ligand L in which one water molecule was encapulated as a guest.[12] In the present work we have extended the work *via* a stepwise synthesis to introduce a 3d metal ion which occupies the position of the water molecule in the cavity. Further d–f heteronuclear cryptates consisting of transition metals [copper(II), nickel(II), *etc*.] and other lanthanide ions have also been synthesized and will be reported elsewhere.

This project was supported by the National Science Foundation of China.

Notes and references

† [DyCuL(DMF)]$(ClO_4)_2$·MeCN yield 40% (Found: C, 38.20; H, 3.75; N, 10.45; $C_{41}H_{46}Cl_5N_{10}O_{12}CuDy$ requires: C, 38.65; H, 3.64; N, 10.99%). λ_{max}/nm (ε/dm^3 mol^{-1} cm^{-1}) (MeCN) 245(75 214), 380(14 511) 490(402). ν_{max}(KBr)/cm^{-1} 1650s(C=N), 1540s(C–O) and 1097(ClO_4^-). Λ_m(DMF, 298 K): 150 s cm^2 mol^{-1}. The complex is soluble in methanol, acentonitrile and DMF.

‡ *Crystal data*: [DyCuL(DMF)]$(ClO_4)_2$·MeCN, $C_{41}H_{46}Cl_5N_{10}O_{12}CuDy$, M = 1274.17; red prism, 0.28 × 0.16 × 0.06 mm, monoclinic, space group $P2_1/c$, a = 19.6358(7), b = 11.8049(4), c = 21.5544(8) Å, β = 98.2600(3)°, V = 4944.4(3) Å^3, Z = 4, D_c = 1.712 Mg m^{-3}, μ = 2.270 mm^{-1}. Using Mo-Ka radiation (λ = 0.71073 Å) at 293(2) K, a total of 17 965 reflections was collected ($1.05 < \theta < 25.05°$), of which 8693 were independent. Refinement converged to R_1 = 0.0658, wR_2 = 0.1109 [$I > 2\sigma(I)$] and R_1 = 0.1570, wR_2 = 0.1450 (all data).

CCDC 182/1622. See http://www.rsc.org/suppdata/cc/a9/a909926n/ for crystallographic files in .cif format.

1 P. Zanello, S. Tamburini, P. A. Vigato and G. A. Mazzocchin, *Coord. Chem. Rev.*, 1987, **77**, 165; J.-P. Costes, A. Dupuis and J.-P. Laurent, *J. Chem. Soc., Dalton Trans*, 1998, 735; C. Fraser and B. Bosnich, *Inorg. Chem.*, 1994, **33**, 338.

2 J. S. Vatentine and D. M. de Freites, *J. Chem. Educ.*,1985, **62**, 990.

3 S. C. Lee and R. H. Holm, *J. Am. Chem. Soc.*, 1993, **115**, 11 789.

4 R. T. Volbeda, M.-H. Charon, C. Piras, E. C. Hatchikian, M. Frey and J. C. Fontecilla-Camps, *Nature*, 1995, **373**, 580.

5 N. H. Pikington and R. Robson, *Aust. J. Chem*, 1970, **23**, 2225.

6 R. R. Gagne, C. L. Spiro, T. J. Smith, C. A. Hamann, W. R. Thies and A. K. Shiemke, *J. Am. Chem. Soc.*, 1981, **103**, 4073; S. Mohanta, K. K Nande, L. K. Tompson, U. Florke and K. Nag, *Inorg. Chem.*, 1998, **37**, 1465.

7 K. Manseki, M. Kumagai, M. Sakamoto, H. Sakiyama, Y. Nishida, A. Matsumoto, Y. Sadaoka, M. Ohba and H. Okawa, *Bull. Chem. Soc. Jpn.*, 1998, **71**, 379.

8 A. Bencini, C. Benelli, A. Caneschi, R. L. Carlin, A. Dei and D. Gatteschi, *J. Am. Chem. Soc.*, 1985, **107**, 8128.

9 F. Avecilla, A. de Blas, R. Bastida, D. E. Fenton, J. Mahia, A. Macias, C. Platas, A. Rodriguez and T. Rodriguez-Blas, *Chem. Commun.*, 1999, 125.

10 F. Avecilla, R. Bastida, A. de Blas, D. E. Fenton, A. Macias, A. Rodriguez, T. Rodriguez-Blas, S. Garcia-Granda and R. Corzo-Suarez, *J. Chem. Soc., Dalton Trans.*, 1997, 409.

11 M. G. B. Drew, O. W. Howarth, G. G. Morgan and J. Nelson, *J. Chem. Soc., Dalton Trans.*, 1994, 3149.

12 C.-J. Feng, Q.-H. Luo, C.-Y. Duan, M.-C. Shen and Y.-J. Liu, *J. Chem. Soc., Dalton Trans.*, 1998, 1377.

The synthesis of angularly fused tricyclic compounds *via* tandem ring closing metathesis reactions†

Martin J. Bassindale,[a] Andrew S. Edwards,[a] Peter Hamley,[b] Harry Adams[a] and Joseph P. A. Harrity*[a]

[a] *Department of Chemistry, University of Sheffield, Brook Hill, Sheffield, UK S3 7HF. E-mail: j.harrity@sheffield.ac.uk*

[b] *Department of Medicinal Chemistry, AstraZeneca Research and Development, Charnwood, Bakewell Road, Loughborough, UK LE11 5RH*

Received (in Liverpool, UK) 14th March 2000, Accepted 3rd May 2000
Published on the Web 25th May 2000

A novel and highly efficient approach to angularly fused tricycles has been developed through the employment of selective tandem ring closing metathesis reactions.

Angularly fused tricycles represent a structurally intriguing unit present in many natural products and have attracted the attention of synthetic chemists for a number of years.[1] Amongst prominent targets of this class of compounds are triquinanes and marine alkaloids, of which there are a plethora of examples with a variety of biological activities. In the process of our investigations into the scope of tandem ring closing metathesis (RCM) reactions[2] for the synthesis of functionalised carbon skeleta,[3,4] we have turned our attention to the application of this technique to the formation of angularly fused tricycles by employing the general strategy outlined in Fig. 1. Specifically, we were interested in observing the relative ease of tricycle formation (mode a cyclisation) *versus* that of spirocyclisation (mode b cyclisation), and additionally, whether spirocycles would themselves participate in tricycle formation. In this regard, the groups of Grubbs[4a] and Mioskowski[4e] have shown that tandem metathesis (mode a type) cyclisation products are highly favoured, and can indeed be generated by ring opening/closing metathesis of mode b type substrates.

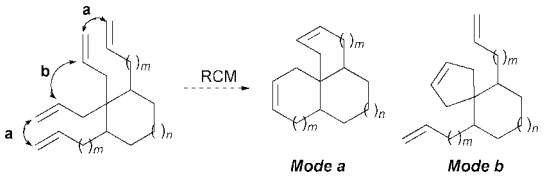

Fig. 1

We prepared a suitable model system through a routine two step procedure, which provided both *syn*- and *anti*-diols **2** and **3** which were readily separated by column chromatography (Scheme 1).

With the desired tetraenes in hand, we turned our attention to the tandem RCM reaction paying particular regard to the selectivity of tricycle *versus* spirocycle formation. Subjection of *syn*-tetraene **2** to 20 mol% Grubbs' catalyst PhCH=Ru(P-$Cy_3)_2Cl_2$ **I** for 48 h gave a complex reaction mixture[5] from

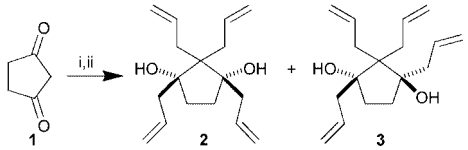

Scheme 1 *Reagents and conditions*: i, CH_2=$CHCH_2OAc$, 0.8% $Pd(PPh_3)_4$, DBU, 74%; ii, CH_2=$CHCH_2MgCl$, 73%, 6:1 *syn*:*anti*.

† Electronic supplementary information (ESI) available: general experimental and synthetic and spectral data for the new compounds. See http://www.rsc.org/suppdata/cc/b0/b002136i/

Table 1 Ru-catalysed preparation of angularly fused tricycles[a]

Entry	Substrate	Product	Yield (%)
1	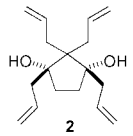 **2**	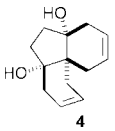 **4**	38[b]
2	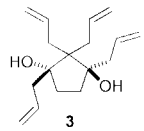 **3**	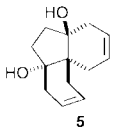 **5**	72
3	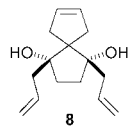 **8**	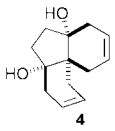 **4**	40[c]
4	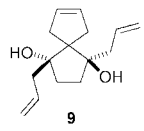 **9**	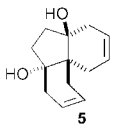 **5**	85

[a] All reactions carried out in dichloroethane at 60 °C for 48 h using 10 mol% **I**. [b] Reaction required 20 mol% **I**. [c] 49% of **8** recovered.

which the desired tricycle **4** could be isolated in 38% yield as a stable crystalline solid (Table 1, entry 1). In contrast to **2**, the *anti*-diol **3** underwent smooth and selective cyclisation to tricycle **5** in high yield (Table 1, entry 2).[6]‡

We were intrigued that the potentially competing spirocyclisation process was not evident under any of the reaction conditions employed, however, we could not rule out the possibility that the spirocycles were formed transiently and reacted *in situ* to furnish the observed tricyclic products. In an attempt to further clarify this issue, we prepared the appropriate spirocycles by the route shown in Scheme 2.

Surprisingly, RCM of diene **6** was rather sluggish and required extensive heating and relatively high catalyst loadings to achieve useful product yield.[7] Nonetheless, the subsequent Grignard alkylation reaction proceeded smoothly to provide a mixture of *syn*- and *anti*-diols in good yield.

Both spirocyclic substrates **8** and **9** were stable to the Ru-catalyst at 25 °C but provided the corresponding tricycles in

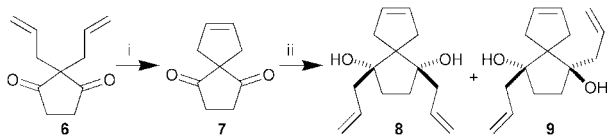

Scheme 2 *Reagents and conditions*: i, 10 mol% **I**, 60 °C, DCE, 48 h, 67%; ii, CH_2=$CHCH_2MgCl$, 66%, 5:1 *syn*:*anti*.

DOI: 10.1039/b002136i

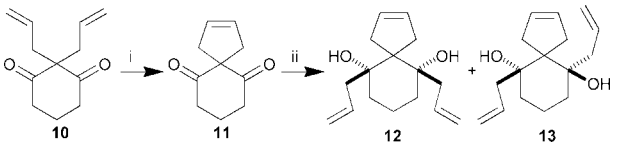

Scheme 3 *Reagents and conditions*: i, 2 mol% **I**, 25 °C, CH_2Cl_2, 16 h, 92%; ii, CH_2=$CHCH_2MgCl$, 85%, 2 : 1 *syn* : *anti*.

comparable yields to those from the appropriate tetraenes in the presence of 10 mol% **I** at elevated temperatures (entries 3 and 4 of Table 1). These results demonstrate that whilst spirocycles **8** and **9** have not been observed in the RCM reactions of **2** and **3**, they cannot be ruled out as intermediates in the reaction process.

In extending this chemistry to six-membered ring analogues we encountered some surprising differences in reactivity. Firstly, all attempts to add allyl magnesium halides to 2,2-diallylcyclohexa-1,3-dione (**10** in Scheme 3) failed to furnish the desired tetraene substrate. We therefore turned our attention to the preparation of the corresponding spirocyclic substrates as outlined in Scheme 3.

In sharp contrast to the RCM reaction of diene **6**, cyclohexane analogue **10** underwent smooth ring closure at room temperature in the presence of 2 mol% **I** to provide the spirocycle **11** in excellent yield. Additionally, this substrate was readily alkylated to give the expected diols **12** and **13** in good yield.

Once again, in contrast to the cyclopentanedione spirocycles, we have found the corresponding cyclohexane analogues to be extremely unreactive towards Ru-catalysed tricycle formation. As outlined in Scheme 4, the *syn*- and *anti*-spirocycles **12** and **13** were inert to metathesis even on prolonged heating with 20 mol% Ru-catalyst. Protection of the diol unit as mono-silyl ether **15** provided bridged bicycle **16** in 64% overall yield, after removal of the TBS-group, as the only metathesis reaction product. In this particular case, it is likely that the increased steric demands of the OTBS unit provides a greater concentration of the diaxial diene conformation and facilitates seven-membered ring closure. We therefore tethered the diol units in the axial position by the preparation of cyclic carbonate **14**,[8] however, once again this substrate was found to be unreactive.

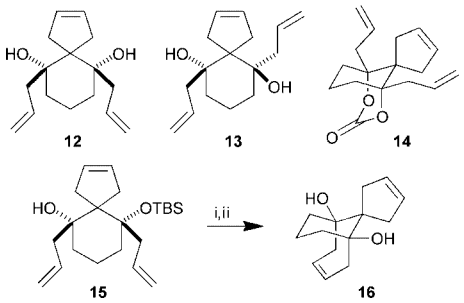

Scheme 4 *Reagents and conditions*: i, 15 mol% **I**, 80 °C, C_6H_6, 48 h; ii, TBAF, 64% overall yield.

The notable difference in reactivity of the cyclopentane-derived spirocycles in comparison to the cyclohexane analogues is unclear at present, however, the relative ease of RCM of diene **10** in comparison to **6** and the ready conversion of spirocycles **8** and **9** *versus* that of **12** and **13** suggests that these differences may originate from the relative strain in the respective cyclopentene moieties.[9] Nonetheless, we have shown that tandem RCM is a viable method for the rapid assembly of *cis,trans*- and *cis,cis*-fused tricyclic skeleta.[10] The application of this methodology in target orientated synthesis and the further study of the selectivity issues raised in this communication are currently under investigation.

We are grateful to the EPSRC for studentships (M. J. B. and A. S. E.) and to AstraZeneca for financial support.

Notes and references

‡ *Crystal data* for $C_{13}H_{18}O_2$ **5** at 150 K: M = 206.27, orthorhombic, space group *Pbca* (no. 61), a = 8.6041(5), b = 13.1932(7), c = 19.0521(10) Å, U = 2162.7(2) Å^3, Z = 8, D_c = 1.267 g cm^{-3}. Mo-Kα radiation (λ = 0.71073 Å), μ(Mo-Kα) = 0.083 mm^{-1}, F(000) = 896. Data were collected in the range 3.02 < θ < 28.27°, 2624 independent reflections (R_{int} = 0.0679), final R = 0.0572, with allowance for the thermal anisotropy of all non-hydrogen atoms.

CCDC 182/1621. See http://www.rsc.org/suppdata/cc/b0/b002136i/ for crystallographic files in .cif format.

1 For representative alkaloid examples, see: K. M. Werner, J. M. de los Santos and S. M. Weinreb, *J. Org. Chem.*, 1999, **64**, 686; W. H. Pearson and Y. Ren, *J. Org. Chem.*, 1999, **64**, 688; C. Sha, F. Lee and C. Chang, *J. Am. Chem. Soc.*, 1999, **121**, 9875; for synthetic approaches to triquinanes, see: G. Mehta and S. Srikrishna, *Chem. Rev.*, 1997, **97**, 671.

2 For recent reviews on the ring closing metathesis reaction in organic synthesis see: S. K. Armstrong, *J. Chem. Soc., Perkin Trans. 1*, 1998, 371; R. H. Grubbs and S. Chang, *Tetrahedron*, 1998, **54**, 4413; M. Schuster and S. Blechert, *Angew. Chem., Int. Ed. Engl.*, 1997, **36**, 2036.

3 M. J. Bassindale, P. Hamley, A. Leitner and J. P. A. Harrity, *Tetrahedron Lett.*, 1999, **40**, 3247.

4 For other examples of tandem diene metathesis reactions, see: (*a*) W. J. Zuercher, M. Hashimoto and R. H. Grubbs, *J. Am. Chem. Soc.*, 1996, **118**, 6634; (*b*) S. D. Burke, K. J. Quinn and V. J. Chen, *J. Org. Chem.*, 1998, **63**, 8626; (*c*) W. J. Zuercher, M. Scholl and R. H. Grubbs, *J. Org. Chem.*, 1998, **63**, 4291; (*d*) M. Lautens and G. Hughes, *Angew. Chem., Int. Ed.*, 1999, **38**, 129; (*e*) C. Baylon, M. Heck and C. Mioskowski, *J. Org. Chem.*, 1999, **64**, 3354; (*f*) A. H. Hoveyda, in *Topics in Organometallic Chemistry*, ed. A. Furstner, Springer-Verlag, Berlin, 1998, vol. 1, pp. 105–132.

5 We have isolated and tentatively assigned (NMR and mass spectrometry) compounds **II** and **III** from the reaction mixture. Their rigorous characterisation is currently underway and will form part of a full account.

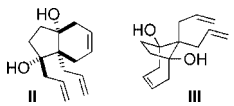

6 The stereochemical assignment of **5** is based on the significant stability of the *cis,cis*-isomer over the alternative *trans,trans*-isomer, calculated to be *ca*. 30 kcal mol^{-1} using AM1 semiempirical methods implemented using Spartan™ software. The assignment of **4** was based on X-ray crystallographic analysis.

7 In the course of this study the RCM reaction of diene **6** was reported to proceed in good yield (77%) at room temperature: S. Kotha, E. Manivannan, T. Ganesh, N. Sreenivasachary and A. Deb, *Synlett*, 1999, 1618. This result could not be reproduced in our hands.

8 Prepared by addition of diol **12** to oxalyl chloride in the presence of pyridine and DMAP catalyst.

9 Additionally, the poor reactivity of the cyclohexane system may originate from the inability of the appropriate alkene units to attain sufficient alignment for metathesis. We thank a referee for this suggestion.

10 All compounds exhibited satisfactory analytical and spectral data.

Formation of a diphosphine: synthesis and molecular structure of bis(tetraphenylbutadienyl)diphosphine, $(Ph_4C_4)P–P(C_4Ph_4)$

Jason K. Vohs, Pingrong Wei, Jianrui Su, Brent C. Beck, Sonya D. Goodwin and Gregory H. Robinson*

Department of Chemistry, The University of Georgia, Athens, GA 30602-2556, USA.
E-mail: robinson@sunchem.chem.uga.edu

Received (in Columbia, MO, USA) 14th February 2000, Accepted 5th April 2000
Published on the Web 25th May 2000

Reaction of 1,4-dilithiotetraphenylbutadiene with phosphorus(III) bromide affords bis(tetraphenylbutadienyl)diphosphine, $(Ph_4C_4)P–P(C_4Ph_4)$, with a phosphorus–phosphorus bond length of 2.2051(11) Å.

Bis(2,4,6-tri-*tert*-butylphenyl)diphosphene, $(Bu^t_3C_6H_2)P{=}P(C_6H_2Bu^t_2)$,[1] the first compound shown to contain a formal phosphorus–phosphorus double bond [P–P 2.034(2) Å], was prepared by the magnesium metal reduction of $(Bu^t_3C_6H_2)PCl_2$. Indeed, alkali (or alkaline earth) metal reduction is one of three general routes to diphosphines (the other two being heating a phosphinous halide, R_2PCl, with a secondary phosphine or with an alkali metal phosphine),[2] a significant development in main group chemistry. Furthermore, as evidenced by subsequent studies concerning $(Bu^t_3C_6H_2)P{=}P(C_6H_2Bu^t_3)$,[3] the chemistry of diphosphenes and diphosphines continues to be of interest to both synthetic and computational chemists. Crucial in the stabilization of $(Bu^t_3C_6H_2)P{=}P(C_6H_2Bu^t_3)$ was the utilization of the sterically demanding 2,4,6-tri-*tert*-butylphenyl ligand. In a related vein, this laboratory has recently examined the organogroup 13 (III) chemistry of 1,4-dilithiotetraphenylbutadiene resulting in two interesting complexes: (a) a spirogallane anion,[4] $[(Ph_4C_4)Ga(C_4Ph_4)]^-$ **I**; and (b) an In_2C_8 ten-membered ring, $(Et_2O)_2Li(Br)_2In\{(C_4Ph_4)\}_2In(Br)_2Li(OEt_2)_2$ **II**.[5]

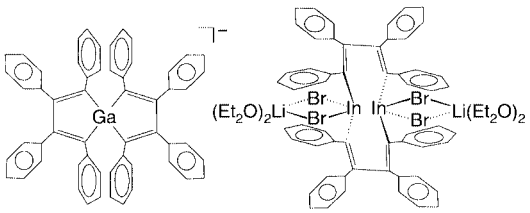

I **II**

Herein, we report the synthesis[6] and molecular structure[7] of bis(tetraphenylbutadienyl)diphosphine, $(Ph_4C_4)P–P(C_4Ph_4)$ **III**, readily isolated from reaction of 1,4-dilithiotetraphenylbutadiene,[8] prepared by the action of an excess of metallic lithium on diphenylacetylene, with phosphorus(III) bromide (Scheme 1). This compound, characterized by ^1H, ^{13}C and ^{31}P NMR spectroscopy elemental analyses and single-crystal X-ray diffraction (Fig. 1), is significant as it represents an interestingly facile, if unexpected, one-pot route to a diphosphine.

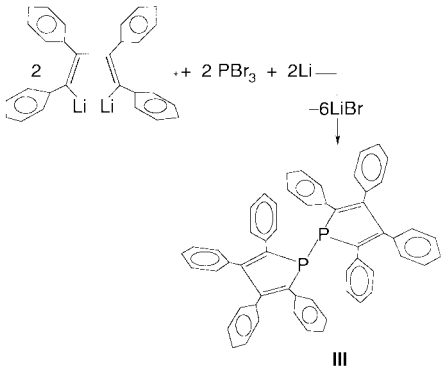

III

Scheme 1

The past two decades have witnessed a number of studies concerning compounds containing phosphorus–phosphorus bonds.[9] Indeed, this laboratory has had an interest in the preparation of diphosphines having previously reported the synthesis and molecular structure of $[(Me_3Si)_2P\{Me_2Ga\}_2PMe]_2$,[10] isolated from reaction of $Me_3P–GaMe_3$ with $P(SiMe_3)_3$, having a P–P single bond length of 2.25(3) Å. Relative to diphosphenes it is important to note the previously reported σ-bonded pentamethylcyclopentadienyl-based diphosphene, bis(pentamethylcyclopentadienyl)diphosphene, $(\sigma\text{-}C_5Me_5)P{=}P(\sigma\text{-}C_5Me_5)$.[11] The phosphorus atoms in $(\sigma\text{-}C_5Me_5)P{=}P(\sigma\text{-}C_5Me_5)$ are two-coordinate (σ-bonding to one of the carbon atoms of the ring and to the other phosphorus atom) with a P–P double bond length of 2.031(3) Å.

A number of points regarding the structure and bonding in $(Ph_4C_4)P–P(C_4Ph_4)$ are relevant. As expected, the five-membered butadienyl rings are planar about the phosphorus atoms with the phenyl rings arranged in a propeller-like fashion. Indeed, the molecule resides in a *trans* configuration. The environment about the phosphorus atoms must be considered distorted pyramidal thereby precluding significant interaction of the phosphorus lone electron pairs with the conjugated system of the tetraphenylbutadienyl moieties. The P–C bond lengths are generally unremarkable. Clearly. the phosphorus–phosphorus bond of 2.2051(11) Å in $(Ph_4C_4)P–P(C_4Ph_4)$ must be considered a single bond. Moreover, the ^{31}P NMR resonance of δ −15.98 in $(Ph_4C_4)P–P(C_4Ph_4)$ is also consistent with a P–P single bond. For comparison, the ^{31}P resonance of $(\sigma\text{-}C_5Me_5)P{=}P(\sigma\text{-}C_5Me_5)$ was reported at δ 504 (121 MHz, C_6D_6)

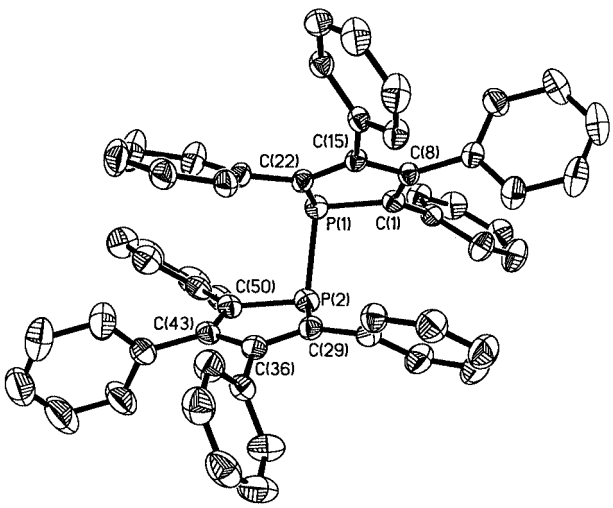

Fig. 1 Molecular structure of $(Ph_4C_4)P–P(C_4Ph_4)$. Bond distances (Å) and angles (°): P(1)–C(22) 1.797(3), P(1)–C(1) 1.799(3), P(1)–P(2) 2.2051(11), P(2)–C(29) 1.796(3), P(2)–C(50) 1.799(3); C(22)–P(1)–C(1) 91.16(12), C(22)–P(1)–P(2) 108.13(9), C(1)–P(1)–P(2) 100.16(9), C(29)–P(2)–C(50) 91.26(14), C(29)–P(2)–P(1) 106.14(10), C(50)–P(2)–P(1) 99.92(10).

DOI: 10.1039/b001257m

while that for the [*trans*-{[Fe(CO_4)]$_2$[PCH($SiMe_3$)$_2$]$_2$}] diphosphene was reported at δ 384.55 (external 85% H_3PO_4) [P–P 2.039(1) Å].[9b]

It is significant that the tetraphenylbutadienyl moiety continues to find utility in main group chemistry. It is noteworthy that the title compound bears some resemblance to the previously reported bis[1-(trimethylsilyl)-2,3,4,5-tetraphenyl-1-silacyclopentadienyl] compound isolated in 54% yield from the sonication of 1,1-dichloro-2,3,4,5-tetraphenyl-1-silacyclopentadiene in the presence of three equivalents of metallic lithium.[12]

We are grateful to the National Science Foundation (G. H. R.: CHE-95-9520162) and to the donors of the Petroleum Research Fund, administered by the American Chemical Society, for support of this work.

Notes and references

1 M. Yoshifuji, I. Shima, N. Inamoto, K. Hirotsu and T. Higuchi, *J. Am. Chem. Soc.*, 1981, **103**, 4578.

2 D. E. C. Corbridge, *Phosphorus: An Outline of its Chemistry, Biochemistry and Technology*, Elsevier, New York, 1985, p. 435.

3 A. H. Cowley, A. Decken, N. C. Norman, C. Krüger, F. Lutz, H. Jacobson and T. Ziegler, *J. Am. Chem. Soc.*, 1997, **119**, 3389.

4 J. Su, S. D. Goodwin, X.-W. Li and G. H. Robinson, *J. Am. Chem. Soc.*, 1998, **120**, 12 994.

5 B. C. Beck, J. Su, P. Wei, X.-W. Li and G. H. Robinson, *Organometallics*, 2000, **19**, 1214.

6 Inside a drybox (M Braun Labmaster 130) a reaction vessel was charged with phosphorus(III) bromide (1.08 g, 4 mmol), and diethyl ether (30 mL). Upon returning to the benchtop, 1,4-dilithiotetraphenylbutadiene, prepared by reaction of lithium (0.09 g, 12.96 mmol) and diphenylacetylene (1.74 g, 9.78 mmol) in diethyl ether, was slowly added to the reaction vessel at −78 °C over a period of 30 min *via* an addition funnel. The system was allowed to warm to room temperature and stir overnight. The solvent was removed *in vacuo*, and the solid was redissolved in hexane (40 mL). The resulting solution was filtered immediately and dried *in vacuo*. The solid was recrystallized in diethyl ether and resulted in yellow–orange crystals (0.56 g, 34% yield): mp 245–246 °C (decomp.). Anal. (E+R Microanalytical Labroatories, Parsipanny, NJ). Calc. (found) for $C_{59}H_{47}P_2$: C, 86.60 (86.51); H, 5.80 (5.76)%. δ_H(300 MHz, 298 K, $CDCl_3$): 0.46 [q, 3H, CH_3 (hexane)], 0.84 [m, 4H, CH_2 (hexane)], 7.26–7.56 [m, 40H, CH (aromatic)] δ_C(300 MHz, 298 K, $CDCl_3$): 14.01, 22.53, 31.47, 126.32, 127.09, 127.82, 129.60, 130.26, 136.52, 137.33, 143.85, 147.82, 151.75. δ_P(300 MHz, 298 K, $CDCl_3$): −15.98.

7 X-Ray intensity data were measured at room temperature on a Bruker SMART™ CCD-based X-ray diffractometer system with graphite-monochromated Mo-Kα radiation (λ = 0.71073 Å). The structure was solved by direct methods using the SHELXTL 5.1 system of computer programs. The non-hydrogen atoms were refined anisotropically while hydrogen atoms were placed in idealized positions with their coordinates and thermal parameters riding on the attached carbon atoms. *Crystallographic data*: monoclinic, space group *C*2/*c* (no. 15), a = 28.092(4), b = 13.6821(16), c = 24.311(2) Å, β = 98.078(5)°, V = 9251.4(19) Å^3 and Z = 8. The asymmetric unit contains one (Ph_4C_4)P–P(C_4Ph_4) molecule and one-half hexane unit (situated about an inversion center). Refinement converged at $R1$ = 0.056 and $wR2$ = 0.132. CCDC 182/1625. See http://www.rsc.org/suppdata/cc/b0/b001257m/ for crystallographic files in .cif format.

8 A. Orechoff, *Chem. Ber.*, 1914, **47**, 89; W. Schlenk and E. Bergmann, *Annales*, 1928, **463**, 71; E. Bergmann and O. Zwecker, *Annales*, 1931, **487**, 155; E. Bergmann and W. Schreiber, *Annales*, 1933, **500**, 118; L. Smith and H. H. Hoehn, *J. Am. Chem. Soc.*, 1941, **63**, 1184.

9 (*a*) J. E. Richman, R. O. Day and R. R. Holmes, *J. Am. Chem. Soc.*, 1980, **102**, 3955; (*b*) K. M. Flynn, M. M. Olmstead and P. P. Power, *J. Am. Chem. Soc.*, 1983, **105**, 2085: (*c*) D. C. Pestana and P. P. Power, *J. Am. Chem. Soc.*, 1989, **111**, 6887; (*d*) M. Drieß, P. Frankhauser, H. Pritzkow and W. Siebert, *Chem. Ber.*, 1991, **124**, 1497.

10 J. A. Burns, W. T. Pennington and G. H. Robinson, *Organometallics*, 1995, **14**, 1533.

11 P. Jutzi, U. Meyer, B. Krebs and M. Dartmann, *Angew. Chem., Int. Ed. Engl.*, 1986, **25**, 919.

12 J.-H. Hong, P. Boudjouk and S. Castellino, *Organometallics*, 1994, **13**, 3387.

Pentamethylmolybdenum

Beatrice Roessler, Sven Kleinhenz and Konrad Seppelt*

Institut für Chemie der Freien Universität Berlin, Fabeckstraße 34-36, D-14195 Berlin, Germany. E-mail: seppelt@chemie.fu-berlin.de

Received (in Cambridge, UK) 4th February 2000, Accepted 30th March 2000

Pentamethylmolybdenum has been prepared and characterized by single crystal structure determination, EPR, and Raman spectroscopy.

The total number of homoleptic[1] neutral metal methyl compounds is small. $Ti(CH_3)_4$ has never been obtained free of donor molecules.[2] $Nb(CH_3)_5$ and $Ta(CH_3)_5$ have been obtained in the pure state,[3] and the structure of the latter has been determined by electron diffraction.[4] $W(CH_3)_6$ and $Mo(CH_3)_6$ are known including their peculiar crystal structures,[5–7] as is $Re(CH_3)_6$.[6,8] Here we describe the formation of $Mo(CH_3)_5$.

In attempts to obtain $Mo(CH_3)_6$ by reacting $MoOCl_4$ with $Zn(CH_3)_2$[7] we have occasionally observed that in high vacuum a blue compound sublimed off into a −196 °C cold trap. We have been able to obtain a single crystal from this material which has been identified as $Mo(CH_3)_5$ by a single crystal structure determination. Subsequently we developed a preparative route from $MoCl_5$ (1.63 mmol) and a slight excess of $Zn(CH_3)_2$ (5.87 mmol) in 20 ml diethyl ether between −78 and −20 °C.[9] After pumping off all volatile materials at −78 °C, 15 ml *n*-pentane was added, and the suspension stirred for 30 min at −78 °C. At −20 °C the solvent was pumped off, and the tail of this vacuum distillation contained a light blue compound. Most of the solvent was pumped off at −78 °C and recrystallisation from $CF_3CH_2CF_3$ between −40 and −60 °C afforded turquoise needles, which turned black upon contact with traces of oxygen or upon warming above −10 °C. $Mo(CH_3)_5$ is thus thermally less stable than $Mo(CH_3)_6$.

The result of the single crystal structure determination is shown in Fig. 1† which shows that the molecule is a square pyramid. For comparison we also prepared $Ta(CH_3)_5$ and succeeded in obtaining single crystals of it by crystallizing a sample from $CF_3CH_2CF_3$ between −40 and −78 °C.† Both molecular structures are virtually identical, in spite of the fact that one is a d^0 and the other a d^1 system. The structural similarity is strikingly different from the $W(CH_3)_6$ ($Mo(CH_3)_6$)/$Re(CH_3)_6$ pair, where the d^1 system is different from the d^0 systems.[5,6]

The only, but still marginal, differences between the $Mo(CH_3)_5$ and $Ta(CH_3)_5$ structures are (i) the larger C_{apical}–M–C_{basal} angles in $Mo(CH_3)_5$, and (ii) the larger bond length difference between apical and basal metal–C bonds for $Ta(CH_3)_5$.

We also calculated the structures of $Mo(CH_3)_5$ and $Ta(CH_3)_5$ using a density functional (DFT) approach, using electron core potentials[10] for Mo and Ta atoms and the 6-311 G(d,p) basis set for C and H.[11] The square pyramidal (*SPY*) structure is energetically strongly favored over the trigonal bipyramidal structure (*TBPY*). For the square pyramidal structures all geometric parameters have been refined independently. In order to obtain energetic and structural data for the trigonal bipyramidal structures one C–M–C angle has been fixed at 180°, while all other variables have been set free. The energy difference between the *SPY* and *TBPY* structures is calculated as 53.4 kJ mol^{-1} for $Ta(CH_3)_5$, (*cf.* 32.2 kJ mol^{-1} in an earlier calculation[12]). For $Mo(CH_3)_5$ the energy difference is even larger at 97.5 kJ mol^{-1}. At present it cannot be said with certainty if this large energy difference is a consequence of imperfect calculations, due to the open shell system. If it is real, this would indicate a strong steric activity of the d^1 electron which would be very unusual. Table 1 gives a summary of experimental and calculated structures of both compounds.

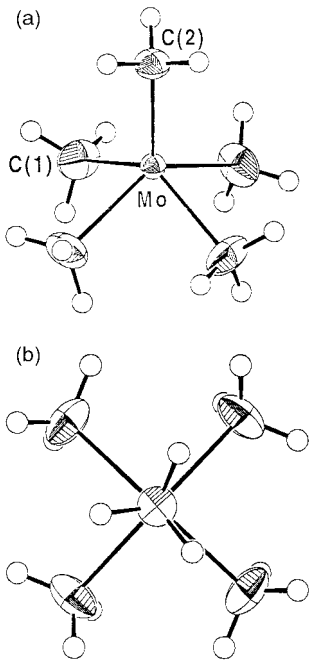

Fig. 1 (a) Crystal structure of $Mo(CH_3)_5$. ORTEP with 50% probability ellipsoids. (b) View along the fourfold axis. The hydrogen positions of the apical methyl group are fourfold disordered and only one orientation is shown. The ORTEP for $Ta(CH_3)_5$ is essentially the same.

Table 1 Bond lengths (pm) and angles (°) for the tetragonal pyramidal structures of $Mo(CH_3)_5$ and $Ta(CH_3)_5$

	$Mo(CH_3)_5$		$Ta(CH_3)_5$			
	X-Ray	DFT calculation[a]	X-Ray	Electron diffraction[b]	DFT calculation	MP2 calculation[c]
M–C_{apical}	206.8(1)	209.9	207.3(14)	211(2)	214.7[a]	215.4
M–C_{basal}	211.1(1)	215.2	215.0(7)	218.0(5)	218.2	218.7
C_{apical}–M–C_{basal}	113.6(2)	114.5	111.1(2)	111.7(13)	112.1	111.6
C_{basal}–M–C_{basal}	80.8(1)	80.0	82.6(2)	82.9(9)	81.8	82.2

[a] For details see text. [b] See ref. 4. [c] See ref. 14.

DOI: 10.1039/b000987n

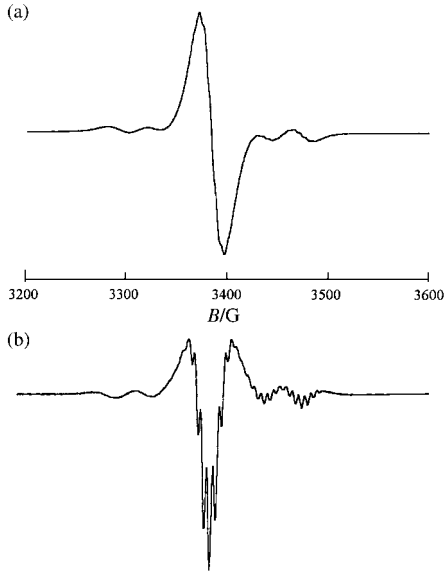

Fig. 2 Isotropic EPR spectrum of $Mo(CH_3)_5$ in *n*-pentane solution at 130 K, 9.44 GHz. g = 1,993, $a(^{95}Mo/^{97}Mo)$ = 4.8(1) mT, a_H' = 0.54(1) mT: (a) first derivative and (b) second derivative spectrum.

The Raman spectrum of $Mo(CH_3)_5$ shows bands (relative intensities in parentheses) at 1181(10), 960(10), 90(50), 882(10), 783(10), 672(60), 620(30), 565(15), 523(100), 507(70), 451(15), 366(25), 308(100), 267(10) and 167(10) cm^{-1} while the region above 2700 cm^{-1} is obscured by the solvent pentane.

$Mo(CH_3)_5$ is paramagnetic and shows an EPR spectrum which is in full agreement with its structure (Fig. 2). Hyperfine splitting due to the two isotopes ^{95}Mo and ^{97}Mo (15.92 and 9.5% natural abundance), both with nuclear spin 5/2 and virtually identical gyromagnetic moments gives rise to six satellite resonances, two of which are obscured by the central line. The further fine structure is well resolved in the second derivative representation, and fits to a ^1H hyperfine structure due to an even number of equivalent hydrogen atoms and particularly well to a binomial distribution of 12th degree. Hyperfine structure due to the three apical hydrogen atoms is not resolved (Fig. 2). In agreement with this the calculation reveals that the unpaired electron has approximately two thirds Mo $4d_{z^2}$ and one third Mo $4d_{x^2-y^2}$ character.

Notes and references

† *Crystal data*: MoC_5H_{15}: M = 171.1, a = 768.0(2), c = 649.0(2) pm, V = 382.8 × 10^6 pm^3, tetragonal, space group *I*4, Z = 2, μ = 1.6 mm^{-1}, 1306 measured, (including Friedel pairs), 340 independent reflections, 25 parameters, R = 0.026, wR^2 = 0.047. Refinement in space group *I*4/*mm* under the assumption of disorder of the C1 atoms gives essentially the same result. Refinement in space group *I*4/*mm* without disorder and C1 in special position *x*,0,*z* results in strongly elongated vibrational amplitudes for these atoms. Keeping the neighborhood of the basal methyl groups in adjacent molecules in mind the non-disordered but twinned solution has been chosen.

TaC_5H_{15}: M = 256.1, a = 784.8(1), c = 647.3(1) pm, V = 398.7 × 10^6 pm^3, tetragonal, space group *I*4, Z = 2, μ = 13.8 mm^{-1}, 883 measured, 802 independent reflections, 20 parameters, R = 0.023, wR^2 = 0.059. In contrast to $Mo(CH_3)_5$ this structure clearly belongs to space group *I*4, the absolute structure has been determined, and there is no indication for twinning.

CCDC 182/1626. See http://www.rsc.org/suppdata/cc/b0/b000987n/ for crystallographic files in .cif format.

1 Homoleptic implies all ligands are the same.
2 $Ti(CH_3)_4$; S. Kleinhenz and K. Seppelt, *Chem. Eur. J*, 1999, **5**, 3573; K. H. Thiele, H. Windisch, H. Schumann and G. Kociok-Kühn, *Z. Anorg. Allg. Chem.*, 1994, **620**, 3829.
3 R. R. Schrock and P. Meakin, *J. Am. Chem. Soc.*, 1974, **96**, 5288.
4 C. Pulham, A. Haaland, A. Hammel, K. Rypdal, H. P. Verne and H. V. Volden, *Angew. Chem.*, 1992, **104**, 1534; *Angew. Chem., Int. Ed. Engl.*, 1992, **31**, 1464.
5 A. J. Shortland and G. Wilkinson, *J. Chem. Soc., Dalton Trans.*, 1973, 872.
6 S. Kleinhenz, V. Pfennig and K. Seppelt, *Chem. Eur. J.*, 1998, **4**, 1687; V. Pfennig and K. Seppelt, *Science*, 1996, **271**, 626.
7 B. Roessler and K. Seppelt, *Angew. Chem.*, 2000, **112**, 1326; *Angew. Chem., Int. Ed.*, 2000, **39**, 1259.
8 K. Mertis and G. Wilkinson, *J. Chem. Soc., Dalton Trans.*, 1976, 1488.
9 The reaction of $MoCl_5$ with $LiCH_2Si(CH_3)_3$ affords $[(CH_3)_3SiCH_2]_3Mo{=}CH{-}Si(CH_3)_3$ and $((CH_3)_3SiCH_2)_3Mo{\equiv}C{-}Si(CH_3)_3$: R. A. Anderson, M. H. Chrisholm, J. F. Gibson, W. W. Reichert, I. P. Rothwell and G. Wilkinson, *Inorg. Chem.*, 1981, **20**, 3934.
10 P. J. Hay and W. R. Wadt, *J. Chem. Phys.*, 1985, **82**, 299.
11 Gaussian 94, Revision E.2, M. J. Frisch, G. W. Trucks, H. B. Schlegel, P. M. W. Gill, B. G. Johnson, M. A. Robb, J. R. Cheeseman, T. Keith, G. A. Petersson, J. A. Montgomery, K. Raghavachari, M. A. Al-Laham, V. G. Zakrzewski, J. V. Ortiz, J. B. Foresman, J. Cioslowski, B. B. Stefanov, A. Nanayakkara, M. Challacombe, C. Y. Peng, P. Y. Ayala, W. Chen, M. W. Wong, J. L. Andres, E. S. Replogle, R. Gomperts, R. I. Martin, D. J. Fox, J. S. Binkley, J. D. Defrees, J. Baker, J. P. Stewart, M. Head-Gordon, C. Gonzalez and J. A. Pople, Gaussian Inc., Pittsburg, PA, 1995.
12 T. A. Albright and H. Tang, *Angew. Chem.*, 1992, **104**, 1532; *Angew. Chem., Int. Ed. Engl.*, 1992, **31**, 1462.

Synthesis and novel reactivity of platinum phosphine–borane complexes *trans*-[PtH(PPhR·BH_3)(PEt_3)$_2$] (R = H, Ph)

Hendrik Dorn, Cory A. Jaska, Ryan A. Singh, Alan J. Lough and Ian Manners*

Department of Chemistry, University of Toronto, 80 St. George Street, Toronto, Ontario, M5S 3H6, Canada. E-mail: imanners@alchemy.chem.utoronto.ca

Received (in Cambridge, UK) 3rd April 2000, Accepted 2nd May 2000
Published on the Web 25th May 2000

The oxidative-addition reaction of $Pt(PEt_3)_3$ with the phosphine–borane adducts $PhPH_2·BH_3$ and $Ph_2PH·BH_3$ leads to regioselective insertion of the $Pt(PEt_3)_2$ fragment into the P–H bond to afford the hydride complexes *trans*-[PtH(PPhR·BH_3)(PEt_3)$_2$] (R = H 1, R = Ph 2); reaction of 2 with $PhPH_2·BH_3$ leads to an unusual ligand exchange reaction which generates 1 and $Ph_2PH·BH_3$.

The discovery of new synthetic methods for the formation of homonuclear or heteronuclear bonds between main group elements is of importance for the construction of inorganic polymer chains and also for the general development of p-block chemistry.[1,2] Transition metal-catalyzed routes represent a particularly attractive approach to this problem.[2,3] Recently we reported a novel metal-catalyzed route to linear and cyclic oligomeric and also high molecular weight poly(phosphinoboranes) which involved dehydrocoupling of phosphine–borane adducts in the presence of late transition metal complexes (Scheme 1).[4,5] A plausible first step in these reactions involves insertion of the transition metal into either the P–H or B–H bond of the adduct. Subsequent steps may involve σ-bond metathesis and/or oxidative addition/reductive elimination processes. Significantly, no homodehydrocoupling products with P–P or B–B bonds have been detected from these reactions to date. It should be noted that the insertion of transition metals into the P–H bonds of secondary phosphines has ample precedent. For example, oxidative addition of P(III)–H bonds at Pt(0) or Pd(0) centers has been demonstrated and such processes are believed to be a key step in the catalytic hydrophosphination of alkenes and alkynes.[6] On the other hand, a range of mono- and dinuclear boryl complexes have recently been reported as a result of the ambient temperature reactions of the B–H bonds in $Me_3P·BH_3$ or $Me_3P·BH_2BH_2·PMe_3$ at metal centers.[7,8] In order to investigate potential pathways during the transition metal mediated P–B bond formation reactions we are studying the hitherto unexplored coordination chemistry of phosphine–borane adducts with both P–H and B–H bonds. Here, we report the oxidative-addition reactions of $Ph_2PH·BH_3$ and $PhPH_2·BH_3$ with the electron rich Pt(0) complex $Pt(PEt_3)_3$ and a preliminary reactivity study of the resulting phosphine–borane complexes.

Reaction of the primary phosphine–borane adduct $PhPH_2·BH_3$ with a stoichiometric amount of $Pt(PEt_3)_3$ in toluene at 60 °C and subsequent crystallization from hexanes resulted in the formation of a yellow solid **1** (23% isolated yield, quantitative by ^{11}B and ^{31}P NMR before workup) which was characterized by multinuclear NMR spectroscopy in $CDCl_3$.† The spectroscopic data for the product was consistent with a structure **1** in which insertion of Pt into a P–H bond rather than the B–H bond had taken place. For example, the product displayed two distinct sets of signals in the ^{31}P NMR spectrum: a doublet at δ 17.9 was assigned to the PEt_3 ligands attached to platinum, showing coupling to another phosphorus nucleus (J_{PP} 19.4 Hz) as well as ^{195}Pt satellite signals (J_{PPt} 2572 Hz). Furthermore, a broad doublet at δ *ca.* −48.7 indicated coupling to a quadrupolar boron nucleus and one hydrogen substituent (J_{PH} 299 Hz) and showed ^{195}Pt satellites with the magnitude J_{PPt} *ca.* 1440 Hz. This signal was assigned to the phosphorus of the fragment Pt–PPhH·BH_3. The ^{11}B NMR spectrum showed a single broad resonance at δ −33.2 which is in the region typical for BH_3 adducts of phosphines. The key ^1H NMR spectroscopic feature is the low-frequency hydride resonance at δ −5.74, which appears as a doublet of triplets with a larger coupling to one phosphorus atom (J_{HP} 124.6 Hz) and a smaller coupling to two phosphorus atoms (J_{HP} 15.4 Hz) as well as ^{195}Pt satellites (J_{HPt} 872 Hz). This suggested the presence of one *trans* substituent (PPhH·BH_3) and two *cis* substituents (PEt_3), with respect to the hydride ligand.

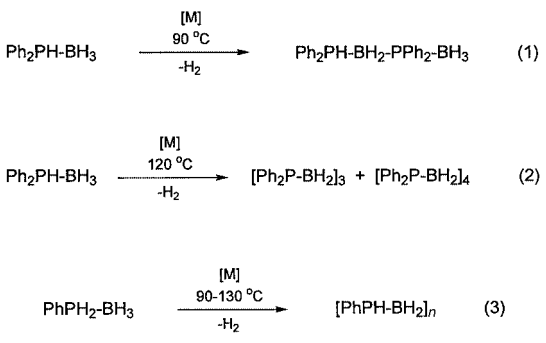

Scheme 1

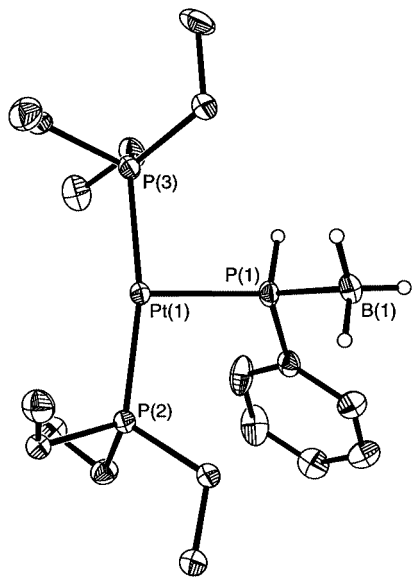

Fig. 1 Molecular structure of **1** (30% displacement ellipsoids). Hydrogen atoms attached to carbon are omitted. Selected bond lengths (Å) and angles (°): Pt(1)–P(1) 2.3477(14), Pt(1)–P(2) 2.2863(13), Pt(1)–P(3) 2.2771(14), P(1)–B(1) 1.953(7), P(1)–H(1P) 1.32(6); P(3)–Pt(1)–P(2) 168.26(5), P(3)–Pt(1)–P(1) 92.83(5), P(2)–Pt(1)–P(1) 98.87(5), B(1)–P(1)–Pt(1) 119.8(2).

DOI: 10.1039/b002615h

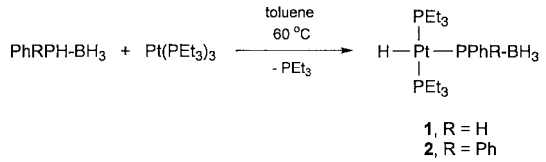

Scheme 2

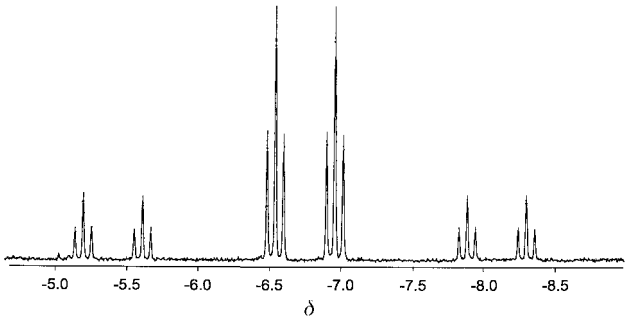

Fig. 2 ^{1}H NMR spectrum (300 MHz, C_6D_6) of the hydride region of **2** [J_{HP}(*trans*) 124.4 Hz, J_{HP}(*cis*) 16.9 Hz, J_{HPt} 805 Hz, PtH].

The molecular structure of compound **1** was confirmed by single crystal X-ray analysis‡ and is consistent with the solution NMR data. A SHELXTL drawing is shown in Fig. 1. The geometry around the Pt(II) center is close to square-planar with *trans* PEt_3 ligands. Although the platinum hydride ligand was not observed in the X-ray study its presence is clearly indicated by the large P(3)–Pt(1)–P(2) angle of 168.26(5)° and, as discussed, from the ^{1}H NMR spectroscopic data. The lengths of the bonds Pt(1)–P(2) [2.2863(13) Å] and Pt(1)–P(3) [2.2771(14) Å] are shorter than the Pt(1)–P(1) bond [2.3477(14) Å], presumably as a consequence of the *trans* influence of the hydride ligand. A similar observation was made in the hydride complex *cis*-[PtH(P(O)Ph_2)(PPh_2(OH))(PEt_3)].[9]

A similar reaction was observed between the secondary phosphine–borane adduct $Ph_2PH{\cdot}BH_3$ and 1 equivalent of $Pt(PEt_3)_3$ (Scheme 2). The orange–yellow platinum complex **2** was isolated in 67% yield. For **2**, signals in the ^{31}P NMR spectrum are observed at δ 16.7 (PEt_3) and δ −3.7 ($PPh_2{\cdot}BH_3$) and in the ^{11}B NMR spectrum at δ −31.4. Fig. 2 shows the hydride region of the ^{1}H NMR spectrum of **2** with the characteristic dt coupling pattern which is flanked by ^{195}Pt satellite signals (J_{HPt} 805 Hz).

Compound **1** represents the first example of a metal complex of a primary phosphine–borane adduct and only two other examples of transition metal complexes of secondary phosphine–borane adducts analogous to **2** are known; a tetrahedral iron complex, [Fe(η^5-C_5Me_5)(CO)$_2$($PPh_2{\cdot}BH_3$)],[10] and a square-planar palladium complex, [Pd(dppp)-(C_6F_5)($PPh_2{\cdot}BH_3$)] [dppp = 1,3-bis(diphenylphosphino)propane], a proposed intermediate in the Pd-catalyzed coupling of secondary phosphine–boranes with aryl halides.[11] However, the synthesis of the latter compounds involved nucleophilic substitution steps rather than insertion of the transition metal fragment.

The isolation of novel complexes **1** and **2** *via* oxidative addition suggests that P–H bond activation may be the key initial step in the late transition metal-catalyzed formation of P–B bonds. In order to explore the reactivity of the complexes, a solution of **2** in C_6D_6 was treated with another equivalent of $PhPH_2{\cdot}BH_3$. After 8 h at room temperature the solution had changed from orange to yellow, however, no P–B coupling reaction was observed by ^{31}P NMR spectroscopy. Surprisingly, a complete exchange of the phosphine–borane ligand had occurred to form exclusively complex **1** together with $Ph_2PH{\cdot}BH_3$ (Scheme 3).

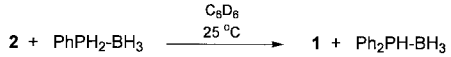

Scheme 3

The demonstration of a novel phosphine–borane ligand exchange reaction at the Pt center indicates that relatively complex reaction chemistry may need to be unravelled if a full mechanistic understanding of late transition metal-catalyzed P–B bond formation reactions is to take place. Detailed studies of the reactivity of novel complexes such as **1** and **2** and analogs directed towards this goal are in progress.

We wish to acknowledge the Petroleum Research Fund administered by the ACS for funding and the Deutsche Forschungsgemeinschaft (DFG) for a postdoctoral fellowship for H. D.

Notes and references

† *Selected spectroscopic data*: for **1**: ^{1}H NMR (300 MHz, $CDCl_3$) δ 7.76–7.70 (m, Ar), 7.26–7.19 (m, Ar), 4.39 (d, J_{HP} 299 Hz, PH), 2.0–0.9 (br q, BH_3), 1.80 (m, CH_2), 1.03 (m, CH_3), −5.74 [dt, J_{HP}(*trans*) = 124.6 Hz, J_{HP}(*cis*) 15.4 Hz, J_{HPt} 872 Hz, PtH]; ^{11}B{^{1}H} NMR (160 MHz, $CDCl_3$) δ −33.2 (br); ^{31}P NMR (121 MHz, $CDCl_3$) δ 17.9 (d, J_{PP} 19.4 Hz, J_{PPt} 2572 Hz, PEt_3), −48.7 (br d, J_{PH} 299 Hz, J_{PPt} 1440 Hz, PHPh); IR (Nujol) 2350 (ν_{BH}), 2022 (ν_{PtH}) cm^{-1}; EIMS *m/z* (%): 541 (1) [M$^+$ − BH_3], 118 (100) [PEt_3]. For **2**: ^{1}H NMR (300 MHz, C_6D_6) δ 8.26–8.14 (m, Ar), 7.26–7.00 (m, Ar), 3.0–1.9 (br q, BH_3), 1.48 (m, CH_2), 0.93 (m, CH_3), −6.75 [dt, J_{HP}(*trans*) 124.4 Hz, J_{HP}(*cis*) 16.9 Hz, J_{HPt} 805 Hz, PtH]; ^{11}B{^{1}H} NMR (160 MHz, C_6D_6) δ −31.4 (br); ^{31}P{^{1}H} NMR (121 MHz, C_6D_6) δ 16.7 (d, J_{PP} 17.4 Hz, J_{PPt} 2648 Hz, PEt_3), −3.7 (br, J_{PPt} 1575 Hz, PPh_2); IR (Nujol) 2341 (ν_{BH}), 2009 (ν_{PtH}) cm^{-1}; EIMS *m/z* (%): 617 (21) [M$^+$ − BH_3], 62 (100) [H_2PEt].

‡ *Crystal data* for **1**: $C_{18}H_{39}BP_3Pt$, M = 554.30, monoclinic, space group $C2/c$, a = 27.1904(13), b = 9.8355(7), c = 19.0955(11) Å, β = 110.777(3)°, U = 4774.6(5) Å^3, Z = 8, D_c = 1.542 g cm^{-3}, μ = 6.077 mm^{-1}, F(000) 2200, T = 150(1) K, crystal size 0.15 × 0.15 × 0.10 mm, 5176 independent reflections, 51791 collected. Goodness-of-fit on F^2 = 1.042, final R indices [$I > 2\sigma(I)$], R_1 = 0.0387, wR_2 = 0.0969. The structures were solved and refined with the SHELXTL-PC V5.1 software package.[12] Refinement was by full-matrix least squares on F^2 using all data (negative intensities included). Hydrogens bonded to carbon atoms were included in calculated positions and treated as riding atoms, hydrogens attached to P(1) and B(1) were refined with isotropic thermal parameters. CCDC 182/1620. See http://www.rsc.org/suppdata/cc/b0/b002615h/ for crystallographic files in .cif format.

1 See, for example: J. E. Mark, H. R. Allcock and R. West, *Inorganic Polymers*, Prentice Hall, Englewood Cliffs, NJ, 1992; I. Manners, *Angew. Chem., Int. Ed. Engl.*, 1996, **35**, 1602.
2 For a recent review on catalytic dehydrocoupling, see: F. Gauvin, J. F. Harrod and H. G. Woo, *Adv. Organomet. Chem.*, 1998, **42**, 363.
3 See, for example: T. Imori, V. Lu, H. Cai and T. D. Tilley, *J. Am. Chem. Soc.*, 1995, **117**, 9931; S. M. Katz, J. A. Reichl and D. H. Berry, *J. Am. Chem. Soc.*, 1998, **120**, 9844.
4 H. Dorn, R. A. Singh, J. A. Massey, A. J. Lough and I. Manners, *Angew. Chem., Int. Ed.*, 1999, **38**, 3321.
5 H. Dorn, R. A. Singh, J. A. Massey, J. M. Nelson, C. A. Jaska, A. J. Lough and I. Manners, *J. Am. Chem. Soc.*, 2000, in press.
6 P. G. Pringle and M. B. Smith, *J. Chem. Soc., Chem. Commun.*, 1990, 1701; L.-B. Han and M. Tanaka, *J. Am. Chem. Soc.*, 1996, **118**, 1571; D. K. Wicht, I. V. Kourkine, B. M. Lew, J. M. Nthenge and D. S. Glueck, *J. Am. Chem. Soc.*, 1997, **119**, 5039; E. Costa, P. G. Pringle and K. Worboys, *Chem. Commun.*, 1998, 49.
7 Y. Kawano, T. Yasue and M. Shimoi, *J. Am. Chem. Soc.*, 1999, **121**, 11 744 and references therein.
8 For further examples of transition metal–boron compounds see: H. Braunschweig, *Angew. Chem., Int. Ed.*, 1998, **37**, 1787; G. J. Irvine, M. J. G. Lesley, T. B. Marder, N. C. Norman, C. R. Rice, E. G. Robins, W. R. Roper, G. R. Whittell and L. J. Wright, *Chem. Rev.*, 1998, **98**, 2685; M. R. Smith III, *Prog. Inorg. Chem.*, 1999, **48**, 505; C. N. Muhoro, X. He and J. F. Hartwig, *J. Am. Chem. Soc.*, 1999, **121**, 5033.
9 L.-B. Han, N. Choi and M. Tanaka, *Organometallics*, 1996, **15**, 3259.
10 W. Angerer, W. S. Sheldrick and W. Malisch, *Chem. Ber.*, 1985, **118**, 1261.
11 A.-C. Gaumont, M. B. Hursthouse, S. J. Coles and J. M. Brown, *Chem. Commun.*, 1999, 63.
12 G. M. Sheldrick, SHELXTL-PC V5.1, Bruker Analytical X-ray Systems Inc., Madison, WI, 1997.

Double fluorescence resonance energy transfer to explore multicomponent binding interactions: a case study of DNA mismatches

Imogen Horsey, W. Scott Furey, Joseph G. Harrison, Mark A. Osborne and Shankar Balasubramanian*

Department of Chemistry, University of Cambridge, Lensfield Road, Cambridge, UK CB2 1EW. E-mail: sb10031@cam.ac.uk

Received (in Liverpool, UK) 30th March 2000, Accepted 26th April 2000
Published on the Web 25th May 2000

A first demonstration, using a four-component system of complementary and single base-mismatched oligonucleotides, that double fluorescence resonance energy transfer (FRET) can be used to interrogate multicomponent interactions in molecular complexes.

The study of intermolecular interactions is key to the understanding of fundamental biological processes. It is well established that many important biological complexes rely upon binding interactions between multiple components. A number of experimental approaches exist for the study of such non-covalent interactions, but few are capable of conveniently providing information about interactions between several components. Fluorescence resonance energy transfer (FRET)[1] between donor and acceptor fluorophores has been usefully employed in the study of molecular interactions in homogeneous solution.[2,3] Furthermore, the theory is sufficiently well understood to carry out inter- or intra-molecular distance mapping experiments,[4] typically in the 10–100 Å range. FRET experiments to study intermolecular interactions are usually carried out for two components (*i.e.* with a single donor and single acceptor). However, if a donor fluorophore is brought in proximity to more than one type of acceptor fluorophore, there exists the possibility of multiple FRET interactions resulting from irradiation at a single wavelength (Fig. 1). In principle it should be possible to simultaneously obtain information about multicomponent binding interactions. FRET has been used to study nucleic acid interactions in examples that include; duplex hybridisation,[5] triple helix[6] and DNA tetraplex formation,[7] and also for DNA diagnostic assays using molecular beacons to analyse point mutations.[8] We report a homogeneous system of oligonucleotides in which double FRET interactions have been used to study specific binding interactions between four components. The studies comprise of sequence-specific nucleic acid interactions and the localisation of single base mismatches, but the general principle will apply more broadly to other mutually binding systems.

The design of this four component system (Fig. 1) comprises a 27mer oligonucleotide (**M**) and three labelled 9mer oligonucleotide sequences (**R**, **F** and **T**), each of which is complementary to discrete, adjacent sections of the 27mer.[9] Each 9mer included a 5-propargylamino-modified thymidine base,[10] which was postsynthetically modified by reaction with the activated *N*-hydroxysuccinimide ester of either rhodamine-X (**R**OX), fluorescein (**F**AM) or carboxy-X-rhodamine (**T**MR) as indicated in Fig. 1. The excitation and emission maxima of these fluorophores are resolvable and the emission spectrum of FAM overlaps significantly with the excitation spectra of both TMR and ROX. On binding of all three 9mers to the target 27mer to give a fully assembled complex, the donor fluorophore (FAM) is *ca.* 20–25 Å from *both* acceptor fluorophores (TMR and ROX) such that excitation of FAM would lead to significant energy transfer to both TMR and ROX.[11] This was monitored by observing both the donor quenching effects and the sensitised emission of the two acceptor fluorophores.

The fluorescence spectrum for the matched four component system (**R**:**F**:**T**:**M**) is shown in Fig. 2(a) along with spectra of

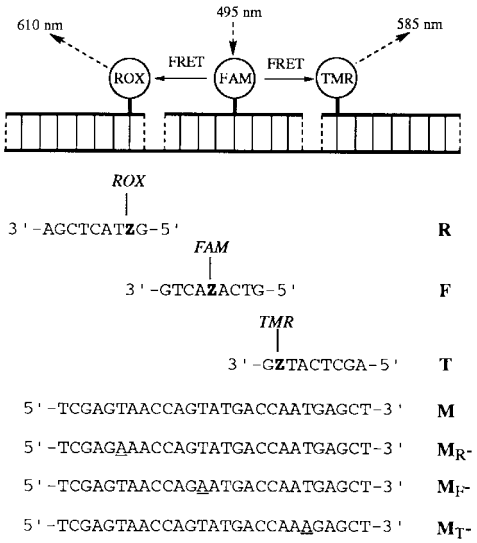

Fig. 1 Schematic of the four-component system, with the sequences used shown below. **Z** = 5-propargylamino dT, ROX = carboxy-X-rhodamine, FAM = carboxyfluorescein, TMR = carboxytetramethylrhodamine. The underlined bases represent T–A single base substitutions. The ROX (**R**), FAM (**F**) and TMR (**T**) labelled oligonucleotide probes bind contiguously on the target (**M**). Oligonucleotide targets $\mathbf{M_R}^-$, $\mathbf{M_F}^-$ and $\mathbf{M_T}^-$ incorporate a single internal A:A mismatch opposite probes **R**, **F** or **T**, respectively.

the individual two component systems (**R**:**M**, **F**:**M**, **T**:**M**) that contribute to the former. Three additional target 27mers ($\mathbf{M_R}^-$, $\mathbf{M_F}^-$ and $\mathbf{M_T}^-$) were designed each with a single central A:A base mismatch to perturb binding of oligonucleotide component **R**, **F** or **T** respectively and examine the effect on energy transfer between the donor and both acceptors (Fig. 1).[12] The fluorescence spectra of these mismatched systems (**R**:**F**:**T**:$\mathbf{M_R}^-$, **R**:**F**:**T**:$\mathbf{M_F}^-$, **R**:**F**:**T**:$\mathbf{M_T}^-$) are presented in Fig. 2(b) where it is clear that mismatches are distinguished by distinct differences

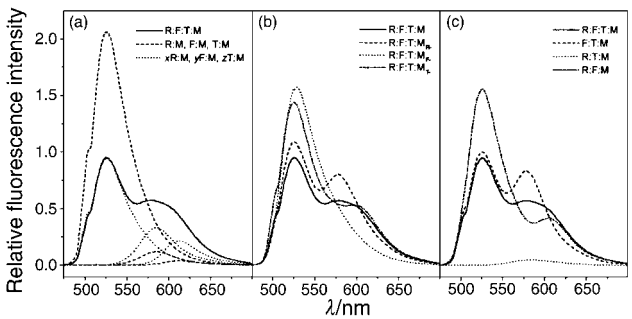

Fig. 2 Relative fluorescence profiles (arbitrary units) for; (a) the basis two-component systems **R**:**M**, **F**:**M**, **T**:**M** (- - - -) and the matched four-component system **R**:**F**:**T**:**M** (——). Also shown is the scaled contributions of **R**:**M**, **F**:**M** and **T**:**M** (· · · · ·) to **R**:**F**:**T**:**M** where $x = 5.33$, $y = 0.46$, $z = 2.75$; (b) mismatched systems **R**:**F**:**T**:$\mathbf{M_R}^-$ (- - -) **R**:**F**:**T**:$\mathbf{M_F}^-$ (· · · · ·) and **R**:**F**:**T**:$\mathbf{M_T}^-$ (··——··——); (c) control systems **F**:**T**:**M** (- - -), **R**:**T**:**M** (· · · · ·) and **R**:**F**:**M** (··—··—).

Table 1 Fluorimeter Assay. Relative fluorescence intensities (arbitrary units) and the contributions from ROX, FAM and TMR to the four component matched and mismatched systems and the three component controls. The relative contributions *x*, *y*, *z* are solved by simultaneous equations[13]

	I_{525}	I_{585}	I_{610}	*x*	*y*	*z*
R:**M**	0	0.01	0.04	1	0	0
F:**M**	2.06	0.36	0.12	0	1	0
T:**M**	0	0.12	0.06	0	0	1
R:**F**:**T**:**M**	0.95	0.56	0.44	5.33	0.46	2.75
R:**F**:**T**:$\mathbf{M_R}^-$	1.08	0.76	0.39	0.96	0.53	4.65
R:**F**:**T**:$\mathbf{M_F}^-$	1.55	0.43	0.19	0.47	0.75	1.26
R:**F**:**T**:$\mathbf{M_T}^-$	1.43	0.52	0.48	7.37	0.69	1.51
F:**T**:**M**	0.99	0.79	0.33	−1.20	0.48	5.26
R:**T**:**M**	0	0.05	0.03	0.23	0	0.38
R:**F**:**M**	1.55	0.37	0.40	7.40	0.75	0.08

in the fluorescence profiles. Melting temperature studies confirmed that the unlabelled (non-fluorescent) 9mers exhibited good discrimination between matched (80–87% bound at 25 °C) and mismatched (< 20% bound at 25 °C) targets.

Control experiments [Fig. 2(c)] were performed on three-component matched systems containing two of the three fluorescent 9mer oligonucleotides bound to the 27mer target. These were the ROX–FAM FRET couple (**R**:**F**:**M**), the TMR–FAM FRET couple (**F**:**T**:**M**) and the ROX–TMR non-FRET pair (**R**:**T**:**M**).

In order to determine the variations in the relative fluorescence contribution of individual fluorophores to each system, the fluorescence spectra were deconvoluted using a set of simultaneous equations.[13] Using this method, each of the three hybridised matched systems **R**:**M**, **F**:**M** and **T**:**M** was assigned a standard value of 1 for the individual contribution to the fluorescence signal of ROX, FAM and TMR, respectively at their respective maximum emission intensities (610, 525, 585, nm). The contributions to the fluorescence resulting from FRET were then determined relative to these values. The relative fluorescence intensities and the calculated contributions from ROX, FAM and TMR to the single four-component matched system, the four-component mismatched systems and controls are summarised in Table 1. The matched system (**R**:**F**:**T**:**M**) exhibited FRET between the donor and *both* acceptors, as indicated by a decrease in the relative fluroescence of FAM (1.0 to 0.46) and an increase in the relative fluroescence of ROX (1.0 to 5.33) and TMR (1.0 to 2.75).

In **R**:**F**:**T**:$\mathbf{M_R}^-$, the mismatch will significantly reduce the proportion of **R** binding. In this case, the system should be very similar to the **F**:**T**:**M** control system. The relative emissions of FAM (0.53) and TMR (4.65) compare well with the **F**:**T**:**M** system (relative emissions of 0.48 and 5.26 respectively). The second mismatch system (**R**:**F**:**T**:$\mathbf{M_F}^-$) will reduce the binding of **F**, which results in no observed FRET between the donor and either acceptor. This resembles the control system **R**:**T**:**M**, in which **F** does not bind, and ROX or TMR produces no significant FRET emission signal. The final system (**R**:**F**:**T**:$\mathbf{M_T}^-$) positions a mismatch that prevents binding of **T**. The result is FRET between FAM and ROX only, as in the control system **R**:**F**:**M**. The two systems compare well, with the relative emissions of FAM (0.69) and ROX (7.37) being very similar to the **R**:**F**:**M** system (relative emissions of 0.75 and 7.40, respectively).

An alternative format for analysis involved fluorescence imaging of samples in a multiwell plate. Samples containing each of the three 9mers (**R**, **F**, **T**) and one of the four matched (**M**) or mismatched ($\mathbf{M_R}^-$, $\mathbf{M_F}^-$, $\mathbf{M_T}^-$) targets were irradiated at 488 nm and emission measured through a 530(±15) nm (FAM), 570(±15) nm (TMR) or 610 nm (ROX) longpass filter. Data were obtained for multiple repeats of each four-component system and analysed using the simultaneous equation method.[13] A plot of relative ROX *vs.* relative TMR emission for each sample from both the earlier fluorimeter studies and fluorimager microtitre plate assays is shown in Fig. 3. Data points were

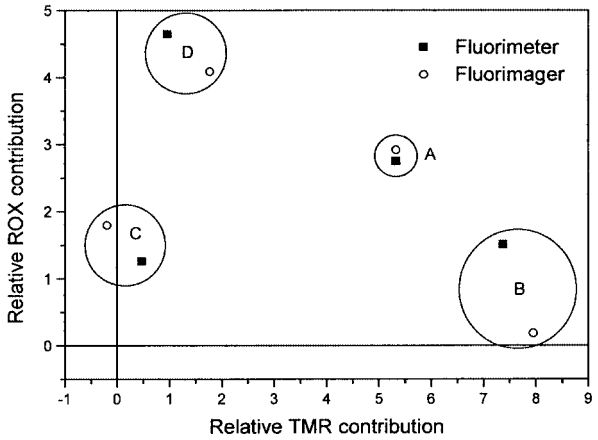

Fig. 3 Relative contributions of both TMR and ROX to fluorescence on binding 9mers to each of the four 27mer targets. Region A corresponds to the matched four component system **R**:**F**:**T**:**M** and regions B, C, D to the mismatched systems **R**:**F**:**T**:$\mathbf{M_R}^-$, **R**:**F**:**T**:$\mathbf{M_F}^-$ and **R**:**F**:**T**:$\mathbf{M_T}^-$ respectively. Fluorimager data (○) have been normalised to the TMR contribution in the matched four-component system of the fluorimeter data (■).

observed to fall into four distinct regions corresponding to the four target types. Region A represents the situation in which both TMR and ROX emission are observed (*i.e.* the matched system, **R**:**F**:**T**:**M**). Region B defines the **R**:**F**:**T**:$\mathbf{M_R}^-$ mismatched system, in which there is TMR emission but no ROX emission. Region C represents the **R**:**F**:**T**:$\mathbf{M_F}^-$ mismatch, which does not exhibit FRET because the donor (FAM) oligonucleotide does not bind. Finally, region D defines the **R**:**F**:**T**:$\mathbf{M_T}^-$ mismatch, in which there is only ROX, but no TMR emission.

These studies provide an insight into the fluorescence behaviour of a double FRET system. The results have shown that a single base mismatch can be detected and mapped in a four component system. Careful design and judicious selection and placement of fluorophores, will enable the general principle to be applied to the study of other multimolecular complexes, and address whether specific combinations of molecules complex under a given set of conditions. The microplate studies also suggest that double FRET can be utilised in a multiplexed format for a more routine analysis of multicomponent interactions.

Notes and references

1 P. R. Selvin, *Methods Enzymol.*, 1995, **246**, 300.
2 R. M. Clegg, *Methods Enzymol.*, 1992, **211**, 353.
3 P. G. Wu and L. Brand, *Anal. Biochem.*, 1994, **218**, 1.
4 L. Stryer, *Annu. Rev. Biochem.*, 1978, **47**, 819.
5 K. M. Parkhurst and L. J. Parkhurst, *Biochemistry*, 1995, **34**, 285.
6 M. S. Yang, S. S. Ghosh and D. P. Millar, *Biochemistry*, 1994, **33**, 15 329.
7 T. Simonsson and R. Sjoback, *J. Biol. Chem.*, 1999, **274**, 17 379.
8 S. Tyagi, *Nature Biotech.*, 1998, **16**, 49.
9 9mers were all of the same base composition so that melt temperatures were similar for the three oligonucleotides.
10 D. J. Allen, P. L. Darke and S. J. Benkovic, *Biochemistry*, 1989, **28**, 4601.
11 Preliminary studies showed FRET was most efficient when the two fluorophores were separated by a distance of seven bases.
12 A:A in the central region of a duplex have the greatest effect on duplex stability: see, for example: F. Aboul-ela, D. Koh and J. J. Tinoco, *Nucleic Acids Res.*, 1985, **13**, 4811; B. L. Gaffney and R. A. Jones, *Biochemistry*, 1989, 5881.
13 Spectra were deconvoluted using the following set of simultaneous equations: $xR_a + yF_a + zT_a = I_a$; $xR_b + yF_b + zT_b = I_b$ and $xR_c + yF_c + zT_c = I_c$ where $R_{a–c}$, $F_{a–c}$ and $T_{a–c}$ are the emission intensities of **R**:**M**, **F**:**M** and **T**:**M**, respectively, at wavelength maxima a–c (a = 610 nm, b = 525 nm, c = 585 nm). $I_{a–c}$ are the observed emission intensities of the sample of interest at wavelengths a–c; *x*, *y* and *z* are unknowns representing the relative contributions to the fluorescence signal by ROX, FAM and TMR, respectively, to the total emission.

ChemComm

A 14-electron ruthenium hydride: the key intermediate in the synthesis of ruthenium carbene complexes; X-ray structure of [RuHCl(PPr$^i_3$)$_2$]

Paul A. van der Schaaf,* Roman Kolly and Andreas Hafner

Ciba Specialty Chemicals, CH-4002 Basel, Switzerland. E-mail: paul.van_der_schaaf@cibasc.com

Received (in Basel, Switzerland) 20th March 2000, Accepted 3rd May 2000

A simple one-pot procedure for the synthesis of ruthenium benzylidenes (Grubbs' catalyst) has been developed in which a novel, highly reactive 14-electron ruthenium monohydride, prepared from [RuCl$_2$(cod)] and two bulky phosphines in boiling propan-2-ol without the use of hydrogen gas, is reacted with hydrogen chloride, an alkyne and styrene.

The discovery and isolation of the first well-defined ruthenium carbenes of the type [RuCl$_2$(=CH–CH=CPh$_2$)(PR$_3$)$_2$][1] by Grubbs and coworkers in 1992 followed by the second generation of the type [RuCl$_2$(=CHPh)(PR$_3$)$_2$][2] have changed the impact of the olefin metathesis reaction in many chemical applications dramatically.[3] Because of our long standing interest in metathesis chemistry,[4] we, as did many others, investigated the use of these well-defined ruthenium carbene catalysts intensively. We found that with these ruthenium carbenes the total catalyst loading in, for example, the polymerization of dicyclopentadiene (DCPD) dropped significantly compared with our recently published method using an arene ruthenium catalyst, such as [(*p*-cymene)RuCl$_2$(PCy$_3$)] (Cy = cyclohexyl).[5] However, the existing syntheses for these ruthenium carbenes rely on barely accessible or unstable and toxic organic compounds which act as the carbene source, *e.g.* phenyl diazomethane for the synthesis of ruthenium benzylidenes. Therefore, for successful commercial applications, new synthetic routes have to be developed which can be scaled-up more easily. Parallel to our efforts, Werner and coworkers developed a new route to benzyl substituted ruthenium carbenes,[6] whereas Grubbs and coworkers developed novel routes to vinyl and phenyl substituted ruthenium carbenes.[7] In both synthetic routes the key intermediate is the ruthenium monohydride dihydrogen species [RuHCl(H$_2$)(PCy$_3$)$_2$], prepared from [RuCl$_2$(cod)] (cod = cycloocta-1,5-diene) and PCy$_3$ in an atmosphere of dihydrogen, which is subsequently reacted with phenyl acetylene or a propargylic chloride, respectively. We now report a simple one-pot procedure for the synthesis of ruthenium carbenes in which the key intermediate, a novel 14-electron species, is prepared starting from [RuCl$_2$(cod)], 2 equivalents of a bulky phosphine, and an appropriate base, but *without* the use of dihydrogen.[8]

Recently, Werner and coworkers published their results on treating a 'red solution' formed upon heating [RuCl$_2$(cod)] with an excess of PPr$^i_3$ in butan-2-ol under an atmosphere of dihydrogen with phenyl acetylene.[6] This reaction led to the formation of [RuCl$_2$(=CHCH$_2$Ph)(PPr$^i_3$)$_2$] in *ca.* 65% yield. The active ruthenium species in the 'magic' red solution, however, was unknown. Addition of diethyl ether to this red solution led to the isolation of the ruthenium(IV) complex [RuH$_2$Cl$_2$(PPr$^i_3$)$_2$]. It was reported that this ruthenium(IV) dihydride species reacts with phenyl acetylene predominantly yielding the five-coordinate vinylidene complex [RuCl$_2$(=C=CHPh)(PPr$^i_3$)$_2$] with the above mentioned benzyl substituted ruthenium carbene [RuCl$_2$(=CCH$_2$Ph)(PPr$^i_3$)$_2$] only as the side product. It was speculated that the active species in the red solution which led to the ruthenium carbene complex was the monohydride–dihydrogen complex [RuHCl(H$_2$)(PPr$^i_3$)$_2$]. Surprisingly, when we carried out the reaction *without* the use of dihydrogen, the reaction worked as well. We prepared a 'red solution' by boiling [RuCl$_2$(cod)] for 3 h with 2 equiv. of PPr$^i_3$ and 1 equiv. of NEt$_3$ in propan-2-ol under an argon atmosphere. ^{1}H NMR investigations on this solution showed a broad triplet at δ −17, indeed indicating the possible presence of the above mentioned ruthenium monohydride dihydrogen species [RuHCl(H$_2$)(PPr$^i_3$)$_2$].[9] By slowly cooling this red solution from 80 °C to room temperature we could isolate the hydride as blocky, orange crystals. Surprisingly, an X-ray structure determination on these crystals revealed the hydride species to be a tetracoordinate, 14-electron d^6 species with formula [RuHCl(PPr$^i_3$)$_2$] **1**.† Fig. 1 shows the molecular geometry of **1** which can be best described as a square-planar structure with the bulky triisopropylphosphines in *trans* positions.‡

Very recently, Caulton and coworkers also described a 14-electron ruthenium monohydride as the intermediate in the synthesis of heteroatom substituted ruthenium carbene complexes using vinyl ethers as the carbene source.[10] However, this hydride, prepared by dehydrohalogenation of [Ru(H)$_2$Cl$_2$(PR$_3$)$_2$] with lithium 2,2,6,6-tetramethylpiperidide, appears to be a halide bridged dimer.[11]

Subsequent addition of phenyl acetylene and styrene to the red solution containing **1** resulted in the isolation of the 'Grubbs' catalyst' [RuCl$_2$(=CHPh)(PPr$^i_3$)$_2$] in moderate yields. However, when we first added an extra equivalent of hydrogen chloride to the hydride solution at −20 °C, subsequently added the acetylene and styrene, warmed the reaction mixture to room temperature and stirred it for an additional hour, the yield could be increased to 75%.§

In the first step of the reaction, the preparation of monohydride **1**, the formation of 3 equivalents of acetone were detected by gas chromatography; 1 equivalent is the result of the hydride formation whereas the other 2 equivalents originate from the reduction of cod to cyclooctane, which was detected by gas chromatography. Upon addition of the HCl solution in diethyl ether the typical sharp ^{1}H NMR hydride signal at δ −17 disappeared and a very broad signal at δ −5 could be observed. Unfortunately, we were unable to isolate a distinct compound. However, in analogy to the previously described HCl addition

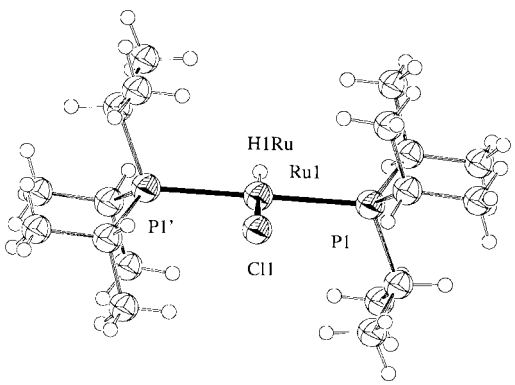

Fig. 1 ORTEP drawing of **1**. Selected bond distances (Å) and angles (°): Ru(1)–P(1) 2.3704(9), Ru(1)–Cl(1) 2.434(3), Ru(1)–H(1Ru) 1.5983; P(1)–Ru(1)–H(1Ru) 90.3, P(1′)–Ru(1)–H(1Ru) 89.7, P(1)–Ru(1)–Cl(1) 89.47(5), P(1′)–Ru(1)–Cl(1) 90.53(5).

DOI: 10.1039/b002298p

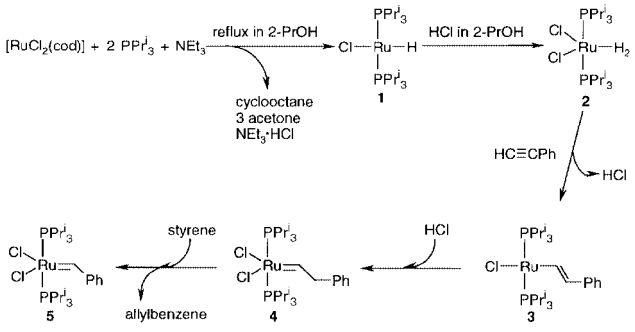

Scheme 1

to a similar osmium carbonyl complex,[12] we propose that the intermediate is the ruthenium(II) dichloride dihydrogen complex **2**. This dihydrogen complex reacts upon addition of phenyl acetylene to generate a short-lived 14-eletron alkenyl complex **3** along with the formation of a molecule HCl. **3** immediately reacts with HCl to form the more stable benzyl substituted ruthenium carbene **4**. A simple metathesis reaction with styrene then gives the Grubbs ruthenium benzylidene catalyst **5** which can be easily isolated by filtration and purified by washing with cold methanol. The complete postulated reaction mechanism is depicted in Scheme 1.

These results demonstrate a very simple one-pot synthesis procedure for the preparation of multigram quantities of the Grubbs catalyst without the use of dihydrogen gas, and utilizing only commercially available starting materials. The novel intermediate monohydride complex was isolated and fully characterized and appeared to be a mononuclear, square-planar, 14-electron species. The reactivity of this monohydride species in other reactions, *e.g.* hydrogen transfer reactions, is currently under investigation.

Notes and references

† An X-ray structure determination of the deuterium analog of **1**, *i.e.* [RuDCl(PPr^i_3)$_2$] **1D** prepared in propan-2-ol-d_8, revealed exactly the same structure. To have absolute proof of this unexpected result we also determined the structure of the tricyclohexylphosphine analogue [RuHCl(PCy_3)$_2$] **1Cy**, prepared using DBU as base instead of NEt_3. This complex also has a square-planar geometry with the two bulky phosphines in *trans* positions.

‡ *Crystal data* for **1**: $C_{18}H_{43}ClP_2Ru$, M = 457.98, monoclinic, space group $P2_1/c$ (no. 14), a = 8.0682(5), b = 8.9506(8), c = 16.6435(12) Å, β = 92.76(1)°, V = 1200.5(2) Å^3, Z = 2, μ(Mo-Kα) = 0.895 mm^{-1}, 9038 reflections measured, 2295 unique (R_{int} = 0.042), observed 1938 [$I > 2\sigma(I)$], Final R_1 = 0.038 (obsd. data), wR_2 = 0.122 (all data).

For **1D**: $C_{18}H_{42}DClP_2Ru$, M = 457.98, monoclinic, space group $P2_1/c$ (no. 14), a = 8.0641(8), b = 8.9361(6), c = 16.6840(15) Å, β = 92.74(1)°, V = 1200.9(2) Å^3, Z = 2, μ(Mo-Kα) = 0.895 mm^{-1}, reflections measured 8559, independent 2272 (R_{int} = 0.022), observed 1977 [$I > 2\sigma(I)$]. Final R_1 = 0.042 (obsd. data), wR_2 = 0.1421 (all data).

For **1Cy**: $C_{36}H_{67}ClP_2Ru$, M = 698.36, triclinic, space group $P\bar{1}$ (no. 2), a = 9.8438(8), b = 10.2011(8), c = 10.8356(9) Å, α = 114.29(1), β = 108.48(1), γ = 90.82(1)°, V = 927.4(13) Å^3, Z = 1, μ(Mo-Kα) = 0.603 mm^{-1}, 6747 reflections measured, 3181 independent (R_{int} = 0.025), observed 2953 [$I > 2\sigma(I)$]. Final R_1 = 0.041 (obsd. data), wR_2 = 0.128 (all data). Twinned crystal with 6% overlapped reflections, which were omitted. Full spheres of intensity data were collected at 223 K on a Stoe Image Plate Diffraction system using Mo-Kα graphite monochromated radiation. Image plate distance 70 mm, ϕ oscillation scans 0–200°, step $\Delta\phi$ = 1°, 2θ range 3.27–52.1°, d_{max}–d_{min} = 12.45–0.81 Å.

The structures were solved by direct methods using the program SHELXS-97.[13] The refinements and all further calculations were carried out using SHELXL-97.[14] The alkyl group H-atoms were included in calculated positions and treated as riding atoms using SHELXL-97 default parameters. In all three compounds the hydride (H1Ru) could be located from a final difference map (*ca.* 1.7 e Å^{-3}), at a distance of 1.6–1.8 Å from the Ru atom. In the final refinement cycles it was held fixed with a U_{iso} = 1.5U_{eq}(Ru) Å^2. The non-H atoms were refined anisotropically, using weighted full-matrix least squares on F^2. An empirical absorption correction was applied for all three compounds but a small amount of residual density was still located near the Cl atoms. All three structures are centrosymmetric implying disordered structures with the Cl and hydride sites being 50% occupied.

CCDC 182/1627. See http//www.rsc.org./suppdata/cc/b0/b002298p/ for crystallographic files in .cif formed.

§ *Synthetic procedure*: a suspension of [$RuCl_2$(cod)] (5.00 g, 17.8 mmol) in 125 ml propan-2-ol was treated with PPr^i_3 (7.0 ml, 36.6 mmol) and NEt_3 (5.0 ml, 36.0 mmol) and refluxed under argon for 3 h. The resulting red coloured, clear solution was cooled to −20 °C and changed to an orange suspension. To this suspension was added dropwise 35 ml of a 1 M HCl solution in diethyl ether over a period of *ca* 15 min keeping the temperature around −20 °C. The reaction mixture was stirred for an additional 10 min, and phenylacetylene (4.0 ml, 36.4 mmol) was added dropwise keeping the reaction mixture below −15 °C. Subsequently, the reaction mixture was stirred for 2 h at between −20 and −15 °C. The resulting purple suspension was treated with styrene (8.0 ml, 70 mmol), the temperature was slowly raised to room temperature and the reaction mixture was allowed to stir for an additional hour. The reaction mixture was partially concentrated and the product filtered off. The purple product was washed with methanol (2 × 10 ml), and dried *in vacuo*. This procedure yielded 7.7 g of [$RuCl_2$(=CHPh)(PPr^i_3)$_2$] (75%). A similar procedure can be used for the synthesis of [$RuCl_2$(=CHPh)(PCy_3)$_2$], except that DBU has to be used as base instead of NEt_3.

1 S. T. Nguyen, L. K. Johnson, R. H. Grubbs and J. W. Ziller, *J. Am. Chem. Soc.*, 1992, **114**, 3974; S. T. Nguyen, R. H. Grubbs and J. W. Ziller, *J. Am. Chem. Soc.*, 1993, **115**, 9858.

2 P. Schwab, M. B. France, J. W. Ziller and R. H. Grubbs, *Angew. Chem., Int. Ed. Engl.*, 1995, **34**, 2039; P. Schwab, R. H. Grubbs and J. W. Ziller, *J. Am. Chem. Soc.*, 1996, **118**, 100.

3 K. J. Ivin and J. C. Mol, *Olefin Metathesis and Metathesis Polymerization*, Academic Press, London, 1997.

4 A. Mühlebach, P. A. van der Schaaf, A. Hafner and F. Setiabudi, *J. Mol. Catal. A: Chem.*, 1998, **132**, 181; A. Hafner, A. Mühlebach and P. A. van der Schaaf, *Angew. Chem., Int. Ed. Engl.*, 1997, **36**, 2121; P. A. van der Schaaf, A. Hafner and A. Mühlebach, *Angew. Chem., Int. Ed. Engl.*, 1996, **35**, 1845; A. Hafner, P. A. van der Schaaf and A. Mühlebach, *Chimia*, 1996, **50**, 131.

5 A. Hafner, A. Mühlebach and P. A. van der Schaaf, *Angew. Chem., Int. Ed. Engl.*, 1997, **36**, 2121.

6 C. Gruenwald, O. Gevert, J. Wolf, P. Gonzales-Herrero and H. Werner, *Organometallics*, 1996, **15**, 1960; J. Wolf, W. Stuer, C. Gruenwald, H. Werner, P. Schwab and M. Schulz, *Angew. Chem., Int. Ed.*, 1998, **37**, 1124.

7 T. E. Wilhelm, T. R. Belderrain, S. N. Brown and R. H. Grubbs, *Organometallics*, 1997, **16**, 3867; T. R. Belderrain and R. H. Grubbs, *Organometallics*, 1997, **16**, 4001; R. H. Grubbs, T. R. Belderrain, S. N. Brown and T. E. Wilhelm, *World Pat., WO 98 21,214* (CalTech) (*Chem. Abstr.*, 1998, **129**, 41513).

8 P. A. van der Schaaf, R. Kolly, A. Hafner and A. Mühlebach, *Eur Pat., EP 839,821* (Ciba SC) (*Chem. Abstr.*, 1998, **129**, 41274).

9 T. Burrow, S. Sabo-Etienne and B. Chaudret, *Inorg. Chem.*, 1995, **34**, 2470.

10 J. N. Coalter III, G. J. Spivak, H. Gerard, E. Clot, E. R. Davidson, O. Eisenstein and K. G. Caulton, *J. Am. Chem. Soc.*, 1998, **120**, 9388.

11 J. N. Coalter III, J. C. Bollinger, J. C. Huffman, U. Werner-Zwanziger, K. G. Caulton, E. R. Davidson, H. Gerard, E. Clot and O. Eisenstein, *New J. Chem.*, 2000, **24**, 9.

12 M. A. Esteruelas, F. J. Lahoz, E. Onate, L. A. Oro, C. Valero and B. Zeier, *J. Am. Chem. Soc.*, 1995, **117**, 7935.

13 G. M. Sheldrick, *Acta Crystallogr., Sect A*, 1990, **46**, 467.

14 G. M. Sheldrick, SHELXL-97, Program for Crystal Structure Determination, Universität Göttingen, Germany, 1999.

Meso–meso-linked porphyrin dimer as a novel scaffold for the selective binding of oligosaccharides†

Masato Ikeda,[a] Seiji Shinkai*[a] and Atsuhiro Osuka[b]

[a] *Department of Chemistry and Biochemistry, Graduate School of Engineering, Kyushu University, Fukuoka 812-8581, Japan. E-mail: seijitcm@mbox.nc.kyushu-u.ac.jp*

[b] *Department of Chemistry, Graduate School of Science, Kyoto University, Sakyo-ku, Kyoto 606-8502, Japan*

Received (in Cambridge, UK) 26th April 2000, Accepted 5th May 2000
Published on the Web 25th May 2000

A meso–meso-linked porphyrin dimer 1 bearing four boronic acid groups shows high selectivity for maltotetraose (*n* = 4) among maltooligosaccharides (*n* = 1–7), indicating that this class of porphyrins acts as a novel scaffold to design oligosaccharide receptors.

The specific interaction between phenylboronic acids and saccharides or related compounds has been attracting increasing attention as a novel force for sugar recognition in aqueous systems.[1–8] Since one phenylboronic acid reacts with two OH groups to form a cyclic boronate ester, monosaccharides usually bearing five OH groups tend to form 1 : 2 monosaccharide–phenylboronic acid complexes.[1,9–13] However, the stability order of these complexes is always the same, which is governed by the inherent structure of monosaccharides.[2–4,14,15] Of such monosaccharides, fructose has a high association constant whereas glucose has a low association constant.[14,15] In contrast, diboronic acids which can react with four of the five OH groups to form intramolecular 1 : 1 complexes show a different stability order, which is related to the specific spatial position of two boronic acid groups. This implies that one can recognise a specific saccharide by appropriate manipulation of two boronic acids in the same molecule and the concept may be extended to the selective binding of oligosaccharides. This idea has been tested with a few diboronic acid systems bearing a 'long' spacer: *e.g.* diphenyl-3,3′-diboronic acid, stilbene-3,3′-diboronic acid and *cis*-5,15-bis[2-(dihydroxyboronyl)phenyl]-10,20-diphenylporphine show some selectivity for certain disaccharides but the selectivity observed so far is not very high.[16–18] We thus considered that one should look for a 'long' and 'rigid' scaffold by which one might finely tune the distance between two boronic acid groups. Recently, it was found that the meso–meso coupling reaction of Zn(II) porphyrinates is efficiently mediated by $AgPF_6$[19] to yield oligomeric porphyrins. These new compounds seem to satisfy the prerequisites mentioned above. As a preliminary step to use these compounds as scaffolds for saccharide recognition, we designed compound **1**. Very interestingly, we have found that **1** shows a high affinity with maltotetraose among maltooligosaccharides. To the best of our knowledge, this is the first artificial saccharide receptor which shows selectivity for oligosaccharides.

Compound **1** was synthesised from 4-(1,3-dioxaborinan-2-yl)benzaldehyde and dipyrrylmethane according to Scheme 1 and identified as its propane-1,3-diol-protected species by ^{1}H NMR and MALDI-TOF mass (*m/z* 1386.9) spectra and elemental analysis.‡ Since ^{1}H NMR spectroscopy showed that the protecting groups are readily eliminated in aqueous media to yield **1**, it was used for the spectroscopic measurements without deprotection treatment. From examination of Lambert–Beer plots, we found that **1** tends to aggregate in water-rich solvents. We thus chose a water (pH 10.5 with 50 mmol dm^{-3} carbonate buffer)–MeOH (2 : 3 v/v) mixture into which **1** was solubilised discretely.

† Electronic supplementary information (ESI) available (i) Fig. A and B (Job plot for **1**+M_4 and possible binding mode for **1**/M_4, respectively). See http://www.rsc.org/suppdata/cc/b0/b003365k/

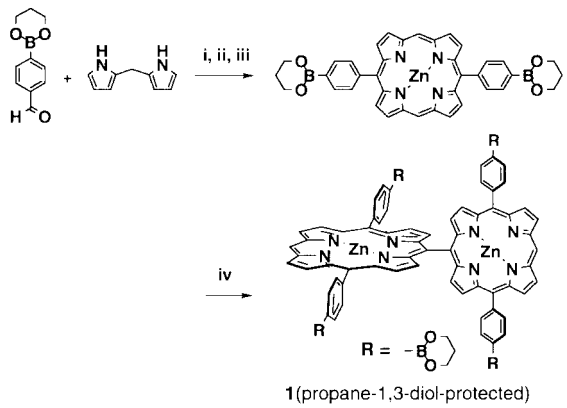

Scheme 1 *Reagents and conditions* [yields]: i, TFA, CH_2Cl_2, r.t. then chloranil, reflux [30%]; ii, $Zn(OAc)_2$, $CHCl_3$–MeOH, r.t. [88%]; iii, propane-1,3-diol, benzene, reflux [98%]; iv, $AgPF_6$/MeCN, $CHCl_3$, r.t. [4%].

The absorption spectrum of **1** showed a split Soret band (412.0 and 448.0 nm) and a few Q bands (516.0, 560.0 and 594.5 nm). When maltooligosaccharides (M_n: α-1,4-linked oligomers of D-glucose) were added, the absorption spectra were scarcely changed, indicating that the skeleton of compound **1** is fairly rigid. In the circular dichrosim (CD) spectra, on the other hand, exciton-coupling-type CD bands appeared in the Soret band region (Fig. 1). It is seen from Fig. 1 that the CD spectra consist of two exciton-coupling bands: for the **1**·M_4 complex (Fig. 1), a negative band at higher wavelength and the positive band at shorter wavelength. The strongest peak appears at 417 nm where two CD bands overlap. The CD intensity at 417 nm is summarised in Table 1. It is seen from Table 1 that: (i) the complex with D-glucose (M_1) is almost CD-silent, (ii) maltose (M_2) and maltotriose (M_3) give a weak negative 417 nm peak whereas maltotetrose and higher-order maltooligosaccharides (M_5–M_7) all give a positive 417 nm peak and (iii) a particularly strong CD band is observed for M_4. The results indicate that (i)

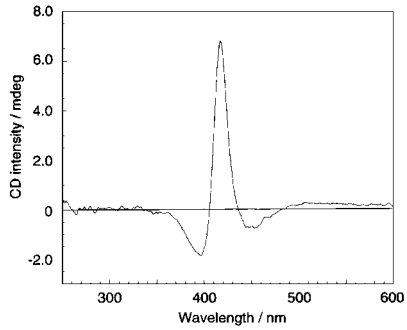

Fig. 1 CD spectrum of **1** (5.00×10^{-6} mol dm^{-3}) with a 1 cm cell in the presence of maltotetraose (50 mmol dm^{-3}) in a water (pH 10.5 with 50 mmol dm^{-3} carbonate)–MeOH (2 : 3) mixture at 25 °C. A similar CD spectral shape was also observed (although the intensity was different) in the presence of other maltooligosaccharides.

Table 1 CD intensity at 417 nm and binding parameters obtained from Hill's plots and substitution methods

Saccharide	CD intensity[a]/ mdeg	K^b/dm^6 mol^{-2}	m^b	K^c/dm^6 mol^{-2}
Glucose (M_1)	0.2	—	—	2.5×10^3
Maltose (M_2)	−0.5	—	—	1.5×10^3
Maltotriose (M_3)	−0.2	—	—	2.0×10^3
Maltotetraose (M_4)	6.8	6.3×10^5	1.7	—
Maltopentaose (M_5)	1.9	1.3×10^4	1.8	—
Maltohexaose (M_6)	1.4	1.6×10^4	1.8	—
Maltoheptaose (M_7)	1.7	2.0×10^3	1.5	—

[a] See caption of Fig. 1. [b] Determined from Hill's plots. [c] The 1:2 to 1:2 substitution (*e.g.* from **1**·$(M_4)_2$ to **1**·$(M_1)_2$) is assumed for the calculation.

D-glucose is too small to bridge two boronic acid groups, (ii) the two porphyrin planes are oriented in opposite directions for the M_2, M_3 complexes and M_4–M_7 complexes, respectively, and (iii) M_4 forms a particularly stable complex with **1**.

To obtain further insights into the binding mode, the complex stoichiometries were estimated by a Job plot method for M_4–M_7 which show measurable CD intensity. A typical example for M_4 is shown in Fig. A(ESI):† a maximum is observed at ([**1**]/([**1**] + [M_4]) = 0.33. This supports the view that **1** binds two M_4 guests to form the stable complex. Similar 1:2 stoichiometries were also observed for M_5, M_6 and M_7. The computational studies (Discover 3/Insight II 98.0) predict that in the most stable conformation the two porphyrin planes cross at 90°, in which the distance between two boron atoms is 1.58 nm. This distance is comparable with that between the 1,2-diol and 4,6-diol in the two terminal D-glucose units of M_4 (*ca.* 1.5–1.8 nm). One may thus illustrate a binding mode for the 1:2 **1**/M_4 complex as shown in Fig. B(ESI).†§

The CD spectra measured as a function of M_4–M_7 concentrations provided several isosbestic points. As typical examples, plots of CD intensity at 417 nm *vs.* [M_4] and [M_5] are shown in Fig. 2. The sigmoidal curvatures indicate that the 1:2 complexes are formed in a cooperative manner. Similar sigmoidal dependences were also observed for M_6 and M_7. The binding of the guest to **1** is cooperative. This cooperative guest binding profile can be analysed with the Hill equation: $\log [y/(1 - y)] = m\log[\text{guest}] + \log K$, where K and m are the association constant and Hill coefficient, respectively, and $y = K/([\text{guest}]^{-m} + K)$.[20] From the slope and the intercept obtained using the linear portion at $\log [y/(1 - y)] = 0$–0.8 we obtained K and m values for M_4–M_7. The determination of K values for M_1–M_3 was difficult because of their weak CD intensity, but measurements were obtained by a substitution method using the **1**·M_4 complex, that is, by the CD intensity decrease induced by addition of M_1–M_3, and the results are summarised in Table 1. Examination of Table 1 reveals that: (i) the magnitude of K is correlated with the CD intensity, (ii) the largest K is observed for M_4, which is 48- and 39-fold larger, respectively, than those of M_5 and M_6 and (iii) the m values are smaller than 2.0, indicating the weak positive allosterism and the presence of the 1:1 species in the low saccharide concentration region. This novel binding mode implies that the binding of the first guest which intramolecularly bridges two boronic acid groups suppresses the rotational freedom of the porphyrin rings and preorganises the two residual boronic acids so that they can easily complex the second guest.

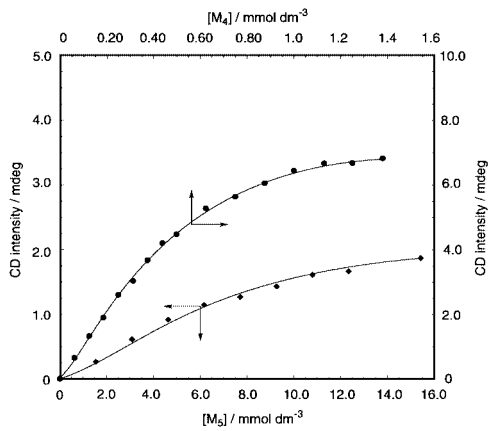

Fig. 2 Plots of CD intensity (417 nm) for **1** (5.00×10^{-6} mol dm^{-3}) *vs.* [M_4] and [M_5].

In conclusion, it was shown that the meso–meso-linked porphyrin dimer is a useful scaffold to separate two boronic acid groups so that they can show selectivity for oligosaccharides. We believe that this study is very important in revealing boronic acid–saccharide interactions toward selective recognition of oligosaccharides.

Notes and references

‡ In step iv (Scheme 1), by-products were detected in which the boronic acid groups were substituted by OH groups. The raw yield of **1** estimated by HPLC was *ca.* 20%.

§ Conformations with low potential energy encountered during a 100 ps MD simulation at 300 K were selected. The system was minimised using conjugate gradient and Newton–Raphson methods until convergence was attained for a gradient of 0.01 kcal mol^{-1} Å^{-1}. The force field used in this study was the ESFF.

1 For recent comprehensive reviews, see: T. D. James, K. R. A. S. Sandanayake and S. Shinkai, *Supramol. Chem.*, 1995, **6**, 141; T. D. James, P. Linnane and S. Shinkai, *Chem. Commun.*, 1996, 281; T. D. James, K. R. A. S. Sandanayake and S. Shinkai, *Angew. Chem., Int. Ed. Engl.*, 1996, **35**, 1910.

2 J. Yoon and A. W. Czarnik, *J. Am. Chem. Soc.*, 1992, **114**, 5874; L. K. Mohler and A. W. Czarnik, *J. Am. Chem. Soc.*, 1993, **115**, 2998.

3 M.-F. Paugam and B. D. Smith, *Tetrahedron Lett.*, 1993, **34**, 3723; G. T. Morin, M. P. Hughes, M.-F. Paugam and B. D. Smith, *J. Am. Chem. Soc.*, 1994, **116**, 8895; P. R. Westmark and B. D. Smith, *J. Am. Chem. Soc.*, 1994, **116**, 9343.

4 Y. Nagai, K. Kobayashi, H. Toi and Y. Aoyama, *Bull. Chem. Soc. Jpn.*, 1993, **66**, 2965.

5 G. Wulff, B. Heide and G. Helfmeier, *J. Am. Chem. Soc.*, 1986, **108**, 1089; G. Wulff and H.-G. Poll, *Makromol. Chem.*, 1987, **188**, 741.

6 C. R. Cooper and T. D. James, *Chem. Commun.*, 1997, 1419.

7 M. Takeuchi, M. Yamamoto and S. Shinkai, *Chem. Commun.*, 1997, 1731.

8 T. Mizuno, M. Takeuchi, I. Hamachi, K. Nakashima and S. Shinkai, *Chem. Commun.*, 1997, 1793.

9 K. Tsukagoshi and S. Shinkai, *J. Org. Chem.*, 1991, **56**, 4089; Y. Shiomi, M. Saisho, K. Tsukagoshi and S. Shinkai, *J. Chem. Soc., Perkin Trans. 1*, 1993, 2111.

10 T. D. James, T. Harada and S. Shinkai, *J. Chem. Soc., Chem. Commun.*, 1993, 857.

11 K. Nakashima and S. Shinkai, *Chem. Lett.*, 1995, 443; K. R. A. S. Sandanayake, T. D. James and S. Shinkai, *Chem. Lett.*, 1995, 503.

12 J. C. Norrild and H. Eggert, *J. Am. Chem. Soc.*, 1995, **117**, 1479.

13 T. D. James, K. R. A. S. Sandanayake, R. Iguchi and S. Shinkai, *J. Am. Chem. Soc.*, 1995, **117**, 8982 and references therein.

14 J. P. Lorand and J. O. Edwards, *J. Org. Chem.*, 1959, **24**, 769.

15 H. Murakami, T. Nagasaki, I. Hamachi and S. Shinkai, *Tetrahedron Lett.*, 1993, **34**, 6273; *J. Chem. Soc., Perkin Trans. 2*, 1994, 975; T. Imada, H. Murakami and S. Shinkai, *J. Chem. Soc., Chem. Commun.*, 1994, 1557; S. Arimori, H. Murakami, M. Takeuchi and S. Shinkai, *J. Chem. Soc., Chem. Commun.*, 1995, 961; S. Arimori, M. Takeuchi and S. Shinkai, *Chem. Lett.*, 1996, 77; *J. Am. Chem. Soc.*, 1996, **118**, 245.

16 K. Kondo, Y. Shiomi, M. Saisho, T. Harada and S. Shinkai, *Tetrahedron*, 1992, **48**, 8239.

17 K. R. A. S. Sandanayake, K. Nakashima and S. Shinkai, *J. Chem. Soc., Chem. Commun.*, 1994, 1621.

18 H. Kijima, M. Takeuchi and S. Shinkai, *Chem. Lett.*, 1998, 781.

19 A. Nakano, A. Osuka, I. Yamazaki, T. Yamazaki and Y. Nishimura, *Angew. Chem., Int. Ed.*, 1998, **37**, 3023; T. Ogawa, Y. Nishimoto, N. Yoshida, N. Ono and A. Osuka, *Angew. Chem., Int. Ed.*, 1999, **38**, 176 and references therein.

20 K. A. Connors, *Binding Constants*, John Wiley, New York, 1987.

Synthesis and structure of the first boron-bridged constrained geometry complexes†

Holger Braunschweig,* Carsten von Koblinski and Ulli Englert

Institut für Anorganische Chemie der Technischen Hochschule, RWTH Aachen, Templergraben 55, D-52056 Aachen, Germany. E-mail: holger.braunschweig@ac.rwth.aachen.de

Received (in Basel, Switzerland) 21st December 1999, Accepted 3rd May 2000
Published on the Web 25th May 2000

In the course of investigations on new Ziegler–Natta-analogous catalyst systems, the first 'constrained geometry' complexes of titanium with a bridging boron atom have been conveniently obtained by a high yield synthesis and were structurally characterized.

Since 1990[1] 'constrained geometry' complexes as catalysts for olefin polymerization have attracted considerable interest, since they show some distinct advantages in comparison to metallocene-based Ziegler–Natta type catalysts,[2] such as formation of copolymers and an increased stability towards MAO even under thermally harsh reaction conditions.[1d]‡ Very recently it was shown by us[3] and others [4] that [1]borametallocenophanes of group 4 elements are easily accessible, highly active catalysts for the polymerization of ethene and propene.

In order to combine the properties of the small and Lewis acidic bridging boron atom with the advantages of constrained geometry catalysts we prepared the compounds [{η^5:η^1-$C_5H_4B(NPr^i_2)NPh$}TiX_2] (X = NMe_2, **1**; X = Cl, **2**).

Similarly to the synthesis of the corresponding [1]boratitanocenophanes [{$(\eta^5$-$C_5H_4)_2BNR_2$}$Ti(NMe_2)_2$],[3a] complex **1** is obtained in a convenient three-step synthesis according to Scheme 1 as an orange, crystalline material in 80% yield. Subsequent treatment of **1** with an excess of Me_3SiCl gave the corresponding dichloro complex **2** in almost quantitative yield as a yellow solid. The structures of **1** and **2** in solution were derived from the multinuclear NMR data.§ In the ^{1}H NMR spectra both compounds show the expected two pseudo-triplets for the cyclopentadienyl protons forming an AA′BB′ spin system. Double sets of signals for the isopropyl groups in the ^{1}H and ^{13}C NMR spectra indicate a hindered rotation with respect to the boron–nitrogen double bond in **1** and **2**. The ^{11}B NMR spectra show signals at δ 27.8 (**1**) and 28.4 (**2**), in the expected range for aryl(diamino)boranes.

Suitable single crystals of **1** (Fig. 1) for an X-ray structural analysis¶ were obtained from hexane at −30 °C. The compound crystallises in the triclinic space group *P*1 and the molecule adopts C_1 symmetry in the crystal. Both atoms B and N2 are trigonal planar, and the planes C20–N2–C23 and N1–B–C1 are almost coplanar with a dihedral angle of 2.2(3)°. The B–N distances of 1.428(3) Å (B–N1) and 1.409(3) Å (B–N2) are in the expected range for B–N double bonds, and the Ti–N distances were found to be *ca*. 1.91 Å for N3 and N4, respectively, while the Ti–N1 distance is markedly longer at 2.020(2) Å.

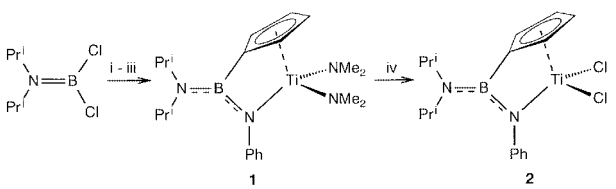

1 2

Scheme 1 *Reagents and conditions*: i, hexane, 0 °C, $Na(C_5H_5)$; ii, toluene, 0 to 25 °C, Li(NPhH); iii, toluene, −78 to 40 °C, $[Ti(NMe_2)_4]$, 78%; iv, hexane, 0 °C, Me_3SiCl, 98%.

† Electronic supplementary information (ESI) available: experimental and polymerisation studies. See http://www.rsc.org/suppdata/cc/b0/b000380h/

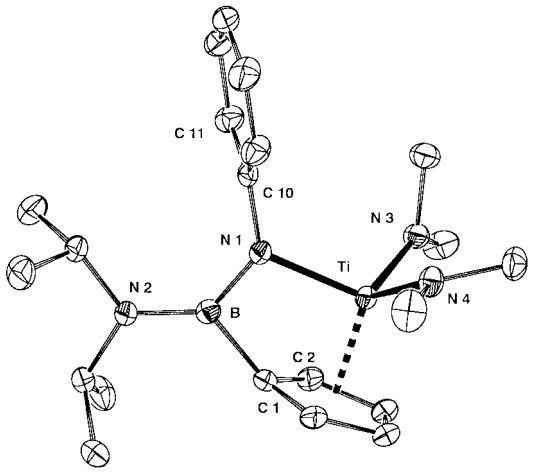

Fig. 1 Molecular structure of **1**. Selected distances (Å) and angles (°): B–N(1) 1.428(3), B–N(2) 1.409(3), Ti–N(1) 2.020(2), Ti–N(3) 1.9045(19), Ti–N(4) 1.913(2), N(3)–Ti–N(4) 103.44(9), N(1)–B–N(2) 131.0(2), C(1)–B–N(1) 103.57(18). Thermal ellipsoids are drawn at the 30% probability level.

Preliminary polymerisation experiments showed compound **2** to be an effective catalyst for the polymerisation of ethene in the presence of MAO. In a typical experiment polyethylene with a molecular weight of *ca*. 470 000 was obtained with an activity of 500 kg polymer (mol cat h)$^{-1}$. As to be expected,[5] complex **1** showed a considerably lower activity towards the polymerisation of olefins. Further investigations of the catalytic properties of compound **2** and related complexes for ethene/styrene-copolymerisation are in progress.

This work was supported by the Deutsche Forschungsgemeinschaft, the Fonds der Chemischen Industrie, and the BASF AG Ludwigshafen.

Notes and references

‡ For a recent review on non-metallocene catalysts see ref. 1(*f*).

§ *Spectroscopic data*: **1**: ^{1}H NMR (499.658 MHz, CD_2Cl_2): δ 0.90 (br, 6H, $CHCH_3$), 1.45 (br, 6H, $CHCH_3$), 2.97 (s, 12H, NMe_2), 3.31 (br, 2H, $CHCH_3$), 5.94 (m, 2H, C_5H_4), 6.44 (m, 2H, C_5H_4), 6.73 (m, 2H, C_6H_5), 6.83 (m, 1H, C_6H_5), 7.14 (m, 2H, C_6H_5). ^{11}B NMR (160.310 MHz, CD_2Cl_2): δ 27.76. ^{13}C NMR (125.639 MHz, CD_2Cl_2): δ 21.36 (br), 27.01 (br), 44.62 (br), 46.11 (br), 47.90 (NMe_2), 120.95 (C_5H_4), 124.00 (C_5H_4), 115.81, 119.99, 128.16, 155.48. MS (EI) (*m*/*z*, %): 402 (M^+, 45), 387 (M^+ − Me, 5), 358 (M^+ − NMe_2, 65), 314 (M^+ − $2NMe_2$, 100), 93 ($C_6H_5NH_2^+$, 95), 64 ($C_5H_4^+$, 45). Correct elemental analysis.

2: ^{1}H NMR (499.658 MHz. CD_2Cl_2): δ 0.90 (d, 6H, ^3J 6.71 Hz, $CHCH_3$), 1.54 (d, 6H, ^3J 6.71 Hz, $CHCH_3$), 3.14 (m, 1H, ^3J 6.71 Hz, $CHCH_3$), 3.41 (m, 1H, ^3J 6.71 Hz, $CHCH_3$), 6.44 (m, 2H, C_5H_4), 7.08 (m, 2H, C_5H_4), 6.91 (m, 2H, C_6H_5), 7.14 (m, 1H, C_6H_5), 7.38 (m 2H, C_6H_5). ^{11}B NMR (160.310 MHz, CD_2Cl_2): δ 28.29. ^{13}C NMR (125.639 MHz, CD_2Cl_2): δ 21.40, 27.72, 45.20, 47.28, 122.52 (C_5H_4), 125.71 (C_5H_4), 124.32, 127.21, 129.62, 152.39. MS (EI) (*m*/*z*, %): 384 (M^+, 15), 369 (M^+ − Me, 30), 348 (M^+ −

Cl, 50), 333 ($M^+ - Cl - Me$, 20), 318 ($M^+ - Cl - 2Me$, 20], 93 ($C_6H_5NH_2^+$, 70), 64 ($C_5H_4^+$, 25). Correct elemental analysis.

¶ *X-Ray structure determination* of **1**: ENRAF-Nonius CAD4 diffractometer, Mo-Kα radiation, incident beam graphite monochromator (λ = 0.71073 Å), T = 213 K, orange platelet of approximate dimensions 0.70 × 0.60 × 0.15 mm directly mounted in dry air flux (Whatman 75-52).

Crystal data: triclinic, space group $P\bar{1}$, a = 9.464(6), b = 9.754(4), c = 13.596 Å, α = 101.94(2), β = 102.32(4), γ = 103.37(4)°, V = 1149 Å^3, Z = 2, D_c = 1.17 g cm^{-3}, μ = 3.8 cm^{-1}. 4351 reflections, 4068 independent, θ_{max} = 26°, solution with direct methods (SHELXS97),[6] refinement on F^2 (SHELXL97),[8] 252 variables, *wR*2 (all data) = 0.1162, *R*1 [for 3347 data with $I > 2\sigma(I)$] = 0.0444, max./min. electron density from final difference Fourier map, 0.437 and −0.200 e Å^{-3}.

CCDC 182/1628. See http://www.rsc.org/suppdata/cc/b0/b000380h/ for crystallographic files in .cif format.

1 (*a*) P. J. Shapiro, E. E. Bunel, W. P. Schaefer and J. E. Bercaw, *Organometallics*, 1990, **9**, 867; (*b*) J. Okuda, *Chem. Ber.*, 1990, **123**, 1649; (*c*) T. Eberle, T. P. Spaniol and J. Okuda, *Eur. J. Inorg. Chem.*, 1998, 237; (*d*) A. L. McKnight and R. M. Waymouth, *Chem. Rev.*, 1998, **98**, 2587 and references therein; (*e*) L. Duda, G. Erker, R. Fröhlich and F. Zippel, *Eur. J. Inorg. Chem.*, 1998, 1153; (*f*) G. J. P. Britovsek, V. C. Gibson and D. F. Wass, *Angew. Chem.*, 1999, **111**, 448; *Angew. Chem., Int. Ed.*, 1999, **38**, 4228.

2 W. Kaminski, *J. Chem. Soc., Dalton Trans.*, 1998, 1413 and references therein.

3 (*a*) H. Braunschweig, C. von Koblinski and R. Wang, *Eur. J. Inorg. Chem.*, 1999, 69; (*b*) H. Braunschweig, C. von Koblinski and M. O. Kristen, Patentschrift, O.Z.0050/49643, 1998, submitted; H. Braunschweig, C. von Koblinski, M. Mamuti, U. Englert and R. Wang, *Eur. J. Inorg. Chem.*, 1999, 1899.

4 A. J. Ashe, III, X. Fang and J. W. Kampf, *Organometallics*, 1999, **18**, 2288; M. T. Reetz, M. Willuhn, C. Psiorz and R. Goddard, *Chem. Commun.*, 1999, 1105.

5 Y. Chen and T. J. Marks, *Organometallics*, 1997, **16**, 3649.

6 G. M. Sheldrick, SHELXL97: Program for Crystal Structure Determination, University of Göttingen, Germany, 1997.

ChemComm

Characterization of imidazolate-bridged Cu(II)–Zn(II) heterodinuclear and Cu(II)–Cu(II) homodinuclear hydroperoxo complexes as reaction intermediate models of Cu,Zn–SOD

Hideki Ohtsu,[a] Shinobu Itoh,[b] Shigenori Nagatomo,[c] Teizo Kitagawa,[c] Seiji Ogo,[c] Yoshihito Watanabe[c] and Shunichi Fukuzumi*[a]

[a] *Department of Material and Life Science, Graduate School of Engineering, Osaka University, CREST, Japan Science and Technology Corporation, Suita, Osaka 565-0871, Japan. E-mail: fukuzumi@chem.eng.osaka-u.ac.jp*
[b] *Department of Chemistry, Faculty of Science, Osaka City University, Sugimoto, Sumiyoshi-ku, Osaka 558-8585, Japan*
[c] *Institute for Molecular Science, Myodaiji, Okazaki 444-8585, Japan*

Received (in Cambridge, UK) 20th March 2000, Accepted 19th April 2000
Published on the Web 25th May 2000

Imidazolate-bridged Cu(II)–Zn(II) heterodinuclear and Cu(II)–Cu(II) homodinuclear hydroperoxo complexes are generated in the reactions between imidazolate-bridged heterodinuclear and homodinuclear complexes and H_2O_2 in the presence of triethylamine base and characterized spectroscopically as reaction intermediate models of Cu,Zn–SOD.

Copper–zinc superoxide dismutase (Cu,Zn–SOD) contains an imidazolate-bridged Cu(II)–Zn(II) heterodinuclear metal center in its active site.[1–6] This enzyme catalyses a very rapid two-step dismutation of superoxide to dioxygen and hydrogen peroxide through an alternate reduction and oxidation of the active-site copper ion as shown in Scheme 1.[5–7] An outer-sphere electron transfer from superoxide to the Cu(II) center occurs to produce O_2 and a Cu(I) center which may be oxidized by another molecule of superoxide in the presence of protons to produce H_2O_2 *via* a hydroperoxo–Cu(II) species (Scheme 1).[6,7] The hydroperoxo–copper(II) species is a key intermediate in biological oxidations catalyzed by copper enzymes including SOD. However, hydroperoxo–copper(II) complexes have been rarely characterized,[8] and there has been no report on the characterization of SOD model hydroperoxo–copper(II) complexes.

Several imidazolate-bridged heterodinuclear complexes have so far been reported as models of Cu,Zn–SOD using two independent mononuclear complexes and a bridging imidazolate ring.[9] However, the lack of binding site of O_2^- in these dinuclear complexes has precluded the characterization of the hydroperoxo–copper(II) intermediate. We have recently prepared imidazolate-bridged Cu(II)–Zn(II) heterodinuclear and Cu(II)–Cu(II) homodinuclear complexes with a newly designed dinucleating ligand, Hbdpi {Hbdpi = 4,5-bis[di(2-pyridylmethyl)aminomethyl]imidazole}.[10]

These SOD model complexes have a pentacoordinate structure at each metal ion including a solvent molecule which

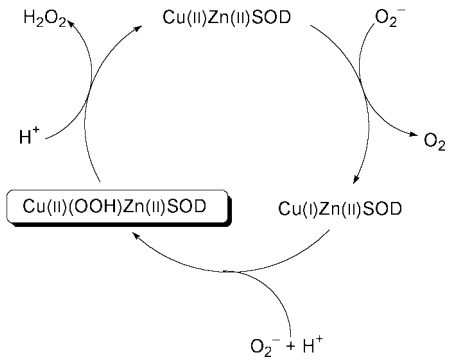

Scheme 1

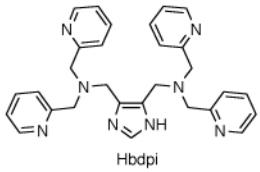

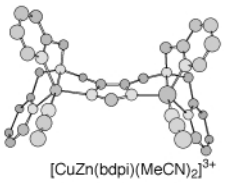

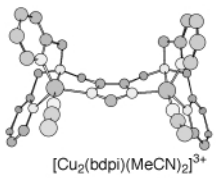

can be readily replaced by a substrate. We report herein the first characterization of SOD model hydroperoxo–Cu(II) intermediates generated by the reactions of hydrogen peroxide with imidazolate-bridged Cu(II)–Zn(II) heterodinuclear and Cu(II)–Cu(II) homodinuclear complexes.

The addition of a large excess of hydrogen peroxide to a MeOH solution of $[CuZn(bdpi)(MeCN)_2](ClO_4)_3 \cdot 2MeCN$ **1** or $[Cu_2(bdpi)(MeCN)_2](ClO_4)_3 \cdot MeCN \cdot 3H_2O$ **2** in the presence of a base such as triethylamine at −80 °C resulted in slight color change from greenish blue to green. The absorption spectra of the resulting solutions are shown in Fig. 1, where an intense band at 360 nm is observed in each case.

No decay of these bands was observed at −80 °C but they disappeared at room temperature. The absorbance of the

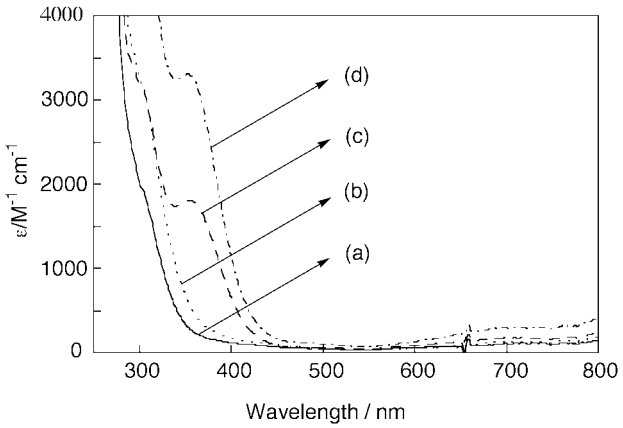

Fig. 1 Absorption spectra of (a) complex **1** (0.2 mM) and (b) **2** (0.2 mM) and those observed upon addition of a large excess of H_2O_2 to a MeOH solution of (c) **1** and (d) **2** in the presence of triethylamine at –80 °C.

DOI: 10.1039/b002208j

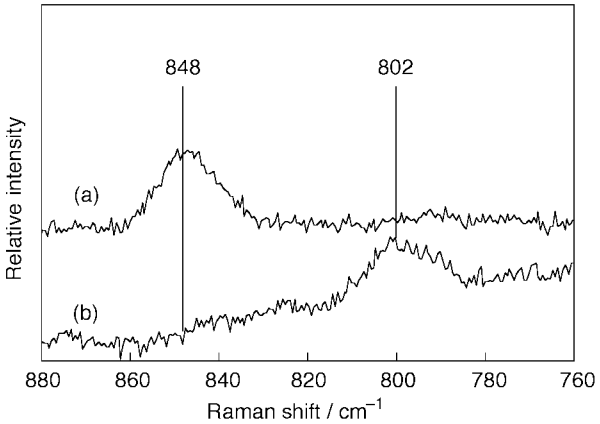

Fig. 2 Resonance Raman spectra obtained with 351 nm excitation of (a) a large excess $H_2{}^{16}O_2$ and (b) $H_2{}^{18}O_2$ in an MeOH solution of complex **1** in the presence of triethylamine at –80 °C.

intermediate **3** derived from complex **1** is about half that of intermediate **4** derived from the same concentration of **2**.

The resonance Raman spectrum of **3** in MeOH measured at −80 °C (laser excitation wavelength 351 nm) shows (Fig. 2) a strong resonance-enhanced Raman band at 848 cm^{-1}, which shifted to 802 cm^{-1} ($\Delta\nu$ = 46 cm^{-1}) when ^{18}O-labeled H_2O_2 was used. The resonance Raman spectrum of **4** was essentially the same as that of **3** ($H_2{}^{16}O_2$: 848 cm^{-1}, $H_2{}^{18}O_2$: 802 cm^{-1}, $\Delta\nu$ = 46 cm^{-1}). The ν value (848 cm^{-1}) of **3** is slightly lower than the value (856 cm^{-1}) reported for the mononuclear hydroperoxo–Cu(II) complex [Cu(II)(bppa)(OOH)](ClO$_4$) [bppa = bis(6-pivalamide-2-pyridylmethyl)(2-pyridylmethyl)amine], which is the only example of a structurally characterized hydroperoxo–Cu(II) complex.[8c] The $\Delta\nu$ value of **3** corresponds exactly to that of [Cu(II)(bppa)(OOH)](ClO$_4$) (46 cm^{-1}) in $H_2{}^{18}O_2$.[8c] The hydroperoxo–Cu(II) complex also has an intense absorption band at 380 nm which is slightly red-shifted as compared to **3** (Fig. 1).[8c] The intense absorption band has been assigned to the charge-transfer transition of the hydroperoxo group to copper(II) ion (LMCT).[8c]

The resonance Raman and absorption spectra in comparison with those of [Cu(II)(bppa)(OOH)](ClO$_4$) strongly indicate formation of hydroperoxo–Cu(II) intermediates, [CuZn(bdpi)(OOH)]$^+$ **3** and [Cu$_2$(bdpi)(OOH)$_2$]$^+$ **4** in the reactions of **1** and **2** with H_2O_2. This assignment is consistent with the half intensity in the absorption band at 360 nm of **3** as compared to **4** (Fig. 1), since **4** contains two Cu–OOH moieties.

Formation of hydroperoxo–Cu(II) intermediates was further confirmed by the ESI mass spectra of **3** and **4** in MeOH at −80 °C, which exhibited signals at *m/z* 651 and 681, respectively.[11] The observed mass and isotope patterns corresponded to the ions [CuZn(bdpi)(OOH)]$^+$ and [Cu$_2$(bdpi)(OOH)$_2$]$^+$, respectively. The use of $H_2{}^{18}O_2$ instead of $H_2{}^{16}O_2$ resulted in the expected change of mass numbers of **3** and **4** to *m/z* 655 and 685, respectively.

The EPR spectrum of **3** was typical of a trigonal-bipyramidal copper complex ($g_{\|}$ = 2.09, $g_{\perp}$ = 2.22, $A_{\|}$ = 8.9 mT and $A_{\perp}$ = 11.3 mT at 77 K in MeOH). These EPR parameters are quite close to those of **1** ($g_{\|}$ = 2.10, $g_{\perp}$ = 2.25, $A_{\|}$ = 10.4 mT and $A_{\perp}$ = 11.5 mT at 77 K in MeOH) and the X-ray structure of **1** shows a trigonal bipyramidal coordination environment of the copper ion.[10] Thus, the copper coordination site of **1** occupied by a solvent molecule may be substituted with hydroperoxide in the reaction with H_2O_2 in the presence of triethylamine base without changing the copper coordination geometry. The EPR spectrum of **4** gave a fairly broad signal centered at $g \cong 2.13$ without hyperfine structure, and this spectral feature is the same as that of **2**. This also indicates that the structure of the intermediate **4** maintains the imidazolate-bridged structure.

These results clearly demonstrate that hydroperoxo–Cu(II) complexes **3** and **4** are generated from imidazolate-bridged Cu(II)–Zn(II) and Cu(II)–Cu(II) SOD model complexes **1** and **2** which utilize their binding sites by reaction with H_2O_2 in the presence of triethylamine base. The hydroperoxo–Cu(II) complexes characterized in this study could serve as SOD intermediate models, providing valuable insight into the SOD catalytic mechanism.

We are grateful to Professor Osamu Yamauchi, Nagoya University, for valuable discussions. This work was partially supported by Grants-in-Aid for Scientific Research Priority Area (Nos. 11228205, 11136229, 11116219 and 11118244) from the Ministry of Education, Science, Culture and Sports of Japan.

Notes and references

1 I. Fridovich, *J. Biol. Chem.*, 1989, **264**, 7761; I. Fridovich, *Annu. Rev. Biochem.*, 1995, **64**, 97.
2 I. Bertini, L. Banci and M. Piccioli, *Coord. Chem. Rev.*, 1990, **100**, 67.
3 J. A. Tainer, E. D. Getzoff, K. M. Beem, J. S. Richardson and D. C. Richardson, *J. Mol. Biol.*, 1982, **160**, 181.
4 J. A. Tainer, E. D. Getzoff, J. S. Richardson and D. C. Richardson, *Nature*, 1983, **306**, 284.
5 P. J. Hart, M. M. Balbirnie, N. L. Ogihara, A. M. Nersissian, M. S. Weiss, J. S. Valentine and D. A. Eisenberg, *Biochemistry*, 1999, **38**, 2167.
6 E. M. Fielden, P. B. Roberts, R. C. Bray, D. J. Lowe, G. N. Mautner, G. Rotilio and L. Calabrese, *Biochem. J.*, 1974, **139**, 49.
7 L. M. Ellerby, D. E. Cabelli, J. A. Graden and J. S. Valentine, *J. Am. Chem. Soc.*, 1996, **118**, 6556.
8 (*a*) K. D. Karlin, R. Ghosh, R. W. Cruse, A. Farooq, Y. Gultneh, R. R. Jacobson, N. J. Blackburn, R. W. Strange and J. Zubieta, *J. Am. Chem. Soc.*, 1988, **110**, 6769; (*b*) R. R. Tahir, N. N. Murthy, K. D. Karlin, N. J. Blackburn, S. N. Shaikh and J. Zubieta, *Inorg. Chem.*, 1992, **31**, 3001; (*c*) A. Wada, M. Harata, K. Hasegawa, K. Jitsukawa, H. Masuda, M. Mukai, T. Kitagawa and H. Einaga, *Angew. Chem., Int. Ed.*, 1998, **37**, 798.
9 M. Sato, S. Nagae, M. Uehara and J. Nakaya, *J. Chem. Soc., Chem. Commun.*, 1984, 1661; Q. Lu, Q. H. Luo, A. B. Dai, Z. Y. Zhou and G. Z. Hu, *J. Chem. Soc., Chem. Commun.*, 1990, 1429; M. Zongwan, C. Dong, T. Wenxia, Y. Kaibei and L. Li, *Polyhedron*, 1992, **11**, 191; J.-L. Pierre, P. Chautemps, S. Refaif, C. Beguin, A. E. Marzouki, G. Serratrice, E. Saint-Aman and P. Rey, *J. Am. Chem. Soc.*, 1995, **117**, 1965; Z.-W. Mao, M.-Q. Chen, X.-S. Tan, J. Liu and W.-X. Tang, *Inorg. Chem.*, 1995, **34**, 2889.
10 H. Ohtsu, Y. Shimazaki, A. Odani, O. Yamauchi, S. Itoh and S. Fukuzumi, *J. Am. Chem. Soc.*, 2000, **122**, in press.
11 The flow pass (fused silica capillary, *ca*. 400 mm long, 0.075 mm inner diameter) in the system was precooled by flushing with MeOH cooled at –80 °C in an acetone/dry ice bath prior to measurements. A solution of **3** or **4** cooled at −80 °C was delivered to the sprayer through the fused silica capillary under a constant Ar pressure (0.1 MPa). The sprayer was held at a potential of −4.5 kV, and compressed N_2 was employed to assist liquid nebulization. The orifice potential was maintained at −25 V. The positive ion ESI mass spectra were measured in the range *m/z* 100–1000.

Nitrous oxide decomposition active site on Ni–MgO catalysts characterized by X-ray absorption fine structure spectroscopy

Yasuo Izumi,* Takehiro Shimizu, Takaaki Kobayashi and Ken-ichi Aika

Department of Environmental Chemistry and Engineering, Interdisciplinary Graduate School of Science and Engineering, Tokyo Institute of Technology, 4259 Nagatsuta, Midori-ku, Yokohama 226-8502, Japan.
E-mail: yizumi@chemenv.titech.ac.jp

Received (in Cambridge, UK) 6th April 2000, Accepted 8th May 2000

A contracted Ni^{2+} coordination site distorted in the direction of Ni···Mg and Ni···Ni was found to be responsible for catalytic N_2O decomposition when Ni^{2+} is diluted in a MgO matrix (Ni^{2+}/Mg^{2+} atomic ratio ≈ 1.0) based on a local structure study by nickel K-edge X-ray absorption fine structure spectroscopy.

Nitrous oxide is one of the gases which affects the environment. Catalysts for nitrous oxide decomposition have not been well developed compared with various catalysts for nitric oxide decomposition.[1] Nickel–MgO[2] and cobalt–MgO[3,4] are reported to form solid solutions. Metal ion-exchanged zeolites have been reported to be unstable to the effects of formed water during NO or N_2O decomposition reactions. A thermally and water-stable Co–MgO solid solution has been applied to N_2O decomposition.[4] The formation of an fcc structure-based solid solution was demonstrated by EXAFS (extended X-ray absorption fine structure) within the range of Co atom% [*i.e.* Co/(Co + Mg) × 100] of 0–5. However, a severe decrease of catalyst surface area and activity was found when the cobalt content exceeded *ca.* 10 atom% owing to the formation of the Co_3O_4 spinel phase.[4] Herein, the structure of Ni–MgO catalysts was investigated by EXAFS, XANES (X-ray absorption near-edge structure) and XRD (X-ray diffraction). Solid solution formation and the correlation between the local coordination structure of Ni ions and N_2O decomposition reactivity are discussed.

Powders were prepared by the impregnation of nickel nitrate into MgO and were heated in air at 1173 K for 24 h and in H_2 at 573 K for 1 h. With increase of nickel concentration, the BET surface area monotonously decreased from 50 $m^2\ g^{-1}$ (MgO) to 14 $m^2\ g^{-1}$ (Ni–MgO, Ni 33.6 atom%) and then remained constant upon further increase of nickel content. The decomposition of N_2O (0.1%) in helium (balance to 101.3 kPa) was monitored at 873 K in a flow system (flow rate 100 ml min^{-1}, 0.2 g catalyst used). The steady-state formation rate of N_2 (and O_2) per unit BET surface area increased linearly from 2 μmol N_2 $h^{-1}\ m^{-2}$ (MgO) to 51 μmol $h^{-1}\ m^{-2}$ (Ni–MgO, Ni 50.0 atom%), and then gradually decreased to 22 μmol $h^{-1}\ m^{-2}$ (NiO). The presence of nickel at the catalyst surface is essential for increased N_2O decomposition, but an excess of nickel (> 50 atom%) was detrimental to the performance of the catalyst.

Normalized Ni K-edge XANES spectra for Ni–MgO catalysts and NiO are shown in Fig. 1A.[5] The rising edge was always within 8339.4–8339.8 eV, demonstrating the valence state of nickel was +2 in the range of Ni 1.5–100 atom%. As the nickel content increases, the two peaks at 8342 and 8355 eV gradually decreased. The peaks at 8362 and 8389 eV for Ni 1.5 atom% [Fig. 1A(a)] gradually shifted, and finally reached 8365 and 8398 eV, respectively, for NiO [Fig. 1A(f)]. The peak intensity at 8389–8398 eV gradually decreased.

These experimental spectra were compared to XANES data generated by *ab initio* calculations. A code FEFF8 was applied to fcc-based model clusters within 6.0 Å from the absorbing Ni atom in self-consistent field (SCF) and multiple scattering calculation modes.[6,7] The imaginary optical potential used in the calculations of the exchange-correlation potential was fixed to 1.5 eV. The XANES spectrum was generated for an isolated Ni^{2+} model which contains only one Ni^{2+} ion at the center of a MgO cluster matrix (Fig. 1B, solid line). The peaks at 8342, 8349 (main peak) and 8389 eV in the XANES of Fig. 1A(a) (Ni 1.5 atom%) were reproduced in the spectra by FEFF8, but the calculated peak at 8359 eV did not correspond to any peaks in Fig. 1A. The gradual decrease in the peaks at 8342 and 8389 eV with increase of Ni^{2+} content was reproduced by FEFF8 (Fig.

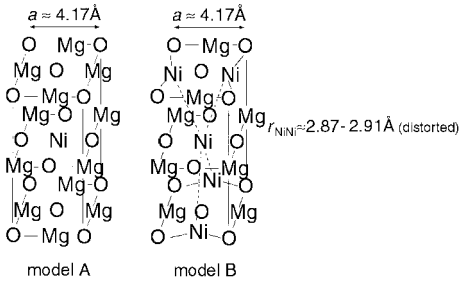

Scheme 1 Ni–MgO models. Model A: Ni 25 atom% unit cell model. Model B: Ni 50 atom% unit cell model. Half of the unit cell is drawn for B. All XANES calculations using FEFF8 were performed for complete (undistorted) fcc coordinates.

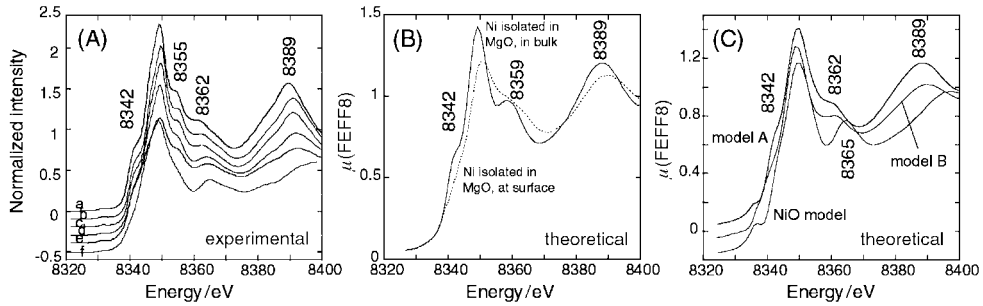

Fig. 1 (A) Ni K-edge XANES for Ni–MgO for Ni atom% of 1.5(a), 4.4(b), 9.5(c), 33.6(d) and 50.0(e) as well as for NiO(f). (B), (C) Ni K-edge XANES generated by FEFF8 for Ni^{2+} isolated in MgO (B, —) or at surface of MgO (B, -----), models A and B and for NiO (C).

Table 1 Ni K-edge EXAFS curve fitting results for Ni–MgO catalysts and NiO

		Ni–O			Ni···Mg			Ni···Ni			
Entry	Ni atom%	*N*	*R*/Å	$\Delta(\sigma^2)/10^{-3}$ Å^2	*N*	*R*/Å	$\Delta(\sigma^2)/10^{-3}$ Å^2	*N*	*R*/Å	$\Delta(\sigma^2)/10^{-3}$ Å^2	R_f[a]
a	1.5	4.7	2.105	0.17	12.0	2.971	2.6				1.9
		(±1.2)	(±0.005)	(±0.93)	(±2.8)	(±0.003)	(±1.4)				
b	4.4	4.9	2.086	0	11.2	2.95	−0.4	1.0	2.94	−2.2	0.92
		(±1.2)	(±0.005)	(±1.1)	(±1.4)	(±0.02)	(±1.7)	(±0.8)	(±0.01)	(±3.2)	
c	9.5	6.0	2.087	1.1	10.0	2.92	0.2	2.2	2.91	0.3	1.7
		(±0.8)	(±0.004)	(±0.8)	(±1.2)	(±0.02)	(±1.3)	(±0.9)	(±0.04)	(±5.4)	
d	33.6	5.1	2.088	1.0	7.6	2.918	0	4.1	2.91	5.8	1.4
		(±0.9)	(±0.005)	(±1.0)	(±1.8)	(±0.007)	(±1.2)	(±1.5)	(±0.02)	(±2.5)	
e	50.0	4.8	2.086	5.3	7.8	2.91	−1.3	4.4	2.872	7.0	0.71
		(±1.1)	(±0.003)	(±1.9)	(±2.0)	(±0.01)	(±2.2)	(±1.3)	(±0.007)	(±3.2)	
f	NiO	5.2	2.093	1.0				12.1	2.954	2.8	1.2
g[b]	NiO	(6)	(2.089)					(12)	(2.954)		

[a] $R_f = \int|k^3\chi(\text{obs.}) - k^3\chi(\text{fit})|^2dk/\int|k^3\chi(\text{obs.})|^2dk$. [b] According to X-ray crystallography.

1B and C). The peak at 8359 eV in Fig. 1B shifted to 8362 eV for models A and B (Scheme 1) and then to 8365 eV for the NiO model (Fig. 1C).

Based on these trends (peak position and intensity), the local structure of Ni^{2+} in Ni–MgO (Ni 1.5 atom%) corresponds to model A. The experimental spectra for Ni–MgO (Ni 4.4 and 9.5 atom%) were similar to theoretical XANES for model B. The spectra for Ni 33.6 and 50.0 atom% [Fig. 1A(d), (e)] were more similar to theoretical XANES for model B than that for NiO (Fig. 1C). Each peak in the theoretical XANES spectra for the surface isolated Ni^{2+} model was smeared out (Fig. 1B, dotted line), and did not resemble any spectra in Fig. 1A. Hence, impregnated nickel appears to be distributed statistically inside the MgO matrix and less appears at the MgO surface. Although imaginary optical potential values and Debye–Waller factors were varied, the shoulder peak at 8355 eV in Fig. 1A was not reproduced in theoretical XANES spectra.[8]

Ni K-edge EXAFS spectra for Ni–MgO catalysts were analyzed.[9] The model parameters of Ni-O, Ni···Mg, and Ni···Ni bonds were generated by FEFF8 in SCF mode. The application of SCF FEFF8 parameters to this system was validated by the curve fit for NiO (Table 1 entry f) which was in accord with crystallographic data (entry g).[10] The coordination number had an error of 12–26% for Ni–O and Ni···Mg and an error of 30–80% for Ni···Ni due to the fit procedure and FEFF theoretical parameters. For Ni–MgO catalysts, the best fit results and fit errors based on 10–20 relatively good fits (R_f < 2.0%) for each spectrum are listed in Table 1. Obtained Ni–O and Ni···Mg distances for Ni 1.5 atom% indicate the same or slightly smaller (< 0.007 Å) coordination distance compared to the pure MgO framework (a = 4.2112 Å). Ni–MgO, (Ni 1.5 atom%) corresponds to either model A (Scheme 1) or an isolated single Ni^{2+} atom model in bulk MgO, in both cases there is no second shell Ni···Ni bond.

With an increase of Ni content above 4.4 atom%, N_{Ni-O} and r_{Ni-O} remained almost constant while the $N_{Ni\cdots Ni}/N_{Ni\cdots Mg}$ ratio gradually increased (Table 1, entries b–e). Model B (Scheme 1) has eight Ni···Mg and four Ni···Ni bonds, corresponding to Table 1, entries d and e. XANES generated for a model with one to two Ni^{2+} at next-nearest sites (intermediate between models A and B) was similar to XANES generated for model B (four next-nearest Ni^{2+}), consistent with obtained local coordination by EXAFS (Table 1, entries b and c). The value of a according to XRD monotonously decreased from 4.211 ± 0.002 Å (Ni 4.4 atom%) to 4.190 ± 0.001 Å (Ni 50.0 atom%).[11] When the Ni^{2+} ion concentration is nearly one per unit cell (Ni–MgO, Ni 4.4 atom%), the Ni^{2+} site is locally contracted in an undistorted cell with $a \approx 4.17$ Å. With two Ni^{2+} ions per unit cell (Ni–MgO, Ni 33.6 and 50.0 atom%), the Ni^{2+} sites are locally contracted and distorted in the direction of Ni···Mg and Ni···Ni (2.87–2.92 ± 0.02 Å), smaller than $\sqrt{2}r_{Ni-O}$ [2.950–2.953 (±0.007 Å)] by 0.03–0.08 Å.

Models with locally contracted Ni^{2+} sites (Table 1, entries c–e) shows significantly different Ni···Mg and Ni···Ni distances (2.97–2.94 Å) in the whole range of Ni (0.02–100 atom%) of ref 12. The lower calcination temperature of Ni–MgO samples (773 K)[12] may be the reason for this discrepancy, compared to the temperature of 1173 K used in this work and 1473 K in ref 3. Solid solution formation from supported NiO particles over MgO was suggested to proceed at > 1073 K.[2]

The reason for the dependence of N_2O decomposition rates on Ni^{2+} content in catalysts can be addressed based on the determined Ni^{2+} local structure. Contracted Ni^{2+} sites at the surface are responsible for the dissociation of the N_2–O bond. As the nickel content increases, the number of contracted Ni^{2+} site increases and therefore the N_2 formation rate per unit BET surface area increases to Ni 50 atom%. The next elementary step, $O(ads) + O \rightarrow O_2$, relates to the activity decrease above Ni 50 atom%. An isotope study utilizing ^{18}O labeling of the catalyst surface and $^{16}O(ads)$ resulted in exclusive $^{16}O^{18}O$ formation, *i.e.* the step $O(ads) + O(surf) \rightarrow O_2$. The Ni^{2+} local coordination for a Ni content of 50.0 atom% (Table 1, entry e) corresponds to model B (Scheme 1). The rate of $^{16}O^{18}O$ formation was in the order, Ni–MgO (Ni 50.0 atom%) > MgO > NiO, suggesting that surface oxygen bonded to Mg^{2+} is more reactive and diagonal distortion of Ni···Mg and Ni···Ni destabilizes lattice oxygen. The nitrous oxide adsorption was weak and not detected by FTIR. Raman and IR spectroscopy may give further insight of distorted lattice vibration around doped Ni^{2+}.[13]

Notes and references

1 M. Shelef, *Chem. Rev.*, 1995, **95**, 209.
2 F. Arena, B. A. Horrell, D. L. Cocke, A. Parmaliana and N. Giordano, *J. Catal.*, 1991, **132**, 58.
3 A. Kuzmin, N. Mironova, J. Purans and A. Sazanov, *Phys. Status Solidi A*, 1993, **135**, 133.
4 Y. Izumi, K. Oshihara and K. Aika, *Chem. Lett.*, 1998, 727.
5 Spectra were measured at the KEK-PF, 7C (99G259) using an Si(111) double crystal monochromator in transmission mode at 290 K.
6 A. L. Ankudinov, B. Ravel, J. J. Rehr and S. D. Conradson, *Phys. Rev. B*, 1998, **58**, 7565.
7 J. J. Rehr, J. Mustre de Leon, S. I. Zabinsky and R. C. Albers, *J. Am. Chem. Soc.*, 1991, **113**, 5135.
8 Theoretical difficulties in incorporating the experimental effects of beamline energy resolution may be the reason for this result.
9 T. Yokoyama, H. Hamamatsu and T. Ohta, EXAFSH 2.1, The University of Tokyo.
10 A. Corrias, G. Mountjoy, G. Piccaluga and S. Solinas, *J. Phys. Chem. B*, 1999, **103**, 10 081.
11 Based on (111), (200), (220), (311) and (222) reflections.
12 T. Yoshida, T. Tanaka, H. Yoshida, T. Funabiki and S. Yoshida, *J. Phys. Chem.*, 1996, **100**, 2302.
13 J. M. Stencel, *Raman Spectroscopy for Catalysis*, Van Nostrand Reinhold, New York, 1990.

ChemComm

Transition metal complexes of the weakly coordinating carborane anion $[CB_{11}H_{12}]^-$: the first isolation and structural characterisation of an intermediate in a silver salt metathesis reaction

Nathan J. Patmore,[a] Jonathan W. Steed[b] and Andrew S. Weller*[a]

[a] *Department of Chemistry, University of Bath, Bath, UK BA2 7AY. E-mail: a.s.weller@bath.ac.uk*
[b] *Department of Chemistry, Kings College London, The Strand, London, UK WC2R 2LS*

Received (in Cambridge, UK) 31st March 2000, Accepted 8th May 2000

Reaction between $CpMo(CO)_3I$ and $Ag[CB_{11}H_{12}]$ eventually affords $CpMo(CO)_3(\eta^1\text{-}CB_{11}H_{12})$, *via* the dimeric compound $[CpMo(CO)_3I{\cdot}Ag\{CB_{11}H_{12}\}]_2$ which represents the first structurally characterised intermediate in a silver salt metathesis reaction.

The ubiquitous silver halide metathesis reaction, used to generate vacant sites on a metal fragment, finds application in many transition metal-mediated reactions, especially *in situ* catalyst generation.[1] Typically, the counter ion paired in such transformations is triflate, $[OTf]^-$, $[BF_4]^-$ or $[PF_6]^-$, and halide metathesis is considered to be rapid. Over ten years ago, Reed and coworkers reported[2] that very weakly coordinating anions, such as the monocarborane $[closo\text{-}CB_{11}H_{12}]^-$,[3] could dramatically slow the rate of metathesis when paired with Ag^+, suggesting that the exceptionally low nucleophilicity of the anion was a limiting factor in these reactions. Reaction between $CpFe(CO)_2I$ ($Cp = \eta^5\text{-}C_5H_5$) and $Ag[CB_{11}H_{12}]$ was proposed (by ^1H NMR and IR data) to proceed through an intermediate adduct, $CpFe(CO)_2I{\cdot}Ag[CB_{11}H_{12}]$, similar to Mattson and Graham's[4] proposed intermediate adduct, formed between $CpFe(CO)_2I$ and $Ag[BF_4]$. However, neither of these transient species (or other related[5] compounds) have been placed on a firm structural footing. Given the widespread use of the silver salt metathesis reaction, the identity of the intermediates in these reactions is of significant interest.

We have a current interest in the transition metal chemistry associated with carboranes such as $[CB_{11}H_{12}]^-$, and as part of this investigation have been studying the reactions of $CpMo(CO)_3X$ (X = Cl, I) with $Ag[CB_{11}H_{12}]$ and derivatives, with the anticipation of forming complexes *via* extrusion of AgX. We report here, the isolation and full characterisation, including the X-ray crystal structure, of the intermediate formed in this silver salt metathesis reaction.

Reaction between $CpMo(CO)_3Cl$ and $Ag[CB_{11}H_{12}]$ in CH_2Cl_2 over 2 days resulted in the precipitation of AgCl and the isolation, in essentially quantitative yield, of $CpMo(CO)_3(\eta^1\text{-}CB_{11}H_{12})$ **2** (Scheme 1). Compound **2** has been fully characterised by multinuclear NMR spectroscopy† and by an X-ray diffraction study[6] and shows the expected[2] 3c–2e Mo–H–B agostic bonding. Compound **2** displays two CO stretching modes in its IR spectrum, at 2071 and 2001 cm^{-1}. Monitoring the reaction by IR spectroscopy showed that the reaction proceeded through an intermediate species [as found for $CpFe(CO)_2I$[2]], but at no time was there a single component observed in the reaction mixture. Moving to $CpMo(CO)_3I$ resulted in a slowing down of the reaction, so that formation of **2** now took 7 days, while after *ca.* 3 h of stirring there was only one component in the reaction mixture, which displayed IR stretches at 2054 and 1973 cm^{-1}, intermediate between the starting material and product. Monitoring this reaction by IR and ^1H NMR spectroscopies showed that this was indeed an intermediate species, continued stirring for 7 days resulting in the clean formation of **2**. Careful recrystallisation of this intermediate overnight at −30 °C afforded small red crystals in reasonable isolated yield (50%), which were pure by IR, microanalysis and NMR spectroscopy,‡ and shown by X-ray diffraction§ to be $[CpMo(CO)_3I{\cdot}Ag\{CB_{11}H_{12}\}]_2$ **1**: the first structurally characterised intermediate in a silver salt metathesis reaction.

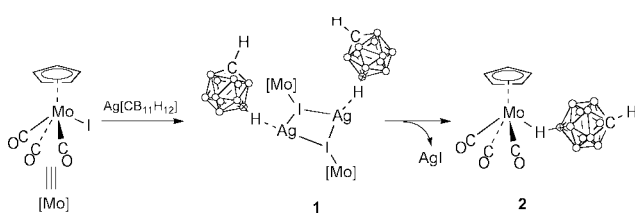

Scheme 1

The solid state structure of **1** is shown in Fig. 1. It is apparent that it adopts a centrosymmetric dimeric structure, with an I–Ag–I–Ag central core hinged around the Mo(1)–I(1)–I(1A)–Mo(1A) vector by 123.2°. The two Ag–I lengths are significantly different, Ag(1)–I(1) 2.9748(10) Å and Ag(1)–I(1A) 2.7599(9) Å. While similar central cores to **1** are known,[7,8] the presence of two additional [M]–I–Ag bridges appended to such a motif is unprecedented. However, there are silver adduct species of transition metal halides that show similar features,[9] such as the recently reported complex $[\{TpRe(NC_6H_4Me\text{-}p)(Ph)I\}_2Ag][PF_6]$[10] [Tp = tris(pyrazolyl)borate] in which silver bridges two {[Re]–I} fragments. The carborane anion is intimately connected with silver, showing a short (1.96 Å) Ag–H–B interaction [Ag(1)–B(12) 2.659(10) Å]. The cages are orientated *syn* to one another with respect to the Mo–I–I–Mo vector, leaving the silver atoms with an apparent vacant coordination site. Inspection of the packing diagram for **1** reveals that this site is occupied by another short (1.96 Å) Ag–H–B interaction arising from an adjacent carborane cage in the lattice, meaning that each cage bridges two silver centres [through H(12) and H(7)]. This results in a chain-like structure

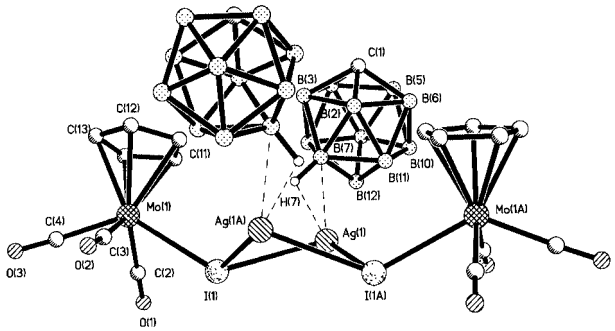

Fig. 1 Structure of the dimeric unit in complex **1**. Atom labels suffixed 'A' are generated crystallographically. Hydrogen atoms [except H(7)] are omitted for clarity. Selected bond lengths (Å) and angles (°): Mo(1)–I(1) 2.8599(8), Ag(1)–I(1) 2.9748(10), Ag(1A)–I(1) 2.7599(9), Ag(1)–B(7) 2.659(10), Ag(1)–H(7) 1.96; Ag(1)–I(1)–Ag(1A) 71.19(3), I(1)–Ag(1)–I(1A) 97.10(3).

DOI: 10.1039/b002585m

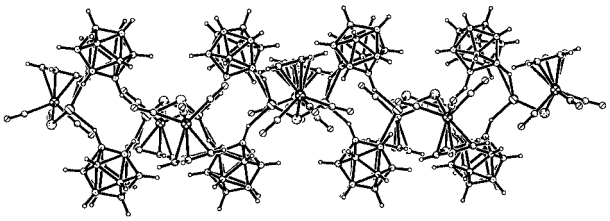

Fig. 2 Extended solid state structure of **1** viewed along the crystallographic '*a*' axis.

along the '*a*' axis in the crystal (Fig. 2). A similar bridging motif has been observed in the simple salt $Ag[CB_{11}H_{12}]\cdot 2C_6H_6$,[2] while dimeric structures formed from single Ag–H–B interactions have also been reported.[11,12]

Although it is unlikely that this polymeric structure persists on dissolution in CH_2Cl_2, evidence for coordination of the carborane cage to Ag in solution comes from inspection of the ^{11}B NMR spectra. The room temperature $^{11}B\{^1H\}$ NMR spectrum (128 MHz) shows two peaks at δ −11.1 and −14.6 in the ratio 1 : 10 (latter peak a 5 + 5 coincidence), significantly different from the free anion (*vide infra*), the unique boron resonance being shifted upfield by *ca.* 5.5 ppm with respect to $Ag[CB_{11}H_{12}]$ [$\delta_{^{11}B}$ −5.4 (1B), −10.6 (5B) and −12.3 (5B) in d_6-acetone]. This chemical shift difference suggests sustained Ag–H–B interaction(s) in solution and is consistent with the observed Ag–H–B contacts in the solid state. In the room-temperature $^1H\{^{11}B\}$ NMR spectrum the unique BH is observed at δ 2.12 and shifts slightly to δ 1.92 on cooling to −90 °C, showing no Ag–H coupling, although such interactions are rarely observed. The ^{109}Ag NMR spectrum displayed a single sharp line at δ 1335, shifted significantly downfield from the normal range ($\delta_{^{109}Ag}$ *ca.* 500) expected for Ag(I) centres.[13]

Overall metathesis can be dramatically suppressed in this system by moving to the less nucleophilic and sterically bulkier carborane anion $Ag[CB_{11}H_6Br_6]$. Stirring for 1 h results in the clean formation of the analogous intermediate complex to **1**,[14] but, surprisingly, no subsequent metathesis was observed, even after extended stirring for 7 days. This result is in accord with the previous observation that the relative nucleophilicity of the conjugate anion in these reactions is rate determining.[2] Nevertheless, the cessation of this reaction at the intermediate stage is, to our knowledge, without precedent. It should be noted, however, that metathesis does not proceed to completion when Vaska's complex and $Ag[CB_{11}H_{12}]$ are combined, but in this system a strong Ag–Ir bond is formed instead,[15] very different from the structure of **1**.

In summary, we have presented here the first fully characterised (NMR, X-ray diffraction) intermediate in a silver salt metathesis reaction, and found it to have a dimeric {[Mo]–I}–Ag–{[Mo]–I}–Ag core in the solid state. This result leads us to speculate upon the motifs accessible using combinations of other $CpML_nX_y$ fragments and monocarborane anions, and we are currently actively pursuing this. Moreover, the lack of metathesis consummation with $Ag[CB_{11}H_6Br_6]$ demonstrates that there is a significant degree of kinetic control in a reaction that is normally considered very facile. This has potential implications for the synthesis of transition metal complexes bearing very weakly coordinating anions *via* silver salt metathesis.

We thank the EPSRC and King's College London for the provision of the X-ray diffractometer and the Nuffield Foundation for the provision of computing equipment (J. W. S.). The Royal Society (A. S. W.) and the University of Bath (N. J. P.) are thanked for financial support. Dr Mary Mahon is thanked for useful discussions and Dr J. P. Rourke is thanked for his assistance in obtaining the ^{109}Ag spectrum of **1**.

Notes and references

† *Spectroscopic data* for **2**: $\delta_{H\{^{11}B\}}$(400 MHz, CD_2Cl_2) 5.86*, 5.79 (5H, s), 2.53 (1H, s, $C_{cage}H$), 1.79 (5H, s, BH), 1.66 (5H, s, BH), −15.11 (1H, s, Mo–H–B). Selected δ_H: −15.11 [1H, partially collapsed quartet, *J*(BH) 90]. $\delta_{^{11}B}$ (128 MHz, CD_2Cl_2) −4.7*, −10.4 (1B, d sh), −11.7 [5B, d, *J*(HB) 151 Hz], −13.9 [5B, d, *J*(HB) 151 Hz], −18.6* (* indicates peaks relating to a minor isomer[6]). Found: C, 28.0; H, 4.4. Calc. for $C_9H_{17}O_3B_{11}Mo$: C, 27.9; H, 4.4%. IR (KBr, cm^{-1}): 2582m, 2549m, 2243w br, 2067s, 1991s, 1980s. (CH_2Cl_2): 2573m, 2230w, vbr, 2071s 2001s br.

‡ *Spectroscopic data* for **1**: 273 K: $\delta_{H\{^{11}B\}}(CD_2Cl_2)$ 5.75 (5H, s), 2.56 (1H, s, $C_{cage}H$), 2.12 (1H, s, BH) and 1.86 (10H, s, BH). $\delta_{^{11}B}(CD_2Cl_2)$ −11.1 [1B, d, *J*(HB) 119 Hz], −14.6 [5B + 5B, app. d, *J*(HB) *ca.* 144 Hz]. 183 K: $\delta_{H\{^{11}B\}}(CD_2Cl_2)$ 5.76 (5H, s), 2.56 (1H, s, $C_{cage}H$), 1.92 (1H, s, BH), 1.73 (5H, s, BH) and 1.68 (5H, s, BH). $\delta_{^{11}B}(CD_2Cl_2)$ −10.1 (1B, br), −14.0 (10B, br). $\delta_{^{109}Ag}$(18 MHz, CD_2Cl_2) 1335 (s). Found: C, 17.8; H, 2.8. Calc. for $C_9H_{17}AgB_{11}IMoO_3$: C, 17.4; H, 2.7%. IR (KBr, cm^{-1}) 2556m, 2531m, 2041s, 1971s, 1950s, (CH_2Cl_2): 2570m, 2054s, 1973s br.

§ *Crystal data* for **1**: $C_9H_{17}AgB_{11}IMoO_3$, M = 622.85, λ = 0.71073 Å, orthorhombic, space group *Pnna*, a = 13.8843(4), b = 15.7193(4), c = 18.1490(6) Å, U = 3961.0(2) $Å^3$, Z = 8, T = 120(2) K, D_c = 2.089 g cm^{-3}, μ = 3.186 mm^{-1}, F(000) = 2336, crystal 0.20 × 0.10 × 0.08 mm, 3870 unique reflections (R_{int} = 0.0476), R_1 = 0.0563, wR_2 = 0.1101 [$I > 2\sigma(I)$].

CCDC 182/1630. See http://www.rsc.org/suppdata/cc/b0/b002585m/ for crystallographic files in .cif format.

1 *Catalytic Asymmetric Synthesis*, ed. I. Ojima, Wiley-VCH, Weinheim, 1993.
2 D. J. Liston, Y. J. Lee, W. R. Scheidt and C. A. Reed, *J. Am. Chem. Soc.*, 1989, **111**, 6643.
3 C. A. Reed, *Acc. Chem. Res.*, 1998, **31**, 133.
4 B. M. Mattson and W. A. G. Graham, *Inorg. Chem.*, 1981, **20**, 3186.
5 D. J. Crowther, S. L. Borkowsky, D. Swenson, T. Y. Meyer and R. F. Jordan, *Organometallics*, 1993, **12**, 2897.
6 N. J. Patmore, M. F. Mahon and A. S. Weller, unpublished results.
7 G. A. Bowmaker, Effendy, P. J. Harvey, P. C. Healy, B. W. Skelton and A. H. White, *J. Chem. Soc., Dalton Trans.*, 1996, 2459 and references therein.
8 B.-K. Teo and J. C. Calabrese, *J. Chem. Soc., Chem. Commun.*, 1976, 185.
9 T. N. Sal'nikova, V. G. Andrianov and Y. T. Struchkov, *Koord. Kkim.*, 1976, **2**, 707.
10 W. S. McNeil, D. D. DuMez, Y. Matano, S. Lovell and J. M. Mayer, *Organometallics*, 1999, **18**, 3715.
11 Y. W. Park, J. Kim and Y. Do, *Inorg. Chem.*, 1994, **33**, 1.
12 H. M. Colquhoun, T. J. Greenhough and M. G. H. Wallbridge, *J. Chem. Soc., Chem. Commun.*, 1980, 192.
13 R. Eujen, B. Hoge and D. J. Brauer, *Inorg. Chem.*, 1997, **36**, 1464.
14 IR ν(CO) cm^{-1}: 2054 and 1975 cm^{-1}. Found: C, 9.28; H, 1.11. Calc.: C, 9.86; H, 1.00%.
15 D. J. Liston, C. A. Reed, C. W. Eigenbrot and W. R. Scheidt, *Inorg. Chem.*, 1987, **26**, 2739.

Novel class of ammonia synthesis catalysts

Claus J. H. Jacobsen

Haldor Topsøe Research Laboratories, Nymøllevej 55, DK-2800 Lyngby, Denmark. E-mail: chj@topsoe.dk

Received (in Oxford, UK) 10th April 2000, Accepted 9th May 2000

Ternary nitrides Fe_3Mo_3N, Co_3Mo_3N and Ni_2Mo_3N, exhibit high catalytic activities in ammonia synthesis; promotion of Co_3Mo_3N with caesium results in higher activity than that of the commercial multi-promoted iron based catalyst.

During the 20th century the catalytic ammonia synthesis has grown to be among the most important industrial processes. More than 1% of the total global energy consumption is currently used for ammonia production. Therefore, improvements in this process could have a significant impact on the consumption of fossil fuels. Consequently, a continuous effort has been made to improve both the Haber–Bosch process and the promoted iron based catalyst discovered by Mittasch and coworkers. Despite these efforts, the preferred industrial ammonia synthesis catalyst is still a multi-promoted iron catalyst very similar to that developed almost a century ago. It was realized by the group of Haber that both osmium and ruthenium catalysts exhibit high ammonia synthesis activities.[1]

Detailed accounts of the previous work on non-iron catalysts have been published.[2,3] Recently, a promoted ruthenium catalyst supported on a special graphite carrier was introduced in commercial operation.[4,5] However, it is not clear whether the improved activity of such catalysts is justified by the significantly higher cost and shorter life-time relative to the traditional iron catalyst. Clearly, it would be very desirable to develop new, active and stable catalysts that do not contain noble metals. We have found that the ternary nitrides Fe_3Mo_3N, Co_3Mo_3N and Ni_2Mo_3N are active and stable ammonia synthesis catalysts at industrially relevant conditions. Addition of a small amount of Cs to Co_3Mo_3N results in a catalyst with a higher activity than that of the commercial multi-promoted iron catalyst.[6]

Ternary nitrides were obtained by two different routes. The first is based on ammonolysis of solid oxide precursors as reported in the literature.[7] The oxide precursors were obtained by mixing a solution of the desired metal nitrate salt (M = Fe, Co, Ni) with a solution of ammonium heptamolybdate. The mixture was evaporated to dryness and calcined at 400 °C for 2 h. The resulting $MMoO_4{\cdot}xH_2O$ was heated at 0.1 °C min^{-1} to 600 °C in a stream of 4.5% NH_3 in 3 : 1 H_2–N_2. After cooling to room-temperature it was confirmed by X-ray powder diffraction that pure Fe_3Mo_3N, Co_3Mo_3N and Ni_2Mo_3N were formed when Fe : Mo = 1, Co : Mo = 1 and Ni : Mo = 2/3, respectively. It was also found that if a Ni : Mo ratio of 1 was used, the X-ray powder patterns could be assigned to a mixture of Ni_2Mo_3N and NiMo alloy and *not* to Ni_3Mo_3N as previously suggested.[8] Alternatively, the ternary nitrides were prepared from high surface area molybdenum nitride obtained by temperature programmed reaction of MoO_3 with NH_3 as described by Volpe and Boudart.[9] The resulting Mo_2N with a surface area of > 200 $m^2\ g^{-1}$ was successively impregnated with saturated solutions (followed by drying) of the desired metal nitrate solution to obtain the correct stoichiometry. Subsequently, the sample was dried and heated at 0.1 °C min^{-1} to 600 °C in a stream of 4.5% NH_3 in 3 : 1 H_2–N_2. It was confirmed by X-ray powder diffraction that Fe_3Mo_3N, Co_3Mo_3N and Ni_2Mo_3N were also formed by this procedure.

Addition of controlled amounts of caesium nitrate to the catalysts could be achieved either by impregnation of the oxide precursors prior to ammonolysis or directly onto the nitride catalyst before testing.

X-Ray powder patterns were recorded by slow scanning on a Philips vertical goniometer equipped with a θ-compensating divergence slit and a diffracted beam graphite monochromator utilizing Cu-Kα radiation. Crystal sizes were estimated from the broadening of the diffraction peaks using the Scherrer equation. *In situ* X-ray powder patterns were obtained as previously described.[10]

Surface areas were obtained from isotherms measured with a Quantachrome Autosorb using N_2 as adsorbant at 77 K.

Catalytic ammonia synthesis activities were recorded at pressures from 1 to 100 bar, temperatures between 320 and 500 °C, and in 3 : 1 and 1 : 1 H_2–N_2 gas mixtures using the set-up previously described.[11] The reported activities are based on the mass of catalyst loaded into the reactor and given as ml ammonia (at STP) produced per hour per gram of catalyst.

In order to conclusively establish that the ternary nitrides are stable under ammonia synthesis, an *in situ* XRPD experiment was conducted. A small amount of $NH_5(CoOHMoO_4)_2$ was loaded into a capillary reactor and transferred to the *in situ* XRPD set-up. A stream of pure ammonia was passed through the sample while it was heated at 0.5 °C min^{-1} to 600 °C at ambient pressure. It was seen that the starting material, $NH_5(CoOHMoO_4)_2$ (prepared by precipitation from a cobalt nitrate and ammonium heptamolybdate solution kept at pH = 8 for 3 days) initially transformed into Co and MoO_2 at 470 °C and a little later MoO_2 transforms into γ-Mo_2N. Finally, Co_3Mo_3N is formed at 600 °C from Co and γ-Mo_2N. From this reaction sequence it was natural to attempt the preparation of Co_3Mo_3N by impregnation of γ-Mo_2N with a metal salt followed by ammonolysis. In principle, this method might be applicable for the preparation of a wide range of ternary or quarternary nitride materials. When formation of Co_3Mo_3N was confirmed in the *in situ* XRPD set-up the sample was cooled to 400 °C and the gas changed to a 3 : 1 mixture of H_2–N_2 at 25 bar. No further changes in the X-ray powder pattern were observed and it was possible to detect formation of ammonia using a Baltzers quadrupole mass spectrometer connected to the exit stream from the capillary reactor.

Fig. 1 shows the X-ray powder pattern obtained at 400 °C, 25 bar in a 3 : 1 mixture of dihydrogen and dinitrogen. All

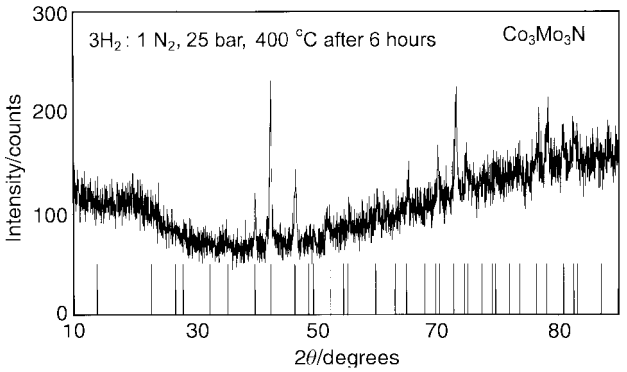

Fig. 1 *In situ* X-ray powder pattern obtained from Co_3Mo_3N at 400 °C, 25 bar in a 3 : 1 mixture of dihydrogen and dinitrogen. Calculated positions of the diffraction lines for Co_3Mo_3N are also shown.

DOI: 10.1039/b002930k

Table 1 Selected properties of molybdenum nitride and ternary nitride catalysts

Catalyst	Space group	BET surface area/m² g^{-1}	Average crystal size/nm
γ-Mo_2N	*Pm*3*m*	203	3.6
Fe_3Mo_3N	*Fdm*	8	45.0
Co_3Mo_3N	*Fd*3*m*	11	39.0
Ni_2Mo_3N	$P4_132$	7	44.0

diffraction lines are assigned to Co_3Mo_3N and it is concluded that Co_3Mo_3N is stable under ammonia synthesis conditions. *In situ* XRPD experiments were not conducted with Fe_3Mo_3N and Ni_2Mo_3N. However, no other compounds or phases were found using XRPD on spent catalyst samples.

Table 1 summarizes selected properties of the ternary nitrides prepared by ammonolysis of mixed oxide precursors. For comparison γ-Mo_2N is also included. It is seen that significantly lower surface areas are obtained for the ternary nitrides compared to that of γ-Mo_2N. The surface areas are in reasonable agreement with those estimated from the average crystal sizes. Promotion of the catalysts with *ca.* 5 wt% caesium did not result in a significant change in crystal size or surface area.

Catalytic activities were measured at 400 °C and 100 bar pressure. The inlet gas contained 4.5% ammonia in 3:1 dihydrogen–dinitrogen. The flow rate was adjusted to obtain 12% ammonia in the exit gas. Table 2 summarizes the activities of the unpromoted and caesium-promoted catalysts. It is observed that the activities are significantly enhanced by caesium promotion. For comparison the activity of a commercial multi-promoted iron catalyst, KM1,[12] is *ca.* 750 ml ammonia h^{-1} g^{-1} under similar conditions but at 410 °C.[13] Fig. 2 directly compares the activity of the caesium-promoted Co_3Mo_3N with that of the commercial catalyst at 400 °C and 50 bar in a 3:1 mixture of dihydrogen and dinitrogen. The feed flow was varied to study the influence of the exit concentration of ammonia on the activity. It is seen that both catalysts are inhibited by ammonia. Under these conditions the Cs/Co_3Mo_3N catalyst is significantly more active than the commercial iron catalyst. An activation energy of 54 kJ mol^{-1} was found for Cs/Co_3Mo_3N at constant conversion using the activity data at 50 bar and 320, 360, 400 and 440 °C. It should be noted that all activities reported here are based on the mass of catalyst. Industrially, the volume-based activities are usually more relevant and in this context it is important to note that the bulk densities of the nitride catalysts are as high as those of iron based catalysts.

Table 2 Catalytic ammonia synthesis activities of molybdenum nitride and ternary nitride catalysts at 400 °C, 100 bar and *ca.* 8% ammonia

Catalyst	Ammonia production/ml h^{-1} g^{-1}
γ-Mo_2N	30
Fe_3Mo_3N	90
Co_3Mo_3N	120
Ni_2Mo_3N	80
Cs/Fe_3Mo_3N	440
Cs/Co_3Mo_3N	1040
Cs/Ni_2Mo_3N	530

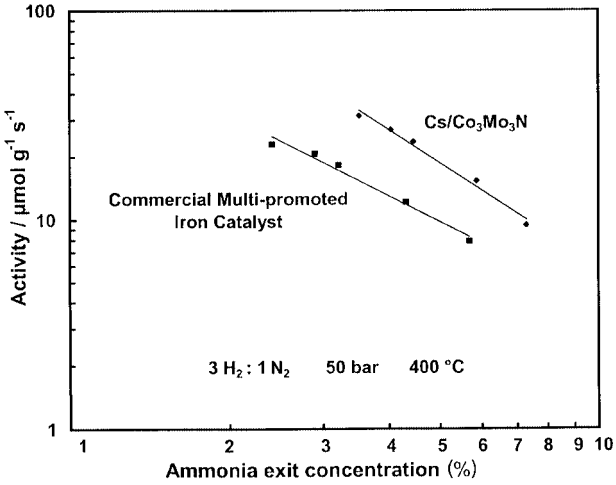

Fig. 2 Catalytic activities of caesium-promoted Co_3Mo_3N and a commercial multi-promoted iron catalyst.

Previously, molybdenum nitride has been reported to exhibit high activity in catalytic ammonia synthesis.[14] However, it is seen that the activities of the ternary nitride catalysts are significantly higher. Particularly, the caesium promoted Co_3Mo_3N catalyst appears interesting. Since the ternary nitride catalysts are formed by ammonolysis at 600 °C they are expected to be very stable during the conditions of ammonia synthesis. The activity shown for Cs/Co_3Mo_3N was unchanged after two weeks at 400 °C and 50 bar. Possibly, other ternary nitrides will also be active ammonia synthesis catalysts.

I would like to thank A. M. Molenbroek for obtaining the *in situ* XRPD patterns and J. Hartvig and L. Jensen for measuring the catalytic activities.

Notes and references

1 A. Mittasch, *Adv. Catal.*, 1950, **2**, 81.
2 A. Ozaki and K. Aika, *Catal. Sci. Technol.*, 1981, **1**, 87.
3 S. Tennison, in *Catalytic Ammonia Synthesis: Fundamentals and Practise*, ed. J. R. Jennings, Plenum Press, New York, 1991, p. 303.
4 *US Pat.*, No. 4,163,775, August 7, 1979 to BP Co.
5 T. A. Czuppon, S. A. Knez, R. W. Schneider and G. Worobets, *Ammonia Plant Saf.*, 1994, **34**, 236.
6 C. J. H. Jacobsen, M. Brorson, J. Sehested, H. Teunissen and E. Törnqvist, Patent Pending, March 12, 1999.
7 J. D. Houmes, D. S. Bem and H.-C. Z. Loye, *Mater. Res. Soc. Symp. Proc.*, 1994, **1**, 153.
8 M. A. Sriram, K. S. Weil and P. N. Kumta, *Appl. Organomet. Chem.*, 1997, **11**, 163.
9 L. Volpe and M. Boudart, *J. Solid State Chem.*, 1985, **59**, 332.
10 B. S. Clausen, G. Steffensen, B. Fabius, J. Villadsen, R. Feidenhans'l and H. Topsøe, *J. Catal.*, 1991, **132**, 524.
11 J. Sehested, C. J. H. Jacobsen, E. Törnqvist, S. Rokni and P. Stoltze, *J. Catal.*, 1999, **188**, 83.
12 A. Nielsen, *An Investigation on Promoted Iron Catalysts for the Synthesis of Ammonia*, Gjellerup, 3rd edn., July 1968.
13 C. J. H. Jacobsen, J. Jiang, S. Mørup, B. S. Clausen and H. Topsøe, *Catal. Lett.*, 1999, **61**, 115.
14 S. T. Oyama, *Catal. Today*, 1992, **15**, 179.

Synthesis and structural characterisation of a magnesium bisenolate: a tetrameric $(Mg_2O_2)_2$ chain terminated by solvating ketone

John F. Allan,[a] Kenneth W. Henderson,*[a] Alan R. Kennedy[a] and Simon J. Teat[b]

[a] *Department of Pure and Applied Chemistry, University of Strathclyde, Glasgow, UK G1 1XL. E-mail: k.w.henderson@strath.ac.uk*

[b] *CCLRC Daresbury Laboratory, Warrington, UK WA4 4AD*

Received (in Cambridge, UK) 11th April 2000, Accepted 9th May 2000

A reactive magnesium enolate intermediate has been identified containing the remarkable composition of four metals, eight enolates (six bridging and two terminally bound) and two unenolised ketones, and its implications in the aldol addition reaction are discussed.

Enolate anions are key intermediates in numerous transformations including alkylations, Michael reactions, protonations, acylations and aldol additions.[1] We have recently begun an investigation into the use of magnesium bisamides, $(R_2N)_2Mg$, as reagents and have found significant differences in their reactivity, and more importantly in their selectivity, compared with their Li analogues. Recently reported uses of Mg-bisamides include the regio- and stereo-selective synthesis of kinetic silyl enol ethers,[2] the formation of secondary and tertiary β-hydroxy ketones *via* aldol addition reactions,[3] and as asymmetric induction reagents in enantioselective deprotonation reactions.[4] Herein, we discuss the formation and structure of a novel magnesium bisenolate and consider its role as a model complex in the aldol addition reaction.

The organometallic complexes produced by the reaction of magnesium bishexamethyldisilazide **1** with 2,4,6-trimethylacetophenone **2** (between 2 and 6 mol equiv.) in hexane solution were initially determined by ^{1}H NMR spectroscopic analysis of the solids precipitated from solution.† Only enolate and unenolised ketone were present in the solids, and the absence of any amide suggested formation of a magnesium bisenolate. This is in marked contrast with our previous studies[3] of the reaction between **1** and 2 mol equiv. of a series of methyl ketones [O=C(Me)R, where R = Bu^t, Ph, Bu^n, Pr^i or cyclohexyl], which undergo aldol addition reactions. Furthermore, the aldol reaction sequence is supported by the structural characterisation of the amido(aldolate) $[\{(Me_3Si)_2NMg(\mu\text{-}OC(Me)^tBuCH_2C(^tBu)=O)\}_2]$ **3**,[3] *i.e.* enolisation followed by aldol addition with retention of one amido unit attached to the metal. Following initial formation of an amido(enolate), two distinct routes are in competition either enolisation or aldol addition (Scheme 1). Formation of a bisenolate in preference to an amido(aldolate) for the reactions involving **2** is most likely due to a combination of the steric crowding and the electronics of the ketone which retard the addition reaction.[5] The presence of an amido(enolate) intermediate in these reactions was confirmed by *in situ* ^{1}H NMR spectroscopic monitoring of the equimolar reaction between **1** and **2**. In addition, bisenolate was also detected in these mixtures demonstrating a competitive reaction even at this stage. Further support for an amido(enolate) reaction intermediate comes from the recent structural elucidation of $[\{(Me_3Si)_2NMg\{\mu\text{-}OC(Ph)=CHMe\}\cdot THF\}_2]$ **4**, formed by reaction of **1** with 1 equiv. of propiophenone.[2b]

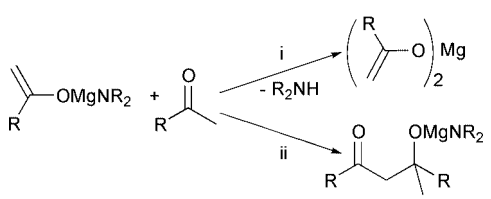

Scheme 1 Formation of (i) bisenolate or (ii) amido(aldolate) *via* an amido(enolate); aggregation state is ignored.

Repeated attempts at crystal growth from the reactions between **1** and **2** resulted in the formation of crystallites too small for conventional single crystal diffraction but were suitable for analysis using synchrotron radiation.‡ This study revealed the complex $[Mg_4\{OC(Mes)=CH_2\}_8\cdot\{O=C(Mes)\text{-}Me\}_2\cdot(C_6H_5(Me)_2)]$ **5** (Mes = 2,4,6-$Me_3C_6H_2$), which is centrosymmetric and contains the novel composition (ignoring the inclusion solvent toluene) of four magnesiums, six bridging enolates, two terminal enolates (O2 and O2*) and two ketones (O1 and O1*) coordinated to the terminal metal centres (Fig. 1). The linear arrangement of the metals in a limited tetrameric complex represents a completely new structural motif in magnesium coordination chemistry.[6] Although rare, tetrameric conformations, where the metals form either rhombohedral or tetrahedral geometries respectively, are known.[6] The structure of **5** can be described as a section of polymeric bisenolate consisting of linked orthogonal Mg_2O_2 rings which has been intersected by donor solvent, interestingly in this case unenolised ketone.

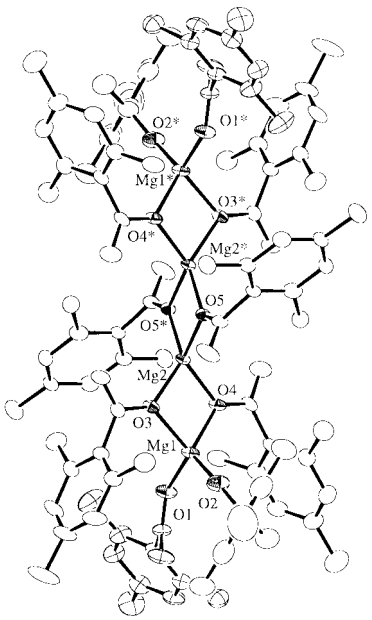

Fig. 1 Molecular structure of **5** with hydrogen atoms and solvents of crystallisation omitted for clarity. The ketone ligands are highlighted with hatched ellipses. Selected bond lengths (Å) and angles (°): Mg(1)–O(1) 2.012(3), Mg(1)–O(2) 1.845(3), Mg(1)–O(3) 1.991(3), Mg(1)–O(4) 1.970(3), Mg(2)–O(3) 1.969(3), Mg(2)–O(4) 1.965(3), Mg(2)–O(5) 1.978(3), Mg(2)–O(5*) 1.963(3); O(1)–Mg(1)–O(2) 110.08(13), O(1)–Mg(1)–O(3) 114.54(12), O(1)–Mg(1)–O(4) 108.28(12), O(2)–Mg(1)–O(3) 117.88(13), O(2)–Mg(1)–O(4) 122.24(14), O(3)–Mg(1)–O(4) 81.16(10), O(3)–Mg(2)–O(4) 81.83(11), O(4)–Mg(2)–O(5) 125.96(12), O(3)–Mg(2)–O(5) 117.87(11), O(3)–Mg(2)–O(5*) 135.08(12), O(4)–Mg(2)–O(5*) 121.39(11). * Indicates the transformation $1-x, 1-y, 1-z$.

DOI: 10.1039/b002892o

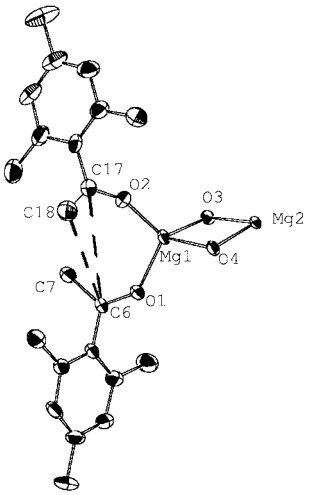

Fig. 2 View of the terminally bound groups in **5**. Important interatomic distances (Å): C(18)–C(6) 4.156(7), C(17)–C(6) 4.164(6), C(18)–O(1) 4.237(6), C(17)–O(1) 4.021(5).

Diphenylmagnesium adopts a polymeric structure[7] similar to the core of **5** but deaggregates only to monomers on addition of either THF or TMEDA.[8] The highly unusual tetrameric framework adopted by **5** may be explained by analysis of the structure. The two central aromatic rings, connected to O(5) and O(5*), are oriented *anti* to one another, whereas the aromatic groups of the terminal rings, connected to O(3) and O(4), are *syn* with respect to each other and are directed towards the terminal metal, Mg(1). If the polymeric form of the bisenolate has a similar structure the steric crowding induced by the *syn* aromatic groups may result in weak links in the polymer chain, leading to preferential scission at these sites. Alternatively, **5** may be the end product of chain growth with the *syn* aromatic groups on O(3) and O(4) blocking any further propagation.

The geometric parameters within **5** are in accord with those expected for Mg-alkoxides.[6] Each metal is four coordinate with no significant interactions to either the arene rings or the olefinic groups (all Mg–C are > 3 Å). The central Mg_2O_2 ring is strictly planar, whereas the two terminal rings are buckled, with each of the atoms deviating from the mean plane by 0.56(1) Å, and with an interplanar angle between the central and outer rings of 80.13(9)°.

A remarkable feature of **5** is the presence of solvating ketone in addition to enolate groups, hence **5** can be considered as a model, aggregated, pre-aldol intermediate. Although there has been much speculation about the importance of pre-solvation in similar transformations, in particular for Li-mediated reactions,[9] surprisingly little direct evidence for its existence has been reported.[10] In part, this is due to the high reactivity of these complexes. In this instance the aldol addition reaction is disfavoured facilitating the isolation of **5**. Nevertheless, the self-coupled tertiary β-hydroxy ketone derived from **2** was detected in low yield (< 5%) on extended reaction times. In contrast, secondary β-hydroxy ketones could be readily prepared (> 80% yield) by reaction of the enolate solutions with aldehydes.

Finally, it is intriguing to speculate on the orientations adopted by the terminally bound enolate and ketone groups within **5**. The olefinic carbons C(17) and C(18) are essentially equidistant to the carbonyl carbon C(6) of the ketone and hence the centre of the π-bond is oriented appropriately for nucleophilic attack of the carbonyl through a six-membered transition state similar to that postulated in the Zimmerman–Traxler model (Fig. 2).[11] Such a mechanism would involve aldol addition *via* the terminal and not the bridging enolate groups of the aggregate.

Notes and references

† **5**: a solution of **1** (3 mmol) in hexane (10 mL) was cooled to −78 °C and **2** (6–18 mmol) was added dropwise by syringe over a period of 2 min. The mixture was allowed to warm to ambient temperature after 15 min and stirred for a further two days. The resulting white solids were filtered off, washed with hexane and analysed by ^{1}H NMR spectroscopy. Subsequent recrystallisation of the solids from hexane–toluene yielded small crystals, which were used for the X-ray diffraction analysis. The varying amount of unenolised ketone present (between 0.1 and 0.8 equiv.) is consistent with more than one type of solvated enolate present, most likely dimers or monomers. However, these could not be separated for unambiguous analysis and limited the analysis of the products to NMR spectroscopy. *In situ* ^{1}H NMR spectroscopic studies indicated complete reaction of **1** with available ketone after several hours at ambient temperature. ^{1}H NMR (400 MHz, [$^2H_5$]pyridine, 25 °C); bisenolate: δ 7.00 (s, 2H, *m*-H, Mes), 3.91, 3.81 [d, ^2J(HH) 1.7 Hz, 1H, C=CH_2] 2.63 (s, 6H, *o*-CH_3), 2.33 (s, 3H, *p*-CH_3); unenolised ketone: δ 6.78 (s, 2H, *m*-H, Mes), 2.42 (s, 3H, *p*-CH_3), 2.19 (s, 9H, *m*-CH_3 and CH_3); amido(enolate): δ 6.89 (s, 2H, *m*-H, Mes), 4.48, 3.91 [d, ^2J(HH) 1.3 Hz, 1H, C=CH_2), 2.59 (s, 6H, *o*-CH_3), 2.27 (s, 3H, *p*-CH_3), 0.29 (s, 18H, $SiMe_3$).

‡ *Crystal data* for **5**: $C_{124}H_{148}Mg_4O_{10}$, M = 1895.66, T = 150(2) K, measurements were performed at Station 9.8, Daresbury SRS with Si111 monochromated radiation (λ = 0.6884 Å). A single crystal of dimensions 0.18 × 0.08 × 0.02 mm was mounted in inert oil and transferred to the cold N_2 gas stream of the diffractometer. Triclinic, space group $P\bar{1}$, a = 11.8142(7), b = 11.8617(7), c = 20.5469(13) Å, α = 74.844(2), β = 84.437(2), γ = 83.078(2)°, U = 2752.5(3) Å^3, Z = 1, μ = 0.185 mm^{-1}, D_c = 1.144 Mg m^{-3}, $2\theta_{max}$ = 45 °, 10156 reflections collected, 7669 unique, (R_{int} = 0.0425) all were used in the calculations. All non-hydrogen atoms were treated anisotropically and all hydrogens included in a riding model. The final $wR(F^2)$ was 0.1823, conventional R was 0.0680 and S = 1.002 for 637 parameters. Highest residual electron density 0.260 e Å^{-3}. Programs were standard (G. M. Sheldrick, University of Göttingen, Germany) diffractometer control software and members of the SHELX family. The structure was solved using direct methods and refined by full-matrix least-squares refinement on F^2. The unit cells of several crystals from different reaction batches were checked to confirm that the synthesis of **5** was reproducible.

CCDC 182/1629. See http://www.rsc.org/suppdata/cc/b0/b002892o/ for crystallographic files in .cif format.

1 H. B. Mekelburger and C. S. Wilcox, in *Comprehensive Organic Synthesis*, ed. B. M. Trost and I. Fleming, Pergamon, Oxford, 1991, vol. 3, ch. 14.

2 (*a*) J. F. Allan, K. W. Henderson and A. R. Kennedy, *Abstracts ACS*, 1999, ORGN 126; (*b*) J. F. Allan, K. W. Henderson and A. R. Kennedy, unpublished results; (*c*) G. Lessène, R. Tripoli, P. Cazeau, C. Biran and M. Bordeau, *Tetrahedron Lett.*, 1999, **40**, 4037.

3 J. F. Allan, K. W. Henderson and A. R. Kennedy, *Chem. Commun.*, 1999, 1325.

4 K. W. Henderson, W. J. Kerr and J. H. Moir, *Chem. Commun.*, 2000, 479.

5 An aluminium enolate derived from **2** has been structurally characterised and its formation investigated by theoretical calculations: J. F. Allan, W. Clegg, M. R. J. Elsegood, K. W. Henderson, A. E. McKeown, P. H. Moran and I. M. Rakov, *J. Organomet. Chem.*, 2000, in press.

6 For a review on the solid-state structures of organomagnesium compounds, see: P. R. Markies, O. S. Akkerman, F. Bickelhaupt, W. J. J. Smeets and A. L. Spek, *Adv. Organomet. Chem.*, 1991, **32**, 147.

7 P. R. Markies, G. Schat, O. S. Akkerman, F. Bickelhaupt, W. J. J. Smeets, P. van der Sluis and A. L. Spek, *J. Organomet. Chem.*, 1990, **315**, 393.

8 D. Thonnes and E. Weiss, *Chem. Ber.*, 1978, **111**, 3381.

9 D. Seebach, R. Amstutz and J. D. Dunitz, *Helv. Chim. Acta*, 1981, **64**, 2622; P. G. Williard and Q.-Y. Liu, *J. Am. Chem. Soc.*, 1993, **115**, 3380.

10 A pinacolone-solvated lithium enolate derived from **2** has been reported but not fully characterised: R. Amstutz, W. B. Schweizer, D. Seebach and J. Dunitz, *Helv. Chim. Acta*, 1981, **64**, 2617; a pinacolone solvated sodium pinacolate has been structurally characterised: P. G. Williard and G. B. Carpenter, *J. Am. Chem. Soc.*, 1986, **108**, 462.

11 H. E. Zimmerman and M. D. Traxler, *J. Am. Chem. Soc.*, 1957, **79**, 1920.

$[Ga_4(C_{10}H_9N_2)_2(PO_4)(H_{0.5}PO_4)_2(HPO_4)_2(H_2PO_4)_2(H_2O)_2]\cdot H_2O$: a novel one-dimensional chain structure containing four different types of monophosphate

Ching-Yeh Chen,[a] Fang-Rey Lo,[a] Hsien-Ming Kao[a] and Kwang-Hwa Lii*[ab]

[a] *Department of Chemistry, National Central University, Chungli, Taiwan 320. E-mail: liikh@cc.ncu.edu.tw*
[b] *Institute of Chemistry, Academia Sinica, Nankang, Taipei, Taiwan 115*

Received (in Cambridge, UK) 17th March 2000, Accepted 8th May 2000

The title compound is unique in such a way that among the vast number of synthetic phosphates and naturally occurring phosphate minerals it is the first example in which four different types of monophosphate, PO_4, $H_{0.5}PO_4$, HPO_4 and H_2PO_4, are present in the same structure.

Metal phosphates have been the subject of intense research owing to their rich structural chemistry and potential applications as ion exchangers, ionic conductors, catalysts and nonlinear optical materials.[1–6] In addition to the metal phosphates prepared in laboratories, phosphate minerals are also found in natural rocks; one example is the well known naturally occurring iron phosphate, cacoxenite, with a remarkable open-framework structure.[7] Some of the synthesized aluminophosphates or derived materials adopt structures that are similar to the naturally occurring aluminosilicates.[8] Anhydrous phosphates such as $LiTi_2P_3O_{12}$ and $LiZr_2P_3O_{12}$ have been prepared using high-temperature solid-state reactions. Many other metal phosphates containing PO_4, HPO_4, H_2PO_4 or combinations of the three have also been synthesized by hydrothermal methods. Hydrogen bonds are often formed in these crystalline hydrogen phosphates and unsymmetrical O–H···O bonds are usually observed. Symmetrical hydrogen bonds, which occur in many dicarboxylates with O···O distances of < 2.5 Å, are rarely found in phosphates. Here, we present the synthesis and characterization of a novel gallophosphate $[Ga_4(C_{10}H_9N_2)_2(PO_4)(H_{0.5}PO_4)_2(HPO_4)_2(H_2PO_4)_2(H_2O)_2]\cdot H_2O$ **1**. Among the vast numbers of metal phosphates that have been synthesized, none has the unique composition of **1** which contains four different types of monophosphates, *viz.* PO_4, $H_{0.5}PO_4$, HPO_4 and H_2PO_4, in the same structure. For $H_{0.5}PO_4$ there is an inversion center at the center of the short, symmetrical O–H–O bonds. We have prepared the monophasic phase and single-crystal X-ray diffraction and ^{31}P magic angle spinning (MAS) NMR have been applied to study the four different coordination environments for phosphorus.

Solvothermal reaction of $Ga(NO_3)_3\cdot 4H_2O$, 4,4′-bipyridine, H_3PO_4, H_2O and butan-1-ol in the molar ratio of 1:3:8:55.5:76.5 in a Teflon-lined acid digestion bomb at 165 °C for 3 d produced compound **1** in 66% yield based on Ga. A suitable colorless crystal was selected for structure determination by single-crystal X-ray diffraction.† The bulk product is monophasic as judged by powder X-ray diffraction (Anal. Calc.: C, 18.25; H, 2.27; N, 4.01. Found: C, 18.21; H, 2.37; N, 4.25%). ^{31}P MAS NMR spectra were acquired at a ^{31}P frequency of 161.73 MHz on a Bruker DSX-400 spectrometer under conditions of high-power proton decoupling. A pulse length of 4 μs ($\pi/4$) and a repetition time of 30 s were used. The ^{31}P chemical shifts were reported relative to 85% H_3PO_4 as external reference. The Hartmann–Hahn condition for ^1H to ^{31}P CP experiments was determined using $(NH_4)_2HPO_4$. The $^1H \rightarrow {}^{31}P$ CP spectra were recorded using a single-contact pulse sequence with reversal of spin temperature in the rotating frame and with proton decoupling during the ^{31}P signal acquisition. This pulse sequence was used for ordinary CP experiments as well as for $T_{1\rho}^{H}$ and $T_{1\rho}^{P}$ relaxation measurements.

Compound **1** has a one-dimensional chain structure. The fundamental building unit consists of two $Ga(1)O_5N$ octahedra, two monoprotonated 4,4′-bipyridine molecules which coordinate to Ga(1), two $Ga(2)O_4$ tetrahedra and seven phosphates of four different types. The connectivity between units is made by $P(1)O_4$ groups that join the GaO_5N and GaO_4 polyhedra to those in the neighboring units and thus form infinite chains parallel to the [001] direction (Fig. 1). $H_{0.5}P(4)O_4$ coordinates to one GaO_4 tetrahedron and two GaO_5N octahedra. The hydrogen atom in $H_{0.5}PO_4$ lies on an inversion center and is shared by two $H_{0.5}P(4)O_4$ groups on the adjacent chains. The O–H bond length in the symmetrical O–H–O bonds is 1.231 Å.[9] $HP(3)O_4$ has one oxygen bridging to GaO_4 and extends away from the chain as a pendant group, which accounts for the relatively larger thermal parameters of the atoms in the group. Of the three remaining P(3)–O bonds, the longest one constitutes the P–OH group, while the other two receive hydrogen bonds from adjacent chains. $H_2P(2)O_4$ is connected to GaO_5N and GaO_4 with the two hydroxo groups being H-bonded to two adjacent chains. All H atoms except those for O_w were found in difference Fourier maps and refined isotropically. The infinite chains are held in position by a network of hydrogen bonds, generating tunnels parallel to [001], within which the monoprotonated 4,4′-bipyridine and lattice water molecules reside (Fig. 2). The lattice water molecule has a site occupancy of 0.5 and is held in the crystal lattice by hydrogen bonds.

Fig. 3 shows the room temperature ^{31}P MAS NMR spectrum of **1**. Four resonances at −0.4, −9.2, −11.3 and −17.9 ppm with relative intensities very close to 1:1:1:0.5 respectively are observed. These signals correspond to the four distinct crystallographic phosphorus sites. In studies of a series of layered Ti, Zr and Al phosphates by MAS NMR spectroscopy, Nakayama *et al*. reported that the isotropic ^{31}P chemical shifts of H_2PO_4, HPO_4 and PO_4 groups appear around −10, −20 and −30 ppm, respectively.[10] Turner *et al.* noted that with increasing radius of the metal ion within one group of elements, the ^{31}P signal shifts downfield (*e.g.* BPO_4: −29.5 ppm, $AlPO_4$:

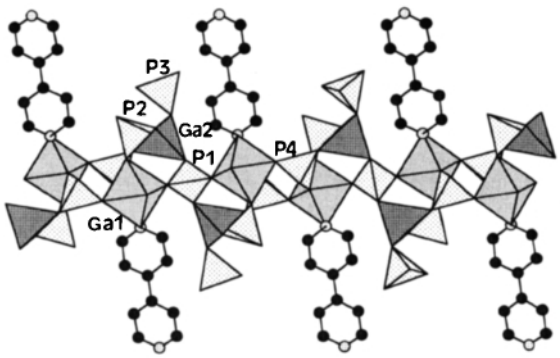

Fig. 1 Section of an infinite chain in **1** viewed along the [010] direction. GaO_5N octahedra are medium gray, GaO_4 tetrahedra are dark gray and PO_4 tetrahedra are light gray. Solid circles and stippled circles are the C and N atoms of 4,4′-bipyridine ligand, respectively.

DOI: 10.1039/b002182m

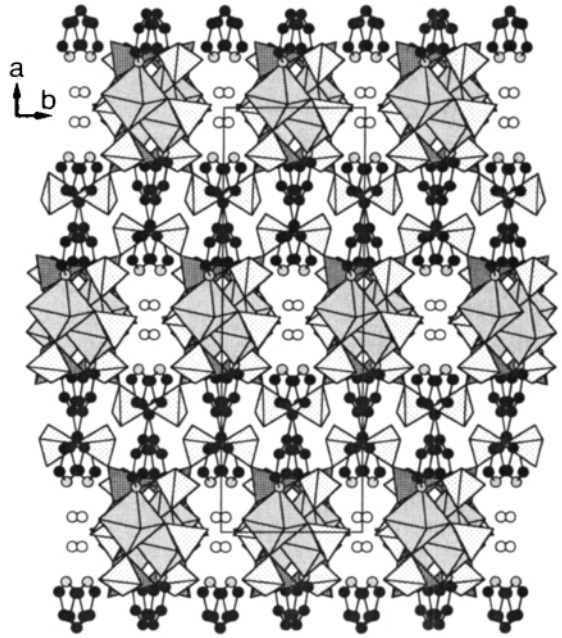

Fig. 2 Structure of **1** viewed along the [001] direction. Open circles are water oxygen atoms.

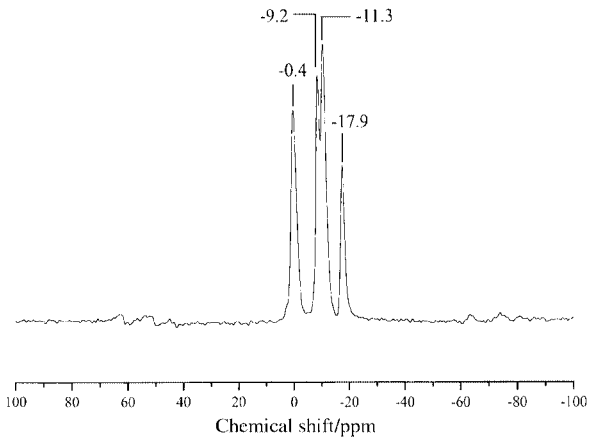

Fig. 3 Proton-decoupled ^{31}P MAS NMR spectrum of **1** acquired at a spinning frequency of 10 kHz. The isotropic chemical shifts are labeled; all other peaks in this spectrum are spinning sidebands. The peaks from left to right are assigned to H_2PO_4, HPO_4, $H_{0.5}PO_4$ and PO_4 groups, respectively.

−24.5 ppm, $GaPO_4$: −9.8 ppm).[11] Wessels *et al.* indicated that for microporous gallophosphates chemical shifts in the range from −10 to −20 ppm generally correspond to Q^4 groups, whereas values close to −5 ppm correspond to Q^3 groups.[12] Based on the above results we conclude that for gallophosphates the isotropic ^{31}P chemical shifts move to high-field values with decreasing protonation and the signals of Q^4 groups shift upfield relative to Q^3 groups. Consequently, the component at −17.9 ppm is assigned to P(1) (PO_4 group), which is also in agreement with the peak intensity. The other three peaks at −0.4, −9.2 and −11.3 ppm can be assigned to the three distinct P sites P(2) (H_2PO_4 group), P(3) (HPO_4 group) and P(4) ($H_{0.5}PO_4$ group), respectively. The HPO_4 peak is located at nearly equal distance from the H_2PO_4 and PO_4 peaks.

$^1H \rightarrow {}^{31}P$ CP experiments at various contact times have been performed to estimate the proximity of the protons and the phosphorus atoms. In theory, the growth of the ^{31}P CP intensity depends on the contact time, the rate constant of magnetization transfer (T_{cp}), the $^{31}P/^1H$ population ratios (ε) and the $T_{1\rho}$ values for both nuclei. The poor CP efficiency for the resonance at −17.9 ppm indicates that the phosphorus atom is not in close proximity to the protons, consistent with the assignment of this resonance to the PO_4 group. On the other hand, the enhancement of signal intensities for the resonances at −0.4, −9.2 and −11.3 ppm at short-contact times is observed. $T_{1\rho}$ values measured for the ^{1}H spins (*ca.* 22 ms) are much shorter than those of the ^{31}P spins in the different phosphate groups (320–580 ms). Fits to these CP intensity data with the measured $T_{1\rho}$ values, using modified versions of the expressions by Mehring[13] and Walter *et al.*[14] and ignoring the contributions from distant water and bipyridyl molecules, demonstrate that the $^{31}P/^1H$ population ratios involved in the CP transfer for the resonances at −0.4, −9.2 and −11.3 ppm are close to 0.5, 1.1 and 2.1, respectively. In addition, T_{cp} values, which are related to the dipolar coupling between ^{1}H and ^{31}P nuclei, are 0.6, 0.85 and 2.15 for the resonances at −0.4, −9.2 and −11.3 ppm, respectively. Both $^{31}P/^1H$ population ratios and T_{cp} values are reasonably in agreement with the above assignment.

In summary, this work illustrates that a novel 1-D gallium phosphate with an unique composition is synthesized under solvothermal conditions and structurally characterized by single-crystal X-ray diffraction and ^{31}P MAS NMR spectroscopy. The compound is unique in that, among the vast number of synthetic phosphates and naturally occurring phosphate minerals it is the first example in which four different types of phosphate, PO_4, $H_{0.5}PO_4$, HPO_4 and H_2PO_4 are present.

Notes and references

† *Crystal data* for $[Ga_4(C_{10}H_9N_2)_2(PO_4)(H_{0.5}PO_4)_2(HPO_4)_2(H_2PO_4)_2(H_2O)_2]\cdot H_2O$: monoclinic, space group *C*2/*c* (no. 15); a = 26.4161(6), b = 8.0416(1), c = 20.3515(4) Å, β = 111.194(1)°; V = 4030.8(1) Å^3, Z = 4, 3120 absorption corrected reflections with $F_o > 4\sigma(F_o)$ out of 4388 unique reflections ($2\theta_{max}$ = 56.1°) measured at 23 °C for a colorless crystal of dimensions 0.135 × 0.063 × 0.027 mm on a Siemens Smart-CCD diffractometer on convergence gave final values of R_1 = 0.0429, $wR_2(F^2)$ = 0.0906, GOF = 1.068, residual electron density between −0.59 and 0.69 e Å^{-3}. Bond-valence calculations indicated that O(3), O(5), O(8), O(9), O(10), O(11) and O(15) had valence sums of 1.33, 1.20, 1.33, 1.17, 1.37, 1.17 and 0.31, respectively, and all other oxygen atoms had values close to 2. The site occupancy factor of O_w is 0.5. All non-hydrogen atoms were anisotropically refined, and all hydrogen atoms except those for O_w were located in difference Fourier maps and refined isotropically. Atoms O(3), O(5) and O(9) are hydroxo oxygens. O(15), which is coordinated to Ga(1), is a water oxygen. The valence sums of O(8) and O(10) are satisfied by forming hydrogen bonds with phosphate groups on different chains.

CCDC 182/1632. See http://www.rsc.org/suppdata/cc/b0/b002182m/ for crystallographic files in .cif format.

1 R. C. Haushalter and L. A. Mundi, *Chem. Mater.*, 1992, **4**, 31.
2 S. L. Suib, *Chem. Rev.*, 1993, **93**, 803.
3 M. E. Davis, *Chem. Eur. J.*, 1997, **3**, 1745.
4 P. Feng, X. Bu and G. D. Stucky, *Nature*, 1997, **388**, 735.
5 G. D. Stucky, M. L. F. Phillips and T. E. Gier, *Chem. Mater.*, 1989, **1**, 492.
6 A. K. Cheetham, G. Ferey and T. Loiseau, *Angew. Chem., Int. Ed.*, 1999, **38**, 3268.
7 P. B. Moore and J. Shen, *Nature*, 1983, **306**, 356.
8 W. M. Meier and D. H. Olson, *Atlas of Zeolite Structure Types*, Butterworth-Heinemann, London, 1992.
9 Short O–H–O bonds that are crystallographically symmetrical range in length from *ca.* 2.4 to 2.6 Å, and it appears that those with O··O distances < *ca.* 2.5 Å have a single potential minimum (A. F. Wells, *Structural Inorganic Chemistry*, Clarendon Press, Oxford, 5th edn., 1984, p. 359.) The O··O distance in **1** is only 2.46 Å, indicating that the H atom is probably at mid-point. However, we cannot exclude the possibility that the H is dynamically disordered between two positions related by the center of symmetry. In that case the formula of the title compound becomes $[Ga_4(C_{10}H_9N_2)_2(PO_4)_2(HPO_4)_3(H_2PO_4)_2(H_2O)_2]\cdot H_2O$.
10 H. Nakayama, T. Eguchi, N. Nakamura, S. Yamaguchi, M. Danjyo and M. Tsuhako, *J. Mater. Chem.*, 1997, **7**, 1063.
11 G. L. Turner, K. A. Smith, R. J. Kirkpatrick and E. Oldfield, *J. Magn. Reson.*, 1986, **70**, 408.
12 T. Wessels, L. B. McCusker, Ch. Baerlocher, P. Reinert and J. Patarin, *Microporous Mesoporous Mater.*, 1998, **23**, 67.
13 M. Mehring, *Principle of High Resolution NMR in Solids*, Springer, Berlin, 1983.
14 T. H. Walter, G. L. Turner and E. Oldfield, *J. Magn. Reson.*, 1988, **76**, 106.

ChemComm

Ag nanowire formation within mesoporous silica

Michael H. Huang, Amer Choudrey and Peidong Yang*

Department of Chemistry, University of California, Berkeley, CA 94720, USA. E-mail: pyang@cchem.berkeley.edu

Received (in Oxford, UK) 27th March 2000, Accepted 9th May 2000

Uniform Ag nanowires have been synthesized within nanoscale channels of mesoporous silica SBA-15 by a simple chemical approach, which involves $AgNO_3$ impregnation, followed by thermal decomposition.

Owing to their high surface areas and uniform pore sizes, mesoporous silica materials have been widely used as host materials for loading catalysts,[1,2] polymers,[3–7] metals[8] and semiconductor nanoparticles[9–13] that have potential catalytic, environmental[14] and optoelectrical applications.[15,16] While there was certain success with the formation of continuous polymer nanofibers within mesoporous silica, inorganic metal or semiconductor nanowire formation within mesoporous MCM-41 materials has been largely elusive and in many cases incomplete filling or nanoparticles were observed. Here we report a simple chemical methodology for the formation of uniform Ag nanowires within mesoporous silica SBA-15.[17] This process involves $AgNO_3$ solution impregnation followed by thermal decomposition. Transmission electron microscopy studies on these samples show unambiguously that these continuous Ag nanowires are made of long polycrystalline domains. They have uniform diameters of 5–6 nm, and large aspect ratios between 100 and 1000. Thus, the current process represents a viable approach for synthesizing uniform metallic nanowires and may be applicable for making other inorganic nanowires with complex compositions.

Mesoporous silica SBA-15 was synthesized in accordance with the published procedure[17] using tri-block copolymer poly(ethylene oxide)–poly(propylene oxide)–poly(ethylene oxide) $EO_{20}PO_{70}EO_{20}$ as template in acidic conditions. Briefly, a solution of $EO_{20}PO_{70}EO_{20}$:2 M HCl:TEOS:H_2O = 2:60:4.25:15 (mass ratio) was prepared, stirred for several hours at 40 °C, and then heated at 100 °C overnight. The solid products were filtered off and calcined at 500 °C for 5 h. Low-angle X-ray diffraction [Fig. 1, inset (a)] and transmission electron microscopy [TEM, Fig. 2(a)] studies on these samples indicate they are mesoporous silica consisting of well-ordered hexagonal packed channels with diameters of 5–6 nm.

To prepare nanowires within these nanoscale channels, 20 mg of SBA-15 powder was soaked in 10 ml of 0.2 M $AgNO_3$ EtOH–H_2O (1:1 v/v) solution and the suspension was stirred overnight at room temperature. The product was filtered off, rinsed with deionized water, and subjected to thermal treatment

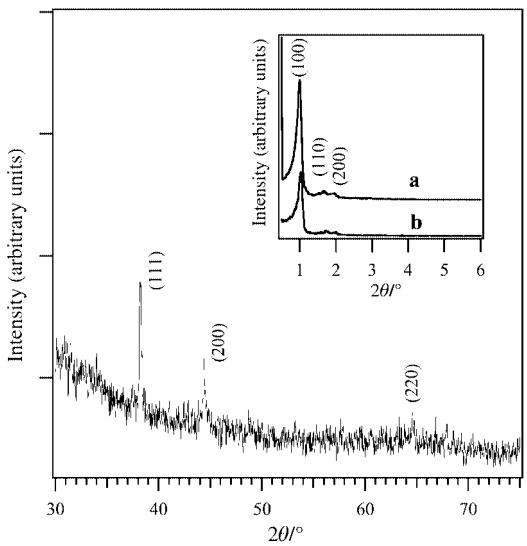

Fig. 1 High-angle X-ray diffraction pattern (Siemens, D5000) of the silver nanowire/SBA-15 composite. The low-angle X-ray diffraction patterns for SBA-15 before (a) and after (b) Ag nanowire loading are shown in the inset.

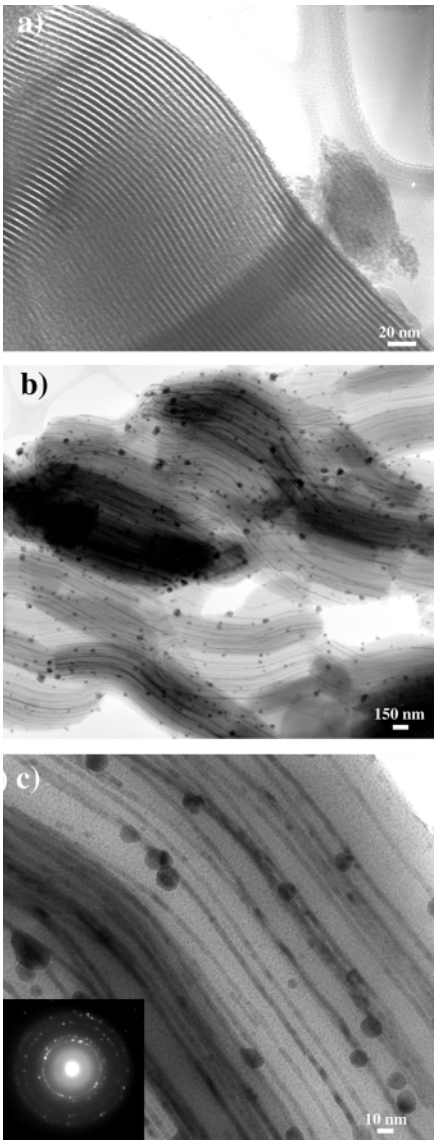

Fig. 2 (a) TEM (Topcon 002B, 200 KeV) image of the as-made SBA-15 mesoporous silica recorded along the [110] zone axis. (b) Low magnification TEM image of SBA-15 mesoporous silica after the Ag nanowire loading; Ag nanowires appear as dark lines in the image. (c) High-magnification TEM image of the Ag nanowires within the SBA-15. A selected area electron diffraction pattern recorded on several Ag nanowires is shown in the inset of (c).

DOI: 10.1039/b002549f

at 300 °C in air for 2 h to decompose the impregnated $AgNO_3$ and form Ag nanowires.

The $AgNO_3$ impregnated sample was colorless while a brown/grey color appeared once the sample was treated at 300 °C. X-Ray diffraction indicates the mesoscopic ordering of SBA-15 was maintained after the $AgNO_3$ loading and the thermal treatment with the observation of low angle peaks that can be indexed as (100), (110) and (200) reflections of the hexagonal mesostructure of SBA-15 [Fig. 1, inset (b)]. Meanwhile, high angle diffraction peaks were observed after the thermal treatment. These diffraction peaks can be readily indexed according to the crystalline Ag structure with cubic lattice constant of $a = 4.07$ Å.

The thermally treated sample was also characterized by TEM [Fig. 2(b), (c)]. While there is a small amount of spherical Ag particles (5–30 nm in diameter) on the external surface of the SBA-15, extensive Ag nanowire formation can be seen in the large area view of the sample [Fig. 2(b)]. A high-magnification image of the sample [Fig. 2(c)] clearly indicates that these nanowires are continuous and essentially follow the curvature of nanoscale channels. They have uniform diameters of 5–6 nm, which are consistent with the sizes of the nanoscale channel templates. These nanowires also possess large aspect ratios from 100 to 1000, which have not been seen previously in many studies using MCM-41,[8] carbon nanotubes[18] or porous alumina[19] as host matrices. By performing an over-focus and under-focus imaging series in the microscope, it is confirmed that these nanowires are actually embedded within the channels instead of being located on the external surface. Furthermore, the highly crystalline nature of the Ag nanowires was confirmed by selected area electron diffraction measurement made on these nanowire arrays [Fig. 2(c) inset]. The diffraction spots/rings can be again indexed as (111), (200), (220) and (311) reflections according to the cubic structure of Ag. The appearance of diffraction rings/spots indicates that the Ag nanowires are comprised of polycrystalline domains with large aspect ratios.

It was found that in order to achieve complete filling of the mesopores within SBA-15, a proper selection of the initial impregnation solution is critical. For example, we attempted using $AgNO_3$ solution in pure water or EtOH–H_2O (3 : 7 or 8 : 2 v/v), in all cases, only spherical Ag particles were obtained after the thermal treatment with a low percentage of channel filling. This incomplete filling is directly related to the very different surface tensions of H_2O and ethanol (71.99 and 21.97 mN m^{-1}, respectively, at room temperature).

N_2 sorption measurements were also carried out on the samples before and after the Ag loading. It was found that the pore volumes decrease from 0.93 cm^3 g^{-1} for as-made SBA-15 to 0.61 cm^3 g^{-1} for Ag-loaded samples. This further confirms that Ag nanowires are indeed located inside the host channels and the loading efficiency is comparable with previous experiments using MCM-41/48.[3,9,11] The capability of nanowire array formation within SBA-15 clearly indicates that the mesopores used to template Ag nanowires are highly ordered with few local defects [Fig. 2(a)] and they are also robust enough to sustain the thermal treatment. Thus we believe SBA-15 should be an ideal host material for making nanowire arrays of metals and many other systems. Initial results indicate that it is possible to form Co, Ni, NiO, Fe_2O_3 and polymer nanowire arrays within the SBA-15 matrix using a similar procedure.

We have also characterized the optical properties of these Ag nanowire arrays. Two plasmon absorption bands (410 and 580 nm) were observed in our preliminary studies. Further studies of the physical properties of these nanowires are currently in progress.

This research was funded by Camille and Henry Dreyfus Foundation, 3M Corporation and University of California, Berkeley. We thank Dr C. Nelson for the help during transmission electron microscopy studies, Professor G. D. Stucky at University of California, Santa Barbara for helpful discussions, Professor J. R. Long for use of the UV–VIS spectrometer and Professor Don T. Tilley for use of the surface area measurement unit. We also thank the National Center for Electron Microscopy for the use of their facilities.

Notes and references

1 W. Zhou, J. M. Thomas, D. S. Shephard, B. F. Johnson, D. Ozkaya, T. Maschmeyer, R. G. Bell and Q. Ge, *Science*, 1998, **280**, 705.
2 S. Kim, S. Son, S. I. Lee, T. Hyeon and Y. K. Chung, *J. Am. Chem. Soc.*, 2000, **122**, 1550.
3 C. Wu and T. Bein, *Science*, 1994, **264**, 1757.
4 K. Kageyama, J. Tamazawa and T. Aida, *Science*, 1999, **285**, 2113.
5 M. J. MacLachlan, P. Aroca, N. Coombs, I. Manners and G. A. Ozin, *Adv. Mater*, 1998, **10**, 144.
6 K. Moller and T. Bein, *Chem. Mater.*, 1998, **10**, 2950.
7 S. A. Johnson, D. Khushalani, N. Coombs, T. E. Mallouk and G. A. Ozin, *J. Mater. Chem.*, 1998, **8**, 13.
8 Y. Plyuto, J. Berquier, C. Jacquiod and C. Ricolleau, *Chem. Commun.*, 1999, 1653.
9 M. Froba, R. Kohn, G. Bouffaud, O. Richard and G. V. Tendeloo, *Chem. Mater.*, 1999, **11**, 2858.
10 J. A. Aggr, M. W. Anderson, M. E. Pemble, O. Terasaki and Y. Nozue, *J. Phys. Chem. B*, 1998, **102**, 3345.
11 V. I. Srdanov, I. Alxneit, G. D. Stucky, C. M. Reaves and S. P. Denbaars, *J. Phys. Chem. B*, 1998, **102**, 3341.
12 G. D. Stucky and J. E. MacDougall, *Science*, 1990, **247**, 669.
13 R. Leon, D. G. Margolese, G. D. Stucky and P. M. Petroff, *Phys. Rev. B*, 1995, **52**, R2285.
14 X. Feng, G. E. Fryxell, L. Q. Wang, A. Y. Kim, J. Liu and K. M. Kemner, *Science*, 1997, **276**, 923.
15 P. Chakraborty, *J. Mater. Sci.*, 1998, **33**, 2235.
16 P. Yang, G. Wirnsberger, H. C. Huang, S. R. Cordero, M. D. McGehee, B. Scott, T. Deng, G. M. Whitesides, B. F. Chmelka, S. K. Buratto and G. D. Stucky, *Science*, 2000, **287**, 465.
17 D. Zhao, J. Feng, Q. Huo, N. Melosh, G. H. Fredrickson, B. F. Chmelka and G. D. Stucky, *Science*, 1998, **279**, 548.
18 J. Sloan, D. M. Wright, H. Woo, S. Bailey, G. Brown, A. P. E. York, K. S. Coleman, J. L. Hutchison and M. L. H. Green, *Chem. Commun.*, 1999, 699.
19 V. M. Cepak and C. R. Martin, *J. Phys. Chem. B*, 1998, **102**, 9985.

Instability of [60]fullerene anions in dichloromethane: a synthetic avenue to $C_{60}>(CH_2)_n$ methanofullerenes

Marcel W. J. Beulen and Luis Echegoyen*

Department of Chemistry, University of Miami, Coral Gables, Florida 33124, USA. E-mail: echegoyen@miami.edu

Received (in Columbia, MO, USA) 29th December 1999, Accepted 26th April 2000

The trianion of C_{60} reacts readily with the commonly used electrochemical solvent dichloromethane to form methanofullerenes of the type $C_{60}>(CH_2)_n$, signaling a cautionary warning against the use of this solvent for electrochemical studies of fullerenes and opening up a new synthetic avenue for these adducts.

Since the discovery of C_{60} in 1985[1] and its subsequent preparation in large scale in 1990[2] the rich electronic properties of this fullerene have been probed by electroanalytical techniques such as cyclic voltammetry (CV) and Osteryoung square wave voltammetry (OSWV).[3] Many different experimental conditions have been used for these studies including a wide variety of supporting electrolytes and solvents (*e.g.* chlorobenzene, tetrahydrofuran, pyridine, nitrobenzene, *N*,*N*,-dimethylformamide and dichloromethane).[4] However, a very common choice has been dichloromethane, and a very large number of fullerene derivatives have been and continue to be investigated in this solvent.[5] Preliminary reports identifying the instability of C_{60}^{3-} in CH_2Cl_2 were published in 1991 and 1992, but no details nor product analyses were presented.[6,7] Since we have also performed electrochemical studies of fullerenes in CH_2Cl_2 and observed quite unusual behavior[8] and since we published the electrosynthesis of [6,6]methanofullerenes by reacting the C_{60} monoanion and dianion with dihalomethano compounds (X_2CRR'; X = Br, I; R = H, R′ = CN or CMe_3),[9] see Scheme 1, we decided to investigate the behavior of the C_{60} anions in this solvent under bulk electrolytic conditions.

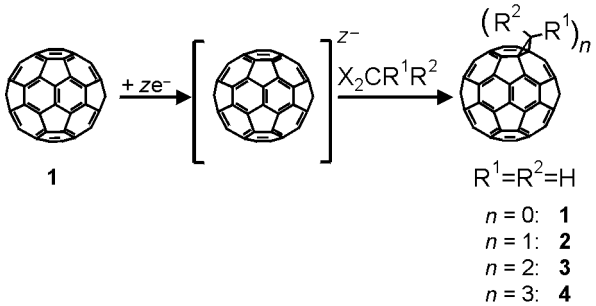

Scheme 1 Formation of methanofullerenes from the anions of C_{60}.

In a typical experiment, *ca.* 2 mg of C_{60} were suspended in dichloromethane and the anions of this fullerene were generated by controlled-potential bulk electrolysis. We followed the stability of these anions *in situ* by CV and OSWV.† The generation of the monoanion (at −0.85 V *vs*. a Ag-wire pseudo-reference electrode) and dianion (at −1.25 V) was straightforward and resulted in well defined electrochemistry [see Fig. 1(a) for the dianion]. No apparent reaction of the mono- or di-anion with the solvent was noted during or after electrolysis.[10] The trianion was generated by controlled potential electrolysis (CPE) applying a potential *ca.* 150 mV more cathodic than the third reduction potential of C_{60} (−1.60 V). This resulted in a steady current after a few minutes, instead of the typical and expected current exponential decay observed during CPE generation of the monoanion and dianion of C_{60}, indicating that a chemical reaction occurs during electrolysis. Arbitrarily, the

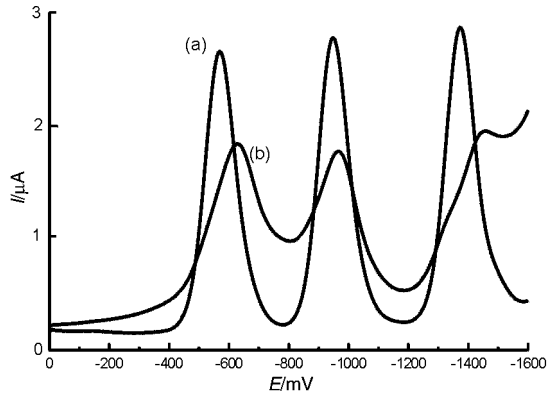

Fig. 1 OSWV of C_{60} in dichloromethane at the dianionic (a) and trianionic (b) states.

electrolysis was interrupted when *ca.* 8 electrons per C_{60} molecule were discharged (reaction time: 30 min). The OSWV was completely changed at this point [Fig. 1(b)] with the waves being much broader. Reoxidation of the reaction mixture and subsequent purification by column chromatography resulted in fullerene products in *ca.* 75% yield. Analysis of the reaction mixture by HPLC, UV–VIS spectroscopy, MALDI-TOF mass spectrometry and NMR spectroscopy showed that scarcely any C_{60} remained. UV–VIS spectroscopy showed a broad peak at *ca.* 425–435 nm while the characteristic C_{60} peak at 406 nm had disappeared. HPLC measurements [eluent hexane–toluene (10 : 1)] indicated the presence of several products, all slightly more polar than C_{60} itself. These products were assigned by MALDI-TOF mass spectrometric analysis (see Fig. 2), which showed the formation of several adducts of C_{60}, with $C_{60}>(CH_2)_2$ as the main product (**1**: 2%; **2**: 20%; **3**: 50%; **4**: 15%, based on HPLC, see Scheme 1 for structure assign-

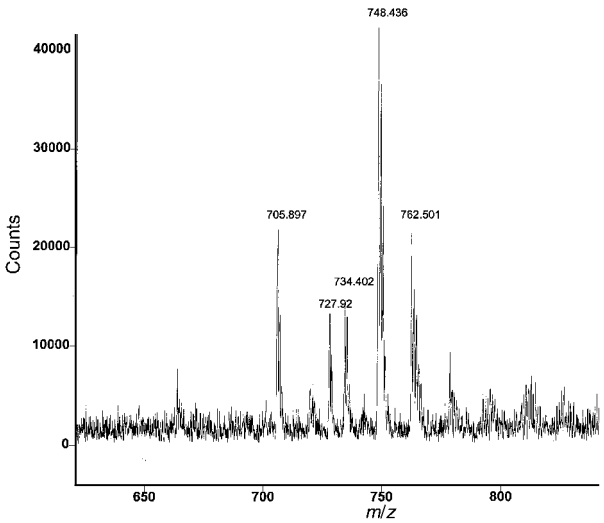

Fig. 2 Maldi-TOF spectrum of the reaction mixture after electrolysis at the trianionic state.

DOI: 10.1039/b001021i

ments).[11] In practice, two different isomers can form in this reaction ([6,6] closed methanofullerenes or [5,6] open methanoannulenes).[12] Based on ^{1}H NMR spectroscopy, which showed several resonances (due to regioisomers of the bis- and tris-adducts) in the range δ 3.4–3.9 for the bridgehead CH_2-protons, but no AB quartets at δ 2.9 and 6.4 (expected for the 5,6 isomer),[12] the isolated isomers were assigned to be of the [6,6] closed methanofullerene type.[13] Therefore, reaction of the C_{60} trianion with the solvent dichloromethane leads to the same type of fullerene derivatives as those formed during the reaction of the C_{60} monoanion and dianion with the diiodo and dibromo reagents previously described.[9] Interrupting the electrolysis at an earlier stage led to the formation of fewer adducts. A reaction time of *ca.* 15 min (*ca.* 4 electrons per C_{60}) resulted in a product ratio of 1 : 1 of C_{60} (**1**) to $C_{60}{>}CH_2$ (**2**) (overall yield: 85%), as determined from HPLC and MALDI-TOF spectrometric measurements.

In conclusion, our experiments clearly showed that C_{60} in its trianionic state is not stable in dichloromethane, and reacts with the solvent to form methanofullerenes. The lower reactivity of this chlorinated compound compared to the corresponding iodo and bromo compounds is compensated by its high abundance. Therefore, this solvent should be used only with extreme caution in the electrochemistry of fullerenes. Additionally, the potential application of the reaction of dichloromethane with the trianion of C_{60} to electrosynthesize methanofullerenes with a variable number of CH_2 groups ranging from one to six is currently under investigation. Of special interest is the regioisomeric distribution observed, to see how it compares with that obtained from other synthetic strategies. Generally, the results described in this study and in previous work show that the anions of C_{60} react with dihaloalkyl compounds in three different ways: the monoanion reacts with activated dihalomethano compounds [$Br_2CH(CN)$],[9b] the dianion reacts with non-activated dihalomethano compounds ($I_2CH[CMe_3]$),[9a] and the trianion reacts with the non-activated and less reactive dihalomethano compounds (Cl_2CH_2).

Financial support for this work from the National Science Foundation through grant CHE-9816503, and the Netherlands Organization for Scientific Research (NWO, talent stipendium, M. W. J. B.) is greatly appreciated.

Notes and references

† *Electrochemistry*: details of the experimental electrochemical set-up for the CV, OSWV and bulk electrolysis measurements have been described elsewhere.[14] Briefly, electrochemical measurements were performed using a BAS 100W Electrochemical Analyzer (Bioanalytical systems). An electrochemical cell designed to carry out CV, OSWV and bulk electrolysis under high vacuum was used. For CV and OSWV, a glassy-carbon working electrode, a silver wire pseudo-reference electrode, and a Pt-mesh counter electrode were used. Bulk electrolysis was carried out using Pt mesh electrodes for both working and counter electrodes. As supporting electrolyte, tetrabutylammonium hexafluorophosphate was used.

General: UV–VIS: Shimadzu UV 2101 PC spectrometer; HPLC: Waters with a SiO_2 column; ^{1}H NMR: Bruker Avance-300 spectrometer; MALDI-TOF MS: PerSeptive Biosystems Voyager-DE STR spectrometer.

1 H. W. Kroto, J. R. Heath, S. C. O'Brien, R. F. Curl and R. E. Smalley, *Nature*, 1985, **318**, 162.
2 W. Krätschmer, L. D. Lamb, K. Fostiropoulos and D. R. Huffmann, *Nature*, 1990, **347**, 354.
3 L. Echegoyen and L. E. Echegoyen, *Acc. Chem. Res.*, 1998, **31**, 593.
4 D. Dubois, G. Moninot, W. Kutner, M. T. Jones and K. M. Kadish, *J. Phys. Chem.*, 1992, **96**, 7137.
5 C. Boudon, J.-P. Gisselbrecht, M. Gross, L. Isaacs, H. L. Anderson, R. Faust and F. Diederich, *Helv. Chim. Acta*, 1995, **78**, 1334; J.-F. Nierengarten, A. Herrmann, R. R. Tykwinski, M. Ruetimann, F. Diederich, C. Boudon, J.-P. Gisselbrecht and M. Gross, *Helv. Chim. Acta*, 1997, **80**, 293.
6 D. Dubois, K. M. Kadish, S. Flanagan, R. E. Haufler, L. P. F. Chibante and L. J. Wilson, *J. Am. Chem. Soc.*, 1991, **113**, 4364.
7 K. M. Kadish and D. Dubois, in *Molecular Electrochemistry of Inorganic, Bioinorganic and Organometallic Compounds*, ed. A. J. L. Pombeiro and J. McCleverty, Kluwer Academic Publishers, Dordrecht, 1992, p. 603.
8 R. Kessinger, J. Crassous, A. Herrmann, M. Ruetimann, L. Echegoyen and F. Diederich, *Angew. Chem., Int. Ed.*, 1998, **37**, 1919.
9 (*a*) P. L. Boulas, Y. Zuo and L. Echegoyen, *Chem. Commun.*, 1996, 1547;(*b*) F. Arias, P. L. Boulas, Y. Zuo, O. Dominguez, M. Gomez-Kaifer and L. Echegoyen, in *Recent Advances in the Chemistry and Physics of Fullerenes and Related Materials*, ed. K. M. Kadish and R. S. Ruoff, The Electrochemical Society, Pennington, NJ, 1996, vol. 3, p. 165.
10 Reoxidation after electrolytically preparing the dianion of C_{60} resulted in the isolation of mainly C_{60} in *ca.* 95% yield.
11 Besides the fullerenes **1**–**4**, some byproducts were formed. The product with *m/z* 706 was tentatively assigned to ($C_{60}CCl_2$–C_8).
12 M. Prato, V. Lucchini, M. Maggini, E. Stimpfl, G. Scorrano, M. Eiermann, T. Suzuki and F. Wudl, *J. Am. Chem. Soc.*, 1993, **115**, 8479.
13 A. B. Smith III, R. M. Strongin, L. Brard, G. T. Furst and W. J. Romanow, *J. Am. Chem. Soc.*, 1993, **115**, 5829; A. B. Smith III, R. M. Strongin, L. Brard, G. T. Furst, W. J. Romanow, K. G. Owens, R. J. Goldschmidt and R. C. King, *J. Am. Chem. Soc.*, 1995, **117**, 5492.
14 M. Diekers, A. Hirsch, S. Pyo, J. Rivera and L. Echegoyen, *Eur. J. Org. Chem.*, 1998, 1111.

ChemComm

Preparation of an MFI-type zeolite membrane on a porous glass disc by substrate self-transformation

Wei-Yang Dong and Ying-Cai Long

Department of Chemistry, Fudan University, Shanghai 200433, P.R. of China. E-mail: yclong@fudan.edu.cn

Received (in Cambridge, UK) 6th March 2000, Accepted 5th May 2000

An MFI-type zeolite membrane containing boron has been prepared on the surface of a boron–silicon porous glass disc by substrate self-transformation in the vapor of ethylamine (EA) and H_2O; both XRD and SEM show that the zeolite crystals on the surface of the porous glass disc were in random orientation; the thickness of the membrane layer was *ca*. 10–20 μm; permeation of O_2 and N_2, and the chemical composition of the membrane were measured.

In the last decade, the study of zeolite membranes has become an important research topic in the area of inorganic membrane materials because of their uniform microporous structure, and high thermal and chemical stability. Many methods for preparing zeolite membranes on various substrates have been developed, including: hydrothermal crystallization;[1] *in situ* hydrothermal synthesis,[2] vapor phase synthesis,[3] sol–gel methods,[4] zeolite-filled (embedded) methods,[5] chemical growth,[6] galvanic metal deposition,[7] leakage-blocked method,[8] synthesis by microwave heating,[9] *etc*. Supports used include porous ceramic discs[2] or tubes,[10] porous glass discs[11] or tubes,[12] porous sintered stainless steel discs,[13] various kinds of metal discs,[1] glass discs or pipes,[4] Teflon slabs and sleeves,[11] single-crystal silicon wafers,[1] filter paper,[14] quartz plate, mica discs, cordierite discs, mullite, stainless steel networks[1] and liquid mercury.[15]

Zeolite ZSM-5 and ZSM-35 membranes were synthesized using the vapor phase method according to Dong *et al.*[3] in which a glass disc or pipe was put on the surface of aluminosilicate gels, or embedded in the gels. These syntheses were carried out at 473 K in amine vapor for 3–7 days. ZSM-35 membranes and ZSM-5 membranes were obtained in the vapor of *n*-propylamine($PrNH_2$)–H_2O and diethylamine(Et_2NH)–H_2O or ethylenediamine(EDA)–triethylamine(Et_3N)–H_2O, respectively. Since this work, zeolite membranes have been synthesized *via* vapor phase methods by many researchers. Here, we report a novel finding related to the synthesis of an MFI-type zeolite membrane in the vapor phase. The zeolite membrane was prepared on the surface of a boron–silicon porous glass disc by substrate self-transformation in ethylamine (EA)–H_2O vapor.

A porous glass disc (18.5 × 17.5 × 2.5 mm, Shanghai Silicate Institute), was used as the starting substrate. The chemical composition of the glass, as measured by chemical titration, was B_2O_3 = 2.5 wt%, Al_2O_3 = 0.37 wt%, SiO_2 = 96.68 wt%, Na_2O = 0.44 wt%. The chemical composition of the membrane was determined with a Field Emission Auger Microprobe, MICROLAB 310F, (VG Scientific, Surface Analysis Company) using Mg-Kα radiation at an X-ray power of 300 W, under a vacuum of 3.0×10^{-8} Mbar. The most probable pore diameter of the substrate was 7.5 nm. The disc was placed in a Teflon holder in a 35 ml stainless steel autoclave, containing *ca*. 10 ml of 50 wt% ethylamine aqueous solution. The porous glass disc was placed in a position so that the disc did not directly contact with the liquid mixture at both room and reaction temperature. The synthesis reaction was carried out in an oven at 180 ± 2 °C for 144 h. After cooling to room temperature, the disc was removed, and dried at 80 °C for 12 h. Both surfaces (A and B) of the disc were transformed to MFI zeolite crystals after this treatment in vapor. Calcination of the membrane was conducted in a crucible oven. One of the two surfaces of the disc (B) was polished before calcination. Permeability of gases on both the calcined zeolite membrane and the substrate was studied at room temperature with the supported membrane and substrate mounted in a special separator. The flow rate of the gas was measured with a soap bubble flowmeter, and the difference of the pressure between two sides of the disc kept at 0.1 MPa.

Fig. 1 shows typical XRD patterns of MFI-type zeolite on both sides of the disc after reaction [Fig. 1(a) and (b)]. The XRD patterns show that the zeolite crystals are in random orientation on the surfaces of the disc. The surfaces of the initial porous glass disc are amorphous [Fig. 1(c)].

SEM shows that the surfaces of the initial porous glass disc are rough and uneven [Fig. 2(a)]. After synthesis, both sides of the disc are covered by MFI zeolite crystals with random orientation [Fig. 2(b)–(d)], consistent with the XRD results. The size of the crystals is *ca*. 15–25 μm [Fig. 2(b)], and the thickness of the membrane layer is *ca*. 10–20 μm [Fig. 2(c) and (d)]. There are no zeolite crystals on the inner surfaces of the disc [Fig. 2(c) and (d)], indicating that the zeolite crystals only formed on the outer surfaces of the disc.

The chemical composition of the membrane, measured by surface analysis, is B_2O_3 = 3.70 wt%, Al_2O_3 = 0.55 wt%, SiO_2 = 95.25 wt%, Na_2O = 0.50 wt%. The permeabilities of O_2 and N_2 through the substrate are 5.06×10^{-8} and 5.56×10^{-8} mol m^{-2} s^{-1} Pa^{-1}, respectively. The calculated ideal selectivity of O_2/N_2 (0.91) is very close to the Knudsen value (0.94), showing

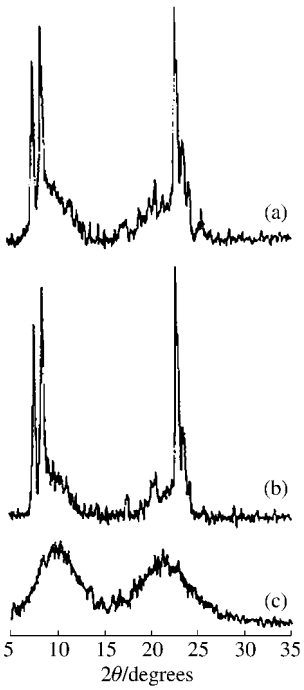

Fig. 1 XRD patterns: (a) surface A of the membrane, (b) surface B of the membrane and (c) surface of the initial porous glass disc.

DOI: 10.1039/b001814g

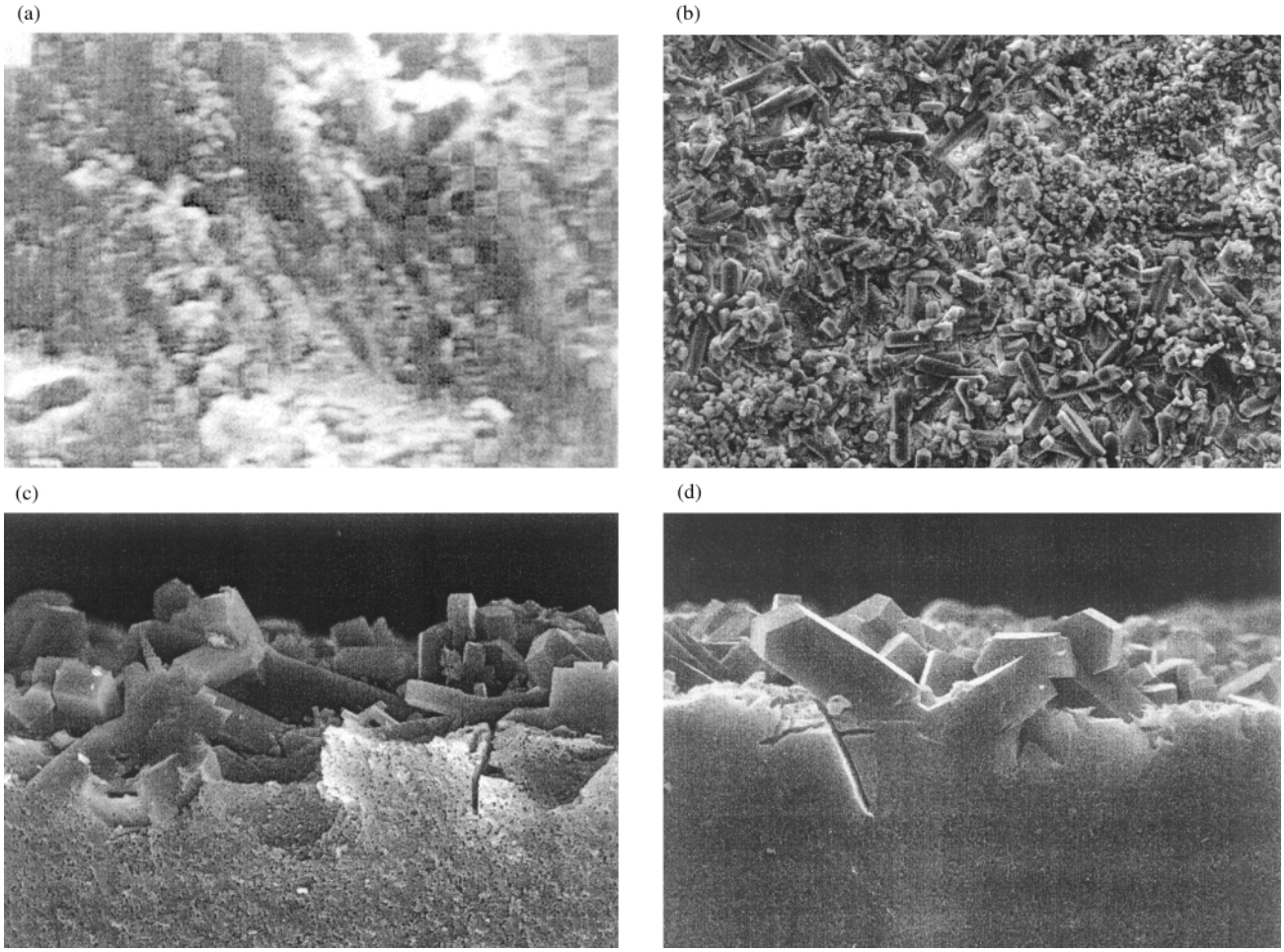

Fig. 2 SEM photographs: (a) the surface of the initial porous glass disc; magnification 1950×, (b) plane view of surface A of the membrane, (c) cross-section of surface A of the membrane, (d) cross-section of surface B of the membrane, before polishing.

that the substrate shows no preferential selectivity for the penetration of O_2 and N_2. On the calcined boron-containing MFI-type zeolite membrane, the permeabilities of O_2 and N_2 are 0.095×10^{-8} and 0.15×10^{-8} mol m^{-2} s^{-1} Pa^{-1}, respectively. The calculated ideal selectivity of O_2/N_2 (0.63) is obviously lower than that for Knudsen behaviour and for the substrate. The fact indicates that the membrane selectively permeates N_2

We are very grateful to Professor Zi Gao for her helpful suggestions and discussions.

Notes and references

1 J. C. Jansen, W. Nugroho and H. van Bekkum, *Proc. 9th Int. Zeolite Conf.*, 1992, **1**, 247.
2 M. D. Jia, K. V. Peinemann and R. D. Behling, *J. Membr. Sci.*, 1993, **82**, 15.
3 J. X. Dong, T. Dou, X. G. Zhao and L. H. Gao, *J. Chem. Soc., Chem. Commun.*, 1992, 1056.
4 T. Bein, K. Brown, P. Enzel and C. J. Brinker, *Mater. Res. Soc. Symp. Proc.*, 1988, **121**, 761.
5 T. Bein, K. Brown and C. J. Brinker, in *Zeolites: Facts, Figures, Future*, ed. P. A. Jacobs and R. A. van Santen, Elsevier Science Publisher BV, Amsterdam, 1989, p. 887.
6 J. Sterte, S. Mintova, G. Zhang and B. J. Schoeman, *Zeolites*, 1997, **18**, 387.
7 P. Kölsch, D. Venzke, M. Noack, P. Toussaint and J. Caro, *J. Chem. Soc., Chem. Commun.*, 1994, 2491.
8 E. R. Geus, J. Schoonman and H. van Bekkum, *Mater. Res. Soc. Symp. Proc.*, 1991, **233**, 231.
9 J. H. Koegler, A. Arafat, H. van Bekkum and J. C. Jansen, *Stud. Surf. Sci. Catal.*, 1997, **105**, 2163.
10 T. Masuda, A. Sato, H. Hara, M. Kouno and K. Hashimoto, *Appl. Catal. A*, 1994, **111**, 143.
11 J. G. Tsikoyiannis and W. O. Haag, *Zeolites*, 1992, **12**, 126.
12 A. Ishikawa, T. H. Chiang and F. Toda, *J. Chem. Soc., Chem. Commun.*, 1989, 764.
13 T. Sano, H. Yanagishita, Y. Kiyozumi, F. Mizukami and K. Haraya, *J. Membr. Sci.*, 1994, **95**, 221.
14 T. Sano, Y. Kiyozumi, K. Maeda, M. Toba, S. Niwa and F. Mizukami, *Proc. 9th Int. Zeolite Conf.*, 1992, **1**, 239.
15 Y. Kiyozumi, F. Mizukami, K. Maeda, M. Toba and S. I. Niwa, *Adv. Mater.*, 1996, **8**, 517.

ChemComm

A general synthesis of aryl phosphines by palladium catalyzed phosphination of aryl bromides using triarylphosphines

Fuk Yee Kwong and Kin Shing Chan*

Department of Chemistry, The Chinese University of Hong Kong, Shatin, New Territories, Hong Kong. E-mail: ksc@cuhk.edu.hk

Received (in Cambridge, UK) 4th April 2000, Accepted 9th May 2000

Palladium catalyzed phosphination of substituted aryl bromides using triarylphosphines as the phosphinating agents has been developed; this method tolerates ketone, aldehyde, ester, nitrile, ether and chloride functional groups.

Triarylphosphines constitute one of the most important class of ligands in transition metal catalyzed reactions.[1] Although there is a necessity to incorporate functional groups in aromatic phosphines in order to tailor the phosphines for modifying catalysis, synthetic methods available are limited in scope. Traditional methods for preparation of these phosphines can be classified into two major categories. The first method involves the reactions of aryl Grignard or organolithium reagents with chlorophosphine, but it is limited to compounds that are not base sensitive.[2] The second method is transition metal catalyzed phosphination. Though it is useful, limitations do exist. Both nickel catalyzed phosphination of aryl triflates using diphenylphosphine[3] or chlorodiphenylphosphine[4] require use of air- and moisture-sensitive phosphinating reagents and the latter method is not tolerant to easily reducible functional groups since Zn metal is used.[4] The Pd/$Ph_2P(O)H$ route requires subsequent reduction by trichlorosilane.[5] The Pd/(trimethylsilyl)diphenylphosphine system is limited to aryl iodides and cannot tolerate aldehyde functional groups.[6] The Pd/phosphine–borane method requires an extra deprotection step and cannot tolerate amine containing functional groups.[7] Generally, the above methods require the use of air-sensitive reagents and are limited in functional group tolerance. Herein, we report palladium catalyzed phosphination using readily available triarylphosphines as the phosphinating agent and functionalized aryl bromides as substrates to synthesize functionalized aromatic phosphines [eqn. (1)].

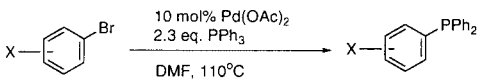

(1)

4-Bromoacetophenone was reacted with 2.3 equivalents of triphenylphosphine in the presence of 10 mol% palladium acetate catalyst in DMF at 110 °C to yield 4-(diphenylphosphino)acetophenone in 40% yield (Table 1, entry 1).† In addition, 4-bromobenzaldehyde can be phosphinated by triphenylphosphine to form 4-(diphenylphosphino)benzaldehyde in 32% yield (Table 1, entry 2). In contrast, the previous method for the preparation[8] of this phosphine, which finds many applications for water soluble polymers[9] and water soluble porphyrins,[10] involved a muti-step synthesis which required protection of the aldehyde.[8] Other functional groups, such as esters, nitriles, methyl ethers and halogens, are tolerant to this phosphination reaction (Table 1, entries 3–7). In contrast, previous syntheses of ester and nitrile containing phosphines required a long synthetic pathway.[11]

Similar rates of reaction were observed for electronically different non-coordinating aryl bromides (Table 1, entries 1,5,7). The rate of the reaction of coordinating substrates which contain ester, aldehyde or nitrile groups (Table 1, entries 2–4), required a longer reaction time. Presumably strongly coordinating substrates rendered the complex coordinatively saturated and hence reduced the catalytic efficiency. For 3- and 4-bromoanisole, the reaction times are similar but the yield of 3-(diphenylphosphino)anisole was higher (Table 1, entries 5 and 6).

Table 1 Palladium catalyzed phosphination of different aryl bromides with triphenylphosphine

Entry	Substrate	Reaction time/h	Yield[a](%)
1[6]	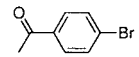	20	40
2[10]	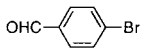	64	32
3[11c]	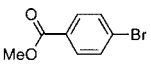	36	30
4[15]	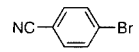	48	36
5[16]	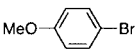	24	27
6[17]	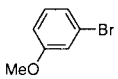	18	38
7[18]	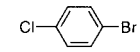	20	51[b]
8	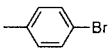	26	58[b]
9[19]	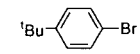	19	59[b]
10[20]		18	51[b]

[a]Isolated yield. [b]GC yield is reported as an average of two runs.

Either $Pd(PPh_3)_4$ or $Pd(OAc)_2$ can catalyze this reaction. $Pd(OAc)_2$ was employed as the catalyst since other triarylphosphines can be used as phosphinating reagents, such as trixylylphosphine, tri(*p*-methoxyphenyl)phosphine and tri(*p*-tolyl)phosphine (Table 2, entries 1–3). Therefore, a variety of different substituted phosphines can be readily prepared through this direct methodology.

A plausible mechanism (Scheme 1) for this phosphination starts with the *in situ* reduction of $Pd(OAc)_2$ by triphenylphosphine to Pd(0).[12] Subsequent oxidative addition with aryl bromide yields a aryl Pd(II) species. Reductive elimination with triphenylphosphine gives a phosphonium salt,[13] which then undergoes oxidative addition with the palladium species to

DOI: 10.1039/b002656p

Table 2 Palladium catalyzed phosphination of *p*-bromoacetophenone with different triarylphosphines

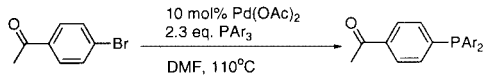

Entry	PAr_3	Product	time/h	Yield[a](%)
1	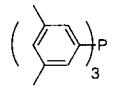	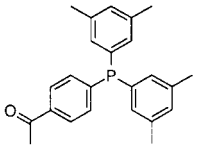	32	34
2	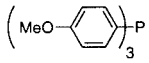	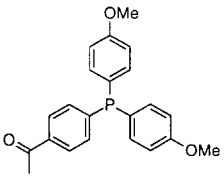	34	33
3	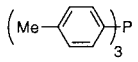	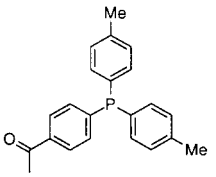	33	39

[a]Isolated yield

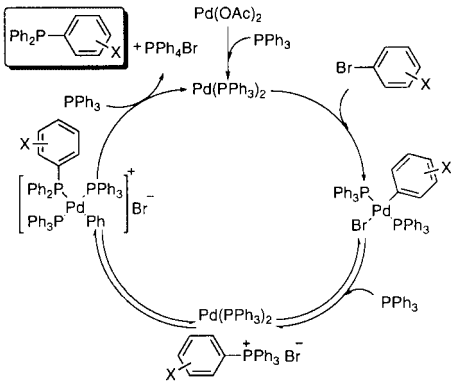

Scheme 1 A plausible mechanism for palladium catalyzed phosphinylation.

generate the coordinated phosphine product.[14] Finally ligand substitution by the other triphenylphosphine regenerates the Pd(0) species and substituted phosphine product.

In conclusion, our phosphination method tolerates a number of functional groups including ketones, aldehydes, esters, nitriles, methyl ethers and chloride. This palladium catalyzed phosphination avoids the problems of traditional raw materials and utilizes the most cost effective triphenylphosphine as the phosphinating reagent. This process has a great potential to tailor a variety of substituted phosphines by using different triarylphosphines as the reagent. Studies are continued to extend the scope of this reaction.

We thank the Research Grants Council of Hong Kong (EI00014) for financial support.

Notes and references

† *General experimental procedure*: 4-bromoacetophenone (100 mg, 0.5 mmol), $Pd(OAc)_2$ (11 mg, 0.05 mmol) and PPh_3 (301 mg, 1.15 mmol) were dissolved in dry DMF (2 mL) under nitrogen in a Telfon stopcock flask. The solution was heated to 110–115 °C and the reaction was monitored by GC–MS. The reaction mixture was then cooled down and DMF was removed by vacuum evaporation. After 20 h, the crude product was purified by column chromatography on silica gel using a solvent mixture of hexane–ethyl acetate (20 : 1) as the eluent to give 4-(diphenylphosphino)acetophenone in 40% yield as a white solid.

1 G. M. Kosolapoff and L. Maier, *Organic Phosphorus Compounds*, vol. 1, Wiley-Interscience, New York, 1972.
2 H. Takaya, K. Mashima, K. Koyano, M. Yagi, H. Kumobayaashi, T. Taketomi, S. Akutagawa and R. Noyori, *J. Org. Chem.*, 1986, **51**, 629.
3 D. Cai, J. F. Payack, D. R. Bender, D. L. Hughes, T. R. Verhoeven and P. J. Reider, *J. Org. Chem.*, 1994, **59**, 7180.
4 D. J. Ager, M. B. East, A. Eisenstadt and S. Laneman, *Chem. Commun.*, 1997, 2359.
5 For recent references, see: A. E. S. Gelpke, H. Kooijman, A. L. Spek and H. Hiemstra, *Chem. Eur. J.*, 1999, **5**, 2472; K. Ding, Y. Wang, H. Yun, J. Liu, Y. Wu, M. Terada, Y. Okubo and K. Mikami, *Chem. Eur. J.*, 1999, **5**, 1734; S. Vyskocil, M. Smrcina, V. Hanus, M. Polásek and P. Kocovsky, *J. Org. Chem.*, 1998, **63**, 7738.
6 S. E. Tunney and J. K. Stille, *J. Org. Chem.*, 1987, **52**, 748.
7 B. H. Lipshutz, D. H. Buzard and C. S. Yun, *Tetrahedron Lett.*, 1999, **40**, 201.
8 J. E. Hoots, T. B. Rauchfuss and D. A. Wrobleski, *Inorg. Synth.*, 1982, **21**, 175; G. P. Schiemenz and H. Kaack, *Liebigs Ann. Chem.*, 1973, 1494.
9 T. Malmstrom, H. Weigl and C. Andersson, *Organometallics*, 1995, **14**, 2593.
10 G. Märkl, M. Reiss, P. Kreitmeier and H. Nöth, *Angew. Chem., Int. Ed. Engl.*, 1995, **34**, 2230.
11 Previous synthesis of 4-(diphenylphosphino)benzonitrile and methyl 4-(diphenylphosphino)benzoate required a three-step route and the overall yields were approximately 11 and 21%, respectively; (*a*) W. N. Chou and M. Pomerantz, *J. Org. Chem.*, 1991, **56**, 2762; (*b*) G. P. Schiemenz and H. U. Siebeneich, *Chem. Ber.*, 1969, **102**, 1883; (*c*) P. S. Aexandrovich, L. P. DeMejo, T. A. Jadwin and J. C. Wilson, *US Pat.*, 4,837,394, 1989.
12 C. Amatore, A. Jutand and M. A. M'Barki, *Organometallics*, 1992, **11**, 3009.
13 Migita *et al*. reported a similar method for preparation of a phosphonium salt (no phosphine product) using toluene or benzene as solvent; presumably the polarity of the solvent alters the products: T. Migita, T. Nagai, K. Kiuchi and M. Kosugi, *Bull. Chem. Soc. Jpn.*, 1983, **56**, 2869; H.-J. Cristau, A. Chene and H. J. Christol, *J. Organomet. Chem.*, 1980, **185**, 283; R. J. Hinkle, P. J. Stang and M. H. Kowalalski, *J. Org. Chem.*, 1990, **55**, 5033.
14 F. E. Goodson, T. I. Wallow and B. M. Novak, *J. Am. Chem. Soc.*, 1997, **119**, 12441; K. C. Kong and C. H. Cheng, *J. Am. Chem. Soc.*, 1991, **113**, 6313; P. E. Garrou, *Chem. Rev.*, 1985, **85**, 171.
15 V. Ravindar, H. Hemling, H. Schumann and J. Blum, *Synth. Commun.*, 1992, **22**, 841.
16 K. Burgess, M. J. Ohimeyer and K. H. Whitmire, *Organometallics*, 1992, **11**, 3588; C. D. Hall, B. R. Tweedy, R. Kayhanian and J. R. Lloyd, *J. Chem. Soc., Perkin Trans 2*, 1992, 775.
17 A. Buhling, P. C. J. Kamer and P. W. N. M. van Leeuwen, *J. Mol. Catal. A: Chem.*, 1995, **98**, 69.
18 D. Bethell, R. Bourne and M. Kasran, *J. Chem. Soc., Perkin Trans. 2*, 1994, 2081.
19 H. A. Brune, M. Falck and R. Hemmer, *Chem. Ber.*, 1984, **117**, 2791.
20 O. Herd, A. Hebler, M. Hingst, M. Tepper and O. Stelzer, *J. Organomet. Chem.*, 1996, **552**, 69.

Isolation and characterisation of C_s-symmetry $C_{60}Me_5O_2OH$, the first methylated fullerenol; a bis-epoxide with two oxygens in a pentagonal ring

Hamad Al-Matar, Peter B. Hitchcock, Anthony G. Avent and Roger Taylor*

The Chemistry Laboratory, CPES School, University of Sussex, Brighton, UK BN1 9QJ. E-mail: r.taylor@sussex.ac.uk

Received (in Cambridge, UK) 21st March 2000, Accepted 11th May 2000

From the reaction between [60]fullerene and MeLi, we have isolated $C_{60}Me_5O_2OH$, which has been characterised by both ^{1}H and ^{13}C NMR spectroscopy and by single-crystal X-ray analysis; uniquely, both epoxide groups bridge 5 : 6-bonds in the same pentagon.

The significance of epoxyfullerenes has yet to be fully recognised. They may be formed by: (i) partial hydrolysis of a halogenofullerene to a *cis* halohydroxy derivative, followed by adjacent elimination of hydrogen halide, giving for example, the abundance of epoxides amongst the products of fullerene fluorination;[1] (ii) ozonolysis;[2] (iii) epoxidation of the fullerene with a peracid;[3] (iv) direct reaction with oxygen, either in the arc-discharge reactors used for fullerene production,[4] or on standing[5] (this can be photochemically accelerated).[6] The extent to which cage addends moderate the latter process is not yet known, but it is probable that all fullerene derivatives undergo this oxidation to some extent.

The formation of the only bis-epoxy fullerenes characterised previously, $C_{60}O_2$, involves addition of oxygen across the 1,2- and 3,4-bonds in a given hexagon;[7] this motif is also believed to be present in $C_{60}O_3$.[8] In the heterocycle $C_{60}Ph_4(C_6H_4)O_2$, we conjectured that one oxygen is present as an epoxide bridging a 5:6-bond in the central pentagon.[9]

There are few reports of the methylation of fullerenes. Olah and coworkers detected the addition of up to 24 methyl groups (with $C_{60}Me_6$ and $C_{60}Me_8$ being prominent) from the reaction of [60]fullerene with Li–MeI.[10] Both 1,2- and 1,4-Me_2C_{60} have been obtained by electrochemical reduction,[11] and we have described preliminary results on the formation of $C_{60}Me_n$ (n = 4, 6, 8) and $C_{70}Me_n$ (n = 2, 4, 6, 8, 10).[12] Polyhydroxyfullerenes have been investigated extensively,[13] but, to date, only one monohydroxyfullerene ($C_{70}Ph_9OH$) has been characterised.[14]

We now report the isolation and full characterisation of the first methylated fullerene, (and methylated fullerenol) and the first bis-epoxide with both oxygens bridging a 5:6-bond. The structure was characterised by NMR spectroscopy, the interpretation of the latter being shown to be correct by single crystal X-ray crystallography.

An xs. of MeLi solution (4 ml of 1.0 M solution in THF–cumene, 110:90) was stirred under N_2 with $C_{60}Cl_6$ (100 mg),[15] at room temp. The orange solution turned brown–black immediately and stirring was continued overnight. Normal work-up followed by column chromatography (70–230 mesh silica gel), gave a major fraction (9:1 cyclohexane–toluene elution) and then a minor fraction (1:1 cyclohexane–toluene elution). This latter was purified further by HPLC using a 10 mm × 25 cm Cosmosil 'Buckyprep' column at a solvent flow rate of 4.7 ml min^{-1} to give $C_{60}Me_5O_2OH$, which eluted after 4.8 (toluene) or 8.8 min (1:1 toluene–heptane), and crystallised as ruby-red hexagonal plates.

The EI mass spectrum (Fig. 1) shows a peak due to the parent ion at 844 amu; notably, the C_{58} fragmentation ion peak at 696 amu is 40% of the intensity of the 720 amu peak. This is much higher than is found in the EI mass spectrum of C_{60} and arises because of the more facile loss of 2 CO molecules, which we have noted previously in the mass spectra of phenylated epoxides of [60]fullerene, where the intensity of the 696 amu peak was 30% of that of the 720 amu peak.[16] When the epoxide functions straddle 5:6-bonds, CO elimination creates a 7/5-membered ring combination, stabilised by the presence of sp^3 carbons bearing the addends.[16]

The IR spectrum (KBr) shows bands at 3520 (broad), 2971, 2924, 2857, 1438, 1384, 1099, 1074, 1047, 1037, 1016, 941, 665, 658, 572, 553, 535 and 513 cm^{-1}.

The ^{1}H NMR spectrum shows peaks at δ_H 3.88 (1 H, s, OH), 1.99 (3 H, s, Me_A), 1.86 (6 H, s, Me_C), 1.75 (6 H, s, Me_B). The peaks were identified by NOE couplings of 2.4, 2.5 and 0.6% between OH and Me_A, Me_B, and Me_C, respectively, and of 0.9 and 0.3% between Me_A and Me_B. Saturation transfer to water confirmed the presence of an OH group; the NOE couplings between OH and *all three* methyls confirmed that OH must be present in the central pentagon.

The ^{13}C NMR spectrum shows 24 2 C and 2 1 C peaks for the cage sp^2-carbons at δ_C (all 2 C except where indicated) 151.56, 148.79, 148.72, 148.69, 148.68, 148.59, 148.49 (1 C), 148.45, 148.44, 148.03, 147.99, 147.90, 147.87, 147.57 (1 C), 147.12, 145.13, 144.39, 144.03, 144.01, 143.97, 143.72, 143.38 (4 C), 143.30, 143.25, 143.08; the half-intensity on-symmetry plane peaks appear in the usual 147–149 ppm range. The sp^3-carbons appear at δ_C 86.60 (2 C, COC), 75.11 (1 C, COH), 72.35 (2 C, COC), 53.12 (1 C, C_1Me), 47.21 (2 C, $C_{15,30}$Me), 46.49 (2 C, $C_{4,11}$Me), 27.38 (1 C, Me_A), 24.88 (2 C, Me_C), 24.20 (2 C, Me_B).

The compound thus has C_s symmetry and was deduced to have the two epoxide functions in the central pentagon, since the only other reasonable locations would be across the 16,17- and 28,29-positions (Fig. 2). However, little difference in the

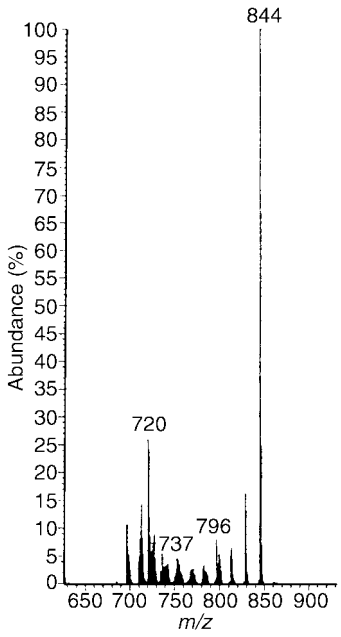

Fig. 1 EI mass spectrum (70 eV) for $C_{60}Me_5O_2OH$.

DOI: 10.1039/b002254n

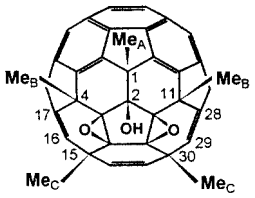

Fig. 2 Structure of symmetrical $C_{60}Me_5O_2OH$, showing numbering.

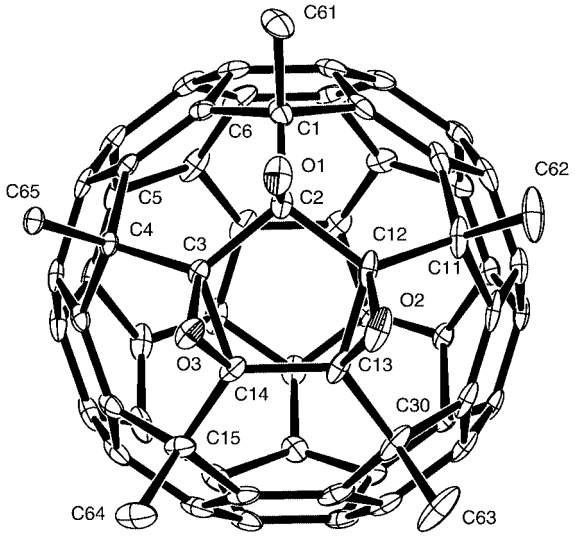

Fig. 3 X-Ray structure of $C_{60}Me_5O_2OH$.

chemical shifts for carbons C-17 and C-28, compared with C-16 and C-29 would then be expected, whereas an experimental difference of 14 ppm is found. This is consistent with two of the epoxide carbons being adjacent to that bearing the OH group (Fig. 2). The structure was confirmed by X-ray crystallography (Fig. 3).†

The structure is thus unique in having two epoxide functions straddling 5 : 6-bonds bonds in the central pentagon. The addend locations in $C_{60}X_6$ structures requires placing two double bonds in the central pentagon, thereby increasing the strain; this can be partially relieved by addition across these bonds. The C–C bonds bridged by the epoxide function are short, at 1.48 Å, whereas all other cage C–C bonds in the central pentagon area and the cage–Me bonds, have an average bond length of 1.55 ± 0.02 Å. The C–O–C bond angles are 61.5°, and some repulsion between the epoxides and the OH group is manifest in the C-3–O-3 bond (1.459 Å), which is longer than the O-3–C-14 bond (1.437 Å).

A notable feature (and one which we have found recently with phenylated [84]fullerene as well) is that on strongly heating the KBr disc (250 °C) of $C_{60}Me_5O_2OH$, a very sharp peak appears at 2170 cm^{-1} after 3 h and grows in intensity with heating during the next 24 h. This is consistent with the presence of matrix-isolated C_5,[17] and parallels earlier work in which similar treatment of KBr discs of insoluble [84]fullerene residues, produced a sharp band at 2035 cm^{-1} attributed to matrix-isolated C_3.[18] We hope to investigate this aspect more fully at a later date.

We thank Kuwait University for a research grant (to H. A.-M.).

Notes and references

† *Crystal data* for $C_{65}H_{16}O_3$: M_r = 844.8, triclinic, $P\bar{1}$ (no. 2), a = 14.6057(3), b = 15.2988(4), c = 15.6144(4) Å, α = 81.596(1), β = 81.663(1), γ = 83.954(2)°, V = 3402.5(1) Å^3, Z = 4, μ(Mo-Kα) = 0.10 mm^{-1}, T = 173 K. R_f = 0.075 for 9548 reflections with $I > 2\sigma(I)$, wR_2 = 0.205 for all 11 740 independent reflections. Two independent molecules were evident: one ordered, the other showing some disorder of the oxygen atoms around the pentagon. CCDC 186/1637. See http://www.rsc.org/suppdata/cc/b0/b002254n/ for crystallographic data in .cif format.

1 O. V. Boltalina, J. H. Holloway, E. G. Hope, J. M. Street and R. Taylor, *J. Chem. Soc., Perkin Trans. 2*, 1998, 1845.
2 D. Heymann and L. P. F. Chibante, *Rec. Trav. Chim.*, 1993, **112**, 531; 639; R. Malhotra, S. Kumar and A. Satyam, *J. Chem. Soc., Chem. Commun.*, 1994, 1339; J. P. Deng, C. Y. Mou and C. C. Han, *Fullerene Sci. Technol.*, 1997, **5**, 1033.
3 A. L. Balch, D. A. Costa, B. C. Knoll and M. M. Olmstead, *J. Am. Chem. Soc.*, 1995, **117**, 8926; M. P. Barrow, N. J. Tower, R. Taylor and T. Drewello, *Chem. Phys. Lett.*, 1998, **293**, 302; A. B. Smith, R. M. Strongin, L. Brard, G. T. Furst, J. H. Atkins, W. J. Romanov, M. Saunders, H. A. Jiménez-Vázquez, K. G. Owens and R. J. Goldschmidt, *J. Org. Chem.*, 1996, **61**, 1904.
4 F. Diederich, R. Ettl, Y. Rubin, R. L. Whetten, R. Beck, M. Alvarez, S. Anz, D. Sensharma, F. Wudl, K. C. Khemani and A. Koch, *Science*, 1991, **252**, 548; V. N. Bezmelnitsin, A. V. Eletskii, N. G. Schepetov, A. G. Avent and R. Taylor, *J. Chem. Soc., Perkin Trans. 2*, 1997, 683.
5 R. Taylor, M. P. Barrow and T. Drewello, *Chem. Commun.*, 1998, 2497.
6 K. M. Creegan, J. L. Robbins, W. K. Robbins, J. M. Millar, R. D. Sherwood, P. J. Tindall, D. M. Cox, A. B. Smith, J. P. McCaulay, D. R. Jones and R. T. Gallagher, *J. Am. Chem. Soc.*, 1992, **114**, 1103.
7 A. L. Balch, D. A. Costa, B. C. Noll and M. M. Olmstead, *J. Am. Chem. Soc.*, 1995, **117**, 8926.
8 T. Hamano, T. Mashino and M. Hiroba, *J. Chem. Soc., Chem. Commun.*, 1995, 1537.
9 A. D. Darwish, A. G. Avent, H. W. Kroto, R. Taylor and D. R. M. Walton, *Chem Commun.*, 1997, 1579.
10 J. W. Bausch, G. K. S. Prakash, G. A. Olah, D. S. Tse, D. C. Lorents, Y. K. Bae and R. Malhotra, *J. Am. Chem. Soc.*, 1991, **113**, 3205.
11 C. Caron, D. Subramanian, F. D'Souza, J. Kim, W. Kutner, M. T. Jones and K. M. Kadish, *J. Am. Chem. Soc.*, 1993, **115**, 8505.
12 H. Al-Matar and R. Taylor, *Recent Adv. Chem. Phys. Fullerenes Relat. Mater.*, 1999, **7**, 163.
13 L. Y. Chiang, in *The Chemistry of Fullerenes*, ed. R. Taylor, World Scientific, Singapore, 1995, ch. 5.
14 P. R. Birkett, A. G. Avent, A. D. Darwish, H. W. Kroto, R. Taylor and D. R. M. Walton, *Chem. Commun.*, 1996, 1231.
15 P. R. Birkett, A. G. Avent, A. D. Darwish, H. W. Kroto, R. Taylor and D. R. M. Walton, *J. Chem. Soc., Chem. Commun.*, 1993, 1230.
16 A. D. Darwish, P. R. Birkett, G. J. Langley, H. W. Kroto, R. Taylor and D. R. M. Walton, *Fullerene Sci. Technol.*, 1997, **5**, 705.
17 J. Szezepanski and M. Vale, *J. Phys. Chem.*, 1991, **95**, 2792.
18 R. Taylor, A. Pénicaud and N. J. Tower, *Chem. Phys. Lett.*, 1998, **295**, 481.

Upper-rim monofunctionalization of calix[4]arene by organometallic diphenylphosphinorhodium complexes†

Martin Vézina, Jonathan Gagnon, Karine Villeneuve, Marc Drouin and Pierre D. Harvey*

Département de Chimie, Université de Sherbrooke, Sherbrooke, P.Q. Canada, J1K 2R1. E-mail: pharvey@courrier.usherb.ca

Received (in Irvine, CA, USA) 17th February 2000, Accepted 1st May 2000

Monofunctionalization of the calix[4]arene upper-rim is achieved by lithiation with Bu^{n}Li, followed by phosphination with Ph_2PCl of monobromotetra-*n*-propoxycalix[4]arene; subsequent reactions with $[Cp^*Rh^{III}Cl_2]_2$ and $Cp^*Rh^I(CO)_2$ provide the corresponding $Cp^*[Ph_2(calix)P]Rh^{III}Cl_2$, which can be converted to $Cp^*[Ph_2(calix)P]Rh^{III}(H)_2$ and $Cp^*[Ph_2(calix)P]Rh^I(CO)$, respectively.

Substituted derivatives of the bowl-like calix[4]arene are easy to synthesize and extremely rich chemistry has emerged from this simple molecule, primarily due to the pioneering work of Gutsche.[1] Many applications in the area of cation binding and transport are now known, and highly selective receptors and novel sensors for polyanionic species have been discovered with this host.[2] Recently, several researchers have prepared transition metal complexes of this platform molecule, mainly *via* the lower-rim section,[3] but some rare upper-rim functionalizations have also appeared in the literature.[4] Of particular interest, Matt and coworkers synthesized conic calix[4]arene complexes using two anchoring phosphine groups placed opposite to each other in the upper-rim.[5] Complexation induced a loop structure where the calix[4]arene cavity was blocked by the transition metal fragment, hence, losing its important hydrophobic hosting function. We now report the first monofunctionalization of the calix[4]arene upper-rim, using the Ph_2P complexing fragment, along with some of its Rh complexes. The complexation of an Rh residue near a hosting device offers the hope of convenient regioselective reactivity in situations where the reacting molecule reversibly binds the calix[4]arene cavity. Many Cp*Rh complexes are known to activate C–H bonds,[6] and anchoring this fragment onto the supramolecular calix[4]arene represents a unique opportunity of potential regioselective C–H bond activation. This work describes the syntheses and characterization of three (η^5-pentamethylcyclopentadienyl)rhodium complexes of diphenylphosphinocalix[4]arene.

The entry into the monofunctionalization proceeds *via* the use of the known monobromotetra-*n*-propoxycalix[4]arene **1**.[7] In this case, simultaneous standard lithiation and phosphination procedures produce the monophosphine ligand: [eqn. (1) and (2)].

$$(PrO)_4calix–Br + Bu^nLi \rightarrow (PrO)_4calix–Li + Bu^nBr \quad (1)$$

$$(PrO)_4calix–Li + Ph_2PCl \rightarrow (PrO)_4calix–PPh_2 + LiCl \quad (2)$$

The latter is easily oxidized to its oxo form in the presence of air in solutions as evidenced from the X-ray structure determination to be described elsewhere, and therefore inert conditions must be used at all times.

The complexation routes of **2** with Cp*Rh complexes are shown in Scheme 1. Complex **3** is conveniently synthesized by directly reacting the known dimeric $[Cp^*RhCl_2]_2$[8] with **2**, and is obtained in 85% isolated yield. Complex **3** is relatively stable and has been structurally characterized by X-ray methods.‡ Fig. 1 shows the X-ray structure and confirms the expected monofunctionalization of the calix[4]arene. The coordination environment of the Rh^{III} metal center is relatively similar to that

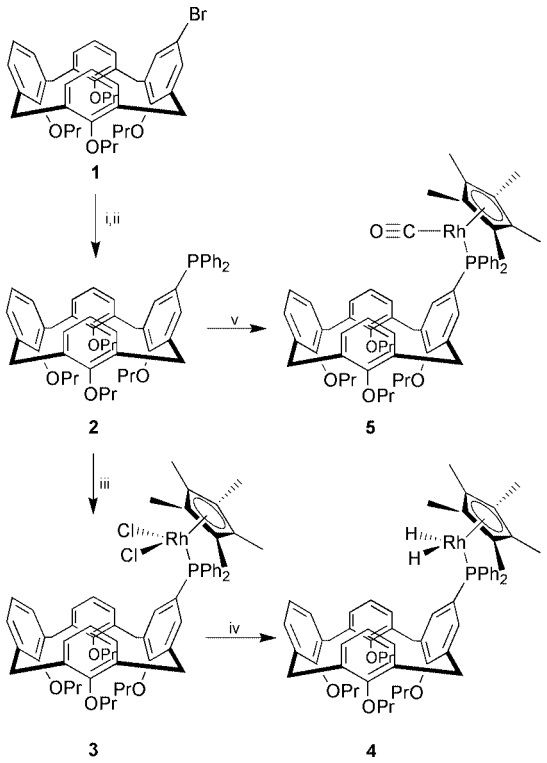

Scheme 1 Synthesis of **2**–**5**. *Reagents and conditions*: i, BuLi/THF/−78 °C; ii, $ClPPh_2$/THF/−78 °C; *iii*, $[Cp^*RhCl_2]_2$/EtOH/reflux 5 h; *iv*, $NaBH_4$/EtOH/reflux 1 h; v, $Cp^*Rh(CO)_2$/benzene/reflux 24 h.

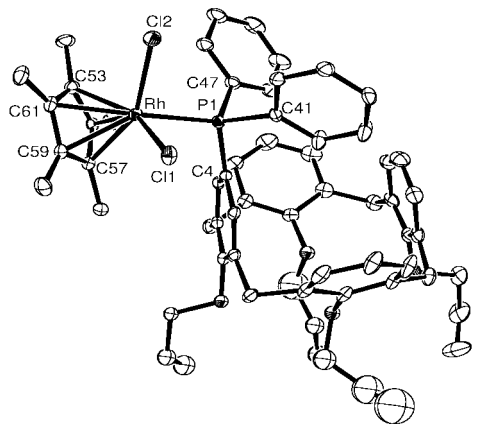

Fig. 1 ORTEP drawing of **3**. Ellipsoids are shown at 10% probability and H atoms are not shown for clarity. Selected bond and distances (Å) and angles (°): Rh–C11 2.3835(18), Rh–C12 2.4053(20), Rh–P 2.3354(18), av. Rh–Cl 2.19(3); C11–Rh–C12 93.54(8), C11–Rh–P 85.71(6), P–Rh–C12 93.50(7).

† Electronic supplementary information (ESI) available: synthesis and characterisation of compounds **2**–**5**. See http://www.rsc.org/suppdata/cc/b0/b001485k/

DOI: 10.1039/b001485k

of the reported less encumbered $[Cp^*Rh(Cl)_2P(Me)_2CH_2]_2$ complex.[9]

The key feature of this structure is that **3** exhibits calix C–P and P–Rh single bonds and at least 12 conformations are possible. Rotation around this C–P bond provides two rotamers where part of the cavity opening is covered by phenyl groups, and one where the metallic residue occupies this specific above position (C_s point group). The single crystal data shows one of the former described rotamers (Ph group on top of the cavity), and the Cp^*RhCl_2 fragment adopts a conformation exhibiting a minimum of steric hindrance between Cp* and Ph, as shown in Fig. 1. ^{1}H NMR spectroscopy clearly established the presence of fluxionality in **3**. Between 218 and 343 K, the spectra exhibit three main regions including the aromatic, methylene and propyl ^{1}H region, which all undergo coalescence processes. The most striking observation is that both the PPh_2 proton and aromatic signals coalesce at the same temperature of *ca.* 268 K, corresponding to $\cong$ 2.2 kJ mol^{-1}. This result strongly indicates that the fluxion must involve cooperative motions of the Ph groups and the calix[4]arene aromatic fragments. The most probable motion is rotation of the $Cp^*(PPh_2)RhCl_2$ group around the calix C–P single bond, where the Ph groups also rotate to pass over the bowlic structure of the calix[4]arene residue. Computer modellings clearly demonstrate that indeed rotations around the calix C–P bond must be accompanied by cooperative rotations of the Ph–P bond, somewhat similar to a 'merry-go-round' motion, allowing the Ph substituents to hop over the calix[4]arene 'walls'.

Complex **3** predictably reacts with $NaBH_4$ in refluxing ethanol to produce the corresponding dihydride **4**. The latter is very reactive, particularly in the presence of light and air, and must be freshly prepared prior to further studies. The presence of hydride groups in **4** is readily illustrated from its ^{1}H NMR and IR spectra which exhibit a characteristic resonance at δ –13.07 ($^1J_{HRh}$ = 28 Hz, $^1J_{HP}$ = 38 Hz), and an absorption at 2080 cm^{-1} (ν_{RhH}), respectively. Complexation of monophosphine ligand **2** can also be performed with the mononuclear $Cp^*Rh^I(CO)_2$ complex[10] *via* a simple thermally induced CO substitution, to form **5**. A single and characteristic ν_{CO} absorption is indeed observed at 1960 cm^{-1} in the solid state, and a complete characterization by standard methods (NMR, FAB mass, chemical analysis), confirms the identity and purity of this novel complex. Complex **5** is somewhat more stable than the dihydride **4**, but decomposition can also be observed upon UV–VIS light irradiation. Preliminary results show that indeed both **4** and **5** either thermally or photochemically eliminate H_2 and CO, respectively, to generate the very reactive species Cp^*Rh^IL (L = phosphine ligand, here **2**).[11] This important intermediate postulated as $Cp^*Rh[Ph_2P(calix)]$, is anticipated to activate C–H bonds,[12] and regioselectivity would be an unprecedented asset. Preparation of the more basic and less encumbered R_2P–calix ligand (R = Pr^i) and its Cp*Rh complex has been successful. Their structural properties and reactivities are under investigation, and will be published in due course.

We acknowledge NSERC (Natural Sciences and Engineering Research Council), FCAR (Fonds Concertés pour l'Avancement de la Recherche) and le Bureau de la Recherche de l'Université de Sherbrooke for funding and graduate scholarships.

Notes and references

‡ *Crystal data* for $C_{62}H_{72}Cl_2O_4PRh$ **3**: M = 1085.98, monoclinic, space group $P2_1/c$, a = 18.009(7), b = 15.401(2), c = 21.996 (5) Å, β = 110.34(2)°, U = 5720(3) Å^3, T = 293 K, Z = 4, μ(Cu-Kα) = 1.54060 Å, 18919 reflections measured, 9703 unique (R_{int} = 0.07) which were used in all calculations. The final $wR(F^2)$ was 0.1897 (all data). Single crystals of $Cp^*[Ph_2P(calix)]RhCl_2$ **3** were obtained from recrystallization in ethanol. These dark red crystals were air-stable and one of them was mounted at 298 K on an Enraf-Nonius CAD-4 automatic diffractometer. The full structure was solved using direct methods and refined by full matrix least-squares on F^2.

CCDC 182/1634.

1 C. D. Gutsche, *Calixarenes*, Royal Society of Chemistry, Cambridge, UK, 1989.

2 *Calixarenes: a versatile class of macrocyclic compounds*, ed. J. Vicens and V. Böhmer, Kluwer Academic Publishers, Dordrecht, 1991; *Calixarenes 50th anniversary: commemorative issue*, ed. J. Vicens, Z. Asfari and J. M. Harrowfield, Kluwer Academic Publishers, Dordrecht, 1994.

3 C. Wieser, C. B. Dieleman and D. Matt, *Coord. Chem. Rev.*, 1997, **165**, 93.

4 P. D. Beer, D. Hesek, K. C. Nam and M. G. B. Drew, *Organometallics*, 1999, **18**, 3933; B. R. Cameron and S. J. Loeb, *Chem. Commun.*, 1996, 2003.

5 I. A. Bagati, D. Matt, H. Thonnessen and P. G. Jones, *Inorg. Chem.*, 1999, **38**, 1585; C. Wieser-Jeunesse, D. Matt and A. De Cian, *Angew. Chem., Int. Ed.*, 1998, **37**, 2861.

6 A. E. Shilov, *Activation of Saturated Hydrocarbons by Transition Metal Complexes*, D. Riedel, Hingham, MA, 1984.

7 A. Ikeda, M. Yoshimura, P. Lhotak and S. Shinkai, *J. Chem. Soc., Perkin Trans. 1*, 1996, 1045.

8 J. W. Kang, K. Moseley and P. M. Maitlis, *J. Am. Chem. Soc.*, 1969, **91**, 5970.

9 W. Keim, P. Kraneburg, G. Dahmen, G. Deckers, U. Englert, K. Linn, T. P. Spaniol, G. Raabe and C. Kruger, *Organometallics*, 1994, **13**, 3085.

10 D. P. Drolet and A. J. Lees, *J. Am. Chem. Soc.*, 1992, **114**, 4186.

11 W. D. Jones and F. J. Feher, *J. Am. Chem. Soc.*, 1986, **108**, 4814; W. D. Jones and F. J. Feher, *J. Am. Chem. Soc.*, 1985, **107**, 620; W. D. Jones and F. J. Feher, *J. Am. Chem. Soc.*, 1984, **106**, 1650; R. A. Periana and R. G. Bergman, *J. Am. Chem. Soc.*, 1984, **106**, 7272; M. J. Wax, J. M. Stryker, J. M. Buchanan, C. A. Kovac and R. G. Bergman, *J. Am. Chem. Soc.*, 1984, **106**, 1121.

12 B. K. McNamara, J. S. Yeston, R. G. Bergman and C. B. Moore, *J. Am. Chem. Soc.*, 1999, **121**, 6437; A. A. Bengali, R. H. Schultz, C. B. Moore and R. G. Bergman, *J. Am. Chem. Soc.*, 1994, **116**, 9585.

ChemComm

The first organoruthenium(IV) complexes containing nitrogen donor ligands by oxidative addition of allylic substrates to coordinatively unsaturated Ru(II) complexes†

Hideo Kondo, Yoshitaka Yamaguchi and Hideo Nagashima*

Institute of Advanced Material Study, Kyushu University, Kasuga, Fukuoka 816-8580, Japan and CREST, Japan Science and Technology Corporation (JST), Japan. E-mail: nagasima@cm.kyushu-u.ac.jp

Received (in Cambridge, UK) 12th April 2000, Accepted 8th May 2000

Oxidative addition of allylic substrates to coordinatively unsaturated ruthenium(II), (η^5-C_5Me_5)Ru(amidinate) complexes, afford cationic ruthenium(IV) compounds, [(η^5-C_5Me_5)Ru(amidinate)(η^3-allyl)]$^+$, which have been characterized by spectroscopic analysis and X-ray structure determination.

Studies on the structures and reactions of coordinatively unsaturated transition metal complexes have received much attention from organometallic chemists, because these compounds are believed to be involved in many transition metal-mediated organic reactions as important intermediates.[1] In particular, the structures and reactions of coordinatively unsaturated ruthenium(II) complexes have been actively investigated recently;[1] these studies contribute to the understanding of the factors leading to the stabilization of these complexes, *e.g.* steric effects, presence of π-donor ligands, metal-bond strength and their tendency towards oxidative addition of H_2 and $HSiR_3$.[1–3] Although the oxidative addition of allylic substrates to ruthenium(II) complexes[4] is an important elementary reaction in the catalytic transformation of an allyl moiety,[5] that to isolated coordinatively unsaturated ruthenium compounds has not, as yet, been studied.[1–3] We have recently reported a novel reactive complex, (η^5-C_5Me_5)Ru(amidinate) **1**, which shows signs of coordinative unsaturation, in which the amidinate ligand contributes to stabilizing the formally 16-electron configuration.[6] The fact that **1** is highly reactive towards the reaction with a variety of two-electron donor ligands stimulated us to explore the possibility that **1** may also be reactive towards oxidative addition reactions.[6] Here, we report that **1** readily reacts with an allylic substrate to give the corresponding cationic Ru(IV) allylic compound as shown in Scheme 1. This is the first example, to the best of our knowledge, of oxidative addition of allylic substrates to isolable coordinatively unsaturated ruthenium complexes. Additionally, the product is a rare example of an organoruthenium(IV) compound coordinated to nitrogen donor ligands.

Complex **1a** was treated with a stoichiometric amount of allyl chloride at −78 °C and the mixture was allowed to warm to room temperature. After 1 h, the solvent was removed *in vacuo*. Spectroscopic evidence suggests that the resulting yellow solid is [(η^5-C_5Me_5)Ru(amidinate)(η^3-allyl)]Cl **2a** (yield of the crude product > 95%) containing *ca.* 5% of (η^5-C_5Me_5)Ru(η^3-allyl)Cl_2.[4a] This new η^3-allyl complex **2a** is not very stable in solution and gradually decomposes to a mixture of intractable products. In contrast, **3a**, a stable analogue of **2a**, was successfully isolated as a yellow solid in 48% yield by exchange in $CHCl_3$ of the counter anion Cl^- to PF_6^- followed by recrystallization of the crude product. Complex **3a** could also be obtained directly from **1a** by treatment with allyl chloride in the presence of $NaPF_6$. The oxidative addition of allyl acetate or allyl methyl carbonate in the presence of $NaPF_6$ offers an alternative synthetic method for **3a** without formation of by-products; **3a** was isolated in quantitative yield. In a similar fashion, **3b**, a methallyl analogue of **3a**, and a compound **3c**, bearing a different amidinate ligand, were successfully prepared and characterized as shown in Table 1.

Table 1

Precursor	R^2	X	Method	Product	Isolated yield (%)
1a	H	Cl	A	**3a**	48
1a	Me	Cl	A	**3b**	55
1c	H	Cl	A	**3c**	62
1a	H	Cl	B	**3a**	64
1a	Me	Cl	B	**3b**	39
1c	H	Cl	B	**3c**	62
1a	H	OCOMe	B	**3a**	97
1a	H	OCO_2Me	B	**3a**	97

Complex **3a** was fully characterized by spectroscopic methods (^{1}H NMR, ^{13}C NMR, IR),‡ elemental analyisis and an X-ray crystal structure determination§ and an ORTEP drawing of **3a** is shown in Fig. 1. Complex **3a** has a square-pyramidal structure, with two nitrogen atoms of the amidinate ligand and terminal carbons of the η^3-allyl ligand at the basal positions. The orientation of the allyl group is *endo*, and variable temperature NMR studies showed that there is no equilibrium with the corresponding *exo* isomer. This *endo* orientation is also seen in (η^5-C_5Me_5)Ru(η^3-allyl)X_2 reported previously.[4a] The crystal structure of **3a**, in comparison with that of the starting

† Electronic supplementary information (ESI) available: typical procedures and spectroscopic data. See http://www.rsc.org/suppdata/cc/b0/b002927k/

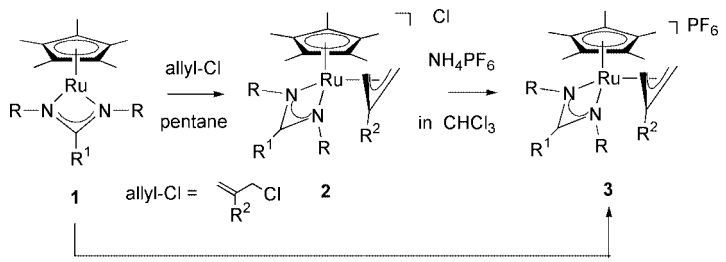

Scheme 1 Method A; allyl–Cl in pentane followed by NH_4PF_6 in $CHCl_3$; method B; allyl–X (X = Cl, OAc, OCO_2Me) and $NaPF_6$ in THF. For **1**–**3**: **a**, R = Bu^t, R^1 = Ph, R^2 = H; **b**, R = Bu^t, R^1 = Ph, R^2 = Me; **c**, R = Pr^i, R^1 = Me, R^2 = H.

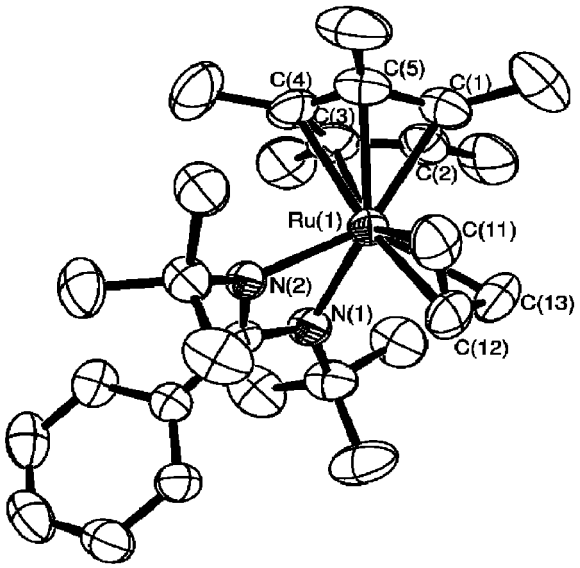

Fig. 1 ORTEP drawing of **3a** showing 50% thermal ellipsoids. PF_6^- omitted for clarity. Selected bond lengths (Å) and angles (°): Ru(1)–C(1–5)$_{av}$ 2.263(4), Ru(1)–N(1), 2.128(3), Ru(1)–N(2) 2.125(3), Ru(1)–C(11) 2.193(5), Ru(1)–C(12) 2.132, Ru(1)–C(13) 2.206, C(11)–C(12) 1.385(8), C(12)–C(13) 1.379(8); N(1)–Ru(1)–N(2) 61.98(12), C(11)–Ru(1)–C(12) 64.1(2), C(11)–C(12)–C(13) 115.2(5).

material **1a** reveals that the Ru–N and Ru–C bonds (average) become longer [**1a**: Ru–N 2.073(3) Å, Ru–C_{av} 2.158(4) Å].

The chemical reactivity of the η^3-allyl moiety is an interesting problem for the exploration of stoichiometric and catalytic reactions mediated by **1** or **2**. Preliminary studies on the reactivity of **3a** revealed that it reacted with nucleophiles such as PhLi and sodium dimethyl methylmalonate but not with electrophiles such as aldehydes and unsaturated molecules such as ethylene and CO. The stoichiometric reaction of **3a** with PhLi in THF gave a mixture of 1-phenylprop-1-ene and 1-phenylprop-2-ene in a ratio of 1:2. Similarly, treatment of **3a** with sodium dimethyl methylmalonate resulted in formation of dimethyl allylmethylmalonate. In both of the reactions, regeneration of **1a** was also observed. The latter allylation reaction can be extended to a catalytic reactions when allyl methyl carbonate is used as the allylic substrate; **1a** (10 mol%) successfully catalyzed the reaction of allyl methyl carbonate with dimethyl methyl malonate in THF at room temperature to give the product in 90% yield (Scheme 2).

In conclusion, oxidative addition of allylic substrates to the isolable coordinatively unsaturated complex (η^5-C_5Me_5)Ru(η-amidinate), has been observed which leads to a new cationic organoruthenium(IV) complex [(η^5-C_5Me_5)Ru(η^3-allyl)(η-amidinate)]$^+$ stabilized by a nitrogen-donor ligand. This oxidative addition is envisioned to be extendable to stoichiometric and catalytic transformations of allylic substrates mediated by **1**–**3**, as already evidenced by our preliminary studies on the reactions of **3a** with nucleophiles.

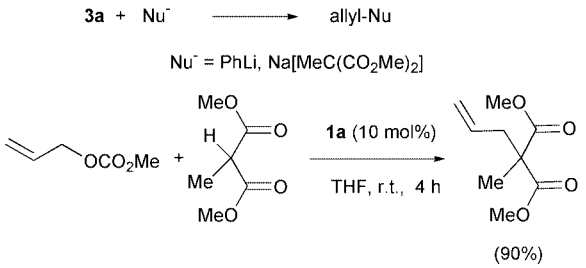

Scheme 2

We are grateful to Kouki Matsubara (Kyushu Univ.) for his help in the X-ray analyses. Part of this work is financially supported by the Japan Society of the Promotion of Science (Grant-in-Aid for Scientific Research 10450343).

Notes and references

‡ Representative spectroscopic evidence: **3a**; ^{1}H NMR ($CDCl_3$): δ 0.95 [s, 18H, $C(CH_3)_3$], 1.81 [s, 15H, $C_5(CH_3)_5$], 2.22 (d, J = 10.2 Hz, 2H, *anti*-CH of the allyl group), 4.53 (d, J = 6.1 Hz, 2H, *syn*-CH of the allyl group), 5.36 (dt, J = 6.1, 10.2 Hz, 1H, central-CH of the allyl group), 7.16 (m, 1H, C_6H_5), 7.24 (m, 1H, C_6H_5), 7.32 (m, 1H, C_6H_5), 7.35 (m, 1H, C_6H_5), 7.44 (m, 1H, C_6H_5). ^{13}C{^{1}H} NMR ($CDCl_3$): δ 10.9 [$C_5(CH_3)_5$], 35.5 [$C(CH_3)_3$], 58.0 [$C(CH_3)_3$], 59.7 (CH_2 of the allyl group), 97.2 (CH of the allyl group), 106.6 [$C_5(CH_3)_5$], 127.4, 127.6, 127.8, 129.9, 132.8, 138.6 (C_6H_5), 178.9 (NCN). Anal. Calc. for $C_{28}H_{43}N_2PF_6Ru$: C, 51.45; H, 6.63; N, 4.29. Found: C, 51.22; H, 6.62; N, 4.34%.

§ *Crystal data* for $C_{28}H_{43}F_6N_2PRu$ **3a**: M = 653.68, orthorhombic, space group *Pbca*, a = 31.771(6), b = 14.038(4), c = 13.366(5) Å, V = 5961(3) Å^3, T = 293 K, Z = 8, μ = 0.637 mm^{-1}, 6849 reflections measured, 6848 unique (R_{int} = 0.0409), 4403 observed ($>2\sigma$), final residuals $R1$ = 0.0492, $wR2$ = 0.1418 [$I > 2\sigma(I)$]; $R1$ = 0.0917, $wR2$ = 0.1620 (all data). CCDC 182/1633. See http://www.rsc.org/suppdata/cc/b0/b002927k/ for crystallographic files in .cif format.

1 For a recent extensive review, see: R. Poli, *Chem. Rev.*, 1996, **96**, 2135 and references therein.
2 For a review on coordinatively unsaturated Ru(II) complexes, see: K. G. Caulton, *New. J. Chem.*, 1994, **18**, 25 and references therein.
3 For recent studies of coordinatively unsaturated ruthenium(II) complexes stabilized by nitrogen donor ligands, see the following literature and references cited therein: C. Gemel, K. Mereite, R. Schmid and K. Kirchner, *Organometallics*, 1997, **16**, 5601; K.-J. Haack, S. Hayashi, A. Fujii, T. Ikariya and R. Noyori, *Angew. Chem., Int. Ed. Engl.*, 1997, **36**, 285; C. Gemel, J. C. Huffman, K. G. Caulton, K. Mauthner and K. Kirchner, *J. Organomet. Chem.*, 2000, **593**, 342.
4 (*a*) H. Nagashima, K. Mukai and K. Itoh, *Organometallics*, 1984, **3**, 1314; H. Nagashima, K. Mukai, Y. Shiota, K. Yamaguchi, K. Ara, T. Fukahori, H. Suzuki, M. Akita, Y. Moro-oka and K. Itoh, *Organometallics*, 1990, **9**, 799; (*b*) M. O. Albers, D. C. Liles, D. J. Robinson, A. Shaver and E. Singleton, *Organometallics*, 1987, **6**, 2347; (*c*) P. J. Fagan, W. S. Mahoney, J. C. Calabrese and I .D. Williams, *Organometallics*, 1990, **9**, 1843; (*d*) E. Rüba, W. Simanko, K. Mauthner, K. M. Soldouzi, C. Slugovc, K. Mereiter, R. Schmid and K. Kirchner, *Organometallics*, 1999, **18**, 3843 and references therein.
5 T. Kondo, H. Ono, N. Sataka, T. Mitsudo and Y. Watanabe, *Organometallics*, 1995, **14**, 1945; T. Kondo, Y. Morisaki, S. Uenoyama, K. Wada and T. Mitsudo, *J. Am. Chem. Soc.*, 1999, **121**, 8657 and references therein.
6 Y. Yamaguchi and H. Nagashima, *Organometallics*, 2000, **19**, 725.

ChemComm

$\{Mn(OH_2)_2[Mn(bpym)(OH_2)]_2[Fe(CN)_6]_2\}_\infty$: a two-dimensional ferrimagnet with a partial cubane motif

Jennifer A. Smith, José-Ramón Galán-Mascarós, Rodolphe Clérac and Kim R. Dunbar*

Texas A&M University, Department of Chemistry, College Station, TX, 77842-3012, USA. E-mail: dunbar@mail.chem.tamu.edu

Received (in Irvine, CA) 23rd February 2000, Accepted 28th April 2000

$\{Mn(OH_2)_2[Mn(bpym)(OH_2)]_2[Fe(CN)_6]_2\}_\infty$, a two-dimensional cyanide-bridged polymer, exhibits canted ferrimagnetism with T_C = 11 K.

Molecule-based magnets are the focus of considerable current research effort, from both the fundamental and device-related perspectives. One of the more exciting developments in recent years is the design of magnets from a consideration of the sign and magnitude of superexchange between adjacent paramagnetic metal centers. The family of magnets based on the 3-D Prussian Blue structural motif nicely illustrates this strategy.[1] In these materials, deliberate choices of metal ions at the two ends of the CN^- bridge lead to well established ground states, and the symmetry of the magnetic orbitals allows for a reasonable prediction of the nature of the superexchange (antiferro- *versus* ferro-magnetic).[2] For example, $V[Cr(CN)_6]_{0.86}\cdot 2.8H_2O$ orders ferrimagnetically at 315 K[1*h*] (due to direct overlap of t_{2g} magnetic orbitals) whereas $CsNi[Cr(CN)_6]\cdot 2H_2O$ orders ferromagnetically at 90 K[1*g*] (due to orthogonality of the t_{2g} and e_g magnetic orbitals). In addition to the high-symmetry Prussian-Blue architectures, hexacyanometallate building blocks are found in other structural motifs, for example in the 3-D ferrimagnet $[Ni(tren)]_3[Fe(CN)_6]\cdot 6H_2O$ synthesized from $[Fe(CN)_6]^{3-}$ and $[Ni(tren)]^{2+}$ [tren is the tetradentate capping ligand tris(2-aminoethyl)amine].[6*e*] A number of 1-D chains,[4] 2-D layered materials[5] and 3-D networks[6] have also appeared in the literature, the common theme among all examples being the incorporation of cyanometallates into networks with metal ions that possess a capping ligand(s).

Our involvement in the chemistry of cyanide compounds is directed at the formation of clusters or low-dimensional materials from specifically tailored precursors.[7] For example, we reasoned that 1:1 reactions between *cis*-$[Mn(bpym)_2(H_2O)_2]^{2+}$ and $[Fe(CN)_6]^{3-}$ would yield a square with *cis*-$[Mn(bpym)_2]^{2+}$ corners linked by $[Fe(CN)_6]^{3-}$ edges or a zigzag bimetallic chain. Both of these hypotheses are based on the expectation that the only leaving groups would be the two water molecules on Mn^{II}. Herein, we report an entirely unexpected result, namely that the 2,2′-bipyrimidine chelates are also very good leaving groups in favor of the nitrogen end of a cyanide group in such reactions.

Brown crystalline needles are formed reproducibly by slow diffusion of a solution of $[Mn(bpym)_2(OH_2)_2][SO_4]$ (bpym = 2,2′-bipyrimidine) in MeCN into a solution of $K_3[Fe(CN)_6]$ in H_2O.[8] X-Ray crystallographic studies† revealed that the product is the neutral, 2-D polymer $\{Mn(OH_2)_2[Mn(bpym)(OH_2)]_2[Fe(CN)_6]_2\}_\infty$ **1**. The asymmetric unit of the structure consists of one $[Fe^{III}(CN)_6]^{3-}$ unit connected to two different types of Mn^{II} centers by cyanide bridges. One Mn atom (Mn2) has retained only one bpym ligand while the other one (Mn1) has lost both of its original bpym ligands. For simplicity in describing the repeat pattern, the building blocks of the layers are defined as $[Fe(CN)_6]^{3-}$ (Fe1), *trans*-$[Mn(OH_2)_2]^{2+}$ (Mn1), and *fac*-$[Mn(bpym)(OH_2)]^{2+}$ (Mn2) units. Each Fe^{III} ion forms bridges to three Mn2 and two Mn1 centers, which leaves one terminal CN^- ligand. The *trans*-$[Mn(OH_2)_2]^{2+}$ units are linked to four Fe^{III} ions, and each *fac*-$[Mn(bpym)(OH_2)]^{2+}$ building block is connected to three independent $[Fe(CN)_6]^{3-}$ anions. The resulting polymeric framework can be described as being composed of individual 1-D chains formed by edge-sharing $\{[Mn(bpym)(OH_2)]_2[Fe(CN)_6]_2\}$ squares. These chains, which exhibit a staircase motif, are stitched into layers by *trans*-$[Mn(OH_2)_2]^{2+}$ bridges that serve to link Fe atoms of adjacent chains and creates two new $\{[Mn(bpym)(OH_2)][Fe(CN)_6]_2[Mn(OH_2)_2]\}$ squares that share a corner (Mn1) [see Fig. 1(a)]. As the simplified diagram in Fig. 1(b) reveals the framework resembles a 2-D array of fused Mn_4Fe_3 cubes that are missing one vertex. It is of further interest to point out that the bpym ligands of adjacent layers are interdigitated to form a stacked column along the *c* axis with a mean spacing of 3.35 Å.

Magnetic studies were performed on a 3.3 mg batch of crystals using a MPMS-XL SQUID magnetometer. Between 50 and 300 K, the molar susceptibility χ_m can be fit to a Curie–Weiss law with C = 13.8 emu K mol^{-1} and θ = −12.8 K (inset in Fig. 2). The Curie constant is in good agreement with the expected spin-only value (13.875 emu K mol^{-1}) for three S = 5/2 Mn(II) and two low spin S = 1/2 Fe(III) centers. The sign of the Weiss constant indicates that local antiferromagnetic interactions dominate as expected for Fe^{III}–CN–Mn^{II} bridges where there is direct overlap of the t_{2g} magnetic orbitals. Below 50 K, χ_m deviates from the Curie–Weiss behavior and undergoes an abrupt increase at *ca*. 11 K which suggests the onset of magnetic ordering (Fig. 3). This state corresponds to a ferrimagnetic ordering, since the Fe^{III} and Mn^{II} spin centers interact antiferromagnetically with non-cancellation of spins. As Fig. 3 shows, the magnetization increases gradually, but saturation is incomplete at 7 T (M = 11.6 μ_B *cf*. the expected value of 13 μ_B). This behavior is a signature of a complicated magnetic structure (competing magnetic interactions with possibly some degree of spin canting), which is not unexpected in view of the crystal structure. No hysteresis was observed in the field dependence of the magnetization. Susceptibility

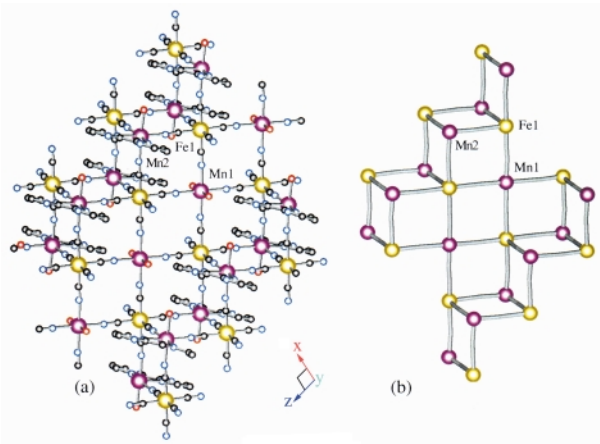

Fig. 1 (a) View of the two-dimensional network down the *b* axis. (b) Scheme emphasizing the partial cubane motif in the 2-D network.

DOI: 10.1039/b001513j

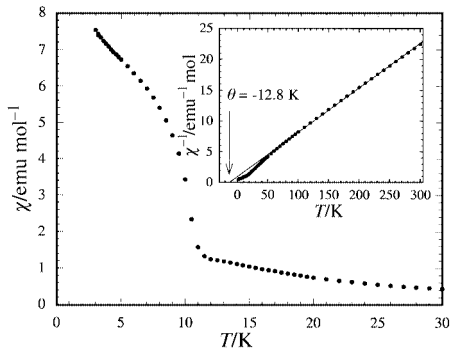

Fig. 2 Thermal dependence below 30 K of χ_m at 100 G for **1**. Inset: temperature dependence of $1/\chi_m$ between 2 and 300 K. The solid line indicates the best fit obtained by the Curie–Weiss law. These measurements were corrected for the sample holder and the diamagnetism contributions estimated from Pascal's constants.

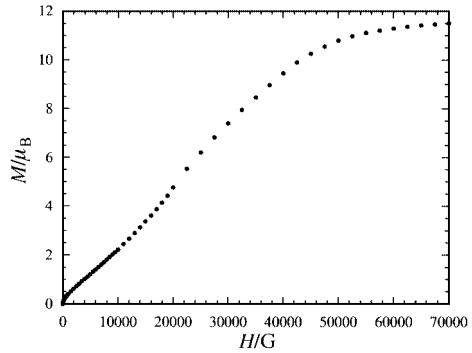

Fig. 3 Field dependence of the magnetization at 2 K.

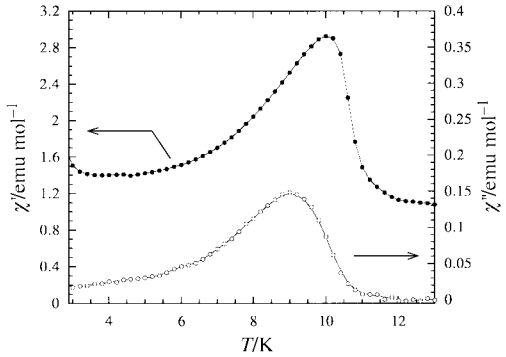

Fig. 4 Temperature dependence of the ac susceptibilities (in-phase, χ', and out-of-phase, χ'') below 13 K [ac measuring field 1 G (10^{-4} T); frequency of 1 Hz; no external dc field].

measurements of the ac type confirm the ferrimagnetic ordering at 11 K (Fig. 4) and reveal no significant frequency dependence.

The result presented here underscores the structural diversity of materials containing cyanometallate building blocks. The slow loss of 2,2′-bipyrimidine ligands from *cis*-$[Mn(bpym)_2(H_2O)_2]^{2+}$ in H_2O–MeCN contributes to the growth of crystals rather than the rapid deposition of powders which is the outcome of reactions that do not involve capping ligands. We are currently investigating reactions of other ligand-protected cations with hexacyanometallate anions, the results of which are forthcoming.

K. R. D. gratefully acknowledges the National Science Foundation for support of this work (NSF CHE-9906583) and for funding the CCD diffractometer (CHE-9807975) and the SQUID instrumentation (NSF-9974899).

Notes and references

† *Crystal data* for $Mn(OH_2)_2[Mn(bpym)(OH_2)]_2[Fe(CN)_6]_2\cdot 9H_2O$: Independent batches produce crystals with the same unit cell dimensions. $C_{28}H_{38}Fe_2Mn_3N_{20}O_{13}$, M_w = 1139.30, monoclinic, space group $P2_1/c$, a = 13.209(3), b = 26.694(5), c = 7.443(2) Å, β = 105.57(3)°, V = 2528.1(10) Å^3, T = 110(2) K, Z = 2, D_c = 1.497 Mg m^{-3}, graphite monochromatized Mo-Kα radiation (λ = 0.71069 Å), Bruker CCD diffractometer, $F(000)$ = 1154, μ = 1.361 mm^{-1}, 0.08 × 0.02 × 0.01 mm, 18980 reflections measured, 6134 of which were unique (R_{int} = 0.2250). The structure was solved by direct methods (SIR97)[9] followed by Fourier synthesis, and refined on F^2 (SHELX-97).[10] All non-hydrogen atoms were refined anisotropically, except for the disordered interstitial water molecules. The final refinement gave $R(F^2)$ = 0.0715 and $R^2_\omega(F^2)$ = 0.1630, by using 1490 reflections [$I > 4\sigma(I)$]. H-atoms are in calculated positions as riding atoms.

CCDC 182/1623. See http://www.rsc.org/suppdata/cc/b0/b001513j/ for crystallographic files in .cif format.

1 (*a*) S. M. Holmes and G. S. Girolami, *J. Am. Chem. Soc.*, 1999, **121**, 5593; (*b*) O. Sato, Y. Einaga, A. Fujishima and K. Hashimoto, *Inorg. Chem.*, 1999, **38**, 4405; (*c*) O. Hatlevik, W. E. Buschmann, J. Zhang, J. L. Manson and J. S. Miller, *Adv. Mater.*, 1999, **11**, 914; (*d*) A. K. Sra, M. Andruh, O. Kahn, S. Golhen, L. Ouahab and J. V. Yakhmi, *Angew. Chem., Int. Ed.*, 1999, **38**, 2606; (*e*) M. Verdaguer, A. Bleuzen, V. Marvaud, J. Vaissermann, M. Seuleiman, C. Desplanches, A. Scuiller, C. Train, R. Garde, G. Gelly, C. Lomenech, I. Roseman, P. Veillet, C. Cartier and F. Villain, *Coord. Chem. Rev.*, 1999, **192**, 1023; (*f*) M. Verdaguer, *Science*, 1996, **272**, 698; (*g*) W. Entley and G. S. Girolami, *Science*, 1995, **268**, 397; (*h*) S. Ferlay, T. Mallah, R. Ouahes, P. Veillet and M. Verdaguer, *Nature*, 1995, **378**, 701; (*i*) V. Gadet, T. Mallah, I. Castro and M. Verdaguer, *J. Am. Chem. Soc.*, 1992, **114**, 9213.

2 K. R. Dunbar and R. A. Heintz, *Prog. Inorg. Chem.*, 1997, **45**, 283.

3 M. Ohba, N. Maruono, H. Okawa, T. Enoki and J.-M. Latour, *J. Am. Chem. Soc.*, 1994, **116**, 11566.

4 A. Marvilliers, S. Parsons, E. Riviére, J.-P. Audiére and T. Mallah, *Chem. Commun.*, 1999, 2217; A. Marvilliers, Y. Pei, J. C. Boquera, K. E. Vostrikora, C. Paulsen, E. Riviére, J.-P. Audiére and T. Mallah, *Chem. Commun.*, 1999, 1951; N. Re, E. Gallo, C. Floriani, H. Miyasaka and N. Matsumoto, *Inorg. Chem.*, 1996, **35**, 6004.

5 J. Larionova, O. Kahn, S. Golhen, L. Ouahab and R. Clérac, *J. Am. Chem. Soc.*, 1999, **121**, 3349; E. Colacio, J. M. Domínguez-Vera, M. Ghazi, R. Kivekäs, F. Lloret, J. M. Moreno and H. Stoeckli-Evans, *Chem. Commun.*, 1999, 987; H.-Z. Kou, W.-M. Bu, D.-Z. Liao, Z.-H. Jiang, S.-P. Yan, Y.-G. Fan and G.-L. Wang, *J. Chem. Soc., Dalton Trans.*, 1998, 4161; N. Re, R. Crescenzi, C. Floriani, H. Miyasaka and N. Matsumoto, *Inorg. Chem.*, 1998, **37**, 2717; M. Ohba, H. N. Fukita and Y. Hashimoto, *J. Am. Chem. Soc.*, 1997, **119**, 1011; S. Ferlay, T. Mallah, J. Vaissermann, F. Bartolomé, P. Veillet and M. Verdaguer, *Chem. Commun.*, 1996, 2481.

6 (*a*) M. Ohba, N. Usuki, N. Fukita and H. Okawa, *Angew. Chem., Int. Ed.*, 1999, **38**, 1795; (*b*) M. P. Shores, L. G. Beauvais and J. R. Long, *J. Am. Chem. Soc.*, 1999, **121**, 775; (*c*) J. L. Heinrich, P. A. Berseth and J. R. Long, *Chem. Commun.*, 1998, 1231; (*d*) N. Fukita, M. Ohba, H. Okawa, K. Matsuda and H. Iwamura, *Inorg. Chem.*, 1998, **37**, 842; (*e*) M. Salah, E. Fallah, E. Rentschler, A. Caneschi, R. Sessoli and D. Gatteschi, *Angew Chem., Int. Ed. Engl.*, 1996, **35**, 1947.

7 $[Mn(bpym)_2(H_2O)_2](SO_4)$ was synthesized by an adaptation of the procedure reported for the perchlorate salt: D. M. Hong, H. H. Wei, L. L. Gan, G. H. Lee and Y. Wang, *Polyhedron*, 1996, **15**, 2335.

8 Alternative synthesis: three equivalents of $[Mn(bpym)_2(H_2O)_2](SO_4)$ in 25 mL of water were added to 2 equivalents of $K_3[Fe(CN)_6]$ in 25 mL of water to yield a brown precipitate within 12 h. The powder was removed by filtration and the filtrate was slowly evaporated to give a brown crystalline material which was washed with water to remove soluble byproducts (64% yield). IR ν_{CN}/cm^{-1} = 2145s, 2110br and 2063w, br. Independent batches exhibit the same IR data.

9 A. Altomare, M. C. Burla, M. Camalli, G. L. Cascarano, C. Giacovazza, A. Guagliardi, A. G. G. Moliterni, G. Polidori and R. Spagna, *J. Appl. Crystallogr.*, 1999, **32**, 115.

10 G. M. Sheldrick SHELX97, Program for Refinement of Crystal Structure, University of Göttingen, Göttingen, Germany, 1997.

ChemComm

Construction of the 11-oxabicyclo[6.2.1]undecane core of the cladiellins by a novel rearrangement reaction

J. Stephen Clark* and Yung-Sing Wong

School of Chemistry, University of Nottingham, University Park, Nottingham, UK NG7 2RD. E-mail: j.s.clark@nottingham.ac.uk

Received (in Cambridge, UK) 29th March 2000, Accepted 8th May 2000

A novel approach to the stereoselective synthesis of the 11-oxabicyclo[6.2.1]undecane system found in the cladiellin (eunicellin) family of marine natural products is described.

Cladiellins (eunicellins) such as litophynin E,[1a] litophynin I[1b] and sclerophytin B[2] are highly oxygenated marine natural products that are part of a much larger family of cembranoids also comprising the briarellins, sacrodictyins and asbestinins.[3] Members of this family of natural products share an oxabicyclo[6.2.1]undecane sub-structure, and many of them possess potent anti-cancer, anti-inflammatory, insecticidal or anti-mollusc activity.[3]

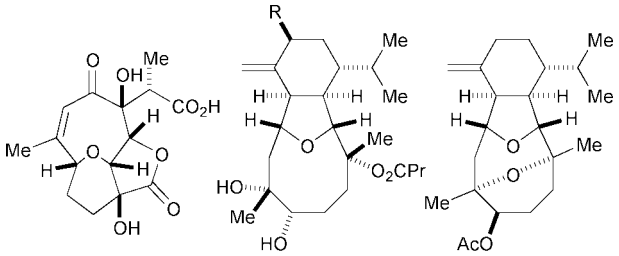

In the course of our research programme directed towards the synthesis of the highly oxygenated sesquiterpene neoliacinic acid,[4,5] we have discovered that it is possible to effect an unusual rearrangement reaction of the oxabicyclo[5.3.1]undecane system of this terrestrial natural product to give the oxabicyclo[6.2.1]undecane system found in the marine cembranoids. We now present the results of our studies and demonstrate that the reaction can be used to prepare the core structure of litophynins E and I.

The (*E*)-bicyclo[5.3.1]bicycloundecene **9**† required for our rearrangement studies was prepared from the commercially available compound (*R*)-γ-butyrolactone-γ-carboxylic acid **1**, which we obtained from (*R*)-glutamic acid (Scheme 1).[6] Ring opening of the lactone **1** was effected using a sub-stoichiometric amount of 10-camphorsulfonic acid (CSA) in a mixture of *n*-butanol and toluene at reflux,[7] and the resulting diester was then converted into the allyl ether **2** by silver(I) oxide promoted alkylation of the free hydroxy group with excess allyl bromide.[8] Saponification of the diester **2** and treatment of the resulting diacid with acetic anhydride provided the substituted glutaric anhydride **3**. Reaction of the cyclic anhydride **3** with a large excess of diazomethane resulted in contrasteric opening of the ring to afford the diazoketone **4** in reasonable yield, without formation of the other possible regioisomeric diazoketone product.‡ The diazoketone **4** was then treated with a sub-stoichiometric amount of $Rh_2(O_2CCPh_3)_4$, which delivered the 3(2*H*)-furanone **5** resulting from intramolecular C–H addition of the intermediate rhodium carbenoid.[4,9] Regioselective and stereoselective introduction of a methyl substituent was accomplished by treatment of the ketone **5** with trimethylaluminium at low temperature.[4,10] At this stage, some of the lactone produced by transesterification of the methyl ester with the tertiary alcohol was obtained, but the process was reversed by treatment of the mixture with triethylamine in methanol at reflux. The tertiary alcohol **6** was converted into the acid **7** by sequential acetylation and selective hydrolysis of the methyl ester, and the carboxylic acid **7** was then transformed into the diazoketone **8**. Treatment of the diazoketone **8** with copper(II) hexafluoroacetylacetonate generated an electrophilic copper carbenoid that underwent tandem oxonium ylide formation and [2,3]-sigmatropic rearrangement with ring expansion.[11] The reaction delivered the strained bridged-bicyclic ether **9** containing an (*E*)-alkene as the key intermediate.[4b] The corresponding (*Z*)-alkene isomer was prepared in 79% yield by treatment of **9** with AIBN and a sub-stoichiometric amount of ethanethiol in benzene at reflux.[4a]

It was immediately apparent that the rather unstable (*E*)-alkene **9** had unusual reactivity. Attempted epoxidation of the alkene **9** with *m*-CPBA in dichloromethane at reflux afforded a complex mixture of products and delivered a major compound that contained an *m*-chlorobenzoate group rather than the expected epoxide. In contrast, the (*Z*)-alkene isomer of **9** underwent conventional epoxidation under identical conditions to deliver the expected product as a *ca.* 3:1 mixture of diastereoisomers. Attempted epoxidation of the (*E*)-alkene **9** with milder oxidants such as DMDO also failed to yield the expected epoxide.

We suspected that the unusual reactivity of the (*E*)-alkene **9** was due to transannular reaction of the bridging ether oxygen,

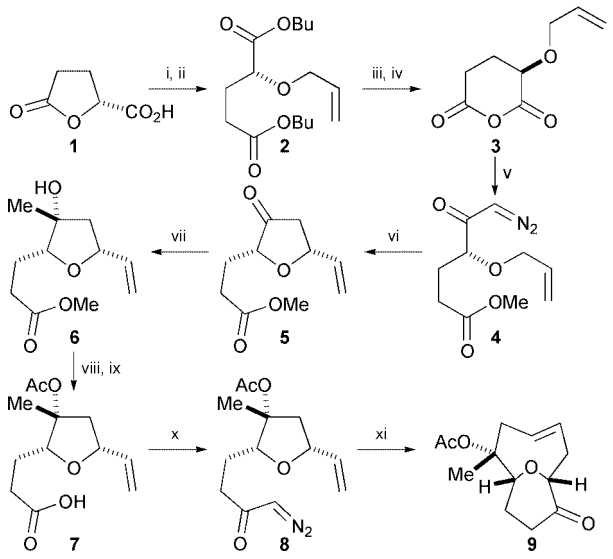

Scheme 1 *Reagents and conditions*: i, Bu^{n}OH, CSA (cat.), PhMe, Dean–Stark, reflux (78%); ii, CH_2CHCH_2Br, Ag_2O, Et_2O, reflux (89%); iii, LiOH, THF, H_2O, reflux; iv, Ac_2O, reflux (83% over two steps); v, CH_2N_2, 0 °C → r.t., CH_2Cl_2–Et_2O (59%); vi, $Rh_2(O_2CCPh_3)_4$, CH_2Cl_2, r.t. (50%); vii, $AlMe_3$, CH_2Cl_2, −78 → −10 °C, then Et_3N, MeOH, reflux (71%); viii, Ac_2O, DMAP, CH_2Cl_2, r.t. (88%); ix, K_2CO_3, MeOH, H_2O, r.t.; x, $(COCl)_2$, CH_2Cl_2, r.t., then CH_2N_2, Et_2O, CH_2Cl_2, 0 °C (67% over two steps); xi, $Cu(hfacac)_2$, CH_2Cl_2, reflux (50%).

DOI: 10.1039/b002511i

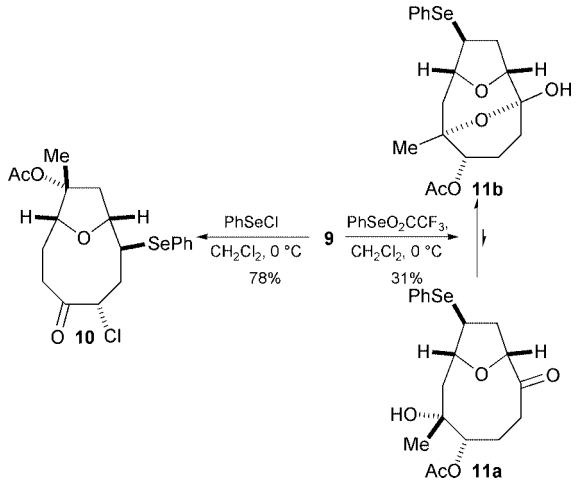

Scheme 2

which is forced to lie in close proximity to the alkene. In order to probe the reactivity of **9**, we investigated the reaction of this compound with electrophilic selenium reagents. Upon treatment with phenylselenenyl chloride, the *E* alkene **9** underwent rearrangement to provide the crystalline oxabicyclo[6.2.1]undecane **10** in good yield. In contrast, treatment of the (*E*)-alkene **9** with phenylselenenyl trifluoroacetate afforded the crystalline rearrangement product **11** in moderate yield. The structures of both the rearrangement products **10** and **11** were confirmed by X-ray crystallography;§ the rearrangement product **11** was found to exist as the hemiacetal **11b**¶ rather than the ring-opened tautomer **11a** in both the solid state and in solution. It is significant that the (*Z*)-isomer of the alkene **9** did not undergo rearrangement when treated with either selenium reagent, but instead reacted to give complex mixtures of products.

The formation of the rearranged bridged-bicyclic ethers **10** and **11** can be accounted for as shown in Scheme 3. Reaction of alkene **9** with either electrophilic selenium reagent results in stereoselective formation of the selenonium ion **12** and subsequent transannular attack of the bridging ether oxygen atom affords the tricyclic oxonium ion **13**. In the presence of chloride ion, nucleophilic attack occurs at the electrophilic site α to the carbonyl group (path *a*) and the bridged-bicyclic ether **10** is produced. In the presence of trifluoroacetate ion, the oxonium intermediate **13** does not suffer immediate attack by the weakly nucleophilic counterion. Instead, the acetate group participates in intramolecular S_N2 opening of the tricyclic oxonium ion (path *b*), and the oxonium intermediate **14** is produced. The ion **14** probably survives until work up, at which

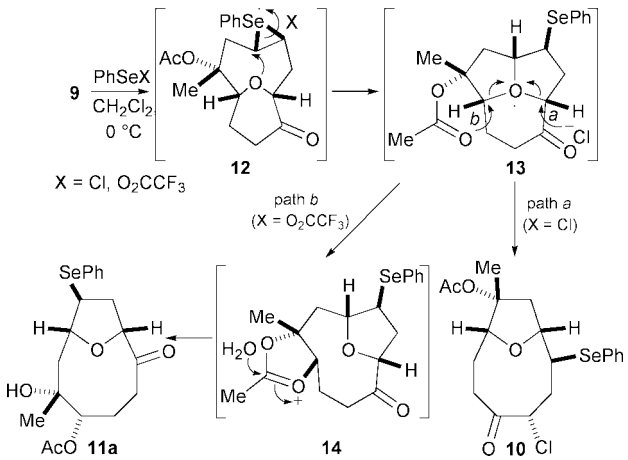

Scheme 3

stage water attacks and the acetate group is transferred from the tertiary site to the less sterically congested secondary hydroxy group.

The rearrangement product **11a** contains most of the functionality that adorns the oxygen-bridged core of litophynins E and I.[1] The compound also possesses the correct absolute and relative configuration at the four oxygen-bearing stereogenic centres. Thus, we have prepared an advanced intermediate for the synthesis of litophynins E and I in 12 steps from the commercially available compound (*R*)-γ-butyrolactone-γ-carboxylic acid **1** (Scheme 1).

We are currently exploring the optimisation of the rearrangement reaction (**9** → **11**, Scheme 3), completion of the synthesis of litophynins E and I, and elaboration of tautomer **11b** to give sclerophytin B. The results of these studies will be reported in due course.

We thank the EPSRC for financial support. We are very grateful to Dr A. J. Blake and Dr C. Wilson for obtaining X-ray crystal data for compounds **10** and **11b**.

Notes and references

† Compound **9** has been prepared by us using an alternative route [see ref. 4*b*)].

‡ The only other product obtained was the dimethyl ester (9%) resulting from hydrolysis of the anhydride **3** and esterification of the resulting diacid.

§ *Crystal data*: **10**: $C_{19}H_{23}ClO_4Se$, M + 429.78, monoclinic, space group $P2_1$, a = 5.2491(2), b = 21.3577(10), c = 16.4109(8) Å, β = 90.709(3)°, V = 1839.66(14) Å^3, Z = 4, μ = 2.207 mm^{-1}, T = 150(2) K, 12 2734 reflections collected of which 6208 (R_{int} = 0.101) were independent and 4081 [$I > 2\sigma(I)$] were observed; $R1$ [$I > 2\sigma(I)$] = 0.0583, $wR2$[$I > 2\sigma(I)$] = 0.0894.

11b: $C_{19}H_{24}O_5Se$, M = 411.34, monoclinic, space group $P2_1$, a = 6.0174(8), b = 20.717(3), c = 7.6596(10) Å, β = 108.215(3)°, V = 907.0(2) Å^3, Z = 2, μ = 2.096 mm^{-1}, T = 150(2) K, 3210 independent reflections collected of which 2792 [$I > 2\sigma(I)$] were observed; $R1$ [$I > 2\sigma(I)$] = 0.0278, $wR2$ [$I > 2\sigma(I)$] = 0.568.

CCDC 182/1635. See http://www.rsc.org/suppdata/cc/b0/b002511i/ for crystallographic data in .cif format.

¶ *Selected data* for **11b**: mp 119–120 °C (Found: C, 55.44; H, 5.73. $C_{19}H_{24}O_5Se$ requires C, 55.48; H, 5.88%); ν_{max}($CHCl_3$)/cm^{-1} 3590, 2938, 1729, 1374, 1103, 1046, 990, 972; δ_H(500 MHz; $CDCl_3$) 1.21 (3H, s), 1.66–1.84 (3H, m), 1.94–2.05 (3H, m), 2.10 (3H, s), 2.38 (1H, br), 2.63–2.70 (1H, m), 2.84 (1H, dd, *J* 8.9, 13.4 Hz), 4.00 (1H, ddd, *J* 3.6, 8.4, 8.4 Hz), 4.19 (1H, d, *J* 7.5 Hz), 4.44–4.47 (1H, m), 4.52–4.54 (1H, m), 7.26–7.30 (3H, m), 7.57–7.59 (2H, m); δ_C(126 MHz; $CDCl_3$) 21.1(q), 22.9(t), 29.9(q), 30.6(t), 35.4(t), 43.4(d), 46.1(t), 72.2(d), 76.1(s), 85.0(d), 87.2(d), 96.8(s), 127.8(d), 129.2(d), 129.6(s), 134.4(d), 170.5(s); MS (EI) *m/z* 412 (M^+, 14%), 410(9), 408(4), 255(22), 195(50), 157(27), 85(53), 43(100) (Found: M^+, 412.0789. $C_{19}H_{24}O_5{}^{80}Se$ requires M, 412.0789).

1 (*a*) M. Ochi, K. Yamada, K. Futatsugi, H. Kotsuki and K. Shibata, *Chem. Lett.*, 1990, 2183; (*b*) M. Ochi, K. Yamada, K. Kataoka, H. Kotsuki and K. Shibata, *Chem. Lett.*, 1992, 155.
2 P. Sharma and M. Alam, *J. Chem. Soc., Perkin Trans. 1*, 1988, 2537.
3 P. Bernardelli and L. A. Paquette, *Heterocycles*, 1998, **49**, 531.
4 (*a*) J. S. Clark, A. G. Dossetter, A. J. Blake, W.-S. Li and W. G. Whittingham, *Chem. Commun.*, 1999, 749; (*b*) J. S. Clark, A. G. Dossetter and W. G. Whittingham, *Tetrahedron Lett.*, 1996, **37**, 5605.
5 D. Takaoka, H. Nozaki and M. Nakayama, *Chem. Commun.*, 1987, 1861.
6 O. H. Gringore and F. P. Rouessac, *Org. Synth.*, 1985, **63**, 121.
7 U. Ravid, R. M. Silverstein and L. R. Smith, *Tetrahedron*, 1978, **34**, 1449.
8 H. G. Aurich and F. Biesemeier, *Synthesis*, 1995, 1171.
9 J. Adams, M.-A. Poupart, L. Grenier, C. Schaller, N. Ouimet and R. Frenette, *Tetrahedron Lett.*, 1989, **30**, 1749.
10 For examples of the stereoselective addition of trimethylaluminium to cyclic ketones see: E. C. Ashby and J. T. Laemmle, *Chem. Rev.*, 1975, **75**, 521; K. C. Nicolaou, M. E. Duggan and C.-K. Hwang, *J. Am. Chem. Soc.*, 1989, **111**, 6666.
11 M. C. Pirrung and J. A. Werner, *J. Am. Chem. Soc.*, 1986, **108**, 6060; E. J. Roskamp and C. R. Johnson, *J. Am. Chem. Soc.*, 1986, **108**, 6062.

ChemComm

Development of new methodology for the synthesis of functionalized α-fluorophosphonates and its practical application to the preparation of phosphopeptide mimetics

Akira Otaka,* Etsuko Mitsuyama, Hideaki Watanabe, Hirokazu Tamamura and Nobutaka Fujii

Graduate School of Pharmaceutical Sciences, Kyoto University, Sakyo-ku, Kyoto 606-8501, Japan. E-mail: aotaka@pharm.kyoto-u.ac.jp

Received (in Cambridge, UK) 20th March 2000, Accepted 10th May 2000

New methodology for the synthesis of functionalized α-fluorophosphonates which utilizes organocopper-mediated reduction has been developed and applied to the preparation of a monofluoromethyl-substituted phosphoserine mimetic-containing peptide.

Naturally occurring phosphate-containing molecules play important roles in various cellular processes, including signal transduction.[1] Therefore, nonhydrolyzable phosphate mimetics have received considerable attention, with α,α-difluorophosphonates serving as potential phosphate mimics,[2] extensive synthetic and biological studies of which have been made.[3] In contrast, evaluation of α-monofluorophosphonates[4] as biological phosphate mimics has been somewhat limited due to lack of flexibility of practical synthetic methodology[5] for this kind of molecule. In our efforts to prepare difluoromethyl (CF_2)-substituted phosphothreonine mimetics,[6] we attempted conjugate addition of a methyl group to 3-(diethylphosphonodifluoromethyl)but-2-enoate **1**† using an organocopper reagent to construct the secondary phosphonate unit. Unexpectedly, the reaction predominantly afforded an organocopper-mediated reduction product, α-fluorovinylphosphonate **3**, and not the corresponding conjugate addition product **2** (Scheme 1). This is the first example of organocopper-mediated reduction of γ-difluoro-α,β-enoates yielding γ-fluoro-β,γ-enoates.

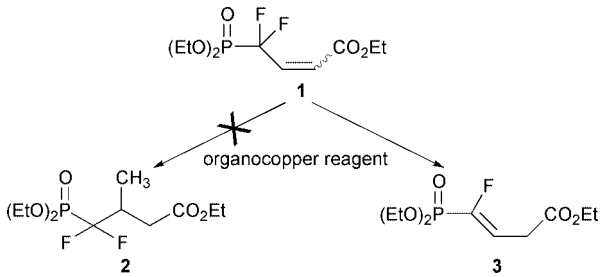

Scheme 1

The α-fluorovinylphosphonate[7] represents a potential synthetic intermediate for the preparation of α-fluorophosphonates. Accordingly, we describe herein the feasibility studies of our newly found reaction and its application to the synthesis of the monofluoromethyl (CHF)-substituted phosphoserine (pSer) mimetic 2-amino-4-fluoro-4-phosphonobutanoic acid (FPab) in a form suitably protected for the preparation of pSer mimetic-containing peptides.

Initially, we chose a difluoromethylphosphonate-bearing conjugate (2*S*)-bornane-[10,2]-sultam (Xs-sultam)-imide[8] **4** as a substrate for the copper-mediated reaction in order to allow subsequent stereoselective introduction of amino functionality under chiral auxiliary control. The sultam-imide **4** was treated under various conditions[9] and the results are shown in Table 1.‡

Reaction of **4** with either MeCu(CN)Li or $Me_2Cu(CN)Li_2$ in the presence of LiCl and/or $AlCl_3$ at −78 °C proceeded without accompanying alkylation, but rather provided the corresponding reduction product **5** with (*E*)-configuration§ in up to 80% isolated yields. Similarly, using methyl copper reagents, the formation of an alkylated product was also not observed. Use of methyl copper reagents was critical for conversion of **4** to **5**, since exposure of **4** to a butyl-copper reagent (run 14) afforded, besides **5**, a Bu-substituted Michael adduct (24%). The reaction presented here, different from other published protocols,[7,10] is conceptually a new methodology for the preparation of α-vinylphosphonates. Hydrogenation of the resulting α-vinylphosphonates affords the corresponding α-monofluorophosphonates, possessing a carboxy functionality which is amenable to further derivatization. Furthermore, starting from a common difluoromethylphosphonate intermediate, both the monofluoro- and corresponding difluoro-methylphosphoryl counterparts can be obtained.

Table 1 Reduction of **4** with several organo copper reagents

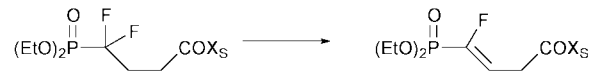

4 X_S = (2*S*)-bornane-[10,2]-sultam **5**

Run	Reagent	Isolated yield (%) of **5**[a]
1	$Me_2CuLi{\cdot}LiI2LiBr$ (1.2 eq.)	49
2	$Me_2CuLi{\cdot}LiI{\cdot}2LiBr$, TMSCl (1.2 eq.)	67
3	$Me_2CuLi{\cdot}LiI2LiBr$ (2.5 eq.), TMSCl (2.0 eq.)	50
4	$MeCu(CN)Li{\cdot}LiBr$ (2.0 eq.)	81
5	$MeCu(CN)Li{\cdot}LiBr$ (5.0 eq.), $AlCl_3$ (2.0 eq.)	84
6	$Me_2Cu(CN)Li_2{\cdot}2LiBr$ (2.5 eq.)	69
7	$Me_2Cu(CN)Li_2{\cdot}2LiBr$ (2.5 eq.), $AlCl_3$ (2.0 eq.)	85
8	$Me_2Cu(CN)Li_2{\cdot}2LiBr$ (1.1 eq.), $BF_3{\cdot}Et_2O$ (1.0 eq.)	52
9	$Me_2Cu(CN)Li_2{\cdot}2LiBr{\cdot}2LiCl$ (1.5 eq.)	87
10	$Me_2Cu(CN)Li_2{\cdot}2LiBr{\cdot}2LiCl$ (2.5 eq.)	92
11	$Me_2Cu(CN)Li_2{\cdot}LiBr{\cdot}2LiCl$, $BF_3{\cdot}Et_2O$ (1.5 eq.)	58
12	$Me_2Cu(CN)Li_2{\cdot}2LiBr{\cdot}2LiCl$, $AlCl_3$ (1.5 eq.)	82
13	$MeLi{\cdot}LiBr$	0[b]
14	$Bu_2Cu(CN)Li_2{\cdot}2LiCl$ (2.5 eq.)	70[c]

[a] Other formed products were not characterized, except for **5** and Michael adduct; [b] no starting material; [c] Michael adduct: 24%

Next, we applied this methodology to the synthesis of CHF-substituted pSer mimetic (FPab) as shown in Scheme 2. Hydrogenation of α-vinylphosphonate **5** over Pd–C in AcOEt proceeded without diastereoselectivity to yield α-monofluorophosphonate **6** in quantitative yield. Reaction of 1-chloro-1-nitrosocyclohexane[11] in THF (blue) with the Na-enolate, resulting from treatment of **6** with NaHMDS in THF at −78 °C, proceeded with high diastereoselectivity to instantaneously afford a colorless solution of nitrone. Treatment of this solution with aqueous 1 N HCl, followed by extractive work-up, gave crude hydroxylamine **7**, which was taken to the next step without further purification. Reduction of **7** with Zn–AcOH in THF, followed by introduction of Boc protection onto the resulting NH_2 group using $(Boc)_2O$, gave Boc-protected **8**. The sultam moiety was then converted to the benzyl ester **9** utilizing

DOI: 10.1039/b002188l

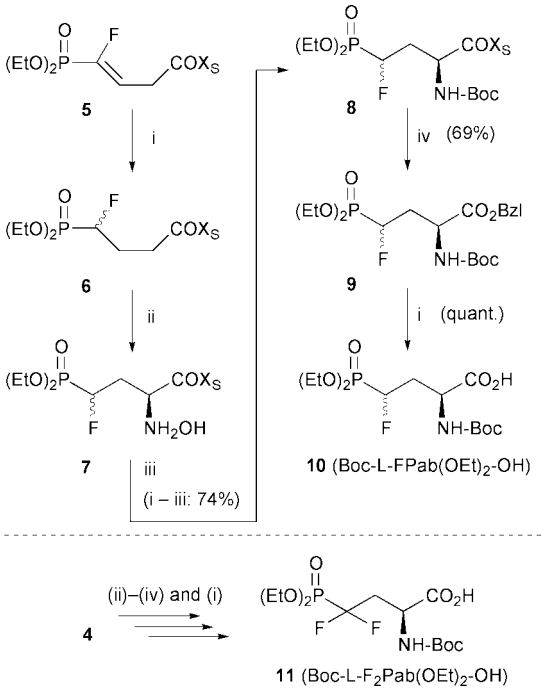

Scheme 2 *Reagents*: (i) H_2/Pd–C, AcOEt; (ii) NaHMDS (1.1 eq.), 1-chloro-1-nitrosocyclohexane (1.1 eq.). THF then **1** N HCl aq.; (iii) Zn (40 eq.). AcOH (50 eq.) then $(Boc)_2O$ (2.0 eq.), CH_3CN; (iv) $Ti(CPr^i)_4$ (2.0 eq.), BzOH (44 eq.), toluene.

$Ti(OPr^i)_4$–benzyl alcohol in toluene at 120 °C. Hydrogenolytic debenzylation (H_2/10% Pd–C in AcOEt) of **9** gave the protected L-CHF-substituted pSer mimetic (Boc-FPab(OEt)$_2$-OH **10**). Application of a similar sequence of reactions to **4** gave enantiometically pure L-CF_2-substituted pSer mimetic[12] (F_2Pab) **11**. We speculate that FPab derivative **10** possesses the 2*S* configuration (L-amino acid), by analogy to F_2Pab derivative **11**, which is obtained from a difluoromethylphosphonate-containing Xs-sultam utilizing a similar reaction sequence and has the 2*S* configuration. To our knowledge, this is the first synthesis of a CHF-substituted pSer mimetic.

In order to examine the general applicability of protected FPab **10** to peptide synthesis, **10** was incorporated into the peptide sequence (H–Gly–FPab–Val–Pro–Met–Leu) using a standard Boc-based solid-phase protocol. The resulting protected peptide resin was treated with a one-pot, two-step deprotection methodology[13] consisting of high-acidity [1 mol dm^{-3} TMSOTf–thioanisole in TFA, *m*-cresol, ethanedithiol (EDT)] and low-acidity (1 mol dm^{-3} TMSOTf–thioanisole in TFA, *m*-cresol, EDT + DMS–TMSOTf), which was developed for practical deprotection of protected phosphoamino acid-containing peptide resins, to yield a crude deprotected peptide without accompanying partially Et-deprotected peptides.¶ After HPLC purification, an FPab-containing peptide was obtained in 63% yield. In order to confirm the 2*S* configuration of FPab, purified peptide was subjected to enzyme digestion using leucine amino peptidase (LAP).‖ Interestingly, it was found that the parent peptides were converted to 5-residue peptides, H–FPab–Val–Pro–Met–Leu–OH, with rates that varied between the diastereomers derived from the fluorine substitution in FPab and with only 10% of FPab being released from the resulting 5-residue peptide after 24 h of LAP treatment. On the other hand, D-FPab-containing peptides remained intact after 24 h digestion using LAP. The present methodology should allow the facile preparation of functionalized α-fluorovinylphosphonates and α-fluorophosphonates. Furthermore, it is tempting to speculate that FPab-containing peptides could serve as inhibitors against both proteases and phosphatases since peptides having FPab residues at the N-terminal position are resistant to the action of LAP.

We thank Dr Terrence R. Burke Jr., NCI, NIH, Bethesda, MD 20892, for proofing the manuscript. This work was supported in part by The Japan Health Sciences Foundation and Grants-in-Aid for Scientific Research from the Ministry of Education, Science and Culture of Japan.

Notes and references

† (*Z*)-3-(diethyldifluoromethyl)but-2-enoate **1** was prepared by coupling of ethyl (*Z*)-3-iodobut-2-enoate with $BrZnCF_2(O)(OEt)_2$ in the presence of CuBr in DMF.[14] The (*E*)-isomer was synthesized according to the literature method.[15] Sultam-imide **4** was synthesized *via* the following sequence of reactions: (i) transesterification of ethyl (*Z*)-3-iodobut-2-enoate to the corresponding *p*-methoxybenzyl (PMB) ester using $Ti(OPr^i)_4$ in PMB-OH; (ii) CuBr-mediated coupling, as mentioned above; (iii) removal of the PMB group with 95% aqueous TFA; (iv) coupling of the sultam.

‡ To a solution of CuCN·2LiCl in THF (1 mol dm^{-3}, 4.2 cm^3) was added MeLi·LiBr in Et_2O (1.5 mol dm^{-3}, 5.6 cm^3) at −78 °C. The mixture was allowed to warm to 0 °C and stirred at this temperature for 1–2 min. After re-cooling to −78 °C, **4** (763 mg, 1.68 mmol) in THF (5 cm^3) was added with a syringe. After being stirred at −78 °C for 1.5 h, the reaction was quenched by addition of sat. NH_4Cl–28% NH_4OH solution. Usual work-up followed by flash chromatography gave **5** (639 mg, 87% yield).

§ Coupling constants of **5** ($^3J_{HF}$ = 38.6, $^3J_{HP}$ = 7.3 Hz) are consistent with those of α-fluorovinylphosphonate possessing (*E*)-configuration ($^3J_{HPtrans}$ = 39–40, $^3J_{HPcis}$ = 7.6–10 Hz).[16]

¶ Protected peptide resin (Boc–Gly–FPab(OEt)$_2$–Val–Pro–Met–Leu–PAM resin, 0.05 mmol) was treated with 1 mol dm^{-3} TMSOTf–thioanisole (molar ratio 1:1) in TFA (2.5 cm^3) in the presence of *m*-cresol (125 mm^3) and EDT (125 mm^3) at 4 °C. After being stirred at 4 °C for 60 min, DMS (0.75 cm^3) and TMSOTf (0.5 cm^3) were successively added to the reaction with additional stirring at room temperature for 2 h. The reaction was quenched by addition of EtOH–H_2O. The aqueous layer was subjected to HPLC purification, yielding 22 mg of the desired peptide. Ion-spray MS *m/z* calcd for $C_{27}H_{49}N_6O_{10}SFP$ (MH^+) 699.76; found 699.50. Purified peptides, consisting of diastereomers derived from FPab, were eluted as two peaks incompletely resolved on HPLC.

‖ Peptides possessing L-phosphotyrosine mimetics as an FPab replacement were completely hydrolyzed by leucine amino peptidase, while D-phosphotyrosine mimetic-containing peptides remained intact.[17]

1 T. Hunter, *Cell*, 2000, **100**, 113.
2 G. M. Blackburn, *Chem. Ind., (London)*, 1981, 134.
3 For a recent review see: M. J. Tozer and T. F. Herpin, *Tetrahedron*, 1996, **52**, 8619; for an updated compilation of references see: J. M. Percy, *Top. Curr. Chem.*, 1997, **193**, 131.
4 L. Schmitt, N. Cavusoglu, B. Spiess and G. Schlewer, *Tetrahedron Lett.*, 1998, **39**, 4009; T. R. Burke Jr., M. S. Smyth, A. Otaka, M. Nomizu, P. P. Roller, G. Wolf, R. Case and S. E. Shoelson, *Biochemistry*, 1994, **33**, 6490.
5 B. Iorga, F. Eymery and P. Savignac, *Tetrahedron*, 1999, **55**, 2671; X. Zhang, W. Qiu and D. J. Burton, *Tetrahedron Lett.*, 1999, **40**, 2681.
6 A. Otaka, E. Mitsuyama, T. Kinoshita, H. Tamamura and N. Fujii, *J. Org. Chem.*, 2000, **65**, in press.
7 G. M. Blackburn and M. J. Parratt, *J. Chem. Soc., Perkin Trans 1*, 1986, 1417.
8 W. Oppolzer, *Pure Appl. Chem.*, 1990, **62**, 1241.
9 *Organocopper Reagents, A Practical Approach*, ed. R. J. K. Taylor, Oxford University Press, Oxford, 1994, pp. 85–28, 143–158, and references cited therein.
10 A. J. Zapata, Y. Gu and G. B. Hammond, *J. Org. Chem.*, 2000, **65**, 227; R. S. Gross, S. Mehdi and J. R. McCarthy, *Tetrahedron Lett.*, 1993, **34**, 7197.
11 W. Oppolzer, O. Tamura and J. Deerberg, *Helv. Chim. Acta*, 1992, **75**, 1965.
12 A. Otaka, K. Miyoshi, T. R. Burke Jr., P. P. Roller, H. Kubota, H. Tamamura and N. Fujii, *Tetrahedron Lett.*, 1995, **36**, 927; D. B. Berkowitz, Q. Shen and J.-H. Maeng, *Tetrahedron Lett.*, 1994, **35**, 6445.
13 A. Otaka, K. Miyoshi, M. Kaneko, H. Tamamura, N. Fujii, M. Nomizu, T. R. Burke Jr. and P. P. Roller, *J. Org. Chem.*, 1995, **60**, 3967.
14 T. Yokomatsu, K. Suemune, T. Murano and S. Shibuya, *J. Org. Chem.*, 1996, **61**, 7207.
15 K. Blades, A. H. Butt, G. S. Cockerill, H. J. Easterfield, T. P. Lequeux and J. M. Percy, *J. Chem. Soc., Perkin Trans 1*, 1999, 3609.
16 R. Waschbüsch, J. Carran and P. Savignac, *Tetrahedron*, 1996, **52**, 14 199.
17 T. R. Burke Jr., M. S. Smyth, M. Nomizu, A. Otaka and P. P. Roller, *J. Org. Chem.*,1993, **58**, 1336.

A new arsenobetaine from marine organisms identified by liquid chromatography–mass spectrometry

Kevin A. Francesconi,*[a] Somkiat Khokiattiwong,[b] Walter Goessler,[c] Søren N. Pedersen[a] and Marija Pavkov[c]

[a] *Institute of Biology, Southern Denmark University, 5230 Odense M, Denmark. E-mail: kaf@biology.ou.dk*
[b] *Phuket Marine Biological Center, Phuket 83000, Thailand*
[c] *Chemistry Institute, Karl-Franzens University Graz, 8010 Graz, Austria*

Received (in Cambridge, UK) 27th March 2000, Accepted 8th May 2000

A new arsenic-containing betaine, trimethyl(2-carboxyethyl)arsonium inner salt 2, has been identified in fish muscle tissue by liquid chromatography–mass spectrometry.

Arsenic is a common constituent of marine organisms where it occurs in a wide range of chemical forms.[1] The major form in marine animals is arsenobetaine **1**, while arsenic containing carbohydrates (dimethylarsinoylribosides) are the predominant forms in marine algae. The biogenesis of the various arsenic compounds is still not known, although plausible pathways have been proposed.[2,3] Unknown arsenic compounds have also been reported in marine samples, the most widespread of these being a cationic arsenical present in fish, molluscs and crustaceans.[4–9] This unknown compound was detected in aqueous (or aqueous methanol) extracts of tissues by HPLC with arsenic-specific detectors, such as an inductively coupled plasma mass spectrometer (ICPMS),[4–8] or an atomic fluorescence spectrometer.[9] Determination of the precise chemical structure of this compound may help elucidate biogenetic

$Me_3As^+CH_2COO^-$ **1** $Me_3As^+CH_2CH_2COO^-$ **2**

pathways for arsenic.

Recently, we analysed (HPLC–ICPMS) aqueous extracts of a range of tropical marine organisms, and found that a coral reef fish, *Abudefduf vaigiensis* (Pomacentridae), contained significant amounts of the unknown compound (8% of the total arsenic), in addition to arsenobetaine, which constituted *ca*. 90% of the arsenic. The extract from *A. vaigiensis* was subjected to TLC (cellulose on a glass plate; butan-1-ol–acetic acid–water 60 : 15 : 25); the cellulose support was then cut into narrow bands (5 mm), each of which was extracted with water (2.0 mL) and a portion (20 μL) of the extract analysed for arsenic by graphite furnace atomic absorption spectrometry. Arsenic was detected in three adjacent fractions in an apparently homogeneous band centred at R_f 0.54, matching the R_f for arsenobetaine. Subsequent HPLC–ICPMS analyses, however, showed that the two slower running TLC fractions contained all their arsenic as arsenobetaine, whereas the faster running fraction contained both arsenobetaine and the unknown arsenical (2 : 1 in terms of arsenic). The concentration of the unknown in this solution (175 ng As cm^{-3}) was now sufficient to enable detection of arsenic (*m/z* 75, As^+) by positive ion LC electrospray MS.[10]

Cation-exchange LC electrospray MS of the solution at 200 V fragmentor voltage and measuring *m/z* 75 yielded only two peaks with retention time 1.83 (arsenobetaine) and 4.31 min (unknown). The analysis was then repeated at 70 V fragmentor voltage and the eluent was analysed in scan mode measuring *m/z* 141–160 (we made the initial assumption that, under these conditions, we were seeing predominantly the $[M + H]^+$ molecular species). This process was repeated scanning from *m/z* 161–180, and so forth, up to *m/z* 400. Only one ion (*m/z* 193), eluting at 4.33 min matched the retention time for the unknown arsenic peak; the closest other ions had retention times of 4.02 (*m/z* 162) and 4.74 min (*m/z* 151). The procedure was then carried out at variable fragmentor voltages,[10] which enabled simultaneous detection of *m/z* 75 (arsenic) and 193 (presumed $[M + H]^+$ for the unknown); the retention times for the two peaks agreed exactly (Fig. 1).

The chromatographic properties and mass spectral data for the unknown were consistent with the structure of the arsenic betaine **2**. An authentic specimen of **2**, prepared[11] by reacting trimethylarsine with 1-bromopropionic acid, was then analysed by LC electrospray MS. It produced retention time and mass spectral data (Fig. 1) matching those obtained for the unknown. Our previous experience with the unknown had revealed a

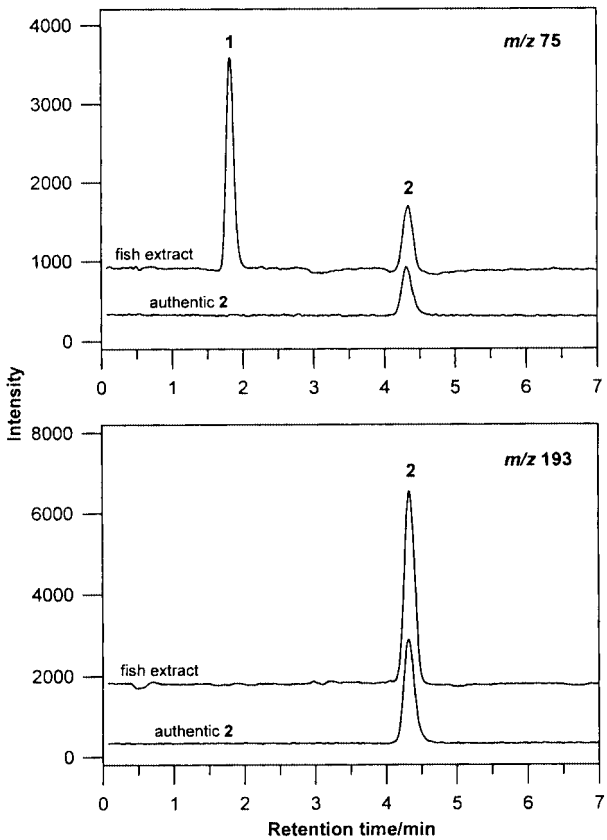

Fig. 1 LC electrospray mass chromatograms of partially purified extract from coral reef fish and authentic compound **2** at *m/z* 75 and 193. Intensity baselines for the fish extract have been offset (600 units for *m/z* 75 and 1500 units for *m/z* 193) to facilitate comparison with chromatograms for authentic compound **2**. LC conditions were: Ionospher C cation-exchange column (3 × 100 mm, 5 μm) from Chrompack; mobile phase was 20 mM aqueous pyridine pH 2.6 (adjusted with HCOOH) mixed with methanol (9 : 1) at 30 °C and flow rate 1.0 mL min^{-1}; 5 μL injection; ions were detected with a G1946A MSD single quadrupole mass spectrometer (Hewlett Packard, Waldbronn, Germany) equipped with an atmospheric pressure ionization (API) LC-MS interface operating at variable fragmentor voltages 70 (*m/z* 193) and 200 V (*m/z* 75).

DOI: 10.1039/b002392m

marked decrease in retention time (cation-exchange) as the pH of the mobile phase was increased, behaviour consistent with a bipolar compound. In the present study, when the chromatography was repeated at pH 4.0, the peaks (*m/z* 75 and 193) for the unknown and for authentic compound **2** both moved to retention time 1.65 min. Characteristic *m/z* fragments for compound **2** were then determined, and the optimal fragmentor voltage was found for the major fragments at *m/z* 120 (Me_3As^+) and 105 (Me_2As^+). LC electrospray MS with variable fragmentor voltages enabling simultaneous detection of the four ions characteristic of compound **2** (*m/z* 75, 105, 120 and 193), was performed on the fish extract, authentic compound **2**, and a co-injected mixture of the two; the mass chromatograms showed coincidence of peaks in all cases (Fig. 2). On the basis of these data, we assigned the new arsenic species from *A. vaigiensis* as trimethyl(2-carboxyethyl)arsonium inner salt **2**. Subsequent HPLC–ICPMS analyses of the sample and authentic material produced data entirely consistent with this assignment.

An unknown cationic arsenic compound (considered to be the same compound) has been reported as a constituent of several certified reference materials[4,5,9] including DORM-2[5] (dogfish muscle tissue from the National Research Council of Canada, Ottawa, Ontario, Canada). LC electrospray MS of an aqueous extract of DORM-2 indicated the presence of compound **2**. However, although the *m/z* 193 molecular species gave a clear signal, the low concentrations of **2** resulted in only a small *m/z* 75 peak. Verification of the new arsenic betaine **2** in DORM-2 was provided by HPLC–ICPMS (a more sensitive technique for determining arsenic ions) by co-chromatography with the authentic standard. The concentration found in this work (0.17 ± 0.05 mg As kg^{-1} dry mass, $n = 3$) is in good agreement with previously published data.[5] Possibly, in future studies on the new arsenic betaine, DORM-2 can serve as a reference sample for those laboratories that do not have access to synthetic material.

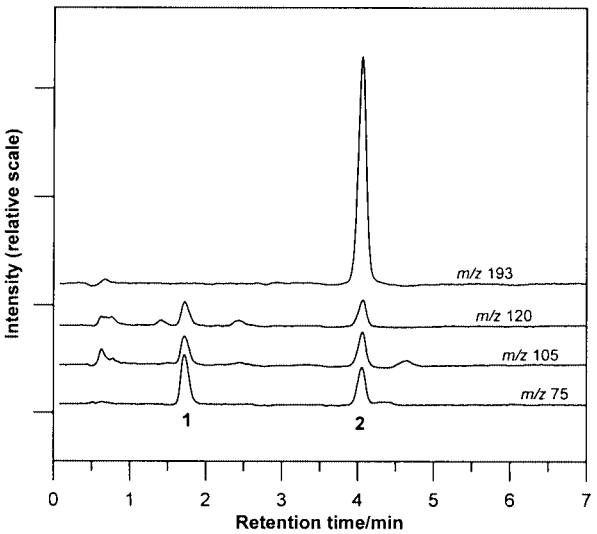

Fig. 2 LC electrospray mass chromatograms of partially purified extract from coral reef fish (5 μL) co-injected with a solution (10 μL) of authentic compound **2** (mixture was 1:1 in terms of concentration of **2**). LC-MS conditions were as described in Fig. 1, except that variable fragmentor voltages were 70 (*m/z* 193), 150 (*m/z* 120, 105), and 200 V (*m/z* 75).

The chromatographic properties of the arsenic betaine **2** match those for the unknown arsenic cation reported in certified reference materials and in a range of marine organisms.[4–9] Consequently, we consider it likely that **2** will prove to be a common constituent of marine animals, in many cases occurring together with arsenobetaine **1**, albeit at much lower concentrations. The presence of the two arsenic betaines **1** and **2** in marine animals offers some insight into the biogenesis of arsenic-containing natural products. A previously proposed pathway[2] suggested that arsenobetaine **1** might be derived from dimethylarsinoylribosides (common metabolites of algae), with the carboxymethyl group of **1** being formed from C4 and C5 of the ribose. Dimethylarsinoylribosides, however, seem less likely to be implicated in the biogenesis of **2** (*i.e.* as a source of the carboxyethyl group) and hence their involvement in the biogenesis of arsenobetaine **1** might also be questioned. A scheme recently proposed by Edmonds[3] may more readily account for the presence of both **1** and **2** in marine organisms. In that scheme, the possible 'arsenylation' of 2-oxo acids by a process analogous to their amination to amino acids was used to explain the origin of several naturally occurring arsenic compounds, including arsenobetaine. The proposed agent for 'arsenylation' was dimethylarsinous acid (Me_2AsOH), the reduced form of the common arsenic metabolite dimethylarsinic acid. Reaction of dimethylarsinous acid with the common 2-oxo compound oxaloacetic acid in the general scheme outlined by Edmonds[3] could give rise to compound **2**.

Identification of other unknown arsenic compounds detected in marine samples will improve our understanding of arsenic-containing natural products. Possibly, these compounds are also arsenic betaines, and structural information might quickly be obtained by mass spectrometric studies (LC–MS and MS/MS) focussing on such compounds.

We thank Jürgen Gailer for synthesising compound **2**, and John Edmonds for making available the contents of ref. 3 before it was published.

Notes and references

1 K. A. Francesconi and J. S. Edmonds, *Adv. Inorg. Chem.*, 1997, **44**, 147.
2 J. S. Edmonds and K. A. Francesconi, *Experientia*, 1987, **43**, 553.
3 J. S. Edmonds, *Bioorg. Med. Chem. Lett.*, 2000, **10**, 1105.
4 E. H. Larsen, G. Pritzl and S. H. Hansen, *J. Anal. At. Spectrom.*, 1993, **8**, 1075.
5 W. Goessler, D. Kuehnelt, C. Schlagenhaufen, Z. Slejkovec and K. J. Irgolic, *J. Anal. At. Spectrom.*,1998, **13**, 183.
6 W. Goessler, A. Rudorfer, E.A. Mackey, P. R. Becker and K. J. Irgolic, *Appl. Organomet. Chem.*, 1998, **12**, 491.
7 K. A. Francesconi, W. Goessler, S. Panutrakul and K. J. Irgolic, *Sci. Total Environ.*, 1998, **221**, 139.
8 V. W. M. Lai, W. R. Cullen and S. Ray, *Mar. Chem.*, 1999, **66**, 81.
9 Z. Slejkovec, J. T. van Elteren and A. R. Byrne, *Talanta*, 1999, **49**, 619.
10 S. N. Pedersen and K. A. Francesconi, *Rapid Commun. Mass Spectrom.*, 2000, **14**, 641.
11 K. A. Francesconi, J. Gailer, J. S. Edmonds, W. Goessler and K. J. Irgolic, *Comp. Biochem. Physiol., C*, 1999, **122**, 131.

ChemComm

Vesicle controlled selectivity in photosensitized oxidation of olefins

Hong Ru Li,[a] Li Zhu Wu[b] and Chen Ho Tung*[a]

[a] *Institute of Photographic Chemistry, Chinese Academy of Sciences, Beijing, 100101, China. E-mail:chtung@ipc.ac.cn*

[b] *Center of Molecular Science, Institute of Chemistry, Chinese Academy of Sciences, Beijing 100080, China*

Received (in Cambridge, UK) 3rd April 2000, Accepted 17th May 2000

The photooxidation of α-pinene (α-PE) and *trans,trans*-1,4-diphenyl-1,3-butadiene (DPB) sensitized by 9,10-dicyanoanthracene (DCA) in mixed surfactant vesicles was selectively directed toward either the singlet oxygen mediated or the superoxide radical anion mediated products by controlling the status and location of the substrate and sensitizer molecules in the reaction media.

Dye-sensitized photooxidation of alkenes has been extensively investigated.[1] There are two well established types of dye-sensitized photooxidation: an energy-transfer pathway and electron-transfer pathway.[2] The energy-transfer pathway involves energy transfer from the triplet sensitizer to ground-state oxygen to generate singlet oxygen ($^1O_2$) which then reacts with the substrate. In the electron-transfer photosensitized oxidation, electron-deficient sensitizers are generally used. Electron transfer from the alkene to the sensitizer in its excited states results in formation of the alkene radical cation and the sensitizer radical anion, which subsequently reduces O_2 to give the superoxide radical anion ($O_2^{\bullet-}$). The generated superoxide radical anion then reacts with the alkene radical cation to yield the oxidation products. Unfortunately, in many cases the two types of photooxidation occur simultaneously, and the selectivity of the oxidation reactions is poor. Of the various approaches to increase selectivity, use of organized and constrained media has shown considerable promise.[3] Here, we report the photooxidation of α-pinene (α-PE) and *trans,trans*-1,4-diphenyl-1,3-butadiene (DPB) sensitized by 9,10-dicyanoanthracene (DCA) in mixed surfactant vesicles. We found that the oxidation could be directed selectively toward the products derived either from the energy transfer pathway or the electron transfer pathway by controlling the status and location of the substrate and sensitizer molecules in the reaction media.

The vesicles used in the present study were prepared by sonicating an equimolar mixture of a cationic surfactant (octyltrimethylammonium bromide, 8.2×10^{-2} M) and an anionic surfactant (sodium laurate, 8.2×10^{-2} M) in buffered solution (pH = 9.2) for 30 min at 50 °C.[4] These vesicles were found to be stable at room temperature and the dispersion solution was optically clear. The photosensitized oxidation was performed in two modes. In the first (mode 1), the sensitizer DCA was incorporated in the bilayer membrane of one set of vesicles and the substrate solubilized in another set of vesicles. Equal volumes of the two sets of vesicle dispersions were then mixed to prepare the samples for photolysis. Although sonication was performed during preparation of the component solutions, the final mixture was not sonicated. In this way intermixing of the solubilizates was prevented. In the second mode (mode 2) both the sensitizer and the substrate were incorporated in the bilayers of the same set of vesicles. Generally, the concentration of the olefins was *ca.* 1.0×10^{-3} M corresponding to thousands of substrate molecules in each vesicle, while the concentration of the sensitizer was generally *ca.* 1.0×10^{-4} M. The samples were irradiated under oxygen by using light with wavelength $\lambda > 400$ nm, ensuring the absence of direct excitation of the alkene substrate. After irradiation, the products were extracted with CH_2Cl_2 and analysed by gas chromatography. The material balance for all the reactions was generally > 95%.

Photooxidation of α-PE sensitized by DCA in homogeneous solution followed by reduction of the reaction mixture with sodium sulfite solution gave the ene product pinocarveol **1** and the non-ene products myrtenal **2**, epoxide **3** and aldehyde **4**, as shown in Scheme 1. The ene and the non-ene products have been proposed to be derived from the energy- and electron-transfer pathways, respectively.[5] The product distributions in acetonitrile and dichloromethane are given in Table 1. The product distribution of the photosensitized oxidation of α-PE in vesicles is dramatically altered compared with that in homogeneous solutions, and is remarkably dependent on the experimental mode. Photooxidation in mode 1 exclusively produced the ene product **1** (Table 1). In contrast, photooxidation in mode 2 only gave the non-ene products **2**–**4** (Table 1). These observations can be easily understood by consideration of the status and location of the substrate and sensitizer molecules in the reaction media. It has been established that DCA can act both as an energy-transfer sensitizer and an electron-transfer sensitizer.[6] In mode 1, the isolation of α-PE in one set of vesicles from DCA in another set of vesicles prevents them from undergoing electron transfer. Thus, no non-ene products were detected. On the other hand, $^1O_2$ can be generated in the DCA-incorporating vesicles by energy transfer from the triplet excited state of DCA to the ground state of oxygen. The species $^1O_2$ is small and uncharged and has a relatively long lifetime and properties which allow it to diffuse freely from one set of vesicles to another set of vesicles where reaction with the

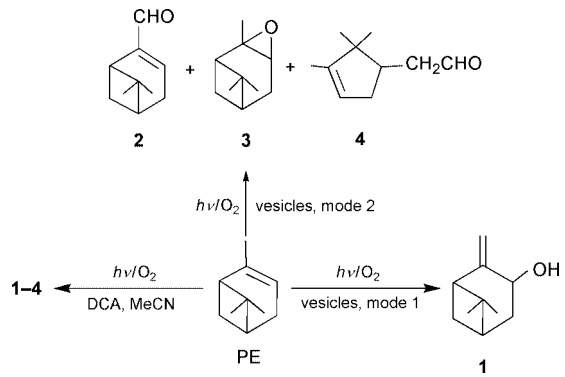

Scheme 1

Table 1 Product distribution in the DCA-sensitized photooxidation of α-PE and DPB in solutions and in vesicles

	PE				DPB					
Media	**1**	**2**	**3**	**4**	**5**	**6**	**7**	**8**	**9**	**10**
MeCH	52	32	13	3	80	80	2	13	0	5
CH_2Cl_2	85	10	5	0	75	75	12	3	5	5
Vesicles (mode 1)	100	0	0	0	100	100	0	0	0	0
Vesicles (mode 2)	0	55	4	41	53	53	23	0	24	0

DOI: 10.1039/b002597f

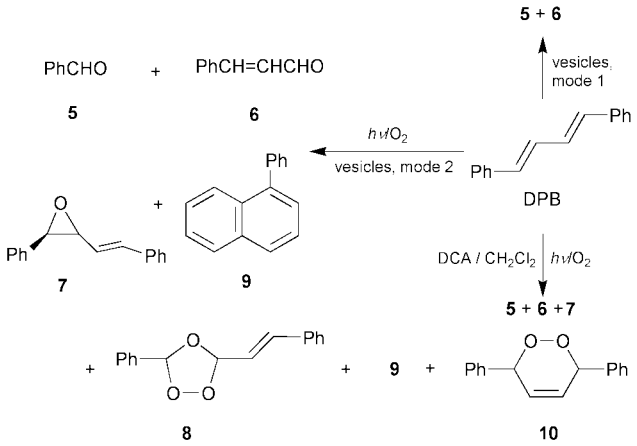

Scheme 2

olefins produces the ene product **1**. In mode 2, the DCA molecule is surrounded by a number of α-PE molecules. The high "local concentration" of α-PE and the close contact between DCA and α-PE molecules in the confined bilayer of vesicles leads to efficient quenching of the singlet excited state of DCA by α-PE *via* an electron-transfer process, generating DCA radical anions and α-PE radical cations. As a result, intersystem crossing from the singlet excited state to the triplet state of DCA can not compete with the quenching process by α-PE. Thus, subsequent triplet energy transfer to O_2 can not occur, and no singlet oxygen mediated product is produced. On the other hand, the generated DCA radical anions will efficiently undergo electron transfer to oxygen to produce superoxide radical anions, which subsequently react with α-PE radical cations located in the same vesicle to yield the non-ene products **2**–**4**.

Photosensitized oxidation of DPB in homogeneous solution has been extensively investigated.[5,7] Irradiation of an oxygen-saturated DPB solution in CH_2Cl_2 containing DCA with visible light gave benzaldehyde **5**, cinnamaldehyde **6**, epoxide **7**, ozonide **8**, 1-phenylnaphthalene **9** and endoperoxide **10** (Scheme 2) and the product distribution is shown in Table 1. **10** is a product of 1,4-cycloaddition of singlet oxygen ($^1O_2$) to DPB. Products **7**–**9** are derived from the electron-transfer pathway. Products **5** and **6** could be produced either *via* an energy- or electron-transfer pathway.[6] The photosensitized oxidation of DPB in vesicles in mode 1 gave **5** and **6** as the unique products (Table 1 and Scheme 2). We believe that these products are derived from the singlet oxygen pathway. In contrast, the photosensitized oxidation of DPB in vesicles in mode 2 only produced the electron-transfer mediated products **5**–**7** and **9** (Table 1) and no singlet oxygen products were detected. These observations demonstrate once again that the selectivity in photosensitized oxidation of alkenes can be directed by incorporation of the sensitizer and substrate in different or the same set of vesicles.

It is of note that the products in the reaction of DPB with singlet oxygen in vesicles are remarkably different from those in homogeneous solutions. The reaction in homogeneous solution yielded endoperoxide **10**, a 1,4-cycloaddition product of the diene to $^1O_2$, as the unique product (Scheme 2). In sharp contrast, the photosensitized oxidation in vesicles produced benzaldehyde **5** and cinnamaldehyde **6** in quantitative yield. Evidently, these products were derived from an intermediate dioxetane, a 1,2-cycloaddition product. It has been established that DPB in solution exists mainly in its transoid conformer,[7] and the cisoid form amounts to *ca.* 1%. The 1,4-cycloaddition of singlet oxygen to the 1,3-diene to form the endoperoxide is concerted and requires a six-membered ring transition state; only the cisoid conformer can satisfy such a requirement. Obviously, the organized semirigid environment in vesicles prevents DPB from undergoing transoid to cisoid conformational change and thus only the 1,2-cycloaddition products were obtained.

In conclusion, vesicles can be used to direct the photosensitized oxidation of olefins either toward the singlet oxygen mediated or the superoxide radical anion mediated products by controlling the status and location of the olefin and sensitizer molecules in the reaction media.

We thank the National Science Foundation of China, and the Bureau for Basic Research, Chinese Academy of Sciences for financial support.

Notes and reference

1 M. Prein and W. Adam, *Angew. Chem., Int. Ed. Engl.*, 1996, **35**, 477.
2 C. S. Foote, *Photochem. Photobiol.*, 1991, **54**, 659.
3 V. Ramamurthy and N. J. Turro, *J. Inclusion Phenom. Mol. Recognit. Chem.*, 1995, **21**, 239.
4 E. W. Kaler, A. K. Murthy, B. E. Rodriguez and J. A. Zasadzinski, *Science*, 1989, **245**, 1371.
5 C. H. Tung and J. Q. Guan, *J. Am. Chem. Soc.*, 1998, **120**, 11874.
6 R. C. Kanner and C. S. Foote, *J. Am. Chem. Soc.*, 1992, **114**, 678; R. C. Kanner and C. S. Foote, *J. Am. Chem. Soc.*, 1992, **114**, 682.
7 C. H. Tung, H. W. Wang and Y. M. Ying, *J. Am. Chem. Soc.*, 1998, **120**, 5179.

ChemComm

Metal-driven self assembly of C_3 symmetry molecular cages

Fulvia Felluga,[a] Paolo Tecilla,*[a] Louise Hillier,[b] Christopher A. Hunter,*[b] Giulia Licini[c] and Paolo Scrimin*[c]

[a] *University of Trieste, Department of Chemical Sciences, via Giorgieri, 1 34127-Trieste, Italy*
[b] *University of Sheffield, Department of Chemistry, Sheffield, UK S3 7HF*
[c] *University of Padova, Department of Organic Chemistry and CNR center CMRO, via Marzolo, 1 35131-Padova, Italy. E-mail: scrimin@mail.chor.unipd.it*

Received (in Liverpool, UK) 24th February 2000, Accepted 10th May 2000

A series of tris(2-aminoethyl)amine (TREN) derivatives functionalized on the arms with pyridine or methylimidazole ligands bind very strongly to a trisporphyrin derivative *via* apical coordination, with formation of molecular cages; the strength of the binding (K_b up to $10^{8.8}$ mol^{-1} dm^3) depends on the structure of the TREN derivative as well as on its coordination to Zn(II).

The self assembly of proteins to elicit new and unique functions is a common feature in the biological world.[1] A case in point is HIV-1 protease, whose activity is dependent on a hydrogen bond-driven dimerization of two protein units.[2] The possibility of realizing molecules of controlled geometry and shape in the laboratory by assembling easily synthesized subunits is an appealing goal which is attracting enormous interest, demonstrated by the continuous flow of contributions appearing in the chemical literature.[3] Such 'supermolecules' may find useful application in molecular recognition and selective substrate transformation, sensing, signal transduction and, eventually, in the realization of miniaturized nanostructures. Metal–ligand coordination is one of the driving forces exploited for the assembly of these structures.[4] Examples are provided by the work of the Stang,[5] Fujita,[6] Hamilton,[7] Sauvage,[8] and Lehn[9] groups. Self-assembling porphyrin oligomers towards macrocycles or polymers have been reported by Hunter *et al.*,[10] while Tabushi and coworkers, as early as 1985,[11] elegantly demonstrated allosteric binding to a Zinc-gable porphyrin.

We report here on the formation of molecular cages driven by apical coordination of the terminal bases of tripodal ligands **1a**–**c** to the three zinc porphyrin units of **2**. The possibility of modifying the conformation of the tris(2-aminoethyl)amine (TREN) platform of derivatives **1a**–**c** *via* metal coordination gives the system a tunable geometry for controlling the binding to **2**.

Ligand **1a** was readily obtained by reaction of 3-pyridinaldehyde with TREN followed by reduction with $NaBH_4$. Ligands **1b**,**c** were prepared *via* condensation of TREN with the 4-formylbenzenamide derivatives, obtained by reaction of 4-formylbenzoyl chloride with 4-aminopyridine (**1b**) or methylhystamine (**1c**), followed by reduction with $NaBH_4$.† The trisporphyrin derivative **2** was prepared by coupling 1,3,5-benzene tricarbonyl trichloride with the corresponding aminoporphyrin,[12] followed by metallation with zinc acetate.† Porphyrin **2**, as well as the free bases **1a**–**c**, are soluble in chlorinated organic solvents. The solubility of the 1:1 Zn(II) complexes of the TREN derivatives in these solvents depends on the nature of the counterions: more hydrophilic nitrates are insoluble, while more lipophilic hexafluorophosphates are freely soluble in these media.

Trisporphyrin **2** shows a typical UV–vis spectrum, with maxima at 420 nm (ε = 430,000 mol^{-1} dm^3 cm^{-1}) and 550 nm (ε = 37,000 mol^{-1} dm^3 cm^{-1}), indicating that there is no intramolecular interaction between the porphyrins. Binding of an apical ligand causes a shift of these peaks to 430 and 565 nm, respectively. The very intense absorptions in the 420–430 nm region can be used for determination of the affinity constant with apical ligands and, in the present case, for the formation of cage complexes between **2** and **1**. Fig. 1 shows the changes in the absorption spectrum of **2** upon addition of increasing amounts of **1a** in CH_2Cl_2. The presence of a well-defined isosbestic point is suggestive of the formation of a single complex, and the fact that all the zinc porphyrin sites are fully complexed after the addition of one equivalent of ligand implies that a 1:1 cage complex has been formed. The complex so formed does not convert into species of different stoichiometry in the presence of up to a twofold excess of the TREN derivative, contrary to recent observations for a bisporphyrin receptor in the presence of multiarmed amines.[13] Clearly, a key role is played here by the complementary structure of the two subunits involved in the formation of the supramolecular cage complex. Analysis of the absorbance *vs.* concentration data‡ leads to a well-behaved complexation curve (Fig. 1, inset) which gives a very high binding constant (log K_b = 8.81) for the 1:1 complex. Similar curves were obtained for tripodal ligands **1b**,**c** and **1a**,**b**–Zn(II) complexes.

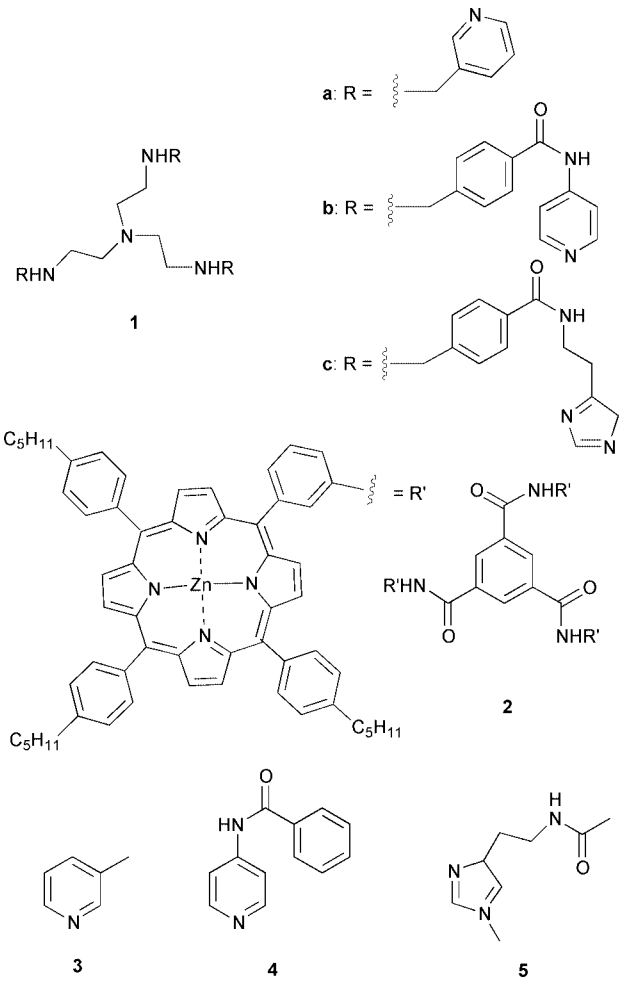

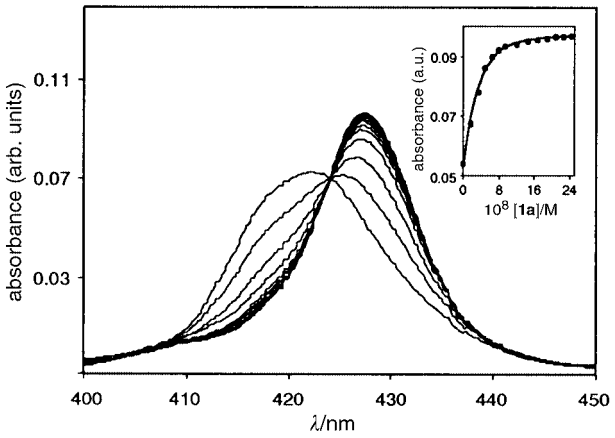

Fig. 1 Change in the absorbance of a 60 μM solution of **2** in CH_2Cl_2 upon addition of **1a**. Inset: binding isotherm of the data at 427 nm. The solid line represents the computer-generated best fit for a 1:1 complex.

The titration data are summarized in Table 1, along with the values determined for model ligands **3**–**5**. The values of the parameters EM and β are also listed in the table. EM§ corresponds to the ratio $\{(K_b)_{cage}/[(K_b)_{model}]^3\}^{0.5}$ and is the effective molarity for the intramolecular cyclizations required to form the cage. β[14] is simply the ratio $(K_b)_{cage}/(K_b)_{model}$ and gives an indication of the absolute strength of binding associated with the formation of the cage, with respect to the single apical coordination of the model compound to one porphyrin. Inspection of Table 1 reveals that tripodal ligand **1a** shows the highest binding constant to **2**, which reduces 30-fold upon Zn(II) binding to TREN. In the case of **1b**, the binding constant is lower and coordination of Zn(II) to TREN does not induce any significant change. Allowing for the stronger binding interaction of methylimidazole to the Zn-porphyrin (compared with pyridine), the least effective ligand is **1c**, with EM and β values significantly lower than those of **1a** and **1b**. The β values indicate that cooperative binding of the tripodal ligands to the three porphyrins leads to a higher affinity than single apical ligands (up to five orders of magnitude in the case of **1a**). Inspection of molecular models reveals that, in the case of **1b**, the length of the tripodal arms and their flexibility is such that coordination of Zn(II) does not significantly affect their binding geometry. However, this flexibility reduces the strength of binding with respect to **1a**, due to the freezing out of conformational mobility on complexation.[14] The disadvantage of flexibility is further evidenced by the relatively low values of EM and β for **1c**, which has even longer arms. For **1a**, the length of the arms¶ is such that apical binding to the porphyrins requires the latter to move out of the plane of the central benzene by rotation around the amide bonds pointing inwards (Fig. 2). Complexation of Zn(II) to the TREN platform further reduces the distance between the three pyridine nitrogens,

Table 1 Binding constants of trisporphyrin **2** to tripodal ligands **1a–c** and model ligands **3–5** in CH_2Cl_2[a] at 25 °C

Ligand	log K_b[b]	EM[c]	β[c]
3[d]	3.75 ± 0.02	—	—
1a	8.81 ± 0.07	6.0×10^{-2}	1.1×10^5
1a·Zn	7.36 ± 0.05	1.1×10^{-2}	4.1×10^3
4[d]	3.98 ± 0.03	—	—
1b	7.75 ± 0.09	8.0×10^{-3}	5.9×10^3
1b·Zn	7.64 ± 0.05	7.1×10^{-3}	4.6×10^3
5[d]	5.37 ± 0.07	—	—
1c[e]	7.50 ± 0.09	5.0×10^{-5}	1.3×10^2

[a] In the presence of 1% CH_3CN. [b] Binding constant are expressed in mol^{-1} dm^3. [c] See the text for the definition of EM and β. The units of EM are mol dm^{-3}, and β is dimensionless. [d] Binding constants of the model ligands are the microscopic values determined assuming independent binding to each porphyrin of **2**. [e] The binding of **1c**·Zn(II) to **2** does not follow a well behaved isotherm; for this reason it has been omitted.

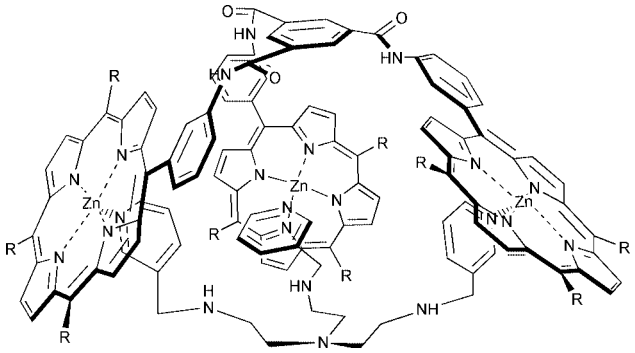

Fig. 2 Schematic diagram of the molecular cage formed by binding of **1a** to **2**.

imposing a more stringent geometric constraint for binding, resulting in a smaller binding constant.

In conclusion, we have shown that tripodal molecules, based on complementary porphyrins and pyridine or imidazole ligands, give highly symmetrical molecular cages with very strong binding constants which are potentially suitable for molecular recognition and selective transformation of substrates trapped in the cavity: work aimed at this goal is ongoing in our laboratories.

This work was supported in part by a grant within the frame of the British–Italian Collaboration in Research and Higher Education.

Notes and references

† All new compounds gave the expected ^{1}H- and ^{13}C-NMR spectra and the correct elemental analyses (C, H, N).

‡ The binding isotherm was fitted using the program HOSTEST II. See: C. S. Wilcox, in *Frontiers in Supramolecular Organic Chemistry and Photochemistry*, H.-J. Schneider and H. Dürr, VCH, Weinheim, 1991.

§ In the cage formation the first binding is intermolecular (K), the second binding is intramolecular ($EM_1 \times K$) and the third binding is also intramolecular ($EM_2 \times K$). Thus, the overall observed binding constant is $EM_1 \times EM_2 \times K^3$. Assuming that $EM_1 = EM_2$, the effective molarity is the square root of the product $EM_1 \times EM_2$.

¶ Energy minimization with the HyperChem program (Hyperchem 2 for Windows, © 1991, Hypercube Inc. and Autodesk Inc.) indicates that two Zn(II) ions in the porphyrin derivative **2** are *ca.* 20 Å apart when the molecule is flat. The distance between two pyridine nitrogens of **1a** is, in the fully stretched conformation, *ca.* 15 Å.

1 W. Stites, *Chem. Rev.*, 1997, **97**, 1233; S. Jones and J. M. Thornton, *Proc. Natl. Acad. Sci. U.S.A.*, 1996, **93**, 13.
2 R. Zutshi, J. Franciskovich, M. Shultz, B. Schweitzer, P. Bishop, M. Wilson and J. Chmielewski, *J. Am. Chem. Soc.*, 1997, **119**, 4841.
3 M. M. Conn and J. Rebek, *Chem. Rev.*, 1997, **97**, 1647.
4 B. Linton and A D. Hamilton, *Chem. Rev.*, 1997, **97**, 1669.
5 P. J. Stang, D. H. Cao, S. Saito and A. M. Arif, *J. Am. Chem. Soc.*, 1995, **117**, 6273.
6 M. Fujita, F. Ibukuro, H. Hagihara and K. Ogura, *Nature*, 1994, **367**, 720.
7 M. S. Goodman, J. Weiss and A. D. Hamilton, *J. Am. Chem. Soc.*, 1995, **117**, 8447.
8 N. Armaroli, F. Diederich, C. O. Dietrich-Buchecker, L. Flamigni, G. Marconi, J.-F. Nierengarten and J.-P. Sauvage, *Chem. Eur. J.*, 1998, **4**, 406.
9 B. Hasenknopf, J.-M. Lehn, B. O. Kneisel, G. Baum and D. Fenske, *Angew. Chem., Int. Ed. Engl.*, 1996, **35**, 1838.
10 X. Chi, A. J. Guerin, R. A. Haycock, C. Hunter and L. D. Sarson, *J. Chem. Soc., Chem. Commun.*, 1995, 2567.
11 I. Tabushi, S. Kugimiya, M. G. Kinnaird and T. Sasaki, *J. Am. Chem. Soc.*, 1985, **107**, 4192.
12 M. Gardner, A. J. Guerin, C. A. Hunter, U. Michelsen and C. Rotger, *New J. Chem.*, 1999, **23**, 309.
13 J. N. H. Reek, A. P. H. J. Schenning, A. W. Bosman, E. W. Meijer and M. J. Crossley, *Chem. Commun.*, 1998, 11.
14 M. Mammen, S.-K. Choi and G. M. Whitesides, *Angew. Chem., Int. Ed.*, 1998, **37**, 2754.

ChemComm

Möbius aromatics arising from a C=C=C ring component†

Sonsoles Martín-Santamaría, Balasundaram Lavan and Henry S. Rzepa*

Department of Chemistry, Imperial College of Science, Technology and Medicine, London, UK SW7 2AY. E-mail: h.rzepa@ic.ac.uk

Received (in Cambridge, UK) 28th March 2000, Accepted 2nd May 2000

Replacement of one planar C=C unit in Hückel 4*n* + 2 aromatic rings by a twisted C=C=C results in chiral 4*n* π Möbius aromatic rings.

The history of aromatic chemistry is dominated by the concept of planar ring systems containing $4n + 2$ conjugated π electrons, the so-called Hückel rule of aromaticity. Heilbronner[1] in 1964 was the first to suggest that applying a Möbius twist to the ring would create an aromatic species if $4n$ π electrons were conjugated. The Möbius concept has been widely applied to considering the aromaticity of pericyclic transition[2] states, but only recently have candidates for stable Möbius aromatics been suggested. Schleyer and coworkers have reported that a Möbius twisted conformation of the $4n$ π system $C_9H_9^+$ is aromatic[3] on the basis of calculated nucleus independent chemical shifts (NICS),[2] a technique which appears reliable and useful at quantifying aromaticity. We recently reported calculations on two conformations of [16]annulene,[4] one being conventionally antiaromatic, but the other having a pronounced Möbius-like twist not associated with any particular region of the ring. This isomer exhibited a NICS value consistent with mild aromaticity rather than antiaromaticity. Here we suggest further candidates for consideration as Möbius aromatics.

Our initial focus was on the chiral species cycloheptatetraene **5**. The presence of a C=C=C substructure in the 7-membered ring reduces the dihedral angle between the 1,3 allene substituents from 90 to 47–50°, which has the effect of breaking the degeneracy of the two highest occupied allene orbitals (Fig. 1; see ESI†). Interaction of both resulting orbitals with the remaining ring π orbitals would create a similar Möbius topology to that envisaged by Heilbronner, the specific case of **5** resulting in what could be termed a [7]Möbius annulene. A NICS calculation (−6.5 ppm, Table 1) establishes that this orbital interaction results in a mildly aromatic system, being rather less so than benzene itself (NICS −10 ppm). NICS calculations on benzannulated derivatives of **5** were reported[5] but the aromaticity of the allene-derived ring was not discussed. The ~40° distortion at the allene unit in **5** is clearly destabilising, since the species is isolable only at low temperatures, dimerising at higher temperatures *via* a $\pi^2 + \pi^2$ cycloaddition (a process known to be inhibited by bulky groups at the 1,3 positions[6]). The calculated bond lengths for **5** also show some alternation, indicative of a reactive species (Fig. 2). The HOMO and HOMO − 1 AM1 orbits computed for **5** are both symmetric with respect to C_2 axis and derive from the twisted allene system, but are now delocalised over the entire ring, and show Möbius topology (Fig. 2). Heilbronner predicted the HOMO for a pure Möbius aromatic would exhibit degeneracy,[1] but purely in a Hückel MO context. No degenerate representations in C_2 symmetry are necessary in **5**, although we do note that the energy difference between HOMO and HOMO − 1 (1.6eV/AM1) is less than that for allene at this twist angle (2.2 eV, Fig. 1†).

As a ligand, **5** is unusual in binding metals to both 'faces' concurrently (*e.g.* **7**),[7] but this is perhaps not unexpected if one considers it having only a single π-face! We also estimate one consequence of **5** (and its metal complexes) being chiral. Thus a typical model chiral auxilliary (*e.g.* R = CHClI or R = camphorsultamil[8]) results in diastereoisomers differing in energy by about 0.4–0.6 kcal mol^{-1} (AM1), a relatively small discrimination, but possibly one capable of being increased by suitable design. **5** interconverts with its mirror image *via* the Hückel $4n + 2$ π aromatic **6** (cycloheptatrienylidene),[9] which at the correlated level (CASPT2) has recently been shown to be the transition state for this process (barrier ~20 kcal mol^{-1}).

Elaborating the theme of substituting C=C=C for C=C (Table 1) we noted that the small ring systems **1** and **2** would be classified as antiaromatic; **2** as a conventional 4π antiaromatic Hückel system with a triplet ground state and **1** as a $4n + 2$ 6π Möbius antiaromatic system. **1** appears not to exist as a minimum at the *ab initio* RHF level, whilst singlet **2** reveals an antiaromatic (positive) NICS value. No minimum for the anion **3** could be located for this putative 8π Möbius aromatic, all optimisations resulting in the aromatic Hückel valence bond isomer **4**, probably because twisting the allene component in **3** to accommodate a 6-membered ring requires too much energy. This is a lesser problem in the larger ring monocation **8**, which appears to be a C_2 symmetric 8π Möbius system exhibiting NICS aromaticity, as is the 8π dication **9**. The singlet neutral form of **9**/**11** as an antiaromatic $4n + 2$ 10π annulene distorts to remove all symmetry and localise the bonds, whereas the triplet neutral **9**/**10** retains C_2 symmetry as might be expected of a $4n + 2$ excited state Möbius aromatic, although the NICS value shows only slight aromaticity (−1.3 ppm).[10] Chiral 12π monoanion **10** and the dianion **11** also show aromatic NICS values and have non-planar twisted geometries (Table 1). Each ring of the chiral bicyclic analogue of naphthalene **12** shows only modestly aromatic NICS values. In this instance, the carbene valence bond isomer **13**, a bridged [10] $4n + 2$ Hückel aromatic annulene, is substantially lower in energy, making it unlikely that **12** is a viable synthetic target. System **14** is derived from the novel Hückel-aromatic S/N systems discovered by Rees and Surtees.[11] As an 8π Möbius, **14** has an aromatic NICS value (Table 1). The 12π system **15** has a much smaller NICS value, which might be related to the larger dihedral angle at the allene termini (75°, Table 1) reducing the Möbius like orbital mixing (*c.f.* Fig. 1†). Our results do imply that optimum Möbius aromaticity may be achieved at allene twists of ~30–60°.

The presence of two or more allene-like chiral Möbius components raises the possibility that these can oppose or cooperate. An even number of the former becomes equivalent to Hückel; but if the latter the topological implications become more complex. For **17** two conformations can indeed be located, one with C_S (Hückel) and the other with C_2 (Möbius) symmetry, the latter being lower in energy and higher in aromaticity (Table 1). In the 10π Hückel aromatic conformation of the alkyne **17**, the triple bond appears to act purely as a two electron contributor whereas in the C_2 form, a possible four-electron alkyne contribution results in 12π Möbius aromaticity. The alkene analogue **18** has smaller NICS aromaticity values and relative energies, due in part to the significant non-planarity of **18**. More intriguingly the higher aromaticity of **17** may be due

† Electronic supplementary information (ESI) available: AM1 allene orbitals (Fig. 1), computed 3D coordinates (as PDB files) and selected orbitals (as 3DMF files). See http://www.rsc.org/suppdata/cc/b0/b002462g/

Table 1 Energies [kcal mol^{-1} for AM1, E_h (Hartree) for RHF/6-31G(d)] and NICS values (ppm) for the ground state structures

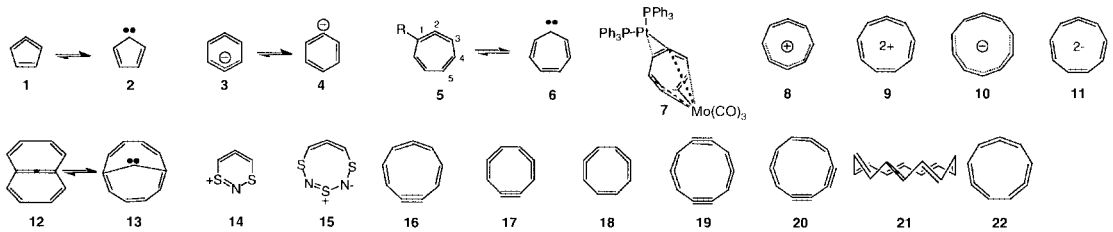

Species	AM1	AM1 relative energy[a]	RHF/6-31G(d)	RHF/6-31G(d) relative energy[a]	NICS	Dihedral angle[b]/°
1	155.3		[c]		—	8
2	147.1		−191.4899728		2.1	—
3	[d]		[d]		—	—
4	57.3		−230.0200		−9.8	—
5	95.7		−268.4477/−270.2424[e]		−6.5/−5.7[e]	51
6	117.0		−268.4241		−7.0	—
8	279.1		−306.6502		−5.6	65
9	575.9[f]		−344.6697		−3.3	86
10	96.8		−383.7313		−5.1	87
11	173.6		−347.4759[g]		−14.2	41
12	200.7		−420.9538		−4.7	37
13	178.5		−420.9954		−14.9	—
14	273.8		−963.7914		−10.9	27
15	72.9		−1415.9675		−0.4[h]	75
16	140.0		−344.1344		−3.3	67
17	229.2/215.3[i]	−13.9	−304.9658/−304.9946[i]	−18.1	−8.0/−11.1	53/50
18	138.7/134.0[i]	−4.7	−306.2419/−306.2556[i]	−8.6	−2.1/−5.0	50/55
19	259.3/251.4[i]	−7.9	−380.6729/−380.6888[i]	−10.0	+3.3/−1.2	48/45
20	270.0/262.2[i]	−7.8	−380.6627/−380.6755[i]	−8.0	−1.9/+3.3	49/61
21a[j]	182.2		−422.0950		−5.7	65
21b[j]	181.0		−499.0069		+0.3	66
21[j]	183.4		−575.9171		−2.2	71
22	175.4/162.2[k]	−13.2	−344.0594/344.0880[k]	−17.9	+0.3/−6.6	50/50

[a] Relative energy in kcal mol^{-1}. [b] Dihedral angle between the two termini of the allene. [c] Converges to **2** on optimisation. [d] Converges to **4** on optimisation. [e] B3LYP/6-31G(d) level. [f] Triplet state energy of neutral form 133.0 kcal mol^{-1}. [g] B3LYP/6-31G(d) values; RHF/6-31G(d) optimisation converges to a planar geometry. [h] Energy/NICS for 1,3,5,2,4-trithiadiazepine: −1378.1686/−9.3 at the RHF/6-31G(d) level. [i] Hückel/Möbius conformations. [j] **21a**, **21b** and **21** are the 12-π, 14-π and 16-π analogues of [10], [12] and [14]-trannulene. [k] C_2/C_3 conformations.

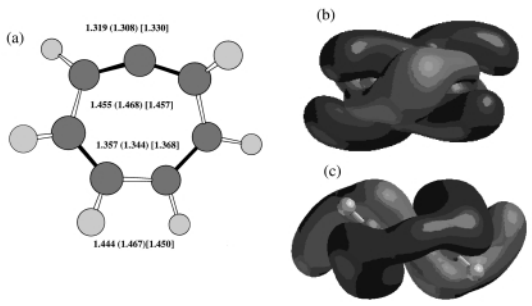

Fig. 2 Calculated geometry (a) (Å, AM1 (RHF-6-31G(d)) [B3LYP/6-31G(d)] and form of the AM1 HOMO (b) and HOMO − 1 (c) orbitals for **5**.

to in-plane trannulene like aromaticity.[12] The alkyne in **16** appears to act as a Möbius contributor, cooperating with the allene component to give a modestly aromatic 12π system. The isomers **19** and **20** also have two conformations. Hückel **19** as an 8 or 12π 4*n* antiaromatic has the expected positive NICS value, whilst C_2 symmetric **19** is slightly Möbius aromatic. Compared to **19**, isomers **20** show reversed NICS values (Table 1), and may be indicative of more complex topological contributions to the aromaticity. A single Möbius component inserted into *e.g.* [14]trannulene **21** appears much less aromatic than the trannulene itself (Table 1), but it does conform to a 4*n* rather than a 4*n* + 2 rule for aromaticity. Finally we note that C_2 symmetric **22** has three allene contributions and as a 12π system it would be expected to be Möbius aromatic. Two isomers were identified, one with C_2 and a lower energy and more aromatic form with C_3 symmetry in which all three allene units cooperate.

We conclude that a diverse range of Möbius 4*n* π aromatic systems can be constructed by using one or more twisted allene fragments as an initiator. The origins of the Möbius and Hückel contributions to the aromaticity and the nominal electron contributions (4*n* *vs.* 4*n* + 2) of these systems may be quite subtle. A dissection of these origins will be reported in a future article.

Notes and references

1 E. Heilbronner, *Tetrahedron Lett.*, 1964, **29**, 1923.
2 H. Jiao and P. v. R. Schleyer, *J. Phys. Org. Chem.*, 1998, **11**, 655.
3 M. Mauksch, V. Gogonea, H. Jiao and P. v. R. Schleyer, *Angew. Chem., Int. Ed.*, 1998, **37**, 2395.
4 S. Martín-Santamaría, B. Lavan and H. S. Rzepa, *J. Chem. Soc., Perkin Trans. 2*, DOI: 10.1039/b002082f.
5 Y. Xie, P. R. Schreiner, P. von R. Schleyer and H. F. Schaefer, *J. Am. Chem. Soc.*, 1997, **119**, 1370; see also: L. Türker, *J. Mol. Struct (THEOCHEM)*, 1998, **454**, 83 for Möbius forms of cyclacenes.
6 C. Mayor and W. M. J. Jones, *J. Org. Chem.*, 1978, **43**, 4498.
7 K. A. Abboud, Zheng Lu and W. M. Jones, *Acta Crystallogr., Sect. C*, 1992, **48**, 909.
8 I. Paterson, J. M. Goodman, M. A. Lister, R. C. Schumann, C. K. McClure and R. D. Norcross, *Tetrahedron*, 1990, **46**, 4663; I. Paterson, J. M. Goodman, M. A. Lister, R. C. Schumann, C. K. McClure and R. D. Norcross, *Tetrahedron*, 1991, **47**, 3471.
9 (*a*) E. V. Patterson and R. J. McMahon, *J. Org. Chem.*, 1997, **62**, 4398; (*b*) M. W. Wong and C. Wentrup, *J. Org. Chem.*, 1996, **61**, 7022; (*c*) P. R. Schreiner, W. L. Karney, P. v. R. Schleyer, W. T. Borden, T. P. Hamilton and H. F. Schaefer, *J. Org. Chem.*, 1996, **61**, 7030.
10 V. Gogonea, P von R. Schleyer and P. R. Schreiner, *Angew. Chem., Int. Ed.*, 1998, **37**, 1945.
11 C. W. Rees and J. R. J. Surtees, *J. Chem. Soc., Perkin Trans. 1*, 1991, **12**, 2945.
12 A. A. Fokin, H. Jiao and H. P. v. R. Schleyer, *J. Am. Chem. Soc.*, 1998, **120**, 9364.

Typeset and printed by Black Bear Press Limited, Cambridge, England

ChemComm
FEATURE ARTICLE

Molecular anatomy of RNA polymerase using protein-conjugated metal probes with nuclease and protease activities

Akira Ishihama

National Institute of Genetics, Department of Molecular Genetics, Mishima, Shizuoka 411-8540, Japan. E-mail: aishaham@lab.nig.ac.jp

Received (in Cambridge, UK) 20th October 1999, Accepted 2nd February 2000
Published on the Web 1st March 2000

Iron (*S*)-1-(*p*-bromoacetamidobenzyl)ethylenediaminetetraacetate (FeBABE) with the sequence-non-specific cleavage activity of nucleic acids and proteins was conjugated to protein Cys residues, and used for mapping the contact sites of both the α-subunit carboxy-terminal domain of *Escherichia coli* RNA polymerase on promoter UP elements and the σ^{70} and σ^{38} subunits on the respective promoters. The same chemical nuclease was also used as a chemical protease for mapping the subunit–subunit contact sites within the RNA polymerase. By using 2-iminothiolane as a linker, FeBABE could be conjugated to protein Lys residues and successfully used for mapping the contact surfaces of some *E. coli* transcription factors on the RNA polymerase holoenzyme.

Most of the biological reactions involved in transfer of genetic information such as replication, transcription and translation are carried out by macromolecular complexes consisting of a large number of proteins and nucleic acids. Regulation of these processes is mediated by rearrangements of protein–DNA, protein–RNA and protein–protein interactions. For instance, the transcription apparatus is composed of the DNA-dependent RNA polymerase, which consists of 4–5 (in the case of prokaryotes) to 12–18 subunits (in the case of eukaryotes), and hundreds of accessory transcription factors. Identification of the protein–DNA, protein–RNA and protein–protein contact networks within the transcription apparatus is crucial for understanding the molecular events carried out in transcription and its regulation. In order to meet the increasing demand for technical innovation for the molecular anatomy of these multi-component assemblies, a variety of new physical, chemical and genetic methods have been developed recently.

Akira Ishihama is Head of the Department of Molecular Genetics, National Institute of Genetics, Mishima, Japan. He obtained his PhD at Nagoya University in 1967, and subsequently worked with Jerard Hurwitz at the Albert Einstein College of Medicine, New York, on the structure–function relationship of bacterial RNA polymerase. He then returned to the Kyoto University Institute for Virus Research in 1970, and worked with the reconstitution of RNA polymerase. In Kyoto, he also began studying the molecular anatomy of viral RNA polymerases. In 1984, he moved to the National Institute of Genetics, and has contributed to the development of the novel research concerned with the molecular interaction between RNA polymerase and transcription factors. In Mishima, he also began studying the molecular anatomy of RNA polymerase II from the fission yeast. His current research interests include the functional modulation of RNA polymerases through protein–DNA, protein–RNA and protein–protein interactions.

Use of metals for cleavage of nucleic acids and proteins

Transition metals are known to catalyze a number of oxidative chemical reactions with deleterious effects in biological systems.[1–5] Iron promotes the formation of reactive radicals such as hydroxyl radicals, which indiscriminately damage all cellular components, even though iron is an indispensable element and the most abundant metal for living organisms. The high reactivities of iron have been put into practical use to explore the properties of macromolecular complexes.[6–11]

Initially free Fe^{2+} or FeEDTA was used to study the conformation of nucleic acids and their complexes.[12–18] The potential value of such reagents for protein mapping was first recognized by using untethered free FeEDTA, and a number of different approaches have been developed to use the metal complexes to map the overall surface of proteins.[19–21] Such methods are often called 'protein footprinting'. The broad specificity of hydroxyl radicals for attack at the backbones of nucleic acids and proteins permitted probing of nearly all the nucleotides and amino acids. FeEDTA complex offers the most general measure of surface accessibility, because its distribution around the target molecule is insensitive to charge, compared with free Fe^{2+}.[4]

The inception and development of methods for site-specific cleavage of nucleic acids and proteins with FeEDTA have led to development of artificial reagents with nucleolytic and proteolytic activities. Various attempts have been made to conjugate FeEDTA to proteins for monitoring of proximity mapping. For this purpose, bifunctional chelating agents were considered as linkers which possess both a strong metal-binding moiety and a group that binds to a biological molecule.[22] Applications of Cys-linked FeEDTA complexes have exploited oxidative chemistry to cut DNA[23] or RNA.[24,25] Most of these procedures are based on the high reactivity of H_2O_2 or O_2 and iron, which depends on the nature of the iron chelate involved.[4,26] For oxidative scission of nucleic acids, the generation of electrophilic species such as hydroxyl radicals is important.[14–16]

Likewise the artificial non-enzyme proteases have been developed in many laboratories.[27–29] It is essential that the protein cutting is only due to the tethered reagent and not to unchelated metal coordinated directly to sites on the protein. Protein-conjugated small metal chelates were shown to cleave polypeptide chains at sites determined by proximity to the chelates, apparently independent of the amino acid residues involved.[10,11,30] The net reaction involves hydrolysis, but not oxidation, of the peptide backbone. The peptide cleavage results from generation of a powerful nucleophile that selectively attacks peptide carbon rather than hydroxyl radicals.[31] The hydrolysis of protein backbones appears to be dominated by nucleophilic iron-peroxo complexes.[31] In the presence of H_2O_2

or O_2 and ascorbate, FeEDTA forms an intermediate oxygen-activated complex that leads to nucleophilic attack by oxygen on the carbonyl carbon of the peptide bond. The reactivities of nucleophiles, $HO–O^-$ and $CH_3O–O^-$, toward carboxylic esters are 100 times higher than hydroxide.

Development of chemical nucleases and proteases

A sulfhydryl-specific EDTA derivative, EDTA-2-aminoethyl 2-pyridyl disulfide (EPD) was developed to tether FeEDTA to protein Cys residues[32] and used for mapping the resolvase-binding site on DNA[23] and the binding sites of some RNA-binding proteins.[33] The newly developed method allowed the identification of regions or surfaces of proteins that are in close proximity to DNA or RNA, and of the portions of DNA or RNA that are closest to each EDTA-derivatized Cys, because the DNA cleavages are highly localized and their efficiency drops rapidly as a function of the distance between the Fe^{2+}EDTA complex and the DNA targets. EPD-Fe has also been applied for analysis of the protein–protein contact network within the non-native equilibrium protein folding intermediate.[32] Cys-linked FeEDTA chelates have since been used to study non-native conformation of Staphylococcal nuclease during folding of the protein.[14,32]

To avoid the need to add iron after conjugation of such metal-chelating reagents as EPD to target molecules, an iron-bound probe, iron (*S*)-1-(*p*-bromoacetamidobenzyl)ethylenediaminetetraacetate (FeBABE) was developed (Fig. 1),[29,34] which can

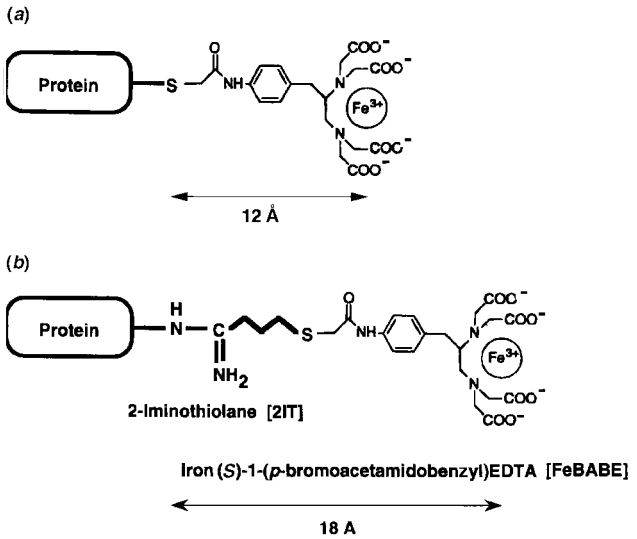

Fig. 1 Chemical probes with nuclease and protease activities. (*a*) Iron (*S*)-1-(*p*-bromoacetamidobenzyl)EDTA [FeBABE] can be conjugated to protein Cys residues.[29] (*b*) FeBABE in combination with 2-iminothiolane (2IT) can be conjugated to protein Lys residues.[53]

be handled in a manner analogous to many other protein-labeling reagents, such as fluorescent probes or cross-linkers. FeBABE can be tethered to proteins preferentially at Cys residues. Protein–FeBABE conjugates are formed under mild reaction conditions and are stable for long periods in the absence of activating reagents. Activation of the chelate iron is accomplished by a brief exposure, for instance for about 10 s, to H_2O_2 in the presence of ascorbate. This generates a highly reactive hydroxyl radical which induces cleavage of the backbones of DNA and RNA. In the presence of H_2O_2 and ascorbate, FeBABE forms an intermediate oxygen-activated complex which leads to nucleophilic attack by oxygen on the carbonyl carbon of the protein peptide bond and causes peptide hydrolysis.[31]

The chemistry of FeBABE was characterized by using proteins of known sequence or structure.[10,11,31] Since direct contact is required between FeBABE and the carbonyl carbon for protein cleavage to take place, the reaction is limited to peptide bonds that are within about 12 Å of the site of attachment of FeBABE (see Fig. 1). Because of this distance limitation and the required orientation for nucleophilic attack on the peptide carbon, it is expected that the number of cleaved sites will be relatively small. Using the human carbonic anhydrase as a model substrate, the efficiency of cleavage was estimated by measuring the cleaved fragments, as determined by the N-terminal sequences, to be 50–70%, indicating most of the cleavage was the hydrolysis of a peptide bond.[31] The high yield of products provides sufficient cleaved materials for sequence analysis. FeBABE is a powerful probe of protein structure, usable with relative ease in any system where Cys-linked reagents are applicable. The cleavage reaction is fast, highly selective, and proceeds in high yield under physiologial conditions. It forms hydrolytic products that are readily characterized by standard N-terminal sequencing of the resolved peptides. The results provide direct information on the proximity of the tethered probe to particular peptide bonds regardless of amino acid residue type, easily exceeding the scope and resolution of chemical cross-linking reagents.

Mapping of RNA polymerase contact sites on promoter DNA

FeBABE has been successfully used for the mapping of protein-bound sequences on DNA and RNA. In particular, a systematic search has been carried out in two cases: the RNA polymerase-contact sites on promoter DNA[35–39] and ribosomal protein-binding sites on rRNA.[40–44] The contact sites of proteins on DNA or RNA can be easily identified from the terminal sequences of fragments generated after cleavage with Fe-BABE.

The RNA polymerase core enzyme of *Escherichia coli* is composed of two α-subunits and one each of the β- and β′-subunits. The carboxy (C)-terminal domain (CTD; amino acid residues 234–329) of the RNA polymerase α-subunit plays a key role in molecular communications with class-I transcription factors and upstream (UP) elements of promoter DNA.[45,46] In order to identify possible differences in the functional roles of the two α-subunits, we established an *in vitro* reconstitution system of hybrid RNA polymerases containing two distinct α-subunit derivatives in a defined orientation.[35] In order to identify the binding sites of two αCTDs on the UP element DNA, a mutant α-subunit without a Cys residue was prepared, from which a number of α-derivatives with a single Cys residue at various positions along the CTD were constructed. After conjugation of FeBABE to the single-Cys mutant α-subunits, each was used, together with untethered wild-type α, for reconstitution of hybrid RNA polymerases containing one intact and one FeBABE-tethered mutant α-subunit. The reconstituted RNA polymerases were used for formation of promoter DNA complexes with or without a UP element, and the complexes were subjected to hydroxyl radical-based DNA cleavage mediated by FeBABE for identification of the contact DNA sequence of each αCTD. In the case of the P1 promoter of *E. coli* ribosomal RNA gene (*rrnB*) promoter, the two α-subunits were found to bind in tandem to two helix turns of the UP element, the β- and β′-associated α-subunits being bound to the promoter proximal and distal regions, respectively (Fig. 2).

The RNA polymerase σ-subunit is responsible for sequence recognition of DNA promoters, and in general bacteria contain multiple molecular species of the σ-subunit, each recognizing a specific set of promoter sequences. For instance, *E. coli* contains seven different σ-subunits.[47] The σ family proteins carry four regions of the conserved sequence. The contact-dependent DNA cleavage method was then applied for mapping spacial relations between the evolutionary conserved regions of various σ-subunits and each DNA strand along the respective promoter DNA. The library of single Cys mutants has been

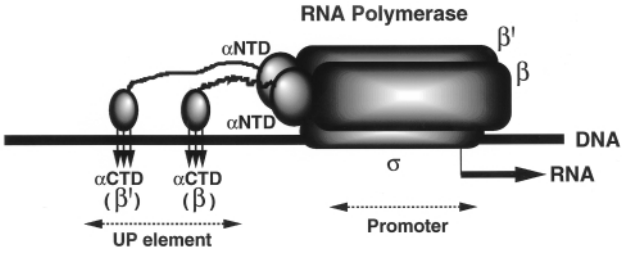

Fig. 2 Identification of the contact sites of RNA polymerase α-subunit on promoter UP element. FeBABE was conjugated at a single Cys residue (position 269) on the UP element contact surface of the α-subunit C-terminal domain (CTD). The reconstituted RNA polymerase holoenzyme containing the FeBABE-tethered α-subunits was used for mapping of the αCTD contact sites on the UP element of the *E. coli* ribosomal RNA (*rrnB*) gene, after sequencing the DNA cleavage sites by hydroxyl radical generated from the protein-tethered FeBABE upon addition of H_2O_2 and ascorbate.[35] The cleavage sites are shown by arrows.

constructed for σ^{70} (the σ major subunit for transcription of growth-related genes) and σ^{38} (the σ-subunit for stationary-phase genes). Results of the DNA cleavage mapping of open complexes using FeBABE-conjugated σ-subunits indicated that each conserved region of both σ^{70} and σ^{38} makes contact with different regions along the promoter DNA (Fig. 3).[37–39] The

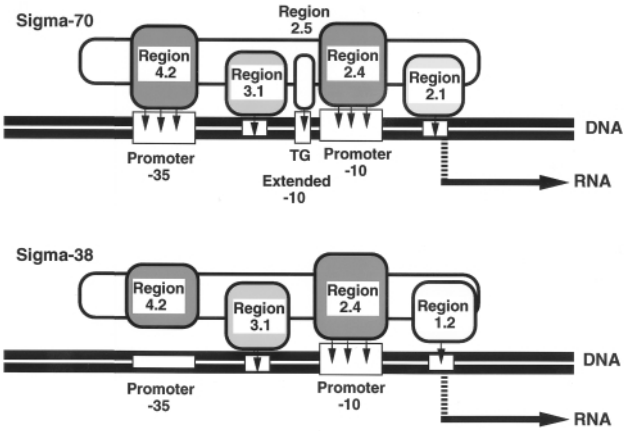

Fig. 3 Identification of the contact sites of RNA polymerase σ-subunits on promoters. FeBABE was conjugated at a single Cys residue located at various positions of single-Cys mutant σ^{70} and σ^{38} subunits of the *E. coli* RNA polymerase. The reconstituted RNA polymerase holoenzymes containing the FeBABE-tethered σ-subunits were used for mapping of the σ-subunit contact sites on the respective promoters, after sequencing the DNA cleavage sites by hydroxyl radical generated from the protein-tethered FeBABE upon addition of H_2O_2 and ascorbate.[37–39] The cleavage sites are shown by arrows. The σ family proteins contain four conserved regions. The regions 2, 3 and 4 are composed of 4, 2 and 2 subregions, respectively. In the case of the major σ^{70} subunit, the region 2.4 is involved in promoter -10 recognition while the region 4.2 recognizes the promoter -35 sequence.

results agreed well with the prediction from mutant studies of essential roles for two hexanucleotide sequences located at promoter -35 and -10. In addition, the determination of direct contact sites by the novel method revealed hitherto unidentified contacts involving sequences other than the -35 and -10 sequences. The comparison of promoter cleavage mapping by σ-conjugated FeBABE also revealed different modes of promoter DNA interaction between different σ-subunits.

Mapping of subunit-subunit contact sites within RNA polymerase

Proximity relationships between the two α-subunits of *E. coli* RNA polymerase were studied using a set of single Cys mutant α-subunits, each harboring a single Cys at various positions along the entire α polypeptide (Fig. 4). FeBABE conjugated to each of these Cys residues introduced both intramolecular and intermolecular cutting of the α-subunit in the presence of

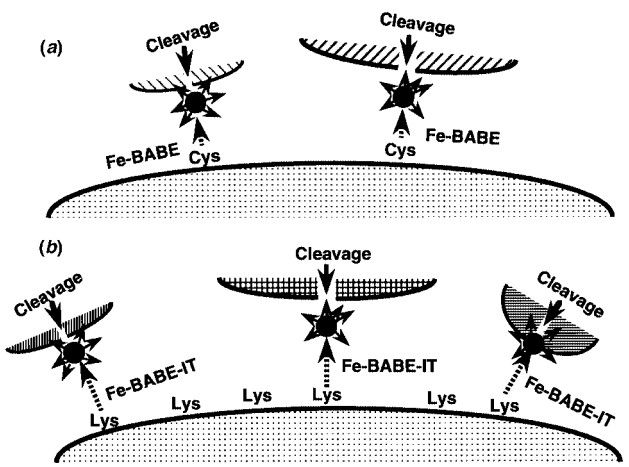

Fig. 4 Contact-dependent cleavage of proteins by the protein-conjugated FeBABE. (*a*) FeBABE can be conjugated to specific Cys residues of proteins (see Fig. 1). The polypeptide backbone of proteins, which are located near the protein-tethered FeBABE, is cleaved in the presence of ascorbate and H_2O_2. The protein–protein contact sites can be identified by tethering FeBABE at specific sites of the proteins using single Cys mutants. (*b*) FeBABE can also be conjugated to Lys residues using 2-iminothiolane (2-IT) as a linker (see Fig. 1). Lys is often involved in protein functions and exposed on protein surfaces. For mapping of protein–protein contact networks, mixtures of FeBABE-tethered proteins, each carrying a single FeBABE conjugation on average at one Lys residue, can be used for the peptide cleavage reaction after addition of H_2O_2 and ascorbate.

ascorbate and H_2O_2.[48] The intramolecular cutting was observed only within an individual N- or C-terminal domain, in agreement with the structural organization of α-subunits.[45,46] From the intermolecular cleavage mapping, the N-terminal assembly domains of two α-subunits were found to be assembled in an antiparallel fashion (Fig. 5).

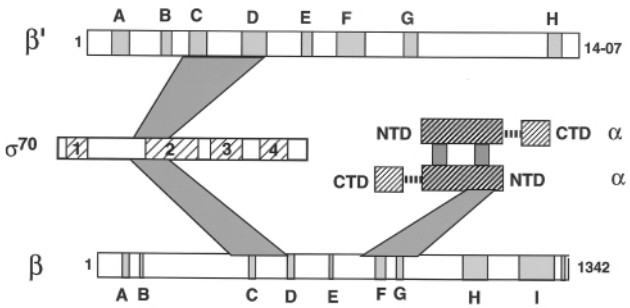

Fig. 5 Subunit–subunit contact sites within the RNA polymerase. FeBABE was conjugated at various positions of the α- or σ-subunits using collections of the respective single Cys mutant derivatives. The contact surfaces of these two small subunits on the two large subunits, β and β′, of the core enzyme were determined after identification of the contact-dependent cleavage sites by FeBABE in the presence of H_2O_2 and ascorbate.[48,49]

The RNA polymerase core enzyme acquires the promoter recognition activity by binding one of the σ-subunits. To characterize the proximity between the core enzyme and various σ-subunits, we analyzed the protein-cutting patterns produced by a set of covalently tethered FeEDTA probes positioned in or near all the four conserved regions. The protein cutting was identified at specific regions of both of the two large subunits, β and β′.[49,50] The σ-contact sites on the core enzyme are essentially the same between σ^{70} (or σ^{D}), the major σ-subunit for recognition of growth-related genes, and σ^{38} (σ^{S}) for recognition of the stationary phase-specific genes (Fig. 5). As proposed by Ghaim *et al.*,[51] Cys residues on the RNA polymerase fall into three categories: a small number of Cys residues are unreactive toward Fe-BABE, some are alkylated but produce no cleavage products upon treatment with ascorbate and peroxide, and some produce intra- and intersubunit cleavages.

The functional specificity of RNA polymerase holoenzymes (core σ-complexes) is further modulated by interaction with one or two of a total of 100–150 transcription factors.[47,52] The contact sites of these factors on RNA polymerase holoenzymes can also be monitored by using FeBABE tethered to each factor protein. For a large scale survey of the holoenzyme–transcription factor contact sites, a bifunctional linker probe, 2-iminothiolane (2-IT), was used for conjugation of FeBABE at Lys residues (see Fig. 1).[53] Transcription factors were conjugated with FeBABE at Lys residues, and the cutting sites of core enzyme subunits were successfully determined after mixing FeBABE-tethered transcription factors and holoenzyme followed by treatment with ascorbate and H_2O_2. The contact sites of σ^{70} and σ^{38} subunits on the β and β′ subunits determined using the newly developed method of a combination of 2IT and FeBABE were essentially the same as by direct conjugation of FeBABE to single Cys mutant σ-subnits. In addition to the σ family proteins, the contact sites have been determined for transcription elongation factors, NusA and GreA, and the RNA polymerase chaperon, owega.[51]

Protein-conjugated chemical probes with nucleolytic or proteolytic activities will be widely used for determining the molecular anatomy of multi-component complexes, in particular those involved in replication, transcription and translation.

The reagent FeBABE was developed in the laboratory of Claude F. Meares (University of California, Davis). The author thanks his many collaborators, whose names are listed in the references, for their contributions to this research. The work in the author's laboratory was financially supported by a Grant-in-Aid for Priority Project 'Biometals' (No. 08249103) from the Ministry of Education, Science, Culture and Sports of Japan, and the CREST (Core Research for Evolutional Science and Technology) fund of the Japan Science and Technology Corporation (JST.)

Notes and references

1 B. Halliwell and J. M. Gutteridge, *Biochem. J.*, 1984, **219**, 1.
2 S. D. Aust, L. A. Morehouse and C. E. Thomas, *Free Radical Biol. Med.*, 1985, **1**, 3.
3 T. P. Ryan and S. D. Aust, *Crit. Rev. Toxicol.*, 1992, **22**, 119.
4 S. Goldstein, D. Meyerstein and G. Czapski, *Free Radical Biol. Med.*, 1993, **15**, 435.
5 S. J. Stohs and D. Bagchi, *Free Radical Biol. Med.*, 1995, **18**, 321.
6 T. D. Tullius and B. A. Dombroski, *Proc. Natl. Acad. Sci. U.S.A.*, 1986, **83**, 5469.
7 C. B. Chen and D. S. Sigman, *Science*, 1987, **237**, 1197.
8 J. A. Latham and T. R. Cech, *Science*, 1989, **245**, 276.
9 J. C. Francois, T. Saison-Behmoaras, C. Barbier, M. Chassignol, N. T. Thuong and C. Helene, *Proc. Natl. Acad. Sci. U.S.A.*, 1989, **86**, 9702.
10 T. M. Rana and C. F. Meares, *J. Am. Chem. Soc.*, 1990, **112**, 2457.
11 T. M. Rana and C. F. Meares, *J. Am. Chem. Soc.*, 1991, **113**, 1859.
12 R. V. Prigodich and C. T. Martin, *Biochemistry*, 1990, **29**, 8017.
13 D. S. Sigman, *Biochemistry*, 1990, **29**, 9097.
14 D. W. Celander and T. R. Cech, *Science*, 1991, **251**, 401.
15 P. B. Dervan, *Methods Enzymol.*, 1992. **208**, 497.
16 M. A. Price and T. D. Tullius, *Methods Enzymol.*, 1992, **212**, 194.
17 M. Zhong and N. R. Kallenbach, *J. Biomol. Struct.*, 1994, **11**, 901.
18 T. Powers and H. F. Noller, *RNA*, 1995, **1**, 194.
19 E. Heyduk and T. Heyduk, *Biochemistry*, 1994, **33**, 9643.
20 R. Goldshleger and S. J. D. Karlish, *Proc. Natl. Acad. Sci., U.S.A.*, 1997, **94**, 9596.
21 H. Nagai and N. Shimamoto, *Genes Cells*, 1997, **2**, 725.
22 M. W. Sundberg, C. F. Meares, D. A. Goodwin and C. I. Diamanti, *Nature (London)*, 1974, **250**, 587.
23 J. M. Mazzarelli, M. R. Ermacora, R. O. Fox and N. D. Grindley, *Biochemistry*, 1993, **32**, 2979.
24 H. Han, A. Schepartz, M. Pellegrini and P. B. Dervan, *Biochemistry*, 1994, **33**, 9831.
25 G. M. Heilek, R. Marusak, C. F. Meares and H. F. Noller, *Proc. Natl. Acad. Sci. U.S.A.*, 1995, **92**, 1113.
26 D. A. Wink, R. W. Nims, J. E. Saavedra, W. E. Utermahlen and P. C. Ford, *Proc. Natl. Acad. Sci. U.S.A.*, 1994, **91**, 6604.
27 L. H. DeRiemer, C. F. Meares, D. A. Goodwin and C. I. Diamanti, *J. Labelled Compd. Radiopharm.*, 1981, **18**, 1517.
28 M. M. Haywartd, J. C. Adrian, Jr. and A. Schepartz, *J. Org. Chem.*, 1995, **60**, 3924.
29 D. P. Greiner, K. A. Hughes, A. H. Gunasekera and C. F. Meares, *Proc. Natl. Acad. Sci., U.S.A.*, 1996, **93**, 71.
30 M. R. Ermacora, D. W. Ledman and R. O. Fox, *Nat. Struct. Biol.*, 1996, **3**, 59.
31 T. M. Rana and C. F. Meares, *Proc. Natl. Acad. Sci. U.S.A.*, 1991, **88**, 10 578.
32 M. R. Ermacora, J. M. Delfino, B. Cuenoud, A. Schepartz and R. O. Fox, *Proc. Natl. Acad. Sci. U.S.A.*, 1992, **89**, 6383.
33 K. B. Hall and R. O. Fox, *Methods Mol. Biol.*, 1999, **18**, 78.
34 J. K. Moran, D. P. Greiner and C. F. Meares, *Bioconjugate Chem.*, 1995, **6**, 296.
35 K. Murakami, M. Kimura, J. T. Owens, C. F. Meares and A. Ishihama, *Proc. Natl. Acad. Sci. U.S.A.*, 1997, **94**, 1709.
36 K. Murakami, J. T. Owens, T. A. Belyaeva, C. F. Meares, S. J. W. Busby and A. Ishihama, *Proc. Natl. Acad. Sci. U.S.A.*, 1997, **94**, 11 274.
37 J. T. Owens, K. Murakami, A. Chmura, N. Fujita, A. Ishihama and C. F. Meares, *Biochemistry*, 1998, **37**, 7670.
38 F. Colland, N. Fujita, D. Kotlarz, J. A. Bown, C. F. Meares, A. Ishihama and A. Kolb, *EMBO J.*, 1999, **18**, 4049.
39 J. A. Bown, J. T. Owens, C. F. Meares, N. Fujita, A. Ishihama, S. J. Busby and S. D. Minchin, *J. Biol. Chem.*, 1999, **274**, 2263.
40 G. M. Heilek and H. F. Noller, *Science*, 1996, **272**, 1659.
41 G. M. Culver and H. F. Noller, *RNA*, 1998, **4**, 1471.
42 K. R. Lieberman and H. F. Noller, *J. Mol. Biol.*, 1998, **284**, 1367.
43 G. M. Culver, G. M. Heilek and H. F. Noller, *J. Mol. Biol.*, 1999, **286**, 355.
44 L. Holmberg and H. F. Noller, *J. Mol. Biol.*, 1999, **289**, 223.
45 A. Ishihama, *Mol. Microbiol.*, 1992, **6**, 3283.
46 A. Ishihama, *J. Bacteriol.*, 1993, **175**, 2483.
47 A. Ishihama, *Nucleic Acids & Molecular Biology, Vol. 11, Mechanism of Transcription*, 1997, ed. F. Eckstein and D. M. J. Lilley, Springer-Verlag, Heidelberg, pp. 53–70.
48 R. Miyake, K. Murakami, J. T. Owens, D. P. Greiner, O. N. Ozoline, A. Ishihama and C. F. Meares, *Biochemistry*, 1998, **37**, 1344.
49 J. T. Owens, R. Miyake, K. Murakami, N. Fujita, A. J. Chmura, A. Ishihama and C. F. Meares, *Proc. Natl. Acad. Sci. U.S.A.*, 1998, **95**, 6021.
50 F. Colland, N. Fujita, D. Kotlarz, A. Ishihama and A. Kolb, submitted for publication.
51 J. B. Ghaim, D. P. Greiner, C. F. Meares and R. B. Gennis, *Biochemistry*, 1995, **34**, 11311.
52 A. Ishihama, *Genes Cells*, 1999, **3**, 135.
53 S. L. Traviglia, S. A. Datwyler, D. Yan, A. Ishihama and C. F. Meares, *Biochemistry*, 1999, **38**, 15774.

ChemComm

An alternative to interpenetration whereby nets with large windows may achieve satisfactory space filling

Stuart R. Batten,[ab] Bernard F. Hoskins,[a] Boujemaa Moubaraki,[b] Keith S. Murray[b] and Richard Robson*[a]

[a] *School of Chemistry, University of Melbourne, Parkville, Victoria 3052, Australia. E-mail: r.robson@chemistry.unimelb.edu.au*

[b] *Department of Chemistry, Monash University, Clayton, Victoria 3800, Australia*

Received (in Cambridge, UK) 20th March 2000, Accepted 8th May 2000
Published on the Web 8th June 2000

A coordination polymer in which copper acetate dimers are bridged by 3-connecting tpt ligands reveals an alternative means to interpenetration whereby frameworks with very large holes may achieve efficient space filling, namely, by forming π–π associations between tpt units of sheets *X* and *X* + 2 inside the holes of sheet *X* + 1.

The promise of ultimately being able to generate by deliberate design new solid materials with useful tailor-made properties provides much of the driving force for the present interest in coordination polymers. An outstanding feature of many coordination polymers is the presence of a number of independent networks which participate in mutual interpenetration, whereby favourable non-bonded interactions can be maximised and more efficient 3D packing achieved.[1] In a very loose and general sense it can be said that the larger the windows in a 2D or 3D net the more likely is interpenetration to occur and the larger is the number of independent nets passing through a particular window likely to be. The coordination polymer we describe below which consists of hexagonal grid (6,3) sheets is unusual in that interpenetration does not occur despite the fact that the hexagonal holes within the sheets are much larger than those present in numerous other (6,3) sheet systems which do participate in interpenetration.[1] The system we describe reveals an alternative means to interpenetration whereby a network with large holes can maximise favourable non-bonded interactions and achieve efficient space filling.

The vast majority of coordination polymers so far investigated have involved single metal centres linked together in a variety of ways by bridging ligands. Relatively little work has focussed on 2D and 3D networks in which bridging ligands link together metal clusters[2] with their interesting electronic, magnetic and catalytic properties. The copper acetate dimer, which we make use of here, is one of the simplest imaginable cluster species with the potential to provide an effectively linear link between donors; indeed, a number of 1D polymeric chains are known.[3] In order to generate 2D and 3D coordination polymers it is obvious that bridging ligands providing the nodes for the network will be required to have connectivity three or higher. We know of only two examples in which metal acetate dimers are connected into 2D or 3D networks.[4,5]

We report here the 2D (6,3) sheet polymer formed when copper acetate dimer units are linked together by the μ_3 bridging ligand 2,4,6-tri(4-pyridyl)-1,3,5-triazine, tpt, which has previously been shown to afford a number of high symmetry 3D coordination polymers.[6] Reaction of $Cu_2(O_2CCH_3)_4(H_2O)_2$ in methanol with tpt in benzyl alcohol yields green crystals of composition $[\{Cu_2(O_2CCH_3)_4\}_3(tpt)_2]\cdot 2MeOH$ (**1**),† whose structure was determined by single crystal X-ray diffraction.‡

Giant hexagonal grid sheets are present, a ring from which is shown in Fig. 1. As can be seen, the tpt units provide the 3-connecting nodes of the net and copper acetate dimers link node to node, the separation between which is *ca.* 18 Å. This generates very large holes.

The way in which efficient 3D packing is achieved without resort to interpenetration is most simply understood by considering the hypothetical stacking of idealised planar (6,3) nets in a manner which parallels that observed in the less regular real system. Any pair of neighbouring sheets are arranged in this idealised situation with half the nodes of one vertically above or below the mid-points of the hexagonal holes of the other, the remaining nodes of both sheets being located vertically above and below each other. By stacking the sheets in this manner to generate the ABCABC... sequence shown in Fig. 2(*a*) all nodes become equivalent (a real example of this arrangement is β rhombohedral graphite). As can be seen in Fig. 2(*a*) three types of columns of nodes perpendicular to the sheets are thereby generated. One type contains nodes from A sheets and B sheets but not from C sheets, which contribute only holes to these particular columns. If we refer to these columns as A/B columns, equal numbers of equivalent A/C and B/C columns are also present. One such column, the central one, is highlighted by the dashed line in Fig. 2(*a*). If the separation between sheets is *d*, the spacings between nodes in any one of the columns follows the sequence *d*, 2*d*, *d*, 2*d*, *d*, 2*d*... as can be seen in Fig. 2(*a*).

By making each of the initially planar trigonal nodes pyramidal in the appropriate direction and to the appropriate degree it is possible to contract each of the 2*d* separations within columns to *d*, as represented in Fig. 2(*b*). The individual sheets thereby acquire an undulating character and the overall structure becomes much more compact, the volume being reduced in the idealised case by close to one third. Pyramidalisation of the 3-connecting nodes allows new attractive node-to-node con-

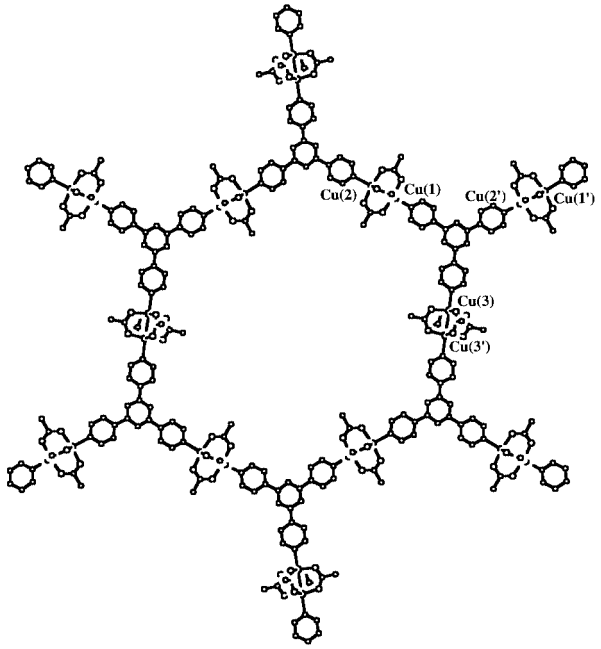

Fig. 1 A single hexagonal window in the (6,3) sheets of **1**. The ring 'diagonals' are *ca.* 34–37 Å.

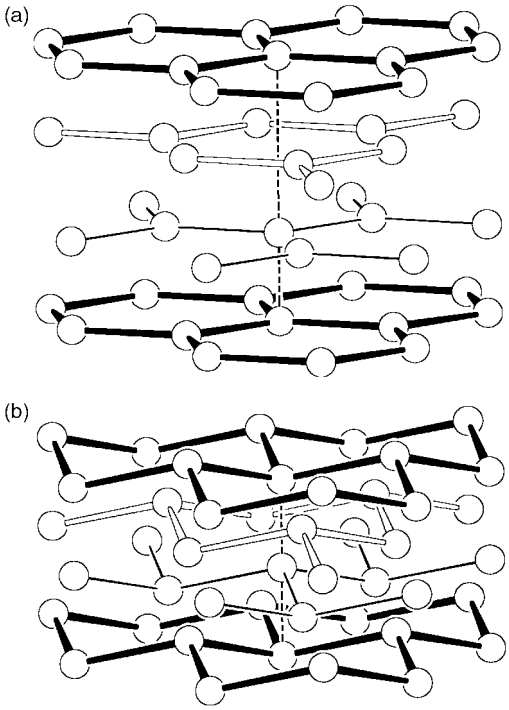

Fig. 2 (*a*) Four idealised planar (6,3) sheets stacked in the ABCA... pattern. (*b*) Hypothetical 'pyramidalisation' of the 3-connecting nodes that were planar in (*a*).

tacts to be made, which, it is interesting to note, involve nodes belonging to sheets that are not immediate neighbours. In effect the holes in any sheet are occupied by nodes belonging to the sheets on each side that come together to make favourable contact with each other around the centre of the hole. This can be easily seen by noting the effect of converting planar nodes in Fig. 2(*a*) to pyramidal nodes in Fig. 2(*b*) whereby the contact, highlighted by the dashed line, between the central node of the upmost sheet and the central node of the sheet depicted with thin bonds becomes shortened from 2*d* to *d*; this contact can be seen to be made through the ring of the intermediate sheet (shown with open bonds).

The 3D arrangement is a deformed version of the idealised structure shown in Fig. 2(*b*). The 3-connecting nodes in this real case are tpt units which remain internally approximately planar despite the fact they constitute pyramidal centres in the sense that lines drawn between triazine centroids make angles significantly less than 120°. The bending required to produce this pyramidalisation occurs mainly not within tpt units but between them; the most pronounced bending is seen at Cu(2) which is located 0.503 Å out of the plane of the coordinated pyridine ring. The node-to-node contacts indicated by a vertical dashed line in the idealised situation shown in Fig. 2(*b*), in the real system are π–π stacks of tpt units. Not only are the individual sheets distorted from hexagonal regularity but the columns are no longer perpendicular to the sheets; in addition the centres of the tpt triazine rings in the columns do not fall on a straight line nor are the average tpt planes perpendicular to the direction of the column. An outstanding feature of some highly symmetrical coordination polymers of tpt reported earlier[6] has been the appearance of tight pairs of tpt units with their triazine rings in close face-to-face π contact, one rotated 60° relative to the other around a 3-fold axis passing through the mid-points of both rings and perpendicular to them; these are examples of Piedfort pairs.[7] In the present structure there appears to be a dominant, structure-determining driving force for each tpt unit to become π-associated not with a single partner but with one on each side to generate an extended π stack. The closest non-hydrogen contacts between tpt units in the columns are not triazine-to-triazine but rather triazine-to-pyridine and the high symmetry of the Piedfort pairs is lost. The closest atom-to-atom contact on one side of a tpt unit to a tpt unit of an adjacent sheet is 3.327 Å, whilst on the other side the closest contact of 3.352 Å is to a tpt unit two sheets removed.

The methanol of solvation is hydrogen bonded to a particular one of the acetate units in the Cu(1)··Cu(2) dimer (O··O, 2.876 Å).

The variation of magnetic susceptibility of **1** with temperature is very much like that of the antiferromagnetically coupled parent complex $Cu_2(O_2CCH_3)_4(H_2O)_2$. Fitting of the data to the Bleaney–Bowers equation[8] for an isolated Cu^{II} dimer yielded parameter values $g = 2.0$, $J = -153$ cm^{-1}, $N\alpha = 60 \times 10^{-6}$ cm^3 mol^{-1}, fraction monomer = 0.02 (*cf.* $Cu_2(O_2CCH_3)_4(H_2O)_2$ $J = -148$ cm^{-1}). Thus there are negligible or very weak dimer–dimer interactions propagated by the tpt group. Related linear chains linked by pyrazines behave similarly.[9]

In conclusion, the structure reported here reveals an alternative means to interpenetration whereby large holes in the individual 2D sheets may be satisfactorily occupied by tpt nodes from the sheets on opposite sides which are attracted together to form π–π associations inside the hole.

Notes and references

† A buffer layer of benzyl alcohol (5 ml) was carefully layered over a solution of tpt (25 mg, 0.080 mmol) in benzyl alcohol (10 ml), and a layer of $Cu(O_2CCH_3)_2{\cdot}H_2O$ (38 mg, 0.19 mmol) in methanol (10 ml) was carefully placed on top of the buffer layer. Green crystalline **1** formed after 3 days (23 mg, 0.013 mmol, 41%). (Found: C, 41.44; H, 3.29; N, 9.79. Calc for $Cu_6C_{62}H_{68}N_{12}O_{26}$: C, 41.47; H, 3.89; N, 9.52%).

‡ *Crystal data* for **1**: $Cu_6C_{62}H_{68}N_{12}O_{26}$, M = 1778.52, green plate, crystal dimensions 0.03 × 0.1 × 0.17 mm, monoclinic, $P2_1/n$ (no. 14), a = 7.976(1), b = 30.996(5), c = 15.559(2) Å, β = 104.47(1)°, U = 3724.5(9) Å^3, T = 150 K, Z = 2, $\mu(Cu_{K\alpha})$ = 2.60 mm^{-1}, 8827 reflections collected, 7634 unique (R_{int} = 0.0618), 4340 observed ($I > 2\sigma(I)$), 482 parameters, R_1 = 0.0739 ($I > 2\sigma(I)$), wR_2 = 0.1952 (all data), S = 1.020. CCDC reference number 182/1631. See http://www.rsc.org/suppdata/cc/b0/b002193h/ for crystallographic files in .cif format.

1 S. R. Batten and R. Robson, *Angew. Chem., Int. Ed.*, 1998, **37**, 1460.
2 (*a*) N. G. Naumov, A. V. Virovets, M. N. Sokolov, S. B. Artemkina and V. E. Fedorov, *Angew. Chem., Int. Ed.*, 1998, **37**, 1943; (*b*) Y. V. Mironov, A. V. Virovets, S. B. Artemkina and V. E. Fedorov, *Angew. Chem., Int. Ed.*, 1998, **37**, 2507; (*c*) D. Hagrman, C. Sangregorio, C. J. O'Connor and J. Zubieta, *J. Chem. Soc., Dalton Trans.*, 1998, 3707; (*d*) M. P. Shores, L. G. Beauvais and J. R. Long, *J. Am. Chem. Soc.*, 1999, **121**, 775; (*e*) M. P. Shores, L. G. Beauvis and J. R. Long, *Inorg. Chem.*, 1999, **38**, 1648; (*f*) S. B. Copp, K. T. Holman, J. O. S. Sangster, S. Subramanian and M. J. Zaworotko, *J. Chem. Soc., Dalton Trans.*, 1995, 2233.
3 (*a*) B. Morosin, R. C. Hughes and Z. G. Soos, *Acta Crystallogr., Sect. B*, 1975, **31**, 762; (*b*) J. Pickardt, *Acta Crystallogr., Sect. B*, 1981, **37**, 1753; (*c*) V. M. Rao, D. N. Sathyanarayana and H. Manohar, *J. Chem. Soc., Dalton Trans.*, 1983, 2167.
4 F. A. Cotton and Y. Kim, *J. Am. Chem. Soc.*, 1993, **115**, 8511.
5 J. Lu, W. T. A. Harrison and A. J. Jacobson, *Chem. Commun.*, 1996, 399.
6 (*a*) B. F. Abrahams, S. R. Batten, H. Hamit, B. F. Hoskins and R. Robson, *Chem. Commun.*, 1996, 1313; *Angew. Chem., Int. Ed. Engl.*, 1996, **35**, 1690; (*b*) S. R. Batten, B. F. Hoskins and R. Robson, *J. Am. Chem. Soc.*, 1995, **117**, 5385; *Angew. Chem., Int. Ed. Engl.*, 1995, **34**, 820; (*c*) B. F. Abrahams, S. R. Batten, M. J. Grannas, H. Hamit, B. F. Hoskins and R. Robson, *Angew. Chem., Int. Ed.*, 1999, **38**, 1475.
7 A. S. Jessiman, D. D. MacNicol, P. R. Mallinson and I. Vallance, *J. Chem. Soc., Chem. Commun.*, 1990, 1619.
8 B. Bleaney and K. D. Bowers, *Proc. Roy. Soc. Ser A*, 1952, **214**, 451.
9 R. Nukada, W. Mori, S. Takamizawa, M. Mikuriya, M. Handa and H. Naono, *Chem. Lett.*, 1999, 367.

ChemComm

Nucleophilic addition reactions of bridged triene η⁶-chromiumtricarbonyl complexes

Rohan E. J. Beckwith,[a] Alexander J. Blake,[a] Michael B. Gravestock,[b] Nigel S. Simpkins*[a] and Claire Wilson[a]

[a] *School of Chemistry, The University of Nottingham, University Park, Nottingham, UK NG7 2RD. E-mail: nigel.simpkins@nottingham.ac.uk*

[b] *AstraZeneca, Mereside, Alderley Park, Macclesfield, Cheshire, UK SK10 4TG*

Received (in Cambridge, UK) 21st March 2000, Accepted 17th May 2000
Published on the Web 8th June 2000

Bridged triene η⁶-chromiumtricarbonyl complexes have been shown to undergo regioselective addition reactions with a range of nucleophiles including organolithium reagents and enolates.

Formation of the corresponding η⁶-chromiumtricarbonyl complex provides a versatile method for enabling nucleophilic addition to aromatic compounds, and can result in the formation of substituted aromatic complexes or non-aromatic products.[1] Less well known are the corresponding seven-membered complexes derived from tropone, cycloheptatriene, and related heterocyclic systems.[2] These compounds have been demonstrated to undergo formal cycloaddition reactions with either alkynes or 1,3-dienes, *e.g.* eqn. (1)[2c,3]

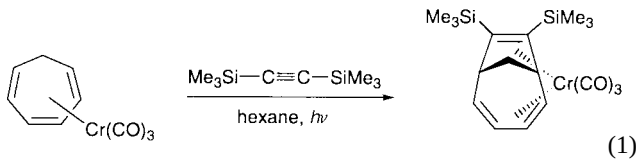

(1)

1 **2**

Cycloheptatriene complex **1** undergoes efficient cycloaddition with bistrimethylsilylacetylene to give the bridged product complex **2** in good yield.† It seemed to us that the type of activation towards nucleophilic substitution seen in the arene complexes might also be operative in triene complexes such as **2**, although, as far as we are aware, this mode of reactivity has not been demonstrated.[4] Here we describe the first examples of additions to such complexes, which occur in a highly regioselective fashion with a range of nucleophiles.

The readily available bis-silylated complex **2** was used for the majority of our initial studies, and also because the vinyl silane functionality in the products could be synthetically useful. Addition of a number of nucleophiles to a solution of **2** in THF at −78 °C, followed by protic work-up, resulted in the formation of the metal-free adducts **3** and/or **4** as shown in Table 1.‡

The complex reacted with several varied alkyllithiums, dimethylcyanocuprate, the lithium enolates derived from ethyl acetate or *N*,*N*-dimethylacetamide, two examples of lithiated nitriles and a lithiated sulfone.§ In every case the initial addition reaction appears to be highly regioselective for the terminus of the complexed diene, whereas the position of subsequent protonation appears to be highly dependent upon the nature of the group being introduced. In most cases the presumed intermediate anionic dienyl complex undergoes protonation distal to the entering substituent, to give exclusively or mainly isomer **3**, whereas in a few cases the alternative isomer **4** predominates.

Although the proposed structures accorded with our expectations, and were supported by high field NMR data, we were concerned by the variable ratios of the two products formed and could not entirely rule out the possibility that the isomers formed were alternative regio- or stereoisomers. Fortunately we were able to obtain X-ray crystal structure determinations of certain derivatives, including the nitrile **3** (R = CH_2CN) and the sulfone **4** (R = CH_2SO_2Ph), which are illustrated in Fig. 1 and 2, respectively.¶

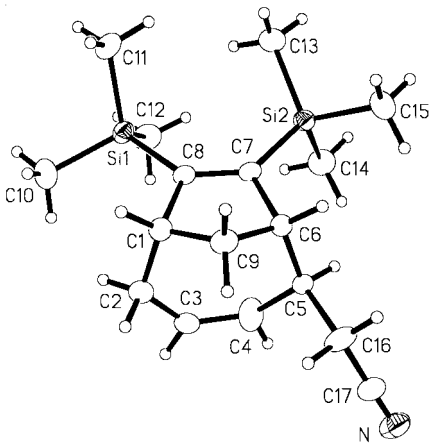

Fig. 1 Crystal structure of nitrile adduct **3** (R = CH_2CN).

Table 1 Nucleophilic addition to complex **2**

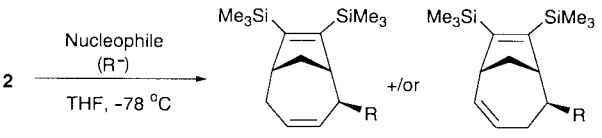

3 **4**

Nucleophile (R⁻)	MeLi	Me_2Cu-$(CN)Li_2$	^{n}BuLi	PhLi	LiC-$(OEt)=CH_2$	CH_2=C-(OLi)OEt	CH_2=C-$(OLi)NMe_2$	$LiCH_2CN$	LiC-$(CH_3)_2CN$	$LiCH_2$-SO_2Ph
Yield (%)	55	30	34	61	84	53	82	50	83	58
3:**4**	7:1	1.3:1	**3**[a]	**3**[a]	**3**[a]	1:2	5:1	5:1	**3**[a]	1:5

[a] Only isomer **3** detected by ^{1}H NMR of crude product.

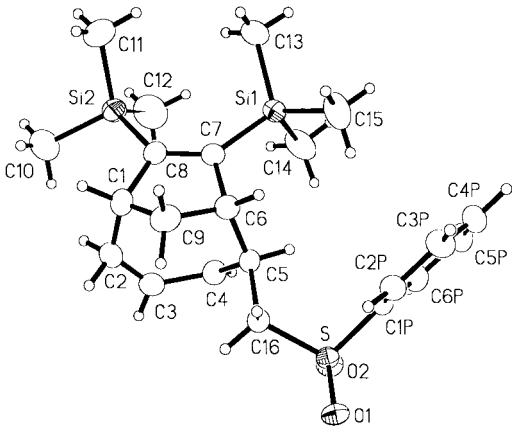

Fig. 2 Crystal structure of sulfone adduct **4** (R = CH_2SO_2Ph).

These two structures confirm that the initial nucleophilic addition to **2** is indeed highly regioselective for the diene terminus, and also that the new substituent is *exo*-orientated in the bridged product. The structures also confirm the contrasting alkene regiochemistry assigned by NMR, but at present we have no convincing explanation for the isomer ratios seen with the different nucleophiles.

It was of interest to briefly examine the transformations possible with these types of product, for example the alkenyl ether product **3** could be converted into the α,β-unsaturated ketone **5** on treatment with dilute acid, eqn. (2).

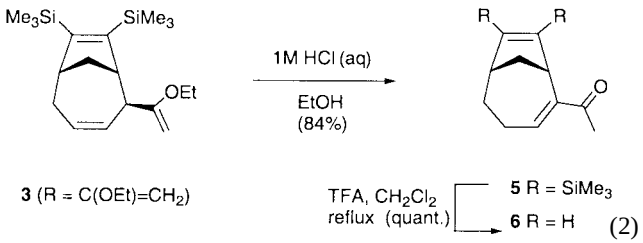

(2)

Treatment of this product under more vigorous acidic conditions (TFA, CH_2Cl_2, reflux) resulted in complete desilylation to give enone **6**. This type of desilylation was also shown to be possible on an alternative type of adduct, compound **3** (R = Ph), on reaction under the same conditions, to give product diene **7**.

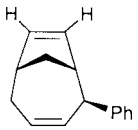

7

In conclusion, we have demonstrated for the first time that efficient nucleophilic addition to bridged chromium complexes is possible. In the near future we hope to extend the chemistry to heterocyclic complexes, which could lead to a novel synthesis of the alkaloid anatoxin-a, and to provide further details of the scope and limitations of the chemistry.‖

We would like to thank the Engineering and Physical Sciences Research Council (EPSRC) and AstraZeneca for support of R. E. J. B. We also acknowledge EPSRC for funding for a diffractometer.

Notes and references

† We obtained a yield of 69%, with even higher yields being possible (80%) according to ref. 3(*b*).

‡ *Typical experimental procedure*: A solution of the appropriate nucleophile in THF was added dropwise to a stirred solution of the bridged triene chromium complex (usually **2**) in THF at −78 °C. The resultant solution was stirred at this temperature until reaction appeared complete by TLC (typically 1 h), and then saturated NH_4Cl(aq) solution was added and the mixture warmed to room temperature prior to extraction with Et_2O (3 × 5 ml). The combined organic extracts were back washed with water, brine, dried ($MgSO_4$) and concentrated *in vacuo*. Flash chromatography on silica gel afforded the addition adducts **3**/**4** as indicated in Table 1.

§ Nucleophiles which did not give clean reactions include the lithium enolate from acetophenone, PhMgCl, and the lithiated derivatives from benzylcyanide, 1,3-dithiane, methoxy methyl ether, *N*-boc-pyrrolidine and 2,3-dihydrofuran. It is unclear why some of these reactions failed, whereas closely related reactions indicated in Table 1 were successful. We have not so far been successful in quenching the intermediate anion with carbon electrophiles.

¶ For both **3** and **4** a crystal was encapsulated in a film of RS3000 perfluoropolyether oil and mounted on a glass fibre before transfer to the diffractometer.

Crystal data for **3**: $C_{17}H_{29}NSi_2$, M = 303.59, monoclinic, a = 11.370(2), b = 16.982(4), c = 19.115(4) Å, β = 103.657(4), U = 3587(2) Å^3, T = 150(2) K, space group $P2_1/c$ (no 14), Z = 8, D_c = 1.125 g cm^{-3}, μ(Mo-Kα) = 0.190 mm^{-1}, 8422 unique reflections measured and used in all calculations. Final R_1 [4937 $F \geqslant 4\sigma(F)$] = 0.0484 and wR (all F^2) was 0.125. For **4**: $C_{22}H_{34}O_2SSi_2$, M = 418.73, triclinic, a = 6.8685(12), b = 9.314(2), c = 19.746(4) Å, α = 102.190(3), β = 95.424(3), γ = 98.875(3), U = 1209.3(6) Å^3, T = 150(2) K, space group $P\bar{1}$ (no. 2), Z = 2, D_c = 1.150 g cm^{-3}, μ(Mo-Kα) = 0.247 mm^{-1}, 4685 unique reflections measured and used in all calculations. Final R_1 [$F \geqslant 4\sigma(F)$] = 0.0510 and wR (all F^2) was 0.148. CCDC 182/1642. See http://www.rsc.org/suppdata/cc/b0/b002256j/ for crystallographic files in .cif format.

‖ One result employing the complex derived from diphenylacetylene indicated that the same type of nuclophilic addition process is possible.

1 (*a*) For a review, see M. F. Semmelhack, in *Comprehensive Organometallic Chemistry II*, ed. E. W. Abel, F. G. A. Stone, G. Wilkinson and L. S. Hegedus, Pergamon, Oxford, 1995, vol. 12, p. 979; (*b*) E. P. Kundig, A. F. Cunningham, P. Paglia and D. P. Simmons, *Helv. Chim. Acta*, 1990, **73**, 386; (*c*) E. P. Kundig, M. Inage and G. Bernadinelli, *Organometallics*, 1991, **10**, 2921.

2 (*a*) C. A. L. Mahaffy and P. L. Pauson, *Inorg. Synth.*, 1979, **19**, 154; (*b*) C. G. Kreiter and S. Z. Ozkar, *Z. Naturforsch., Teil B*, 1977, **32**, 408; (*c*) J. H. Rigby, H. S. Ateeq, N. R. Charles, S. V. Cuisiat, M. D. Ferguson, J. A. Henshilwood, A. C. Krueger, C. O. Ogbu, K. M. Short and M. T. Heeg, *J. Am. Chem. Soc.*, 1993, **115**, 1382.

3 (*a*) I. Fischler, F.-W. Grevels, J. Leitich and S. Ozkar, *Chem. Ber.*, 1991, **124**, 2857; (*b*) K. Chaffee, P. Huo, J. B. Sheridan, A. Barbieri, A. Aistars, R. A. Lalancette, R. L. Ostrander and A. L. Rheingold, *J. Am. Chem. Soc.*, 1995, **117**, 1900.

4 For related additions to iron complexes, see: W. A. Donaldson, in *Comprehensive Organometallic Chemistry II*, ed. E. W. Abel, F. G. A. Stone, G. Wilkinson and L. S. Hegedus, Pergamon, Oxford, 1995, vol. 12, p. 623; for additions to cycloheptatriene complexes, see: M.-C. P. Yeh and C.-N. Chuang, *J. Chem. Soc., Chem. Commun.*, 1994, 703; W. Chen, J. B. Sheridan, M. L. Coté and R. A. Lalancette, *Organometallics*, 1996, **15**, 2700.

Isolation and structural determination of two derivatives of the elusive carbamic acid†

Michele Aresta,[a] Danielle Ballivet-Tkatchenko,[b] Daniela Belli Dell'Amico,[c] Michel C. Bonnet,[d] Daniele Boschi,[c] Fausto Calderazzo,*[c] René Faure,[d] Luca Labella[c] and Fabio Marchetti[e]

[a] *Dipartimento di Chimica, Campus Universitario, Università di Bari, I-70126 Bari, Italy*
[b] *Institut de Recherches sur la Catalyse-CNRS, 2 av. Einstein, F-69626 Villeurbanne, France*
[c] *Dipartimento di Chimica e Chimica Industriale Università di Pisa, Via Risorgimento 35, I-56126 Pisa, Italy. E-mail: facal@dcci.unipi.it*
[d] *Laboratoire de Chimie Analytique 2, Université Claude Bernard, 43 bd du 11 novembre 1918, F-69622-Villeurbanne cédex, France*
[e] *Dipartimento di Ingegneria Chimica, dei Materiali, delle Materie Prime e Metallurgia Università degli Studi 'La Sapienza', via del Castro Laurenziano 7, I-00185 Roma, Italy*

Received (in Oxford, UK) 28th March 2000, Accepted 18th April 2000
Published on the Web 8th June 2000

The dibenzyl-substituted carbamic acid $(PhCH_2)_2NC(O)OH$ (1), its deprotonation product $[(PhCH_2)_2NH_2][(PhCH_2)_2NCO_2]$ (2) and $CoCl(NO)_2[PhP(OCH_2CH_2)_2N$-$C(O)OH]\cdot 2MeCOMe$(3·2MeCOMe) are reported, the diffractometric study showing the carbamic acids 1 and 3 to be paired through hydrogen bonds.

Carbamic acids $R_2NC(O)OH$ (R = alkyl, aryl) have been until now elusive compounds, even for primary amines,[1] owing to their tendency to undergo decarbonation[2] under reduced pressure of carbon dioxide [eqn. (1)] or deprotonation in the presence of amine [eqn. (2)]. Carbamic acid itself, $H_2NC(O)OH$, has not been isolated so far although it has been detected by IR at low temperature,[2] and some of its properties have been calculated theoretically.[3,4]

$$R_2NH + CO_2 \rightleftarrows R_2NC(O)OH \quad (1)$$

$$R_2NC(O)OH + R_2NH \rightleftarrows [R_2NH_2][R_2NCO_2] \quad (2)$$

Thus, although *N*-substituted carbamic species are believed to be key intermediates in biological carbonations,[5] and in the photosynthetic carbon cycle promoted by Rubisco (ribulose 1,5-biphosphate carboxylase),[6] no simple member of this class has been isolated and no crystal data are available. This paper covers this gap.

Secondary amines R_2NH (R = Bu^n, Pr^i, *c*-C_6H_{11}) as neat liquids were reacted with CO_2 at atmospheric pressure over reaction times of several hours up to constant volume, gas volumetric measurements showing the CO_2/R_2NH molar ratio to be close to 0.5, namely 0.56 (Bu^n, 9.6 °C), 0.44 (Pr^i, 19.3 °C) and 0.53 (*c*-C_6H_{11}, 24.9 °C). Accordingly, the corresponding dialkylammonium dialkylcarbamate is the predominant product of the reaction. By contrast, for R = $PhCH_2$, a $CO_2/(PhCH_2)_2NH$ molar ratio close to 1 was observed at 10.3 °C, showing the preferential formation of *N*,*N*-dibenzylcarbamic acid $(PhCH_2)_2NC(O)OH$ **1**. By operating in heptane at *ca.* 9 °C, the carbonation, monitored by gas volumetry, corresponded to the complete conversion to **1**. Well formed crystals of **1** were obtained from heptane (*vide infra*).

The carbonation of dibenzylamine was monitored by IR in a PCTFE medium. When dibenzylamine was submitted to a CO_2 atmosphere at room temperature, the spectrum corresponded to the formation of **2**. Cooling the PCTFE mull at *ca.* 5 °C under CO_2 led to the almost exclusive formation of **1** after several hours. The process can be reversed by increasing the temperature and/or reducing the partial pressure of CO_2. The ν(CO) band of the carbamic function at 1640 cm^{-1} suggests the presence of intermolecular hydrogen bonds, in substantial agreement with theoretical calculations and spectroscopic data at low temperature[2–4] for the NH_3/CO_2 system.

When the carbonation of dibenzylamine was conducted with a CO_2/amine molar ratio not exceeding 0.5, **2** was obtained.‡ The corresponding IR spectrum shows bands centred at 1530, 1432, 1410, 1330 and 1316 cm^{-1}. The 1530 cm^{-1} band is assigned to ν_{as}(CO) of the O_2CN moiety, which compares well with those at 1525 and at 1550 cm^{-1} for $[NH_4]O_2CNH_2]$[9] (thin film, −190 °C), and $[Me_2NH_2][O_2CNMe_2]$ (neat liquid), respectively.[10]

The structure of **1** consists of two crystallographically independent molecules‡ (Fig. 1), whose main bond distances and angles are listed in the figure legend. In agreement with earlier theoretical studies,[3] the molecule does not crystallize as its zwitterionic form. The adopted conformation meets the requirement of maintaining the bulky benzyl groups relatively far from the $–CO_2H$ function. The main difference between the two molecules is in the torsion angles N(1)–C(9)–C(10)–C(11) and N(2)–C(24)–C(25)–C(26) differing by 34°. Within the same molecule, the C–O bond distances differ by 0.08 or 0.06 Å, the longer distance being connected with the oxygen carrying the hydrogen. The carbamate moieties are substantially

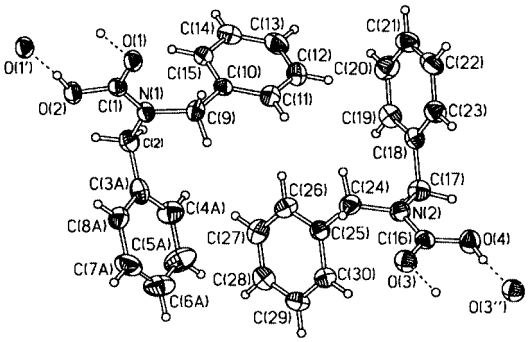

Fig. 1 The asymmetric unit of **1**. Thermal ellipsoids are at 50% probability. The hydrogen-bonded pairs are represented, together with the most populated positions of the disordered C(3)–C(8) ring. Relevant bond distances (Å) and angles (°). N(1)–C(2) 1.461(3), N(1)–C(9) 1.464(2), N(1)–C(1) 1.345(3), C(1)–O(1) 1.246(3), C(1)–O(2) 1.321(3), O(2)···O(1′) 2.556(2), N(2)–C(17) 1.465(3), N(2)–C(24) 1.468(3), N(2)–C(16) 1.340(3), C(16)–O(3) 1.254(3), C(16)–O(4) 1.315(3), O(3)···O(4″) 2.590(3); C(1)–N(1)–C(2) 123.5(2), C(1)–N(1)–C(9) 119.1(2), C(2)–N(1)–C(9) 117.5(2), O(1)–C(1)–N(1) 122.1(2), O(2)–C(1)–N(1) 115.1(2), O(1)–C(1)–O(2) 122.8(2), C(16)–N(2)–C(17) 123.1(2), C(16)–N(2)–C(24) 119.7(2), C(17)–N(2)–C(24) 116.8(2), O(3)–C(16)–N(2) 121.4(2), O(4)–C(16)–N(2) 115.8(2), O(3)–C(16)–O(4) 122.8(2). ′ = 3/2 − *x*, −1.2 − *y*, 1 − *z*; ″ = 2 − *x*, −*y*, 2 − *z*.

† Dedicated to Professor Heinrich Vahrenkamp on the occasion of his 60th birthday anniversary in recognition of his outstanding contributions to inorganic chemistry.

DOI: 10.1039/b002479l

planar (maximum deviation from planarity 0.07 Å). The N(1)–C(1) and N(2)–C(16) bond distances of 1.345 and 1.340 Å to the –C(O)OH function are substantially identical to the distance of 1.34 Å indicated by *ab initio* calculations.[3]

As in carboxylic acids, each molecule is connected through two end-on hydrogen bonds, which are shown in Fig. 1, in pairs related by an inversion centre.

Single crystals of **3** were obtained from an acetone solution of $CoCl(NO)_2[PhP(OCH_2CH_2)_2NH]$[11] upon carbonation at atmospheric pressure at −30 °C. The carbamic acid fragment‡ is paired through two end-on hydrogen bonds, similarly to **1**. The intermolecular O···O bond distance of 2.580 Å implies the existence of hydrogen atoms in between. The N–C(O)OH fragments in **1** and **3** do not differ significantly in bond distances and angles and, as expected, the C–O bonds are not equivalent.

Computational studies on the decomposition of ammonium carbamate[3,4] favour carbamic acid $H_2NC(O)OH$ as the intermediate, and its zwitterionic form as the transition state. The isolation of carbamic acids **1** and **3**, in the present study, shows for the first time that, under carbon dioxide at *atmospheric* pressure, carbonation of the secondary amine to the corresponding carbamic acid can be in fact a thermodynamically favourable process provided the appropriate substituents and reaction conditions are chosen, probably a determining factor in the stabilisation of the system being the hydrogen-bond network in the solid state, as previously observed in $Ag(O_3SOH)$.[12] The dialkylammonium carbamate may further slowly undergo carbonation to the acid or be kinetically or thermodynamically stabilized as such, depending on the nature of the group R. The zwitterionic form of the acid, $\{R_2NH^+CO_2^-\}$, may be a kinetically relevant intermediate undergoing fast deprotonation in the presence of amine.

The present findings are believed to be relevant, *inter alia*, to the problem of carbon dioxide fixation by amino groups in biopolymers in the solid state.[13]

We wish to thank the Ministero dell'Università e della Ricerca Scientifica e Tecnologica (MURST), Programmi di Ricerca Scientifica di Rilevante Interesse Nazionale (Cofinanziamento 1998–9), and the Centre National de la Recherche Scientifique for financial support.

Notes and references

‡ *Crystallography*: reflection intensities were collected on a Siemens P4 diffractometer for **1** and **2**, and on a Nonius CAD-4 diffractometer for **3**, both equipped with graphite-monochromatized Mo-Kα radiation (λ = 0.71073 Å). All data were collected in the ω–2θ scan mode.

Crystal data: for **2** at 173(2) K: $C_{29}H_{30}N_2O_2$; colourless monoclinic prisms. Cell parameters: a = 15.339(1), b = 8.850(1), c = 18.402(2) Å, β = 101.68(1)°, V = 5057.8(14) Å^3, Z = 4, D_c = 1.192 Mg m^{-3}, μ(Mo-Kα) = 0.084 mm^{-1}, space group $P2_1/n$ (no. 14), 3575 intensities collected between θ = 2.26 and 24.0° in the range $-17 \leqslant h \leqslant 0$, $0 \leqslant k \leqslant 8$, $-20 \leqslant l \leqslant 21$, and corrected for Lorentz and polarization effects; after merging (R_{int} = 0.0215), 3438 independent reflections; structure solved by direct methods (SIR92),[7] and refined (SHELXTL).[8] The nitrogen-bonded hydrogen atoms of the cation were located in the difference Fourier map, and were not refined; the other hydrogen positions were allowed to ride on the corresponding carbon atoms, obtaining R_1 [$I > 2\sigma(I)$] = 0.0447 and wR_2 = 0.1039 (298 parameters, without restraints).

For **1** at 173(2) K: $C_{15}H_{15}NO_2$; colourless needle-like prisms. Cell dimensions: a = 39.397(7), b = 5.545(1), c = 24.783(3) Å, β = 110.90(1)°, V = 2443.7(4) Å^3; monoclinic crystal, Z = 16, D_c = 1.267 Mg m^{-3}, μ(Mo-Kα) = 0.075 mm^{-1}, space group $C2/c$ (no. 15) or Cc, 4675 intensities collected between θ = 2.21 and 24.0° in the range $-44 \leqslant h \leqslant 1$, $-5 \leqslant k \leqslant 1$, $-26 \leqslant l \leqslant 28$, and corrected for Lorentz and polarization effects; after merging ($R_{int} = [\Sigma|F_o^2 - F_o^2(\text{mean})|/\Sigma(F_o^2)]$ = 0.0260), 3557 independent reflections; structure solved in the centrosymmetric space group (SIR92),[7] and refined (SHELXTL).[8] The abnormally large thermal ellipsoids of the aromatic ring suggested the presence of local rotational disorder. Two different phenyl rings of fixed geometry and rotated by slightly different angles around the C(2)–C(3) bond were then introduced in the same position, by fixing to unity the total occupancy of the site. The hydrogen within the C(O)OH group was located on the difference Fourier map and introduced in the calculations without refining; the other hydrogen atoms were introduced in calculated positions and allowed to ride on the corresponding carbon atoms. The final refinement cycles (353 parameters, no restraints) gave the reliability factors R_1 [$I > 2\sigma(I)$] = 0.0411 and wR_2 = 0.1012 (all data).

For **3** at 243(2) K: $C_{17}H_{26}ClCoN_3O_8P$; dark-brown prisms. Cell parameters: a = 9.612(2), b = 11.936(3), c = 12.371(4) Å, α = 73.34(2), β = 69.94(2), γ = 66.18(2)°, V = 1201.4(6) Å^3, Z = 2, D_c = 1.453 Mg m^{-3}, μ(Mo-Kα) = 0.937 mm^{-1}, triclinic, space group $P\bar{1}$ (no. 2), 3918 independent observed intensities collected between θ = 1.89 and 30.0° in the range $-12 \leqslant h \leqslant 13$, $-16 \leqslant k \leqslant 16$, $0 \leqslant l \leqslant 10$, and corrected for Lorentz, polarization effects and absorption (ψ-scan method); structure solution by direct methods and refined (SHELXTL).[8] The asymmetric unit turned out to contain two acetone molecules, one of them being affected by some orientational disorder. The hydrogen atoms were introduced in calculated positions and allowed to ride on the connected atoms. The final refinement cycles with anisotropic thermal factors for heavy atoms and isotropic ones for hydrogen atoms (280 parameters, no restraints) gave R_1 [$I > 2\sigma(I)$] = 0.0915 and wR_2 = 0.1321.

CCDC 182/1613. See http://www.rsc.org/suppdata/cc/b0/b002479l/ for crystallographic files in .cif format.

1 M. Aresta and E. Quaranta, *Tetrahedron*, 1992, **48**, 1515.
2 R. K. Khanna and M. H. Moore, *Spectrochim. Acta, Part A*, 1999, **55**, 961.
3 N. Wen and M. H. Brooker, *J. Phys. Chem.*, 1995, **98**, 359.
4 M. Remko and B. M. Rode, *J. Mol. Struct. (THEOCHEM)*, 1995, **339**, 125.
5 A. S. Midvan, D. C. Fry and E. H. Serpesu, in *Enzymatic and Model Carboxylations and Reactions for Carbon Dioxide Utilization*, ed. M. Aresta and J. V. Schloss, Kluwer, Dordrecht, 1990, p. 211.
6 W. W. Cleland, T. J. Andrews, S. Gutteridge, F. C. Hartman and G. H. Lorimer, *Chem. Rev.*, 1998, **98**, 549.
7 A. Altomare, G. Cascarano, C. Giacovazzo, A. Guagliardi, M. C. Burla, G. Polidori and M. Camalli, *J. Appl. Crystallogr.*, 1994, **27**, 435.
8 G. M. Sheldrick, SHELXTL-PLUS, Report 5.03, Siemens Analytical X-Ray Instruments Inc., Madison, WI, USA, 1994.
9 D. L. Frasco, *J. Chem. Phys.*, 1964, **41**, 2134.
10 W. Schroth, H. D. Schädler and J. Andersch, *Z. Chem.*, 1989, **29**, 129.
11 M. Aresta, D. Ballivet-Tkatchenko, M. C. Bonnet, R. Faure and H. Loiseleur, *J. Am. Chem. Soc.*, 1985, **107**, 2994.
12 D. Belli Dell' Amico, F. Calderazzo, F. Marchetti and S. Merlino, *Chem. Mater.*, 1998, **10**, 524.
13 V. Schimming, C.-G. Hoelger, G. Buntkowsky, I. Sack, J.-H. Fuhrhop, S. Rocchetti and H.-H. Limbach, *J. Am. Chem. Soc.*, 1999, **121**, 4892.

Cyclodextrin–fullerenes: a new class of water-soluble fullerenes

Shashadhar Samal and Kurt E. Geckeler*

Laboratory of Applied Macromolecular Chemistry, Department of Materials Science and Engineering, Kwangju Institute of Science and Technology, 1 Oryong-dong, Puk-gu, Kwangju 500-712, South Korea.
E-Mail: keg@kjist.ac.kr

Received (in Cambridge, UK) 24th January 2000, Accepted 9th May 2000
Published on the Web 8th June 2000

Solubilization of fullerenes in water by nucleophilic addition of cyclodextrin-R-monoamines to C_{60}, where R represents iminoalkyl and iminoaryl residues, is reported and studies involving the host–guest characteristics, free radical scavenging and DNA-cleaving properties indicate that this class of compounds has potential for a number of biological and medical applications.

Fullerenes are extraordinarily susceptible to attack by a variety of chemical reagents.[1] They exhibit high reactivity towards multiple addition of organic free radicals[2] and have been demonstrated to cleave DNA in the presence of light.[3] It has been reported recently that certain mutagenic and carcinogenic properties, and a number of neurodegenerative diseases, are associated with free radicals.[4] Hence, water-soluble fullerene compounds are suitable for potential biomedical applications. Previous approaches to the preparation of water-soluble fullerenes,[5] such as inclusion complexation with cyclodextrin or cyclodextrin prepolymers, multi-hydroxylation, 1,3-dipolar cycloaddition, nucleophilic cyclopropanation, polymer embedding *etc.*, are characterized by significant alteration of the fullerene molecule by modification. Our approach involves covalent binding of fullerenes with cyclodextrins (CD) leading to high water solubility and biocompatibility.

Nucleophilic additions of primary and secondary amines are known reactions and have been investigated for functionalization of the fullerene cage.[6] Preparation of fullerenylated aminopolymers has also been reported.[7] Synthesis of the fullerene–cyclodextrin conjugate (**4**) (Scheme 1)† was achieved by adding small volumes of a cyclodextrin monoamine (**3**) solution to a C_{60} solution at intervals of six hours, until about 30% of the fullerene remained unreacted.[7] The CD-amine–fullerene was purified by subsequent membrane filtration.[8] Separation from any higher derivatives was achieved by using membranes with a molar mass cut-off (MMCO) of 2000 g mol^{-1} and low-molecular weight components, if any, by membrane of MMCO of 1000 g mol^{-1}. FT-IR spectra of a model compound [60]fullerene-deoxy-6-(1,4-diiminophenyl)-β-cyclodextrin (**4a**) display the distinct features of the fullerene component. The UV–Vis spectrum (Fig. 1) shows considerable peak broadening beyond 350 nm for **4a**. Several authors have ascribed this behavior to aggregation of the molecules in water, confirmed further from dynamic light scattering studies.[5f,g] The ^{13}C NMR spectrum showed resonances due to the fullerene carbons at *ca.* 140 ppm.

To rule out the possibility of a competitive host–guest complexation reaction typical of cyclodextrins,[9] we synthesized the β-CD-1,4-diaminobenzene host–guest complex and characterized the material by various spectral techniques. Though the IR of both the inclusion complex and the covalently bonded CD-diamine (**3a**) did not show any significant differences, there were typical distinguishing patterns in the UV–Vis, ^1H NMR, TGA, and DSC data.

Cyclodextrin cage compounds have been demonstrated to be useful for several medical applications involving the host–guest complexation strategy and controlled release of the guest drug molecule.[10] In order to prove that the CD ring is still available for formation of inclusion complexes, we used *p*-nitrophenol (PNP) as a model molecule. The reaction between **4a** and PNP was monitored and compared with the reaction between β-CD and PNP by recording the change in the UV–Vis absorption pattern. It was seen that, with time, the peak at 405 nm gradually

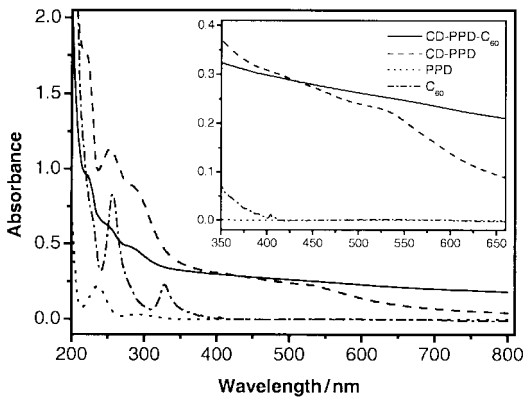

Fig. 1 UV–Vis spectra of C_{60} in hexane and *p*-phenylenediamine (PPD), mono-6-deoxy-6-(1,4-diiminodiphenyl)-β-cyclodextrin (CD-PPD), and [60]fullerene-deoxy-6-(1,4-diiminodiphenyl)-β-cyclodextrin (CD-PPD-C_{60}, **4a**) in water.

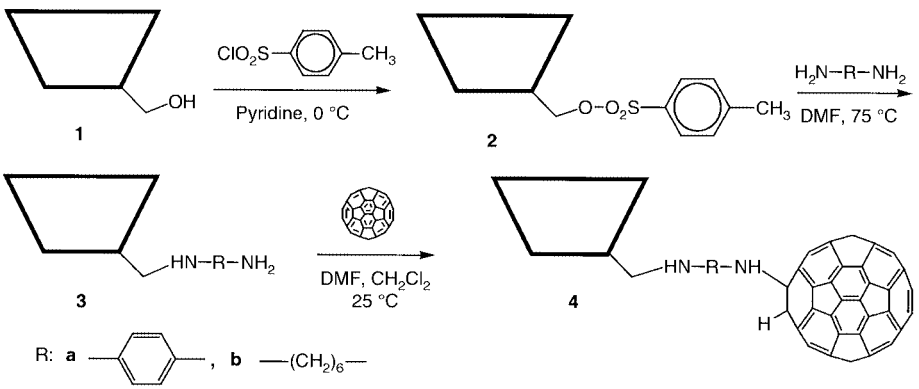

Scheme 1 Synthesis of fullerene–cyclodextrin conjugates.

increased in intensity for both the **4a**–PNP and β-CD–PNP experiments, whereas this absorption for PNP alone was not significant. The molar ratios **4a**:β-CD:PNP for **4a**–PNP and β-CD–PNP inclusion experiments were 1:2:8. It was observed that the rate of increase in the absorption intensity for β-CD–PNP complexation was nearly twice than that for the **4a**–PNP reaction, which means that the CD ring in **4a** is as active as that in free CD molecules.

It is known that C_{60} readily adds simple alkyl and aryl radicals[2] and undergoes radical polyreactions.[11] The stable free radical 1,1-diphenyl-2-picrylhydrazyl (DPPH) has been used to study the antioxidant activities of phenols and catechol.[12] We utilized this radical for the reaction with **4a** in ethanolic solution and monitored the absorbance at 517 nm. The reaction proceeded with a gradual decrease of absorbance at 517 nm, with a visual bleaching of the pink color of the radical solution, indicating that **4a** is an effective radical scavenger.

The interaction potential of fullerenes with biological molecules has been recently recognized, especially their ability to cleave DNA nucleotides[3b,c] *via* a singlet oxygen transfer at the guanosine base sequence.[3d] We conducted a screening experiment in which a sample of DNA oligonucleotide, which was purified by membrane filtration prior to use, was treated with **4a** in aqueous media. The UV–Vis spectrum of the solution mixture shows two peaks, one at 260 nm, characteristic of the DNA component, and another broad absorption with a maximum at 343 nm due to the fullerene compound. It was observed that the fullerene peak intensity gradually decreased, indicating that there had been a reaction with the DNA in which **4a** was gradually consumed. There was no noticeable decrease in the intensity of the DNA peak.

Upon diafiltration of the fullerene compound–DNA solution mixture (20 mL) through the membrane (MMCO 10 000 g l^{-1}, used for purification of crude DNA) with 800 mL water (filtration factor, $Z = 40$), the amount of DNA in the permeates sharply decreased and only a very small quantity of the DNA component was left in the retentate. This was ascertained from a rapid decrease in the characteristic DNA absorbance at 260 nm in the permeates. The molar mass of the DNA in these samples was measured by GPC. It was found that almost the entirity of the DNA had undergone cleavage, leaving behind no high molecular mass species.

We are grateful to KOFST and K-JIST, Korea, for partial financial support and to B. J. Choi and S. J. Choi for technical assistance.

Notes and references

† General procedure for synthesis of [60]fullerene-β-cyclodextrin conjugate (**4**): Amine **3** (0.02 mmol) dissolved in 10 mL DMF was added in small portions, keeping a gap of 6 h between each addition, to the fullerene (C_{60}) (14 mg, 0.02 mmol) dissolved in 100 mL methylene chloride, until 30% of the theoretical amount of fullerene remained unreacted. The mixture was stirred at 25 °C under N_2 (3–10 d), after which the organic solvent was removed. Then 200 mL water was added, the insoluble black residue filtered off and the filtrate freeze-dried. The crude sample was purified further by membrane filtration (details in the text). The yield and solubility of the fullerene–cyclodextrin conjugates varied, representing the characteristics of the amine component and the macrocycles, respectively.

1 F. Diederich and C. Thilgen, *Science*, 1996, **271**, 317; F. Wudl, *Acc. Chem. Res.*, 1992, **25**, 157; *ACS Symp. Ser. 481*, ed. G. S. Hammond and V. J. Kuck, American Chemical Society, Washington, DC, 1992; R. Taylor and D. R. M. Walton, *Nature*, 1993, **363**, 685; K. E. Geckeler, *Trends Polym. Sci.*, 1994, **2**, 355; A. Hirsch, *Synthesis*, 1995, 895; *Fullerene Chemistry, Tetrahedron Symposia-in-Print Number 60*, ed. A. B. Smith III, 1996; K. E. Geckeler and S. Samal, *Polym. Int.*, 1999, **48**, 743.

2 P. J. Krusic, E. Wasserman, P. N. Keizer, J. R. Morton and K. F. Preston, *Science*, 1991, **254**, 1183.

3 (*a*) Y. N. Yamakoshi, T. Yagami, S. Sueyoshi and N. Miyata, *J. Org. Chem.*, 1996, **61**, 7236; (*b*) E. Nakamura, H. Tokuyama, S. Yamago, T. Shiraki and Y. Sugiura, *Bull. Chem. Soc. Jpn.*, 1996, **69**, 2143; (*c*) I. Atsushi, H. Tsukasa, K. Masaru, S. Hikaru and S. Seiji, *Chem. Commun.*, 1999, 1403; (*d*) N. Higashi, T. Inoue and M. Niwa, *Chem. Commun.*, 1997, 1507.

4 C. E. Beyer, J. D. Steketee and D. Saphire, *Biochem. Pharm.*, 1998, **56**, 1265.

5 (*a*) J. P. Mittal, *Pure Appl. Chem.*, 1995, **67**, 103; (*b*) K. I. Priyadarsini, H. Mohan and J. P. Mittal, *Fullerene Sci. Technol.*, 1995, **3**, 479; (*c*) T. Andersson, K. Nilsson, M. Sundahl, G. Westman and O. Wennerstrom, *J. Chem. Soc. Chem. Commun.*, 1992, 604; (*d*) H.-C. Hu, Y. Liu, D.-D. Zhang and L.-F. Wang, *J. Inclusion Phenom. Macromol. Chem.*, 1999, **33**, 295; (*e*) L. Y. Chiang, J. B. Bhonsle, L. Wang, S. F. Shu, T. M. Chang and J. R. Hwu, *Tetrahedron*, 1996, **52**, 4963; (*f*) T. Da Ros, M. Prato, F. Novello, M. Maggini and E. Banfi, *J. Org. Chem.*, 1996, **61**, 9070; (*g*) M. Brettreich and A. Hirsch, *Tetrahedron Lett.*, 1998, **39**, 2731.

6 A. Hirsch, Q. Li and F. Wudl, *Angew. Chem., Int. Ed. Engl.*, 1991, **30**, 1309; K. E. Geckeler and N. Arsalani, *Fullerene Sci. Technol.*, 1997, **5**, 127.

7 K. E. Geckeler and A. Hirsch, *J. Am. Chem. Soc.*, 1993, **115**, 3850; A. O. Patil, G. W. Schriver, B. Cartensen and R. Lundberg, *Polym. Bull.*, 1994, **30**, 187.

8 K. E. Geckeler, in *Bioanalytical and Biochemical Laboratory Methods*, (German), ed. K. E. Geckeler and H. Eckstein, Vieweg, Wiesbaden, Germany, 1998, ch. 1.6.

9 M. L. Bender and M. Komiyama, *Cyclodextrin Chemistry*, Springer, Berlin, 1978; *Cyclodextrin Technology*, ed. J. Szejtli, Kluwer Academic Publishers, London, 1988; *Comprehensive Supramolecular Chemistry, Vol. 3, Cyclodextrins*, Ex. ed. J. L. Atwood, J. E. D. Davies, D. D. Macnicol and F. Vogtle, vol. ed. J. Szejtli and T. Osa, Elsevier, New York, 1996.

10 L. Szente and J. Szejtli, *Adv. Drug Delivery Rev.*, 1999, **36**, 17.

11 K. E. Geckeler and N. Arsalani, *Fullerene Sci. Technol.*, 1996, **4**, 897; W. T. Ford, T. D. Graham and T. H. Mourey, *Macromolecules*, 1997, **30**, 6422.

12 L. R. C. Barclay, C. E. Edwards and M. R. Vinqvist, *J. Am. Chem. Soc.*, 1999, **121**, 6226.

ChemComm

Preparation of highly active NiW hydrotreating model catalysts with 1,2-cyclohexanediamine-*N*,*N*,*N*′*N*′-tetraacetic acid (CyDTA) as a chelating agent

G. Kishan, L. Coulier, V. H. J. de Beer, J. A. R. van Veen and J. W. Niemantsverdriet*

Schuit Institute of Catalysis, Eindhoven University of Technology, 5600 MB Eindhoven, The Netherlands. E-mail: j.w.niemantsverdriet@tue.nl

Received (in Oxford, UK) 25th April 2000, Accepted 16th May 2000
Published on the Web 8th June 2000

Changing the order in which oxidic W and Ni convert to sulfides by adding 1,2-cyclohexanediamine-*N*,*N*,*N*′,*N*′-tetraacetic acid (CyDTA) as a chelating agent for nickel in the preparation of NiWS–SiO_2 catalysts is the key ingredient in obtaining a high activity for thiophene hydrodesulfurization.

Stringent future legislation for low-sulfur diesel fuel places increasingly higher demands on the performance of hydrotreating catalysts.[1,2] Supported sulfides of molybdenum or tungsten promoted with nickel or cobalt are widely applied to this end.[2] In the preparation, sulfidation of the oxidic precursors in a mixture of H_2S–H_2 or in the sulfur-containing hydrocarbon feed is an essential step. The sulfidation of supported MoO_3 and oxidic CoMo and NiMo catalysts has received considerable attention.[3–10] The generally accepted view is that in order to obtain active CoMoS and NiMoS catalysts, sulfidation of molybdenum should precede that of cobalt and nickel, such that the reactive edges of the MoS_2 slabs can serve as anchoring sites for the promoter atoms.[8–10] Chelating agents such as nitrilotriacetic acid (NTA)[9,10] and ethylenediaminetetraacetic acid (EDTA)[4,5] assist in stabilizing nickel and cobalt, such that their conversion to sulfides is retarded with respect to molybdenum.

Much less is known about tungsten sulfidation. Tungsten oxide is more difficult to convert to sulfides than molybdenum.[3,11] Shimizu *et al.*[12] report that chelating agents improve the activity of NiW–Al_2O_3 catalysts in hydrodesulfurization of benzothiophene and hydrogenation of *o*-xylene. The origin of the promotional effect is not clear, however.

Our purpose is to demonstrate that addition of 1,2-cyclohexanediamine-*N*,*N*,*N*′,*N*′-tetraacetic acid (CyDTA) as a chelating agent for Ni in the preparation of NiWS–SiO_2 catalysts leads to a 2.3-fold increase in thiophene hydrodesulfurization activity, as compared to a standard NiWS–SiO_2 catalyst. We correlate the catalytic activity with the order in which nickel and tungsten convert to sulfides, as measured by X-ray photoelectron spectroscopy (XPS). To measure XPS spectra at improved resolution, we used model supports consisting of a thin hydrophilic SiO_2 layer on a silicon substrate.[13]

SiO_2 supports were prepared by oxidizing Si(100) at 750 °C for 24 h in air. Oxidized wafers were cleaned in H_2O_2–NH_3(aq) (3 : 2 v/v) at 65 °C and hydroxylated in boiling water for 30 min. The sample was covered with an aqueous solution of ammonium metatungstate (Merck), nickel nitrate [$Ni(NO_3)_2{\cdot}6H_2O$; Merck] and 1,2-cyclohexanediamine-*N*,*N*,*N*′,*N*′-tetraacetic acid ($C_{14}H_{22}N_2O_8{\cdot}H_2O$; Merck) and spin coated under N_2 at 2800 rpm.[14] Concentrations were adjusted to result in loadings of 6 W atoms nm^{-2} and variable Ni loading between 1 and 6 atoms nm^{-2}. The amount of CyDTA added was equal to the amount of Ni present. Catalysts prepared without CyDTA were calcined (500 °C, 30 min), whereas NiW-CyDTA–SiO_2 catalysts were used without calcination. Sulfidation was carried out in a glass tube reactor with 10% H_2S in H_2 at a heating rate of 5 °C min^{-1} (2 °C min^{-1} for NiW-CyDTA–SiO_2) to the desired temperature, after which samples were kept at that temperature for 30 min. Next, the sample was cooled to room temperature under helium and transported to the XPS under N_2 atmosphere.

XPS spectra were obtained on a VG Escalab 200MK spectrometer, at a constant pass energy of 20 eV. Binding energies were corrected with reference to the Si 2p peak of SiO_2 at 103.3 eV.

Thiophene hydrodesulfurization was carried out with 5 cm^2 of model catalyst in a microflow reactor operating in batch mode (1.5 bar, 400 °C, with 4% thiophene in H_2), after sulfidation at 400 °C. Gas samples were taken with a syringe for gas chromatograph (GC) analysis of the products. All activity results presented are the average of at least six different measurements, which showed good reproducibility.

Fig. 1 shows W 4f and Ni 2p XPS spectra of the NiW-CyDTA–SiO_2 model catalyst after sulfidation at the indicated temperatures. The W 4f spectrum of the fresh catalyst shows a doublet at 35.6 eV characteristic of W(VI) oxide.[15] The small peak at 41.6 eV corresponds to the W $5p_{3/2}$ state. As Fig. 1 shows, sulfidation of W starts at 150 °C and is completed at 300 °C, where the W 4f spectrum shows a doublet at 32.6 eV, characteristic of WS_2.[15] Sulfidation of a Ni-free W–SiO_2 sample (not shown) proceeded similarly to the progression shown in Fig. 1A. Addition of CyDTA to W–SiO_2 in the preparation had no measurable effect on the sulfidation rate of tungsten.

Sulfidation of Ni, however, is greatly affected by CyDTA. The Ni 2p spectrum of fresh NiW-CyDTA–SiO_2 (Fig. 1B) exhibits the pattern characteristic of Ni^{2+}, with the Ni $2p_{3/2}$ peak at 855.4 eV accompanied by shake-up features.[15] The Ni $2p_{3/2}$ binding energy, however, is 1.5 eV lower than that of Ni in CyDTA-free Ni–SiO_2 and NiW–SiO_2 catalysts, evidencing complexation of nickel by CyDTA. As Fig. 1B shows, the complexed nickel is stable in H_2S–H_2 upto temperatures just below 250 °C. In contrast, NiO reacts in H_2S at room temperature, and conversion to nickel sulfide (Ni $2p_{3/2}$ binding energy of 854.0 eV[15]) is complete at 100 °C. The same is true for Ni sulfidation in NiW–SiO_2 catalysts, however, the Ni $2p_{3/2}$ peak shifts to a higher binding energy of 854.5 eV after complete sulfidation of W at sulfidation temperatures around 300 °C. We take the additional 0.5 eV shift of the Ni $2p_{3/2}$ peak as evidence that the initially formed Ni_3S_2 rearranges, and redisperses over the reactive edges of the WS_2 slabs, as proposed by Reinhoudt *et al.*[11]

Fig. 1B shows that CyDTA retards the sulfidation of Ni to *ca.* 250–300 °C. This temperature range coincides with the disappearance of the N 1s signal characteristic of the CyDTA ligand, indicating that the decomposition of the latter determines the rate of Ni sulfidation.

The activity of the catalysts for thiophene hydrodesulfurization is shown in Fig. 2. The blank silica support in the reactor has an order of magnitude lower activity than W–SiO_2, and shows mainly cracking products. The W–SiO_2 catalyst calcined at 500 °C is detectably active, with a product distribution showing predominantly 1-butene as the primary product. The Ni–SiO_2 catalyst calcined at 500 °C exhibits lower activity. Synergism is clearly observed in the standard NiW–SiO_2 model

DOI: 10.1039/b003272g

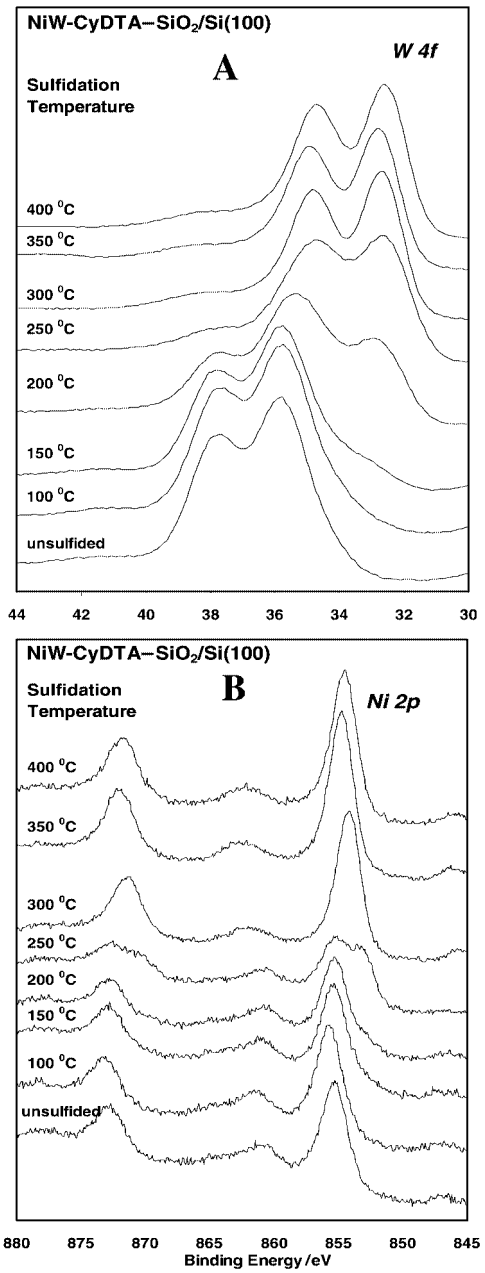

Fig. 1 (A) W 4f and (B) Ni 2p XP spectra of NiW-CyDTA–SiO_2/Si(100) model catalysts during sulfidation at various temperatures. The spectra show that CyDTA retards the sulfidation of Ni such that the sulfidation of W precedes that of Ni.

catalyst, for which the total activity is more than twice that of Ni–SiO_2 and W–SiO_2 combined. The highest activity is observed with NiW-CyDTA–SiO_2, which is about 2.3 times more active than a standard NiW–SiO_2 sample of the same nominal composition. The C_4-product distribution of this catalyst is: 40% 1-butene, 36% *trans*-2-butene and 24% *cis*-2-butene. Optimum activity was observed with NiW–SiO_2 catalysts containing 4 Ni atoms or more, in addition to 6 W atoms nm^{-2} on SiO_2. This level of conversion corresponds to a pseudo-turnover frequency of 4×10^{-2} mol (thiophene) mol(W + Ni)$^{-1}$ s^{-1}. Increasing the Ni loading further did not influence the activity significantly. Interestingly, the optimum Ni/W atomic ratio of 0.66 equals that in commercial NiW–Al_2O_3 catalysts.[2]

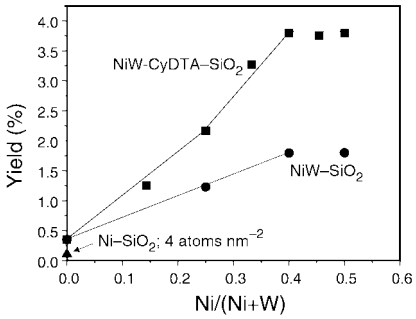

Fig. 2 Thiophene HDS activity as a function of Ni-content in NiWS–SiO_2/Si(100) model catalysts containing 6 W atoms nm^{-2} (batch reaction at 400 °C, runtime 1 h).

We attribute the high HDS activity of NiW-CyDTA–SiO_2 to the retardation of nickel sulfidation by the chelating agent to temperatures where WS_2 has already formed. As a result, Ni atoms released by CyDTA can move to the edges of WS_2 to form a finely dispersed NiW sulfide. A similar phase, commonly referred to as CoMoS, has been identified as the active phase in sulfided CoMo catalysts by Topsøe and coworkers.[2] A similar structure may be invoked to explain the high activity of sulfided NiW catalysts. The reason that standard NiW–SiO_2, in which Ni-sulfidation is not retarded by complexing agents, shows appreciable promotion of desulfurization activity is that the Ni_3S_2 phase which forms at low temperatures redisperses at higher temperatures and may still end up in the form of suboptimal clusters on the edges of WS_2, as recently proposed by Reinhoudt *et al.*[11] However, application of sufficiently stable chelating agents such as CyDTA, that retard Ni sulfide formation to temperatures where WS_2 has formed, results in the most active form of the NiWS catalyst, as demonstrated in this paper.

Notes and references

1 J. W. Gosselink, *CatTech.*, 1998, **4**, 127.
2 H. Topsøe, B. S. Clausen and F. E. Massoth, *Hydrotreating Catalysis*, Springer-Verlag, Berlin, 1996.
3 B. Scheffer, P. J. Mangnus and J. A. Moulijn, *J. Catal.*, 1990, **121**, 18.
4 L. Medici and R. Prins, *J. Catal.*, 1996, **163**, 38.
5 R. Cattaneo, T. Shido and R. Prins, *J. Catal.*, 1999, **185**, 199.
6 A. M. de Jong, H. J. Borg, L. J. van IJzendoorn, V. G. M. F. Soudant, V. H. J. de Beer, J. A. R. van Veen and J. W Niemantsverdriet, *J. Phys. Chem.*, 1993, **97**, 6477.
7 Th. Weber, J. C. Muijsers, J. H. M. C. van Wolput, C. P. J. Verhagen and J. W. Niemantsverdriet, *J. Phys. Chem.*, 1996, **100**, 14 144.
8 L. Coulier, V. H. J. de Beer, J. A. R. van Veen and J. W. Niemantsverdriet, *Top. Catal.*, 2000, in press.
9 J. A. R. van Veen, E. Gerkema, A. M. van der Kraan and A. Knoester, *J. Chem. Soc., Chem. Commun.*, 1987, 1684.
10 A. M. de Jong, V. H. J. de Beer, J. A. R. van Veen and J. W Niemantsverdriet, *J. Phys. Chem.*, 1996, **100**, 17 722.
11 H. R. Reinhoudt, Y. van der Meer, A. M. van der Kraan, A. D. van Langeveld and J. A. Moulijn, *Fuel. Process. Technol.*, 1999, **61**, 43.
12 T. Shimizu, K. Hiroshima, T. Honma, T. Mochizuki and M. Yamada, *Catal. Today*, 1998, **45**, 271.
13 P. L. J. Gunter, J. W. Niemantsverdriet, F. H. Ribeiro and G. A. Somorjai, *Catal. Rev.-Sci. Eng.*, 1997, **39**, 77.
14 R. M. van Hardeveld, P. L. J. Gunter, L. J. van IJzendoorn, W. Wieldraaijer, E. W. Kuipers and J. W. Niemantsverdriet, *Appl. Surf. Sci.*, 1995, **84**, 339.
15 J. F. Moulder, W. F. Stickle, P. E. Sobol and K. D. Bomben, *Handbook of XPS*, Perkin-Elmer Corporation, Eden Prairie, MN, 1992.

ChemComm

A porphyrin square: synthesis of a square-shaped π-conjugated porphyrin tetramer connected by diacetylene linkages

Ken-ichi Sugiura, Yoshinobu Fujimoto and Yoshiteru Sakata*

The Institute of Scientific and Industrial Research (ISIR), Osaka University, Mihogaoka 8-1, Ibaraki, Osaka 567-0047, Japan. E-mail: sakata@sanken.osaka-u.ac.jp

Received (in Cambridge, UK) 5th April 2000, Accepted 9th May 2000
Published on the Web 8th June 2000

A square-shaped π-conjugated porphyrin tetramer has prepared: the excitation energies of both the Soret and Q bands, 19 880 (503) and 15 180 cm^{-1} (659 nm), respectively, are quite low compared with those for the monomer and reported cyclic porphyrin oligomers.

Interdisciplinary research on porphyrin oligomers (POs) has been attracting much attention over the last two decades.[1] Studies are focused on the elucidation of the function of naturally occurring POs, such as the cyclophane-like dimeric *special pair* in the photosynthetic reaction center,[1] as well as the creation of component molecules for novel advanced materials.[2–8] Recently, many efforts have been made to prepare cyclic porphyrin oligomers (CPOs) motivated by the wheel-shaped oligomeric porphyrinoid architecture found in the light harvesting proteins.[9] After the pioneering work of Sanders and Anderson in 1989,[10] several CPOs have been reported, in which each porphyrin is connected by covalent[11–13] or coordination bonds.[14] However, the linkages are only limited to aryl-based *meso*-groups in which the porphyrin and linker π-systems are orthogonal. Therefore, the electronic interaction between the neighbouring chromophores in the ground state remains small.[7] With the aim of creating a highly conjugated CPO, we chose a diacetylene unit to connect porphyrins directly at the *meso*-position.[4–8, 15] Here we report the synthesis and some basic properties of a new cyclic π-conjugated porphyrin tetramer **1** (Fig. 1).

The synthetic route to **1** is shown in Scheme 1. An important key intermediate, 5,10-bis(3,5-di-*tert*-butylphenyl)porphyrin **3**, which acts as the corners of the square **1** was prepared in 3% yield by the coupling reaction of 3,5-di-*tert*-butylphenylbenzaldehyde and pyrrole with tripyrrane **2**, as reported by Taniguchi and coworkers,[16] in the presence of powdered NaCl.[17] After metallation of **3**, functionalization reactions were performed at the *meso*-positions, *i.e.* bromination (affording **5**), introduction of acetylene groups (to give **6**), and the removal of the TMS groups (providing **7**).† Glaser–Hay coupling[4] of **7** at a 2.6 mM concentration gave moderately soluble, brown coloured crude products. The resulting reaction mixture was analyzed by matrix-assisted laser desorption ionization time-of-flight mass spectrometry to give a main peak for M^+ at *m/z* 3160, along with a weak one at *m/z* 2371. This clearly indicates the tetramer was formed exclusively (*m/z* calc. for M^+ of the cyclic tetramer, $C_{208}H_{200}N_{16}Ni_4$: 3159; *m/z* calc. for M^+ of the acyclic trimer, $C_{156}H_{152}N_{12}Ni_3$: 2371). Separation of the tetramer was successfully achieved using preparative gel permeation chromatography. The absence of C≡C–H and asymmetric C≡C stretching bands in the IR spectrum of **1**, characteristically observed for **7** at 3310s and 2106m cm^{-1}, respectively, suggest the tetramer to be cyclic. The simple pattern of ^{1}H-NMR peaks† also supports the cyclic structure having D_{4h} symmetry (*vide infra*). In a

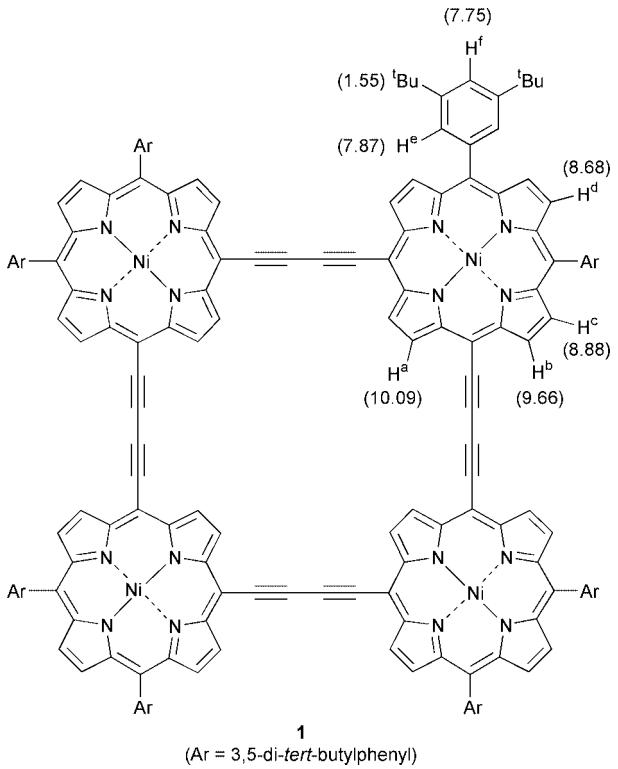

Fig. 1 Compound **1** along with ^{1}H-NMR assignments.

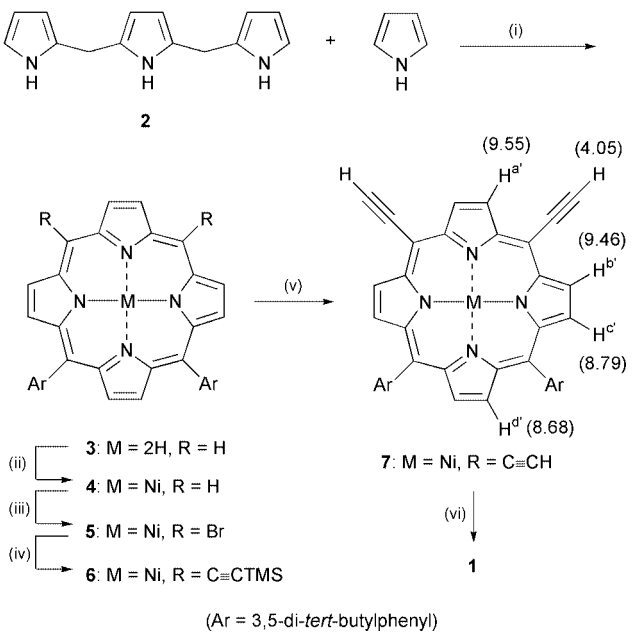

Scheme 1 *Reagents and conditions*: (i) 2.0 eq. 3,5-di-*tert*-butylphenylbenzaldehyde, TFA, NaCl, CH_2Cl_2; (ii) excess $Ni(CH_3CO_2)_2{\cdot}4H_2O$, $(CH_2Cl)_2$, reflux; (iii) 2.05 eq. NBS, CH_2Cl_2, −20 °C, (iv) 3.0 eq. TMS–C≡CH, Cu_2Cl_2, $Pd(PPh_3)_4$, NEt_2H, (v) $^nBu_4NF$, CH_2Cl_2 (vi) Cu_2Cl_2, TMEDA, CH_2Cl_2. The values in parentheses for **7** are ^{1}H-NMR assignments.

DOI: 10.1039/b002699i

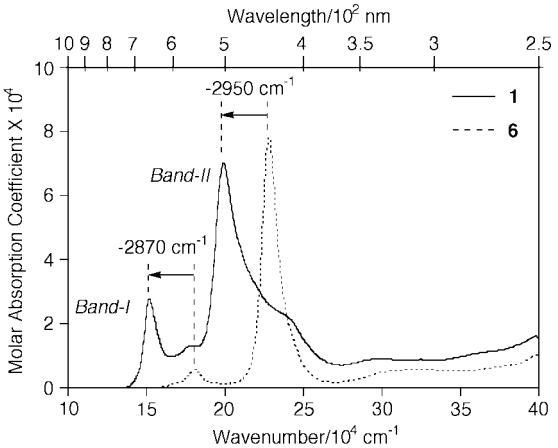

Fig. 2 Absorption spectra of **1** (solid line) and **6** (dotted line) in $CHCl_3$.

typical reaction, 41.3 mg of **7**, 400.0 mg of Cu_2Cl_2, 0.55 mL of TMEDA, and 50 mL of dry CH_2Cl_2 gave 8.9 mg of the tetramer **1** as a lustrous dark-green solid (22% yield). It should be emphasised that this relatively high yielding formation of cyclic **1** occurred in the absence of template;[12] the isolated yield of the structurally similar square was 7% at most.[11]

The ^{1}H-NMR chemical shift of the internal protons (H^a: 10.09 ppm) is informative about the structure of **1** from the following two view points. First, compared to the corresponding protons of **7** ($H^{a'}$: 9.55 ppm), H^a is shifted to low field by +0.54 ppm. Although a similar downfield shift was observed for the linear porphyrin oligomers connected by the diacetylene linkages, *e.g.* +0.22 ppm for the dimer,[8] the shift for **1** is more than double this value. Second, the difference in the chemical shifts of the internal (H^a) and the external protons (H^b: 9.66 ppm) adjacent to the diacetylene units of **1** is +0.43 ppm. This value is also larger than that observed for **7** (+0.09 ppm: 9.55 ppm for $H^{a'}$ and 9.46 ppm for $H^{b'}$). These results suggest that the H^a-protons of **1** are affected by the ring current, not only of the two adjacent porphyrin rings, but also of the diagonal porphyrin in the square and also clearly suggests **1** to be cyclic.

The electronic spectra of **1** and **6** are shown in Fig. 2. The spectrum of **1** is composed of two main bands: Q-band-like band I and Soret-band-like band II.† Reflecting the highly conjugated structure, band I and band II appear at 15 180 (659) and 19 880 cm^{-1} (503 nm), respectively. Both band I and band II are shifted to lower energy compared with those of the monomer **6** by about 2900 cm^{-1}. Although these bands appear at much longer wavelengths than those of the porphyrin square connected by *meso*-aryl-based linkages reported by Lindsey and coworkers (λ_{max} = 23 260 cm^{-1}; 430 nm),[11] these wavelengths are similar to the corresponding linear tetramer.[6] The intensity of band I normalized per chromophore was increased compared with that of **6**. Conversely, the intensity of band II was decreased. This phenomenon suggests that the degeneracy of the a_{1u} and a_{2u} orbitals of the porphyrins is lifted[7] and that a new π-electronic system in the square is formed.

In conclusion, a novel and highly conjugated porphyrin square was prepared. In addition to the expanded π-system of the molecule, our square has a central cavity corresponding to the size of molecules such as hexamethylbenzene.[18] These characteristics will allow us to use the square as an advanced host molecule. We are currently investigating the photochemistry of the corresponding free base and zinc complex, as well as contraction and expansion of the square by replacing the diacetylene units with –C≡C– and –(C≡C–)$_n$ (n > 3) linkers, respectively, keeping the π-conjugation between the four porphyrins.

This work was supported in part by a Grant-in-Aid for Scientific Research on Priority Areas (no. 11136222 'Metal-assembled Complexes' to K-i. S., no. 11166238 'Molecular Physical Chemistry' to K-i. S., and no. 10146103 'Creation of Characteristic Delocalized Electronic Systems' to Y. S.) from the Ministry of Education, Science, Sports and Culture, Japan. We appreciate the technical assistance provided by the Materials Analysis Centre of ISIR, Osaka University as well as helpful discussions with Professor S. Taniguchi, Ibaraki National College of Technology, Japan.

Notes and references

† *Data*: **3**: ^{1}H-NMR ($CDCl_3$) δ 10.21 (s, 2H), 9.44 (s, 2H), 9.33 (d, J = 5, 2H), 9.06 (d, J = 5, 2H), 8.97 (s, 2H), 8.09 (d, J = 2, 4H), 7.81 (t, J = 2 Hz, 2H), 1.54 (s, 36H), −3.27 (bs, 2H). **4**: ^{1}H-NMR ($CDCl_3$) δ 9.88 (s, 2H), 9.23 (s, 2H), 9.17 (d, J = 5, 2H), 8.98 (d, J = 5, 2H), 8.90 (s, 2H), 7.92 (d, J = 2, 4H), 7.76 (t, J = 2 Hz, 2H), 1.50 (s, 36H). **5**: ^{1}H-NMR ($CDCl_3$) δ 9.39 (s, 2H), 9.34 (d, J = 5, 2H), 8.69 (d, J = 5, 2H), 8.62 (s, 2H), 7.72 (d, J = 2, 4H), 7.64 (t, J = 2 Hz, 2H), 1.39 (s, 36H). **6**: ^{1}H-NMR ($CDCl_3$) δ 9.50 (s, 2H), 9.41 (d, J = 5, 2H), 8.75 (d, J = 5, 2H), 8.64 (s, 2H), 7.79 (d, J = 2, 4H), 7.70 (t, J = 2, 2H), 1.45 (s, 36H), 0.54 (s, 18H). UV–vis λ_{max} ($CHCl_3$): 310 (log ε = 3.77), 438 (4.89), 554 (3.76) nm. **7**: ^{1}H-NMR ($CDCl_3$) δ 9.55 (s, 2H), 9.46 (d, J = 5, 2H), 8.79 (d, J = 5, 2H), 8.68 (s, 2H), 7.81 (d, J = 2, 4H), 7.72 (t, J = 2, 2H), 4.05 (s, 2H), 1.46 (s, 36H) ppm. **1**: ^{1}H-NMR ($CDCl_3$) δ 10.09 (s, 8H), 9.66 (d, J = 5, 8H), 8.88 (d, J = 5, 8H), 8.68 (s, 8H), 7.87 (d, J = 2, 16H), 7.75 (t, J = 2, 8H), 1.55 (s, 144H). UV–vis λ_{max} ($CHCl_3$): 324 (log ε = 3.94), 423 (sh, 4.37), 503 (4.85), 562 (4.12), 659 (4.44) nm.

1 Reviews: M. R. Wasielewski, *Chem. Rev.*, 1992, **92**, 435; H. Kurreck and M. Huber, *Angew. Chem., Int. Ed. Engl.*, 1995, **34**, 849.
2 J. D. Spence and T. D. Lash, *J. Org. Chem.*, 2000, **65**, 1530.
3 K.-i. Sugiura, H. Tanaka, T. Matsumoto, T. Kawai and Y. Sakata, *Chem. Lett.*, 1999, 1193.
4 H. L. Anderson, S. J. Martin and D. D. C. Bradley, *Angew. Chem., Int. Ed. Engl.*, 1994, **33**, 655.
5 H. L. Anderson, *Inorg. Chem.*, 1994, **33**, 972.
6 P. N. Taylor, J. Huuskonen, G. Rumbles, R. T. Aplin, E. Williams and H. L. Anderson, *Chem. Commun.*, 1998, 909.
7 H. L. Anderson, *Chem. Commun.*, 1999, 2323.
8 V. S.-Y. Lin, S. G. DiMagno and M. J. Therien, *Science*, 1994, **264**, 1105; V. S.-Y. Lin and M. J. Therien, *Chem. Eur. J.*, 1995, **1**, 645.
9 T. Pullerits and V. Sundström, *Acc. Chem. Res.*, 1996, **29**, 381.
10 H. L. Anderson and J. K. M. Sanders, *J. Chem. Soc., Chem. Commun.*, 1989, 1714.
11 R. W. Wagner, J. Seth, S. I. Yang, D. Kim, D. F. Bocian, D. Holten and J. S. Lindsey, *J. Org. Chem.*, 1998, **63**, 5042.
12 S. Anderson, H. L. Anderson and J. K. M. Sanders, *Acc. Chem. Res.*, 1993, **26**, 469.
13 J. Li, A. Ambroise, S. I. Yang, J. R. Diers, J. Seth, C. R. Wack, D. F. Bocian, D. Holten and J. S. Lindsey, *J. Am. Chem. Soc.*, 1999, **121**, 8927; O. Mongin, A. Schuwey, M.-A. Vallot and A. Gossauer, *Tetrahedron Lett.*, 1999, **40**, 8347.
14 C. M. Drain and J.-M. Lehn, *J. Chem. Soc., Chem. Commun.*, 1994, 2313 (corrigendum: *J. Chem. Soc., Chem. Commun.*, 1995, 503); K. Funatsu, A. Kimura, T. Imamura and Y. Sasaki, *Chem. Lett.*, 1995, 765.
15 To the best of our knowledge, the introduction of the acetylene group on the *meso*-position was first proposed by Arnold and coworkers in 1978. D. P. Arnold, A. W. Johnson and M. Mahendran, *J. Chem. Soc., Perkin Trans. 1*, 1978, 366; D. P. Arnold and L. J. Nitschinsk, *Tetrahedron*, 1992, **48**, 8781; D. P. Arnold and D. A. James, *J. Org. Chem.*, 1997, **62**, 3460; D. P. Arnold, G. A. Heath and D. A. James, *J. Porphyrins Phthalocyanines*, 1999, **3**, 5.
16 S. Taniguchi, H. Hasegawa, M. Nishimura and M. Takahashi, *Synlett*, 1999, 73.
17 F. Li, K. Yang, J. S. Tyhonas, K. A. MacCrum and J. S. Lindsey, *Tetrahedron*, 1997, **53**, 12 339.
18 J. D. Ferrara, C. Tessier-Youngs and W. J. Youngs, *J. Am. Chem. Soc.*, 1985, **107**, 6719.

Encapsulation of Et_3N^+–H···OH_2 in a hydrogen-bonded resorcarene capsule

Alexander Shivanyuk,* Kari Rissanen* and Erkki Kolehmainen

Department of Chemistry, University of Jyväskylä, PO Box 35, Jyväskylä, FIN-40351, Finland. E-mail: shivan@jyu.fi and kari.rissanen@jyu.fi

Received (in Cambridge, UK) 16th March 2000, Accepted 15th May 2000
Published on the Web 8th June 2000

In the crystalline state a resorcarene dimer linked by ten hydrogen-bonding water molecules encapsulates the hydrogen-bonded complex Et_3N^+–H···OH_2 while bromide anions are positioned outside the cavity.

Supramolecular encapsulation is a topic of considerable current interest.[1] Designed self-complementary molecules form dimeric[2] or tetrameric[3] hydrogen-bonded capsules including charged and neutral guest species. Resorcarenes **1** linked by smaller hydrogen-bonding molecules assemble into dimeric[4] and hexameric[5] hollow structures in the solid state**.** Molecular encapsulation of dimeric hydrogen-bonded complexes has been discovered recently in apolar solutions[6] however much less is known about such complexation in the crystalline state.[7]

Herein we describe the first single crystal X-ray structure of a hydrogen-bonded molecular capsule encapsulating the hydrogen-bonded heterocomplex Et_3N^+–H···OH_2.

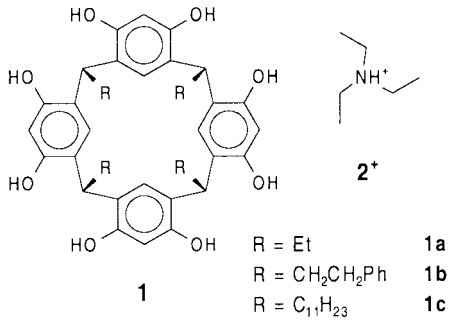

Co-crystallization of **1a** with a ten-fold excess of Et_3NHBr from aqueous EtOH results in cubic crystals which, although unstable without solvent, were suitable for single crystal X-ray analysis.† The resorcarene molecules adopt a perfect cone conformation stabilized by four intramolecular hydrogen bonds between neighboring hydroxy groups. Two molecules of **1a**, sitting on a two fold crystallographic rotation axis, form a dimer held together by ten hydrogen-bonded water molecules disordered over 16 sites (Fig. 1). One $\mathbf{2}^+$ and one hydrogen-bonded water molecule [N1A···O12a 2.735(7) Å] are encapsulated in such a dimeric cavity.[8] Two opposite orientations occur for the encapsulated Et_3N^+–H···OH_2 with occupancy factors of 0.7 and 0.3. Furthermore, in each orientation the ethyl groups are strongly disordered owing to the fact that the three-fold axis of $\mathbf{2}^+$ coincides with the two-fold axis of the capsule. Encapsulated $\mathbf{2}^+$ is shifted by 0.28 Å from the center of the cavity[9] towards resorcarene molecule B. Several close non-bonded contacts (3.49–3.67 Å) were found between carbon atoms of Et_3N^+–H and resorcinol rings of **1a** which manifest C–H··π attractions. The encapsulated water molecule (O12a) is located deep in the resorcarene socket of molecule A forming four close non-bonded contacts to the aromatic C–H atoms of the resorcinol rings with O–C distances of 3.327(4) and 3.335(4) Å.[10] Such an arrangement allows O–H··π interactions between the encapsulated water molecule and the resorcinol rings. The hydrogen bonding in Et_3N^+–H···OH_2 should theoretically increase the positive charge on the hydrogen atoms of the water molecule and thus facilitate O–H··π attractions.

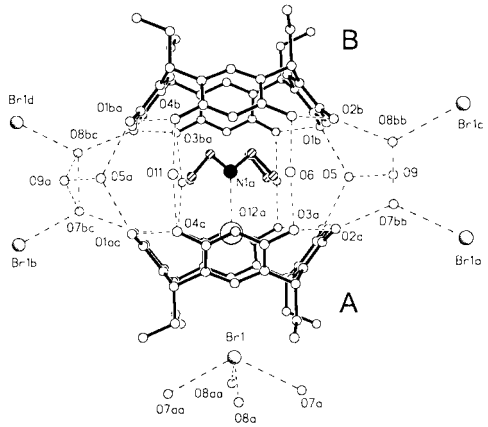

Fig. 1 Single-crystal X-ray structure of [(**1a**$_2$·10H_2O)-@($\mathbf{2}^+$·H_2O)]Br^-·4.8H_2O. All hydrogen atoms are omitted for clarity. Hydrogen bonds are indicated by dotted lines. The most populated orientation of the disordered cation and water molecule is indicated. The nitrogen atom of $\mathbf{2}^+$ and oxygen atom of encapsulated water molecule are shown with arbitrary radii. Distances between hydrogen-bonding oxygen atoms are between 2.606(3) and 2.791(5) Å. Distances between the hydrogen-bonded Br anion and water molecules are between 3.323(6) and 3.348(5) Å.

The bromide anion is positioned outside the cavity and lies within the shallow pocket formed by four pendant CH_2 groups of molecule A[11] and is solvated by four disordered hydrogen-bonded water molecules (Fig. 1). The shortest N···Br distance [8.212(6) Å] is *ca.* 2.5 times longer than in $\mathbf{2}^+$ Br^-.[12] The distance of the bromide anion to the carbon atom of the CH_2 group is 4.004(4) Å reflecting weak C–H···Br^- interactions. The hydrogen-bonded array of the resorcarene dimer is not saturated and therefore four symmetry related bromide anions are hydrogen bonded to the bridging water molecules (Fig. 1).

^{1}H NMR spectroscopy shows that no complex is formed between **1** and $\mathbf{2}^+$ in polar solvents such as methanol-d_4 or DMSO-d_6. However, in $CDCl_3$ saturated with H_2O, lipophilic resorcarenes **1b,c** strongly interact with $\mathbf{2}^+$ X^- (X^- = Cl^-, Br^-, ClO_4^-). At [$\mathbf{2}^+$ X^-]/[**1b,c**] ≥ 0.5, ^{1}H NMR spectra show sharp signals of methyl and methylene protons of the complexed cation which are both shifted upfield by *ca.* 1.3 ppm (Fig. 2). The exchange of complexed and free $\mathbf{2}^+$ is slow on the NMR timescale at 303 K (500 MHz) and the integration shows that two resorcarene molecules complex one cation $\mathbf{2}^+$. The signal of the water protons (5–6 H per **1c**) is shifted downfield ($\Delta\delta$ = 1.9 ppm) and the multiplet of resorcinol OH groups is centered at δ 9.5 owing to strong hydrogen-bonding. These results suggest that hydrogen-bonded water molecules participate in the formation of the 2:1 capsule also in $CDCl_3$.[13] These results are also in agreement with the fact that in dry $CDCl_3$ the systems **1b,c** + *n* $\mathbf{2}^+X^-$ exhibit broad ^{1}H NMR spectra, most probably owing to the formation of ill defined hydrogen-bonded aggregates. Detailed NMR investigations of these complex systems in apolar solvents are currently in progress and will be reported in due course.

In conclusion, the solid-state encapsulation of ammonium cations by a water linked dimer of **1a** is strongly dependent on

DOI: 10.1039/b002144j

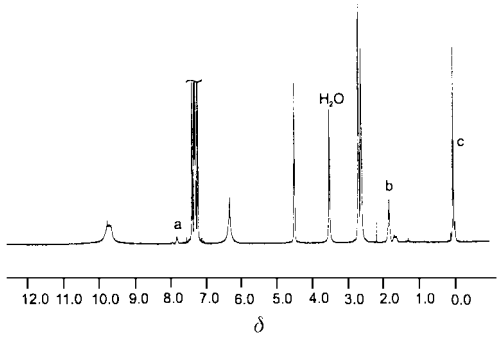

Fig. 2 ^{1}H NMR spectrum of 2 **1b** + **2**$^+$Cl$^-$ {[**1b**] = 3×10^{-2} M, 500 MHz, 303 K, $CDCl_3$}. The signals of the complexed cation are: a, NH; b, CH_2; c, CH_3.

the structure of the guest. For the previously studied complex with Et_4N^+[14] no anion is found while the negative charge was distributed over all oxygen atoms of the capsule. The smaller volume of Et_3NH^+ and the presence of the hydrogen bonding N–H group seem to be crucial for the encapsulation of Et_3N^+–H··OH_2 in the cavity of the resorcarene dimer. The incomplete saturation of the hydrogen-bonded array within the hydrogen bonded shell determines the strong hydrogen-bonding interaction of the capsule with external bromide anions. This feature is being currently explored for the rational design of externally tuned supramolecular containers.

Notes and references

† *X-Ray crystal structure analysis*: Data were recorded with a Kappa CCD difractometer using graphite monochromatised Mo-Kα radiation [λ(Mo-Kα) = 0.71073 Å]. The data was processed with Denzo-SMN v0.93.0 [Z. Otwinowski and W. Minor, *Processing of X-ray Diffraction Data Collected in Oscillation Mode*, *Methods in Enzymology*, vol. 276: *Macromolecular Crystallography*, Part A, ed. C. W. Carter, Jr. and R. M. Sweet, Academic Press, New York, 1997, pp. 307–326]. The structures were solved by direct methods (SHELXS-97: G. M. Sheldrick, *Acta Crystallogr., Sect. A*, 1990, **46**, 467) and refinements, based on F^2, were made by full-matrix least-squares techniques (SHELXL-97, G. M. Sheldrick, *A program for crystal structure refinement*, 1997, University of Göttingen, Germany). The hydrogen atoms were placed in calculated idealized positions with isotropic temperature factors (1.2 times the C temperature factor) and refined as riding atoms. The hydrogen atoms of water molecules and disordered cation were not located. The atoms of the cation in the less populated orientation as well as two strongly disordered water molecules were treated isotropically.

Crystal data: [(**1a**$_2$·10H_2O)@(**2**$^+$·H_2O)]Br^-·4.8H_2O: crystal size 0.4 × 0.3 × 0.25 mm, tetragonal, space group $I4_1/a$, a = 20.2620(5), c = 43.1040(7), V = 17696.3(7) Å^3, Z = 8, D_c = 1.214 g cm^{-3}, μ = 0.542 mm^{-1}, $2\theta_{max}$ = 49.44 °, F(000) = 6824, $R1$ = 0.0539, $wR2$ = 0.15875 [for 5042 reflections with $I > 2\sigma(I)$], R_{int} = 0.0525, $R1$ = 0.0792, $wR2$ = 0.1800 (for all 7537 reflections), 590 parameters, S = 1.106.

CCDC 182/1639. See http://www.rsc.org/suppdata/cc/b0/b002144j/ for crystallographic files in .cif format.

1 M. M. Conn and J. Rebek, Jr., *Chem. Rev.*, 1997, **97**, 1647.
2 B. C. Hamman, K. D. Shimizu and J. Rebek, Jr., *Angew. Chem., Int. Ed.*, 1999, **35**, 1326; O. Mogck, E. F. Paulus, V. Böhmer, I. Thondorf and W. Vogt, *Chem. Commun.*, 1996, 2533; R. G. Chapman, G. Olovsson, J. Trotter and J. C. Sherman, *J. Am. Chem. Soc.*, 1998, **120**, 6252.
3 C. Nuckolls, F. Hof, T. Martín and J. Rebek, Jr., *J. Am. Chem. Soc.*, 1999, **121**, 10281.
4 K. N. Rose, L. J. Barbour, G. W. Orr and J. L. Atwood, *Chem. Commun.*, 1998, 407; L. R. MacGillivray, P. R. Diamente, J. L. Reid and J. A. Ripmeester, *Chem. Commun.*, 2000, 359.
5 L. R. MacGillivray and J. L. Atwood, *Nature*, 1997, **389**, 469.
6 T. Heinz, D. M. Rudkevich and J. Rebek, Jr., *Angew. Chem., Int. Ed.*, 1999, **38**, 1136.
7 For encapsulation of a hydrogen bonded dimer of sulfuric acid in a dimeric calixarene capsule, see: M. J. Hardie, M. Makha and C. L. Raston, *Chem. Commun.*, 1999, 2409.
8 The 2:1 ratio between **1a** and Et_3NH^+ was additionally established by ^{1}H NMR spectroscopy. Crystals were removed from the mother liquor, cleaned with filter paper, and dissolved in DMSO-d_6.
9 The center of the cavity is determined as the gravity center of the bridging methine atoms of the resorcarene molecules forming the dimer.
10 For inclusion of water molecules in the cavity of calixarenes, see: J. L. Atwood, F. Hamada, K. D. Robinson, G. W. Orr and R. L. Vincent, *Nature (London)*, 1991, **349**, 683; A. Drjaca, M. Hardie and C. L. Raston, *J. Chem. Soc., Dalton. Trans.*, 1999, 3639.
11 Compare with: A. Shivanyuk, E. F. Paulus and V. Böhmer, *Angew. Chem., Int. Ed.*, 1999, **38**, 2906.
12 M. A. James, T. S. Cameron, O. Knop, M. Neuman and M. Falk, *Can. J. Chem.*, 1985, **63**, 1750.
13 The encapsulation of β-methyl glucoside by a resorcarene dimer in $CDCl_3$ has been described, however, the detailed structure of the complex could not be established: Y. Kikuchi, Y. Tanaka, S. Sutarto, K. Kobayashi, H. Toi and Y. Aoyama, *J. Am. Chem. Soc.*, 1992, **114**, 10 302.
14 K. Murayama and K. Aoki, *Chem. Commun.*, 1998, 607.

ChemComm

A versatile approach to the total synthesis of the pseudomonic acids

Catherine Mckay,[a] Thomas J. Simpson,[a] Christine L. Willis,*[a] Andrew K. Forrest[b] and Peter J. O'Hanlon[b]

[a] *School of Chemistry, University of Bristol, Cantock's Close, Bristol, UK BS8 1TS. E-mail: chris.willis@bristol.ac.uk*

[b] *SmithKline Beecham Pharmaceuticals, New Frontiers Science Park, Third Avenue, Harlow, UK CM19 5AW*

Received (in Liverpool, UK) 17th April 2000, Accepted 12th May 2000
Published on the Web 8th June 2000

The total synthesis of pseudomonic acid C is described using an approach which gives access to analogues and putative biosynthetic precursors; the key step is installation of the C_7 side-chain *via* alkylation of a trisubstituted δ-lactone with complete stereocontrol and in 85% yield under conditions which avoid the possible competing elimination of a protected hydroxy group β to the carbonyl.

Pseudomonic acid C is one of a family of *C*-glycopyranosides produced by *Pseudomonas fluorescens*.[1] These compounds are potent inhibitors of Gram positive bacterial and mycoplasmal pathogens[2] and pseudomonic acid A (with a 10,11-epoxide) is used clinically for the treatment of bacterial skin infections. More recently new pseudomonic acid derivatives such as thiomarinol have been isolated from marine organisms.[3]

Despite their biological importance, the biosynthesis of these polyketide derived secondary metabolites[4] has not been established. Results of feeding studies with oxygen-18 precursors indicate that the oxygens attached to C-1, C-5, C-7 and C-13 are all derived from acetate whereas the oxygen at C-6 must originate from either the atmosphere or water.[5] These results are in accord with the proposal that the tetrahydropyran ring is formed either *via* an intramolecular conjugate addition of 5-OH to an enone or *via* an intramolecular S_N2 type attack of the 5-OH onto an activated 16-hydroxy group. However, the mechanism of cyclisation has not been established and its timing relative to other steps such as hydroxylation at C-6 or esterification at C-1 is not known. Therefore our goal was to develop a new and flexible approach to the synthesis of pseudomonic acid which would give access to acyclic compounds to examine these processes as well as to analogues for biological assessment. Previous routes have involved either elaboration of carbohydrates or the modification of dihydropyrans.[6] These approaches do not give access to the required putative biosynthetic intermediates and hence a new strategy was required.

The key features of this strategy (Scheme 1) are: (i) the enantioselective synthesis of a suitably protected functionalised δ-lactone **II** from the bicyclic lactone **I**; (ii) preparation of the C_7 side-chain **III** with a good leaving group to act as the electrophile for reaction with the enolate of **II**; (iii) installation of the C_7 side-chain with complete stereocontrol under conditions which avoid the possible competing elimination of a protected hydroxy group β to the carbonyl in **II** to give **IV**; (iv) reduction of the lactone **IV** to a tetrahydropyran followed by further manipulation of the side chain to methyl ketone **V** and chain extension with a known phosphonate[7] to the target compound. Lactone **IV** would be the precursor of the acyclic compounds required to examine the ring closure reactions.

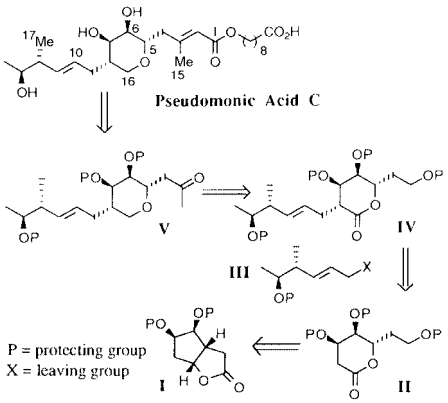

Scheme 1

The first step was introduction of a *cis*-vicinal diol which was achieved *via* treatment of *cis*-bicyclo[3.2.0]hept-7-en-2-one **1** with catalytic osmium tetroxide giving a 9:1 mixture of *exo*:*endo* vicinal diols.[8] (−)-(1*S*,5*R*)-Bicyclic ketone **1** required as the starting material was prepared with 95% ee *via* resolution of the bisulfite adduct.[9] The *syn* diols could be protected as either the acetonide or benzyl ethers but, for ease of manipulation at later stages of the synthesis, the *tert*-butyldimethylsilyl (TBS) ether **2** was preferred (Scheme 2) Baeyer–Villiger oxidation proceeded as expected[10] with complete regiocontrol giving the required lactone **3** in 68% yield over the three steps from **1**.

Elaboration of bicyclic lactone **3** to the required δ-lactone **7** was accomplished by a straightforward sequence involving initial reduction of **3** with $LiAlH_4$ to diol **4**. Selective protection of the primary alcohol of **4** as either the benzoate, trityl ether or TBDPS ether proceeded in excellent yields (> 90%), but the best protecting group for later stages of the synthesis proved to be the TBS ether. Oxidation of alcohol **5** with TPAP[11] followed by treatment of the resultant cyclopentanone **6** with MCPBA gave δ-lactone **7** possessing the stereogenic centres which would become C-5, C-6 and C-7 of pseudomonic acid.

The key stage of the total synthesis was the alkylation to introduce selectively the C_7 side chain of pseudomonic acid. Examples of alkylation of δ-lactones have been reported,[12] and Seebach *et al.*[13] showed that stereocontrol of the methylation of a δ-lactone possessing a free hydroxy group β to the carbonyl could be achieved using chelation control with the alkoxide. However, we found no literature precedents for alkylation of a δ-lactone possessing a β-silyl ether and it was anticipated that β-elimination to give the α,β-unsaturated lactone may be a competing process.

Allylic bromides have been used as electrophiles in the alkylation of simple δ-lactones in natural product synthesis[14]

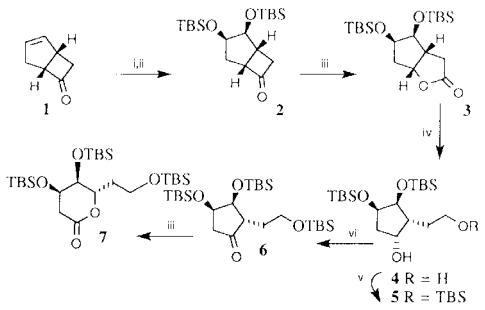

Scheme 2 *Reagents and conditions*: i, OsO_4, NMO (*N*-methylmorpholine *N*-oxide), Me_2CO; ii, TBSOTf, CH_2Cl_2, pyridine; iii, *m*-CPBA, $NaHCO_3$, CH_2Cl_2; iv, $LiAlH_4$, THF; v, TBSCl, imidazole, CH_2Cl_2; vi, TPAP (tetrapropylammonium perruthenate), NMO, CH_2Cl_2.

DOI: 10.1039/b003094p

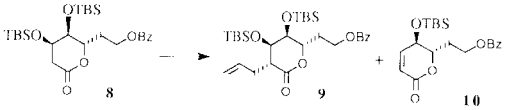

Scheme 3

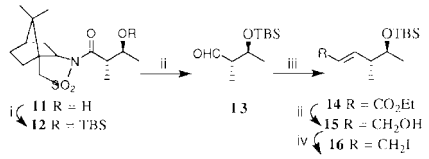

Scheme 4 *Reagents and conditions*: i, TBSOTf, pyridine, CH_2Cl_2; ii, DIBAL-H, CH_2Cl_2, −78 °C; iii, $(EtO)_2POCHCO_2Et$, BuLi, THF; iv, DIPHOS (1,2-bis(diphenylphosphino)ethane), I_2, 0 °C.

and so we carried out model studies using allyl bromide. Treatment of trisubstituted δ-lactone **8** with LDA followed by addition of allyl bromide gave, at best, 20% yield of the alkylated product **9** (Scheme 3). HMPA has been used to improve yields in the alkylation of δ-valerolactone,[15] but on addition of HMPA to our reaction, β-elimination occurred giving the α,β-unsaturated lactone **10** as the major product. However, when the reaction was repeated with the more reactive allyl iodide as the electrophile, **9** was obtained in 84% yield. From NMR studies it was evident that a single product had been isolated and the X-ray crystal structure confirmed that the allyl group in **9** was indeed on the opposite face to the protected vicinal diol as required for the synthesis of pseudomonic acid.

The next stage was the preparation of the C_7 side chain **III** with iodide as the leaving group. The enantioselective synthesis of the analogous alcohol **15** (92% de) has been described by Keck and Tafesh.[16] We adopted a similar approach to **15** (Scheme 4) but used the known alcohol **11**[17] to establish the two asymmetric centres. Protection as the TBS ether **12** and reductive cleavage of the auxiliary using DIBAL-H at −78 °C gave aldehyde **13** in 93% yield over the two steps. Chain extension of **13** to **14** followed by reduction with DIBAL-H gave the required allylic alcohol **15** (> 99% de). Reaction of **15** with DIPHOS and I_2 at 0 °C[18] gave allylic iodide **16** in quantitative yield. The key alkylation of the lithium enolate of δ-lactone **7** with allylic iodide **16** in the presence of HMPA led to the required tetrasubstituted δ-lactone **17** in 85% yield after purification (Scheme 5).

Having created all the necessary asymmetric centres around the central δ-lactone core, the next goal was reduction to the analogous tetrahydropyran using a modification of the procedure described by Kraus *et al.*[19] Treatment of lactone **17** with

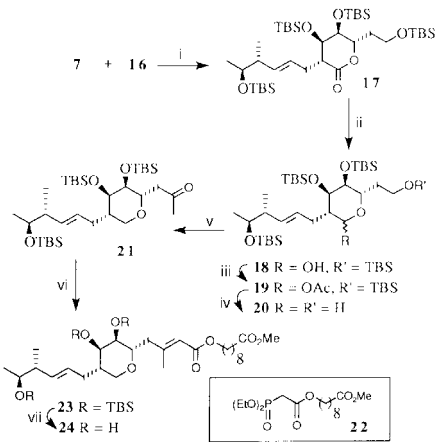

Scheme 5 *Reagents and conditions*: i, LDA, HMPA, −78 to 5 °C; ii, DIBAL-H, CH_2Cl_2, −78 °C; iii, Ac_2O, pyridine; iv, Et_3SiH, $BF_3{\cdot}Et_2O$, CH_2Cl_2, −78 °C; v, PDC, CH_2Cl_2 then MeMgBr, Et_2O, −5 °C then TPAP, NMO, CH_2Cl_2; vi, **22**, KHMDS, THF; viii, TBAF, THF.

DIBAL-H in CH_2Cl_2 at −78 °C gave lactol **18** which could be reduced directly to the tetrahydropyran with triethylsilane in the presence of $BF_3{\cdot}Et_2O$. However, an improved yield was obtained by acetylation to **19** prior to the triethylsilane reduction. The reaction conditions led to the concommitant selective removal of the TBS ether to unmask the primary alcohol **20** required for the next stage of the synthesis. Oxidation of **20** with PDC to the corresponding aldehyde, introduction of C-17 using MeMgBr and a second oxidation with TPAP then gave methyl ketone **21** in 74% yield from **20**.

The final carbon–carbon bond forming reaction was the Horner–Emmons coupling of ketone **21** with phosphonate **22** (prepared in 75% yield by the DCC/DMAP mediated coupling methyl 9-hydroxynonanoic acid with diethyl phosphonoacetic acid) giving the *E*-unsaturated ester **23**. Deprotection of the TBS ethers with TBAF gave methyl pseudomonate C **24**, with spectroscopic data in accord with those previously reported[7,20] and with $[\alpha]_D$ +10.0 (*c* 0.15, $CHCl_3$). Interestingly our literature search revealed no $[\alpha]_D$ value for methyl pseudomonate C derived from natural sources and only that for material prepared by total synthesis.[20] Hence a sample of pseudomonic acid C isolated from *Ps. fluorescens* was methylated giving ester **24** with $[\alpha]_D$ +10.7 (*c* 0.3, $CHCl_3$), in good agreement with the value obtained for our synthetic sample. The methyl ester may be hydrolysed[20] to pseudomonic acid C.

We are grateful to the EPSRC and SB for funding (to C. M.), Dr T. M. Peakman for NOE studies and to Ms K. M. Anderson and Professor A. G. Orpen for X-ray studies.

Notes and references

1 P. J. O'Hanlon, N. H. Rogers and J. W. Tyler, *J. Chem. Soc., Perkin Trans. 1*, 1983, 2655.
2 M. J. Basker, K. R. Comber, J. P. Clayton, P. C. T. Hannan, L. W. Mizen, N. H. Rogers, B. Slocombe and R. Sutherland, *Curr. Chemother. Infect. Dis.; Proc. Int. Congr. Chemother.*, 1979, **1**, 471; J. Hugher and G. Mellows, *Biochem. J.*, 1978, **176**, 305.
3 H. Shiozawa, T. Kagasaki, T. Kinoshita, H. Haruyama, H. Domon, Y. Utsui, K. Kodama and S. Takahashi, *J. Antibiotics*, 1993, **46**, 1834.
4 E. B. Chain and G. J. Mellows, *J. Chem. Soc., Perkin Trans. 1*, 1977, 294; T. C. Feline, R. B. Jones, G. Mellows and L. Philips, *J. Chem. Soc., Perkin Trans. 1*, 1977, 309.
5 F. M. Martin and T. J. Simpson, *J. Chem. Soc., Perkin Trans. 1*, 1989, 207.
6 For a review, see: Y. J. Class and P. DeShong, *Chem. Rev.*, 1995, **95**, 1843.
7 G. E. Keck, D. F. Kachensky and E. J. Enholm, *J. Org. Chem.*, 1985, **50**, 4317.
8 N. Broom, P. J. O'Hanlon, T. J. Simpson, R. Stephen and C. L. Willis, *J. Chem. Soc., Perkin Trans. 1*, 1995, 3067.
9 H. Greuter, J. Dingwall, P. Martin and D. Beelus, *Helv. Chim Acta*, 1981, **64**, 2812; R. Newton, personal communication.
10 P. A. Grieco, *J. Org. Chem.*, 1972, **37**, 2363.
11 S. V. Ley, J. Norman, W. P. Griffiths and S. P. Marsden, *Synthesis*,1994, 639.
12 See, for example: D. Askin, T. R. Verhoevan, T. M. H. Liu and I. Shinkai, *J. Org. Chem.*, 1991, **56**, 4929; J. H. Hutchinson and T. Money, *J. Chem. Soc., Chem. Commun.*, 1986, 288; K. Tomioka, H. Kawasakai, K. Yasuda and K. Koga, *J. Am. Chem. Soc.*, 1988, **110**, 3597; S. Takane, M. Morimoto, K. Matsuda and K. Ogasawara, *Chem. Pharm. Bull.*, 1982, **30**, 4238.
13 D. Seebach, H. Chow, R. F. W. Jackson, A. Sutter, S. Thaisrivongs and J. Zimmermann, *Liebigs Ann. Chem.*, 1986, 1281.
14 I. Paterson, *Tetrahedron Lett.*, 1979, **17**, 1519; L. Poppe, L. Novak, P. Kolonitz, A. Bata and C. Szantay, *Tetrahedron*, 1988, **44**, 1477.
15 R. Walton and B. Fraser-Reid, *J. Am. Chem. Soc.*, 1991, **113**, 5791.
16 G. E. Keck and A. M. Tafesh, *J. Org. Chem.*, 1989, **54**, 5845.
17 W. Oppolzer, J. Blagg, I. Rodriguez and E. Walther, *J. Am. Chem. Soc.*, 1990, **112**, 2767; W. Oppolzer, C. Starkemann, I. Rodriguez and G. Bernardinelli, *Tetrahedron Lett.*, 1991, **32**, 61.
18 S. P. Schmidt and D. Brooks, *Tetrahedron Lett.*, 1987, **28**, 767.
19 G. A. Kraus, K. A. Frazier, B. D. Roth, M. J. Taschner and K. Neuenschwander, *J. Org. Chem.*, 1981, **46**, 2417.
20 J. C. Barrish, H. L. Lee, T. Mitt, G. Pizzolato, E. G. Bagglioni and M. R. Uskokvic, *J. Org. Chem.*, 1988, **53**, 4282.

ChemComm

Mesomorphic phase transition of a cyclotetraphosphazene containing Schiff base moieties: comparison with the corresponding cyclotriphosphazene

Keiichi Moriya,*[a] Yasuyuki Kawanishi,[a] Shinichi Yano[a] and Meisetsu Kajiwara[b]

[a] *Department of Chemistry, Faculty of Engineering, Gifu University, Yanagido, Gifu 501-1193, Japan. E-mail: moriya@apchem.gifu-u.ac.jp*

[b] *School of Dentistry, Aichigakuin University, Kusumoto-cho, 1-100 Chikusa-ku 464-0074, Japan*

Received (in Oxford, UK) 13th January 2000, Accepted 10th May 2000
Published on the Web 8th June 2000

Newly prepared octakis{4-[*N*-(4′-heptyloxyphenyl)iminomethyl]phenoxy}cyclotetraphosphazene, consisting of a cyclotetraphosphazene ring backbone and Schiff base side-chain groups has been found to generate an enantiotropic smectic A phase; this is a first example of a mesomorphic cyclotetraphosphazene.

Cyclotetraphosphazenes are cyclic compounds of general formula $(PNX_2)_4$, in which tetracoordinated phosphorus atoms alternate regularly with the nitrogen atoms (Fig. 1). Several cyclotetraphosphazenes have been synthesized by introducing functional side chains into them.[1,2] Although some examples of mesomorphic transitions in cyclotriphosphazenes have been described[3–7] no liquid crystalline phases of cyclotetraphosphazenes have been observed.[5,7] In particular, in a previous paper, we reported our studies on phase transitions of cyclotetraphosphazenes and cyclotriphosphazenes with the same 4-octyloxybiphenyl mesogenic side groups.[5] We found no liquid crystalline phase for octakis[4-(4′-octyloxy)biphenoxy]-cyclotetraphosphazene **1** but an enantiotropic smectic C phase was observed for hexakis[4-(4′-octyloxy)biphenoxy]cyclotriphosphazene **2**. These results were interpreted in terms of the X-ray single crystal structure analyses of octakis(4-biphenoxy)-cyclotetraphosphazene (OBCP) and hexakis-(4-biphenoxy)cyclotriphosphazene (HBCP), which have shown the side chains lining-up randomly in the former but in a relatively regular fashion for the latter.[8] A similar situation might be assumed for compounds **1** and **2**. In tetramer **1**, the eight side chains are directed essentially randomly so preventing the formation of a mesomorphic layer structure. However, in trimer **2**, each of the three side chains of the cyclotriphosphazene molecules point almost perpendicularly upwards and downwards from the cyclotriphosphazene ring plane, which aids in the formation of a mesomorphic layer structure. The molecular structure of compound **2** assuming an all *trans* conformation for the octyloxy side chains based on the crystal structure of HBOP.[4] The architecture of the mesomorphic phase is reminiscent of arrangements of the mesomorphic phase in a cyclotetrasiloxane,[9] a dendric octasilsesquioxane,[10] and a fullerene derivative.[11]

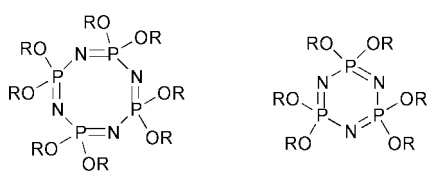

1, **3**

2, **4**

1, **2** R = $C_6H_4C_6H_4OC_8H_{17}$

3, **4** R = $C_6H_4CH{=}NC_6H_4OC_7H_{15}$

Fig. 1 Chemical formulae of octakis{4-[*N*-(4′-heptyloxyphenyl)iminomethyl]phenoxy}cyclotetraphosphazene **3** and hexakis{4-[*N*-(4′-heptyloxyphenyl)iminomethyl]phenoxy}cyclotriposphazene **4**, octakis[4-(4′-octyloxy)biphenoxy]cyclotetraphosphazene **1** and hexakis[4-(4′-octyloxy)biphenoxy]cyclotriphosphazene **2**.

Schiff bases have a strong tendency to produce mesomophic phases.[6,12,13] Therefore, for attempted generation of liquid crystalline behavior, we synthesized octakis{4-[*N*-(4′-heptyloxyphenyl)iminomethyl]phenoxy}cyclotetraphosphazene **3** (Fig. 1), with side chains containing Schiff bases with long alkoxy tails, laterally linked to the cyclotetraphosphazene ring. We studied its phase transitions and mesogenicity using polarizing microscopy and DSC measurements, and the obtained results were compared with those for the cyclotriphosphazene, hexakis{4-[*N*-(4′-heptyloxyphenyl)iminomethyl]phenoxy}cyclotriphosphazene **4** with similar mesogenic side groups (Fig. 1). This paper presents the first evidence for the formation of a mesophase in cyclotetraphosphazenes.

Compound **1** was synthesized as follows. 4-Heptyloxyacetanilide **5** was prepared from 4-hydroxyacetanilide (25 g, 0.16 mol), bromoheptane (28.5 g, 0.16 mol) and KOH (11 g, 0.17 mol) in ethanol (200 ml) under reflux for 6 h. 4-Heptyloxyaniline **6** was synthesized from **5** (20 g, 83 mmol) and KOH (15 g, 0.23 mol) in ethanol (200 ml) under reflux for 24 h. Hexakis(4-formylphenoxy)cyclotetraphosphazene **7** was prepared from hexachlorocyclotetraphosphazene (5.0 g, 10.6 mmol) (Nihon Soda Co., Ltd.) and the sodium salt of 4-hydroxybenzaldehyde in THF (125 ml) under reflux for 3 h. The sodium salt was prepared from 4-hydroxybenzaldehyde (17.5 g, 0.143 mol) and NaH (5.73 g, 0.143 mol) in THF under reflux for 2 h. Finally, compound **3** was prepared by the reaction of **6** (2.7 g, 13 mmol) and **7** (1.0 g, 0.87 mmol) in benzene (50 ml) under reflux for 6 h. Water produced in the solution was removed by molecular sieves in a Dean–Stark tube. The obtained crude products were separated by filtration and recrystallized three times from benzene and once from THF–cyclohexane (1:1) after being separated by filtration. Compound **3** was characterized by ^{1}H and ^{31}P NMR, IR spectroscopy and elemental analysis.[14] Phase transitions were studied using Seiko DSC 210 and SSC 5500 systems from room temperature to above the melting point at heating/cooling rates of 5 K min^{-1}. The textures of the mesophase were observed using a polarizing microscope (Nikon, Optiphot-pol XTP-11) with a temperature controlled hot stage (Mettler, FP-80) at heating/cooling rates of 5 K min^{-1}.

The DSC thermograms of octakis{4-[*N*-(4′-heptyloxyphenyl)iminomethyl]phenoxy}cyclotetraphosphazene **3** for the first cooling (1c) and second heating (2h) processes are shown in Fig. 2. For the first cooling process, two exothermic peaks were observed at 429 and 422 K. According to polarizing microscopy, upon cooling from an isotropic liquid, batonnets were observed at 429 K which grew into a fan texture at *ca.* 428.8 K, suggesting the presence of a smectic A phase.[15] In the first heating process, two endothermic peaks were observed at 428 and 430 K. According to polarizing microscopy, melting of compound **3** was observed at 428 K and between 428 and 430 K a fan texture similar to that in the first cooling process was seen, which establishes the existence of the smectic A phase. The view become black at 430 K, which corresponds to the SmA–I phase transition. This is the first case of a mesomorphic phase in cyclotetraphosphazenes.

DOI: 10.1039/b000497i

Table 1 Phase transition temperatures (T/K) and (in parentheses) phase transition enthalpies (ΔH/kJ mol^{-1}) and entropies (ΔS/J K^{-1} mol^{-1}) of compound **1**–**4**

Compound	Side chain	Backbone	Cr		Sm1		SmC		SmA		I
1	$C_8H_{17}OC_6H_4C_6H_4O$	P_4N_4	·	411(76,185)	—		—		—		·
2	$C_8H_{17}OC_6H_4C_6H_4O$	P_3N_3	·	440(79,180)	—		·	457(15,33)	—		·
3	$C_7H_{15}OC_6H_4N{=}CC_6H_4O$	P_4N_4	·	428(77,180)	—		—		·	430(28,66)	·
4	$C_7H_{15}OC_6H_4N{=}CC_6H_4O$	P_3N_3	·	460(74,161)	·	482(1,3)	·	499(0.5,1)	·	512(18,35)	·

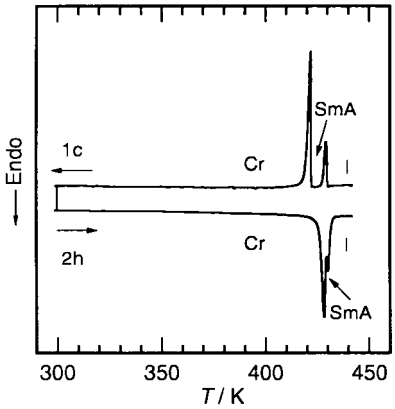

Fig. 2 DSC thermograms of octakis{4-[*N*-(4′-heptyloxyphenyl)iminomethyl]phenoxy}cyclotetraphosphazene **3** for the first cooling (1c) and second heating (2h) processes.

Table 1 shows a comparison of the phase transition temperatures, phase transition enthalpies and entropies for the pairs of tetramers (**1**, **3**) and trimers (**2**, **4**) bearing the same mesogenic substituents: octyloxybiphenoxy (**1**, **2**) and 4-{*N*-[4′-heptyloxyphenyl]iminomethyl}phenoxy groups (**3**, **4**). The thermodynamic values were obtained from the second heating process *via* DSC measurements. For the tetramers, the derivative **3** with substituents containing the Schiff base (compound **3**) has a narrow enantiotropic liquid crystalline phase with a temperature range of only 2 K, while no mesomorphic phase was observed for the derivative with octyloxybiphenoxy side chains (compound **1**).[5] The trimer with the Schiff base substituents (compound **4**) shows the enantiotropic mesomorphic phase transition sequence Cr–Sm1–SmC–SmA–I.[6] It displays a high SmA–I transition temperature (512 K) and wide mesomorphic phase transition region (ΔT = 52 K). By contrast, the trimer with octyloxybiphenoxy side chains (compound **2**) undergoes an enantiotropic mesomorphic phase transition, Cr–SmC–I.[3–5] The SmC phase was confirmed by X-ray photography under a magnetic field.[3] The SmC–I transition temperature (457 K) is lower, and the mesomorphic phase transition region (ΔT = 17 K) is narrower than those for the trimer with the Schiff base substituents (compound **4**). The compounds with the Schiff base side chains appear to have a higher thermal stability in the mesomorphic phase and higher mesomorphic phase generation ability than those with 4-octyloxybiphenoxy side chains. Two possible interpretations for the observed differences may be considered. In the first, the molecular structure of the tetramer with Schiff base side chains is assumed to differ significantly from that of the tetramer with octyloxybiphenoxy side chains. The other possible interpretation is that the intermolecular interactions might be much stronger for the Schiff base derivative **3** than for the octyloxybiphenoxy derivative **1** even if the molecular structures do not differ very much from each other. Based on this assumption, the mesomorphic ability of the compounds with Schiff base side chains would be high. Assuming this, and that compound **3** retains this molecular structure after melting, it would appear to be difficult to form a mesomorphic phase because of the random orientation of the side groups. Probably, the cyclotetraphosphazene rings would soften and the Schiff base side chains can form a smectic A layer structure. This behavior was observed in the SmA phase of the cyclotriphosphazene with dodecylbiphenoxy side groups, in which the local order parameter around the P atom obtained by ^{31}P NMR spectroscopy was *ca.* 0.44.[4] This value is lower than that in a typical sectic A phase and suggests the presence of disorder in the cyclotriphosphazene. The difference in the mesogenicity of tetramers and trimers is a result of their differing molecular structure.

In conclusion, we have introduced mesogenic side groups containing Schiff base functionalities onto the cyclotetraphosphazene ring and obtained the first N_4P_4 derivative capable of generating a mesomorphic smectic A phase. The liquid crystalline behavior results from assistance from the Schiff base to the formation of a layer structure due to the favorable intermolecular interactions of the laterally linked mesogenic units, which may override the formation of random orientations of the side chains typical in cyclotetraphosphazenes.

We are grateful to Nihon Soda Co., Ltd. for providing octachlorocyclotetraphosphazene.

Notes and references

1 H. R. Allcock, *Chem. Rev.*, 1972, **72**, 319.
2 C. W. Allen, in *The Chemistry of Inorganic Homo- and Heterocycles*, Academic Press, New York, 1987, ed. I. Haiduc and D. B. Sowerby, vol. 2, pp. 501.
3 A. M. Levelut and K. Moriya, *Liq. Cryst.*, 1996, **20**, 119.
4 K. Moriya, H. Mizusaki, M. Kato, T. Suzuki, S. Yano, M. Kajiwara and K. Tashiro, *Chem. Mater.*, 1997, **9**, 255.
5 K. Moriya, T. Suzuki, H. Mizusaki, S. Yano and M. Kajiwara, *Chem. Lett.*, 1997, 1001.
6 K. Moriya, T. Masuda, T. Suzuki, S. Yano and M. Kajiwara, *Mol. Cryst. Liq. Cryst.*, 1998, **318**, 267.
7 K. Moriya, T. Suzuki, Y. Kawanishi, T. Masuda, H. Mizusaki, S. Nakagawa, H. Ikematsu, K. Mizuno, S. Yano and M. Kajiwara, *Appl. Organomet. Chem.*, 1998, **12**, 771.
8 H. R. Allcock, D. C. Ngo, M. Parvez, R. R. Whittle and W. J. Birdsall, *J. Am. Chem. Soc.*, 1991, **113**, 2628.
9 G. H. Mehl and J. W. Goody, *Chem. Ber.*, 1996, **129**, 521.
10 I. M. Saez and J. W. Goodby, *Liq. Cryst.*, 1999, **26**, 1101.
11 T. Chuard, R. Deschenaux, A. Hirsch and H. Schönberger, *Chem. Commun.*, 1999, 2103.
12 W. Spratte and G. M. Schneider, *Mol. Cryst. Liq. Cryst.*, 1979, **51**, 101.
13 A. Wregeleben, L. Richter, J. Deresch and D. Demus, *Mol. Cryst. Liq. Cryst.*, 1980, **59**, 329.
14 *Characterization data* for compound **3**: mp 425 K; IR (KBr) 2932, 2856, 1625, 1604, 1578, 1251, 1220, 1174, 1161, 985, 846 cm^{-1}; ^{1}H NMR ($CDCl_3$) δ 0.9 (t, *J* 7.0 Hz, 3H), 1.3–1.8 (m, 10H), 3.9 (t, *J* 6.6 Hz, 2H), 6.8 (d, *J* 9.0 Hz, 2H), 7.0 (d, *J* 9.0 Hz, 2H), 7.1 (d, *J* 9.0 Hz, 2H), 7.7 (d, *J* 8.8 Hz, 2H), 8.4 (s, 1H); ^{31}P NMR δ −12.7 (s). Anal. Calc. for $C_{160}H_{192}O_{16}N_4P_4$: C, 72.16; H, 7.27; N, 6.31 Found: C, 71.94; H, 7.08; N, 6.25%. ^{1}H NMR (solvent $CDCl_3$) and ^{31}P NMR (solvent $CDCl_3$) spectra were recorded on a JEOL A-400 spectrometer using TMS as the internal standard for the former and 85% H_3PO_4 as the external standard for the latter.
15 D. Demus and D. Richter, in *Textures of Liquid Crystals*, Verlag Chemie, Weinheim, 1978, p. 32.

ChemComm

First successful enantiomeric discrimination of chiral alkanes using NMR spectroscopy

Muriel Sarfati, Jacques Courtieu and Philippe Lesot*

Laboratoire de Chimie Structurale Organique, CNRS ESA 8074, ICMO, Bât. 410, Université de Paris-Sud, 91405 Orsay, France. E-mail: philesot@icmo.u-psud.fr

Received (in Cambridge) 7th April 2000, Accepted 17th May 2000
Published on the Web 8th June 2000

Natural abundance deuterium NMR spectroscopy in a chiral polypeptide liquid crystal solvent (PBLG) is used to successfully discriminate between chiral alkanes.

The enantiomeric differentiation of saturated chiral hydrocarbons is an interesting but difficult task using NMR spectroscopy. Among this class of compounds, 3-methylhexane **1**, -heptane **2** and -octane **3** are excellent illustrative examples.

Although the separation of 3-methylhexane by gas chromatography using undiluted cyclodextrin derivatives as a chiral stationary phase is noteworthy,[1] to the best of our knowledge, all isotropic NMR techniques have failed to discriminate between such chiral alkanes, as no successful results have been reported to date. This situation occurs mainly because these compounds do not possess any functional groups, making the derivatisation of the chiral molecule or the preparation *in situ* of specific complexation agents impossible.[2] Consequently, only NMR analytical approaches in which shape recognition plays an important role in the chiral discrimination mechanisms, compared with the electrostatic interaction contributions, are likely to produce successful results.

In this preliminary work, we demonstrate for the first time that enantiomeric discrimination of chiral alkanes is possible using natural abundance deuterium (NAD) NMR spectroscopy in a chiral polypeptide liquid-crystalline solvent composed of poly-γ-benzyl-L-glutamate (PBLG) dissolved in chloroform.[3,4]

Four different reasons justify the use of this unusual NMR tool. First, we have recently shown that the shape of solutes plays a important role in the differential orientation effect (DOE) of two enantiomers in the PBLG phase.[5,6] Second, since it may be expected that the difference in the interaction between the *R* and *S* isomers and the polypeptide helices will generate a rather small DOE, it is necessary to observe a very sensitive order-dependent NMR interaction, such as the quadrupolar interaction for deuterium ($I = 1$) nuclei.[3] Indeed, when the orientational difference between the *R* and *S* isomers is small, the relatively large magnitude of the deuterium quadrupolar coupling constant for a C–D bond (QCC ≈ 170 kHz)[7] can give a sufficiently large difference in their residual quadrupolar splittings ($\Delta\nu_Q^R - \Delta\nu_Q^S$), enabling their observation. Third, since the detection of rare spins such as deuterons in natural abundance is not an insurmountable obstacle in terms of sensitivity (*i.e.* detection using standard NMR equipment and reasonable experimental time), the site-specific labelling of the chiral molecules is not required, avoiding time-consuming synthetic work.[3] Finally, all possible deuterated sites of the molecule can be simultaneously probed, thus increasing the probability of observing a chiral differentiation.[3]

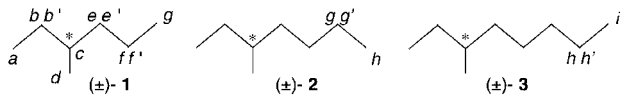

Proton-decoupled NAD NMR spectra in organic solutions of PBLG consist of the superposition of independent quadrupolar doublets, $\Delta\nu_{Q_i}$, corresponding to all non-equivalent deuterons in each of the two enantiomers.[3,4] Thus, in the case of (±)-**1**, (±)-**2**, and (±)-**3**, 20, 24 and 28 different chiral isotopomers exist in the mixture respectively, and a maximum of 20, 24 and 28 doublets, respectively, are expected to be detected if all deuterated sites show a chiral discrimination. Consequently, even if dipolar couplings between two rare atoms cannot be detected, the correlation between the two components for each quadrupolar doublet is not always simple, mainly due to overlapping of peaks, and requires the use of proton-decoupled deuterium 2D-NMR experiments.[4]

Fig. 1 reports the NAD 2D Q-COSY spectrum† of (±)-**1**‡ in the PBLG–$CHCl_3$ phase recorded at 298 K over 16 h at 61.4 MHz.[4] In this 2D spectrum, we can observe 12 different quadrupolar doublets. This result clearly indicates that two deuterons in the molecule are differentiated between, as only 10 doublets would be observed if no chiral separation occured. To confirm this result, we have recorded the NAD 2D Q-COSY spectrum of (±)-**1** in a racemic mixture of PBLG and PBDG (the enantiomer of PBLG) in $CHCl_3$.[6,8] In this mixture, the fast exchange between chiral solutes and the vicinity of PBLG and PBDG eliminates the chiral discrimination, hence only 10 quadrupolar doublets can be (and were) observed. The assignment of each doublet is non-trivial because all deuterons in methylene groups are diasteorotopic (non-equivalent),[3,4] and deuterium chemical shift dispersion in apolar alkanes is rather small. However, we can indirectly identify them from analysis of HMQC (^1H–^{13}C) and INADEQUATE (^{13}C–^{13}C) 2D spectra of (±)-**1** in an isotropic state, which enable a clear assignment of ^{13}C and ^1H signals. Assuming that deuteron chemical shifts in

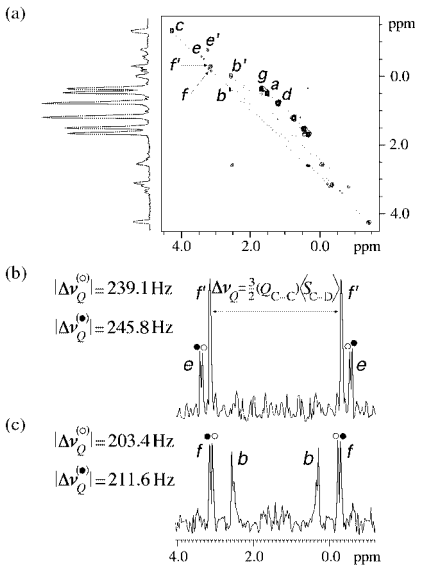

Fig. 1 2D contour plot of a NAD Q-COSY experiment obtained for (±)-**1** (a). The two columns extracted after tilting of the 2D spectrum show a chiral discrimination of the deuterons denoted *e*(b) and *f*(c). The doublet due to each enantiomer is arbitrarily labelled with (●) and (○). The chloroform doublet is not shown in the spectrum.

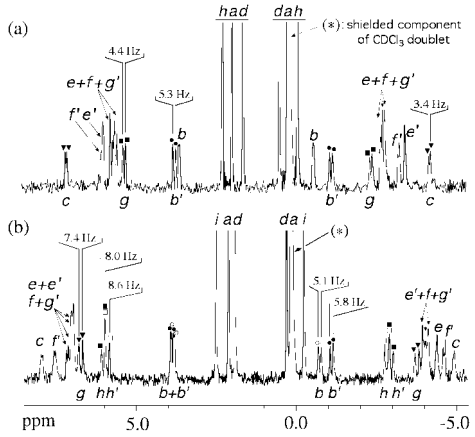

Fig. 2 NAD 1D spectra of (±)-**2** (a) and (±)-**3** (b). All clearly discriminated deuterons are labelled with different symbols.

PBLG are similar to those of protons measured in neat $CHCl_3$, it becomes possible to unambiguously assign almost all deuterium quadrupolar doublets. In addition, this assignment can be confirmed by measuring the proton–carbon dipolar couplings, $D_{C\text{-}H}$, in the carbon-13 spectrum of (±)-**1** in PBLG.[9] Since the ratio $|\Delta\nu_{Q_{C-D}}/D_{C-H}|$ can be quantified as 11.8 ± 0.2 (because $S_{C-D} = S_{C-H}$), we may *a priori* calculate the magnitude of $\Delta\nu_{Q_{C-D}}$ of the deuterons for a given assigned carbon and then compare with experimental values. Using this procedure, we were able to confirm that the deuterons *e* and *f* are discriminated between [Fig. 1(*b*) and (*c*)], while deuterons *b*, *b*' and *c* show broad peaks, indicating an unresolved chiral discrimination. In contrast, no chiral discrimination was detected between the methyl signals (*a*, *d*, *g*).

Fig. 2 reports the NAD 1D-NMR spectra† of (±)-**2**‡ and (±)-**3**‡ recorded at 298 K in the PBLG–$CHCl_3$ phase. Notably, we can unambiguously observe the doubling of numerous peaks, indicating that enantiomers of (±)-**2** and (±)-**3** are discriminated between in the PBLG–$CHCl_3$ phase. Here again, the assignment procedure previously described shows that the largest chiral separations are measured for the diastereotopic deuterons denoted *b*' and *g*, and *b*,*b*',*h*,*h*' and *g* for (±)-**2** and (±)-**3**, respectively. As for (±)-**1**, none of the methyl groups is discriminated between, but a small chiral separation has been observed on the deuteron attached to the asymmetric carbon on these compounds.

The successful enantiomeric differentiation of chiral flexible alkanes using deuterium NMR spectroscopy in PBLG is possible because the polypeptide helices are able to interact enantioselectively with non-functionalized enantiomers and because the sensitivity of the quadrupolar interaction to the DOE is sufficiently large to reveal small orientational differences. This result establishes the significant role of shape recognition in chiral discrimination mechanisms involved in the PBLG phase. An evaluation of the potential of this approach on a wide range of saturated and unsaturated chiral hydrocarbons is currently underway and will be extensively discussed in a subsequent publication.

We thank Professor Henri B. Kagan for stimulating discussions and Dr Claude Brevard from Bruker SA, France for the loan of a 5 mm selective ^2H probe with ^{19}F lock.

Notes and references

† NMR experiments: NMR experiments were performed on a Bruker DRX-400 using a 5 mm selective deuterium probe. The sample was not spun in the field and the temperature was controlled by the BVT 2000 system. Due to the good long term stability of the magnet, no field-frequency lock was used. The WALTZ-16 sequence was applied as broad-band proton decoupling. The 2D Q-COSY spectrum of (±)-**1** was recorded using 300 (t_1) × 1700 (t_2) data points. 400 transients for each t_1 increment were added, leading to a total of 120 000 scans. Gaussian filtering was applied in both dimensions. The 1D interferograms of (±)-**2** and (±)-**3** were acquired using a pulse angle of *ca*. 70°, a recycle delay of *ca*. 0.5 s and 1.7 k of data points, summing over 230 000 and 140 000 scans, respectively. No digital filtering was used.

‡ Sample composition: The liquid-crystalline NMR samples of (±)-**1**, (±)-**2**, (±)-**3** were prepared from 80, 50 and 60 mg of racemic material, 81 mg [degree of polymerisaton (DP) = 562(50%)+1078(50%)], 100 mg (DP = 562) and 100 mg (DP = 562) of PBLG (purchased from Sigma corp.) and 445, 400 and 400 mg of $CHCl_3$, respectively. For sample preparation, see refs. 4 and 5.

1 W. A. Köning, R. Krebber, S. Evers and G. Bruhn, *J. High Resolut. Chromatogr., Chromatogr., Commun.*, 1990, **13**, 702.
2 D. Parker, *Chem. Rev.*, 1991, **91**, 1441.
3 P. Lesot, D. Merlet, A. Loewenstein and J. Courtieu, *Tetrahedron: Asymmetry*, 1998, **9**, 1871.
4 D. Merlet, B. Ancian, J. Courtieu and P. Lesot, *J. Am. Chem. Soc.*, 1999, **121**, 5249.
5 P. Lesot, D. Merlet, T. P. Rantala, J. Jokisaari, J. W. Emsley and J. Courtieu, *J. Phys. Chem. A*, 1997, **101**, 5719.
6 C. Canlet, D. Merlet, P. Lesot, A. Meddour, A. Loewenstein and J. Courtieu, *Tetrahedron: Asymmetry*, 2000, **11**, 1911.
7 J. W. Emsley and J. C. Lindon, *NMR Spectroscopy Using Liquid Crystal Solvents*, Pergamon Press, Oxford, 1975.
8 K. Czarniecka and E. T. Samulski, *Mol. Cryst. Liq. Cryst.*, 1981, **63**, 205.
9 P. Lesot, D. Merlet, A. Loewenstein and J. Courtieu, *J. Chem. Soc., Faraday Trans.*, 1998, **91**, 1371.

Low-temperature, clean catalytic combustion of N-bearing gasified biomass using a novel NH_3 trapping catalyst

Robert Burch and Barry W. L. Southward*

School of Chemistry, The Queen's University of Belfast, Belfast, UK BT9 5AG. E-mail: b.w.l.southward@qub.ac.uk

Received (in Cambridge, UK) 3rd April 2000, Accepted 11th May 2000
Published on the Web 8th June 2000

Substantially reduced NO_x emissions are obtained in the low temperature catalytic combustion of NH_3-bearing simulated biogas by use of a novel 1%Pt/20%CuO/Al_2O_3-trapping catalyst and cyclic operation between fuel lean and rich conditions.

The exploitation of renewable energy sources to both limit CO_2 emissions and extend fossil fuel reserves is a subject of considerable interest with the former aspiration being embodied in the landmark Kyoto agreement.[1] This interest is exemplified by the various attempts to harness biomass-derived fuels for combined heat and power generation.[2–7] However, during gasification, biogenic nitrogen, fixed during plant growth, is converted into significant quantities of NH_3 (600–4000 ppm) in addition to the main fuel components, CO (9.8–17.2%) and H_2 (9.8–13.2%) as well as CH_4, CO_2, H_2O and N_2.[2] The presence of this NH_3 is a particular obstacle to the exploitation of biogas as a fuel since its combustion in a conventional burner results in the formation of significant amounts of nitrogen oxides (NO_x) which are well-known atmospheric pollutants.[8]

Attempts to overcome this problem by catalytic combustion of the NH_3/fuel mix have met with limited success with N_2 yields of $< 70\%$ being typical.[3,4] In contrast, we have demonstrated substantially improved performance using either redox-acid catalysts, such as 12-tungstophosphoric acid which yield *ca*. 85% N_2,[5] or by use of a catalyst which can couple NH_3 oxidation and NO_x reduction using the fuel components of the biogas mixture[6] giving close to 100% N_2 selectivity. However, in order to achieve these high conversions of NH_3 to N_2, both catalysts must be operated at temperatures $\geqslant 600$ °C. We have now discovered for the first time a procedure for the selective oxidation of NH_3 to N_2 in simulated biogas, which can operate at temperatures as low as 200 °C.

The catalyst used was 1%Pt/20%CuO/Al_2O_3 (hereafter referred to as PtCu) prepared by sequential incipient wetness impregnation of Al_2O_3 (Criterion CK300, surface area 200 $m^2\ g^{-1}$). The dried Al_2O_3 (120 °C, 24 h) was first impregnated with $CuSO_4{\cdot}5H_2O$ (ex Aldrich 98%) dried (24 h at room temperature, 24 h at 120 °C), and calcined (500 °C, 24 h). The process was repeated for the addition of 1% Pt ($PtDNDA_{aq}$ ex Johnson Matthey, 2.28% Pt). The preparation of 1%Pt/Al_2O_3 was performed in an identical manner. Catalyst testing (60 mg) was performed in a standard quartz flow microreactor described previously[7] at a gas flow rate of 300 $cm^3\ min^{-1}$, (GHSV of *ca*. 240 000 h^{-1}). NO_x emissions and residual NH_3 levels were determined using an external NH_3 oxidation reactor (with independent oxygen supply) coupled to a NO_x chemiluminescence detector (Signal series 4000 with data logging at 1 s intervals using Signal SIGLOG). Switching between lean and rich fuel conditions was achieved using a pressure-balanced three-way valve immediately prior to the O_2 mass flow controller. This enabled the oxidant to be 'switched' from 20% O_2/He (lean conditions) to 1%O_2/He (rich conditions).

Fig. 1 illustrates both the lean steady state and switching activity of the PtCu for the oxidation of NH_3 under comparatively mild conditions (1000 ppm NH_3, 1.02% CO, 0.68% H_2). The steady-state N_2 yield was *ca*. 94%, already a significant improvement upon previous data[3,4] and is ascribed to the establishment of an *internal selective catalytic reduction* (*i*SCR) mechanism[5,7]

However, unlike previous metal and metal oxide systems for NH_3 oxidation, the PtCu catalyst is unique and may be considered to be a composite material with a strong synergy between two very specific but different active sites. Pt provides the first site whose function is the activation of NH_3, which has been shown to be the rate limiting step of the *i*SCR reaction.[7,9,10] The second site then resides on the Cu, which adsorbs NH_3 to produce an NH_x(ads) species (as shown by NH_3 TPD[11]) These NH_x(ads) species then react with the NO_x formed on the Pt to give N_2, consistent with the proposals of Janssen *et al*.[12]

The synergistic effect is particularly apparent when comparing the activity of the PtCu with both 10%Cu/Al_2O_3 and 1%Pt/Al_2O_3. 10%Cu/Al_2O_3 was found to require temperatures of *ca*. 400 °C to produce high yields of N_2 ($> 90\%$) while although 1%Pt/Al_2O_3 was active at lower temperatures it gave only a very low selectivity (*ca*. 29% N_2 at 200 °C).

The high N_2 yields of the PtCu were further improved by transient switching of the oxidant (15 s rich, 45 s lean). Indeed, by switching it was possible to obtain peak N_2 yields of 100% before N_2 production decreased over some 500 s to the values obtained under steady state conditions. This reflects the buffering of the system *via* the reservoir of NH_x(ads) species on the Cu. Under lean conditions these species are 'titrated' by *in situ* NO but in the absence of sufficient O_2 for full reaction the Cu accumulates an NH_x(ads) adsorbate layer, thus preventing NH_3 'slip'.

The importance of transient operation is seen even more clearly when we compare the activities of 1%Pt/Al_2O_3 with the PtCu catalyst in a more realistic feed stream containing high levels of the fuel components (5.1% CO and 3.4% H_2) (Fig. 2). In this case under lean conditions NH_3 conversion was again 100%, but in both cases NH_3 was predominantly converted into NO, reflecting an interception of any NO–NH_3 reaction. Moreover, as can be seen in Fig. 2 (filled diamonds) oxidant

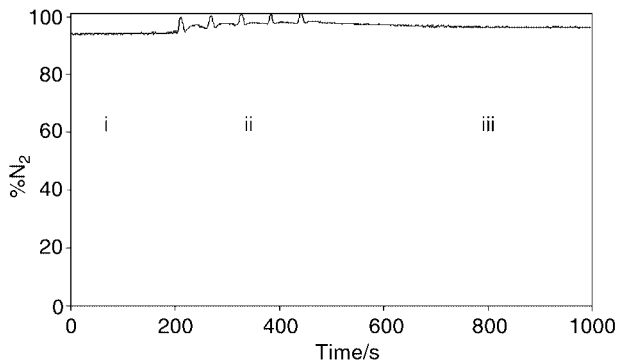

Fig. 1 N_2 production from the selective catalytic oxidation of NH_3/CO/H_2 over 1%Pt/20%CuO/Al_2O_3 at 200 °C (1000 ppm NH_3, 1.02% CO, 0.68% H_2, with either 2.1% O_2 (lean conditions) or 0.1% O_2 (rich conditions), balance He). Key: i, first 200 s of operation is under lean conditions; ii, cyclic operation 15 s rich/45 s lean for 300 s; iii, final 500 s operation is under lean conditions.

DOI: 10.1039/b002594l

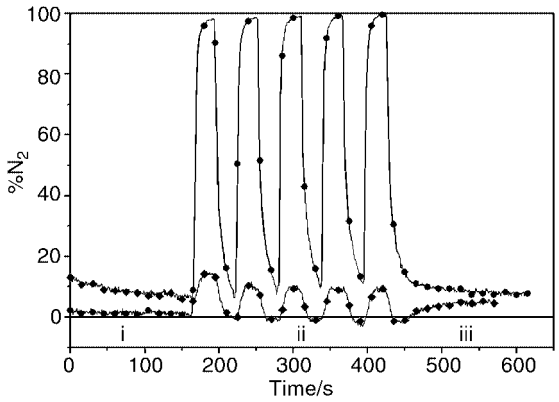

Fig. 2 N_2 production from the selective catalytic oxidation of $NH_3/CO/H_2$ over $1\%Pt/Al_2O_3$ and $1\%Pt/20\%CuO/Al_2O_3$ at 200 °C (1000 ppm NH_3, 5.1% CO, 3.4% H_2, 9.3% O_2 (lean conditions) or 0.5% O_2 (rich conditions), balance He). Key: i, first 180 s operation is lean; ii, cyclic operation 30 s rich/30 s lean for 300 s; iii, final operation under lean conditions. (◆) $1\%Pt/Al_2O_3$, (●) $1\%Pt/20\%CuO/Al_2O_3$.

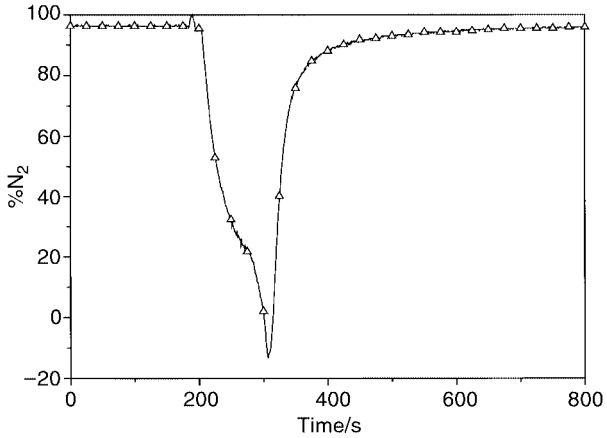

Fig. 3 N_2 production from the selective catalytic oxidation of $NH_3/CO/H_2$ over $1\%Pt/20\%CuO/Al_2O_3$ at 200 °C (1000 ppm NH_3, 1.02% CO, 0.68% H_2, with either 2.1% O_2 (lean conditions) or 0.1% O_2 (rich conditions), balance He). Key: i, first 180 s of operation is under lean conditions; ii, rich operation for 120 s; iii, final 500 s operation is under lean conditions.

cycling had a minimal effect on N_2 yields for the $1\%Pt/Al_2O_3$ catalyst. In contrast, with the PtCu catalyst (filled circles), under transient conditions there was a sudden and dramatic improvement in catalyst selectivity, with > 98% N_2 production being recorded.

These observations are entirely consistent with the proposed *i*SCR reaction, and may be rationalised as follows: in the case of the PtCu sample only, on switching to rich operation, the CuO was partially reduced by NH_3 to produce a reservoir of NH_x(ads). Then, on switching to lean conditions, all the gas phase NH_3 was again fully oxidised to NO on the Pt, but the NO formed is reduced to N_2 by NH_x(ads) on the Cu. However, this reduction process is limited by the concentration of NH_x(ads) and once these species are consumed excess NO is observed, in agreement with our experimental observations.

Further evidence of the trapping mechanism is found by examination of the effect of switching time on activity. Fig. 3 illustrates the activity of PtCu, under dilute fuel conditions at 200 °C when the rich phase is extended to 120 s. Again the initial increase in N_2 is observed (*cf.* Fig. 1). However, extending the period under rich conditions leads to a saturation of the trap and the breakthrough of NH_3/loss of N_2, clearly demonstrating the link between cyclic operation and high N_2 yields.

In conclusion, we have developed a potential strategy for the low-temperature removal of NH_3 from biomass-derived gases by the cyclic operation of a regenerable NH_3 trap catalyst which facilitates an *i*SCR-type reaction. Experiments have demonstrated that the concept is viable and provides a further novel method to overcome the environmental problems associated with the direct combustion of biogas. The strategy may be equally applicable to any comparable gasification gas derived from coal, or other renewable source. The concept is a further example of the advantages which may be gained by forcing catalysts to work harder by periodic perturbation of the reaction conditions.[13–15]

We are pleased to acknowledge the financial support of ABB-Alstom power, DTI, and EPSRC through the FORESIGHT Challenge initiative. Helpful discussions with colleagues at Lens (Dr M. Amblard), Cranfield University (Mr J. J. Witton, Professor B. Moss, Mr J. M. Przybylski and Dr E. Noordally) and at ABB-Alstom Power (Mr M. Cannon, G. J. Kelsall) are gratefully acknowledged.

Notes and references

1 *Kyoto Protocol to the United Nations Framework Convention on Climate Change*, Kyoto, Japan, 1–10 December, 1997.
2 *Development of Improved Stable Catalysts and Trace Element Capture for Hot Gas Cleaning*, DTI / ETSU / Clean Coal Power Generation Group, Project Profile 178, Harwell, Oxfordshire, 1996.
3 L. Lietti, C. Groppi and C. Ramella, *Catal. Lett.*, 1998, **53**, 91.
4 M. F. M. Zwinkels, G. M. Eloise Heginuz, B. H. Gregertsen, K. Sjöström and S. G. Järås, *Appl. Catal. A Gen.*, 1997, **148**, 325.
5 R. Burch and B. W. L. Southward, *Chem. Commun.*, 1999, 1475.
6 R. Burch and B. W. L. Southward, *Br. Pat. Appl.*, 98238879.3, 1998; R. Burch and B. W. L. Southward, *Chem. Commun.*, 2000, 703.
7 M. Amblard, R. Burch and B. W. L. Southward, *Appl. Catal. B Environ.*, 1999, **22**, L159.
8 P. J. Millington, PhD Thesis, University of Reading, 1995.
9 M. Amblard, PhD Thesis, University of Reading, 1999.
10 N. I. Il'chenko and G. I. Golodets, *J. Catal.*, 1975, **39**, 57; N. I. Il'chenko and G. I. Golodets, *J. Catal.*, 1975, **39**, 73.
11 R. Burch and B. W. L. Southward, *J. Catal.*, submitted.
12 F. J. J. G. Janssen, F. M. G. van den Kerkhof, H. Bosch and J. R. H. Ross, *J. Phys. Chem.*, 1987, **91**, 5921; F. J. J. G. Janssen, F. M. G. van den Kerkhof, H. Bosch and J. R. H. Ross, *J. Phys. Chem.*, 1987, **91**, 6633.
13 R. Burch, P. Fornasiero and B. W. L. Southward, *J. Catal.*, 1999, **182**, 234.
14 D. J. Crittle, PhD Thesis, University of Reading, 1999.
15 *Eur. Pat.*, EP 573 672A1, 1992 (to Toyota).

ChemComm

Electrophilic halogenation of thioethers: 5-chloro- and 5,6-dichloro-5,6-dihydro-1,3-dithiolo[4,5-*b*][1,4]dithiine-2-one and an efficient synthesis of vinylenedithiotetrathiafulvalene (VDT-TTF)

Olivier J. Dautel, Jan Larsen and Marc Fourmigué*

Sciences Moléculaires aux Interfaces, FRE 2068 CNRS, 2, rue de la Houssinière, BP32229 44322 Nantes, France. E-mail: fourmigue@cnrs.imn.fr

Received (in Liverpool, UK) 10th March 2000, Accepted 16th May 2000
Published on the Web 8th June 2000

The SO_2Cl_2 chlorination of 5,6-dihydro-1,3-dithiolo[4,5-*b*]-[1,4]dithiine-2-one affords the corresponding mono- and *trans*-di-chloro derivatives which eliminate HCl upon treatment with KF/18-crown-6 or LiBr/HMPA, offering an easy route to the unsaturated vinylenedithiotetrathiafulvalene (VDT-TTF).

Halogen···halogen intermolecular interactions[1] have been recently used for the resolution of racemic bromoalkanes[2] and for the elaboration of novel organic conductors based on bromo- or iodo-tetrathiafulvalenes.[3,4] The strongly decreased donor ability of the analogous chlorinated TTFs prompted us to look for novel derivatives where the halogen atoms are not conjugated with the π-redox TTF core. Since the direct halogenation of the ethylenedithio moieties of the oxidation-sensitive bis(ethylenedithio)tetrathiafulvalene (BEDT-TTF) is not possible, we investigated the electrophilic halogenation of its precursor, *i.e.* 5,6-dihydro-1,3-dithiolo[4,5-*b*][1,4]dithiine-2-one[5] **1** and report here on the synthesis and reactivity of the mono- and dichloro derivatives of **1**.

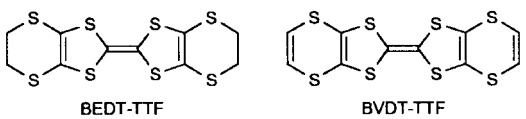

The chlorination of **1** was efficiently performed with 1 equiv. of SO_2Cl_2 in refluxing CCl_4 to afford racemic (*R*,*S*)-**2** in 91% yield (Scheme 1).† With two equiv. of sulfuryl chloride, *trans*-5,6-dihydro-5,6-dichloro-1,3-dithiolo[4,5-*b*][1,4]dithiine-2-one **3** was obtained in 60% yield as a racemic mixture of (*R*,*R*) and (*S*,*S*) enantiomers without any (*R*,*S*) isomer, as confirmed by the presence of a single ^{1}H NMR signal and the X-ray crystal structure resolution of **3** (Fig. 1).‡ The molecule is located on an *mm*2 site in which the two chlorine atoms adopt axial positions while the carbon atoms are disordered, a consequence of the (*R*,*R*) and (*S*,*S*) racemic mixture. This *trans* addition, also observed in the dichlorination of 1,4-dithiane,[6] derives from the lowered nucleophilicity of the sulfur atom of **2**, α to the CHCl group (Scheme 2). The electrophilic reagent thus reacts on the second sulfur atom and the migration of the Cl^+ moiety occurs on the less hindered side, followed by HCl elimination to afford **3**. Note also that only traces of the trichloro derivative were obtained with an excess of chlorinating agent, while prolonged refluxing only led to product degradation.

In an attempt to obtain the corresponding mono- and difluoro derivatives of **1** by substitution of the chlorine atoms, **2** and **3** were reacted with KF/18-crown-6 as described, for example, in the reaction of $PhSCH_2Cl$ to give $PhSCH_2F$.[7] Under those conditions however, we observed that HCl elimination took place instead, affording in both cases the corresponding vinylic derivatives **4** and **5** in 50 and 60% yield, respectively (Scheme 1). This reaction thus provides easy access to the vinylic dithiolone **4**, otherwise prepared in low yield from the $dmit^{2-}$ dianion.[8,9] This is all the more appealing since **4** can be used as a starting material for a number of attractive target molecules, such as bisvinylenedithiotetrathiafulvalene (BVDT-TTF),[10] the unsymmetrically substituted vinylenedithiotetrathiafulvalene (VDT-TTF) as well as metal dithiolene complexes which can now be prepared from **4**.

A first illustration of this potential is given here by the chloro diester derivative **7**, obtained by $P(OMe)_3$ cross-coupling of **2** with **6**,[11] which directly affords VDT-TTF in 60% yield upon treatment with LiBr/HMPA in a one-pot reaction (Scheme 3) in which the two ester groups are hydrolysed and decarboxylated

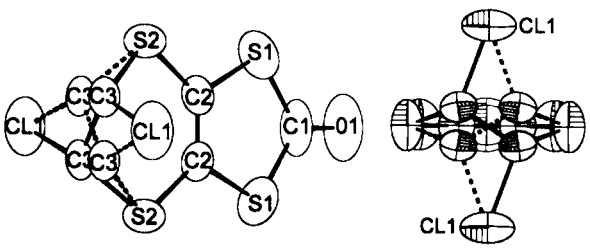

Fig. 1 Two views of the dichloro derivative **3**, showing the statistical distribution of the (*R*,*R*) (unbroken line bonds) and (*S*,*S*) (dashed line bonds) enantiomers in the crystalline form.

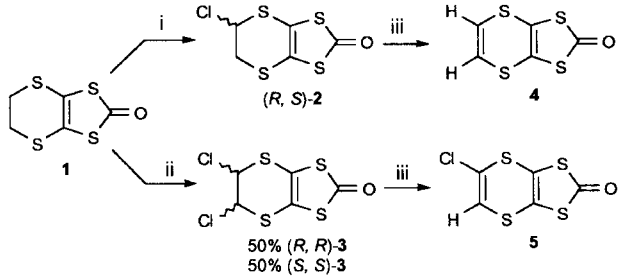

Scheme 1 *Reagents and conditions:* i, 1 equiv. SO_2Cl_2, CCl_4, reflux, 24 h; ii, 2 equiv. SO_2Cl_2, CCl_4, reflux, 24 h; iii, 4 equiv. KF, 0.2 equiv. 18-crown-6, MeCN, reflux, 18 h.

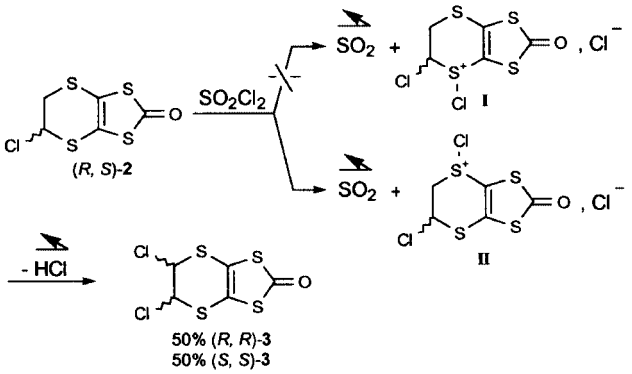

Scheme 2 Postulated mechanism for the chlorination of **2**.

DOI: 10.1039/b001996h

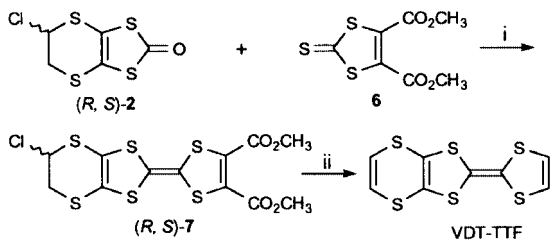

Scheme 3 *Reagents and conditions:* i, $P(OMe)_3$, reflux, 3 h; ii, 11 equiv. LiBr, HMPA, 80 °C, 30 min, 150 °C, 60 min.

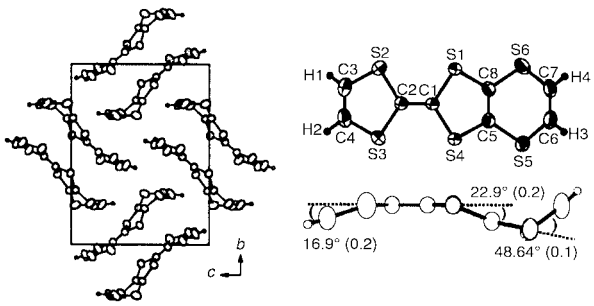

Fig. 2 The X-ray crystal structure of VDT-TTF. Left: projection view of the unit cell along *a*. Right: ORTEP view and numbering scheme of the VDT-TTF molecule (with 50% probability displacement ellipsoids) and folding angles of the dithiole and dithiine rings.

while HCl is simultaneously eliminated under these basic conditions. Note that the reported synthesis of VDT-TTF involved the coupling of **4** with **6** in 8% yield and further decarboxylation in 18% yield.[12] Recrystallization from toluene afforded red crystals the X-ray crystal structure of which prove them to be isostructural with the saturated EDT-TTF analogue (Fig. 2).‡ Of particular note are the folding angles of the five- and six-membered rings along the S···S axes, 16.9(2) and 22.9(2)° in the dithiole rings along S2···S3 and S1···S4, respectively and 48.6(1)° along S5···S6 in the dithiine ring.[13] The availability of VDT-TTF will allow thorough investigations of its radical cation salts with various counter anions as well as reactivity studies, particularly in lithiation experiments where both types of vinylic hydrogen atoms of VDT-TTF might compete for metallation.

The efficient halogenation reactions described here, and the reactivity of the chlorinated species will prompt us to investigate the preparation of the corresponding halogenated tetrathiafulvalenes and their radical cation salts. Furthermore, other chlorinating agents are also being investigated with **1** for the synthesis of the tetrachloro derivative, while preliminary results on its direct fluorination showed the Selectfluor® reagent to be effective.

Notes and references

† *Selected data* for **2**: white crystals; mp 84 °C (CCl_4), δ_H(200 MHz, $CDCl_3$): 3.39 (dd, ^3J 13.5, 6.9 Hz, 1H), 3.66 (dd, ^3J 13.5, 3.3 Hz, 1H), 5.79 (dd, ^3J 6.9; 3.3 Hz, 1H). δ_C(50 MHz, $CDCl_3$): 188.7, 114.4, 114.1, 59.2, 39.7. ν_{max}(KBr)/cm^{-1}: 1675 (C=O). MS (70 eV, EI): *m/z* (%) 244 (6), 243 (52), 242 (13, $M^{\bullet+}$), 241 (91), 213 (57), 88 (63), 76 (100) (Anal. Calc for $C_5H_3ClOS_4$ (242.795): C, 24.73; H, 1.25; Cl, 14.60. Found: C, 24.80; H, 1.11; Cl, 14.88%). For **3**: light yellow platelets; mp 157 °C (CCl_4), δ_H(200 MHz, $CDCl_3$): 5.52 (s, 2H). δ_C(50 MHz, $CDCl_3$): 187.1 (1C), 110.5 (2C), 62.1 (2C). ν_{max}(KBr)/cm^{-1}: 1670 (C=O). MS (70 eV, EI): *m/z* (%) 278 (17), 276 (54, $M^{\bullet+}$), 247 (45), 151 (49), 88 (90), 76 (100). (Anal. Calc. for $C_5H_2Cl_2OS_4$ (277.240): C, 21.66; H, 0.73; Cl, 25.58; S, 46,26. Found: C, 21.68; H, 0.76; Cl, 25.36; S, 45.64%). For **4**: light yellow needles; mp 99 °C (MeCN), δ_H(200 MHz, $CDCl_3$): 6.61 (s, 2H). δ_C(50 MHz, $CDCl_3$): 192.3 (1C), 123.9 (2C), 117.2 (2C). ν_{max}(KBr)/cm^{-1}: 1665 (C=O). MS (70 eV, EI): *m/z* (%) 206 (84, $M^{\bullet+}$), 178 (100), 88 (78), 76 (78) (Anal. calc. for $C_5H_2OS_4$ (206.334): C, 29.11; H, 0.98; S, 62.16. Found: C, 29.07; H, 0.92; S, 60.30%). For **5**: white crystals; mp 160 °C (CCl_4), δ_H(200 MHz, $CDCl_3$): (s, 1H). δ_C(50 MHz, $CDCl_3$): 191.2, 127.7, 120.1, 119.0, 118.4. ν_{max}(KBr)/cm^{-1}: 1663 (C=O). MS (70 eV, EI): *m/z* (%) 239 (96, $M^{\bullet+}$), 211 (88), 136 (100), 76 (57) (Anal. Calc for C_5HClOS_4 (239.860): C, 24.94; H, 0.42; Cl, 14.72; S, 53.27. Found: C, 25.07; H, 0.52; Cl, 14.84; S, 51.77%). For **7**: black needles; mp 128 °C (toluene–cyclohexane, 3:7), δ_H(200 MHz, $CDCl_3$): 3.30 (dd, ^3J 13.4, 7.0 Hz, 1H), 3.50 (dd, ^3J 13.4, 3.6 Hz, 1H), 3.83 (s, 6H), 5.72 (dd, ^3J 3.6, 7.0 Hz, 1H). δ_C(50 MHz, $CDCl_3$): 159.8 (2C), 131.9, 129.0, 116.0 (2C), 115.4 (2C), 59.1, 53.5 (2C), 39.5. ν_{max}(KBr)/cm^{-1}: 1720 (C=O). MS (70 eV, EI): *m/z* (%) 444 (28, $M^{\bullet+}$), 381 (63), 261 (100), 218 (38), 76 (29) (Anal. Calc. for $C_{12}H_9ClO_4S_6$ (445.046): C, 32.39; H, 2.04; Cl, 7.97; O, 14.38; S, 43.23. Found: C, 32.88; H, 1.99; Cl, 8.00; O, 14.23; S, 42.04%). For VDT-TTF: red platelets; mp 185 °C (toluene), δ_H(200 MHz, $CDCl_3$): 6.34 (s, 2H), 6.54 (s, 2H). δ_C(50 MHz, $CDCl_3$): 129.0, 128.3, 125.3, 124.7 (2C), 118.9 (2C). MS (70 eV, EI): *m/z* (%) 291 (59, $M^{\bullet+}$), 146 (100), 88 (38) (Anal. Calc. for $C_8H_4S_6$ (291.864): C, 32.85; H, 1.38; S, 65.77. Found: C, 33.05; H, 1.32; S, 65.73%).

‡ X-Ray data for **3** and VDT-TTF were collected on a Stoe Imaging Plate Diffractometer (IPDS) with Mo-Kα radiation, λ = 0.71073 Å at T = 293(2) K. The structures were solved by direct methods and refined against F^2 using the SHELXTL5.04 set of programs. Hydrogen atoms in VDT-TTF were found in the Fourier difference map and refined isotropically.

Crystal data for **3**: $C_5H_2Cl_2OS_4$, M = 277.240, orthorhombic, space group *Pmmn*, a = 7.0595(21), b = 7.4252(20), c = 9.3827(22) Å, V = 491.8(4) Å^3, Z = 2, D_c = 1.875 g cm^{-3}, μ = 1.456 mm^{-1}, data collected = 2833, unique data = 2091 (R_{int} = 0.0337) of which 323 with $I > 2\sigma(I)$, $R(F)$ = 0.0357, $R_w(F^2)$ = 0.0871.

For VDT-TTF: $C_8H_4S_6$, M = 292.47, monoclinic, space group $P2_1/n$, a = 6.4203(13), b = 14.905(3), c = 11.648(2) Å, V = 1112.4(4) Å^3, Z = 4, D_c = 1.746 g cm^{-3}, μ = 1.182 mm^{-1}, data collected = 8649, unique data = 2142 (R_{int} = 0.0515) of which 5988 with $I > 2\sigma(I)$, $R(F)$ = 0.0268, $R_w(F^2)$ = 0.0565.

CCDC 182/1640. See http://www.rsc.org/suppdata/cc/b0/b001996h/ for crystallographic data in .cif format.

1 G. R. Desiraju, in *Crystal Engineering, The Design of Organic Solids*, Elsevier, Amsterdam, 1989, ch. 6; G. R. Desiraju, *Chem. Commun.*, 1997, 1475.
2 A. Farina, S. V. Meille, M. T. Messina, P. Metrangelo, G. Resnati and G. Vecchio, *Angew. Chem., Int. Ed.*, 1999, **38**, 2433.
3 M. Jørgensen and K. Bechgaard, *Synthesis*, 1989, 208; M. R. Bryce and G. Cooke, *Synthesis*, 1991, 263; U. Kux, H. Suzuki, S. Sasaki and M. Iyoda, *Chem. Lett.*, 1995, 183.
4 R. Gompper, J. Hock, K. Polborn, E. Dormann and H. Winter, *Adv. Mater.*, 1995, **7**, 41; Y. Kuwatani, E. Ogura, H. Nishikawa, I. Ikemoto and M. Iyoda, *Chem. Lett.*, 1997, 817; T. Imakubo, T. Maruyama, H. Sawa and K. Kobayashi, *Chem. Commun.*, 1998, 2021.
5 K. Hartke, T. Kissel, J. Quante and R. Matusch, *Chem. Ber.*, 1980, **113**, 1898.
6 H. T. Kalff and C. Romers, *Recl. Trav. Chim. Pays-Bas*, 1966, **85**, 637; H. T. Kalff and C. Romers, *Acta Crystallogr.*, 1965, **18**, 164.
7 K. M. More and J. Wemple, *Synthesis*, 1977, 791.
8 T. Nakamura, S. Iwasaka, H. Nakano, K. Inoue, T. Nogami and H. Mikawa, *Bull. Chem. Soc. Jpn.*, 1987, **60**, 365.
9 G. C. Papavassiliou, V. C. Kakoussis, D. J. Lagouvardos and G. A. Mousdis, *Mol. Cryst. Liq. Cryst.*, 1990, **181**, 171.
10 H. Kobayashi, A. Kobayashi, T. Nakamura, T. Nogami and Y. Shirota, *Chem. Lett.*, 1987, 559.
11 M. V. Lakshmikantham and M. P. Cava, *J. Org. Chem.*, 1980, **45**, 2632.
12 G. C. Papavassiliou, J. S. Zambounis, G. A. Mousdis, V. Gionis and S. Y. Yiannopoulos, *Mol. Cryst. Liq. Cryst.*, 1988, **156**, 269.
13 Similar folding angles are observed in the structure of the neutral BVDT-TTF. See ref. 8.

ChemComm

A biomimetic model reaction for the extradiol catechol dioxygenases

Gang Lin,[a] Gillian Reid[b] and Timothy D. H. Bugg*[a]

[a] *Department of Chemistry, University of Warwick, Coventry, UK CV4 7AL. E-mail: mssgv@csv.warwick.ac.uk*
[b] *Department of Chemistry, University of Southampton, Highfield, Southampton, UK SO17 1BJ*

Received (in Liverpool, UK) 7th February 2000, Accepted 16th May 2000
Published on the Web 8th June 2000

A model reaction is described for extradiol catechol cleavage involving $FeCl_2$ or $FeCl_3$, 1,4,9-triazacyclononane (TACN), pyridine and dioxygen which shows similar cofactor and regio-selectivity to the extradiol catechol dioxygenases.

The oxidative cleavage of catechol and other dihydroxy aromatics is a key step in the biodegradation by soil bacteria of naturally occurring aromatic molecules and many aromatic environmental pollutants.[1]

The catechol dioxygenases are a class of non-haem iron enzymes that catalyse the oxidative cleavage of catechols. These enzymes can be divided into two subclasses (Scheme 1): the intradiol dioxygenases, which utilise a non-haem iron(III) cofactor, catalyse the cleavage of the carbon–carbon bond between the two catechol oxygens; and the extradiol dioxygenases, which utilise a non-haem iron(II) cofactor, catalyse the cleavage of the carbon–carbon bond adjacent to the catechol oxygens.[2]

The intradiol cleaving enzymes require non-haem Fe^{3+} to effect oxygen activation, which is ligated by two His and two Tyr moieties.[3] The extradiol cleaving enzymes require non-haem Fe^{2+} as an active site cofactor,[2,4] ligated by two His and one Glu ligands. Many attempts to model the catechol dioxygenases have been reported, but most catalysts give intradiol cleavage products.[5] However, there are three reported examples of extradiol cleavage by synthetic iron complexes. Funabiki *et al.*[6] found that $FeCl_2$ or $FeCl_3$ in THF–H_2O cleaves 3,5-di-*tert*-butylcatechol to substituted 2-pyrones, which were believed to derive from decarboxylation of the extradiol-cleavage intermediate α-keto lactone. Dei *et al.* found that the complex [Fe^{III}(TACN)Cl(dbc)] afforded 2-pyrone upon exposure to O_2 in 35% yield.[7] Ito and Que used the same complex to give an almost quantitative yield of 2-pyrone using a modified procedure.[8] However, none gave the authentic extradiol reaction product. Here, we report the first observation of extradiol ring fission product 2-hydroxymuconic aldehyde by an iron-dependent model reaction shown in Scheme 2. An investigation of the catalytic properties of $FeCl_2$ and $FeCl_3$ in the presence of a series of macrocyclic ligands, namely 1,4,7-triazacyclononane ([9]aneN_3, TACN), 1-oxo-4,7,10-triazacyclododecane ([12]aneN_3O), 1-oxo-4,7-diazacyclononane ([9]aneN_2O), 1,5,9-triazacyclododecane ([12]aneN_3), for extradiol catechol cleavage was carried out in methanol by UV–VIS spectroscopy (0.1 mM of catechol in methanol). Reaction of $FeCl_2$ or $FeCl_3$ in the presence of 1.0 equiv. TACN gave a new product absorbing at 315 nm. Upon addition of NaOH, the absorption maximum shifted immediately to 405 nm (Fig. 1), then over a

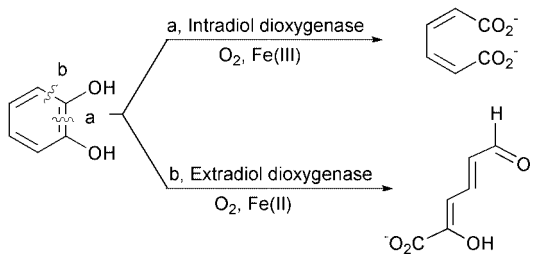

Scheme 1

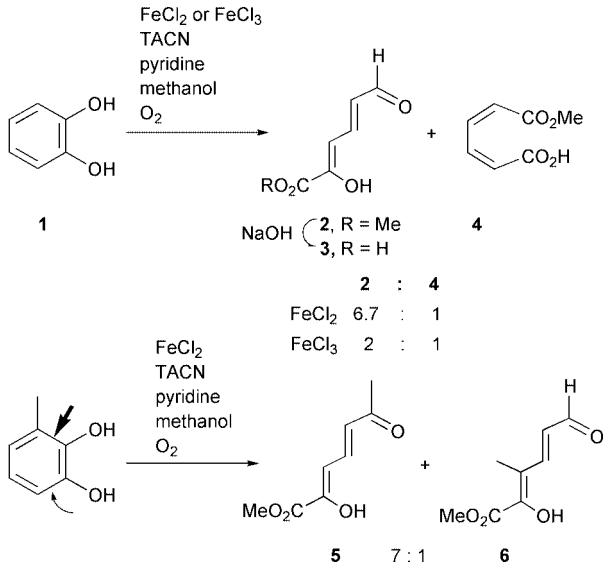

Scheme 2

period of 2 h to 378 nm, the characteristic λ_{max} for the extradiol ring fission product. The free acid form **3** of ring fission product **2** is reported to show an absorption maximum shift from 322 nm (pH 3) to 378 nm (pH 8) on passing from the enol to the enolate form.[9] The UV–VIS data suggested that the initial product was the methyl ester enol **2**, which was converted into the corresponding enolate, then hydrolysed to give the disodium salt of acid **3**. Reaction of $FeCl_2$ or $FeCl_3$ in the presence of each of the other macrocyclic ligands gave no absorbance above 300 nm, indicating no extradiol cleavage.

To confirm the identity of the reaction product, a large scale model reaction of catechol with O_2 in the presence of $FeCl_2$ or $FeCl_3$, pyridine and TACN with a ratio of 1 : 1 : 3 : 1 (cat : Fe : py- : TACN) was carried out in methanol by bubbling dioxygen gas into the solution for 3 h (for $FeCl_2$) or 5 h (for $FeCl_3$).† The ^{1}H NMR spectrum of the reaction product displayed signals

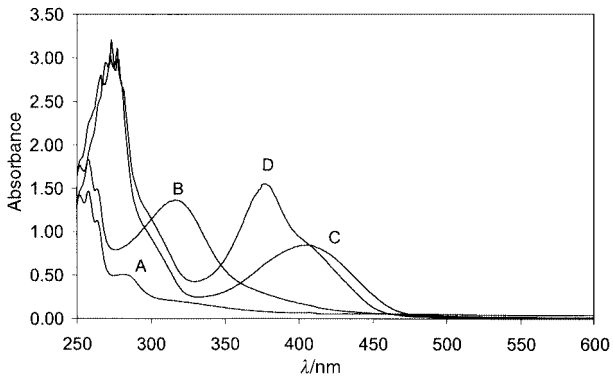

Fig. 1 UV–VIS spectra of (A) mixture of 0.1 mM catechol, 0.1 mM TACN, 0.3 mM pyridine, 0.1 mM $FeCl_2$ in methanol(recorded immediately after mixing), (B) the product **2** formed after 1 h, (C) methyl ester enolate upon adding NaOH (0.3 mM, final conc.) to B(recorded immediately after adding NaOH), (D) hydrolysis product **3** (recorded 2 h after addition of NaOH).

DOI: 10.1039/b003625k

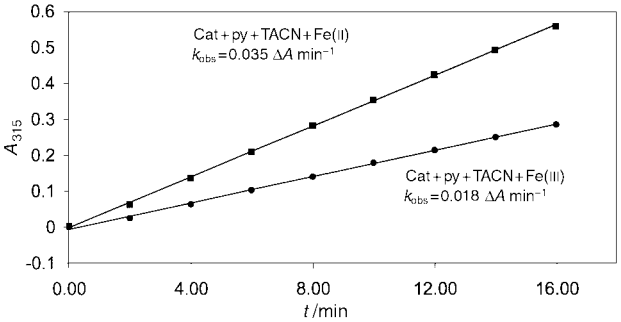

Fig. 2 Kinetic study of the reaction at 23 °C (0.1 mM catechol, 0.1 mM $FeCl_2$ or $FeCl_3$, 0.1 mM TACN, 0.3 mM pyridine in methanol). Absorbance at 315 nm was measured every 2 min for a total of 16 min.

corresponding to 2-hydroxymuconic semialdehyde methyl ester **2** as the major product, by comparison with NMR data for an enzymatic extradiol cleavage product,[11] and muconic acid monomethyl ester **4** as the minor product confirmed by comparison with authentic NMR spectral data (Scheme 2).[12]

This is the first reported reaction to give 2-hydroxymuconic semialdehyde as the major product from a biomimetic model reaction of extradiol dioxygenase. Its derivative 3,5-dibutyl-2-hydroxymuconic semialdehyde has been detected as a minor product previously from a reaction of 3,5-di-*tert*-butylcatechol, identified by Funabiki.[6] The extradiol cleavage product has also been generated using KO_2/DMSO.[10]

No ring fission was observed when either TACN, pyridine or Fe(II)/Fe(III) was omitted, indicating that all these reagents are essential for this reaction. The reaction was found to proceed using DBU in place of pyridine at a lower rate, but not using 2,6-lutidine or 4-dimethylaminopyridine. The absorption maximum at 315 nm was still observed using ethanol instead of methanol, but was not observed when the reaction was attempted in aqueous buffer. No activity was observed using $CuCl_2$, $CoCl_2$ or $MnCl_2$. Similarly, no activity was observed using $FeSO_4$ or $Fe(NH_4)_2(SO_4)_2$.

Interestingly, the reaction in the presence of $FeCl_2$ gave extradiol product **2** (50% yield by NMR spectroscopy using DMF as internal standard) and intradiol product **4** (7.5%) in a ratio of 6.7 : 1, while the reaction in the presence of $FeCl_3$ gave the products in a ratio of 2 : 1. Monitoring of A_{315} (corresponding to extradiol cleavage product only) revealed the reaction is twice as fast in the presence of 0.1 mM $FeCl_2$ (k_{obs} = 0.035 ΔA min^{-1}) than 0.1 mM $FeCl_3$ (k_{obs} = 0.018 ΔA min^{-1}) (Fig. 2). These observations imply that there is some intrinsically higher activity and specificity of Fe^{2+} for extradiol cleavage, which gives some insight into the fact that Fe^{2+} is the cofactor for the extradiol dioxygenase family.[2]

Furthermore, the treatment of 3-methylcatechol under the same conditions gave ketone **5** and aldehyde **6** in a ratio of 7 : 1 (only a trace amount of intradiol cleavage product) by NMR, which demonstrates that the model reaction also shows regioselectivity for the site of C–C cleavage. It is of interest that the model reaction shows the same selectivity as is found for extradiol dioxygenases which cleave 3-substituted catechols,[2] for example, 2,3-dihydroxyphenylpropionate 1,2-dioxygenase (MhpB) from *Escherichia coli*, which cleaves in the same way to give a ketone ring fission product whose ^{1}H NMR spectrum is almost identical to **5**.[11]

These observations raise the question of what the active iron-containing species during the reaction are. TACN has previously been shown to form a mononuclear, octahedral iron(III) complex with 3,5-di-*tert*-butylcatechol.[7] Monitoring of the $FeCl_3$-containing reaction at 0.4 mM TACN concentration by UV–VIS spectroscopy reveals the immediate formation of a complex (λ_{max} 456, 712 nm), which decays as product is formed, and whose UV–VIS spectrum matches that of the complex formed anaerobically between $FeCl_3$, TACN and catechol, indicating that an Fe(III)–TACN-catechol complex is formed. Monitoring of the $FeCl_2$-containing reaction at 0.4 mM TACN concentration by UV–VIS spectroscopy reveals immediate product formation at 315 nm, but only gradual formation of the Fe(III)–TACN-catechol complex, indicating that some oxidation of iron(II) is taking place during the reaction, but that a separate iron(II) complex is responsible for the majority of extradiol product formation. The formation of distinct iron(II) and iron(III) complexes, whose structures remain to be determined, would account for the different product distributions formed by $FeCl_2$ *cf.* $FeCl_3$.

In conclusion, this model reaction shows several features which closely mimic the extradiol dioxygenases. The extradiol ring fission product **2** is obtained as the major product; the reaction shows an inherent preference in extradiol selectivity for Fe^{2+} over Fe^{3+}, shows a similar regioselectivity to the extradiol dioxygenases, and demonstrates a selectivity for the TACN ligand which parallels the facial tridentate coordination found in the extradiol dioxygenase active site. It will be of interest to study the scope and the mechanism of this model reaction, and compare its properties with the enzyme-catalysed reaction.

This work was supported by a grant (B10351) from BBSRC.

Notes and references

† 11 mg (0.1 mmol) of catechol, 20 mg (0.1 mmol) of $FeCl_2 \cdot 4H_2O$, 24 mg (0.3 mmol) of pyridine and 12.9 mg (0.1 mmol) of TACN were dissolved in 500 mL of methanol in a single-necked round bottom flask. Oxygen gas was bubbled through the reaction mixture with stirring for 3 h. After removing the solvent, 2 mL of 10% HCl was added, and the products was extracted with diethyl ether and dried (Na_2SO_4). 2-hydroxymuconic semialdehyde methyl ester **2**: yield 50% (by NMR based on DMF as the internal standard): δ_H(300 MHz, $CDCl_3$) 9.55 (d, 1H, *J* = 7.8 Hz, 6-CHO), 7.51 (dd, 1H, *J* 15.3, 11.5 Hz, 4-H), 6.31 (d, 1H, *J* 11.5 Hz, 3-H), 6.21 (dd, 1H, *J* 15.3, 7.8 Hz, 5-H), 3.86 (s, 3H, 1-CO_2CH_3); δ_C(75 MHz, $CDCl_3$) 205.1, 194.1, 164.2, 144.6, 139.6, 133.3, 51.2. Muconic acid monomethyl ester **4**: yield 7.5% (by NMR based on DMF as the internal standard): δ_H (300 MHz, $CDCl_3$) 7.93 (dd, 0.15H, *J* 10.8, 10.8 Hz, 3-H), 7.80 (dd, 0.15H, *J* 10.8, 10.8 Hz, 4-H), 6.0 (m, 2- and 5-H), 3.7 (s, 0.45 H, 1-CO_2CH_3).

1 S. Dagley, *Essays Biochem.*, 1975, **11**, 81.
2 For reviews of the catechol dioxygenases, see: L. Que, Jr. and R. Y. N. Ho, *Chem. Rev.*, 1996, **96**, 2607; T. D. H. Bugg and C. J. Winfield, *Nat. Prod. Rep.*, 1998, **15**, 513.
3 D. H. Ohlendorf, J. D. Lipscomb and P. C. Weber, *Nature*, 1988, **336**, 403.
4 S. Han, L. P. Eltis, K. N. Timmis, S. W. Muchmore and J. T. Bolin, *Science*, 1996, **270**, 976; K. Sugimoto, T. Senda, H. Aoshima, E. Masai, M. Fukuda and Y. Mitsui, *Structure*, 1999, **7**, 953.
5 L. Que, Jr., R. C. Kolanczyk and L. S. White, *J. Am. Chem. Soc.*, 1987, **109**, 5373; H. G. Jang, D. D. Cox and L. Que, Jr., *J. Am. Chem. Soc.*, 1991, **113**, 9200; S. Fuji, H. Ohya-Nishiguchi, N. Hirota and A. Nishinaga, *Bull. Chem. Soc. Jpn.*, 1993, **66**, 1408; M. Duda, M. Pascaly and B. Krebs, *Chem. Commun.*, 1997, 835.
6 T. Funabiki, A. Mizoguchi, T. Sugimoto, S. Tada, M. Tsugi, H. Sakamoto and S. Yoshida, *J. Am. Chem. Soc.*, 1986, **108**, 2921.
7 A. Dei, D. Gatteschi and L. Pardi, *Inorg. Chem.*, 1993, **32**, 1389.
8 M. Ito and L. Que, Jr., *Angew. Chem., Int. Ed. Engl.*, 1997, **36**, 1342.
9 F. Terradas and W. Hugo, *Helv. Chim. Acta*, 1991, **74**, 124.
10 R. Muller and F. Lingens, *Z. Naturforsch., Teil C*, 1989, **44**, 207.
11 W. W. Y. Lam and T. D. H. Bugg, *J. Chem. Soc., Chem. Commun.*, 1994, 1163.
12 Muconic acid monomethyl ester **4** was prepared by a known method: D. Bankston, *Org. Synth.*, 1988, **66**, 180.

ChemComm

High temperature calcination for a highly efficient and regenerable B_2O_3/ZrO_2 catalyst for the synthesis of ε-caprolactam

Bo-Qing Xu,*[a] Shi-Biao Cheng,[b] Xin Zhang,[a] Shuang-Feng Ying[a] and Qi-Ming Zhu[a]

[a] *State Key Lab of C_1 Chemical Technology and Department of Chemistry, Tsinghua University, Beijing 100084, China. E-mail: bqxu@mailtsinghua.ed.cn*

[b] *Research Institute of Petroleum Processing, SINOPEC, Beijing 100083 China*

Received (in Cambridge, UK) 20th April 2000, Accepted 16th May 2000
Published on the Web 8th June 2000

High temperature calcination of boria-supported zirconia leads to highly selective and regenerable B_2O_3/ZrO_2 catalysts for the synthesis of ε-caprolactam by Beckmann rearrangement of cyclohexanone oxime.

The Beckmann rearrangement of cyclohexanone oxime is an important industrial reaction for the production of ε-caprolactam. The conventional technology makes use of fuming sulfuric acid as the catalyst in the liquid phase.[1] This technique is not environmentally friendly and is considered to be one of the most inefficient chemical processes, since it produces 2–5 equivalents of valueless by-product (ammonium sulfate) for every unit of the desired lactam product. It has long been hoped that this process could be replaced with one based on a solid acid catalyst.[2] However, the development of such a specific solid catalyst has proven to be a big challenge in heterogeneous catalysis. Borias supported on oxide supports are reported to be efficient catalysts for the Beckmann reaction.[3–7] The main obstacle to the practical use of these catalysts comes from the rapid deactivation and poor regeneration properties of these catalysts.[8,9] Since supported boria was believed to be volatile above 400 °C, the preparation of supported boria catalysts in the literature was deliberately developed in order to avoid using high calcination temperatures to activate the impregnated boria catalysts. Thus, calcination at 350 °C has become a 'standard' activation procedure for preparing supported boria catalysts.[3–7] Following the 'standard' preparation, we reported recently that boria supported on zirconia, B_2O_3/ZrO_2, was highly active and selective for lactam synthesis; the average lactam yield during a 6 h reaction over properly prepared B_2O_3/ZrO_2 catalyst was greater than 90%.[10,11] 'Pure' zirconia containing no boria showed very poor selectivity for the lactam synthesis.[11] Here, we show that activation of boria-loaded zirconia with high temperature (600–700 °C) calcinations produces highly selective (96–98%) catalysts for the Beckmann reaction. Although the loading of boria affects the catalyst activity and selectivity, deactivated catalysts can be regenerated, regardless of the boria loading, to their initial activity and selectivity by calcination at 600 °C.

Samples of B_2O_3/ZrO_2 were prepared by impregnation of the zirconia support with an aqueous solution of boric acid.[10,11] The boria loading in the catalyst was determined by ICP-MS analysis, and is expressed as a weight percentage of the catalyst sample. Zirconyl hydroxide, which was obtained by hydrolysis of $ZrOCl_2 \cdot 8H_2O$ with an aqueous solution of ammonia (25–28 wt% NH_3), was used as the precursor for the support. Before introduction of the boria, this support precursor was precalcined in air at various temperatures. After the support had been loaded with boria, the catalyst sample was activated by a further calcination at elevated temperatures in air. Both the calcination of the support and of the catalyst was carried out for 10 h. The Beckmann rearrangement reaction was performed on a down-flow fixed bed reactor at 300 °C with 10wt% cyclohexanone oxime in benzene (solvent), and with N_2 as the carrier gas. The weight hourly space velocity (WHSV) of the oxime reactant was 0.32 h^{-1}. Experimental details for the catalyst preparation and the gas-phase Beckmann reaction have been described elsewhere.[10,11] Regeneration of the deactivated catalyst was performed by calcination in air at 600 °C for 8 h.

The precalcination temperature (PCT) of the support precursor [$ZrO(OH)_2 \cdot xH_2O$] before loading with boria, the loading of boria, and the catalyst activation (calcination) temperature (CAT) after the loading are important parameters for catalyst preparation.[12,13] When the CAT is fixed for the preparation, the catalyst activity and selectivity at a fixed loading of boria can be significantly modified by changing the PCT. When the temperature for the catalyst activation is kept at or below 500 °C (CAT $\leqslant$ 500 °C), support precalcination at 300 °C (*i.e.* PCT = 300 °C) leads to the highest oxime conversion activities among 10% B_2O_3/ZrO_2 samples with various PCT histories.[13] Catalysts with PCT $\geqslant$300 °C also effectively reduce the formation of undesirable by-products when compared with samples prepared using lower PCTs.[13] In this work, the PCT is fixed at 300 °C for the catalyst samples to examine the effect of varying the CAT on the Beckmann reaction. A catalyst loaded with 9.5% B_2O_3 has been used for this prupose. This loading of boria is close to the optimum load with the 'standard' preparation (CAT = 350 °C) on a zirconia support precalcined at 500 °C (PCT = 500 °C).[11] Table 1 shows that oxime conversion and the selectivity and yield of the lactam are little affected over the entire period on an 8 h reaction time on stream (TOS) when the CAT is increased from the 'standard' activation temperature (350 °C) to 500 °C over this 9.5% B_2O_3/ZrO_2 catalyst. However, a further increase in the CAT to 600 °C results in dramatically improved selectivity and yield of the desired lactam; the selectivity increases from 70–80% to values greater than 95%, and the average lactam yield increases from *ca.* 70% to 92%. The last group of data at the bottom of the Table 1 gives the results of the reaction over a 'pure' zirconia support that was activated at 600 °C. Except at the very beginning of the reaction, the desired lactam product is basically not produced. This observation agrees with our conclusions from earlier work that the active catalytic sites for the Beckmann reaction are connected with boria in the sample.[13] ICP-MS analysis showed that the B_2O_3 loading in the three samples with CAT = 350, 500 and 600 °C are in the range 9.0–9.7%, which indicates that no significant loss of boron occurs during catalyst activation (calcination) with CAT > 400 °C. It is, therefore, clear that high temperature activation (calcination) is essential for the preparation of highly efficient B_2O_3/ZrO_2 catalysts. The ability of B_2O_3 to withstand the high temperature calcinations suggests a strong interaction between B_2O_3 and the support surface.

With CAT = 600 °C for the catalyst preparation, samples of B_2O_3/ZrO_2 catalysts were prepared with various loadings of boria. Fig. 1 presents the time course of the oxime conversion over two B_2O_3/ZrO_2 samples with 5 and 13.5% B_2O_3 by weight, respectively. While the oxime conversion decreases more or less with reaction time, no significant change (< 2%) in the lactam selectivity is observed over both catalysts; the lactam selectivity is 81–83% with the 5% B_2O_3/ZrO_2 sample and 96–97% with the 13.5% B_2O_3/ZrO_2 sample (not shown in the figure). Experiments were undertaken in order to ascertain the

Table 1 Effect of catalyst activation/calcination temperature (CAT) on the Beckmann rearrangement of cyclohexanone oxime[a]

Sample	TOS/h 1	2	3	4	5	6	7	8	Average
CAT = 350 °C									
Oxime conv. (%)	98.2	100	100	100	100	98.9	85.3	88.0	96.3
Lactam selec. (%)	76.5	73.6	70.9	74.5	75.7	74.4	81.6	80.0	76.5
Lactam yield (%)	75.1	73.6	70.9	74.5	75.7	73.6	69.6	70.4	73.7
CAT = 500 °C									
Oxime conv. (%)	100	100	100	100	100	97.4	89.6	80.9	96.0
Lactam selec. (%)	71.4	68.7	69.0	69.0	69.4	69.3	74.7	79.3	71.4
Lactam yield (%)	71.4	68.7	69.0	69.0	69.4	67.5	66.9	64.2	68.5
CAT = 600 °C									
Oxime conv. (%)	100	100	100	100	100	96.1	89.9	81.8	96.0
Lactam selec. (%)	96.7	96.1	96.3	96.2	96.0	95.8	95.7	95.0	96.0
Lactam yield (%)	96.7	96.1	96.3	96.2	96.0	92.1	86.0	77.7	92.1
ZrO_2-600[b]									
Oxime conv. (%)	73.5	—	16.9	—	0.2	—	0.1	0	18.2
Lactam selec. (%)	4.2	—	0	—	0	—	0	0	0.9
Lactam yield (%)	3.1	—	0	—	0	—	0	0	0.6

[a] Catalyst: 9.5% B_2O_3/ZrO_2; reaction temperature: 300 °C; WHSV: 0.32 h^{-1}; solvent/carrier: benzene/N_2. [b] Zirconia support calcined at 600 °C.

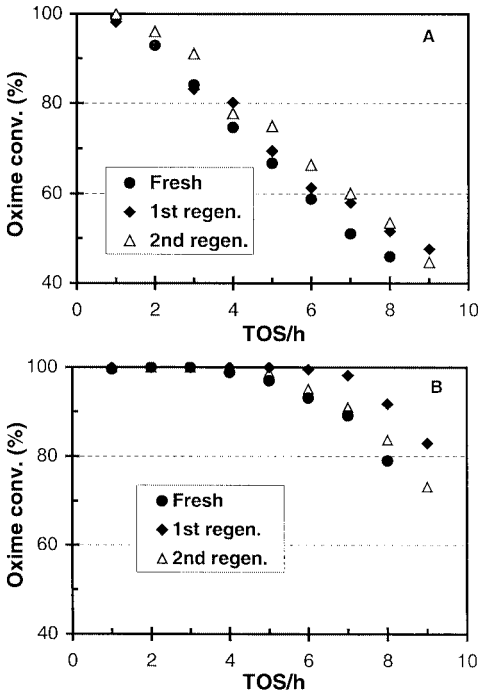

Fig. 1 Time course of cyclohexanone oxime conversion over fresh and regenerated 5% B_2O_3/ZrO_2 (A) and 13.5% B_2O_3/ZrO_2 (B) catalysts.

reusability of the deactivated catalyst when regenerated by calcination in air at 600 °C for 8 h. Quantitative measurement of boron in the samples revealed that the difference in boria loading between the fresh and corresponding regenerated samples is less than 6% of the loading in the fresh sample.

It is evident from Fig. 1 that these two catalysts do not lose any activity for the Beckmann reaction, even after two repeated deactivation–regeneration cycles. Also, no meaningful change in the lactam selectivity was detected over these two catalysts in the deactivation–regeneration cycles. Very similar behavior was also observed with samples containing higher boria loadings, *e.g.* 20% B_2O_3. These observations may be very important, since complete restoration of catalyst activity and selectivity could prove attractive for industrial application. The effect of boria loading on the catalytic performance of 'fresh' B_2O_3/ZrO_2 catalysts has been a focus of discussion in other publications.[11,13]

For the 10% B_2O_3/ZrO_2 catalysts prepared with CAT = 600 °C, it has been shown that the precalcination temperature (PCT = 110–500 °C) of the support precursor has little effect on the catalytic efficiency for the lactam synthesis.[13] Attempts were therefore made to impregnate boric acid directly onto zirconyl hydroxide that had been dried at 110 °C, but with an even higher temperature (700 °C) used for the catalyst activation. This preparation produced even more efficient B_2O_3/ZrO_2 catalysts (boria loading 8–15%) that are able to yield 98% ε-caprolactam for longer than 10 h TOS, which further demonstrates that high temperature catalyst activation/calcination is beneficial for the production of highly efficient and regenerable solid acid catalysts based on supported boria. This conclusion could be important for the development of a practical boria catalyst for industrial application. Additionally, the discovery that zirconia-supported boria catalysts are able to withstand high temperature (600–700 °C) calcination seems of interest for fundamental research. Further study is required to understand the chemistry of the interaction between boria and the surface of the zirconia support.

Financial support of this work is provided by the Foundation for Fundamental Research of Tsinghua University and NSFC (grant no. 2890018).

Notes and references

1 J. E. Kent and S. Riegel, *Handbook of Industrial Chemicals*, 8th edn., van Nostrand, New York, 1983, p. 402.
2 K. Tanabe, *Appl. Catal.*, 1994, **113**, 147.
3 BASF, *Ger. Pat.*, 1,227,028, 1967.
4 W. F. Yates, R. O. Downs and J. C. Burleson, *US Pat.*, 3,639,391, 1972.
5 H. Sato, K. Urabe and Y. Izumi, *J. Catal.*, 1986, **102**, 99.
6 H. Sato, S. Hasebe, H. Sakurai, K. Urabe and Y. Izumi, *Appl. Catal.*, 1987, **29**, 107.
7 T. Curtin, J. B. McMonagle and B. K. Hodnett, *Appl. Catal., A*, 1992, **93**, 91.
8 T. Curtin, J. B. McMonagle and B. K. Hodnett, *J. Catal.*, 1993, **142**, 172.
9 T. Ushikubo and K. Wada, *J. Catal.*, 1994, **148**, 138.
10 S. B. Cheng, B. Q. Xu, D. Q. Wang, F. Wang, T. X. Cai and X. S. Wang, *Chin. J. Catal. (Cuihua Xuebao)*, 1996, **17**, 282.
11 B. Q. Xu, S. B. Cheng, S. Jiang and Q. M. Zhu, *Appl. Catal., A*, 1999, **188**, 361.
12 S. B. Cheng, B. Q. Xu, T. X. Cai and X. S. Wang, *Chin. J. Catal. (Cuihua Xuebao)*, 1996, **17**, 330; S. B. Cheng, B. Q. Xu, T. X. Cai and X. S. Wang, 1996, **17**, 404.
13 B. Q. Xu, S. B. Cheng, X. Zhang and Q. M. Zhu, *Catal. Today*, in press.

The addition of isocyanides to ReS_4^-: [3 + 1] cycloaddition to S=M=S

Daniel E. Schwarz and Thomas B. Rauchfuss*

School of Chemical Sciences and the Frederick Seitz Materials Research Laboratory, University of Illinois at Urbana-Champaign, Urbana, IL 61801 USA. E-mail: rauchfuz@uiuc.edu

Received (in Irvine, CA, USA) 27th January 2000, Accepted 3rd May 2000
Published on the Web 8th June 2000

Isocyanides undergo [3 + 1] cycloadditions to ReS_4^- to give dithiocarboimidate derivatives, $Re(S)(S_4)(S_2CNR)^-$ and $Re_2S_5(S_2CNR)_2^{2-}$, which undergo S-atom transfer and, in the case of the monometallic species, *N*-alkylation.

Cycloadditions to oxo- and thio-metallates represent an important class of reactions related to atom transfer catalysis, *e.g.* by OsO_4.[1] In these transformations, the substrate adds wholly or in part to the main group atom, the metal playing a secondary role. Such cycloadditions to metal sulfides are relevant to catalyst–substrate interactions in hydrodesulfurization (HDS) catalysis.[2] Virtually all metal-based cycloadditions proceed *via* 2 + 2 or, more commonly, 3 + 2 pathways,[3,4] 3 + 1 pathways have not been observed.

Metal sulfides have been shown to catalyze the conversion of CO into thioesters and other biologically significant functionalities, although the mechanisms of such reactions are unclear.[5,6] The pathways for such reactions might be elucidated through studies on the interactions of isoelectronic analogues of CO with soluble metal sulfides under well defined conditions. Of all the soluble metal sulfides,[7] ReS_4^- **1** exhibits the greatest

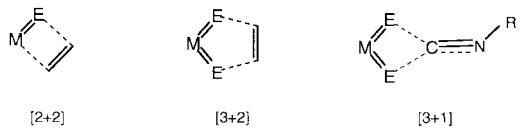

reactivity toward alkenes and alkynes.[8–11] Compound **1** was therefore selected for an investigation of the reactions of metal sulfides with isocyanides, which are isoelectronic with CO.

With rigorous exclusion of light and adventitious oxidants, solutions of **1**, as its NEt_4^+ or PPh_4^+ salts, are unreactive towards MeNC. The reaction of MeNC and **1**, however, proceeds briskly when in the presence of elemental sulfur. Addition of 1–2 equivalents of elemental sulfur to solutions of (PPh_4)**1** and MeNC afforded brown microcrystalline **2** whose (−)ESI-MS spectrum shows molecular ions at *m/z* 372 ($z = 2-$) and 743 ($z = 1-$) corresponding to $Re_2S_9(CNMe)_2^{2-}$ (isolated yield: 35%).† The IR spectrum of **2** exhibits peaks at 1586 and 526 cm^{-1} for $\nu_{C=N}$ and $\nu_{Re=S}$, respectively. The ^1H NMR spectrum in CD_3CN shows a PPh_4^+/Me ratio of 1; a pair of equally intense Me signals (δ 3.25 and 3.274) is attributed to the unsymmetrical environment of the square-pyramidal Re centers such that the Me can be *trans* to persulfide or sulfide (Scheme 1). In part due to its low solubility, $(PPh_4)_2$ **2** was not obtained as X-ray quality crystals.

The addition of further equivalents of S_8 to MeCN slurries of **2** gave $(PPh_4)[Re(S)(S_4)(S_2CNMe)]$ **3a** over the course of several hours at room temperature. In this reaction, the two isomers of **2** are consumed at comparable, but not identical rates. The new species can be more easily prepared by treatment of **1** with MeNC in the presence of an excess of sulfur, the yields being *ca.* 60%. The poorly soluble side products in this reaction absorb at *ca.* 1580 cm^{-1} ($\nu_{C=N}$); (−)ESI-MS of these solids revealed ions corresponding to $[ReS_4]_m[MeNC]_n^{m-}$ (where *m* and *n* = 1 and 2). The structure of **3a** was established by single crystal X-ray diffraction (Fig. 1).‡ The rhenium atom is square pyramidal; the square base is defined by the tetrasulfido bridge and the dithiocarboimidate ($MeNCS_2^{2-}$) ligands, a terminal sulfur atom occupying the apical position. The rhenium atom lies 0.4570 Å out of the plane formed by the basal sulfur ligands. The C=N distance is 1.24 Å, which is consistent with a double bond, and resembling previously described dithiocarbodimidate complexes.[12,13]

Analogues of **3** were prepared using *tert*-butyl isocyanide (Bu^tNC) and cyclohexyl isocyanide (CyNC) to give the corresponding derivatives **3b** and **3c**, respectively.§ No RNC exchange was observed when solutions of **3a** were treated with an excess of Bu^tNC or solutions of **3b** were exposed to MeNC. Warm solutions of **3a** react with **1** and 1 equiv. of MeNC to give **2**, indicating that intermetallic S-atom transfer is facile.

Methylation of **3a** with MeOTf gave the dithiocarbamate $Re(S)(S_4)(S_2CNMe_2)$ **4**, confirming the relationship between dithiocarboimidate and the more familiar dithiocarbamate ligands. Dithiocarbamate complexes are usually prepared from preformed dithiocarbamates or thiuram disulfides,[14] not by *N*-alkylation routes.

The mechanism by which **2** and **3** arise involves generation of a reactive derivative by the addition of sulfur atoms to **1** followed by trapping with RNC. We have previously shown that such solutions bind nitriles (*via* a 3 + 2 cycloaddition process[9]). Further work is underway to identify this reactive intermediate.

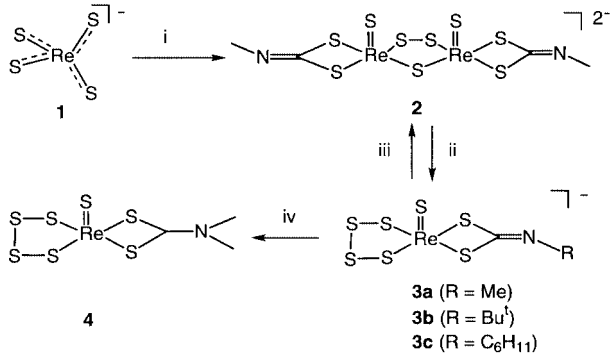

Scheme 1 *Reagents and conditions*: i, S_8, MeNC (25 °C); ii, excess S_8; iii, **1**, MeNC; iv, MeOTf.

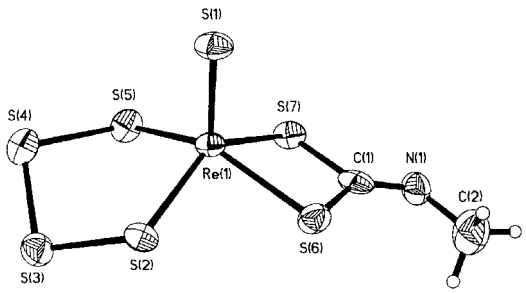

Fig. 1 Structure of **3a** with thermal ellipsoids drawn at the 50% probability level. Selected distances (Å) and angles (°): Re–S(1) 2.088(1), Re–S(2) 2.257(1), Re–S(5) 2.291(1), Re–S(6) 2.355(1), Re–S(7) 2.344(1), C(1)–S(7) 1.776(7), C(1)–S(6) 1.802(7), C(1)–N 1.248(8), N–C(2) 1.467(10); S(6)–C(1)–N 131.2(6), S(7)–C(1)–N 125.0(6), C(1)–N–C(2) 118.2(7), S(2)–Re–S(5) 92.41(7), S(6)–Re–S(7) 73.66(6).

DOI: 10.1039/b000932f

The important conclusion is that isocyanides add across the S=M=S functionality[7] *via* an unprecedented 3 + 1 cycloaddition process. Isocyanides have been shown to add to μ-S ligands in binuclear molybdenum compounds.[15]

This research was sponsored by the U.S. National Science Foundation.

Notes and references

† Satisfactory CHN analyses were obtained for **2**, **3a**–**c**, and **4**.

‡ *Crystallographic data* for **3a**: $C_{26}H_{23}NPReS_7$, M 791.12, T 193(2) K, monoclinic space group $P2_1/c$ a = 11.0148(7), b = 19.6065(13), c = 13.6281(9) Å, β = 98.89°, V = 2907.8(3) Å^3, Z = 4, μ = 4.755 mm^{-1}, 18817 reflections (R_{int} = 0.1019), 6944 independent reflections, for observed data R_1 = 0.0427, wR_2 = 0.0898, for all data R_1 = 0.0947, wR_2 = 0.1043.

CCDC 182/1636. See http://www.rsc.org/suppdata/cc/b0/b000932f/ for crystallographic files in .cif format.

§ **3b**: ^{1}H NMR (CD_3CN, 500 MHz): δ 1.43 (s). (−)ESI-MS: *m/z* 494. **3c**: ^{1}H NMR (CD_3CN, 500 MHz): δ 1.3–1.9(m). (−)ESI-MS: *m/z* 520.

1 W. A. Nugent and J. M. Mayer, *Metal–Ligand Multiple Bonds*, J. Wiley, New York, 1988.

2 R. J. Angelici, in *Hydrodesulfurization and Hydrodenitrification*, ed. R. B. King, J. Wiley, New York, 1994.

3 R. S. Pilato, K. A. Eriksen, E. I. Stiefel and A. L. Rheingold, *Inorg. Chem.*, 1993, **32**, 3799.

4 Z. K. Sweeney, J. L. Polse, R. A. Andersen, R. G. Bergman and M. G. Kubinec, *J. Am. Chem. Soc.*, 1997, **119**, 4543.

5 C. Huber and G. Wächtershäuser, *Science*, 1998, **281**, 670.

6 C. Huber and G. Wächtershäuser, *Science*, 1997, **276**, 245.

7 D. Coucouvanis, *Adv. Inorg. Chem.*, 1998, **45**, 1.

8 J. T. Goodman, S. Inomata and T. B. Rauchfuss, *J. Am. Chem. Soc.*, 1996, **118**, 11 674.

9 J. T. Goodman and T. B. Rauchfuss, *Angew. Chem., Int. Ed. Engl.*, 1997, **36**, 2083.

10 J. T. Goodman and T. B. Rauchfuss, *Inorg. Chem.*, 1998, **37**, 5040.

11 J. T. Goodman and T. B. Rauchfuss, *J. Am. Chem. Soc.*, 1999, **121**, 5017.

12 F. A. Cotton and C. B. Harris, *Inorg. Chem.*, 1968, **7**, 2140.

13 S. B. Schougaard, T. Pittelkow, F. Krebs, S. Larsen, H. O. Sørensen, D. R. Greve and T. Bjørnholm, *Acta Crystallogr. Sect. C*, 1998, **54**, 470.

14 L. Wei, T. R. Halbert, H. H. Murray III and E. I. Stiefel, *J. Am. Chem. Soc.*, 1990, **112**, 6431.

15 D. J. Miller and M. Rakowski DuBois, *J. Am. Chem. Soc.*, 1980, **102**, 4925.

Synthesis and coordinative properties of a hybrid bis(diphenylphosphino)methane–terpyridine

Guillaume Pickaert,[a] Michèle Cesario,[b] Laurent Douce[a] and Raymond Ziessel*[a]

[a] *Laboratoire de Chimie, d'Electronique et Photonique Moléculaires, Ecole Européenne de Chimie, Polymères et Matériaux, Université Louis Pasteur, 25 rue Becquerel, F-67087 Strasbourg Cedex 02, France. E-mail: ziessel@chimie.u-strasbg.fr*

[b] *Institut de Chimie des Substances Naturelles, CNRS, F-91128 Gif-sur-Yvette, France*

Received (in Cambridge, UK) 31st March 2000, Accepted 15th May 2000

A newly-synthesized 4′-[bis(diphenylphosphino)methane]–2,2′:6′,2″-terpyridine-based (dppm–terpy) ligand forms complexes by selective complexation of the terpy or diphos segment, respectively, with Fe(II) or Pd(II) salts; in the latter case, an X-ray structural analysis reveals the formation of a neutral square-planar complex assembled from the deprotonated ligands.

The 2,2′:6′,2″-terpyridine (terpy) molecule is widely used in transition metal chemistry as a meridionally coordinating and tridentate chelating ligand. Multiple applications have been found in the areas of analysis and the design of molecular electronic devices.[1] Phosphine-functionalized terpy entities, such as terpyPPh_2[2] and terpyPO_3H_2,[3] readily complex many different transition metals and bind strongly to certain semiconductors. We have shown recently that terpy$CH_2P(O)Ph_2$ can be deprotonated under mild conditions to produce a useful synthon for the preparation of carotenoid-based photoactive molecular-scale wires.[4] In light of the rich coordination chemistry of bis(diphenylphosphino)methane (dppm), a species well known in organometallic chemistry as a monodentate, bidentate or bridging ligand,[5] it was anticipated that the hitherto unreported terpy analogue (dppm–terpy) might be a valuable building block for the construction of multimetallic networks. Interest in such polynuclear assemblies is stimulated by the study of intramolecular electron or energy transfer processes[6] as well as by the coupling of luminophoric metal centers to photoactive catalytic sites.

We present here, the synthesis and coordination behaviour of a hybrid diphos/terpy ligand where the complexation behaviour is governed by the choice of the metal precursor. Ligand **L** is prepared in a stepwise fashion from the deprotonated monophosphine-terpy ligand **1**, followed by nucleophilic substitution with PPh_2Cl as illustrated in Scheme 1. The dppm–terpy ligand **L** is characterized by a ^{31}P NMR signal at δ −3.7 (singlet), compared to intermediate **1** which gives a singlet at δ −8.5. The corresponding phosphine oxide $\mathbf{L(O)_2}$, obtained under phase transfer conditions with $NaIO_4$ as oxidant, shows a ^{31}P NMR signal at δ 29.5, with the CH proton appearing as a triplet at δ = 5.00, J_{HP} 14.4 Hz. A strong IR absorption band is found at 1210 cm^{-1} ($\nu_{P=O}$).

The ambivalent reactivity of dppm–terpy is demonstrated by virtue of its interaction with Fe and Pd precursors. Thus, reaction of **L** with $Fe(ClO_4)_2{\cdot}6H_2O$ gives a deep-violet complex whose structure is assigned as $\mathbf{C^1}$.† Both the intense MLCT absorption band centred at 562 nm (ε = 20450 $dm^3\ mol^{-1}\ cm^{-1}$) and the slightly shifted singlet observed (δ 3.2 in $CDCl_3$) in the ^{31}P NMR spectrum are indicative of complexation at the terpy segment. Note that the related Fe(II) complex formed from $\mathbf{L(O)_2}$ gives a singlet at δ 30.0 (CD_3CN). In contrast, ligand **L** reacts with [Pd(acac)$_2$] (acac = acetylacetonate) to form a sparingly soluble, deep-yellow compound (λ_{max} = 407 nm, ε = 43450 $dm^3\ mol^{-1}\ cm^{-1}$) that lacks the signal characteristic of the CH fragment in the proton NMR spectrum but displays a ^{31}P NMR signal at δ −29.9 (singlet in CD_2Cl_2). The presence of uncomplexed terpy fragments within this latter complex, labelled as $\mathbf{C^2}$ in Scheme 2, was confirmed by an X-ray diffraction study (*vide infra*). The dppm–terpy ligands are deprotonated during the process so that the overall product is a neutral palladium(II) complex. It is likely that the acac anion operates as a buffer to deprotonate the ligand.[7]

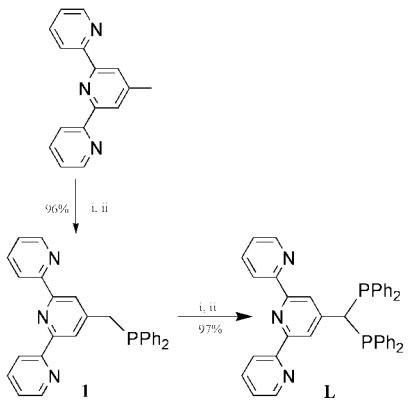

Scheme 1 *Reagents and conditions*: i, Bu^nLi, Pr^i_2NH, THF, −78 °C; ii, Ph_2PCl, THF.

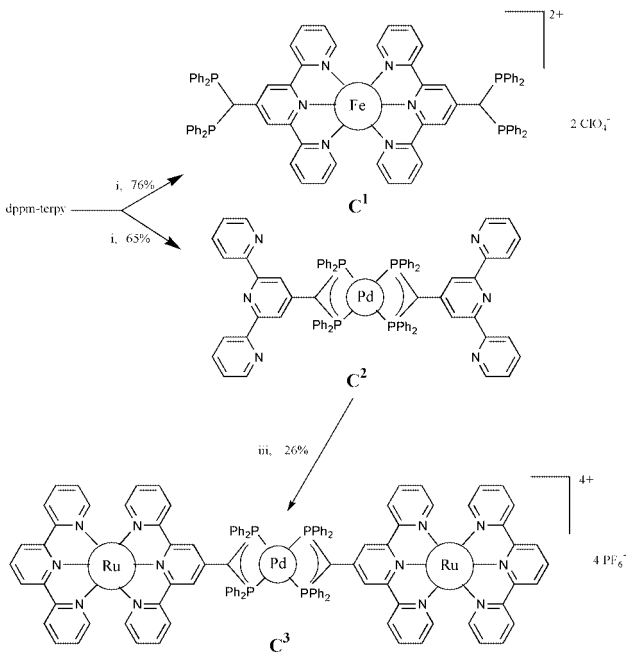

Scheme 2 *Reagents and conditions*: i, $Fe(ClO_4)_2{\cdot}6H_2O$, methanol–dichloromethane; ii, [Pd(acac)$_2$], THF; iii, [Ru(terpy)(dmso)Cl_2], methanol, $AgBF_4$, 80 °C; all reactions were carried out using argon degassed solutions.

DOI: 10.1039/b002586k

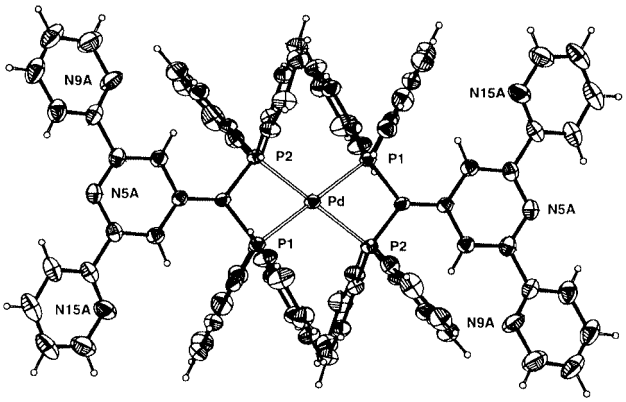

Fig. 1 ORTEP drawing of complex **C**[2] (Displacement ellipsoids are shown at the 50% probability level); Hydrogen atoms have been omitted for clarity. Selected bond lengths (Å) and angles (°): Pd–P(1) 2.317(2), Pd–P(2) 2.315(2), P(1)–C(terpy) 1.756(4), P(1)–C(phenyl) 1.826(5), P(1)–C(phenyl) 1.822(5), P(2)–C(terpy) 1.764(4), P(2)–C(phenyl) 1.818(4), P(2)–C(phenyl) 1.823(5), P(2)*–Pd–P(2) 180.0, P(2)–Pd–P(1)* 109.09(5), P(2)–Pd–P(1) 70.91(5), P(1)–C(terpy)–P(2) 99.5(2).

The single-crystal X-ray analysis‡ (Fig. 1) indicates that the palladium atom is in a square-planar environment with the four P atoms coordinated to the metal centre and with two uncoordinated terpyridines. The crystals consist of discrete neutral centrosymmetric molecules, the Pd atom being located on an inversion centre. As expected, all six N-atoms are in a transoidal arrangment that minimizes electronic interactions.[8] An angle of 16.0(0)° between the planes defined by the two pyridine rings containing N(5A) and N(15A) and a dihedral angle of 16.8(0)° between the planes of the external rings containing N(15A) and N(9A) illustrate twisting about the interannular C–C bonds, as well as the slight distortion within the terpy subunit. Owing to the anionic nature of the coordinated diphos–terpy ligands the C–P bond distances (*ca*. 1.76 Å) are shorter than in related Pd(II)-phosphine complexes.[9] The bite angle P(1)–Pd–P(2) of 70.91(5)° and the twist of the phenyl rings around the P atom *versus* the plane defined by the square containing the palladium (71–75°) are in good agreement with values expected for a regular square-planar coordination polyhedron.

This mononuclear Pd(II) complex is of interest as a potential *metallo-synthon* for the construction of more elaborate molecular architectures in which the electronic interaction between both sites could, in principle, be tuned by the oxidation state of the central metal. In order to demonstrate this principle, we chose to complex the free terpy moieties with [Ru(terpy)(dmso)Cl_2][10] under mild conditions. The heterotrinuclear complex **C**[3] has a characteristic MLCT absoption band at 482 nm (ε = 43000 $dm^3\ mol^{-1}\ cm^{-1}$), and exhibits a singlet in the ^{31}P NMR spectra at δ −10.6 (CD_3CN). The MALDI-TOF mass spectra is in keeping with the proposed structure.†

The redox behaviour of these complexes was studied by cyclic voltammetry in MeCN (for **C**[1] and **C**[3]) or dichloromethane (for **C**[2]) containing $NBu^n_4PF_6$ (0.1 mol dm^{-3}) as supporting electrolyte. The Pd(II) complex **C**[2] exhibits two irreversible oxidation waves at $E_{pa}(1)$ = 0.69 and $E_{pa}(2)$ = 1.04 V *vs*. SCE using ferrocene as internal reference (Fc/Fc^+ = 0.41 V). No peaks are seen upon reductive scans, at least above −2.0 V *vs*. SCE. The oxidative processes can be ascribed to the successive oxidation of the anionic terpy–diphos ligands. Within the mixed Ru/Pd complex **C**[3], ligand-based oxidation steps are found at $E_{pa}(1)$ = 0.87 and $E_{pa}(2)$ = 1.06 V *vs* SCE. This complex also exhibits a single metal-based oxidation at 1.34 V *vs*. SCE (ΔE_p = 80 mV) and two irreversible terpy-based reductions at $E_{pc}(1)$ = −1.28 V and $E_{pa}(2)$ = −1.49 V. It is surmised that the unusual irreversibility of the ligand reduction is due to the strong electron density provided by the anionic Ph_2PCPPh_2 fragment appended to the terpy units. As expected, complex **C**[1] exhibits three well-defined and reversible redox processes; namely, a single oxidation at 1.26 V (ΔE_p = 70 mV) and two ligand-centered reductions at −1.20 V (ΔE_p = 74 mV) and −1.39 V *vs*. SCE (ΔE_p = 66 mV). The easier Fe(II) oxidation *vs*. Ru(II) in **C**[3] is in keeping with related unsubstituted terpy complexes.[11]

Preliminary steady-state emission studies show that complex **C**[2], in the solid state (0.5% dispersed in $MgSO_4$), exhibits an intense but structureless emission band at 590 nm when excited at 400 nm. This emission is not observed in deoxygenated acetonitrile solution. Additional photophysical measurements will be carried out in order to explore the photoreactivity of **C**[3].

In summary, we describe a simple strategy for the synthesis of hybrid ligands carrying hard and soft complexation centres. The diphos or the terpy part of the ligand can be complexed with good selectivity, using either Pd(II) or Fe(II), respectively. Further complexation of the free terpy centers with redox-active Ru(II) fragments facilitates preparation of linear heterotrinuclear complexes in a controlled manner. On-going experiments will study the chemistry of these novel multitopic systems.

Notes and references

† Synthetic details will be reported elsewhere. All new compounds gave satisfactory elemental analyses and were authenticated by ^1H and ^{13}C NMR, FTIR and MS. All ^{31}P NMR chemical shift are referenced using H_3PO_4 (85% in water) as internal standard. *Selected data*: for **C**[1]; FAB *m*/*z* (*m*-NBA) 1386.0 $[M - ClO_4]^+$. Found: C, 64.49, H, 4.13, N, 5.41. $C_{80}H_{62}N_6O_8P_4Cl_2Fe$ requires C, 64.66; H, 4.21; N, 5.66%. For **C**[2]; FAB^+ (*m*-NBA): *m*/*z* 1335.0 $[M+H]^+$. Found: C, 71.85, H, 4.47, N, 6.17. $C_{80}H_{60}N_6P_4Pd$ requires C, 71.94; H, 4.53; N, 6.29%. For **C**[3]; MALDI-TOF *m*/*z* 2439.4 $[M - PF_6]^+$, 2294.9 $[M - 2PF_6]$. Found: C, 51.57, H, 3.48, N, 7.53. $C_{110}H_{82}N_{12}P_8PdRu_2F_{24}.2C_2H_3N$ requires C, 51.35; H, 3.33; N, 7.35%.

‡ *Crystal data* for **C**[2]: $C_{80}H_{60}N_6P_4Pd$, M = 1335.62, monoclinic, space group $P2_1/n$, yellow crystals, a = 11.477(4), b = 25.327(9), c = 11.595(5) Å, β = 98.54(4)°, V = 3333(2) $Å^3$, Z = 2, T = 293 K, D_c = 1.331 g cm^{-3}, μ = 0.425 mm^{-1}, $F(000)$ = 1376. The final conventional R_1 factor is 0.0705 for 4185 data and 398 parameters, and 0.11 for all data, wR_2 = 0.1423 (all data), goodness of fit = 1.068; largest peak and hole in the final difference map were within +0.59 and −0.45 e $Å^3$. CCDC 182/1638. See http//www.rsc.org/suppdata/cc/b0/b002586k for crystallographic files in .cif format.

1 E. C. Constable, *Transition Metals in Supramolecular Chemistry*, Kluwer, Dordrecht, 1994, p. 81; R. Ziessel, *J. Chem. Educ.*, 1997, **74**, 673; R. Ziessel, *Synthesis*, 1999, 1839.
2 E. C. Constable, C. E. Housecroft, M. Neuburger, A. G. Schneider and M. Zehnder, *J. Chem. Soc., Dalton Trans.*, 1997, 2427.
3 S. M. Zakeeruddin, M. K. Nazeeruddin, P. Pechy, F. P. Rotzinger, R. Humphry-Baker, K. Kalyanasundaram and M. Grätzel, *Inorg. Chem.*, 1997, **36**, 5937.
4 G. Pickaert and R. Ziessel, *Tetrahedron Lett.*, 1998, **39**, 3497.
5 R. J. Puddephatt, *Chem. Soc. Rev.*, 1983, **12**, 99.
6 B. Whittle, N. S. Everest, C. Howard and M. D. Ward, *Inorg. Chem.*, 1995, **34**, 2025.
7 H. Hashimoyo, S. Okeya and Y. Nakamura, *Bull. Chem. Soc. Jpn.*, 1988, **61**, 1593.
8 A. Harriman, M. Hissler, R. Ziessel, A. De Cian and J. Fisher, *J. Chem. Soc., Dalton Trans.*, 1995, 4067 and references therein.
9 J. Barkley, M. Ellis, S. J. Higgins and M. K. McCart, *Organometallics*, 1998, **17**, 1725.
10 V. Grosshenny and R. Ziessel, *J. Organomet. Chem.*, 1993, **453**, 19.
11 D. E. Morris, K. W. Hanck and M. Keith DeArmond, *J. Electroanal. Chem.*, 1983, **149**, 115.

ChemComm

Cyclodextrin-appended myoglobin as a tool for construction of a donor–sensitizer–acceptor triad on a protein surface

Itaru Hamachi,*†[a] Hiroshi Takashima,[a] Yi-Zhen Hu,[a] Seiji Shinkai[a] and Shigero Oishi[b]

[a] *Department of Chemistry and Biochemistry, Graduate School of Engineering, Kyushu University, Fukuoka 812-8581, Japan. E-mail: itarutcm@mbox.nc.kyushu-u.ac.jp*

[b] *Department of Chemistry, School of Science, Kitasato University, Sagamihara, 228-8520, Japan*

Received (in Cambridge, UK) 13th March 2000, Accepted 18th May 2000

A protein-based and noncovalently-linked donor–sensitizer–acceptor triad has been prepared by self-assembly *via* mechanical linkages and hydrophobic interactions, and its photoinduced electron transfer properties have been studied.

Multi-step electron transfer (ET) in protein matrices is the key process of biological energy transduction in photosynthetic and mitochondrial respiratory systems.[1,2] A number of efforts have shown that model proteins suitably modified with an electron donor or acceptor are valuable for understanding such complicated ET mechanisms.[3] Most of the models reported so far, however, are simple donor–acceptor diads because of serious limitations for modifying native protein matrices. We recently reported a donor–sensitizer–acceptor triad attached to protein matrices using cofactor reconstitution methods.[4] Here, we describe a novel strategy for the construction of a triad by self-assembly. The protein-based triad, which consists of cyclodextrin(CD)–appended Zn–myoglobin (Zn-Mb-CD), an adamantane-modified $Ru(bpy)_3$ and a bis(viologen)cyclophane (BXV^{4+}), is noncovalently connected by elaborately employing mechanical linkages[5] and hydrophobic interactions.

The β-CD-modified protoporphyrins IX (**1a** and **1b**) were synthesized according to Scheme 1. Protoporphyrin IX (PP) mono-ethylester was condensed with 6-monoamino-peracetylated-β-CD in the presence of BOP to yield a CD-appended heme **2**. Subsequent metal insertion into the heme center followed by hydrolysis of the ester groups gave the target compound **1**. Tris-heteroleptic $Ru(bpy)_3$ derivatives (**3**, **4**) used

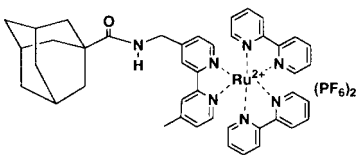

3

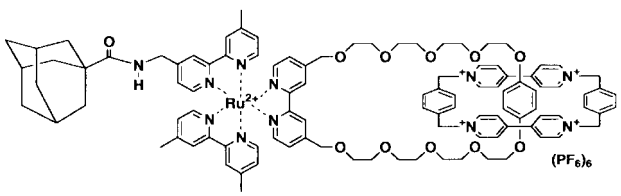

4

herein were synthesized according to the synthetic route reported previously by us.[4,5] All of the compounds were characterized by FT-IR, NMR, MALDI-TOF mass spectrometry, and elemental analysis.

Reconstitution of **1a** and **1b** with apo-Mb were carried out according to the literature reported by us.[4] The yield of Zn-Mb-CD and Fe(III)-Mb (Fe-Mb-CD) were 36% and 40%, respectively. The absorption and/or fluorescence spectra of Zn-Mb-CD and Fe-Mb-CD are very similar to those of their corresponding native forms, Zn-Mb and Fe-Mb.[6] Spectroscopic titration experiments clearly show that 1 equiv. of **1** is quantitatively complexed with apo-Mb (data not shown). In Fe-Mb-CD, the spectroscopic changes due to the ligand exchange and redox and oxygen-binding reactions were almost identical to native Mb.[6] These results undoubtedly imply that the heme unit of **1** is located in the natural heme crevice of Mb.

Binding of $Ru(bpy)_3$ derivatives bearing adamantane units to the CD-appended Mb's was monitored by emission quenching of $Ru(bpy)_3$ of **3** by Fe-Mb-CD. The emission lifetime of **3** was determined to be *ca*. 500 ns in the absence of Fe-Mb-CD. By addition of Fe-Mb-CD (10 μM) to a solution of **3** (1 : 1 ratio), we observed a faster decay (64%, the lifetime of 100 ns) of the emission at 600 nm, as well as the normal lifetime of 500 ns (36%). The shorter lifetime is attributable to the fraction of **3** bound to Fe-Mb-CD.[7] Based on these fractions, the binding constant of the adamantane unit of **3** with the CD unit of Fe-Mb-CD was estimated to be *ca*. 5×10^5 M^{-1}, suggesting that the

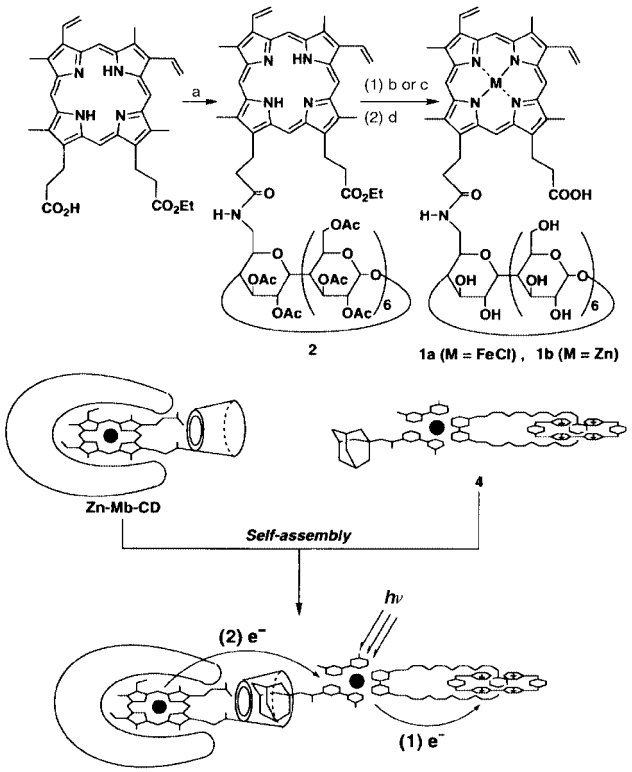

Scheme 1 *Reagents and conditions*: a, 6-monoamino-peracetylated-β-CD, BOP (1 equiv.), DIEA (1 equiv.), dry DMF, N_2, r.t., 9 h, 35%; b, $Zn(OAc)_2$ (10 equiv.), $CHCl_3$–MeOH (1 : 1, v : v), r.t., 5 h, 95%; c, $FeCl_2$ (12 equiv.), dry DMF, N_2, 65 °C, 5 h, 48%; d, 1 N NaOH (42 equiv.), MeOH–THF (1 : 1, v : v), r.t., 17 h, 89% (**1a**) and 76% (**1b**).

† Visiting professor at the Institute of Molecular Science, Myodaiji, Okazaki, 444-8585, Japan.

DOI: 10.1039/b001997f

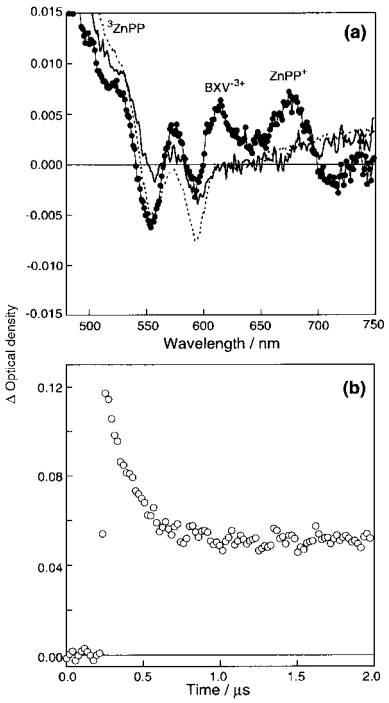

Fig. 1 (a) Transient absorption spectra observed after laser excitation of Zn-Mb-CD (10 μM)/**4** (20 μM) and Zn-Mb (10 μM)/**4** (20 μM) complexes in deaerated phosphate buffer (pH 7.0, 50 mM) solution at the delay time of 50 ns. (—●—) Zn-Mb-CD/**4**, λ_{ex} = 460 nm; (·····) Zn-Mb-CD/**4**, λ_{ex} = 596 nm; (——) Zn-Mb/**4**, λ_{ex} = 460 nm. (b) Time profile monitored at 670 nm in Zn-Mb-CD/**4** after laser excitation at 460 nm.

$Ru(bpy)_3$ derivatives **3** and **4** can form tight complexes with Zn-Mb-CD or Fe-Mb-CD.

Next, a donor–sensitizer–acceptor triad system was prepared by spontaneous assembly of Zn-Mb-CD with the $Ru(bpy)_3$-based diad **4**. Fig. 1a shows the transient absorption spectrum obtained by photoexcitation of an aqueous solution containing Zn-Mb-CD (10 μM)/**4** (20 μM) at 460 nm (MLCT band of $Ru(bpy)_3$; —●—) and 596 nm (Q-band of ZnPP; ·····): Photolysis at 460 nm led to the immediate appearance of absorption bands due to the viologen radical and the ZnPP radical at 610 nm and 670 nm, respectively, in addition to the ZnPP triplet absorption at 470 nm.[4,5,8] In contrast, the viologen and ZnPP radicals are not photo-produced in a mixture of native Zn-Mb and **4** (*i.e.* without CD; ——) under the same conditions. This is direct evidence for the formation of a pseudo intramolecular Zn-Mb-CD/**4** complex, in which a charge-separated (CS) state between ZnPP and cyclic viologen is generated by photolysis of the MLCT band of $Ru(bpy)_3$ (460 nm). Interestingly, the CS state was not observed by photoexcitation of Zn-Mb-CD/**4** at 596 nm excitation, indicating that a direct electron transfer from the excited ZnPP to cyclic viologen does not occur. Moreover, both the excited singlet and triplet states of the ZnPP unit of Zn-Mb-CD were not considerably quenched by **4**. This implies that an energy transfer from excited ZnPP to $Ru(bpy)_3$ does not take place in the Zn-Mb-CD/**4** complex. Conceivably, the CS is photogenerated by a stepwise electron transfer as shown in Fig. 2. Initial electron transfer occurs from the photo-excited $Ru^{II}(bpy)_3$ to the cyclic viologen,[5] followed by reduction of the produced $Ru^{III}(bpy)_3$ by ZnPP to yield the final CS state.[4] It is noteworthy that both ET steps occur in noncovalently linked donor–acceptor pairs.

The kinetic behavior of the CS state of Zn-Mb-CD/**4** was monitored at 670 nm. As shown in Fig. 1b, the absorbance at 670 nm appears within 50 ns, indicating that steps 2 and 3 of Fig. 2 proceed faster than 50 ns. Unfortunately, the precise rate constants for steps 2 and 3 have not been determined due to instrumental limitations. The lifetime of the CS state was determined to be *ca.* 640 ns from the decay process shown in Fig. 1b.[9] The quantum yield of the CS state was estimated to be 0.03 by using 5,10,15,20-tetraphenylporphyrin as a reference.[10]

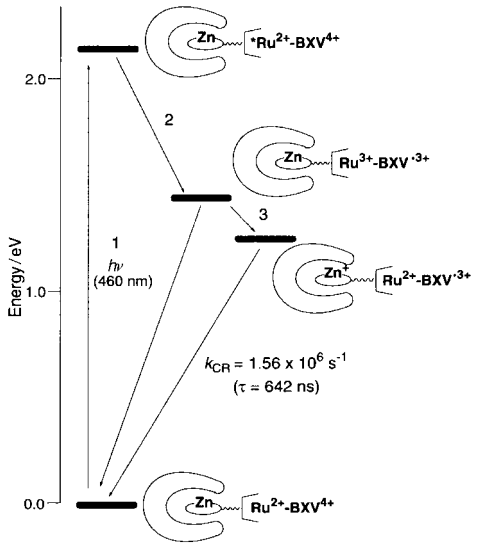

Fig. 2 Schematic energy diagram for the photoinduced reactions in the Zn-Mb-CD/**4** complex.

In conclusion, we have successfully prepared a noncovalently linked donor–sensitizer–acceptor triad on a myoglobin surface using a rational combination of mechanical bonding and hydrophobic interactions. The present approach may extend to the utilization of various kinds of donors and/or acceptors in semisynthetic systems, by which one can obtain valuable insight into ET events occurring in a protein matrix.

H. Takashima is a fellow of the Japan Society for the Promotion of Science (JSPS) for Japanese Junior Scientists and Y.-Z. Hu is a JSPS postdoctoral fellow. This research was partially supported by a specially promoted area (Biotargeting, No. 11132261) and a COE formation program (Molecular Assembly) from the Ministry of Education, Science, Sports and Culture of Japan.

Notes and references

1 (*a*) J. Deisenhofer and H. Michel, *Angew. Chem., Int. Ed. Engl.*, 1989, **28**, 829; (*b*) R. Huber, *Angew. Chem., Int. Ed. Engl.*, 1989, **28**, 848.
2 (*a*) G. McLendon and R. Hake, *Chem. Rev.*, 1992, **92**, 481; (*b*) L. Qin and N. M. Kostic, *Biochemistry*, 1992, **31**, 5145; (*c*) J. M. Nocek, J. S. Zhou, S. D. Forest, S. Priyadarshy, D. N. Beratan, J. N. Onuchic and B. M. Hoffman, *Chem. Rev.*, 1996, **96**, 2459.
3 I. Hamachi and S. Shinkai, *Eur. J. Org. Chem.*, 1999, 539.
4 (*a*) Y.-Z. Hu, S. Tsukiji, S. Shinkai and I. Hamachi, *Chem. Lett.*, 1999, 517; (*b*) Y.-Z. Hu, S. Tsukiji, S. Shinkai, S. Oishi and I. Hamachi, *J. Am. Chem. Soc.*, 2000, **122**, 241; (*c*) Y.-Z. Hu, H. Takashima, S. Tsukiji, S. Shinkai, T. Nagamune, S. Oishi and I. Hamachi, *Chem. Eur. J.*, 2000, **6**, 1907.
5 (*a*) Y.-Z. Hu, D. Van Loyen, O. Schwarz, S. Mossmann, H. Dürr, V. Huch and M. Veith, *J. Am. Chem. Soc.*, 1998, **120**, 5822; (*b*) Y.-Z. Hu, S. Bossmann, D. van Loyen, O. Schwarz and H. Dürr, *Chem. Eur. J.*, 1999, **5**, 1267.
6 (*a*) T. Yonetani and H. Schleyer, *J. Biol. Chem.*, 1967, **242**, 3926; (*b*) D. Puett, *J. Biol. Chem.*, 1973, **248**, 4623.
7 The emission of the $Ru(bpy)_3$ unit in the Fe-Mb-CD/**3** complex is quenched by intracomplex electron transfer from $Ru(bpy)_3$ to Fe-Mb. see: I. Hamachi, S. Tanaka, S. Tsukiji, S. Shinkai and S. Oishi, *Inorg. Chem.*, 1998, **37**, 4380.
8 The appearance of the ZnPP triplet absorption is due to the weak light absorption by the ZnPP moiety at 460 nm (*ca.* 10%) which decays with a lifetime of 2 ms. Since the emission of **3** was not quenched in the presence of Zn-Mb-CD, energy transfer from excited $Ru(bpy)_3$ to ZnPP can be ruled out.
9 On the time scale detected (2 μs), the decay curve in Fig. 1b does not reach zero because the ZnPP triplet state exhibits an absorption residue at 670 nm. The remaining fraction decays with a lifetime similar to that of the ZnPP triplet state of Zn-Mb-CD (*ca.* 2 ms).
10 T. S. Moore, D. Gust, J.-C. M. Mathis, C. Chachaty, R. V. Bensasson, E. J. Land, D. Doizi, P. A. Liddell, W. R. Lehman, G. A. Nemeth and A. L. Moore, *Nature*, 1984, **307**, 630.

ChemComm

Fluoride recognition in 'super-extended cavity' calix[4]pyrroles†

Salvatore Camiolo and Philip A. Gale*

Department of Chemistry, University of Southampton, Southampton, UK SO17 1BJ. E-mail: philip.gale@soton.ac.uk

Received (in Cambridge) 20th April 2000, Accepted 18th May 2000

Extended cavity ester (4) and amide (5) calix[4]pyrrole macrocycles have been synthesised and shown to bind fluoride exclusively in deuteriated DMSO solution.

The coordination chemistry of anionic species by abiotic receptor species is an area of supramolecular chemistry that continues to attract the attention of coordination chemists.[1] One of the major goals in molecular recognition is to produce receptors that are highly selective in their guest binding properties. The discovery that calix[4]pyrroles (such as *meso*-octamethylcalix[4]pyrrole (**1**)) are effective anion binding agents[2] in solution has led to the synthesis of a variety of new calixpyrrole macrocycles that have been used for anion binding,[3] sensing[4] and in new anion separation technologies.[5] Recently Sessler and co-workers[6] and Floriani and co-workers[7] have independently reported the syntheses of extended cavity calix[4]pyrroles derived from 4-hydroxyacetophenone. The αααα-isomer of this species (**2**) possesses an array of phenol moieties that resembles that present in lower-rim unfunctionalised calix[4]arenes in the cone conformation. Sessler and co-workers have studied the anion recognition properties of the isomers of **2** together with OMe derivatives (**3**) and found anion selectivity trends in line with those observed for other calix[4]pyrrole species.[6] We have modified the phenol groups of compound **2** with a variety of 'longer' and bulkier functional groups than methyl and have obtained tetra-ester (**4**) and -amide (**5**) macrocycles with 'super-extended cavities'. These macrocycles show interesting highly selective anion coordination properties in solution that are atypical of calix[4]pyrrole macrocycles.

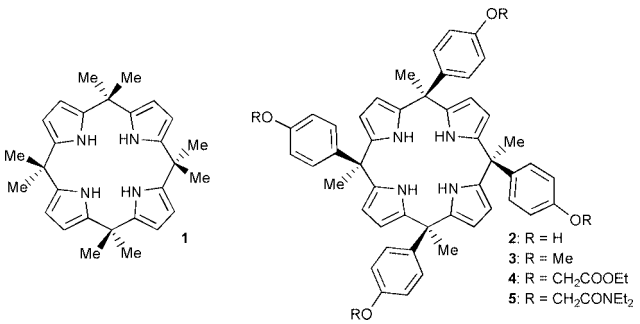

Compound **4** was synthesised by reaction of compound **2** with ethylbromoacetate in dry acetone in the presence of K_2CO_3 with heating at reflux for 5 days. The tetra-ester derivative was isolated as a white powder in 76.5% yield. Compound **5** was synthesised by reaction of compound **2** with 2-chloro-*N*,*N*-diethylacetamide and potassium iodide in dry acetone with stirring for 5 days and was isolated in 50% yield. These compounds may be regarded as pyrrolic analogues of the lower-rim functionalised calix[4]arenes synthesised and studied in the 1980s by McKervey, Ungaro and co-workers.[8]

Solution binding properties of **4** and **5** were investigated using ^{1}H NMR titration techniques in deuteriated DMSO solution. Previous studies in deuteriated dichloromethane with compound **1**[2] and deuteriated acetonitrile with compounds **1**, **2** and **3**[6] have shown downfield shifts of the calix[4]pyrrole NH proton on addition of chloride and dihydrogen phosphate anions consistent with the formation of 1:1 receptor–anion solution complexed species. However, it was found that addition of 20 equivalents of Cl^-, Br^-, I^-, $H_2PO_4^-$ or HSO_4^- anions (as tetrabutylammonium salts) to deuteriated DMSO solutions of **4** and **5** caused *no changes* in the NMR spectra of these calixpyrroles.[9] Compounds **4** and **5** therefore *do not interact* with these putative anionic guests in DMSO solution. On the other hand, upon addition of fluoride anions, new resonances (for the N*H*, Ar*H*, pyrrole C*H* and ArOCH_2C protons) were observed in the ^{1}H NMR spectra of **4** and **5** corresponding to the formation of fluoride complexes with slow complexation/decomplexation kinetics relative to the NMR timescale (Fig. 1). In addition, coupling is observed between the NH protons of the calixpyrroles and the bound fluoride anions (confirmed by ^{19}F NMR spectroscopy) at room temperature (21 °C) with coupling constants of 47 Hz for both compounds **4** and **5**. This coordination coupling has only previously been observed in a

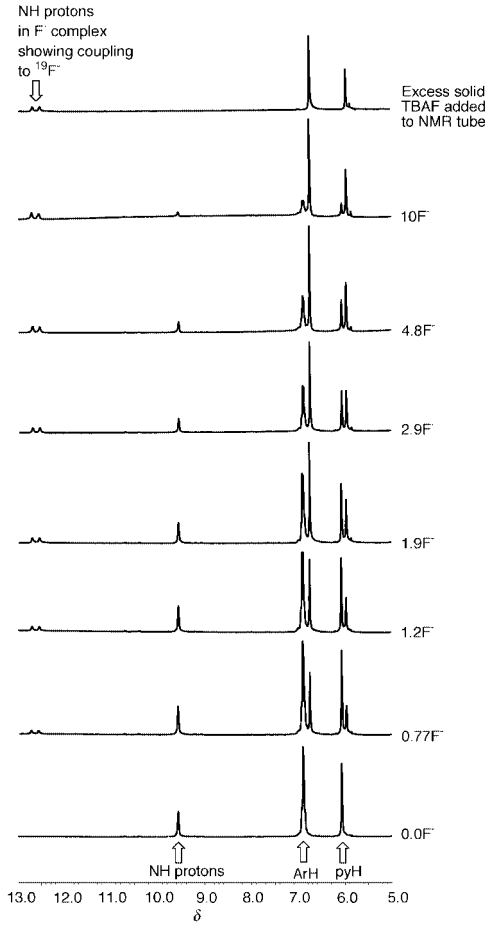

Fig. 1 NMR spectra of compound **5** in deuteriated DMSO solution on addition of aliquots of tetrabutylammonium fluoride. Proton resonances corresponding to the free receptor and fluoride complex can be seen in addition to coupling between the NH proton and $^{19}F^-$ nucleus.

† Electronic supplementary information (ESI) available: synthesis details, NMR and MS, and titration curves. See http://www.rsc.org/suppdata/cc/b0/b003229h/

DOI: 10.1039/b003229h

calix[4]pyrrole–fluoride complex at low temperature (193 K) in deuteriated dichloromethane solution.[10] The concentration profiles of compounds **4** and **5** and their fluoride complexes during the NMR titrations (calculated by integration of the relevant NH resonances in the NMR spectra) are shown in Fig. 2.

In order to compare the solution binding properties of **4** and **5** with *meso*-octamethylcalix[4]pyrrole **1** and the extended cavity calix[4]pyrrole **2**, titrations of these species with fluoride and chloride anions were conducted in deuteriated DMSO solution. In the case of compound **1**, upon addition of fluoride anions, a broadening of the 'free' NH resonance at 9.4 ppm occurred and the appearance of a new resonance at 12.8 ppm (after the addition of 1.4 equivalents of fluoride) was observed. Upon addition of chloride anions to solutions of **1** in the same solvent, shifts of the NH proton were observed with a maximum shift to 11.1 ppm after 3.3 equivalents of chloride. Least squares non-linear fitting of the titration results (pyrrole CH protons) with fluoride and chloride to a 1:1 anion/calixpyrrole binding model with the EQNMR computer program[11] afforded stability constants of 1060 and 1025 M^{-1} (errors estimated to be < 15%) with compound **1** and fluoride and chloride respectively. Similar behaviour was observed with compound **2** and chloride, however the shift of the NH proton was small (a downfield shift of 0.1 ppm after seven equivalents of chloride) and the binding profile did not reach a plateau. This suggests that only a weak interaction is occurring with chloride, making the accurate calculation of a stability constant difficult. The evolution of new resonances corresponding to a solution complexed species was observed upon addition of fluoride anions to compound **2** in deuteriated DMSO solution.

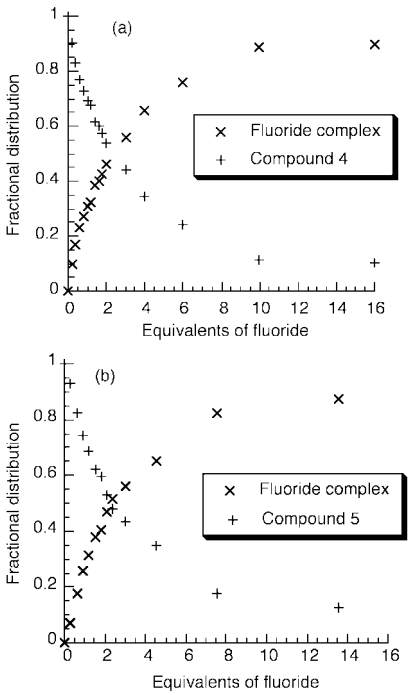

Fig. 2 Concentration profiles for (a) compound **4** and its fluoride complex and (b) compound **5** and its fluoride complex during ^{1}H NMR titrations in deuteriated DMSO solution at room temperature (21 °C).

Compounds **4** and **5** therefore show unique solution anion binding properties in that they *only bind fluoride* in deuteriated DMSO solution. These receptors do not interact with the other anions studied, behaviour not observed with other calix[4]pyrroles. It appears that the presence of an extended cavity in compound **2** and a 'super-extended' cavity in compounds **4** and **5** serves to decrease (**2**) and switch off (**4** and **5**) the affinity of this class of receptor for anions other than fluoride in DMSO solution. We are currently continuing to study the unusual coordination properties of these and other new calix[4]pyrroles in deuteriated DMSO. The results of this work will be reported in due course.

P. A. G. would like to thank the Royal Society for a University Research Fellowship and the EPSRC for a project studentship (to S. C.). Helpful discussions with Dr Pavel Anzenbacher, Jr. (present address: Bowling Green State University, Ohio, USA) are gratefully acknowledged.

Notes and references

1 P. A. Gale, *Coord. Chem. Rev.*, 2000, **199**, 181; P. D. Beer and P. A. Gale, *Angew. Chem., Int. Ed.*, 2000, in press; M. M. G. Antonisse and D. N. Reinhoudt, *Chem. Commun.*, 1998, 443; F. P. Schmidtchen, *Nachr. Chem. Tech. Lab.*, 1988, **36**, 8.
2 P. A. Gale, J. L. Sessler, V. Král and V. Lynch, *J. Am. Chem. Soc.*, 1996, **118**, 5140; J. L. Sessler and P. A. Gale, in *The Porphyrin Handbook*, vol. 6, ed. K. M. Kadish, K. M. Smith and R. Guilard, Academic Press, San Diego, CA and Burlington, MA, 2000, pp. 257–278.
3 P. A. Gale, J. L. Sessler, W. E. Allen, N. A. Tvermoes and V. Lynch, *Chem. Commun.*, 1997, 665.
4 H. Miyaji, P. Anzenbacher Jr., J. L. Sessler, E. R. Bleasdale and P. A. Gale, *Chem. Commun.*, 1999, 1723; P. A. Gale, L. J. Twyman, C. I. Handlin and J. L. Sessler, *Chem. Commun.*, 1999, 1851.
5 J. L. Sessler, P. A. Gale and J. W. Genge, *Chem. Eur. J.*, 1998, **4**, 1095.
6 P. Anzenbacher Jr., K. Jursíková, V. M. Lynch, P. A. Gale and J. L. Sessler, *J. Am. Chem. Soc.*, 1999, **121**, 11 020.
7 L. Bonomo, E. Solari, G. Toraman, R. Scopelliti, M. Latronico and C. Floriani, *Chem. Commun.*, 1999, 2413.
8 A. Arduini, A. Pochini, S. Reverberi and R. Ungaro, *J. Chem. Soc., Chem. Commun.*, 1984, 981; F. Arnaud-Neu, E. M. Collins, M. Deasy, G. Ferguson, S. J. Harris, B. Kaitner, A. J. Lough, M. A. McKervey, E. Marques, B. L. Ruhl, M. J. Schwing-Weill and E. M. Seward, *J. Am. Chem. Soc.*, 1989, **111**, 8681.
9 Solubility problems prevented anion binding studies being conducted with compound **5** in deuteriated acetonitrile solution. It was therefore decided to conduct all binding studies in deuteriated DMSO (estimated water content approx. 0.02%) in order to give a consistent set of results and to minimise the chances of ion-pair formation in solution (which may occur with low polarity and poor donor/acceptor solvents such as dichloromethane). It should be noted however that ^{1}H NMR titrations of compound **4** with fluoride or chloride anions in deuteriated acetonitrile solution resulted in the appearance of new resonances corresponding to solution complexed species (slow exchange conditions in contrast to compound **2** which displays fast exchange with anions under these conditions (see ref. 6)).
10 P. A. Gale, J. L. Sessler and V. Král, *Chem. Commun.*, 1998, 1.
11 M. J. Hynes, *J. Chem. Soc., Dalton Trans.*, 1993, 311.

Oxygenation of alkanes with hydrogen peroxide catalysed by osmium complexes

Georgiy B. Shul'pin,*[a] Georg Süss-Fink[b] and Lidia S. Shul'pina[c]

[a] *Semenov Institute of Chemical Physics, Russian Academy of Sciences, ul. Kosygina, dom 4, Moscow 117977, Russia. E-mail: shulpin@chph.ras.ru*
[b] *Institut de Chimie, Université de Neuchâtel, Avenue de Bellevaux 51, CH-2000, Neuchâtel, Switzerland*
[c] *Nesmeyanov Institute of Organoelement Compounds, Russian Academy of Sciences, ul. Vavilova, dom 28, Moscow 117813, Russia*

Received (in Basel, Switzerland) 9th March 2000, Accepted 18th May 2000

Efficient oxidation of alkanes, including methane and ethane, with H_2O_2 in the presence of catalytic amount of an Os complex in MeCN (addition of nitrogen-containing heterocycles significantly enhances the yield of the products) or in $MeCO_2H$ gives the corresponding ketones and alcohols.

Unlike aromatic and olefinic hydrocarbons, alkanes are known to exhibit only negligible reactivity in reactions with a variety of normal reagents and the yields of the products are usually low, especially in the case of light saturated hydrocarbons (methane, ethane and propane).[1] Osmium compounds, particularly OsO_4, oxidize unsaturated hydrocarbons and some other organic compounds stoichiometrically and catalyse their oxygenations with various reagents.[2,3]

Here, we report that soluble osmium derivatives, especially $OsCl_3$, catalyse efficiently the oxygenation of saturated hydrocarbons with hydrogen peroxide. All reactions[4] were carried out at 80 °C. The oxidation of cycloheptane (0.4 mol dm^{-3}) in MeCN with H_2O_2 (1.0 mol dm^{-3}) in the presence of $OsCl_3$ (1.0×10^{-3} mol dm^{-3}) gave after 3 h cycloheptanol (0.05 mol dm^{-3}) and cycloheptanone (0.013 mol dm^{-3}), the total turnover number (TON) being 63. Addition of a small amount of pyridine (0.125 mol dm^{-3}) gave rise to a noticeable increase in the yield and to the predominant formation of the ketone (after 90 min: cycloheptanol, 0.020 mol dm^{-3}; cycloheptanone, 0.092 mol dm^{-3}; TON, 112). Other nitrogen-containing heterocycles also promote the oxidation: for example, the reaction with *n*-heptane in the presence of 3-methylpyrazole (Fig. 1) affords predominantly isomeric ketones (after 60 min total concentration 0.028 mol dm^{-3}) as well as isomeric alcohols (total 0.04 mol dm^{-3}). Heptanal has been detected only in negligible concentration. The reaction is accompanied by non-productive H_2O_2 decomposition to give molecular oxygen, and the oxidation decreases when hydrogen peroxide concentration becomes low (after approximately 1 h, as shown in Fig. 1). By varying the additive, it is possible to control the ketone/alcohol ratio (Table 1). Lower alkanes can be easily oxidized in MeCN, if pyridine is added to the reaction solution (Table 2). In contrast to methane which is the least reactive hydrocarbon in this reaction and affords methanol as the main product, ethane and propane give mainly carbonyl compounds and only smaller amounts of alcohols with TON values of 102 and 150, respectively.

The selectivities of the alkane oxidations catalysed by $OsCl_3$ are higher than those determined for analogous hydroxylations by the systems 'H_2O_2–*h*ν' and 'H_2O_2–$FeSO_4$' as well as 'H_2O_2–VO_3^-–pyrazinecarboxylic acid (PCA)'[7] which are believed to produce free hydroxyl radicals (Table 3). It is noteworthy that selectivities significantly increase when pyridine is added to the reaction solution. Moreover, while the oxidation of *cis*-decalin with H_2O_2–$OsCl_3$ in MeCN occurs without retention of the configuration (the *trans/cis* ratio of the products formed being more than unity), in the presence of

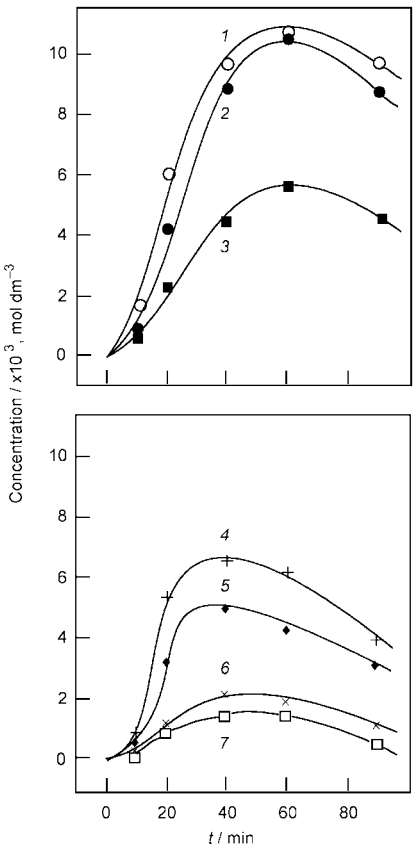

Fig. 1 Accumulation of heptan-2-one (*1*), heptan-3-one (*2*), heptan-4-one (*3*), heptan-2-ol (*4*), heptan-3-ol (*5*), heptan-4-ol (*6*) and heptan-1-ol (*7*) in the *n*-heptane (0.4 mol dm^{-3}) oxidation with H_2O_2 (1.0 mol dm^{-3}) catalysed by $OsCl_3$ (10^{-3} mol dm^{-3}) in MeCN in the presence of 3-methylpyrazole (0.12 mol dm^{-3}) at 80 °C.

Table 1 Oxidation of cycloheptane (0.4 mol dm^{-3}) with H_2O_2 (1.0 mol dm^{-3}) in MeCN (80 °C, 2 h)[4]

		Products/mol dm^{-3}		
Catalyst	Additive	Cyclo-heptanol (OL)	Cyclo-heptanone (ONE)	Ratio OL/ONE
$OsCl_3$	2,5-Dichloropyridine	0.076	0.014	5.4
$OsCl_3$	None	0.049	0.010	4.9
$OsCl_3$	2,2′-Bipyridine	0.059	0.026	2.3
Na_2OsCl_6	3,5-Dimethylpyrazole	0.022	0.026	0.85
Na_2OsCl_6	3-Methylpyrazole	0.030	0.070	0.45
$OsCl_3$	3-Methylpyrazole	0.035	0.077	0.45
$OsCl_3$	Pyridine	0.020	0.092	0.2

DOI: 10.1039/b002015j

Table 2 Oxygenation of lower alkanes (H_2O_2 = 1 mol dm^{-3}, $OsCl_3$ = 1 × 10^{-3} mol dm^{-3}, py = 0.125 mol dm^{-3}; MeCN 80 °C, 1.5 h)[4]

Alkane (pressure/bar)	Products/mol dm^{-3}
Methane (40)	CH_3OH (0.017); HCHO (3.0×10^{-5})
Ethane (20)	CH_3CHO (0.08); CH_3CH_2OH (0.022)
Propane (6)	CH_3CH_2CHO (0.034); CH_3COCH_3 (0.054); $CH_3CH(OH)CH_3$ (0.018); $CH_3CH_2CH_2OH$ (0.044)
n-Butane (2)	$CH_3CH_2CH_2CHO$ (0.011); $CH_3COCH_2CH_3$ (0.026); $CH_3CH(OH)CH_2CH_3$ (0.011); $CH_3CH_2CH_2CH_2OH$ (0.002)

Table 3 Selectivities of alkane oxidations by various systems

Substrate	System	Selectivity[a]
n-Heptane		C(1):C(2):C(3):C(4)
	H_2O_2–*hν* in MeCN	1.0:7.3:6.3:8.1
	H_2O_2–$FeSO_4$ in MeCN–H_2O	1.0:5.0:4.8:4.6
	H_2O_2–$OsCl_3$ in MeCN	1.0:11.8:9.8:3.5
2,2,4-Trimethyl-pentane		1°:2°:3°
	H_2O_2–*hν* in MeCN	1.0:1.75:6.2
	H_2O_2–$FeSO_4$ in MeCN–H_2O	1.0:2.75:6.0
	H_2O_2–Bu_4NVO_3–PCA in MeCN	1.0:3.0:4.8
	H_2O_2–$OsCl_3$ in MeCN	1.0:2.2:8.7
	H_2O_2–$OsCl_3$ in MeCN–py (0.125 mol dm^{-3})	1.0:2.1:18.3
cis-Decalin		*trans*/*cis*
	H_2O_2–*hν* in MeCN	1.3
	H_2O_2–*hν* in py	1.9
	H_2O_2–$FeSO_4$ in MeCN–H_2O	3.4
	H_2O_2–Bu_4NVO_3–PCA in MeCN	2.1
	H_2O_2–$OsCl_3$ in MeCN–py (0.125 mol dm^{-3})	1.2
	H_2O_2–$OsCl_3$ in MeCN–py (6.25 mol dm^{-3})	0.56
	H_2O_2–$OsCl_3$ in $MeCO_2H$	0.26

[a] Parameter C(1):C(2):C(3) is normalized (*i.e.* calculated taking into account the number of hydrogen atoms at each position) relative reactivities of hydrogens at carbon atoms 1, 2 and 3 of the alkane chain, respectively; parameter 1°:2°:3° is normalized relative reactivities of hydrogen atoms at primary, secondary and tertiary carbons, respectively; parameter *trans*/*cis* = [*trans*-decal-9-ol]/[*cis*-decal-9-ol], where [*trans*- and *cis*-decal-9-ol] are concentrations of *trans*- and *cis*-decal-9-ol formed in the oxidation, respectively.

pyridine the reaction becomes more selective, the *trans/cis* ratio decreasing with increasing pyridine concentration. It is important to note that in $MeCO_2H$ the reaction exhibits a high value of the *trans/cis* parameter (0.26) and the parameter RC_{cis} = $100(c_{cis} - c_{trans})/(c_{cis} + c_{trans})$ = 58%. The value of the *trans/cis* parameter for the system 'H_2O_2–$OsCl_3$' in $MeCO_2H$ is only slightly higher than that (*trans/cis* = 0.12) for the hydroxylation in MeCN by the system 'H_2O_2–$LMn^{IV}(O)_3$-$Mn^{IV}L^+$–$MeCO_2H$ (L = 1,4,7-trimethyl-1,4,7-triazacyclononane)' described recently.[8]

On the basis of the results obtained and especially taking into account the selectivity parameters, one may assume that oxidation by the system H_2O_2–$OsCl_3$ starts with hydrogen atom abstraction from the alkane by an oxo osmium complex, and the reaction occurs in a solvent cage. The alkyl radicals formed react then with dioxygen to generate the corresponding alkyl hydroperoxide which decomposes to afford the corresponding ketone and alcohol. The system described here can be considered as a model for the oxidations of C–H compounds catalysed by iron-containing enzymes, osmium being an iron homologue in the Periodic System. Indeed, oxidations with participation of cytochrome P-450, methane monooxygenase and chloroperoxidase are believed to begin with hydrogen atom abstraction by a high-valent iron oxo species.[1,9] Coordination of a nitrogen-containing heterocycle (and/or acetate) to osmium may produce a catalytically active oxo species surrounded with voluminous ligands, and the relatively high bond- and stereoselectivities of the alkane oxidation may be due in this case to the bulkiness of the ligands at the reaction centre.

We thank the Russian Basic Research Foundation and the Swiss National Science Foundation for support.

Notes and references

1 (*a*) A. E. Shilov and G. B. Shul'pin, *Activation and Catalytic Reactions of Saturated Hydrocarbons in the Presence of Metal Complexes*, Kluwer, Dordrecht, 2000; (*b*) A. E. Shilov and G. B. Shul'pin, *Chem. Rev.*, 1997, **97**, 2879; (*c*) R. H. Crabtree, *Chem. Rev.*, 1995, **95**, 987; (*d*) G. B. Shul'pin, *Organic Reactions Catalysed by Metal Complexes*, Nauka, Moscow, 1988.

2 Reviews: T. Wirth, *Angew. Chem., Int. Ed.*, 2000, **39**, 334; R. A. Sánchez-Delgado, M. Rosales, M. A. Esteruelas and L. A. Oro, *J. Mol. Catal. A: Chem.*, 1995, **96**, 231; Y. Gao, in *Encyclopedia of Reagents for Organic Synthesis*, ed. L. A. Paquette, J. Wiley & Sons, Chichester, 1995, vol. 6, pp. 3801–3810; H. C. Kolb, K. B. Sharpless and M. S. Van Nieuwenhze, *Chem. Rev.*, 1994, **94**, 2483; *Catalytic Oxidations with Hydrogen Peroxide as Oxidant*, ed. G. Strukul, Kluwer, Dordrecht, 1992; K. A. Jørgensen, *Chem. Rev.*, 1989, **89**, 431; A. H. Haines, *Methods for the Oxidation of Organic Compounds*, Academic Press, London, 1985; M. Schroeder, *Chem. Rev.*, 1980, **80**, 187; *Oxidation*, ed. R. L. Augustine, Marcel Dekker, Inc., New York, 1969.

3 Recent original papers: P. C. B. Page, M. J. MacKenzie and D. R. Burkle, *Tetrahedron*, 1998, **54**, 14 581; K. Bergstad, J. J. N. Piet and J.-E. Bäckvall, *J. Org. Chem.*, 1999, **64**, 2545; A. J. Pearson and I. B. Neagu, *J. Org. Chem.*, 1999, **64**, 2890; T. J. Donohoe, K. Blades, M. Helliwell, P. R. Moore and J. J. G. Winter, *J. Org. Chem.*, 1999, **64**, 2980; P. Barthazy, M. Wörle and A. Mezetti, *J. Am. Chem. Soc.*, 1999, **121**, 480; K. S. Coleman, M. Coppe, C. Thomas and J. A. Osborn, *Tetrahedron Lett.*, 1999, **40**, 3723; J. Eames, H. J. Mitchell, A. Nelson, P. O'Brien, S. Warren and P. Wyatt, *J. Chem. Soc., Perkin Trans. 1*, 1999, 1095; F. Ahmed, E. H. Al-Mutairi, K. L. Avery, P. M. Cullis, W. U. Primrose, G. C. K. Roberts and C. L. Willis, *Chem. Commun.*, 1999, 2049; W. A. Herrmann, R. M. Kratzer, J. Blümel, H. B. Friedrich, R. W. Fischer, D. C. Apperley, J. Mink and O. Berkesi, *J. Mol. Catal. A: Chem.*, 1997, **120**, 197.

4 The oxidations of higher hydrocarbons were carried out in air in thermostated Pyrex cylindrical vessels with vigorous stirring. The total volume of the reaction solution was 5 or 10 mL. In a typical experiment, initially, a portion of 35% aqueous solution of hydrogen peroxide (Fluka) was added to the solution of the catalyst, substrate and heterocycle in acetonitrile (Fluka). The oxidations of lower alkanes were carried out in an stainless steel autoclave with intensive stirring (volume of the reaction solution was 5 mL and total volume of autoclave was 100 mL). Before the oxidation the autoclave was charged with the alkane under appropriate pressures. The reactions were stopped by cooling with ice and the reaction solution was analysed by GC (DANI-86.10; fused silica capillary column 25 m × 0.32 mm × 0.25 mm, CP-WAX52CB; integrator SP-4400). Comparison of the chromatograms of the reaction samples before and after their treatment with PPh_3 (for this method, see refs. 1(*a*),(*b*),5–8) demonstrated that concentrations of alkyl hydroperoxides were very low. The concentration of formaldehyde was measured spectrophotometrically after its transformation into 2,6-dimethyl-3,5-diacetyl-1,4-dihydropyridine as described previously.[6]

5 G. B. Shul'pin, M. M. Bochkova and G. V. Nizova, *J. Chem. Soc., Perkin Trans. 2*, 1995, 1465; G. B. Shul'pin, G. V. Nizova and Yu. N. Kozlov, *New. J. Chem.*, 1996, **20**, 1243.

6 G. V. Nizova, G. Süss-Fink and G. B. Shul'pin, *Chem. Commun.*, 1997, 397; G. V. Nizova, G. Süss-Fink and G. B. Shul'pin, *Tetrahedron*, 1997, **53**, 3603; G. Süss-Fink, G. V. Nizova, S. Stanislas and G. B. Shul'pin, *J. Mol. Catal. A: Chem.*, 1998, **130**, 163.

7 G. B. Shul'pin, D. Attanasio and L. Suber, *J. Catal.*, 1993, **142**, 147; G. V. Nizova and G. B. Shul'pin, *Russ. Chem. Bull.*, 1994, **43**, 1146; G. B. Shul'pin, M. C. Guerreiro and U. Schuchardt, *Tetrahedron*, 1996, **52**, 13 051; M. C. Guerreiro, U. Schuchardt and G. B. Shul'pin, *Russ. Chem. Bull.*, 1997, **46**, 749.

8 J. R. Lindsay Smith and G. B. Shul'pin, *Tetrahedron Lett.*, 1998, **39**, 4909; G. B. Shul'pin and J. R. Lindsay Smith, *Russ. Chem. Bull.*, 1998, **47**, 2379; G. B. Shul'pin, G. Süss-Fink and J. R. Lindsay Smith, *Tetrahedron*, 1999, **55**, 5345.

9 F. Hino and D. Dolphin, *Chem. Commun.*, 1999, 629; K. Chen and L. Que, Jr., *Chem. Commun.*, 1999, 1375; E. Baciocchi, O. Lanzalunga and L. Manduchi, *Chem. Commun.*, 1999, 1715.

Direct conversion of aromatics into a synthetic steamcracker feed using bifunctional zeolite catalysts

Jens Weitkamp,*[a] Andreas Raichle,[a] Yvonne Traa,[a] Martin Rupp[b] and Franz Fuder[b]

[a] *Institute of Chemical Technology, University of Stuttgart, D-70550 Stuttgart, Germany. E-mail: jens.weitkamp@po.uni-stuttgart.de*
[b] *VEBA OEL AG, D-45876 Gelsenkirchen, Germany*

Received (in Cambridge, UK) 28th April 2000, Accepted 19th May 2000

Aromatics with 6 to 9 carbon atoms can be converted catalytically with hydrogen on bifunctional zeolites, such as Pd/H-ZSM-5, into a high-quality steamcracker feed, thereby opening a direct route for the utilisation of surplus pyrolysis gasoline.

In view of the predicted over-supply of aromatics,[1] novel catalytic routes for their conversion into valuable products are urgently needed. One of the major sources of aromatics is so-called pyrolysis gasoline, a by-product of steamcracking in which ethylene and propylene are made from light hydrocarbons, such as straight-run naphtha,[2] LPG[3] or ethane. In a preceding communication[4] we have shown that cycloalkanes (which are readily obtained from aromatics by catalytic ring hydrogenation) can be converted on acidic zeolite catalysts, such as H-ZSM-5, into a high-quality steamcracker feed consisting mainly of ethane, propane and *n*-butane. Here, we demonstrate that, as an alternative to this two-stage route (ring hydrogenation followed by ring opening), aromatics can be *directly* converted with hydrogen into the same type of synthetic steamcracker feed, if *bifunctional* zeolite catalysts, *e.g.*, Pd/H-ZSM-5, are used. The literature on catalytic ring opening of aromatics in an excess of hydrogen is very scarce,[5–8] and on the catalysts used so far, the yields of *n*-alkanes with two or more carbon atoms, *i.e.* the most desirable hydrocarbons for a synthetic steamcracker feed, are reported to be low.

Results of the conversion of toluene[9] on 0.2Pd/H-ZSM-5[10] are displayed in Fig. 1. Whereas the conversion of toluene is 100% throughout the temperature range covered, the types of reaction occurring vary drastically: at 200 °C, hydrogenation to methylcyclohexane is the predominant reaction, and part of the methylcyclohexane is isomerised in consecutive reactions *via* the well known[11] bifunctional mechanism into ethylcyclopentane and dimethylcyclopentanes. With increasing temperature, more and more ring opening occurs. At 320 °C, virtually all cyclic hydrocarbons are converted into alkanes,[12] and increasing the temperature further brings about a diminution of the yield of isoalkanes which undergo secondary cracking reactions into propane and ethane. At 400 °C toluene is converted with a yield of 72.8% into C_{2+}-*n*-alkanes (*cf.* Table 1, column 4). It is noteworthy that no aromatics occur in the product under any reaction conditions, and very little methane is formed even at 400 °C. For various reasons (high hydrogen consumption and exothermicity, methane does not form ethylene or propylene in the steamcracker), methane is a very undesired product.

Upon increasing the palladium content of the catalyst from 0.2 to 0.5 and 1.0 wt.%, the yields at a reaction temperature of 400 °C do not change significantly. From this we conclude that, under the conditions applied in this work, ring opening and the formation of light alkanes proceed *via* the bifunctional hydrocracking mechanism[13] and Haag–Dessau cracking,[14] rather than *via* hydrogenolysis[15] on the noble metal.

Table 1 shows results obtained at 400 °C with different feed hydrocarbons. No products other than alkanes were found with any feed hydrocarbon under these conditions. The yields of methane are low throughout (around 3–4%, Table 1, entry 2). Interestingly, the yields of the desired C_{2+}-*n*-alkanes (Table 1, entry 7) do vary significantly with the nature of the aromatic

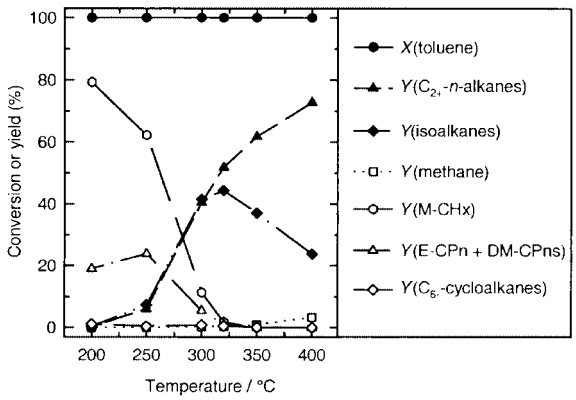

Fig. 1 Conversion of toluene on 0.2Pd/H-ZSM-5 at various temperatures (*X*: conversion; *Y*: yield; M-CHx: methylcyclohexane; E-CPn: ethylcyclopentane; DM-CPns: dimethylcyclopentanes).

Table 1 Conversion of aromatics on 0.2Pd/H-ZSM-5 at 400 °C

		Feed					
Entry		Benzene	Toluene	*o*-Xylene	*p*-Xylene	Ethylbenzene	1,2,4-Trimethylbenzene
1	X^a (%)	100	100	100	100	100	100
2	$Y_{methane}{}^b$ (%)	3.7	3.3	4.0	4.1	2.5	3.0
3	$Y_{ethane}{}^b$ (%)	14.4	7.9	15.6	14.9	30.6	13.6
4	$Y_{propane}{}^b$ (%)	62.8	48.6	49.1	46.7	49.0	49.4
5	$Y_{n\text{-butane}}{}^b$ (%)	11.9	15.9	14.2	15.0	9.5	15.2
6	$Y_{C_{5+}\text{-}n\text{-alkanes}}{}^b$ (%)	1.2	0.4	3.4	3.8	1.1	2.7
7	$Y_{C_{2+}\text{-}n\text{-alkanes}}{}^{b,c}$ (%)	90.3	72.8	82.3	80.4	90.2	80.9
8	$Y_{isoalkanes}{}^b$ (%)	6.0	23.9	13.7	15.5	7.3	16.1

[a] *X* is the conversion of the aromatic feed hydrocarbon. [b] *Y* is the yield of the product indicated and defined in the usual manner, *e.g.*, $Y_{n\text{-butane}} = (4/7) \times (\dot{n}_{n\text{-butane, out}}/\dot{n}_{toluene, in})$, $\dot{n}$ being the molar flux. [c] Sum of entries 3 to 6.

DOI: 10.1039/b003422n

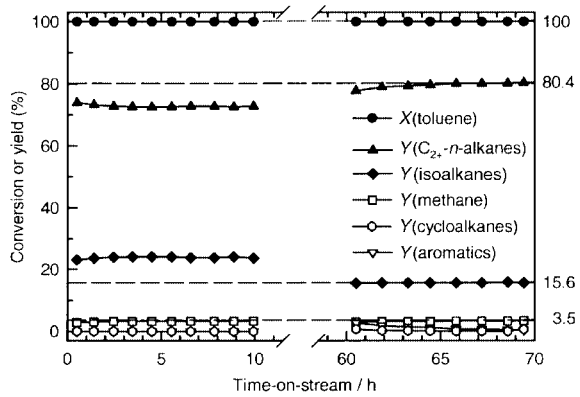

Fig. 2 Coke selectivation in the conversion of toluene on 0.2Pd/H-ZSM-5. (During the initial 10 h and from 60 to 70 h on-stream time, the reaction temperature was 400 °C. In the period between 10 h and 60 h, lower reaction temperatures in the range from 200 to 350 °C were applied; *X*: conversion; *Y*: yield.)

feed hydrocarbon. This yield is lowest for toluene and above 90% for both benzene and ethylbenzene. Note also that very large amounts of propane are formed from benzene (which can be rationalized in terms of a so-called type C β-scission[16,17] of hexyl cations), while an unusually high yield of ethane is observed in the product from ethylbenzene (which we tentatively ascribe to a deethylation reaction).

Regardless of the hydrocarbon used as feed, there was no significant change in the product yields with time-on-stream. In Fig. 2, results are shown which were obtained with toluene as feed on 0.2Pd/H-ZSM-5. During the initial 10 h, the yield of C_{2+}-*n*-alkanes amounted to *ca*. 73%. For the next 50 h (not shown in Fig. 2) toluene was converted on this catalyst sample at lower temperatures in the range 200–350 °C. Thereafter, the reaction temperature was again raised to 400 °C for 10 h. Significantly better yields of the desired C_{2+}-*n*-alkanes (*ca*. 80%) were attained than with the fresh catalyst. We interpret this selectivity gain in terms of a so-called coke selectivation, *i.e.* at the lower reaction temperatures between the two runs at 400 °C, some dimerization and/or disproportionation reactions of methylcyclohexane[18] or toluene inside the zeolite pores must have taken place, whereby larger product molecules were formed which ultimately led to some carbonaceous deposits with a concomitant narrowing of the pores. Similar effects have been observed by others, *e.g.* in the disproportionation of toluene on H-ZSM-5.[19]

In conclusion, we have demonstrated that aromatics can be *directly* converted with hydrogen into a high-quality steamcracker feed on bifunctional zeolite catalysts of the Pd/H-ZSM-5 type. This direct route will have to compete with the two-stage variant consisting of ring hydrogenation in the aromatics over a hydrogenation catalyst followed by ring opening of cycloalkanes on monofunctional zeolites.[4] The main technological advantage of the direct route described here is a single catalytic reactor for the manufacture of synthetic steamcracker feed from pyrolysis gasoline. On the other hand, advantageous features of the two-stage variant are (i) the possibility to optimise the ring hydrogenation of aromatics and the ring opening of the resulting cycloalkanes separately and (ii) the generation of the exothermic heat in two separate reactors and, hence easier removal of this heat. It remains to be seen whether the direct route or the two-stage variant is economically more attractive.

Notes and references

1 W. J. Petzny and C.-P. Hälsig, in *DGMK Tagungsbericht 9903, Proc. DGMK Conference: The Future Role of Aromatics in Refining and Petrochemistry, October 13-15, 1999, Erlangen, Germany*, ed. G. Emig, M. Rupp and J. Weitkamp, DGMK, Hamburg, 1999, p. 7.

2 Straight-run naphtha is a light petroleum fraction composed essentially of C_5 and C_6 hydrocarbons.

3 LPG stands for Liquefied Petroleum Gas, the C_3 and C_4 hydrocarbons from petroleum.

4 J. Weitkamp, A. Raichle, Y. Traa, M. Rupp and F. Fuder, *Chem. Commun.*, 2000, 403.

5 T. Sano, K. Okabe, H. Hagiwara and H. Takaya, *J. Mol. Catal.*, 1987, **40**, 113.

6 J.-K. Chen, A. M. Martin, Y. G. Kim and V. T. John, *Ind. Eng. Chem. Res.*, 1988, **27**, 401.

7 L. P. Poslovina, V. G. Stepanov, L. V. Malysheva, E. A. Paukshtis, L. A. Vostrikova and K. G. Ione, *Stud. Surf. Sci. Catal.*, 1997, **105**, 997.

8 A. Chambellan, O. Cairon and T. Chevreau, in *Proc. 12th Int. Zeolite Conf., Warrendale, USA, July 5–10, 1998*, ed. M. M. J. Treacy, B. K. Marcus, M. E. Bisher and J. B. Higgins, Materials Research Society, Baltimore, 1999, p. 1025.

9 Toluene is a major constituent of pyrolysis gasoline, other typical aromatics in pyrolysis gasoline are ethylbenzene, xylenes and benzene.

10 Zeolite ZSM-5 (n_{Si}/n_{Al} = 20) was hydrothermally synthesised after S. Ernst and J. Weitkamp, *Chem. Ing. Tech.*, 1991, **63**, 748, ion-exchanged with aqueous solutions of NH_4NO_3 and $Pd(NH_3)_4Cl_2$ and pre-treated successively in flows of air (12 h), nitrogen (1 h) and hydrogen (7 h) at 400 °C to yield bifunctional catalysts with $m_{Pd}/m_{dry\ zeolite}$ = 0.2, 0.5 or 1.0% referred to as 0.2Pd/H-ZSM-5, 0.5Pd/H-ZSM-5 and 1.0Pd/H-ZSM-5, respectively. The experiments were performed in a flow-type stainless steel apparatus with a fixed-bed reactor. The mass of dry catalyst (particle size between 0.20 and 0.32 mm), the total pressure (which was virtually equivalent to the partial pressure of hydrogen), the partial pressure of the aromatic feed hydrocarbon at the reactor inlet and the weight hourly space velocity (WHSV) amounted to 500 mg, 6.0 MPa, 65 kPa and 0.68 h^{-1}, respectively. Product analysis was achieved by capillary gas chromatography.

11 J. Weitkamp, P. A. Jacobs and S. Ernst, *Stud. Surf. Sci. Catal.*, 1984, **18**, 279.

12 The product yields at 320 °C are: methane 0.5%, ethane 1.0%, propane 41.3%, *n*-butane 7.4%, *n*-pentane 1.7%, *n*-hexane 0.5%, isobutane 40.7%, isopentane 2.3%, isohexanes 1.3%, isoheptanes 0.1%, cycloalkanes 3.3%.

13 J. Weitkamp, in *Ketjen Catalysts Symposium 1988: Fluid Catcracking, Hydrocracking, Hydrotreating, Pt-Reforming*, ed. H. J. Lovink, Akzo Chemicals, Amersfoort, 1988, p. G-3 1.

14 (*a*) W. O. Haag and R. M. Dessau, in *Proc. 8th Int. Congr. Catal., July 2–6, 1984, Berlin, Germany*, vol. 2, Verlag Chemie, Weinheim, 1984, p. 305; (*b*) S. Kotrel, H. Knözinger and B. C. Gates, *Microporous Mesoporous Mater.*, 2000, **35–36**, 11.

15 F. G. Gault, *Adv. Catal.*, 1981, **30**, 1.

16 β-Scission of alkylcarbenium ions—a scission of the carbon–carbon bond in the β-position with respect to the positively charged carbon atom—is the key step in the bifunctional hydrocracking mechanism.

17 J. Weitkamp, P. A. Jacobs and J. A. Martens, *Appl. Catal.*, 1983, **8**, 123.

18 H. Schulz, J. Weitkamp and H. Eberth, in *Proc. 5th Int. Congr. Catalysis*, ed. J. W. Hightower, North-Holland, Amsterdam, 1973, vol. 2, p. 1229.

19 L.-Y. Fang, S.-B. Liu and I. Wang, *J. Catal.*, 1999, **185**, 33.

ChemComm

Estradiol binding synthetic polypeptides

G. Giraudi,* C. Giovannoli, C. Tozzi, C. Baggiani and L. Anfossi

Department of Analytical Chemistry, University of Torino, Via P. Giuria 5, 10125 Torino, Italy. E-mail: giraudi@ch.unito.it

Received (in Cambridge, UK) 14th December 1999, Accepted 19th May 2000

We have synthesised polypeptides that mimic the binding properties of natural receptors with high affinity and selectivity towards the steroid hormone estradiol, performing a template polymerisation in aqueous medium and without creating rigid structures.

Selective recognition systems are usually created in synthetic polymers obtaining a three-dimensional structure that has been shaped to match the template, after its removal. As a consequence, artificial systems of recognition are available for nucleotides,[1] inorganic ions,[2] amino acids[3,4] and herbicides.[5] We employed the template polymerisation method to synthesise oligopeptides that were templated with the steroid hormone estradiol. The application of this technique is completely new because until now the literature only gave examples on cross-linked organic macroporous polymers, whereas we performed the polymerisation in aqueous medium without the formation of rigid structures. The initial idea was that an amino acid mixture could generate polypeptidic systems, thus establishing non-covalent bonds with molecular species present in the polymerisation mixture. Polypeptides are structures that are well suited for the design of systems with molecular recognition properties, above all for the large structural heterogeneity in the amino acid lateral chain that gives rise to a great variety of chemical properties and non-covalent interactions useful in template polymerisation.

The amino acid composition of the mixtures that we polymerised is similar to bovine serum albumin. Two different amino acid mixtures were polymerised: the first—branched mixtures— contained branched monomers (Gly, Ala, Leu, Pro, Phe, Tyr, Trp, Ser, Met, Arg, His, Lys, Asp, Asn, Gln, Glu, Cys-Cys), the second—linear mixtures— contained the same amino acids apart from Lys, Asp, Glu, Cys-Cys and were richer in Leu and Gly. This enabled us to study the binding properties of both cross-linked and linear structures. Furthermore, for each mixture the polymerisation was performed in the presence (template mixtures) and in the absence (blank mixtures) of estradiol to compare the binding properties, and were performed for different reaction times (1, 3 and 30 h) to evaluate the influence of this variable on the binding constants.[6]

To remove the estradiol we used anion exchange chromatography on a DEAE-Sephacel column.[7]

The concentration of the oligopeptides was determined by spectrophotometric measurements, and the recoveries were between 94 and 97%.

After purification of the mixtures, we characterised the oligopeptides by determining the average molecular weights by HPLC using an Alltech Macrosphere GPC 60 A 7 μm (250 mm × 4.6 mm).[8] The average M_w was between 2000 and 6000 Da, increasing with the polymerisation time, and so, considering an average amino acid M_w of 130 Da, the degree of polymerisation was between 15 and 46, with an average value of 30.

The spectrophotometric titration of the template oligopeptides with estradiol performed at 274 nm shows that the stoichiometry of binding is close to 1 : 1, but an evaluation of the binding constant was not possible due to the absence of curvature in the equivalence region.

To evaluate the binding affinity of the oligopeptides we used immunocompetition where the oligopeptides competed with an immobilised anti-estradiol antibody for tritium labelled estradiol. The anti-estradiol antibody was immobilised into the wells of microtitre plates previously coated with goat anti-rabbit IgG antibodies, according to the literature.[9] The measurement of estradiol bound to the antibody in the presence of the oligopeptides allowed us to determine the binding constants K (by fitting a proper mathematical equation to the experimental data) of the oligopeptide mixtures. This defines the ratio between the binding of the tritium labelled estradiol with the antibody in the presence of the oligopeptides and without the oligopeptides, as a function of the binding constant of the antibodies for estradiol, the concentration of the solid phase, binding site antibodies, the tritium labelled estradiol concentration, the concentration of the oligopeptides and the binding constant of the oligopeptides for the estradiol. The first two parameters were determined in separate experiments as reported in the literature,[9] thus, knowing the tritium labelled estradiol concentration and the concentration of the oligopeptides we could obtain the binding constants of the oligopeptide mixtures for estradiol from the competition curves (Fig. 1). The binding constants are shown in Table 1.

As all these results could be affected by contributions from residual estradiol, we performed a template and blank polymer-

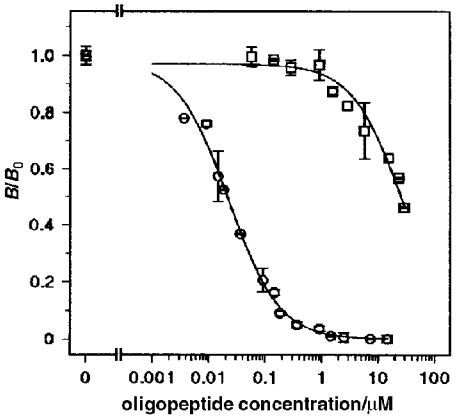

Fig. 1 Immunocompetition of branched mixtures polymerised for 1 hour. The plot of B/B_0, where B is the binding of the tritium labelled estradiol with the antibody in the presence of the oligopeptides and B_0 without the oligopeptides, *vs*. the oligopeptide concentration, gives competition curves from which the binding constant of the oligopeptides towards estradiol can be calculated. The branched template oligopeptides (○) and the branched blank oligopeptides (□) are shown.

Table 1 Binding constants of oligopeptide mixtures

Oligopeptide mixtures	Polymerisation time/h	Template K/M^{-1}	Blank K/M^{-1}
Branched	1	9.0×10^8	9.0×10^6
	3	1.2×10^9	1.5×10^7
	30	6.6×10^9	1.3×10^9
Linear	1	4.4×10^8	2.2×10^6
	3	5.8×10^8	2.8×10^6
	30	1.4×10^9	3.6×10^8

DOI: 10.1039/a909798h

isation in the presence of labelled estradiol.[10] After purification, the amount of bound estradiol was determined by this method, and only 3–4% of the template polypeptides contained bound estradiol. Control experiments were therefore carried out to investigate the effect of bound estradiol. Therefore, we corrected the mathematical equation, including a parameter that allowed us to take into account the presence of some residual estradiol. Fitting this last equation to the experimental data, we observed that the binding constants were essentially unchanged. So, the reported results are not affected by any contribution from residual estradiol, as the great excess of high affinity oligopeptides prevents the effective displacement of labelled estradiol from antibody binding sites by the residual template molecule.

To further verify the absence of artefacts in the evaluation of binding constants (due to the presence of residue template molecules), we performed some preliminary ultrafiltration experiments.[11] All values of binding constants obtained are about one order of magnitude lower than those obtained by competitive binding experiments, both for blank and template mixtures, but are affected by great imprecision. The reason for this is related to the partial adsorption of estradiol on the ultrafiltration membrane and also to the partial ultrafiltration of the oligopeptides, as determined in separate experiments with tritium labelled oligopeptides. The method is thus insensitive to residual estradiol but the partial ultrafiltration of oligopeptides leads to an underestimation of the binding. For these reasons we abandoned the ultrafiltration technique in favour of the competitive binding assay, which is simple to perform and gives better results.

In order to verify that there were no interactions between the rabbit anti-estradiol antibodies or the goat anti-rabbit γ-globulin antibodies and the oligopeptides, we checked the interactions of labelled oligopeptides (template and blank mixtures) with the immobilised antibodies.[12] In both cases we registered no significant binding to the solid phase. So, the inhibition of binding between labelled estradiol and its antibody is caused only by the binding properties of the oligopeptide mixtures that bind the steroid.

From the previously reported results, we note the very high affinity of the oligopeptides for the templating molecule. The difference between the binding constants of the template and blank mixtures shows the importance of the template effect on the amino acid mixtures and the efficacy of these systems as competitors of the antibodies themselves. For all mixtures the binding constants increase with the polymerisation time; this effect can be explained by the formation of more and more complex structures which are able to interact better with estradiol. The ratio between template and blank decreases when we increase the polymerisation time, probably because in the blank mixtures a longer reaction time increases the formation of more complex oligopeptide structures able to rearrange themselves around the steroid molecule to obtain a greater interaction. Instead, in the template mixtures this effect is less important as the binding properties are mainly due to the imprint.

An important parameter to consider is the specificity of binding. We performed an immunocompetition using the branched oligopeptides (1 h, 30 h) to evaluate the binding constant of this mixture for structural homologues, such as the steroids, testosterone and progesterone. The experimental procedure was similar to those used previously.[13] The results indicate that the oligopeptides do not have significant affinity for these molecules. For template branched oligopeptides (1 h) the binding constant for the testosterone is 1.2×10^5 M^{-1} *vs.* 9.0×10^8 M^{-1} for the estradiol, whereas for the blank ones K is 3.3×10^4 M^{-1} *vs.* 9.0×10^6 M^{-1}. The binding constants obtained for the branched oligopeptides polymerised for 30 h (template: 7.7×10^5 M^{-1}; blank: 4.8×10^6 M^{-1} for testosterone) confirm the hypothesis that longer reaction times can result in structures which can rearrange themselves to better match the steroid molecule without loss of selectivity (this remains unchanged), thus indicating that the imprinting effect is operative in all cases. For progesterone it is possible only to estimate an upper limit for the binding constant (1.0×10^4 M^{-1}). This is further evidence of the high affinity and high specificity of recognition toward the templating molecule. Moreover the template mixtures have selectivities similar not only to usual antisera, but also to the molecular imprinted polymers.[14]

Notes and references

1 C. Andreu, A. Galan, K. Kobiro, J. De Mendosa, T. K. Park, J. Rebek, A. Salmeron and N. Usman, *J. Am. Chem. Soc.*, 1994, **116**, 5501.
2 M. Yoshida, K. Uezu, M. Goto and S. Furusaki, *J. Appl. Polym. Sci.*, 1999, **73**, 1223.
3 M. Kempe, *Anal. Chem.*, 1996, **68**, 1948.
4 Y. Liao, W. Wang and B. Wang, *Bioorg. Chem.*, 1998, **26**(6), 309.
5 T. Takeuchi, D. Fukuma and J. Matsui, *Anal. Chem.*, 1999, **71**, 285.
6 The polymerisation was performed in mixed aqueous/organic media (carbonate buffer 0.2 M pH 9/DMF, 1 + 1) using carbodiimide as a condensing agent. The mixtures were shaken according to the different reaction times at room temperature in the dark. Then the oligopeptide mixtures were filtered on 0.45 μm sintered glass.
7 We washed the resin with carbonate buffer (20 mM, pH 8.5) until the absorbance had returned to the baseline. After reversing the direction of the flow, the elution was performed by running a phosphate buffer (50 mM phosphate, 1 M NaCl, 1 mM EDTA, pH 7).
8 K. Stulik, V. Pacakova, J. Suchankova and H. A. Claessens, *Anal. Chim. Acta*, 1997, **352**, 1.
9 G. Giraudi, I. Rosso, C. Baggiani and C. Giovannoli, *Anal. Chim. Acta*, 1999, **381**, 133.
10 Labelled estradiol (2.8×10^{-2} μM) was added to the estradiol and the amino acid mixtures before polymerisation. During the purification, we followed the absorbance of the oligopeptides with a spectrophotometric detector and the eluate was fractionated every 5 cm^3 to check the signal of the labelled estradiol.
11 We added the oligopeptides at increasing concentrations to a constant amount of labelled estradiol, and after centrifugation in an Amicon MPS-1 device, equipped with YM1 membranes (nominal molecular weight cut-off of 1000 Da), we measured the ultrafiltered estradiol in the filtrate. The fraction of estradiol in the retentate plotted *vs.* the oligopeptide concentration allowed us to estimate the value of binding constants.
12 For the synthesis of the labelled oligopeptides we added volumes of labelled Ser, Leu, Gly, Glu (each amino acid was 1.0 mCi cm^{-3}) to the amino acid solution, and then we performed the polymerisation as previously described. These quantities were proportional to the percentage of the corresponding amino acid in the polymerisation mixture and assured a significant measure of radioactivity. The small volumes added can be considered negligible in comparison to the volume of the whole polymerisation mixture.
13 We used antibodies directly against testosterone and tritium labelled testosterone for the affinity measurement of this steroid, and anti-progesterone antibodies and tritium labelled progesterone for the determination of the affinity for this one.
14 O. Ramstroem and K. Mosbach, *Chem. Biol.*, 1996, **3**, 471.

ChemComm

The unexpected head-to-head dimerisation of 1*H*-phosphirenes

Ngoc Hoa Tran Huy, Louis Ricard and François Mathey

Laboratoire "Hétéroéléments et Coordination" UMR CNRS 7653, DCPH, Ecole Polytechnique, 91128, Palaiseau Cedex, France. E-mail: dcph@poly.polytechnique.fr

Received (in Basel, Switzerland) 14th February 2000, Accepted 16th May 2000

Both 1*H*-phosphirenes and their P-W(CO)$_5$ complexes readily dimerise in the presence of Ni(II) or Pd(0) catalysts to give the corresponding 1,2-dihydro-1,2-diphosphinines.

The ready dimerisation of borirenes into 1,4-diboracyclohexadienes is well documented and has been studied in some depth from a theoretical standpoint.[1] Similarly, silirenes readily give 1,4-disilacyclohexadienes in the presence of a palladium catalyst.[2] In both cases, no head-to-head dimers were detected. In the silicon case, although no mechanism was proposed for the dimerisation, the intermediacy of a 1-metalla-2-silacyclobutene appeared likely.[3] Since we knew from preceding experiments that both Pd(0) and Pt(0) readily insert into the P–C bonds of 1*H*-phosphirenes and phosphirene complexes,[4,5] it was tempting to explore the possible dimerisation of these phosphirenes in the presence of palladium catalysts.

Preliminary experiments were carried out with 1,2,3-triphenylphosphirene[6] and its P-W(CO)$_5$ complex.[7] Heating 1,2,3-triphenylphosphirene with [Pd(PPh$_3$)$_4$] in toluene at 85 °C overnight led only to decomposition products. After several experiments, we finally found that clean dimerisation was achieved with a Ni(II) catalyst at room temperature (Scheme 1).

The structure of **2**† unexpectedly corresponds to a head-to-head dimer (Fig. 1).‡ The ring is highly distorted with two *trans* phosphorus lone pairs and some strain as indicated by the rather small P–P–C(ring) angles of 91.09(5) and 91.27(5)°. The P–P bond is short for a single bond at 2.193(2) Å. Compound **2** displays surprising instability. It decomposes completely upon heating at 65 °C for 20 min in toluene. Looking for more stable derivatives, we decided to investigate the dimerisation of phosphirene P-W(CO)$_5$ complexes. The complex of **1** appeared to be rather inert. We reasoned that a 1,2-disubstituted species would be more reactive. Accordingly, we prepared the (1-phenyl-2-trimethylsilylphosphirene)pentacarbonyltungsten complex **3**† by the usual technique[7] and studied its evolution in toluene at 85 °C in the presence of [Pd(PPh$_3$)$_4$]. Overnight we observed the formation of the head-to-head dimer **4**† which was isolated in 60% yield (Scheme 2).

The dimerisation is regio- and stereo-selective (Fig. 2).‡ The regioselectivity can be easily explained by a preferential insertion of Pd(0) into the less hindered P–CH intracyclic bond.

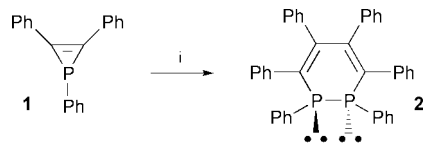

Scheme 1 *Reagents and conditions*: (i) 150 mg of **1**, 10 mg of [NiCl$_2$(Ph$_2$PCH$_2$CH$_2$PPh$_2$)], CH$_3$CN, 25 °C, 2 d, 70% yield.

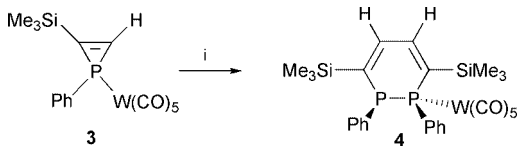

Scheme 2 *Reagents and conditions*: (i) 530 mg of **3**, 30 mg of [Pd(PPh$_3$)$_4$], toluene, 85 °C, 16 h.

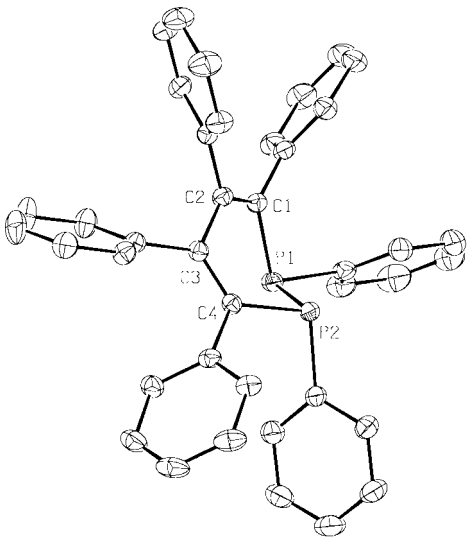

Fig. 1 Crystal structure of **2**. Significant bond distances (Å) and angles (°): P(1)–C(1) 1.857(2), P(1)–C(5) 1.831(2), P(1)–P(2) 2.193(2), P(2)–C(35) 1.839(2), P(2)–C(4) 1.855(1), C(1)–C(2) 1.357(2), C(2)–C(3) 1.493(2), C(3)–C(4) 1.355(2); C(5)–P(1)–C(1) 102.67(6), C(5)–P(1)–P(2) 101.38(5), C(1)–P(1)–P(2) 91.09(5), C(35)–P(2)–C(4) 102.04(6), C(35)–P(2)–P(1) 101.19(5), C(4)–P(2)–P(1) 91.27(5), C(2)–C(1)–P(1) 118.9(1), C(1)–C(2)–C(3) 123.1(1), C(4)–C(3)–C(2) 122.7(1), C(3)–C(4)–P(2) 119.9(1).

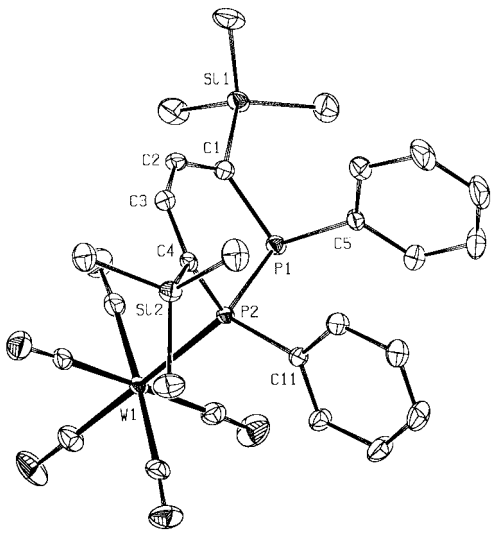

Fig. 2 Crystal structure of **4**. Significant bond distances (Å) and angles (°): P(1)–C(1) 1.817(3), P(1)–C(5) 1.828(3), P(1)–P(2) 2.227(1), P(2)–C(4) 1.815(3), P(2)–C(11) 1.824(3), P(2)–W(1) 2.5277(7), Si(1)–C(1) 1.896(3), Si(2)–C(4) 1.905(3), C(1)–C(2) 1.352(4), C(2)–C(3) 1.463(4), C(3)–C(4) 1.351(4); C(1)–P(1)–P(2) 101.3(1), C(1)–P(1)–C(5) 102.3(1), C(5)–P(1)–P(2) 105.7(1), C(4)–P(2)–C(11) 106.7(1), C(4)–P(2)–P(1) 105.7(1), C(11)–P(2)–P(1) 100.9(1), C(4)–P(2)–W(1) 114.2(1), C(11)–P(2)–W(1) 119.2(1), P(1)–P(2)–W(1) 108.52(3).

DOI: 10.1039/b001304h

The ring is almost undistorted. The intracyclic angles at phosphorus are normal at 101.3(1) (P_{III}) and 105.7° (P_W). The P–P bond is also in the normal range at 2.227 Å. In contrast to **2**, the stereochemistry at the phosphorus atoms is *cis* and **4** is quite stable.

At the moment, we have no precise explanation for this unexpected head-to-head dimerisation. The only argument which can be pointed out has a thermodynamic basis. The formation of one P–P and one C–C bond is more energetically favourable than the formation of two P–C bonds: 61 + 88 > 2 × 65 kcal mol^{-1}.[8] Unlike phosphorus, both silicon and boron have much lower electronegativities than carbon and the dimerisation of silirenes and borirenes is probably controlled by the polarity of the Si–C and B–C ring bonds. Whatever its origin, this head-to-head dimerisation of phosphirenes provides a direct access to the almost unknown 1,2-dihydro-1,2-diphosphinine ring. At the moment, only a 1,2-disulfide has appeared in the literature, prepared by a low-yield multi-step procedure.[9] The chemistry of this ring is now open for investigation.

Notes and references

† Selected analytical and spectroscopic data: **2**: Precipitates as yellow crystals from CH_3CN; ^{31}P NMR (CH_2Cl_2): δ −45.5; *m/z* 573 (M + H, 14%), 465 (M + H − PPh, 100). **3**: ^{31}P NMR (toluene): δ −185.6, $^1J_{PW}$ 275 Hz; ^{1}H NMR ($CDCl_3$): δ 0.29 (s, $SiMe_3$), 8.89 (d, $^2J_{PH}$ 24.9 Hz, ring H); ^{13}C NMR ($CDCl_3$): δ −1.15 (s, $SiMe_3$), 136.95 (d, $^1J_{CP}$ 15.5 Hz, ring CH), 139.48 (d, $^1J_{CP}$ 7.6 Hz, Ph-C_{ipso}), 142.83 (d, $^1J_{CP}$ 36.6 Hz, *C*-$SiMe_3$), 196.54 (d, $^2J_{CP}$ 9.1 Hz, *cis*-CO), 198.34 (d, $^2J_{CP}$ 32.5 Hz, *trans*-CO); *m/z* (^{184}W) 530 (M, 23%), 388 (M − 5CO, 100); Anal. Calc. for $C_{16}H_{15}O_5PSiW$: C, 36.25; H, 2.85. Found: C, 36.87; H, 2.68%. **4**: Purified by chromatography on silica gel (hexane–CH_2Cl_2, 10:1); yellow crystals (60%): ^{31}P NMR ($CDCl_3$): δ −68.0 (P_{III}) and 26.3 (P-W), $^1J_{PP}$ 277 Hz; ^{1}H NMR ($CDCl_3$): δ 0.00 (s, $SiMe_3$), 0.08 (s, $SiMe_3$); ^{13}C NMR ($CDCl_3$): δ −0.87 (d, $^3J_{CP}$ 3.7 Hz, $SiMe_3$), 0.57 (s, $SiMe_3$), 140.59 (d, $^2J_{CP}$ 28.0 Hz, ring CH), 142.38 (s, ring CH), 197.58 (pseudo t, *cis*-CO); *m/z* (^{184}W) 709 (M − CO, 22%), 596 (M − 5CO, 100); Anal. Calc. for $C_{27}H_{30}O_5P_2Si_2W$: C, 44.03; H, 4.11. Found: C, 43.94; H, 4.13%.

‡ *Crystal data* for **2**: $C_{40}H_{30}P_2 \cdot 1/2CH_2Cl_2$, M = 615.04 g mol^{-1}, triclinic, a = 6.069(5) Å, b = 12.180(5) Å, c = 22.035(5) Å, α = 97.030(5)°, β = 92.580(5)°, γ = 96.690(5)°, V = 1602.7(15) Å^3, T = 150.0(1) K, space group $P\bar{1}$, Z = 2, μ(Mo-Kα) = 0.247 cm^{-1}. 14341 reflections measured, 9228 unique (R(int) = 0.0285) which were used in all calculations. The final $wR(F^2)$ was 0.1472 (all data), $R1$ = 0.0482. For **4**: $C_{27}H_{30}O_5P_2Si_2W$, M = 736.48 g mol^{-1}, monoclinic, a = 12.6004(3) Å, b = 12.2493(3) Å, c = 20.1311(5) Å, β = 96.1640(10)°, V = 3089.19(13) Å^3, T = 150.0(1) K, space group $P2_1/c$, Z = 4, μ(Mo-Kα) = 3.953 cm^{-1}. 16625 reflections measured, 8897 unique (R(int) = 0.0578) which were used in all calculations. The final $wR(F^2)$ was 0.0928 (all data), $R1$ = 0.0247. CCDC 182/1641. See http://www.rsc.org/suppdata/cc/b0/b001304h/ for crystallographic files in .cif format.

1 P. H. M. Budzelaar, S. M. van der Kerk, K. Krogh-Jesperson and P. v. R. Schleyer, *J. Am. Chem. Soc.*, 1986, **108**, 3960.
2 M. Ishikawa, H. Sugisawa, M. Kumada, T. Higuchi, K. Matsui and K. Hirotsu, *Organometallics*, 1982, **1**, 1473.
3 M. Ishikawa, J. Ohshita, Y. Ito and J. Iyoda, *J. Am. Chem. Soc.*, 1986, **108**, 7417; J. Ohshita, Y. Isomura and M. Ishikawa, *Organometallics*, 1989, **8**, 2050.
4 S. S. Al Juaid, D. Carmichael, P. B. Hitchcock, S. Lochschmidt, A. Marinetti, F. Mathey and J. F. Nixon, *J. Chem. Soc., Chem. Commun.*, 1988, 1156; S. S. Al Juaid, D. Carmichael, P. B. Hitchcock, A. Marinetti, F. Mathey and J. F. Nixon, *J. Chem. Soc., Dalton Trans.*, 1991, 905.
5 D. Carmichael, P. B. Hitchcock, J. F. Nixon, F. Mathey and A. Pidcock, *J. Chem. Soc., Chem. Commun.*, 1986, 762.
6 S. Lochschmidt, F. Mathey and A. Schmidpeter, *Tetrahedron Lett.*, 1986, **27**, 2635.
7 A. Marinetti, F. Mathey, J. Fischer and A. Mitschler, *J. Am. Chem. Soc.*, 1982, **104**, 4484.
8 W. W. Schoeller, in *Multiple Bonds and Low Coordination in Phosphorus Chemistry*, ed. M. Regitz and O. J. Scherer, Thieme, Stuttgart, 1990, pp. 5–32.
9 T. Kawashima, M. Shimamura and N. Inamoto, *Heterocycles*, 1982, **17**, 341. A 3,6-di(*tert*-butyl)-1,2-dihydro-1,2-diphosphinine has also been isolated as a byproduct from the reaction of phenylphosphine with 1,4-di(*tert*-butyl)buta-1,3-diyne: D. Carmichael and F. Mathey, unpublished results, 1993.

Photochemical synthesis and structural properties of high membered thiohelicenes

Tullio Caronna,*[a] Roberta Sinisi,[a] Marinella Catellani,[b] Luciana Malpezzi,[a] Stefano V. Meille[a] and Andrea Mele[a]

[a] *Dipartimento di Chimica del Politecnico, Via Mancinelli 7, 20131 Milano, Italy. E-mail: tullio.caronna@polimi.it*
[b] *Istituto di Chimica delle Macromolecole-CNR, Via Bassini 15, 20133 Milano, Italy*

Received (in Liverpool, UK) 29th March 2000, Accepted 23rd May 2000

A general photochemical synthesis of large thiohelicenes containing nine and eleven rings is discussed along with the organisation of racemic thiohelicenes in crystals: heterochiral assembling is dominant except in the nine-ring system where interactions involving terminal ring S atoms favour the segregation of close-packed homochiral molecules in planes.

Helicenes are intrinsically chiral helical molecules structurally characterised by *ortho*-fusion of aromatic rings. Nonracemic, appropriately substituted systems exhibit a spontaneous organisation in macroscopic fibrous structures in the solid state, while in concentrated solutions and thin films a gigantic rotation of the plane of polarised light was evidenced.[1–3] The polyconjugated chiral structure of helicenes makes them interesting candidates for optoelectronic applications[4] and molecular devices.[5] Higher carbohelicenes are endowed with an inherent propensity to homochiral molecular recognition.[6]

Some studies on lower heterohelicenes containing thiophene rings were published long ago.[7–9] Here, we report on a general synthetic approach we used to prepare a series of heterohelicenes formed by alternate thiophene and benzene rings: trithia[5]heterohelicene **4**, tetrathia[7]heterohelicene **7** and, for the first time, large molecules such as pentathia[9]heterohelicene **10** and esathia[11]heterohelicene **13.** We also investigated the electronic and self assembling properties of these systems with the aim of establishing whether the preference for heterochiral molecular aggregation shown by the racemic five- and seven-member thiaheterohelicenes in crystals[8,9] persists in higher members of the series, specifically with reference to the crystal structure of **10**.

Substituted helicenes are obtained in good yield by chemical synthesis both in racemic or enantiomeric form.[11,12] We obtained a series of unsubstituted thiohelicenes using a general procedure for the preparation of racemic molecules, shown in Scheme 1, where the photochemical cyclisation represents the final step. With this synthetic route it was possible to obtain molecules as large as the nine- and eleven-membered thiohelicenes.

Two approaches were in principle possible to synthesise large condensed systems. The first consists of the double photochemical ring closure of a molecule containing two 1,2-disubstituted ethylenes. In this case the bis-ethylene molecule needs only to contain a heteroaryl moiety that does not exceed three members and can be easily prepared. The second possibility, preferable in the case of higher thiohelicenes, consists of a single photochemical cyclisation of a 1,2-diheteroarylethylene and larger heteroaryl substituents, such as thio[5]heterohelicenes, are necessary.

The synthesis of thio[*n*]helicene (n = 7, 9 condensed rings) starts by reacting thio[$n - 4$]helicene with Vilsmeier reagent [$POCl_3$ and PhN(Me)CHO in boiling toluene] in order to obtain the corresponding 2-carbaldehyde. The phosphonium salt **5** is produced from the 2-carbaldehyde **2** with a sequence of reactions illustrated in Scheme 1 and described elsewhere.[13] The Wittig reaction between the phosphonium salt and the 2-carbaldehyde of the thio[$n - 4$]helicene gives a 1,2-diheteroarylethylene. The racemic thio[*n*]helicene can be easily obtained in high yield by the photoinduced cyclodehydrogenation of appropriate 1,2-diheteroarylethylenes.† The synthesis of the larger esathia[11]helicene **13** begins with the reaction between the 2-carbaldehyde-thio[5]helicene **8** and the phosphonium salt of the thio[5]helicene **11**, followed by photocyclisation of the 1,2-diheteroarylethylenes **12**.†

Electronic absorption spectra of the thiohelicene series in solution are shown in Fig. 1. Upon increasing the number of condensed rings, the absorption bands shift to lower energy owing to the lengthening of the π-conjugation in the helical

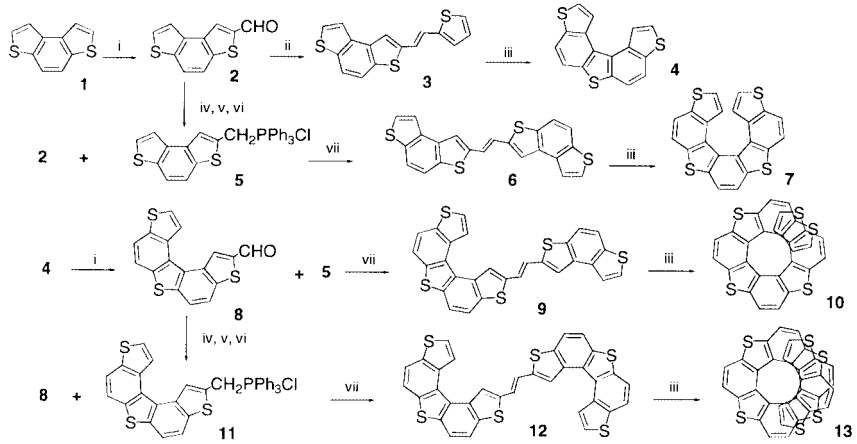

Scheme 1 *Reagents and conditions*: i, $POCl_3$, PhN(Me)CHO, toluene; ii, $(C_4H_3S)CH_2PPh_3Br$, NaOMe, anhydrous MeOH; iii, *hν*: 350 nm or visible light; iv, $NaBH_4$, EtOH–THF; v, $SOCl_2$, benzene–Py; vi, PPh_3, benzene; vii, NaOMe, anhydrous MeOH.

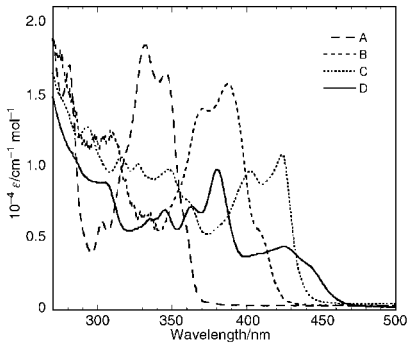

Fig. 1 Electronic molar absorption spectra of molecules in chloroform solution: A trithia[5]heterohelicene, B tetrathia[7]heterohelicene, C pentathia[9]heterohelicene and D esathia[11]heterohelicene.

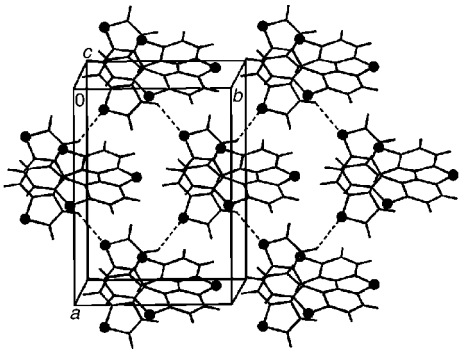

Fig. 3 Packing of pentathia[9]heterohelicene showing the arrangement of isochiral molecules in *quasi*-hexagonal planar assemblies parallel to the *ab* plane. Short S···H interactions are evidenced.

system. The photoluminescence spectra show a similar behaviour, with emissions that are red-shifted increasing the molecular size.‡

Fig. 2 and 3 show views of the packing of the nine ring helicene **10** as obtained by single crystal X-ray diffraction.§ The structure of the eleven ring system **13** will be presented elsewhere.[14] The tendency to stacking of antipodes[9] in interdigitated columnar structures is apparent (Fig. 2) for all of the thiohelicene racemic structures including **10**. The stacking interactions involve especially the third and/or the fourth rings (from the molecular ends) of enantiomeric pairs, and vary depending upon the particular molecule. In all the systems investigated specific interactions engaging sulfur[15,16] and hydrogen atoms at distances slightly shorter than the sum of the van der Waals radii (1.80 Å for S and 1.20 Å for H) were found. They always involve atoms of terminal rings and are quite probably attractive playing a role in molecular recognition and self assembly. The contacts are S···S 3.544 Å and S···H 2.89 Å in the case of the five- and seven-ring systems respectively. In the case of **10** S···H interactions§ at 2.87 Å appear a key feature of the microsegregation of homochiral, tubular molecules in planes parallel to the *ab* lattice plane (*ca*. Fig. 3). The helical axes of all molecules within a plane are parallel and form an angle of *ca*. 40° with *c*, while the twofold intramolecular axes are all parallel to *b*. The adopted *C*2/*c* space group corresponds to that predicted to yield best packing for racemic molecules preserving their C_2 symmetry in the crystal.[17]

We can conclude that for larger oligomers of thiohelicenes homochiral lateral aggregation of helices becomes more favourable. Interactions between terminal units are still important in the recognition pattern also for the nine- and eleven-ring systems. In the supermolecular tubular structures formed in racemic systems the two enantiomers alternate along a tube (Fig. 2). The role played by sulfur in the intermolecular interactions allows rationalisation of the different behaviour as compared to carbohelicenes. Attempts at optically resolving **10** and **13** are in progress to determine their chiroptical properties and characterise the self assembling properties of large homochiral thiohelicenes.

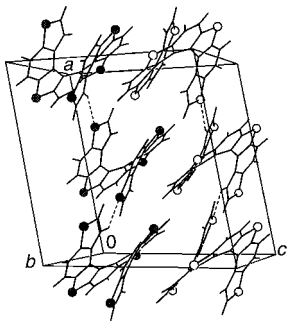

Fig. 2 Crystal packing of pentathia[9]heterohelicene evidencing both the stacking of enantiomers along the *c* axis direction and planes of isochiral molecules parallel to the *ab* plane. The molecular chirality is made apparent by the graphic codes of the sulfur atoms.

Notes and references

† *Tetrathia[7]heterohelicene*: photochemical cyclisation yield 85%; *m*/*z* 402; δ 6.76 for the α hydrogen of thiophene. *Pentathia[9]heterohelicene*: photochemical reaction quantitative; *m*/*z* 508; δ 5.52 for the α hydrogens. *Esathia[11]heterohelicene*: photochemical reaction yield 60%; *m*/*z* 614; δ 5.25 for the α hydrogens.

‡ Emission spectra of chloroform solutions: tetrathia[5]heterohelicene emission maximum 360 nm; tetrathia[7]heterohelicene 410 nm; pentathia-[9]heterohelicene 440 nm; esathia[11]heterohelicene 480 nm.

§ *Crystal data* for **10**: $C_{28}H_{12}S_5$, M_r = 508.68, monoclinic, space group *C*2/*c* (no. 15), a = 14.655(1), b = 10.656(1), c = 13.976(1) Å, β = 100.25(1)°, V = 2147.7(3) Å^3, Z = 4, D_c = 1.57 g cm^{-3}, μ = 5.098 mm^{-1}, 3662 reflections (1875 unique, R_{int} = 0.078) were collected on a Siemens P4 diffractometer. The structure was solved by direct methods using the SIR97 program and refined by full-matrix least squares with SHELXL97. The final stage converged to $wR(F^2)$ = 0.048 (R_w = 0.123). To better evaluate intermolecular contacts standard neutron C–H distances of 1.08 Å were used. CCDC 182/1649. See http://www.rsc.org/suppdata/cc/b0/b002581j/ for crystallographic files in .cif format.

1 C. Nuckolls, T. J. Katz and L. Castellanos, *J. Am. Chem. Soc*., 1996, **118**, 3767.
2 C. Nuckolls, T. J. Katz, T. Verbiest, S. Van Elshocht, H.-G. Kuball, S. Kiesewalter, A. J. Lovinger and A. Persoons, *J. Am. Chem. Soc*., 1998, **120**, 8656.
3 C. Nuckolls and T. J. Katz, *J. Am. Chem. Soc.*, 1998, **120**, 9541.
4 D. Beljonne, Z. Shuai, J. L. Brédas, M. Kauranen, T. Verbiest and A. Persoons, *J. Chem Phys.*, 1998, **108**, 1301.
5 T. R. Kelly, J. P. Sestelo and I. Tellitu, *J. Org. Chem.*, 1998, **63**, 3655.
6 R. Kuroda, *J. Chem. Soc., Perkin Trans. 2*, 1982, 789.
7 H. Wynberg, *Acc. Chem. Res.*, 1971, **4**, 65.
8 H. Nakagawa, K. Yamada, H. Kawazura and H. Miyamae, *Acta Crystallogr., Sect. C*, 1984, **40**, 1039.
9 H. Nakagawa, A. Obata, K. Yamada, H. Kawazura, M. Konno and H. Miyamae, *J. Chem. Soc., Perkin Trans. 2*, 1985, 1999.
10 M. B. Groen, H. Schadenberg and H. Wynberg, *J. Org. Chem.*, 1971, **36**, 2797.
11 J. Larsen and K. Bechgaard, *J. Org.Chem.*, 1996, **61**, 1151.
12 K. Tanaka, H. Suzuki and H. Osuga, *J. Org. Chem.*, 1997, **62**, 4465.
13 K. Tanaka, H. Osuga, H. Suzuki, Y. Shogase and Y. Kitahara, *J. Chem. Soc., Perkin Trans. 1*, 1998, 935.
14 T. Caronna, R. Sinisi, M. Catellani, L. Malpezzi and S. V. Meille, *Chem. Mater.*, submitted.
15 G. Desiraju, *Crystal Engineering*, Elsevier, Amsterdam, 1989, ch. 7.
16 R. Taylor and O. Kennard, *J. Am. Chem. Soc.*, 1982, **104**, 5063.
17 I. Kitaigorodsky, *Molecular Crystals and Molecules*, Academic Press, London, 1973, ch. 1.

ChemComm

Synthesis of enantiopure isoprene epoxides from (*S*)-lactic acid *via* 'dispoke' intermediates

Daping Zhang,[a] Christine Bleasdale,[a] Bernard T. Golding*[a] and William P. Watson[b]†

[a] *Department of Chemistry, Bedson Building, University of Newcastle upon Tyne, Newcastle upon Tyne, UK NE1 7RU. E-mail: b.t.golding@ncl.ac.uk*

[b] *Shell International Chemicals BV, Shell Research and Technology Centre Amsterdam, Toxicology Department, PO Box 38000, 1030BN Amsterdam, The Netherlands*

Received (in Liverpool, UK) 14th March 2000, Accepted 9th May 2000

'Dispoke protected lactate' derived from (*S*)-lactic acid was converted into the enantiopure isoprene epoxides (*S*)-2-ethenyl-2-methyloxirane and (2*R*,2′*S*)-2-methylbioxirane.

The mechanistic toxicology of isoprene is a subject of considerable current importance.[1] In this context, samples of single enantiomers of isoprene epoxides are required for the preparation of reference standards of DNA adducts. We describe efficient syntheses of enantiomerically pure (*S*)-2-ethenyl-2-methyloxirane **1** and (2*R*,2′*S*)-2-methylbioxirane **2**, using as starting material the 'dispoke protected lactate' **3** derived from (*S*)-lactic acid.[2] An eight-step synthesis of (*S*)-2-(1-methylethenyl)oxirane (88% ee) from D-mannitol has been reported.[3] This was oxidised with MCPBA to a mixture of (2*S*,2′*R*)- and (2*R*,2′*R*)-2-methylbioxirane.

There is concern about the toxicology of isoprene because of its structural similarity to buta-1,3-diene, which is a multi-organ carcinogen in rodents.[4,5] This has raised the question of the effect of the methyl group in isoprene on its toxicity and carcinogenic potential. Studies with isoprene have shown that its carcinogenicity towards rodents is much lower than buta-1,3-diene.[6] It is therefore important to determine the significance of these findings for the cancer risk from human exposures to isoprene, which are unavoidable because isoprene is produced during normal metabolism.[7,8] Human exposures can also occur due to the presence of isoprene in tobacco smoke,[9] automobile exhaust gases,[9] emissions from plants and trees[10] and industrial sources.[11]

In vitro studies have shown that the mammalian metabolism of isoprene is similar to that of buta-1,3-diene and involves cytochrome P450 oxidation to mono- and then di-epoxides, which may be metabolites responsible for toxicity. It is important to clarify the influence of the stereochemistry of these epoxides on isoprene's toxicology, as well as determining the effect of the methyl group. We have previously shown stereochemical differences between rat, mouse and human in the formation of the mono-epoxides of isoprene by liver preparations *in vitro*.[13]

A key intermediate for the preparation of (*S*)-2-ethenyl-2-methyloxirane **1** is (*S*)-2-hydroxy-2-methylbutenoic acid **4**. Several approaches to prepare **4** in enantiopure form were tried using Evans' chiral oxazolidinone chemistry,[14] but none were successful. Furthermore, we were unable to resolve racemic 2-hydroxy-2-methylbutenoic acid, either *via* diastereoisomeric salts with optically active amines, or by lipase-catalysed hydrolysis of its esters. The failure of these approaches may be due to the similarity of the methyl and vinyl groups, which leads to diastereoisomers derived from 2-hydroxy-2-methylbutenoic acid having similar physical and chemical properties. However, (*S*)-2-hydroxy-2-methylbutenoic acid **4** could be readily prepared from the 'dispoke protected lactate' **3** (Scheme 1).‡ Ley and his coworkers[2] have shown that condensation with acetaldehyde of the carbanion derived by deprotonation of **3** with LDA gives predominately diastereoisomer **5**. We converted **5** into its triflate **6**, which underwent smooth DBU-induced elimination to **7**. Deprotection of **7** by treatment with 95% TFA gave (*S*)-2-hydroxy-2-methylbutenoic acid **4**. The synthesis of **1** was completed by reduction of **4** to (*S*)-2-methylbut-3-ene-1,2-diol **8**, tosylation of **8** to **9**, treatment of **9** with base and direct distillation of **1** from the reaction mixture in the manner described.[15] The high enantiomeric purity of **1** {$[\alpha]_D$ + 17.6 (*c* 6.2 g/100 ml in ethyl acetate at 19 °C)} was confirmed using ^{1}H NMR spectroscopy in conjunction with the chiral shift reagent europium tris[3-(heptafluoropropylhydroxymethylene)-(−)-camphorate] in deuterioacetonitrile.

(2*R*,2′*S*)-2-Methylbioxirane **2**, was also readily prepared from the 'dispoke protected lactate' **3**. Condensation of the carbanion derived by deprotonation of **3** with LDA with 2-(4-methoxybenzyloxy)acetaldehyde[16] gave predominately diastereoisomer **10**, which was converted into lactone **11** by treatment with 95% TFA. Reduction of **11** to tetraol **12** was

† Present address: AstraZeneca Central Toxicology Laboratory, Alderley Park, Alderley Edge, Cheshire, UK SK10 4TJ.

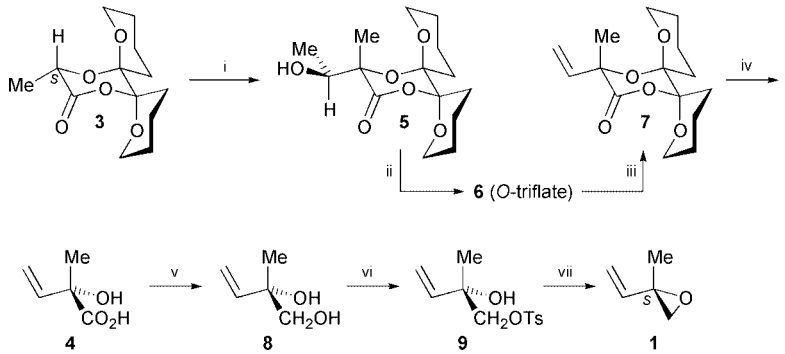

Scheme 1 Synthesis of (*S*)-2-ethenyl-2-methyloxirane **1**. *Reagents and conditions*: i, LDA + DMPU/Bu^{n}Li in THF; MeCHO, 93% (*cf.* ref. 2); ii, triflic anhydride/pyridine in CH_2Cl_2, 100%; iii, DBU in CH_2Cl_2 71%; iv, 95% TFA, 88%; v, $LiAlH_4$ in diethyl ether, 100%; vi, TsCl/pyridine in toluene, 51%; vii, $NaOCH_2CH_2OH$ in $HOCH_2CH_2OH$, 80%.

DOI: 10.1039/b002133o

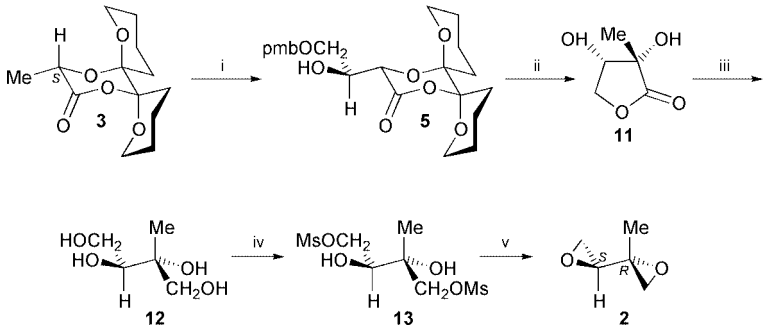

Scheme 2 Synthesis of (2*R*,2′*S*)-2-methylbioxirane **2**. *Reagents and conditions*: i, LDA + DMPU/Bu^{n}Li in THF; pmbOCH$_2$CHO, 73%; ii, 95% TFA, 78%; iii, NaBH$_4$ in MeOH, 100%; iv, MsCl in pyridine, 37%; v, NaOCH$_2$CH$_2$OH in HOCH$_2$CH$_2$OH, 49% (pmb = *p*-methoxybenzyl).

followed by selective mesylation of the primary hydroxy groups to give **13** and finally base-induced ring closures to diepoxide **2**. The resulting **2** {[α]$_D$ −0.4 (*c* 5.8 g/100 ml ethyl acetate at 19 °C)} was shown to be enantiomerically and diastereomerically pure using ^{1}H NMR spectroscopy with the same chiral shift reagent as above. A racemic reference sample of both diastereoisomers of 2-methylbioxirane was prepared from *rac*-2-ethenyl-2-methyloxirane by oxidation with MCPBA in dichloromethane.[3]

The work described herein makes the isoprene epoxides **1** and **2** available in sufficient amounts for the preparation of adduct standards from proteins and DNA. The kinetics and mechanisms of biologically relevant reactions of isoprene epoxides are currently under study in our laboratory.

This work was supported by Shell International Chemicals BV. We thank Professor S. V. Ley for a helpful discussion.

Notes and references

‡ All new compounds gave analytical and spectroscopic data in accord with their assigned structure.

1 National Toxicology Programme TR-486, Toxicology and Carcinogenesis Studies of Isoprene (CAS No. 78-79-5) in F344/N Rats, 1997.
2 G.-J. Boons, R. Downham, K. S. Kim, S. V. Ley and M. Woods, *Tetrahedron*, 1994, **50**, 7157.
3 D. Wistuba, K. Weigand and H. Peter, *Chem. Res. Toxicol.*, 1994, **71**, 336; [this paper refers to (*S*)-2-ethenyl-2-methyloxirane, prepared from (*S*)-2-methylbut-3-ene-1,2-diol, but gives no information on the source of the latter compound].
4 P. E. Owen and J. R. Glaister, *Environ. Health Perspect.*, 1990, **86**, 19.
5 R. L. Melnick and M. C. Kohn, *Carcinogenesis*, 1995, **16**, 157.
6 P. G. Gervasi, L. Citti, M. Del Monte, V. Longo and D. Benetti, *Mutat. Res.*, 1985, **156**, 77.
7 J. P. Conkle, B. J. Camp and B. E. Welsch, *Arch. Environ. Health*, 1975, **30**, 290.
8 Isoprene is detectable in human breath (0.15 μmol kg^{-1} h^{-1}): D. Gelmont, R. D. Stein and J. F. Mead, *Biochem. Biophys. Res. Commun.*, 1981, **99**, 1456.
9 T. E. Graedel, D. T. Hawkins and L. D. Claxton, *Atmospheric Chemical Compounds. Sources, Occurrence and Bioassay*, Academic Press, Orlando, FL, p. 145.
10 F. Loreto and T. D. Sharkey, *Plants Cell Environ.*, 1993, **16**, 563.
11 US National Institute for Occupational Safety and Health (1993) National Occupational Exposure Survey (1981–1983), Cincinnati, OH.
12 P. Gervasi and V. Longo, *Environ. Health. Perspect.*, 1990, **86**, 85.
13 R. D. Small, B. T. Golding and W. P. Watson, *Xenobiotica*, 1997, **27**, 1155.
14 D. A. Evans, T. C. Britton, J. A. Ellman and R. L. Dorow, *J. Am. Chem. Soc.*, 1990, **112**, 4011.
15 M. K. Ellis, B. T. Golding, A. B. Maude and W. P. Watson, *J. Chem. Soc., Perkin Trans. 1*, 1991, 747.
16 Prepared from *rac*-2,2-dimethyl-1,3-dioxolane-4-methanol (‘solketal’) by a sequence of *p*-methoxybenzylation, acidic hydrolysis and periodate oxidation.

Inner C-arylation of a doubly N-confused porphyrin–Pd complex in toluene—the possibility of a Pd^{3+} intermediate†

Hiroyuki Furuta,*[ab] Hiromitsu Maeda,[a] Atsuhiro Osuka,*[a] Mikio Yasutake,[c] Teruo Shinmyozu[c] and Yuichi Ishikawa[c]

[a] *Department of Chemistry, Graduate School of Science, Kyoto University, Kyoto 606-8502, Japan. E-mail: hfuruta@kuchem.kyoto-u-ac.jp; osuka@kuchem-kyoto-u.ac.jp*
[b] *PRESTO, Japan Science of Technology Corporation (JST), Japan*
[c] *Institute for Fundamental Research of Organic Chemistry, Kyushu University, Fukuoka 812-8581, Japan*

Received (in Cambridge, UK) 14th April 2000, Accepted 18th May 2000

An inner C-tolyl substituted Pd^{2+} complex of a doubly N-confused porphyrin (N_2CP) was obtained from the reaction of N_2CP and $Pd(OAc)_2$ in toluene and the structure was revealed by a single crystal X-ray analysis.

'N-Confused porphyrin' (NCP) or 'inverted porphyrin' is a porphyrin isomer wherein one of the pyrrolic rings is inverted.[1,2] Owing to the inner core carbon and outward pointing nitrogen, NCP coordination chemistry differs greatly from that of normal porphyrins.[3–5] For example, NCP can serve as both a

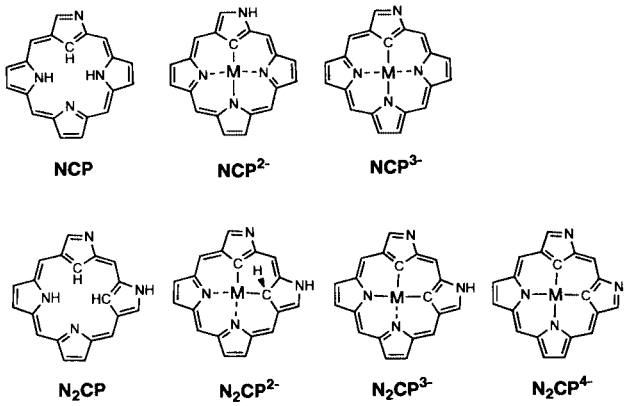

divalent (NCP^{2-}) and a trivalent (NCP^{3-}) ligand with d^8 metals such as Ni^{2+} and Ag^{3+}.[2,5] Recently, we have succeeded in synthesizing 'doubly N-confused porphyrin (N_2CP)' and disclosed its trivalent (N_2CP^{3-}) ligand nature in the complexation of Cu^{3+} and Ag^{3+}.[6] If the multi-valence property observed in NCP was common in all NCP families,[7] other valences, such as N_2CP^{2-} or N_2CP^{4-}, could be expected for divalent (M^{2+}) or tetravalent (M^{4+}) metal coordination. By keeping this point in mind, we have examined Pd complexation with N_2CP because square planar coordination of Pd^{2+} and/or Pd^{4+} is well known.[8] Interestingly, the synthesized complex was Pd^{2+}–N_2CP bearing a solvent molecule at an inner core carbon. In this communication, the X-ray structure and absorption spectrum of a novel Pd complex, Pd^{2+}–N_2CP–Tol (**2**), are reported.

When N_2CP, 2-ethoxy-5,10,15,20-tetrakis(pentafluorophenyl)-3,7-diaza-21,22-dicarbaporphyrin (**1**), [6] was treated with 2 equiv. of $Pd(OAc)_2$ in refluxing toluene for 5 h, a yellow-greenish product was obtained in 18% yield. A FABMS peak at *m/z* 1217.8 indicated the attachment of a tolyl group to the Pd–N_2CP complex. The ^1H NMR signals of the complex showed distinctly in the range from 11 to 1 ppm in CD_2Cl_2, which suggested that the Pd oxidation state of the complex was diamagnetic, either Pd^{2+} (d^8) or Pd^{4+} (d^6). The tolyl signals derived from the solvent were observed in the high field region (5.61–6.36 ppm), which indicated that the tolyl group was located on the porphyrin core, presumably at an inner carbon or nitrogen. The methyl groups on the tolyl substituent were found to occur at the *para* and *meta* positions in a 1 : 2 ratio. Moreover, an outer NH signal was observed at 10.37 ppm, which suggested N_2CP^{2-} type ligand formation, that is, Pd^{2+} coordination. Pd^{2+}–N_2CP–Tol (**2**) was isolated as a single product and the formation of neither Pd^{3+}–N_2CP nor Pd^{4+}–N_2CP was observed (Scheme 1). By using $CHCl_3$ or C_6H_6 as the solvent, the complexation reaction did not proceed and N_2CP (**1**) was recovered. However, in the presence of C_6H_6 and toluene (1/1 v/v), both C-phenyl and C-tolyl Pd–N_2CP complexes were formed. Furthermore, the formation of a C-arylated complex was observed in *m*-xylene but not in *p*-xylene in which the steric hindrance was significant.

The explicit structural details of the Pd^{2+}–N_2CP–Tol (**2**) complex was derived from a single crystal X-ray diffraction analysis (Fig. 1).[9] Surprisingly, a solvent tolyl group is bound to the inner carbon of a confused pyrrole ring which does not have an ethoxy group. The tolyl-substituted confused pyrrole ring is bent at 56.3° and the tolyl group stands almost vertically (88.6°) at the opposite side of a mean N_2C_2 plane consisting of core

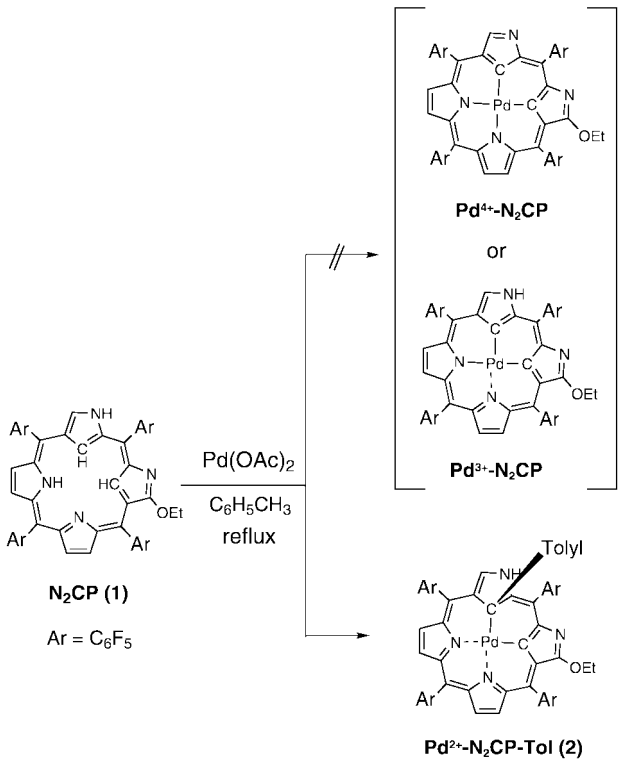

Scheme 1 Reaction of N_2CP (**1**) and $Pd(OAc)_2$.

† Electronic supplementary information (ESI) available: synthesis details, ^1H and ^{13}C NMR spectra, thermal ellipsoid plot showing all atoms, unit cell packing diagram for **2**. See http://www/rsc.org/suppdata/cc/b0/b003022h/

DOI: 10.1039/b003022h

nitrogens and carbons. The Pd–C bond distances are 1.97(1) and 2.202(9) Å, and the Pd–N distances are 2.09(1) and 2.056(8) Å.[10] Reflecting the tilting of the confused pyrrole ring and the different carbon atom types, sp^2 and sp^3, the two Pd–C bond distances differ greatly (0.23 Å). On the other hand, the Pd–N bond distances are slightly longer than in Pd^{2+}–tetraphenylporphyrin, 2.009 Å.[11] In the single crystal, the tolyl group was disordered and refinement of the structure was well performed with the assumption of a *para*:*meta* ratio of 2:3, in agreement with the ^{1}H NMR data. Similar structures, such as a perpendicular orientation of the C-substituted group and/or the strong tilting of the coordinating 5-membered ring, have been observed in N-alkylporphyrin and Pd–thiaporphyrin complexes.[4,12] The absorption spectrum of **2** displays three broad bands with peak maxima at 318.0, 410.0 and 662.0 nm indicating the distortion of the porphyrin ring (Fig. 2).

Mechanistically, it is not clear which Pd oxidation state, either Pd^{2+}, Pd^{3+} or Pd^{4+}, is formed before the tolyl group is incorporated at the inner carbon. One of the possible mechanisms is the initial formation of the unstable Pd^{3+}–N_2CP complex, like Ag^{3+} and Cu^{3+}, which is then attacked successively by a toluene molecule at either Pd or the Pd-connected carbon. As the Pd^{3+} (d^7) species is paramagnetic, a radical mechanism could be involved in the formation of **2** (Scheme 2).[13] Supporting this, the ratio of the obtained tolyl complex shows the statistical distribution, $p:m = 1:2$.[14] The H-radical derived from toluene would change to H^+ eventually, because

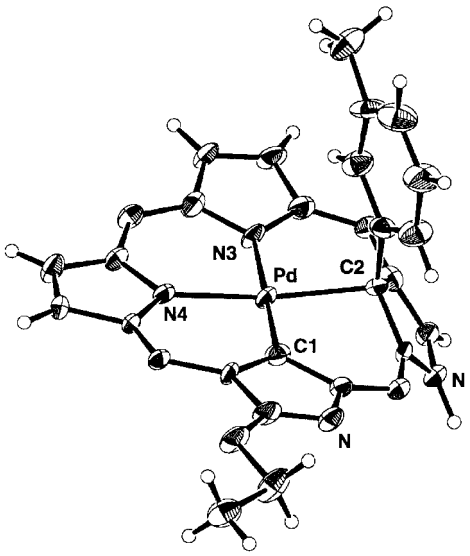

Fig. 1 X-Ray structure of Pd–N_2CP–Tol (**2**). Solvents and pentafluorophenyl groups are omitted for clarity. Selective bond lengths (Å) and angles (°): Pd–C1, 1.97(1); Pd–C2, 2.202(9); Pd–N3, 2.09(1); Pd–N4, 2.056(8); C1–Pd–C2, 90.1(5); C2–Pd–N3, 90.6(4); N3–Pd–N4, 90.1(4); N4–Pd–C1, 89.2(4); C1–Pd–N3, 179.1(3); C2–Pd–N4, 170.5(3).

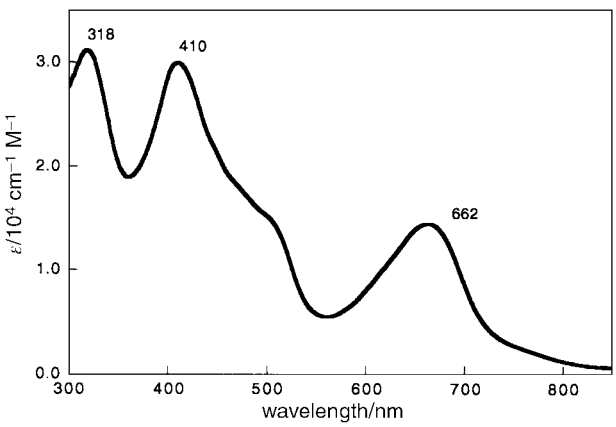

Fig. 2 Absorption spectrum of Pd–N_2CP–Tol (**2**) in $CHCl_3$.

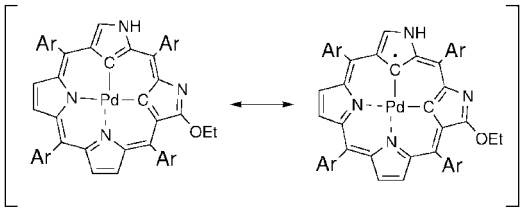

Scheme 2 A possible intermediate Pd^{3+}–N_2CP.

palladium black (Pd^0) is always associated with this reaction. It is reported that $Pd(OAc)_2$ causes the facile palladation of aromatic compounds to afford biaryls.[15,16] Although we have not detected bitolyl in this reaction, the other mechanism involving a tolyl–Pd complex before the formation of a Pd–carbon bond with the confused pyrrole can not be excluded. As this reaction implies the possibility of aromatic C–H activation, detailed study of the mechanism in addition to investigations with other group 10 metals is currently underway.[17]

Notes and references

1 H. Furuta, T. Asano and T. Ogawa, *J. Am. Chem. Soc.*, 1994, **116**, 767.

2 P. J. Chmielewski, L. Latos-Grażyński, K. Rachlewicz and T. Glowiak, *Angew. Chem., Int. Ed. Engl.*, 1994, **33**, 779.

3 L. Latos-Grażyński, in *The Porphyrin Handbook*, ed. K. M. Kadish, K. M. Smith and R. Guilard, Academic Press, San Diego, 1999, vol. 2, ch. 14.

4 P. J. Chmielewski, L. Latos-Grażyński and T. Glowiak, *J. Am. Chem. Soc.*, 1996, **118**, 5690; P. J. Chmielewski and L. Latos-Grażyński, *J. Chem. Soc., Perkin Trans. 2*, 1995, 503; P. J. Chmielewski and L. Latos-Grażyński, *Inorg. Chem.*, 1997, **36**, 840.

5 H. Furuta, T. Ogawa, Y. Uwatoko and K. Araki, *Inorg. Chem.*, 1999, **38**, 2676.

6 H. Furuta, H. Maeda and A. Osuka, *J. Am. Chem. Soc.*, 2000, **122**, 803.

7 There are 15 members in the NCP family according to the number and position of the confused pyrroles, see ref. 6.

8 C. F. J. Barnard and M. J. H. Russell, in *Comprehensive Coordination Chemistry*, ed. G. Wilkinson, Pergamon Press, Oxford, 1987, vol. 5, ch. 51.

9 *Crystal data*: **2**, violet prism, $C_{53}H_{18}F_{20}N_4OPd\cdot0.5C_6H_{14}\cdot0.3H_2O$, M_w = 1261.62, monoclinic, space group $P2_1/n$ (no. 14), a = 15.780(1), b = 22.179(2), c = 15.618(1) Å, β = 118.743(2)°, V = 4792.5(7) Å^3, Z = 4, D_{calc} = 1.7496 g cm^{-3}, T = −180 °C. Final R = 0.078 (GOF = 0.84) for 3178 observed reflections with $I > 2\sigma(I)$, R_w = 0.248 for 17002 all unique data. CCDC 182/1644. See http://www.rsc.org/suppdata/cc/b0/b003022h/ for crystallographic files in .cif format.

10 Similar Pd coordination with two C–Pd σ-bonds and two N–Pd coordinate bonds, has been observed in the 2,2′-biphenyl-2″,2‴-bipyridyl palladium complex, Pd(bph)(bpy). C. Cornioley-Deuschel and A. von Zelewsky, *Inorg. Chem.*, 1987, **26**, 3354.

11 E. B. Fleisher, C. K. Miller and L. E. Webb, *J. Am. Chem. Soc.*, 1964, **86**, 2342.

12 A. L. Balch, C. R. Cornman, L. Latos-Grażyński and M. M. Olmstead, *J. Am. Chem. Soc.*, 1990, **112**, 7552; L. Latos-Grażyński, J. Lisowski, P. Chmielewski, M. Greszczuk, M. M. Olmstead and A. L. Balch, *Inorg. Chem.*, 1994, **33**, 192.

13 ESR spectra of a Pd(III) trithiacyclononane complex have been reported. A. J. Blake, A. J. Holder, T. I. Hyde, Y. V. Roberts, A. J. Lavery and M. Schröder, *J. Organomet. Chem.*, 1987, **323**, 261.

14 Partial rate factors for *meta* and *para* positions are known to be comparable in radical reactions, see J. March, in *Advanced Organic Chemistry*, Wiley, New York, 1985, p. 618.

15 J. M. Davidson and C. Triggs, *Chem. Ind. (London)*, 1966, 457; J. M. Davidson and C. Triggs, *J. Chem. Soc. A*, 1968, 1324.

16 J. Tsuji, in *Palladium Reagents and Catalysts*, Wiley, Chichester, 1995, p. 74.

17 It is noteworthy that such a C-arylation reaction has not been observed in NCP. When NCP was subjected to the Pd complexation reaction under similar conditions, Pd^{2+}–NCP and Pd bridged dimer formation were observed. H. Furuta, N. Kubo, H. Maeda, T. Ishizuka, A. Osuka, H. Nanami and T. Ogawa, *J. Am. Chem. Soc.*, submitted.

A new class of hybrid mesoporous materials with functionalized organic monolayers for selective adsorption of heavy metal ions

A. M. Liu,[a] K. Hidajat,[a] S. Kawi*[a] and D. Y. Zhao[b]

[a] *Department of Chemical and Environmental Engineering, National University of Singapore, 10 Kent Ridge Crescent, Singapore 119260, Singapore. E-mail: chekawis@nus.edu.sg*
[b] *Department of Chemistry, Fudan University, Shanghai 200433, P.R. China*

Received (in Cambridge, UK) 4th April 2000, Accepted 19th May 2000

Thiol- and amino-functionalized SBA-15 silicas with uniform mesoporosities were prepared and employed for removing heavy metal ions from waste water; the thiolated SBA-15 adsorbent exhibited a higher complexation affinity for Hg^{2+}, while the other metal ions (Cu^{2+}, Zn^{2+}, Cr^{3+} and Ni^{2+}) showed exceptional binding ability with its aminated analogue.

To synthesize improved adsorbents for the removal of toxic heavy metal ions from waste water is a continuing research objective of environmental pollution control processes. Considerable efforts have been devoted to the preparation of mesoporous silica-based adsorbents due to their unique large surface area, well-defined pore size and pore shape and well-modified surface properties.[1–5] This application generally requires the materials to exhibit specific binding sites for heavy metal ions, but most mesoporous materials themselves do not have such surface properties. Accordingly, an efficient approach has been developed so that functional monolayers are chemically bonded to the surfaces of supports. The functionalized hybrid materials show great adsorption capacity and specificity for metal ions. For instance, a few metal ion adsorbents have been prepared by grafting thiol ligands onto the surface of a MCM-41 support, which are extremely efficient in removing mercury and other heavy metal ions.[1,2] The effectiveness of such adsorbents has been ascribed to the complexation chemistry of grafted ligands with metal ions. Continuing our efforts in synthesizing and improving the hydrothermal stability of mesoporous materials and in investigating their applications,[6–8] we prepared in this study two novel thiol- and amino-functionalized SBA-15 materials and investigated their complexation affinities for heavy metal ions. The more regular structure and much thicker silica walls of SBA-15 (31–64 Å) may impart significant hydrothermal stability in comparison to MCM-41. In addition, amino groups grafted on an SBA-15 support are expected to show considerably higher binding ability to relatively harder metal ions such as Cu^{2+}, Zn^{2+}, Cr^{3+} and Ni^{2+}.

Synthesis of the parent mesoporous SBA-15 was achieved by the use of a triblock copolymer surfactant in acidic media.[9] The calcined material has a surface area of 814 $m^2\ g^{-1}$ and an average pore size of 76 Å, as determined using the nitrogen adsorption technique and transmission electron microscopy (TEM). The X-ray powder diffraction pattern of this material shows a very intense peak (100) and two additional high order peaks with lower intensities, indicating a significant degree of long range ordering of the structure and well formed hexagonal pore arrays of the sample. SBA-15 functionalized with 3-mercaptopropyl groups [SBA-15(SH)] (5.6% C, S_{BET} 461 $m^2\ g^{-1}$ and V_t 0.66 $m^3\ g^{-1}$) and primary 3-aminopropyl groups [SBA-15(NH_2)] (9.5% C, S_{BET} 279 $m^2\ g^{-1}$ and V_t 0.45 $m^3\ g^{-1}$) were obtained through the treatment with chloroform solution of 3-mercaptopropyltriethoxysilane and 3-aminopropyltriethoxysilane, respectively. It was found that, upon functionalization, the surface area, total pore volume and pore size decreased significantly, revealing that the surface modification indeed occurred inside the primary mesopores of the SBA-15. However, the XRD analysis indicated that, in addition to a very intense peak (100), two higher order peaks were still observed. Therefore, the chemical bonding procedure did not diminish the structural ordering of SBA-15.

The ^{29}Si and ^{13}C NMR spectra and peak assignments for functionalized samples SBA-15(SH) and SBA-15(NH_2) are depicted in Fig. 1 and 2, respectively. In the ^{29}Si NMR spectrum of SBA-15(SH) (Fig. 1(a)), the three peaks at −113.8, −105.6 and −96.3 ppm are attributed to silicon in the siloxane binding environment without hydroxyl groups [$(SiO)_4Si$], isolated silanol groups [$(SiO)_3Si$-OH] and to geminal silanol groups [$(SiO)_2Si$-$(OH)_2$] of the silica support. In addition to these signals, two additional signals can be observed at −71.9 and −63.4 ppm, which correspond to two different environments for the siloxane groups in the functionalized monolayers:[10] (i)

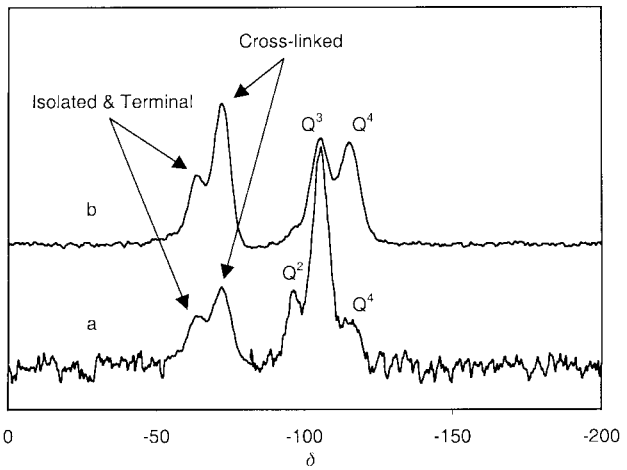

Fig. 1 ^{29}Si NMR spectra of organic monolayers on SBA-15: (a) SBA-15(SH) and (b) SBA-15(NH_2).

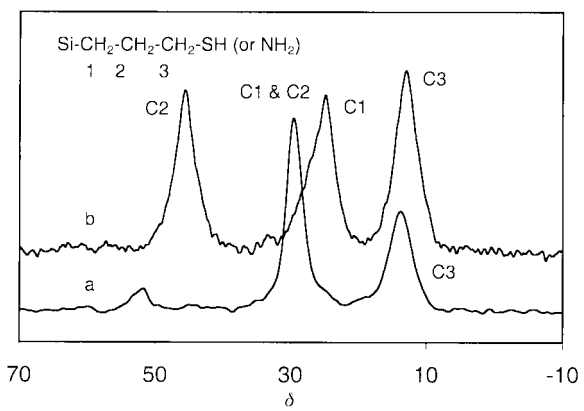

Fig. 2 ^{13}C NMR spectra of organic monolayers on SBA-15: (a) SBA-15(SH) and (b) SBA-15(NH_2).

DOI: 10.1039/b002661l

Table 1 Analyzed concentrations of toxic metal ions in waste water solutions before and after adsorption treatment (concentration in ppm)[a]

	Hg	Cu	Zn	Cr	Ni
No treatment	10.1	5.21	10.1	5.21	10.2
After treatment with SBA-15	10.2	5.12	10.2	5.13	10.3
After treatment with SBA-15(SH)	0	3.18	9.91	4.72	5.10
After treatment with SBA-15(NH_2)	2.15	0.01	0	0	0

[a] 10 mL of waste solution was mixed with 100 mg of adsorbent at room temperature with agitation overnight. The remaining metal concentrations in solution were analyzed using inductively coupled plasma spectroscopy (ICP).

cross-linked groups bound to two neighboring siloxanes and (ii) isolated groups and terminal groups bound to only one neighboring siloxane. In the case of sample SBA-15(NH_2) (Fig. 1(b)), only two distinguishable peaks at −115.0 and −105.5 ppm were recorded for the silica support. An increase of the Q^4 peak intensity was also observed, along with a reduction in the signal intensity of the Q^3 site. In agreement with higher coverage of amino monolayers for SBA-15(NH_2) (9.5% C), these observations indicate that, compared with the mercaptopropyl groups in SBA-15(SH) (5.6% C), more aminopropyl groups have been grafted onto Si-OH groups of the silica support, and thus more Q^4 silica sites are subsequently formed. It should be noted that relative peak intensities in the ^{29}Si NMR spectra are not strictly quantifiable due to differences in relaxation behavior. In the ^{13}C NMR spectrum of SBA-15(SH) (Fig. 2(a)), the peak at 13.8 ppm is ascribed to the methylene carbon group C3 that is directly bonded to the silicon atom. The strong signal at 29.6 ppm is attributed to the other two methylene carbons (C2 and C1). However, for sample SBA-15(NH_2), three distinct peaks are clearly observed at 13.1, 24.9 and 45.6 ppm, which can be assigned to the carbons C3, C1 and C2, respectively. We believe that the better resolution of the peaks for the three carbons in SBA-15(NH_2) is associated with the higher ordering orientation of the carbon chains with respect to the silica surface.[1]

The functionalized materials exhibited unique selective affinity for binding heavy metal ions. Table 1 lists the ion concentrations of simulated waste water solutions before and after treatment with SBA-15(SH) and SBA-15(NH_2). It can be seen that a single treatment with SBA-15(SH) reduced the mercury concentration to below the detection limit, but it exhibited little or no affinity for other metal ions. On the other hand, the aminated SBA-15 adsorbent efficiently removed the metal ions from the waste solution with the exception of Hg^{2+}. Note that no significant concentration change for all metal ions was observed when unmodified SBA-15 was directly treated with the waste water solution under identical conditions. Thus, the concentration change is indeed attributed to the complexation reactions between metal ions with grafted ligands. It has been well recognized that softer transition metal ions are prone to forming stable complexes with ligands carrying softer donor atoms, and *vice versa*. Sulfur has been regarded as a softer donor atom compared with nitrogen, and therefore it is understandable that the thiolated adsorbent exhibited higher complexation affinity for the softer metal ion Hg^{2+}, while the other relatively harder metal ions (Cu^{2+}, Zn^{2+}, Cr^{3+} and Ni^{2+}) demonstrated considerably higher binding ability with its aminated analogue.

The hydrolytic stability was tested by treating mercury-loaded SBA-15(SH) and copper-loaded SBA-15(NH_2) in water at 70 °C for 12 h. Elemental analysis indicated that only a very small amount of metal was released during this process (0.5% Hg and 0.8% Cu were released from SBA-15(SH) and SBA-15(NH_2), respectively). To regenerate the used adsorbents, the metal-loaded functionalized SBA-15 adsorbents were washed with conc. HCl, resulting in complete removal of the loaded metal. The regenerated SBA-15(SH) and SBA-15(NH_2) materials were treated with $Hg(NO_3)_2$ and $Cu(NO_3)_2$ solutions, respectively. An Hg loading of 292 mg g(SBA-15(SH))$^{-1}$ and a Cu loading of 46 mg g(SBA-15(NH_2))$^{-1}$ were obtained, corresponding to about 60% of the original loading capacities. Similar results were obtained for a third regeneration and reuse cycle. These results indicated that both adsorbents remained effective even after extended regeneration and reuse cycles. In good agreement with the results, BET analyses of the regenerated adsorbents indicated that the surface area and pore volume for both adsorbents only slightly decreased (*ca*. 5% decrease), while the pore size essentially remained unchanged [68 Å for SBA-15(SH) and 63 Å for SBA-15(NH_2)]. IR spectra showed that the bonds corresponding to grafted ligands were still present. This result clearly demonstrates that both the mesoporous SBA-15 silica and the organic monolayers appear to essentially retain their structures even after extended use.

For the purpose of comparison, thiolated and aminated MCM-41 were also prepared and tested in this study. The effectiveness of these adsorbents is comparable to their SBA-15 analogues. However, the regeneration process resulted in a significant decrease in surface area and pore volume for both functionalized MCM-41 adsorbents: the surface area and pore volume of the regenerated MCM-41(SH) are 465 (665) $m^2\ g^{-1}$ and 0.41 (0.61) $cm^3\ g^{-1}$; for MCM-41(NH_2), 282 (460) $m^2\ g^{-1}$ and 0.26 (0.41) $cm^3\ g^{-1}$ (the corresponding original values are indicated in parentheses). This result is in good agreement with the report that SBA-15 is much more stable than MCM-41.[9] A great loss in adsorption capacity to heavy metal ions was observed accordingly: an Hg loading of 160 mg g(MCM-41(SH))$^{-1}$ and a Cu loading of 28 mg g(MCM-41(NH_2))$^{-1}$ were obtained, corresponding to about 35% of the original loading capacities.

Less attention has been focused on the synthesis and applications of SBA-15 mesoporous silica since it was discovered in 1998.[11–13] However, we believe that this unique mesoporous material can provide more possibilities for the design and synthesis of open pore structures because of its high surface area and easily controllable uniform pore size that may be extended to *ca*. 300 Å. In addition, compared with MCM-41, the more uniform pore structure and thicker silica walls of SBA-15 (31–64 Å) are shown to impart significant stability to the material under hydrothermal conditions.[9]

We are grateful to the National University of Singapore and the National Science and Technology Board of Singapore for the support of this research (Grant No. RP960608A).

Notes and references

1 X. Feng, G. E. Fryxell, L.-Q. Wang, A. Y. Kim, J. Liu and K. M. Kemner, *Science*, 1997, **276**, 923.
2 J. Liu, X. Feng, G. E. Fryxell, L.-Q. Wang, A. Y. Kim and M. Gong, *Adv. Mater.*, 1998, **10**, 161.
3 L. Mercier and T. J. Pinnavaia, *Adv. Mater.*, 1997, **9**, 500.
4 L. Mercier and T. J. Pinnavaia, *Environ. Sci. Technol.*, 1998, **32**, 2749.
5 J. Brown, L. Mercier and T. J. Pinnavaia, *Chem. Commun.*, 1999, 69.
6 S. Kawi and M. W. Lai, *Chem. Commun.*, 1998, 1407.
7 S. C. Shen and S. Kawi, *J. Phys. Chem. B*, 1999, **103**, 8870.
8 G. J. Li and S. Kawi, *Sens. Actuators B: Chem.*, 1999, **59**, 1.
9 D. Y. Zhao, J. L. Feng, Q. S. Huo, N. Melosh, G. H. Fredrickson, B. F. Chmelka and G. D. Stucky, *Science*, 1998, **279**, 548.
10 D. W. Sindorf and G. E. Macier, *J. Am. Chem. Soc.*, 1983, **105**, 3765.
11 Z. H. Luan, M. Hartmann, D. Y. Zhao, W. Z. Zhou and L. Kevan, *Chem. Mater.*, 1999, **11**, 1621.
12 Y. H. Yue, A. Gedeon, J. L. Bonardet, N. Melosh, J. B. DíEspinose and J. Fraissaed, *Chem. Commun.*, 1999, 1967.
13 Z. H. Luan, E. M. Maes, P. A. W. van der Heide, D. Y. Zhao, R. S. Czernuszewicz and L. Kevan, *Chem. Mater.*, 1999, **11**, 3680.

Arylchlorocarbenes in the synthesis of heterocycles containing two nitrogen atoms

Yuri N. Romashin,[a] Michael T. H. Liu,*[a] Satnam S. Nijjar[a] and Orazio A. Attanasi[b]

[a] *Department of Chemistry, University of Prince Edward Island, P.E.I., Canada C1A 4P3. E-mail: Liu@upei.ca*
[b] *Instituto di Chimica Organica, Università di Urbino, 61029 Urbino, Italy*

Received (in Corvallis, OR, USA) 10th April 2000, Accepted 10th May 2000

Substituted pyrazoles and pyrrolo[1,2-*c*]pyrimidines were prepared from the reaction of arylchlorocarbenes with 1,2-diazabuta-1,3-dienes and 4-vinylpyrimidines, respectively.

We recently reported the successful application of arylchlorocarbenes generated from arylchlorodiazirines to the synthesis of indolizines and pyrroles (Scheme 1, reactions (i) and (ii)).[1,2] The key step of the described approach produces a nitrogen ylide, followed by 1,5-intramolecular cyclization and HCl elimination. We now report further application of this methodology to the synthesis of a wider array of heterocycles containing two nitrogen atoms, such as pyrazoles and pyrrolo[1,2-*c*]pyrimidines (Scheme 1, reactions (iii) and (iv)). Pyrazoles have attracted the attention of many chemists because of their applications in organometallic chemistry as ligands, in synthesis, in particular of bioactive compounds, as well as their thermal reactions, spectroscopic applications and theoretical calculations.[3] Pyrrolo[1,2-*c*]pyrimidines, the aza analogues of indolizines, have attracted substantial interest because of their ability to facilitate easy ring cleavage, their variety of ring transformations and recyclizations,[4] and for their role as starting materials to N-bridged heteroaromatics.[5] However, the known synthetic routes to these compounds are lengthy and result in poor yields.[5,6] In this respect, these highly reactive carbenes have been harnessed and utilized to achieve difficult synthetic tasks which other reactive intermediates cannot easily perform.

The arylchlorocarbenes **2a–c** were generated from arylchlorodiazirines **1a–c**[7] by thermolysis. Phenylazostilbene **7** was prepared from acetoxydeoxybenzoin and phenylhydrazine.[8] Thermolysis of arylchlorodiazirines **1a–c** in the presence of phenylazostilbene **7** leads to 1,3,4,5-tetrasubstituted pyrazoles **5a-c** in good yield (74–83%). Attanasi and coworkers have developed an effective approach to pyrazoles based on a preliminary 1,4-addition of a nucleophilic reagent to the 1,2-diazabuta-1,3-diene substrates, which also gave a 70–80% product yield.[9] Vinylpyrimidines **8a,b** were prepared from 4-methylpyrimidine according to previously described procedures.[10,11] Thermolysis of arylchlorodiazirines **1a-c** in the presence of vinylpyrimidines **8a**,**b** leads to 6,7-disubstituted pyrrolo[1,2-*c*]pyrimidines **6a–c** in a 17–22% yield. The yields and physical data of obtained pyrazoles **5a–c** and pyrrolopyrimidines **6a–c** are given in ref. 12.†

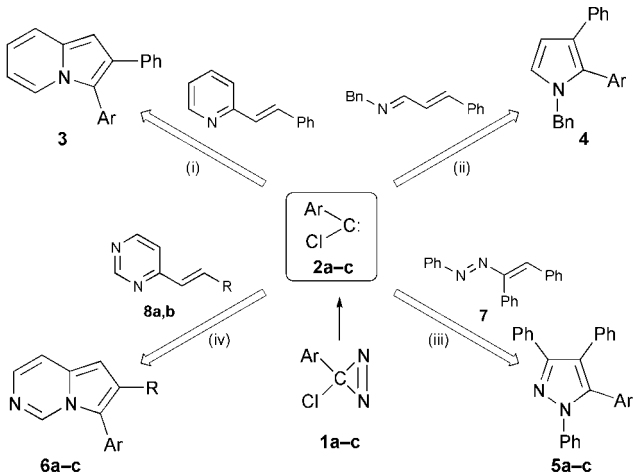

1,2,5: **a** Ar = Ph, **b** Ar = *p*-MeC_6H_4, **c** Ar = *p*-ClC_6H_4
6: **a** R = H, Ar = *p*-ClC_6H_4, **b** R = Ph, Ar = *p*-MeC_6H_4, **c** R = Ph, Ar = *p*-ClC_6H_4
8: **a** R = H, **b** R = Ph

Scheme 1

In general, solutions of chlorodiazirine **1a–c** (2 mmol) and phenylazostilbene **7** or vinylpyrimidine **8a**,**b** (1 mmol) were refluxed in absolute benzene (10 mL) for 24 h. After workup, the pyrazoles **5a–c** were purified by column chromatography on silica gel with 10 : 1 hexane–diethyl ether eluent, followed by crystallization from propan-2-ol–hexane (1 : 3); pyrrolopyrimidines **6a–c** were purified by column chromatography on Al_2O_3 (basic) with 4 : 1 hexane–diethyl ether eluent.

Vinylpyrimidines **8a**,**b** are transparent at 351 nm, which is not the case for phenylazostilbene **7**. In order to learn whether the reaction of chlorodiazirines **1a–c** with vinylpyrimidines **8a**,**b** goes through an N-ylide intermediate, we undertook laser flash photolysis (LFP) studies[14] of this system to examine the kinetics of nitrogen ylide formation and the rate of 1,5-dipolar cyclization.

LFP irradiation at 351 nm of a solution of chlorophenyldiazirine **1a** in benzene (A = 1.0 at λ = 376, 392 nm) at 25 °C produces a transient absorption at 310 nm due to the formation of the chlorophenylcarbene **2a**, whose decay rate constant is 2.02×10^5 s^{-1}. In the presence of pyrimidine derivative **8b**, a new transient attributed to the pyrimidinium ylide appears at 550 nm. The plot of the observed pseudo-first-order rate constants for the growth of the absorption at 550 nm *vs.* concentration of **8b** is linear, and the rate constant for the reaction of chlorophenylcarbene **2a** and pyrimidine **8b** at 25 °C is $k_{ylide} = 3.24 \times 10^8$ $M^{-1}s.^{-1}$ The intercept of the straight line (2.78×10^5 s^{-1}) is the chlorophenylcarbene **2a** decay rate constant in the absence of **8b**, which is similar to that detected at 310 nm (2.02×10^5 s^{-1}). The pyrimidinium ylide (at 550 nm) decays in benzene with a lifetime equal to 102.2 μs at 22 °C, independent of the concentration of **8b**. Therefore, the rate constant for the 1,5-dipolar cyclization of pyrimidinium ylide is $k_{1,5\text{-cycl}} = 9.78 \times 10^3$ s^{-1}. The temperature dependence (0–55 °C) of the pyrimidinium ylide decay to form the

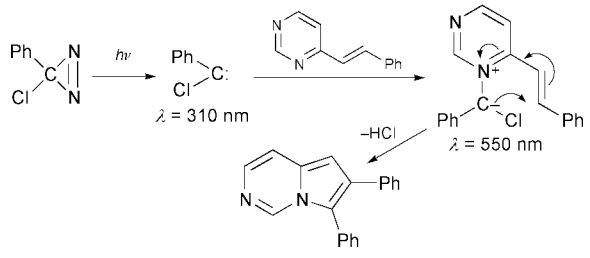

Scheme 2

DOI: 10.1039/b002940h

1,5-cyclization product yielded the following Arrhenius parameters: E_a = 10.0 kcal mol^{-1} and A = 2.36 × 10^{11} s^{-1}.

We have shown that chlorocarbenes can be successfully applied to the synthesis of 1,3,4,5-tetrasubstituted pyrazoles and 6,7-disubstituted pyrrolo[1,2-*c*]pyrimidines. This methodology is simple and effective. We have also demonstrated the existence of nitrogen ylides as intermediates in these reactions. The kinetics of the 1,5-dipolar cyclizations of pyrimidinium ylides to yield pyrrolo[1,2-*c*]pyrimidines are reminiscent of the cyclization of 2-vinylpyridinium ylides to indolizines[1] and azomethine ylides to pyrroles.[2]

M. T. H. L. and Yu. N. R. wish to thank the NSERC of Canada for its generous financial support. We also thank Dr Wei Ma, Rutgers University, for assistance with the LFP experiments.

Notes and references

† All compounds reported herein gave satisfactory microanalysis data.

1 M. T. H. Liu, Yu. N. Romashin and R. Bonneau, *Int. J. Chem. Kinet.*, 1994, **26**, 1179; R. Bonneau, Yu. N. Romashin, M. T. H. Liu and S. E. MacPherson, *J. Chem. Soc., Chem. Commun.*, 1994, 509.

2 Yu. N. Romashin, M. T. H. Liu and R. Bonneau, *Chem. Commun.*, 1999, 447; R. Bonneau, Yu. N. Romashin and M. T. H. Liu, *J. Photochem. Photobiol., A*, 1999, **126**, 31; Yu. N. Romashin, M. T. H. Liu, W. Ma and R. A. Moss, *Tetrahedron Lett.*, 1999, **40**, 7163.

3 E. L. Moyano, G.I. Yranzo and J. Elguero, *J. Org. Chem.*, 1998, **63**, 8188.

4 D. A. Maiboroda, E. V. Babaev and K. Jug, *J. Org. Chem.*, 1997, **62**, 7100.

5 J. M. Minguez, M. I. Castellote, J. J. Vaquero, J. L. Garcia-Navio, J. Alvarez-Builla, O. Castaño and J. L. Andres, *J. Org. Chem.*, 1996, **61**, 4655.

6 J. L. Wong, S. M. Brown and H. Rapoport, *J. Org. Chem*, 1965, **30**, 2398.

7 W. H. Graham, *J. Am. Chem. Soc.*, 1965, **87**, 4396.

8 B. F. Bonini, G. Maccagnani, G. Mazzanti, G. Rosini and E. Foresti, *J. Chem. Soc., Perkin Trans. 1*, 1981, 2322.

9 O. A. Attanasi and P. Filippone, *Synlett*, 1977, 1128; A. Attanasi, P. Filippone, C. Fiorucci, E. Foresti and F. Mantellini, *J. Org. Chem.*, 1998, **63**, 9880; O. A. Attanasi, P. Filippone, C. Fiorucci and F. Mantellini, *Tetrahedron Lett.*, 1999, **40**, 3891.

10 C. G. Overberger and I. C. Kogon, *J. Am. Chem. Soc.*, 1954, **76**, 1879.

11 H.-H. Perkampus and Th. Bluhm, *Tetrahedron*, 1972, **28**, 2099.

12 Data for 1,3,4,5-tetraphenylpyrazole **5a**: 78% yield; mp 217.5–218.5 °C [lit.[13]: mp 217–218 °C]; ^{1}H NMR (300 MHz, $CDCl_3$): δ 7.0–7.4 (18H, m), 7.5–7.6 (2H, m). For 1,3,4-triphenyl-5-(*p*-methylphenyl)pyrazole **5b**: 83% yield; mp 173–174 °C; ^{1}H NMR (300 MHz, $CDCl_3$): δ 2.31 (3H, s), 6.9–7.4 (17H, m), 7.5–7.6 (2H, m); MS: *m*/*z* 386 (100), 385 (51%). For 1,3,4-triphenyl-5-(*p*-chlorophenyl)pyrazole **5c**: 74% yield; mp 178–179 °C; ^{1}H NMR (300 MHz, $CDCl_3$): δ 6.9–7.4 (17H, m), 7.5–7.6 (2H, m); MS: *m*/*z* 408 (33), 406 (100%). For 7-(*p*-chlorophenyl)pyrrolo[1,2-*c*]pyrimidine **6a**: 17% yield; ^{1}H NMR (300 MHz, $CDCl_3$): δ 6.53 (1H, d, J = 3.5, 5-H_{pyr}), 6.90 (1H, J = 3.5 Hz, 6-H_{pyr}), 7.2–7.3 (2H, m, C_6H_4), 7.4–7.6 (4H, m, 3-H_{pyr}, 4-H_{pyr}, C_6H_4), 9.04 (1H, s, 1-H_{pyr}); MS: *m*/*z* 230 (34), 228 (100), 193 (16), 192 (18%). For 6-phenyl-7-(*p*-methylphenyl)pyrrolo[1,2-*c*]pyrimidine **6b**: 17% yield; ^{1}H NMR (300 MHz, $CDCl_3$): δ 2.43 (3H, s, Me), 6.65 (1H, s, 5-H_{pyr}), 7.1–7.5 (11H, m, 3-H_{pyr}, 4-H_{pyr}, Ph, C_6H_4), 8.76 (1H, s, 1-H_{pyr}). For 6-phenyl-7-(*p*-chlorophenyl)pyrrolo[1,2-*c*]pyrimidine **6c**: 22% yield; ^{1}H NMR (300 MHz, $CDCl_3$): δ 6.70 (1H, s, 5-H_{pyr}), 7.2–7.5 (11H, m, 3-H_{pyr}, 4-H_{pyr}, Ph, C_6H_4), 8.79 (1H, s, 1-H_{pyr}); MS: *m*/*z* 306 (33), 304 (100).

13 M. E. Kuehne, S. J. Weaver and P. Franz, *J. Org. Chem.*, 1964, **29**, 1582.

14 These experiments were performed with a Lambda Physik COMPex model 120 excimer laser using a Spectra Gases filled with 0.1875% F_2, 0.468% Xe, and 99.334% Ne. The sample in a 10 × 10 mm cell was excited at 351 nm by single light pulses (10 ns; 40 mJ). The detection unit comprised a 1000 W Oriel xenon arc lamp, a 1 in. Uniblitz shutter, Instruments SA grating monochromator, and a RCA 4840 photomultiplier tube wired in a 5-dynode configuration. The data collection and analysis system included a Stanford Research Systems model DG535 4-channel digital delay/pulse generator and a Tektronix TDS 320 2-channel oscilloscope.

ChemComm

Liquid-crystalline Abrikosov flux phase with an antiferroelectric structure

J. W. Goodby,*[a] A. Petrenko,[a] M. Hird,[a] R. A. Lewis,[a] J. Meier[b] and J. C. Jones[c]

[a] *Department of Chemistry, University of Hull, Hull, UK HU6 7RX. E-mail: j.w.goodby@chem.hull.ac.uk*
[b] *School of Physics and Engineering Physics, Chalmers University of Technology and Göteborg University, SE-41296 Göteborg, Sweden*
[c] *DERA, St Andrews Road, Gt Malvern, Worcs. UK WR14 3PS*

Received (in Cambridge, UK) 12th April 2000, Accepted 8th May 2000

(*S*)-1-Methylheptyl 2-[4-(4-dodecyloxybenzoyloxy)phenyl]-pyrimidine-5-carboxylate and its racemic modification are synthesised; miscibility studies, investigations of defect textures, differential scanning calorimetry and electrical field studies show that this material exhibits an antiferroelectric twist grain boundary TGBC*$_A$ analogue of the Abrikosov flux phase found in superconductors.

The prediction[1,2] and discovery[3,4] of the twist grain boundary smectic A* (TGBA*) phase led to the unification of phase transition theory in liquid crystals with those of superconductors. Subsequent to these seminal contributions, TGB phases were found to be ubiquitous in the field of self-organising systems where they have been encountered at transitions from either the isotropic liquid or the chiral nematic (N*) phase to the lamellar, smectic (Sm) state.[5–7] At the normal chiral nematic to smectic transition, the helical ordering of the chiral nematic phase collapses to give the layered structure of the smectic phase. However, for strongly chiral systems, there can be competition between the need of the molecules, due to their chiral packing requirements, to form a helical macro-structure and the need for the formation of a lower energy layered structure. This frustration is relieved by the formation of a helical structure with its heli-axis parallel to the planes of the layers. The helix and lamellar structures are, however, incompatible with one another and cannot co-exist without the formation of defects. The co-existence is achieved by having small blocks/sheets of molecules, with a local smectic structure, which are rotated with respect to one another *via* sets of screw dislocations located at their interfaces, thereby giving a quasi-helical structure.[2] In this way the twist distortions are localised in defects that periodically punctuate the normal smectic state which is analogous to how lines of flux punctuate the Abrikosov vortex state in type II superconductors.

Frustrated equivalents of the smectic A* and C* phases have been found, with both having commensurable or incommensurable variants that are dependent on the rational number of smectic blocks/sheets with respect to the pitch of the phase.[8,9] For the TGBC modification a number of subphases have been discovered which are dependent on; (i) the presence (TGBC*) or expulsion (TGBC) of the local heli-axis of the smectic C* phase which is oriented perpendicular to the layers of molecules and to the heli-axis of the TGB phase; (ii) the direction of the local spontaneous polarization relative to the heli-axis (parallel or perpendicular); (iii) the inversion of the handedness of the helix in the TGBC phase as a function of temperature;[10] and (iv) the formation of a 2D modulated structure with respect to the tilt.[11]

Here we report on the liquid crystal properties of (*S*)-1-methylheptyl 2-[4-(4-dodecyloxybenzoyloxy)phenyl]pyrimidine-5-carboxylate **A**, and its racemic modification **B**. Through miscibility studies, investigations of defect textures, differential scanning calorimetry, and electrical field studies, we suggest this material exhibits the first example of a twist grain boundary (TGBC*$_A$) phase that has a local antiferroelectric structure.

The transition temperatures, and the associated enthalpies for each phase transition, for (*S*)-1-methylheptyl 2-[4-(4-dodecyloxybenzoyloxy)phenyl]pyrimidine-5-carboxylate **A**, and its racemate **B**, were determined by thermal polarized microscopy and differential scanning calorimetry, and are given together in Table 1. Firstly, we note from the Table 1 there are considerable differences in transition temperatures between the enantiomer and the racemate, however, we also emphasise that the purities of the materials were found to be better than 99.5%. Therefore the differences in temperatures are real, as are the variances in phase sequences and phase types, and both are associated with the effects of chirality on the self-organising processes. Importantly the isotropization temperature for the racemate is higher than that for the enantiomer, whereas the transition to a tilted smectic phase is lower, these results are at variance with problems associated with the effects of impurities.

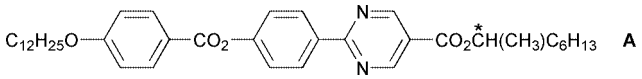

Homogenous, homeotropic, uncovered droplets, and free-standing film specimens of **A** were examined by transmitted, polarized-light, thermal microscopy. The phase first formed from the isotropic liquid was iridescent and clearly helical. The phase did not exhibit either focal-conic, platelet or *schlieren* defect textures, and was not typical of either the TGBA or TGBC phase. Nevertheless, at lower temperatures the transition to and from the smectic C*$_A$ phase was characterised by the formation of filaments typical of a TGB phase.[12] A Grandjean plane texture, typical of a helical phase was obtained for **A** in a homogeneously aligned (perpendicularly oriented layers) cell with a *ca.* 5 μm spacing that had been antiparallel-buffed. The fact that the heli-axis forms normal to the glass substrates of the cell indicates that the twist is in the direction of the planes of the layers, *i.e.* typical of a TGB phase. The presence of filaments and a heli-axis in the plane of the layers confirm that the phase formed first on cooling the isotropic liquid of the enantiomer is a twist grain boundary phase, however, the lack of a characteristic texture suggested that the phase was not of the same class as those characterised so far.

Table 1 The transition temperatures (°C) and the associated enthalpies of transition [ΔH/kJ g^{-1}] for (*S*)-1-methylheptyl 2-[4-(4-dodecyloxybenzoyloxy)phenyl]pyrimidine-5-carboxylate **A** and its racemic modification **B**; * denotes the enthalpies that were too small to be evaluated.

Chiral compound **A**

Iso–TGBC*$_A$	TGBC*$_A$–SmC$_A$*	SmC$_A$*–Cryst	Mp/°C
93 [−0.87]	91.6 [−0.22]	68.3 [−28.8]	86.4

Racemic modification **B**

I–SmA	SmA–SmC	SmC–SmC$_{alt}$	SmC$_{alt}$–Cryst	Mp/°C
96 [−9.12]	90.5 [−]*	89.2 [−]*	43.6 [−34.8]	72.6 [75.6]

DOI: 10.1039/b002941f

Comparing the results obtained for racemate **B** with those for enantiomer **A** yields some interesting and contrasting observations. The mesophase formed first on cooling the isotropic liquid of the racemic modification exhibits a focal-conic texture that is characterised by its elliptical and hyperbolic lines of optical discontinuity, and a homeotropic optically extinct texture. The presence of these defect textures characterises the mesophase as smectic A. Subsequent cooling leads to the homeotropic areas becoming *schlieren*, and the focal-conic domains becoming broken, both of these textures are characteristic of the formation of a smectic C phase. As the temperature is lowered there is the formation of a third phase, again characterised by the presence of a *schlieren* texture, but this time the focal-conic domains are not as broken as they were in the smectic C phase. These observations are in keeping with the third phase being an *anticlinic* smectic C_{alt} phase, where the tilt directions of the molecules alternate on passing from one layer to the next, *i.e.* the tilt direction rotates through an angle of 180° on passing from one layer to the next. Thus racemate **B** appears to exhibit a SmA, SmC, SmC_{alt} phase sequence, whereas the enantiomer **A** exhibits a TGB and SmC^*_A sequence.

Differential scanning calorimetry was used to investigate the nature of the phase transitions and to determine their associated enthalpy values, see Table 1. Fig. 1 shows the cooling scans for both the racemate and the enantiomer. For the racemate (dotted line) the smectic A phase forms first on cooling from the isotropic liquid at 96 °C. On further cooling a smectic C phase is formed at 90.5 °C, but as the transition is second order it is detected only as a baseline step in the DSC. As the temperature is lowered a weak first order transition is found for smectic C to smectic C_{alt} at 89.2 °C.

A, solid line in Fig. 1, shows strong pretransitional effects in the isotropic liquid just before the transition to the TGB phase. Transitional effects in the isotropic liquid are typical for systems that are about to form TGB phases and are associated, like those of superconductors, with entangled or disentangled flux phases, *i.e.* the amorphous liquid has some long range order associated with it.[13] The transition to the TGB phase is strongly first order, but the associated enthalpy is much lower than that obtained for the clearing point of the racemate. However, the enthalpy for the isotropic liquid to smectic A transition is approximately equal to the sum of the enthalpies associated with the pretransitional effect in the liquid and the isotropic liquid to TGB phase of the enantiomer.[3,4]

The magnitude of the spontaneous polarization for **A**, determined using the triangular wave method, was found to reach a maximum value of approximately 60 nC cm^{-2}. Examination of the current flow as a function of temperature and time showed that as the material is switched from one stable ferroelectric state to the other, two separate events occur which correspond to switching from one ferroelectric state to the antiferroelectric state and on to the other ferroelectric state. As

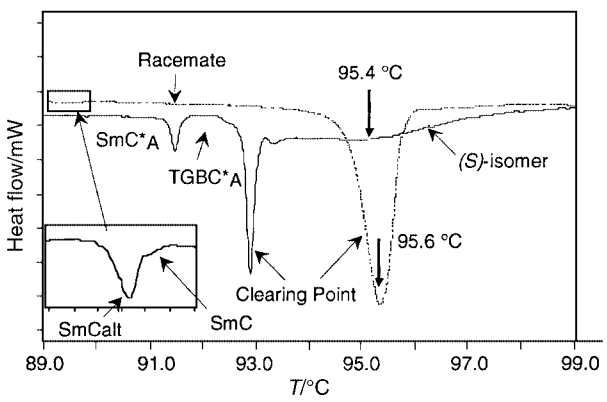

Fig. 1 Differential scanning thermograms obtained on cooling for the (*S*)-enantiomer, **A** (solid lines) and its racemic modification, **B** (dotted lines), the scan rate was 2 °C min^{-1}.

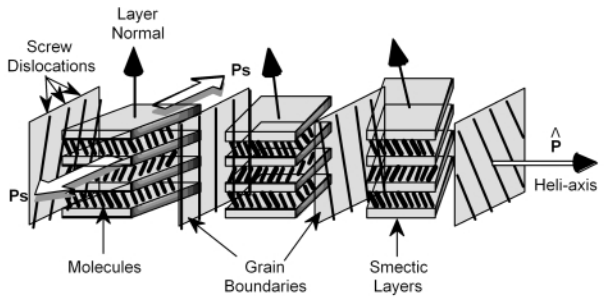

Fig. 2 A cartoon of the proposed structure of the antiferroelectric $TGBC^*_A$ phase.

the temperature is reduced, so the antiferroelectric state becomes more stable, which is probably reflected in a higher viscosity. At the transition to the TGB phase there is no appreciable change in the switching process indicating that the phase formed from the TGB phase on cooling is indeed antiferroelectric, confirming the observations made from the miscibility studies, *i.e.* that enantiomer **A** does not exhibit either a smectic A* or smectic C* phase that corresponds to the achiral phases of the racemate. It is also interesting to note the events that take place prior to and during the switching of the TGB phase. When the cell is filled from the isotropic liquid the homogeneous alignment causes the formation of a helical macrostructure, associated with the TGB phase, perpendicular to the glass substrates. As the field is applied the helix unwinds to give a bookshelf-like geometry, as the field is increased a helix, associated with an antiferroelectric phase, now forms perpendicular to the layers and parallel to the planes of the glass substrates. Increasing the field induces this phase to unwind to give a stable unwound antiferroelectric phase, which as the field is increased gives way to a stable switched ferroelectric phase. These investigations suggest that the polarization vector associated with the ferroelectric layers in the antiferroelectric phase lies perpendicular to the heli-axis as shown in Fig. 2.

In conclusion, we have demonstrated that (*S*)-1-methylheptyl 2-[4-(4′-dodecyloxybenzoyloxy)phenyl]pyrimidine-5-carboxylate exhibits a novel TGB which we believe to be antiferroelectric. This result represents the addition of a new frustrated state of matter to the family of twist grain boundary phases.

We thank the University of Hull Overseas Research Student Scheme, the Department of Chemistry, University of Hull, the EU TMR programme (Optical Research of Chiral Systems ORCHIS), and DERA for financial support.

Notes and references

1 P. G. de Gennes, *Solid State Commun.*, 1972, **10**, 753.
2 S. R. Renn and T. C. Lubensky, *Phys. Rev. A*, 1988, **38**, 2132.
3 J. W. Goodby, M. A. Waugh, S. M. Stein, E. Chin, R. Pindak and J. S. Patel, *Nature*, 1989, **337**, 449.
4 J. W. Goodby, M. A. Waugh, S. M. Stein, E. Chin, R. Pindak and J. S. Patel, *J. Am. Chem. Soc.*, 1989, **111**, 8119.
5 A. J. Slaney and J. W. Goodby, *J. Mater. Chem.*, 1991, **1**, 5.
6 A. J. Slaney and J. W. Goodby, *Liq. Cryst.*, 1991, **9**, 849.
7 A. Bouchta, H. T. Nguyen, M. F. Achard, F. Hordouin, C. Destrade, R. J. Tweig, A. Maaroufi and N. Isaert, *Liq. Cryst.*, 1992, **12**, 575.
8 G. Strajer, R. Pindak, M. A. Waugh, J. W. Goodby and J. S. Patel, *Phys. Rev. Lett.*, 1990, **64**, 1545.
9 L. Navailles, P. Barois and H. T. Nguyen, *Phys. Rev. Lett.*, 1993, **71**, 545; L. Navailles, R. Pindak, P. Barois and H. T. Nguyen, *Phys. Rev. Lett.*, 1995, **74**, 5224; L. Navailles, P. Barois and H. T. Nguyen, *Phys. Rev. Lett.*, 1994, **72**, 1300.
10 K. Takatoh, A. G. M. Lamb and J. W. Goodby, *Proceedings of the Annual British Liquid Crystal Society Conference*, Hull, 1994.
11 P. A Pramod, R. Pratibha and N. V. Madhusudana, *Curr. Sci.*, 1997, **73**, 761.
12 J. M. Gilli and M. Kamayé, *Liq. Cryst.*, 1992, **12**, 545.
13 J. W. Goodby, D. A. Dunmur and P. J. Collings, *Liq. Cryst.*, 1995, **19**, 703.

ChemComm

Water-soluble platinum and palladium nanoparticles modified with thiolated β-cyclodextrin†

Julio Alvarez, Jian Liu, Esteban Román and Angel E. Kaifer*

Center for Supramolecular Science and Department of Chemistry, University of Miami, Coral Gables, FL 33124-0431, USA. E-mail: akaifer@miami.edu

Received (in Columbia, MO, USA) 23rd March 2000, Accepted 17th May 2000

Pt and Pd nanoparticles can be modified with surface-attached cyclodextrin receptors leading to water-soluble materials that exhibit catalytic activity for the hydrogenation of allylamine.

The modification of metal[1] and semiconductor[2] nanoparticles with organic monolayers has become a very fruitful and active field of research in modern chemistry. An attractive aspect of recent developments in this area is that the final materials may exhibit combined properties from their inorganic nuclei and their organic surfaces. Our group is particularly interested in the modification of metal nanoparticles (metal clusters or colloids) with organic monolayers prepared with suitable, synthetic molecular hosts. We have recently reported several examples illustrating the use of cyclodextrins (CDs) for the modification of gold colloidal[3] or cluster[4] particles. In this report, we demonstrate the surface attachment of CDs to platinum and palladium nanoparticles that catalyze the hydrogenation of allylamine. As opposed to classical Pt and Pd catalytic materials, these novel nanocomposites are soluble in aqueous media and can be easily recovered by precipitation with ethanol.

Ulman and coworkers have recently reported the preparation of platinum nanoparticles protected with alkanethiol monolayers.[5] Inspired by this report, we decided to adapt our published procedure for the preparation of CD-modified gold clusters[4] to the synthesis of Pt and Pd nanoparticles derivatized with chemisorbed CD hosts. To this end, solutions of $PtCl_4^{2-}$ or $PdCl_4^{2-}$ sodium salts in DMSO–H_2O were readily reduced with BH_4^- in the presence of *per*-6-thio-β-cyclodextrin[6] (HS-β-CD, see structure below), leading to the isolation of dark precipitates.‡ These materials show FTIR spectra which are very similar to that exhibited by free HS-β-CD, indicating the

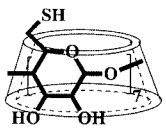

HS-β-CD

presence of the thiolated CD in the dark solids (ESI, Fig. S1†). Furthermore, close inspection of these IR spectra reveals that the weak S–H stretching peak at *ca*. 2560 cm^{-1}, which is clearly visible in the spectrum of free HS-β-CD, disappears in the spectrum of the dark precipitates collected from the reduced Pt and Pd complex solutions. This is consistent with the anticipated conversion of the H–S bonds in HS-β-CD to metal–thiolate bonds as the CD host chemisorbs on the surface of the metal nanoparticles.[3b] ^1H NMR spectroscopy also provides experimental evidence that supports the presence of HS-β-CD in the dark precipitates. However, the proton resonances from the CD receptors appear as broad peaks, a result of their relative proximity to the metal particles.[4,7] These spectroscopic features must result from the presence of HS-β-CD molecules attached to the metal nanoparticles, since any free HS-β-CD molecules were washed away before spectroscopic analysis.‡

TEM measurements recorded on the precipitates collected from the reduction of the Pt (or Pd) complex in the presence of HS-β-CD verified that these solids materials are composed of metal particles with dimensions in the nanometer range. Typical TEM images are shown in Fig. 1 and histograms showing the particle size distributions (obtained from individual measurements on at least 100 particles) are given as ESI (Fig. S2).† The average diameters were 14.1 ± 2.2 and 15.6 ± 1.3 nm for the Pt and Pd particles, respectively. Both the Pt and Pd nanoparticles exhibit limited polydispersity and their sizes fall clearly into the colloidal particle domain.

All these results clearly indicate that the derivatization of the Pt and Pd nanoparticles with surface-attached, thiolated β-CD receptors proceeds smoothly, yielding reasonably monodisperse, CD-modified Pt (or Pd) colloidal particles. Unlike modification with alkanethiols,[5] which passivates the particle surfaces and renders them catalytically inactive, we anticipated that these CD-covered Pt (and Pd) nanoparticles will exhibit catalytic activity. Therefore, in order to substantiate this hypothesis, we selected the hydrogenation of allylamine as a

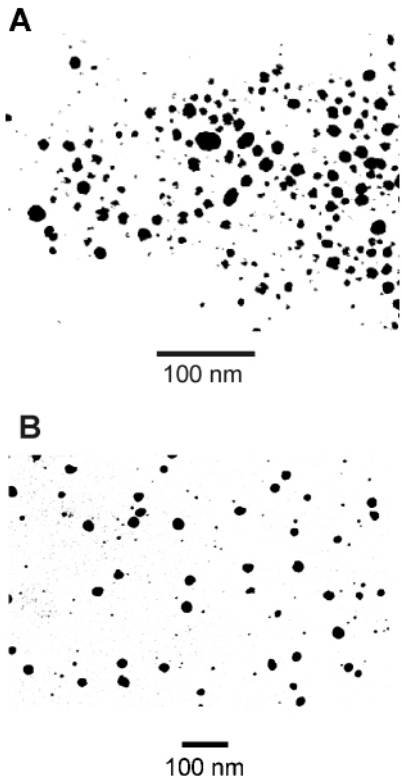

Fig. 1 TEM images of (a) CD-modified Pt nanoparticles and (b) CD-modified Pd nanoparticles.

† Electronic supplementary information (ESI) available: Fig. S1 (FTIR spectra) and S2 (size distribution histograms). See http://www.rsc.org/suppdata/cc/b0/b002423f/

DOI: 10.1039/b002423f

Table 1 Percentage conversion from allylamine (1.8 mmol) to propylamine under 1.0 atm H_2(g) at room temperature in D_2O solution (2.0 mL)

Catalyst	Amount/mg	*t*/h	Conversion (%)
CD-mod. Pt	10	6	> 95
CD-mod. Pd	10	6	100
None	—	6	0
CD-mod. Pt	5	1	10
CD-mod. Pd	5	1	30

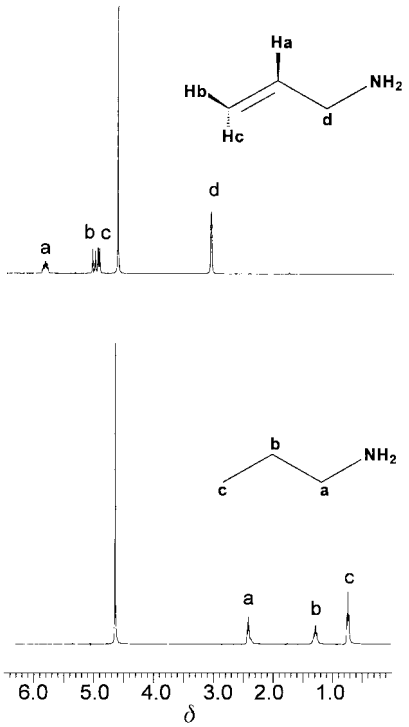

Fig. 2 ^{1}H NMR spectra of a 0.9 M solution of allylamine in D_2O containing 10 mg of CD-modified Pd colloids before (top) and after (bottom) 6 h of exposure to an H_2(g) atmosphere at 760 mm Hg.

straightforward test reaction. Our experimental results clearly verified the activity of these nanoparticles as 'homogeneous' catalysts[8] (Table 1). Under the surveyed reaction conditions,‡ both CD-modified Pt and Pd colloids catalyzed the hydrogenation of allylamine to propylamine. In a set of experiments, using 10 mg of each catalyst and 6 h reaction time, the surface modified Pt and Pd colloids achieved full conversion. In a second series of experiments, using 5 mg of each catalyst and a shorter reaction time of 1 h, the CD-modified Pd nanoparticles were more efficient than the CD-modified Pt nanoparticles. As an illustrative example, Fig. 2 shows the ^{1}H NMR spectra recorded before and after 6 h of hydrogenation catalyzed by 10 mg of the CD-modified Pd nanoparticles. We should note here that both types of CD-modified metal nanoparticles were soluble in the reaction medium and could be easily recovered at the end of the reaction by precipitation with ethanol.

In conclusion, we have demonstrated that the surface modified Pt and Pd colloidal particles reported in this work are active catalysts for the hydrogenation of allylamine in aqueous solution. These novel materials may find applications in 'green chemistry' and, perhaps, lead to 'selective' catalytic activity,[9] modulated by the molecular recognition properties of the surface-attached hosts. We are currently working towards this important goal.

We are grateful to the National Science Foundation for the support of this research work (to A. E. K., CHE-9982014). E. R. thanks the University of Miami for a graduate Maytag fellowship.

Notes and references

‡ *Preparation of modified metal colloids*: a DMSO–H_2O (1 : 4 v/v) solvent mixture was used to dissolve the metal complex. A sample of 0.125 mmol of Na_2PtCl_4 (or Na_2PdCl_4) was dissolved in 20 mL of the solvent mixture and placed in a 100 mL round bottom flask under vigorous stirring. Another 20 mL aliquot of solvent containing 12.5 mg (0.0096 mmol) of HS-β-CD and 75.5 mg (40 mmol) of $NaBH_4$ was prepared and carefully homogenized. The latter solution was added through an addition funnel to the metal complex solution, while maintaining the stirring rate. The reaction mixture was allowed to run its course overnight. After this, 10–15 mL of absolute ethanol was added to precipitate the metal particles. The dark precipitate was collected by centrifugation and washed several times, first with DMSO to remove free HS-β-CD and then with ethanol to remove the DMSO. Complete removal of the thiolated cyclodextrin was verified by thin layer chromatography (TLC). Once this was achieved, the sample was dried under vacuum at 60 °C during 24 h. The resulting dried powder was submitted for characterization by spectroscopic analysis or transmission electron microscopy (TEM) and used in the catalytic experiments.

Catalytic experiments: the CD-modified Pd and Pt colloids prepared in this work were tested for catalytic activity under identical reaction conditions. A solution of a measured amount of the catalyst in 2 mL of D_2O was stirred in a 5 mL peak-shaped flask and saturated with hydrogen gas for 10 min. Allylamine (136 μL, 1.8 mmol) was added with a microsyringe and a ^{1}H NMR spectrum was recorded just prior to the hydrogenation reaction. The flask was then sealed with a rubber septum under a hydrogen atmosphere (760 mm Hg) and left for the selected reaction time. At the end of this time, another ^{1}H NMR spectrum was recorded to monitor the extent of conversion from allylamine to propylamine.

1 M. J. Hostetler and R. W. Murray, *Curr. Opin. Colloid Interface Sci.*, 1997, **2**, 42; C. R. Martin, *Anal. Chem.*, 1998, **70**, A322.
2 M. Bruchez Jr., M. Moronne, P. Gin, S. Weiss and A. P. Alivisatos, *Science*, 1998, **281**, 2013; W. C. W. Chan and S. Nie, *Science*, 1998, **281**, 2016.
3 (*a*) J. Liu, R. Xu and A. E. Kaifer, *Langmuir*, 1998, **14**, 7337; (*b*) J. Liu, S. Mendoza, E. Román, M. J. Lynn, R. Xu and A. E. Kaifer, *J. Am. Chem. Soc.*, 1999, **121**, 4304.
4 J. Liu, W. Ong, E. Roman, M. J. Lynn and A. E. Kaifer, *Langmuir*, 2000, **16**, 3000.
5 C. Yee, M. Scotti, A. Ulman, H. White, R. Rafailovich and J. Sokolov, *Langmuir*, 1999, **15**, 4314.
6 M. T. Rojas, R. Königer, J. F. Stoddart and A. E. Kaifer, *J. Am. Chem. Soc.*, 1995, **117**, 336.
7 R. H. Terrill, T. A. Postlethwaite, C.-H. Chen, C.-D. Poon, A. Terzis, A. Chen, J. E. Hutchison, M. R. Clark, G. Wignall, J. D. Londono, R. Superfine, M. Falvo, C. S. Johnson Jr., E. T. Samulski and R. W. Murray, *J. Am. Chem. Soc.*, 1995, **117**, 12 537.
8 The term *homogeneous* catalyst is usually reserved for molecular species. We use this term liberally in order to emphasize the soluble character of these Pt and Pd nanoparticles. These systems lie along the borderline between homogeneous and heterogeneous catalysts as a natural reflection of their colloidal character.
9 For a recent example of novel Pt- and Pd-based catalysts that exhibit some degree of selectivity, see: M. Zhao and R. M. Crooks, *Angew. Chem., Int. Ed.*, 1999, **38**, 364.

ChemComm

Hydroxamic acids are nitric oxide donors. Facile formation of ruthenium(II)-nitrosyls and NO-mediated activation of guanylate cyclase by hydroxamic acids

Celine J. Marmion,[a] Terry Murphy,[a] James R. Docherty[b] and Kevin B. Nolan*[a]

[a] *Department of Chemistry, Royal College of Surgeons in Ireland, 123, St. Stephen's Green, Dublin 2, Ireland. E-mail: kbnolan@rcsi.ie*

[b] *Department of Physiology, Royal College of Surgeons in Ireland, 123, St. Stephen's Green, Dublin 2, Ireland*

Received (in Cambridge, UK) 29th February 2000, Accepted 18th May 2000

Hydroxamic acids are shown for the first time to be effective NO donors by their ability to readily form ruthenium(II)-nitrosyls, and to cause vascular relaxation of rat aorta by NO-mediated activation of the iron-containing guanylate cyclase.

Hydroxamic acids, a group of weak organic acids of general formula RC(O)N(R′)OH, fulfil a variety of roles in biology and medicine, for example, as siderophores for iron(III),[1] as potent and selective inhibitors of enzymes such as peroxidases,[2] ureases,[3] and matrix metalloproteinases,[4] and as hypotensive,[5] anti-cancer, anti-tuberculous and antifungal agents.[6] While some of these roles are undoubtedly due to the chelating ability of the hydroxamate group, others, such as the hypotensive effects (a known nitric oxide property), may be due to their ability to release nitric oxide, a view strengthened by the now established importance of NO in many physiological processes.[7] We report herein the first evidence that hydroxamic acids can indeed act as NO donors, as shown by the fact that they readily transfer NO to ruthenium(III) and cause vascular relaxation in rat aorta by activation of the iron-containing guanylate cyclase enzyme.

Reaction of K[Ru(Hedta)Cl]·2H_2O (200 mg, 0.40 mmol), with benzohydroxamic acid (177 mg, 1.29 mmol) in aqueous solution (30 cm^3) at room temperature resulted in an immediate colour change from straw-yellow to red. A brown product was obtained (*ca.* 55% yield without attempted optimisation) following purification on a Sephadex LH 20 column and removal of solvent. The unambiguous formation of a ruthenium nitrosyl complex was confirmed by microanalysis,† IR, mass and ^{1}H NMR spectra, which were consistent with the formulation K_2[Ru(edta)(NO)Cl], containing a linear, diamagnetic Ru^{2+}–NO^+ group[8] (IR: distinctive ν_{NO} at 1880 cm^{-1}, broad, strong ν_{CO} at 1660 cm^{-1}, no absorption at 1730 cm^{-1}, confirming fully depronated edta[9] and ν_{Ru-Cl} at 300 cm^{-1}; ESI-MS: mass peaks at 420 and 390 amu, corresponding to $[Ru(edta)(NO)]^-$ and $[Ru(edta)]^-$, respectively, with correct isotopic abundances; ^{1}H NMR: δ 3.6 due to ethylenic protons, 3.8, 4.1, 4.3 and 4.4 due to CH_2COO^- protons, in D_2O solution). This complex is similar to the previously reported six-coordinate Ru(H_2edta)(NO)Cl·2H_2O,[9] but contains fully deprotonated tetradentate edta with two pendant carboxylate groups. A related complex, $[Ru(edta)NO]^-$, is formed in solution by reaction of NO with K[Ru(Hedta)Cl].[10] Similar reactions of K[Ru(Hedta)Cl]·2H_2O with acetohydroxamic acid and salicylhydroxamic acid also gave the same product in high yields. The products of the denitrosylation reactions were shown to be the corresponding carboxylic acids by TLC, UV and ^{1}H NMR analysis.‡§ Reaction of $RuCl_3$·xH_2O with aceto-, benzo-, salicyl- and anthranilic hydroxamic acids in ethanol followed by purification on Sephadex LH 20 columns also gave ruthenium(II) nitrosyl complexes, all of which have very distinctive ν_{NO} bands at *ca.* 1885 cm^{-1}.¶

The ability of hydroxamic acids to release nitric oxide in simple biological systems was shown by vascular relaxation of endothelium-denuded rings of rat aorta.[11] These were set up in organ baths for isometric tension recording. Rings were contracted with the α_1-adrenoreceptor agonist phenylephrine (1 μM), and the ability of increasing concentrations of hydroxamic acid derivatives to produce relaxation was examined; the results are shown in Fig. 1. Of the hydroxamic acids investigated, benzohydroxamic acid proved most effective, causing approximately 45% relaxation of rat aorta at a concentration of 300 μM. Although this value is higher than that quoted for the well known NO donor 3-morpholinosydnonimine, SIN-1 (1 μM), it compares favourably with that of another NO donor 4-(3-butoxy-4-methoxybenzo)-2-imidazolidilone, Ro-20-1724 (100 μM).[12] Relaxation occurred by activation of the enzyme guanylate cyclase (a definitive receptor for NO),[13] as shown by the fact that methylene blue (10 μM), a known inhibitor of this enzyme,[14] prevented the relaxation (*e.g.* relaxation to 300 μM acetohydroxamic acid: vehicle (distilled water) treated, 31.4±10.9% relaxation; methylene blue treated, 6.4±3.1% relaxation, $n = 4$, $P < 0.05$).

In this work, we have shown conclusively that hydroxamic acids can act as effective NO donors by demonstrating that they can readily transfer NO to ruthenium(III), the first reported metal nitrosyl complexes formed from hydroxamic acids. Furthermore, hydroxamic acids can cause vascular relaxation in rat aorta by NO-mediated activation of the iron-containing enzyme guanylate cyclase, thus confirming the biological relevance of our novel results.

We thank Mr Brendan Harhen, Department of Clinical Pharmacology, RCSI, for mass spectra, The Microanalytical Laboratory, University College Dublin for the microanalysis, Dublin Institute of Technology for ^{1}H NMR and far IR spectra, and the Irish Government for financial support under its 'Programme for Research In Third Level Institutions' and EU COST D8.

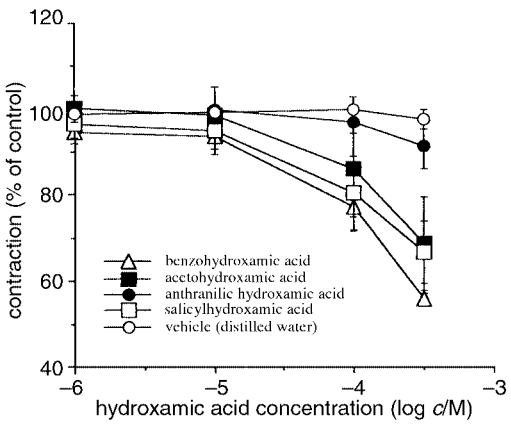

Fig. 1 The effects of hydroxamic acids on relaxation of rat aorta.

Notes and references

† Microanalysis: found: C, 21.03; H, 2.78; N, 7.51; Cl, 9.11. K_2[Ru(edta)-(NO)Cl]·0.5HCl·H_2O ($C_{10}H_{14.5}N_3O_{10}Cl_{1.5}K_2Ru$) requires C, 21.10; H, 2.57; N, 7.39; Cl, 9.34%.

‡ An aqueous mixture of benzohydroxamic acid and an excess of [Ru(Hedta)Cl]$^-$, after completion of the reaction, was analysed by TLC [silica plates and a toluene–ether–acetic acid–methanol (120:60:18:1) or ethanol–water–ammonia (8:1:1) solvent mixture] which confirmed the presence of benzoic acid and the absence of benzohydroxamic acid. The UV spectrum in H_2O has a band at 224 nm due to benzoic acid which is not present in the spectrum of the nitrosyl complex. The ^{1}H NMR spectrum of a D_2O solution containing [Ru(Hedta)Cl]$^-$ and a twofold excess of benzohydroxamic acid, to ensure complete removal of the paramagnetic ruthenium(III) complex, showed a signal at δ 8.01 which is characteristic of benzoic acid, but not of benzohydroxamic acid. The acid-catalysed hydrolysis of hydroxamic acids to carboxylic acids (half-life *ca*. 1 h at 88 °C) has previously been reported.[15]

§ A possible mechanism for the denitrosylation of the hydroxamic acid (RC(O)NHOH) involves aquation of [Ru(Hedta)Cl]$^-$, followed by nucleophilic attack by the hydroxo conjugate base ligand on the hydroxamic acid carbonyl group, giving an intermediate from which hydroxylamine is eliminated. Abstraction of NO from this causes displacement of the carboxylate ligand ($RCOO^-$) and this, together with displacement of coordinated edta carboxylate by chloride in the work up procedure, gives [Ru(edta)(NO)Cl]$^{2-}$.

¶ IR(Nujol mull): strong ν_{NO} at 1885 cm^{-1} (acetohydroxamate complex), 1885 cm^{-1} (benzohydroxamate), 1883 cm^{-1} (salicylhydroxamate) and 1885 cm^{-1} (anthranilic hydroxamate).

1 B. Kurzak, H. Kozlowski and E. Farkas, *Coord. Chem. Rev.*, 1992, **114**, 169.
2 S. S. C. Tam, D. H. S. Lee, E. Y. Wang, D. G. Munroe and C. Y. Lau, *J. Biol. Chem.*, 1995, **270**, 13948.
3 M. Arnold, D. A. Brown, O. Deeg, W. Errington, W. Haase, K. Herlihy, T. J. Kemp, H. Nimir and R. Werner, *Inorg. Chem.*, 1998, **37**, 2920.
4 I. Botos, L. Scapozza, D. Zhang, L. A. Liotta and E. F. Meyer, *Proc. Natl. Acad. Sci. USA*, 1996, **93**, 2749.
5 R. Zamora, A. Grzesiok, H. Weber and M. Feelisch, *Biochem. J.*, 1995, **312**, 33.
6 M. J. Miller, *Chem. Rev.*, 1989, **89**, 1563 and references therein.
7 D. R. Adams, M. Brochwicz-Lewinski and A. R. Butler, *Nitric Oxide: Physiological Roles, Biosynthesis and Medical Uses*, in *Progress in the Chemistry of Organic Natural Products*, ed. W. Herz, H. Falk, G. W. Kirby, R. E. Moore and Ch. Tamm, Springer, Wien, New York, 1999, No. 76.
8 S. P. Fricker, *Platinum Met. Rev.*, 1995, **39**, 150.
9 A. A. Diamantis and J. V. Dubrawski, *Inorg. Chem.*, 1981, **20**, 1142.
10 N. A. Davies, M. T. Wilson, E. Slade, S. P. Fricker, B. A. Murrer, N. A. Powell and G. R. Henderson, *Chem. Commun.*, 1997, 47.
11 C. Connolly, P. A. McCormick and J. R. Docherty, *Eur. J. Pharmacol.*, 1998, **352**, 53.
12 D. H. Maurice, D. Crankshaw and R. J. Haslam, *Eur J. Pharmacol.*, 1991, **192**, 235.
13 J. W. Denninger and M. A. Marletta, *Biochim Biophys Acta*, 1999, **1411**, 334.
14 W. Martin, G. M. Villani, D. Jothianandan and R. F. Furchgott, *J. Pharmacol. Exp. Ther.*, 1985, **232**, 708.
15 D. C. Berndt, *J. Chem. Educ.*, 1971, **48**, 200.

ChemComm

3-Bromobarekoxide, an unusual diterpene from *Laurencia luzonensis*

Masayuki Kuniyoshi,[a] Mong S. Marma,[a] Tatsuo Higa,[a] Gérald Bernardinelli[b] and Charles W. Jefford[b]*

[a] *Department of Chemistry, Biology and Marine Science, University of the Ryukyus, Nishihara, Okinawa 903-0213, Japan*

[b] *Laboratory of Crystallography and Department of Organic Chemistry, University of Geneva, 1211 Geneva 4, Switzerland. E-mail: jefford@sc2a.unige.ch*

Received (in Liverpool, UK) 28th March 2000, Accepted 18th May 2000

A new, rare diterpene characterized by a cycloheptane ring *trans*-fused to a *trans*-decalin moiety was isolated from *Laurencia luzonensis* and its absolute structure determined by X-ray crystallography.

The red alga of the genus *Laurencia* and the sea hares that feed upon it have been a bountiful source of metabolites. So far more than 300 have been characterized, most of which are sesquiterpenes and C_{15} acetogenins. However a few di- and triterpenes have also been described.[1] We now report on a rare diterpene consisting of a seven-membered ring fused to decalin (**1**) which

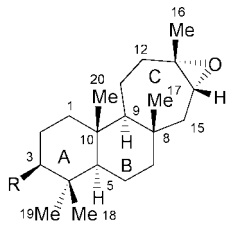

1 R = Br
3 R = H

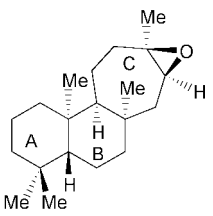

2

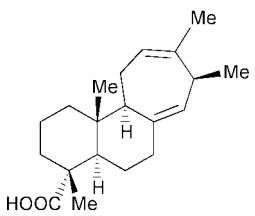

4

was obtained from the hitherto unexamined species *Laurencia luzonensis*.

A sample (3.5 kg), collected off the coast of Kudaka Island, Okinawa, in May 1998, was extracted by steeping with 95% ethanol. Concentration of the extracts and partitioning between water and ethyl acetate gave an oil (12.5 g). Successive chromatography over silica gel with solvent mixtures ranging from hexane, dichloromethane, and ethyl acetate afforded a fraction which was purified by HPLC (LiChrosorb Si60, hexane/AcOEt, 10:1). Subsequent recrystallization from CCl_4 furnished **1** (58.5 mg) as colorless crystals, mp 165 °C, $[\alpha]_D^{24}$ = 6.18 (*c* 0.3, $CHCl_3$).

The molecular formula $C_{20}H_{33}OBr$ was deduced from the ^{13}C NMR spectrum and LR EIMS. The monobrominated nature of the compound was immediately evident from the molecular ion peak which appeared as a doublet of equal intensity (*m/z* 368, 370). The absence of olefinic and carbonyl signals in the NMR spectrum suggested a tetracyclic entity. The carbon signals at δ 60.52 (s) and 60.45 (d) together with the proton signal at δ 2.70 (dd, *J* = 7.5, 7.5 Hz) indicated an epoxide (Table 1). Therefore the remaining three rings are carbocyclic. Analysis of the 1D and 2D NMR spectra (COSY, HMQC, HMBC, NOESY) led to a diterpene structure composed of *trans*-decalin and an epoxide fused to a common seven-membered ring. Comparison of the NMR data of **1** (Table 1) with those reported for barekoxide (**2**), a related terpene isolated from the sponge *Chelonaplysilla erecta*,[2] revealed good agreement apart from the obvious differences between the A rings. Therefore, we initially assumed that **1** was simply the 3β-bromo derivative of **2** in which the A/B and B/C junctions are *trans* and *cis*-fused respectively. However, as the absolute configuration of **2** was unknown, determining that of **1** would provide an convenient proof of structure for both molecules. Accordingly, a single crystal of **1** was submitted to X-ray analysis.† It is immediately seen that the decalin moiety is certainly *trans*, but that the B/C ring junction is *trans* as well (Fig. 1). Despite the *syn*-axially disposed methyl groups, the cyclohexane and cycloheptane rings adopt chair conformations. Evidently, the structure previously assigned to **2** is doubtful. Clarification was secured by treating **1** with tributyltin hydride and AIBN in DMSO.‡ Reductive debromination gave the parent hydrocarbon **3** as colorless crystals, mp 140 °C, $[\alpha]_D^{24}$ = 5.2 (*c* 0.256, $CHCl_3$). The ^1H and ^{13}C NMR spectra of **3** were essentially the same as those recorded for barekoxide (**2**).§ We therefore conclude that structure **2** is incorrect and should be revised to that of **3**. Furthermore, the sign of the specific rotation indicates that barekoxide of sponge origin¶ must have the same absolute configuration as the alga-derived product **3**.

Table 1 ^1H and ^{13}C NMR chemical shifts (ppm) of 3-bromobarekoxide (**1**) and long range CH correlations as obtained in the HMBC experiment

Carbon number	δ_C	δ_H (multiplicity, *J* in Hz)	CH correlation
1	41.68 t	1.80 (dt, 13.0, 3.5) 1.00 (br dd, 13.0, 3.5)	H2, H20
2	31.00 t	2.18 (dq, 12.5, 3.5) 2.07 (m)	H1, H3
3	69.52 d	3.98 (dd, 13.0, 4.5)	H1, H2, H18, H19
4	39.80 s		H2, H3, H18, H19
5	56.77 d	0.90 (dd, 11.5, 3.0)	H1, H6, H18, H19, H20
6	20.10 t	1.50 (m), 1.25 (m)	H5, H7
7	44.04 t	1.60 (m), 1.50 (m)	H5, H6, H15, H17
8	37.32 s		H7, H9, H15, H17
9	64.28 d	0.82 (br d, 10.0)	H11, H12, H15, H17, H20
10	38.82 s		H1, H2, H5, H9, H20
11	19.97 t	1.70 (m), 1.50 (m)	H9, H12
12	35.92 t	2.00 (m), 1.35 (m)	H9, H11, H16
13	60.52 s		H12, H15, H16
14	60.45 d	2.70 (dd, 7.5, 7.5)	H15, H16
15	47.07 t	1.85 (dd, 14.0, 7.5) 1.20 (dd, 14.0, 7.5)	H7, H9, H17
16	22.42 q	1.32 (s)	H12, H14
17	19.55 q	1.02 (s)	H9, H15
18	18.13 q	0.93 (s)	H3, H5, H19
19	30.50 q	1.05 (s)	H3, H5, H18
20	15.93 q	0.87 (s)	H1, H5, H19

DOI: 10.1039/b002530p

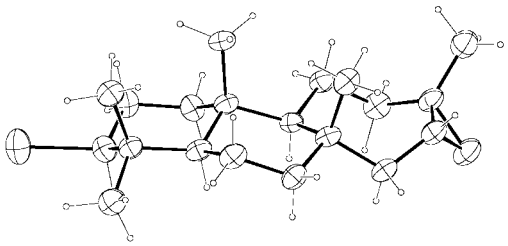

Fig. 1 Perspective view of the crystal structure of **1**. Ellipsoids are represented with 40% probability.

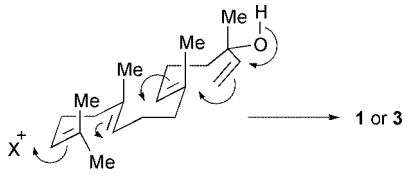

5 X = Br or H

Scheme 1

The present findings correctly establish the absolute structure and confirm the novelty of the diterpene framework of the barekoxides. The tricyclic entity of *trans*-decalin fused to cycloheptane is extremely rare in nature and is only encountered in strobal[3] and strobic acid (**4**).[4] Significantly, the configuration of the C(5), C(9) and C(10) atoms in **1** and **3** is the same as in **4**. Clearly, all three metabolites arise by a similar stereoselective biogenetic pathway. Bromination or protonation of geranyllinalool (**5**) creates a steroid-like tetracyclic array affording **1** or **3**, whereas proton-initiated cyclization followed by oxidation of the C(19) methyl group, 1,3 methyl shift, and elimination accounts for **4** (Scheme 1).

Notes and references

† *Crystal data* for **1**: $C_{20}H_{33}OBr$, M = 369.4, orthorhombic, $P2_12_12_1$, Z = 4, a = 7.6677(6), b = 11.419(1), c = 21.001(1) Å, U = 1838.8(2) Å^3, $F(000)$ = 784, μ(Cu-Kα) = 3.029 mm^{-1}, D_c = 1.334 g cm^{-3}, T = 200 K, 2651 measured reflections, of which 2141 were observable ($|F_o| > 4\sigma(F_o)$). R_{int} for equivalent reflections 0.022. Data were corrected for Lorentz and polarization effects, and for absorption ($T_{min,max}$ = 0.4460, 0.5262). The structure was solved by direct methods and refined (on F) by full matrix least squares. The absolute configuration was determined (Flack parameter x = 0.02(3)).[5] R = 0.031, wR = 0.030 for 255 variables and 2141 contributing reflections. Non-Me hydrogen atoms were observed and refined with a fixed value of isotropic displacement parameters (U = 0.05 Å^2); Me-hydrogen atoms were refined with restraints on bond lengths and bond angles (free rotation) and blocked in the final cycles. Calculations were carried out using the XTAL system.[6] CCDC 182/1646. See http://www.rsc.org/suppdata/cc/b0/b002530p/ for crystallographic files in .cif format.

‡ 3-Bromobarekoxide (**1**, 6 mg) was treated with tributyltin hydride (50 μL) and AIBN (3 mg) in DMSO (0.2 mL) at room temperature overnight. The reaction mixture was worked up in the usual manner and the product purified by HPLC (Lichrosorb Si60, hexane/AcOEt, 10 : 1) to yield **3** (4.2 mg, 88%).

§ Some of the proton signals cited in ref. 2 for **2** were incorrectly assigned. Our assignments for semi-synthetic **3** (formerly **2**) are as follows: ^{1}H NMR (C_6D_6) δ 2.59 (t, J = 7.5 Hz, H-14), 1.88 (dd, J = 14.0, 8.0 Hz, H-12), 1.71 (dd, J = 13.5, 6.0 Hz, H-15), 1.58 (m, H-1), 1.55 (m, H-2), 1.55 (m, H-6), 1.50 (m, H-11), 1.42 (br t, J = 13.0 Hz, H-12), 1.38 (m, H-1), 1.35 (m, H-2), 1.30 (m, H-3), 1.29 (m, H-7), 1.25 (m, H-6), 1.22 (m, H-15), 1.22 (s, H-16), 1.15 (m, H-11), 1.10 (m, H-3), 1.02 (m, H-7), 0.86 (s, H-17), 0.84 (s, H-18), 0.80 (s, H-19), 0.70 (s, H-20), 0.60 (m, H-9), 0.58 (m, H-5).

¶ We thank Professor Y. Kashman and Dr A. Rudi of Tel Aviv University, Israel, for kindly measuring the optical rotation ($[\alpha]_D$) of an old, stored sample of sponge-derived barekoxide which they found to be 13.9.

1 K. L. Erickson, in *Marine Natural Products: Chemical and Biological Pespectives*, ed. P. J. Scheuer, Academic Press, New York, 1983, vol. 5, pp. 131–257.
2 A. Rudi and Y. Kashman, *J. Nat. Prod.*, 1992, **55**, 1408.
3 D. F. Zinkel and B. B. Evans, *Phytochemistry*, 1972, **11**, 3387.
4 D. F. Zinkel and B. P. Spalding, *Tetrahedron*, 1973, **29**, 1441.
5 H. D. Flack, *Acta Crystallogr., Sect. A*, 1983, **39**, 876; H. D. Flack and G. Bernardinelli, *Acta Crystallogr., Sect. A*, 1999, **55**, 908.
6 S. R. Hall, H. D. Flack and J. M. Stewart, XTAL3.2 User's Manual, Universities of Western Australia and Maryland, 1992.

ChemComm

Triphenylphosphine-mediated olefination of aldehydes with (*Z*)-(2-acetoxyalk-1-enyl)phenyl-λ³-iodanes: generation and reaction of (2-oxoalkyl)phenyl-λ³-iodanes

Masahito Ochiai,* Yoshio Nishi, Junichi Nishitani, Da-Wei Chen, Sakiko Hashimoto and Yoshimi Tsuchimoto

Faculty of Pharmaceutical Sciences, University of Tokushima, 1-78 Shomachi, Tokushima 770-8505, Japan. E-mail: mochiai@ph2.tokushima-u.ac.jp

Received (in Cambridge, UK) 17th April 2000, Accepted 22nd May 2000

(*Z*)-(2-Acetoxyalk-1-enyl)phenyl-λ³-iodanes, on treatment with triethylamine in methanol in the presence of triphenylphosphine, undergo Wittig olefination with aldehydes, which involves the intermediacy of α-iodanyl ketones generated by *in situ* protonation of monocarbonyl iodonium ylides.

Recently, we reported that the ester exchange reaction of (*Z*)-(2-acetoxyalk-1-enyl)phenyl-λ³-iodanes **1** with EtOLi quantitatively generates the unstabilized monocarbonyl iodonium ylides **2** in THF at −78 °C with the liberation of ethyl acetate (Scheme 1).[1] In a marked contrast to the stable iodonium ylides derived from β-dicarbonyl compounds,[2] the monocarbonyl iodonium ylides **2** are moderately nucleophilic and undergo nucleophilic attack towards carbonyl compounds and activated imines. In general, ylides react with carbonyl compounds in either of two possible reaction modes, Wittig type reaction yielding alkenes and Corey type reaction leading to the formation of epoxides, depending on the nature of ylides and carbonyl compounds.[3] Because of the very high reductive nucleofugality of the λ³-phenyliodanyl groups,[4] monocarbonyl iodonium ylides **2** exclusively undergo alkylidene transfer reactions (Corey type) with aldehydes yielding epoxides:[1a] thus, the reaction of **1** with aldehydes in the presence of EtOLi gives α,β-epoxy ketones **3** in good yields with *trans*-isomers as the major product. No formation of the Wittig type olefination products **5** was observed in this reaction. The reaction course, however, was dramatically altered to the Wittig olefination pathway, when both the base and the solvent were changed to triethylamine and methanol, and the reaction was carried out in the presence of triphenylphosphine. We report herein triphenylphosphine-mediated Wittig olefination of aldehydes with (*Z*)-(2-acetoxyalk-1-enyl)phenyl-λ³-iodanes **1**, which involves an efficient generation of (2-oxoalkyl)phenyl-λ³-iodanes **4** under mild conditions.

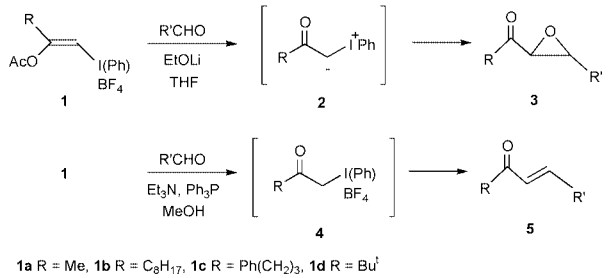

1a R = Me, **1b** R = C_8H_{17}, **1c** R = $Ph(CH_2)_3$, **1d** R = Bu^t

Scheme 1

To a stirred solution of (*Z*)-2-acetoxydec-1-enyl(phenyl)-λ³-iodane **1b** and triphenylphosphine (2 equiv.) in MeOH was added triethylamine (1.3 equiv.) at room temperature under nitrogen and the mixture was stirred for 30 min. A solution of benzaldehyde (1.5 equiv.) in MeOH was added and the mixture was heated at 60 °C for 24 h. After usual workup, preparative TLC [hexane–ethyl acetate (10 : 1)] afforded a 98 : 2 mixture of (*E*)- and (*Z*)-1-phenylundec-1-en-3-one **5c** in 73% yield. No evidence for formation of the epoxide **3** (R = C_8H_{17}, R′ = Ph) was observed in this reaction. The results of the Wittig type reaction of aldehydes with the vinyl(phenyl)-λ³-iodanes **1** are summarized in Table 1. The vinyl-λ³-iodanes **1a**–**c** readily undergo Wittig olefinations with aromatic aldehydes containing electron-withdrawing or -donating substituents as well as with aliphatic aldehydes to give α,β-unsaturated ketones **5** with high *trans* selectivity. With α,β-unsaturated aldehydes, selective reaction at the carbonyl group was observed with no evidence for Michael addition yielding cyclopropanes (entries 9 and 16). With the use of the sterically demanding λ³-iodane, β-*tert*-butylvinyliodane **1d**, the Wittig olefination becomes sluggish (entry 17).

Table 1 Wittig olefinations of aldehydes with β-acetoxyvinyl(phenyl)-λ³-iodanes **1**[a]

				Product (yield (%))[b]	
Entry	**1**	R′CHO (R′)	*t*/h	**5**	Ratio[c]
1	**1a**	Ph	24[d]	**5a** (62)	93 : 7
2	**1a**	*n*-C_9H_{19}	48[d]	**5b** (60)	100 : 0
3	**1b**	Ph	24	**5c** (73)	98 : 2
4	**1b**	*p*-$MeOC_6H_4$	24	**5d** (45)	99 : 1
5	**1b**	*p*-MeC_6H_4	24	**5e** (64)	99 : 1
6	**1b**	*p*-ClC_6H_4	24[d]	**5f** (85)	91 : 9
7	**1b**	*p*-$NO_2C_6H_4$	40[d]	**5g** (86)	93 : 7
8	**1b**	*n*-C_9H_{19}	48	**5h** (65)	100 : 0
9	**1b**	*E*-MeCH=CH	42[d]	**5i** (57)	100 : 0
10	**1c**	Ph	24	**5j** (58)	92 : 8
11	**1c**	*p*-MeC_6H_4	24	**5k** (62)	100 : 0
12	**1c**	*p*-$MeOC_6H_4$	24	**5l** (75)	95 : 5
13	**1c**	*p*-ClC_6H_4	24	**5m** (60)	99 : 1
14	**1c**	*p*-$NO_2C_6H_4$	24	**5n** (82)	> 99 : 1
15	**1c**	*n*-C_9H_{19}	24	**5o** (53)	100 : 0
16	**1c**	*E*-MeCH=CH	24	**5p** (48)	100 : 0
17	**1d**	*p*-ClC_6H_4	24	**5q** (10)	99 : 1

[a] Reactions were carried out at 60 °C under N_2. [b] Isolated yields. [c] *Trans* : *cis* ratio. [d] Reactions were carried out at 25 °C under N_2.

As illustrated in Scheme 2, a mechanism for the Wittig olefination of aldehydes upon reaction with (*Z*)-(2-acetoxyalk-1-enyl)-λ³-iodanes **1** in the presence of triethylamine and triphenylphosphine in MeOH might be assumed to involve the following key steps: (i) ester exchange of β-acetoxyvinyl-λ³-iodanes **1** with MeOH under basic conditions generating the monocarbonyl iodonium ylides **2** with the liberation of methyl acetate, (ii) formation of (2-oxoalkyl)-λ³-iodanes **4** *via* protonation of the ylides **2** with the resulting Et_3NHBF_4, (iii) bimolecular nucleophilic substitution of **4** with triphenylphosphine yielding (2-oxoalkyl)phosphonium salts **6**, and (iv) Wittig olefination of aldehydes with β-acylphosphonium ylides **7** produced from **6** by reaction with regenerated triethylamine. This mechanism involves the *in situ* generation and conversion of the monocarbonyl iodonium ylides **2** which undergo Corey type reaction to the monocarbonyl phosphonium ylides **7** which

DOI: 10.1039/b003090m

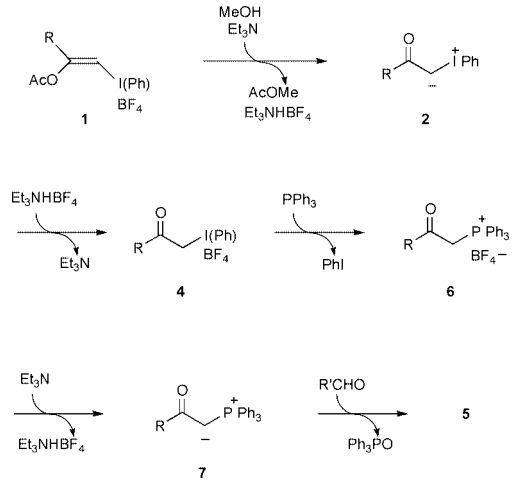

Scheme 2

undergo Wittig olefination. Alternatively, the (2-oxoalkyl)iodanes **4** might be directly produced *via* triethylamine-mediated ester exchange of vinyliodanes **1** with MeOH.

Several experimental observations are in line with this proposed mechanism. Reaction of **1b** with triethylamine (1.1 equiv.) in MeOH (25 °C, 1 h) afforded a mixture of α-methoxy ketone **8** (43%), hydroxy dimethylacetal **9** (35%) and methyl acetate (91%) (Scheme 3). Without triethylamine, **1b** was recovered unchanged in MeOH. High yield formation of methyl acetate clearly indicates the intervention of the ester exchange between β-acetoxyvinyliodane **1b** and MeOH under basic conditions. Bimolecular nucleophilic substitution of (2-oxoalkyl)iodane **4b** with MeOH will produce the α-methoxy ketone **8**. Furthermore, formation of the hydroxy dimethylacetal **9** under basic conditions strongly suggests the intermediacy of the (2-oxoalkyl)iodane **4b** in this reaction (Scheme 3), as reported by Moriarty *et al.*[5] It has been reported that the presence of the λ^3-phenyliodanyl group raises the CH acidity of malonic esters

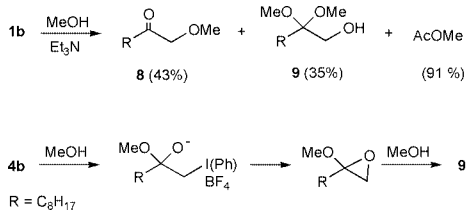

Scheme 3

by eight orders of magnitude.[6] Based on these data, the acidity (pK_a) of α-methylene protons of (2-oxoalkyl)iodanes **4** is estimated to be *ca.* 12. Therefore, it seems reasonable to assume that Et_3NHBF_4 with similar acidity (pK_a = 11.0),[7] undergoes proton transfer to the monocarbonyl iodonium ylides **2** yielding the (2-oxoalkyl)iodanes **4**.

It is possible to isolate the intermediate (2-oxoalkyl)phosphonium salts **6**: treatment of **1b** with triethylamine and triphenylphosphine in MeOH at room temperature, after acidification of the reaction mixture with 5% aqueous HBF_4 solution, afforded the phosphonium tetrafluoroborate **6b** in 89% yield. Without acid treatment, the monocarbonyl phosphonium ylide **7b** was obtained, thereby illustrating the occurrence of transylidation between iodonium and phosphonoim ylides under such conditions. The formation of phosphonium ylides **7** is compatible with the reported acidity of acetonyl(triphenyl)-phosphonium salt **6a** (R = Me, pK_a = 6.6), *i.e.* more acidic than Et_3NHBF_4.[8]

In conclusion, we have developed an efficient one-pot procedure for Wittig olefination of aldehydes with (*Z*)-(2-acetoxyalk-1-enyl)phenyl-λ^3-iodanes **1**. In addition to the reported Corey type alkylidene-transfer reaction of the monocarbonyl iodonium ylides to aldehydes, this new strategy developed here makes vinyl-λ^3-iodanes **1** valuable progenitors in monocarbonyl onium ylide chemistry.

Notes and references

1 (*a*) M. Ochiai, Y. Kitagawa and S. Yamamoto, *J. Am. Chem. Soc.*, 1997, **119**, 11 598; (*b*) M. Ochiai and Y. Kitagawa, *Tetrahedron Lett.*, 1998, **39**, 5569; (*c*) M. Ochiai and Y. Kitagawa, *J. Org. Chem.*, 1999, **64**, 3181.

2 G. F. Koser, in *The Chemistry of Functional Groups, Supplement D*, Wiley, New York, 1983; A. Varvoglis, *The Organic Chemistry of Polycoordinated Iodine*, VCH, New York, 1992; P. J. Stang and V. V. Zhdankin, *Chem. Rev.*, 1996, **96**, 1123.

3 T. Naito, S. Nagase and H. Yamataka, *J. Am. Chem. Soc.*, 1994, **116**, 10 080; Y. Matano, *J. Chem. Soc., Perkin Trans. 1*, 1994, 2703; B. E. Maryanoff and A. B. Reitz, *Chem. Rev.*, 1989, **89**, 863; A. W. Johnson, W. C. Kaska, K. A. O. Starzewski and D. A. Dixon, *Ylides and Imines of Phosphorus*, Wiley, New York, 1993; B. M. Trost and L. S. Melvin, *Sulfur Ylides*, Academic Press, New York, 1975; S. Oae, *Organic Chemistry of Sulfur*, Plenum, New York, 1977.

4 T. Okuyama, T. Takino, T. Sueda and M. Ochiai, *J. Am. Chem. Soc.*, 1995, **117**, 3360.

5 R. M. Moriarty, H. Hu and S. C. Gupta, *Tetrahedron Lett.*, 1981, **22**, 1283; R. M. Moriarty and O. Prakash, *Acc. Chem. Res.*, 1986, **19**, 244.

6 O. Y. Neiland and B. Y. Karele, *Zh. Org. Khim.*, 1971, **7**, 1611.

7 D. R. Lide, *CRC Handbook of Chemistry and Physics*, CRC, Boca Raton, FL, 1992.

8 S. Fliszar, R. F. Hudson and G. Salvadori, *Helv. Chim. Acta*, 1963, **46**, 1580; A. W. Johnson and R. T. Amel, *Can. J. Chem.*, 1968, **46**, 461.

Synthesis of highly ordered mesoporous silica materials using sodium silicate and amphiphilic block copolymers

Ji Man Kim and Galen D. Stucky*

Department of Chemistry, University of California at Santa Barbara, Santa Barbara, CA 93106, USA. E-mail: stucky@chem.ucsb.edu

Received (in Columbia, MO, USA) 22nd March 2000, Accepted 17th May 2000

A commercially important synthetic approach to highly ordered mesoporous silica materials (SBA-family) with 2-D hexagonal (*P6mm*), 3-D hexagonal (*P6*$_3$*/mmc*) and cubic (*Im3m* and *Pm3m*) structures, using sodium silicate as the silica source and amphiphilic block copolymers as the structure-directing agents is demonstrated.

It is well known that mesoporous silica materials are synthesised by synergistic self-assembly between surfactant and silica species to form mesoscopically ordered composites.[1,2] Generally, two types of surfactants are used for the formation of mesoporous silica materials: ionic surfactants such as alkyltrimethylammonium bromide[1,3] and nonionic surfactants such as alkylamine[4] and poly(ethylene oxide)-type copolymers.[5–7] The ionic surfactants interact electrostatically with inorganic species, whereas the nonionic surfactants result in the formation of mesocomposites through hydrogen bond or van der Waals interaction. The nonionic surfactants give commercially important advantages compared with the ionic surfactants. They are easily removable, nontoxic, biodegradable and relatively inexpensive. Pinnavaia and coworkers[6] have reported the synthesis of MSU-*X* mesoporous materials with several nonionic surfactants. These materials are composed of worm-like channels, which are disorderedly arrayed. Stucky and coworkers[7] have reported the synthesis of SBA mesoporous silica materials, which have well-ordered channel and cage structures, using amphiphilic di- and triblock copolymers as the structure directing agents at or below the isoelectric point (pH $\leqslant$ 3). However, these synthetic procedures using nonionic surfactants are not as commercially viable as they might be due to the use of tetraethyl orthosilicate (TEOS) as a silica source. Recently, Guth and coworkers[8] have pointed this out and reported the synthesis of mesoporous silica material using nonionic surfactant and sodium silicate in the pH range 3–10.5. However, the mesoporous materials thus obtained exhibit irregular or disordered channel connectivity and broad pore size distributions.

Here, we report the synthesis of highly ordered mesoporous silica materials that include 2-dimensional (2-D) hexagonal SBA-15 (*P6mm*), 3-dimensional (3-D) hexagonal SBA-12 (*P6*$_3$*/mmc*) and cubic SBA-16 and SBA-11 (*Im3m* and *Pm3m*) using sodium metasilicate as the silica source and nonionic amphiphilic block copolymers as the structure-directing agents.

Triblock copolymers such as Pluronic P123 ($EO_{20}PO_{70}EO_{20}$, M_{av} = 5800) and Pluronic P85 ($EO_{26}PO_{39}EO_{26}$, M_{av} = 4600) and diblock copolymer, $C_nH_{2n+1}(OCH_2CH_2)_xOH$ (C_nEO_x, n = 12–18, x = 9–23), were used as received from BASF, Aldrich and Sigma. Sodium metasilicate ($Na_2SiO_3{\cdot}9H_2O$) and concentrated hydrochloric acid (c-HCl, 37.6%) were obtained from Fisher Scientific. In a typical synthesis batch, 3.0 g of $C_{18}EO_{10}$ was dissolved in 57.4 g of distilled water and then 8.8 g of sodium metasilicate was added at room temperature with magnetic stirring, giving a clear solution. To this reaction mixture, 17.7 g of c-HCl was quickly added with vigorous magnetic stirring. The resulting gel mixture was stirred for 1 day at room temperature and subsequently heated for 1 day at 373 K in an oven to increase the degree of silanol group condensation. In the case of Pluronic triblock polymers, the reaction temperature was 313 K before heating to 373 K. The solid product was filtered off and dried at 373 K. The product was then slurried in ethanol–HCl mixture, filtered off, washed with ethanol, dried in an oven, and calcined in air under static conditions at 823 K. The product yield in a typical synthesis batch was above 90% on the basis of the silica recovery.

Fig. 1a–c show powder X-ray diffraction (XRD) patterns for SBA-15 materials, obtained from $C_{12}EO_9$, $EO_{26}PO_{39}EO_{26}$ and $EO_{20}PO_{70}EO_{20}$, after calcination. All exhibit XRD patterns with a very intense diffraction peak and two or more weak peaks, which are characteristic of a 2-D hexagonal (*P6mm*) structure.[1,5,7] The SBA-15 obtained from $EO_{20}PO_{70}EO_{20}$ shows (210) and (300) peaks, which indicates excellent textural uniformity of the material. There were no significant changes upon calcination, except for the expected increase in XRD peak intensity and lattice contraction (7–12%). Fig. 2a is a transmission electron microscopic (TEM) image for SBA-15 (Fig. 1c). The TEM image also indicates that the material has a highly ordered 2-D hexagonal structure, similar to that of SBA-15 obtained from TEOS.[7] Other 2-D hexagonal silica materials in Fig. 1a and b give similar TEM images except for their different channel sizes. The N_2 adsorption–desorption isotherms and pore size distribution curves for the present SBA-15 materials are essentially the same as those of SBA-3 and SBA-15.[3,7] Lattice parameters and pore sizes are listed in Table 1.

Fig. 1d and e show XRD patterns for the mesoporous silica materials obtained from $C_{12}EO_{23}$ and $C_{16}EO_{20}$, respectively. The XRD patterns can be indexed as cubic *Im3m* for Fig. 1d and cubic *Pm3m* for Fig. 1e.[7] It is interesting and important that cubic *Im3m* mesoporous silica (SBA-16) can be obtained using

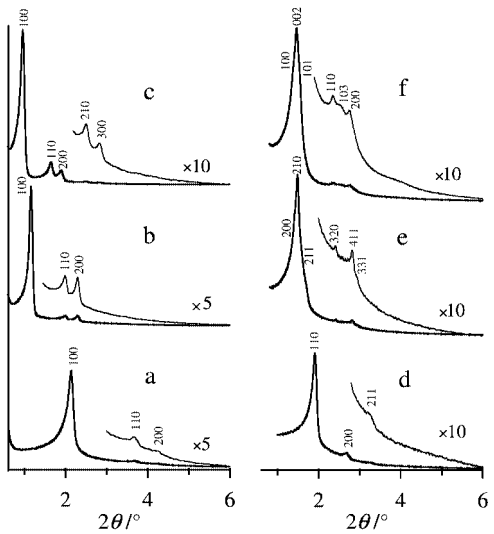

Fig. 1 XRD patterns for the mesoporous silicas obtained from (a) $C_{12}EO_9$, (b) $EO_{26}PO_{39}EO_{26}$, (c) $EO_{20}PO_{70}EO_{20}$, (d) $C_{12}EO_{23}$, (e) $C_{16}EO_{20}$ and (f) $C_{18}EO_{10}$. XRD patterns were collected with a Cu-Kα X-ray source using a Sintag X_2 instrument.

DOI: 10.1039/b002362k

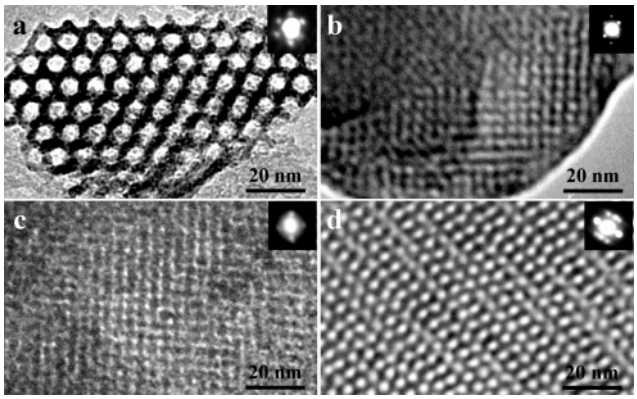

Fig. 2 TEM images and ED patterns for the calcined mesoporous silicas obtained from (a) $EO_{20}PO_{70}EO_{20}$, (b) $C_{12}EO_{23}$, (c) $C_{16}EO_{20}$ and (d) $C_{18}EO_{10}$. The TEM image was taken with a 2000 FX JEOL instrument operating at 200 kV.

Table 1 Lattice parameter, pore diameter and BET surface area of mesoporous silicas

Polymer	Mesophase	Cell parameter/nm[a]	Pore size nm[b]	Surface area/m^2 g^{-1}
$C_{12}EO_9$	2-D hexagonal	4.79	3.8	1055
$C_{12}EO_{23}$	cubic *Im*3*m*	6.70	3.5, 4.3[c]	701
$C_{16}EO_{20}$	cubic *Pm*3*m*	13.25	4.2, 5.0[c]	637
$C_{18}EO_{10}$	3-D hexagonal	7.43, 12.02[d]	4.5, 5.4[c]	572
$EO_{26}PO_{39}EO_{26}$	2-D hexagonal	8.83	5.6	849
$EO_{20}PO_{70}EO_{20}$	2-D hexagonal	10.68	7.6	600

[a] Lattice parameters calculated from *d* spacings in XRD patterns. [b] Pore size distribution obtained from N_2 adsorption–desorption isotherms following the BdB analysis with cylindrical and spherical models.[9,10] [c] Numbers denote pore opening size and largest diameter in spherical cage structure, respectively. [d] Numbers represent lattice parameters *a* and *c*, respectively.

the $C_{12}EO_{23}$ diblock copolymer as well as with the triblock copolymer $EO_{106}PO_{70}EO_{106}$ (Pluronic F127).[7] TEM images for the cubic materials are shown in Fig. 2b and c. The images show well-ordered structures viewed along the [001] direction, suggesting that both mesoporous silica materials have highly ordered cubic structures.

Fig. 1f and Fig. 2d are the XRD pattern and TEM image, respectively, for the mesoporous silica obtained from $C_{18}EO_{10}$. The XRD pattern can be indexed as a 3-D hexagonal ($P6_3/mmc$) structure with cell parameters a = 7.43, 12.03 nm. The cell parameter ratio (c/a) is 1.62, which is very similar to ideal ratio (1.633) for a typical hexagonal close-packed (hcp) phase and those of SBA-12[7] and SBA-2.[3] Fig. 3 shows N_2 adsorption–desorption isotherms and pore size distribution curves for the 3-D hexagonal material. The N_2 isotherm is of type IV with a H2 hysteresis loop, which indicates this material has bottle shaped pores similar to those of SBA-2.[3]

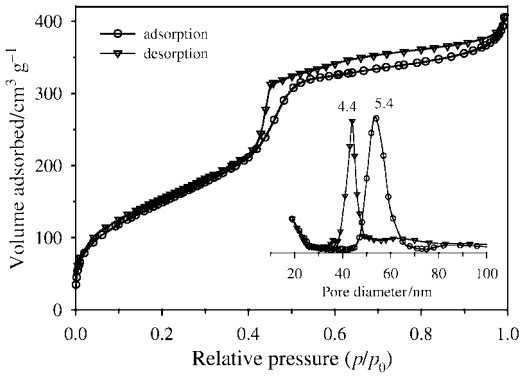

Fig. 3 N_2 adsorption–desorption isotherms for the mesoporous silica material obtained from $C_{18}EO_{10}$ and the corresponding pore size distribution curves. N_2 adsorption isotherms were obtained at liquid N_2 temperature using a Micromeritics ASAP 2000 instrument and pore size distributions were calculated by the BdB (Broekhoff and de Boer) method[9,10] with a spherical model.

In conclusion, we have developed a new synthetic method for highly ordered mesoporous silicas using sodium metasilicate as the silica source and amphiphilic block copolymers as the structure-directing agents. The replacement of TEOS by sodium metasilicate leads to the low cost production of mesoporous silica materials for practical applications. In addition, other substituents such as aluminium, titanium, *etc.* can be incorporated into the silica framework of the present SBA materials for applications such as catalysis and ion exchange.

This work is supported by the National Science Foundation and the Army Research Office.

Notes and references

1 Q. Hou, D. I. Margolese, U. Ciesla, P. Feng, T. E. Gier, P. Sieger, R. Leon, P. M. Petroff, F. Schüth and G. D. Stucky, *Nature*, 1994, **368**, 317.
2 A. Firouzi, D. Kumar, L. M. Bull, T. Besier, P. Sieger, Q. Hou, S. A. Walker, J. A. Zasadzinski, C. Glinka, J. Nicol, D. Margolese, G. D. Stucky and B. F. Chmelka, *Science*, 1995, **267**, 1138.
3 Q. Huo, R. Leon, P. M. Petroff and G. D. Stucky, *Science*, 1995, **268**, 1324.
4 P. T. Tanev, M. Chlbwe and T. J. Pinnavaia, *Nature*, 1994, **368**, 321; P. T. Tanev and T. J. Pinnavaia, *Science*, 1995, **267**, 865.
5 G. Attard, J. C. Glyde and C. G. Göltner, *Nature*, 1995, **378**, 366.
6 S. A. Bagshaw, E. Prouzet and T. J. Pinnavaia, *Science*, 1995, **269**, 1242.
7 D. Zhao, J. Feng, Q. Huo, N. Melosh, G. H. Fredrickson, B. F. Chmelka and G. D. Stucky, *Science*, 1998, **279**, 548; D. Zhao, Q. Hou, J. Feng, B. F. Chmelka and G. D. Stucky, *J. Am. Chem. Soc.*, 1998, **120**, 6024.
8 L. Sierra, B. Lopez, H. Gil and J.-L. Guth, *Adv. Mater.*, 1999, **11**, 307; L. Sierra and J.-L. Guth, *Microporous Mesoporous Mater.*, 1999, **27**, 243.
9 J. C. P. Broekhoff and J. H. de Boer, *J. Catal.*, 1967, **9**, 8.
10 W. W. Lukens, P. Schmidt-Winkel, D. Zhao and G. D. Stucky, *Langmuir*, 1999, **15**, 5403.

ChemComm

A predictive computational study of $AlPO_4$-14: crystal structure and framework stability of the template-free $AlPO_4$-14 from its as-synthesised templated form

Stéphanie Girard,[a] Caroline Mellot Draznieks,*[a] Julian D. Gale[b] and Gérard Férey[a]

[a] *Institut Lavoisier, UMR CNRS 8637, Université de Versailles St-Quentin, 45 avenue des Etats-Unis, Versailles Cedex, 78035 France. E-mail: mellot@chimie.uvsq.fr*

[b] *Department of Chemistry, Imperial College of Science Technology and Medicine, South Kensington, UK SW7 2AY*

Received (in Oxford, UK) 25th April 2000, Accepted 25th May 2000

The crystal structure of $AlPO_4$-14 in its calcined form was predicted using lattice energy minimisation and an initial model derived from its as-synthesised templated form, highlighting the possibility of using computational approaches for exploring thermodynamic stabilities of as-synthesised open-framework structures upon template extraction.

The evergrowing field of open-framework inorganic materials is in part related to the extensive development of synthetic routes involving organic amines.[1] The template molecules or structure-directing agents are incorporated in the final structure, acting as compensating charges or allowing the production of micropores with tailored size and shape. In a number of cases, for example aluminophosphates (AlPOs), the non-framework species may be removed, leaving behind an open-framework structure with potential adsorption or catalytic properties. However, the removal of the template is often a critical step and the production of the related stable open-framework compound cannot be easily anticipated.

In the recent years, computational tools have played a key role in the study of the structure and energetics of open-framework materials,[2] with the widespread use of energy minimisation techniques. For example, in the field of zeolites, energy minimisations have made it possible to locate extra-framework cations,[3] elucidate the adsorption sites of sorbate molecules[4] and to solve structures.[5] Also, the relative thermodynamic framework stabilities of various inorganic systems, such as silica polymorphs[6] and aluminophosphates,[7] have been successfully studied using appropriate forcefields.

Here we present an attempt to use energy minimisation to anticipate the calcined crystal structure of an as-synthesised aluminophosphate structure. Our main interest is to predict the stability and the crystal structure of the inorganic framework in the absence of the structure directing agent or template, starting from the knowledge of the as-synthesised structure only. We describe illustrative results for the $AlPO_4$-14 system, for which validating experimental structural data are available, both for the as-synthesised and calcined forms, from a synchrotron powder X-ray diffraction study.[8]

Diffraction results[8] show that the as-synthesised $AlPO_4$-14 structure comprises alternating Al and P atoms, linked by bridging oxygen atoms, with P atoms in a tetrahedral environment and the Al atoms possessing various coordinations (IV, V and VI) as a consequence of the extra-framework species becoming bonded. While two of the four inequivalent Al atoms are in tetrahedral coordination, one is in fivefold coordination and the other in octahedral coordination. The arrangement of AlO_x and PO_4 polyhedra constructs a three-dimensional 8-ring channel system in the *a* and *b* directions. The structure also contains hydroxy groups and non-framework species, *i.e.* protonated isopropylamine templating agents and water molecules. Each hydroxy group bridges three Al atoms: a five coordinate one and two six coordinate aluminium atoms. The isopropylamine template is protonated and balances the charge on the hydroxy group. Fig. 1 shows the above features in a selected view of the as-synthesised $AlPO_4$-14. The calcination of $AlPO_4$-14 leads to a zeotype open-framework structure where all Al and P atoms are in tetrahedral coordination, that retains the three-dimensional 8-ring channel system.

Our calculations were carried out using the lattice energy minimisation code GULP.[9] The interatomic potentials used were those developed by Gale and Henson using an empirical fit to the crystal structure plus elastic and dielectric properties of berlinite.[10] This formal charge shell model forcefield has been shown to reproduce the experimentally determined structures of aluminophosphates with good accuracy and to yield estimates of their relative framework stabilities that are consistent with thermodynamic data.[7]

The experimental crystal structure of the as-synthesised $AlPO_4$-14, $Al_8P_8O_{32}(OH)_2(C_3H_{10}N)_2(H_2O)_2$, proposed by Wilson *et al.*[8] was taken as a starting point for our calculations. This structure was then modified prior to energy minimisation as follows: atoms that are presumed to evacuate upon calcination, *i.e.* bridging hydroxy groups, isopropylamine templates and water molecules, were removed, leaving behind a neutral open-framework structure, namely, $Al_8P_8O_{32}$. This results in a structure where all four inequivalent Al atoms are in tetrahedral coordination, retaining two Al atoms in highly distorted environments (with O–Al–O angles ranging from 90 to 167°) that emanate from the two six-fold and five-fold coordinated Al atoms of the as-synthesised structure (see Fig. 2). In a final step, the modified structure was submitted to a constant pressure (*i.e.* allowing both cell parameters and fractional coordinates to relax) minimisation in space group *P*-1 since this was the space group of the as-synthesised structure.

In Fig. 3(*a*), we show the calcined structure of $AlPO_4$-14 as predicted by our energy minimisation. Clearly, the agreement with the observed calcined structure [Fig. 3(*b*)] proposed by Wilson *et al.*[8] is very good. In Table 1, we show a comparison

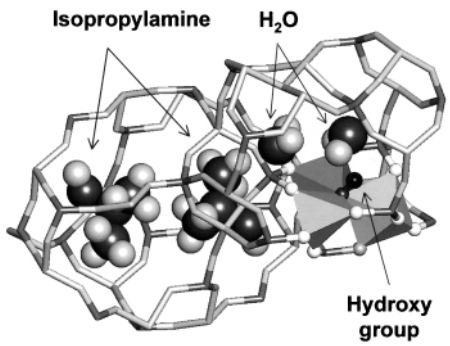

Fig. 1 Partial view of the as-synthesised $AlPO_4$-14 structure, $Al_8P_8O_{32}(OH)_2(C_3H_{10}N)_2(H_2O)_2$ from crystal data in ref. 7. Water molecules and organic template molecules are trapped in adjacent cages. A selection of three Al atoms with bipyramidal and sixfold coordination is represented with solid polyhedra, where the bridging hydroxy group participates in the coordination of all three Al atoms.

DOI: 10.1039/b003344h

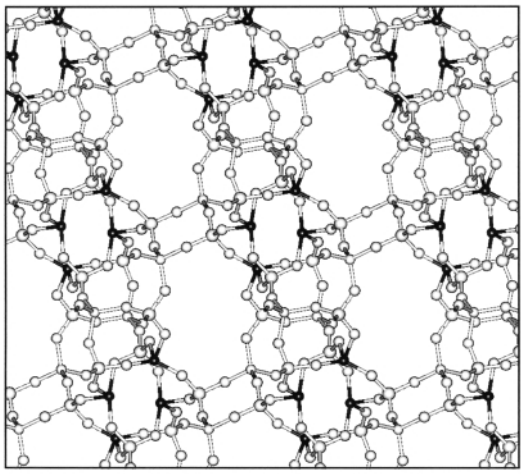

Fig. 2 Initial model for calcined $AlPO_4$-14, $Al_8P_8O_{32}$, used in our calculations and constructed from its as-synthesised form, removing the templating agent, water molecules and bridging hydroxy groups. The so-modified structure is left with Al atoms in highly distorded tetrahedral environment (shown in black).

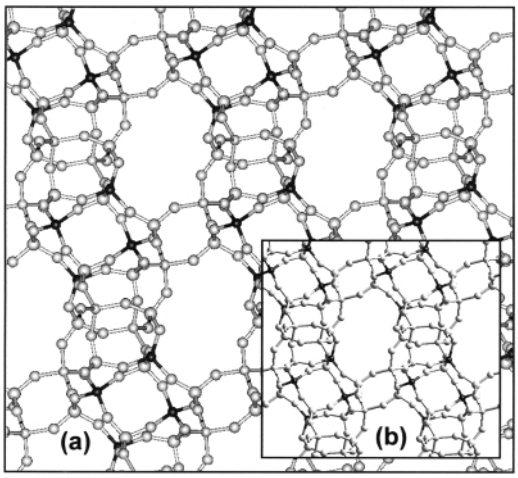

Fig. 3 (*a*) Predicted structure for calcined $AlPO_4$-14 from energy minimisation of the initial model, $Al_8P_8O_{32}$. (*b*) Observed structure of calcined $AlPO_4$-14 proposed by Wilson *et al*.[8]

Table 1 Cell dimensions of the observed and predicted $AlPO_4$-14 structure in its calcined form

	Observed structure of calcined $AlPO_4$-14 from diffraction[8]	Predicted structure of calcined $AlPO_4$-14 from its as-synthesised form[a]
Cell dimensions (*P*-1)		
a/Å	9.704	9.674
b/Å	9.736	9.751
c/Å	10.202	10.269
α/°	77.81	77.46
β/°	77.50	76.50
γ/°	87.69	87.14

[a] This work

of our calculated lattice parameters for the predicted calcined $AlPO_4$-14 with those of the observed structure. Interestingly, our initial model of calcined $AlPO_4$-14, with an initial lattice energy of 12374.8 kJ mol^{-1} per tetrahedral unit, converged rapidly towards the structure where all Al atoms are in regular tetrahedral environment, with a final lattice energy of 12924.9 kJ mol^{-1} per tetrahedral unit. This makes the structure of $AlPO_4$-14 11.7 kJ mol^{-1} less stable than α-berlinite per T site. For comparison, the work of Henson *et al.*[7] demonstrates that the most pure aluminophosphates are between 4 and 13 kJ mol^{-1} less stable than the thermodynamically favoured polymorph under ambient conditions, making $AlPO_4$-14 a relatively unstable structure. Our energy minimisation predicts the observed calcined structure of $AlPO_4$-14 remarkably well, especially as the initial model had large distorsions arising from the deletion of ligand atoms in the coordination spheres of the Al atoms from the as-synthesised form. Also, we checked that minimisations from both points, the initial model of calcined $AlPO_4$-14 or the observed calcined structure, lead to the same structure.

Another important use of potentials is that they can test space groups for possible lower symmetry distortions, as found for other AlPOs.[7] The phonon spectrum at the Γ point of the calcined structure of $AlPO_4$-14 was calculated to check the space group as *P*-1. The structure was found to be phonon stable in this space group verifying that the symmetry is at least *P*-1.

In summary, energy minimisation allows us to estimate the thermodynamic stability of calcined $AlPO_4$-14 and to predict its crystal structure, starting with the knowledge of the as-synthesised structure and anticipating the species removed during the calcination process. The further viability of this approach has been recently demonstrated through the prediction of the calcined form of a newly synthesised templated aluminophosphate, where atomic coordinates of the calcined form, which has a structure different from the as-synthesised form, were obtained from the simulation, allowing their direct use for future powder diffraction refinement.[11]

We are grateful to Dr T. Loiseau and C. Sassoye for helpful discussions.

Notes and references

1 A. K. Cheetham, G. Férey and T. Loiseau, *Angew. Chem., Int. Ed.*, 1999, **38**, 3268.
2 *New Methods for Modelling Processes within Solids and at their Surfaces*, ed. C. R. A. Catlow, Oxford University Press, London, 1993; *Computer Modelling in Inorganic Crystallography*, ed. C. R. A. Catlow, Academic Press, London, 1997.
3 J. M. Newsam, C. M. Freeman, A. M. Gorman and B. Vessal, *Chem. Commun.*, 1996, 1945; G. Vitale, C. F. Mellot, L. M. Bull and A. K. Cheetham, *J. Phys. Chem. B*, 1997, **101**, 4559.
4 C. F. Mellot, A. Davidson and A. K. Cheetham, *J. Phys. Chem. B*, 1998, **102**, 2530.
5 B. J. Campbell, G. Bellussi, L. Carluccio, G. Perego and A. K. Cheetham, *Chem. Commun.*, 1998, 1725.
6 M. J. Sanders, M. Leslie and C. R. A. Catlow, *J. Chem. Soc., Chem. Commun.*, 1984, 1271; J. D. Gale, *J. Phys. Chem. B*, 1998, **102**, 5423; N. H. Henson, A. K. Cheetham and J. D. Gale, *Chem. Mater.*, 1994, **6**, 1647.
7 N. H. Henson, A. K. Cheetham and J. D. Gale, *Chem. Mater.*, 1996, **8**, 664.
8 R. W. Broach, S. T. Wilson, R. M. Kirchner, MRS Series, *Proceeding of the 12th International Zeolite Conference*, ed. M. M. J. Treacy, B. K. Marcus, M. E. Bisher and J. B. Higgins, 1999.
9 J. D. Gale, *J. Chem. Soc., Faraday Trans.*, 1997, **93**, 629.
10 J. D. Gale and N. J. Henson, *J. Chem. Soc., Faraday Trans.*, 1994, **90**, 3175.
11 C. Sassoye, S. Girard, C. Mellot Draznieks, F. Taulelle, T. Loiseau and G. Férey, manuscript in preparation.

ChemComm

First synthesis and characterization of vinylselenols and vinyltellurols

Jean-Claude Guillemin,* Asmae Bouayad and Dange Vijaykumar

Laboratoire de Synthèse et Activation de Biomolécules, UMR CNRS 6052, ENSCR, Avenue du Général Leclerc, 35700 Rennes, France. E-mail: jean.claude.guillemin@ensc-rennes.fr

Received (in Liverpool, UK) 11th April 2000, Accepted 24th May 2000

Vinylselenols and vinyltellurols have been prepared by slow addition of tributyltin hydride to the corresponding divinyldiselenide or divinylditelluride in tetraglyme.

Several α,β-unsaturated heterocompounds bearing one or several hydrogen atom(s) on the heteroatom exhibit interesting properties. For instance, base-induced keto–enol or imine–enamine tautomerism is a consequence of the high acidity of the hydrogen linked to the heteroatom.[1] Recently, evidence for a similar increase of acidity between saturated and α,β-unsaturated phosphines and arsines was provided by FT-ICR mass spectrometry and theoretical calculations.[2] From a synthetic viewpoint, the rearrangement of such α,β-unsaturated compounds provides an efficient method for the preparation or the chemical trapping of the corresponding carbon–heteroatom multiple bond derivatives.[3] Although primary α,β-unsaturated derivatives of mercury, silicon, germanium, tin, nitrogen, phosphorus, arsenic, antimony, oxygen and sulfur have been reported,[4] no primary α,β-unsaturated selenol or tellurol derivatives have been isolated so far.[5] Such compounds, which are probably unstable in a variety of experimental conditions, cannot be easily prepared by conventional approaches used for other heterocompounds.

Flash vacuum pyrolysis is an efficient technique to prepare derivatives of the elements of the first and second rows of the periodic table and vinylthiols have also been prepared by this method.[6] However, with the elements of subsequent rows, the energy of the carbon–heteroatom bond is often too low to withstand high temperatures. The preparation of thiols, selenols or tellurols *via* LAH or other reducing agents such as borohydrides requires an acidolysis of the resulting salt to isolate the free product.[7] Although quite stable compounds such as vinylthiols have been prepared in this manner,[8] such approaches are not viable for sensitive α,β-unsaturated derivatives of selenols and tellurols.

Since 1994, we have been involved in the synthesis of primary low boiling α,β- or β,γ-unsaturated phosphines, arsines, stibines, stannanes and mercury hydrides.[3,9–12] We have developed an efficient procedure for the preparation of these compounds using vacuum line techniques, *via* the reduction of the corresponding halo derivatives with excess tributyltin hydride. This approach cannot be used to prepare SH, SeH or TeH derivatives because these products would quickly react with the tin hydride to form the corresponding S–Sn, Se–Sn or Te–Sn derivatives. However, Crich *et al.* have recently shown that a selenol (PhSeH) can be detected for a short time by addition of Bu_3SnH to a solution of diphenyldiselenide.[13] By combining this approach with the experimental technique developed in our laboratory, we looked into the preparation of kinetically unstable selenols and tellurols. We now report here, the synthesis of low boiling vinylselenols and tellurols starting from the corresponding divinyldiselenides or ditellurides.

The synthesis of divinylditellurides has been reported by Dabdoub and Comasseto.[14] The arial oxidation of the product formed by insertion of tellurium in vinyl Grignard reagents led to compounds **1a**–**c** (Scheme 1). Starting from a mixture of *Z*- and *E*-isomers of 1-bromopropene, only the *Z*-dipropenylditelluride **1b** was obtained. The simple divinyldiselenides have never been reported before. We prepared the divinyldiselenides

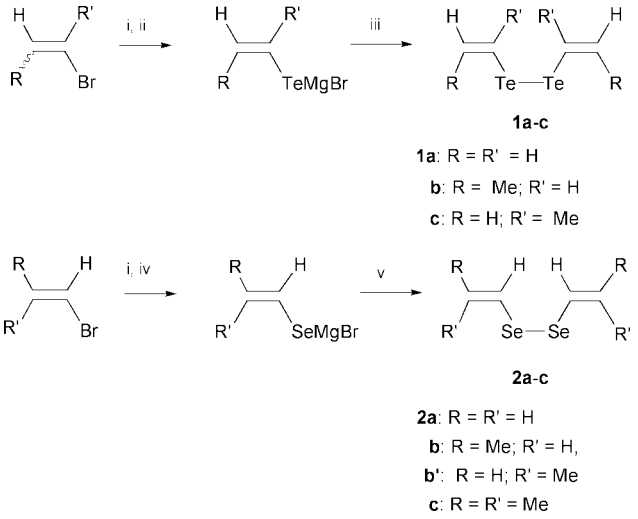

Scheme 1 *Reagents and conditions*: i, Mg; ii, Te, reflux, 30 min; iii, air; iv, Se, room temp.; v, Br_2, −20 °C.

2a–**c** starting from selenium and vinyl Grignard reagents using dibromine as the oxidizing reagent (yields: 52–73%). Compounds **2a**–**c** have been unambiguously characterized by ^1H, ^{13}C, ^{77}Se NMR and high resolution mass spectrometry (HRMS). The ^{77}Se NMR signals were observed between δ 236 (**1c**) and δ 407 (**1b′**).[15]

The vinylselenols **3a**–**c** and vinyltellurols **4a**–**c** were prepared by slow addition of 1.5 equiv. of Bu_3SnH to a solution of **2a**–**c** or **1a**–**c**, respectively, in tetraglyme (Scheme 2).† The products were continuously distilled *in vacuo* from the reaction mixture and condensed in a cold trap. They were thus isolated before their reaction with the tin hydride. Vinylselenols **3a**–**c** were obtained in good yields (73–83%) but only moderate yields

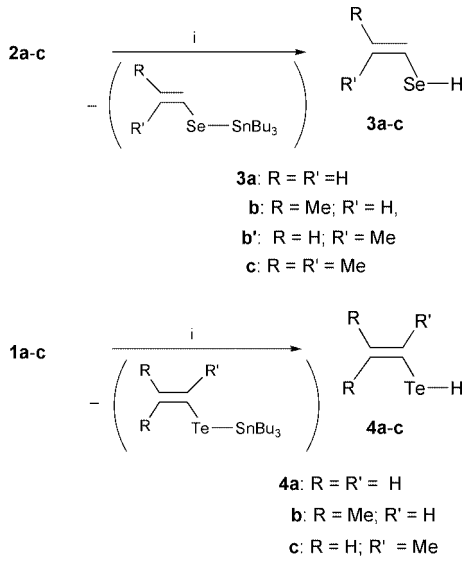

Scheme 2 *Reagents*: i, Bu^n_3SnH.

DOI: 10.1039/b002886j

Table 1 Yield and selected NMR data for the ethyl and ethenyl selenium and tellurium derivatives

	Yield[a]	δ_H			δ_C		
	(%) (lit.)	X-H	XCH	$^1J_{X-H}$	$\delta_{C\alpha}$	$\delta_{C\beta}$	δ_X
EtSH	96	1.39	2.53	-	19.5	18.9	-
EtSeH	89 (86)[b]	-0.56	2.62	47.5	12.1	20.1	29[c]
EtTeH	83 ()[d,e]	-4.68	2.65	45.7	-9.7	21.1	-44.7
	(50-70)[f]	-	6.25	-	131.4	114.4	-
	87 (≈60)[g]	2.97	6.30	-	123.9	115.7	-
	63 (crude)	-	6.69	-	119.7	124.9	388.8
	73	1.06	6.61	59.8	118.4	120.5	113.6
	(67)[h]	-	7.13	-	101.8	131.3	282.9
	32	-2.97	6.93	25.6	100.0	130.5	70.4

[a] This work. [b] Ref. 16. [c] Ref. 15. [d] Yield not given, ref. 17. [e] Ref. 18. [f] Ref. 19. [g] Ref. 8. [h] Ref. 14.

(32–43%) were observed for the more reactive tellurols **4a**–**c**.‡

All compounds **3a**–**c**, **4a**–**c** were unambiguously characterized by ^{1}H, ^{13}C, ^{77}Se or ^{125}Te NMR spectroscopy and HRMS.§ In the ^{1}H NMR spectrum, the presence of an unsaturated group on a heteroatom usually leads to a downfield shift of the signals of hydrogen(s) attached to the heteroatom and an increase in the coupling constants.[9,11] In the ^{1}H NMR spectra of selenols **3a**–**c**, the signal of the hydrogen on the selenium atom was observed *ca*. 1.5 ppm downfield to that of the saturated derivative (Table 1). A similar downfield effect was observed for the tellurols. The $^1J_{SeH}$ and $^1J_{SeC}$ coupling constants of the unsaturated compounds **3a**–**c** are higher than those of the saturated compounds [$^1J_{SeC}$ (**3a**): 93.2 Hz, $^1J_{SeC}$ (EtSeH): 45.0 Hz]. This can be attributed to an increase of the s character of the Se–H and Se–C bonds. Although a similar increase was observed for the $^1J_{TeC}$ coupling constant of tellurols [$^1J_{TeC}$ (**4a**): 247.3 Hz, $^1J_{TeC}$ (EtTeH): 114.9 Hz], an opposite effect was observed for the $^1J_{TeH}$ coupling constants. To the best of our knowledge although a upfield signal has been observed for the proton on the mercury atom of the vinyl derivative,[12] such a decrease of a $^1J_{XH}$ coupling constant for a vinylic derivative has never been reported.

Vinylselenols and vinyltellurols exhibit a low stability at room temperature: the half-life of selenols **3a**–**c** diluted in $CDCl_3$ is *ca*. one day and *ca*. 60 min for the tellurols **4a**–**c**. Only insoluble black decomposition products were observed after a few days.

In conclusion, we have successfully prepared vinylselenols and tellurols by reaction of Bu_3SnH with the corresponding diselenide or ditelluride derivatives. By reaction with a hydride (Bu^n_3SnH), compounds bearing an acidic hydrogen (RSH, RSeH, RTeH) were prepared *via* a radical reaction thus providing a new route which is an alternative to the hydrolytic method. Further investigation into the synthesis of other unsaturated selenols and tellurols, and spectroscopic studies are currently under progress in our lab.

We thank the PNP (INSU-CNRS) and the CNES for financial support and Dr M. Davies for helpful suggestions in writing the paper.

Notes and references

† *Typical experimental procedure*: (**CAUTION:** *Selenols and tellurols are potentially highly toxic compounds and must be used with great care under a well-ventilated hood*). The apparatus already described for the reduction of dichlorostibines was used.[10] The flask containing the precursor [2 mmol of **1a**–**c** or **2a**–**c** diluted in tetraglyme (5 mL)] was fitted on a vacuum line and degassed. Bu^n_3SnH (3 mmol) was then slowly added (30 min) at room temperature with a syringe through the septum. During and after the addition, vinylselenols **3a**–**c** or tellurols **4a**–**c** was distilled off *in vacuo* (10^{-1} mbar) from the reaction mixture. A cold trap (−60 °C) removed selectively the less volatile products and compounds **3a**–**c**, **4a**–**c** were condensed on a cold finger (−196 °C) connected at the bottom to a flask or an NMR tube. A co-solvent can be added at this step. After disconnecting from the vacuum line by stopcocks, the apparatus was filled with dry nitrogen; liquid nitrogen was subsequently removed. The product was collected in a Schlenk flask or a NMR tube and kept at low temperature (< −50 °C) before analysis.

‡ Under these experimental conditions, we have also prepared alkylthiols (EtSH, yield: 96%), vinylthiols (MeCH=CHSH, yield: 91%), arylthiols (PhSH, yield: 77%), alkylselenols (EtSeH, yield: 89%) and alkyltellurols (EtTeH, yield: 83%). The reaction with EtSeSEt led to ethanethiol (yield: 92%) and traces of EtSeH suggesting that the ethylseleno group acts as a protecting group for the thiol.

§ *Selected data:* **3b,b′**: bp (0.1 Torr) ≈ −70 °C. Yield: 83%. $\tau_{1/2}$ (5% in $CDCl_3$) ≈ 25 h. (*E*)-**3b**: δ_H(400 MHz, $CDCl_3$, −40 °C) 0.78 [d, 1H, *J* 5.3, $^1J_{SeH}$ 60.7 Hz (d), SeH], 1.72 (d, 3H, *J* 6.4 Hz, CH_3), 5.98 (dq, 1H, *J* 15.3, 6.4 Hz, CH), 6.10 (m, 1H, CH). δ_C(100 MHz, $CDCl_3$, −40 °C) 20.2, 107.4, 133.7. δ_{Se}(57.2 MHz, $CDCl_3$, −40 °C) 31.0. (*Z*)-**3b′**. δ_H(400 MHz, $CDCl_3$, −40 °C) 0.69 (d, 1H, *J* 6.9 Hz, SeH), 1.67 (d, 3H, *J* 6.6 Hz, CH_3); 6.04 (dq, 1H, *J* 8.7, 6.6 Hz, CH), 6.31 (dd, 1H, *J* 8.7, 6.9 Hz, CH). δ_C(100 MHz, $CDCl_3$, −40 °C) 16.0, 110.6, 128.4. δ_{Se} (57.2 MHz, $CDCl_3$, −40 °C) 75.4. HRMS: calc. for ($C_3H_6{}^{80}Se\cdot$)$^+$ (*Z* + *E*): *m*/*z* 121.9634; found: 121.963. **3c**: bp (0.1 Torr) ≈ −60 °C. Yield: 77%. $\tau_{1/2}$ (5% in $CDCl_3$) ≈ 20 h. δ_H(400 MHz, $CDCl_3$, −40 °C) 0.61 [d, 1H, *J* 5.9, $^1J_{SeH}$ 60.5 Hz (d), SeH]; 1.72 (s, 3H, CH_3), 1.80 (s, 3H, CH_3), 5.95 (d, 1H, *J* 5.9 Hz, CH). δ_C(100 MHz, $CDCl_3$, −40 °C) 20.9, 26.0, 101.8, 138.3. δ_{Se}(57.2 MHz, $CDCl_3$, −40 °C) 26.0. HRMS calc. for ($C_4H_8{}^{80}Se\cdot$)$^+$: *m*/*z* 135.9791; found: 135.979. **4b**: bp (0.1 Torr) ≈ −50 °C. Yield: 43%. $\tau_{1/2}$ (5% in $CDCl_3$): 1 h. δ_H (400 MHz, $CDCl_3$, −40 °C) −3.43 [d, 1H, *J* 5.4, $^1J_{TeH}$ 26.2 Hz (d), TeH], 1.71 (d, 3H, *J* 6.3 Hz, CH_3), 6.33 (dq, 1H, *J* 9.0, 6.3 Hz, CH), 6.61 (dd, 1H, *J* 9.0, 5.4 Hz, CH). δ_C (100 MHz, $CDCl_3$, −40 °C) 20.6, 94.5, 136.0. δ_{Te}(94.7 MHz, $CDCl_3$, −40 °C) −95.4. HRMS: calc. for ($C_3H_5{}^{130}Te.$)$^+$: *m*/*z* 171.9539; found: 171.953. **4c**: bp (0.1 Torr) ≈ −50 °C. Yield: 34%. $\tau_{1/2}$ (5% in $CDCl_3$): 1 h. δ_H (400 MHz, $CDCl_3$, −40 °C) −2.78 [s, 1H, $^1J_{TeH}$ 28.5 Hz (d), TeH], 2.34 (t, 3H, *J* 1.3 Hz, CH_3); 5.40 (q, 1H, *J* 1.3 Hz, H*C*H); 5.75 (q, 1H, *J* 1.3, *H*CH). δ_C(100 MHz, $CDCl_3$, −40 °C) 34.1, 116.3, 125.6. δ_{Te} (94.7 MHz, $CDCl_3$, −40 °C) 182.5. HRMS: calc. for ($C_3H_6{}^{128}Te\cdot$)$^+$: *m*/*z* 171.9539; found: 171.954.

1 A. J. Kresge, *Acc. Chem. Res.*, 1990, **23**, 43; B. J. Smith and L. Radom, *J. Am. Chem. Soc.*, 1989, **111**, 8297.
2 O. Mó, M. Yáñez, M. Decouzon, J.-F. Gal, P.-C. Maria and J.-C. Guillemin, *J. Am. Chem. Soc.*, 1999, **121**, 4653.
3 L. Lassalle, S. Legoupy and J.-C. Guillemin, *Organometallics*, 1996, **15**, 3466; J.-C. Guillemin, L. Lassalle, P. Dréan, G. Wlodarczak and J. Demaison, *J. Am. Chem. Soc.*, 1994, **116**, 8930.
4 A. Chrostowska, V. Métail, G. Pfister-Guillouzo and J.-C. Guillemin, *J. Organomet. Chem.*, 1998, **570**, 175 and references therein.
5 Ethynylselenol has been detected by IR spectroscopy among other products in an argon matrix at 8 K: J. Laureni, A. Krantz and R. A. Hajdu, *J. Am. Chem. Soc.*, 1976, **98**, 7872.
6 Y. Vallée, M. Khalid, J.-L. Ripoll and A. Hakiki, *Synth. Commun.*, 1993, **23**, 1267.
7 H. C. Brown, P. B. Weissman and N. M. Yoon, *J. Am. Chem. Soc.*, 1966, **88**, 1458; C. F. Allen and D. D. MacKay, *Org. Synth.*, 1943, **Coll. Vol. II**, 580; L. E. Overman, J. Smoot and J. D. Overman, *Synthesis*, 1974, 59.
8 L. Brandsma, *Recl. Trav. Chim. Pays-Bas*, 1970, **89**, 593.
9 J.-C. Guillemin and K. Malagu, *Organometallics*, 1999, **18**, 5259.
10 S. Legoupy, L. Lassalle, J.-C. Guillemin, V. Metail, A. Senio and G. Pfister-Guillouzo, *Inorg. Chem.*, 1995, **35**, 1466.
11 L. Lassalle, T. Janati and J.-C. Guillemin, *J. Chem. Soc., Chem. Commun.*, 1995, 699.
12 J.-C. Guillemin, N. Bellec, S. Kiz-Szétsi, L. Nyulászi and T. Veszprémi, *Inorg. Chem.*, 1996, **35**, 6586.
13 D. Crich, J.-T. Hwang, S. Gastaldi, F. Recupero and D. J. Wink, *J. Org. Chem.*, 1999, **64**, 2877.
14 M. J. Dabdoub and J. V. Comasseto, *J. Organomet. Chem.*, 1988, **344**, 167.
15 For ^{77}Se NMR data, see: H. Duddeck, *Prog. NMR Spectrosc.*, 1995, **27**, 1.
16 L. Brandsma and H. E. Wijers, *Recl. Trav. Chim. Pays-Bas*, 1963, **82**, 68.
17 A. Baroni, *Atti Accad. Naz. Lincei Cl. Sci. Fis. Mater. Nat. Rend.*, 1938, **6**, 238.
18 H. C. E. McFarlane and W. McFarlane, *NMR Newly Accessible Nucl.*, 1983, **2**, 275.
19 H. E. Wijers, H. Boelens, A. Van der Gen and L. Brandsma, *Recl. Tav. Chim. Pays-Bas*, 1969, **88**, 519.

ChemComm

Methyltrioxorhenium-catalyzed epoxidations in ionic liquids

Gregory S. Owens and Mahdi M. Abu-Omar*

Department of Chemistry and Biochemistry, University of California, Los Angeles, CA 90095-1569, USA. E-mail: mao@chem.ucla.edu

Received (in Irvine, CA, USA) 28th February 2000, Accepted 11th May 2000

Alkenes and allylic alcohols have been epoxidized in an ambient-temperature ionic liquid for the first time using methyltrioxorhenium (MTO) and urea hydrogen peroxide; excellent conversions and selectivities for the epoxides of a wide number of substrates were observed.

One of the pressing issues for chemists in the twenty-first century is the pursuit of 'clean' or 'green' chemical transformations.[1] A particular source of chemical waste that is often taken for granted is the use of volatile molecular solvents.[2,3] The use of non-volatile ionic liquids, or molten salts, in chemical synthesis and catalysis has received attention in recent years;[2] however, the utility of these compounds remains largely unexplored. We report the first catalytic epoxidation system that makes use of a room-temperature ionic liquid as the solvent. Alkenes and allylic alcohols have been oxidized to their corresponding epoxides using the well studied methyltrioxorhenium (MTO) catalyst and urea hydrogen peroxide (UHP) with the ionic liquid 1-ethyl-3-methylimidazolium tetrafluoroborate, [emim]BF_4, as the solvent.

Numerous low-melting ionic salts are known, including chlorocuprates, halogenoaluminates, and alkylphosphonium, *N*-alkylpyridinium, alkylammonium, and *N*,*N*′-alkylimidazolium cations with various anions.[2] Chlorocuprates are not suitable for catalytic oxidations because of their oxygen sensitivity, and halogenoaluminates are difficult to work with because of their instability in the presence of water. We chose to use the 1-ethyl-3-methylimidazolium cation because: (i) its synthesis is facile,† and (ii) it is neither oxygen nor water sensitive (but is hygroscopic). Furthermore, with BF_4^- as the counteranion, the salt melts at 15 °C.[4]

The discovery by Herrmann in 1991 of MTO's ability to catalyze the epoxidation of olefins has led to a wealth of information regarding the efficiency and versatility of this catalyst.[5] This discovery has also fueled many efforts aimed at developing 'environmentally friendly' oxidation systems, as the only byproduct of the MTO–peroxide system is water. The creation of two active oxygen-transfer complexes, a monoperoxo- and a diperoxorhenium species, during the catalytic cycle has been well established, as have the mechanisms of oxygen transfer (Scheme 1). We refer the reader to the many reviews that have been written on the subject of MTO-catalyzed oxidations, for further information.[6–9]

Urea hydrogen peroxide has been shown to be a water-free peroxide source for MTO-catalyzed epoxidations.[10] The only disadvantage, thus far, to using UHP is that it is insoluble in organic solvents, such as chloroform, methylene chloride, and acetonitrile. Hence, the MTO–UHP system in organic media is heterogeneous.

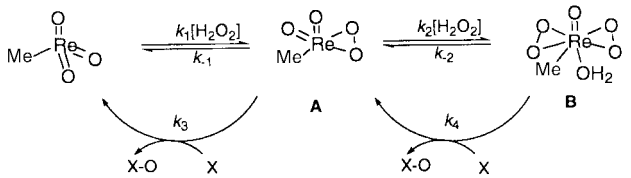

Scheme 1

In this work, the advantageous properties of the MTO–UHP oxidation system and [emim]BF_4 have been combined to give an exceptionally clean environment for catalytic oxidations. One major advantage of this system is that both UHP and MTO are soluble in the ionic liquid, as are the peroxorhenium species. This gives an oxidation solution that is completely homogeneous. The formation of the peroxorhenium species is evident by the appearance of an intense yellow color in the solution; this color is attributable to the monoperoxo- and the diperoxorhenium intermediates. UV–Vis experiments have confirmed the presence of the diperoxorhenium complex, as indicated by its absorption maximum at 360 nm.

The results in Table 1 show that several different olefinic substrates have been oxidized to epoxides, with yields ranging from fair (in the case of 1-decene) to excellent. Aqueous hydrogen peroxide (30%) was used in one experiment (entry 4) to illustrate the ring-opening of sensitive epoxides in the presence of large amounts of water, as previously reported in molecular solvents.[5,11,12] In contrast, the reaction in entry 3 was performed with molecular sieves to ensure the complete removal of water from the system. As a result, only the epoxide

Table 1 Epoxidations of various substrates with MTO–peroxide in [emim]BF_4[a]

Entry	Substrate	Oxidant	Conversion (%)[b]	Epoxide yield (%)[b]
1		UHP	≥95	≥99
2		UHP	≥95	≥95
3		UHP	≥95	≥95
4		H_2O_2 (30%)	≥95	≤5[c]
5		UHP	>99	95[d]
6		UHP	95	≥95
7	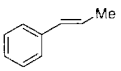	UHP	≥95	≥95
8		UHP	≥95	≥95
9		UHP	>99	85[e]
10		UHP	46[f]	>99

[a] *Reaction conditions*: 0.5 mol substrate, 1.0 mol oxidant, 2% MTO, room temperature, 8 h. [b] Yields determinded by ^{1}H NMR and GC–MS. [c] The majority of the product is the diol. [d] Major products are 2,3-epoxycyclohexanol (62%) and 2,3-epoxycyclohexanone (32%). [e] This yield represents the diepoxide. The remainder of the product is the monoepoxide. The same results are obtained when 2.0 mol oxidant is used. [f] This conversion was obtained after 72 h.

DOI: 10.1039/b001661f

was obtained. It is also interesting to note the poor conversion in the reaction of 1-decene (entry 10). Better conversions for this reaction have been obtained with other MTO–peroxide epoxidation systems;[11–13] however, after 72 h, we observed that the reaction mixture was still intensely yellow, indicating that the catalyst is still active and, apparently, highly stable in this ionic medium. The poor conversion of 1-decene may be the result of heterogeneity in the solution; 1-decene was the least soluble substrate in the ionic liquid. The results in Table 1 also indicate that the time required for the epoxidation of these substrates is quite comparable to that required for previously reported results.[5,11,12] Additionally, as shown in previous work,[10] the use of UHP eliminates the epoxide ring-opening that is commonly observed when using aqueous hydrogen peroxide. This is because the urea that is produced during the consumption of UHP modulates the pH of the solution and prevents acid-catalyzed ring opening.

As shown in Table 1, two equivalents of UHP were used relative to the substrate. Although two equivalents of oxidant leads to faster epoxidation rates, only a single equivalent is required, as evidenced by experiments with 1,5-cyclooctadiene using one and two equivalents of UHP per double bond, which yield the same product distributions.

Remaining reactants and products are both easily removed from the reaction mixture *via* extraction with diethyl ether, which is immiscible with the ionic liquid used in this work. This method of removing reactants and products is also advantageous because MTO, the peroxorhenium species, and the urea byproduct are insoluble in diethyl ether. Careful evaporation of the ether extracts gives the reactant–product mixture, which can then be analyzed by NMR and GC–MS.

In summary, the advantages of this oxidation system are numerous: (i) urea hydrogen peroxide and MTO are completely soluble in [emim]BF_4, giving a homogeneous oxidation solution. (ii) The oxidation solution is nearly water-free, so conversion of the substrates yields only the epoxides and not the diols. (iii) Left-over reactants, if any, and products are easily separated from the oxidation solution by extraction with an immiscible solvent. (While it is true that molecular solvents have been used for isolation of the reactants/products in this work, one can easily imagine a large-scale system in which the reactants and products are distilled from the reaction mixture, thereby completely eliminating the use of organic solvents.) (iv) Most rates of epoxidation in this system are at least comparable to previously published data. Current work in progress includes the determination of equilibrium constants K_1 and K_2 (Scheme 1) in [emim]BF_4 and characterization of the kinetics. We also hope to expand the use of this oxidation solution to substrates other than olefins, such as amines, alcohols, hydrocarbons, and aromatics.

We are grateful to the National Science Foundation (CAREER Grant CHE-9874857), the Arnold and Mabel Beckman Foundation for a Young Investigator Award to M. M. A. O., and the University of California Toxic Substances Research and Teaching Program (UCTSR&TP) for financial support of this research. We would like to thank Professor Thomas Welton for helpful discussions.

Notes and references

† The 1-ethyl-3-methylimidazolium cation is readily synthesized from 1-methylimidazole and bromoethane. Subsequent metathesis with sodium tetrafluoroborate gives the desired ionic liquid, which is purified by passage through neutral alumina.[14] The conversion in the metathesis step is rather important, as bromide competes with alkenes for oxidation to hypobromite.[15]

1 R. T. Baker and W. Tumas, *Science*, 1999, **284**, 1427.
2 T. Welton, *Chem. Rev.*, 1999, **99**, 2071.
3 M. J. Earle, P. B. McCormac and K. R. Seddon, *Green Chem.*, 1999, **1**, 23.
4 J. S. Wilkes and M. J. Zaworotko, *J. Chem. Soc., Chem. Commun.*, 1992, 965.
5 W. A. Herrmann, R. W. Fischer and D. W. Marz, *Angew. Chem., Int. Ed. Engl.*, 1991, **30**, 1638.
6 W. A. Herrmann and F. E. Kuhn, *Acc. Chem. Res.*, 1997, **30**, 169.
7 C. C. Romao, F. E. Kuhn and W. A. Herrmann, *Chem. Rev.*, 1997, **97**, 3197.
8 J. H. Espenson, *Chem. Commun.*, 1999, 479.
9 G. S. Owens, J. Arias and M. M. Abu-Omar, *Catal. Today*, 2000, **55**, 317.
10 W. Adam and C. M. Mitchell, *Angew. Chem., Int. Ed. Engl.*, 1996, **35**, 533.
11 J. Rudolph, K. L. Reddy, J. P. Chiang and K. B. Sharpless, *J. Am. Chem. Soc.*, 1997, **119**, 6189.
12 A. K. Yudin and K. B. Sharpless, *J. Am. Chem. Soc.*, 1997, **119**, 11 536.
13 C. Coperet, H. Adolfsson and K. B. Sharpless, *Chem. Commun.*, 1997, 1565.
14 T. Welton, personal communication, 1999.
15 J. H. Espenson, O. Pestovsky, P. Huston and S. Staudt, *J. Am. Chem. Soc.*, 1994, **116**, 2869.

A new and versatile diamide–diamine donor ligand set in early transition metal chemistry†

Michael E. G. Skinner, David A. Cowhig and Philip Mountford*

Inorganic Chemistry Laboratory, South Parks Road, Oxford, UK OX1 3QR.
E-mail: philip.mountford@chemistry.oxford.ac.uk

Received (in Cambridge, UK) 28th March 2000, Accepted 22nd May 2000

Straightforward, multigram synthesis of the new diamide–diamine proligand H_2N_2NN' [N_2NN' = (2-NC_5H_4)-$CH_2N(CH_2CH_2NSiMe_3)_2$] is described along with a preliminary survey of the five- and six-coordinate, neutral and cationic, single- and multiply-bonded complexes of groups 3, 4 and 5 that it can support; the related bis(alkoxide)–diamine proligand H_2O_2NN' is also described where H_2O_2NN' = (2-NC_5H_4)$CH_2N(CH_2CMe_2OH)_2$.

The bis(cyclopentadienyl) ligand set has been the dianionic environment *par excellence* for organotransition metal chemistry for *ca*. four decades.[1] Driven by the search for new fundamental and catalytic chemistry, the last ten years in particular have established the importance of polydentate di- and tri-anionic N-donor ligands as environments for early- to mid-transition metal coordination and organometallic complexes.[2]

Among the tetradentate 'N_4' donor ligands, the porphyrins[2b] and tetraaza[14]annulenes[2c] are probably the best established *di*anionic ligands. They provide a really quite rigid, square-base donor environment. In contrast, the *tri*anionic triamidoamine 'tren' systems generally provide four vertices of a trigonal bipyramid or octahedron. Such ligands have been extremely successful in developing p-block, early-mid transition metal, lanthanide and actinide chemistry.[2d,3] Despite these successes, however, as a trianionic species the versatility of this ligand is hampered in certain regards for developing new lanthanide, and groups 3 and 4 chemistry in particular since there is only one (group 4) or no (lanthanide, group 3) metal electrons remaining for binding additional anionic ligands. Dianionic 'N_4' analogues of the tren systems will help advance early transition metal and lanthanide chemistry, and compliment the extensive studies of *tri*dentate diamido-donor systems.[2a] Indeed, it was recently reported that addition of an extra donor arm to bis(alkoxide)-donor systems can lead to enhanced ethylene polymerisation capability.[4]

The straightforward syntheses of the new proligands H_2N_2NN' **2**-H_2 and H_2O_2NN' **3**-H_2 are shown in Scheme 1.‡ The intermediate tetra-amine **1** has been previously described,[5] but we have found that the alternative synthesis shown from 2-aminomethylpyridine is more convenient on a large scale. The proligand **2**-H_2 is conveniently converted (Bu^nLi) to its lithiated derivative Li_2N_2NN' **2**-Li_2. The new proligands can all be prepared in multigram quantities: *e.g.* 5.4 g of **1** yields 7.1 g (75%) of **2**-H_2 and lithiation of this gives 4.2 g (57%) of Li_2N_2NN' **2**-Li_2.

The ready availability of H_2N_2NN' **2**-H_2 and Li_2N_2NN' **2**-Li_2 has allowed us to develop a representative range of new five- and six-coordinate, neutral and cationic, single- and multiply-bonded complexes of groups 3, 4 and 5 (Scheme 2). They are formed by salt- (for **4**–**6**), and alkane- or amine- (for **7** and **8**) elimination reactions; the applicability of a range of such protocols will clearly permit these new ligands to be incorporated into a wide range of transition, lanthanide and main group metal derivatives. Thus reaction of Li_2N_2NN' **2**-Li_2 with $[Ti(NAr)Cl_2(py)_3]$[6a] (Ar = $C_6H_3Pr^i_2$-2,6) or $[Ta(NBu^t)Cl_3(py)_2]$[6b] gives the five- and six-coordinate imides, $[Ti(NAr)(N_2NN')]$ **4** and $[Ta(NBu^t)Cl(N_2NN')]$ **5**, respectively. Transition metal imides continue to attract considerable interest,[7] and those of group 4 with π-donor coligands can have a particularly rich reaction chemistry.[2a,7,8] Reaction of **2**-Li_2 with YCl_3 in pyridine affords the 'ate' complex **6**, formulated as '$[YCl(N_2NN')(py)]\cdot 1.5LiCl$' on the basis of elemental analyses and ^{7}Li NMR spectroscopy. Nonetheless, preliminary reactivity studies of **6** show that it behaves as though it were simply $[YCl(N_2NN')(py)]$, and that it is a useful synthon with the Y-bound Cl ligand being readily substituted by bulky monoanionic donors.

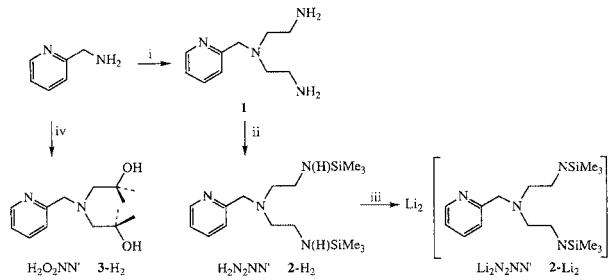

Scheme 1 *Reagents and yields*: i, *N*-tosylaziridine (74% for this step) then conc. H_2SO_4 83% (61% overall); ii, 2 Me_3SiCl, 4 Et_3N, 75%; iii, 2.2 Bu^nLi, 57%; iv, 3-isobutylene oxide, 25%.

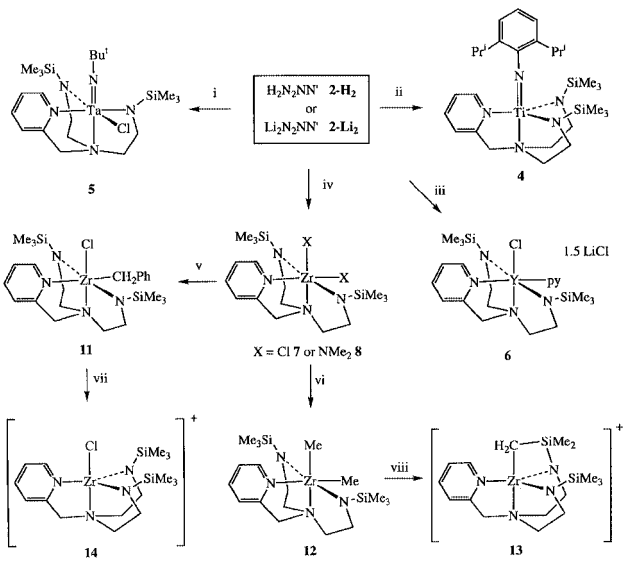

Scheme 2 *Reagents and yields*: i, (with **2**-Li_2) $[Ta(NBu^t)Cl_3(py)_2]$, 36 h, 29%; ii, (with **2**-Li_2) $[Ti(NC_6H_3Pr^i_2\text{-}2,6)Cl_2(py)_3]$, 58%; iii, (with **2**-$Li_2$) YCl_3, 71%; iv, (with **2**-H_2) for **7**: $[ZrCl_2(CH_2SiMe_3)_2\cdot 2Et_2O]$, 87%; for **8**: $[Zr(NMe_2)_4]$, 55%; v, $PhCH_2MgCl$, 87%; vi, LiMe (2 equiv.), 88%; vii, $B(C_6F_5)_3$, 61% [counter ion = $B(CH_2Ph)(C_6F_5)_3^-$]; viii, $B(C_6F_5)_3$, 60% [counter ion = $BMe(C_6F_5)_3^-$].

† Electronic supplementary information (ESI) available: experimental details and characterisation. See http://www.rsc.org/suppdata/cc/b0/b002455o/

DOI: 10.1039/b002455o

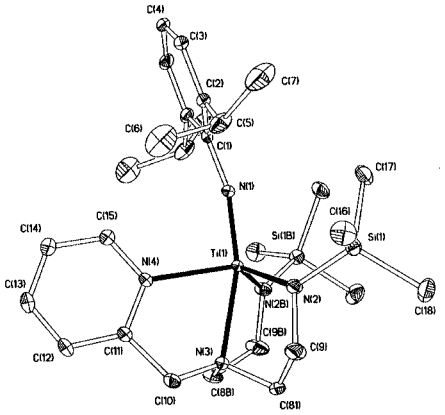

Fig. 1 Displacement ellipsoid plot of [Ti(N_2NN′)($NC_6H_3Pr^i_2$-2,6)] **4**.

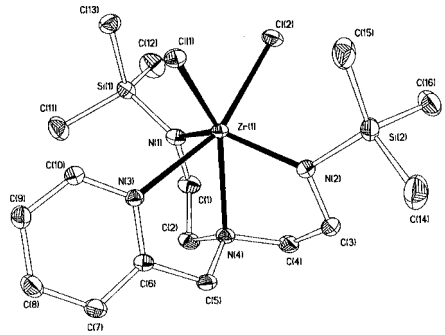

Fig. 2 Displacement ellipsoid plot of [Zr(N_2NN′)Cl_2] **7**.

The group 4 compounds [Zr(X)$_2$(N_2NN′)] (X = Cl **7** or NMe_2 **8**) are readily obtained from **2**-H_2 and [Zr(CH_2SiMe_3)$_2Cl_2$·2Et_2O][9] or [Zr(NMe_2)$_4$], respectively. Such *cis*-X_2 complexes are of great importance in the study of new stoichiometric and catalytic group 4 reaction chemistry.[10] The bis(alkoxide) analogues of **7** and **8**, namely [Zr(X)$_2$(O_2NN′)] [X = Cl **9** or NMe_2 **10**, eqn. (1)] can be similarly prepared from

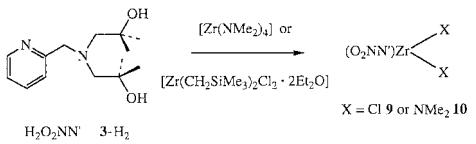

(1)

H_2O_2NN′ **3**-H_2. The compounds **9** and **10** will provide interesting comparisons with their more sterically-shielded tetraaza homologues **7** and **8**, and with very recent bis(phenoxide)–diamine ligands that are active ethylene polymerisation catalysts.[4]

We have structurally confirmed that the N_2NN′ ligand can readily accommodate both five- and six-coordinate metal centres. Views of the X-ray structures of [Ti(NAr)(N_2NN′] **4** and [$ZrCl_2$(N_2NN′)] **7** are shown in Fig. 1 and 2, respectively.§ The structure of **4** reveals an approximately trigonal bipyramidal geometry at the five-coordinate Ti centre. The structure of **7** reveals an approximately octahedral Zr centre; the chloride ligands are mutually *cis*. In both **4** and **7**, and indeed in all the derivatives to date of the N_2NN′ ligand, including the crowded bis(dimethylamide) complex **8**, the pyridyl donor is firmly bound to the metal centre and establishes a well defined coordination environment.

One or both chloride ligands in [$ZrCl_2$(N_2NN′)] **7** can be substituted using organo-magnesium or -lithium reagents forming the mono- and di-alkyl derivatives [Zr(CH_2Ph)Cl(N_2NN′)] **11** and [$ZrMe_2$(N_2NN′)] **12** in *ca*. 90% yield. There is no evidence in any of the reaction chemistry herein for metallation or other attack at the pyridyl donor group. *cis*-Dialkyl compounds such as **12** are potential precursors to Ziegler–Natta olefin polymerisation catalysts.[10] Treatment of **12** with $B(C_6F_5)_3$ or [CPh_3][$B(C_6F_5)_4$], however, affords the TMS-metallated cation **13** with counter anion [$MeB(C_6F_5)_3$]$^-$ or [$B(C_6F_5)_4$]$^-$; there is no evidence for interaction between **13** and the [$MeB(C_6F_5)_3$]$^-$ anion in solution. The [$MeB(C_6F_5)_3$]$^-$ salt of **13** is thermally stable at r.t. in both the solid state and CD_2Cl_2 solution, and has been fully characterised by NMR and elemental analysis. Cation **13** presumably forms *via* an intermediate cation [ZrMe(N_2NN′)]$^+$ (not observed) followed by σ-bond metathesis with one of the $SiMe_3$ C–H bonds. Similar reactions have been seen in group 4 triamidoamine chemistry,[11] but can, in principle, be circumvented by use of alternative amide N-substituents: such protocols are well established.[2a,12] Indirect evidence for a five-coordinate cationic intermediate comes from the formation of the cation [ZrCl(N_2NN′)]$^+$ **14** from the monobenzyl complex [Zr(CH_2Ph)Cl(N_2NN′)] **11** and $B(C_6F_5)_3$. Salts of the cation **13** react sluggishly with ethylene (1 atm), but work is in progress to develop analogues of H_2N_2NN′ with other, more robust amide N-substituents.

In summary, we have described the new diamido–diamine ligand H_2N_2NN′ and a survey of its versatile complexation chemistry.

This work was supported by the EPSRC and Royal Society. We thank Dr G. A. Vaughan (Exxon Chemical Co.) for a gift of [Zr(NMe_2)$_4$] and Dr D. J. Watkin for help with the X-ray data collection.

Notes and references

‡ Full spectroscopic data and elemental analyses have been obtained as far as possible for all the new compounds.

§ *Crystal data* for **4**: $C_{28}H_{49}N_5Si_2Ti$, M = 559.80, orthorhombic, space group *Pbcm*, a = 9.8632(4), b = 18.413(1), c = 17.507(1) Å, U = 3179.4(8) Å^3, Z = 4, T = 170 K, μ = 0.36 mm^{-1}, 3688 independent reflections (R_{merge} = 0.035), 3240 with $I > 3\sigma(I)$ used in refinement, final R indices: R = 0.0574, R_w = 0.0434. For **7**·0.5C_6H_6: $C_{16}H_{32}Cl_2N_4Si_2Zr$·0.5$C_6H_6$, M = 537.81, monoclinic, space group $P2_1/n$, a = 8.4280(1), b = 14.3380(4), c = 21.5020(6) Å, β = 93.295(2)°, U = 2594.0 Å^3, T = 150 K, μ = 0.73 mm^{-1}, 5550 independent reflections (R_{merge} = 0.030), 4506 with $I > 3\sigma(I)$ used in refinement, final R indices: R = 0.0278, R_w = 0.0269. CCDC 182/1648. See http://www.rsc.org/suppdata/cc/b0/b002455o/ for crystallographic files in .cif format.

1 *Metallocenes: synthesis, reactivity, applications*, ed. A. Togni and R. L. Halterman, Wiley-VCH, New York, 1998, vol. 1 & 2.

2 Recent reviews: (*a*) diamide-donors in general; L. H. Gade, *Chem. Commun.*, 2000, 173 (Feature Article); (*b*) porphyrins: H. Brand and J. Arnold, *Coord. Chem. Rev.*, 1995, **140**, 137; (*c*) tetraaza[14]annulenes: P. Mountford, *Chem. Soc. Rev.*, 1998, **27**, 105; (*d*) triamidoamines: R. R. Schrock, *Acc. Chem. Res.*, 1997, **30**, 9; J. G. Verkade, *Acc. Chem. Res.*, 1993, **26**, 483.

3 P. Roussel, N. W. Alcock and P. Scott, *Chem. Commun.*, 1998, 801; P. Roussel, N. W. Alcock, R. Boaretto, A. Kingsley, I. J. Munslow, C. P. Sanders and P. Scott, *Inorg. Chem.*, 1999, **38**, 3651 and references therein.

4 E. Y. Tshuva, I. Goldberg, M. Kol, H. Weitman and Z. Goldschmidt, *Chem. Commun.*, 2000, 379.

5 H. Adams, N. A. Bailey, W. D. Carlisle, D. E. Fenton and G. Rossi, *J. Chem. Soc., Dalton Trans.*, 1990, 1271.

6 (*a*) A. J. Blake, P. E. Collier, S. C. Dunn, W.-S. Li, P. Mountford and O. V. Shishkin, *J. Chem. Soc., Dalton Trans.*, 1997, 1549; (*b*) J. Sundermeyer, J. Putterlik, M. Foth, J. S. Field and N. Ramesar, *Chem. Ber.*, 1994, **127**, 1201.

7 D. E. Wigley, *Prog. Inorg. Chem.*, 1994, **42**, 239; P. Mountford, *Chem. Commun.*, 1997, 2127 (Feature Article).

8 J. L. Bennett and P. T. Wolczanski, *J. Am. Chem. Soc.*, 1997, **119**, 10 696 and references therein.

9 H. Brand, J. A. Capriotti and J. Arnold, *Organometallics*, 1994, **13**, 4469.

10 G. J. P. Britovsek, V. C. Gibson and D. F. Wass, *Angew. Chem., Int. Ed.*, 1999, **38**, 429 and references therein.

11 C. Morton, N. W. Alcock and P. Scott, *Organometallics*, 1999, **18**, 4608; C. C. Cummins, R. R. Schrock and W. M. Davis, *Organometallics*, 1992, **11**, 1452.

12 G. E. Greco, A. I. Popa and R. R. Schrock, *Organometallics*, 1998, **17**, 5591.

ChemComm

Formation of nanorods by self-assembly of alkyl-substituted polyphenylene dendrimers on graphite

Simona Loi,[a] Uwe-Martin Wiesler,[b] Hans-Jürgen Butt*[a] and Klaus Müllen[b]

[a] *Institut für Physikalische Chemie, Universität Mainz, 55099 Mainz, Germany. E-mail: butt@wintermute.chemie.uni-mainz.de*
[b] *Max-Planck-Institut für Polymerforschung Mainz, 55126 Mainz, Germany*

Received (in Cambridge, UK) 17th April 2000, Accepted 11th May 2000

Alkyl-substituted polyphenylene dendrimers with a tetrahedral or disk-like shape form self-assembled monolayers on graphite (HOPG) which show complex supramolecular structures, such as parallel rods of 6 nm diameter or two-dimensional crystals.

The construction of supramolecular structures by self-assembly of molecules is a topic of great current interest in relation to the fabrication of new materials.[1–3] Dendrimers are attractive building blocks to form such materials because they are monodisperse macromolecules with well-defined shapes and dimensions.[4,5] In this paper, we report on the structure of self-assembled dendritic monolayers on the basal plane of graphite. Dendrimers binding to graphite are the ideal model system to study the adsorption of macromolecules to surfaces because adsorbant and adsorbent are well defined.

Different dodecyl-substituted polyphenylene dendrimers were synthesized (Fig. 1) and monolayers were formed by spontaneous adsorption from solution on the basal plane of graphite. The structure of these monolayers was imaged with an atomic force microscope (AFM). Formation of self-assembled dendritic monolayers is possible because the alkyl chains adsorb strongly to graphite; the adsorption energy is roughly 7 kJ mol^{-1} per methylene unit.[6,7] In addition, each phenylene subunit in close contact with the graphite surface is expected to contribute an adsorption energy of roughly 15 kJ mol^{-1}.[8]

Dendrimers **1** and **2** were prepared divergently *via* reiterative Diels–Alder cycloaddition according to the procedure described in ref. 9. The synthesis starts from a polyfunctional central building block, tetra(4-ethynylphenyl)methane for **1**, and 1,3,5-triethynylbenzene for **2**. To introduce dodecyl alkyl chains on the periphery of the dendrimer, tetraphenylcyclopentadienones alkylated with dodecyl chains were added by Diels–Alder cycloaddition as the last layer of the dendrimer. The dendrimers were characterized by MALDI-TOF mass spectrometry, NMR spectroscopy and GPC, and revealed that the products were pure. Due to the polyphenylene backbone and the high number of twisted, interlocked benzene rings, these dendrimers show a high shape persistence, with diameters of 5.5 and 3.8 nm for dendrimers **1** and **2**, respectively.[10] According to force field calculations and X-ray diffraction studies, dendrimer **1** shows a tetrahedric structure, whereas dendrimer **2** has a more planar propeller-like structure (Fig. 1).[11,12]

Dendrimer layers were prepared with the spin coating technique. A drop of solution was deposited on a freshly cleaved HOPG (highly oriented pyrolytic graphite) substrate and the

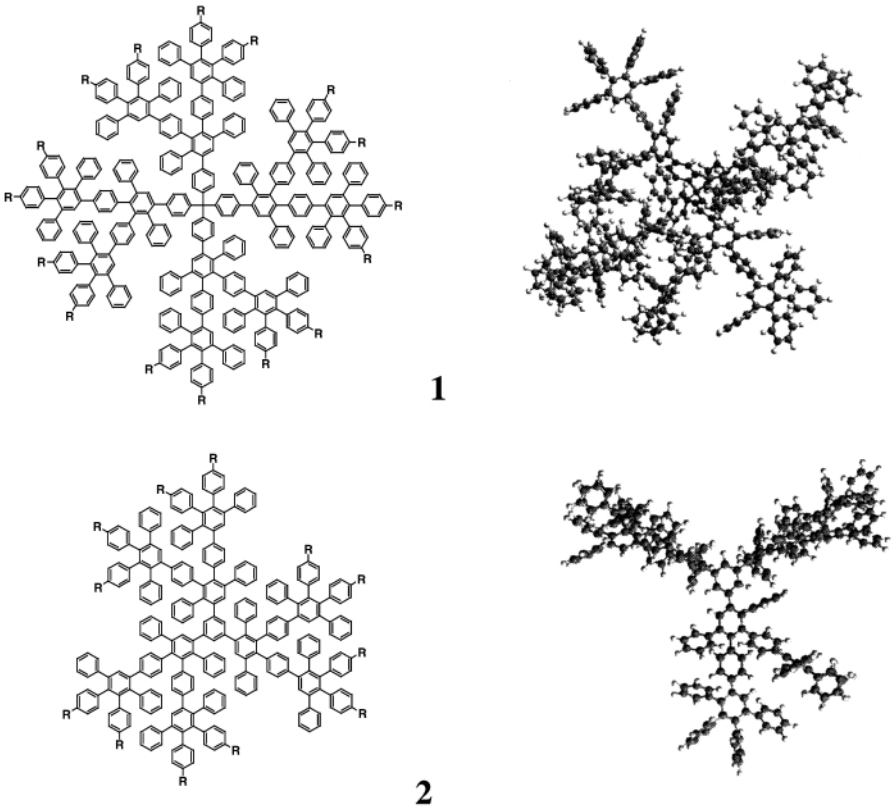

Fig. 1 2D- and 3D-structure (MM2 molecular mechanic simulation with CERIUS2 program package, Molecular Simulations Inc., Waltham, MA, USA) of the investigated alkyl-substituted polyphenylene dendrimers; R=$C_{12}H_{25}$.

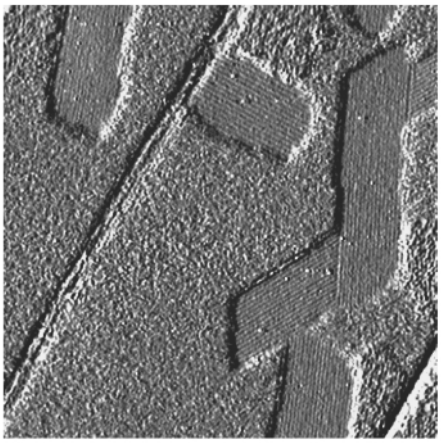

Fig. 2 AFM amplitude image (scan size 639 nm) of a dendrimer **1** layer on HOPG.

sample was rotated at 810 rpm for 10 s. Dendrimers were dissolved in dichloromethane at a concentration of 0.002 mg ml^{-1} ($2.7–4 \times 10^{-7}$ M). Samples were imaged at room temperature with a commercial AFM (Nanoscope III, Digital Instruments, Santa Barbara, California) in tapping mode using rectangular silicon cantilevers (Nanosensors, 125 μm long, 30 μm wide, 4 μm thick) with an integrated tip, a nominal spring constant of 42 N m^{-1}, and a resonance frequency of 330 kHz.

When preparing layers of dendrimer **1**, most of the graphite surface was covered with a diffuse layer. In addition, some distinct structures were observed. Some of the most remarkable structures were regions covered by parallel rows of 5.9 ± 0.7 nm spacing (Fig. 2). Typically, the regions were 50–100 nm wide and 70–800 nm long. Usually only a few percent of the total surface area was covered with a rod-like structure. However, in 2 out of 11 experiments, almost the whole surface was covered by rods. The rods were stable and could be imaged for several hours. Different rod-like regions were oriented parallel (0°) or at 60 or 120° with respect to each other. This indicates that the underlying graphite with its hexagonal structure determines the orientation of the dendrimer rods.

When forming monolayers from dendrimer **2**, in 4 out of 6 experiments, two-dimensional crystals (Fig. 3) were formed. The primitive unit cell can be described by the lattice constants $a = 10.2 \pm 0.3$, $b = 7.4 \pm 0.4$ nm and an angle of 122.8 ± 2°. Like the rod-like regions, these lattices were oriented parallel (0°) or at 60 or 120° with respect to each other, indicating that the underlying graphite determines their orientation. Each unit cell probably contains at least two molecules. This is indicated by the unit cell area of 63 nm^2. An upper limit for the area occupied by one dendrimer can be estimated from the extension of a polyphenylene chain with 10 phenylene rings plus two dodecyl chains, which is roughly 6 nm. When hexagonally close packed, circles of 6 nm diameter would occupy an area of 31 nm^2. In addition, each protrusion in a unit cell had an elongated, oval and not spherical shape. This shows that individual molecules do not form separate units, but that real supramolecular structures are formed. The two-dimensional crystals were stable and could be scanned many times. In one experiment we observed rod formation, as with dendrimer **1**. The spacing between the rods was again 6 nm. The rods were not stable and disappeared after scanning them few times.

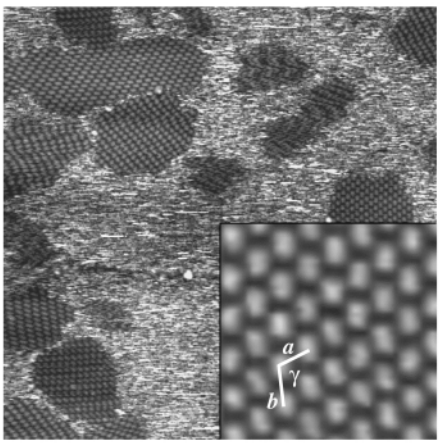

Fig. 3 AFM height image of a dendrimer **2** layer on HOPG showing a region with two-dimensional crystals (scan size 578 nm, 1 nm height). The insert shows details of a crystal. The lattice constants are indicated.

The formation of rods on surfaces has been observed from dendritic nanorods.[13] However, to the best of our knowledge, this is the first observation of rod formation from the self-assembly of dendrimers which are tetrahedral (dendrimer **1**) or shaped like a disc (dendrimer **2**) in solution.

Since it is a requirement for the formation of regular structures, it is ideally that single dendrimers on bare graphite are mobile. Hydrocarbon chains are strongly adsorbed to graphite and, once they are adsorbed, it is unlikely that they can leave the surface spontaneously. They can, however, diffuse laterally. Computer simulations of individual alkyl chains on graphite revealed negligible activation energy for translation along the chain.[6] The same is true for the polyphenylene subunits, because benzene molecules are able to diffuse laterally, even at temperatures of 85 K.[14] Hence, the dendrimers can probably diffuse on bare graphite. This explains why we were never able to image half-covered graphite. Either the surface was totally clean (this was the case when preparing layers from concentrations of < 0.002 mg ml^{-1}) or an almost complete monolayer was observed.

The requirement of high lateral mobility also explains why thiol-substituted dendrimers on gold do not form regular structures.[2] They bind to gold and remain at the point of first encounter, held by the strong localised thiol–gold bond. In contrast, dendrimers which form a monolayer at the air–water interface and which are laterally mobile also show two-dimensional crystalline packing.[15]

This project was supported by the Deutsche Forschungsgemeinschaft Graduiertenkolleg 'Physik und Chemie Supramolekularer Systeme' (S. L.) and the Fonds der Chemischen Industrie (U.-M. W.). We also acknowledge the financial support of the Bundesministerium für Bildung und Forschung (03C0299 7).

Notes and references

1 J. Massey, K. N. Power, I. Manners and M. A. Winnik, *J. Am. Chem. Soc.*, 1998, **120**, 9533.
2 V. Chechik and R. M. Crooks, *Langmuir*, 1999, **15**, 6364.
3 J. W. Kriesel and T. D. Tilley, *Chem. Mater.*, 1999, **11**, 1190.
4 A. P. H. J. Schenning, C. Elissen-Roman, J. W. Weener, M. W. P. L. Baars, S. J. van der Gaast and E. W. Meijer, *J. Am. Chem. Soc.*, 1998, **120**, 8199.
5 A. J. Berresheim, M. Müller and K. Müllen, *Chem. Rev.*, 1999, **99**, 1747.
6 R. Hentschke, B. L. Schürmann and J. P. Rabe, *J. Chem. Phys.*, 1992, **96**, 6213.
7 A. A. Isirikyan and A. V. Kiselev, *J. Phys. Chem.*, 1961, **65**, 601.
8 A. Vernov and W. A. Steele, *Langmuir*, 1991, **7**, 2817.
9 F. Morgenroth, E. Reuther and K. Müller, *Angew. Chem., Int. Ed. Engl.*, 1997, **36**, 631.
10 T. Pakula, personal communication..
11 F. Morgenroth, C. Kübel and K. Müllen, *J. Mater. Chem.*, 1997, **7**, 1207.
12 U.-M. Wiesler, A. J. Berresheim, F. Morgenroth and K. Müllen, *Macromolecules*, submitted..
13 W. Stocker, B. Karakaya, B. L. Schürmann, J. P. Rabe and A. D. Schlüter, *J. Am. Chem. Soc.*, 1998, **120**, 7691.
14 A. Vernov and W. A. Steele, *Langmuir*, 1991, **7**, 3110.
15 G. Cui, Y. Xu, M. Liu, F. Fang, T. Ji, Y. Chen and Y. Li., *Macromol. Rapid Commun.*, 1999, **20**, 71.

ChemComm

A new diastereoselective approach to simplified Dynemicin analogues

Giuseppe Guanti* and Renata Riva*

Università di Genova, Dipartimento di Chimica e Chimica Industriale, and C.N.R., CSCCCA, via Dodecaneso 31, I-16146 Genova, Italy. E-mail: guanti@chimica.unige.it, riva@chimica.unige.it

Received (in Liverpool, UK) 10th March 2000, Accepted 23rd May 2000

The stereoselective synthesis of new simplified Dynemicin analogues is reported: key steps of the sequence are the regio- and diastereo-selective functionalization of a quinoline nucleus, bearing a substituent with a stereogenic centre, and the formation of the 10-membered cyclic enediyne system by Pd-catalyzed Stille-like reaction.

Enediynes constitute an important family of recently discovered natural derivatives. Owing to their unusual molecular structure and strong cytotoxic activity, *via* unique double strand cleavage of DNA, in recent years these compounds have attracted the attention of many research groups. Dynemicin A **1** is certainly one of the most representative examples of this class of substances and the synthesis of this enediyne has been reported.[1] However, since its molecular structure is complex, many efforts have been made to synthesize simplified analogues, hopefully mimicking the activation mechanism.[2]

We recently performed a regio- and diastereo-selective nucleophilic addition of magnesium acetylides onto 2-(4-quinolyl)propan-1-ol and showed that the extent of induction was determined by the nature of the hydroxy protecting group.[3] Based on this methodology, compounds such as **5** and **6** (see Scheme 2) could be prepared in high chemical yield and moderate to good diastereomeric ratio.

Within our project in the enediyne field,[4] we planned to transform these adducts into enediynes **2a**,**b**, which are simplified analogues of **1** (Scheme 1). Although compounds with similar structure have been recently prepared by Isobe and coworkers,[5] we focused our attention on a completely different synthetic approach. The most critical step of our plan was undoubtedly the formation of the 10-membered cyclic enediyne system. For this purpose two different strategies were envisaged: (1) route A, in which the acyclic system already bears all the required ten carbon atoms; in this case the ring closure could be induced by the base-induced coupling of a bis(propargyl bromide)[6] or by an intramolecular pinacol coupling performed on a bis(aldehyde);[4b] (2) route B, in which the acyclic system, bearing only eight carbon atoms of the incoming enediyne, is coupled with a suitable two-carbon unit.[1a,7]

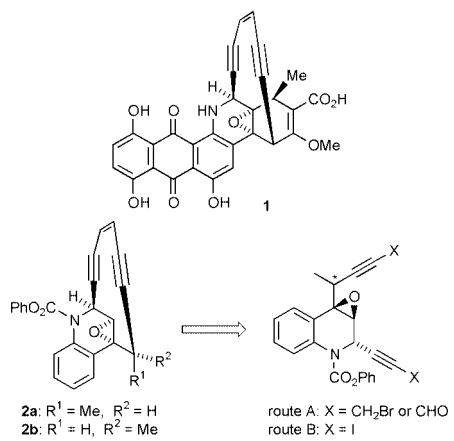

Scheme 1

We first explored route A. For this purpose, after deprotection of the alcoholic function of **5** (R^1 = TBDMS) and **6** (R^1 = triphenylmethyl (Tr)), obtained as 68:32 and 87:13 diastereomeric mixtures respectively, and chromatographic separation of the epimeric **7a** and **7b**, we separately transformed them into the diacetylenic intermediates **11** and **12**, following the procedure reported in Scheme 2. Owing to the propensity of **8a**,**b** to epimerize, the oxidation of the primary alcoholic function to the aldehyde was troublesome, either under Dess–Martin conditions, which were successfully used for the preparation of enediyne intermediates,[8] or under standard Swern conditions. Finally, we succeeded in performing the reaction under slightly modified Swern conditions[9] and **8a**,**b** were used just after aqueous work-up. The homologation of the aldehyde function of **8a** was first attempted through the one-pot sequence proposed by Ohira,[10] which directly allowed the preparation of **11a** in quite good yield (59%), but with extended epimerization, leading to a 7:3 mixture of **11a** and **11b**, probably due to the basic reaction conditions. We then examined the possibility to utilize the Corey–Fuchs[11] procedure. While the preparation of dibromides **9a**,**b** was realized without problems, the transformation of them to give alkyne moieties was more difficult than expected: after many attempts, in which all the possible factors affecting this transformation were examined, the optimal conditions were found to be treatment of **9a**,**b** with Bu^nLi for 15 min at low temperature under argon; on the other hand, working under nitrogen, the reaction was sluggish and the isolated yields of **10a**,**b** were never higher than 40%! C-Desilylation under basic conditions gave **11a**,**b**, and the overall chemical yield from **7a**,**b** was higher (72 and 76% respectively) than that obtained by the previously attempted one-step sequence and, most importantly, no epimerization was observed. Epoxidation of the double bond to give **12a**,**b** was straightforward and completely stereoselective, as expected from literature data.[5a]

With **10a**,**b**, **11a**,**b** and **12a**,**b** in hand, we tried to perform the homologation of the acetylenic functions. However, all attempts to substitute the acetylenic hydrogens with an alkoxymethyl moiety or a synthetic equivalent were unsuccessful.

At this point we turned our attention to route B and examined the possibility to build the enediynic system through a Stille double coupling reaction. This approach was not straightforward; indeed this methodology has been applied only in a few cases to generate cyclic 3-ene-1,5-diyne systems,[1a,7] but always on partially rigid systems, for which the ring closure should be easier than in our case. For this purpose we prepared the diastereomeric bis(iodides) **13a** and **13b** by simultaneous iodination with *N*-iodosuccinimide/$AgNO_3$[12] of both alkyne functions of **12a**,**b** and then performed the Pd(0)-catalyzed cross-coupling reaction with (*Z*)-bis(trimetylstannyl)ethylene. The first attempts were unsuccessful, but eventually, after a careful optimization of reaction conditions [solvent, temperature, choice of Pd(0) source, use of additives, high dilution in order to minimize intermolecular attack of tin reagent], we were able to obtain the epimeric enediynes **2a**,**b** in satisfactory yields. The different yields (60% for **2a** *cf.* 76% for **2b**)

DOI: 10.1039/b002031l

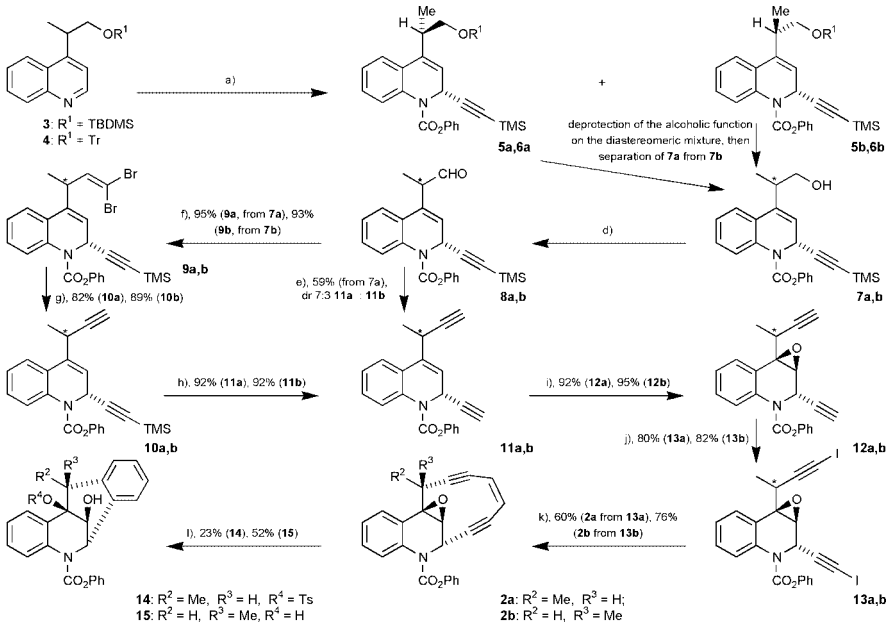

Scheme 2 *Reagents and conditions*: (a) TMS–C≡C–MgBr, $PhCO_2Cl$, THF, −78 °C, R^1 = TBDMS: 87%, 68 : 32 **5a** : **5b**, R^1 = Tr: 98%, 87 : 13 **6a** : **6b**; (b) R^1 = TBDMS: HF, MeCN, −20 → 10 °C, 91%; (c) R^1 = Tr: *p*-TSA, MeOH, 0 °C, 99%; (d) $(COCl)_2$, DMSO, Pr^1_2EtN, −78 °C; (e) $MeCOCN_2P(O)(OMe)_2$, K_2CO_3, MeOH, 0 °C; (f) CBr_4, PPh_3, THF, −78 → −50 °C; (g) Bu^nLi, toluene, −78 °C, Ar; (h) $NaHCO_3$, MeOH, 60 °C; (i) *m*-CPBA, CH_2Cl_2, 0 °C; (j) NIS, $AgNO_3$, THF, r.t., dark; (k) (*Z*)-$Me_3SnCH{=}CHSnMe_3$, $Pd(PPh_3)_4$, LiCl, DMF, 70 °C; (l) i, *p*-TSA (0.5 M sol. in THF), benzene, cyclohexa-1,4-diene, r.t., 30 min; ii, Et_3N, r.t., 24 h.

confirmed our expectations, based on molecular mechanics calculations performed with the CS Chem3D program (Cambridge Soft, Cambridge, MA, USA, version 4.0). For both iodides we found about eight further stable conformations with similar energy, as expected for systems which are not conformationally blocked. The distance between the two iodine bearing sp carbons is in the range 5.0–6.0 Å for **13a** and 4.1–4.4 Å for **13b**. As a result, **13b** is therefore best suited for the new C–C bond forming reaction, owing to the proximity of the two terminal sp carbons.

Finally, we tested the propensity of these compounds to undergo Bergman cycloaromatization, which is responsible for the biological activity of most enediyne derivatives. On Dynemicin and analogues, cycloaromatization usually takes place as soon as the epoxide is opened.[1,2,5*a*,7*a*,13] For this reason we submitted both **2a**,**b** to epoxide opening in the presence of *p*-toluenesulfonic acid.[5*a*,13*a*] To our surprise, after a reaction time of one day, we isolated two different compounds, the monotosylate **14** from **2a** and diol **15** from **2b**, for which the relative configuration at the benzylic carbon is only tentatively assigned based on literature data[5*a*,13*a*] and molecular mechanics studies. At the moment we do not have an explanation for the different behaviour of the two epimers during the acid-induced cycloaromatization process, although we think that different mechanisms could take place, probably due to a different conformation of the molecule in the two epimers.

From our results it seems clear that a relative configuration like that of **7b** seems to be preferable for the synthesis of the enediyne moiety, although this is not the preferred stereoisomer in the initial stereoselective addition step. However, we believe that this is not a real problem, since, thinking to extend our protocol on (*S*)-3-acetoxy-2-(4-quinolyl)propan-1-ol derivatives,[14] the enantiodivergency of this chiral synthon and the diastereodivergency of compounds analogous to **5** and **6** should be exploited to obtain the most useful diastereoisomer for the transformation into the corresponding enediyne. Studies in this field are still in progress in our laboratories.

We thank Ms Sara Perrozzi and Ms Dina Cavallo for their contribution to this work and C.N.R., University of Genova, and MURST (COFIN 98) for financial support.

Notes and references

1 (*a*) M. D. Shair, T. Y. Yoon, K. K. Mosny, T. C. Chou and S. J. Danishefsky, *J. Am. Chem. Soc.*, 1996, **118**, 9509; (*b*) A. G. Myers, N. J. Tom, M. E. Fraley, S. B. Cohen and D. J. Madar, *J. Am. Chem. Soc.*, 1997, **119**, 6072; (*c*) J. Taunton, J. L. Wood and S. L. Schreiber, *J. Am. Chem. Soc.*, 1993, **115**, 10 378.
2 M. E. Maier, F. Boße and A. J. Niestroj, *Eur. J. Org. Chem.*, 1999, 1.
3 G. Guanti, S. Perrozzi and R. Riva, *Tetrahedron: Asymmetry*, 1998, **9**, 3923.
4 (*a*) L. Banfi, A. Basso and G. Guanti, *Tetrahedron*, 1997, **53**, 3249; (*b*) L. Banfi, G. Guanti and A. Basso, *Eur. J. Org. Chem.*, 2000, 939.
5 (*a*) T. Nishikawa, A. Ino and M. Isobe, *Tetrahedron*, 1994, **50**, 1449; (*b*) T. Nishikawa, M. Yoshikai, K. Obi, T. Kawai, R. Unno, T. Jomori and M. Isobe, *Tetrahedron*, 1995, **51**, 9339.
6 R. S. Huber and G. B. Jones, *Tetrahedron Lett.*, 1994, **35**, 2655.
7 (*a*) T. Takahashi, Y. Sakamoto, H. Yamada, S. Usui and Y. Fukazawa, *Angew. Chem., Int. Ed. Engl.*, 1995, **34**, 1345; (*b*) H. Tanaka, H. Yamada, A. Matsuda and T. Takahashi, *Synlett*, 1998, 381; (*c*) D. L. J. Clive, Y. Bo, Y. Tao, S. Daigneault, Y.-J. Wu and G. Meignan, *J. Am. Chem. Soc.*, 1998, **120**, 10 332; (*d*) D. K. Moss, J. D. Spence and M. H. Nantz, *J. Org. Chem.*, 1999, **64**, 4339.
8 R. Unno, H. Michishita, H. Inagaki, Y. Suzuki, Y. Baba, T. Jomori, T. Nishikawa and M. Isobe, *Bioorg. Med. Chem.*, 1997, **5**, 883.
9 G. Guanti, L. Banfi, R. Riva and M. T. Zannetti, *Tetrahedron Lett.*, 1993, **34**, 5483.
10 S. Ohira, *Synth. Commun.*, 1989, **19**, 561.
11 E. J. Corey and P. L. Fuchs, *Tetrahedron Lett.*, 1972, **13**, 3769.
12 T. Nishikawa, S. Shibuya, S. Hosokawa and M. Isobe, *Synlett*, 1994, 485; in our hands the direct transformation of TMS–alkyne moiety into iodide was sluggish and overall yields lower.
13 (*a*) K. C. Nicolaou, A. L. Smith, S. V. Wendeborn and C.-K. Hwang, *J. Am. Chem. Soc.*, 1991, **113**, 3106; (*b*) K. C. Nicolaou and W.-M. Dai, *Angew. Chem., Int. Ed. Engl.*, 1991, **30**, 1387; (*c*) P. A. Wender, S. Beckham and J. G. O'Leary, *Synthesis*, 1994, 1278.
14 L. Banfi, G. Guanti, A. Mugnoli and R. Riva, *Tetrahedron: Asymmetry*, 1998, **9**, 2481.

Photosensitization of a porous TiO_2 electrode with merocyanine dyes containing a carboxyl group and a long alkyl chain

Kazuhiro Sayama,[a] Kohjiro Hara,[a] Nahoko Mori,[b] Makoto Satsuki,[b] Sadaharu Suga,[b] Shingo Tsukagoshi,[c] Yoshimoto Abe,[c] Hideki Sugihara[a] and Hironori Arakawa*[a]

[a] *National Institute of Materials and Chemical Research (NIMC), Higashi 1-1, Tsukuba, Ibaraki 350-8565, Japan. E-mail: h.arakawa@home.nimc.go.jp*
[b] *Hayashibara Biochemical Laboratories, Inc., Fujita 564-176, Okayama 701-0221, Japan*
[c] *Facility of Science and Technology, Science University of Tokyo, Yamazaki 2641, Noda, Chiba 278, Japan*

Received (in Cambridge, UK) 24th February 2000, Accepted 22nd May 2000

Porous TiO_2 electrodes sensitized using merocyanine dyes containing a carboxyl group and a long alkyl chain, in particular 3-carboxymethyl-5-[2-(3-alkyl-2-benzothiazolinyldene)ethylidene]-2-thioxo-4-thiazolidinone, showed remarkably high solar–energy efficiency (4.2%, AM-1.5, 100 mW cm^{-2}).

Since Grätzel *et al.* reported a highly efficient solar cell (incident solar light–power conversion efficiency, η_{sun} = 10%) based on a nanocrystalline TiO_2 semiconductor electrode sensitized by a Ru complex,[1,2] the studies on dye sensitization of porous oxide semiconductors have been actively investigated. Most papers on the Grätzel type solar cell so far have focused on metal complex dyes such as bipyridyl and porphyrin derivatives, and little attention has been shown to the use of organic dyes as photosensitizers. There are some early works on the spectral sensitization of non-porous semiconductors using organic dyes,[3] however, the efficiencies were quite low. It is worthwhile to develop highly efficient organic dye sensitizers from the standpoint of low cost, saving of limited precious metal resources and the easy handling for cell recycling without removal of metal, however, the efficiencies of Grätzel type cells sensitized by organic dyes were relatively low (η_{sun} < 1.3%).[4–10] Here we investigated various kinds of merocyanine organic dyes containing a carboxyl group as an anchor to attach the dye on the semiconductor surface. Merocyanine dyes have been studied on dye multi-layer photovoltaic cells based on a Shottky-type barrier at the metal/dye film contact,[11–13] but have been rarely investigated on Grätzel cells. We report here, for the first time, that some merocyanine dyes show excellent efficiencies up to η_{sun} = 4.2% on porous TiO_2 semiconductor electrodes, and also investigate the relationship between solar cell efficiency and the structure of the dyes.

All dyes were synthesized by Hayashibara Biochemical Laboratories Inc. The preparation of the porous TiO_2 film electrode on a conducting glass support (F-SnO_2,10 Ω sq^{-1}) was *via* the published procedure.[2] TiO_2 powder (Nihon Aerosil, P-25) was mainly used in order to prepare a TiO_2 paste for coating. Adsorption of a dye on the TiO_2 surface was carried out by soaking the TiO_2 electrode in a 220 mg dm^{-3} dry ethanol solution of the dye at 80 °C for 1 h, and the electrode was washed with ethanol. The dye-sensitized TiO_2 electrode was incorporated into a thin-layer sandwich-type solar cell with a Pt/conducting glass as counter electrode and electrolyte solution. To investigate the efficiency of dyes (Table 1), an Xe lamp with suitable band pass filters (3–4 mW cm^{-2}) and UV cut off filter was used as the light source. The incident solar light–electric energy conversion efficiency (η_{sun}) was measured with a solar simulator (AM-1.5, WACOM Co.).

We mainly investigated the photoelectrochemical properties of indole type [Ma, X = $C(CH_2)_2$] and benzothiazole type (Mb, X = S) merocyanines, a widely used merocyanine dye, as shown in Scheme 1. Both Ma(2)-N and Mb(2)-N dyes containing a carboxyl group adsorbed strongly on the TiO_2 surface, and showed significantly high efficiencies. On the other hand, the Mb(2)′ dye containing no carboxyl group scarcely adsorbed on TiO_2 and the cell efficiency was negligible, suggesting that the presence of anchoring groups to adsorb on the semiconductor surface is essential for efficient dye-sensitization. In the studies of solid photovoltaic cells using dye multi-layer electrodes without semiconductors,[11,13] various kinds of merocyanine dyes including Ma and Mb dyes were examined, and the carboxyl group was not essential in contrast to the dye-sensitized semiconductor cells studied here. The

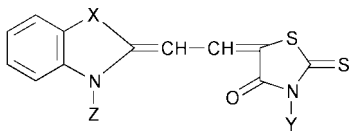

Scheme 1 Structure of merocyanine dyes; for the identity of X, Y and Z see Table 1.

Table 1 Photoelectrochemical properties of porous TiO_2 semiconductor solar cells sensitized with various merocyanine dyes[a]

	Dye structure									
Dye	X	Y	Z	λ_{max}[b]/nm	$\lambda_{threshold}$[b]/nm	IPCE[c] (%)	Isc[d]/mA	Voc[d]/V	ff[d] (%)	η_{Xe}[d] (%)
Ma(2)-N	CMe_2	CH_2CO_2H	C_2H_5	490(520)	550(600)	38.0	3.50	0.61	60	1.6
Mb(2)-N	S	CH_2CO_2H	C_2H_5	520(560)	570(660)	33.3	3.92	0.62	60	1.8
Mb(5)-N	S	CH_2CO_2H	C_5H_{11}	520(560)	570(660)	36.7	4.68	0.68	60	2.4
Mb(10)-N	S	CH_2CO_2H	$C_{10}H_{21}$	520(570)	570(660)	41.7	5.35	0.68	60	2.7
Mb(18)-N	S	CH_2CO_2H	$C_{18}H_{37}$	520(590)	580(670)	41.8	5.50	0.62	54	2.3
Mb(2)′	S	Me	Et	520(—)	570(—)	< 0.1	< 0.01	—	—	< 0.1
Mb(2)-M	S	Et	CH_2CO_2H	520(550)	570(650)	45.7	4.28	0.52	58	1.6
Ma(2)-NM	CMe_2	CH_2CO_2H	CH_2CO_2H	500(540)	580(630)	26.5	2.30	0.50	63	0.9

[a] TiO_2 film (thickness 7 μm, area 1 cm^2) prepared from P-25. The electrolyte solution was a mixture of tetrapropylammonium iodide (0.5 M) and iodine (0.05 M) in ethylene carbonate–dry acetonitrile (60:40 v/v). [b] In ethanol; values in parentheses were measured on TiO_2. [c] IPCE was measured by monochromatic light at near λ_{max} using band pass filters. [d] Under white light from an Xe lamp > 420 nm (80 mW cm^{-2}).

DOI: 10.1039/b001517m

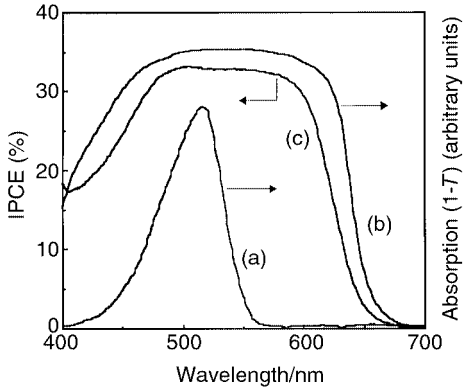

Fig. 1 Absorption spectra of Mb(2)-N in ethanol solution (a), Mb(2)-N on TiO_2 electrode (b) and IPCE action spectrum of the Mb(2)-N/TiO_2 cell (c). The TiO_2 electrode and the electrolyte were same as indicated in Table 1.

incident photon–current efficiencies (IPCE) of the dye-sensitized semiconductor cells in our study were superior to those of solid photovoltaic cells (IPCE < 22%).[11–13]

Fig. 1 shows the light absorption spectra of Mb(2)-N in ethanol solution (a) and Mb(2)-N on a TiO_2 electrode (b), in addition to the IPCE action spectrum of the Mb(2)-N/TiO_2 cell (c). The absorption peak maximum (λ_{max}) and the absorption threshold ($\lambda_{threshold}$) of various dyes in ethanol and on TiO_2 are also shown in Table 1. All merocyanine dyes had a narrow absorption band in ethanol solution, and the peak at around 500 nm was assigned to the monomer.[12] By adsorbing the dye on the TiO_2 electrode, a broadening of the absorption spectrum and a large red shift of the absorption threshold were observed in all electrodes. The IPCE action spectrum was as broad as the absorption spectrum on TiO_2. Similar broadening and red shifts have been reported on several merocyanine multi-layer electrodes without semiconductors.[11,12] Therefore, it is suggested that the interaction between neighboring dyes causes the red shift and the broadening of the absorption. The changes of absorption on the merocyanine multilayer electrode are explained on the basis of exciton phenomena, calculated from the molecular packing structure of the dye aggregate and the coupling of transition dipoles.[11] It was reported that a J-aggregate of Mb(2)-N, which showed a large red shift and a sharp absorption peak at 610 nm, was formed in the TiO_2 mesoporous network after aqueous solution treatment.[14] In our experiments, while a large red shift of the absorption was observed, no sharp absorption peak at *ca.* 610 nm was observed. Therefore, we speculate that small J-like aggregates were formed on the TiO_2, and that chemical anchoring on the TiO_2 surface restricted the formation of large and highly oriented J-aggregates.

We investigated the merocyanines [Mb(*m*)-N] with long straight alkyl chains (carbon number: m = 2, 5, 10 and 18) in detail, since it has been reported that the formation of J-aggregates is more facile with increasing length of alkyl chain in the study of dye multi-layer electrodes.[12,13] The peak maximum and threshold of absorption for Mb(*m*)-N on TiO_2 were slightly shifted to the longer wavelength with an increase in *m* (Table 1). In addition the rise of absorption at the threshold became sharp with increasing *m*. The IPCE of Mb(*m*)-N/TiO_2 cells at *ca.* 520 nm increased with an increase of *m*, and these electrodes had the same values of light harvesting efficiency at 520 nm. Therefore, it is suggested that the intrinsic sensitization efficiency, *i.e.* quantum efficiency, increased with the length of alkyl chain.

In discussing the relationship between the sensitization efficiency and the presence of long alkyl chains the electron injection process from the excited state of the dye to the TiO_2 generally competes with other undesirable processes, and photo-isomerization is one of the major decay pathways for merocyanine.[10] The presence of long alkyl chains and aggregate formation probably prevents isomerization by the restriction of rotation around the methine chain. Moreover, in the J-aggregate crystal structure of Mb(2)-N sodium salt octahydrate,[14] the alkyl chain is located at the opposite side of the carboxyl group, and the formation of single isomers and uniform orientation of the dye seem to be important factors for good J-aggregation. It is speculated that the repulsion between long alkyl chains and the TiO_2 surface might help form the predominant isomer, in which the alkyl chain lies far apart from the carboxyl group anchoring on the TiO_2 surface. Mb(2)-M, which has a carboxyl group at another position Z instead of position Y, showed almost same efficiency as Mb(2)-N. On the other hand, the photocurrent of Ma(2)-NM containing two carboxyl groups was very low compared with that of Ma(2)-N containing one carboxyl group. The configuration and aggregation of Ma(2)-NM on TiO_2 were very restricted by two anchors, and this might affect the photocurrent. From all the results, it is concluded that the control of configuration and aggregation of the merocyanine dye are very important factors in improving the solar cell efficiency.

Finally, we improved the efficiency of the Mb(18)-N/TiO_2 solar cell using thicker TiO_2 films (*ca.* 13 μm thickness) prepared by the alkoxide method using a different electrolyte solution consisting of a mixture of LiI (0.1 M), 1,2-dimethyl-3-propylimidazolium iodide (0.6 M), iodine (0.05 M), 4-*tert*-butylpyridine (1 M) and methoxyacetonitrile as solvent.[2,15] The maximum η_{sun} value under solar simulated light (100 mW cm^{-2}, AM-1.5, 0.25 cm^2) was *ca.* 4.2% (Isc: 9.7 mA cm^{-2}, Voc: 0.62 V, ff: 69%), the best value among organic dye systems reported so far.[3–10] The stability of these dyes in a sealed solar cell is now under investigation.

Notes and references

1 B. O'Regan and M. Grätzel, *Nature*, 1991, **353**, 737.
2 M. Nazeeruddin, A. Kay, I. Rodicio, R. Humphry-Baker, E. Muller, P. Liska, N. Vlachopoulos and M. Grätzel, *J. Am. Chem. Soc.*, 1993, **115**, 6382.
3 H. Gerischer, M. E. Michel-Beyerle, F. Rebentrost and H. Tributsch, *Electrochim. Acta*, 1968, **13**, 1509; T. Watanabe, A. Fijishima, O. Tatsuoki and K. Honda, *Bull. Chem. Soc. Jpn.*, 1976, **1**, 49.
4 H. Tsubomura, M. Mastumura, Y. Nomura and T. Amamiya, *Nature*, 1976, **261**, 402.
5 T. N. Rao and L. Bahadur, *J. Electrochem. Soc.*, 1997, **144**, 179; C. Nasr, D. Liu, S. Hotchandani and P. V. Kamat, *J. Phys. Chem.*, 1996, **100**, 11 054.
6 S. Ferrere, A. Zaban and B. A. Gregg, *J. Phys. Chem. B*, 1997, **101**, 4490.
7 K. Tennakone, G. R. Kumara, A. Kumarasinghe, K. Wijayantha and P. Sirimanne, *Semicond. Sci. Technol.*, 1995, **10**, 1689.
8 N. J. Cherepy, G. P. Smestad, M. Grätzel and J. Z. Zhang, *J. Phys. Chem. B*, 1997 **101**, 9342.
9 K. Sayama, M. Sugino, H. Sugihara, Y. Abe and H. Arakawa, *Chem. Lett.*, 1998, 753.
10 A. C. Khazraji, S. Hotchandani, S. Das and P. V. Kamat, *J. Phys. Chem. B*, 1999 **103**, 4693.
11 D. L. Morel, E. L. Stogryn, A. K. Ghosh, T. Feng, P. E. Purwin, R. F. Shaw, C. Fishman, G. R. Bird and A. P. Piechowski, *J. Phys. Chem.*, 1984, **88**, 923; A. P. Piechowski, G. R. Bird, D. L. Morel and E. L. Stogryn, *J. Phys. Chem.*, 1984, **88**, 934.
12 K. Irikama, F. Mizutani and M. Yoshiura, *Chem. Lett.*, 1980, 1399.
13 F. Mizutani, S. Iijima and K. Tsuda, *Bull. Chem. Soc. Jpn.*, 1982, **55**, 1295; F. Mizutani, S. Iijima, K. Sasaki and Y. Shimura, *Ber. Bunsenges. Phys. Chem.*, 1982, **86**, 907.
14 F. Nüesch, J. E. Moser, V. Shklover and M. Grätzel, *J. Am. Chem. Soc.*, 1996, **118**, 5420.
15 C. J. Berbé, F. Arendse, P. Comte, M. Jirousek, F. Lenzmann, V. Shklover and M. Grätzel, *J. Am. Ceram. Soc.*, 1997, **80**, 3157; S. Yanagida, S. Kambe, W. Kubo, K. Murakoshi, Y. Wada and T. Kitamura, *Z. Phys. Chem.*, 1999, **212**, 31.

Two photochemical pathways in competition: matrix isolation, time-resolved and NMR studies of *cis*-[Ru(PMe$_3$)$_4$(H)$_2$]†

Virginia Montiel-Palma,[a] Robin N. Perutz,*[a] Michael W. George,[b] Omar S. Jina[b] and Sylviane Sabo-Etienne[c]

[a] *University of York, Heslington, York, UK YO10 5DD. E-mail: rnp1@york.ac.uk*
[b] *University of Nottingham, University Park, Nottingham, UK NG7 2RD*
[c] *Laboratoire de Chimie de Coordination du C. N. R. S., 205 Route de Narbonne, 31077 Toulouse Cedex 04, France*

Received (in Basel, Switzerland) 20th March 2000, Accepted 8th May 2000

cis-[Ru(PMe$_3$)$_4$(H)$_2$] (1) reacts by two distinct photochemical pathways resulting in the formation of [Ru(PMe$_3$)$_4$] and [Ru(PMe$_3$)$_3$(H)$_2$]; derivatives of these intermediates are generated in the presence of CO and Ph$_2$SiH$_2$.

Photochemical loss of H_2 from *cis*-metal dihydride complexes is a general phenomenon widely employed to generate reactive unsaturated species.[1] We have demonstrated by laser flash photolysis, matrix isolation and steady state photolysis of the complexes [Ru(R$_2$PCH$_2$CH$_2$PR$_2$)$_2$H$_2$] (R = Me, Et, Ph, C$_2$F$_5$) that irradiation induces efficient loss of H_2 and formation of square-planar [Ru(R$_2$PCH$_2$CH$_2$PR$_2$)$_2$] intermediates.[2] It is therefore puzzling that UV irradiation of *cis*-[Ru(PMe$_3$)$_4$(H)$_2$] (**1**) in the presence of R$_3$SiH (R = Me, Ph) results in quantitative loss of PMe$_3$ and formation of [Ru(PMe$_3$)$_3$(SiR$_3$)(H)$_3$].[3,4] Here we present an investigation of the low-temperature matrix, transient-solution and steady-state photochemistry of **1**. We show that the reaction with R$_3$SiH creates the illusion of a single pathway. Our evidence reveals two photochemical pathways involving 16-electron intermediates, one gives rise to [Ru(PMe$_3$)$_4$] (**2**) and the other to [Ru(PMe$_3$)$_3$(H)$_2$] (**3**).

When **1** was irradiated under CO in [$^2H_6$]benzene (or [$^2H_8$]-toluene), two monocarbonyls *cis, mer*-[Ru(PMe$_3$)$_3$(CO)(H)$_2$] (**4**)[5] and [Ru(PMe$_3$)$_4$(CO)] (**5**)[6] and two dicarbonyls [Ru(PMe$_3$)$_2$(CO)$_2$(H)$_2$] (**6**)[7] and [Ru(PMe$_3$)$_3$(CO)$_2$] (**7**),[8,9] were identified by their characteristic ^{1}H and ^{31}P NMR as well as their solution IR spectra (ESI†). The number of CO groups in each species was counted *via* the ^{31}P NMR spectrum with ^{13}CO labelled material.[10] The identity of the products obtained by steady-state solution photolysis suggests the occurrence of photochemical loss of H_2 in competition with the loss of PMe$_3$ established previously.[3,4] In order to test this hypothesis, we turned to matrix isolation in conjunction with time-resolved spectroscopy in solution.

Complex **1** was isolated in an Ar matrix at 12 K.[11] After UV irradiation (17 min, 273 < λ < 400 nm), the originally colourless matrix turned purple and the area of the ν(Ru–H) bands (1820 cm^{-1}) decreased by 11%. A weak new band in the ν(Ru–H) region was observed at *ca*. 1790 cm^{-1}. The UV–VIS spectrum showed new bands at 543 and *ca*. 304 nm (Fig. 1). Subsequent selective photolysis (λ > 520 nm) depleted the principal initial photoproduct leaving bands of another species with λ_{max} = 503, *ca*. 610 nm. UV irradiation (273 < λ < 400 nm, 30 min) of **1** in an Ar + 1.5% CO matrix, resulted in new bands in the ν(CO) region assigned to **4**, **5** and **7** (Table 1, ESI†).

Laser flash photolysis (308 nm)[12] of **1** in cyclohexane solution under argon generated a transient within the instrumental response time, which decayed by second order kinetics ($k_2/\varepsilon l$ = 2.9 × 10^5 s^{-1}). The spectrum under 400 Torr of H_2 recorded by this method (λ_{max} = 550 ± 5 nm) greatly resembled the one obtained after photolysis in inert matrices (Fig. 1). The transient reacted with a variety of reagents giving pseudo-first order rate constants which varied linearly with the concentration of added quencher (Fig. S1, ESI†). The resulting second order rate constants are: k(CO) = (8.9 ± 0.4) × 10^8 > k(H$_2$) = (5.6 ± 0.4) × 10^8 > k(Et$_2$SiH$_2$) = (2.2 ± 0.1) × 10^7 > k(PMe$_3$) = (1.1 ± 0.1) × 10^6 > k(Et$_3$SiH) = (2.8 ± 0.1) × 10^5 > k(PEt$_3$) = (2.7 ± 0.8) × 10^5 > k(C$_2$H$_4$) = (1.8 ± 0.1) × 10^5 dm^3 mol^{-1} s^{-1}.[13]

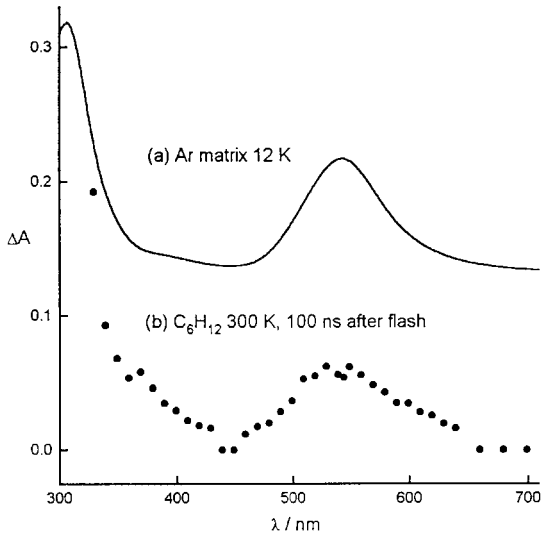

Fig. 1 (*a*) UV–VIS spectrum following photolysis of **1** in an argon matrix at 12 K (17 min, 273 < λ < 400 nm). (*b*) Point-by-point transient spectrum at 300 K measured 100 ns after laser flash photolysis (308 nm) of **1** in cyclohexane under 400 Torr H_2.

When the decay of the transient generated under H_2 was complete, no net change in absorbance was observed at any wavelength from 350 to 800 nm. In contrast, a high net change in absorbance at 350 nm in the presence of PMe$_3$ (< 0.1 mol dm^{-3}) implicated a longer-lived photoproduct.[14] This behaviour can be understood if the extinction coefficient in the visible region of **2** greatly exceeds that of **3**. The principal transient species observed by UV–VIS spectroscopy is then **2**. Reaction of **2** with H_2 would regenerate **1**, while treatment with PMe$_3$ would result in [Ru(PMe$_3$)$_5$] (probably unstable).

Further kinetic information was obtained by time-resolved infrared (TRIR) spectroscopy. A cyclohexane solution of **1** under CO was irradiated with a pulsed laser (266 nm) and the IR spectrum measured in a point-by-point fashion.[15] The TRIR spectrum showed a well-defined band at 1929 cm^{-1} due to **4** (Fig. 2). The second order rate constant for formation of **4** was determined [p(CO) = 150 to 760 Torr] as k_2 = (5.1 ± 0.6) × 10^7 dm^3 mol^{-1} s^{-1}. Since this value is about 17 times smaller than the rate constant for reaction of the UV–VIS transient with CO (see above), we postulate that **2** is the only transient *observable* by flash photolysis with UV–VIS detection.[16]

† Electronic supplementary information (ESI) available: IR spectral data for **4**–**7** (Table 1) and kinetic data (Fig. S1). See http://www.rsc.org/suppdata/cc/b0/b002297g/

DOI: 10.1039/b002297g

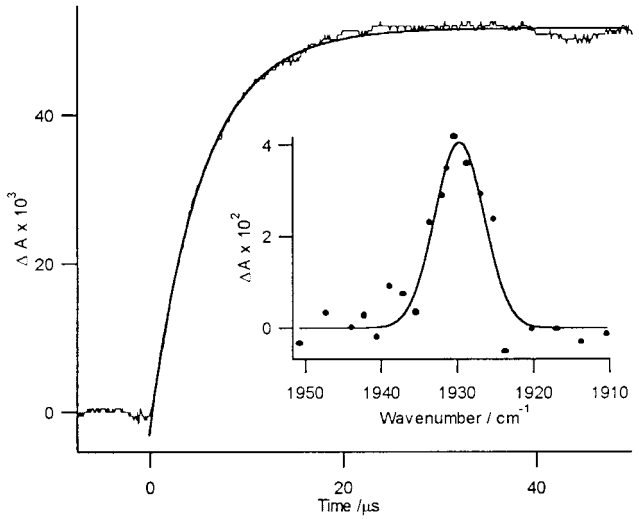

Fig. 2 Growth of ν(CO) band at 1929 cm^{-1} of **4** measured by TRIR spectroscopy after flash photolysis (266 nm) of **1** in cyclohexane under 300 Torr CO. Inset shows partial spectrum 23 μs after flash.

At this stage, we knew that laser flash photolysis of **1** generates **2** which reacts with Et_3SiH, presumably to give $[Ru(PMe_3)_4(SiEt_3)H]$. In apparent contradiction, steady state photolysis of **1** with Me_3SiH or Ph_3SiH only gives $[Ru(PMe_3)_3(SiR_3)(H)_3]$ (R = Me, Ph), derived from loss of PMe_3.[3,4] We therefore investigated the products of irradiating **1** with silanes by NMR spectroscopy. Low temperature photolysis in [$^2H_8$]toluene at 195 K in the presence of $HSiMe_3$ or $HSiEt_3$ generated the trihydrides but did not reveal the anticipated H_2-loss products. Reasoning that silanes with a smaller cone angle would stabilise $[Ru(PMe_3)_4(SiR_3)H]$, we irradiated **1** in the presence of dihydridosilanes. Photolysis of **1** with Ph_2SiH_2 yielded *cis*-$[Ru(PMe_3)_4(SiPh_2H)H]$ and $[Ru(PMe_3)_3(SiPh_2H)(H)_3]$[17] with an initial ratio of quantum yields of *ca.* 1:4.5 respectively.[18] Similar results were obtained with Et_2SiH_2, $HSi(OMe)_2$(allyl) and $HSiMe_2$(allyl).

Our evidence from a variety of methods now provides a consistent view of the photochemistry of **1** (Scheme 1). Two photochemical pathways act in competition: loss of PMe_3 occurs with a quantum yield *ca.* 4.5 times that for loss of H_2 in solution. We postulate that the H_2-loss products, *cis*-$[Ru(PMe_3)_4(SiR_3)H]$, are generated initially with all silanes, but if the silane is bulky (R = Me, Et, Ph), these products are labile and are converted to $[Ru(PMe_3)_3(SiR_3)(H)_3]$. Rapid displacement of PMe_3 by H_2 from *cis*-$[Ru(PMe_3)_4(SiR_3)H]$ has also been observed by Berry.[19] Competitive photodissociation of dihydrogen and phosphine has been encountered in the tetrahydride system $[Os(H)_4(PMe_2Ph)_3]$,[20] but H_2 photodissociation is the sole pathway in $[Ir(\eta^5\text{-}C_5Me_5)(PMe_3)(H)_2]$.[21]

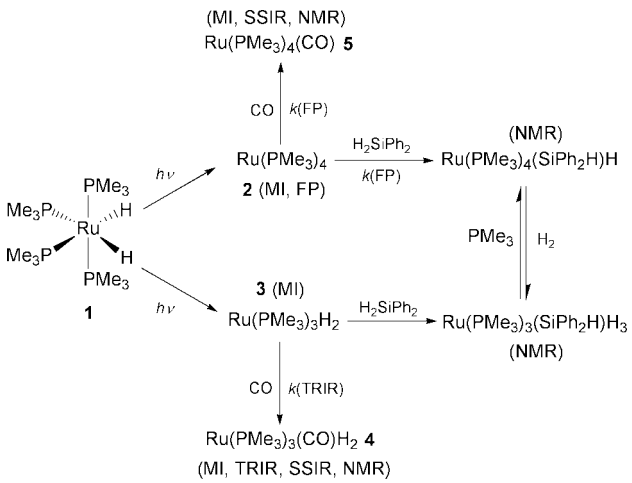

Scheme 1 The photoreactivity of **1** showing the reactions of the primary photoproducts with CO and Ph_2SiH_2. The methods employed for detection are indicated: MI = matrix isolation, FP = flash photolysis, TRIR = time resolved IR, SSIR = IR spectroscopy following steady-state irradiation and NMR = NMR spectroscopy following steady-state irradiation.

We are grateful for support from CONACYT (México), ORS Awards, The British Council-Alliance Programme and to Professor D. H. Berry, Dr J. N. Moore and Dr S. B. Duckett for helpful discussions.

Notes and references

1 R. N. Perutz, *Pure Appl. Chem.*, 1998, **70**, 2211.
2 L. Cronin, M. C. Nicasio, R. N. Perutz, R. G. Peters, D. M. Roddick and M. K. Whittlesey, *J. Am. Chem. Soc.*, 1995, **117**, 10 047.
3 (*a*) D. H. Berry and L. J. Procopio, *J. Am. Chem. Soc.*, 1991, **113**, 8627; (*b*) J. A. Reichl and D. H. Berry, *Adv. Organomet. Chem.*, 1998, **43**, 197.
4 M. J. Burn and R. G. Bergman, *J. Organomet. Chem.*, 1994, **472**, 43.
5 W. Kohlmann and H. A. Werner, *Naturforsch, Teil B*, 1993, **48**, 1499 ($\nu_{(CO)}$ of **4** (C_6H_6) = 1940 cm^{-1} is inconsistent with our measurements).
6 **5**: $^{31}P\{^1H\}$ NMR (121.5 MHz, C_6D_6, 300 K): δ −10.1 (s). IR $\nu(^{13}CO)$ (C_6D_6): 1760 cm^{-1}.
7 R. J. Mawby, R. N. Perutz and M. K. Whittlesey, *Organometallics*, 1995, **14**, 3268.
8 R. Boese, W. B. Tolman and K. P. C. Vollhardt, *Organometallics*, 1986, **5**, 582. Note that **7** adopts a fluxional C_{2v} structure.[9]
9 M. Ogasawara, F. Maseras, N. Gallego-Planas, K. Kawamura, K. Ito, K. Toyota, W. E. Streib, S. Komiya, O. Eisenstein and K. G. Caulton, *Organometallics*, 1997, **16**, 1979.
10 $^{31}P\{^1H\}$ NMR (121.5 MHz, [$^2H_8$]toluene, 300 K). $[Ru(PMe_3)_3(^{13}CO)(H)_2]$: δ 1.0 (dd, $^2J_{PP}$ 25.4 and $^2J_{PC}$ 10.5 Hz), δ −9.3 (td, $^2J_{PP}$ 24.7 and $^2J_{PC}$ 9 Hz); $[Ru(PMe_3)_2(^{13}CO)_2(H)_2]$: δ −0.8 (t, $^2J_{PC}$ 9.5 Hz); $[Ru(PMe_3)_3(^{13}CO)_2]$: δ −4.3 (t, $^2J_{PC}$ 8.4 Hz); $[Ru(PMe_3)_4(^{13}CO)]$: δ −9.8 (d, $^2J_{PC}$ 2.9 Hz).
11 Compound **1** was sublimed at 328 K and cocondensed with argon onto a window cooled to 20 K. The matrix was cooled to 12 K, see D. M. Haddleton, A. McCamley and R. N. Perutz, *J. Am. Chem. Soc.*, 1988 **110**, 1810.
12 Laser flash photolysis experiments were performed using a XeCl excimer laser (λ_{exc} = 308 nm, pulse width *ca.* 50 ns).[2]
13 E. Wilhelm and R. Battino, *Chem. Rev.*, 1973, **73**, 1. The solubilities of CO, H_2 and C_2H_4 in cyclohexane were taken as 9.3×10^{-3}, 3.8×10^{-3} and 1.4×10^{-1} mol dm^{-3} atm^{-1} respectively. Errors in rate constants are quoted to 95% confidence limits.
14 The rate constant for reaction with PMe_3 did not vary significantly with the wavelength of measurement.
15 Nd:YAG laser (λ_{exc} = 266 nm, detection with diode IR laser, CaF_2 windows, 1 mm pathlength), see M. W. George, M. Poliakoff and J. J. Turner, *Analyst*, 1994, **119**, 551.
16 The detection of the ν(CO) band of **5** by TRIR spectroscopy proved difficult due to overlap with the Ru–H stretching mode of **1** and its low IR extinction coefficient. To our surprise, bands were observed at 1828 and 1881 cm^{-1} (rise time < 1 μs) which correspond to the multiple substitution product **7** even when using an open-flow system. They were confirmed to result from a single-photon process. This species may be derived from hot **2** (full details will be published elsewhere).
17 Selected NMR data [$^2H_8$]toluene, 294 K. $[Ru(PMe_3)_4H(SiPh_2H)]$ ^1H NMR (400.1 MHz): δ −10.3 (dq, 1 H, $^2J_{HP}$ 67, 22.5 Hz, RuH), 5.9 (tt, 1H, $^3J_{PH}$ 14.6, 4.7 Hz, $SiPh_2H$). ^{31}P NMR (162 MHz): ABX_2 δ -0.1 (m, $^2J_{PP}$ 25, 23.7 Hz, X_2), −10.2 (m, $^2J_{PP}$ 25, 16 Hz, A) and −10.7 (m, $^2J_{PP}$ 25, 16 Hz, B. $[Ru(PMe_3)_3(H)_3(SiPh_2H)]$ ^1H NMR: δ −9.5 (m, 3 H, RuH_3), 6.7 (m, 1 H, $SiPh_2H$). ^{31}P NMR: δ −10.4 (br s) J_{SiH} by ^{29}Si filtered $^1H\{^{31}P\}$ spectroscopy: 64.5 Hz.
18 Relative quantum yields were calculated from the integrations of the dangling Si–H protons of both products in the ^1H NMR spectra recorded after short photolysis times in the presence of 3 equiv. of silane. On more prolonged photolysis, the ratio of the yields approaches unity, as a result of thermal/photochemical interconversion of the products.
19 (*a*) D. H. Berry, personal communication; V. K. Dioumaev, K. Plössl, P. J. Carroll and D. H. Berry, *J. Am. Chem. Soc.*, 1999, **121**, 8391; (*b*) We further tested this hypothesis by placing a 1:1 solution of *cis*-$[Ru(PMe_3)_4(SiPh_2H)H]$ and $[Ru(PMe_3)_3(SiPh_2H)(H)_3]$ under dihydrogen and heating to 80 °C. After 2 h the ratio of the products changed to 1:3.9 respectively.
20 J. W. Bruno, J. C. Huffman, M. A. Green, J. D. Zubkowski, W. E. Hatfield and K. G. Caulton, *Organometallics*, 1990, **9**, 2556.
21 A. Arndtsen, R. G. Bergman, T. A. Mobley and T. H. Peterson, *Acc. Chem. Res.*, 1995, **28**, 154.

ChemComm

Polymerisation of acrylonitrile with di(organoimido)chromium(VI) complexes

Ulrich Siemeling,*†[a] Lars Kölling,[a] Anja Stammler,[a] Hans-Georg Stammler,[a] Eric Kaminski[b] and Gerhard Fink[b]

[a] *Fakultät für Chemie, Universität Bielefeld, Universitätsstraße 25, D-33615 Bielefeld, Germany*
[b] *Max-Planck-Institut für Kohlenforschung, Kaiser-Wilhelm-Platz 1, D-45470 Mülheim an der Ruhr, Germany*

Received (in Basel, Switzerland) 20th March 2000, Accepted 25th May 2000

$[(Bu^tN)_2Cr(CH_2Ph)_2]$ 1 and $[(NCMe_2CH_2CH_2CMe_2N)Cr(CH_2Ph)_2]$ 2 are robust single-component catalysts for the polymerisation of acrylonitrile, which afford high-molecular-weight PAN and also allow acrylonitrile–methyl methacrylate copolymerisation; owing to its strained seven-membered chelate ring, 2 exhibits exceptionally small imido bond angles.

The polymerisation of α-olefins by titanocene- and zirconocene-based catalysts is of great technological relevance.[1] Nevertheless, there is increasing interest in the development of novel non-metallocene catalysts for olefin polymerisation, since these may allow, *inter alia*, an even greater control over polymer properties. Several new catalyst families have been described in this context,[2] one of them being di(organoimido)-chromium(VI) complexes of the type $(RN)_2CrX_2$ (X = Cl, Me, CH_2Ph),[3] which have proved to be excellently suited to the polymerisation of ethylene in the presence of a cocatalyst.[4] Owing to their comparatively low Lewis acidity, catalysts based on group 6 metals may be more tolerant towards polar, functionalised olefins than group 4 metal systems. For example, complexes of the type $(RN)_2CrCl_2$ have been shown to tolerate ester groups in the cyclopropanation of olefins.[5] We report here on the polymerisation of acrylonitrile by di(organoimido)chromium(VI) complexes.

We have utilised $[(Bu^tN)_2Cr(CH_2Ph)_2]$[3a] **1** and the novel *ansa*-di(organoimido) complex $[(NCMe_2CH_2CH_2CMe_2N)Cr(CH_2Ph)_2]$ **2**‡ as catalysts. **2** bears an isolobal relationship to group 4 *ansa*-metallocene derivatives.[6] Its structure has been determined by single-crystal X-ray diffraction (Fig. 1)§ and resembles that of **1**.[3b] Both compounds contain an η^1- and an η^2-benzyl ligand. In solution, however, only one set of ^{1}H NMR resonances is observed for the two benzyl ligands even at low temperatures owing to rapid averaging. The most striking differences between **1** and **2** are due to the strained seven-membered chelate ring present in **2**, which causes exceptionally small imido bond angles (Table 1). A similar structural effect was recently observed in the chemistry of molybdenum.[6a] A variable-temperature ^{1}H NMR study (500.1 MHz, $[^2H_8]$toluene solvent) reveals that the chelate ring is moderately flexible in solution. At room temperature, a single, averaged signal at δ 1.82 is observed for the four protons of the CH_2CH_2 unit, which is compatible with an averaged C_{2v}-symmetric structure. The singlet shows coalescence at *ca.* −10 °C. At −70 °C two well separated signals (2 × 2 lines) are observed at δ 1.25 and 2.35, which is in agreement with the AA′BB′ spin system expected for a rigid C_2-symmetric ligand framework. $\Delta G^{\#}$ is *ca.* 48 kJ mol^{-1} for the ring inversion.

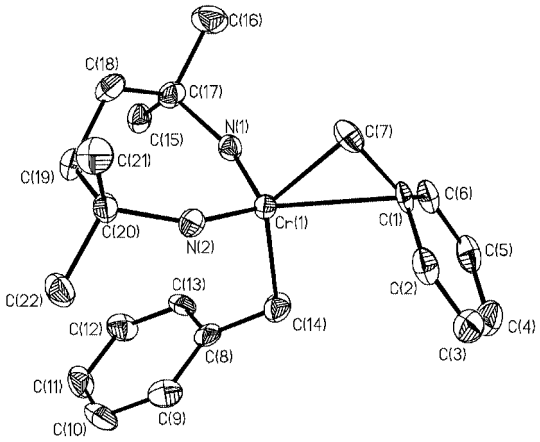

Fig. 1 Molecular structure of **2** in the crystal. Selected bond lengths (pm) and angles (°): Cr(1)–C(1) 242.0(4), Cr(1)–C(7) 207.0(4), Cr(1)–C(14) 208.5(4), N(1)–C(17) 146.6(5), N(2)–C(20) 145.9(5); C(1)–Cr(1)–C(7) 37.03(14), Cr(1)–C(7)–C(1) 84.6(2), C(7)–Cr(1)–C(14) 130.89(16), Cr(1)–C(14)–C(8) 113.9(3).

Table 1 Comparison of bond lengths (pm) and angles (°) in **1** and **2**

	1	**2**
Cr–N	162.5(2)/163.2(2)	163.1(3)/163.3(3)
N–Cr–N	116.09(8)	104.19(16)
Cr–N–C	166.07(13)/160.60(13)	146.8(3)/147.3(3)

Complexes **1** and **2** are active catalysts for the polymerisation of the polar, functionalised olefin acrylonitrile (AN). No cocatalyst is needed.¶ In all cases studied the polymerisation started immediately and continued for an extended period of time (Fig. 2). Initially, the polyacrylonitrile (PAN) yield increased linearly, and during the course of the reaction it approached an upper limit. After a while the clear solution became cloudy and a white precipitate was observed. At the same time the viscosity started to increase. The molecular weight reached remarkably high values, and the polydispersity (M_w/M_n) decreased slightly with the conversion (Fig. 2). The PAN produced by **1** and **2** had approximately the same tacticity (Table 2).[7] Copolymerisation experiments were performed with acrylonitrile and methyl methacrylate (MMA). The low glass

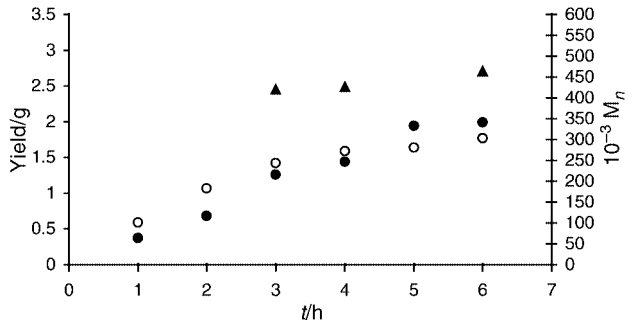

Fig. 2 Polymerisation of acrylonitrile with **1** and **2** {PAN yields [(●) **1**, (○ **2**] and molecular weights [(▲) **2**]}: Molecular weights and polydispersity for **2** after 3/4/6 h: M_n = 420 000/427 000/464 000; M_w = 1 200 000/1 200 000/1 300 000; M_w/M_n = 2.9/2.8/2.8.

† New address: Fachbereich 18 (Physik), Universität Gesamthochschule Kassel, Heinrich-Plett-Str. 40, D-34132 Kassel, Germany. E-mail: siemeling@uni-kassel.de.

DOI: 10.1039/b002310h

Table 2 The triad microtacticity of polyacrylonitrile as obtained from 75.5 MHz ^{13}C NMR spectra in $[^2H]_6$DMSO

	Triad tacticity (%)		
Specified group	mm	mr	rr
Cyano	31[a]	45[a]	24[a]
	25[b]	48[b]	27[b]
Methine	27[a]	53[a]	20[a]
	27[b]	52[b]	21[b]

[a] **1**. [b] **2**.

Table 3 Results of acrylonitrile–methyl methacrylate copolymerisation runs using **1** and **2**

Run	AN/mmol	MMA/mmol	Yield/g	T_g[a]/°C
1[b]	400	100	2.02	84.64
2[b]	100	400	4.57	92.04
3[c]	200	100	0.94	78.63
4[c]	75	150	0.71	87.49

[a] T_g (PMMA) = 128 °C and T_g (PAN) = 144 °C with **1** and **2**. [b] **1**. [c] **2**.

transition temperature T_g in comparison with T_g of the respective homopolymer PAN and PMMA indicates that the products obtained must be copolymers (Table 3).

The metal-catalysed polymerisation and copolymerisation of acrylonitrile is unprecedented. We are currently investigating the polymerisation mechanism. We note that with rigid ligand architectures of appropriate symmetry the formation of stereoregular functionalised polyolefins may be feasible, if the polymerisation mechanism is essentially metal-centered.

This work was generously supported by the Bundesministerium für Bildung und Wissenschaft, Forschung und Technologie.

Notes and references

‡ Complex **2** was synthesised in analogy to the three-step route developed for **1**, starting from the silylated diamine $(Me_3Si)HNCMe_2CH_2CH_2$-$CMe_2NH(SiMe_3)$ and CrO_2Cl_2. *Selected spectroscopic data:* δ_H(500.1 MHz, $CDCl_3$, 298 K) 7.00 (m, 10 H, Ph) 2.53 (s, 4 H, CH_2Ph) 1.83 [br s, 4H, $(CH_2)_2$], 0.99 (s, 12H, Me). δ_C(125.8 MHz, $CDCl_3$, 298 K) 141.0 (C_{ipso} Ph) 130.8 (C_{ortho} Ph) 129.0 (C_{meta} Ph) 124.9 (C_{para} Ph) 74.2 (CMe_2) 43.7 (CH_2Ph) 40.6 [$(CH_2)_2$] 27.4 (Me). MS (CI) *m/z* 375 (100%) $[M]^+$.

§ *Crystal data* for **2**: $C_{22}H_{30}CrN_2$, M = 374.5, monoclinic, space group $P2_1/n$, a = 8.471(4), b = 16.716(10), c = 14.781(6) Å, β = 100.21(3)°, V = 2059.9(18) Å^3, Z = 4, μ(Mo-Kα) = 0.561 mm^{-1}, F(000) = 800, orange plate (0.6 × 0.4 × 0.1 mm), $2\theta_{max}$ = 50.0°, 3886 reflections measured, 3627 unique (R_{int} = 0.0558) which were used in all calculations; $R(F)$ = 0.0570 for 2346 reflections with $I > 2\sigma(I)$, $wR(F^2)$ = 0.1222 for all data. A single crystal was mounted in inert oil and transferred to the cold gas stream of a Siemens $P2_1$ four-circle diffractometer. The structure was solved using direct methods and the non-hydrogen atoms were refined anisotropically using full-matrix least-squares based on F^2 (programmes used: Siemens SHELXTL PLUS and SHELXL 97).

CCDC 182/1659. See http://www.rsc.org/suppdata/cc/b0/b002310h/ for crystallographic files in .cif format.

¶ *Experimental procedures*: polymerisations of acrylonitrile were carried out under argon in a 100 ml flask equipped with a magnetic stirrer and a cooling jacket. Typically, polymerisations were run with 0.012 mmol of **1** or **2** and 300 mmol of acrylonitrile in toluene solution (40 ml) at 20 °C. The reactions were carried out in the dark to exclude radical formation, since usually polyacrylonitrile is prepared by radical polymerisation. The reactions were quenched with methanol. The white fine powder which precipitated was filtered off and dried *in vacuo* at 60 °C for 12 h. Copolymerisation experiments with acrylonitrile and methyl methacrylate were made under essentially identical conditions, utilising 0.02 mmol of **1** or **2** in toluene solution.

1 For leading reviews, see: W. Kaminsky, *J. Chem. Soc., Dalton Trans.*, 1998, 1413; C. Janiak, in *Metallocenes*, ed. A. Togni and R. Halterman, Wiley-VCH, Weinheim, 1998, vol. 2, pp. 547–623; M. Bochmann, *J. Chem. Soc., Dalton Trans.*, 1996, 255; H. H. Brintzinger, D. Fischer, R. Mülhaupt, B. Rieger and R. Waymouth, *Angew. Chem.*, 1995, **107**, 1255; H. H. Brintzinger, D. Fischer, R. Mülhaupt, B. Rieger and R. Waymouth, *Angew. Chem., Int. Ed. Engl.*, 1995, **34**, 1143; *Ziegler Catalysts*, ed. G. Fink, R. Mülhaupt and H. H. Brintzinger, Springer, Berlin, 1995.

2 For a recent review, see: G. J. P. Britovsek, V. C. Gibson and D. F. Wass, *Angew. Chem.*, 1999, **111**, 448; G. J. P. Britovsek, V. C. Gibson and D. F. Wass, *Angew. Chem., Int. Ed.*, 1999, **38**, 428.

3 (*a*) M. P. Coles, C. I. Dalby, V. C. Gibson, I. R. Little, E. L. Marshall, M. H. Ribeiro da Costa and S. Mastoianni, *J. Organomet. Chem.*, 1999, **591**, 78; (*b*) M. P. Coles, C. I. Dalby, V. C. Gibson, W. Clegg and M. R. J. Elsegood, *J. Chem. Soc., Chem. Commun.*, 1995, 1709; (*c*) M. P. Coles and V. C. Gibson, *Polym. Bull.*, 1994, **33**, 529.

4 Homogeneous chromium catalysts for olefin polymerisation have been reviewed, see: K. H. Theopold, *Eur. J. Inorg. Chem.*, 1998, 15.

5 D. Jan, F. Simal, A. Demonceau, A. F. Noels, K. A. Rufanov, N. A. Ustynyuk and D. N. Gourevitch, *Tetrahedron Lett.*, 1999, **40**, 5695.

6 Related complexes have already been described for Mo and W, see: (*a*) E. A. Kretzschmar, J. Kipke and J. Sundermeyer, *Chem. Commun.*, 1999, 2381; (*b*) U. Siemeling, T. Türk, W. W. Schoeller, C. Redshaw and V. C. Gibson, *Inorg. Chem.*, 1998, **37**, 4738; (*c*) C. Redshaw, V. C. Gibson, W. Clegg, A. J. Edwards and B. Miles, *J. Chem. Soc., Dalton Trans.*, 1997, 3343; (*d*) V. C. Gibson, C. Redshaw, W. Clegg, M. R. J. Elsegood, U. Siemeling and T. Türk, *J. Chem. Soc., Dalton Trans.*, 1996, 4513.

7 M. Minagawa, K. Ute, T. Kitayama and K. Hatada, *Macromolecules*, 1994, **27**, 3669.

ChemComm

α-LNA, locked nucleic acid with α-D-configuration

Poul Nielsen* and Jakob Kragh Dalskov

Department of Chemistry, University of Southern Denmark, Odense University, 5230 Odense M, Denmark. E-mail: pon@chem.sdu.dk

Received (in Cambridge, UK) 18th April 2000, Accepted 16th May 2000

The bicyclic thymine monomer of α-LNA (αT^L) was efficiently synthesised and used in the synthesis of α-LNA sequences: incorporation of single αT^L-monomers in α-configured oligothymidylates destabilises the affinity towards both complementary DNA and RNA, whereas a fully modified α-LNA sequence displays a very efficient recognition of complementary RNA.

Conformationally restricted oligonucleotide analogues have been intensively investigated for their abilities in high affinity nucleic acid recognition.[1] As a prime example, LNA (locked nucleic acid)† has recently been introduced as a nucleic acid analogue displaying unprecedented affinity towards DNA and RNA.[2] The anomeric inverted analogue of DNA (α-DNA) has been demonstrated to hybridise efficiently with complementary DNA and RNA with a parallel strand orientation, and to be highly resistant towards degradation by nucleases.[3] Chemically modified analogues of α-DNA have also been investigated,[4] including the introduction of α-configured bicyclic nucleoside monomers.[5]

The α-2′-deoxynucleoside monomers in α-DNA as well as the β-2′-deoxynucleoside monomers in DNA exist in an equilibrium between the two low-energy N- and S-type conformational ranges.[6,7] In none of the α-DNA analogues, investigated so far,[4,5] have the monomers been efficiently restricted towards N-type conformations. Hoping to obtain an unprecedented parallel nucleic acid recognition and, thereby, a new tool in the development of diagnostic probes and antisense therapeutics, we therefore decided to examine the incorporation into oligonucleotides of an α-nucleoside analogue which is conformationally locked in an N-type conformation, *i.e.* α-LNA.‡

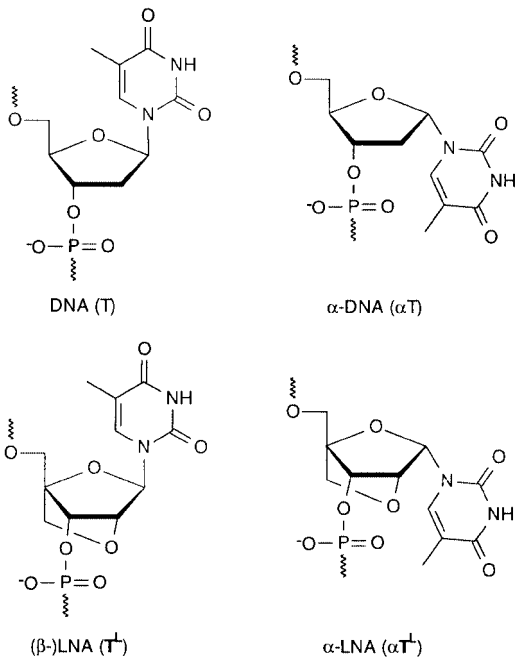

In order to synthesise the α-LNA thymine monomer (αT^L, **4**, Scheme 1) we first investigated the coupling of thymine to appropriate bicyclic carbohydrate precursors.[9] However, this approach has never been optimised to give the target compound in a satisfactory yield, and we hereby introduce an alternative synthetic strategy. The starting methyl furanoside **1** was obtained, as described previously,[9] and used in a modified Vorbrüggen nucleobase coupling reaction (Scheme 1). After varying the reaction conditions, the best result in terms of yield and ratio of products was obtained by using *in situ* TMS-protection of both the 2′- hydroxy functionality in **1** and the thymine, followed by coupling by using TMS-triflate as the Lewis acid in refluxing acetonitrile for seven days. After desilylation, the mixture of nucleosides was reacted with sodium hydride to give the anomeric mixture **2** (α:β ≈ 1.3:1 according to ^{1}H NMR) in 57% overall yield. After removal of the benzyl groups by hydrogenation, the β- and α-LNA monomers (**3**[2] and **4**,[9] respectively) were obtained in 98% yield and separated. The configuration of **4** was confirmed by comparison of NMR data with its exact enantiomer[8d] and by NOE-difference spectra as mutual contacts were observed between H-1′ and H-3′ and between H-5″ and H-6, respectively. The αT^L monomer **4** was prepared for incorporation into oligonucleotide sequences by protection, by using the dimethoxytrityl (DMT) group to give **5**, followed by phosphitylation to give the phosphoramidite synthon **6**.§ This compound was used in automated solid phase synthesis of oligonucleotides by using the phosphoramidite approach.[10] In connection with the α-thymidine (αT) phosphoramidite, the α-LNA sequences were obtained (Table 1) by using tetrazole activation and 10 min coupling times giving > 98% stepwise coupling yields. The modified oligomers **8**–**10** and **12**, **13** were synthesised by using the DMT-*ON* mode on universal CPG-support (Biogenex), which allowed the synthesis of fully modified sequences after cleavage from the solid support by using LiCl in aqueous

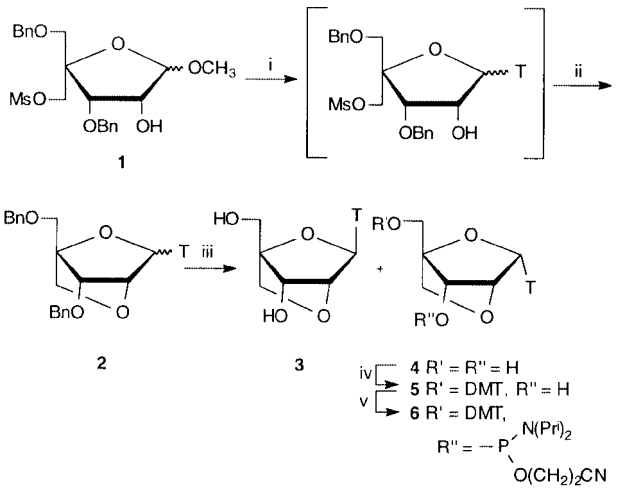

Scheme 1 *Reagents and conditions*: i, (a) TMS-Cl, *N*,*O*-bistrimethylsilylacetamide, thymine, MeCN, then TMS-OTf, (b) TBAF, THF; ii, NaH, DMF (57%, three steps); iii, H_2, $Pd(OH)_2$/C, EtOH (98%); iv, DMT-Cl, $AgNO_3$, Py, THF, DMF (80%); v, $EtN(Pr^i)_2$, $NC(CH_2)_2OP(Cl)N(Pr^i)_2$, CH_2Cl_2 (79%). T = thymine-l-yl.

DOI: 10.1039/b003104f

Table 1 Hybridisation data for α-LNA sequences and reference strands

	Sequence	dA_{14} complement		rA_{14} complement		rA_6CA_7 complement
		T_m/°C[a]	ΔT_m/°C[b]	T_m/°C[a]	ΔT_m/°C[b]	T_m/°C[a]
7	5′-T_{14}	33.0		30.0		n.d.[c]
8	5′-αT_{14}	32.0		43.0		n.d.[c]
9	5′-αT_7**T**$^{\mathbf{L}}$$T_6$	25.5	−6.5	35.0	−8.0	n.d.[c]
10	5′-αT_5**T**$^{\mathbf{L}}$$_4T_5$	26.0	−1.5	24.5	−4.6	n.d.[c]
11	5′-T_{10}	22.0		20.0		n.d.[c]
12	5′-αT_{10}	18.0		33.5		22.0
13	5′-α**T**$^{\mathbf{L}}$$_{10}$	no T_M[d]		45.0	+1.2[e]; +2.5[f]	37.0

[a] Melting temperatures (T_m) obtained from the maxima of the first derivatives of the melting curve (A_{260} *vs.* temperature) recorded in a buffer containing 10 mM Na_2HPO_4, 100 mM NaCl, 0.1 mM EDTA, pH 7.0 using 1.5 μM concentrations of the two complementary sequences, assuming identical extinction coefficients for all thymine nucleotides. [b] The change in T_m value per modification compared with the reference strand **8**. [c] Not determined. [d] No clear cooperative transition was seen. [e] Compared with **12**. [f] Compared with **11**.

ammonia. The oligomers were purified by using disposable reverse phase chromatography cartridges (Cruachem), which yielded products with > 90% purity, as judged from capillary gel electrophoresis. The compositions of α-LNA sequences were verified from MALDI-MS spectra.¶

The α-LNA sequences **9**, **10** and **13**, as well as their α-DNA counterparts **8** and **12**, were mixed with their DNA and RNA complements and the resulting hybridisation data are shown in Table 1. Compared to the unmodified sequence **7**, the affinity of the unmodified α-sequence **8** towards dA_{14} is, as expected,[3] similar. However, the introduction of one or four α-LNA monomers (**9** or **10**, respectively) results in strongly decreased affinities towards dA_{14}. Towards complementary RNA, rA_{14}, **8** has a higher affinity than **7** and the destabilising effect of one or four α-LNA monomers is even more pronounced. However, in both cases, the introduction of a block of α-LNA monomers diminishes the combined destabilising effect (comparing ΔT_m for **9** and **10**). This suggests that the N-type conformation α-LNA monomers do not have the ability to alter neighbouring nucleosides and, thereby, change the overall single strand conformation towards a form which is more preferable for duplex formation. As judged from NMR studies, this is an important feature of the original (β-)LNA.[11]

The fully modified α-LNA sequence **13** displays strong recognition of the complementary RNA-strand (ΔT_m = +1.2 °C per monomer compared to α-DNA **12** and +2.5 °C compared to the unmodified oligodeoxynucleotide sequence **11**). On the other hand, no clear cooperative transition was seen when **13** was mixed with dA_{14}. This indicates either that α-LNA is unable to recognise DNA and is thereby extraordinarily RNA-selective or, alternatively, that the two sequences might form a secondary structure not detectable by UV-spectroscopy at 260 nm. Thus, a broad non-cooperative transition at 40–45 °C is seen in the mixture, but a similar transition is also observed for **13** alone. Even though the possibility of self-melting has been described earlier for longer α-oligothymidylate sequences,[12] the broad transition and low hyperchromicity observed for **13** alone does not indicate the melting process of a duplex structure, but rather a transition between secondary forms of single strands. The presence of a duplex between **13** and rA_{14} was confirmed by the fact that a clear melting transition of a duplex between **13** and a mis-matching complementary sequence was observed with T_m decreased by 8 °C (Table 1). Furthermore, thermal stabilities measured at higher ionic concentrations (data not shown) were increased, as expected, for all the duplexes involving **11**–**13** and RNA-complements as well as **11** and **12** with dA_{14}, whereas no clear cooperative transitions at increased temperature were observed with **13**:dA_{14} or with **13** alone.

In conclusion, α-LNA is able to form a duplex with complementary RNA with a high thermal stability comparable to other stereoisomers of LNA,[8] even though the original (β)LNA still displays the highest affinity towards complementary nucleic acids. Nevertheless, α-LNA in the present oligothymidylate sequence displays the highest affinity towards RNA of any α-D-configured oligonucleotide analogue. However, from the sequences presented here we are not able to determine whether α-LNA prefers a parallel strand orientation upon hybridisation. This subject is under investigation in our laboratories *via* the synthesis of α-LNA sequences with mixed nucleobase compositions, in addition to further examination of the properties and applications of α-LNA.

The Danish Natural Science Research Council is thanked for financial support. Ms. Britta M. Dahl, Department of Chemistry, University of Copenhagen, is thanked for synthesising oligonucleotide sequences. Dr Henrik M. Pfundheller, Exiqon A/S, is thanked for recording MALDI-MS spectra.

Notes and references

† LNA is defined as an oligonucleotide containing one or more LNA monomers which are bicyclic nucleosides preorganized in N-type conformations. α-LNA is therefore defined as an oligonucleotide containing one or more monomeric α-D-LNA nucleosides in connection to unmodified α-D-nucleosides.

‡ Three other stereoisomers of LNA have been recently introduced[8] and their affinities towards both complementary RNA and the enantiomeric L-RNA have been investigated.[8c] In that sense, an α-LNA sequence has been examined in form of the duplex between its enantiomer α-L-LNA and L-RNA, but only as an (almost) fully modified sequence and only against RNA.[8c]

§ Selected data for **6**: δ_P($CDCl_3$, 121.5 MHz with 85% H_3PO_4 as external standard) 150.9, 151.1.

¶ MALDI-MS: *m/z* ([M − H]$^-$ (found/calc.): **9** (4227.1/4223.8); **10** (4309.2/4307.8); **13** (3261.6/3260.1).

1 P. Herdewijn, *Liebigs Ann. Chem.*, 1996, 1337; P. Herdewijn, *Biochim. Biophys. Acta*, 1999, **1489**, 167.

2 S. K. Singh, P. Nielsen, A. A. Koshkin and J. Wengel, *Chem. Commun.*, 1998, 455; A. A. Koshkin, S. K. Singh, P. Nielsen, V. K. Rajwanshi, R. Kumar, M. Meldgaard, C. E. Olsen and J. Wengel, *Tetrahedron*, 1998, **54**, 3607; S. Obika, D. Nanbu, Y. Hari, J. Andoh, K. Morio, T. Doi and T. Imanishi, *Tetrahedron Lett.*, 1998, **39**, 5401; A. A. Koshkin, P. Nielsen, M. Meldgaard, V. K. Rajwanshi, S. K. Singh and J. Wengel, *J. Am. Chem. Soc.*, 1998, **120**, 13 252; J. Wengel, *Acc. Chem. Res.*, 1999, **32**, 301.

3 F. Morvan, B. Rayner, J.-L. Imbach, S. Thenet, J.-R. Bertrand, J. Paoletti, C. Malvy and C. Paoletti, *Nucleic Acids Res.*, 1987, **15**, 3421; M. Durand, J. C. Maurizot, N. T. Thuong and C. Helene, *Nucleic Acids Res.*, 1988, **16**, 5039.

4 C. H. Gotfredsen, J. P. Jacobsen and J. Wengel, *Bioorg. Med. Chem.*, 1996, **4**, 1217; K. Pongracz and S. M. Gryaznov, *Nucleic Acids Res.*, 1998, **26**, 1099; F. Morvan, J. Zeidler and B. Rayner, *Tetrahedron*, 1998, **54**, 71; A. Laurant, M. Laval, F. Debart, J.-J. Vasseur and B. Rayner, *Nucleic Acids. Res.*, 1999, **27**, 4151.

5 M. Bolli, P. Lubini and C. Leumann, *Helv. Chim. Acta*, 1995, **78**, 2077; R. Zou and M. D. Matteucci, *Bioorg. Med. Chem. Lett.*, 1998, **8**, 3049.

6 W. Saenger, *Principles of Nucleic Acid Structure*, Springer, New York, 1984.

7 C. Thibaudeau and J. Chattopadhyaya, *Nucleosides Nucleotides*, 1997, **16**, 523.

8 (*a*) V. K. Rajwanshi, A. E. Håkansson, B. M. Dahl and J. Wengel, *Chem. Commun.*, 1999, 1395; (*b*) V. K. Rajwanshi, A. E. Håkansson, R. Kumar and J. Wengel, *Chem. Commun.*, 1999, 2073; (*c*) V. K. Rajwanshi, A. E. Håkansson, M. D. Sørensen, S. Pitsch, S. K. Singh, R. Kumar, P. Nielsen and J. Wengel, *Angew. Chem., Int. Ed.*, 2000, **39**, 1656; (*d*) A. E. Håkansson and J. Wengel, personal communication.

9 P. Nielsen and J. Wengel, *Chem. Commun.*, 1998, 2645.

10 M. H. Caruthers, *Acc. Chem. Res.*, 1991, **24**, 278.

11 M. Petersen, C. B. Nielsen, K. E. Nielsen, G. A. Jensen, K. Bondensgaard, S. K. Singh, V. K. Rajwanshi, A. A. Koshkin, B. M. Dahl, J. Wengel and J. P. Jacobsen, *J. Mol. Recognit.*, 2000, **13**, 44.

12 U. Neidlein and C. Leumann, *Tetrahedron Lett.*, 1992, **33**, 8057.

Ligand assisted dimerisation of a diplatinum(2+) system: a straightforward high yield access to tetranuclear platinum clusters

Walter Schuh, Helmuth Wachtler, Gerhard Laschober, Holger Kopacka, Klaus Wurst and Paul Peringer*

Institut für Allgemeine, Anorganische und Theoretische Chemie Universität Innsbruck, A-6020 Innsbruck, Austria. E-mail: paul.peringer@uibk.ac.at

Received (in Basel, Switzerland) 13th April 2000, Accepted 24th May 2000

The iodide induced dimerisation of a dppm-/diphenylphosphido-bridged Pt_2^{2+} system leads to a 56 CVE Pt_4 butterfly cluster which is diprotonated by HO_3SCF_3 to give a 60 CVE rectangular Pt_4 cluster.

An electron count of 56 or 54 for tetranuclear platinum clusters in tetrahedral geometry with a latitudinal or longitudinal ligand arrangement is predicted by theoretical studies based on $Pt(PH_3)_2$ fragments.[1] 54-electron CVE clusters are proposed to be stabilised by bridging dppm or phosphido ligands, which might be able to retain the less favourable longitudinal ligand arrangement. Taking into account that two additional electrons lead to a butterfly geometry of the Pt_4 core, we report here on a ligand controlled stabilisation of an unusual cluster electron count: a Pt_4 butterfly cluster with the hitherto unknown valence electron count of 56 is readily accessible *via* dimerisation of the diplatinum(2+) system in a suitable ligand sphere. The protonation of the cluster is associated with a novel structural rearrangement of the cluster core to a rectangular 60 CVE Pt_4 skeleton.

Treatment of $[Pt_2(\mu\text{-dppm})(\mu\text{-}PPh_2)\{\eta^2\text{-bicyclo(2.2.1)hept-2-ene}\}_2](O_3SCF_3)_2$ **1**, (Scheme 1) with 1 mol equiv. of NBu_4I in toluene–dichloromethane (4/1) produces quantitatively the tetranuclear cluster $[Pt_4(\mu\text{-dppm})_2(\mu\text{-}PPh_2)_2I_2]$ **2** (Scheme 1, Fig. 1†) as dark red red crystals which are sparingly soluble in all common organic solvents. The reaction proceeds *via* the substitution of one bicyclo(2.2.1)hept-2-ene by iodide‡ which may in turn induce the dissociation of the remaining bicyclo-(2.2.1)hept-2-ene resulting in a reactive intermediate. The formation of **2** represents a ring opening dimerisation, the overall oxidation state of the platinum centres of +1 is maintained. We do not know whether the $Pt_2(\mu\text{-}PPh_2)$ or the $Pt_2(\mu\text{-dppm})$ ring is opened. The molecular structure of **2** exhibits a butterfly shaped Pt_4 skeleton. Complying with a crystallographically imposed C_2 symmetry, the two dppm and two diphenylphosphido ligands alternately bridge between the hinge and wingtip platinum atoms. One terminal iodide ligand is attached to each wingtip.

The wingtip to hinge Pt–Pt distances are 274.03(8) pm for the dppm-bridged and 287.40(8) pm for the diphenylphosphido-bridged platinum atoms. The distance between the two hinge Pt atoms of the butterfly framework amounts to 269.33(11) pm. The dihedral angle between the two wings [144.27(2)°] is substantially larger compared with other Pt_4 butterfly clusters

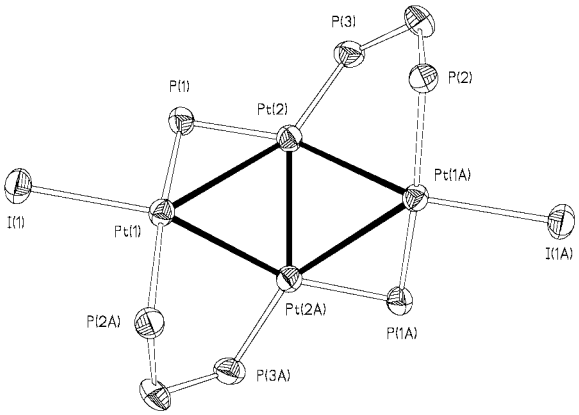

Fig. 1 Molecular structure of **2**. The phenyl groups have been omitted for clarity.

(83.7–96.8°).[3] The Pt_2P_2C rings formed by the dppm ligands adopt twist conformations. The structure seems to be retained in solution according to ^{31}P NMR spectroscopy.§

The protonation of **2** with 50% aqueous trifluoromethanesulfonic acid quantitatively produces the yellow tetranuclear dihydrido cluster $[Pt_4(\mu\text{-dppm})_2(\mu\text{-}PPh_2)_2(\mu_2\text{-}H)_2(\mu_2\text{-}I)_2](O_3SCF_3)_2$ **3** (Scheme 1, Fig. 2†) which is slightly soluble in CH_2Cl_2. The formation of **3** is accompanied by a rearrangement of the Pt_4 shape to a rectangle, a change of the geometry of the phosphido phosphorus relative to the dppm phosphorus atoms from *cis/trans* in **2** to *cis/cis* in **3** and a change to a bridging bonding mode of the iodide ligands. The phosphido bridged edges of the Pt_4 rectangle involve relatively short Pt–Pt distances [279.92(3) and 277.28(3) pm], whilst the distances of the dppm bridged platinum atoms [296.85(3) and 300.58(3) pm] indicate that the Pt–Pt interactions are weak. All sides are doubly bridged, either by dppm and iodide or by diphenylphosphido and hydride ligands making a 60-electron CVE. The hydride and iodide ligands are on the same side of the Pt_4 plane. The hydride ligands could be located *via* X-ray structure analysis and their position is confirmed by NMR spectroscopy:¶ the intensity of the hydride signal of the isotopomer containing one ^{195}Pt nucleus demonstrates a μ_2-H bonding. The P–H coupling constants involving the dppm and phosphido phospho-

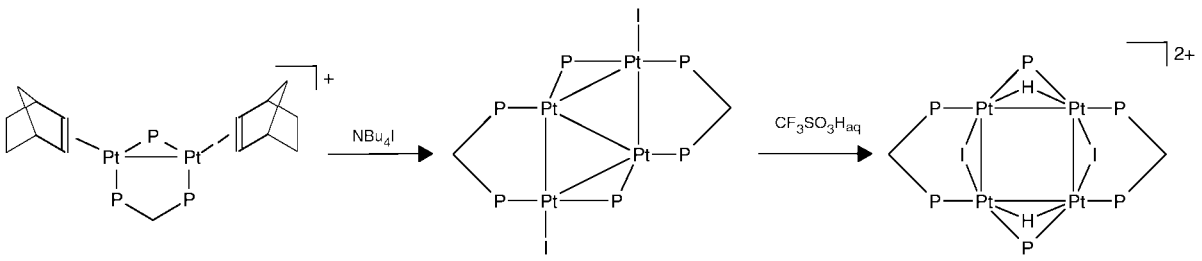

1 **2** **3**

Scheme 1

DOI: 10.1039/b003101l

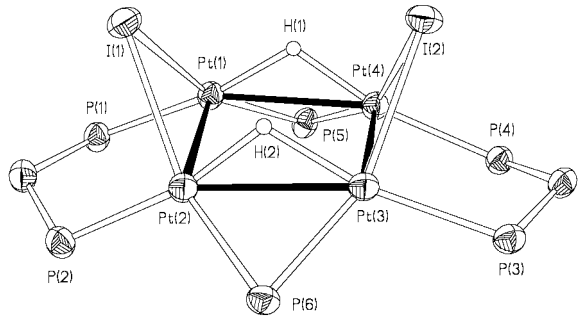

Fig. 2 Structure of the cation of **3**. The phenyl groups have been omitted for clarity.

rus atoms are 87.7 and 13.2 Hz respectively. This indicates the H–Pt–P_{dppm} angle to be distinctly larger compared with the H–Pt–$P_{phosphido}$ angle and this requires the hydride ligands to bridge the same edge as the phosphido ligands. The hydride ligands are kinetically stable on the NMR time scale at ambient temperature.

Dimerisation reactions related to the formation of **2** exist for the dipalladium(2+) system: the product of $[Pd_2(\mu\text{-dppm})_2Cl_2]$ and $NaBH_4$ was recently identified as $[Pd_4(\mu\text{-dppm})_4(\mu_4\text{-H})_2]^{2+}$ and the reaction with $[Cu(MeCN)_4]^+$ gave $[Pd_4(\mu\text{-dppm})_4(\mu_2\text{-Cl})_2]^{2+}$.[4,5] The X-ray structure of the latter product showed a rectangular Pd_4 skeleton [Pd–Pd 259.4(2) and 374.2(3) pm] consisting of two isolated Pd_2 moieties whereas no solid state structure of $[Pd_4(\mu\text{-dppm})_4(\mu_4\text{-H})_2]^{2+}$ is available. Analogous reactions of the platinum congener $[Pt_2(\mu\text{-dppm})_2Cl_2]$ leave the $[Pt_2(\mu\text{-dppm})_2]$ arrangement unchanged.[6] The different reactivities of the platinum and palladium $[M_2(\mu\text{-dppm})_2Cl_2]$ complexes have been attributed to different M–P bonding strengths. The reactivity of **1** in contrast to $[Pt_2(\mu\text{-dppm})_2Cl_2]$ is apparently due to the presence of both dppm and diphenylphosphido ligands.

Notes and references

† *Crystal data* for **2**: $C_{74}H_{64}I_2P_6Pt_4$, M = 2173.23, monoclinic, a = 1272.88(5), b = 2578.7(2), c = 2115.80(10) pm, β = 97.689(4)°, V = 6.8824(7) nm^3, T = 218(2) K, space group $C2/c$ (no. 15), Z = 4, Mo-Kα radiation (λ = 71.073 pm), 15160 reflections measured, 4166 reflections unique (R_{int} = 0.0597), reflections with $I > 2\sigma(I)$ 3670, $R1$ [$I > 2\sigma(I)$] = 0.0478, $wR2$ [$I > 2\sigma(I)$] = 0.1055, Goodness of fit 1.253. The structure was solved by direct methods (SHELXS-86),[7] and refined by full matrix least squares methods on F^2 (SHELXL-93).[8]

For **3**: $C_{76}H_{66}F_6I_2O_6P_6Pt_4S_2{\cdot}2.5HO_3SCF_3{\cdot}4H_2O{\cdot}0.5CH_2Cl_2$, M = 2963.11, triclinic, a = 1452.98(2), b = 1850.66(2), c = 1873.47(3) pm, α = 104.854(1), β = 96.059(1), γ = 99.961(1)°, V = 4.73613(11) nm^3, T = 218 (2) K, space group $P\bar{1}$ (no. 2), Z = 2, Mo-Kα radiation (λ = 71.073 pm), 83252 reflections measured, 14013 reflections unique (R_{int} = 0.0661), reflections with $I > 2\sigma(I)$ 12327, $R1$ [$I > 2\sigma(I)$] = 0.0326, $wR2$ [$I > 2\sigma(I)$] = 0.0767, Goodness of fit 1.017. The structure was solved by direct methods (SHELXS-86),[7] and refined by full matrix least squares methods on F^2 (SHELXL-93).[8]

CCDC 182/1656. See http://www.rsc.org/suppdata/cc/b0/b003101l/ for crystallographic files in .cif format.

‡ *NMR data* for $[Pt_2(\mu\text{-dppm})(\mu\text{-}PPh_2)\{\eta^2\text{-bicyclo(2.2.1)hept-2-ene}\}I]$. ^{31}P NMR (CD_2Cl_2): δ 198.3 [P^1 (phosphido), $J(P^1P^2)$ 332.1, $J(P^1P^3)$ 181.3, $J(Pt^1P^1)$ 2422, $J(Pt^2P^1)$ 3152 Hz], 7.3 [P^2 (dppm, phosphorus *cis* to I), $J(P^2P^3)$ 62.8, $J(Pt^1P^2)$ 54, $J(Pt^2P^2)$ 3493 Hz], −2.7 [P^3 (dppm, phosphorus *cis* to bicyclo(2.2.1)hept-2-ene), $J(Pt^1P^3)$ 2896, $J(Pt^2P^3)$ 105.9 Hz]; ^{195}Pt NMR (CD_2Cl_2): δ −5807 [Pt^1 (Pt bound to bicyclo(2.2.1)hept-2-ene), $J(Pt^1Pt^2)$ 3137 Hz], −5240 [Pt^2 (Pt bound to I)].

§ *NMR data* for **2** (labelling of the atoms as in Fig. 1). ^{31}P NMR (CD_2Cl_2): δ 170.0 [P^1, $J(PtP^1)$ 2563, 2343, 238 Hz], 9.5 [P^3, $J(PtP^3)$ 3865, 813 Hz], −2.4 [P^2, $J(PtP^2)$ 2824 Hz].

¶ *NMR data* for **3** (labelling of the atoms as in Fig. 2). ^{31}P NMR (CD_2Cl_2): δ 142.2 [P^5, $J(Pt^1P^5)$ 3236, $J(Pt^2P^5)$ 54 Hz], 17.3 [P^1, $J(Pt^1P^1)$ 3974, $J(Pt^4P^1)$ 274 Hz]; ^1H NMR (CD_2Cl_2): δ −7.39 [^2J(PH) 13.2 (PPh_2), 87.7 (dppm), ^1J(PtH) 403 Hz].

1 D. G. Evans, *J. Organomet. Chem.*, 1987, **319**, 265.
2 H. Wachtler, W. Schuh, K.-H. Ongania, K. Wurst and P. Peringer, *Organometallics*, 1998, **17**, 5640.
3 T. Zhang, M. Drouin and P. D. Harvey, *J. Cluster Sci.*, 1998, **9**, 165 and references therein; G. Douglas, L. Manojlovic-Muir, K. W. Muir, M. C. Jennings, B. R. Lloyd, M. Rashidi, G. Schoettel and R. J. Puddephatt, *Organometallics*, 1991, **10**, 3927 and references therein; K. H. Dahmen, A. Moor, R. Naegeli and L. M. Venanzi, *Inorg. Chem.*, 1991, **30**, 4285 and references therein.
4 I. Gauthron, J. Gagnon, T. Zhang, D. Rivard, D. Lucas, Y. Mugnier and P. D. Harvey, *Inorg. Chem.*, 1998, **37**, 1112.
5 P. Braunstein, M. A. Luke, A. Tiripicchio and M. Camellini, *Angew. Chem., Int. Ed. Engl.*, 1987, **26**, 768.
6 M. C. Grossel, J. R. Batson, R. P. Moulding and K. R. Seddon, *J. Organomet. Chem.*, 1986. **304**, 391.
7 G. M. Sheldrick, SHELXS-86: program for crystal structure solutions, Göttingen, 1986.
8 G. M. Sheldrick, SHELXL-93: program for refinement of crystal structures, Göttingen, 1993.

Porphyrin sensitization of circularly polarised near-IR lanthanide luminescence: enhanced emission with nucleic acid binding†

Andrew Beeby,*[a] Rachel S. Dickins,[a] Simon FitzGerald,[a] Linda J. Govenlock,[a] Christine L. Maupin,[b] David Parker,*[a] James P. Riehl,[b] Giuliano Siligardi[c] and J. A. Gareth Williams[a]

[a] *Department of Chemistry, University of Durham, South Road, Durham, UK DH1 3LE. E-mail: david.parker@durham.ac.uk*
[b] *Department of Chemistry, Michigan Technological University, Houghton, Michigan 4993 11295, USA*
[c] *Department of Pharmacy, King's College London, Stamford Street, London, UK SE1 8WA*

Received (in Cambridge, UK) 25th March 2000, Accepted 23rd May 2000

A palladium porphyrin has been covalently linked to a chiral lanthanide complex and effectively sensitises near-IR emission from Nd and Yb; sensitisation is enhanced in the absence of oxygen and in the presence of a nucleic acid.

The use of 'antennae' chromophores (such as substituted aryl,[1] bipyridyl[2] and phenanthridyl[3] groups) to sensitize lanthanide emission is now well established, particularly for lanthanide complexes which emit in the visible region of the spectrum, *e.g.* Eu(III) and Tb(III). The triplet energies of porphyrins (typically 12 000–17 000 cm^{-1}) render them suitable chromophores for sensitization of the relatively low-lying excited state(s) of lanthanide ions such as Yb(III) (10 200 cm^{-1}) and Nd(III) (11 360 cm^{-1}). Lanthanides with emission bands in the near-IR region of the spectrum have a variety of potential applications, including time-resolved luminescence imaging,[4] beyond the range of biological absorption or emission (*e.g.* from NADPH, haematoporphyrin). Previous work has demonstrated that Yb–porphyrin complexes possess rapid rates of energy transfer ($> 10^7$ s^{-1}) from the porphyrin antennae to the bound Yb ion[5] and the Yb emission intensity is primarily limited by quenching of the $^2F_{5/2}$ excited state involving vibrational energy transfer to bound OH oscillators.[6] In these cases, the Yb emission is insensitive to oxygen quenching of the intermediate excited porphyrin triplet. When an Yb ion is further away from the sensitising chromophore, the energy transfer step is less efficient and deactivation of the intermediate triplet state by oxygen may compete. Palladium porphyrin complexes possess particularly long-lived triplet states[7] and are subject to quite efficient oxygen quenching in polar media. Tetracationic Pd–porphyrins have been shown to bind to DNA[8] and the intercalation suppresses oxygen quenching, enhancing the phosphorescence by factors of up to 20.

With this background in mind, we have prepared a set of Pd–porphyrin conjugates which are linked to a well defined cationic, chiral lanthanide moiety. The strongly helical tetraamide complexes of Eu, Tb and Yb, incorporating an intercalating phenanthridinium moiety, have recently been shown to bind to DNA stereoselectively and with a factor of 50 in GC *vs.* AT base-pair differentiation.[9] The aim of the work described herein was to explore the sensitising ability of the proximate Pd–porphyrin chromophore for Nd and Yb emission and the effect of oxygen in the presence and absence of a simple oligonucleotide.

2-Aminoporphyrin **1** was prepared following the method described by Crossley and King.[10] Amide coupling of **1** with chloroacetic acid, using standard amide coupling conditions, followed by Pd complexation afforded the corresponding porphyrin chloroacetamide, which was then treated with an excess of KI in THF–MeCN to give the porphyrin iodoacetamide **2**. Reaction of **2** with an excess of cyclen in THF at 50 °C

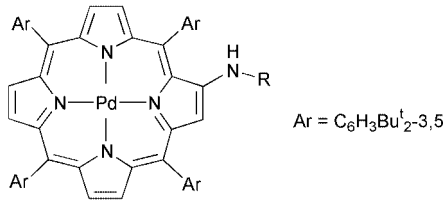

1 R = H
2 R = $COCH_2I$

gave an almost quantitative yield of the monosubstituted-{Pd–porphyrin}-12-N_4. Introduction of the three chiral pendant arms onto the remaining ring nitrogens was carried out by reaction with either (*S*)- or (*R*)-2-chloro-*N*-(methylbenzyl)ethanamide to afford (*SSS*-*S*)-L^1 and the (*RRR*-*R*) isomer, respectively. Alkylation also occurred at the rather acidic amide NH position on the porphyrin periphery. Reaction of L^1 with lanthanide trifluromethanesulfonates (Yb, Nd, Gd) afforded cationic complexes which were purified by alumina preparative plate chromatography. Complexes gave ESMS, microanalyses and ^1H NMR spectra in accord with the proposed structures. For example, for $[YbL^1]^{3+}$, ESMS analysis revealed peaks at *m/z* 738 $[M]^{3+}$ and 1181 $[M + CF_3SO_3]^{2+}$ and the ^1H NMR spectrum in CD_3OD(293 K, 200 MHz) showed a single set of resonances (> 87%) for the most shifted ring axial proton for both stereoisomers at δ +100.8, 95.5, 78.2 and 72.9. Such chemical shift values are in a similar range to those observed for related tetraamide Yb complexes with a capping water molecule, in which the complex adopts a square antiprismatic coordination environment.[11]

The circular dichroism spectra for the (*RRR*)-$[NdL^1]^{3+}$, (*RRR*)-$[YbL^1]^{3+}$ and (*SSS*)-$[YbL^1]^{3+}$ complexes, in the visible range, are shown in Fig. 1. The CD spectra are dominated by the porphyrin chromophore, with the characteristic Soret band at *ca.* 422 nm (log ε = 5.36 M^{-1} cm^{-1}), and the α and β bands at 520 (log ε 4.37) and 560 nm (log ε 3.57), respectively (295 K, MeOH). The weak induced CD obtained for the (*RRR*)-Yb

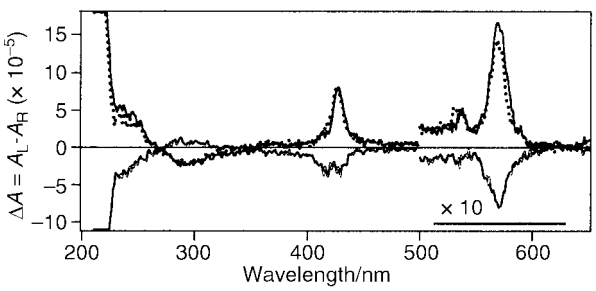

Fig. 1 CD spectra of (*RRR*-*R*)-YbL^1 (upper bold), (*RRR*-*R*)-NdL^1 (dashed) and (*SSS*-*S*)-YbL^1 (lower) (295 K, MeOH).

† Electronic supplementary information (ESI) available: emission spectra. See http://www.rsc.org/suppdata/cc/b0/b002452j/

DOI: 10.1039/b002452j

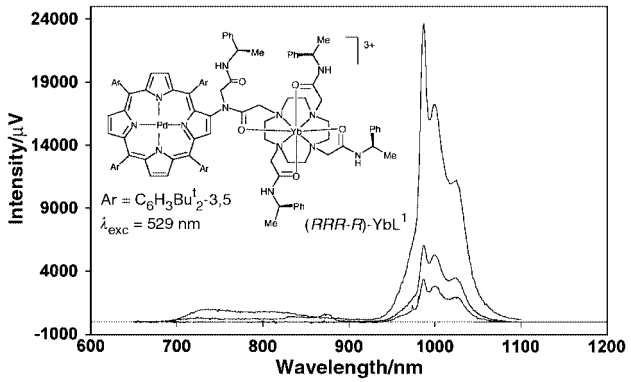

Fig. 2 Emission spectra for (*RRR*-*R*)-YbL[1] (295 K, 20% D_2O–CD_3OD, 5 μM) in degassed solution (top), in aerated solution (bottom) and in the presence of 0.1 mM $[(CG)_6]_2$.

complex resembles that of the Nd complex, with g_{abs} values of $+1.7 \times 10^{-4}$ (560 nm) and $+0.8 \times 10^{-4}$ (423 nm). Intriguingly the CD spectrum of the (*SSS*) stereoisomer showed a split Soret band (perhaps related to the change in the tertiary amide configuration in the two complexes, giving a different orientation of the porphyrin chromophore with respect to the Yb ion) and a reduced ICD at 420 and 566 nm. The chirality of the excited state of the lanthanide centre is conveniently probed using circularly polarised luminescence spectroscopy (CPL);[12] the first examples of CPL in the near-IR, following sensitised excitation in the near-UV, have only recently been reported.[13] With (*RRR*)-$[YbL^1]^{3+}$, weak CPL was observed following excitation at 529 nm, with $g_{em} = -0.04$ (985 nm) and $+0.05$ (963 nm) and a very similar spectrum, with the opposite polarisation was observed for the (*SSS*) complex. CPL spectra were also measured for the (*RRR*)-Nd complex and, for the first time, small, but measurable, CPL was observed for the $^4F_{3/2} - {}^4I_{9/2}$ transitions [*e.g.* $g_{em} = +0.015$ (884 nm)] and for the $^4F_{3/2}$–$^4I_{11/2}$ transition [$g_{em} = -0.006$ (1055 nm)].

The total emission spectra for the Yb and Nd porphyrin conjugates were measured in aerated and degassed MeOH and CD_3OD (Fig. 2), following excitation at 529 nm. Enhanced emission from the Ln ion was observed in the deuteriated solvent (a factor of 4 for Yb and 2.5 for Nd), reflecting the known sensitivity of the excited ion to quenching by OH oscillators.[6] In the absence of oxygen, the phosphorescence from the Pd–porphyrin appeared as a broad emission with maxima at *ca*. 735 and 800 nm, while that due to the lanthanide was also enhanced (a factor of 7 for Yb and 2 for Nd). The excitation spectra of degassed samples, observing the emission from Yb at 980 nm and Nd at 1064 or 870 nm, revealed the same spectrum which matched the porphyrin absorption spectrum of the separate complexes. Taken together such behaviour is consistent with competitive rates of energy transfer and triplet quenching by oxygen. The energy transfer to Nd is considerably more efficient than to Yb, as a consequence of the better spectral overlap integral (Nd: absorption maxima at 740, 794 and 865 nm (with ε values of 6, 9 and 3 $dm^3\ mol^{-1}\ cm^{-1}$, respectively) overlap well with the porphyrin emission band, but poorly with Yb at 980 nm (2 $M^{-1}\ cm^{-1}$). The absence of the porphyrin emission in aerated solution reflects the efficiency of the bimolecular quenching process (values of $k_q[O_2]$ of *ca*. 1×10^9 s^{-1} have been reported for palladium porphyrins).[8] In addition, the very presence of Ln emission is an indication that the rate of intramolecular energy transfer is relatively fast. The Yb emission from the stereoisomeric (*SSS*)-YbL[1] complex was identical in form but was 40% lower in intensity.

Preliminary time resolved studies have allowed the decay of the porphyrin triplet and the grow-in and decay of the Nd or Yb emission to be monitored. The rate constant for oxygen quenching was calculated to be $5 \times 10^8\ M^{-1}\ s^{-1}$ for the Nd complex. Complex decay profiles were observed consistent with the similar rates of decay of the Yb excited state and the rate of dissociative solvent exchange.[11] However, qualitative agreement between the rate of triplet decay and the rate of Ln 'grow-in' was observed, consistent with the conventional mechanism of triplet-mediated lanthanide sensitisation.[2,6]

In the presence of a 20 mol excess of $[(CG)_6]_2$ oligonucleotide or calf-thymus DNA, in aerated solution {20% D_2O–CD_3OD, 296 K, 5 μM (*RRR*)-$[YbL^1]^{3+}$, λ_{exc} 529 nm}, the porphyrin emission re-appeared to 30% of its value in deoxygenated media; the Yb emission also increased by a factor of 2, *i.e.* also to *ca*. 30% of the value in deoxygenated solution. Very similar behaviour was observed with the (*SSS*) stereoisomer. Evidently binding to the nucleic acid inhibits quenching of the porphyrin triplet by oxygen. That the porphyrin moiety might be interacting with the CG base pairs was suggested by the observation of a red-shift (9 nm) and a pronounced hypochromicity of the Soret band (40%) on binding.

The behaviour reported here is of interest with respect to time-resolved near-IR imaging studies. The sensitivity of the Nd and especially Yb emission to pO_2 may also be of interest in defining regions of low oxygen tension.

We thank EPSRC, the Royal Society, the Commissioners of the Exhibition of 1851 (L. J. G.), and BBSRC for support.

Notes and references

1 A. Casnati, C. Fischer, M. Guardigli, A. Isernia, I. Manet, N. Sabbatini and R. Ungaro, *J. Chem. Soc., Perkin Trans. 2*, 1996, 395; M. P. Oude-Wolbers, F. C. J. M. Van Veggel, B. H. M. Snellink-Ruel, J. W. Hofstraat, F. A. J. Guerts and D. N. Reinhoudt, *J. Am. Chem. Soc.*, 1997, **119**, 138.
2 N. Sabbatini, M. Guardigli and J.-M. Lehn, *Coord. Chem. Rev.*, 1993, **123**, 201.
3 D. Parker, K. Senanayake and J. A. G. Williams, *J. Chem. Soc., Perkin Trans. 2*, 1998, 2129.
4 M. I. Gaiduk, V. V. Grigoryants, A. F. Mironov, V. D. Rumyantseva, V. I. Chissov and G. M. Sukhin, *J. Photochem. Photobiol. B*, 1990, **7**, 15.
5 T. F. Kachura, A. N. Sevchenko, K. N. Solov'ev and M. P. Tsvirko, *Dokl. Akad. Nauk SSSR*, 1974, **217**, 1121; M. Gauterman, C. D. Schumaker, T. S. Srivastava and T. Yaneta, *Chem. Phys. Lett.*, 1976, **40**, 456.
6 A. Beeby, I. M. Clarkson, R. S. Dickins, S. Faulkner, D. Parker, L. Royle, A. S. de Sousa, J. A. G. Williams and M. Woods, *J. Chem. Soc., Perkin Trans. 2*, 1999, 493; M. P. Oude-Wolbers, F. C. J. M. van Veggel, B. H. M. Snellink-Ruel, J. W. Hofstraat, F. A. J. Guerts and D. N. Reinhoudt, *J. Chem. Soc., Perkin Trans. 2*, 1998, 2141; M. H. V. Werts, J. W. Verhoeven and J. W. Hofstraat, *J. Chem. Soc., Perkin Trans. 2*, 2000, 433.
7 P. M. Gewehr and D. T. Delpy, *Med. Biol. Eng. Comput.*, 1993, **31**, 2; P. M. Gewehr and D. T. Delpy, *Med. Biol. Eng. Comput.*, 1993, **31**, 11; D. B. Papkovsky, *Anal. Chem.*, 1995, **67**, 4112; P. Hartmann and W. Trettnak, *Anal. Chem.*, 1996, **68**, 2615; A. Beeby and S. Faulkner, *Chem. Phys. Lett.*, 1997, **266**, 116 and references therein.
8 A. M. Brun and A. Harriman, *J. Am. Chem. Soc.*, 1994, **116**, 10 383.
9 L. J. Govenlock, C. E. Mathieu, C. L. Maupin, D. Parker, J. P. Riehl, G. Siligardi and J. A. G. Williams, *Chem. Commun.*, 1999, 1699.
10 M. J. Crossley and L. J. King, *J. Chem. Soc., Chem. Commun.*, 1984, 920.
11 A. S. Batsanov, A. Beeby, J. I. Bruce, J. A. K. Howard, A. M. Kenwright and D. Parker, *Chem. Commun.*, 1999, 1011.
12 J. P. Riehl and F. S. Richardson, *Chem. Rev.*, 1986, **86**, 1; J. P. Riehl and F. S. Richardson, *Methods Enzymol.*, 1993, **226**, 539.
13 C. L. Maupin, D. Parker, J. P. Riehl and J. A. G. Williams, *J. Am. Chem. Soc.*, 1998, **120**, 10 563.

ChemComm

Excited-state interconversion between emissive MLCT levels in a dinuclear Ru(II) complex containing a bridging ligand with an extended π system

Lucia Flamigni,*[a] Susana Encinas,[a] Francesco Barigelletti,[a] Frederick M. MacDonnell,*[b] Kahn-Jong Kim,[b] Fausto Puntoriero[c] and Sebastiano Campagna*[c]

[a] *Istituto FRAE-CNR, Via Gobetti 101, I-40129 Bologna, Italy. E-mail: photochem@chem.unime.it*
[b] *Department of Chemistry and Biochemistry, University of Texas at Arlington, Arlington, Texas 76019, USA*
[c] *Dipartimento di Chimica Inorganica, Chimica Analitica e Chimica Fisica, Università di Messina, Via Sperone 31, I-98166 Messina, Italy*

Received (in Basel, Switzerland) 17th April 2000, Accepted 22nd April 2000

For a diruthenium complex, charge migration between different moieties of a bridging ligand with extended conjugation is directly monitored for the first time by using time-resolved emission and absorption spectroscopy.

In recent years, luminescent Ru(II) complexes containing bpy-like polypyridine ligands with extended conjugation have received extensive attention because of their possible use as building blocks for multicomponent systems. These include stereochemically pure metallodendrimers,[1] molecular wires,[2–4] topologically controlled dyads and triads,[5] and compounds designed to behave as luminescent DNA probes.[6–11]

During the progress of these studies, some interesting and somewhat unexpected results have been obtained, in particular: (i) a dramatic effect of solvent or microenvironment on the luminescence properties of these species, which led to the so-called 'light-switching' behaviour of some of these species with respect to DNA interations;[6,7,10] (ii) a relatively small electronic coupling between metal-based chromophores connected by large and conjugated planar bridges,[1–4] implying relatively slow photoinduced electron and energy transfers across the bridges.

Recent investigations[1,10] pointed out that most of these results could be rationalised by taking into account the presence of multiple metal-to-ligand charge-transfer (MLCT) excited states (Fig. 1). According to this view, these states are localised on different moieties of the polypyridine ligands with extended conjugation, with their relative energy ordering and interconversion rates subject to the influence of the microenvironment. This assumption however relies on dynamics of interconversion between states which have been only marginally addressed.[10,11]

Here, we present direct evidence for the excited state interconversion between luminescent MLCT levels involving the tetrapyrido[3,2-*a*:2′,3′-*c*3″,2″-*h*:2‴,3‴-*j*]phenazine bridging ligand (tpphz). The interplay of these MLCT levels is responsible for the photophysical properties of the dinuclear complex $[(phen)_2Ru(\mu\text{-tpphz})Ru(phen)_2](PF_6)_4$ **1** (phen = 1,10-phenanthroline; the structural formula of **1** is shown in Fig. 2),[1] and the dynamics of the process are described on the basis of the results obtained from time-resolved absorption and luminescence spectroscopy.

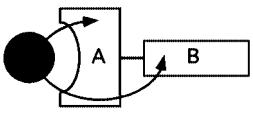

Fig. 1 Schematic representation of the MLCT transitions (arrows) from a metal M (solid circle) to a planar ligand A–B with extended conjugation, which give rise to multiple MLCT excited states. To underline the different localization of the two ligand orbitals involved in the transitions, the ligand A–B is represented as a segmented species, in which A and B are different moieties. Additional ligands and complex charges are neglected. M-to-A CT may convert into M-to-B CT by an A-to-B electron-transfer process.

The redox behavior, ground state absorption spectra, and steady-state luminescence spectra of **1** in acetonitrile fluid solution at room temperature and in a MeOH–EtOH (4:1, v/v) rigid matrix at 77 K have been previously reported.[1] The results are consistent with the following description. Direct irradiation first leads to population of the singlet Ru → tpphz CT state involving the phenanthroline moiety of the tpphz ligand, which very rapidly decays to the corresponding triplet state. At 77 K in rigid matrix, this latter state deactivates to the ground state, giving rise to a ^{3}MLCT luminescence peaking at 585 nm. By contrast, in fluid solution at room temperature a charge reorganization process occurs within the (formally) reduced tpphz bridging ligand. Here, the extra electron initially localized on the phen moiety migrates towards the central, pyrazine-based part of the bridge. Thus, the charge-reorganization process leads to population of a triplet Ru → tpphz CT state involving the pyrazine moiety of tpphz, which is the lowest energy excited state of **1**.[1] In turn, this level deactivates to the ground state (λ_{em}^{max} = 710 nm, τ = 100 ns; data in argon-purged acetonitrile).

In an attempt to study in further detail the dynamics of the excited-state interconversion taking place in **1**, we have performed time-resolved studies in different solvents.[12] In acetonitrile solution at room temperature the shape of the luminescence spectrum, as registered at the end of a 35 ps laser pulse, is constant in a time window of 7 ns, and essentially similar to that obtained from steady-state experiments. A possible explanation can be sought in the rate constant of the process, which could be faster than our experimental resolution time (30 ps). If this is the case, the interconversion process has to be slowed down to be detectable. For this reason, we decided to perform the experiments in dichloromethane because in this low-polarity solvent, CT levels are expected to be destabilized with respect to what happens in acetonitrile. Because of the different donor–acceptor separation in the two possible MLCT states involving the large bridging ligand, the extent of this effect should be larger for the final, lower-lying MLCT level (with reference to Fig. 1, this level could be described as a M-to-B CT state) than for the upper-lying MLCT state initially populated (which may be described as M-to-A CT, Fig. 1). As a consequence, in dichlomethane and with respect to acetonitrile, the lower-lying MLCT level should be destabilized (or less

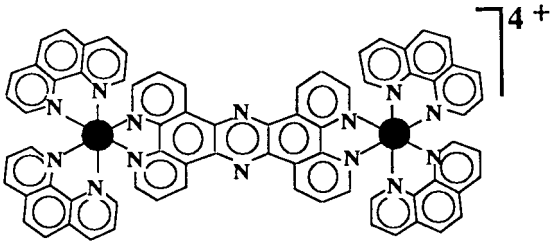

Fig. 2 Structural formula of **1**.

DOI: 10.1039/b004109m

stabilized) with respect to the upper-lying level, so that the driving force of the interconversion process between the two MLCT states is expected to be less favourable and the related rate constant slower and accessible to the time resolution of our equipment.

Actually, the luminescence properties of **1** are time-dependent in dichloromethane solution at room temperature (Fig. 3). In this solvent, the luminescence spectrum registered within the time gate 0–250 ps peaks at *ca.* 610 nm, while the spectrum registered within the time interval 1200–1450 ps is significantly red-shifted, peaking at *ca.* 630 nm (this spectrum is substantially similar to the steady-state emission spectrum in dichloromethane). These results suggest that at least two excited states contribute to the emission of **1** in dichloromethane at room temperature. The kinetic analysis of the streak image in the high- and low-energy wavelength regions of the emission spectra clearly indicates that the lower-energy emissive state is produced from the excited state responsible for the higher-energy emission. Actually, this latter emission decays with a lifetime of 220 ps, whereas the lower-energy emission exhibits a risetime of 200 ps, Fig. 3. Further evidence for the two-state interconversion comes from transient absorption spectroscopy, Fig. 4. Here we see that the absorption spectrum which is present at the end of the laser pulse, exhibiting a maximum around 625 nm, evolves to a new spectrum with a slightly blue shifted maximum, 620 nm, and a higher extinction coefficient. The rate of formation of the new species is 230 ps, see inset of Fig. 4, in good agreement with the luminescence results.

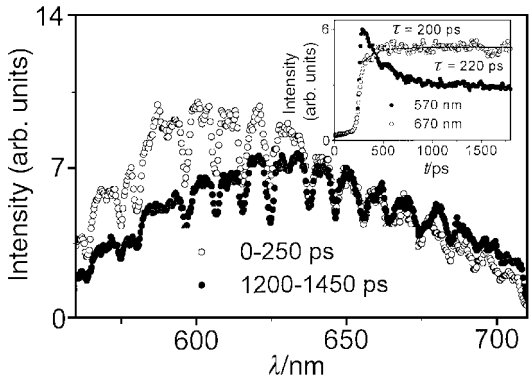

Fig. 3 Time-resolved luminescence spectra of **1** in CH_2Cl_2 following a 35 ps laser pulse (355 nm, 4 mJ); (○) integrated spectrum in the time interval 0–250 ps after the laser pulse; (●) integrated spectrum in the time interval 1200–1450 ps after the laser pulse. The inset shows the luminescence time profiles at 570 nm (●) and 670 nm (○) with the fitted exponential functions.

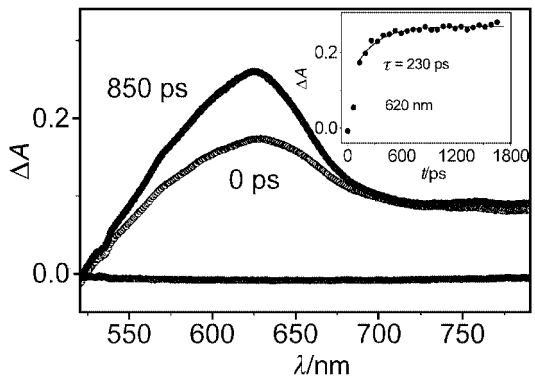

Fig. 4 Time resolved absorption spectra of **1** in CH_2Cl_2 following a 35 ps laser pulse (532 nm, 7 mJ); absorbance at the end of the laser pulse (○) and at 850 ps after the laser pulse (●). The inset shows the time evolution of the absorbance at 620 nm with the fitted exponential function.

On the basis of the spectroscopic results as observed for the time windows of Fig. 3 and 4, we assign the detected process to formation of the Ru → tpphz CT state involving the pyrazine moiety of the tpphz bridging ligand ($MLCT_0$) from the initially produced Ru → tpphz CT level involving the phenanthroline moiety of tpphz ($MLCT_1$). Over longer timescales, subsequent decay of the $MLCT_0$ state to the ground state takes place (not shown in the Figures). From the time evolution of the spectra the rate constant for the charge-migration process leading the interconversion from $MLCT_1$ to $MLCT_0$ is found to be 5×10^9 s^{-1}. Given that rate constants of the order of 10^{12}–10^{13} s^{-1} might be expected for an intramolecular conversion step between states of the same multiplicity, this suggests that a non-negligible energy barrier exists.

In conclusion, we have reported on the experimental observation of the interconversion dynamics of two MLCT excited states localised on the tpphz ligand, a bridge with an extended conjugation incorporated within a Ru(II) dinuclear species. We believe that our results may provide a useful basis for studies concerned with photoinduced intramolecular energy and electron transfer processes occurring in multinuclear species and across large-sized ligands.

This work was supported by MURST (Progetto 'Dispositivi Supramolecolari'), CNR, EC-TMR Program (Contract no. FMRX-CT-980226), and the Robert A. Welch Foundation (Grant Y-1301).

Notes and references

1 S. Campagna, S. Serroni, S. Bodige and F. M. MacDonnell, *Inorg. Chem.*, 1999, **38**, 692 and references therein.
2 K. Warnmark, O. Heyke, J. A. Thomas and J.-M. Lehn, *Chem. Commun.*, 1996, 2603.
3 E. Ishow, A. Gourdon, J.-P. Launay, C. Chiorboli and F. Scandola, *Inorg. Chem.*, 1999, **38**, 1504 and references therein.
4 C. Chiorboli, C. A. Bignozzi, F. Scandola, E. Ishow, A. Gourdon and J. P. Launay, *Inorg. Chem.*, 1999, **38**, 2402.
5 R. López, A. M. Leiva, F. Zuloaga, B. Loeb, E. Norambuena, K. M. Omberg, J. R. Schoonover, D. Striplin, M. Devenney and T. J. Meyer, *Inorg. Chem.*, 1999, **38**, 2924 and references therein.
6 E. Amouyal, A. Homsi, J. C. Chambron and J. P. Sauvage, *J. Chem. Soc., Dalton Trans.*, 1990, 1841.
7 A. E. Friedman, J. C. Chambron, J. P. Sauvage, N. J. Turro and J. K. Barton, *J. Am. Chem. Soc.*, 1990, **112**, 4960.
8 E. Tuite, P. Lincoln and B. Nórden, *J. Am. Chem. Soc.*, 1997, **119**, 239.
9 R. B. Nair, B. M. Cullum and C. J. Murphy, *Inorg. Chem.*, 1997, **36**, 962.
10 E. J. C. Olson, D. Hu, A. Hörmann, A. M. Jonkman, M. R. Arkin, E. D. A. Stemp, J. K. Barton and P. F. Barbara, *J. Am. Chem. Soc.*, 1997, **119**, 11 458 and references therein.
11 G. Albano, P. Belser, L. De Cola and M. T. Gandolfi, *Chem. Commun.*, 1999, 1171.
12 The system for time-resolved luminescence experiments is based on a Nd:YAG laser (PY62-10 Continuum, 35 ps pulse) and a streak camera (C1587 Hamamatsu). Excitation was performed at 355 nm, and the absorbance of the solutions at the excitation wavelength was around 1. Time-resolved absorption spectra were detected by a pump and probe system based on the same 35 ps laser and an OMA. Excitation was performed at 532 nm and the absorbance of the solutions at the excitation wavelength was 0.2. For further details see ref. 13.
13 L. Flamigni, N. Armaroli, F. Barigelletti, V. Balzani, J.-P. Collin, J.-O. Dalbavie, V. Heitz and J.-P. Sauvage, *J. Phys. Chem. B*, 1997, **101**, 5936 and references therein.

A double-helix generated from a ferrocenyl-thiosemicarbazato metallo-synthon and its novel hydrogen-bonding cavities

Fang Chen-jie, Duan Chun-ying,* He Cheng and Meng Qing-jin*

Coordination Chemistry Institute, The State Key Laboratory of Coordination Chemistry, Nanjing University, Nanjing, 210093, P. R. China. E-mail: duancy@nju.edu.cu

Received (in Cambridge, UK) 17th April 2000, Accepted 23rd May 2000

A double helical architecture generated from a readily prepared ferrocenyl-containing bisthiosemicarbazone ligand is described together with its application to the self-assembly of novel supramolecular hydrogen-bonding cavities.

A theme of considerable interest in supramolecular chemistry is the spontaneous and selective formation of organized supramolecular architectures *via* self-assembly.[1] The double-helical structures generated by the complexation of two ligands around metal ions lying on the helical axis retain a unique fascination since life itself is encoded within a double-helical architecture. While the basic features of the design necessary to assemble a double helix are now fairly well established,[2,3] challenges in defining the precise topography or conformation of the helical superstructure remain.

Here, we introduce a ferrocene bridged bisthiosemicarbazone ligand (Fig. 1) to generate a double-helical zinc complex *via* self-assembly. The ferrocene group was chosen as a spacer to separate the two metal binding sites, not only because this spacer is suitable to assemble double-helices,[3] but also because host molecules containing metallocene units can accommodate metal ions at their coordination sites and undergo redox changes.[4]

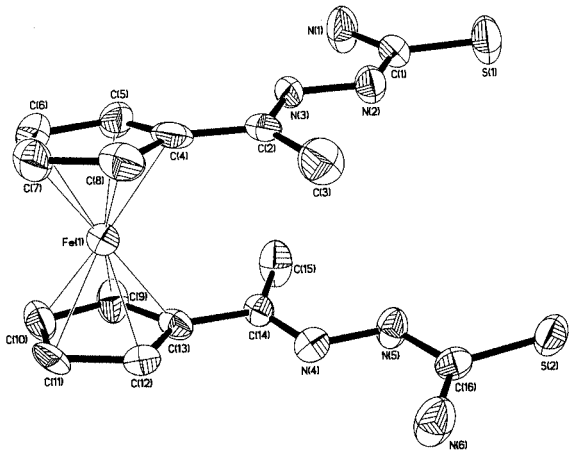

Fig. 1 ORTEP[8] plot of the ligand H_2L, showing the non-hydrogen atoms as 50% probability thermal ellipsoids. Selected bond lengths (Å): S(1)–C(1) 1.686(6), N(1)–C(1) 1.336(8), N(2)–C(1) 1.349(7), N(2)–N(3) 1.386(6), C(2)–C(3) 1.494(8), S(2)–C(16) 1.693(5), N(6)–C(16) 1.322(7), N(5)–C(16) 1.343(7), N(4)–N(5) 1.375(6).

Thiocarbazones and thiosemicarbazones have been used to assemble supramolecular architectures.[5] The hydrogen atoms attached to the amino nitrogen atoms of the thiosemicarbazone moiety have the ability to form donor hydrogen bonds. This kind of non-covalent bond has the potential to assemble smaller, simpler fragments into the desired cavities under favourable conditions, which is important in host–guest chemistry and has applications in chemistry, biology and materials science.[6]

When diacetylferrocene was treated with thiosemicarbazide in ethanol, a red crystalline solid formed readily.‡ Elemental analysis and crystal structure analysis‡ indicated the formation of a bisbidentate ligand $NH_2C(S)N(H)N{=}CMe(C_5H_4)$-$Fe(C_5H_4)CMe{=}NN(H)C(S)NH_2$ H_2L.† The ligand shows a *cis*-configuration with two thiosemicarbazone moieties positioned at the same side with the torsion angle C(2)–C(4)···C(13)–C(14) being −10.8°. Each thiosemicarbazone moiety is coplanar with the Cp ring to which it is attached (the mean deviation from the best plane is 0.09 Å on average). The C–S bond lengths of 1.69 Å agree well with those in related compounds, indicating that the Schiff-base compound H_2L remains as the *thione* tautomer. The two thiosemicarbazone moieties of the ligand adopt a configuration in which the hydrazone nitrogen atoms N(3) and N(6) are *trans* to S(1) and S(2), respectively. Rotation of the H_2NCS fragment by 180° about the C(1)–N(2) and C(16)–N(5) bonds places each pair of the sulfur atoms and the hydrazone nitrogen atoms on the same side, thus enabling H_2L to function as a double anionic N_2S_2 ligand.

Reaction of H_2L with $Zn(MeCO_2)_2{\cdot}2H_2O$ in methanol at reflux gives the binuclear neutral complex Zn_2L_2 **1** *via* self-assembly.† Complex **1** is a stable pale-orange precipitate which is insoluble in most organic solvents. Recrystallization of the compound from DMF by dichloromethane diffusion afforded X-ray quality crystals.‡ The structure of one of the two enantiomers is shown in Fig. 2 and confirms the formation of a double-helix composed of two anionic ligands L^{2-} wrapped around two Zn(II) ions which are separated by 7.74 Å. The complex possesses a crystallographic C_2 axis perpendicular to the helical Zn···Zn axis, with the four coplanar metal atoms forming a slightly distorted rhombus with sides of 5.0 Å and interior angles of 79 and 101°. Each zinc center occupies a four-

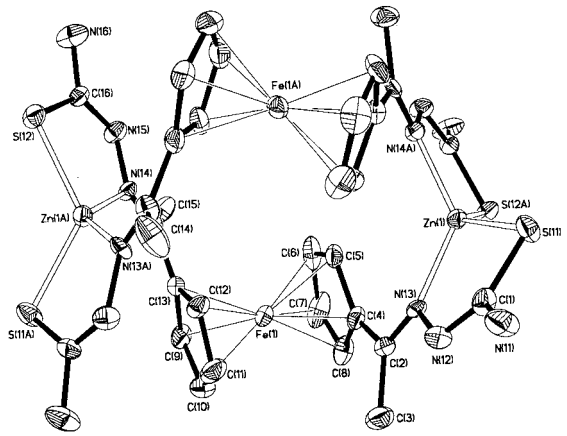

Fig. 2 ORTEP plot of the coordinated zinc(II) complex Zn_2L_2, showing the non–hydrogen atoms as 50% probability thermal ellipsoids. The solvent molecules and hydrogen atoms are omitted for clarity. Selected bond lengths (Å) and angles (°): Zn(1)–N(13) 2.073(9), Zn(1)–S(11) 2.280(3), S(11)–C(1) 1.730(1), S(12)–C(16) 1.739(1), N(11)–C(1) 1.348(2), N(12)–C(1) 1.289(2), N(12)–N(13) 1.401(1), N(14)–N(15) 1.396(1), N(15)–C(16) 1.305(1), N(16)–C(16) 1.350(2); N(14A)–Zn(1)–N(13) 130.4(3), S(12A)–Zn(1)–S(11) 125.4(8), N(13)–Zn(1)–S(11) 86.6(3), N(14A)–Zn(1)–S(12A) 87.5(2), N(13)–Zn(1)–S(12A) 116.3(3), N(14A)–Zn(1)–S(11) 115.3(3), Symmetry code A: 1−*x*, *y*, 1−*z*.

DOI: 10.1039/b003072o

coordinated pseudo-tetrahedral environment bound to atoms S(1) and N(3) from one L^{2-} ligand, and S(2A) and N(4A) from a second ligand (Fig. 2). The dihedral angle between the two coordinated planes is 77°. The Zn–S distances of 2.266(3)–2.274(4) Å and Zn–N distances of 2.059(9)–2.068(9) Å agree well with those in related compounds. The thiosemicarbazone moieties are twisted by *ca*. 50° from the Cp rings to which they are attached with dihedral angles between the two thiosemicarbazone moieties of 73.5°. Coordination to the metal center also forces twisting between the two side chains with a torsion angle C(2)–C(4)···C(13)–C(14) of 128°. No significant deformation of the almost parallel Cp ring is observed. The measured C–S bond distances range from 1.736(11) to 1.748(11) Å and are within the normal range of a C–S single bond,[7] indicating that the thiosemicarbazone moieties L^{2-} adopt the *thiol* tautomeric form in acting as a doubly charged negative ligand. The C–N and N–N bond distances in L^{2-} are intermediate between formal single and double bonds, pointing to extensive electron delocalization over the entire molecular skeleton.

While both the dichloromethane molecules and water molecules lie outside the cavity of the helix, X-ray diffraction analysis of the complex reveals that helices of each enantiomer interact with each other through hydrogen bonds forming an infinite tube as shown in Fig. 3. The imino nitrogen atoms of the thiosemicarbazone moieties act as H-bond acceptors while the amino nitrogen atoms act as donors, these pair up with the corresponding imino and amino nitrogen atoms of a parallel helix forming hydrogen bonds. The N···N separations are 3.18(1) and 3.16(1) Å for N(11)···N(15B) (1−*x*, 1+*y*, 1−*z*) and N(16)···N(12C) (1−*x*, −1+*y*, 1−*z*), respectively, while N–H···N angles are 156(1) and 171° for N(11)–H(11B)···N(15B) and N(16)–H(16A)···N(12C), respectively. The one-dimensional tube contains alternate cavities and walls (the double-helix molecules) reminiscent of a train. Each 'coach' includes two hydrogen bonded dimeric water molecules with an O···O separation of *ca*. 2.93 Å. The O···O vector occupies a C_2 axis perpendicular to the helical Zn···Zn axis. No obvious hydrogen bonds are seen between the guest molecules and the host.

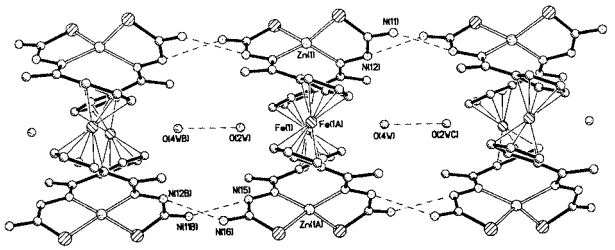

Fig. 3 View of the hydrogen-bonding one-dimensional tube with included water molecules. Symmetry code B: 1−*x*, 1+*y*, 1−*z*; C: 1−*x*, −1+*y*, 1–*z*.

The ferrocene-bridged double-helical complex derived here from an inexpensive and readily prepared bisthiosemicarbazone ligand and its novel hydrogen-bonding supramolecular 'train-like' system with each 'coach' of the train including two water molecules is interesting in that it provides an unusual example in metallo-supramolecular chemistry. This self-assembled nano-structure showing host–guest interactions shows potential for broadening the scope for further work in self-assembly. The development of new ligand systems containing the functional ferrocene group and application to assemble supramolecular cavities are in progress.

This work is supported by the National Natural Science Foundation of China.

Notes and references

† *Preparations*: H_2L: five drops of glacial acetic acid were added to a mixture of thiosemicarbazide (0.36 g, 4 mmol) and diacetylferrocene (0.54 g, 2 mmol) in ethanol solution (15 mL). A red solid formed after refluxing for 4 h which was isolated, washed with ethanol and dried under vacuum. $C_{16}H_{20}FeN_6S_2{\cdot}CH_3CH_2OH$: Calc. C, 46.8; H, 5.7; N, 18.2. Found: C, 46.3; H, 5.5; N, 17.9%.

Zn_2L_2: thiosemicarbazone (0.42 g, 1 mmol) and zinc acetate (0.22 g, 1 mmol) were mixed in 25 mL methanol. After refluxing for 4 h, a pale-orange solid formed which was isolated, washed with methanol and dried under vacuum. $C_{32}H_{36}Fe_2N_{12}S_4Zn_2{\cdot}H_2O{\cdot}CH_3OH$: Calc: C, 39.4; H, 4.2; N, 16.7. Found: C, 40.0; H, 4.4; N, 16.3%.

‡ *Crystal data*: for H_2L: $C_{16}H_{22}FeN_6OS_2$, M = 434.37, monoclinic, space group: *C*2/*c*, a = 29.0219(14), b = 8.797(2), c = 18.447(2) Å, β = 125.94(1)°, U = 3812.7(11) Å^3, Z = 8, D_c = 1.513 Mg m^{-3}, μ = 1.029 mm^{-1}, F(000) = 1808, T = 293(2) K. 3350 independent reflections measured, 2297 observed [$F > 4\sigma(F)$]. Refinement on all data and 323 parameters converged at $R1$ = 0.0647, $wR2$ = 0.1512, respectively.

For **1**·$2CH_2Cl_2{\cdot}2H_2O$: $C_{34}H_{44}Cl_4Fe_2N_{12}O_2S_4Zn_2$, monoclinic, space group *C*2, a = 30.076(6), b = 9.6742(18), c = 21.693(5) Å, U = 4675.4(17) Å^3, Z = 4, D_c = 1.655 Mg m^{-3}, F(000) = 2368, μ = 2.075 mm^{-1}. 4849 independent reflections measured, 4240 observed [$F > 4\sigma(F)$]. Refinement on all data and 553 parameters converged at $R1$ = 0.070, $wR2$ = 0.177, respectively.

Intensities were collected on a Siemens P4 four circle diffractometer with graphite-monochromated Mo-Kα radiation (λ = 0.71073 Å) using the ω–2θ scan mode. Data were corrected for Lorentz-polarization effects during data reduction using XSCANS,[9] and a semi-empirical absorption correction from ψ-scans was applied. The structures were solved by direct methods and refined on F^2 *via* full-matrix least-squares methods using SHELXTL version 5.0.[10]

CCDC 182/1653. See http://www.rsc.org/suppdata/cc/b0/b003072o/ for crystallographic files in .cif format.

1 J. M. Rivera, T. Martin and J. Rebek, Jr, *Science*, 1998, **279**, 1021; M. Fujita, D. Oguro, M. Miyazawa, H. Oka, K. Yamaguchi and K. Ogura, *Nature*, 1995, **378**, 469; L. J. Prins, J. Huskens, F. D. Jong, P. Timmerman and D. N. Reinhoudt, *Nature*, 1999, **398**, 498; P. J. Stang and B. Olenyuk, *Acc. Chem. Res.*, 1997, **30**, 502; D. Philp and J. F. Stoddart, *Angew. Chem., Int. Ed. Engl.*, 1996, **35**, 1154.

2 J.-M. Lehn, *Supramolecular Chemistry—Concept and Perspectives*, VCH, Weinheim, 1995; *Comprehensive Supramolecular Chemistry*, ed. J.-M. Lehn, J. L. Atwood, J. E. D. Davies, D. D. MacNicol and F. Vögtle, Pergamon, Oxford, 1996, vol. 9, pp. 213–252; C. Piguet, G. Bernardinelli and G. Hopfgartner, *Chem. Rev.*, 1997, **97**, 2005; A. Bilyk, M. M. Harding, P. Turner and T. W. Hambley, *J. Chem. Soc., Dalton Trans.*, 1994, 2783.

3 M. J. Hannon, S. Bunce, A. J. Clarke and N. W. Alcock, *Angew. Chem., Int. Ed.*, 1999, **38**, 1277; N. Yoshida, H. Oshio and T. Ito, *Chem. Commun.*, 1998, 63; M. J. Hannon, C. L. Painting, A. Jackson, J. Hamblin and W. Errington, *Chem. Commun.*, 1997, 1807; M. J. Hannon, C. L. Painting and N. W. Alcock, *Chem. Commun.*, 1999, 2023.

4 P. D. Beer, P. A. Gale and G. Z. Chen, *J. Chem. Soc., Dalton Trans.*, 1999, 1897; M. Buda, J.-C. Moutet, E. Saint-Aman, A. De Cian, J. Fischer and R. Ziessel, *Inorg. Chem.*, 1998, **37**, 4146.

5 C. Y. Duan, B. M. Wu and T. C. W. Mak, *J. Chem. Soc., Dalton Trans.*, 1996, 3485; C. Y. Duan, Z. H. Liu, X. Z. You, F. Xue and T. C. W. Mak, *Chem. Commun.*, 1997, 381; C. He, C. Y. Duan, C. J. Fang, Y. J. Liu and Q. J. Meng, *J. Chem. Soc., Dalton Trans*, 2000, 1207.

6 J. De Mendoza, *Chem. Eur. J.*, 1998, **4**, 1373; J. Rebek Jr., *Acc. Chem, Res.*, 1999, **32**, 278; L. R. MacGillivray and J. L. Atwood, *Angew. Chem. Int. Ed.*, 1999, **38**, 1018.

7 A. G. Orpen, L. Brammer, F. H. Allen, O. Kennard, G. G. Watson and R. Taylor, in *Structure Correlation*, ed. H. B. Buigi and J. D. Dunitz, VCH, Weinheim, 1994, vol. 2, Appendix A., pp. 751–778.

8 C. K. Johnson, ORTEP, Report ORNL-3794, Oak Ridge National Laboratory, TN, USA, 1965.

9 XSCANS, Version 2.1, Siemens Analytical X-ray Instruments, Inc., Madison, WI, 1994.

10 Siemens, SHELXTL, Version 5.0, Siemens Industrial Automation, Inc. Analytical Instrumentation, Madison, WI, 1995.

ChemComm

Unusually high *ortho*-selectivity in electrophilic aromatic substitution promoted by $GaCl_3$†

Fumi Yonehara, Yoshiyuki Kido and Masahiko Yamaguchi

Department of Organic Chemistry, Graduate School of Pharmaceutical Sciences, Tohoku University, Aoba, Sendai 980-8578, Japan. E-mail: yama@mail.pharm.tohoku.ac.jp

Received (in Cambridge, UK) 20th April 2000, Accepted 23rd May 2000

1,4-Bis(trimethylsilyl)buta-1,3-diyne in the presence of $GaCl_3$ reacts with aromatic hydrocarbons at −90 to −100 °C yielding 2-arylbut-1-en-3-ynes; the reactions exhibit an unusually high tendency to alkenylate the *o*-position of alkyl substituents; toluene, ethylbenzene and isopropylbenzene react predominantly to exclusively at the *o*-position while *o*-xylene and 1,2,3,4-tetrahydronaphthalene react at the 3 and 5-position, respectively.

Ortho–para selectivity in electrophilic aromatic substitution is an issue still not fully understood. Particularly, selective *o*-alkylation is rare, since a slight increase in the steric bulk of the substituent directs the reaction to the *p*-position.[1] Several benzene derivatives possessing heteroatom functionalities are known to exhibit such *o*-selectivity, which is ascribed to the interactions between the electrophile and the substituent.[2] Only modest levels of *o*-selectivity are observed in some reactions of toluene, where such an interaction is unavailable[3] while *o*-selectivity is rare for ethylbenzene or isopropylbenzene. Described here is an *o*-selective aromatic alkenylation reaction using $GaCl_3$ and 1,4-bis(trimethylsilyl)buta-1,3-diyne **1**. We previously reported the β-silylethenylation reaction of arenes with trimethylsilylethyne **2** in the presence of $GaCl_3$[4] involving C–C bond formation between an organogallium ethenyl cation and an arene exhibiting *para*-selectivity. By contrast, examination revealed that the electrophile derived from **1** shows an unusually high tendency to alkenylate the *o*-position of alkyl substituents.

Arene (5 mol equiv.) and **1** (1 mol equiv.) were reacted with $GaCl_3$ (2 mol equiv.) in CH_2Cl_2 at −90 to −100 °C for 1–2 h.‡ THF was then added, and the mixture stirred for 0.5 h at −90 to −100 °C. Aqueous workup gave (*Z*)-1,4-bis(trimethylsilyl)-2-arylbut-1-en-3-yne **3** and 4-trimethylsilyl-2-arylbut-1-en-3-yne **4** (method A) as shown in Scheme 1.[5] For some arenes such as *p*-xylene or *m*-xylene, addition of another portion of $GaCl_3$ (2 mol equiv.) increases the total yield (method B). The reaction can be carried out using an equimolar amount of *p*-xylene and **1** with only a slight decrease in the yield. Addition of THF prior to the water improves the yield of the products. The (*Z*)-stereochemistry of **3** was determined by NOE studies. The reaction sites of the arenes were confirmed unambiguously by spectroscopic methods. The isomer distribution of **3** is similar to that of **4**. The olefinic trimethylsilyl group of **3** can be removed producing **4** by careful treatment with CF_3CO_2H in a mixture of diethyl ether and water with the temperature gradually increased from −78 °C to room temperature. For example, (*Z*)-1,4-bis(trimethylsilyl)-2-(2,5-dimethylphenyl)-but-1-en-3-yne **7** was monodesilylated in 70% yield. Reactions of **1**, which is a stable alternative to buta-1,3-diyne, have attracted considerable attention in organic synthesis. For example, silicon substitution with electrophiles occurs in the presence of Lewis acids or methyllithium giving diyne compounds.[6] Organometal addition producing enynes has also been reported.[7] Electrophilic addition to **1** as well as to the parent buta-1,3-diyne has been little studied.[8]

† Electronic supplementary information (ESI) available: full experimental and spectroscopic data. See http://www.rsc.org/suppdata/cc/b0/b003215h/

It may be reasonably assumed, based on the employment of similar reagents and reaction conditions, that the present reaction and the β-silylethenylation[4] involve similar electrophilic substitution mechanisms. However, several differences are noted. First, the orientation of these reactions differs considerably. The directing effect of the methyl group to its *o*-position is unusually high in the present reaction; indeed toluene

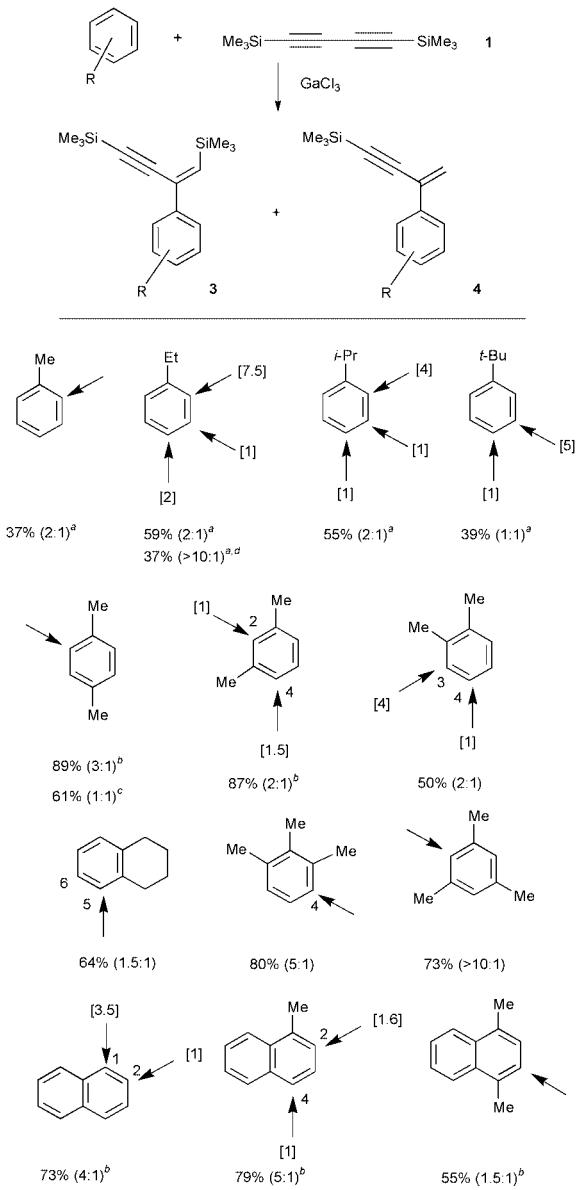

Scheme 1 Yield of **3** + **4** is shown. Figures in parentheses indicate the ratio of **3**:**4**. →: Reaction site. [ ]: Isomer ratio of **3**. [a] 20 mol equiv. of arene used. [b] Method B employed. [c] 1 mol equiv. of arene used. [d] 1,4-Bis(triethylsilyl) buta-1,3-diyne used, the isomer ratio is very similar to the reaction of **1**.

DOI: 10.1039/b003215h

reacts exclusively at the *o*-position. This is in contrast to the observation that the β-silylethenylation predominantly occurs at the *p*-position.[4] Ethylbenzene and isopropylbenzene also predominantly react at the *o*-position. Notably, *tert*-butylbenzene gives the *m*-isomer as the major product. Disubstituted benzenes also show a tendency to react at positions adjacent to the alkyl substituents; *o*-xylene is predominantly alkenylated at the 3-position, 1,2,3,4-tetrahydronaphthalene exclusively reacts at the 5-position while a considerable proportion of *m*-xylene reacts at the 2-position. The dominant reaction sites in β-silylethenylation are at the 4-, 6- and 4-positions for these three substrates, respectively.[4] It is known from detritiation experiments that the *p*-position in toluene is about twice as reactive as the *o*-position.[9] Similarly, the 4-position of *o*-xylene, the 6-position of 1,2,3,4-tetrahydronaphthalene and the 4-position of *m*-xylene are more reactive than the others.[9] Detritiation is considered to reflect the reactivity of the aromatic sites excluding steric effects. The orientation of β-silylethenylation using **2**, therefore, can be understood by taking into account both electronic and steric effects. The orientation of the present reaction using **1** is unusual with reaction at the less reactive and more hindered sites predominating. The following examples also show the anomalous orientation of this reaction. 1-Methylnaphthalene predominantly reacts at the 2-position. While 1,3,5-trimethylbenzene is inert to β-silylethenylation, the reaction of **1** proceeds smoothly. The substituent on the silicon atom of **1** is not essential for *o*-selectivity, since 1,4-bis(triethylsilyl)buta-1,3-diyne reacts with ethylbenzene also at the *o*-position.

Second, a difference in the behavior of **1** and **2** is observed in deuteration experiments. When the reaction of *p*-xylene and **1** was quenched with D_2O, product **7** was not deuterated at the olefin moiety. Whereas β-silylethenylation using **2** produced a β-deuterated product.[4] Since the reaction of **1**, as for **2**, is likely to proceed *via* the organogallium electrophile **5**, an arenium cation **6** should be formed (Scheme 2). The above result of the deuteration experiment suggests that protodegallation of **6** takes place in the reaction mixture, regenerating $GaCl_3$. Unfortunately, 10 or 50 mol% of $GaCl_3$ does not effectively promote the catalytic reaction.§

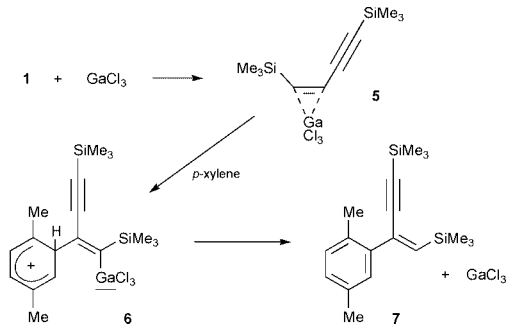

Scheme 2

Third, the present reaction proceeds at a temperature lower than that for β-silylethenylation.[4] While the latter reaction does not take place at −90 °C, the former reaction occurs efficiently even at −100 °C. The electrophilic species derived from **1** appears to be more reactive than that from **2**.

A higher polyyne compound can also be used for alkenylation. Reaction of 1,8-bis(triethylsilyl)octa-1,3,5,7-tetrayne **8**[10] and toluene yields 2-aryloct-1-en-3,5,7-triyne **9** (Scheme 3). Since the *p*-product predominated here, the anomalous orientation in the reaction of **1** can be attributed, at least in part, to its diyne structure.

This work was supported by grants from the Japan Society of Promotion of Science, Ministry of Education, Science and Culture, Japan, and the Naito Science Foundation. A fellowship to Y. K. from the JSPS for young Japanese scientists is gratefully acknowledged.

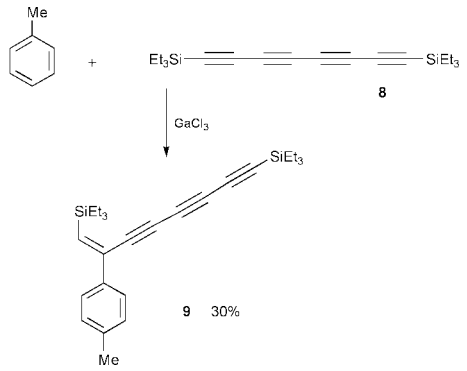

Scheme 3

Notes and references

‡ *Typical procedure*: under an argon atmosphere, to a stirred solution of *p*-xylene (0.31 mL, 2.5 mmol) in CH_2Cl_2 (4 mL) was added dropwise a solution of $GaCl_3$ (1.0 M in methylcyclohexane, 1.0 mL) at −98 °C. To this mixture, **1** (97 mg, 0.5 mmol) in CH_2Cl_2 (1 mL) was added slowly, and stirring was continued for 1 h at this temperature. Then THF (3 mL) was added, and after 30 min water was added. A standard workup gave **7** (74 mg, 49%) and 4-trimethylsilyl-2-(2,5-dimethylphenyl)but-1-en-3-yne (10 mg, 9%).

§ There are lines of evidence for product inhibition: (i) When **7** (2 mol equiv.) was added to the reaction mixture of *m*-xylene (2 mol equiv.), **1** (2 mol equiv.) and $GaCl_3$ (1 mol equiv.) at −90 °C, alkenylation was totally inhibited with recovery of **7** in 84% yield. In contrast, 17% of the product derived from *m*-xylene was obtained in the absence of **7** under the same conditions. (ii) Compound **7** and $GaCl_3$ react to form an orange solution in methylcyclohexane at −100 °C, which fades on addition of THF. Reversible complex formation was also detected by *in situ* IR. **7**: IR (methylcyclohexane, −95 °C) 1248, 843 cm^{-1}. **7**•$GaCl_3$ complex: IR (methylcyclohexane, −95 °C) 1252, 839 cm^{-1}. For complex formation of $GaCl_3$ and aromatic hydrocarbons, see ref. 11.

1 G. A. Olah, *Friedel-Crafts Chemistry*, John Wiley & Sons, New York, 1973; R. Taylor, *Electrophilic Aromatic Substitution*, John Wiley & Sons, New York, 1990.
2 See, for example; F. Krausz and R. Martin, *Bull. Soc. Chim. Fr.*, 1965, 2192; B. M. Lynch, C. M. Chen and Y.-Y. Wigfield, *Can. J. Chem.*, 1968, **46**, 1141; S. R. Hartshorn, R. B. Moodie and K. Schofield, *J. Chem. Soc. B*, 1971, 2454.
3 G. A. Olah, S. J. Kuhn and S. H. Flood, *J. Am. Chem. Soc.*, 1961, **83**, 4571; R. O. C. Norman and G. K. Radda, *J. Chem. Soc.*, 1961, 3610; G. A. Olah, S. H. Flood, S. J. Kuhn, M. E. Moffatt and N. A. Overchuck, *J. Am. Chem. Soc.*, 1964, **86**, 1046; G. A. Olah, S. J. Kuhn and B. A. Hardie, *J. Am. Chem. Soc.*, 1964, **86**, 1055; A. J. Davidson and R. O. C. Norman, *J. Chem. Soc.*, 1964, 5404; An exception using Me_3Te^+ was reported: K. Laali, H. Y. Chen and R. J. Gerzina, *J. Organomet. Chem.*, 1988, **348**, 199.
4 M. Yamaguchi, Y. Kido, A. Hayashi and M. Hirama, *Angew. Chem., Int. Ed. Engl.*, 1997, **36**, 1313; Y. Kido, S. Yoshimura, M. Yamaguchi and T. Uchimaru, *Bull. Chem. Soc. Jpn.*, 1999, **72**, 1445.
5 Synthesis of 2-arylbut-1-en-3-ynes: G. Sartori, A. Pastorio, R. Maggi and F. Bigi, *Tetrahedron*, 1996, **52**, 8287; F. Bigi, S. Carloni, R. Maggi, C. Muchetti and G. Sartori, *J. Org. Chem.*, 1997, **62**, 7024.
6 P. J. Stang and M. Ladika, *Synthesis*, 1981, 29; T. Tsukiyama, S. C. Peters and M. Isobe, *Synlett*, 1993, 413; A. B. Holmes, C. L. D. Jennings-White and A. H. Schulthess, *J. Chem. Soc., Chem. Commun.*, 1979, 840.
7 J. A. Miller and G. Zweifel. *J. Am. Chem. Soc.*, 1983, **105**, 1383; T. Kusumoto, K. Ando and T. Hiyama, *Bull. Chem. Soc., Jpn.*, 1992, **65**, 1280; A. Tillack, S. Pulst, W. Baumann, H. Baudisch, K. Kortus and U. Rosenthal, *J. Organomet. Chem.*, 1997, **532**, 117.
8 F. Öztürk, G. Baykut, M. Moini and J. R. Eyler, *J. Phys. Chem.*, 1987, **91**, 4360; F. Öztürk, M. Moini, F. W. Brill, J. R. Eyler, T. J. Buckley, S. G. Lias and P. J. Ausloos, *J. Phys. Chem.*, 1989, **93**, 4038.
9 R. Baker, C. Eaborn and R. Taylor, *J. Chem. Soc.*, 1961, 4927; H. V. Ansell and R. Taylor, *J. Chem. Soc. B*, 1968, 526; J. Vaughan and G. J. Wright, *J. Org. Chem.*, 1968, **33**, 2580.
10 Synthesized by the reported method; M. Yamaguchi, H.-J. Park, M. Hirama, K. Torisu, S. Nakamura, T. Minami, H. Nishihara and T. Hiraoka, *Bull. Chem. Soc. Jpn.*, 1994, **67**, 1717.
11 S. Ulvenlund, A. Wheatley and L. Bengtsson, *J. Chem. Soc., Dalton Trans.*, 1995, 255.

Switching stereocontrol in the high pressure-induced hetero-Diels–Alder reaction

Hashim Al-Badri,[a] Noël Collignon,[b] Jacques Maddaluno*[a] and Serge Masson[c]

[a] *Laboratoire des Fonctions Azotées et Oxygénées Complexes de l'IRCOF, UPRES-A 6014 CNRS, Université de Rouen, 76821 Mont-Saint-Aignan Cedex, France. E-mail: jmaddalu@crihan.fr*

[b] *Laboratoire d'Hétérochimie Organique de l'IRCOF, UPRES-A 6014 CNRS, INSA de Rouen, Place E. Blondel, BP 08, 76131 Mont-Saint-Aignan Cedex, France*

[c] *Laboratoire de Chimie Moléculaire et Thioorganique, UMR 6507 CNRS, Université de Caen et ISMRA, 6 Boulevard du Maréchal Juin, 14050 Caen Cedex, France*

Received (in Cambridge, UK) 17th April 2000, Accepted 19th May 2000

The formation of a transient Michael adduct, triggering an *in-situ* isomerization of the heterodiene, is postulated to explain the reversal of the diastereoselectivity of high pressure-promoted hetero-Diels–Alder reactions carried out in the presence of pyridine.

Application of high pressure in organic synthesis is a rapidly developing research area.[1] In particular, the use of these extreme conditions in [4+2] cycloadditions not only causes a marked acceleration of the reactions due to negative volumes of activation, but also often imposes efficient stereocontrol by favouring the more compact transition state, namely the *endo* state.[2]

Pursuing our work on the hetero-Diels–Alder reaction of α-phosphono-substituted heterodienes **1** [W = $(RO)_2P(O)$] with electron-rich dienophiles **2** (Scheme 1),[3] we recently observed an unexpected reversal of the diastereoselectivity of the resulting cycloadduct **3**, at high pressure, when the β-phenyl group of the diene was replaced by a pyridyl group.[4] Having postulated a possible *in situ* (*E*)- to (*Z*)-isomerization of the pyridyl-substituted diene, we decided to study, more generally, the possibility of modifying the selectivity of such high pressure-promoted cycloadditions by adding pyridine to the reaction mixture. We report here our first significant results (Table 1).

The synthesis of the phosphono-heterodienes (*E*)-**1a**–**c** were previously described.[3,4] The non-phosphonic diene **1d** was prepared according to a modification of the literature procedure,[5] giving a *ca.* 40:60 mixture of (*E*)/(*Z*)-isomers, which could be separated by HPLC. [6] Dienophiles **2a**,**b** are commercially available. The reactions of **1** with a ten-fold excess of **2** (acting also as solvent), at 20 °C and 11 kbar, led to the cycloadduct **3** as a mixture of two diastereomers, whose relative configuration was deduced from ^{1}H–^{1}H NOESY, ^{1}H and ^{13}C NMR spectra.[3,4] In the first set of experiments, we studied the reaction of the pair (*E*)-**1a**/**2a**. As we reported,[4] in the absence of pyridine the expected cycloadduct **3a** was obtained in very good yield after 72 h, with a predominent *trans*-diastereoselectivity (Table 1, entry 1), in agreement with the expectation of a preferred *endo*-transition state. In the presence of 1 equiv. of pyridine (entry 3), the reaction was complete after 24 h, giving **3a** in excellent yield, and with a high *cis*-selectivity (de = 82%), which was not altered by using an excess of pyridine (4 equiv., entry 4). However, with 0.5 equiv. of pyridine, the *cis*-selectivity of the cycloaddition dropped significantly (entry 2). At this stage, we checked that the 68/32 *t*-**3a**/*c*-**3a** mixture obtained in the first experiment was unchanged in the presence of 1 equiv. of pyridine for 48 h at 20 °C and 11 kbar. In addition, we verified that pure (*E*)-**1a** was configurationally stable at high pressure in the absence of pyridine, whereas we noticed that, in the presence of 1 equiv. of pyridine at 20 °C and 11 kbar for 48 h, it was partially isomerized into a 98:2 (*E*)-**1a**/(*Z*)-**1a** mixture. These accumulated results led us to think that the predominent *cis*-diastereoselectivity of the cycloaddition observed in the presence of pyridine was due to an equilibrated *in situ* isomerization of the (*E*)-heterodiene into its (*Z*)-isomer,[7] whose rate constant k_2 (reaction path b) should be higher, for steric reasons, than that (k_1) of its (*E*)-partner (reaction path a), *via* an *endo*-transition state assumed to be predominent in both cases (Scheme 2). We propose that such an unusual pyridine-promoted (*E*) ↔ (*Z*) isomerization[8] could take place through the formation, in hyperbaric conditions, of a transient adduct **4** resulting from a Michael-type addition of pyridine to (*E*)-**1a**.[9] The progressive decrease of the *trans*-selectivity from entry 1 to entries 3 and 4 seems to be in agreement with stoichiometric consumption of the (*E*)-heterodiene by the pyridine, to give the stabilized ionic adduct **4**, which likely decomposes into the (*Z*)-isomer by a retro-Michael release of pyridine, the overall process being equilibrated. Moreover, in order to account for the global selectivity of the cycloaddition, a minor contribution of the *exo*-approach mechanism (reaction paths c and d, in Scheme 2) could also be considered.

The results obtained in the following seem to agree with the mechanism proposed in Scheme 2 and illustrate the advantage and easiness of the method. In particular, the phosphono-heterodienes **1a**–**c**, for which only the (*E*)-isomers are available,[3,4] were efficiently transformed, as depicted in Scheme 1, into very interesting dihydro-pyrans or -thiopyrans **3**, usually obtained as their predominent *trans*-diastereoisomers, but often with a modest selectivity (Table 1, entries 1, 5, 7, 9 and 11).[10] The addition of 1 equiv. of pyridine to the reaction mixture, under the same conditions, allowed us to accelerate the reaction, as well as to reverse its selectivity, giving access to the less common *cis*-isomer (entries, 3, 6, 8, 10 and 12), occasionally with a diastereomeric excess up to 97% (entry 6).

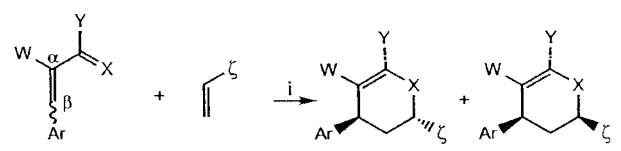

1a X = S, Y = SEt, W = $(EtO)_2P(O)$, Ar = Ph
b X = S, Y = SEt, W = $(EtO)_2P(O)$, Ar = 4-NO_2-C_6H_4
c X = O, Y = Me, W = $(MeO)_2P(O)$, Ar = 4-NO_2-C_6H_4
d X = O, Y = Me, W = EtOC(O), Ar = Ph

2a ζ = OEt
b ζ = SEt

3a X = S, Y = SEt, W = $(EtO)_2P(O)$, Ar = Ph, ζ = OEt
b X = S, Y = SEt, W = $(EtO)_2P(O)$, Ar = Ph, ζ = SEt
c X = S, Y = SEt, W = $(EtO)_2P(O)$, Ar = 4-NO_2-C_6H_4, ζ = SEt
d X = O, Y = Me, W = $(MeO)_2P(O)$, Ar = 4-NO_2-C_6H_4, ζ = OEt
e X = O, Y = Me, W = $(MeO)_2P(O)$, Ar = 4-NO_2-C_6H_4, ζ = SEt
f X = O, Y = Me, W = EtOC(O), Ar = Ph, ζ = OEt

Scheme 1 *Reagents and conditions*: i, without solvent, **2** in ten-fold excess, *n* equiv. of pyridine, 11 kbar, 20 °C.

DOI: 10.1039/b003060k

Table 1 Selectivity and yield of the high pressure-promoted synthesis of cycloadducts **3a–f**, in the presence or absence of pyridine

Entry	Diene	Dienophile	Equiv. Py (*n*)	Products[a]	Selectivity[b] *trans/cis*	Yield[c] (%)
1[d]	(*E*)-**1a**	**2a**	0	*t*-**3a**/*c*-**3a**	68:32	88
2			0.5		16:84	87
3			1		8:92	90
4			4		9:91	88
5	(*E*)-**1a**	**2b**	0	*t*-**3b**/*c*-**3b**	66:34	84
6			1		1.5:98.5	88
7[d]	(*E*)-**1b**	**2b**	0	*t*-**3c**/*c*-**3c**	86:14	83
8			1		6.5:93.5	86
9[e]	(*E*)-**1c**	**2a**	0	*t*-**3d**/*c*-**3d**	75:25	95
10			1		30:70	93
11	(*E*)-**1c**	**2b**	0	*t*-**3e**/*c*-**3e**	93:7	89
12			1		18:82	91
13	(*E*)-**1d**	**2a**	0	*t*-**3f**/*c*-**3f**	64:36	92
14			1		14:86	93
15	(*Z*)-**1d**	**2a**	0		13:87	92
16			1		15:85	92

[a] The experimental procedure was described in ref. 3. [b] Determined after pressure release, on the crude mixture, by ^{31}P and/or ^{1}H NMR integration measurements. [c] Yields of purified oily products. Purification by flash chromatography over silica gel [eluent: ether/MeOH (95:5) for **3a** and **3e**; ether/CH_2Cl_2 (70:30) for **3b** and **3c**; ether for **3d**; heptane/AcOEt (80:20) for **3f**]. Purity checked and structures established by ^{1}H and ^{13}C NMR spectroscopy. Satisfactory microanalyses or HRMS were obtained. [d] Results taken from ref. 4. [e] Results taken from ref. 3.

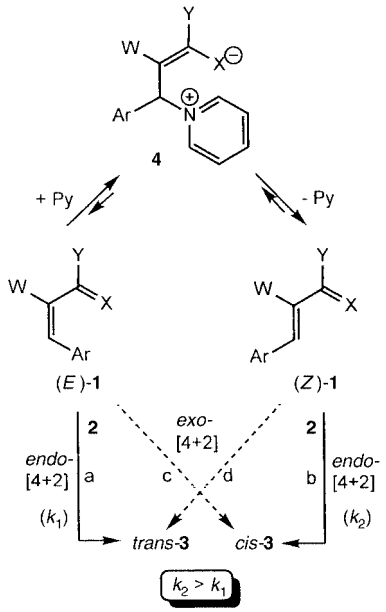

Scheme 2 Proposed mechanism for the pyridine-induced *cis*-diastereoselectivity of the [4+2] cycloaddition of **1** to **2**, at high pressure.

Finally, we report the cycloaddition of the cetoester **1d** with the dienophile **2a**, leading to the dihydropyran **3e** (entries 13–16). As observed above, in the absence of pyridine the diene (*E*)-**1d** gave **3e** with modest *trans*-diastereoselectivity (entry 13),[10] whereas in the presence of 1 equiv. (or an excess) of pyridine the *cis*-isomer became greatly predominant (entry 14). Interestingly, the same selectivity was obtained by using the diene (*Z*)-**1d** in the absence (entry 15) as well as in the presence of pyridine (entry 16). The remarkable similarity of these last three results suggests that in these three cases, and in particular for the first of them, the main reaction path was path b (Scheme 2). Moreover, we found that when pure diene (*E*)-**1d** was treated with 1 equiv. of pyridine in an inert solvent at 20 °C and 11 kbar for 48 h, it was isomerized into a 43:57 (*E*)-**1d**/(*Z*)-**1d** mixture. The same ratio was obtained when starting from pure (*Z*)-**1d**, indicative of a thermodynamic (*E*)/(*Z*) equilibration of **1d** at high pressure in the presence of pyridine.

In conclusion, this communication describes a straightforward method allowing, by addition of pyridine, the reversal of the diastereoselectivity of some high pressure-promoted hetero-Diels–Alder reactions, giving access, at room temperature, to unusual cycloadduct isomers. This method is especially useful when only the (*E*)-isomer of the heterodiene is available. In order to explain the observed results, a mechanism involving a transient Michael addition of pyridine to the starting (*E*)-diene,[11] and allowing the *in situ* formation of the more reactive (*Z*)-isomer, is proposed.

Notes and references

1 Review: G. Jenner, *Tetrahedron*, 1997, **53**, 2669: for recent important results, see: (*a*) S. Hillers and O. Reiser, *Chem. Commun.*, 1996, 2197; (*b*) F.-G. Klärner and V. Breitkopf, *Eur. J. Org. Chem.*, 1999, 2757; (*c*) G. J. Kuster and H. W. Scheeren, *Tetrahedron Lett.*, 2000, **41**, 515.

2 L. F. Tietze, M. Henrich, A. Niklaus and M. Buback, *Chem. Eur. J.*, 1999, **5**, 297 and references therein.

3 H. Al-Badri, J. Maddaluno, S. Masson and N. Collignon, *J. Chem. Soc., Perkin Trans. 1*, 1999, 2225.

4 H. Al-Badri, N. Collignon, J. Maddaluno and S. Masson, *Tetrahedron*, 2000, **56**, 3909.

5 We prepared **1d** by condensing methyl acetoacetate with benzaldehyde bis(morpholino)aminal (following the procedure described in ref. 3), instead of benzaldehyde used by: C. A. Kingsbury, D. Draney, A. Sopchik, W. Rissler and D. Durham, *J. Org. Chem.*, 1976, **41**, 3863.

6 The separation of the isomers was achieved by using a Waters HPLC chromatograph, a Nova Pack (L = 10 cm, Φ = 0.8 cm) silica gel column and heptane/AcOEt (97:3) as eluent.

7 An example of light-promoted (*E*)/(*Z*)-heterodiene isomerization preceding the cycloaddition has been reported by: L. F. Tietze, T. Brumby, M. Pretor and G. Remberg, *J. Org. Chem.*, 1988, **53**, 810.

8 (*E*)-**1a** was configurationally stable in the presence of pyridine, at 20 °C and atmospheric pressure for several days.

9 High pressure-induced hetero-Michael additions of primary amines have been described in the literature [see for example: (*a*) J. d'Angelo and J. Maddaluno, *J. Am. Chem. Soc.*, 1986, **108**, 8112; (*b*) F. Dumas, B. Mezrhab, J. d'Angelo, C. Riche and A. Chiaroni, *J. Org. Chem.*, 1996, **61**, 2293], and are currently under study in our laboratories (A. Y. Rulev, J. Maddaluno, G. Plé, J. C. Plaquevent and L. Duhamel, *J. Chem. Soc., Perkin Trans. 1*, 1998, 1397, and work in preparation).

10 In each case, we verified, first, that the starting diene was configurationally stable at 11 kbar in the absence of pyridine, and secondly that the obtained cycloadduct mixture did not isomerize, at 11 kbar, in the presence of pyridine.

11 The postulated addition of the nucleophilic pyridine to the heterodiene is to be considered in relation to the first step of the Baylis–Hillman reaction, which is known to be very sensitive to pressure; see for instance: A. Gilbert, T. W. Heritage and N. S. Isaacs, *Tetrahedron: Asymmetry*, 1991, **2**, 969; I. E. Markó, P. R. Giles and N. J. Hindley, *Tetrahedron*, 1997, **53**, 1015.

ChemComm

Carbon parity affecting the packing state of azobenzene–urea monolayers

Toru Kobayashi, Takahiro Seki* and Kunihiro Ichimura

Photofunctional Chemistry Division, Chemical Resources Laboratory, Tokyo Institute of Technology, 4259 Nagatsuta, Midori-ku, Yokohama 226-8503, Japan. E-mail: tseki@res.titech.ac.jp

Received (in Cambridge, UK) 8th March 2000, Accepted 19th May 2000

The monolayers of azobenzene (Az)-containing urea amphiphiles show clear odd–even effects of the alkylene spacer length in respect of the spreading behavior on water and the packing state of the Az chromophore on a quartz substrate.

The urea moiety is very simple in structure but provides a particularly useful building block[1] in supramolecular chemistry.[2,3] Urea derivatives associate *via* intermolecular bifurcated NH···O=C hydrogen bonds (see Fig. 1) and these paired hydrogen bonds afford a robust and highly directional intermolecular joint. On the surface of water, the monolayers of long chain alkylureas are known to exhibit a unique thermally-induced area change.[4] The monolayer of alkylureas, unlike other amphiphiles, exhibits a sudden contraction at an intrinsic transition temperature on heating. It is assumed that the rupture of the bifurcated hydrogen bonds among the urea heads is responsible for this thermal change in the molecular packing.

Our recent work using an azobenzene (Az)-containing long chain urea showed that this monolayer on the surface of water adopts a characteristic packing structure in which the *trans*-to-*cis* photoisomerization is completely prevented.[5] More interestingly, when the monolayer is transferred onto a hydrophilic substrate, the atmospheric humidity change sharply switches the assembled state and hence the photoreactivity of Az in the assembly.[6] We report herein a new aspect of the molecular design of the Az–urea monolayer system. It is found here that the carbon parity (odd/even number) of the alkylene spacer connecting the urea and the Az unit obviously results in the alternation of the spreading behavior and the molecular packing nature. Examples of odd–even effects affecting the thermal properties in thermotropic liquid crystals are widely known.[7] In two dimensional monolayer or bilayer assembly systems, various surface-mediated phenomena, such as wetting of liquid,[8] ice nucleation,[9] liquid crystal alignment[10] and electrochemical properties[11] are altered by the carbon parity. This paper presents a new example involving the photochromic monolayer.

The family of Az–urea compounds, *N*-(5-{4-[(4-hexylphenyl)azo]phenoxy})alkylurea (**1**, n = 3–7), used in this work are shown in Fig. 1. These compounds were synthesized in a similar manner to that described in ref. 5 for n = 10. The corresponding Az-containing carboxylic acid derivatives, the starting compounds, were converted to isocyanates and then a subsequent reaction with ammonia gas was performed.[12] The spreading behavior of Az-containing monolayers was evaluated on pure water (Milli-Q grade, 18 MΩ cm^{-1}, pH = 5.8) using a Lauda FW1 film balance in subdued red light. After evaporation of the solvent, monolayers were compressed at a speed of 30 cm^2 min^{-1}, and the surface pressure was recorded *versus* the molecular area. The absorption spectra were taken on a JASCO MAC-1 spectrophotometer, which was principally designed for low absorbance measurements.

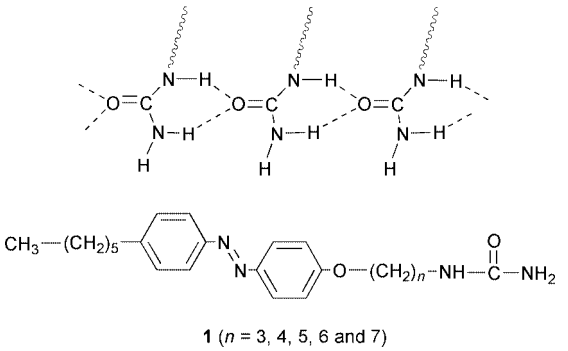

1 (n = 3, 4, 5, 6 and 7)

Fig. 1 Schematic representation of the bifurcated hydrogen bonds between the urea units (above), and the chemical structure of the Az–urea amphiphiles used in this study (below).

Surface pressure–area (π–A) isotherms of **1** (n = 3–7) in the *trans* form obtained at 20 ± 0.5 °C are shown in Fig. 2. As indicated, the limiting area per molecule, which was estimated by extrapolating the steepest slope to zero pressure, indicated systematic alternation with n (see Fig. 2 inset). For the compounds with an odd number of carbons in the spacer (n = 3, 5 and 7), the limiting area was in the range 0.29–0.30 nm^2. On the other hand, the monolayers of **1** having an even numbered spacer (n = 4 and 6) showed significant area expansions with higher compressibility. Since the cross section of vertically aligned Az is 0.25 nm^2, as estimated from the X-ray diffraction data of crystals,[13] it can be thus interpreted that the molecules in these monolayers are tilted with respect to the surface normal. The degree of molecular tilting for the even numbered carbon spacers should be greater than that of the odd numbered ones.

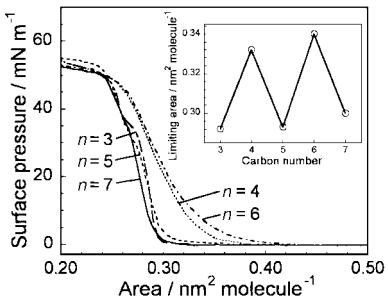

Fig. 2 Surface pressure–area isotherms of monolayers of **1** (n = 3–7) on pure water at 20 °C. In the inset, the limiting occupying area is plotted against the alkylene spacer length (n).

The shape of π–A curves also showed regular changes with n. The even numbered (n = 4 and 6) compounds gave a continuous smooth slope in the π–A curves. In contrast, monolayers of the odd carbon series (n = 3, 5 and 7) showed a sharper increase in the curve, indicative of lower compressibility. Furthermore, a characteristic inflecting region around 33 mN m^{-1} was observed for the odd numbered series only. We have not yet elucidated the process involved in this phase transition.

Single layers of **1** (n = 3–7) on water were deposited onto a clean quartz plate by the vertical lifting procedure at 20 mN m^{-1}. The transfer ratio was 1.0 ± 0.1 in all cases. Fig. 3 displays the transmission UV–vis absorption spectra of the monolayers of **1** on both sides of the quartz plate measured in the dry state. From these spectral features, the effect of the carbon parity of

DOI: 10.1039/b001867h

the spacer on the packing state of Az can be evaluated as follows.

Firstly, the aggregation state of Az was altered by the carbon number. The peak position of the π–π* band attributed to the long axis transition of Az (λ_{max}), which indicates the aggregation state of the chromophore,[14] showed a zigzag change with increasing *n* (open circles in Fig. 3 inset). The Az units in the transferred monolayers formed H-aggregates in all cases, judging from the considerable hyprochromic shifts of λ_{max} (317–327 nm) from the value in chloroform solution (352 nm).[5] As a general tendency, λ_{max} shifted to shorter wavelengths with increasing spacer length, indicating that a stronger H-type aggregation is formed in the monolayer with the longer spacers, due to stronger van der Waals interactions. Among these, λ_{max} for the odd numbered series showed significant hypsochromic shifts.

Secondly, the molecular orientation was altered. The absorption ratios of the two π–π* bands, *i.e.* the absorption intensity of the short-axis transition (peaking below 250 nm) relative to that of the long-axis transition (300–400 nm) (A_{short}/A_{long}), are plotted as a function of *n* (filled squares in Fig. 3 inset). The value of A_{short}/A_{long} was less than 1.0 for the even numbered series, whereas it exceeded 1.0 for the odd numbered series. This absorbance ratio can be related to the degree of molecular tilting. In the transmission mode measurements, the smaller value of A_{short}/A_{long} indicates a larger molecular tilt from the surface normal. Therefore, the monolayers of **1** with the even numbered spacers should be tilted to a greater extent than those of the odd numbered series. This observation is in good agreement with the above mentioned results of (i) the larger expansion in the spreading behavior on water (Fig. 2) and (ii) the less hypsochromic shifts of the π–π* band in the absorption spectrum (open circles in Fig. 3 inset) for the even numbered series.

We assume the origin of the odd–even effects observed here is as follows. The formation of the bifurcated hydrogen bonds fixes the head groups firmly and molecular motion is thereby strongly hindered. When the alkylene spacer chain takes the all-*trans* zigzag conformation, then the orientation of the Az moiety should be affected alternately by the carbon parity. A precise understanding of the packing state requires further exploration using techniques such as X-ray analysis, Fourier transform infrared spectroscopy and microscopy observations, which will be the subject of future investigations.

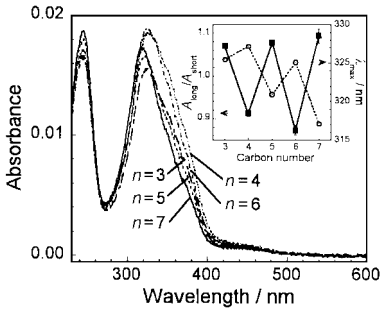

Fig. 3 UV–Vis absorption spectra of monolayers of **1** (n = 3–7) transferred at 20 mN m^{-1} onto both sides of a quartz plate. The inset shows λ_{max} (open circles) and A_{short}/A_{long} (filled squares, see text for definition) plotted against the alkylene spacer length (n).

In conclusion, this work revealed a new carbon parity effect observed in the packing state of photochromic Az units in a monolayer assembly. Since the packing state of Az governs the *trans*-to-*cis* photoisomerization behavior,[5] the findings observed here may have implications for the design of various photochromic functions.

Notes and references

1 See for example: J. C. MacDonald and G. M. Whitesides, *Chem. Rev.*, 1994, **94**, 2383; and references therein; X. Zhao, Y.-L. Chang, F. W. Fowler and J. W. Lauher, *J. Am. Chem. Soc.*, 1990, **112**, 6627.

2 K. Hanabusa, K. Shimura, K. Hirose, M. Kimura and H. Shirai, *Chem. Lett.*, 1996, 885.

3 J. van Esch, S. De Feyter, R. M. Kellog, F. DeSchryver and B. L. Ferringa, *Chem. Eur. J.*, 1997, **3**, 1287.

4 J. Glazer and A. E. Alexander, *Trans. Faraday Soc.*, 1951, **47**, 401; T. Kato, H. Akiyama and M. Yoshida, *Chem. Lett.*, 1992, 565.

5 T. Seki, T. Fukuchi and K. Ichimura, *Bull. Chem. Soc. Jpn.*, 1998, **71**, 2807.

6 T. Seki, T. Fukuchi and K. Ichimura, *Langmuir*, 2000, **16**, 3564

7 For example: D. Demus, in *Handbook of Liquid Crystals*, ed. D. Demus, J. Goodgy, G. W. Gray, H.-W Spiess and V. Vill, Wiley-VCH, Weinheim, 1998, vol. 1, pp. 133–187, and references therein.

8 Y. T. Tao, *J. Am. Chem. Soc.*, 1993, **115**, 4350; R. Colorado, Jr., R. J. Villazana and T. R. Lee, *Langmuir*, 1998, **14**, 6337.

9 M. Gavish, R. Popovitz-Biro, M. Laahav and L. Leiserowitz, *Science*, 1990, **250**, 972.

10 V. K. Gupta and N. L. Abbot, *Phys. Rev. E*, 1996, **54**, R4541.

11 M. Shimomura, K. Utsugi, J. Horikoshi, K. Okuyama, O. Hatozaki and N. Oyama, *Langmuir*, 1991, **7**, 760.

12 Detailed procedures and analytical data for this series will be reported elsewhere. Only the melting points and elemental analysis data are listed here. *N*-(3-{4-[(4-Hexylphenyl)azo]phenoxy})propylurea (n = 3): mp = 163–165 °C; found: C: 68.70; H: 7.80; N: 14.57; calcd for $C_{22}H_{30}N_4O_2$: C: 69.08; H: 7.91; N: 14.65%. *N*-(4-{4-[(4-Hexylphenyl)azo]phenoxy})butylurea (n = 4); mp = 154–156 °C; found: C: 69.80; H: 7.85; N: 14.30; calcd for $C_{23}H_{32}N_4O_2$: C: 69.67; H: 8.13; N: 14.13%. *N*-(5-{4-[(4-Hexylphenyl)azo]phenoxy})pentylurea (n = 5): mp = 148–149 °C; found: C: 70.09; H, 8.62; N: 13.60; calcd for $C_{24}H_{34}N_4O_2$: C: 70.24; H: 8.29; N: 13.66%. *N*-(6-{4-[(4-Hexylphenyl)-azo]phenoxy})hexylurea (n = 6): mp = 154–155 °C; found: C: 70.64; H: 8.69; N: 13.22; calcd for $C_{25}H_{36}N_4O_2$: C: 70.72; H: 8.55; N: 13.20%. *N*-(7-{4-[(4-Hexylphenyl)azo]phenoxy})heptylurea (n = 7): mp = 141–143 °C; found: C: 71.05; H: 8.67; N: 12.81; calcd for $C_{26}H_{38}N_4O_2$: C: 71.20; H: 8.73; N: 12.77%.

13 C. J. Brown, *Acta Crystallogr.*, 1966, **21**, 146.

14 M. Shimomura, R. Ando and T. Kunitake, *Ber. Bunsen-Ges. Phys. Chem.*, 1983, **87**, 1134.

Novel *N,S*- and *N,Se*-planar chiral [2,2]paracyclophane ligands: synthesis and application in Pd-catalyzed allylic alkylation

Xue-Long Hou,*[ab] Xun-Wei Wu,[a] Li-Xin Dai,[a] Bo-Xun Cao[a] and Jie Sun[a]

[a] *Laboratory of Organometallic Chemistry, Shanghai Institute of Organic Chemistry, Chinese Academy of Sciences, 354 Fenglin Lu, Shanghai 200032, China. E-mail: xlhou@pub.sioc.ac.cn*

[b] *Shanghai-Hong Kong Joint Laboratory in Chemical Synthesis, Shanghai Institute of Organic Chemistry, Chinese Academy of Sciences, 354 Fenglin Lu, Shanghai 200032, China*

Received (in Cambridge, UK) 4th April 2000, Accepted 19th May 2000

Novel *N,S*- and *N,Se*-ligands with planar chirality derived from [2.2]paracyclophane have been synthesized and applied in palladium-catalyzed allylic alkylation reaction, in which ligands 5 and 9 with the two substituents at benzylic and benzene ring positions give the highest ee values.

The design and synthesis of new chiral ligands play a crucial role in transition metal catalyzed asymmetric reactions.[1] Recently, ligands possessing planar chirality have attracted greater interest amongst various chiral ligands in asymmetric catalysis. In comparison with ferrocene derivatives[2] and arene transition metal complexes,[3] little attention has been paid to ligands derived from [2.2]paracyclophane, a structural framework capable of introducing planar chirality, and only a limited number of reports have appeared on studies of chiral [2.2]paracyclophanes,[4] especially their uses in asymmetric catalysis,[4e–h,k] although these ligands are linearly chiral,[5] chemically stable[6] and undergo racemization only at relatively high temperature.[7] As part of a program aimed at the applications of planar chirality in asymmetric synthesis[8] we studied the role of [2.2]paracyclophane-type planar chirality in asymmetric induction. Herein we disclose our results on the synthesis of novel *N,S*- and *N,Se*-ligands with planar chirality and central chirality based on the [2.2]paracyclophane backbone and their use in the palladium-catalyzed allylic alkylation reaction.[9]

From racemic 4-carboxy[2.2]paracyclophane **1** as starting material[10] and by using literature procedures[11] oxazoline **3** was obtained as a mixture of two diastereoisomers. Direct *ortho*-lithiation of oxazoline **3** with Bu^{n}Li and an equimolar amount of TMEDA followed by quenching with PhSSPh gave rise to the expected products **4a** and **4b** (Scheme 1). To our surprise, a third product **5** was obtained in addition to the expected *ortho*-lithiation/electrophile quenching products **4a** and **4b**. The structure of **5** was determined by ^{1}H NMR spectroscopy and confirmed by X-ray crystallography.† The planar chirality of these three products were readily determined by comparison with that of products obtained by using optically pure **1a** and **1b**[10] as starting materials and repeating the same procedure. In addition, the absolute configuration of C-2 in **5** was assigned as (*R*) based on the (*S*)-configuration of C-19 in the oxazoline moiety (Fig. 1). Possibly the benzylic substituted cyclophane **5** was produced owing to the nonplanarity of benzene ring of the cyclophane[12] and the steric effect of isopropyl group of the oxazoline.[13]

To examine the efficiency of these planar chiral *N,S*-ligands in asymmetric synthesis, palladium-catalyzed allylic alkylation was chosen as the model reaction (Scheme 2). The experiment was carried out at r.t. in the presence of $[Pd(\eta^3\text{-}C_3H_5)Cl]_2$ and the ligands. A nucleophile was generated from dimethyl malonate in the presence of *N,O*-bis(trimethylsilyl)acetamide (BSA) and a catalytic amount of salt. The results were summarized in Table 1. It was found that all ligands **4a**, **4b** and **5** can catalyze the reaction to afford the substitution product **7** in almost quantitative yields. In comparison with the results

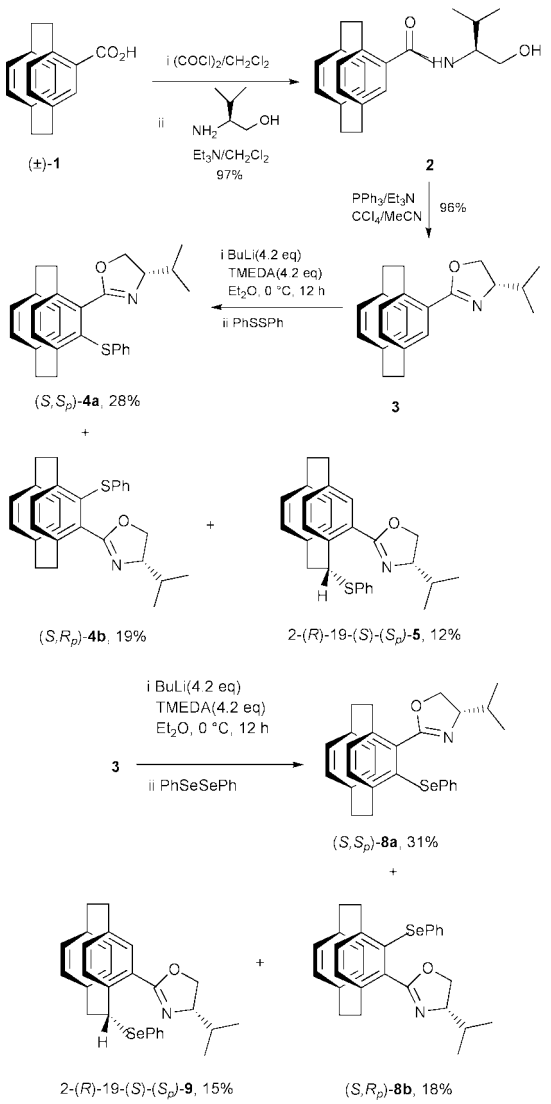

Scheme 1

obtained by using benzene ring substituted compounds **4a** and **4b** as ligands, the reaction using the benzylic substituted cyclophane **5** provided far better enantioselectivity, and the reactivity of **5** was also much higher than that of **4a** and **4b** (entries 4, 5 *cf.* entry 6).

The structure of ligand **5** is unique in the planar chiral cyclophane family. Its enantioselectivity and reactivity are also notable. Therefore similar *N,Se*-ligands **8a**, **8b** and **9**, with the latter having the same skeleton as **5**, were prepared by using similar procedures from intermediate **3** (Scheme 1) and tested further for the efficiency of planar chiral ligands with the two

DOI: 10.1039/b002679o

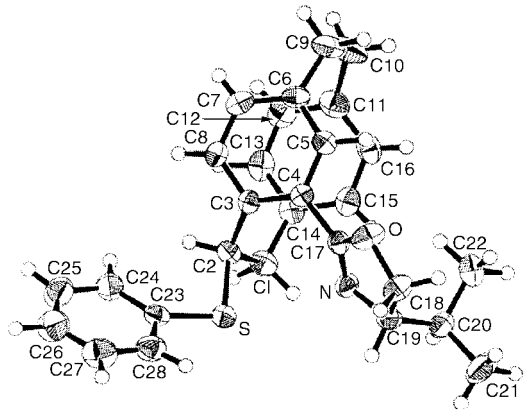

Fig. 1 ORTEP drawing of 2-(*R*)-19-(*S*)-(S_p)-**5** with the atomic numbering.

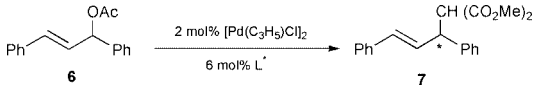

Scheme 2

Table 1 The effect of different ligands on the enantioselective palladium-catalyzed allylic substitution reaction using planar chiral *N,S*- and *N,Se*-ligands[a]

Entry	Ligand	Solvent	Salt	*t*/h	Yield (%)[b]	Ee (%)[c]	Configuration[d]
1	**4a**	PhMe	LiOAc	40	98	54	*R*
2	**4a**	CH_2Cl_2	LiOAc	24	98	50	*R*
3	**4a**	CH_2Cl_2	KOAc	36	98	53	*R*
4	**4a**	MeCN	KOAc	32	98	54	*R*
5	**4b**	MeCN	KOAc	21.5	98	63	*S*
6	**5**	MeCN	KOAc	1.5	98	94	*S*
7	**8a**	MeCN	KOAc	20	98	57	*R*
8	**8b**	MeCN	KOAc	30	98	73	*S*
9	**9**	MeCN	KOAc	2	98	93	*S*

[a] Molecular ratio: $[Pd(\eta^3\text{-}C_3H_5)Cl]_2$: ligand : **6** : dimethyl malonate : BSA : salt = 2 : 6 : 100 : 300 : 300 : 3. [b] Isolated yield after flash chromatography. [c] Ee determined by HPLC (chiralel OJ column). [d] Absolute configuration of the product **7** was assigned by comparison with the sign of specific rotation according to literature data.[14]

coordinating atoms at benzylic and benzene ring positions in asymmetric synthesis. It can be seen that a higher ee value was obtained for benzylic substituted ligand **9** relative to **8a** and **8b** (entry 9 *cf.* entries 7,8 in Table 1). As for the *N, S*-ligand, the reactivity of the benzylic derivative (**9**) as ligand is higher than that using ring-substituted cyclophanes **8a** and **8b** as ligands. These results clearly show that the ligand with the two coordinating atoms at benzylic and benzene ring-positions is more effective than that with both the coordinating atoms at benzene ring-positions. This is presumably due to the increased tether length between the donor atoms which coordinate palladium in **5** and **9**, bringing the asymmetric environment closer to the allyl species during the reaction.[15] Interestingly, **4a** and **8a** with the same S_p planar chirality afforded **7** in (*R*)-configuration, whereas **4b**, **8b** with R_p planar chirality gave rise to **7** in (*S*)-configuration, even though all of these ligands showed the same central chirality at the oxazoline. It seems that the central chirality is not a decisive factor in controlling the absolute configuration of the product in our reaction.[8b,e]

In summary, novel *N,S*- and *N,Se*-ligands bearing the two coordinating atoms at benzylic and benzene ring positions showed excellent enantioselectivity and reactivity in palladium-catalyzed allylic alkylation reaction. The synthesis of further similar ligands *via* introduction of other coordinating atoms at the benzylic position and further investigations on the role of these in asymmetric reactions in more detail are in progress.

Financial support from the National Natural Science Foundation of China (Project 29790127 and 29872045), National Outstanding Youth Fund, Chinese Academy of Sciences, and Shanghai Committee of Science and Technology is gratefully acknowledged.

Notes and references

† *Crystal data* for **5**: M = 427.60, orthorhombic, space group $P2_12_12$, a = 14.633(2), b = 19.668(4), c = 7.749(2) Å, V = 2230.0(8) Å^3, Z = 4, D_c = 1.274 g cm^{-3}, T = 293 K, λ(Mo-Kα) = 0.7107 Å, μ = 1.657 cm^{-1}, 2938 measured reflections, 2555 observed reflections, R = 0.0430, R^1 = 0.0540, S = 1.800, p_{max}, p_{min} = 0.431, −0.344 e Å^{-3}. CCDC 182/1650. See http://www.rsc.org/suppdata/cc/b0/b002679o/ for crystallographic files in .cif format.

1 *Catalytic Asymmetric Synthesis*, ed. I. Ojima, VCH, New York, 1993; R. Noyori, *Asymmetric Catalysis In Organic Synthesis*, Wiley, New York, 1994.
2 For reviews, see: *Ferrocenes*, ed. A. Togni and T. Hayashi, VCH, Weinheim, 1995; C. J. Richards and A. J. Locke, *Tetrahedron: Asymmetry*, 1998, **9**, 2377.
3 C. Bolm and K. Muniz, *Chem. Soc. Rev.*, 1999, **28**, 51.
4 (*a*) H. J. Reich and K. E. Yelm, *J. Org. Chem.*, 1991, **56**, 5672; (*b*) R. Yanada, M. Higashikawa, Y. Miwa, T. Taga and F. Yoneda, *Tetrahedron: Asymmetry*, 1992, **11**, 1387; (*c*) D. Y. Antonov, Y. N. Belokon, N. S. Ikonnikov, S. A. Orlova, A. P. Pisarevsky, N. I. Raevski, V. I. Rozenberg, E. V. Sergeeva, Y. T. Struchkov, V. I. Tararov and E. V. Vorontsov, *J. Chem. Soc., Perkin Trans. 1*, 1995, 1873; (*d*) V. V. Sergeeva, V. I. Rozenberg, E. V. Vorontsov, T. D. Danilova, Z. A. Starikova, A. I. Yanovsky, Y. N. Belokon and H. Hopf, *Tetrahedron: Asymmetry*, 1996, **12**, 3445; (*e*) Y. Belokon, M. Moscalenko, N. Ionnikov, L. Yashkina, D. Antonov, E. Vorontsov and V. Rozenberg, *Tetrahedron: Asymmetry*, 1997, **19**, 3245; (*f*) P. J. Pye, K. Rossen, R. A. Reamer, N. N. Tsou, R. P. Volante and P. J. Reider, *J. Am. Chem. Soc.*, 1997, **119**, 6207; (*g*) K. Rossen, P. J. Pye, A. Maliakal and R. P. Volante, *J. Org. Chem.*, 1997, **62**, 6462; (*h*) A. H. Vetter and A. Berkessel, *Tetrahedron Lett.*, 1998, **39**, 1741; (*i*) P. J. Pye, K. Rossen, R. A. Reamer, R. P. Volante and P. J. Reider, *Tetrahedron Lett.*, 1998, **39**, 4441; (*j*) V. I. Rozenberg, N. V. Dubrovina, E. V. Vorontsov, E. V. Sergeeva and Y. N. Belokon, *Tetrahedron: Asymmetry*, 1999, **10**, 511; (*k*) U. Wörsdörfer, F. Vögtle, M. Nieger, M. Waletzke, S. Grimme, F. Glorius and A. Pfaltz, *Synthesis*, 1999, **4**, 597.
5 R. S. Cahn, C. K. Ingold and V. Prelog, *Experientia*, 1956, **12**, 81; *Angew. Chem., Int. Ed. Engl.*, 1966, **5**, 385.
6 D. J. Cram and N. Allinger, *J. Am. Chem. Soc.*, 1955, **77**, 6289.
7 H. J. Reich and D. J. Cram, *J. Am. Chem. Soc.*, 1969, **91**, 3517.
8 (*a*) X. D. Du, L. X. Dai, X. L. Hou, L. J. Xia and M. H. Tang, *Chin. J. Chem.*, 1998, **16**, 90; (*b*) S. L. You, Y. G. Zhou, X. L. Hou and L. X. Dai, *Chem. Commun.*, 1998, 2765; (*c*) W. P. Deng, X. L. Hou and L. X. Dai, *Tetrahedron: Asymmetry* 1999, **10**, 4689; (*d*) L. X. Dai, X. L. Hou, W. P. Deng, S. L. You and Y. G. Zhou, *Pure Appl. Chem.*, 1999, **71**, 1401; (*e*) W. P. Deng, X. L. Hou, L. X. Dai, Y. H. Yu and W. Xia, *Chem. Commun.*, 2000, 285; (*f*) S. L. You, X. L. Hou and L. X. Dai, *Tetrahedron: Asymmetry*, 2000, **11**, 1495.
9 For reviews, see: B. M. Trost and D. L. Van Vranken, *Chem. Rev.*, 1996, **96**, 395; B. M. Trost, *Acc. Chem. Res.*, 1996, **29**, 355; G. J. Helmchen, *J. Organomet. Chem.*, 1999, **576**, 203.
10 V. Rozenberg, N. Dubrovvina, E. Sergeeva, D. Antonov and Y. Belokon, *Tetrahedron: Asymmetry*, 1998, **9**, 653.
11 H. Vorbruggen and K. Krolikliewicz, *Tetrahedron Lett.*, 1981, **22**, 4471.
12 P. M. Keehn and S. M. Rosenfeld, *Cyclophanes*, Academic Press, New York, 1983, p. 71.
13 A similar result was obtained in the diastereomeric deprotonation of chiral ferrocenyl oxazolines: see: C. J. Richards, T. Damalidis, D. E. Hibbs and M. B. Hursthouse, *Synlett*, 1995, 74; T. Sammakia and H. A. Latham, *J. Org. Chem.*, 1995, **60**, 6002.
14 P. Wimmer and M. Widhalm, *Tetrohedron: Asymmetry*, 1995, **6**, 657.
15 B. M. Trost and D. L. Van Vranken, *Angew. Chem., Int. Ed. Engl.*, 1992, **31**, 228; G. J. Dawson, C. G. Frost, C. J. Martin, J. M. J. Williams and S. J. Coote, *Tetrahedron Lett.*, 1993, **34**, 7793; A. Chesney, M. R. Bryce, R. W. J. Chubh, A. S. Batsancy and J. A. K. Howard, *Tetrahedron: Asymmetry*, 1997, **8**, 2337.

Facile electronic communication between bimetallic termini bridged by elemental carbon chains

Tong Ren,* Gang Zou and Julio C. Alvarez

Department of Chemistry and Center for Supramolecular Science, University of Miami, Coral Gables, FL 33124 USA. E-mail: tren@miami.edu

Received (in Columbia, MO, USA) 4th April 2000, Accepted 23rd May 2000

Rich electrochemistry and strong electronic couplings across the carbon bridges are revealed for compounds composed of two tetra(μ-*N*,*N*′-2-anilinopyridinate)diruthenium(II,III) termini bridged by either butadiynediyl (1) or ethynediyl (2) ligands.

The proposal of constructing molecular wires from linear arrays of covalently-linked metal-complexes (M) and elemental carbon chain (C_m) has been inspired by the pioneering work of Nast[1] and Hagihara.[2] Extensive electronic delocalization along the $-(M-C_m)_\infty-$ backbone holds the promise for new generation electronic and optoelectronic materials.[3] Much of the work during this decade has focused on the M–C_m–M type molecular compounds.[4,5] The degree of delocalization between two equivalent termini M is gauged by the comproportionation constant K_{com} for the following equilibrium:

$$[M-C_m-M]+[M-C_m-M]^{2+} \overset{K_{com}}{\rightleftharpoons} 2[M-C_m-M]^{+} \quad (1)$$

K_{com} (= $\exp\{F[E_{1/2}(2+/1+)-E_{1/2}(1+/0)]/RT\}$) can be computed from the electrode potentials $E_{1/2}(2+/1+)$ and $E_{1/2}(1+/0)$.[6] Significant delocalization along the C_m-bridge (K_{com} *ca.* 10^8–10^{12}) has been achieved with termini of CpFe(P–P),[7] CpRe(P)(NO),[8] $CpRu(P)_2$[9] and $Mn(P–P)_2I$[10] (P and P–P are mono- and bi-dentate phosphines, respectively), all mononuclear transition metal complexes. We report the first examples of capping elemental carbon chains (C_2 and C_4) with a bimetallic terminus, $[Ru_2(\mu\text{-ap})_4]^+$ (ap = 2-anilinopyridinate), which is the valence-averaged (not mix-valence!) diruthenium species with a 2.5 Ru–Ru bond order.[11,12]

It has been established that the mono-capped complexes $[Ru_2](C{\equiv}CR)$ (**3**) with R as Ph, H (**3a**), $SiMe_3$ (**3a**) and CH_2OCH_3 (**3c**) can be obtained from the transmetalation reaction between $[Ru_2]Cl$ and $LiC{\equiv}CR$.[12,13] Similarly, treating $[Ru_2]Cl$ with either 0.5 equiv. of $LiC{\equiv}CC{\equiv}CLi$ or 1 equiv. of $LiC{\equiv}CLi$ yields **1** and **2**, respectively.† Formulation of $(C{\equiv}C)_n$-

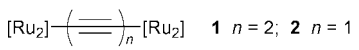

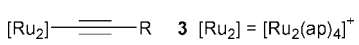

bridged dimers was established by both the elemental analysis and FAB-mass spectrometry.† Further confirmation of $(C{\equiv}C)_n$-bridging structural motif is provided by an X-ray diffraction study of molecule **1**.‡ Asymmetric unit of the crystal **1** contains the halves of two independent molecules, and each is related to the other half *via* a crystallographic inversion center. Metric parameters of the two independent molecules are very similar, and the structural plot of one of them is presented in Fig. 1, where a linear array formed by the bridging C_4-chain and two $[Ru_2]$ termini is clear.

Compared with $[Ru_2](C{\equiv}CSiMe_3)$ (**3b**),[13] the 'half' molecule of **1**, the coordination geometry of the 2-anilionopyridinates around the Ru_2 core in **1** is essentially unchanged as evidenced by the averaged Ru(II)–N and Ru(III)–N bond lengths 2.050 and 2.095 Å in **1**, and 2.046 and 2.096 Å in **3b**. Room temperature effective magnetic moments of **1** and **2** are respectively 4.2 and

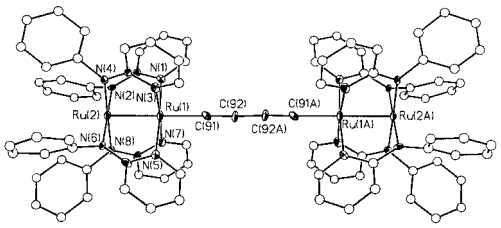

Fig. 1 ORTEP of **1** at 20% probability level. Selected bond lengths and angles: Ru(1)–C(91), 2.047(14) Å; C(91)–C(92), 1.258(16) Å; C(92)–C(92A), 1.33(2) Å; Ru(1)–Ru(2), 2.3311(15) Å; Ru(2)–Ru(1)–C(91), 179.5(4)°; Ru(1)–C(91)–C(92), 177.8(12)°; C(91)–C(92)–C(92A), 176.1(19)°.

3.8 μ_B per $[Ru_2]$, indicating a S = 3/2 ground state that has been observed for many Ru_2(II,III) compounds including **3** and $[Ru_2]Cl$.[11–13] Hence, the termini of both **1** and **2** are globally isoelectronic with **3** and $[Ru_2]Cl$. Some small but notable differences, however, do exist between **1** and **3b**: the Ru–Ru (2.331(2) Å) and $C_\alpha{\equiv}C_\beta$ (1.258(16) Å) distances in **1** are elongated from that of **3b** (2.3162(5) and 1.207(6) Å), while the Ru–C_α distance is shortened (2.047(14) Å in **1** and 2.077(4) Å in **3b**). The C_β–$C_\beta{}'$ (≡C–C≡) distance, 1.33(2) Å, is identical to that found for the highly delocalized $[Mn(dmpe)_2I]_2(\mu\text{-}C_4)$,[10] but shorter than 1.367[9] Å found for *trans*-$[Pt(PPh_3)_2Cl]_2(\mu\text{-}C_8)$, a molecule lacking delocalization.[14] Although barely significant, all these changes are consistent with the strengthening of the Ru–C π interaction and concurrent weakening of the π(C≡C) bond. The valence structure of the $[Ru_2]_2(\mu\text{-}C_4)$ backbone may contain a significant contribution of cumulenic resonance structure **B** in addition to the predominant resonance structure **A** depicting the localized carbon–carbon triple bonds.

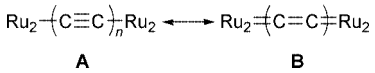

Cyclic voltammograms (CV) of **3** indicate two quasireversible redox processes (CV for **3a** shown in Fig. 2): an oxidation (**3a**$^+$/**3a**) around 462 mV and a reduction (**3a**/**3a**$^-$) around −873 mV and an irreversible couple at more positive potential (*ca.* 1300 mV). Upon a change from simple axial coordination of C≡CR to $(C{\equiv}C)_n$-bridge, both **1** and **2** undergo four quasireversible and one irreversible one-electron redox processes between −1600 and +1200 mV (Fig. 2). Therefore, there are six accessible oxidation states in both molecules **1** and **2**, surpassing the record of five established for $[CpRu(P)_2]_2(\mu\text{-}C_4)$.[9]

Based on the established electrochemistry of **3**,[13] the quasireversible redox couples in both **1** and **2** can be unambiguously assigned as:

Redox couples I and II correspond to the one electron reduction couple in **3**, and III and IV correspond to the oxidation couple in **3**. $\Delta E_{1/2}$(II/I) and $\Delta E_{1/2}$(IV/III), the differences in electrode

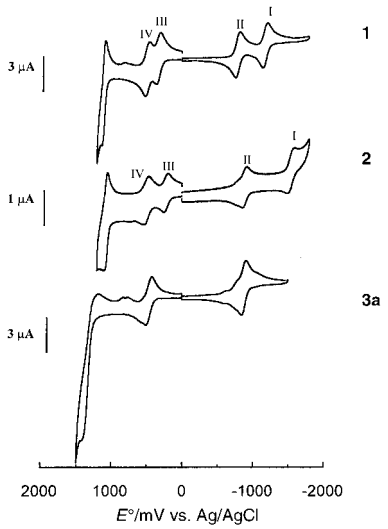

Fig. 2 Cyclic voltammograms of compounds **1**, **2** and **3a** recorded at a scan rate of 100 mV/s in 0.20 M $(Bu^n)_4NPF_6$ solution (THF, N_2-degassed) on a BAS CV-100W voltammetric analyzer with a glassy carbon working electrode, a Pt-wire auxiliary electrodes, and a Ag/AgCl reference electrode.

potentials, are respectively 389 and 157 mV in **1**, and 667 and 285 mV in **2**, which are undoubtedly the result of strong electronic coupling between two [Ru_2] termini mediated by the $(C{\equiv}C)_n$-bridges. Corresponding comproportionation constants K_{com}(red) and K_{com}(ox) are 3.8×10^6 and 506 for **1**, and 1.9×10^{11} and 6.6×10^4 for **2**, and K_{com}(red) for **2** is comparable to the largest K_{com} determined for other $(C{\equiv}C)_n$-bridged complexes with CpFe(P–P) (1.6×10^{12}),[7] CpRe(P)(NO) (1.1×10^9),[8] $CpRu(P)_2$ (1.5×10^{11}),[9] and $Mn(P–P)_2I$ (5.4×10^{10})[10] termini. Distance-dependence of the coupling is evident: K_{com} of C_4-bridged **1** is several orders of magnitude smaller than that of C_2-bridged **2**. Furthermore, K_{com}(red) is much larger than K_{com}(ox) in the same molecule, indicating that the Ru–C π-bonding is much stronger in the reduced form than in the oxidized form. Both linear and square arrays of bimetallic units covalently linked by dicarboxylates have been reported recently,[15] and K_{com} as high as 1.3×10^{12} was determined for $[W_2(O_2C^tBu)_3]_2$(μ-oxalate).

Effect of electronic delocalization over the C_m-bridge is also evident from the UV–VIS–NIR spectra (Fig. 3). The 'half' molecule **3a** absorbs strongly at 465 (**A**) and 745 nm (**B**), which may be respectively attributed to σ(Ru–C) to δ*(Ru_2) and π(Ru_2) to π*(Ru–N) transitions in analogy to the case of $Ru_2(O_2CR)_4Cl$.[16] Upon establishing the C_m bridge, each band is 'split' into two intensified bands (A1 and A2; B1 and B2), and the emergence of bands A2 and B2 accounts for the color change from the dark green for all $Ru_2(ap)_4(C{\equiv}CR)$ species[12,13] to the dark blue and red–purple colors for **1** and **2**, respectively. Clearly, the strong electronic coupling across the C_m bridge results in a significant orbital mixing between two [Ru_2] termini. The energy splitting of either the ground state or the excited state due to the mixing is sufficiently large that each of transitions **A** and **B** evolves into two bands.

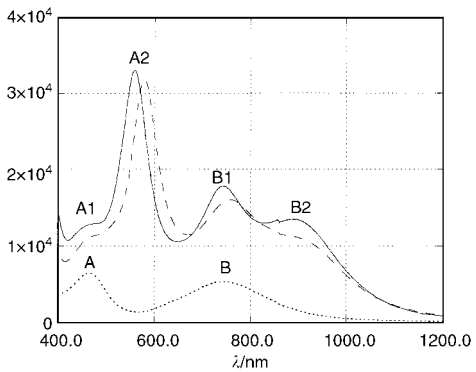

Fig. 3 UV–VIS spectra of compounds **1** (dash), **2** (solid) and **3a** (dot) recorded in THF.

The unprecedented number of accessible oxidation states in a C_m-bridged complex discovered for **1** and **2** clearly demonstrates the advantage of using bimetallic units as terminal electron reservoirs in constructing molecular conductors. The presence of multiple reversible redox couples in **1** and **2** may furthermore allow access to both the anionic (*e.g.* $\mathbf{1}^-$ and $\mathbf{1}^{2-}$) and cationic derivatives ($\mathbf{1}^+$ and $\mathbf{1}^{2+}$). Isolations of these derivatives and the analogs with longer C_m bridges are being explored in our laboratory.

Generous support from the University of Miami (Start-up fund, CCD-diffractometer fund, and General Research Award) is gratefully acknowledged. We also thank Professor A. Kaifer for the access of electrochemical apparatus.

Notes and references

† **1** and **2** were obtained by treating $Ru_2(ap)_4Cl$ with either LiCCCCLi (0.6 equiv.) or LiCCLi (1 equiv.) in THF at room temperature for 12 h under argon. After the mixture was washed with brine, the solvent was removed from the organic layer to yield a purple solid. Residual starting material was removed *via* rinsing with CH_2Cl_2 till the washings became colorless. Recrystallization in THF yield dark purple microcrystalline solids (53% for **1** and 42% for **2**). Compound **1**: Anal. for $C_{92}H_{72}N_{16}Ru_4$, Found (calcd.): C, 61.24 (61.18); H, 4.06 (4.02); N, 12.37(12.41); MS-FAB (*m/z*, based on ^{101}Ru): 1808 [M^+]. UV–VIS in THF λ, nm (ε/M^{-1} cm^{-1}): 467(sh), 578(31 900), 757(16 100), 910(sh). CV data ($E_{1/2}$(mV)/ΔE_p(mV)/(i_{pa}/i_{pc})): I, −1173/61/0.94; II, −784/64/1.10; III, 334/59/1.65; IV, 491/63/0.66; third oxidation, 1115/71/4.72. Compound **2**: Anal. for $C_{90}H_{72}N_{16}Ru_4$, Found (calcd.): C, 60.64 (60.66); H, 4.05 (4.07); N, 12.35 (12.58). MS-FAB (*m/z*, based on ^{101}Ru): 1784 [M^+]. UV–VIS in THF λ, nm (ε/M^{-1} cm^{-1}): 465(sh), 558(33 000), 743(17 900), 892(13 500). Cyclic voltammetry data ($E_{1/2}$(mV)/ΔE_p(mV)/(i_{pa}/i_{pc})): I, −1555/75/1.97; II, −888/57/1.142; III, 223/58/1.22; IV, 508/78/1.45; third oxidation, 1079/63/5.40.

‡ *Crystal data* for **1**·$8H_2O$: $C_{92}H_{88}N_{16}O_8Ru_4$, M = 1933.94, triclinic, $P\bar{1}$, a = 10.0838(17), b = 20.023(3), c = 22.504(4) Å, α = 95.518(3), β = 95.250(3), γ = 93.827(4)°, U = 4490.7(13) $Å^3$, Z = 2, μ(MoKα) = 0.723 mm^{-1}, T = 300 K, 19970 reflections measured, 12401 unique (R_{int} = 0.0696), final $R1$ = 0.075, w$R2$ = 0.159. CCDC 182/1662. See http://www.rsc.org/suppdata/cc/b0/b002777o/ for crystallographic files in .cif fomat.

1 R. Nast, *Coord. Chem. Rev.*, 1982, **47**, 89.
2 N. Hagihara, K. Sonogashira and S. Takahashi, *Adv. Polym. Sci.*, 1980, **40**, 149.
3 R. P. Kingsborough and T. M. Swager, *Prog. Inorg. Chem.*, 1999, **48**, 123.
4 For recent reveiws/perspectives: (*a*) M. H. Chisholm, *Angew. Chem., Int. Ed. Engl.*, 1991, **30**, 673; (*b*) H. Lang, *Angew. Chem., Int. Ed. Engl.*, 1994, **33**, 547; (*c*) U. H. F. Bunz, *Angew. Chem., Int. Ed. Engl.*, 1996, **35**, 969; (*d*) F. Paul and C. Lapinte, *Coord. Chem. Rev.*, 1998, **178**–**180**, 431.
5 R. E. Martin and F. Diederich, *Angew. Chem., Int. Ed.*, 1999, **38**, 1350.
6 C. Creutz, *Prog. Inorg. Chem.*, 1983, **30**, 1.
7 N. Le Narvor, L. Toupet and C. Lapinte, *J. Am. Chem. Soc.*, 1995, **117**, 7129.
8 M. Brady, W. Weng, Y. Zou, J. W. Seyler, A. J. Amoroso, A. M. Arif, M. Bohme, G. Frenking and J. A. Gladysz, *J. Am. Chem. Soc.*, 1997, **119**, 775.
9 M. I. Bruce, L. I. Denisovich, P. J. Low, S. M. Peregudova and N. A. Ustynyuk, *Mendeleev Commun.*, 1996, 200.
10 S. Kheradmandan, K. Heinze, H. W. Schmalle and H. Berke, *Angew. Chem., Int. Ed.*, 1999, **38**, 2270.
11 F. A. Cotton and R. A. Walton, *Multiple Bonds between Metal Atoms*, Oxford University Press, Oxford, 1993.
12 A. R. Chakravarty and R. A. Cotton, *Inorg. Chim. Acta*, 1986, **113**, 19.
13 G. Zou, J. C. Alvarez and T. Ren, *J. Organomet. Chem.*, 2000, **596**, 152.
14 T. P. Peters, J. C. Bohling, A. M. Arif and J. A. Gladysz, *Organometallics*, 1999, **18**, 3261.
15 (*a*) R. H. Cayton, M. H. Chisholm, J. C. Huffman and E. B. Lobkovsky, *J. Am. Chem. Soc.*, 1991, **113**, 8709; (*b*) F. A. Cotton, L. M. Daniels, C. Lin and C. A. Murillo, *J. Am. Chem. Soc.*, 1998, **121**, 4538.
16 V. M. Miskowski and H. B. Gray, *Inorg. Chem.*, 1988, **27**, 2501.

ChemComm

A chiral Eu^{3+}–thienoyltrifluoroacetone complex on an avidin tetramer: luminescence and CD studies on the supramolecular protein–metal chelate complex

Masumi Taki, Hiroshi Murakami and Masahiko Sisido*

Department of Bioscience and Biotechnology, Faculty of Engineering, Okayama University, 3-1-1 Tsushimanaka, Okayama 700-8530, Japan. E-mail: sisido@cc.okayama-u.ac.jp

Received (in Cambridge, UK) 8th March 2000, Accepted 23rd May 2000

A chiral Eu^{3+}–chelate complex was built into the biotin-binding sites of an avidin tetramer by the binding of biotin-linked thienoyltrifluoroacetones.

Eu^{3+}–β-diketone complexes are known to exhibit distinct luminescence when irradiated under UV light.[1] The emission properties have been intensively studied and have found a variety of chemical and biological applications, *e.g.* as sensitive fluorometric probes.[2] However, conventional bidentate β-diketone chelators form rather unstable complexes with Eu^{3+}, and their luminescence intensity is often very weak, especially in aqueous media. In order to overcome this problem, Matsumoto and coworkers synthesized a new type of Eu^{3+} chelate in which two bidentate β-diketone moieties are covalently linked.[3,4] The tetradentate ligand formed a very stable complex with Eu^{3+}, and the complex emitted strong luminescence.[4]

The finding of luminescence enhancement in the above tetradentate chelate motivated us to build a supramolecular Eu^{3+} complex of two bidentate ligand molecules arranged on a protein framework. A tetrameric avidin was chosen as the protein framework, since it strongly binds biotin[5] or biotin derivatives[6] through non-covalent interactions. The X-ray crystallographic data of the avidin tetramer[7] indicates that two of the four biotin-binding sites face one side of the tetramer and the two biotins in the binding sites take a right-handed screw configuration with a chirality factor of 0.90.[8] The dissymmetrically arranged biotin-binding pockets can be used to incorporate two biotin-labeled bidentate ligands in a chiral configuration. The structure and synthesis of the biotin-linked bidentate ligand **2** (Bi-TTA), are shown in Scheme 1.

Complexation of the Bi-TTA with avidin was confirmed by the fluorescence quenching of tryptophan in avidin. Fig. 1 shows the fluorescence spectra of avidin in the presence of different amounts of Bi-TTA. The peak position of tryptophan fluorescence shifted to a shorter wavelength[9] and decreased upon addition of Bi-TTA. The decrease stopped when the avidin units were saturated by the Bi-TTA molecules. The extent of fluorescence quenching was much larger than the quenching by biotin,[6] presumably owing to an energy transfer process from the singlet excited state of the tryptophan to the triplet state of the β-diketone group.

The formation of the Bi-TTA–Eu^{3+} complex on the protein framework was monitored by the increase of luminescence intensity of a solution of Bi-TTA and Eu^{3+} upon addition of avidin. As shown in Fig. 2, the narrow luminescence band at 613 nm increased with the addition of avidin, and the increase ceased after almost all the Bi-TTA molecules were bound to avidin. The luminescence intensity of the Bi-TTA–Eu^{3+} complex in the presence of avidin is 25 times larger than that of the free Bi-TTA and Eu^{3+} mixture in the absence of avidin. No luminescence band at 613 nm was observed for a mixture of Eu^{3+} and avidin in the absence of Bi-TTA.

When an excess of avidin was quickly added to a fresh mixture of Bi-TTA and Eu^{3+} up to a tetrameric avidin : Bi–TTA ratio of 5 : 1, the luminescence emission at 613 nm decreased to 17% of the intensity for the tetrameric avidin : Bi-TTA ratio of 1 : 4. The reduced Eu^{3+} emission in the presence of an excess of avidin suggests that the emission enhancement at 613 nm originates from interactions between the metal chelates on the avidin tetramer and Eu^{3+} that are most effective when the tetrameric avidin : Bi-TTA ratio is 1 : 4.

The ligand : Eu^{3+} ratio was determined to be 1 : 1 from the luminescence titration curve of the mixture of tetrameric avidin:Bi-TTA (1 : 4) with the addition of Eu^{3+}. The luminescence intensity at 613 nm increased with the addition of Eu^{3+}, and the increase ceased when the Eu^{3+} : Bi-TTA ratio reached

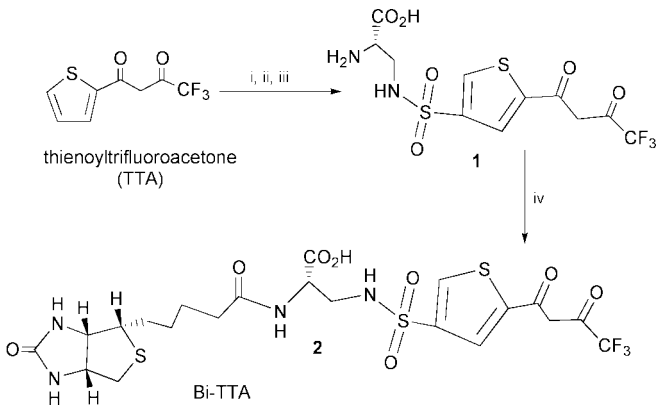

Scheme 1 *Reagents and conditions*: i, chlorosulfuric acid, 0 °C → room temp., 30%; ii, *N*-α-Boc-L-α,β-diaminopropionic acid, DMF, carbonate buffer (pH 9.3), r.t., 80%; iii, TFA, 0 °C, 100%; iv, *N*-hydroxysuccinimidobiotin, TEA, DMF, r.t., 100%.

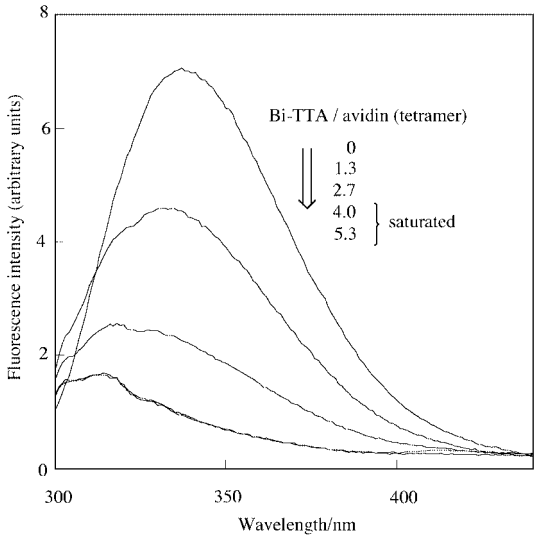

Fig. 1 Fluorescence spectra of avidin–Bi-TTA mixtures in PIPES–NaCl buffer at pH = 6.5. λ_{ex} = 290 nm. The molar ratios are indicated: [avidin (tetramer)] = 7.8×10^{-8} M.

DOI: 10.1039/b001908i

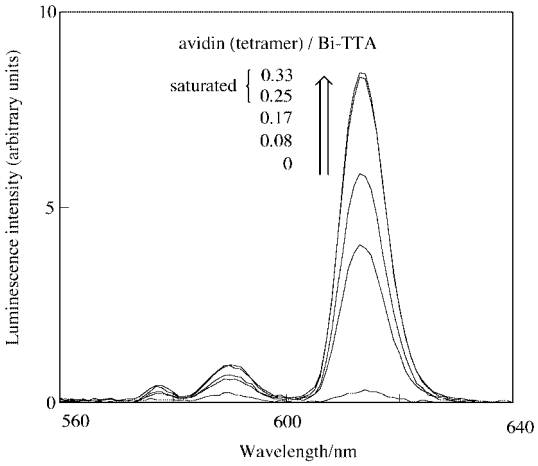

Fig. 2 Luminescence spectra of avidin–Bi-TTA mixtures in the presence of $EuCl_3$ in PIPES–NaCl buffer at pH = 6.5. The molar ratios of avidin (tetramer)/Bi-TTA are indicated: λ_{ex} = 343 nm. The TTA moiety is selectively excited under the conditions: [Bi-TTA] = 3.1×10^{-7} M, [$EuCl_3$] = 1.2×10^{-4} M.

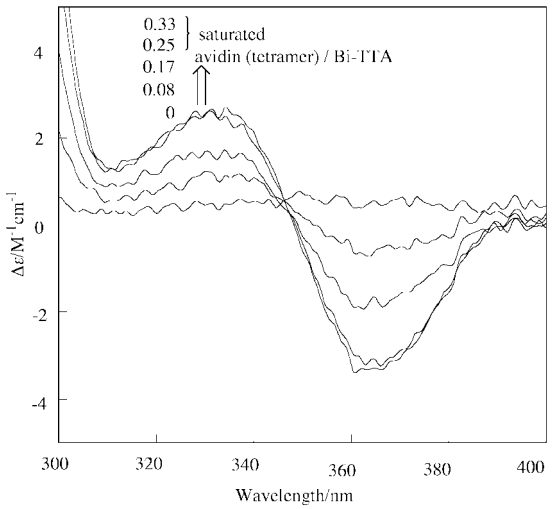

Fig. 3 CD spectra of Bi-TTA in the presence of $EuCl_3$ and different amounts of avidin in PIPES–NaCl buffer at pH = 6.5. The molar ratios are indicated; [Bi-TTA] = 4.0×10^{-4} M, [$EuCl_3$] = 3.0×10^{-3} M.

4:4. The Eu^{3+}:ligand ratio indicates that each TTA moiety binds a single Eu^{3+} ion, and the luminescence intensity increases when two TTA–Eu^{3+} complexes self-assemble on one side of the tetrameric avidin framework.

The formation of the two TTA–Eu^{3+} complexes was also confirmed from CD spectra. As shown in Fig. 3, a marked CD doublet appeared at 333 and 365 nm with the addition of avidin to a mixture of Bi-TTA and Eu^{3+}. The CD peak was saturated when all the Bi-TTA molecules were bound to avidin. No CD signal was observed in a tetrameric avidin:Bi-TTA (1:4) solution in the absence of Eu^{3+}. When Eu^{3+} was added to the latter solution, a similar CD spectrum as in Fig. 3 appeared, indicating the formation of the ligand–Eu^{3+} complex.

The luminescence and CD data indicate the formation of a chiral dimeric ligand–Eu^{3+} complex on the protein framework. The chiral lanthanide complex may find applications in enantioselective catalysis for the cleavage of nucleic acids[10] or proteins.[11]

This work was supported by a Grant-in-Aid for Specially Promoted Research from the Ministry of Education, Science, Sports and Culture, Japan (No. 11102003). M. T. and H. M. are also grateful to the Japan Society for the Promotion of Science (JSPS) for research fellowship grants.

Notes and references

1 S. I. Weissman, *J. Chem. Phys.*, 1942, **10**, 214.
2 F. S. Richardson, *Chem. Rev.*, 1982, **82**, 541.
3 J. Yuan and K. Matsumoto, *Anal. Sci.*, 1996, **12**, 695.
4 J. Yuan, K. Matsumoto and H. Kimura, *Anal. Chem.*, 1998, **70**, 596.
5 N. M. Green, *Adv. Protein Chem.*, 1975, **29**, 85.
6 M. Kuragaki and M. Sisido, *Bull. Chem. Soc. Jpn.*, 1997, **70**, 261.
7 P. C. Weber, D. H. Orlendorf, J. J. Wendoloski and F. R. Salemme, *Science*, 1989, **243**, 85.
8 The chirality factor is defined by $\zeta = \boldsymbol{r}_{12} \cdot (\boldsymbol{m}_1 \times \boldsymbol{m}_2)$, where $\boldsymbol{r}_{12}$ is a unit vector from the center of first biotin site to the second biotin site and $\boldsymbol{m}_1$, $\boldsymbol{m}_2$ are unit vectors that are fixed on the two biotin molecules, respectively. ζ takes a value from +1 for a right-handed screw configuration to −1 for a left-handed one. ζ = 0 for an achiral configuration: see, N. Harada and K. Nakanishi, *Circular Dichroic Spectroscopy, Exciton Coupling in Organic Stereochemistry*, University Science Books, New York, 1982; Y. Inai, M. Sisido and Y. Imanishi, *J. Chem. Phys.*, 1990, **94**, 8365.
9 G. P. Kurzban, G. Gitlin, E. A. Bayer, M. Wilchek and P. M. Horowitz, *Biochemistry*, 1989, **28**, 8537.
10 M. Komiyama, N. Takeda and H. Shigekawa, *Chem. Commun.*, 1999, 1443.
11 Y. Yamamoto and M. Komiyama, *Nucleic Acids, Symp. Ser.*, 1992, **27**, 33.

ChemComm

A novel photocycloaddition of substituted pyridines with benzofuran†

Masami Sakamoto,*[a] Ai Kinbara,[a] Tadao Yagi,[a] Takashi Mino,[a] Kentaro Yamaguchi[b] and Tsutomu Fujita[a]

[a] *Department of Materials Technology, Faculty of Engineering, Chiba University, Yayoi-cho, Inage-ku, Chiba 263-8522, Japan. E-mail: saka@galaxy.tc.chiba-u.ac.jp*

[b] *Chemical Analysis Center, Chiba University, Yayoi-cho, Inage-ku, Chiba 263-8522, Japan*

Received (in Cambridge, UK) 27th March 2000, Accepted 23rd May 2000

Irradiation of a benzene solution containing 3-cyano-2-methoxypyridine (0.02 M) and benzofuran (0.5 M) resulted in the formation of stereo-isomeric 1:1 adducts, *endo* and *exo*-7-cyano-2-methoxy-4-methyl-9-oxa-3-aza-10,11-benzotricyclo[6.3.0.0^{4,7}]undeca-2,5-diene, accompanied by 5-cyano-2-methoxypyridine and a pyridine dimer; the structures of the adducts were established by X-ray structural analyses.

The photochemistry of heteroaromatics is an underdeveloped area compared with the carbon aromatics, such as benzene, naphthalene and anthracene derivatives, the photochemical behavior of which has been extensively studied from both mechanistic and synthetic perspectives.[1–7] In particular, the ring expansion or transformation of a pyridine ring with photochemical 4 + 4 or 2 + 2 cycloaddition is quite difficult.[8] We are interested in investigating the photochemical aspects of heteroaromatics and their utilization for the synthesis of new heterocycles. Recently, we reported that 2-alkoxy-3-cyanopyridines show comparatively high photochemical reactivity for promoting a variety of photochemical reactions, such as dimerization and 4 + 4 cycloaddition with furan.[9–11] The high reactivity of these pyridines compared with a simple pyridine is dependent on the polarization within the pyridine ring from the conjugate relationship of the cyano and alkoxy groups. We have identified a new photochemical 2 + 2 cycloaddition reaction between two heteroaromatics, pyridine and benzofuran.

When a benzene solution of 3-cyano-2-methoxy-6-methylpyridine **1a** (0.02 M) containing 0.05 M of benzofuran was irradiated with Pyrex filtered light, two types of 1 : 1 adducts of **1a** and benzofuran (**2a**, 32%; **3a**, 25%) were obtained, accompanied by **4a** and the pyridine dimer **5a**, in 7 and 33% yields, respectively, at 59% conversion (Table 1). The structures of the adducts, **2a** and **3a**, were determined on the basis of elemental analyses and the spectral data. Finally, the stereoisomeric structures were established by X-ray structural analyses (Fig. 1 and 2).‡ In the cases of the transpositional isomer **4a** and the dimer **5a**, we have already reported their formation by the direct irradiation of **1a**.[9] Irradiation of **1b** and **1c** also gave two stereoisomeric adducts as shown in Table 1, their structures were determined by comparison of the spectral data of **2a** and **3a**.

Usually, an electronically excited pyridine is not observed to undergo any radiative relaxation; however, this pyridine **1** shows strong emission of fluorescence at 310 nm. The emissive singlet excited state of pyridine reacts with the ground state of benzofuran, because the addition reaction was not quenched by triplet quenchers, such as 2,5-dimethylhexa-2,4-diene, penta-1,3-diene or stilbene, and also the sensitization by benzophenone or xanthone was quite inefficient. The formation of the adducts **2** and **3** is explainable in terms of the 2 + 2 cycloaddition taking place at the C-2 and C-3 positions of the singlet excited state of the pyridine ring with the C-3 and C-2 positions of benzofuran leading to **6** (Scheme 1). A subsequent ring-opening reaction gives cyclooctatriene **7**, which is followed by electrocyclization to the tricyclic adducts **2** and **3**.

The mechanism is also supported by Frontier-MO calculations using the PM3 Hamiltonian.[12] The orbital energies and coefficients of the singlet excited state for **1a** (HSOMO and LSOMO) and those of the ground state of benzofuran (LUMO and HOMO) were obtained (Fig 3). The energy gap (ΔE) between the LSOMO and HOMO is smaller than that between the HSOMO and LUMO, and this frontier orbital interaction is most important in this photocycloaddition. The coefficients at

Table 1 Photoreaction of the pyridine–benzofuran system

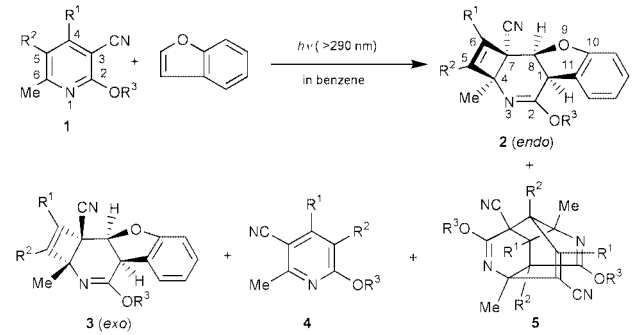

					Yield (%)[a]			
Pyridine	R^1	R^2	R^3	conv.(%)	**2**	**3**	**4**	**5**
1a	H	H	Me	59	32	25	7	33
1b	H	H	Et	64	34	27	3	34
1c	Me	H	Me	46	31	11	56	0

[a] Isolated yield. A benzene solution 0.02 M in pyridine **1** and 0.05 M in benzofuran was irradiated with a high-pressure mercury lamp.

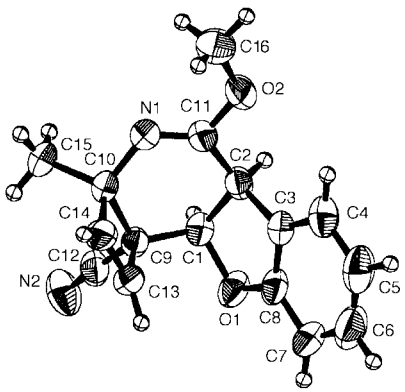

Fig. 1 ORTEP drawing of pyridine–benzofuran adduct **2a**. Selected bond lengths (Å) and angles (°); N(1)–C(10) 1.442(6), C(1)–C(9) 1.663(7), C(9)–C(10) 1.698(7), C(9)–C(13) 1.618(7), C(10)–C(14) 1.617(7), C(13)–C(14) 1.322(7), C(10)–C(9)–C(13) 84.3(4), C(9)–C(10)–C(14) 85.1(4), C(9)–C(13)–C(14) 95.6(4), C(10)–C(14)–C(13) 94.8(4), O(1)–C(1)–C(9)–C(13) 47.1(6), N(1)–C(10)–C(9)–C(13) 107.6(6), N(1)–C(10)–C(14)–C(13) −115.0(6), C(1)–C(9)–C(10)–C(14) 124.1(5), C(1)–C(9)–C(13)–C(14) 120.1(5), C(2)–C(1)–C(9)–C(13) −70.3(6).

† Electronic supplementary information (ESI) available: experimental section. See http://www.rsc.org/suppdata/cc/b0/b002396p/

the 3-position in the LSOMO of the singlet excited state of the pyridine ring and those at the 2-position of the HOMO in the ground state of furan are larger than those at any other positions. It is concluded that the initial bond formation occurs between the C2–C3 positions of pyridine and the C3–C2 positions of benzofuran, leading to **6**.

Gilbert and Heath reported the photochemical addition of 2-cyanoanisole to vinyl ether leading to a 2 + 2 adduct, and subsequently followed by ring-opening to a cylcooctatriene.[13]

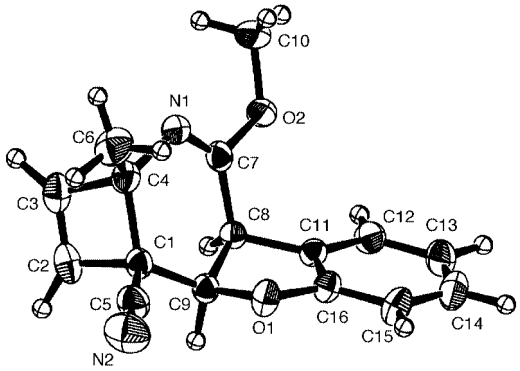

Fig. 2 ORTEP drawing of pyridine–benzofuran adduct **3a**. Selected bond lengths (Å) and angles (°); O(1)–C(9) 1.459(4), N(1)–C(4) 1.453(4), C(1)–C(2) 1.526(4), C(1)–C(4) 1.610(4), 1.521(4), C(2)–C(3) 1.317(6), C(3)–C(4) 1.526(4), C(2)–C(1)–C(4) 84.4(2), C(1)–C(2)–C(3) 95.6(3), C(2)–C(3)–C(4) 95.4(3), C(1)–C(4)–C(3) 84.6(2), O(1)–C(9)–C(1)–C(2) 170.3(3), O(1)–C(9)–C(1)–C(4) 93.0(3), O(1)–C(9)–C(1)–C(6) −40.4(3), N(1)–C(4)–C(1)–C(2) −111.6(3), N(1)–C(4)–C(1)–C(5) 136.2(3), N(1)–C(4)–C(3)–C(2) 117.1(3), C(1)–C(4)–C(3)–C(2) −0.3(3), C(2)–C(1)–C(4)–C(3) 0.2(2), C(3)–C(2)–C(1)–C(4) −0.3(3).

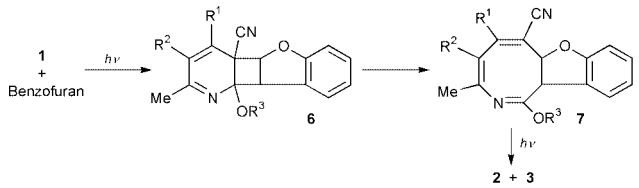

Scheme 1

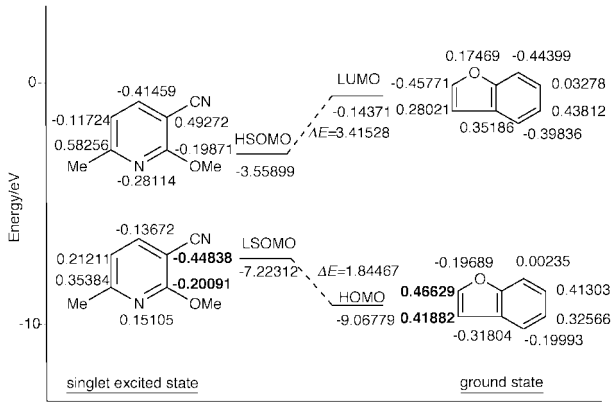

Fig. 3 Estimated energies and coefficients of 3-cyano-2-methoxy-6-methylpyridine **1a** and benzofuran obtained from the PM3 Hamiltonian contained within the MOPAC program.

The cyclooctatriene cyclizes to a secondary photoproduct, a bicyclo[4.2.0]octa-2,7-diene structure, upon irradiation. The reversibility of the photochemical reaction and the thermal conversion between the cyclooctatriene and the bicyclo-[4.2.0]octa-2,7-diene were confirmed. In our present reaction, the thermal and photochemical reactions of **2** and **3** were carried out to obtain further supporting information on the reaction. However, the pyrolysis and the photolysis at 254 nm of the photoadducts gave polymerized materials, furthermore, when the addition reaction was followed by ^{1}H NMR spectroscopy, primary cyclobutane **6** or cyclooctatriene **7** could not be detected on irradiation in an NMR tube. The high reactivity of **6** may be due to steric crowding or the bond-weakening character of the cyano and methoxy groups facilitates the ring opening to the cyclooctatriene, subsequently leading to **7**.[14]

In conclusion, we have detailed the first example of a photochemical reaction between two heteroaromatic compounds, a pyridine and benzofuran system, leading to 1:1 cycloadducts. Attempts at photoaddition with benzothiophene, indole or *N*-methylindole instead of benzofuran proved unsuccessful. We are continuing to explore the details and the scope of the photochemical reactions of heteroaromatics.

Notes and references

‡ *Crystal data*: for **2a**; colorless prismatic crystal, $C_{16}H_{14}N_2O_2$, orthorhombic space group *Fdd*2, a = 17.024(6), b = 29.192(7), c = 11.183(4) Å, V = 5557(3) Å^3, Z = 16, D_c = 1.273 g cm^{-3}, μ(Cu-Kα) = 6.93 cm^{-1}. The structure was solved by the direct method and refined by full-matrix least squares, where the final R and R_w were 0.057 and 0.065 for 1410 reflections.

For **3a**; colorless prismatic crystal, $C_{16}H_{14}N_2O_2$, triclinic space group $P\bar{1}$, a = 9.903(2), b = 10.132(2), c = 7.430(1) Å, α = 91.75(1), β = 105.73(2), γ = 108.74(1)°, V = 673.8(2) Å^3, Z = 2, D_c = 1.312 g cm^{-3}, μ(Cu-Kα) = 7.14 cm^{-1}. The structure was solved by the direct method and refined by full-matrix least squares, where the final R and R_w were 0.055 and 0.066 for 2777 reflections.

CCDC 182/1655. See http://www.rsc.org/suppdata/cc/b0/b002396p/ for crystallographic files in .cif format.

1 D. Bryce-Smith and A. Gilbert, *Tetrahedron*, 1976, **32**, 1309.
2 A. Gilbert, *Synthetic Organic Photochemistry*, ed. W. M. Horspool, Plenum, New York, 1984.
3 J. J. McCullough, *Chem. Rev.*, 1987, **87**, 811.
4 H. Bouas-Laurent, A. Castellan and J.-P. Desvergne, *Pure Appl. Chem.*, 1980, **52**, 2633.
5 H.-D. Becker, K. Sandros and K. Anderson, *Angew. Chem., Int. Ed. Engl.*, 1983, **22**, 495.
6 C. Kowala, G. Sugowdz, W. H. F. Sasse and J. A. Wunderlich, *Tetrahedron Lett.*, 1972, 4721.
7 B. K. Seliger and M. Sterns, *Chem. Commun.*, 1969, 978.
8 For the photocycloaddition of pyridines with alkenes, pentafluoropyridine reacts with ethylene at the C3–C4 bond leading to cyclobutane, see: M. G. Barlow, D. E. Brown and R. N. Haszeldine, *J. Chem. Soc., Chem. Commun.*, 1977, 669.
9 M. Sakamoto, M. Kimura, T. Fujita, T. Nishio, I. Iida and S. Watanabe, *J. Am. Chem. Soc.*, 1991, **113**, 5859.
10 M. Sakamoto, T. Sano, M. Takahashi, K. Yamaguchi, T. Fujita and S. Watanabe, *Chem. Commun.*, 1996, 1349.
11 M. Sakamoto, A. Kinbara, T. Yagi, M. Takahashi, K. Yamaguchi, T. Mino, S. Watanabe and T. Fujita, *J. Chem. Soc., Perkin Trans. 1*, 1999, 171.
12 J. J. P. Stewart, *J. Comput. Chem.*, 1989, **10**, 221.
13 A. Gilbert and P. Heath, *Tetrahedron Lett.*, 1987, **47**, 5909.
14 P. J. Wagner, M. Sakamoto and A. E. Madkour, *J. Am. Chem. Soc.*, 1992, **114**, 7298.

ChemComm

Facile construction of the oxaphenalene skeleton by *peri* ring closure. Formal synthesis of mansonone F

Young-Ger Suh,* Dong-Yun Shin, Kyung-Hoon Min, Soon-Sil Hyun, Jae-Kyung Jung and Seung-Yong Seo

College of Pharmacy, Seoul National University, San 56-1, Shinrim-Dong, Kwanak-Gu, Seoul 151-742, Korea. E-mail: YGSUH@plaza.snu.ac.kr

Received (in Cambridge, UK) 7th March 2000, Accepted 16th May 2000

A concise and divergent total synthesis of mansonone F has been accomplished *via* an efficient construction of the oxaphenalene skeleton by facile *peri* ring closure of the naphthol ether, and an effective preparation of the cyclization precursor starting from readily available 5-methoxy-1-tetralone by employing a palladium-induced aromatization of the naphthalinol.

Mansonone F (**1**) and biflorin, which are members of the naturally occurring *ortho*-naphthoquinone family, contain the unusual oxaphenalene skeleton.[1] Biflorin, the first oxaphenalene natural product, was found to have antibiotic properties.[2] More interestingly, mansonone F, a tricyclic sesquiterpenoid, has been reported as a phytoalexin[3–5] which is accumulated in the heartwood of the genus *Ulmus* in response to infections. Recently, mansonone F has also been isolated from the root bark of *Ulmus davidiana*, which has been traditionally used as a medicinal plant for treatment of infections in Korea. In addition, the highly potent anti-MRSA activity of mansonone F, comparable to that of vancomycin, has been studied in our laboratory.[6] However, the paucity of natural mansonone F, as well as its inherent structural constraint, has limited the optimization of its biological properties by structural modification and its therapeutic application. These reasons prompted us to develop a practical and divergent synthetic route to mansonone F, although an elegant synthesis of mansonone F employing intramolecular Diels–Alder addition of benzynes to furans has already been reported.[7] We report herein a concise and divergent synthesis of mansonone F starting from readily available 5-methoxy-1-tetralone.

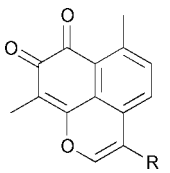

1 Mansonone F R=CH_3

Biflorin R=$CH_2CH_2CHC(CH_3)_2$

Our synthetic strategy (Scheme 1) envisions a highly efficient construction of the tricyclic oxaphenalene skeleton *via peri* ring closure[8] by an intramolecular Friedel–Crafts acylation of the dimethylnaphthol ether **2** or **3**. The cyclization precursors **2** and **3** are readily accessible from the commercially available methoxytetralone **5** by sequential introduction of the alkyl substituents and an effective aromatization of the tetralinol intermediate.

Our synthesis (Scheme 2) commenced with preparation of the methylnaphthol **4**. The first methyl substituent, corresponding to the C6-methyl of mansonone F, was conveniently introduced by methyl Grignard addition to the carbonyl of the tetralone **5**. Aromatization[9] of the resulting carbinol by palladium-induced concurrent dehydration and dehydrogenation and then demethylation of the resulting methoxynaphthalene by boron tribromide provided the methylnaphthol **4**. The methylnaphthol **4** was transformed in a straightforward manner into the cyclization precursor **2** by a three step sequence. The second methyl substituent corresponding to the C9-methyl of mansonone F was effectively introduced by benzeneboronic acid-assisted hydroxymethylation[10] followed by hydrogenolysis of the resulting benzyl alcohol. *O*-alkylation of the naphthol **6** with bromoacetate afforded the dimethylnaphthol ether **2** as a cyclization precursor. The key tricyclic oxaphenalene skeleton of mansonone F was efficiently constructed by a facile *peri* ring closure[8] of the dimethylnaphthol ether **2**. Conversion of the ester **2** to an acid halide and then intramolecular Friedel–Crafts

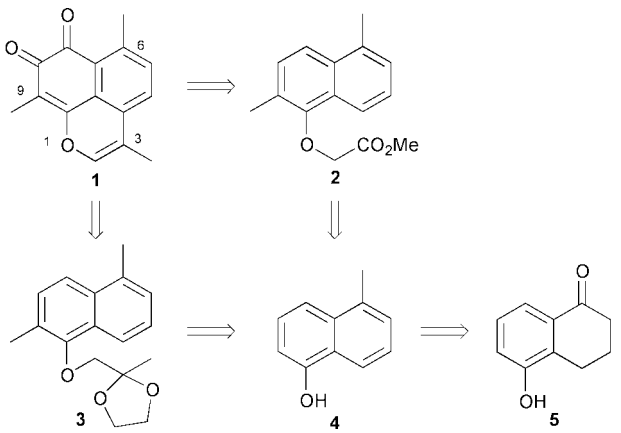

Scheme 1 Synthetic strategy.

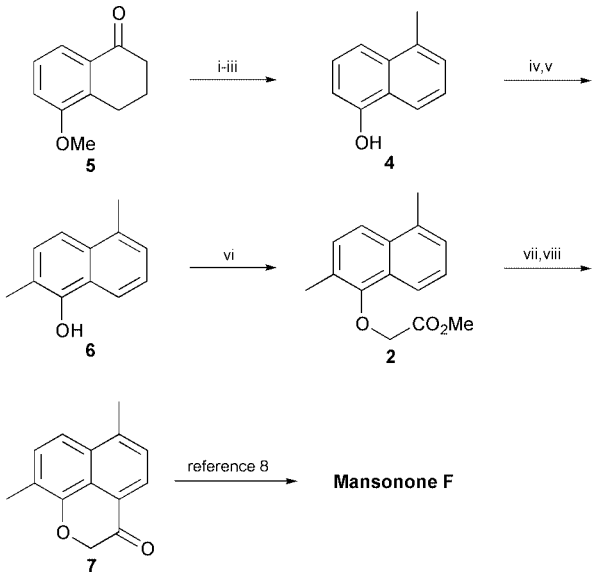

Scheme 2 First synthetic route to mansonone F. *Reagents and conditions*: i, MeMgI, Et_2O, reflux, 1 h; ii, 10% Pd/C, triglyme, reflux, 2 days; iii, BBr_3, CH_2Cl_2, −78 °C, then warm to room temp. (94% in 3 steps); iv, $PhB(OH)_2$, $(CHO)_n$, propionic acid, PhH, reflux, 1 h, then H_2O_2, THF; v, 10% Pd/C, H_2, MeOH, 5 h (63% in 2 steps); vi, $BrCH_2CO_2Me$, K_2CO_3, acetone, reflux (82%); vii, $LiOH·H_2O$, THF–H_2O, 10 min; viii, $(COCl)_2$, PhH, reflux, 1 h, then $AlCl_3$, CH_2Cl_2 (74% in 2 steps).

DOI: 10.1039/b001859g

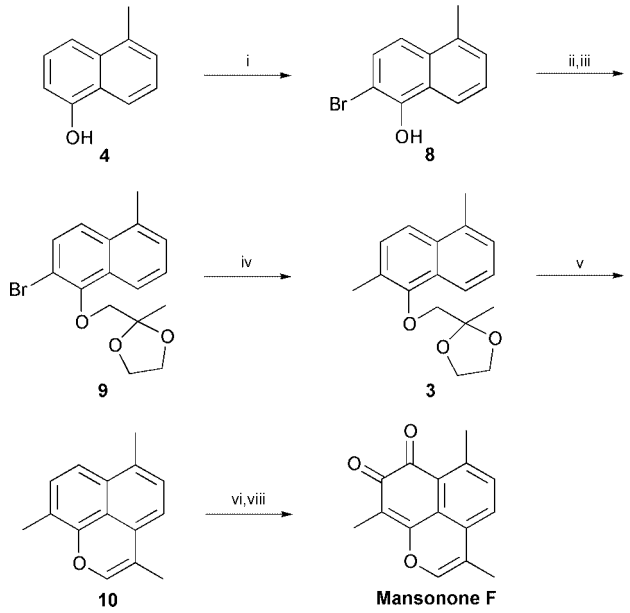

Scheme 3 Alternative synthetic route to mansonone F. *Reagents and conditions*: i, NBS, CH_2Cl_2, 0 °C (60–70%); ii, $BrCH_2COMe$, K_2CO_3, acetone, reflux (96%); iii, $(CH_2OH)_2$, PTSA, PhH, reflux (89%); iv, Bu^nLi, MeI, THF, −78 °C, then warm to room temp. (95%); v, PPA, 100 °C (87%); vi, $Cu(NO_3)_2{\cdot}xH_2O$, Ac_2O (83%); vii, 10% Pd/C, $NaBH_4$, MeOH, then Fremy's salt, 0.06 M NaH_2PO_4, acetone (41%).

acylation of the acid halide afforded the advanced intermediate **7**, which was transformed into mansonone F by a known procedure.[7]

Our alternative synthetic route for the transformation of methylnaphthol **4** into mansonone F is summarized in Scheme 3. The tether for *peri* ring closure was introduced to the bromonaphthol **8** by sequential *O*-alkylation with bromoacetone and carbonyl protection. Addition of the methyl substituent corresponding to the C9-methyl of mansonone F was achieved by halogen–metal exchange followed by methylation. Finally, construction of the oxaphenalene skeleton was executed by facile *peri* ring closure induced by polyphosphoric acid, to give the key intermediate **10**. In order to complete the synthesis, the ortho-quinone moiety of mansonone F was elaborated by application of the reported procedure.[7] The synthetic mansonone F was identical in all aspects to the naturally occuring compound.[1,10]

In summary, the total synthesis of mansonone F has been accomplished *via* a 10 step sequence, starting from the readily available 5-methoxy-1-tetralone (**5**). The key part of this synthesis involves the efficient preparation of 1,6-dimethyl-5-alkoxynaphthalene as a divergent cyclization precursor and its facile conversion to form the oxaphenalene skeleton by *peri* ring closure. This concise and practical synthetic procedure, providing a variety of substituents at the C3, C6 and C9 positions, offers a useful synthetic route to this important prospective anti-MRSA drug.

This research was supported by grant CHMP-00-CH-15-0014 from the Ministry of Health & Welfare and in part by 1999 BK21 project for Medicine, Dentistry and Pharmacy.

Notes and references

1 R. H. Thomson, *Naturally Occurring Quinones*, Academic Press, London, 1971, 198.
2 O. Goncalves de Lima, W. Keller-Schierlein and V. Prelog, *Helv. Chim. Acta*, 1958, **41**, 1386.
3 J. C. Overeem and D. M. Elgersma, *Phytochemistry*, 1970, **9**, 1949.
4 M. T. Dumas, G. M. Strunz, S. M. Hubbes and R. S. Jeng, *Experimentia*, 1983, **39**, 1089.
5 L. C. Duchesne, R. S. Jeng and M. Hubbes, *Can. J. Bot.*, 1984, **63**, 678.
6 Unpublished results. H. S. Kim, PhD dissertation, Seoul National University, 1999.
7 W. M. Best and D. Wege, *Aust. J. Chem.*, 1986, **39**, 647.
8 R. Adams, *Org. React.*, 1957, **2**, 114.
9 W. Dai, E. Abu-Shqara and R. G. Harvey, *J. Org. Chem.*, 1995, **60**, 4905.
10 G. B. M. Bettòlo, C. G. Casinovi and C. Galeffic, *Tetrahedron Lett.*, 1965, 4857.

Generation of $C_{10}H_4$ species in a low-temperature argon matrix: consecutive photolysis of 1,2;5,6-naphthalenetetracarboxylic dianhydride†

Tadatake Sato, Hiroyuki Niino and Akira Yabe*

National Institute of Materials and Chemical Research (NIMC), Higashi 1-1, Tsukuba, Ibaraki 305-8565, Japan. E-mail: yabe@nimc.go.jp

Received (in Cambridge, UK) 30th March 2000, Accepted 30th May 2000

1,2;5,6-Naphthalenetetracarboxylic dianhydride has been consecutively photolyzed in a low-temperature argon matrix by wavelength-selective irradiation; dec-5-ene-1,3,7,9-tetrayne, which is the second $C_{10}H_4$ isomer, was generated as the final product.

Benzdiyne and naphthdiyne, in which two triple bonds are contained within one aromatic system, are challenging reactive intermediates. Recently, we reported the direct observation of a benzdiyne derivative by photolysis of 1,4-bis(trifluoromethyl)-2,3;5,6-benzenetetracarboxylic anhydride in a low-temperature argon matrix, which was the first finding that a benzdiyne could be trapped by the matrix isolation method.[1] However, we were unable to confirm the generation of parent benzdiynes (C_6H_2) by the consecutive photolysis of the corresponding precursors.[2–4] In a series of experiments, we confirmed the generation of hexa-1,3,5-triyne, the most stable C_6H_2 isomer, as a final photoproduct. This final product was formed by the ring opening of the benzdiynes.[4] Ring-opening reactions resulting in the generation of an acetylenic compound have also been reported in the case of benzyne.[5] These findings suggested that arynes containing diyne species are good precursors for acetylenic compounds, which are difficult to prepare by normal synthetic methods.

These acetylenic compounds, oligoynes and the compounds with a cross-conjugated π-system, have attracted much attention in the past. For example, Diederich *et al.* have thoroughly investigated such compounds in a series of research on molecular and polymeric carbon allotropes,[6,7] reporting the synthetic preparation of tetraethnylethene,[8] which is the only isomer with a $C_{10}H_4$ molecular formula identified so far. The acetylenic compounds are of interest as a building block for novel carbon networks.

Here, we report the consecutive photolysis of 1,2;5,6-naphthalenetetracarboxylic dianhydride **1**[9] in a low-temperature argon matrix (Scheme 1). The photolysis, which used several lasers, was carried out in an attempt to generate naphth-1,5-diyne. A novel acetylenic compound with a cross-conjugated π-system was observed as the final product, as well as stepwise-produced reactive intermediates.

Crystallites of **1** were vaporized at 145 °C and co-deposited with argon (99.9999%) onto a CsI or CaF_2 plate in a sample chamber whose pressure was kept at $< 10^{-5}$ Torr.[10] Precursor **1** was photolyzed using a XeCl excimer laser (308 nm, 5 Hz, *ca.* 10 mJ cm^{-2} $pulse^{-1}$). The photolysis was followed by FTIR and UV–VIS absorption spectroscopies. Upon irradiation, new IR bands ascribable to photogenerated species appeared, while the IR bands of **1** decreased. The appearance of IR bands arising from CO and CO_2 indicated that decarboxylation and decarbonylation of **1** were induced upon irradiation at 308 nm. This photolysis resulted in the generation of an intermediate having a naphthyne structure, **2**. Prolonged irradiation at 308 nm caused the formation of ketene species **3** by the addition of CO

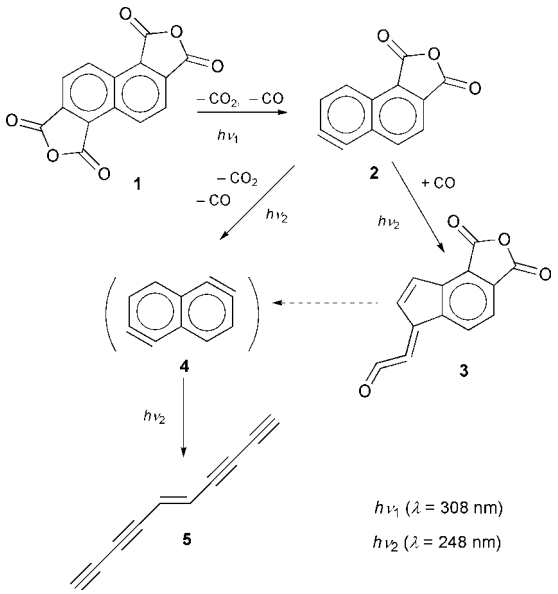

Scheme 1

to **2**, which was confirmed by the appearance of the characteristic IR bands at 2082 and 2087 cm^{-1}.[11] The intermediates **2** and **3** were identified on the basis of their FTIR spectra being in good agreement with the theoretical IR spectra calculated by density functional theory (B3LYP/6-31G** level).[12] The obtained intermediate **2** was photolyzed upon irradiation at 248 nm (KrF excimer laser, 5 Hz, 8 mJ cm^{-2} $pulse^{-1}$). During the initial stage of irradiation, generation of **3** was the dominant process. However, upon prolonged irradiation, the generation of **3** was diminished and the generation of CO and CO_2 became the dominant process. Since the IR bands of **2** decreased upon irradiation, it was suggested that this process resulted in the formation of naphth-1,5-diyne ($C_{10}H_4$, **4**). However, IR bands ascribable to **4** were not observed. Upon irradiation, only two weak IR bands at 621 and 3323 cm^{-1} appeared, other than the increasing peaks of CO and CO_2. These weak bands were ascribable to the C–H bending and stretching modes of acetylenic compounds. Moreover, upon further irradiation at 248 nm, **3** was also photolyzed slowly. Even at this stage, increases in the IR bands of CO, CO_2 and the acetylenic species was still observed.

Taking into account benzyne[5] and benzdiynes,[2–4] it is plausible that acetylenic compounds may be generated by ring-opening of **4**. Certainly, the acetylenic C–H stretching band at 3323 cm^{-1} was observed at almost the same position as that of butadiyne (3324–6, 3340 cm^{-1}), hexatriyne (3324–7 cm^{-1}), or hex-1-ene-3,5-diyne (3324 cm^{-1}), which were formed by ring-opening reactions of benzyne[5] and/or benzdiynes[2–4] or the photo-decomposition of benzene.[13] It should be noted that several peaks were observed when several kinds of acetylenic compounds were formed simultaneously.[3,13] In our experiment, one C–H stretching peak accompanied by a shoulder on its higher wavenumber side was observed at 3323 cm^{-1} as shown in Fig. 1. Moreover, no peaks ascribable to other photo-

† Electronic supplementary information (ESI) available: synthesis of **1**, theoretically estimated IR data for *cis*- and *trans*-dec-5-ene-1,3,7,9-tetrayne and details of TD-DFT calculations. See http://www.rsc.org/suppdata/cc/b0/b002555k/

DOI: 10.1039/b002555k

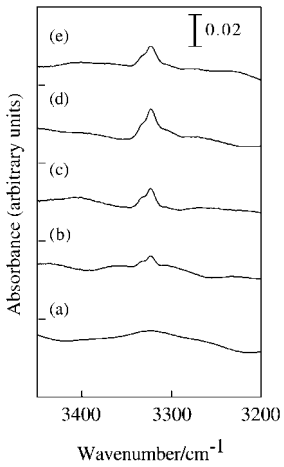

Fig. 1 FTIR spectra (C–H stretching band) upon photoirradiation of **1** with a KrF excimer laser: (a) before irradiation, (b) after 9000 pulses, (c) after 21000 pulses, (d) after 66000 pulses and (e) after 1800 pulse irradiation with the ArF excimer laser.

generated species were observed. Thus, the acetylenic $C_{10}H_4$ species was solely or dominantly generated: fragmentation of the $C_{10}H_4$ species can be excluded as a minor process. The species formed upon irradiation at 248 nm showed specific UV–VIS absorption bands as shown in Fig. 2. After irradiation by the XeCl excimer laser, absorption bands at 305, 296, 250 and 205 (broad) nm were observed. The bands at 250 and 205 nm were assigned to **2**, which was the major species existing upon irradiation at 308 nm and photolyzed upon irradiation at 248 nm. In contrast, the bands at 305 and 296 nm were assigned to **3**, since these bands also grew up in the initial irradiation at 248 nm. During this stage, increases in the bands at 372, 354, 338 and 305 nm were clearly observed, which were also assigned to **3**. Under prolonged irradiation, the absorption bands of **3** decreased slowly, and other bands emerged at 317, (296), 280, 213, 203 and 195 nm. These bands were assigned to the acetylenic $C_{10}H_4$ compound showing the C–H stretching band at 3323 cm^{-1}. Similar vibronic absorption bands have frequently been observed in acetylenic compounds.[14,15] As mentioned above, it was assumed that the acetylenic $C_{10}H_4$ compound was generated by ring-opening of **4**. Compound **4** has C_{2h} structure, in which two *o*-benzyne molecules are symmetrically fused. Considering that hex-1-ene-3,5-diyne was formed by ring-opening of benzyne,[5] we tentatively assigned the compound to dec-5-ene-1,3,7,9-tetrayne ($C_{10}H_4$, **5**), which has not been isolated before. This assignment was supported by the following discussions. The theoretical prediction shows two

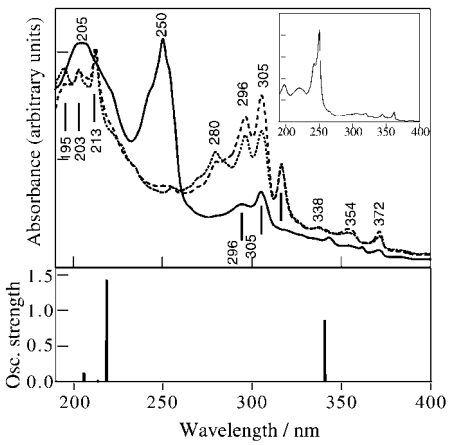

Fig. 2 (Top) UV spectra of the photolysis of **1** with a Nd:YAG laser (THG), XeCl and KrF excimer lasers in an argon matrix at 11 K: (——) after irradiation with Nd:YAG laser (THG) and XeCl excimer laser, (– – –) after successive irradiation with 3000 pulses and (····) 9000 pulses of the KrF excimer laser. Inset: UV spectra of **1** observed before irradiation in the argon matrix. (Bottom) transition energies and oscillator strengths of **5** calculated by the TD-DFT method.

C–H bending bands (581 and 587 cm^{-1}) and one C–H stretching band (3354 cm^{-1}) with intensities > 90 km mol^{-1}. On the other hand, the experimental results showed one C–H bending band (621 cm^{-1}) and one C–H stretching band (3323 cm^{-1}) with a shoulder as described above. Only one bending band would be ascribed to two neighboring bands and the appearance of the shoulder on the stretching band would be explained by matrix splitting.[16] Although tetraethynylethene, which is also a $C_{10}H_4$ species, would seem to be a possible candidate, it can be dismissed because it shows a quite different UV–VIS absorption spectrum.[8] The lowest transition band of the acetylenic $C_{10}H_4$ compound (317 nm) was seen in a longer wavelength region than that of hex-1-ene-3,5-diyne (275 nm in an Ne matrix).[5] This indicated that the π-conjugation system of the observed acetylenic compound was extended more than that of hex-1-ene-3,5-diyne. Electronic absorption spectra can be well described by time-dependent density functional theory (TD-DFT) calculations.[17] Transition energies and oscillator strengths of **5** calculated by the TD-DFT method are shown by bars in Fig. 2, which show favorable correspondences with the experimental result.[18] Thus, the observed acetylenic $C_{10}H_4$ compound was assigned to dec-5-ene-1,3,7,9-tetrayne.

In conclusion, the reactive intermediates **2** and **3** were identified on the basis of their FTIR spectra being in good agreement with calculated IR spectra. The aromatic $C_{10}H_4$ species, naphth-1,5-diyne, converted to a $C_{10}H_4$ species with acetylenic C–H moieties by ring-opening reactions. The acetylenic $C_{10}H_4$ species was dec-5-ene-1,3,7,9-tetrayne, the second $C_{10}H_4$ isomer, which has not previously been prepared.

Notes and references

1 M. Moriyama, T. Ohana and A. Yabe, *J. Am. Chem. Soc.*, 1997, **119**, 10 229.
2 M. Moriyama, T. Ohana and A. Yabe, *Chem. Lett.*, 1995, 557.
3 M. Moriyama and A. Yabe, *Chem. Lett.*, 1998, 337.
4 M. Moriyama, T. Sato, T. Uchimaru and A. Yabe, *Phys. Chem. Chem. Phys.*, 1999, **1**, 2267.
5 J. G. Radziszewsky, B. A. Hess, Jr. and R. Zahradnik, *J. Am. Chem. Soc.*, 1992, **114**, 52.
6 F. Diederich, *Nature*, 1994, **369**, 199.
7 F. Diederich, *Pure Appl. Chem.*, 1999, **71**, 265.
8 Y. Rubin, C. B. Knobler and F. Diederich, *Angew. Chem., Int. Ed. Engl.*, 1991, **30**, 698.
9 Compound **1** was synthesized from 2,6-dimethylnaphthalene following the literature procedure [Y. Dozen and S. Fujishima, *Yukigoseigaku*, 1972, **30**, 964 (Japanese)]. Details of the synthesis are provided as ESI†.
10 *Spectroscopic data* for **1** (Ar matrix, 11 K) UV–VIS λ/nm: 362, 355, 350, 329, 319, 306, 250, 242, 221, 198. FTIR ν/cm^{-1} 3094vw, 1862s, 1790vs, 1625w, 1389w, 1385w, 1292s, 1231w, 1175m, 1132m, 921vs, 869m, 790vw, 749m, 707w, 635w, 598w, 565m, 531w.
11 T. Sato, M. Moriyama, H. Niino and Y. Akira, *Chem. Commun.*, 1999, 1089.
12 This data will be published elsewhere.
13 J. L. Laboy and B. S. Ault, *J. Photochem. Photobiol. A: Chem.*, 1993, **74**, 99.
14 T. Böhm-Gössl, W. Hunsmann, L. Rohrschneider, W. M. Schneider and W. Ziegenbein, *Chem. Ber.*, 1963, **96**, 2504.
15 E. Kloster-Jensen, H. Haink and H. Christen, *Helv. Chim. Acta*, 1974, **57**, 1731.
16 In the results on DFT calculations for **5** (C_{2h} structure), another symmetrically forbidden C–H stretching mode (A_g 3354.6 cm^{-1}, 0 km mol^{-1}) was observed at higher wavenumber than that of the symmetrically allowed mode (B_u 3354.2 cm^{-1}, 341 km mol^{-1}). In the argon matrix, compound **5** may not be able to form an ideal symmetrical structure because it confined within a matrix cavity. In this case, the IR band corresponding to the A_g mode could be observed as a weak shoulder on the high wavenumber side of main C–H stretching band. As another possibility, we should consider the *trans*-confomer formed by *cis–trans* isomerization of the central C=C bond under photoirradiation (two acetylenic C–H stretching modes of the *trans*-conformer are predicted at higher wavenumbers: B_2 3355.2 cm^{-1}, 138 km mol^{-1}; A_1 3355.7 cm^{-1}, 120 km mol^{-1}).
17 M. E. Casida, C. Jamorski, K. C. Casida and D. R. Salahub, *J. Chem. Phys.*, 1998, **108**, 4439.
18 TD-DFT calculations were performed: see ESI.†

The complexation of halide ions by a calix[6]pyrrole

Grazia Cafeo,[a] Franz H. Kohnke,*[a] Giovanna L. La Torre,[a] Andrew J. P. White[b] and David J. Williams*[b]

[a] *Università di Messina, Salita Sperone 31, 98166 Messina, Italy. E-mail: franz@scirocco.unime.it*
[b] *Chemical Crystallography Laboratory, Department of Chemistry, Imperial College of Science, Technology and Medicine, South Kensington, London, UK SW7 2AY*

Received (in Cambridge) 20th March 2000, Accepted 23rd May 2000

The X-ray crystal structures of the 1 : 1 complexes formed by calix[6]pyrrole 1b with Bu$^n_4$NCl and Bu$^n_4$NBr show the macrocycle to adopt D_{3d} symmetry and to encapsulate the halide ions within the macroring cavity *via* six N–H···X$^-$ hydrogen bonds; the macrocycle subtly adjusts its conformation to accommodate the differently sized anions; preliminary extraction experiments indicate that 1b is a dramatically stronger chloride ion complexing agent than its smaller analogue calix[4]pyrrole 1a.

Molecular receptors for cations and neutral guests have been extensively studied for many years.[1] In contrast, macrocycles capable of binding anions have attracted considerably less attention. However, because of the key role of anions in fundamental aspects of chemistry and biology, the search for novel and selective hosts for anions is a rapidly developing area of supramolecular chemistry.[2]

Significant progress in this field has been made by the discovery that, for example, pyrrole-based analogues of the calix[4]arenes such as **1a** are capable of binding fluoride and

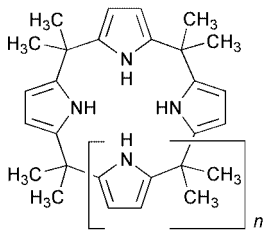

n = 1 **1a** *n* = 3 **1b**

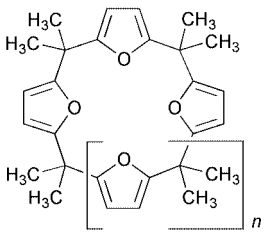

n = 3 **2**

chloride ions.[3–5] However, complexation occurs by means of a facial arrangement involving hydrogen bonding interactions between the four pyrrole N–H and the anions and not by inclusion within the macrocyclic cavity, which is too small for either the fluoride or the chloride ions.

These observations led us to synthesise[6] the larger calix[6]pyrrole **1b** from the known furan-based analogue **2**. This new synthesis provided a novel route to **1b** which, unlike its smaller analogue **1a**, is not readily isolated from the mixture of compounds obtained by the previously employed condensation reaction of pyrrole and acetone.[3b] We were thus able to investigate, for the first time, the behaviour of **1b** as a molecular receptor for halide ions. We expected **1b** to be an appreciably better complexing agent for the halide ions than **1a** both in terms of strength (it has the potential to form an additional two N–H···X$^-$ hydrogen bonds) and selectivity (owing to the possible inclusion of the ion within the larger macroring cavity—and hence achieve size-discrimination).

In order to estimate the improved binding of **1b** towards chloride and bromide with respect to that of **1a**, we compared the ability of the two macrocycles to complex and transfer these ions from a water phase to a lipophilic dichloromethane phase. The tests were extended to include also fluoride and iodide. In a series of extraction experiments, solutions of Bu$^n_4$NF, Bu$^n_4$NCl, Bu$^n_4$NBr and Bu$^n_4$NI in D_2O (10^{-2} M) were extracted with equal volumes of solutions containing **1a** or **1b** (10^{-2} M) in CD_2Cl_2 under identical conditions and temperature (16 °C). After separation of the two phases, the amount of anion transferred in each case was calculated from the ^{1}H NMR spectra of the CD_2Cl_2 solutions using the ratios between the integration values for the resonances of the protons of the macrocycles and those of the ammonium ion (which has to follow the halogen ion into the organic phase).† The values obtained were also confirmed by the corresponding decrease of the amount of salt in the D_2O phase which was measured by integration of ^{1}H NMR peak profiles with respect to a known amount of dioxane added as an internal standard.

In order to single out the contributions of the macrocycles to the phase transfer of the anions from other factors (halogen lipophilicity and phase transfer due to the Bu$^n_4$N$^+$ cation) the partition of these salts between the two phases was also determined in the absence of **1a** or **1b**. Macrocycles **1a** and **1b** are insoluble in water.

The results obtained (Table 1) indicate that the contribution of **1a** to the phase transfer of fluoride, chloride, bromide and iodide (if it exists) is marginal and its magnitude is at most within the experimental error. On the other hand, **1b** can effectively bind and transfer both chloride and bromide ions into a DCM phase and shows a *ca*. six-fold selectivity factor for chloride with respect to bromide.

The ^{1}H NMR spectra of **1b** in the presence of chloride and bromide (at the percentage concentration extracted) also show significant shifts of the pyrrole N–H resonances from its uncomplexed value of δ 7.67 towards higher values (up to δ 10.93 for chloride and δ 8.40 for bromide) which are certainly due to the involvement of the N–H protons in hydrogen bonding interactions with the halogen ions. A line broadening of the C–H resonances is also observed especially for the chloride complex.

Encouraged by these results, and to test the potential for inclusion as a function of the anion size, as well as to gain information on the mode of binding, we subjected 1 : 1 solutions of **1b** with Bu$^n_4$NCl and with Bu$^n_4$NBr in DCM to slow evaporation of the solvent to give, in each case, single crystals of 1 : 1 complexes suitable for X-ray analysis (mp 232–234 and 189–191 °C, respectively).

Table 1 Transfer of Bu$^n_4$NF, Bu$^n_4$NCl, Bu$^n_4$NBr and Bu$^n_4$NI (%) between D_2O and CD_2Cl_2 at 16 °C with and without **1a** and **1b**. The figures indicate the percentage variation in the concentration of salt in each phase after equilibration and were reproducible within a ±2% error

	Macrocycle					
	None		**1a**		**1b**	
	D_2O	CD_2Cl_2	D_2O	CD_2Cl_2	D_2O	CD_2Cl_2
Bu$^n_4$NF	[a]	[b]	[a]	[a]	[a]	[a]
Bu$^n_4$NCl	−4	[b]	−4	+4	−65	+65
Bu$^n_4$NBr	−20	[b]	−22	+22	−31	+31
Bu$^n_4$NI	−86	[b]	−86	+86	−86	+86

[a] Value within experimental error (< 2%). [b] The percentage variation was not measured.

DOI: 10.1039/b002239j

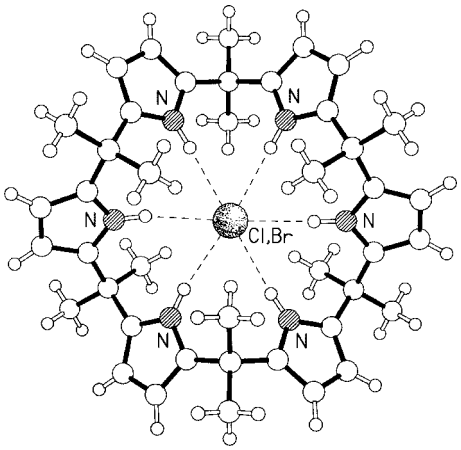

Fig. 1 Plan view of the X-ray structure of the 1:1 complexes formed between calix[6]pyrrole **1b** and Cl^- and Br^-. The hydrogen bonding geometries: N··X, H··X distances (Å), and N–H··X angles (°) are in the ranges 3.265(5)–3.305(5), 2.39–2.42 and 166–177 in the chloride and 3.344(5)–3.404(5), 2.46–2.51 and 170–178 in the bromide.

The X-ray analysis of the 1:1 complex‡ formed between the calix[6]pyrrole **1b** and chloride shows (Fig. 1), that to achieve binding, the host macrocycle undergoes a substantial conformational change from that observed for the 1:1 complex with water.[6] In the water complex the macrocycle adopts a tennis-ball-seam (D_{2d}) conformation whereas here with chloride the symmetry approximates closely to D_{3d}. The chloride anion is positioned centrally with respect to the six pyrrole nitrogen atoms (which are coplanar to within 0.02 Å) and displaced out of this plane by 0.37 Å along the molecular C_3 axis. Binding is *via* six N–H··Cl hydrogen bonds for which the N··Cl and H··Cl distances (Å) range between 3.265(5) and 3.305(5) [*cf.* a range of 3.264(7)–3.331(7) in the tetrapyrrole structure[7]], and 2.39 and 2.42 respectively; the N–H··Cl angles are in the range 166–177°. The small displacement of the chloride ion out of the plane of the six pyrrole nitrogens is accompanied by a slight 'flowering' of the macrocycle, the mean C··C separations between the inwardly directed methyl groups of the 'upper' and 'lower' set of isopropylidene groups being 5.25 and 4.40 Å, respectively.

The expectation that this 'flowering' in the case of the bromide complex would be more pronounced than in the chloride, owing to the larger anion size, was confirmed by X-ray analysis‡ (Fig. 2). Surprisingly, despite the inclusion in both structures of substantial amounts of disordered solvent, the structures are isomorphous. In the bromide complex the anion is again centrally positioned within the macrocycle which adopts a more distorted conformation but one which still approximates to D_{3d}. The bromide ion is bound by six N–H··Br hydrogen bonds with N··Br and H··Br distances ranging between 3.344(5) and 3.404(5), and 2.46 and 2.51 Å respectively; the N–H··Br angles are in the range 160–178°. Accompanying the increase in anion size (and lengthening of the hydrogen bonds) is an increase in the displacement of the anion (Br^-) from the plane of the six pyrrole nitrogen atoms (0.69 Å) and 'flowering' of the macrocycle, the Br^- adopting a 'perching' geometry analogous to that of, for example, ammonium ions with 18-crown-6. Here, the mean C··C separations (**a**–**f** in Fig. 2) between the inwardly directed methyl groups of the 'upper' and 'lower' set of isopropylidene groups are 5.62 and 4.31 Å, respectively. The anions, cations and solvent are, in both structures, well separated and there are no significant intermolecular interactions. The differences in the two solid state structures are consistent with the ability of **1b** to discriminate by size between the two halogen anions chloride and bromide.

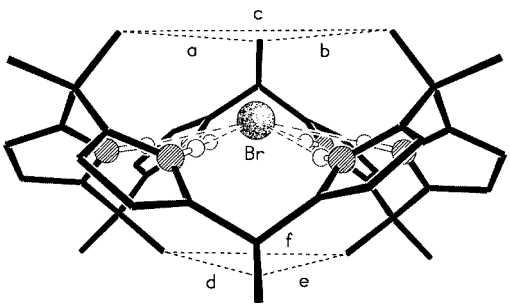

Fig. 2 Elevation of the X-ray structure of the 1:1 complex between calix[6]pyrrole **1b** and Br^- showing the 'perching' geometry of the hydrogen bonded Br^- ion within the 'flowered' macrocyclic conformation. The distances **a**–**c** and **d**–**f** between the inwardly directed isopropylidene methyl carbon atoms are in the ranges 5.46–5.72 and 4.26–4.38 Å respectively (*cf.* 5.11–5.37 and 4.34–4.48 Å respectively, in the chloride complex).

Work is in progress in our laboratory to determine the values of the association constants of **1b** with the halogen ions. Selectivity tests will include competitive binding experiments and transport across liquid membranes.

Notes and references

† The equilibrium of transfer between the two phases was always achieved within 10 min of vigorous stirring. The amount of $Bu^n_4N^+$ transferred between the two phases was not affected by the addition of NaOH to the water phase.

‡ *Crystal data for* [**1b**–Cl^-][$Bu^n_4N^+$]: $[C_{42}H_{54}N_6{\cdot}Cl][C_{16}H_{36}N]{\cdot}4CH_2Cl_2$, M = 1260.5, monoclinic, *Pn* (no. 7), a = 17.592(1), b = 9.970(1), c = 20.050(1) Å, β = 90.55(1)°, V = 3516.4(4) Å^3, Z = 2, D_c = 1.191 g cm^{-3}, μ(Cu-Kα) = 35.8 cm^{-1}, F(000) = 1344, T = 293 K; Siemens P4/RA diffractometer, ω-scans, 4370 independent reflections refined on F^2 to give R_1 = 0.053, wR_2 = 0.147 for 3700 independent observed absorption corrected reflections [$|F_o| > 4\sigma(|F_o|)$, $2\theta \leq 124°$] and 704 parameters. The polarity of the structure could not be unambiguously determined from either an *R*-factor test (R_1^+ = 0.0544, R_1^- = 0.0545) or by use of the Flack parameter [x^+ = +0.49(5), x^- = +0.51(5)]; evidence suggested a degree of racemic twinning. For [**1b**·Br^-][$Bu^n_4N^+$]: $[C_{42}H_{54}N_6{\cdot}Br][C_{16}H_{36}N]{\cdot}4CH_2Cl_2$, M = 1298.9, monoclinic, *Pn* (no. 7), a = 17.472(2), b = 9.801(1), c = 20.037(1) Å, β = 90.00(1)°, V = 3431.1(5) Å^3, Z = 2, D_c = 1.257 g cm^{-3}, μ(Cu-Kα) = 40.0 cm^{-1}, F(000) = 1368, T = 183 K; Siemens P4/RA diffractometer, ω-scans, 5380 independent reflections refined on F^2 to give R_1 = 0.054, wR_2 = 0.142 for 5253 independent observed absorption corrected reflections [$|F_o| > 4\sigma(|F_o|)$, $2\theta \leq 128°$] and 704 parameters. The polarity of the structure was determined by a combination of an *R*-factor test (R_1^+ = 0.0540, R_1^- = 0.0568) and by use of the Flack parameter [x^+ = +0.15(4), x^- = +0.85(4)]. CCDC 182/1654. See http://www.rsc.org/suppdata/cc/b0/b002239j/ for crystallographic files in .cif format.

1 B. Dietrich, in *Comprehensive Supramolecular Chemistry*, ed. G. W. Gokel, Elsevier, Exeter, 1996, vol. 1, p. 153.

2 For recent examples and reviews, see: P. D. Beer, *Chem. Commun.*, 1996, 689; J. L. Atwood, K. T. Holman and J. W. Steed, *Chem. Commun.*, 1996, 1401; D. M. Rudkevich, W. Verboom, Z. Brzozka, M. J. Palys, W. P. R. V. Stauthamer, G. J. van Hummel, S. M. Franken, S. Harkema, J. F. J. Engbersen and D. N. Reinhoudt, *J. Am. Chem. Soc.*, 1994, **116**, 4341; W. Xu, J. J. Vittal and R. J. Puddephatt, *J. Am. Chem. Soc.*, 1995, **117**, 8362; *Supramolecular Chemistry of Anions*, ed. A. Bianchi, E. García-España and K. Bowman-James, Wiley–VCH, Weinheim, 1997; J. Scheerder, J. F. J. Engbersen and D. N. Reinhoudt, *Recl. Trav. Chim. Pays-Bas*, 1996, **115**, 307; R. Vilar, D. M. P. Mingos, A. J. P. White and D. J. Williams, *Chem. Commun.*, 1999, 229.

3 (*a*) P. A. Gale, J. L. Sessler and V. Král, *Chem. Commun.*, 1998, 1 and references therein; (*b*) P. A. Gale, J. L. Sessler, J. W. Genge, V. Kral, A. Andrievsky, V. Lynch, P. I. Samsom, W. E. Allen, C. T. Brown and A. Gebauer, *World Pat.*, WO97/37995 (*Chem. Abstr.*, 1997, **127**, 346236).

4 For recent examples of calix[4]pyrrole derivatives as anion sensors see: H. Miyaji, P. Anzenbacher, Jr., J. L. Sessler, E. R. Bleasdale and P. A. Gale, *Chem. Commun.*, 1999, 1723; P. A. Gale, L. J. Twyman, C. I. Handlin and J. L. Sessler, *Chem. Commun.*, 1999, 1851.

5 For a recent example of chloride binding by means of C–H··Cl hydrogen bonding, see: E. Alcade, C. Alvarez-Rúa, S. Garcia-Granada, E. Garcia-Rodriguez, N. Mesquida and L. Pérez-García, *Chem. Commun.*, 1999, 295.

6 G. Cafeo, F. H. Kohnke, G. L. La Torre, A. J. P. White and D. J. Williams, *Angew. Chem., Int. Ed.*, 2000, **39**, 1496.

7 P. A. Gale, J. L. Sessler, V. Král and V. Lynch, *J. Am. Chem. Soc.*, 1996, **118**, 5140.

ChemComm

Oligomerization–transmetalation reactions of $Cp^*CrMe_2(PMe_3)$/methylaluminoxane catalysts

Jonathan S. Rogers and Guillermo C. Bazan*

Department of Chemistry, University of California, Santa Barbara, CA 93106, USA. E-mail: bazan@ucsb.edu

Received (in Irvine, CA, USA) 15th March 2000, Accepted 18th May 2000

Chain growth in the reaction of ethylene with $Cp^*CrMe_2(PMe_3)$ activated with methylaluminoxane is restricted by a fast Cr/Al transmetalation process.

A range of metal ligand combinations exists for catalyzing the polymerization[1] and oligomerization[2] of olefins. The varying structures control the polymerization process to different extents and provide a means to tailor the polymer structure and the ensuing physical properties. The 'single site' technology is making a profound impact in the manufacture of this important class of commodity materials.[3]

Within this context, we recently reported that boratabenzene complexes of chromium(III), such as $(C_5H_5B–Me)CrMe_2(PMe_3)$ **1**, lead to active ethylene polymerization catalysts

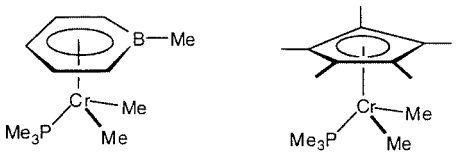

upon activation with methylaluminoxane (MAO).[4] Since the reactivity of boratabenzene catalysts differs from the performance of their isoelectronic cyclopentadienyl-based counterparts,[5] it was of interest to compare **1**/MAO against $Cp^*CrMe_2(PMe_3)$/MAO (**2**/MAO). Compound **2** has been prepared previously and investigated because complexes of this type exhibit extreme ^1H and ^2H NMR parameters,[6] however little is known on its reactivity potential. In this contribution we show that the **2**/MAO catalysts react with ethylene to produce a distribution of low molecular weight oligomers with an *odd* number of carbon atoms.

Addition of a solution of **2** to MAO in toluene (50 μmol Cr; [Cr] = 1×10^{-3} M; Al/Cr = 1000, 23 °C) results in a color change from dark purple to red. Fast consumption of ethylene is observed when this solution is exposed to 1 atm of the monomer.[7] An activity of 87 kg[product]/(mol Cr h)$^{-1}$ was determined by measuring the amount of ethylene incorporated into the reaction vessel over a 30 min period. No precipitate was observed under these conditions. Using the same experimental setup, the Cp_2ZrCl_2/MAO catalyst system consumed 85 kg[ethylene]/(mol Zr h)$^{-1}$ to give high molecular weight polyethylene. Thus, under these conditions the affinity of **2**/MAO toward ethylene is comparable to those that characterize group 4 metallocene catalysts.

The mixture obtained from the **2**/MAO reaction was quenched with water and worked up with aqueous base. Analysis of the organic product by GCMS [Fig. 1(a)] reveals that the major product (*ca.* 98%) is a distribution of straight chain *n*-alkanes with an *odd* number of carbon atoms. The minor component corresponds to the homologous progression of *even* numbered alkanes.

Scheme 1 provides a plausible reaction pathway for the formation of the main product. In analogy to metallocene-type catalysts,[8] and taking into consideration the known reactivity of **1**[4] and the work of Theopold and coworkers,[9] it is likely that the

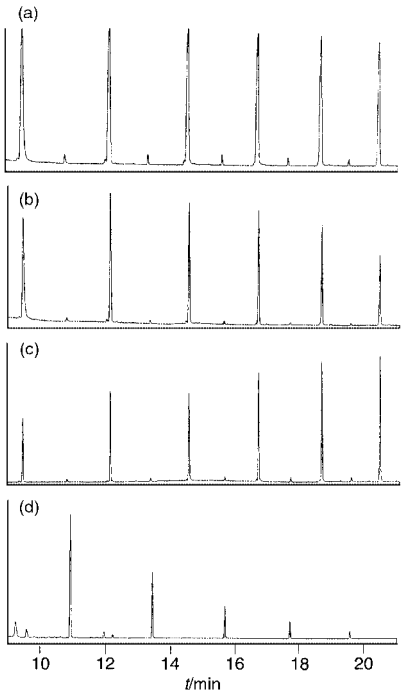

Fig. 1 GCMS analysis of C_{13} through to C_{23} products obtained from the following reactions: (a) **2**/MAO/C_2H_4; (b) **2**/MAO/C_2H_4 with 415 equiv. Al_2Me_6; (c) **2**/MAO/C_2H_4, after removal of volatiles from MAO *in vacuo*; (d) **2**/MAO/C_2H_4 with 830 equiv. '$AlEt_3$'. For all reactions: 50 μmol Cr; [Cr] = 1 X 10^{-3} M; Al/Cr = 1000; 1 atm C_2H_4.

reaction between MAO and **2** leads to catalytic species of the type $[Cp^*(Me_3P)Cr–Me]^+$ ([Cr]–Me in Scheme 1). Insertion of ethylene leads to the propagating chain **I** in Scheme 1. Transfer to aluminium gives the aluminium alkyl **II** and regenerates $[Cp^*(Me_3P)Cr–Me]^+$. The reaction sequence shown in Scheme 1 provides odd carbon alkanes upon hydrolysis of **II**.

The chemical structure of '[Al]–Me' in Scheme 1 is not precise, in part because of the complex and poorly defined structure of MAO and because commercially available MAO contains varying amounts of trimethylaluminium. To explore the effect of increasing the concentration of '[Al]–Me' an additional 415 equiv. of Al_2Me_6 were added to the catalyst solution and the reactivity with ethylene measured. As shown by the GCMS chromatogram in Fig. 1(b), the additional Al_2Me_6

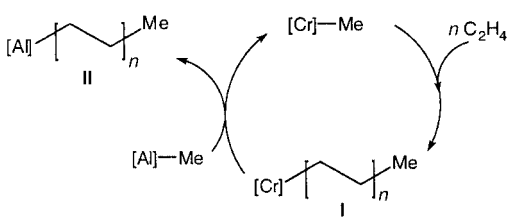

Scheme 1

DOI: 10.1039/b002146f

shifts the distribution in favor of the shorter alkanes, however the overall activity decreases to 34 kg[product]/(mol Cr h)$^{-1}$.

To examine the effect of reduced Al_2Me_6 concentration, the commercially available MAO solution was placed under vacuum for 16 h.[10] The resulting MAO solids were redissolved in toluene and the reaction with **2** and ethylene was carried out as before. Under these conditions, the activity was measured at 133 kg[product]/(mol Cr h)$^{-1}$ and polyethylene precipitates out of solution, accounting for *ca.* 85% of the product. The distribution of soluble alkanes gives a greater proportion of the heavier products [Fig. 1(c)]. Also relevant in this context is that only polyethylene is produced when **2** is activated by $B(C_6F_5)_3$.[4]

The overall trends illustrated in Fig. 1(a)–(c) are consistent with the mechanism proposed in Scheme 1. Additional Al_2Me_6 increases the rate of chain transfer to aluminium and gives rise to a distribution of shorter chain alkanes. The slower rate of ethylene consumption with the additional Al_2Me_6 may be due to the formation of bridging species such as **III**. It is anticipated

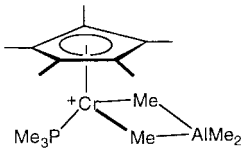

III

that the coordination of $AlMe_3$ to [Cr]–Me in **III** decreases the concentration of the active species thereby decreasing overall ethylene uptake. Removing free trimethylaluminium from MAO has the opposite effects—longer chains are obtained and more ethylene is consumed. Finally, we propose that the small fraction of even alkanes observed in the product results from a small fraction of ethyl and/or hydride found in the MAO.[11] When triethylaluminium is added (830 equiv. of '$AlEt_3$') to **2**/MAO (50 μmol Cr; [Cr] = 1×10^{-3} M; Al/Cr = 1000, 23 °C) the product is a homologous distribution of *n*-alkanes with an *even* number of carbon atoms [Fig. 1(d), activity = 97 kg[product]/(mol Cr h)$^{-1}$].

In summary, the **2**/MAO combination is an active catalyst for the oligomerization of olefins. Chain growth is limited by efficient Cr/Al transmetalation reactions.[12] After aqueous workup the product is a distribution of linear alkanes. The overall cycle shown in Scheme 1 reduces to the Cr-catalyzed insertion of ethylene into the Al–C bond.[13] It is also noteworthy that the isoelectronic boratabenzene–cyclopentadienyl substitution for the chromium catalysts (**1** *vs.* **2**), has a different effect than in zirconium catalysts. Under similar reaction conditions, the combination $Cp^*_2ZrCl_2$/MAO gives high molecular weight polyethylene, while $[C_5H_5B–OEt]_2ZrCl_2$/MAO[2b] produces low molecular weight 1-alkenes. In the zirconium case differences in reactivity stem from faster rates of β-hydride elimination for the boratabenzene complexes. For chromium, boratabenzene complexes exhibit slower rates of transmetalation with aluminium functionalities in MAO, leading to higher molecular weight polymer.

We are grateful to the Department of Energy for financial assistance.

Notes and references

1 *Transition Metals and Organometallics as Catalysts for Olefin Polymerization*, ed. W. Kaminsky and H. Sinn, Springer-Verlag, Berlin, 1988; *Ziegler Catalysts*, ed. G. Fink, R. Mülhaupt and H. H. Brintzinger, Springer-Verlag, Berlin, 1995; G. J. P. Britovsek, V. C. Gibson and D. F. Wass, *Angew. Chem., Int. Ed.*, 1999, 429; M. Bochmann, *J. Chem. Soc., Dalton Trans.*, 1996, **3**, 255.

2 (*a*) C. M. Killian, L. K. Johnson and M. Brookhart, *Organometallics*, 1997, **16**, 2005; (*b*) J. S. Rogers, G. C. Bazan and C. K. Sperry, *J. Am. Chem. Soc.*, 1997, **119**, 9305; (*c*) B. L. Small and M. Brookhart, *J. Am. Chem. Soc.*, 1998, **120**, 7134; (*d*) G. J. P. Britovsek, V. C. Gibson, B. S. Kimberley, P. J. Maddox, S. J. McTavish, G. A. Solan, A. J. P. White and D. J. Williams, *Chem. Commun.*, 1998, 849.

3 D. Rotman, *Chem. Week*, 1996, **158**(36), 37; M. M. Paige, *Chem. Eng. News*, 1998, **76**(49), 25.

4 J. S. Rogers, X. Bu and G. C. Bazan, *J. Am. Chem. Soc.*, 2000, **122**, 730.

5 G. C. Bazan, G. Rodriguez, A. J. Ashe, III S. Al-Ahmad and J. W. Kampf, *Organometallics*, 1997, **16**, 2492; J. S. Rogers, R. J. Lachicotte and G. C. Bazan, *J. Am. Chem. Soc.*, 1999, **121**, 1288; G. C. Bazan, G. Rodriguez, A. J. Ashe, III, S. Al-Ahmad and C. Müller, *J. Am. Chem. Soc.*, 1996, **118**, 2291.

6 A. Grohmann, F. H. Kohler, G. Müller and H. Zeh, *Chem. Ber.*, 1989, **122**, 897.

7 *General polymerization procedure*: in a nitrogen filled glovebox, 50 μmol of **2** was weighed to the nearest 0.1 mg and dissolved in toluene. This solution was combined with the appropriate amount of MAO (10.3 wt% Al, 1.000 Al/Cr) and placed inside a 100 mL round bottom flask with a magnetic stir bar. Sufficient toluene was added to bring the total volume to 50 mL. The flask was fitted with a needle valve assembly and removed from the glovebox. The apparatus was weighed to the nearest 0.001 g and attached on a vacuum line. Vacuum was applied for 5 s and the flask was immersed in a water bath at room temperature. The flask was then exposed to an ethylene source which was vented to a mercury bubbler. After 30 min, the ethylene feed was stopped, the flask was cleaned, and weighed again to the nearest 0.001 g for activity determinations. The reaction was quenched using 3 mL of water and alumina salts were dissolved in aqueous base. The toluene layer was extracted to give the product.

8 R. F. Jordan, C. S. Bajgur, R. Willet and B. Scott, *J. Am. Chem. Soc.*, 1986, **108**, 7410; G. G. Hlatky, H. W. Turner and R. R. Eckman, *J. Am. Chem. Soc.*, 1989, **111**, 2728; X. Yang, C. L. Stern and T. J. Marks, *J. Am. Chem. Soc.*, 1991, **113**, 3623; R. F. Jordan, *Adv. Organomet. Chem.*, 1991, **32**, 325; X. Yang, C. L. Stern and T. J. Marks, *J. Am. Chem. Soc.*, 1994, **116**, 10015.

9 B. J. Thomas, S. N. Noh, G. K. Schulte, S. C. Sendlinger and K. H. Theopold, *J. Am. Chem. Soc.*, 1991, **113**, 893; K. H. Theopold, *Acc. Chem. Res.*, 1990, **23**, 263; K. H. Theopold, *Chemtech*, 1997, **26** and references cited therein.

10 For leading references on the removal of trimethylaluminium from MAO, see: L. Resconi, S. Bosssi and L. Abis, *Macromolecules*, 1990, **23**, 4489; I. Tritto, M. C. Sacchi, P. Locatelli and S. X. Li, *Macromol. Chem. Phys.*, 1996, **197**, 1537; A. R. Barron, *Organometallics*, 1995, **14**, 3581.

11 The hydrolysis product of MAO is known to contain *ca.* 98% methane, as well as hydrogen and lighter hydrocarbons: D. B. Malpass, *Aluminoxanes from Akzo Nobel*, Akzo Nobel Chemicals Inc., Chicago, 1999.

12 Chain transfer to aluminium also occurs with iron-based catalysts, see: G. J. P. Britovsek, M. Bruce, V. C. Gibson, B. S. Kimberley, P. J. Maddox, S. Mastroianni, S. J. McTavish, C.Redshaw, G. A. Solan, S. Strömberg, A. J. P. White and D. J. Williams, *J. Am. Chem. Soc.*, 1999, **121**, 8728.

13 Analogous reactivity can be found in samarium mediated ethylene insertion into Mg–C bonds, see: J.-F. Pelletier, A. Mortreux, X. Olonde and K. Bujadoux, *Angew. Chem., Int. Ed. Engl.*, 1996, **35**, 1854.

ChemComm

The metal-directed self-assembly of three-dimensional porphyrin arrays†

Kelly Chichak and Neil R. Branda*

Department of Chemistry, University of Alberta, Edmonton, AB, Canada T6G 2G2. E-mail: neil.branda@ualberta.ca

Received (in Columbia, MO, USA) 25th February 2000, Accepted 16th May 2000

Six metalloporphyrins spontaneously assemble into octahedral arrays through a metal-directed synthesis; ^{1}H NMR provides a convenient means for tracking the progress of the self-assembly process and highlights that the rates in which the octahedral complexes form are influenced by the steric demands of the building blocks.

The power of self-assembly synthesis lies in its ability to rapidly generate large and sophisticated molecular architectures from readily accessible building blocks with maximum efficiency. Extensive hands-on synthetic steps are minimized because the pathway to the formation of the assemblies is guided by the nature of the recognition surfaces programmed into the components. This provides access to high yields under thermodynamic control. Self-assembly synthesis has been applied to the area of coordination chemistry to produce a variety of elegant structures including helicates,[1] squares,[2] closed-shell capsules,[3] linear ribbons, two-dimensional nets and three-dimensional weaves.[4] We are taking advantage of this strategy to create molecular arrays with well-defined architectures based on metalloporphyrins and other transition metal complexes.[5] Porphyrins are particularly attractive supramolecular building blocks as they have rich photo- and redox properties and, to date, numerous polymolecular assemblies held together by covalent or non-covalent interactions have been used to model solar energy capture and transfer in naturally occurring photosystems, as well as to create artificial photoactive molecular devices.[6]

We recently reported the preparation of linear multicomponent porphyrin arrays in which a central metal atom positions two pyridyl Lewis bases that, in turn, axially coordinate to ruthenium-based metalloporphyrins.[5,7] The terpyridine scaffold, however, is restricted in its use. Only linear arrays can be conveniently synthesized. A ligand displaying multiple, divergent Lewis basic sites provides a means to extend the self-assembly strategy to three-dimensional metal-templated porphyrin arrays. The tetrapyridyl ligand [4,4′-di(4″-pyridyl)-2,2′-bipyridine, **1**][8] is ideal for this purpose. We report here the spontaneous assembly of three-dimensional ruthenium arrays **2**(TTP) and **2**(OEP) *via* axial coordination of ruthenium(II) porphyrin building blocks to a modified tris(bipyridine)ruthenium(II) metal template where the Lewis basic lone pair vectors are extensions of the octahedral geometry of the central metal–ligand complexes. We also describe a one-pot

† Electronic supplementary information (ESI) available: synthesis and spectral data for **2**, **2**(TTP), **2**(OEP) and **3**(TTP). See http://www.rsc.org/suppdata/cc/b0/b002562n/

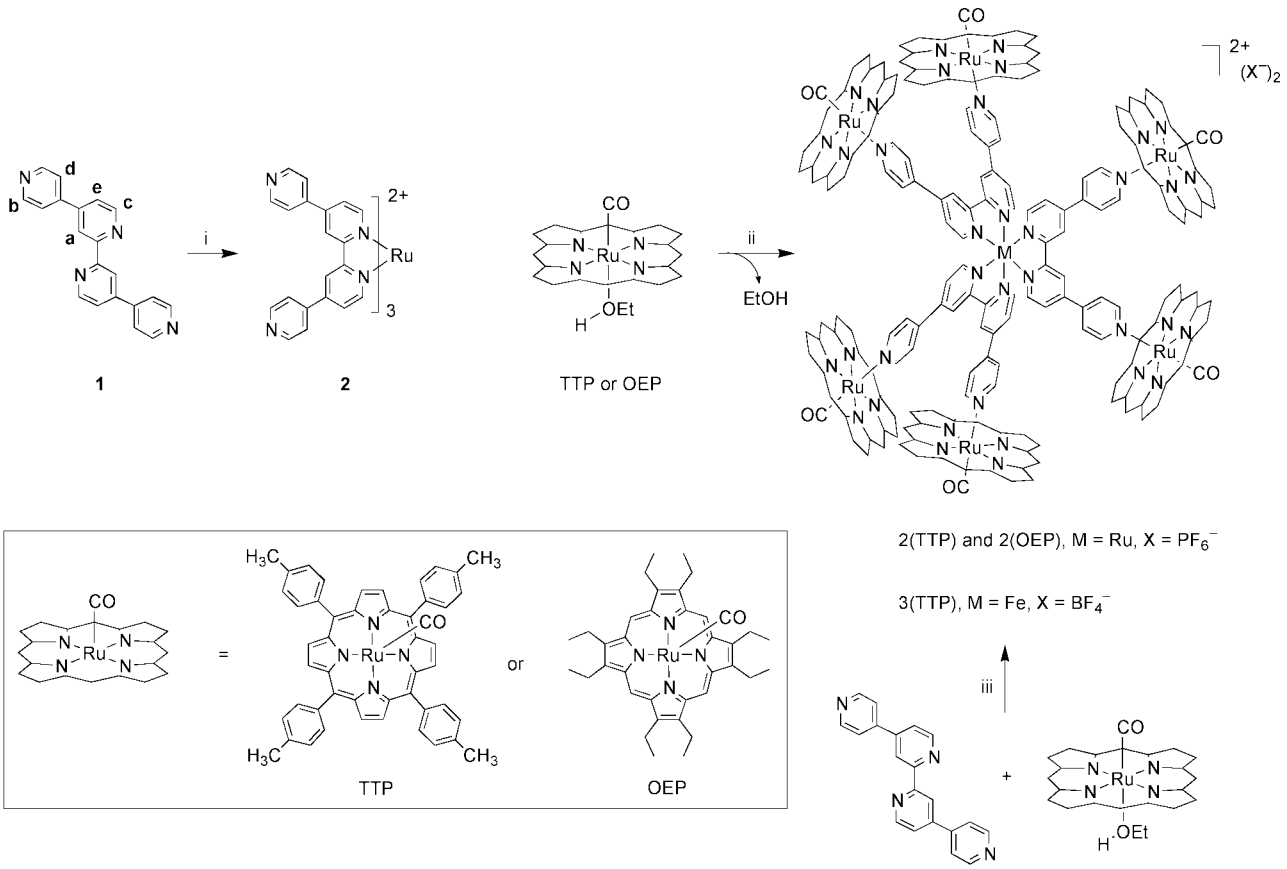

Scheme 1 *Reagents and conditions*: i, $RuCl_3 \cdot xH_2O$, ethylene glycol, reflux, then excess NH_4PF_6; ii, **2**, acetone, room temp; iii, $FeBF_4 \cdot 6H_2O$, acetone–methylene chloride, room temp.

synthesis of an octahedral iron analog **3**(TTP) from its simplest molecular components.

Multigram quantities of ligand **1** can be conveniently prepared in one step by dehydrogenating 4,4′-bipyridine according to known methods.[8] The octahedral ruthenium core unit **2** was prepared by heating $RuCl_3 \cdot xH_2O$ with three molar equivalents of **1** and was isolated as its hexafluorophosphate salt (Scheme 1). Arrays **2**(TTP) and **2**(OEP) were synthesized by treating the core template with six equivalents of [Ru(TTP)(CO)(EtOH)] and [Ru(OEP)(CO)(EtOH)], respectively, in acetone with gentle heating (Scheme 1). Arrays **2**(TTP) and **2**(OEP) were isolated as air-stable red solids in yields greater than 95% and characterized by UV–VIS, IR and ^{1}H NMR spectroscopy, and mass spectrometry.†

All arrays exhibit significantly upfield-shifted signals in their ^{1}H NMR spectra, corresponding to the protons on the core unit which are completely surrounded by the shielding cones of as many as six porphyrin building blocks. The most significant shift corresponds to the protons directly adjacent to the axially directed nitrogen atoms ($\Delta\delta$ as much as 8.3 ppm upfield), as it is these hydrogen atoms that are buried deepest within each porphyrin's shielding cone and experience the greatest anisotropic effect.

The most notable feature of the self-assembly process arises from the steric bulk expressed by the porphyrinic building blocks and is highlighted by the different rates at which **2**(TTP) and **2**(OEP) form in solution. ^{1}H NMR studies of **2**(TTP) reveal that the self-assembling process is slow on the NMR time scale and sharp peaks for the statistical mixture of fully assembled and lower-generation arrays were clearly visible, even when six molar equivalents of [Ru(TTP)(CO)(EtOH)] were added [Fig. 1(b)]. Only upon heating to 45 °C did the spectrum simplify to signals that correspond to **2**(TTP) alone [Fig. 1(c)].‡ On the other hand, despite the fact that the ruthenium atom in the octaethylporphyrin is a weaker Lewis acid,[9] complex **2**(OEP) assembles at a significantly greater rate than **2**(TTP), as illustrated by the immediate appearance of major signals for the fully assembled array [Fig. 1(d)]. We attribute these phenomena to the relative steric bulk of the tolyl and ethyl groups. The need to input additional energy in the case of **2**(TTP) was not unexpected as the tetratolylporphyrin traces out a circle of a diameter that is significantly larger than that inscribed by the octaethyl analog (18.5 *vs.* 12.7 Å). The result is that the CH_3 groups on the tolyl overlap with those on adjacent porphyrin rings in **2**(TTP).

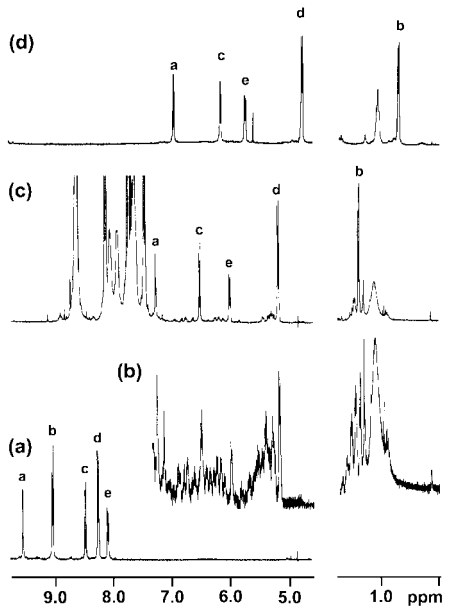

Fig. 1. ^{1}H NMR (300 MHz, acetone-d_6) spectra of (a) **2**, (b) **2** + 6 equiv. [Ru(TTP)(CO)(EtOH)] before and (c) after heating at 45 °C for 2 h, and (d) **2** + 6 equiv. [Ru(OEP)(CO)(EtOH)] at room temperature. Peak assignments correspond to the atom labels in Scheme 1.

The octahedral iron analog **3**(TTP) is readily synthesized in greater than 70% isolated yield in one step when a 1 : 2 mixture of solid **1** and solid [Ru(TTP)(CO)(EtOH)] is dissolved in a acetone-d_6/CD_2Cl_2 solution of $Fe(BF_4)_2 \cdot 6H_2O$ with gentle heating. This particular iron synthon was chosen for these studies because the highly labile nature of the metal's ligands allows for the rapid generation of the octahedral core fragment in high purity at room temperature, avoiding the harsh conditions required to form the ruthenate counterpart. Here, ten molecular species must organize and form twelve dative metal–ligand bonds in this assembly pathway. It is clear that, under these conditions, the self-assembly process results from the reading of both ruthenium and iron's inherent coordination algorithms and from the binding information stored in ligand **1**.

The absorption spectra in the UV–VIS region of **2**(TTP) and **2**(OEP) are essentially the sums of the spectra of the arrays' constituents. Initial steady-state emission spectra of these complexes, however, argue that there is a significant difference between the excited states of each array and their building blocks. Detailed results of the photophysical studies will be described elsewhere.

This work was supported by a grant from the Natural Sciences and Engineering Research Council of Canada and the University of Alberta.

Notes and references

‡ The spectra of both **2**(TTP) and **2**(OEP) generated *in situ* are identical to those of the corresponding isolated compounds.

1 J.-M. Lehn, *Supramolecular Chemistry—Concepts and Perspectives*, VCH, Weinheim, 1995; M. Albrecht, *Chem. Soc. Rev.*, 1998, **27**, 281 and references therein.
2 M. Fujita, *Chem. Soc. Rev.*, 1998, **27**, 417; P. J. Stang, *Chem. Eur. J.*, 1998, **4**, 19.
3 N. Takeda, K. Umemoto, K. Yamaguchi and M. Fujita, *Nature*, 1999, **398**, 794; D. L. Caulder and K. N. Raymond, *J. Chem. Soc., Dalton Trans.*, 1999, 1185 and references cited therein.
4 S. R. Batten and R. Robson, *Angew. Chem., Int. Ed.*, 1998, **37**, 1460 and references cited therein.
5 K. Chichak and N. Branda, *Chem. Commun.*, 1999, 523.
6 A. Osuka, M. Ikeda, H. Shiratori, Y. Nishimura and I. Yamazaki, *J. Chem. Soc., Perkin Trans. 2*, 1999, 1019; R. W. Wagner, J. Seth, S. I. Yang, D. Kim, D. F. Bocian, D. Holten and J. S. Lindsey, *J. Org. Chem.*, 1998, **63**, 5042; L. Flamigni, F. Barigelletti, N. Armaroli, J.-P. Collin, J.-P. Sauvage and J. A. G. Williams, *Chem. Eur. J.*, 1998, **4**, 1744; J. L. Sessler, C. T. Brown, D. O'Connor, S. L. Springs, R. Wang, M. Sathiosatham and T. Hirose, *J. Org. Chem.*, 1998, **63**, 7370; C. C. Mak, N. Bampos and J. K. M. Sanders, *Angew. Chem., Int. Ed.*, 1998, **37**, 3020.
7 For examples of other porphyrin arrays assembled through axial coordination, see: M. Gardner, A. J. Guerin, C. A. Hunter, U. Michelsen and C. Rotger, *New J. Chem.*, 1999, **23**, 309; S. L. Darling, C. C. Mak, N. Bampos, N. Feeder, S. J. Teat and J. K. M. Sanders, *New J. Chem.*, 1999, **23**, 359.
8 R. J. Morgan and A. D. Baker, *J. Org. Chem.*, 1990, **55**, 1986.
9 S. S. Eaton and G. R. Eaton, *Inorg. Chem.*, 1977, **16**, 72.

ChemComm

Frameworks of amino acids: synthesis and characterization of two zinc phosphono-amino-carboxylates with extended structures

Stacy J. Hartman, Evgeny Todorov, Carlos Cruz and Slavi C. Sevov*†

Department of Chemistry and Biochemistry, University of Notre Dame, Notre Dame, IN 46556, USA. E-mail: ssevov@nd.edu

Received (in Columbia, MO, USA) 7th February 2000, Accepted 18th May 2000

Two α-amino acids, 3-phosphono-2-aminopropionic and 4-phosphono-2-aminobutyric, are used to link zinc atoms in three-dimensional structures where the three phosphonic and one of the carboxylic oxygen atoms coordinate to the metal, while the protonated amino groups and the second carboxylic oxygen atom are not coordinated and remain terminal in the voids of the framework.

Multifunctional ligands have attracted much interest in recent years mainly due to the possibility to build infinite frameworks by coordination to metal centers.[1] Such hybrid inorganic–organic compounds have the potential for use in shape recognition,[2] and more importantly, in stereoselectivity when chiral linkers are used.[3] Linkers with two or more different functional groups are even more interesting since they can provide different modes of coordination, different stability, and different structural dimensionality and motifs. Extended structures of such organic moieties with two different end groups that are both coordinated to the metal centers are actually quite rare. Known and structurally characterized are one such amino-phosphonate with a zeolite-like structure,[4] three carboxylate-phosphonates with layered structures,[5] and three of the latter type but with three-dimensional framework structures.[6] We have now taken one step further in the complexity, and have studied organic linkers with three different functional groups, *i.e.* species with an amino, carboxylic and phosphonic groups. Reported here are the structures and the IR and TGA characteristics of two framework compounds of zinc and phosphonated α-amino acids, $Zn(O_3PCH_2CH(NH_3)COO)$ (**1**) and $Zn(O_3PCH_2CH_2CH(NH_3)COO)$ (**2**), where the zinc atoms are coordinated by oxygen from the phosphonic and the carboxylic groups. Our ultimate goal is to achieve layered compounds with non-coordinated carboxylic and amino groups that are potential candidates for stereoselective intercalation due to the chiral α-carbon. In the pursuit of this same goal, layered inorganic compounds such as zirconium phosphate have been intercalated with amino acids where the latter interact electrostatically or van der Waals-like with the host.[7]

Compounds **1** and **2** were synthesized hydrothermally in autoclaves at 130 °C (2 d) from $Zn(NO_3)_2{\cdot}6H_2O$, and DL-2-amino-3-phosphonopropionic or DL-2-amino-4-phosphono-butyric acids (from Sigma), respectively, in molar ratio 1 : 4 and resulting pH of about 1.5. The latter is perhaps very near the isoelectric point of these very acidic amino acids, and as a result they exist as zwitterions in the product. The resulting solids were filtered, washed with water, ethanol and acetone, and were dried at room temperature. Compound **1** crystallizes as large polyhedral crystals, while the crystals of **2** are extremely small and very thin rectangular plates. Correspondingly, the structure of **1** was determined from X-ray diffraction data collected on a regular four-circle diffractometer, while a CCD area detector was used for the structure of **2**.†

The structure of compound **1** is a hybrid of alternating inorganic and organic layers (Fig. 1). The inorganic layers, made of oxygen-connected tetrahedra centered by phosphorus and zinc, are linked by the amino acid molecules. The connectivity is achieved *via* the carbon–phosphorus bond of the phosphonated amino acid and with the coordination of one of the carboxylic oxygens to Zn (Fig. 1 and in the TOC). The other oxygen of the latter is noncoordinated as is the protonated amino group of the amino acid. Thus, unlike other examples of bi-coordinated organic moieties such as diphosphonates or carboxylates-phosphonates and poly-carboxylates, the organic species here are highly functionalized with hydrophilic groups, *i.e.* with the $>C{=}O$ and NH_3^+ functionalities. These functional groups point toward the one-dimensional inter-linker apertures (4.36 Å O–O diameter) that exist along the *b* direction (Fig. 1), and are hydrogen bonded between themselves.

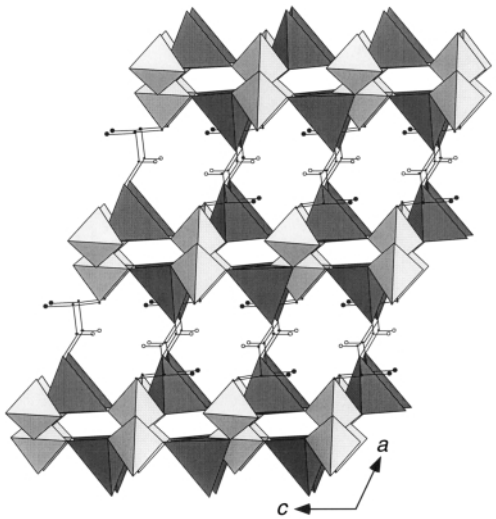

Fig. 1 A general view of the structure of compound **1**, $Zn(O_3PCH_2CH(NH_3)COO)$, along the *b* axis. The carbon and nitrogen atoms are shown as small and large black circles, respectively, while the non-coordinated oxygen of the carboxylic group is shown as an open circle. The darker and lighter shaded tetrahedra are centered by Zn and P, respectively.

The structure of compound **2** presents very similar features. Its carboxylic groups are also coordinated *via* only one oxygen atom, and therefore, the second one is terminal, and the amino groups are again protonated to $-NH_3^+$ (Fig. 2 and in the TOC). Crystallographically, there are two different phosphono-amino acids as well as zinc atoms in this structure but they are all nearly identical in coordination, bond distances and angles. Similar to **1**, the structure of **2** (Fig. 2) contains phosphonate–zinc inorganic layers that are grafted by the amino acid moieties. Nevertheless, there is an additional feature in this structure, inorganic chains of PO_3/ZnO_4 running along the *a* axis (the viewing direction of Fig. 2). The chains are positioned between the inorganic layers and are linked to the two neighboring layers by the amino acids. This leads to increased separation between the layers, 17.5 Å (half the *b* axis), since they are formally connected by amino acid–PO_3–ZnO_4–amino acid composite linker. These linkers are not perpendicular to the layers but are rather tilted, most likely due to the rigidity of the carbon angles, and give the impression that the layers are offset or shifted along the *c* direction with respect to each other. Long narrow gaps of about 19.3 Å (measured in O–O distance) are formed between

DOI: 10.1039/b001275k

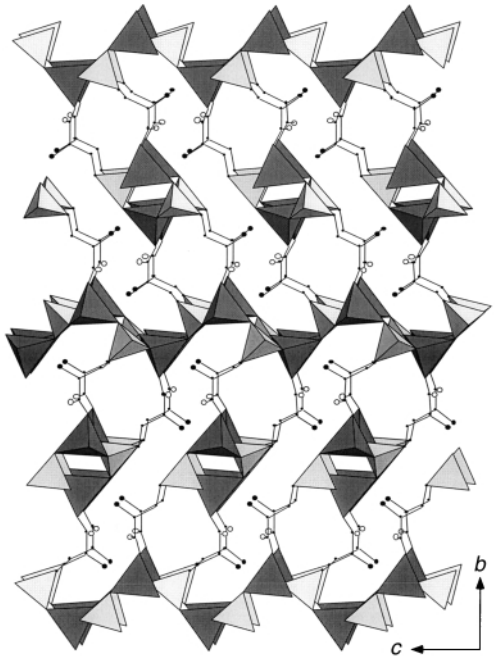

Fig. 2 A general view of the structure of compound **2**, $Zn(O_3PCH_2CH_2CH(NH_3)COO)$, along the *a* axis. The carbon and nitrogen atoms are shown as small and large black circles, respectively, while the non-coordinated oxygen of the carboxylic group is shown as an open circle. The darker and lighter shaded tetrahedra are centered by Zn and P, respectively.

the composite linkers. All pendant amino groups and carboxyl oxygen atoms point into these gaps and are extensively hydrogen bonded through that space (3 bonds per amino group and one bond per carboxylic oxygen). Both structures are centrosymmetric and contain racemic mixtures of the corresponding amino acids.

The compounds are thermally stable up to about 350 °C in a flow of air, according to TGA measurements. At this temperature, in a single sharp step, they lose the organic fraction in the form of CO_2, NH_3 and H_2O, and end up as $ZnHPO_4$. The IR spectra of the compounds (in KBr pressed pellets) show the antisymmetric and symmetric vibrations of the carboxylic groups. For compound **1** they are observed at 1627 and 1414 cm^{-1}, respectively, while doublets at 1636 and 1621 cm^{-1} for the antisymmetric and at 1446 and 1429 cm^{-1} for the symmetric vibrations are observed for compound **2**. The splitting is due to the two crystallographically different amino acids, *i.e.* the two slightly differently bonded carboxylic groups in the compound. The vibrations of the phosphonic groups are observed in the region 900–1200 cm^{-1}, as expected.

The existence of these framework compounds proves that it is possible sometimes to teach 'an old dog', the amino acids, 'new tricks'. The next step is to find a way to anchor only the phosphonic groups in a layer-type compound, and use the two functionalities COOH and NH_3, and the chiral α-carbon for a variety of intercalation and chiral molecular recognition reactions.

Such supported amino acids can be used for a number of organic reactions in the interlayer spacing, including formation of peptide bonds and longer chains of different residues. The two compounds presented here are not layered or microporous, and guest molecules can not access the inside of the structures, but they clearly have the right structural motifs and are on the right track towards more open frameworks.

We thank Chris Cahill for help with the data collection, and the National Science Foundation (DMR-9701550) for the financial support and for the Summer Program in Solid State Chemistry.

Notes and references

† *Crystal data* for $Zn(O_3PCH_2CH(NH_3)COO)$ **1**: Mw = 232.4, monoclinic, $P2_1/c$, Z = 4, a = 8.234(1), b = 9.768(2), c = 8.850(2) Å, β = 109.5(1)°, V = 670.9(2) Å^3, μ = 38.69 cm^{-1}. A hemisphere of data was collected on a CAD4 single crystal diffractometer with graphite-monochromated Mo-Kα radiation at room temperature (crystal size 0.35 × 0.25 × 0.20 mm, ω-2θ scans, $2\theta_{max}$ = 50°, 2328 and 1182° collected and independent reflections, respectively). *Crystal data* for $Zn(O_3PCH_2CH_2CH(NH_3)COO)$ **2**: Mw = 246.4, monoclinic, $P2_1/n$, Z = 8, a = 5.2022(6), b = 35.000(3), c = 8.1165(4) Å, β = 94.16(1)°, V = 1473.9(2) Å^3, μ = 35.30 cm^{-1}. Nearly a full sphere of data was collected on a Bruker SMART system with a CCD area detector (graphite-monochromated Mo-Kα radiation, room temperature, crystal size 0.16 × 0.06 × < 0.01 mm, 60 seconds/frame, $2\theta_{max}$ = 56.5°, 9719 and 3549 collected and independent reflections, respectively). The structures were solved by direct methods and refined with the aid of the SHELXTL-V5.1 package. XABS empirical absorption corrections were applied to the data of **2** after the structure was refined with isotropic thermal parameters. Final residual values: compound **1**, $R1/wR2$ = 4.74/14.30% for 968 reflections with $I \geqslant 2\sigma I$ and 99 refined parameters; compound **2**, $R1/wR2$ = 8.45/15.95% for 1092 reflections with $I \geqslant 2\sigma I$ and 225 refined parameters. The somewhat higher R-values for **2** are due to absorption problems resulting from the extremely anisotropic crystals (plates, 0.16 × 0.06 × < 0.01 mm). CCDC 182/1661. See http://www.rsc.org/suppdata/cc/b0/b001275k/ for crystallographic files in .cif format.

1 *Comprehensive Supramolecular Chemistry*, ed. J. L. Atwood, J. E. D. Davis, D. D. MacNicol and F. Vogtle, Pergamon, New York, 1996, vol. 6 (Solid-state supramolecular chemistry: crystal engineering) and vol. 7 (Solid-state supramolecular chemistry: two- and three-dimensional inorganic networks); A. Clearfield, in *Progress in Inorganic Chemistry*, ed. K. D. Karlin, Wiley, New York, 1998, vol. 47, pp. 371–510.
2 G. Cao and T. E. Mallouk, *Inorg. Chem.*, 1991, **30**, 1434.
3 G. Cao, M. E. Garcia, M. Alcala, L. F. Burgess and T. E. Mallouk, *J. Am. Chem. Soc.*, 1992, **114**, 7574; T. E. Mallouk and J. A. Gavin, *Acc. Chem. Res.*, 1998, **31**, 209.
4 S. Drumel, P. Janvier, D. Deniaud and B. Bujoli, *J. Chem. Soc., Chem. Commun.*, 1995, 1051.
5 S. Drumel, P. Janvier, P. Barboux, M. Bujoli-Doeuff and B. Bujoli, *Inorg. Chem.*, 1995, **34**, 148; S. Drumel, P. Janvier, M. Bujoli-Doeuff and B. Bujoli, *New J. Chem.*, 1995, **19**, 239; G. B. Hix, D. S. Wragg, P. A. Wright and R. E. Morris, *J. Chem. Soc., Dalton Trans.*, 1998, 3359.
6 A. Distler and S. C. Sevov, *Chem. Commun.*, 1998, 959; F. Serpaggi and G. Ferey, *Inorg. Chem.*, 1999, **38**, 4741; S. Ayyappan, G. D. de Delgado, A. K. Cheetham, G. Ferey and C. N. R. Rao, *J. Chem. Soc., Dalton Trans.*, 1999, 2905.
7 Y. Ding, D. J. Jones, P. Maireles-Torres and J. Roziere, *Chem. Mater.*, 1995, **7**, 562.

Typeset and printed by Black Bear Press Limited, Cambridge, England

ChemComm
FEATURE ARTICLE

Asymmetric epoxidation of electron-deficient olefins

Michael J. Porter[a] and John Skidmore[b]

[a] *Department of Chemistry, University College London, Christopher Ingold Laboratories, 20 Gordon Street, London, UK WC1H 0AJ. E-mail: m.j.porter@ucl.ac.uk*
[b] *Department of Chemistry, University of Liverpool, Liverpool, PO Box 147, UK L69 7ZD. E-mail: johnskid@liv.ac.uk*

Received (in Cambridge, UK) 6th March 2000, Accepted 26th April 2000
Published on the Web 9th June 2000

In recent years, methods for the asymmetric epoxidation of electron-deficient olefins, particularly α,β-enones, have attracted widespread attention. A critical review is presented of these methods, which include epoxidations with chiral metal hydroperoxides, asymmetric phase-transfer methods, the use of polyamino acid catalysts and the use of chiral dioxiranes.

1. Introduction

Epoxidation holds a venerable place in the history of catalytic asymmetric synthesis. The development by Sharpless in the early 1980s of a system which can efficiently and predictably produce either enantiomer of an epoxide from an allylic alcohol using substoichiometric quantities of titanium and tartrate, paved the way for much of today's catalytic asymmetric synthesis.[1] Following this discovery, much progress has been made towards the asymmetric epoxidation of other classes of olefins; in particular the manganese–salen reagents of Jacobsen and Katsuki perform admirably in the asymmetric epoxidation of unfunctionalised, and particularly conjugated (*Z*)-disubstituted olefins.[2] More recently, the work of several groups has indicated that dioxiranes generated *in situ* from Oxone® and chiral ketones show great promise as asymmetric epoxidation reagents for a range of alkenes.[3]

On the other hand, no system for the asymmetric epoxidation of electron-deficient olefins has gained widespread popularity amongst synthetic organic chemists. Indeed, only recently have systems been described which allow the epoxidation of a wide range of enones with high enantioselectivity. This review introduces and compares the most significant and general of these epoxidation methods.

Most of the methods for the enantioselective epoxidation of electron-deficient alkenes are essentially asymmetric variants of the Weitz–Scheffer epoxidation[4] using alkaline H_2O_2; they are thus selective for electron-deficient alkenes in the presence of other olefins. A number of more general epoxidation methods have been applied to electron-poor olefins, and these are presented towards the end of this review.

As this survey is designed to cover those methods which may be generally applicable and synthetically useful for a range of olefins, we have chosen to exclude methods which rely on a different structural feature (such as an allylic alcohol) for the asymmetric epoxidation of an electron-deficient alkene.[5] In addition, isolated reports of epoxidations not developed with synthetic utility in mind, such as the isolation of a cell-free extract with quinone mono-oxygenase activity,[6] have been omitted.

2. Chiral ligand–metal peroxide systems

Several methods for the asymmetric epoxidation of electron-deficient alkenes rely on the use of a chiral ligand coordinated to the metal atom of a metal peroxide, which then executes a Weitz–Scheffer reaction. A number of metals, including zinc, lithium, magnesium and various lanthanides, have been used for this purpose and these methods are discussed in further detail below. In addition, Strukul and coworkers have described an asymmetric epoxidation process mediated by a platinum–diphosphine–peroxide complex, but the yields and enantioselectivities obtained in this reaction are moderate at best.[7]

a. Zinc-mediated asymmetric epoxidation

In 1996, Enders *et al*. disclosed that (*E*)-α,β-unsaturated ketones can be epoxidised in asymmetric fashion using stoichiometric quantities of diethylzinc and a chiral alcohol, under an oxygen atmosphere, to give *trans*-epoxides (Scheme 1).[8] Following screening of 35 optically active alcohols, (1*R*,2*R*)-*N*-methylpseudoephedrine (**1**) was selected as the alcohol which gave the best enantioselectivities. Furthermore, it was found that **1** could be recovered in almost quantitative yield from the reaction mixture.

More recently, Pu and coworkers have reported the use of a chiral polybinaphthyl **2** in similar reactions;[9] slightly in excess of 1 equivalent (based on the monomer binaphthyl unit) of **2** was necessary for the reaction to proceed.

As can be seen from Table 1, Enders' system gives excellent yields for several classes of enone for which the Pu conditions lead to much lower yields.[10] Furthermore, while the two methods are comparable in giving a moderate ee for the

Mike Porter was born in Harrogate, UK, in 1970. From 1988, he studied at Merton College, Oxford, where he received his BA degree in 1992. He remained in Oxford for his DPhil studies under the supervision of Professor Sir Jack Baldwin. Following postdoctoral positions at the University of Texas with Professor Philip Magnus and at the University of Liverpool with Professor Stan Roberts, he was appointed in 1999 to a lectureship at University College London. His research interests include the use of metal carbenes in synthesis, and the biomimetic synthesis of natural products.

John Skidmore was born in Macclesfield, UK, in 1972. He studied for his BA degree at St. Peter's College, Oxford, graduating in 1994. His DPhil studies were carried out under the supervision of Dr J. M. Peach in the Dyson Perrins Laboratory at Oxford. Since 1997 he has been investigating polyamino acid catalysed asymmetric reactions in collaboration with Professor Stan Roberts at the University of Liverpool, initially as a Senior Research Assistant and currently as a Principal Scientist funded by Degussa-Hüls AG.

DOI: 10.1039/b001780i

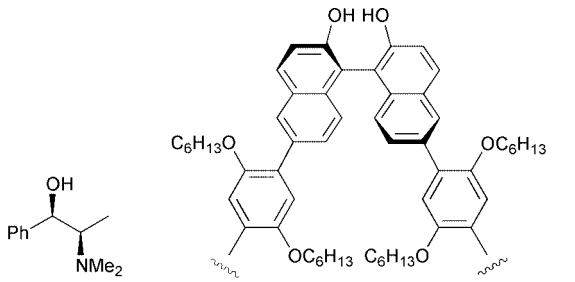

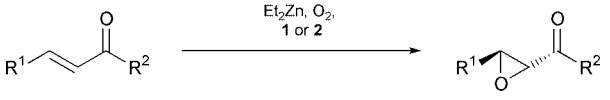

Scheme 1

Table 1 Comparison of the Enders[8] and Pu[9] ligands

R^1	R^2	Method[a]	Yield (%)	Ee (%)
Ph	Ph	A	94	61
		B	41	71[b]
Pr^i	Ph	A	97	92
		B	18	25[b]
Me	Ph	A	96	85
$Ph(CH_2)_2$	Bu^t	A	99	90

[a] A = **1** (2.4 equiv.), Et_2Zn (1.1 equiv.), O_2; B = **2** (1.1 equiv.), Et_2Zn (1.05 equiv.), O_2. [b] The predominant isomer was the enantiomer of that illustrated.

epoxidation of chalcone, Enders' system also shows high asymmetric induction for alkyl-substituted enones.

Enders' reagent has also been used for the asymmetric epoxidation of a series of β-alkylidene-α-tetralones (Scheme 2, Table 2).[8b] It appears that the enantioselectivity of the process generally increases as the substituent, R, increases in size. The reaction, however, fails for other α-substituted enones; it was surmised that this may be due to the requirement for an *s-cis* conformation of the enone moiety.

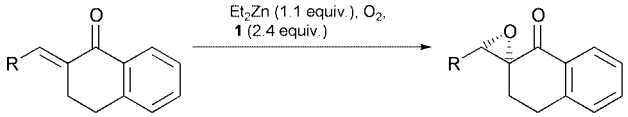

Scheme 2

Table 2 Epoxidation of alkylidenetetralones using Enders' ligand[8b]

R	Yield (%)	Ee (%)
H	40	3
Me	85	80
Et	65	90
Pr^i	98	> 99
Ph	62	64

In addition to enones, the diethylzinc/oxygen/**1** system has been used for epoxidation of some (*E*)-nitroalkenes (Scheme 3, Table 3).[11] The absolute stereochemistry of the nitroepoxides was assumed by analogy with the enone substrates.

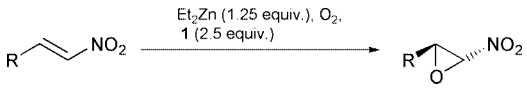

Scheme 3

Both Enders and Pu have proposed similar reaction pathways, based on the Weitz–Scheffer mechanism, for their

Table 3 Epoxidation of nitroalkenes using Enders' ligand[11]

R	Yield (%)	Ee (%)
$Ph(CH_2)_2$	64	37
Pr^i	53	42
Bu^t	57	82

asymmetric epoxidations (Scheme 4). It is suggested that diethylzinc reacts with the chiral ligand (**1** or **2**) to give a zinc alkoxide **3**, with the loss of ethane. Reaction of **3** with molecular oxygen then gives rise to a chiral metal peroxide **4**. Stereoselective conjugate addition of this peroxide to an enone **5** affords intermediate zinc enolate **6**, which then collapses to the chiral epoxide **7** and a zinc dialkoxide.

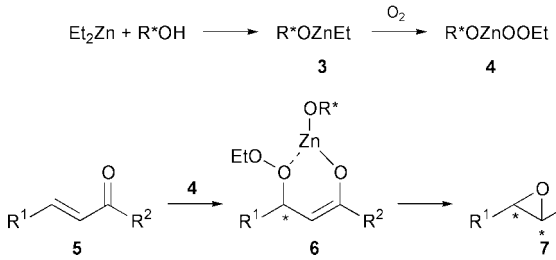

Scheme 4

Improving upon the stoichiometric process described above, Pu and coworkers have developed a variant which is catalytic in zinc and ligand, using the modified polybinaphthyl **8**.[9] In this epoxidation process, oxygen is replaced as the stoichiometric oxidant by *tert*-butyl hydroperoxide (TBHP) (Scheme 5, Table 4). Under these adapted conditions, both chalcone derivatives and alkyl-substituted enones are epoxidised with high yields and acceptable levels of enantiocontrol.

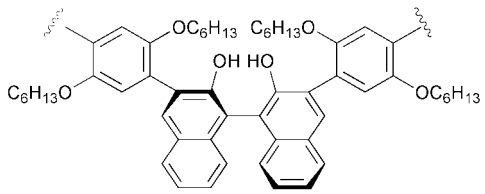

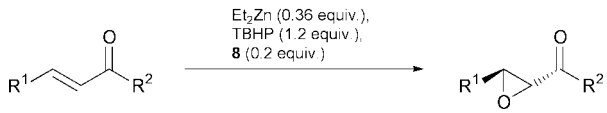

Scheme 5

Table 4 Catalytic asymmetric epoxidation using Pu's ligand[9]

R^1	R^2	Yield (%)	Ee (%)
Ph	Ph	95	74
p-ClC_6H_4	Ph	81	79
Pr^i	Ph	94	81
Bu^t	Ph	67	64

For this catalytic process, a slight modification of the mechanism in Scheme 4 has been proposed (Scheme 6). In this case, the initially formed chiral zinc alkoxide **3** reacts with TBHP to give zinc peroxide species **9**, with the loss of a second ethane molecule. Following formation of the epoxide, ligand exchange of *tert*-butyl alcohol for a TBHP molecule regenerates the chiral zinc peroxide **9**.

b. Lanthanide-BINOL systems

Shibasaki *et al*. have developed a series of complexes of general form $LnM_3(BINOL)_3$, $AlM(BINOL)_2$ and $GaM(BINOL)_2$ (Ln

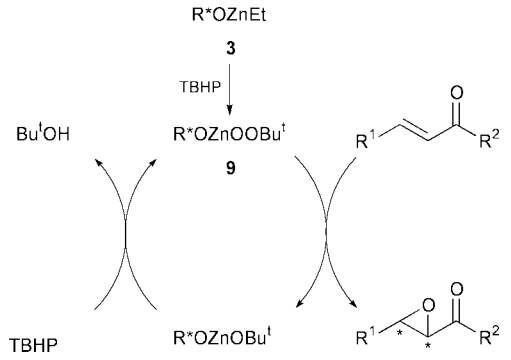

Scheme 6

= lanthanide, M = alkali metal) which have been shown to catalyse a range of transformations, such as Diels–Alder cyclisation, aldol condensation and Michael addition, in an asymmetric fashion.[12] It is believed that these bimetallic catalysts are effective owing to the presence of a Brønsted basic and a Lewis acidic site which serve to orientate the substrate and reagent in a chiral environment such that reaction may occur; Shibasaki compares this to the behaviour of some enzymes.

It was found that $LaNa_3[(R)\text{-BINOL}]_3$ catalyses the epoxidation of chalcone by *tert*-butyl hydroperoxide (TBHP) to afford (2*S*,3*R*)-epoxychalcone in 92% yield and 83% ee. Unfortunately, this epoxidation method did not prove to be generally applicable to other enones.[13*a*]

In the case of some Michael additions, Shibasaki and coworkers had previously found that alkali metal-free complexes were effective catalysts. Following this precedent, it was found that reaction of an equimolar mixture of (*R*)-BINOL **10** and $La(OPr^i)_3$ in the presence of 4 Å molecular sieves generates a complex capable of catalysing the asymmetric epoxidation of a range of (*E*)-enones. In this case, cumene hydroperoxide (CMHP) proved to be the most effective oxidant (*e.g.* chalcone was epoxidised in 93% yield and 83% ee). Alternative ligands were investigated and a substantial improvement in enantioselectivity was observed with 3-hydroxymethyl-BINOL **11**

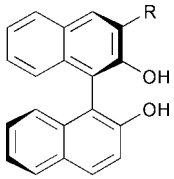

10 R = H
11 R = CH_2OH

($Ln(OPr^i)_3$: **11** = 1:1.25). It was found that the optimum lanthanide was dependent on the nature of the enone; aryl ketones were more effectively epoxidised using a La–**11**–CMHP system whilst alkyl ketones responded better to Yb–**11**–TBHP (Scheme 7, Table 5, methods A and B).[13*a*] Recently, Shibasaki and coworkers used this method for a diastereoselective epoxidation as part of a synthesis of some prostaglandins.[13*b*]

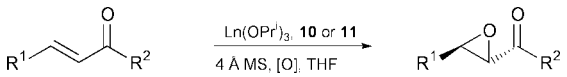

Scheme 7

Shibasaki has made some interesting observations concerning the mode of action of these catalysts. He suggests (citing ^{13}C NMR evidence) that they adopt an oligomeric structure, allowing one Ln–BINOL moiety to act as a Brønsted base to deprotonate the hydroperoxide whilst a second Ln–BINOL unit

Table 5 Comparison of lanthanide–BINOL based epoxidation systems[13*a*,14,15]

R^1	R^2	Method[a]	Yield (%)	Ee (%)
Ph	Ph	A	93	91
		C	99	81
		D	99	96
Pr^i	Ph	A	95	94
		D	89	93
Ph	Me	B	83	94
		C	92	94
		D	92	93
n-C_5H_{11}	Me	B	71	91
Ph	Pr^i	B	55	88
		C	82	93
		D	67	96

[a] A = ($La(OPr^i)_3$–**11**) (5 mol%), CMHP (1.5 equiv.), 4 Å sieves;[13*a*] B = ($Yb(OPr^i)_3$–**11**) (5–8 mol%), TBHP (1.5 equiv.), 4 Å sieves;[13*a*] C = ($Yb(OPr^i)_3$–**10**) (5 mol%), TBHP (1.5 equiv.), 4 Å sieves, water (22.5 mol%);[14] D = ($La(OPr^i)_3$–**10**) (5 mol%), TBHP (1.5 equiv.), 4 Å sieves, triphenylphosphine oxide (15 mol%).[15]

acts a Lewis acid, activating and controlling the orientation of the enone. A chiral amplification effect, whereby the ee of the product epoxide can exceed that of the ligand, was provided as evidence for this dual role.[13*a*]

More recently, Shibasaki and coworkers[14] have reported a method for improving the activity of the Yb–BINOL **10**–TBHP system allowing enantioselectivities to be attained which are comparable with the more expensive Yb–**11** catalyst. Addition of water (4.5 equivalents relative to $Yb(OPr^i)_3$) to a catalyst generated from $Yb(OPr^i)_3$: BINOL **10** (2 : 3) was found to give optimal results (Scheme 7, Table 5, method C). Surprisingly, it was found still to be necessary to add molecular sieves to this system in order to obtain effective catalysis. The catalysts generated from ligand **11** are not improved by the addition of water in an analogous manner and it should be noted that, as the above modification is of the ytterbium-based catalyst, ees are lower in the case of aryl ketones. Shibasaki has advanced an explanation for the effect of water, suggesting that it coordinates to ytterbium and controls the orientation of the hydroperoxides to form an appropriate asymmetric environment for the epoxidation.

Inanaga and coworkers have investigated the effect of a range of additives on Shibasaki's La–BINOL **10** catalyst. Comparison of lutidine-*N*-oxide, 1,3-dimethyl-2-imidazolidinone, tri-*n*-butylphosphine oxide, triphenylphosphine oxide, tri-*o*-tolylphosphine oxide, tri-*p*-tolylphosphine oxide and HMPA revealed that triphenylphosphine oxide is the most effective additive.[15] For the epoxidation of chalcone the addition of triphenylphosphine oxide (15 mol%) produced an improvement in ee from 73 to 96%. Similarly high ees were found for three alkyl ketones; unlike Shibasaki's lanthanum complexes, this catalytic system is applicable to alkyl and aryl enones (Scheme 7, Table 5, method D). It was suggested that the activation is due to the disruption of the oligomeric structure of the catalyst by coordination of the phosphorus-based ligand.

Shibasaki has shown that the unmodified Yb–**11** catalyst is also effective for the epoxidation of (*Z*)-enones to the corresponding *cis*-epoxides (Scheme 8, Table 6).[16] The trans-

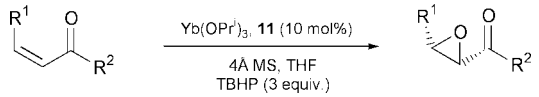

Scheme 8

formation proceeds with good yields and high stereoselectivity for aliphatic enones. In the case of aromatic enones, the reaction is less effective owing to formation of substantial (up to 32%) amounts of the unwanted *trans*-epoxide. Interestingly the use of a given enantiomer of the BINOL derived ligand **11** generates

Table 6 Epoxidation of (*Z*)-olefins to afford *cis*-epoxides[16]

R^1	R^2	Yield (%)	Ee (%)
n-C_5H_{11}	Me	74	94
Pr^n	$(CH_2)_2Ph$	78	93
n-C_5H_{11}	Pr^n	80	96
Me	Ph	60	82
Pr^n	Ph	51	88

the opposite sense of stereochemistry at the β-carbon compared to the epoxidation of (*E*)-enones; thus the (*R*)-**11** catalyst converts (*Z*)-enones to the (2*S*,3*S*)-epoxides. The Yb–**11** catalyst also proved effective in the epoxidation of a trisubstituted enone, $Me_2C=CHCOPh$ being converted to the corresponding epoxide in 78% yield and 87% ee.[16]

c. Diethyl tartrate-metal peroxides

Jackson and coworkers have reported the epoxidation of enones using metal peroxides modified by chiral ligands.[17] Initial work investigated the effect of stoichiometric quantities of a range of chiral ligands on the addition of lithium *tert*-butyl peroxide (generated *in situ* from *tert*-butyl hydroperoxide (TBHP) and *n*-butyllithium) to chalcone. Diethyl tartrate (DET) was found to be the most effective ligand and an equivalent of lithium *tert*-butoxide was required for the reaction to proceed. The use of 1.1 equivalents of (+)-DET in a non-coordinating solvent, typically toluene, afforded the (2*R*,3*S*)-epoxide in 71–75% yield and 62% ee.

Attempts to use substoichiometric quantities of the ligand in this reaction were ineffective; however, replacement of *n*-butyllithium by dibutylmagnesium gave a system in which the use of only 11 mol% of DET and 10 mol% of the base was necessary for high levels of asymmetric induction on a range of chalcone-type enones (Scheme 9, Table 7). Interestingly the catalytic magnesium system generates epoxides antipodal with those obtained using the stoichiometric lithium system.

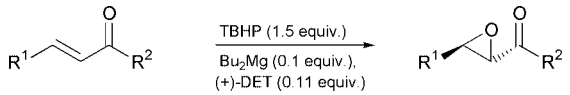

Scheme 9

Table 7 Asymmetric epoxidation using Jackson's system[17]

R^1	R^2	Yield (%)	Ee (%)
Ph	Ph	61	94
p-ClC_6H_4	Ph	54	81
p-MeC_6H_4	Ph	36	84
Ph	2-Naphthyl	46	92

3. Phase-transfer catalysis

Phase-transfer catalysis, developed initially in the mid-1960s, typically uses an organic salt (such as a quaternary ammonium salt) to transport inorganic ions into an organic phase. By using chiral ammonium salts, it is possible to induce asymmetry in reactions such as enolate alkylations, Michael additions and Darzens reactions.[18]

The most common phase-transfer reagents used for the asymmetric epoxidation of enones are alkylated *Cinchona* alkaloids. A handful of papers using other chiral phase-transfer salts has appeared,[19] but ees for these epoxidations are low (≤37%).

The possibility of using a chiral phase-transfer salt in a biphasic Weitz–Scheffer epoxidation was first investigated by Wynberg and coworkers in the mid-1970s. A series of papers was published in which phase-transfer catalysts **12** and **13** were

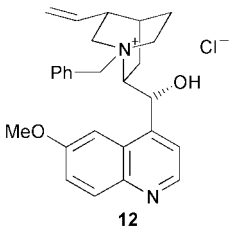

12

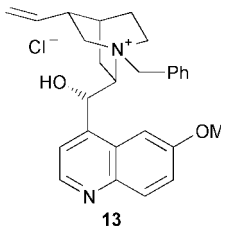

13

produced by *N*-benzylation of quinine and quinidine respectively.[20]

These compounds proved capable of catalysing the asymmetric epoxidation of a wide range of enones using aq. H_2O_2, *tert*-butyl hydroperoxide (TBHP) or sodium hypochlorite as oxidant; the ees obtained were in the range 0–54%. In an isolated example, an ee of 78% was obtained by Harigaya *et al.*, using **12** as the catalyst in the epoxidation of a 2-aryl naphthoquinone.[21]

Kawaguchi and coworkers have reported phase-transfer epoxidation using a related set of catalysts: a C_2-symmetrical pair, **14** and **15**, derived by reaction of the alkaloids cinchonidine and cinchonine respectively with α,α'-dibromo-*o*-xylene; and *N*-(9-fluorenyl)quininium bromide (**16**). These salts catalyse the epoxidation of cyclohexenone with ees up to 63%.[22]

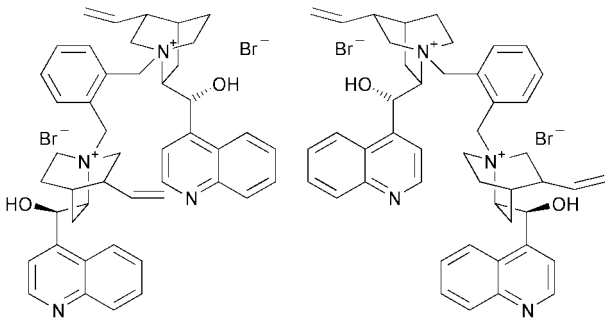

14 **15**

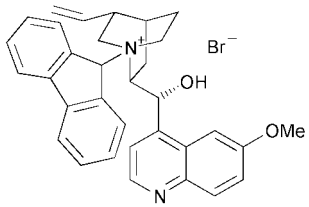

16

More recently, **12** and similar phase-transfer catalysts based on *Cinchona* alkaloids have been utilised by Taylor and coworkers for the asymmetric synthesis of the manumycin class of natural products. Best results were obtained using *N*-benzylcinchonidinium chloride (**17**), which mediated the epoxidation of enone **18** in 32% yield and 89% ee (Scheme 10).[23]

Two recent reports have shown significant improvements in phase-transfer catalysed asymmetric epoxidation. In 1998, Lygo and Wainwright described the use of catalysts **20** and **21**, derived from cinchonidine and cinchonine respectively; these differ from catalysts of the Wynberg type (**12** and **13**) as they incorporate a 9-anthracenylmethyl group in place of the benzyl group on the quinuclidine nitrogen, and bear a benzyl group on the secondary alcohol. In the presence of sodium hypochlorite as stoichiometric oxidant, these catalysts mediate the epoxidation of a wide range of substituted chalcones and alkyl-substituted enones with complete diastereoselectivity and with ees in the range 69–90% (Scheme 11, Table 8, method A); **12** and **13** provide products with opposite senses, but similar magnitudes, of stereoinduction.[24]

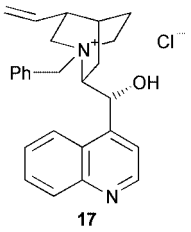

17

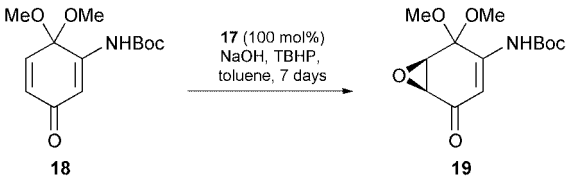

18 19

Scheme 10

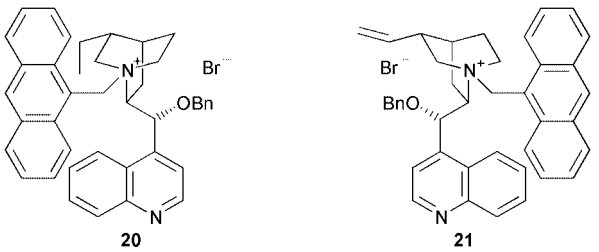

20 21

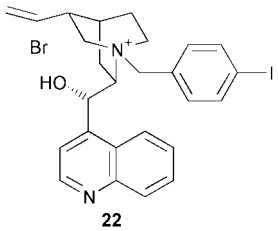

22

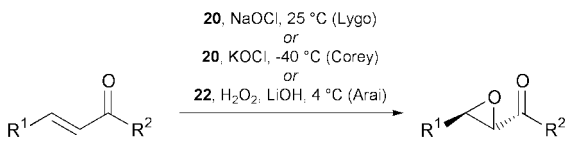

Scheme 11

Table 8 Comparison of the Lygo,[24] Corey[25] and Arai[26] epoxidations

R^1	R^2	Method[a]	Yield (%)	Ee (%)
Ph	Ph	A	90	86
		B	96	93
		C	97	84
Ph	*p*-BrC_6H_4	A	99	88
		B	92	93
p-$MeOC_6H_4$	Ph	A	87	82
		B	70	95
Cy	Ph	B	85	94
m-MeC_6H_4	Ph	C	100	92
n-C_6H_{13}	*p*-BrC_6H_4	A	89	84
n-C_5H_{11}	*p*-FC_6H_4	B	90	91
Ph	Bu^t	A	40	85
Bu^t	Ph	C	90	55

[a] A = **20** (0.1 equiv.), NaOCl (2 equiv.), 25 °C; B = **20** (0.1 equiv.), KOCl (5 equiv.), −40 °C; C = **22** (0.05 equiv.), aq. H_2O_2 (10 equiv.), LiOH (3 equiv.), 4 °C.

More recently, Corey and Zhang have shown that the use of catalyst **20** with potassium hypochlorite as the stoichiometric oxidant and a reaction temperature of −40 °C, gives epoxidation of a range of enones with ees of 90–99% (Scheme 11, Table 8, method B).[25] Epoxidation of β-alkylidene-α-tetralones, however, gives ees of only 61 and 76%; Corey interprets this as an indication that a non-planar enone geometry is favoured in the epoxidation reaction (*vide infra*).

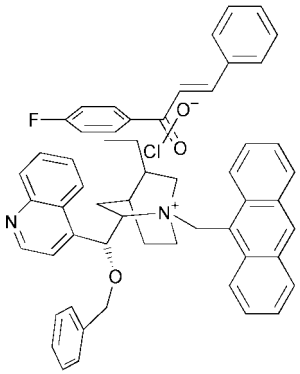

Fig. 1

Further *Cinchona* catalysts have been developed by Arai *et al.*, who surveyed the alkylation of cinchonine with a range of substituted benzyl bromides.[26] Notably, *N*-(4-iodobenzyl)cinchoninium bromide (**22**) allows highly stereoselective oxidation of chalcone derivatives, although the ees are lower for alkyl-substituted enones (Scheme 11, Table 8, method C). Intriguingly, the epoxides obtained using this cinchonine-derived catalyst are generated with the opposite sense of stereoinduction to those from Lygo's cinchonine-derived catalyst **21**. The same authors also described a quinidine-based phase-transfer catalyst which was used to epoxidise substituted naphthoquinones and acyclic enones with ees ranging from 17 to 76%.[27]

Corey and Zhang[25] have posited a three-dimensional arrangement of ammonium cation **20**, benzal-4-fluoroacetophenone and hypochlorite ion to account for the observed stereoselectivity (Fig. 1). In this model, the fluorophenyl ring of the substrate is twisted out of conjugation with the carbonyl group and is wedged between the ethyl and quinoline substituents of the catalyst. The hypochlorite ion is contact ion-paired with the charged nitrogen and the carbonyl oxygen is placed as close to the N^+ as is permitted by van der Waals forces. This arrangement places the nucleophilic oxygen of the hypochlorite ion in proximity to the β-carbon of the enone, and positioned such that only one face of the enone is accessible.

4. Polyamino acid catalysed epoxidation[28]

In 1980 Juliá *et al*. reported the poly-L-alanine catalysed asymmetric epoxidation of chalcone (Scheme 12).[29] The Juliá reaction conditions were triphasic, consisting of the insoluble polyamino acid catalyst, an aqueous solution of NaOH and H_2O_2 and a solution of chalcone in an organic solvent. The polyamino acid catalyst could readily be prepared from the corresponding amino acid *via* conversion to the *N*-carboxy-anhydride (NCA) and then treatment with an initiator such as water, a simple primary amine or a polystyrene-bonded amine.[30] It was found that enantioselectivity of the epoxidation increased as the average chain length increased from 10 to 30 residues. Over a series of papers the group of Juliá and Colonna investigated this method for the epoxidation of chalcone and simple analogues.[29,31] Their contribution to this field has recently been reviewed elsewhere.[28c] An important feature of the Juliá–Colonna epoxidation is that the insoluble catalyst may be readily separated from the reaction products, washed and reused. It was reported, however, that on reuse the catalyst frequently gave reduced enantioselectivity, a phenomenon ascribed to degradation of the catalyst under the strongly basic reaction conditions.[31c] A limitation of the Juliá-Colonna methodology is the length of reaction; even relatively reactive substrates such as chalcone and simple derivatives require 24 hours for complete conversion.[31a] Less reactive substrates

either generate products in low yield and ee or fail to form any epoxide. In particular enolisable substrates such as **23** (60% yield, 62% ee)[32] and **24** (decomposition)[33] are poor substrates for the triphasic reaction conditions.

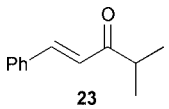

23

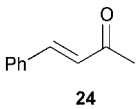

24

Nonetheless, a reasonable range of epoxides has been prepared using the triphasic reaction conditions by Juliá and Colonna and by others (Scheme 12, Table 9).

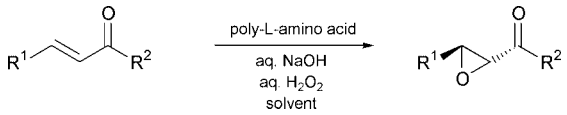

Scheme 12

Table 9 Substrates epoxidised under Juliá–Colonna conditions

R^1	R^2	Catalyst[a]	Yield (%)	Ee (%)	Ref.
Ph	Ph	PLA	85	93	29
Ph	*o*-$MeOC_6H_4$	PLA	54	50	31*a*
Ph	2-Naphthyl	PLL	90	93	34
Ph	2-Furyl	PLL	85	87	34
Ph	2-Pyridyl	PLL	74	79	34
o-[$Ph(CH_2)_8$]C_6H_4	2-Naphthyl	PLL	82	95	35
p-$MeSC_6H_4$	2-Naphthyl	PLL	65	96	36
Ph	2-Thienyl	PLA	96	80	31*a*
2-Furyl	2-Naphthyl	PLL	75	> 96	34
2-Pyridyl	Ph	PLL	84	72	34
4-Pyridyl	2-Naphthyl	PLL	67	> 96	34
p-$MeOC_6H_4$	*o*-MOMO-C_6H_4	PLA	64	66	37
Ph	Bu^t	PLL	92	> 98	34
Ph	Cyclopropyl	PLL	85	77	38
Bu^t	Ph	PLL	85	90	34
β-Styryl	2-Naphthyl	PLL	78	> 96	34
β-Styryl	Bu^t	PLL	90	> 97	34
PhCO	Ph	PLL	76	76	38
Bu^tCO	Bu^t	PLL	> 95	> 95	38
Bu^tO_2C	Ph	PLL	66	≥95	38
$Bu^n{}_3Sn$	Ph	PLL	90	> 99	39

[a] PLL = poly-L-leucine, PLA = poly-L-alanine; see references for examples using poly-D-amino acids.

The limitations of poor catalyst recycling and low reactivity have been overcome in modifications reported by Roberts and coworkers. Two biphasic procedures have been developed which reduce reaction times for chalcone to under 30 minutes. The first of these is essentially anhydrous in nature.[33,40] Peroxide is delivered in the form of an anhydrous complex, typically urea–H_2O_2. Such complexes are cheap, stable and easy to handle and are safer than concentrated solutions of H_2O_2 in organic or aqueous solvents.[41] The inorganic base employed by Juliá and Colonna is replaced with a strong amidine base, 1,8-diazabicyclo[5.4.0]undec-7-ene (DBU) and the reaction is performed in an organic solvent such as THF. Under these conditions enolisable substrates, such as simple alkyl ketones, can be readily epoxidised.[33] These biphasic conditions constitute the most widely tested and reliable of the new class of polyamino acid catalysed epoxidation systems (Scheme 14, Table 12, method A). Examples reported by Roberts and coworkers typically use polyleucine, however it has recently been disclosed that poly-L-neopentylglycine can offer advantages of increased reaction rate and enantioselectivity.[42]

In order to maximise both rate and stereoselectivity for the biphasic reaction it is necessary to activate the catalyst under conditions analogous to the triphasic procedure. This activation procedure consists of stirring the polyamino acid in a mixture of 4 M aq. NaOH and toluene for 1–5 days (the exact activation time appears to depend on the batch of catalyst), before filtering, washing and drying the catalyst.[43]

It has been demonstrated that the poly-L-leucine catalyst can readily be recycled under these conditions; for example it has been shown that for the epoxidation of chalcone, catalyst used for five previous reactions still afforded epoxide in 96% ee, albeit with increased reaction time. For less reactive substrates the activity of the catalyst was found to drop more rapidly with recycling, however it was found that the original activity could be recovered by submitting the recycled material to the activation procedure.[44]

A disadvantage of the aforementioned biphasic conditions is that they are rather more expensive than the triphasic conditions owing to the use of a more costly oxidant and of 1.5 equivalents of DBU (attempts to use substoichiometric quantities have proved unsuccessful); thus these conditions are not ideal for large-scale work. An alternative procedure employs inexpensive sodium percarbonate (NaPc) as both oxidant and base.[43] Screening of a range of solvent systems for this oxidant revealed that organic–water mixtures are most effective, in particular DME–water gives rates and enantioselectivities comparable with the urea–H_2O_2/THF/DBU system (Scheme 14, Table 12, method B). The non-catalysed background reaction under these conditions was found to be considerably slower than under the urea–H_2O_2/THF/DBU conditions; thus increased substrate to catalyst ratios may be employed with minimal reduction in ee (Table 10).

Table 10 Epoxidation of chalcone using poly-L-leucine[43]

	10 mol% catalyst[a]		2 mol% catalyst[a]	
Conditions	Yield (%)	Ee (%)	Yield (%)	Ee (%)
Urea–H_2O_2/DBU/THF	85	> 95	92	89
NaPc/DME/H_2O	—	96	87	94

[a] Based on a single polymer chain as the catalytic unit.

The sodium percarbonate–DME–water conditions have proved particularly useful for the diastereoselective epoxidation of enones with an oxy-substituted γ-chiral centre. Use of sodium percarbonate–DME–water at −3 to 0 °C gives reasonable selectivity for the epoxidation of such substrates in both the matched and mismatched sense (Scheme 13, Table 11).[45]

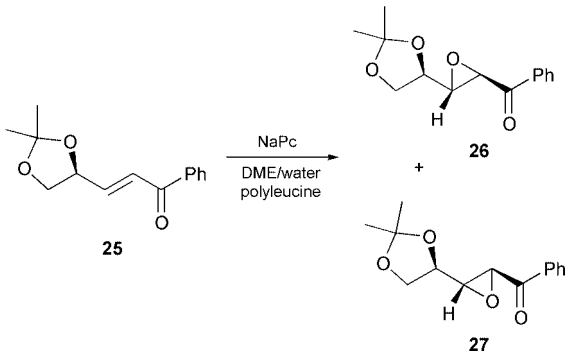

25 **26** + **27**

Scheme 13

Table 11 Diastereoselective epoxidation of **25**[45]

Catalyst	*syn* **26**:*anti* **27**	Yield (%)	Matching
None	1:3.0	94	None
Poly-D-leucine	1:34	97	Matched
Poly-L-leucine	3.8:1	98	Mismatched

One further improvement reported by Roberts and coworkers is the introduction of a silica-supported polyamino acid catalyst.[46] It has been shown in the field of biotransformations that the immobilisation of enzymes on silica affords material

more active than the native enzyme when used in organic solvents. In addition, it has been found that this material is more readily recycled. Polyleucine was stirred as a suspension in THF with a range of solid supports and the properties of the resultant adsorbed materials were investigated. It was found that silica provided the best combination of improved activity and ease of filtration/recycling. Generally the silica-adsorbed material is active enough to allow as little as 2.5 mol% catalyst (based on 1 equivalent being a single polyamino acid chain) to be used without any reduction in enantioselectivity (Scheme 14, Table 12, method C).[46]

The polyleucine catalysed epoxidation shows some interesting selectivity. For example, the diene **28** is selectively epoxidised on the disubstituted double bond to afford the monoepoxide **29** in reasonable yield and good ee (Scheme 15).[48]

Generally α-substituted enones, such as α-methylchalcone are unreactive under polyleucine catalysed conditions. One exception to this is the case of cyclic enones derived from tetralone, indanone or benzosuberone (Scheme 16).[49] A similar explanation to that proposed by Enders *et al*., in which an *s-cis* conformation is required for epoxidation to occur, may account for this difference in reactivity.[8b]

Of all the epoxidation methods discussed in the current article the polyamino acid catalysed reaction is probably the one which is the least well understood from a mechanistic standpoint. A number of fundamental questions remain to be answered. The primary issues are the nature of the interaction between polyamino acid, substrate and/or oxidant and the relationship between the structure and the activity of the catalyst. Of these, the latter question is the more readily addressed. Studies by Juliá, Colonna and coworkers[31c] and by Roberts and coworkers[42] have found that polyleucine, polyalanine, polyisoleucine and poly(neopentylglycine) are effective catalysts. Of these the first two are known to favour an α-helical structure whilst polyisoleucine is reported to form a β-sheet. This seems to suggest that the secondary structure of the polyamino acid is not directly related to the catalysis. Less effective polyamino acids include polyvaline,[31c] polyphenylalanine[31c] and polyproline.[31d]

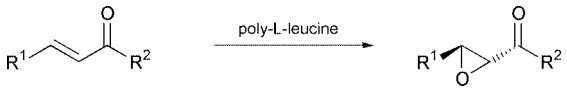

Scheme 14

Polyamino acids containing mixtures of L- and D-leucine have been prepared with a view to examining the importance of different regions of the polyamino acid chain. Investigation of material prepared by sequential polymerisation of D- and L-leucine *N*-carboxyanhydrides (NCAs) suggested that the amino terminal region plays a dominant role in determining which enantiomer of the product is generated.[50] In order to investigate this phenomenon further, Roberts and coworkers first demonstrated that a 20-mer of polyleucine prepared using a peptide synthesiser exhibits catalytic behaviour like that of the material prepared by NCA polymerisation. Such material is bound at the *C*-terminus *via* a hydroxymethyl phenoxyacetic acid linker and a polyethylene glycol graft to a polystyrene resin and is thus termed H-(L-Leu)$_{20}$-PEG-PS.[51] A series of oligopeptides of defined primary structure was then prepared and their behaviour as catalysts was examined.[52] It was shown that as few as five D-leucine residues at the *N*-terminus of a 20-mer of polyleucine is sufficient to overcome any catalytic effect of the 15 L-leucine residues which make up the rest of the polymer chain. Under the urea–H_2O_2/DBU/THF conditions the catalyst H-(D-Leu)$_5$-(L-Leu)$_{15}$-PEG-PS generated the epoxide corresponding to that afforded in the presence of poly-D-leucine in 52% ee. Moreover, the peptide H-(D-Leu)$_7$-(L-Leu)$_{13}$-PEG-PS catalysed formation of the same epoxide in 83% ee. In order to confirm that the bias towards the *N*-terminal region is not a reflection of the polymer support bound to the *C*-terminus the H-(D-Leu)$_5$-(L-Leu)$_{15}$-PEG-PS catalyst was cleaved from the support using TFA, recovered and tested again; although the ee was somewhat diminished by this procedure (21%), the major product was still the epoxide configured by a poly-D-leucine catalyst.

5. Bovine serum albumin catalysed epoxidation

In a series of papers, Colonna *et al*. have reported the use of bovine serum albumin (BSA) as an additive to Weitz–Scheffer

Table 12 Substrates epoxidised under Roberts' conditions

R^1	R^2	Method[a]	Yield (%)	Ee (%)	Ref.
Ph	Ph	A	85	> 95	33
		B	87	94	43
		C	*100*[b]	⩾93	46*a*
Ph	*o*-$O_2NC_6H_4$	A	91	91	47
Ph	*o*-MeC_6H_4	A	94	81	47
Ph	*o*-$MeNHC_6H_4$	A	62	96	47
Ph	*o*-$NH_2C_6H_4$	A	81	> 98	47
		C	85	93	46*a*
Ph	*p*-$NH_2C_6H_4$	A	0	—	47
Ph	2-Naphthyl	A	91	91	44
p-ClC_6H_4	Ph	A	62	62	47
p-ClC_6H_4	*o*-$NH_2C_6H_4$	A	91	> 98	47
Ph	Me	A	70	80	33
Ph	Pr^i	A	56	89	46*a*
		C	78	93	46*a*
Ph	Bu^t	A	76	94	33
		B	94	94	43
p-$MeOC_6H_4$	Bu^t	A	⩾90	⩾96	33
Ph	Bu^i	A	87	96	44
Ph	Pr^n	A	85	94	44
Ph	Et	A	80	82	44
Cy	Ph	A	91	89	33
β-(*E*)-Styryl	2-Naphthyl	A	85	96	48
(*E*)-ClCH=CH	Ph	A	57	86	48
(*E*)-Bu^tO_2CCH=CH	Ph	A	95	90	48
(*E*)-MeO_2CCH=CH	Ph	A	90	90	48
(*E*,*E*)-MeCOCH=CHCH=CH	Ph	A	43	90	48

[a] A = poly-L-leucine, urea–H_2O_2, DBU, THF; B = poly-L-leucine, sodium percarbonate, DME, water; C = poly-L-leucine–SiO_2, urea–H_2O_2, DBU, THF. [b] Italicised values refer to conversion rather than yield.

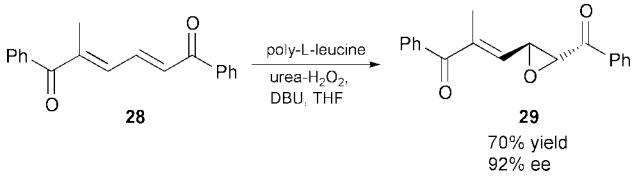

28 **29**

Scheme 15

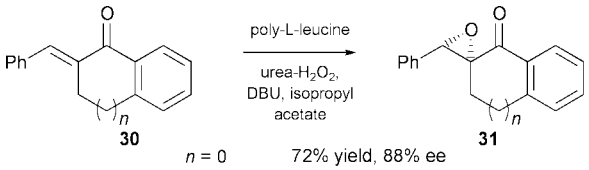

30 **31**

$n = 0$ 72% yield, 88% ee
$n = 1$ 76% yield, 84% ee
$n = 2$ 74% yield, 59% ee

Scheme 16

epoxidations of naphthoquinones.[53] Both the magnitude and the sense of enantioselectivity in the reaction were found to be strongly dependent on the nature of the side chains R and R′ (Scheme 17, Table 13). The best enantioselectivities were obtained using *tert*-butyl hydroperoxide (TBHP) as the oxidant,

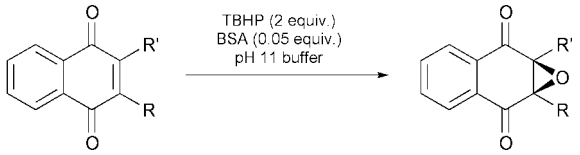

Scheme 17

in an alkaline buffer solution (slightly higher ees were obtained in pH 9 buffer than in pH 11 buffer).[53b] Further improvements in enantioselectivity could be obtained by addition of small amounts of isooctane to the reaction mixture.[53c]

Table 13 Epoxidation of naphthoquinones in the presence of BSA[53]

R	R′	Yield (%)	Ee (%)
Me	H	34	20
Bu^i	H	62	77
		56[a]	90[a]
Bu^n	H	35	14[b]
n-C_6H_{13}	H	29	30[b]
n-C_8H_{17}	H	66	100[b]
Cy	H	64	70
Et	Me	22	54[c]

[a] Epoxidation performed in the presence of 5 mol% isooctane. [b] The predominant isomer was the enantiomer of that illustrated. [c] The absolute stereochemistry was not determined.

6. Epoxidation with chiral dioxiranes

The first attempts to effect asymmetric epoxidation using chiral dioxiranes were reported by Curci *et al.* in the mid-1980s.[54] It is only recently, however, that chiral ketones, the precursors of the corresponding dioxiranes, have been developed which will allow the epoxidation of a wide range of alkenes with good enantioselectivity.

While chiral dioxiranes can, in theory, epoxidise most classes of olefin, Baeyer–Villiger reaction of the chiral ketone from which the dioxirane is derived frequently competes with epoxidation for unreactive substrates. As a result, only a few chiral dioxiranes have been used successfully to epoxidise electron-deficient alkenes. In particular, the ketones **32** and **33**, derived from (−)-quinic acid, have been developed by Shi and coworkers; on treatment with Oxone® these are believed to generate chiral dioxiranes which then epoxidise the enones shown in Scheme 18 and Table 14, regenerating the chiral ketones.[3,55] An ester, ethyl cinnamate, was also epoxidised with good enantioselectivity, albeit in low yield.

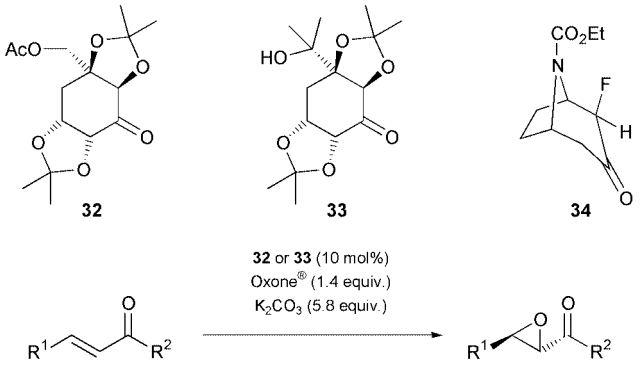

32 **33** **34**

Scheme 18

Table 14 Epoxidation using Shi's chiral dioxiranes[3,55]

R^1	R^2	Ketone	Yield (%)	Ee (%)
Ph	Ph	**32**	80	94
		33	85	96
Ph	Me	**33**	75	82
Ph	Pr^i	**33**	70	89
Ph	OEt	**32**	34	86
		33	35	89

The tropinone derivative **34**, developed by Armstrong and Hayter[56] as a chiral dioxirane precursor, has also been applied to the epoxidation of an electron-deficient olefin; methyl cinnamate was epoxidised with 33% yield and 64% ee using this catalyst under conditions similar to those employed by Shi and coworkers.[3,55]

7. Miscellaneous methods

Among the numerous substrates which have been epoxidised using manganese–salen catalyst **35** are several electron-deficient alkenes. A series of (*Z*)-cinnamate esters has been studied by Jacobsen *et al.*; on epoxidation with sodium hypochlorite in the presence of **35**, both *cis*- (**36**) and *trans*-epoxides (**37**) are obtained (Scheme 19, Table 15).[57] Two general trends can be extracted from these data: the presence of electron-donating groups (R^1) on the aromatic ring minimises the extent of 'leakage' to the *trans*-epoxide **37**, but gives the lowest enantiopurity in the *cis*-product **36**; and for a given R^1, increasing the bulk of R^2 increases the enantioselectivity.

Furthermore, various isoflavones have been epoxidised by Lévai *et al.* using catalyst **35** and its enantiomer (Scheme 20, Table 16);[58] in this case, although good ees were obtained for certain substrates, the yields are disappointing.

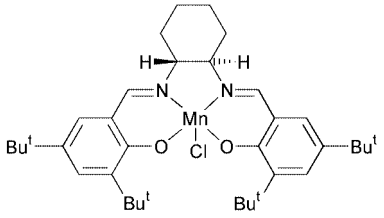

35

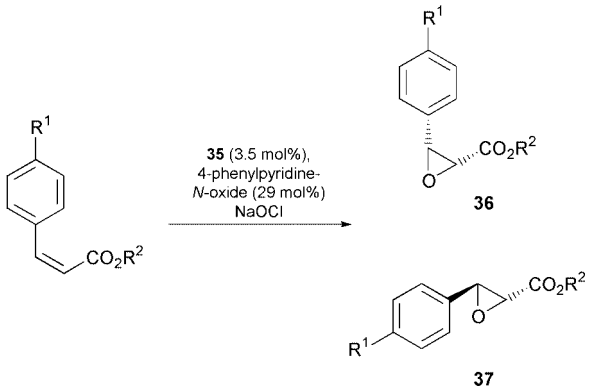

Scheme 19

Table 15 Epoxidation of cinnamate esters using Jacobsen's catalyst[57c]

R^1	R^2	*cis* **36**:*trans* **37**	*cis* **36** Ee (%)	*trans* **37** Ee (%)
OMe	Me	11.7:1	72	66
Me	Me	7.0:1	79	41
H	Me	5.7:1	85	62
CF_3	Me	1:1.25	79	55
NO_2	Me	1:3.7	91	53
H	Et	—	92	—
H	Pr^i	—	96	—

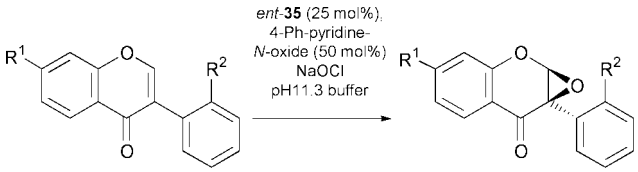

Scheme 20

Table 16 Epoxidation of isoflavones using Jacobsen's catalyst[58]

R^1	R^2	Yield (%)	Ee (%)
H	H	25	65
OMe	H	26	77
OMs	H	23	56
OMe	OMe	30	90
OMs	OMe	31	94

An isolated report by Kumar and Bhakuni in 1996 outlined the use of MCPBA localised in a chiral liposomal bilayer as a reagent for asymmetric epoxidation.[59] Five electron-deficient olefins were oxidised with moderate to good enantioselectivity using this reagent, with esters displaying higher ees than ketones (Scheme 21, Table 17).

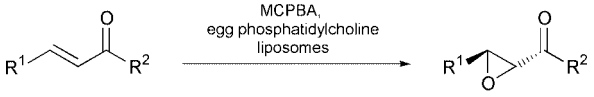

Scheme 21

Table 17 Epoxidation using liposomised MCPBA[59]

R^1	R^2	Yield (%)	Ee (%)
Ph	OMe	75	92
m-$MeOC_6H_4$	OMe	70	95
Ph	Ph	65	70
o-ClC_6H_4	Ph	63	68
Ph	*m*-ClC_6H_4	67	62

The groups of Colonna[60] and Takahashi[61] have both reported on the modification of Weitz–Scheffer conditions by the addition of cyclodextrins. Under Colonna's optimised conditions, the ees recorded for the epoxidation of a range of naphthoquinones and chalcone derivatives were below 48%; the highest ee observed by Takahashi and coworkers in the epoxidation of cinnamaldehyde was 2.5%.

In a related study, Sakuraba and Tanaka have shown that crystalline chalcone–cyclodextrin complexes, when dispersed in water, can be epoxidised by sodium hypochlorite with high yield and *ca.* 30% ee.[62]

8. Summary

It is clear from the above review that no single approach for the epoxidation of electron deficient olefins stands out from the methods discussed. The variation in selectivity observed between the different approaches means that they should all be considered as potential candidates for a given synthetic transformation. In order to aid this selection process Table 18 compares the effectiveness of the different methodologies for the epoxidation of various key classes of olefin. For the sake of clarity, it has not been possible to include all of the methods, and we have chosen to concentrate on a representative selection of the most general and effective. One caveat which should be borne in mind when consulting Table 18 is the tendency for a range of yields or ees to reflect unrepresentative, extreme results, particularly when a larger number of examples has been reported.

Despite the lack of a general method a number of high yielding and highly stereoselective methods exist; with judicious choice the chemist can epoxidise a wide range of electron deficient olefins. This fact, coupled with the potential of epoxides substituted with electron withdrawing groups as synthetic intermediates,[28c] should ensure that these methods gain increasing acceptance amongst the synthetic organic community. Moreover, it seems likely that we will witness many new and interesting developments in this field over the coming years. It remains to be seen, however, whether one single method will be developed to such an extent that it dominates epoxidation of enones in the way that the Sharpless reaction has become the pre-eminent method for the epoxidation of allylic alcohols.

Table 18 Comparison of epoxidation methods for various classes of olefin[a]

Olefin class[b]	Enders[c]	Shibasaki[d]	Jackson[e]	Lygo[f]	Corey[g]	Roberts[h]	Shi[i]
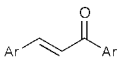	94% yd 61% ee 1 example	78–93% yd 83–91% ee 2 examples	36–61% yd 81–94% ee 5 examples	77–99% yd 71–89% ee 9 examples	70–97% yd 92–98.5% ee 12 examples	21–98% yd 53–99% ee 18 examples	85% yd 96% ee 1 example
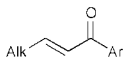	94–99% yd 82–92% ee 5 examples	81–95% yd 71–94% ee 3 examples	—	79–94% yd 77–90% ee 7 examples	85–90% yd 91–95% ee 3 examples	91% yd 89% ee 1 example	—
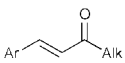	— —	55–83% yd 88–94% ee 2 examples	— —	40% yd 85% ee 1 example	—	70–90% yd 80–96% ee 6 examples	70–75% yd 82–89% ee 2 examples
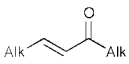	99% yd 90% ee 1 example	71–91% yd 88–91% ee 2 examples	—	—	—	—	—
	—	51–80% yd 82–96% ee 5 examples	—	—	—	—	—
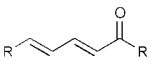	—	—	—	—	—	43–95% yd 86–98% ee 7 examples	—
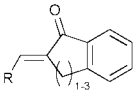	62–99% yd 64–99% ee 5 examples	—	—	—	no yd reported 61–76% ee 2 examples	63–85% yd 59–96% ee 8 examples	—
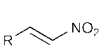	47–74% yd 37–82% ee 5 examples	—	—	—	—	—	—
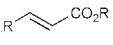	—	—	—	—	—	—	35% yd 89% ee 1 example

[a] Values given are the range reported, yd = yield. [b] Alk = alkyl group. [c] **1**, Et_2Zn, O_2 (refs. 8, 11). [d] **11**, $Ln(OPr^i)_3$, CMHP or TBHP (refs. 13a, 16). [e] (+)-DET, Bu_2Mg,TBHP (ref. 17). [f] **20**, NaOCl (ref. 24). [g] **20**, KOCl (ref. 25). [h] poly-L-leucine, DBU, UHP (refs. 33, 47–49, 63). [i] **33**, K_2CO_3, Oxone® (ref. 3).

Acknowledgements

We thank Professor S. M. Roberts for helpful advice and discussions and JS would like to acknowledge Degussa-Hüls AG for the funding of a Principal Scientist position.

Notes and references

1 R. A. Johnson and K. B. Sharpless, in *Comprehensive Organic Synthesis*, ed. B. M. Trost and I. Fleming, New York, 1991, vol. 7, p. 389.
2 T. Katsuki, *Coord. Chem. Rev.*, 1995, **140**, 189.
3 Z.-X. Wang, S. M. Miller, O. P. Anderson and Y. Shi, *J. Org. Chem.*, 1999, **64**, 6443 and references therein.
4 E. Weitz and A. Scheffer, *Ber. Dtsch. Chem. Ges.*, 1921, **54**, 2327.
5 M. Bailey, I. E. Markó and W. D. Ollis, *Tetrahedron Lett.*, 1991, **32**, 2687; D. A. Clark, F. De Riccardis and K. C. Nicolaou, *Tetrahedron*, 1994, **50**, 11391.
6 S. J. Gould, B. Shen and Y. G. Whittle, *J. Am. Chem. Soc.*, 1989, **111**, 7932.
7 C. Baccin, A. Gusso, F. Pinna and G. Strukul, *Organometallics*, 1995, **14**, 1161.
8 (*a*) D. Enders, J. Zhu and G. Raabe, *Angew. Chem., Int. Ed. Engl.*, 1996, **35**, 1725; (*b*) D. Enders, J. Zhu and L. Kramps, *Liebigs Ann./Recueil*, 1997, 1101.
9 H.-B. Yu, X.-F. Zheng, Z.-M. Lin, Q.-S. Hu, W.-S. Huang and L. Pu, *J. Org. Chem.*, 1999, **64**, 8149.
10 Yields could be increased to >90% by use of additional diethylzinc or of a modified, monomethylated binaphthol ligand; in either case, the ees dropped precipitously.
11 D. Enders, L. Kramps and J. Zhu, *Tetrahedron: Asymmetry*, 1998, **9**, 3959.
12 M. Shibasaki, H. Sasai and T. Arai, *Angew. Chem., Int. Ed. Engl.*, 1997, **36**, 1237.
13 (*a*) M. Bougauchi, S. Watanabe, T. Arai, H. Sasai and M. Shibasaki, *J. Am. Chem. Soc.*, 1997, **119**, 2329; (*b*) K. Yamada, T. Arai, H. Sasai and M. Shibasaki, *J. Org. Chem.*, 1998, **63**, 3666.
14 S. Watanabe, Y. Kobayashi, T. Arai, H. Sasai, M. Bougauchi and M. Shibasaki, *Tetrahedron Lett.*, 1998, **39**, 7353.
15 K. Daikai, M. Kamaura and J. Inanaga, *Tetrahedron Lett.*, 1998, **39**, 7321.
16 S. Watanabe, T. Arai, H. Sasai, M. Bougauchi and M. Shibasaki, *J. Org. Chem.*, 1998, **63**, 8090.
17 C. L. Elston, R. F. W. Jackson, S. J. F. MacDonald and P. J. Murray, *Angew. Chem., Int. Ed. Engl.*, 1997, **36**, 410.
18 A. Nelson, *Angew. Chem., Int. Ed.*, 1999, **38**, 1583.
19 M. Shi and Y. Masaki, *J. Chem. Res. (S)*, 1994, 250; M. Shi, K. Kazuta, Y. Satoh and Y. Masaki, *Chem. Pharm. Bull.*, 1994, **42**, 2625; J. P. Mazaleyrat, *Tetrahedron Lett.*, 1983, **24**, 1243.
20 R. Helder, J. C. Hummelen, R. W. P. M. Laane, J. S. Wiering and H. Wynberg, *Tetrahedron Lett.*, 1976, 1831; H. Wynberg and B. Greijdanus, *J. Chem. Soc., Chem. Commun.*, 1978, 427; J. C. Hummelen and H. Wynberg, *Tetrahedron Lett.*, 1978, 1089; H. Wynberg and B. Marsman, *J. Org. Chem.*, 1980, **45**, 158; H. Pluim and H. Wynberg, *J. Org. Chem.*, 1980, **45**, 2498.
21 Y. Harigaya, H. Yamaguchi and M. Onda, *Heterocycles*, 1981, **15**, 183.
22 N. Baba, J. Oda and M. Kawaguchi, *Agric. Biol. Chem.*, 1986, **50**, 3113; N. Baba, J. Oda, S. Kawahara and M. Hamada, *Bull. Inst. Chem. Res., Kyoto Univ.*, 1989, **67**, 121.
23 L. Alcaraz, G. Macdonald, J. P. Ragot, N. Lewis and R. J. K. Taylor, *J. Org. Chem.*, 1998, **63**, 3526; G. Macdonald, L. Alcaraz, N. J. Lewis and R. J. K. Taylor, *Tetrahedron Lett.*, 1998, **39**, 5433.
24 B. Lygo and P. G. Wainwright, *Tetrahedron Lett.*, 1998, **39**, 1599; B. Lygo and P. G. Wainwright, *Tetrahedron*, 1999, **55**, 6289.
25 E. J. Corey and F.-Y. Zhang, *Org. Lett.*, 1999, **1**, 1287.
26 S. Arai, H. Tsuge and T. Shioiri, *Tetrahedron Lett.*, 1998, **39**, 7563.

27 S. Arai, M. Oku, M. Miura and T. Shioiri, *Synlett*, 1998, 1201.
28 For recent reviews, see: (*a*) S. Ebrahim and M. Wills, *Tetrahedron: Asymmetry*, 1997, **8**, 3163; (*b*) L. Pu, *Tetrahedron: Asymmetry*, 1998, **9**, 1457; (*c*) M. J. Porter, S. M. Roberts and J. Skidmore, *Bioorg. Med. Chem.*, 1999, **7**, 2145.
29 S. Juliá, J. Masana and J. C. Vega, *Angew. Chem., Int. Ed. Engl.*, 1980, **19**, 929.
30 H. R. Kricheldorf, *α-Aminoacid-N-Carboxy-Anhydrides and Related Heterocycles*, Springer-Verlag, Berlin, 1987; S. Itsuno, M. Sakakura and K. Ito, *J. Org. Chem.*, 1990, **55**, 6047.
31 (*a*) S. Juliá, J. Guixer, J. Masana, J. Rocas, S. Colonna, R. Annuziata and H. Molinari, *J. Chem. Soc., Perkin Trans. 1*, 1982, 1317; (*b*) S. Julia, J. Masana, J. Rocas, S. Colonna, R. Annunziata and H. Molinari, *Anal. Quim.*, 1983, **79**, 102; (*c*) S. Colonna, H. Molinari, S. Banfi, S. Juliá, J. Masana and A. Alvarez, *Tetrahedron*, 1983, **39**, 1635; (*d*) S. Banfi, S. Colonna, H. Molinari, S. Juliá and J. Guixer, *Tetrahedron*, 1984, **40**, 5207.
32 W. Kroutil, M. E. Lasterra-Sánchez, S. J. Maddrell, P. Mayon, P. Morgan, S. M. Roberts, S. R. Thornton, C. J. Todd and M. Tüter, *J. Chem. Soc., Perkin Trans. 1*, 1996, 2837.
33 B. M. Adger, J. V. Barkley, S. Bergeron, M. W. Cappi, B. E. Flowerdew, M. P. Jackson, R. McCague, T. C. Nugent and S. M. Roberts, *J. Chem. Soc., Perkin Trans. 1*, 1997, 3501.
34 M. E. Lasterra-Sánchez, U. Felfer, P. Mayon, S. M. Roberts, S. R. Thornton and C. J. Todd, *J. Chem. Soc., Perkin Trans. 1*, 1995, 343.
35 J. R. Flisak, K. J. Gombatz, M. M. Holmes, A. A. Jarmas, I. Lantos, W. L. Mendelson, V. J. Novack, J. J. Remich and L. Snyder, *J. Org. Chem.*, 1993, **58**, 6247.
36 M. E. Lasterra Sánchez and S. M. Roberts, *J. Chem. Soc., Perkin Trans. 1*, 1995, 1467.
37 J. A. N. Augustyn, B. C. B. Bezuidenhoudt and D. Ferreira, *Tetrahedron*, 1990, **46**, 2651.
38 W. Kroutil, P. Mayon, M. E. Lasterra-Sánchez, S. J. Maddrell, S. M. Roberts, S. R. Thornton, C. J. Todd and M. Tüter, *Chem. Commun.*, 1996, 845.
39 J. R. Falck, R. K. Bhatt, K. M. Reddy and J. H. Ye, *Synlett*, 1997, 481.
40 P. A. Bentley, S. Bergeron, M. W. Cappi, D. E. Hibbs, M. B. Hursthouse, T. C. Nugent, R. Pulido, S. M. Roberts and L. E. Wu, *Chem. Commun.*, 1997, 739.
41 M. S. Cooper, H. Heaney, A. J. Newbold and W. R. Sanderson, *Synlett*, 1990, 533.
42 A. Dhanda, K.-H. Drauz, T. P. Geller and S. M. Roberts, *Chirality*, 2000, in press.
43 J. V. Allen, K.-H. Drauz, R. W. Flood, S. M. Roberts and J. Skidmore, *Tetrahedron Lett.*, 1999, **40**, 5417.
44 J. V. Allen, S. Bergeron, M. J. Griffiths, S. Mukherjee, S. M. Roberts, N. M. Williamson and L. E. Wu, *J. Chem. Soc., Perkin Trans. 1*, 1998, 395.
45 P. C. Ray and S. M. Roberts, *Tetrahedron Lett.*, 1999, **40**, 1779.
46 (*a*) T. Geller and S. M. Roberts, *J. Chem. Soc., Perkin Trans. 1*, 1999, 1397; (*b*) L. Carde, H. Davies, T. P. Geller and S. M. Roberts, *Tetrahedron Lett.*, 1999, **40**, 5421.
47 W.-P. Chen, A. L. Egar, M. B. Hursthouse, K. M. A. Malik, J. E. Mathews and S. M. Roberts, *Tetrahedron Lett.*, 1998, **39**, 8495.
48 J. V. Allen, M. W. Cappi, P. D. Kary, S. M. Roberts, N. M. Williamson and L. E. Wu, *J. Chem. Soc., Perkin Trans. 1*, 1997, 3297.
49 P. A. Bentley and S. M. Roberts, unpublished results.
50 P. A. Bentley, W. Kroutil, J. A. Littlechild and S. M. Roberts, *Chirality*, 1997, **9**, 198.
51 M. W. Cappi, W.-P. Chen, R. W. Flood, Y.-W. Liao, S. M. Roberts, J. Skidmore, J. A. Smith and N. M. Williamson, *Chem. Commun.*, 1998, 1159.
52 P. A. Bentley, M. W. Cappi, R. W. Flood, S. M. Roberts and J. A. Smith, *Tetrahedron Lett.*, 1998, **39**, 9297.
53 (*a*) S. Colonna and A. Manfredi, *Tetrahedron Lett.*, 1986, **27**, 387; (*b*) S. Colonna, A. Manfredi, R. Annunziata and M. Spadoni, *Tetrahedron*, 1987, **43**, 2157; (*c*) S. Colonna, A. Manfredi and M. Spadoni, *Tetrahedron Lett.*, 1987, **28**, 1577; (*d*) S. Colonna, N. Gaggero, A. Manfredi, M. Spadoni, L. Casella, G. Carrea and P. Pasta, *Tetrahedron*, 1988, **44**, 5169.
54 R. Curci, M. Fiorentino and M. R. Serio, *J. Chem. Soc., Chem. Commun.*, 1984, 155.
55 Z. X. Wang and Y. Shi, *J. Org. Chem.*, 1997, **62**, 8622.
56 A. Armstrong and B. R. Hayter, *Chem. Commun.*, 1998, 621.
57 (*a*) E. N. Jacobsen, W. Zhang, A. R. Muci, J. R. Ecker and L. Deng, *J. Am. Chem. Soc.*, 1991, **113**, 7063; (*b*) L. Deng and E. N. Jacobsen, *J. Org. Chem.*, 1992, **57**, 4320; (*c*) E. N. Jacobsen, L. Deng, Y. Furukawa and L. E. Martínez, *Tetrahedron*, 1994, **50**, 4323.
58 A. Lévai, W. Adam, R. T. Fell, R. Gessner, T. Patonay, A. Simon and G. Tóth, *Tetrahedron*, 1998, **54**, 13105.
59 A. Kumar and V. Bhakuni, *Tetrahedron Lett.*, 1996, **37**, 4751.
60 S. Banfi, S. Colonna and S. Juliá, *Synth. Commun.*, 1983, **13**, 1049; S. Colonna, S. Banfi and A. Papagni, *Gazz. Chim. Ital.*, 1985, **115**, 81; S. Colonna, A. Manfredi, R. Annunziata, N. Gaggero and L. Casella, *J. Org. Chem.*, 1990, **55**, 5862.
61 Y. Hu, A. Harada and S. Takahashi, *Synth. Commun.*, 1988, **18**, 1607.
62 H. Sakuraba and Y. Tanaka, *Org. Prep. Proced. Int.*, 1998, **30**, 226.
63 R. J. J. Nel, H. van Rensburg, P. S. van Heerden, J. Coetzee and D. Ferreira, *Tetrahedron*, 1999, **55**, 9727.

ChemComm

Reaction of tris-arylgallium(III) with water: biaryl coupling *versus* Ga–C hydrolysis

Peter J. Nichols, Stavroula Papadopoulos and Colin L. Raston*

Department of Chemistry, Monash University, Clayton, Melbourne, Victoria 3800 Australia

Received (in Columbia, MO, USA) 24th March 2000, Accepted 12th May 2000
Published on the Web 20th June 2000

Reaction of toluene solutions of tris(aryl)gallium(III) compounds with water results in intra-molecular biaryl coupling (70% yield) and an oligomeric organogallium(III) hydroxide/oxide $[Ga_{12}O_{14}H_4(aryl)_{12}]$, whereas reaction in THF with water leads to hydrolysis, formation of arylH, and for aryl = Ph the trimeric THF hydrogen bonded trimer, $[Ph_2Ga(\mu\text{-}OH)]_3\cdot 3THF$.

Recent years have seen major developments in the synthesis and characterisation of galloxane (organogallium(III) oxide) and organogallium(III) hydroxide/oxide compounds.[1–13] Controlled hydrolysis reactions of organogallium(III) compounds, GaR_3, and reactions with excess water lead to the formation of hydroxide or mixed hydroxide/oxide species. These include (a) dimeric species, $[Ga(Mes)_2(\mu\text{-}OH)]_2$, Mes = 1,3,5-trimethylphenyl,[11] and $[Ga_2\{C(SiMe_3)_3\}_2Me_2(OH)(\mu\text{-}OH)(H_2O)]$,[8] (b) trimeric species, $[RR'Ga(\mu\text{-}OH)]_3$, R = R′ = Bu^t,[4,5] = Me,[6] and R = Me, R′ = $C(SiMe_3)_3$,[8] and (c) clusters, $[Ga_6(Mes)_6(\mu_3\text{-}O)_4(\mu_3\text{-}OH)_4]$,[7] $[Ga_{12}Bu^t_{12}(\mu_3\text{-}O)_8(\mu\text{-}O)_2(\mu\text{-}OH)_4]$,[2] and $[Ga_4\{C(SiMe_3)_3\}_4(\mu\text{-}O)_2(\mu\text{-}OH)_4]$.[8] Thermolysis of $[Ga(Mes)_2(\mu\text{-}OH)]_2$ gives $[Ga_9(Mes)_9O_9]$ as a unique, structurally authenticated galloxane.[8]

All of the condensation reactions of GaR_3 with water arise from hydrolysis of one or more of the Ga–C bonds. We now show that treatment of tris-arylgallium(III) compounds, $Ga(aryl)_3$,† in toluene with water results in the formation of C–C bi-aryl coupled compounds and oligomeric arylgallium(III) hydroxide/oxide species. In contrast, treatment of the same compounds with excess water using tetrahydrofuran as a phase transfer reagent leads to Ga–C hydrolysis of one or two aryl groups with only a trace of the bi-aryl coupled compound being formed. These results are summarised in Scheme 1. The formation of bi-aryl coupled compounds has implications in organic synthesis, and is relevant to the actively pursued Suzuki aryl coupling reactions involving boronic acids and esters,[14,15] which require a transition metal catalyst in the presence of oxygen, unlike in the present reactions. Moreover, the reaction of organometallics with water is of interest in the search for environmentally benign synthetic protocols.[16]

For the two phase toluene/water reactions the bi-aryl coupled compounds are isolated from the organic phase, and the gallium(III) hydroxide/oxide cluster compounds are isolated from the aqueous phase. The bi-aryls are formed in yields exceeding 70% (based on two aryl groups being converted to the bi-aryl) with a trace of the expected hydrolysis product, R = H, Me (*o*-, *m*-, *p*-), and *p*-Ph (GC). Conversely the single phase

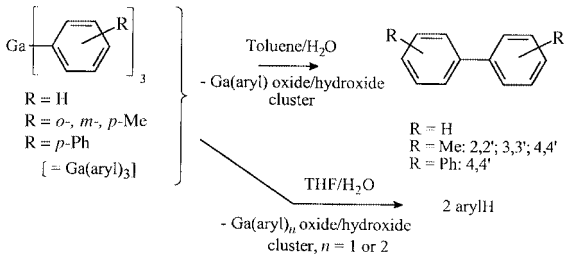

Scheme 1

reaction in THF gives mainly hydrolysis products and a trace of the bi-aryl product.

The metal containing by-products of these reactions were investigated as part of a detailed understanding of the mechanism of the reactions. Mass spectrometry (electrospray: methanol/methylene chloride) of the rapidly formed white micro-crystalline product obtained from the coupling reactions revealed the formation of singly and positively charged clusters of composition $[Ga_{12}O_{14}H_4(aryl)_{12}]$, **1**. The dominance of these

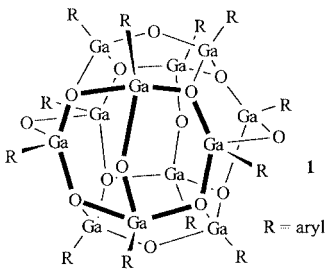

1

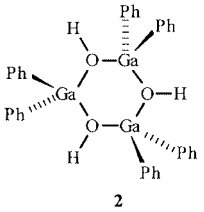

2

ions in the mass spectra shows the stability of the ions, and that the dominant species in solution is a single cluster. The same clusters are also formed in mildly acidic and basic solutions. A likely structure for these clusters is a central polyhedral core of twelve fused six-membered rings, **1**, as found in the structure of $[Ga_{12}Bu^t_{12}(\mu_3\text{-}O)_8(\mu\text{-}O)(\mu\text{-}OH)_4]$,[2] albeit with the position of hydrogen atoms on the bridging hydroxy groups not defined. For the reaction of $GaPh_3$ with water in THF we were able to intercept and isolate some of the intermediate hydrolysis species, trimeric $[Ph_2Ga(\mu\text{-}OH)]_3$, **2**, the final product being **1**. Compound **2** was authenticated using X-ray diffraction data as the hydrogen bonded tris-THF adduct.‡ While bis-alkyl analogues of the trimer are known,[4–6,8] this is the first example of a bis-aryl system. $[Ph_2Ga(\mu\text{-}OH)]_3$ crystallises in the monoclinic space group *C*2/*c*, and consists of diphenylgallium bridged to two other diphenylgallium units *via* two μ-OH bridges with each gallium in a distorted tetrahedral geometry, Fig. 1. THF molecules are H-bonded to the OH bridges with two THF molecules related by a crystallographic C_2 symmetry axis disordered equally over two positions. Phenyl groups are close to being co-planar with an adjacent Ga–O bond and this allows maximum access to the OH groups for hydrogen bonding to THF.

As to the mechanism of the bi-aryl coupling reactions we have established that it is an intra-molecular process since hydrolysis of a mixture of the two compounds, $Ga(aryl)_3$, aryl = Ph or *p*-tolyl, in toluene gave exclusively the symmetrical bi-aryls. This also implies that $Ga(aryl)_3$ species themselves are non-labile and that the synthesis of mixed tris-arylgallium(III) species is possible which would be a route to unsymmetrical bi-aryl compounds on hydrolysis. Competition experiments, bi-aryl coupling *versus* hydrolysis, were investigated for the reaction of $Ga(C_6H_4Ph\text{-}p)_3$ in THF with excess water with increasing amounts of toluene relative to THF. The bi-aryl coupling diminishes dramatically only when the THF concentration is *ca.* 30% in toluene, even for two-phase reactions. Thus the THF plays an important role in initially coordinating to the

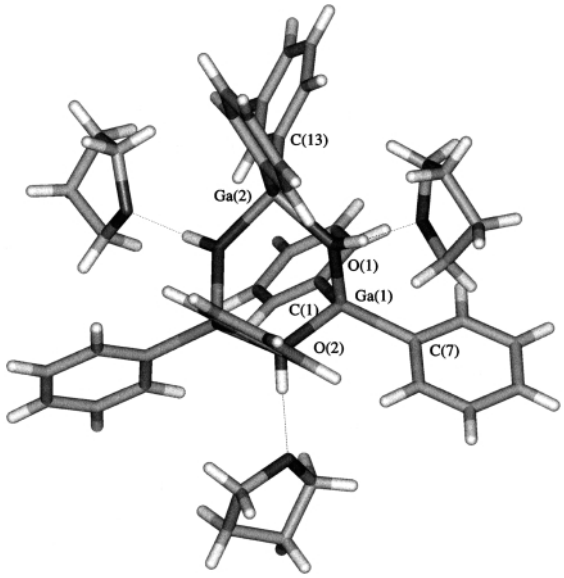

Fig. 1 Molecular structure of $[Ph_2Ga(\mu\text{-}OH)]_3\cdot 3THF$; important bond distances (Å) and angles (degrees): Ga(1)–O(1), 1.908(3); Ga(1)–O(2), 1.916(2); Ga(2)–O(1), 1.911(3); Ga(1)–C(1), 1.993(5); Ga(1)–C(7), 1.977(5); Ga(2)–C(13), 1.962(5); O(1)–Ga(1)–O(2), 97.9; O(1)–Ga(1)–C(7), 111.7; O(1)–Ga(1)–C(1), 110.8(2); C(1)–Ga(1)–C(7), 122.4(2). THF oxygen to hydroxy oxygen distances are 2.64(1) and 2.69(1) Å. (Corresponding $Ga_2OH\cdots O$ 1.71, 1.74 Å).

metal centre and/or hydrogen bonding to a water molecule on the metal centre as found in $[Ga(Mes)_3(OH_2)]\cdot 2THF$[11] and in the structure of **2**. The oxidant in the aryl coupling reactions is water with evolution of one equivalent of hydrogen gas (experimentally determined); note also that controlled experiments excluding oxygen afforded the same products. The hydrolysis reactions are rapid and under these conditions there would be insufficient oxygen delivered to account for the bi-aryl formation. The bi-aryl coupling is likely to proceed through a five coordinate bis-water adduct, $[Ga(aryl)_3(OH_2)]$, at the interface between the water and toluene, leading to a bis-hydroxide, $[Ga(aryl)(OH)_2]$, on elimination of the biphenyl, which then oligomerizes. However a reductive elimination of bi-aryl leading to a Ga(I) species which is then oxidized by water cannot be ruled out. In the presence of THF competition between complexation of THF and water would block such a bi-molecular water process.

Roesky *et al.*[11] have established that the controlled reaction of $[Ga(Mes)_3]$ in THF with water initially gives a four coordinate adduct of water, then a proposed five coordinate bis-adduct, followed by $[Ga(Mes)_2(\mu\text{-}OH)]_2$ then $[Ga_6(Mes)_6(\mu_3\text{-}O)_4(\mu_3\text{-}OH)_4]$, and that the latter compound is formed on reaction of $[Ga(Mes)_3]$ with water in toluene. The lack of aryl coupling here presumably relates to the steric impediment of two bulky aryl groups connecting at the metal centre and/or two water molecules coordinating to the metal centre necessary to effect a bimolecular water process for aryl coupling. Steric hindrance is also noteworthy in giving a smaller cluster, $[Ga_6(Mes)_6(\mu_3\text{-}O)(\mu_3\text{-}OH)_4]$,[7] either as an unstable hexa-tetrahydrofuran solvate[7] or its mono-tetrahydrofuran solvate which was isolated in the present study.§ We note that substitution of one of the *o*-positions of the aryl groups by Me still gives the biaryl, R = Me, Scheme 1. For *o*-OMe and *o*-Ph, however, the amount of coupling is reduced, 40 and 35% respectively. Substitution in both positions (aryl = mesitylene) gives arylH. This is consistent with some steric influence, including the formation of chelate rings in the gallium complex which may shut down the coupling reaction by blocking binding of two water molecules to the metal centre.

It is thus possible to prepare symmetrical bi-aryl compounds from tris-arylgallium(III) species. An inherent problem from the organic synthesis perspective, however, is the loss of one of the aryl groups to the gallium(III) hydroxide/oxide species. This aspect is being addressed along with developing the method for the synthesis of unsymmetrical bi-aryls.

We are grateful to the Australian Research Council for support of this work.

Notes and references

† Compounds $Ga(aryl)_3$, aryl = Ph, *o*-, *m*-, *p*-tolyl, were prepared by reacting the Grignard or lithium reagent of an arylbromide with $GaCl_3$ in diethyl ether (yields 65–80%), and melting points checked with the same compounds prepared from $Hg(aryl)_2$ and gallium metal.[17,18] $Ga(aryl)_3$, aryl = C_6H_4OMe-*o*, C_6H_4Ph-*o* and C_6H_4Ph-*p*, were similarly prepared from their corresponding lithium reagents but were difficult to obtain pure. The hydrolysis reactions involved addition of a $Ga(aryl)_3$ toluene solution at *ca.* 25 °C to excess water followed by stirring for 5 min. The two layers were separated and the respective products isolated; $Ga_{12}O_{10}(OH)_4(aryl)_{12}$, aryl = Ph, C_6H_4Me-*o*, -*m*, -*p*, from the aqueous layer, yields 30–40%, $M/2^+$ and M^+ (FTMS) 995.81, 1990.64, Ph; 1079.7, 2158.8, *o*-tolyl, *m*-tolyl, *p*-tolyl; 1175.6, 2350.7, C_6H_4OMe-*o*; M^+ 1549.0, C_6H_4Ph-*p*, C_6H_4Ph-*o*.

‡ *X-Ray crystallography*. A prismatic crystal of dimensions 0.15 × 0.15 × 0.1 mm was mounted under a stream of argon onto a glass capillary under oil. X-Ray data were collected at 123(1) K on an Enraf-Nonius KappaCCD single crystal diffractometer with Mo-Kα radiation (λ = 0.71073 Å). Data were corrected for Lorentzian and polarisation effects, but not absorption. The structure was solved using Fourier techniques with teXsan and refined by full matrix least-squares on *F* using teXsan: $[Ph_2Ga(\mu\text{-}OH)]_3\cdot 3THF$ $C_{48}H_{57}O_6Ga_3$, M_r = 939.13 g mol^{-1}, monoclinic, *C*2/*c* (no. 15), a = 16.3050(3), b = 17.6498(3), c = 15.9096(2) Å, β = 100.777(1)°, V = 4497.7(1) Å^3, ρ_{calc} = 1.387 g dm^{-3}, μ = 18.30 cm^{-1} (no correction), Z = 4, 33253 reflections were collected (6400 unique), $2\theta_{max}$ = 60.1° (4917 observed, $I > 3\sigma(I)$, R = 0.067, Rw = 0.082). The non-hydrogen atoms were refined anisotropically and hydrogen atoms were included at geometrically estimated positions but not refined. CCDC 182/1643. See http://www.rsc.org/suppdata/cc/b0/b002422h/ for crystallographic files in .cif format.

§ *Crystal structure* of $[Ga_6(Mes)_6(\mu_3\text{-}O)_4(\mu_3\text{-}OH)_4]\cdot THF$, the same cluster being previously authenticated as the hexakis-THF adduct;[7] crystals were obtained from THF: M_r = 1121.37 g mol^{-1}, trigonal $R\bar{3}$ (no. 148), a = 22.5232(2), c = 20.8835(2) Å, V = 9174.7(0.1) Å^3, ρ_{calc} = 1.218 g dm^{-3}, μ = 26.41 cm^{-1} (no correction), Z = 6, 45092 reflections, $2\theta_{max}$ = 60.1° (3576 observed, $I > 3\sigma(I)$, R = 0.061, Rw = 0.060). The THF molecule is disordered over two positions.

1 J. Storre, A. Klemp, H. W. Roesky, R. Fleischer and D. Stalke, *Organometallics*, 1997, **16**, 3074.
2 C. C. Landry, C. J. Harlan, S. G. Bott and A. R. Barron, *Angew. Chem., Int. Ed. Engl.*, 1995, **34**, 1201.
3 A. R. Barron, *Comments Inorg. Chem.*, 1993, **14**, 123.
4 A. A. Naiini, V. Young, Y. Han, M. Akinc and J. G. Verkade, *Inorg. Chem.*, 1993, **32**, 3781.
5 D. A. Atwood, A. H. Cowley, P. R. Harris, R. A. Jones, S. U. Koschmieder, C. M. Nunn, J. L. Atwood and S. G. Bott, *Organometallics*, 1993, **12**, 24.
6 Q. Zhao, H. Sun, W. Chen, C. Duan, Y. Liu, Y. Pan and X. You, *Organometallics*, 1998, **17**, 156; P. D. Croucher, A. Drlijaca, S. Papadopoulos and C. L. Raston, *Chem. Commun.*, 1999, 153.
7 J. Storre, T. Belgardt, D. Stalke and H. W. Roesky, *Angew. Chem., Int. Ed. Engl.*, 1994, **33**, 1244.
8 C. Schnitter, H. W. Roesky, T. Albers, H.-G. Schmidt, C. Ropken, E. Parisini and G. M. Sheldrick, *Chem. Eur. J.*, 1997, **3**, 1783.
9 R. D. Schlueter, H. S. Isom, A. H. Cowley, D. A. Atwood, R. A. Jones, F. Olbrich, S. Corbelin and R. J. Lagow, *Organometallics*, 1994, **13**, 4058.
10 M. B. Power, W. M. Cleaver, A. W. Apblett, A. R. Barron and J. W. Ziller, *Polyhedron*, 1992, **11**, 477.
11 J. Storre, A. Klemp, H. W. Roesky, H.-G. Schmidt, M. Noltemeyer, R. Fleischer and D. Stalke, *J. Am. Chem. Soc.*, 1996, **118**, 1380, and references therein.
12 J. Storre, C. Schnitter, H. W. Roesky, H.-G. Schmidt, M. Noltemeyer, R. Fleischer and D. Stalke, *J. Am. Chem. Soc.*, 1997, **119**, 7505.
13 A. H. Cowley, F. P. Gabbai and D. A. Atwood, *J. Am. Chem. Soc.*, 1994, **116**, 1559.
14 A. Suzuki, *J. Organomet. Chem.*, 1999, **576**, 147, and references therein.
15 D. F. O'Keefe, M. C. Dannock and S. M. Marcuccio, *Tetrahedron Lett.*, 1992, **33**, 6679, and references therein.
16 Y. Yang and T. H. Chan, *J. Am. Chem. Soc.*, 2000, **122**, 402, and references therein.
17 D. A. Atwood, A. H. Cowley and R. A. Jones, *J. Coord. Chem.*, 1992, **26**, 69.
18 J. H. Smith and T. B. Brill, *Inorg. Chem.*, 1977, **16**, 20.

ChemComm

The origin of the 'spike' in the EPR spectrum of C_{60}^-

Parimal Paul,† Robert D. Bolskar,‡ Alex M. Clark and Christopher A. Reed*

Department of Chemistry, University of California, Riverside, California 92521-0403, USA. E-mail: chris.reed@ucr.edu

Received (in Cambridge, UK) 28th April 2000, Accepted 26th May 2000
Published on the Web 20th June 2000

The long-debated origin of the narrow line-width signal in the EPR spectrum of C_{60}^- is shown to be $C_{120}O^-$, arising from unavoidable $C_{120}O$ impurity in air-exposed samples of C_{60}.

A vexing problem in C_{60} chemistry has been the origin of a narrow line-width signal or "spike" superimposed on the broad EPR spectrum of C_{60}^- (Fig. 1). In the nine years since it was first observed, no fewer than six different hypotheses have been forwarded to explain its existence, but none has been confirmed. In a recent comprehensive review of the literature on this subject,[1] we concluded that the most likely explanation lies in $C_{120}O$, a recently discovered, inevitable impurity in air-exposed samples of C_{60}.[2] In this communication, we provide data that confirm this hypothesis.

If $C_{120}O$ impurity is the source of the sharp signal, three experiments of proof suggest themselves. (a) The EPR characteristics of pure $C_{120}O^-$ should match those reported for the narrow line-width signal. (b) Addition of an authentic sample of $C_{120}O$ to a standard sample of C_{60}^- should enhance the sharp signal at precisely the same g value and line width. (c) The preparation of high purity C_{60}, free of detectable $C_{120}O$, should allow a spike-free EPR spectrum of C_{60}^- to be obtained.

A sample of $C_{120}O$ was prepared by literature methods[3] and purified by standard HPLC methods.[2] One-electron reduction to $C_{120}O^-$ was achieved with <1 equiv. of cobaltocene in *o*-dichlorobenzene. As shown in Fig. 2, the EPR spectrum at 100 K is characterized by a sharp signal at $g = 2.0013$ and $\Delta H_{pp} = 1.42$ G (calibrated against DPPH). These parameters closely match those of the major signal observed when a two-electron electrochemical reduction of $C_{120}O$ is carried out in *o*-dichlorobenzene ($g = 2.0016$, $\Delta H_{pp} = 1.1$ G at 77 K).[4] This suggests that $C_{120}O^{2-}$ may be EPR silent (or weak) under these conditions and that the observed sharp signal results from $C_{120}O^-$, present because of the difficulty of carrying out a precise, quantitative two-electron reduction. The temperature dependence of the line width of the $C_{120}O^-$ signal is minimal, decreasing to 1.33 G at 225 K. The variation of signal parameters with solvent is also small. For example, in 2-methyltetrahydrofuran at 100 K, $g = 2.0005$ and $\Delta H_{pp} = 2.0$ G. In tetrahydrofuran at 100 K, the values are $g = 1.9988$ and $\Delta H_{pp} = 2.6$ G. The signal characteristics of $C_{120}O^-$ are clearly compatible with the 'spike' in C_{60}^- where, depending on conditions, g values are reported in the range 1.9995–2.0012 and $\Delta H_{pp} = 0.1$–3.5 G.[5]

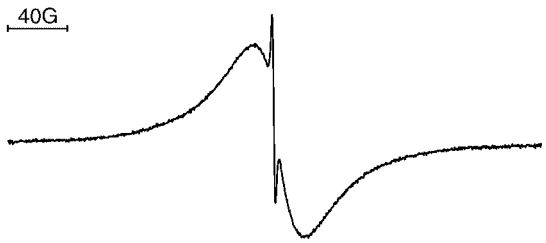

Fig. 1 Typical EPR spectrum of C_{60}^- prepared from off-the-shelf C_{60} showing the broad signal (major) and the sharp signal or 'spike' (minor). Conditions: $[Co(Cp)_2][C_{60}]$ in tetrahydrofuran at 140 K, microwave power 5.7 mW, modulation 5 G.

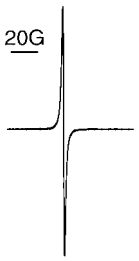

Fig. 2 EPR spectrum of $[Co(Cp)_2][C_{120}O]$ in *o*-dichlorobenzene at 100 K (microwave power 5.7 mW, modulation 1.25 G).

To explore whether this compatibility means identity, small additions of $[Co(Cp)_2^+][C_{120}O^-]$ were made to solutions of $[Co(Cp)_2^+][C_{60}^-]$ to ascertain whether the sharp signal increased relative to the broad signal. As shown in Fig. 3, this is exactly what happens. Moreover, the peak positions are *precisely* those of the spike. Experimental error and reproducibility variances are <0.08 G. The data in Fig. 3 provide

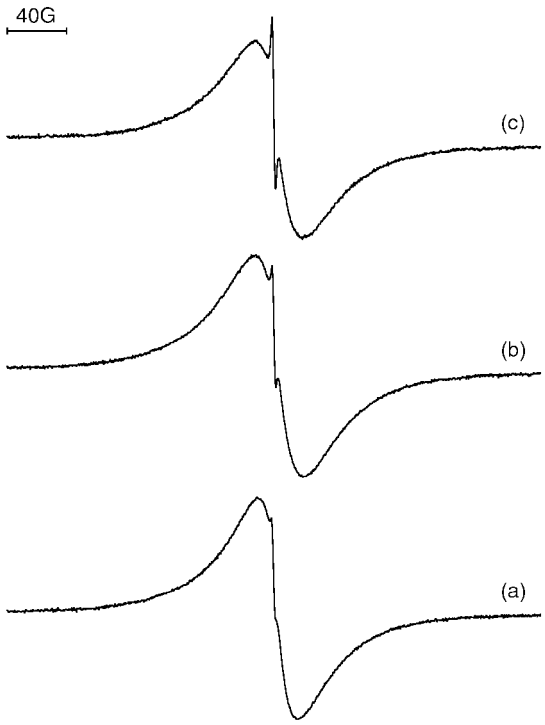

Fig. 3 EPR spectrum of C_{60}^-, prepared by cobaltocene reduction of freshly purified C_{60}, (a) and as a function of increasing increments of added $C_{120}O^-$ (b and c) (conditions same as Fig. 1).

† Visiting Scientist from the Central Salt and Marine Chemicals Research Institute, Bhagnavar, India.
‡ Present address: TDA Research, 12345 West 52nd Ave., Wheat Ridge, Colorado 80033, USA.

DOI: 10.1039/b003428m

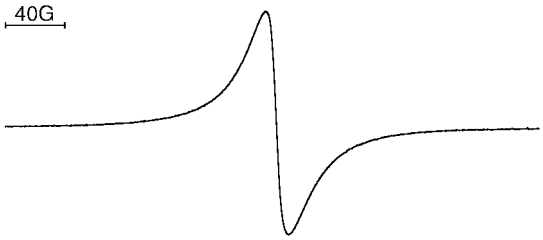

Fig. 4 EPR spectrum of C_{60}^- prepared from twice HPLC-purified C_{60} (conditions same as Fig. 1).

compelling evidence that the spike in C_{60}^- is due to $C_{120}O$ impurity.

Finally, we purified C_{60} by HPLC to try to obtain a spike-free EPR spectrum of C_{60}^-. Purification of C_{60} was carried out using a Cosmosil Buckyprep column with toluene as eluent. Double passage gave C_{60} with essentially undetectable quantities of $C_{120}O$ (monitoring at 330 nm) and a middle cut was collected anaerobically with exclusion of light. As shown in Fig. 4, the EPR spectrum of a cobaltocene-reduced sample of this material gave a spike-free spectrum at 100 K (g = 1.9963, ΔH_{pp} = 16.4 G). Interestingly, however, when we chose measurement conditions which optimized the observation of the sharp signal relative to the broad signal (higher temperatures where the broad signal becomes even broader and the use of the lowest possible microwave powers because the spike saturates more easily than the broad signal), traces of the $C_{120}O^-$ signal could still be detected as shoulders in the inflection region. This is partly a reflection of the extraordinary sensitivity of the EPR technique but it also shows how difficult it is to rid C_{60} entirely of $C_{120}O$. Traces of O_2 convert C_{60} to $C_{120}O$ with extraordinary ease.[2]

In summary, it now appears certain that all air-exposed samples of C_{60} contain $C_{120}O$ and that all EPR work using such samples has been compromised by its presence. It is likely that most (if not all) of the sharp signals observed in the EPR spectra of discrete C_{60}^{n-} fulleride ions (n = 1–4) arise from $C_{120}O^{n-}$ species (n = odd) or decomposition products therefrom. Further studies are in progress to investigate the full extent of the $C_{120}O$ influence in spectra of the more highly charged fulleride anions.

There have been a number of reports of sharp signals increasing significantly at the expense of broad signals upon aging of C_{60}^- salts.[1] We do not find this to be the case with the present samples. The solution of $[Co(Cp)_2][C_{60}]$ that gave rise to Fig. 1 was kept in a torch-sealed quartz EPR tube for several weeks. Its spectrum has remained essentially unchanged, even with exposure to laboratory light. It is likely that release of oxygen from the walls of containers or aerobic leakage are responsible for reports to the contrary. C_{60}^- would be preferentially oxidized (to EPR silent C_{60}) giving the *appearance* of an increase in $C_{120}O^-$ concentration. (The overlay of the two signals, and their very different line-widths, has typically precluded reliable measurements of absolute intensities). In the extreme (*i.e.* room temperature, low reduction levels, low signal-to-noise ratios) the observation of *only* a sharp signal[6,7] can be explained. Even the metal-intercalated fulleride materials such as A_3C_{60} (A = Na, K, *etc.*) are reported to have the sharp signal of an 'impurity phase' superimposed on the broad signal arising from conduction electrons.[8] Perhaps it also arises from $C_{120}O^{n-}$ defects (n = 5 or 7). Indeed, a number of complex explanations for multiple signals in fullerides[9] may have more straightforward interpretations.

We thank the US National Institutes of Health for financial support.

Notes and references

1 C. A. Reed and R. D. Bolskar, *Chem. Rev.*, 2000, **100**, 1075.
2 R. Taylor, M. P. Barrow and T. Drewello, *Chem. Commun.*, 1998, 2497.
3 S. Lebedkin, S. Ballenweg, J. Gross, R. Taylor and W. Kratchmer, *Tetrahedron Lett.*, 1995, **36**, 4971.
4 A. L. Balch, D. A. Costa, W. R. Fawcett and K. Winkler, *J. Phys. Chem.*, 1996, **100**, 4823.
5 S. S. Eaton and G. R. Eaton, *Appl. Magn. Reson.*, 1996, **11**, 155.
6 H. Moriyama, H. Kobayashi, A. Kobayashi and T. Watanabe, *J. Am. Chem. Soc.*, 1993, **115**, 1185.
7 A. Stasko, V. Brezová, S. Biskupic, K.-P. Dinse, P. Schweitzer and M. Baumgarten, *J. Phys. Chem.*, 1995, **99**, 8782.
8 A. Janossy, O. Chauvet, S. Pekker, J. R. Cooper and L. Forro, *Phys. Rev. Lett.*, 1993, **71**, 1091.
9 M. C. B. L. Shohoji, M. L. T. M. B. Franco, M. C. R. L. R. Lazana, S. Nakazawa, K. Sato, D. Shiomi and T. Takui, *J. Am. Chem. Soc.*, 2000, **122**, 2962.

Neutron diffraction study of a very short O–H···N hydrogen bond: crystalline adduct of 2-methylpyridine and pentachlorophenol

Thomas Steiner,*[a] Chick C. Wilson[b] and Irena Majerz*[c]

[a] *Institut für Chemie—Kristallographie, Freie Universität Berlin, Takustraße 6, D-14195 Berlin, Germany. E-mail: steiner@chemie.fu-berlin.de*
[b] *ISIS Facility, CLRC Rutherford Appleton Laboratory, Didcot, Oxon, UK OX11 0QX*
[c] *Institute of Chemistry, University of Wroclaw, 50-383 Wroclaw, Poland*

Received (in Cambridge, UK) 11th February 2000, Accepted 23rd May 2000
Published on the Web 20th June 2000

In the neutron diffraction study of the 1:1 adduct 2-methylpyridine–pentachlorophenol, a very short O–H···N hydrogen bond is found with a sharply defined proton position, and distances of O–H = 1.068(7), H···N = 1.535(7) and O···N = 2.588(3) Å; the bond order of H···N is about 0.24 valence units.

There is great current interest in the strongest types of hydrogen bonds, in particular in the context of chemical reactivity.[1] Whereas strong homonuclear hydrogen bonds O–H···O are today quite well investigated,[2] the experimental material on the very important heteronuclear N–H···O and O–H···N hydrogen bonds is still far from satisfactory. N–H···O and O–H···N hydrogen bonds are in most cases only of moderate strength, but can in some situations also become very strong. An interesting example are adducts of amines and phenols with suitably small values of ΔpK_a [$\Delta pK_a = pK_a(NH^+) - pK_a(OH)$].[3] In a certain 'critical' range of ΔpK_a, the systems can be found in crystals as molecular adducts linked by hydrogen bonds O–H···N, as ionic adducts linked by N^+–H···O^- interactions, or even as an equilibrium between the two.[4] In all these situations, hydrogen bond distances N···O can be < 2.6 Å. Strong intramolecular N–H···O and O–H···N hydrogen bonds have been described for resonance-assisted cases,[5] but they suffer from steric restrictions and have longer H···O separations than the more linear interactions in molecular adducts. Some of the most poorly described properties of strong heteronuclear hydrogen bonds are the distance characteristics at the H-atom, which cannot be deduced from X-ray diffraction data, but require neutron diffraction experiments. For strong O/N–H···N/O hydrogen bonds, not even one neutron diffraction study has been published as yet (for a survey, see ref. 6).

To perform a neutron diffraction study of a strong O–H···N hydrogen bond, we have selected as a model system the adduct of 2-methylpyridine and pentachlorophenol, **1**, which grows crystals of the large size that is required. X-Ray diffraction crystal structures of several related compounds have been published, as found surveyed in ref. 4. Neutron diffraction data on a single crystal of **1** were collected at 30 K at the instrument SXD of the ISIS facility.[7]† In the crystal, a molecular (not an ionic) adduct is formed, as is shown in Fig. 1. The hydrogen bond connecting the molecules has a geometry of O–H = 1.068(7), H···N1′ = 1.535(7), O···N1′ = 2.588(3) Å, O–H···N1′ = 167.5(6)°, and is directed almost ideally at the electron lone-pair of the pyridyl N-atom [H···N1′···C4′ = 172.7(3)°]. This is by far the shortest O-H···N bond for which neutron diffraction data are available. The H(O) atom is a relatively short distance from one of the methyl H-atoms, H···H72′ = 2.33(1) Å; this probably repulsive interaction might be responsible for a significant rotation of the methyl group out of the minimum energy conformation [torsion angle N1′–C2′–C7′–H72′ = 17.8(7)°; note that H and H72′ are displaced in opposite directions from the pyridyl plane, Fig. 1(b)]. Some further parameters of the molecular geometries are given in the legend of Fig. 1.

With very short hydrogen bonds, an important question is how sharply the hydrogen atom is located, and if there possibly is proton disorder. A look at Fig. 1 shows that the mean square displacement of the proton in the hydrogen bond is small, even smaller than those of the protons of the hydrogen atoms bonded to C. Numerically, its mean square displacement U_{eq} is 0.021(1) Å^2 compared to an average U_{eq} = 0.025(1) Å^2 of the C(sp^2)–H and 0.038(2) Å^2 of the methyl protons. This means that the proton in the hydrogen bond is very sharply located. To study the possibility of hydrogen atom disorder, O–H···N ↔ O^-···H–N^+, a hypothetical and partially occupied proton position at the N-atom was included in test refinements (compare the related

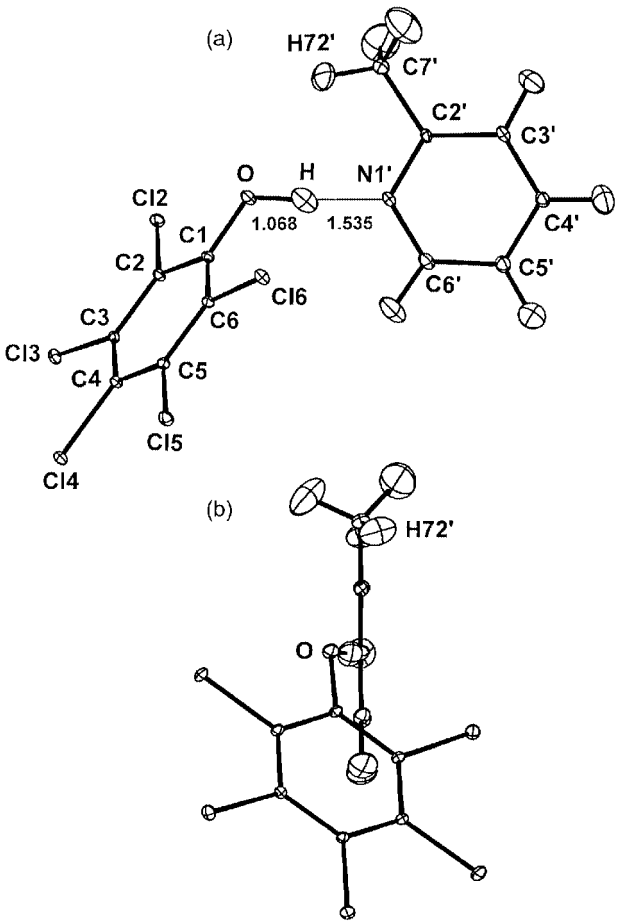

Fig. 1 Structure of **1** at 30 K, displacement ellipsoids are drawn at the 50% probability level. (a) View on the pyridine plane, (b) view perpendicular to the pyridine plane. Relevant geometrical parameters: O–H = 1.068(7), C1–O = 1.317(3) Å, C–O–H = 117.1(5), C2–C1–O–H = −140.3(6)°, N1′–C2′ = 1.338(3), N1′–C6′ = 1.335(4) Å, C2′–N1′–C6′ = 119.2(2)°, H···N1′ = 1.535(7), O···N1′ = 2.588(3) Å, O–H···N1′ = 167.5(6)°, H···Cl6 = 2.728(6), O···Cl6 = 2.963(3) Å, O–H···Cl6 = 91.9(4)°.

DOI: 10.1039/b001179g

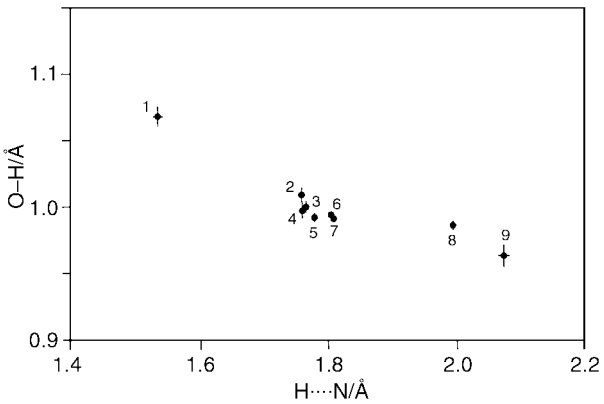

Fig. 2 Plot of O–H against H···N distances in O–H···N hydrogen bonds studied by neutron diffraction. Standard uncertainties are shown as bars, unless they are smaller than the central graphical symbol. **1**: this work. **2**, **3**: 3-aminophenol and 2-aminophenol, respectively.[12a] **4**: 3-amino-1,6-anhydro-3-deoxy-β-D-glucopyranose.[12b] **5**, **8**: adenosine.[12c] **6**: ethanedial dioxime.[12d] **7**: formamide oxime.[12e] **9**: sodium 6-nitrosaccharin tetrahydrate.[12f]

refinement of a disordered hydrogen bond in benzoic acid, ref. 8). In free refinement, the occupancy of the proton at the O-atom remained at 1.0, whereas that of the hypothetical proton at N dropped to −0.02. This means that an ionic adduct, if present in the crystal, at 30 K can only be populated spuriously.

An important general feature of X–H···Y hydrogen bonds is an elongation of the X–H bond compared to free X–H groups. This points at the hydrogen bond being an incipient proton transfer reaction.[9] In Fig. 2, the dependence of the O–H from the H···N distance is shown for all published neutron diffraction data (substances and references given in the Figure legend). The elongation of the O–H bond in **1** exceeds by far that in all previous studies, following trends that are much better studied in homonuclear hydrogen bonds.[9] If bond orders *s* of the O–H and H···N bonds are calculated from the distances using the Pauling approximation with the most recent set of numerical parameters,[6] one obtains $s_{OH} = 0.71$ and $s_{H\cdots N} = 0.24$. The rule of bond order conservation ($s_{OH} + s_{H\cdots N} = 1.0$) is not ideally fulfilled, indicating that the parameters in ref. 6 are only roughly valid for very short hydrogen bonds. Nevertheless, it becomes clear that the bond order of H···N is about ¼ of a valence unit, meaning that the 'incipient proton transfer' characterizing a hydrogen bond has reached already quite an advanced stage in **1**. This gives particular importance to the observation of a sharply located proton with a small vibration amplitude, and disfavours widespread concepts that in very short hydrogen bonds, the proton would oscillate in a potential that is deep but relatively flat at the bottom. Published views that heteronuclear hydrogen bonds cannot be very short (in H···X) by principle are disfavoured too, and it may be assumed that O–H···N hydrogen bonds can be made even shorter by suitably tuning the pK_a values of the donor and/or acceptor molecules.

Notes and references

† *Crystal data*: Single crystals of **1** ($C_6H_7N{\cdot}C_6HCl_5O$, M = 359.47) were obtained by slow evaporation of a CCl_4 solution of pentachlorophenol (Fluka) and an excess of 2-methylpyridine (Merck). A single crystal of dimensions 2.5 × 2 × 1 mm, *V ca.* 5 mm^3, was wrapped in aluminium foil and mounted on the time-of-flight Laue diffractometer SXD of the ISIS spallation neutron source.[7a] Crystals are sensitive to atmosphere of high humidity, requiring swift handling. Diffraction data were collected at 30(1) K, and reduced to 4303 independent structure factors[7b] (wavelength range 0.5–5.0 Å, total of 48 frames with a three weeks interruption after seven frames due to a failure of the source; because of continued cooling only 20% reduction in the sacttering after this delay). Unit cell dimensions at 30 K are a = 9.227(5), b = 11.668(6), c = 6.849(4) Å, α = 104.61(3), β = 105.06(3), γ = 99.87(3)°, U = 666.5(6) Å^3, with space group $P\bar{1}$ (no. 2). The structure was solved by molecular replacement methods,[10a] using the phenol and pyridine moieties in the related crystal structure of 4-methylpyridine–pentachlorophenol[11] as the search fragment. Anisotropic refinement with standard methods[10b] (245 parameters) proceeded smoothly, and converged at an R value of 0.0735 [$wR(F^2)$ = 0.1830].

CCDC 182/1663. See http://www.rsc.org/suppdata/cc/b0/b001179g/ for crystallographic files in .cif format.

1 F. Hibbert and J. Emsley, *Adv. Phys. Org. Chem.*, 1990, **26**, 255; G. A. Jeffrey, *Introduction to Hydrogen Bonding*, Oxford University Press, Oxford, 1997.
2 V. Bertolasi, P. Gilli, V. Ferretti and G. Gilli, *Chem. Eur. J.*, 1996, **2**, 925.
3 Z. Malarski, M. Rospenk, L. Sobczyk and E. Grech, *J. Phys. Chem.*, 1982, **86**, 401.
4 I. Majerz, Z. Malarski and L. Sobczyk, *Chem. Phys. Lett.*, 1997, **274**, 361.
5 V. Bertolasi, P. Gilli, V. Ferretti, G. Gilli and K. Vaughan, *New J. Chem.*, 1999, **23**, 1261; A. Filarowski, A. Koll and T. Glowiak, *Monatsh. Chem.*, 1999, **130**, 1097.
6 T. Steiner, *J. Phys. Chem. A*, 1998, **102**, 7041.
7 (*a*) C. C. Wilson, in *Neutron Scattering Data Analysis*, ed. M. W. Johnson, Adam Hilger, Bristol, 1990, ch. 2; (*b*) C. C. Wilson, *J. Mol. Struct.*, 1997, **405**, 207.
8 C. C. Wilson, N. Shankland and A. J. Florence, *J. Chem. Soc., Faraday Trans.*, 1996, **92**, 5051.
9 H. B. Bürgi and J. D. Dunitz, *Acc. Chem. Res.*, 1983, **16**, 153.
10 (*a*) E. Egert and G. M. Sheldrick, *Acta Crystallogr., Sect. A*, 1985, **41**, 262; (*b*) G. M. Sheldrick, SHELXL97, University of Göttingen, 1997.
11 Z. Malarski, I. Majerz and T. Lis, *J. Mol. Struct.*, 1987, **158**, 369.
12 (*a*) F. H. Allen, V. J. Hoy, J. A. K. Howard, V. R. Thalladi, G. R. Desiraju, C. C. Wilson and G. J. McIntyre, *J. Am. Chem. Soc.*, 1997, **119**, 3477; (*b*) J. H. Noordik and G. A. Jeffrey, *Acta Crystallogr., Sect. B*, 1977, **33**, 403; (*c*) W. T. Klooster, J. R. Ruble, B. M. Craven and R. K. McMullan, *Acta Crystallogr., Sect. B*, 1991, **47**, 376; (*d*) G. A. Jeffrey, J. R. Ruble and J. A. Pople, *Acta Crystallogr., Sect. B*, 1982, **38**, 1975; (*e*) G. A. Jeffrey, J. R. Ruble, R. K. McMullan, D. J. DeFrees and J. A. Pople, *Acta Crystallogr., Sect. B*, 1981, **37**, 1381; (*f*) R. Rudert, J. Buschmann, P. Luger, D. Gregson and G. Trummlitz, *Acta Crystallogr., Sect. C*, 1989, **45**, 1013.

From major to minor and back—a decisive assessment of $C_{60}H_{36}$ with respect to the Birch reduction of C_{60}

Yury Vasil'ev,[a] Darren Wallis,[a] Matthias Nüchter,[b] Bernd Ondruschka,[b] Anatolii Lobach[c] and Thomas Drewello*[a]

[a] *Department of Chemistry, University of Warwick, Coventry, UK CV4 7AL. E-mail: t.drewello@warwick.ac.uk*
[b] *Friedrich-Schiller-Universität Jena, Institut für Technische Chemie und Umweltchemie, Lessingstrasse 12, D-07743 Jena, Germany*
[c] *Institute of Problems of Chemical Physics, Russian Academy of Sciences, 142432 Chernogolovka, Moscow Region, Russia*

Received (in Oxford, UK) 11th May 2000, Accepted 26th May 2000
Published on the Web 20th June 2000

Hydrogenated fullerenes derived from the Birch reduction and from hydrogen transfer reduction of [60]fullerene have been examined by matrix-assisted laser desorption ionization; applying 9-nitroanthracene as the matrix, it has been possible to desorb and ionise the samples with such a low degree of fragmentation as to enable the establishment of the amount of hydrogen bound to the fullerene; in contrast to the currently assumed polyhydrofullerene distribution featuring $C_{60}H_{36}$ only as a minor component, evidence has been obtained which re-establishes $C_{60}H_{36}$ as the major product of the Birch reduction.

The hydrogenation of fullerenes has been achieved by a large variety of synthetic methods including the Birch reduction,[1] transfer hydrogenation,[2] reactions with elemental hydrogen,[3] reduction in metal/acid systems[4] and others.[5] Thirty-six often represents a 'magic number' for the quantity of hydrogen attached to [60]fullerene. According to semiempirical and *ab initio* SCF calculations, the thermodynamically most stable structure of $C_{60}H_{36}$ possesses *T* symmetry.[6] This structure was initially suggested by Taylor[7] and is characterised by four isolated benzenoid rings located at the corners of a tetrahedron. A recent X-ray investigation provides evidence for the existence of the benzenoid rings in $C_{60}H_{36}$.[8] Two isomers in a ratio of 2 : 1 have been found applying ^{3}He NMR[9] and their structures have been proposed to exhibit C_3 and *T* symmetry. The coexistence of the C_3 isomer, which is thermodynamically less stable than the *T* isomer, probably indicates that kinetic factors play an important role in the hydrogenation of C_{60}. It seems reasonable to assume that variations in the way the reduction is achieved can lead to the formation of alternative structures of $C_{60}H_{36}$. It has even been proposed that in the case of the Birch reduction,[1] $C_{60}H_{36}$, which is commonly referred to as the first ever synthesised fullerene derivative, is only a minor product of the obtained distribution of hydrogenated [60]fullerenes of the type $C_{60}H_x$, with *x* ranging from 18 to 36.[10] These conclusions were derived from mass spectrometry-based experiments in which the reaction product resulting from the Birch reduction of C_{60} has been laser-desorbed into the gas phase to be in a second step, subsequently laser-ionised. A distribution of $C_{60}H_x^+$ ions was obtained which was centred at $x = 30$ and 32 with only a minor contribution attributed to $C_{60}H_{36}$. The fact that signals due to C_{60}^+ fragment ions were entirely absent was taken as evidence for the softness of the method revealing the true distribution of the hydrogenated [60]fullerenes. A similar distribution was obtained using liquid secondary ion mass spectrometry (LSIMS) and an almost perfect fit to a theoretical distribution based on Monte Carlo calculation supported the experimental findings. The comparison with other approaches for ionization, especially when electron impact (electron ionization, EI) was used, for which the sample had to be heated to achieve evaporation, revealed a clear shift in the observed $C_{60}H_x^+$ distribution towards $C_{60}H_{36}$. However, since C_{60}^+ was also prominently observed under these conditions, it was concluded that the excitation of the sample resulted in the dissociation of the initial $C_{60}H_x$ species with *x* being centred at around 30 and that the observed ions with a larger hydrogen content represent more stable species which resist dissociation. Interestingly, for the transfer hydrogenation of [60]fullerene by 9,10-dihydroanthracene (DHA), $C_{60}H_{36}$ has been established beyond any doubt as the major product utilising field desorption mass spectrometry.[2] Roger, Birkett and Campbell (RBC) have recently re-examined the hydrogenated product from transfer reduction of C_{60} with DHA by matrix-assisted laser desorption/ionization (MALDI) mass spectrometry.[11] A matrix combination of 5-methoxysalicylic acid and $NaBF_4$ was found to provide the softest conditions, and a spectrum was recorded which consisted almost entirely of only one signal arising from $C_{60}H_{35}^+$, which can be taken as direct evidence for the exclusive production of $C_{60}H_{36}$. The Birch reduction[1] and the hydrogen transfer reduction[2] differ in the actual reaction mechanism. The Birch reduction proceeds *via* anionic intermediates and the transfer reduction most probably involves neutral radicals, so that the findings by RBC[11] are not necessarily in conflict with those obtained by Banks *et al.*[10] In order to reveal whether or not the two reductions lead to different product distributions, we investigated the products derived from both reactions by MALDI time-of-flight mass spectrometry. In line with recently reported experiments by others,[12] our own initial efforts to apply the above mentioned matrix combination were unsuccessful, as the desorption/ionization process was always accompanied by efficient fragmentation. The reason for this has to be seen as due to slightly differing experimental conditions from those reported originally,[11] rather than in a failure of the method as such. RBC pointed out that the wavelength of the laser light, the laser fluence and the pulse duration were of crucial importance.[11] Employing a nitrogen laser of 337 nm wavelength with a variable laser fluence, the most pronounced difference in the present experiments is the pulse duration of 3 ns, which is two orders of magnitude longer and is probably the cause of the enhanced fragmentation. Unexpectedly, a much simpler approach was found to be more suitable for the present study. Using 9-nitroanthracene (9-NA) as the matrix (using a matrix : analyte ratio of 50 : 1) led to conditions which allow conclusive insight. Although there exists no comprehensive screening of matrices for the analysis of fullerene derivatives by MALDI, 9-NA has been used successfully in several earlier investigations involving related compounds.[13–17] The signals obtained at the threshold for ion formation from hydrogenated [60]fullerene, derived by transfer reduction[2] from DHA for which the synthetic details have been published elsewhere,[18] are depicted in Fig. 1(a). The base peak corresponds to $C_{60}H_{35}^+$ in line with the findings reported by RBC[11] and very little fragmentation is observed. The same experiment performed with the sample derived from the Birch reduction[1] gave rise to the spectrum shown in Fig. 1(b), which is almost identical to the

DOI: 10.1039/b003882m

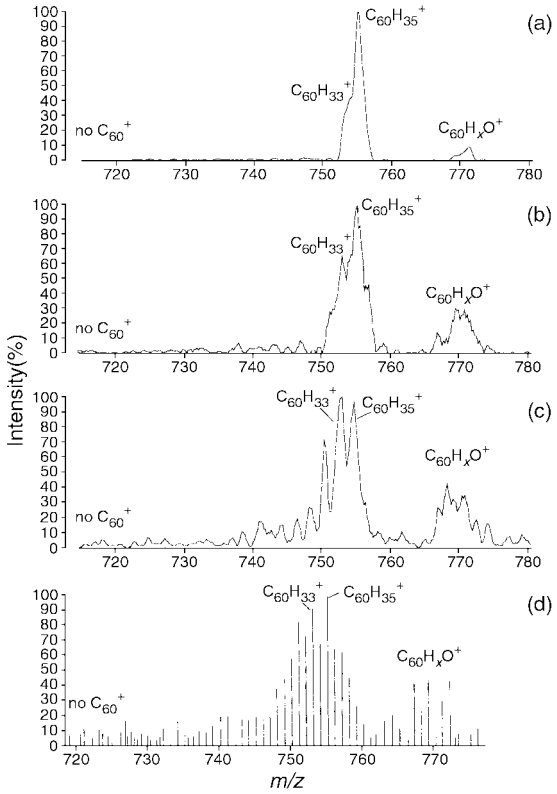

Fig. 1 (a) Threshold positive-ion MALDI mass spectrum of $C_{60}H_{36}$ derived from transfer reduction. (b) Threshold positive-ion MALDI mass spectrum of Birch-reduced C_{60}. (c) Positive-ion MALDI mass spectrum of Birch-reduced C_{60} at slightly higher laser fluence than in (b). (d) Positive-ion liquid secondary ion mass spectrum of Birch-reduced C_{60}.

spectrum in Fig. 1(a). When the laser fluence is only slightly increased, the spectrum depicted in Fig. 1(c) results. Caused by enhanced fragmentation, a clear shift of the ion distribution is observed with $C_{60}H_{33}^+$ now prevailing. Fig. 1(d) shows the liquid secondary ion mass spectrum (LSIMS) of Birch-reduced C_{60} using 3-nitrobenzyl alcohol (3-NBA) as the matrix. With $C_{60}H_{35}^+$ as the major signal and no evident C_{60}^+ peak, LSIMS confirms the MALDI findings. In all spectra, small satellite peaks are observed, arising from oxygenated species. We assume that these are indicative of a partial oxidation of the hydrogenated samples, although we have recently established[19] that oxygen transfer from 9-NA to the analyte can be very pronounced during the desorption/ionization process in MALDI. The observation of these satellite peaks does not affect the interpretation of the present findings, as these species were also observed in the work performed by Banks *et al.*[10] In contrast to the assumption that $C_{60}H_{35}^+$ results under these conditions from protonation of $C_{60}H_{34}$,[10] RCB have provided evidence, that at least in the MALDI experiments, the $C_{60}H_{35}^+$ is directly formed from $C_{60}H_{36}$.[11] A comprehensive MALDI investigation on related, organic ligand-bearing fullerene derivatives confirms that protonation is not important for the ion formation in the present experiments.[19] The observed $C_{60}H_x^+$ ions (with *x* representing an odd number of hydrogen atoms) are thus indicative for the neutral $C_{60}H_{x+1}$ species. In contrast, the close match reported earlier[10] for the experimental distribution and the distribution derived from a Monte Carlo simulation was based on the assumption that the odd numbered $C_{60}H_x^+$ ions would represent $C_{60}H_{x-1}$ neutrals. On the basis of the present experiments it has to be concluded that the earlier experiments suffered from the partial dissociation of $C_{60}H_{36}$. Obviously, conditions were met by which a certain amount of hydrogen was readily evaporated from $C_{60}H_{36}$ without the complete loss of all attached hydrogen atoms, suggesting soft ionization conditions and leading to a distribution of ions which do not represent the neutrals which were initially present. In this context it is interesting to note that, in line with the assumptions made by Banks *et al.*,[10] fragment ions such as C_{60}^+ are primarily the result of neutral dissociation followed by ionization, rather than caused by fragmentation of energised ions. Recent investigations into the dissociation behaviour of size-selected, hydrogenated fullerene ions reveal that cage rupture efficiently competes with hydrogen losses in these cases.[20] This means the direct formation of C_{60}^+ from $C_{60}H_{36}^+$ is unlikely.

In summary, using 9-NA as the chosen matrix for the MALDI analysis of hydrogenated fullerenes creates desorption/ionization conditions which are sufficiently free of fragmentation to allow the establishment of the hydrogen content. These findings re-establish $C_{60}H_{36}$ as the major product derived by Birch reduction of C_{60}.

The work at Warwick was financially supported by The Leverhulme Trust.

Notes and references

1 R. E. Haufler, J. Conceicao, L. P. F. Chibante, Y. Chai, N. E. Byrne, S. Flanagan, M. M. Haley, S. C. O'Brien, C. Pan, Z. Xiao, W. E. Billups, M. A. Ciufolini, R. H. Hauge, J. L. Margrave, L. J. Wilson, R. F. Crul and R. E. Smalley, *J. Phys. Chem.*, 1990, **94**, 8634.

2 C. Rückhardt, M. Gerst, J. Ebenhoch, H.-D. Beckhaus, E. E. B. Campbell, R. Tellgmann, H. Schwarz, T. Weiske and S. Pitter, *Angew. Chem., Int. Ed. Engl.*, 1993, **32**, 584.

3 C. Jin, R. Hettich, R. Compton, D. Joyce, J. Blencoe and T. Burch, *J. Phys. Chem.*, 1994, **98**, 4215.

4 A. D. Darwich, A. K. Abdul-Sada, G. L. Langley, H. W. Kroto, R. Taylor and D. R. M. Walton, *J. Chem. Soc., Perkin Trans. 2*, 1995, 2359.

5 N. F. Gol'dshleger and A. P. Moravskii, *Russ. Chem. Rev.*, 1997, **66**, 323.

6 L. D. Book and G. E. Scuseria, *J. Phys. Chem.*, 1994, **98**, 4283.

7 R. Taylor, *J. Chem. Soc., Perkin Trans. 2*, 1992, 1667.

8 A. V. Okotrub, L. G. Bulusheva, I. P. Asanov, A. S. Lobach and Yu. M. Shulga, *J. Phys. Chem. A*, 1999, **103**, 716.

9 O. V. Boltalina, M. Bühl, A. Khong, M. A. Saunders, J. M. Street and R. Taylor, *J. Chem. Soc., Perkin Trans. 2*, 1999, 1475.

10 M. R. Banks, M. J. Dale, I. Gosney, P. K. G. Hodgson, R. C. K. Jennings, A. C. Jones, J. Lecoultre, P. R. R. Langridge-Smith, J. P. Maier, J. H. Scrivens, M. J. C. Smith, C. J. Smyth, A. T. Taylor, P. Thorburn and A. S. Webster, *J. Chem. Soc., Chem. Commun.*, 1993, 1149.

11 I. Rogner, P. Birkett and E. E. B. Campbell, *Int. J. Mass Spectrom. Ion Processes*, 1996, **156**, 103.

12 L. Zhou, A. A. Tuinman, R. N. Compton and A. S. Lahamer, *Electrochem. Soc. Proc.*, 1998, **98**, 493.

13 A. Gromov, S. Lebedkin, S. Ballenwag, A. G. Avent, R. Taylor and W. Krätschmer, *Chem. Commun.*, 1997, 209.

14 S. G. Penn, D. A. Costa, A. L. Balch and C. B. Lebrilla, *Int. J. Mass Spectrom. Ion Processes*, 1997, **169**, 371.

15 R. Taylor, M. P. Barrow and T. Drewello, *Chem. Commun.*, 1998, 2497.

16 M. P. Barrow, N. J. Tower, R. Taylor and T. Drewello, *Chem. Phys. Lett.*,1998, **293**, 302.

17 M. S. Al-Jafari, M. P. Barrow, R. Taylor and T. Drewello, *Int. J. Mass Spectrom.*, 1999, **184**, L1.

18 A. S. Lobach, A. A. Perov, A. I. Rebrov, O. S. Roshchupkina, V. A. Tkacheva and A. N. Stepanov, *Russ. Chem. Bull.*, 1997, **46**, 641.

19 T. Brown, N. L. Clipston, N. Simjee, H. Hungerbühler and T. Drewello, in preparation.

20 M. Möder, M. Nüchter, B. Ondruschka, G. Czira, K. Vekey, M. P. Barrow and T. Drewello, *Int. J. Mass Spectrom.*, 2000, **195**/**196**, 599.

Dissociation of O_2 on the reduced SnO_2 (110) surface

Ben Slater,*[ab] C. Richard A. Catlow,[a] David E. Williams[b] and A. Marshall Stoneham[c]

[a] *The Davy-Faraday Research Laboratory, The Royal Institution of Great Britain, 21 Albemarle Street, London, UK W1X 4BS. E-mail: ben@ri.ac.uk*
[b] *Department of Chemistry, University College London, 20 Gordon St, London, UK WC1H OAJ*
[c] *Department of Physics and Astronomy, University College London, Gower St, London, UK WC1E 6BT*

Received (in Oxford, UK) 13th March 2000, Accepted 12th May 2000
Published on the Web 20th June 2000

We report evidence from plane-wave (PW) pseudo-potential calculations, which suggests that neutral, molecular oxygen dissociates exothermically at bridging oxygen vacancies on the SnO_2 (110) surface, supporting recent experimental data.

Stannic oxide (SnO_2) is widely used industrially as a selective catalyst in oxidative dehydrogenation and is also a highly tuneable gas sensor, used in the detection of reducing gases. Although a wealth of experimental literature exists on SnO_2 reaction kinetics and profiles,[1,2] speculations on reaction mechanisms are a subject of contention. One such area of debate is the question of how oxygen gas effects the observed, substantial increase in surface conductivity. Of general interest is the need to establish how feasible homolysis of O_2 is at the surface. We have established previously that the adsorption energy of neutral oxygen at the surface is extremely small[3] (< 0.02 eV). Here, we describe a theoretical study to elucidate the thermodynamic viability of the dissociation of O_2 with the reduced (110) SnO_2 surface. On a reduced surface, the bridging oxygen vacancies can facilitate the first step in the Mars and van Krevelen[4] reaction, which underpins its catalytic and sensing properties.

Experiment[1] and previous calculations (including atomistic[5–7] and PW studies[8–10]) have shown the (110) surface to be energetically the most stable surface under ambient conditions. To generate a model for the surface, we first performed a constant pressure relaxation of the bulk unit cell using the VASP[11–13] code. We used an energy cut-off of 495 eV, an ultrasoft pseudo-potential for the Sn and O ions and the Ceperley–Alder expansion for local exchange. The resulting relaxed lattice parameters of $a = b = 4.725$ and $c = 3.180$ Å, are in excellent agreement with the experimentally measured values of 4.737 and 3.186 Å, respectively, and reproduce the experimental c/a ratio of 0.673. We then constructed a cell to describe the (110) surface, containing three cell layers forming a slab, comprising a total of 72 ions. We selected a vacuum width of 5.0 Å having verified complete convergence of the surface energy at 4.51 Å. Upon relaxation of the surface, we obtained a surface energy of 1.19 J m^{-2} in close agreement with previous atomistic[5–7] and PW studies.[8–10]

We verified the quality of the oxygen pseudo-potential by calculating the spin-polarised, relaxed bond length and binding energy for the molecular oxygen triplet. The oxygen bond length of 1.225 Å compares well with the measured value of 1.216 Å.[14] The binding energy (BE) of oxygen is overestimated at 7.0 eV compared with the experimental value of 5.1 eV;[14] this is a generic feature of LDA based methods. Although we would expect gradient corrections to improve the agreement with experiment for the molecular binding energy, we in fact obtained considerably poorer lattice constants for SnO_2 using GGA pseudo-potentials. Therefore, for methodological consistency, we have used LDA pseudo-potentials throughout.

Fig. 1 shows a schematic of the dissociation process. Light spheres indicate oxygen, dark spheres represent tin and black spheres signify dissociated oxygen. Site A is a bridging oxygen, whilst Site B is a five coordinate tin site and C is the oxygen vacancy. The first step in this process is the formation of a bridging oxygen vacancy; the second is the dissociation of oxygen at the vacancy with encapsulation of an oxygen atom in the vacancy, and the adsorption of the monoatom at a neighbouring five-fold Sn site.

Table 1 summarises the total energy of formation for the configurations calculated using an identical cell geometry.

The energy of dissociation can be expressed as the difference between the undissociated and dissociated surfaces, where the initial configuration is simply one where oxygen is non-interacting with the defective surface, *i.e.* the energy of the isolated oxygen molecule plus the energy of the defect-containing surface. Thus, the dissociation of oxygen is exothermic, releasing a net energy of 0.59 eV. In considering the equilibrium between molecular and atomised oxygen, we note that the energy of adsorption of the monoatom to the five-fold Sn site is −1.25 eV, whilst the vacancy formation energy is +2.84 eV. (We have assumed the vacating oxygen atom combines with another gaseous oxygen monoatom to form paramagnetic molecular oxygen). The monoatom is adsorbed 2.02 Å above the five-fold tin site, and its spin is reduced to a singlet.

Using these calculations, we can consider the end-points of dissociation for two other reactions; first that where oxygen dissociates to occupy two adjacent bridging oxygen vacancies

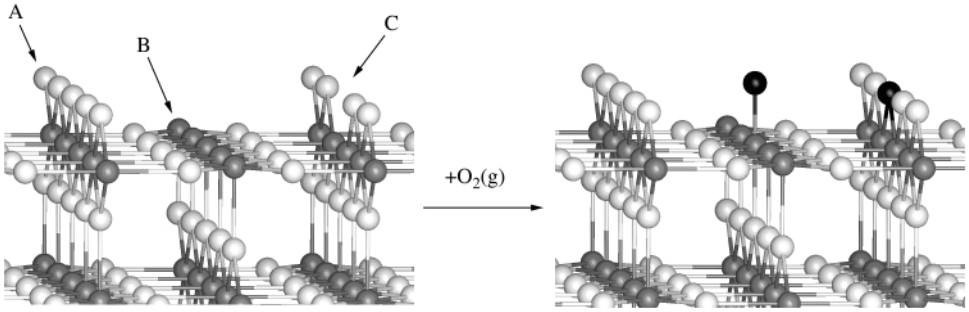

Fig. 1 Schematic oxygen dissociation process. The darker atoms in the final state come from the O_2 molecule: one atom fills the O vacancy (C), and the other is adsorbed on the five-coordinated Sn site (B).

DOI: 10.1039/b002039g

Table 1 Total energies of formation

Configuration	Energy/eV
SnO_2 perfect surface	−496.388
SnO_2 with bridging defect	−488.386
O_2 molecule	−10.332
O atom	−1.678
SnO_2 with bridging defect + dissociated O_2	−499.312

(A) and secondly, where two adjacent adatoms are formed (B) and compare with the main study here, where one bridging vacancy is occupied and one adatom is formed (C). Reactions A and C are exothermic; −5.68 and −0.59 eV, respectively, whereas reaction B is endothermic, +4.48 eV. Therefore, in the absence of specific activation barrier heights, we would expect reaction A to proceed more quickly than C and that reaction B will not occur at low temperatures.

The fact that the dissociation process is predicted to be exothermic for reaction C is our fundamental result, since this strongly supports the proposition that oxygen dissociates at bridging oxygen vacancies, filling the vacancy and producing an oxygen adatom. This evidence corroborates the recent postulate of Henderson and coworkers[15] who reported TPD (temperature programmed desorption) measurements with isotopically labelled oxygen. The authors suggested that below 600 K, oxygen on TiO_2 dissociates at bridging oxygen vacancy sites to fill oxygen vacancies and form adsorbed oxygen monoatoms at adjacent in-plane titanium sites on the TiO_2 (110) surface, a surface which is isostructural with the SnO_2 surface considered here. In addition, we have shown how two reactions (A and C) are concerted first steps in the generalised Mars and van Krevelen oxidative process.

We are grateful to EPSRC for providing time on the T3E facility at Manchester.

Notes and references

1 V. E. Henrich and P. A. Cox, *The Surface Science of Metal Oxides*, Cambridge University Press, Cambridge, 1994.
2 D. E. Williams, in *Solid State Gas Sensing*, ed. P. T. Moseley and B. C. Tofield, Adam Hilger, Bristol, 1987.
3 C. R. A. Catlow, C. M. Barker, R. G. Bell, S. T. Bromley, D. S. Coombes, F. Cora, S. French, B. Slater, A. A. Sokol, L. Whitmore and S. M. Woodley, NATO ASI Series, Kluwer Academic Press, in press.
4 P. Mars and D. W. van Krevelen, *Chem. Eng. Sci.*, 1954, **41**, 3.
5 B. Slater, D. H. Gay, C. R. A. Catlow, V. Dusastre and D. E. Williams, *J. Phys. Chem. B*, 1999, **103**, 10 644.
6 P. A. Mulheran and J. H. Harding, *Modelling. Mater. Sci. Eng.*, 1992, **1**, 39.
7 R. I. Hines, N. L. Allan and W. R. Flavell, *J. Chem. Soc. Faraday Trans.*, 1996, **92**, 2057.
8 I. Manassidis, J. Goniakowski, L. N. Kantorovich and M. J. Gillan, *Surf. Sci.*, 1995, **339**, 258.
9 J. Goniakowski and M. J. Gillan, *Surf. Sci.*, 1996, **350**, 145.
10 J. Goniakowski, J. M. Holender, L. N. Kantorovich, M. J. Gillan and J. A. White, *Phys. Rev. B*, 1996, **53**, 957.
11 G. Kresse and J. Hafner, *Phys. Rev. B*, 1993, **48**, 13115.
12 G. Kresse and J. Furthmüller, *Comput. Mater. Sci.*, 1996, **6**, 15.
13 G. Kresse and J. Furthmüller, *Phys. Rev. B*, 1996, **54**, 11169
14 K. P. Huber and G. Herzberg, *Constants of Diatomic Molecules*, Van Nostrand Reinhold, New York, 1979.
15 W. S. Epling, C. H. F. Peden, M. A. Henderson and U. Diebold, *Surf. Sci.*, 1998, **412/413**, 333.

ChemComm

Copper(I) mediated living radical polymerisation in an ionic liquid

Adrian J. Carmichael,[a] David M. Haddleton,*[a] Stefan A. F. Bon[a] and Kenneth R. Seddon[b]

[a] *Department of Chemistry, University of Warwick, Coventry, UK CV4 7AL. E-mail: D.M.Haddleton@warwick.ac.uk*
[b] *The QUILL Centre, The Queen's University of Belfast, Stranmillis Road, Belfast, UK BT9 5AG*

Received (in Cambridge, UK) 26th April 2000, Accepted 31st May 2000
Published on the Web 20th June 2000

1-Butyl-3-methylimidazolium hexafluorophosphate, a room temperature ionic liquid, has been used as solvent for the copper(I) mediated living radical polymerisation of methyl methacrylate; the rate of reaction is enhanced and narrow polydispersity polymers are obtained which are easily isolated from the catalyst.

Transition metal mediated living radical polymerisation is rapidly developing as an efficacious new route for the controlled polymerisation of vinyl monomers.[1–3] We have been utilising a system based on $Cu^{I}X$ with alkylpyridylmethanimine ligands.[4,5] These Schiff base ligands are easily synthesised, and can be readily manipulated in order to vary the properties of the catalyst (*e.g.* solubility). One of the main constraints of this chemistry is the high level of catalyst required for acceptable rates of polymerisation, often equimolar with respect to initiator. This leads to contamination of products necessitating catalyst removal. Although this is relatively easily achieved in a laboratory, for most polymers, it would be advantageous for this extra process to be eliminated, especially with regards to exploitation of the technology. In order to achieve this we have been examining a number of routes including the use of solid supported catalysts[6,7] and fluorous biphasic conditions.[8]

Room temperature ionic liquids have been found to be excellent solvents for a number of chemical reactions, *e.g.* hydrogenation, alkylation, Diels–Alder reactions, *etc.*[9,10] However, the only polymerisation reactions reported in ionic liquids, to date, are the Ziegler–Natta polymerisation of ethylene,[11] the oligomerisation of butene[12] and the formation of conducting films by the electropolymerisation of arenes.[13] All of which have been carried out in water sensitive chloroaluminate(III) ionic liquids.

Imidazolium ionic liquids have been developed as air and water-stable reaction media which are tolerant to many functional groups.[14] This permits the use of a wide range of monomers in polymerisation reactions. As such it offers an excellent alternative method to address the problems of transition metal mediated living polymerisation. We have used the room temperature ionic liquid, 1-butyl-3-methylimidazolium hexafluorophosphate, [bmim][PF_6],[15] as a solvent for the Cu^{I} catalysed living radical polymerisation of methyl methacrylate (MMA). Our initial findings are reported which represent the first example of an ionic liquid being used for living radical polymerisation and indeed the first example of a new generation non-hygroscopic ionic liquid used as a polymerisation medium.

The addition of *N*-propyl-2-pyridylmethanimine to a deoxygenated suspension of $Cu^{I}Br$ in [bmim][PF_6] in a 1:1 molar ratio results in the formation of a dark brown homogenous solution at room temperature. Mixtures in toluene, the more normal solvent, only become homogeneous at, or near, reaction temperature (typically 90 °C). Polymerisation of MMA, with ethyl-2-bromoisobutyrate, as initiator, in this solution proceeds readily, reaching 87% conversion after 90 min at 70 °C (Table 1).† This is a fast reaction when compared to polymerisation in non-polar solvents. The increase in rate is manifested by a broadening of the polydispersity to 1.43, ascribed to free radical–free radical termination reactions. A similar increase in the rate has been observed with other polar/co-ordinating solvents, including water[16] and is thought to be due to co-ordination of the solvent to Cu^{I}. This is highly likely in the present case where only one equivalent of *N*-propyl-2-pyridylmethanimine with respect to copper is used precluding the exclusive presence of tetrahedral L_2Cu species. These observations led us to lower the reaction temperature, in an attempt to avoid excessive premature termination. Polymerisation proceeds efficiently at 50 and 30 °C reaching 45% conversion after 180 min at 30 °C.

Table 1 Final molecular mass and conversion data for PMMA synthesised in this work

Reaction[a]	Temperature/°C	Time/min	Conversion (%)[b]	M_n[c]	PDI[c]	k_p[pol*] × 10^4/s^{-1} [d]
1[e]	70	90	87	6440	1.43	5.67
2[e]	50	90	89	7390	1.41	4.13
3[e]	30	180	45	6420	1.30	0.56
4[f]	30	150	69	8390	1.36	1.36
5[g]	30	300	90	15 500	1.35	1.33

[a] All reactions carried were 50% v/v MMA in [bmim][PF_6]. [b] Conversion from integration of ^{1}H NMR. [c] Determined using SEC against pMMA standards. [d] From slope of first order kinetic plot. [MMA]–[$Cu^{I}Br$]–[Ligand]–[Initiator]: [e] = 50:1:1:1; [f] = 50:1:2:1; [g] 100:1:2:1.

Increasing the ratio of *N*-propyl-2-pyridylmethanimine to Cu^{I} to 2:1 (entries 4 and 5, Table 1) results in the rate of polymerisation approximately doubling indicating the reaction is approximately first order in ligand over this range. All reactions at 30 °C show very good first-order kinetic behaviour (Fig. 1) indicating a low amount of termination under these conditions. This taken together with the relatively low PDI values and low M_n of the products indicates that the polymerisation shows living characteristics as observed in more conventional organic solvents. When the [M]/[I] was doubled from 50 to 100 (reactions 4 and 5) an approximate doubling of the M_n is observed, as would be expected for a living polymerisation. Fig. 2 shows the evolution of the M_n as a function of conversion for reaction 4, which increases linearly again as would be expected for living polymerisation. Polymer produced at early stages in the reaction is of higher mass than

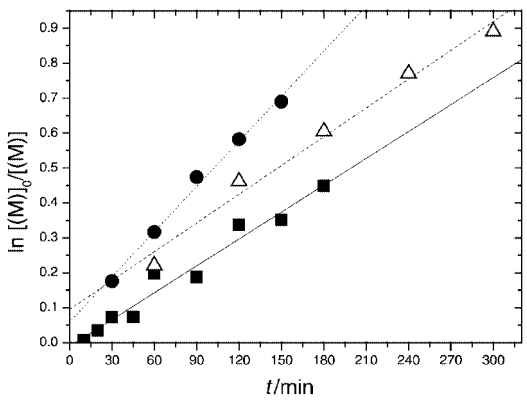

Fig. 1 First order rate plots for the polymerisation of MMA in [bmim][PF_6] at 30 °C. (■) reaction 3, (●) reaction 4 and (▲) reaction 5.

DOI: 10.1039/b003335i

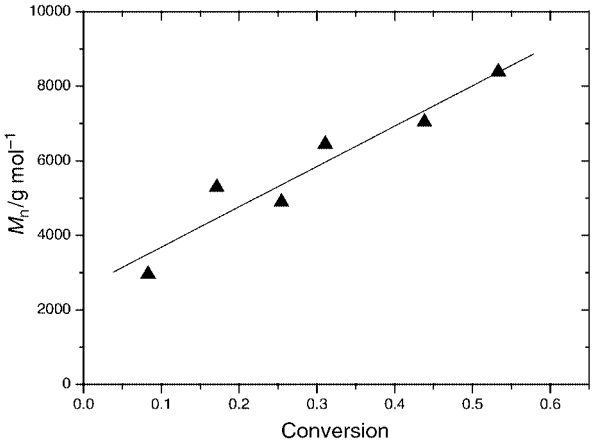

Fig. 2 Evolution of molar mass with conversion for reaction 4, line drawn is the linear regression fit through the data.

would be predicted which is ascribed to radical–radical coupling which occurs efficiently with low mass species as is often observed with living radical polymerisation.[5]

The Cu^{I} catalyst is very soluble in [bmim][PF_6], which in turn is immiscible with organic solvents, such as toluene. This allows the reaction solution to be washed with toluene so as to extract the poly(methyl methacrylate) (PMMA) product. The catalyst remains in the ionic liquid layer allowing isolation of the polymer product whilst leaving the catalyst solution for potential re-use. Analysis of the PMMA (reaction 4) for residual copper by ICP, shows a copper content of 3.4×10^{-3}% (2% expected if no copper is removed).

In summary, the room temperature ionic liquid [bmim][PF_6] has been demonstrated to be an excellent solvent for Cu^{I}–*N*-propyl-2-pyridylmethanimine mediated living radical polymerisation of MMA. Reactions are relatively fast as has been observed for other polar/co-ordinating solvents. The polymer is recovered essentially copper free by a simple solvent wash. Optimisation of this process and the potential to recycle the recovered ionic liquid–catalyst mixture are currently in progress.

Notes and references

† In a typical polymerisation reaction [bmim][PF_6] (10 cm^3) and Cu^{I}Br (0.142 g, 0.990 mmol) were placed in a Schlenk tube and degassed by pumping *in vacuo* for 30 min. MMA (5.34 cm^3, 49.9 mmol) was added and the mixture freeze–pump–thawed three times. *N*-Propyl-2-pyridylmethanimine ligand (0.309 cm^3, 1.98 mmol) was added to give a brown solution and a final freeze–pump–thaw cycle carried out. The Schlenk tube was immersed in a thermostated oil bath at 30 °C. When the contents stabilised at the reaction temperature, ethyl-2-bromoisobutyrate (0.146 cm^3, 0.995 mmol) was added *via* a degassed syringe. The polymerisation was sampled at suitable time periods throughout the reaction. Polymer for SEC analysis was obtained by an extraction of the reaction mixture with toluene followed by removal of the toluene *in vacuo*. Copper content of extracted polymer was obtained by ICP analysis at Warwick.

1 J. S. Wang and K. Matyjaszewski, *J. Am. Chem. Soc.*, 1995, **117**, 5614.
2 T. E. Patten and K. Matyjaszewski, *Acc. Chem. Res.*, 1999, **32**, 895.
3 M. Kato, M. Kamigaito, M. Sawamoto and T. Higashimura, *Macromolecules*, 1995, **28**, 1721.
4 D. M. Haddleton, C. B. Jasieczek, M. J. Hannon and A. J. Shooter, *Macromolecules*, 1997, **30**, 2190.
5 D. M. Haddleton, M. C. Crossman, B. H. Dana, D. J. Duncalf, A. M. Heming, D. Kukulj and A. J. Shooter, *Macromolecules*, 1999, **32**, 2110.
6 D. M. Haddleton, D. Kukulj and A. P. Radigue, *Chem. Commun.*, 1999, 99.
7 D. M. Haddleton, D. J. Duncalf, D. Kukulj and A. P. Radigue, *Macromolecules*, 1999, **32**, 4769.
8 D. M. Haddleton, S. G. Jackson and S. A. F. Bon, *J. Am. Chem. Soc.*, 2000, **122**, 1542.
9 M. J. Earle, P. B. McCormac and K. R. Seddon, *Chem. Commun.*, 1998, 2245.
10 M. J. Earle, P. B. McCormac and K. R. Seddon, *Green Chem.*, 1999, **1**, 23.
11 R. T. Carlin and J. S. Wilkes, *J. Mol. Catal.*, 1990, **63**, 125.
12 A. A. K. Abdul-Sada, P. W. Ambler, P. K. G. Hodgson, K. R. Seddon and N. J. Stewart, *World Patent*, 1995, WO 95/21871.
13 V. M. Kobryanskii and S. A. Arnautov, *J. Chem. Soc., Chem. Commun.*, 1992, 727.
14 J. S. Wilkes, J. A. Levisky, R. A. Wilson and C. L. Hussy, *Inorg. Chem.*, 1982, **21**, 1263.
15 J. G. Huddleston, H. D. Willauer, R. P. Swatloski, A. E. Visser and R. D. Rogers, *Chem. Commun.*, 1998, 1765.
16 E. J. Ashford, V. Naldi, R. O'Dell, N. C. Billingham and S. P. Armes, *Chem. Commun.*, 1999, 1285.

Highly active water-soluble palladium catalyst for the regioselective carbonylation of vinyl aromatics to 2-arylpropionic acids

S. Jayasree, A. Seayad and R. V. Chaudhari*

Homogeneous Catalysis Division, National Chemical Laboratory, Pune-411 008, India. E-mail: rvc@ems.ncl.res.in

Received (in Cambridge, UK) 12th April 2000, Accepted 30th May 2000
Published on the Web 20th June 2000

A novel water-soluble Pd complex containing pyridine carboxylate and TPPTS as ligands is a highly active catalyst for the carbonylation of vinyl aromatics under biphasic conditions and provides high regioselectivity to 2-arylpropionic acids.

Biphasic catalytic reactions using water-soluble transition metal complexes are of much current interest since they provide the unique advantages of homogeneous catalysis as well as facilitating the easy separation of the catalyst from the products.[1] While biphasic hydroformylation of olefins using water-soluble Rh catalysts has been practiced industrially,[2] the biphasic hydrocarboxylation of olefins is still at an exploratory stage, mainly due to the low catalytic activity and selectivity offered by most of the catalyst systems studied so far. An important application of hydrocarboxylation is in the synthesis of 2-arylpropionic acids, a class of non-steroidal anti-inflammatory agents, from the corresponding vinyl aromatic compounds[3] or aryl ethanols.[4] Biphasic carbonylation using *in situ* prepared $Pd(TPPTS)_3$ catalyst along with acidic promoters provided only very low catalytic activity (TOF = 1.5–50 h^{-1}) and 2-arylpropionic acid selectivity (50–70%) under mild reaction conditions of 60–120 °C and 40–60 bar.[5] A maximum regioselectivity of 90.2% was reported at higher CO pressure (140 bar), but with very low catalytic activity (TOF = 5 h^{-1}).[5a] Cationic water-soluble Pd complexes containing bidentate diphosphine 2,7-bis(SO_3Na)-Xantphos was reported recently to catalyse the hydrocarboxylation of olefins, which also provided low catalytic activity (TOF = 5 h^{-1}) and 2-arylpropionic acid (35%) selectivity.[6] Here we report for the first time a novel water-soluble Pd catalyst system for the biphasic carbonylation of vinyl aromatic compounds, which provides significantly improved turnovers and 2-arylpropionic acid regioselectivity.

Recently, we have reported a novel Pd^{II} complex containing pyridine carboxylate, PPh_3 and TsO^- ligands (**I**), which was found to be an efficient carbonylation catalyst under homogeneous conditions.[7] Here, we demonstrate that a novel water-soluble Pd catalyst prepared† by exchanging the PPh_3 ligand of complex **I** with TPPTS [tris(*m*-sulfophenyl)phosphine trisodium salt] (Scheme 1), is a highly active catalyst for the carbonylation of vinyl aromatics under biphasic conditions (Scheme 2). For instance, in the case of carbonylation of styrene, high catalytic activities (TOF) up to 550 h^{-1} (*ca.*10 times higher than the previously reported catalyst systems) were achieved with high regioselectivity to $CH_3CHPhCO_2H$ (up to 95%) at lower CO pressure (54 bar). The catalyst system $PdCl_2$–4TPPTS gave only a very low reaction rate (TOF = 34 h^{-1}) and $CH_3CHPhCO_2H$ selectivity (41%) under the present set of conditions. In a typical carbonylation experiment,‡ the aqueous catalyst, LiCl, TsOH and the substrate dissolved in toluene were charged to a stirred pressure reactor and the reaction was carried out at 54 bar of CO partial pressure at 115 °C under 1100 rpm for a specified time. The reaction mixture was analyzed by GC§ and the products were confirmed by GC-MS and NMR.

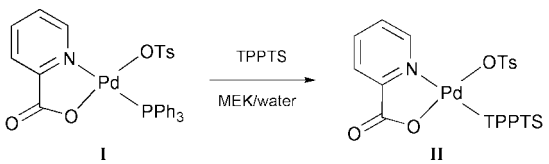

I II

Scheme 1 Synthesis of water-soluble Pd complex **II**.

An attempt was made to characterize the water-soluble Pd complex formed after the exchange of PPh_3 with TPPTS, by isolation from H_2O by precipitation using EtOHl.¶ The pale yellow complex obtained was stable in the solid state and in solution under Ar but its aqueous solution gradually decomposed to a red solution within 2–3 days on exposure to air. IR of the isolated complex showed C=O stretching vibrations at 1636 cm^{-1} and Pd–N vibrations at 524 cm^{-1}. ^{31}P NMR in D_2O showed a strong signal at 35.31 ppm and a weak signal at 36.13 ppm, which may be due to the *trans* (N *trans* to TPPTS) and *cis* (N *cis* to TPPTS) isomers respectively. ^1H NMR and elemental analysis were consistent with the structure of **II** given in Scheme 1.‖

The typical results of carbonylation of styrene are presented in Table 1. The best catalytic activity and selectivity was achieved with 2 equiv. of TPPTS to Pd, unlike the classical $PdCl_2$–TPPTS system where 4–6 equiv. TPPTS to Pd were required to obtain the highest catalytic activity. Further increase in TPPTS concentration lowered the catalytic activity as well as the $CH_3CHPhCO_2H$ selectivity significantly.

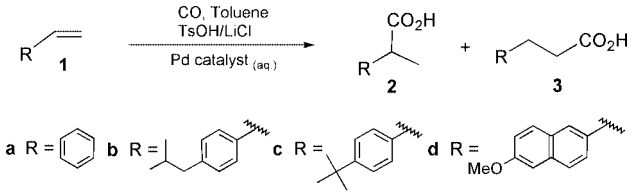

Scheme 2 Carbonylation of vinyl aromatics to 2-arylpropionic acids.

Table 1 Biphasic carbonylation of vinyl aromatics using the novel water-soluble Pd catalyst[a]

Run	Substrate	Time/h	Conversion (%)	TOF/h^{-1}	Selectivity[b] (%) 2	3
1[c]	1a	1.42	94.5	302	92	7.2
2	1a	1.5	93	282	90.7	8.7
3[d]	1a	4	78	89	45	54.6
4[e]	1a	1.42	93	100	88	11.8
5[f]	1a	1.5	91	550	95	4
6[f,g]	1a	4	30	34	41.2	58
7[h]	1a	2.5	76.5	139	76.5	23
8[i]	1a	3.5	78	102	41	59
9[f]	1b	5	81	147	98	1.5
10[f]	1c	3	90	273	96.6	2.8
11[j]	1d	12	45.5	10	93	6.5
12	4b	5	20	18	98	2

[a] *Conditions:* Pd (0.0629 mmol), TPPTS/Pd = 3, substrate (28.8 mmol), TsOH (11.2 mmol), LiCl (11.2 mmol), H_2O (6 ml), toluene (15.5 ml), P_{CO} (54 bar), *T* (388 K). [b] Traces of bis(α-methylbenzyl) ether was also detected. [c] TPPTS/Pd = 2. [d] TPPTS/Pd = 6. [e] Substrate (9.62 mmol). [f] Substrate (57.7 mmol). [g] Catalyst = $PdCl_2$–4TPPTS. [h] HCl instead of TsOH–LiCl. [i] In the absence of LiCl. [j] Substrate (16.67 mmol).

DOI: 10.1039/b002940o

Reaction rates were highly dependent on substrate concentration as well as promoters. The TOF increased steadily with styrene concentration of up to 32% (57.7 mmol), presumably due to the increase in concentration of styrene in the aqueous catalytic phase in equilibrium with organic phase. The concentration of promoters (TsOH–LiCl) also showed a significant effect on the reaction rates; at lower concentrations the TOF and yields being extremely low. In the absence of LiCl the catalytic activity and selectivity decreased considerably (see run 8, Table 1), suggesting a possible role of LiCl in the formation of phenylethyl chloride as the active carbonylation substrate. The formation of phenylethyl chloride was also confirmed by the analysis of intermediate organic phase samples. In addition, a small amount of phenylethyl alcohol was also detected in the intermediate samples, which may form by the acid catalyzed reversible hydration of the olefin. However, in the final reaction mixture only negligible amounts of the alcohol were detected.

Substituted vinyl aromatic compounds such as 4-isobutylstyrene (TOF = 147 h^{-1}), and 4-*tert*-butylstyrene (TOF = 273 h^{-1}) also gave good reaction rates though comparatively lower than that of styrene. 4-Isobutylstyrene gave high Ibuprofen selectivity of 98% while 6-methoxy-2-vinylnaphthalene gave 93% selectivity to Naproxen under these conditions (TOF = 10 h^{-1}). Since secondary arylethanols can be dehydrated to vinyl aromatic compounds under acidic reaction conditions, carbonylation of 1-(4-isobutylphenyl)ethanol (*p*-IBPE)[8] (**4b**) was also studied. TOF up to 18 h^{-1} was achieved with an Ibuprofen selectivity of 98%. Such a lower rate is expected considering the sluggish dehydration of IBPE to 4-isobutylstyrene under biphasic conditions.

In order to check whether the catalyst was reusable after the reaction, a few recycle experiments were carried out after phase separation. The recycle of catalyst after a reaction at 115 °C showed only very low catalytic activity (TOF = 25 h^{-1}). However, recycle experiments under lower temperatures (100–105 °C) showed only negligible loss in catalytic activity. In all these cases analysis of Pd content in the organic phase after a reaction showed only < 0.05–0.1 ppm of Pd indicating negligible leaching of Pd to the organic phase. The catalyst was efficiently reusable even at 115 °C when fresh styrene was added to the reaction mixture under CO atmosphere. The analysis of the organic layer for Pd content after two such recycles also showed only < 0.1 ppm of Pd. These observations indicate that the catalyst is stable during an experiment and efficient recycle of the catalyst can be carried out under CO. High conversions (91%) achieved even at higher substrate concentrations (32%, see run 5, Table 1) also support this argument. Traces of colloidal Pd formation were observed under certain conditions mainly at higher temperatures (> 115 °C). Since the reaction is passing through the Cl derivative as the active carbonylation substrate, either of the two catalytic cycles involving Pd^0/Pd^{II} or Pd^{II}/Pd^{IV} seems to be possible. However, further studies on the nature of catalytic species under reaction conditions are essential to understand the actual reaction mechanism, which are currently in progress at our laboratory.

In conclusion, we have demonstrated a novel water-soluble Pd catalyst system, which is highly active for the regioselective carbonylation of vinyl aromatics to 2-arylpropionic acids under biphasic conditions and provides significant improvement over the current state of art for the biphasic carbonylation of vinyl aromatics.

S. J. and A. S. thank CSIR (Council of Scientific and Industrial Research), India for a research fellowship.

Notes and references

† **I** was dissolved in methyl ethyl ketone (MEK) (10 ml) and shaken vigorously with 2 or 3 equiv. of TPPTS in H_2O (6 ml). The yellow colour of the MEK layer disappears and the aqueous layer becomes yellow indicating the formation of **II** in water. For carbonylation reactions the aqueous layer was used after washing with pure MEK a few times (traces of MEK remain in the aqueous layer). All the solvents were degassed with Ar before use.

‡ The carbonylation reactions were carried out in a Parr Hastelloy C autoclave (50 ml). In a typical reaction, the substrate (28.8 mmol), catalyst (0.0629 mmol) (prepared as above) in 6 ml degassed water, LiCl–TsOH (11.2 mmol) and toluene (15.5 ml) (degassed) were charged to the autoclave. The contents were flushed a few times with N_2 followed by CO and heated to the desired temperature (115 °C). The autoclave was then pressurized with CO (54 bar) and the reaction was started by agitation (1100 rpm) and was continued for the specified time. TOF = Turnover Frequency = number of moles of carbonylation product formed per mole of Pd per hour.

§ The analysis of the liquid samples was carried out using a gas chromatograph (HP 5890) using a HP-FFAP capillary column.

¶ A yellow fine powder was precipitated as a suspension, which was allowed to settle, and the supernatant solution decanted. The precipitate was washed many times with EtOH and then with Et_2O and dried under vacuum. All the solvents used were degassed with Ar prior to use.

‖ *Selected data* for **II**: IR (KBr) 1636s ($\nu_{C=O}$), 1397s ($\nu_{O=C-O}$), 524s (ν_{Pd-N}). ^{31}P (D_2O, ppm) δ 35.31s (N *trans* to PPh_3), δ 36.13w (N *cis* to PPh_3). ^1H (D_2O, ppm) δ 2.25s (3H, tolyl CH_3), δ 7.2–8m (Ph and pyridyl). (Found: C, 34.05; H, 3.28; N, 1.33; S, 12.32; P, 2.50. Calc. For $C_{31}H_{23}NNa_3O_{14}PPdS_4 \cdot 6H_2O$: C, 34.598; H, 3.278; N, 1.301; S, 11.916; P, 2.878). Presence of H_2O was also confirmed by ^1H NMR and IR.

1 (*a*) Aqueous phase organometallic catalysis: *Concepts and applications*, ed. B. Cornils and W. A. Herrmann, Wiley-VCH, Weinheim, 1998; (*b*) F. Bertoux, E. Monflier, Y. Castanet and A. Mortreux, *J. Mol. Catal. A: Chem.*, 1999, **143**, 11; (*c*) G.-J. ten Brink, I.W.C.E. Arends and R.A. Sheldon, *Science*, 2000, **287**, 1636; (*d*) B. Zimmermann, J. Herwig and M. Beller, *Angew. Chem., Int. Ed. Engl.*, 1999, **38**, 2372.

2 (*a*) B. Cornils and E. Kuntz, *J. Organomet. Chem.*, 1995, **502**, 177; (*b*) *Eur. Chem. News*, 1995, Jan 15, 29.

3 (*a*) H. Alper and N. Hamel, *J. Am. Chem. Soc.*, 1990, **112**, 2803; (*b*) A. Seayad, S. Jayasree and R.V. Chaudhari, *Org. Lett.*, 1999, **1**, 459.

4 (*a*) V. Elango, M. A. Murphy, G. N. Mott, E. G. Zey, B. L. Smith and G. L. Moss, EP 400 892, 1990; (*b*) A. Seayad, S. Jayasree and R. V. Chaudhari, *Catal. Lett.*, 1999, **61**, 99; (*c*) H. Zhou, J. Cheng, S. Lu, H. Fu and H. Wang, *J. Organomet. Chem.*, 1998, **556**, 239; (*d*) S. Jayasree, A. Seayad and R. V. Chaudhari, *Chem. Commun.*, 1999, 1067.

5 (*a*) G. Papadagianakis, G. Verspui, L. Matt and R.A. Sheldon, *Catal. Lett.*, 1997, **47**, 43; (*b*) S. Tilloy, E. Monflier, F. Bertoux, Y. Castanet and A. Mortreux, *New J. Chem.*, 1997, **21**, 529; (*c*) F. Bertoux, S. Tilloy, E. Monflier, Y. Castanet and A. Mortreux, *J. Mol. Catal. A: Chem.*, 1999, **138**, 53; (*d*) F. Bertoux, E. Monflier, Y. Castanet and A. Mortreux, *J. Mol. Catal. A: Chem.*,1999, **143**, 23.

6 M. S. Goedheijt, J. N. H. Reek, P. C. J. Kamer and P. W. N. M. van Leeuwen, *Chem. Commun.*, 1998, 2431.

7 (*a*) R. V. Chaudhari, S. Jayasree and A. Seayad, Indian Patent Appl. 3697 DEL 98 March, 1999, US 6,069,253 Dt. 31-05-2000; (*b*) S. Jayasree, A. Seayad and R.V. Chaudhari, *Org. Lett.*, 2000, **2**, 203.

8 G. Papadogianakis, L. Maat and R. A. Sheldon, *J. Chem. Tech. Biotech.*, 1997, **70**, 83.

The spectroscopic identification and characterisation of carbonyl telluride (OCTe)†

Adam J. Bridgeman, Neil Harris and Nigel A. Young*

Department of Chemistry, The University of Hull, Hull, UK HU6 7RX. E-mail: n.a.young@chem.hull.ac.uk

Received (in Cambridge, UK) 9th May 2000, Accepted 25th May 2000
Published on the Web 20th June 2000

Photolysis of H_2Te in CO or 1% CO/Ar matrices at *ca.* 10 K results in the formation of carbonyl telluride; the assignment of the ν_{CO} modes of OCTe (1965.3 cm^{-1}), O^{13}CTe (1920.0 cm^{-1}) and ^{18}OCTe (1921.3 cm^{-1}) in neat CO matrices is confirmed by DFT calculations.

Carbonyl telluride (OCTe) is the only member of the carbonyl chalcogenides (apart from carbonyl polonide) that has not been spectroscopically identified or characterised, either in the solid, vapour or in cryogenic matrices. Reference to it in the chemical literature is very fleeting, including the first report of its preparation in 1944 which contained no experimental or characterisation details, but which did indicate that it was less stable than the analogous carbonyl selenide.[1] In 1993 Sonoda[2] reported that carbonyl telluride had not yet been identified, and we cannot find any subsequent reports. There are however, a couple of earlier papers containing predictions of its vibrational modes,[3] and calculations of its proton affinity and structural parameters.[4] As carbonyl selenide has been identified as the catalytic intermediate in the selenium assisted carbonylation of amines,[2] and it is also known that tellurium catalyses this reaction[5] we have initiated a study of the interaction of tellurium atoms with carbon monoxide to spectroscopically identify and characterise carbonyl telluride so that its presence in tellurium mediated organic transformations can be identified. One of the most common ways of stabilising reactive species is matrix isolation, but there is a distinct paucity of tellurium atom cryochemistry because the predominant vapour phase species above heated elemental tellurium are dimers, tetramers, *etc.*, and even when the vapour is superheated, the fraction of tellurium atoms remains low.[6] In this work we report the photolysis of H_2Te as an alternative source of tellurium atoms, and whilst this has been used previously to obtain tellurium atoms in argon matrices for Mössbauer experiments,[7] it has not been exploited as a cryochemical synthetic tool. In addition to being a source of atomic tellurium, Donovan *et al.*[8] have shown that when H_2Te is photolysed by UV light, some of the resultant Te atoms are in a $^1D_2$ excited state rather than the $^3P_2$ ground state expected from thermal evaporation, and this may result in lower activation barriers for subsequent reactions.

When H_2Te was matrix isolated in solid N_2 and photolysed with UV radiation,[9] the intensities of the three IR active bands at 2085.2 cm^{-1} (ν_1), 865.1 cm^{-1}(ν_2) and 2092.0 cm^{-1} (ν_3), (in good agreement with the previous high resolution[10] and nitrogen matrix[11] IR data) were reduced considerably, with no sign of the growth of any other bands. We have noted that this photobleaching is much more efficient using UV rather than visible irradiation, and that photolysis during deposition also increased the photobleaching of the H_2Te bands. In a neat CO ($^{12}C^{16}O$) matrix, the H_2Te stretching modes were obscured by the bands due to the various CO isotopomers. On UV photolysis in neat CO the ν_2 mode of H_2Te at 863.0 cm^{-1} decreased, and a new band (in the ν_{CO} region associated with carbonyl complexes) grew in at 1965.3 cm^{-1}, as well as features[12] due to HCO (*ca.* 1860 cm^{-1}) and H_2CO (*ca.* 1740 cm^{-1}) [Fig. 1(a)]. When ^{13}CO was used [Fig. 1(b)] the 1965.3 cm^{-1} band shifted to 1920.0 cm^{-1} and the use of ^{12}CO:^{13}CO ($\approx$1:1) mixed matrices [Fig. 1(c)] confirmed the presence of only one CO group in the moiety giving rise to these bands. With the use of $C^{18}O$ [Fig. 1(d)], the shift from a CO (1965.3 cm^{-1}) to a $C^{18}O$ matrix (1921.3 cm^{-1}) was less than that for a ^{13}CO matrix (1920.0 cm^{-1}). When H_2Te was trapped in a 1% CO/Ar matrix, the only band observed after photolysis in the 2000–1680 cm^{-1} region was at 1970.7 cm^{-1}, which is the counterpart of the 1965.3 cm^{-1} feature in the neat CO matrices, with no evidence of any HCO or H_2CO. When D_2Te was isolated and photolysed in a 1% CO/Ar matrix, the band at 1970.7 cm^{-1} was also present with no sign of any deuterated analogue, and photolysis of H_2Te in 1% ^{13}CO/Ar yielded a new feature at 1924.7 cm^{-1}.

The presence of HCO and H_2CO in the neat CO matrices confirms that the photolysis of H_2Te yields hydrogen and tellurium. The assignment of the features at 1965.3, 1920.0 and 1921.3 cm^{-1} in neat CO matrices to the ν_{CO} modes of the isotopomers of a monocarbonyl species is straightforward on the basis of the mixed CO:^{13}CO experiments, and the fact that in 1% CO/Ar matrices the 1970.7 cm^{-1} band is not affected by deuteration confirms the lack of hydrogen in the species giving rise to these features. As OCS is one of the products formed when H_2S is photolysed in solid CO,[12] it is reasonable to assign the features at 1965.3, 1920.0 and 1921.3 cm^{-1} to the ν_{CO} modes of OCTe, O^{13}CTe and ^{18}OCTe, respectively. The lack of bands other than these in the 1% CO/Ar matrices confirms this assignment as it has been noted previously that HCO is only observed in dilute CO/Ar matrices when vac-UV photolysis rather than UV–VIS photolysis is employed.[13] The isotopic ratios, in conjunction with the experimental data for the ν_{CO} modes of OCSe (OC^{80}Se, 2023.525064 cm^{-1}; O^{13}C^{80}Se,

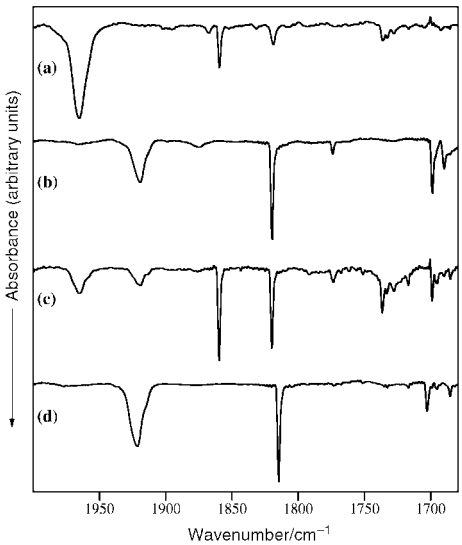

Fig. 1 Matrix isolation IR spectra of the photolysis products of H_2Te in neat CO matrices at *ca.* 10 K: (a) $^{12}C^{16}O$ (CO); (b) ^{13}CO; (c) CO:^{13}CO (~1:1); (d) $C^{18}O$.

† Electronic supplementary information (ESI) available: DFT calculations for OCTe, COTe and $(OC)_2Te$. See http://www.rsc.org/suppdata/cc/b0/b003721o/

DOI: 10.1039/b003721o

1973.82425 cm^{-1}; ^{18}OC^{80}Se, 1983.54657 cm^{-1})[14] and our DFT calculated[15] frequencies of the ν_{CO} modes of OCTe (OCTe, 1981 cm^{-1}; O^{13}CTe, 1933 cm^{-1}; ^{18}OCTe, 1939 cm^{-1}), all reinforce the conclusion that these bands are the ν_{CO} modes of carbonyl telluride. The DFT calculations also indicated that the intensity of the ν_{CTe} and δ_{OCTe} modes would be too low to be observed in the experimental spectra.[16]

Our previous DFT calculations[17] have shown that the bonding between a main group metal and CO can be described in an analogous way to the synergic mechanism used for conventional transition metal carbonyls. In the case of OCTe the DFT calculations predict that the Te σ-accepts *ca.* 0.6 e$^-$ and π-backdonates *ca.* 0.7 e$^-$ to CO, resulting in a lengthening of the CO bond and a reduction of the CO bond order and ν_{CO} frequency. The Te–CO bond energy for OCTe with respect to Te(^{3}P) and CO($^1\Sigma^+$) was calculated to be −187 kJ mol^{-1}, and OCTe was favoured over the COTe isomer by 152 kJ mol^{-1} with markedly different values for ν_{CO} of 1981 and 1835 cm^{-1}, respectively. The linear dicarbonyl telluride [$(OC)_2Te$] was found to be 36 kJ mol^{-1} less stable than OCTe, and $(OC)_3Te$ was unstable with respect to decomposition.

Therefore, using the first spectroscopic identification and characterisation of carbonyl telluride, this work has demonstrated that the photolysis of hydrogen telluride is an excellent source of both hydrogen and tellurium atoms for use in cryochemical synthesis. The identification of the ν_{CO} modes of OCTe will be useful in identifying whether this is an intermediate in organic transformations.

We gratefully acknowledge the support of The University of Hull and the EPSRC for an award of a studentship (NH) and for equipment (GR/H 29117, GR/K 17514).

Notes and references

1 P. L. Robinson and K. R. Stainthorpe, *Nature*, 1944, **153**, 24.
2 N. Sonoda, *Pure Appl. Chem.*, 1993, **65**, 699.
3 L. H. Jones, *Inorg. Chem.*, 1967, **6**, 429.
4 P. G. Jasien and W. J. Stevens, *J. Chem. Phys.*, 1985, **83**, 2984.
5 N. Kambe, K. Kondo, H. Ishii and N. Sonoda, *Bull. Chem. Soc. Jpn.*, 1981, **54**, 1460.
6 P. Hassanzadeh, C. Thompson and L. Andrews, *J. Phys. Chem.*, 1992, **96**, 8246 and references therein.
7 P. H. Barrett, P. A. Montano and J. B. Mann, *Phys. Rev. B*, 1976, **14**, 4755; P. A. Montano, H. M. Nagarathna, D. Newlin and G. W. Stewart, *J. Chem. Phys.*, 1981, **74**, 5558; M. van der Heyden, M. Pasternak and G. Langouche, *J. Phys. Chem. Solids*, 1985, **46**, 1221.
8 R. J. Donovan, D. J. Little and J. Konstantatos, *J. Photochem.*, 1972/73, **1**, 86; D. J. Little, R. J. Donovan and R. J. Butcher, *J. Photochem.*, 1973/74, **2**, 451; R. J. Donovan, D. J. Little and J. Konstantatos, *J. Chem. Soc., Faraday Trans. 2*, 1972, **68**, 1812.
9 The H_2Te (D_2Te) was prepared by the addition of H_2O (D_2O) to powdered Al_2Te_3 (Strem) and was flushed out of the reaction vessel by N_2, through an ice-salt trap to remove residual moisture before condensation at 77 K and purification by vacuum sublimation and storage at either 77 or 195 K. During the matrix isolation experiments the H_2Te was kept at 147 K (methylcyclohexane slush) and the vapour condensed in an excess of matrix gas for *ca.* 1 h on a CsI plate maintained at *ca.* 10 K by an APD Cryogenic DE204SL Displex cryostat. IR spectra were acquired using a Bruker IFS66 FTIR spectrometer with a KBr beamsplitter and DTGS detector operating at 1 cm^{-1} resolution. The photolysis utilised an Oriel 200 W Hg–Xe lamp. The matrix gases were supplied and used as received from Distillers MG (N_2, 99.999%; CO, 99.997%), Cambridge Isotope Laboratories (^{13}CO, 99%) and Euroisotop (C^{18}O, 99%).
10 J.-M. Flaud, Ph. Arcas, H. Bürger and O. Polanz, *J. Mol. Spectrosc.*, 1997, **182**, 315; J.-M. Flaud, M. Betrencourt, Ph. Arcas, H. Bürger, O. Polanz and W. J. Lafferty, *J. Mol. Spectrosc.*, 1997, **182**, 396; J.-M. Flaud, Ph. Arcas, H. Bürger, O. Polanz and L. Halonen, *J. Mol. Spectrosc.*, 1997, **183**, 310.
11 N. A. Young, PhD Thesis, Southampton University, 1988.
12 D. E. Milligan and M. E. Jacox, *J. Chem. Phys.*, 1964, **41**, 3032.
13 D. E. Milligan and M. E. Jacox, *J. Chem. Phys.*, 1969, **51**, 277; D. E. Milligan and M. E. Jacox, *J. Chem. Phys.*, 1971, **54**, 927.
14 K. Sueoka, Y. Hamada and H. Uehara, *J. Mol. Spectrosc.*, 1988, **127**, 370.
15 DFT calculations were carried out as described in ref. 17 using the DeFT code.[18] The detailed DFT calculation output is available as ESI.†
16 In addition to the bands assigned to OCTe, HCO and H_2CO in the neat CO matrices, there was a variable intensity band at 1819 cm^{-1} that shifted to 1774 cm^{-1} in ^{13}CO. In C^{18}O matrices, the band was of very very low intensity at 1773 cm^{-1}. In the 1% CO/Ar matrices these bands were absent. The isotopic behaviour in mixed CO:^{13}CO matrices was characteristic of a monocarbonyl species and the isotopic ratios are very similar to those of HCO, but different to both the observed and calculated isotopic shifts of OCTe. Therefore, we believe that these features are due to interaction between the formyl radicals and adventitious impurities in the matrix, for example, previous workers[19] have assigned bands at *ca.* 1820 cm^{-1} in neat O_2 matrices to the formylperoxy radical [HC(O)OO].
17 A. J. Bridgeman, *J. Chem. Soc., Dalton Trans.*, 1997, 1323.
18 A. St-Amant, DeFT, a FORTRAN program, University of Ottawa, 1994.
19 T.-L. Tso and E. K. C. Lee, *J. Phys. Chem.*, 1984, **88**, 5465.

One-step synthesis of size tuned zinc selenide quantum dots *via* a temperature controlled molecular precursor approach

Young-wook Jun, Ja-Eung Koo and Jinwoo Cheon*

Department of Chemistry and School of Molecular Science – BK21, Korea Advanced Institute of Science and Technology (KAIST), Taejon 305-701, Korea. E-mail: jcheon@kaist.ac.kr

Received (in Cambridge, UK) 13th April 2000, Accepted 30th May 2000
Published on the Web 20th June 2000

One-step size-controlled synthesis of ZnSe quantum dots is studied and the obtained QDs are luminescent with the emission wavelength varying over a wide range (up to 100 nm) depending on the particle size; the single-molecular precursor is an air-stable bis(phenylselenolato)zinc *N*,*N*,*N*′,*N*′-tetramethylethylenediamine (TMEDA) complex, which effectively affords different sizes of ZnSe QDs depending on growth temperatures.

Nanomaterials are of great interest owing to the novel optical, electronic and catalytic properties that arise from the quantum size effects and large surface areas that are characteristic of these species. In particular, quantum dots (QDs) of semiconducting materials have received special attention because their electronic band gaps can be tuned, thus varying their optical response from the IR to the UV depending on the size of the dots.[1–5] The tunability of the band gap makes QDs useful for many applications such as light emitting diodes[5] and as ultrasmall luminescent tags for biological studies.[6]

Bulk materials that absorb or emit in the blue to near-UV regions of the electromagnetic spectrum are being extensively studied owing to their potential uses in optical sensors and lasers.[7,8] The best known bulk semiconductors with band gaps in this region are GaN (E_{gap} = 3.4 eV) and ZnSe (E_{gap} = *ca.* 2.7 eV). Synthetic studies on QDs of these two materials with decent electronic band tunings, however, have been very limited.[9,10] For isolated colloidal ZnSe QDs, the use of a diselenocarbamate single-source precursor and a dual source precursor system are two successful demonstrations.[10]

One of the important current issues of nanomaterials research is the controlled synthesis of QDs. In many cases, however, successful nanostructured materials syntheses[1,11] with desired size and shape criteria, require multi-step processes and thus developing a simple and controlled method of synthesizing QDs is of particular interest.

Here we present a one-step synthesis of ZnSe QDs the sizes of which can be precisely tuned by simple temperature control. We demonstrate that these are luminescent in the blue region and that the emission wavelength varies over a very wide range (up to 100 nm) depending on the particle size. The key to this synthesis is the proper choice of a molecular precursor which has good solubility, adequate thermal stability, and simple ligand elimination processes that produce desired materials. Notably, our obtained QDs have a high monodispersity without size selective precipitation.

The compound bis(phenylselenolato)zinc, $Zn(SePh)_2$,[12] is polymeric and poorly soluble in organic solvents, and is thus not particularly convenient as a precursor for the synthesis of QDs. We observe, however, that the polymer reacts with *N*,*N*,*N*′,*N*′-tetramethylethylenediamine (TMEDA) to form a soluble, air-stable, monomeric adduct of stoichiometry $Zn(SePh)_2$-(TMEDA) (Fig. 1).[13–15] As similarly observed by Yamamoto and Steigerwald in related work on alkyl- or phenyl-chalcogenolate ligand systems, this ligand is more thermally stable than other bulky selenolate ligands such as $SeSi(SiMe_3)_3$, and thermolysis of its complexes produces clean QDs with reduced contamination caused by undesired ligand fragmentation processes.[16]

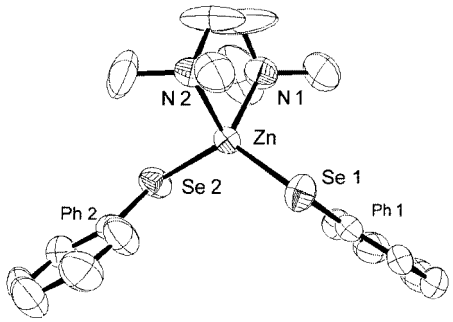

Fig. 1 ORTEP drawing of $Zn(SePh)_2$(TMEDA). Selected bond distances (Å) and angles (°): Se(1)–Zn(1) 2.398(2), Se(2)–Zn(1) 2.399(2), Zn(1)–N(1) 2.120(9), Zn(1)–N(2) 2.147(9); Se(1)–Zn–Se(2) 125.54(6), N(1)–Zn(1)–N(2) 86.3(3).

One-step size controlled synthesis of QDs was carried out by the thermolysis of $Zn(SePh)_2$(TMEDA) (eqn. 1).[17,18]

$$[Zn(SePh)_2][TMEDA] \xrightarrow{heat} ZnSe + TMEDA + Ph_2Se \quad (1)$$

In a typical QD synthesis, $Zn(SePh)_2$(TMEDA) (0.5 g, 0.101 mmol) was dissolved in trioctylphosphine (10 ml) and the resulting solution injected into hot trioctylphosphine oxide (3.92 g, 10.1 mmol). The latter solution is kept at one of four different temperatures: 320, 340, 367 or 385 °C. After 1 h, the resulting yellow solution was cooled to 80 °C and treated with an excess of methanol to generate a yellow flocculate, which is separated by centrifugation and washed with methanol. The resulting pale yellow powder was readily redispersed in toluene. No further size selection is carried out.

The QDs obtained are highly monodispersed with sizes that depend on the growth temperature. Relative to the position of the 460 nm (2.7 eV) absorption band edge for bulk ZnSe, the absorption band edges of the ZnSe QDs are blue-shifted. Larger shifts are seen for higher growth temperatures. Thus, the absorption band shifts are 0.95, 0.37, 0.29 and 0.17 eV for QDs grown at 385, 367, 340 and 320 °C, respectively. Similar blue shifts are also observed in the photoluminescence spectra: the band maxima are 387 (3.20 eV), 429 (2.89 eV), 443 (2.80 eV) and 451 nm (2.75 eV) for samples grown at 385, 367, 340 and 320 °C, respectively (Fig. 2). These results show that smaller quantum dots are obtained at higher growth temperatures where more nucleation sites are present and relatively less ZnSe material is available for each nucleus during growth kinetics. High resolution transmission electron micrographs show that the ZnSe QDs are roughly spherical and that the particles within a single sample have relatively uniform sizes (Fig. 3). The average sizes of the ZnSe QDs are 2.7 ± 0.2, 4.0 ± 0.35 nm, 4.4 ± 0.35 and 4.9 ± 0.29 nm for samples grown at 385, 367, 340, 320 °C, respectively (Fig. 2C). The ZnSe particles are in the cubic phase, as determined by X-ray diffraction and selected area electron diffraction.[18] Energy dispersive X-ray emission analysis of the QDs confirms that the particles have a 1 : 1 Zn : Se stoichiometry.

The results above demonstrate that monodispersed ZnSe QDs can be prepared by means of a simple and convenient one-pot

DOI: 10.1039/b002983l

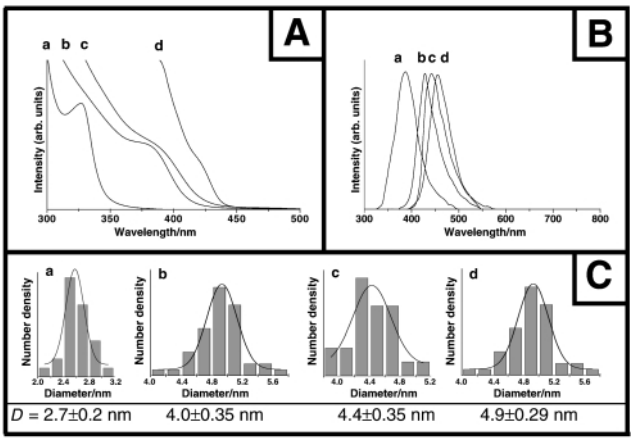

Fig. 2 Optical spectra and size distribution of ZnSe QDs grown at (a) 385 (b) 367 (c) 340 (d) 320 °C. (A) UV–VIS absorption spectra, (B) photoluminescence spectra and (C) size distribution.

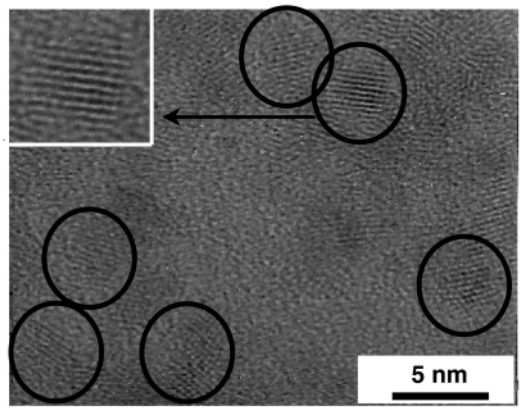

Fig. 3 HRTEM images of ZnSe QDs grown at 340 °C.

synthesis from an air-stable monomeric molecular precursor. The growth of QDs follows a simple ligand elimination reaction and by varying the growth temperature it is possible to control their size. The results constitute a good demonstration of controlling the size of semiconductor QDs with band gaps in the blue region of the electromagnetic spectrum. We believe that this strategy can be extended to facile size controlled synthesis of QDs of other materials that, at present, are difficult or complicated to prepare.

This work was supported by the KOSEF (1999-1-122-001-5) and we thank KBSI and KRISS for the TEM analyses.

Notes and references

1 C. D. Murray, D. J. Norris and M. G. Bawendi, *J. Am. Chem. Soc.*, 1993, **115**, 8706.
2 J. E. Bowen Katari, V. L. Colvin and A. P. Alivisatos, *J. Phys. Chem.*, 1994, **98**, 411.
3 (a) N. Chestnoy, R. Hull and L. E. Brus, *J. Chem. Phys.*, 1986, **85**, 2237; (b) M. L. Steigerwald and L. E Brus, *Acc. Chem. Res.*, 1990, **23**, 183.
4 A. L. Rogach, A. Kornowski, M. Gao, A. Eychmüller and H. J. Weller, *J. Phys. Chem. B*, 1999, **103**, 3065.
5 B. O. Dabbousi, M. G. Bawendi, O. Onitsuka and M. F. Rubner, *Appl. Phys. Lett.*, 1995, **66**, 1316.
6 A. P. Alivisatos, X. Peng, T. E. Wilson, K. P. Johnsson, C. J. Loweth, M. P. Bruchez, Jr. and P. G. Schultz, *Nature*, 1996, **382**, 609.
7 S. Strite and H. Morkoc, *J. Vac. Sci. Technol. B*, 1992, **10**, 1237.
8 S. V. Ivanov, A. A. Toropov, S. V. Sorokin, T. V. Shubina, I. V. Sedova, P. S. Kop'ev, Z. I. Alferov, A. Waag, H. J. Lugauer, G. Reuscher, M. Keim, F. F. Fischer and G. Landwehr, *Semiconductors*, 1999, **33**, 1016.
9 A. C. Frank, F. Stowasser, C. R. Miskys, O. Ambacher and R. A. Fischer, *J. Am. Chem. Soc.*, 1998, **120**, 3512.
10 (*a*) N. Revaprasadu, M. A. Malik, P. O'Brien, M. M. Zulu and M. Wakefield, *J. Mater. Chem.*, 1998, **8**, 1885; (*b*) B. Ludolph, M. A. Malik, P. O'Brien and N. Revaprasadu, *Chem. Commun.*, 1998, 1849; (*c*) M. A. Hines and P. Guyot-Sionnest, *J. Phys. Chem.*, 1998, **102**, 3655.
11 C. G. Wu and T. Bein, *Science*, 1994, **264**, 1757; L. Z. Wang, J. L. Shi, W. H. Zhang, M. L. Ruan, J. Yu and D. S. Yan, *Chem. Mater.*, 1999, **11**, 3015.
12 $Zn(SePh)_2$ was prepared according to a modification of literature procedure (M. Bochmann, G. Bwembya and K. J. Webb, *Inorg. Synth.*, 1997, **31,** 19). Selenophenol (2.14 g, 13.54 mmol) was slowly added to $Zn[N(SiMe_3)_2]_2$ (2.61 g, 6.76 mmol) in toluene (50 ml) for 30 min. A white precipitate began to form and the mixture was stirred at room temp. for 12 h, after which heptane (10 ml) was added. The precipitate was collected by filtration, washed with heptane (5 ml), and dried *in vacuo*, to give a white powder (2.32 g, 90%).
13 TMEDA (1.07 g, 9.17 mmol) was added to a suspension of $Zn(SePh)_2$ (1.81 g, 6.11 mmol) in toluene (50 ml). The mixture was stirred for 24 h to give a pale yellow solution, which was filtered, treated with pyridine (5 ml) and heptane (30 ml), and cooled to −24 °C to give colorless crystals (1.765 g, 59%), mp 137–138 °C. Anal. Calc. for $C_{18}H_{26}N_2Se_2Zn$: C, 43.8; H, 5.27; N, 5.67. Found: C, 43.1; H, 5.34; N, 5.37%. $\delta_H(CDCl_3$, 25 °C): 7.90 (t, 2H, J_{HH} 7 Hz, *o*-CH), 6.86 (*m*, 3H, *m*-CH and *p*-CH), 2.67 (s, 2H, NCH_2), 2.48 (s, 6H, NMe_2).
14 An X-ray crystallographic study of $Zn(SePh)_2$(TMEDA) (Fig. 1) shows that the zinc center adopts a distorted tetrahedral geometry with a large Se–Zn–Se angle of 125.55° and a small N–Zn–N angle of 86.33°. The Zn–Se and Zn–N bond lengths are 2.398 and 2.134 Å, respectively. The bond lengths and angles are similar to those seen for other zinc complexes with organochalcogen and amine ligands.[15] *Crystal data*: $C_{22}H_{16}N_2Se_2Zn$, M_r = 531.69, monoclinic, space group $P2_1/c$, a = 11.202(2), b = 12.7326(14), c = 15.125(3) Å, β = 107.050(18)°, U = 2062.5(6) Å^3, Z = 4, D_c = 1.340 g cm^{-3}, $F(000)$ = 1040, μ(Mo-Kα) = 47.2 cm^{-1}, R_1 = 0.0623, wR_2 = 0.1634. CCDC 182/1665. See http://www.rsc.org/suppdata/cc/b0/b002983l/ for crystallographic files in .cif format.
15 M. Bochmann, G. C. Bwembya, R. Grinter, A. K. Powell, K. J. Webb, M. B. Hursthouse, K. M. Abdul Malik and M. A. Mazid, *Inorg. Chem.*, 1994, **33**, 2290; N. Ueyama, T. Sufawara, K. Sasaki, A. Nakamura, S. Yamashita, Y. Wakatsuki, H. Yamazaki and N. Yasuoka, *Inorg. Chem.*, 1988, **27**, 741; G. Mugesh, H. B. Singh, R. P. Patel and R. J. Butcher, *Inorg. Chem.*,1998, **37**, 2263.
16 Molecular precursor strategies with chalcogenolate ligands have been similarly used to prepare other II/VI semiconducting materials. See: (*a*) J. G. Brennan, T. Siegrist, P. J. Carrol, S. M. Stuczynski, L. E. Brus and M. L. Steigerwald, *J. Am. Chem. Soc.*, 1989, **111**, 4141; (*b*) J. G. Brennan, T. Siegrist, P. J. Carrol, S. M. Stuczynski, P. Reynders, L. E. Brus and M. L. Steigerwald, *Chem. Mater.*, 1990, **2**, 403; (*c*) K. Osakada and T. Yamamoto, *J. Chem. Soc., Chem. Commun.*, 1987, 1117.
17 Upon themolysis of $Zn(SePh)_2$(TMEDA), the generation of Ph_2Se was identified by ^{1}H NMR spectroscopy.
18 X-Ray diffraction spectra show three broad peaks at 2θ = 27.41 (111), 48.04 (200) and 68.76° (311), similar to the cubic phase observed in CdSe.[4] Interestingly, the synthesis of hexagonal ZnSe QDs has previously been reported.[10*a*]

ChemComm

Palladium(II)-supported hydrotalcite as a catalyst for selective oxidation of alcohols using molecular oxygen

Takahiro Nishimura, Nobuyuki Kakiuchi, Masashi Inoue and Sakae Uemura*

Department of Energy and Hydrocarbon Chemistry, Graduate School of Engineering, Kyoto University, Sakyo-ku, Kyoto 606-8501, Japan. E-mail: uemura@scl.kyoto-u.ac.jp

Received (in Cambridge, UK) 28th March 2000, Accepted 30th May 2000
Published on the Web 20th June 2000

Palladium(II)-supported hydrotalcite acts as a reusable catalyst for the oxidation of alcohols to aldehydes and ketones in the presence of pyridine under atmospheric pressure of oxygen.

Heterogeneous catalysts are currently receiving considerable attention from the standpoint of environmental and economical concerns because of their unique properties such as easy handling, simple separation and reusability.[1] Hydrotalcite [$Mg_6Al_2(OH)_{16}CO_3{\cdot}4H_2O$] is a naturally produced basic clay mineral which has a layered structure consisting of positively charged brucite-like layers and negatively charged counter ions located in the interlayers.[2] It has been used as a solid base catalyst in several reactions[3] and also some modified hydrotalcites have been prepared and used for aerobic oxidation of alcohols.[4] The utility of hydrotalcite as a support for transition metals has also been investigated[5] and further elaboration of its use in organic synthesis is awaited.

Recently we have reported the palladium-catalysed oxidation of alcohols to aldehydes and ketones using a catalytic amount of $Pd(OAc)_2$, pyridine and 3 Å molecular seives (MS3A) under atmospheric pressure of oxygen.[6] In order to construct a high-performance catalytic system, we have attempted heterogenization of this system to produce a reusable and efficient solid catalyst. Among several clay supports examined, we found that hydrotalcite was an effective support for Pd(II) in the oxidation of alcohols. We report here, the synthesis of a new heterogeneous catalyst, a palladium(II) salt supported hydrotalcite [Pd(II)-hydrotalcite] from commercially available reagents, and its application as a catalyst for aerobic oxidation of alcohols under oxygen.[7]

Pd(II)-hydrotalcite† (1.56 mmol g^{-1} Pd) was prepared by mixing $Pd(OAc)_2$, pyridine and hydrotalcite in toluene at 80 °C for 1 h, followed by filtration, washing and drying under reduced pressure at room temperature.[8] A residue was scarcely observed in the filtrate after removing solvents under reduced pressure, showing that virtually all of the $Pd(OAc)_2$ initially employed was adsorbed on hydrotalcite. The basal spacing (d_{003}) of the commercially available hydrotalcite was 7.8 Å as estimated by a sharp peak obtained from X-ray diffraction (XRD) analysis, while that of the prepared Pd(II)-hydrotalcite was essentially the same with no differences of peak pattern between hydrotalcite and Pd(II)-hydrotalcite being observed. This result suggests that the palladium salt is immobilised on the surface of hydrotalcite.[9]

Initially the catalytic oxidation of benzyl alcohol **1a** using Pd(II)-hydrotalcite‡ was performed (Scheme 1), and typical results are listed in Table 1. The oxidation of benzyl alcohol **1a** (1 mmol) in toluene at 80 °C for 2 h in the presence of 5 mol% Pd(II)-hydrotalcite (0.05 mmol Pd) under O_2 afforded benzaldehyde **2a** in 62% yield (Table 1, entry 1). By further addition of pyridine (0.2 mmol) in the reaction media, efficient oxidation proceeded to give a quantitative yield of **2a** (entry 2). The amount of the catalyst could be reduced to 1 mol%, although a longer reaction time was required to achieve the complete conversion of **1a** (entries 3 and 4). Other benzylic alcohols (**1b** and **1c**) were also smoothly oxidized to the corresponding aldehydes in high yields (entries 5 and 6). Non-activated primary and secondary aliphatic alcohols **3a–c** were easily transferred to the corresponding aldehydes and ketones in high yields (entries 7–9). In the latter case, however, the reaction was slower and an excess of pyridine (1.0 mmol) was required (entries 8 and 9). The reactions of alkenic alcohols using Pd(II)-hydrotalcite or $Pd(OAc)_2$/pyridine/MS3A (homogeneous catalytic system; abbreviated as MS-system)[6] were then carried out and compared, the results of which are summarized in Table 2. In the oxidation of geraniol **5** and nerol **7**, the presence of an excess of pyridine was required (entries 1–3). When the reaction of **5** was carried out using the MS-system, the yield of the corresponding aldehyde **6** was low (56%) even after long

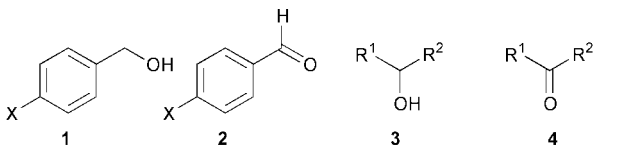

Scheme 1

Table 1 Pd(II)-hydrotalcite-catalysed oxidation of alcohols by molecular oxygen[a]

Entry	Substrate	Catalyst	Pyridine/ mmol	Reaction time/h	Product	Conversion (%)	Isolated yield (%)[b]
1	**1a**	0.30 g, 5 mol%	—	2	**2a**	74	62[c]
2	**1a**	0.30 g, 5 mol%	0.2	2	**2a**	100	quant.[c]
3	**1a**	0.06 g, 1 mol%	0.2	12	**2a**	98	91[c]
4[d]	**1a**	0.60 g, 1 mol%	2.0	12	**2a**	94	87[c]
5	**1b**	0.30 g, 5 mol%	0.2	2	**2b**	97	90
6	**1c**	0.30 g, 5 mol%	0.2	2	**2c**	98	92
7	**3a**	0.30 g, 5 mol%	0.2	6	**4a**	97	86
8	**3b**	0.30 g, 5 mol%	1.0	11	**4b**	100	93
9	**3c**	0.30 g, 5 mol%	1.0	11	**4c**	100	92

[a] *Reaction conditions*: Pd(II)-hydrotalcite (1.56 mmol g^{-1} Pd), alcohol (1.0 mmol), pyridine, toluene (10 mL), 80 °C, O_2. [b] Based on alcohol employed. [c] GLC yield. [d] 10-Fold scale reaction.

DOI: 10.1039/b002447n

Table 2 Catalytic oxidation of geraniol and nerol using Pd(II)-hydrotalcite and $Pd(OAc)_2$/pyridine/MS3A[a]

Entry	Substrate	Product	Pd(II)-hydrotalcite[b] Time/h	Pd(II)-hydrotalcite[b] Isolated yield (%)[d]	$Pd(OAc)_2$/pyridine/MS3A[c] Time/h	$Pd(OAc)_2$/pyridine/MS3A[c] Isolated yield (%)[d]
1[e]	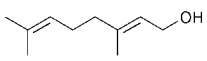	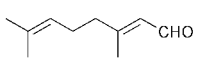	12	45 (58) *E* : *Z* = 95 : 5		
2	**5** *E* : *Z* = 98 : 2	**6**	4.5	91 (98) *E* : *Z* = 96 : 4	15	56 (76) *E* : *Z* = 63 : 37
3	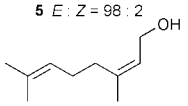 **7** *E* : *Z* = 2 : 98	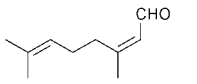 **8**	4.5	89 (100) *E* : *Z* = 6 : 94	15	39 (71) *E* : *Z* = 31 : 69

[a] *Reaction conditions*: alcohol (1.0 mmol), pyridine (5.0 mmol), O_2, 80 °C. [b] Pd(II)-hydrotalcite (1.56 mmol g^{-1} Pd; 300 mg, 0.05 mmol Pd). [c] $Pd(OAc)_2$ (0.05 mmol), MS3A (500 mg). [d] The value in parentheses is the conversion of alcohol (%). *E*:*Z* ratio determined by ^{1}H NMR. [e] Pyridine (0.2 mmol) used.

reaction times and the *E*:*Z* ratio was seriously disturbed (*E*:*Z* = 63:37), while the Pd(II)-hydrotalcite catalysed reaction smoothly proceeded to give **6** in 91% isolated yield without geometrical isomerization (*E*:*Z* = 96:4, entry 2). Similarly, aldehyde **8** was obtained highly selectively from **7** in high yield using Pd(II)-hydrotalcite (89%, *E*:*Z* = 6:94), while both product yield and selectivity were low using the MS-system (entry 3).[10] Although the reason for this high catalytic activity and selectivity arising from immobilisation of a palladium(II) salt on hydrotalcite is not yet clear,[10] this catalyst is shown to be especially effective for the oxidation of unsaturated alcohols.

The catalyst could be easily separated from the reaction mixture by simple filtration and recycled. For example, Pd(II)-hydrotalcite could be recycled at least three times in the oxidation of benzyl alcohol **1a** although the catalytic activity decreased with the third use (1st: 98%, 2nd: 93%, 3rd: 77%).

In summary, we have demonstrated that a novel Pd(II)-supported hydrotalcite worked as an efficient catalyst for the oxidation of alcohols under oxygen. Especially, in the oxidation of geometrically isomerizable allylic alcohols such as geraniol and nerol, the corresponding aldehydes were obtained in high yield without any isomerization. The catalyst can be easily separated and recycled. Further characterization of this catalyst and application to other reactions are now in progress.

We gratefully thank Kyowa Chemical Ind., Ltd. for the gift of hydrotalcite [$Mg_6Al_2(OH)_{16}CO_3{\cdot}4H_2O$, brand name ALCAMAC < L > ®]. T. N. gratefully thanks a Fellowship of the Japan Society for the Promotion of Science for Young Scientists.

Notes and references

† *Procedure for the preparation of Pd(II)-hydrotalcite*: to a mixture of $Pd(OAc)_2$ (375 mg, 1.67 mmol) and toluene (100 mL) in a 200 mL two-necked flask was added pyridine (331 mg, 4.18 mmol) at 80 °C during which the brown suspension turned yellowish white. Then, hydrotalcite (ALCAMAC < L > ®, 10.0 g) was added and the mixture was stirred vigorously for 1 h at 80 °C. The obtained slurry was cooled to 0 °C, followed by filtration and washing with diethyl ether (20 mL × 2). The resulting solid was dried *in vacuo* at room temp. to give a yellowish white powder of Pd(II)-hydrotalcite. Elemental analysis; found: N, 0.35% [calc. N, 0.44% assuming that $Pd(OAc)_2{\cdot}2C_5H_5N$ formed *in situ* was completely adsorbed].

‡ *Procedure for Pd(II)-hydrotalcite catalysed oxidation of alcohols using molecular oxygen*: to a suspension of Pd(II)-hydrotalcite (300 mg, 0.05 mmol Pd) in toluene (6 mL) in a 20 mL two-necked flask was added pyridine (0.2–5.0 mmol) and the resulting mixture was stirred. Oxygen was then introduced into the flask from an O_2 balloon under atmospheric pressure and the mixture was heated to 80 °C for *ca.* 10 min with stirring. Then, an alcohol (1.0 mmol) in toluene (4 mL) was added and the mixture was stirred vigorously for 2 h (or appropriate time) at 80 °C under oxygen. After the reaction the catalyst was separated by filtration through a glass filter. Removal of the solvent from the filtrate under reduced pressure left an oily residue which was subjected to column chromatography (Merck silica gel 60; hexane–diethyl ether as eluent) to give the product.

1 M. Balogh and P. Laszlo, *Organic Chemistry Using Clays*, Springer-Verlag, New York, 1993; J. H. Clark, *Catalysis of Organic Reactions by Supported Inorganic Reagents*, VCH, New York, 1994; R. L. Augustine, *Heterogeneous Catalysis for the Synthetic Chemist*, Dekker, New York, 1996.
2 F. Cavani, F. Trifiró and A. Voccari, *Catal. Today*, 1991, **11**, 173.
3 Recent examples of the reactions catalysed by hydrotalcite, see: B. M. Choudary, M. Lakshmi Kantam, Ch. Venkat Reddy, K. Koteswara Rao and F. Figueras, *J. Mol. Catal. A*, 1999, **146**, 279; T. Raja, T. M. Jyothi, K. Sreekumar, M. B. Talawar, J. Santhanalakshmi and B. S. Rao, *Bull. Chem. Soc. Jpn.*, 1999, **72**, 2117 and references therein.
4 K. Kaneda, T. Yamashita, T. Matsushita and K. Ebitani, *J. Org. Chem.*, 1998, **63**, 1750; T. Matsushita, K. Ebitani and K. Kaneda, *Chem. Commun.*, 1999, 265.
5 For example: T. Tatsumi, K. Yamamoto, H. Tajima and H. Tominaga, *Chem. Lett.*, 1992, 815; B. F. Sels, D. E. D. Vos and P. A. Jacobs, *Tetrahedron Lett.*, 1996, **37**, 8557; M. P. Kapoor and Y. Matsumura, *Chem. Commun.*, 2000, 95.
6 T. Nishimura, T. Onoue, K. Ohe and S. Uemura, *Tetrahedron Lett.*, 1998, **39**, 6011; T. Nishimura, T. Onoue, K. Ohe and S. Uemura, *J. Org. Chem.*, 1999, **64**, 6750.
7 For recent examples of aerobic oxidation using heterogeneous palladium catalysts, see: M. Hronec, Z. Cvengrosová and J. Kizlink, *J. Mol. Catal.*, 1993, **83**, 75; K. Kaneda, M. Fujii and K. Morioka, *J. Org. Chem.*, 1996, **61**, 4502; G. Noronha and P. M. Henry, *J. Mol. Catal. A*, 1997, **120**, 75; K. Kaneda, Y. Fujie and K. Ebitani, *Tetrahedron Lett.*, 1997, **38**, 9023; K. Ebitani, Y. Fujie and K. Kaneda, *Langmuir*, 1999, **15**, 3557.
8 The $Pd(OAc)_2(py)_2$ complex is formed by the reaction of $Pd(OAc)_2$ with pyridine, see: S. V. Kravtsova, I. P. Romm, A. I. Stash and V. K. Belsky, *Acta Crystallogr., Sect. C*, 1996, **52**, 2201; T. A. Stephenson, S. M. Morehouse, A. R. Powell, J. P. Heffer and G. Wilkinson, *J. Chem. Soc.*, 1965, 3632.
9 The presence of pyridine in Pd(II)-hydrotalcite was detected by TG/MS analysis, while desorption of pyridine was not observed from hydrotalcite which was treated with pyridine in toluene and washed by the same procedure as in the preparation of Pd(II)-hydrotalcite. We postulate that the Pd(II)-pyridine complex was adsorbed on the surface (not between layers) by ionic bonding between the Pd(II)-pyridine complex and hydroxy groups on the surface of the hydrotalcite.
10 Low catalytic activity of the MS-system might be due to strong complexation of palladium by the olefin. In Pd(II)-hydrotalcite, however, such complexation may be inhibited because of the steric bulk of hydrotalcite surface and this may be a reason for very low geometric isomerizations observed with the Pd(II)-hydrotalcite system.

ChemComm

Pyridine functionalised N-heterocyclic carbene complexes of palladium

Arran A. D. Tulloch,[a] Andreas A. Danopoulos,*[a] Robert P. Tooze,[b] Sean M. Cafferkey,[a] Sven Kleinhenz[a] and Michael B. Hursthouse*[a]

[a] *Department of Chemistry, University of Southampton, Highfield, Southampton, UK SO17 1BJ. E-mail: ad1@soton.ac.uk*
[b] *Ineos Acrylics, Wilton, PO Box 90, Middlesbrough, Cleveland, UK TS90 8JE*

Received (in Basel, Switzerland) 28th March 2000, Accepted 26th May 2000
Published on the Web 20th June 2000

The pyridine functionalised N-heterocyclic carbene complexes (C–N)PdMeBr, C–N = 3-R-1-(2-picolyl)imidazolin-2-ylidene, (R = Bu^t 1a, R = mes 1b, mes = mesityl) are described; they are excellent catalysts for the Heck arylation; 1b is monomeric with a chelating C–N ligand; the product obtained by interaction of 1a with AgO_2CCF_3 shows a $[Pd(C–N)]_4$ framework with bridging C–N ligands.

N-heterocyclic carbenes have recently emerged as a new family of ligands with electronic characteristics similar to those of the phosphines.[1] The great interest in their complexes with transition metals has been stimulated by the realisation that they can act as catalysts or catalyst precursors to important transformations, such as Pd-catalysed Heck and Suzuki couplings, CO–ethylene copolymerisations, Ru-catalysed olefin metathesis and Rh catalysed hydrosilylations.[2] Furthermore, electronic and steric optimisation of the catalytic site should be achievable *via* ligand design. Recent reports on the synthesis of functionalised hemilabile N-heterocyclic carbene complexes[3,4] and their use as catalyst precursors prompted us to communicate our results describing the full characterisation of three novel pyridine functionalised N-heterocyclic carbene complexes of palladium, including two crystal structures and preliminary studies on their catalytic activities in Heck coupling and amination reactions.

The complexes (C–N)PdMeBr, C–N = 3-R-1-(2-picolyl)-imidazolin-2-ylidene, (R = Bu^t **1a**, R = mes **1b**, Scheme 1) were prepared in good yields by careful deprotonation at low temperatures of 3-R-1-(2-picolyl)imidazolium bromide, [H(C–N)] Br, (R = Bu^t, mes), with $LiNPr^i_2$ in THF, followed by trapping of the *in situ* formed carbene with (cod)PdMeBr. Complexes **1a**,**b** are air-stable solids and **1b** can be crystallised from CH_2Cl_2 by slow evaporation.† The structure of **1b** was determined by X-ray crystallography and is shown in Fig. 1.‡ The chelating ligand is coordinated to the square planar palladium centre with the carbene end disposed *trans* to the bromide. The carbene plane forms an angle of 64.2° with the square plane of the palladium. The resulting six-membered ring is puckered to release conformational strain.

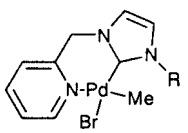

R=Bu^t, **1a**; R=mes, **1b**

Scheme 1

Abstraction of the halide from **1a** by $Ag(O_2CCF_3)$ in acetonitrile results in isolation of complex **2**† the structure of which is shown in Fig. 2.‡ In this case the C–N ligand is bridging with carbene and pyridine ends occupying mutually *trans* positions. The four Pd atoms occupy the corners of a distorted tetrahedron and the ligands bridge four of the six sides in a way which leaves two opposite sites free.

Compounds analogous to **1** (R = Me) have recently been reported by McGuinness and Cavell,[4] however, they could not obtain crystallographic data. In the absence of such data for comparison, we note with interest that there are several other aspects of their paper, which point towards important differences between their complexes and the ones reported herein. Mention is made of the unselective reaction of bases with the precursor imidazolium salts, which precludes the use of the simple synthetic technique employed by us to synthesise the palladium complexes. They also note that their complexes once formed are unstable towards strong bases,which limits their use in amination catalysis. Both problems are believed to arise from

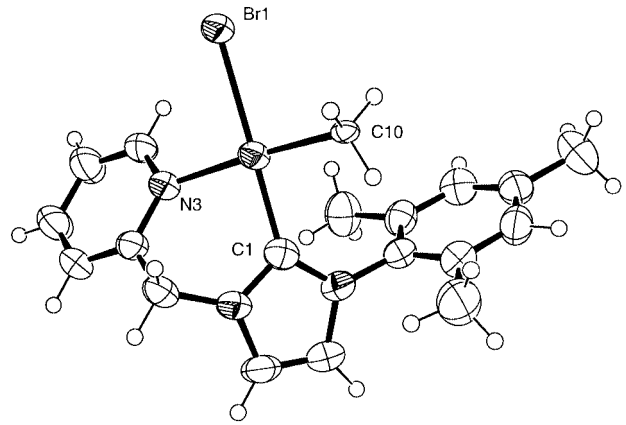

Fig. 1 Molecular structure of **1b**. Selected bond lengths (Å) and angles (°): Pd1–C1 1.964(4), Pd1–C10, 2.147(3), Pd11–N3 2.183(3), Pd1–Br1 2.4969(6); Br1–Pd1–C1 177.5(1), Br1–Pd1–C10 90.51(8), Br1–Pd1–N3 92.59(8).

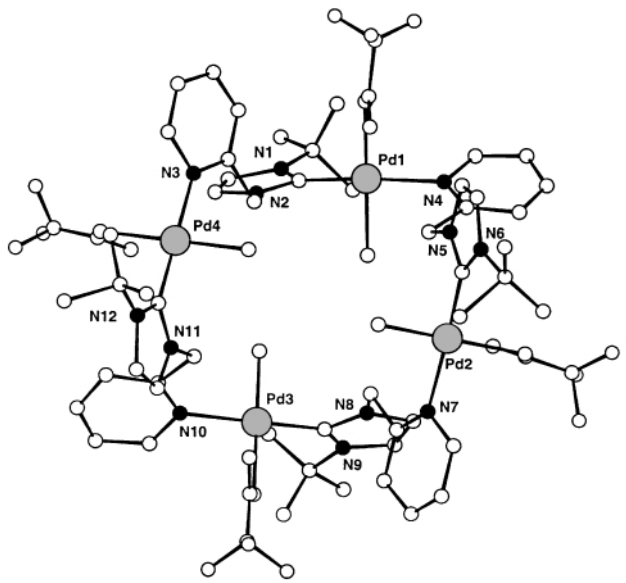

Fig. 2 Molecular structure of **2**. Selected bond lengths (Å): Pd–N 1.99(2)–2.11(2), Pd–O 2.145(15)–2.170(15), Pd–C_{methyl} 1.94(2)–2.10(2), Pd–$C_{carbene}$ 1.89(3)–1.96(3).

DOI: 10.1039/b002645j

Table 1 Selected results of Heck reactions catalysed by **1a**

Aryl halide[a]	Alkene[b]/amine	*t*/h	*T*/°C	Catalyst (mol %)	Base	Yield (%)[d]	TON
PhI	mac	3	130	7×10^{-3}	Na_2CO_3	90	12 900
PhI	mac	1	130	7×10^{-4}	NEt_3	85	121 400
PhI	mac	2	130	7×10^{-4}	NEt_3	95	135 700
PhI	mac	3	130	7×10^{-4}	NEt_3	100	142 900
PhI	mac	6	130	3.5×10^{-4}	NEt_3	100	285 800
PhI	mac	18	140	7×10^{-5}	NEt_3	98	1400 000
PhI	mac	38	140	3.5×10^{-5}	NEt_3	100	2858 000
4-$NO_2C_6H_4Br$	bac	18	140	0.5	NaOAc	95	190
4-$MeCOC_6H_4Br$	bac	18	140	0.5	NaOAc	100	200
PhBr[c]	PhNHMe	24	65	7×10^{-4}	NEt_3	10	14 300
PhBr	mac	75	130	7×10^{-3}	NEt_3	10	1 400
PhBr	mac	152	130	7×10^{-3}	NEt_3	20	2 900

[a] ArX, 5 mmol; alkene/amine, 6 mmol; NEt_3, 7 mmol; NaOAc, 7 mmol; Na_2CO_3, 3.5 mmol; *N*-methylpyrrolidone used as solvent. [b] mac = Methyl acrylate; bac = *n*-butyl acrylate. [c] Determined by GC, based on the aryl halide. [d] THF used as solvent.

undesired deprotonation of the methylene protons linking the carbene to the heterocyclic donor, or even the methyl substituent of the carbene. We believe these initial observations may presage structure–property relationships in similar catalysts.

Complexes **1a** and **1b** are excellent precatalysts for the Heck coupling and show good activity for amination reactions (see Table 1). The activity of **1a** does not seem to decrease with time, implying high thermal stability under the reaction conditions. It is highest in *N*-methylpyrrolidone and *N*,*N*′-dimethylacetamide but is dependent on reaction temperature. The highest turnover frequencies are observed when triethylamine is used as base; other bases such as Na_2CO_3 or NaO_2CMe have also been used successfully but require longer reaction times. The results for the coupling of aryl iodides with acrylates are comparable to the best systems known.[5] Although the mechanism and the nature of the active species in the Heck reaction is far from clear,[6] our results show that (i) highly active palladium catalysts are obtained by using hemilabile carbene complexes, (ii) the presence of other labile ligands in the coordination sphere of the metal makes predictions of the nature of the catalytic species difficult and (iii) higher nuclearity complexes such as **2** may be precursors to the active catalyst which could be obtained by dissociation of the labile end of the ligand. Catalysis by higher nuclearity complexes, especially under Heck conditions, is less likely.

Studies on the reactivity of the new complexes, extension of the methodology to other transition metals and the synthesis of other functionalised N-heterocyclic carbene ligands with a variety of other donor functionalities is under way.

We are indebted to Ineos Acrylics, EPSRC and the University of Southampton for support.

Notes and references

† *Spectroscopic data*: **1a**: MS (ES): *m/z* 377, $[Pd(C–N)Me(MeCN)]^+$. ^1H NMR (300 MHz, $CDCl_3$): δ 9.14 (d, 1H, α-*N*-pyridyl H), 7.70 (dt, 1H, γ-*N*-pyridyl H), 7.33 (t, 1H, β-*N*-pyridyl H), 7.24 (d, 1H, *H*CCH), 7.14 (d, 1H, HCC*H*), 6.66 (m, 1H, β-*N*-pyridyl H), 5.23 (m, 1H,NCH*H*), 5.92 (m, 1H, NC*H*H), 1.95 [s, 9H, $C(CH_3)_3$], 0.56 (s, 3H, $PdCH_3$). $^{13}C\{^1H\}$ NMR (100.5 MHz, $CDCl_3$): δ 175.2 (NCN), 159.7, 152.7, 137.9 (pyridyl C), 123.6, 122.2, 120.4, 119.1 (pyridyl C, NCCN), 59.3 (NCH_2), 54.3 [$C(CH_3)_3$], 30.2 [$C(CH_3)_3$], −7.5 ($PdCH_3$).

1b: MS (ES): *m/z* 439, $[Pd(C–N)Me(MeCN)]^+$. ^1H NMR (300 MHz, $CDCl_3$): δ 9.33 (d, 1H, α-*N*-pyridyl H), 7.76 (dt, 1H, γ-*N*-pyridyl H), 7.50 (d, 1H, β-*N*-pyridyl H), 7.34 (m, 1H, β-*N*-pyridyl H), 7.27 (d, 1H, HCCH), 6.93 (s, 2H, mes CH), 6.78 (d, 1H, *H*CCH), 5.50 (br, 2H, CH_2), 2.31 (s, 3H, mes CH_3), 2.08 (s, 6H, mes CH_3), 0.22 (s, 3H, $PdCH_3$). $^{13}C\{^1H\}$ NMR (100.5 MHz, $CDCl_3$): δ 174.4 (NCN), 153.3, 152.8, 138.7 (pyridyl C), 135.6, 134.9 (mes C), 129.2, 128.8 (mes CH), 124.5, 124.2, 122.2, 121.7 (pyridyl C, NCCN), 55.5 (NCH_2), 21.2, 18.5 (mes CH_3), −13.9 ($PdCH_3$).

2: MS (ES): *m/z* 377, $[Pd(C–N)Me(MeCN)]^+$. ^1H NMR (300 MHz, CD_3CN): δ 8.8 (d, 1H, α-*N*-pyridyl H), 7.5 (dt, 1H, γ-*N*-pyridyl H), 7.2 (m, 1H, β-*N*-pyridyl H), 7.1 (d, 1H, β-*N*-pyridyl H), 7.0 (d, 1H, *H*CCH), 6.4 (d, 1H, HCC*H*), 5.3 (br, CH_2), 0.56 (s, 3H, $PdCH_3$), 1.7 [s, 9H, $C(CH_3)_3$]. $^{13}C\{^1H\}$ NMR (100.5 MHz, $CDCl_3$): δ 174.0 (NCN), 158.5 (pyridyl C), 151.5 ($PdCO_2CF_3$), 150.5, 138.2 (pyridyl C), 123.3, 122.8, 121.4, 120.3 (pyridyl C, NCCN), 97.6 (CF_3), 58.4 (NCH_2), 56.1 [$C(CH_3)_3$], 31.8 [$C(CH_3)_3$], −9.2 ($PdCH_3$).

‡ *Crystal data*: for **1b**: $C_{19}H_{22}BrN_3Pd$, M = 478.71, rhombohedral, space group $R\bar{3}h$ (no. 148), a = 24.521(4), c = 20.201(4) Å, U = 10519(3) Å^3, T = 150 K, Z = 18, μ(Mo-Kα) = 2.507 mm^{-1}, 25874 reflections measured, 4782 unique (R_{int} = 0.047) which were used in all calculations. The final $wR(F^2)$ was 0.1142 (all data) and R = 0.0439 [$F > 2\sigma(F)$]. The structure contains highly disordered solvent CH_2Cl_2 which is located in channels along the c axis (1035 e cell^{-1}) and was treated in the manner described by Sluis and Spek.[7]

For **2**: crystals were obtained by layering of CH_2Cl_2 solution of **2** with ether: $C_{60}H_{80}F_{12}N_{12}O_8Pd_4 \cdot (x$ THF ($x \approx 4$), M_r = 1749.04, triclinic, space group $P\bar{1}$ (no. 2), a = 9.852(2), b = 20.026(4), c = 21.056(4) Å, α = 89.95(3), β = 90.19(3), γ = 90.04(3) °, U = 4154.2(14) Å^3, Z = 2, T = 150 K, μ = 0.935, 34221 reflections measured, 10208 reflections observed, R = 0.1095, R_w = 0.2539. The crystals were of particularly poor quality, and the data reported is the best of four data collections and refinements tried. Recognising the approximate C_2 symmetry of the molecule and orthorhombic cell geometry, we have explored the possibility of higher symmetry structure. Whilst strong data merge reasonably well for orthorhombic (R_{int} = 0.13), monoclinic (R_{int} = 0.062; *cf.* R_{int} = 0.056 for triclinic) we were not able to solve or refine in the higher symmetries.

CCDC 182/1666. See http://www.rsc.org/suppdata/cc/b0/b002645j/ for crystallographic files in .cif format.

1 Review: W. A. Herrmann and C. Køcher, *Angew. Chem., Int. Ed. Engl.*, 1997, **36**, 2162.
2 For Heck and Suzuki coupling reactions, see: W. A. Herrmann, in *Applied Homogeneous Catalysis with Organometallic Compounds*, ed. B. Cornils and W. A. Herrmann, Wiley-VCH, Weinheim, 2000, p. 725; C. Zhang, J. Huang, M. L. Trudell and S. P. Nolan, *J. Org. Chem.*, 1999, **64**, 3804; for CO–ethylene copolymerisations, see: M. G. Gardiner, W. A. Herrmann, C.-P. Reisinger, J. Schwarz and M. Spiegler, *J. Organomet. Chem.*, 1999, **572**, 239; for olefin metathesis reactions, see: T. Weskamp, W. C. Schattenmann, W. C. Spiegler and W. A. Herrmann, *Angew. Chem., Int. Ed.*, 1998, **37**, 2490; M. Scholl, T. M. Trnka, J. P. Morgan and R. H. Grubbs, *Tetrahedron Lett.*, 1999, **40**, 2247; for catalytic hydrosilations, see: W. A. Herrmann, L. J. Goossen, C. Køcher and G. R. J. Artus, *Angew. Chem., Int. Ed. Engl.*, 1996, **35**, 2805.
3 W. A. Herrmann, C. Køcher, L. Goossen and G. R. J. Artus, *Chem. Eur. J.*, 1996, **2**, 1627; W. A. Herrmann, L. Goossen and M. Spiegler, *Organometallics*, 1998, **17**, 2162.
4 D. S. McGuinness and K. J. Cavell, *Organometallics*, 2000, **19**, 741.
5 M. Ohff, A. Ohff and D. Milstein, *Chem. Commun.*, 1999, 357.
6 B. L. Shaw, S. D. Perera and E. A. Staley, *Chem. Commun.*, 1998, 1361; B. L. Shaw, *New J. Chem.*, 1998, **22**, 77.
7 P. van der Sluis and A. L. Spek, *Acta Crystallogr., Sect. A.*, 1990, **46**, 194.

Palladium catalysed Suzuki cross-coupling reactions in ambient temperature ionic liquids

Christopher J. Mathews,[a] Paul J. Smith[b] and Thomas Welton*[b]

[a] *ZENECA Agrochemicals, Jealotts International Research Centre, Bracknell, UK RG42 6ET*
[b] *Department of Chemistry, Imperial College of Science Technology and Medicine, London, UK SW7 2AY. E-mail: t.welton@ic.ac.uk*

Received (in Cambridge, UK) 6th April 2000, Accepted 30th May 2000
Published on the Web 20th June 2000

Palladium catalysed Suzuki cross-coupling reactions have been conducted in the ambient temperature ionic liquid,1-butyl-3-methylimidazolium tetrafluoroborate ([bmim][BF_4]), exhibiting unprecedented reactivities in addition to easy product isolation and catalyst recycling.

The continuing depletion of natural resources and growing environmental awareness has necessitated changes in the practices of both the chemical industry and academia. One strategy that addresses these issues is the replacement of deleterious molecular solvents with environmentally more benign, reaction enhancing alternatives. Of the novel solvents that have emerged, ambient temperature ionic liquids consisting of 1,3-dialkylimidazolium cations have shown great promise (Fig. 1).[1] Their negligible vapour pressure, ease of handling and potential for recycling, circumvent many of the problems associated with volatile organic solvents. Furthermore, their high compatibility with transition metal catalysts and limited miscibility with common solvents, enables easy product and catalyst separation with the retention of the stabilised catalyst in the ionic phase. These and related ionic liquids have been successfully employed as the media in a number of reactions, which include hydrogenations,[2] alkene dimerizations,[3] Diels–Alder[4] and Friedel–Crafts[5] reactions.

The Suzuki[6] cross-coupling reaction is an extremely versatile methodology for the generation of new carbon–carbon bonds and is employed most successfully in the synthesis of biaryls.[7] The reaction, however, suffers from a number of drawbacks such as catalyst loss into the product, catalyst decomposition and poor reagent solubilities. We postulated that these problems might be resolved by the use of ionic liquids. Recently, the closely related Heck[8] and Trost–Tsuji[9] coupling reactions have been conducted in ionic liquids with great success. We report herein the first examples of the more complex palladium catalysed Suzuki cross-coupling reactions in the ambient temperature ionic liquid, [bmim][BF_4]. [bmim][BF_4] has a liquid range in the order of 300 °C, it is stable in air and is known to solubilize many organometallic compounds.[10] These properties, in addition to its controllable miscibility with water and immiscibility with ether, make [bmim][BF_4] a potential solvent for Suzuki reactions.

The reaction of 4-bromotoluene with phenylboronic acid in [bmim][BF_4] was initially investigated using the original Suzuki conditions.[11] This afforded 4-methylbiphenyl in a 30% yield after 6 h, with catalyst decomposition evidenced by the precipitation of a black solid (Table 1, entry 6). Further investigation revealed that modifying the original conditions significantly boosted yields of the desired products, enhanced reaction rates and prevented catalyst decomposition. The new conditions involved heating the catalyst with the arylhalide in [bmim][BF_4] at 110 °C with vigorous stirring until complete solution occurred. The catalytic solution is cooled to ambient temperature and the reaction started by the addition of the arylboronic acid and an aqueous solution of Na_2CO_3.[12] Adopting this procedure with a reduced catalyst concentration, $Pd(PPh_3)_4$ (1.2 mol%, based on arylhalide), afforded 4-methylbiphenyl in a 69% yield after 10 min, without catalyst decomposition (Table 1, entry 7). The reaction can also be achieved with one-tenth the catalyst concentration generally required, $Pd(PPh_3)_4$ (0.3 mol%, Table 1, entry 8). Once the catalytic solution has been generated the reaction can be conducted under air with analogous results and no catalyst decomposition (Table 1, entry 9).

The scope of the reaction in [bmim][BF_4] was investigated with electron-rich and electron-deficient arylhalides (Table 1). The reactivity exhibits dramatic enhancements over the conditions generally employed. For example, conducting the reaction of bromobenzene with phenylboronic acid under the original Suzuki conditions affords biphenyl with an 88% yield in 6 h (5 TON h^{-1}).[11] In [bmim][BF_4] a 93% yield is achieved in 10 min (455 TON h^{-1}, Table 1, entry 2), which is over 90 times the original reactivity. Notably, 4-methoxybiphenyl is afforded in a 40% yield in 6 h (2 TON h^{-1}) applying the original conditions.[11] In [bmim][BF_4] an 81% yield is afforded in

Cationic Components

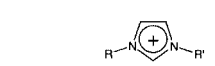

R = ^{n}Bu; R' = Me, 1-*n*-Butyl-3-methylimidazolium, ([bmim]$^+$)
R = Et; R' = Me, 1-Ethyl-3-methylimidazolium, ([emim]$^+$)

Anionic Components

Cl^-
$[AlCl_4]^-$
$[TfO]^-$
$[BF_4]^-$
$[PF_6]^-$

Fig. 1

Table 1 Scope of the Suzuki cross-coupling reaction in [bmim][BF_4]: variation of the arylhalide

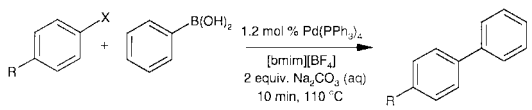

Entry	X	R	Yield (%)[a]	TON	TON h^{-1}
1	I	H	86 (95)	72	430
2	Br	H	93 (95)	78	465
3	Cl	H	1 (1)	1	5
4	Br	Cl	17	14	85
5	Br	$COCH_3$	67 (97)	56	335
6	Br	CH_3	30 [b]	25	150
7	Br	CH_3	69 (92)	58	345
8	Br	CH_3	72 [d]	60	360
9	Br	CH_3	68 [c]	57	340
10.1	Br	OCH_3	81 (92)	67	401
10.2	Br	OCH_3	89	73	441
10.3	Br	OCH_3	77	64	381
10.4	Br	OCH_3	82	68	406

[a] Isolated yields of corresponding cross coupled product based on arylhalide. Purity confirmed by GC, GC-MS and ^{1}H NMR. Isolated yields after 3 h in parentheses. [b] Suzuki reaction without prior activation of catalyst. Original catalyst concentration employed, $Pd(PPh_3)_4$ (3 mol%). Catalyst decomposition observed. [c] Reaction performed under air. [d] Lower catalyst concentration, $Pd(PPh_3)_4$ (0.3 mol%). Reaction time 1 h.

DOI: 10.1039/b002755n

Table 2 Scope of the Suzuki cross-coupling reaction in [bmim][BF_4]: variation of the arylboronic acid

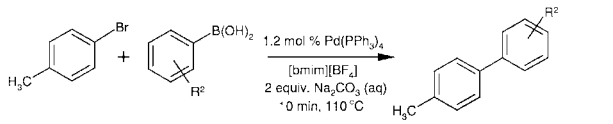

Entry	R^2	Product	Yield (%)[a]	TON	TON h^{-1}
1	4-CH_3	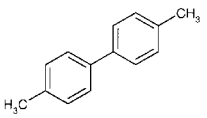	68	57	340
2	2-CH_3	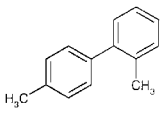	68	57	340
3	4-OMe	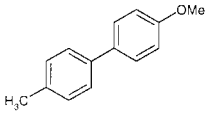	81	68	405
4	4-$COCH_3$	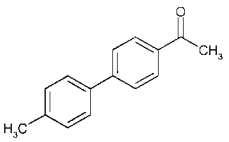	45	38	225

[a] Isolated yields of corresponding cross coupled product based on arylhalide. Purity confirmed by GC-MS and ^{1}H NMR.

10 min (401 TON h^{-1}, Table 1, entry 10.1), which is in the order of 200 times the original reactivity. We are continuing to explore the generality of this result. Despite these enhancements, chlorobenzene was still inactive even after 3 h, with only a trace of biphenyl being detected, presumably due to *homo*-coupling of the arylboronic acid (Table 1, entry 3).[13]

The effect of the arylboronic acid partner on the Suzuki reactions in [bmim][BF_4] was also investigated (Table 2). The results of the functionalised arylboronic acids seem to parallel those obtained with the same functional groups on the arylhalide. This suggests that both the nature of the arylhalide and the arylboronic acid affect the reaction, apparently in an analogous manner. We are continuing to investigate these interesting results.

Isolation of the biaryl products from the [bmim][BF_4] reaction mixture can be achieved by extraction with diethyl ether, sublimation or precipitation by the addition of water, all without any apparent leaching of palladium species into the product. Extraction with diethyl ether was found to be a generally applicable method for all biaryls and led to the highest yields. Biphenyl, mono-, and di-functionalised biaryls can easily be sublimed from the reaction mixture by heating at 80 °C *in vacuo*. With water insoluble products, isolation and catalytic solution recovery and recycling was most effective with water. Typically, the reaction mixture was allowed to cool to *ca.* 60 °C, warm water was added and the mixture left to cool to ambient temperature whereupon the biaryl products crystallised out. These were collected by filtration and washed with cold water to afford the desired product with a purity > 98% (determined by GC). The only impurity being the *homo*-coupled product. The negligible amount of *homo*-coupled products detected in the reactions can be avoided by adding the phenylboronic acid to the reaction mixture over a period of an hour.

The by-products ($NaHCO_3$ and $Na[XB(OH)_2]$) generated in the reaction modify the miscibility of water with [bmim][BF_4] such that two phases are formed at ambient temperature. The by-products are preferentially soluble in the large excess of added water. This enables the removal of the by-products with the water, affording the cleaned, ionic liquid, catalytic solution. The ability to isolate product and recover the catalytic solution permits repetitive catalytic runs. The catalytic solution was re-used three times without loss of activity in the reaction of 4-bromoanisole with phenylboronic acid (Table 1, entries 10.2–10.4. Once the catalytic solution has been prepared in the first run, it can be re-used with no further modification. The product was extracted with diethyl ether and the catalytic solution washed with water after each run.

In summary, we have demonstrated that Suzuki cross-coupling reactions can be successfully conducted in the ambient temperature ionic liquid, [bmim][BF_4], with a number of advantages: (i) The reactions show a significant increase in reactivity at reduced catalyst concentration, especially with respect to non-activated arylbromides. (ii) Homo-coupled products can be eliminated, affording isolated products in high purity avoiding laborious purification procedures. (iii) The reactions can be performed under air without loss of yield or catalyst decomposition. (iv) The procedures developed permit repetitive catalytic runs without loss of catalyst activity. Further investigations concerning the nature of the active catalytic species and the mechanism of reaction are currently in progress.

This work was supported by EPRSC and a ZENECA CASE award (P. J. S.). We would like to thank Karsten Tonn (Imperial College) for performing GC-MS analysis and Dr Michael A. Carroll (Imperial College) for informative discussions. We would also like to thank Johnson Matthey for the kind loan of palladium.

Notes and references

1 K. R. Seddon, *J. Chem. Tech. Biotechnol.*, 1997, **68**, 351; K. R. Seddon, *Kinet. Catal. (Engl. Transl.)*, 1996, **37**, 693.
2 P. J. Dyson, D. J. Ellis, D. G. Parker and T. Welton, *Chem. Commun.*, 1999, 25.
3 B. Ellis, W. Keim and P. Wasserscheid, *Chem. Commun.*, 1999, 336.
4 T. Fisher, A. Sethi, T. Welton and J. Woolf, *Tetrahedron Lett.*, 1999, **40**, 793.
5 A. Stark, B. L. MacLean and R. D. Singer, *J. Chem. Soc., Dalton Trans.*, 1999, 63.
6 N. Miyaura and A. Suzuki, *Chem. Rev.*, 1995, **95**, 2457 and references therein.
7 S. P. Stanforth, *Tetrahedron*, 1998, **54**, 263 and references therein.
8 V. P. W. Böhm and W. A. Herrmann, *Chem. Eur. J.*, 2000, **6**, 1017; A. J. Carmichael, M. J. Earle, J. D. Holbrey, P. B. McCormac and K. R. Seddon, *Org. Lett.*, 1999, **1**, 997; L. Xu, W. Chen and J. Xiao, *Organometallics*, 2000, **19**, 1123; W. A. Herrmann and V. P. W. Böhm, *J. Organomet. Chem.*, 1999, **572**, 141.
9 C. De Beelefon, E. Pollet and P. Grenouillet, *J. Mol. Catal. A.*, 1999, **145**, 121; W. Chen, L. Xu, C. Chatterton and J. Xiao, *Chem. Commun.*, 1999, 1247.
10 T. Welton, *Chem. Rev.*, 1999, **99**, 2071.
11 The original Suzuki conditions employ: arylhalide (2.5 mmol, 1 equiv.); arylboronic acid (2.75 mmol, 1.1 equiv.); $Pd(PPh_3)_4$ (3 mol%, based on arylhalide); Na_2CO_3 (5.3 mmol, 2 equiv.) and toluene–H_2O–EtOH 4:2:1, heated at 110 °C for 6 hours. N. Miyaura, T. Yanagi and A. Suzuki, *Synth. Commun.*, 1981, **11**, 513.
12 Typical procedure for the Suzuki reaction in [bmim][BF_4]: aryl halide (2.5 mmol, 1 equiv.) was added to a suspension of $Pd(PPh_3)_4$ (34.7 mg, 0.03 mmol, 1.2 mol%) in degassed [bmim][BF_4] (5 cm^3) at ambient temperature under nitrogen. The mixture was slowly heated to 110 °C with vigorous stirring affording a yellow–orange solution. The solution was cooled to ambient temperature and the arylboronic acid (2.75 mmol, 1.1 equiv.) and a solution of Na_2CO_3 (560 mg, 5.28 mmol, 2.1 equiv.) in water (2.5 cm^3) was added. The mixture was reheated at 110 °C with vigorous stirring for a further 10 min, then cooled and extracted with diethyl ether (3 × 15 cm^3). The combined extracts were washed first by brine (2 × 10 cm^3), then water (2 × 10 cm^3) and dried ($MgSO_4$). Filtering through a silica pad and evaporation to dryness afforded the Suzuki biaryl product as characterised by GC-MS, ^{1}H-NMR and IR spectroscopy. The reaction mixture was washed with water (2 × 10 cm^3) and dried under *vacuo* to recover the catalytic solution.
13 The low reactivity of aryl chlorides in cross-coupling reactions is well documented. For discussions, see V. V. Grushin and H. Alper, *Chem. Rev.*, 1994, **94**, 1047.

ChemComm

Synthesis and structure of the first open-framework cadmium oxalate possessing channels

P. A. Prasad, S. Neeraj, Srinivasan Natarajan and C. N. R. Rao*

Chemistry and Physics of Materials Unit and CSIR Centre of Excellence in Chemistry, Jawaharlal Nehru Centre for Advanced Scientific Research, Jakkur P.O., Bangalore 560 064, India. E-mail: cnrrao@jncasr.ac.in

Received (in Cambridge, UK) 4th April 2000, Accepted 31st May 2000
Published on the Web 20th June 2000

A three-dimensional open-framework cadmium oxalate, $K[C_3N_2H_5][Cd(C_2O_4)_2]$, in which both the amine and the K^+ ion participate in the formation of the structure, has been synthesized and characterized for the first time.

Amongst the variety of open-framework inorganic materials, those of the metal carboxylates constitute a new family.[1–3] While the literature abounds in reports of the synthesis and characterization of aluminosilicates and metal phosphates with open architectures,[4] recent studies of metal carboxylates have also brought out certain novel structural features.[1,2] For example, OZn_4 clusters have been observed in zinc benzenedicarboxylates[2a] and Co–O–Co layers in a cobalt succinate.[1c] Metal oxalates synthesized hydrothermally in the presence of organic amines exhibit two- and three-dimensional architectures.[5,6] In the latter type of metal oxalates, the oxalate units lie in the plane of honeycomb-type layers and also provide the out-of-plane bridges to form the three-dimensional structure. The oxalate unit also plays a dual role in metal oxalate–phosphates where it forms an integral part of the layer structure predominantly constituted by the phosphate network and also acts as the link to create the third dimension.[7] Up to now open-framework metal oxalates synthesized in the presence of structure-directing amines have been restricted to those of Sn(II) and Zn. We have been exploring ways of preparing open-framework cadmium oxalates for some time. Here, we report the first successful synthesis and characterization of a Cd oxalate of the formula $K[C_3N_2H_5][Cd(C_2O_4)_2]$ **I**, with open architecture and possessing channels.

The cadmium oxalate **I** was synthesized by employing hydrothermal methods. Typically, 0.5 g of cadmium oxalate was dispersed in a mixture of 4.3 ml of butan-2-ol (BuOH) and 1.1 ml of water. To this, 0.328 ml of glacial acetic acid and 0.24 g of imidazole were added, followed by a small quantity of KCl (0.04 g). The approximate molar ratio of the reaction mixture was $5CdC_2O_4:KCl:5.5C_3N_2H_4:9MeCO_2H:75BuOH:100H_2O$. The mixture was homogenized for 30 min at room temperature (298 K), sealed in a 23 ml Teflon-lined acid digestion bomb and heated at 110 °C for 46 h. The product, a crop of tiny colorless diamond-shaped crystals, was recovered by suction filtration, washed with deionized water and dried at ambient temperature and conditions. Powder X-ray diffraction (XRD) indicated that the product was a new material, the pattern being entirely consistent with the structure determined by single crystal X-ray diffraction. Thermogravimetric analysis (TGA) under a nitrogen atmosphere (50 ml min^{-1}) from room temperature to 700 °C (heating rate = 10 °C min^{-1}) shows only one mass loss in the region 280–380 °C. The mass loss of 53.2% corresponds well with the loss of the oxalate and amine (calc. 55.6%). The powder X-ray diffraction pattern of the decomposed sample indicated that it was amorphous.

A suitable single crystal was carefully selected and subjected to X-ray diffraction using a Siemens SMART diffractometer with a CCD detector† and the structure was solved by direct methods. The asymmetric unit contains 20 independent non-hydrogen atoms. The structure of **I** consists of a network of cadmium and oxalate units forming an anionic framework with formula $[Cd(C_2O_4)_2]^{2-}$. Charge neutrality is achieved by the monoprotonated amine and potassium ions. Two K^+ ions occupy special positions with a site occupancy factor (SOF) of 0.5 per framework formula unit. The framework is built-up of four oxalate units, linked *via* the oxygens to the cadmium atoms with Cd–O distances in the range 2.327(3)–2.528(3) Å [$(Cd–O)_{av}$ = 2.422 Å] and O–Cd–O angles in the range 67.5(1)–151.3(1)° [$(O–Cd–O)_{av}$ = 88.6°]. The cadmium atoms are eight-coordinated with respect to oxygens forming a dodecahedral arrangement as shown in Fig. 1(a). The dodecahedral arrangement of oxygen atoms around the cadmium is of note since Cd atoms are generally octahedrally coordinated.

The complex framework structure of **I** can be understood in terms of simpler building units. Thus, the *in-plane* connectivity between the oxalate units [C(2)–C(3)O_4 and C(4)–C(4)O_4] and Cd results in the formation of honeycomb-like layers with twelve-membered apertures (six Cd and six oxalate units) along the [011] direction, as shown in Fig. 1(b). The remaining oxalate unit [C(1)–C(1)O_4] bridges (out-of-plane connection) these layers giving rise to one-dimensional elliptical channels (10.4 ×

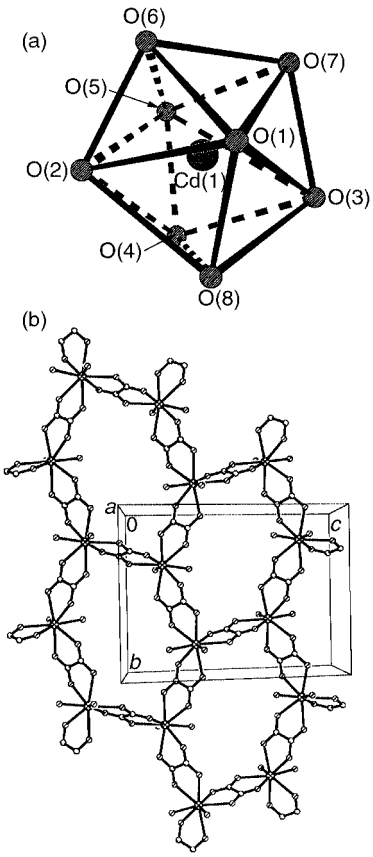

Fig. 1 (a) The environment of cadmium atoms in **I**. Note that the oxygen atoms form a dodecahedral arrangement around Cd. (b) In-plane connectivity between the oxalates and cadmium in **I**, along the *bc* plane, showing honeycomb-like layers.

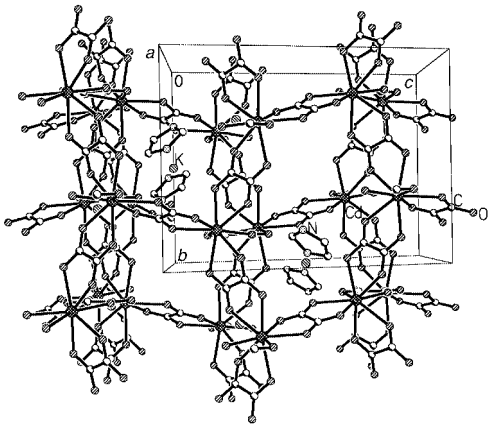

Fig. 2 Structure of $K[C_3N_2H_5][Cd(C_2O_4)_2]$ **I** along the *a* axis, showing one-dimensional channels. Note that both K^+ and imidazolium cations occupy the same channels.

7.2 Å, shortest atom–atom contact distances not including the van der Waals radii), along the *a* axis. The imidazolium and K^+ ions reside in these channels (Fig. 2). The linkages between $C(2)–C(3)O_4$ and $C(1)–C(1)O_4$ oxalates and Cd (in-plane) result in a layer with twelve-membered rectangular apertures, along the *ab* plane. These layers are pillared by the $C(4)–C(4)O_4$ oxalate units (out-of-plane) forming another one-dimensional channel of width (4.1 × 11.3 Å) along the *c* axis. To our knowledge, **I** is the first example of an open-framework cadmium oxalate possessing channels.

The structure of **I** shows close similarity to that of $[NH_4][Ti(C_2O_4)_2]·2H_2O$.[8] In the latter, the Ti atom is surrounded by eight oxygens forming a square antiprism. Connectivity between the Ti and oxalate units results in a three-dimensional structure with channels containing $[NH_4]^+$. Connectivity between Cd and the two oxalates in **I** leads to layers, which are then connected by another oxalate leading to three-dimensional connectivity.

In summary, the synthesis and structure of a novel open-framework cadmium oxalate **I** has been accomplished. It is likely that the formation of such an architecture is facilitated by the presence of two types of structure-directing species, the protonated organic amine and the alkali metal cation. The formation of channels in the presence of alkali metal cations is reminiscent of aluminosilicate zeolites,[9] and paves the way for possible ion-exchange and related studies. Since **I** is the first example of an open-framework cadmium oxalate it would be profitable to explore the formation of similar or related compounds by employing structure-directing agents. Work in this direction is in progress.

Notes and references

† *Crystal data* for **I**: $K[C_3N_2H_5][Cd(C_2O_4)_2]$, M = 396.6, crystal dimensions 0.2 × 0.2 × 0.16 mm, monoclinic, space group $C2/c$, a = 13.016(1), b = 11.291(1), c = 15.754(1) Å, β = 105.04(1)°, V = 2236.01(9) Å^3, Z = 8, D_c = 2.356 g cm^{-3}, μ(Mo-Kα) = 2.37 mm^{-1}, λ = 0.71073 Å. Structure solved by direct methods (SHELXTL-PLUS). A total of 4641 reflections were collected at 298 K in the θ range 2.42–23.25° and merged to give 1617 unique data (R_{int} = 0.033) of which 1463 with $I > 2\sigma(I)$ were considered to be observed. The structure was solved by direct methods with SHELXS-86[10] and difference Fourier synthesis. Final R_1 = 0.02 and wR_2 = 0.049 and S = 1.07 were obtained for 174 parameters. All the hydrogen atoms were located initially in the difference Fourier maps and for the final refinements, hydrogen atoms for the amine molecule were placed geometrically and held in the riding mode. Final Fourier map minimum and maximum: −0.664/0.359 e Å^{-3}. Full-matrix least-squares structure refinement against $|F^2|$ were carried out with SHELXTL-PLUS program package.[11]

CCDC 182/1668. See http://www.rsc.org/suppdata/cc/b0/b002684k/ for crystallographic files in .cif format.

1 (*a*) F. Serpaggi and G. Ferey, *J. Mater. Chem.*, 1998, **8**, 2737; F. Serpaggi and G. Ferey, 1998, **8**, 2749; (*b*) C. Livage, C. Egger, M. Nogues and G. Ferey, *J. Mater. Chem.*, 1998, **8**, 2743; (*c*) C. Livage, C. Egger and G. Ferey, *Chem. Mater.*, 1999, **11**, 1546.

2 (*a*) H. Li, M. Eddaoudi, M. O'Keefe and O. M. Yaghi, *Nature*, 1999, **402**, 276; (*b*) M. Reineke, M. Eddaoudi, M. Fehr, D. Kelly and O. M. Yaghi, *J. Am. Chem. Soc.*, 1999, **121**, and references therein; (*c*) S. S.-Y. Chui, S. M.-F. Lo, J. P. H. Charmant, A. G. Orpen and I. D. Williams, *Science*, 1999, **283**, 1148.

3 S. Romero, A. Mosset and J. C Trombe, *Eur. J. Solid State Inorg. Chem.*, 1997, **34**, 209; V. Kiritsis, A. Michaelides, S. Skoulika, S. Golhen and L. Quahab, *Inorg. Chem.*, 1998, **37**, 3407; S. O. H. Gutschke, D. J. Price, A. K. Powell and P. T. Wood, *Angew. Chem., Int. Ed.*, 1999, **38**, 1088.

4 J. M. Thomas, *Philos. Trans. R. Soc. London A*, 1990, **333**, 173; M. E. Davis, *Chem. Eur. J.*, 1997, **3**, 1745; A. K. Cheetham, G. Ferey and T. Loiseau, *Angew. Chem., Int. Ed.*, 1999, **38**, 3268.

5 S. Ayyappan, A. K. Cheetham, S. Natarajan and C. N. R. Rao, *Chem. Mater.*, 1998, **10**, 3746; S. Natarajan, R. Vaidhyanathan, C. N. R. Rao, S. Ayyappan and A. K. Cheetham, *Chem. Mater.*, 1999, **11**, 1633.

6 R. Vaidhyanathan, S. Natarajan, A. K. Cheetham and C. N. R. Rao, *Chem. Mater.*, 1999, **11**, 3636.

7 A. Choudhury, S. Natarajan and C. N. R. Rao, *Chem. Eur. J.*, 2000, **6**, 1168.

8 H. S. Sheu, J. C. Wu, T. Wang and R. B. English, *Acta Crystallogr., Sect. B*, 1996, **52**, 458.

9 W. M. Meier, D. H. Olson and Ch. Baerlocher, *Altas of Zeolite Structural Types*, Elsevier, New York, 4th edn., 1996.

10 G. M. Sheldrick, SHELXS-86 Program for Crystal Structure Determination, Universität Göttingen, 1986, *Acta Crystallogr., Sect. A*, 1990, **46**, 467.

11 G. M. Sheldrick, SHELXTL-PLUS Program for Crystal Structure Solution and Refinement, Universität Göttingen, 1993.

A novel class of cationic *gemini* surfactants showing efficient *in vitro* gene transfection properties

Patrick Camilleri,*[a] Andreas Kremer,[a] Andrew J. Edwards,[a] Kevin H. Jennings,[a] Owen Jenkins,[a] Ian Marshall,[a] Caroline McGregor,[b] William Neville,[a] Simon Q. Rice,[a] Richard J. Smith,[a] Mike J. Wilkinson[a] and Anthony J. Kirby[b]

[a] *SmithKline Beecham Pharmaceuticals, New Frontiers Science Park, Third Avenue, Harlow, Essex, UK CM19 5AW*
[b] *University Chemical Laboratory, Lensfield Road, Cambridge, UK CB2 1EW.*
E-mail: Patrick_Camilleri@sbphrd.com

Received (in Cambridge, UK) 3rd March 2000, Accepted 2nd June 2000
Published on the Web 20th June 2000

Five novel peptide-based cationic *gemini* surfactants have been synthesised and their ability to transfect plasmid DNA containing the luciferase gene has been examined. Three of these detergents, differing in the number of positive charges per molecule at neutral pH, mediated transfection on their own. However, their efficiency increased markedly on the addition of a neutral colipid and a basic polypeptide.

Over the last ten years various cationic lipids have been synthesised for complexation with DNA and the *in vitro* delivery of genes to mammalian cells, leading to successful expression of the corresponding proteins.[1–3] The hydrophobic 'tails' of the majority of these cationic detergents consist of one or two saturated or mono-unsaturated hydrocarbon chains containing 16 to 18 carbon atoms; examples are cetyltrimethylammonium bromide (CTAB) and 2,3-dioleoyloxy-*N*-{2-[1,4-bis(3-aminopropymino)-2-butylcarboxamido]ethyl}-*N*,*N*-dimethyl-1-propylammonium bromide (DOSPA).[4]

The polar 'head-groups' of cationic lipid vectors have generally consisted of monovalent quaternary ammonium salts (as in CTAB and 1,2-dioleoyloxypropyl-*N*,*N*,*N*-trimethylammonium chloride, DOTAP). However, lipids such as DOSPA with a multivalent 'head-group' have been found to transfer genes *in vitro* more efficiently than the monovalent analogues.[5]

We report a novel class of non-viral gene-transfer vectors based on *gemini* surfactants (Fig. 1). Unlike several cationic lipids used in gene transfection studies, GS1 to GS5 *gemini* surfactants are solids, easy to handle and readily soluble in aqueous media over a wide range of pH. We use a thioether rather than the disulfide linkage for reasons of chemical stability. However, the amide linkages in the 'head-groups' and between the 'head-groups' and the hydrophobic alkyl chains confer a degree of biodegradability, reducing the potential cytotoxicity of these detergents.

Complexation of cationic lipids with DNA is a key design factor for these vehicles. The binding interaction between the cationic *gemini* molecules and DNA was confirmed by agarose gel electrophoresis studies (Fig. 2). Various concentrations of *gemini* surfactants were incubated with the pCMV-luciferase

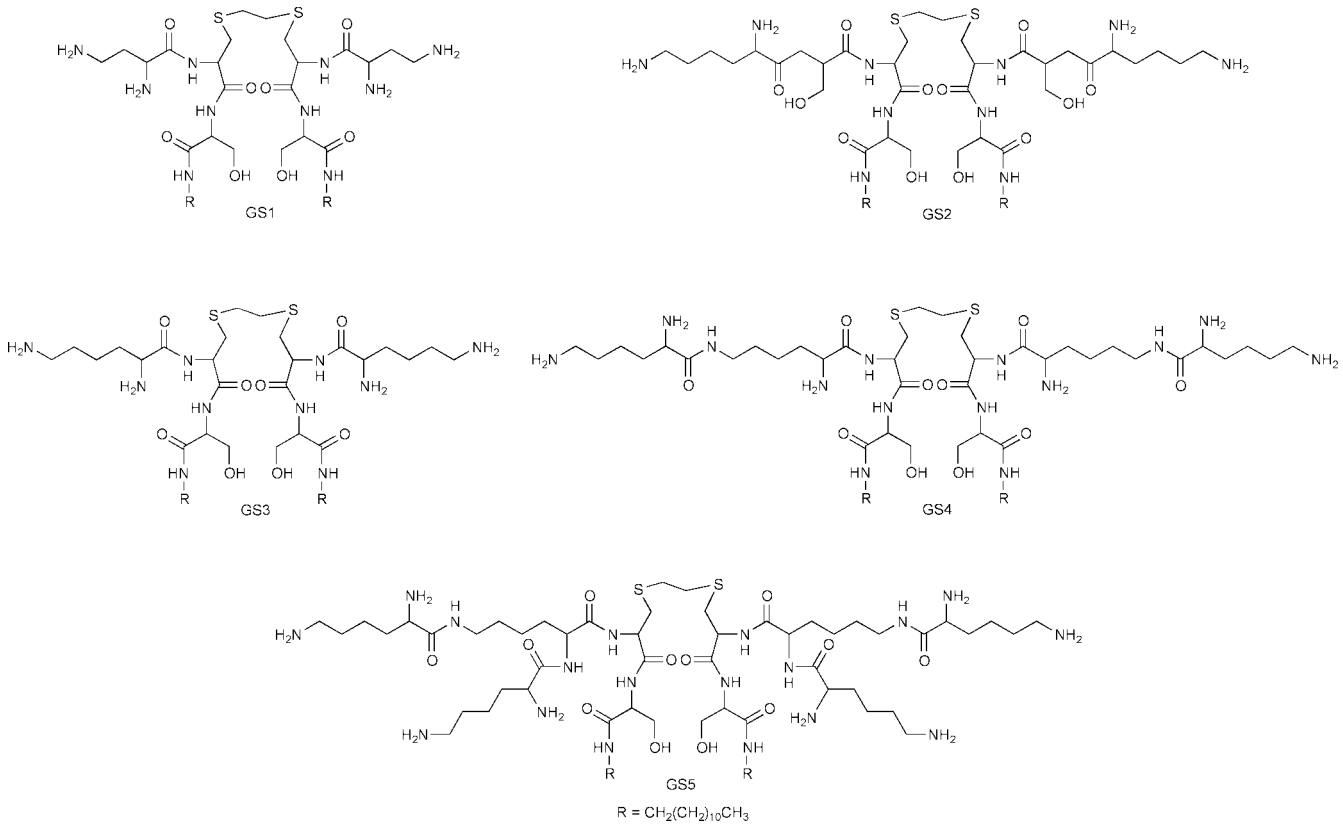

Fig. 1 Chemical structures of *gemini* surfactants GS1 to GS5. All details on the synthesis of these surfactants are provided in patent application, WO 99-29712 (SmithKline Beecham plc).

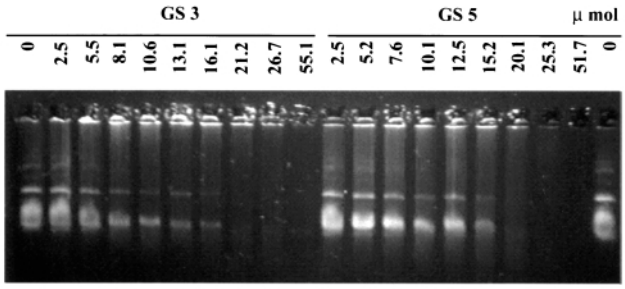

Fig. 2 Interaction of *gemini* surfactants with DNA in the presence of ethidium bromide. Agarose gel electrophoresis assay with GS3 and GS5.

plasmid DNA complexed with ethidium bromide.† These mixtures were then electrophoresed in agarose gel, and subsequently visualised under ultraviolet light. These experiments indicate that all five molecules were effective in releasing the nucleic acid from the DNA–ethidium bromide complex, consistent with binding of the cationic *gemini* to the DNA.

Relative transfection efficiencies for surfactants GS2, GS4 and GS5 are shown in Fig. 3. GS2 and GS5 are most efficient at about 10 μM, whereas for *gemini* GS4 the optimal concentration is slightly higher, at 13 μM. Concentrations used in the transfection experiments are well below the cmc values (0.3 ± 0.1 mM) so that the formation of micelles or liposomes (multilamellar forms) does not appear to be necessary for transfection to occur. Although the electrostatic nature of complex formation of these *gemini* molecules with DNA is likely to be important for complexation with DNA, it is not the only factor that influences gene transfection. Thus surfactants GS1 and GS3 complex with DNA, but do not mediate transfection. It may be that the complexes formed by these two surfactants are too strong to release DNA at a critical point, or that interactions other than electrostatic contribute to transfection efficiency.

It is well known that the DNA transfection efficiency of cationic lipids improves in the presence of a neutral colipid ('helper') and/or a basic polypeptide.[6,7] Thus LIPOFECTAMINE PLUS™ (Life Technologies), one of the leading commercial products for *in vitro* gene transfection, consists of a mixture of DOSPA, dioleoylphosphatidylethanolamine

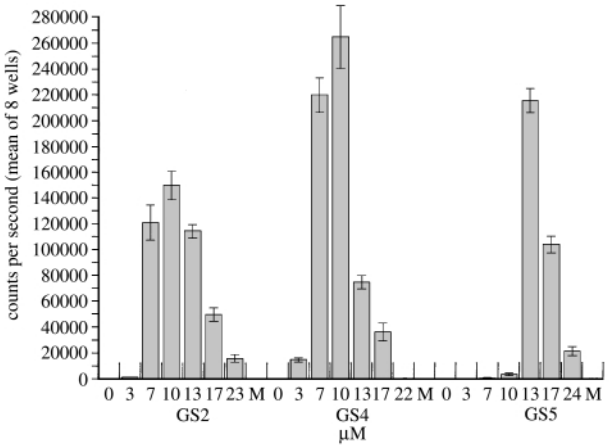

Fig. 3 Transfection experiment in CHO-K1 cells. The cells were incubated overnight at 37 °C with DNA and different concentrations of GS2, GS4 and GS5 or GS without DNA (M). Luciferase activity was measured using the stable light signal reporter gene assay and the counts per second from eight wells were averaged.

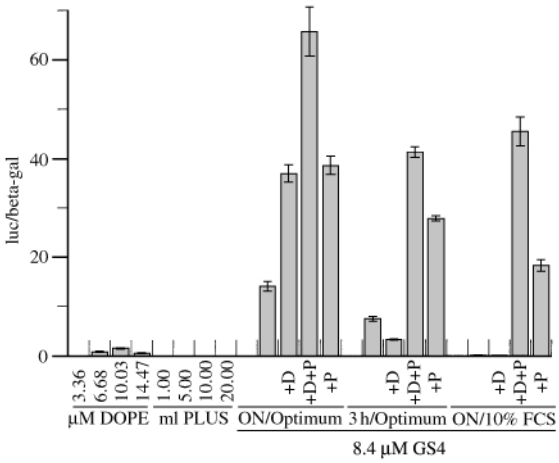

Fig. 4 Transfection experiment in CHO-K1 β-gal cells. The cells were incubated in Opti-MEM® or complete medium with the transfection mixtures overnight (ON) or 3 h at 37 °C. GS4 was used alone or in combination with DOPE (+D), with 'PLUS'-reagent (+P) or in a combination of both (+D+P). The luciferase activity of eight wells was normalized against the corresponding β-galactosidase activity. As controls, various amounts of DOPE and 'PLUS'-reagent alone were incubated with DNA and used for transfection (over night/Opti-MEM®).

(DOPE) and a basic peptide. The transfection efficiencies of GS4 alone and in the presence of (i) DOPE, (ii) the 'Plus' reagent (a basic peptide) and (iii) DOPE and the 'Plus' reagent is shown in Fig. 4. Addition of either the neutral lipid or the basic peptide increases transfection efficiency more than twofold. However, the biggest increase in efficiency occurs when both neutral lipid and basic peptide are added to GS4. It is remarkable that overnight incubation of the DNA with serum in the presence of GS4, DOPE and the 'Plus' reagent gave the maximum protection from degradation by serum nucleases. A similar result was reported recently for the transfection vehicle 3β-[*N*-(*N*′,*N*′-dimethylaminoethyl)carbamyl]cholesterol in the presence of polylysine.[7] In the majority of experiments, the observed expression level with GS4 was of the same order of magnitude as that with LIPOFECTAMINE PLUS™ (data not shown).

Notes and references

† The IUPAC name for ethidium bromide is 3,8-diamino-5-ethyl-6-phenylphenanthridinium bromide.

1 J. H. Felgner, R. Kumar, C. N. Sridhar, C. J. Wheeler, Y. J. Tsai, R. Border, P. Ramsey, M. Martin and P. L. Felgner, *Proc. Natl. Acad. Sci. USA*, 1987, **84**, 7413.
2 C. Y. Wang and L. Huang, *Biochemistry*, 1989, **28**, 9508.
3 J. H. Felgner, R. Kumar, C. N. Sridhar, C. J. Wheeler, Y. J. Tsai, R. Border, P. Ramsey, M. Martin and P. L. Felgner, *J. Biol. Chem.*, 1994, **269**, 2550.
4 R. J. Lee and L. Huang, *Crit. Rev. Ther. Drug Carrier Syst.*, 1997, **14**, 173.
5 J. G. Lewis, K. Y. Lin, A. Kothavale, W. M. Flanagan, M. D. Matteucci, D. DePrince, R. A. Mook, R. W. Hendren and R. W. Wagner, *Proc. Natl. Acad. Sci. USA*, 1996, **93**, 3176.
6 C. W. Pouton, P. Lucas, B. J. Thomas, A. N. Uduehi, D. A. Milroy and S. H. Moss, *J. Controlled Release*, 1998, **53**, 289.
7 J.-P. Yang and L. Huang, in *Self-assembling Complexes for Gene Delivery: From Laboratory to Clinical Trials*, eds. A. V. Kabanov, P. L. Felgner and L .W. Seymour, John Wiley & Sons, New York, 1998, ch. 6.

ChemComm

Practicable regiospecific bifunctionalization on the secondary face of α- and β-cyclodextrins†

Katsunori Teranishi

Faculty of Bioresources, Mie University, Kamihama, 1515, Tsu, Mie, 514-8507, Japan.
E-mail: teranisi@bio.mie-u.ac.jp

Received (in Cambridge, UK) 28th March 2000, Accepted 10th May 2000
Published on the Web 20th June 2000

Practicable regiospecific bifunctionalization onto the A,B-secondary hydroxyl face of α- and β-cyclodextrins, such as diepoxidation and diamination, has been made possible by staple-disulfonation with benzophenone-3,3′-disulfonyl imidazole and molecular sieves in DMF.

Regiospecific multifunctionalization techniques on the primary and secondary hydroxyl groups of cyclodextrins have been investigated in order to enhance the ability of cyclodextrins to act as acceptors or artificial enzymes. Several significant regiospecific disulfonations on the primary hydroxyl groups have been developed to modify the primary face[1] and, as a result, some elegant bifunctional catalyses have been achieved.[2] However, regioselective bifunctionalization on the secondary face has proven more difficult to accomplish.[3] Hence, no absolutely regioselective bifunctionalizations have, as yet, been developed. Two reported disulfonations on two secondary hydroxyl groups of α-, and β-cyclodextrins were not absolutely regiospecific, but afforded mixtures of the regioisomeric $2^A,2^B$-, $2^A,2^C$-, and $2^A,2^D$-disulfonates in extremely low yields.[4] Additionally, inconvenient separation techniques were necessary to isolate the products. Accordingly, an investigation into the bifunctionalization of the secondary hydroxyl groups was undertaken and led to the development of a very useful and efficient method for the exclusively regiospecific preparation of $2^A,2^B$-disulfonates of α- and β-cyclodextrins, with no $2^A,2^C$- and $2^A,2^D$-disulfonate isomers. This preliminary communication details the new method and shows that the $2^A,2^B$-disulfonates are effectively converted to the corresponding A,B-dimannoepoxido and $3^A,3^B$-diamino compounds, useful for the functionalization of cyclodextrins.

Recently, an interesting regiospecific monosulfonation on the secondary hydroxyl groups of cyclodextrins using a combination of sulfonyl imidazole and molecular sieves has been reported,[5] although the mechanism of the sulfonation is not yet clear. This method is extremely encouraging in practical cyclodextrin chemistry because the mild non-alkaline reaction conditions do not induce decomposition of the sulfonates. Furthermore, the reaction occurs independently of the nature of the sulfonyl groups. In this study, the use of benzophenone-3,3′-disulfonyl imidazole,† easily prepared from benzophenone-3,3′-disulfonyl chloride, imidazole and triethylamine,[6] as a $2^A,2^B$-disulfonation 'stapling' reagent (see Scheme 1) has been investigated. A mixture of α- or β-cyclodextrin (0.01 mol), benzophenone-3,3′-disulfonyl imidazole (0.01 mol), and freshly activated powdered molecular sieves 4 Å (10 g) in *N*,*N*-dimethylformamide (DMF) (200 ml) was stirred at 30 °C for 20 h. The molecular sieves were removed by filtration and the filtrate concentrated under reduced pressure. Warm 20% aqueous MeOH (400 ml) was added to the residue and the insoluble solid, containing a small amount of **1-α** or **1-β** and more complex sulfonated cyclodextrins, was removed by filtration. The filtrate was passed through a simple open reverse-phase chromatography column (50 × 120 mm, Fuji Silisia Chromatorex-ODS DM1020T). Elution with water and 10% aqueous MeOH removed the remaining unreacted cyclodextrin. Stepwise gradient elution to 50% aqueous MeOH gave pure 'staple-$2^A,2^B$-disulfonate' **1-α** and **1-β** in 30 and 33% yields, respectively. No other mono- or disulfonate isomers, such as staple-$2^A,2^C$-disulfonates, staple-$2^A,2^D$-disulfonates, 6-sulfonates or 3-sulfonates, resulting from the reaction were observed by HPLC analysis of the reaction mixture and ^{1}H NMR spectroscopy on the reaction products. The structural assignments of **1-α** and **1-β** were made from ^{1}H NMR, H–H COSY, ROESY, HOHAHA, ^{13}C NMR, H–C COSY, and FAB-MS spectra,† and by further derivatisations. The FAB-MS spectra of **1-α** and **1-β** indicated that the disulfonation of each cyclodextrin molecule was performed by a single benzophenone-3,3′-disulfonyl molecule. The ^{1}H NMR spectra, assigned from the H–H COSY experiments, exhibit an appreciable downfield shift of the resonances due to the H-1, H-2 and H-3 protons of the two glucose units of **1-α** and **1-β**, as shown in Fig. 1. In particular, the chemical shifts of the H-2 protons show a larger downfield shift than do the H-3 protons. The ^{13}C NMR spectra, assigned from the H–C COSY experiments, show an upfield shift of the C-1 and C-3 carbon resonances and a downfield shift of the C-2 carbon peaks of the two glucose units of **1-α** and **1-β**. These data show that the two sulfonyl groups of

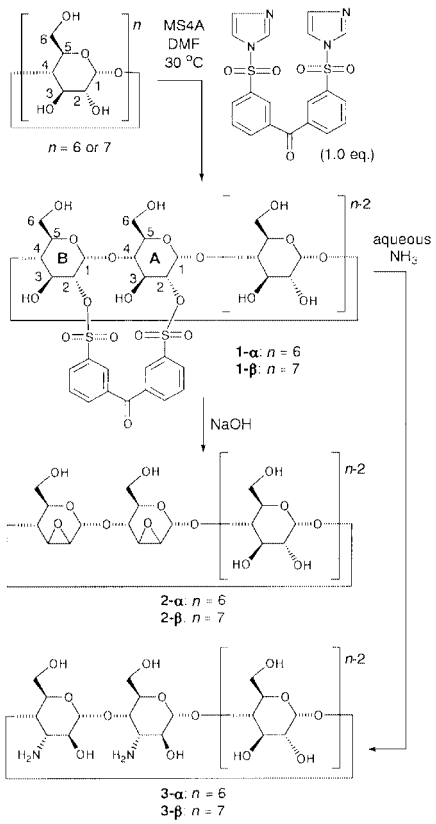

Scheme 1

† Electronic supplementary information (ESI) available: spectroscopic data. See http://www.rsc.org/suppdata/cc/b0/b002445g/

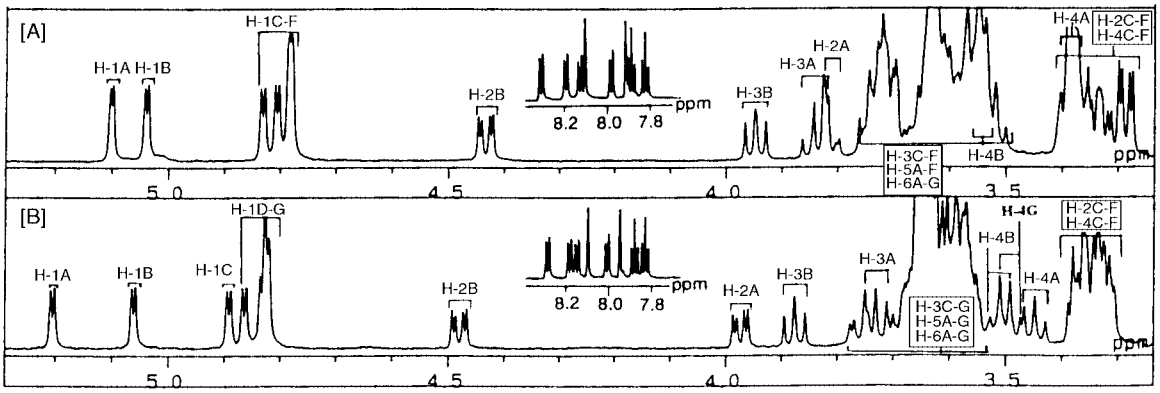

Fig. 1 [A] ^{1}H NMR spectrum of **1-α** [500 MHz, DMSO-d_6 containing 5% D_2O, 60 °C, ref. DMSO (δ 2.49)]. [B] ^{1}H NMR spectrum of **1-β** [500 MHz, DMSO-d_6 containing 5% D_2O, 80 °C, ref. DMSO (δ 2.49)]. The assigned signals are numbered according to the usual convention, shown in Scheme 1, and the glucose units are lettered A to F or G. The letters A and B refer to the sulfonated glucose units.

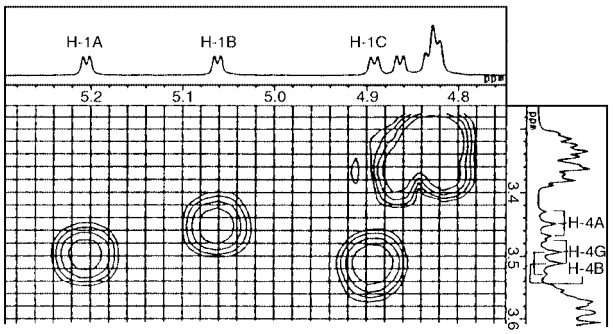

Fig. 2 Partial 2D ROESY NMR spectrum of **1-β** [500 MHz, DMSO-d_6 containing 5% D_2O, 80 °C, ref. DMSO (δ 2.49)].

the benzophenone-3,3′-disulfonyl molecule are located at the C-2 oxygen of the two glucose units. The regiochemistry of the disulfonyl groups of **1-β** was determined using a 2D ROESY NMR experiment (Fig. 2), whereas for **1-α**, this could not be done because the H-4 protons of the sulfonated glucose units and those of adjoining glucose units could not be assigned definitely (see Fig. 1[A]). The 2D ROESY NMR spectrum of **1-β** shows that the H-1B proton of one sulfonated glucose unit has a cross peak with the H-4A proton of another sulfonated glucose unit, indicating that the two units adjoin. Therefore, the structure of **1-β** is 2^A,2^B-disulfonated β-cyclodextrin, as shown in Scheme 1. Treatment of **1-α** and **1-β** with 0.1 mol l^{-1} aqueous NaOH (10 equiv.) at 20 °C for 1 h followed by simple open reverse-phase column chromatography afforded the corresponding pure di-2,3-manno-epoxides **2-α** and **2-β** in 87 and 90% yields, respectively. Their ^{1}H and ^{13}C NMR spectra were seen to be identical with published spectra for authentic A,B-di-2,3-mannoepoxides.[4] Hence **1-α** was assigned as 2^A,2^B-disulfonated α-cyclodextrin, as shown in Scheme 1, and furthermore, the structure of **1-β** was reconfirmed as 2^A,2^B-disulfonated β-cyclodextrin.

The conversion of the hydroxyl groups of cyclodextrins to amino groups is one of the important techniques for the modification of cyclodextrins. Hence, the transformation of 2-mono- or di-*O*-sulfonylcyclodextrins to 3-amino-3-deoxy-2(*S*),(3*R*)-cyclodextrins *via* 2,3-mannoepoxidocyclodextrins has been investigated.[7] However, a straightforward method for absolutely regiospecific A,B-diamination on the secondary face has never been reported.

Investigation into selective A,B-diamination on the secondary face showed that the staple-A,B-disulfonates prepared in the present study were very useful substrates for diamination. The treatment of **1-α** and **1-β** in 28% aqueous NH_3 at 37 °C for 5 days, followed by ion-exchange column chromatography (Sephadex CM-25) efficiently yielded the corresponding pure 3^A,3^B-diamino-3^A,3^B-dideoxy-(2*S*),(3*R*)-cyclodextrins **3-α** and **3-β** in 86 and 84% yields, respectively. The ^{1}H and ^{13}C NMR spectra of **3-α** were seen to be thoroughly identical with authentic published spectra[7b] and the structure of **3-β** was confirmed by ^{1}H and ^{13}C NMR and FAB mass spectroscopies (ESI†).

Studies on the scope and limitations of the present strategy for the absolutely regiospecific disulfonation are currently in progress.

The author thanks the Japanese Ministry of Education, Science, and Culture for a Grant-in-Aid for Scientific Research [(C) 10640520 and 11660106] and the Naito Foundation. The NMR instrument used in this research was installed at the Cooperative Research Center of Mie University.

Notes and references

1 I. Tabushi, K. Shimokawa, N. Shimizu, H. Shirakata and K. Fujita, *J. Am. Chem. Soc.*, 1976, **98**, 7855; I. Tabushi, Y. Kuroda and K. Shimokawa, *J. Am. Chem. Soc.*, 1979, **101**, 1614; I. Tabushi, Y. Kuroda, K. Yokota and L. C. Yuan, *J. Am. Chem. Soc.*, 1981, **103**, 711; I. Tabushi, T. Nabeshima, H. Kitaguchi and K. Yamamura, *J. Am. Chem. Soc.*, 1982, **104**, 2017; I. Tabushi, K. Yamamura and T. Nabeshima, *J. Am. Chem. Soc.*, 1984, **106**, 5267; K. Fujita, A. Matsunaga and T. Imoto, *J. Am. Chem. Soc.*, 1984, **106**, 5740; I. Tabushi, T. Nabeshima, K. Fujita, A. Matsunaga and T. Imoto, *J. Org. Chem.*, 1985, **50**, 2638; R. Breslow, J. W. Canary, M. Varney, S. T. Waddell and D. Yang, *J. Am. Chem. Soc.*, 1990, **112**, 5212.

2 R. Breslow, J. B. Doherty, G. Guillot and C. Lipsey, *J. Am. Chem. Soc.*, 1978, **100**, 3227; R. Breslow, P. Bovy and C. L. Hersh, *J. Am. Chem. Soc.*, 1980, **102**, 2115; I. Tabushi, Y. Kuroda and A. Mochizuki, *J. Am. Chem. Soc.*, 1980, **102**, 1152; I. Tabushi, Y. Kuroda, M. Yamada, H. Higashimura and R. Breslow, *J. Am. Chem. Soc.*, 1985, **107**, 5545; E. Anslyn and R. Breslow, *J. Am. Chem. Soc.*, 1989, **111**, 8931; E. Anslyn and R. Breslow, *J. Am. Chem. Soc.*, 1989, **111**, 5972; R. Breslow and A. Graff, *J. Am. Chem. Soc.*, 1993, **115**, 10 988; J. Desper and R. Breslow, *J. Am. Chem. Soc.*, 1994, **116**, 12 081; R. Breslow and C. Schmuck, *J. Am. Chem. Soc.*, 1996, **118**, 6601; R. Breslow, J. Desper and Y. Huang, *Tetrahedron Lett.*, 1996, **37**, 2541.

3 A. R. Khan, P. Forgo, K. J. Stine and V. T. D'Souza, *Chem. Rev.*, 1998, **98**, 1977.

4 K. Fujita, S. Nagamura, T. Imoto, T. Tahara and T. Koga, *J. Am. Chem. Soc.*, 1985, **107**, 3233; K. Fujita, T. Ishizu, K. Oshiro and K. Obe, *Bull. Chem. Soc. Jpn.*, 1989, **62**, 2960.

5 K. Teranishi, K. Watanabe, M. Hisamatsu and T. Yamada, *J. Carbohydr. Chem.*, 1998, **17**, 489; K. Teranishi, S. Tanabe, M. Hisamatsu and T. Yamada, *Biosci., Biotechnol., Biochem.*, 1998, **62**, 1249.

6 J. L. Work and J. E. Herweh, *J. Polym. Sci., Part A*, 1968, 2022; Y. A. Berlin, O. G. Chakhmakhcheva, V. A. Efimov, M. N. Kolosov and V. G. Korobko, *Tetrahedron Lett.*, 1973, 1353.

7 (*a*) T. Murakami, K. Harata and S. Morimoto, *Chem. Lett.*, 1988, 553; (*b*) K. Fuita, Y. Egashira, T. Imoto, T. Fujioka, K. Mihashi, T. Tahara and T. Koga, *Chem. Lett.*, 1989, 429; (*c*) H. Ikeda, Y. Nagano, Y. Du, T. Ikeda and F. Toda, *Tetrahedron Lett.*, 1990, **31**, 5045; (*d*) K. Fuita, K. Ohta, Y. Ikegami, H. Shimada, T. Tahara, Y. Nogami, T. Koga, K. Saito and T. Nakajima, *Tetrahedron Lett.*, 1994, **35**, 9577.

ChemComm

Probing the internal structure of a cobalt aluminophosphate catalyst. An inelastic neutron scattering study of sorbed dihydrogen molecules behaving as one- and two-dimensional rotors

Anibal J. Ramirez-Cuesta,*[ab] Philip C. H. Mitchell,*[a] Stewart F. Parker[c] and Philip A. Barrett[d]

[a] *Department of Chemistry, University of Reading, Reading, UK RG6 6AD. E-mail: a.j.ramirez-cuesta@reading.ac.uk*
[b] *Departamento de Fisica, Universidad Nacional de San Luis, 5700 San Luis, Argentina*
[c] *ISIS Facility, Rutherford Appleton Laboratory, Chilton, Didcot, Oxon, UK OX11 0QX*
[d] *The Royal Institution, 21 Albemarle Street, London, UK W1X 4BS*

Received (in Cambridge, UK) 31st March 2000, Accepted 2nd June 2000
Published on the Web 20th June 2000

Analysis of the inelastic neutron scattering rotational spectrum of sorbed dihydrogen in a cobalt aluminophosphate catalyst shows that dihydrogen molecules confined in the internal space of the CoAlPO behave as 1D rotors, rotating with the H–H axis aligned with the internal electric field, and as 2D rotors, rotating in a plane and bound sideways at surface sites.

As part of a continuing study[1] of the binding and activation of dihydrogen at catalytic centres and hydrogen atom spillover, we report the interaction of H_2 with the compound CoAlPO-18. The inelastic neutron scattering (INS) spectrum (energy loss vibrational spectrum) of the bound H_2 molecule enables us to observe and assign the H_2 rotational transitions and to describe the H_2 interactions. The H_2 molecule through its INS spectrum may be used as a local structural probe of a porous material.

Cobalt containing microporous materials are important selective oxidation catalysts in, for example, liquid phase oxidation of alkenes with dioxygen[2] and selective oxidation of cyclohexane to cyclohexanone.[3] The synthesis of the CoAlPO-18 catalyst is accomplished by standard hydrothermal sol–gel techniques.[4] Removal of the template is effected by calcination in oxygen; the cobalt(II) is oxidised to cobalt(III).[5] The catalyst is subsequently reduced in hydrogen to generate Brönsted acid sites. The interaction of the hydrogen molecule with the Co(III) centre is therefore crucial. The CoAlPO provided an opportunity to study the binding and activation of the H_2 molecule at a well defined site since the cobalt is known to reside in the framework before and after calcination and reduction. Here we report a study of the interaction of the dihydrogen molecule with the Co(III) site, both experimentally with inelastic neutron scattering (INS) on the TOSCA spectrometer at the Rutherford Appleton Laboratory, and theoretically with perturbation theory.

Inelastic Neutron Scattering Spectra (INS) measurements on the compound CoAlPO-18 were made on the TOSCA instrument at the ISIS Facility at the Rutherford Appleton Laboratory,[6] and cover the molecular vibrational range (16–4000 cm^{-1}) in one spectrum. A sample of CoAlPO-18 (15.7 g) was contained in a standard zirconium INS cell. This was heated in oxygen at 773 K to ensure conversion of Co to Co(III) and complete removal of the template. The sample was then dosed *in situ* with hydrogen at 20 K to a concentration of *ca.* 1 H_2 per cavity. When the CoAlPO-18 dosed with hydrogen was evacuated at 30 K the peaks at 58 and 168 cm^{-1} both disappeared. This is entirely consistent with them being associated with H_2 adsorbed on the same site.

The INS spectrum (0–250 cm^{-1}) after background subtraction (CoAlPO and the cell) is shown in Fig. 1. We observe sharp rotational transitions of the H_2 molecule and a broad recoil tail. The peaks have been fitted as Lorentzians.

In solid dihydrogen, the molecules rotate freely and have almost the same value for the rotational constant, B, as in the gas phase (B = 59.3 cm^{-1}). The energy level scheme is that of a linear rotor in three dimensional space [eqn. (1)].[7] For

$$E_J = J(J + 1)B \quad (1)$$

dihydrogen adsorbed on graphite the rotational states are slightly hindered but they can still be represented as perturbed three-dimensional rotor states.[8–10] The rotational ground state is nearly pure J = 0. The lowest band of excited states, nominally J = 1, is separated from the ground state by an average energy of $2BJ$ and is split by *ca.* 20.2–21.8 cm^{-1}. In our previously reported INS spectrum of H_2 on a Ru/C catalyst the lowest energy transition was seen as a sharp strong band at 120 cm^{-1} (B = 60 cm^{-1}).[1] This was the J(0–1) rotational transition (*para*- to *ortho*-H_2, allowed in INS although strongly forbidden in photon spectroscopy).[11] It is striking, however, that in the spectrum of H_2 adsorbed on CoAlPO-18 (Fig. 1) the *lowest* energy band is at 58.4 cm^{-1}, generally a featureless region of the spectrum. Clearly we cannot treat all our sorbed H_2 as an unconstrained rotor.

As the out-of-plane forces securing the H_2 to the surface increase in strength the molecule becomes more constrained. Ultimately these rotational states will, themselves, become hindered.[12] Here, however, we shall assume that translations and rotations parallel to the surface are unhindered; a potential that governs the rotational motion of the molecule is given by eqn. (2),[13] where θ is the angle between the H–H bond and the

$$V(\theta,\phi) = \sin^2(\theta)[a + b\cos(2\phi)] \quad (2)$$

preferred orientation in space (z axis), ϕ is the azimuthal angle in spherical coordinates, and a, b are constants. For $b \approx 0$, if a

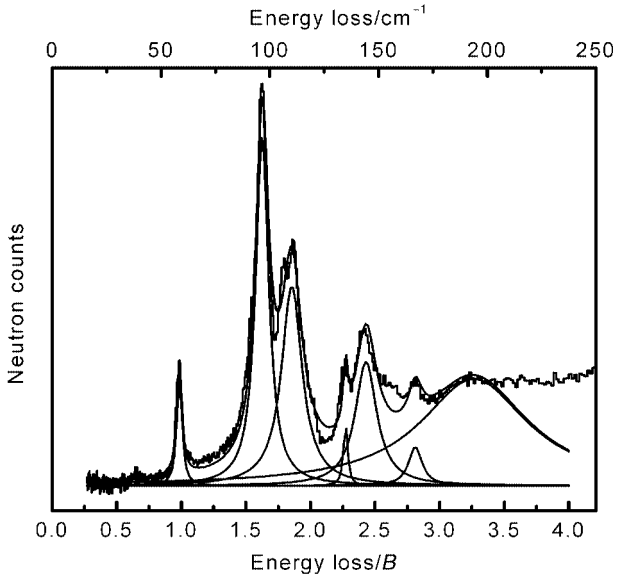

Fig. 1 Inelastic neutron scattering spectrum of H_2 in CoAlPO-18 showing the rotational modes. The peaks are deconvoluted as Lorentzians.

DOI: 10.1039/b002587i

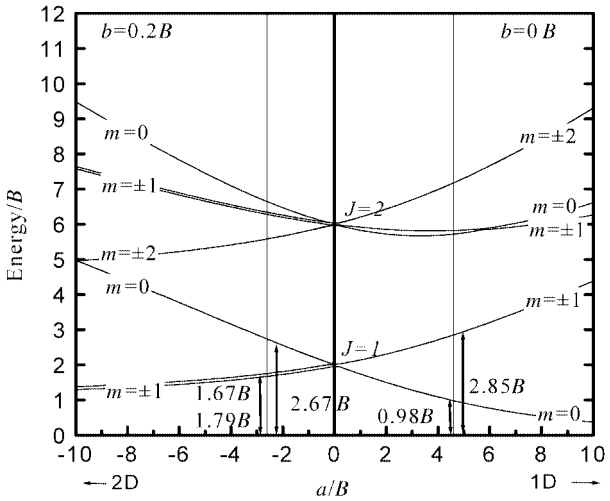

Fig. 2 Rotational states of constrained H_2: energy in units of the rotational constant B *vs.* the perturbation parameter a of Fig. 1 with $b = 0.2B$. Vertical arrows locate peaks in the INS spectrum.

> 0 the molecule will tend to align with the z axis (1D case) whereas if $a < 0$ the molecule will tend to lie in a plane perpendicular to that axis (2D case). Different values of b correspond to different hindrances to rotation within the plane perpendicular to the z axis. If the value of $a < 0$ is large enough, the rotor is effectively constrained to rotate in a plane, the so called two-dimensional rotor.[14] The energy levels are $E_J = J^2B$ and the lowest energy band appears at B. To obtain the transition energies from the ground state to excited rotational states, the Schrodinger equation for a quantum rotor in a potential given by eqn. (2) was solved numerically with a spherical harmonic basis set, $Y_{lm,}$ for values of the parameters a/B and b/B.[13] The parameters were evaluated by fitting to the INS spectrum.

Fig. 2 shows the behaviour of the rotational energy transitions from the ground state as a function of the value of a for $b = 0B$ and $0.2B$. For $a = 0$ we have the three-dimensional free rotor (3D rotor); negative values of a correspond with the 2D case and positive values with the 1D case. Transitions in agreement with the INS spectrum are shown by vertical arrows in Fig. 2 and assignments are given in Table 1. The fitted values of the parameters a and b [eqn. (2)] are for the 1D rotor ($a = 4.6B$ and $b = 0$), whereas for the the 2D rotor, $a = 2.8B$ and $b = 0.2B$.

Table 1 Assignment of the rotational modes in the INS spectrum of H_2 in CoAlPO-18

Peak					
cm^{-1}	B	Relative area	Width/ cm^{-1}	Transition	Assignment
58.4	0.985	0.125	2.77	$\|0,0\rangle \rightarrow \|1,0\rangle$	1D rotor
96.4	1.63	1.000	7.27	$\|0,0\rangle \rightarrow \|1,1\rangle$	2D rotor
110	1.86	0.896	11.4	$\|0,0\rangle \rightarrow \|1,-1\rangle$	2D rotor
134	2.26	0.055	2.28	$\|0,0\rangle \rightarrow \|1,0\rangle$	2D rotor
145	2.45	0.584	2.28	$\|0,0\rangle \rightarrow \|1,0\rangle$	2D rotor
168	2.83	0.116	7.59	$\|0,0\rangle \rightarrow \|1,1\rangle$	1D rotor

Finally we consider whether it is possible to associate features of the INS spectrum with particular components of the CoAlPO-18. We note that the intensity ratio of the 58 cm^{-1} peak to the 96 and 100 cm^{-1} peaks is *ca.* 1/17, the same as the Co/Al ratio if one Al^{3+} in each unit cell is replaced by one Co^{3+}. It is, therefore, possible that it is the Co^{3+} which aligns the H_2 molecule as the 1D rotor (58 cm^{-1} peak) (*cf.* the perpendicular orientation towards Co^{3+} of acetonitrile in CoAlPO-18).[15] The 2D rotor peaks then derive from H_2 molecules rotating in a plane and bound sideways at surface sites comprising Co^{3+} or framework AlPO. Density functional theory calculations are in hand to calculate the rotational frequencies of H_2 molecules bound at various sites of the CoAlPO-18.

We thank the EPSRC for funding (GR/M90627) and access to the ISIS neutron beam (GR/L13834); Professor Richard Catlow for his interest; Dr G. Sankar (Royal Institution) for helpful comments on the CoALPO structure and Dr J. Tomkinson (ISIS) on the hydrogen INS. Dr John Turner (Royal Institution) was involved in the initial planning of the project.

Notes and references

1 P. C. H. Mitchell, S. F. Parker, J. Tomkinson and D. Thompsett, *J. Chem. Soc., Faraday Trans.*, 1998, **94**, 1489.
2 H. F. W. L. van Breukelen, M. E. Gerritsen, V. M. Ummels, J. S. Broens and J. H. C. van Hooff, *Stud. Surf. Sci. Catal.*, 1997, **105**, 1029; M. Hartmann and L. Kevan, *Chem. Rev.*, 1999, **99**, 635.
3 T. Maschmeyer, R. D. Oldroyd, G. Sankar, J. M. Thomas, I. J. Shannon, J. A. Klepetko, A. F. Masters, J. K. Beattie and C. R. A. Catlow, *Angew. Chem., Int. Ed. Engl.*, 1997, **36**, 1639.
4 P. A. Barrett, G. Sankar, C. R. A. Catlow and J. M. Thomas, *J. Phys. Chem.*, 1996, **100**, 8977.
5 J. M. Thomas, G. N. Greaves, G. Sankar, P. A. Wright, J. Chen, A. J. Dent and L. Marchese, *Angew. Chem., Int. Ed. Engl.*, 1994, **33**, 1871.
6 S. F. Parker, C. J. Carlile, T. Pike, J. Tomkinson, R. J. Newport, C. Andreani, F. P. Ricci, F. Sachetti and M. Zoppi, *Physica B*, 1998, 241.
7 K. Svensson, L. Bengtsson, J. Bellman, M. Hassel, M. Persson and S. Andersson, *Phys. Rev. Lett.*, 1999, **83**, 124; I. F. Silvera, *Rev. Mod. Phys.*, 1980, **52**, 393.
8 W. Langel, D. L. Price, R. O. Simmons and P. E. Sokol, *Phys. Rev. B*, 1988, **38**, 11 275.
9 A. D. Novaco, *Phys. Rev. B: Condens. Matter*, 1992, **46**, 8178; *Phys. Rev. Lett.*, 1988, **60**, 2058.
10 A. D. Novaco and J. P. Wroblewski, *Phys. Rev. B: Condens. Matter*, 1989, **39**, 11 364.
11 J. M. Nicol, J. Eckert and J. Howard, *J. Phys. Chem.*, 1988, **92**, 7117.
12 D. White and E. N. Lassettre, *J. Chem. Phys.*, 1960, **32**, 72.
13 A. P. Smith, R. Benedeck, F. R. Trouw, M. Minkoff and L. H. Yang, *Phys. Rev. B*, 1996, **53**, 10187.
14 P. W. Atkins, *Physical Chemistry*, Oxford University Press, Oxford, 6th edn., 1998, p. 475.
15 P. A. Barrett, G. Sankar, R. H. Jones, C. R. A. Catlow and J. M. Thomas, *J. Phys. Chem.*, 1997, **101**, 9555.

Molecular rods based on a ruthenium(II) macrocyclic bis(acetylide) building block†

Mei-Yuk Choi,[a] Michael C. W. Chan,[a] Shie-Ming Peng,[b] Kung-Kai Cheung[a] and Chi-Ming Che*[a]

[a] *Department of Chemistry, The University of Hong Kong, Pokfulam Road, Hong Kong SAR, China. E-mail: cmche@hku.hk*

[b] *Department of Chemistry, National Taiwan University, Taipei, Taiwan*

Received (in Cambridge, UK) 4th April 2000, Accepted 22nd May 2000
Published on the Web 20th June 2000

The prototype of an organometallic linear-rod building block incorporating the saturated σ-donating 16-TMC macrocycle, peripheral pyridine moieties for versatile ligation, and the π-conjugated *trans*-[Ru(C≡Cpy-4)$_2$] fragment along the molecular axis, is described and applied to the assembly of trimetallic arrays.

The development of molecular rods and wires[1,2] has gained importance in view of their potential applications in the emerging fields of molecular-scale electronics and devices.[3] An attractive pursuit in this area is the design of rigid building blocks with readily tuneable electronic, steric and photophysical characteristics.[4] In this context, we became interested in metal–acetylide units as components in organometallic supermolecules. The unique nature of the M–C≡CR interaction allows delocalisation of electron density in principle and has been harnessed in several active areas of material science,[5] but reports of supramolecular metal–acetylide systems are relatively sparse.[6]

We present the bis(σ-pyridylacetylide) derivative *trans*-Ru(16-TMC)(C≡Cpy-4)$_2$ (**Ru**, 16-TMC = 1,5,9,13-tetramethyl-1,5,9,13-tetraazacyclohexadecane) as a supramolecular bridging module for multinuclear rod-like assemblies.[7] The unique combination of properties that has been incorporated into the design of the neutral complex **Ru** include: (a) enhanced d_π(Ru) → π*(C≡Cpy) back-bonding due to the saturated σ-donating 16-TMC amine ligand, as observed for the arylacetylide analogues;[8] (b) versatile coordination to adjacent units by the pendant pyridine moieties, to yield multicomponent systems with well-defined structures; (c) the electronic effect conferred upon **Ru** by the 16-TMC macrocycle and the π-overlapping Ru–C≡Cpy interaction can afford anisotropic properties.

Reaction of a methanolic solution of [Ru(16-TMC)Cl$_2$]Cl with zinc amalgam, sodium methoxide and 4-ethynylpyridine yielded **Ru** as a yellow crystalline solid.‡ We suggest that the sterically bulky nature of the 16-TMC ligand leads to preferential ligation of acetylide groups at the Ru(II) centre rather than pyridyl moieties. Treatment of **Ru** with two equivalents of [Re(N–N)(CO)$_3$(MeCN)]OTf (OTf = CF_3SO_3) under reflux in THF afforded the trimetallic complexes [{Re(N–N)(CO)$_3$}$_2${μ-(4-pyC≡C)$_2$Ru(16-TMC)}](OTf)$_2$ (**[a–c]Re$_2$Ru**, see Fig. 1) as dark red solids in moderate yields (50–60%).‡ These derivatives are thermally stable > 200 °C (*e.g.* decomposition occurs at 220–222 °C for **Ru**; 207–210 °C for **[b]Re$_2$Ru**).

The IR spectrum of **Ru** displays an intense band at 1990 cm^{-1} for the asymmetric C≡C stretch. This value is slightly lower than that for the arylacetylide congeners (2002–2012 cm^{-1}),[8] and is one of the lowest ever reported for a simple metal bis(σ-acetylide) derivative.[5] The strongly electron-donating nature of 16-TMC is apparent, resulting in improved π back-bonding from the electron-rich Ru(II) core. The ν_{as}(C≡C) values for **[a–c]Re$_2$Ru** are shifted to 2028–2030 cm^{-1} upon coordination of Re(I) centres at the pyridyl sites. The FT Raman spectra of the trimetallic complexes show a symmetric C≡C stretch at 2010–2024 cm^{-1}. The electrospray mass spectra for **[a–c]Re$_2$Ru** are all dominated by two clusters of signals, the intensities of which correspond to the calculated isotope patterns of the $[M]^{2+}$ (peaks separated by 0.5 u) and $[M + OTf]^+$ species respectively. The ^{13}C NMR resonance for the α-acetylide carbon in **[a–c]Re$_2$Ru** (assigned by ^{1}H–^{13}C COSY, DEPT-135 and by comparison with precursors) appears at δ 155.4–156.7. This downfield shift compared to related Ru σ-acetylide complexes[5,7] again indicates strong ruthenium-to-acetylide π back-bonding. The cyclic voltammograms for **Ru** and **[a–c]Re$_2$Ru** all exhibit a well-defined reversible/quasi-reversible couple at −0.28 to −0.40 V *vs*. $Cp_2Fe^{0/+}$ (ΔE_p 50–130 mV), which is assigned to the Ru(III/II) couple.

While numerous multinuclear molecular rods have been described, structural elucidations are rarely provided. X-Ray crystallographic analyses have been performed on **Ru** and **[a]Re$_2$Ru**·Et$_2$O,§ and their molecular structures are shown in Fig. 2. The metal atoms in **Ru** and **[a]Re$_2$Ru** all reside in distorted octahedral environments. The salient features of these structures are their linearity along the molecular axis and the coplanarity of the pyridine ring systems. The former illustrates the potential application of **Ru** as a linear rigid-rod motif, while the latter implies that the π orbitals within the *trans*-[Ru(C≡Cpy-4)$_2$] fragment are able to undergo favourable overlap in the crystal lattice. For **[a]Re$_2$Ru**, a facial arrangement of the carbonyl ligands is observed, while the end-to-end Re···ReA distance is 19.1 Å. The Ru–C [**Ru**: 2.065(7) Å, **[a]Re$_2$Ru**: 2.040(10) Å] and C≡C [**Ru**: 1.20(1) Å, **[a]Re$_2$Ru**: 1.207(13) Å] bond lengths are comparable to those reported for related Ru(II) σ-acetylide[5] and σ-pyridylacetylide[7] derivatives.

The UV-Vis absorption spectrum of **Ru** in dichloromethane (Fig. 3) contains an intense absorption band at λ_{max} 430 nm (ε = 4.7 × 10^4 dm^3 mol^{-1} cm^{-1}). Because the saturated 16-TMC ligand is optically transparent in the UV-Vis spectral region, this absorption is assigned to a d_π(Ru)→π*(C≡Cpy) metal-to-ligand charge transfer (MLCT) transition. The trimetallic derivatives **[a–c]Re$_2$Ru** display characteristic UV-Vis absorptions at λ_{max} 355–430 (sh, $\varepsilon \approx 1 \times 10^4$ dm^3 mol^{-1} cm^{-1}) and 516 ($\varepsilon \approx 7 \times 10^4$ dm^3 mol^{-1} cm^{-1}) nm (Fig. 3 for **[a]Re$_2$Ru**). With

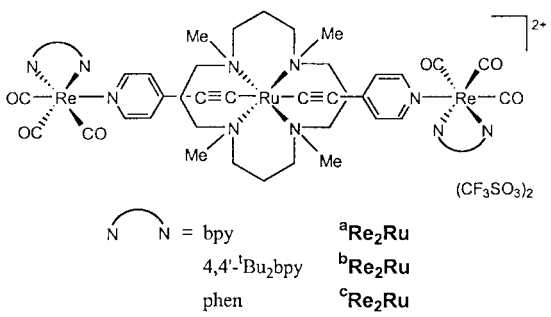

Fig. 1

† Electronic supplementary information (ESI) available: experimental details, characterisation details. See http://www.rsc.org/suppdata/cc/b0/b002674n/

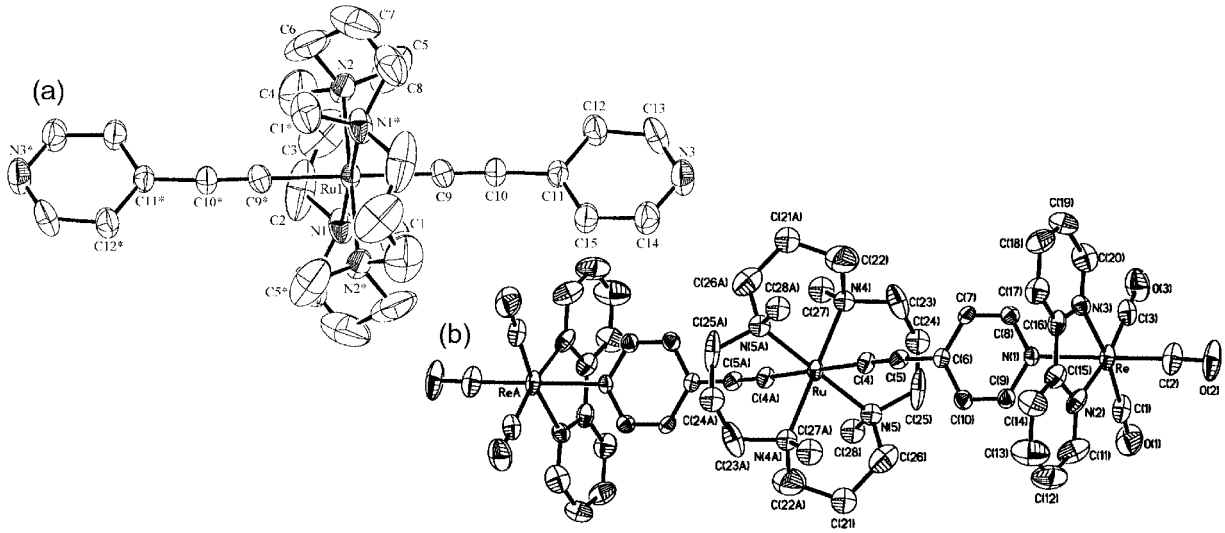

Fig. 2 (a) Perspective view of **Ru** (40% probability ellipsoids). Selected bond distances (Å) and angles (°): Ru–N(1) 2.249(6), Ru–N(2) 2.292(6), Ru–C(9) 2.065(7), C(9)–C(10) 1.20(1), C(10)–C(11) 1.43(1); N(1)–Ru–C(9) 92.0(3), Ru–C(9)–C(10) 173.5(7), C(9)–C(10)–C(11) 174.1(9). (b) Perspective view of cation in ^{a}**Re$_2$Ru**·Et$_2$O (30% probability ellipsoids). Selected bond distances (Å) and angles (°): Ru–N(4) 2.28(2), Ru–C(4) 2.040(10), C(4)–C(5) 1.207(13), C(5)–C(6) 1.410(13), Re–N(1) 2.208(7); N(4)–Ru–C(4) 88.0(5), Ru–C(4)–C(5) 174.0(9), C(4)–C(5)–C(6) 172.9(11).

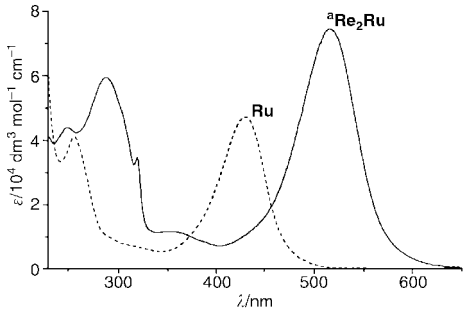

Fig. 3 UV-Vis absorption spectra of **Ru** (CH_2Cl_2) and ^{a}**Re$_2$Ru** (CH_3CN) at 298 K.

reference to previous spectroscopic studies on rhenium(I) diimine systems,[9] the former are attributed to d_π(Re) → π*(diimine) MLCT transitions. The highly intense 516 nm absorption band is tentatively assigned to be d_π(Ru)→π*(C≡Cpy) MLCT in nature. The observed red shift from **Ru** is in accordance with the Lewis acidity of the pyridine-bound Re(I) centres. Furthermore, the identical λ_{max} value of this band for $^{a-c}$**Re$_2$Ru** suggests that the transition concerned contains negligible contribution from the different diimine ligands. Complex **Ru** is non-emissive in solution or solid states. While [Re(diimine)(CO)$_3$(py)]$^+$ complexes are known to exhibit a long-lived Re→π*(diimine) MLCT excited state in solution at room temperature, this photoluminescence is quenched in the trinuclear arrays $^{a-c}$**Re$_2$Ru**. A possible mechanism for the quenching process involves fast intercomponent energy transfer (Re^{I*}–Ru^{II}–Re^{I} → Re^{I}–Ru^{II*}–Re^{I}), leading to a non-radiative Ru→π*(C≡Cpy) charge transfer excited state.[10]

We are grateful for financial support from The University of Hong Kong and the Research Grants Council of the Hong Kong SAR, China [HKU 501/96P]. We thank Prof. K. Y. Wong for assistance in electrochemical measurements.

Notes and references

‡ Satisfactory elemental analyses were obtained for all new complexes. Detailed characterisation is provided in the electronic supplementary information.

§ *Crystal data* for **Ru**: $C_{30}H_{44}N_6Ru$, M = 589.79, monoclinic, $P2_1/c$, a = 8.763(2), b = 10.534(2), c = 15.243(2) Å, β = 97.31(2)°, V = 1395.6(5) Å^3, Z = 2, D_c = 1.403 g cm^{-3}, μ = 5.92 cm^{-1}, T = 301 K. A total of 2741 unique reflections (R_{int} = 0.074) was collected on a MAR diffractometer ($2\theta_{max}$ = 56°). The structure was solved by direct methods and refined by least-squares treatment on F^2 using the TeXsan program: R = 0.064, wR = 0.078 for 1530 reflections with $I > 3\sigma(I)$ and 169 parameters. For ^{a}**Re$_2$Ru**·Et$_2$O: $C_{62}H_{70}F_6N_{10}O_{13}Re_2RuS_2$, M = 1814.89, triclinic, $P\bar{1}$, a = 8.3284(2), b = 10.5843(3), c = 20.8961(5) Å, α = 84.370(1), β = 84.973(1), γ = 88.998(1)°, V = 1826.0(1) Å^3, Z = 1, D_c = 1.650 g cm^{-3}, μ = 3.65 mm^{-1}, T = 295 K. A total of 7455 unique reflections (R_{int} = 0.097) were collected on a Siemens SMART CCD diffractometer (ω scans, $2\theta_{max}$ = 53°). The structure was solved by direct methods and refined by least-squares treatment on F^2 using the SHELXL-93 program (the 16-TMC ligand is disordered, with major and minor occupancies of 0.6:0.4 respectively for positions rotated by 45°): R = 0.065, wR = 0.133 for 4349 absorption-corrected (SADABS, transmission 0.379–0.648) reflections with $I > 2\sigma(I)$ and 416 parameters.

CCDC 182/1600. See http://www.rsc.org/suppdata/cc/b0/b002674n/ for crystallographic files in .cif format.

1 P. F. H. Schwab, M. D. Levin and J. Michl, *Chem. Rev.*, 1999, **99**, 1863.

2 A. El-ghayoury, A. Harriman, A. Khatyr and R. Ziessel, *Angew. Chem., Int. Ed.*, 2000, **39**, 185; L. De Cola and P. Belser, *Coord. Chem. Rev.*, 1998, **177**, 301; M. Brady, W. Weng, Y. Zhou, J. W. Seyler, A. J. Amoroso, A. M. Arif, M. Böhme, G. Frenking and J. A. Gladysz, *J. Am. Chem. Soc.*, 1997, **119**, 775; F. Coat, M. A. Guillevic, L. Toupet, F. Paul and C. Lapinte, *Organometallics*, 1997, **16**, 5988; V. Balzani, A. Juris, M. Venturi, S. Campagna and S. Serroni, *Chem. Rev.*, 1996, **96**, 759; E. C. Constable, C. E. Housecroft, E. R. Schofield, S. Encinas, N. Armaroli, F. Barigelletti, L. Flamigni, E. Figgemeier and J. G. Vos, *Chem. Commun.*, 1999, 869.

3 *Molecular Electronics*, ed. J. Jortner and M. A. Ratner, Blackwell, Cambridge, 1997.

4 A. Mayr, M. P. Y. Yu and V. W. W. Yam, *J. Am. Chem. Soc.*, 1999, **121**, 1760.

5 J. Manna, K. D. John and M. D. Hopkins, *Adv. Organomet. Chem.*, 1995, **38**, 79.

6 Y. Zhu, O. Clot, M. O. Wolf and G. P. A. Yap, *J. Am. Chem. Soc.*, 1998, **120**, 1812; O. Lavastre, J. Plass, P. Bachmann, S. Guesmi, C. Moinet and P. H. Dixneuf, *Organometallics*, 1997, **16**, 184; M. C. B. Colbert, J. Lewis, N. J. Long, P. R. Raithby, A. J. P. White and D. J. Williams, *J. Chem. Soc., Dalton Trans.*, 1997, 99; V. Grosshenny, A. Harriman, M. Hissler and R. Ziessel, *J. Chem. Soc., Faraday Trans.*, 1996, **92**, 2223; W. Weng, T. Bartik, M. Brady, B. Bartik, J. A. Ramsden, A. M. Arif and J. A. Gladysz, *J. Am. Chem. Soc.*, 1995, **117**, 11922.

7 Reports on related complexes have focused on their non-linear optical properties, *e.g.* I. Y. Wu, J. T. Lin, J. Luo, S. S. Sun, C. S. Li, K. J. Lin, C. Tsai, C. C. Hsu and J. L. Lin, *Organometallics*, 1997, **16**, 2038.

8 M. Y. Choi, M. C. W. Chan, S. Zhang, K. K. Cheung, C. M. Che and K. Y. Wong, *Organometallics*, 1999, **18**, 2074.

9 For example, see: L. Sacksteder, A. P. Zipp, E. A. Brown, J. Streich, J. N. Demas and B. A. DeGraff, *Inorg. Chem.*, 1990, **29**, 4335.

10 See cyano-bridged [Re^{I}–N≡C–Ru^{II}–C≡N–Re^{I}] systems: K. Kalyanasundaram, M. Grätzel and Md. K. Nazeeruddin, *Inorg. Chem.*, 1992, **31**, 5243; C. A. Bignozzi, R. Argazzi, C. G. Garcia, F. Scandola, J. R. Schoonover and T. J. Meyer, *J. Am. Chem. Soc.*, 1992, **114**, 8727.

Reversible olefin complexation by silver ions in dry poly(vinyl methyl ketone) membrane and its application to olefin/paraffin separations

Hoon Sik Kim,*[ab] Jae Hee Ryu,[b] Honggon Kim,[a] Byoung Sung Ahn[a] and Yong Soo Kang*[b]

[a] *CFC Alternatives Research Center, Korea Institute of Science and Technology, PO Box 131, Cheongryang, Seoul 130-650, Korea*

[b] *Center for Facilitated Transport Membrane, Korea Institute of Science and Technology, PO Box 131, Cheongryang, Seoul 130-650, Korea. E-mail: khs@kist.re.kr*

Received (in Cambridge, UK) 26th April 2000, Accepted 5th June 2000
Published on the Web 22th June 2000

Rapid and reversible olefin coordination to silver ions in $AgBF_4$–poly(vinyl methyl ketone) membrane has been characterized using FTIR and UV spectroscopy.

Olefin/paraffin separation by facilitated transport membrane using silver salts as carriers has been considered as a promising alternative to the conventional energy intensive distillation process.[1,2] The basis for the separation is the ability of silver ions to react reversibly with olefins forming silver–olefin complexes.[1–4] In general, facilitated transport phenomena have been mostly observed in supported liquid membranes and ion exchange membranes.[5] However, such membranes show facilitated olefin transport only in the presence of water, which is a serious drawback for practical application.[5] A solution to this problem is the development of dry polymer membranes in which silver ions can interact with olefins even in the absence of water.[6] Despite the extensive research on facilitated olefin transport phenomena in the water-free state, only a few dry polymer membranes have been developed. Accordingly, very little information has been obtained about phenomena occurring on the solid polymer membrane such as reversible interactions of silver salts with olefins and/or the polymer matrix, which is of pivotal importance in the development of high performance dry polymer membranes.[7]

It is well known that silver–olefin complexes are extremely unstable and lose olefin easily upon exposure to air.[8] Therefore, in order to characterize reversible olefin coordination to silver ions in a solid polymer membrane, the polymer matrix should contain some functional group(s) to stabilize the silver–olefin complexes to a certain extent. In addition, appropriate equipment should be used for the spectroscopic measurements in an inert or olefin atmosphere. Antonio and Tsou suggested that the stability of silver–olefin complexes could be enhanced by weak interaction between silver ions and oxygen atoms.[9] Among various oxygen-containing polymers, poly(vinyl methyl ketone) (PVMK) was chosen since it has a relatively simple structure and contains carbonyl functional groups the absorption peaks of which can be clearly seen by IR spectroscopy. A pressure cell is employed for the spectroscopic characterization of reversible interactions of silver salts with olefins and/or the polymer matrix in an inert or olefin atmosphere.[10]

We report the direct spectroscopic observation of rapid and reversible coordination of olefins to silver ions in dry PVMK membranes and of the interaction of silver ions with carbonyl groups in PVMK using FTIR and UV spectroscopy. We also report that the facilitated transport membrane consisting of $AgBF_4$ and PVMK exhibits excellent performance for olefin/paraffin separation.

All the samples for spectroscopic characterization[11] and permeation tests[12] were prepared in a dry box under argon to avoid contact with water. Spectroscopic characterization was carried out using a pressure cell equipped with two CaF_2 or quartz windows[10] and permeation tests were performed in a stainless steel separation module described elsewhere.[13]

The series of IR spectra in Fig. 1 demonstrate the solid state interaction of $AgBF_4$ with PVMK and reversible olefin coordination to silver ions dissolved in the solid $AgBF_4$–PVMK membranes. The peak at 1709 cm^{-1} in Fig. 1(a), associated with the C=O stretching frequency of uncoordinated PVMK, shifts to a lower frequency upon incorporation of $AgBF_4$, demonstrating the coordination of carbonyl groups to silver ions. The membrane with a molar ratio $AgBF_4$:PVMK = 1:4 shows a strong carbonyl absorption peak at 1681 cm^{-1} and a shoulder peak at *ca.* 1709 cm^{-1} which are assigned to coordinated and free carbonyl groups, respectively [Fig. 1(b)]. However, the membrane with a molar ratio of 1:2 shows a single absorption band implying that the maximum coordination number of silver ion by carbonyl groups is approximately two.

When the membrane ($AgBF_4$:PVMK = 1:2) was exposed to 30 psig of propylene and then purged with N_2, a new IR absorption peak at 1586 cm^{-1} appeared [Fig. 1(d)]. This new peak represents the C=C stretching vibration of coordinated propylene (*cf.* $\nu_{C=C}$ of free hex-1-ene = 1640 cm^{-1}).[7] It is interesting that the peak at 1586 cm^{-1} remains even after outgassing at 10^{-5} Torr for 4 h at room temperature. However, exposure of the propylene coordinated membrane to 30 psig of buta-1,3-diene and subsequent treatment with N_2 gives a new peak at 1558 cm^{-1} with concomitant disappearance of the peak at 1586 cm^{-1}. The peak at 1558 cm^{-1} can be assigned to the C=C stretching frequency of coordinated buta-1,3-diene [Fig. 1(e)]. The peak at 1558 cm^{-1} is replaced by a peak at 1586 cm^{-1} upon introduction of propylene into the gas cell containing the buta-1,3-diene-coordinated $AgBF_4$–PVMK

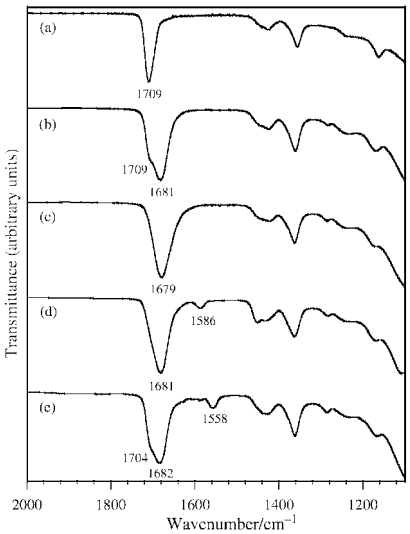

Fig. 1 IR spectra for the solid state interactions of $AgBF_4$ with PVMK and olefins: (a) PVMK, (b) $AgBF_4$:PVMK = 1:4, (c) $AgBF_4$:PVMK = 1:2, (d) propylene-coordinated membrane, (e) buta-1,3-diene-coordinated membrane.

DOI: 10.1039/b003373l

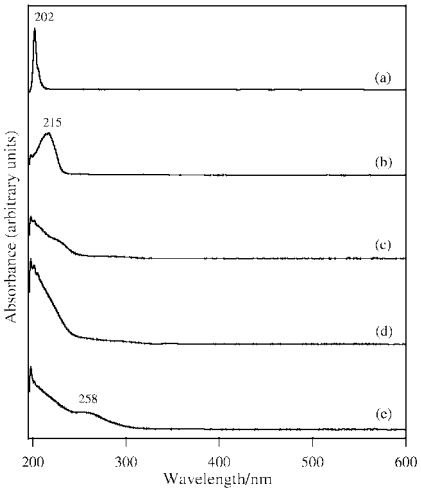

Fig. 2 UV spectra of olefin coordinated $AgBF_4$–PVMK membranes: (a) propylene, (b) buta-1,3-diene, (c) $AgBF_4$–PVMK ($AgBF_4$:PVMK = 1:2), (d) propylene-coordinated membrane, (e) buta-1,3-diene-coordinated membrane.

membrane. These results strongly indicate that the coordinated olefins are not rigidly held to silver ions in the membranes. Therefore, olefins can diffuse from the feed stream across the membrane to the permeate side thereby resulting in selective separation of olefins from the olefin/paraffin mixture.

The coordination of olefins to silver ions in the $AgBF_4$–PVMK membrane results in some significant changes in the absorption band of the coordinated carbonyl groups. As shown in Fig. 1(e), the IR spectrum of the buta-1,3-diene-coordinated membrane shows two carbonyl stretching bands at 1682 and *ca*. 1704 cm^{-1}. The shoulder peak at *ca*. 1704 cm^{-1} can be tentatively assigned to free carbonyl groups of PVMK, and this result strongly suggests that olefins and carbonyl groups compete with each other for coordination to silver ions.

Reversible olefin coordination was also observed by spectral changes in the UV absorption as shown in Fig. 2. Fig. 2(d) shows a strong and broad absorption band at 220–230 nm for propylene coordinated $AgBF_4$–PVMK ($AgBF_4$:PVMK = 1:2). When the propylene coordinated membrane was exposed to buta-1,3-diene atmosphere followed by an N_2 purge, the absorption band at 220–230 nm disappeared and a new band appeared at *ca*. 258 nm associated with coordinated buta-1,3-diene [Fig. 2(e)]. This result again indicates that co-ordinated propylene is labile enough to be readily replaced by other olefins. In the same manner, the absorption band of coordinated propylene at 220–230 nm reappeared when propylene was introduced into the cell containing the buta-1,3-diene coordinated membrane.

The separation of an olefin/paraffin mixture (1:1, v/v) was performed to evaluate the facilitated transport effect of silver ions in PVMK. Fig. 3 shows the effect of the molar ratio of $AgBF_4$/PVMK on the selectivity for olefins over paraffins. The selectivity for propylene (ethylene) over propane (ethane) increases with increasing molar ratio of $AgBF_4$:PVMK up to

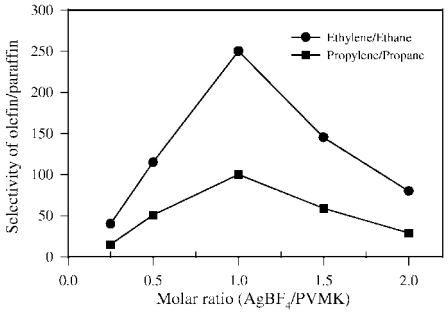

Fig. 3 Effect of molar ratio of $AgBF_4$/PVMK on the selectivity for olefins over paraffin selectivity.

1:1 and then decreases with further increases in the molar ratio. Such a selectivity dependence on the molar ratio of $AgBF_4$:PVMK implies that the coordination environment of silver ions in PVMK has a significant effect on the facilitated transport of olefins. The higher selectivity for ethylene/ethane in comparison with that for propylene/propane can be ascribed to the difference in diffusion rates of the mixture gas and/or to the difference in affinities for the olefins to silver ions in the membrane.

XPS analysis of $AgBF_4$–PVMK membranes is under way to characterize the chemical states of silver, carbon and oxygen atoms in $AgBF_4$–PVMK membranes.

We acknowledge financial support from the Ministry of Science and Technology of Korea through the Creative Research Initiatives Program.

Notes and references

1 H. Jarvelin and J. R. Fair, *Ind. Eng. Chem. Res.*, 1993, **32**, 2201.
2 C. D. M. Beverwijk, G. J. M. van der Kerk, A. J. Leusink and J. G. Noltes, *Organomet. Chem. Rev. A*, 1970, **5**, 215.
3 J.-S. Yang and G.-H. Hsiue, *J. Membr. Sci.*, 1996, **120**, 69.
4 D. J. Safarik and R. B. Eldridge, *Ind. Eng. Chem. Res.*, 1998, **37**, 2571.
5 W. S. Ho and D. C. Dalrymple, *J. Membr. Sci.*, 1994, **91**, 13; J.-S. Yang and G.-H. Hsiue, *J. Membr. Sci.*, 1996, **111**, 27; T. Yamaguchi, C. Baertsch, C. A. Koval, R. D. Noble and C. N. Bowman, *J. Membr. Sci.*, 1996, **117**, 151.
6 S. Sunderrajan, B. D. Freeman and I. Pinnau, in *Proceedings of the American Chemical Society Division of Polymeric Materials: Science and Engineering*, American Chemical Society, Washington DC, 1997, vol. 99, pp. 267–268.
7 S. Sunderrajan, B. D. Freeman and C. K. Hall, *Ind. Eng. Chem. Res.*, 1999, **38**, 4051.
8 H. W. Quinn, J. S. McIntyre and D. J. Peterson, *Can. J. Chem.*, 1965, **43**, 2896.
9 M. R. Antonio and D. T. Tsou, *Ind. Eng. Chem. Res.*, 1993, **32**, 273.
10 J. Haver and M. Wojciechowska, *J. Catal.*, 1988, **110**, 23.
11 Polymer membranes for IR and UV measurements were prepared as follows: a THF solution containing $AgBF_4$ and PVMK was coated onto a CaF_2 (IR) or quartz (UV) window and dried under vacuum. The coated and uncoated windows were then placed in a pressure cell.
12 A $AgBF_4$–PVMK solution in THF was cast onto a microporous polyester membrane using a casting knife.
13 S. Bai, A. Scridhar and A. A. Khan, *J. Membr. Sci.*, 1998, **147**, 131.

ChemComm

Asymmetric synthesis of (+)-loline

Paul R. Blakemore, Volker K. Schulze and James D. White*

Department of Chemistry, Oregon State University, Corvallis, Oregon 97331-4003 USA. E-mail: james.white.orst.edu

Received (in Cambridge, UK) 18th April 2000, Accepted 22nd May 2000
Published on the Web 22th June 2000

The first asymmetric synthesis of (+)-loline has been achieved in 20 steps from (−)-malic acid by a route incorporating intramolecular hetero-Diels–Alder cycloaddition of an acylnitrosodiene.

The lolium alkaloids comprise a small group of pyrrolizidine bases which possess a unique ether linkage bridging C2 and C7.[1] The principal member of the lolium group, (+)-loline **1**, was first isolated in 1955 from the rye grass *Lolium cuneatum* and its structure was initially misassigned.[2] Subsequently, lolium alkaloids were also found in the pasture grass tall fescue (*Festuca arundinacea*),[3] and most recently have been discovered in the roots of the tropical liana *Argyreia mollis*.[4] Acylated derivatives of loline are toxic to larvae of the horn fly (*Haematobia irritans*), an important arthopod ectoparasite of cattle.[5] A previous synthesis of (±)-loline **1** was reported in 1986 by Tufariello *et al.*[6]

Our plan for the synthesis of (+)-**1** envisioned formation of the bridging ether of loline at a late stage from a suitably functionalized pyrrolizidine core **2** (Scheme 1). Appropriate substituents X and Y could, in principle, be installed by oxidation of an unsaturated pyrrolizidine precursor. The latter was envisioned from a 3,6-dihydro-1,2-oxazine, itself accessible *via* intramolecular hetero-Diels–Alder cycloaddition of acylnitrosodiene **3**. Acylnitroso compounds are highly reactive dienophiles[7] and their cycloaddition chemistry has been exploited in several pyrrolizidine[8] and indolizidine[9] alkaloid syntheses.

The synthesis of a suitable precursor for **3**, hydroxamic acid **10**, began with (*S*)-(−)malic acid **4** (Scheme 2). Conversion of **4** to diene **7** was accomplished in six steps by modification of an existing route to the analogous (*R*)-benzyl ether.[10] Thus, reduction of **4** with $BH_3{\cdot}SMe_2$ was followed by acid catalyzed acetalization of the resulting triol to yield dioxane **5**, $[\alpha]_D^{23}$ + 9.9 (*c* 0.96, $CHCl_3$), as a single diastereoisomer in 64% overall yield. Swern oxidation of the remaining free hydroxy group yielded an unstable aldehyde which was immediately reacted with allylidene triphenylphosphorane to afford diene **6** (*E*:*Z* = 3:7) in 40% yield (two steps). Since only two isomers were observable in both the ^{1}H and ^{13}C NMR spectra of **6** it was concluded that no epimerization of the aldehyde had occurred during the Wittig reaction. Treatment of **6** with 5 equivalents of DIBAL-H selectively reduced the less hindered acetal C–O bond to yield a primary alcohol with concomitant formation of an internal *p*-methoxybenzyl ether. Subsequent iodine (1 mol%) catalyzed photoisomerization (medium pressure mercury lamp, no filter) yielded diene **7** (63% from **6**), $[\alpha]_D^{23}$ −60.3 (*c* 1.10, $CHCl_3$), with *E*:*Z* ≥ 95:5 by ^{1}H NMR analysis. A second Swern oxidation gave an aldehyde which was further oxidized to the carboxylic acid **8** with buffered sodium chlorite. The latter was converted to *O*-succinimidyl ester **9**, and the activated ester was then amidated with hydroxylamine to yield hydroxamic acid **10**, $[\alpha]_D^{23}$ −30.2 (*c* 0.97, $CHCl_3$), in 75% overall yield from **7**.[9a]

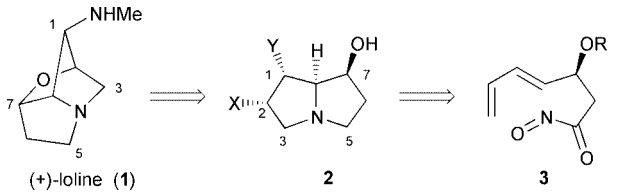

Scheme 1

Initial studies of the hetero-Diels–Alder reaction were carried out with the protected hydroxamic acid **12**, previously prepared from diacetone-D-glucose.[11] Oxidation of **12** with a periodate salt generates a highly reactive acylnitroso intermediate which is trapped by the pendant diene to afford a mixture of the diastereomeric oxazines, **13*c*** and **13*t***. A range of reaction conditions for **12** was surveyed in the hope that good selectivity for the desired *cis* oxazine **13*c*** could be achieved (Table 1). Initial results in non-polar solvents were encouraging (entries 1–3) in that **13*c*** was the major product of the cycloaddition; however, the yield and selectivity were only moderate. Changes in temperature generally had little effect, although carrying out the reaction in refluxing benzene (entry 4) improved the overall yield at the expense of *cis* selectivity. The latter conditions are similar to those employed in the dienophile transfer technique reported by Keck and Nickell,[8] which gave very similar results. More polar solvents (entries 5–7) afforded better yields, but the reaction was not selective. Addition of water to the reaction medium resulted in a preference for the unwanted *trans* oxazine **13*t*** (entry 8); the effect of water on selectivity in an analogous reaction was noted previously by Kibayashi and coworkers.[10] The most practical conditions for preparation of **13*c*** (entry 7), when applied to **10** (entry 9), gave a 57:43 mixture of **11*c***:**11*t***. The oxazines **11*c***, $[\alpha]_D^{23}$ + 86.0 (*c* 0.71, $CHCl_3$), and **11*t***, $[\alpha]_D^{23}$ −75.5 (*c* 2.45, $CHCl_3$), were readily separated by silica gel chromatography.

Conversion of oxazine **11*c*** into pyrrolizidine lactam **14** was readily accomplished in three steps (Scheme 3). Reductive scission of the N–O bond of **11*c*** with excess sodium amalgam afforded a monocyclic allylic alcohol in 91% yield. After quantitative mesylation of the hydroxy group, exposure to LDA resulted in smooth cyclization to bicycle **14** (88%), mp 55–56 °C, $[\alpha]_D^{23}$ −72.0 (*c* 0.50, $CHCl_3$), upon warming.

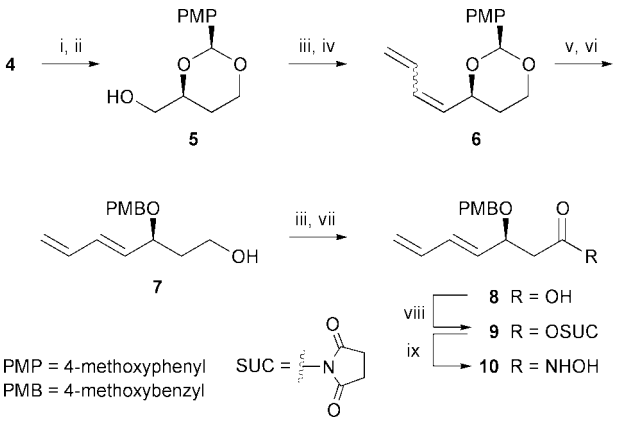

Scheme 2 *Reagents and conditions*: i, $BH_3{\cdot}SMe_2$, $B(OMe)_3$, THF, 0 °C to r.t.; ii, $PMPCH(OMe)_2$, PPTS, CH_2Cl_2, reflux; iii, $(COCl)_2$, DMSO, CH_2Cl_2, −60 °C, then Et_3N, −60 °C to r.t.; iv, allyltriphenylphosphonium bromide, BuLi, THF, −30 °C to r.t.; v, DIBAL-H, CH_2Cl_2, 0 °C to r.t.; vi, I_2, *hν*, C_6H_6, r.t.; vii, $NaClO_2$, $NaH_2PO_4{\cdot}H_2O$, 2-methylbut-2-ene, Bu^tOH–H_2O, 0 °C to r.t.; viii, CF_3CO_2SUC, Py, THF, r.t.; ix, $HONH_2{\cdot}HCl$, Et_3N, CH_2Cl_2, 0 °C.

DOI: 10.1039/b003121f

Table 1 Effect of solvent and temperature on the intramolecular hetero-Diels–Alder reaction of acylnitrosodienes[a] to yield 3,6-dihydro-1,2-oxazines

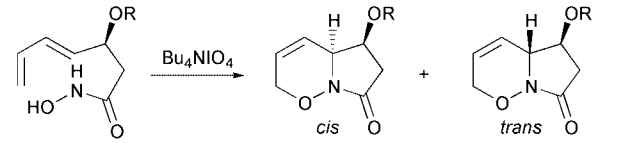

10 R = PMB
12 R = TBDMS

11c R = PMB
13c R = TBDMS

11t R = PMB
13t R = TBDMS

Entry	R	Solvent	*T*/°C	Yield[c] (%)	*Cis*:*trans*[d]
1	TBDMS	PhMe	−20	49	70:30
2	TBDMS	C_6H_6	0	60	71:29
3	TBDMS	C_6H_6	22	64	70:30
4	TBDMS	C_6H_6	80	80	60:40
5	TBDMS	CH_2Cl_2	−78	86	50:50
6	TBDMS	CH_2Cl_2	0	73	45:55
7	TBDMS	$CHCl_3$	22	91	55:45
8[b]	TBDMS	THF–H_2O (1:1)	0	97	27:73
9	PMB	$CHCl_3$	22	87	57:43

[a] The acylnitroso intermediate was generated *in situ* by slow addition of the hydroxamic acid (**10** or **12**) to a solution of $Bu^n_4NIO_4$ (2 equiv., *ca.* 0.03 M). [b] $NaIO_4$ used. [c] Isolated yield of oxazine products. [d] Determined by ^1H NMR integration of the mixture.

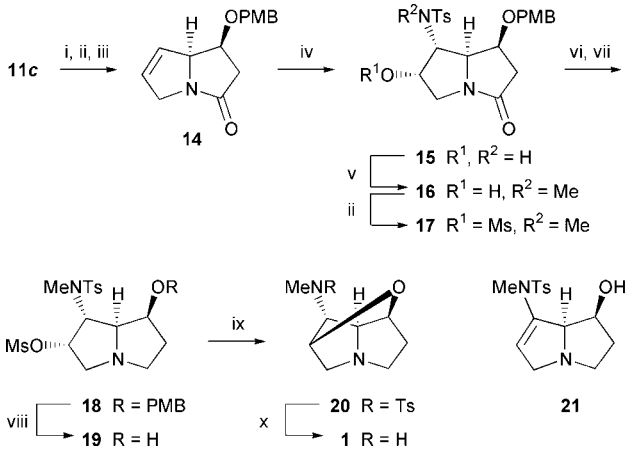

Scheme 3 *Reagents and conditions*: i, 6% Na(Hg), NaH_2PO_4, EtOH, 0 °C; ii, MsCl, Et_3N, CH_2Cl_2, 0 °C; iii, LDA, THF, −78 °C to r.t.; iv, $K_2OsO_2(OH)_4$, $(DHQD)_2PHAL$, chloramine-T, Bu^tOH-H_2O (1:1), r.t.; v, MeI, Bu^tOK, Bu^tOH, 50 °C; vi, $BH_3{\cdot}SMe_2$, THF, r.t.; vii, $Pd(OH)_2/C$, MeOH, r.t.; viii, DDQ, CH_2Cl_2–H_2O (20:1), r.t.; ix, *o*-$Cl_2C_6H_4$, 180 °C; x, sodium naphthalenide, DME, −60 °C.

Exploratory attempts to functionalize the olefinic bond of **14** led us to the discovery that **14** could be aminohydroxylated with the desired regioselectivity under the conditions used by Chang and Sharpless.[12] Thus, treatment of a mixture of **14** and chiral ligand $(DHQD)_2PHAL$ (25 mol%) in Bu^tOH–H_2O (1:1) with chloramine-T (2 equiv.), followed by portionwise addition of potassium osmate (1 mol% every 24 h for 3 days), afforded 40–52% of readily separated amino alcohols, **15** and its regioisomer, in a ratio of 3:1, respectively, together with 21% of a diol. All products were the result of oxidation of **14** from the *exo* face.

Selective methylation of the sulfonamide NH of **15** yielded 76% of **16**, $[\alpha]_D^{23}$ + 49.0 (*c* 0.55, $CHCl_3$); mesylation of the free alcohol then gave a 99% yield of the crystalline lactam **17**, mp 187–190 °C, $[\alpha]_D^{23}$ + 66.1 (*c* 0.70, $CHCl_3$). The latter was reduced with a large excess of $BH_3{\cdot}SMe_2$ (30 equiv.), and the resulting pyrrolizidine–borane complex was decomposed by the combined action of Pearlman's catalyst and methanol to give **18**, $[\alpha]_D^{23}$ + 73.3 (*c* 0.51, $CHCl_3$), in 73% overall yield. Oxidative removal of the PMB ether of **18** with DDQ was sluggish and required over 60 h to afford **19**, mp 175 °C (decomp.), $[\alpha]_D^{22}$ + 45.8 (*c* 0.28, $CHCl_3$), in 70% yield.

Unexpectedly, **19** failed to cyclize to the cage structure of loline under a variety of basic reaction conditions, giving only the elimination product **21** instead. In contrast, direct thermolysis of the hydroxy mesylate in the absence of a base afforded *N*-tosylloline **20**, $[\alpha]_D^{22}$ + 40.9 (*c* 0.11, $CHCl_3$), in 74% yield with no trace of **21**. *N*-Tosylloline prepared by tosylation of a sample of natural loline had $[\alpha]_D^{22}$ +38.0 (c 0.10, $CHCl_3$). Reductive removal of the tosyl substituent from **20** was effected with sodium naphthalenide and afforded (+)-loline **1**, isolated as its dihydrochloride salt in 48% yield. The ^1H and ^{13}C NMR spectra of synthetic material matched exactly those reported for the natural material.[13]

We are grateful to Professor Lowell P. Bush, University of Kentucky, for a sample of loline dihydrochloride and to Professor Joseph J. Tufariello, State University of New York at Buffalo, for the NMR spectra of (±)-loline and its dihydrochloride. One of us (V. K. S.) thanks the Deutsche Forschungsgemeinschaft for a Fellowship. Financial support was provided by the U.S. National Institutes of Health (GM58889).

Notes and references

1 L. P. Bush, F. F. Fannin, M. R. Siegel, D. L. Dahlman and H. R. Burton, *Agric., Ecosystems Environ.*, 1993, **44**, 81.
2 S. Y. Yunusov and S. T. Akramov, *J. Gen. Chem. USSR (Engl. Transl.)*, 1955, **25**, 1765; S. Y. Yunusov and S. T. Akramov, *J. Gen. Chem. USSR (Engl. Transl.)*, 1960, **30**, 3105.
3 S. G. Yates and H. L. Tookey, *Aust. J. Chem.*, 1965, **18**, 53.
4 B. Tofern, M. Kaloga, L. Witte, T. Hartmann and E. Eich, *Phytochemistry*, 1999, **51**, 1177.
5 C. T. Dougherty, F. W. Knapp, L. P. Bush, J. E. Maul and J. Van Willigen, *J. Med. Entomol.*, 1998, **35**, 798.
6 J. J. Tufariello, H. Meckler and K. Winzenberg, *J. Org. Chem.*, 1986, **51**, 3556.
7 For a review of acylnitroso compounds, see: G. W. Kirby, *Chem. Soc. Rev.*, 1977, **6**, 1.
8 G. E. Keck and D. G. Nickell, *J. Am. Chem. Soc.*, 1980, **102**, 3632; G. E. Keck, *Tetrahedron Lett.*, 1978, 4767.
9 For some examples, see: (*a*) G. E. Keck and D. R. Romer, *J. Org. Chem.*, 1993, **58**, 6083; (*b*) C. Kibayashi and S. Aoyagi, *Synlett*, 1995, 873; (*c*) H. Abe, S. Aoyagi and C. Kibayashi, *Tetrahedron Lett.*, 2000, **41**, 1205.
10 M. Naruse, S. Aoyagi and C. Kibayashi, *J. Org. Chem.*, 1994, **59**, 1358.
11 S. Kim and J. D. White, unpublished results.
12 G. Li, H.-T. Chang and K. B. Sharpless, *Angew. Chem., Int. Ed. Engl.*, 1996, **35**, 451.
13 R. J. Petroski, S. G. Yates, D. Weisleder and R. G. Powell, *J. Nat. Prod.*, 1989, **52**, 810.

A simple, general and robust function for equilibria in aqueous electrolyte solutions to high ionic strength and temperature†

Peter M. May

A. J. Parker Cooperative Research Centre for Hydrometallurgy, School of Mathematical and Physical Sciences, Murdoch University, Murdoch, WA 6150, Australia. E-mail: may@murdoch.edu.au

Received (in Cambridge) 19th April 2000, Accepted 1st June 2000
Published on the Web 22th June 2000

A novel function is proposed to calculate the conditional equilibrium constants of reactions in aqueous solution; two parameters characterise a non-electrolyte-specific response to increasing ionic strength (< 5 M) and temperature (< 250 °C).

How chemical equilibria in solution respond to changing experimental conditions is of considerable theoretical and practical importance. A good function is needed to model natural and industrial systems and to analyse the vast array of experimental data on which such models depend. Since electrolyte solutions depart strongly from ideality, this has proved elusive[1] and, consequently, many different functions have been employed.[2]

Among the most common approaches nowadays are the Pitzer,[3] the Brønsted–Guggenheim–Scatchard Specific Ion Interaction (SIT),[1] the Helgeson–Kirkham–Flowers (HKF)[4] and the Density[5] models. However, none is the obvious method of choice and, of the many tens of thousands of reactions of interest, only a small fraction have been characterised using these functions.[6]

The main problem with the Pitzer, SIT and HKF models lies in the numerical fitting of parameters that they use to describe individual chemical systems. Although very good agreement with experimental data can be achieved, many 'interaction coefficients' are typically involved. Predictions are then put in doubt because (a) the fitted parameters do not capture the essence (*i.e. only* the predominant factors) of the underlying *general* physicochemical behaviour and (b) unique characterisation becomes difficult, and extrapolations thwarted, by mathematical correlation (covariance).

In contrast, the parameters of the Density model are much fewer, are entirely fundamental and can be measured independently. The Density model thus provides an excellent means for assessing and predicting data under ideal conditions, *i.e.* at infinite dilution. It has been used extensively for these purposes at the U.S. Oak Ridge National Laboratories (ORNL),[8] whose results comprise by far the largest single body of reliable equilibrium constants in aqueous electrolyte solutions, especially at higher temperatures.[7]

Unfortunately, the Density model as described by Andersen *et al*.[5] does not deal directly with the effects of ionic strength. Extraneous and varied means are invoked to extrapolate measurements to infinite dilution, a notoriously difficult task even at ambient temperatures with plenty of data. A failure to record properly in databases the particular smoothing function used, and the parameters so obtained, exacerbates the problem. Sometimes more than ten fitting parameters are employed.

To extend the Density model to finite concentrations, I propose here, a novel function that calculates the conditional equilibrium constants of reactions in aqueous solution. The function is based on just two additional semi-empirical parameters that characterise the effects of increasing ionic strength and temperature in a non-electrolyte-specific manner. The need for, and magnitude of, specific interaction coefficients is thus much reduced.

The scientific description of the effect of ionic strength on equilibria in electrolyte solutions has recently been reviewed.[2] Soon after Debye and Hückel demonstrated the dominance in dilute solutions of coulombic interactions between ions, Hückel suggested that the expression for the mean ionic activity coefficient, $\gamma_{\pm}$, could be extended to higher concentrations by introducing a linear term, ascribed to 'ion-solvent interactions'. Guggenheim then proposed a formula for mixtures in which this linear term is expanded into a summation involving the so-called 'ion interaction coefficients'. This formula underpins the SIT model in current use today.

There is considerable experimental evidence showing that activity coefficients (and, hence, conditional equilibrium constants) vary in a way that accords with this linear behaviour. However, no theoretical explanation has prevailed, allowing the proliferation of correction functions described above.

An equation that works satisfactorily[8] at constant temperature (t) has the form

$$\log_{10} K' = \log_{10} K^0 + \left(\frac{-\Delta Z^2 A\sqrt{I}}{1+1.5\sqrt{I}} \right) + BI \qquad (1)$$

where K' is the conditional equilibrium constant at finite ionic strength, K^0 is the equilibrium constant (at infinite dilution), and A and ΔZ^2 are the usual Debye–Hückel factors. Both B and the factor in the denominator, shown here as 1.5 to accord with the SIT model,[1] must be nearly constant to maintain thermodynamic consistency but their exact values are somewhat arbitrary on account of the covariance between them.

The key observation of the present work is simply that the value of B itself changes linearly with temperature. To represent this behaviour in accord with the Density model (for which all parameters refer to a reference temperature) this variation is conveniently expressed as $B = G_C + G_M (t - 25)$, where the symbols G_C and G_M refer to the intercept and slope respectively of the Guggenheim factor B at 25 °C.

The linearity of the expression for B is important in the maintenance of thermodynamic consistency when the function is applied to reactions in general. Also important is the low correlation between the five parameters of the extended Density model (log K^0, ΔH^0, ΔC_p^0, G_C and G_M).

The new function has been applied in the characterisation of reaction data in the JESS Thermodynamic database.[6] Although much is still to be done, it is clear that in this way the vast majority of compiled equilibrium constants can be rationalised to well within their experimental error. Very few exceptions have been encountered and these exhibit no discernable pattern, leaving experimental error as their most likely explanation.

A very demanding test was provided by the ORNL data, comprising more than 700 equilibrium constants of unsurpassed precision and accuracy for over 30 reactions. All these chemical systems were fitted satisfactorily. The median deviations between observed and calculated data were typically better than 0.05 log K units and the worst rarely greater than 0.1 units.

† Electronic supplementary information: plots for 38 chemical systems of conditional equilibrium constants as a function of ionic stength and temperature. See http://www.rsc.org/suppdata/cc/b0/b003157g/

DOI: 10.1039/b003157g

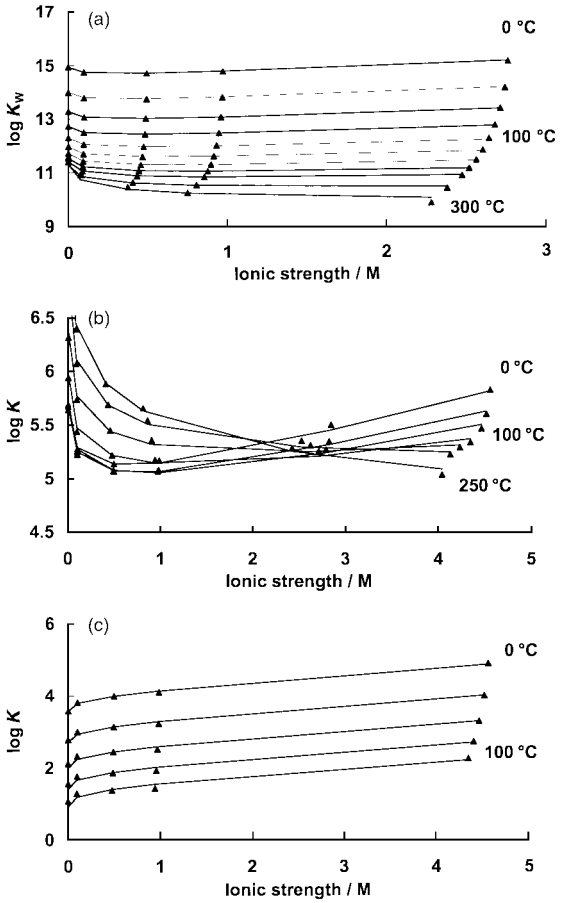

Fig. 1 Illustrative plots of observed and predicted values for conditional equilibrium constants as a function of ionic strength and temperature with three different types of chemical reaction: (a) the hydrolysis of water,[10] (b) the first protonation of succinate[11] and (c) the solubility of gibbsite.[12]

These differences are small compared to the changes in the measured equilibrium constants which over the intervals $0 \leqslant I \leqslant 5.0$ M and $0 \leqslant t \leqslant 250$ °C typically vary by as much as 3 log K units. It may even be possible to improve on these predictions for data at higher temperatures by taking account of density change in the electrolyte medium, but this remains to be done.

Three examples, representing quite different types of behaviour, are shown in Fig. 1. Plots for 38 chemical systems have been deposited as ESI.†

Despite the formal mathematical similarity between the function being proposed here and that of the SIT method, the two approaches differ diametrically. Whereas the (temperature-dependent) SIT parameters are many (one for each ion–counter ion, ion–neutral and neutral–neutral interaction[1]) and represent *specific* interactions, just two values, G_C and G_M, are used in this work to characterise the *non-specific* response of the reaction to changing conditions. It seems much better to attribute specific properties only to the *differences* in equilibrium constants observed in different background electrolytes at the same ionic strength and temperature: this isolates behaviour that is common to all electrolytes, such as caused by the general reduction in water activity with increasing concentration, and it keeps the magnitude of the specific factors to a minimum. The effects of individual electrolytes can then simply be described as a direct association between species (see *e.g.* ref. 9), which generally yields even better fits of the data.

The observed data are nonetheless modelled well, albeit not exactly, by the non-specific function on its own. This has all the flexibility needed to follow the main trends exhibited by equilibria to high concentrations (≈ 5 M) and high temperature (≈ 250 °C). It also possesses the three chief attributes necessary to rationalise diverse experimental data and to predict values beyond the range of parameterisation, namely it (a) appears applicable to all types of reaction, (b) involves only a few parameters and (c) offers a reasonable physicochemical basis for avoiding optimisation of values when this is not warranted by the data available.

Financial support from Murdoch University and from the Australian Government under its Cooperative Research Centres Program is gratefully acknowledged.

Notes and references

1 I. Grenthe, A. V. Plyasunov and K. Spahiu, in *Modelling in Aquatic Chemistry*, ed. I. Grenthe and I. Puigdomenech, OECD, Paris, 1997, pp. 325–426.
2 M. E. Sastre de Vincente, *Curr. Top. Solution Chem.*, 1997, **2**, 157.
3 K. S. Pitzer, in *Activity Coefficients in Electrolyte Solutions*, ed. K. S. Pitzer, CRC Press, Boca Raton, FL, 1991, pp. 75–153.
4 D. A. Sverjensky, E. L. Shock and H. C. Helgeson, *Geochim. Cosmochim. Acta*, 1997, **61**, 1359.
5 G. M. Anderson, S. Castet, J. Schott and R. E. Mesmer, *Geochim. Cosmochim. Acta*, 1991, **55**, 1769.
6 P. M. May and K. Murray, *Talanta*, 1993, **40**, 819 and preceding parts of this series.
7 R. E. Mesmer, W. L. Marshall, D. A. Palmer, J. M. Simonson and H. F. Holmes, *J. Solution Chem.*, 1988, **17**, 699.
8 P. W. Linder and K. Murray, *Talanta*, 1982, **29**, 377.
9 S. G. Capewell, G. Hefter and P. M. May, *J. Solution Chem.*, 1998, **27**, 865.
10 F. H. Sweeton, R. E. Mesmer and C. F. Baes, *J. Solution Chem.*, 1974, **3**, 191.
11 R. M. Kettler, D. A. Palmer and D. J. Wesolowski, *J. Solution Chem.*, 1995, **24**, 65.
12 D. J. Wesolowski and D. A. Palmer, *Geochim. Cosmochim. Acta*, 1994, **58**, 2947.

An *in situ* time-resolved neutron diffraction study of the hydrothermal crystallisation of barium titanate

Richard I. Walton,[a] Ronald I. Smith,[b] Franck Millange,[a] Iain J. Clark,[c] Derek C. Sinclair[c] and Dermot O'Hare*[a]

[a] *Inorganic Chemistry Laboratory, University of Oxford, South Parks Road, Oxford, UK OX1 3QR. E-mail: dermot.ohare@chem.ox.ac.uk*
[b] *ISIS Facility, Rutherford Appleton Laboratory, Chilton, Didcot, Oxon, UK OX11 0QX*
[c] *Department of Engineering Materials, University of Sheffield, Mappin Street, Sheffield, UK S1 3JD*

Received (in Cambridge, UK) 27th April 2000, Accepted 30th May 2000
Published on the Web 22th June 2000

The hydrothermal crystallisation of barium titanate, $BaTiO_3$, has been studied for the first time by *in situ* time-resolved neutron powder diffraction; we deduce that $BaTiO_3$ is formed from solution by reaction between $[Ti(OH)_x]^{(4-x)+}_{(aq)}$ and $[Ba(OH)_x]^{(2-x)+}_{(aq)}$ species, rather than by a heterogeneous reaction between solid TiO_2 and $Ba^{2+}_{(aq)}$ ions.

Tetragonal barium titanate, t-$BaTiO_3$, finds widespread application in the electroceramics industry. The ferroelectric properties and high permittivity of t-$BaTiO_3$ are exploited in, for example, thermistors, capacitors, and electro-optic devices. Traditional routes to the synthesis of the material employ direct solid-state reaction between barium carbonate and titanium dioxide at elevated temperature (> 900 °C). Hydrothermal routes to $BaTiO_3$ have been the focus of much recent research as an efficient low temperature method for its manufacture (see, for example, refs. 1–3). The reaction of a number of barium and titanium sources in water at temperatures as low as 80 °C has enabled the production of t-$BaTiO_3$ and by varying reaction conditions and choice of starting materials it has proved possible to change the particle size and morphology of the material produced. Particular attention has been paid to the production of ultrafine (submicron) powders[1–4] and to the production of thin films[5–7] by the hydrothermal method. Such control of morphology is extremely desirable and has huge potential value, both in the manufacture of miniaturised devices[8,9] and in the production of dense fine-grained ceramics by sintering of the fine powders initially prepared.[10]

An understanding of the formation mechanism will be vital if controlled growth of t-$BaTiO_3$ is to be performed and the potential applications described above are to be exploited. Although the kinetics and mechanism of hydrothermal barium titanate production have been discussed by several authors,[11–14] no agreed description of its formation mechanism has been reached. Two extreme models have been postulated: one involving a homogenous solution phase reaction between titanium and barium hydroxy anions (the dissolution–precipitation mechanism) and another involving the reaction between solid TiO_2 and soluble barium species (the *in situ* heterogeneous transformation mechanism).[12] The data previously used to probe the kinetics of barium titanate crystallisation were derived entirely from quenching experiments, whereby material was removed from the reaction cell after given period of time and examined.

Because of the absorbing nature of the sample, we were unfortunately unable to probe the barium titanate crystallisation using *in situ* time-resolved synchrotron X-ray diffraction experiments, which are now well established.[15,16] Powder neutron diffraction, however, offers an alternative means of following the crystallisation. In recent months we have developed a gold coated, null-scattering (67.7 atom% Ti, 32.3 atom% Zr) environmental cell that enables us to record *in situ* high-resolution powder neutron diffraction patterns of highly reactive and/or corrosive materials reacting under hydrothermal conditions.[17] Only one previous report of the use of neutron diffraction to follow reactions under hydrothermal conditions appears in the literature, and this did not overcome the problem of significant scattering from the reaction vessel appearing in the diffraction patterns, which seriously limited the amount of quantitative and structural information that could potentially be extracted.[18] Here, we describe the first use of the Oxford-ISIS hydrothermal cell to study a hydrothermal synthesis using *in situ* neutron diffraction.

Fig. 1(a) shows the time-of-flight powder neutron diffraction patterns of the crystalline starting materials [TiO_2 (2.12 g) $Ba(OD)_2{\cdot}8D_2O$ (9.81 g), Ba : Ti ratio of 1.1 : 1] as a suspension in 10 ml D_2O in the hydrothermal cell before heating.† The cell was then heated to 125 °C and neutron diffraction patterns

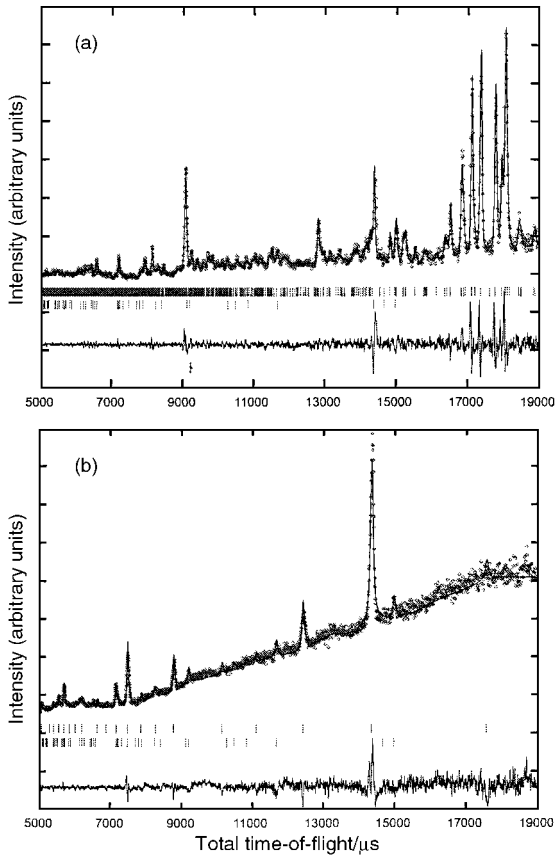

Fig. 1 Powder neutron diffraction data obtained from within the hydrothermal cell. for (a) $Ba(OD)_2{\cdot}8D_2O$ (upper tick marks) and TiO_2 (lower tick marks) in D_2O and (b) for the barium titanate produced by heating the mixture at 125 °C for 12 h (lower tick marks are unreacted TiO_2). The points are the experimental data, the full line the result of the whole pattern fitting, and the lower line the difference curve.

DOI: 10.1039/b003386n

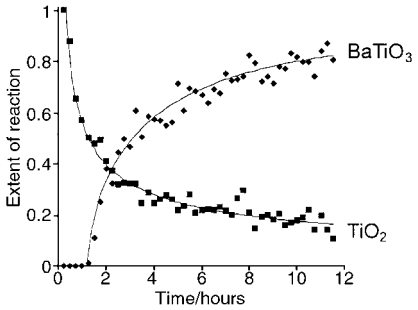

Fig. 2 Changes in integrated Bragg peak intensities for TiO_2 and $BaTiO_3$ during reaction at 125 °C. Line are guides to the eye and have no physical significance.

recorded every 15 min for a period of 12 h. Fig. 1(b) shows the sum of the four final diffraction patterns obtained, *i.e.* 1 h of data in total. These data can be successfully modelled as arising from cubic $BaTiO_3$. At 125 °C we would have expected t-$BaTiO_3$ to have formed since at temperatures below 130 °C the lower symmetry form is thermodynamically more stable. These synthesis conditions, however, produce submicron-sized particles of $BaTiO_3$ and as has previously been pointed out, it is very difficult to identify the $BaTiO_3$ polymorph using diffraction methods when the Bragg reflections are considerably broadened by the small particle size.[2,19]

Integrated intensities of the well resolved Bragg reflections were determined by Gaussian-fitting and this enabled decay and growth curves of both the starting materials and products to be quantitatively determined. Fig. 2 shows the extent of reaction ($\alpha = I/I_\infty$) curves *vs.* time derived from integrated intensities of TiO_2 and $BaTiO_3$ as a typical reaction mixture was heated at 125 °C. The growth curves for all the resolved Bragg reflections of $BaTiO_3$ were identical suggesting that crystal growth is isotropic, which is not unexpected given the spherical morphology of particles typically produced by this hydrothermal synthesis. We also have investigated the use of amorphous $TiO_2{\cdot}H_2O$ as a titanium source, which has recently been used to prepare submicron $BaTiO_3$ particles,[2] and confirmed that the rate of reaction is considerably more rapid compared to the crystalline source.

The neutron diffraction data clearly show that the crystalline barium source, barium deuteroxide octahydrate dissolves rapidly before any other changes in crystallinity are apparent in the reaction mixture; in all cases the Bragg reflections of $Ba(OD)_2{\cdot}8D_2O$ disappear in less than 1 h and always before the appearance of any $BaTiO_3$. All previously discussed mechanisms for the hydrothermal crystallisation of barium titanate suggest that the barium source is in solution and our *in situ* results provide clear evidence for this assumption. Most significantly, when crystalline TiO_2 is used as the titanium source its initial decay is rapid and more than 50% of the TiO_2 dissolves before the appearance of any of the $BaTiO_3$ product. This strongly suggests that a dissolution–precipitation mechanism is taking place, *i.e.* that barium titanate is formed by reaction between dissolved $Ba^{2+}_{(aq)}$ and $[Ti(OH)_x]^{(4-x)+}_{(aq)}$ species. If reaction between Ba^{2+} ions in solutions and solid TiO_2 particles was taking place, then we would expect the rate of formation of $BaTiO_3$ to mirror the decay of TiO_2. Some previous studies have assumed the latter *in situ* heterogeneous transformation mechanism,[11] but more recent studies using electron microscopy techniques find no evidence for this model; for example Pinceloup *et al.* examined the quenched material from barium titanate crystallisations after various periods of time and always observed distinct titania or barium titanate particles, and that there was no relationship between particle size distribution in the titanium oxide starting material and the barium titanate product.[14] Our study thus provides independent evidence for the dissolution–precipitation mechanism by a novel technique.

The kinetic crystallisation curves can be analysed quantitatively using the Avrami–Erofe'ev expression for a nucleation-growth mechanism.[20–23] We find that the power dependence (n) of the rate expression is 1.1 ± 0.5. A value of $n = 1$ suggests that the rate determining step of reaction is the reaction at the phase boundary, *i.e.* the chemical reaction taking place at the nucleation sites between solution Ba^{2+} and $[Ti(OH)_x]^{(4-x)+}$ anions. This study has thus provided a firm foundation on which to base a mechanism for the hydrothermal crystallisation of barium titanate.

In summary, we have demonstrated in this paper that neutron diffraction has the potential to be a powerful technique for the study of chemical processes under non-ambient conditions. It offers the potential for collecting new data not available using other sources and also data complementary to that available from analogous *in situ* synchrotron X-ray diffraction experiments. We believe with the ongoing improvements in available neutron flux and in detector technology it will be possible to collect data of higher quality in shorter time intervals from reaction vessels such as we have described.

We thank the EPSRC for financial support and provision of beam-time at the ISIS Facility.

Notes and references

† Neutron diffraction patterns presented were recorded in the high resolution backscattering detector bank [2θ(av.) = 45°] of the POLARIS diffractometer at the UK pulsed spallation neutron source ISIS, Rutherford Appleton Laboratory. The hydrothermal autoclave was loaded with TiO_2 (2.12 g), $Ba(OD)_2{\cdot}8D_2O$ (9.81 g) and D_2O (10 g) under a dry nitrogen atmosphere and rapidly heated under autogeneous pressure at 125 °C. The TiO_2 was purely in the anatase polymorph, and this was confirmed by the good fit achieved to the neutron diffraction data. The structure of barium hydroxide octahydrate has been determined using single crystal X-ray diffraction methods[24] and using the cell parameters previously found as a starting point for refinement against the neutron data allowed confirmation of the identity of the barium source [X-ray values: a = 9.274 Å, b = 9.260 Å, c = 11.817 Å, β = 98.95°,[24] neutron refined values: a = 9.3137(3) Å, b = 9.3043(3) Å, c = 11.860(8) Å, β = 98.995(3)°].

1 R. Asiaie, W. Zhu, S. A. Akbar and P. K. Dutta, *Chem. Mater.*, 1996, **8**, 226.
2 I. J. Clark, T. Takeuchi, N. Ohtori and D. C. Sinclair, *J. Mater. Chem.*, 1999, **8**, 83.
3 M. Wu, J. Long, G. Wang, A. Huang, Y. Luo, S. Feng and R. Xu, *J. Am. Ceram. Soc.*, 1999, **82**, 3254.
4 M. H. Um and H. Kumazawa, *J. Mater. Sci.*, 2000, **35**, 1295.
5 E. B. Slamovich and I. A. Aksay, *J. Am. Ceram. Soc.*, 1996, **79**, 239.
6 C. F. Kao and C. L. Yang, *J. Eur. Ceram. Soc.*, 1999, **19**, 1365.
7 J. Zeng, C. Lin, Z. Song, K. Li and J. Li, *Philos. Mag. Lett.*, 2000, **80**, 119.
8 T. Hoffman, T. Doll and V. M. Fuenzalida, *J. Electrochem. Soc.*, 1997, **144**, L293.
9 S. Venigalla, D. J. Clancy, D. V. Miller, J. A. Kerchner and S. A. Costantino, *Am. Ceram. Soc. Bull.*, 1999, **78**, 51.
10 P. Pinceloup, C. Courtois, A. Leriche and B. Thierry, *J. Am. Ceram. Soc.*, 1999, **82**, 3049.
11 W. Hertl, *J. Am. Ceram. Soc.*, 1988, **71**, 879.
12 J. O. Eckert, C. C. Hung-Houston, B. L. Gerstan, M. M. Lenka and R. E. Riman, *J. Am. Ceram. Soc.*, 1996, **79**, 2929.
13 J. A. Kernchner, J. Moon, R. E. Chodelka, A. A. Morrone and J. H. Adair, *ACS Symp. Ser.*, 1998, **681**, 106.
14 P. Pinceloup, C. Courtois, J. Vicens, A. Leriche and B. Thierry, *J. Eur. Ceram. Soc.*, 1999, **19**, 973.
15 J. S. O. Evans, R. J. Francis, D. O'Hare, S. J. Price, S. M. Clark, J. Flaherty, J. Gordon, A. Nield and C. C. Tang, *Rev. Sci. Instrum.*, 1995, **66**, 2442.
16 A. K. Cheetham and C. F. Mellot, *Chem. Mater.*, 1997, **9**, 2269.
17 R. I. Walton, R. J. Francis, P. S. Halasyamani, D. O'Hare, R. I. Smith, R. Done and R. Humpreys, *Rev. Sci. Instrum.*, 1999, **70**, 3391.
18 E. Polak, J. Munn, P. Barnes, S. E. Tarling and C. Ritter, *J. Appl. Crystallogr.*, 1990, **23**, 258.
19 E. W. Shi, C. T. Xia, W. Z. Zhong, B. G. Wang and C. D. Feng, *J. Am. Ceram. Soc.*, 1997, **80**, 1567.
20 M. Avrami, *J. Chem. Phys.*, 1939, **7**, 1103.
21 M. Avrami, *J. Chem. Phys.*, 1940, **8**, 212.
22 M. Avrami, *J. Chem. Phys.*, 1941, **9**, 177.
23 B. V. Erofe'ev, *C. R. Dokl. Acad. Sci. URSS*, 1946, **52**, 511.
24 M. Sacerdoti, V. Bertolasi, V. Ferretti and C. A. Accorsi, *Z. Kristallogr.*, 1990, **192**, 111.

ChemComm

An unprecedented coordination mode for hemilabile pendant-arm 1,4,7-triazacyclononanes and the synthesis of cationic organoaluminium complexes

David A. Robson,[a] Leigh H. Rees,[a] Philip Mountford*[a] and Martin Schröder*[b]

[a] *Inorganic Chemistry Laboratory, South Parks Road, Oxford, UK OX1 3QR. E-mail: philip.mountford@chemistry.oxford.ac.uk*

[b] *School of Chemistry, University of Nottingham, University Park, Nottingham, UK NG7 2RD. E-mail: martin.schroder@nott.ac.uk*

Received (in Cambridge, UK) 14th April 2000, Accepted 24th May 2000
Published on the Web 26th June 2000

Reaction of $AlMe_3$ or [$AlMe_3$·py] with the pendant arm OH-funtionalised 1,4,7-triazacyclononane proligands, HL^1 or HL^2, affords the four- and five-coordinate derivatives [Al(L^1)Me_2] 1 or [$Al_2(L^2)_2Me_4$] 2 in which the pendant alkoxide O-donor and only *one* macrocycle N-donor is bound to Al; methyl anion abstraction from 1 yields cationic, pentacoordinate [Al(L^1)Me]$^+$ in which L^1 has a tetradentate coordination mode [L^1 = 1-(2-hydroxy-3,5-di-*tert*-butylbenzyl)-4,7-diisopropyl-1,4,7-triazacyclononane; L^2 = 1-(2-hydroxy-2-methylethyl)-4,7-diisopropyl-1,4,7-triazacyclononane].

Pendant-arm macrocycles offer the ability to modify and tune the electronic and stereochemical properties of a range of metal centres,[1] and may be regarded as potent protecting groups for catalytic reactions. We were therefore interested to explore the potential of pendant arm triazacyclononane ligands in neutral and cationic organoaluminium chemistry, for which there is no precedent in the literature, although several examples of compounds involving N-substituted 1,4,7-triazacyclononane ligands with the group 13 elements are known. Aluminium compounds in general are widely used as reagents or catalysts across a range of organic and inorganic chemistry, and cationic complexes, in particular, can lead to enhanced reactivity through more effective substrate coordination and activation.[2] We report herein preliminary results, including the first structurally authenticated examples of complexes having a triazacyclononane ligand coordinated through only *one* nitrogen, together with the first example of a cationic *p*-block organometallic complex of a triazacyclononane ligand.

Reaction of $AlMe_3$ or $AlMe_3$·py with HL^1 or HL^2 causes elimination of methane and affords the mono- or bi-nuclear

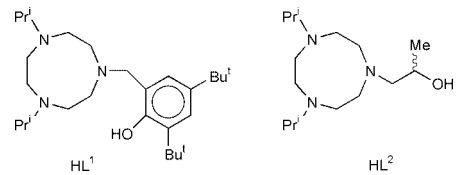

compounds [Al(L^1)Me_2] **1** and [$Al_2(L^2)_2Me_4$] **2** in good to fair yield (Scheme 1).†[3a] The molecular structures of **1** and **2** are shown in Figs. 1 and 2, respectively.‡ The compound [Al(L^1)Me_2] **1** possesses an approximately tetrahedral Al(III) centre [range of angles subtended at Al(1): 95.0(2)–119.8(2)°], the coordination sphere of which comprises two methyl groups, the oxygen atom of the pendant phenoxide group and only one N-donor of the triazacyclononane ligand. The compound [$Al_2(L^2)_2Me_4$] **2** features two approximately trigonal bipyramidal Al(III) centres [*e.g.* N(1)–Al(1)–O(28) 151.0(2)°; sum of the angles subtended at Al(1) by O(13), C(14), C(15) = 360.1°] with the pendant oxygen donors bridging them. The most important and highly unusual feature of **1** and **2** is that only *one* of the three macrocyclic N-donors binds to the Al(III) centre. That **2** forms a binuclear, μ-O-bridged complex is attributed to steric factors, the greater steric bulk of L^1 stabilising the mononuclear complex.

The low temperature, high-field NMR spectra of the highly fluxional compounds **1** and **2** are consistent with the solid state structures.† Of special note for both compounds is the presence of two low-field multiplets in the range δ 4–5 of the ^{1}H NMR spectra; these are assigned to two of the macrocylic ring methylene hydrogens. These shifts appear to be particularly diagnostic of the mono-N-coordinated mode of ligation of the ligands L^1 and L^2, as such features are absent from the ^{1}H NMR spectra of structurally authenticated tri-N-coordinated transition and main group metal complexes of pendant arm derivatives of triazacyclononanes.[3a,4]

The reaction of HL_2 or [$Al_2(L^2)_2Me_4$] **2** with 2 equiv. of $AlMe_3$ cleaves the dimer and gives binuclear [Al(L^2·AlMe_3)Me_2] **3** (Scheme 1) in which $AlMe_3$ is bound to the pendant alkoxide oxygen,‡§ rather than forming a product with the $AlMe_3$ bound to a nitrogen lone pair of L^2. As for **1** and **2**, the triazacyclononane ring in **3** binds through only one nitrogen, and the ^{1}H NMR spectrum shows a diagnostic pair of multiplets in the region δ 4–5. In contrast, [Al(L^1)Me_2] **1** does not react at all with $AlMe_3$, suggesting that neither the phenoxide oxygen nor the macrocycle nitrogen lone pairs are accessible.

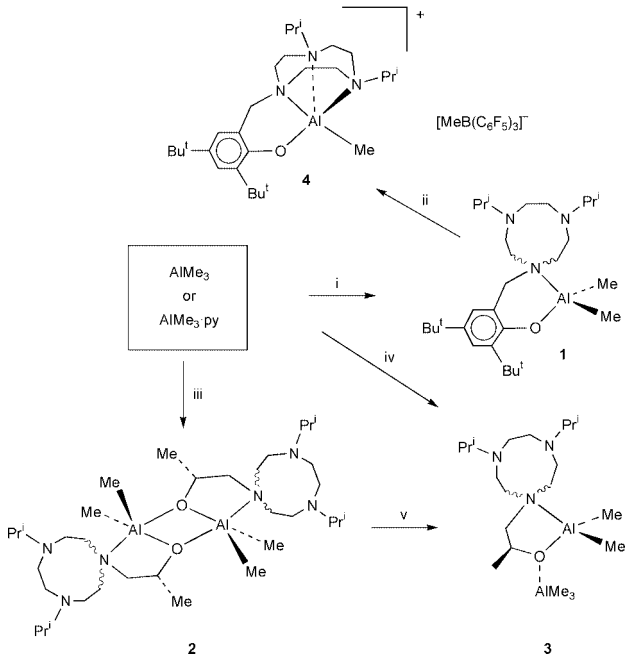

Scheme 1 *Reagents and conditions*: i, HL^1, hexane, r.t., 2 h, 57%; ii, $B(C_6F_5)_3$, CH_2Cl_2, r.t., 30 min, quantitative; iii, HL^2, hexane, r.t., 2 h, 30%; iv, 0.5 HL^2, hexane, r.t., 2 h, 71%; v, 2 $AlMe_3$, C_6D_6, r.t., 5 min, quantitative.

DOI: 10.1039/b003019h

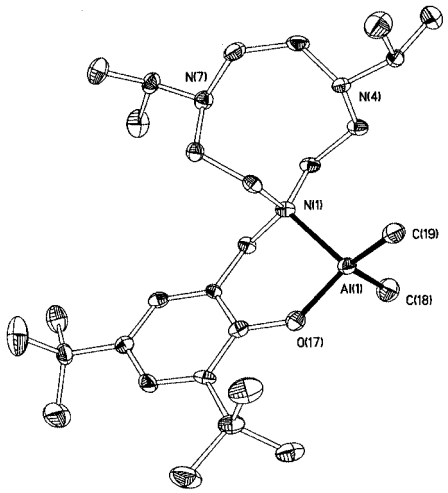

Fig. 1 Displacement ellipsoid plot of $[Al(L^1)Me_2]$ **1**. Hydrogen atoms are omitted for clarity and displacement ellipsoids are drawn at the 40% probability level. Selected bond lengths (Å): Al(1)–O(17) 1.759(4), Al(1)–N(1) 2.011(4), Al(1)–C(18) 1.965(5), Al(1)–C(19) 1.953(5).

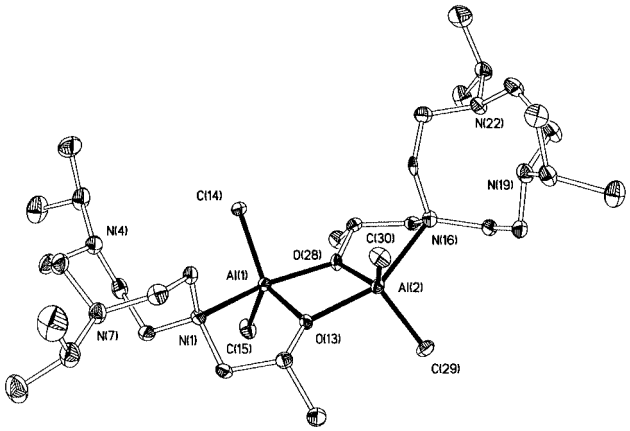

Fig. 2 Displacement ellipsoid plot of $[Al_2(L^2)_2Me_4]$ **2** Hydrogen atoms are omitted for clarity and displacement ellipsoids are drawn at the 40% probability level. Selected bond lengths (Å): Al(1)–O(13) 1.849(3), Al(1)–N(1) 2.245(4), Al(1)–C(14) 1.977(5), Al(1)–C(15) 1.972, Al(1)–O(28) 1.935(3), Al(2)–O(28) 1.845(3), Al(2)–N(16) 2.265(4), Al(2)–C(29) 1.966(5), Al(2)–C(30) 1.983(5), Al(2)–O(13) 1.946(3).

The mono-N-coordination modes for L^1 and L^2 in compounds **1**–**3** are unique in the now very extensive and important field of triazacyclononane ligand coordination (transition and main group metal) chemistry.[1,3] While there are a few examples of triazacyclononane ligands bonding through only two nitrogen ligands, these are found only for later transition metals where ligand field effects (*e.g.* those associated with d^8 square planar complexes) are particularly dominant.[5] Only one triazacyclononane complex of aluminium has been previously structurally characterised, namely six-coordinate [Al(L)] where L is the tris(pendant arm) ligand 1,4,7-$(O_2CCH_2)_3$[9]aneN_3.[6]

As mentioned above, there is considerable current interest in well defined, cationic organoaluminium compounds.[2c–g] Reaction of $[Al(L^1)Me_2]$ **1** with $B(C_6F_5)_3$ gives $[Al(L^1)Me][MeB(C_6F_5)_3]$ **4** (Scheme 1). We have not yet obtained diffraction-quality crystals of **4** and so this complex has been characterised by non-crystallographic techniques.† The ^1H and ^{19}F NMR data for the $[MeB(C_6F_5)_3]^-$ anion show that there is no interaction with the $[Al(L^1)Me]^+$ cation in which L^1 now bonds to Al through *all three* macrocyclic nitrogens.[7] This coordination mode is suggested by the *ca*. 0.3–0.9 ppm downfield ^1H NMR shifts of the NPr^i group resonances compared to those in **1**–**3** (consistent with bonding to a cationic metal centre) and the absence of any macrocyclic ring methylene resonances in the region δ 4–5 which would be expected for a mono-N-coordinated L^1. Analogous trigonal bipyramidal coordination modes have been reported for $[Zn(L^1)Cl]$ and its homologues.[3a]

Compound **4** is the first example of a cationic *p*-block organometallic complex of any triazacyclononane ligand. Moreover, the interconversion of coordination modes (mono-N-bound in **1** to tri-N-bound in **4**) has never before been observed for triazacyclononane complexes, and the current work suggests that the hemilability of functionalised [9]ane_3 ligands can be used to control and tune the reactivity of the Al centre. Preliminary studies of the reactions of other complexes $[Al(L)Me_2]$ (L = monopendant arm functionlised triazacyclononane) with $B(C_6F_5)_3$ show that other examples of organoaluminium cations related to **4** can be prepared, and reactivity studies of these cations towards organic substrates are in progress.

This work was supported by the EPSRC and Royal Society. We thank Dr N. A. H. Male for helpful discussions.

Notes and references

† Full spectroscopic data and elemental analyses have been obtained for all the new compounds which were prepared under dry, anaerobic conditions.

‡ *Crystal data* for **1**: $C_{29}H_{54}AlN_3O$, M = 487.73, orthorhombic, $P2_12_12_1$, a = 10.3380(4), b = 13.9560(7), c = 20.8520(11) Å, U = 3008.5(2) Å^3, Z = 4, T = 150(2) K, μ = 0.091 mm^{-1}, 7450 refelections measured, 3926 (R_{int} = 0.0338) used in refinement, final R indices: R_1 = 0.0715 [data with $I > 2\sigma(I)$], $wR_2(F^2)$ = 0.1466 (all data). *For* **2**: $C_{34}H_{76}Al_2N_6O_2$, M = 654.97, monoclinic, $P2_1$, a = 12.2690(5), b = 13.4100(6), c = 12.4290(4) Å, β = 95.998(2)°, U = 203.71(14) Å^3, Z = 2, T = 150(2) K, μ = 0.106 mm^{-1}, 4232 independent reflections measured and used in refinement, final R indices: R_1 = 0.0691 [data with $I > 2\sigma(I)$], $wR_2(F^2)$ = 0.174 (all data).

CCDC 182/1658. See http://www.rsc.org/supp data/cc/b0/b003019h/ for crystallographic files in .cif format.

§ The X-ray structure of $[Al(L^2{\cdot}AlMe_3)Me_2]$ **3** has been determined and will be reported in full elsewhere.[4]

1 For leading references, see: P. V. Bernhardt and G. A. Lawrence, *Coord. Chem. Rev.*, 1990, **104**, 297; J. P. Danks, N. R. Chapmness and M. Schröder, *Coord. Chem. Rev.*, 1998, **174**, 417; P. Chaudhuri and K. Wieghardt, *Prog. Inorg. Chem.*, 1987, **25**, 329.

2 For leading references in neutral and cationic aluminium chemistry, see: (*a*) J. J. Eisch, in *Comprehensive Organometallic Chemistry II*, ed. E. W. Abel, F. G. A. Stone and G. Wilkinson, 1995, vol. 11, ch. 6; (*b*) K. B. Starowieyski, in *Chemistry of Aluminium, Gallium, Indium and Thallium*, ed. A. J. Downs, Chapman & Hall, London, UK, 1993, pp. 322–371; (*c*) S. Dagorne, I. A. Guzei, M. P. Coles and R. F. Jordan., *J. Am. Chem. Soc.*, 2000, **122**, 274; (*d*) P. A. Cameron, V. C. Gibson, C. Redshaw, J. A. Segal, M. D. Bruce, A. J. P. White and D. J. Williams, *Chem. Commun.*, 1999, 1883; (*e*) J. P. Corden, W. Errington, P. Moore and M. G. H. Wallbridge, *Chem. Commun.*, 1999, 323; (*f*) J. A. Jegier and D. A. Atwood, *Inorg. Chem.*, 1997, **36**, 2034; (*g*) M. Bochmann and D. M. Dawson, *Angew. Chem., Int. Ed. Engl.*, 1996, **35**, 2226.

3 (*a*) J. A. Halfen, B. A. Jazdzewski, S. Mahapatra, L. M. Berreau, E. C. Wilkinson, L. Que and W. B. Tolman, *J. Am. Chem. Soc.*, 1997, **119**, 8217; (*b*) S. Mahapatra, J. A. Halfen, E. C. Wilkinson, G. Pan, X. Wang, V. G. Young, C. J. Cramer, L. Que and W. B. Tolman, *J. Am. Chem. Soc.*, 1996, **118**, 11 555.

4 S. Y. Bylikin, N. A. H. Male, L. H. Rees, D. A. Robson, P. Mountford and M. Schröder, unpublished results.

5 For examples, see: A. J. Blake, I. A. Fallis, S. Parsons, S. A. Ross and M. Schröder, *J. Chem. Soc., Dalton Trans.*, 1996, 525; G. Schlager, K. Weighardt and B. Nuber, *Inorg. Chem.*, 1995, **34**, 6449 and references therein.

6 U. Bossek, D. Hanke, K. Weighardt and B. Nuber, *Polyhedron*, 1993, **12**, 1.

7 D. J. Gillis, M. J. Turodet and M. C. Baird, *J. Am. Chem. Soc.*, 1993, **115**, 2543; A. D. Horton, J. d. With, J. v. d. Linden and H. v. d. Weg, *Organometallics*, 1996, **15**, 2672.

ChemComm

Metallic nanoparticles from heterometallic Co–Ru carbonyl clusters in mesoporous silica xerogels and MCM-41-type materials†

Fanny Schweyer,[abc] Pierre Braunstein,*[a] Claude Estournès,[b] Jean Guille,*[b] Henri Kessler,*[c] Jean-Louis Paillaud[c] and Jacky Rosé[a]

[a] *Laboratoire de Chimie de Coordination, UMR 7513 CNRS, Université Louis Pasteur, 4 rue Blaise Pascal, 67070 Strasbourg Cedex, France. E-mail: braunst@chimie.u-strasbg.fr*

[b] *Groupe des Matériaux Inorganiques, Institut de Physique et Chimie des Matériaux, 23 rue du Loess, 67037 Strasbourg Cedex, France*

[c] *Laboratoire des Matériaux Minéraux, UPRES-A 7016 CNRS, Ecole Nationale Supérieure de Chimie de Mulhouse, 3 rue Alfred Werner, F-68 093 Mulhouse, France*

Received (in Cambridge, UK) 4th April 2000, Accepted 31st May 2000
Published on the Web 26th June 2000

Impregnation of a mesoporous xerogel or of MCM-41 with an organic solution of the heterometallic cluster $[NEt_4][Co_3Ru(CO)_{12}]$, followed by thermal treatment under an inert atmosphere, leads to highly dispersed magnetic nanoparticles under milder conditions than when conventional metal salts are used as precursors.

The confinement of molecular clusters in the cavities of meso- or nano-porous inorganic matrices is attracting increasing interest as a way to stabilise highly dispersed metals in the form of atoms, clusters or colloids and prevent their coalescence into larger, ill defined aggregates. There are obvious implications for the fabrication of microelectronic devices[1] and for catalytic reactions whose selectivity will critically depend on the size and dispersion of the metal particles and also on the shape of the cavity in which they are embedded.[2] Numerous recent reports have emphasised the specific magnetic, optical, electrochemical, chemical and catalytic properties of nanostructures constructed from molecular clusters or colloids.[3] The sol–gel process is being increasingly applied to the design of new materials using functional building blocks[4] and it has already been used to incorporate mono- and bi-metallic species into inorganic matrices.[2c,5] Furthermore, solids with a template-based morphology control, such as zeolites and MCM-41, are currently attracting increasing attention as a way to stabilise highly dispersed metal particles endowed with unique properties (*e.g.* magnetic, catalytic, *etc.*).[6] A challenging development concerns the use of molecular mixed-metal clusters since microalloy particles could be obtained that would not be accessible by other, more conventional approaches.

With the aims of studying the influence of the structure of the inorganic matrix on the metal particles obtained after thermal treatment of confined molecular Ru/Co clusters, we have compared a mesoporous silica of the MCM-41 type with mesoporous silica xerogels.

A sample of MCM-41[7a] (pore diameter *ca.* 27 Å, specific surface area 1000 $m^2\ g^{-1}$) was impregnated with a dark red saturated THF solution of $[NEt_4][Co_3Ru(CO)_{12}]$,[8] resulting in a Co/Si molar ratio of 0.07 (EDX analysis). When a 1×10^{-3} M solution of the cluster was used, its discoloration from dark red to light red optically indicated adsorption of the cluster onto MCM-41. The solid was then rinsed with THF until the filtrate was colourless and drying under primary vacuum at room temperature (24 h) afforded an ochre powder which was kept under argon. The IR spectrum in the ν(CO) region contained the fingerprint absorptions of the molecular cluster.[8] X-Ray powder diffraction showed the absence of crystallised $[NEt_4][Co_3Ru(CO)_{12}]$, consistent with a high dispersion of the molecular cluster. The typical IR ν(CO) pattern was lost around 200 °C whereas the unsupported cluster decomposes at *ca.* 150 °C, which is consistent with a stabilising effect of the matrix. Furthermore, for the first time to our knowledge, the thermal evolution of the impregnated MCM-41 was followed by magnetic measurements in original lab-built equipment allowing heating of the sample under either reducing (H_2, N_2–5% H_2) or inert atmospheres (Ar). Magnetisation at 1 Tesla progressively increases above 250 °C to reach a maximum at *ca.* 550 °C [Fig. 1(a)]. Further heating results in a decrease of the magnetisation consistent with a Curie point at *ca.* 980 °C. In comparison, a similar experiment on the pure cluster showed an increase in the magnetisation by 180 °C and a Curie temperature around 650 °C. In both cases, the Curie temperature is lower than in pure bulk cobalt (*ca.* 1115 °C), which may be interpreted as resulting from the formation of Co/Ru alloys and/or from the small size of the particles. This will be further investigated by variable temperature XRD experiments under an inert atmosphere.

A crushed mesoporous xerogel[9] (pore diameter *ca.* 35 Å along with microporous domains, specific surface area 750 $m^2\ g^{-1}$) was impregnated, dried and thermally treated in the same manner. The Co/Si molar ratio was *ca.* 0.025 (EDX analysis). Magnetisation at 1 Tesla increases above 200 °C in a stepwise manner and reaches a maximum around 550 °C with a Curie temperature around 1000 °C [Fig. 1(b)]. For consistency, the magnetisation is expressed as per gram of cobalt to account for the different metal content in the samples.

Thermal treatments under argon were realised at 250, 350 and 500 °C on both materials. In all cases, TEM observations showed metal particles which for MCM-41 were well dispersed with a narrow size distribution (Table 1) whereas in the xerogels, the dispersion is less regular. At 500 °C, the small particles (*ca.* 30 Å) coalesce to form larger, ill defined aggregates (*ca.* 200 Å). This clearly points to a structural effect

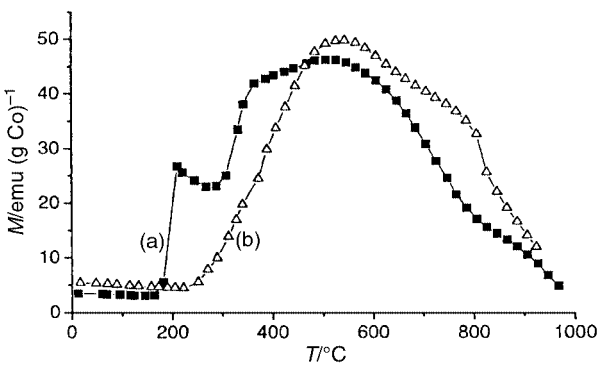

Fig. 1 Dynamic magnetic measurements under Ar of MCM-41 (a) and silica xerogels (b) impregnated with a saturated THF solution of $[NEt_4][Co_3Ru(CO)_{12}]$.

† Dedicated to the memory of Professor O. Kahn, who made so many brilliant contributions to inorganic chemistry.

Table 1 Sizes of the particles (Å) observed by TEM on MCM-41 and xerogels, after 1 h treatment under Ar at different temperatures

	T/°C		
	250	350	500
MCM-41	10	15	80
Xerogel	30	60	30/200

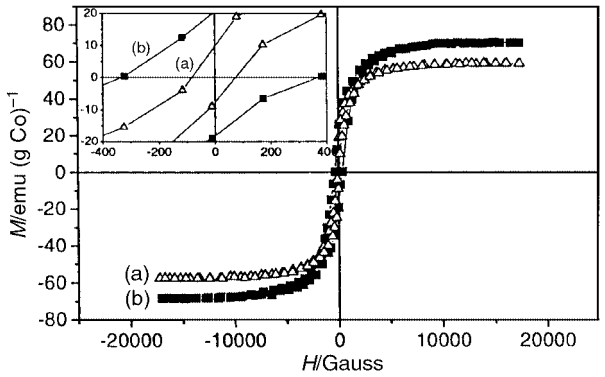

Fig. 2 Isothermal magnetic measurements at room temperature of MCM-41 (a) and silica xerogels (b) impregnated with a saturated THF solution of $[NEt_4][Co_3Ru(CO)_{12}]$, after 1 h treatment under Ar at 500 °C. Inset: expansion near zero shows an increase of the coercitivity for the monoliths.

of the inorganic matrix. Electron diffraction patterns performed on the particles observed after a thermal treatment at 500 °C show the presence of three different metallic phases: pure hexagonal cobalt, pure fcc cobalt, and pure hexagonal ruthenium; no alloy was formed at such low temperature. In contrast, X-ray diffraction after thermal treatment at 900 °C showed that a Co/Ru hexagonal alloy is also present besides pure metallic fcc cobalt and hexagonal ruthenium. Using Vegard's law, we have determined the composition of this alloy to be 86 atom% Co.

Hysteresis loops recorded at ambient temperature on the different samples are consistent with the particles sizes, since no open loop is observed for the doped MCM-41 treated below 350 °C. The xerogels show a ferromagnetic behaviour when treated at or above 350 °C (Fig. 2). In the other samples, superparamagnetic behaviour is observed. Particularly noteworthy is that, irrespective of the matrix, metal particles could be obtained at such a low temperature, without the use of a reductive atmosphere, which cannot be achieved when metal salts [*e.g.* cobalt(II) nitrate][10] are used since a hydrogen atmosphere is required to generate metallic behaviour. This is clearly due to the low oxidation state of the molecular precursor used.

Finally, the differences observed, on the one hand between the impregnated and the unsupported precursor and on the other, between the two impregnated materials, clearly indicate that the magnetic properties originate from particles inside the porous materials and not from intact molecular precursor or metal salts resulting from its decomposition, present at the external surface of the grains.

The approach presented here, which involves in the impregnation of well defined heterometallic, low oxidation-state, organometallic clusters into a given porous silica matrix, followed by thermal treatment under an inert atmosphere leads to the formation of magnetic metal particles at temperatures as low as 250 °C. The differences observed between the two kinds of materials concerning the repartition and sizes of the nanoparticles, as well as their magnetic behaviour highlights the structural effect of the inorganic matrix that should allow control of the particle size in the nanometer range and, accordingly, their magnetic properties.

We are grateful to Dr M. Drillon for valuable discussions and the Centre National de la Recherche Scientifique and the Région Alsace for support (Doctoral grant to F. S).

Notes and references

1 U. Simon, *Adv. Mater.*, 1998, **10**, 1487; G. Schmid and L. F. Chi, *Adv. Mater.*, 1998, **10**, 515; U. Simon, in *Metal Clusters in Chemistry*, ed. P. Braunstein, L. A. Oro and P. R. Raithby, Wiley–VCH, Weinheim, 1999, vol. 3, p. 1342.

2 (*a*) P. Braunstein, R. Devenish, P. Gallezot, B. T. Heaton, C. J. Humphreys, J. Kervennal, S. Mulley and M. Ries, *Angew. Chem., Int. Ed. Engl.*, 1988, **27**, 927; (*b*) S. Kawi and B. C. Gates, in *Clusters and Colloid. From Theory to Applications*, ed. G. Schmid, Wiley–VCH, Weinheim, 1994, ch. 4, p. 298; (*c*) D. S. Shephard, T. Mashmeyer, B. F. G. Johnson, J. M. Thomas, G. Sankar, D. Ozkaya, W. Zhou, R. Oldroyd and R. G. Bell, *Angew. Chem., Int. Ed. Engl.*, 1997, **36**, 2242; (*d*) B. F. G. Johnson, S. A. Raynor, D. S. Shephard, T. Mashmeyer, J. M. Thomas, G. Sankar, S. Bromley, R. Oldroyd, L. Gladden and M. D. Mantle, *Chem. Commun.*, 1999, 1167; (*e*) R. Raja, G. Sankar, S. Hermans, D. S. Shephard, S. Bromley, J. M. Thomas, B. F. G. Johnson and T. Maschmeyer, *Chem. Commun.*, 1999, 1571; (*f*) E. Lindner, T. Schneller, F. Auer and H. A. Mayer, *Angew. Chem., Int. Ed.*, 1999, **38**, 2154; (*g*) M. Sasaki, M. Osada, N. Higashimoto, T. Yamamoto, A. Fukuoka and M. Ichikawa, *J. Mol. Catal. A: Chem.*, 1999, **141**, 223.

3 N. Toshima and T. Yonezawa, *New J. Chem.*, 1998, 1179; *Metal Clusters in Chemistry*, ed. P. Braunstein, L. A. Oro and P. R. Raithby, Wiley–VCH, Weinheim, 1999.

4 R. J. P. Corriu and D. Leclercq, *Angew. Chem., Int. Ed. Engl.*, 1996, **35**, 1420; N. Hüsing and U. Schubert, *Angew. Chem., Int. Ed.*, 1998, **37**, 22, and references therein.

5 P. Braunstein, D. Cauzzi, G. Predieri and A. Tiripicchio, *Chem. Commun.*, 1995, 229; J. P. Carpenter, C. M. Lukehart, S. B. Milne, S. R. Stock, J. E. Wittig, B. D. Jones, R. Glosser and J. G. Zhu, *J. Organomet. Chem.*, 1998, **557**, 121.

6 C. T. Kresge, M. E. Leonowicz, W. J. Roth, J. C. Vartuli and J. S. Beck, *Nature*, 1992, **359**, 710; J. S. Beck, J. C. Vartuli, W. J. Roth, M. E. Leonowicz, C. T. Kresge, K. D. Schmitt, C. T.-W. Chu, D. H. Olson, E. W. Sheppard, S. B. McCullen, J. B. Higgins and J. L. Schlenker, *J. Am. Chem. Soc.*, 1992, **114**, 10 834; A. Corma, *Chem. Rev.*, 1997, **97**, 2373; J. H. Clark and D. J. Macquarrie, *Chem. Commun.*, 1998, 853; J. Y. Ying, C. P. Mehnert and M. S. Wong, *Angew. Chem., Int. Ed.*, 1999, **38**, 56.

7 (*a*) A. C. Voegtlin, A. Matijasic, J. Patarin, C. Sauerland, Y. Grillet and L. Hure, *Microporous Mater.*, 1997, **10**, 137; (*b*) Molar composition: 1 SiO_2: 0.8 NaOH: 0.2 C_{16}TMABr: 135 H_2O: 0.59 HCl.

8 P. Braunstein and J. Rosé, *Inorg. Synth.*, 1989, **26**, 356.

9 N. Viart and J. L. Rehspringer, *J. Non-Cryst. Solids*, 1996, **195**, 223; molar composition: 1 TMOS: 4 MeOH: 1 $HCONH_2$: 0.45 HNO_3: 4.5 H_2O.

10 T. Lutz, C. Estournes and J. L. Guille, *J. Sol–Gel Sci. Technol.*, 1998, **13**, 929.

ChemComm

Nano-size stripes of self-assembled bolaform amphiphiles

Song Gao,[a] Bo Zou,[a] Lifeng Chi,[ab] Harald Fuchs,[b] Junqi Sun,[a] Xi Zhang*[a] and Jiacong Shen[a]

[a] *Key Lab of Supramolecular Structure and Spectroscopy, Department of Chemistry, Jilin University, Changchun 130023, P.R. China*

[b] *Physikalisches Institut, Westfälische Wilhelms-Universität, D-48149, Münster, Germany*

Received (in Cambridge, UK) 2nd May 2000, Accepted 6th June 2000
Published on the Web 26th June 2000

Self-assembled nano-sized stripes are obtained spontaneously by electrostatic adsorption of bolaform amphiphiles onto mica sheets. The ordered stripes are separated from each other by about 10 nm, and the ordered region can extend over macroscopic areas.

Amphiphiles at interfaces are a traditional but challenging topic in colloid chemistry, and now especially in supramolecular science.[1,2] Bolaform amphiphiles are molecules containing two hydrophilic moieties connected by a hydrophobic chain.[3] It is shown that bolaform amphiphiles have different aggregation behaviors,[4] and cationic bolaform amphiphiles can form a self-assembled monolayer on negatively charged substrates.[5,6] Surface patterning with microscopically defined structures is another rapidly developing topic.[7] Some interesting results have recently been reported concerning the regular packing of two-dimensional aggregates formed by amphiphilic molecules at the air–water interface and transferred onto solid substrates.[8,9] The self-assembled monolayer of the polyether dendron can lead to the formation of a patterned surface with nanometer-sized features and the nanostructure can be controlled by the size of the dendron.[10,11]

Combining the above two fields, we herein report not only the interfacing self-assembly of bolaform amphiphiles, but also an approach for creating ordered nano-sized surface structures. They are obtained spontaneously by electrostatic adsorption of bolaform amphiphiles containing rigid hydrophobic azobenzene groups and hydrophilic pyridinium head groups onto mica slides. The size of the structure is in the nanometer region and it is formed by molecular self-assembly at the liquid–solid interface. Our main interest is to establish a method for surface patterning and to understand how the experimental conditions or chemical structure influence the molecular packing in the self-assembled nano-structures.

The bolaform amphiphiles included in this work are azobenzene-4,4′-dicarboxylic acid bis(pyridiniohexyl ester) dibromide (**azo-11**), and azobenzene-4,4′-dicarboxylic acid bis(pyridinioundecyl ester) dibromide (**azo-6**) (Scheme 1). The syntheses of the substances are described elsewhere.[4] Scanning force microscopy (SFM) observation of the self-assembled nano-structures was carried with commercial instruments (Digital Instrument, Nanoscope III, Dimension 3000™ and Multimode™), operating in tapping mode.

To construct nano-sized stripes on mica a clean mica sheet was immersed into aqueous solution of **azo-11** (*c*. = 1.0×10^{-4} M, unless given otherwise). After adsorption for a certain time, the mica sheet was taken out and dried for about 30 min in a desiccator (P_2O_5). Except for the kinetics study, adsorbing time was 30 min for **azo-11** and **azo-6**.

Confocal Raman of the mica sheet after immersion in **azo-11** solution for 30 min confirmed that dicationic **azo-11** was

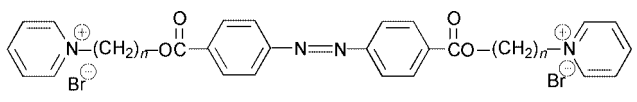

n = 6, **azo-6**; *n* = 11, **azo-11**

Scheme 1 Chemical structures of bolaform amphiphiles.

successfully adsorbed. We observed four peaks at 1403, 1457, 1497 and 1602 cm^{-1}, where the former two peaks corresponded to azo Fermi, and the latter two peaks were attributed to benzene.

The adsorption kinetics were studied by analyzing the film coverage from SFM images. This increases rapidly for **azo-11** with adsorption time initially. From SFM, within about 2 min, the film coverage reaches equilibrium and remains almost constant thereafter. It is conjectured that electrostatic attraction between the substrate and adsorbing molecules is the driving force for adsorbtion of cationic molecules onto the negatively charged surface.

SFM observation reveals that **azo-11** forms well-ordered stripes on a freshly cleaved mica sheet (Fig. 1A). The mean distance of ordered stripes is about 10 nm. They show a preferred orientation (Fig. 1B). The dark areas seen here are uncovered regions. The stripes are packed parallel to the elongated defects. The ordered regions with the same orientation can extend to large areas, up to centimeters. The nanometer size of the ordered stripes indicates that such an ordered structure is not formed by regular packing of single molecules but rather by molecular assemblies. Considering the fact that the **azo-11** concentration used for adsorption is above the critical micelle concentration (cmc), we speculate that the formation of the structure should be related to the micelle in the solution.

In order to confirm the above speculation, we varied the **azo-11** concentration systematically. We found that stripe structures are formed for concentrations of 5.0×10^{-5} M and above, even at 1.0×10^{-3} M, although the ordered structure shows a slight change at this concentration compared with the normal one. However, there is a critical concentration, 3.3×10^{-5} M, at which ordered structures and irregular aggregates co-exist (Fig. 1C). Below this, *e.g.* at 2.5×10^{-5} M, stripe structures may be completely lost. Instead, only irregular aggregates exist on the mica sheet (Fig. 1D). The cmc of **azo-11** was measured to be 3.4×10^{-5} M by the dramatic change of fluorescence with concentration.

Ourselves and others have used similar bolaform amphiphiles to fabricate the layer-by-layer assemblies previously, but no such nano-sized structure has been found. The reason could be that the concentration of bolaform amphiphile used for assemblies is often chosen to be lower than the critical concentration in order to avoid micelles and to ensure isotropic monomer deposition for multilayer construction.[5,6] Further evidence to support the above argument is given by UV/Vis irradiation experiments. After the **azo-11** solution was exposed to UV/Vis irradiation for up to 30 min, the film was prepared under the same conditions as above. Although mostly ordered regions were observed, we found that there are also some irregular regions. One possible reason is the *trans–cis* isomerization of azobenzene in between the bolaform amphiphile, which could partially destroy the structure of elongated micelles in solution. The UV/Vis absorption spectra support our assumption that the *trans–cis* isomerization can not be complete for the system, and some *cis–trans* mixture exists even after UV/Vis irradiation for 30 min.

For a similar bolaform amphiphile but with a shorter spacer, **azo-6**, we cannot find any similar structures even when we vary

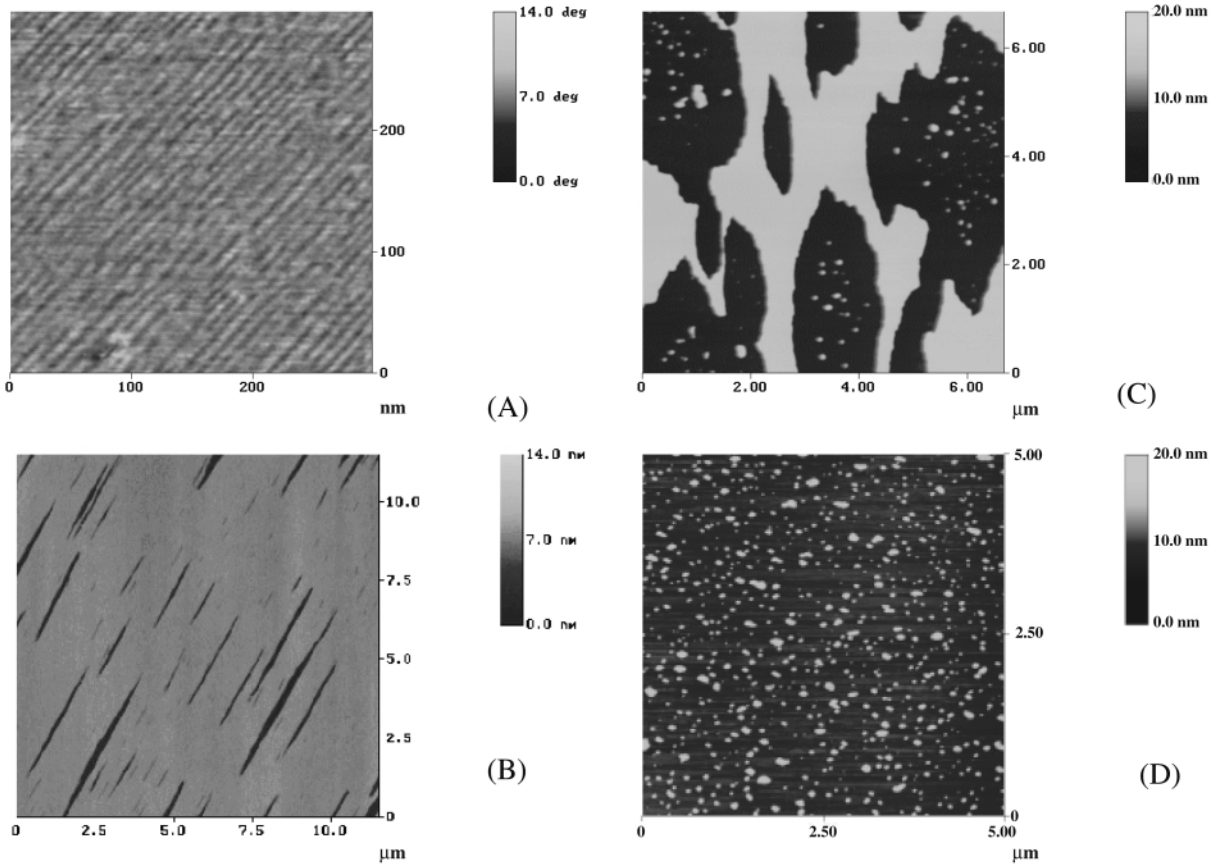

Fig. 1 SFM images of **azo-11** on a mica sheet. Self-assembled nano-sized stripes are formed by immersion of mica sheet into an aqueous solution of **azo-11** (*c.* 1.0×10^{-4} M), as shown in (A) in small areas and (B) in large areas. Ordered structures and irregular aggregates co-exist when the concentration of **azo-11** reaches a critical value, 3.3×10^{-5} M (C). Only irregular aggregates exist on mica sheet when the concentration of **azo-11** is as low as 2.5×10^{-5} M (D).

the concentration and prolong adsorbing time. It is inferred that the compromise between aggregation behavior of the compounds in solution, electrostatic interaction and van der Waals forces *etc*. plays an important role in molecular organization at the liquid–solid interface.

It is also found that the ordered packing of stripes could not form without a crystalline template *i.e*. a mica sheet. By depositing two layers of polyelectrolytes of diazo-resin and poly(sodium styrene sulfonate) alternately onto the mica sheet, a modified mica sheet with a negative charge but an amorphous surface was obtained. With this modified mica sheet, we repeated the previous experiments and found that the bolaform amphiphile **azo-11** can adsorb onto the negative charged surface. Unfortunately, no regular supramolecular structures were formed. Furthermore, by replacing the mica sheet by a glass slide, **azo-11** spread well onto the glass slide, but did not form any ordered structures.

In conclusion, we have demonstrated a very simple way to create ordered surface structures, based on the self-assembly of bolaform amphiphiles at the liquid–solid interface. As a result, it enhances many of the unique features of the ordered structure, like stability on a nanometer scale and over very large areas. Considering the great diversity of bolaform amphiphiles, we anticipate that this type of pattern fabricating method might open up other possibilities for surface modification.

This project is supported by the Outstanding Youth Fund, Overseas Youth Co-Operation Fund, and the National Natural Science Foundation of China. X. Z. thanks DAAD (German Academic Exchange Service) for support during his two-month visit at the University of Muenster, Germany. The compounds are from Professor H. Ringsdorf (Institut fur Organische Chemie, Universitat Maniz), and the authors appreciate his helpful comments.

Notes and references

1 J. M. Lehn, *Supramolecular Chemistry—Concepts and Perspectives*, VCH, Weinheim, 1995.
2 H. Ringsdorf, B. Schlarb and J. Venzmer, *Angew. Chem., Int. Ed. Engl.*, 1988, **23**, 113.
3 J. H. Fuhrhop, U. Liman and H. H. David, *Angew. Chem., Int. Ed. Engl.*, 1985, **24**, 339.
4 V. Hessel, H. Ringsdorf, R. Laversanne and F. Nallet, *Recl. Trav. Chim. Pays-Bas*, 1993, **112**, 339.
5 G. Decher, in *Comprehensive Supramolecular Chemistry*, vol. 9, ed. J. P. Sauvage and M. W. Hosseini, Pergamon, Oxford, 1996, pp. 507–528.
6 X. Zhang and J. C. Shen, *Adv. Mater.*, 1999, **11**, 1139.
7 Y. Xia, J. A. Rogers, K. E. Paul and G. M. Whitesides, *Chem. Rev.*, 1999, **99**, 1823.
8 S. Manne and H. E. Gaub, *Science*, 1995, **270**, 1480.
9 T. Kato, M. Kameyama, M. Ehara and K. I. Iimura, *Langmuir*, 1998, **14**, 1786.
10 Z. S. Bo, L. Zhang, X. Zhang, J. C. Shen, S. Höppene, L. F. Chi and H. Fuchs, *Chem. Lett.*, 1998, 1197.
11 L. Zhang, F. W. Huo, Z. Q. Wang, L. X. Wu, X. Zhang, S. Höppener, L. F. Chi, H. Fuchs, J. W. Zhao, L. Niu and S. J. Dong, *Langmuir*, 2000, **16**, 3813.

Boronate linker for 'traceless' solid-phase synthesis

Christelle Pourbaix,[a] François Carreaux,*[a] Bertrand Carboni,*[a] and Hervé Deleuze[b]

[a] *Synthèse et Electrosynthèse organiques, UMR 6510 CNRS, Université de Rennes 1, Campus de Beaulieu, 35042 Rennes Cedex, France. E-mail: francois.carreaux@univ-rennes1.fr*

[b] *Laboratoire de Chimie Organique et Organométallique, UMR 5802 CNRS, Université de Bordeaux 1, 351, Cours de la libération, 33405 Talence, France*

Received (in Liverpool, UK) 2nd May 2000, Accepted 2nd June 2000
Published on the Web 26th June 2000

The development of a new boron-based strategy for 'traceless' solid-phase synthesis of aromatic compounds is reported. A resin capture process can precede the cleavage step.

The combinatorial library approach is increasingly used for the discovery and development of new drugs, catalysts and materials.[1] Most of the organic chemical libraries reported to date have been constructed using solid-phase methods. A key aspect of these strategies is the linkage element, which acts as a tether to the polymeric support material. Typically, linkage to the polymeric support is based on a protecting group. However, after cleavage from the support, the presence of the functional group previously used for the attachment may have a negative effect on the biological or chemical properties of the target compounds. To overcome this disadvantage, alternative approaches were developed where linkage through a functional group can be excised efficiently, when desired, leaving behind no trace or 'memory' of the solid-phase synthesis (formation of a new C–H or C–C bond).

Only a few 'traceless' linkers have been reported so far for the synthesis of aromatic compounds, none of which are general.[2] As part of a program to develop new solid-phase synthetic methodologies, we became interested in exploring the use of polymer-supported arylboronates. We have prepared recently a macroporous support **1** which was found to be efficient in immobilizing a wide variety of arylboronic acids under mild and neutral conditions.[3,4] Since protonolysis of arylboranes is a well-documented reaction,[5] we planned to use the boronate functionality as a new traceless linker for the solid-phase synthesis of aromatic compounds. Furthermore, since the polymer **1** is extremely selective in its reactions with boronic acids, the boronate linker can be used in another strategy where the synthesis is initiated in solution and the material is subsequently captured by solid support before performing 'traceless' cleavage. In each approach, the cleavage step is associated with the regeneration of the resin **1** (Scheme 1).

In order to find an efficient procedure for the traceless cleavage of supported arylboronates, preliminary experiments have been performed on the resin-bound *m*-nitrophenylboronic acid (Table 1). Protodeboronation of arylboranes usually occurs under drastic hydrolytic conditions, catalysed by conc NaOH[6] or conc HCl.[7] Due to the incompatibility of these procedures with various acid or base sensitive functional groups, transition metal salts have attracted our attention as mild protonolysing reagents.[8] After some unsuccessful experiments, it was found that nitrobenzene can be obtained using an aqueous solution of $Ag(NH_3)_2NO_2$ in EtOH at rt (entry 1)[9] and that the use of THF instead of EtOH significantly improved the yield (entry 2). The optimized conditions required 10 equiv. of 0.5 M aq. $Ag(NH_3)_2NO_3$ in THF at 75–80 °C for 8 h (yield 75%, purity > 95%)(entry 4). The use of a gel-type glycerol-PS resin[10] led to < 50% of deboronation under the same conditions, clearly underlining the benefit of macroporous resin **1**. This cleavage was further examined with different aryl ring systems and the liberated products were isolated in moderate to good yields (entries 5–7).

The solutions obtained after filtration of the resin were evaporated to dryness, the residue was taken up in a mixture of EtOAc and H_2O, and, after separation of the layers, the organic solvent was evaporated. In all cases, the remaining products were > 85% pure as determined by GC or NMR.[11]

Of particular interest to combinatorial chemistry is the use of resin **1** to immobilize functionalized boronic acid templates and carry out different solid-phase transformations. As an example, butan-1-ol was coupled to resin-bound *p*-carboxyphenylboronic acid **2**, to afford the corresponding ester **3** in 56% after cleavage. Similarly, resin-bound *m*-aminophenylboronic acid **4** was

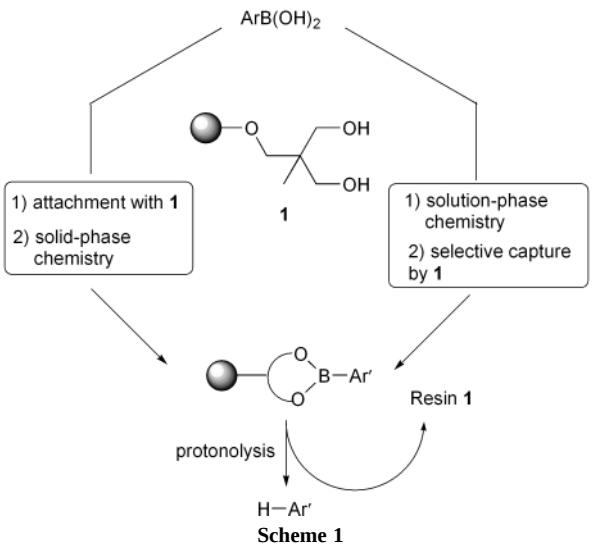

Scheme 1

Table 1 Protodeboronation of resin-bound arylboronic acids using an aqueous silver ammonium nitrate complex[a]

Entry	Ar	Conditions	Yield (%)[b]	Purity (%)[c]
1	3-NO_2-C_6H_4	$Ag(NH_3)_2NO_3$ (2 equiv.), EtOH–H_2O (1:1), 48 h, rt	36	> 95
2	3-NO_2-C_6H_4	$Ag(NH_3)_2NO_3$ (2 equiv.), THF–H_2O (1:1), 48 h, rt	60	> 95
3	3-NO_2-C_6H_4	$Ag(NH_3)_2NO_3$ (10 equiv.), THF–H_2O (1:1), 48 h, rt	75	> 95
4	3-NO_2-C_6H_4	$Ag(NH_3)_2NO_3$ (10 equiv.), THF–H_2O (1:1), reflux, 8 h	77	> 95
5	1-Naphthyl	$Ag(NH_3)_2NO_3$ (10 equiv.), THF–H_2O (1:1), reflux, 8 h	95	> 95
6	3,4-OCH_2O-C_6H_4	$Ag(NH_3)_2NO_3$ (10 equiv.), THF–H_2O (1:1), reflux, 8 h	80	85
7	4-MeO-C_6H_4	$Ag(NH_3)_2NO_3$ (10 equiv.), THF–H_2O (1:1), reflux, 8 h	35	86

[a] Aqueous silver diamine nitrate (0.5 M) was prepared by titrating silver nitrate solution with sufficient ammonia to dissolve all precipitate (pH 7–8). [b] Yields of isolated product (based upon loading of resin **1**, 1 mmol g^{-1}). [c] GC purity of the crude reaction mixture.

DOI: 10.1039/b003487h

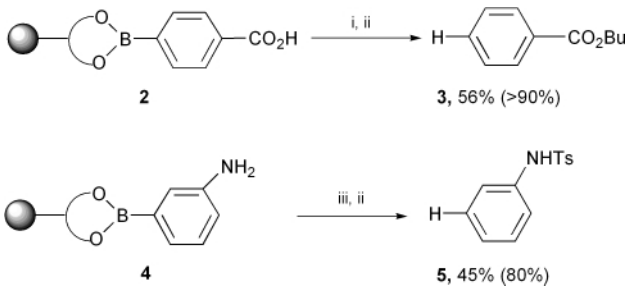

Scheme 2 GC or NMR purities are given in brackets. *Reagents and conditions*: i, $SOCl_2$ (15 equiv.), toluene, 70 °C, 12 h, then filtration and washing, then BuOH (10 equiv.), pyridine (15 equiv.), toluene, 25 °C, 24 h; ii, $Ag(NH_3)_2NO_3$ (0.5 M in water, 10 equiv.), THF, reflux, 8h; iii, 4-$MePhSO_2Cl$ (5 equiv.), $EtN(Pri)_2$ (10 equiv.), CH_2Cl_2, 25 °C, 12 h.

transformed into sulfonamide **5** upon treatment with *p*-methylphenylsulfonyl chloride (Scheme 2).

The exact mechanism of the silver ion catalyzed proto-deboronation has not been clearly demonstrated, but the hypothesis of an arylmetal intermediate is strongly favoured.[8] Note that, after washing (water, THF and Et_2O), the filtered slightly green resin can be reused for another attachment without requiring a regeneration step and with no apparent loss of activity.

The resin capture strategy is very promising for library generation since it combines the flexibility of solution synthesis with the purity of solid-phase products. In this regard, resin **1** could be very useful in capturing only organoboron products from complex reaction mixtures and, subsequently, to perform 'traceless' cleavage. For example, some transformations in the solution-phase of functionalized boronic acids have been realized using an excess of various reagents. *m*-Aminophenylboronic acid **6** was transformed into anilide by treatment with benzoyl chloride and *p*-formylphenylboronic acid **9** was subjected to a reductive amination with benzylamine. The crude products of these reactions were combined with resin **1** at reflux in THF to afford **7** and **10**. The desired products **8** and **11** were obtained in excellent purities and yields after cleavage. As another significant demonstration of the interest of such an approach, an UGI four-component condensation[12] was carried out with **12**, benzylamine, benzylisonitrile and isobutyraldehyde in MeOH at 60 °C for 12 h. After evaporation of the solvent, the crude product was treated with **1** to selectively afford **13**. After cleavage, the α-(acylamino) amide **14** was obtained in 57% yield and with a high purity (> 90%), as shown in Scheme 3. To the best of our knowledge, this constitutes the first example of resin capture which releases product with formation of a carbon–hydrogen bond in place of the resin attachment.

In conclusion, we have developed a new 'traceless' linker technology for solid-phase chemistry. The conditions of cleavage are compatible with the presence of functional groups such as amines, amides, esters, ethers and sulfonamides.[13] The boronate linker system is distinct from the existing alternatives by its ability to regenerate the polymer, and its use in a resin capture process. Other reactions of polymer-supported boronates in the formation of a new carbon–carbon bond instead of the initial boron–carbon bond are currently in progress in our laboratory.

We thank Dr B. Maillard (Université de Bordeaux 1) for fruitful discussions.

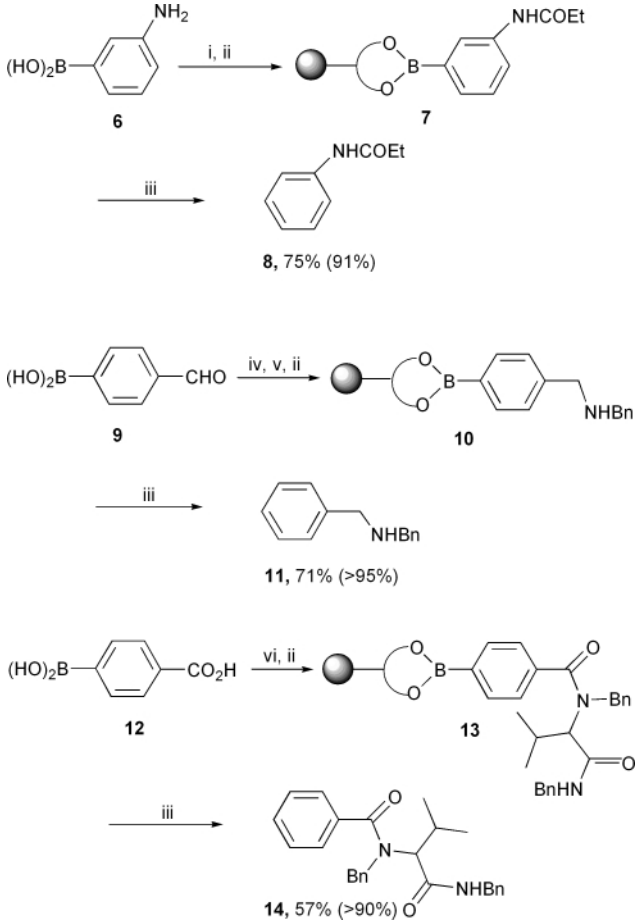

Scheme 3 In brackets are given the GC or NMR purities. *Reagents and conditions*: i, EtCOCl (7 equiv.), pyridine (7 equiv.), CH_2Cl_2, rt, 20 h; ii, resin **1** (1 equiv.), THF, reflux, 16 h; iii, $Ag(NH_3)_2NO_3$ (0.5 M in water, 10 equiv.), THF, reflux, 8 h; iv, propanediol (1.2 equiv.), Et_2O, rt, 30 min; v, $PhCH_2NH_2$ (4 equiv.), $NaBH(OAc)_3$ (4 equiv.), CH_2Cl_2–DMF (1 : 1), rt, 24 h; vi, $PhCH_2NH_2$ (1.2 equiv.), PriCHO (1.2 equiv.), $PhCH_2NC$ (1.2 equiv.), MeOH, 60 °C, 12 h.

Notes and references

1 For selected reviews, see: D. Obrecht and J. M. Villalgordo, *Solid Supported Combinatorial and Parallel Synthesis of Small-Molecular-Weight Compounds Libraries*, Pergamon, New York, 1998; L. A. Thompson and J. A. Ellman, *Chem. Rev.*, 1996, **96**, 555; B. Jandeleit, D. J. Schaefer, T. S. Power, H. W. Turner and W. H. Weinberg, *Angew. Chem., Int. Ed.*, 1999, **38**, 2494.

2 For a recent review, see: B. Reitz, *Curr. Opin. Drug Discovery Dev.*, 1999, **2**, 358.

3 B. Carboni, C. Pourbaix, F. Carreaux, H. Deleuze and B. Maillard, *Tetrahedron Lett.*, 1999, **40**, 7979.

4 For other preparations of resin bound boronic acids, see: D. G. Hall, J. Taylor and M. Gravel, *Angew. Chem., Int. Ed.*, 1999, **38**, 3064; W. Li and K. Burgess, *Tetrahedron Lett.*, 1999, **40**, 6527.

5 M. Vaultier and B. Carboni, in *Comprehensive Organometallic Chemistry II*, eds. G. Wilkinson, F. G. A. Stone and V. E. Abel, Pergamon Press, Oxford, 1995, Vol. 11, p. 191.

6 A. D. Ainley and F. Challenger, *J. Chem. Soc.*, 1930, 2171.

7 H. G. Kuivila and K. V. Nahabedian, *J. Am. Chem. Soc.*, 1961, **83**, 2159.

8 H. G. Kuivila, J. F. Reuwer Jr. and J. A. Mangravite, *J. Am. Chem. Soc.*, 1964, **86**, 2666.

9 D. S. Kemp and D. C. Roberts, *Tetrahedron Lett.*, 1975, **52**, 4629.

10 The glycerol-PS resin (Purchased from Novabiochem. Inc.) was coupled to *m*-nitrophenylboronic acid in THF, under the same conditions as with resin **1**.

11 A small amount of boronic acid can be detected in some cases, (5–10%). This by-product results from the hydrolysis of the boronate linker and is easily removed by treating the crude of the reaction after cleavage with the diol resin **1** under the immobilization conditions of boronic acids. The polymer **1** is then used as solid-supported scavenger of boronic acids.

12 I. Ugi, S. Lohberger and R. Karl, in *Comprehensive Organic Synthesis*, eds. B. M. Trost and I. Fleming, Pergamon, New York, 1991, Vol. 2, p. 1083.

13 All new, nonpolymeric compounds were completely characterized (1H NMR, 13C NMR, IR, MS, elemental analysis, or HRMS).

ChemComm

Rhodium(I) complexes of unsymmetrical diphosphines: efficient and stable methanol carbonylation catalysts†

Charles-Antoine Carraz,[a] Evert J. Ditzel,[b] A. Guy Orpen,[a] Dianne D. Ellis,[a] Paul G. Pringle*[a] and Glenn J. Sunley[b]

[a] *School of Chemistry, University of Bristol, Cantocks Close, Bristol, UK BS8 1TS. E-mail: paul.pringle@bristol.ac.uk*

[b] *BP Chemicals, Hull Research and Technology Centre, Saltend, Hull, UK HU12 8DS*

Received (in Cambridge) 7th April 2000, Accepted 17th May 2000

Rhodium complexes of unsymmetrical diphosphines of the type $Ph_2PCH_2CH_2PAr_2$ are catalysts for the carbonylation of methanol; several features of the catalysis are reminiscent of iridium carbonylation catalysts.

Methanol carbonylation (eqn. (1)) is one of the most successful industrial applications of homogeneous catalysis and is currently carried out on a scale of several million tonnes per annum.[1] The rhodium–iodide catalysed process gives acetic acid in better than 99% selectivity and the mechanism has been thoroughly reviewed by Maitlis *et al.*[2] The new *Cativa* process uses an iridium–iodide catalyst and offers many advantages over the rhodium system.[3] The conditions shown in eqn. (1) limit the use of phosphine modified catalysts because of the potential problem of quaternisation of the ligand.[1] Thus, while the rhodium complexes of P,O-, P,N- and P,S-donor ligands have all been reported[4–8] to be methanol carbonylation catalysts, either the conditions used were not the industrial conditions of eqn. (1) and therefore the process would not be viable,[4–6] or the catalysts were found to be unstable.[7,8] Here we report that rhodium complexes of unsymmetrical ethylene diphosphine ligands are more efficient catalysts than their symmetrical dppe analogues for methanol carbonylation and longer-lived than any previously reported ligand-modified catalysts under the harsh conditions of eqn. (1).[9]

$$\mathrm{MeOH} + \mathrm{CO} \xrightarrow[\text{[cat] / HI}]{\text{150-200 °C, 10-60 bar}} \mathrm{MeCOOH} \qquad (1)$$

The diphosphines **1a–f**, some of which are known,[10,11] were made according to eqn. (2) and fully characterised. The

$$Ph_2P\!\!\smile\!\!PCl_2 \xrightarrow{\text{ArLi or ArMgBr}} Ph_2P\!\!\smile\!\!PAr_2 \qquad (2)$$

Ar = C_6H_4OMe-4 **1a**, C_6H_4F-3 **1b**, $C_6H_4CF_3$-3 **1c**, $C_6H_3F_2$-3,5 **1d**, $C_6H_2F_3$-3,4,5 **1e**, $C_6H_3(CF_3)_2$-3,5 **1f**

catalysts were prepared by addition of diphosphines **1a–f** or **2a–d** to $[Rh_2(\mu\text{-}Cl)_2(CO)_4]$ in methanol [eqn. (3)]. Under these conditions the complexes **3a–f** and **4a–f** are formed in approximately 1 : 1 ratio in each case; these isomeric mixtures have been isolated and fully characterised. Similarly the iodo analogues **5e** and **6e** have been prepared and characterised as a 1 : 1 mixture.

The carbonylation catalysis was carried out under the conditions given in eqn. (1) and the results are presented in Table 1.† In each case the conversion of methanol was greater than 98% and the selectivity for acetic acid was greater than 99%; the rates for the diphos systems (entries 1–11) were all lower than the commercial $[RhI_2(CO)_2]^-$ catalyst. The following observations suggest that the catalyst is a diphosphine–

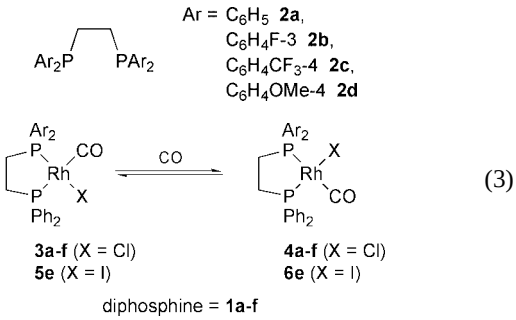

(3)

rhodium complex throughout and not $[RhI_2(CO)_2]^-$. IR spectra obtained *in situ* during catalysis with ligand **1e** showed the absence of the intense ν(CO) bands for $[RhI_2(CO)_2]^-$ at 2059 and 1988 cm^{-1}. At the end of the catalysis, when the solution cooled, a homogeneous orange solution or red crystalline precipitate was present and ^{31}P NMR and IR spectra showed the presence of a mixture of diphosphine rhodium(III) carbonyl complexes (^1J(RhP) *ca.* 100 Hz, ν(CO) *ca.* 2090 cm^{-1}). The product *fac*-$[RhI_3(CO)$(**1b**)$]$ **7** was isolated from the reaction mixture using the catalyst derived from **1b** and the crystal structure of its pentane solvate was determined (see Fig. 1). The octahedral geometry at the rhodium(III) centre is somewhat distorted (iodine atoms I(1) and I(2) lie 0.140 and 0.184 Å respectively from the RhP_2 plane). The carbonyl ligand lies *cis* to the diphosphine phosphorus atoms, which show identical Rh–P bond lengths, any difference in the values being masked by the disorder.‡ The rate of catalysis is constant throughout a run and, after all the methanol was consumed, a second aliquot of methanol was injected and the rate was the same as in the first run. This final observation not only confirms the integrity of the

Table 1 Methanol carbonylation data†

Entry	Ligand	Rate[a]	$CH_3CH_2CO_2H$[b]
1	**1a**	2.0	6
2	**1b**	5.0	45
3	**1c**	5.6	50
4	**1d**	8.5	79
5	**1e**	7.6	54
6	**1f**	2.9	31
7	**1b** + Ru[c]	13.7	188
8	**2a**	1.9	4
9	**2b**	2.0	13
10	**2c**	2.3	20
11	**2d**	1.7	12
12[d]	—	18.5	276

[a] At 10% conversion, in mol l^{-1} h^{-1} with estimated errors of 5–10%. [b] Concentration in ppm. [c] $[RuI_2(CO)_4]$ (0.576 g, 1.23 mmol) added to the catalyst mixture. [d] Catalyst is $[RhI_2(CO)_2]^-$.

† Electronic supplementary information (ESI) available: typical experimental procedure for catalysis. See http://www.rsc.org/suppdata/cc/b0/b002802i/

DOI: 10.1039/b002802i

catalyst but also shows its longevity is greater than any previous rhodium–phosphine catalyst under these conditions[7] since it shows that all the diphosphine catalysts undergo over 500 turnovers without noticable diminution of activity.

In the following respects, the rhodium–diphosphine catalysts resemble the iridium *Cativa* catalysts. The main inefficiencies in traditional rhodium-catalysed methanol carbonylation are the water gas shift reaction and the formation of by-products such as MeCHO, EtI and $CH_3CH_2CO_2H$; this problem is much reduced with the iridium catalysts.[3] The amount of propionic acid reported in Table 1 for the diphosphine catalysts (entries 1–10) is significantly less than with $[RhI_2(CO)_2]^-$ as catalyst under these conditions (entry 12). ^{31}P NMR studies in CH_2Cl_2 show that oxidative addition of MeI to **5e**/**6e** is very rapid. The greater nucleophilicity of [RhI(CO)(diphosphine)] complexes[12] than $[RhI_2(CO)_2]^-$ may partly explain the similarities between the rhodium–diphosphine and the iridium catalysts.

Since the iridium catalysts are promoted by iodide-abstracting ruthenium complexes,[3] we investigated whether $[RuI_2(CO)_4]$ would also promote the rhodium catalyst from diphosphine **1b**; by comparing entries 7 and 2 in Table 1, it is clear that the addition of the Ru complex has more than doubled the rate.

From the data in Table 1, it can be deduced that the influence of the phosphorus substituents is complicated. The rate data are plotted in Fig. 2 as a function of the Hammett constants for the aryl substituents. The plot shows that increasing the electron-withdrawing power of the substituents on the aryl rings in the unsymmetrical diphosphines generally increases the catalyst activity up to a point, beyond which the rate decreases. The significance of the maximum in the curve might be interpreted in terms of a balance of σ-donor and π-acceptor qualities being required to optimise the rate. However entries 4 and 9 in Table 1 are with ligands **1d** and **2b** which would be expected to have similar overall donor/acceptor properties by virtue of the same number of *meta*-fluoro substituents and yet they show very different catalytic performance. In fact, all of the symmetrical diphosphines **2a**–**d** yield catalysts of similarly low activity (entries 8–11). Thus the *asymmetry* of the diphosphine is apparently crucial. Casey *et al.*[10] have shown that unsymmetrical diphosphines are superior to the symmetrical analogues for hydroformylation catalysis and associated this with a preference of the better σ-donor for the axial site in the trigonal bipyramidal intermediates. It is notable that P,O-, P,N- and P,S-donor ligands used previously[4–8] for methanol carbonylation are all unsymmetrical with one strong and one medium or weak donor. For the best one ($Ph_2PCH_2CH_2P(S)Ph_2$), Baker *et al.*[7] showed that only one isomer (with the S-donor *trans* to CO) is formed in the reaction of $[Rh_2I_2(CO)_4]$ with the ligand. By contrast, we find no such diastereoselectivity in the reaction of diphosphines **1a**–**f** with $[Rh_2X_2(CO)_4]$ (X = Cl or I). In the presence of CO, ^{31}P NMR spectroscopy shows that the diastereoisomers **3**/**4** and **5**/**6** interconvert rapidly (eqn. (3) and thus the *ca.* 1:1 mixtures observed represent the thermodynamic proportions. Hence there is little difference in the stability of the [RhI(CO)(diphos)] precursors under ambient conditions in CH_2Cl_2 but it is possible that under the radically different conditions of the catalysis, one of the isomers is preferred or one is significantly more reactive.

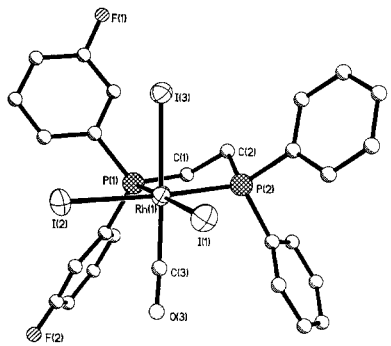

Fig. 1 The molecular structure of **7** showing one of the two orientations of the *meta*-C_6H_4F groups. Important molecular dimensions include: bond lengths (Å) Rh(1)–C(3) 1.885(6), Rh(1)–P(1) 2.335(2), Rh(1)–P(2) 2.3370(15), Rh(1)–I(1) 2.7337(7), Rh(1)–I(2) 2.7296(7), Rh(1)–I(3) 2.6869(6); bond angle (°) P(1)–Rh(1)–P(2) 86.03(6).

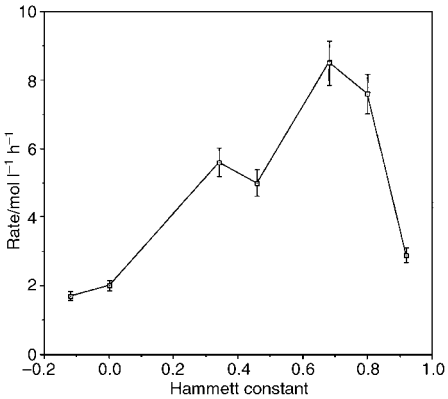

Fig. 2 Plot of the rate of methanol carbonylation (from Table 1) as a function of the Hammett substituent constant, σ for the Ar substituents in the ligands $Ph_2PCH_2CH_2PAr_2$. The error bars represent a 7.5% error in the rate measurement.

In conclusion we have established that unsymmetrical diphosphine–rhodium complexes are very active and selective catalysts for methanol carbonylation under industrially significant conditions and these catalysts have several features in common with the iridium *Cativa* catalysts.

We thank BP Chemicals and the EPSRC for financial support.

Notes and references

‡ *Crystal structure analysis* of $[Rh(CO)I_3[Ph_2P(C_2H_4)P(3\text{-}C_6H_4F)_2]\cdot 0.5C_5H_{12}$, **7**·$0.5C_5H_{12}$. *Crystal data*: $C_{29.5}H_{22}F_2I_3OP_2Rh$, M = 976.02, orthorhombic, space group *Pbca* (no. 61), a = 18.850(3), b = 15.338(4), c = 20.992(4)Å, T = 173 K, U = 6069(6) Å^3, Z = 8, μ = 3.755 mm^{-1}, 6885 unique data, $R1$ = 0.038. The fluorine atoms are disordered occupying one *meta* site on each of the four aryl rings equally as a consequence of the enantiomers of **7** crystallising at the same site in the unit cell. CCDC 182/1645. See http://www.rsc.org/suppdata/cc/b0/b002802i/ for crystallographic files in .cif format.

1 (*a*) M. Gauss, A. Seidel, P. Torrence and P. Heymans, in *Applied Homogeneous Catalysis with Organometallic Compounds*, ed. B. Cornils and W. A. Herrmann, VCH, New York, 1996; (*b*) M. J. Howard, M. D. Jones, M. S. Roberts and S. A. Taylor, *Catal. Today*, 1993, **18**, 325.

2 P. M. Maitlis, A. Haynes, G. J. Sunley and M. J. Howard, *J. Chem. Soc., Dalton Trans.*, 1996, 2187.

3 (*a*) M. J. Howard, G. J. Sunley, A. D. Poole, R. J. Watt and B. K. Sharma, *Stud. Surf. Sci. Catal.*, 1999, **121**, 61; (*b*) T. Ghaffar, H. Adams, P. M. Maitlis, G. J. Sunley, M. J. Baker and A. Haynes, *Chem. Commun.*, 1998, 1023; (*c*) see also ref 3 in J. Yang, A. Haynes and P. M. Maitlis, *Chem. Commun.*, 1999, 179.

4 R. W. Wegman, A. G. Abatjoglou and A. M. Harrison, *J. Chem. Soc., Chem. Commun.*, 1987, 1891.

5 A. Bader and E. Lindner, *Coord. Chem. Rev.*, 1991, **108**, 27.

6 M. S. Balakrishna, R. Klein, S. Uhlenbrock, A. A. Pinkerton and R. G. Cavell, *Inorg. Chem.*, 1993, **32**, 5676.

7 M. J. Baker, M. G. Giles, A. G. Orpen, J. Taylor and R. J. Watt, *J. Chem. Soc., Chem. Commun.*, 1995, 197.

8 J. R. Dilworth, J. R. Miller, N. Wheatley, M. J. Baker and G. Sunley, *J. Chem. Soc., Chem. Commun.*, 1995, 1579.

9 M. J. Baker, E. Ditzel, G. Sunley, C. A. Carraz and P. G. Pringle, *Br. Pat.*, 1999, 9907447.8.

10 C. P. Casey, E. L. Paulsen, E. W. Beuttenmueller, B. R. Proft, B. A. Matter and D. R. Powell, *J. Am. Chem. Soc.*, 1999, **121**, 63 and references therein.

11 H. Brunner and A. Stumpf, *J. Organomet. Chem.*, 1993, **459**, 139; P. N. Kapoor, D. D. Pathak, G. Gaur and M. Kutty, *J. Organomet. Chem.*, 1984, **276**, 167.

11 L. Gonsalvi, H. Adams, G. J. Sunley, E. Ditzel and A. Haynes, *J. Am. Chem. Soc.*, 1999, **121**, 11 233.

A three-dimensional neutral framework of a novel decavanadium cluster bridged by an AsO_4 tetrahedron: $[AsV^{IV}_8V^{V}_2O_{26}(\mu\text{-}H_2O)]\cdot 8H_2O$

Wei-Ming Bu,[a] Ling Ye,[a] Guo-Yu Yang,[b] Mei-Cheng Shao,[c] Yu-Guo Fan*[a] and Ji-Qing Xu[a]

[a] *Key Lab of Supramolecular Structure and Spectroscopy, Jilin University, Changchun 130023, P.R. China. E-mail: xray@mail.jlu.edu.cn*
[b] *Department of Chemistry of Biochemistry, University of Notre Dame, IN 46556, USA*
[c] *Department of Chemistry, Peking University, Beijing 100871, P.R. China*

Received (in Cambridge, UK) 26th April 2000, Accepted 2nd June 2000

A three-dimensional neutral framework of a novel decavanadate ion $[V^{IV}_8V^{V}_2O_{26}(\mu\text{-}H_2O)]$ containing an AsO_4 tetrahedral bridge has been synthesized hydrothermally and structurally characterized by X-ray diffraction.

One of the great challenges of modern chemistry is to create multifunctional structures which have well defined cavities and surfaces with sites or areas of different reactivity by linking preorganised robust building blocks.[1] Given the significance of transition metal oxide surfaces[2] and proven roles of polyoxometalates and their derivatives in catalysis and materials science,[3] it is conceivably valuable to attempt to design and prepare transition metal oxide based materials with desired and controllable properties by assembling metal oxide clusters which provide remarkably diverse and well defined building blocks.[4] Although the mechanism by which the assembly is organised remains elusive, a popular strategy in the realisation of materials engineering involves combined applications of the hydrothermal synthesis method and structure-directing templates.[5] On-going research has demonstrated that transition metal (*e.g.* Fe, Co, Ni, Cu, Zn and Mn) coordination complexes may serve as inorganic bridging ligands linking polyoxoanion clusters into one-, two- and three-dimensional networks.[6]

Owing to their exceptional ability to form mixed-valence compounds that exhibit rich electronic and magnetic properties, polyoxovanadates have been extensively studied with many structurally characterized examples now known.[7] Recently, a decavanadium cluster with a $[V^{V}_{10}O_{22}]^{6-}$ core has been reported, and an X-ray structural analysis shows that it is a discrete ion with a chiral framework formed by nine square-pyramidal VO_5 polyhedra surrounding one VO_4 tetrahedron linked through the vertices.[8] Although decavanadate ions as discrete entities are common, synthetically prepared examples of extended structures with decacavanadate ions are relatively rare. According to our literature search, only one example, $[Cu(en)_2]_2[V^{IV}_4V^{V}_6O_{25}]$, has been reported, which consists of $Cu(en)_2^{2+}$ groups linked through layered vanadium oxides into a three-dimensional network.[9] Khan *et al.* reported several three-dimensional frameworks which consist of spherical $[V_{18}O_{42}(XO_4)]$ clusters linked by bridging $[M(H_2O)_4]$ groups (X : V, S; M : Fe, Co, Mn, Zn).[10] Here, we report an entirely new type of mixed-valence decavanadate ion $[V^{IV}_8V^{V}_2O_{26}(H_2O)]$ as a building block which is bridged by AsO_4 tetrahedra leading to a three-dimensional neutral network $[AsV^{IV}_8V^{V}_2O_{26}(\mu\text{-}H_2O)]\cdot 8H_2O$ **1**. There are many structures reported in which AsO_4 terahedra are encapsulated in mixed-valence V^{IV}/V^{V} as well as V^{IV} polyoxoanions. To our knowledge, AsO_4 tetrahedra linking polyoxoanions in a bridging mode has not been described to date.

Compound **1** was prepared hydrothermally from a mixture of V_2O_5, H_3AsO_4, $H_2C_2O_4$, en and H_2O heated to 160 °C for three days.† The en is not incorporated into the structure of **1**, but is necessary to maintain the pH of the reaction. $H_2C_2O_4$ was employed as a reducing agent. The IR spectrum of the product exhibits characteristic bands at 972 and 958 cm^{-1} assigned to $\nu(V{=}O_t)$ and a number of bands in the range 750–900 cm^{-1} associated with ν(V–O–V) and ν(V–O–As).

The extended highly symmetrical structure of **1**‡ (Fig. 1), consists of a three-dimensional neutral network of $[V^{IV}_8V^{V}_2O_{27}]$ cages with crystallographic T_d symmetry, with each cage connected to four other neighboring units *via* AsO_4 bridging groups. This generates a network of $[-\{V_{10}O_{27}\}-AsO_4-\{V_{10}O_{27}\}-]_\infty$ arrays running along two mutually perpendicular directions. The building block units in the structure of **1** may be viewed as a 'rugby ball'-like $[V^{IV}_8V^{V}_2O_{26}]$ shell encapsulating a central water molecule which is covalently bonded to two V(1) atoms in a μ-bridging mode with a V(1)–O(6) distance of 2.450 Å. The symmetry at O(6) is 222. Indeed, an unusual property of reduced polyvandates is their tendency to form cages encapsulating a guest molecule.[11] Compound **1** represents a most unusual member of this class of clusters with the central bridging encapsulated water molecule.

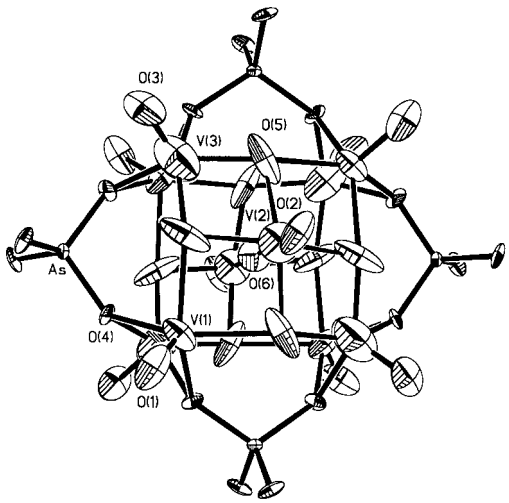

Fig. 1 Unit cell of structure **1** down the crystallographic *a* axis showing the rectangular channels parallel to this axis. Water molecules have been omitted for clarity.

The $[V^{IV}_8V^{V}_2O_{27}]$ unit is a new type of decavanadium ion. The vanadium exhibits two types of coordination: pyramidal [V(1) and V(3)] and octahedral [V(2)]. The octahedral geometry around vanadium V(2) is defined by a terminal oxo group [O(1)], four μ-oxygen atoms [O(5)] of the shell, and one μ-oxygen atom [O(6)]. The square-pyramidal geometry around V(1) and V(3) is formed by four basal μ_3-oxo [O(4), O(5)] groups from the shell and an apical terminal oxo groups. Two $V(1)O_5$ and two $V(3)O_5$ pyramids are corner-shared by a μ_3-O(5) atom to form a $[V_4O_{16}]$ ring. These vanadium atoms are all co-planar. Two such $[V_4O_{16}]$ rings are joined to each other by sharing edges in a parallel manner with two $V(2)O_6$ octahedra capping oppositely disposed faces of these two rings, respectively, forming a rugby ball-like structure. The surface of

DOI: 10.1039/b003359f

the cluster exhibits four open windows. Curiously, the four AsO_4 tetrahedra cap on the windows by edge-sharing through a μ_3-oxo group [O(4)] leading to a three-dimensional neutral network.

According to bond valence sum (BVS) calculations[12] and charge balance, compound **1** is formulated as $[AsV^{IV}{}_8V^{V}{}_2O_{26}(H_2O)]\cdot 8H_2O$. The assignment of oxidation state for the vanadium and arsenic atoms are consistent with their coordination geometries and are confirmed by valence sum calculations which gives values for V1, V2, V3 and As of 4.06, 5.06, 4.15 and 5.10, respectively. The valence sum calculations associated with O(6) (BVS = 0.28) identify it as a water molecule, a feature consistent with the significant lengthened bond distance.

It is noteworthy that the structure of **1** possesses large rectangular and hexagonal channels, which are filled with water molecules of crystallization (eight water molecules per unit cell) (Fig. 1 and 2). The rectangular channels run along all three crystallographic axes with mean diameters of 10.508 Å while hexagonal channels extend along the diagonal direction of the unit cell with a mean diameter of 11.986 Å. The arsenic atoms reside on a $\bar{4}$ axis. In addition, two perpendicular $\bar{4}$ axes pass through the center of the $[V_{10}O_{27}]$ unit. Owing to the crystallographically imposed $\bar{4}$ symmetry, these channels may be viewed as a cylinder, not observed previously in other metal oxide cluster frameworks. Whereas transition metal coordination complexes acting as bridges are well established, it is seen here that AsO_4 tetrahedra may play an important role in the assembly of a specific structural motif.

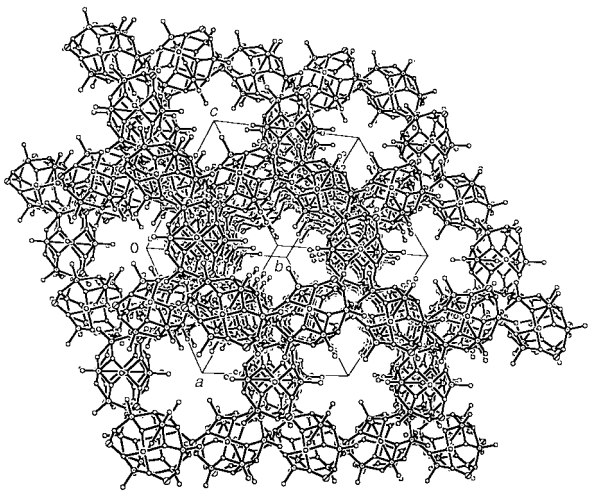

Fig. 2 The hexagonal channels viewed along the diagonal direction of the unit cell.

The room-temperature EPR spectrum of a crystalline sample of **1** consists of one signal (g 2.034), indicating the presence of V^{IV} centers. Although no hyperfine structure was observed, the linewidth was extremely narrow, which suggests significant exchange coupling.

The magnetic susceptibility χ_m of **1** was measured between 2 and 300 K. The value of $\chi_m T$ shows a gradual decrease as the temperature is decreased, indicative of weak antiferromagnetic exchange coupling. Because no suitable theoretical model is available in the literature[13] for such a complex system, detailed magnetic analyses were not performed for the present compound.

This work has important implications for the conversion of discrete cluster anions into three-dimensional networks[14] and demonstrates that the use of hydrothermal techniques is a vital tool for the realisation of materials design. This novel structure and building principle may provide further insight into designing new porous materials as well as other supramolecular architectures.

We thank National Natural Science Foundation of China, and Key Lab of Supramolecular Structure and Spectroscopy for financial support.

Notes and references

† A mixture of V_2O_5 (5.5 g), H_3AsO_4 (1.5 g), $H_2C_2O_4$ (1 g) and H_2O (20 ml) was neutralized to pH = 8 with en (2 ml). The sample was then sealed in a Teflon-lined reactor which was heated to 160 °C for three days. After cooling to room temperature, black prism-shaped crystals were isolated in *ca*. 40% yield (based on vanadium). Anal. Calc. for $H_{18}As_2V_{10}O_{35}$: As, 12.11; V, 41.17; H, 1.47. Found: As, 11.92; V, 41.10; H, 1.52%.

‡ *Crystal data* for **1**: $[AsV^{IV}{}_8V^{V}{}_2O_{26}(H_2O)]\cdot 8H_2O$: cubic, space group: $I\bar{4}3m$ (no. 217), a = 16.7083 Å, V = 4360.6 Å^3, Z = 4. A black crystal of dimensions 0.23 × 0.21× 0.11 mm was mounted on a glass fiber. Data were collected on Siemens P4 four circle diffractometer at room temperature in the range $2 < 2\theta < 50°$ using the ω scan technique. A total of 4600 reflections was collected of which 978 with $I > 2\sigma(I_o)$ were used. No attempt was made to locate the water hydrogen atoms. The structure was solved by direct methods and refined using SHELXTL (Version 5.01). Attempts to resolve the structure in the centric space group *Im*3*m* proved unsatisfactory. Structure solution and refinement based on 587 reflections and 31 parameters gave $R(R_w)$ = 0.0567 (0.1098).

CCDC 182/1671. See http://www.rsc.org/suppdata/cc/b0/b003359f/ for crystallographic files in .cif format.

1 C. A. C. Sequeira and M. J. Hudson, *Multifunctional Inorganic Solids*, Kluwer, Dordrecht, 1993; *Comprehensive Supramolecular Chemistry*, Vol. 6, *Solid-State Supramolecular Chemistry: Crystal Engineering*, and Vol. 7, *Solid-State Supramolecular Chemistry: Two- and Three-dimensional Inorganic Networks*, ed. J. L. Atwood, J. E. D. Davies, D. D. MacNicol, F. Vögtle and J.-M. Lehn, Elsevier, Oxford, 1996.

2 M. T. Pope and A. Müller, *Angew. Chem., Int. Ed. Engl.*, 1991, **30**, 34; *Polyoxometalates: From Platonic Solids to Anti-Retroviral Activity*, ed. M. T. Pope and A. Müller, Kluwer, Dordrecht, 1994; A. Müller, F. Peters, M. T. Pope and D. Gatteschi, *Chem. Rev.*, 1998, **98**, 239; A. Müller, *Nature*, 1991, **352**, 115.

3 G. Alberti, U. Constantino, M. Cascila and R. Vivani, *Adv. Mater.*, 1996, **8**, 291; P. A. Cox, *Transition Metal Oxides*, Clarendon Press, Oxford, 1995.

4 E. Coronado and C. J. Gomez-Garcia, *Chem. Rev.*, 1998, **98**, 273; M. T. Pope and A. Muller, *Angew. Chem., Int. Ed. Engl.*, 1991, **30**, 34.

5 J. R. DeBord, R. C. Haushalter, L. M. Meyer, D. J. Rose, P. J. Zapf and J. Zubieta, *Inorg. Chim. Acta*, 1997, **256**, 165; Y. Xu, B. Zhang, N. Goh and L. Chia, *Inorg. Chim. Acta.*, 1998, **282**, 10.

6 W. Bu, G. Yang, L. Ye and Y. Fan, *Chem. Lett.*, 2000, 462; J. Xu, R. Wang, Y. Yang, W. Bu and Y. Fan, *Chem. Commun.*, 1999, 983; Y. Xu, N. Goh and L. Chia, *Chem. Commun.*, 1998, 1709; D. Hagrman, P. J. Zapf and J. Zubieta, *Chem. Commun.*, 1998, 1283; D. Hagrman and J. Zubieta, *Chem. Commun.*, 1998, 2005; R. L. LaDuca, R. Finn and J. Zubieta, *Chem. Commun.*, 1999, 1669.

7 M. T. Pope and A. Muller, *Angew. Chem., Int. Ed. Engl.*, 1991, **30**, 29; M. T. Pope, *Comprehensive Coordination Chemistry*, ed. G. Wilkinson, J. A. McCleverty and R. Gillard, Pergaman Press, Oxford, 1987, vol. 3, p. 1023.

8 K. Oyaizu and E. Tsuchida, *Angew. Chem., Int. Ed.*, 1999, **38**, 1292.

9 Y. Zhang, J. R. D. Debord, C. J. O'Conor, R. C. Haushalter, A. Clearfield and J. Zubieta, *Angew. Chem., Int. Ed. Engl.*, 1996, **35**, 989.

10 M. I. Khan, E. Yohames and D. Powell, *Chem. Commun.*, 1999, 23; M. I. Khan, E. Yohames and R. J. Doedens, *Angew. Chem., Int. Ed.*, 1999, **38**, 1292; M. I. Khan, E. Yohames and D. Powell, *Inorg. Chem.*, 1999, **38**, 212.

11 A. Muller, R. Rohlfing, E. Krickemeyer and H. Bögge, *Angew. Chem., Int. Ed. Engl.*, 1993, **32**, 90; W. G. Klemperer, T. A. Marquart and O. M.Yaghi, *Angew. Chem., Int. Ed. Engl.*, 1992, **31**, 49; A. J. Jacobson and D. P. Goshorn, *J. Am. Chem. Soc.*, 1991, **113**, 3188.

12 M. O'Keeffe and A. Navrotsky, *Structure and Bonding in Crystals*, Academic Press, New York, 1981, vol. II, p. 1.

13 O. Kahn, *Molecular Magnetism*, VCH, Weinheim, Germany, 1993.

14 A. Stein, S. W. Keller and T. E. Mallouk, *Science*, 1993, **259**, 1558; G. M. Whitesides, J. P. Mathias and C. T. Seto, *Science*, 1991, **254**, 1312.

ChemComm

Solid phase lipid synthesis (SPLS) for construction of an artificial glycolipid library†

Itaru Hamachi,*‡ Shigeki Kiyonaka and Seiji Shinkai

Department of Chemistry and Biochemistry, Graduate School of Engineering, Kyushu University, Fukuoka 812-8581, Japan. E-mail: itarutcm@mbox.nc.kyushu-u.ac.jp

Received (in Cambridge, UK) 30th March 2000, Accepted 24th May 2000
Published on the Web 26th June 2000

A simple solid phase lipid synthesis (SPLS) is proposed for construction of an artificial glycolipid library; this method is so convenient and flexible that we have efficiently constructed a glycolipid library; some of these glycolipids formed into stable bilayer aggregates in aqueous solution, suggesting that the glycolipids obtained by SPLS are useful as a suitable model of naturally occurring glycolipids.

Recent development in the field of glycobiology has clearly established that naturally occurring glycolipids have various key functions in biological systems.[1] Despite such important roles, fundamental questions on the relationship of the functions to the molecular structures are poorly understood. This is partially due to the complicated and diverse structures of natural glycolipids. An appropriate model and synthetic scheme are now required.[2] We describe herein a simple and convenient strategy for synthesis of artificial glycolipids based on a solid phase method (SPLS). Using the present method we efficiently constructed a small glycolipid library.

Typical examples of the designed artificial glycolipids are shown in Fig 1. Since the artificial glycolipids can be divided into several structural modules to provide flexibility to SPLS,[3] we planned to combine these modules on a resin in sequence (Scheme 1). The Merrifield resin modified with a 3-hydoxymethyl-4-nitrophenoxy linker was employed as a solid support.[4] Initially, phenylisopropyl Fmoc-aspartate as a connector part is attached to the resin using a condensation reagent (DIC). After deprotection of the Fmoc group, succinic anhydride was reacted with the amine site to introduce succinic amide as a spacer, followed by condensation of dialkylamine with the remaining carboxylic acid site to form a hydrophobic tail.[5] Then, the phenylisopropyl group was cleaved by 2% TFA to afford a free β-carboxylic acid of the aspartic acid connector,[6] which was next connected with aminoethyl glycoside,[7, 8] a polar head group. Finally, the artificial glycolipid thus synthesized, was released from the solid support. Two distinct methods were used for the cleavage from the resin, (i) hydrazinolysis,[9] or (ii) photolysis followed by methanolysis.[4] In the hydrazinolysis, cationic lipids bearing a hydrazide were afforded,† whereas anionic lipids bearing a carboxylate were obtained in the photolysis sequence.† All glycolipids were purified by gel chromatography [Sephadex LH20, eluent : $CHCl_3$–MeOH (1/1)], and identified by MALDI-TOF mass and NMR spectroscopies.† The overall yield for the six or seven steps ranges from 33 to 91%. Using this SPLS method, a small library was prepared as summarized in Table 1.

In order to confirm the fundamental capability to form a lipid membrane, we next investigated aggregation properties of the artificial glycolipids using conventional physicochemical measurements. Glc-asp(NH_2)-$2C_2$ and Glc-asp(NH_2)-$2C_6$ were solu-

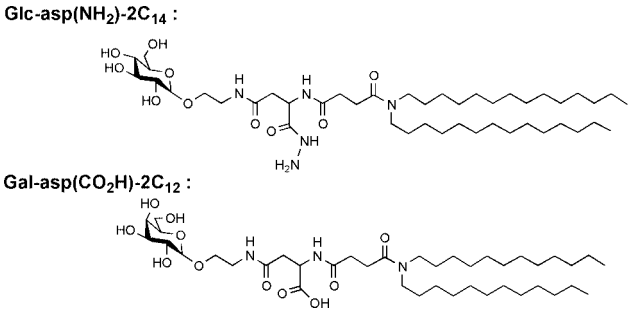

Fig. 1 Typical examples of artificial glycolipids. The glycolipids are abbreviated as 'sugar–connector(charge)–tail'. Sugar denotes the sugar head structure (Glc, Gal, Man), connector denotes the connection part of the lipid (asp), charge denotes the surface charge [NH_2 (cationic) or CO_2H (anionic)], and tail denotes the hydrophobic tail group ($2C_{12}$, $2C_{14}$, $2C_{16}$ *etc.*).

† Details of the release of Glc-asp(NH_2)-$2C_{12}$ from resin **5** and the synthesis of Glc-asp(CO_2H)-$2C_{12}$ are available as electronic supplementary information (ESI). See http://www.rsc.org/suppdata/cc/b0/b002545n/

‡ Visiting professor at the Institute of Molecular Science, Myodaiji, Okazaki, Japan.

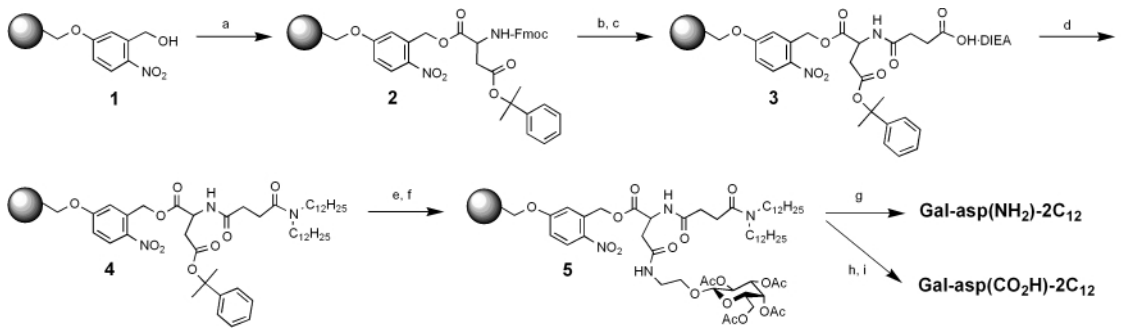

Scheme 1 Typical synthetic route towards artificial glycolipids (Gal-asp(NH_2)–$2C_{12}$, and Gal-asp(CO_2H)–$2C_{12}$). *Reagents and conditions*: (a) Fmoc-Asp(Pip)-OH (3.0 equiv.), DIC (3.0 equiv.), DMAP (3.0 equiv.), HOBT (4.0 equiv.), DMF, 25 °C, 10 h, 83%; (b) piperidine (20%), DMF, 25 °C, 30 min.; (c) succinic anhydride (4.0 equiv.), DIEA (4.0 equiv.), DMF, 25 °C, 14 h; (d) didodecylamine (3.0 equiv.), pyBOP (3.0 equiv.), DIEA (3.0 equiv.), DMF, 25 °C, 10 h; (e) TFA (2%), CH_2Cl_2, 25 °C, 3 h; (f) 2-aminoethyl-*O*-tetraacetyl glucopyranoside (3.0 equiv.), pyBOP (3.0 equiv.), DIEA (3.0 equiv.), DMF, 25 °C, 10 h; (g) $NH_2NH_2·H_2O$ (50 equiv.), THF–MeOH (4/1, v/v), 25 °C, 5 h, 67% over six steps; (h) *hν*, THF, 25 °C, 24 h; (i) NaOMe (1.0 equiv./unit), CH_2Cl_2–MeOH (3/1, v/v), 25 °C, 3 h, 39% over seven steps. Pip = phenylisopropyl, DIC = *N*,*N*′-diisopropylcarbodiimide, DMAP = 4-dimethylaminopyridine, HOBT = 1-hydroxybenzotriazole, DIEA; = *N*,*N*′-diisopropylethylamine, pyBOP = benzotriazol-1-yl-oxytrispyrrolidinophosphonium hexafluorophosphate.

DOI: 10.1039/b002545n

Table 1 Yields and aggregation properties of artificial glycolipids synthesized by SPLS

Compound	Total yield (%)	Aggregation properties in water		
		Diameter[a]/nm	Morphology[b]	T_c[c]/°C
Gal-asp(CO_2H)-2C_{12}	39	40–350	Vesicles	< 0
Gal-asp(NH_2)-2C_{12}	67	120–690	Vesicles	< 0
Man-asp(NH_2)-2C_{12}	91	660–1230	Vesicles	< 0
Glc-asp(NH_2)-2C_2	49	< 5	No aggregates	Not measured
Glc-asp(NH_2)-2C_6	56	< 5	No aggregates	Not measured
Glc-asp(NH_2)-2C_{10}	68	170–810	Vesicles	< 0
Glc-asp(NH_2)-2C_{12}	81	50–90, 200–810	Vesicles	< 0
Glc-asp(NH_2)-2C_{14}	59	90–370	Vesicles, helical rods	4–5
Glc-asp(NH_2)-2C_{16}	60	140–430	Vesicles, helical rods, tubes	23–25
Glc-asp(NH_2)-2C_{18}	33	Not dispersed		

[a] The aggregates were assumed to be spherical in calculation of diameters. [b] All samples were negatively-stained with uranyl acetate. [c] Phase transition behaviors of the bilayer membrane were estimated by DSC.

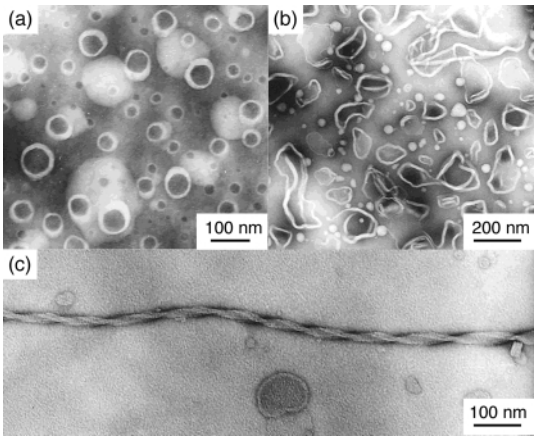

Fig. 2 TEM images of aggregates formed in 1.0 mM aqueous dispersions of artificial glycolipids. All samples were incubated at 35 °C for 12 h, followed by staining with uranyl acetate. The pH of the dispersed solution was *ca.* 6.2. (a) Gal-asp(NH_2)–2C_{12}, (b) Glc-asp(NH_2)–2C_{12}, (c) Glc-asp(NH_2)–2C_{14}.

ble in water without sonication whereas Glc-asp(NH_2)-2C_{18} was not dispersed even by prolonged sonication. Other glycolipids swelled in water, and then yielded a homogeneous dispersion displaying light-scattering properties upon sonication. The size distribution of the glycolipid aggregates in aqueous solution was studied by dynamic light scattering measurement (DLS, Otsuka DLS 7000). For Glc-asp(NH_2)-2C_2 and Glc-asp(NH_2)-2C_6, no or less than a few nm diameter of aggregates was determined, suggesting that these were dissolved as monomers or small micelles. DLS for the other lipids dispersed in aqueous solutions showed aggregate sizes is in the range 40–1230 nm.

Direct observation of these aggregates was conducted by transmission electron microscopy (TEM). No aggregates were observed for Glc-asp(NH_2)-2C_2 or Glc-asp(NH_2)-2C_6, consistent with data of their solubilities and DLS measurements. Fig. 2 shows typical TEM images of the artificial glycolipids. Both Glc-asp(NH_2)-2C_{12} and Glc-asp(CO_2H)-2C_{12} predominantly form into unilamellar vesicles. The layer width of these vesicles was roughly estimated to be 10 nm, which corresponds to the bimolecular length of Glc-asp(NH_2)-2C_{12}. Similarly, spherical vesicles were observed for Gal-asp(NH_2)-2C_{12} and Man-asp(NH_2)-2C_{12}, indicating that the morphology of these aggregates is not dependent on the head group structure of the monosaccharide. When the tail part becomes longer as for Glc-asp(NH_2)-2C_{14} and Glc-asp(NH_2)-2C_{16}, more developed structures such as helical rods and/or long tubes were observed, as well as vesicles.

Membrane fluidity of these aggregates was estimated by differential scanning calorimetry (DSC). The glycolipids bearing didodecylamine [Glc-asp(CO_2H)-2C_{12} and Glc-, Gal- or Man-asp(NH_2)-2C_{12}], do not show any endothermic peaks, suggesting that the phase transition temperature (T_c) is lower than 0 °C. Glc-asp(NH_2)-2C_{14} shows a rather broad peak at *ca.* 4–5 °C and the T_c of Glc-asp(NH_2)-2C_{16} was determined as 23–25 °C. The corresponding phase transition enthalpy (ΔH) was also determined to be 4–5 kcal mol^{-1} for Glc-asp(NH_2)-2C_{14} and 8–9 kcal mol^{-1} for Glc-asp(NH_2)-2C_{16}, comparable to that of typical natural phospholipids. It is clear that T_c gradually rises with an increase in the hydrophobic chain length, but these artificial glycolipids are still in the fluidic liquid crystal phase at room temperature.

In conclusion, we have developed a convenient SPLS method and successfully applied it to the construction of a small library of artificial glycolipids. All physicochemical data clearly demonstrated that some glycolipids form into stable aggregates consisting of bilayer membranes in aqueous solution. The proposed SPLS scheme is so flexible that we may envision a large library of glycolipids which confers valuable insights for the design of novel saccharide-based biomaterials, as well as elucidation of biological functions of natural glycolipids.

We are grateful to Professor K. Fukase (Osaka University) for his helpful comments on *O*-glycoside synthesis at the initial stage of this research. This research was financially supported by a Germinating Research grant (11878109) from the Ministry of Education, Science, Sports and Culture of Japan, and TERUMO life science foundation.

Notes and references

1 S. Hakomori, *Annu. Rev. Biochem.*, 1981, **50**, 733; S. Hakomori, *Pure Appl. Chem.*, 1991, **63**, 473; A. Varki, *Glycobiology*, 1993, **3**, 97; R. A. Dwek, *Chem. Rev.*, 1996, **96**, 683; K. J. Yarema and C. R. Bertozzi, *Curr. Opin. Chem. Biol.*, 1998, **2**, 49.

2 Several types of artificial glycolipids have been prepared recently: M. Hato and H. Minamikawa, *Langmuir*, 1996, **12**, 1658; Z. Zhang, K. Kukunaga, Y. Sugimura, K. Nakao and T. Shimizu, *Carbohydr. Res.*, 1996, **292**, 47; Y. Hisaeda, E. Ohshima, J. Kikuchi and Y. Murakami, *Tetrahedron Lett.*, 1997, **38**, 6713; S. Takeoka, K. Sou, C. Boettcher, J. H. Fuhrhop and E. Tsuchida, *J. Chem. Soc., Faraday Trans.*, 1998, **94**, 2151; J. Song and R. I. Hollingsworth, *J. Am. Chem. Soc.*, 1999, **121**, 1851; H. C. Hansen and G. Magnusson, *Carbohydr. Res.*, 1999, **322**, 181.

3 The validity of module-combination for artificial lipids has been established by Kunitake *et al.*: T. Kunitake, *Angew. Chem., Int. Ed. Engl.*, 1992, **31**, 709.

4 K. C. Nicolaou, N. Watanabe, J. Li, J. Pastor and N. Winssinger, *Angew. Chem., Int. Ed.*, 1998, **37**, 1559.

5 L. Schmitt, C. Dietrich and R. Tampe, *J. Am. Chem. Soc.*, 1994, **116**, 8485.

6 C. Yue, J. Thierry and P. Potier, *Tetrahedron Lett.*, 1993, **34**, 323.

7 J. Dahmén, T. Frejd, G. Grönberg, T. Lave, G. Magnusson and G. Noori, *Carbohydr. Res.*, 1983, **116**, 303.

8 H. C. Hansen, S. Haataja, J. Finne and G. Magnusson, *J. Am. Chem. Soc.*, 1997, **119**, 6974.

9 H. Kunz and H. Waldmann, *Helv. Chim. Acta*, 1985, **68**, 618.

10 ^{1}H NMR spectra of the final products obtained by hydrazinolysis suggest that the glycolipids were partially racemized at the connector site (8/2 = L-asp/D-asp).

The first fluorescent sensor for boronic and boric acids with sensitivity at sub-micromolar concentrations

Wei Wang, Greg Springsteen, Shouhai Gao and Binghe Wang*

Department of Chemistry, North Carolina State University, Raleigh, NC 27695-8204, USA. E-mail: binghe_wang@ncsu.edu

Received (in Cambridge, UK) 15th March 2000, Accepted 15th May 2000
Published on the Web 26th June 2000

An anthracene-based PET sensor which uses a diethanolamine recognition site is selective for boronic and boric acids, showing up to a 19-fold fluorescent intensity enhancement upon binding.

Boronic acids and boric acid are ubiquitous compounds in chemistry and biology. Boronic acids are important organic intermediates that have been widely used in Suzuki cross-coupling reactions,[1] protection of diols,[2] Diels–Alder reactions[3] and asymmetric synthesis of amino acids.[4] In addition, this class of compounds has been used for the development of sensors for carbohydrates and amino acids;[5,6] selective transporters of nucleosides, saccharides and nucleotides;[7] inhibitors of proteases;[8] and therapeutic agents in boron neutron capture therapy (BNCT) of certain brain tumors.[9] Therefore, fluorescent sensors for boronic acids could be used for the analysis and detection of such compounds in a variety of applications. Boric acid plays an essential role in plant growth.[10] However, the cellular and molecular mechanisms through which boric acid functions in plant cells are far from clear. Appropriately designed sensors could be used for probing the detailed biological functions of boric acid at the cellular and molecular levels. To the best of our knowledge, no fluorescent sensors for either boronic or boric acids have been reported.

The design presented here takes advantage of the known high affinity binding of boronic and boric acid moieties with diethanolamine through boronate formation.[11] This boronate is stabilized by the donation of the nitrogen lone pair electrons to the open shell of the boron atom,[12] which allows for the formation of two five-membered rings (*e.g.* **2**, Scheme 1). Such binding has been used for the stabilization, purification and characterization of boronic acids.[13] Furthermore, it is known that the nitrogen lone pair electrons of 9-aminomethylanthracene can quench the fluorescence of the anthracene moiety through photoinduced electron transfer (PET).[5,6,14] Masking of the nitrogen lone pair electrons causes a suppression of this fluorescence quenching and, therefore, results in fluorescence intensity increases.[6,12] We envisioned that the diethanolamine recognition motif could be incorporated into an anthracene molecule so that its binding with boronic and boric acids would lead to the formation of boronate/borate **2**, which has a boron atom ideally positioned to accept, and therefore mask the nitrogen lone pair electrons. This masking of the nitrogen lone pair electrons could then lead to a fluorescence increase of the anthracene moiety. A fluorescent sensor, *N*-(9-anthrylmethyl)diethanolamine **1**, was designed, synthesized, and evaluated for its binding with boronic and boric acids (Scheme 1). In the absence of boronic and boric acids, the sensor displayed very weak fluorescence. However, upon addition of boronic or boric acid, the fluorescence intensity of the sensor increased by > 16-fold, at saturation concentrations (data not shown).

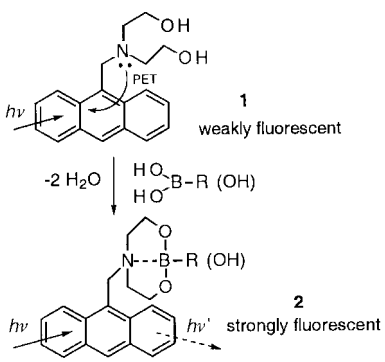

Scheme 1 The tight binding of boronic acid/boric acid with sensor **1**.

N-(9-Anthrylmethyl)diethanolamine **1** was readily synthesized from 9-(chloromethyl)anthracene through reaction with diethanolamine (6.0 equiv.) in the presence of K_2CO_3 (10.0 equiv.) and a catalytic amount of KI (0.3 equiv.) in a mixture of $CHCl_3$ and MeCN under reflux for 2.5 h (97% yield). In a typical binding experiment, the sensor was dissolved in methanol and was added to the solutions of different concentrations of boronic or boric acid in MeOH. The final concentration of the sensor was fixed at 10^{-5} M.

In the absence of boric or boronic acids, the sensor exhibited very low fluorescence owing to the quenching of the anthracene fluorescence through PET. For the boronic acid binding studies, phenylboronic acid was used as a model compound. Upon addition of phenylboronic acid, the sensor solution showed concentration-dependent fluorescence intensity increases from 34% at 10^{-6} M (Table 1, Fig. 1) to 16-fold at saturation (50 mM, data not shown). The sensor responded to boric acid with a 107% intensity increase at 10^{-7} M (Table 1, Fig. 1) and a 19-fold increase at saturation (500 mM, data not shown).

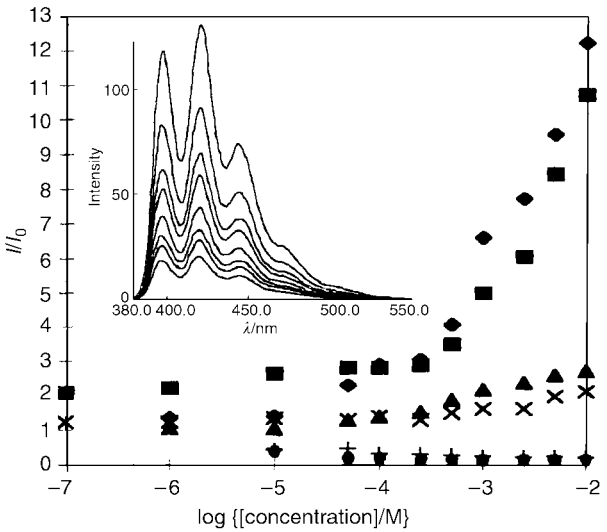

Fig. 1 Relative fluorescence intensity changes (I/I_0) as a function of log[boronic or boric acid] with **1** or **3** (1.0×10^{-5} M) in MeOH at room temperature, λ_{ex} = 370 nm, λ_{em} = 419 nm. $PhB(OH)_2$ with sensor **1** (◆); $B(OH)_3$ with sensor **1** (■); $PhB(OH)_2$ with control **3** (▲); $B(OH)_3$ with control **3** (×); $PhCO_2Na$ with sensor **1** (●); $PhOP(O)(ONa)_2$ with sensor **1** (+). *Inset:* a typical set of fluorescence emission spectra of sensor **1** (1.0×10^{-5} M) with $PhB(OH)_2$ in MeOH from 0 M to 1×10^{-3} M.

Table 1 The effect of $PhB(OH)_2/B(OH)_3$ on the fluorescent intensity of **1** and **3**

	I/I_0[a]			
	$PhB(OH)_2$[b]		$B(OH)_3$[b]	
Conc(M)	**1**	**3**	**1**	**3**
1.0×10^{-7}	—	—	2.07 ± 0.17	1.22 ± 0.10
1.0×10^{-6}	1.34 ± 0.17	1.05 ± 0.07	2.20 ± 0.29	1.23 ± 0.16
1.0×10^{-5}	1.38 ± 0.01	1.04 ± 0.02	2.63 ± 0.38	1.32 ± 0.06
5.0×10^{-5}	2.28 ± 0.22	1.28 ± 0.04	2.79 ± 0.37	1.28 ± 0.10
1.0×10^{-4}	2.88 ± 0.43	1.37 ± 0.14	2.79 ± 0.40	1.36 ± 0.13
2.5×10^{-4}	3.03 ± 0.31	1.50 ± 0.15	2.86 ± 0.33	1.27 ± 0.08
5.0×10^{-4}	4.04 ± 0.37	1.85 ± 0.07	3.48 ± 1.18	1.47 ± 0.11
1.0×10^{-3}	6.58 ± 0.21	2.15 ± 0.08	4.96 ± 0.24	1.59 ± 0.25

[a] I_0: the intensity of **1** or **3** (1.0×10^{-5} M) in the absence of phenylboronic/boric acid; I the intensity of **1** or **3** (1.0×10^{-5} M) in the presence of phenylboronic/boric acid. [b] The ratio is listed as the average of three runs with the standard deviation.

It is well known that aminomethylanthracene-based fluorescent sensors are sensitive to pH changes.[15] Therefore, incidental changes in pH due to the addition of the boric or boronic acids were a possible contributing factor in the fluorescence intensity changes observed with sensor **1**, which could complicate the interpretation of the results. To examine whether the fluorescence intensity changes were due to unintended changes in the pH of the solution, we also synthesized compound **3** as a control by following the same procedure for the preparation of **1**. If incidental pH changes were not the reason for the fluorescence intensity changes observed with **1**, we would not expect **3** to be sensitive to boronic and boric acids because compound **3** lacks the two hydroxy groups (Scheme 2), which are critical for the formation of the tight complex of **1** with boronic and boric acids (Scheme 1). Indeed, it was found that compound **3** showed minimal fluorescence intensity changes upon addition of boric or boronic acids at concentrations up to 10^{-5} M (Fig. 1, Table 1). Even at 10 mM, the fluorescence intensity changes were small [1.6- to 2.2-fold *cf.* 5.0- to 6.0-fold with **1,** (Table 1)]. Such results indicate that the fluorescence intensity changes observed with sensor **1** are not primarily due to unintended changes in pH. Furthermore, the minor changes in the fluorescence intensity of **3** may be due to the non-specific weak complexation of the nitrogen atom of **3** with boronic or boric acid (**4**, Scheme 2).

To examine the selectivity of the sensor for boronic and boric acids in the presence of other anions, we also studied the effect of sodium benzoate and disodium phenyl phosphate on the fluorescence intensity of sensor **1**. These anions were not able to increase the fluorescence intensity of the sensor and actually caused a slight lowering of the intensity (Fig. 1). A ^{1}H NMR spectral comparison of the complexed and uncomplexed forms of sensor **1** shows that the sensor/analyte binding is in a 1:1 molar ratio for both phenylboronic acid and boric acid.

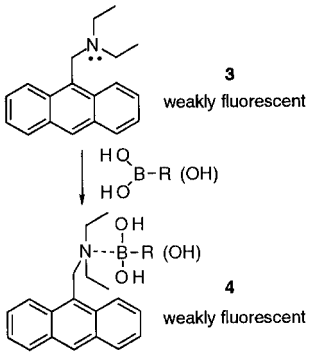

Scheme 2 The weak interaction of boronic acid/boric acid with control compound **3**.

In conclusion, the first fluorescent sensor **1** for boronic and boric acids shows high sensitivity and selectivity. Further work in this area may be beneficial to chemical process monitoring, impurity detection, examination of the intracellular functions of boric acid in plant cells, and biological analysis of medicinally useful boronic acid compounds.

This research has been supported by the National Institutes of Health (DK55062).

Notes and references

1 N. Miyaura and A. Suzuki, *Chem. Rev.*, 1995, **95**, 2457.
2 R. J. Ferrier, *Adv. Carbohydr. Chem. Biochem.*, 1978, **35**, 31.
3 K. Ishihara and H. Yamamoto, *Eur. J. Org. Chem.*, 1999, 527.
4 N. A. Petasis and I. A. Zavialov, *J. Am. Chem. Soc.*, 1997, **119**, 445.
5 T. D. James, P. Linnane and S. Shinkai, *Chem. Commun.*, 1996, 281.
6 J. Yoon and A. W. Czarnik, *J. Am. Chem. Soc.*, 1992, **114**, 5874.
7 P. R. Westmark, S. J. Gardiner and B. Smith, *J. Am. Chem. Soc.*, 1996, **118**, 11 093.
8 D. H. Bao, W. P. Huskey, C. A. Kettner and F. Jordan, *J. Am. Chem. Soc.*, 1999, **121**, 4684.
9 G. W. Kabalka, *Expert Opin. Ther. Pat.*, 1998, **8**, 545.
10 *Boron and Its Role in Crop Production*, ed. U. C. Gupta, CRC Press, Boca Raton, FL, 1993.
11 D. G. Hall, J. Tailor and M. Gravel, *Angew. Chem. Int. Ed.*, 1999, **38**, 3064.
12 T. Burgemeister, R. Grobe-Einsler, R. Grotstollen, A. Mannschreck and G. Wulff, *Chem. Ber.*, 1981, **114**, 3403.
13 P. B. Tripathy and D. S. Matteson, *Synthesis*, 1990, 200.
14 T. D. James, K. R. A. S. Sandanayake and S. Shinkai, *Angew. Chem., Int. Ed. Engl.*, 1996, **35**, 1910.
15 R. S. Atkinson, D. R. G. Brimage, R. S. Davidson and E. Gray, *J. Chem. Soc., Perkin Trans. 1*, 1973, 960.

Formation of novel conjugated polycarbon–metal systems *via* metal migration on a M–C≡C–C≡C–M linkage

Munetaka Akita,* Min-Chul Chung, Aizoh Sakurai and Yoshihiko Moro-oka

Chemical Resources Laboratory, Tokyo Institute of Technology, 4259 Nagatsuta, Midori-ku, Yokohama 226-8503, Japan. E-mail: makita@res.titech.ac.jp

Received (in Cambridge, UK) 9th May 2000, Accepted 1st June 2000

Reactions of butadiynediyldimetal complexes, Fp*–C≡C–C≡C–M(η^5-C_5R_5)$(CO)_2$ 1 [M = Fe, Ru; R = Me, H; Fp* = FeCp*$(CO)_2$], with group 8 metal carbonyls result in migration of a σ-bonded metal fragment along the C_4 rod to form novel highly conjugated polycarbon–metal systems; the zwitterionic μ-but-2-yn-1-ylidene-4-ylidyne complex $Ru_3(CO)_{10}$(μ_3-C–C≡C–μ-C)Fe_2Cp*$_2(CO)_3$ 2, and the dimerized product with a cumulenic μ-C_8 ligand $(Cp^*Fe)_4$-$Ru_2(CO)_{13}$[μ_6-C_8–C(=O)] 3, *via* 1,4-migration and the zwitterionic acetylide cluster-type product Fp*$^+$[$Cp(CO)_2$Ru-(η^2-C≡C)–(μ_3-C≡C)$Fe_3(CO)_9$]$^-$ 4, *via* 1,3-migration.

Increasing attention focused on polycarbon–transition metal complexes stems originally from their relevance to surface bound carbide intermediates[1] and recently from their intriguing chemical and physical properties which are potentially applicable to new molecular devices.[2] However, neither interaction modes nor synthetic methods have been thoroughly exploited. During the course of our synthetic study of polycarbon cluster compounds derived from polyynediyldimetal complexes M–$(C\equiv C)_n$–M [n = 1–6; M = Fe or Ru(η^5-C_5R_5)(CO_2)],[3] we observed formation of novel highly conjugated polycarbon–transition metal systems resulting from migration of a σ-bonded metal fragment along the carbon rod. Herein we report results of interaction of butadiynediyl complexes **1** (n = 2) with group 8 metal carbonyl species.

Reaction of the butadiynediyldiiron complex **1a** [Scheme 1, Fp* = FeCp*$(CO)_2$; Cp* = η^5-C_5Me_5][3b] with $Ru_3(CO)_{12}$ in refluxing CH_2Cl_2 gave a mixture of products, from which two compounds **2** and **3a** were isolated after TLC separation (silica gel). For the purple red product **2**,† the single Cp* NMR signal and the highly deshielded ^{13}C NMR signal (δ_C 347.1) suggested formation of a symmetrical cluster compound **2′** bearing a cumulenic >C=C=C=CFe_2 fragment but X-ray crystallography of its η^5-C_5Me_4Et derivative **2**#‡ [Fig. 1(a)] revealed a mirror symmetrical zwitterionic but-2-yne-1-ylidene-4-ylidyne structure[5] with (i) a C_4 bridge showing long–short–long bond alternation and (ii) μ_3-coordination of the C4 and C23 atoms. Contribution of the neutral butatrienetetrayl structure **2′**, however, is evident, since (i) the C_4 rod is slightly tilted toward Ru3 as indicated by the C3–C4–Ru bond angles and (ii) the C–C distances of the μ-C–C≡C–C moiety are averaged to some extent. It should be noted that the (μ-C_4)Fe_2Cp*$_2(CO)_3$ structure results from 1,4-migration of the iron fragment along the C_4 rod, *i.e.* the FeCp*$(CO)_n$ fragment is shifted from one end of the C_4 bridge to the other upon interaction with $Ru_3(CO)_{12}$. The NMR spectrum of the other deep purple red complex **3a**† contained four sets of Cp* signals indicating oligomerization of **1a**, and X-ray crystallography‡ [Fig. 1(b)] revealed a hexanuclear structure with a dimerized C_8 skeleton. Again, formation of the new C_8 carbon linkage involves 1,4-migration (C5 → C8) of the iron fragment. The migration induces a change of part of the polyyne structure into a cumulenic moiety (C8=C7=C6=C5) with similar C–C distances. Although the pentatetraenylidene structure **3a′** π-bonded to the two ruthenium atoms is a possible canonical structure of **3a**, the bent C5–

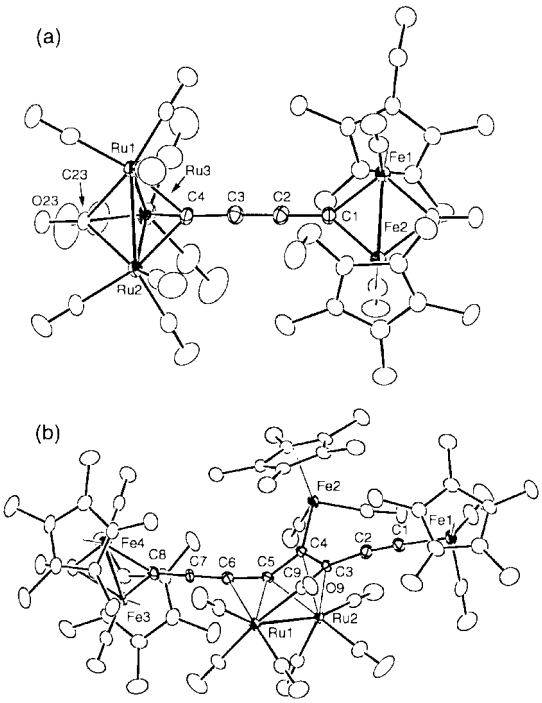

Fig. 1 Molecular structures of **2**# (a) and **3a** (b) drawn at the 30% probability level. Selected parameters: **2**#: Fe–C1 1.906(6), 1.885(9), C1–C2 1.31(1), C2–C3 1.25(1), C3–C4 1.34(1), C4–Ru 2.093–2.120(9), Ru–Ru 2.749–2.781(1), Fe1–Fe2 2.530(2) Å; Fe–C1–C2 137.4(6), 138.8(7), C1–C2–C3 179(1), C2–C3–C4 177.4(8), Ru1–C4–C3 133.4(6), Ru2–C4–C3 132.3(7), Ru3–C4–C3 126.0(6)°. **3a**: C1–C2 1.202(8), C2–C3 1.443(8), C3–C4 1.408(7), C3–C9 1.538(8), C4–C5 1.415(7), C5–C6 1.315(8), C6–C7 1.308(7), C7–C8 1.285(7), Fe1–C1 1.912(6), Ru2–C3 2.291(5), Fe2–C4 2.024(5), Ru2–C4 2.279(5), Ru1–C5 2.228(5), Ru2–C5 2.128(5), Ru1–C6 2.458(5), Fe3–C8 1.934(6), Fe4–C8 1.924(6), Ru1–C9 2.118(6), Ru1–Ru2 2.7453(7), Fe3–Fe4 2.542(1) Å; Fe1–C1–C2 176.4(5), C1–C2–C3 168.7(6), C2–C3–C4 128.2(5), C2–C3–C9 114.7(4), C4–C3–C9 113.0(4), C3–C4–C5 112.5(5), C4–C5–C6 144.1(5), Ru1–C5–Ru2 78.1(2), C5–C6–C7 168.4(6), C6–C7–C8 176.4(6), Ru1–C9–C3 110.3(3)°.

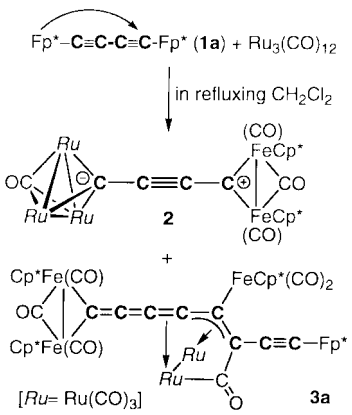

Scheme 1

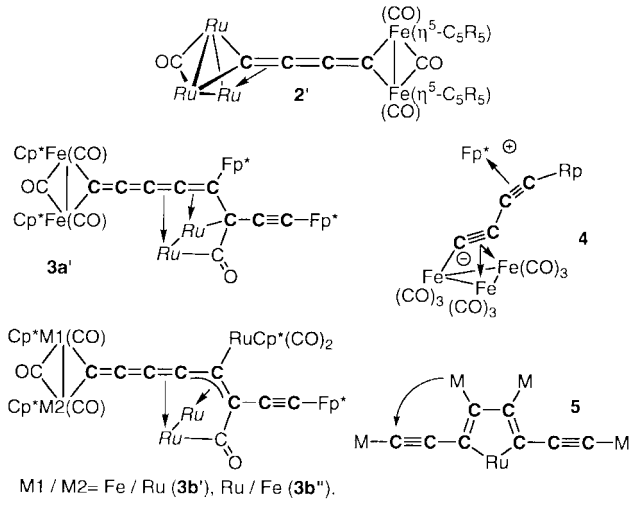

Chart 1

C4–C3 moiety with similar C–C and Ru2–C distances reveals η^3-allyl coordination to Ru2. The linear C3–C2–C1–Fe1 moiety is a normal η^1-acetylide structure. Coordination of the perpendicularly projected, adjacent cumulenic π orbitals of the C6–C5 and C5–C4 bonds to the two ruthenium atoms connected by a Ru–Ru bond[6] leads to strain, which is relieved by formation of a larger membered ring structure *via* CO-insertion [CO(9)]. The C_8 bridge was also characterized by ^{13}C NMR spectroscopy.† Except for the deshielded C8 signal (δ_C 254.7), the other signals appeared in a rather narrow range (δ_C 157–107).

The isostructural C_8 complex **3b**† was obtained from the Fe, Ru-mixed metal butadiynediyl complex, Fp*–C≡C–C≡C–RuCp*$(CO)_2$ **1b**,[4] upon treatment with $Ru_3(CO)_{12}$.§ Complex **3b** consisted of a mixture of two inseparable isomers, **3b′** and **3b″** (Chart 1), as indicated by NMR data containing two sets of signals as well as the successful X-ray structural analysis taking into account a disordered structure containing two components. It should be noted that no homometallic complexes (M1 = M2 = Ru or Fe) were detected by NMR and FD-MS analyses suggesting an intramolecular mechanism for the migration.

Another example of metal migration was observed for reaction of Fp*–C≡C–C≡C–RuCp$(CO)_2$ **1c** [Cp(η^5-C_5H_5) derivative of **1b**] with $Fe_2(CO)_9$, a group 8 metal carbonyl.§ The deshielded ^{13}C NMR signal (δ_C 193.7) of the resultant purple Fe_3-adduct **4** (Chart 1)† suggested formation of a μ-acetylide cluster compound,[7] and X-ray crystallography‡ revealed a pentanuclear structure consisting of a cationic dinuclear μ–η^1:η^2-acetylide complex part and an anionic trinuclear μ_3-acetylide cluster type structure. The structure of each component is normal, and the diamagnetic nature of **4** can be interpreted in terms of the zwitterionic structure, each metal center in which is coordinatively saturated.

In conclusion, interaction of the butadiynediyl complexes **1** with group 8 metal carbonyls results in the formation of novel highly conjugated polycarbon–metal cluster systems. The structures of **2** and **3** suggest the occurrence of stepwise metal migration along the carbon rod, and the C_8 linkage in **4** is formed *via* 1,4-migration on a ruthenacyclopentadiene intermediate **5** resulting from oxidative metallacyclization of **1** (Chart 1).[8] Noteworthy features of the present system are as follows. The formation of zwitterionic structures such as **2** and **4** are regarded as typical of electron transfer through unsaturated carbon rods. Another feature is the flexible coordination mode of the $C(sp)_n$ system. For example, in the case of interaction with trimetallic species, the C_4 ligand can behave as a three- (μ_3-η^1-C_4 like C4 in **2**) to seven-electron donor (μ-η^3-propargylidene-ketene).[3c] When combined with coordination of CO ligands, which can act as either one- or two-electron donors, various intermediates have many opportunities to attain coordinative saturation by switching coordination modes of the C_4 and/or CO ligands.

We are grateful to the Yamada Science Foundation for financial support of this research.

Notes and references

† *Selected spectroscopic data*: **2** (7%): $\delta_H(CD_2Cl_2)$ 1.71 (Cp*). $\delta_C(CD_2Cl_2$, −90 °C) 347.1 (C1), 216.7 (C4), 119.0, 118.4 (C3≡C4); 269.1 (μ_3-CO), 268.3 (μ-CO), 211.1 (Fe–CO), 196.9 (Ru–CO). IR(CH_2Cl_2) ν(C≡C) 2081; ν(CO) 2047, 2008, 1961, 1903; ν(μ-CO) 1801; ν(μ_3-CO) 1700 cm^{-1}. **3a** (10%) $\delta_H(CDCl_3)$ 1.92, 1.86, 1.73, 1.68 (Cp*). $\delta_C(CDCl_3)$ 254.7 (μ-C=); 157.3, 134.0, 129.0, 128.9, 111.5, 108.8, 106.8 (C1–C7); 274.9 (μ-CO); 225.7 (>C=O); 218.0, 216.0, 215.6, 214.5, 213.2, 200.0, 198.6, 197.1, 193.7 (CO). IR(CH_2Cl_2) ν(C≡C) 2060; ν(CO) 2030, 1801, 2015, 1996, 1961, 1954, 1895, ν(μ-CO) 1780, ν(>C=O) 1575 cm^{-1}. **3b** (12%):§ $\delta_H(CD_2Cl_2)$ 2.04, 1.97, 1.90, 1.88, 1.86, 1.80, 1.75, 1.69 (Cp*). **5** (11%):§ $\delta_H(CDCl_3)$ 5.56 (Cp), 1.97 (Cp*). $\delta_C(CDCl_3)$ 193.7, 144.0, 123.3, 104.8 (C_4); 216.0, 215.0, 196.8 (CO). IR(CH_2Cl_2) ν(CO) 2047, 2036, 1995, 1982, 1962, 1939; ν(C=C) 1606 cm^{-1}.

‡ X-Ray diffraction measurements were made on a Rigaku RAXIS IV imaging plate area detector with graphite-monochromated Mo-Kα radiation (λ = 0.71069 Å) at −60 °C. *Crystal data*: **2**#: $C_{42}H_{41}O_{13}Fe_2Ru_3$, M = 1168.7, monoclinic, space group $P2_1/c$, a = 15.445(1), b = 16.481(2), c = 18.873(3) Å, β = 112.60(1)°, V = 4435.2(10) $Å^3$, Z = 4, D_c = 1.75 g cm^{-3}, μ = 17.0 cm^{-1}, $R1$ = 0.068 for the 8584 unique data with $F > 4\sigma(F)$ ($wR2$ = 0.212 for all 9332 data) and 552 parameters. **3a**: $C_{68}H_{74}O_{14}Fe_4Ru_2$, M = 1540.9, monoclinic, space group $P2_1/n$, a = 13.323(2), b = 18.681(9), c = 26.420(4) Å, β = 93.023(7)°, V = 6566(2) $Å^3$, Z = 4, D_c = 1.56 g cm^{-3}, μ = 13.7 cm^{-1}, $R1$ = 0.064 for the 10696 unique data with $F > 4\sigma(F)$ ($wR2$ = 0.173 for all 11815 data) and 815 parameters. Details of **4** are included in the supplementary material. CCDC 182/1669.

§ Other products: from **1b**: Fp*–C≡C–(μ_4-C≡C)Ru_4Cp*$(CO)_{11}$ **6** (43%); from **1c**: Fp*–C≡C–(μ_3-C≡C)Fe_2RuCp*$(CO)_9$ **7** (7%) and $(CO)_2$Cp*Ru–(μ-η^3-C_3)[$Fe_2(CO)_6$]–C(=C=O)–Fp* **8** (15%). Complexes **6** and **7** are acetylide cluster-type compounds and complex **8** contains a μ-η^3-propargylidene-ketene ligand.[3c] No characterizable product was obtained from Fp*–C≡C–C≡C–FeCp$(CO)_2$.

1 M. Tachikawa and E. L. Muetterties, *Prog. Inorg. Chem.*, 1981, **28**, 203; J. S. Bradley, *Adv. Organomet. Chem.*, 1983, **22**, 1; D. F. Shriver and M. J. Sailor, *Acc. Chem. Res.*, 1988, **21**, 374; W. Beck, B. Niemer and M. Wieser, *Angew. Chem., Int. Ed. Engl.*, 1993, **32**, 923; H. Lang, *Angew. Chem., Int. Ed. Engl.*, 1994, **33**, 547; U. Bunz, *Angew. Chem., Int. Ed. Engl.*, 1996, **35**, 969; A. L. Balch and M. M. Olmstead, *Chem. Rev.*, 1998, **98**, 2133; M. I. Bruce, *Chem. Rev.*, 1998, **98**, 2797.

2 R. Dembinski, T. Bartik, B. Bartik, M. Jaeger and J. Gladysz, *J. Am. Chem. Soc.*, 2000, **122**, 810; M. Brady, R. Dembinski and J. A.Gladysz, *Angew. Chem., Int. Ed. Engl.*, 1996, **35**, 414; M. Brady, W. Weng, Y. Zhou, J. W. Seylet, A. J. Amoroso, A. M. Arif, M. Böhme, G. Frenking and J. A. Gladysz, *J. Am. Chem. Soc.*, 1997, **119**, 775; T. Bartik, W. Weng, J. A. Ramsden, S. Szafert, S. B. Falloon, A. M. Arif and J. A. Gladysz, *J. Am. Chem. Soc.*, 1998, **120**, 11 071; M. Guillemot, L. Toupet and C. Lapinte, *Organometallics*, 1998, **17**, 1928; M. I. Bruce, B. D. Kelly, B. W. Skelton and A. H. White, *J. Chem. Soc., Dalton Trans.*, 1999, 847.

3 Reviews: for C_2 complexes: (*a*) M. Akita and Y. Moro-oka, *Bull. Chem. Soc. Jpn.*, 1995, **68**, 420; C_4–C_{12} complexes: (*b*) M. Akita, M.-C. Chung, A. Sakurai, S. Sugimoto, M. Terada, M. Tanaka and Y. Moro-oka, *Organometallics*, 1997, **16**, 4882; (*c*) M. Akita, M.-C. Chung, M. Terada, M. Miyauti, M. Tanaka and Y. Moro-oka, *J. Organomet. Chem.*, 1998, **565**, 49; (*d*) M. Akita, A. Sakurai and Y. Moro-oka, *Chem. Commun.*, 1999, 101; (*e*) A. Sakurai, M. Akita and Y. Moro-oka, *Organometallics*, 1999, **18**, 3241; (*f*) M.-C. Chung, A. Sakurai, M. Akita and Y. Moro-oka, *Organometallics*, 1999, **18**, 4684.

4 Fp#–C_4–Fp# [Fp# = Fe(η^5-C_5Me_4Et)$(CO)_2$] and **1b**,**c** were prepared by Cu-catalyzed coupling between Fp*– or Fp#–C_4H and the appropriate metal chloride according to ref. 3(*b*).

5 Zwitterionic complexes formed by electron transfer through C_x bridges have been reported: S. B. Falloon, A. M. Arif and J. A. Gladysz, *Chem. Commun.*, 1997, 629.

6 Related structurally characterized μ–η^2:η^2-allene complexes: E. L. Hoel, G. B. Ansell and S. Leta, *Organometallics*, 1986, **5**, 585.

7 E. Sappa, A. Tiripicchio and P. Braunstein, *Chem. Rev.*, 1983, **83**, 203; P. R. Raithby and M. J. Rosales, *Adv. Inorg. Chem. Radiochem.*, 1985, **29**, 169.

8 R. J. Haines, in *Comprehensive Organometallic Chemistry II*, ed. E. W. Abel, F. G. A. Stone and G. Wilkinson, Pergamon, Oxford, 1995, vol. 7, ch. 11.2.3.

ChemComm

Unusual radical *ipso*-substitution reaction of an aromatic methoxy group induced by tris(trimethylsilyl)silane-AIBN or SmI_2

Tetsuaki Tanaka,* Ryutaro Wakayama, Shin-ichiro Maeda, Hidenori Mikamiyama, Naoyoshi Maezaki and Hiroaki Ohno

Graduate School of Pharmaceutical Sciences, Osaka University, 1-6 Yamadaoka, Suita, Osaka 565-0871, Japan. E-mail: t-tanaka@phs.osaka-u.ac.jp

Received (in Cambridge, UK) 10th May 2000, Accepted 6th June 2000
Published on the Web 26th June 2000

While conformationally favourable thiocarbamates bearing an aromatic methoxy group undergo intramolecular *ipso*-substitution of the methoxy group by treatment with tris(trimethylsilyl)silane (TTMSS) and AIBN, either conformationally flexible or favourable ketones easily cyclise into a five- or six-membered rings by treatment with SmI_2.

Radical cyclisation is one of the most useful methodologies for formation of a wide variety of carbon skeletons.[1] Particularly, the intramolecular reaction of the radical with an aryl group would provide an efficient synthetic route for constructing polycyclic systems containing an aromatic ring. During the course of our program directed toward the synthesis of macrocarpals,[2] we observed an unusual *ipso*-substitution of an aromatic methoxy group by treatment of the thiocarbamate **1** with TTMSS[3] and AIBN, yielding a cyclised product **2** (Scheme 1). A search of the literature revealed that there is no report describing the successful radical aromatic *ipso*-substitution of a methoxy group.[4] Accordingly, we undertook an investigation to identify the essential factor for the progress of this unusual cyclisation.[5]

First, we prepared racemic thiocarbamates **3**–**6** bearing the substituted phenyl group, and exposed them to the radical cyclisation conditions described above. As shown in Scheme 2,

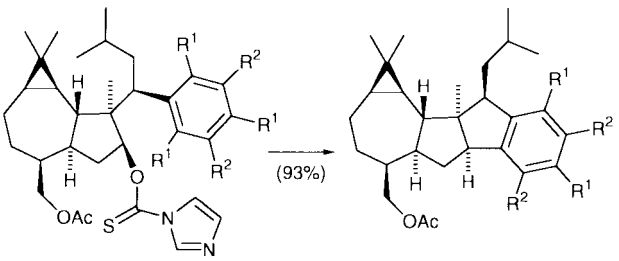

Scheme 1

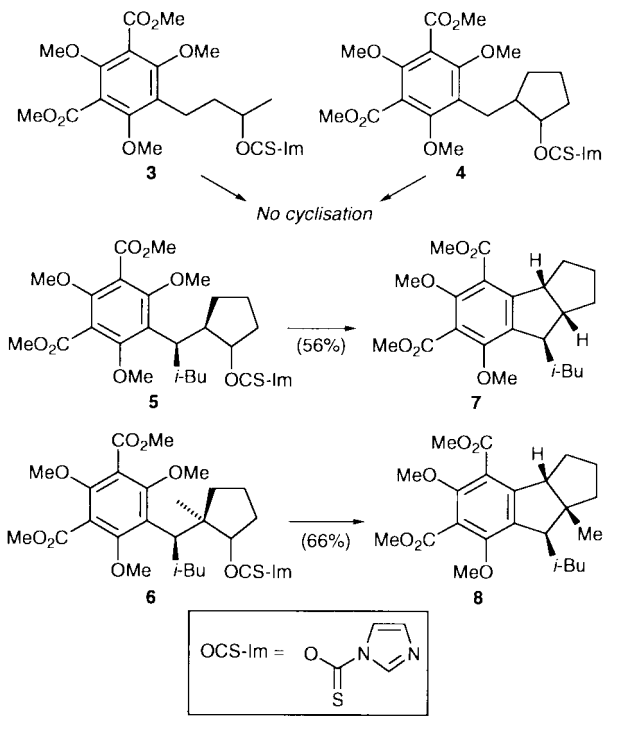

Scheme 2

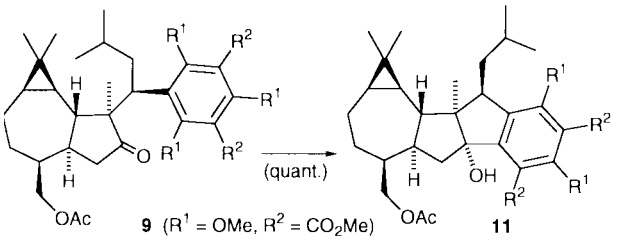

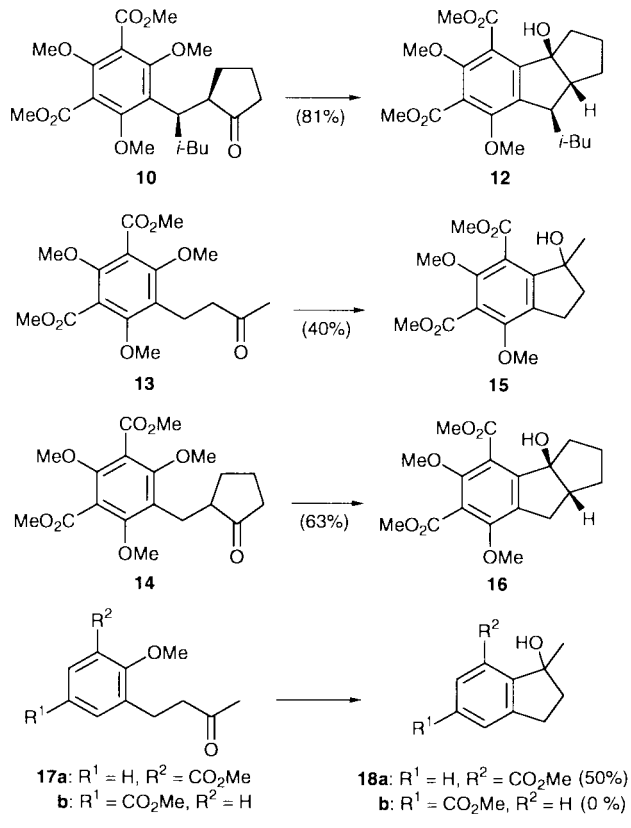

Scheme 3

DOI: 10.1039/b003742g

we observed no cyclisation by treatment of **3** or **4** with TTMSS–AIBN. However, conformationally more restricted thiocarbamates **5** and **6** gave the desired cyclised products **7** and **8**, respectively. In sharp contrast, the respective epimers of **5** and **6** at the benzylic position led to undesired reduction (deoxygenation or removal of thiocarbamate) under identical reaction conditions.

Based on these results, it is apparent that TTMSS-induced *ipso*-substitution is highly dependent on the steric nature of the starting thiocarbamates. Although the ground state and the reactive conformer are not necessarily the same, the conformation of radical intermediates, because of their low activation energy, is understood to have a significant effect on the course of the reaction. According to calculations,[6] the location of the alkyl radical generated from **5** and **6** is close to the reaction site (3.46 and 3.49 Å, respectively) in the most stable conformer.

This novel cyclisation is expected to be applicable to a wide range of substrates if the distance between the radical and aryl methoxy group could be shortened in some way. We then turned our attention to the strong chelating ability of samarium.[7] Since no information was available as to whether the aromatic methoxy group could be appropriately replaced by a ketyl radical, we initially explored SmI_2-induced cyclisation of the conformationally favoured ketones **9** and **10**. As shown in Scheme 3, these ketones were treated with 3.5 equivalents of SmI_2 in THF at room temperature, affording cyclised products **11** and **12**, respectively. Next, it was found that sterically more flexible ketones **13** and **14** could also be cyclised into **15** and **16** by exposure to SmI_2, as we expected. It should be clearly noted that in the TTMSS-induced reaction, we could obtain no cyclised products using the thiocarbamates **3** or **4** derived from the ketones **13** and **14** (Scheme 2). Interestingly, while **17a** gave the cyclised product **18a** in 50% yield, the ketone **17b** led to recovery of the unchanged starting material (64%) along with isolation of a small amount of the alcohol as a reduction product (22%).

Based on these observations, we propose the mechanism of chelation-induced cyclisation, as shown in Fig. 1. The ketyl radical intermediate **A**, generated by the reaction of the ketone **17a** with SmI_2, would be folded like **B** by the chelation of Sm(III) with the oxygen of both the methoxy and the ester group. Such chelation might attract the ketyl radical close to the reaction site, which enables the ketyl radical to attack the aromatic carbon. The resulting dienyl radical **C** was then reduced to the anionic species **D** by single electron transfer by SmI_2, followed by elimination of methoxide and hydrolysis to give **18a**.

In conclusion, we have developed a novel cyclisation reaction by radical *ipso*-substitution of an aromatic methoxy group. While TTMSS-induced cyclisation is highly dependent on the structure of the starting materials, SmI_2-mediated cyclisation was found to be applicable to conformationally flexible substrates. The scope and limitation of this novel cyclisation, and application to the synthesis of natural products are now being investigated in this laboratory.

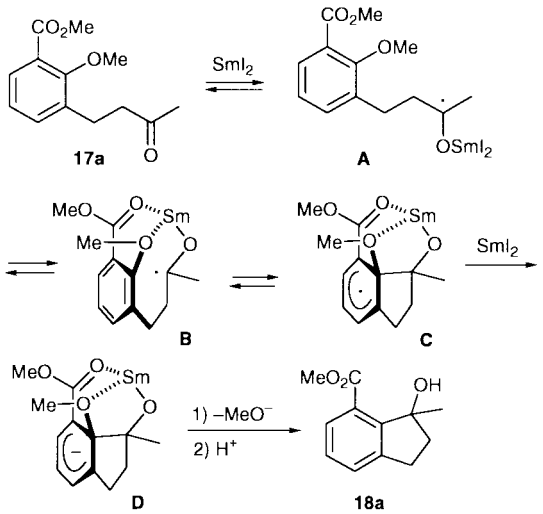

Fig. 1

This work was supported by a Grant-in-Aid for Scientific Research from the Ministry of Education, Sports, and Culture, Japan, for which the author's thanks are due.

Notes and references

1 B. Giese, in *Organic Chemistry Series, Vol. 5, Radicals in Organic Synthesis: Formation of Carbon–Carbon Bonds*, ed. J. E. Baldwin, Pergamon, Oxford, 1986, pp. 141–266; D. P. Curran, in *Comprehensive Organic Synthesis, Vol. 4*, ed. B. M. Trost and I. Fleming, Pergamon, Oxford, 1991, pp. 779; P. A. Baguley and J. C. Walton, *Angew. Chem., Int. Ed. Engl.*, 1998, **37**, 3072; A. Krief and A.-M. Laval, *Chem. Rev.*, 1999, **99**, 745; W. R. Bowman, C. F. Bridge and P. Brookes, *J. Chem. Soc., Perkin Trans. 1*, 2000, 1.

2 T. Tanaka, H. Mikamiyama, K. Maeda, T. Ishida, Y. In and C. Iwata, *Chem. Commun.*, 1997, 2401; T. Tanaka, H. Mikamiyama, K. Maeda and C. Iwata, *J. Org. Chem.*, 1998, **63**, 9782.

3 M. Ballestri, C. Chatgilialoglu, K. B. Clark, D. Griller, B. Giese and B. Kopping, *J. Org. Chem.*, 1991, **56**, 678.

4 Demethoxylative C–C bond formation is known to occur in very limited cases, see: W. S. Lee, I.-Y. Jeong, M. Shiro, S. Sano and Y. Nagao, *Tetrahedron Lett.*, 1997, **38**, 611; R. Yanada, N. Negoro, M. Okaniwa, Y. Miwa, T. Taga, K. Yanada and T. Fujita, *Synlett*, 1999, 537; for C–O bond formation, see: K. Nowada, H. Sakuragi, K. Tokumaru and M. Yoshida, *Chem. Lett.*, 1976, 1243.

5 For related works, see: H.-G. Schmalz, S. Siegel and J. W. Bats, *Angew. Chem., Int. Ed. Engl.*, 1995, **34**, 2383; O. Hoffmann and H.-G. Schmalz, *Synlett*, 1998, 1426; C. U. Dinesh and H.-U. Reissig, *Angew. Chem., Int. Ed.*, 1999, **38**, 789; D. Crich and J.-T. Hwang, *J. Org. Chem.*, 1998, **63**, 2765; J. Boivin, M. Yousfi and S. Z. Zard, *Tetrahedron Lett.*, 1997, **38**, 5988; A. Citterio, R. Sebastiano, A. Maronati, R. Santi and F. Bergamini, *J. Chem. Soc., Chem. Commun.*, 1994, 1517.

6 MD and MO calculations were performed by SPARTAN (Ver. 5.1.1) using MM 2 method and PM 3 Hamiltonian.

7 P. Girard, J. L. Namy and H. B. Kagan, *J. Am. Chem. Soc.*, 1980, **102**, 2693; G. A. Molander, *Chem. Rev.*, 1992, **92**, 29; G. A. Molander and C. R. Harris, *Chem. Rev.*, 1996, **96**, 307; A. Krief and A.-M. Laval, *Chem. Rev.*, 1999, **99**, 745.

ChemComm

A new procedure for the synthesis of *C*-glycosides of nojirimycin

Laura Cipolla, Barbara La Ferla, Francesco Peri and Francesco Nicotra*

Department of Biotechnology and Biosciences, University of Milano-Bicocca, Piazza della Scienza 2, I-20126 Milano, Italy. E-mail: francesco.nicotra@unimib.it

Received (in Cambridge) 15th May 2000, Accepted 30th May 2000
Published on the Web 26th June 2000

Reaction with allylmagnesium bromide of *N*,2,3,4,6-penta-benzyl-D-glucopyranosylamine 2, obtained from tetrabenzylglucose and benzylamine, afforded stereoselectively the open chain amino alcohol 3, which was converted into the *C*-glycoside of nojirimycin 6 by full protection of the amino function by Fmoc, oxidation of the free hydroxy group, hydrolysis of the Fmoc group and final intramolecular reductive amination with $NaBH(OAc)_3$; compound 6 was also converted into methyl ketone 7, by manipulation of the allylic appendage.

Deoxynojirimycin (1,5-dideoxy-1,5-imino-D-glucitol, DNJ) is a sugar-like plant alkaloid with inhibitory activity of a variety of glucosidases.[1] In particular, the capacity of deoxynojirimycin to inhibit trimming glucosidase I and II, interfering in N-linked oligosaccharide processing,[2] makes this molecule particularly attractive as a potential drug. It is well established that many pathological processes such as viral infections[3] and adhesion of tumour metastasis to endothelial cells,[4] involve complex N-linked oligosaccharides. Furthermore, inhibitors of glucosidases can find application in regulation of carbohydrate metabolic disorders.[5] In view of current interest in anti-HIV activity, the synthesis of DNJ derivatives and their analogues, which can reduce replication and infectivity of HIV, has attracted particular attention. Homologues,[6] deoxygenated,[7] *N*-alkylated,[7,9] *O*-glycosylated[7] and other DNJ derivatives have been synthesised by chemical[8] and enzymatic[9] methods. Investigation of their activity led to the interesting observation that short lipophylic appendages, *e.g.* a butyl group, at the N atom, strongly enhance the biological response.[10]

We wanted to find an efficient method for the introduction of a lipophylic substituent at position 1 of protected DNJ instead of at the N atom, particularly one affording stereoselectively the α-derivative, since the trimming α-glucosidases are the most interesting enzymes to be inhibited. We identified the allyl group as the substituent of choice, since its transformation into other functional groups, and its exploitation in the synthesis of neoglycoconjugates and *C*-disaccharides is widely described.[11]

Protected α-1-allyl-1-deoxynojirimycin has already been synthesised[12] from glucose through the key intermediate 1-fluoro-1-deoxynojirimycin, using a complex multistep sequence. We herein report an efficient approach allowing the stereoselective synthesis of protected α-1-allyl-1-deoxynojirimycin in 6 steps and 36% overall yield, using tetrabenzylglucose (**1**) as commercially available starting material (Scheme 1). This requires first the introduction of the amino function, secondly of the allylic appendage and finally the cyclisation to the desired piperidine derivative. From a stereochemical point of view, the allylation reaction and the cyclization are crucial to the effectiveness of the synthesis, and must be highly stereoselective. The amino group was introduced by reaction of **1** with benzylamine in CH_2Cl_2, in the presence of 4 Å molecular sieves and 1 equiv. of toluene-*p*-sulfonic acid. The resulting glycosylamine **2** (80% yield) was then treated with allylmagnesium bromide (10 equiv., Et_2O), in order to introduce stereoselectively the allylic appendage. The Grignard reaction occurs at the imino function, in equilibrium with the glycosylamine, *via* a Cram-chelated intermediate, affording stereoselectively the *threo* isomer **3** (81% yield, 90% de).[13] The cyclisation of **3** to the 'allyl-α-*C*-glycoside' of **6**, was accomplished by oxidation followed by reductive amination,[14] which turned out to be troublesome. Oxidation of the free –OH group of **3** with PCC resulted in over-oxidation and partial degradation of the product.[15] Swern oxidation with DMSO–Ac_2O provided the desired ketone with concomitant acetylation of the amine, and failed when Ac_2O was replaced with P_2O_5 or oxalyl chloride. These results clearly suggested that the amino group must be fully protected in order to perform a successful oxidation, and then deprotected to afford the cyclic azasugar by reductive amination. Both the protection/deprotection and the reductive amination reactions were difficult. Different protecting groups and reducing agents were tested. In terms of yields and stereoselection, the best results were obtained as follows: **3** was protected as **4** (FmocCl, Na_2CO_3, dioxane–H_2O, 89% yield), oxidised with PCC (CH_2Cl_2, 4 Å molecular sieves, 90% yield) to ketone **5**, then the amino group of **5** was deprotected with piperidine in DMF. Reductive amination of the crude product with $Na(OAc)_3BH$ (AcOH, dry Na_2SO_4, 1,2-dichloroethane, −35 °C) afforded **6**,† the protected allyl-α-*C*-glycoside of nojirimycin, in 78% yield and 90% de.‡ As an example of manipulation of the allylic appendage, **6** was treated with catalytic Na_2PdCl_4 (0.3 equiv.) and $CuCl_2$ (1 equiv.) in DMF–THF–H_2O (8/5/1) affording **7**§ in 50% yield. Alternatively, the allylic appendage can undergo a 5-*exo* iodocyclization–debenzylation, involving the benzyloxy group in the γ position.[16] Treatment of **6** with NIS in THF, afforded stereoselectively the bicyclic compound **8**¶ (2′*R*, determined by NOE experiments, as the only detected isomer) in 42% yield. Deprotection of **6** by

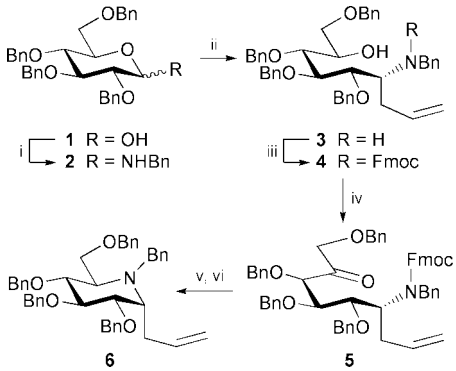

Scheme 1 *Reagents and conditions*: i, $PhCH_2NH_2$ 10 equiv., PTSA 1 equiv., CH_2Cl_2, 4 Å m.s., 80% yield, 5 days; ii, CH_2=$CHCH_2MgBr$ 10 equiv., dry Et_2O, 81% yield, 90% de; iii, FmocCl, dioxane–10% aq. Na_2CO_3, 89% yield; iv, PCC 3 equiv., CH_2Cl_2, 4 Å m.s., 90% yield; v, piperidine, DMF; vi, $NaHB(OAc)_3$, AcOH, dry Na_2SO_4, 1,2-dichloroethane, −35 °C, 78% yield, 90% de.

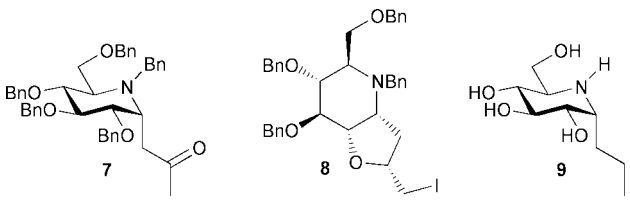

DOI: 10.1039/b003877f

hydrogenolysis [H_2, $Pd(OH)_2$, AcOH, AcOEt–EtOH 1:1] afforded **9**[12] in quantitative yield.

The procedure herein reported allows the synthesis of protected allyl-α-*C*-glycoside of nojirimycin through a highly stereoselective (80% de) and high yielding procedure (36%, 6 steps), from commercially available tetrabenzylglucose. The manipulation of the allylic appendage, widely reported in *C*-glycosides and to some extent also in iminosugars, allows the synthesis of a variety of functional groups and derivatives. The reported approach will be exploited in future projects devoted to the synthesis of imino-*C*-disaccharides.

We thank the Ministero dell'Università e della Ricerca Scientifica e Tecnologica (MURST) for financial support and Paolo Petroni for contributing to the experimental work.

Notes and references

† *Selected data* for **6**: oil, $[\alpha]_D$ + 21.4 (*c* 1, $CHCl_3$); δ_H(500 MHz, C_6D_6): 2.39 (dt, 1H, *J* 14.0, 8.1, H-1′a), 2.53 (dt, 1H, *J* 14.0, 5.8, H-1′b), 3.11 (ddd, 1H, *J* 9.5, 4.9, 2.1, H-5), 3.16 (dt, 1H, *J* 8.6, 5.4, H-1), 3.63 (dd, 1H, *J* 10.3, 2.1, H-6a), 3.75–3.83 (m, 2H, H-2, H-6b), 3.84–3.90 (m, 3H, PhC*H*N, H-3, H-4), 4.04 (d, 1H, *J* 14.0, PhC*H*N), 4.14, 4.20 (ABq, 2H, *J* 11.9, PhCH_2O), 4.34 (s, 2H, PhCH_2O), 4.65, 5.04 (ABq, 2H, *J* 11.4, PhCH_2O), 4.84, 5.03 (ABq, 2H, *J* 11.2, PhCH_2O), 4.98–5.13 (m, 2H, H-3′), 5.78–5.92 (m, 1H, H-2′), 7.00–7.41 (m, 25H, Ph-H); δ_C(75.43 MHz, $CDCl_3$, aromatic C omitted) 29.11 (t, C-1′), 52.95 (t, NCH_2Ph), 57.19 and 57.53 (2d, C-1 and C-5), 68.57 (t, C-6), 72.17, 72.90, 75.09 and 75.38 (4t, OCH_2Ph), 78.72, 79.31, 83.99 (3d, C-2, C-3, C-4), 115.30 (t, C-3′), 137.76 (d, C-2′). Anal. Calcd. for $C_{44}H_{47}NO_4$: C 80.82, H 7.25, N 2.14%; Found C 80.77, H 7.28, N 2.11%.

‡ Determined by ^{13}C NMR of the crude reduction product, in comparison with the spectrum of the epimer at C-5 (ref. 8).

§ *Selected data* for **7**: oil, $[\alpha]_D$ + 9.6 (*c* 1, $CHCl_3$); δ_H(300 MHz, C_6D_6): 1.76 (s, 3H, H-3′), 2.23 (dd, 1H, *J* 15.3, 5.0, H-1′a), 2.57 (dd, 1H, *J* 15.3, 7.1, H-1′b), 2.83–2.94 (m, 1H, H-5), 3.61 (dd, 1H, *J* 10.2, 1.6, H-6a), 3.64–3.82 (m, 5H, H-2, H-3, H-4, H-6b, PhC*H*N), 3.84–3.90 (m, 2H, H-1, PhC*H*N), 4.10, 4.15 (ABq, *J* 11.8, PhCH_2O), 4.24, 4.32 (ABq, *J* 11.8, PhCH_2O), 4.61, 5.02 (ABq, *J* 11.4, PhCH_2O), 4.84, 5.03 (ABq, *J* 11.2, PhCH_2O), 7.01–7.48 (m, 25H, Ph-H); Anal. Calcd. for $C_{44}H_{47}NO_5$: C 78.89, H 7.0, N 2.09%; Found C 78.92, H 7.08, N 2.06%.

¶ *Selected data* for **8**: yellow oil, $[\alpha]_D$ + 11 (*c* 0.65, $CHCl_3$); δ_H(300 MHz, $CDCl_3$): 1.66 (bq, 1H, *J* 11.0, H-1′a), 2.24 (ddd, 1H, *J* 11.0, 5.7, 5.7, H-1′b), 2.98–3.03 (m, 1H, H-5), 3.21 (dd, 1H, *J* 9.9, 6.8, H-3′a), 3.30 (dd, 1H, *J* 9.9, 4.8, H-3′b), 3.55 (dd, 1H, *J* 8.1, 5.1, H-4), 3.60–3.72 (m, 4 H, H-1, H-6a, H-6b, PhC*H*N), 3.86 (t, 1H, *J* 8.3. H-3), 3.90–3.97 (m, 2H, H-2′, PhC*H*N), 4.15 (t, 1H, *J* 8.3. H-2), 4.41 (s, 2H, PhCH_2O), 4.43, 4.61 (ABq, *J* 11.0, PhCH_2O), 4.78, 4.97 (ABq, *J* 11.4, PhCH_2O); δ_C(75.43 MHz, $CDCl_3$, aromatic C omitted) 9.92 (t, C-3′), 36.20 (t, C-1′), 59.34, 60.83 (2d, C-1 and C-5), 54.76 (t, NCH_2Ph), 67.02 (t, C-6), 72.84, 73.26 and 74.06 (3t, OCH_2Ph), 77.56, 80.00, 80.75 and 84.16 (4d, C-2, C-3, C-4 and C-2′); Calcd. for $C_{37}H_{40}INO_4$: C 64.44, H 5.85, I 18.40, N 2.03%; Found C 64.60, H 5.70, I 18.55, N 1.99%.

1 *Carbohydrate Analogues as Glycosidase Inhibitors—Nojirimycin and Beyond*, ed A. Stütz, VCH, Weinheim, 1998; S. V. Evans, L. E. Fellows, T. K. M. Shing and G. W. Fleet, *Phytochemistry*, 1985, **24**, 1953.
2 A. D. Elbein, *FASEB J.*, 1991, **5**, 3055.
3 R. A. Gruters, J. J. Neefjes, M. Tersmette, R. E. Y. De Goede, A. Tulp, H. G. Huisman, F. Miedema and H. L. Ploegh, *Nature*, 1987, **330**, 74.
4 See for example: R. J. Bernacki, M. J. Niedbala and W. Korytnyk, *Cancer Metastasis Rev.*, 1985, **4**, 81; R. Pili, J. Chang, R. A. Patris, R. A. Mueller, F. J. Chrest and A. Passaniti, *Cancer Res.*, 1995, **55**, 2920.
5 See for example: B. Junge, M. Matzke and J. Stoltefuss, *Handbook of Experimental Pharmacology*, 1996, **119**, 411.
6 G. C. Kite, L. E. Fellows, G. W. J. Fleet, P. S. Liu, A. M. Scofield and N. G. Smith, *Tetrahedron Lett.*, 1988, **29**, 6483; I. Bruce, G. W. Fleet, I. Cenci di Bello and B. Winchester, *Tetrahedron*, 1992, **48**, 183; K. E. Holt, F. J. Leeper and S. Handa, *J. Chem. Soc., Perkin Trans. I*, 1994, 231; C.-H. Wong, L. Provencher, J. A. Porco, Jr., S.-H. Jung, Y.-F. Wang, L. Chen, R. Wang and D. H. Steensma, *J. Org. Chem.*, 1995, **60**, 1492.
7 For a comprehensive review see: C. W. Ekhart, M. H. Fechter, P. Hadwiger, E. Mlaker, A. E. Stütz, A. Tauss and T. Wrodnigg in *Carbohydrate Analogues as Glycosidase Inhibitors—Nojirimycin and Beyond*, ed. A. Stütz, VCH, Weinheim, 1998, p. 254.
8 For a recent review of synthetic methods see: B. La Ferla and F. Nicotra in *Carbohydrate Analogues as Glycosidase Inhibitors—Nojirimycin and Beyond*, ed. A. Stütz, VCH, Weinheim, 1998, p. 68.
9 See for example: K. K.-C. Liu, T. Kajimoto, L. Chen, Z. Zhong, Y. Ichikawa and C.-H. Wong, *J. Org. Chem.*, 1991, **56**, 6280; T. Kajimoto, K. K.-C. Liu, R. L. Pederson, Z. Zhong, Y. Ichikawa, J. A. Porco, Jr. and C.-H. Wong, *J. Am. Chem. Soc.*, 1991, **113**, 6187.
10 See for example: A. Karpas, G. W. Fleet, R. A. Dwek, S. Petursson, S. K. Namgoong, N. G. Ramsden, G. S. Jacob and T. W. Rademacher, *Proc. Natl. Acad. Sci. USA*, 1988, **85**, 9229; A. Tan, L. van der Boek, S. van Boeckel, H. Ploegh and J. Bolscher, *J. Biol. Chem.*, 1991, **266**, 14 504; G. B. Karlsson, T. D. Butters, R. A. Dwek and F. M. Platt, *J. Biol. Chem.*, 1993, **268**, 570; F. M. Platt, G. R. Neises, R. A. Dwek and T. D. Butters, *J. Biol. Chem.*, 1994, **269**, 8362.
11 C. Bertozzi and M. Bednarski, *Carbohydr. Res.*, 1992, **223**, 243; K. H. Mortell, R. V. Weatherman and L. L. Kiessling, *J. Am. Chem. Soc.*, 1996, **118**, 2297; L. Lay, F. Nicotra, C. Pangrazio, L. Panza and G. Russo, *J. Chem. Soc., Perkin 1*, 1994, 333; F. Peri, L. Cipolla, B. La Ferla, P. Dumy and F. Nicotra, *Glycoconjugates J.*, 1999, **16**, 399; L. Cipolla, F. Nicotra, E. Vismara and M. Guerrini, *Tetrahedron*, 1997, **53**, 6163
12 T. Fuchss, H. Streicher and R. R. Schmidt, *Liebigs Ann. Rec.*, 1997, 1315.
13 L. Cipolla, L. Lay, F. Nicotra, C. Pangrazio and L. Panza, *Tetrahedron*, 1995, **51**, 4679.
14 H. S. Overkleeft, J. Van Wiltenburg and U. K. Pandit, *Tetrahedron*, 1994, **50**, 4215; R. Hoos, A. B. Naughton and A. Vasella, *Helv. Chim. Acta*, 1993, **76**, 2666.
15 L. Cipolla, F. Nicotra and C. Pangrazio, *Gazz. Chim. Ital.*, 1996, **126**, 663.
16 L. Cipolla, L. Lay and F. Nicotra, *J. Org. Chem.*, 1997, **62**, 6678.

Synthesis and ionic properties of nematic compounds bearing an ether-crown moiety: an NMR approach†

K. Leblanc,[a] P. Berdagué,[a] J. Rault,[b] J.-P. Bayle[a] and P. Judeinstein*[a]

[a] *R.M.N. en Milieu Orienté, ESA 8074, Bâtiment 410, Université Paris-Sud, 91405 Orsay, France. E-mail: pjudeins@icmo.u-psud.fr*

[b] *Laboratoire de Physique des Solides, LA 2, Bâtiment 510, Université Paris-Sud, 91405 Orsay, France*

Received (in Oxford, UK) 13th January 2000, Accepted 25th May 2000
Published on the Web 26th June 2000

Thermotropic ionic nematics with moderate transition temperatures are obtained by dissolving alkali metal salts within nematogens bearing a crown ether moiety; in these media, the ions show a significant 'apparent ionic order' as measured by quadrupolar NMR spectroscopy.

Functionalized liquid crystals, which show the ordered structures of solids and the mobility of liquids, provide a combination of very innovative properties for numerous applications.[1] It is with this intent that grafting of poly(ethylene oxide)[2–6] or crown ether moieties has been already researched.[6–10] These segments are intriguing because they can dissolve organic molecules and ionic compounds.[11] However, when these polar units are linked to nematogen cores, microsegregation occurs between the different segments and leads to highly ordered self-organized phases.[12] The nematic phase is most suitable for NMR studies owing to its easy orientation in the magnetic field.

In this work we show that liquid crystals CBS_n, CHA_n and CRA_6 containing lateral chains and terminal crown ethers display a nematic phase at moderate temperatures over a wide temperature range, even when significant amounts of salt are dissolved within the phase. The cation binding ability of these new nematogens was analysed by thermal analysis and NMR studies. The three series of compounds were synthesized following standard steps which have already been reported.[4,13]

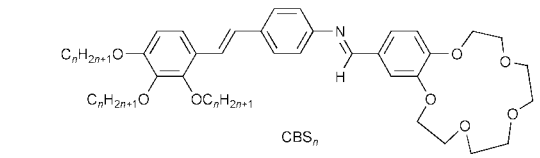

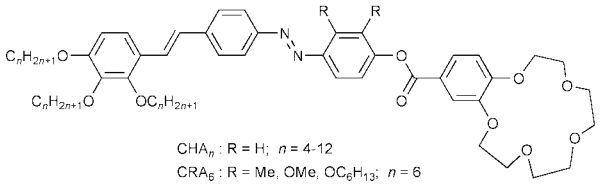

The transition temperatures of the compounds CBS_n and CHA_n are plotted in Fig. 1. The CBS_n compounds show monotropic behaviour while all compounds in the CHA_n and CRA_6 families show an enantiotropic nematophase over a wide temperature range. As expected, the mesogenic behaviour is very sensitive to the properties of the rigid core. The CBS_n series is based on three conjugated aromatic units. The balance between the mobility induced by the three alkoxy chains, the rigidity of the conjugated core and the relative rigidity of the crown ether leads to compounds presenting monotropic behaviour with a large temperature difference between the melting and the isotropic–nematic transitions.[13] Lenghtening of the rigid core in the CHA_n series leads to the formation of enantiotropic nematophases at fairly high temperatures relative to the CBS_n series.

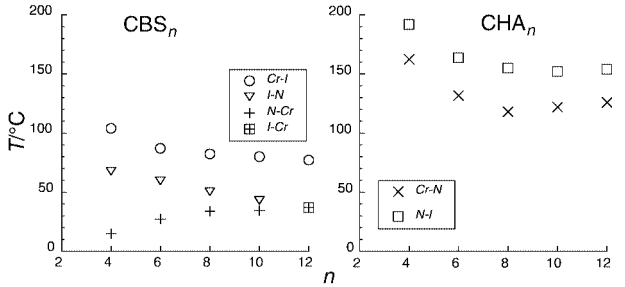

Fig. 1 Nematic range for CBS_n and CHA_n; transition temperatures measured by DSC (10 °C min^{-1}) (Cr: crystalline, N: nematic, I: isotropic).

To our knowledge, molecules of the CHA_n series are the first nematogens containing a crown ether moiety which show a large liquid crystalline range and reasonably low transition temperatures. This can be explained by the presence of three alkyl chains which increases the fraction of the mobile components which perturb the molecular cooperative packing by decreasing the segregation between aromatic, polyether and aliphatic fragments.[13] This effect has been also observed in polycatenar compounds.[14] In order to decrease the transition temperatures we have introduced lateral substituents. The liquid-crystalline properties of the CRA_6 compounds are listed in Table 1. As expected, the presence of lateral substituents substantially decreases the transition temperatures.

Crown ether derivatives are widely studied for their ability to dissolve salts by complexing cations leading to 'host–guest' entities.[11] Consequently, Li^+ and Na^+ salts were introduced inside the CHA_4 compound. Measured quantities of salt and nematogen were dissolved in $CHCl_3$–THF and heated for 1 h. Then the solvents were removed *in vacuo* and further dried (0.1 mm Hg, 70 °C, 3 h). The mixtures were then studied by DSC and polarizing microscopy. The phase diagrams are shown in Fig. 2 as a function of the molar ratio x (x = cation/crown ether moiety). CHA_4 mixed with $LiBF_4$ or $NaCF_3SO_3$ behave similarly with a nematic phase observed for x up to 0.5, and a more ordered smectic phase for higher values of x.

This molecule shows an unexpected nematic phase for a wide range of x, whereas molecules described elsewhere in the literature always show very ordered phases, even for low values of x. These ordered phases are generally explained by the

Table 1 Nematic range for CRA_6 compounds

R		Cr		N		I	
H	131.7	•	163.9	•	158.8	•	65
Me	137.5	•	159.8	•	157.5	•	119
OMe	120.7	•	129.3	•	126.1	•	< 30
OC_6H_{13}	75.9	•	88.4	•	83.7	•	< 30

† Electronic supplementary information (ESI) available: synthesis of CBS_n and CRA_6. See http://www.rsc.org/suppdata/cc/b0/b000501k/

DOI: 10.1039/b000501k

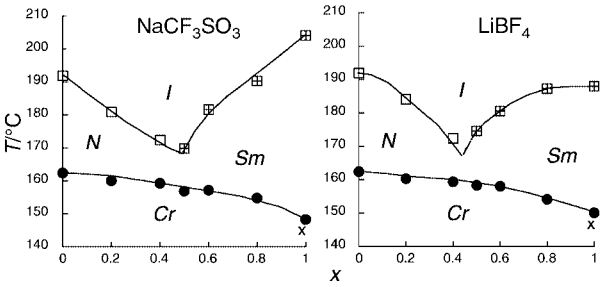

Fig. 2 Phase diagrams for CHA_4 alkali salt mixtures.

stacking of two molecules sharing one cation or by the segregation of the ionic motives in columnar mesostructures.[6] In these new systems, the observation of nematic phases over a large compositional range (x) can be explained by the three alkyl chains which prevent ionic interactions between cations, counter anions and molecules. The size of the crown cavity is larger than Li^+ but fits Na^+ ions well, while larger cations such as Cs^+ do not fit[11] and attempts to obtain mesogenic phases with this ion failed.

NMR of quadrupolar nuclei (*i.e.* with nuclear spin $I > \frac{1}{2}$) is a very sensitive method for probing the local anisotropy inside oriented media.[15] In isotropic solvents the averaged electric field gradient (*efg*) is zero and each non-equivalent nucleus gives a single line in the fast reorientation regime. In contrast, when ions are dissolved in anisotropic media, host–guest interactions may lead to the partial orientation of the dissolved entities and to a polarization of the electronic cloud, leading to a partially ordered *efg* of the cation which leads to $2I$ equally spaced lines. The existence of a quadrupolar splitting indicates that ions are effectively distorted and oriented inside anisotropic media. The measured quadrupolar splitting, $\Delta\nu_Q^{(ion)}$, represents the so-called 'apparent ionic order'.[16]

^7Li and ^{11}B ($I = \frac{3}{2}$) NMR spectra obtained for CRA_6 (R = Me) mixed with 0.2 equivalents of $LiBF_4$ [nematic range 136.6–152.4 °C (heating cycle) and down to 85 °C (cooling step)] are shown in Fig. 3. At 433 K, single lines are observed, thus showing the isotropy of the medium. Narrow linewidths were measured for both ions (*ca*. 20 Hz) which indicates their high mobility inside the fluid system. In the nematic state (400 K), triplets (intensities 3:4:3) were observed for both nuclei, indicating that both cations and anions experience the anisotropy of the media. The quadrupolar splittings, $\Delta\nu_Q^{(Li)}$ and $\Delta\nu_Q^{(B)}$ are ten times larger than those measured in swollen oriented DNA fibers[17] or lyotropic liquid crystals.[18] An enlargement of the ^{11}B central signal also indicates a quintet structure, which corresponds to the dipolar splitting $T_{B-F}^1 = 66$ Hz. An 'apparent ionic order' $S = 5 \times 10^{-3}$ was calculated for the anion inside these structures. This low value may be attributed to anisotropic tumbling and distortion of the anion from its initial T_d symmetry.[18]

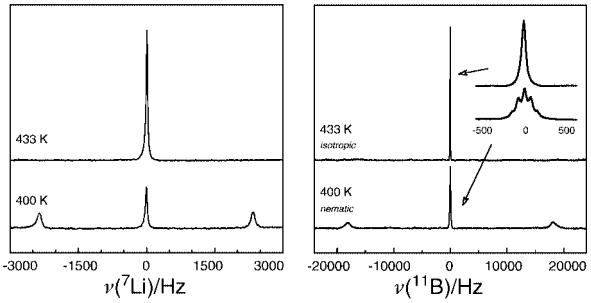

Fig. 3 ^7Li and ^{11}B NMR spectra of $LiBF_4$ (0.2 mol dm^{-3}) dissolved in $CMeA_6$, in the isotropic and nematic state. Spectra are shown to an absolute scale.

Further studies are in progress to understand the orientation inside these systems and to correlate these values with ion-crown complexation and ion-pairing.

Notes and references

1 B. Bahadur, in *Liquid Crystal—Applications and Uses*, World Scientific Publishing Co, Pte. Ltd., Singapore, vol. 1–3, 1990–1992.
2 M. Lee, N.-K. Oh and H. K. Lee, *J. Mater. Chem.*, 1996, **6**, 1079.
3 V. Percec, D. Tomazos, J. Heck, H. Blackwell and G. Ungar, *J. Chem. Soc., Perkin Trans. 2*, 1994, 31.
4 V. Rayssac, P. Judeinstein, J. P. Bayle, D. Kuwahara, H. Ogata and S. Miyajima, *Liq. Cryst.*, 1998, **25**, 427.
5 M. Kölbel, T. Beyersdorff, I. Sletvold, C. Tschierske, J. Kain and S. Diele, *Angew. Chem.*, 1999, **38**, 1077.
6 G. Johannson, V. Percec, G. Ungar and D. Abramic, *J. Chem. Soc., Perkin Trans. I*, 1994, 447.
7 V. Percec, G. Johannson, G. Ungar and J. Zhou, *J. Am. Chem. Soc.*, 1996, **118**, 9855.
8 G. X. He, F. Wada, K. Kikukawa, S. Shinkai and T. Matsuda, *J. Org. Chem.*, 1990, **55**, 541.
9 J. W. Goodby, G. H. Mehl, I. M. Saez, R. P. Tuffin, G. Mackenzie, R. Auzély-Velty, T. Benvegnu and D. Plusquellec, *Chem. Commun.*, 1998, 2057.
10 Qing Jiang, L. Z. Li, M. G. Xie and J. W. Ran, *Mol. Cryst. Liq. Cryst., Sect. A*, 1997, **302**, 323.
11 J. M. Lehn, *Supramolecular Chemistry*, Verlag, Weinheim, 1995.
12 C. Tschierske, *J. Mater. Chem.*, 1998, **8**, 1485.
13 P. Berdagué, M. Munier, P. Judeinstein, J. P. Bayle, C. S. Nagaraja and K. V. Ramanathan, *Liq. Cryst.*, 1999, **26**, 211.
14 H. T. Nguyen, C. Destrade and J. Malthête, *Adv. Mater.*, 1997, **9**, 375.
15 E. T. Samulski, *Polymer*, 1985, **26**, 177.
16 V. Dessolle, J. P. Bayle, J. Courtieu, J. Rault and P. Judeinstein, *J. Phys. Chem. B*, 1999, **103**, 2653.
17 J. Schultz, L. Nordenskiöld and A. Rupprecht, *Biopolymers*, 1992, **32**, 1631.
18 F. Fujiwara, L. W. Reeves and A. S. Tracey, *J. Am. Chem. Soc.*, 1974, **96**, 5250.

ChemComm

Novel synthesis of alkali and quaternary onium hydroxides *via* liquid anion exchange; an alternative concept for the manufacture of KOH and other hydroxide salts

Gadi Rothenberg,† Harold Wiener, Zohar Lavie and Yoel Sasson*

Casali Institute of Applied Chemistry, Hebrew University of Jerusalem, 91904, Israel. E-mail: ysasson@vms.huji.ac.il

Received (in Cambridge, UK) 19th April 2000, Accepted 7th June 2000
Published on the Web 26th June 2000

Alcohols enhance the extraction of a basic potential through a liquid membrane in the presence of quaternary ammonium salts, thus enabling preparation of caustic solutions without direct transport of hydroxide ions.

Production of potassium hydroxide (KOH) in the US in 1993 was 276 kilotons.[1] It is used principally in the manufacturing of K_2CO_3 and $KMnO_4$, and for the production of pesticides, fertilizers, soaps and detergents.[1] Quaternary onium hydroxides are mainly used as phase-transfer catalysts and as templating agents in the synthesis of molecular sieves.[2]

Currently, KOH is produced industrially by the electrolysis of KCl, using diaphragm cells, mercury cells, or ion-exchange membrane cells. Because of high energy costs and product impurities associated with diaphragm cells, most of the KOH is produced using ion-exchange membrane cells or mercury cells. Obviously, environmental awareness is a prime concern in KOH plants employing the latter protocol. Other electrolytic and electrodialytic methods are known for the preparation of MOH-type salts[3,4] and quaternary onium hydroxides[5] on a small and medium scale, but all of these alternatives are capital and energy intensive, with product cost very sensitive to plant size.

We have previously shown that quaternary ammonium hydroxides could also be produced on a laboratory scale in a batch solid-liquid extraction process.[6] However, since it was necessary to use a methanolic solution, no phase separation was obtained, leading to a complicated protocol which precluded large-scale applications.‡

It is well known that direct liquid/liquid extraction of hydroxide anions using onium salts is practically impossible.[7] However, we have now discovered[8] that contacting a weak organic acid ($pK_a > 16$; *e.g.* an alcohol) with a quaternary onium halide in a hydrophobic medium, creates a liquid membrane that can selectively extract and release a basic potential between two aqueous solutions. This enables the preparation of various hydroxide salts, in good yields and purities, without physically transferring hydroxide ions through the membrane. The process requires only simple extraction equipment and utilises NaOH, the cheapest and most widely available caustic source.

Our process is based on two extraction stages. First, a concentrated aqueous solution of NaOH is contacted with a hydrophobic solvent which contains a quaternary onium halide QX (X = Cl, Br, I) and a lypophilic alcohol, ROH. The differences in lipophilicity between the alkoxide ion, RO^-, and the halide, result in the formation of QOR in the organic phase, with concurrent extraction of the halide into the aqueous phase [eqns. (1) and (2)].

$$NaOH_{(aq)} + ROH_{(org)} \overset{K_1}{\rightleftharpoons} NaOR_{(int)} + H_2O_{(aq)} \quad (1)$$

$$NaOR_{(int)} + QX_{(org)} \overset{K_2}{\rightleftharpoons} NaX_{(aq)} + QOR_{(org)} \quad (2)$$

In the second stage, the phases are separated, and the organic phase is contacted with an aqueous solution of the appropriate alkali (or alkali-earth or quaternary onium) halide salt. The basicity potential is extracted into the aqueous phase as the QOR moiety reacts with the *water* and MX to form ROH and QX in the organic phase and MOH in the aqueous phase [eqn. (3)]. The organic phase is then recycled, with no further treatment, back to stage 1.

$$QOR_{(org)} + MX_{(aq)} + H_2O \overset{K_3}{\rightleftharpoons} QX_{(org)} + ROH_{(org)} + MOH_{(aq)} \quad (3)$$

Successive extractions increase OH^-/X^- ratios in the product solution after each pass, depending on the total equilibrium constant for the above reactions (*i.e.* the extraction

Table 1 Two-stage hydroxide extraction under various conditions[a]

Entry	Parameter changed	KOH formed (% per cycle)	Extractant capacity (% per cycle)[b]	NaOH used (% per cycle)
Alcohol				
1[c]	Hexan-1-ol	4.5	18.0	0.6
2[c]	Octan-2-ol	2.5	10.0	0.5
3[c]	Pentan-2-ol	2.5	10.0	0.5
Aliquat 336 concentration[d]				
4[e]	0.5 mol kg^{-1}	4.5	18.0	0.6
5[e]	1 mol kg^{-1}	7.7	15.0	1.5
6[e]	1.5 mol kg^{-1}	13.2	17.3	2.6
Alcohol				
7	Hexan-1-ol	7.7	15.0	1.5
8	Octan-2-ol	4.5	11.0	1.1
9	None	4.1	8.0	0.8
NaOH concentration				
10[d,e]	10 mol kg^{-1}	4.5	18.0	0.6
11[d,e]	10 mol kg^{-1}	4.6	18.0	0.7
12[e]	10 mol kg^{-1}	7.7	15.0	1.5
13[e]	12.5 mol kg^{-1}	8.5	17.0	1.4
Alcohol				
14[f]	Hexan-1-ol	8.5	17.0	1.4
15[f]	Octan-1-ol	8.6	17.0	1.4
16[f]	Pinacol	19.2	37.9	3.1
17[f]	Octanane-1,2-diol	16.4	33.0	2.6

[a] *Reaction conditions* (unless noted otherwise): 10 mol kg^{-1} NaOH; 2 mol kg^{-1} KCl; 1 mol kg^{-1} extracting agent in hexane. [b] Extracted hydroxide concentration relative to the theoretical hydroxide concentration that would have been obtained if the first extraction stage [eqns. (1) and (2)] was shifted completely to the right. [c] 0.5 mol kg^{-1} extracting agent. [d] Tricaprylmethylammonium chloride. [e] Hexan-1-ol used. [f] 12.5 mol kg^{-1} NaOH.

† Current address: York Green Chemistry Group, Chemistry Department, The University of York, Heslington, York, UK YO10 5DD. E-mail: gr8@york.ac.uk

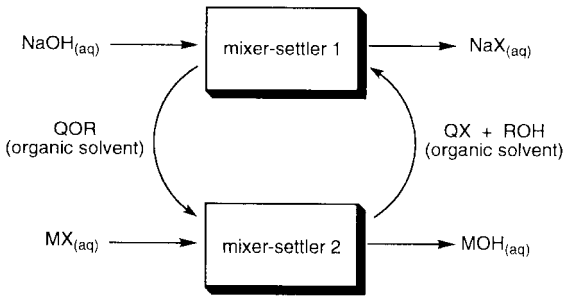

Scheme 1 Schematic representation of continuous MOH production.

is better for systems where K_1K_2 and K_3 are large). This can be explained by considering the selectivity constants§ of the various anions involved. Since the second extraction equilibrium is readily shifted to the right, the overall equilibrium constant ($K_1K_2K_3$) is determined by the selectivity constant of the alkoxide anion formed in the organic solvent. In the absence of the alcohol, the miniscule selectivity constants of the hydrophilic hydroxide anions lead to the relatively poor basicity extraction during the first extraction stage. However, the much higher selectivity constants of the alkoxide anions enhance the desired basicity extraction into the organic phase.[9,10]

The synthesis of KOH from KCl and NaOH, using different extracting agents, was chosen as a typical case study.¶ The results of extraction experiments under various conditions are summarized in Table 1. Repeated experiments showed that good yields of KOH were obtained from KCl using this method. 6–8 cycles were typically required to reach equilibrium. CsOH, LiOH and NMe_4OH, were similarly prepared from the corresponding chloride salts. Ammonium salt losses were typically $<2\%$ after 20 cycles, depending on solvent and concentration.

It can be seen that the extraction efficacy depends on the type of alcohol, in the order diols > primary alcohols > secondary alcohols. The high activity of diols may be attributed to possible formation of an intramolecular hydrogen-bonded complex.[10]

In conclusion, we present here a novel concept for the preparation of hydroxide salts, which is effected through a series of simple liquid anion exchange extractions. This concept may be conveniently adapted into a continuous process using mixer-settler techniques, as shown in Scheme 1, and may therefore constitute a practicable, cheap, and eco-friendly alternative to existing mercury-cell technologies.

Notes and references

‡ Lipophilic ammonium hydroxides (with at least two alkyl chains above C_8) may be obtained by extraction of hydroxide ions into an alcohol organic phase with lipophilic ammonium chlorides.[11] However, this method cannot be used for the manufacture of hydrophilic ammonium hydroxides.

§ For a given pair of anions Y^- and Z^-, the selectivity constant, $K^{sel}_{(Z/Y)}$ is defined as the equilibrium constant for the biphasic exchange reaction $QY_{(org)} + Z^-_{(aq)} \rightleftharpoons QZ_{(org)} + Y^-_{(aq)}$, *i.e.* $K^{sel}_{(Z/Y)} = \{[Y^-_{(aq)}][QZ_{(org)}]\}/\{[Z^-_{(aq)}][QY_{(org)}]\}$.[12]

¶ Representative experimental procedure: a source solution **A** was prepared by dissolving 50 g of NaOH in 50 g of water (50% w/w soln, 12.5 mol kg^{-1} NaOH). An extractant solution **B** was prepared by dissolving 40 g of Aliquat-336 and 12 g of pinacol in 48 g of hexane (1 mol kg^{-1} A-336 and pinacol). A destination solution **C** was prepared by dissolving 15 g of KCl in 85 g water (15% w/w soln, 2 mol kg^{-1} KCl). Solutions **A** and **B** were contacted at 25 °C, and, following phase separation, the organic (lighter) phase **B** was contacted with solution **C** at 25 °C. The phases were separated and solution **C** was analyzed for Cl^- and OH^- content by volumetric titration (HNO_3 0.01 mol kg^{-1} for titrating OH^- ions, using phenolphthalein as indicator; $AgNO_3$ 0.05 M for titrating chloride ions, using K_2CrO_4 as indicator). After the first cycle, the KCl solution contained 20 mol% KOH. The process was repeated until analysis of the chloride content of solution **C** showed that an equilibrium was reached (*ca.* 80 mol% KOH after eight cycles). Evaporation and filtration of the destination solution **C** precipitated the remaining KCl to yield up to >98% pure KOH soln.[13]

1 M. B. Freilich and R. L. Petersen, in *Kirk–Othmer Encyclopaedia of Chemical Technology*, ed. J. I. Kroschwitz and M. Howe-Grant, Wiley-Interscience, New York, 4th edn., 1996, vol. 19, pp. 1083–1084.
2 A. Tuel, Y. Ben Taârit and C. Naccache, *Zeolites*, 1993, **13**, 454.
3 T. A. Sedneva, I. P. Tyulyunov, I. A. Fedina, V. A. Masloboev, E. P. Lokshin and N. B. Voskobojnikov, *RU Pat.*, 2070426, 1996 (*Chem. Abstr.*, 1997, 127:52985).
4 P. M. Brown, *US Pat.*, 4036713, 1976 to Foote Mineral Co., 1976.
5 F. Buonomo, G. Bellussi and B. Notari, *Eur. Pat.*, 127201, 1984 (*Chem. Abstr.*, 1985, 102:102490).
6 L. Toib, S. Dermaik, M. Michman and Y. Sasson, *Synlett*, 1995, 245.
7 C. M. Starks, C. L. Liotta and M. Halpern, *Phase Transfer Catalysis*, Chapman and Hall, New York, 1994.
8 G. Rothenberg, H. Wiener, Y. Sasson and Z. Lavie, *Isr. Pat. Appl.*, 133622 (December 20, 1999).
9 B. R. Agarwal and R. M. Diamond, *J. Phys. Chem.*, 1963, **67**, 2785.
10 E. V. Dehmlow, R. Thieser, Y. Sasson and E. Pross, *Tetrahedron*, 1985, **41**, 2927.
11 L. E. Walker, *US Pat.*, 5559155, 1996.
12 J. E. Gordon and R. E. Kutina, *J. Am. Chem. Soc.*, 1977, **99**, 3903; J. de la Zerda and Y. Sasson, *J. Chem. Soc., Perkin Trans. 2*, 1987, 1147.
13 G. Åkerlöf and O. Short, *J. Am. Chem. Soc.*, 1937, **59**, 1912; W. J. Moore, *Physical Chemistry*, Prentice-Hall, Englewood Cliffs, 4th edn., 1962, pp. 157–158.

ChemComm

Acylation of activated aromatics without added acid catalyst

James S. Brown, Roger Gläser, Charles L. Liotta and Charles A. Eckert*

Schools of Chemical Engineering, Chemistry and Biochemistry, and Specialty Separations Center, Georgia Institute of Technology, Atlanta, GA 30332-0100, USA. E-mail: cae@che.gatech.edu

Received (in Covallis, OR, USA) 24th February 2000, Accepted 15th May 2000
Published on the Web 26th June 2000

Phenol and resorcinol can be acetylated to the corresponding esters and ketones in aqueous and neat acetic acid at high temperature (250–300 °C) to substantial equilibrium conversion without any added acid catalyst.

Friedel–Crafts and other acylations generally require stoichiometric quantities of strong mineral acids, such as H_2SO_4, H_3PO_4, and HCl, or nonregenerable Lewis acids, such as $AlCl_3$.[1] These acids require neutralization and disposal, and disposal costs can be considerable. The conventional acylation of one mol of phenol with acetic acid consumes stoichiometric quantities of $AlCl_3$. Neutralizing this $AlCl_3$ requires land-filling several pounds of $Al(OH)_3$ salt for every pound of product produced.[2,3] In addition, many of these reactions require polar organic solvents, such as methylene chloride, that can simultaneously dissolve the reactants as well as the reactant–catalyst complex.[1,3]

Aromatic acylations have also been performed successfully without salt production over solid acids, such as zeolites,[4] as well as polymer supported alkyl sulfonic acid.[5] Heterogeneous catalysis of this type, however, generally requires the operating expense of vaporizing the reactant and the increased capital cost of the large vessels needed for solid–vapor contacting. In addition, the need for periodic regeneration or replacement of the rapidly deactivating zeolite catalysts may preclude their use in commercial applications where reactants readily form coke. Ghibaudi and Colassi attempted the Fries rearrangement of phenyl acetate at low pressure and very high temperatures (T > 675 °C) without catalyst, but only phenol and ketene were detected as products.[6] Photo-Fries rearrangements of phenyl acetate[7] and 2,5-dimethylphenyl acetate[8] have been run successfully to produce the corresponding ketones.

Another alternative to acid catalysts that require neutralization and disposal are polar-protic solvents at elevated temperature that can simultaneously act as the solvent, catalyst, and, in certain cases, the reactant. Liquid water (T_c = 374 °C) in the nearcritical region (250–300 °C) exhibits some beneficial properties that make it a good solvent and catalyst for acid-catalyzed organic reactions. As the temperature is increased from room temperature to 275 °C, the dieletric constant decreases from 80 to 20, and nearcritical water readily dissolves both organic and ionic compounds. Even non-polar organics, such as toluene, become miscible above 300 °C.[9–10] In addition, the dissociation constant of water increases by three orders of magnitude from room temperature to 275 °C, making it a source of hydronium and hydroxide ions that may catalyze reactions. Nearcritical water has been used as a solvent, catalyst, and reactant for a number of hydrolyses that require added mineral acid at ambient conditions.[9,12–15] It has also been successfully used for the Friedel–Crafts alkylation of phenol and *p*-cresol with *tert*-butyl alcohol.[16]

Nearcritical acetic acid (T_c = 319 °C) is another polar, protic solvent that may simulatenously act as the solvent, catalyst, and reactant in some reactions. Similar to nearcritical water, nearcritical acetic acid readily dissolves organics, and it has a higher acid strength and dissociation constant than water. Acetic acid can also be distilled from reaction products unlike other Lewis acid catalysts, such as $AlCl_3$, that require neutralization to salts and subsequent disposal.

We have successfully acetylated phenol and resorcinol in nearcritical water, as well as in neat acetic acid, in the temperature range 250–300 °C without any added acid catalyst or UV light. Performing Friedel–Crafts acylations and Fries-rearrangements in neat or aqueous acetic acid at elevated temperatures is also attractive as no additional organic solvent is required, and any unused acetic acid may be recycled for further reaction.

The reactions were performed in 3.2 ± 0.2 ml titanium batch vessels as described elsewhere.[16] Each vessel was loaded with phenol or resorcinol, an excess of acetic acid (Aldrich, HPLC grade), and, in certain experiments, deoxygenated water (Aldrich, HPLC grade). For reactions in neat acetic acid, the molar ratio of reactant to acetic acid was 1:50. For reactions in aqueous acetic acid, the molar ratio of reactant to acetic acid to water was 1 : 12 : 47, respectively. Products were identified by GC–MS (EI mode) and by comparison of the GC retention times and EI mass spectra to those of commercially available compounds. The composition of the each product mixture was quantified by GC-FID.

The Friedel–Crafts alkylations of phenol and *p*-cresol with *tert*-butyl alcohol in nearcritical water previously reported[16,17] were found to be reversible, with equilibrium yields of *ca.* 20 mol%. In this work, we report that the acetylations of phenol and resorcinol are also reversible at high temperature in the presence of water, but with less favorable equilibrium yields. These acylations are generally irreversible with traditional Friedel–Crafts catalysts due to the complexation of the acid catalyst with the carbonyl oxygen of the product. In this work, however, products were not stabilized by complexation with catalyst and were free to react back to starting material. In aqueous acetic acid at 290 °C, phenol was primarily converted to 2′-hydroxyacetophenone, 4′-hydroxyacetophenone, and phenyl acetate in roughly equal amounts, with a combined equilibrium yield of less than 1%. Under the same conditions, resorcinol was converted to primarily 2,4-dihydroxy-acetophenone (Scheme 1) with a modest equilibrium yield of 4%.

To determine the effect of water on the equilibrium limitation of these reactions, the stability of the products was checked in water at nearcritical conditions. The product of the forward reaction of resorcinol and acetic acid, 2,4-dihydroxyacetophenone, was placed in liquid water at 250 °C. The concentration

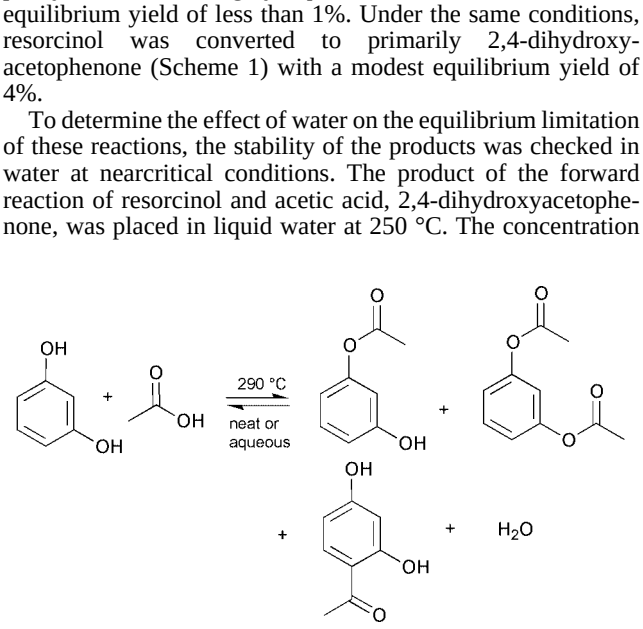

Scheme 1

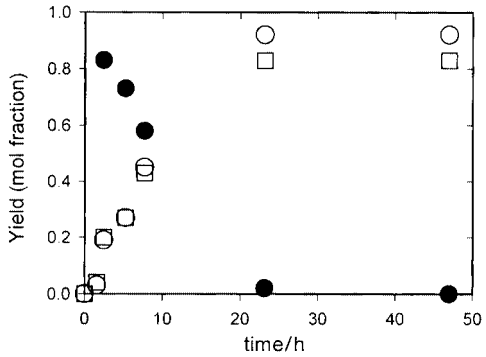

Fig. 1 Back reaction of 2,4-dihydroxyacetophenone (●) to resorcinol (□) and acetic acid (○) using water at 250 °C as solvent.

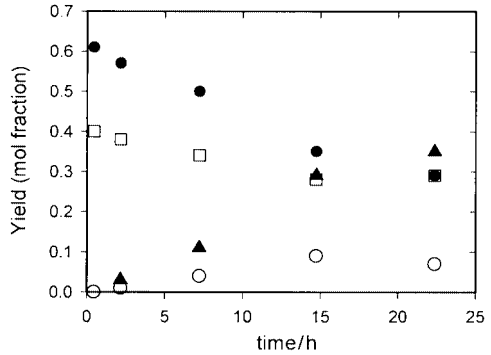

Fig. 2 Reaction of phenol (□) and acetic acid to phenyl acetate (●), 2′-hydroxyacetophenone + 4′-hydroxyacetophenone (○), and byproducts (▲) at 290 °C.

vs. time data of the almost complete conversion of 2,4-dihydroxyacetophenone back to the corresponding amounts of resorcinol and acetic acid are shown in Fig. 1. The products of the phenol acetylation, 2′-hydroxyacetophenone, 4′-hydroxyacetophenone, were also converted to phenol and acetic acid when high-temperature water was used as a solvent.

The tunable solvent properties of nearcritical water allow for the facile separation of products upon cooling, but excess water imposes too severe an equilibrium limitation on this reaction. To overcome the equilibrium limitation in the presence of excess water, the acetylations of phenol and resorcinol were run in neat acetic acid. Unlike water, acetic acid does not require elevated temperature to solubilize organics, so phenol was first refluxed in neat acetic acid for 24 h (*ca*. 117 °C). This resulted in an equilibrium conversion of 16% entirely to phenyl acetate with no detectable quantities of 2′-hydroxyacetophenone or 4′-hydroxyacetophenone. In neat acetic acid at 290 °C, however, phenol was converted to 2′-hydroxyacetophenone, 4′-hydroxyacetophenone, and phenyl acetate, with a combined equilibrium yield of 8 mol% (Fig. 2). Byproducts included 2-methyl chromone and 4-methyl coumarine. These same byproducts have been found in the Fries rearrangement of phenyl acetate over zeolites and are a result of the intramolecular reaction of 2-acetoxyacetophenone.[18] Under the same conditions, resorcinol was successfully converted to primarily 2,4-dihydroxyacetophenone, with an equilibrium yield of more than 50%, in less than 12 h. The yield of 2,4-dihydroxyacetophenone *vs*. time is shown in Fig. 3.

Although no water was added initially, the reactions in neat acetic acid remain equilibrium limited. In contrast to the Fries rearrangement of phenyl acetate, however, water is produced from the reaction of acetic acid and phenol or resorcinol. This implies that the water produced by the forward reactions in neat acetic acid may also promote the reverse reaction to phenol or

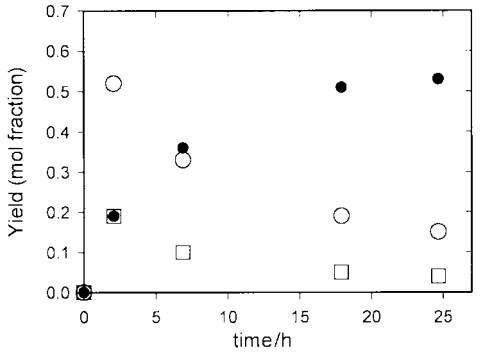

Fig. 3 Reaction of resorcinol and acetic acid to 2,4-dihydroxyacetophenone (●), resorcinol monoacetate (○), and resorcinol diacetate (□) at 290 °C.

resorcinol and acetic acid. The production of water could be avoided by starting the reaction with the corresponding monoesters of phenol and resorcinol.

In summary, Friedel–Crafts acylations of activated aromatic compounds can be run homogeneously at high temperature in nearcritical water without added Lewis acid catalysts, which have an undesirable environmental impact. While nearcritical water allows for subsequent separation of products upon cooling, it limits the reaction equilibrium yield of desired products when present in excess. Running the same reaction in neat acetic acid allows for a ten-fold increase in yield, while still avoiding the unwanted salt byproducts associated with strong mineral and Lewis acid catalysts.

We are grateful for the financial support of Kosa, Celanese, the Environmental Protection Agency, the National Science Foundation, and the Deutsche Forschungsgemeinschaft. We would like to thank Carla Moopenn, Griffin Smith, and Lee Suber for their help collecting data.

Notes and references

1 G. A. Olah, *Friedel–Crafts and Related Reactions*, Interscience Publishers, New York, London, Sydney, 1964, vol. III, p. 1606.
2 P. J. Harrington and E. Lodewijk, *Org. Process Res. Dev.*, 1997, **1**, 72.
3 H.-J. Kabbe and A. Widdig, *Angew. Chem., Int. Ed. Engl.*, 1982, **21**, 247.
4 I. Neves, F. Jayat, P. Magnoux, G. Perot, F. R. Ribeiro, M. Gubelmann and M. Guisnet, *J. Mol. Catal.*, 1994, **93**, 169.
5 M. G. Hitzler, F. R. Smail, S. K. Ross and M. Poliakoff, *Chem. Commun.*, 1998, 359.
6 E. Ghibaudi and A. J. Colussi, *Int. J. Chem. Kinet.*, 1984, **16**, 1575.
7 H. Shizuka, T. Morita, Y. Mori and I. Tanaka, *Bull. Chem. Soc. Jpn.*, 1969, **42**, 1831.
8 R. Suau, G. Torres and M. Valpuesta, *Tetrahedron Lett.*, 1995, **36**, 1311.
9 F. E. Anderson and J. M. Prausnitz, *Fluid Phase Equilib.*, 1986, **32**, 63.
10 K. Chandler, B. Eason, C. L. Liotta and C. A. Eckert, *Ind. Eng. Chem. Res.*, 1998, **37**, 3515.
11 J. F. Connolly, *J. Chem. Eng. Data*, 1966, **11**, 13.
12 B. Kuhlmann, E. Arnett and M. Siskin, *J. Org. Chem.*, 1994, **59**, 3098.
13 D. Bröll, C. Kaul, A. Kramer, P. Krammer, T. Richter, M. Jung, H. Vogel and P. Zehner, *Angew. Chem., Int. Ed.*, 1999, **38**, 2998.
14 H. P. Lesutis, R. Glaeser, C. L. Liotta and C. A. Eckert, *Chem. Commun.*, 1999, **20**, 2063.
15 S. D. Iyer and M. T. Klein, *J. Supercrit. Fluids*, 1997, **10**, 191.
16 K. Chandler, F. Deng, A. K. Dillow, C. L. Liotta and C. A. Eckert, *Ind. Eng. Chem. Res.*, 1997, **36**, 5175.
17 K. Chandler, C. L. Liotta, C. A. Eckert and D. Schiraldi, *AIChE J.*, 1998, **44**, 2080.
18 Y. Pouilloux, N. S. Gnep, P. Magnoux and G. Perot, *J. Mol. Catal.*, 1987, **40**, 231.

ChemComm

An unusual three-dimensional porous framework complex $\{[Cu(en)_2][KCr(CN)_6]\}_\infty$ (en = ethylenediamine) from a template self-assembly reaction

Aihua Yuan,†[a] Jianzhong Zou,[b] Baolong Li,[a] Zhenggen Zha,[a] Chunying Duan,[a] Yongjian Liu,[a] Zheng Xu*[a] and Steven Keizer[c]

[a] *Coordination Chemistry Institute, State Key Laboratory of Coordination Chemistry, Nanjing University, Nanjing 210093, P.R. China. E-mail: sklc@netra.nju.edu.cn*
[b] *Department of Chemistry and Chemical Engineering, Southeast University, Nanjing 210096, P.R. China*
[c] *Department of Chemistry, University of Western Ontario, London, Ontario, Canada N6A 5B7*

Received (in Cambridge, UK) 10th April 2000, Accepted 26th May 2000

The crystal structure of $\{[Cu(en)_2][KCr(CN)_6]\}_\infty$ reveals a novel three-dimensional porous framework in which $[Cu(en)_2]^{2+}$ acts as a template and K^+ as a connecting unit.

For years, chemists have devoted their efforts and have dreamt about the ability to assemble compounds, by using building units and connecting units in similar way that a bricklayer would erect a building. With the development of crystallography and synthesis chemistry, the assembly of polymer compounds[1] on the basis of simply adding building units and connecting them, is now achievable. Recently, a successful example of this process was construction of cyano bridged complexes[2] in which the cyanometallate anion behaves as the bridging moiety to build a multidimensional structure with a second coordination center and the resulting complexes demonstrated unique properties. These complexes are usually composed of a cyanometallate $[M(CN)_n]^{m-}$ (building unit), and a guest molecule and/or a complementary ligand. In general, the choice of the cyanometallate is limited, since the geometry of the complexes are restricted to, *e.g.* linear as in $[Ag(CN)_2]^-$,[2a] trigonal as in $[Cu(CN)_3]^{2-}$,[3] tetrahedral as in, $[Cd(CN)_4]^{2-}$,[4] square planar as in $[Ni(CN)_4]^{2-}$,[5] and octahedral $[M(CN)_6]^{3-}$.[2b,c] The second coordination center, however, can be almost any metal ion in the Periodic Table. Usually, the transition metal ion is selected because of the existence of a σ–π feedback bond between the selected metal ion and the cyano group which enables production of more stable complexes. The guest ion is often associated with organic molecules or other ions,[4,5] such as H_2O, unidentate aliphatic amines, ambidentate α,ω-diaminoalkanes, aromatic amines, pyrazine or piperazine. These compounds are necessary to fill up the void space so stabilizing the crystal structure.

We have recently prepared and structurally characterized a new polymeric supramolecular compound $\{[Cu(en)_2][KCr(CN)_6]\}_n$ **1**[9] (en = ethylenediamine) through a one-step self-assembly reaction of the complex $[Cu(en)_2](ClO_4)_2$ and $KCr(CN)_6$ in aqueous solution. The compound assembles itself *via* hexacyanochromium $\{[Cr(CN)_6]^{3-}\}$ as the building unit, and potassium cations as the connecting units. The copper(II) complex $[Cu(en)_2]^{2+}$ acts as the template/guest molecule. This is also a novel example where the potassium ion acts as a connecting unit to form a three-dimensional porous framework with the $[Cr(CN)_6]^{3-}$ ion. It is uncommon that the complex ion $[Cu(en)_2]^{2+}$ acts both as a special template, whose size, shape and charge match that of the cavity in the host lattice, and as a guest which stabiizes the crystal lattice. In fact, without $[Cu(en)_2]^{2+}$, $K_3[Cr(CN)_6]$ cannot form a three dimensional porous structure.

The IR spectra of complex **1** shows two sharp ν_{CN} bands at 2124 and 2111 cm^{-1} which are at lower wavenumber than that of the bridging cyano group (2150 cm^{-1} for the linear Cr–CN–Ni moiety[2c]) or a non-bridging cyano group {2128 cm^{-1} for the complex $K_3[Cr(CN)_6]$[6]} and indicates that these two cyano groups are neither linear bridging linked to two transition metals (Cr^{3+}, Cu^{2+}), nor non-bridging. Indeed the cyano group coordinates to potassium ions, as has been established by crystallography.

The asymmetric unit of **1** consists of a $[Cr(CN)_6]^{3-}$ ion, a K^+ and a $[Cu(en)_2]^{2+}$ ion and the structure is shown in Fig. 1. The geometry of the Cr^{3+} ion is octahedral with coordination of six carbon atoms of the cyano groups. The Cr–C bond lengths are 2.065(3), 2.080(2) and 2.085(2) Å, similar to values found in $K_3[Cr(CN)_6]$ (2.057, 2.075, 2.100 Å)[7] and $PPh_4[Ni(pn)_2][Cr(CN)_6]\cdot H_2O$ (pn = 1,3-propanediamine) (2.062, 2.083 and 2.087 Å).[2c] The six nitrogen atoms of the cyano groups coordinate to a potassium cation. According to the bond lengths (K–N) and bond angles (C–N–K) the six cyano groups can be divided into two groups. The first group is found in linear Cr–C–N–K chains, with K–N distances of 2.846 and 2.766 Å, and C–N–K bond angles of 172.3 and 178.6°. The

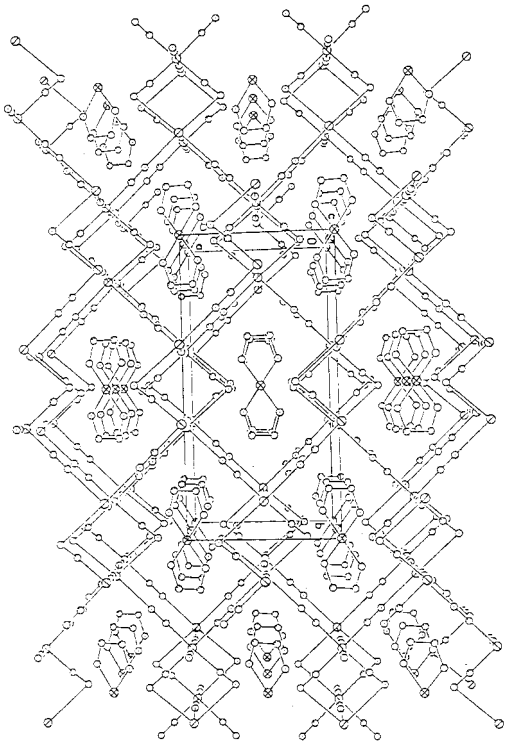

Fig. 1 Projection of the 3-D network structure of **1** in which the $[Cu(en)_2]^{2+}$ cations act as templates.

† Present address: Department of Welding and Material Engineering, East China Shipbuilding Institute, Zhengjiang 210093, P.R. China.

DOI: 10.1039/b002913k

second group comprises non-linear Cr–C–N–K chains with the CN group coordinating sideways,[8] with K–N distance of 3.229 Å, much longer than the linear bond distance. IR spectroscopy provides additional evidence with two ν_{CN} bands being observed with the intensity of the low wavenumber band at 2111 cm^{-1} being more intense than that of the high wavebumber band at 2124 cm^{-1}. The first band is due to the four σ bonded cyano groups linearly attached to a potassium cation while the second band results from the two cyano groups bonded sideways to potassium cations. This assignment is consistent with the molecular structure, in which four cyano groups donate their σ bonding electrons to the empty d^2sp^3 hybrid orbitals of the K^+ ions to form four σ-bonds which decreases the wavenumber, ν_{CN}. Another two cyano groups, which are part of the same hexacyanochromium ion, coordinate to K^+ ions sideways,[8] which owing to the orientation of the frontier orbitals, leads to poorer overlap. Consequently, the wavenumber of the cyano group is higher for the sideways coordination mode than for a linear σ bond.

The spontaneous assembly process of $Cu(en)_2(ClO_4)_2$ and $K_3[Cr(CN)_6]$ is a very specific one-step reaction. The $[Cu(en)_2]^{2+}$ ion acts both as a template and a guest while the structure of the host $\{[KCr(CN)_6]^{2-}\}_\infty$ is dependant upon the shape, size and charge of the guest ion. The cavity is very tight, and use of bulkier substituents $\{[Cu(nmen)_2]^{2+}$, $[Cu(dmen)_2]^{2+}$, $[Cu(tmen)_2]^{2+}$, $[Cu(pn)_2]^{2+}$; nmen = *N*-methylethylenediamine, dmen = *N*,*N*-dimethylethylenediamine, tmen = tetramethylethylenediamine, led to different types of complexes. In the self-assembly process of **1**, other than its shape, size and charge, the chemical properties of the $[Cu(en)_2]^{2+}$ ion is another important factor. Using $[Ni(en)_2]^{2+}$ (same symmetry) in place of $[Cu(en)_2]^{2+}$ ion, led to a different polymer complex $\{[Ni(en)_2]_3[Cr(CN)_6]\}_\infty$.

This work was supported by the National Nature Science Foundation of China for key project No. 29823001.

Notes and references

1 K. Biradha, D. Dennis, V. A. MacKinnon, C. Seward and M. J. Zaworotko, in *Current Challenges on Large Scale Supramolecular Assemblies*, NATO Advanced Research Workshop, ed. G. Tsoucaris, Kluwer Academic Publishers, Dordrecht, The Netherlands, 1999, pp. 115–132; B. F. Abrahams, S. R. Batten, M. J. Grannas, H. Hamit, B. F. Hoskins and R. Robson, *Angew. Chem., Int. Ed.*, 1999, **38**, 1475; P. J. Hagrman, D. Hagrman and J. Zubieta, *Angew. Chem., Int. Ed.*, 1999, **38**, 2638.

2 (*a*) G. A. Bowmaker, B. J. Kennedy and J. C. Reid, *Inorg. Chem.*, 1998, **37**, 3968; (*b*) M. Ohba, N. Usuki, N. Fukita and H. Okawa, *Angew. Chem., Int. Ed.*, 1999, **38**, 1795; (*c*) M. Ohba, N. Usuki, N. Fukita and H. Okawa, *Inorg. Chem.*, 1998, **37**, 3349.

3 D. J. Chesnut and J. Zubieta, *Chem. Commun.*, 1998, 1707.

4 T. Iwamoto, *Supramolecular Chemistry in Cyanometallate Systems*, in *Comprehensive Supramilecular Chemistry*, ed. D. D. MacNicol, F. Toda and R. Bishop, Pergamon, Oxford, 1996, vol. 6, ch. 19, pp. 643–690; T. Kitazawa, *Chem. Commun.*, 1999, 891.

5 D. W. Knoeppel and S. G. Shore, *Inorg. Chem.*, 1996, **35**, 1747; I. Muga, J. M. Gutierrez-Zorrilla, A. Luque, P. Roman and F. Lloret, *Inorg. Chem.*, 1997, **36**, 743.

6 L. H. Jones, *Inorg. Chem.*, 1963, **2**, 777.

7 S. Jagner, E. Ljungstrom and N.-G. Vannerberg, *Acta. Chem. Scand., Ser. A*, 1974, **28**, 623.

8 G.-C. Guo and T. C. W. Mak, *Angew. Chem., Int. Ed.*, 1998, **37**, 3183.

9 X-Ray crystallographic structure determination of **1**: all data were measured on a Siemens P4 four-circle diffractometer with monochromated Mo-Kα radiation (λ = 0.71073 Å) using the θ–2θ scan mode. The data were corrected for Lorentz and polarization effects during data reduction using XSCANS. The structure was solved by the direct method and refined on F^2 by full-matrix least-squares methods using SHELXTL Version 5.0. All non-hydrogen atoms were refined anisotropically. All hydrogen atoms were placed in calculated positions (C–H 0.96 Å, N–H 0.90 Å) assigned fixed isotropic thermal parameters at 1.2 times the equivalent isotropic *U* of the atoms to which they are attached and allowed to ride on their respective parent atoms. The contributions of these hydrogen atoms were included in the structure factor calculations. All computations were carried out on a PC-586 computer using the SHELXTL-PC program package. Analytical anomalous dispersion corrections were incorporated. *Crystal data*: $C_{10}H_{16}CrCuKN_{10}$, M = 430.97, monoclinic, space group $C2/c$, a = 8.5237(12), b = 17.014(3), c = 12.103(2) Å, β = 98.70(2)°, V = 1735.0(5) Å^3, Z = 4, D_c = 1.650 g cm^{-3}, 4.70 < θ < 60.00°, crystal size 0.6 × 0.6 × 0.1 mm; 2540 unique reflections and 108 variables converged to $R1$ = 0.0505, $wR2$ = 0.1492. CCDC 182/1670. See http://www.rsc.org/suppdata/cc/b0/b002913k/ for crystallographic files in .cif format.

Synthesis and structures of half-sandwich W(VI) tri(selenido) and W(II) selenolato complexes

Hiroyuki Kawaguchi[a] and Kazuyuki Tatsumi*[b]

[a] *Coordination Chemistry Laboratories, Institute for Molecular Science, Myodaiji, Okazaki 444-8595, Japan*
[b] *Research Center for Materials Science, Nagoya University, Furo-cho, Chikusa-ku, Nagoya 464-8602, Japan. E-mail: i45100a@nucc.cc.nagoya-u.ac.jp*

Received (in Cambridge, UK) 25th April 2000, Accepted 5th June 2000

The reaction of Cp^*WCl_4 with $LiSeBu^t$ in THF in the presence of Bu^tNC gave rise to $Cp^*W(SeBu^t)(CNBu^t)_3$ 3, while treatment of the $Cp^*WCl_4/LiSeBu^t$ reaction mixture with Li_2Se_2 followed by cation exchange with PPh_4Br in MeCN afforded $(PPh_4)[Cp^*WSe_3]$ 1.

The chemistry of terminal selenido complexes is much less developed than that of the familiar metal oxides and sulfides.[1] This is mainly because many of the traditional reagents used in metal oxo and sulfido chemistry are not simply transferable to their selenido congeners.[2] In the course of our studies of group 6 transition metal chalcogenido chemistry, we previously isolated the half-sandwich tri(sulfido) complexes $[Cp^*MS_3]^-$ (M = Mo, W).[3,4] Carbon–sulfur bond rupture of thiolato complexes gives ready access to thiolato/sulfido derivatives and eventually $[Cp^*MS_3]^-$. Here we report the synthesis of $(PPh_4)[Cp^*WSe_3]$ **1** *via* C–Se bond cleavage.

For the selenolation reagent, the readily accessible $LiSeBu^t$ was employed, which is prepared by the reaction of $LiBu^t$ with 1 equiv. of selenium in THF at −78 °C. We have reported facile C–S bond cleavage of *tert*-butylthiolato complexes of group 5 and 6 metals,[3] and C–Se bond activation was expected to occur for the analogous selenolato complexes. Addition of 4 equiv. of $LiSeBu^t$ to Cp^*WCl_4 in THF at −78 °C gave a red solution. After stirring for 30 min, the solution turned brown, from which $Cp^*_2W_2Se_2(\mu\text{-}Se)_2$ **2** was obtained in 40% yield (Scheme 1). Spectral data show that **2** is a mixture of *syn*- and *anti*-isomers. In a separate experiment, a freshly prepared $Cp^*WCl_4/LiSeBu^t$ mixture was quickly transferred into a THF solution of Li_2Se_2 to give a dark red suspension. Cation exchange with PPh_4Br in MeCN provided the intriguing tri(selenido) complex **1** as dark red crystals in 23% yield concomitant with **2** (14%).† This synthetic route to **1** is reminiscent of the preparation of $[Cp^*MoS_3]^-$ by the reaction of $Cp^*MoS_2(SBu^t)$ with Li_2S_2 and supports the generation of the hypothetical $Cp^*WSe_2(SeBu^t)$ intermediate in the $Cp^*WCl_4/LiSeBu^t$ reaction.[3] While the reaction of Cp^*WCl_4 with $LiSBu^t$ afforded $Cp^*W(SBu^t)_3$, $Cp^*WS_2(SBu^t)$, and $Cp^*_2W_2S_2(\mu\text{–}S)_2$, all attempts to isolate the expected Se analogues, such as $Cp^*W(SeBu^t)_3$ and $Cp^*WSe_2(SeBu^t)$, have failed.

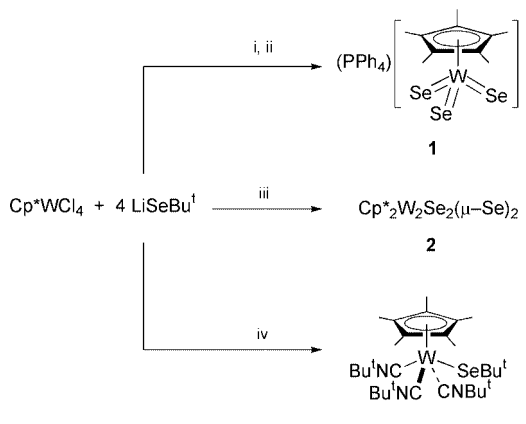

Scheme 1 *Reagents and conditions:* i, Li_2Se_2, THF; ii, PPh_4Br, MeCN; iii, 30 min, −78 °C, THF; iv, Bu^tNC, THF.

Fig. 1 shows the three-legged piano-stool structure of the anion of **1**.‡ The average W–Se distance of 2.322 Å in **1** is similar to that of $(PPh_4)_2[WSe_4]$ [2.314(1) Å].[5] The IR spectrum of **1** shows the W=Se stretching frequency at 284 cm^{-1} comparable to that of $[WSe_4]^{2-}$.[6] The ^{77}Se NMR signal (δ 1437) lies in the range of chemical shifts for terminal selenido ligands.[7] The UV–VIS spectra of **2** and its sulfur congener $(PPh_4)[Cp^*WS_3]$ are similar, showing a strong absorption at 437 and 377 nm, respectively, assignable to charge-transfer transitions from selenium and sulfur to the vacant d orbital of tungsten. The red shift on going from sulfide to selenide (0.45 eV) compares well with the difference in the first ionization potentials of S and Se.[8]

In another experiment, we carried out the $Cp^*WCl_4/LiSeBu^t$ reaction in the presence of Bu^tNC, from which $Cp^*W(SeBu^t)(CNBu^t)_3$ **3** was isolated as brown crystals in 41% yield (Scheme 1).§ The X–ray structure of **3**‡ shows the metal surrounded in a distorted trigonal-bipyramidal geometry wherein the Se and C(20) atoms occupy axial positions, if the Cp* ligand is viewed as a monodentate ligand (Fig. 1). While two of the three Bu^tNC ligands are nearly linear [C–N–C = 175.8(8), 164.3(7)°], the other contains essentially an sp^2–type N atom with a C(15)–N(1)–C(16) angle of 128.7(6)° amongst the smallest of known bent isocyanides (122–156°).[9] The presence of the bent isocyanide is ascribed to extensive π–back donation from the electron-rich W(II) metal ion to the isocyanide. The bent isocyanide also has a shorter W–C bond [1.984(7) Å] and a longer C_{ipso}–N bond [1.220(9) Å] relative to the corresponding values in two linear isocyanides (mean 2.032 and 1.151 Å). This structural feature is consistent with the two N–C stretching frequencies at 2038 and 1813 cm^{-1} observed in the IR spectrum. The W–Se distance of 2.6271(7) Å is comparable to that of $CpW(CO)_3(SeCH_2Ph)$ [2.623(1) Å].[10] On the other hand, the ^1H NMR spectrum of **3** in C_6D_6 at room temperature shows three singlets assignable to *tert*-butyl groups in an intensity ratio of 2:1:1, indicating that the complex is fluxional in solution. Previously, we reported the isolation of

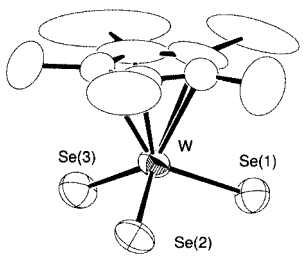

Fig. 1 Molecular structure of the anion of **1**. Selected bond lengths (Å) and angles (°): W–Se(1) 2.322(1), W–Se(2) 2.326(1), W–Se(3) 2.319(1); Se(1)–W–Se(2) 105.42(4), Se(1)–W–Se(3) 103.87(4), Se(2)–W–Se(3) 104.25(4).

DOI: 10.1039/b003303k

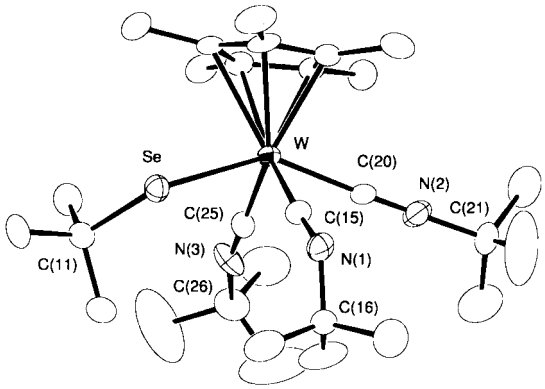

Fig. 2 Molecular structure of **3**. Selected bond lengths (Å) and angles (°): W–Se 2.6271(7), W–C(15) 1.984(7), W–C(20) 2.039(7), W–C25 2.025(8), Se–C(11) 2.019(8), N(1)–C(15) 1.220(9), N(2)–C(20) 1.148(9), N(3)–C(25) 1.153(9); Se–W–C(5) 82.9(2), Se–W–C(15) 73.3(2), Se–W–C(20) 140.7(2), Se–W–C(25) 88.9(2), C(15)–W–C(20) 73.6(3), C(15)–W–C(25) 103.9(3), C(20)–W–C(25) 79.1(3).

the W(IV) thiolato complex $Cp^*W(SBu^t)_3(CNBu^t)$ from the Cp^*WCl_4/LiS^tBu reaction in the presence of Bu^tNC.[4] The isolation of a W(II) selenolato complex, **3**, is in accord with the tendency of selenolato complexes to favor lower oxidation states.

Notes and references

† All manipulations were carried out under an atmosphere of argon using solvents purified by standard methods. A mixture of $LiSeBu^t$ (7.60 mmol) and Cp^*WCl_4 (0.86 g, 1.87 mmol) in THF (50 mL) was quickly added to a slurry of Li_2Se_2 (1.40 mmol) in THF (20 mL) at −78 °C. The solution was warmed up to room temperature and stirred for 2 h. After centrifugation, the solution was evaporated to dryness. The residue was dissolved in MeCN (30 mL) to give a dark red solution and a brown solid. A solution of PPh_4Br (0.47 g, 1.12 mmol) in MeCN (20 mL) was added to the dark red supernatant. Concentration and cooling to −20 °C afforded 0.38 g of **1** as dark red crystals in 23% yield. The brown solid which was insoluble in MeCN was recrystallized from toluene to provide **2** in 14% yield. Data for **1**: ^{1}H NMR (500 MHz, $CDCl_3$), δ 2.20 (s, 15H, Cp*), 7.6–8.0 (m, 20H, PPh_4). ^{77}Se NMR (95.3 MHz, $CDCl_3$, Me_2Se), δ 1437. IR ν/cm^{-1}: 284m (W=Se). UV–VIS (MeCN): λ_{max}/nm(ε/M^{-1} cm^{-1}) 299 (19000), 350 (sh), 437 (38000), 530 (sh). Anal. calc.: C, 45.61, H, 3.94. Found: C, 45.57; H, 3.98%. Data for **2**: ^{1}H NMR (500 MHz, $CDCl_3$), δ 2.27 (s, Cp*), 2.33 (s, Cp*). IR ν/cm^{-1}: 315m, 298m (W=Se). FAB-MS: 954 (M^+). Anal. calc.: C, 25.18; H, 3.17. Found: C, 25.01; H, 3.30%.

‡ *Crystal data*: for **1**: $C_{34}H_{35}Se_3PW$, M = 895.35, orthorhombic, space group *Pbca*, a = 18.284(5), b = 20.171(7), c = 17.758(5) Å, V = 6549(2) Å^3, Z = 8, T = 293 K, μ(Mo-Kα) = 69.37 cm^{-1}, Rigaku-AFC7R, 6360 measured reflections ($2\theta_{max}$ = 50°). The structure was solved by Patterson methods and refined by full-matrix least squares. At convergence, R = 0.057, R_w = 0.058, and GOF = 1.44 for 352 variables refined against 4341 unique reflections [$I > 1\sigma(I)$].

For **3**: $C_{29}H_{51}N_3SeW$, M = 704.55, monoclinic, space group $P2_1/n$, a = 9.7349(8), b = 18.9776(5), c = 17.4477(3) Å, β = 97.1791(7) °, V = 3198.1(2) Å^3, Z = 4, T = 173 K, μ(Mo-Kα) = 47.74 cm^{-1}, Rigaku-AFC7 equipped with a MSC/ADSC Quantum1 CCD detector, 20472 measured reflections ($2\theta_{max}$ = 55°). The structure was solved by Patterson methods and refined by full-matrix least squares (TEXSAN). At convergence, R = 0.077, R_w = 0.063, and GOF = 1.47 for 307 variables refined against all 7147 unique reflections.

CCDC 182/1672. See http://www.rsc.org/suppdata/cc/b0/b003303k/ for crystallographic files in .cif format.

§ Bu^tNC (1.0 mL, 8.8 mmol) was added to a mixture of Cp^*WCl_4 (0.46 g, 1.06 mmol) and $LiSeBu^t$ (4.24 mmol) in THF (30 mL) at −78 °C. The solution was warmed to room temperature and stirred for 0.5 h. The resulting brown solution was evaporated to dryness. The residue was crystallized from hexane to give **3** (0.31 g, 41%). ^{1}H NMR (400 MHz, C_6D_6), δ 1.36 (s, 18H, Bu^t), 1.44 (s, 9H, Bu^t), 1.86 (s, 9H, Bu^t), 1.93 (s, 15H, Cp*); IR ν/cm^{-1}, 2038s, 1813s. Anal. calc.: C, 49.44; H, 7.30; N, 5.96. Found: C, 49.07; H, 7.31; N, 5.61%.

1 T. M. Trnka and G. Parkin, *Polyhedron*, 1997, **16**, 1031; G. Parkin, *Prog. Inorg. Chem.*, 1998, **47**, 1.
2 L. C. Roof and J. W. Kolis, *Chem. Rev.*, 1993, **93**, 1037; K. Tatsumi, H. Kawaguchi and K. Tani, *Angew. Chem., Int. Ed. Engl.*, 1993, **32**, 591.
3 H. Kawaguchi and K. Tatsumi, *J. Am. Chem. Soc.*, 1995, **117**, 3885; H. Kawaguchi, K. Yamada, J.-P. Lang and K. Tatsumi, *J. Am. Chem. Soc.*, 1997, **119**, 10 346; K. Tatsumi, A. Tahara and A. Nakamura, *J. Organomet. Chem.*, 1994, **471**, 111.
4 T. Nagasawa, H. Kawaguchi and K. Tatsumi, *J. Organomet. Chem.*, 1999, **592**, 46.
5 S. C. O'Neal and J. W. Kolis, *J. Am. Chem. Soc.*, 1988, **110**, 1971.
6 A. Müller, E. Diemann, R. Jostes and H. Bögge, *Angew. Chem., Int. Ed. Engl.*, 1981, **20**, 934.
7 R. W. M. Wardle, S. Bhaduri, C.-N. Chau and J. A. Ibers, *Inorg. Chem.*, 1988, **27**, 1747; J. H. Shin and G. Parkin, *Organometallics*, 1995, **14**, 1104.
8 C. E. Moore, *Atomic Energy Levels, National Bureau of Standards*, Washington DC, 1949.
9 D. Rabinovich and G. Parkin, *Inorg. Chem.*, 1995, **34**, 6341; E. M. Carnahan, R. L. Rardin, S. G. Bott and S. J. Lippard, *Inorg. Chem.*, 1992, **31**, 5193; W. D. Jones, G. P. Foster and J. M. Putinas, *Inorg. Chem.*, 1987, **26**, 2120; T. Adachi, N. Sasaki, T. Ueda, M. Kamikawa and T. Yoshida, *J. Chem. Soc., Chem. Commun.*, 1989, 1320; J. Chatt, A. J. L. Pombeiro, R. L. Richards, G. H. D. Royston, K. W. Muir and R. Walker, *J. Chem. Soc., Chem. Commun.*, 1975, 708.
10 W. Eikens, C. Kienitz, P. G. Jones and C. Thöne, *J. Chem. Soc., Dalton Trans.*, 1994, 3329.

Unusual alkali metal α- or β-phenyl(trimethylsilyl)amides†‡

Floria Antolini, Peter B. Hitchcock, Michael F. Lappert* and Philippe Merle

The Chemistry Laboratory, University of Sussex, Brighton, UK BN1 9QJ. E-mail: m.f.lappert@sussex.ac.uk

Received (in Cambridge, UK) 19th April 2000, Accepted 24th May 2000

The synthesis (1–3 and 5) and structures (1–5) of the crystalline, hydrocarbon-soluble metal amides [M{μ-N(SiMe$_3$)(SiMe$_2$Ph)}(NCBu^t)$_n$]$_2$ [*n* = 0 and M = Li 1 (*cis*), M = Na 2 (*trans*) having intermolecular Na···C contacts, or *n* = 1 and M = Na (*cis*) 3], [Li{μ-N(SiMe$_3$)Ph}-*cis*]$_2$[μ-{N(SiMe$_3$)Ph}Li-*cis*]$_2$ 4 and *trans*-[Na{μ-N(SiMe$_3$)Ph}(tmen)] 5 are reported.

Bulky crystalline metal amides display a diversity of structures.[1] In the absence of a neutral coligand, they are polymers, *e.g.* [Na{μ-N(SiMe$_3$)$_2$}]$_\infty$, trimers, *e.g.* [M{μ-N(SiMe$_3$)$_2$}]$_3$ (M = Li or Na),[2] or, for [M{μ-NC(Me)$_2$(CH$_2$)$_3$CMe$_2$}]$_4$,[3] tetramers. Crystalline bis(trimethylsilyl)amides of the heavier alkali metals are dimers.[2] Addition of tmen to a bulky Li or Na amide results in its fragmentation into a crystalline mono- or binuclear compound, such as [Li{N(SiMe$_3$)$_2$}(tmen)],[4] *trans*-[Li{μ-N(Me)Ph}(tmen)]$_2$,[5] or *trans*-[Na{μ-N(Pr^i)C$_6$H$_{11}$-c}(tmen)]$_2$.[6]

We now report on the synthesis (**1**–**5**) (Schemes 1 and 2) and structures (**1**, **2** and **4**) of the crystalline Li and Na trimethylsilylamides having an additional α- or β-phenyl *N*-centered substituent: *cis*-[Li{μ-N(SiMe$_3$)(SiMe$_2$Ph)}]$_2$ **1**, *trans*-[Na{μ-N(SiMe$_3$)(SiMe$_2$Ph)}]$_2$ **2**, *trans*-[Na{μ-N(SiMe$_3$)(SiMe$_2$Ph)}(NCBu^t)]$_2$ **3**, [Li{μ-N(SiMe$_3$)Ph}-*cis*]$_2$[μ-{N(SiMe$_3$)Ph}Li-*cis*]$_2$ **4** and [Na{μ-N(SiMe$_3$)Ph}(tmen)]$_2$ **5**.

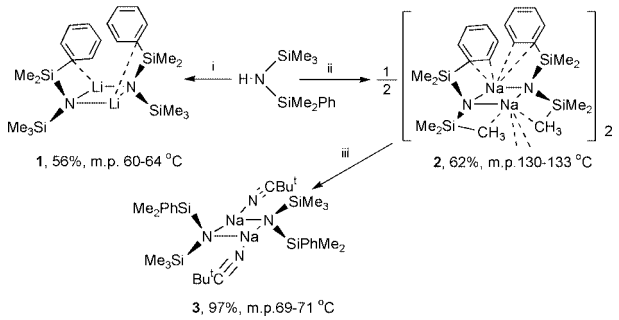

Scheme 1 Synthesis of the crystalline Li and Na amides **1**–**3** (yields are for crystals, from C_6H_6). *Reagents and conditions:* i, LiBu^n in C_6H_{14}, C_5H_{12}, −70 to 20 °C; ii, NaCH$_2$Ph, C_6H_{14}, −78 to 35 °C; iii, 2 Bu^{t}CN, C_5H_{12}, −78 to 20 °C.

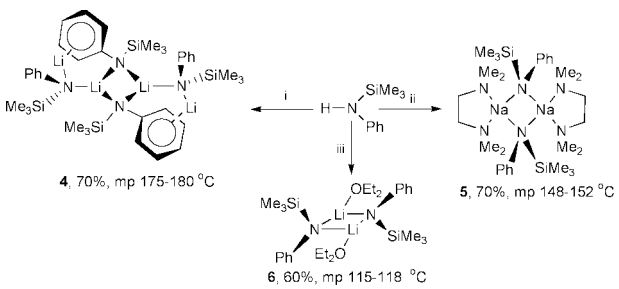

Scheme 2 Synthesis of the crystalline Li and Na amides **4**–**6** (yields are for crystals, from PhMe **4**, C_5H_{12} for **5** and Et$_2$O for **6**). *Reagents and conditions:* i, LiBu^n, C_6H_{14}, 0 to 20 °C (*cf.* ref. 8); ii, NaN(SiMe$_3$)$_2$, Et$_2$O, 0 to 20 °C; then tmen to the precipitate in C_5H_{12}–PhMe; iii, LiBu^n, Et$_2$O, 0 to 20 °C.

Treatment of {phenyl(dimethyl)silyl}(trimethylsilyl)amine[7] with *n*-butyllithium or benzylsodium in pentane or hexane at low temperature yielded **1** or **2**, respectively. Addition of 2-cyano-2-methylpropane to **2** in pentane, irrespective of stoichiometry, afforded the 1 : 1 adduct **3**. Each of **1**–**3** furnished X-ray quality crystals from hexane for **1** and **3** or benzene for **2**.

Similar low temperature reactions between *N*-trimethylsilylaniline[8] and *n*-butyllithium in hexane or bis(trimethylsilyl)amidosodium in diethyl ether yielded **4**, or a white precipitate of the presumed sodium analogue which with tmen in pentane–toluene gave **5**. X-Ray quality crystals of **4** (from toluene) or **5** (from pentane) were obtained upon recrystallisation. Compound **4** had previously been made similarly[8] and used to make corresponding amides of Zn, Cd and Hg.[9] A material related to **4**, and believed to have been [Li{N(SiMe$_3$)Ph}]$_2$·OEt$_2$, was used *in situ* for the synthesis of [M′{N(SiMe$_3$)Ph}$_3$Cl] (M′ = Zr or Hf); it was obtained from aniline and successively LiBu^n, Me$_3$SiCl, LiBu^n and Et$_2$O.[10] In our hands, this procedure afforded *trans*-[Li{μ-N(SiMe$_3$)Ph}(OEt$_2$)]$_2$ **6**.

The new colourless (**1**–**4** and **6**) or pale pink (**5**), air-sensitive, benzene-soluble, compounds **1**–**3**, **5** and **6** gave satisfactory analyses and ambient temperature benzene solution multinuclear NMR spectra. Such data for **4** were similar to those in the literature,[10] but ^{29}Si and ^{7}Li spectral details are new (ESI†). The X-ray structures of each of **1**–**5** have been elucidated; those for **3** and **5** will be reported in the full paper.§

Numerous neutral donor-free lithium amide crystals structures are known; those for **1** and **4** display new features.

As for **1** (Fig. 1), only a single previous example of a dinuclear complex, albeit of opposite stereochemistry, *trans*-[Li{μ-N(SiMe$_3$)C$_6$H$_3$Pr$^i_2$-2,6}]$_2$ **7** was known.[11] Each Li atom in **1** and **7** has a close (< 2.45 Å) contact to its *ipso*-carbon, which is γ- in **1** but β- in **7**; in the latter there are two further more distant [2.76(2) Å] contacts to the γ- and δ- (*C*HMe$_2$) carbon atoms.[11] The LiNLiN core in **1**, unlike in **7**, deviates from a planar rhombus, the Li–N bonds ranging from 1.980(3) to 2.019(3) Å, the four atoms alternating above and below the plane by *ca.* 0.033 Å. The amide **1** has a two-fold symmetry axis; **7** is centrosymmetric.

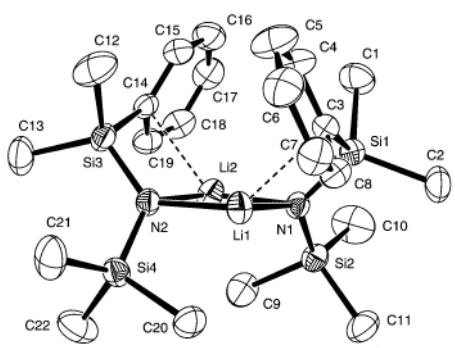

Fig. 1 Molecular structure (ORTEP) of **1** with atom labelling, H omitted for clarity.

† Electronic supplementary information (ESI) available: spectroscopic and analytical data, details of crystallography, and comparative data for **1**–**4**, **7** and **8**. See http://www.rsc.org/suppdata/cc/b0/b003169k/

‡ No reprints available.

DOI: 10.1039/b003169k

The tetranuclear, crystalline lithium amide **4** (Fig. 2) has an unprecedented structure. Unlike its only prior tetranuclear neutral donor-free complex, the planar octacyclic [L{μ-$\overline{NC(Me)_2(CH_2)_3CMe_2}$}]$_4$,[12] the centrosymmetric **4** has two distinct and different lithium atom environments. The four lithium atoms are arranged in a stair-like fashion, the central two, Li(1) and Li(2), are separated by 2.601(9) Å, while the two terminal, Li···Li(1 or 2) distances are longer at 3.121(9) Å, the Li–Li(1 or 2)–Li angles being 118(1)°. The atoms Li(1) and Li(2) are each bound to three nitrogen atoms at distances of 2.057(9) to 2.183(9) Å. Each of the terminal lithium atoms is bound slightly more tightly to a terminal nitrogen atom [Li(3 or 4)–N(3 or 4) 2.004(9) or 1.983(10) Å] and also has close η^6-contacts to the phenyl ring attached to a bridging nitrogen atom [av. Li(3 or 4)···M(1 or 2) 2.17(2) Å], the N–Li–M angle being 128.8(5) or 134.1(5)° at Li(3) or Li(4), respectively [M(1) and M(2) are the centroids of the phenyl rings attached to N(1) and N(2), respectively]. The Li(1)–N(1)–M(1) and Li(2)–N(2)–M(2) angles are 95.1 and 97.2°, respectively, compared with Li(1)–N(1)–C(1) and Li(2)–N(2)–C(10) angles of 95.6 and 98.0°, respectively; hence the Ph rings are essentially flat. The central $(LiN)_2$ ring is puckered, the torsion angle between the Li(1)N(1)Li(2) and Li(1)N(2)Li(2) planes being 14.6(4)°. The substituents at N(1) and N(2) are arranged in a *cis* fashion, while the two terminal {N(SiMe$_3$)Ph}Li(3 or 4) fragments attached to Li(1 or 2) also have the *cis*-orientation.

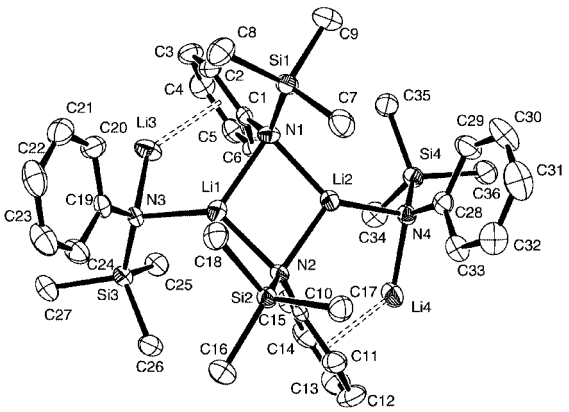

Fig. 2 Molecular structure (ORTEP) of **4** with atom labelling, H omitted for clarity.

The crystalline sodium amide **2** (Fig. 3) is a polymer made up of linked dinuclear units; each is attached to its neighbour by close intermolecular Na···C contacts. Neutral donor-free dinuclear Na amides are, we believe, unprecedented. Like its isoleptic complex **1**, each monomer unit of **2** has a two-fold rotation axis along Na(1)Na(2), but differs from **1** in having a *trans*-arrangement of the substituents at the N atoms and in having different environments for each of the alkali metal atoms. Each sodium atom has four additional Na···C close contacts: for Na(2) from the *ipso*-[2.686(1) Å] and one of the adjacent *ortho*-[2.884(2) Å] carbon atoms of the aromatic rings and for Na(1) from the C(1) carbon atoms of the *trans*-SiMe$_3$ groups [2.948(2) Å] and from the C(3) carbon atoms of an inversion centered related molecule [3.060(2) Å]. The Si–N–Si′ angle is slightly wider in **2** [av. 126.3(1)°] than in **1** [av. 123.9(5)°], but narrower than in its Bu^{t}CN complex **3** [129.9(1)°].[13] As for [Li{μ-N(SiMe$_3$)$_2$}(NCBu^t)]$_2$,[14] **3** may be regarded as a model MR′(NCR) intermediate for reaction of RCN with an organometallic compound MR′.

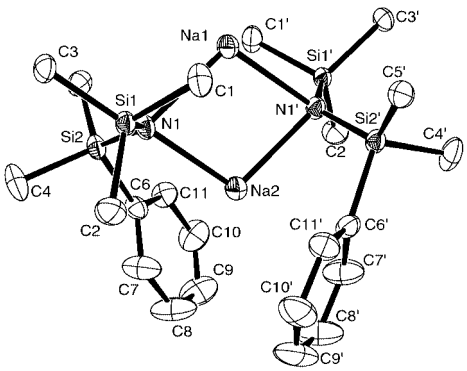

Fig. 3 Molecular structure (ORTEP) of **2** with atom labelling, H omitted for clarity.

The crystalline, dinuclear *trans*-sodium amide **5** is broadly similar to others, such as *trans*-[Na{μ-N(Pr^i)C$_6$H$_{11}$-c}-(tmen)]$_2$.[6] Comparative data on **1**–**4**, **7** and **8** are listed (ESI†).

The tetranuclear lithium amide **4** at 163 K in toluene-d$_8$ showed two ^{7}Li environments of equal intensity at δ 0.89 and −4.6, corresponding to the central and terminal lithium atoms in the crystal, whereas at higher temperatures various exchange processes (2D ^{7}Li EXSY) were observed.

The present results serve to highlight (*cf.* also ref. 1) the diversity of structural motifs available to alkali metal amides; the role of complexes **1**–**5** as reagents is being explored.

We thank the European Commission for the award of a Marie Curie fellowship for P. M. and the EPSRC for other support.

Notes and references

§ *Crystallographic data* for each of **1**, **2** and **4** were collected at 173(2) K on an Enraf-Nonius Kappa CCD (**1** and **2**) or CAD4 (**4**) diffractometer (ESI†).

1: $C_{22}H_{40}Li_2N_2Si_4$, M = 458.8, monoclinic, space group $P2_1/n$ (no. 14), a = 14.2980(3), b = 13.6936(3), c = 15.2530(3) Å, β = 98.635(1)°, U = 2952.6(1) Å^3, Z = 4, D_c = 1.03 g cm^{-3} μ(Mo-Kα) = 0.21 mm^{-1}. Final residual was R_1 = 0.041 for the 5613 reflections with $I > 2\sigma(I)$ and wR_2 = 0.113 for all the 6948 reflections. **2**: $C_{22}H_{40}N_2Na_2Si_4$, M = 491.0, monoclinic, space group $C2/c$ (no. 15), a = 16.6414(6), b = 14.6700(5), c = 11.6899(4) Å, β = 93.187(2)°, U = 2849.4(1) Å^3, Z = 4, D_c = 1.14 g cm^{-3} μ(Mo-Kα) = 0.25 mm^{-1}. Final residual was R_1 = 0.038 for the 2958 reflections with $I > 2\sigma(I)$ and wR_2 = 0.103 for all the 3364 reflections. **4**: $C_{36}H_{56}Li_4N_4Si_4$, M = 684.97, triclinic, space group $P\bar{1}$ (no. 2), a = 10.103(4), b = 10.873(5), c = 20.223(7) Å, α = 99.82(3), β = 91.76(3), γ = 113.16(3)°, U = 2001(1) Å^3, Z = 2, D_c = 1.14 g cm^{-3} μ(Mo-Kα) = 0.18 mm^{-1}. Final residual was R_1 = 0.073 for the 4136 reflections with $I > 2\sigma(I)$ and wR_2 = 0.194 for all the 7003 reflections. CCDC 182/1657. See http://www.rsc.org/suppdata/cc/b0/b003169k/ for crystallographic files in .cif format.

1 (*a*) K. Gregory, P. v. R. Schleyer and R. Snaith, *Adv. Inorg. Chem.*, 1991, **37**, 47; (*b*) R. E. Mulvey, *Chem. Soc. Rev.*, 1991, **20**, 167.
2 S. Neander and U. Berhens, *Z. Anorg. Allg. Chem.*, 1999, **625**, 1429 and references therein to Li, Na and K bis(trimethylsilyl)amides.
3 B. Gehrhus, P. B. Hitchcock, A. R. Kennedy, M. F. Lappert, R. E. Mulvey and P. J. A. Rodger, *J. Organomet. Chem.*, 1999, **587**, 88.
4 J. L. Atwood, M. F. Lappert, W.-P. Leung and H. Zhang, unpublished results cited in ref. 1(*b*).
5 D. Barr, W. Clegg, R. E. Mulvey, R. Snaith and D. S. Wright, *J. Chem. Soc., Chem. Commun.*, 1987, 716.
6 P. C. Andrews, N. D. R. Barnett, R. E. Mulvey, W. Clegg, P. A. O'Neil, D. Barr, L. Cowton, A. J. Dawson and B. J. Wakefield, *J. Organomet. Chem.*, 1996, **518**, 85.
7 K. A. Andrianov, A. M. Komonov and N. A. Makarova, *Zh. Obshch. Khim. II*, 1966, **36**, 895.
8 H. Schumann, J. Winterfeld, E. C. E. Rosenthal, H. Hemling and L. Esser, *Z. Anorg. Allg. Chem.*, 1995, **621**, 122.
9 H. Schumann, J. Gottfriedsen, S. Dechert and F. Girgsdies, *Z. Anorg. Allg. Chem.*, 2000, **626**, 747.
10 J. R. Galsworthy, M. L. H. Green, N. Maxted and M. Müller, *J. Chem. Soc., Dalton Trans.*, 1998, 387.
11 D. K. Kennepohl, S. Brooker, G. M. Sheldrick and H. W. Roesky, *Chem. Ber.*, 1991, **124**, 2223.
12 M. F. Lappert, M. J. Slade, A. Singh, J. L. Atwood, R. D. Rogers and R. Shakir, *J. Am. Chem. Soc.*, 1983, **105**, 302.
13 F. Antolini, P. B. Hitchock and M. F. Lappert, unpublished work.
14 G. Boche, I. Langlotz, M. Marsch, K. Harms and G. Frenking, *Angew. Chem., Int. Ed. Engl.*, 1993, **32**, 1171.

Towards mapping of functional group distributions in functional polymers by AFM force titration measurements

Holger Schönherr,[a] Menno T. van Os,[ab] Zdenek Hruska,[c] Jamal Kurdi,[d] Renate Förch,[b] Farzaneh Arefi-Khonsari,[d] Wolfgang Knoll[b] and G. Julius Vancso*[a]

[a] *University of Twente, MESA+ Research Institute and Faculty of Chemical Technology, Materials Science and Technology of Polymers, PO Box 217, 7500 AE Enschede, The Netherlands. E-mail: g.j.vancso@ct.utwente.nl*
[b] *Max-Planck-Institute for Polymer Research, Ackermannweg 10, 55128 Mainz, Germany*
[c] *Alkor GmbH Kunststoffe, Morgensternstrasse 9, 81479 München, Germany*
[d] *Laboratoire de Genie des Procedes Plasma et Traitement de Surface, ENSCP, 11 rue Pierre & Marie Curie, 75231 Paris Cedex 05, France*

Received (in Oxford, UK) 8th May 2000, Accepted 31st May 2000

We report on the mapping of functional group distributions at flat, functionalised polymer surfaces with a sub-50 nm resolution by means of pH-dependent AFM force titration measurements using chemically modified tips.

The presence *and* spatial distribution of functional groups in polymer coatings or surface-treated bulk polymers play an important role in determining the interfacial properties of these materials.[1] While there are numerous techniques available which allow one to identify and analyse the functional groups introduced by, *e.g.* a surface modification reaction, the determination of the lateral spatial distribution of these functional groups, and the characterisation of their local environment on a sub-100 nm scale remains difficult to impossible with these techniques.[2,3]

As shown here for the first time, atomic force microscopy (AFM) with chemically functionalised tips was successfully applied to tackle this problem. The work described here combines the strategies of AFM tip modification[4] and *active* external control of tip–sample interactions in nanometer-scale AFM adhesion measurements on polymers which contain ionisable functional groups.[5–8] In particular, it is shown that pH-dependent force titration measurements allow one to map functional group distributions with a sub-50 nm resolution. The results obtained on three different polymer model systems, *i.e.* oxyfluorinated isotactic polypropylene (iPP),[9] plasma polymerised allylamine (PPAA),[10] and ammonia plasma modified polypropylene (PP), will be discussed.[11]

The interfacial properties of three different types of polymer surfaces were investigated in AFM force-distance measurements. The model surfaces differ in the type and local environment of the functional groups which are exposed at the free film surface. As shown in previous studies, PPAA contains amino groups,[10] oxyfluorinated iPP carboxylic acid groups,[12] and ammonia plasma modified PP basic (amino) groups.[11] The adhesion properties of these samples can be expected to differ strongly as a result of the different surface chemistry.

Gold-coated AFM tips were functionalised with ω-hydroxy-substituted thiols in order to adjust the interactions between tip and sample surface.[4,5,7–9,13] In an aqueous medium, hydroxy-terminated tips were previously shown to possess pH independent adhesion properties.[5] In these experiments the ionisation state of the exposed functional groups in the polymer films was varied systematically *in situ* by adjusting the pH of the aqueous medium while maintaining a constant ionic strength.[14]

Pull-off forces were evaluated from 100 force–distance curves for each pH.[15] Depending on the pH exclusively repulsive, both attractive and repulsive, or exclusively attractive interactions were detected.

The average pull-off force as a sum of attractive (van der Waals and dipolar) and repulsive (electrostatic) forces was calculated as peak maximum of a Gaussian distribution fitted to the corresponding histograms. The mean value found depended on the pH of the aqueous solution. As is shown in Fig. 1, the average pull-off forces exhibited a behaviour similar to conventional titration experiments. Force titration experiments have been performed previously by Lieber and coworkers[5] and van der Vegte and Hadziioannou,[7] without being accompanied by force volume imaging. For low pH values the PPAA and PP samples, which contain basic amino groups, showed negligible pull-off forces, while at pH >5 the adhesion was quite pronounced. An opposite trend was observed for the carboxylic acid-containing oxyfluorinated iPP, while the untreated iPP (without functional groups) showed no pH dependent pull-off forces.

The reduction of the pull-off forces as a result of repulsive interactions can be attributed to the presence of protonated amino groups for the PPAA and PP (low pH), and deprotonated

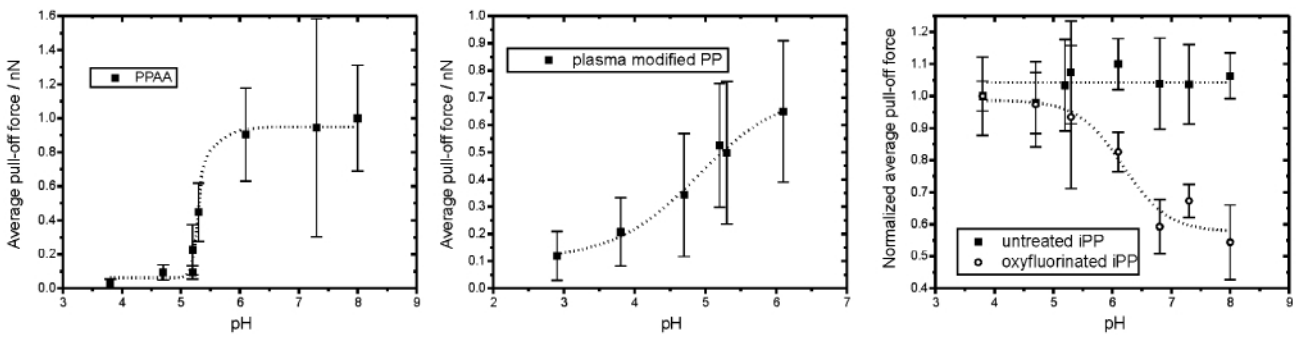

Fig. 1 Force titration data acquired with hydroxy-terminated tips for representative samples of the three model surfaces studied. For PPAA (left) and ammonia plasma modified PP (middle) the average pull-off forces are shown, for the untreated and oxyfluorinated iPP (right) the values were normalised to the values found for pH 3.8 (errors bars correspond to the standard deviation of the mean determined from the pull-off force distribution histograms). The dotted lines have been added to guide the eye.

DOI: 10.1039/b003756g

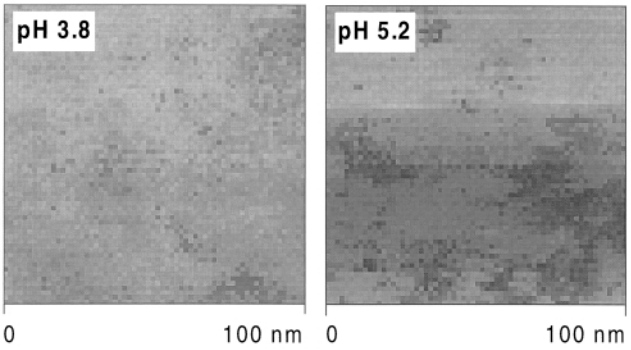

Fig. 2 Pull-off force images of a plasma polymerised allylamine film (peak power 175 W, duty cycle 10/10)[10] at different pH. In the force images dark regions indicates high adhesion (−0.1, −0.5 nN for pH 3.8 and 5.2, respectively), bright regions indicates low adhesion (*ca.* 0 and −0.1 nN for pH 3.8 and 5.2, respectively).

carboxylic acid groups in the iPP (high pH), respectively. The inflection points (force pK_a) are closely related to the thermodynamic surface pK_a values.[16] It is obvious that the force pK_a values are shifted relative to the known p*K*a values (in solution) for carboxylic acids and amino groups (acetic acid: pK_a 4.8; ethylamine: pK_a 10.7). The force pK_a values are shifted to a higher pH for the acidic groups, while for basic groups they are lower. Similar shifts were previously observed experimentally[5,17] and were related to the hydrophobicity of the local environment of the corresponding functional groups. This general interpretation is corroborated by recent simulations.[18] The more hydrophobic the local environment, the more difficult it becomes to create a charge due to the lower dielectric constant of the environment.

The shift of the force pK_a values observed in average force measurements can be used to differentiate between functional groups in different local environments. Depending on the hydrophobicity of the environment and on the local density of (electrostatically interacting) functional groups, these will either be ionised or neutral at pH values close to complete ionisation/neutrality. As indicated in the average adhesion measurements (*vide supra*) the adhesion properties are dramatically different for these two cases. Thus, by carefully adjusting the pH of the solution, areas where ionisation begins can be detected with a spatial resolution of 20 nm or better. This is shown in Fig. 2.

At pH 3.8 the amino groups of the PPAA are completely deprotonated which results in negligible adhesive forces. When the pH of the solution is adjusted to values close to the force pK_a, the spatial distribution of the pull-off forces is inhomogeneous. In the areas with pronounced adhesion the amino groups are neutral (dark patches in Fig. 2, right), while in the other areas repulsive or only weakly adhesive force are detected (bright areas in Fig. 2, right). The observed inhomogeneous distribution of amino groups at the surface of PPAA is most probably related to inhomogeneous temperature distribution in the plane of the film during the polymerization or different reaction pathways due to inhomogeneous initial coverage or *initially* deposited reaction products. This may lead to a heterogeneous restructuring of the polymer and the reorientation of the amino groups upon initial aging of the films in air similar to the processes observed previously.[19]

The data shown here constitute to our knowledge the first results on laterally resolved *imaging* of functional group distributions on polymers on a *sub*-50 nm level using scanning force microscopy with chemically modified tips ('chemical force microscopy'). pH-dependent pull-off force measurements carried out on various functional polymers using OH-functionalised tips revealed laterally inhomogeneous pull-off forces. These inhomogeneous forces can be related to variations of local 'pK_a' values and different local hydrophobicity, and thus to inhomogeneous distribution of the polar functional groups present at the polymer surface.

The oxyfluorinated iPP samples were kindly provided by SOLVAY S.A. and SOLVAY ALKOR-DRAKA Snc. The authors acknowledge financial support by the Council for Chemical Sciences of the Netherlands Organisation for Scientific Research (CW-NWO) in the priority program materials (PPM).

Notes and references

1 G. S. Ferguson and G. M. Whitesides, in *Modern Approaches to Wettability*, ed. M. E. Schrader and G. I. Loeb, Plenum, New York, 1992, p. 143 and references therein; B. Hupfer and H. Ringsdorf, in *Surface and Interfacial Aspects of Biomedical Polymers*, ed. J. D. Andrade, Vol. 1, *Surface Chemistry and Physics*, ch. 4, Plenum, New York, 1985, p. 77; C. J. van Oss, in *Polymers and Interfaces II*, ed. W. J. Feast, H. S. Munro and R. W. Richards, Wiley & Sons, New York, 1993, ch. 11, pp. 268–290; A. Ulman, *An Introduction to Ultrathin Organic Films: From Langmuir–Blodgett to Self-Assembly*, Academic Press, New York, 1991.
2 *Practical Surface Analysis*, ed. D. Briggs and M. P. Seah, Wiley, Chichester, 1992.
3 C.-M. Chan, *Polymer Surface Modification and Characterization*, Hanser Publishers, Munich, 1994, p. 100.
4 C. D. Frisbie, L. F. Rozsnyai, A. Noy, M. S. Wrighton and C. M. Lieber, *Science*, 1994, **265**, 2071.
5 A. Noy, D. V. Vezenov and C. M. Lieber, *Annu. Rev. Mater. Sci.*, 1997, **27**, 381.
6 S. K. Sinniah, A. B. Steel, C. J. Miller and J. E. Reutt-Robey, *J. Am. Chem. Soc.*, 1996, **118**, 8925.
7 E. W. van der Vegte and G. Hadziioannou, *J. Phys. Chem.*, 1997, **101**, 9563.
8 H. Schönherr and G. J. Vancso, *J. Polym. Sci. B, Polym. Phys.*, 1998, **36**, 2486.
9 H. Schönherr, Z. Hruska and G. J. Vancso, *Macromolecules*, 1998, **31**, 3679.
10 M. T. van Os, B. Menges, R. Förch, W. Knoll, R. B. Timmons and G. J. Vancso, *Mater. Res. Soc. Symp. Proc.*, 1999, **544**, 45; M. T. van Os, B. Menges, R. Förch, G. J. Vancso and W. Knoll, *Chem. Mater.*, 1999, **11**, 3252.
11 N. Shahidzadeh, F. Arefi-Khonsari, M. M. Chehimi and J. Amouroux, *Surf. Sci.*, 1996, **352**–**354**, 888.
12 G. Kranz, R. Lüschen, T. Gesang, V. Schlett, O. D. Hennemann and W. D. Stohrer, *Int. J. Adhes. Adhes.*, 1994, **14**, 243.
13 K. Feldmann, T. Tervoort, P. Smith and N. D. Spencer, *Langmuir*, 1998, **14**, 372.
14 The data presented here were acquired at an ionic strength of 1.87×10^{-3}. Phosphate and acetate buffers were used. It should be noted that the force titration curves and the corresponding inflection points were found to be independent of the ionic strength (in the range of 2×10^{-1} to 2×10^{-4}).
15 Triangular shaped silicon nitride cantilevers with silicon nitride tips (Digital Instruments (DI), Santa Barbara, CA, USA), which were coated with 2 nm Ti and 75 nm Au in high vacuum (Balzers), were functionalised with 11-hydroxyundecanol following the procedures described in refs. 8 and 9. The SFM measurements were carried out with a NanoScope III multimode SFM (DI) with modified tips in buffered aqueous solutions of constant ionic strength utilising a liquid cell (DI). The force distance curves used for construction of force titration curves were obtained with at least 10 different positions for each sample. For laterally resolved pull-off force measurements the AFM was operated in the force volume (FV, DI) mode. Only subsequent up and down scans which showed the same force characteristics were considered.
16 A strict quantitative evaluation, such as described by Hu and Bard (K. Hu and A. J. Bard, *Langmuir*, 1997, **13**, 5114), is at this point not possible due to uncertainties of the tip shape (granular gold coating) and the unknown effect of the morphology of the polymer films.
17 C. D. Bain and G. M. Whitesides, *Langmuir*, 1989, **5**, 1370; T. R. Lee, R. I. Carey, H. A. Biebuyck and G. M. Whitesides, *Langmuir*, 1994, **10**, 741; S. E. Creager and J. Clark, *Langmuir*, 1994, **10**, 3675; R. C. Chatelier, C. J. Drummond, D. Y. C. Chan, Z. R. Vasic, T. R. Gengenbach and H. J. Griesser, *Langmuir*, 1995, **11**, 4122.
18 J. L. Smart and J. A. McCammon, *J. Am. Chem. Soc.*, 1996, **118**, 2283.
19 T. R. Gengenbach, Z. R. Vasic, S. Li, R. C. Chatelier and H. J. Griesser, *Plasmas Polym.*, 1997, **2**, 91.

ChemComm

Remarkable carbene-induced transformation of 2,4,6-tri-*tert*-butyl-1,3,5-triphosphabenzene, $P_3C_3Bu^t_3$, to the 1,2,4-triphosphole, $P_3C_2Bu^t_2CBu^t$(carbene). Crystal and molecular structure of the planar triphosphole complex $[Mo(CO)_3(\eta^5\text{-}P_3C_2Bu^t_2CBu^t(carbene))]$ [carbene = C(N(Me)C(Me) = C(Me)N(Me))]†

Scott B. Clendenning,[a] Peter B. Hitchcock,[a] John F. Nixon*[a] and László Nyulászi[b]

[a] *School of Chemistry, Physics and Environmental Science, University of Sussex, Brighton, Sussex, UK, BN1 9QJ. E-mail: j.nixon@sussex.ac.uk*

[b] *Department of Inorganic Chemistry, Technical University of Budapest, H-1521 Budapest Gellért tér 4, Hungary*

Received (in Cambridge, UK) 16th February 2000, Accepted 22nd May 2000

Treatment of 2,4,6-tri-*tert*-butyl-1,3,5-triphosphabenzene, $P_3C_3Bu^t_3$, with the stable carbene 1,3,4,5-tetramethylimidazol-2-ylidene affords the planar 1,2,4-triphosphole, $P_3C_2Bu^t_2CBu^t$(carbene), [carbene = C(N(Me)C(Me)=C(Me)N(Me))] which has been structurally characterised as its η^5- ligated $[Mo(CO)_3]$ complex; theoretical calculations are presented on the mechanism of this novel reaction.

The synthesis and ligating properties of compounds containing P–C multiple bonds is of considerable current interest.[1–4] The availability[5–7] of 2,4,6-tri-*tert*-butyl-1,3,5-triphosphabenzene $P_3C_3Bu^t_3$ **1** has enabled its chemistry to be developed and we recently described an unusual [1+4]-cycloadditon reaction with a stable silylene.[8] We now describe the remarkable reaction of **1** with the stable 'Arduengo' type carbene 1,3,4,5-tetramethylimidazol-2-ylidene **2**[9] which involves extrusion of a CBu^t fragment from the six-membered aromatic ring to quantitatively afford the 1,2,4-triphosphole, $P_3C_2Bu^t_2CBu^t$(carbene) **3** (carbene = 1,3,4,5-tetramethylimidazol-2-ylidene). (Scheme 1) This type of behaviour is unprecedented and has no parallel in conventional organic chemistry.

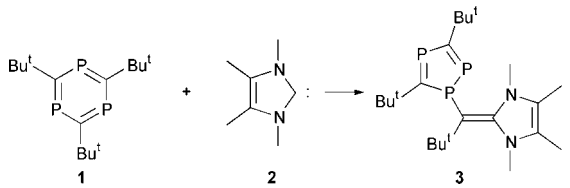

Scheme 1

To our knowledge, contractions from aromatic six-membered rings to aromatic five-membered rings are unknown in organic chemistry. In sulfur chemistry, reactions with electrophiles are known to cause six- to five-membered ring contractions in nonaromatic systems with S–S bond formation.[10,11] While ring expansion of arenes[12] and aromatic phosphabenzenes[13,14] are known to occur with carbenes, no ring contractions have been reported to date.

Thus, addition of the 1,3,5-triphosphabenzene **1** to the carbene **2** in solutions of benzene, toluene or THF immediately led to a deep red solution of the 1,2,4-triphosphole **3** which could be isolated as an air and moisture-sensitive red oil.‡ **3** is highly soluble in benzene, toluene, THF and diethyl ether but only sparingly soluble in saturated hydrocarbon solvents.

The structure of **3** was established by its mass spectrum and its characteristic ^{1}H, ^{13}C and ^{31}P NMR spectra, the latter exhibiting a very similar pattern of lines to that of the known, structurally characterised, triphosphole $P_3C_2Bu^t_2CH(SiMe_3)_2$.[15] The ^{31}P NMR spectrum of the triphosphole **3** consists of three doublets of doublets in the unsaturated region at δ 209.2, 163.3 and 121.4 with the expected large ^1J(PP) coupling of 519.6 Hz, indicating a highly delocalised π-system, and the two smaller ^2J(PP) couplings of 40.3 and 27.2 Hz. While the ^{13}C and ^{1}H NMR specta are in good agreement with the proposed structure, several accidental coincidences should be noted. Though chemically inequivalent, in both the ^{13}C and ^{1}H NMR spectra, the two N-methyl groups and two carbene backbone methyl groups appear as singlets at their respective chemical shifts.

Confirmation of the proposed structure came from a single crystal X-ray diffraction study of the η^5-ligated molybdenum tricarbonyl complex **4** which was made by treatment of **3** with $[Mo(CO)_3$(cycloheptatriene)] at room temperature.‡ Crystals suitable for single crystal X-ray diffraction were grown at –25 °C from a saturated toluene solution layered with light petroleum (bp 40–60 °C).§

The molecular structure of **4**, shown in Fig. 1, reveals the following interesting features which are strongly indicative of a significantly delocalised system: (i) the sum of the bond angles at the tricoordinate phosphorus P(2) is 358.5°, (ii) the sum of the bond angles within the triphosphole ring is 539.97°, (iii) the C(14)=C(19) bond is 1.452(3) Å, (iv) the P(2)–C(14) bond outside the triphosphole ring is very short [1.7130(19) Å], (v) the P–C bond distances within the triphosphole ring are almost identical, [1.760(2), 1.7623(19), 1.763(2) and 1.774(2) Å, respectively].

The molybdenum tricarbonyl complex **4** was also characterised by ^{31}P, ^{13}C and ^{1}H NMR spectroscopy and mass

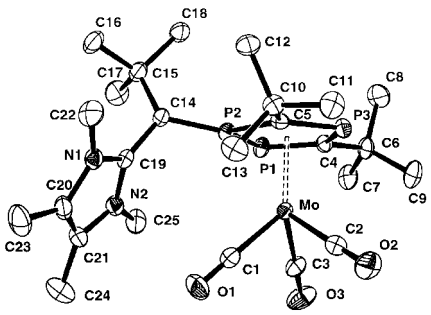

Fig. 1 Molecular structure of **4**. Selected bond lengths (Å) and angles (°): P(1)–C(4) 1.774(2), P(1)–P(2) 2.1214(7), P(2)–C(14) 1.7130 (19), P(2)–C(5) 1.760(2), P(3)–C(5) 1.7623(19), P(3)–C(4) 1.763(2), Mo–M(1) 1.986(2), C(1)–O(1) 1.161(3), C(14)–C(19) 1.452(3), N(1)–C(19) 1.361(2), N(1)–C(20) 1.388(3), N(1)–C(22) 1.456(3), N(2)–C(19) 1.356(3), N(2)–C(21) 1.388(3), N(2)–C(25) 1.461(3), C(20)–C(21) 1.350(3); C(4)–P(1)–P(2) 95.20(6), C(14)–P(2)–C(5) 129.43(9), C(5)–P(2)–P(1) 104.64(7), C(5)–P(3)–C(4) 101.40(9), P(3)–C(4)–P(1) 122.73(11), P(2)–C(5)–P(3) 116.00(10), C(19)–C(14)–C(15) 119.50(16), C(15)–C(14)–P(2) 119.68(14), C(14)–P(2)–P(1) 124.44(7).

† Electronic Supplementary information (ESI) available: spectroscopic data for **3** and **4**, B3LYP/6-31+G* level generated structure of **3**, and reaction of **3** with $[PtCl_2(PR_3)]_2$. See http://www.rsc.org/suppdata/cc/b0/b001285h/

DOI: 10.1039/b001285h

spectrometry. As was observed in the η^5-ligated $Mo(CO)_3$ complex of the triphosphole $P_3C_2Bu^t_2CH(SiMe_3)_2$,[16] we observe a large upfield shift for the ring phosphorus resonances as well as an inversion in the chemical shifts of the two formally unsaturated P centres. Furthermore, the ^{13}C and ^1H NMR spectra of **4** revealed that the chemical shift coincidences of methyl groups in the parent triphosphole mentioned above, were no longer present.

We have investigated the mechanism of the above transformation of **1** to **3** by theoretical calculations[17] at the B3LYP/6-31+G* level. The parent 1,3,5-triphosphabenzene, $P_3C_3H_3$, and the diaminocarbene, $C(NH_2)_2$, were used initially to model the entire reaction path. In order to take the most important steric effects into account, additional new calculations were performed at all the minima (product and intermediates), to find the corresponding structures derivable from 2,4-dimethyl-6-*tert*-butyl-1,3,5-triphosphabenzene and 1,3-dimethylimidazol-2-ylidene. Since no significant changes were observed in the relative energies of the minima on the reaction path, apart from some destabilisation of the first intermediate, we consider that the transition structures are not significantly affected.

From the reaction of the diaminocarbene and the triphosphabenzene a complex **5** (Fig. 2) is obtained in which the charge of the carbon atom of the diaminocarbene unit becomes more positive by 0.6 than in the free diaminocarbene, while each of the three phosphorus ring atoms become more negative by *ca.* 0.2 electrons. Thus **5** can be described as an ylid in which the negative charge is delocalised over the PCPCP unit. Intermediate **7** is formed from **5** *via* the transition state **6TS** as a result of a ring closure and the product **9** is formed *via* transition state **8TS**. Despite a careful search, no transition state linking **5** directly to **9** was found. Furthermore, the Gibbs free energies of **5**, **6TS**, **7**, **8TS** and **9** are lowered by 4.4, 3.0, 6.6, 4.7 and 21.5 kcal mol^{-1}, respectively, from that of the reactants and since the transition structures lie just slightly higher in energy than the intermediates, the reaction should proceed smoothly.

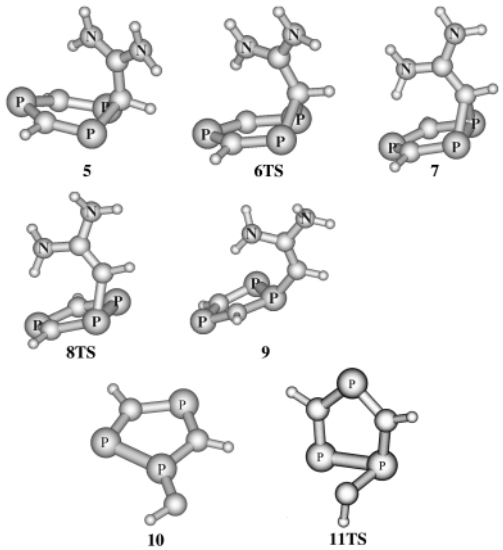

Fig. 2 B3LYP/6-31+G* level generated structures of intermediates and transition states generated in the transformation of **1** to **3**.

The structure of the experimentally observed **3** has also been optimised at the B3LYP/6-31G* level (neglecting the two β methyl groups on the imidazole ring). The calculated structural parameters are very similar to those obtained for the molybdenum complex **4**, except that the tricoordinate phosphorus atom is somewhat less planar (Σ bond angles 348.6 °). The calculated C(14)=C(19) bond length for the uncomplexed triphosphole system is 1.413 Å and the P(2)–C(14) bond length is 1.780 Å, while the remaining bonding distances are even closer to those obtained from the X-ray structure.

Finally, of special interest is the *reversible* nature of the triphosphabeneze–(triphosphole-carbene) interconversion. Thus treatment of **3** with $[PtCl_2(PR_3)]_2$ (PR_3 = PMe_3 or PMe_2Ph), at room temperature over 4 days leads to removal of the carbene, forming mixtures of the Pt(II) complexes *trans*-$[PtCl_2(PR_3)$(carbene)], *cis*-$[PtCl_2(PR_3)_2]$ and $[PtCl_2(carbene)_2]$ with simultaneous regeneration of the triphosphabenzene ring **1**, as the major product, as evidenced by ^{31}P NMR spectroscopy. Mechanistic information comes from theoretical calculations on the parent system which suggest that triphosphabenzene, $P_3C_3H_3$, which arises from loss of the carbene $C(NH_2)_2$ from **9** by metal complexation, results from the isomerisation of the planar compound **10** (Fig. 2), which has a singlet ground state and is less stable than triphosphabenzene by 59.3 kcal mol^{-1}. The Gibbs free energy of the transition state **11TS** for this reaction lies 17.5 kcal mol^{-1} higher than that of **10**.

We thank NSERC of Canada for a scholarship (for S. B. C.), the Royal Society and OTKA TO 26335 (for joint funding of J. F. N. and L. N.), EPSRC for their continuing support (to J. F. N.) for phospha-organometallic chemistry and Lisa Titcomb for the sample of 1,3,4,5-tetramethylimidazol-2-ylidene.

Notes and references

‡ *Preparations*: $P_3C_2Bu^t_2CBu^t$(carbene) **3**: to a solution of $C\{N(Me)\}_2C_2Me_2$ (63.6 mg, 0.512 mmol) in THF (5 mL) was added a solution of $P_3C_3Bu^t_3$ (153.8 mg, 0.512 mmol) in THF (5 mL) with stirring. The resulting red solution was stirred for 2 h before removing the solvent *in vacuo* to afford a red oil in quantitative yield by ^1H and ^{31}P NMR spectroscopy.

$[Mo(CO)_3P_3C_2Bu^t_2CBu^t$(carbene)] **4**: to a solution of $C\{N(Me)\}_2C_2Me_2$ (83.0 mg, 0.668 mmol) in benzene (10 mL) was added a solution of $P_3C_3Bu^t_3$ (200.7 mg, 0.668 mmol) in benzene (10 mL) with stirring. The resulting red solution was stirred for 1 h prior to the addition of a red solution of $[Mo(CO)_3$(cycloheptatriene)] (190.3 mg, 0.699 mmol) in benzene (10 mL) with no colour change. After a further 72 h stirring, the reaction mixture was filtered and the solvent removed *in vacuo* to give an orange solid, which was washed with hexane (10 mL) at −50 °C to afford **4** as a fine orange powder (313.1 mg, 78%).

§ *Crystal data* for **4**: $C_{25}H_{39}MoN_2O_3P_3$, M = 604.3, triclinic, space group $P\bar{1}$(no. 2), a = 10.5667(3), b = 10.9262(3), c = 13.8900(4) Å, α = 90.436(2), β = 96.562(2), γ = 114.401(2)°, U = 1448.18(7) $Å^3$, Z = 2, D_c = 1.39 Mg m^{-3}, crystal dimensions 0.4 × 0.3 × 0.2 mm, $F(000)$ = 628, T = 173(2) K, Mo-Kα radiation (λ = 0.71073 Å) Data collection: Kappa CCD. Of the total 5046 independent reflections measured, 4645 having $I > 2\sigma(I)$ were used in the calculations. The final indices [$I > 2\sigma(I)$] were $R1$ = 0.024, $wR2$ = 0.058 and $R1$ = 0.028, $wR2$ = 0.059 (for all data). CCDC 182/1651. See http://www.rsc.org/suppdata/cc/b0/b001285h/ for crystallographic files in .cif format.

1 K. B. Dillon, F. Mathey and J. F. Nixon, *Phosphorus: The Carbon Copy*, John Wiley, Chichester, 1998, pp. 366 and references therein.
2 J. F. Nixon, *Coord. Chem. Rev.*, 1995, **145**, 201.
3 J. F. Nixon, *Chem. Rev.*, 1988, **88**, 1327.
4 *Multiple Bonds and Low Coordination in Phosphorus Chemistry*, ed. M. Regitz and O. J. Scherer, Georg Thieme Verlag, Stuttgart, 1990, p. 496 and references therein.
5 P. Binger, S. Leininger, J. Stannek, B. Gabor, R. Mynott, J. Bruckmann and C. Kruger, *Angew. Chem., Int. Ed. Engl.*, 1995, **34**, 2227.
6 F. Tabellion, A. Nachbauer, S. Leininger, C. Peters, M. Regitz and F. Preuss, *Angew. Chem., Int. Ed.*, 1998, **37**, 1233.
7 R. Gleiter, H. Lange, P. Binger, J. Stannek, C. Kruger, J. Bruckmann, U. Zenneck and S. Kummer, *Eur. J. Inorg. Chem.*, 1998, 1619.
8 S. B. Clendenning, B. Gehrhus, P. B. Hitchcock and J. F. Nixon, *Chem. Commun.*, 1999, 2451.
9 A. J. Arduengo III, *Acc. Chem Res.*, 1999, **32**, 913 and references therein.
10 C. G. Marcellus, R. T. Oakley, A. W. Cordes and W. T. Pennington, *Can. J. Chem.*, 1984, **62**, 1822.
11 J. E. Ellis, J. H. Fried, I. T. Harrison, E. Rapp and C. H. Ross, *J. Org. Chem.*, 1977, **42**, 2891.
12 J. March, *Advanced Organic Chemistry*, John Wiley, Chichester, 4th edn., 1992, p. 869 and references therein.
13 G. Keglevich, *Synthesis*, 1993, **93**, 931.
14 G. Keglevich, *Rev. Heteroat. Chem.*, 1996, **14**, 119.
15 V. Caliman, P. B. Hitchcock and J. F. Nixon, *J. Chem. Soc., Chem. Commun.*, 1995, 1661.
16 V. Caliman, P. B. Hitchcock, J. F. Nixon, L. Nyulaszi and N. Sakarya, *Chem. Commun.*, 1997, 1305.
17 Quantum chemical calculations were carried out using the Gaussian 98 package (Gaussian 98, Revision A.5).

ChemComm

Control of the iodination reaction on activated aromatic residues in peptides†

Gemma Espuña,[a] Gemma Arsequell,[a] Gregorio Valencia,*[a] José Barluenga,*[b] Marta Pérez[b] and José M. González[b]

[a] *Unit for Glycoconjugate Chemistry, I.I.Q.A.B.-C.S.I.C., Jordi Girona 18-26, E-08034 Barcelona, Spain*
[b] *Instituto Universitario de Química Organometálica 'Enrique Moles'-Unidad Asociada al C.S.I.C., Universidad de Oviedo E-33071, Oviedo, Spain. E-mail: barluenga@sauron.quimica.uniovi.es*

Received (in Cambridge, UK) 17th April 2000, Accepted 31st May 2000

By using a slight molar excess of the IPy_2BF_4 reagent in an acid containing medium, activated aromatic residues on Tyr derivatives and peptides selectively react yielding, as major products, the monoiododerivatives; this level of reaction control cannot be achieved by other iodinating methods.

The methods available for either labeling complex biomolecules throughout radioiodination[1] or extending the reactivity of organic molecules by iodination[2] share similar problems. For most applications of iodinated aromatic compounds, monoiodination will be ideal, but known iodinating methods usually yield mixtures of mono-, diiodinated and unreacted species.[3] Accordingly, efficient control of the iodination of phenol-like compounds[4] at room temperature, that would result in a practical approach to monoiodinate target Tyr containing peptides still remains to be developed. The iodonium reagent IPy_2BF_4 that we are currently investigating[5] is very effective at iodinating aromatic functions of both simple organic molecules[6] and more complex polyfunctional peptides.[7] The performance of IPy_2BF_4 is dependent on factors such as reagent to substrate stoichiometry, the solvent and the presence of acid.[8]

In searching for conditions for the selective and direct preparation of monoiodinated Tyr derivatives as new building blocks for use in combinatorial chemistry and Tyr containing peptides, starting from **1** we have established conditions for its regioselective conversion to **2** at rt, as outlined in Scheme 1. Thus, mixing HBF_4 with **1** in CH_2Cl_2 prior to the addition of stoichiometric amounts of IPy_2BF_4 results in the formation of **2** in 90% yield (the presence of minor amounts of the 2-regioisomer was noticed by ^1H NMR analysis of the crude reaction mixture). Next, we explored the iodination of **3** under the same conditions and **4** was obtained in 93% isolated yield (Scheme 2).

Then, we examined the reaction conditions shown in Table 1 on the protected Tyr derivative Fmoc-Tyr-OH **5**. As expected, if no acid was present, the sole reaction product was the diiodinated derivative when an excess of IPy_2BF_4 was added to a CH_3CN solution of Fmoc-Tyr-OH. Under the same conditions, stoichiometric amounts of the reagent produced mixtures of mono-, diioiodinated and unreacted species. However, addition of an equimolar quantity of HBF_4, in CH_3CN or CH_2Cl_2, or 10% TFA in CH_2Cl_2, and a slight excess of the reagent, the monoiodinated building block Fmoc-Tyr(3′-I)-OH **6** was the exclusive reaction product (Scheme 3).

For comparison to the traditional Chloramine T iodinating method,[9] Fmoc-Tyr-OH was reacted in CH_3CN with excess of both NaI and Chloramine T and the diiodinated derivative was produced. However, in conditions involving stoichiometric amounts of the iodinating reagents,[9c] low yields of Fmoc-Tyr(3′-I)-OH were obtained.

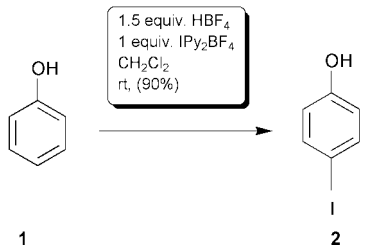

Scheme 1

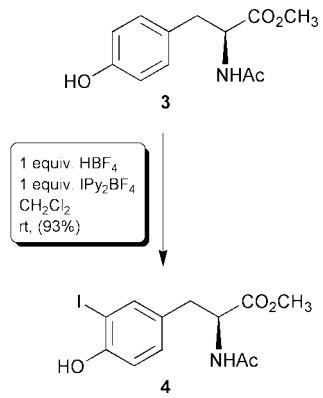

Scheme 2

Table 1 Conditions assayed for the monoiodination of Fmoc-Tyr-OH

Entry	IPy_2BF_4 (equiv.)	Acid	Solvent
1	2.2	—	CH_3CN
2	1.1	—	CH_3CN
3	1.1	1 equiv. HBF_4	CH_3CN
4	1.1	1 equiv. HBF_4	CH_2Cl_2
5	1.5	10% TFA	CH_2Cl_2

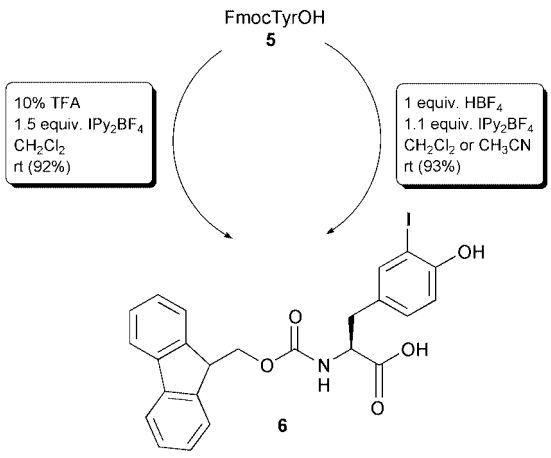

Scheme 3

† Electronic supplementary information (ESI) available: experimental and characterization data for compounds **4**, **6**, **7**–**13**. See http://www.rsc.org/suppdata/cc/b0/b003064n/

DOI: 10.1039/b003064n

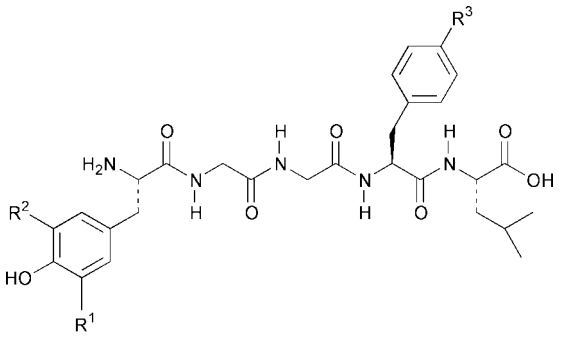

R^1 = H	R^2 = H	R^3 = H	**7** Leu-Enk
R^1 = I	R^2 = H	R^3 = H	**8** [**Tyr(I)**]-I-Leu-Enk
R^1 = H	R^2 = H	R^3 = I	**9** [**Phe(*p*-I)**]-I-Leu-Enk
R^1 = I	R^2 = I	R^3 = H	**10** [**Tyr(I,I)**]-di-I-Leu-Enk

Scheme 4

The potential of this method was also explored on different peptides. The opioid pentapeptide (Leu-enkephalin: H-Tyr-Gly-Gly-Phe-Leu-OH **7**) provided a simple model, showing both Tyr and Phe residues with aromatic side chains that may react towards aromatic electrophilic iodination with our reagent in acidic conditions. To facilitate the identification of the possible iodination products, a series of reference peptides were synthesized from commercially available building blocks. Thus, peptides **8**, **9** and **10** (Scheme 4) were prepared and characterized by RP-HPLC, MALDI-TOF-MS and ^{1}H-NMR. Reaction of **7** in 10% TFA in CH_2Cl_2, which are conditions frequently applied in peptide chemistry, with 1.5 equiv. IPy_2BF_4, afforded the Tyr monoiodinated species **8** as a major product (Scheme 5). The monoiodinated derivative, with an approximate conversion of 60%, was isolated by RP-HPLC and was further characterized by MALDI-TOF-MS and ^{1}H-NMR. After HPLC and NMR data comparison with **8**, **9** and **10** (Scheme 4), no trace of iodination on Phe residues could be observed, which confirmed the selectivity of the reagent towards Tyr side chains.

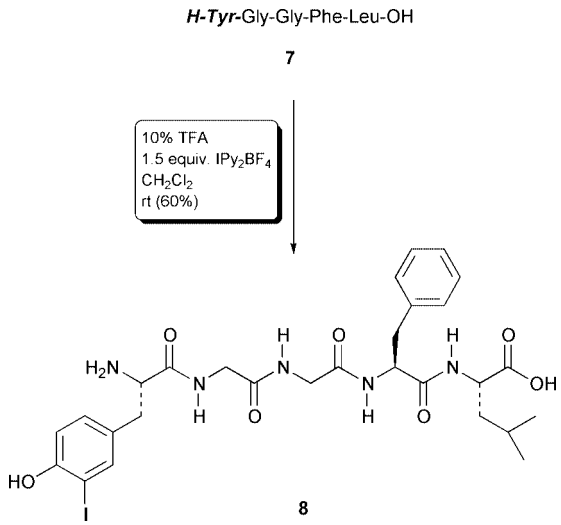

Scheme 5

These reaction conditions were also successfully tested on biologically active peptides with acid labile post-translational modifications such as in the case of glyco- and phosphopeptides,[10] **11** and **12**, (containing *O*-glycosyl and phosphoseryl residues, respectively) (Scheme 6). This method may also be of potential application on larger and water-soluble peptides and proteins; preliminary evidence was gathered after assaying these iodination conditions on **13** in aqueous solution. Thus, oxytocin, which has only one Tyr residue in its sequence

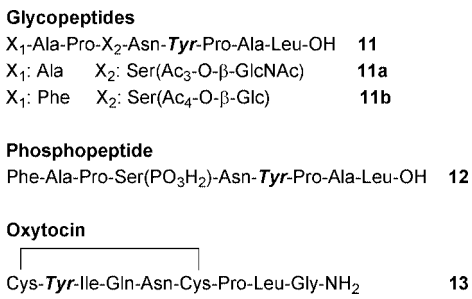

Scheme 6

(Scheme 6), was reacted in 10% TFA aqueous media with 1.3 equiv. IPy_2BF_4 and the monoiodinated derivative was observed as a major product with 50% conversion. HPLC and MALDI-TOF-MS analysis confirmed the identity of this product, which holds its disulfide bridge in place.

In summary, a method for controlling iodination reactions on activated aromatic residues of peptides is proposed for the first time. The procedure can be carried out in aqueous media and reaction conditions are mild enough for application to acid-labile glyco- and phosphopeptides. Work is in progress to extend these procedures to protein chemistry.

Financial support from the Spanish DGES (PB97-1271), and CICYT and the European Commission (1FD97-1041) is gratefully acknowledged. G. E. thanks CIRIT, Generalitat de Catalunya, Barcelona (Spain), for a fellowship.

Notes and references

1 (*a*) D. S. Wilbur, *Bioconjugate Chem.*, 1992, **3**, 433; (*b*) A. C. Patel and S. R. Matthewson, in *Molecular Biomethods Handbook*, ed. R. Rapley and J. M. Walker, Humana, Totowa, NJ, 1998, ch. 31, pp. 401–411; (*c*) G. Hermanson, in *Bioconjugate Techniques*, Academic Press, NY, 1996, ch. 8.4, pp. 400–416.

2 As a general review: (*a*) E. B. Merkushev, *Synthesis*, 1988, 923.

3 Some selected examples for peptides are given. Using Iodobeads: (*a*) T. J. Tsomides and H. N. Eisen, *Anal. Biochem.*, 1993, **210**, 129; (*b*) K. C. Lee, T. S. Kang, B. H. Woo, J. T. Lee, H. S. Lee and P. P. DeLuca, *J. Chromat. B*, 1997, **694**, 31; Using Iodogen: (*c*) E. S. Kozlowski, G. Johnson, D. D. Dischino, S. I. Dworetzky, C. G. Boissard and V. K. Gribkoff, *Int. J. Pep. Protein Res.*, 1996, **48**, 194; Using the enzymatic method of lactoperoxidase: (*d*) A. Clerico, G. Iervasi, C. Manfredi, S. Salvadori, M. Marastoni, M. G. Del Chicca, D. Giannessi, S. Del Ry, M. G. Andreassi, L. Sabatino, M. R. Iascone, A. Biagini and L. Donato, *Eur. J. Nucl. Med.*, 1995, **22**, 997.

4 (*a*) D. S. Wilbur, W. E. Stone and K. W. Anderson, *J. Org. Chem.*, 1983, **48**, 1542; (*b*) K. J. Edgar and S. N. Falling, *J. Org. Chem.*, 1990, **55**, 5287; (*c*) M. Zupan, J. Iskra and S. Stavber, *Tetrahedron Lett.*, 1997, **38**, 6305.

5 (*a*) J. Barluenga, *Pure Appl. Chem.*, 1999, **71**, 431; (*b*) J. Barluenga and J. M. González, in *Current Trends in Organic Synthesis*, ed. C. Scolastico and F. Nicontra, Kluwer Academic/Plenum Publishers, NY, 1999, pp. 145–151.

6 (*a*) J. Barluenga, J. M. González, M. A. García-Martín, P. J. Campos and G. Asensio, *J. Chem. Soc., Chem. Commun.*, 1992, 1016; (*b*) T. L. Hudgens and K. D. Turnbull, *Tetrahedron Lett.*, 1999, **40**, 2719.

7 (*a*) J. Barluenga, M. A. García-Martín, J. M. González, P. Clapés and G. Valencia, *Chem. Commun.*, 1996, 1505; (*b*) G. Arsequell, G. Espuña, G. Valencia, J. Barluenga, R. Pérez Carlón and J. M. González, *Tetrahedron Lett.*, 1998, **39**, 7393; (*c*) G. Arsequell, G. Espuña, G. Valencia, J. Barluenga, R. Pérez Carlón and J. M. González, *Tetrahedron Lett.*, 1999, **40**, 7279.

8 (*a*) J. Barluenga, J. M. González, M. A. García-Martin, P. J. Campos and G. Asensio, *J. Org. Chem.*, 1993, **58**, 2058; (*b*) J. Barluenga, J. M. González, M. A. García-Martin and P. J. Campos, *Tetrahedron Lett.*, 1993, **34**, 3893.

9 (*a*) W. M. Hunter and F. C. Greenwood, *Nature*, 1962, **194**, 495; (*b*) F. C. Greenwood, W. M. Hunter and J. S. Glover, *Biochem. J.*, 1963, **89**, 114; (*c*) T. Kometani, D. S. Watt and T. Ji, *Tetrahedron Lett.*, 1985, **26**, 2043.

10 Immunological glyco- and phosphopeptides: (*a*) G. Arsequell, J. S. Haurum, T. Elliot, R. A. Dwek and A. C. Lellouch, *J. Chem. Soc. Perkin Trans. 1*, 1995, 739; (*b*) M. A. Andersen, J. Espuny, A. Neisig, G. Arsequell, I. Søndergaard, J. Neefjes, J. Zeuthen, T. Elliot and J. S. Haurum, *J. Immunol.*, 1999, **163**, 3812.

A cyano-bridged molecular magnet with a novel two-dimensional brick wall structure

Hui-Zhong Kou,[a] Song Gao,*[a] Bao-Qing Ma[a] and Dai-Zheng Liao[b]

[a] *State Key Laboratory of Rare Earth Materials Chemistry and Applications, PKU-HKU Joint Laboratory on Rare Earth Materials and Bioinorganic Chemistry, College of Chemistry, Peking University, Beijing 100871, P.R. China. E-mail: gaosong@chemms.chem.pku.edu.cn*

[b] *Department of Chemistry, Nankai University, Tianjin 300071, P.R. China*

Received (in Cambridge, UK) 17th April 2000, Accepted 6th June 2000

Slow diffusion of $K_3[Fe(CN)_6]$ and $[NiL](ClO_4)_2$ (L = 3,10-diethyl-1,3,5,8,10,12-hexaazacyclotetradecane) yields a novel cyano-bridged 2D brick wall-like assembly which is ferromagnetically ordered below 9.1 K with considerably strong hard magnetic behaviour.

It is well known that the cyanide ion can coordinate to one metal ion through the carbon atom acting as a monodentate ligand or connect two metal ions as a bridging ligand through both the carbon and nitrogen atoms. Recently, magnetic interactions between paramagnetic metal ions through the cyanide bridge have been extensively investigated. In particular, the cyanide-bridged 3D bimetallic assemblies of Prussian Blue type, derived from $[M(CN)_6]^{3-}$ (M = Cr^{III}, Fe^{III}) and simple transition metal ions $[M']^{n+}$, have attracted great attention owing to the fact that many of them exhibit a considerably high magnetic critical (Curie) temperature.[1] However, the difficulty in obtaining single crystals suitable for X-ray diffraction analysis precludes the clarification of the magneto–structural correlation. Furthermore, the face-centred cubic structures (based on powder XRD results) they usually possess result in low or no magnetic anisotropy, which would give low or no magnetic coercivity.[1] To overcome these problems, hybrid Prussian Blue analogues have been synthesized by the reaction of coordinately unsaturated transition metal complexes $[M'L]^{m+}$ (L = polydentate ligand) with hexacyanometalate building blocks $[M(CN)_6]^{3-}$ (M = Fe, Cr or Mn).[2,3] Consequently, the introduction of organic ligands could lower the symmetry of the lattice, and afford various molecular structures.[2,3]

Most recently, stair-shaped 2D honeycomb networks, $[Ni(cyclam)]_3[Cr(CN)_6]_2\cdot 20H_2O$,[3a] $[Ni(cyclam)]_3[Fe(CN)_6]_2\cdot xH_2O$,[3b,c] $[NiL^1]_3[Fe(CN)_6]_2\cdot 9H_2O$[3d] and $[NiL^1]_3[Cr(CN)_5(NO)]_2\cdot 10H_2O$[3e] ($L^1$ = 3,10-dimethyl-1,3,6,8,10,12-hexaazacyclotetradecane 3,10-dimethyl-1,3,6,8,10,12-hexaazacyclotetradecane) have been reported. According to Mallah *et al.*, for Ni_3M_2 systems containing *trans* nickel macrocyclic complexes a meridional arrangement might lead to either a 2D flat brick wall-like layer or a double chain stair-like structure. However, this arrangement of five moieties [two $M(CN)_6$ and three Ni(macrocycle)] in a plane imposes a steric hindrance between the macrocycle ligands.[4] Therefore, only stair-shaped 2D honeycomb networks have been obtained so far. We have found, however, that the reaction between a bulky planar macrocyclic nickel(II) complex $[NiL](ClO_4)_2$[5] (L = 3,10-diethyl-1,3,5,8,10,12-hexaazacyclotetradecane) and $K_3[Fe(CN)_6]$ afforded a complex of similar formula, $[NiL]_3[Fe(CN)_6]_2\cdot 12H_2O$ **1**, which does have the flat brick wall-like structure.

Well shaped red–brown crystals of **1** for X-ray structure analysis† and magnetic measurements were grown at room temperature by the slow diffusion of an orange DMF solution (30 mL) of $[NiL](ClO_4)_2$ (0.15 mmol) and a yellow aqueous solution (30 mL) of $K_3[Fe(CN)_6]$ (0.15 mmol) in an H-tube.‡

The structure consists of neutral flat layers with slightly distorted rectangles. Unlike the honeycomb-like complexes mentioned above, in which three [Ni(cyclam)] or $[NiL^1]$ groups connect with three cyanide groups in a *fac* arrangement at an iron(III), chromium(II) or chromium(III) cation,[3] in the present complex each $[Fe(CN)_6]^{3-}$ unit uses three cyanide groups in a meridional arrangement to connect with three *trans*-$[NiL]^{2+}$ units [Fig. 1(a)]. This particular local molecular disposition extends to give rise to a brick wall-like structure [Fig. 1(b)], as predicted by Mallah *et al.*[4] The bridging cyanide ligands coordinate to the nickel(II) ions in a considerably bent fashion with Ni–N≡C bond angles of 148.5(9)° for C(1)–N(1)–Ni(2), 151.4(9)° for C(4)–N(4)–Ni(1) and 152.1(9)° for C(3)–N(3)–Ni(3), which prevents the steric hindrance of L. The coordination environment of the nickel ions can be described as axially elongated octahedral. Adjacent Fe···Ni distances are 5.003(2) Å for Fe···Ni(1), 4.987(2) Å for Fe···Ni(2) and 4.985(2) Å for Fe···Ni(3), respectively. In the crystal, the layers align along the

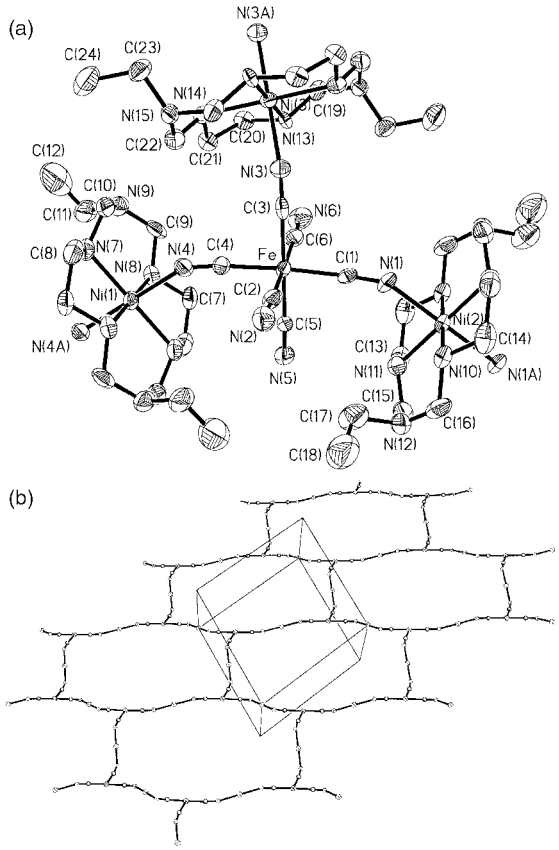

Fig. 1 (a) ORTEP plot of complex **1**. Selected bond distances (Å): Ni(2)–N(10) 2.050(9), Ni(2)–N(11) 2.053(9), Ni(2)–N(1) 2.126(8), Ni(3)–N(13) 2.064(8), Ni(3)–N(14) 2.066(8), Ni(3)–N(3) 2.111(9), Ni(1)–N(8) 2.072(10), Ni(1)–N(7) 2.074(8), Ni(1)–N(4) 2.139(10). (b) Projection along the *a* axis showing the brick wall-like backbone containing Fe_6Ni_6 rectangles.

DOI: 10.1039/b003089i

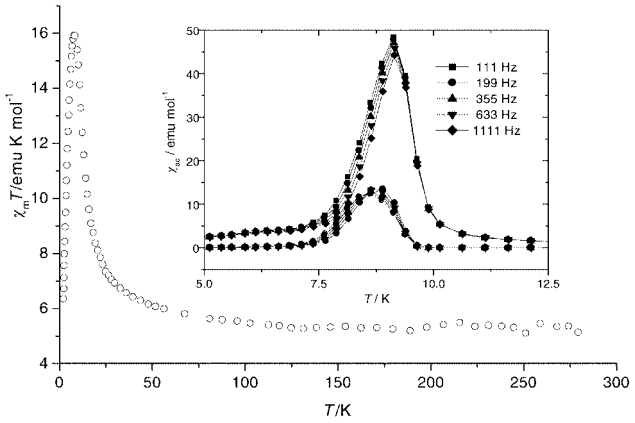

Fig. 2 Temperature dependence of $\chi_M T$ for **1**. Real (χ') and imaginary (χ'') ac magnetic susceptibilities in zero applied dc field and an ac field of 2 Oe at different frequencies for **1** are shown in the inset.

[110] direction with a separation of *ca*. 8.33 Å, and the nearest interlayer metal–metal distance is 8.53 Å for Ni(2)···Fe. Water molecules are positioned between the layers and are linked to the terminal CN^- ligands of $Fe(CN)_6^{3-}$ and other water molecules *via* hydrogen bonding.

The magnetic susceptibility of **1** has been measured on a crystalline sample confined within a gelatine capsule under a field of 10 kOe in the temperature range 2–280 K. A plot of $\chi_m T$ *vs*. T is shown in Fig. 2, where χ_m is the magnetic susceptibility per Ni_3Fe_2 unit. The $\chi_m T$ value at 280 K is *ca*. 5.3 emu K mol^{-1} (6.5 μ_B) which increases smoothly and then sharply with decreasing temperature, reaching a maximum value of 15.9 emu K mol^{-1} (11.3 μ_B) at 7.8 K, strongly suggestive of the occurrence of magnetic ordering. Below 7.8 K, $\chi_m T$ decreases rapidly, which may be due to interlayer antiferromagnetic interactions, a saturation effect and/or the zero-field splitting effect of nickel(II) ions in axially elongated octahedral surroundings. The magnetic susceptibility above 8.4 K obeys the Curie–Weiss law with a positive Weiss constant, θ, of +7.0 K.

The onset of a long-range magnetic phase transition is confirmed by the temperature dependence of the ac magnetic susceptibility displayed in the inset of Fig. 2. The real part of the ac magnetic susceptibility, χ', has a maximum at *ca*. 9.1 K for a frequency of 111 Hz, suggesting that T_c of complex **1** is *ca*. 9.1 K. The weak frequency dependence of χ_{ac}' and χ_{ac}'' suggests a degree of glassy behaviour.

The field dependence of the magnetization (0–50 kOe) measured at 1.6 K shows rapid saturation of magnetization reaching a value of 7.4 $N\beta$ at 50 kOe which is close to the expected $S = 4$ value of 8 $N\beta$ for a ferromagnetic Ni_3Fe_2 system. A hysteresis loop at 1.6 K was observed with a coercive field as large as 1500 Oe and a remnant magnetization of *ca*. 1.36 $N\beta$ per Ni_3Fe_2 unit, typical of a hard ferromagnet. To our knowledge, the coercivity in **1** is the highest measured for hybrid Prussian Blue analogues, probably due to the presence of the magnetic anisotropy of the paramagnetic ions, the grain size of the sample used and/or irreversible movements of the domain walls.[1a,2b,6] Magnetic studies on samples of different sizes should bring some insights into the origins of the large coercive field and remnant magnetization. Further work to this end is in progress in our laboratory.

In conclusion, we have obtained a hybrid Prussian Blue analogue with a unique brick wall-like molecular structure which serves as a new molecule-based ferromagnet showing hard magnetic behaviour.

This work was supported by the State Key Project of Fundamental Research (G1998061306), the National Natural Science Foundation of China (29771001 and 29831010) and the Excellent Young Teachers Fund of MOE, P.R.C.

Notes and references

† *Crystal data* for **1**: $C_{48}H_{114}N_{30}O_{12}Ni_3Fe_2$, $M = 1591.52$, triclinic, space group $P\bar{1}$, $a = 10.018(2)$, $b = 13.861(3)$, $c = 15.162(3)$ Å, $\alpha = 102.06(3)$, $\beta = 101.24(3)$, $\gamma = 92.67(3)°$, $V = 2011.0(7)$ Å^3, $Z = 1$, $D_c = 1.314$ g cm^{-3}, μ(Mo-Kα) = 1.018 mm^{-1}, $T = 293$ K. A total of 7004 unique reflections were collected in the range $3.47 < \theta < 25°$, of which 2227 were considered observed [$I \geqslant 2\sigma(I)$] and used in the calculations. The final conventional R factor (on F^2) was 0.0850 [*wR2* = 0.2492 (all data)].

‡ Yield 9 mg. IR (KBr): ν/cm^{-1} = 2150, 2130 and 2110 (C≡N).

CCDC 182/1673. See http://www.rsc.org/suppdata/cc/b0/b003089i/ for crystallographic files in .cif format.

1 See, for example: (*a*) V. Gadet, T. Mallah, I. Castro and M. Verdaguer, *J. Am. Chem. Soc.*, 1992, **114**, 9213; (*b*) Ø. Hatlevik, W. E. Bushmann, J. Zhang, J. L. Manson and J. S. Miller, *Adv. Mater.*, 1999, **11**, 914; (*c*) S. M. Holmes and G. S. Girolami, *J. Am. Chem. Soc.*, 1999, **121**, 5593; (*d*) O. Sato, T. Iyoda, A. Fujishima and K. Hashimoto, *Science*, 1996, **272**, 704.

2 See, for example: (*a*) K. V. Langenberg, S. R. Batten, K. J. Berry, D. C. R. Hockless, B. Moubaraki and K. S. Murray, *Inorg. Chem.*, 1997, **36**, 5006; (*b*) M. S. El Fallah, E. Rentschler, A. Caneschi, R. Sessoli and D. Gatteschi, *Angew. Chem., Int. Ed. Engl.*, 1996, **35**, 1947; (*c*) M. Ohba, N. Usuki, N. Fukita and H. Okawa, *Angew. Chem., Int. Ed. Engl.*, 1999, **38**, 1795; (*d*) H.-Z. Kou, W.-M. Bu, D.-Z. Liao, P. Cheng, Z.-H. Jiang, S.-P. Yan, Y.-G. Fan and G.-L. Wang, *J. Chem. Soc., Dalton Trans.*, 1998, 4161; (*e*) A. Marvilliers, S. Parsons, E. Riviere, J. P. Audiere and T. Mallah, *Chem. Commun.*, 1999, 2217.

3 (*a*) S. Ferlay, T. Mallah, J. Vaissermann, F. Bartolome, P. Veillet and M. Verdaguer, *Chem. Commun.*, 1996, 2481; (*b*) E. Colacio, J. M. Dominguez-Vera, M. Ghazi, R. Kivekas, F. Lloret, J. M. Moreno and H. Stoeckli-Evans, *Chem. Commun.*, 1999, 987; (*c*) B. Nowicka, M. Hagiwara, Y. Wakatsuki and H. Kisch, *Bull. Chem. Soc. Jpn.*, 1999, **72**, 441; (*d*) H.-Z. Kou, S. Gao, W.-M. Bu, D.-Z. Liao, B.-Q. Ma, Z.-H. Jiang, S.-P. Yan, Y.-G. Fan and G.-L. Wang, *J. Chem. Soc., Dalton Trans.*, 1999, 2477; (*e*) H.-Z. Kou, S. Gao, B.-Q. Ma and D.-Z. Liao, *Chem. Commun.*, 2000, 713.

4 T. Mallah, A. Marvilliers and E. Riviere, *Phil. Trans. R. Soc. London A*, 1999, **357**, 3139.

5 M. P. Suh and S.-G. Kang, *Inorg. Chem.*, 1988, **27**, 2544.

6 H. O. Stumpf, Y. Pei, C. Michaut, O. Kahn, J. P. Renard and L. Ouahab, *Chem. Mater.*, 1994, **6**, 257.

ChemComm

Observations on the transition-metal catalysed oxidation of alkanes in trifluoroacetic acid: urea–hydrogen peroxide/TFA as a convenient method for the oxidation of unactivated C–H bonds

Christopher J. Moody and Jenny L. O'Connell

School of Chemistry, University of Exeter, Stocker Road, Exeter, UK EX4 4QD. E-mail: c.j.moody@ex.ac.uk

Received (in Liverpool, UK) 17th April 2000, Accepted 22nd May 2000

Oxidation of cyclohexane in TFA using 30% aqueous H_2O_2 or urea–H_2O_2 (UHP) gives cyclohexyl trifluoroacetate in good yield, although the reaction is not accelerated by rhodium or ruthenium catalysts casting doubt on earlier claims on the role of transition-metals in oxidations in TFA.

The oxidation of unactivated C–H bonds in alkanes is often regarded as one of the Holy Grails of organic chemistry.[1] Whereas in Nature such oxidations are efficiently carried out by enzymes, there exists no single general laboratory or industrial method, despite the undoubted commercial importance of such a process. Nevertheless a number of methods have been developed which do effect the oxidation of unactivated C–H bonds: these include oxidations in superacid media,[2] using peroxide type reagents (including peracids, dioxiranes and oxaziridines),[3] ozone,[4] various cytochrome P450 models,[5] and a range of metal mediated oxidations,[6] including Gif chemistry.[7] Much of the current work in this area focuses on the use of transition-metal catalysed processes, and in view of our own interest in reactions catalysed by dirhodium(II) carboxylates,[8] we were intrigued to see a *Chemical Communication* in which dirhodium tetraacetate was reported to catalyse the oxidation of cyclohexane by hydrogen peroxide in TFA.[9] As a prelude to investigating the role of dirhodium(II) catalysts in other oxidation reactions, we have reinvestigated this original work, and report our results herein.

In their communication, Nomura and Uemura reported that a variety of rhodium salts (0.1–0.3 mol%) catalysed the oxidation of cyclohexane by 30% aqueous hydrogen peroxide in TFA. The yields of cyclohexyl trifluoroacetate were consistently 62–65% irrespective of the rhodium salt used, and the authors suggested a mechanism involving a highly reactive oxorhodium species.[9] The use of strongly acidic media is quite common in metal catalysed oxidations of hydrocarbons since (a) the conjugate base of a strong acid is a poor σ-donor and therefore enhances the electrophilicity of the metal ion, and (b) the esterification of the alcohol, the primary product of alkane oxidation, protects it from further oxidation.[10] However, it appears that the authors did not carry out a blank reaction in TFA in the absence of the rhodium salt.[9] This is somewhat surprising since many years earlier Deno and Messer also reported the oxidation of cyclohexane to cyclohexyl trifluoroacetate (73% yield) under more or less identical conditions (30% aqueous H_2O_2 in TFA) but in the *absence* of any metal salt.[11] Therefore our initial experiments were designed to investigate this apparent anomaly (Scheme 1). When cyclohexane (5 mmol) was treated with 30% aqueous H_2O_2 (15 mmol) in TFA (12 ml) in the presence of dirhodium tetraacetate (1 mol%) at room temperature, oxidation to cyclohexyl trifluoroacetate did indeed occur as evidenced by gas chromatographic analysis which clearly showed disappearance of the hydrocarbon and formation of the ester over 12 h (Fig. 1). When the blank experiment was run under identical conditions but in the absence of the rhodium complex a very similar plot was obtained (Fig. 1). The results show that this particular oxidation of cyclohexane clearly proceeds in the absence of the metal complex, and furthermore dirhodium tetraacetate does not catalyse the reaction.

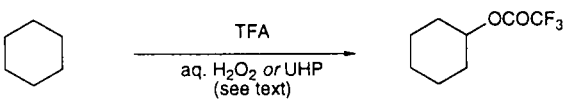

Scheme 1

In order to obtain rate constants for the oxidation of cyclohexane in TFA, aqueous H_2O_2 was replaced by the urea hydrogen peroxide complex (UHP), a convenient solid source of anhydrous H_2O_2. This enabled the use of a large excess of peroxide to create pseudo-first order reaction conditions. Under these conditions (2.5 mmol cyclohexane in 2 ml CH_2Cl_2, 22 mmol UHP, 10 ml TFA), rates for the oxidation of cyclohexane in the presence ($k = 2.9 \times 10^{-5}$ M^{-1} s^{-1}) and absence ($k = 3.3 \times 10^{-5}$ M^{-1} s^{-1}) of dirhodium tetraacetate were readily obtained (Fig. 2). Given the error in the determination of rate constants (estimated as ±10%), the rates of these two reactions are clearly similar. In both the 30% aqueous H_2O_2–TFA and UHP–TFA oxidations, trace amounts of cyclohexanol were also observed. In a separate blank experiment it was shown that cyclohexanol is readily esterified in TFA, and therefore the alcohol is presumably the initial product of oxidation.

We also investigated the use of ruthenium catalysts based on the $RuCl_3$–TFA system reported by Murahashi *et al.*,[12] which was also thought to involve a metal oxo complex as the oxidant. Again it was evident that $RuCl_3$ also had no effect on the rate of cyclohexane oxidation in TFA ($k = 3.1 \times 10^{-5}$ M^{-1} s^{-1}). Therefore, we conclude that claims of transition-metal catalysed oxidations of hydrocarbons in peroxide–TFA systems should be viewed with caution in cases where the appropriate blank experiments have not been carried out. This view concurs with that of Hogan and Sen who have independently concluded that the role of the metal in C–H oxidation reactions carried out in TFA needs to be reassessed.[10,13]

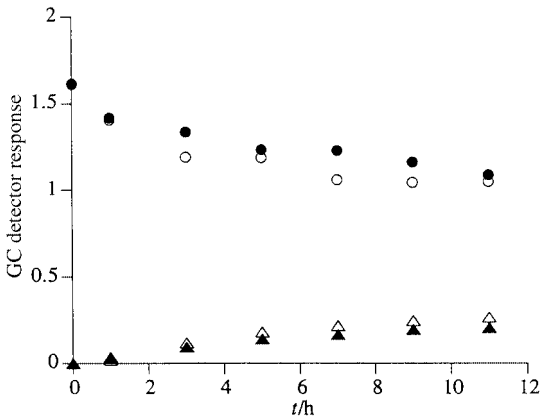

Fig. 1 Cyclohexane consumption and cyclohexyl trifluoroacetate formation *vs.* time in 30% aqueous hydrogen peroxide–TFA in the absence (○/△) or presence (●/▲) of dirhodium tetraacetate.

DOI: 10.1039/b003074k

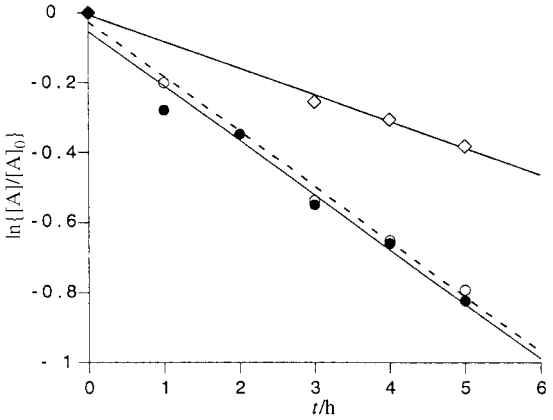

Fig. 2 Oxidation of cyclohexane by UHP–TFA in absence (○) or presence (●) (1 mol%) of dirhodium tetraacetate, and oxidation of cyclohexane-d_{12} (◇), where $[A]_0$ is the initial concentration of cyclohexane.

In the work of Deno *et al.* using 30% aqueous H_2O_2 in TFA,[11,14] it was assumed that the active oxidant was peroxytrifluoroacetic acid which participated in a concerted oxidation mechanism *via* a cyclic transition state, the electrophilic nature of the oxidant being further enhanced by protonation (Scheme 2). To shed further light on the mechanism of the UHP–TFA oxidation, we compared the rate of oxidation of cyclohexane with its perdeuterated analogue ($k = 1.4 \times 10^{-5}$ M^{-1} s^{-1}) (Fig. 2). The observed kinetic isotope effect of 2.3 ± 0.2 is in accord with previous studies using peracids as oxidants, and is possibly indicative of a concerted (*cf.* Scheme 2) or oxenoid type mechanism.[3a] Unfortunately alternative mechanisms involving radical hydrogen abstractions cannot be completely ruled out, since although such reactions usually exhibit a significantly larger deuterium isotope effect ($k_H/k_D \approx 4$–8),[15] the isotope effect can be as low as 1.[16]

The preparative oxidation of hydrocarbons was briefly investigated, and some illustrative examples are shown in Table 1. Cyclohexane, cycloheptane ($k = 6.4 \times 10^{-5}$ M^{-1} s^{-1}) and cyclooctane were all oxidized to the corresponding esters; norbornane gave the ester of *exo*-norborneol as the major product, and although adamantane was rapidly oxidized to the tertiary ester, with no sign of the secondary ester by GC, the product was unstable under the reaction conditions. *n*-Hexane gave a mixture of 2- and 3-hexyl trifluoroacetates (ratio = 47:53) with no evidence for oxidation at the terminal methyl group. Compounds containing aromatic rings (*n*-propylbenzene, cumene, tetralin) were completely decomposed in either 30% aqueous H_2O_2–TFA or in UHP–TFA.[17]

In summary, we have shown that UHP–TFA is a simple system for the oxidation of unactivated C–H bonds in alkanes; such reactions are not accelerated by rhodium or ruthenium catalysts, and therefore claims of metal catalysis of related reactions in TFA should be viewed with caution.

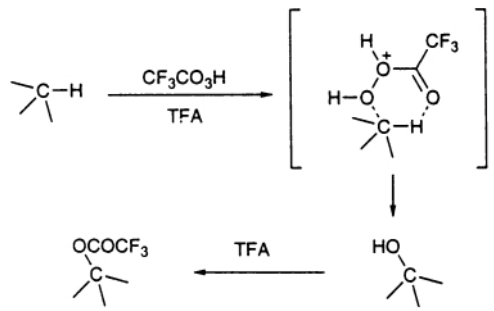

Scheme 2

Table 1 Preparative scale hydrocarbon oxidation using UHP–TFA

Alkane	Product	Yield (%)
	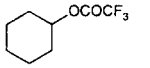	80
	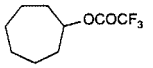	78
	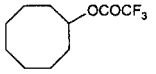	45[a]
	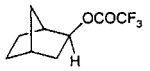	67[a,b]
	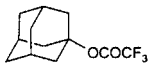	[c]

[a] GC yield; the reaction mixture is more complex. [b] Only the *exo*-product was observed. [c] Product not stable under reaction conditions; identified by GC by comparison with an authentic sample; 2-adamantyl trifluoroacetate was not present (GC).

This work was supported by the EPSRC.

Notes and references

1 For recent reviews: O. Reiser, *Angew. Chem., Int. Ed. Engl.*, 1994, **33**, 69; B. A. Arndtsen, R. G. Bergman, T. A. Mobley and T. H. Peterson, *Acc. Chem. Res.*, 1995, **28**, 154.

2 G. A. Olah, D. G. Parker and N. Yoneda, *Angew. Chem., Int. Ed. Engl.*, 1978, **17**, 909.

3 (*a*) H.-J. Schneider and W. Muller, *J. Org. Chem.*, 1985, **50**, 4609; (*b*) G. Asensio, R. Mello, M. E. Gonzalez-Nunez, G. Castellano and J. Corral, *Angew. Chem., Int. Ed. Engl.*, 1996, **35**, 217; (*c*) R. Mello, M. Florentino, C. Fusco and R. Curci, *J. Am. Chem. Soc.*, 1989, **111**, 6749; (*d*) A. Bravo, H. R. Bjorsvik, F. Fontana, F. Minisci and A. Serri, *J. Org. Chem.*, 1996, **61**, 9409; (*e*) A. Arnone, S. Foletto, P. Metrangolo, M. Pregnolato and G. Resnati, *Org. Lett.*, 1999, **1**, 281.

4 D. H. Giamalva, D. F. Church and W. A. Pryor, *J. Org. Chem.*, 1988, **53**, 3429.

5 B. Meunier, *Chem. Rev.*, 1992, **92**, 1411.

6 A. E. Shilov and G. B. Shul'pin, *Chem. Rev.*, 1997, **97**, 2879.

7 D. H. R. Barton and D. Doller, *Acc. Chem. Res.*, 1992, **25**, 504.

8 R. T. Buck, D. M. Coe, M. J. Drysdale, C. J. Moody and N. D. Pearson, *Tetrahedron Lett.*, 1998, **39**, 7181; C. J. Moody, S. Miah, A. M. Z. Slawin, D. J. Mansfield and I. C. Richards, *Tetrahedron*, 1998, **54**, 9689.

9 K. Nomura and S. Uemura, *J. Chem. Soc., Chem. Commun.*, 1994, 129.

10 A. Sen, *Acc. Chem. Res.*, 1998, **31**, 550.

11 N. C. Deno and L. A. Messer, *J. Chem. Soc., Chem. Commun.*, 1976, 1051.

12 S. Murahashi, Y. Oda, N. Komiya and T. Naota, *Tetrahedron Lett.*, 1994, **35**, 7953.

13 T. Hogan and A. Sen, *J. Am. Chem. Soc.*, 1997, **119**, 2642.

14 N. C. Deno, E. J. Jedziniak, L. A. Messer, M. D. Meyer, S. G. Stroud and E. S. Tomezsko, *Tetrahedron*, 1977, **33**, 2503.

15 S. Murahashi, Y. Oda, T. Naota and T. Kuwabara, *Tetrahedron Lett.*, 1993, **34**, 1299; A. S. Goldstein, R. H. Beer and R. S. Drago, *J. Am. Chem. Soc.*, 1994, **116**, 2424; Z. Wan and W. S. Jenks, *J. Am. Chem. Soc.*, 1995, **117**, 2667.

16 B. Singh, J. R. Long, F. F. deBiani, D. Gatteschi and P. Stavropoulos, *J. Am. Chem. Soc.*, 1997, **119**, 7030.

17 *Cf.* N. C. Deno, B. A. Greigger, L. A. Messer, M. D. Meyer and S. G. Stroud, *Tetrahedron Lett.*, 1977, 1703.

Formation of carbene and cyclopentadienyl ligands from phenylacetylene *via* oligomerisation and C≡C bond scission at a mixed-metal W–Co centre

John E. Davies,[a] Martin J. Mays,*[a] Paul R. Raithby,[a] Koshala Sarveswaran[a] and Gregory A. Solan[b]

[a] *Department of Chemistry, Lensfield Road, Cambridge, UK CB2 1EW. E-mail: mjm14@cam.ac.uk*
[b] *Department of Chemistry, University of Leicester, University Road, Leicester, UK LE1 7RH*

Received (in Cambridge, UK) 25th April 2000, Accepted 9th June 2000

The 1,2,4-triphenylcyclopentadienyl ligand and the CHR carbene ligand, bound respectively to the Co and W atoms in [(η⁵-C_5H_5)W{μ-CBu^{t}CC(CO_2Me)=C(CO_2Me)CH}(μ-PPh_2)Co(η⁵-$C_5Ph_3H_2$)], are derived from the oligomerisation and cleavage of three molecules of phenylacetylene in the reaction of [(OC)(η⁵-C_5H_5)W{μ-C(CO_2Me)CC(C≡CBu^t)(OMe)O}(μ-PPh_2)Co($CO)_2$] with this acetylene.

The catalytic cyclo-oligomerisation of alkynes mediated by mononuclear, binuclear and polynuclear transition metal complexes to give organic compounds such as benzenes, fulvenes and cyclooctatetraenes has been well documented.[1–4] Sometimes stable organometallic complexes can be isolated in which the metal atom is ligated by the cyclised oligomer or is incorporated in a metallocyclic ring with the oligomeric moiety as in [(η⁴-Ph_4C_4)RhCl]$_2$ (from the dimerisation of diphenylacetylene),[5] [(η⁶-C_6Me_6)Co(η⁵-C_5H_5)] (from the trimerisation of dimethylacetylene)[6] or [$Co_2(CO)_4${μ-C(Bu^t)-CHCHCHCHC(Bu^t)}] (from the co-trimerisation of *tert*-butylacetylene and acetylene).[7] Reports of the oligomerisation and cleavage of an acetylene to give a C_5R_5-ring and CR unit (R = H, alkyl or aryl) are considerably more scarce. The few examples that have been reported all feature reactions of trinuclear or higher nuclearity homometallic cluster complexes and furnish organometallic products only in low[8] to very low yields.[9]

Recently, we have been interested in C–C coupling reactions of alkynes or acetylides on mixed-metal dinuclear transition metal centres. For example, the reaction of the alkyne-bridged complex [(OC)$_2$(η⁵-C_5H_5)W{μ-C(CO_2Me)C(CO_2Me)}Co-($CO)_3$] with PPh_2C≡CBu^t leads to [(OC)(η⁵-C_5H_5)W{μ-C-(CO_2Me)CC(C≡CBu^t)(OMe)O}(μ-PPh_2)Co($CO)_2$] **1** in which an acetylide fragment, generated from P–C bond cleavage within the PPh_2C≡CBu^t ligand, has coupled with the bridging alkyne.[10] Here, we report that phenylacetylene undergoes C≡C bond scission and oligomerisation on reaction with **1** to form a tungsten–cobalt complex containing an η⁵-bound triphenylcyclopentadienyl ligand and a terminal CHR carbene ligand (Scheme 1) both derived from phenylacetylene.

Treatment of **1** with excess phenylacetylene in toluene at 383 K for 6 h affords air stable [(η⁵-C_5H_5)W{μ-CBu^{t}CC(CO_2-Me)=C(CO_2Me)CH}(μ-PPh_2)Co(η⁵-$C_5Ph_3H_2$)] **2** as the sole product in 46% yield.† The product was isolated by TLC on silica [hexane–ethylacetate (3:1) as eluent] as a brown crystalline solid and characterised on the basis of ^{1}H, ^{13}C and ^{31}P NMR spectroscopy,‡ FAB-MS and X-ray diffraction.§

The molecular structure of compound **2** is depicted in Fig. 1. The molecule comprises a tungsten–cobalt core [W–Co 2.704(1) Å] with both metal atoms being bound terminally by mutually *cis* η⁵-cyclopentadienyl ligands [C_5H_5 on W and 1,2,4-$C_5Ph_3H_2$ on Co] and bridged by a PPh_2 group and a six-electron donor CBu^{t}CC(CO_2Me)=C(CO_2Me)CH ligand. The organic bridging ligand can be considered as a η^2:η$^{2\prime}$-bridging alkyne [*via* C(45) and C(46)] with one of the alkyne substituents being a Bu^t group and the other a C(CO_2Me)=C(CO_2Me)CH group. This latter group further coordinates to W *via* the CH carbene carbon atom [W=C(53) 2.000(7) Å]. The metallocyclopentadienyl ring so formed, [W(1)–C(46)–C(47)=C(50)–C(53)=], is almost planar [maximum deviation from plane 0.039 Å, C(46)] with the other end of the bridging alkyne [C(45)], sitting out of this plane. Both cyclopentadienyl groups are essentially planar with the phenyl rings in the 1,2,4-triphenylcyclopentadienyl ligand being located slightly out of the plane of the C_5 ring [C(11) elevation 0.243 Å, C(17) elevation 0.335 Å, C(23) elevation 0.297 Å] and tilted with torsion angles of 28.9° [C(24)–C(23)–C(9)–C(10)], 34.9° [C(12)–C(11)–C(6)–C(10)] and 49.9° [(C(18)–C(17)–C(7)–C(8)] with respect to the plane of the ring.

The key features of the structure of **2** are the presence of the 1,2,4-$C_5Ph_3H_2$ ligand and the W(1)=C(53) double bond. The formation of the carbene and the substituted cyclopentadienyl ring requires the cleavage of the C≡C triple bond in phenylacetylene to give PhC and CH fragments. The C_5 ring is formed by the linking of two unbroken phenylacetylene ligands with the C–Ph fragment, whereas the CH fragment inserts into the W–C bond of the bridging ligand in **1**, with resultant displacement of the coordinated vinyl and ester groups, to form a μ-CBu^{t}CC-(CO_2Me)=C(CO_2Me)CH ligand. Examples of crystallographically characterised homo- and hetero-bimetallic tungsten complexes containing a terminally bound carbene ligands are rare[11] with the W(1)=C(53) bond distance [2.000(7) Å] in **2** falling in the mid-range. It is noteworthy that the organic transformation mediated by **1** has resulted in the loss in **2** of all the terminal carbonyl groups in **1**.

The spectroscopic data for **2** is consistent with the solid state structure being maintained in solution. In the IR spectrum two weak bands at 1727 and 1698 cm^{-1} can be attributed to the ketonic carbonyls of the MeO_2CC=CCO_2Me unit. The ^{1}H NMR spectrum of **2** displays, in addition to phenyl and alkyl resonances, a downfield singlet at δ 11.8 which is assigned to the carbene CH proton. Similarly, a downfield shift is observed for the carbene carbon atom in the ^{13}C NMR spectrum at δ 234.3

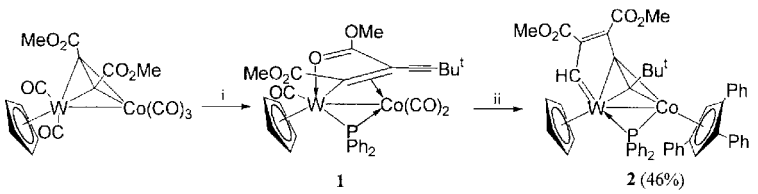

Scheme 1 *Reagents and conditions*: i, Ph_2PC≡CBu^t, heat; ii, PhC≡CH, heat, 6 h.

DOI: 10.1039/b003296o

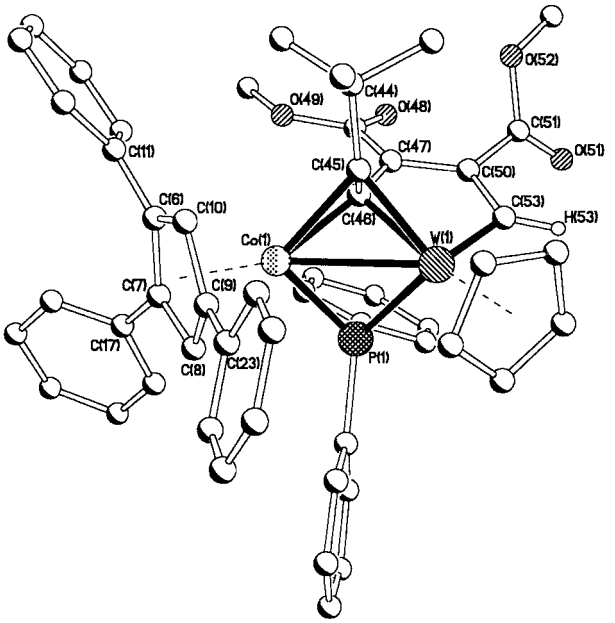

Fig. 1 The molecular structure of $[(\eta^5\text{-}C_5H_5)W\{\mu\text{-}CBu^tCC(CO_2Me)\text{=}C(CO_2Me)CH\}(\mu\text{-}PPh_2)Co(\eta^5\text{-}C_5Ph_3H_2)]$ **2** with all hydrogen atoms except for H(53) omitted for clarity. Selected bond lengths (Å) and angles (°): W(1)–Co(1) 2.704(1), W(1)–C(53) 2.000(7), W(1)–C(46) 2.157(6), W(1)–C(45) 2.045(6), W(1)–P(1) 2.354(2), W(1)–$(C_5H_5)_{centroid}$ 2.053(6), Co(1)–C(46) 2.007(6), Co(1)–$(C_5Ph_5H_2)_{centroid}$ 1.739(6), Co(1)–C(45) 2.096(6), Co(1)–P(1) 2.187(2), C(45)–C(46) 1.443(8), C(46)–C(47) 1.429(8), C(47)–C(50) 1.383(8), C(50)–C(53) 1.431(9); Co(1)–P(1)–W(1) 72.98(5), C(53)–W(1)–Co(1) 120.1(2), C(45)–W(1)–Co(1) 50.1(2), C(46)–Co(1)–W(1) 52.0(2).

while the carbon atoms of the 1,2,4-substituted cyclopentadienyl ring are seen as upfield singlets at δ 106.7 (*C*–Ph) and 87.0 (C–H).

The mechanism by which the transformation of **1** to **2** occurs is uncertain but it is remarkable that only one product is formed in significant yield from such a complex reaction. A notable feature is that the acetylenic-based bridging ligand in **1** does not participate in the formation of the substituted cyclopentadienyl ligand.[12] Although the yield for the reaction of **1** to give **2** has not been fully optimised it still represents a considerable enhancement of the low yields previously obtained in the cluster-mediated formation of cyclopentadienyl and carbene ligands from acetylenes.[8,9,13] Further work is underway to assess the scope of the transformation and this will be the subject of a future publication.

We wish to thank the Cambridge Commonwealth Trust and Professor B. F. G. Johnson for funding (to K. S.).

Notes and references

† *Synthesis* of **2**: phenylacetylene (0.2 cm^3, 1.80 mmol) was added dropwise to a solution of $[(\eta^5\text{-}C_5H_5)(OC)W\{\mu\text{-}C(CO_2Me)\text{=}C(CCBu^t)C(OMe)O\}(\mu\text{-}PPh_2)Co(CO)_2]$ **1** (0.30 g, 0.37 mmol) in toluene (50 cm^3) and heated at 383 K for 6 h. After the removal of volatiles under reduced pressure, the residue was loaded on to the base of silica TLC plates and eluted with hexane–ethylacetate (3:1) to give **2** as a brown crystalline complex (0.18 g, 46%). FAB mass spectrum, *m/z* 1022 [M$^+$]. Found: C, 63.02; H, 5.11. Calc. for $C_{53}H_{48}CoO_4PW$ **2**: C, 62.24, H, 4.73%).

‡ *Selected spectroscopic data* for **2**: IR (hexane) ν(CO)/cm^{-1}: 1727w, 1698w: NMR ($CDCl_3$): ^{1}H, δ 11.8 (s, 1H, =CH), 8.0–6.7 (m, 25H, Ph), 5.5 (s, 7H, C_5H_5 and $C_5Ph_3H_2$), 3.4 (s, 3H, CO_2Me), 3.3 (s, 3H, CO_2Me), 0.82 (s, 9H, Bu^t): ^{13}C-{^{1}H}, δ 234.2 (s, =CH), 167.7 (s, *C*O_2Me), 167.1 (s, *C*O_2Me), 153.6 (s, *C*CO_2Me), 146.0 (s, *C*CO_2Me), 137–125 (m, Ph), 106.7 (s, *C*Ph), 95.7 (s, Cp), 87.0 (s, CH), 50.9 (s, CO_2*Me*), 50.6 (s, CO_2*Me*), 44.9 (s, *C*Me_3), 33.0 (s, C*Me*$_3$): ^{31}P-{^{1}H}, δ 89.3 (s, μ-PPh_2).

§ *Crystal data* for **2**: $C_{53}H_{48}CoO_4PW$, M = 1022.66, monoclinic, space group $P2_1/n$, a = 10.402(5), b = 21.565(5), c = 19.623(5) Å, β = 100.70(2)°, V = 4325(3) Å^3, Z = 4, D_c = 1.570 g cm^{-3}, μ(Mo-Kα) = 3.125 mm^{-1}, F(000) = 2056, T = 180(2) K; orange/red prisms, 0.10 × 0.10 × 0.10 mm, Rigaku RAXIS-IIC imaging plate, three sets of 35, 25 and 60 frames (each with crystal in a different orientation), 3° rotation per frame and 30 min exposure per frame, 7611 (R_{int} = 0.0780) independent reflections. The structure was solved by direct methods and the non-hydrogen atoms of the complex were refined anisotropically using full-matrix least squares based on F^2 to give R_1 = 0.0491, wR_2 = 0.0949 for 5765 independent observed reflections [$I > 2\sigma(I)$] and 562 parameters.

CCDC 182/1680. See http://www.rsc.org/suppdata/cc/b0/b003296o/ for crystallographic files in .cif format.

1 N. E. Schore, *Chem. Rev.*, 1988, **88**, 1081; M. J. Winter, in *The Chemistry of Metal–Carbon Bond*, ed. F. R. Hartley and S. Patai, John Wiley & Sons, Chichester, 1985, vol. 3, p. 259.
2 G. Süss-Fink and G. Meister, *Adv. Organomet. Chem.*, 1993, **35**, 41.
3 R. E. Colborn and K. P. C. Vollhardt, *J. Am. Chem. Soc.*, 1986, **108**, 5470; W. Reppe, O. Schlichting, K. Klager and T. Toepel, *Justus Liebigs Ann. Chem.*, 1948, **560**, 1.
4 A. D. Burrows, M. Green, J. C. Jeffery, J. M. Lynam and M. F. Mahon, *Angew. Chem., Int. Ed.*, 1999, **38**, 3043; E. S. Johnson, G. J. Balaich, P. E. Fanwick and I. P. Rothwell, *J. Am. Chem. Soc.*, 1997, **119**, 11 086; J. M. O'Connor, K. Hiibner, R. Merwin, P. K. Gantzel, B. S. Fong, M. Adams and A. L. Rheingold, *J. Am. Chem. Soc.*, 1997, **119**, 3631.
5 A. Efraty, *Chem. Rev.*, 1977, **77**, 691; M. Maitlis, *Acc. Chem. Res.*, 1976, **9**, 93.
6 K. Jonas, E. Deffense and D. Habermann, *Angew. Chem., Int. Ed. Engl.*, 1983, **22**, 716.
7 R. S. Dickson and P. J. Fraser, *Adv. Organomet. Chem.*, 1974, **12**, 323; E. M. Arnett, *J. Am. Chem. Soc.*, 1964, **86**, 4729.
8 J. L. Haggitt, B. F. G. Johnson, A. J. Blake and S. Parsons, *J. Chem. Soc., Chem. Commun.*, 1995, 1263.
9 S. Aime, L. Milone, E. Sappa and A. Tiripicchio, *J. Chem. Soc., Dalton Trans.*, 1977, 227; E. Sappa, A. Tiripicchio and A. M. M. Lanfredi, *J. Chem. Soc., Dalton Trans.*, 1978, 552.
10 J. E. Davies, M. J. Mays, P. R. Raithby, K. Sarveswaran and G. P. Shields, *J. Organomet. Chem.*, 1999, **573**, 180.
11 H. Adams, N. A. Bailey and M. J. Winter, *J. Chem. Soc., Dalton Trans.*, 1984, 273; D. Hodgson, J. A. K. Howard, F. G. A. Stone and M. J. Went, *J. Chem. Soc., Dalton Trans.*,1985, 1331; M. J. Breen, P. M. Shulmann, G. L. Geoffroy, A. L. Rheingold and W. C. Fultz, *Organometallics*, 1984, **3**, 782.
12 For comparison see, A. J. Blake, J. L. Haggitt, B. F. G. Johnson and S. Parsons, *J. Chem. Soc., Dalton Trans.*, 1997, 991; G. Brauer, F. J. Feher, M. Green, J. K. Hogg and A. G. Orpen, *J. Chem. Soc., Dalton Trans.*, 1996, 3387.
13 R. D. Adams and W. Wily, *J. Cluster Sci.*, 1993, **4**, 245.

ChemComm

Phosphodiester bond cleavage mediated by a cyclic β-sheet peptide-based dinuclear zinc(II) complex

Keiichi Yamada,†[a] Yu-ichi Takahashi,[a] Hatsuo Yamamura,[a] Shuki Araki,[a] Kazuki Saito[b] and Masao Kawai*[a]

[a] *Department of Applied Chemistry, Nagoya Institute of Technology, Gokiso-cho, Showa-ku, Nagoya 466-8555, Japan. E-mail: kawai@ach.nitech.ac.jp*

[b] *Yokoyama CytoLogic Project, ERATO, Japan Science and Technology Corporation, Tsukuba 300-2635, Japan*

Received (in Cambridge, UK) 26th April 2000, Accepted 5th June 2000

A dinuclear Zn(II) complex of $N^{2\delta}$,$N^{2\delta}$,$N^{2'\delta}$,$N^{2'\delta}$-tetrakis(2-pyridylmethyl) derivative of cyclic peptide gramicidin S markedly accelerated the cleavage of the phosphodiester linkage of the RNA model substrate 2-hydroxypropyl *p*-nitrophenyl phosphate.

Rational design of functional molecules mimicking biologically important species such as enzymes is one of the most challenging fields in modern chemistry. Peptides and peptidomimetics are promising building blocks for the construction of such systems. While numerous studies using α-helical peptides as well-defined structural units were reported, functional molecules based on β-structured peptides were few. The cyclic decapeptide gramicidin S (GS, Fig. 1) possesses a stable antiparallel β-sheet conformation with two type II′ β-turns at the D-Phe-Pro sequences.[1] The amino groups of the two Orn residues of GS are located at one side of the β-sheet, and are suitable for the introduction of various functional groups.

It has been shown that the active sites of many enzymes contain two metal ions which operate cooperatively.[2] Artificial models for the dinuclear metalloenzymes were reported in which pyridine-containing ligand groups were linked to a molecular scaffold such as a calix[4]arene framework.[3] Since the dinuclear Zn(II) complex of the simple diamine derivative $[(PyCH_2)_2NCH_2]_2CHOH$ was shown to promote hydrolysis of the phosphodiester linkage of a diribonucleotide,[4] we have prepared a GS derivative containing two bis(2-pyridylmethyl) amino groups in place of free amino groups, namely [Orn$(PyCH_2)_2^{2,2'}$]GS (**1**). In the present study, the Zn(II) ion-chelating behavior of **1** and phosphodiester bond cleavage mediated by the dinuclear Zn(II) complex have been examined.

$N^{2\delta}$,$N^{2\delta}$,$N^{2'\delta}$,$N^{2'\delta}$-Tetrakis($PyCH_2$) derivative **1** was prepared from GS•2HCl in 57% yield by treatment with 2-PyCHO and $NaBH_3CN$ in MeOH.[5] For comparison, a GS derivative containing only one $(PyCH_2)_2N$ group, namely [Orn$(PyCH_2)_2^2$, Orn(Tfa)$^{2'}$]GS (**2**), was prepared in a similar manner from the singly protected [Orn(Tfa)^2]GS.[6] An alternative bis($PyCH_2$) derivative in which each Orn side chain carries a $PyCH_2NH$ group, namely [Orn$(PyCH_2)^{2,2'}$]GS (**3**), was also prepared by treatment of GS•2HCl with PyCHO followed by catalytic hydrogenation in 70% yield.

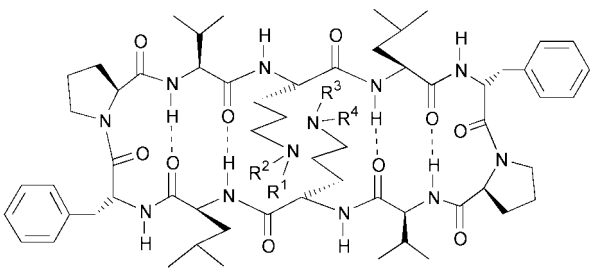

GS	$R^1 = R^2 = R^3 = R^4 = H$
1	$R^1 = R^2 = R^3 = R^4 = PyCH_2$
2	$R^1 = R^2 = PyCH_2$, R^3 = Tfa, $R^4 = H$
3	$R^1 = R^3 = PyCH_2$, $R^2 = R^4 = H$

Fig. 1 The structures of gramicidin S (GS) and the 2-pyridylmethyl ($PyCH_2$) derivatives **1**–**3**.

The pyridylmethyl derivatives **1**–**3** exhibited similar CD spectra to that of the parent GS, although the molecular ellipticity of **1** was slightly smaller than GS (Fig. 2a). The ^1H NMR spectral characteristics of **1** in DMSO-d_6 were also similar to those of GS, but the NH proton signal of the D-Phe residue of **1** (δ 8.59, d, J = 4.8) was more shielded, possessing a larger $N^{\alpha}H$–$C^{\alpha}H$ J value compared with the corresponding signal for GS (δ 9.04, d, J = 2.8). A similar spectral feature was observed for the GS derivatives lacking a main chain-side chain H-bonding interaction between $N^{\delta}H$(Orn) and C=O (D-Phe).[7,8] Therefore **1** was assumed to adopt essentially the same β-sheet conformation as that of GS, although the conformation was slightly distorted or disordered due to the absence of the H-bonding stabilization.

Zn(II) ion-binding properties of these pyridylmethyl derivatives were studied by spectrometric titrations. A CD spectral change between 245 and 280 nm upon the addition of aliquots of $ZnCl_2$ to the solution of **1** in MeOH as shown in Fig. 2b suggested stepwise formation of the 1:1 and 1:2 complexes between **1** and Zn^{2+}. A similar spectral change was also observed in buffered aqueous CH_3CN (pH 7.0) which was employed as the solvent for kinetic experiments described later. Formation of the stable dinuclear complex **1**•$(Zn^{2+})_2$ was further supported by UV spectroscopic titration. The CD spectrum of the dinuclear complex‡ in MeOH below 250 nm which was assumed to reflect the main chain conformation was similar to the CD spectral curve of unmodified GS (Fig. 2a). ^1H NMR analysis in DMSO-d_6 indicated a C_2 symmetrical structure for the dinuclear Zn(II) complex **1**•$(Zn^{2+})_2$. ROESY experiments revealed steric proximity of one of the pyridyl groups in each side chain of the Orn residues and the α-protons in the Pro-Val sequences. The NH proton of the D-Phe residue exhibited a similar signal (δ 9.06, d, J < 3.0) to that of natural GS. Taking into account these spectral characteristics the dinuclear complex was assumed to adopt the stable GS-type β-sheet conformation. Instead of the *i* to *i* + 2 type

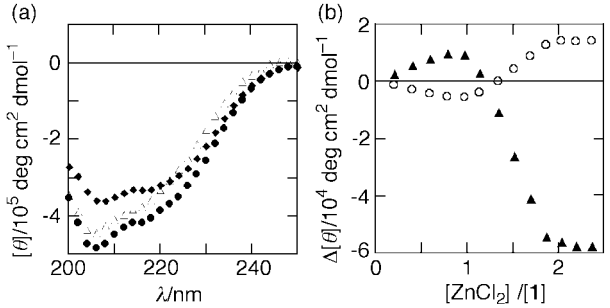

Fig. 2 (a) CD spectra in MeOH of GS•2HCl (●), **1** (◆) and **1** with Zn^{2+}: $[ZnCl_2]/[\mathbf{1}]$ = 2.4 (△). (b) Change of [θ] at 250 nm (○) and 271 nm (▲) upon the addition of $ZnCl_2$ to **1** in MeOH.

DOI: 10.1039/b003370g

Table 1 Pseudo-first-order rate constant of Zn(II) complex-mediated phosphodiester bond cleavage of HPNP[a]

Complex	k_{obs}/s^{-1}	Relative rate
None	0.51	1
1•$(Zn^{2+})_2$	3300	6500
2•Zn^{2+}	11	22
4•$(Zn^{2+})_2$	41	80

[a] Assays were carried out in 50% CH_3CN–20 mM HEPES buffer (pH 7.0) except **2**•Zn^{2+} (80% CH_3CN–20 mM HEPES buffer).

$N^{\delta}H$(Orn)··· C=O(D-Phe) H-bonding found in GS and its derivatives[8] the metal ions might play some role in the conformational stabilization. As expected, the bis($PyCH_2$) derivative **2** formed only the mononuclear 1 : 1 complex and no complex-forming tendency with Zn^{2+} was observed for the other derivative **3**.

Activity of the Zn(II) complexes of **1** and **2** for the cleavage of the linkage of 2-hydroxypropyl *p*-nitrophenyl hydrogen phosphate (HPNP) as an RNA model substrate was examined. For comparison, a dinuclear Zn(II) complex of the propanediamine derivative $[(PyCH_2)_2NCH_2]_2CH_2$ **4** lacking the peptide moiety was prepared and was also subjected to the kinetic study. The complexes were generated *in situ* in buffered aq. CH_3CN solution (pH 7.0) and the reaction progress was monitored by the absorbance at 400 nm due to the liberated *p*-nitrophenolate ion from HPNP.§ The obtained pseudo-first-order rate constants (k_{obs}) of the Zn(II) complex-mediated reaction are summarized in Table 1. The dinuclear complex **1**•$(Zn^{2+})_2$ was found to accelerate the reaction drastically. The effect of the mononuclear complex **2**•Zn^{2+} was much lower, indicating the importance of the cooperative participation of the two Zn(II) centers in the reaction process. Since the rate constant of the dinuclear complex **4**•$(Zn^{2+})_2$ lacking the peptide moiety was the same order as that of the mononuclear complex, the relative arrangement of the two Zn(II) centers linked to the rigid β-sheet framework by a moderately flexible trimethylene chain was considered to furnish a desirable reaction site enabling cooperative functioning of the two metal ions.

The pH dependence study of the reaction rate using **1**•$(Zn^{2+})_2$ demonstrated the optimal activity at pH 7.0. Metal ion-bound water in a hydrophobic environment is known to be highly acidic ($pK_a \approx 7$ to 8)[9] and in our case the Zn^{2+}–OH^- species generated near the antiparallel β-strands of GS moiety acts as a nucleophile, attacking the β-OH group of HPNP. As shown in Fig. 3 another Zn(II) ion was assumed to coordinate to phosphate oxygen, assisting the nucleophilic attack of the resulting anionic β-oxygen atom in HPNP to accomplish the intramolecular transesterification. The presence of the neighbouring hydroxy group was essential since the complex did not enhance the hydrolysis of di(*p*-nitrophenyl) hydrogen phosphate examined as a DNA model substrate.

In summary, we have demonstrated that the dinuclear Zn(II) complex **1**•$(Zn^{2+})_2$ possessing a β-sheet framework remarkably promoted phosphodiester bond cleavage of the RNA model substrate HPNP.¶ Very recently, Scrimin *et al.* reported transesterification of HPNP by a dinuclear Zn(II) catalyst based on water-soluble 3[10]-helical peptide.[10] A cyclodextrin-based dinuclear Cu(II) complex which hydrolyzes an amide bond was reported by Fujita's group.[11]

We are grateful to Dr Taka-aki Okamura (Department of Macromolecular Science, Osaka University) for mass spectral measurements and to Nikken Kagaku, Co. Ltd. for the supply of GS•2HCl. This work was supported by Grants-in-Aid from the Ministry of Education, Science, and Culture, Japan.

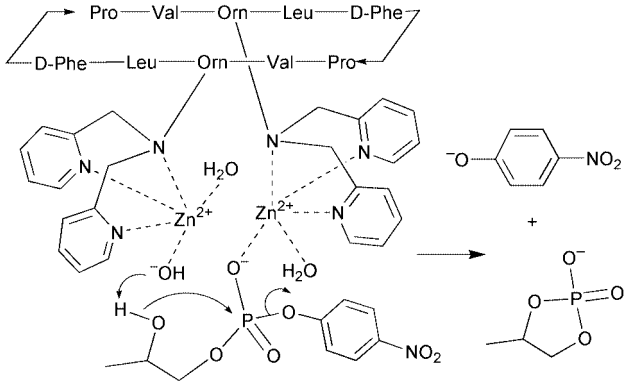

Fig. 3 A possible mechanism for the transesterification of HPNP mediated by the dinuclear Zn(II) complex of **1**.

Notes and references

† Present address: Faculty of Engineering, Gunma University, Kiryu 376-8515, Japan.

‡ **1**•$(Zn^{2+})_2$ was prepared from a MeOH solution of **1** (26 mg, 0.017 mmol) and $Zn(NO_3)_2$•$6H_2O$ (17 mM, 2 ml) by evaporating the solvent and lyophilization as a white solid (33 mg). ESI-MS: *m/z* 817.4 [**1** + 2Zn − 2H]$^{2+}$, $(C_{84}H_{111}N_{16}O_{10}Zn_2)^{2+}$ requires *m/z* 817.4. The complex thus obtained was water-soluble although **1** itself was almost insoluble in water.

§ A typical kinetic experiment was undertaken in 50% CH_3CN–20 mM HEPES buffer (pH 7.0) as follows: After mixing the solutions of **1** (0.5 mM, 3.0 ml) and $Zn(NO_3)_2$ (50 mM, 60 μl) for 1 min, HPNP (75 mM, 10 μl) was added and the pseudo-first-order rate constant k_{obs} was calculated by initial slope method using the absorbance at 400 nm.

¶ The corresponding D-Tyr analog of **1**, namely [Orn$(PyCH_2)_2^{2,2'}$, D-Tyr$^{4,4'}$]GS, possessing phenolic hydroxy groups to which a variety of functional groups (*e.g.* substrate binding sites) could be introduced was also prepared. The dinuclear Zn(II) complex exhibited similar activity to **1**•$(Zn^{2+})_2$ (k_{obs} = 2200 s^{-1}).

1 N. Izumiya, T. Kato, H. Aoyagi, W. Waki and M. Kondo, in *Synthetic Aspects of Biologically Active Cyclic Peptides: Gramicidin S and Tyrocidines*, Kodansya, Tokyo, 1979.
2 D. E. Wilcox, *Chem. Rev.*, 1996, **96**, 2435; N. Straeter, W. N. Lipscomb, T. Klabunde and B. Krebs, *Angew. Chem., Int. Ed. Engl.*, 1996, **35**, 2054.
3 For example, P. Molenveld, S. Kapsabelis, J. F. J. Engbersen and D. N. Reinhoudt, *J. Am. Chem. Soc.*, 1997, **119**, 2948.
4 M. Yashiro, J. Sumaoka and M. Komiyama, *J. Chem. Soc., Chem. Commun.*, 1995, 1793.
5 T. Kayatani, Y. Hayashi, M. Suzuki and A. Uehara, *Bull. Chem. Soc. Jpn.*, 1994, **67**, 2980.
6 K. Yamada, K. Ando, Y. Takahashi, H. Yamamura, S. Araki and M. Kawai, *J. Pept. Res.*, 1999, **54**, 168.
7 H. Sakamoto, Y. Shimohigashi, H. Yoshitomi, M. Ohno and K. Kawano, *Peptide Chemistry 1990*, ed. Y. Shimonishi, Protein Research Foundation, Osaka, 1991, p. 291; M. Tamaki, S. Akabori and I. Muramatsu, *Int. J. Pept. Protein Res.*, 1996, **47**, 369.
8 M. Kawai, T. Yamamoto, K. Yamada, S. Kurobe, H. Yamamura, S. Araki, Y. Butsugan, K. Kobayashi, R. Katakai, K. Saito and T. Nakajima, *Lett. Pept. Sci.*, 1998, **5**, 5.
9 J. H. Coates, G. J. Gentle and S. F. Lincoln, *Nature (London)*, 1974, **249**, 773.
10 P. Rossi, F. Felluga, P. Tecilla, F. Formaggio, M. Crisma, C. Toniolo and P. Scrimin, *J. Am. Chem. Soc.*, 1999, **121**, 6948.
11 J. Yan, M. Atsumi, D. Yuan and K. Fujita, *Tetrahedron Lett.*, 2000, **41**, 1825.

ChemComm

Electron-beam induced formation of nanoparticle chains and wires from a ruthenium cluster polymer

Brian F. G. Johnson,*[a] Katharine M. Sanderson,[a] Douglas S. Shephard,[a] Dogan Ozkaya,[a] Wuzong Zhou,[a] Haroon Ahmed,*[b] Michael D. R. Thomas,[b] Lynne Gladden[c] and Michael Mantle[c]

[a] *Department of Chemistry, The University of Cambridge, Lensfield Road, Cambridge, UK CB2 1EW. E-mail: bfgj1@cam.ac.uk*
[b] *Cavendish Lab., The University of Cambridge, Madingley Road, Cambridge, UK CB3 0HE*
[c] *Department of Chemical Engineering, The University of Cambridge, New Museums Site, Cambridge, UK CB2 3QZ*

Received (in Cambridge, UK) 15th December 1999, Accepted 2nd May 2000
Published on the Web 13th June 2000

The novel organometallic cluster polymer of probable formula $[Ru_6C(CO)_{15}Ph_2PC_2PPh_2]_n$ (n = *ca.* 1000) 1 has been prepared and, on irradiation in an electron beam, forms first nanoparticle chains and then conducting wires.

The potential of simple organic and inorganic molecules as precursors in the formation of electronic devices by direct chemical synthesis is substantial. Well-studied examples include carbon nanotubes,[1] novel resists,[2] metal[3] and semiconducting colloids[4] and conducting and semiconducting polymers.[5] A wealth of physical phenomena have been observed for these examples varying from zero-dimensional electronic confinement[6] to a wide variety of field-effect transition (FET) structures.[7]

Here we report a further type of compound which offers considerable potential in its application to new electronic devices. Until recently, carbonyl clusters have received little attention in this connection, partly because of their relatively small size, and partly because of the difficulty in performing standard microelectronic fabrication. We now report that these difficulties may be largely overcome by the use of materials containing clusters bonded *within* a polymer backbone.

A number of organometallic polymers have been reported previously. These range from those with pendant organometallic fragments attached to polymeric organic backbones[8] to those with metallic species incorporated into the backbone.[9] A common method of incorporation of a metal as a pendant is by performing a polymerisation on a functionalised unit, *e.g.* the free radical polymerisation of vinylferrocene.[10] Other polymers in this class include rigid-rod transition metal–acetylide polymers which usually involve group 10 metals or gold; these polymers consist of metals linked by organic spacers with a minimum capacity to bend. This is achieved by using alkyne or aromatic groups alternately to form rigid rods. In these systems the metal has been shown to coordinate in a *trans* fashion.[11] The electrical and electrochemical properties of such materials have not been investigated in detail.

Here, we report: (i) the synthesis and characterisation of the first organometallic polymer with carbonyl clusters in the backbone formulated as $[Ru_6C(CO)_{15}Ph_2PC_2PPh_2]_n$ and (ii) the processing of this material by electron beam exposure into nanowires with tunable conduction characteristics.

The new cluster based polymer $[Ru_6C(CO)_{15}(Ph_2PC_2PPh_2)]_n$ was synthesised from the direct reaction of $[Ru_6C(CO)_{17}]$ with the alkyne linking reagent $[Ph_2PC_2PPh_2]$ in tetrahydrofuran under reflux. After 5 h, removal of the solvent, followed by precipitation from dichloromethane, hexane gives the polymeric derivative $[Ru_6C(CO)_{15}Ph_2PC_2PPh_2]_n$ **1** as a dark brown powder which is soluble in dichloromethane.† Other products **2**–**4** may also be separated from other reaction stoichiometries. These have been identified as $[Ru_6C(CO)_{16}PPh_2C_2PPh_2]$ **2**, $Ru_6C(CO)_{15}\{PPh_2C_2PPh_2\}_2]$ **3** and $[Ru_5C(CO)_{13}PPh_2C_2PPh_2]$ **4**.† Significantly, in a separate experiment, we have observed that compound **3** undergoes reaction with a stoichiometric amount of $[Ru_6C(CO)_{17}]$ to yield polymer **1**. We believe that the polymer consists of $[Ru_6C(CO)_{15}]$ units linked by $[Ph_2PCCPPh_2]$ ligands (Fig. 1). The polymer **1** has been identified by routine chemical analysis. Elemental analyses (C, H) are totally in accord with the proposed empirical formula, and the presence of phosphorus is further confirmed by the solid state ^{31}P NMR† which exhibits a broad band at $\delta -20$. In the IR spectrum a broad ν(CO) band is observed† consistent with a polymer containing a large number of bonded CO ligands. A molecular weight of 1000–1020 has been estimated from electon microscopy carried out on several samples. This technique has been developed from our TEM studies of other systems.[12] In brief, a monolayer of polymer was deposited from solution onto holey carbon microscopy grids. The images over

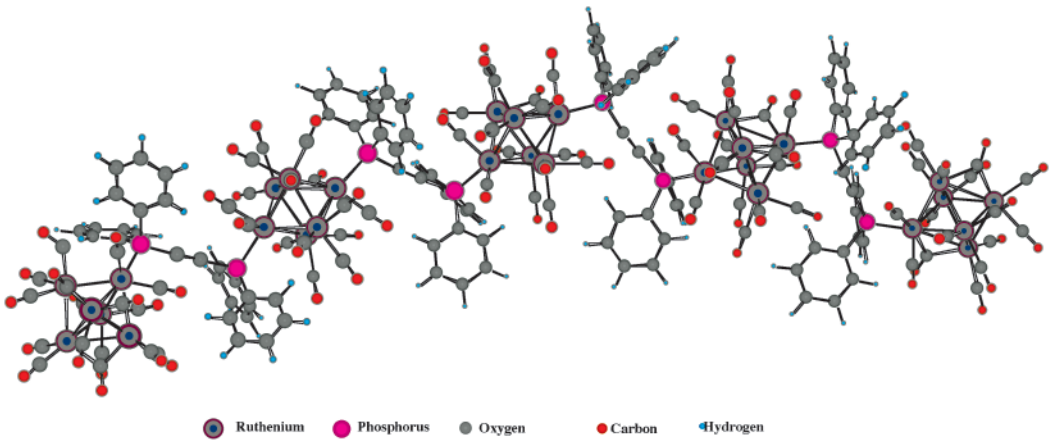

Fig. 1 The proposed structure of $[Ru_6C(CO)_{15}(Ph_2PC_2PPh_2)]_n$.

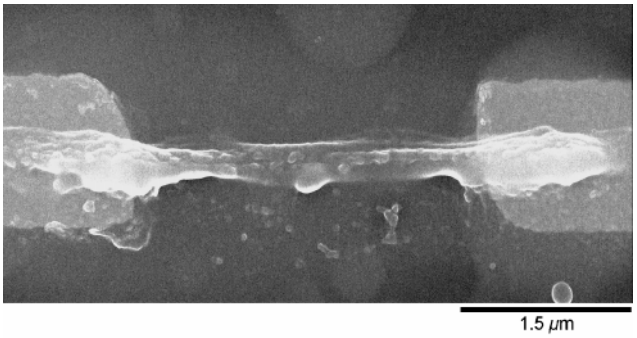

Fig. 2 SEM micrograph of a typical device. The polymeric nanowire (300 nm in width) lies on top of the gold contacts.

time showed that the polymer was very beam sensitive but from the initial images of chains of clusters an estimate of chain length could be determined. Further studies were made on the polymer supported on silica spheres (*ca.* 5 nm in diameter) to confirm and follow the nanoparticle growth induced by the electron beam (*vide infra*). This work will also be dealt with in a more detailed manner in a full paper.

Silicon substrates coated with 200 nm of high-quality oxide were prepared with micro-fabricated contacts composed of 10 nm Cr and 30 nm of Au (Fig. 2). The contacts defined a region for investigation of 4 × 5 μm, orientated with the shorter direction along the current path. A freshly prepared solution of polymer **1** in dichloromethane (200 mg ml^{-1}) was filtered through Teflon (200 nm pore size) and then spin-coated onto the substrate forming a layer *ca.* 120 nm thick. The layers were smooth and uniform and largely free from visible imperfections. Following preparation, exposures were performed on the samples in the usual way by electron-beam lithography (accelerating voltage 60 kV, current 1 nA, beam diameter *ca.* 250 nm). Exposures were conducted at 25 °C in a vacuum of 10^{-4} Pa or better. After development for 1 min, the polymeric material was observed to behave as a negative electron beam resist, with a sensitivity of 400 C m^{-2}. Atomic force microscopy (AFM) was used to determine the thickness of the material after development. At this stage the conductivity of the material was found to be immeasurably small. However, after more extensive electron beam exposures (accelerating voltage 60 kV, current 10 nA, beam diameter 1 μm at doses ranging from 10^3 to 4 × 10^6 C m^{-2}) the films showed conductivity increasing in a power law as a function of dose. The conduction mechanism was found to be variable range hopping in two dimensions[13] (Fig. 3). Using a finely focussed electron beam, it was possible to make wires as small as 100 nm in width. A typical device is shown in Fig. 2. The current–voltage characteristics near room temperature are well fitted by a hyperbolic sine, as predicted by variable-range hopping theory. However, at low temperatures, the current is strongly suppressed at low bias voltage.

We postulate that in the initially formed polymer the cluster units are surrounded by the non-conducting carbonyl sheath but that on initial irradiation with the electron-beam this sheath is lost to produce nanoparticle chains thus accounting for the observed contraction in volume. Weight loss as measured by tga tends to support this view. Further irradiation is then considered to bring about the fusion of groups of these particles into larger clusters, forming a conducting chain. We consider that this conductivity is brought about by an electron hopping process between nanoparticle groups rather than through the formation of a continuous metal wire. At low temperature, the device characteristics observed are consistent with charging-suppressed transport through these groups.

We thank the EPSRC and ICI for a CASE award (K. M. S.).

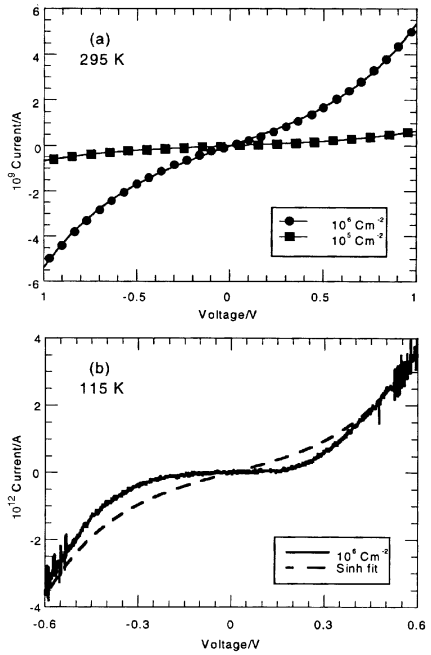

Fig. 3 Conductance/dose characteristics for two nanowires. All fits are hyperbolic sine functions.

Notes and references

† Compound **1** identified as $[Ru_6C(CO)_{15}Ph_2PC_2PPh_2]_n$ [FTIR: υ(CO) 2009br cm^{-1} br; **2** identified as $[Ru_6C(CO)_{16}PPh_2CCPPh_2)]$ [*m/z* 1492.26 (M + MeO$^-$); FTIR: υ(CO) 2084.6w cm^{-1}, 2032.8s cm^{-1}]; **3** identified as $Ru_6C(CO)_{15}[PPh_2CCPPh_2]_2$ [*m/z* 1859.43 (M + MeO$^-$); $\delta_P(H_3PO_4$ −30.4(s), 12.3 (s); FTIR: υ(CO) 2065.9m, 2018.4vs, 1970.2 (sh) cm^{-1}]; **4** identified as $Ru_5C(CO)_{13}PPh_2CCPPh_2$ by X-Ray crystal analysis. [*m/z* 1306.9 (M + MeO$^-$); FTIR: υ(CO) 2075.3w, 2053 s, 2016.5 cm^{-1} s, 1991.7 (sh) cm^{-1}; solid state MAS NMR: δ_P −20 (s, br) with side bands at δ −80 and +40; δ_C 125 (qnt, br)]

1 M. Bockrath, D. H. Cobden, P. L. McEuen, N. G. Chopra, A. Zettl, A. Thess and R. E. Smalley, *Science*, 1997, **275**, 1922.
2 J. Fujita, Y. Onishi, Y. Ochiai and S. Matsui, *Appl. Phys. Lett.*, 1996, **68**, 1297.
3 T. Sato, H. Ahmed, D. Brown and B. F. G. Johnson, *J. Appl. Phys.*, 1997, **82**, 696; L. Clarke, M. N. Wybourne, M. Yan, S. X. Cai and J. F. W. Keana, *Appl. Phys. Lett.*, 1997, **71**, 617.
4 D. L. Klein, R. Roth, A. K. L. Lim, A. P. Alivisatos and P. L. McEuen, *Nature*, 1997, **389**, 699.
5 C. J. Drury, C. M. J. Mutsaers, C. M. Hart, M. Matters and D. M. de Leeuw, *Appl. Phys. Lett.*, 1998, **73**, 108.
6 V. Erokhin, S. Carrara, H. Amenitch, S. Bernstorff and C. Nicolini, *Nanotechnology*, 1998, **9**, 158.
7 S. J. Tans, A. R. M. Verschueren and C. Dekker, *Nature*, 1998, **393**, 49.
8 C. E. Carraher, Jr. and C. U. Pittman, Jr., in *Metal Containing Polymeric Systems*, ed. J. E. Sheats, C. E. Carraher, Jr. and C. U. Pittman Jr., Plenum, New York, 1985
9 P. Nguyen, P. Gómez-Elipe and I. Manners, *Chem. Rev.*, 1999, **99**, 1515.
10 F. S. Arimoto and C. H. Haven Jr., *J. Am. Chem. Soc.*, 1955, **77**, 6295.
11 T. B. Marder, G. Lesley, Z. Yuan, H. B. Fyfe, P. Chow, G. Stringer, I. R. Jobe, N. J. Taylor, I. D. Williams and S. K. Kurtz, in *Materials for Nonlinear Optics: Chemical Perspectives*, ed. S. R. Marder, J. E. Sohn and G. D. Stucky, ACS, Washington DC, 1991.
12 W. Zhou, D. S. Shephard, J. M. Thomas, T. Maschmeyer, B. F. G. Johnson and R. G. Bell, *Science*, 1998, **280**, 705; D. S. Shephard, W. Zhou, T. Maschmeyer, J. M. Matters, C. L. Roper, S. Parsons, B. F. G. Johnson and M. J. Duer, *Angew. Chem., Int. Ed.*, 1998, **37**, 2718.
13 M. D. R. Thomas, H. Ahmed, K. M. Sanderson, D. S. Shephard, B. F. G. Johnson and W. Zhou, *Applied Phys. Lett.*, 2000, **76**, 1773.

ChemComm

Chiral packing of chiral quintuple layers polycatenated to give a three-dimensional network in the coordination polymer $[Co_5(bpe)_9(H_2O)_8(SO_4)_4](SO_4)\cdot 14H_2O$ [bpe = 1,2-bis(4-pyridyl)ethane]

Lucia Carlucci,[a] Gianfranco Ciani,*[b] Davide M. Proserpio[b] and Silvia Rizzato[b]

[a] *Dipartimento di Biologia Strutturale e Funzionale, Università dell'Insubria, Via J. H. Dunant 3, 21100 Varese, Italy*

[b] *Dipartimento di Chimica Strutturale e Stereochimica Inorganica and Centro CNR, Via G. Venezian 21, 20133 Milano, Italy. E-mail: davide@csmtbo.mi.cur.it*

Received (in Basel, Switzerland) 13th March 2000, Accepted 26th May 2000
Published on the Web 21st June 2000

The reaction of cobalt(II) sulfate with 1,2-bis(4-pyridyl)-ethane gives a crystalline polymeric species comprised of chiral quintuple layers with five decks of linear chains rotated by 120° from level to level, that are perpendicularly joined *via* five-metal helical motifs; furthermore, each of these two-dimensional frames is catenated by the neighbouring layers to give an overall three-dimensional chiral nanoporous architecture.

There is much current interest for the crystal engineering of coordination frameworks,[1] not only because of their potential applications as zeolite-like materials, for molecular selection, ion exchange and catalysis, but also for their intriguing architectures, new topologies and intertwining *phenomena*. Some recent examples have shown that topological types unprecedented in inorganic chemistry and in minerals can be achieved within the area of networked coordination polymers.[2] Moreover, new types of supramolecular intertwinings of infinite motifs have been discovered, that open interesting perspectives in the study of these materials. Particularly attractive are polymeric systems sustained by supramolecular entanglements reminiscent of the mechanical bonds in molecular rotaxanes and catenanes, exhibiting constituent motifs of dimensionality lower than that of the resulting overall architecture. Known examples include polyrotaxanes[3] and polycatenated one-dimensional[4] and two-dimensional motifs.[5] Species like these are expected to be of comparable robustness but more flexible than the usual networks entirely based on coordinative bonds with similar ligands.[6] We report here on a new member of this class of polycatenated motifs, $[Co_5(bpe)_9(H_2O)_8(SO_4)_4](SO_4)\cdot 14H_2O$ [bpe = 1,2-bis(4-pyridyl)ethane] **1**, that presents a new remarkable chiral three-dimensional architecture sustained by the catenation of chiral five-fold decked layers.

Compound **1** forms as beautiful flat hexagonal pink crystals by slow evaporation of solutions obtained on mixing bpe in ethanol and Co(II) sulfate in water, with metal-to-ligand molar ratios from 1:1.7 to 1:2. The crystals are stable in the air at room temperature for an extended time but start to lose solvated water molecules when heated above *ca.* 40 °C. The powdered material obtained in good yields by fast evaporation of more concentrated solutions of the reagents corresponds to almost pure **1**, as confirmed by X-ray powder diffraction methods.

The crystal structure of **1**† shows the presence of multiple layers containing five levels of one-dimensional linear polymers, all lying perpendicular to the crystallographic *c* axis, that are formed by Co(II) ions joined by bpe ligands in a *trans* conformation (Co···Co distances of 13.69 Å). These polymers run on the five decks in different directions rotated by 120° about the *c* axis on passing from one level to the successive one, thus resulting in a *ABCAB* sequence. The decks are connected along the normal direction *via* five-metal helical motifs, illustrated in Fig. 1, all exhibiting homochirality (left handed chirality for the crystal examined). The resulting chiral multilayer thus formed is schematically shown in Fig. 2.

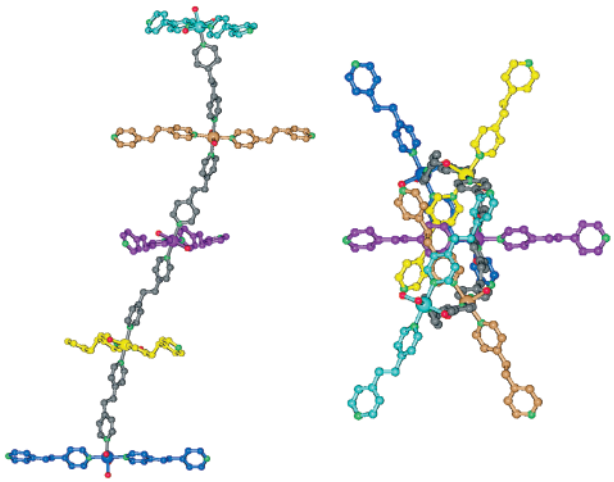

Fig. 1 A lateral (left) and a top (right) view of a single helical motif joining perpendicularly the quintuple layer (different colours are used to evidence the five decks). A two-fold axis passes through the central metal.

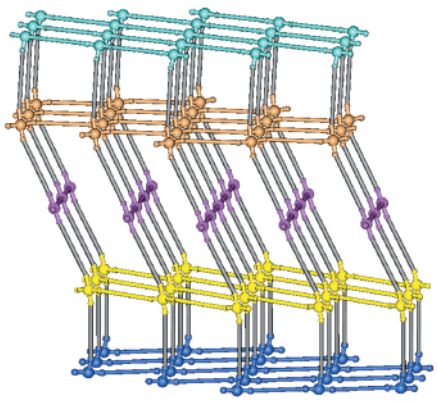

Fig. 2 A schematic view of a single five-decked layer with the same colours as in Fig. 1.

The cobalt ions of the two external levels are three-connected to bpe ligands (T-shaped geometry) while those of the three internal levels are four-connected to such ligands (square-planar geometry). The coordination spheres of the cobalt ions are completed by oxygen atoms of the sulfates and by water molecules (three *mer* H_2O for the two external Co, two sulfates for the central cobalt, one H_2O and one sulfate for the other two metal ions), resulting in all cases in distorted octahedral geometries. The five-metal helical chains are terminated at both ends by axial H_2O ligands, *i.e.* the external 'surfaces' of the multilayers are covered by coordinated water molecules. Though other examples of multiple layers are known within coordination polymers,[7] the two-dimensional motif of **1** is

unique in terms of topology, number of decks and thickness (see Fig. 2). To our knowledge, it is the largest two-dimensional coordination polymer ever reported.

We can rationalize this two-dimensional polymeric motif as a five-layer section of the chiral three-dimensional four-connected framework described by O'Keeffe as the 'dense' net.[8] This shows an *ABCABC* infinite sequence of levels and exhibits the unusual ($7^5 9$) topology. The first real example of this frame-work (three-fold interpenetrated) has been recently observed in a copper(II) polymeric species.[2a]

The stacking distance between two adjacent levels of each quintuple layer lies in the range 12.26–13.10 Å, so that the resulting overall height is as large as 50.5 Å. Identical layers are superimposed along the *c* crystallographic axis, with an interlayer gap of 13.4 Å (see Fig. 3). Two other sets of quintuple layers are generated by the 3_1 symmetry axis, exhibiting sequences of their five levels of the *BCABC* and *CABCA* type, respectively, resulting in an overall chiral packing. The three sets are entangled in such a way that each layer is catenated not only by the two nearest neighbouring (upper and lower) layers but also by the two second nearest neighbouring ones, as illustrated in Fig. 3. Thus each layer is intertwined in a 'parallel fashion'[1b] with the other four, to give a fascinating polycatenated array. Infinite catenation of polymeric motifs represents a type of supramolecular entanglement that is still quite uncommon. Known examples include polycatenated one-dimensional ladders that give two-dimensional[4b] or three-dimensional arrays,[4a,c] as well as two-dimensional simple,[5c] double[5a] and quadruple layers,[5b] resulting in three-dimensional architectures. We have very recently reported also on a catenated three-dimensional system based on different polymeric motifs, *i.e.* one-dimensional ribbons of rings and two-dimensional (4,4)-layers, that exhibits a peculiar sponge-like nanoporous behaviour.[6b]

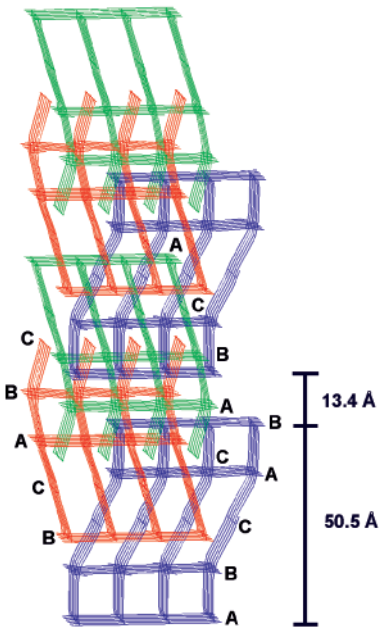

Fig. 3 The catenation of the two-dimensional quintuple layers. Three colours are used to evidence the different sets of layers generated by the 3_1 axis. Inside one layer the two interpenetrating nearest neighbours are also entangled between themselves (the inner red and blue layers inside the central green one).

The polycatenation in compound **1** is not sufficient to fill all the free voids, corresponding to *ca.* the 19.6% of the cell volume (calculated by neglecting the chlatrated H_2O molecules and the uncoordinated sulfates). These spaces are comprised of isolated cavities (three major cavities each of volume *ca.* 450 Å^3) containing solvated water molecules that can be removed by heating. Thermogravimetric analyses of **1**, under a nitrogen flux, show that both the solvated and the coordinated water molecules are completely lost in a continuous fashion in the range 40–120 °C. Above this point the product loses crystallinity and becomes unstable,‡ but if the samples are heated only up to *ca.* 80 °C the solvent loss (*ca.* 8% of the total weight, corresponding approximately to the solvated water molecules) can be regained by exposure to water vapour overnight, as confirmed by TGA and XRPD.

Since catenation of polymeric frameworks can allow a certain flexibility of the whole architecture, it can potentially favour solvent exchange processes, as observed in previous examples.[6] Compound **1** can be, therefore, considered as a model species for nanoporous arrays that present the additional features of non rigidity and chirality.

Notes and references

† *Crystal data* for compound **1**: $[Co_5(bpe)_9(H_2O)_8(SO_4)_4](SO_4)\cdot 14H_2O$, M = 2829.43, trigonal, $P3_121$ (no. 152), $a = b$ = 13.690(2), c = 63.880(9) Å, U = 10368(3) Å^3, Z = 3, D_c = 1.359 Mg m^{-3}, Mo-Kα radiation (λ = 0.71073 Å), μ(Mo-Kα) = 0.745 mm^{-1}, 61444 reflections measured, 9999 unique (R_{int} = 0.043), final $R1$ = 0.088 for 9343 independent reflections [$I > 2\sigma(I)$]. The data collection was performed at 293 K on an SMART-CCD Bruker diffractometer, by the ω-scan method, within the limits $2 < \theta < 24°$. The structure was solved by direct methods (SIR97) and refined by full-matrix least squares (SHELX97). The non coordinated sulfate anion is statistically distributed over two positions and was refined with half occupancy. One bpe ligand is statistically disordered by a two-fold axis passing through N1 and N2 and was refined using a half weight model. The handedness of the crystal was determined by testing the two enantiomeric models.

CCDC 182/1664. See http://www.rsc.org/suppdata/cc/b0/b002021o/ for crystallographic files in .cif format.

‡ Two other weight losses are observed. The first in the range 120–250 °C (*ca.* 19%) corresponds approximately to three ligand molecules. The corresponding XRPD spectrum shows a completely different pattern arising from a new violet anhydrous phase. The second weight loss (*ca.* 36–37%), occurs in the range 280–430 °C and leads to a final residue of $CoSO_4$, as evidenced by XRPD.

1 (*a*) B. F. Hoskins and R. Robson, *J. Am. Chem. Soc.*, 1990, **112**, 1546; (*b*) S. R. Batten and R. Robson, *Angew. Chem., Int. Ed.*, 1998, **37**, 1460; (*c*) O. M. Yaghi, H. Li, C. Davis, D. Richardson and T. L. Groy, *Acc. Chem. Res.*, 1998, **31**, 474; (*d*) M. Munakata, L. P. Wu and T. Kuroda-Sowa, *Adv. Inorg. Chem.*, 1999, **46**, 173; (*e*) P. J. Hagrman, D. Hagrman and J. Zubieta, *Angew. Chem., Int. Ed.*, 1999, **38**, 2638; (*f*) A. J. Blake, N. R. Champness, P. Hubberstey, W.-S. Li, M. A. Withersby and M. Schröder, *Coord. Chem. Rev.*, 1999, **183**, 117.

2 See *e.g.*: (*a*) L. Carlucci, G. Ciani, P. Macchi and D. M. Proserpio, *Chem. Commun.*, 1998, 1837; (*b*) B. F. Abrahams, S. R. Batten, M. J. Grannas, H. Hamit, B. F. Hoskins and R. Robson, *Angew. Chem., Int. Ed.*, 1999, **38**, 1475.

3 B. F. Hoskins, R. Robson and D. A. Slizys, *J. Am. Chem. Soc.*, 1997, **119**, 2952.

4 See, *e.g.*: (*a*) M. Fujita, Y. J. Kwon, O. Sasaki, K. Yamaguchi and K. Ogura, *J. Am. Chem. Soc.*, 1995, **117**, 7287; (*b*) A. J. Blake, N. R. Champness, A. Khlobystov, D. A. Lenenovkii, W.-S. Li and M. Schröder, *Chem. Commun.*, 1997, 2027; (*c*) L. Carlucci, G. Ciani and D. M. Proserpio, *J. Chem. Soc., Dalton Trans.*, 1999, 1799.

5 (*a*) F.-Q. Liu and T. D. Tilley, *Inorg. Chem.*, 1997, **36**, 5090; (*b*) L. Carlucci, G. Ciani, P. Macchi, D. M. Proserpio and S. Rizzato, *Chem. Eur. J.*, 1999, **5**, 237; (*c*) M.-L. Tong, X.-M. Chen, B.-H. Ye and L.-N. Ji, *Angew. Chem., Int. Ed.*, 1999, **38**, 2237.

6 (*a*) M. Fujita, O. Sasaki, K. Watanabe, K. Ogura and K. Yamaguchi, *New J. Chem.*, 1998, **22**, 189; (*b*) L. Carlucci, G. Ciani, D. M. Proserpio and S. Rizzato, *Angew. Chem., Int. Ed.*, 2000, **40**, 1506.

7 L. Carlucci, G. Ciani, D. M. Proserpio and A. Sironi, *Angew. Chem., Int. Ed. Engl.*, 1995, **34**, 1895; M. Kondo, T. Joshitomi, K. Seki, H. Matsuzaka and S. Kitagawa, *Angew. Chem., Int. Ed. Engl.*, 1997, **36**, 1725; K. N. Power, T. L. Hennigar and M. J. Zaworotko, *New J. Chem.*, 1998, **22**, 177.

8 M. O'Keeffe, *Z. Kristallogr.*, 1991, **196**, 21; M. O'Keeffe and B. G. Hyde, *Crystal structures I: patterns and symmetry*, Mineralogical Society of America, Washington, DC, 1996; see also M. O'Keeffe, *Nature*, 1998, **392**, 879.

ChemComm

Solid state coordination chemistry of oxovanadium phosphates: hydrothermal syntheses and structures of the network and chain phosphate phases $[\{Cu(bpy)\}_2(VO)_3(PO_4)_2(HPO_4)_2]\cdot 2H_2O$ and $[\{Cu(terpy)\}_2(VO_2)_3(PO_4)(HPO_4)_2]$

Robert Finn and Jon Zubieta*

Department of Chemistry, Syracuse University, Syracuse, NY 13244, USA. E-mail: jazubiet@mailbox.syr.edu

Received (in Columbia, MO, USA) 8th December 1999, Accepted 16th May 2000
Published on the Web 26th June 2000

The hydrothermal reactions of Cu_2O, the appropriate polypyridine ligand, Na_3VO_4, H_3PO_4 and H_2O at 200 °C yield the two-dimensional material $[\{Cu(bpy)\}_2(VO)_3(PO_4)_2(HPO_4)_2]\cdot 2H_2O$ and the one-dimensional phosphate $[\{Cu(terpy)\}_2(VO_2)_3(PO_4)(HPO_4)_2]$, examples of the structure-directing role of secondary metal–ligand subunits on the architectures of vanadium phosphates.

One approach to the design of novel materials exploits the often dramatic influence of organic molecules on inorganic microstructures.[1,2] Zeolites,[3,4] mesoporous materials of the MCM-41 class,[5] and open framework metal phosphates[6,7] are examples of families of materials which incorporate organic cations as structure-directing agents. An alternative approach introduces the organic component as a ligand, linking metal sites into complex metal–organic scaffoldings.[8,9] A variant of this strategy as applied to molybdenum oxides employs secondary metal–ligand complex subunits, not only as charge-compensating and space-filling components, but also as intimate structural components of bimetallic oxide composite materials, exemplified by copper–molybdenum oxides such as [Cu(4,4′-bipyridylamine)MoO_4], [Cu(*o*-phen)MoO_4] and [Cu(tetraphenylporphyrin)$Cu_2Mo_3O_{11}$].[10–12] Since both the ligand geometry and spatial extension, as well as the coordination preferences of the secondary metal site can be manipulated, considerable flexibility may be achieved in the spatial transmission of the structural information inherent at the ligated metal site. The success of this approach in the evolution of a wealth of new materials in the molybdenum oxide family encouraged us to explore the structure-directing role of copper–organonitrogen subunits in the industrially significant oxovanadium phosphate family of materials. The coordination preferences of the copper and the consequences of increased ligand bulk and denticity are evident in the structure of two novel bimetallic oxide phosphate materials, two dimensional $[\{Cu(2,2'\text{-bipyridyl})\}_2(VO)_3(PO_4)_2(HPO_4)_2]\cdot 2H_2O$ (**1**) and one-dimensional $[\{Cu(terpyridyl)\}_2(VO_2)_3(PO_4)(HPO_4)_2]$ (**2**).

Compound **1** was prepared as dark green rhombi in 40% yield from the hydrothermal reaction of Cu_2O, 2,2′-bipyridine, Na_3VO_4, H_3PO_4 and H_2O at 200 °C for 95 h.† Substitution of terpyridine for bipyridine in the reaction mixture and heating at 200 °C for 50 h yielded **2** as emerald green rhombi in 50% yield. The infrared spectra of **1** and **2** exhibit strong bands in the 920–970 cm^{-1} range attributed to ν(V=O) and a series of bands characteristic of the phosphate group in the 1100–1600 cm^{-1} range.

As shown in Fig. 1, the structure of **1**‡ consists of copper–vanadium oxide–phosphate layers, decorated with 2,2′-bipyridyl groups projecting above and below into the interlamellar region. The network is constructed from the corner- and edge-sharing polyhedral connectivity of copper(II) square pyramids, vanadium(IV) octahedra and square pyramids and phosphate tetrahedra. The Cu(II) coordination geometry is defined by the nitrogen donors of the bpy ligand and three oxygen donors from each of two $\{PO_4\}^{3-}$ groups and the –OH group of the $\{HPO_4\}^{2-}$ unit. The Cu–O and P–O bond lengths of 2.35 and 1.61 Å, respectively, and valence sum calculations[13] establish this as the protonation site. The square pyramidal V(IV) site consists of a terminal apical oxo-group and four phosphate oxygen donors from each of four $\{PO_4\}^{3-}$ or $\{HPO_4\}^{2-}$ groups, while the octahedral V(IV) site features a terminal oxo-group and five oxygen donors from four $\{PO_4\}^{3-}$ groups. One phosphate group bridges three vanadium centers and a copper site, while the second bridges three vanadium and two copper sites, sharing two vertices with both vanadium and copper centers.

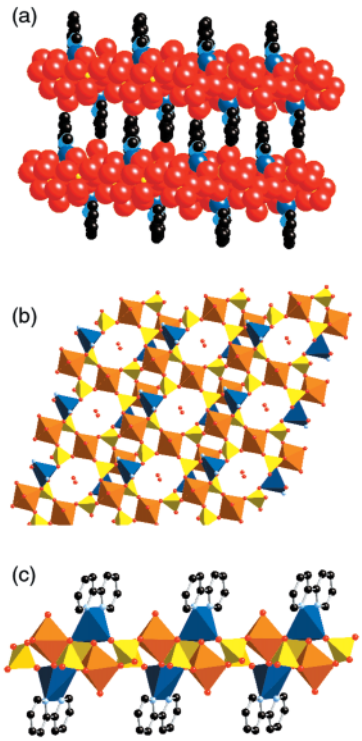

Fig. 1 (a) A space-filling view of the structure of **1**, parallel to the oxide layer. Red spheres, oxygen; dark blue spheres, copper; black spheres, carbon; light blue spheres, nitrogen. Hydrogen atoms have been omitted for clarity. (b) A view of the structure of **1**, normal to the plane of the bimetallic phosphate layer. The square pyramidal vanadium sites are represented as yellow polyhedra linking the $\{Cu_2(bpy)_2(VO)_2(PO_4)_2(HPO_4)_2\}$ chains with the vanadium octahedra in yellow, the copper sites in blue and the phosphate groups in violet. (c) A polyhedral representation of the $\{Cu_2(bpy)_2(VO)_2(PO_4)_2(HPO_4)_2\}$ chain. Selected bond lengths (Å): V1–O_t, 1.586(4); V1–$O_{phosphate}$, 1.964(3), av. of 4; V2–O_t, 1.607(2); V2–$O_{phosphate}$, 2.071(4), av. of 5; P–O, 1.531(4), av.; P–O(H), 1.605(2); Cu–O, 1.975(4), av; Cu–O(H), 2.349(2).

The structure of **1** may be best described as $\{Cu_2(bpy)_2(VO)_2(PO_4)_2(HPO_4)_2\}$ chains linked through square pyramidal $\{VO_5\}$ units into a 2-D network. Embedded within the chain are $\{Cu_2(bpy)_2(VO)_2(PO_4)_2\}$ clusters, constructed of a central ring of edge- and corner-sharing $\{VO_6\}$ octahedra and $\{PO_4\}$ tetrahedra capped by two $\{CuO_3N_2\}$ square pyramids. The phosphate groups of this cluster motif each link two copper and two vanadium sites, participating in edge-sharing with a

DOI: 10.1039/a909743k

vanadium polyhedron and contributing two triply-bridging oxygen donors. The fourth vertex of each of these phosphate groups serves to bridge to the square pyramidal vanadium site. The individual clusters are linked into the chain motif through four corner-sharing $\{PO_4\}$ tetrahedra. The fourth vertex of each of these phosphate sites again bridges to the square pyramidal vanadium center. One consequence of this unprecedented polyhedral connectivity is to generate eight polyhedral connect rings $[V_4P_4O_8]$ which create network cavities. The water molecules of crystallization are situated within these cavities and strongly hydrogen-bonded to the phosphate oxygens and the protonated phosphate oxygen. Since these intralamellar cavities are contained within hydrophobic regions defined by the bipyridyl groups, there is no facile pathway for removal of H_2O from the crystal. This observation is confirmed by the thermal gravimetric analysis of **1** which exhibits no weight loss below 250 °C, whereupon water is lost in two steps (250–275 °C and 310–375 °C). Ligand loss occurs above 400 °C to give an amorphous gray powder at 650 °C.

The structural consequences of increasing ligand bulk and denticity are apparent in the one-dimensional structure of **2**, shown in Fig. 2. The chain consists of exclusively corner-sharing vanadium(v) tetrahedra, square pyramids and trigonal bipyramids, copper square pyramids and $\{PO_4\}^{3-}$ and $\{HPO_4\}^{2-}$ tetrahedra. There are three distinct vanadium centers: an 'isolated' $\{VO_4\}$ tetrahedra site (*i.e.* no V–O–V linkages) and a binuclear site consisting of an oxo-bridged $\{VO_5\}$ trigonal bipyramid and $\{VO_5\}$ square pyramid. The $\{PO_4\}^{3-}$ group participates in corner-sharing to bridge the vanadium sites of the binuclear unit, the tetrahedral vanadium site and the copper. The remaining phosphate sites each bridge three metal centers and exhibit a pendant and protonated oxygen site. The terpy ligand occupies three coordination sites on the copper and introduces significant steric constraints, leaving two coordination sites available for linking to the oxovanadium phosphate chain. One copper site coordinates to two oxygen donors from two phosphorus tetrahedra, while the second bonds to a phosphorus oxygen and a bridging oxo-group of the trigonal bipyramidal vanadium site. The presence of three distinct vanadium polyhedra in **2** is a structurally unique feature for the oxovanadium phosphate family of materials.

Oxovanadium phosphates have received considerable attention as a result of their catalytic properties in organic oxidations[14,15] and their intercalation properties.[16] Significant activity has focused on structural modification and design of vanadyl phosphates through the introduction of organic substructures as templates and charge-compensating cations.[6,17] The approach to hybrid oxometal–phosphate/organic solids illustrated by the isolation of **1** and **2** employs secondary metal–organic ligand subunits as covalent linkers to the oxometal phosphate substructure. This strategy not only yields novel structural types, but appears to afford primitive control over the dimensionality of the solid through manipulation of the steric requirements and denticity of the ligand. The evolution of synthetic design in such solids appears inherent in the systematic variation of the secondary metal and its coordination preferences, the organic ligand, and the hydrothermal reaction conditions.

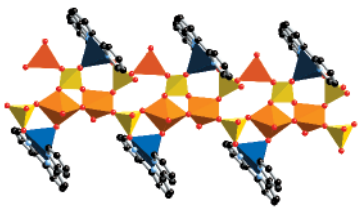

Fig. 2 A polyhedral representation of the structure of **2** using the same color scheme as for Fig. 1. Selected bond lengths (Å): tetrahedral vanadium: V1–O_t, 1.614(4) and 1.633(3); V1–O_b, 1.838(3) and 1.861(3); trigonal bipyramidal vanadium: V2–O_t, 1.594(4); V2–O_b(–Ve), 1.703(3); V2–$O_{phosphate}$, 1.956(5), av.; square pyramidal vanadium: V3–O_t, 1.620(3); V3–O_b(–Cu), 1.647(3); V3–O_b(–V2), 1.987(3); V3–$O_{phosphate}$, 1.985(4), av.; Cu1–$O_{phosphate}$, 1.923(3) and 2.099(3); Cu1–N, 2.052(6), av.; Cu2–O_b(–V3), 2.241(3); Cu2–$O_{phosphate}$, 1.921(4); Cu2–N, 1.993(6), av.

This work was supported by NSF grant CHE9617232. The thermogravimetric analyzer was purchased with a grant from Allen Trust and Deluxe Check Corporation.

Notes and references

† Reactions were carried out in Teflon-lined Parr acid-digestion bombs at 30% fill volume. Reaction conditions summary: **1**, mole ratio for Cu_2O: 2,2′-bipy: terpy: Na_3VO_4: H_3PO_4: H_2O of 1.4: 1.1: 1.0: 1.3: 15.3: 1750; 200 °C, 95 h, **2**, Cu_2O: terpy: Na_3VO_4: H_3PO_4: H_2O of 1.9: 1.0: 2.2: 19.6: 2060; 200 °C, 50 h.

‡ *Crystal data* for: $C_{10}H_{11}N_2O_{10.5}P_2CuV_{1.5}$ **1**: triclinic $P\bar{1}$, a = 8.1496(5), b = 9.7211(6), c = 11.9472(7) Å, α = 106.811(1), β = 98.943(1), γ = 110.429(1)°, V = 813.64(9) Å^3, $R1$ = 0.040 for 3665 reflections. For $C_{30}H_{24}N_6O_{18}P_3Cu_2V_3$ **2**: triclinic $P\bar{1}$, a = 8.9915(5), b = 11.3011(6), c = 19.4556(11) Å, α = 106.762(1), β = 91.208(1), γ = 103.984(1)°, V = 1828.0(2) Å^3, $R1$ = 0.0519 for 8486 reflections. CCDC 182/1679.

1 S. I. Stupp and P. V. Braun, *Science*, 1997, **277**, 1242.
2 P. V. Braun, P. Osenar, V. Tohver, S. B. Kennedy and S. I. Stupp, *J. Am. Chem. Soc.*, 1999, **121**, 7302.
3 D. E. W. Vaughan, *Properties and Applications of Zeolites*, Chem. Soc. Special Publ. No. 33, ed. R. P. Townsend, The Chemical Society, London, 1979, p. 294.
4 M. E. Davis and R. F. Lobo, *Chem. Mater.*, 1992, **4**, 756.
5 C. T. Kresge, M. E. Leonowicz, W. J. Roth, J. C. Vartuli and J. S. Beck, *Nature*, 1992, **359**, 710.
6 M. I. Khan, L. M. Meyer, R. C. Haushalter, C. L. Sweitzer, J. Zubieta and J. L. Dye, *Chem. Mater.*, 1996, **8**, 43.
7 P. Feng, X. Bu and G. D. Stucky, *Nature*, 1997, **388**, 735.
8 C. Janick, *Angew. Chem., Int. Ed. Engl.*, 1997, **36**, 1431.
9 O. M. Yaghi, M. Li, C. Davis, D. Richardson and T. L. Groy, *Acc. Chem. Res.*, 1998, **31**, 474.
10 P. J. Hagrman, D. Hagrman and J. Zubieta, *Angew. Chem., Int. Ed.*, 1999, **38**, 2638.
11 D. J. Chesnut, D. Hagrman, P. J. Zapf, R. P. Hammond, R. LaDuca, Jr., R. C. Haushalter and J. Zubieta, *Coord. Chem. Rev.*, 1999, **190–192**, 737.
12 D. Hagrman, P. J. Hagrman and J. Zubieta, *Angew. Chem., Int. Ed.*, 1999, **38**, 2638.
13 I. D. Brown and D. Altermatt, *Acta Crystallogr., Sect. C*, 1985, **41**, 244.
14 G. Centi, *Catal. Today*, 1993, **16**, 5.
15 M. T. Sananes, G. J. Hutchings and J.-C. Volta, *J. Chem. Soc., Chem. Commun.*, 1995, 243.
16 J. Kalousova, J. Votinsky, L. Benés, K. Meláová and V. Zima, *Collect. Czech. Chem. Commun.*, 1998, **63**, 1.
17 X. Bu, P. Feng and G. Stucky, *J. Chem. Soc., Chem. Commun.*, 1995, 1337.

ChemComm

Solvent directing immediate fluorination of aromatic ketones using 1-fluoro-4-hydroxy-1,4-diazoniabicyclo[2.2.2]octane bis(tetrafluoroborate)†

Stojan Stavber,* Marjan Jereb and Marko Zupan

Laboratory for Organic and Bioorganic Chemistry, 'Jožef Stefan' Institute and Department of Chemistry, University of Ljubljana, Jamova 39, 61000 Ljubljana, Slovenia. Fax: +386 61 1773 811; E-mail: stojan.stavber@ijs.si

Received (in Liverpool, UK) 2nd May 2000, Accepted 12th June 2000

Reactions of aryl alkyl ketones with 1-fluoro-4-hydroxy-1,4-diazoniabicyclo[2.2.2]octane bis(tetrafluoroborate) (Accufluor™ NFTh) in methanol result in selective and almost quantitative formation of the corresponding α-fluoroketones, while in acetonitrile exclusive fluorofunctionalisation of the activated aromatic ring take place.

The strategic introduction of a fluorine atom into organic molecules has attracted considerable current interest in related fields of chemistry[1] since this element often induces beneficial changes in the physicochemical and biological properties[2] of organic compounds. The ever increasing application of these fluorofunctionalised compounds has given a strong impetus to the academic as well as the industrial evaluation of new reagents and methods for selective fluorination under mild reaction conditions. In the last decade the introduction of numerous organic molecules incorporating a reactive N–F bond as versatile, mild, electrophilic fluorinating reagents[3] has created new challenges and revolutionarily influenced achievements in this field of organic chemistry.

Fluorofunctionalisation of organic compounds bearing a carbonyl functional group has been of special interest,[1] since this reactive moiety is often present in bioactive molecules or in potentially valuable building blocks for the synthesis of more sophisticated organofluorine derivatives. The position α to the carbonyl seems to be the most strategic one for the introduction of fluorine,[4] but when using electrophilic fluorinating reagents prior activation through enolate anions or enol ethers is necessary, except for sufficiently activated 1,3-dicarbonyl substrates. The presence of other active sites, such as an activated aromatic ring, in a target molecule often provokes lower regioselectivity of fluorofunctionalisation, thus making the task considerably more difficult. We now report the reactions of 1-fluoro-4-hydroxy-1,4-diazoniabicyclo[2.2.2]octane bis(tetrafluoroborate) (Accufluor™ NFTh[5]) with alkyl aryl ketones bearing a strongly activated aromatic ring.

In a typical experiment we treated 6-methoxy-1-indanone with NFTh in acetonitrile solution under reflux and in the crude reaction mixture established a high yield (68%) of 7-fluoro-6-methoxyindan-1-one (**3a**, Scheme 1). The observed regioselectivity of the reaction was quite different from that in the case of the same reaction of unsubstituted indan-1-one where regiospecific fluorination of the α-carbonyl position was observed.[6] Although the result of this reaction was expected since the aromatic part of the substrate is strongly activated and suitable for fluorofunctionalisation,[3] we checked the effect of the solvent on the course of the reaction and found that by using methanol as the reaction medium, the regiochemistry of the fluorination process changed dramatically, leading the reaction towards quantitative formation of 2-fluoro-6-methoxyindan-1-one (**2a**, Scheme 1). Encouraged by the possibility that the regioselectivity of fluorination of these types of ketones could be regulated only by the solvent used, we further investigated the reactions of NFTh with a series of methoxy substituted benzocycloalkan-1-one derivatives‡ and found that in methanol 7-methoxy-3,4-dihydronaphthalen-1(2*H*)-one was transformed to 2-fluoro-7-methoxy-3,4-dihydronaphthalen-1(2*H*)-one (**2b**) in over 90% yield, while in acetonitrile the fluorofunctionalisation of the aromatic ring took place regioselectively at position 8, thus forming 8-fluoro-7-methoxy-3,4-dihydronaphthalen-1(2*H*)-one (**3b**). Solvent directed regioselective fluorination was also observed in the case of 5-methoxyindan-1-one or 6-methoxy-3,4-dihydronaphthalen-1(2*H*)-one: 2-fluoro derivatives **4** were exclusively formed in methanol, while in acetonitrile fluorination of the aromatic ring was again found to be favoured but not regiospecific and two isomers **5** and **6** in a relative ratio of 3:1 were isolated from the crude reaction mixture.

Direct fluorination of methyl aryl ketones in the α-carbonyl position was found to be considerably less effective than the corresponding functionalisation of dialkyl or alkyl aryl ketones,[6] but by using methanol as reaction medium the NFTh mediated transformation of acetophenone to fluoromethyl phenyl ketone was readily accomplished in over 80% yield. This fact encouraged us to also use the protocol described for the fluorofunctionalisation of methyl aryl ketones bearing an activated aryl part of the molecule. 1-Acetylnaphthalene was, following reaction with NFTh in methanol, thus effectively and regioselectively transformed to fluoromethyl 1-naphthyl ketone **7**, while the reaction in acetonitrile was in this case found to be unselective and up to six mono and difluoro isomers of the substrates were detected in the crude reaction mixture. On the other hand, the analoguous reaction of 9-acetylphenanthrene resulted in the formation of high yield fluoromethyl 9-phenanthryl ketone **9** if methanol was used as the solvent, while exclusive formation of 9-acetyl-10-fluorophenanthrene **10** was established when the reaction was performed in acetonitrile. We further found that strong electron donating substituents on the *para* position of acetophenone did not interfere with the effectiveness of the reactions. Fluorination of 4-hydroxy- or 4-methoxyacetophenone resulted in the high yield formation of the corresponding fluoromethylacetophenones **11** and 3-fluoro substituted derivatives **12**, respectively, depending on the solvent used. Similar results were also obtained with *ortho* substituted acetophenones: fluoromethyl-2-methoxyacetophenone **13** was formed in methanol and a 1:1 mixture of 3-fluoro- (**14**) and 5-fluoro-2-methoxyacetophenone (**15**) in acetonitrile mediated reactions. Unfortunately, derivatisation of acetophenone with an electron donating substituent at the *meta* position caused complete loss of the selectivity of the reaction, and in both solvents only a complex mixture of fluorinated products was observed.

Considering the results obtained, we can point out some important facts which in general facilitate the task of fluorofunctionalisation of ketones considerably. Using Accufluor™

† The results of characterisation of **2a**, **2b**, **3a**, **3b**, **4a**, **4b**, **5a**, **6a** and **9** are available as electronic supplementary information (ESI). See http://www.rsc.org/suppdata/cc/b0/b003488f/

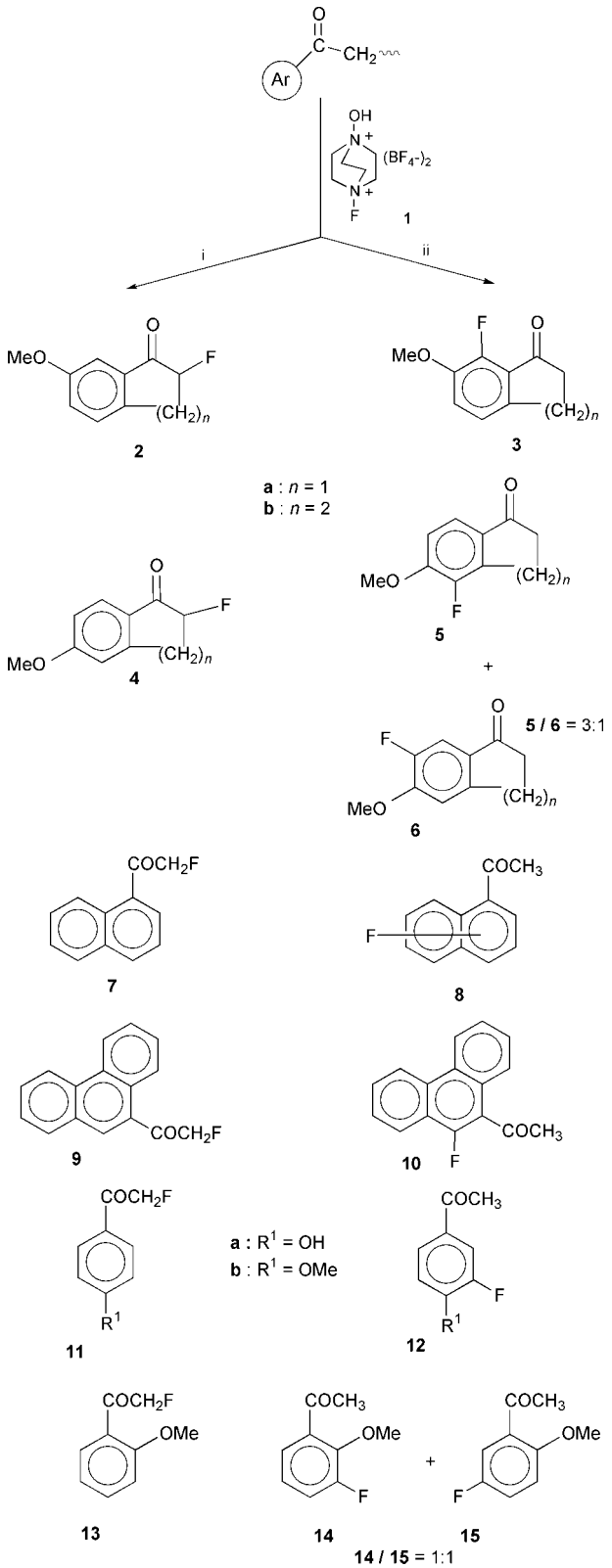

Scheme 1 *Reaction conditions*: i, MeOH, reflux for 0.5–4 h, if necessary hydrolysis with 10% HCl in MeCN; ii, MeCN, reflux for 0.5–4 h.

NFTh direct and selective fluorination can be effectively achieved even of those ketones bearing an activated aromatic part of the molecule, while alkyl aryl regioselectivity of fluorofuctionalisation could be regulated by the solvent. When methanol is used as solvent the substrate is regioselectively fluorinated at the α-carbonyl position, while in acetonitrile medium the same molecule reacts as an activated aromatic substrate and fluorination of the aryl ring is favoured. In addition, reaction is also effective with methyl aryl ketones, which makes the method convenient for direct α-carbonyl fluorination of a comprehensive range of ketones. Mechanistic elucidation of these reactions is in progress and on the basis of preliminary results we can assume that a subtle interplay of keto–enol tautomerism of the studied ketones plays a crucial role on the course of these reactions. In methanol, the keto–enol equilibrium lies sufficiently on the side of an enol form and a substrate reacts with NFTh as an alkene, following the reaction pathway similar to our recent observations,[7] resulting in α-fluoroketones. This assumption is reasonable since we already established that in the case of fluorination with N–F reagents activated alkenes[7] are for several decades more reactive than activated aromatics.[8] In acetonitrile keto–enol equilibrium is less favourable and the activated aromatic ring became the most reactive part of the substrate.

The authors are grateful to the Ministry of Science and Technology of the Republic of Slovenia for financial support, and to T. Stipanovič and Professor B. Stanovnik for elemental combustion analysis.

Notes and references

‡ To a solution of 2 mmol of ketone in 20 mL of methanol or acetonitrile 1.35 g of Accufluor™ NFTh (2.1 mmol of active compound) was added and the suspension heated under reflux for 0.5 to 4 h until KI starch paper showed the consumption of the fluorinating reagent. The reaction solvent was removed under reduced pressure and the crude reaction mixture dissolved in CH_2Cl_2 (50 mL), insoluble material filtered off, the solution washed with water (50 mL), dried over Na_2SO_4 and the solvent evaporated. The isolated crude reaction mixtures were analysed by ^{1}H and ^{19}F NMR. The amounts of fluorinated products were determined from the ^{19}F NMR spectra of crude reaction mixtures using octafluoronaphthalene as an additional standard and yields between 90–95% for α-fluoro carbonyl products or 70–75% of fluoro aromatics (**3**, **5** + **6**, **10**, **12** and **14** + **15**) were obtained. Since crude α-fluoro carbonyl derivatives were often formed mainly in dimethylketal form, hydrolysis with 10% HCl solution in MeCN, followed by crystallisation of α-fluoro ketone was necessary in order to obtain pure products (75–85% yield) **2**, **4**, **7**, **9**, **11**, and **13**, while fluoro aromatic derivatives were purified by preparative TLC (SiO_2, CH_2Cl_2) and 55–65% yield of satisfactory pure products obtained. New compounds were fully characterised by NMR, MS, and IR spectroscopy and their purity verified by combustion analysis.†

1 *Methods of Organic Chemistry (Houben-Weyl) Vol E 10a and 10b: Organo-Fluorine Compounds*, ed. B. Baasner, H. Hagemann and J. C. Tatlow, Thieme, New York, 1999; *Chemistry of Organic Fluorine Compounds II. A Critical Review*, ed. M. Hudlicky and A. E. Pavlath, ACS Monograph 187, ACS, Washington DC, 1995.
2 *Organofluorine Compounds in Medicinal Chemistry and Biomedicinal Application*, ed. R. Filler, Y. Kobayashi and L. M. Yagupolskii, Elsevier, Amsterdam, 1993.
3 G. S. Lal, G. P. Pez and R. G. Syvret, *Chem. Rev.*, 1996, **96**, 1737; G. G. Furin and A. A. Fainzilberg, *Russ. Chem. Rev.*, 1999, **68**, 653; S. D. Taylor, C. C. Kotoris and G. Hum, *Tetrahedron*, 1999, **55**, 12 431.
4 F. A. Davis and P. V. N. Kasu, *Org. Prep. Proced. Int.*, 1999, **31**, 125 and references therein.
5 Accufluor™ NFTh is commercially available as 50% w/w on alumina. We are indebted to Dr George Shia from AlliedSignals, Inc. for providing us with free samples of the reagent.
6 S. Stavber and M. Zupan, *Tetrahedron Lett.*, 1996, **37**, 3591.
7 S. Stavber, T. Sotler-Pečan and M. Zupan, *Tetrahedron*, 2000, **56**, 1929.
8 M. Zupan, J. Iskra and S. Stavber, *Tetrahedron*, 1996, **52**, 11 341.

$C_{60}F_{18}O$, the first characterised intramolecular fullerene ether

Olga V. Boltalina,[a] Benoit de La Vaissière,[b] Patrick W. Fowler,[b] Peter B. Hitchcock,[c] John P. B. Sandall,[b] Pavel A. Troshin[a] and Roger Taylor[c]

[a] *Chemistry Department, Moscow State University, Moscow 119899, Russia*
[b] *School of Chemistry, Exeter University, Stocker Road, Exeter, UK EX4 4QD*
[c] *The Chemistry Laboratory, CPES School, Sussex University, Brighton, UK BN1 9QJ*

Received (in Cambridge, UK) 10th May 2000, Accepted 12th June 2000

A single-crystal X-ray structure determination of the main isomer of $C_{60}F_{18}O$ shows it to be an intramolecular fullerene ether rather than an epoxide, and thus the first example of an oxa-homo[60]fullerene.

Formation of oxides is a major feature of fullerene chemistry. Hitherto, these oxides have been either characterised (*e.g.* $C_{60}O$,[1] $C_{70}O$,[2] $C_{60}O_2$,[3] $C_{60}O_3$,[4], $C_{60}O_n$,[5] $C_{60}Me_5O_2OH$[6]), or conjectured (*e.g.* $C_{60}Ph_4C_6H_4O_2$,[7] fluorofullerene oxides[8,9]) as epoxides. Strong circumstantial evidence for the epoxy form of fluorofullerene oxides was provided by identification of components in the moisture-induced reactions: $C_{60}F_n \rightarrow C_{60}F_{n-1}OH \rightarrow C_{60}F_{n-2}O$ (for various values of n), HF loss being manifest also in container etching. It was also notable that the isolated oxides were associated with precursors which possessed two additional fluorine atoms. A further indication of the presence of epoxides was the dramatic increase in oxide content when either fluoro[60]- or [70]fullerenes were reacted with aq. MeOH.[9]

Recently we described the isolation and ^{19}F NMR characterisation of the main isomer of $C_{60}F_{18}O$.[10] This has C_s symmetry, and the data were consistent with the presence of an in-plane epoxy oxygen atom (addition across a 6,6-double bond, **1**), but we also considered the possibility of insertion into various 6,5-single bonds. Insertion of oxygen into 6,6- and 6,5-bonds of [60]fullerene is predicted to be quasi-isoenergetic,[11] though no example of the latter has been observed; one of us conjectured that this was the first step in the spontaneous formation of $C_{60}Ph_8O_4$ from $C_{60}Ph_8$.[12]

However, three features seemed somewhat anomalous regarding the structure **1**. First, for the oxide to be an epoxide, there should be evidence of a precursor $C_{60}F_{20}$ molecule, and although traces of a component of this formula were seen, the amount was very small.[10] Secondly, the necessary precursor structure required the addition of two fluorine atoms remote from the rest, which contradicts the pattern for which we are finding increasing evidence (see *e.g.* ref. 13), that addition take places in a contiguous fashion. Thirdly, although traces of other oxides appeared to be present, there was no obvious energetic reason for **1** to be preferred; indeed, calculations indicated that an epoxide was not the structure of overall lowest energy for the formula.

We recently have scaled up our production of $C_{60}F_{18}$ (100–200 mg yield) and found that substantial quantities (*ca.* 50 mg) of the previously described isomer[10] of $C_{60}F_{18}O$ are also produced. This was separated by HPLC as described previously, but using a larger column of 10 mm diameter and 4.7 mol min^{-1} toluene flow rate. On standing, a toluene solution of this material deposited lemon-coloured plates, which single crystal X-ray characterisation† (Fig. 1) showed to be **2**.

This is thus the first intramolecular fullerene ether to be characterised and also the first having oxygen inserted into a 6,5-bond. The numbering of $C_{60}F_{18}$ is shown in **3** and hence this

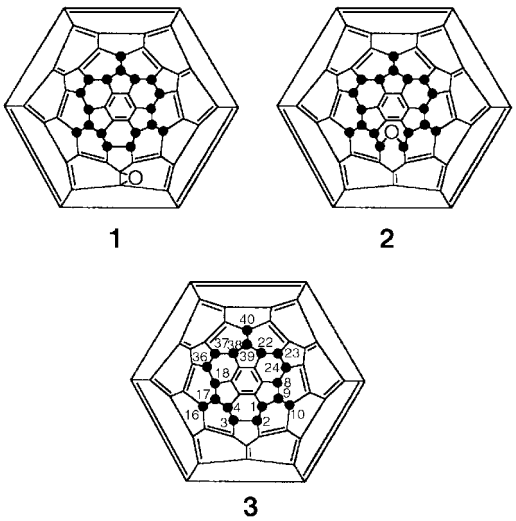

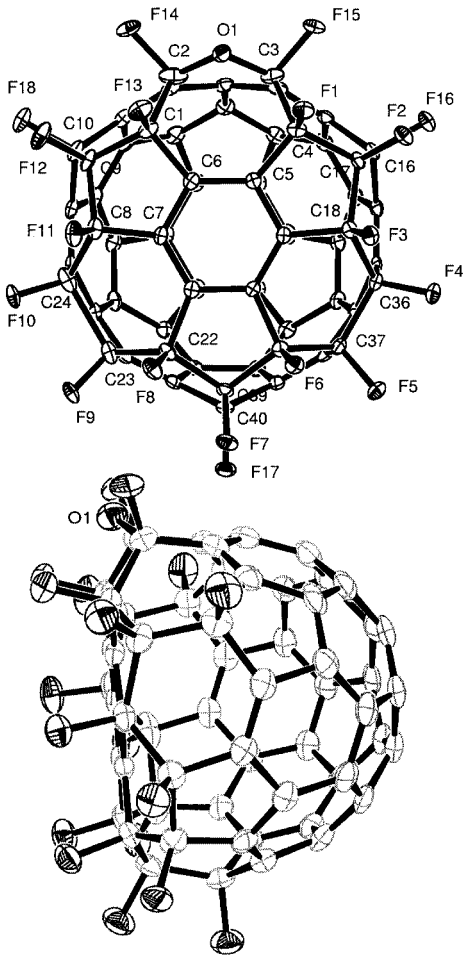

Fig. 1 Two projections (ORTEP) of $C_{60}F_{18}O$.

DOI: 10.1039/b003753m

Table 1 Heats of formation (kcal mol^{-1}) for C_s $C_{60}F_{18}O$ structures

	MNDO	AM1
(i) Epoxides 6,6-bond to which oxygen is added		
5,6	*−63.9*	*17.8*
13,30	*−111.7*	*−18.0*
58,59	*−122.4*	*−27.3*
11,12	−113.5	23.2
28,29	−117.4	23.2
(ii) Ethers 6,5-bond in which oxygen is inserted		
20,21	*−56.7*	*21.2*
55,56	*−115.8*	*−29.2*
47,48	*−130.1*	*−41.7*
1,6	−43.9	−17.9
2,12	−113.5	−34.1
9,10	−122.8	−43.5
10,11	−129.2	−50.3
1,2	−129.3	−50.5
1,9	−142.3	−66.2
2,3	−150.9	−74.5

ether is 1,2,3,4,8,9,10,16,17,18,22,23,24,36,37,38,39,40-octadecafluoro-1,2,3,4,8,9,10,16,17,18,22,23,24,36,37,38,39,40-octadecahydro-2a-oxa-2(3)a-homo[60]fullerene. This compound complements the homofullerenes and aza-homofullerenes, which have -CR_2- and -NR-, respectively, inserted into 5,6-bonds; these were first reported in 1991–1993[14] and numerous examples are now known.

The preference for this insertion may have a simple rationalisation. Recently we reported the single crystal X-ray structure for $C_{60}F_{18}$[15] which showed that the lengths (Å) of the FC–CF bonds in the molecule are: 1.557 (1,2); 1.672 (2,3); 1.623 (1,9); 1.558 (9,10). Semi-empirical calculations on this structure give the same ordering of bond lengths with the 2,3-bond at 1.69 Å (AM1), 1.71 Å (MNDO) exceeding the 1,9-bond by 0.4 Å (AM1), 0.3 Å (MNDO). Thus the 2,3-bond being the longest should also be the weakest, and hence the most amenable to oxygen insertion. In **2** the long (2,3) bond of $C_{60}F_{18}$ has opened out by 0.53 Å. The fact that oxides are major by-products of fullerene fluorination suggests that the reaction is also enhanced by electron withdrawal.

Previously, we compared the experimental results with semi-empirical calculations of the stability of C_s $C_{60}F_{18}O$ isomers involving incorporation of oxygen at various epoxide and ether sites. For the latter we considered only those bonds which connect carbons having no fluorine addends. These calculations (italicised data) are reproduced in Table 1.

One epoxide and one ether, involving addition to the central benzenoid ring, were clearly ruled out by their extremely low stabilities. The remaining data showed that the ethers should be the more stable, but each was ruled out by the ^{19}F NMR data (which consisted of 8×2 F + 2×1 F peaks, as follows: (i) one of the 2 F peaks was shifted substantially downfield (*ca.* 40 ppm) and this could not be accounted for by the remote oxygen in the 47,48-isomer. (ii) The 55,56-isomer required a downfield shift of one of the 1 F peaks, which was not observed. The data were however fully consistent with the 13,30-epoxide (**1**).

We have now calculated the heats of formation for all of the possible epoxides and ethers, including for the latter, insertion between carbons each or both of which are bonded to fluorine. The results (non-italicised) are given in Table 1 and it is very satisfying to see that of all the possible isomers, the one that is isolated in by far the largest yield is the one that is predicted to be the most stable. MNDO has a known tendency to favour ether over epoxide formation even in the bare [60]fullerene,[11] but the differences here should be more reliable indications of a real chemical preference, as they are much larger and stem from a clear geometric effect.

One unexpected feature however is the relatively small downfield shift for the resonances of the fluorines immediately adjacent to the oxygen. We have obtained significantly greater downfield shifts of some fluorine resonances in other fluorofullerene oxides, which may be attributable to differential electron withdrawal as a function of the number of sp^3 addend-bearing carbons. Further work on isolation and characterisation of oxides of fluorofullerenes is in hand.

O. V. B. thanks the RSC for an authors grant, and O. V. B. and R. T. thank the Royal Society for a Joint Project award. The TMR networks USEFULL (CT 960126) and BIOFULL (CT 980192) are thanked for financial support.

Notes and references

† *Crystal data*: $C_{60}F_{18}O\cdot(C_7H_8)$, M = 1170.7, Monoclinic, $P2_1/n$ (no. 14), a = 11.4675(4), b = 21.2128(9), c = 16.9247(6) Å, β = 101.769(3)°, V = 4030.5(3) Å^3, z = 4, μ(Mo-Kα) = 0.17 mm^{-1}, T = 173 K. 27044 reflections measured on an Enraf-Nonius Kccd diffractometer, 5545 unique (R_{int} = 0.103), refinement on all F^2, R^1 = 0.052 [for 4276 reflections with $I > 2\sigma(I)$], wR^2 = 0.114 (for all reflections). CCDC 182/1682. See http://www.rsc.org/suppdata/cc/b0/b003753m/ for crystallographic data in .cif format.

1 K. M. Creegan, J. L. Robbins, W. K. Robbins, J. M. Millar, R. D. Sherwood, P. J. Tindall, D. M. Cox, A. B. Smith, J. P. McCaulay, D. R. Jones and R. T. Gallagher, *J. Am. Chem. Soc.*, 1992, **114**, 1103.

2 A. B. Smith, R. M. Strongin, L. Brard, G. T. Furst, J. H. Atkins, W. J. Romanov, M. Saunders, H. A. Jiménev-Vázquez, K. G. Owens and R. J. Goldschmidt, *J. Org. Chem.*, 1996, **61**, 1904; V. N. Bezmelnitsin, A. V. Eletskii, N. G. Schepetov, A. G. Avent and R. Taylor, *J. Chem. Soc., Perkin Trans. 2*, 1997, 683.

3 A. L. Balch, D. A. Costa, B. C. Noll and M. M. Olmstead, *J. Am. Chem. Soc.*, 1995, **117**, 8926.

4 T. Hamano, T. Mashino and M. Hiroba, *J. Chem. Soc., Chem. Commun.*, 1995, 1537; C. Fusco, R. Seraglia and R. Curci, *J. Org. Chem.*, 1999, **64**, 8363.

5 M. P. Barrow, N. J. Tower, R. Taylor and T. Drewello, *Chem. Phys. Lett.*, 1998, **293**, 302.

6 H. Al-Matar, P. B. Hitchcock, A. G. Avent and R. Taylor, *Chem. Commun.*, 2000, 1071.

7 A. G. Avent, P. R. Birkett, A. D. Darwish, H. W. Kroto, R. Taylor and D. R. M. Walton, *Chem. Commun.*, 1997, 1579.

8 R. Taylor, J. H. Holloway, E. G. Hope, G. J. Langley, A. G. Avent, T. J. Dennis, J. P. Hare, H. W. Kroto and D. R. M. Walton, *J. Chem. Soc., Chem. Commun.*, 1992, 665; R. Taylor, G. J. Langley, J. H. Holloway, E. G. Hope, A. K. Brisdon, H. W. Kroto and D. R. M. Walton, *J. Chem. Soc., Perkin Trans.2*, 1995, 181; O. V. Boltalina, J. H. Holloway, E. G. Hope, J. M. Street and R. Taylor, *J. Chem. Soc., Perkin Trans. 2*, 1998, 1845.

9 R. Taylor, G. J. Langley, J. H. Holloway, E. G. Hope, H. W. Kroto and D. R. M. Walton, *J. Chem. Soc., Chem. Commun.*, 1993, 875.

10 A. G. Avent, O. V. Boltalina, P. W. Fowler, A. Yu. Lukonin, V. K. Pavlovich, J. P. B. Sandall, J. M. Street and R. Taylor, *J. Chem. Soc., Perkin Trans. 2*, 1998, 1319.

11 K. Raghavachari, *Chem. Phy. Lett.*, 1992, **195**, 221; K. Raghavachari and C. Sosa, *Chem. Phys. Lett.*, 1993, **209**, 223.

12 P. R. Birkett, A. G. Avent, A. D. Darwish, H. W. Kroto, R. Taylor and D. R. M. Walton, *J. Chem. Soc., Chem. Commun.*, 1995, 1869.

13 O. V. Boltalina, M. Bühl, A. Khong, M. Saunders, J. M. Street and R. Taylor, *J. Chem. Soc., Perkin Trans. 2*, 1999, 1475.

14 T. Suzuki, Q. Li, K. C. Khemani, F. Wudl and O. Almarsson, *Science*, 1991, **254**, 1186; M. Prato, Q. Li, F. Wudl and V. Lucchini, *J. Am. Chem. Soc.*, 1993, **115**, 1148.

15 I. S. Neretin, K. A. Lyssenko, M. Yu. Antipin, Y. L. Slovokhotov, O. V. Boltalina, P. Troshin, A. Lukonin, L. V. Sidorov and R. Taylor, *Angew. Chem., Int. Ed.*, in the press.

Enantio- and chemoselective reduction of 2,4-diketo acid derivatives with cinchona modified Pt-catalyst—Synthesis of (*R*)-2-hydroxy-4-phenylbutyric acid ethyl ester

Martin Studer,* Stefan Burkhardt, Adriano F. Indolese and Hans-Ulrich Blaser

Solvias AG, R-1055.616, Postfach, 4002, Basel, Switzerland. Fax: +41-61-686-6311; E-mail: martin.studer@solvias.com

Received (in Liverpool, UK) 30th March 2000, Accepted 5th June 2000

The enantio- and chemoselective hydrogenation of several 2,4-diketo acid derivatives to the corresponding 2-hydroxy compounds with cinchona modified Pt catalysts can be carried out with chemoselectivities of > 99% and enantioselectivities up to 86% (*R*) and 68% (*S*), respectively, and enrichment to > 98% ee was possible for several compounds by one crystallization, opening up an efficient technical synthesis of (*R*)-2-hydroxy-4-phenylbutyric acid ethyl ester, a building block for several ACE inhibitors.

Chiral 2-hydroxy-4-keto acid derivatives are interesting starting materials for the synthesis of a wide variety of intermediates and active substances.[1–3] Considering that many different 2,4-dioxo keto esters are easily synthesized *via* a Claisen condensation of methyl ketones with oxalate esters,[4] a chemo- and enantioselective reduction would give direct access to the desired compounds (Scheme 1). However, this enantioselective hydrogenation has not been reported until recently[2] due to the difficulty of discriminating between the two keto functions. The Pt–cinchona system is known to be very specific for the enantioselective hydrogenation of 2-keto esters[5] and a few other activated C=O bonds,[6–8] whereas unfunctionalized ketones are not suitable substrates. This high specificity is usually a disadvantage, but this paper shows that the underlying chemoselectivity can also be used to good advantage. Here, we report the hydrogenation of various 2,4-diketo acid derivatives with excellent chemoselectivity and medium to high ee's, and describe a new synthesis of enantiomerically pure (*R*)-2-hydroxy-4-phenylbutyric acid ethyl ester (HPB-ester), a building block for the synthesis of several commercially important ACE inhibitors[1] (Scheme 2).†

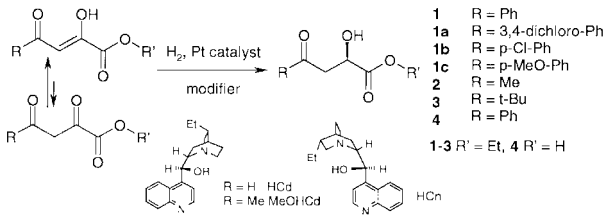

Scheme 1 Hydrogenation of 2,4-diketo acid derivatives, structure of substrates and modifiers.

Because **1** and **4** are cheap and easily accessible precursors for the HPB-ester,[4] their hydrogenation was investigated in some detail (selected results are summarized in Table 1). Based on our experience with the enantioselective hydrogenation of 2-keto acid derivatives,[5] heterogeneous Pt catalysts modified by 10,11-dihydrocinchonidine (HCd) and 10,11-dihydrocinchonine (HCn) were our favorites to obtain the (*R*)- and (*S*)-HPB-ester. With these modifiers, an extensive screening of the influence of catalyst type, solvent and reaction conditions was carried out. As hoped for, the chemoselectivity of all modified systems was always > 95% at 25 °C, regardless of catalyst type and solvent, provided that the reaction was stopped after the uptake of one mole of hydrogen. It is well known that for ethyl pyruvate or 4-phenyl-2-oxobutyric acid ethyl ester, by far the highest ee's are obtained with *O*-methyl-10,11-dihydrocinchonidine (MeOHCd) in AcOH.[5] In contrast, the highest ee for **1** of 86% (*R*) as well as the highest rate were observed in toluene with HCd and 5% Pt–Al_2O_3 catalysts. Pt on SiO_2 or other supports always gave lower ee's and most of the time lower rates. Other apolar or slightly polar solvents like benzene, xylene, cyclohexane, hexane, ethyl acetate, or diisopropyl ether led to ee's between 85 and 71%. In protic solvents like *t*-BuOH, AcOH or EtOH ee's between 40 and 61%, and in DMF an ee of

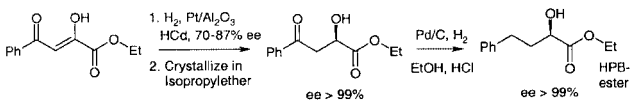

Scheme 2 Synthesis of (*R*)-2-hydroxy-4-phenyl butyric acid ethyl ester.

Table 1 Screening of support and solvents for the enantioselective hydrogenation of **1** and **4** with supported Pt catalysts modified with HCd, MeOHCd and HCn: effect on ee and rate

Entry	Substrate	Solvent	Catalyst	Pressure/bar	Modifier	Ee (%)	Rate/mmol g^{-1} min^{-1}
1	1	Toluene	JMC 94[a]	60	HCd	86 (*R*)	6.4
2	1	AcOH	JMC 94[a]	60	HCd	45 (*R*)	3.6
3	1	EtOH	JMC 94[a]	60	HCd	40 (*R*)	5.2
4	1	Toluene	E 4759[b]	60	HCd	86 (*R*)	3.4
5	1	Toluene	E 4759[b]	5	HCd	80 (*R*)	1.5
6	1	Toluene	E 4759[b]	135[d]	HCd	87 (*R*)	4.0
7	1	Toluene	F 340[c]	60	HCd	74 (*R*)	1.9
8	1	Toluene	E 4759[b]	60	HCn	59 (*S*)	0.9
9	1	AcOH	E 4759[b]	60	HCn	48 (S)	0.8
10	4	Toluene	JMC 94[a]	60	MeOHCd	23 (*R*)	0.2
11	4	EtOH	JMC 94[a]	60	MeOHCd	52 (*R*)	3.4
12	4	THF	JMC 94[a]	60	MeOHCd	56 (*R*)	0.9

Conditions: See experimental. [a] 5% Pt/Al_2O_3 (Johnson Matthey). [b] 5% Pt–Al_2O_3 (Engelhard). [c] 5% Pt–SiO_2 (Degussa). [d] 0 °C.

DOI: 10.1039/b002538k

25% were obtained. Temperature and pressure affected the results only slightly. The optimal modifier concentration was 5.3×10^{-4} M at a modifier to catalyst ratio of 1:10 (w/w), similar to the results obtained with ethyl pyruvate.[9] Analogous experiments were carried out with the pseudoenantiomeric HCn as modifier. All trends were similar, but the best ee's in toluene were always lower by about 20%. Furthermore, the reactions were always slower by a factor of about three and a doubling of the modifier concentration was necessary for the highest ee. Surprisingly, the ee's in AcOH were comparable, as described by LeBlond *et al.* for ethyl pyruvate.[10] Obviously the small difference between HCd and HCn (attachment point of the side chain in the quinuclidine unit) is quite important in toluene but not so much in AcOH. For the 2,4-diketo acid **4**, the ee's were significantly lower than for the corresponding ethyl ester **1**. More polar solvents gave better results as observed for mono keto acids, where the highest ee's were obtained in a EtOH–H_2O mixture.[11]

To obtain the HPB-ester with the desired ee of > 99%, further enrichment of the 2-hydroxy-4-keto ester was necessary. This worked remarkably well: a single crystallization from $^{i}Pr_2O$ brought the ee from > 72% to > 99% with a chemical yield of approx. 50–60%. Hydrogenolysis of the keto group with Pd–C in EtOH–HCl finally gave the desired HPB-ester in high yield with an ee of > 99% (overall yield starting from **1** approx. 50–60%).[12]

In order to expand the scope of this chemo- and enantioselective reaction, substrates **1a**–**c**, **2** and **3** were also tested (Table 2), and proved to be highly chemoselective. This is remarkable considering that only a few of the homogenous catalysts mentioned above showed high chemoselectivity for **2** and **3**, and even fewer both high chemo- and enantioselectivity.[2] As observed for **1**, the highest ee's (70–80%) were usually obtained in toluene. The only exception was **3**, where AcOH gave 74% and toluene 63% ee. For all esters investigated, the reactions in EtOH proceeded with the lowest ee's but often the highest rates. Comparing **1**, **1a**, **1b** and **1c**, it seems that electron withdrawing groups on the Ph groups give slightly higher ee's and rates. For all these substrates, HCn was also investigated as modifier to give the (*S*)-2-hydroxy-4-keto esters. The ee's were again lower by 20–30%. Enrichment by recrystallization to > 98% ee was possible for **1a**, **1b** and **1c** but not for **2** and **3** which are not crystalline at rt.

Table 2 Screening of solvents and modifiers for the enantioselective hydrogenation of various 2,4-diketo esters with Pt–Al_2O_3 catalysts: effect on ee and rate

Entry	Substrate	Solvent	Modifier	Ee/(%)	Rate/mmol g^{-1} min^{-1}
13	1a	Toluene	HCd	84 (*R*)	Nd
14	1a	Toluene	HCn	68 (*S*)	1.3
15	1b	Toluene	HCd	82 (*R*)	5.0
16	1b	Toluene	HCn	64 (*S*)	Nd
17	1c	Toluene	HCd	79 (*R*)	2.0
18	1c	Toluene	HCn	49 (*S*)	Nd
19	2	EtOH	—	0[a]	0.3
20	2	EtOH	HCd	56 (*R*)	13
21	2	Toluene	HCd	78 (*R*)[b]	3.5
22	2	Toluene	HCn	57 (*S*)	Nd
23	2	AcOH	MeOHCd	65 (*R*)	7.5
24	2	AcOH	HCn	63 (*S*)	Nd
25	3	EtOH	—	0[c]	0.1
26	3	EtOH	HCd	34 (*R*)	0.7
27	3	Toluene	HCd	63 (*R*)	0.5
28	3	Toluene	HCn	42 (*S*)	Nd
29	3	AcOH	MeOHCd	74 (*R*)	1.5
30	3	AcOH	HCn	54 (*S*)	Nd

Conditions see Experimental. Catalyst for **1a**—E 4759, for **2** and **3**—JMC 94, 60 bar, 25 °C. [a] 4% diol. [b] 5 °C. [c] Diol not detectable by NMR.

The hydrogenation of all 2,4-diketo esters with the unmodified Pt catalysts was slower than the modified systems, typically by a factor of 3–60 (ligand accelerated catalysis[5,10]). However, all rates were relatively low compared to ethyl pyruvate (rates up to 300 mmol g^{-1} min^{-1}) or 4-phenyl-2-oxobutyric acid ethyl ester (rates up to 40 mmol g^{-1} min^{-1}).[13] For ethyl pyruvate it was demonstrated by reaction with D_2 that hydrogenation occurs by addition across the C=O bond.[5] In contrast to mono keto esters where only the keto form is observed, diketo esters showed > 80% enol in the solvents used for the hydrogenation (NMR results). Therefore, one possible explanation for these rate differences between mono and diketo esters could be the different keto–enol ratio. Unfortunately, a reaction with D_2 was not conclusive due to a massive exchange of H/D in the starting material and product, and it is uncertain whether the keto or the enol form is hydrogenated. In addition, the modified catalyst gave significantly less 2,4-dihydroxy ester than unmodified catalyst. This improved chemoselectivity is mainly due to the acceleration of the hydrogenation of the 2-keto group, but there are also indications that the reaction of the 4-keto group is slowed down.

In conclusion, the scope of the cinchona modified Pt catalysts has been expanded to the enantio- and chemoselective hydrogenation of various 2,4-diketo ester derivatives. For a range of 2-hydroxy-4-keto esters enrichment to > 98% ee is possible by a simple crystallization thereby enabling an efficient technical access to enantiomerically pure building blocks for ACE inhibitors and related compounds.

This project was carried out for and in collaboration with the Life Science Molcules Unit of Ciba Specialty Chemicals (Ciba LSM). We thank P. Herold, H. P. Jalett, F. Spindler and A. Hafner for valuable discussions and G. Thoma for careful experimental work.

Notes and references

† Hydrogenations were carried out as described in ref. 6. Example for ethyl (*R*)-2,4-dioxo-4-phenylbutyrate **1**: 2.0 g diketo ester **1** in 30 ml toluene were hydrogenated at 25 °C and 60 bar H_2 pressure in a 50 ml stainless steel autoclave in the presence of 50 mg 5% Pt–Al_2O_3 (pretreated for 2 h in H_2 at 400 °C) and 5 mg HCd. After H_2 uptake had stopped (*ca.* 160 min), the catalyst was filtered and the solution was evaporated to dryness at reduced pressure. Yield: 1.97 g (98%), product content > 97% (NMR), ee 86% (HPLC, OD-H, hexane–EtOH 98.5:1.5, flow 0.7 ml min^{-1}; retention time: (*S*)-enantiomer 46.0 min, (*R*)-enantiomer 49.6 min).

The experiments with the other substrates were carried out in a similar manner. In cases with low activity, higher catalyst loadings were used (constant catalyst–modifier ratio). With HCn, a modifier–catalyst ratio of 1:5 was normally used. All new substrates and products gave satisfactory analytical results (^{13}C, ^{1}H, and MS).

1 M. Studer, P. Herold, A. Indolese and S. Burkhardt, *WO 9950223 (31.03.1998, assigned to Ciba LSM).*
2 V. Blandin, J. F. Carpentier and A. Mortreux, *Eur. J. Org. Chem.*, 1999, 1787.
3 P. G. Baraldi, S. Manfredi, G. P. Pollini, R. Romagnoli, D. Simoni and V. Zanirato, *Tetrahedron Lett.*, 1992, **33**, 2871.
4 C. Beyer and L. Claisen, *Berichte*, 1887, **20**, 2178.
5 H. U. Blaser, H. P. Jalett, M. Müller and M. Studer, *Catal. Today*, 1997, **37**, 441.
6 M. Studer, S. Burkhardt and H. U. Blaser, *Chem. Commun.*, 1999, 1727.
7 B. Török, K. Felfödi, K. Balazsik and M. Bartok, *Chem. Commun.*, 1999, 1725.
8 M. Studer, V. Okafor and H. U. Blaser, *Chem. Commun.*, 1998, 1053.
9 M. Garland and H. U. Blaser, *J. Am. Chem. Soc.*, 1990, **112**, 7048.
10 C. LeBlond, J. Wang, J. Liu, A. T. Andrews and Y.-K. Sun, *J. Am. Chem. Soc.*, 1999, **121**, 4920.
11 H. U. Blaser and H. P. Jalett, *Stud. Surf. Sci. Catal.*, 1993, **78**, 139.
12 For more details see P. Herold, A. Indolese, M. Studer, H. P. Jalett, U. Siegrist and H. U. Blaser, accepted by *Tetrahedron Lett.*
13 M. Studer, unpublished results.

ChemComm

HF–pyridine promoted Friedel–Crafts type arylation of 2-acetoxy-D-glucal. Stereoselective synthesis of 1-arylhex-3-enopyranosiduloses

Masahiko Hayashi,* Shu-zo Nakayama and Hirotoshi Kawabata

Department of Chemistry, Faculty of Science, Yamaguchi University, Yamaguchi 753-8512, Japan.
E-mail: hayashi@po.cc.yamaguchi-u.ac.jp

Received (in Cambridge, UK) 25th April 2000, Accepted 7th June 2000

A variety of aromatic substrates were treated with 2-acetoxy-D-glucal in the presence of HF–pyridine to give 1-arylhex-3-enopyranosiduloses in high yield and in high α-selectivity.

C-Glycosylarenes or *C*-aryl glycosides are *C*-glycosides found in natural products.[1] These compounds often exhibit interesting biological activity, such as antibacterial, anti-tumor, enzyme inhibitory effects, and inhibition of platelet aggregation.[2] Therefore, the study of the synthesis of *C*-glycosylarenes is of interest to synthetic organic chemists. The most straightforward synthesis of *C*-glycosylarenes should be the Friedel–Crafts type reaction between glycosyl donors and aromatic compounds.[3,4]

We recently reported the reaction of acetylated and unprotected D-glucal with trimethylsilyl cyanide which led to the synthesis of 2,3-unsaturated glycosyl cyanides.[5] During the course of this study, we became interested in the reaction of D-glucal with aromatic compounds, which should be an efficient synthetic route to *C*-aryl glycosides.[6] Here we would like to report the Friedel–Crafts type reaction of acetylated D-glucal with aromatic compounds.

First, we examined the reaction of 3,4,6-tri-*O*-acetyl-D-glucal with mesitylene (1,3,5-trimethylbenzene) in the presence of a variety of Lewis acids such as Me_3SiOTf, $BF_3{\cdot}OEt_2$ and $Sc(OTf)_3$. However, all reactions resulted in the formation of complex mixtures and the desired 1-aryl glycoside was not obtained. Then we employed the reaction of 2,3,4,6-tetra-*O*-acetyl-D-glucal (**1**) with mesitylene using the above Lewis acids. In these cases, 1-arylated hex-3-enopyranosidulose (**6**) was obtained in high yield.[7] Some of the results are summarized in Table 1. Among the Lewis acids we examined, Me_3SiOTf showed the best results (20 mol%, 0 °C, 1 h, 90% yield, α:β = 88:12). The configuration of the major anomeric center was determined as α by ^{1}H NMR spectral analysis.

Table 1 Reaction of 2,3,4,6-tetra-*O*-acetyl-D-glucal with mesitylene[a]

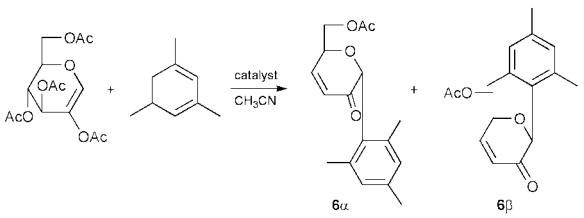

6α 6β

	Conditions			Product	
Entry	Catalyst (mol%)	*T*/°C	*t*/h	Yield (%)[b]	α:β[c]
1	Me_3SiOTf (20)	0	1	90	88:12
2	$BF_3{\cdot}OEt_2$ (20)	15	20	58	80:20
3	$Sc(OTf)_3$ (10)	20	24	65	79:21
4	HF–pyridine	0	1	90	90:10

[a] All reactions were carried out in acetonitrile except for entry 4. [b] Isolated yield after silica-gel column chromatography. [c] ^{1}H NMR analysis.

Interestingly, rare-earth metal triflates other than $Sc(OTf)_3$, such as $Sm(OTf)_3$, $Y(OTf)_3$ and $Yb(OTf)_3$ were inactive in the above reaction. HF–pyridine was found to work as an effective promoter and to be superior to the conventional Lewis acids as for a variety of aromatic compounds (Table 2). HF–pyridine is used as a fluorinating agent,[8] for example in the synthesis of glycosyl fluorides.[9] However, in the present case, HF–pyridine worked as a promoter in the Friedel–Crafts coupling reaction. As shown in Table 2, a variety of α-1-arylated hex-3-enopyranosidulose products were obtained in high yields. As for the relative reactivity, among the aromatic compounds we examined, anisole reacted with **1** faster than the other aromatic compounds. For methylated benzene derivatives, the order of the reactivity is as follows; mesitylene > *m*-xylene > *o*- and *p*-xylene, toluene. Isomerization was not observed under the reaction conditions, indicating that the observed stereochemical outcome resulted from kinetic control.

The reactions proceed *via* a Ferrier type reaction.[10] The reaction is initiated by the reaction of 2-acetoxy-D-glucal with HF–pyridine to generate an oxocarbenium ion which then reacts with aromatic substrates such as xylene and mesitylene to give 1-aryl-2,3-unsaturated glycosides, though these compounds were not isolated. Then deacetoxylation at the 4-position affords the 1-arylhex-3-enopyranosiduloses. In the case of the reaction of 3,4,6-tri-*O*-acetyl-2-bromo-D-glucal with mesitylene, a Ferrier type product, that is, the 2,3-unsaturated 1-arylated product was obtained in 86% yield (α:β = 77:23).

A typical experimental procedure is as follows: In a 50 mL polyethylene vessel, 2,3,4,6-tetra-*O*-acetyl-D-glucal (1.0 g, 3.04 mmol) and mesitylene (0.84 mL) were placed. To this mixture was added 70% HF–pyridine (1.5 mL) at 0 °C and the whole mixture was stirred for 1 h at 0 °C. After the confirmation of the completion of the reaction by TLC, the mixture was poured into saturated $NaHCO_3$ solution and extracted with ethyl acetate (20 mL × 3). The combined organic layer was washed with brine (20 mL × 3), and then evaporated. Chromatography of the residue on a silica gel column afforded **6** (777 mg, 90%). Separation of the anomers was effected by column chromatography on silica gel (1:2 ethyl acetate–hexane as an eluent): **6**α (less polar) $[\alpha]_D^{23}$ −149.1° (*c*. 1.2, $CHCl_3$); **6**β (more polar) $[\alpha]_D^{22}$ −53.1° (*c*. 1.2, $CHCl_3$).

In conclusion, we have developed a HF–pyridine promoted Friedel–Crafts type arylation of 2-acetoxy-D-glucal with a variety of aromatic compounds which facilitated the synthesis of 1-aryl-2-hex-3-enopyranosiduloses.

We would like to acknowledge Dr Hidemitsu Uno of the Center for Advanced Chemical Analysis and Instrumentation of Ehime University for his help in the structure determination of compound **6**. Support from Monbusho (Grant-in-Aid for Scientific Research on Priority Areas, No. 706: Dynamic Control of Stereochemistry), the Shorai Foundation for Science

Table 2 HF–pyridine promoted reaction of 2,3,4,6-tetra-*O*-acetyl-D-glucal (**1**) with some aromatic compounds[a]

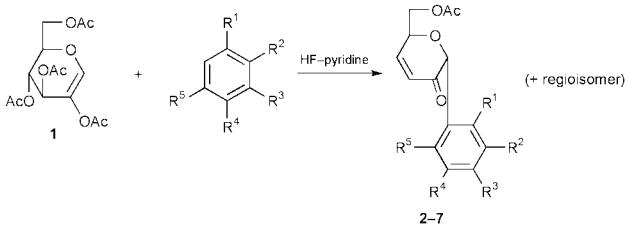

	Aromatic compound					HF–pyridine mL/g of substrate	Conditions		Product[b] Yield (%)[c] (regioisomer ratio)[d]	α:β[d]
	R^1	R^2	R^3	R^4	R^5		T/°C	t/h		
1	H	H	CH_3	H	H	2.2	18	15	**2** 88 ($o:p$ = 25:75)[e]	α
2	H	CH_3	CH_3	H	H	2.5	20	23	**3** 76 (86:14)[f]	α
3	CH_3	H	CH_3	H	H	2.6	20	2	**4** 100 (91:9)[g]	α
4	CH_3	H	H	CH_3	H	2.3	16	7	**5** 76	α
5	CH_3	H	CH_3	H	CH_3	1.4	0	1	**6** 90	90:10
6	OCH_3	H	H	H	H	2.4	0	0.5	**7** 84 ($o:p$ = 57:43)	α

[a] All reactions were carried out in a polyethylene vessel. [b] The structures of major isomers are given above. [c] Isolated yield after silica gel column chromatography. [d] Determined by ^{1}H NMR (400 MHz) analysis. [e] Isomers not separated. [f] minor isomer:  [g] minor isomer: 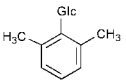 [h] Minor isomer was β.

and Technology and the Nagase Science and Technology Foundation is gratefully acknowledged.

Notes and references

1 D. E. Levy and C. Tang, *The Chemistry of* C-*Glycosides*, Pergamon, Oxford, 1995; M. H. D. Postema, C-*Glycoside synthesis*, CRC Press: Boca Raton, 1995; K. Suzuki and T. Matsumoto, in *Preparative Carbohydrate Chemistry*, ed. S. Hanessian, Marcel Dekker, Inc.: New York, 1997, pp. 527–542; M. H. D. Postema, *Tetrahedron*, 1992, **48**, 8545.

2 U. Hacksell and G. D. Daves, Jr., *Prog. Med. Chem.*, 1985, **22**, 1.

3 R. R. Schmidt and G. Effenberger, *Carbohydr. Res.*, 1987, **171**, 59; R. R. Schmidt and M. Hoffmann, *Tetrahedron Lett.*, 1982, **23**, 409; A. O. Stewart and R. M. Williams, *J. Am. Chem. Soc.*, 1985, **107**, 4289; For the synthesis of *C*-glycosylarenes, see also, N. C. Chaudhuri and E. T. Kool, *Tetrahedron Lett.*, 1995, **36**, 1795; B. A. Schweitzer and E. T. Kool, *J. Org. Chem.*, 1994, **59**, 7238; D. S. Brown and S. V. Ley, *Tetrahedron Lett.*, 1988, **29**, 4869.

4 For the *O*→*C* rearrangement method; T. Matsumoto, M. Katsuki and K. Suzuki, *Tetrahedron Lett.*, 1988, **29**, 6935; T. Matsumoto, T. Hosoya and K. Suzuki, *Tetrahedron Lett.*, 1990, **31**, 4629; T. Matsumoto, M. Katsuki, H. Jona and K. Suzuki, *Tetrahedron Lett.*, 1989, **30**, 6185; T. Matsumoto, M. Katsuki, H. Jona and K. Suzuki, *J. Am. Chem. Soc.*, 1991, **113**, 6982; T. Matsumoto, T. Hosoya and K. Suzuki, *Synlett*, 1991, 709; K. Suzuki, *Pure Appl. Chem.*, 1994, **66**, 1557; T. Kometani, H. Kondo and Y. Fujimori, *Synthesis*, 1988, 1005; K. Toshima, G. Matsuo, T. Ishizuka, M. Nakata and M. Kinoshita, *J. Chem. Soc., Chem. Commun.*, 1992, 1641; J.-A. Mashling and R. R. Schmidt, *Synthesis*, 1993, 325.

5 M. Hayashi, H. Kawabata and O. Arikita, *Tetrahedron Lett.*, 1999, **40**, 1729.

6 S. Czernecki and V. Dechavanne, *Can. J. Chem.*, 1983, **61**, 533; G. Casiraghi, M. Cornia, L. Colombo, G. Rassu, G. G. Fava, M. F. Belicchi and L. Zetta, *Tetrahedron Lett.*, 1988, **29**, 5549; G. Casiraghi, M. Cornia, G. Rassu, L. Zetta, G. G. Fava and F. Belicchi, *Carbohydr. Res.*, 1989, **191**, 243.

7 R. J. Ferrier and P. M. Petersen, *J. Chem. Soc., Perkin Trans. 1*, 1992, 2023; T. Tsukiyama and M. Isobe, *Tetrahedron Lett.*, 1992, **33**, 7911.

8 G. A. Olah, J. T. Welch, Y. D. Vankar, M. Nojima, I. Kerekes and J. A. Olah, *J. Org. Chem.*, 1979, **44**, 3872.

9 M. Hayashi, S. Hashimoto and R. Noyori, *Chem. Lett.*, 1984, 1747; W. A. Szarek, G. Grynkiewics, B. Doboszewski and G. W. Hay, *Chem. Lett.*, 1984, 1751.

10 R. J. Ferrier, *Adv. Carbohydr. Chem. Biochem.*, 1965, **20**, 67; R. J. Ferrier, *Adv. Carbohydr. Chem. Biochem.*, 1969, **24**, 199.

ChemComm

Chemical tuning of ferromagnetism and superconductivity in $RuSr_2GdCu_2O_8$†

A. C. Mclaughlin,[ab] V. Janowitz,[ab] J. A. McAllister[ab] and J. P. Attfield[ab]

[a] *Department of Chemistry, University of Cambridge, Lensfield Road, Cambridge, UK CB2 1EW. E-mail: acm43@cus.cam.ac.uk*

[b] *Interdisciplinary Research Centre in Superconductivity, University of Cambridge, Madingley Road, Cambridge UK CB3 0HE*

Received (in Cambridge, UK) 11th April 2000, Accepted 12th June 2000

When substituted for Ru in the ferromagnetic superconductor $RuSr_2GdCu_2O_8$, both Sn^{4+} and Nb^{5+} suppress the ferromagnetism in the RuO_2 layers, but they respectively enhance and diminish superconductivity in the CuO_2 planes through hole transfer to and from the CuO_2 layers, showing that these materials are underdoped with an estimated maximum T_c of 65 ± 10 K.

Ferromagnetism and superconductivity are considered to be incompatible in homogenous solids, but a remarkable coexistence of these properties has recently been discovered in the mixed oxide $RuSr_2GdCu_2O_8$.[1–10] This has a tetragonal '1212' type structure, similar to that of $YBa_2Cu_3O_7$, with layers stacked in the sequence …RuO_2.SrO.CuO_2.Gd.CuO_2.SrO…[6,9,10] Resistivity measurements show that this material displays bulk superconductivity in the CuO_2 planes, with a critical temperature (T_c) of up to 46 K, whilst the ferromagnetic transition at T_M = 136 K results from ordering of moments in the RuO_2 planes.[4,5,7] The presence of ferromagnetism is confirmed by hysteresis loops in magnetisation *vs.* field measurements, with remnant and saturated moments of 0.1 and 1.0 μ_B per Ru atom. However, recent neutron diffraction measurements detected only an antiferromagnetically ordered component,[8] so that the overall magnetic arrangement may be canted with both ferro- and antiferro-magnetic components. This canting may result from antisymmetric exchange between Ru moments as a result of local rotations and tilts of the RuO_6 octahedra owing to a size mismatch between the ruthenate and cuprate layers.[6,9,10] $RuSr_2GdCu_2O_8$ is cation and oxygen stoichiometric, and the hole-doping (oxidation) of the CuO_2 planes needed to induce superconductivity arises from the overlap of the Ru t_{2g} and the Cu $d_{x^2-y^2}$ bands. The formula may thus be written as $Ru^{5-2p_0}Sr_2Gd(Cu^{2+p_0})_2O_8$ to show the average Ru and Cu oxidation states. Transport measurements suggest that the intrinsic hole doping is $p_0 \approx 0.07$,[7] showing that this material is strongly underdoped, as optimum superconductivity in copper oxides is generally found for a hole-doping of $p \approx 0.16$. The average oxidation states are thus $Ru^{4.86+}$ and $Cu^{2.07+}$.

To investigate the relationship between the charge distribution, superconductivity and magnetism in $RuSr_2GdCu_2O_8$ further, we have attempted to replace Ru by non-magnetic, fixed valent cations. Samples of $Ru_{1-x}Sn_xSr_2GdCu_2O_8$ were previously prepared with nominal compositions x = 0–0.4.[11] Tin doping was found to suppress T_M and enhance T_c, but firm conclusions about the origin of this effect could not be drawn as the samples were not phase pure. We have subsequently prepared phase pure Sn-doped samples for $x < 0.1$, and a series of > 98% pure Nb doped samples, as summarised here.

Ceramic samples of $Ru_{1-x}M_xSr_2GdCu_2O_8$ (M = Sn: x = 0, 0.025, 0.05, 0.075; M = Nb: x = 0, 0.05, 0.1, 0.15, 0.2) were prepared by solid state reaction of stoichiometric powders of RuO_2, SnO_2, Nb_2O_5, $SrCO_3$, Gd_2O_3 and CuO. These were ground, die-pressed into pellets and reacted in flowing nitrogen at 1010 °C for 20 h, in flowing oxygen at 1050 °C and at 1055 °C for 10 h each, then at 1060 °C for 4 days, and finally slow cooled to room temperature. X-Ray diffraction patterns demonstrated that the $Ru_{1-x}Sn_xSr_2GdCu_2O_8$ solid solutions were phase pure, however there was a trace of $SrRuO_3$ in the $Ru_{1-x}Nb_xSr_2GdCu_2O_8$ samples. The greatest amount was estimated to be 2.2(1)% $SrRuO_3$ in the x = 0.20 sample by Rietveld analysis. Thermogravimetric analyses gave oxygen contents between 7.95 and 8.05 for all samples, showing them to be stoichiometric within the experimental error of ±0.05.

Magnetisations were measured on a Quantum Design SQUID magnetometer in an applied field of 1 kOe after zero-field cooling. A broadening of the magnetic transition and a reduction in the Curie temperature T_M (Table 1) is observed with increasing Nb [Fig. 1(a)] or Sn substitution. Variable field measurements between ±50 kOe at 10 K revealed hysteresis loops for all samples. The hysteretic parameters all decrease smoothly with Nb or Sn substitution; the coercivity falls from 410 Oe in the undoped material to 320 Oe for 7.5% Sn substitution and 240 Oe for 20% Nb substitution and the remnant Ru moments are 0.13, 0.09 and 0.05 μ_B, respectively. The saturated Ru moments, estimated by subtracting the Gd contribution following a procedure described elsewhere,[11] are 1.0, 0.8 and 0.6 μ_B in the same three samples. These results are all in keeping with a dilution of the ferromagnetism in the RuO_2 layers by substitution of diamagnetic Sn^{4+} or Nb^{5+}.

The resistivities of sintered polycrystalline bars were measured between 7 and 300 K using the standard four-probe ac technique. Superconducting transitions are observed for the $Ru_{1-x}Nb_xSr_2GdCu_2O_8$ samples with x = 0–0.15 [Fig. 1(b)] but not for x = 0.2 down to 7 K. All the $Ru_{1-x}Sn_xSr_2GdCu_2O_8$ samples are superconducting and the onset T_c increases up to 50 K for x = 7.5%. The thermoelectric powers of the same sintered bars were measured at 290 K. The derived Seebeck coefficient decreases from 80 μV K^{-1} in the undoped material to 70 μV K^{-1} in $Ru_{0.925}Sn_{0.075}Sr_2GdCu_2O_8$ but increases to 120 μV K^{-1} in $Ru_{0.8}Nb_{0.2}Sr_2GdCu_2O_8$. The proportion (< 2%) of $SrRuO_3$ is too small to affect these bulk transport measurements.

The charge distribution in the doped materials may be written as $(Ru^{5-2p_0})_{1-x}M^q{}_xSr_2Gd(Cu^{2+p^+\Delta p})_2O_8$ where the extrinsic

Table 1 Variations of the hole doping level p, the onset superconducting critical temperature T_c, and the Curie temperature T_M for $Ru_{1-x}M_xSr_2GdCu_2O_8$ solid solutions with values of x for Nb and Sn substitution as shown

p	x_{Nb}(%)	x_{Sn}(%)	T_c/K	T_M/K
0.064	20	—	—	103
0.068	15	—	19	110
0.072	10	—	19	118
0.076	5	—	29	127
0.080	0	—	37	136
0.080	—	0	38	136
0.091	—	2.5	45	126
0.101	—	5	46	117
0.112	—	7.5	50	103

† Electronic supplementary information (ESI) available: Rietveld refinement patterns [Fig. 1(a)–(c)] and characterisation data (Table 1). See http://www.rsc.org/suppdata/cc/b0/b002669g

DOI: 10.1039/b002669g

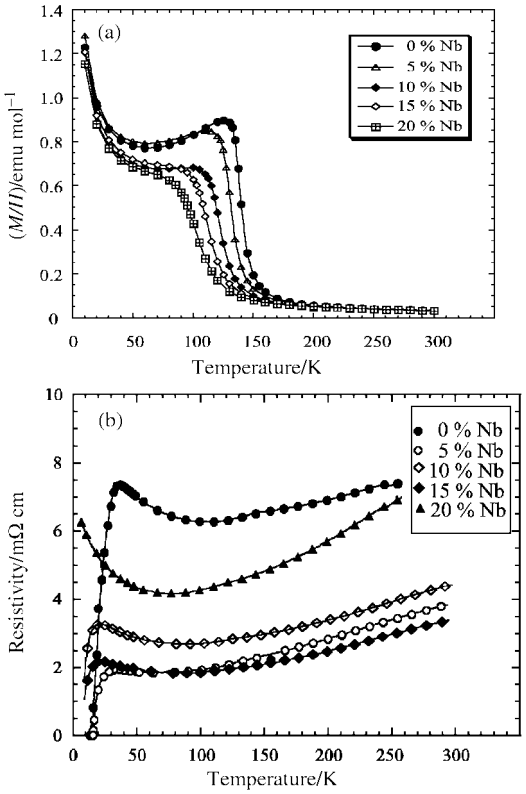

Fig. 1 Temperature variations of (a) magnetisation/field and (b) electronic resistivity for $Ru_{1-x}Nb_xSr_2GdCu_2O_8$ solid solutions.

doping introduced by the substituents M of charge q is $\Delta p = (5 - q - 2p_0)x/2$. This assumes that the substituent does not change the intrinsic band structure. This description is verified by the transport data for the $Ru_{1-x}M_xSr_2GdCu_2O_8$ solid solutions, which show that the electronic doping can be increased or decreased relative to the intrinsic level. Substitution of $Ru^{4.86+}$ by Nb^{5+} leads to removal of holes from the CuO_2 planes (chemical reduction), so that the materials become more underdoped and T_c decreases. This is supported by the increase of the 290 K Seebeck coefficient with x in the $Ru_{1-x}Nb_xSr_2GdCu_2O_8$ series, as this is known to increase from ≈ 0 in optimally doped materials with $p \approx 0.16$ to $\approx 10^2$ μV K^{-1} in very underdoped materials.[12] $NbSr_2GdCu_2O_8$ was previously reported to be non-superconducting and could not be doped sufficiently to induce superconductivity,[13] but we note that this is achieved for > 85% replacement of Nb by Ru. The trend in superconductivity of the $Ru_{1-x}Sn_xSr_2GdCu_2O_8$ solid solutions is opposite to that of the $Ru_{1-x}Nb_xSr_2GdCu_2O_8$ series. The replacement of $Ru^{4.86+}$ by Sn^{4+} transfers more holes into the CuO_2 planes (chemical oxidation), so T_c increases and the Seebeck coefficient decreases.

The variation of T_c with doping level has been established in many cuprate superconductors and to a good approximation varies quadratically as $T_c = T_c^{max}[1 - 82.6(p - 0.16)^2]$.[14] This equation has been fitted to the onset T_c values in Table 1 by writing $p = p_0 + \Delta p$, giving values of $p_0 = 0.080(5)$ for the intrinsic doping, in good agreement with the previous value of 0.07,[7] and $T_c^{max} = 65(10)$ K as an estimate for the maximum T_c at optimum doping. This is somewhat lower than the highest T_c of ≈105 K in comparable 1212 cuprates such as $(Tl_{0.5}Pb_{0.5})Sr_2(Ca,Y)Cu_2O_7$.[15] This suppression could reflect a pairbreaking interaction with the ferromagnetic moments in the RuO_2 plane, but this effect should be greater in the undoped compound than in the less ferromagnetic $Ru_{1-x}M_xSr_2GdCu_2O_8$ derivatives, leading to a greater reduction of T_c at $p \approx p_0$ which is not observed in Fig. 2. Lattice strain from the mismatch of the cuprate and ruthenate layers is a more probable explanation for the low T_c's in this system. This has previously been evidenced by the unusually short apical Cu–O bond of 2.16 Å in

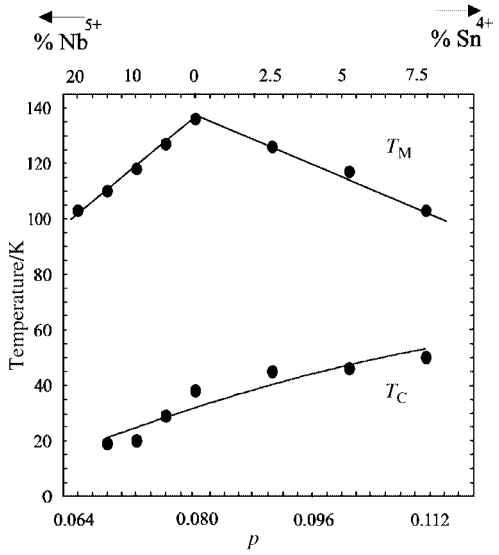

Fig. 2 The variation of the superconducting critical temperature (T_c) and the Curie temperature (T_M) with doping level p (lower scale) and %Nb or Sn substitution (upper scale) in the $Ru_{1-x}M_xSr_2GdCu_2O_8$ solid solutions. The T_c values are fitted by the quadratic expression given in the text.

$RuSr_2GdCu_2O_8$,[6] suggesting that the geometry of the structure is not optimal for superconductivity.

In conclusion, this study shows that up to 20% Nb^{5+} or 7.5% Sn^{4+} can be substituted for Ru in $RuSr_2GdCu_2O_8$. These diamagnetic substituents tune the physical properties by lowering the magnetic ordering temperature and ferromagnetic moment of the ruthenate layers, and respectively removing or adding holes to the copper oxide planes. The $Ru_{1-x}M_xSr_2GdCu_2O_8$ materials behave as typical underdoped cuprates and the maximum T_c that could be obtained at optimum doping is estimated to be 65 ± 10 K, which is less than those in comparable materials. This could reflect a magnetic pairbreaking effect but more probably results from lattice strains in the cuprate layers.

We thank EPSRC for provision of Research Grant No. GR/M59976 and a studentship for A. C. M., and S. Rycroft and J. R. Cooper for help with transport measurements.

Notes and references

1 L. Bauernfeind, W. Widder and H. F. Braun, *Physica C*, 1995, **254**, 151.
2 K. B. Tang, Y. T. Qian, L. Yang, Y. D. Zhao and Y. H. Zhang, *Physica C*, 1997, **282–287**, 947.
3 I. Felner, U. Asaf, S. Reich and Y. Tsabba, *Physica C*, 1999, **311**, 163.
4 J. L. Tallon, C. Bernhard, M. E. Bowden, P. W. Gilberd, T. M. Stoto and D. J. Pringle, *IEEE Trans. Appl. Superconduct.*, 1999, **9**, 1696.
5 C. Bernhard, J. L. Tallon, C. Niedermayer, T. Blasius, A. Golnik, E. Brucher, R. K. Kremer, D. R. Noakes, C. E. Stronach and E. J. Ansaldo, *Phys. Rev. B*, 1999, **59**, 14099.
6 A. C. Mclaughlin, W. Zhou, J. P. Attfield, A. N. Fitch and J. L. Tallon, *Phys. Rev. B*, 1999, **60**, 7512.
7 J. L. Tallon, J. W. Loram, G. V. M. Williams and C. Bernhard, *Phys. Rev. Lett.*, 2000, **61**, R6471.
8 J. W. Lynn, B. Keimer, C. Ulrich, C. Bernhard and J. L. Tallon preprint.
9 A. C. Mclaughlin, J. P. Attfield and J. L. Tallon, *Int. J. Inorg. Mater.*, 2000, **2**, 95.
10 O. Chmaissam, J. D. Jorgensen, H. Shaked, P. Dollar and J. L. Tallon, *Phys. Rev. B*, 2000, **61**, 6401.
11 A. C. Mclaughlin and J. P. Attfield, *Phys. Rev. B*, 1999, **60**, 14605.
12 S. D. Obertelli, J. R. Cooper and J. L. Tallon, *Phys. Rev. B*, 1992, **46**, 14928.
13 M.Vybornov, W. Perthold, H. Michor, T. Holubar, G. Hilscher, P. Rogl, P. Fischer and M. Divis, *Phys. Rev. B*, 1995, **52**, 1389.
14 M. R. Presland, J. L. Tallon, R. G. Buckley, R. S. Liu and N. E. Flower, *Physica C*, 1991, **176**, 95.
15 R. S. Liu, P. P. Edwards, Y. T. Huang, S. F. Wu and P. T. Wu, *J. Solid State Chem.*, 1990, **86**, 334.

Enantioselective hydroboration of olefins catalysed by cationic rhodium complexes of 2-phenylquinazolin-4-yl-2-(diphenylphosphino)naphthalene†

Mary McCarthy,[a] Mark W. Hooper[b] and Patrick J. Guiry*[a]

[a] *Department of Chemistry, University College Dublin, Belfield, Dublin 4, Ireland*
[b] *Dyson Perrins Laboratory, University of Oxford, South Parks Road, Oxford, UK OX1 3QY. E-mail: p.guiry@ucd.ie*

Received (in Liverpool, UK) 9th May 2000, Accepted 7th June 2000

Cationic rhodium complexes of 2-phenylquinazolin-4-yl-2-(diphenylphosphino)naphthalene catalyse the hydroboration of indene, tetrahydronaphthalene and a range of styrenes in high yields, regioselectivities and with enantiomer excesses of up to 97%

The report by Männig and Nöth[1] that Rh–phosphine complexes successfully catalysed the hydroboration of olefins added a new dimension to the hydroboration methodology developed by Brown.[2] With catecholborane as the borane source, the catalysed variant offered potential advantages in terms of chemo-, regio- and enantioselectivity.[3] Burgess[4] first reported catalytic enantioselective hydroboration and Hayashi subsequently used Rh–BINAP complexes for the hydroboration of styrene in ees of up to 96%.[5] Togni applied Rh complexes of the diphosphine Josiphos **1** (92% ee) and the related pyrazole-

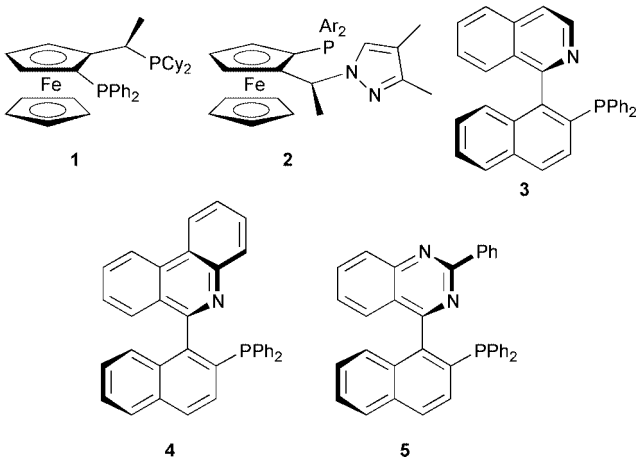

1 **2** **3** **4** **5**

containing phosphinamine **2** (98% ee).[6,7] Brown used the axially chiral phosphinamine ligands QUINAP **3** (91% ee)[8] and PHENAP **4** (67% ee)[9] and also extended the standard hydroboration–oxidation sequence to include hydroboration–amination.[10] We have recently reported the synthesis and resolution of the related ligand, 2-phenylquinazolin-4-yl-2-(diphenylphosphino)naphthalene **5**, and, in view of the success of **3** and **4**, we wished to test its enantiodifferentiating ability in Rh-catalysed olefin hydroboration and we now report our preliminary results.[11]

The required cationic Rh catalyst was prepared in a standard manner from TMS triflate and (cycloocta-1,5-diene)(pentane-2,4-dionato)rhodium(I) and (*R*)-**5**.[12] Because of its susceptibility to oxidation, the catalyst was freshly made *in situ* and we also used freshly distilled catecholborane. We focused on vinylarene substrates, paying particular attention to those which would highlight the effect on reactivity and enantioselectivity of different aryl substituents and β-substitution, as exemplified by olefins **6**–**12**. In each of the reactions the catalysed hydroboration was followed by direct oxidation with H_2O_2 to afford the corresponding alcohol. The results of our investigations are given in Table 1.

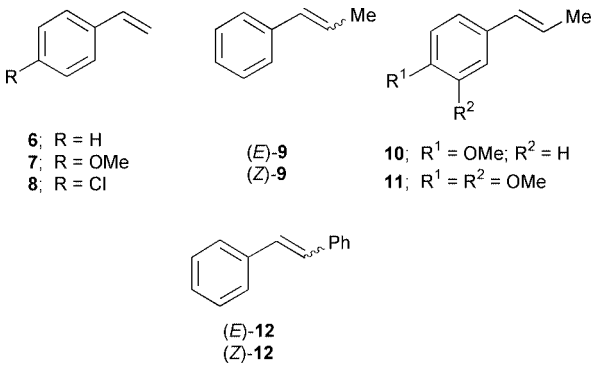

6; R = H
7; R = OMe
8; R = Cl

(*E*)-**9**
(*Z*)-**9**

10; R^1 = OMe; R^2 = H
11; R^1 = R^2 = OMe

(*E*)-**12**
(*Z*)-**12**

The α:β regioselectivity obtained using phenylethene **6** was found to increase using lowered reaction temperatures and the optimised values obtained were 80:20 with an ee value of 79% after a reaction time of 2 h. This ee value compares favourably with PHENAP **4** (67%) but is lower than that obtained with QUINAP **3** (88%) and our regioselectivity was poorer than both **3** and **4** (97:3 and 90:10, respectively).[8a,9] The sense of

Table 1 Catalytic hydroboration of stilbenes[a]

Entry	Olefin	*T*/°C	α:β[b]	Conversion (%)[b]	Ee (%) (*R*)[c]
1	**6**	25	68:32	100	63[d]
2	**6**	0	80:20	100	79[d]
3	**7**	25	75:25	100	77[d]
4	**7**	0	77:23	91	81[d]
5	**8**	25	78:22	100	46[d]
6	**8**	0	83:17	100	49[d]
7	(*E*)-**9**	25	91:9	100	94[d]
8	(*Z*)-**9**	25	92:8	100	91[d]
9	**10**	25	88:12	87	88[d]
10	**10**	0	89:11	72	92[d]
11	**11**	25	93:7	75	97[d]
12	**11**	0	91:9	65	93[d]
13	(*E*)-**12**	25	—	—	—
14	(*Z*)-**12**	25	—	100	59[e]
15	(*Z*)-**12**	0	—	100	62[e]

[a] *Typical procedure*: Freshly distilled catecholborane (0.5 mmol) in THF (1 ml) was added dropwise to a solution of olefin (0.5 mmol) and [(*R*)-diphenyl[1-(2-phenylquinazolin-4-yl)(2-naphthyl)]phosphine]rhodium(cycloocta-1,5-diene)trifluoromethanesulfonate (5 μmol) in THF (1 ml). The solution turned brown and was stirred at room temp. for 2 h. The reaction was placed in an ice bath and quenched with EtOH (1 ml). 30% H_2O_2 (aq.) (3 ml) and 1 M NaOH (aq.) (3 ml) were added and the mixture was allowed to warm and stirred for 1 h at room temp. The mixture was transferred to a separating funnel and Et_2O was added (10 ml). The organic extracts were washed with 1 M NaOH (aq.), brine and then dried over $MgSO_4$. The solvent was removed *in vacuo* to give the product as an oil. ^{1}H NMR obtained gave % conversion and regioselectivity. Enantioselectivities were determined by either GC or HPLC. [b] Regioselectivities and conversions by ^{1}H NMR. [c] Absolute configuration assigned by similarity in order of elution in the GC analysis and from the sign of the optical rotation.[8] [d] Enantiomeric excesses were determined by GC (β-Dex®120 column, 30 m × 0.25 mm, 0.25 μm film thickness). [e] Enantiomeric excesses were determined by HPLC (Chiralcel OD column 99.5:0.5 Hex–*i*PrOH.

DOI: 10.1039/b004014m

asymmetry was identical to **3** and **4**, *i.e*. the (*R*)-ligand affords the (*R*)-product alcohol. The more electron-rich 4-methoxyphenylethene **7** gave similar regioselectivities and an increased ee of 81%, but again lower than the 94% ee value observed with QUINAP **3**.[8a] The electron-deficient substrate, 4-chlorophenylethene **8**, afforded similar regioselectivities but significantly lowered ees of 46–49%, which is in agreement with trends observed employing QUINAP **3** and analogues.[8b] More promising results in terms of regio- and stereoselectivity were obtained using β-substituted arylethenes. Both the (*E*)- and (*Z*)-isomers of propenylbenzene **9** demonstrated a preference for reaction at the benzylic position and similarly in high ees of 94 and 91%, respectively. Similar values were obtained with QUINAP **3** and PHENAP **4**[9] whereas BINAP afforded an ee of 42% for (*E*)-**9** and 18% for (*Z*)-**9**.[5] (*Z*)-Propenyl-4-methoxybenzene **10** was a similarly successful substrate giving up to 92% ee in 72% yield after reaction for 6 days at 0 °C. The combination of an even more electron-rich arene and β-substituted olefin **11** gave the best ee of 97% using ligand **5**. Again it was noted that increasing the electron richness of the arene was beneficial in terms of enantioselectivity but led to a retardation of the reaction as seen by the poorer yields obtained. In order to determine the effect of increasing the bulk at the β-position we tested (*E*)- and (*Z*)-stilbene **12** and found that (*E*)-**12** was an unreactive substrate whereas (*Z*)-**12** afforded up to 62% ee in excellent yield. This result is similar to that obtained with QUINAP **3** where high ees (85–91%) were obtained with both isomers, although it was noted that (*E*)-**12** reacted at a significantly lower rate (45 turnovers after 20 h).[8b] The best ee reported for (*Z*)-**12** using BINAP was significantly lower at 16%.[5]

The cyclic olefins, indene **13** and 1,2-dihydronaphthalene **14**, are two of the most challenging substrates in Rh-catalysed

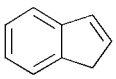

13

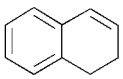

14

hydroboration. We tested Rh complexes of **5** with these substrates and the results are shown in Table 2. Excellent conversions and regioselectivities were obtained and optimised ees of 84% and 89% were obtained with **13** and **14**, respectively. The result for **13** is slightly lower than that reported for QUINAP **3** (86%),[8b] but compares favourably to PHENAP **4** (64%)[9] and even more so when compared to BINAP (19%).[5] A similar trend is observed for substrate **14** as our result of 89% is again lower than that reported for QUINAP **3** (96%),[8b] but is higher than the value obtained with PHENAP **4** (84%)[9] and in this case no result has been quoted for BINAP.

All the reactions noted in Table 1 were run on a 0.5 mmol scale with 1 mol% catalyst. In a further study, the hydroboration of (*E*)-propenylbenzene **9** was carried out using 0.5 mol% catalyst and our results are given in Table 3. Using 0.5 mol% catalyst, the ee obtained after 15 min was slightly lower than the values obtained after 1 h (94% ee), 4 h (96% ee), and 16 h (95% ee) which were not lowered in comparison with the value obtained with 1 mol% catalyst (Table 1, entry 7).

In conclusion, our results demonstrate that **5**, applied in Rh catalysed hydroboration of substituted arylethenes, β-substituted arylethenes and cyclic olefins, gives excellent conversions, good regioselectivities and ees of up to 97%. For substituted arylethenes our ligand, 2-phenylquinazolin-4-yl-2-(diphenylphosphino)naphthalene **5**, as with QUINAP **3** and PHENAP **4**, afforded lower ees than both BINAP and Josiphos **1**. However, for β-substituted arylethenes and cyclic olefins these axially chiral phosphinamine ligands are far superior. This can be explained by inferring that the increased steric demand of the olefin is more easily accommodated by these less sterically demanding ligands. Further hydroboration studies employing structurally related quinazoline-containing ligands[13] are in progress and will be reported in due course from these laboratories.[14]

Table 2 Catalytic hydroboration of cyclic olefins

Entry	Olefin	*T*/°C	α:β[a]	Conversion (%)[a]	Ee (%) (*R*)[b]
1	**13**	25	98:2	98	84[c]
2	**13**	0	98:2	99	81[c]
3	**14**	25	>99:1	100	89[d]
4	**14**	0	>99:1	>99	88[d]

[a] Regioselectivities and conversions by ^{1}H NMR. [b] Absolute configuration assigned by similarity in order of elution in the GC analysis and from the sign of the optical rotation.[8] [c] Enantiomeric excesses were determined by GC (Supelco 2-4310 α-Dex®120 column, 30 m × 0.25 mm, 0.25 μm film thickness). [d] Enantiomeric excesses were determined by GC (β-Dex®120 column, 30 m × 0.25 mm, 0.25 μm film thickness).

Table 3 Variation of catalyst concentration in the hydroboration of (*E*)-**9**

Entry	Mol % Catalyst	Time/h	Conversion (%)	Ee (%) (*R*)
1	0.5	0.25	17	92
2	0.5	1	31	94
3	0.5	4	75	96
4	0.5	16	100	95

We are indebted to Dr John Brown, University of Oxford, for his interest in this work and for supporting the visit of M. McC. to his laboratories where the initial hydroboration studies were performed. Financial support from Enterprise Ireland [Basic Research Award (SC/94/565) and a Research Scholarship (BR/94/158) to M. McC.] is gratefully acknowledged as is the award of the 1997 BOC Gases Postgraduate Bursary to M. McC. We thank the EPSRC for the award of a studentship to M. W. H. Many thanks to Shane Robinson of this department for his help with ee determinations using HPLC.

Notes and references

† This compound has previously been published under the name 2-phenylquinazolinap.

1 D. Männig and H. Nöth, *Angew. Chem., Int. Ed. Engl.*, 1985, **24**, 878.
2 H. C. Brown, in *Hydroboration*, W. A. Benjamin, New York, 1962.
3 I. Beletskaya and A. Pelter, *Tetrahedron*, 1997, **53**, 4957; K. Burgess and M. J. Ohlmeyer, *Chem. Rev.*, 1991, **91**, 1179.
4 K. Burgess and M. J. Ohlmeyer, *J. Org. Chem.*, 1988, **53**, 5178.
5 T. Hayashi, Y. Matsumoto and Y. Ito, *Tetrahedron: Asymmetry*, 1991, **2**, 601.
6 A. Togni, C. Breutel, A. Schnyder, F. Spindler, H. Landert and A. Tijani, *J. Am. Chem. Soc.*, 1994, **116**, 4062.
7 A. Schnyder, L. Hintermann and A. Togni, *Angew. Chem., Int. Ed. Engl.*, 1995, **34**, 931; H. C. L. Abbenhuis, U. Burckhardt, V. Gramlich, A. Martelletti, J. Spencer, I. Steiner and A. Togni, *Organometallics*, 1996, **15**, 1614.
8 (*a*) J. M. Brown, D. I. Hulmes and T. P. Layzell, *J. Chem. Soc., Chem. Commun.*, 1993, 1673; (*b*) H. Doucet, E. Fernandez, T. P. Layzell and J. M. Brown, *Chem. Eur. J.*, 1999, **5**, 1320.
9 J. M. Valk, G. A. Whitlock, T. P. Layzell and J. M. Brown, *Tetrahedron: Asymmetry*, 1995, **6**, 2593.
10 E. Fernandez, M. W. Hooper, F. I. Knight and J. M. Brown, *J. Chem. Soc., Chem. Commun.*, 1997, 173.
11 (*a*) M. McCarthy, R. Goddard and P. J. Guiry, *Tetrahedron: Asymmetry*, 1999, **10**, 2797; (*b*) M. McCarthy and P. J. Guiry, *Polyhedron*, 2000, **19**, 541.
12 J. M. Brown, P. L. Evans and P. A. James, *Org. Synth.*, 1989, **68**, 64.
13 P. M. Lacey, C. M. McDonnell and P. J. Guiry, *Tetrahedron Lett.*, 2000, **41**, 2475.
14 P. M. Lacey, C. P. Saunders, S. Kelly and P. J. Guiry, unpublished results.

ChemComm

Pseudopolyrotaxane composed of an azobenzene polymer and γ-cyclodextrin. Reversible and irreversible photoisomerization of the azobenzene groups in the polymer chain

Isao Yamaguchi, Kohtaro Osakada* and Takakazu Yamamoto*

Research Laboratory of Resources Utilization, Tokyo Institute of Technology, 4259 Nagatsuta, Midori-ku, Yokohama 226-8503 Japan

Received (in Cambridge, UK) 3rd April 2000, Accepted 6th June 2000

A polyrotaxane composed of γ-cyclodextrin and azobenzene containing polyester undergoes UV light induced isomerization of *trans*- to *cis*- azobenzene, whereas the reverse isomerization does not occur under the usual conditions of irradiation with visible light.

Interactions of various compounds with photoisomerizable azobenzene groups with cyclodextrins have been investigated to develop new photoresponsive materials.[1] Much attention has been directed toward cyclodextrin-based polyrotaxanes and pseudopolyrotaxanes of azobenzenes.[2] Recently, a rotaxane system composed of cyclodextrin (CD) and an azobenzene-containing polymer exhibited quick and reversible molecular shuttle type behavior induced by photoisomerization of the azobenzene group.[3] In the course of our study of the preparation and properties of various pseudopolyrotaxanes with cyclodextrins,[4] we observed a significant influence of the host CD molecules on the photoinduced *cis*–*trans* isomerization of the azobenzenes. Here we report syntheses of a new pseudopolyrotaxane of polyazobenzene and of a corresponding CD free polyazobenzene, as well as the effect of CD on the photoisomerization of polyazobenzene.

A 1:1 inclusion complex of butane-1,4-diol diglycidyl ether (BDGE) [1,4-bis(2,3-epoxypropoxy)butane] and γ-CD (**1**)[5] reacts with azobenzene-4,4′-dicarboxylic acid (ABDA) in the presence of a catalytic amount of $[Et_3NCH_2Ph]^+Cl^-$ to afford the pseudopolyrotaxane **2**(*trans*), which, on average, contains 0.21 γ-CD unit per repeating unit as evaluated from elemental analysis and NMR spectroscopy (Scheme 1). The azobenzene groups in the polymer take the *trans* configuration, as revealed by UV-vis spectroscopy. The pseudopolyrotaxane **2**(*trans*) gives a DSC scan which is quite different from that of a physical mixture of **2**(*trans*) and γ-CD. Analysis by GPC gives values for M_n of 9500 and M_w of 17 100 (*vs.* polystyrene standards).

Cyclodextrin-free polyester (**3**(*trans*)) having azobenzene groups with M_n = 8750 and M_w = 15100 was also obtained as an orange solid (76%) in a similar fashion from the polyaddition of BDGE to ABDA (Scheme 2). The ratio of –CH(CH$_2$OH)– and –CH$_2$–CH(OH)– linkages formed *via* α- and β-cleavage of the oxirane ring, respectively, is determined to be 0.62:0.38. Similar ratios have been reported for polymers obtained by the ring-opening polyaddition of diglycidyl ethers and dicarboxylic acids.[6] An attempt to prepare **2**(*trans*) from a mixture of γ-CD and **3**(*trans*) was not successful, indicating that the polymers, once formed, do not form the supramolecular system with γ-CD, presumably due to the presence of the bulky azobenzene units.

Photoisomerization of the azobenzene group[7] of **2**(*trans*) and **3**(*trans*) was investigated, and the results were compared. Upon irradiation of a DMSO solution of **2**(*trans*) with UV light (245 nm), the absorption peak at 331 nm due to the π–π* transitions of the *trans* azobenzene unit decreased accompanied by growth of the peak at 433 nm due to the n–π* transition of the *cis* azobenzene unit.[8] Fig. 1 shows changes in the absorption spectrum during the reaction, which follows first-order kinetics with a rate constant of 1.7×10^{-3} s^{-1} at 30 °C and 1.5×10^{-3} s^{-1} at 25 °C. The γ-CD free polyester **3**(*trans*) undergoes a similar *trans* to *cis* photoisomerization under irradiation with UV light (245 nm) and gives a first-order rate constant (1.3×10^{-3} s^{-1}, 25 °C) comparable to that of **2**(*trans*). These results clearly indicate the occurrence of the photoinduced isomerization of **2**(*trans*) and **3**(*trans*) to **2**(*cis*) and **3**(*cis*), respectively.

As for **3**(*cis*), irradiation with visible light (> 440 nm) causes a reverse isomerization, increasing the strength of the peak at 330 nm and decreasing the strength of the peak at 432 nm. It has been reported that various azobenzenes undergo a similar reverse photoisomerization under irradiation with visible light. However, irradiation of the DMSO solution of **2**(*cis*) with visible light (> 440 nm) caused no observable isomerization of **2**(*cis*) to the original **2**(*trans*). Heating of **3**(*cis*) at 50 °C also leads to its isomerization to **3**(*trans*) within 15 min, whereas **2**(*cis*) does not undergo such thermally induced isomerization. Since **2** and **3** have similar molecular weights and polydispersities, the large difference in the photo and thermally induced isomerization may be ascribed to a difference in the molecular structure or aggregation behavior between **2** and **3** in solution.

Fig. 2 shows plots of η_{sp}/c against c for **2**(*trans*), **3**(*trans*), **2**(*cis*), and **3**(*cis*). As shown in Fig. 2, **2**(*cis*) gave a larger η_{sp}/c value and a larger slope in the η_{sp}/c *vs.* c plots, compared with

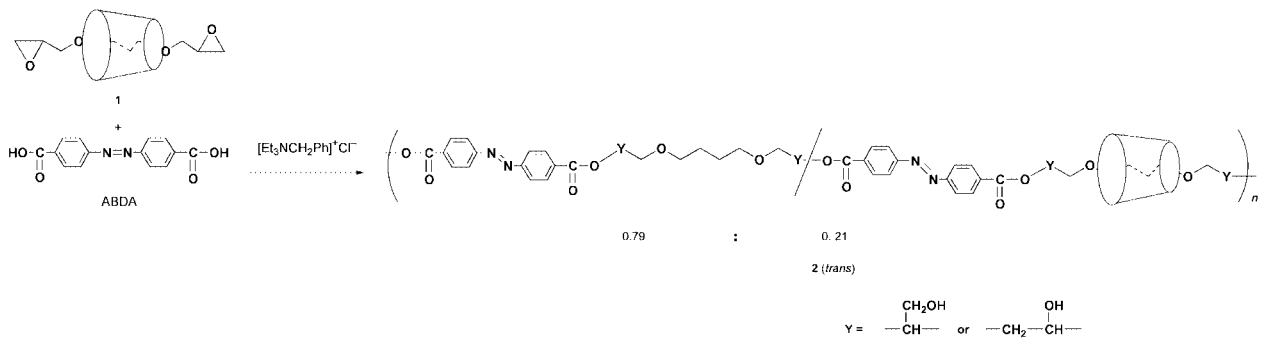

Scheme 1

DOI: 10.1039/b002642p

the other three polymers. The larger slope suggests the presence of intermolecular interactions between the polymer molecules. On the other hand, for polyamide type polyazobenzenes –(amide unit–N=N–)$_n$–, it is reported that the *cis* and *trans* polymers give the same slope in the η_{sp}/c *vs. c* plots.[9] In this case, photoinduced *cis* to *trans* isomerization proceeds smoothly. The viscometric results of **2**(*cis*) suggest the presence

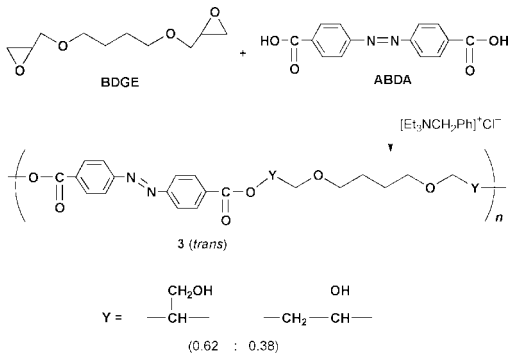

Scheme 2

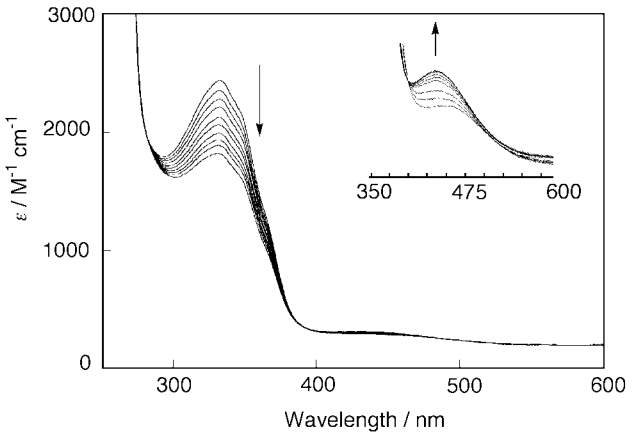

Fig. 1 Change of the absorption spectra of DMSO solution of **2** during isomerization from the *trans* to the *cis* form irradiated with UV light (245 nm) at 30 °C. The spectra were recorded at t = 0, 2, 4, 6, 8, 10, 12, 14, 16 and 18 min.

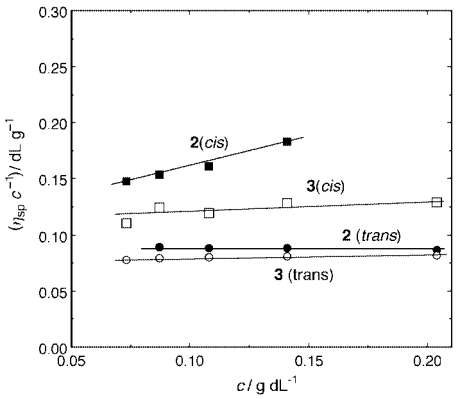

Fig. 2 Viscosity of **2**(*trans*) and **3**(*trans*) in DMSO at 25 °C before and after irradiation with UV light (245 nm).

of significant intermolecular interactions between **2**(*cis*) molecules assisted by CD, which may effect the *cis* to *trans* isomerization of the azobenzene group. Chart 1 depicts a

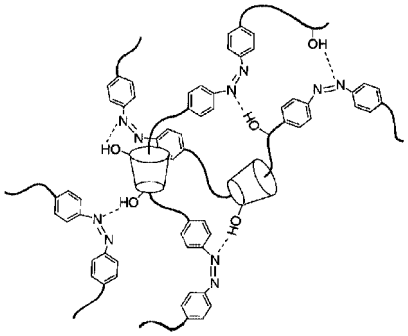

schematic drawing of intermolecular interactions between the pseudopolyrotaxane molecules caused by N···H–O hydrogen bonds. The *cis* azobenzene group is sterically less crowded and has a higher proton affinity than the *trans*-azobenzene groups. By forming the hydrogen bond, the cis form of azobenzene seems stabilized. Addition of large excess amounts of γ-CD to a DMSO solution of **3**(*cis*) retards the photoinduced *cis* to *trans* isomerization, but γ-CD contained in **2** (0.21 molarity of the monomer units) blocks the isomerization much more effectively. This may also be due to stabilization of the *cis*-azobenzene unit by hydrogen bonding with γ-CD. The retardation effect appears to be more effective in **2**(*cis*) which has the γ-CD unit in its own polymer chain.

The authors are grateful to Professor Takahiro Seki and Dr Shinya Morino in our laboratory for their helpful discussions. This work was supported by a Grant-in-Aid for Scientific Research from the Ministry of Education, Science, Culture, and Sports, Japan.

Notes and references

1 (*a*) H. Tachibana and M. Matsumoto, *Adv. Mater.*, 1993, **5**, 796; (*b*) M. Tanaka, R. Azumi, H. Tachibana, T. Nakamura, Y. Kawabata, M. Matsumoto, T. Miyasaka, W. Tagaki, H. Nakahara and K. Fukuda, *Thin Solid Films*, 1994, **244**, 832; (*c*) S. Anderson, T. D. W. Claridge and H. L. Anderson, *Angew. Chem., Int. Ed. Engl.*, 1997, **36**, 1310; (*d*) M. R. Craig, T. D. W. Cloridge, M. G. Hutchings and H. L. Anderson, *Chem. Commun.*, 1999, 1537 and references therein.

2 (*a*) A. Harada, *Acta Polymer.*, 1998, **49**, 3; (*b*) S. A. Nepegodiev and J. F. Stoddart, *Chem. Rev.*, 1998, **98**, 1959.

3 H. Murakami, A. Kawabuchi, K. Kotoo, M. Kunitake and N. Nakashima, *J. Am. Chem. Soc.*, 1997, **119**, 7605.

4 I. Yamaguchi, K. Osakada and T. Yamamoto, *J. Am. Chem. Soc.*, 1996, **118**, 1811.

5 I. Yamaguchi, H. Ishii, K. Osakada, T. Yamamoto and S. Fukuzawa, *Bull. Chem. Soc. Jpn.*, 1999, **72**, 1541.

6 (*a*) P. A. Martínez, V. Cádiz, A. Mantecón and A. Serra, *Angew. Makromol. Chem.*, 1985, **133**, 97; (*b*) A. Serra, V. Cádiz and A. Mantecón, *Angew. Makromol. Chem.*, 1987, **155**, 93.

7 G. Zimmerman, L. Chow and U. Paik, *J. Am. Chem. Soc.*, 1958, **80**, 3528.

8 (*a*) J. Ronayette, R. Arnaud and J. Lemaire, *Can. J. Chem.*, 1974, **52**, 1858; (*b*) H. Rau, *J. Photochem.*, 1984, **26**, 221.

9 (*a*) M. Irie, Y. Hirano, S. Hashimoto and K. Hayashi, *Macromolecules*, 1981, **14**, 262; (*b*) M. Irie and W. Schnabel, *Macromolecules*, 1981, **14**, 1246.

ChemComm

Dopamine interaction with a polyamine cryptand of 1*H*-pyrazole in the absence and in the presence of Cu(II) ions. Crystal structure of $[Cu_2(H_{-1}L)(ClO_4)_3{\cdot}2H_2O$

Laurent Lamarque,[a] Carlos Miranda,[a] Pilar Navarro,*[a] Francisco Escartí,[b] Enrique García-España,*[b] Julio Latorre[b] and José A. Ramírez*[b]

[a] *Instituto de Química Médica, Centro de Química Orgánica Manuel Lora Tamayo, CSIC, Juan de la Cierva 3, 28006 Madrid, Spain*

[b] *Departamento de Química Inorgànica, Facultat de Química, Universitat de València, C/Dr. Moliner 50, 46100 Burjassot, València, Spain. E-mail: enrique.garcia-es@uv.es*

Received (in Cambridge, UK) 20th April 2000, Accepted 5th June 2000

The crystal structure of the binuclear Cu^{2+} complex $[Cu_2(H_{-1}L)](ClO_4)_3{\cdot}2H_2O$ of the cryptand L = 1,4,7,8,11,14,17,20,21,24,29,32,33,36-tetradecaazapentacyclo[12.12.12.1^{6,9}.1^{19,22},1^{31,34}]hentetraconta-6,9(41),19(40),21,31,34(39)-hexaene is presented; evidence for the formation in solution of binary L–dopamine and ternary Cu^{2+}–L–dopamine complexes is presented.

Supramolecular chemistry has developed through the preparation of sophisticated molecular receptors which are able to discriminate and induce characteristic properties in given substrates.[1] Tridimensional cryptand-like receptors with appropriate arrangements of binding sites have yielded interesting patterns in many aspects of molecular recognition like metal ion or anion coordination chemistry.[1,2] We have previously reported the synthesis, basicity and complexing properties of polyamine coronands of 1*H*-pyrazole able to form Zn^{2+} and Cu^{2+} pyrazolate salts.[3,4] Herein we report on a polyamine cryptand of related structure.[5] We advance the results of a study on its interaction with Cu^{2+} and on the formation of mixed complexes with the biologically relevant neurotransmitter dopamine.[6]

Ligand L was prepared as reported in ref. 5 by reacting 3,5-pyrazoledicarbaldehyde and tris(2-aminoethyl)amine in 3:2 molar ratio in MeOH, followed by reaction *in situ* with $NaBH_4$. Crystals of $[Cu_2(H_{-1}L)(ClO_4)_3]{\cdot}2H_2O$ **1** were prepared

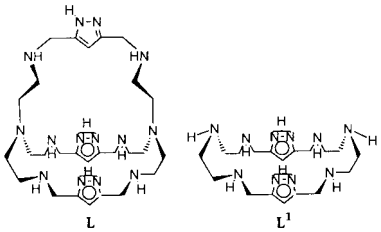

L L^1

mixing methanolic solutions of free L (57 mg, 0.1 mmol) and $Cu(ClO_4)_2{\cdot}6H_2O$ (74 mg, 0.2 mmol). Evaporation of the solution gave a blue solid that after re-dissolution in a minimum amount of hot water, gave crystals of $[Cu_2(H_{-1}L)(ClO_4)_3]{\cdot}2H_2O$ **1** suitable for X-ray diffraction analysis.† The crystal structure of **1** consists of $[Cu_2(H_{-1}L)]^{3+}$ cations, ClO_4^- anions and water molecules. The coordination geometry around each Cu^{2+} is square pyramidal, the base of the pyramid being formed by two secondary nitrogens of the bridge and two nitrogen atoms of two different pyrazolate moieties which act as exobidentate ligands. The axial positions are occupied by the bridgehead nitrogen atoms, with distortion being more pronounced in one of the two sites [Cu(1)–N(1) 2.29(2) Å, Cu(2)–N(6) 2.403(9) Å]. The Cu^{2+}–L distances involving the sp^2 pyrazolate nitrogen atoms [Cu(1)–N(3) 1.90(1) Å, Cu(1)–N(9) 1.93(1) Å, Cu(2)–N(4) 1.92(1) Å, Cu(2)–N(8) 1.91(1) Å] are much shorter than those of the secondary nitrogen atoms [Cu(1)–N(2) 2.11(1) Å, Cu(1)–N(10) 2.06(1) Å, Cu(2)–N(5) 2.08(1) Å, Cu(2)–N(7) 2.11(2) Å]. The Cu(1)···Cu(2) distance is 3.960(3) Å. Similar coordination features were observed in the crystal structure of the binuclear complex $[Cu_2(H_{-2}L^1)](ClO_4)_2$, in which L^1 is the coronand ligand that constitutes the base of cryptand L,[3] and in several crystal structures of pyrazole containing ligands.[7] Interestingly, we have observed that Cu^{2+} leads to the ready deprotonation of the two pyrazole fragments involved in the coordination, without requiring any addition of base (*vide infra*). However, the pyrazole in the non-coordinating bridge of L (see Fig. 1) does not deprotonate, and lies to one side of the macrocyclic cavity. One of the nitrogen atoms of the aliphatic chains is protonated and hydrogen bonded to a water molecule [N(11)···O(1) 2.79(2) Å] placed at one side of the macrocyclic cavity and further connected to the sp^2 nitrogen of the pyrazole group through an additional hydrogen bond [N(12)···O(1) 3.12(2) Å]. The distances of the water molecule to the non-protonated nitrogen atom of the bridge and to the other pyrazole nitrogen are much longer (5.38 and 3.79 Å, respectively). The other water molecule, which is located completely outside of the cavity, is hydrogen bonded to N(10) [N(10)···O(2) 2.98(2) Å].

The coordination arrangement keeps both Cu^{2+} metal ions close to one face of the cage [the elevation of the Cu atoms over the mean plane defined by the nitrogen donors of the base of the square pyramid are 0.142(7) and 0.272(7) Å for Cu(1) and

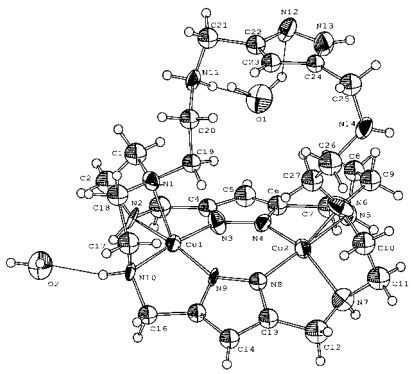

Fig. 1 ORTEP drawing of the $[Cu_2(H_{-1}L)]^{3+}$ complex cation also showing the hydrogen bonds to the water molecules. Selected distances (Å) and angles (°): Cu(1)–N(3) 1.90(1), Cu(1)–N(9) 1.93(1), Cu(1)–N(10) 2.06(1), Cu(1)–N(2) 2.11(1), Cu(1)–N(1) 2.29(2), Cu(1)–Cu(2) 3.96(3), Cu(2)–N(8) 1.91(1), Cu(2)–N(4) 1.92(1), Cu(2)–N(5) 2.08(1), Cu(2)–N(7) 2.11(2), Cu(2)–N(6) 2.403(9), O(1)–N(11) 2.79(2), O(1)–N(12) 3.12(3), O(2)–N(10) 2.98(2); N(10)–Cu(1)–N(2) 103.7(5), N(2)–Cu(1)–N(3) 81.4(6), N(3)–Cu(1)–N(9) 94.7(6), N(9)–Cu(1)–N(10) 79.6(6), N(1)–Cu(1)–N(2) 82.0(5), N(10)–Cu(1)–N(1) 81.4(5), N(3)–Cu(1)–N(1) 102.9(6), N(9)–Cu(1)–N(1) 111.3(5), N(8)–Cu(2)–N(4) 94.6(5), N(4)–Cu(2)–N(5) 80.2(6), N(5)–Cu(2)–N(7) 101.4(7), N(8)–Cu(2)–N(7) 81.4(6), N(4)–Cu(2)–N(6) 123.7(6), N(5)–Cu(2)–N(6) 81.1(4), N(7)–Cu(2)–N(6) 81.7(5), N(8)–Cu(2)–N(6) 105.6(5).

DOI: 10.1039/b003231j

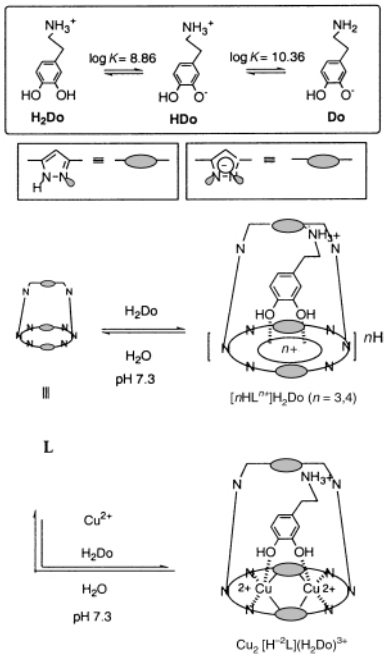

Scheme 1

Cu(2), respectively] leaving enough free room within the cavity to allow the encapsulation of further substrates as exogenous ligands. Owing to the biological relevance that ternary Cu^{2+}–dopamine complexes have in enzyme mimicking and neurotransmitter regulation, we have preliminarily studied this system.

pH-Metric analysis shows that free L displays up to six protonation steps in the pH range 2.5–10.5 with pK_a values in the range 9.5–5.2.[8] This makes this compound highly charged in solution at physiological pH and a promising receptor for encapsulating anionic or polar substrates.

The cryptand heterocyclophane L displays high affinity for Cu^{2+} forming in aqueous solution very stable binuclear complexes of stoichiometries $[Cu_2L]^{4+}$, $[Cu_2H_{-1}L]^{3+}$ and $[Cu_2H_{-2}L]^{2+}$,[9] at a molar ratio Cu^{2+}:L = 2:1, which are the only species over a wide pH range ($[Cu_2L]^{4+}$ from pH 3 to 5, $[Cu_2H_{-1}L]^{3+}$ from pH 5.5 to 8 and $[Cu_2H_{-2}L]^{2+}$ above pH 8.5). Taking into account that in the crystal structure of **1**, the two pyrazole groups involved in the coordination of Cu^{2+} are deprotonated and that the constant of the equilibrium $[Cu_2L]^{4+}$ = $[Cu_2H_{-1}L]^{3+}$ + H^+ is log K = −5.37, Cu^{2+} coordination to L induces a decrease of more than six pH units in the protonation constant of pyrazole with respect to the free heterocycle. A similar behaviour has also been observed in the system Cu^{2+}–L[1],[10] and in a related system containing two 1,4,7-triazacyclononane units linked by a 3,5-pyrazole bridge.[7]

The interaction of L with dopamine (Do) has been analysed in the pH range 2.5–9.0 with 1:1 dopamine:receptor species being detected with degrees of protonation varying between 7 and 1. Around physiological pH, the magnitude of the interaction reaches values close to 5 logarithm units (K_{app} = $\Sigma[DoH_{i+j}\cdot L]/\Sigma[H_jDo]\Sigma[H_iL]$ = 10^5:[11] therefore, the neurotransmitter forms a remarkably stable complex with the receptor. UV studies confirm this interaction. UV spectra of solutions containing a constant amount of L and variable amounts of dopamine at pH 7 show an increase in absorptivity and eventual saturation of an absorption band centred at 214 nm. Fitting of the absorbance *vs.* [Do]/[L] plots confirms the 1.1 Do:L stoichiometry and allows an estimation of an affinity constant of *ca.* 5 logarithmic units, in agreement with the pH-metric studies. Molecular models suggest the possibility of a partial inclusion of the dopamine molecule in the cavity of the receptor and its stabilisation by a variety of intermolecular forces such as electrostatic and/or hydrogen bonding interactions (Scheme 1).

Finally, we comment on the formation of ternary complexes Cu^{2+}–L-dopamine of stoichiometry $[Cu_2H_2LDo]^{5+}$, $[Cu_2HLDo]^{4+}$, $[Cu_2LDo]^{3+}$ and $[Cu_2H_{-1}LDo]^{3+}$ which, taking into account the pH range of their formation, can be formulated formally as deriving from the following equilibria: H_2Do^+ + $[Cu_2L]^{4+}$ = $[Cu_2H_2LDo]^{5+}$, log K = 3.7; H_2Do^+ + $[Cu_2H_{-1}L]^{3+}$ = $[Cu_2HLDo]^{4+}$, log K = 4.0; H_2Do^+ + $[Cu_2H_{-2}L]^{2+}$ = $[Cu_2LDo]^{3+}$, log K = 3.7; HDo + $[Cu_2H_{-2}L]^{2+}$ = $[Cu_2H_{-1}LDo]^{2+}$, log K = 4.0.

The formation of the ternary complexes implies breaking of the Cu–N axial bonds and their replacement by strong Cu–phenolate bonds[12] as suggested by modelling of the system. An interaction of the ammonium group of dopamine with the sp^2 bond of the pyrazole moiety might also contribute to the final stabilisation of the complexes (Scheme 1).

The observed recognition patterns and crystal structure suggest interesting developments of this receptor in the fields of medicinal chemistry and enzyme mimicking.

We thank SAF 96-0242-CO2 y SAF99-0063 and PB96-0796-CO2 for financial support.

Notes and references

† *Crystal data* for **1**: $C_{27}H_{51}N_{14}O_{14}Cl_3Cu_2$, M = 1029.25, monoclinic, space group $C2/c$, a = 44.667(5), b = 9.124(5), c = 20.050(5) Å, β = 97.687(5), V = 8098(5) Å^3, Z = 4, 6579 reflections collected of which 3411 were independent (R_{int} = 0.1348), D_c = 1.687 Mg m^{-3}, $R(R_w)$ = 0.0625(0.1621). CCDC 182/1674.

1 J.-M. Lehn, *Angew. Chem., Int. Ed. Engl*, 1988, **27**, 89; J.-M. Lehn, *Supramolecular Chemistry, Concepts and Perspectives*, VCH, Weinheim, 1995.

2 *Supramolecular Chemistry of Anions*, ed. A. Bianchi, K. Bowman-James and E. García-España, Wiley-VCH, New York, 1997.

3 M. Kumar, V. J. Arán and P. Navarro, *Tetrahedron Lett.*, 1993, **34**, 3159; M. Kumar, V. J. Arán, P. Navarro, A. Tamos-Gallardo and A. Vega, *Tetrahedron Lett.*, 1995, **35**, 5723; V. J. Arán, M. Kumar, J. Molina, L. Lamarque, P. Navarro, E. García-España, J. A. Ramírez, S. V. Luis and B. Escuder, *J. Org. Chem.*, 1999, **64**, 6135.

4 J. Elguero, *Pyrazoles in Comprehensive Heterocyclic Chemistry II, A Review of the Literature 1982–1995*, ed. A. R. Katritzky, C. V. Ress and S. F. V. Scriven, Pergamon, New York, 1997, vol. 3.

5 M. Kumar, V. J. Arán and P. Navarro, *Tetrahedron Lett.*, 1995, **36**, 2161.

6 E. J. Nestler, *J. Neurosci.*, 1992, **12**, 2439; M. Giros, M. Jaber, R. S. Jones, R. M. Wightman and M. G. Caron, *Nature*, 1996, **379**, 606; B. B. Hoffman and R. J. Lefkowitz, *Goodmas&Gilman's The Pharmacological Basis of Therapuetics*, ed. J. G. Hardman and I. Limbird, MacGraw Hill, New York, 1996, ch. 10.

7 L. Behle, M. Neuburger, M. Zehnder and T. A. Kaden, *Helv. Chim. Acta*, 1995, **78**, 693; S. S. Tandon, L. K. Thompson and J. N. Bridson, *J. Chem. Soc., Chem. Commun.*, 1993, 804.

8 Potentiometry was carried out in 0.15 mol dm^{-3} NaCl at 298.1 K using concentrations of L, Cu^{2+} and dopamine in the range 1–3 × 10^{-3} mol dm^{-3}. The program HYPERQUAD (A. Sabatini, A. Vacca and P. Gans, *Coord. Chem. Rev.*, 1992, **120**, 389) was used to derive the values of the protonation and stability constants. Protonation constants of L under the same experimental conditions: log $K_{HL/H.L}$ = 9.54(2), log $K_{H_2L/HL.H}$ = 8.71(1); log $K_{H_3L/H_2L.H}$ = 7.72(2); log $K_{H_4L/H_3L.H}$ = 6.55(3), log $K_{H_5L/H_4L.H}$ = 6.51(3), log $K_{H_6L/H_5L.H}$ = 5.23(3). Protonation constants of dopamine (Do, see Scheme 1): log $K_{HDo/Do.H}$ = 10.36(1), log $K_{H_2Do/HDo.H}$ = 8.86(1).

9 At a molar ratio of 2:1 the species $[Cu_2HL]^{5+}$, $[Cu_2L]^{4+}$, $[Cu_2H_{-1}L]^{3+}$ and $[Cu_2H_{-2}L]^{2+}$ are found in solution with stability constants: $2Cu^{2+}$ + H^+ + L = $[Cu_2HL]^{5+}$, log K = 38.73(7); $2Cu^{2+}$ + L = $[Cu_2L]^{4+}$, log K = 36.61(3), $2Cu^{2+}$ + L = $[Cu_2H_{-1}L]^{3+}$ + H^+, log K = 31.39(3); $2Cu^{2+}$ + L = $[Cu_2H_{-2}L]^{2+}$ + $2H^+$, log K = 24.24(4).

10 P. Navarro and E. García-España, work in preparation.

11 Potentiometric titrations indicate that between pH 3 and 9.5 the formation of the species H_jDoL with j = 1–7: Do + H^+ + L = $HDoL^+$, log K = 16.19(2); Do + $2H^+$ + L = H_2DoL^{2+}, log K = 25.72(2); Do + $3H^+$ + L = H_3DoL^{2+}, log K = 34.57(2); Do + $4H^+$ + L = H_4DoL^{4+}, log K = 43.04(2); Do + $5H^+$ + L = H_5DoL^{2+}, log K = 50.39(2); Do + $6H^+$ + L = H_6DoL^{2+}, log K = 57.08(2); Do + $7H^+$ + L = H_7DoL^{7+}, log K = 63.40(2). Conditional constants defined as K_{app} = $\Sigma[DoH_{i+j}L]/\Sigma[H_jDo]\Sigma[H_iL]$ range from 2 to 5.5 logarithmic units in the pH range studied.

12 A. Gergerly, T. Kiss and G. Deak, *Inorg. Chim. Acta*, 1979, **36**, 113; B. Grass-Küznar, V. I. Simeon and O. A. Weber, *J. Inorg. Nucl. Chem.*, 1974, **36**, 2151.

ChemComm

Photochromism of chromene crystals; a new property of old chromenes†

Jonathan Hobley,*[a] Vincenzo Malatesta,*[b] Roberto Millini,[c] William Giroldini[b] Lucia Wis,[b] Masahiro Goto,[a] Maki Kishimoto[a] and H. Fukumura[d]

[a] *Advanced Science Research Centre, Japan Atomic Energy Research Institute, 25-1, Mii-Minami-Machi, Neyagawa, Osaka 572-0019, Japan. Tel: +81 728 31 0943; Fax: +81 728 31 0596; E-mail: j.hobley@apr.jaeri.go.jp*
[b] *Great Lakes Technology, Via Maritano 26, 20097, San Donato Milanese, Italy*
[c] *Enitecnologie, Via Maritano 26, 20097, San Donato Milanese, Italy*
[d] *Department of Chemistry, School of Science, Tohoku University, Sendai, Miyagi 980-8578, Japan*

Received (in Cambridge, UK) 2nd May 2000, Accepted 12th June 2000

Of the four chromene compounds; 3,3-diphenyl-5,10a-dihydro-3*H*-benzo[*f*]chromene (CHR1), 6-methoxy-2,2-diphenyl-2*H*-benzo[*h*]chromene (CHR2), 2,2-diphenyl-2*H*-benzo[*h*]chromene (CHR3) and 6,7-dimethoxy-2,2-diphenyl-2*H*-chromene (CHR4), CHR2–4 exhibited crystalline state photochromism.

Solution and dispersed state photochromism are well known phenomena, however there are relatively fewer examples of crystalline state photochromism.[1–5] Photochromic crystals are especially unusual, although not unknown,[3–5] when the photochromism involves large structural changes such as *cis–trans* isomerisation. This is due to the small free volume in a crystal lattice. In the case of spiropyrans and spirooxazines such crystalline photochromism, involving a minimum of two isomerisation steps, has been reported using femtosecond laser pulses where there is a laser fluence threshold that must be reached before any colouration reaction is observed.[5] Prior to our work, photochromic chromene (CHR) crystals, having a similar photochemistry to the spirooxazines, had not been reported.[6] The CHR reaction mechanism in solution[7,8] is shown in Scheme 1 exemplified for CHR1. As can be seen the reaction is complex involving several isomerisation steps.

CHR1–4 were synthesised by Great Lakes Technology using the standard synthetic routes.[6,9] UV/VIS spectra were measured using a Hewlett Packard HP8452 diode array spectrophotometer in reflectance mode. Macroscopic UV irradiation was carried out using a nitrogen laser at 337 nm (10 nanosecond pulse duration, repetition rate 100 Hz, 0.1 mW pulse^{-1} cm^{-2}) or a 100 W Hg lamp emitting in the visible and UV. HPLC was used to assign CHR2 photochromic reaction products with a reverse phase C-18 column on an HP 1090 chromatograph with a 1 : 9 ratio of water to acetonitrile at a flow rate of 1 mL min^{-1}

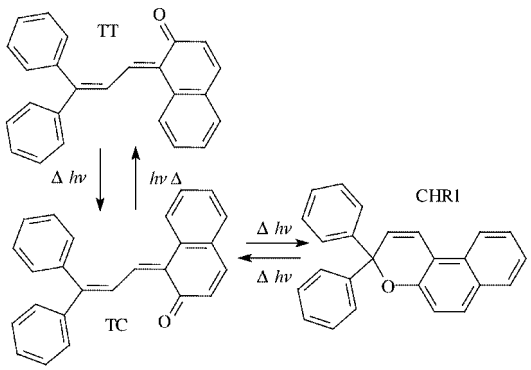

Scheme 1

† Microscopic colour images showing photo-colouration and bleaching are available as electronic supplementary information (ESI). Microscopic images were obtained with a Nikon Eclipse E800 Fluorescence microscope using the microscope's Hg lamp excitation source to photo-convert the crystals. See http://www.rsc.org/suppdata/cc/b0/b003480k/

with diode array UV/VIS detection. X-Ray diffraction data[10] were collected before and after 1 h of irradiation of a single CHR2 crystal (0.5 × 0.5 × 0.4 mm) using the nitrogen laser.

After UV irradiation (nitrogen laser or CW source) pale yellow CHR2 crystals turned deep orange. The orange colour was partially photobleachable with visible light, but did not thermally bleach. This is shown in Fig. 1. The non-permanent component of the CHR2 colouration could be cycled between photocoloured and photobleached states.

For CHR2 it is possible to isolate the TT isomer from the TC isomer since it can crystallise in a mixed lattice with the CHR2 form.[12] From solutions of such mixed crystals HPLC retention times were established for the CHR2-form (5.45 min) and the TT isomer (6.55 min). From HPLC on mixtures of the TT, TC and CHR2-form, produced photochemically in acetonitrile, the TC isomer retention time (8.31 min) was also found. The λ_{max} of the TT isomer was blue shifted by only 10 nm with respect to that of the TC isomer. Retention times from HPLC carried out on dissolved photocoloured crystals (nitrogen laser 1 h) showed that the crystals contained a mixture of mainly the CHR2 form, but with TT and TC isomers also present. The integrated absorption/elution time profiles of TT and TC were approximately equal, implying similar fractional conversion to TT and TC if we assume similar extinction coefficients. The overall fraction of photoconversion to TT and TC suggested from this HPLC and separately determined by ^{1}H NMR was < 1% even after prolonged irradiation (nitrogen laser 1 h). Also from X-ray analysis of a single CHR2 crystal we found no detectable increase in the bulk lattice disorder even after prolonged irradiation (nitrogen laser 1 h). We must therefore conclude that under these conditions photoisomerisation is probably not a feature of every lattice site, although this may be because conversion is concentrated at the surfaces by consideration of Beers Law.

Using HPLC on photoconverted and subsequently photobleached CHR2 we found that photobleaching reduces the

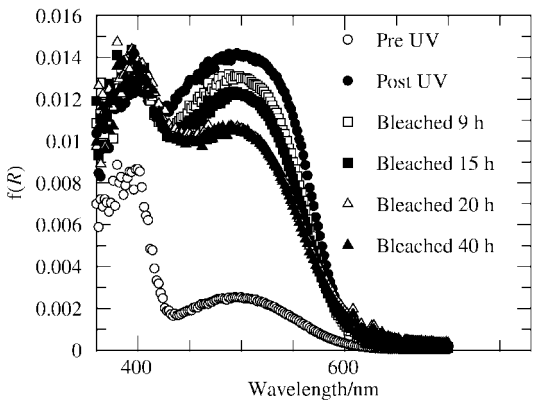

Fig. 1 Diffuse reflectance spectra (Kubelka Munk)[11] of CHR2 crystals before and after UV irradiation and during and after photobleaching.

DOI: 10.1039/b003480k

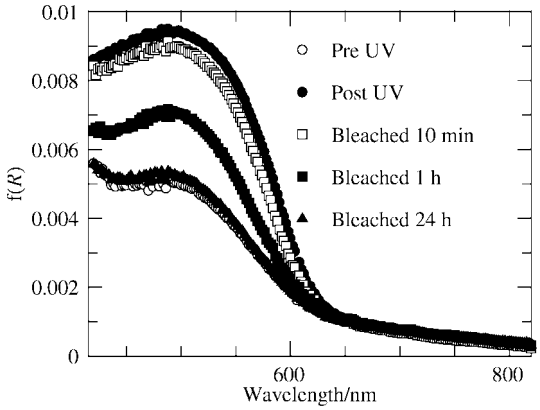

Fig. 2 Diffuse reflectance spectra (Kubelka Munk)[11] of CHR3 crystals before and after UV irradiation and during and after photobleaching. For microscopic colour images showing photo-colouration and bleaching see http://www.rsc.org/suppdata/cc/b0/b003480k/

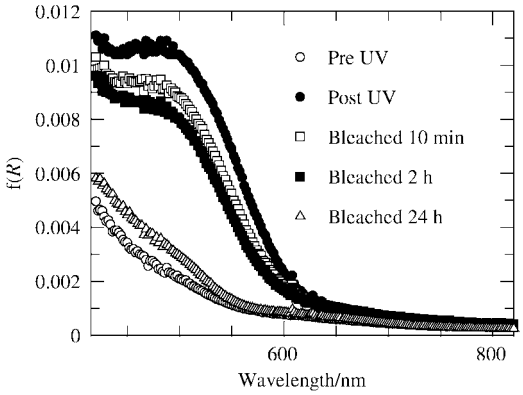

Fig. 3 Diffuse reflectance spectra (Kubelka Munk)[11] of CHR4 crystals before and after UV irradiation and during and after photobleaching.

proportion of the TC isomer relative to the TT form. The TT isomer is persistent both photochemically and thermally. Conversely CHR3 and CHR4 crystals photocoloured with UV light could be almost fully photo and thermally bleached back to the CHR-form. This is shown in Figs. 2 and 3.

All of the compounds CHR2–4 could be photoconverted with relatively weak CW UV irradiation sources. For example, photocolouration was even observed after irradiating the samples with the excitation beam from a standard fluorimeter (Shimadzu RF5300PPC 350 nm). From this we conclude that this colouration reaction is activated by a single photon non-cooperative (no simultaneous excitation of adjacent sites required[5]) solid-state reaction. We also note that CHR1 did not exhibit any photochromism in its the crystalline state.

This work was funded by the European commission (J. H., BRITE EURAM contract No. BRPR-CT96-0328, project No. BE-3380, fellowship No. BRMA-CT 97-5041 and by JISTEC (J. H., STA fellowship).

Notes and references

1 M. Irie, K. Uchida, T. Eriguchi and H. Tsuzuki, *Chem. Lett.*, 1995, 899.
2 M. Irie, *Pure Appl. Chem.*, 1996, **68**, 1367.
3 M. D. Cohen and G. M. J. Schmidt, *J. Phys. Chem.*, 1962, **66**, 2442.
4 J. Harada, H. Uekusa and Y. Ohashi, *J. Am. Chem. Soc.*, 1999, **121**, 5809.
5 T. Asahi and H. Masuhara, *Chem. Lett.*, 1997, 1165.
6 J. Hobley, V. Malatesta and W. Giroldini, Italian Patent Application MI200A000435, March 7th 2000.
7 S. Delbaere, B. Luccioni-Houze, C. Bochu, Y. Zerral, M. Campredon and G. Vermeersch, *J. Chem. Soc., Perkin Trans, 2*, 1998, 1153.
8 G. Ottavi, G. Favaro and V. Malatesta, *J. Photochem. Photobiol., A, Chem.*, 1998, **115**, 123.
9 R. Guglielmetti, *Photochromism Molecules and Systems*, ed. H. Durr and H. Bouas-Laurent, Elsevier, N.Y., 1990, p. 314.
10 Data collected on Siemens AED automated diffractometer with Mo-Kα radiation (l0.71069 Å, $q/2q$ scan, q_{max} = 30°.
11 F. Wilkinson and G. Kelly, *Handbook of Organic Photochemistry*, vol. 1, ed. J. C. Scaiano, CRC. Press Inc., 1989, 293.
12 J. Hobley, V. Malatesta, W. Giroldini, R. Millini and H. Fukumura unpublished results.

Typeset and printed by Black Bear Press Limited, Cambridge, England

Synthetic studies on calicheamicin γ_1^I—synthesis of (−)-calicheamicinone and models representing the four sugars and the aromatic system

Derrick L. J. Clive,* Yong Tao, Yunxin Bo, Yong-Zhou Hu, Natesan Selvakumar, Shaoyi Sun, Sylvain Daigneault and Yong-Jin Wu

Department of Chemistry, University of Alberta, Edmonton, Alberta, Canada T6G 2G2. E-mail: derrick.clive@ualberta.ca

Received (in Cambridge, UK) 14th February 2000, Accepted 2nd May 2000
Published on the Web 29th June 2000

The synthesis of (−)-calicheamicinone (2), the carbohydrates 88, 101, 111, 119 and 120, and the hexasubstituted benzene 139, is described; these compounds formally represent the subunits of the antitumor antibiotic calicheamicin γ_1^I (1).

Professor Derrick Clive was born in London and received his B.Sc. and Ph.D. (D. H. R. Barton and J. E. Baldwin) from Imperial College.

Dr Yong Tao was born in Ningbo and educated at Zhejiang Medical University (B. Pharm. Sci.) and the Shanghai Institute of Materia Medica, Chinese Academy of Sciences (Ph.D., Dr Jiasen Liu). He is now a Senior Research Scientist at Pfizer (Groton, Conn.).

Dr Yunxin Bo comes from Jiangsu and was educated at Suzhou University (B.Sc.) and the Shanghai Institute of Materia Medica (Ph.D., Professor Donglu Bai). He is a Research Scientist at Amgen Inc. (California).

Professor Yong-Zhou Hu was born in Zhejiang Province and obtained his B.Sc. at the Zhejiang Medical University and his Ph.D. (Professor Donglu Bai) at the Shanghai Institute of Materia Medica. He is Professor and Dean in the School of Pharmaceutical Science, Zhejiang University, Hangzhou.

Dr Natesan Selvakumar was born in Salem (Tamil Nadu State) and studied for his B.Sc. at Periyar E.V.R. College. He obtained his Ph.D. (Professor G. S. R. Subba Rao) from the Indian Institute of Science (Bangalore), and is now a Senior Scientist at Dr Reddy's Research Foundation (Hyderabad).

Dr Shaoyi Sun is from Qingdao and was educated at Qufu Normal University (B.Sc.) and the Chinese Academy of Medical Sciences and Peking Union Medical College (Ph.D., Professor Dequan Yu). He is currently a postdoctoral fellow in Professor Clive's group..

Dr Sylvain Daigneault is from Montreal and obtained his B.Sc. at the University of Sherbrooke and Ph.D. (D. Clive) at the University of Alberta. He is a Senior Research Scientist at Ayerst Canada (Montreal).

Dr Yong-Jin Wu is from Hunan and was educated at Hunan Normal University (B.Sc.) and Memorial University of Newfoundland (Ph.D., Professor D. J. Burnell). He is a Research Scientist at Bristol–Myers–Squibb.

The antitumor antibiotic calicheamicin γ_1^I (**1**)[1] has attracted much attention as a synthetic target.[2] Two syntheses have been reported,[3] but the structure is so complicated that further synthetic work will surely provide many opportunities for new discoveries.

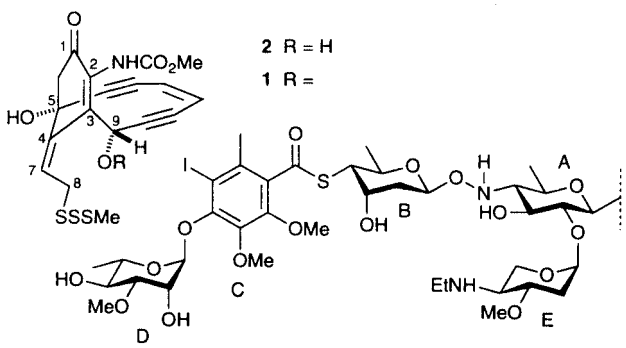

Synthesis of calicheamicin γ_1^I is a major undertaking—both chemical and financial—and a suitably cautious approach would be guided by the dominant structural characteristic that the compound is composed of several subunits—the aglycone (**2**), four carbohydrates, and a hexasubstituted benzene ring. Accordingly, synthetic work would first involve construction of each subunit, and the information thus gained might then be used in the more complex task of modifying the routes so that they can be integrated harmoniously into a composite synthesis of the whole structure. We describe here our own work[4–6] on the simpler of these tasks—synthesis of the subunits.[7,8]

Synthesis of (−)-calicheamicinone

The aglycone, (−)-calicheamicinone (**2**), presented the most difficult synthetic problem among the subunits of calicheamicin γ_1^I, because the substance is a rare structural type which had not been made before when we began our studies; in contrast, the carbohydrate segments and the aromatic unit—unusual though they are—did at least possess much in common with well-known compound classes.

Synthetic plan

Exploratory work by the Magnus group[9] had indicated that the allylic trisulfide of **2** should be accessible from the corresponding alcohol. Further analysis of the synthetic problem showed that two very suggestive features of calicheamicinone are the tertiary and secondary acetylenic alcohols. Their presence suggested that they might be assembled by acetylide addition to a suitably protected form of the hypothetical dicarbonyl subunit **3** (see arrows). It was then obvious that the enediyne might be

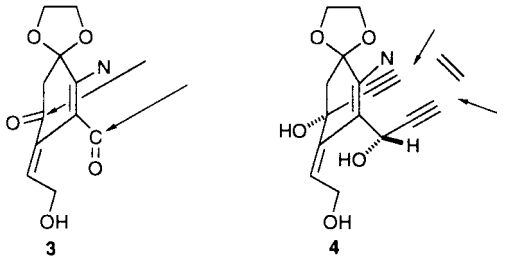

added in several ways: as an intact six-carbon enediyne unit, as an acetylene and an enyne, or as two acetylenes, followed by addition of a two-carbon unit and, in the event, this last process (see **4**, arrows), was the one we eventually used.

Although the above analysis is straightforward, the proper choice of dicarbonyl compound (*cf.* **3**) required a great deal of experimental effort before a promising structure was identified. This was based on the Diels–Alder reaction summarized (without stereochemical implications) in Scheme 1.

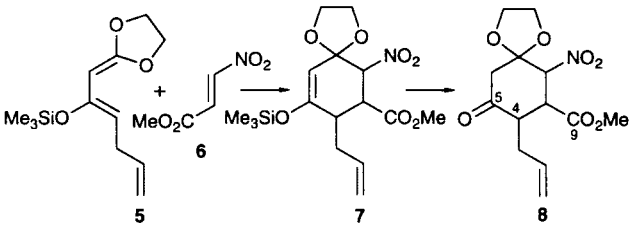

Scheme 1

Mild hydrolysis of the initial adduct **7** would be expected to afford **8**, which has many of the features of the schematic structure **3**: the carbonyl groups at C(5) and C(9) could serve as points of attachment for the acetylene units, the nitro group could eventually provide part of the carbamate, and the chain at C(4) would serve as the precursor to the allylic trisulfide. The choice of a cyclic ketal (see **8**) was based on the expectation that this form of protection would be more stable than the corresponding dimethyl ketal.

A number of ketene acetals (*cf.* **5**) had been reported[10] and an analogy for the proposed cycloaddition (*cf.* **5** + **6** → **7**) was also available.[11] On the basis of this encouraging background, we then proceeded with work along the lines of Scheme 1.

Formation of the central ring by Diels–Alder reaction

The readily available β-keto ester **9**[12] was subjected to ester exchange with 2-chloroethanol (**9** → **10**), and the resulting (2-chloroethyl) ester was converted into the required acyl ketene acetal **11** by the action of anhydrous potassium carbonate in DMF (Scheme 2).[10b] Attempts to effect the cyclization with sodium hydride were unsuccessful.

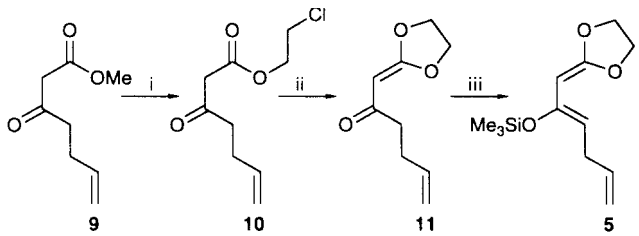

Scheme 2 *Reagents and conditions*: i, 2-chloroethanol, Ti(OPr-*i*)$_4$, 55 °C, 16 h, 75 °C, 24 h, 63%; ii, K_2CO_3, DMF, 80%; iii, $(Me_2PhSi)_2NLi$, Me_3SiCl, THF, −78 °C.

The next task was to convert the acyl ketene acetal into the *Z* silyl enol ether **5**, the *Z* geometry being preferred to facilitate the intended Diels–Alder reaction. For generating the silyl enol ether, LDA, lithium hexamethyldisilazide, and the very hindered base $(Me_2PhSi)_2NLi$ were evaluated, but only the latter produced the required geometry, which it did exclusively, and silylation *in situ* then gave **5**. This compound is not very stable but, fortunately, it can be used without purification, as even in the presence of $(Me_2PhSi)_2NH$ it reacts (Scheme 3) with the

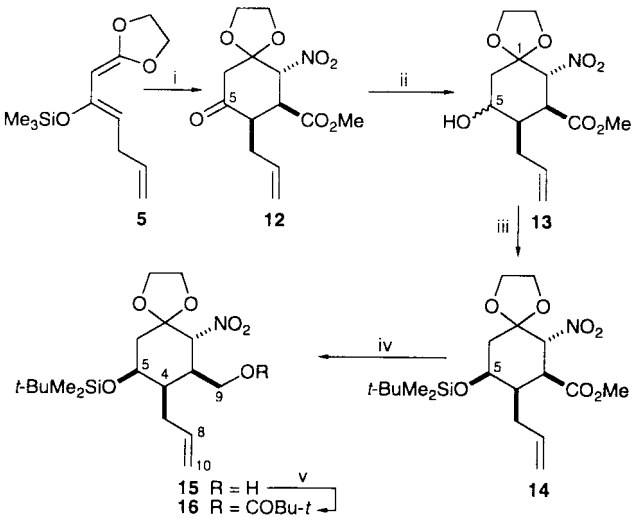

Scheme 3 *Reagents and conditions*: i, methyl (*E*)-2-nitropropenoate (**6**), THF, 0 °C, 1.5 h; aqueous NH_4Cl, 2 h, room temperature, 56% from **11**; ii, $NaBH_4$, MeOH, 0 °C, 99%; iii, *t*-$BuMe_2SiOTf$, 2,6-lutidine, CH_2Cl_2, 65% 5β epimer, 33% 5α epimer from **12**; iv, DIBAL-H, CH_2Cl_2, 99% for 5β, 99% for 5α; v, *t*-BuCOCl, DMAP, PhMe, 99% for 5β, 99% for 5α.

nitro ester **6**, and mild acidic workup affords crystalline ketone **12** in 56% yield overall from the acyl ketene acetal **11**.

Keto ester **12** is a key intermediate, and its structure was confirmed by X-ray analysis. From **12**, the first task was to protect the C(5) carbonyl. This was best done by simple reduction to give, in the event, a 2 : 1 mixture of alcohols, which were then silylated and separated (**12** → **13** → **14**). Although efficient *and* stereoselective ketone reduction was not possible, both of the C(5) epimers could be used; they were each subjected to the same reactions and, after several steps, both epimeric series converge to a single compound. These circumstances make the whole process quite efficient.

Next, the ester group in **14** (and in its 5α epimer) was reduced and the resulting alcohol protected by pivaloylation (**14** → **15** → **16**). At that point, with the C(5) and C(9) oxygen functions protected, it was appropriate to remove C(10) and introduce an oxygen at C(8), as these operations would adjust the side chain to the correct length and appropriate functionality.

Cleavage of the C(8)-C(10) double bond under classical conditions (Scheme 4), with osmium tetraoxide and sodium periodate, and reduction of the resulting aldehyde **17** gave the

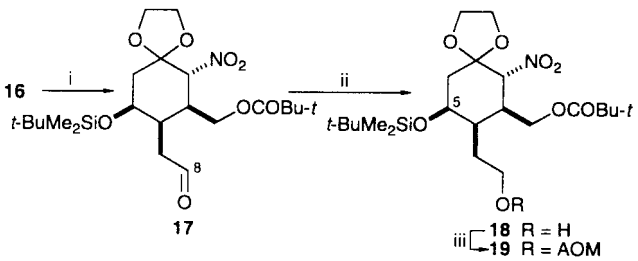

Scheme 4 AOM = $CH_2OC_6H_4OMe$-*p*. *Reagents and conditions*: i, OsO_4, $NaIO_4$, CCl_4, H_2O, *t*-BuOH, 73% for 5β, 77% for 5α; ii, $NaBH_4$, MeOH, 96% for 5β, 92% for 5α; iii, *p*-$MeOC_6H_4OCH_2Cl$, *i*-Pr_2NEt, DMAP, PhMe, 91% for 5β, 89% for 5α.

expected alcohol; this was protected with *p*-anisyloxymethyl chloride (**16** → **17** → **18** → **19**). Each of these steps was efficient in both the 5β series shown in Scheme 4, and in the corresponding 5α series.

With **19** and its 5α epimer in hand, the time had come to reduce the nitro group. Reduction of aliphatic nitro compounds is not as easy as in the aromatic series, but we found that the reagent generated by sonication of nickel(II) chloride hexahydrate and sodium borohydride[13] works very well (Scheme 5,

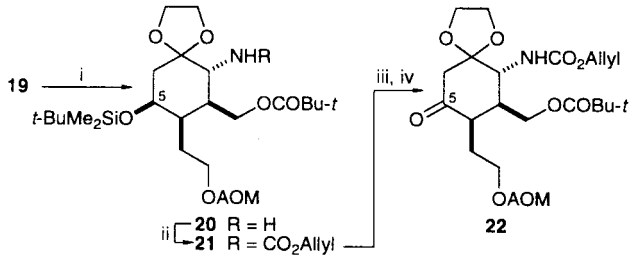

Scheme 5 AOM = $CH_2OC_6H_4OMe$-*p*. *Reagents and conditions*: i, $NaBH_4$, $NiCl_2.6H_2O$, MeOH, sonication, 95% for 5β, 95% for 5α; ii, allyl chloroformate, pyridine, THF, 82% for 5β, 82% for 5α; iii, Bu_4NF, THF, 95% for 5β, 96% for 5α; iv, CrO_3, pyridine, CH_2Cl_2, 95% for 5β, 90% for 5α.

19 → **20**) for both C(5) epimers. In each case, the resulting amine was protected as its allyl carbamate and, finally, the C(5) oxygen function was deprotected and oxidized by the Collins procedure (**21** → **22**).

At the stage of the resulting ketone (**22**) both of the C(5) epimers converge to the same product, and in both series identical reactions have been used, with almost identical results.

Attachment of two acetylene units

Ketone **22** gave a complex mixture with lithium trimethylsilylacetylide—a result that was very worrying—but we quickly found that it reacts cleanly (91%) with the corresponding cerium salt[14] to afford alcohol **23** (Scheme 6), in which the

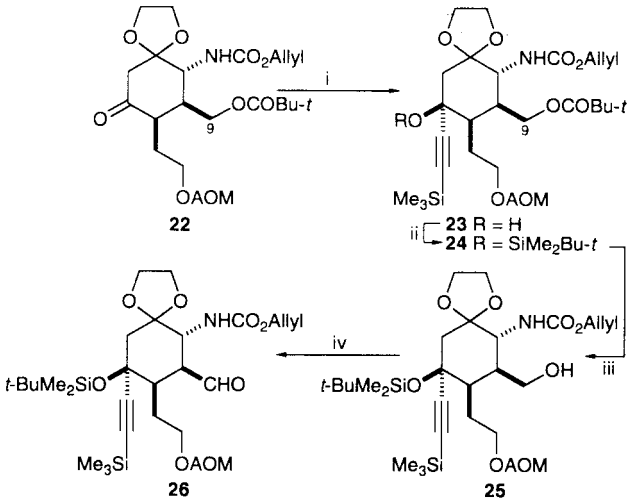

Scheme 6 AOM = $CH_2OC_6H_4OMe$-*p*. *Reagents and conditions*: i, $Me_3SiC{\equiv}CLi$, $CeCl_3$, THF, −78 °C, 91%; ii, *t*-$BuMe_2SiOTf$, 2,6-lutidine, CH_2Cl_2, 97%; iii, DIBAL-H, CH_2Cl_2, 95%; iv, CrO_3, pyridine, CH_2Cl_2, 90%.

acetylide has added from the same face as the nitrogen substituent. The hydroxy group was then protected by silylation (**23** → **24**), and preparations could now be made to introduce the second acetylene.

To that end, the pivaloyl group at C(9) was removed by the action of DIBAL-H, and the resulting alcohol was oxidized by the Collins procedure (**24** → **25** → **26**), with all the steps proceeding in high yield.

Treatment of aldehyde **26** with the cerium salt of trimethylsilylacetylene at −90 °C gave a 7:2 separable mixture of the required alcohol **27** and its C(9) epimer **28** (Scheme 7).

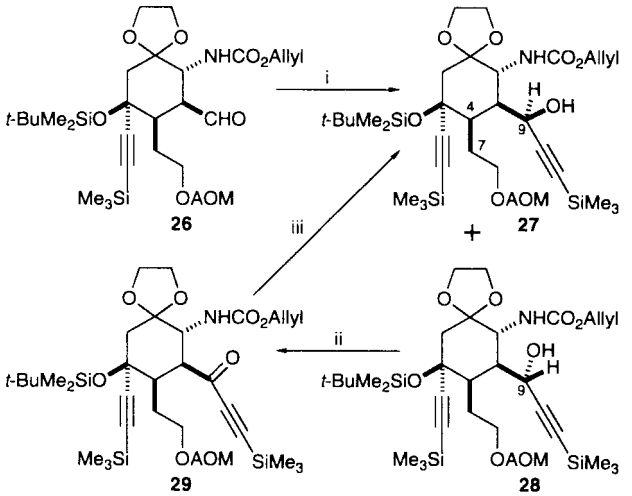

Scheme 7 AOM = $CH_2OC_6H_4OMe$-*p*. *Reagents and conditions*: i, $Me_3SiC{\equiv}CLi$, $CeCl_3$, THF, −90 °C, 79% for **27**, 16% for **28**; ii, PCC, 4 Å molecular sieves, CH_2Cl_2, 93%; iii, $NaBH_4$, MeOH, 0 °C, 88%

Attempts to improve the stereoselectivity by running the reaction at an even lower temperature, or by use of the ytterbium salt[15] of the acetylene were not successful. Fortunately, oxidation of the undesired isomer **28** gave a ketone that was reduced stereoselectively (11.6:1) to **27**, by sodium borohydride; thus, the overall transformation of **26** into **27** is quite efficient (92%), but required several experiments.

Introduction of the C(4)–C(7) double bond

With both acetylenic units in place, the next task was to incorporate the two-carbon chain at C(4) into a ring, so as to be able to generate the C(4)-C(7) double bond with the correct geometry (see **2**). Ring formation was accomplished by the straightforward operations summarized in Scheme 8.

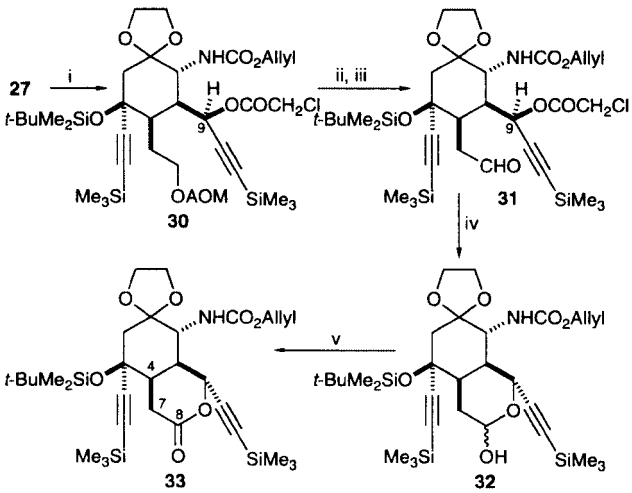

Scheme 8 AOM = $CH_2OC_6H_4OMe$-*p*. *Reagents and conditions*: i, $(ClCH_2CO)_2O$, pyridine, 99%; ii, $(NH_4)_2Ce(NO_3)_6$, pyridine, MeOH, H_2O, 89%; iii, CrO_3, pyridine, CH_2Cl_2, 91%; iv, NH_3(aq), MeOH, 0 °C; v, CrO_3, pyridine, CH_2Cl_2, 92% from **31**.

Protection of the C(9) hydroxy as a chloroacetate (**27** → **30**), followed by removal of the *p*-anisyloxymethyl group by exposure of the chloroacetate to ceric ammonium nitrate, gave an alcohol that was oxidized with the Collins reagent. Treatment of the resulting aldehyde **31** with dilute aqueous ammonium hydroxide released the C(9) hydroxy group, and this closed spontaneously onto the aldehyde group, so as to afford a mixture of lactols **32**. Another Collins oxidation then gave lactone **33**.

At this point the C(4)–C(8) chain is restrained within a ring so that the C(4)–C(7) double bond could be introduced (see Scheme 9) with the required *E* geometry. Phenylselenenylation

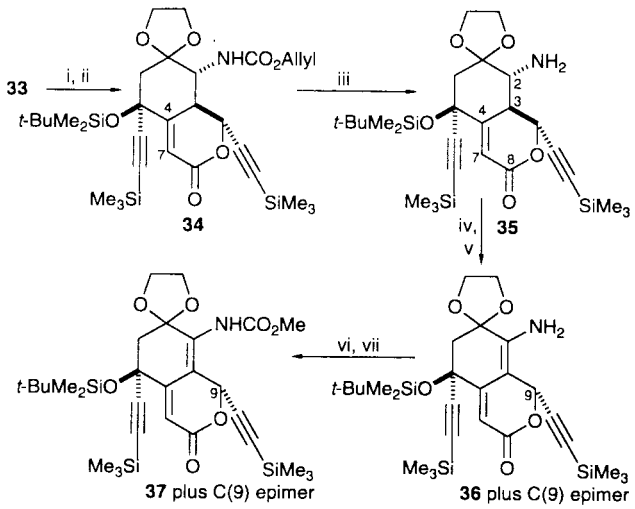

Scheme 9 *Reagents and conditions*: i, LDA, THF, PhSeBr, −78 °C; ii, dimethyldioxirane, −42 °C, 67% from **33**; iii, $(Ph_3P)_4Pd$, dimedone, THF, 80%; iv, *t*-BuOCl, Et_2O–THF; v, DABCO, PhMe; vi, $Cl_3COCO_2CCl_3$, pyridine, CH_2Cl_2; vii, MeOH, 78% (as an 8:1 isomer mixture) from **35**.

at C(7) and oxidation with dimethyldioxirane—an excellent reagent for use in selenoxide elimination—gave the desaturated lactone **34**. The intermediate phenyl selenide is not very stable and was not characterized, but the fact that it undergoes the selenoxide fragmentation indicates that the phenylseleno group must be on the same face as the C(4) hydrogen. We next removed the nitrogen protecting group by the action of tetrakis(triphenylphosphine)palladium(0) in the presence of dimedone,[16] the latter nucleophile being the best of several we tried. The resulting amine (**35**) was crystalline, and X-ray analysis confirmed the structure.

Introduction of the C(2)–C(3) double bond

Introduction of the C(2)–C(3) double bond required a great deal of exploratory work before we identified the structural features that would allow efficient desaturation. This exploratory work guided many details of the synthetic plan discussed so far and directed us to the route leading ultimately to **35**, which has the two features we identified as important: the presence of a C(4)–C(7) double bond and incorporation of C(7) and C(8) into a ring.

Freshly prepared *t*-butyl hypochlorite converted **35** into its *N*-chloro derivative, and treatment with an excess of DABCO generated the corresponding imine, which underwent tautomerization to afford the fully conjugated enamide **36** and its C(9) epimer in an 8:1 ratio. The mixture of enamides is not very stable, and it was necessary to convert them promptly into the corresponding isocyanates, by treatment with triphosgene; the isocyanates, in turn, were immediately quenched with methanol. These operations gave carbamate **37** as an 8:1 mixture of C(9) epimers, the predominant one being that shown in Scheme 9. Neither of the epimer mixtures—enamide or carbamate—could be separated, but separation and isomerization of the *anti* isomer into the desired *syn* compound was easily achieved after the next step.

We assume that isomerization occurs by ring opening (see arrows in **37′**), followed by reclosure.

Formation of the enediyne ring

Our plan for closing the enediyne ring called for use of a double Stille reaction, and so we had first to remove the acetylenic silicon groups from **37**. Treatment with tetrabutylammonium fluoride did indeed give the corresponding terminal acetylene (Scheme 10), but under the reaction conditions further epimerization occurred at C(9). Fortunately, the epimeric acetylenes **38** and **39** were very easily separated, and the *anti* bisacetylene

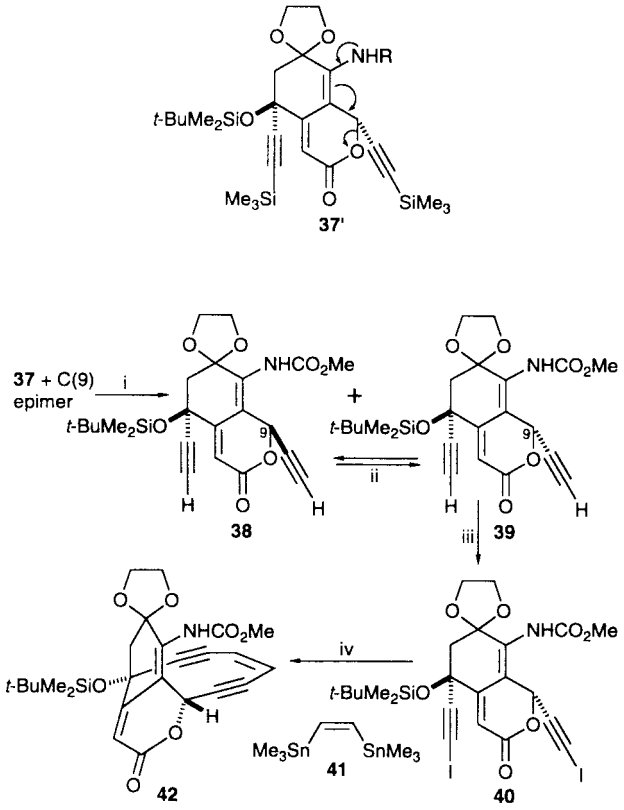

Scheme 10 *Reagents and conditions*: i, Bu_4NF, THF, 39% for **38**, 46% for **39**; ii, Bu_4NOAc, 100% of a 4:6 mixture of **38** and **39**; iii, NIS, $AgNO_3$, acetone, 89%; iv, **41**, $(Ph_3P)_4Pd$, DMF, 60 °C, 72%.

could be converted in 100% yield into a 4:6 mixture in favor of **39**. After one recycling the yield of **39** was 69% from the mixture of **37** and its C(9) epimer. X-Ray analysis of the desired *syn* bisacetylene showed that the distance between the terminal acetylenic carbons is 4.154 ± 0.005 Å.

The acetylenic hydrogens were next replaced by iodine (**39** → **40**), using *N*-iodosuccinimide in the presence of silver nitrate.[17] Finally, a double Stille coupling of the diiodide with (*Z*)-1,2-bis(trimethylstannyl)ethene (**41**) gave the cyclic enediyne **42** in 72% yield, bringing the synthesis to a point where we needed to build up the allylic trisulfide and remove any remaining protecting groups.

Second route to the *syn* bisacetylene 39

During our development of the above route to **39** we encountered so many unexpected difficulties that we took the precaution of seeking another route to the same compound; in the event, this additional work had unusual and beneficial consequences.

The second route begins with the same Diels–Alder adduct used earlier and, as before, this was converted into alcohol **15** (see Scheme 3) and its C(5) epimer. In the first route the C(9) hydroxy group was protected before cleavage of the pendant double bond, but in the present case (Scheme 11), the double bond was cleaved without hydroxyl group protection and, as expected, the lactols **43** were formed. These were then protected by treatment with pivaloyl chloride. During the reaction epimerization of **43** occurs at C(8), so as to give only the product **44**, with the pivaloyl group equatorial. The nitro group was then reduced in high yield, again using the sodium borohydride–nickel chloride combination, and the resulting amine was protected as its allyl carbamate (**44** → **45**).

Finally, the C(5) oxygen was desilylated and oxidized, just as before (**45** → **46**). An identical set of reactions was done in the 5α series, and, at the stage of ketone **46**, both series converge to the same product, just as in the earlier route. Although both C(5) epimers were processed individually, the same reaction condi-

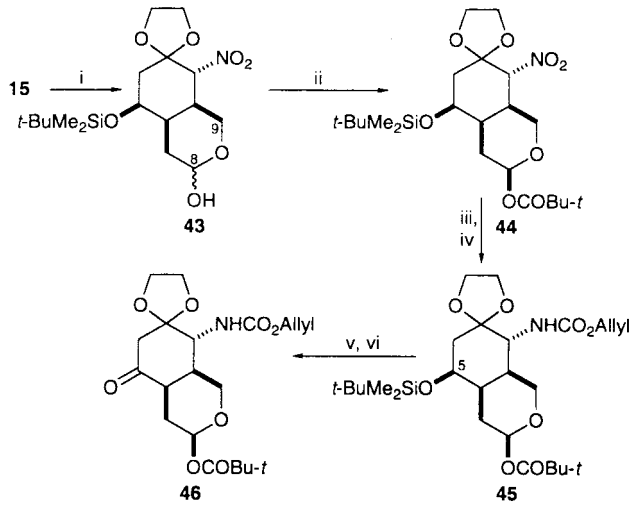

Scheme 11 *Reagents and conditions*: i, OsO_4, $NaIO_4$, CCl_4, H_2O, *t*-BuOH, 98% for 5α, 98% for 5β; ii, *t*-BuCOCl, pyridine, CH_2Cl_2, 96% for 5α, 96% for 5β; iii, $NaBH_4$, $NiCl_2{\cdot}6H_2O$, MeOH, sonication, 95% for 5β, 91% for 5α; iv, allyl chloroformate, pyridine, THF, 94% for 5β, 93% for 5α; v, Bu_4NF, THF, 97% for 5β, 95% for 5α; vi, PCC, 4 Å molecular sieves, CH_2Cl_2, 91% for 5β, 92% for 5α.

tions were used for both, and in each step the corresponding yields were almost identical.

Second route—introduction of the first acetylene

For introducing the first acetylene unit we again used the cerium salt of trimethylsilylacetylene and obtained, in high yield, alcohol **47** (Scheme 12), in which the acetylide had entered *anti*

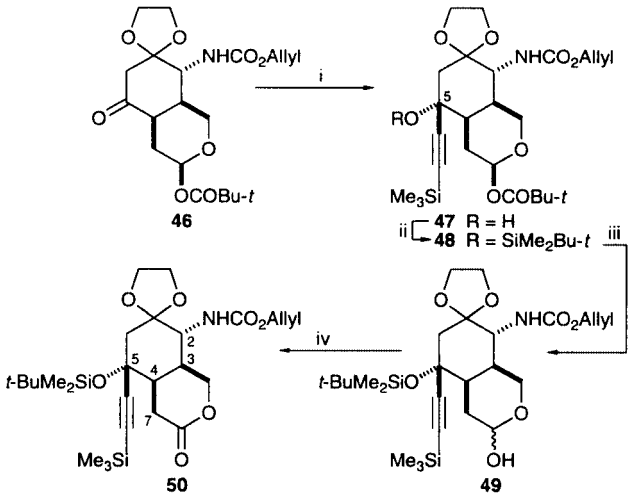

Scheme 12 *Reagents and conditions*: i, $Me_3SiC{\equiv}CLi$, $CeCl_3$, THF, −78 °C, 91%; ii, *t*-$BuMe_2SiOTf$, 2,6-lutidine, CH_2Cl_2, 93%; iii, DIBAL-H, CH_2Cl_2, 96%; iv, CrO_3, pyridine, CH_2Cl_2, 97%.

to the nitrogen, in contrast to the result in the first route (*cf.* **22** → **23**, Scheme 6). The stereochemical assignment in the present case was made by X-ray analysis. The alcohol was protected by silylation (**47** → **48**), and the pivaloyl group was then removed by treatment with DIBAL-H. Oxidation of the resulting lactols took the route to a point (**50**) where we had again to introduce double bonds at C(4)–C(7) and at C(2)–C(3). Both of these operations were done by the methods that had worked well in the first route.

The C(4)–C(7) double bond was introduced by phenylselenenylation and dimethyldioxirane oxidation of the intermediate selenide (Scheme 13, **50** → **51**), for which we again assume on mechanistic grounds that the phenylseleno group is *syn* to the C(4) hydrogen. Removal of the allyloxycarbonyl group (**51** → **52**) by the action of a palladium catalyst in the

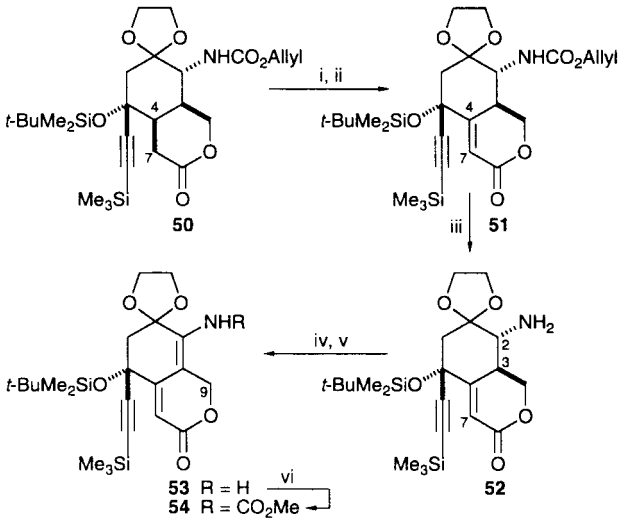

Scheme 13 *Reagents and conditions*: i, LDA, THF, PhSeBr, −78 °C; ii, dimethyldioxirane, 85%; iii, $(Ph_3P)_4Pd$, dimedone, THF, 93%; iv, *t*-BuOCl, Et_2O–THF; v, DBU, PhMe, 81% from **52**; vi, $Cl_3COCO_2CCl_3$, pyridine, CH_2Cl_2, then MeOH, 91%.

presence of dimedone liberated the free amine and, once again, that was chlorinated with *tert*-butyl hypochlorite. Exposure to a hindered base—in this case DBU—gave an imine, which immediately isomerized to the fully conjugated enamide **53**. This was converted into its isocyanate, which was quenched with methanol, thereby generating the required methyl carbamate **54**.

Second route—introduction of the second acetylene

Introduction of the second acetylene—that at C(9) in lactone **54**—required, of course, that the C(9) carbon be oxidized. In the event, we were very pleased to find that our first attempt at oxidation was successful (Scheme 14). We took advantage of

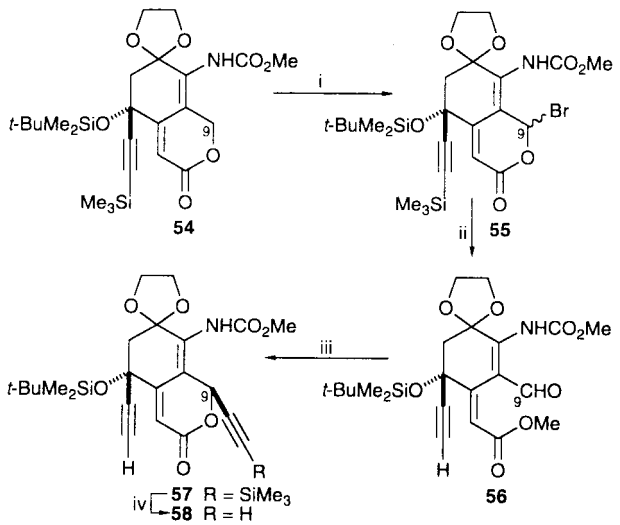

Scheme 14 *Reagents and conditions*: i, NBS, $(PhCO)_2O_2$, light, CCl_4; ii, $AgNO_3$, THF, H_2O, pyridine; then CH_2N_2, 77% from **54**; iii, $Me_3SiC{\equiv}CLi$, $CeCl_3$, THF, −78 °C, 91%; iv, Bu_4NF, THF, 46% for **58**, 42% of the C(9) epimer of **58**.

the fact that the C(9) hydrogens are allylic and are part of an ether subunit; consequently, these hydrogens should be susceptible to free radical reactions, and treatment with NBS under standard bromination conditions (dibenzoyl peroxide, tungsten lamp irradiation) gave a mixture of epimeric bromides **55**. These were hydrolyzed with aqueous silver nitrate to an aldehyde acid which, though it existed largely as a mixture of epimeric hydroxy lactones (OH instead of Br in **55**), was easily trapped as the methyl ester **56** by reaction with diazomethane.

During hydrolysis the acetylenic trimethylsilyl group is lost, but it would eventually have had to be removed and so its loss at this stage was of no consequence. The overall yield from **54** to **56** was 77%—a value that is most satisfactory in view of the fact that several transformations have been performed in one operation on a rather complex and sensitive structure.

We were now ready to introduce the second acetylene. Naturally, we intended to use the cerium salt of trimethylsilylacetylene, but we had no idea of what stereochemical outcome to expect, and so we really were very pleased to find that a single compound (**57**) was formed in excellent yield (91%) and with the desired *syn* stereochemistry. When we removed the acetylenic trimethylsilyl group, the product (**58**) was, of course, identical to the material obtained by the first route. Two points need to be made about the formation of **58**. The first is that, during the desilylation, epimerization occurs at C(9), but this problem was handled in the same way as in the first route: the undesired *anti* bisacetylene was treated with tetrabutylammonium acetate to obtain an equilibrium mixture of the *syn* and *anti* isomers, so that the yield of the desired *syn* material was 71% from **57** after one recycling.

The second point also concerns stereochemistry. Up to this point we have been dealing with racemic compounds, but representing them by a single enantiomer. In the two routes, the first acetylene [at C(5)] has a different stereochemical relationship to the nitrogen function, being in one case *syn* (*cf.* **23**) and in the other *anti* (*cf.* **47**). However, all the stereogenic centers in **47** except C(5) are ultimately converted into sp^2 hybridization, and so both racemic monoacetylenes give the same *racemic* product, *i.e.* **58** and **39** are identical, but are drawn in different ways merely to emphasize the *initial* relationship between the C(5) acetylene and the nitrogen. Later on we were able to make good use of this stereochemical outcome in order to prepare optically pure material.

Formation of (±)-calicheamicinone

By the time we had made the cyclic enediyne **42** Danishefsky and coworkers[7a] and Nicolaou and coworkers[8] had shown how substances of very similar structure could be converted into calicheamicinone, and we used a method similar to theirs.

Lactone **42** was first reduced with DIBAL-H (Scheme 15) to a mixture of lactols (**59**) and then the silicon protecting group was removed in the usual way (**42** → **59** → **60**). The DIBAL-H

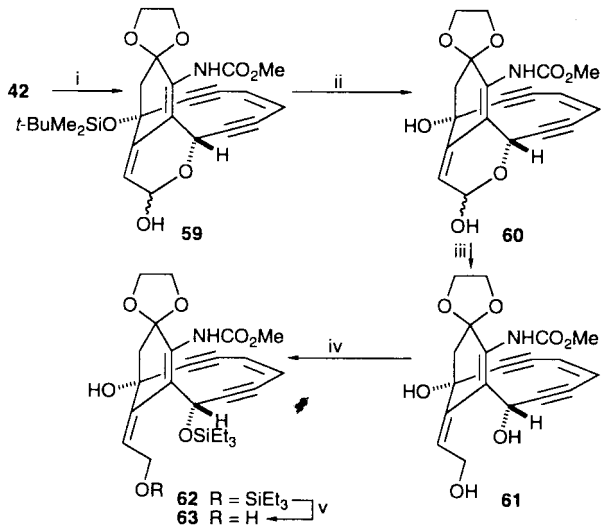

Scheme 15 *Reagents and conditions*: i, DIBAL-H, CH_2Cl_2, 98%; ii, Bu_4NF, THF, 94%; iii, $NaBH_4$, MeOH, 76%; iv, Et_3SiOTf, 2,6-lutidine, CH_2Cl_2, 95%; v, AcOH, THF, H_2O, 94%.

reduction must be done before desilylation in order to avoid solubility problems with the desilylated lactone and, in turn, desilylation must precede installation of the trisulfide because the latter is sensitive to tetrabutylammonium fluoride. Thus, the timing of the last two reactions is critical. Lactols **60** were further reduced with sodium borohydride to triol **61**, and at this point it was necessary to protect the secondary hydroxy group so as to block its participation in a subsequent Mitsunobu reaction. Selective protection was achieved by silylating both the primary and secondary hydroxy groups and then storing the resulting product (**62**) in a mixture of acetic acid, THF and water. Under these conditions the primary allylic hydroxy group was released (**62** → **63**), and the stage was set to introduce the trisulfide unit.

The primary hydroxy group was replaced by a thioacetyl group, under typical Mitsunobu conditions (Scheme 16, **63** → **64**), and the free thiol was then liberated by treatment with

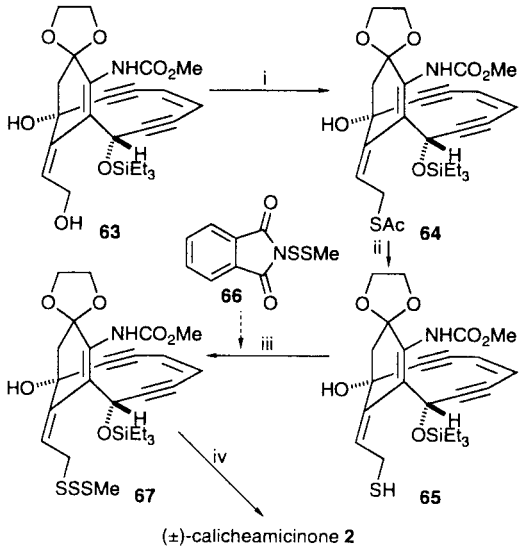

Scheme 16 *Reagents and conditions*: i, *i*-PrO_2CN = NCO_2Pr-*i*, Ph_3P, AcSH, 94%; ii, DIBAL-H, CH_2Cl_2; iii, *N*-(methyldithio)phthalimide, CH_2Cl_2, 88% from **64**; iv $TsOH·H_2O$, THF, H_2O, 84%.

DIBAL-H. The next step proved to be troublesome until we recognized that freshly chromatographed thiol must be used. As soon as that was established, we found that treatment of **65** with an eight-fold excess of reagent **66** gave the desired trisulfide **67** in 88% yield over the two steps from **64**. Finally, the remaining protecting groups were removed by mild acid hydrolysis, affording (84%) racemic calicheamicinone as a white foam.

Synthesis of optically pure and crystalline (−)-calicheamicinone

In the two syntheses of racemic calicheamicinone described above, the stereochemical relationship between the first acetylene and the nitrogen is different, but both modes of acetylide addition ultimately lead to the same *racemic* product. However, if the initial Diels–Alder adduct is made optically pure, then each route would give a different enantiomer of calicheamicinone. Moreover, the *absolute* stereochemistry of the initial Diels–Alder adduct is immaterial—provided it is known—since calicheamicinone of natural or unnatural stereochemistry can be reached from either enantiomer of the Diels–Alder adduct simply by selecting one or other of the two routes. With this unusual situation as background, we set out to prepare optically pure calicheamicinone,[5] a task for which the only new problem was the preparation of the Diels–Alder adduct in optically pure form and the determination of its absolute configuration.

In our initial Diels–Alder reaction (*cf.* Scheme 1) we had used the *methyl* ester of β-nitroacrylic acid; consequently, nitroacrylates such as **68** and **69** were obvious candidates for use in an asymmetric Diels–Alder reaction.

Our first choice was the oxazolidinone derivative **68**, but we were unable to prepare it. Perhaps we were too impatient but, in

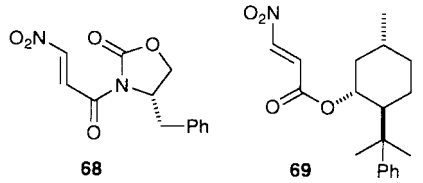

any event, our second choice—the 8-phenylmenthol derivative **69**—served the desired purpose admirably. Preparation of **69** was initially problematic, but it did not take long to devise an acceptable route (Scheme 17).

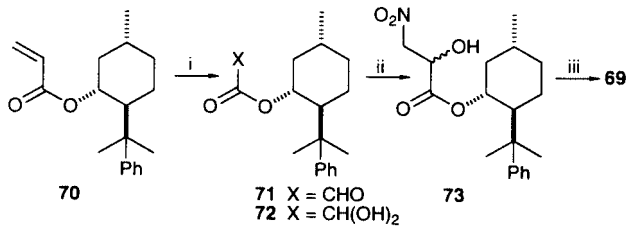

Scheme 17 *Reagents and conditions*: i, $NaIO_4$, OsO_4, H_2O, dioxane, 98%; ii, $MeNO_2$, alumina, 90%; iii, MsCl, Et_3N, 89%.

Optically pure 8-phenylmenthol[18] was acylated with acryloyl chloride and the double bond in the product **70**[19] was cleaved by the Lemieux–Johnson method to provide a mixture of the glyoxylate **71** and its hydrate **72**. This mixture underwent a Henry reaction with nitromethane in the presence of neutral alumina[20] to give a mixture of nitro alcohols (**71**, **72** → **73**), which was easily dehydrated by mesylation and spontaneous elimination.

For the asymmetric Diels–Alder reaction the diene component **5** was again generated *in situ*; it reacts smoothly with the optically pure nitroacrylate to give, after mild acid workup, the ketone **74** in slightly higher yield than for the *methyl* ester—64 versus 56%. X-Ray analysis of the ketone showed that the absolute configuration was as drawn in Scheme 18. The C(5)

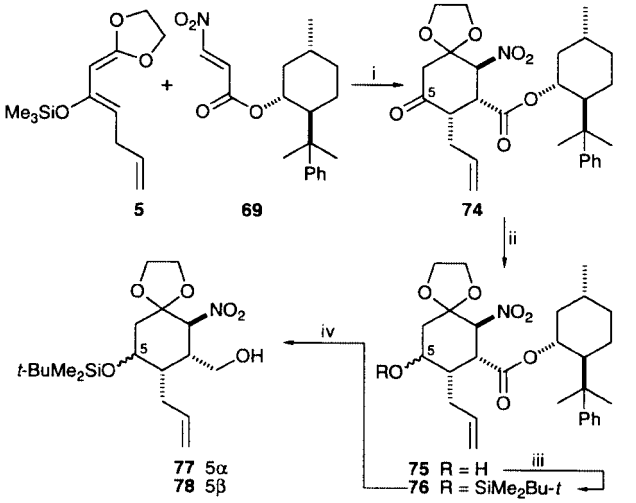

Scheme 18 *Reagents and conditions*: i, THF, −78 °C, 35 min, then aqueous NH_4Cl, 4 h, 64% based on **11**; ii, $NaBH_4$, MeOH, 99%; iii, *t*-$BuMe_2SiOTf$, 2,6-lutidine, CH_2Cl_2, 100%; iv, DIBAL-H, CH_2Cl_2, −78 to −30 °C, 52% for **77** and 27% for **78**.

carbonyl was reduced as before to a mixture of epimeric alcohols, and these were then silylated (**74** → **75** → **76**). Finally, the chiral auxiliary was removed by treatment with DIBAL-H, first at −78 °C and then at −30 °C. With proper temperature control the two optically pure alcohols **77** (52% from ketone **74**) and **78** (27%) can be obtained, and the chiral auxiliary is recovered (96%). Alcohols **77** and **78** correspond to the racemic compounds used earlier (see Scheme 3), and the absolute configuration of ketone **74** indicated that the second route (Schemes 11–14) developed with racemic material would lead to calicheamicinone of natural configuration. Accordingly, the earlier experiments were repeated using both **77** and **78**; the sequence afforded (−)-calicheamicinone. Our material was crystalline, and we were able to obtain the first X-ray crystallographic data for calicheamicinone.

Synthesis of model compounds representing the sugar units

Once the aglycone had been completed we began work on the sugars and the aromatic unit. We arbitrarily decided to make each of the sugars from materials in the chiral pool—but excluding other sugars—or by asymmetric synthesis.

Synthesis of a ring E model

Our starting material for the ring E unit (see structure **1**) was serine, which is easily converted[21] into the *N*-ethyl ester **79**. *N*-Carbamoylation and silylation of the remaining hydroxy group (see Scheme 19) gave the fully protected derivative **81** (**79** → **80** → **81**). DIBAL-H reduction furnished aldehyde **82**, and

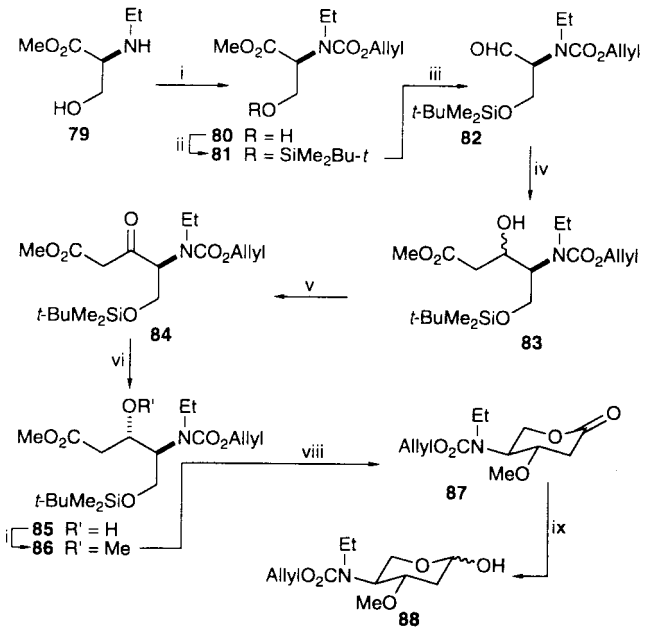

Scheme 19 *Reagents and conditions*: i, allyl chloroformate, K_2CO_3, THF, water, 0 °C, 94%; ii, *t*-$BuMe_2SiOTf$, imidazole, DMF, 97%; iii, DIBAL-H (added over 1 h), CH_2Cl_2, −78 °C, 30 min; iv, SmI_2, THF, −78 °C, MeO_2CCH_2Br, 1 h, 56% from **81**; v, PCC, 4 Å molecular sieves, CH_2Cl_2, 1 h; vi, $NaBH_4$, MeOH, 0 °C, 83% from **83**; vii, $MeOSO_2CF_3$, 2,6-di-*tert*-butyl-4-methylpyridine, CH_2Cl_2, reflux, 82%; viii, 3:1:1 AcOH–THF–water, 24 h; azeotrope with PhMe; PhMe, AcOH, 80 °C, 5 h, 86%; ix, DIBAL-H, CH_2Cl_2, −78 °C, 88%.

condensation with methyl bromoacetate, mediated by samarium iodide,[22] served to generate the required carbon skeleton (**82** → **83**). The condensation gave a mixture of isomers with the major one having a stereochemistry at the hydroxy-bearing carbon opposite[23] to that required. Consequently, an oxidation-reduction sequence (**83** → **84** → **85**) was needed to adjust the stereochemistry; alcohol **85** was obtained in 89% ee. Methylation and desilylation then led directly to lactone **87**, and DIBAL-H reduction gave the lactols **88**, corresponding to a protected version of the ring E sugar of calicheamicin γ_1^I.[24]

Synthesis of a ring B model

Synthesis of the ring B unit began with methyl (*R*)-lactate, which was converted by silylation and reduction into aldehyde **89** (Scheme 20), following a literature procedure.[25] Addition of the magnesium acetylide derived from ethyl propiolate afforded

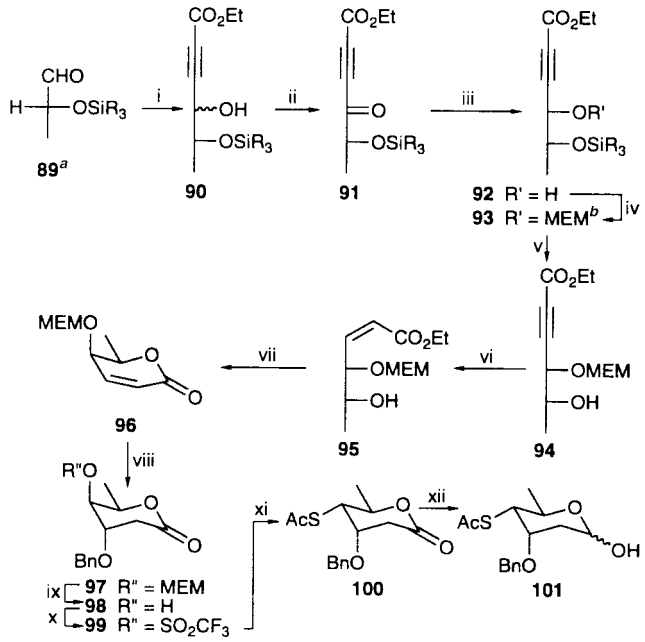

Scheme 20 [a]R_3 = Me_2Bu-*t*. [b]MEM = $CH_2OCH_2CH_2OMe$. *Reagents and conditions*: i, $EtO_2CC{\equiv}CMgBr$, THF, HMPA, **89** in CH_2Cl_2, −78 °C, 72%; ii, Jones reagent; iii, K-Selectride, THF, −78 °C, 68% from **90**; iv, MEMCl, *i*-Pr_2NEt, CH_2Cl_2, 86%; v, 48% aqueous HF, MeCN, 94%; vi, 5% Pd–$BaSO_4$, quinoline, H_2, 1 atm, 86%; vii, PhMe, AcOH, 80 °C, 95%; viii, BnOH, $Hg(OAc)_2$, $HClO_4$, 2 days; then THF, aqueous pH 8 buffer, $NaBH_4$, 52% overall, 71% corrected for recovered **96**; ix, Me_3SiCl, NaI, MeCN, 86%; x, $(CF_3SO_2)_2O$, pyridine, CH_2Cl_2; xi, AcSK, DMF, 48% from **98**; xii, DIBAL-H, CH_2Cl_2, −95 °C, 90%.

a 9.6 : 1 mixture of alcohols **90**, in which the minor isomer was the desired one.[25] Accordingly, the alcohols were subjected to Jones oxidation (**90** → **91**) and then treated with K-Selectride, so as to generate the required stereochemistry (**91** → **92**).[25] The hydroxy group was now protected as its MEM ether, and the other oxygen was deprotected with aqueous HF in acetonitrile (**92** → **93** → **94**). Semihydrogenation gave the *Z* alkene **95**, which lactonized (**95** → **96**) on heating in the presence of acetic acid. At this point, treatment with benzyl alcohol and mercuric acetate served to effect alkoxymercuration of the double bond, and reduction with sodium borohydride released the desired benzyloxy lactone **97**.[26] The C(4) oxygen was next deprotected with iodotrimethylsilane, generated *in situ*, and sulfonylated with triflic anhydride (**97** → **98** → **99**). These operations took the route to a point where a thioacetyl group could be introduced by S_N2 inversion, using potassium thioacetate in DMF (**99** → **100**). Finally, DIBAL-H reduction at −95 °C gave the lactols **101** (94%), the thioacetyl group remaining intact. Lactols **101** represent a model of the ring B sugar unit of calicheamicin γ_1^I.[27]

Synthesis of a ring A model

Our ring A model is one having a hydroxy group at C(4) that can be converted into a leaving group (for displacement by a hydroxylamine nitrogen), a C(2) hydroxy group for glycosylation with a suitable ring E precursor, and C(1) blocked as a methyl glycoside. Structure **111** satisfies these requirements, and the route we used to prepare it should allow differential protection of the C(2) and C(3) oxygen functions.

Intermediate **93**, used in the synthesis of the ring B model, served as the starting point for the ring A model. The acetylenic ester unit was converted by reduction ($LiAlH_4$) and oxidation into aldehyde **103** (see Scheme 21), and the latter was converted in one step into the *E* olefinic ester **104**. The double bond was then hydroxylated, giving as the major product (80% yield) the desired diol **105**, this structural assignment being made after ring closure. Selective benzoylation of the C(2) hydroxy group

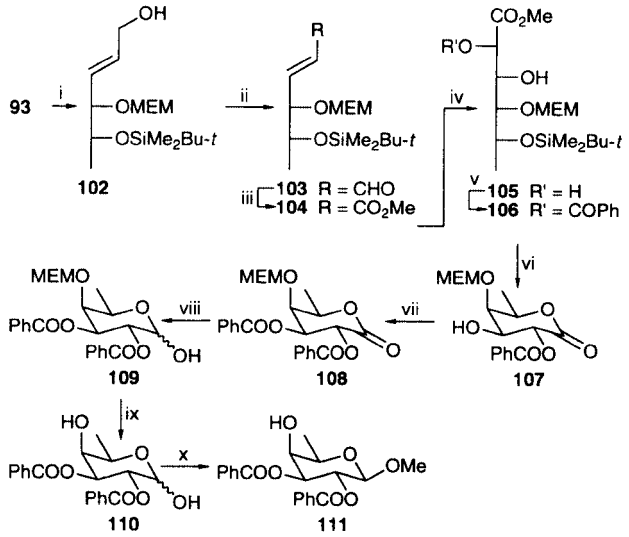

Scheme 21 *Reagents and conditions*: i, $LiAlH_4$, THF, 83%; ii, MnO_2, hexane; iii, MnO_2, NaCN, MeOH, AcOH, 87% from **102**; iv, OsO_4, NMO, *t*-BuOH, 8:1 acetone–water, 78% (isolated) plus an isomer (16%); v, PhCOCl, Et_3N, DMAP, CH_2Cl_2, 0 °C, room temperature, 84%; vi, Bu_4NF, THF, AcOH, 92%; vii, PhCOCl, pyridine, DMAP, CH_2Cl_2, 98%; viii, DIBAL-H in CH_2Cl_2, THF, −78 °C, 87%; ix, Me_3SiCl, NaI, MeCN, −20 °C; x, $(MeO)_3CH$, camphorsulfonic acid, MeOH, reflux, 78% from **109**.

afforded **106** and, when the silyl group was removed, under standard conditions, spontaneous lactonization occurred, generating lactone **107**. For convenience in this model study we chose to mask the C(3) hydroxy group as a benzoate (**107** → **108**). At that point, DIBAL-H reduction selectively modified the lactone carbonyl, providing a mixture of lactols (**109**), and the C(4) oxygen was deprotected, using iodotrimethylsilane, generated as before, *in situ*. Finally, the anomeric position was blocked as a methyl glycoside (**110** → **111**).[28]

Synthesis of a ring D model

We arbitrarily decided to prepare our ring D model by asymmetric synthesis rather than from rhamnose; consequently, our route, which is closely related to prior methods,[24f] is longer than that starting with a preformed sugar, but does offer additional possibilities for incorporating isotopic labels.

The (*S*) furyl alcohol **112**[29] (Scheme 22) was prepared by asymmetric[29,30] transfer hydrogenation from the corresponding

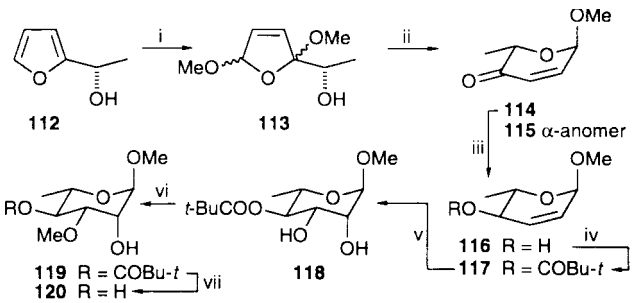

Scheme 22 *Reagents and conditions*: i, Br_2, MeOH, −40 °C, 89%; ii, HCO_2H, MeOH, 61% **114**, 20% **115**; iii, $LiAlH_4$, Et_2O, −50 °C, then warm to room temperature, 94%; iv, *t*-BuCOCl, pyridine, DMAP, CH_2Cl_2, 93%; v, OsO_4, *t*-BuOH, NMO, 9:1 acetone–water, 97%; vi, Bu_2SnO, 10 : 1 MeOH–PhH, reflux 70 min, cool, MeI, 45 °C, 17 h, 95%; vii, $LiOH{\cdot}H_2O$, 4 : 1 MeOH–water, 5 days, 85 or 95%, corrected for recovered **119**.

ketone. Following a literature procedure,[31] bromination in methanol (**112** → **113**) and treatment with formic acid then gave a mixture of the desired pyranosidulose **114**[32] (61%) and the α-anomer (20%), both of which were used in the synthesis, as described below.

Reduction of the ketone with lithium aluminium hydride proceeded[31] with the required stereochemical result in high yield (**114** → **116**, 94%). At this point, the optical purity of the compound was confirmed by NMR comparison of its Mosher ester with corresponding material made from racemic **112**. The C(3) hydroxy group was now protected as its pivaloyl ester, and dihydroxylation, under standard conditions, produced diol **118**, which could be selectively and efficiently (95%) methylated[33] (Bu_2SnO, MeI) on the C(3) oxygen (**118** → **119**). Mild basic hydrolysis gave diol **120**. Both **119** and **120** serve as models for the D ring.[34]

The ring closure step from **113** afforded as a byproduct the α-anomer **115** in 20% yield, but the stereochemistry could be adjusted (Scheme 23), so that some of this material could be used for the main sequence of Scheme 22.

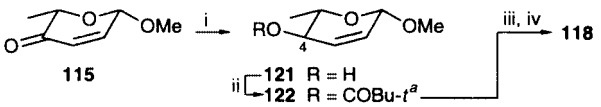

Scheme 23 [a]Yield of C(4) epimer 22%. *Reagents and conditions*: i, $NaBH_4$, THF, water, 0 °C; ii, *t*-BuCOCl, pyridine, DMAP, $CHCl_3$, 66% **116**, 22% for the C(4) anomer; iii, camphorsulfonic acid, MeOH; iv, OsO_4, *t*-BuOH, NMO, 9:1 acetone–water, 75% from **115**.

Reduction of ketone **115** with sodium borohydride, and pivaloylation gave **122** as the predominant product. Without purification, this was subjected to conditions for acetal exchange, so as to form mainly the α-glycal. Finally, dihydroxylation gave pure **118** in 75% overall yield from **122**. We did not investigate the use of other hydride agents, in an attempt to improve the isomer ratio (*ca*. 3:1) in the first step.

Synthesis of the aromatic unit

The carbohydrate domain of calicheamicinone is interrupted by the hexasubstituted benzene, which is flanked by a monosaccharide and a trisaccharide. Before we began our own work,[6] methods had been published for making the parent aromatic system **123** (R = H),[35] the corresponding ester **123** (R = Me),[21,35] and the nitrile **124**.[24f] We prepared ester **123** (R = Me) by two routes, using very simple reactions. Both routes lead to compound **130** (Scheme 24), from which the target is easily reached, as described below.

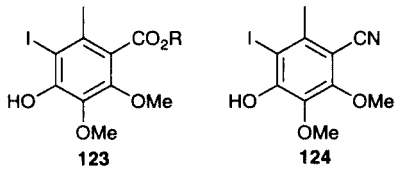

Our first route begins with the known nitro acetate **125**[36] (Scheme 24), which is available in good yield from vanillin by acetylation (Ac_2O, aqueous NaOH; 94%) and nitration (fuming HNO_3; 83%). Catalytic hydrogenation served to reduce both the nitro and formyl groups, and in this way the required methyl and amino functions are introduced (**125** → **126**). Sandmeyer reaction, acetate hydrolysis, and allylation of the resulting phenol then gave the bromo allyl ether **127**. This rearranged in high yield when heated in refluxing decalin, to produce the *ortho* allyl phenol **128**, which was methylated under standard conditions. Finally, halogen–metal exchange and acylation with methyl chloroformate gave **130**, which is an advanced intermediate common to both the routes we developed to the aromatic ring.

The second route (Scheme 25) starts with piperonal. The derived cyclohexylimine (*ca*. 97%) is easily converted into aldehyde ester **131** by lithiation and treatment with methyl chloroformate (88%).[37] Hydrogenolysis again converts the formyl group into a methyl, and then the phenolic hydroxy

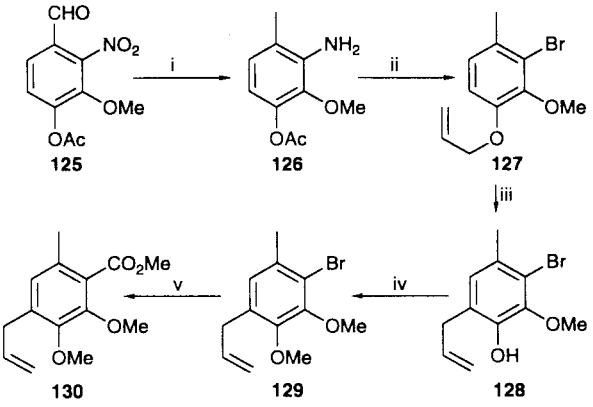

Scheme 24 *Reagents and conditions*: i, AcOH, MeOH, Pd-C, H_2, 93%; ii, (a) $NaNO_2$, HCl, CuBr, (b) MeOH, KOH, heat, 81%, (c) K_2CO_3, allyl bromide, acetone, 96%; iii, refluxing decalin (*ca*. 190 °C), 91%; iv, K_2CO_3, Me_2SO_4, acetone, 92%; v, *n*-BuLi, THF, MeOCOCl, 81%.

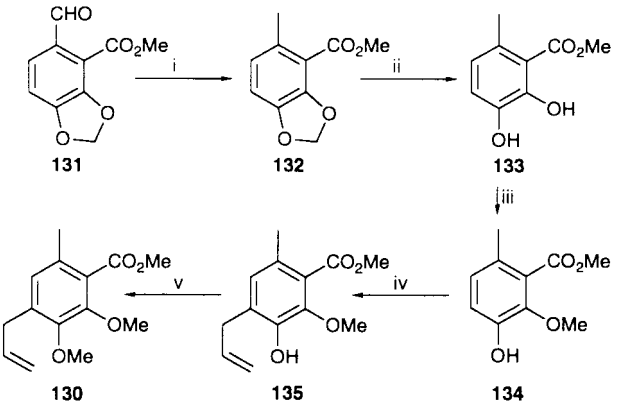

Scheme 25 *Reagents and conditions*: i, AcOH, MeOH, Pd–C, H_2, 93%; ii, $AlBr_3$, EtSH, 93%; iii, Li_2CO_3, MeI, DMF, 71%, after correction for recovered **133** (30%); iv, (a) K_2CO_3, allyl bromide, acetone, 92%, (b) refluxing decalin (*ca*. 190 °C), 86%; v, K_2CO_3, Me_2SO_4, acetone, 97%.

groups were released by the action of aluminium tribromide in ethanethiol. The critical next step (**133** → **134**) involved selective methylation of the C(2) hydroxy group. This was accomplished[38] by using methyl iodide and lithium carbonate in DMF at room temperature and, under these conditions, it was possible to isolate the desired monomethyl ether **134** in acceptable yield (50%, or 71%, after correction for recovered **133**). The remaining hydroxy group was then allylated as before, and Claisen rearrangement gave the new phenol **135**. This was then methylated (**135** → **130**), bringing the sequence to a point that overlaps with the first route.

Having a supply of **130** in hand, we had next to degrade the allyl pendant to a formyl group (Scheme 26). To this end, the

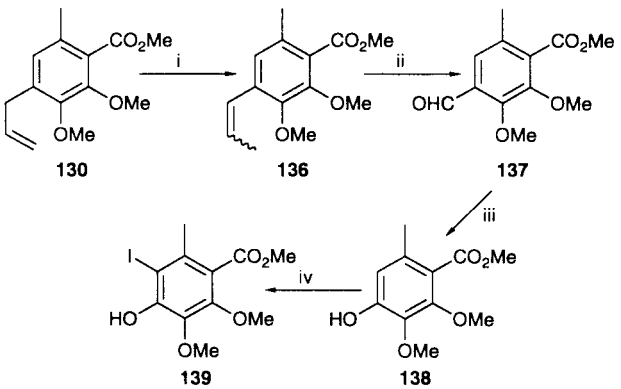

Scheme 26 *Reagents and conditions*: i, $RhCl_3·3H_2O$, EtOH, heat, 89%; ii, OsO_4, $NaIO_4$, *t*-BuOH, CCl_4, H_2O, 83%; iii, MCPBA, CH_2Cl_2, then MeOH, KOH, water, 81%; iv, ICl, CH_2Cl_2, 95%.

double bond was shifted into conjugation with the aromatic ring, using rhodium trichloride in refluxing ethanol,[39] and oxidative cleavage of the product (**136**) under Lemieux–Johnson conditions gave aldehyde **137**. At that point, Baeyer–Villiger oxidation and base hydrolysis produced the known phenol **138**,[35] which reacted with iodine monochloride to afford in 95% yield the target **139**—a substance that represents the aromatic unit of calicheamicin.

Conclusion

Our synthetic work has led to each of the subunits of calicheamicin γ_1^I, including the first preparation of *crystalline* (−)-calicheamicinone, for which the molecular dimensions were established by X-ray analysis. At several points a remarkable level of stereoselectivity was observed with alkynyl cerium reagents, and the stereochemical aspects of the synthesis of **2** are very unusual.

Acknowledgements

We thank Natural Sciences and Engineering Research Council of Canada, the Merck Frosst Therapeutic Research Centre, and the Alberta Cancer Board for financial support. Y. T. held an AHFMR Postdoctoral Fellowship, Y.-J. W. an NSERC Postdoctoral Fellowship, and S. D. a 1967 NSERC Graduate Fellowship.

Notes and references

1 Representative reviews on the chemistry and mode of action: K. C. Nicolaou and W.-M. Dai, *Angew. Chem., Int. Ed. Engl.*, 1991, **30**, 1387; S. J. Danishefsky and M. D. Shair, *J. Org. Chem.*, 1996, **61**, 16; A. C. Weymeth-Wilson, *Nat. Prod. Rep.*, 1997, **14**, 99; J. A. Murphy and J. Griffiths, *Nat. Prod. Rep.*, 1993, **10**, 551.

2 Reviews on synthesis: H. Lhermitte and D. S. Grierson, *Contemp. Org. Synth.*, 1996, **3**, 41; H. Lhermitte and D. S. Grierson, *Contemp. Org. Synth.*, 1996, **3**, 93.

3 K. C. Nicolaou, C. W. Hummel, M. Nakada, K. Shibayama, E. N. Pitsinos, H. Saimoto, Y. Mizuno, K.-U. Baldenius and A. L. Smith, *J. Am. Chem. Soc.*, 1993, **115**, 7625; S. A. Hitchcock, M. Y. Chu-Moyer, S. H. Boyer, S. H. Olson and S. J. Danishefsky, *J. Am. Chem. Soc.*, 1995, **117**, 5750.

4 D. L. J. Clive, Y. Bo, Y.; Y. Tao, S. Daigneault, Y.-J. Wu and G. Meignan, *J. Am. Chem. Soc.*, 1998, **120**, 10 332.

5 D. L. J. Clive, Y. Bo, N. Selvakumar, R. McDonald and B. D. Santarsiero, *Tetrahedron*, 1999, **55**, 3277.

6 Y.-Z. Hu and D. L. J. Clive, *J. Chem. Soc., Perkin Trans. 1*, 1997, 1421.

7 Synthesis of racemic calicheamicinone: (*a*) J. N. Haseltine, M. Paz Cabal, N. B. Mantlo, N. Iwasawa, D. S. Yamashita, R. S. Coleman, S. J. Danishefsky and G. K. Schulte, *J. Am. Chem. Soc.*, 1991, **113**, 3850; (*b*) I. Churcher, D. Hallet and P. D. Magnus, *J. Am. Chem. Soc.*, 1998, **120**, 10350.

8 Synthesis of optically pure calicheamicinone: A. L. Smith, E. N. Pitsinos, C.-K. Hwang, Y. Mizuno, H. Saimoto, G. R. Scarlato, T. Suzuki and K. C. Nicolaou, *J. Am. Chem. Soc.*, 1993, **115**, 7612; J. Aiyer, S. A. Hitchcock, D. Denhart, K. K. C. Liu, S. J. Danishefsky and D. M. Crothers, *Angew. Chem., Int. Ed. Engl.*, 1994, **33**, 855.

9 P. Magnus, R. T. Lewis and F. Bennett, *J. Chem. Soc., Chem. Commun.*, 1989, 916 and references therein.

10 *Cf.* (*a*) J. Banville and P. Brassard, *J. Chem. Soc., Perkin Trans. 1*, 1976, 1852; (*b*) M. D. Broadhurst, *J. Org. Chem.*, 1985, **50**, 1117; (*c*) C. N. Eid, Jr. and J. P. Konopelski, *Tetrahedron*, 1991, **47**, 975; (*d*) J. P. Konopelski and R. A. Kasar, *Tetrahedron Lett.*, 1993, **34**, 4587.

11 *Cf.* S. Danishefsky, M. P. Prisbylla and S. Hiner, *J. Am. Chem. Soc.*, 1978, **100**, 2918; S. Danishefsky, *Acc. Chem. Res.*, 1981, **14**, 400.

12 S. N. Huckin and L. Weiler, *J. Am. Chem. Soc.*, 1974, **96**, 1082.

13 J. O. Osby and B. Ganem, *Tetrahedron Lett.*, 1985, **26**, 6413.

14 Stoichiometry: $Me_3SiC{\equiv}CLi : CeCl_3 = 1:1$.

15 *Cf.* K. Utimoto, A. Nakamura and S. Matsubara, *J. Am. Chem. Soc.*, 1990, **112**, 8189.

16 H. Kunz and C. Unverzagt, *Angew. Chem., Int. Ed. Engl.*, 1984, **23**, 436.

17 H. Hofmeister, K. Annen, H. Laurent and R. Wiechert, *Angew. Chem., Int. Ed. Engl.*, 1984, **23**, 727.

18 O. Ort, *Org. Synth.*, 1987, **65**, 203.

19 J. K. Whitesell, A. Bhattacharya, C. M. Buchanan, H. H. Chen, D. Deyo, D. James, C.-L. Liu and M. A. Minton, *Tetrahedron*, 1986, **42**, 2993.

20 G. Rosini, R. Ballini and P. Sorrenti, *Synthesis*, 1983, 1014.

21 R. D. Groneberg, T. Miyazaki, N. A. Stylianides, T. J. Schulze, W. Stahl, E. P. Schreiner, T. Suzuki, Y. Iwabuchi, A. L. Smith and K. C. Nicolaou, *J. Am. Chem. Soc.*, 1993, **115**, 7593.

22 *Cf.* G. A. Molander, J. B. Etter, L. S. Harring and P.-J. Thorel, *J. Am. Chem. Soc.*, 1991, **113**, 8036.

23 *O*-Methylation, DIBAL-H reduction of the ester to an aldehyde and acid-catalyzed desilylation and ring closure gave a pyranose with *cis* nitrogen and OMe groups, indicating that the hydroxy stereochemistry in **83** (major isomer) required inversion.

24 (*a*) For synthesis of a model from D-glucose, see: F. L. Van Delft, G. A. Van Der Marel and J. H. Van Boom, *Carbohydrate Lett.*, 1996, **2**, 53; (*b*) for synthesis from serine, see: W. R. Roush and J. A. Hunt, *J. Org. Chem.*, 1995, **60**, 798; (*c*) D. Kahne, D. Yang and M. D. Lee, *Tetrahedron Lett.*, 1990, **31**, 21; (*d*) ref. 21; (*e*) for synthesis from methyl 2-deoxy-β-D-ribofuranoside, see: E. A. Mash, S. K. Nimkar and S. M. DeMoss, *J. Carbohydr. Chem.*, 1995, **14**, 1369. (*f*) R. H. Halcomb, S. H. Boyer, M. D. Wittman, S. H. Olson, D. J. Denhart, K. K. C. Liu and S. J. Danishefsky, *J. Am. Chem. Soc.*, 1995, **117**, 5720; (*g*) P. Crotti, V. Di Bussolo, L. Favero, F. Macchia and M. Pineschi, *Tetrahedron: Asymmetry*, 1996, **7**, 779; (*h*) F. Badalassi, P. Crotti, L. Favero, F. Macchia and M. Pineschi, *Tetrahedron*, 1997, **53**, 14 369.

25 M. Hirama, I. Nishizaki, T. Shigemoto and S. Itô, *J. Chem. Soc., Chem. Commun.*, 1986, 393.

26 *Cf.* S. Thaisrivongs and D. Seebach, *J. Am. Chem. Soc.*, 1983, **105**, 7407.

27 (*a*) For synthesis of a model from methyl α-D-galactopyranoside, see: A. Classen and H.-D. Scharf, *Liebigs Ann. Chem.*, 1993, 183; (*b*) for synthesis from 2,6-dideoxy-α-D-ribohexopyranose, see: K. Van Laak and H.-D. Scharf, *Tetrahedron Lett.*, 1989, **30**, 4505; (*c*) for synthesis based on Sharpless kinetic resolution, see: W. R. Roush and D. Gustin, *Tetrahedron Lett.*, 1994, **35**, 4931; (*d*) for synthesis from D-fucose, see: S.-H. Kim, D. Augeri, D. Yang and D. Kahne, *J. Am. Chem. Soc.*, 1994, **116**, 1766; (*e*) for synthesis from 4,6-*O*-benzylidene-D-allal (R. U. Lemieux, E. Fraga and K. A. Watanabe, *Can. J. Chem.* 1968, **46**, 61), see ref 21.

28 For synthesis of a model from D-galactose, see: H. Rainer and H.-D. Scharf, *Liebigs Ann. Chem.*, 1993, 117; ref. 21; for synthesis from crotonaldehyde, see: W. R. Roush and B. C. Follows, *Tetrahedron Lett.*, 1994, **35**, 4935; for synthesis from di-*O*-actyl-d-fucal, see ref. 24(*f*).

29 A. Fujii, S. Hashiguchi, N. Uematsu, T. Ikariya and R. Noyori, *J. Am. Chem. Soc.*, 1996, **118**, 2521.

30 M. A. Bennet and A. K. Smith, *J. Chem. Soc., Dalton Trans.*, 1974, 233.

31 P. G. Sammes and D. Thetford, *J. Chem. Soc., Perkin Trans. 1*, 1988, 111.

32 The route from **114** is similar to that reported by Danishefsky and coworkers [see ref. 24(*f*).

33 J. Mariño-Albernas, V. Verez-Bencomo, L. Gonzalez-Rodriguez, C. S. Perez-Martinez, E. Gonzalez-Abreu Castell and A. Gonzalez-Segredo, *Carbohydr. Res.*, 1988, **183**, 175.

34 For synthesis from D-rhamnose, see ref. 27(*d*); ref. 21; for synthesis from di-*O*-acetyl-L-rhamnal, see ref. 24(*f*).

35 K. van Laak and H.-D. Scharf, *Tetrahedron*, 1989, **45**, 5511.

36 A. P. N. Burge, E. V. Brandt and D. G. Roux, *Phytochemistry*, 1983, **22**, 2813.

37 F. E. Ziegler and K. W. Fowles, *J. Org. Chem.*, 1976, **41**, 1564.

38 *Cf.* W. E. Wymann, R. Davis, J. W. Patterson, Jr. and J. R. Pfister, *Synth. Commun.*, 1988, **18**, 1379.

39 *Cf.* J. Andrieux, D. H. R. Barton and H. Patin, *J. Chem. Soc., Perkin Trans. 1*, 1977, 359.

ChemComm

Novel organic porous solids with channel and layered structures from 1,3,5-triazine-2,4,6-triaminehexaacetic acid and its calcium salt

S. N. Ghanashyam Acharya,[a] R. Srinivasa Gopalan,[b] G. U. Kulkarni,[b] K. Venkatesan[a] and Santanu Bhattacharya*[a]

[a] *Department of Organic Chemistry, Indian Institute of Science, Bangalore, India 560 012. E-mail: sb@orgchem.iisc,ernet.in; Fax: +91-80-360-0529*

[b] *Chemistry and Physics of Materials Unit, Jawaharlal Nehru Centre for Advanced Scientific Research, Jakkur, Bangalore, India 560 064*

Received (in Cambridge, UK) 13th March 2000, Accepted 6th June 2000
Published on the Web 30th June 2000

Single crystals of a symmetrically substituted molecule, 1,3,5-triazine-2,4,6-triaminehexaacetic acid, (TTHA) and its Ca^{2+} salt have been synthesized, the analysis of which reveals the existence of novel channel type cavities and helical packing organizations in the crystals.

Nanoporous inorganic structures of widely varying three-dimensional arrangements are well known.[1] However, organic molecules are generally more amenable to chemical functionalization. Consequently there has been a steady rise in attempts to design organic molecules that can self-assemble *via* non-covalent interactions.[2] Indeed, intelligent use of the directional nature of the hydrogen bonding and other structure directing forces have generated solids with a whole variety of structural motifs from man-made organic templates.[3,4]

Due to our continuing interest in the synthesis of organic solids[5] with controllable crystalline packing, we considered the design of solids with framework structures, in which the building blocks within the individual infinite networks are linked either *via* H-bonds, or through metal-to-ligand bonds. One way to develop solids with predictable 3D organization requires design of a molecule with a symmetrical and well-defined spatial arrangement of subunits, that can associate through one or more non-covalent interactions. For this purpose we chose the aromatic triazine nucleus in melamine as a core which possesses -NH_2 substituents at the 2-, 4- and 6-positions. The ability of the melamine pendant residues to undergo H-bonding interactions with other molecules or ions has been exploited in both solution and the solid state.[3] It occurred to us that the -NH_2 groups in melamine could be replaced by -$N(CH_2CO_2H)_2$ moieties, giving a core triazine nucleus with three symmetrically placed, strongly metal-complexing bidentate sites. The resulting ligand, 1,3,5-triazine-2,4,6-triamine hexaacetic acid (**TTHA**, **1**)† provides a symmetrical array of

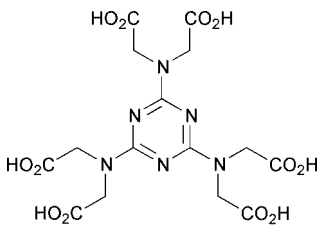

TTHA (1)

three bidentate sites at which selected metal ions can be strongly bound, each site closely resembling those in the 'textbook' chelating agent EDTA and related derivatives. One important feature of the connecting ligands providing three bidentate residues on the triazine hub is that when a metal ion binds to three of them, the metal itself adopts the role of three nodal points from which further connections could be engineered. Therefore ligands like **TTHA** should be well poised to generate a range of supramolecular framework structures in the solid state.

Crystallization of **TTHA** from its aqueous solution yields a solid which could be examined by single-crystal X-ray diffraction.‡ In monoclinic crystals of **1** four molecules of **TTHA** were found to be packed in the unit cell in the space group *C*2/*c*, the molecular symmetry in the crystal lattice being $C_2(2)$ which passes through the atoms N(11), C(12) and N(22) (not shown). The nature of the intramolecular bond lengths in the aromatic core is indicative of extensive π-electron delocalization, which results in the planarity of this molecular entity. From the values of the torsional angles it is clear that the conformations of each -$N(CH_2CO_2H)_2$ side-chain are slightly different. These conformations adjust according to the need to accommodate efficient intermolecular H-bonding interactions in the lattice and deviate out of the plane of the triazine rings.

TTHA forms H-bonded (O–H···O) dimers through the CO_2H residues. Other weak interactions such as C–H···O and C–H···N also exist. The supramolecular architecture produced upon non-covalent association of **TTHA**, results in a 'crinkled' molecular tape supported by O–H···O H-bonds, which extend in the direction of the *c*-axis (not shown). All six CO_2H groups in **TTHA** participate in such interactions and this association extends infinitely (Fig. 1). Such supramolecular sheets of **TTHA** are stacked along the *a*-axis giving exquisite channels of various sizes. While the polar CO_2H ends maintain the channels, the columns in the channels in such aggregates are made of triazine rings. The arrangement is reminiscent of pillared inorganic layered structures, the CO_2H residues

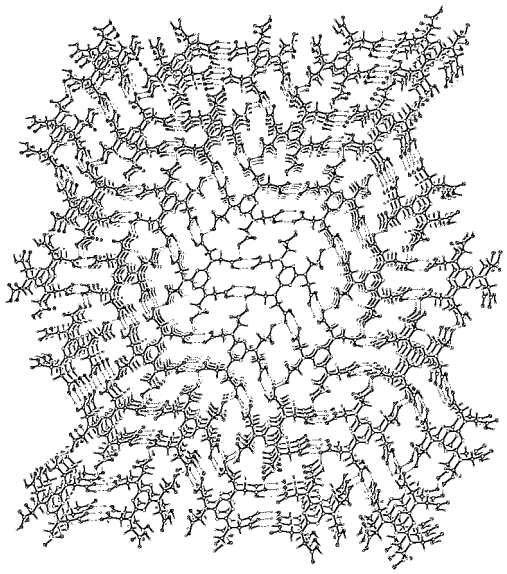

Fig. 1 Crystal packing of layers of **TTHA** in 3D showing the superposition of eight layers of **TTHA** molecules leading to the formation of channels.

DOI: 10.1039/b002016h

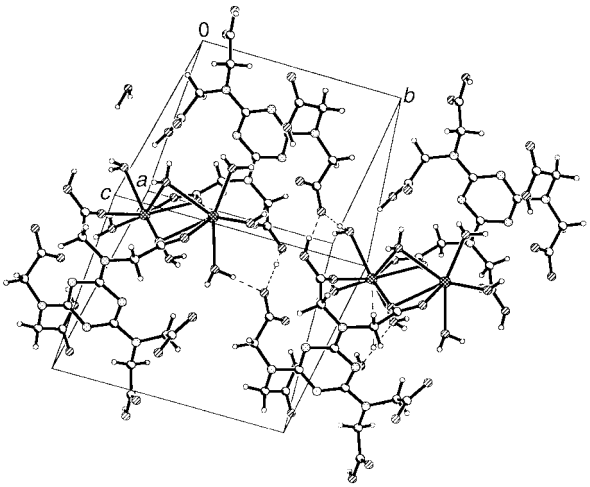

Fig. 2 Ca^{2+} ion induced supramolecular motif of **TTHA** showing the helical organization.

forming pillars between the layers formed by **TTHA** in **TTHA**.

This observation prompted us to explore the possibilities of generating an open-framework metal-coordination polymer of **TTHA**, using an oxophilic metal such as the Ca^{2+} ion. Indeed, crystals of a suitable quality for single-crystal X-ray diffraction of the Ca^{2+} salt of **TTHA**‡ were obtained upon prolonged incubation in water. The structure of the Ca^{2+} salt of **TTHA** consists of two molecules of **TTHA**, bound to two Ca^{2+} ions in the asymmetric unit (not shown). The two crystallographically independent **TTHA** molecules are related by an approximate non-crystallographic centre of symmetry. However, the side-arm $-N(CH_2CO_2^-)_2$ anions projecting from the same triazine hub show appreciable differences in their conformations.

From the crystal structure it is also evident that the two Ca^{2+} ions, Ca1 and Ca2 are octa-coordinated and are bridged by two carboxy groups maintaining a distance of 4.84 Å. As many as eight water molecules in the asymmetric unit are also found to be involved in the formation of a 3D network of O–H···O H-bonds. The most predominant feature of the solid state organization is that Ca^{2+} and the water molecules are confined to the crystal space between the two independent **TTHA** molecules. This feature is shown in Fig. 2, which omits the intermolecular H-bond connectivities for clarity. This also shows that the supramolecular architecture of the molecules along the *b*-axis is stabilized by O–H···O H-bonds. The planar triazine part of the **TTHA** moieties is essentially perpendicular to the *c*-axis of the unit cell. In this situation, the side-arms of **TTHA** project out in such a manner that its terminal carboxy groups not only participate in the intermolecular O-H···O H-bonds but are also able to ligate with the Ca^{2+} ions. The planar rings of the crystallographically independent triazines are parallel to one another, separated by ~3.5 Å. However, the triazine rings do not overlap completely and are partially displaced from one another. Further inspection shows that a helical organization exists in this polymeric network where multiple, short triazine–triazine π or C–H···π triazine contacts probably assist in stabilizing such helical organizations.

In summary, we were able to design a new supramolecular scaffold utilizing **TTHA** as a central tecton which can form self-organized entities in the solid state. The results presented herein augur well for the future generation of a whole variety of crystalline coordination polymers based on templates bearing aminediacetic acid (EDTA and related ligands) with a wide choice of metal centers, in some cases with channel-like organizations. In view of the increasing demand for the synthesis of planar molecular templates with trigonal and hexagonal symmetry for materials design,[6] **TTHA** should provide convenient routes to prepare a new family of solids, the packing organizations of which could be controlled by crystal engineering. Other metal substitution may allow the generation of porous solids with redox or charged subsites and these might offer new matrices with altered physical properties for specific catalytic and separation science applications. Synthesis and investigation of the properties of these novel solid materials are underway.

We thank Professor C. N. R. Rao for helpful discussions. This work was supported by the Swarnajayanti Fellowship Grant of the Department of Science and Technology, Govt. of India.

Notes and references

† **TTHA** and its precursors have been characterized spectroscopically and also by elemental analysis and the corresponding data were consistent with their proposed structures.

‡ Single crystal X-ray diffraction studies. X-Ray diffraction intensities were measured at room temperature by ϖ scans using a Siemens three-circle diffractometer attached to a CCD area detector and a graphite monochromator for the Mo-Kα radiation (50 kV, 40 mA). The crystal structures were solved by direct methods using the SHELXTL program[7] and refined by full matrix least squares on F^2. All the non-hydrogen atoms were refined anisotropically. H atoms were located by the difference Fourier method and were refined isotropically. CCDC 182/1677.

Crystal data: $C_{15}H_{18}O_{12}N_6$ (**TTHA**), M = 474.3, monoclinic, space group $C2/c$, a = 5.057(1), b = 21.607(2), c = 17.406(2) Å, β = 91.69(1)°, V = 1900.0(0) Å^3, Z = 4, $D_{calcd.}$ = 1.797 g cm^{-3}, μ(Mo-K$_\alpha$) = 0.07 mm^{-1}, F(000) = 492. Crystal dimensions 0.35 × 0.35 × 0.20 mm. The final R-values were R_1 = 0.0464, R_w = 0.1267 and GOF = 1.162 for 1386 reflections.

$C_{30}H_{32}O_{24}N_{12}Ca_2{\cdot}8H_2O$ (Ca^{2+} salt of **TTHA**), M = 1168.9, triclinic, space group $P1$, a = 10.407(1), b = 10.990(2), c = 20.543(8) Å, α = 92.82 (2), β = 98.82 (2), γ = 95.43 (2)°, V = 2306.5(8) Å^3, Z = 4, $D_{calcd.}$ = 1.68 g cm^{-3}, μ(Mo-K$_\alpha$) = 0.37 mm^{-1}, F(000) = 1212.0, Crystal dimensions 0.63 × 0.60 × 0.43 mm. The final R-values were R_1 = 0.0403, R_w = 0.1334 and GOF = 1.148 for 4911 reflections.

1 S. Oliver, A. Kuperman and G. A. Ozin, *Angew. Chem., Int. Ed.*, 1998, **37**, 46; J. M. Thomas, *Chem. Eur. J.*, 1997, **3**, 1557; M. E. Davies, *Chem. Eur. J.*, 1997, **3**, 1745; W. M. Meier, D. H. Olson and Ch. Baerlocher, *Atlas of Zeolite Structure Types*, Elsevier, Boston, 1996.

2 J.-M. Lehn, *Supramolecular Chemistry: Concepts and Perspectives*, VCH, Weinheim, 1995; J. R. Fredericks and A. D. Hamilton, *Comprehensive Supramolecular Chemistry*, ed. J. L. Atwood, J. E. D. Davies, D. D. MacNicol and F. Vogtle, Pergamon, Oxford, 1996, pp. 565.

3 G. M. Whitesides, E. E. Simanek, J. P. Mathies, C. T. Seto, D. N. Chin, M. Mammen and D. M. Gordon, *Acc. Chem. Res.*, 1995, **28**, 37; V. R. Pedireddi, S. Chatterjee, A. Ranganathan and C. N. R. Rao, *J. Am. Chem. Soc.*, 1997, **119**, 10 867; A. Ranganathan, V. R. Pedireddi and C. N. R. Rao, *J. Am. Chem. Soc.*, 1999, **121**, 1752.

4 S. S.-Y. Chin, S. M. F. Lo, J. P. H. Charemant, A. G. Orpen and I. D. Williams, *Science*, 1999, **283**, 1148; K. Biradha, C. Seward, M. J. Zaworotko and B. F. Abrahams, *Angew. Chem., Int. Ed.*, 1999, **38**, 492; G. R. Desiraju, *Angew. Chem., Int. Ed. Engl.*, 1995, **34**, 2311.

5 S. S. Mandal, R. Kadirvelraj, T. N. Guru Row and S. Bhattacharya, *Chem. Commun.*, 1996, 2725; S. Bhattacharya, P. Dastidar and T. N. Guru Row, *Chem. Mater.*, 1994, **5**, 531.

6 F. Cherioux, P. Audebest and P. Hapiot, *Chem. Mater.*, 1998, **10**, 1984; D. C. Talmassebi and T. Sasaki, *J. Org. Chem.*, 1998, **63**, 728; P. V. Bernhardt and E. J. Hays, *J. Chem. Soc., Dalton Trans.*, 1998, 3539; G. A. Downing, C. S. Franapton, J. H. Gall and D. D. MacNicol, *Angew. Chem., Int. Ed. Engl.*, 1996, **35**, 1547.

7 SHELXTL (SGI version) Siemens Analytical X-ray Instruments Inc. 1995, Madison, Wisconsin, USA.

ChemComm

Synthesis of a stable stibabismuthene; the first compound with an antimony–bismuth double bond

Takahiro Sasamori,[a] Nobuhiro Takeda†[b] and Norihiro Tokitoh*†[b]

[a] *Department of Chemistry and Physics of Condensed Matter, Graduate School of Science, Kyushu University, Japan*
[b] *Institute for Fundamental Research of Organic Chemistry, Kyushu University, 6-10-1 Hakozaki, Higashi-ku, Fukuoka 812-8581, Japan. E-mail: tokitoh@boc.kuicr.kyoto-u.ac.jp*

Received (in Cambridge, UK) 8th March 2000, Accepted 14th June 2000
Published on the Web 30th June 2000

The condensation reaction of an overcrowded dihydrostibine with dibromobismuthine using 1,8-diazabicyclo[5.4.0]undec-7-ene as a base afforded the first stable stibabismuthene, the formation of which was evidenced by UV–VIS and Raman spectra and its chemical reactivity.

In recent years there has been much interest in compounds with a double bond between heavier group 15 elements. Since the first isolation of a stable diphosphene (Mes*P=PMes*; Mes* = 2,4,6-tri-*tert*-butylphenyl) in 1981,[1] a number of examples of kinetically stabilized diphosphenes (RP=PR)[2] and diarsenes (RAs=AsR)[2c,3] have been isolated and fully characterized. Recently, we have succeeded in the synthesis and characterization of the first stable distibene (TbtSb=SbTbt)[4] and dibismuthene (TbtBi=BiTbt),[5] even heavier congeners of azo compounds, by taking advantage of an efficient steric protection group, Tbt = 2,4,6-tris[bis(trimethylsilyl)methyl]phenyl.[6] Very recently, Power and coworkers also synthesized another type of stable distibene and dibismuthene substituted by bulky 2,6-$Ar_2C_6H_3$ groups (Ar = mesityl or 2,4,6-triisopropylphenyl).[7] As for the case of heteronuclear double-bond compounds between heavier group 15 elements, several phosphaarsenes[3a,8] and phosphastibenes[8,9] have been synthesized as stable compounds. However, there are no examples of a heteronuclear doubly bonded system between antimony and bismuth, *i.e.* stibabismuthene. Although the successful results on the kinetic stabilization of distibene and dibismuthene (TbtE=ETbt; E = Sb, Bi) naturally prompted us to apply the Tbt group to the synthesis of stable stibabismuthene, we were apprehensive that the extremely low solubility of the Tbt-substituted doubly bonded system of heavier group 15 elements may prevent us from utilising the possible synthetic approaches or spectroscopically detecting the reaction products. On the other hand, during the course of our investigation on the kinetic stabilization of low-coordinated highly reactive species we have developed another bulky aromatic substituent, 2,6-bis[bis(trimethylsilyl)methyl]-4-[tris(trimethylsilyl)methyl]phenyl (Bbt),[10] which is expected to be a potentially more useful steric protecting

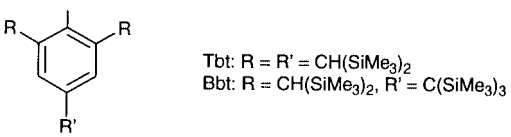

group than TbT. In fact, a new distibene and dibismuthene substituted by Bbt groups, which have relatively high solubility compared with TbtE=ETbt (E = Sb, Bi), have been successfully synthesized and characterized.[11] We now report the successful application of the Bbt group to the synthesis of the first stable stibabismuthene, BbtSb=BiBbt **1**.

† *Present address*: Institute for Chemical Research, Kyoto University, Gokasho, Uji, Kyoto 611-0011, Japan. E-mail: tokitoh@boc.kuicr.kyoto-u.ac.jp

The condensation reaction of $BbtBiBr_2$ with $BbtSbH_2$, which was prepared by the reaction of $BbtSbBr_2$ with $LiAlH_4$, in the presence of 1,8-diazabicyclo[5.4.0]undec-7-ene (DBU) in THF at −95 °C afforded stibabismuthene **1**‡ as red–purple crystals quantitatively (Scheme 1). Stibabismuthene **1** showed satisfactory spectral data, as discussed below.

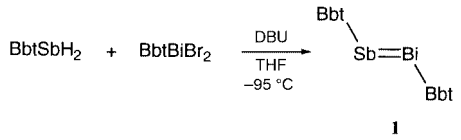

Scheme 1

In the Raman spectrum (in the solid state) of **1**, a strong line attributable to the Sb–Bi stretching was observed at 169 cm^{-1}. This wavenumber lies between the value of the Sb–Sb stretching vibration in TbtSb=SbTbt (207 cm^{-1})[4] and that of the Bi–Bi stretching vibration in TbtBi=BiTbt (135 cm^{-1}),[5] and is higher than the Sb–Sb and Bi–Bi stretching frequencies for Ph_2E–EPh_2 (E = Sb, Bi).[12] The UV–VIS spectrum of **1** in hexane shows two absorption maxima at 709 nm (ε 200 dm^3 mol^{-1} cm^{-1}) and 516 (7500), which are most likely assignable to the forbidden n → π* and the allowed π→ π* transitions of the Sb=Bi chromophore, respectively.

These results are consistent with the characteristic red-shifts in the electronic spectra of previously reported heavier congeners of azo compounds, and the λ_{max} value for the π → π* transition of **1** lies between those of BbtSb=SbBbt **2** [λ_{max} 490 nm (ε 6000 dm^3 mol^{-1} cm^{-1})][11] and BbtBi=BiBbt **3** [λ_{max} 537 nm (ε 6000 dm^3 mol^{-1} cm^{-1})].[11] These spectral data suggest that **1** features a double bond between antimony and bismuth in solution as well as in the solid state. The reason for the additional red-shift for the n → π* transition of **1**, which is 39 nm longer than that of **3** [λ_{max} 670 nm (sh, ε 20)], is not clear at present.

The molecular structure of stibabismuthene **1** was also supported by X-ray crystallographic analysis, but definite structural parameters for **1** have not been obtained yet owing to the inevitable disorder of the antimony and bismuth atoms, which cannot be solved by data collection with a number of different single crystals of **1** even at low temperature (−180 °C).§

Stibabismuthene **1** is stable at ambient temperature in hydrocarbon solvents in the absence of air and light. When a solution of **1** in benzene-d_6 was heated at 70 °C, **2** and **3** were formed very slowly as judged by ^{1}H NMR spectroscopy

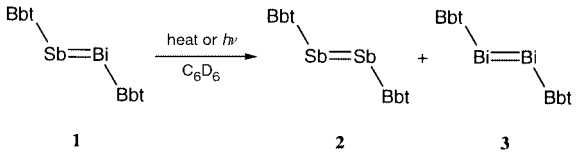

Scheme 2

DOI: 10.1039/b001900n

(Scheme 2). Heating a solution of **1** at 80 °C for 20 days led to the formation of a mixture of **1**, **2** and **3** with the ratio of 1:1.4:1.1, respectively. On the other hand, when a solution of **1** in benzene-d_6 was irradiated with a medium pressure mercury lamp (100 W) in a sealed Pyrex NMR tube at room temperature, the disproportionation reaction was complete in 4 h to give a 1:1 mixture of **2** and **3**. The results of the thermal and photochemical disproportionation reactions of **1** into the homonuclear double-bond species **2** and **3** can be regarded as chemical evidence for the formation of stibabismuthene **1**.

Taking the previous reports on the reactivities of diphosphenes[2,13] into consideration, two different pathways can be postulated for the disproportionation reactions of stibabismuthene **1** (Scheme 3). The first is the dimerization of **1** by heating or irradiation followed by decomposition of the resulting four-membered dimer **4** into the homonuclear double-bond species **2** and **3** (path A), while the other is based on the dissociation of **1** giving the corresponding monovalent species, *i.e.* stibinidene **5** and bismuthinidene **6**, both of which might undergo ready dimerization leading to the formation of **2** and **3**, respectively (path B).

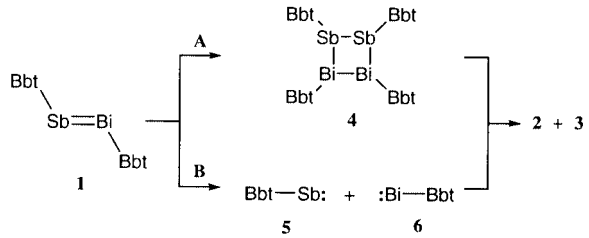

Scheme 3

Although we have examined the thermolysis and photolysis of **1** in the presence of 2,3-dimethylbuta-1,3-diene in expectation of trapping the intermediary monovalent species **5** and **6**, no [4 + 1] cycloadducts of **5** and **6**, but only distibene **2** and dibismuthene **3**, were obtained in high yields. Since we have already found that the stibinidene **5** generated by thermal cycloreversion of the corresponding overcrowded stibolene derivative readily undergoes [4 + 1] cycloaddition with 2,3-dimethylbuta-1,3-diene to give the stable stibinidene adduct,[10,11] the disproportionation reaction of stibabismuthene is not rationalized by the mechanism *via* stibinidene and bismuthinidene intermediates but most likely interpreted in terms of the association–dissociation mechanism *via* the head-to-head dimerization of **1**.

In summary, we have succeeded in the synthesis of the first stable stibabismuthene **1** by taking advantage of kinetic stabilization afforded by a new and effective steric protecting group, Bbt. Further investigations on the physical and chemical properties of stibabismuthene and syntheses of other variations of heteronuclear doubly bonded systems between heavier main group elements are currently in progress.

This work was partially supported by Grants-in-Aid for Scientific Research on Priority Areas (No. 09239101 and 11166250) from the Ministry of Education, Science, Sports and Culture of Japan. T. S. thanks Research Fellowships of the Japan Society for the Promotion of Science for Young Scientists. We acknowledge Professor Y. Furukawa of Waseda University for measuring the Raman spectra. We are also grateful to Shin-Etsu Chemical Co. Ltd., for the generous gifts of chlorosilanes.

Notes and references

‡ *Spectral data* for **1**: red–purple crystals, mp 259–260 °C (decomp.); ^{1}H NMR (400 MHz, C_6D_6) δ 0.31 (s, 36H), 0.34 (s, 36H), 0.39 (s, 27H), 0.40 (s, 27H), 1.98 (s, 2H), 2.07 (s, 2H), 7.19 (s, 2H), 7.53 (s, 2H); ^{13}C NMR (100 MHz, C_6D_6) δ 1.37 (q), 2.42 (q), 2.82 (q), 5.76 (q), 21.42 (s), 22.15 (s), 41.35 (d), 43.64 (d), 124.23 (d), 128.95 (d), 145.48 (s), 148.54 (s), 151.81 (s), 152.20 (s), 153.70 (s), 195.34 (brs). FT-Raman (Nd:YAG laser 1064 nm) 169 cm^{-1} ($\nu_{Sb=Bi}$). UV–VIS (hexane) λ_{max}/nm (ε/dm^3 mol^{-1} cm^{-1}) 709 (200), 516 (7500). FAB-MS: *m*/*z* 880 ([BbtBiSb − Si(CH$_3$)$_3$]$^+$), 832 ([BbtBi]$^+$), 745 ([BbtSb + H]$^+$).

§ *Crystal data* for **1**: $C_{60}H_{134}Si_{14}BiSb$, M = 1579.64, triclinic, space group $P\bar{1}$ (no. 2), a = 12.574(2), b = 18.056(2), c = 9.318(1) Å, α = 92.756(3), β = 98.623(4), γ = 88.678(8)°, V = 2088.9(5) Å^3, Z = 1, D_c = 1.256 g cm^{-3}, Mo-Kα (λ = 0.71069 Å) radiation, μ(Mo-Kα) = 26.54 cm^{-1}, T = −180 °C, 13387 reflections measured, 8279 unique (R_{int} = 0.048).

CCDC 182/1683. See http://www.rsc.org/suppdata/cc/b0/b001900n/ for crystallographic files in .cif format

1 M. Yoshifuji, I. Shima, N. Inamoto, K. Hirotsu and T. Higuchi, *J. Am. Chem. Soc.*, 1981, **103**, 4587.
2 For reviews see: (*a*) L. Weber, *Chem. Rev.*, 1992, **92**, 1839; (*b*) M. Yoshifuji, in *Multiple Bonds and Low Coordination in Phosphorus Chemistry*, ed. M. Regitz and O. J. Scherer, George Thieme Verlag, Stuttgart, Germany, 1990, p. 321; (*c*) A. H. Cowley, J. E. Kilduff, J. G. Lasch, S. K. Mehrotra, N. C. Norman, M. Pakulski, B. R. Whittlesey, J. L. Atwood and W. E. Hunter, *Inorg. Chem.*, 1984, **23**, 2582.
3 (*a*) A. H. Cowley, J. G. Lasch, N. C. Norman and M. Pakulski, *J. Am. Chem. Soc.*, 1983, **105**, 5506; (*b*) C. Couret, J. Escudié, Y. Madaule, H. Ranaivonjatovo and J.-G. Wolf, *Tetrahedron Lett.*, 1983, **24**, 2769; (*c*) A. H. Cowley, N. C. Norman and M. Paulski, *J. Chem. Soc., Dalton Trans.*, 1985, 383.
4 N. Tokitoh, Y. Arai, T. Sasamori, R. Okazaki, S. Nagase, H. Uekusa and Y. Ohashi, *J. Am. Chem. Soc.*, 1998, **120**, 433.
5 N. Tokitoh, Y. Arai, R. Okazaki and S. Nagase, *Science*, 1997, **277**, 78.
6 R. Okazaki, M. Unno and N. Inamoto, *Chem. Lett.*, 1987, 2293; R. Okazaki, N. Tokitoh and T. Matsumoto, in *Synthetic Methods of Organometallic and Inorganic Chemistry*, ed. W. A. Herrmann, vol. ed. N. Auner and U. Klingebiel, Thieme, New York, 1996, vol. 2, p. 260.
7 B. Twamley, C. D. Sofield, M. M. Olmstead and P. P. Power, *J. Am. Chem. Soc.*, 1999, **121**, 3357.
8 A. H. Cowley, J. G. Lasch, N. C. Norman, M. Pakulski and B. R. Whittlesey, *J. Chem. Soc., Chem. Commun.*, 1983, 881.
9 B. Twamley and P. P. Power, *Chem. Commun.*, 1998, 1979.
10 N. Tokitoh, T. Sasamori and R. Okazaki, *Chem. Lett.*, 1998, 725 and references therein.
11 T. Sasamori, N. Takeda, N. Tokitoh and R. Okazaki, unpublished results.
12 H. Bürger and R. Eujen, *J. Mol. Struct.*, 1983, **98**, 265; A. Ashe III, E. Ludwig Jr. and J. Oleksyszyn, *Organometallics*, 1983, **2**, 1859.
13 M. Yoshifjui, T. Sato and N. Inamoto, *Bull. Chem. Soc. Jpn.*, 1989, **62**, 2394.

ChemComm

Electrocatalytic four-electron reduction of oxygen to water by a highly flexible cofacial cobalt bisporphyrin

Christopher J. Chang,[a] Yongqi Deng,[a] Chunnian Shi,[b] C. K. Chang,*[c] Fred C. Anson*[b] and Daniel G. Nocera*[a]

[a] *Department of Chemistry, 6-335, Massachusetts Institute of Technology, 77 Massachusetts Avenue, Cambridge, Massachusetts 02139, USA. E-mail: nocera@mit.edu*
[b] *Division of Chemistry and Chemical Engineering, Arthur Amos Noyes Laboratory, California Institute of Technology, Pasadena, California 91125, USA*
[c] *Department of Chemistry, Michigan State University, East Lansing, Michigan 48824, USA*

Received (in Bloomington, IN, USA) 16th February 2000, Accepted 11th April 2000
Published on the Web 5th July 2000

Dicobalt(II) cofacial bisporphyrins anchored by dibenzofuran (DPD) and xanthene (DPX) are efficient electrocatalysts for the four-electron reduction of oxygen to water despite their *ca*. 4 Å difference in metal–metal distances, suggesting that the considerable longitudinal 'Pac-Man' flexibility of the pillared platforms is the origin for the similar catalytic reactivity of these structurally disparate systems.

Enzymatic systems are remarkable in their ability to accommodate the large range of motion required for the binding and catalysis of small molecules. In many cases, the kinetic steps of the processes involved are ultimately predicated on conformational changes of the active site upon substrate binding, activation, and/or product release. An outstanding example is the binding and biological reduction of dioxygen to water by cytochrome *c* oxidase (C*c*O).[1] The critical O–O bond cleavage chemistry is mediated by a flexible, dinuclear iron–heme/copper (Fe_{a3}/Cu_B) assembly.[1,2] Nevertheless, the pursuit of structural and functional models for O_2 activation have emphasized, for the most part, bimetallic reaction centers poised within well-defined, rigid pockets.[3–7] For example, pillared cofacial dicobalt bisporphyrins bridged by anthracene (DPA) and biphenylene (DPB)[8–11] impair ring slippage, and as a result, these complexes efficiently electrocatalyze the direct four-electron reduction of oxygen to water (as opposed to the two-electron pathway involving peroxide) with little structural reorganization of juxtaposed subunits. Can efficient oxygen-activation chemistry be preserved when this cofacial structural motif exhibits a large range of motion? To address this issue, we have developed methods for the facile assembly of new cofacial bisporphyrins, incorporating dibenzofuran (DPD)[12] or xanthene (DPX)[13] pillars that exhibit variable pocket sizes with minimal lateral displacements. Herein, we report that dicobalt(II) complexes of both DPD and DPX efficiently mediate the direct four-electron reduction of oxygen to water despite a *ca.* 4 Å difference in their metal–metal distances (as determined from their X-ray crystal structures), suggesting that the longitudinal 'Pac-Man' flexibility of these molecular clefts allows the designed binding pocket to structurally accommodate reaction intermediates during multielectron catalysis.

Co_2(DPD) **1** was obtained in excellent yield (91%) from reaction of the corresponding free base bisporphyrin with $CoCl_2$ and 2,6-lutidine.† Crystals suitable for X-ray diffraction studies were grown from dichloromethane–methanol solutions.‡ The structure of **1** (Fig. 1) shows that two methanol solvent molecules are coordinated *inside* the bisporphyrin pocket to the two cobalt(II) centers. In order to accommodate the two exogeneous ligands, the DPD framework opens its 'bite' considerably. The interplanar angle between the two macrocycles is 56.5°, resulting in metal–metal (8.624 Å) and center-to-center (8.874 Å) distances that are markedly larger than found in Zn_2(DPD) ($d_{Zn–Zn}$ = 7.775 Å, $d_{Ct–Ct}$ = 7.587 Å).[12]

The Co(II) cores adopt an approximate square-pyramidal geometry, as the N–Co–N bond angles are 90 ± 1.3° and the N–Co–O bond angles are 90 ± 5.3°. The Co centers are displaced slightly from the porphyrin meanplane (d_{av} = 0.1355 Å) toward the axial ligand. The average axial Co–O bond length (2.272 Å) is significantly longer than that of the average equatorial Co–N bond (1.982 Å), owing to the occupancy of the d_{z^2} orbital by a single unpaired electron in Co(II). A conformational analysis of the two macrocycles indicates inequivalent ring systems. The porphyrin ring containing Co(1) exhibits an S_4 ruffle with a mean deviation from planarity of 0.1416 Å. In contrast, the ring with Co(2) is essentially flat (average deviation 0.0307 Å). Lastly, the most important structural feature of **1** in relation to its O_2 reactivity (*vide infra*) is the small tortional twist (9.3°, defined as the torsion angle between the two *meso*-carbon to

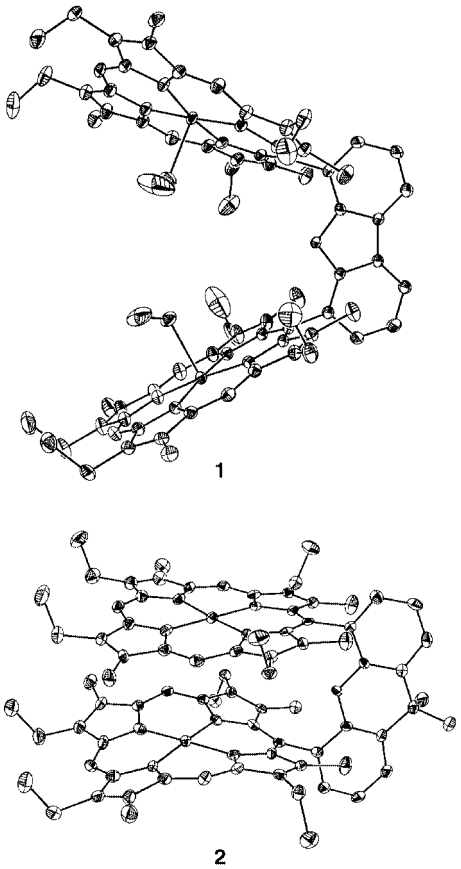

Fig. 1 Molecular structures of **1** and **2** with hydrogen atoms omitted for clarity. Thermal ellipsoids are drawn at the 30% probability level.

DOI: 10.1039/b001620i

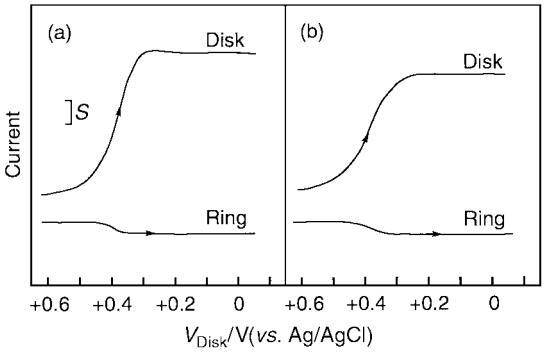

Fig. 2 Rotating Pt ring-disk voltammograms for reduction of O_2 at pyrolytic graphite disks coated with (a) **1** and (b) **2**. Rotation rate, 100 rpm; disk current, S = 10 μA; ring current, S = 5 μA; supporting electrolyte, 0.5 M $HClO_4$–1.5 M CF_3CO_2H saturated with air.

spacer bonds) between the porphyrinic subunits, giving a cofacial binding pocket with a directed longitudinal reaction coordinate for substrate binding and activation.

Cyclic voltammograms of **1** in nitrobenzene give a single, reversible oxidative wave at +0.33 V (*vs*. AgCl/Ag), consistent with two non-interacting metal centers. The complex was screened as an electrocatalytst for the reduction of dioxygen.[14,15] Fig. 2(a) displays a rotating ring-disk voltammogram for the reduction of O_2 at a graphite electrode coated with **1**. Remarkably, **1** catalyzes the reduction of oxygen at the unusually positive potential of 0.37 V (*vs*. AgCl/Ag) with 80% of the O_2 reduction proceeding along the four-electron pathway to produce water; the longitudinal 'Pac-Man' flexibility of this molecular cleft apparently allows it to 'bite' down on the O_2 substrate resulting in efficient catalytic activation.

We sought to compare the reactivity of **1** to a dicobalt(II) cofacial complex where the bite size of the cleft is preorganized for oxygen activation. The six-membered center ring of the xanthene spacer of Co_2DPX **2**† causes the two porphyrin macrocycles to bend slightly in toward each other (Fig. 1), giving a mean interplanar distance of 3.519 Å between the two porphyrin rings,‡ which is quite similar to that found in Co_2DPB (3.381 Å).[10,11] However, the torsional twist (21.1°) between the two rings results in a metal–metal distance of 4.582 Å (Co_2DPB, 3.726 Å). The square geometry for the Co(II) cores is confirmed by the N–Co–N bond angles of 90 ± 1.7°. As observed for **1** and for other structurally characterized DPX metal complexes,[13] the two ring systems of **2** are structurally inequivalent in the solid state. The macrocycle with Co(1) exhibits a pronounced ruffled conformation with a mean deviation from planarity of 0.2227 Å, while the macrocycle containing Co(2) has a less pronounced ruffle with a mean deviation from planarity of 0.1118 Å. The more compressed structure of **2** engenders mixed-valence behavior, as two reversible electrochemical oxidations are observed at +0.28 and +0.17 V; the Co(II)/Co(III) DPX complex reacts with dioxygen in the presence of 1,5-dicyclohexylimidazole to give a 15-line EPR spectrum typical of a symmetrical biscobalt(III) superoxo complex (g = 2.02, A_{Co} = 11.14 G).[8–10] Nevertheless, **2** efficiently catalyzes the reduction of oxygen at a potential (0.38 V *vs*. AgCl/Ag) and with a selectivity for the four-electron pathway to produce water (72%) commensurate to **1** [Fig. 2(b)].

The observation that both complexes are efficient catalysts for the four-electron reduction of oxygen to water, despite their notable differences in structure and redox behavior, is striking. The results suggest that the longitudinal open-to-closed conformational change in the presence of oxygen, especially dramatic in the DPD framework, involves only a small change in conformational energy. The structure of the bisiron(III) μ-oxo complex of DPD provides further evidence of the 'Pac-Man' effect, as the framework readily closes its structure to give a complex with a compressed metal–metal distance of 3.504 Å.[12] Accordingly, the conformational flexibility of these 'Pac-Man' porphyrins provides a directed reaction coordinate for facile substrate activation and product release. With the synthetic availability of both the DPD and DPX frameworks, we are poised to incisively investigate structural and electronic effects on the small-molecule reactivity of these pillared cofacial bisporphyrins. Current studies are aimed at photoactivating the dioxygen molecule to address mechanistic issues concerning the proton-coupled O–O bond cleavage chemistry[16] of these and related complexes.

C. J. C. gratefully acknowledges the National Science Foundation for a predoctoral fellowship. We thank A. Heyduk for help with the X-ray crystallography. This work was supported by the National Institutes of Health GM 47274.

Notes and references

† Complexes **1** and **2** were prepared by metallation of the appropriate cofacial bisporphyrin with $CoCl_2$ and 2,6-lutidine in refluxing THF. X-Ray quality crystals were obtained from slow evaporation of dichloromethane/methanol solutions. *Characterization data*: **1**: $C_{76}H_{76}Co_2N_8O$: calc. C, 73.89; H, 6.20; N, 9.54; found C, 73.82; H, 6.26; N, 8.94%. HRFABMS (M^+): calc. *m*/*z* 1234.4806; found: 1234.4801. **2**: $C_{79}H_{82}Co_2N_8O$: calc. C, 74.24; H, 6.47; N, 8.77; found: C, 73.86; H, 6.42; N 8.71%. HRFABMS (M^+): calc. *m*/*z* 1276.5276; found 1276.5257.

‡ *Crystal data*: **1**: $C_{80}H_{84}Cl_2Co_2N_8O_4$, M = 1410.31, triclinic, space group $P\bar{1}$, a = 10.9872(2), b = 13.0824(2), c = 27.2127(10) Å, α = 84.68, β = 87.2850(10), γ = 71.8840(10)°, U = 3700.93(9) Å^3, Z = 2, D_c = 1.266 g cm^{-3}. A total of 15393 reflections were collected in the θ range 1.50–23.68° at 183(2) K on a Siemens SMART CCD diffractometer, of which 10494 were unique (R_{int} = 0.0334). The largest peak and hole in the difference map were 1.651 and −0.756 e Å^{-3}, respectively. The least squares refinement converged normally giving residuals of R = 0.0795, *wR*2 = 0.2186, and GOF = 1.121. **2**: $C_{79}H_{82}Co_2N_8O_2$, M = 1277.39, monoclinic, space group $C2/c$, a = 24.1310(5), b = 10.6260(2), c = 50.2717(10) Å, β = 99.5120(10)°, V = 12713.2(4) Å^3, Z = 8, D_c = 1.335 g cm^{-3}. A total of 25472 reflections were collected in the θ range 1.64–23.42° at 183(2) K, of which 9225 were unique (R_{int} = 0.1088). The largest peak and hole in the difference map were 0.445 and −0.461 e Å^{-3}, respectively. The least squares refinement converged normally giving residuals of R = 0.0829, *wR*2 = 0.1479, and GOF = 1.149.

CCDC 182/1685. See http://www.rsc.org/suppdata/cc/b0/b001620i/ for crystallographic files in .cif format

1 H. Michel, J. Behr, A. Harrenga and A. Kannt, *Annu. Rev. Biophys. Biomol. Struct.*, 1998, **27**, 329.
2 S. Ferguson-Miller and G. T. Babcock, *Chem. Rev.*, 1996, **96**, 2889.
3 J. P. Collman, M. Rapta, M. Bröring, L. Raptova, R. Schwenninger, B. Boitrel, L. Fu and M. L'Her, *J. Am. Chem. Soc.*, 1999, **121**, 1387.
4 J. P. Collman, L. Fu, P. C. Herrmann, Z. Wang, M. Rapta, M. Broring, R. Schwenninger and B. Boitrel, *Angew. Chem., Int. Ed.*, 1998, **37**, 3397.
5 J. O. Baeg and R. H. Holm, *Chem. Commun.*, 1998, 571.
6 H. C. Liang, M. Dahan and K. D. Karlin, *Curr. Opin. Chem. Biol.*, 1999, **3**, 168.
7 D. Ricard, B. Andrioletti, M. L'Her and B. Boitrel, *Chem. Commun.*, 1999, 1523.
8 C. K. Chang and I. Abdalmuhdi, *Angew. Chem., Int. Ed. Engl.*, 1984, **23**, 164.
9 C. K. Chang, H. Y. Liu and I. Abdalmuhdi, *J. Am. Chem. Soc.*, 1984, **106**, 2725.
10 J. P. Collman, J. E. Hutchinson, M. A. Lopez, A. Tabard, R. Guilard, W. K. Seok, J. A. Ibers and M. L'Her, *J. Am. Chem. Soc.*, 1992, **114**, 9869.
11 J. P. Collman, P. S. Wagenknecht and J. E. Hutchinson, *Angew. Chem., Int. Ed. Engl.*, 1994, **33**, 1537.
12 Y. Deng, C. J. Chang and D. G. Nocera, *J. Am. Chem. Soc.*, 2000, **122**, 410.
13 C. J. Chang, Y. Deng, A. F. Heyduk, C. K. Chang and D. G. Nocera, *Inorg. Chem.*, 2000, **39**, 959.
14 F. C. Anson, C. Shi and B. Steiger, *Acc. Chem. Res.*, 1997, **30**, 437.
15 M. Yuasa, B. Steiger and F. C. Anson, *J. Porphyrins Phthalocyanines*, 1997, **1**, 181.
16 R. I. Cukier and D. G. Nocera, *Annu. Rev. Phys. Chem.*, 1998, **49**, 337.

ChemComm

Synthesis and characterization of 2,6-di-*tert*-butyl-1-thio-1,4-benzoquinone, the first isolable monothio-1,4-benzoquinone

Riho Suzuki, Kouzou Matsumoto, Hiroyuki Kurata and Masaji Oda*

Department of Chemistry, Graduate School of Science, Osaka University, Toyonaka, Osaka 560-0043, Japan. E-mail: moda@chem.sci.osaka-u.ac.jp

Received (in Cambridge, UK) 26th April 2000, Accepted 14th June 2000
Published on the Web 30th June 2000

The title compound, a labile but isolable substance owing to appreciable steric protection, shows substantially higher electron affinity than the corresponding 1,4-benzoquinone and is reduced by water.

While *p*-benzoquinones have been extensively studied,[1] little has been known about the corresponding sulfur analogues. A major reason may be the general lability of thiocarbonyl compounds that makes their handling and isolation in pure form difficult.[2] Bock and co-workers have reported the pyrolytic generation and spectroscopic characterization of the parent dithio- and monothio-1,4-benzoquinones, **1** and **2**, in low temperature matrices.[3] Recently 2,6-dialkyl-4-thio-1,4-benzoquinones **3** have been generated and trapped by cycloaddition with 1,3-dienes.[4] The only isolable, related monothioquinone so far known is monothioanthraquinone **4**.[5] We have recently reported the synthesis and properties of thioquinone methides **5** in which *tert*-butyl groups give steric protection to a considerable extent.[6] Here we report the synthesis and characterization of 2,6-di-*tert*-butyl-1-thio-1,4-benzoquinone **6**, the first isolable, monothio-1,4-benzoquinone.

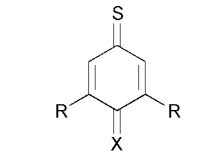

1: X = S; R = H
2: X = O; R = H
3: X = O; R = alkyl

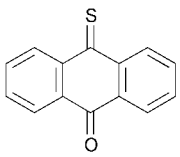

4

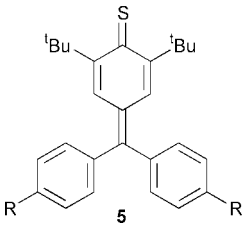

5

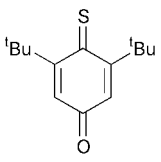

6

We have already described the generation of lithium 2,6-di-*tert*-butyl-4-lithiothiophenoxide **7** as the key synthon for **5**.[6] The exposure of a THF solution of **7** to O_2 at −70 °C followed by the usual work-up afforded bisphenol disulfide **8**† in 50% yield. A major byproduct was 2,6-di-*tert*-butylthiophenol, a reduction product. Obviously, the two *tert*-butyl groups at the *ortho*-positions are not bulky enough to hinder the coupling of the intermediate thiophenoxy radical as reported for the 2,6-di-*tert*-butylthiophenoxy radical itself.[7] The initially expected mercaptophenol **9**† was obtained by reduction of **8** with zinc powder in acetic acid (60%). The attempted oxidation of **9** to **6** with DDQ in benzene or acetone resulted, however, in the formation of **8**. We therefore expected that oxidation of **8** to its bis(phenoxy radical) **10** would cause cleavage of the rather weak disulfide bond, leading to the generation of **6**. In fact, NMR monitoring of a mixture of **8** and excess DDQ (3.5 equiv.) in deaerated benzene-d_6 in a sealed tube at room temperature gave rise to new proton signals as singlets at δ 1.14 and 6.48 and a ^{13}C signal at δ 233.45 (C=S) which are reasonable for the desired **6**. However, in spite of the use of excess DDQ, the reaction seemed to form a 2:1 equilibrium mixture of **6** and **8** probably by mediation of DDQ and its hydroquinone. Although the signals of **6** remained almost unchanged in the solution for at least two months, the attempted isolation of **6** from the mixture failed because of its lability. This failure suggests that the isolation of **6** from solutions should be difficult. In the end, the isolation of **6** in almost pure form was achieved in 70% yield by its sublimation to a water-cooled cold finger from a solid-state mixture of **8** and PbO_2 (1:30 w/w) heated at 140 °C under vacuum.

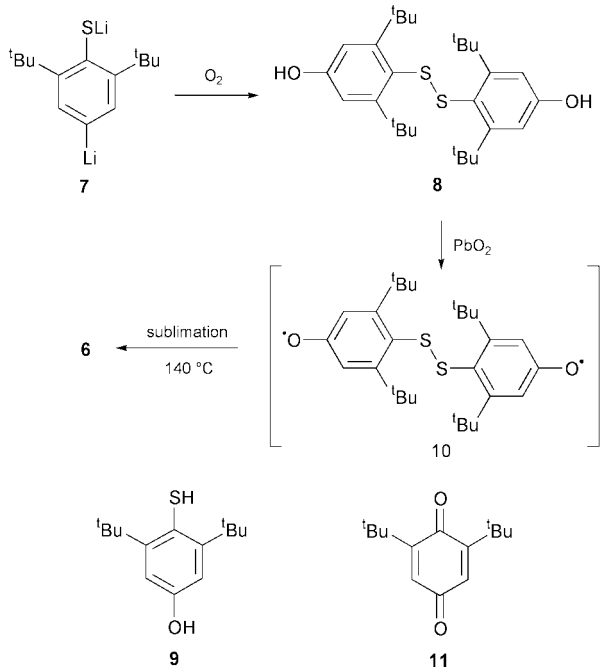

The monothiobenzoquinone **6**† thus obtained is a greenish yellow solid. Although relatively stable in the solid state as well as in neutral aprotic solvents such as benzene and acetone at room temperature, **6** is sensitive to moisture and other protic substances. The IR spectrum of **6** shows an intense carbonyl absorption at 1639 cm^{-1} and a less intense thiocarbonyl absorption (intense in the Raman spectrum) at 1141 cm^{-1}. This thiocarbonyl stretching frequency is considerably lower than that of **4** (1212 cm^{-1})[5] and even lower than the significantly dipolar 4*H*-pyran-4-thione (1168 cm^{-1}).[8] The electronic spectrum of **6** exhibits a weak absorption (ε = 32) at 758 nm, which is assignable to the n → π* transition of the thiocarbonyl group, as well as a strong absorption at 321 nm. The visible absorption of **6** is at an appreciably longer wavelength than those of **2** (500 nm)[3] and **4** (697 nm).[5] The IR and visible absorption spectral

DOI: 10.1039/b003330h

results suggest a substantial polarization of the thiocarbonyl group of **6**. In this context, a semiempirical theoretical calculation (PM3) predicts that **6** should take the boat form, due to steric congestion, with bow and stern angles of 50° and 27°, respectively. This molecular deformation from planarity could be responsible for the enhanced polarization (elongation) of the thiocarbonyl bond.

Thiocarbonyl compounds are usually more easily reduced than the corresponding carbonyl compounds.[9] Upon cyclic voltammetry, **6** shows two irreversible reduction waves at −0.60 and −1.33 V (both peak potentials *vs*. Ag/Ag^+, in 0.1 M *n*-Bu_4NClO_4–CH_3CN, ferrocene/ferrocene$^+$ = 0.10 V). These reduction potentials are about 0.5 V lower than those of 2,6-di-*tert*-butyl-1,4-benzoquinone **11** (the corresponding peak potentials: 1.07 and 1.88 V) measured under the same conditions, indicating that **6** is a substantially strong electron acceptor. Surprisingly, **6** was found to be reduced rather than hydrolysed by water: when a small amount of D_2O was added into an acetone solution of **6** either in the dark or light at room temperature, the signals of **6** at δ 1.37 (s) and 6.46 (s) disappeared within 1 h with the concurrent appearance of new signals at δ 7.00 (s), 6.93 (br s), 6.73 (br s) and 6.52 (s) in the olefinic to aromatic region. The products were identified to be monothiohydroquinone **9**, disulfide **8** and benzoquinone **11**, formed in a 45 : 50 : 5 ratio (^{1}H NMR and TLC comparison with those of the authentic samples). The formation of **8** (probably also **9**) points to the intermediate formation of the corresponding thiophenoxy radical. In addition, the ferricyanide test as a preliminary qualitative test afforded a positive result, conforming the formation of hydrogen peroxide in the solution. Thus, hydrolysis of **6** to **11** is a very minor process, different from the usually easy hydrolysis of thioketones to ketones.

In conclusion, although the two *tert*-butyl groups at the *ortho* positions are not bulky enough for steric protection, 2,6-di-*tert*-butyl-1-thio-1,4-benzoquinone **6** was synthesized as a labile but isolable compound at around room temperature and was found to show a considerably high electron affinity and to undergo an unusual reaction with water. We are now investigating the detailed chemical properties of **6**.

This work was supported by a Grant-in-Aid for Scientific Research of Special Field (No.10146102) from the Ministry of Education, Science, Sports and Culture, Japan.

Notes and references

† *Selected physical and spectroscopic data*; **6**: mp 87–88 °C; MS (EI) *m/z* 238 (M^+ + 2H, 100%), 236 (M^+, 20), 221 ($M^+ - CH_3$, 27), 180 ($M^+ - C_4H_8$, 25), 165 (M^+ − 71, 69); IR: ν (KBr)/cm^{-1} 2963 (s), 1639 (s, C=O), 1556 (m), 1456 (m), 1366 (m), 1302 (m), 1261 (m), 1232 (m), 1200 (m), 1141 (m, C=S), 1096 (m), 1072 (m), 1022 (m), 910 (m), 801 (m); δ_H (400 MHz, C_6D_6) 1.13 (s, 18H), 6.49 (s, 2H); δ_C(100 MHz, C_6D_6) 30.98, 36.87, 121.94, 163.58, 189.94 (C=O), 233.45 (C=S); UV–Vis (cyclohexane) λ_{max}/nm (ε) 321 (14 300), 456 sh, 758 (32); **8**: mp 210–213 °C; MS (EI) *m/z* 474 (M^+, 12%), 238 ($M^+/2$ + 1, 100), 181 ($M^+/2 - C_4H_9$, 16); δ_H(270 MHz, CD_2Cl_2) 1.04 (s, 18H), 1.60 (s, 18H), 4.84 (br s, 2H, OH), 6.65 (s, 2H), 6.86 (s, 2H); The NMR spectra show restricted rotation of the S–S or C–S bond with an estimated energy barrier of $\Delta G^{\ddagger}$ = 16.5 ± 0.2 kcal mol^{-1} (T_c = 75 °C in benzene); see also ref. 10; **9**: mp 124–127 °C; MS (EI) *m/z* 238 (M^+, 100%), 181 ($M^+ - C_4H_9$, 17); δ_H(270 MHz, $CDCl_3$) 1.58 (s, 18H), 3.24 (s, 1H), 4.57 (s, 1H), 6.89 (s, 2H).

1 *The Chemistry of the Quinonoid Compounds*, ed. S. Patai and Z. Rappoport, Wiley, 2nd edn., 1988.
2 M. V. Lakshmikantham, M. Levinson, M. Menachery and M. P. Cava, *J. Org. Chem.*, 1986, **51**, 411; M. V. Lakshmikantham, M. S. Raasch, M. P. Cava, S. G. Bott and J. L. Atwood, *J. Org. Chem.*, 1987, **52**, 1874.
3 H. Bock, S. Mohmand, T. Hirabayashi, G. Maier and H. P. Reisenauer, *Chem. Ber.*, 1983, **116**, 273.
4 B. Cantini, G. Capozzi, S. Menichetti and C. Nativi, *Synthesis*, 1999, 1046.
5 M. S. Raasch, *J. Org. Chem.*, 1979, **44**, 632.
6 R. Suzuki, H. Kurata, T. Kawase and M. Oda, *Chem. Lett.*, 1999, 571.
7 W. Rundel, *Chem. Ber.*, 1968, **101**, 2956.
8 Á. Somogyi, G. Jalsovszky, C. Fülop, J. Stark and J. E. Boggs, *Spectrochim. Acta, Part A*, 1989, **45**, 679.
9 J. Simonet, in *The Chemistry of Sulfur-Containing Functional Groups*, ed. S. Patai and Z. Rappoport, Wiley, 1993, pp. 440–448.
10 H. Kessler and W. Rundel, *Chem. Ber.*, 1968, **101**, 3350; N. Ueyama, T. Okamura, Y. Yamada and A. Nakamura, *J. Org. Chem.*, 1995, **60**, 4893.

ChemComm

Unique chains of alternating octahedral and tetrahedral cobalt(II) sites: crystal structures of the novel chloro-bridged complexes $[Co_4(\mu\text{-}Cl)_6Cl_2(thf)_4(MeOH)_2]_n$ and $[\{Co_4(\mu\text{-}Cl)_6Cl_2(thf)_4(H_2O)_2\}\cdot 2THF]_n$†

Jean-Cyrille Hierso,[a] Dianne D. Ellis,[b] Anthony L. Spek,[b] Elisabeth Bouwman*[a] and Jan Reedijk[a]

[a] *Leiden Institute of Chemistry, Gorlaeus Laboratories, Leiden University, PO Box 9502, 2300 RA Leiden, The Netherlands. E-mail: bouwman@chem.leidenuniv.nl*

[b] *Bijvoet Centre for Biomolecular Research, Crystal and Structural Chemistry, Utrecht University, Padualaan 8, 3584 CH Utrecht, The Netherlands*

Received (in Cambridge, UK) 20th April 2000, Accepted 7th June 2000
Published on the Web 4th July 2000

$[Co_4(\mu\text{-}Cl)_6Cl_2(thf)_4(MeOH)_2]_n$, a *catena*-polycobalt(II) complex with an unusual linear chain of octahedral/tetrahedral/octahedral cobalt sites, is obtained quantitatively from the reaction between cobalt chloride hydrate and trimethylorthoformate in THF.

Literature reports on infinite polymeric chains based on copper, manganese or cobalt, indicate the most common routes to obtaining *catena*-complexes are to use polydentate ligands as bridges between metallic units,[1–5] or to take advantage of potential intermolecular hydrogen bonding.[6] Numerous copper complexes,[2,6] and a few cobalt compounds were obtained in these ways.[1,3–5] Halide-bridged polymeric structures have also been characterised for these metals.[7] Interestingly, X-ray structure determinations describing chain-type cobalt complexes still remain scarce, apparently because these polymeric structures are difficult to grow as single crystals.[8] Of the reported structures the majority feature repeating linear chloro-bridged chains of monomeric cobalt octahedra,[7b] or elegant halide-bridged 'zigzag' chains (non-linear) as the polymeric network.[8–10] We report the isolation and structural characterisation of a new family of inorganic polymers of cobalt, showing an unprecedented chain of three different cobalt sites.

$[Co_4(\mu\text{-}Cl)_6Cl_2(thf)_4(MeOH)_2]_n$ **1** was obtained in quantitative yield from a mixture of $CoCl_2\cdot 6H_2O$ and trimethylorthoformate in tetrahydrofuran solution.‡ Crystals used for X-ray diffraction were kept under dry diethyl ether to prevent any decomposition before measurements.§ The structure of **1** consists of an infinite regular chain of three distinct successive cobalt sites (Fig. 1) connected in different ways. Co(1) and Co(3) are located on crystallographic inversion centres linked, respectively, by two and one bridging chloride ions to Co(2) centres. This creates a *repeating* pattern of tetranuclear units $[-Co(thf)_2(\mu\text{-}Cl)_2CoCl(\mu\text{-}Cl)Co(MeOH)_2(thf)_2(\mu\text{-}Cl)CoCl(\mu\text{-}Cl)_2-]$, or more simply $[Co_4(\mu\text{-}Cl)_6Cl_2(thf)_4(MeOH)_2]$. The strict asymmetric unit, from which the entire chain can be built, is formulated $[Co_2Cl_4(thf)_2(MeOH)]$. The geometry around Co(1) is octahedral having four μ-chloro bridges in equatorial sites, linked to two symmetry related Co(2) centres, and two thf molecules in axial positions, Co(1) thus being part of a $CoCl_4O_2$ chromophore. Each Co(2) centre is in a distorted tetrahedral environment made up of a terminal chloride and three μ-chloro bridges; two connected to Co(1) and the third bridged to Co(3). The bridging properties force the tetrahedral Cl(1)–Co(2)–Cl(2) angle to contract to 97.31(3)°, whilst the mono-bridged angle Cl(2)–Co(2)–Cl(4) has opened to 118.44(3)°. The coordination sphere around Co(3) consists of four oxygen donors atoms from two *trans*-thf and two *trans*-methanol molecules located at the equatorial positions. The axial positions are occupied by the bridging atoms Cl(4) producing a $CoCl_2O_4$ chromophore. The longer Co(3)–Cl(4) distances relative to Co(3)–O, result in a tetragonal *elongation* along the pseudo-four-fold axis of the Co(3) octahedral environment. The Co(1)–Cl(2) bond length is very long, 2.5488(7) Å, so that in this case a pronounced compressed octahedral geometry, *i.e.* a tetragonal *contraction* along the pseudo-four-fold axis is suggested around the Co(1) atom.

The Co–Cl bond distances are in agreement with the values reported for tetrahedral and octahedral chloride geometries in related cobalt/chloride complexes.[7,11,12] The terminal chloride on Co(2) is involved in a O–H···Cl hydrogen bond interaction to the *cis*-methanol molecule coordinated to Co(3). A closely related trinuclear cobalt chloride anion, $[Co_3Cl_8(thf)_2]^{2-}$, has recently been described.[13] The X-ray structure determination revealed three successive cobalt sites: tetrahedral/octahedral/tetrahedral each connected *via* di-μ-chloro bridges. The molecular structure of $[\{Co_4(\mu\text{-}Cl)_6Cl_2(thf)_4(H_2O)_2\}\cdot 2THF]_n$ **2**§ (Fig. 2) is very similar to **1**, except that the methanol molecules coordinated to Co(3) are replaced by water molecules, and two additional thf molecules per tetranuclear unit have cocrystallised in the lattice. The most significant difference between the two complexes involves the hydrogen bonding network; both complexes form an intramolecular OH···Cl(terminal) interaction [O(1)···Cl(3) 3.041(2) Å, O(1)–H(1)···Cl(3) 170(4)° in **1**; O(1)···Cl(3) 3.117(2) Å, O(1)–H(1B)···Cl(3) 168(3)° in **2**]. In **2** the water molecule forms an additional strong intermolecular bond with the thf molecule in the lattice. This results

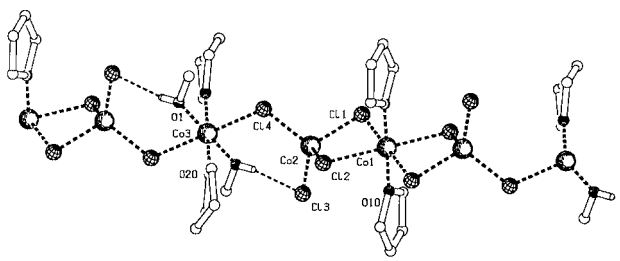

Fig. 1 Schematic representation of the crystal structure of **1**: H atoms omitted for clarity. Selected bond lengths (Å) and bond angles (°): Co(1)–Cl(1) 2.4600(6), Co(1)–Cl(2) 2.5488(7), Co(1)–O(10) 2.0381(18), Co(2)–Cl(1) 2.2918(8), Co(2)–Cl(2) 2.2861(7), Co(2)–Cl(3) 2.2533(8), Co(2)–Cl(4) 2.2898(8), Co(3)–Cl(4) 2.5049(7), Co(3)–O(1) 2.067(2), Co(3)–O(20) 2.0696(19); Cl(1)–Co(1)–Cl(2) 86.64(2), Cl(1)–Co(1)–O(10) 88.43(5), Cl(2)–Co(1)–O(10) 89.97(6), Cl(1)–Co(2)–Cl(2) 97.31(3), Cl(1)–Co(2)–Cl(3) 115.20(3), Cl(1)–Co(2)–Cl(4) 108.37(3), Cl(2)–Co(2)–Cl(3) 110.39(3), Cl(2)–Co(2)–Cl(4) 118.44(3), Cl(3)–Co(2)–Cl(4) 107.24(3), Cl(4)–Co(3)–O(1) 89.72(6), Cl(4)–Co(3)–O(20) 89.52(6), O(1)–Co(3)–O(20) 91.22(8), Co(1)–Cl(1)–Co(2) 86.29(3), Co(1)–Cl(2)–Co(2) 84.34(2), Co(2)–Cl(4)–Co(3) 119.47(3), Co(3)–O(1)–H(1) 112(3). Hydrogen bonding geometries : distances (Å), O(1)–H(1)···Cl(3) 2.33(4), O(1)···Cl(3) 3.041(2); angle (°), O(1)–H(1)–Cl(3) 170(4).

† Electronic supplementary information (ESI) available: elemental analysis, FTIR, VIS–NIR, temperature dependence of magnetic moment, data and apparatus for **1**. See http://www.rsc.org/suppdata/cc/b0/b003213l/

DOI: 10.1039/b003213l

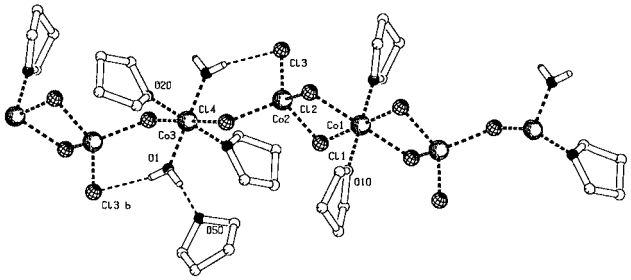

Fig. 2 Schematic representation of the crystal structure of **2**: hydrogen bonding geometries: distances (Å), O(1)–H(1B)···Cl(3) 2.36(3), O(1)···Cl(3) 3.117(2), O(1)–H(1A)···O(50) 1.81(3), O(1)···O(50) 2.625(3); angles (°), O(1)–H(1B)–Cl(3) 168(3), O(1)–H(1A)–O(50) 174(3). Bond lengths and angles generally differ from **1** by < 0.05 Å and 2° respectively, except for Cl(2)–Co(2)–Cl(4) 109.57(3)° [118.44(3)° in **1**].

in a slight contraction of the tetranuclear unit in **2** compared to **1** [intra Co(1)···Co(3) distances in the two complexes: 7.3608(2) Å for **1** and 7.0407(3) Å for **2**].

VIS–NIR spectroscopy in diffuse reflectance of **1** shows the dominance in intensity of tetrahedral coordination typical bands (a broad band at 6600 cm^{-1}, and a more intense band at 15000 cm^{-1}). The bands corresponding to an octahedral environment around cobalt are present but partially obscured (shoulders at 12000 and 19000 cm^{-1}). Temperature dependent solid-state magnetic susceptibility (χ_m) measurements on crystals of **1** were performed. The effective magnetic moment (μ_{eff}/Co_2) slowly decreases from 7.27 μ_B at 260 K to 6.91 μ_B at 80 K, and then more steeply to 4.72 μ_B at 12 K. It then increases rapidly to 6.66 μ_B at 5 K. The observed μ_B of 7.27 at 260 K is close to the spin-only value of 6.93 μ_B for a dinuclear high-spin Co^{II}_2 (S = 3) system. Octahedral and tetrahedral Co^{II} ions can behave as spin-1/2 and spin-3/2 depending on temperature and spin–orbit coupling. The temperature dependence of μ_{eff} is thus consistent with linear repeating Co^{II} dimers with S = 3/2 at higher temperatures. The decrease of μ_{eff} between 100 and 12 K is likely due to depopulation of higher Kramers levels, and the increase at 12 K is ascribed to weak ferromagnetic interactions possibly occurring between di-μ-chloro linked Co^{II}.[7a]

Previously, tetranuclear $[M_4(\mu_3\text{-}Cl)_2(\mu\text{-}Cl)_4Cl_2(thf)_6]$ species (M = Co, Fe) have been synthesised from anhydrous metal chlorides in THF, and only in the case of manganese was a polymeric compound isolated.[9] It has now been shown that cobalt in presence of THF can also form polymeric species. Compound **2** has been isolated repeatedly from attempts of recrystallisation of a cobalt chloride oxime microcrystalline powder,[14,15] in a mixture of THF–diethyl ether as solvent; experiments are ongoing to obtain the product by a more direct route. The mechanisms of formation of **2**, and especially the insertion of residual water molecules are not yet completely understood; nevertheless, we assume that the weak oxime ligands are readily replaced by water and THF molecules during the time of crystallisation. From the previous observations, it is clear that the thermodynamic driving force leading to this family of self-assembly compounds should be important. If we consider **1**, MeOH is generated *in situ* from the action of trimethylorthoformate on water following the global equation:

$$HC(OMe_3)_3 + H_2O \rightarrow 2\ MeOH + O{=}CHOMe$$

as a consequence the MeOH:THF molar ratio is *ca.* 1:20. Assuming the coordination abilities of THF and MeOH are similar, the explanation for the formation of the complex should be self-assembly likely continuously carried out in the coordination sphere of cobalt or at least in a close vicinity to the metal centres. This means that methanol molecules should be readily accessible to grow the structure, despite their poor ratio relative to THF. These two examples show that unusual self-assembly can occur even in the absence of polydentate ligands. Further studies are in progress to extend this class of compounds.

Financial support has been provided by the Dutch Ministry of Economic Affairs (BTS 98141). This work was also supported (A. L. S., D. D. E.) by the Council for Chemical Sciences of the Netherlands Foundation for Scientific Research (CW-NWO). We are grateful to Mr O. Roubeau for working on magnetic susceptibilities measurements. We thank Dr S. T. Warzeska, Mr A. Eikelboom and Dr J. Bieleman for fruitful discussions.

Notes and references

‡ Although the synthesis can be carried out in air, experiments under inert atmosphere using Schlenk techniques and a vacuum line ensure the protection of the sensitive final product. To 0.2 g (0.85 mmol) of $CoCl_2{\cdot}6H_2O$ was added an excess of trimethylorthoformate (1.5 ml). The mixture was gently heated (50 °C) in 15 ml of THF until complete dissolution of the solid. After cooling to ambient temperature for 30 min, the deep blue solution was evaporated to dryness resulting in a shiny blue powder which is very moisture sensitive (0.17 g, 0.39 mmol, yield 92%). From a diethyl ether–tetrahydrofuran two layer recrystallisation, nice shiny blue prisms suitable for X-ray diffraction can be obtained after a few hours.

§ Data were collected on a Nonius Kappa CCD area detector, using Mo-Kα radiation with a graphite monochromator (λ = 0.71073 Å), on a rotating anode at 150 K. Lorentz polarisation and absorption corrections were applied in both instances. Refinement was carried out using full-matrix least squares on F^2 (SHELXL-97).

Crystal data: for **1**: $C_9H_{20}Cl_4O_3Co_2$, M_r = 435.91, monoclinic, space group $P2_1/c$ (no. 14), a = 10.9390(3), b = 12.1510(4), c = 12.6313(3) Å, β = 103.068(2)°, V = 1635.47(8) Å^3, F(000) = 880, Z = 4, μ(Mo-Kα) = 2.677 mm^{-1}. 15654 reflections measured, 3728 independent, R_{int} = 0.0501. Refinement converged at $wR2$ value of 0.0682, $R1$ = 0.0330 [for 2975 reflections with $F_o > 4\sigma(F_o)$].

For **2**: $C_8H_{18}Cl_4O_3Co_2{\cdot}C_4H_8O$: M_r = 493.99, triclinic, space group $P\bar{1}$ (no. 2), a = 8.6714(3), b = 10.8418(3), c = 11.8514(5) Å, α = 76.563(2), β = 77.804(2), γ = 68.245(2)°, V = 996.81(6) Å^3, F(000) = 504, Z = 2, μ(Mo-Kα) = 2.210 mm^{-1}. 10959 reflections measured, 4520 independent, R_{int} = 0.0381. Refinement converged at $wR2$ value of 0.0651, $R1$ = 0.0314 [for 3674 reflections with $F_o > 4\sigma(F_o)$].

CCDC 182/1676. See http://www.rsc.org/suppdata/cc/b0/b003213l/ for crystallographic files in .cif format.

1 G. R. Clark and G. J. Palenik, *Cryst. Struct. Commun.*, 1979, **8**, 261; S. I. Al-Resayes, P. B. Hitchcock and J. F. Nixon, *J. Chem. Soc., Chem. Commun.*, 1991, 78.
2 See, for example: E. Bouwman, P. Evans, R. A. G. de Graaff, H. Kooijman, R. Poinsot, P. Rabu, J. Reedijk and A. L. Spek, *Inorg. Chem.*, 1995, **34**, 6302; X.-M. Chen, X.-L Feng, X.-L. Yu and T. C. W. Mak, *Inorg. Chim. Acta*, 1997, **266**, 121; G. A. van Albada, R. C. Guijt, J. G. Haasnoot, M. Lutz, A. L. Spek and J. Reedijk, *Eur. J. Inorg. Chem.*, 2000, 121 and references therein.
3 D. Poleti and L. Karanović, *Acta Crystallogr., Sect. C*, 1989, **45**, 1002.
4 G. Smith, D. E. Lynch, T. C. W. Mak, W.-H. Yip and C. H. L. Kennard, *Polyhedron*, 1993, **12**, 203.
5 W. L. Driessen and T. X. Neenan, *Acta Crystallogr., Sect. C*, 1996, **52**, 59.
6 See for example: M. M. Chowdhry, D. M. P. Mingos, A. J. P. White and D. J. Williams, *Chem. Commun.*, 1996, 899; M. Munakata, L. P. Wu, M. Yamamoto, T. Kuroda-Sowa and M. Maekawa, *J. Am. Chem. Soc.*, 1996, **118**, 3117 and references therein.
7 For a review see: (*a*) W. E. Hatfield, W. E. Estes, W. E. Marsh, M. W. Pickens, L. W. der Haar and R. R. Weller, *Extended Linear Chain Compounds*, ed. J. S. Miller, Plenum Press, New York, 1982, vol. 3, p. 89; (*b*) D. B. Losee, J. N. McElearney, G. E. Shankle, R. L. Carlin, P. J. Cresswell and W. T. Robinson, *Phys. Rev. B*, 1973, **8**, 2185.
8 F. S. Keij, R. A. G. de Graaff, J. G. Haasnoot, A. J. Oosterling, E. Pedersen and J. Reedijk, *J. Chem. Soc., Chem. Commun.*, 1988, 424.
9 P. Sobota, Z. Olejnik, J. Utko and T. Lis, *Polyhedron*, 1993, **12**, 613; P. Sobota, J. Utko and L. B. Jerzykiewicz, *Inorg. Chem.*, 1998, **37**, 3428.
10 B. W. Dockum and W. M. Reiff, *Inorg. Chem.*, 1982, **21**, 391; B. W. Dockum, G. A. Eisman, E. H. Witten and W. M. Reiff, *Inorg. Chem.*, 1983, **22**, 150.
11 P. T. Moseley and H. M. M. Shearer, *J. Chem. Soc., Dalton Trans.*, 1973, 61.
12 N. Thorup and H. Soling, *Acta Chem. Scand.*, 1969, **8**, 2933; A. Herweijer, W. J. M. de Jonge, A. C. Botterman, A. L. M. Bongaarts and J. A. Cowen, *Phys. Rev. B*, 1973, **8**, 2185.
13 C. von Hänisch, D. Fenske, F. Weigend and R. Ahlrichs, *Chem. Eur. J.*, 1997, **3**, 1494.
14 Results to be published.
15 J.-C. Hierso, D. D. Ellis, A. L. Spek, E. Bouwman and J. Reedijk, *Eur. J. Inorg. Chem.*, submitted.

ChemComm

Guest-dependent novel photochromism of 7-bromo-1,4,8-triphenyl-2,3-benzo[3.3.0]octa-2,4,7-trien-6-one in its inclusion crystals

Koichi Tanaka,*[a] Tomoyuki Watanabe[a] and Fumio Toda[b]

[a] *Department of Applied Chemistry, Faculty of Engineering, Ehime University, Matsuyama, Ehime 790-8577, Japan. E-mail: tanaka@en3.ehime-u.ac.jp*

[b] *Department of Chemistry, Faculty of Science, Okayama University of Science, 1-1 Ridai-cho, Okayama 700-0005, Japan*

Received (in Cambridge, UK) 18th May 2000, Accepted 14th June 2000
Published on the Web 4th July 2000

Inclusion crystals of 7-bromo-1,4,8-triphenyl-2,3-benzo[3.3.0]octa-2,4,7-trien-6-one (1) showed a reversible color change from yellow to green on exposure to UV-light, and this depends on the guest molecules present.

Organic photochromic compounds have received considerable attention in recent years due to their potential applications such as information storage, electronic display systems, optical switching devices, ophthalmic glasses, and so on.[1] Several types of organic photochromic compounds such as naphthopyrans, spiropyrans, fulgides (dialkylidenesuccinic anhydrides), anils (*N*-phenyl imines), hydrazones, stilbenes, and diarylethenes have been discovered and their properties investigated.[2] Recently, we have reported the novel photochromism of crystalline biindenylidene, which shows a reversible color change from yellow to reddish-purple upon photoirradiation.[3] We have now found that the title compound **1**[4] forms inclusion complex crystals with various kinds of organic guest molecules and some of these inclusion crystals show a reversible color change from yellow to green upon photoirradiation in the solid state (Scheme 1). It was also found that the stability of the photochromism depends on the type of guest molecule included. This is the first example of guest-dependent photochromism in host–guest inclusion crystals.

When a mixture of **1** and various kinds of guest compounds was recrystallized from AcOEt solution, inclusion complex crystals of **1** were obtained† (Table 1). Some of these inclusion crystals show a reversible color change from yellow to green upon photoirradiation in the solid state, although **1** itself does not show any photocoloration. For example, upon photoirradiation yellow crystals of the 2 : 1 inclusion compound of **1** with *p*-dimethoxybenzene turned green. These crystals revert to yellow on storage in the dark for 6 h at room temperature or quickly on heating at 60 °C. The UV spectral change of the 2 : 1 inclusion crystals is shown in Fig. 1. Similarly, the inclusion crystals with acetone (1 : 1), butan-2-one (1 : 1), cyclopentanone (1 : 1), cyclohexanone (1 : 1), dioxane (1 : 1), carbon tetrachloride (1 : 1), 1,1-dichloroethane (1 : 1), 1,1,2,2-tetrachloroethane (1 : 1), benzene (1 : 1), *o*-xylene (1 : 1), *p*-xylene (2 : 1), anisole (2 : 1), *m*-dimethoxybenzene (2 : 1) and 2-picoline (1 : 1) showed photochromism in the solid state. Interestingly, the photochromism of the inclusion crystals of **1** was very sensitive to the structure of the guest compounds. For example, cyclopentanone shows photochromism, while pentan-3-one does not. Similar structural effects were observed in the following cases: dioxane *vs*. tetrahydropyran, 1,1-dichloroethane *vs*. 1,2-dichloroethane, *o*-dimethoxybenzene *vs*. *m*- and *p*-dimethoxybenzene and 2-picoline *vs*. 3- and 4-picoline. An electronic effect of the guest compounds may be important, because the dimethoxybenzene derivatives as guest showed photochromism, while dichlorobenzene derivatives did not (Table 1).

It is also remarkable that the stability of the photochromism depends on the type of guest molecule. For example, the bleaching times of the green color which developed upon photoirradiation of the various inclusion crystals of **1** were 3 h (benzene), 4 h (cyclopentanone), 5 h (2-methylpyridine), 6 h (*p*-dimethoxybenzene), 9 h (*m*-dimethoxybenzene), 10 h (cyclohexanone and 1,1-dichloroethane), 12 h (anisol and *o*-xylene), 24 h (*p*-xylene), 164 h (butan-2-one), and 504 h (acetone and dioxane), respectively.

The solid-state IR spectrum of the green crystals was identical with that of the yellow crystals, and no EPR signal developed upon photoirradiation. The photochromic properties of **1** are probably due to π–π interactions owing to its suitable molecular packing in the inclusion crystals, because photoirradiation of **1** in solution did not show any photochromic properties. Further detailed studies of the relationship between crystal structures and photochromic properties of the inclusion complexes of **1** are in progress.

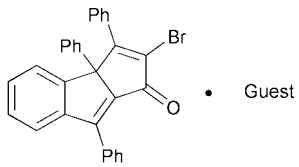

1

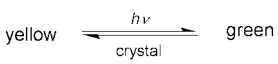

Scheme 1

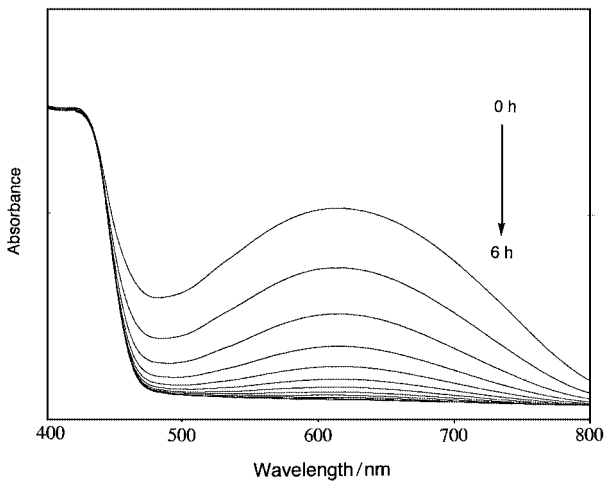

Fig 1 UV spectral changes of the 1 : 1 inclusion complex of **1** with *p*-dimethoxybenzene in the solid state. Successive measurements were recorded every 30 min from the top (after irradiation) to the bottom (after keeping 6 h in the dark).

DOI: 10.1039/b004007j

Table 1 Inclusion complex of **1** (host : h) with various guest (g) compounds

Guest	h : g[a]	Photochromism	Bleaching time/h	Guest	h : g[a]	Photochromism	Bleaching time/h
Acetone	1 : 1	yes	504		1 : 1	no	
Butan-2-one	1 : 1	yes	164				
Pentan-3-one	1 : 1	no			1 : 1	no	
	1 : 1	yes	4				
	1 : 1	yes	10		1 : 1	no	
	1 : 1	no		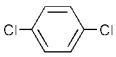	1 : 1	no	
	1 : 1	no		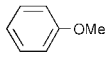	2 : 1	yes	12
	1 : 1	yes	504	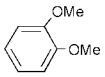	2 : 1	no	
CH_2Cl_2	1 : 1	no		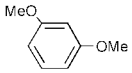	2 : 1	yes	9
$CHCl_3$	1 : 1	no					
CCl_4	1 : 1	yes	9	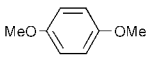	2 : 1	yes	6
CH_3CHCl_2	1 : 1	yes	10				
CH_2ClCH_2Cl	1 : 1	no			1 : 1	no	
$CHCl_2CHCl_2$	1 : 1	yes	10				
	1 : 1	yes	3		1 : 1	yes	5
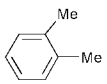	1 : 1	yes	12		2 : 1	no	
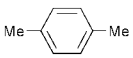	2 : 1	yes	24	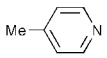	1 : 1	no	

[a] The host : guest ratios were determined by TG, NMR and elemental analysis.

Notes and references

† Representative procedure for preparation of inclusion crystals and measurement of the diffuse reflectance UV spectra: When a mixture of **1**[4] and *p*-dimethoxybenzene was recrystallized from ethyl acetate in the dark, a 2 : 1 inclusion crystal of **1** and *p*-dimethoxybenzene was obtained as pale yellow prisms (mp 165–169 °C). The colored inclusion crystals were developed by photoirradiation with a high-pressure Hg lamp through a Pyrex filter for 10 min under aerobic conditions, and their diffuse reflectance UV spectra monitored by using a Shimadzu MPS-2000 spectrophotometer.

1 B. V. Gemert, in *Organic Photochromic and Thermochromic Compounds*, ed. J. C. Crano and R. J. Guglielmetti, Plenum Press, New York, 1999.

2 H. Yoshikawa and S. Nishikiori, *Chem. Lett.*, 2000, 142; M. Nanasawa, M. Miwa, M. Hirai and T. Kuwabara, *J. Org. Chem.*, 2000, **65**, 593; L. Dinescu and Z. Y. Wang, *Chem. Commun.*, 1999, 2497; S. Kobatake, M. Yamada, T. Yamada and M. Irie, *J. Am. Chem. Soc.*, 1999, **121**, 2380 and 8450; T. Arai and M. Ikegami, *Chem. Lett.*, 1999, 965; H. Kurata, T. Tanaka and M. Oda, *Chem. Lett.*, 1999, 749; S. Delbaere, B. L-Houze, C. Bochu, Y. Teral, M. Campredon and G. Vermeersch, *J. Chem. Soc., Perkin Trans 2*, 1998, 1153; Y. Eichen, J.-M. Lehn, M. Scherl, D. Haarer, J. Fischer, A. DeCian, A. Corval and P. Trommsdorff, *Angew. Chem., Int. Ed. Engl.*, 1995, **34**, 2530; H. Koyama, T. Kawato, H. Kanatomi, H. Hatsushita and K. Yonetani, *J. Chem. Soc., Chem. Commun.*, 1994, 579; V. Amarendra and K. Venkatesan, *J. Chem. Soc., Perkin Trans. 2*, 1991, 829; Y. Mori, Y. Ohashi and K. Maeda, *Bull. Chem. Soc. Jpn.*, 1989, **62**, 3171; H. Kamogawa and T. Suzuki, *J. Chem. Soc., Chem. Commun.*, 1985, 525; S. D. Cox, C. W. Dirk, F. Moraes, D. E. Wellman, F. Wudl, M. Soltis and C. Strouse, *J. Am. Chem. Soc.*, 1984, **106**, 7131; K. Ichimura and S. Watanabe, *Bull. Chem. Soc. Jpn.*, 1976, **49**, 2220.

3 K. Tanaka and F. Toda, *J. Chem. Soc., Perkin Trans. 1*, 2000, 873.

4 F. Toda, M. Sasaoka, Y. Todo, K. Iida, T. Hino, Y. Nishiyama, H. Ueda and T. Oshima, *Bull. Chem. Soc. Jpn.*, 1983, **56**, 3314.

Selective hydroformylation of *N*-allylacetamide in an inverted aqueous two-phase catalytic system, enabling a short synthesis of melatonin†‡

Göran Verspui, Guido Elbertse, Frank A. Sheldon, Michiel A. P. J. Hacking and Roger A. Sheldon*

Delft University of Technology, Laboratory for Organic Chemistry and Catalysis, Julianalaan 136, NL-2628 BL Delft, The Netherlands. E-mail: r.a.sheldon@tnw.tudelft.nl

Received (in Liverpool, UK) 5th May 2000, Accepted 13th June 2000
Published on the Web 4th July 2000

Water increases the selectivity in the Rh–phosphine catalysed hydroformylation of *N*-allylacetamide; an aqueous–organic biphasic system, containing a hydrophobic Rh-catalyst, provided facile catalyst/product separation, after which the aqueous product phase could be used in a one-pot synthesis of *N*-acetyl-5-methoxytryptamine (melatonin).

Olefin hydroformylation is one of the most commercially important reactions that makes use of a homogeneous catalyst.[1] Rh–phosphine complexes are active catalysts for this reaction with high selectivities towards linear aldehydes and a number of successful methods for the recycling of these catalysts have been developed.[2] Unfortunately, the feedstock is mainly restricted to linear, non-functionalised α-olefins, such as propene, styrene, *etc*.

Aldehydes bearing various functional groups are widely applied in the synthesis of, for example, flavours, fragrances and pharmaceuticals.[3] Their preparation by hydroformylation of a hetero-atom functionalised olefin, however, is not straightforward since these substrates react slowly, require high catalyst loadings and harsh reaction conditions, which leads to the formation of condensation products, such as acetals, hemiacetals, imines, *etc*.[4]

In connection with an alternative synthesis of *N*-acetyl-5-methoxytryptamine (melatonin), a human hormone which regulates sleep,[5] we required 4-acetamidobutanal. When combined with 4-methoxyphenylhydrazine this aldehyde affords an intermediate hydrazone, which in the presence of an acid undergoes a Fischer-indole reaction (Scheme 1).[6] 4-Acetamidobutanal was previously prepared by hydroformylation of *N*-allylacetamide in THF using 1% of $HRh(CO)(PPh_3)_3$.[7] After 18 h at 80 °C and 83 bar ($CO:H_2 = 1:1$), a conversion of 76% was reached with the product distribution: 4-acetamidobutanal (11%), 3-acetamido-2-methylpropanal (63%), *N*-acetylpyrrolidine (13%) and 2-formyl-*N*-acetylpyrrolidine (13%).

We found that the $Rh–PPh_3$ catalysed hydroformylation of *N*-allylacetamide gave the best results in a polar, protic solvent, such as methanol. Since *N*-allylacetamide is also soluble in water, we decided to carry out the hydroformylation in a one-phase aqueous medium, employing the water-soluble Rh–tppts catalyst (tppts = $P(C_6H_4$-*m*-$SO_3Na)_3$). To our surprise we found that the reaction proceeded smoothly under mild conditions. At 70 °C and a 10 bar pressure of a H_2–CO (1:1) mixture, the reaction was completed in 45 min using as little as 0.04% catalyst (Table 1, Exp. 2), with an initial rate of 3891 turnovers h^{-1}. The isomeric aldehydes were obtained in 99% selectivity. It was demonstrated by Mortreux and co-workers previously that the hydroformylation of acrylesters, such as methylacrylate, into their α- and β-formylesters also proceeds at a faster rate in a toluene–water two-phase system, employing the Rh–tppts catalyst, compared to the rate of $Rh–PPh_3$ in toluene alone (initial TOF = 545 *vs*. 225 h^{-1} (50 °C, 50 bar)).[8]

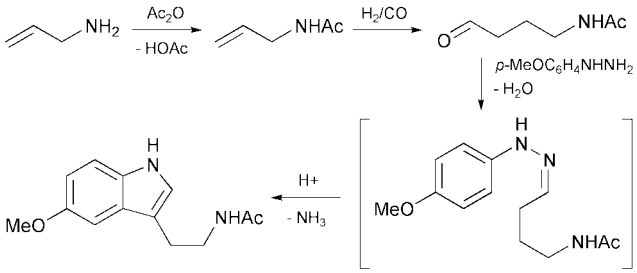

Scheme 1 Alternative synthesis of *N*-acetyl-5-methoxytryptamine.

In a series of $MeOH–H_2O$ mixtures we found that both the reaction rate and the selectivity towards the aldehydes increased with the water content. A direct comparison of the two catalysts in neat MeOH showed that $Rh–PPh_3$ is slightly more active than Rh–tppts and yields a product mixture with a slightly higher linear/branched (l/b) ratio (1.15 *vs*. 1.05, Table 1). The rather low regioselectivity compared to non-functionalised linear olefins, such as propene (l/b = 23),[2] suggests that coordination of the amide may take place during the insertion of the olefin into the Rh–hydride bond. The possible formation of a 6-membered chelate ring (Scheme 2) is expected to enhance the formation of the branched aldehyde.

† Catalytic conversions in water, part 18. (Part 17: G. J. ten Brink, I. W. C. E. Arends and R. A. Sheldon, *Science*, 2000, **287**, 1636.)
‡ Experimental details are available as electronic supplementary information (ESI). See http://www.rsc.org/suppdata/cc/b0/b003715j/

Table 1 The hydroformylation of *N*-allylacetamide in organic, aqueous and biphasic media

Exp.[a]	Catalyst	Solvent	Time/min	Conv./%	Yield/%	1/b ratio	TOF[f]/h^{-1}
1	$Rh–PPh_3$	MeOH	180	98.6	92.3	1.15	1342
2	Rh–tppts	H_2O	45	98.9	97.9	1.30	3891
3	Rh–tppts	$MeOH–H_2O$[d]	120	99.9	95.3	1.09	1459
4	Rh–tppts	MeOH	180	99.9	93.4	1.05	1239
5	Rh–tppts	Toluene–H_2O[e]	60	97.4	96.8	1.34	2946
6	$Rh–PPh_3$	Toluene–H_2O[e]	270	81.6	80.2	1.54	578
7[b]	Rh–Xantphos	Toluene–H_2O[e]	1320	26.4	24.4	20.0	31
8[c]	Rh–Xantphos	Toluene–H_2O[e]	600	99.6	96.4	15.3	177

[a] Reaction conditions: 0.010 mmol $Rh(acac)(CO)_2$, 0.25 mmol ligand, 25 mmol *N*-allylacetamide, 70 °C, 10 bar H_2O–CO (1/1), 1000 rpm, 125 ml total reaction volume. [b] 0.010 mmol [$Rh(acac)(CO)_2$], 0.050 mmol Xantphos. [c] 0.050 mmol [$Rh(acac)(CO)_2$], 0.250 mmol Xantphos, 90 °C. [d] $MeOH–H_2O$ = 1/1 (v/v), 125 ml total. [e] 100 ml toluene, 100 ml H_2O. [f] TOF = initial turnover frequency in mol aldehyde per mol catalyst per hour.

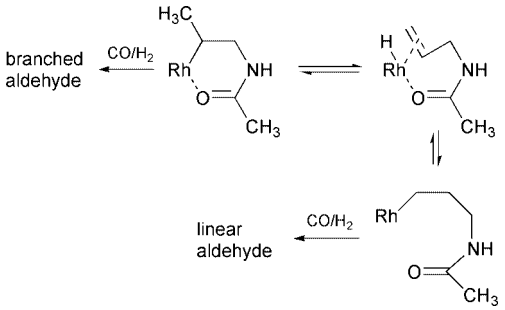

Scheme 2 Proposed intermediates in the Rh/tppts catalysed hydroformylation of *N*-allylacetamide.

The high partition coefficients of 4-acetamidobutanal and 3-acetamido-2-methylpropanal in the water layers forestalled our attempts to extract them from the aqueous reaction mixtures with an organic solvent. Especially in the synthesis of pharmaceuticals the presence of traces of heavy metals is undesirable. In order to achieve efficient product/catalyst separation, we turned to an 'inverse two-phase catalyst system', containing the hydrophobic Rh–PPh_3 catalyst in a toluene–water mixture. In such a system the catalyst remains dissolved in the organic phase, while the products will move to the water layer; the opposite of standard aqueous biphasic catalysis.

In the biphasic system, the Rh–PPh_3 catalysed reaction (Exp. 6) proceeded considerably slower compared to Rh–tppts (Exp. 5), consistent with our observation (see above) that the reaction rate decreases when the hydroformylation is carried out in an apolar solvent, such as toluene. In addition, due to mass transfer limitations, the reaction rate decreased substantially after *ca.* 50% conversion (see Fig. 1). Such a decrease was less pronounced in the case of Rh–tppts, that operates in the aqueous layer, where the substrate concentration remains sufficiently high, resulting in a zero-order reaction profile until *ca.* 80% conversion. Nevertheless, due to the presence of water, the selectivity towards the aldehydes remained high (98%, Exp. 6) and the Rh–PPh_3 catalyst could conveniently be separated from the aqueous product phase.

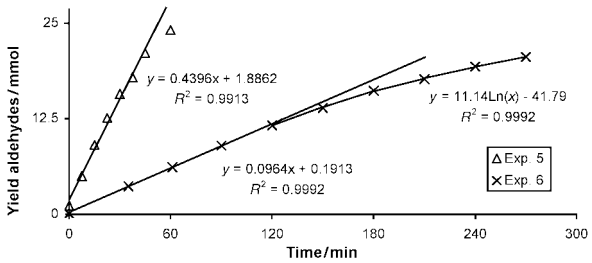

Fig. 1 Reaction profiles of Exp. 5 and Exp. 6.

To increase the regioselectivity towards the linear aldehyde, generally, rigid diphosphine ligands with a large bite angle are used.[9] We tested the Rh–Xantphos combination[10] (Xantphos = 4,5-bis(diphenylphosphino)-9,9-dimethylxanthene) in our inverted two-phase system and, indeed, the l/b ratio increased to 20. The reaction rate, however, decreased dramatically to 31 h^{-1} (Table 1, Exp. 7). At 90 °C, in the presence of 0.2% catalyst, a nearly quantitative conversion was reached in 10 h reaction time with a small compromise in the l/b ratio. The organic catalyst phase could be recycled in 5 consecutive runs without loss in activity. Rh-analysis of the water layers by means of atomic absorption spectrometry confirmed a quantitative (> 99%) catalyst/product separation.

N-Acetyl-5-methoxytryptamine was subsequently prepared in a one-pot procedure starting from allylamine (see ESI). By successive acetylation of allylamine, selective hydroformylation, hydrazone formation with 4-methoxyphenylhydrazine (HCl salt) and a Fischer indole reaction, melatonin was isolated from the aqueous reaction mixture in 44% yield (not optimised).

In conclusion, we have demonstrated that the hydroformylation of *N*-allylacetamide proceeds smoothly in a one-phase aqueous medium, as well as in an aqueous–organic two-phase protocol under mild reaction conditions. Although we could not take full advantage of the rate accelerating effect of water in the inverted two-phase catalyst system, the linear aldehyde was obtained in high selectivity and efficient catalyst/product separation was achieved. The organic soluble catalyst was recycled and the aqueous product phase was applied without purification in the synthesis of *N*-acetyl-5-methoxytryptamine. Mechanistic details and the scope of the inverted two-phase system are currently under investigation.

We thank Dr G. Papadogianakis and Dr G. Besenyei for the fruitful discussions and Mr J. Padmos for the Rh-analysis. Financial support by NWO-CW is also gratefully acknowledged.

Notes and references

1 K. Weissermel and H. J. Arpe, *Industrial Organic Chemistry, 3rd edn.* VCH, Weinheim, 1997; *Applied Homogeneous Catalysis with Organometallic Compounds*, ed. B. Cornils and W. A. Herrmann, vol. 1, VCH, Weinheim, 1996.

2 E. G. Kuntz, *CHEMTECH*, 1987, 570; Y. Chauvin, L. Mussmann and H. Olivier, *Angew. Chem., Int. Ed. Eng.*, 1995, **34**, 2698; I. T. Horváth, G. Kiss, R. A. Cook, J. E. Bond, P. A. Stevens, J. Rabai and E. J. Mozeleski, *J. Am. Chem. Soc.*, 998, **120**, 3133; E. Lindner, T. Schneller, F. Auer and H. A. Mayer, *Angew. Chem., Int. Ed. Eng.*, 1999, **38**, 2155.

3 H. H. Szmant, *Organic building blocks of the chemical industry*, Wiley, New York, 1989; *Ullmann's Encyclopedia of Ind. Chem.*, Vol. A11, VCH, Weinheim, Germany, p. 141.

4 C. Botteghi, R. Ganzerla, M. Lenarda and G. Moretti, *J. Mol. Catal.*, 1987, **40**, 129; P. Eilbracht, L. Bärfacker, C. Buss, C. Hollmann, B. E. Kitsos-Rzychon, C. L. Kranemann, T. Rische, R. Roggenbuck and A. Schmidt, *Chem. Rev.*, 1999, **99**, 3329.

5 H. M. Hugel and D. J. Kennaway, *Org. Prep. Proced. Int.*, 1995, **27**, 1.

6 W. Marais and C. W. Holzapfel, *Synth. Commun.*, 1998, **28**, 3681.

7 I. Ojima and Z. Zhang, *J. Org Chem.*, 1988, **53**, 4422; I. Ojima and Z. Zhang, *J. Organomet. Chem.*, 1991, **417**, 253; I. Ojima, A. Korda and W. R. Shay, *J. Org. Chem.*, 1991, **56**, 2024; I. Ojima, Z. Zhang, A. Korda, P. Ingallina and N. Clos, *Adv. Chem.*, 1991, **56**, 278; see also: S. Sato, M. Takesada and H. Wakamatsu, *Nippon Kagaku Zasshi*, 1969, **90**, 579; Y. Becker, A. Eisenstadt and J. K. Stille, *J. Org. Chem.*, 1980, **45**, 2145.

8 G. Fremy, E. Monflier, J. F. Carpentier, Y. Castanet and A. Mortreux, *Angew. Chem., Int. Ed. Engl.*, 1995, **34**, 1474.

9 For the hydroformylation of functionalised olefins in THF: G. D. Cuny and S. L. Buchwald, *J. Am. Chem. Soc.*, 1993, **115**, 2066.

10 M. Kranenburg, Y. E. M. van der Burgt, P. C. J. Kamer, P. W. N. M. van Leeuwen, K. Goubitz and J. Fraanje, *Organometallics*, 1995, **14**, 3081.

ChemComm

Theanaphthoquinone, a novel pigment oxidatively derived from theaflavin during tea-fermentation

Takashi Tanaka, Yayoi Betsumiya, Chie Mine and Isao Kouno*

School of Pharmaceutical Sciences, Nagasaki University, 1-14 Bunkyo-machi, Nagasaki 852-8521, Japan. E-mail: ikouno@net.nagasaki-u.ac.jp

Received (in Cambridge, UK) 2nd May 2000, Accepted 15th June 2000
Published on the Web 4th July 2000

Treatment of a mixture of epicatechin and epigallocatechin with extracts of fresh tea leaf or banana fruit generated a new pigment named theanaphthoquinone, which has a 1,2-naphthoquinone moiety oxidatively derived from the benzotropolone unit of theaflavin.

Theaflavins and thearubigins are major pigments of black tea and it is generally accepted that these are formed from flavan-3-ols (catechin) during tea fermentation.[1] Although structures and biogenesis of theaflavins having a benzotropolone unit are well studied, little is known about thearubigins despite many spectroscopic and chemical studies on these heterogeneous polymers.[2] Biochemical studies on tea fermentation indicated that oxidation of theaflavins might participate in thearubigin formation.[1]

For the purpose of clarification of the oxidative metabolism of flavan-3-ols in tea fermentation and characterization of thearubigins, a mixture of (−)-epicatechin (EC) and (−)-epigallocatechin (EGC), the major flavan-3-ols of tea leaf, was treated with aqueous extract of fresh tea leaf (*Camellia sinensis* var. *sinensis*). Prior to the reaction, almost all flavan-3-ols in the tea extract were removed by homogenization with Polyclar AT and subsequent filtration.[3] Analysis of the reaction mixture by HPLC equipped with a photodiode-array detector showed accumulation of theaflavin (**2**) at the initial stage (5 h). Subsequently, a peak due to an unknown product (**1**) having an absorption maximum at 440 nm appeared (10–20 h). Although an attempt to isolate **1** from the reaction mixture failed owing to the presence of many minor products, we found that **1** and **2** were also synthesized in a similar reaction using banana fruit instead of tea leaves.

Separation of **1** and **2** from the reaction mixture treated with banana fruit was much easier than that in the tea leaf experiment (isolation yield from EGC: **1**, 16%; **2**, 39%).[4] Extracts of apple, potato, sweet potato, persimmon and black mushroom were also examined and found to be capable of synthesizing **2**; however, **1** was not detected in their reaction mixtures.

Structure elucidation of the dark yellow pigment **1**, named theanaphthoquinone, was as follows: ^{1}H and ^{13}C NMR spectra[5] resembled those of **2** and showed signals arising from two sets of A and C rings of flavan-3-ols. The ^{13}C NMR spectrum indicated the presence of two conjugated carbonyl groups [δ_C 180.62 (C-a) and 183.38(C-b)] and 8 sp^2 carbons besides those of the A and C rings. The HMBC correlation[6] of these carbons with three aromatic protons [δ_H 6.789 (H-c), 7.327 (H-g), 7.441(H-e)] and H-2 (δ_H 5.377) and H-2′ (δ_H 5.163) of the two C-rings revealed the presence of a 1,2-naphthoquinone structure. In addition, the appearance of a signal due to a phenolic hydroxy group at very low field (δ_H 12.28) indicated an intramolecular H bond with one of the C=O groups. The negative FABMS showed a pseudo-molecular ion peak at *m/z* 535, which was two mass units larger than that expected (*m/z* 533 [M − H]$^-$), and probably arose from a reduction product of **1**, because similar phenomena are known for some quinones with low redox potentials.[7] The final confirmation for the structure was made by condensation with *o*-phenylenediamine affording a phenazine derivative **1a** (*m/z* 605 [M − H]$^-$) and its spectral analysis (Scheme 1).[8]

1 and **2** were not detected when EC and EGC were treated separately with banana extract, and it was clear that **2** was

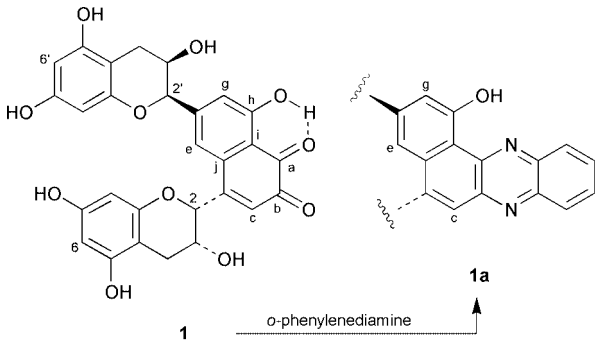

Scheme 1

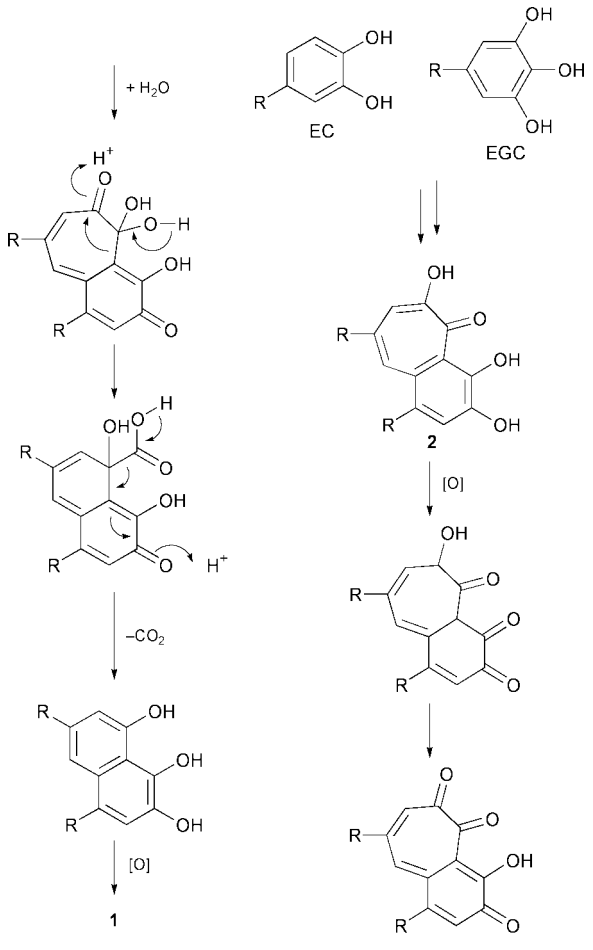

Scheme 2

DOI: 10.1039/b003510f

synthesized from a combination of EC and EGC.[1] Therefore, it is suggested that **1** is biosynthesized from **2** with the aid of polyphenol oxidase as shown in Scheme 2. The discovery of **1**, the first pigment generated by oxidation of **2**, is of great interest from the viewpoint of food manufacturing. In addition, a prolonged experiment using tea leaf extract until 30 h showed a decrease of **1** and **2** and an increase of polymeric substances, since only a broad peak was detected on HPLC analysis, suggesting that **1** was further metabolized during tea fermentation and might be related to thearubigin formation.

This work was supported by a Grant-in-aid for Scientific Research No. 12680594 from the Japan Society for the Promotion of Science.

Notes and references

1 A. P. Davies, C. Goodsall, Y. Cai, A. L. Davis, J. R. Lewis, J. Wilkins, X. Wan, M. N. Clifford, C. Powell, A. Parry, A. Thiru, R. Safford and H. E. Nursten, in *Plant Polyphenols 2: Chemistry, Biology, Pharmacology, Ecology*, ed. G. G. Gross, R. W. Hemingway and T. Yoshida, Kluwer Academic/Plenum Publishers, 1999, p. 697.

2 T. Ozawa, M. Kataoka, K. Morikawa and O. Negishi, *Biosci. Biotech. Biochem.*, 1996, **60**, 2023.

3 Fresh tea leaves (30 g) were homogenized with 150 ml of water in the presence of Polyclar AT (10g). After filtration, the filtrate (3 ml) was mixed with an aqueous solution (0.5 ml) of EC (10 mg) and EGC (10 mg) and vigorously stirred at 20 °C. An aliquot of the mixture was extracted with aqueous acetone and analyzed by reverse phase HPLC.

4 Isolation of **1**: Banana fruit flesh (*Musa acuminata* Colla cv. giant cavendish) (200 g) was homogenized with water (600 ml) in a Warring blender and filtered with four layers of muslin. The filtrate (300 ml) was mixed with an aqueous solution (50 ml) of EC (1.0 g, 3.45 mmol) and EGC (1.0 g, 3.27 mmol) and stirred vigorously for 5 h at 20 °C. The mixture was poured into acetone (800 ml) and filtered. The filtrate was concentrated and extracted with AcOEt (300 ml × 4) and the extract was applied to a column of Sephadex LH-20. Elution with EtOH afforded **1** (280 mg, 0.524 mmol) and **2** (728 mg, 1.29 mmol).

5 *Selected data* for **1**: red amorphous powder, $[\alpha]_D$ − 386.9° (*c*. 0.2, MeOH), λ_{max}^{EtOH}(log ε): 249 (4.29), 440 (3.70); δ_H(500 MHz, acetone-d_6) 5.377 (br s, H-2), 4.396 (br d, *J* 2.7, H-3), 2.955 (dd, *J* 4.6, 16.5, H-4), 2.815 (br d, *J* 16.5, H-4), 5.163 (br s, H-2′), 4.429 (ddd, *J* 1.9, 3.7, 4.6, H-3′), 2.713 (dd, *J* 3.7, 16.6, H-4′), 2.899 (dd, *J* 4.6, 16.6, H-4′), 6.062 and 6.065 (each d, *J* 2.3, H-6 and H-6′), 6.005 and 6.006 (each d, *J* 2.3, H-8 and H-8′) and 12.28 (s, OH); δ_C(125 MHz, acetone-d_6 + D_2O) 180.62 (C-a), 183.38 (C-b), 126.97 (C-c), 152.16 (C-d), 118.05 (C-e), 152.88 (C-f), 120.13 (C-g), 166.97 (C-h), 115.27 (C-i), 133.91 (C-j), 75.40 (C-2), 64.84 (C-3), 28.92 (C-4), 99.68 (C-4), 156.15 (C-8a), 78.85 (C-2′), 66.30 (C-3′), 28.78 (C-4′), 99.38 (C-4a′), 156.09 (C-8a′); (calc. for $C_{28}H_{22}O_{11}\cdot 7/4H_2O$: C, 59.42; H, 4.54. Found: C, 59.78; H, 4.98%).

6 *Selected HMBC correlations* for **1**: H-c to C-b, C-d, C-j and C-2; H-e to C-d, C-j, C-i, C-f, C-g and C-2′; H-g to C-e, C-f, C-h, C-i and C-2′; H-2 to C-c, C-d, C-j and C-4; H-2’ to C-e, C-f, C-g, C-4′ and C-8a′.

7 L. D. Detter, O. W. Hand, R. G. Cooks and R. A. Walton, *Mass Spectrom. Rev.*, 1988, **7**, 465.

8 Synthesis of **1a**: A solution of **1** (15mg) and *o*-phenylenediamine (10 mg) in EtOH (3 ml) containing 10% acetic acid was stirred at 45 °C for 2 h. The mixture was separated by Sephadex LH-20 column chromatography using EtOH to yield **1a** (16.0 mg) as a red amorphous powder. $[\alpha]_D$ −361.3° (*c*. 0.1, MeOH), λ_{max}^{EtOH}(log ε): 266 (4.563), 438 (4.03); δ_H (500 MHz, acetone-d_6 + D_2O) 8.243 (m), 7.983 (m), 8.048 (d, *J* 0.9, H-c), 7.756 (d, *J* 1.1, H-e), 7.465 (br s, H-g), 5.757 (br s, H-2), 4.565 (m, H-3), 3.100 (dd, *J* 4.5, 16.5 H-4), 2.927 (br d, *J* 16.5, H-4), 5.373 (br s, H-2′), 4.565 (m, H-3′), 2.996 (dd, *J* 4.5, 16.3, H-4′) and 2.770 (dd, *J* 3.9, 16.3, H-4′). Long-range H–C correlations observed in the HMBC spectrum were entirely consistent with the structure **1a**.

ChemComm

Alcohol dehydrogenase is active in supercritical carbon dioxide

Tomoko Matsuda,*[a] Tadao Harada[a] and Kaoru Nakamura[b]

[a] *Department of Materials Chemistry, Faculty of Science and Technology, Ryukoku University, Otsu, Shiga 520-2194, Japan*
[b] *Institute for Chemical Research, Kyoto University, Uji, Kyoto 611-0011, Japan*

Received (in Cambridge, UK) 22nd May 2000, Accepted 14th June 2000
Published on the Web 5th July 2000

Alcohol dehydrogenase from *Geotrichum candidum* was found to be active in supercritical carbon dioxide at 10 MPa; high activities and excellent enantioselectivities were observed for the asymmetric reduction of aromatic and cyclic ketones.

Supercritical fluids have been used as solvents for organic synthesis as well as for extraction and chromatography by taking advantage of both their gas-like low viscosities and high diffusivities and their liquid-like solubilizing power.[1] Moreover, the tunability of these properties is unique to supercritical fluids; small changes in pressure or temperature lead to significant changes in density-dependent solvent properties such as the relative permittivity, the solubility parameter, and the partition coefficient.[1] Among many fluids, supercritical carbon dioxide ($scCO_2$) has the added benefits of an environmentally benign nature, nonflammability, low toxicity, high availability, and ambient critical temperature (T_c = 31.0 °C) that make it suitable for biotransformations.[1] The attraction of combining natural catalysts with a natural solvent has been the driving force behind a growing body of literature[2] on the stability, activity and specificity of enzymes in $scCO_2$.[1] Since the first report on biotransformations in supercritical fluids in 1985 by Randolph *et al.*,[3] Hammond *et al.*[4] and Nakamura *et al.*,[5] the benefits of using supercritical fluids for biotransformations have been demonstrated by Mori *et al.*[6] and Kamat *et al.*:[7] *e.g.* improved reaction rates, control of selectivities by pressure, *etc.*

However, most of the biocatalysts used in supercritical fluids are hydrolytic enzymes[1–7] such as lipases and proteases with the exception of cholesterol oxidase,[8] and no report on the use of alcohol dehydrogenases in supercritical fluids has yet been published, despite the fact that they are an important class of enzymes for the asymmetric reduction of ketones to produce chiral alcohols. There is growing demand for such alcohols as the chiral synthones for natural products, pharmaceuticals, agrochemicals, and ferroelectric liquid crystals. Here we report the first achievement of a highly enantioselective reduction of ketones by alcohol dehydrogenase in $scCO_2$ (Scheme 1).

The resting cells of a fungus, *Geotrichum candidum*[9] IFO 5767, were employed for the reduction of ketones owing to its high reactivity with unnatural substrates and the simplicity of its growth. The whole-resting cell instead of an isolated enzyme was used for the reduction, and thus the addition of expensive coenzyme was not necessary and the solubilities of the coenzymes in $scCO_2$ did not need to be considered. The cell was immobilized on a water-absorbing polymer[9c] to spread it on the large surface of the polymer. At first, the reduction of *o*-fluoroacetophenone in $scCO_2$ at 10 MPa was conducted, which resulted in (*S*)-1-(*o*-fluorophenyl)ethanol at 81% after 12 h. A control experiment to prove that the reduction did not proceed before the supercritical condition was also conducted.[10] The time course of the reaction (Fig. 1) shows that the yield increased with the reaction time, which proved that the alcohol dehydrogenase catalyzed the reduction even in the supercritical condition.

The substrate specificity was investigated, and as listed in Table 1, the biocatalytic reduction in $scCO_2$ proceeded for various ketones. Acetophenone, acetophenone derivatives, benzyl acetone and cyclohexanone were used as substrates, and it was found that all of them were reduced by the alcohol dehydrogenase in $scCO_2$. The effects of fluorine substitution at the *ortho*, *para* and α positions of acetophenone were obvious. Compared with the unsubstituted analogue, substitution at the *ortho* or α position increased the yield, whereas substitution at the *para* position decreased the yield. Systematic study of the relationship between the effect of the fluorine substituent and the effect of properties of $scCO_2$ as well as isolation of the enzyme responsible for the reduction, tasks which are in progress in our laboratory, would give a better understanding of the fluorine recognitions by the protein.

The finding that the alcohol dehydrogenase is active in $scCO_2$ is significant, but not sufficient for practical use; high enantioselectivity of the reduction is also necessary for synthetic purposes. In our case, very high enantioselectivities (> 99% ee) were obtained for the reduction with the majority of the substrates tested, while slightly lower enantioselectivities (96, 97% ee) were observed for a few of them. The enantioselectivities obtained in this system are superior to or at least equal to those for most other biocatalytic and chemical systems.[11]

In a typical experiment, *G. candidum* IFO 5767 was grown as described previously.[9d] The freshly prepared cell (0.25 g wet wt) was suspended in H_2O (0.75 mL) and propan-2-ol (0.050 mL), and immobilized on water absorbing polymer (BL-100®, 0.125 g) as described previously.[9c] In the experiment, we used a stainless steel pressure-resistant vessel (Taiatsu Techno, Co., Osaka, TVS-N2 type, 10 mL) equipped with a stop valve (Whitey Co. SS3NBS4G), manometer (Taiatsu Techno, Co., Osaka, 15 MPa), and HPLC pump (Jasco PU-1580 pump) connected to a cooler (−5 °C) and CO_2 gas cylinder. In this vessel, the immobilized cell, a magnetic stirrer, and a ketone (0.017 mmol, placed in a glass tube to prevent it from contacting the biocatalyst before achieving the supercritical conditions) were charged. Then the vessel was warmed to 35 °C, and CO_2 preheated to 35 °C was introduced until a pressure of 10 MPa was reached. The mixture was stirred at 35 °C for 12 h, and the CO_2 was liquefied at −10 °C and then the gas pressure was

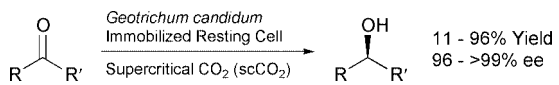

Scheme 1

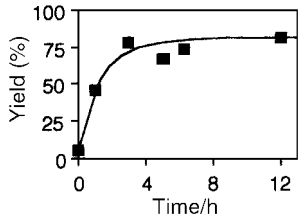

Fig. 1 Time course of reduction of *o*-fluoroacetophenone in $scCO_2$ at 10 MPa.

DOI: 10.1039/b004069j

Table 1 Reduction of various ketones by immobilized cell in $scCO_2$

Substrate	Yield (%)	Ee (%)	Config.
	51	> 99	*S*
	81	> 99	*S*
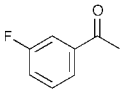	53	> 99	*S*
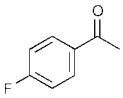	11	97	*S*
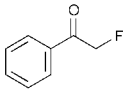	96	96	*R*
	22	> 99	*S*
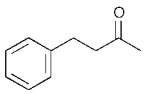	61	> 98	*S*
	96	—	—

Conditions are described in text.

released. The resulting residue was dissolved in ether, and the mixture was put on Extrelut and quickly eluted with ether. Chemical yield and ee were measured using a chiral GC-column (Chirasil-DEX CB; 25 m; He 2 mL min^{-1}). The absolute configurations were determined by comparing the GC retention times with those of authentic samples.

In conclusion, the alcohol dehydrogenase from *G. candidum* was found to be active in $scCO_2$ at 35 °C and 10 MPa and to catalyze asymmetric reduction of various ketones with excellent enantioselectivities. For practical use, there has so far been some hesitation to use alcohol dehydrogenases in spite of their high enantioselectivities because of the difficulties in extracting the product from aqueous solvents. We believe that this report opens up new possibilities for asymmetric reduction by an enzyme with a natural and easily-removable solvent.

The authors greatly appreciate the advice and technical support in assembling the $scCO_2$ reactor given by Professor Okamoto at Kyoto Institute of Technology, Professor Okahata and Dr Mori at Tokyo Institute of Technology, Dr Ozaki at Osaka University and Professor Hori and Dr Tabata at Fukui University. This work was supported by a Grant-in-Aid for Encouragement of Young Scientists (No. 12740400) and a Grant-in-Aid for Scientific Research (C) (No. 11640602) from the Ministry of Education, Science, Sports and Cultre of Japan. The authors are grateful to Osaka Yuki Kagaku Kogyo Co., Ltd. for providing BL-100® (water-absorbing polymer).

Notes and references

1 A. J. Mesiano, E. J. Beckman and A. J. Russell, *Chem. Rev.*, 1999, **99**, 623; Y. Ikushima, *Adv. Colloid Interface Sci.*, 1997, **71–72**, 259; E. Cernia and C. Palocci, in *Methods in Enzymology*, ed. J. N. Abelson and M. I. Simon, Academic Press, San Diego, 1997 , vol. 286, p. 495; S. V. Kamat, E. J. Beckman and A. J. Russell, *Crit. Rev. Biotechnol.*, 1995, **15**, 41; O. Aaltonen and M. Rantakylä, *CHEMTECH*, 1991, 240; P. G. Jessop, T. Ikariya and R. Noyori, *Chem. Rev.*, 1999, **99**, 475; A. Baiker, *Chem. Rev.*, 1999, **99**, 453; J. F. Brennecke and J. E. Chateauneuf, *Chem. Rev.*, 1999, **99**, 433; T. Moriyoshi, T. Kita and Y. Uosaki, *Ber. Bunsenges. Phys. Chem.*, 1993, **97**, 589.

2 S.-H. Yoon, H. Nakaya, O. Ito, O. Miyawaki, K.-H. Park and K. Nakamura, *Biosci. Biotechnol. Biochem.*, 1998, **62**, 170; S. H. Yoon, O. Miyawaki, K.-H. Park and K. Nakamura, *J. Ferment. Bioeng.*, 1996, **82**, 334; Y. Ikushima, N. Saito, M. Arai and H. W. Blanch, *J. Phys. Chem.*, 1995, **99**, 8941; J. C. Erickson, P. Schyns and C. L. Cooney, *AIChE J.*, 1990, **36**, 299; N. Fontes, M. C. Almeida, C. Peres, S. Garcia, J. Grave, M. R. Aires-Barros, C. M. Soares, J. M. S. Cabral, C. D. Maycock and S. Barreiros, *Ind. Eng. Chem. Res.*, 1998, **37**, 3189; N. Fontes, E. Nogueiro, A. M. Elvas, T. C. d. Sampaio and S. Barreiros, *Biochim. Biophys. Acta*, 1998, **1383**, 165.

3 T. W. Randolph, H. W. Blanch, J. M. Prausnitz and C. R. Wilke, *Biotechnol. Lett.*, 1985, **7**, 325.

4 D. A. Hammond, M. Karel, A. M. Klibanov and V. J. Krukonis, *Appl. Biochem. Biotechnol.*, 1985, **11**, 393.

5 K. Nakamura, Y. M. Chi, Y. Yamada and T. Yano, *Chem. Eng. Commun.*, 1986, **45**, 207.

6 T. Mori and Y. Okahata, *Chem. Commun.*, 1998, 2215; T. Mori, A. Kobayashi and Y. Okahata, *Chem. Lett.*, 1998, 921.

7 S. Kamat, J. Barrera, E. J. Beckman and A. J. Russell, *Biotechnol. Bioeng.*, 1992, **40**, 158; S. V. Kamat, B. Iwaskewycz, E. J. Beckman and A. J. Russell, *Proc. Natl. Acad. Sci. USA*, 1993, **90**, 2940; S. V. Kamat, E. J. Beckman and A. J. Russell, *J. Am. Chem. Soc.*, 1993, **115**, 8845; A. K. Chaudhary, S. V. Kamat, E. J. Beckman, D. Nurok, R. M. Kleyle, P. Hajdu and A. J. Russell, *J. Am. Chem. Soc.*, 1996, **118**, 12 891.

8 T. W. Randolph, D. S. Clark, H. W. Blanch and J. M. Prausnitz, *Science*, 1988, **239**, 387; T. W. Randolph, H. W. Blanch and J. M. Prausnitz, *AIChE J.*, 1988, **34**, 1354.

9 (*a*) R. Azerad and D. Buisson, in *Microbial Reagents in Organic Synthesis, NATO ASI Series C*, ed. S. Servi, Kluwer Academic Publishers, Dordrecht, 1992, p. 421; (*b*) T. Matsuda, T. Harada, N. Nakajima, T. Itoh and K. Nakamura, *J. Org. Chem.*, 2000, **65**, 157; (*c*) K. Nakamura, Y. Inoue, T. Matsuda and I. Misawa, *J. Chem. Soc., Perkin Trans. 1*, 1999, 2397; (*d*) K. Nakamura and T. Matsuda, *J. Org. Chem.*, 1998, **63**, 8957.

10 The reaction was stopped as soon as the pressure reached 10 MPa by cooling at −10 °C, then a negligible amount of the reaction proceeded (yield 5%), which was probably due to the reaction during the time between the critical pressure and 10 MPa.

11 S. M. Roberts, *J. Chem. Soc., Perkin Trans. 1*, 2000, 611; S. M. Roberts, *J. Chem. Soc., Perkin Trans. 1*, 1999, 1; S. M. Roberts, *J. Chem. Soc., Perkin Trans. 1*, 1998, 157; T. Benincori, E. Cesarotti, O. Piccolo and F. Sannicolo, *J. Org. Chem.*, 2000, **65**, 2043; Y.-J. Cherng, J.-M. Fang and T.-J. Lu, *J. Org. Chem.*, 1999, **64**, 3207; T. Ohkuma, M. Koizumi, H. Doucet, T. Pham, M. Kozawa, K. Murata, E. Katayama, T. Yokozawa, T. Ikariya and R. Noyori, *J. Am. Chem. Soc.*, 1998, **120**, 13 529.

ChemComm

Lanthanide co-ordination frameworks of 4,4′-bipyridine-*N*,*N*′-dioxide†

De-Liang Long, Alexander J. Blake, Neil R. Champness* and Martin Schröder*

School of Chemistry, The University of Nottingham, University Park, Nottingham, UK NG7 2RD. E-mail: M.Schroder@nottingham.ac.uk, Neil.Champness@nottingham.ac.uk

Received (in Cambridge, UK) 24th March 2000, Accepted 19th May 2000
Published on the Web 5th July 2000

Metal–ligand co-ordination frameworks of 4,4′-bipyridine-*N*,*N*′-dioxide (L) have been prepared; $\{[Sm(L)_2(NO_3)_3]\cdot 0.5H_2O\}_\infty$ 1, $\{[Er_2(L)_3(NO_3)_6]\cdot 2CH_3OH\}_\infty$ 2; 1 shows rare two-fold interpenetrating three-dimensional $CdSO_4$-like nets, and 2 shows an unprecedented two-dimensional 4.8^2 network.

The construction of inorganic co-ordination networks and crystal engineering have developed rapidly in recent years, the vast majority of reported work being based upon the use of polydentate ligands bound to d-block transition metal ions.[1] Ligands based upon aromatic N-donor ligands, such as 4,4′-bipyridine, have been particularly studied as they can be readily varied, giving a high degree of control over co-ordination framework structure. Aspects of such ligands that can be tuned include: denticity, ligand donor-atom separation, and, consequently, the degree of interpenetration, steric and electronic properties, and even the degree of inter-ligand interaction.

Far less common has been the use of lanthanide ions as nodes in the construction of co-ordination framework polymers.[2] Such structures can be expected to be more difficult to control than their d-block metal analogues due to the higher co-ordination numbers of lanthanide ions. However, the inherent flexibility of their co-ordination geometry is particularly attractive for the preparation of new network types as this greater structural ambivalence will lead to the synthesis of unprecedented structures. Based on the fact that lanthanide ions have a high affinity for hard oxygen-containing ligands, we have developed a new, widely applicable strategy using, for the first time, 4,4′-bipyridine-*N*,*N*′-dioxide (L) as a bridging ligand in the construction of fully characterised co-ordination networks. This strategy using poly(*N*-oxide) ligands offers exciting possibilities as the degree of structural manipulation seen in d-block coordination frameworks can now be developed for networks based upon f-block metals.

Although the co-ordination of pyridine-*N*-oxides to lanthanide ions in discrete molecular compounds is reasonably well established,[3] we are aware of only one report in the literature of a complex of 4,4′-bipyridine-*N*,*N*′-dioxide,[4] with another of a copper(II) co-ordination polymer of the related azobis(pyridine-4,4′-dioxide).[5] We now report two compounds with very different structures, $\{[Sm(L)_2(NO_3)_3]\cdot 0.5H_2O\}_\infty$ **1** and $\{[Er_2(L)_3(NO_3)_6]\cdot 2CH_3OH\}_\infty$ **2** (L = 4,4′-bipyridine-*N*,*N*′-dioxide).

Yellow crystals of **1**, and pale pink crystals of **2**, were prepared‡ by slow diffusion of $Sm(NO_3)_3$ or $Er(NO_3)_3$ and 4,4′-bipyridine-*N*,*N*′-dioxide in a MeOH–CH_2Cl_2 solvent mixture, the latter component acting to slow the rate of diffusion and thus the reaction. The crystals of **1** were very stable in air and did not decay upon continuous exposure to moisture, but crystals of **2** lost crystallinity quickly following removal from the mother liquor. Single crystal X-ray analyses§ confirm that these materials have polymeric structures, based on networks of ten-co-ordinate lanthanide centres for **1** and nine-co-ordinate centres for **2**, with L bridging the metal centres. Whereas the Sm(III) ions in **1** have a regular SmO_{10} co-ordination environment with the oxygen atoms forming a hexadecahedron (Fig. 1a), the Er(III) ions in complex **2** have an ErO_9 co-ordination environment, with nine oxygen atoms forming a distorted tricapped trigonal prism (Fig. 1b), reflecting the reduction in the ionic radius from Sm(III) to Er(III).

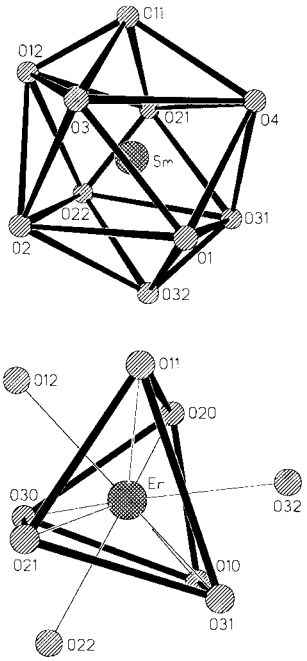

Fig. 1 Metal co-ordination environments in **1** (a) and **2** (b).

1 adopts a two-fold interpenetrating three-dimensional $CdSO_4$-like framework (a in Scheme 1, Fig. 2). The 4,4′-bipyridine-*N*,*N*′-dioxide ligands sustain a 3-D framework motif through two different linkages. The first propagates along the two diagonal directions of the *ab* face; the ligand is slightly bent, with the two pyridyl rings twisted at an angle of 14.8° and bridging two Sm(III) centres at a distance of 12.7 Å. The other linkage exists as a zigzag line propagating along the *c* axis; in this case the ligand is more bent, with the two pyridyl rings twisted at an angle of 29.9° and bridging the two Sm(III) centres at a much shorter distance of 11.6 Å. The framework found here

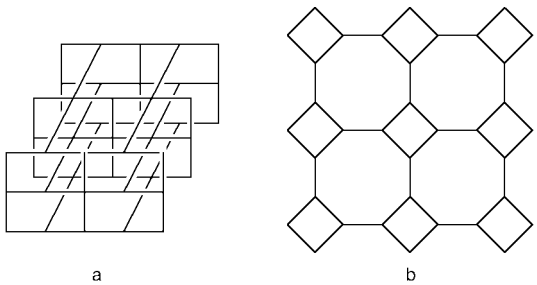

Scheme 1 Schematic representation of (a) a $CdSO_4$ 3D-net and (b) a 2D 4.8^2 net.

† Electronic supplementary information (ESI) available: colour version of Fig. 2 and 3. See http://www.rsc.org/suppdata/cc/b0/b002363j/

DOI: 10.1039/b002363i

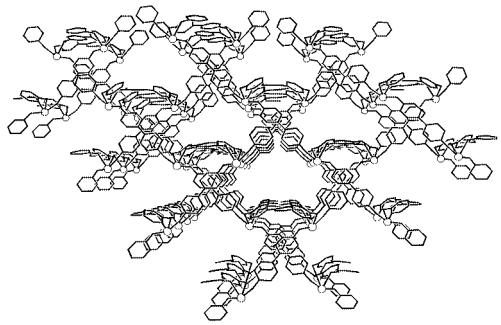

Fig. 2 Packing diagram of compound **1** showing one component of the two interpenetrating frameworks (viewed down the *c* axis). Nitrate groups, solvent molecules and hydrogen atoms are omitted for clarity.

is a severely distorted $CdSO_4$-like net,[6,7] The previous examples of $CdSO_4$-type nets, $\{Cu[1,2\text{-bis}(4\text{-pyridyl})ethane]_2(NO_3)_2\}_\infty$ reported by Zaworotko *et al*.[6] and the related 'dense-net' structure of copper complexed with 1,2-bis(4-pyridyl)ethyne reported by Ciani *et al*.,[7] are both constructed from *d*-metal junctions. As the conformation of the linking ligands is flexible, the junction at Sm(III) is distorted from square-planarity causing the connection propagating along the *c* direction to develop into a zigzag line. When viewed along the *c* direction, the structure is seen to contain 12.0 × 12.0 Å channels (Fig. 2). However, these channels are occupied by a second interpenetrating independent framework.

The smaller ionic radius for Er(III) compared to Sm(III) results in nine-co-ordinate Er(III) centres in **2** *via* six oxygen donors from three nitrates and three from three 4,4′-bipyridine-*N*,*N*′-dioxide ligands. These latter ligands link the Er(III) ions to form a 2-D sheet of 4.8^2 topology (b in Scheme 1, Fig. 3). This type of net, predicted by Wells[8] but not previously observed for co-ordination frameworks, consists of three connected nodes shared by one tetragonal square unit and two octagons. The octagonal unit forms an 88-membered ring, comprising eight metal ions and eight ligands, of *ca.* 2.6 nm diameter. This large cavity is occupied by the four-membered ring motif of an adjacent layer thus inhibiting interpenetration. When viewed along the *c* axis, tetragonal channels with dimensions of 10.0 × 10.0 Å can be seen (Fig. 3), in which methanol solvent molecules are accommodated.

The isolation of complexes **1** and **2** suggests the possibility of constructing designed inorganic networks with lanthanide metal salts and bridging pyridine-*N*-oxide ligands. We have every reason to believe that, in the same way that polypyridines are important for d-block metal ions, poly(pyridine-*N*-oxides) may become equally important for f-block metal ions, thus leading to a new family of inorganic co-ordination networks and framework materials.

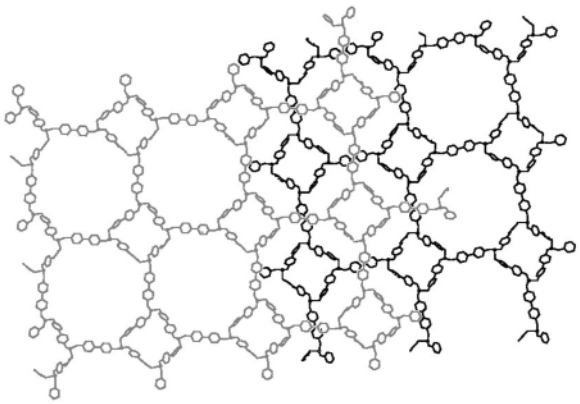

Fig. 3 View of the 4.8^2 nets in compound **2** with two adjacent layers in different colours. Nitrate groups, solvent molecules and hydrogen atoms are omitted for clarity.

This work was supported by the Royal Society (K. C. Wong Fellowship to D.-L. L.) and the Engineering and Physical Sciences Research Council.

Notes and references

‡ *Experimental procedure*: $\{[Sm(4,4'\text{-bipyridine-}N,N'\text{-dioxide})_2(NO_3)_3]\cdot 0.5H_2O\}$ **1**. Solid $Sm(NO_3)_3\cdot 6H_2O$ (44 mg, 0.10 mmol) at the bottom of a vial was covered with CH_2Cl_2 (4 cm³) over which a solution of 4,4′-bipyridine-*N*,*N*′-dioxide hydrate (44 mg, 0.20 mmol) in MeOH (6 cm³) was layered. Over a period of 15 days, the solid $Sm(NO_3)_3\cdot 6H_2O$ gradually dissolved with concomitant formation of yellow crystals of the product on the wall of the vial. $\{[Er_2(4,4'\text{-bipyridine-}N,N'\text{-dioxide})_3(NO_3)_6]\cdot 2CH_3OH\}$ **2** was prepared by an analogous method, forming pale pink columnar crystals. Satisfactory spectroscopic and analytical data were obtained for both compounds.

§ *X-Ray experimental, general procedures*: data for both compounds were collected on a Stoe Stadi-4 four-circle diffractometer, graphite monochromated Mo-Kα radiation (λ = 0.71073 Å), ω–θ scans. Both structures were solved by direct methods[9] and refined using full-matrix least squares techniques on F^2.[10] All non-hydrogen atoms were refined anisotropically and hydrogen atoms were placed in geometrically calculated positions and allowed to ride on their parent atoms.

Crystal data for $[Sm(4,4'\text{-bipyridine-}N,N'\text{-dioxide})_2(NO_3)_3]\cdot 0.5H_2O$ **1**: $C_{20}H_{17}N_7O_{13.5}Sm$, M = 721.76, orthorhombic, space group *Pbcn* (no. 60), a = 16.529(4), b = 17.616(5), c = 17.244(5) Å, U = 5021(2) Å³, T = 150(2) K, Z = 8, D_c = 1.907 Mg m^{-3}, μ(Mo-Kα) = 2.424 mm^{-1}. 4919 unique reflections [R_{int} = 0.0852] [4144 with $I > 2\sigma(I)$]. Final R_1 = 0.033, wR_2(all data) = 0.077.

$\{[Er_2(4,4'\text{-bipyridine-}N,N'\text{-dioxide})_3(NO_3)_6]\cdot 2CH_3OH\}$ **2**: $C_{32}H_{32}Er_2N_{12}O_{26}$, M = 1335.22, tetragonal, space group $P\bar{4}2_1c$ (no. 114), a = 26.435(6), c = 7.584(2) Å, U = 5300(2) Å³, T = 220(2) K, Z = 4, D_c = 1.673 Mg m^{-3}, μ(Mo-Kα) = 3.235 mm^{-1}. 4422 unique reflections, [3542 with $I > 2\sigma(I)$]. Final R_1 = 0.076, wR_2 (all data) = 0.179.

CCDC 182/1647. See http://www.rsc.org/suppdata/cc/b0/b002363i/ for crystallographic files in .cif format.

1 P. J. Hagrman, D. Hagrman and J. Zubieta, *Angew. Chem., Int. Ed.*, 1999, **38**, 2638; A. J. Blake, N. R. Champness, P. Hubberstey, W.-S. Li, M. A. Withersby and M. Schröder, *Coord. Chem. Rev*., 1999, **183**, 117; O. M. Yaghi, H. Li, C. Davis, D. Richardson and T. L. Groy, *Acc. Chem. Res.*, 1998, **31**, 474; S. R. Batten and R. Robson, *Angew. Chem., Int. Ed.*, 1998, **37**, 1460.

2 For example, see: D. M. L. Goodgame, S. Menzer, A. M. Smith and D. J. Williams, *Chem. Commun.*, 1997, 339; J. G. Mao, H. J. Zhang, J. Z. Ni, S. B. Wang and T. C. W. Mak, *Polyhedron*, 1999, **18**, 1519; T. M. Reineke, M. Eddaoudi, M. Fehr, D. Kelley and O. M. Yaghi, *J. Am. Chem. Soc.*, 1999, **121**, 1651; T. M. Reineke, M. Eddaoudi, M. O'Keeffe and O. M. Yaghi, *Angew. Chem., Int. Ed.*, 1999, **38**, 2590; D. D. Wu, Z. Y. Zhou, S. L. Li and T. C. W. Mak, *Polyhedron*, 1997, **16**, 749; D. M. L. Goodgame, S. P. W. Hill and D. J. Williams, *Inorg. Chim. Acta*, 1998, **272**, 131; L. Ma, O. R. Evans, B. M. Foxman and W. Lin, *Inorg. Chem.*, 1999, **38**, 5837.

3 For example, see: L. R. Melby, N. J. Rose, E. Abramason and J. C. Caris, *J. Am. Chem. Soc.*, 1964, **86**, 5117; A. R. Al-Karaghouli and J. S. Wood, *Inorg. Chem.*, 1979, **18**, 1177 and 1184; A. R. Al-Karaghouli, R. O. Day and J. S. Wood, *Inorg. Chem.*, 1978, **17**, 3702; G. S. Conary, A. A. Russell, R. T. Paine, J. H. Hall and R. R. Ryan, *Inorg. Chem.*, 1988, **27**, 3242; B. M. Rapko, E. N. Duesler, P. H. Smith, R. T. Paine and R. R. Ryan, *Inorg. Chem.*, 1993, **32**, 2164; C. Rodellas, G. Vicentini and L. B. Zinner, *Acta Chem. Scand. Ser. A*, 1987, **41**, 294; J. Lipkowski, K. Suwinska and G. D. Andreetti, *J. Coord. Chem.*, 1990, **22**, 83; J. W. Steed, C. P. Johnson, C. L. Barnes, R. K. Juneja, J. L. Atwood, S. Reilly, R. L. Hollis, P. H. Smith and D. L. Clark, *J. Am. Chem. Soc.*, 1995, **117**, 11 426; C. O. Paul-Roth, J.-M. Lehn, J. Guilhem and C. Pascard, *Helv. Chim. Acta*, 1995, **78**, 1895.

4 H. W. Lin and W. X. Zhu, *Chem. J. Chin. Univ.*, 1996, **17**, 1516; M. J. Plater, M. R. S. Foreman and A. M. Z. Slawin, *Inorg. Chim. Acta*, 2000, **303**, 132.

5 N. R. Stemple and W. H. Watson, *Cryst. Struct. Commun.*, 1975, **4**, 25; J. G. Mao, H. J. Zhang, J. Z. Ni, S. B. Wang and T. C. W. Mak, *Polyhedron*, 1998, **17**, 3999.

6 K. N. Power, T. L. Hennigar and M. J. Zaworotko, *Chem. Commun.*, 1998, 595.

7 L. Carlucci, G. Ciani, P. Macchi and D. M. Proserpio, *Chem. Commun.*, 1998, 1837.

8 A. F. Wells, *Structural Inorganic Chemistry*, 5th edn., Clarendon Press, Oxford, 1984.

9 G. M. Sheldrick, SHELXS-97, University of Göttingen, Germany, 1997.

10 G. M. Sheldrick, SHELXL-97, University of Göttingen, Germany, 1997.

Photocatalytic H_2 evolution under visible light irradiation on Ni-doped ZnS photocatalyst

Akihiko Kudo* and Masahiko Sekizawa

Department of Applied Chemistry, Faculty of Science, Science University of Tokyo, 1-3 Kagurazaka, Shinjuku-ku, Tokyo 162-8601, Japan. E-mail: a-kudo@ch.kagu.sut.ac.jp

Received (in Cambridge, UK) 25th April 2000, Accepted 15th June 2000
Published on the Web 5th July 2000

$Zn_{0.999}Ni_{0.001}S$ photocatalysts (energy gap = 2.3 eV) heat-treated at 773 K in an N_2 flow showed activity for hydrogen evolution from aqueous solutions containing K_2SO_3 and Na_2S as reducing reagents under visible light irradiation without co-catalysts such as Pt.

Water splitting using photocatalysts is an important reaction from the viewpoint of global energy and environmental concerns. Although some photocatalysts have been reported to show high activities for the water splitting, they are active only under UV-light irradiation.[1,2] However, photocatalysts which are active for the water splitting under visible light irradiation have not been developed. Even in the presence of sacrificial reagents, the only well-known photocatalysts that can produce hydrogen or oxygen from aqueous solutions under visible light irradiation are Pt/CdS and WO_3.[3–5] Therefore, development of new visible-light-driven photocatalysts is a priority. One of us has recently found that $BiVO_4$ prepared in an aqueous process showed high activity for oxygen evolution from aqueous solutions containing Ag^+ as an electron scavenger.[6,7] On the other hand, it is important to develop new and less harmful visible-light-driven photocatalysts than Pt/CdS for hydrogen evolution from aqueous solutions. We have studied the development of new visible-light-driven photocatalysts based on ZnS and have previously reported a CuS–ZnS solid solution photocatalyst.[8] However, this CuS–ZnS photocatalyst has poor thermal and chemical stability. The present work reports thermally and chemically stable Ni-doped ZnS photocatalysts for hydrogen evolution from aqueous K_2SO_3 and Na_2S solutions under visible light irradiation.

Ni-doped ZnS photocatalysts were prepared by mixing an aqueous $Zn(NO_3)_2$ and $Ni(NO_3)_2$ solution with an aqueous Na_2S solution. The obtained precipitates were washed with distilled water using a centrifuge and then were heat-treated at 773 K in an N_2 flow. Photocatalytic reactions were carried out in a closed gas circulation system by using a 300 W Xe illuminator (CERMAX, LX300) and optical cut-off filters. The Ni-doped ZnS photocatalyst (1 g) was dispersed in aqueous K_2SO_3 and Na_2S solutions in a Pyrex reaction cell. The amounts of H_2 evolved were determined by using a gas chromatograph (Ohkura, Model 802, TCD, Ar carrier). Quantum yields were measured using an interference filter (λ_{max}: 420 nm, half width; 11 nm) and chemical actinometry measured using ammonium ferrioxalate.

Fig. 1 shows photocatalytic H_2 evolution from an aqueous solution containing K_2SO_3 and Na_2S as reducing reagents on $Zn_{0.999}Ni_{0.001}S$ powder heat-treated at 773 K in an N_2 flow under visible light irradiation. H_2 efficiently evolved even without co-catalysts such as Pt. The rate of H_2 evolution was 280 μmol h^{-1}, a relatively large value under the present experimental conditions (300W Xe lamp, λ > 420 nm). The turnover number of reacted electrons to the amount of Ni doped reached 170 at 8 h of the reaction time and the quantum yield at 420 nm was 1.3%. More than 7500 μmol of H_2 was formed in a prolonged experiment (> 50 h). The number of electrons reacted exceeded the amount of the catalyst (10 mmol),

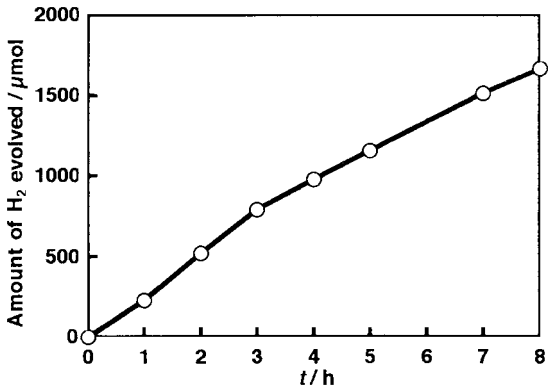

Fig. 1 Photocatalytic H_2 evolution from an aqueous K_2SO_3 (0.5 mol l^{-1})–Na_2S (0.005 mol l^{-1}) solution (300 ml) on $Zn_{0.999}Ni_{0.001}S$ powder (1 g) heat-treated at 773 K in an N_2 flow under visible light irradiation (λ > 420 nm). Light source: 300 W Xe lamp.

indicating the reaction proceeded photocatalytically with negligible photocorrosion.

Fig. 2 shows diffuse reflectance spectra of non-doped ZnS and $Zn_{0.999}Ni_{0.001}S$ heat-treated powders. The spectrum of $Zn_{0.999}Ni_{0.001}S$ showed a visible light absorption band with the onset around 540 nm in addition to the UV light absorption band derived from ZnS. The energy gap estimated from the onset of the visible light absorption band was 2.3 eV. The color of the photocatalyst was pale yellow and did not change after photocatalytic reactions. The shape of the diffuse reflectance spectrum of $Zn_{0.999}Ni_{0.001}S$ indicates that the doped nickel forms a new energy level in the band structure of ZnS. The visible light absorption band is assigned as due to the transition from the Ni 3d level to the conduction band level of ZnS, since the $Zn_{0.999}Ni_{0.001}S$ photocatalyst possesses highly active H_2 evolution sites as well as ZnS. Unless the conduction band was not derived from that of ZnS, such a high activity for the H_2 evolution without co-catalysts as evidenced in Fig. 1 would not be obtained. The photoexcitation of electrons from the Ni 3d level to the conduction band suggests that the photocorrosion

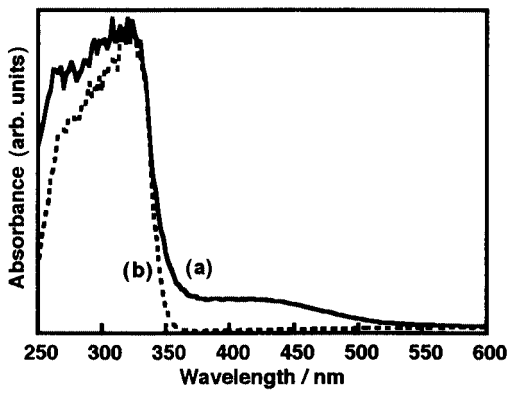

Fig. 2 Diffuse reflectance spectra of $Zn_{0.999}Ni_{0.001}S$ (a) and ZnS (b) powder heat-treated at 773 K in an N_2 flow.

DOI: 10.1039/b003297m

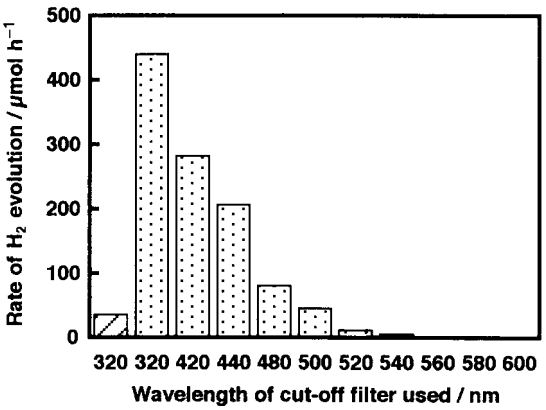

Fig. 3 The dependence of photocatalytic activities for H_2 evolution from an aqueous K_2SO_3 (0.5 mol l^{-1})–Na_2S (0.005 mol l^{-1}) solution (300 ml) over $Zn_{0.999}Ni_{0.001}S$ (dotted bar) and ZnS (hatched bar) powder heat-treated at 773 K in an N_2 flow upon wavelength (controlled *via* cut-off filters). Light source: 300 W Xe lamp.

observed for ZnS photocatalysts under band gap irradiation should be suppressed in the present system.

The wavelength dependence of the photocatalytic H_2 evolution on the $Zn_{0.999}Ni_{0.001}S$ photocatalysts was investigated as shown in Fig. 3. The number of incident photons was increased as the wavelength of cut-off filters was shortened. Although Fig. 3 is different from an ordinary action spectrum, it indicates the following points. When a cut-off filter of 540 nm was used, H_2 evolution was clearly observed. This wavelength corresponds to the onset of the diffuse reflectance spectrum as shown in Fig. 2. The $Zn_{0.999}Ni_{0.001}S$ photocatalyst showed considerably higher activity than non-doped ZnS even under full-arc irradiation ($\lambda > 320$ nm). It is often observed that doping transition metals with partly-filled d orbitals into photocatalysts such as TiO_2 strongly decreases the photocatalytic activities. However, such an suppression effect by the doping was not predominant in the present metal ion-doped ZnS photocatalyst system.

There were some problems concerning the thermal and chemical stability for the previously reported Cu-doped ZnS photocatalyst.[8] When the Cu-doped ZnS photocatalyst was dried or heat-treated to obtain good crystallinity, the photocatalytic activity for H_2 evolution was drastically decreased and the color of the photocatalyst changed after the photocatalytic reaction. In contrast to the Cu-doped ZnS photocatalyst, although the activity of the Ni-doped ZnS photocatalyst was lower, it was thermally and chemically stable. Moreover, the energy gap of Ni-doped ZnS (2.3 eV) was smaller than that of Cu-doped ZnS (2.5 eV) indicating that Ni-doped ZnS can utilize a wider spectral region of visible light than Cu-doped ZnS. The Ni-doped ZnS photocatalyst can produce H_2 using reducing reagents of sulfur compounds which are formed as by-products in petrochemical industries. Therefore, the Ni-doped photocatalyst is expected to be a practically useful photocatalyst.

In conclusion, Ni-doped ZnS has been developed as a new visible-light-driven photocatalyst for H_2 evolution from aqueous solutions. The development seems to suggest a way in making UV respondent photocatalysts respondent also to visible light.

This work was supported by New Energy and Industrial Technology Development Organization (NEDO)/Research Institute of Innovate Technology for the Earth (RITE), Core Research for Evolutional Science and Technology (CREST), and a Grant-in-Aid (No. 11640601) from the Ministry of Education, Science, Sports, and Culture, Japan.

Notes and references

1 A. Kudo, *Hyomen (Surface)*, 1998, **36**, 625.
2 K. Domen, T. Takata, M. Hara and J. N. Kondo, *Bull. Chem. Soc. Jpn*, 2000, **73**, 1307.
3 T. Sakata, in *Photocatalysis: fundamentals and applications*, ed. N. Serpone and E. Pelizzetti, Wiley, New York, 1989, ch. 10, p. 311.
4 J. R. Darwent and A. Mills, *J. Chem. Soc., Faraday Trans. 2*, 1982, **78**, 359.
5 W. Erbs, J. Desilvestro, E. Borgarello and M. Grätzel, *J. Phys. Chem.*, 1984, **88**, 4001.
6 A. Kudo, K. Ueda, H. Kato and I. Mikami, *Catal. Lett.*, 1998, **53**, 229.
7 A. Kudo, K. Omori and H. Kato, *J. Am. Chem. Soc.*, 1999, **121**, 11459.
8 A. Kudo and M. Sekizawa, *Catal. Lett.*, 1999, **58**, 241.

ChemComm

The first water-soluble main-chain polyfullerene†

Shashadhar Samal, Bum-Jin Choi and Kurt E. Geckeler*

Laboratory of Applied Macromolecular Chemistry, Department of Materials Science and Engineering, Kwangju Institute of Science and Technology, 1 Oryong-dong, Puk-gu, Kwangju 500-712, South Korea. E-mail: keg@kjist.ac.kr

Received (in Cambridge, UK) 15th May 2000, Accepted 12th June 2000
Published on the Web 5th July 2000

The synthesis of the first water-soluble polyfullerene is accomplished by nucleophilic reaction of a diamine supramolecularly shielded in a cyclodextrin cavity with fullerene, leading to a versatile new field for main-chain fullerene polymers.

Although a versatile derivatization chemistry of fullerenes has been developed,[1] solubilizing fullerenes in water while preserving the intrinsic properties of the carbon allotropes has met with limited success and consequently only a few reports are available in this field.[2] Previous attempts to synthesize fullerene main-chain polymers have been based on multi-step synthetic concepts and resulted in water-insoluble products.[3] In view of the potential biological and biomedical applications of water-soluble fullerene compounds,[4] we synthesized polyfullerenes following a general strategy, which we call the supramolecular masking concept, in which fullerene molecules are connected in the polymer main chain with bifunctional guest compounds that are supramolecularly shielded by a macrocyclic host. In a typical experiment, the cyclodextrin–amine complex (**2**), dissolved in dimethylformamide, was treated with a solution of [60]fullerene in dichloromethane, at room temperature, facilitating a nucleophilic polyaddition reaction between the accessible amino groups of the diamine moiety in the cyclodextrin cavity and C_{60}, leading to the water-soluble polyfullerene (**3**) (Scheme 1).

Initially, we thought of using *p*-phenylenediamine (PPD) as the simplest aromatic diamine for complexation with β-cyclodextrin (CD), the cyclic glucose hepta-oligomer, and subsequent use of the complex (CD–PPD) as the monomeric precursor for the synthesis of the fullerene main-chain polymer. The result was a species with a molecular mass of ~2.8 kg mol^{-1} (GPC data). Spectral data provided evidence of reaction between the inclusion complex and C_{60}. Formation of a short segment instead of a polymer was ascribed to the low probability of reaction of C_{60} with the PPD nitrogens (N–N distance 576 pm) embedded in the depth of the CD cavity (780 pm).

A similar reaction between the inclusion complex CD–bis(*p*-aminophenyl) ether (CD–BPE, N–N distance 968 pm) and C_{60} resulted in polymer **3**, (poly[(β-cyclodextrin–bis(*p*-aminophenyl) ether)-*co*-[60]fullerene], M_n = 18.9, M_w = 20.0 kg mol^{-1}; polydispersity 1.06) that exhibited a high solubility in water (> 10 mg ml^{-1}). The inclusion complex registered absorption peaks in the UV-Vis spectrum at 243 and 295 nm, whereas **3** registered peaks at 243, 286, and 343 nm (Fig. 1). Additionally there was substantial peak broadening beyond 350 nm (inset). Dynamic light scattering studies of water-soluble fullerenes have established that this peak broadening is due to scattering

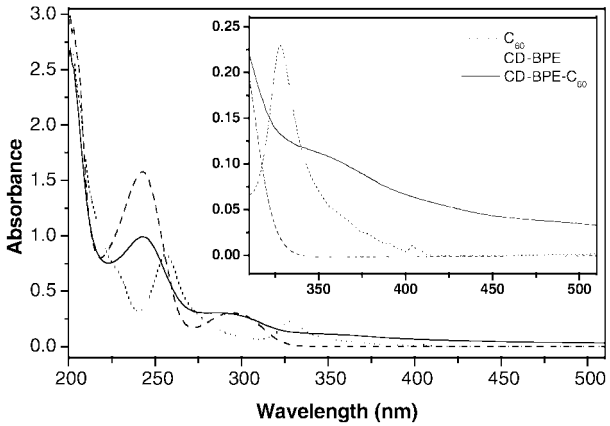

Fig. 1 UV-Vis spectra of C_{60} inclusion complex CD–BPE, and the polyfullerene CD–BPE–C_{60} (**3**).

† A colour version of the space-filling model of the supramolecularly shielded polyfullerene (Fig. 2) is available as electronic supplementary information (ESI). See http://www.rsc.org/suppdata/cc/b0/b003881o/

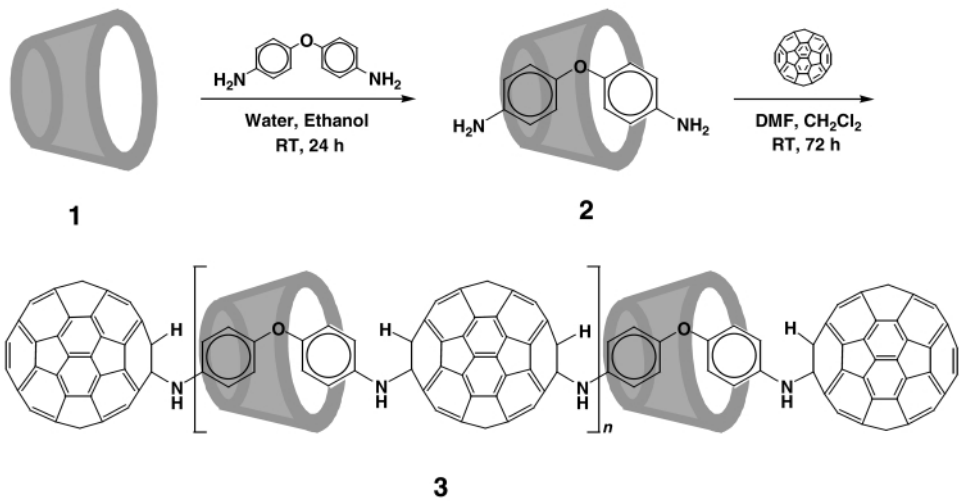

Scheme 1 Reaction scheme for the synthesis of polyfullerene (**3**).

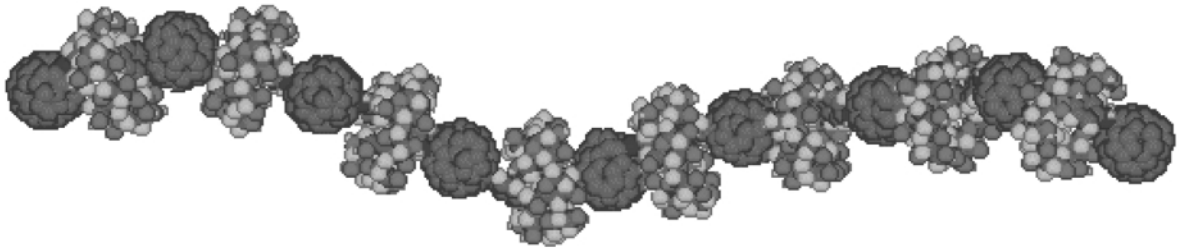

Fig. 2 Space-filling model of the supramolecularly shielded polyfullerene. For colour version, see http://www.rsc.org/suppdata/cc/b0/b003881o/

by fullerene aggregates.[5] The FT-IR spectra of the polyfullerene had distinct differences from the inclusion complex. In the case of the species from the reaction of CD–PPD and C_{60}, the fullerene peak was seen at 527 cm^{-1}, whereas for **3**, this peak was prominent at 513 cm^{-1}.

The ^1H NMR spectrum of the complex CD–BPE was well-defined, with the aromatic protons at 6.48, 6.51, 6.59, 6.62 ppm, contrary to the weak aromatic proton peaks of the CD–PPD complex, possibly due to the guest being deeply embedded in the CD cavity. The aromatic ring carbon atoms were registered at 114.7, 118.8, 144.0 and 148.3 ppm. All the characteristic peaks of the CD and BPE components were present in the polyfullerene **3**. Additionally, in the ^{13}C NMR spectra, there were peaks between 139–144 ppm assigned to the fullerene component.

In a comparative study without CD, C_{60} and BPE reacted to furnish a water-insoluble product. The material was characterized and found to be a polysubstituted fullerene, as could be expected of fullerene–amine reactions. Interestingly, such polysubstitution could be effectively prevented by the simple routine of placing the amine moiety within a cyclodextrin ring. The spatial dimensions of the macrocycle effectively prevented multifunctionalization of the fullerene units. At the moment we have not ascertained if C_{60} is connected at the *trans*-1 positions with the diamine and if there is any branching. Branching would mean strong stereochemical constraints, since each fullerene ball in the copolymer chain is already flanked by two CD units (see Fig. 2 for a space-filling model). Studies in this direction are being pursued, examining the spatial dimensions of the macrocycle and the fullerene in the molecular models.

In exploring the application potential of this novel polymer, preliminary experiments have shown that the material could be useful in biological and biomedical fields. The polyfullerene was found to strongly scavenge a living free radical, 1,1-diphenyl-2-picrylhydrazyl, even more strongly than [60]fullerene itself. Furthermore, the polymer was also found to cleave DNA oligonucleotide in the presence of light, which was ascertained from the GPC studies in conjunction with membrane filtration of the nucleotide before and after cleaving experiments. These preliminary results indicate that the polymer has retained the properties of the pristine [60]fullerene.

Although the above model reaction involves β-cyclodextrin and [60]fullerene, it is rather unlikely that the results described here are confined to these specific molecules. It might also allow the direct use of other fullerenes of the fullerene family such as higher homologues and exo- and endohedrally modified species, and the macrocyclic part may also be modified using a great variety of building units. The materials are expected to have a strong application potential in the biomedical area due to their hydrophilicity, but also many other applications of these interesting molecules can be envisaged such as their use as building blocks for molecular machines and robotics.[6] Further studies to elucidate the full potential of the approach are in progress.

Financial support from KOFST and K-JIST, Korea, is gratefully acknowledged.

Notes and references

1 R. Taylor and D. R. M. Walton, *Nature*, 1993, **363**, 685; K. E. Geckeler, *Trends Polym. Sci.*, 1994, **2**, 355; A. Hirsch, *Synthesis*, 1995, 895; F. Diederich and C. Thilgen, *Science*, 1996, **271**, 317; K. E. Geckeler and S. Samal, *Polym. Int.*, 1999, **48**, 743.

2 K. E. Geckeler and A. Hirsch, *J. Am. Chem. Soc.*, 1993, **115**, 3850; H.-C. Hu, Y. Liu, D.-D. Zhang and L.-F. Wang, *J. Inclusion Phenom. Macrocyclic Chem.*, 1999, **33**, 295.

3 A. M. Rao, P. Zhou, K.-A. Wang, G. T. Hager, J. M. Holden, Y. Wang, W.-T. Lee, X.-X. Bi, P. C. Eklund, D. S. Cornett, M. A. Ducan and I. Amster, *Science*, 1993, **259**, 955; A. Gügel, P. Belik, M. Walter, A. Kraus, H. Harth, M. Wagner, J. Spickermann and K. Müllen, *Tetrahedron*, 1996, **52**, 5007; M. Taki, S. Takigami, Y. Watanabe, Y. Nakamura and J. Nishimura, *Polym. J.*, 1996, **29**, 1020; M. Ozawa, J. Li, K. Nakahara, L. Xiao, H. Sugawara, K. Kitazawa, K. Kinbara and K. Saigo, *J. Polym. Sci., Part A, Polym. Chem.*, 1998, **36**, 3139.

4 S. H. Friedman, D. L. De Camp, R. P. Sijbesma, G. Srdanov, F. Wudl and G. L. Kenyon, *J. Am. Chem. Soc.*, 1993, **115**, 6506; S. Yamago, H. Tokuyama, E. Nakamura, K. Kikuchi, S. Kananishi, K. Sueki, H. Nakahara, S. Enomoto and F. Ambe, *Chem. Biol.*, 1995, **2**, 385; E. Nakamura, H. Tokuyama, S. Yamago, T. Shiraki and Y. Sugiura, *Bull. Chem. Soc. Jpn.*, 1996, **69**, 2143; H. H. C. Chen, C. Yu, T. H. Ueng, S. Chen, B. J. Chen, K. J. Huang and L. Y. Chiang, *Toxicol. Pathol.*, 1998, **26**, 143; R. Bernstein, F. Prat and C. S. Foote, *J. Am. Chem. Soc.*, 1999, **121**, 464; I. Atsushi, H. Tsukasa, K. Masaru, S. Hikaru and S. Seiji, *Chem. Commun.*, 1999, 1403.

5 M. Brettreich and A. Hirsch, *Tetrahedron Lett.*, 1998, **39**, 2731; T. Da Ros, M. Prato, F. Novello, M. Maggini and E. Banfi, *J. Org. Chem.*, 1996, **61**, 9070.

6 J. Howard, *Nature*, 1997, **389**, 561; N. Koumura, R. W. J. Zijlstra, R. A. van Delden, N. Harada and B. L. Feringa, *Nature*, 1999, **401**, 152.

Iminophosphorane-mediated carbodiimide metathesis

Stephen A. Bell, Steven J. Geib and Tara Y. Meyer*

Department of Chemistry, University of Pittsburgh, Pittsburgh, Pennsylvania 15260, USA. E-mail: tmeyer+@pitt.edu

Received (in Irvine, CA, USA) 10th April 2000, Accepted 5th June 2000
Published on the Web 5th July 2000

Iminophosphorane Cl_3P=NAr (Ar = 2-fluorophenyl) is an active carbodiimide metathesis catalyst and the cycloaddition product, a 1,3-diaza-2-phosphetidine, is an intermediate in the reaction.

We study the metathesis of C=N bonds with the intention of developing the diverse synthetic and polymerization applications that depend on a single, well-defined reaction site. Until now, both our efforts[1–3] and those of others[4] have focused on metal–imide-mediated process. There are intriguing examples in the literature of stoichiometric metathesis of iminophosphoranes with carbodiimides as well as catalytic disproportionation of isocyanates using phosphine oxides.[5–9] These examples of heterocumulene reactivity inspired us to extend our search for C=N metathesis catalysts to include phosphorus systems. Here, we describe our discovery that iminophosphoranes can act as catalysts for metathesis of carbodiimides, and we provide evidence for a diazaphosphetidine intermediate.

Trichloroiminophosphoranes can self-dimerize in solution, a behavior that should, theoretically, correlate with a potential for reactivity with the similarly polarized C=N bond. In particular, we have focused on the *o*-fluorophenyl derivative, **1** which is known[10] to exist as an equilibrium mixture of dimer and monomer (K_{eq} = 0.17 dm^3 mol^{-1} at 50 °C, Scheme 1). ^{31}P NMR spectroscopy easily differentiates the two forms: −45.2 ppm (monomer) and −76.4 ppm (dimer).

The addition of an equivalent of diisopropylcarbodiimide to the iminophosphorane equilibrium mixture, followed by heating to 50 °C for 24 h gives a single product† by ^{31}P NMR spectroscopy (−58.2 ppm). ^1H NMR spectroscopic data‡ are consistent with the formulation of diazaphosphetidine **2** arising from the addition of the C=N bond across the P=N bond, with the expected N-to-P regiochemistry. The observed 31 Hz phosphorus coupling of the methyne proton of one of the two inequivalent isopropyl groups is diagnostic for this product.

X-Ray diffraction studies of a single crystal,§ isolated from a preparative scale reaction, confirmed the guanidinate-type structure (Fig. 1). Complex **2** crystallized into a pseudo-*TBPY* geometry with one chlorine and the aryl-substituted nitrogen located in axial positions. Although electronegativity arguments would predict two axial chlorines, the small guanidinate ring size dictates that the more electronegative of the two nitrogens, the N-2-fluorophenyl, will occupy one axial site. The notably unsymmetric ring can then be explained by normal axial/equatorial bond length differences.

Although one example of a similar guanidinate-type structure was found in a search of the Cambridge Crystal Database,[11] the compound was not prepared by cycloaddition. Analogous urea-derived structures are more common.[12] It is interesting to note

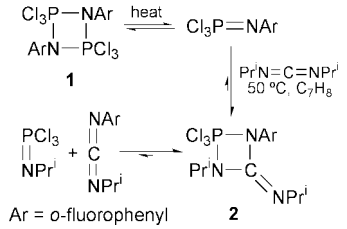

Scheme 1

that Molina *et al*., as part of their extensive studies on the preparation of heterocycles from carbodiimides, isocyanates and iminophosphoranes, isolated and characterized crystallographically an example of a zwitterionic, betaine form of this type of intermediate.[13]

Heating diisopropylcarbodiimide and di(*p*-tolyl)carbodiimide at 120–125 °C in toluene in the presence of iminophosphorane **1** (10 mol%) induced metathesis of the carbodiimides as indicated by the growth of ^1H NMR resonances associated with the mixed carbodiimide (Scheme 2). No =NR exchange was noted when the carbodiimides were heated without catalyst present. The reaction proceeded in < 24 h to give equilibrium mixtures of the carbodiimides. In an independent experiment, the same carbodiimides were metathesized at a similar rate in the presence of 10 mol% of the guanidinate complex **2**. The parallel activity of the guanidinate complex is consistent with its role as an intermediate in the catalytic process, although further studies will be required before other mechanisms, such as acid- or amine-catalyzed reactions,[4a] can be ruled out.

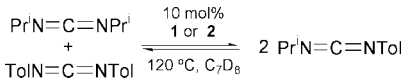

Scheme 2

The similarities of Wittig chemistry and metal-catalyzed metathesis are interesting. Until now, however, phosphorus-ylide and -imine reactions have nearly always exploited the formation of a thermodynamically more stable P=E (E = O,S) bond as a driving force. In contrast, the preliminary results described here establish that truly catalytic metathetical processes are also possible for phosphorus. We are currently investigating the generality of these reactions.

This research was supported by the National Science Foundation (CAREER 9624138 and POWRE 9624139). We

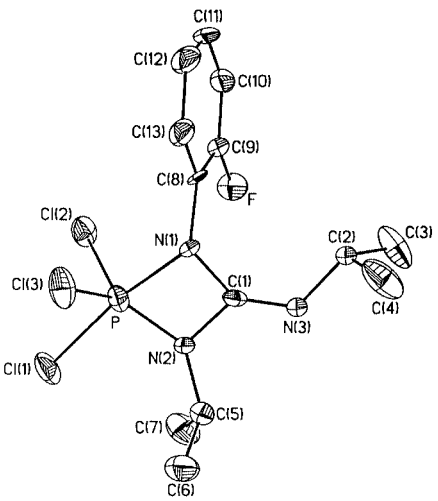

Fig. 1 Molecular structure of **2** indicating the atomic numbering scheme. Selected bond lengths (Å) and angles (°): P–Cl(1) 2.1029(12), P–Cl(3) 2.0352(12), P–N(1) 1.783(3), P–N(2) 1.6511(4), N(1)–C(1) 1.398(4), N(2)–C(1) 1.432(4); Cl(1)–P–Cl(3) 90.95(5), Cl(2)–P–Cl(3) 108.06(6), N(1)–P–Cl(1) 170.44(13), N(2)–P–Cl(1) 94.93(11), N(1)–C(1)–N(3) 138.5(3), N(1)–C(1)–N(2) 96.4(3), N(2)–C(1)–N(3) 125.1(3).

DOI: 10.1039/b003148h

also gratefully acknowledge support from the DuPont Educational Aide Grant Program. T. Y. M. is a fellow of the Alfred P. Sloan Foundation.

Notes and references

† *Synthetic procedure* for **2**: 1,3-diisopropylcarbodiimide (0.400 mL, 2.56 mmol) was added to a toluene solution (20 mL) of **1** (0.631 g, 2.56 mmol), in a reaction vessel equipped with a Teflon stopcock. After stirring for 48 h at 50 °C, the solvent was removed to give a white solid. Recyrstallization from CH_2Cl_2–hexanes (1 : 6) at −35 °C gave a 50.2% yield of **2**. Anal. Calc. for $C_{13}H_{18}N_3PFCl_3$: C, 41.90; H, 4.88; N, 11.27. Found: C, 41.71; H, 4.93; N, 11.09%.

‡ *Spectral data* for **2**: ^{1}H NMR (300 MHz, C_7D_8): δ 6.64–6.75 (m, aromatics), 4.35 (d/sept, PNCH), 3.35 (sept, NC=NCH), 1.49 (d, NC=NCHCH_3), 1.02 (d, PNCHCH_3), 0.91 (d, PNCHC′H_3). ^{31}P{^{1}H} NMR (121 MHz, C_7D_8): δ −58.2 (s).

§ *Crystallographic data* for **2** at 210(2) K: $C_{13}H_{18}Cl_3FN_3P$, M = 372.62, monoclinic, space group $P2_1/n$, a = 9.2930(19), b = 17.376(4), c = 10.822(2) Å, β = 93.02 (3)°, V = 1745.1(6) Å^3, D = 1.418 g cm^{-3}, Z = 4, μ = 0.622 mm^{-1}. Of the 2503 reflections collected ($2.22 \leqslant 2\theta \leqslant 26.00°$) with Mo-K$\alpha$ radiation (λ = 0.71073 Å), the 2288 with $F_o^2 > 2\sigma(F_o^2)$ were used in the final least-squares refinement to yield $R(F_o)$ = 0.0360 and $R_w(F_o^2)$ = 0.0931.

CCDC 182/1681.

1 G. K. Cantrell and T. Y. Meyer, *J. Am. Chem. Soc.*, 1998, **120**, 8035.
2 G. K. Cantrell and T. Y. Meyer, *Chem. Commun.*, 1997, 1551.
3 G. K. Cantrell and T. Y. Meyer, *Organometallics*, 1997, **16**, 5381.
4 (*a*) J. M. McInnes and P. Mountford, *Chem. Commun.*, 1998, 1669; (*b*) K. R. Birdwhistell, J. Lanza and J. Pasos, *J. Organomet. Chem.*, 1999, **584**, 200; (*c*) R. L. Zuckerman, S. W. Krska and R. G. Bergman, *J. Am. Chem. Soc.*, 2000, **122**, 751.
5 R. Huisgen and J. Wulff, *Chem. Ber.*, 1969, **102**, 1848; J. Bodeker, P. Kockritz and K. Courault, *Z. Chem.*, 1979, **19**, 59; P. Molina, M. Alajarin and A. Vidal, *J. Org. Chem.*, 1993, **58**, 1687.
6 A. W. Johnson, *Ylides and Imines of Phosphorus*, John Wiley & Sons, Inc., New York, 1993, pp. 403–484.
7 T. W. Campbell, J. J. Monagle and V. Foldi, *J. Am. Chem. Soc.*, 1962, **84**, 3673.
8 J. J. Monagle and J. V. Mengenhauser, *J. Org. Chem.*, 1966, **31**, 2321.
9 R. C. Hall and D. J. H. Smith, *J. Chem. Soc., Perkin Trans. 2*, 1977, 1373.
10 E. Fluck and D. Wachtler, *Liebigs. Ann. Chem.*, 1980, 1651.
11 M. Farkens, P. G. Jones, A. Fischer and R. Schmutzler, *Phosphorus, Sulfur Silicon*, 1992, **73**, 195.
12 G. I. Derkach and A. V. Narbut, *Zh. Obsch. Khim Eng. Ed.*, 1965, **35**, 937; H. Ulrich and A. A. R. Sayigh, *Angew. Chem., Int. Ed. Engl.*, 1964, **3**, 585.
13 P. Molina, M. Alajarin, C. Lopez-Leonardo, R. M. Claramunt, M. C. Foces-Foces, F. H. Cano, J. Catalan, J. L. G. de Paz and J. Elguero, *J. Am. Chem. Soc.*, 1989, **111**, 355.

Linking of metal centres through boryl ligands: synthesis, spectroscopic and structural characterisation of a symmetrically bridged boryl complex $CpFe(CO)_2BO_2C_6H_2O_2BFe(CO)_2Cp$

S. Aldridge,*[a] R. J. Calder,[a] A. A. Dickinson,[a] D. J. Willock[a] and J. W. Steed[b]

[a] *Department of Chemistry, Cardiff University, PO Box 912, Park Place, Cardiff, UK CF10 3TB. E-mail: AldridgeS@cardiff.ac.uk*

[b] *Department of Chemistry, King's College London, Strand, London, UK WC2R 2LS*

Received (in Basel, Switzerland) 12th May 2000, Accepted 14th June 2000
Published on the Web 5th July 2000

The synthesis, spectroscopic and structural characterisation of the symmetrically bridged boryl complex $CpFe(CO)_2BO_2C_6H_2O_2BFe(CO)_2Cp$ are reported, together with analysis of the bonding by structural and DFT methods.

Transition metal boryl complexes (L_nMBR_2) have been the subject of considerable recent research effort,[1] in part because of their involvement in versatile organic transformations such as the metal-catalysed hydroboration and diboration of multiple bonds.[1,2] Furthermore, derivatives of the type $(C_5R_5)M(CO)_n$-$BO_2C_6H_2Me_2$ (M = Fe, Ru, n = 2; M = W, n = 3) have been shown to functionalise alkanes under photolytic conditions, with the unusual activity and regiochemistry of the reaction being tentatively ascribed to the presence of a ligand with Lewis acidic properties.[3,4] Recent studies have sought to probe the nature of the metal–boron interaction in metal boryl complexes by spectroscopic and crystallographic methods.[1] Almost exclusively,[5] such studies have focussed on monodentate boryl ligands adopting a terminal mode of coordination with respect to the metal centre.[1] Here, we describe a novel synthetic route to metal complexes featuring bidentate boryl ligands together with the structural and spectroscopic characterisation of the symmetrically bridged (μ_2,η^1,η^1) boryl system $CpFe(CO)_2$-$BO_2C_6H_2O_2BFe(CO)_2Cp$ **4**. Comparison of the mode of coordination of the bridging boryl ligand with that found for terminally bound analogues allows significant insight into the nature of the metal–boron interaction.

In our recent work we have been seeking to develop synthetic approaches to multifunctional boranes and boron halides based on polyhydroxybenzene frameworks (*e.g.* **3**) as potential precursors to multinuclear metal boryl complexes.[6] The synthetic route to compound **4** is outlined in Scheme 1; fuller details of the preparation of the trimethylsilyl and chloroborane precursors have been reported recently.[6] Addition of a toluene solution of **3** to 2 equivalents of $CpFe(CO)_2Na$ suspended in toluene at −30 °C, followed by warming to room temperature and stirring for 1 week led to the formation of an orange–red solution and a beige precipitate. Removal of the supernatent by filtration, extraction of the beige precipitate with CH_2Cl_2 and subsequent crystallisation by layering with 40/60 petroleum led to the formation of **4** in 45% yield. This compound is air sensitive, although thermally robust enough to survive unchanged at room temperature for several weeks under an argon atmosphere. It is sparingly soluble in non-polar organic media and decomposes rapidly in donor solvents such as thf or diethyl ether. Compound **4** has been characterised† by ^{1}H, ^{13}C and ^{11}B NMR, IR spectroscopy, high-resolution mass spectrometry, elemental analysis and single crystal X-ray diffraction.

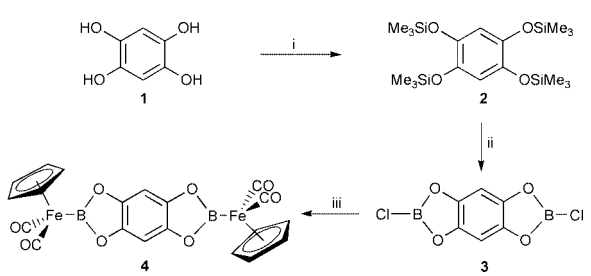

Scheme 1 Synthesis of the bridged boryl complex **4**. *Reagents and conditions*: i, Me_3SiCl (10 equiv.), Et_3N, toluene, 12 h at room temp., 78%; ii, BCl_3 (2 equiv.), 40/60 petroleum, 3 h at 50 °C, 89 %; iii, $CpFe(CO)_2Na$ (2 equiv.), toluene, 1 week at room temp., 45%.

The single ^{11}B NMR shift at δ_B 48 is entirely consistent with the formation of a symmetrically bridged molecule in which both of the B–Cl linkages in **3** have been replaced by Fe–B bonds, being very similar to those reported by Hartwig *et al*. for the terminally coordinated Bcat (cat = *ortho*-$O_2C_6H_4$) complexes $(C_5R_5)Fe(CO)_2Bcat$ [δ_B 51.8 (R = H)[4] and 54.3 (R = Me),[4] respectively]. Similar chemical shifts have also been reported by Braunschweig *et al*. for other terminal boryl ligands bound to iron.[7,8]

A single crystal X-ray diffraction study was undertaken on **4**,‡ the results of which confirm the formulation predicted on the basis of spectroscopic data and are illustrated in Fig. 1. The molecular structure consists of two piano-stool $CpFe(CO)_2X$ fragments linked in μ_2,η^1,η^1 fashion by the $BO_2C_6H_2O_2B$ ligand.

The synthesis and structural characterisation of **4** allows, for the first time, the opportunity to compare the coordination behaviour of a bridging boryl ligand ($BO_2C_6H_2O_2B$) with that of the analogous terminally bound ligand (Bcat). The complex $CpFe(CO)_2Bcat$ features near co-planarity of O–B–O and B–Fe–Cp centroid moieties consistent with the existence of a Fe–B π interaction involving the $CpFe(CO)_2$ HOMO and the ligand-based LUMO.[4] In the case of **4**, however, the crystal structure reveals a near orthogonal relationship [82.2(1)°] between the corresponding planes and implies no π interaction between ligand LUMO and Fp HOMO. This observation is consistent with the fact that the ν(CO) stretching frequencies for **4** are somewhat lower than those observed for $CpFe(CO)_2Bcat$ (2006 and 1954 cm^{-1} *vs*. 2024 and 1971 cm^{-1}).[4] Given that the steric

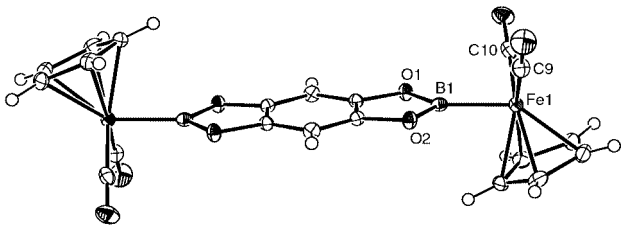

Fig. 1 Molecular structure of $CpFe(CO)_2BO_2C_6H_2O_2BFe(CO)_2Cp$, **4**. Relevant bond lengths (Å) and angles (°): Fe(1)–B(1) 1.971(2), Fe(1)–C(10) 1.751(2), Fe(1)–C(9) 1.758(2), Fe–Cp(centroid) 1.721(2), B(1)–O(1) 1.406(2), B(1)–O(2) 1.406(2); C(9)–Fe–C(10) 93.97(8), B(1)–Fe–C(9) 88.32(8), B(1)–Fe–C(10) 87.35(8), O(1)–B(1)–O(2) 109.15(14), O(1)–B(1)–Fe(1) 121.94(12), O(2)–B(1)–Fe(1) 125.79(13), O(1)–B(1)–Fe(1)–Cp(centroid) 82.2(1).

DOI: 10.1039/b003901m

requirements at the iron centre of the terminal Bcat and bridging $BO_2C_6H_2O_2B$ ligands are likely to be very similar it seems evident that the difference in ligand coordination is due to electronic factors. The presence of two extra oxygen-based substituents on the central benzene ring in **4** might be expected to render the ring more electron rich, thereby increasing the degree of O–B π interaction and reducing the π acidity of the boron centre with respect to the iron.

Interestingly, although these structural and spectroscopic observations imply a weaker Fe–B interaction, the Fe–B bond length is lengthened only marginally in **4** compared to the terminally bound $CpFe(CO)_2Bcat$ system [1.971(2) *vs.* 1.959(6) Å].[4] Conceivably this may reflect the fact that the bond length in such systems is relatively insensitive to the π contribution to bonding. However, the Fe–B distance in **4** is also significantly shorter than that found in any other terminally bound iron boryl complex for which the B–Fe–Cp centroid and BR_2 planes are close to orthogonal [average 2.048(5) Å§]. Such a shortening of the Fe–B bond might also be consistent with a weak π interaction between the boryl LUMO and the Fp HOMO − 2 (a 1a′ π type MO which is perpendicular to the HOMO[9]). Such an interaction has been suggested for the complex $CpFe(CO)_2BPh_2$ [which, at 2.034(3) Å,[4] has a markedly longer Fe–B bond than **4**] and has been discussed by Hoffmann and coworkers in their analysis of ligand orientation in Fp–carbene complexes.[9]

Comparison of the bonding in **4** and $CpFe(CO)_2Bcat$ was further aided by DFT calculations[10] carried out for the model compound $CpFe(CO)_2BO_2C_2H_2$, **5**, the preliminary results of which are reported here.¶ Total energies were calculated for various rotamers of the molecule **5** in which the angle between the B–Fe–Cp centroid and O–B–O planes was varied by rotation about the Fe–B bond in 10° intervals between 0 and 90°. Energy minima are found for θ = *ca.* 10 and 80°. These observations are indeed consistent with the presence of weak π type interactions between the Fp HOMO and boryl-based LUMO for the near parallel orientation of the B–Fe–Cp centroid and O–B–O planes and between the Fp HOMO − 2 and boryl LUMO for the perpendicular orientation. The calculated energy difference between these two minima is very small (0.1 kJ mol^{-1} at the gradient corrected DFT level of theory), such that the adoption of one particular orientation in the solid state may well be influenced by crystal packing forces.

The structure of **4** illustrates the coordination behaviour of a symmetrical μ_2,η^1,η^1 boryl ligand and demonstrates significant differences in metal–boron interaction compared to terminal η^1 analogues. The synthetic methodology outlined in Scheme 1, together with the recent synthesis of the *bis*(borane) $HBO_2C_6H_2O_2BH$,[6] open up routes to a wide range of bridging boryl complexes *via* metathetical or oxidative addition pathways.

The support of the Nuffield Foundation, the Royal Society and Cardiff University are gratefully acknowledged. We would also like to thank the EPSRC National Mass Spectrometry Service. The calculations presented in this paper were carried out with the help of support from the EPSRC, Synetix and OCF. In addition, J. W. S thanks the EPSRC and King's College London for the provision of the X-ray diffractometer and the Nuffield Foundation for the provision of computing equipment.

Notes and references

† *Spectroscopic data* for **4**: MS(EI): M^+ = 514, isotopic pattern corresponding to 2 B, 2 Fe atoms, fragment ion peaks at *m/z* 486, 458, 430, 402 corresponding to sequential loss of four CO molecules, exact mass (calculated) *m/z* 513.9417, (observed) 513.9424. ^{1}H NMR ([$^2H_6$]benzene, 21 °C), δ 4.95 (s, 10H, Cp), 6.99 [s, 2H, $CpFe(CO)_2BO_2C_6H_2O_2BFe(CO)_2Cp$]. ^{13}C NMR ([$^2H_6$]benzene, 21 °C), δ 82.85 (Cp), 94.68 (aromatic *C*H), 143.83 (aromatic quaternary), 212.54 (CO). ^{11}B NMR (toluene, 21 °C), δ 48 (br). IR(KBr disk, cm^{-1}) ν(CO) 2006s, 1954s. Elemental analysis: calc. for $C_{20}H_{12}B_2Fe_2O_8$, C, 46.74, H, 2.35. Found: C, 46.22, H 2.14%.

‡ *Crystallographic data* for **4**: $C_{20}H_{12}B_2Fe_2O_8$, monoclinic, space group $P2_1/n$, a = 6.4542(3), b = 12.2543(4), c = 12.4180(6) Å, β = 93.604(3)°, U = 980.22(7) Å^3, Z = 2, D_c = 1.740 Mg m^{-3}, M = 513.94, T = 100 K. 6704 reflections collected, 2243 independent (R_{int} = 0.0340) which were used in all calculations. R_1 = 0.0257, wR_2 = 0.0582 for observed unique reflections [$I > 2\sigma(I)$] and R_1 = 0.0315, wR_2 = 0.0605 for all 2243 unique reflections. The max. and min. residual electron densities on the final difference Fourier map were 0.331 and −0.255 e Å^{-3}, respectively.

CCDC 182/1684. See http://www.rsc.org/suppdata/cc/b0/b003901m/ for crystallographic data in .cif format.

§ Reported Fe–B distances (Å) for iron boryl complexes in which B–Fe–Cp centroid and BR_2 planes are close to orthogonal [torsion angle (°) in square brackets]: $CpFe(CO)_2BPh_2$ 2.034(3) [75],[4] $CpFe(CO)_2B(NMe_2)B(NMe_2)Cl$ 2.090(3) [92.4],[7] $Cp^*Fe(CO)_2B(NMe_2)Cl$ 2.027(5) [87.4],[8] $[CpFe(CO)_2]_2B_3N_3H_3Cl$ 2.041(1) [90.6 and 94.5].[5] The complex $Cp^*Fe(CO)_2BH_2{\cdot}PMe_3$, containing four-coordinate boron[11] was not included in this analysis.

¶ *Details of DFT calculations*: The ADF 1999.02[12,13] suite of programs was used for DFT calculations, employing Becke's gradient-corrected exchange functional[14] and Lee–Yang–Parr's correlation functional (BLYP).[15] Triple-zeta Slater type orbitals were used as basis functions with a polarisation function added for H through Ar and Ga through Kr. The level of frozen core approximation for C and O was the 1s orbital and for Fe orbitals up to 2p were fixed. The geometry of each molecule was optimised at the BLYP level of theory with no symmetry restrictions.

1 G. J. Irvine, M. J. G. Lesley, T. B. Marder, N. C. Norman, C. R. Rice, E. G. Robins, W. R. Roper, G. Whittell and L. J. Wright, *Chem. Rev.*, 1998, **98**, 2685; M. R. Smith, *Prog. Inorg. Chem.*, 1999, **48**, 505; H. Braunschweig, *Angew. Chem., Int. Ed.*, 1998, **37**, 1787; H. Wadepohl, *Angew. Chem., Int. Ed. Engl.*, 1997, **36**, 2441.
2 See, for example, K. Burgess and M. J. Ohlmeyer, *Chem. Rev.*, 1991, **91**, 1179.
3 K. M. Waltz and J. F. Hartwig, *Science*, 1997, **277**, 211.
4 J. F. Hartwig and S. Huber, *J. Am. Chem. Soc.*, 1993, **115**, 4908; K. M. Waltz, C. N. Muhoro and J. F. Hartwig, *Organometallics*, 1999, **18**, 3383.
5 Two examples of highly asymmetric μ_2,η^1 Bcat derivatives of platinum have been reported by Norman and coworkers: D. Curtis, M. J. G. Lesley, N. C. Norman, A. G. Orpen and J. Starbuck, *J. Chem. Soc., Dalton Trans*, 1999, 1687; Braunschweig *et al*. have reported bridged complexes based on a central borazine moiety: H. Braunschweig, C. Kollann and M. Müller, *Eur. J. Inorg. Chem.*, 1998, 291.
6 S. Aldridge, R. J. Calder, M. H. Cunningham, K. M. A. Malik and J. W. Steed, *J. Organomet. Chem.*, 2000, in press.
7 H. Braunschweig, B. Ganter, M. Koster and T. Wagner, *Chem. Ber.*, 1996, **129**, 1099.
8 H. Braunschweig, C. Kollann and U. Englert, *Eur. J. Inorg. Chem.*, 1998, 465.
9 B. E. R. Schilling, R. Hoffmann and D. Lichtenberger, *J. Am. Chem. Soc.*, 1979, **101**, 585.
10 The use of DFT methods to study bonding in boryl complexes is precedented: D. G. Musaev and K. Morokuma, *J. Phys. Chem.*, 1996, **100**, 6509.
11 T. Yasue, Y. Kawano and M. Shimoi, *Chem. Lett.*, 2000, **1**, 58.
12 ADF 1999, E. J. Baerends, A. Bérces, C. Bo, P. M. Boerrigter, L. Cavallo, L. Deng, R. M. Dickson, D. E. Ellis, L. Fan, T. H. Fischer, C. Forseca Guerra, S. J. A. van Gisbergen, J. A. Groeneveld, O. V. Gritsenko, F. E. Harris, P. van den Hoek, H. Jacobsen, G. van Kessel, F. Kootstra, E. van Lenthe, V. P. Osinga, P. H. T. Philipsen, D. Post, C. C. Pye, W. Ravenek, P. Ros, P. R. T. Schipper, G. Schreckenbach, J. G. Snijders, M. Sola, D. Swerhone, G. te Velde, P. Vernooijs, L. Versluis, E. van Wezenbeek, G. Wiesenekker, S. K. Wolff, T. K. Woo and T. Ziegler, was obtained from *Theoretical Chemistry*, Vrije Universiteit, Amsterdam, The Netherlands.
13 C. Forseca Guerra, J. G. Snijders, G. te Velde and E. J. Baerends, *Theor. Chem. Acc.*, 1998, **99**, 391.
14 A. D. Becke, *Phys. Rev. A*, 1988, **38**, 3098.
15 C. Lee, W. Yang and R. G. Parr, *Phys. Rev. B*,1988, **37**, 785.

ChemComm

Photocontrol of Na^+ transport across a phospholipid bilayer containing a bisanthroylcalix[4]arene carrier

Takashi Jin

Section of Intelligent Materials and Devices, Research Institute for Electronic Science, Hokkaido University, Sapporo 060-0812, Japan. E-mail: jin@imd.es.hokudai.ac.jp

Received (in Cambridge, UK) 13th March 2000, Accepted 13th June 2000
Published on the Web 5th July 2000

Photocontrol of Na^+ transport across a phospholipid bilayer membrane can be undertaken by using a new calix[4]arene carrier bearing two anthracene moieties.

Photoresponsive compounds are of great interest for the development of photocontrolled transport systems where ion and electron fluxes across membranes can be regulated by light.[1] Since a first report[2] of photoresponsive crown ethers, a number of the photocontrolled ion transport systems using bulky liquid membranes have been reported.[3] However, there are very limited studies of photocontrol of ion fluxes across lipid bilayer membranes.[4] The photoresponsive ionophores, by which ion fluxes across lipid bilayers can be controlled, are expected to be useful for the study of the response of cellular systems to ion concentrations. Here, we report the first example of photocontrol of Na^+ transport across a phospholipid bilayer containing a bisanthroylcalix[4]arene carrier **1**.

Calix[4]arene esters are known to have selective complexing abilities[5] toward Na^+ ions, and act as selective Na^+ carriers[6–8] in lipid bilayer membranes. It has been shown that the rates of Na^+ transport by a calix[4]arene ester across a phospholipid bilayer membrane are comparable to the rates by an antibiotic ionophore, monensin.[6] To synthesize a phoresponsive calix[4]arene-based Na^+ carrier, we introduced two photo-dimerizable anthracenes into the terminal positions (-OCH_2COR) of sodium binding sites in a calix[4]arene ester.[9] Anthracene

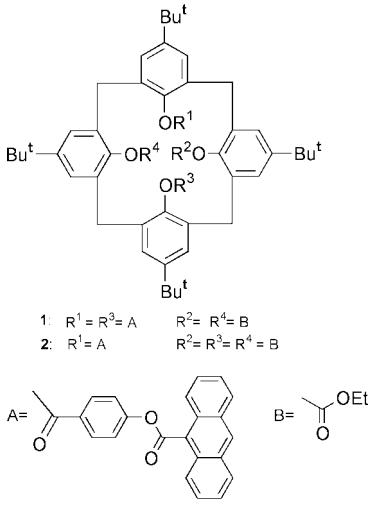

appended calix[4]arenes **1** and **2** were prepared from the reaction of *p*-(9-anthroyloxy)phenacyl bromides (Molecular Prob. Inc.) and bis- or trisethoxycarbonylmethyl ether[10] of *p*-*tert*-butylcalix[4]arene in the presence of K_2CO_3 in THF. The compounds were identified by ^1H NMR and field desorption mass spectroscopy.† The signal patterns in $ArCH_2Ar$ protons confirmed that both **1** and **2** adopted cone conformations in $CDCl_3$. The Na^+ complexing abilities of **1** and **2** were checked by the ^1H NMR titration experiments.[5]

Photoirradiations were carried out in THF at 25 °C using a 150 W Xe lamp through a band pass filter (λ 360 nm). As shown in Fig. 1(a), the UV irradiation of the solution of the bisanthroylcalix[4]arene **1** caused a decrease in the absorbance of anthracene moieties with two isosbestic points. However, the UV irradiation of the solution of the monoanthroyl calix[4]arene **2** did not cause a significant spectral change (Fig. 1(b)). These results indicate that the photodimerization of the two anthracene moieties in **1** readily takes place in THF (Scheme 1), but not in **2**. The slight decrease in the absorption of **2** may be explained by the photobreaching of the anthracene moiety. In the case of **1**, the thermal decomposition of the photodimeric form was hardly observed even after 24 h in the dark, suggesting that the photodimeric form of **1** is very stable compared to the monomeric form of **1**.

The ion transport experiments were conducted by a planar bilayer membrane[11] (soybean phospholipid) with the aid of a voltage-clamp technique.‡ The ion transport selectivity of **1** was evaluated by the measurements of the current–voltage relationships in the unsymmetrical ionic conditions of LiCl (*cis*)–NaCl (*trans*) and KCl (*cis*)–NaCl (*trans*), where the salt concentrations in two chambers were set to 100 mM containing 25 mM HEPES–Tris Buffer (pH 7.2). The reverse potentials were obtained as −80 and −37 mV for the LiCl–NaCl and KCl–NaCl systems at 25 °C. From the Goldman–Hodgkin–Katz equation,[12] the ion permeability ratios (P_{X^+}/P_{Na^+}) across the bilayer membrane were calculated as P_{Li^+}/P_{Na^+} = 0.044 and P_{K^+}/P_{Na^+} = 0.24, showing that **1** can act as a selective Na^+ carrier in a phospholipid bilayer membrane.

Fig. 2 shows the effect of UV (> 310 nm) irradiation on the membrane currents resulting from Na^+ transport by **1** and **2**. Upon UV irradiation of the bilayer membrane containing **1**, the Na^+ currents (at 100 mV) immediately decreased (Fig. 2(a)), while UV irradiation of the membrane containing **2** did not cause any change (Fig. 2(b)). This behavior is consistent with the results of the spectral change of **1** and **2** in THF by UV irradiation. In the case of **1**, it should be noted that the Na^+ currents are going to recover after the light-off, which can be explained by the increase in the concentration of the monomeric

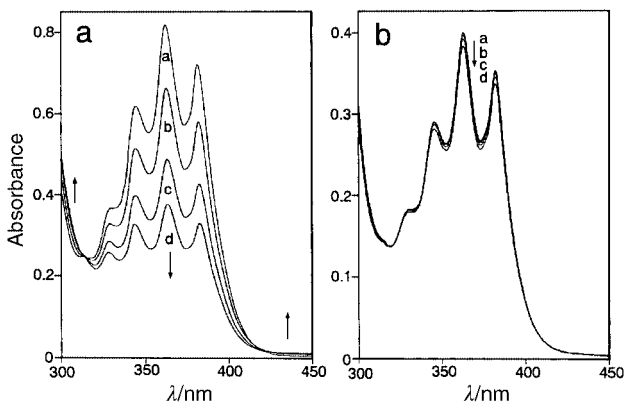

Fig. 1 The absorption spectra of **1** (a) and **2** (b) in THF before and after UV irradiation (360 nm) : (a) 0 s; (b) 30 s; (c) 1 min; (d) 5 min.

DOI: 10.1039/b002034f

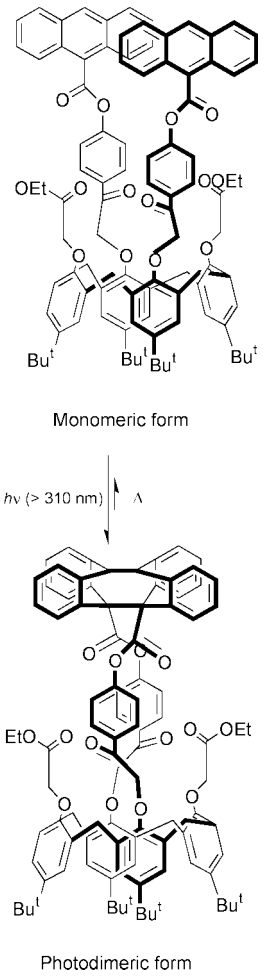

Scheme 1

form of **1** in the membrane region at the aperture in a Teflon film. This may be due to the lateral diffusion of the monomeric form of **1** from the membrane which is not irradiated by light. In fact, after a long irradiation time (*ca*. 30 min), the membrane current decreased to be the current (0.5 pA) of a control level. The increase in Na^+ currents, which result from the thermal decomposition of the dimeric form of **1**, was not observed within 1 h. These results indicate that the photodimerization of two anthracene moieties in **1** takes place in the lipid membrane and the Na^+ transport activity diminishes in the photodimetric form of **1**.

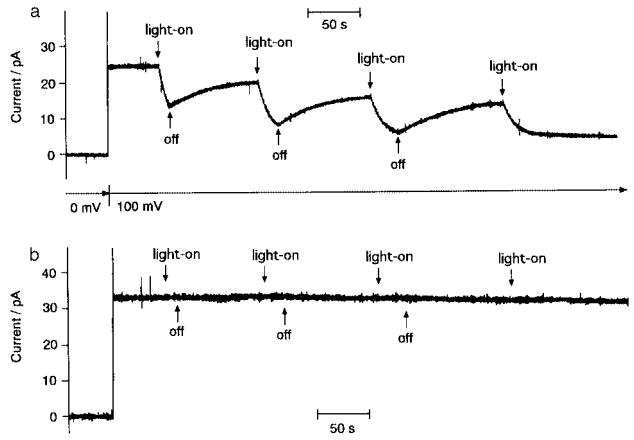

Fig. 2 The changes in Na^+ currents across the lipid bilayer membrane containing **1** (a) or **2** (b) at 100 mV by UV irradiation (> 310 nm). Two chambers were filled with 100 mM NaCl aq. solutions (pH 7.2, 25 mM HEPES–Tris buffer). The bilayer membranes were prepared by the lipid–calix[4]arene mixtures (lipid: **1** or **2** = 100: 1 w/w). The UV irradiation (3.2 mW mm^{-2}) was performed through a glass fiber, where the spot of the light was *ca*. 5 mm diameter.

In conclusion, we have demonstrated that photocontrol of Na^+ fluxes across a bilayer membrane can be undertaken by using a bisanthroylcalix[4]arene **1**. This is the first report of a photoresponsive Na^+ carrier which is active in a phospholipid bilayer. We believe that the new calix[4]arene **1** has potential for use as a photoresponsive Na^+ carrier for the regulation of Na^+ concentrations in biological membrane systems.

The author thanks Dr G. Nishimura and Mr T. Ohta for technical support. The author also thanks Mr E. Yamada for the measurements of ^{1}H NMR spectra.

Notes and references

† *Selected data* for **1**: δ_H(400 MHz, $CDCl_3$), 1.06 and 1.24 (s, 18H, CMe_3), 1.30 (t, 6H, CH_2CH_3), 3.32 (d, 4H, $ArCH_2Ar$, *J* 13.0), 4.19 (q, 4H, CH_2CH_3), 4.87 (s, 4H, OCH_2CO_2), 5.09 (d, 4H, $ArCH_2Ar$, *J* 13.0), 5.83 (s, 4H, OCH_2COPh), 6.76 and 7.00 (s, 4H, ArH), 7.36–8.49 (26H, COPh and anthracene); field desorption mass spectrum, *m/z* 1497 (M^+).

‡ Planar bilayer membranes were formed at an aperture (diameter, 0.2 mm) in a Teflon film (thickness, 12.5 μm) which separated two Teflon chambers (internal volume of each chamber is 1.7 ml with surface area of 1 cm^2). The side to which compounds were added was defined as the '*cis*' chamber and the opposite side was the '*trans*' chamber. A patch clamp amplifier (CEZ-2300; Nihon Kohden, Ltd., Tokyo, Japan) was used in a voltage clamp mode to amplify the currents and to control the voltages across the bilayer membranes. The command voltage was fed to the *trans* chamber *via* an Ag/AgCl electrode through an agar bridge and the *cis* chamber was grounded *via* an Ag/AgCl electrode through an agar bridge. The voltage was referenced to the *cis* side with respect to the *trans* side.

1 J.-M. Lehn, *Supramolecular Chemistry—Concepts and Perspectives*, VCH, Weinheim, 1995.
2 S. Shinkai, T. Nakaji, Y. Nishida, T. Ogawa and O. Manabe, *J. Am. Chem. Soc.*, 1980, **102**, 5860.
3 See for example: S. Shinaki, T. Nakaji, T. Ogawa, K. Shigematsu and O. Manabe, *J. Am. Chem. Soc.*, 1981, **103**, 111; M. Irie and M. Kato, *J. Am. Chem. Soc.*, 1985, **107**, 1024; S. Shinkai, T. Ogawa, K. Shigematsu and O. Manabe, *J. Chem. Soc., Perkin Trans. 1*, 1987, 449; M. Sato, T. Kinoshita, A. Takizawa and Y. Tsujita, *Polym. J. (Tokyo)*, 1989, **21**, 369; M. G. Kodzwa and D. G. Rethwisch, *Polym. Mater. Sci. Engl.*, 1997, **76**, 279.
4 K. Kano, Y. Tanaka, T. Ogawa, M. Shimomura, Y. Okahata and T. Kunitake, *Chem. Lett.*, 1980, 421; J. Sunamoto, K. Iwamoto, Y. Mohri and K. Kominato, *J. Am. Chem. Soc.*, 1982, **104**, 5502; H. Nakanishi and H. Yamaguchi, *Kagaku Kogyo*, 1992, **43**, 198; M. Tanaka and Y. Yonezawa, *J. Phys. Chem.*, 1996, **100**, 5160; Y. Lei and J. K. Hurst, *Langmuir*, 1999, **15**, 3424.
5 F. Arnaud-Neu, E. M. Collins, M. Deasy, G. Ferguson, S. J. Harris, B. Kaitner, A. J. Lough, M. A. McKervey, E. Marques, B. L. Ruhl, M. J. Schwing-Weill and E. M. Seward, *J. Am. Chem. Soc.*, 1989, **111**, 8681; T. Jin and K. Ichikawa, *J. Phys. Chem.*, 1991, **95**, 2601; T. Jin, *Phys. Chem. Chem. Phys.*, 2000, **2**, 1401.
6 T. Jin, K. Kinjo, T. Koyama, Y. Kobayashi and H. Hirata, *Langmuir*, 1996, **12**, 2684.
7 N. Kimizuka, T. Wakiyama, A. Yanai, S. Shinkai and T. Kumitake, *Bull. Chem. Soc. Jpn.*, 1996, **69**, 3681.
8 T. Jin, M. Kinjo, Y. Kobayashi and H. Hirata, *J. Chem. Soc., Faraday Trans.*, 1998, **94**, 3135.
9 A similar design of ionophoric calix[4]arenes for the photocontrol of metal-binding activity has been reported: G. Gang, T. Sasaki, K. Nakashima and S. Shinkai, *Chem. Lett.*, 1992, 1287; G. Gang, T. Sasaki, Y. Kawahara and S. Shinkai, *Tetrahedron. Lett.*, 1992, **33**, 2163; T. Tsudera, A. Ikeda and S. Shinkai, *Tetrahedron*, 1997, **53**, 13 609.
10 K. Iwamoto and S. Shinkai, *J. Org. Chem.*, 1992, **57**, 7066.
11 M. Montal and P. Mueller, *Proc. Natl. Acad. Sci. USA*, 1972, **69**, 3561.
12 *Membrane Transport*, ed. S. L. Bonting and J. J. H. H. M. de Pont, Elsvier, New York, 1981.

ChemComm

Quantitative extraction of aqueous alkali metal ions using supercritical carbon dioxide and polyethylene glycol ligands

Shunsuke Mochizuki, Richard L. Smith, Jr. and Hiroshi Inomata*

Department of Chemical Engineering, Research Center of Supercritical Fluid Technology, Tohoku University, Aoba-ku, Aramaki-Aza, Aoba 07, Sendai 980-8579, Japan. E-mail: inomata@scf.che.tohoku.ac.jp

Received (in Cambridge) 27th April 2000, Accepted 15th June 2000
Published on the Web 5th July 2000

Quantitative extraction (30–70%) of alkali metal ions (K^+, Na^+: 1.7×10^{-4} mol dm^{-3}) from aqueous solutions with supercritical carbon dioxide (40 °C, 10–18 MPa) could be achieved using glymes (triethylene glycol dimethyl ether (triglyme: 3G), tetraethylene glycol dimethyl ether (tetraglyme: 4G)) and the addition of pentadecafluoro-*n*-octanoic acid (HPFOA) that supplies a CO_2-philic counter ion and makes the metal–ligand complex soluble in the CO_2 solvent *via* counter ion exchange.

CO_2 in its supercritical state ($scCO_2$) is being proposed for many analytical and industrial applications. Although $scCO_2$ can dissolve many non-polar organic compounds,[1–3] it has difficulty in solubilizing metal ions due to its low relative permitivity. To address this, many researchers have examined the use of added ligands, surfactants or microemulsions. Some success in extracting transition metals such as Cu^{2+}, Pb^{2+}, Hg^{2+}, and lanthanoids, has been found using ligands (β-diketones, dithiocarbamates, organic phosphorus acids, *etc.*) *via* chelation,[4–6] but this technique seems unsuitable for alkali metals, since these do not form coordinate bonds with the above-mentioned ligands. Alkali metal ions, *e.g.* Na^+ or K^+, form complexes with only a few ligands, *e.g.* crown ethers or non-macrocyclic compounds such as surfactants having polyoxyethylene (POE) groups.[7–9] The polyethylene glycol compounds, glymes ($CH_3(OCH_2CH_2)_nOCH_3$), are attractive because of their ability to coordinate to metal ions. Darr *et al.* synthesized Ag^+(fluorinated-β-diketone)(glyme) complexes[10] and Pollard *et al.* examined Ce^{3+}(fluorinated-β-diketone)$_3$(glyme)[11] with the hope of obtaining $scCO_2$ soluble complexes. However, there are no reports of using glymes for extracting alkali metal ions with $scCO_2$.

In previous work, we developed a technique whereby alkali metal ions could be extracted with $scCO_2$, using an appropriate ligand with the addition of a small amount of additive that supplies a CO_2-philic counter ion.[12,13] The technique was applied to the extraction of Na^+ and K^+ using crown ether ligand and perfluorocarboxylic acid additive. Semi-quantitative (*ca.* 50%) recoveries were obtained. The perfluorocarboxylic acid additive made the metal ion–ligand complex soluble in $scCO_2$ by generating a CO_2-philic counter anion that exchanged with the anion of the metal–ligand complex. In this work, we report the experimental results on glymes, which are a new class of ligands that have not previously been identified as being applicable to alkali metal extractions with $scCO_2$ and which provide an inexpensive and practical alternative to crown ethers.

Materials NaCl (99.5%), KCl (99.5%), triethylene glycol dimethyl ether (triglyme: 3G, 93%), tetraethylene glycol dimethyl ether (tetraglyme: 4G, 98%), pentadecafluoro-*n*-octanoic acid (HPFOA, 95.0%) and HCl (analytical grade) were purchased from Wako Pure Chemical and used without further purification. The extraction apparatus used in this work has been previously described.[10] Briefly, an aqueous solution (6 ml) of the alkali metal salt (1.7×10^{-4} mol dm^{-3}; ionic strength (I) = 1.0×10^{-1} mol dm^{-3} (H, Cl)), a given amount of ligand and HPFOA (molar ratio; metal : ligand : HPFOA = 1 : 30–300 : 30–300) were loaded into an extraction cell (internal volume: 50 ml). The cell was immersed in a water bath (40 °C) and then pressurized by introducing CO_2 (99.9%). The solution in the cell was stirred by a magnetic stirrer for about 30 min to ensure complex formation and phase partitioning equilibrium. After equilibration, a vapor phase sample was taken by opening the stop valve and depressurizing. The extract in the vapor phase was trapped in a collection vessel that contained 10 ml of EtOH. After sampling, the residual aqueous phase in the cell was analyzed by HP 4500 ICP-MS to determine the metal ion concentration. The pH of the aqueous phase after extraction was also measured. The amount of metal in the collection vessel was analyzed to check the mass balance. The extraction recovery was determined by the difference in concentration of metal ions in the cell before and after extraction and was calculated by the following equation: Recovery = $([\text{metal}]_{\text{init}} - [\text{metal}]_{\text{resid}})/[\text{metal}]_{\text{init}}$, where $[\text{metal}]_{\text{init}}$ and $[\text{metal}]_{\text{resid}}$ represent the initial and residual concentration of metal ion in the cell, respectively.

Fig. 1 shows the extraction results for K^+ using 3G with $scCO_2$ at 40 °C. The recovery was negligibly small with only 3G, indicating that glymes may form complexes with K^+ but that their equilibrium constant is either very small or their solubility in $scCO_2$ is low. On the other hand, the addition of HPFOA gave a recovery that was between 10 and 20%. This can be explained by the fact that glymes form a complex with K^+, which has a low solubility in $scCO_2$. When HPFOA is added, the acid dissociates and gives a CO_2-philic $PFOA^-$ anion. The $PFOA^-$ anion undergoes exchange with the Cl^- anion of the complex in the aqueous phase, and consequently the affinity of the complex for $scCO_2$ increases due to the $scCO_2$-philic PFOA chain. This mechanism seems to be similar to that described in our previous work on crown ether ligands.[10,11] More importantly, the recoveries are semi-quantitative for this type of ligand. However, for the case of 3G, the recoveries were not as high as those obtained for the crown ether ligands, which could be attributed to the difference in the formation constants (K) between the alkali metal ion and glymes or crown ethers, those logarithmic values in MeOH at 25 °C were reported as 1.72 and 6.10, respectively.[14]

We examined the concentration dependence of HPFOA on the complex. The metal ion concentration ratio (D) between the

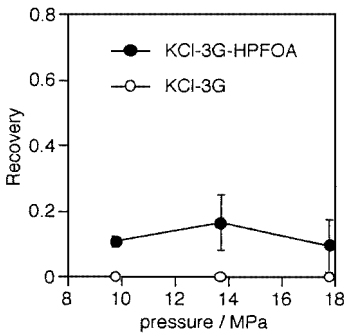

Fig. 1 Variation of recovery with pressure for K^+ using 3G. Extraction conditions: 40 °C, molar ratio; alkali metal : ligand = 1 : 100.

DOI: 10.1039/b003411h

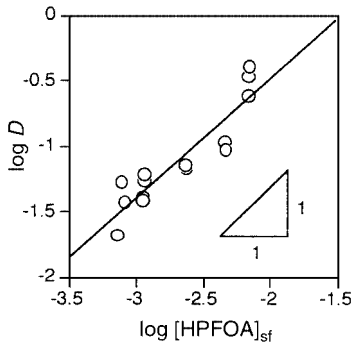

Fig. 2 Variation of log *D* with [HPFOA] using 3G. Extraction conditions: 40 °C, 13.7 MPa, molar ratio; alkali metal : ligand : HPFOA = 1 : 100 : 30–300.

supercritical phase and aqueous phase was calculated from the data and plotted on a logarithmic scale against $[HPFOA]_{(sf)}$ for the KCl–3G–HPFOA system as shown in Fig. 2, where (sf) refers to species in the supercritical phase. The log *D* increased proportionally with an increase in $[HPFOA]_{(sf)}$ and its slope was found to be about unity, indicating that one HPFOA molecule took part in the extraction for each alkali metal ion–glyme complex. This trend is similar to that observed for extractions made with crown ether ligands in $scCO_2$.[13] However, when we plotted log *D versus* log [ligand] as in the previous work, a linear relationship was not obtained as shown in Fig. 3.

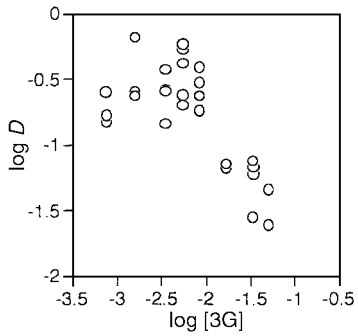

Fig. 3 Variation of log *D* with 3G concentration. Extraction conditions: 40 °C, 13.7 MPa, molar ratio; alkali metal : ligand : HPFOA = 1 : 30–300 : 100.

We considered that the range of ligand and additive concentrations studied might affect the observed recoveries. Since the ligand and additive concentrations were higher than that of the metal ions, strong HPFOA–glyme interactions in the liquid phase may occur. To check this, UV measurements of aqueous samples were made at 20 °C and atmospheric pressure. The spectra did not provide any evidence for HPFOA–glyme interaction. Another possibility is consecutive complex formation that might occur between alkali metal ion and glyme in aqueous phase such as 1 : 2 (metal : glyme), 1 : 3, *etc*. This would lead to a decrease in metal ion recovery since the larger complex would make ions unavailable for extraction if only the 1 : 1 complex was assumed to be extracted *via* counter ion exchange. Regardless of the solution interaction, at 3G concentrations of log [3G] from −2 to −2.7, the recovery increased remarkably up to around 80%.

Table 1 Recoveries (%) for alkali metal ions using 3G and 4G ligands and HPFOA additive. Extraction conditions: 40 °C, 13.7 MPa

Molar ratio[a]	Alkali metal	3G	4G
1 : 100 : 100	Na^+	14.8	20.5
	K^+	16.5	23.6
1 : 33 : 100	Na^+	36.0	40.9
	K^+	71.8	32.9

[a] Metal : glyme : HPFOA.

We ran additional experiments with a longer oxyethylene chain glyme, 4G (see Table 1). Two molar ratios were considered at 40 °C and 13.7 MPa. At conditions of 1 : 100 : 100 (metal : glyme : HPFOA), recoveries were higher for K^+ than Na^+ for both glymes and it was found that 4G gave higher recoveries than 3G for the corresponding Na^+ and K^+ extractions. These results can be explained to some extent by the difference in complex formation ability. For the Na^+–4G and K^+–4G systems, the 1 : 1 (metal : ligand) formation constants (log *K*) in MeOH at 25 °C are 1.28 and 1.72, respectively.[14] However, when we changed the ligand concentration to 1 : 33 : 100, the recoveries did not follow the formation constant data. In conclusion, the molar ratios are not optimized for the highest recoveries, but with the use of glyme ligands and a CO_2-philic counter ion exchange technique, we demonstrate quantitative extraction. Our next step in this research is to perform more detailed measurements and to develop a model based on successive complex formation.

The authors wish to acknowledge the financial assistance of the New Energy and Industrial Technology Development Organization (NEDO), the Intelligent Cosmos Research (ICR) and the Ministry of Education, Science, Sports and Culture. This research was partly performed as part of the Regional Consortium Energy Project.

Notes and references

1 S. B. Hawthorne and D. J. Miller, *Anal. Chem.*, 1987, **59**, 1705.
2 J. J. Langenfeld, S. B. Hawthorne, D. J. Miller and J. Pawllszyn, *Anal. Chem.*, 1994, **66**, 909.
3 M. Johansson, T. Berglof, D. C. Baxter and W. Frech, *Analyst*, 1995, **120**, 755.
4 M. Ashraf-Khorassani, M. T. Combs and L. T. Taylor, *J. Chromatogr. A*, 1997, **774**, 37.
5 C. M. Wai and S. Wang, *J. Chromatogr. A*, 1997, **785**, 369.
6 J. M. Murphy and C. Erkey, *Environ. Sci. Technol.*, 1997, **31**, 1674.
7 S. Yanagida, K. Takahashi and M. Okahara, *Bull. Chem. Soc. Jpn.*, 1977, **50**, 1386.
8 A. M. Y. Jaber, G. J. Moody and J. D. R. Thomas, *J. Inorg. Nucl. Chem.*, 1977, **39**, 1689.
9 D. C. W. Siew, R. P. Cooney, M. J. Taylor and A. J. Easteal, *J. Chem. Soc., Faraday Trans.*, 1990, **86**, 1109.
10 J. A. Darr, M. Poliakoff, A. J. Blake and W. Li, *Inorg. Chem.*, 1998, **37**, 5491.
11 K. D. Pollard, H. A. Jenkins and R. J. Puddephatt, *Chem. Mat.*, 2000, **12**, 701.
12 S. Mochizuki, N. Wada, R. L. Smith, Jr. and H. Inomata, *Anal. Commun.*, 1999, **36**, 51.
13 S. Mochizuki, N. Wada, R. L. Smith, Jr. and H. Inomata, *Analyst*, 1999, **124**, 1507.
14 G. Chaput, G. Jeminet and J. Jullard, *Can. J. Chem.*, 1975, **53**, 2240.

ChemComm

Oxygen initiated unprecedented condensation of propargylamine into the 1,3-di(propargylimino)propylateanion coordinated to cobalt(III)

Aleksei A. Sidorov,[a] Marina O. Ponina,[a] Sergei M. Deomidov,[a] Vladimir M. Novotortsev,[a] Albert Demonceau,[b] Sergei E. Nefedov,[a] Igor L. Eremenko*[a] and Ilya I. Moiseev[a]

[a] *N.S. Kurnakov Institute of General and Inorganic Chemistry, Russian Academy of Sciences, 117907 Moscow, GSP-1, Leninsky prosp., Russia. E-mail: ilerem@ionchran.rinet.ru*

[b] *Laboratory of Macromolecular Chemistry and Organic Catalysis, C.E.R.M. University of Liege, Sart-Tilnam (B.6a) B-4000 Liege, Belgium*

Received (in Cambridge, UK) 4th January 2000, Accepted 23rd May 2000
Published on the Web 5th July 2000

Condensation of coordinated propargylamine into the unprecedented 1,3-di(propargylimino)propylateanion, an analogue of the acetylacetonate anion, is initiated by dioxygen in the Co(II) polymeric trimethylacetate complex/ $NH_2CH_2C{\equiv}CH$ system; molecular structures of the intermediate complex, $Co(O_2CCMe_3)_2(H_2NCH_2C{\equiv}CH)_4$ and final product $Co(O_2CCMe_3)_2(NH_2CH_2C{\equiv}CH)_2[N,N'$-$(HC{\equiv}CCH_2NCHCHCHNCH_2C{\equiv}CH)]$ were established by X-ray analysis.

The chemistry of transition metal complexes with propargylic amines is rather poorly studied. Here, we describe unexpected condensation of Co(II) coordinated propargylamine into the unprecedented 1,3-di(propargylimino)propylateanion bound to a Co(III) centre.

Upon reacting the cobalt(II) containing polymeric complex $[Co(OH)_n(O_2CCMe_3)_{2-n}]_x$ or oligomeric complex $Co_6(\mu_3$-$OH)_2(O_2CCMe_3)_{10}(HO_2CCMe_3)_4$[1] with propargylamine under an anaerobic atmosphere, the paramagnetic mononuclear complex $Co(O_2CCMe_3)_2(H_2NCH_2C{\equiv}CH)_4$ **1** was obtained as the main product (95% yield)†. The four propargylamine molecules occupy the four positions in the equatorial plane [Co–N 2.206(2)–2.214(2) Å] of the octahedral Co(II) atom according to X-ray diffraction data‡ as shown in Fig. 1.

Complex **1** is fairly stable under Ar atmosphere in toluene solution containing an excess of propargylamine up to the solvent boiling point. However, complex **1** readily transforms in the diamagnetic cobalt(III) complex, $Co(O_2CCMe_3)_2(NH_2CH_2C{\equiv}CH)_2[N,N$-$(HC{\equiv}CCH_2NCHCHCHN$-$CH_2C{\equiv}CH)]$ **2**, upon reaction with an excess of propargylamine (CH_2Cl_2, 20 °C) in air; even traces of air initiate the reaction (Scheme 1).§

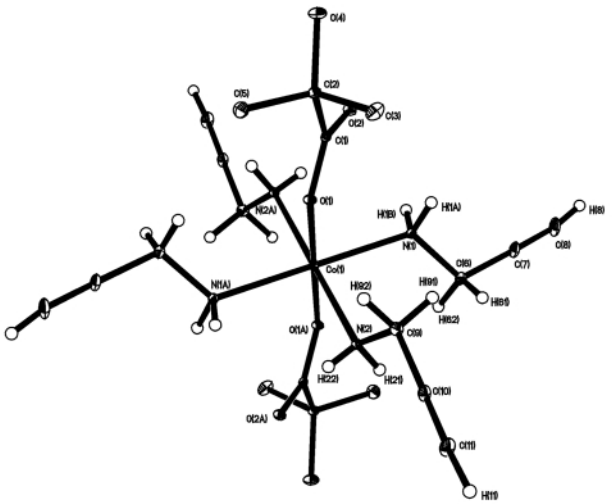

Fig. 1 Molecular structure of $Co(O_2CCMe_3)_2(H_2NCH_2C{\equiv}CH)_4$ **1**; Co–O 2.064(1), C–N 1.452(3)–1.453(3), C≡C 1.158(4)–1.162(4) Å.

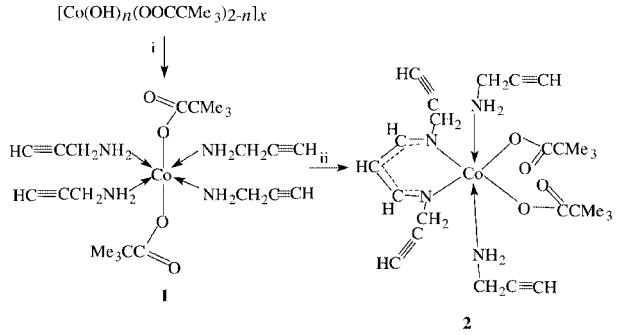

Scheme 1 Interconversions of cobalt(II/III) complexes. *Reagents and conditions*: i, 4 equiv. propargylamine, CH_2Cl_2, Ar atmosphere; ii, 1–2 equiv. propargylamine, CH_2Cl_2 or toluene, in air.

According to an X-ray diffraction study‡ the Co(III) atom has an octahedral environment with two propargylamine ligands occupying apical positions [Co–N 1.974(2) Å] and three anionic ligands [two O_2CCMe_3 groups (Co–O 1.976(2) Å) and one *N*,*N*′- coordinated RNCHCHCHNR (R = propargyl) fragment (Co–N 1.936(2)Å)] in the equatorial plane of the complex coordination sphere as shown in Fig. 2. The metal atom and the planar C–N=CHCHCH=N–C fragment lie in the same plane

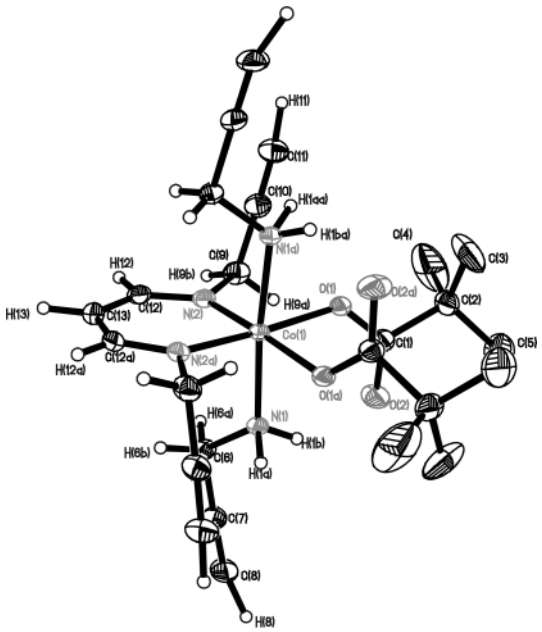

Fig. 2 Molecular structure of $Co(O_2CCMe_3)_2(NH_2CH_2C{\equiv}CH)_2[N,N$-$(HC{\equiv}CCH_2NCHCHCHNCH_2C{\equiv}CH)]$ **2**: C≡C 1.167(5) Å in the propargylamine ligands and 1.172(6) Å in the 1,3-di(propargylimino)propylateanion).

forming an aromatic system with shortened C=N bonds [1.303(4) Å] lying in the same plane of the H atoms [C–C–H 118.4(9)°] and equivalent C(H)–C(H) bonds [1.375(4) Å]. This geometry is very similar to that observed in six-membered metal–acetylacetonate rings.[2,3]

Complex **2** could be also prepared *via* direct reaction between a cobalt trimethylacetate polymer and propargylamine (reagent ratio Co: L = 1: 5–6) in air in toluene solution at 20 °C.

The reaction of an oligomeric nonanuclear nickel(II) complex and an excess of propargylamine gives rise to the complex $Ni(O_2CCMe_3)_2L_4$ **3**.[4] Geometric parameters of complex **3** are very similar to those of complex **1**. Unlike cobalt complex **1**, the nickel compound **3** is stable in air and does not react with propargylamine present in excess even at elevated temperature in solution. This fact suggests that the redox properties of the metal centre and its capability to be involved in one-electron transfer reactions are of importance for the observed amine condensation to form complex **2**. A study addressed toward mechanistic aspects of the reaction is in progress.

We thank Professor AndrewWojcicki for fruitful discussions and the Russian Foundation for Basic Research (Projects 99-03-33091 and 99-03-32805) for financial support.

Notes and references

† Propargylamine (11.58 mmol, 0.638 g) was added gradually to an CH_2Cl_2 solution (40 ml) of $Co_6(\mu_3\text{-}OH)_2(O_2CCMe_3)_{10}(HO_2CCMe_3)_4$ (0.322 mmol, 0.583 g) or 0.5 g of the polymeric complex $[Co(OH)_n(O_2CCMe_3)_{2-n}]_x$ (ratio propargylamine : Co = 4 : 1) under Ar atmosphere and the solution was stirred at 20 °C. Then the solvent was evaporated *in vacuo* to 10 ml and cooled to −5 °C. Pale-pink crystals of complex **1** which formed were separated and dried *in vacuo* (yield 95%). Single crystals suitable for X-ray investigation were prepared by slow cooling of the hot concentrated solution of **1** in CH_2Cl_2. $[Co(O_2CCMe_3)_2(H_2NCH_2C{\equiv}CH)_4]$ **1**. Anal. Calc for $C_{22}H_{38}CoN_4O_4$: C, 54.89; H, 7.90; N, 11.64. Found: C, 55.1; H, 8.0; N, 11.7%. IR, (KBr pellet), ν/cm^{-1}: 3450m, 3352m, 3308s, 3234m, 2963s, 2944s, 2870m, 1672s, 1579vs, 1481vs, 1419vs, 1363s, 1221s, 1098m, 1011s, 980w, 894m, 795w, 645m, 635s, 610s, 570m. μ_{eff} = 4.96 μ_B (293 K).

‡ *Crystal data*: for **1**: $C_{22}H_{38}CoN_4O_4$, M = 481.49, triclinic, space group $P\bar{1}$, μ(Mo-Kα) = 6.63 cm^{-1}, R_1 = 0.0463, wR_2 = 0.1310; a = 6.528(3), b = 10.634(4), c = 11.041(4) Å, α = 66.36(2), β = 79.60(2), γ = 75.89(2)°; V = 678.0(5) Å^3; T = 20 °C; Z = 1, collected/independent reflections 3675/3388 (R_{int} = 0.0265). For **2**: $C_{25}H_{37}CoN_4O_4{\cdot}0.5C_6H_6$, M = 555.58; monoclinic space group, $C2/c$, μ(Mo-Kα) = 6.63 cm^{-1}; R_1 = 0.0483, wR_2 = 0.1214; a = 14.830(3), b = 15.354(3), c = 15.282(3) Å, β = 94.83(3)°, V = 3467.4(12) Å^3; T = 20 °C; Z = 4, collected/independent reflections: 3101/3101.

§ Propargylamine (19.91 mmol, 1.095 g) was added gradually to an toluene solution (40 ml) of $Co_6(\mu_3\text{-}OH)_2(O_2CCMe_3)_{10}(HO_2CCMe_3)_4$ (0.553 mmol, 1 g) or 0.9 g of polymeric complex $[Co(OH)_n(O_2CCMe_3)_{2-n}]_x$ (ratio propargylamine : Co = 5–6 : 1) and the pink suspension of complex **1** was stirred in air at 100 °C for 1–2 h. until formation of a red–brown solution. This solution was kept at 20 °C for 7–9 days after which brown prisms of $Co(O_2CCMe_3)_2(NH_2CH_2C{\equiv}CH)_2[N,N\text{-}(HC{\equiv}CCH_2NCHCHCHNCH_2\text{-}C{\equiv}CH)]$ **2** were formed. Crystals of complex **2** were separated and dried *in vacuo* (yield 18%). Anal. Calc for $C_{25}H_{37}CoN_4O_4$: C, 58.14; H, 7.17; N, 10.85. Found: C, 57.8; H, 7.4; N, 10.5%. IR, (KBr pellet), ν/cm^{-1}: 3296m, 3222m, 3024m, 2963m, 2938m, 2887m, 1771w, 1740w, 1672w, 1610s, 1592s, 1573s, 1511vs, 1462w, 1407s, 1376s, 1345s, 1221s, 1036s, 894w, 746m, 63 vs, 542m. Single crystals suitable for X-ray investigation were prepared by slow cooling of a hot concentrated solution of **2** in benzene.

CCDC 182/1652. See http://www.rsc.org/suppdata/cc/b0/b000004n/ for crystallographic files in .cif format.

1 M. A. Golubnichaya, A. A. Sidorov, I. G. Fomina, M. O. Ponina, S. M. Deomidov, S. E. Nefedov, I. L. Eremenko and I. I. Moiseev, *Russ. Chem. Bull.*, 1999, **53**, 1773.
2 T. M. Suzuki, S. Ohba, S. Sato, V. Saito and K. Saito, *Inorg. Chem.*, 1983, **22**, 2048.
3 M. Atoh, K. Kashiwabara and J. Fujita, *Bull. Chem. Soc. Jpn.*, 1985, **58**, 3492.
4 A. A. Sidorov, S. M. Deomidov, S. E. Nefedov, I. G. Fomina, P. V. Danilov, V. M. Novotortsev, O. G. Volkov, V. N. Ikorskii and I. L. Eremenko, *Russ. J. Inorg. Chem.*, 1998, **43**, 846.

New versatile approach to α-hydrazonoesters and amino acid derivatives through a modified Japp–Klingemann reaction

V. Atlan, L. El Kaim* and C. Supiot

Laboratoire Chimie et Procédés, Ecole Nationale Supérieure de Techniques Avancées, 75015 Paris, France. E-mail: elkaim@ensta.fr

Received (in Liverpool, UK) 25th April 2000, Accepted 22nd May 2000
Published on the Web 5th July 2000

Addition of diazonium tetrafluoroborates to an acyl chloride pyridine mixture affords hydrazonoacid derivatives in smooth conditions; this new Japp–Klingemann reaction emphasizes the synthetic potential of electrophilic addition to ketenes.

Hydrazones are associated with a wealth of well-known reactions such as the Wolff–Kishner,[1] the Shapiro[2] reactions or the Eschenmoser rearrangement.[3] Numerous asymmetric catalytic reductions of compounds with carbon–nitrogen double bonds have been carried out,[4] among these α-hydrazonoesters have shown a great potential as enantiopure amino acid precursors.[5] The importance of these reductions has given us the impetus to search for new selective access to these valuable intermediates.

α-Hydrazonoesters are usually prepared by a Japp–Klingemann[6] reaction between an arenediazonium salt and a malonic acid derivative. It is a two step process involving coupling of the active methylene compounds followed by a final decarboxylation. Simple acid derivatives are not acidic enough and their use as starting materials for Japp–Klingemann reactions often requires preliminary carboethoxylation of the compound. Recently Sakakura *et al.*[7] described a direct preparation of α-hydrazonoester from ester *via* ketene silyl ketals but their reaction requires the use of a strong base (*e.g.* LDA) which may not be compatible with sensitive substrates.

In connection with our previous study on the trifluoroacetic anhydride additions to ketenes,[8] we believed that α-hydrazonoesters could be prepared in one step directly from the acid chloride. This reaction would involve electrophilic diazonium salt attack on the corresponding ketene generated under weak base treatment. Electrophilic attacks on ketenes are well precedented[9] but this reactivity has been poorly explored in comparison to nucleophilic attack. Indeed, by adding diazonium salt **2b** to a mixture of acid chloride **1a** and pyridine, we observed the formation of α-hydrazonoester **3b** with a yield of 63% (Scheme 1, Table 1).

The interest of this method lies in the generation of the ketene with a large excess of pyridine (3 equiv.) which avoids ketene dimerisation by forming zwitterion **A**. The latter can be attacked by the diazonium giving the azocompound **B** and **C** through further deprotonation (Scheme 2); ethanolysis of **C** finally gives hydrazonoesters **3**.

The reaction is performed at room temperature in dichloromethane using 3 equiv. of pyridine and 1.1 equiv. of diazonium salt (added 10 min after the ketene–pyridine adduct formation).

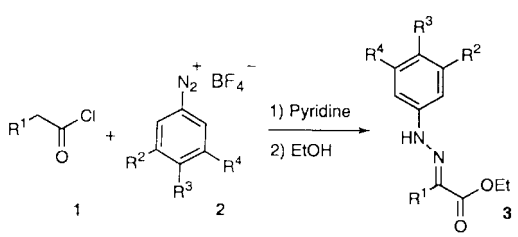

Scheme 1 Addition of diazonium salts to acyl chlorides.

Table 1 Formation of hydrazones **3** from diazonium salts **2**

Chloride **1**	Diazonium **2**	Product **3**[a]	Yield (%)
1a	**2a**	**3a**	33
1a	**2b**	**3b**	63
1a	**2c**	**3c**	66
1a	**2d**	**3d**	56
1a	**2e**	**3e**	55.5
1b	**2b**	**3f**	78
1b	**2c**	**3g**	67
1c	**2b**	**3h**	83
1d	**2b**	**3i**	40
1e	**2b**	**3j**	65
1f	**2b**	**3k**	41
1g	**2b**	**3l**[b]	63
1g	**2c**	**3m**[b]	55
1h	**2c**	**3n**[b]	57

[a] To a dichloromethane solution of acid chloride (0.25 M) was added pyridine (3 equiv.) and after 10 min the diazonium salt **2** (1.1 equiv.). [b] Same procedure but with 0.12 M concentration.

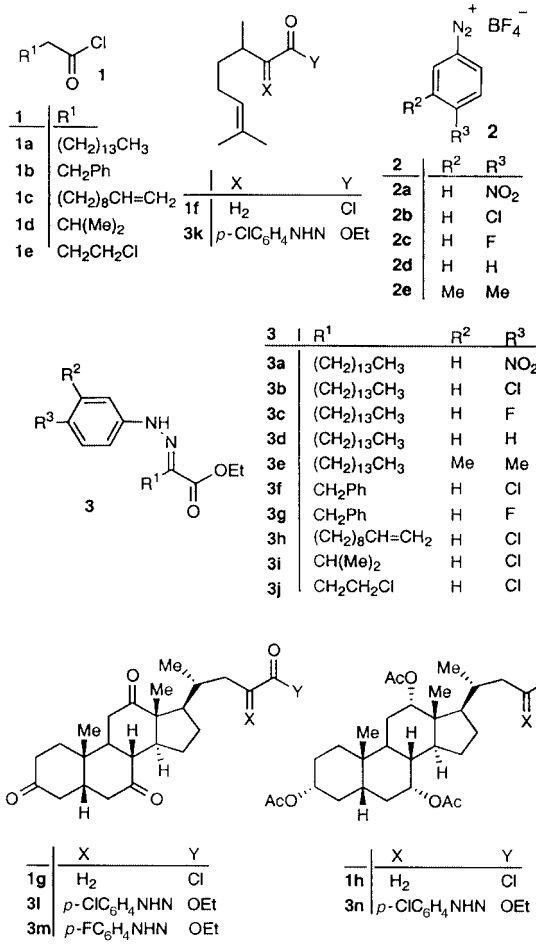

DOI: 10.1039/b003361h

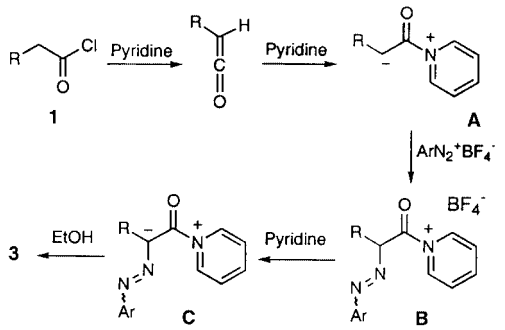

Scheme 2 Possible intermediates in α-hydrazono ester formation.

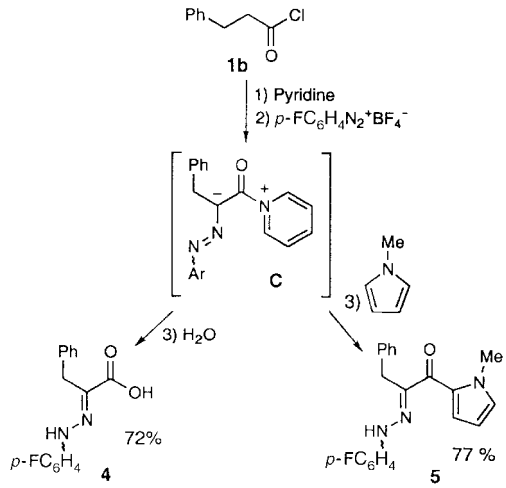

Scheme 3 Acid chloride–diazonium manifold.

The reaction is best carried out at 0.25 M concentration except for steroids **3n**, **3o**, **3p** for which it was reduced to 0.12 M. The results, reported in Table 1, show that moderate to good yields were obtained for most diazonium salts tested and that this new method is compatible with various sensitive functions such as esters and ketones (**3n**, **3o**, **3p**).

The strength of this approach is further underlined by the manifold provided by the final treatment: when ethanolysis gives esters, hydrolysis can form directly free α-hydrazonoacids whereas addition of *N*-methylpyrrole in the mixture forms pyrrole substituted derivatives in a Friedel–Craft acylation type reaction (Scheme 3).

The potential of this new reaction as well as other additions of electrophiles to ketenes are still under investigation in our research group.

We wish to thank Drs Samir Zard and Jean Boivin for help and encouragement.

Notes and references

1 R. O. Hutchins and M. K. Hutchins, *Comprehensive Organic Synthesis*, ed. B. M. Trost, Pergamon Press, 1991, vol. 8, pp. 327–362, and references therein.
2 R. M. Adlington and A. G. M. Barret, *Acc. Chem. Res.*, 1983, **16**, 55.
3 A. Eschenmoser, D. Felix and G. Ohloff, *Helv. Chim. Acta*, 1967, **50**, 708.
4 K. Harada and T. Munegumi, *Comprehensive Organic Synthesis*, ed. B. M. Trost, Pergamon Press, 1991, vol. 8, pp. 139–158, and references therein.
5 E. J. Corey, R. J. McCaully and H. S. Sachdev, *J. Am. Chem. Soc.*, 1970, **92**, 2476; M. J. Burk and M. F. Gross, *Tetrahedron Lett.*, 1994, **50**, 9363.
6 R. R. Phillips, *Organic Reaction*, ed. R. Adams, John Wiley and Sons, 1959, vol. 10, pp. 144–178.
7 T. Sakakura and M. Tanaka, *Chem. Commun.*, 1985, 1309; T. Sakakura, M. Hara and M. Tanaka, *J. Chem. Soc., Perkin Trans 1*, 1994, 289.
8 J. Boivin, L. El Kaim and S. Z. Zard, *Tetrahedron*, 1995, **51**, 2573; J. Boivin, L. El Kaim and S. Z. Zard, *Tetrahedron*, 1995, **51**, 2585.
9 S. Bowadt and P. B. Rasmussen, *Synthesis*, 1989, 114; P. D. Bartlett and L. B. Gortler, *J. Am. Chem. Soc.*, 1963, **85**, 1864; H. G. Viehe, B. Le Clef and A. Elgavi, *Angew. Chem., Int. Ed. Engl.*, 1977, **16**, 182.

ChemComm

Metal-promoted assembly of organic-based cages into a porous material

Roger G. Harrison,* N. Kent Dalley and Alex Y. Nazarenko

Department of Chemistry and Biochemistry, Brigham Young University, Provo, Utah 84602, USA. E-mail: rogerharrison@byu.edu

Received (in Cambridge, UK) 19th April 2000, Accepted 15th June 2000
Published on the Web 6th July 2000

Metal-assembled cages form grids in the solid-state and pack into a manner that creates a material with pores and channels.

Zeolites are very valuable because of their extensive use as molecular sieves, catalysts, and ion exchange materials.[1] One essential feature to zeolites is their porous structure. We have synthesized a porous material, $Ca_4Co_4\mathbf{1}_2{\cdot}xH_2O$, composed of metal and organic components that has a zeolite like porous structure and adsorbs water. This material is a part of an expanding area of metal–organic frameworks which have porous structures, but are not based on silicates or aluminates.[2] These new materials are important because they have different properties than those of zeolites, and may be used as specific catalysts for organic transformations or selective trapping agents. Even though part of their framework is organic, these materials retain their structure after water or solvent molecules are removed and up to temperatures of 300 °C.[2]

Similar to porous metal–organic materials are the metal-assembled supramolecular compounds that form squares, arrays, grids, ladders, sheets and even cages.[3] The assembly of nonporous metal compounds, like the formation of porous metal–organic frameworks, relies on the coordination ability of metal ions and the proper choice of organic ligand. Both of these classes of compounds may have infinite structures, however, the porous materials have often been investigated for adsorptivity. The non-porous metal-assembled compounds sometimes have cavities that encapsulate guests or solvent molecules.[4] The metal-assembled cages act as molecular boxes that bind guests until the cages are signaled by pH change to open and allow guest release.

During our research on metal-assembled cage molecules (Scheme 1), we have discovered that the cages assemble into arrays linked by coordinating cations. The array formation is promoted by the presence of carboxylate groups on four sides of the cages, which are positioned 90° apart in a nearly planar arrangement. Carboxylate groups, having two oxygens and more than one lone pair of electrons on each oxygen, can bind to more than one metal ion and in some cases help create porous materials. Examples of bridging carboxylate groups are very common in metalloproteins and small molecule models of metalloproteins, where metal centers are linked by carboxylates from amino acids or alkyl carboxylates.[5] The four carboxylate groups in $Ca_4Co_4\mathbf{1}_2{\cdot}xH_2O$ come from **1**, which is a cup-shaped resorcinarene molecule that has four pairs of carboxylates positioned on its upper rim. These carboxylates coordinate to transition metal ions and, in the process, form octaanionic cage complexes.[6] One can think of the carboxylate groups on the cages as four metal binding sites equally spaced from each other around the middle of an ellipsoid.

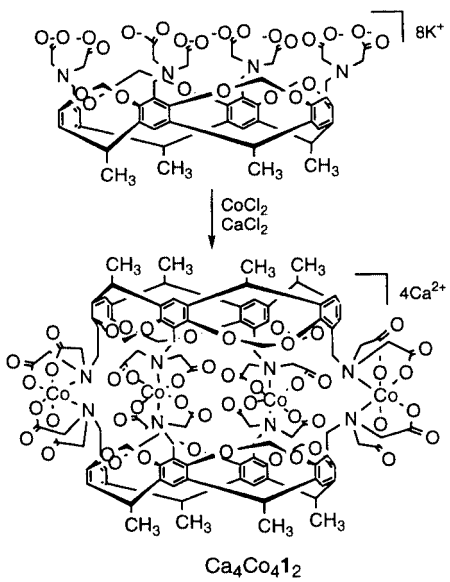

Scheme 1

Owing to the anionic nature of these metal-assembled cages, counter cations are associated with them. When calcium is the counter cation and an aqueous solution of cobalt-assembled cages is allowed to crystallize by slow diffusion of isopropyl alcohol, the calcium ions coordinate to oxygen atoms of the carboxylates and in so doing form $Ca_4Co_4\mathbf{1}_2{\cdot}xH_2O$.† This bonding of oxophilic calcium ions to carboxylate oxygens is not unusual, but what is novel is that the calcium ions coordinate to carboxylates from two cages and create a bridge between two cages. In addition to coordinating to carboxylate oxygens, the calcium ions also coordinate to water molecules, which complete their coordination sphere. As the calcium ions bring together two cages, they assemble a two-dimensional array of cages (Fig. 1)‡ The cages are *ca*. 18 Å apart from each other (center of one cage to the center of the next nearest cage). When the rows of cages line up, voids are formed which would have diameters of *ca*. 15 Å, except that they contain water molecules that are a part of a ring of molecules hydrogen-bonded together around the cages. Thus, the voids have edge lengths of *ca*. 9.5 Å (Ca to Ca van der Waals radii).

The placement of the next layer of cages is also of interest. Though the voids of one layer would seem to be the optimum place for the cages of the next layer, the cages do not position themselves there, but rather lie over the cation bridges of the first layer.[7] In so doing, rhombic pores and channels form

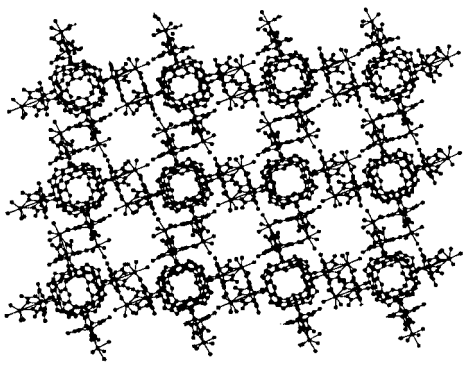

Fig. 1 A top view of $Ca_4Co_4\mathbf{1}_2$ from the X-ray crystal structure showing the packing of the cages into two-dimensional arrays with linking calcium ions. Note the four carboxylate groups are on the exterior of the cages, 90° apart, and help connect the cages together.

DOI: 10.1039/b003187i

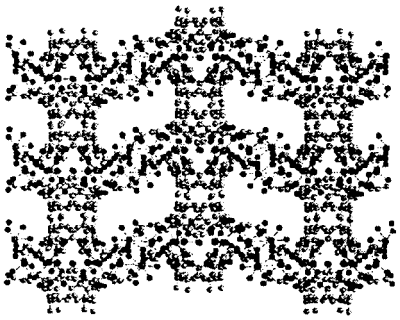

Fig. 2 A side view of $Ca_4Co_4\mathbf{1}_2$ showing the packing of three layers of cages and the channels connecting the pores. The cages in the middle layer are behind the first and third layers. The first and third layers are separated by carboxylate groups of the middle layer. The water molecules within the channels have been omitted for clarity.

(Fig. 2). Cages line two sides of the pores while carboxylates and calcium ions occupy the other four sides. Owing to the presence of both phenyl, methyl, and carboxylate groups on the cages, the pores have both a nonpolar and polar nature. Since the carboxylates do not fill the whole side of a pore as the cages do, channels lead into the pores from two directions. The pores are roughly shaped like hexagons, 9.5 × 9.5 × 21 Å, with two of the long sides occupied by cages. The connecting channels have 5 × 12 Å edges and since they are lined with carboxylate oxygens and water molecules bound to calcium ions, they are expected to be hydrophilic and variable in size depending on the amount of water bound to calcium. Fig. 2 shows that a line of cages is linear in one direction and zigzaged in the other. This is because the bridging carboxylate arms of the cages are side-by-side or one on top of the other.

An important property of porous materials is their ability to retain molecules within their pores. The pores of $Ca_4Co_4\mathbf{1}_2{\cdot}xH_2O$ are occupied by water and isopropyl alcohol molecules. Some water molecules are bound to the counter cations, some hydrogen bonded around the cages, and others disordered within the pores. This is similar to zeolites, where water is bound to cations within a silica or alumina framework. In an attempt to understand the material's affinity for water, we used thermogravametric analysis to measure the change in mass of the material as a function of temperature. When the temperature of the material is raised at a rate of 1 °C min^{-1} from 25 to 250 °C, initially, a fast rate of weight loss is observed up to 120 °C, after which weight is lost more slowly until the weight of the material becomes constant. The total weight loss accounts for 20% of the material and gives a 40 : 1 water to $Ca_4Co_4\mathbf{1}_2$ ratio. A composition of 20% water ranks this material with zeolites in water content.[1] The water to complex ratio of 40 : 1 is in good agreement with the ratio found by X-ray crystallography: 43 : 1.

Not surprisingly, after releasing water, this material adsorbs water. When the dehydrated material is cooled in the presence of a stream of water vapor (20 mm Hg), an initial fast rate of water uptake is observed below 90 °C, which leads into a slower rate of water adsorption as the temperature reaches ambient. The amount of water that was lost is regained. This process of dehydration and adsorption can be repeated without a significant change to the amount of water adsorbed. This is an indication that the material's internal structure remains intact and that heating and water removal do not cause decomposition. Another indication of retention of structural integrity is that the external block-shape of the crystals does not change during adsorption and dehydration. Further studies on the retention of structure are under way.

In conclusion, $Ca_4Co_4\mathbf{1}_2{\cdot}xH_2O$ is a new metal–organic porous material composed of elaborate organic cage molecules and cations. Four perpendicular carboxylate-binding groups on the cage part of $Co_4\mathbf{1}_2{}^{8-}$ provide sites for calcium binding and the assembly of the cages into arrays. The packing of the layers of cages over the bridges of other layers creates pores and channels within the material. Metal-assembled cages and water molecules line the channels that link the pores. These pores and channels contain water, which can be removed and adsorbed. Future research will focus on the use of $C_4CO_4\mathbf{1}_2$ as a small molecule trapping agent, and the affect on pore size by the substitution of the calcium ions by other metal ions.

We thank Brigham Young University for supporting this research.

Notes and references

† *Synthesis* of $Ca_4Co_4\mathbf{1}_2{\cdot}xH_2O$: this is performed in a similar manner to the synthesis of $Ba_4Co_4\mathbf{1}_2$, see ref. 6. To a solution of $Ba_4\mathbf{1}{\cdot}24H_2O$ (33 mg, 0.016 mmol) dissolved in 1 M hydrochloric acid (1 mL) and water (2 mL) was added K_2SO_4 (17 mg). The white precipitate of $BaSO_4$ that formed was removed by filtration. Cobalt(II) chloride hexahydrate (9.0 mg, 0.038 mmol) and $CaCl_2$ were added to the solution and the pH raised to 5 by addition of K_2CO_3. Isopropyl alcohol was then layered over the solution. After two days, pink prismatic crystals of $Ca_4Co_4\mathbf{1}_2$ formed (18 mg, 36% yield). Anal. Calc. for $C_{112}H_{104}N_8O_{48}Ca_4Co_4{\cdot}24H_2O$: C, 42.58; H, 4.82; N, 3.55. Found: C, 42.83; H, 4.57; N, 3.31%.

‡ *Crystallographic data* for $Ca_4Co_4\mathbf{1}_2{\cdot}2(CH_3)_2CHOH{\cdot}43H_2O$: M = 3618, pink color, dimensions 0.5 × 0.4 × 0.25 mm, monoclinic, space group $C2/c$ (no. 15), Z = 4, a = 18.598(4), b = 27.575(8), c = 37.106(8) Å, β = 92.318(10)°, V = 19 014(8) Å^3, D_c = 1.199 g cm^{-3}, T = 292(2) K; Mo-Kα radiation (λ = 0.71073 Å); 9469 total data, 6209 [$F > 4\sigma(F)$] observed independent reflections with 2.1 < θ < 21° collected: R = 0.0890, R_w = 0.1352, GOF = 1.055. Crystals were mounted in a sealed capillary and immersed in mother liquor during analysis. Disordered water molecules were located in the crystal.

CCDC 182/1690. See http://www.rsc.org/suppdata/cc/b0/b003187i/ for crystallographic files in .cif format.

1 D. W. Breck, *Zeolite Moleculear Sieves*, Wiley, New York, 1974; R. Szostak, *Molecular Sieves Principles of Synthesis and Identification*, Thomas Science, New York, 2nd edn., 1998.

2 P. J. Hagrman, D. Hagrman and J. Zubieta, *Angew. Chem., Int. Ed.*, 1999, **38**, 2638; T. M. Reineke, M. Eddaoudi, M. Fehr, D. Kelley and O. M. Yaghi, *J. Am. Chem. Soc.*, 1999, **121**, 1651; H. Li, M. Eddaoudi, M. O'Keeffe and O. M. Yaghi, *Nature*, 1999, **402**, 276; C. J. Kepert and M. J. Rosseinsky, *Chem. Commun.*, 1999, 375; T. Niu and A. J. Jacobson, *Inorg. Chem.*, 1999, **38**, 5346; H. Gudbjartson, K. Biradha, K. M. Poirier and M. J. Zaworotko, *J. Am. Chem. Soc.*, 1999, **121**, 2599; D. M. L. Goodgame, D. A. Grachvogel and D. J. Williams, *Angew. Chem., Int. Ed.*, 1999, **38**, 153; J. Heo, S.-Y. Kim, D. Whang and K. Kim, *Angew. Chem., Int. Ed.*, 1999, **38**, 641; L. R. MacGillivray, R. H. Groeneman and J. L. Atwood, *J. Am. Chem. Soc.*, 1998, **120**, 2676; M. Kondo, T. Yoshitomi, K. Seki, H. Matsuzaka and S. Kitagawa, *Angew. Chem., Int. Ed. Engl.*, 1997, **36**, 1725; G. B. Gardner, D. Venkataraman, J. S. Moore and S. Lee, *Nature*, 1995, **374**, 792.

3 B. Olenyuk, J. A. Whiteford, A. Fechtenkötter and P. J. Stang, *Nature*, 1999, **398**, 796; N. Takeda, K. Umenmoto, K. Yamaguchi and M. Fujita, *Nature*, 1999, **398**, 794; T. N. Parac, D. L. Caulder and K. N. Raymond, *J. Am. Chem. Soc.*, 1998, **120**, 8003; E. J. Enemark and D. P. Stack, *Angew. Chem., Int. Ed.*, 1998, **37**, 932; P. N. W. Baxter, in *Comprehensive Supramolecular Chemistry*, ed. J. P. Sauvage and M. W. Hosseini, Pergamon, Oxford, 1996, vol. 9, pp. 165–211; B. Linton and A. D. Hamilton, *Chem. Rev.*, 1997, **97**, 1669.

4 O. D. Fox, J. F. Leung, J. M. Hunter, N. K. Dalley and R. G. Harrison, *Inorg. Chem.*, 2000, **39**, 783; J. S. Fleming, K. L. Mann, C.-A. Carraz, E. Psillakis, J. C. Jeffery, J. A. McCleverty and M. C. Ward, *Angew. Chem., Int. Ed.*, 1998, **37**, 1279; D. L. Caulder, R. E. Powers, T. N. Parac and K. N. Raymond, *Angew. Chem., Int. Ed.*, 1998, **37**, 1840; M. Fujita, S.-Y. Yu, T. Kusukawa, J. Funaki, K. Ogura and K. Yamaguchi, *Angew. Chem., Int. Ed.*, 1998, **37**, 2082; R. W. Saalfrank, V. Seitz, D. L. Caulder, K. N. Raymond, M. Teichert and D. Stalke, *Eur. J. Inorg. Chem.*, 1998, 1313.

5 S. J. Lippard and J. M. Berg, *Principles of Bioinorganic Chemistry*, University Science Books, Mill Valley, CA, 1994, pp. 291–319.

6 O. D. Fox, N. K. Dalley and R. G. Harrison, *J. Am. Chem. Soc.*, 1998, **120**, 7111.

7 For a calixarene assembled into layers, see: A. W. Coleman, S. G. Bott, S. D. Morley, C. M. Means, K. D. Robinson, H. Zhang and J. L. Atwood, *Angew. Chem., Int. Ed. Engl.*, 1988, **27**, 1361.

Antenna functions of 5,15-bis(imidazol-4-yl)-10,20-bis(4-dodecyloxyphenyl)-porphyrin supramolecular assembly through imidazole–imidazole hydrogen bonding†

Naoto Nagata, Shin-ichi Kugimiya and Yoshiaki Kobuke*

Graduate School of Materials Science, Nara Institute of Science and Technology, CREST, Japan Science and Technology Corporation (JST), 8916-5 Takayama, Ikoma City, 630-0101, Japan. E-mail: kobuke@ms.aist-nara.ac.jp

Received (in Cambridge, UK) 25th April 2000, Accepted 19th June 2000
Published on the Web 6th July 2000

The title bis(imidazol-4-yl)porphyrin 1 gave supramolecular assemblies through hydrogen bonding; efficient excited energy transfer followed by electron transfer to quenchers has been observed in toluene.

Chromophore assemblies play important roles in light-harvesting antenna functions of photosynthesis. In bacterial antenna complexes, 18[1a] or 16[1b] bacteriochlorophylls are arranged in a macro-ring with slipped cofacial structures by coordination of imidazolyl side chains from transmembrane α-helices in B850,[1a,b] and 9[1a] or 8[1b] bacteriochlorophylls are arranged in a macro-ring of coplanar orientation in B800.[1a,b] In contrast to these well-organized structures in bacterial antennae, antenna complexes from plant sources are more or less disordered.[1c] In both cases the arrangements are provided by non-covalent interactions, and supramolecular assembly formation by hydrogen bonding and metal-to-ligand coordination is thought to be a promising way to achieve the construction of artificial antenna models.[2,3]

In this communication, we introduce the use of bis(imidazolyl)porphyrin **1** to mimic light-harvesting antenna function by supramolecular assembly formation through hydrogen bonds between imidazol-4(5)-yls substituted at two facing *meso* positions of the porphyrin ring.[4] 5,15-Bis(imidazolyl)porphyrin **1** was prepared conventionally[5] from imidazol-4(5)-yl-2,2′-dipyrrylmethane and 4-dodecyloxybenzaldehyde as shown in Scheme 1.

The ^{1}H NMR spectrum of **1** in $CDCl_3$ gave broad peaks, which were sharpened gradually by the addition of CD_3OD.

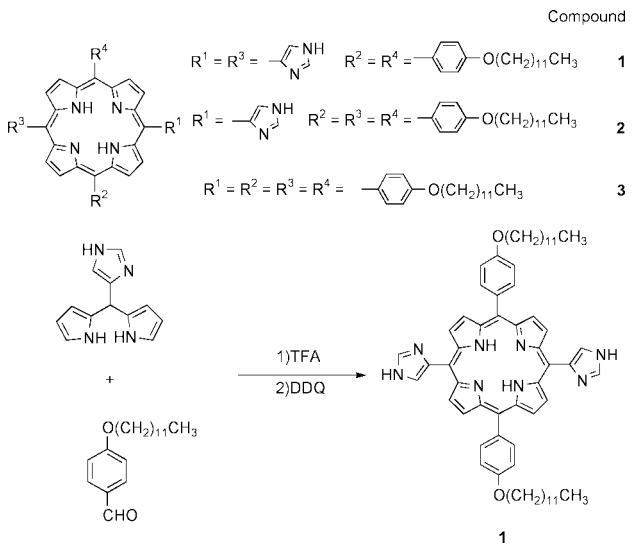

Scheme 1 Preparation of bis(4-imidazolyl)porphyrins.

† Electronic supplementary information (ESI) is available: experimental details and ^{1}H NMR of **1** in $CDCl_3$. See http://www.rsc.org/suppdata/cc/b0/b003267k/

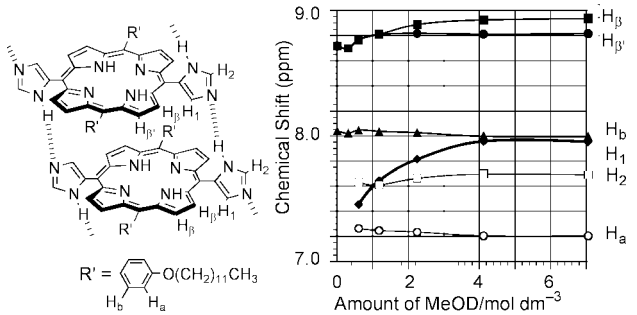

Fig. 1 NMR Titration of **1** (4 mmol dm^{-3}) in $CDCl_3$ with CD_3OD at 20 °C.

Fig. 1 shows the titration behaviour of the imidazolyl, pyrrolic and aromatic protons. The characteristic up-field shift with decreasing CD_3OD concentration was observed most specifically at the *meso*-imidazol-4-yl proton (H_1),[6] and less significantly at one of the β-pyrrolic protons (H_β). Other peaks were insensitive to CD_3OD addition. The shift behaviour is accounted for by the breaking of hydrogen bonds between imidazolyl substituents by the addition of CD_3OD. The selective shielding of the H_1 proton compared to H_2 in the aggregate suggests that H_1 is brought above the facing porphyrin plane by hydrogen bond formation between imidazolyl substituents of different porphyrins. Therefore, the slipped cofacial arrangement **1** is proposed as the structural unit of hydrogen bonded porphyrin rather than the head-to-tail one. The former orientation can be stabilized by cooperative interaction of maximal hydrogen bonds of imidazolyls and π-stacking of porphyrins and is thought to be the more stable. In accord with this orientation, the H_β proton received the second largest up-field shift with decreasing CD_3OD concentration. In contrast, monoimidazolyl-substituted porphyrin **2**, gave quite a normal NMR spectrum without any specific shielding or peak broadening.

This porphyrin–porphyrin interaction is sensitively reflected in their UV spectra. Characteristics of the Soret band of **1** are compared with those of mono- and non-imidazolyl substituted porphyrins **2** and **3**, respectively, in Table 1. The half bandwidth of **1** (29 nm) in a $CHCl_3$ solution (free from EtOH) is significantly broadened compared with that of **2** (16 nm) at the same concentration in the same solvent. A further broadening is

Table 1 Comparison of absorption spectral characteristics of **1** and porphyrin analogs in various solvents

	λ_{max} (Half band width)/nm			
Compound	MeOH	$CHCl_3$[a]	Toluene	Cyclohexane
1	418(24)	424(29)	426(34)	426(84)
2	419(16)	424(16)	424(16)	422(18)
3	421(13)	420(13)	420(13)	420(13)

[porphyrin] = 1.6 μmol dm^{-3}; [a] EtOH free, $CHCl_3$ was used.

Table 2 Comparison of fluorescence intensities of **1** in various solvents

Compound	Relative intensity at peak maximum (λ_{max}/nm)			
	MeOH	$CHCl_3$[a]	Toluene	cyclohexane
1	507 (662)	442 (668)	428 (669)	36 (664)

[**1**] = 1.6 μmol dm^{-3}; [a] EtOH free, $CHCl_3$ was used.

observed in toluene for **1**, but there is observed solvent dependence in the halfwidth of the Soret band observed for **2**. This behaviour is explained by exciton coupling theory for two porphyrin chromophores in a slipped cofacial orientation,[7] where two transition moments interact in face-to-face and parallel orientations to give rise to blue and red shifts, respectively. The peak splitting could not be observed in the present case and the overall spectral maxima shifted to longer wavelengths. The increased broadening of Soret bands of **1** in increasingly less polar solvents was incompatible with the idea that they contained split absorptions as components. In the case of **3**, having no hydrogen bonding group, no solvent dependence was observed for MeOH, $CHCl_3$ and toluene either for absorption maxima or half bandwidths. Monoimidazolyl-substituted porphyrin **2** seemed to be too weak to interact significantly in this fashion and showed behaviour similar to unsubstituted porphyrin **3** in the range 2×10^{-3}–4 mmol dm^{-3}. This may suggest the cooperation of hydrogen bonds and π-stacking interaction in the present supramolecular structure formation.[8] Interestingly, the fluorescence intensity of bis(imidazolyl)porphyrin **1** remained almost constant for the change of solvent from MeOH to toluene as shown in Table 2. This result indicates that bis(imidazolyl)porphyrin **1** in the supramolecular assembly showed no significant self-quenching by supramolecular complex formation.

In order to obtain direct evidence of assembly formation, the toluene solution of **1** was analyzed by static light scattering at 26 °C. From a Zimm plot[9] of the data obtained at 3.3, 6.6, 9.9 and 13 μmol dm^{-3}, the radius of gyration was estimated as 23 nm. Although the molecular weight could not be obtained because the refractive indices of the solution and pure solvent were too close, we could observe particles from **1** in similarly dilute concentrations (3.3–13 μmol dm^{-3}) in toluene.

The efficiency of energy–electron transfer from the assembly to external acceptors was estimated by fluorescence quenching experiments. Stern–Volmer plots for two acceptor molecules, chloranil and tetraphenylporphyrinatoMn(III) chloride (ClMntpp) in toluene, are illustrated in Figs. 2a and b, respectively, together with the plot obtained by using non-imidazolyl substituted porphyrin **3** as the reference.

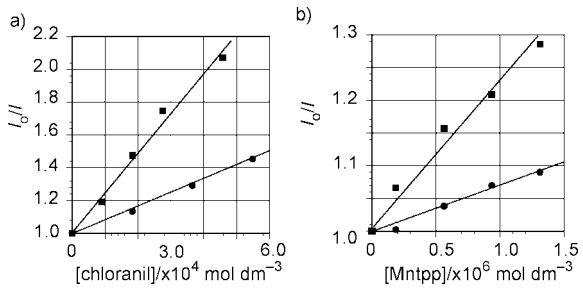

Fig. 2 Stern–Volmer plots for **1** (1.6 μmol dm^{-3}, ■) and **3** (1.6 μmol dm^{-3}, ●) with (a) chloranil and (b) ClMntpp in toluene.

Chloranil quenched the fluorescence of **1** 2.9 times faster than that of **3**. This result suggests that the supramolecule **1** is a more efficient energy–electron donor than the monomeric species. There is a possibility, however, that chloranil becomes a better acceptor through the formation of a hydrogen bonded complex with the imidazolyl part of **1**, but not with **3**. This possibility was excluded by experiment: ClMntpp, having no hydrogen bond site, quenched the fluorescence of **1** more efficiently than that of **3** by the same factor of 2.9. The possibility that **1** specifically interacts with ClMntpp through coordination of an imidazolyl group to Mn was safely excluded by there being no shift of the Soret band of ClMntpp, in accord with the small coordination equilibrium constant reported for imidazole and ClMntpp.[8] A possible explanation for efficient energy transfer and/or electron transfer from the supramolecule may be based on the idea that the excitation energy is delocalized over the whole supramolecule and transferred to acceptors from any components of the supramolecule as in the oxinylporphyrin.[10] These results establish the usefulness of the supramolecular porphyrin assembly as a mimic of the energy storage function of light harvesting antenna complexes (see Scheme 2).

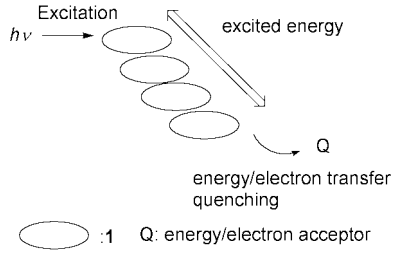

Scheme 2 Excitation energy storage in supramolecular bis(imidazolyl)porphyrin assembly.

In conclusion, imidazolyl porphyrin is a useful component for obtaining porphyrin assemblies, not only through hydrogen bonding but also by metal coordination.[3] Further applications for bis(imidazolyl)porphyrin **1** and its derivatives are now under active investigation.

Notes and references

1 (*a*) G. McDermott, S. M. Prince, A. A. Free, A. M. Hawthornthwaite-Lawless, M. Z. Papiz, R. J. Cogdell and N. W. Isaacs, *Nature*, 1995, **374**, 517; (*b*) J. Koepke, X. Hu, C. Muenke, K. Schulten and H. Michel, *Structure*, 1996, **4**, 581; (*c*) W.-D. Schubert, O. Klukas, N. Krauss, W. Saenger, P. Fromme and H. T. Witt, *J. Mol. Biol.*, 1997, **272**, 741.

2 J. L. Sessler, B. Wang, S. L. Spring and C. T. Brown, in *Comprehensive Supramolecular Chemistry*, ed. Y. Murakami, Pergamon, UK, 1996, vol. 4, ch. 9, pp 311 and references therein; J. L. Sessler, C. T. Brown, D. O'Connor, S. L. Springs and R. Wang, *J. Org. Chem.*, 1998, **63**, 7370 and references therein; A. Osuka, R. Yoneshima, H. Shiratori, T. Okada, S. Taniguchi and N. Mataga, *Chem. Commun.*, 1998, 1567; C. Ikeda, N. Nagahara, E. Motegi, N. Yoshioka and H. Inoue, *Chem. Commun.*, 1999, 1759; Y. Aoyama, T. Kamohara, A. Yamagishi, H. Toi and H. Ogoshi, *Tetrahedron Lett.*, 1987, **28**, 2143; X. Chi, A. J. Guerin, R. A. Haycock, C. A. Hunter and L. Sarson, *Chem. Commun.*, 1995, 2567; R. T. Stibrany, J. Vasudevan, S. Knapp, J. A. Potenza, T. Emge and H. J. Schugar, *J. Am. Chem. Soc.*, 1996, **118**, 3980; R. K. Kumar, S. Balasubramanian and I. Goldberg, *Chem. Commun.*, 1998, 1435; T. Miyatake, H. Tamiaki, A. R. Holzwarth and K. Schaffner, *Photochem. Photobiol.*, 1999, **69**, 448; S. Knapp, B. Huang, T. J. Emge, S. Sheng, K. Krgh-Jespersen, J. A. Potenza and H. J. Schugar, *J. Am. Chem. Soc.*, 1999, **121**, 7977.

3 Supramolecular assemblies of imidazolylporphyrin: Y. Kobuke and H. Miyaji, *J. Am. Chem. Soc.*, 1994, **116**, 4111; Y. Kobuke and H. Miyaji, *Bull. Chem. Soc. Jpn.*, 1996, **69**, 3563.

4 Strong hydrogen bondings and π stacking of imidazol-2-yl substituted Pd porphyrins and their proton conductivity have been reported in the solid state: L. R. Milgrom, S. Bone, D. W. Bruce and M. P. Macdonald, *J. Mol. Electronics*, 1991, **7**, 95.

5 C.-H. Lee and J. S. Lindsey, *Tetrahedron*, 1984, **39**, 11427.

6 The imidazolyl H_1 and H_2 protons were assigned unequivocally by observing the ^{1}H ^{13}C COSY spectrum, where N–*CH*=C and N–*CH*=N carbons appeared at 135 and 120 ppm, respectively.

7 M. Kasha, H. R. Rawls and M. A. El-Bayoumi, *Pure Appl. Chem.*, 1965, **11**, 371.

8 The coordination equilibrium constant K_{eq} between imidazole and ClMntpp is reported in S. Banfi, F. Montaniri and S. Quici, *J. Org. Chem.*, 1989, **54**, 1850 as 182 ± 15 mol^{-1} dm^3 in CH_2Cl_2 at 25 °C. Contribution of possible coordination species is calculated as less than 0.1% of free [ClMntpp].

9 B. H. Zimm, *J. Chem. Phys.*, 1948, **16**, 1099.

10 I. V. Rubtsov, Y. Kobuke, H. Miyaji and K. Yoshihara, *Chem. Phys. Lett.*, 1999, **308**, 323. Another possibility was suggested by a referee, who pointed out that lowering of S_1 or even S_0 could affect either the pre-exponential or Marcus like terms and mediate the rate favourably. Photophysical studies may address the mechanism and will be reported elsewhere.

Chalcogen atom transfer reactions. Kinetics of terminal bonded sulfur atom transfer between main group metal centers

Stephen R. Foley and Darrin S. Richeson*

Department of Chemistry, University of Ottawa, Ottawa, ON, Canada, K1N 6N5. E-mail: darrin@science.uottawa.ca

Received (in Irvine, CA, USA) 17th April 2000, Accepted 7th June 2000
Published on the Web 6th July 2000

The first comprehensive investigation of S atom transfer between two different metal centers is presented using the reaction of the terminal chalcogen atom bearing complex $[CyNC(^tBu)NCy]_2SnS$ with $[CyNC(^tBu)NCy]_2Ge^{II}$; this multielectron redox reaction between Ge^{II} and Sn^{IV} proceeds *via* a second-order process with an inner sphere mechanism involving a μ-S intermediate as the proposed pathway; results of S and Se atom transfer between $[CyNC(^tBu)NCy]_2Ge$ and PPh_3 are also presented.

Atom transfer reactions are an active area of fundamental investigation that have attracted considerable attention in large part due the manifest role of oxygen atom transfer in many oxidation processes and in several biological processes.[1,2] The oxygen atom transfer reactions that have been studied are dominated by metal–oxo donor reactions with a non-metal acceptor. In comparison, transfer of heavier group 16 elements and/or complete inter-metal transfer of a multivalent atom are less established.[3,4] Some chalcogen complexes of Ti(IV) are known to function as effective sources of chalcogen atoms. However, the atom transfer reactivity of Cp_2TiE_5 (E = S, Se)[5] and of (OEP)TiE_2 (OEP = octaethylporphyrinato; E = O, S, Se)[6] are based on ligand reduction and are therefore categorized as secondary atom transfer reactions. When attention is focussed on main group metal complexes the number of clear examples of this class of reaction dwindles to a single detailed investigation.[7] In fact this example, shown by eqn. (1), represents the sole comprehensive study for inter-metal two electron transfer mediated by heavy elements of group 16 (*i.e.* S or Se) and involved the reversible transfer of sulfur and selenium atoms between tin porphyrin complexes of *meso*-tetraphenylporphyrinato (TPP) and *meso*-tetra-*p*-tolylporphyrinato (TTP) ligands.

$$(TTP)Sn^{II} + (TPP)Sn{=}S \rightleftarrows (TTP)Sn{=}S + (TPP)Sn^{II} \quad (1)$$

The limited examples of primary atom transfer reactions involving sulfur and selenium atoms include the exchange between the terminal chalcogenido complexes [η⁴-Me_8taa]SnE (E = S, Se; Me_8taa = octamethyldibenzotetraazaannulene) and the Ge(II) species [η⁴-Me_8taa]Ge [eqn. (2)].[8] More recently the preparation of terminal selenido complexes of gallium and indium supported by tris(3,5-di-*tert*-butylpyrazolyl)hydroborato (^{tBu}Tp) ligation allowed for the observation of selenium atom transfer from indium to gallium [eqn. (3)].[9] Kinetic parameters have not been established for either of these systems.

$$[\eta^4\text{-}Me_8taa]SnE + [\eta^4\text{-}Me_8taa]Ge^{II} \rightarrow [\eta^4\text{-}Me_8taa]Sn^{II} + [\eta^4\text{-}Me_8taa]GeE \quad (2)$$

$$[^{tBu}Tp]InSe + [^{tBu}Tp]Ga^{I} \rightarrow [^{tBu}Tp]In^{I} + [^{tBu}Tp]GaSe \quad (3)$$

Our interest in the formation of multiple bonds between main group elements and the subsequent reactivity of these unusual species led us to prepare a family of amidinato complexes of Ge and Sn $[CyNC(^tBu)NCy]_2ME$ [M = Sn, E = S (**1S**); M = Ge, E = S (**2S**), Se (**2Se**)] that possess terminal chalcogenido functions.[10,11] These compounds were prepared by oxidative addition of styrene sulfide or elemental selenium to the corresponding M(II) precursors, $[CyNC(^tBu)NCy]_2M$ [M = Sn (**1**), Ge(**2**)]. These results now allow us to report the first comprehensive study of heteronuclear inter-metal sulfur atom transfer reactions.

When the bis(amidinato)tin(IV) sulfide species **1S** and bis(amidinato)germanium(II) complex **2** are mixed at room temperature complete sulfur atom exchange between these complexes can be achieved according to eqn. (4) in Scheme 1.

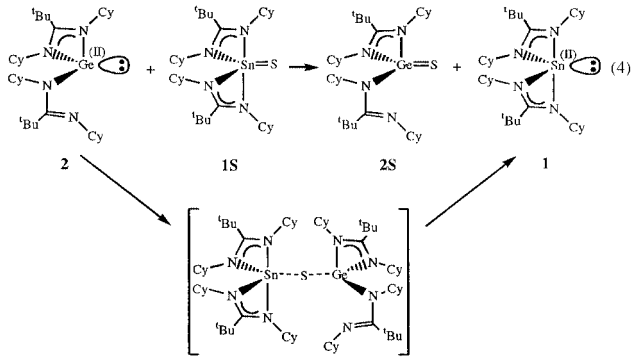

Scheme 1

At room temperature this reaction proceeded smoothly over several days and could be conveniently monitored by ^{1}H NMR in C_6D_6. The ^{t}Bu groups for the four different amidinate complexes provided an excellent spectroscopic handle to monitor this reaction. For example, as the reaction progresses, the ^{t}Bu resonances of **1S** at δ 1.17 continuously decrease in intensity concomitant with the appearance of new ^{t}Bu resonances at δ1.35, signifying the formation of **1**.

The corresponding ^{t}Bu resonances for the germanium complexes are slightly more complicated. Instead of having both amidinate ligands bidentate and equivalent as with compounds **1** and **1S**, both **2** and **2S** are known to exhibit one bidentate and one monodentate ('dangling') ligand as shown in Scheme 1. This feature has been demonstrated through structural and spectroscopic characterization for both **2** and **2S** and is a general feature for a number of other germanium amidinate complexes that we have prepared.[12] As a result, the two amidinate ligands in the Ge complexes are inequivalent and two separate ^{t}Bu signals are observed for **2** and for **2S**. Thus, during the progress of the reaction, two new ^{t}Bu resonances appear at δ 1.70 and 1.07 signifying the formation of **2S** while the two resonances for the ^{t}Bu groups of **2** (δ1.61, 1.16) simultaneously decrease in intensity.

The progress of S atom transfer between **1S** and **2** can be monitored by following the changes in integration of the ^{t}Bu resonance of any of the four complexes in Scheme 1. In all kinetic runs, the data for this transfer reaction was found to obey an integrated rate law for second-order reactions.† Plots of reciprocal concentration *vs.* time were linear for more than two half lives. In all cases the data indicated a complete, non-reversible transfer of a terminally bonded sulfur atom from Sn to Ge.

Rate constants for this reaction could be determined over a temperature range of 40 °C and a summary of this data is given in

DOI: 10.1039/b003146l

Table 1. Measurements from 25 to 65 °C resulted in k values that ranged from 1.18×10^{-3} to 2.14×10^{-2} M^{-1} s^{-1} with resulting half-lives of 18 h to 31 min. The thermal decomposition of **2S** precluded studies at higher temperatures. An Eyring plot of these results indicated a linear relationship with associated activation parameters of $\Delta H^{\ddagger} = 17.6 \pm 0.2$ kcal mol^{-1} and $\Delta S^{\ddagger} = -14.4 \pm 0.3$ cal K^{-1} mol^{-1}.

The first-order dependence of the reactants was confirmed by imposing pseudo-first-order conditions on the reaction by having **1S** in large excess compared to **2**. Under these circumstances the disappearance of **2** and subsequent formation of **2S** exhibited first order behavior.

The only comparable system for which kinetic information is available is given by eqn. (1). In this case the kinetic analysis was consistent with a reversible second-order reaction.[7] The equilibrium constant for this reaction was near unity between −40 and −10 °C in toluene-d_8. Kinetic measurements for eqn. (1) at temperatures ranging from 30 to 60 °C resulted in k_f values from 0.40 to 2.39 M^{-1} s^{-1}.

The rate law and activation parameters that we obtained for eqn. (4) in Scheme 1 support an inner-sphere mechanism which likely proceeds *via* interaction of the chalcogen atom on tin and the Ge(II) center resulting in a sulfur bridged intermediate (Scheme 1). While this species was not observed in our experiments, the negative entropy of activation ($\Delta S^{\ddagger} = -14.4$ cal K^{-1} mol^{-1}) is consistent with an associative type reaction involving a μ-sulfido intermediate. This observation is in line with the value of $\Delta S^{\ddagger}$ (-24.1 cal K^{-1} mol^{-1}) determined for eqn. (1) for which a similar μ-S species was suggested.[7] Consistent with this proposition is the low $\Delta H^{\ddagger}$ value, which suggests that significant bond formation between Ge and the bridging sulfido ligand that offsets the energy are required for the cleavage of the Sn=S during the transfer. Again the $\Delta H^{\ddagger}$ value obtained for eqn. (4) is similar to that obtained for the homonuclear exchange reaction shown in eqn. (1) ($\Delta H^{\ddagger} = 10.9 \pm 0.9$ kcal mol^{-1}).[7]

The direction of this sulfur atom exchange reaction demonstrates the thermodynamic stability of the terminal GeS bond relative to the corresponding SnS bond. This is consistent with the notions that both the tendency to engage in multiple bonding and the stability of M(IV) *vs.* M(II)[13] decreases for the heavier congeners of the group 14 elements (Ge > Sn > Pb). This is further supported by the fact that the π-bond energy associated with the Sn=S bond has been estimated to be 31.8 kcal mol^{-1} which is considerably lower than that of the Ge=S bond (40.0 kcal mol^{-1}).[14]

Keeping in mind that the common acceptors for oxygen atom transfer reactions are tertiary phosphines[1,2] we also examined the chalcogen atom exchange reactions between the germanium complexes **2**, **2S** and **2Se** and Ph_3PE/Ph_3P (E = S, Se). This should also provide some indication of the relative bond strengths for these species. Complex **2** reacts with 1 equiv. of triphenylphosphine selenide‡ in C_6D_6 according to eqn. (5). ^1H NMR spectroscopy indicated a complete conversion of Ph_3P=Se to Ph_3P while germylene **2** was converted to **2Se**. Under these conditions complete selenido atom exchange was achieved from the phosphorus to the germanium in < 4 min at room temperature with no indication of remaining starting materials. However, when the same reaction was performed with Ph_3PS in place of the Ph_3PSe, no reaction with **2** was observed even at elevated temperatures.

Table 1 Rate constants for eqn. (4) in C_6D_6

T/°C	k M^{-1} s^{-1}
25	$(6.28 \pm 0.84) \times 10^{-4}$
35	$(1.46 \pm 0.13) \times 10^{-3}$
45	$(4.19 \pm 0.06) \times 10^{-3}$
55	$(1.08 \pm 0.04) \times 10^{-2}$
60	$(1.53 \pm 0.06) \times 10^{-2}$
65	$(2.14 \pm 0.05) \times 10^{-2}$

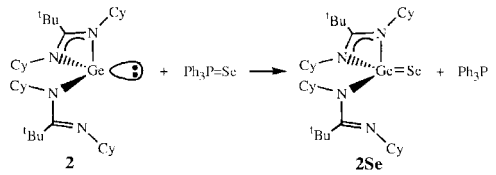

(5)

We have found complete primary sulfur atom exchange between tin and germanium amidinates can be achieved and the kinetic parameters of this reaction have been fully determined. This represents the first comprehensive study of a heteronuclear inter-metal two-electron sulfur atom transfer. The data indicate an inner-sphere mechanism with μ-S formation. Chalcogen atom exchange between PPh_3 and **2** provide results that are consistent with increasing strength of interaction for the terminal sulfido species in the order $[CyNC(^tBu)NCy]_2SnS$ **1S** < $[CyNC(^tBu)NCy]_2GeS$ **2S** < Ph_3PS while for terminal selenido species the order appears to be Ph_3PSe < $[CyNC(^tBu)NCy]_2GeSe$ **2Se**. Our current efforts are directed at extending this investigation of inter-metal chalcogen atom transfer and exploring transfer to non-metal acceptors.

Notes and references

† All kinetic measurements were carried out in duplicate and were monitored by NMR spectroscopy using a Bruker 500 MHz or a Gemini 200 MHz spectrometer. Benzene-d_6 was distilled from Na/K alloy and used as solvent and internal standard. $[CyNC(^tBu)NCy]_2Sn$=S **1S** and $[CyNC(^tBu)NCy]_2Ge$ **2** were prepared according to literature procedures.[10,11]

Solutions of **1S** and **2** were prepared at concentrations ranging from 0.011 to 0.075 M and in ratios from 1 : 1 to 7 : 1. Samples were monitored in a temperature controlled NMR probe for at least two half lives. During remote ^1H NMR experiments, spectra were obtained at regular intervals that varied with temperature (*e.g.* 45 min at 35 °C and 3 min at 65 °C). For measurements at 25 °C, a temperature controlled water bath set at 25.0 °C was used and spectra were recorded manually every 2 h. Pseudo-first-order conditions were investigated at 35 °C where the initial concentrations were: $[(CyNC(^tBu)NCy)_2Sn=S] = 0.075$ M and $[(CyNC(^tBu)NCy)_2Ge] = 0.011$ M.

‡ Ph_3P=Se was prepared by dissolving triphenylphosphine (2.038 g, 7.78 mmol) in 35 ml THF followed by addition of excess elemental selenium (1.023 g, 13 mmol). The mixture was stirred for 24 h and filtered. The product was subsequently recrystallized from THF in 66% yield (1.66 g).

1 R. H. Holm, *Chem. Rev.*, 1987, **87**, 1401.
2 L. K. Woo, *Chem. Rev.*, 1993, **93**, 1125.
3 For recent studies of inter-metal nitrogen atom transfer reactions see: C. E. Laplaza, A. R. Johnson and C. C. Cummins, *J. Am. Chem. Soc.*, 1996, **118**, 709; L. A. Bottomley and F. L. Neeley, *Inorg. Chem.*, 1997, **36**, 5435; C. J. Chang, D. W. Low and H. B. Gray, *Inorg. Chem.*, 1997, **36**, 270; J. Bendix, T. Weyhermuller, E. Bill and K. Wieghardt, *Angew. Chem., Int. Ed.*, 1999, **38**, 2766; T. Agapie, A. L. Odom and C. C. Cummins, *Inorg. Chem.*, 2000, **39**, 174.
4 M. J. A. Johnson, P. M. Lee, A. L. Odom, W. M. Davis and C. C. Cummins, *Angew. Chem., Int. Ed. Engl.*, 1997, **36**, 87.
5 C. M. Bolinger, J. E. Hoots and T. B. Rauchfuss, *Organometallics*, 1982, **1**, 223; R. Guilard, C. Ratti, A. Tabard, P. Richard, D. Dubois and K. M. Kadish, *Inorg. Chem.*, 1990, **29**, 2532; C. Ratti, P. Richard, A. Tabard and R. Guilard, *J. Chem. Soc., Chem. Commun.*, 1989, 69; R. Guilard, C. Ratti, J.-M. Barbe, D. Dubois and K. M. Kadish, *Inorg. Chem.*, 1991, **30**, 1537.
6 L. K. Woo and J. A. Hayes, *Inorg. Chem.*, 1993, **32**, 2228.
7 L. M. Berreau and L. K. Woo, *J. Am. Chem. Soc.*, 1995, **117**, 1314.
8 M. C. Kuchta and G. Parkin, *J. Am. Chem. Soc.*, 1994, **116**, 8372.
9 M. C. Kuchta and G. Parkin, *Inorg. Chem.*, 1997, **36**, 2492.
10 Y. Zhou and D. S. Richeson, *J. Am. Chem. Soc.*, 1996, **118**, 10 850.
11 S. R. Foley, C. Bensimon and D. S. Richeson, *J. Am. Chem. Soc.*, 1997, **119**, 10 359.
12 S. R. Foley, G. P. A. Yap and D. S. Richeson, *Dalton Trans.*, accepted for publication.
13 F. A. Cotton, G. Wilkinson, C. A. Murillo and M. Bochmann, *Advanced Inorganic Chemistry*, Wiley, New York, 6th edn., 1999.
14 Y. Matsuhashi, N. Tokitoh, R. Okazaki and M. Goto, *Organometallics*, 1993, **12**, 2573.

ChemComm

Novel aluminium– and gallium–nitrogen heteronorbornanes†

Christian Lustig and Norbert W. Mitzel*

Anorganisch-chemisches Institut, Technische Universität München, Lichtenbergstr. 4, 85747 Garching, Germany. E-mail: n.mitzel@lrz.tu-muenchen.de

Received (in Basel, Switzerland) 5th May 2000, Accepted 16th June 2000
Published on the Web 6th July 2000

Selective formation of 2,5-dialumina-3,6-diaza- and 2,5-digalla-3,6-diaza-norbornane is achieved by reaction of bis(lithiomethyl-methylamino)methane with dimethylaluminium and dimethylgallium chloride by simultaneous formation of two metal–carbon and two metal–nitrogen bonds accompanied by two ring closure reactions; the norbornane-basket structures are favoured over potential isomers containing three-membered rings and over polymeric aggregation.

Small molecule nitrogen compounds of aluminium and gallium are the subjects of recent interest owing their potential as molecular precursors for III/V materials.[1] Investigations on both donor–acceptor adducts and metal amides have been intensely pursued.[2] Recent interest in compounds with acceptor and donor atoms in geminal position revealed various types of possible aggregates, either intramolecular *via* formation of three-membered ring systems as in compounds containing *BCN*,[3] *BNN*,[4] *AlCN*[5] and *AlNN*[6] but also *SiON*,[7] *GeON*[8] and *SnON*[9] units or intermolecular *via* formation of dimers with cyclohexane-like six-membered rings as in $[(H_2BCH_2SMe)_2]$,[10] $[Me_2Al(CH_2PMe_2)]_2$ and $[Al(CH_2PMe_2)_3]_2$,[11] and $[(Me_3C\text{-}CH_2)_2InCH_2PPh_2]_2$.[12] We intended to construct systems with two *ECN* functions joined by a bridging unit which have at least three possibilities for aggregation as depicted in Scheme 1 two three-membered rings (**A**), six-membered rings in either polymeric aggregation (**B**) or aggregated to form a norbornane-like structure (**C**).

In this contribution we demonstrate by preparation of the first alumina- and galla-azanorbornanes that the structural motif **C** is preferred for the saturated AlCN and GaCN systems. The reaction of a slurry of Karsch's dilithiated aminale $[LiCH_2(Me)N]_2CH_2$[13] with 2 equiv. of dimethylaluminium chloride or dimethylgallium chloride in toluene at −78 °C leads to a simultaneous formation of four chemical bonds and two ring closures to give the norbornane-like aggregates depicted in Scheme 2.‡ The reactions proceeds uniformly, and no sign of structures of type **A** and **B** were observed.

Compounds **1** and **2** show the typical NMR spectra of norbornane units with two non-equivalent signals for the two geminal methyl groups at Al or Ga (E) and the geminal hydrogen atoms at the carbon atom connecting E and N. These signals do not coalesce upon heating toluene solutions to 110 °C, proving the absence of rapid rearrangement reactions involving cleavage of the donor acceptor bonds, required for a positional exchange of the metal bound methyl groups.

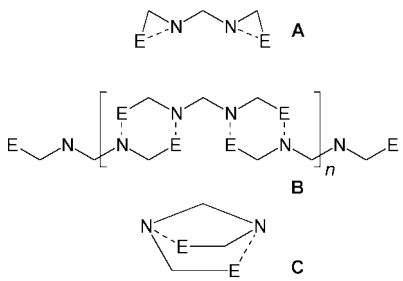

Scheme 1

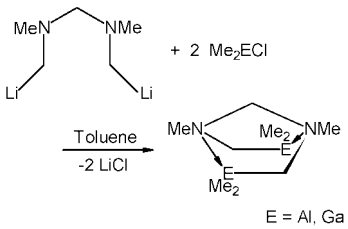

Scheme 2

Single crystals of both compounds, obtained from toluene solutions upon cooling, were examined by X-ray diffraction, and the structure of **1** is shown in Fig. 1.‡§ Compound **1** and the isostructural **2** are the first structurally characterised aminomethyl-aluminium and -gallium compounds. The molecules reside on C_2 axes passing through the aminal carbon atom and are chiral, but occur in the crystal as a racemate. The methylene bridge between the two N atoms causes the $E_2C_2N_2$ six-membered ring to adopt a boat conformation with compressed angles at the metal centres [**1**: 86.2(1)°, **2**: 85.1(1)°] and widened angles at the methylene groups in the six-membered ring [**1**: 105.8(1), **2**: 106.3(2)°] relative to the C_{2v} symmetric hydrocarbon norbornane where the C–C–C angles at the methylene groups in the six-membered ring are 102.7°.[14] This leads to a geometry at the metal atoms which deviates drastically from an ideal tetrahedron. The endocyclic E–N and E–C bond lengths are long when compared to the gas phase values of simple reference compounds such as Me_3Al–NMe_3 [Al–N 2.099(10), Al–C 1.987(5) Å][15] and Me_3Ga–NMe_3 [Ga–N 2.09(3), Ga–C 1.992(6) Å].[16]

The N–C bonds involving the metallated carbon atoms in the norbornane cages of **1** and **2** (N–C2) are *ca*. 3 pm longer than the N–C1 and N–C2 bonds. This elongation of bonds within the ring system indicates the presence of some strain. B3LYP/6-311G(d) calculations were conducted to obtain an estimate for

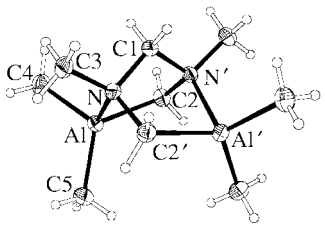

Fig. 1 Molecular structure of $(Me_2AlCH_2MeN)_2CH_2$ **1**. Selected interatomic distances (Å) and angles (°) for **1**: Al–C2 2.020(1), Al–C4 1.971(1), Al–C5 1.962(1), Al–N 2.028(1), N–C1 1.481(1), N–C2 1.514(1), N–C3 1.482(1); Al′–C2–N 105.8(1), Al–N–C2′ 110.2(1), N–C1–N′ 106.2(1), N–Al–C2 86.2(1), C1–N–Al 102.2(1), C1–N–C2 107.1(1), C2–Al–C4 112.3(1), C2–Al–C5 120.6(1). Selected interatomic distances (Å) and angles (°) for isostructural **2**: Ga–C2 2.026(3), Ga–C4 1.991(4), Ga–C5 1.977(4), Ga–N 2.124(3), N–C1 1.476(4), N–C2 1.503(4), N–C3 1.475(4); Ga′–C2–N 106.3(2), Ga–N–C2′ 110.7(2), N–C1–N′ 106.7(3), N–Ga–C2 85.1(1), C1–N–Ga 100.7(2), C1–N–C2 108.5(2), C2–Ga–C4 112.9(2), C2–Ga–C5 122.0(2).

† Electronic supplementary information (ESI) available: selected geometry parameters for **1** and **2** (X-ray and DFT). See http://www.rsc.org/suppdata/cc/b0/b003813j/

the difference in energy between the monomolecular structures **A** and **C**, which were predicted to be 162 and 206 kJ mol^{-1} for **1** and **2**, respectively, and their three-membered ring isomers. As the norbornane structures of **1** and **2** cannot be regarded as strain-free, although much less strained than the three-membered-ring isomers, these values indicate that the *AlCN* units in the three-membered-ring isomers contain at least 80 kJ mol^{-1} more strain energy relative to their six-membered ring dimers. The observation of compounds containing *AlCN* and also *AlNN* three-membered rings can therefore only be rationalised by steric shielding of the small ring unit.

The compact structures of **1** and **2** leads to their comparatively high volatility, and both can be sublimed at *ca*. 90 °C under a pressure of 0.01 mbar without decomposition. The volatility of **1** and **2** leads to the expectation of a small molecular dipole moment for **1** and **2**. Calculations give estimates for dipole moments of 3.95 and 3.43 D for **1** and **2**. The value for **1** is higher than for its three-membered-ring isomer (2.14 D).

We have shown that introduction of two linkages containing acceptor and donor atoms in geminal positions are useful for the synthesis of organometallic heterocyclic systems without the necessity for sterically demanding ligands. Variations of the donor and acceptor centres and the bridging unit opens a field for many novel structural motifs generated through intra- and inter-molecular coordination and for the construction of new macrocyclic compounds.

We are grateful to the Deutsche Forschungsgemeinschaft, the Leonhard–Lorenz-Stiftung and the Fonds der Chemischen Industrie for financial support. Selected geometry parameters for crystalline **1** and **2** accompanied by the results of B3LYP/6-311G(d) calculations is available as ESI.†

Notes and references

‡ *Preparation of* **1** and **2**: Me_2ECl (E = Al, Ga) (10 ml of a 1 M solution in *n*-hexane, 10 mmol) was slowly added at −78 °C to a stirred suspension of $[LiCH_2N(Me)]_2CH_2$ (0.57 g, 5.00 mmol) in toluene (40 ml). The reaction mixture was gradually warmed to room temperature and stirred for 1 day. The solvents were evaporated under reduced pressure and the residue was dissolved in *n*-hexane (20 ml) and filtered. Storage at −20 °C afforded colourless crystals.

Compound **1**: yield: 0.72 g (67%), mp 118–119 °C. CI-MS [*m/z* (%)]: 198 (100), [$M^+ - CH_3$]; ^{1}H NMR (400.05 MHz, 298 K, C_6D_6): δ −0.67 (s, 6 H, $AlCH_3$), −0.34 (s, 6 H, $AlCH_3$), 0.97 (d,$^1J_{HH}$ 12.8 Hz, 2 H, $AlCH_2N$), 1.82 (s, 6 H, NCH_3), 2.11 (d,$^1J_{HH}$ 12.8 Hz, 2 H, $AlCH_2N$), 2.16 (s, 2 H, NCH_2N); ^{13}C{^{1}H} NMR(100.50 MHz, 298 K, C_6D_6): δ −10.50 ($AlCH_3$), −8.92 (s, $AlCH_3$), 45.88 (NCH_3), 47.52 ($AlCH_2N$), 81.71 ($AlCH_2N$); ^{27}Al NMR (104.05 MHz, 298 K, C_6D_6): δ 178 ($\nu_{\frac{1}{2}}$ 1700 Hz).

Compound **2**: yield: 1.11 g (74%), mp 114–116 °C. CI-MS [*m/z* (%)]: 284 (100), [$M^+ - CH_3$]; ^{1}H NMR(400.05 MHz, 298 K, C_6D_6): δ −0.35 (s, 6 H, $GaCH_3$), −0.09 (s, 6 H, $GaCH_3$), 1.16 (d,$^1J_{HH}$ 11.35 Hz, 2 H, $GaCH_2N$), 1.88 (s, 6 H, NCH_3), 2.11 (s, 2 H, NCH_2N), 2.26 (d,$^1J_{HH}$ = 11.35, 2 H, $GaCH_2N$), ^{13}C{^{1}H} NMR (100.50 MHz)): δ −7.32 ($GaCH_3$), −5.93 ($GaCH_3$), 45.73 (NCH_3), 49.21 ($GaCH_2N$), 82.32 ($GaCH_2N$).

§ *Crystal data*: **1**, $C_9H_{24}Al_2N_2$, M = 214.26, monoclinic, space group $P2/n$, a = 7.802(2), b = 7.351(1), c = 11.923(2) Å, β = 101.36(1)°, V = 670.4(2) Å^3, D_c(Z = 2) = 1.061 g cm^{-1}. 2067 reflections collected on a Turbo-CAD4 four circle diffractometer [ω-scan, $2\theta_{max}$ = 54°, Mo-Kα radiation, λ = 0.71073 Å, T = 143(2) K] merged to 1463 unique (R_{int} = 0.036) refining to R_1 = 0.023 for 1347 data [$F_o > 4\sigma(F_o)$] and wR_2 = 0.069 for all 1463 data. Anisotropic refinement of all thermal displacement parameters for non-H-atoms, isotropic for H-atoms.

2, $C_9H_{24}Ga_2N_2$, M = 299.74, monoclinic, space group $P2/n$, a = 7.7786(3), b = 7.4037(3), c = 11.8506(6) Å, β = 101.475(3)°, V = 668.8(2) Å^3, D_c(Z = 2) = 1.488 g cm^{-1}. 2447 reflections collected on a Nonius DIP2020 image plate diffractometer [$2\theta_{max}$ = 53°, Mo-Kα radiation, λ = 0.71073 Å, T = 133(2) K] merged to 1372 unique (R_{int} = 0.011) refining to R_1 = 0.034 for 1220 data [$F_o > 4\sigma(F_o)$] and wR_2 = 0.090 for all 1372 data. Anisotropic refinement of all thermal displacement parameters for non-H-atoms, isotropic for H-atoms.

CCDC 182/1689. See http://www.rsc.org/suppdata/cc/b0/b003813j/ for crystallographic files in .cif format.

1 A. H. Cowley and R. A. Jones, *Angew. Chem., Int. Ed. Engl.*, 1989, **28**, 1208.
2 *Chemistry of Aluminum, Gallium and Indium*, ed. A. J. Downs, Blackie–Chapman Hall, London, 1993; *Coordination Chemistry of Aluminum*, ed. G. H. Robinson, VCH Publishers, Weinheim, 1993.
3 T. H. Hseu and L. H. Larsen, *Inorg. Chem.*, 1975, **14**, 330.
4 S. Diemer, H. Nöth and W. Storch, *Eur. J. Inorg. Chem.*, 1999, 1765.
5 W. Uhl, U. Schütz, W. Hiller and M. Heckel, *Chem. Ber.*, 1994, **127**, 1587.
6 W. Uhl and F. Hannemann, *Eur. J. Inorg. Chem.*, 1999, 201.
7 N. W. Mitzel and U. Losehand, *Angew. Chem., Int. Ed. Engl.*, 1997, **36**, 2807; N. W. Mitzel and U. Losehand, *J. Am. Chem. Soc.*, 1998, **120**, 7320.
8 N. W. Mitzel and U. Losehand, *Eur. J. Inorg. Chem.*, 1998, 2023.
9 N. W. Mitzel, U. Losehand and A. Richardson, *Organometallics*, 1999, **18**, 2610.
10 H. Nöth and D. Sedlak, *Chem. Ber.*, 1983, **116**, 1479.
11 H. H. Karsch and A. Appelt, *Phosphorus Sulfur Relat. Elem.*, 1983, **18**, 287; H. H. Karsch, A. Appelt, F. H. Köhler and G. Müller, *Organometallics*, 1985, **4**, 231.
12 O. T. Beachley, M. A. Banks, M. R. Churchill, W. G. Feighery and J. C. Fettinger, *Organometallics*, 1991, **10**, 3036.
13 H. H. Karsch, *Chem. Ber.*, 1996, **129**, 483.
14 N. L. Allinger, H. J. Geise, W. Pyckhout, L. A. Paquette and J. C. Gallucci, *J. Am. Chem. Soc.*, 1989, **111**, 1106.
15 G. A. Anderson, F. R. Forgaard and A. Haaland, *Acta Chem. Scand.*, 1972, **26**, 1947.
16 V. S. Mastryukov, V. P. Novikov, L. V. Vilkov, A. V. Golubinskii, L. M. Golubinskaya and V. I. Bregadze, *Zh. Strukt. Khim.*, 1987, **28**, 143; *J. Struct. Chem. (Engl. Transl.)*, 1987, **28**, 122.

Photoelectron transfer from excited-state ruthenium(II) tris(bipyridyl) to methylviologen in an ionic liquid

Charles M. Gordon*[a] and Andrew J. McLean*[b]

[a] *Department of Pure and Applied Chemistry, University of Strathclyde, 295 Cathedral Street, Glasgow, UK G1 1XL. E-mail: c.m.gordon@strath.ac.uk*

[b] *Department of Chemistry and Chemical Engineering, University of Paisley, Paisley Campus, Paisley, UK PA1 2BE. E-mail: mcle-ch0@paisley.co.uk*

Received (in Cambridge, UK) 10th May 2000, Accepted 19th June 2000
Published on the Web 6th July 2000

The temperature dependence of bimolecular rate constant and product cage escape yields for the photoelectron transfer reaction between $[Ru(bpy)_3]^{2+}$ and MV^{2+} in the ionic liquid 1-butyl-3-methylimidazolium hexafluorophosphate is reported.

Ionic liquids have been the subject of considerable interest in recent years. Potential applications include battery electrolytes,[1] solvents for homogeneous catalysis or other organic reactions,[2] novel extraction solvents[3] and liquid crystals.[4] The interest is stimulated in particular by their potential application as 'green' solvents in industrial processes.[5] However, there is very little quantitative information regarding their influences on chemical reactions. To date there are also only three papers that describe the use of ionic liquids as solvents for photochemical reactions.[6]

The simplest of all chemical reactions is electron transfer; this type of process occurred in the photochemical systems so far investigated in ionic liquids.[6] We decided to start a quantitative examination of the influence of ionic liquids on reaction rates in one of the most thoroughly investigated of photoinduced electron transfer systems: the ruthenium tris(4,4′-bipyridyl)/methylviologen ($[Ru(bpy)_3]^{2+}/MV^{2+}$) couple. The effects of the medium on this reaction have been studied extensively with variation in temperature, solvent, pH and ionic strength.[7] These results may be summarised with reference to Schemes 1 and 2.

$$*R^{2+} + MV^{2+} \underset{k_{-d}}{\overset{k_d}{\rightleftharpoons}} [*R^{2+}\cdots MV^{2+}] \xrightarrow{k_e} [R^{3+}\cdots MV^{\bullet+}]$$

Scheme 1

$$\begin{array}{ccc} [R^{3+}\cdots MV^{\bullet+}] & \underset{k_d}{\overset{k_{-d}}{\rightleftharpoons}} & R^{3+} + MV^{\bullet+} \\ \Big\downarrow k_b & & \\ [R^{2+}\cdots MV^{2+}] & \underset{k_d}{\overset{k_{-d}}{\rightleftharpoons}} & R^{2+} + MV^{2+} \end{array}$$

Scheme 2

First there is the forward electron transfer step (Scheme 1) involving the reaction between the photoexcited $[Ru(bpy)_3]^{2+}$, $*R^{2+}$, and methylviologen, MV^{2+}, forming an encounter complex/exciplex $[*R^{2+}\cdots MV^{2+}]$. This occurs with a bimolecular rate constant corresponding to diffusion control, k_d. Once formed, $[*R^{2+}\cdots MV^{2+}]$ can either regenerate reactants with a unimolecular rate constant k_d, or electron transfer may occur from $*R^{2+}$ to MV^{2+} with a rate constant k_e. The composite bimolecular rate constant for the overall luminescence quenching reaction, k_q, is given by eqn. (1)

$$k_q = k_d k_e/(k_{-d} + k_e) \quad (1)$$

After forward electron transfer has occurred within the encounter complex, there are two competing reaction pathways as summarised in Scheme 2.

Back electron transfer within the $[R^{3+}\cdots MV^{+}]$ cage, with a rate constant k_b, competes with diffusion apart of R^{3+} and $MV^{\cdot+}$, which occurs with a rate constant k_{-d}. The cage escape efficiency, η_{ce}, is given by eqn. (2)

$$\eta_{ce} = k_{-d}/(k_b + k_{-d}) \quad (2)$$

This photochemical system has a number of features that could be influenced by a purely ionic environment. It has previously been shown that ion pairing of the encounter complexes with a variety of solvated anions in aqueous solution increases k_q and decreases η_{ce}.[8] In an ionic liquid, there is the question as to the extent to which solvent anions will reduce electrostatic repulsion between the two reactant cations *via* a charge screening effect on formation of an encounter complex. Such effects may also reduce k_{-d}. Furthermore, k_b could be affected by alterations in electronic coupling between caged donor/acceptor pairs, or changes in ΔG and solvent reorganisation energy. A combination of these effects would be expected to result in significantly different k_q and η_{ce} values in ionic liquids.

We have examined the temperature dependence of k_q and η_{ce} in the ionic liquid 1-butyl-3-methylimidazolium hexafluorophosphate ([bmim][PF_6]) using laser flash photolysis methods.[9] The value of k_q was determined from plots of the first order rate constant for the decay of $*R^{2+}$, k_{obs}, as a function of MV^{2+} concentration at a series of temperatures over the range 6–70 °C. The concentrations of MV^{2+} employed ranged from 5 to 15 mM. The results are shown in Fig. 1 together with the resulting Arrhenius plot. The Arrhenius behaviour fits the equation $\ln k_q = 33.98\ (\pm 1.7) - 5003\ (\pm 480)/T$, giving an activation energy (E_a) of 41.6 (±4) kJ mol^{-1} and a pre-exponential factor of 5.72×10^{14} mol^{-1} dm^3 s^{-1} for the luminescence quenching reaction. At 20 °C, this corresponds to a k_q value of 2.19×10^7 mol^{-1} dm^3 s^{-1}. This should be compared with values of 1.7×10^9 and 2.2×10^7 mol^{-1} dm^3 s^{-1} previously recorded at this temperature in water and acetonitrile respectively.[10] The viscosity of [bmim][PF_6] at 20 °C is 0.330 Pa s, compared with 0.001 and 0.00036 Pa s for water and acetonitrile, respectively. Given the high viscosity of [bmim][PF_6], we would anticipate that this reaction becomes diffusion controlled, *i.e.* $k_e \gg k_{-d}$, and therefore $k_q = k_d$. To this end, we determined an E_a for viscous flow of 37.6 kJ mol^{-1} in [bmim][PF_6] over the temperature range 10–70 °C. Clearly, E_a for the reaction between MV^{2+} and $*R^{2+}$ is very close to that of viscous flow. Electrostatic repulsions should result in an increase in the barrier to formation of an encounter complex/exciplex between two divalent cations in a typical, non-ionic solvent. This leads us to conclude that such repulsions contribute no more than *ca.* 4 kJ mol^{-1} to our observed activation energy in [bmim][PF_6], which is effectively our estimated error in E_a. Finally, the pre-exponential factor is extremely large for a bimolecular reaction,

DOI: 10.1039/b003754k

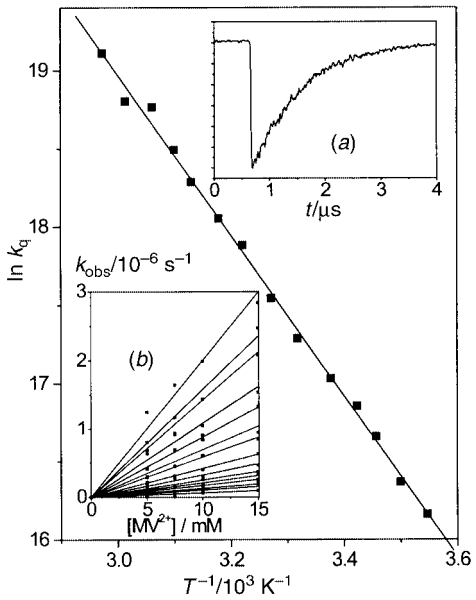

Fig. 1 Arrhenius plot for the bimolecular rate constant for the reaction between *[Ru(bpy)$_3$]$^{2+}$ and Mv^{2+} in [bmim][PF$_6$]. Insert (a) *[Ru(bpy)$_3$]$^{2+}$ emission recorded at λ = 630 nm (λ_{ex} = 355 nm) and 19 °C under N_2-saturated conditions; (b) plot of k_{obs} as a function of [MV^{2+}] over the temperature range 5–70 °C.

and corresponds to a value of ΔS = 29.3 (±14) J K^{-1} mol^{-1} at 298 K. Such a positive $\Delta S^{\ddagger}$ value suggests a structure-breaking process involving the freeing up of solvent ions on formation of the encounter complex. This in turn suggests that the solvent itself is a significantly ordered environment, as has previously been indicated from NMR studies on related ionic liquid systems.[11] We are currently investigating the influence of solute charges on diffusion-controlled reaction rates within ionic liquids and will report our results in due course.

Values of η_{ce} were calculated by measuring the intensity of the signal observed for MV$^{\cdot+}$ at 605 nm relative to that of *R^{2+} at 450 nm (values previously reported in acetonitrile of 1.37 × 10^4 and −1.0 × 10^4 mol^{-1} dm^3 cm^{-1} respectively were used for the difference molar absorptivities).[10] The rate of formation of MV$^{\cdot+}$ was always the same as the rate of decay of *R^{2+} fluorescence. The calculated values of η_{ce} range from 0.35 at 25 °C to 0.8 at 60 °C, compared with 0.29 at 20 °C and 0.45 at 65 °C in acetonitrile.[10] Such large values of η_{ce} are unexpected in a viscous ionic solvent due to the much larger E_a reducing k_{-d} in the ionic liquid with respect to that a non-viscous solvent such as acetonitrile. Previous studies have clearly shown that η_{ce} decreases with increasing ionic strength, primarily because of the anionic counter ions counteracting the electrostatic repulsion between R^{3+} and MV$^{\cdot+}$ within the encounter complex. This leads to k_{-d} decreasing with respect to k_b as ionic strength increases, which in turn results in a decrease in η_{ce}.[8] Clearly, our results are in complete contrast to these earlier studies. Our assumption that the relative molar absorptivities of *R^{2+} and MV$^{\cdot+}$ are independent of solvent may of course be incorrect; nonetheless we do not expect such ratios to alter greatly in different solvents. For comparable cage escape yields to be observed in [bmim][PF$_6$] and acetonitrile at room temperature (assuming Schemes 1 and 2 are valid), k_b must decrease in the ionic liquid relative to acetonitrile in order to compensate for the lower k_{-d} value in the former solvent. Back electron transfer from MV$^{\cdot+}$ to R^{3+} is thought to occur in the so-called Marcus inverted region.[12] Therefore reduction in k_b in [bmim][PF$_6$] with respect to acetonitrile must either be due to ΔG becoming more negative, or else a smaller solvent reorganisation energy in [bmim][PF$_6$], or a combination of both. At this stage we do not have reliable estimates of ΔG in this solvent, nor can we reliably estimate the reorganisation energies; these are usually estimated using the dielectric continuum model. Using pyrenecarbonaldehyde fluorescence as a probe of solvent dielectric, ε, we estimate ε < 10 for [bmim][PF$_6$] at 20 °C.[13] It is quite possible that ΔG is more negative and the solvent reorganisation energy is smaller in [bmim][PF$_6$] than acetonitrile, given such a low dielectric in the former solvent. We are currently determining the temperature dependence of ΔG in a range of ionic liquids, and will report our results in full at a later date.

However, there may be a non-electrochemical explanation for the large η_{ce} values in the ionic liquid. A weak dependence of k_b on ΔG has been reported for a number of [Ru(diimine)$_3$]$^{2+}$/MV^{2+} systems;[12] a suggested explanation is that significant molecular reorientation is required within the solvation sphere *prior* to back electron transfer. In such a situation the reorientation step is rate determining and competes with diffusion apart of the products. Our results are consistent with this hypothesis: both the diffusion apart of the charge separated pair and geometric reorganisation could be expected to require significant contributions from those processes driving viscous flow. The activation energies of both k_{-d} and k_b would then be affected by [bmim][PF$_6$] solvation to a similar extent, and therefore cage escape yields are not greatly altered with respect to less viscous solvents such as acetonitrile.

In conclusion, we have been able to show that the photoelectron transfer reaction between *R^{2+} and MV^{2+} in [bmim][PF$_6$] occurs, within experimental error, at a diffusion-controlled rate. We believe this is the first detailed report of quantified reaction kinetics in an ionic liquid, and also the first indication of the magnitude of diffusion-controlled rate constants in such media. The yield of MV$^{\cdot+}$ is surprisingly larger than expected for such a viscous medium. We are currently investigating the influence of solvent viscosity on diffusion-controlled processes and cage escape yields with a range of ionic liquids, and will report our results in due course.

We thank the Royal Society of Edinburgh for the award of a BP Research Fellowship (C. M. G.), EPSRC (C. M. G.) and the University of Paisley (A. M.) for financial support, Mr Jim Morrow for assistance with viscosity measurements, and Mr David Stirling for assistance with the flash photolysis measurements.

Notes and references

1 See for example: A. B. McEwen, H. L. Ngo, K. LeCompte and J. L. Goldman, *J. Electrochem. Soc.*, 1999, **146**, 1687.
2 T. Welton, *Chem. Rev.*, 1999, **99**, 2071.
3 J. G. Huddleston, H. D. Willnauer, R. P. Swatloski, A. E. Visser and R. D. Rogers, *Chem. Commun.*, 1998, 1765.
4 C. M. Gordon, J. D. Holbrey, A. R. Kennedy and K. R. Seddon, *J. Mater. Chem.*, 1998, **8**, 2627.
5 J. D. Holbrey and K. R. Seddon, *J. Chem. Soc., Dalton Trans.*, 1999, 2133.
6 H. L. Chum, D. Koran and R. A. Osteryoung, *J. Am. Chem. Soc.*, 1978, **100**, 310; G. Hondrogiannis, C. W. Lee, R. M. Pagni and G. Mamantov, *J. Am. Chem. Soc.*, 1993, **115**, 9828; C. Lee, T. Winston, A. Unni, R. M. Pagni and G. Mamantov, *J. Am. Chem. Soc.*, 1996, **118**, 4919.
7 C. D. Clark and M. Z. Hoffmann, *Coord. Chem. Rev.*, 1997, **159**, 359 and references therein.
8 C. D. Clark and M. Z. Hoffmann, *J. Phys. Chem.*, 1996, **100**, 7526.
9 *Experimental details*: [bmim][PF$_6$] was prepared according to literature procedures, and dried thoroughly under vacuum before use.[3] In all experiments the concentration of [Ru(bpy)$_3$]$^{2+}$ was 4 × 10^{-5} M. The laser flash photolysis setup is based around a Spectron Nd-YAD laser, combined with an Applied Photophysics optical bench.
10 H. Sun, A. Yoshimura and M. Hoffmann, *J. Phys. Chem.*, 1994, **98**, 5058.
11 (*a*) K. M. Dieter, C. J. Dymek Jr, N. E. Heimer, J. W. Rovang and J. S. Wilkes, *J. Am. Chem. Soc.*, 1988, **110**, 2722; (*b*) P. Bonhôte, A.-P. Dias, N. Papageorgiou, K. Kalyanasundaram and M. Grätzel, *Inorg. Chem.*, 1996, **35**, 1168.
12 T. Ohno, A. Yoshimura, D. R. Prasad and M. Z. Hoffmann, *J. Phys. Chem.*, 1991, **95**, 4723.
13 We would like to thank a referee for drawing attention to the empirical correlation between the wavelength of maximum fluorescence intensity of the probe and ε for a wide range of solvents. See ref. 11(*b*) for details.

ChemComm

Thermally stable fatigue resistant near infrared active photochromic compounds, exemplified by 6-amino-7-cyano-3-(dicyclopropylmethylene)-4-(2,5-dimethyl-3-furyl)-benzofuran-2(3*H*)-one

Harry G. Heller,* David S. Hughes, Michael B. Hursthouse and Neil G. Rowles

Chemistry Department, Cardiff University, PO Box 912, Cardiff, UK CF1 3TP. E-mail: heller@cardiff.ac.uk

Received (in Cambridge, UK) 2nd May 2000, Accepted 15th June 2000
Published on the Web 7th July 2000

The title pale yellow photochromic compound 11b in toluene, on irradiation at 366 nm, cyclises to the thermally stable infrared active blue–green photochrome, 8-amino-7-cyano-4,4-dicyclopropyl-3a,4-dihydro-6-hydroxy-2,3a-dimethylnaphtho[2,1-*b*]furan-5,6-carbolactone, 12b which has a λ_{max} value of 720 nm for its broad long wavelength absorption band.

E-Fulgides, (*E*)-3-[1-(2,5-dimethyl-3-furyl)ethylidene]-4-isopropylidenetetrahydrofuran-2,5-dione **1a**, (*E*)-3-[1-(2,5-dimethyl-3-furyl)ethylidene]-4-(cyclopropylmethylene)tetrahydrofuran-2,5-dione **1b**, (*E*)-3-[2,5-dimethyl-3-thienyl)-ethylidene-4-isopropylidene tetrahydrofurandione **1c** and (*E*)-3-[2-methyl-5-phenyl-3-thienyl)ethylidene-4-(dicyclopropylmethylene)tetrahydrofuran-2,5-dione **1d** reacted with malononitrile and diethylamine in THF to give exclusively (*E*)-2-dicyanomethylene derivatives **3a–d** which, in toluene, cyclised to photochromes **4a–d** on irradiation at 366 nm. The thermally stable blue photochromes **4a–d** underwent reverse reactions on exposure to white light. Previous papers[1,2] reported erroneously that *E*-fulgides (*e.g.* **1a**) gave the corresponding (*E*)-5-dicyanomethylene derivatives (*e.g.* **8a)** on reaction with malononitrile (1 equiv.) and diethylamine (2 equiv.) in THF, followed by cyclisation with acetyl chloride.

Z-Fulgides **6a–d** gave exclusively the corresponding pale yellow (*Z*)-5-dicyanomethylene derivatives **7a–d** under similar experimental conditions. The latter, in toluene, isomerised to *E*-isomers **8a–d** and cyclised to photochromes **9a–d** on irradiation at 366 nm. The thermally stable blue photochromes **9a–d** underwent reverse reactions to pale yellow *E*-isomers **8a–d** on exposure to white light.

Deprotonation of the methyl group *syn* to the dicyanomethylene group in (*Z*)-2-dicyanomethylene derivative **3b**, by boiling with diisopropylamine in THF, gave anion **5b**, which reacted with the adjacent cyano group to form imine **10b**, which isomerised to 6-amino-7-cyano-3-(dicyclopropylmethylene)-4-(2,5-dimethyl-3-furyl)-1-benzofuran-2(3*H*)-ones **11b**,† obtained as bright yellow crystals (from chloroform–petrol). Its structure was confirmed by X-ray crystallographic analysis (Fig. 1). Amines **11a–d** were prepared in a similar manner.

All new compounds were fully characterised. Spectral data, melting points and yields are given in Table 1.

On irradiation at 366 nm, amines **11a–d** in toluene cyclised to thermally stable blue-green photochromes **12a–d** (Table 2) which underwent the reverse reactions on exposure to white light.

Photochromes **2a–d**, **4a–d**, and **9a–d** showed bathochromic shifts when the push-pull effect is enhanced, as reported for infrared active dyes.[3] Photochromes **12a–d** have increased intramolecular charge-transfer character, due to the tendency to

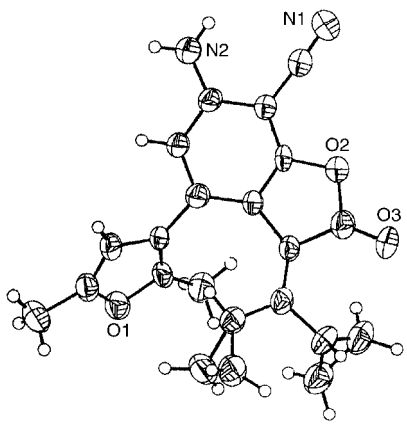

Fig. 1 The X-ray structure of the photochromic compound **11b**.

DOI: 10.1039/b003496g

Table 1 λ_{max} Values for solutions in toluene after photocyclisation, melting points, and yields of photochromic compounds[a]

Compound	**3a**	**3b**	**3c**	**3d**	**7a**	**7b**	**7c**	**7d**	**11a**	**11b**	**11c**	**11d**
λ_{max}/nm	318	323	323	341	353	358	335	333	349	374	348	378
Mp/°C	153–154	155–156	177–178	150–151	184–185	182–183	177–178	151–152	227–229	180–181	212–214	237–238
% Yield	62	62	35	49	39	67	35	90	39	65	31	47

[a] **a** X = O, R^1 = R^2 = Me; **b** X = O, R^1 = Me; R^2 = cyclopropyl; **c** X = S, R^1 = R^2 = Me; **d** X = S, R^1 = Ph, R^2 = cyclopropyl.

Table 2 λ_{max} Values for the long wavelength absorption bands of photochromes in toluene after the photocyclisation of precursors, illustrating the major bathochromic shifts that can be achieved by molecular tailoring[a]

Photochrome	**2a**	**2b**	**2c**	**2d**	**4a**	**4b**	**4c**	**4d**	**9a**	**9b**	**9c**	**9d**	**12a**	**12b**	**12c**	**12d**
λ_{max}/nm	496	514	520	566	601	594	598	653	610	634	642	669	698	720	681	776

[a] **a** X = O, R^1 = R^2 = Me; **b** X = O, R^1 = Me; R^2 = cyclopropyl; **c** X = S, R^1 = R^2 = Me; **d** X = S, R^1 = Ph, R^2 = cyclopropyl.

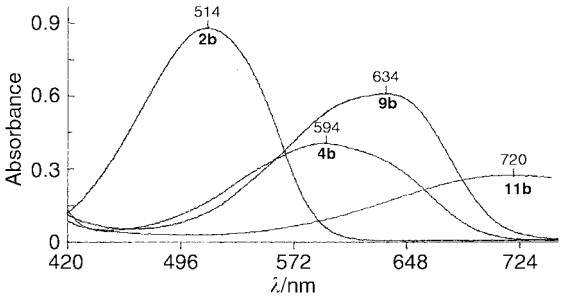

Fig. 2 The spectra of compounds **2b**, **4b**, **9b** and **12b** (1×10^{-4} molar solutions in toluene) after irradiation at 366 nm to the photostationary state.

retain the benzene ring, as indicated by resonance forms **13a**–**d**, which results in the broad absorption band in the region 750–800 nm. The spectra of coloured forms, thermal stability, fatigue resistance and high efficiencies for colouring and bleaching make the photochromic system based on compounds **11a**–**d** well suited for optical memory devices and security printing. The major changes in the spectra of these photochromes by molecular tailoring are illustrated in Fig. 2.

We thank Philips Research, Eindhoven, The Netherlands and at Redhill, UK and EPSRC for a CASE studentship to N. G. R. and for support of the X-ray crystallographic work.

Notes and references

† *Crystal data* for **11b**: $C_{22}H_{20}N_2O_3$, M_r 360.4, monoclinic, space group $P(2)\,1/c$, a = 9.372(8), b = 11.198(7), c = 17.679(7) Å, β = 101.06 (4)°, V = 18212 A^3, T = 293(2) K, Z = 4, D_c = 1.315 g cm^{-3}, R_1 = 0.0380, wR_2 = 0.0676 for all 2655 points data and 248 parameters. Data were recorded using a FAST TV area detector diffractometer and Mo-Kα radiation. CCDC 182/1692. See http://www.rsc.org/suppdata/cc/b0/b003496g/ for crystallographic files in .cif format.

1 H. G. Heller, D. S. Hughes, M. B. Hursthouse and K. V. S. Koh, *J. Chem. Soc. Chem. Commun.*, 1994, 2713.
2 Z. Sun, R. S. Hosmane and M. Tadros, *Tetrahedron Lett.*, 1995, **36**, 3453.
3 Y. Kubo, F. Mori, K. Komatsu and K. Yoshida, *J. Chem. Soc., Perkin Trans. 1*, 1988, 2439.

ChemComm

Side chain elongation causes a change from enthalpy driven to entropy driven binding in the molecular recognition of tetraanionic peptides†

Xavier Salvatella,[a] Mark W. Peczuh,[b] Margarida Gairí,[c] Rishi K. Jain,[b] Jorge Sánchez-Quesada,[d] Javier de Mendoza,[d] Andrew D. Hamilton*[b] and Ernest Giralt*[a]

[a] *Departament de Química Orgànica, Universitat de Barcelona, Martí i Franqués 1-11, 08028 Barcelona, Spain. E-mail: giralt@qo.ub.es*
[b] *Department of Chemistry, Yale University, New Haven, CT 06520, USA. E-mail: andrew.hamilton@yale.edu*
[c] *Unitat de Ressonància Magnètica Nuclear, Serveis Científico-Tècnics, Universitat de Barcelona, Martí i Franqués 1-11, 08028 Barcelona, Spain*
[d] *Departamento de Química Orgánica, Universidad Autónoma de Madrid, Cantoblanco, 28049 Madrid, Spain*

Received (in Cambridge) 10th May 2000, Accepted 21st June 2000
Published on the Web 7th July 2000

In binding to tetraguanidinium compounds, the average side chain length of tetraanionic peptides determines the thermodynamics of binding, the degree of helix induction and the rigidity of the complex formed.

Protein–protein interactions play an essential role in the regulation of biochemical events in living organisms.[1] Although the increasing number of structures deposited in the structural databases reveals some interesting trends in the biophysical properties of protein–protein interfaces,[2] the design of protein surface receptors able to disrupt such interactions remains a challenge. However, peptide surface binding by synthetic receptors has been studied intensively and is providing interesting candidates for protein surface recognition.[3,4] We have reported the association between tetraguanidinium receptor **1** and peptide **2** with an *i*, *i* + 3, *i* + 6, *i* + 9 arrangement

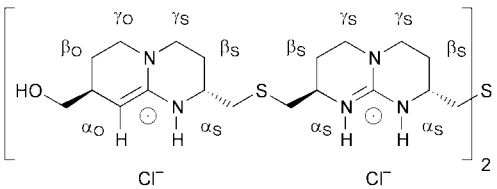

1

of aspartate residues in 10% aqueous methanol.[4] Although side chain length has been shown to affect important properties of amino acids such as helical propensity[5] and the ability to make side chain-to-backbone hydrogen bonds[6] little attention has been paid to its importance in peptide and protein recognition.

† Electronic supplementary information (ESI) available: isothermal titration calorimetry, ^{1}HNMR and NOE data. See http://www.rsc.org/suppdata/cc/b0/b003728l/

With the aim of further developing the approach to protein surface receptors we have now investigated the effect of increasing side chain length. We have sequentially replaced aspartate by glutamate so that the Asp–Glu ratio spans gradually from the all aspartate peptide **2** to the all glutamate peptide **6**. This family of peptides has been studied by CD, NMR and isothermal titration calorimetry (ITC) in order to explore which molecular recognition parameters are affected by increasing side chain length. As reported below we have found that lengthening the side chain has a dramatic effect on the thermodynamics of binding, which shifts from enthalpically driven to entropically driven.

The helical content of the peptides in solution was assessed by circular dichroism spectroscopy and showed (Table 1) that replacement of aspartate by glutamate gradually increases the helical content of the peptide (Hel_i) as predicted from their helix propensities.

Binding of **1** to **2** causes a large increase in the helicity of the peptide because the alignment of atoms necessary for intermolecular hydrogen bond formation requires that the peptide adopts a helical conformation. CD binding[7] titrations of **3** to **6** were carried out to assess the effect of side chain length on helix induction. The results (Table 1) show that the effect of the stepwise replacement of aspartate by glutamate is a gradual decrease in the helical induction due to complex formation (ΔHel). The absolute increase of fractional helicity decreases from 24% for **2** to nearly no conformational change for **5** and **6**.

ITC was used to detect binding and measure affinity constants in the cases where there was no change in ellipticity at 222 nm. The data confirm the 1 : 1 stoichiometry of complexation and give an independent measurement of K_a for peptide **2**, validating the results previously reported by CD. Peptide **2** shows an overall negative enthalpy change (−5.64 kcal mol^{-1}) whereas **6** shows a positive enthalpy change upon binding (3.68 kcal mol^{-1}). Peptide **4**, which has an equal number of aspartate and glutamate residues in its surface shows an enthalpically

Table 1 Thermodynamic and binding data for **1** with tetracarboxylate peptides[14]

Sequence	Hel_i	Hel_f	ΔHel	K_a (M^{-1})	ΔG_a (kcal mol^{-1})	ΔH_a (kcal mol^{-1})	$T\Delta S_a$ (kcal mol^{-1})
2 Ac-A-A-A-**D**-Q-L-**D**-A-L-**D**-A-Q-**D**-A-A-Y-NH_2	21	45	24	CD 3.4 ± 1.2 × 10^5 ITC 1.2 ± 0.2 × 10^5	−7.23	−5.64	1.29
3 Ac-A-A-A-**E**-Q-L-**D**-A-L-**D**-A-Q-**D**-A-A-Y-NH_2	20	40	20	CD 5.6 ± 1.0 × 10^4			
4 Ac-A-A-A-**E**-Q-L-**E**-A-L-**D**-A-Q-**D**-A-A-Y-NH_2	26	36	10	CD 5.3 ± 2.2 × 10^4 ITC [a]	−6.44	0	6.44
5 Ac-A-A-A-**E**-Q-L-**E**-A-L-**E**-A-Q-**D**-A-A-Y-NH_2	27	26	−1	CD 2.2 ± 1.5 × 10^4			
6 Ac-A-A-A-**E**-Q-L-**E**-A-L-**E**-A-Q-**E**-A-A-Y-NH_2	33	30	−3	CD [a] ITC 1.5 ± 0.4 × 10^5	−7.06	3.68	10.74

[a] No observed change by the noted technique.

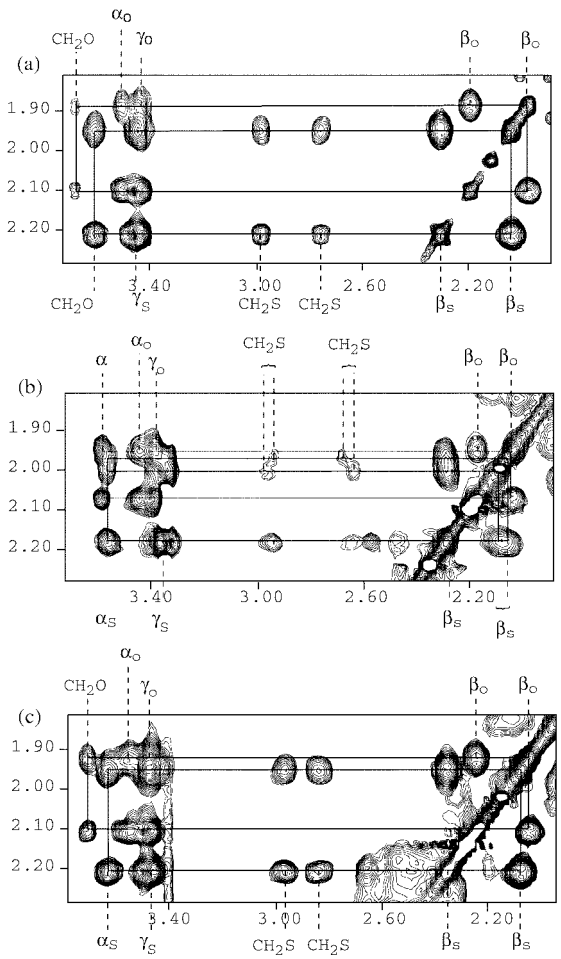

Fig. 1 Expansion of the TOCSY spectrum of **1** (a). Equivalent spectrum in the presence of peptide **2** (b), and in the presence of peptide **6** (c).

neutral binding curve. Despite this variation in thermodynamic behavior, the affinity constants obtained by the combination of CD and ITC methods reveal that affinity does not greatly depend on the individual nature of the residues involved with complex formation, as shown in Table 1.

Chemical shift changes in **1** upon complexation of **2** and **6** have been monitored by NMR spectroscopy.[8] Unbound **1** has a C_2 axis of symmetry which simplifies its spectrum and is no longer present in the complex with tetra acid peptides. Fig. 1(a) shows an expansion of the TOCSY spectrum of unbound **1**. The splitting of resonances in **1** due to the asymmetry of the **1**:**2** complex can be observed in Fig. 1(b). However, this splitting is not observed in the NMR spectrum of **1** bound to **6**. Although chemical shift changes occur, no loss of symmetry is detected as shown in Fig. 1(c). Further evidence for the different rigidity of the complexes is provided by the existence of intermolecular NOEs between the CH_2S and α_S protons of **1** and the methyl groups of leucine 6 and/or leucine 9 of **2** which are not observed in the complex formed between **1** and **6**.

Recognition of **2** is enthalpy driven. Because of the relative rigidity of the aspartate side chains in contact with the receptor, a change in the backbone conformation of **2** towards higher helicity is necessary as shown in Table 1. Despite the entropic penalty associated with preorganization, complex formation takes place due to the large negative enthalpy of α-helix formation[9] and the entropy of liberation of counterions and solvent. Complexation of **6** is however entropy driven. The longer side chain of glutamate allows complex formation to take place without major re-organization: the overall conformation does not change as observed by CD (Table 1). The large entropy change on complexation is probably due to the liberation of solvent and counterions initially bound to the peptide and the receptor. The rigidity of the complex, related to the change in entropy, is also side chain length dependent: close proximity of **1** and the all aspartate peptide **2** in the **1**:**2** complex is indicated by the existence of intermolecular NOEs and the extent of chemical shift changes compared to **1**. The lack of intermolecular NOEs and the less pronounced chemical shift changes suggest that **1**:**6** is significantly less rigid. Binding of **4**, which displays two Asp and two Glu residues on its anionic surface, is enthalpically neutral (Table 1), confirming that side chain length modulates to a great extent the features of recognition between **1** and tetraanionic peptides.

Although the binding of sulfate anions by guanidinium receptors has recently been reported to be entropy driven,[10] in our case the thermodynanic behavior can be tuned by changing side chain length. These results can be analyzed in the context of enthalpy–entropy compensation.[11] This phenomenon has often been described in ligand–protein interactions and is defined as a compensating behavior of the relative changes to ΔH and $T\Delta S$ of binding within a series of ligands or receptors of similar structure.[12]

In summary, we have shown how recognition of *i*, *i* + 3, *i* + 6, *i* + 9 tetra-carboxylate peptides by **1** is a general phenomenon that takes place both with Asp and Glu containing peptides but that length of the side chain has a dramatic impact on the thermodynamics of binding. A recent survey of 'hot spots' shows that Asp is 2–3 times more likely than Glu to contribute to the stability of protein–protein complexes.[13] Our results suggest that this may be due to the tighter nature of Asp *vs.* Glu complexation.

Work in our laboratories was supported by grants from the US–Spain Science & Technology Program, CICYT (PB93-0283, BIO99-484 and 2FD97-0267), Generalitat de Catalunya (Grup Consolidat and Centre de Referència en Biotecnologia), NATO and the National Institutes of Health (GM35208). X.S. acknowledges a Bruker graduate fellowship.

Notes and references

1 J. Janin and C. Chothia, *J. Biol. Chem.*, 1990, **265**, 16027.
2 L. Lo Conte, C. Chothia and J. Janin, *J. Mol. Biol.*, 1999, **285**, 2177.
3 M. W. Peczuh and A. D. Hamilton, *Chem Rev.*, 2000, in press.
4 M. W. Peczuh, A. D. Hamilton, J. Sánchez-Quesada, J. de Mendoza, T. Hack and E. Giralt, *J. Am. Chem. Soc.*, 1997, **119**, 9327; T. Haack, M. W. Peczuh, X. Salvatella, J. Sánchez-Quesada, J. de Mendoza, A. D. Hamilton and E. Giralt, *J. Am. Chem. Soc.*, 1999, **121**, 11 813.
5 S. Padmanabhan, E. J. York, J. M. Stewart and R. L. Baldwin, *J. Mol. Biol.*, 1996, **257**, 726.
6 M. Vijayakumar, H. Qian and H.-X. Zhou, *Proteins: Struct., Funct., Genet.*, 1999, **34**, 497.
7 CD experiments were carried out by increasing the concentration of **1** while keeping the concentration of peptide constant (T = 278 K). Ellipticity at 222 nm (Θ_{obs}) was used to calculate the percentage helicity f, $f = 100[(\Theta_{obs} - \Theta_0)/(\Theta_{100}-\Theta_0)]$ where Θ_0 is the ellipticity of the denatured peptide and Θ_{100} is the ellipticity of the 100% helical peptide [$\Theta_{100} = -40\,000(1 - 2.5/n)$; n is the number of amide bonds].
8 NMR samples were 1 mM in CD_3OH–H_2O (9:1), the experiments were carried out on a Bruker Avance DMX-500 spectrometer at 278 K. Experiments used for the assignment included COSY, TOCSY, NOESY, [^{13}C, ^{1}H]-HSQC and [^{13}C, ^{1}H]-HMBC.
9 J. M. Scholtz, S. Marqusee, R. L. Baldwin, E. J. York, J. M. Stewart, M. Santoro and D. W. Bolen, *Proc. Natl. Acad. Sci. USA.*, 1991, **88**, 2854.
10 M. Berger and F. P. Schmidtchen, *J. Am. Chem. Soc.*, 1999, **121**, 9986.
11 E. Gallichio, M. M. Kubo and R. M. Levy, *J. Am. Chem. Soc.*, 1998, **120**, 4526; V. L. TlapakSimmons and G. D. Reinhart, *Biophys. J.*, 1998, **75**, 1010.
12 H. Qian, *J. Chem. Phys.*, 1998, **109**, 10015.
13 A. A. Bogan and K. S. Thorn, *J. Mol. Biol.*, 1998, **280**, 1.
14 Binding constants fittings were made using either the CD titration curves or the enthalpy evolution curves. In the first case the fittings were done by non-linear regression analysis (C. S. Wilcox in *Frontiers in Supramolecular Chemistry and Photochemistry*, eds. H. J. Schneider and H. Durr, VCH, Weinheim, **1990**, pp.123–143) and in the latter using Microcal Origin software.

ChemComm

Synthesis and cross-coupling reactions of solid-supported alkylzinc reagents

Richard F. W. Jackson,*[a] Leslie J. Oates[a] and Michael H. Block[b]

[a] *Department of Chemistry, Bedson Building, The University of Newcastle, Newcastle upon Tyne, UK NE1 7RU. E-mail: r.f.w.jackson@newcastle.ac.uk*

[b] *Astra Zeneca Pharmaceuticals, Mereside, Alderley Park, Macclesfield, Cheshire, UK SK10 4TG*

Received (in Liverpool, UK) 10th May 2000, Accepted 15th June 2000
Published on the Web 7th July 2000

Hydroboration of Wang-supported pent-4-enoic acid 1, followed by transmetallation with Et_2Zn, gives a solid-supported zinc reagent, 2, which undergoes palladium-catalysed coupling with aryl iodides, to give the corresponding 5-arylpentanoic acids 3 in moderate to good yields, after cleavage from the resin using TFA.

Solid phase synthesis has developed into one of the main methods used in the construction of libraries of compounds in the search for biological activity. While a vast amount is known about the formation of carbon–heteroatom bonds on solid phase, the area of carbon–carbon bond formation has been less well-developed.[1] More specifically, the application of organometallic chemistry to carbon–carbon bond formation in solid phase synthesis has not been extensively investigated. There are examples of reaction of solid supported electrophiles with solution phase organometallic reagents, for example stannanes[2] and organozinc halides,[3] and this approach offers the advantage of being able to use a large excess of the organometallic reagent to ensure high conversion of the solid-supported electrophile. However, this approach has the dual disadvantages that each electrophile has to be loaded separately onto solid support, and also that the limited number of 'off-the-shelf' organometallic reagents means that most would need to be prepared separately. This clearly militates against the use of this chemistry in real library synthesis. By contrast, the large number of readily available electrophiles means that the preparation of solid-supported organometallic reagents has the potential to be much more generally applicable.

The preparation of solid-supported organometallic reagents was originally limited to the lithiation of cross-linked polystyrene, and this approach is widely used for the synthesis of modified polystyrene resins.[4] The use of solid-supported stannanes has been reported,[5] but these reagents are only appropriate for the transfer of unsaturated functionality. More recently, both aryl Grignard reagents[6] and aryl zincates[7] have been prepared from iodobenzoic acid derivatives supported on Wang resin. There is clearly a great need for the development of methods for the preparation of solid-supported alkylmetal derivatives, and the well-established functional group tolerance of alkylzinc reagents suggested that these might be good candidates.[8,9]

Organozinc reagents have most often been prepared by the heterogeneous reaction of alkyl iodides with metallic zinc, a process which is clearly not applicable to solid phase. A very attractive alternative is the overall conversion of an alkene into a dialkylzinc compound by initial hydroboration with diethylborane, followed by transmetallation with diethylzinc.[10] We have therefore prepared Wang-supported pent-4-enoic acid **1** (using 3 equivalents of pent-4-enoic acid relative to Wang resin). This material was subsequently treated with an equivalent of Et_2BH in THF, and after washing, an excess of Et_2Zn was added at 0 °C. Subsequent reaction with iodobenzene under palladium catalysis,† followed by cleavage from the resin using TFA,‡ gave 5-phenylpentanoic acid **3a** (78%, based on resin loading of pent-4-enoic acid as determined by cleavage using TFA–CH_2Cl_2 from a sample of the resin **1**), Scheme 1. A brief survey of the applicability of the process established that other substituted aromatic iodides are also appropriate coupling partners (Table 1).

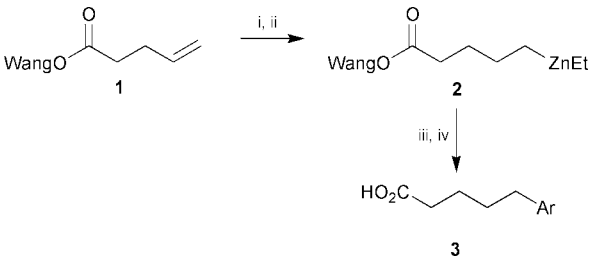

Scheme 1 *Reagents and conditions:* i, Et_2BH (1 equiv.), 5 °C, 30 min; ii, Et_2Zn (10 equiv.), 0 °C, 30 min; iii, ArI (2 equiv.), $Pd_2(dba)_3$ (2.5 mol.%), P(*o*-tol)$_3$ (10 mol.%), room temp., 16 h; iv, TFA, CH_2Cl_2, room temp, 1 h.

Table 1 Preparation of 5-aryl valeric acids

Ar–I	Product	Ar	Yield (%)
Ph–I	**3a**	Ph	78
4-MeC_6H_4–I	**3b**	4-MeC_6H_4	42
4-$O_2NC_6H_4$–I	**3c**	4-$O_2NC_6H_4$	58
3-$O_2NC_6H_4$–I	**3d**	3-$O_2NC_6H_4$	44
2-$O_2NC_6H_4$–I	**3e**	2-$O_2NC_6H_4$	42
1-Naphthyl–I	**3f**	1-Naphthyl	49

The usual product of zinc–boron exchange reactions is the symmetrical dialkylzinc species **4**,[10] towards which the equilibrium is shifted by removal of the triethylborane by distillation, although it is likely that the ethylalkylzinc species **2** is also formed in the presence of an excess of diethylzinc. On solid phase, the distinction between these two species is not important, since the ethylbenzene arising from coupling of the ethyl group in **2** with the electrophile is removed during the washing process after the coupling reaction and before the cleavage with trifluoroacetic acid.

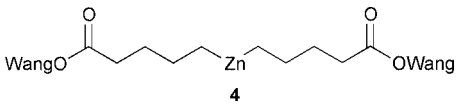

This demonstration that simple functionalised alkylzinc reagents can be prepared on solid-support opens the possibility of the use of such reagents in library synthesis.

We thank Astra Zeneca for support (L. J. O.)

Notes and references

† Wang pent-4-enoate resin (500 mg, 0.55 meq) was allowed to swell with dry (distilled) THF (5 cm^3) under N_2 in dry glassware. This mass of resin typically absorbed 3.8 cm^3 of THF. The excess solvent was decanted *via* a syringe, and the resin washed with THF (2 × 5 cm^3). THF (2 cm^3) was added, and the reaction cooled in ice–water before addition of diethylborane (80 μl, 0.56 mmol), prepared from triethylborane and borane–dimethyl sulfide complex. After 30 min the solvent was decanted, and the resin washed with THF (5 cm^3). THF (2 cm^3) was added and the suspension cooled to 0 °C, followed by the addition of Et_2Zn (400–500 μl, 4–5 mmol).

After 30 min the solvent was decanted, and the resin washed with THF (2 × 5 cm^3). THF (5 cm^3) was added, followed by Pd_2dba_3 and P(*o*-tolyl)$_3$ (1:4 molar ratio 20–25 μmol Pd) and the electrophile (1.1 mmol). The reaction was allowed to proceed overnight at rt (20–22 °C). The resin was poured into a sintered-funnel, drained in air, and washed thoroughly with THF until the washings ran clear. The resin was then treated with acetic acid–THF (50:50, 50 cm^3, 30 min), washed with THF (3 × 20 cm^3) and then with CH_2Cl_2 (4 × 20 cm^3).

‡ The resin was placed in a sintered-funnel and washed with dry (distilled) CH_2Cl_2 (3 × 10 cm^3). The funnel was covered with aluminium foil, a mixture of CH_2Cl_2 (1.5 cm^3) and TFA (5 cm^3) was added and the mixture allowed to stand for 1 h. The solvent was drained into a flask under N_2, and the resin washed with dry CH_2Cl_2 (2 × 20 cm^3). The solvent(s) were evaporated to give the crude products as oils, from which the products crystallised upon standing. All products were recrystallised from petroleum ethers or petroleum ether–$CHCl_3$ systems.

1 B. A. Lorsbach and M. J. Kurth, *Chem. Rev.*, 1999, **99**, 1549.
2 M. S. Deshpande, *Tetrahedron Lett.*, 1994, **35**, 5613.
3 S. Marquais and M. Arlt, *Tetrahedron Lett.*, 1996, **37**, 5491; M. Rottländer and P. Knochel, *J. Comb. Chem.*, 1999, **1**, 181; A. E. Jensen, W. Dohle and P. Knochel, *Tetrahedron*, 2000, **56**, 4197.
4 For example, C. Halm, J. Evarts and M. J. Kurth, *Tetrahedron Lett.*, 1997, **38**, 7709, and references therein.
5 F. W. Forman and I. Sucholeiki, *J. Org. Chem.*, 1995, **60**, 523; H. Kuhn and W. P. Neumann, *Synlett*, 1994, 123; M. J. Plunkett and J. A. Ellmann, *J. Am. Chem. Soc.*, 1995, **117**, 3306; M. S. Brody and M. G. Finn, *Tetrahedron Lett.*, 1999, **40**, 415.
6 L. Boymond, M. Rottländer, G. Cahiez and P. Knochel, *Angew. Chem., Int. Ed. Engl.*, 1998, **37**, 1701.
7 Y. Kondo, T. Komine, M. Fujinami, M. Uchiyama and T. Sakamoto, *J. Comb. Chem.*, 1999, **1**, 123.
8 P. Knochel and R. D. Singer, *Chem. Rev.*, 1993, **93**, 2117.
9 S. Gair and R. F. W. Jackson, *Curr. Org. Chem.*, 1998, **2**, 527.
10 F. Langer, L. Schwink, A. Desasagayaraj, P.-Y. Chavant and P. Knochel, *J. Org. Chem.*, 1996, **61**, 8229.

A novel ATRP initiating system $Fe(dtc)_3/FeCl_3/PPh_3$ for MMA polymerization

Xiao-Ping Chen and Kun-Yuan Qiu*

Department of Polymer Science and Engineering Chemistry Building, Peking University, Beijing 100871, China. E-mail: kyqiu@chemms.chem.pku.edu.cn

Received (in Cambridge, UK) 5th June 2000, Accepted 14th June 2000
Published on the Web 7th July 2000

A 'living'/controlled radical polymerization of MMA was carried out with a novel ATRP initiation system: iron(III) tri(diethyldithiocarbamate) $[Fe(dtc)_3]/FeCl_3/PPh_3$, where neither an organic halide nor a radical initiator was used.

As we know, atom transfer radical polymerization (ATRP) is one of the effective controlled/'living' radical polymerization systems to synthesize well-defined polymers with low polydispersities and complex architectures;[1,2] and up to now, two types of ATRP, *i.e.* (conventional) ATRP and reverse ATRP,[3–5] have been known.

In ATRP, organic halides (RX) are used as initiators, transition-metal compounds in their lower oxidation state (M^n) are used as catalysts and electron-donating compounds are used as ligands (L). In reverse ATRP, a radical initiator and a higher oxidation state transition-metal catalyst complex $M^{n+1}XL_m$ are used instead of an organic halide initiator RX and lower oxidation state catalyst complex M^nL_m. As in ATRP, a controlled/'living' radical polymerization can also be carried out in a reverse ATRP system, under which a dynamic equilibrium is established, where the dormant polymer chains are reversibly activated *via* a halogen atom transfer reaction.

More recently, we have first reported a third ATRP process, *i.e. in situ* ATRP of MMA polymerization using the tetraethylthiuram disulfide (TD)/$FeCl_3/PPh_3$ system.[6] In the *in situ* ATRP process, RX and M^{n+} are both created *in situ* from the reaction between a radical initiator TD and $FeCl_3$ at a given polymerization temperature. The polymerization proceeds following a conventional ATRP and is well-controlled.

So far, from the reported literature, one of components in an ATRP initiating system must be either an organic halide[1,2] (in ATRP) or a radical initiator[3–5] (in reverse ATRP or *in situ* ATRP). Recently, however, a paper concerning a living radical polymerization of styrene with $Fe(dtc)_3$/AIBN system in a halogen-free living process was published.[7]

Here we report a novel initiating system $Fe(dtc)_3/FeCl_3/PPh_3$, in which neither an organic halide nor a radical initiator as the initiator for ATRP was used. The polymerization of MMA with this initiating system proceeded *via* an ATRP process.

The bulk polymerization of MMA was carried out using the $Fe(dtc)_3/FeCl_3/PPh_3$ initiation system at 80 °C. With $[MMA]_0:[Fe(dtc)_3]_0:[FeCl_3]_0:[PPh_3]_0 \approx 300:1:30:90$, a plot of $\ln([M]_0/[M])$ *vs.* time as shown in Fig. 1, showed a straight line, indicating that the kinetics was first order in monomer and that the concentration of propagating radicals was unchanged during the polymerization. It can be seen in Fig. 2 that the $M_{n\,(GPC)}$, number-average molecular weight measured by GPC, increased linearly with conversion from 1300 to 7200. A quite narrow polydispersity index (1.10–1.16) was obtained as the monomer conversion increased from 11 to 79% in 40 min. The value of $M_{n\,(GPC)}$ was almost equal to $M_{n(th)}$, a theoretical number-average molecular weight calculated from $M_{n(th)} = ([MMA]_0/3[Fe(dtc)_3]_0) \times MW_{MMA} \times$ conversion. The efficiencies (f) of initiator as computed from $f = M_{n(th)}/M_{n(GPC)}$ were ≈ 1.0.

When the ratio of feeds in a separate experiment was the same as in bulk, similar results of solution polymerization of MMA in anisole were obtained although with a lower rate of polymerization, *e.g.* the conversion was 52% at 40 min, $M_{n(GPC)}$ was 4700 and M_w/M_n was 1.19.

Accordingly, the above results clearly suggested that the MMA polymerization with the $Fe(dtc)_3/FeCl_3/PPh_3$ initiation system at 80 °C exhibited some 'living'/controlled radical polymerization characteristics.

We investigated the effects of initial initiator concentration on the polymerization of MMA under fixed conditions: $[MMA]_0 = 9.38$ mol l^{-1}, $[Fe(dtc)_3]_0:[FeCl_3]_0:[PPh_3]_0 = 1:30:90$, at 80 °C. When $[Fe(dtc)_3]_0$ is 3.13×10^{-3} mol l^{-1}, the conversion was 62%, $M_n = 55\,800$, $M_w/M_n = 1.23$, while when $[Fe(dtc)_3]_0$ was increased to 6.25×10^{-3} mol l^{-1}, the conversion was 68.7%, $M_n = 28\,100$, $M_w/M_n = 1.32$ after the same polymerization time of 5 h. This indicated that PMMA with higher number-average molecular weight and narrow polydispersity can be obtained using a lower initial concentration of $Fe(dtc)_3$.

The polymers obtained are well-defined PMMA with α-Et_2NCS_2– and ω-chlorine groups according to FTIR, UV and

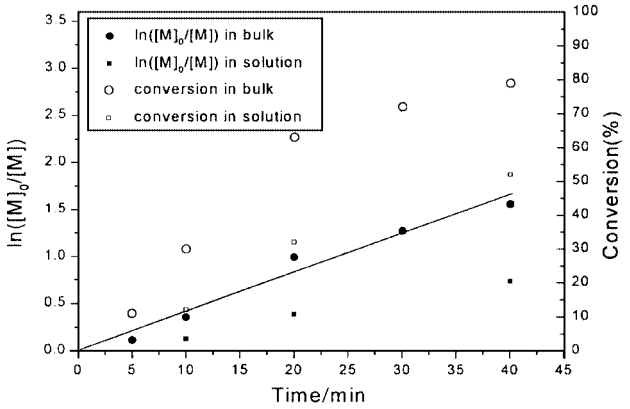

Fig. 1 Time dependence of $\ln[M]_0/[M]$ and conversion at 80 °C, where $[M]_0$ and [M] are the MMA concentration at times 0 and t, respectively. *Conditions*: in bulk, $[MMA]_0 = 9.38$ mol l^{-1}, $[Fe(dtc)_3]_0 = 3.13 \times 10^{-2}$ mol l^{-1}, $[FeCl_3]_0 = 9.38 \times 10^{-1}$ mol l^{-1}, $[PPh_3]_0 = 2.81$ mol l^{-1}; in anisole, $[MMA]_0 = 5.25$ mol l^{-1}, $[Fe(dtc)_3]_0 = 1.75 \times 10^{-2}$ mol l^{-1}, $[FeCl_3]_0 = 5.25 \times 10^{-1}$ mol l^{-1}, $[PPh_3]_0 = 1.57$ mol l^{-1}.

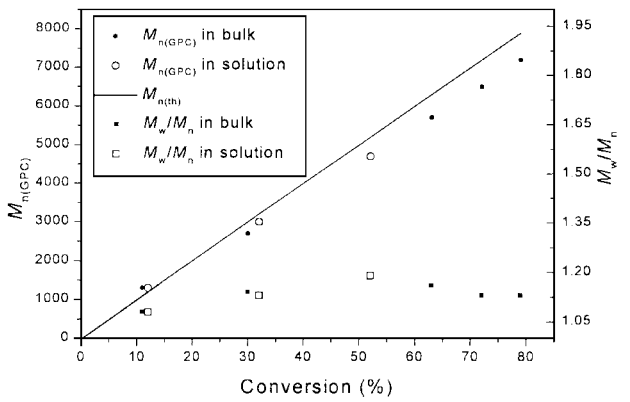

Fig. 2 Dependence of the molecular weight and polydispersity of PMMA on the monomer conversion at 80 °C (conditions as in Fig. 1).

DOI: 10.1039/b004471g

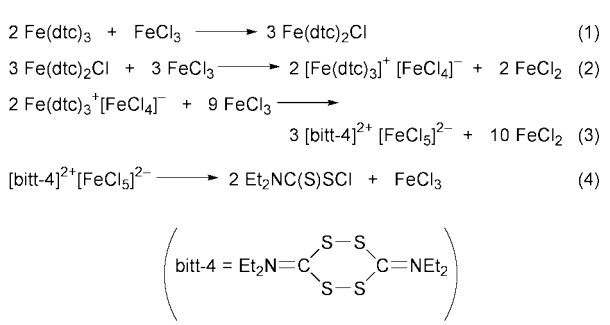

Scheme 1

NMR spectra. In the FTIR spectrum of the PMMA, signals at 1272 and *ca.* 3440 cm^{-1} are characteristic absorption bands of the Et_2NCS_2– group while the UV spectrum of the PMMA powder identifies Et_2NCS_2– (*ca.* 276.8 nm) as an end group. In the ^1H NMR spectrum, the chemical shift at δ 3.07 corresponds to the methylene protons $Et_2NCS_2CH_2$, whilst that at δ 3.70 is due to $(CH_3CH_2)_2NCS_2$–. A signal at δ 3.79 arises from protons of the methoxy group, whilst that at δ 2.50 arises from the methylene protons of the terminal MMA unit capped with an ω-end chlorine, similar to that reported by Sawamoto and coworkers[8] and by us.[6] The $M_{n(NMR)}$ value (5100) is close to $M_{n(GPC)}$ (4700), indicating that all the polymer chains have chlorine ends. The presence of an ω-chlorine end group at the polymer chains suggests the polymerization proceeds in an ATRP process.

Some control experiments were carried out to clarify the polymerization mechanism. The polymerization of MMA with $Fe(dtc)_3$ alone did not take place after 160 minutes at 80 °C or after 60 min at 100 °C indicating that $Fe(dtc)_3$ was not a thermal radical initiator. Addition of PPh_3 did not modify the observed behavior, and polymerization only occurred in the presence of all three components $Fe(dtc)_3$, $FeCl_3$ and PPh_3, *e.g.* the conversion was 11% after 5 min at 80 °C. Using $Fe(dtc)_3$ and $FeCl_3$ in the absence of PPh_3 at 80 °C, led to precipitation of $FeCl_2$ after *ca.* 10 min whilst no polymer was obtained even after 15.5 h.

According to the above results and the reaction of $Fe(dtc)_3$ with $FeCl_3$ reported in the literature[9] and our previous work,[6] we propose the reaction of $Fe(dtc)_3$ with $FeCl_3$ as shown in Scheme 1.

Reactions (1) and (2) are the same as the results reported by Victoriano *et al.*,[9] whilst in the step (3), bis(dialkylimonium)tetrathiolane (bitt-4) is possibly formed instead of bis(dialkylimonium)trithiolane (bitt-3)[9] in the presence of the monomer MMA and PPh_3. Bitt-4 may discompose into (diethylthiocarbamoyl)sulfur chloride (Et_2NCS_2Cl) as shown in step (4).

Therefore, the mechanism of polymerization proposed is as depicted in Scheme 2.

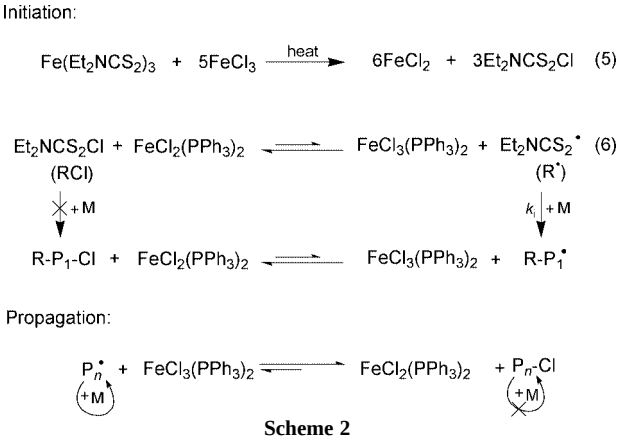

Scheme 2

At the temperature of polymerization, $Fe(dtc)_3$ reacts with $FeCl_3$ *via* a redox process to form an organic halide, (Et_2NCS_2Cl) and $FeCl_2$ [eqn. (5) in Scheme 2; simplified from the combination of the reactions in Scheme 1]. Thus, the initiator (Et_2NCS_2Cl) and the transition-metal catalyst in the lower oxidation state ($FeCl_2$) for an ATRP system are created *in situ*. The primary radical $Et_2NCS_2^{\cdot}$, formed from the reaction of Et_2NCS_2Cl with $FeCl_2(PPh_3)_2$, probably initiates MMA polymerization [eqn. (6) in Scheme 2]. with subsequent reactions following a conventional ATRP.

Chain extension polymerization of PMMA with an ω-chlorine end group can be carried out using the ATRP catalyst system. For a bulk process at 100 °C, using PMMA with M_n = 2500, M_w/M_n = 1.14, $[PMMA]_0 = 2.73 \times 10^{-2}$ mol l^{-1} and $[MMA]_0$ = 8.32 mol l^{-1}, $[CuCl]_0 = 2.73 \times 10^{-2}$ mol l^{-1}, $[2,2'\text{-bipyridine}]_0 = 8.19 \times 10^{-2}$ mol l^{-1}; a conversion of 96.4% was achieved after 12 h, with M_n of the chain-extended PMMA = 41900, M_w/M_n = 1.12.

Notes and references

1 M. Kato, M. Kamigaito, M. Sawamoto and T. Higashimura, *Macromolecules*, 1995, **28**, 1721.
2 J. S. Wang and K. Matyjaszewski, *J. Am. Chem. Soc.*, 1995, **117**, 5614.
3 G. Moineau, Ph. Dubois, R. Jérôme, T. Senninger and Ph. Teyssié, *Macromolecules*, 1998, **31**, 545.
4 J. S. Wang and K. Matyjaszewski, *Macromolecules*, 1995, **28**, 7572.
5 X. P. Chen and K. Y. Qiu, *Macromolecules*, 1999, **32**, 8711.
6 X. P. Chen and K. Y. Qiu, *Chem. Commun.*, 2000, **3**, 233.
7 M. Nishimura, M. Kamigaito and M. Sawamoto, *Polym. Prepr.*, 1999, **40**, 470.
8 T. Ando, M. Kamigaito and M. Sawamoto, *Macromolecules*, 1998, **31**, 6708.
9 L. I. Victoriano, J. A. Gnecco and H. V. Carbacho, *Polyhedron*, 1996, **15**, 1315.

Regioselective iron-mediated C–C coupling reactions: role of the iodide anion†

Karine Ferré,[a] Philippe Le Mignot,[a] Sourisak Sinbandhit,[b] Loïc Toupet[c] and Véronique Guerchais*[a]

[a] *UMR 6509 CNRS-Université de Rennes 1 'Organométalliques et Catalyse: Chimie et Electrochimie Moléculaires', Campus de Beaulieu, Université de Rennes 1, 35042 Rennes Cedex, France. E-mail: guerchai@univ-rennes1.fr*

[b] *Centre Régional de Mesures Physiques de l'Ouest (C.R.M.P.O.), Campus de Beaulieu, Université de Rennes 1, 35042 Rennes Cedex, France*

[c] *UMR CNRS 6626 Groupe Matière Condensée et Matériaux, Campus de Beaulieu, Université de Rennes 1, 35042 Rennes Cedex, France*

Received (in Cambridge, UK) 12th April 2000, Accepted 16th June 2000
Published on the Web 6th July 2000

The chelate iron(allyloxy)carbene complexes [Fe(C_5H_5)(CO){η^3-C(OCHR^{1}CH=CR^{2}R^3)(C_6H_4-*o*-Cl)}][BF_4] (2a-e) yield in the presence of [*n*Bu_4N][I] the corresponding β,γ-unsaturated ketones R^{3}R^{2}C=CHCHR^{1}C(O)(C_6H_4-*o*-Cl) (3); this reaction proceeds with high regioselectivity without rearrangement of the allyl fragment.

The design of transition metal complexes capable of selective C–C bond formation under mild conditions is highly desirable. Such a reaction can be achieved by carbene complexes which are good candidates to promote processes within the coordination sphere of the metal. For instance, chelate (allyloxy)carbene complexes have been postulated as key intermediates in the [Ru(Cp)(PPh_3)$_2$Cl)]-catalysed coupling of allylic alcohol and terminal alkynes, affording β,γ-unsaturated ketones.[1,2] Although [Ru](allyloxy)carbene ([Ru] = Ru(Tp)(Cl)) complexes have been recently described,[3] no direct evidence of such transformation from these species has been reported.[4] The related chelate iron (allyloxy)carbene complexes[5] can be useful models for providing an insight into the mechanism of this reaction, and this is likely to be important in the development and design of new catalysts. Iron (alkoxy)carbene complexes [Fe(C_5H_5)(CO)$_2${C(OR)R′}] are known to undergo facile *O*-dealkylation reactions in the presence of iodide anions,[6] regenerating the starting acyl precursor [Fe(C_5H_5)(CO)$_2${C(O)R′}] along with RI. This prompted us to examine the deallylation reaction of *chelate* (allyloxy)carbene complexes under the same conditions, the coordinated allyl fragment thus generated is expected to be involved in a metal-mediated C–C coupling. We report herein the reactivity of the chelate (allyloxy)carbene complexes [Fe(C_5H_5)(CO){η^3-C(OCHR^{1}CH=CR^{2}R^3)(C_6H_4-*o*-Cl)}][BF_4] (**2**) towards iodide salts, and the formation of the corresponding β,γ-unsaturated ketones **3**. Since the iron moiety is not sterically encumbered, this facilitates the study of different substituted allyloxy derivatives, showing that this transformation is efficient and proceeds with excellent regioselectivity.

The *chelate* (allyloxy)carbene complexes (η^3-*C,C,C*) [Fe(C_5H_5)(CO){η^3-C(OCHR^{1}CH=CR^{2}R^3)(C_6H_4-*o*-Cl)}][BF_4] (**2a**–**e**), are readily accessible from the methoxycarbene complexes containing a labile CH_3CN ligand [Fe(C_5H_5)(CO)(CH_3CN){C(OMe)(C_6H_4-*o*-Cl)}][BF_4] (**1**).[5] The structure of **2c**, containing a trisubstituted C=C fragment, has been confirmed by X-ray crystallography (Fig. 1).§ The reaction of **2** (**a**, R^2 = Ph, R^1 = R^3 = H; **b**, R^2 = Me, R^1 = R^3 = H; **c**, R^2 = R^3 = Me, R^1 = H; **d**, R^1 = Me, R^2 = R^3 = H; **e**, R^1 = R^2 = R^3 = H) with [*n*Bu_4N][I] in CH_2Cl_2 gives quantitatively the ketones R^{3}R^{2}C=CHCHR^{1}C(O)(C_6H_4-*o*-Cl) (**3**) (Scheme 1). If the reaction is carried out in the presence of CO (1 atm), the organometallic fragment is recovered as [Fe(C_5H_5)(CO)$_2$(I)].[7] The *E*-configuration of **3a**–**b** is confirmed by the ^{1}H NMR data. The resonances of the olefinic protons of

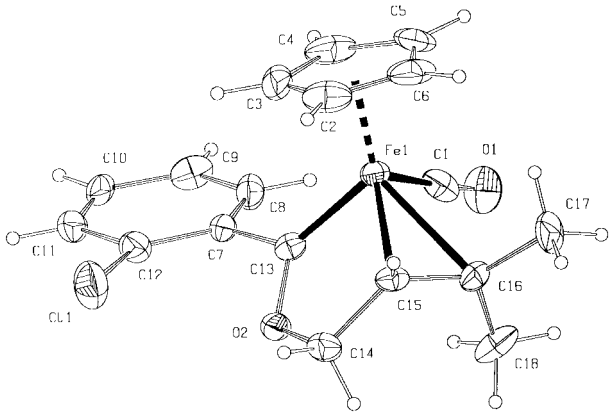

Fig. 1 ORTEP drawing of **2c**. Selected bond distances (Å) and angles (°): O2–C13 1.344(14), O2–C14 1.430(14), Fe–C13 1.828(11), C15–C16 1.41(2), C17–C16–C18 117.8(14), O2–C13–C7 108.9(9), C13–O2–C14 115.4(8).

3a are located at δ 6.54 (=CH) and 6.41 (=C*H*Ph) with a typical coupling constant ^3J(H,H) = 16 Hz, whereas those of **3b** appear at δ 5.66 (=CH, ^3J(H,H) = 15.3 Hz) and 5.35 (=C*H*Me). Moreover, the formation of the conjugated isomer *i.e.* the α-enone, which would result from isomerisation of the C=C double bond, does not occur. Remarkably, no rearrangement of the initial allyl group is observed. Depending on the precursor used, the α- and γ-methyl substituted ketones **3d** and **3b** are formed, respectively. The above data indicate that the carbon atom of the allyl substituent, which is involved in the C–O bond cleavage, recombines to form the new C–C bond. The proposed mechanism showing the participation of the iodide is depicted in Scheme 2. Rupture of the C–O bond[8,9] by nucleophilic attack of I^- on the carbon atom yields a coordinated allyl iodide fragment, which then could oxidatively add to the iron center, inducing the decoordination of the olefinic unit. Then, the transient 18-electron Fe(IV) species reductively eliminates the acyl and the η^1-allyl ligands to afford the observed ketone **3**, and the iron-containing compounds. The first step has been already

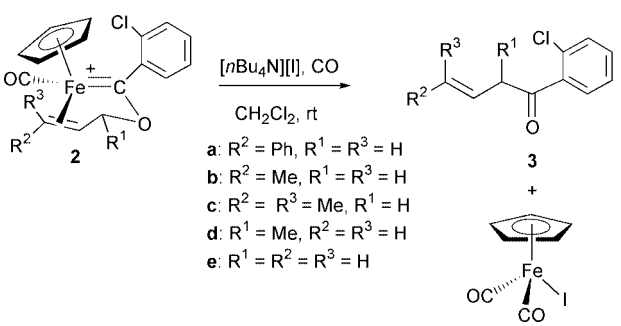

Scheme 1

† Electronic supplementary information (ESI) available: experimental data for compound **3**. See http://www.rsc.org/suppdata/cc/b0/002921l/

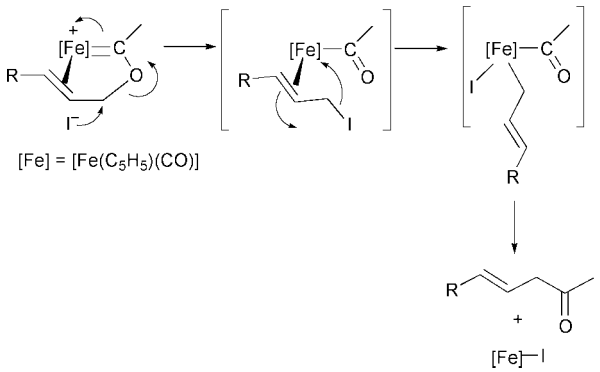

Scheme 2

observed for unchelated iron (alkoxy)carbene complexes,[6] it can be explained by the substantial contribution of the resonance oxonium form, in which the C–O bond is weakened. Moreover, this shows that the C–C bond forming reaction occurs within the co-ordination sphere of the metal, and this requires pre-coordination of the allyloxy group, as previously suggested.[1,10]

These results provide the direct evidence of the formation of β,γ-unsaturated ketones from *chelate* (allyloxy)carbene complexes. Moreover, the role of the iodide is crucial to initiate this process. Finally, the above data on the $[Fe(Cp)(CO)]^+$ iron moiety, capable to coordinate tri- and disubstituted C=C bonds, show that the arrangement of the allyl group is maintained during this transformation, allowing regioselective reactions.

This work was supported by the CNRS. We thank the MENRT for a grant to K. F.

Notes and references

§ *Crystal data* for **2c**: $C_{18}H_{18}O_2ClFeBF_4$, M = 444.43 orthorhombic space group $P2_12_12_1$, a = 7.462(7), b = 11.991(3), c = 21.169(7) Å, V = 1894(2) Å^{-3}, Z = 4, ρ = 1.558 g cm^{-3}. CAD4 NONIUS diffractometer, MoKα radiation, μ = 9.85 cm^{-1}, $F(000)$ = 1064, T = 293 K. 1972 reflections, 1240 with $I > 2\sigma(I)$ observed ($\omega/2\theta$ = 1, *hkl*: 0.6, 0.15, 0.27. R = 0.0798, R_w = 0.152, $w = 1/[\sigma^2(F_o)^2 + (0.1757P)^2]$, S_w = 1.019 (residual $\Delta\rho$ < 0.58 eÅ^{-3}). CCDC 182/1695. See http://www.rsc.org/suppdata/cc/b002921l/ for crystallographic files in .cif format.

1 B. M. Trost, G. Dyker and R. J. Kulawiec, *J. Am. Chem. Soc.*, 1990, **112**, 7809; B. M. Trost and R. J. Kulawiec, *J. Am. Chem. Soc.*, 1992, **114**, 5579; Y. Nishibayashi, I. Takei and M. Hidaï, *Organometallics*, 1997, **16**, 3091.

2 B. M. Trost and J. A. Flygare, *J. Am. Chem. Soc.*, 1992, **114**, 5476; B. M. Trost and J. A. Flygare, *Tetrahedron Lett.*, 1994, **35**, 4059.

3 E. Rüba, C. Gemel, C. Slugovc, K. Mereiter, R. Schmid and K. Kirchner, *Organometallics*, 1999, **18**, 2275.

4 The formation of a ketone by thermolysis of a tungsten (allyloxy)-carbene complex has been described: C. P. Casey and A. J. Shusterman, *Organometallics*, 1985, **4**, 736.

5 C. Schulz, M. Tohier, M. S. Sinbandhit and V. Guerchais, *Inorg. Chim. Acta*, 1999, **291**, 449.

6 A. R. Cutler, *J. Am. Chem. Soc.*, 1979, **101**, 604; A. R. Cutler, P. K. Hanna and J. C. Vites, *Chem. Rev.*, 1988, **88**, 1363; A. Davison and D. L. Reger, *J. Am. Chem. Soc.*, 1972, **94**, 9237.

7 If the reaction is carried out in the absence of CO, the iodo derivative is formed along with ferrocene and unidentified inorganic iron-compounds.

8 Halide ions are powerful nucleophiles capable of C–O bond cleavage of ethers: see, M. V. Bhatt and S. U. Kulkarni, *Synthesis*, 1983, **4**, 249.

9 Examples of selective Csp^3–O bond activation by anions acting as dealkylation reagents have been previously reported, a process promoted by Lewis acid metal centres, see: M. E. van der Boom, S.-Y. Liou, Y. Ben-David, A. Vigalok and D. Milstein, *Angew. Chem., Int., Ed. Engl.*, 1997, **36**, 625; M. E. van der Boom, S.-Y. Liou, Y. Ben-David, L. J. W. Shimon and D. Milstein, *J. Am. Chem. Soc.*, 1998, **120**, 6531; G. Poignant, S. Nlate, V. Guerchais, A. J. Edwards and P. R. Raithby, *Organometallics*, 1997, **16**, 124.

10 For unchelated Ruthenium-(allyloxy)carbene complexes, see: D. Pilette, H. Le Bozec, A. Romero and P. H. Dixneuf, *J. Chem. Soc., Chem. Commun.*, 1992, 1220; M. A. Estuerelas, A. V. Gómez, A. M. López, E. Oñate and N. Ruiz, *Organometallics*, 1998, **17**, 2297; M. A. Estuerelas, A. V. Gómez, A. M. López, M. Oliván, E. Oñate and N. Ruiz, *Organometallic*, 2000, **19**, 4.

ChemComm

Cluster stabilization by an open-chain tetrapyrrolic ligand: first evidence for NH activation as an initial step in tetrapyrrole metalation processes

Martin Bröring,* Andreas Pfister and Kerstin Ilg

Institut für Anorganische Chemie, Universität Würzburg, Am Hubland, D-97074 Würzburg, Germany. E-mail: Martin.Broering@mail.uni-wuerzburg.de

Received (in Basel, Switzerland) 5th May 2000, Accepted 15th June 2000
Published on the Web 10th July 2000

Bisdipyrrin 1 reacts with $Ru_3(CO)_{12}$ to yield the pentanuclear cluster 2; the X-ray structure of 2 sheds new light on the metalation processes of oligopyrrolic ligands.

The coordination chemisty of bile pigments and related ligands,[1] an emerging branch of porphyrin research, has been developed mainly in the last decade.[2] Most of the structurally characterized complexes of this class were found to exhibit metalloporphyrin-like structures with the metal ion bound to the four central nitrogen atoms of the ligand. The higher flexibility of the open-chain tetrapyrroles with respect to the porphyrins, however, also allows other coordination modes, and some examples of M_2L_2 arrangements[3] as well as complexes coordinated through donor atoms of the ligand periphery[4] were obtained. In our efforts to explore the coordination chemistry of open-chain oligopyrroles and to apply helical chiral chelates in catalytic processes, ruthenium complexes have become a major goal. This communication reports the unprecedented coordination of ruthenium to the bile pigment analogue bisdipyrrin **1**[5] and provides the first example for the role of NH activation in tetrapyrrole metalation processes.

The method most widely used to introduce a ruthenium ion into a porphyrin is the reaction of the ligand with an excess of $Ru_3(CO)_{12}$ in a high boiling solvent.[6] When applying these conditions (Scheme 1) to the bisdipyrrin **1** (twofold molar excess of ruthenium carrier, toluene, 130 °C), a single defined product was observed by TLC and could subsequently be isolated using radial chromatography (13% yield). Upon slow evaporation from hexane–CH_2Cl_2, dark red crystals suitable for X-ray diffraction were obtained. As the structural analysis[7] revealed, the product was not the anticipated (carbonyl)ruthenium bisdipyrrin, but the pentanuclear cluster **2**.[8]

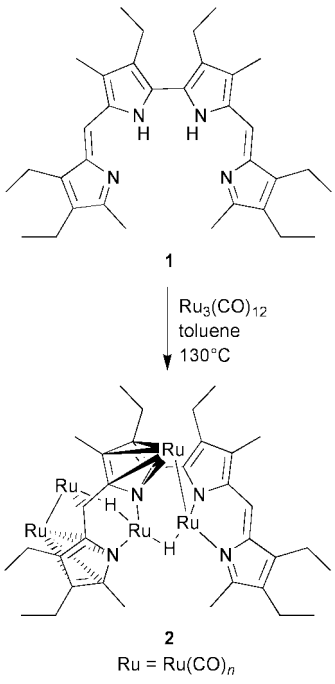

Scheme 1

The complicated arrangement of the Ru_5H_2 cluster core found in **2** can best be understood as composed from three subunits. Two Ru_2 moieties are located above and below the tetrapyrrolic ligand. While one of these is bound through a normal dipyrrin N_2 chelate and a η^5-coordinated pyrrole [Ru(2)–Ru(5)], the other is found to bind to the *meso*-carbon atom C(34) of the second dipyrrolic half of the bisdipyrrin, supported by another η^5 coordination [Ru(3)–Ru(4)].[9] Finally, the fifth ruthenium center Ru(1) is situated in between the two remaining nitrogen atoms N(3) and N(4) and acts as a central unit, connecting the two Ru_2 fragments *via* μ-hydrido bridges to Ru(2) and Ru(3), respectively. Fig. 1 demonstrates the action of the flexible and severely twisted bisdipyrrin ligand on the Ru_2–H–Ru–H–Ru_2 moiety. In addition, eleven surrounding CO ligands serve to saturate the coordination spheres of the ruthenium centers of cluster **2**, allowing octahedral geometries for all five metal atoms (Fig. 2). The cluster core and the tetrapyrrolic ligand thus both adopt conformations optimized for the stabilization of the uncommon structure. This synergysm accounts for the surprising fact that **2** shows enhanced resistance against thermal cluster degradation and decomposition.

Since the assignment of hydride ligands bound to heavy metal atoms through X-ray diffraction is generally problematic, a ^{1}H NMR spectroscopic investigation of **2** was undertaken which showed signals at −15.30 and −18.40 corresponding to the two hydrido ligands in **2** (Fig. 3). The coupling (4 Hz) between these hydrides is in accord with them both being bound to the same ruthenium center. In addition, the signal at δ −18.40 shows a coupling of 1 Hz with the resonance of the *meso* proton

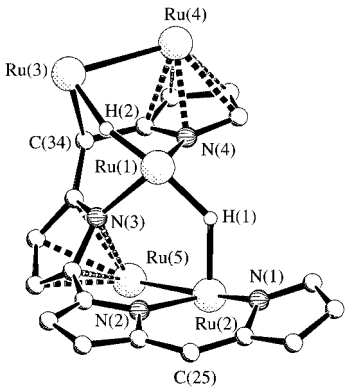

Fig. 1 Schakal plot of the molecular structure of **2** (alkyl groups and CO ligands omitted for clarity). Selected bond lengths (Å) and bond angles (°): Ru(1)–Ru(2) 3.26, Ru(1)–Ru(3) 3.27, Ru(3)–Ru(4) 2.778(13), Ru(2)–Ru(5) 2.793(12), Ru(3)–C(34) 2.209(10), Ru(1)–N(3) 2.086(7), Ru(1)–N(4) 2.205(8), Ru(2)–N(1) 2.149(7), Ru(2)–N(2) 2.119(8), C(33)–C(34) 1.482(13), C(34)–C(35) 1.470(13), C(24)–C(25) 1.361(15), C(25)–C(26) 1.415(14); Ru(1)–H(1)–Ru(2) 130.7, Ru(1)–H(2)–Ru(3) 154.7, N(1)–Ru(2)–N(2) 84.3(3), N(3)–Ru(1)–N(4) 89.0(3).

DOI: 10.1039/b003815f

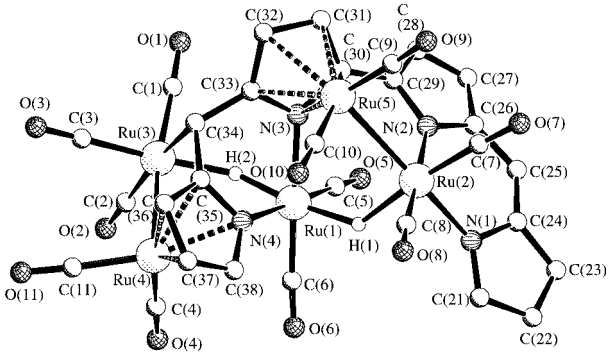

Fig. 2 View of the octahedral coordination geometries of the five ruthenium metal centers in **2** (alkyl groups omitted for clarity).

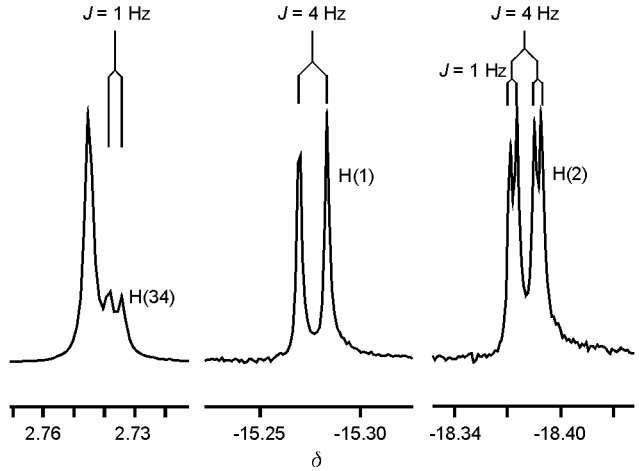

Fig. 3 Details of the ^{1}H NMR spectrum of **2** (300 MHz, benzene-d_6).

H(34), indicative of the close vicinity of H(2) and H(34), so strongly supporting the structural findings.

The bridging hydrides originate from the NH functionalities of the bisdipyrrin ligand and indicates that the well-established mechanism for tetrapyrrole metalation, deformation of the macrocycle, subsequent binding of a metal ion to two nitrogen donors, and insertion into the porphyrin cavity with concomitant deprotonation,[10] is not the only plausible mechanistic pathway. Obviously, a route involving the oxidative addition of an NH moiety on an appropriate metal carrier constitutes a suitable alternative, especially if carriers with metal centers in low oxidation states are employed.[11] For porphyrins, the initial structures formed during metalation processes using metal carbonyls probably resemble cluster fragment complexes similar to that found for bisdipyrrin **2**; owing to the rigid macrocyclic character of porphyrins, however, cluster degradation should be fast and inevitably result in the well-known N_4-coordinated metal porphyrins.[12]

This work was funded by the Deutsche Forschungsgemeinschaft (Emmy-Noether-Programm Brö 2010/1-1). We thank Christian Galka for fruitful discussions and Professor Helmut Werner for his generous support.

Notes and references

1 H. Falk, *The Chemistry of Linear Oligopyrrols and Bile Pigments*, Springer, Wien, 1989.

2 J. V. Bonfiglio, R. Bonnett, D. G. Buckley, D. Hamzetash, M. B. Hursthouse, K. M. Abdul Malik, A. F. McDonagh and J. Trotter, *Tetrahedron*, 1983, **39**, 1865; A. L. Balch, M. Mazzanti, B. C. Noll and M. M. Olmstead, *J. Am. Chem. Soc.*, 1993, **115**, 12 206; S. Attar, A. Ozarowski, P. M. Van Calcar, K. Winkler and A. L. Balch, *Chem. Commun.*, 1997, 1115; A. Gossauer, F. Fehr, F. Nydegger and H. Stöckli-Evans, *J. Am. Chem. Soc.*, 1997, **119**, 1599; P. A. Lord, M. M. Olmstead and A. L. Balch, *Inorg. Chem.*, 2000, **39**, 1128.

3 G. Struckmeier, U. Thewalt and J.-H. Fuhrhop, *J. Am. Chem. Soc.*, 1976, **98**, 278; W. S. Sheldrick and J. Engel, *J. Chem. Soc., Chem. Commun.*, 1980, 5; R. G. Khoury, L. Jaquinod and K. M. Smith, *Tetrahedron*, 1998, **54**, 2339; Y. Zhang, A. Thompson, S. J. Rettig and D. Dolphin, *J. Am. Chem. Soc.*, 1998, **120**, 13 537.

4 A. L. Balch, M. Mazzanti, B. C. Noll and M. M. Olmstead, *J. Am. Chem. Soc.*, 1994, **116**, 9115; R. G. Khoury, M. O. Senge, J. E. Colchester and K. M. Smith, *J. Chem. Soc., Dalton Trans.*, 1996, 3937; R. Koerner, M. M. Olmstead, A. Ozarowski and A. L. Balch, *Inorg. Chem.*, 1999, **38**, 3262; P. Lord, M. M. Olmstead and A. L. Balch, *Angew. Chem., Int. Ed.*, 1999, **38**, 2761.

5 A. W. Johnson and R. Price, *J. Chem. Soc.*, 1960, 1649; D. Dolphin, R. L. N. Harris, J. L. Huppatz, A. W. Johnson, I. T. Kay and J. Leng, *J. Chem. Soc. C.*, 1966, 98; M. Bröring, *Synthesis*, 2000, in press.

6 B. C. Chow and I. A. Cohen, *Bioinorg. Chem.*, 1971, **1**, 57; M. Tsutsui, D. Ostfeld, J. N. Francis and L. M. Hoffman, *J. Coord. Chem.*, 1971, **1**, 115; D. P. Rilemma, J. K. Nagle, L. F. Barringer and T. J. Meyer, *J. Am. Chem. Soc.*, 1981, **103**, 56; M. Barley, J. Y. Becker, G. Domazetis, D. Dolphin and B. R. James, *Can. J. Chem.*, 1983, **61**, 2389.

7 *Crystal data* for $C_{45}H_{46}N_4O_{11}Ru_5$ **2**: red prisms, M = 1324.21, monoclinic, space group $P2_1/c$, a = 19.633(4), b = 15.226(3), c = 17.809(4) Å, β = 89.76(3)°, U = 5323.7(18) Å^3, Z = 4, D_c = 1.652 g cm^{-3}, μ = 1.441 mm^{-1}, F(000) = 2608, 54724 reflections collected (2.47 < θ < 25.10°) at 173(2) K, 9374 independent (R_{int} = 0.1057), 4350 used in the structure refinement; R_1 = 0.0542 [$I > 2\sigma(I)$], wR_2 = 0.1526 (all data), GOF = 0.815 for 623 parameters and 12 restraints, largest difference peak, hole = 0.434, −0.074 e Å^{-3}. CCDC 182/1687. See http://www.rsc.org/suppdata/cc/b0/b003815f/ for crystallographic files in .cif format.

8 *Spectroscopic data* for **2**: mp 132 °C (decomp.); MS(DCI, isobutane): m/z 1325.8, [M + H]$^+$; $\delta_H$benzene-d_6): 7.08 [s, 1H, H(25)], 2.72 (s, 3H, CH_3), 2.71 [d, J (HH) 1 Hz, 1H, H(34)], 2.62–2.11 (m, 10H, 5 × CH_2CH_3), 2.57, 2.20 (2 × s, 6H, 2 × CH_3), 1.97–1.88 (m, 2H, CH_2CH_3), 1.89 (s, 3H, CH_3), 1.17–0.81 (m, 18H, 6 × CH_3), −15.30 [d, J(HH) 4 Hz, 1H, H(1)], −18.40 [dd, 1H, H(2)]; $\delta_C$benzene-d_6): 208.2, 208.1, 206.6, 199.8, 198.11, 198.10, 196.0, 193.1, 192.4, 191.8, 191.0 (11 × CO); 164.9, 147.2, 144.9, 141.2, 138.4, 137.1, 134.2, 134.0, 133.6, 120.8, 117.1, 117.0, 115.5, 108.8, 105.9, 96.3 (16 × C_{quat}); 123.8 [C(25)]; 19.9, 19.7, 19.6, 19.1, 18.8, 18.4 (6 × CH_2CH_3); 19.3, 18.5, 17.6, 16.4, 16.3, 15.9, 15.8, 15.6, 11.0, 10.4 (10 × CH_3); 3.5 [C(34)]; IR (KBr): ν/cm^{-1} 2969, 2933, 2873 (s, ν_{C-H}); 2072, 2053 (sh), 2045, 2024, 2003 (sh), 1997, 1971, 1953, 1927, 1920 (sh) (s, $\nu_{C\equiv O}$); 1607 (s, $\nu_{C=C}$) (Calc. for $C_{45}H_{46}N_4O_{11}Ru_5$: C, 40.82; H, 3.50; N, 4.23. Found: C 39.81, H 3.40, N 3.95%).

9 K. K. Dailey, G. P. A. Yap, A. L. Rheingold and T. B. Rauchfuss, *Angew. Chem., Int. Ed. Engl.*, 1996, **35**, 1833; C. Floriani, *Pure Appl. Chem.*, 1996, **68**, 1.

10 P. Hambright, in *Porphyrins and Metalloporphyrins*, ed. K. M. Smith, Elsevier, New York, 1975, p. 247.

11 J. W. Buchler, in *The Porphyrins*, ed. D. Dolphin, Academic Press, New York, 1979, vol. I, p. 389.

12 For an interesting exception, see: Y.-W. Chan, F. E. Wood, M. W. Renner, H. Hope and A. L. Balch, *J. Am. Chem. Soc.*, 1984, **106**, 3380; A. L. Balch, Y.-W. Chan, M. M. Olmstead, M. W. Renner and F. E. Wood, *J. Am. Chem. Soc.*, 1988, **110**, 3897.

ChemComm

Stereoselective *cis* glycosylation of 2-*O*-allyl protected glycosyl donors by intramolecular aglycon delivery (IAD)

Christopher M. P. Seward,[a] Ian Cumpstey,[a] Mahmoud Aloui,[a] Seth C. Ennis,[a] Alison J. Redgrave[b] and Antony J. Fairbanks*[a]

[a] *Dyson Perrins Laboratory, Oxford University, South Parks Road, Oxford, UK OX1 3QY. Email: antony.fairbanks@chemistry.ox.ac.uk*

[b] *Glaxo Wellcome Research and Development, Medicines Research Centre, Gunnels Wood Road, Stevenage, UK SG1 2NY*

Received (in Liverpool, UK) 6th June 2000, Accepted 19th June 2000
Published on the Web 10th July 2000

2-*O*-Allyl protected glycosyl donors may be glycosylated stereoselectively *via* a three step sequence involving double bond isomerization, *N*-iodosuccinimide mediated tethering to a glycosyl acceptor and subsequent intramolecular glycosylation (intramolecular aglycon delivery, IAD).

Stereoselective intramolecular glycosylation of glycosyl acceptors temporarily tethered to the 2-hydroxy group of the glycosyl donor is a synthetically useful technique allowing access to a range of *cis*-1,2-glycosides which can otherwise be problematic to synthesise. A number of methods have been developed for the temporary linking of donor and acceptor prior to glycosylation.[1–4] Modification of the donor 2-hydroxy protecting group commonly provides a tethering site. Thus the Hindsgaul approach involves Tebbe methylenation of a 2-*O*-acetate to produce a vinyl ether which is then coupled with the acceptor using acid catalysis to produce a mixed ketal.[3] Alternative methodology developed by Ogawa and co-workers employs oxidation of a *p*-methoxybenzyl (PMB) protecting group, which allows linking of donor and acceptor as a mixed acetal.[4] We would herein like to report the first use of the 2-*O*-allyl protecting group as the means of tethering donor to acceptor. It was envisaged that Wilkinson's catalyst mediated isomerisation of the double bond would efficiently produce a vinyl ether, which could then be subjected to tethering with *N*-iodosuccinimide (NIS) and subsequent intramolecular glycosylation according to our recently reported procedure.[5]

The 2-*O*-allyl protected glycosyl donors **1** and **2**, which are readily available through standard manipulations,† were isomerized using a combination of Wilkinson's catalyst and n-butyllithium according to a procedure recently reported by Boons and Isles.[6] This straightforward method proceeded extremely efficiently to yield the enol ethers **3** and **4** respectively in quantitative yield (Scheme 1). NIS mediated tethering was then undertaken for both *manno* and *gluco* donors **3** and **4** with a series of alcohols (ROH, Table 1) in the presence of 4 Å molecular sieves.‡ In all cases tethering proceeded efficiently in either THF or 1,2-dichloroethane (DCE) as solvent to yield mixed acetal intermediates **5a–e**, **6a–d**,**f** as diastereomeric mixtures.§ Subsequent intramolecular glycosylation proved more sluggish than we had previously experienced.[5] In the case of the less reactive anomeric thiophenyl *manno* mixed acetals **5a–e**, efficient reaction required the addition of silver triflate and more protracted reaction times at either room temperature or higher. However in all cases intramolecular glycosylation occurred in a stereospecific fashion to furnish the corresponding β-mannosides **7a–e**. The more reactive thiomethyl *gluco* mixed acetals **6a-d**,**f** were efficiently activated by the addition of methyl triflate, yielding α-glucosides **8a–d**,**f** again as single anomers following work-up.¶‖

Attention then turned to the potential one-pot reaction, whereby tethering and glycosylation are achieved in a single reaction vessel. Unlike our previous results[5] which were obtained with the Hindsgaul mixed ketal system, attempted one-pot glycosylation of donors **3** and **4** with an excess of cyclohexanol (typically 3 equivalents) produced anomeric mixtures, clearly indicating competitive intermolecular reaction by the excess of acceptor in solution. In order to find a solution to this problem, and also to overcome the sluggishness of the thiophenyl *manno* glycosylation reaction, attention turned to the use of the readily available thiomethyl substituted *manno* glycosyl donor **9**.† Isomerisation of **9** proceeded efficiently to yield the enol ethers **10** which were subsequently examined as

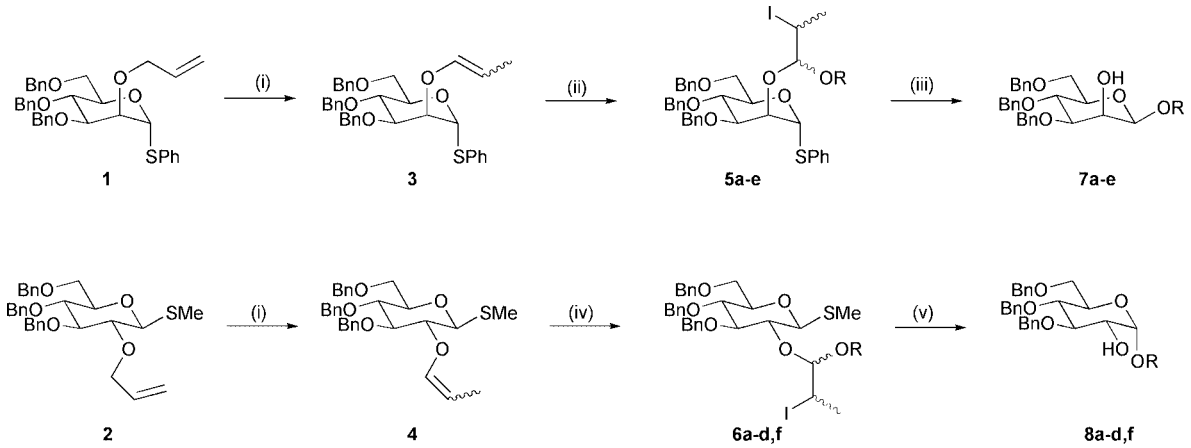

Scheme 1 *Reagents and conditions*: (i) $(Ph_3P)_3RhCl$, *n*-BuLi, THF, reflux, > 99%; (ii) ROH, *N*-iodosuccinimide, 4 Å molecular sieves, 1,2-dichloroethane, −40 °C to RT, 76–100%; (iii) *N*-iodosuccinimide, AgOTf, 2,6-di-*tert*-butyl-4-methylpyridine, 4 Å molecular sieves, 1,2-dichloroethane, RT (or 50 °C), 59–81%; (iv) ROH, *N*-iodosuccinimide, 4 Å molecular sieves, 1,2-dichloroethane, −40 °C to RT, 63–98%; (v) MeOTf, 2,6-di-*tert*-butyl-4-methylpyridine, 1,2-dichloroethane, RT, 65–77%.

DOI: 10.1039/b004522p

Table 1 Yields for tethering and glycosylation

Alcohol ROH	Product/yield of mixed acetals	Product/yield of glycosylation[7]
MeOH	**5a**/93% **6a**/98%	**7a**/77% **8a**/65%
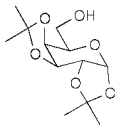	**5b**/95% **6b**/84%	**7b**/81% **8b**/70%
	**5c**/76% **6c**/80%	**7c**/68% **8c**/77%
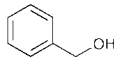	**5d**/ > 99% **6d**/95%	**7d**/76% **8d**/67%
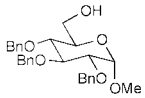	**5e**/90%	**7e**/57%
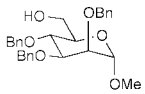	**6f**/63%	**8f**/72%

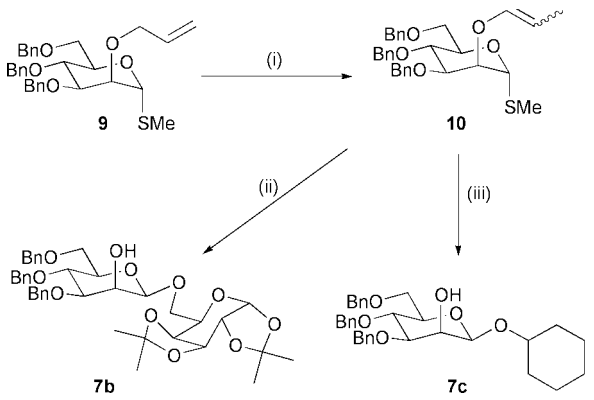

Scheme 2 *Reagents and conditions*: (i) $(Ph_3P)_3RhCl$, *n*-BuLi, THF, reflux, > 99%; (ii) diacetone galactose, *N*-iodosuccinimide, 4 Å molecular sieves, CH_3CN, −40 °C to RT, then MeOTf, 72%; (iii) cyclohexanol, *N*-iodosuccinimide, 4 Å molecular sieves, 1,2-dichloroethane, −40 °C to RT, then MeOTf, 67%.

substrates for tethering and glycosylation. Conditions initially employed for the one-pot reactions of **10**, involving NIS mediated tethering with cyclohexanol and subsequent glycosylation by the addition of methyl triflate to the reaction mixture, again resulted in the formation of anomeric mixtures. The β : α ratio could be increased from 2 : 1 to a respectable 5 : 1 by simple dilution of the reaction mixture once tethering was complete before the addition of the methyl triflate, but α products could not be entirely eliminated. However by the use of an excess of glycosyl donor any competing intermolecular reaction could be avoided. Thus reaction of the donor **10** (2.0 equivalents) with either diacetone galactose or cyclohexanol (in acetonitrile and 1,2-dichloroethane respectively) produced the corresponding β-mannosides **7b** and **7c** as single anomers in 72% and 67% yield respectively (Scheme 2).

In summary we have demonstrated that 2-*O*-allyl protected glycosyl donors may be employed for the synthesis of a variety of *cis*-1,2-glycosides. Of particular note is that isomerization of the allyl group is a very efficient process, and is superior to the often troublesome and messy Tebbe methylenation reaction. In addition the use of an excess of glycosyl donor allows both tethering and glycosylation to be performed in a single reaction vessel, obviating the need for handling of sensitive mixed acetal intermediates. Further investigations into the use of allyl derived enol ethers for *cis* glycosylation procedures, particularly employing hindered secondary carbohydrate glycosyl acceptors are currently in progress, and the results will be reported in due course.

We gratefully acknowledge financial support from the Leverhulme Trust (Postdoctoral Fellowship to M. A.), the EPSRC (Quota award to C. M. P. S.) and Glaxo Wellcome (CASE award to I. C.), and also the use of the Chemical Database Service (CDS) at Daresbury, UK and the EPSRC National Mass Spectrometry Service at Swansea.

Notes and references

† 2-*O*-Allyl protected donor **1** was prepared from the corresponding 2-*O*-acetate[5] *via* deprotection with sodium methoxide in methanol and allylation with sodium hydride and allyl bromide in DMF. 2-*O*-Allyl protected donors **2** and **9** were prepared from the corresponding 2-*O*-acetyl-1-bromo and 2-*O*-acetyl-1-chloro glycosides respectively by reaction with dimethyl disulfide and butyllithium in THF followed by allylation as above.[8] Full experimental details will be published in due course.

‡ Typical procedure for *manno*/*S*-phenyl tethering: the vinyl ether (0.15 mmol), the alcohol (3 equiv.) and powdered 4 Å molecular sieves (*ca*. 500 mg) were stirred in 3.5 ml dry DCE under argon at −40 °C. NIS (2.5 equiv.) was added and the mixture was allowed to warm slowly to room temperature. After 16 h, dichloromethane was added, the mixture was filtered through Celite®, washed with aqueous sodium thiosulfate, dried, filtered and concentrated *in vacuo*. The resulting residue was purified by flash column chromatography to give the mixed acetal as a clear oil.

§ No attempt was made at separation, and the mixtures were used as such for subsequent glycosylation.

¶ In line with our previous observations, the oxonium ion produced after aglycon delivery may be trapped, either by any available alcohol in solution or alternatively by succinimide. Simple treatment of the crude reaction mixture with either aqueous TFA or aqueous lithium hydroxide respectively efficiently hydrolyses these trapped products, typically increasing the yield of glycosylated product by 10–15%.

‖ Typical procedure for *manno*/*S*-phenyl glycosylation: the mixed acetals (0.1 mmol), NIS (5 equiv.), silver triflate (1 equiv.), 2,6-di-*tert*-butyl-4-methyl pyridine (DTBMP) (5 equiv.) and powdered 4 Å molecular sieves (*ca*. 250 mg) were dissolved in dry DCE under argon. The solution was then stirred at room temperature (or 50 °C) until TLC indicated disappearance of the starting material. TFA (10 ml), methanol (4 ml) and water (2 ml) were added and the solution was stirred for a further 1–4 h. Dichloromethane was added, the mixture filtered through Celite®, washed with saturated aqueous sodium bicarbonate and the aqueous layers were re-extracted with dichloromethane. The combined organic extracts were washed with aqueous sodium thiosulfate, dried ($MgSO_4$), filtered and concentrated *in vacuo*. The resulting residue was purified by flash column chromatography to give the pure β-mannoside.

1 G. Stork and J. J. La Clair, *J. Am. Chem. Soc.*, 1996, **118**, 247; G. Stork and G. Kim, *J. Am. Chem. Soc.*, 1992, **114**, 1087.
2 M. Bols, *J. Chem. Soc., Chem. Commun.*, 1993, 791; M. Bols, *Tetrahedron*, 1993, **49**, 10 049; M. Bols, *J. Chem. Soc., Chem. Commun.*, 1992, 913.
3 F. Barresi and O. Hindsgaul, *Can. J. Chem.*, 1994, **72**, 1447; F. Barresi and O. Hindsgaul, *Synlett*, 1992, 759; F. Barresi and O. Hindsgaul, *J. Am. Chem. Soc.*, 1991, **113**, 9376.
4 M. Lergenmüller, T. Nukada, K. Kuramochi, A. Dan, T. Ogawa and Y. Ito, *Eur. J. Org. Chem.*, 1999, 1367; Y. Ito, Y. Ohnishi, T. Ogawa and Y. Nakahara, *Synlett*, 1998, 1102; A. Dan, Y. Ito and T. Ogawa, *J. Org. Chem.*, 1995, **60**, 4680; Y. Ito and T. Ogawa, *Angew. Chem., Int. Ed. Engl.*, 1994, **33**, 1765.
5 S. C. Ennis, A. J. Fairbanks, R. J. Tennant-Eyles and H. S. Yeates, *Synlett*, 1999, 1387.
6 G.-J. Boons and S. Isles, *J. Org. Chem.*, 1996, **61**, 4262.
7 Data for β-mannosides **7a**–**d** and α-glucosides **8a**–**d** was consistent with that reported by us previously.[5] Selected data for **7e**: a white solid, mp 105–108 °C (Et_2O–petrol), $[\alpha]_D^{22}$ +22.2 (*c*, 0.91, $CHCl_3$), [lit.[1b] $[\alpha]_D^{25}$ +24.0 (*c*, 1.0, $CHCl_3$); **8f**: a colourless oil, $[\alpha]_D^{22}$ +65.5 (*c*, 1.1, $CHCl_3$), (HRMS+H^+: 897.4229. $C_{55}H_{61}O_{11}$ requires: 897.4214).
8 F. Yamazaki, S. Sato, T. Nukada, Y. Ito and T. Ogawa, *Carbohydr. Res.*, 1990, **201**, 31; Y. Ito, O. Kanie and T. Ogawa, *Angew. Chem., Int. Ed. Engl.*, 1996, **35**, 2510; F. W. Lichtentaler and T. Schneider-Adams, *J. Org. Chem.*, 1994, **59**, 6728.

The formation of sulfur macrocycles containing dialkyne units

John E. Davies, Louisa J. Hope-Weeks, Martin J. Mays* and Paul R. Raithby

Department of Chemistry, Lensfield Road, Cambridge, UK CB2 1EW. E-mail: mjm14@cus.cam.ac.uk

Received (in Cambridge, UK) 9th May 2000, Accepted 14th June 2000
Published on the Web 10th July 2000

Treatment of the dialkyne complex [{$Co_2(CO)_6$}$_2${μ-η^2:μ-η^2-$HOCH_2C{\equiv}CC{\equiv}CCH_2OH$}] with $HBF_4{\cdot}OEt_2$ at −78 °C and the subsequent addition of $[HS(CH_2)_2]_2X$ (X = S or O) affords the novel macrocyclic complexes [{$Co_2(CO)_5$}{$Co_2(CO)_6$}{(μ-η^2-$C{\equiv}CCH_2SCH_2CH_2)_2S$}] 1a, [{$Co_2(CO)_6$}$_2${(μ-η^2-$C{\equiv}CCH_2SCH_2CH_2)_2O$ }] 2a and [{$Co_2(CO)_6$}$_2${(μ-η^2-$C{\equiv}CCH_2SCH_2CH_2)_2X$}]$_2$ [X = S 1b or O 2b].

Crown thioethers and related sulfur macrocycles have been the subject of numerous studies owing to their ability to bind metal ions more strongly than mono- or bi-dentate thioethers.[1] Structural studies on uncoordinated sulfur macrocycles have shown that the sulfur atoms tend to adopt an exodentate conformation in which all the sulfur lone pairs are orientated out of the macrocyclic cavity.[2] Therefore these macrocycles must undergo substantial conformational change in order to coordinate to an added metal ion. Several sulfur macrocycles undergo this type of conformational change on reaction with added metal ions such as Pd(II),[3] Hg(II),[4] Ni(II)[5] or Ag(I)[6,7] to give cyclic systems in which at least two of the sulfur atoms have co-ordinated to the metal and are in an endodentate configuration.

We now report the synthesis of several new sulfur macrocycles† (Fig. 1) and, in particular, of the novel complex [{$Co_2(CO)_5$}{$Co_2(CO)_6$}{(μ-η^2-$C{\equiv}CCH_2SCH_2CH_2)_2S$}] **1a** which contains a dialkyne unit and three sulfur donor atoms of which only one is endodentate and coordinated to a metal.

The X-ray crystal structure‡ of **1a** (Fig. 2) confirms that a 13-membered macrocyclic ring has formed. Two of the sulfur atoms are exodentate to the ring but the central sulfur atom is endodentate and coordinated axially to one of cobalt atoms already present in the molecule rather than to an added metal ion. This mode of coordination of a sulfur macrocycle containing three sulfur atoms is unprecedented. In contrast complex **1b** (Fig. 3),‡ the dimer of **1a**, contains no Co–S interactions.

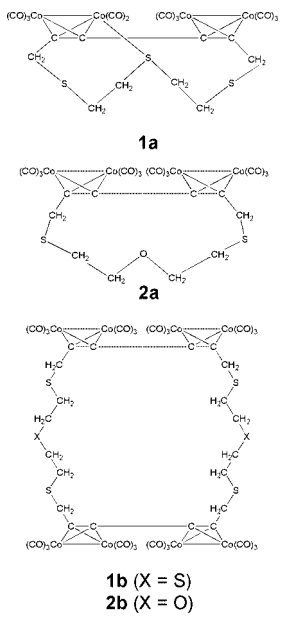

Fig. 1 The new sulfur macrocycles containing dialkyne units.

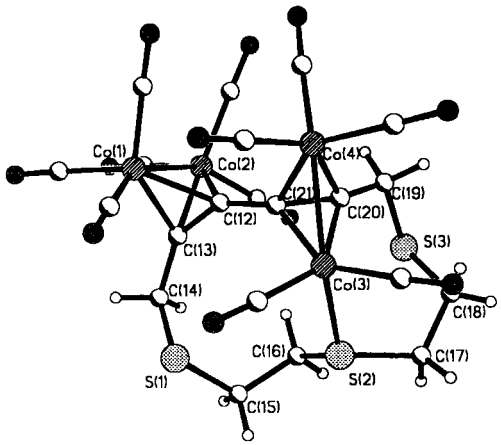

Fig. 2 Molecular structure of **1a**. Selected bond lengths (Å) and angles (°): Co(3)–S(2) 2.2702(8), S(2)–C(16) 1.820(3), S(2)–C(17) 1.824(3), C(16)–C(15) 1.531(4), S(1)–C(15) 1.812(3), C(17)–C(18) 1.526(4), S(3)–C(18) 1.815(3), C(12)–C(13) 1.351(4), C(21)–C(20) 1.354(3), S(2)–Co(3)–Co(4) 154.30(2), C(15)–C(16)-S(2) 110.3(2), C(17)–C(18)-S(3) 115.4(2), C(16)–C(15)–S(1) 114.0(2), C(18)–C(17)-S(2) 117.7(2), C(20)–C(19)-S(3) 113.5(2).

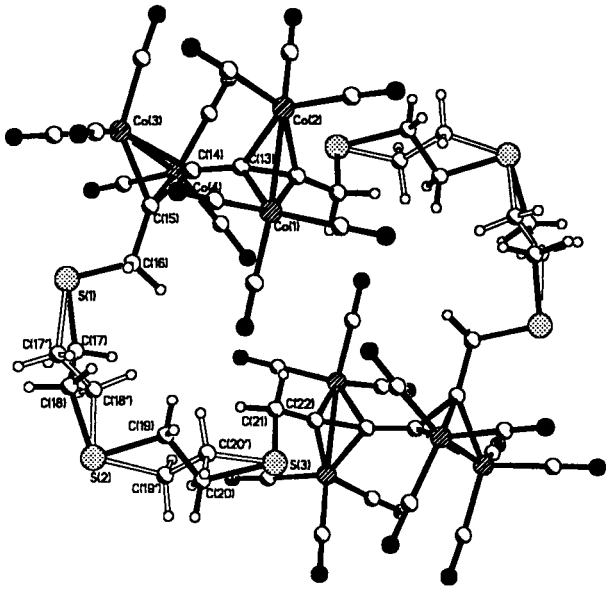

Fig. 3 Molecular structure of **1b** showing the two orientations of the disorder within the ring system. Selected bond lengths (Å) and angles (°): S(1)–C(17) 1.793(6), S(1)–C(17') 1.976(14), S(2)–C(19) 1.823(9), S(2)–C(19') 1.846(9), S(2)–C(18) 1.817(6), S(2)–C(18′) 1.831(13), S(3)–C(20) 1.847(9), S(3)–C(20') 1.807(9), C(17)–C(18) 1.518(9), C(17′)–C(18′) 1.48(2), C(19)–C(20) 1.523(10), C(19′)–C(20′) 1.490(12), C(22)–C(13) 1.356(5), C(14)–C(15) 1.359(5), C(16)–S(1)–C(17) 100.0(3), C(16)-S(1)–C(17′) 95.5 (5), C(17)–C(18)-S(2) 115.1(4), C(17′)–C(18′)–S(2) 104.9(10), C(18)–S(2)–C(19) 90.1(3), C(18′)–S(2)–C(19′) 96.2(5), S(2)–C(19)–C(20) 107.3(6), S(2)–C(19′)–C(20′) 112.0(6), C(19)–C(20)–S(3) 111.4(6), C(19′)–C(20′)–S(3) 110.8(6), C(20)–S(3)–C(21) 99.7(3), C(20′)–S(3)–C(21) 101.9(3). (Primed atoms refer to the second orientation of the disordered ring system).

DOI: 10.1039/b003720f

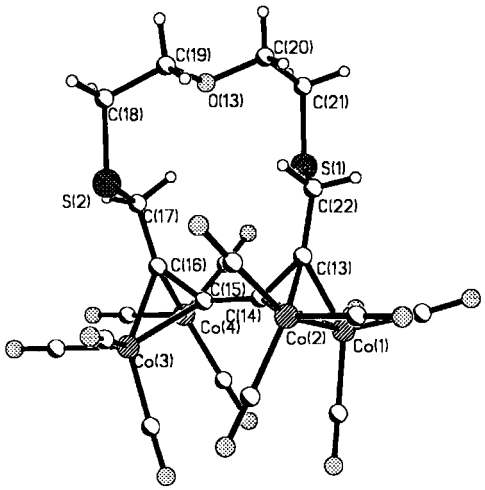

Fig. 4 Molecular structure of **2a**. Selected bond lengths (Å) and angles (°): O(13)–C(19) 1.420(4), O(13)–C(20) 1.419(4), C(20)–C(21) 1.508(5), C(19)–C(18) 1.516(4), S(1)–C(21) 1.809(3), S(2)–C(18) 1.815(3), S(1)–C(22) 1.813(3), S(2)–C(17) 1.824(3), C(16)–C(15) 1.345(4), C(14)–C(13) 1.343(4), C(18)–C(19)–O(13) 108.6(3), C(21)–C(20)–O(13) 109.0 (3), C(19)–C(18)–S(2) 115.0(2), C(20)–C(21)-S(1) 115.3(2), C(13)–C(22)–S(1) 108.7(2).

All the carbon–sulfur bond lengths in **1a** and **1b** fall within the expected range for macrocylic thioethers, ranging from 1.793(6) to 1.846(9), as do all the carbon–carbon single bond lengths which range from 1.48(2) to 1.531(4).[1] The carbon–carbon triple bond lengths range from 1.351(4) to 1.359(5), typical of coordinated alkynes.[6,8] The cobalt–sulfur bond distance of 2.2702(8) in **1a** is also typical of other reported values.[9]

The novel macrocycle **1a** and its dimer **1b** are synthesized† by the reaction of $[\{Co_2(CO)_6\}_2\{\mu\text{-}\eta^2\text{:}\mu\text{-}\eta^2\text{-}HOCH_2C{\equiv}CC{\equiv}C\text{-}CH_2OH\}]$ with 1 equiv. of $[HS(CH_2)_2]_2S$ in the presence of catalytic amounts of $HBF_4{\cdot}OEt_2$ at −78 °C and separated by chromatography in an analogous manner to that reported by Went and coworkers for the related mono-alkyne complexes.[6] Substitution of $[HS(CH_2)_2]_2S$ by $[HS(CH_2)_2]_2O$ affords the related macrocyclic compounds **2a**, **2b** in which the central sulfur atom in **1a**, **1b** is replaced by an oxygen atom. The combined yields of the monomer (**a**) and the dimer (**b**) are in excess of 90% in each case.

The X-ray crystal structure‡ of **2a**, (Fig. 4), again confirms the presence of a 13- membered macrocyclic ring as in **1a**.

The central oxygen atom of the ring, although it is endodentate as is typical of crown ethers, does not coordinate to a cobalt centre in contrast to the central sulfur atom in **1a** and, as a consequence, there is no loss of a carbonyl group from either of the $Co_2(CO)_6$ units in **2a** both of which remain intact. The two sulfur atoms in **2a** adopt the same geometry as the corresponding sulfur atoms in **1a** and are exodentate. All carbon–sulfur bonds in **2a** fall within the expected range of values, as do the carbon–carbon single bonds of the crown thioether.[1]

An inspection of the crystal structures reveals that in each case the CH_2 protons are in different environments; this results in complicated ^{1}H NMR spectra in the SCH_2 and OCH_2 regions comprising of overlapping multiplets. The ^{13}C NMR spectra exhibit only one resonance due to a CO group, as is common for alkyne-bridged dicobalt complexes; localized site exchange[10] or a trigonal twist[11] has been proposed previously to explain this fluxionality.

In linear diyne complexes containing two coordinated dicobalt hexacarbonyl fragments these fragments are co-ordinated *trans* to each other such that the two Co-Co vectors are almost parallel.[12] The steric demands of the cyclic diynes in **1a**, **1b** and **2a** do not allow this relative orientation and the two fragments are twisted to varying degrees such that the two Co–Co vectors approach an orthogonal configuration.

The influence of the nature of the linking groups and of the donor atoms on the geometry of these macrocyclic dialkyne complexes is under further study.

We gratefully acknowledge the financial support of EPSRC, DERA and the Isaac Newton Trust (to L. J. H). EPRSC support for the purchase of the Nonius Kappa CCD diffractometer is also gratefully acknowledged.

Notes and references

† *Selected spectroscopic data*: [IR (ν_{CO}/cm^{-1}) measured in hexane; ^{1}H NMR and ^{13}C{^{1}H}NMR spectra were recorded in $CDCl_3$ solution relative to $SiMe_4$; *J* in Hz].

1a: 1983.7w, 2013.7(sh), 2020.5s, 2031.2vs, 2058.6vs, 2082.8s, 2101.7s cm^{-1}; ^{1}H NMR ($CDCl_3$),δ4.33(s, 4H, CCH_2), 2.96–3.00(m, 8H, CH_2CH_2); ^{13}C{^{1}H} NMR, δ 199.2(CO), 101.2, 94.3 (C_2), 37.3 (CCH_2), 34.9, 33.3(SCH_2); FAB MS: *m*/*z* 772 (M^+) and $M^+ - n$CO (*n* = 2–11). **1b**: 2026.2m, 2058.8s, 2082.2m, 2100.9w cm^{-1}; ^{1}H NMR, δ 4.11(s, 8H, CCH_2), 2.82–2.92(m, 16H, CH_2CH_2); ^{13}C{^{1}H} NMR, δ199.4(CO), 101.6(C_2), 34.68 (CCH_2), 30.96(SCH_2); FAB MS: *m*/*z* 1600 (M^+) and $M^+ - n$CO (*n* = 2–24); **2a**: 2026.5m, 2059.3s, 2081.8m, 2100.8m cm^{-1}; ^{1}H NMR, δ 4.50(s, 4H, CCH_2), 3.68–3.80 (m, 4H, OCH_2), 2.71–2.85 (m, 4H, SCH_2); ^{13}C{^{1}H} NMR, δ 199.6(CO), 101.6(C_2), 71.7(OCH_2), 31.6, 32.9, 36.7(SCH_2); FAB MS: 784 (M^+) and $M^+ - n$CO (*n* = 1–12). **2b**: 2025.3m, 2057.3s, 2081.9m, 2100.7m cm^{-1}; ^{1}H NMR, δ 4.09(s, 8H, CCH_2), 3.70–3.77 (m, 8H, OCH_2), 2.83–3.00 (m, 8H, SCH_2); ^{13}C{^{1}H} NMR 198.9(CO), 99.6(C_2), 71.4, 70.9(OCH_2), 31.6, 34.6(SCH_2); FAB M/S: 1568 (M^+) and $M^+ - n$CO (*n* = 6–24).

‡ *Crystal data*: all data collected at 180(2) K using an Oxford Cryosteam cooling apparatus.

Crystal data: for **1a**: $C_{21}H_{12}Co_4O_{11}S_3$, *M* = 772.21, triclinic, space group $P\bar{1}$ (no. 2), *a* = 10.3957(3), *b* = 10.4236(3), *c* = 12.7370(3) Å, α = 97.388(2), β = 93.166(2), γ = 96.499(2)°, *U* = 1356.52(6) Å^3, *Z* = 2, μ(Mo-Kα) = 2.690 mm^{-1}, 10450 reflections measured, 6217 unique (R_{int} = 0.0263); R_1 = 0.0253, wR_2 = 0.0736.

For **1b**: $C_{44}H_{24}Co_8O_{24}S_6$, *M* = 1600.43, triclinic, space group $P\bar{1}$ (no. 2), *a* = 9.2401(4), *b* = 10.6059(4), *c* = 15.5957(5) Å, α = 102.693(2), β = 101.976(2), γ = 91.827(2)°, *U* = 1453.75(10) Å^3, *Z* = 1, μ(Mo-Kα) = 2.516 mm^{-1}, 10079 reflections measured, 6587 unique (R_{int} = 0.0287); R_1 = 0.0389, wR_2 = 0.1098.

For **2a**: $C_{22}H_{12}Co_4O_{13}S_2$ *M* = 784.16, monoclinic, space group $P2_1/c$, *a* = 9.3920(2), *b* = 16.3920(7), *c* = 18.5020(7) Å, β = 90.255(2), *U* = 2848.42(17) Å^3, *Z* = 4, μ(Mo-Kα) = 2.498 mm^{-1}, 8990 reflections measured, 4999 unique (R_{int} = 0.0391); R_1 = 0.0349, wR_2 = 0.0573.

CCDC 182/1686. See http://www.rsc.org/suppdata/cc/b0/b003720f/ for crystallographic files in .cif format.

1 S. R. Cooper, *Acc. Chem. Res.*, 1988, **21**, 141.
2 R. E. Wolf, J. R. Hartman, J. M. E. Storey, B. M. Foxman and S. R. Cooper, *J. Am. Chem. Soc.*, 1987, **109**, 4328.
3 A. J. Blake, D. Fenske, W. Li, V. Lippolis and M. Schröder, *J. Chem. Soc., Dalton Trans.*, 1998, 3961.
4 A. J. Blake, W. Li, V. Lippolis, A.Taylor and M. Schröder, *J. Chem. Soc., Dalton Trans.*, 1998, 2931.
5 L. Escriche, M. Almajano, J. Casabó, F. Teixidor, J. Rius, C. Maravitles, R. Kivekäs and R. Sillampää, *J. Chem. Soc., Dalton Trans.*, 1993, 2969.
6 F. Demirhan, A. Gelling, S. Irisli, J. C. Jeffery, S. N. Salek, O. S. Senturk and M. J. Went, *J. Chem. Soc., Dalton Trans.*, 1993, 2765; S. C. Bennett, J. C. Jeffrey and M. J. Went, *J. Chem. Soc., Dalton Trans.*, 1994, 3171.
7 R. Alberto, W. Nef, A. Smith, T. A. Kaden, M. Neuburger, M. Zehnder, A. Frey, U. Abram and A. Schubiger, *Inorg. Chem.*, 1996, **35**, 3420.
8 C. E. Housecroft, B. F. G. Johnson, M. S. Khan, J. Lewis, P. R. Raithby, M. E. Robson and D. A. Wilkinson, *J. Chem. Soc., Dalton Trans.*, 1992, 3171.
9 A. J. Edwards, S. R. Mack, M.J . Mays, C. Mo, P. R. Raithby and M. Rennie, *J. Organomet. Chem.*, 1996, **519**, 243.
10 S. Aime, L. Milone, R. Rossetti and P. L. Stanghellini, *Inorg. Chim. Acta*, 1977, **22**, 155.
11 A. J. M. Caffyn, M. J. Mays, G. Conole, M. McPartlin and H. R. Powell, *J. Organomet. Chem.*, 1992, **436**, 83.
12 C. J. McAdam, N. W. Duffy, B. H. Robinson and J. Simpson, *Organometallics*, 1996, **15**, 3935.

Pt(0) and Pd(0) based metallocryptands: metallophilic hosts for Pb(II) ion†

Vincent J. Catalano,*[a] Byron L. Bennett[a] and Bruce C. Noll[b]

[a] *Department of Chemistry, University of Nevada, Reno, NV 89557, USA. E-mail: vjc@unr.edu*
[b] *Department of Chemistry, University of Colorado, Boulder, CO 80309, USA*

Received (in Irvine, CA, USA) 9th May 2000, Accepted 16th June 2000

Metallocryptands based on trigonally coordinated Pt(0) or Pd(0) with P_2phen [2,9-bis(diphenylphosphino)-1,10-phenanthroline] bind Pb(II) ion through very strong, closed-shell metallophilic interactions; their syntheses, characterization and X-ray crystallography are presented.

The bonding interaction between closed-shell, heavy metal ions is gaining increasing attention.[1] In the absence of unpaired electrons to form covalent bonds or opposite charges to form strong ionic bonds, the close approach of closed-shelled species might be expected to exhibit no net attraction or be repulsive; however, there are numerous examples of heavy metal ions like Au(I), Tl(I) or Pb(II) associating with other metals or aggregating with short separations.[2] The origin of this metallophilic attraction is not completely understood, but relativistic effects appear to be important.[3]

Recently (Scheme 1), we reported the application of a unique Au(I)-based inorganic host complex to probe the resulting aurophilic interactions between the capping metal and the encapsulated guest ion.[4] In this work we observed a very strong and short (*ca*. 2.9 Å) Au(I)–Tl(I) interaction. The highly luminescent Tl(I) containing species is substitution inert and stable in solution while the Na^+ containing species readily dissociates the sodium ion indicating that the Au–Tl interaction is strong enough to maintain this assembly. We were unable to explore any Au(I)–Pb(II) interactions using this system probably because of the higher charge on the purported complex leads to dissociation and ultimately decomposition.

We now have extended this system to include zero-valent d^{10} metals and report the synthesis and characterization of the Pd(0)- and Pt(0)-based metallocryptates with exceptionally short Pd(0)–Pb(II) and Pt(0)–Pb(II) interactions. To our knowledge this is the first report of an unsupported Pd(0) or Pt(0)–Pb(II) bond. Further, these metallocryptands represent a new type of host complex that employ attractive metallophilic interactions for metal ion binding rather than Lewis acid–base interactions.

The deep green–brown, air-stable $[Pd_2(P_2phen)_3Pb](ClO_4)_2$ **1** or $[Pt_2(P_2phen)_3Pb](ClO_4)_2$ **2** [P_2phen = 2,9-bis(diphenylphosphino)-1,10-phenanthroline], are easily synthesized in good yield in acetonitrile according to eqns. (1) and (2).‡ Although the

$$Pd_2(dba)_3{\cdot}CHCl_3 + 3\ P_2phen + Pb(ClO_4)_2 \rightarrow [Pd_2(P_2phen)_3Pb](ClO_4)_2 + 3dba + CHCl_3 \quad (1)$$

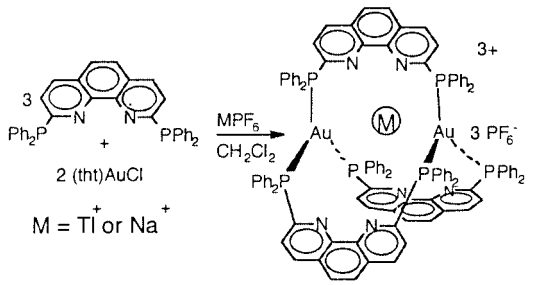

Scheme 1

† Electronic supplementary information (ESI) available: preparation, spectral data and MALDI-TOF spectrum for compound **2**. See http://www.rsc.org/suppdata/cc/b0/b003758n/

$$2\ Pt(dba)_2 + 3\ P_2phen + Pb(ClO_4)_2 \rightarrow [Pd_2(P_2phen)_3Pb](ClO_4)_2 + 2dba \quad (2)$$

solutions of **1** or **2** are stable, the Pb(II) can be replaced by addition of an excess of Tl(I) ion. The $^{31}P\{^1H\}$ NMR spectra contain a single resonance at +29.8 ppm for **1** and +48.1 ppm ($^1J_{Pt-P}$ 4085 Hz) for **2**. Interestingly coupling to ^{207}Pb (22% spin 1/2) is not observed. A similar phenomena is observed in the Tl^+ containing species reported elsewhere.[5] The ^{195}Pt NMR spectrum of **2** shows the anticipated quartet at 2916 ppm without resolvable $^1J_{Pt-Pb}$ coupling. For comparison, Balch *et al*.[6] reported a $^1J_{Pt-Pb}$ coupling of 214 Hz for the Pt(II) containing species, $[(MeCO_2)Pb(P_2\text{-crown})Pt(CN)_2]^+$ (P_2-crown = 1,10-bis[(diphenylphosphino)methyl]-1,10-diaza-4,7,13,16-tetraoxaoctadecane). Direct observation of a ^{207}Pb resonance was unsuccessful likely due to the low receptivity and natural abundance of ^{207}Pb coupled with the moderate solubility of **2**.

The X-ray crystal structure§ of **1** (Fig. 1) confirms the formulation. The Pb atom resides in the center of the D_3 symmetric cavity formed by the P_2phen ligands coordinated to the two trigonal Pd(0) centers. The Pd(1)–Pb(1) and Pd(2)–Pb(1) separations are nearly identical at 2.7095(6) and 2.6902(6) Å respectively, and a Pb center is nearly linearly bonded with the Pd(1)–Pb(1)–Pd(2) angle of 178.75(1)° indicating the lone pair is stereochemically inactive. The Pb–N separations range from 3.095(1) to 3.215(1) Å (av. Pb–N 3.142(1) Å] and are considered non-bonding. Each Pd atom is slightly displaced out of the respective trigonal plane towards the central Pb atom by *ca*. 0.2 Å.

As shown in Fig. 1, the molecule crystallizes in a non-centrosymmetric space group with an overall helical geometry. However, the bulk material is racemic because both enantio-

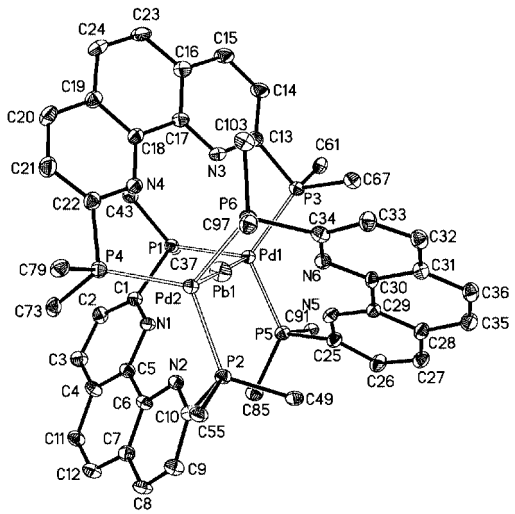

Fig. 1 Thermal ellipsoid plot for the cation of **1**. Hydrogen atoms and phenyl rings are removed for clarity. Selected distances (Å) and angles (°): Pd1–Pb(1) 2.7095(6), Pd2–Pb1 2.6902(6), Pb1–N1 3.090(2), Pb1–N2 3.095(2), Pb1–N3 3.090(2), Pb1–N4 3.215(2), Pb1–N5 3.156(2), Pb1–N6 3.166(2); Pd1–Pb1–Pd2 178.75(1), P1–Pd1–P3 119.41(5), P1–Pd1–P5 117.27(4), P3–Pd1–P5 121.30(5), P2–Pd2–P4 120.15(4), P2–Pd2–P6 116.42(4), P4–Pd2–P6 120.21(5).

DOI: 10.1039/b003758n

mers are present in the crystal. The helicity is reflected in the large P(1)–Pd(1)–Pd(2)–P(2), P(3)–Pd(1)–Pd(2)–P(4) and P(5)–Pd(1)–Pd(2)–P(6) torsion angles of 116.9, 123.1 and 115.9°, respectively. This twisting of the trigonal planes compresses the metallocryptate to accommodate the requisite Pd(1)···Pd(2) separation of 5.399(1) Å.

Crystals of **2** were obtained but did not produce satisfactory refinement.§ However, reliable Pt–Pb separations of 2.7469(6) and 2.7325(6) Å were measured, and the cation is nearly identical to **1** in every other respect.

Pd– or Pt–Pb bonding is rare, and a search of the Cambridge Crystallographic Data Centre produced only a few examples of structurally characterized Pd– or Pt–Pb bonds,[5,7] and none of these contained a formally zero-valent transition metal. Most of these are formed either through strong ligand interaction or through insertion reactions producing covalently bonded M–Pb complexes;[8] however, a few cases exist for unsupported Pb(II)–M bonds.[9] For example, Usón *et al*. reported the structure of $Pb[Pt(C_6F_5)_4]_2^{2-}$ that contains short Pb(II)–Pt(II) separations of 2.769(2) and 2.793(2) Å along with short Pb···F contacts believed to stabilize the complex. In contrast, neither **1** or **2** have any stabilizing Pb···ligand interactions.

The MALDI-TOF mass spectra of **1** and **2** (not shown here) confirm the presence of Pb in each complex. Molecular ion peaks corresponding to $[M_2Pb(P_2phen)_3]^+$ (M = Pt or Pd) with and without the perchlorate counter ion are easily identified. Interestingly, the intensity of the peak corresponding to the empty metallocryptand is very small, indicating that the Pb ion is strongly held in the gas phase.

The attractive metal–metal interactions observed here can be rationalized by employing a qualitative MO diagram (Fig. 2) similar to that proposed by Balch *et al*.[10] by combining the filled d_{z^2} and empty p_z orbitals on the transition metals with the filled Pb 6s and empty Pb 6p_z orbitals. Mixing between levels stabilizes the filled orbitals relative to their unfilled counterparts leading to an attractive interaction between these metals. Further, Fackler and coworkers[11] have employed a similar model with additional relativistic contributions from the 6s orbital to describe attractive Au–Tl interactions.

The electronic absorption spectra of **1** and **2** in acetonitrile contain absorptions attributable to ligand π–π* transitions between 230 and 310 nm. Both complexes exhibit a low energy band at 481 for **1** and 470 for **2** tentatively assigned to the $M_{d\sigma^*} \rightarrow M_{p\sigma^*}$ transition depicted in the MO scheme. For comparison, both $Pd(PPh_3)_3$ and $Pt(PPh_3)_3$ exhibit weak absorptions in the same region,[12] but unlike these trigonal complexes, neither **1** or **2** are luminescent in solution, nor do these complexes exhibit reversible cyclic voltammetry.

The compounds reported here are examples of a rapidly expanding class of easily synthesized inorganic host complexes that employ strong, closed-shell attractive interactions for metal ion binding. By eliminating ligand–ion interactions these metallocryptands provide a simple probe the metal–metal bonding both in solution and in the solid state. Substitution of Pb(II) for other heavy metal ions should provide a numerous combination of heavy metal interactions for further study. We are currently probing these systems.

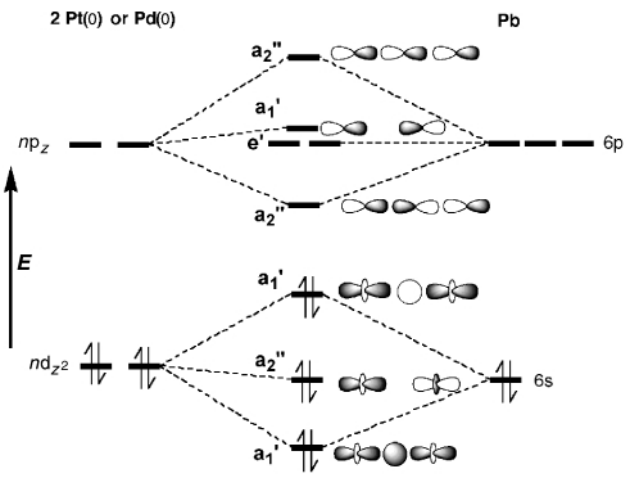

Fig. 2 Simplified molecular orbital diagram depicting the interaction between two trigonally coordinated d^{10} metal ions with the filled s and empty p_z orbital on a Pb^{2+} ion in the D_{3h} point group.

Acknowledgment is made to the National Science Foundation (CHE-9624281), to the Donors of The Petroleum Research Fund, administered by the American Chemical Society for their generous financial support of this research.

Notes and references

‡ *Preparations*: $[Pd_2Pb(P_2phen)_3](ClO_4)_2$ **1**: a 100 mL Schlenk flask was charged with 0.100 g (0.182 mmol) of 2,9-bis(diphenylphosphino)-1,10-phenanthroline dissolved in 10 mL of CH_2Cl_2. To this solution was added 1.39 g (0.304 mmol) of $Pb(ClO_4)_2$ (dissolved in 5 mL of 1 : 1 DCM–MeOH) with stirring. After 10 min the vessel was capped and the contents subjected to two freeze-pump-thaw cycles and moved to a glovebox. A suspension of 0.063 g of $Pd_2(dba)_3{\cdot}CHCl_3$ (0.0061 mmol) in MeCN (10 mL) was added dropwise affording an dark solution. After stirring an additional 30 min and volatiles were removed and the residue dissolved in a minimum amount of MeCN. Flash chromatography (alumina) eluting with MeCN and precipitation with Et_2O afforded a brown solid. Yield: 100 mg (73 %). $C_{108}H_{78}N_8Cl_2O_8P_6PbPd_2{\cdot}2DCE$ Calc. C, 54.63; H, 3.52; N, 3.41. Found: C, 55.21; H, 3.43; N, 3.52%. ^{1}H NMR (300 MHz, CD_3CN, 25 °C) δ 8.246 (d, *J* 8.0 Hz), 7.879 (s), 7.470 (d, *J* 8.0 Hz), 7.292 (m), 7.023 (m), 6.858 (m), 6.439 (m), 6.163 (m); $^{31}P\{^1H\}$ (121 MHz, CH_2Cl_2–$CDCl_3$, 25 °C): δ 29.8 (s br).

$[Pt_2Pb(P_2phen)_3](ClO_4)_2$, **2** (see ESI†).

§ *Crystal data*: for $C_{112}H_{78}Cl_6N_6O_8P_6PbPd_2$ **1**·2DCE, *M* = 2454.31, orthorhombic, *a* = 26.665(7), *b* = 14.449(3), *c* = 25.967(5) Å, *V* = 10 005(4) Å^3, *T* = 140 K, space group $Pna2_1$, *Z* = 4, μ(Mo-K) = 2.353 mm^{-1}, 87 599 reflections measured, 28 762 unique (R_{int} = 0.0452) were used in all calculations. The final *R*1(all data) was 0.057 and *wR*2 (all data) was 0.0815. Single crystals of $[Pd_2(P_2phen)_3Pb](ClO_4)_2{\cdot}2DCE$ were grown by slow diffusion of benzene into a DCE solution of the complex.

CCDC 182/1694. See http://www.rsc.org/suppdata/cc/b0/b003758n/ for crystallographic data in .cif format.

For nitrate salt of **2**: $[Pt_2Pb(P_2phen)_3]_2(NO_3)_4{\cdot}Pb(NO_3)_2{\cdot}4DCE{\cdot}MeOH$, *M* = 5493, triclinic, *a* = 18.2425(3), *b* = 25.6650(4), *c* = 29.2485(6) Å, α = 64.932(1), β = 79.399(1), γ = 78.724(1)°, *V* = 12054(4) Å^3, *T* = 140 K, space group $P\bar{1}$, *Z* = 2, 81 238 reflections measured, 30591 unique (R_{int} = 0.0533) were used in all calculations. The final *R*1(all data) was 0.1074 and *wR*2 (all data) was 0.1433. The anions were severely disordered and could not be reliably located.

1 P. Pyykkö, *Chem. Rev.*, 1997, **97**, 597; P. Pyykkö, N. Runeberg and F. Mendizabal, *Chem. Eur. J.*, 1997, **3**, 1451.

2 O. Crespo, E. J. Fernandez, P. G. Jones, A. Laguna, J. M. Lopez-de-Luzuriaga, A. Mendia, M. Monge and E. Olmos, *Chem. Commun.*, 1998, 2233; S. Wang, G. Garzón, C. King, J.-C. Wang and J. P. Fackler, Jr., *Inorg. Chem.*, 1989, **28**, 4623; S. Wang, J. P. Fackler, Jr., C. King and J. C. Wang, *J. Am. Chem. Soc.*, 1988, **110**, 3308; M. Maliarik, K. Berg, J. Claser, M. Sandström and I. Tróth, *Inorg. Chem.*, 1998, **37**, 2910.

3 N. Kaltsoyanis, *J. Chem. Soc., Dalton Trans.*, 1997, 1; E. J. Fernandez, J. M. Lopez-de-Luzuriaga, M. Monge, M. A. Rodriguez, O. Crespo, M. C. Gimeno, A. Laguna and P. G. Jones, *Inorg. Chem.*, 1998, **37**, 6002; K. Balasubramanian, *Relativistic Effects in Chemistry, Part A*, Wiley-Interscience, New York, 1997.

4 V. J. Catalano, B. B. Bennett, H. M. Kar and B. C. Noll, *J. Am. Chem. Soc.*, 1999, **121**, 10 235.

5 V. J. Catalano, B. B. Bennett, R. L. Yson and B. C. Noll, *J. Am. Chem. Soc.*, 2000, (submitted).

6 A. L Balch, E. Y. Fung, J. K. Nagle, M. M. Olmstead and S. P. Rowley, *Inorg. Chem.*, 1993, **32**, 3295.

7 V. G Albano, C. Castellari, M. Monari, V. De Felice, M. L. Ferrara and F. Ruffo, *Organometallics*, 1995, **14**, 4213; J. M. Casas, J. Fornies, A. Martin, V. M. Orera, A. G. Orpen and A. J. Rueda, *Inorg. Chem.*, 1995, **34**, 6514.

8 B. Crociani, M. Nicolini, D. A. Clemente and G. Bandoli, *J. Organomet. Chem.*, 1973, **49**, 249; G. Carturan, G. Deganello, T. Boschi and U. Belluco, *J. Chem. Soc. A*, 1969, 1142.

9 R. Usón, J. Forniés, L. R. Ralvello, M. A. Usón and I. Usón, *Inorg. Chem.*, 1992, **31**, 3697.

10 A. L. Balch, V. J. Catalano, M. A. Chatfield, J. K. Nagle, M. M. Olmstead and P. E. Reedy, Jr., *J. Am. Chem. Soc.*, 1991, **113**, 1252.

11 S. Wang, G. Garzón, C. King, J.-C. Wang and J. P. Fackler, Jr., *Inorg. Chem.*, 1989, **28**, 4623.

12 P. D. Harvey and H. B. Gray, *J. Am. Chem. Soc.*, 1988, **110**, 2145.

ChemComm

Selective synthesis of anatase and rutile *via* ultrasound irradiation

Weiping Huang, Xianghai Tang, Yanqin Wang, Yuri Koltypin and Aharon Gedanken*

Department of Chemistry, Bar-Ilan University, Ramat-Gan 52900, Israel. E-mail: gedanken@mail.biu.ac.il

Received (in Oxford, UK) 25th April 2000, Accepted 12th June 2000

A simple and efficient methodology has been established for the selective synthesis of anatase and rutile as well as their mixtures with various precursors using ultrasound irradiation; the products, the particle sizes of which are nanometric (< 9 nm), are dependent both upon the reaction temperature and the precursor used; a substantial reduction in reaction time as well as reaction temperature is observed as compared to the corresponding hydrothemal processes.

Since Fujishima and Honda[1] discovered the photocatalytic splitting of water on titania electrodes, intensive, world-wide research activity based on titania has ensued. Titania has three crystalline phases: rutile, anatase and brookite, of which rutile is the most stable while anatase exhibits the highest photocatalytic activity.[2] Up to now, many methods have been established for the synthesis of titania,[3–8] the sol–gel technique being the most often used. Unfortunately, the sol–gel derived precipitates are amorphous in nature, which requires further treatment to induce crystallization.[9,10] The hydrothermal technique is widely employed to enhance crystallinity in laboratory and commercial preparations. However, many factors, *e.g.* reaction temperature, reaction time and the medium, may influence the crystallization process. A recent paper demonstrated that the optimum temperature for the hydrothermal treatment is 473–493 K.[11] In order to obtain crystalline titania at lower temperature, a longer aging time is required. On the other hand, the photocatalytic activity of titania is particle size dependent, *i.e.* the smaller the titania particles, the higher their photocatalytic activity.[12] Hence, it is of great importance to improve the synthesis methodology. Here we describe a new, simple route for the direct, selective synthesis of nanosized anatase and rutile employing ultrasound irradiation for a short reaction time.

The sonochemical synthesis has been described elsewhere,[13] which has been employed to prepare amorphous metals[14,15a] and oxides.[15b] In the present work, it has been found that ultrasound irradiation can also accelerate the crystallization process of titania. The most important result of this investigation is the dependence of the product phase on both the used precursor and the reaction temperature. Under the same reaction conditions, anatase was formed when tetraisopropyltitanate (TPT) was employed as the precursor, rutile was obtained when titanium tetrachloride (TTC) was used, while a mixture of anatase and rutile was obtained when the precursor was a mixture of TPT and TTC.

In a typical synthesis, 110 mL of deionized water was sonicated by employing a direct immersion titanium horn (Sonics and Materials, VC-600, 20 kHz, 100 W cm^{-2}) for 10 min. At this stage 10 mL of the precursor (TPT, TTC or TPT+TTC, Aldrich) was injected into the sonication cell. The mixture was further sonicated continuously for 3 h. The sonication was conducted without cooling so that a temperature of 353 K was reached at the end of the reaction. The precipitates were separated by centrifugation and washed twice with deionized water and once with ethanol. The product was further dried under vacuum overnight. The detailed synthesis conditions for various samples are summarized in Table 1.

The powder X-ray diffraction (PXRD) patterns of the as-prepared samples are presented in Fig. 1. The reflections in Fig. 1(a) can be indexed to rutile (JCPDS 21-1276) while those in Fig. 1(b) are indexed to anatase (JCPDS 21-1272), which correspond to the as-prepared products using TTC and TPT as precursors, respectively. The sonication of a TPT and TTC mixture yielded sample C, which was a mixture of anatase and rutile [Fig. 1(c)]. Unlike the sol–gel method, the as-prepared products of the sonication process are always perfectly crystalline. For comparison, sample D was synthesized by employing the same precursor and reaction conditions (353 K) as sample C except that the reaction was carried out without sonication. Sample D is poorly crystalline or amorphous as shown in Fig. 1(d).

By employing the well-known formula[16] $X_A = [1 + 1.26(I_R/I_A)]^{-1}$, where X_A is the fraction of anatase in the mixture, and I_R and I_A are the intensities of reflections (110) of rutile and (101) of anatase, respectively, it is estimated that sample C contains 47.6% anatase and 52.4% rutile. This is quite surprising because the molar ratio of TPT to TTC in the irradiated solution is 63.4 : 36.6. Taking into account that rutile and anatase were the sole corresponding products when TTC and TPT acted as the precursors, separately, it is obvious that part of rutile formed at the expense of TPT.

The strong influence of the reaction temperature and the acidity of the medium on the crystallization of titania were further demonstrated in the syntheses of samples E–H. When TPT was used as precursor and sonication was carried out at 303 K, sample E was obtained as a mixture of brookite (JCPDS 29-1360) and anatase [Fig. 1(e)] while for TTC sonicated at *ca.* 283 K the product obtained (*i.e.* sample F) was mainly rutile [Fig. 1(f)]. However, at the same temperature when TTC was

Table 1 Synthesis conditions for samples A–H and their crystalline phases

Sample	Precursor	Synthesis conditions[a]	Sample phase	Particle size[b]/nm	$S_{BET}/m^2\ g^{-1}$
A	TTC	Hydrolyzed in water, sonicated for 3 h	Rutile	8.2	103.5
B	TPT	Hydrolyzed in water, sonicated for 3 h	Anatase	3.5	201.5
C	TPT+TTC	Hydrolyzed in water, sonicated for 3 h, TPT : TTC = 63.4 : 36.6 (molar ratio)	Rutile + anatase (52.4 : 47.6)	6.8	
D	TPT+TTC	Hydrolyzed in water, aged at 353 K for 3 h	Poorly crystalline	—	
E	TPT	Hydrolyzed in water, sonicated at 303 K for 3 h	Brookite + anatase	2.5	
F	TTC	Hydrolyzed in water, sonicated at *ca.* 283 K for 3 h	Rutile	5.9	
G	TPT	Hydrolyzed in 0.2 mol/L HCl (pH = 0.7), sonicated for 3 h	Rutile + anatase	6.5	
H	TPT	Precipitated the supernatant of G at pH 8.6 with $NH_3 \cdot H_2O$ (24% aq.), sonicated for 3 h	Anatase	2.9	289.8

[a] Sonication was carried out under atmospheric pressure without cooling if no other conditions are specified. [b] Average particle size was estimated from PXRD line-broadening employing Scherrer formula.

DOI: 10.1039/b003349i

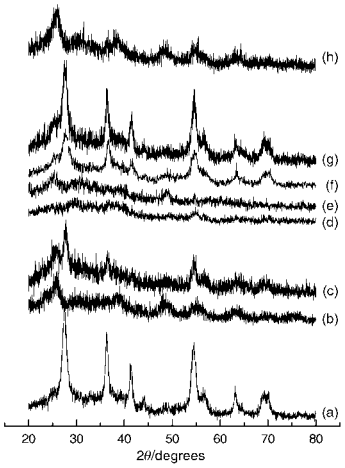

Fig. 1 PXRD patterns of the as-prepared samples A–H (from bottom to top).

hydrolyzed and aged, no precipitates appeared without sonication. It is interesting that when TPT was dissolved in a dilute HCl solution (pH = 0.7) and sonicated, only little solid product (sample G) was obtained showing a rutile phase [Fig. 1(g)]. However, after adjustment of the pH of the above supernatant to 8.6 by addition of ammonia, a white precipitate appeared, and further sonication resulted in the formation of sample H, which was pure anatase [Fig. 1(h)]. These results imply that, although the ultrasonic irradiation promotes the crystallization process of titania, the final crystalline phase of the product is also determined by the acidity of the medium. The particle sizes of samples A, B, C, E, F, G and H, were below 9 nm (Table 1) and were calculated using the Scherrer formula. A TEM image of sample H is shown in Fig. 2, and reveal particles of 4–6 nm diameter.

The results from liquid-N_2 adsorption measurements may aid understanding of the formation of the products. Fig. 3 shows the N_2 adsorption isotherms and pore size distributions of samples A, B and H. The isotherms are characteristic of types H2 (for samples B and H) and H3 (for sample A).[17] Many porous absorbents tend to give a type H2 loop. For sample B a very broad pore size distribution with an average pore size of 5.0 nm was measured, while for sample H a narrower pore size distribution was observed. However, unlike the mesoporous samples B and H (anatase) the results obtained for sample A (rutile) indicate its non-mesoporous nature. The mesopores in samples B and H may be constructed through the aggregation of particles.

A close examination of the PXRD patterns reveals a curious phenomenon. The reflections assigned to anatase are always broader than those for rutile, which implies smaller mean

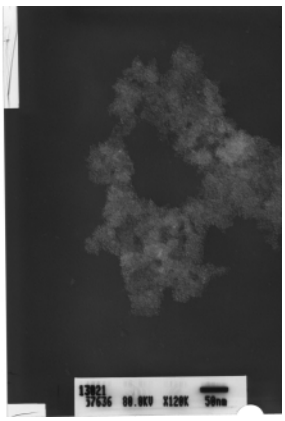

Fig. 2 TEM image of sample H obtained on a JEOI-JEM1200EX electron microscope.

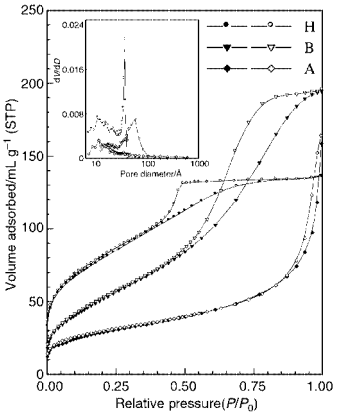

Fig. 3 Adsorption (filled)–desorption (open) isotherms of N_2 for samples A, B and H. Inset: pore size distributions of samples A, B and H.

particle sizes of the bulk anatase products. In fact, according to the Scherrer formula, the particle sizes of all rutile samples are almost twice that of the anatase samples (Table 1). As TTC hydrolyzes violently in water, part of the titanium hydroxide precipitates before dissolving in the acidic solution. Meanwhile, some of the titanium ions that exist as titanyl can be further coordinated by chloride anions. In contrast, the hydrolysis of TPT in water is slower, which results in a nearly neutral, partly condensed and more homogeneous gel. In the latter case, ultrasound irradiation generates many localized hot spots within the gel, outside which the polycondensation of ≡Ti–OH species is promoted. This further causes the homogeneous formation of a large number of seed nuclei, which leads to a smaller particle size. We propose that the interactions caused by sonication amongst the titanium species in the gel is stronger than those in the mixture containing ≡Ti–Cl species, which leads to the formation of anatase, a less condensed metastable phase.

W. H. and X. T. thank the Fred and Barbara Kort Sino–Israel Postdoctoral Fellowships Foundation for financial support and the China Scholarship Council for its support.

Notes and references

1 A. Fujishima and K. Honda, *Nature*, 1972, **37**, 238.
2 J. Ovenstone and K. Yanagisawa, *Chem. Mater.*, 1999, **11**, 2770.
3 R. W. Siegel, S. Ramasamy, H. Hahn, Z. Li, T. Lu and R. Gronsky, *J. Mater. Res.*, 1988, **2**, 1367.
4 P. W. Morrison, Jr., R. Raghavan, A. J. Timpone, C. P. Artelt and S. E. Pratsinis, *Chem. Mater.*, 1997, **9**, 2702.
5 Q. Chen, Y. Qian, Z. Chen, G. Zhou and Y. Zhang, *Mater. Lett.*, 1995, **22**, 77.
6 Y. Murakami, T. Matsumoto and Y. Takasu, *J. Phys. Chem. B*, 1999, **103**, 1836.
7 P. D. Moran, J. R. Bartlett, G. A. Bowmaker and J. L. Woolfrey, *J. Sol–Gel Sci. Technol.*, 1999, **15**, 251.
8 S. Komarneni, R. K. Rajha and H. Katsuki, *Mater. Chem. Phys.*, 1999, **61**, 50.
9 C. C. Wang and J. Y. Ying, *Chem. Mater.*, 1999, **11**, 3113.
10 E. A. Barringer and H. K. Bowen, *J. Am. Ceram. Soc.*, 1982, **65**, c199.
11 H. Cheng, J. Ma and L. Qi, *Chem. Mater.*, 1995, **7**, 663.
12 Z. Zhang, C. C. Wang, R. Zakaria and J. Y. Ying, *J. Phys. Chem. B*, 1998, **102**, 10 871.
13 K. S. Suslick, *Ultrasound: its Chemical, Physical and Biological Effects*, VCH, Weinheim, 1988.
14 K. S. Suslick, S. B. Choe, A. A. Cichowlas and M. W. Grinstaff, *Nature*, 1991, **353**, 414.
15 (*a*) Yu. Koltypin, X. Cao, G. Kataby, R. Prozorov and A. Gedanken, *J. Non-Cryst. Solids*, 1996, **201**, 159. (*b*) X. Cao, Yu. Koltypin, R. Prozorov, G. Kataby and A. Gedanken, *J. Mater. Chem.*, 1997, **7**, 2447.
16 R. A. Spurr and H. Myers, *Anal. Chem.*, 1957, **29**, 760.
17 K. S. W. Sing, D. H. Everett, R. A. W. Haul, L. Moscou, R. A. Pierotti, J. Rouquerol and T. Siemieniewska, *Pure Appl. Chem.*, 1985, **57**, 603.

Silica grain labelling and EDX spectroscopy; evidence for inter-grain diffusion of $Pt(NH_3)_4^{2+}$ species during Pt/SiO_2 catalyst preparation by ionic exchange

Alexandre Goguet,[a] Mimoun Aouine,[b] Francisco J. Cadete Santos Aires,[b] Daniel Schweich[a] and Jean-Pierre Candy*[c]

[a] *Laboratoire de Génie des Procédés Catalytiques (URA-CNRS), CPE Lyon, 69616 Villeurbanne, France*
[b] *Institut de Recherches sur la Catalyse (UPR 5401-CNRS), 2 Av. Albert Einstein, 69626 Villeurbanne, France*
[c] *Laboratoire de Chimie Organométallique de Surface (UMR-CNRS), CPE Lyon, 69616 Villeurbanne, France. E-mail: candy@mulliken.cpe.fr*

Received (in Oxford, UK) 10th March 2000, Accepted 26th June 2000

Labelling of silica grains and energy dispersive X-ray spectroscopy (EDX) in a TEM-FEG (field emission gun) were used to demonstrate the migration of $Pt(NH_3)_4^{2+}$ species from one grain to another during Pt/SiO_2 catalyst preparation by the ion-exchange procedure.

The reaction of $Ti(OPr)_4$ with the surface of silica grains can be used to graft Ti species. It is therefore possible to mark out some grains incorporated into a silica grains population in order to trace their behavior during for example, the adsorption processes of metal precursors in aqueous media.

The concept of interfacial coordination chemistry was proposed by Che[1] to describe the interaction of transition metal ions with oxide surfaces. In aqueous solution, the transition metal ions are complexed and interaction occurs frequently *via* ionic exchange. For platinum supported on silica, the silica surface protons are exchanged by $Pt(NH_3)_4^{2+}$ ions to form a surface complex $(SiO^-)_2Pt(NH_3)_4^{2+}$.[2] The decomposition of this complex under oxygen or hydrogen leads to Pt particles.[3] Although this method is commonly used, the fixation and dispersion processes of the species are not well-characterized. The aim of this work is to show that the use of Ti labelled silica grains demonstrates that the exchanged species migrate from one silica grain to another when impregnated and non-impregnated silica grains are mixed.

The concentration of Pt in aqueous solution for increasing interaction time with silica[4] is reported in Table 1. Clearly, the adsorption equilibrium of $Pt(NH_3)_4^{2+}$ on the silica surface is reached within < 1 min. For low metal loading (*ca.* 1 wt%), one may thus wonder whether the adsorbed platinum complex is homogeneously distributed all over the silica surface and among the silica particles.

In an initial experiment,[5] EDX analyses[6] of 1 wt% Pt/SiO_2 samples (Fig. 1) demonstrate that after 5 min of contact between the solution and silica, some of the silica grains do not support any Pt whilst others exhibit Pt/Si ratios far from the expected value corresponding to 1 wt% (*ca.* 0.003). Conversely, after 24 h, most of the particles exhibit a Pt/Si atomic ratio close to 0.004. This is most certainly due to the fast fixation of $Pt(NH_3)_4^{2+}$ ions on some silica grains and subsequent redistribution to the other grains. The migration of $Pt(NH_3)_4^{2+}$ can occur either on the silica surface or *via* the liquid phase.

In a second experiment,[7] Ti-labelled[8] silica grains were mixed with previously impregnated unlabelled silica. EDX analysis of the sample clearly shows (Fig. 2) that the migration of species from previously impregnated grains to other grains occurs even at low contact times (5 min) since all Ti-labelled grains that were analyzed contain Pt. After 24 h, the Pt content tends to become homogeneously distributed over all the grains and the average atomic ratio Pt/Si reaches 0.004. Before addition of unlabelled silica, the amount of $Pt(NH_3)_4^{2+}$ present in solution (3.3 μmol) is much smaller than the amount of Pt complex adsorbed on silica (48.0 μmol), and thus these results clearly demonstrate that $Pt(NH_3)_4^{2+}$ ions can migrate between silica grains, even at low metal loading and thus at very low liquid phase concentration, at the adsorption equilibrium.

This is, to our knowledge, the first time that Ti labelled silica grains and EDX analysis have been used for the study of the migration of adsorbed species from one grain to another.

Table 1 Concentration of $Pt(NH_3)_4^{2+}$ in solution for increasing times of interaction with 1 g of silica

Time/min	0	1	10	40
[Pt]/mmol l^{-1}	0.97	0.13	0.11	0.11
pH of solution	11.8	8.2	7.9	7.9

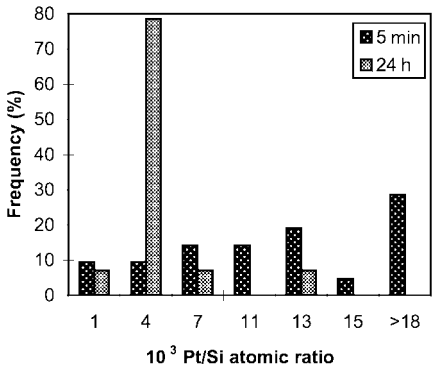

Fig. 1 Pt/Si atomic ratio obtained by EDX on silica grains after 5 min and 24 h of contact during the preparation of the Pt (1 wt%) catalyst.

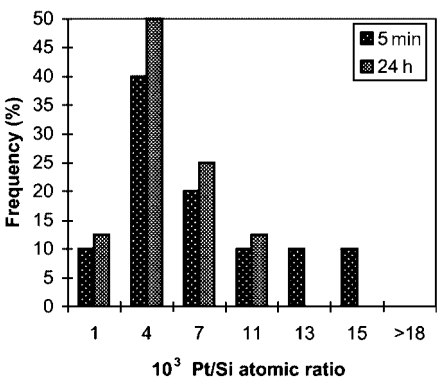

Fig. 2 Pt/Si atomic ratio obtained by EDX on Ti-labelled silica grains after 5 min and 24 h of contact between unlabelled and Ti-labelled silica.

DOI: 10.1039/b001955k

Notes and references

1 M. Che, *Proc. 10th Int. Congr. Catal.*, 19–24 July 1992, Budapest, Hungary, ed. L. Guczi, F. Solymosi and P. Tetenyi, Elsevier Science Publishers, Amsterdam, 1993, p. 31.

2 A. H. Benesis, R. M. Curtis and H. P. Studer, *J. Catal.*, 1968, **10**, 328.

3 W. Zou and R. D. Gonzalez, *J. Catal.*, 1992, **133**, 202.

4 Aérosil Degussa silica grains (SiO_2, 200 $m^2\ g^{-1}$, 10–20 nm) were used as the support. These were freshly treated under flowing dry air at 520 °C for 5 h (heating rate 2 °C min^{-1}) before use. Platinum tetraamine hydroxide [$Pt(NH_3)_4(OH)_2$], prepared from $Pt(NH_3)_4Cl_2$ (Aldrich) by ionic exchange[1] was used as the platinum precursor. 1 g of silica was introduced into a magnetically stirred flask with 30 ml of deionized H_2O and 51.3 mmol of $Pt(NH_3)_4(OH)_2$ at 20 °C. The amount of Pt introduced corresponds to an expected loading value of 1 wt% of dry silica. The adsorption rate of $Pt(NH_3)_4^{2+}$ ions onto the silica surface was measured by elemental (Pt) analysis of samples of the solution taken at regular time intervals. Elemental analysis was performed with a ICP Jovin Yvo apparatus.

5 1 g of silica was impregnated in a solution of 51.3 μmol of $Pt(NH_3)_4(OH)_2$ in 30ml of deionized H_2O at 20 °C. Samples taken after 5 min and 24 h of contact were analyzed.

6 EDX analysis of solid samples: EDX experiments where performed with a Pentafet-LinK ISIS (Oxford Instruments) spectrometer in a JEOL JEM 2010-F TEM (200 kV) equipped with a high resolution pole piece. The samples were dried in an oven at 80 °C before EDX measurement. The probe size was adjusted to the grain size of *ca.* 10 nm. Only isolated grains were analyzed in order to avoid simultaneous analysis of two different grains.

7 0.5 g of silica was impregnated in a solution of 51.3μmol of $Pt(NH_3)_4(OH)_2$ in 30ml of deionized H_2O at 20 °C for 1 h. Then 0.5 g of Ti-labelled silica was mixed with 0.5 g of unlabelled impregnated silica and samples corresponding to 5 min and 24 h of contact between the two silica populations were analyzed.

8 Ti labelled silica grains: 1 g of silica was treated at 500 °C under vacuum during 24 h, then $Ti(OPr)_4$ in hexane solution was introduced at room temperature under flowing argon and the suspension stirred for 4 h at room temperature. Next, the solid was extracted by filtration under argon, dried under vacuum for 24 h and then treated at 500 °C under flowing O_2–N_2 (20 : 80) for 2 h. The Ti loading, measured by elemental analysis, was 0.4 wt%. EDX measurements indicated that the silica grains were labelled with Ti. It was also established that the loading of 1 g of Ti labelled silica does not vary when it is impregnated with 30 ml of deionized H_2O and NH_4OH (pH 10) at 20 °C, stirred for 24 h and then washed four times with deionized water. The Ti loading of the sample is low with only 3% of the silica surface being covered by TiO_2. Two samples of Pt/SiO_2 prepared in the same manner, using unlabelled and Ti labelled silica exhibit the same Pt loading (1 wt%) and the same metallic particle size distribution. We thus concluded that Ti labelling did not influence the results.

ChemComm

Hydroformylation of epoxides catalyzed by cobalt and hemilabile P–O ligands

R. Weber,[a] U. Englert,[b] B. Ganter,[b] W. Keim[a] and M. Möthrath*[a]

[a] *Institute of Technical and Macromolecular Chemistry, RWTH Aachen, Worringer Weg 1, 52074 Aachen, Germany. E-mail: moethrath@itc.rwth-aachen.de*

[b] *Institute of Anorganic Chemistry, RWTH Aachen, Professor-Pirlet-Straße 1, 52056 Aachen, Germany*

Received (in Cambridge, UK) 5th April 2000, Accepted 7th June 2000

Complexes of cobalt efficiently catalyze the hydroformylation of epoxides in the presence of hemilabile P–O chelating ligands to give β-hydroxyaldehydes in high selectivities and yields.

The hydroformylation of epoxides provides an elegant and inexpensive pathway to β-hydroxyaldehydes which may easily be hydrogenated to 1,3-diols which have a wide variety of uses.[1] Lately propane-1,3-diol has attracted considerable industrial interest as an intermediate in the production of polyester fibers and films.[2]

For the hydroformylation of epoxides, special catalysts and ligands are needed to suppress side reactions such as isomerization and hydrogenation.

Previously, chelating diphosphine ligands have been reported for the cobalt catalyzed hydroformylation of epoxides.[3] For the rhodium catalyzed hydroformylation of olefins and for carbonylation reactions P–O ligands have been found to be superior to their phosphine analogues.[4] This fact prompted us to apply P–O ligands to the hydroformylation of epoxides. To the best of our knowledge, P–O ligands have not been reported for the hydroformylation of epoxides, whereas various diphosphine ligands such as dppm, dppe, dppp and dppb have been reported for this process (Scheme 1).

$Ph_2P(CH_2)_nP(=O)Ph_2$		$Ph_2P(CH)_nPPh_2$	
	n		*n*
dppmO	1	dppm	1
dppeO	2	dppe	2
dpppO	3	dppp	3
		dppb	4

Scheme 1 Structures of investigated ligands.

Using a catalyst prepared *in situ* under the applied reaction conditions from $Co_2(CO)_8$ and dppmO (for abbreviations see Scheme 1) in toluene, ethylene oxide **1** was converted to 3-hydroxypropanal **2** with 89% selectivity. Hydrogenation of **2** yielded 32% of propane-1,3-diol (1,3-PDO), **3** (Scheme 2).†

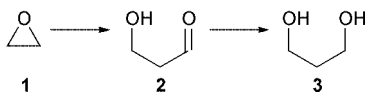

Scheme 2

In comparison to dppe (Table 1, run 2) the dppmO system proved to be much more efficient in terms of higher selectivities and yields. The reaction with diphosphines strongly depends on the solvents applied. Performing the reaction in a mixture of toluene and chlorobenzene, which is known to yield the best results for dppe, we could only achieve a 17% maximum yield of 1,3-PDO under the conditions selected.

To examine the role of the chelate effect of the ligands, the reaction was run with monodentate triphenylphosphine ($Co:PPh_3$ = 1:2) and with triphenylphosphine and diphenylmethylphosphine oxide ($Co:PPh_3:Ph_2MeP(O)$ = 1:1:1) as ligands (Table 1, runs 3 and 4). Scarcely any 1,3-PDO was observed after hydrogenation. Obviously, the presence of a chelating ligand is an important condition for a catalytically active system.

The use of dppeO and dpppO (Table 1, runs 5 and 6) as ligands led to a significant decrease in selectivity and yield, indicating that ligands which are capable of forming a five-membered chelate ring are preferred. A similar trend was observed employing dppm, dppp and dppb (Table 1, runs 7, 8, 9) as ligands.

As is well known in homogeneous catalysis, the variation of the ligand to metal ratio can have a strong influence on the activity and selectivity of the reaction. We thus varied the dppmO to cobalt ratio (Table 1, runs 10–14) and found that an increase of the amount of dppmO employed led to a steady enhancement of the 1,3-PDO yield, whereas an inverse relationship was observed for dppe.[5] The maximum yield of 1,3-PDO was obtained for a 1:1 ratio of dppe to cobalt and increasing the ligand to cobalt ratio resulted in a dramatic loss of activity. An explanation for the different behavior of the dppmO–Co system may be understood from ^{31}P NMR investigations of the reaction mixture after a pre-formation period. For a dppmO to cobalt ratio > 1, free ligand can be detected. It is known that triphenylphosphine oxide is used as a promoter for the hydroformylation of ethylene oxide[6] and excess dppmO may act in a similar manner. By increasing the amount of the free ligand the activity of the system is improved and therefore, dppmO can act as ligand and promoter at the same time.

We were able to isolate a stable cobalt complex $[(dppmO)Co(CO)_3]_2$, a single crystal X-ray analysis of which confirmed the dimeric structure (Fig. 1). The coordination geometry around cobalt is trigonal bipyramidal.‡

A comparison of the catalytic behavior of the isolated complex (Table 1, run 15) to the *in situ* system gave nearly

Table 1 Cobalt catalyzed hydroformylation of ethylene oxide **1**

Run	Ligand	Ligand:Co	GC yield of **3**[a](%)	Selectivity toward **2**[b] (%)
1	dppmO	1:1	32	89
2	dppe	1:1	10	76
3	PPh_3	2:1	< 1	—
4	PPh_3, $Ph_2MeP(O)$	1:1:1	≈ 2	—
5	dppeO	1:1	9	63
6	dpppO	1:1	5	51
7	dppm	1:1	—	—
8	dppp	1:1	4	52
9	dppb	1:1	3	58
10	—	—	3	—
11	dppmO	1:2	22	59
12	dppmO	3:4	26	89
13	dppmO	3:2	47	84
14	dppmO	2:1	54	84
15	$[(dppmO)Co(CO)_3]_2$	1:1	31	90

[a] Yields are based on the substrate and were determined by gas chromatography with standard compounds. For simpler GC detection all samples were hydrogenated. [b] Selectivity = products/(by-products + products).

DOI: 10.1039/b002703k

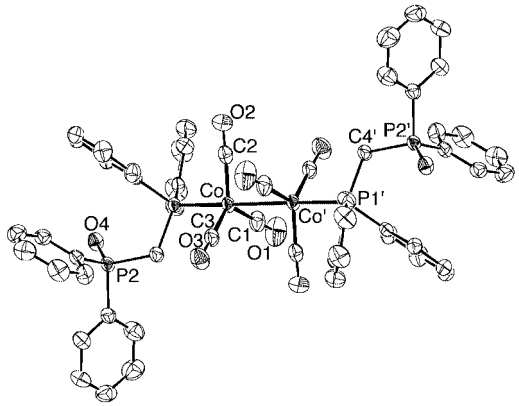

Fig. 1 Displacement ellipsoid plot (PLATON[11]) of the molecular structure of $[(dppmO)Co(CO)_3]_2$ in the crystal. Ellipsoids are drawn at 50% probability with hydrogen atoms omitted. Primed atoms are related to unprimed ones by the symmetry operation $-x, -y, -z$. Selected bond distances (Å) and angles (°): Co–Co′ 2.660(1), Co–P1 2.185(1), P1–C4 1.836(3), C4–P2 1.818(3), P2–O4 1.481(2); Co–Co′–P1′ 178.45(4), P1–C4–P2 121.6(2).

identical results and thus it can be assumed that for both runs the same catalytically active species are formed. The reaction sequence shown in Scheme 3 is proposed for this catalytic system.

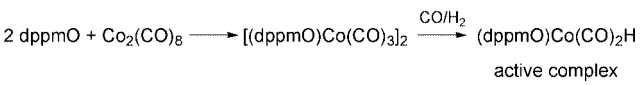

Scheme 3 Proposed catalytic sequence.

Cobalt catalyzed hydroformylation with dppmO as ligand can be readily applied to other epoxides affording the corresponding 1,3-diols after hydrogenation of the 3-hydroxyaldehydes (Table 2).

Propylene oxide and *trans*-2,3-epoxybutane (Table 2, runs 1, 2) are especially suitable for hydroformylation. The poorer results for styrene oxide and cyclohexene oxide can be explained in terms of increased isomerization to the corresponding aldehydes. It is known that $Co_2(CO)_8$ may catalyze those isomerization reactions.[7] Assuming that the isomerization occurs *via* an ionic mechanism and that the stabilization of the intermediate carbocation is of importance, the extent of the isomerization of styrene oxide becomes understandable.

Table 2 Cobalt catalyzed hydroformylation of different epoxides with dppmO

Run	Epoxide	Yield of 1,3-diol[a] (%)	Selectivity toward 3-hydroxyaldhyde[b] (%)
1	Propylene oxide	30	75
2	*trans*-2,3-butene oxide	66	79
3	Cyclohexene oxide	39	52
4	Styrene oxide	7	4

[a] Yields are based on the substrate and were determined by gas chromatography with standard compounds. For simpler GC detection all samples were hydrogenated. [b] Selectivity = products/(by-products + products).

In conclusion, the hydroformylation of epoxides employing hemilabile P–O ligands and cobalt metal salts has been successfully carried out for the first time. Suitable hemilabile ligands must be able to form a chelate ring with cobalt, preferably a five membered-ring chelate. An excess of the hemilabile ligands further enhances the yield of the β-hydroxyaldehydes. The reaction can be extended to different epoxides establishing a new route to synthesize 1,3-diols or 3-hydroxyaldehydes.

We thank Degussa Hüls AG and the DFG for support of our work.

Notes and references

† All reactions were carried out in a 100 ml steel autoclave with all manipulations carried out under argon. In a typical experiment, the appropriate amount of ligand in 10 ml of toluene was added to a Schlenk tube containing a stirring bar and 68.4 mg (0.2 mmol) of $Co_2(CO)_8$ in 10 ml of toluene. The mixture was transferred into the autoclave and the dropping funnel of the autoclave was filled with 50 mmol of the epoxide. The charged autoclave was pressurized with CO and H_2 (100 bar) and stirred at 100 °C for 1 h. The epoxide was dropped into the reaction mixture and the reaction carried out for 3 h, with temperature and pressure being constantly monitored throughout. After the reaction, the autoclave was allowed to cool in an ice-bath to room temperature, and the gases were vented. The liquid reaction mixture was collected in methanol and analyzed by GC. A small part of the reaction mixture (1 ml) was hydrogenated and analyzed by GC.

‡ X-Ray structure determination of $[(dppmO)Co(CO)_3]_2$. ENRAF-Nonius CAD4 diffractometer, Mo-Kα radiation (λ = 0.71073 Å), incident beam graphite monochromator, T = 203 K, platelet of approximate dimensions 0.74 × 0.66 × 0.24 mm³ mounted in dry dinitrogen flux. *Crystal data*: triclinic, space group $P\bar{1}$, a = 9.040(3), b = 10.619(2), c = 14.119(6) Å, α = 80.74(3), β = 72.79(3), γ = 89.43(2)°, V = 1276.8(9) Å³, Z = 1, D_c = 1.25 g cm^{-3}, μ = 7.5 cm^{-1}. 4795 reflections, θ_{max} = 25°, empirical absorption correction by azimuthal scans.[8] Solution with direct methods (SHELXS86[9]), refinement on F (SDP[10]), 404 variables, R_w = 0.040, R = 0.036 for 3822 independent data with $I > 1.0\sigma(I)$. Residual electron density from final difference Fourier synthesis 0.91 e Å^{-3}. CCDC 182/1675.

1 *Shell Chemicals Magazine*, no 10, 2nd Quarter 1998; *CD Roempp Chemie Lexikon*, version 1.0, Georg Thieme Verlag, Stuttgart, New York, 1995; *Ullman's Encyclopedia of Industrial Chemistry*, 5th completely revised edn., VCH, Weinheim, Basel, New York, 1985–1995.
2 J. G. Smith, C. J. Kibler and B. J. Sublett, *J. Polym. Sci., Part A-1*, 1966, **4**, 1841; *ECN Chemscope*, May 1998, **40**.
3 L. H. Slaugh, *US Pat.*, 5 256 827, 1993 (Shell); L. H. Slaugh, *US Pat.*, 5 304 686, 1994 (Shell); L. H. Slaugh, *US Pat.*, 5 304 691, 1994 (Shell); L. H. Slaugh, *US Pat.*, 5 344 993, 1993 (Shell); L. H. Slaugh, *World Pat.*, WO 94/18149, 1994 (Shell); C. W. Smith, *US Pat.*, 3 456 017, 1969 (Shell).
4 C. Abu-Gnim and I. Amer, *J. Organomet. Chem.*, 1996, **516**, 235.
5 R. Weber, Diplomarbeit, RWTH Aachen, 1996.
6 P. R. Weider, *US Pat.*, 5 563 302, 1996.
7 R. E. Parker and N. S. Isaac, *Chem. Rev.*, 1950, **59**, 737.
8 A. C. T. North, D. C. Phillips and F. S. Mathews, *Acta Crystallogr., Sect. A*, 1968, **24**, 351.
9 G. M. Sheldrick, SHELXS86, Program for Structure Solution, University of Göttingen, 1986.
10 ENRAF-Nonius, SDP Version 5.0, 1989.
11 A. L. Spek, PLATON-98, University of Utrecht, The Netherlands, 1998.

The new catalytic property of supported rhenium oxides for selective oxidation of methanol to methylal

Youzhu Yuan, Takafumi Shido and Yasuhiro Iwasawa*

Department of Chemistry, Graduate School of Science, The University of Tokyo, Hongo, Bunkyo-ku, Tokyo 113-0033, Japan. E-mail: iwasawa@chem.s.u-tokyo.ac.jp

Received (in Cambridge, UK) 15th May 2000, Accepted 23rd June 2000

A new catalytic property of supported rhenium oxides has been found for selective methanol oxidation to methylal; high performances for the selective catalytic oxidation are observed with V_2O_5-, ZrO_2-, Fe_2O_3- and TiO_2-supported Re–oxide catalysts, which are characterized by pulse experiments, XRD and XPS.

Numerous efforts have been made to develop selective oxidation catalysts for methanol conversions to formaldehyde, methyl formate and dimethoxymethane (methylal). Methanol oxidation to formaldehyde has been extensively studied and commercialized on silver and ferric molybdate catalysts.[1] High-yield production of methyl formate from methanol has also been accomplished on mixed metal oxides such as V–Ti oxides,[2] Sn–Mo oxides,[3] and Bi-based oxides.[4] Methylal is used as a gasoline additive, a solvent in perfume industry, a key intermediate for preparing high concentration formaldehyde, and a reagent in organic synthesis. The catalytic methylal synthesis from methanol ($3\ MeOH + 1/2\ O_2 \rightarrow CH_2(OMe)_2 + 2\ H_2O$) has been reported on V/TiO_2,[1] V–Mo–O,[5] PMoH–5.75/SiO_2,[6,7] Mo/MCM-41,[8] and MoO_3(100),[9,10] but the selectivities to methylal on those catalysts were low. Recently, we found a crystalline binary oxide compound SbR_2O_6 which was selective for the methylal formation.[11] The selectivity reached 93.5% at a conversion of 6.5% at 573 K. However, the crystalline oxide $SbRe_2O_6$ has a very low surface area (1 $m^2\ g^{-1}$), resulting in insufficient activity for methylal production. The performance of SbR_2O_6 was attributed to the Re–oxide octahedra connecting with Sb–O chains.[11] The property of Re species capable of adopting a variety of oxidation states that are illustrated in both binary and ternary oxides,[12–14] may provide rich and interesting chemistry. Nevertheless, Re oxides have not widely been used as catalysts for selective oxidation reactions owing to sublimation under pretreatment and reaction conditions.[15] In this study we have found the new catalytic property of supported and unsupported Re oxides for the selective methanol oxidation to methylal.

Inorganic oxide-supported Re oxide catalysts were prepared by an incipient wetness impregnation method using an aqueous solution of ammonium perrhenate (NH_4ReO_4), followed by drying at 383 K for 12 h. The samples were put into a glass-made fixed-bed reactor in a flow system and heated to 673 K at a heating rate of 4 K min^{-1} in a He flow and held at 673 K for 6 h. The samples thus obtained were further treated *in situ* in the fixed-bed flow reactor under the He flow at 573 K for 1 h before use as catalysts. A typical Re loading was 10 wt% as Re/support. Methanol (Wako, purity 99.8%) was introduced to the flow reactor by bubbling He gas through a glass saturator filled with methanol. Unsupported Re oxides were also pretreated at 673 K in a similar way. The catalytic reactions on the supported and unsupported Re–oxide catalysts were carried out at 513 K under the reaction conditions GHSV = 40 000 ml h^{-1} g_{cat}^{-1} and $He:O_2:MeOH = 86.3:9.7:4.0$ (mol%) at 1 atm. The products were analyzed by an on-line gas chromatograph using Porapak N and Unibeads C columns.

Table 1 shows the performances of the supported Re–oxide catalysts for the selective methanol oxidation to methylal. The performances of unsupported Re oxides (ReO_3 and ReO_2) and two typical supports (α-Fe_2O_3 and V_2O_5) are also listed in Table 1 for comparison.

It was found that Re oxides supported on TiO_2 (rutile and anatase), V_2O_5, ZrO_2 (monoclinic), Fe_2O_3 (α and γ) and α-Al_2O_3 were active in order of the reaction rates per g_{Re} for the supports, TiO_2(anatase) > TiO_2(rutile) > γ-Fe_2O_3 > ZrO_2 > V_2O_5 > α-Fe_2O_3. Among them, Re/V_2O_5, Re/γ-Fe_2O_3, Re/α-Fe_2O_3, Re/ZrO_2 and Re/α-Al_2O_3 showed selectivities of 88–94% to methylal (Table 1). When the conversion for Re/γ-Fe_2O_3 was further increased by decreasing the space velocity, the methylal selectivity decreased a little, while the formaldehyde selectivity increased. Re oxides supported on SiO_2

Table 1 Catalytic methanol oxidation on supported Re–oxide catalysts at 513 K[a]

		MeOH conversion		Selectivity (mol%)				
Catalyst	$S_{BET}/m^2\ g^{-1}$	mol%	Rate/mmol h^{-1} g^{-1}	$CH_2(OMe)_2$	HCHO	Me_2O	HCO_2Me	CO_x[b]
Re/TiO_2-rutile	5	53.7	351.2	83.1	1.9	0.7	9.1	5.2
Re/TiO_2-anatase	50	59.5	389.1	78.5	4.1	1.1	11.7	4.6
Re/V_2O_5	6	21.5	140.6	93.7	0.0	4.3	0.0	2.0
Re/ZrO_2	9	35.8	234.1	89.4	2.0	Trace	7.6	1.0
Re/α-Fe_2O_3	3	15.5	101.4	90.5	2.0	1.0	6.0	0.5
Re/γ-Fe_2O_3	16	48.4	319.2	91.0	2.4	1.0	4.6	1.0
Re/SiO_2	36	15.1	98.8	60.7	1.3	Trace	11.9	26.1
Re/α-Al_2O_3	10	16.3	106.6	88.3	2.8	Trace	5.9	2.9
Re/Sb_2O_3	1	0.0	0.0	0.0	0.0	0.0	0.0	0.0
Re/Bi_2O_3	1	0.0	0.0	0.0	0.0	0.0	0.0	0.0
Re/MoO_3	5	9.1	59.5	80.0	0.0	19.0	0.0	1.0
α-Fe_2O_3	3	0.0	0.0	0.0	0.0	0.0	0.0	0.0
V_2O_5	6	9.3	10.8[c]	1.0	91.5	7.4	0.0	Trace
ReO_3	1	12.4	10.2	99.0	0.0	0.5	0.5	0.0
ReO_2	7	65.3	50.0	64.6	6.4	2.0	10.2	16.8

[a] Re loading: 10.0 wt%, GHSV = 40 000 ml h^{-1}·g_{cat}, $He:O_2:MeOH = 86.3:9.7:7:4$ (mol%). [b] $CO_x = CO_2 + CO$. [c] mmol h^{-1} g_V^{-1}.

DOI: 10.1039/b003870i

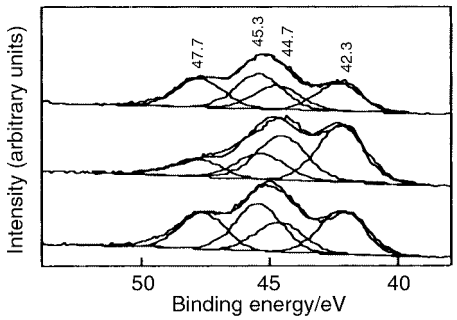

Fig. 1 Re 4f XPS spectra for 10.0 wt% Re/α-Fe_2O_3 catalysts: (a) after pretreatment at 673 K for 6 h in He, (b) after ten methanol pulses at 513 K and (c) after catalytic methanol oxidation at 513 K for 2 h in the presence of O_2. The XPS binding energies were referred to 284.6 eV for C 1s.

produced a significant amount of CO_x and those supported on Sb_2O_3 and Bi_2O_3 showed no activity at 513 K (Table 1). α-Fe_2O_3 and V_2O_5 themselves were almost inactive for methylal formation though V_2O_5 produced formaldehyde. When these oxides were supported by Re oxides, the obtained Re/α-Fe_2O_3 and Re/V_2O_5 showed selectivities to methylal as high as 91–94%. ReO_3 was most selective (99%), while the selectivity of ReO_2 was much lower (64.6%). When the mixture of He–MeOH–O_2 was admitted to Re_2O_7 at 513 K, the color changed from yellow (Re_2O_7) to read (ReO_3) in <3 min, accompanied with sublimation of some of the Re_2O_7, and showed a selectivity to methylal $>90\%$ after 10 min of time-on-stream. Under the reaction conditions below 553 K, there was no loss of Re oxides by sublimation in Re/TiO_2, Re/V_2O_5, Re/Fe_2O_3, Re/ZrO_2, Re/SiO_2, Re/Al_2O_3 and Re/MoO_3. It indicates that bulk Re_2O_7 is not a stable phase in the methylal synthesis conditions. It was concluded from plots of the selectivities against the reaction rates per surface area or the conversions in Table 1 that Re/α-Fe_2O_3, Re/γ-Fe_2O_3, Re/V_2O_5 and Re/ZrO_2 exhibit high catalytic selectivity on Re/α-Fe_2O_3 increased with increasing Re loading and reached saturation values at 2.0 wt% Re (15.5 and 92.0%, respectively). The highest reaction rates per g_{Re} of the supported Re–oxide catalysts were thus achieved in the range of Re loadings 1–3 wt%.

Recently, a high selectivity of 76.2% was reported on 2 mol% Mo supported on MCM-41, but it was achieved at a very low conversion of 0.7% at 543 K.[8] Further, the Mo/MCM-41 catalyst was rapidly deactivated owing to a significant leaching of Mo species from the channels of MCM-41.[8] On the other hand, no deactivation of the supported Re oxides occurred for 6 h of time-on-stream at 513 K. Methylal formation from methanol was also reported on PMoH–5.75/SiO_2[6,7] and V/TiO_2,[1] but the selectivities toard methylal were as low as 40–56%.[11]

The XPS spectrum [Fig. 1(a)] for the as-pretreated Re/α-Fe_2O_3 showed a peak at 42.3 eV which is assigned to the Re $4f_{7/2}$ level for Re^{4+} species (also deconvolued at 44.7 eV for $4f_{5/2}$). The XPS spectrum also showed peaks at 45.3 and 47.7 eV assigned to Re $4f_{7/2}$ and $4f_{5/2}$ levels possibly for a Re^{6+} species, respectively [Fig. 1(a)]. The Re $4f_{7/2}$ binding energy (45.3 eV) is lower by 1.2–1.6 eV than that reported for Re_2O_7 (R^{7+}), but higher by 0.8–1.0 eV than that for ReO, (Re^{6+}).[17,18] We measured XPS spectra for the Re/α-Fe_2O_3 catalysts with different Re loadings in the range 0.1–10.0 wt%. The Re^{6+} peaks at 45.3 and 47.7 eV were observed in all the samples, while the Re^{4+} peaks at 42.3 and 44.7 eV developed only for the catalysts with Re > 2.0 wt%. The XRD lines for ReO_2 appeared for the Re/α-Fe_2O_3 catalysts with Re > 3.0 wt%, while no diffraction lines due to Re_2O_7 and ReO_3 were detected. It is most likely from these results that the initial Re^{7+} precursors were reduced to Re^{6+} and also to Re^{4+} for Re loadings above 2.0 wt% under the pretreatment conditions.[16] We estimate 2 wt% of Re as a monolayer of Re oxides at the α-Fe_2O_3 surface. The fact that neither Re^{4+} (XPS) nor ReO_2 (XRD) were detected on the catalysts with Re loadings below 2.0 wt% indicates that dispersed Re oxides are scarcely reduced to Re^{4+} under He at 673 K probably because of interaction with the α-Fe_2O_3 surface.

When pulses of 1 ml of He–MeOH = 96.0 : 4.0 (mol%) were introduced onto the 10.0 wt% Re/α-Fe_2O_3 catalyst at 513 K, methylal was formed during the course of the first to fourth methanol pulses with decreasing selectivities, and after the fifth pulse no methylal was produced. It is evident from the pulse experiments in the absence of gaseous O_2 that lattice oxygen atoms of the Re oxides work as active oxygen species for the selective oxidation of methnol. From the pulse experiments where the 10 wt% Re/α-Fe_2O_3 catalyst reacted with the methanol pulses at 513 K, we estimated that the amount of lattice oxygen atoms incorporated into the produced methylal was 1.88×10^{19} atom m^{-2}. Exhaustion of the active oxygen atoms increased the formation of H_2, CH_4 and CO_2 in a molar ratio of nearly 2 : 1 : 1 probably through decomposition of HCO_2Me produced preferable on the reduced Re oxides. After ten methanol pulses at 513 K, the intensities of the XPS peaks at 45.3 and 47.7 eV assigned to Re^{6+} species decreased drastically, while the Re^{4+} peak intensities increased significantly [Fig. 1(b)]. The consumed lattice oxygen atoms were regenerated by gaseous O_2 as established by XPS spectroscopy [Fig. 1(c)].

In summary, we have developed supported Re–oxide catalysts which show high performances for selective catalytic oxidation of methanol to methylal. The high performances of the Re oxides were obtained when V_2O_5, ZrO_2 and Fe_2O_3 were used as supports. The redox capability of Re oxides at the support surfaces (possibly $Re^{6+} \leftrightharpoons Re^{4+}$) may be responsible for the selective oxidation of methanol to formaldehyde, while the appropriate acidy Re oxides may also be necessary for the acetalization of formaldehyde with methanol to form methylal.

This work was supported by Core Research for Evolutional Science and Technology (CREST) of Japan Science and Technology Corporation (JST).

Notes and references

1 J. M. Tatibouët, *Appl. Catal. A: Gen.*, 1997, **148**, 213.
2 G. Busca, A. S. Elmi and P. Forzatti, *J. Phys. Chem.*, 1987, **91**, 5236.
3 M. Ai, *J. Catal.*, 1982, **77**, 279.
4 N. Arora, G. Deo, I. E. Wachs and A. M. Hirt, *J. Catal.*, 1996, **159**, 1.
5 J. M. Tatibouët and J. E. Germain, *Bull. Soc. Chem. Fr. I*, 1980, **9**–**10**, 343.
6 M. Fournier, A. Aouissi and C. Rocchiccioli-Deltchff, *J. Chem. Soc., Chem. Commun.*, 1994, 307.
7 C. Rocchiccioli-Deltcheff, A. Aoussi, S. Launary and M. Fournier, *J. Mol. Catal. A: Chem.*, 1996, **114**, 331.
8 I. J. Shannon, T. Maschmeyer, R. D. Oldroyd, G. Sankar, J. M. Thomas, H. Pernot, J. P. Baalikdjian and M. Che, *J. Chem. Soc., Faraday Trans.*, 1998, **94**, 1495.
9 J. M. Tatibouët and J. E. Germain, *J. Catal.*, 1981, **72**, 375.
10 J. M. Tatibouët, J. E. Germain and J. C. Volta, *J. Catal.*, 1983, **32**, 240.
11 Y. Yuan, H. Liu, H. Imoto, T. Shido and Y. Iwasawa, *Chem. Lett.*, 2000, 674.
12 H. Liu, E. C. Gaigneaux, H. Imoto, T. Shido and Y. Iwasawa, *J. Phys. Chem.*, 2000, **104**, 2033.
13 H. Watanebe, H. Imoto and H. Tanaka, *J. Solid State Chem.*, 1998, **138**, 245.
14 A. Butz, G. Miehe, H. Paulus, P. Strauss and H. Fuess, *J. Solid State Chem.*, 1998, **138**, 232.
15 S. Albonetti, F. Cavani and F. Trifiro, *Catal. Rev.-Sci. Eng.*, 1996, **38**, 413.
16 Y. Yuan, T. Shido and Y. Iwasawa, to be published.
17 E. S. Shpiro, V. I. Avaev, G. V. Antoshin, M. A. Ryashentseva and K. M. Minachev, *J. Catal.*, 1978, **44**, 402.
18 A. Cimino, B. A. De Angelis, D. Gazzoli and M. Valigi, *Z. Anorg. Allg. Chem.*, 1980, **460**, 86.

ChemComm

Synthesis and structure of a nitrogen/sulfur-ligated zinc hydroxide complex†

Lisa M. Berreau,*[a] Russell A. Allred,[a] Magdalena M. Makowska-Grzyska[a] and Atta M. Arif[b]

[a] *Department of Chemistry and Biochemistry, Utah State University, 0300 Old Main Hill, Logan, UT 84322-0300, USA. E-mail: berreau@cc.usu.edu*

[b] *Department of Chemistry, University of Utah, 315 S. 1400 E., Salt Lake City, Utah 84112 USA*

Received (in Irvine, CA, USA) 12th April 2000, Accepted 20th June 2000

Using a novel secondary amine-appended nitrogen/sulfur ligand, the first example of a nitrogen/sulfur-ligated zinc hydroxide complex, a species relevant to the active forms of several zinc-containing metalloenzymes, has been prepared and structurally characterized.

Zinc-containing metalloenzymes utilize active site structural motifs of varying nuclearity and supporting primary and secondary coordination environments to catalyze a diverse array of chemical transformations.[1] Distinctive among active site structures in these enzymes are those which have sulfur ligation to a Zn(II) ion that also binds a water/hydroxo moiety that is directly involved in catalysis.[1a] Specifically, the presence of cysteine sulfur ligation at the mononuclear Zn(II) active site ions of alcohol dehydrogenase,[2] peptide deformylase,[3] cytidine deaminase,[4] spinach carbonic anhydrase,[5] and at one of the two active site Zn(II) ions found in the metallo-β-lactamases from *B. fragilis*, *B. cereus*, and *A. hydrophila*,[6] has prompted research efforts toward the goal of generating Zn(II) complexes, supported by a mixed nitrogen/sulfur coordination environment, that possess an available coordination position for water/hydroxo binding.[7] However, despite the construction of several new ligand systems, a discrete zinc hydroxide species supported by a metal coordination sphere possessing sulfur donors has remained elusive, in part because of the tendency of thiolate ligands to produce oligomeric structures.[8] Herein we describe the synthesis and structural characterization of the first zinc hydroxide complex supported by a mixed nitrogen/sulfur ligand environment.

Reasoning that hydrogen bonding interactions might prove useful toward the stabilization and isolation of a nitrogen/sulfur-ligated zinc hydroxo species,[9] we prepared a new ligand system, *N*-bis-2-(methylthio)ethyl-*N*-(6-neopentylamino-2-pyridylmethyl)amine (bmnpa, Scheme 1), that combines a nitrogen/sulfur coordination environment with a secondary amine functionality that may serve as a hydrogen bond donor in metal complexes. As shown in Scheme 1, this ligand was prepared *via* a two-step reaction sequence. Treatment of 2-pivalolylamido-6-aminomethylpyridine[10] with 2 equivalents of 1-bromo-2-methylthioethane yielded *N*-bis-2-(methylthio)ethyl-*N*-(6-pivalolyamido-2-pyridylmethyl)amine (bmppa) in 61% yield.‡ Reduction of bmppa with $LiAlH_4$ in THF-pyridine followed by purification by column chromatography yielded the desired bmnpa ligand.‡ Zinc complexation of bmnpa was achieved *via* admixture of equimolar amounts of bmnpa, $Zn(ClO_4)_2·6H_2O$ and KOH (Scheme 2) in methanol at ambient temperature followed by crystallization from MeCN–Et_2O, which produced a colorless crystalline material with an analytical composition consistent with the empirical formula $[(bmnpa)Zn(OH)]ClO_4$ **1**.§¶ It is notable that in the absence of added KOH, a different zinc complex is generated. Specifically, treatment of bmnpa with $Zn(ClO_4)_2·6H_2O$ in MeOH followed by crystallization from MeCN–Et_2O yielded $[(bmnpa)Zn(ClO_4)](ClO_4)$ **2** (Scheme 2), which deposited as plate-type crystals.§¶

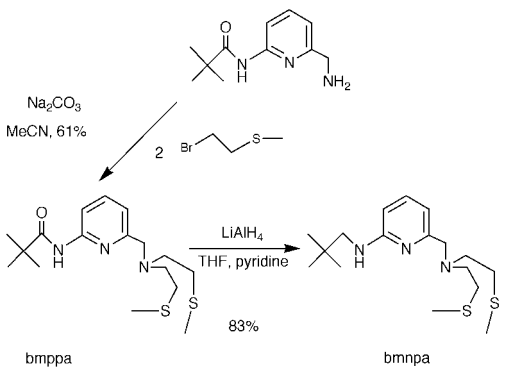

Scheme 1

X-Ray crystallographic analysis of **1** revealed an asymmetric, dinuclear nitrogen/sulfur-ligated zinc hydroxide structure (Fig. 1, top), with only one of the two available thioether sulfur donors ligated to each Zn(II) center. The five-coordinate zinc ions, which are related by an inversion center, exhibit a slightly distorted trigonal bypyramidal geometry (τ = 0.80)[11] with the pyridyl nitrogen [Zn(1)–N(2) 2.068(3) Å], a thioether sulfur [Zn(1)–S(1) 2.514(1) Å] and a hydroxide oxygen atom [Zn(1)–O(1) 1.974(3) Å] occupying equatorial positions. The observed Zn(1)–O(1) bond length falls within the range (*ca.* 1.9–2.3 Å) of distances previously reported for bridging hydroxo moieties in multinuclear zinc complexes.[12] The second zinc oxygen bond [Zn(1)–O(1′)] is slightly longer [2.028(3) Å] and is a structural component of a six-membered ring [Zn(1)-O(1′)···H-N(3)–C(9)–N(2)][13] created by a hydrogen bonding interaction between the secondary amine hydrogen [N(3)–H] and a lone pair on the hydroxyl oxygen [O(1′)···N(3) 2.82 Å, O(1′)···H–N(3) 161.0°].[14] Because this intramolecular hydrogen bonding interaction involves the longer Zn(1)–O(1′) bond, it appears to contribute toward the stabilization of the asymmetric dinuclear $Zn_2(OH)_2$ core.

Complex **2** is mononuclear in the solid state (Fig. 1, bottom), adopting a distorted trigonal bipyramidal geometry (τ = 0.65)

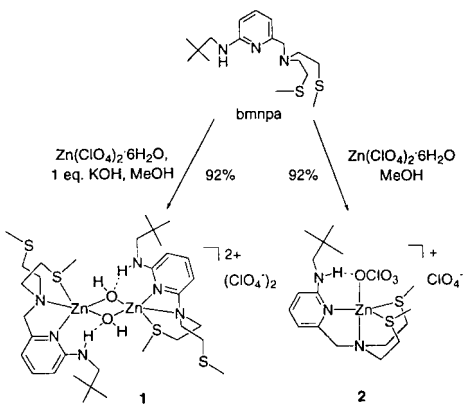

Scheme 2

† Electronic supplementary information (ESI) available: synthesis and characterization of ligands and complexes. See http://www.rsc.org/suppdata/cc/bo/b003144p/

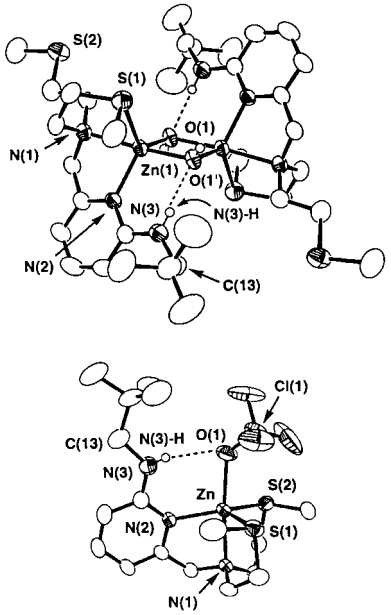

Fig. 1 Drawings of the cationic portions of the X-ray crystal structures of **1** (top) and **2** (bottom). All ellipsoids are drawn at the 50% probability level. Selected bond lengths (Å) and angles (°): **1**: Zn(1)–O(1) 1.974(3), Zn(1)–S(1) 2.514(1), Zn(1)–N(1) 2.189(3), Zn(1)–N(2) 2.068(3), Zn(1)–O(1′) 2.028(3); S(1)–Zn(1)–N(1) 82.8(1), N(1)–Zn(1)–N(2) 80.70(12), N(2)–Zn(1)–O(1) 114.2(1), N(2)–Zn(1)–O(1′) 102.6(1), N(1)–Zn(1)–O(1) 98.7(1), N(1)–Zn(1)–O(1′) 174.5(1), S(1)–Zn(1)–O(1) 126.8(1), S(1)–Zn(1)–O(1′) 91.7(1); **2**: Zn–O(1) 2.174(3), Zn–S(1) 2.432(1), Zn–S(2) 2.390(1), Zn–N(1) 2.191(3), Zn–N(2) 2.042(3); O(1)–Zn–N(1) 174.8(1), N(2)–Zn–S(2) 136.1(1), N(2)–Zn–S(1) 109.3(1), S(1)–Zn–S(2) 111.8(1).

with both thioether sulfur atoms of the ligand bound to the Zn(II) center [Zn–S(1) 2.432(1) Å, Zn–S(2) 2.390(1) Å] in the equatorial plane. The Zn–S bond distances of **2** fall between those reported for the monomeric, four-coordinate [$(Ph_2CHS)Bp^{But,Pri}$]ZnI [2.460(2) Å][7b] and [$HB(tim^{Me})_2pz$]ZnI [2.320(2), 2.352(2) Å][7c] complexes, but are slightly shorter than the Zn–S(1) distance found in **1** [2.514(1) Å]. Located *trans* to the apical nitrogen atom in **2** is a coordinated perchlorate anion [Zn–O(1) 2.174(3) Å]. An intramolecular hydrogen bonding interaction between the zinc-bound oxygen atom of this anion and the secondary amine donor [O(1)···N(3) 2.93 Å, N(3)–H···O(1) 158°] is present in the solid state.

Importantly, the isolation of complex **1** confirms the feasibility of using ligand systems possessing a single hydrogen bond donor to stabilize biologically relevant metal hydroxide species. Evidence for the hydrogen bonding interaction found in the solid state between the metal-bound hydroxide and the secondary amine proton [N(3)–*H*] in **1** remaining intact in solution is derived from examination of ^{1}H NMR spectra of the complex obtained in dry CD_3CN. Specifically, the N(3)–*H* resonance of **1**, which is found as a broad triplet at δ 8.97 (*J* 6.3 Hz), with the observed multiplicity being indicative of a slow rate of exchange and coupling with the adjacent methylene unit [C(13)-H_2, δ 2.71, d, *J* 6.3 Hz], is shifted significantly downfield from the position of the same resonance in the free ligand [N(3)–*H*, δ 5.01]. This deshielding of the N(3)–*H* resonance in **1** indicates a decrease in the electron density surrounding this proton due to its involvement in a hydrogen bonding interaction. It is also intriguing that the chemical shift of the secondary amine proton of the bmnpa ligand is highly dependent upon the nature of the anions present in zinc complexes, as **2** exhibits a N(3)–*H* resonance at δ 5.79.

In summary, we have synthesized a new secondary amine-appended nitrogen/sulfur ligand system and have utilized it to prepare and structurally characterize the first example of a nitrogen/sulfur-ligated zinc hydroxide complex. As such, it the first relevant synthetic complex for the catalytic site of several nitrogen/sulfur-ligated zinc enzymes that possess a water/hydroxo moiety that is directly involved in catalysis. The results outlined herein lay the groundwork for extensive reactivity studies directed at examining the influence of sulfur ligation on the reactivity of a zinc hydroxide moiety toward a variety of biologically-relevant substrates including alcohols, amides and CO_2.

We thank Utah State University for financial support and John C. Price and Peter Jeppson for assistance in ligand preparation.

Notes and references

‡ Characterized by ^{1}H and ^{13}C NMR, FTIR, HRFAB-MS and CHN analysis.

§ Characterized by ^{1}H and ^{13}C NMR, FTIR and CHN analysis.

¶ *Crystal data:* for **1**: $C_{17}H_{32}ClN_3O_5S_2Zn$, M = 523.4, monoclinic, space group $P2_1/n$, a = 11.5830(3), b = 17.1392(6), c = 12.1278(5) Å, β = 98.964(2)°, V = 2378.25(14) Å^3, Z = 4, T = 200 K, μ = 1.352 mm^{-1}. Using Mo-Kα radiation (0.71073 Å), a total of 9424 reflections were collected (5.94 < 2θ < 54.98°), of which 5303 were independent. Refinement converged to R_1 = 0.0507, wR_2 = 0.1180 (I > 2σI) and R_1 = 0.0764, wR_2 = 0.1317 (all data). The perchlorate anion was disordered over more than two orientations, with some overlapping of the oxygen positions. For **2**: $C_{17}H_{31}Cl_2N_3O_8S_2Zn$, M = 605.8, monoclinic, space group $P2_1/a$, a = 16.0431(9), b = 9.2753(3), c = 19.5165(11) Å, β = 111.1170(16)°, V = 2709.1(2) Å^3, Z = 4, T = 200 K, μ = 1.301 mm^{-1}. Using Mo-Kα radiation (0.71073 Å), a total of 14106 reflections were collected (6.16 < 2θ < 65.24°), of which 8382 were independent. Refinement converged to R_1 = 0.0602,wR_2 = 0.1481 (I > 2σI) and R_1 = 0.1009, wR_2 = 0.1688 (all data). The noncoordinated perchlorate anion and the *tert*-butyl group both exhibit *ca*. 60% orientational disorder.

CCDC 182/1700. See http://www.rsc.org/suppdata/cc/b0/b003144p/ for crystallographic files in .cif format.

1 (*a*) W. N. Lipscomb and N. Sträter, *Chem. Rev.*, 1996, **96**, 2375; (*b*) R. H. Holm, P. Kennepohl and E. I. Solomon, *Chem. Rev.*, 1996, **96**, 2239.

2 H. Eklund and C.-I. Brändén, in *Zinc Enzymes*, ed. T. G. Spiro, John Wiley and Sons, New York, 1983, pp. 125–152.

3 M. K. Chan, W. Gong, P. T. R. Rajagopalan, B. Hao, C. M. Tsai and D. Pei, *Biochemistry*, 1997, **36**, 13 904.

4 L. Betts, S. Xiang, S. A. Short, R. Wolfenden and C. W. Carter, Jr., *J. Mol. Biol.*, 1994, **235**, 635.

5 M. H. Bracey, J. Christiansen, P. Tovar, S. P. Cramer and S. G. Bartlett, *Biochemistry*, 1994, **33**, 13 126.

6 (*a*) Z. Wang, W. Fast, A. M. Valentine and S. J. Benkovic, *Curr. Opin. Chem. Biol.*, 1999, **3**, 614 and references therein; (b) M. H. Valladares, M. Kiefer, U. Heinz, R. P. Soto, W. Meyer-Klaucke, H. F. Nolting, M. Zeppezauer, M. Galleni, J-M. Frère, G. M. Rossolini, G. Amicosante and H-W. Adolph, *FEBS Lett.*, 2000, **467**, 221.

7 (*a*) C. Kimblin, B. M. Bridgewater, D. G. Churchill and G. Parkin, *Chem. Commun.*, 1999, 2301; (*b*) P. Ghosh and G. Parkin, *Chem. Commun.*, 1998, 413; (c) C. Kimblin, T. Hascall and G. Parkin, *Inorg. Chem.*, 1997, **36**, 5680; (*d*) B. Müller, A. Schneider, M. Tesmer and H. Vahrenkamp, *Inorg. Chem.*, 1999, **38**, 1900; (*e*) B. S. Hammes and C. J. Carrano, *Inorg. Chem.*, 1999, **38**, 4593; (*f*) S.-J. Chiou, P. Ge, C. G. Riordan, L. M. Liable-Sands and A. Rheingold, *Chem. Commun.*, 1999, 159.

8 R. Burth, A. Stange, M. Schäfer and H. Vahrenkamp, *Eur. J. Inorg. Chem.*, 1998, 1759.

9 (*a*) S. Ogo, S. Wada, Y. Watanabe, M. Iwase, A. Wada, M. Harata, K. Jitsukawa, H. Masuda and H. Einaga, *Angew. Chem., Int. Ed.*, 1998, **37**, 2102; (*b*) Z. Shirin, B. S. Hammes, V. G. Young, Jr. and A. S. Borovik, *J. Am. Chem. Soc.*, 2000, **122**, 1836; (*c*) B. S. Hammes, V. G. Young, Jr. and A. S. Borovik, *Angew. Chem., Int. Ed.*, 1999, **38**, 666; (*d*) Z. Shirin, V. G. Young, Jr. and A. S. Borovik, *Chem. Commun.*, 1997, 1967.

10 2-Pivalolylamido-6-aminomethylpyridine: M. Harata, K. Jitsukawa, H. Masuda and H. Einaga, *Chem. Lett.*, 1995, 61.

11 A. W. Addison, T. N. Rao, J. Reedijk, J. van Rijn and G. C. Verschoor, *J. Chem. Soc., Dalton Trans.*, 1984, 1349.

12 (*a*) I. B. Gorrell, A. Looney, G. Parkin and A. L. Rheingold, *J. Am. Chem. Soc.*, 1990, **112**, 4068; (*b*) S. S. Al-Juaid, N. H. Buttrus, C. Eaborn, P. B. Hitchcock, A. T. L. Roberts, J. D. Smith and A. C. Sullivan, *J. Chem. Soc., Chem. Commun.*, 1986, 908; (*c*) A. M. Arif, A. H. Cowley, R. A. Jones and S. U. Koschmieder, *J. Chem. Soc., Chem. Commun.*, 1987, 1319.

13 Average deviation from planarity of the atoms in the six-membered ring is 0.0965 Å.

14 A hydrogen-bonding interaction was also found between the hydroxyl proton [O(1)–*H*] and oxygen atoms of the disordered, non-coordinated perchlorate anion.

Enhanced mobility of the cluster $Ru_3(CO)_{12}$ in the solid state formed *in situ* by the reaction of CO and $Ru_3(CO)_6(\mu\text{-}CO)(\mu_3:\eta^2:\eta^3:\eta^5\text{-}C_{12}H_8)$ on silica

Silvio Aime,*[a] Alejandro Arce,[b] Roberto Gobetto,[a] Daniela Giusti[a] and Marc Stchedroff[a]

[a] *Dipartimento di Chimica Inorganica, Chimica Fisica dei Materiali, Università degli Studi di Torino, via Pietro Giuria 7, 10125 Torino, Italy. E-mail: aime@ch.unito.it*

[b] *Centro de Quimica Instituto Venezolano de Investigaciones Cientificas (IVIC), Apartado 21827, Caracas 1020-A, Venezuela*

Received (in Basel, Switzerland) 28th March 2000, Accepted 20th June 2000

The reaction of $Ru_3(CO)_6(\mu\text{-}CO)(\mu_3:\eta^2:\eta^3:\eta^5\text{-}C_{12}H_8)$ (physisorbed on SiO_2) with CO in the solid state leads to $Ru_3(CO)_{12}$ and acenaphthylene in quantitative yields; the $Ru_3(CO)_{12}$ generated *in situ* is highly mobile leading to a reduced chemical shielding anisotropy.

The large magnetic anisotropy of carbonyl groups makes the solid state ^{13}C MAS NMR spectra of metal carbonyls highly characteristic,[1,2] as they show a large number of spinning sidebands (SSBs) flanking the isotropic peaks. The onset of molecular motion in the solid state is indicated by the disappearance of these SSB manifolds. This effect is neatly illustrated by the comparison of the ^{13}C MAS spectra of $(C_6H_6)Cr(CO)_3$ as bulk crystals and included in the cavity of β-cyclodextrin.[3,4] The large mobility of $(C_6H_6)Cr(CO)_3$ inside the β-CD cavity appears to be the result of a lack of strong intermolecular interactions which usually lock organometallic molecules rigidly in the crystalline state.[5]

We have previously attempted many solid gas reactions with clusters. However, in almost all cases the products were disordered but static on the NMR timescale.[6] The subject of this communication, is the novel enhanced mobility of $Ru_3(CO)_{12}$ on a silica surface, occurring solely when the $Ru_3(CO)_{12}$ is deposited by the solid state, *in situ*, carbonylation of $Ru_3(CO)_6(\mu\text{-}CO)(\mu_3:\eta^2:\eta^3:\eta^5\text{-}C_{12}H_8)$ leading to substantial reduction in the chemical shift anisotropy.

$Ru_3(CO)_6(\mu\text{-}CO)(\mu_3:\eta^2:\eta^3:\eta^5\text{-}C_{12}H_8)$ is synthesised by the previously reported method.† All the samples used were synthesised using *ca.* 30% ^{13}CO enrichment.‡ At low temperature the solution spectrum of $Ru_3(CO)_6(\mu\text{-}CO)(\mu_3:\eta^2:\eta^3:\eta^5\text{-}C_{12}H_8)$ shows seven ^{13}CO absorptions, one (269.3 ppm) in the bridging region and six (205.0, 202.7, 201.7, 193.9, 190.0 and 186.8 ppm) in the terminal region, consistent with the structure previously proposed.[7] $Ru_3(CO)_6(\mu\text{-}CO)(\mu_3:\eta^2:\eta^3:\eta^5\text{-}C_{12}H_8)$ reacts readily in solution with CO quantitatively affording $Ru_3(CO)_{12}$ and free acenaphthylene. However, this reaction is considerably inhibited in the solid state at room temperature. Contrastingly, by physisorbing $Ru_3(CO)_6(\mu\text{-}CO)(\mu_3:\eta^2:\eta^3:\eta^5\text{-}C_{12}H_8)$ on a surface of SiO_2 (Sigma; 450–550 $m^2\ g^{-1}$ surface area, 10% coverage of the silica surface) the same reaction occurs readily. After 5 min at RT under 100 Torr of CO, 7 mg of $Ru_3(CO)_6(\mu\text{-}CO)(\mu_3:\eta^2:\eta^3:\eta^5\text{-}C_{12}H_8)$ was transformed into $Ru_3(CO)_{12}$ and acenaphthylene (IR spectrum, KBr disk).[8]

Therefore we decided to further investigate this process by ^{13}C solid state NMR spectroscopy. The ^{13}C CP-MAS spectrum of $Ru_3(CO)_6(\mu\text{-}CO)(\mu_3:\eta^2:\eta^3:\eta^5\text{-}C_{12}H_8)$ shows the bridging carbonyl at 270 ppm while the six terminal CO resonances overlap in three broad signals at 205, 190 and 185 ppm respectively. As has been previously observed for a number of examples the SSB pattern of bridging CO resonances is quite different from that of the terminal CO resonances.[9] This difference may be explained in terms of the reduced chemical shift anisotropy of the bridging CO ligands in respect to the terminal CO ligands, thus providing further confirmation for the assignments.

The ^{13}C CP-MAS spectrum of $Ru_3(CO)_6(\mu\text{-}CO)(\mu_3:\eta^2:\eta^3:\eta^5\text{-}C_{12}H_8)$, physisorbed on SiO_2 displays close similarity with the corresponding ^{13}C CP-MAS spectrum of the crystalline compound [Fig. 1]. On following the reaction of CO with $Ru_3(CO)_6(\mu\text{-}CO)(\mu_3:\eta^2:\eta^3:\eta^5\text{-}C_{12}H_8)/SiO_2$ by $^{13}C\text{-}\{^1H\}$ HPPD-MAS (high power proton decoupled—magic angle spinning) there is a progressive decrease in the intensity of the resonances of the starting material, which are in turn replaced by an intense peak at 199.8 ppm which is unambiguously assigned to $Ru_3(CO)_{12}$.

The most striking feature of the ^{13}C MAS spectrum of the reaction products is the totally unprecedented absence of any SSB manifold flanking the carbonyl resonance of $Ru_3(CO)_{12}$ [Fig. 2(c)]. This indicates that $Ru_3(CO)_{12}$ produced *in situ* on the surface of the silica possesses a very high mobility on the NMR time scale as compared with that of the normal bulk $Ru_3(CO)_{12}$ [Fig. 2(a)].[10] In order to gain a fuller understanding of the causes and the generality of this uniquely enhanced mobility we carried out further experiments: (a) the physisorbtion of $Ru_3(^{13}CO)_{12}$ and acenaphthylene on silica; (b) the reaction of $Ru_3(CO)_{11}(MeCN)$ on silica with CO to form $Ru_3(CO)_{12}$ *in situ*; (c) the physisorbtion of an identical amount of $Ru_3(CO)_{12}$ to that used in (a) directly onto silica. In all three cases the presence of $Ru_3(CO)_{12}$ was confirmed by solid state IR spectra (KBr disk). However, in none of the three cases was the absence of sidebands, in the MAS spectra, reproduced. This indicates that the fast molecular motion was absent in the $Ru_3(CO)_{12}$ obtained in all three of these experiments. The most striking spectrum is that obtained from the direct physisorbtion of $Ru_3(CO)_{12}$ onto silica: the ^{13}C MAS experiment [Fig. 2(b)] carried under identical conditions to highly mobile $Ru_3(CO)_{12}$ on silica produces no discernible signal. This is due to two factors; firstly all the signals of crystalline $Ru_3(CO)_{12}$ (dispersed over 350 ppm) are averaged into one signal in the highly mobile $Ru_3(CO)_{12}$, and secondly the relaxation properties of the highly mobile $Ru_3(CO)_{12}$ are more favourable. The most plausible explanation for the motion of $Ru_3(CO)_{12}$ obtained

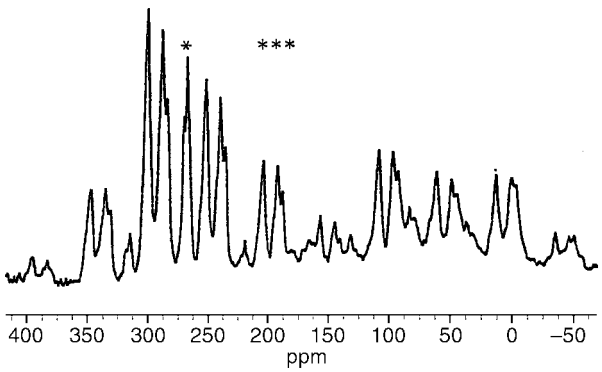

Fig. 1 ^{13}C HPPD MAS spectrum of a ^{13}CO enriched sample of $Ru_3(CO)_6(\mu\text{-}CO)(\mu_3:\eta^2:\eta^3:\eta^5\text{-}C_{12}H_8)$ supported on SiO_2: 67.8 MHz, spinning speed 3200 Hz, 500 scans (* denotes isotropic peaks).

DOI: 10.1039/b002641g

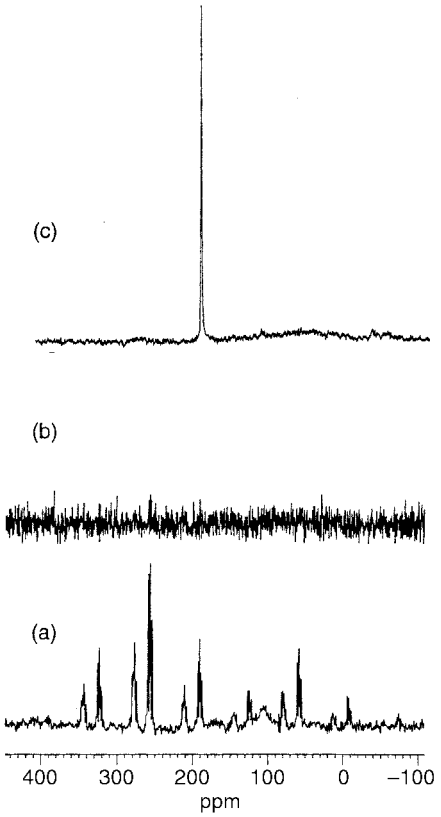

Fig. 2 ^{13}C HPPD MAS spectrum of (a) crystalline $Ru_3(CO)_{12}$, 240 transients, 5 kHz; (b) $Ru_3(CO)_{12}$ physisorbed on silica, 240 transients, 5 kHz; (c) $Ru_3(CO)_{12}$ on silica obtained by the reaction of $Ru_3(CO)_6(\mu\text{-}CO)(\mu_3:\eta^2:\eta^3:\eta^5\text{-}C_{12}H_8)$ physisorbed on SiO_2 with ^{13}CO: 67.8 MHz, spinning speed 5300 Hz, 24 scans. The net amount of $Ru_3(CO)_{12}$ on the silica in samples (b) and (c) is identical.

from $Ru_3(CO)_6(\mu\text{-}CO)(\mu_3{:}\eta^2:\eta^3:\eta^5\text{-}C_{12}H_8)$ with CO on SiO_2 surface is that $Ru_3(CO)_{12}$ and $C_{12}H_8$ formed are unable to yield microcristalline aggregates. This would fully account for the lack of the observed SSB manifold in the solid state experiments.

T_1 measurements on a ^{13}CO enriched sample of the highly mobile $Ru_3(^{13}CO)_{12}$/acenaphthylene/silica samples were carried out. The experiments, although carried out in the solid state, were performed using a commercial solution spectrometer (operating frequency 100.5 MHz for ^{13}C) in normal 5 mm solution tubes and a standard solution probehead. The fact that the signal was observable in this way indicates just how fast the molecular motion is in order to average the shielding anisotropy to this extent. At ambient temperature the measured T_1 is markedly shorter than that found for the same compound in solution at the same magnetic field strength (350 ms *vs.* 4280 ms) indicating that the extent of motion occurring in the solid state system is significantly lower than that occurring in a highly mobile liquid phase.

An analysis of T_1 *versus* temperature shows that there is an incipient minimum value at 250 K, from which it is possible to obtain an estimate of the molecular reorientation time. By using this calculated τ_c value and assuming that the observed T_1 is determined mainly by the chemical shift relaxation pathway,[11] it is possible to obtain a $\Delta\sigma$ value of 350 ppm that is not dissimilar to the values reported in literature measured respectively from wideline,[1] MAS[12] and variable field-solution state experiments.[10] On fitting the observed T_1 *vs.* temperature data an activation energy of 16.9 kJ mol^{-1} for the molecular reorientational motion of $Ru_3(CO)_{12}$ in this system is obtained.

This project was supported by TMR contract number ERBFMRXCT960091, by MURST (COFIN 98) and by CIRCMSB, Italy and a sabbatical for A. J. A. from IVIC Venezuela. We thank Dr Abil Aliev and the ULIRS solid state NMR service.

Notes and references

† $Ru_3(CO)_6(\mu\text{-}CO)(\mu_3:\eta^2:\eta^3:\eta^5\text{-}C_{12}H_8)$ is recovered in 91% yield from the reaction of $Ru_3(CO)_{12}$ and $C_{12}H_8$ for 24 h in refluxing heptane followed by separation by preparative TLC. IR (CO, KBr, cm^{-1}) 2042, 2030, 2010, 1996, 1953, 1770.

‡ ^{13}CO was obtained from Isotec Inc 99% ^{13}C; enrichment of $Ru_3(CO)_{12}$ using the standard technique of exchange in cyclohexane solution at 80 °C. Gas reactions were carried out using the neat ^{13}CO gas.

1 J. W. Gleeson and R. V. Vaughan, *J. Chem. Phys.*, 1983, **78**, 5384.
2 S. Aime, W. Dastru, R. Gobetto and G. E. Hawkes, *Advanced Applications of NMR to Organometallic Chemistry*, ed. M. Gielen, R. Willem and B. Wrackmeyer, John Wiley, New York, 1996.
3 P. J. Barrie, C. A. Mitsopoulou, M. Motevalli and E. W. Randall, *J. Chem. Soc., Dalton Trans.*, 1997, 353.
4 S. Aime, H. Canuto, R. Gobetto and F. Napolitano, *Chem. Commun.*, 1999, 281.
5 D. Braga, *Chem. Rev.*, 1992, **92**, 633.
6 S. Aime, W. Dastru, R. Gobetto, J. Krause and E. Sappa, *Organometallics*, 1995, **14**, 3224.
7 H. Nagashima, T. Fukahori, K. Aoki and K. Itoh, *J. Am. Chem. Soc.*, 1993, **115**, 10430.
8 G. A. Battiston, G. Bor, U. K. Dietler, S. F. A. Kettle, R. Rossetti, G. Sbrignadello and P. L. Stanghellini, *Inorg. Chem.*, 1980, **19**, 1961.
9 G. E. Hawkes, K. D. Sales, S. Aime, R. Gobetto and Lu-Yun Lian, *Inorg. Chem.*, 1991, **30**, 1489.
10 S. Aime, W. Dastru, R. Gobetto, J. Krause and L. Milone, *Organometallics*, 1995, **14**, 4435.
11 R. K. Harris, *Nuclear Magnetic Resonance Spectroscopy*, Pittman, London, 1983.
12 T. H. Walter, L. Reven and E. Oldfield, *J. Phys. Chem.*, 1989, **93**, 1320.

The diverse reactions of the silylene Si[(NCH$_2$Bu^t)$_2$C$_6$H$_4$-1,2] with Li[Si(SiMe$_3$)$_3$](thf)$_3$ and K[N(SiMe$_3$)$_2$]†

Barbara Gehrhus,* Peter B. Hitchcock, Michael F. Lappert* and J. Chris Slootweg

The Chemistry Laboratory, University of Sussex, Brighton, UK BN1 9QJ. E-mail: B.Gehrhus@sussex.ac.uk

Received (in Cambridge, UK) 15th May 2000, Accepted 15th June 2000

The silylene Si[(NCH$_2$Bu^t)$_2$C$_6$H$_4$-1,2] 1 inserts into the Li–Si bond of Li[Si(SiMe$_3$)$_3$](thf)$_3$ to afford the new silyllithium compound Li[(1)Si(SiMe$_3$)$_3$](thf)$_2$ 2, whereas 1 with K[N(SiMe$_3$)$_2$] yields the amidopotassium compound K[N(SiMe$_3$){(1)(SiMe$_3$)}](thf)$_x$ [x = 0 (3a) or 3 (3b)]; the X-ray structures of the crystalline mononuclear complex 2 and the polymeric aggregate 3a are reported, and NMR spectra show that in solution 2 is in equilibrium with its factors.

We report the first examples of reactions of a divalent, two-coordinate group 14 element compound EX_2, which with an anionic reagent MX′ yield four-coordinate E-atom adducts. For the present, they relate to systems in which EX_2 is the thermally stable silylene **1**[1] and MX′ is Li[Si(SiMe$_3$)$_3$](thf)$_3$ **A** or K[N(SiMe$_3$)$_2$]. Although these reactions took place under mild conditions, their outcome was different (Scheme 1). Thus, the 1:1-adduct was the product of insertion in the former case, but a rearranged product in the latter. They were isolated as (i) the crystalline, mononuclear bis(thf)[(sisyl)silyl]lithium complex **2**; and (ii) the solid bis(thf)potassium amide **3**, which upon recrystallisation gave the polymeric neutral donor-free potassium amide **3a** and the tris(thf) complex **3b**. The molecular structures of **2**, **3a** and **3b** have been determined;‡ discussion of **3b** is deferred to the full paper, as is the formation of the Li analogue of **3** from Li[N(SiMe$_3$)$_2$] and **1**.

Each of the yellow (**2**) or colourless (**3** and **3b**) complexes gave satisfactory microanalyses. The EI-mass spectra of **3** and **3a** were identical and, as for **2**, the major *m/z* peaks corresponded to the appropriate fragments: [anion]$^+$ and [anion − Bu^t]$^+$.

In solution, the lithium complex **2** was shown to be in equilibrium with its precursors, as demonstrated particularly clearly by VT ^{29}Si{^{1}H}-NMR spectra. Thus, dissociation was complete at ambient temperature, but was negligible at 213 K; a ^1J(^{29}Si^{7}Li) was not observed, probably due to the fast exchange process. Complex **3b** retained its structural integrity at 298 K. The data, with those for **1**,[1] Li[Si(SiMe$_3$)$_3$](thf)$_3$,[2]

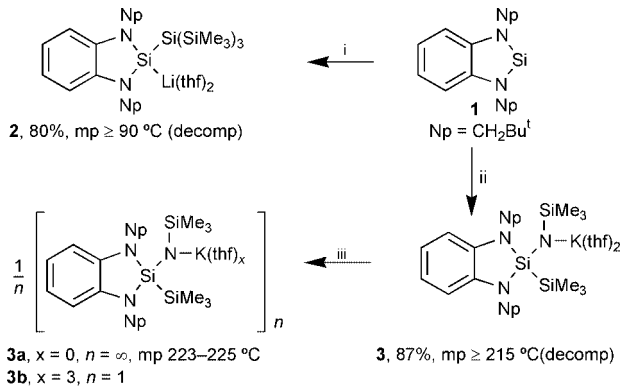

Scheme 1 Synthesis of the alkali metal complexes **2**, **3**, **3a** and **3b**. *Reagents and conditions*: i, [Li{Si(SiMe$_3$)$_3$}(thf)$_3$], C$_6$H$_{14}$, −30 °C; ii, ½ [KN(SiMe$_3$)$_2$]$_2$, thf, −30 °C; C$_6$H$_{14}$–thf, 0 °C (**3a**), −25 °C (**3b**); iii, **3a** (at *ca*. 20 °C), **3b** (at −25 °C) recrystallised from hexane–thf solution.

† No reprints available.

Table 1 ^{29}Si NMR spectroscopic chemical shifts for **1**–**3** and related compounds

	δ(^{29}Si)		
Complex (conditions[a])	α-Si	β-Si	γ-Si
[Li{Si(SiMe$_3$)$_3$}(thf)$_3$]^2 **A**	−189.4	−5.2	
1	96.2		
2	60.1	−9.35	−4.5
	[94.5 (**1**)	−5.3]	
3a	−19.5	−23.0	−26.2
Li[N(SiMe$_3$){Si(SiMe$_3$)$_3$}]^3 **B**	−7.1	−49.3	−18.0
Li[Si(Ph)(NEt$_2$)$_2$](thf)$_3$[4] **C**	27.9		

[a] Solvent (*T*/K): **A**, C$_7$D$_8$ (298); **1**, C$_6$D$_6$ (298); **2**, C$_7$D$_8$–thf (213, [298]); **3a**, C$_7$D$_8$–thf (298); **B**, C$_6$D$_6$ (303); **C**, thf (273).

Li[N(SiMe$_3$){Si(SiMe$_3$)$_3$}]^3 **B** and Li[Si(Ph)(NEt$_2$)$_2$](thf)$_3$,[4] are shown in Table 1.

Complex **2** (Fig. 1) has the lithium atom in a three-coordinate, distorted trigonal-planar environment. The silyl anion is pyramidal at the Si(1) atom with respect to its contiguous Si(2), N(1) and N(2) atoms; the sum of the angles subtended by these three neighbouring atoms is low, 295.4°, as a consequence of the small bite angle of the adjacent chelating ligand; *cf*. 307.2° in Li[Si(SiMe$_3$)$_3$](thf)$_3$ **A**[2] and 309.8° in Li[Si(Ph)(NEt$_2$)$_2$](thf)$_3$ **C**.[4] The Li–Si(1) distance of 2.609(4) Å in **2** is slightly shorter than the 2.644(12) Å in **A** or 2.732(7) Å in **B**. The Si(1)–Si(2) bond length of 2.493(1) in **2** is longer than the mean Si$_\alpha$–Si$_\beta$ bond length of 2.330(2) Å in **A**. The mean Si–N bond length of 1.801(3) Å in **2** [1.800(4) Å in **3a**] is longer than the 1.75(1) Å in **1**, and the N(1)–Si(1)–N(2) bond angle of 87.25(8)° is slightly more acute than the 88.2(1)° in **1**, or the 88.15(6)° in **3a**.

The potassium amide **3a** comprises mononuclear units (Fig. 2), each linked to its neighbours by close K···*C*(17)H$_3$ [3.268(2) Å] and K··η^3-C$_6$H$_4$ [mean K···*C*(*o, m, m'*) 3.17 Å] contacts (Fig. 3). Similar intermolecular contacts are known in various potassium amides and alkyls.[5] Associated with K···*C*(17)H$_3$ is

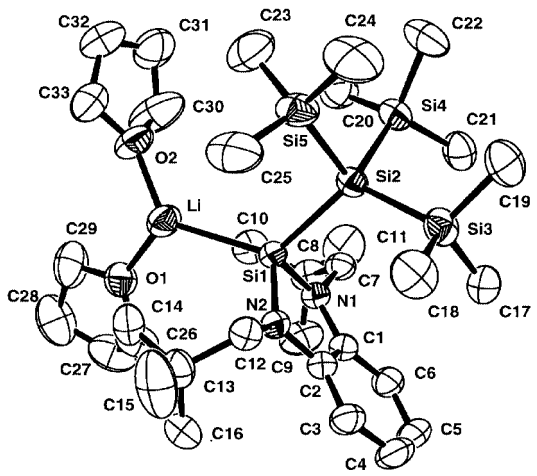

Fig. 1 Crystal structure of **2**.

DOI: 10.1039/b003833o

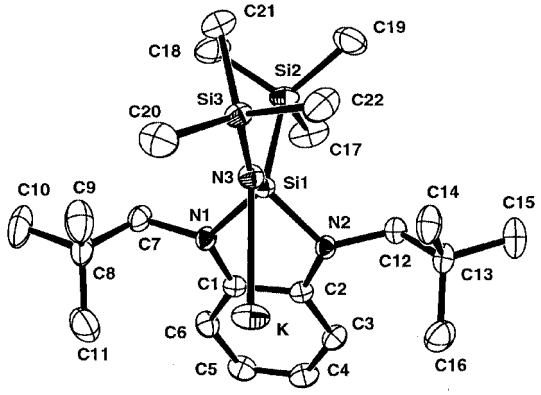

Fig. 2 Crystal structure of **3a**.

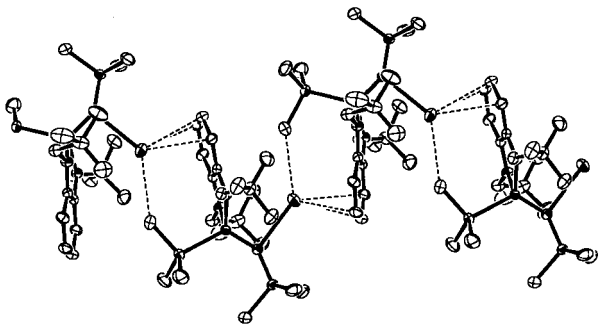

Fig. 3 Intermolecular contacts in **3a**.

the narrower Si(1)–Si(2)–C(17) angle of 105.84(7)°, compared with the mean of Si(1)–Si(2)–C(18 or 19) of 113.7(3)°. The amido nitrogen atom N(3) is in a planar environment, the Si(1)–N(3)–Si(3) angle of 144.40(9)° being only *ca.* 10° narrower than that in the separated $[N(SiPh_3)_2]^-$ anion of $[Li(12\text{-crown-}4)_2][N(SiPh_3)_2]\cdot thf$,[6] but much wider than the 136(1)° in $[K\{N(SiMe_3)_2\}(thf)_2]$.[7] The N–Si bond lengths of 1.64(1) Å in the latter is close to the 1.6302(13) Å for Si(1)–NK in **3a**, but is significantly shorter than the Si(3)–NK bond length, 1.6739(14) Å. The N–K distance of 2.6938(14) Å in **3a** is unexceptional; *cf.* 2.70(2) Å in $[K\{N(SiMe_3)_2\}(thf)_2]$.[7]

The pathways to **2** or **3**, from **1** and $Li[Si(SiMe_3)_3](thf)_3$ or $K[N(SiMe_3)_2]$, probably require that in the first step the silylene **1** behaves as a nucleophile yielding the appropriate adduct

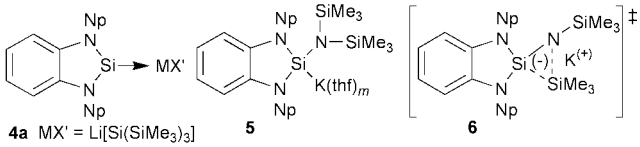

$X_2E{:}MX'$ (**4a** or **4b**). Complex **2** is presumed to arise from **4a** by insertion of X′ into the E–M bond, and a similar step from **4b** would yield **5**. Complex **3** is believed to be formed by a final Me_3Si shift from the N to Si, either from **5** (a 1,2-shift; *cf.* the transition state **6**) or **4b** (a 1,3-shift). Although anionic trimethylsilyl shifts are well documented,[8] this, we believe, is the first N→Si example. Precedents for $X_2E{:}MX'$ adducts in group 14 element chemistry include (i) silylene–(Ni^0 or Pt^{II}) complexes such as $[Ni(\mathbf{1})_4]$ and *trans*-$[Pt\{(\mathbf{1})Cl_2\}_2(\mathbf{1})_2]$[9] and (ii) carbene–(MX′) complexes such as $[Li\{C[N(Bu^t)CHCHN\text{-}Bu^t]\}\{\eta^5\text{-}C_5H_2(SiMe_3)_3\text{-}1,2,4\}]$[10] and $[K\{C[N(Pr^i)(CH_2)_3N\text{-}Pr^i]\}\{\mu\text{-}N(SiMe_3)_2\}]_2$,[11] and (iii) stannylene–MCp complexes such as $SnCp_2(\mu\text{-}Cp)Na$ from $SnCp_2$ + NaCp.[12] Alternative EX_2/MX' reactions have led to X/X′ exchange as in (i) $SnCp_2$ + $LiN(SiMe_3)_2$ yielding $Sn(Cp)[N(SiMe_3)_2](\mu\text{-}Cp)Li(pmdeta)$,[13] and (ii) $SnCp^*_2$ + $Li[CH(SiMe_3)_2]$ affording $Sn[CH(SiMe_3)_2]_2$ + $LiCp^*$.[14] Insertion reactions of **1** into O–H, C–I, Ge^{II}–N, Sn^{II}–C, Sn^{II}–N or Pb^{II}–N bonds have been reported, as with $M'[N(SiMe_3)_2]_2$ to give $M'[\mathbf{1}\{N(SiMe_3)_2\}]_2$ (M′ = Sn **7** or Pb).[15] The rearrangement **5**→ **3** cannot be due to the lability of the anion $\{(\mathbf{1})\{N(SiMe_3)_2\}\}^-$, since it is found in **7** as a ligand. We suggest that **3** may be favoured, at least in part, by the strong Si–Si bond, as evident by its short [2.359(1) Å in **3a**] bond length, comparable with the av. Si–Si bond distance of 2.379 Å in **2**. However, according to bond dissociation energy data a migration of Me_3Si from nitrogen to silicon is unexpected.[16] The facile dissociation of **2** is probably due to steric constraints, consistent with the long Si–Si($SiMe_3$) bond of 2.493(1) Å and the narrow N–Si–Si angles, av. 103.9(6)°.

The present results significantly extend the already substantial boundaries of silylene reaction types. From work in progress, we anticipate that several new silicon-centred ligands $[(\mathbf{1})X']^-$ (that in **2** being a forerunner) will become available for use for a wide range of metals, and that the exceedingly bulky amido ligand present in **3** will find a useful role.

We thank the EPSRC for an Advanced Fellowship for B. G., the Free University of Amsterdam for support for J. C. S., and Dr A. G. Avent for the ^{29}Si NMR spectroscopic data.

Notes and references

‡ *Crystallographic data*: for **2**: $C_{33}H_{69}LiN_2O_2Si_5$, M = 673.29, monoclinic, space group $P2_1/n$ (no. 14), a = 12.8306(11), b = 18.4336(13), c = 18.7237(15) Å, β = 96.161(4)°, U = 4402.8(6) Å^3, Z = 4, μ = 0.19 mm^{-1}, T = 173(2) K, 7659 unique reflections (R_{int} = 0.060), $R1$ = 0.052 for 5962 reflections with $I > 2\sigma(I)$, $wR2$ = 0.138 for all reflections.

3a: $C_{22}H_{44}KN_3Si_3$, M = 473.97, monoclinic, space group $P2_1/n$ (no. 14), a = 13.4645(4), b = 12.7533(3), c = 16.5858(3) Å, β = 91.759(2)°, U = 2846.7(1) Å^3, Z = 4, μ = 0.33 mm^{-1}, T = 173(2) K, 6689 unique reflections (R_{int} = 0.044), $R1$ = 0.039 for 5363 reflections with $I > 2\sigma(I)$, $wR2$ = 0.097 for all reflections.

CCDC 182/1688. See http://www.rsc.org/suppdata/cc/b0/b003833o/for crystallographic files in .cif format.

1 B. Gehrhus, P. B. Hitchcock, M. F. Lappert, J. Heinicke, R. Boese and D. Bläser, *J. Organomet. Chem.*, 1996, **521**, 211.
2 A. Heine, R. Herbst-Irmer, G. M. Sheldrick and D. Stalke, *Inorg. Chem.*, 1993, **32**, 2694.
3 M. Westerhausen and W. Schwarz, *Z. Anorg. Allg. Chem.*, 1993, **619**, 1053.
4 A. Kawachi and K. Tamao, *J. Am. Chem. Soc.*, 2000, **122**, 1919.
5 *E.g.*, see K. W. Klinkhammer, *Eur. J. Chem.*, 1997, **3**, 1418; W. Clegg, S. Kleditzsch, R. E. Mulvey and P. O'Shaughnessy, *J. Organomet. Chem.*, 1998, **558**, 193.
6 H. Chen, R. A. Bartlett, H. V. R. Dias, M. M. Olmstead and P. P. Power, *J. Am. Chem. Soc.*, 1989, **111**, 4338.
7 A. M. Domingos and G. M. Sheldrick, *Acta Crystallogr., Sect. B.*, 1974, **30**, 517.
8 A. G. Brook and A. R. Bassindale, *Molecular Rearrangements of Organosilicon Compounds*, in *Rearrangements in Ground and Excited States*, Academic Press, New York, 1980, vol. 2.
9 B. Gehrhus, P. B. Hitchcock, M. F. Lappert and H. Maciejewski, *Organometallics*, 1998, **17**, 5599.
10 A. J. Arduengo, M. Tamm, J. C. Calabrese, F. Davidson and W. J. Marshall, *Chem. Lett.*, 1999, 1021.
11 R. W. Alder, M. E. Blake, C. Bortolotti, S. Bufali, C. P. Butts, E. Linehan, J. M. Oliva, A. G. Orpen and M. J. Quayle, *Chem. Commun.*, 1999, 241.
12 D. R. Armstrong, M. J. Duer, M. G. Davidson, D. Moncrieff, C. A. Russell, C. Stourton, A. Steiner, D. Stalke and D. S. Wright, *Organometallics*, 1997, **16**, 3340.
13 M. A. Paver, C. A. Russell, D. Stalke and D. S. Wright, *J. Chem. Soc., Chem. Commun.*, 1993, 1349.
14 P. Jutzi and B. Hielscher, *Organometallics*, 1986, **5**, 2511.
15 B. Gehrhus, P. B. Hitchcock and M. F. Lappert, *Angew. Chem., Int. Ed. Engl.*, 1997, **36**, 2514.
16 R. Becerra and R. Walsh, *Thermochemistry*, in *The Chemistry of Organic Silicon Compounds*, ed. Z. Rappoport and Y. Apeloig, Wiley, Chichester, 1998, vol. 2.

Novel tripodal chelating ligand for appending and encapsulating metal ions. Crystal structure of a parachute-like hydrogen bonded complex

Wei-Yin Sun,*[a] Jin Xie,[a] Taka-aki Okamura,[b] Chang-Kang Huang[a] and Norikazu Ueyama[b]

[a] *Coordination Chemistry Institute, State Key Laboratory of Coordination Chemistry, Nanjing University, Nanjing 210093, China. E-mail: sunwy@netra.nju.edu.cn*

[b] *Department of Macromolecular Science, Graduate School of Science, Osaka University, Toyonaka, Osaka 560, Japan*

Received (in Cambridge, UK) 9th May 2000, Accepted 19th June 2000

Tripodal ligand 1,3,5-tris(1-methylimidazol-2-ylmethyl)-2,4,6-trimethylbenzene (3) forms a parachute-like non-covalent complex with zinc tetrachloride, 5·[Zn_2Cl_6]$_{0.5}$, where the imidazoles of the ligand are protonated and bind to the metal ion through NH···Cl hydrogen bonds.

Although biological systems efficiently organize simple units into aggregates with intricate and wonderful functions by non-covalent interactions, self-assembly of frameworks with specific topology, interesting properties and functions is still a challenge for chemists.[1] A number of hydrogen-bonded aggregates have been obtained by self-organization of organic or organic–inorganic components.[1–3] We herein report a parachute-like complex obtained by assembly of organic tripodal ligand 1,3,5-tris(1-methylimidazol-2-ylmethyl)-2,4,6-trimethylbenzene (**3**) and inorganic zinc tetrachloride. In this complex, protonation of the imidazoles of the ligand and its binding to the metal ion through NH···Cl hydrogen bonds provides a good example of a dual role for a single ligand.

We are currently engaged in the systematic study of self-assembly of tripodal ligands **1**–**4** (Scheme 1) with various metal ions and are investigating the influence of linkage mode of bridging ligands on the assembly process of supramolecular complexes.[4] Up to now, tripodal ligands **1** and **2**, and others also having benzene or other arene as the ring core such as 2,4,6-tris(4-pyridyl)-1,3,5-triazine, 1,3,5-tris(pyrazol-1-ylmethyl)-2,4,6-triethylbenzene have been reported to form polymeric networks or multinuclear metallocages with metal ions.[4,5] The ligand **3** was demonstrated for the first time to form a parachute-like non-covalently bonded complex with zinc tetrachloride. [$ZnCl_4$]$^{2-}$ has been used as a counterion for crystallization of Ru(II) and Co(II) complexes.[6,7] In the present complex, this anion binds to **3** through NH···Cl interactions in which the Cl atom acts as an acceptor of hydrogen bonds.

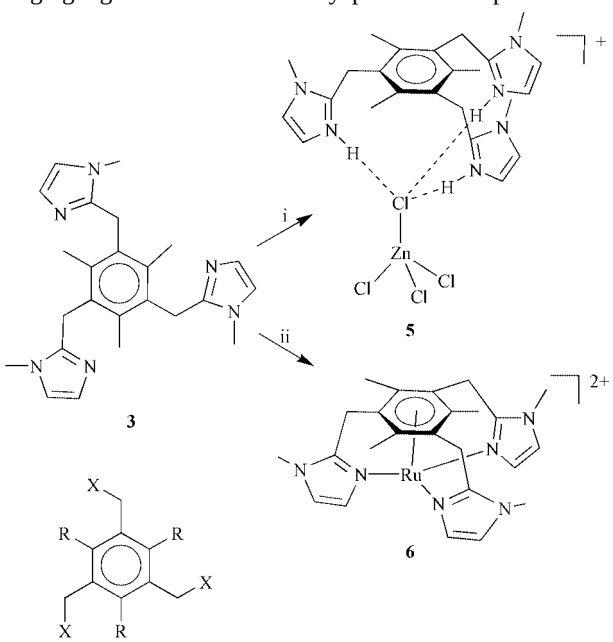

	R	X
1	CH_3	Imidazol-1-yl
2	H	Imidazol-1-yl
3	CH_3	1-Methylimidazol-2-yl
4	H	Benzimidazol-2-yl

Scheme 1 *Reagents*: i, $ZnCl_2$ + HCl; ii, $Ru(DMSO)_4Cl_2$. For details see notes of preparations.

Assembly of **3**† with $ZnCl_2$ in hydrochloric acid solution gave the hydrogen bonded complex, **5**·[Zn_2Cl_6]$_{0.5}$ (Scheme 1).‡ As shown in Fig. 1,§ all three imidazole groups of **3** are protonated which was confirmed by IR spectral measurements. The distances between each imidazole proton and Cl(12) ranges from 2.32 to 2.45 Å which indicates the presence of triple N–H···Cl hydrogen bonds. Therefore, **5** looks like a parachute in which [$ZnCl_4$]$^{2-}$ acts as an appending group. The atom Cl(12) is located under **3** with a distance of 3.43 Å between Cl(12) and the center of the benzene ring plane. Two adjacent molecules of **5** with normal and upside down orientations linked by hydrogen bonds are illustrated in Fig. 2(a). There are four additional hydrogen bonds in each [$ZnCl_4$]$^{2-}$ unit excluding the triple N–H···Cl(12) bonds described above: C(14)–H···Cl(11) [$r_{C(14)–Cl(11)}$ = 3.517(8) Å], C(11A)–H···Cl(11) [$r_{C(11A)–Cl(11)}$ = 3.707(6) Å], C(54)–H···Cl(13) [$r_{C(54)–Cl(13)}$ = 3.602(7) Å] and C(101A)–H···Cl(14) [$r_{C(101A)–Cl(14)}$ = 3.768(8) Å]. The unit shown in Fig. 2(a) can be repeated and joined by

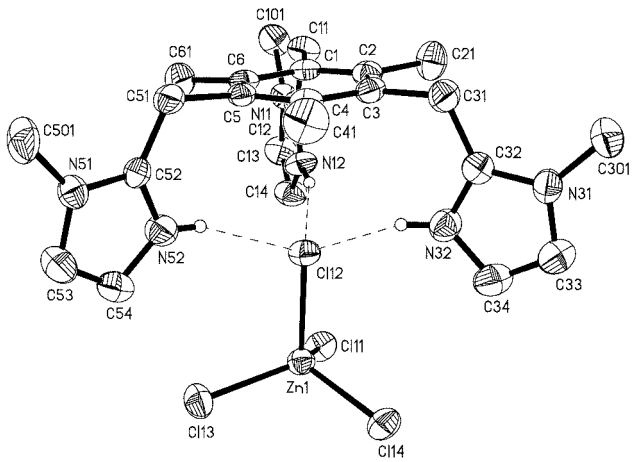

Fig. 1 Crystal structure of **5**, thermal ellipsoids are drawn at 50% probability and the N–H···Cl hydrogen bonds are indicated by dashed lines. Selected bond lengths (Å) and angles (°): Zn1–Cl11 = 2.269(1), Zn1–Cl12 = 2.360(1), Zn1–Cl13 = 2.242(2), Zn1–Cl14 = 2.249(2), N12–Cl12 = 3.199(4) [H1–Cl12 = 2.32], N32-Cl12 = 3.194(5) [H2-Cl12 = 2.40], N52–Cl12 = 3.254(5) [H3–Cl12 = 2.45]; N12–H1–Cl12 = 163, N32–H2–Cl12 = 154, N52–H3–Cl12 = 162, Cl12–Zn1–Cl11 = 104.64(5), Cl12–Zn1–Cl13 = 105.86(6), Cl12–Zn1–Cl14 = 108.23(6), Cl11–Zn1–Cl13 = 113.71(6), Cl11–Zn1–Cl14 = 110.28(6), Cl13–Zn1–Cl14 = 113.49(6).

DOI: 10.1039/b003694n

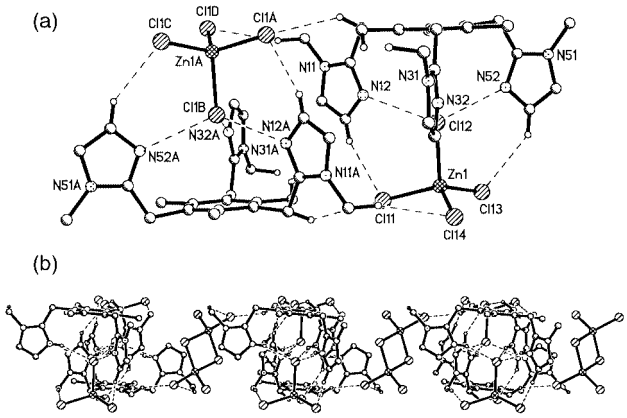

Fig. 2 Two adjacent parachute-like molecules with normal and upside down orientations (a) and one-dimensional chain (b) linked by hydrogen bonds.

$[Zn_2Cl_6]^{2-}$ through hydrogen bonds to generate an infinite one-dimensional chain [Fig. 2(b)]: C(301A)–H···Cl(22) [$r_{C(301A)–Cl(22)}$ = 3.620(8) Å] and C(21A)–H···Cl(22) [$r_{C(21A)–Cl(22)}$ = 3.530(8) Å].

Another coordination mode of such a tripodal ligand is the encapsulation of the metal ion with additional coordination to the benzene ring as demonstrated by Hartshorn and Steel.[6] We are also studying the reactions of **3** with other metal salts. The reaction between **3** and $Ru(DMSO)_4Cl_2$ was investigated by electrospray mass (ES-MS) spectrometry and NMR spectroscopy.¶ Four main peaks at *m*/*z* 202.3, 252.3, 403.4 and 420.8 were observed which correspond to $[\mathbf{3} + 2H]^{2+}$, $[Ru(\mathbf{3})]^{2+}$, $[\mathbf{3} + H]^+$ and $[\mathbf{3} + H_2O + H]^+$, respectively. All these assignments were confirmed by good agreements between the observed and calculated isotopic distributions. The results of ES-MS imply that only the mononuclear Ru(II) complex is formed by the reaction of **3** with $Ru(DMSO)_4Cl_2$. In the ^{13}C NMR spectrum of **6**·Cl_2, the benzene ring carbons were shifted upfield by *ca.* 32 ppm compared with the corresponding signals of **3**. The NMR study suggests the coordination of Ru to the benzene ring of **3**.[6]¶ This means that **3** may encapsulate the Ru(II) ion (**6**) as shown in Scheme 1.

In conclusion, the present study shows that the novel tripodal ligand **3** can append to the metal ion through non-covalent interactions and encapsulate the metal ion through chelation and η^6-arene coordination.

The authors are grateful for funding from the National Nature Science Foundation of China for financial support of this work.

Notes and references

† The ligand **3** was prepared from 1,3,5-tris(bromomethyl)-2,4,6-trimethylbenzene, 1-methylimidazole and *n*-BuLi using standard Schlenk techniques in 45% isolated yield. $\delta_H(CDCl_3)$: 7.05 (s, 3H), 6.91 (s, 3H), 4.24 (s, 6H), 3.90 (s, 9H), 2.07 (s, 9H).

‡ *Experimental*: a solution of **3** (40.2 mg, 0.1 mmol) in MeOH (5 ml) was added to a 1 M HCl (10 ml) solution of $ZnCl_2$ (40.8 mg, 0.3 mmol) at room temperature. The mixture was filtered after stirring for about 10 min and the filtrate was stood at *ca*. 40 °C for several days. Light yellow crystals were collected in *ca*. 60% yield. Macroanal. Found: C, 36.64; H, 4.22; N, 10.66. $C_{24}H_{33}N_6Cl_7Zn_2$ requires C, 36.75; H, 4.24; N, 10.71%. $\delta_H(D_2O$, 298 K): 7.32 (s, 3H), 7.12 (s, 3H), 4.42 (s, 6H), 3.83 (s, 9H), 2.05 (s, 9H).

§ *Crystal data* for **5**·$[Zn_2Cl_6]_{0.5}$ ($C_{24}H_{33}N_6Cl_7Zn_2$): M = 784.50, triclinic, space group $P\bar{1}$, a = 13.593(4), b = 13.788(4), c = 10.821(3) Å, α = 108.41(2), β = 112.25(2), γ = 104.09(2)°, U = 1621(1) Å^3, Z = 2, D_c = 1.606 g cm^{-3}, μ = 2.081 mm^{-1}, $F(000)$ = 796, T = 296(1) K. The data collection was carried out on a Rigaku AFC5R four-circle diffractometer by $\omega - 2\theta$ scan techniques using graphite-monochromated Mo-Kα radiation (λ = 0.7107 Å). Total 7720 reflections were collected of which 7408 are independent (R_{int} = 0.017). The structure was solved by direct methods with SIR92 and refined by full-matrix least-squares calculations. The final $R1$ = 0.0431[$I > 2\sigma(I)$], max., min. residual density: +0.80, −0.96 e Å^{-3}. CCDC 182/1693. See http://www.rsc.org/suppdata/cc/b0/b003694n/ for crystallographic files in .cif format.

¶ A solution of **3** (40.2 mg, 0.1 mmol) and $Ru(DMSO)_4Cl_2$ (48.9 mg, 0.1 mmol) in EtOH–H_2O (1 : 3, 15 ml) was refluxed for 10 h. After filtration, the filtrate was stood at room temperature for several days and a brown powder was obtained. $\delta_H(D_2O$, 313 K): 7.36 (s, 3H), 7.03 (s, 3H), 4.47 (s, 6H), 3.96 (s, 9H), 2.25 (s, 9H).

1 See, for example: F. Zeng and S. C. Zimmerman, *Chem. Rev.*, 1997, **97**, 1681.
2 For example: A. Marsh, M. Silvestri and J.-M. Lehn, *Chem. Commun.*, 1996, 1527; O. Félix, M. W. Hosseini, A. De Cian and J. Fischer, *Angew. Chem., Int. Ed. Engl.*, 1997, **36**, 102; D. J. Pesak and J. S. Moore, *Angew. Chem., Int. Ed. Engl.*, 1997, **36**, 1633; A. Kraft and R. Fröhlich, *Chem. Commun.*, 1998, 1085.
3 For example: D. S. Lawrence, T. Jiang and M. Levett, *Chem. Rev.*, 1995, **95**, 2229; G. M. Whitesides, E. E. Simanek, J. P. Mathlas, C. T. Seto, D. N. Chin, M. Mammen and D. M. Gordon, *Acc. Chem. Res.*, 1995, **28**, 37; P. N. W. Baxter, J.-M. Lehn, J. Fischer and M.-T. Youinou, *Angew. Chem., Int. Ed., Engl.*, 1994, **33**, 2284; Y. Zhang, L. Jianmin, M. Nishiura and T. Imamoto, *Chem. Lett.*, 1999, 543.
4 H. K. Liu, W. Y. Sun, W. X. Tang, T. Yamamoto and N. Ueyama, *Inorg. Chem.*, 1999, **38**, 6313; H. K. Liu, W. Y. Sun, D. J. Ma, K. B. Yu and W. X. Tang, *Chem. Commun.*, 2000, 591.
5 C. M. Hartshorn and P. J. Steel, *Chem. Commun.*, 1997, 541; M. Fujita, D. Oguro, M. Miyazawa, H. Oka, K. Yamaguchl and K. Ogura, *Nature*, 1995, **378**, 469.
6 C. M. Hartshorn and P. J. Steel, *Angew. Chem., Int. Ed., Engl.*, 1996, **35**, 2655, and references therein.
7 D. A. House and P. J. Steel, *Inorg. Chim. Acta*, 1999, **288**, 53.

A novel open-framework aluminophosphate $[AlP_2O_6(OH)_2][H_3O]$ containing propeller-like chiral motifs

Wenfu Yan, Jihong Yu, Zhan Shi and Ruren Xu*

Key Lab of Inorganic Synthesis and Preparation Chemistry, Department of Chemistry, Jilin University, Changchun 130023, P.R. China. E-mail: rrxu@mail.jlu.edu.cn

Received (in Cambridge, UK) 25th May 2000, Accepted 21st June 2000

A new open-framework aluminophosphate containing propeller-like chiral motifs has been synthesized solvothermally using 2-aminopyridine as the structure-directing agent and its structure is determined by single-crystal X-ray diffraction.

During recent decades, a large number of microporous aluminophosphates have been synthesized which exhibit various novel framework topologies, as well as analogous structures with known zeolites.[1–3] However, the preparation of chiral open-framework aluminophosphates, of potentially important application in asymmetric synthesis and separation, has been less successful. The introduction of chirality into the open-framework using traditional template molecules, such as chiral organic amines, is found to be particularly difficult. However, recently the employment of chiral metal complexes as template agents has promoted the formation of a few layered compounds with chirality or chiral motifs in their porous sheets, such as GeTex1,[4] GeTex2,[5] GeTex3[6] and d-$Co(en)_3 \cdot Al_3P_4O_{16} \cdot 3H_2O$.[7] To our knowledge, there are no three-dimension (3D) open-framework aluminoposphates with chirality or chiral structural subunits. Here, we report a novel 3D open-framework aluminophosphate (denoted AlPO-CJ4) synthesized using 2-aminopyridine as a structure-directing agent. It consists of propeller-like chiral motifs with both Δ and Λ configurations.

Large single crystals of AlPO-CJ4 were prepared in a gel system with molar composition 1.0 $Al(OPr^i)_3$: 2.4 H_3PO_4: 2.0 2-aminopyridine: 20 2-BuOH. Typically, 1.0 g of finely ground aluminium triisopropoxide was first dispersed into 9 mL butan-2-ol solvent with stirring, followed by addition of 0.9 g of 2-aminopyridine. Phosphoric acid (85 wt%, 0.8 mL) was finally added dropwise to the above reaction mixture with stirring. A sticky gel was formed, and was transferred into a Teflon-lined stainless autoclave and heated at 180 °C for 8 days under autogeneous pressure. The product was filtered off and washed thoroughly with deionized water and dried at 70 °C. X-Ray powder diffraction patterns were recorded on a Simens D5005 X-ray diffractometer with Cu-Kα radiation (λ = 1.5418 Å). The experimental powder X-ray diffraction (XRD) pattern of AlPO-CJ4 accords with the simulated pattern derived from structural data (Fig. 1), establishing the as-synthesized product as a single phase.

Inductively coupled plasma (ICP) analysis performed on a Perkin-Elmer Optima 3300 DV ICP instrument gives Al and P contents in the product as 11.7 and 25.3%, respectively. This is in agreement with calculated values of 11.3% and 26.1% based on the formula of $[AlP_2O_6(OH)_2][H_3O]$ revealed by single-crystal structure analysis. Single crystal structure analysis, as well as elemental analysis, shows that no 2-aminopyridine is involved in the product. However, 2-aminopyridine is found to be necessary for the formation of AlPO-CJ4. If other organic amines such as 2-methylpyridine are used instead to 2-aminopyridine in the reaction mixture, only the dense phase berlinite is obtained. This demonstrates that the organic additive plays an important structure-directing role as in case of VPI-5.[8]

A single crystal of AlPO-CJ4 with dimensions of 0.08 × 0.06 × 0.04 mm was glued to a fine glass fiber and mounted on a three-circle fixed Siemens diffractometer fitted with a Bruker SMART CCD detector.

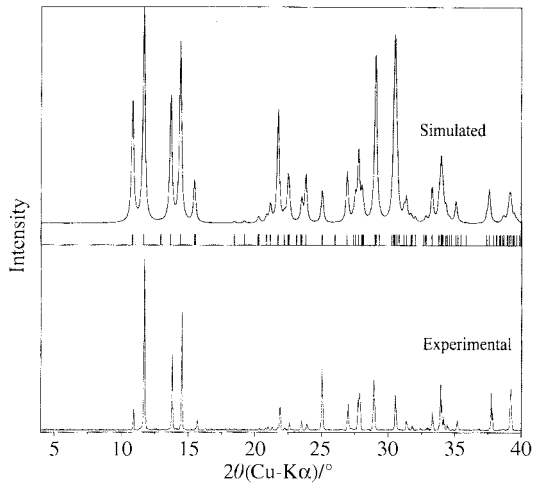

Fig. 1 Experimental and simulated powder X-ray diffraction patterns of AlPO-CJ4.

Structure analysis† indicates that AlPO-CJ4 crystallizes in the $P\bar{1}$ space group. The structure of AlPO-CJ4 is constructed by alternation of AlO_6 octahedra and $PO_3(OH)$ tetrahedra *via* vertex oxygen atoms. To our knowledge, this is the first open-framework AlPO, in which the primary Al building unit is solely made up of AlO_6 octahedra with all six oxygen vertices being shared by adjacent P atoms. Also, it is the first 3D aluminophosphate with an Al:P ratio of 1:2, distinct from previous $AlP_2O_8^{3-}$ aluminophosphates with 1D chain[9,10] and 2D layer structures.[11–13]

Interestingly, the structure of AlPO-CJ4 features chiral propeller-like motifs as found for $Co(en)_3^{3+}$, as can be seen in Fig. 2. This chiral motif is formed by Al(2)-centered octahedra with three cyclic four-membered rings. The O–Al–O bond

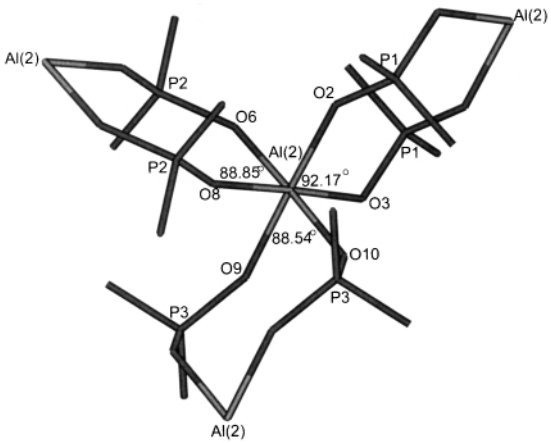

Fig. 2 A propeller-like chiral motif formed by three cyclic four-membered rings.

angles for the three blades of the propeller are 88.85, 88.54 and 92.17°. These chiral motifs are connected with each other to form a puckered 2D layer parallel to the *ab* plane, which contains double crown-like 12-membered rings as shown in Fig. 3. Each 12-membered ring is surrounded by six chiral motifs with three of Δ- and three of Λ-configuration. The 2D layers are connected *via* Al(1) atoms lying at inversion centers to form the 3D open-framework ofAlPO-CJ4 (Fig. 4), with interconnecting 8-MR channels along the [100], [010] and [001] directions.

The protonated water molecules, which balance the negative charge of the framework, are trapped in the channels, and interact with the terminal oxygens attached to P atoms through

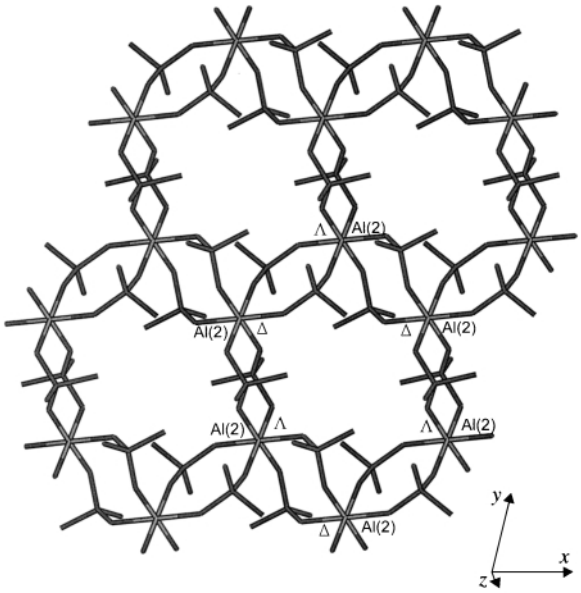

Fig. 3 2D layer formed by connecting the chiral motifs; Δ and Λ indicate the absolute configurations of the motifs.

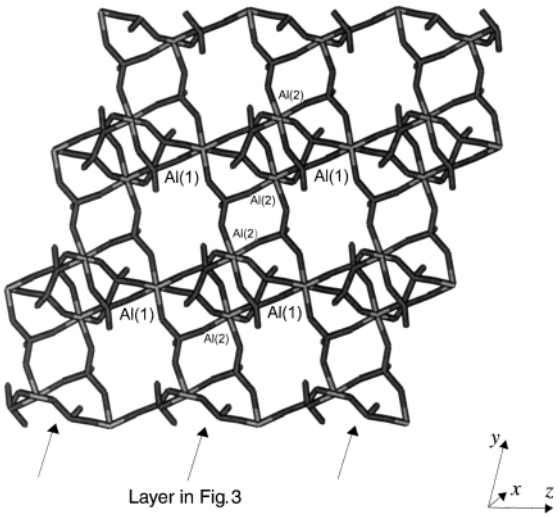

Fig. 4 3D open-framework forming by connecting the 2D layers *via* Al(1) atoms, viewed along the [100] direction. Water molecules in the channel are not shown.

H-bonds with $O_W \cdots O_{terminal}$ distances in the range 2.853–3.086 Å. Energy calculations employing Cerius[2] using the Burchart 1.01-Dreiding 2.21 force field[14,15] gives the H-bonding interaction energy between the framework and occluded water molecules as −10.0 kcal mol^{-1} per unit cell. It is believed that the water molecules play an important role in the stabilization of the open-framework of AlPO-CJ4. By contrast, the structure-directing agent 2-aminopyridine is too large to be accommodated in the 8-MR channel of AlPO-CJ4 and may be the reason why 2-aminopyridine is not involved in the structure.

In summary, a novel 3D aluminophosphate compound consisting of chiral motifs was synthesized from a solvethermal system using 2-aminopyridine as a structure-directing agent. Propeller-like chiral motifs are connected to each other and form a 2D layer and further construct a 3D open-framework *via* Al(1) atoms. The discovery of such chiral structural motifs will open up the possibility for the rational design of chiral microporous materials.

This work was supported by the National Natural Science Foundation and Pangdeng Project of China.

Notes and references

† *Crystal data* for $[AlP_2O_6(OH)_2][H_3O]$: M = 237.96, triclinic, space group $P\bar{1}$ (no. 2), a = 7.1177(2), b = 8.6729(2), c = 9.2200(3) Å, α = 65.108(2), β = 70.521(1), γ = 68.504(2)°, U = 469.4(2) Å^3, T = 293(2) K, Z = 3, μ(Mo-Kα) = 0.859 mm^{-1}, D_c = 2.525 g cm^{-3}, 1114 reflections measured, 1107 observed (R_{int} = 0.0115) which were used in all calculations. The final $wR(F^2_{all\ data})$ was 0.1098 and $R(F_{all\ data})$ was 0.0445. The structure was solved by direct methods using SHELXL 97.

CCDC 182/1697. See http://www.rsc.org/suppdata/cc/b0/b004200p/ for crystallographic files in .cif format.

1 S. T. Wilson, B. M. Lok, C. A. Messina, T. R. Cannan and E. M. Flanigen, *J. Am. Chem. Soc.*, 1982, **104**, 1146.
2 J. M. Bennett, W. J. Dytrych, J. J. Pluth, J. W. Richardson Jr. and J. V. Smith, *Zeolites*, 1986, **6**, 349.
3 W. H. Meier, D. H. Olson and Ch. Baerlocher, *Atlas of Zeolite Structure Types*, Elsevier, London, 1996.
4 K. Morgan, G. Gainsford and N. Milestone, *J. Chem. Soc., Chem. Commun.*, 1995, 425.
5 D. A. Bruce, A. P. Wilkinson, M. G. White and J. A. Bertrand, *J. Chem. Soc., Chem. Commun.*, 1995, 2059.
6 D. A. Bruce, A. P. Wilkinson, M. G. White and J. A. Bertrand, *J. Solid State Chem.*, 1996, **125**, 228.
7 M. J. Gray, J. D. Jasper, A. P. Wilkinson and J. C. Hanson, *Chem. Mater.*, 1997, **9**, 976.
8 M. E. Davis, C. Saldarriaga, C. Montes, J. Garces and C. Crowder, *Nature*, 1988, **331**, 698.
9 R. H. Jones, J. M. Thomas, R. Xu, Q. Huo, Y. Xu, A. K. Cheetham and D. Bieber, *J. Chem. Soc., Chem. Commun.*, 1990, 1170.
10 I. D. Williams, J. Yu, Q. Gao, J. Chen and R. Xu, *Chem. Commun.*, 1997, 1273; A. M. Chippindale and C. Turner, *J. Solid State Chem.*, 1997, **128**, 318.
11 K. R. Morgan, G. J. Gainsford and N. B. Milestone, *Chem. Commun.*, 1997, 61.
12 M. A. Leech, A. R. Cowley, K. Prout and A. M. Chippindale, *Chem. Mater.*, 1998, **10**, 451.
13 B. Wei, J. Yu, Z. Shi, S. Qiu and J. Li, *J. Chem. Soc., Dalton Trans.*, 2000, **13**, 1979.
14 Cerius[2]©Molecular simulations/Biosym corporation, San Diego, 1995.
15 J. Li, J. Yu, W. Yan, Y. Xu, W. Xu, S. Qiu and R. Xu, *Chem. Mater.*, 1999, **11**, 2600.

Nanoreactors based on (polymerized) ABA-triblock copolymer vesicles

Corinne Nardin,[a] Sandra Thoeni,[a] Jörg Widmer,[a] Mathias Winterhalter[b] and Wolfgang Meier*[b]

[a] *Department of Physical Chemistry, University of Basel, Klingelbergstrasse 80, CH-4056 Basel, Switzerland*
[b] *IPBS-CNRS UPR 9062, University Paul Sabatier, 31077, Toulouse, France. E-mail: wolfgang.meier@unibas.ch*

Received (in Oxford, UK) 23rd May 2000, Accepted 21st June 2000

A new kind of nanoreactor has been prepared by the incorporation of a channel protein into the shell of (polymerized) vesicles formed from an amphiphilic ABA-triblock copolymer.

A major goal in material science is to miniaturize processes down to the nanometer level. One typical example is the formulation of hollow nanoparticles of reproducible size. For such nanocontainers a widespread range of applications have been suggested. For example, one can think about chemistry in a confined volume under controlled conditions, or protection of guest molecules like enzymes against an hostile outside environment (*e.g.* protease). Such an environment requires a stable shell with a selective permeability.[1] In recent years considerable progress has been made in developing synthetic approaches to control the size and morphology of such particles.[2] Recently we reported a mild procedure for the preparation of stable nanocapsules from an amphiphilic poly(2-methyloxazoline)-block–poly(dimethylsiloxane)-block–poly(2-methyloxazoline) triblock copolymer (PMOXA-PDMS-PMOXA) which carried polymerizable groups at both ends.[3]

This polymer aggregates spontaneously in dilute aqueous solution into vesicular structures, the sizes of which can be controlled in the range 50 to 500 nm.[3] These aggregates can be considerably stabilized by a subsequent crosslinking polymerization of the reactive end groups of the underlying triblock copolymers. In the resulting nanocapsules all the individual block copolymers are interconnected *via* covalent bonds to a giant 'supermacromolecule'. Fig. 1 shows a characteristic cryogenic transmission electron micrograph (Cryo-TEM) of polymerized triblock copolymer vesicles. The thickness of the triblock copolymer shells is estimated to be about 10 nm, in good agreement with previous findings.[3,4]

Prior to any use of these polymer shells as nanosized reactors one had to find ways to control their permeability. Here we suggest the encapsulation of an enzyme. The enzyme should stay trapped in the interior of the particles while the substrates should be able to diffuse into, and the products out of, the nanoreactors. However, owing to their higher hydrophobic thickness, the triblock copolymer shells are even less permeable to small hydrophilic solutes than conventional phospholipid bilayers.[4–7]

Nature provides a great variety of passive or specific channels which allow the permeation of specific substrates across biological membranes. The lipid bilayer serves as a matrix for such channel proteins. However, many of the membrane proteins require a specific lipid composition, hydrophobic thickness or change distribution to be fully functional. The PMOXA-PDMS-PMOXA triblock copolymer behaves in aqueous solution in many respects like a higher molecular weight analogue of conventional lipids.[3,4] Therefore, in order to control the permeation we wanted to make use of such natural membrane proteins and tried to reconstitute them into our polymeric nanocapsules. (See Fig. 2 for a schematic representation of the resulting nanoreactor).

The block copolymer membranes are considerably thicker than conventional lipid bilayers ($d \approx 5$ nm)[3–7] due to the larger size of the underlying block copolymer molecules. The hydrophobic–hydrophilic pattern of membrane proteins are naturally optimized with respect to the thinner biological membranes and the hydrophobic part of channel forming proteins may therefore be too small to fit through the polymer membranes. This raises the question of whether the proteins can preserve their activity within a block copolymer membrane. However, the high flexibility and the conformational freedom of the polymer molecules may allow a block copolymer membrane to adapt to the specific geometric and dynamic requirements of membrane proteins without considerable loss of free energy. In such a case it is expected that the protein will remain functional.

To control the permeability of the nanocapsules we used a well-characterized nonspecific membrane channel, the bacterial porin OmpF.[8,9] Porins are transmembrane proteins which form trimeric channels in the outer membrane of Gram-negative bacteria. These water-filled channels allow passive diffusion of small solutes like ions, nutrients or antibiotics across the

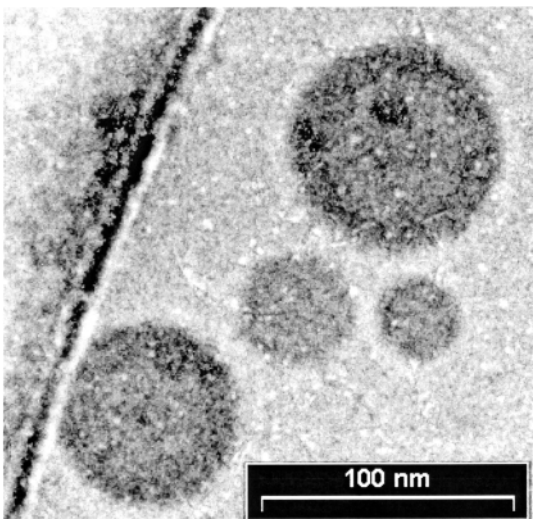

Fig. 1 Cryo-transmission electron micrograph of polymerized triblock copolymer vesicles.

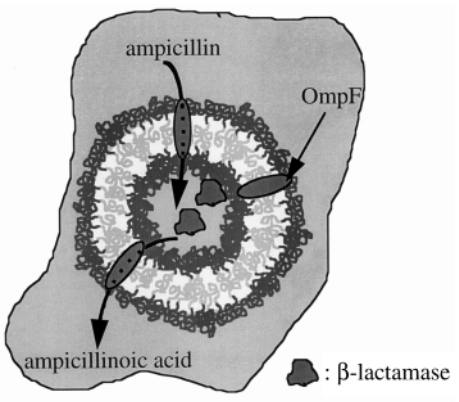

Fig. 2 Schematic representation of a β-lactamase-containing nanoreactor prepared from an amphiphilic triblock copolymer and the porin OmpF.

DOI: 10.1039/b004280n

membrane. Molecules with a molecular weight above 400 Da are sterically excluded.

The procedure used to prepare the nanoreactors was analogous to that of the (polymerized) triblock copolymer vesicles described previously.[3] Although the porin could also be incorporated into performed vesicles the following procedure turned out to be more convenient. A stock solution of the porin (13.3 mg mL^{-1} in 1 wt% octylpolyoxyethylene, 100 nM NaCl and 10 mM HEPES,† pH 7.4) was mixed with a 17 wt% solution of the triblock copolymer (M_n = 9000 Da) in ethanol to a final molar ratio of 1:1000 (protein:polymer). For encapsulation of the enzyme in the interior of the porin-containing vesicles, the clear and homogeneous solution was slowly added to an aqueous β-lactamase solution (0.024 mg mL^{-1} in 10 mM HEPES, 100 mM NaCl, pH 7.4) to a final triblock copolymer concentration of 1 wt%. Then the resulting dispersion was repeatedly extruded through filters of a defined pore size (Nucleopore filters (Millipore); pore width 200 nm). This gave rather monodisperse triblock copolymer vesicles with an average diameter of 250 nm.[3] Non-encapsulated protein was removed chromatographically (Sephadex G-200) from the porin-containing vesicles. If desired, a crosslinking polymerization of the methacrylate end-groups of the underlying triblock copolymers could subsequently be initiated by irradiating the vesicles dispersion for 2 min with UV-light. Previous investigation had shown that under these conditions the conversion of the methacrylate end-groups is > 90%.[3]

It is well-known that the enzyme β-lactamase is able to hydrolyze β-lactam antibiotics like ampicillin. This reaction can be used to assay, *via* a secondary reaction, the activity of the enzyme.[10,11] In contrast to ampicillin, the product of the hydrolysis (the ampicillinoic acid) can reduce iodine to iodide. This can readily be monitored by micro-iodometry, *i.e. via* the decolorization of a starch–iodine complex.[10,11]

In the present system the enzyme is immobilized in the aqueous core domain of the nanocapsules. Consequently, prior to hydrolysis the ampicillin has to enter the interior of the polymer particles. To check the functionality of the system we added 10 μL of a 1 mM ampicillin solution (in 10 mM HEPES, 100 mM NaCl, pH 7.4) to the nanoreactor dispersion and incubated the resulting mixture for 30 min. Starch-iodine reagent was prepared by mixing 5 mL of a 8 mM iodine, 320 mM potassium iodide solution with 20 mL 1 M sodium wolframate in 2 M acid acetic and then adding 5 mL of 2 wt% soluble starch which had been dissolved in 1 M acetic acid by gentle boiling for 3 min. Subsequently 0.5 mL of the starch–iodine reagent was added to the reaction mixture and the absorbance of the starch–iodine complex at 623 nm was measured as a function of time.[10,11] The results are shown in Fig. 3 together with the control experiments for the free, non-encapsulated enzyme and nanocapsules without OmpF channels. It is important to note that within the experimental error the results before and after polymerization of the triblock copolymer shells were always the same and subsequently discussed together.

For the nanocapsules made in the absence of porin the absorbance remained constant over the time course of the experiment. As expected, the ampicillin is not able to diffuse across the thick triblock copolymer shells. It is not therefore hydrolyzed by the enzyme and the iodine is not reduced. In contrast to that for the OmpF-containing nanoreactors the absorbance of the complex decreases slowly with time due to the reduction of the iodine. Obviously the channel protein remains functional despite the extreme thickness of the triblock copolymer shells and even the crosslinking polymerization of the reactive triblock copolymers does not affect its conformation. This is in agreement with systematic investigations on membrane proteins reconstituted into planar triblock copolymer membranes.[4]

Inspection of Fig. 3 shows that the reaction rate of encapsulated enzyme is lower than in the control experiment using free enzyme. This is due to the slow diffusion of the ampicillin and the ampicillinoic acid through the rather limited

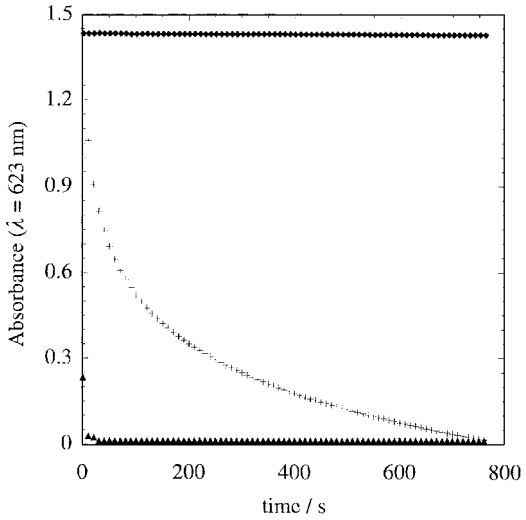

Fig. 3 Time profile of the absorbance of the starch–iodine complex at 623 nm after 30 min incubation in the presence of 10 μL of a 1 mM ampicillin solution (10 mM HEPES, 100 mM NaCl, pH 7.4). +: poly(2-methyloxazoline)–poly(dimethylsiloxane)–poly(2-methyloxazoline) triblock copolymer (PMOXA-PDMS-PMOXA) nanoreactors; ▲: control with free, non encapsulated enzyme; ◆: control with PMOXA-PDMS-PMOXA nanocapsules without OmpF channels.

number of narrow OmpF channels in the shells of the reactors.

In conclusion, we have shown that functional OmpF channels can be incorporated into the shells of triblock copolymer vesicles. Despite the artificial surrounding within such a polymerized triblock copolymer shell the functionality of the membrane protein is fully preserved. These channels therefore allow a direct access to enzymes encapsulated in the interior of these vesicles. We are currently investigating the extension of this principle to other enzymes and other transport proteins, with the goal of substrate-specific nanoreactors which could find interesting applications in areas like drug delivery or catalysis.

We thank Drs Patrick van Gelder and Alexandra Graff for stimulating discussions. Financial support to the Swiss National Science Foundation is gratefully acknowledged.

Notes and references

† HEPES = 4-(2-hydroxyethyl)-1-piperazine ethanesulfonic acid.

1 T. M. S. Chang, 'Microencapsulation (Artificial Cells)', in *Polymeric Materials Encyclopedia*, ed. J. C. Salemone, CRC Press, New York, 1996, Volume 6, 4351.
2 See for example: J. Ding and G. Liu, *J. Phys. Chem. B*, 1998, **102**, 6107; E. Donath, B. Sukhoruskov, F. Caruso, S. A. Davis and H. Möhwald, *Angew. Chem., Int. Ed. Engl.*, 1998, **37**, 2201; O. Emmerich, N. Hugenberg, M. Schmidt, S. S. Sheiko, F. Baumann, B. Deubzer, J. Weis and J. Ebenhock, *Adv. Mater.*, 1999, **11**, 1299; S. Stewart and G. J. Liu, *Chem. Mater.*, 1999, **11**, 1048; H. Huang. E. E. Remsen, T. Kowalewski and K. L. Wooley, *J. Am. Chem. Soc.*, 1999, **121**, 3805.
3 C. Nardin, T. Hirt, J. Leukel and W. Meier, *Langmuir*, 2000, **16**, 1035.
4 C. Nardin, M. Winterhalter and W. Meier, *Angew. Chem.*, submitted.
5 B. M. Disher, Y.-Y. Won, D. S. Ege, J. C. M. Lee, F. S. Bates, D. E. Disher and D. A. Hammer, *Science*, 1999, **284**, 1143.
6 D. D. Lasic, in *Liposomes: From Physics to Application*, Elsevier Science Publications B. V., Amsterdam, 1993.
7 A. Diederich, M. Strobel, W. Meier and M. Winterhalter, *J. Phys. Chem.*, 1999, **B103**, 1402.
8 H. Nikdaido, *Molecular Microbiology*, 1992, **6(4)**, 435.
9 B. Eisenberg, *Acc. Chem. Res.*, 1998, **31**, 117.
10 W. Zimmermann and A. Rosselet, *Antimacrobial Agents and Chemotherapy*, 1977, **12(3)**, 368.
11 R. P. Novick, *Biochem. J.*, 1962, **83**, 236.

Novel layer-type triple salts of silver(I), $AgCN{\cdot}AgF{\cdot}4AgCF_3CO_2{\cdot}2L$ (L = MeCN or H_2O)†

Quan-Ming Wang and Thomas C. W. Mak*

Department of Chemistry, The Chinese University of Hong Kong, New Territories, Hong Kong SAR, P.R. China. E-mail: tcwmak@cuhk.edu.hk

Received (in Cambridge, UK) 12th May 2000, Accepted 19th June 2000

The novel silver(I) triple salts $AgCN{\cdot}AgF{\cdot}4AgCF_3CO_2{\cdot}2L$ (L = MeCN or $2H_2O$) exhibit the same type of layer structure, in which [F@Ag_6] units each representing a fluoride-centred octahedral silver cage are interconnected by μ_4-κ*C*,κ*C*:κ*N*,κ*N*-cyanide and μ_4-*O*,*O*:*O*′,*O*′-trifluoroacetato bridges.

Current interest in cyanide-bridged one-, two- and three-dimensional complexes is focused on not only their structural variety but also their unusual magnetic and electrical properties.[1] In contrast to the common usage of soluble $[Ag(CN)_2]^-$ in the construction of coordination networks, we choose to combine AgCN with soluble silver salts to form crystalline double salts, anticipating that in such a silver-rich environment the cyanide ligand may display unusual bridging modes that lead to the formation of novel 2D or 3D coordination networks. This strategy has yielded a variety of silver(I) double salts of the general formula *m*AgY·*n*AgZ·*x*L (Y, Z = anions; L = solvate molecule that may be present).[2–5] Interestingly, when we attempted to synthesize double salts of the type *m*AgCN·*n*-$AgCF_3CO_2$, an unexpected product $AgCN{\cdot}AgF{\cdot}4AgCF_3CO_2{\cdot}$2MeCN **1** was obtained and structurally characterized. Subsequently, another closely related triple salt $AgCN{\cdot}AgF{\cdot}4AgCF_3$-$CO_2{\cdot}2H_2O$ **2** was accessible by a simple route.

Compound **1** was obtained by dissolving AgCN in an aqueous solution of CF_3CO_2Ag and $AgBF_4$ in the presence of acetonitrile.‡ Deliberate addition of $AgBF_4$ into the solution was intended to increase the Ag^+ concentration to the threshold that is necessary for dissolving AgCN. Although thermal decomposition of CF_3CO_2Ag can release AgF,[6] $AgBF_4$ is more likely the source of F^- in the product. It has been demonstrated that, in some instances, decomposition of BF_4^- into F^- and BF_3 (presumably coordinated to ligand or solvent molecules) can occur in the reactions of transition metal (also including silver) tetrafluoroborate derivatives.[7] Repeating the preparative procedure using AgF instead of $AgBF_4$ improved the yield of **1** and resulted in the formation of **2**.

Single crystal X-ray analysis§ revealed that **1** has a layer structure, a portion of which is illustrated in Fig. 1. The F^- ion located at an inversion center is surrounded by six Ag(I) atoms in the form of a slightly elongated octahedron. The Ag–F distances in the equatorial plane are almost the same at 2.4520(4) and 2.4490(4) Å, whereas the significantly longer axial distance of 2.5759(5) Å can be ascribed to the attachment of a terminal acetonitrile ligand to an axial Ag(I) atom. This [F@Ag_6] octahedron may be compared with the regular one in rock salt-type AgF with Ag–F 2.46 Å.[8] In the 3D framework of $Ag_2C_2{\cdot}8AgF$, in which the fluoride ions act as bridges between [C_2@Ag_9]Ag moieties, the Ag–F distances fall in the range 2.196(2)–2.571(2) Å.[5c] It is noteworthy that there are very few examples of metal polyhdedra enclosing a fluoride ion,[9,10] and to our knowledge the [F@Ag_6] octahedron occurs only in AgF and the present triple salts.

The trifluoroacetato ligand usually acts as a μ_2-bridge in its metal complexes,[11a] and the μ_3-coordination mode is much less common.[11b] In contrast, each trifluoroacetato ligand in **1** functions in an asymmetric μ_4-*O*,*O*:*O*,*O*′ mode [Ag(1)–O(4) 2.455(4), Ag(3)–O(4) 2.562(4) Å, Ag(2)–O(3) 2.458(4), Ag(3)′–O(3) 2.537(3) Å], with its carboxylato group bridging an edge of a [F@Ag_6] octahedron while linking the vertices of two adjacent octahedra (see Fig. 1). Compound **1** thus provides the first example of a trifluoroacetato ligand coordinated to four metal centers, although several carboxylato complexes (especially oxalates) containing a μ_4-carboxylato group have been reported.[12]

The four equatorial Ag(I) atoms of each [F@Ag_6] octahedron are connected to neighboring octahedra through bridging cyanide ligands to generate a 2D $\{[(F@Ag_6)(CN)]^{4+}\}_\infty$ coordination network, as shown in Fig. 2. This linkage pattern is different from those in the double salts $Ag_2C_2{\cdot}2AgClO_4{\cdot}2H_2O$[5a] and $Ag_2C_2{\cdot}AgNO_3$,[5b] in which the [C_2@Ag_6] octahedra share vertices or edges to generate a 2D or 3D network, respectively. The cyanide ion is disordered about a $\bar{1}$ site, and is modeled by atom C1 with an assigned site-occupancy factor of $(6 + 7)/(6 \times 2) = 1.083$ [Ag1–C1 2.232(5) and Ag2–C1 2.234(5)]. The cyanide ligand with C–N bond length 1.108(9) Å bridges four [F@Ag_6] octahedra in a rare μ_4-κ*C*,κ*C*:κ*N*,κ*N* ligating mode, the only precedent being found in $3AgCN{\cdot}2AgF{\cdot}3H_2O$,[2] in which bent Ag_2F_2 and triangular [$Ag_3(H_2O)_3$] units are interconnected by μ_4- and μ_3-cyanide groups.

The 2D network lies in the (100) plane, and the acetonitrile ligands and hydrophobic tails of trifluoroacetato groups are accommodated in the interlayer region with a layer-to-layer separation of $a\sin\beta$ = 13.90 Å.

The layer structure of **2**§ is formally derived from that of **1** with each acetonitrile ligand replaced by a smaller aqua ligand. The [F@Ag_6] octahedron in **2** exhibits some distortion in the equatorial plane with Ag–F bond lengths of 2.371(3), 2.379(3), 2.464(3) and 2.484(3) Å, whereas the axial Ag–F distances are 2.585(3) and 2.589(3) Å. The more condensed packing of layers

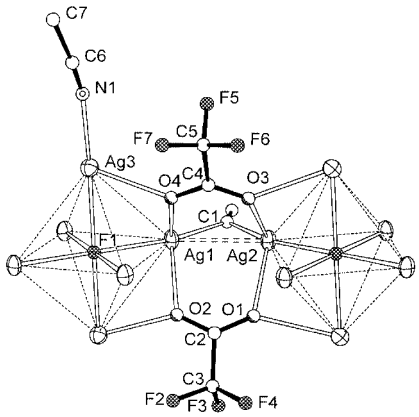

Fig. 1 A portion of the layer structure of $AgCN{\cdot}AgF{\cdot}4AgCF_3CO_2{\cdot}2$MeCN **1** with labeling of atoms in the independent unit. Ag(I) atoms are drawn as 30% thermal ellipsoids and the remaining atoms are differentiated by size and shading. The edges of each Ag_6 octahedron, which lie in the range 3.463–3.562 Å, are outlined by dotted lines. The Ag1···Ag2 distance is 2.8835(8) Å.

† Dedicated to the memory of Professor George Alan Jeffrey (1915–2000).

DOI: 10.1039/b003821k

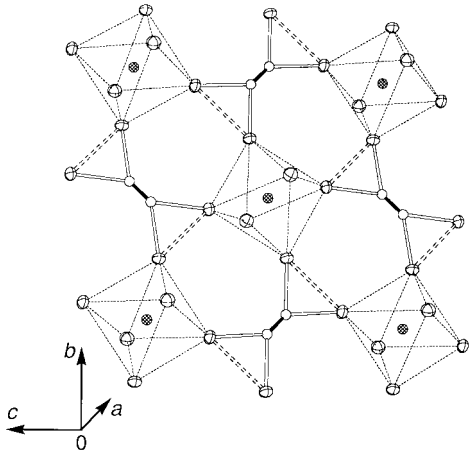

Fig. 2 A two-dimensional $\{[(F@Ag_6)(CN)]^{4+}\}_\infty$ network in **1**.

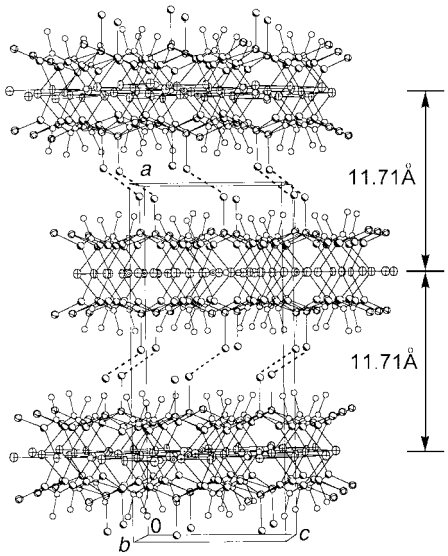

Fig. 3 Crystal structure of $AgCN{\cdot}AgF{\cdot}4AgCF_3CO_2{\cdot}2H_2O$ **2** viewed approximately in the *b* direction. Hydrogen bonds between aqua ligands of adjacent layers are represented by broken lines. All F atoms have been omitted for clairty.

in **2** yields an interlayer separation of $(a\sin\beta)/2$ = 11.71 Å, shorter by *ca.* 2.1 Å than that in **1**. Adjacent layers are related by a 2_1 axis along the *b* direction, which leads to the ABAB··· packing shown in Fig. 3 This is different from the case in **1**, where the layers are related by lattice translation *a*. The outstretched aqua ligands of adjacent layers in **2** form weak hydrogen bonds of the type O1w··O1w′ = 3.020 and O2w··O2w′ = 3.027 Å in successive interlayer regions, linkings the layers into a 3D network. This kind of packing may account for equatorial distortion of the $[F@Ag_6]$ unit in **2**, in contrast to that in **1**.

The present work describes the first structural characterization of novel silver(I) triple salts of the type *l*AgX·*m*AgY·*n*AgZ·*x*L, in which octahedral $\{F@Ag_6\}$ units are consolidated by μ_4-κ*C*,κ*C*:κ*N*,κ*N*-cyanide and μ-*O*,*O*:*O*′,*O*′-carboxylato groups. Notably, the propensity of all three anions to attain their highest ligation numbers,[4a] along with agentophilicity [attractive interaction between silver(I) atoms to form aggregates],[2,13] provide the driving force to assemble the robust $[(F@Ag_6)(CN)(CF_3CO_2)_2]_\infty$ layer from its components.

Dissolving AgCN in a concentrated silver salt solution may lead to the formation of some $[Ag_n(CN)]^{(n-1)+}$ species, which is comparble to the complexation of CuI to yield $[CuI_4]^{3-}$. The self-assembly of such polynuclear species to generate a 2D network in **1** and **2** is envisaged to be a complex process in which the fluoride ion draws six Ag(I) atoms together, the cyanide ion bridges the resulting $[F@Ag_6]$ octahedra, and the trifluoroacetato ligand further stabilizes the octahedra while providing for charge balance. The terminally coordinated, neutral ligand L plays a secondary role as either acetonitrile or aqua ligand can be attached to each layer with little effect on its structural integrity. Extension of this work by inserting other solvent molecules such as fumaronitrile or succinonitrile between the layers is in progress.

This project is supported by Hong Kong Research Grants Council Earmarked Grant CUHK 4022/98P.

Notes and references

‡ *Synthesis*: AgCN was added to 1 mL of a concentrated aqueous solution of $AgCF_3CO_2$ and $AgBF_4$ (molar ratio *ca.* 1:1) in a plastic beaker with stirring until saturated. The excess amount of AgCN was filtered off, and a few drops of MeCN were added to the filtrate. (Note: excess MeCN would lead to deposition of AgCN as a white precipitate.) The resulting solution was placed in a desiccator charged with P_2O_5. Colorless plate-like crystals of **1** were obtained in *ca.* 10 yield after several days.

Using AgF instead of $AgBF_4$ in the above preparation produced colorless plate-like crystals of **1** in *ca.* 20% yield as the first crop, and a second crop of colorless block-like crystals of **2** was obtained in *ca.* 40% yield. Both complexes are light-sensitive and decompose readily in common solvents such as water, methanol and acetonitrile. IR (KBr pellet)/cm^{-1}: 2138w, 1682vs, 1434m, 1208vs, 1135vs, 839s, 804s, 724s, 518vw for **1**; 2139w, 1682vs, 1433m, 1135vs, 839s, 804s, 724s, 518vw for **2**.

§ *Crystal data*: compound **1**: $C_{13}H_6Ag_6F_{13}N_3O_8$, M = 1226.43, monoclinic, space group $P2_1/c$ (no. 14), a = 14.484(1), b = 10.0013(7), c = 9.9918(7) Å, β = 106.259(2)°, V = 1389.5(2) Å^3, Z = 2, D_c = 2.931 Mg m^{-3}, $F(000)$ = 1136, μ(Mo-Kα) = 4.275 mm^{-1}. 9031 reflections measured, 3346 unique (R_{int} = 0.0448), final $R1$ = 0.0343, $wR2$ = 0.0809 for 2584 independent reflections [$I > 2\sigma(I)$].

Compound **2**: $C_9H_4Ag_6F_{13}NO_{10}$, M = 1180.35, monoclinic, space group $P2_1/c$, a = 23.446(2), b = 9.9378(7), c = 9.8962(7) Å, β = 90.002(2)°, V = 2305.8(3) Å^3, Z = 4, D_c = 3.400 Mg m^{-3}, $F(000)$ = 2176, μ(Mo-Kα) = 5.149 mm^{-1}. 17536 reflections measured, 6532 unique (R_{int} = 0.0399), final $R1$ = 0.0385, $wR2$ = 0.0867 for 3986 independent reflections [$I > 2\sigma(I)$]. Data collection was performed at 293 K on a Bruker SMART 1000 CCD diffractometer using frames of oscillation range 0.3°, with $3 < \theta < 28°$ for **1** and $3 < \theta < 30°$ for **2**.

CCDC 182/1691. See http://www.rsc.org/suppdata/cc/b0/b003821k/ for crystallographic files in .cif format.

1 T. Iwamoto, in *Comprehensive Supramolecular Chemistry*, ed. D. D. MacNicol, F. Toda and R. Bishop, Pergamon, Oxford, 1996, vol. 6, ch. 19, p. 643; K. R. Dunbar and R. A. Heintz, *Prog. Inorg. Chem.*, 1997, **45**, 283.

2 G.-C. Guo and T. C. W. Mak, *Angew. Chem., Int. Ed.*, 1998, **37**, 3183.

3 D. Britton and J. D. Dunitz, *Acta Crystallogr.*, 1965, **19**, 815.

4 (*a*) G.-C. Guo and T. C. W. Mak, *Chem. Commun.*, 1999, 813; (*b*) G.-C. Guo and T. C. W. Mak, *Angew. Chem., Int. Ed.*, 1998, **37**, 3246.

5 (*a*) G.-C. Guo, Q.-G. Wang, G.-D. Zhou and T. C. W. Mak, *Chem. Commun.*, 1998, 339; (*b*) G. C. Guo, G.-D. Zhou and T. C. W. Mak, *J. Am. Chem. Soc.*, 1999, **121**, 3136; (*c*) G.-C. Guo, G.-D. Zhou, Q.-G. Wang and T. C. W. Mak, *Angew. Chem., Int. Ed.*, 1998, **37**, 630.

6 E. V. Karpova, A. I. Boltalin, Y. M. Korenev and S. I. Troyanov, *Russ. J. Coord. Chem.*, 1999, **25**, 65.

7 R. H. Crabtree, G. G. Hlatky and E. M. Holt, *J. Am. Chem. Soc.*, 1983, **105**, 7302; P. B. Hitchcock, M. F. Lappert and R. G. Tayler, *J. Chem. Soc., Chem. Commun.*, 1984, 1082; R. W. M. Ten Hoedt and J. Reekijk, *Inorg. Chim. Acta*, 1981, **51**, 23.

8 R. W. G. Wyckoff, *Crystal Structures*, Interscience, New York, 1963, vol. 1.

9 D. L. Thorn, R. L. Harlow and N. Heron, *Inorg. Chem.*, 1995, **34**, 2629.

10 D. Stalke, F.-Q. Liu and H. W. Roesky, *Polyhedron*, 1996, **15**, 2841.

11 (*a*) R. G. Griffin, J. D. Ellett Jr., M. Mehring, J. G. Bullitt and J. S. Waugh, *J. Chem. Phys.*, 1972, **57**, 2147; J. Feldman and J. Calabrese, *Inorg. Chem.*, 1994, **33**, 5955; (*b*) G. Bruno, G. Tresoldi, S. L. Schiavo, S. Sergi and P. Piraino, *Inorg. Chim. Acta*, 1992, **197**, 9; J. Powell, M. J. Horvath, A. Lough, A. Phillips and J. Brunet, *J. Chem. Soc., Dalton Trans.*, 1998, 637; F. A. Cotton, E. V. Dikarev and X.-J. Feng, *Inorg. Chim. Acta*, 1995, **237**, 19.

12 V. W. Day, M. R. Thompson, C. S. Day, W. G. Klemperer and R.-S. Liu, *J. Am. Chem. Soc.*, 1980, **102**, 5971; T. C. W. Mak, W.-H. Yip, C. H. L. Kennard, G. Smith and E. J. O.'Reilley, *J. Chem. Soc., Dalton Trans.*, 1988, 2353; Q. Chen, S.-C. Liu and J. Zubieta, *Inorg. Chem.*, 1989, **28**, 4433.

13 M. A. Omary, T. R. Webb, Z. Assefa, G. E. Shankle and H. H. Patterson, *Inorg. Chem.*, 1998, **37**, 1380.

$La_{24}Li_{18.67}Ti_{5.33}O_{56}$: a novel columnar intergrowth structure of perovskite and distorted, cation-excess zinc blende†

Caroline A. Kirk,[a] Eric E. Lachowski[b] and Anthony R. West[a]

[a] *Department of Engineering Materials, University of Sheffield, Mappin Street, Sheffield, UK S1 3JD. E-mail: a.r.west@sheffield.ac.uk*

[b] *Department of Chemistry, University of Aberdeen, Meston Walk, Aberdeen, UK AB24 3UE*

Received (in Cambridge, UK) 14th February 2000, Accepted 16th June 2000
Published on the Web 6th July 2000

The structure of the new phase, $La_{24}Li_{18.67}Ti_{5.33}O_{56}$, tetragonal, space group *P*4/*mbm*, a = 13.2443(13), c = 14.9258(20) Å, consists of alternating columns, rotated by 45° relative to each other, of perovskite-like structure, with Ti and Li in alternate octahedral sites, and twinned, distorted, zinc blende-like structure.

Distorted crystal structures commonly occur when one type of atom is too small for the sites available to it. The perovskite family, ABO_3, provides many examples of structural distortions involving either distorted octahedra, BO_6 if the B cation is slightly too small or tilted octahedra if the A cation is too small. In the latter case, the A cations and oxygen, collectively, form close packed, *cp*, layers but the A cation may be too small to occupy a site surrounded by 12 equidistant oxygens. Additional complications occur, in, for example, the tungsten bronzes, $A_{1-x}BO_3$, when vacancies are introduced into the A cation array.

We report here, the crystal structure of $La_{24}Li_{18.67}Ti_{5.33}O_{56}$ which represents a new kind of distorted, partially-collapsed, *cp* structure. The structure contains large packing atoms, La, and smaller atoms, Li and Ti, which can occupy either tetrahedral or octahedral sites, but the La : O ratio is 1 : 2.33 rather than 1 : 3 as in perovskite. Consequently, instead of a uniformly distorted structure, as in, *e.g.* $GdFeO_3$, the structure separates into infinite columns of relatively undistorted *cp* structure.

The new phase, $La_{24}Li_{18.67}Ti_{5.33}O_{56}$ was synthesised during an investigation of compound formation in the system La_2O_3–Li_2O–TiO_2; this system is of interest as it contains the perovskite-related phase $La_{1/2+x}Li_{1/2-3x}TiO_3$[1] which exhibits exceptionally high lithium ion conductivity, 1×10^{-3} Ω^{-1} cm^{-1} at room temperature. At the outset, the composition of the new phase was uncertain since volatilisation of Li_2O was significant under the conditions used, *viz.* 12–24 h at 900 °C in Au foil boats. Nevertheless, a sample which was essentially phase-pure by powder X-ray diffraction, (XRD), was obtained on reacting the mixture ($7La_2O_3$+$10Li_2CO_3$+$3TiO_2$); this had the same La : Ti ratio as deduced in the final formula, but an excess of Li. Its powder XRD pattern could not be indexed by trial-and-error methods but it was found by selected area electron diffraction, SAED, to be tetragonal, which then enabled the XRD pattern to be indexed on a primitive cell with a = 13.2443(13) and c = 14.9258(20) Å.

For the structure determination, a sub-cell with halved c, was used since all observed XRD lines as well as the neutron diffraction (ND) data could be satisfactorily indexed on a tetragonal cell with a = 13.2443(13) and c = 7.4629(10) Å, in the space group *P*4/*mbm* (no. 127); hence the structure contains a weak supercell that is observed only by SAED. It was not possible to solve the structure from either XRD or ND data alone. Using electron density maps obtained by applying 'Direct Methods' to the XRD data set, La positions were located and this enabled an iterative solution and refinement of the structure to be carried out using combined XRD and ND data as input to the Rietveld programme GSAS.[2] After refinement of partial structure models at each stage, difference Fourier maps were constructed for both XRD and ND data and this gradually allowed the positions of more atoms to be identified, which were then inputted into the Rietveld refinement and the process repeated. This process was continued until a model corresponding to the stoichiometry '$La_{24}Ti_6O_{48}$' was obtained, at which point the difference maps became relatively featureless. The remainder of the structure was determined using a combination of crystal chemical intuition, based on examination of coordination environments of the various atoms and their bond distances and bond valence analysis to indicate which oxygens were underbonded and whether Ti, Li sites contained Ti or Li alone or had mixed occupancy. A comparison of the goodness-of-fit parameter (χ^2) and R values of the partial structure $La_{24}Ti_6O_{48}$ with those of $La_{24}Li_{18.67}Ti_{5.33}O_{56}$ is given in Table 1, showing a clear improvement in the fit when the extra O site and Li sites are added. The observed, calculated and difference profiles of the XRD and ND data from the refinement of $La_{24}Li_{18.67}Ti_{5.33}O_{56}$ are provided as ESI†. Full details of the structure determination will be reported elsewhere together with a detailed description of the crystal structure.

During the final stages of refinement, the composition of the new phase was determined from site occupancy factors. The absolute Li,Ti contents are slightly uncertain since some sites contained mixed Li,Ti occupancy; it was assumed that overall, these sites were full, but it is also possible that they contain some vacancies, compensated by a higher Ti/Li ratio.

The structure contains layers perpendicular to c (not shown) of La and O atoms that are alternately planar and buckled. The layers at z = ¼ and 0, ½, shown in projection in Fig. 1 and Fig. 2 are not *cp* in this orientation: for them to be *cp*, each packing atom (La, O) should be surrounded by a hexagonal ring of six other packing atoms. It is, however, possible, if we consider for a moment La and O to be equivalent, to identify fragments of *cubic close packed, ccp*, unit cells, *e.g.* four La(1) atoms around O(8) at both corner and face centre positions, Fig. 1, giving rise to the 'domino-five' arrangement of a *ccp* cell face; in addition, parallel to c, the 'domino-fives' alternate with square arrangements of O(7), Fig. 2, which represent side face centres of the *ccp* unit cells. Centred at corner and face centre positions,

Table 1 Comparison of χ^2 and R values[a]

	$La_{24}Ti_6O_{48}$	$La_{24}Li_{18\ 2/3}Ti_{5\ 1/3}O_{56}$
χ^2	16.31	5.393
wR_p (ND)	6.28	3.43
R_p (ND)	11.61	6.39
wR_p (XRD)	6.83	6.46
R_p (XRD)	4.91	4.73
wR_p (overall)	6.30	3.62
R_p (overall)	5.44	4.86

[a] % Value.

† Electronic supplementary information (ESI) available: observed, calculated and difference plots of XRD and ND data of $La_{24}Li_{18.67}Ti_{5.33}O_{56}$. See http://www.rsc.org/suppdata/cc/b0/b001196g/

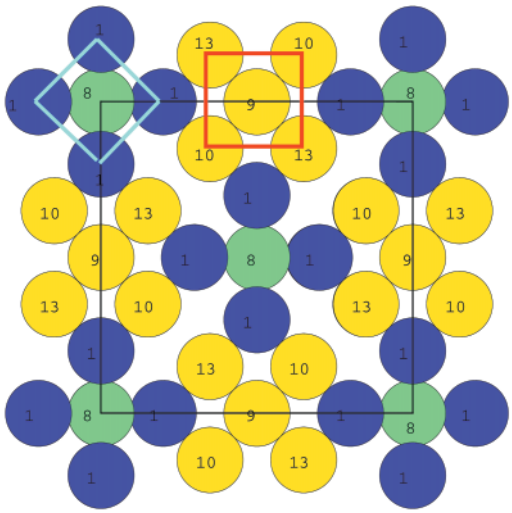

Fig. 1 *ab* Section at $z = 0.25$, with idealised La–O and O–O bond lengths: La(1): purple; O(9), O(10), O(13): yellow; O(8): green. The zinc blende-related columns are yellow, with the subcell outlined in red; the perovskite columns are green/purple with the subcell outlined in blue.

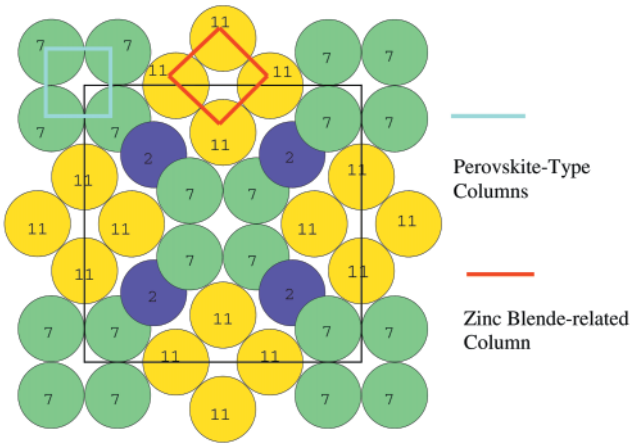

Fig. 2 *ab* Section at $z = 0$, with Idealised La–O and O–O bond lengths. La(2): purple; O(11): yellow; O(7): green. Column colours as in Fig. 1. Section at $z = \frac{1}{2}$ (not shown) is very similar, but with La(3) instead of La(2), O(5) instead of O(11) and O(6) instead of O(7).

therefore, columns of mixed La,O *ccp* cells run parallel to *c*. These have the perovskite structure, not only as regards the La, O distribution but also the octahedral positions at, *e.g.* 000 and $00\frac{1}{2}$, which are occupied, alternately, by Ti and Li.

A second set of *ccp* columns is centred on the edge-centre positions, *i.e.* in Fig. 1 oxygens O(10), O(13), around O(9) at $0\frac{11}{24}$ and $\frac{1}{2}0\frac{1}{4}$, with oxygens O(11) at $z = 0$, Fig. 2, and O(5) at $z = \frac{1}{2}$ (not shown). These columns are somewhat distorted from the idealised, square symmetry. An *ab* projection of one such

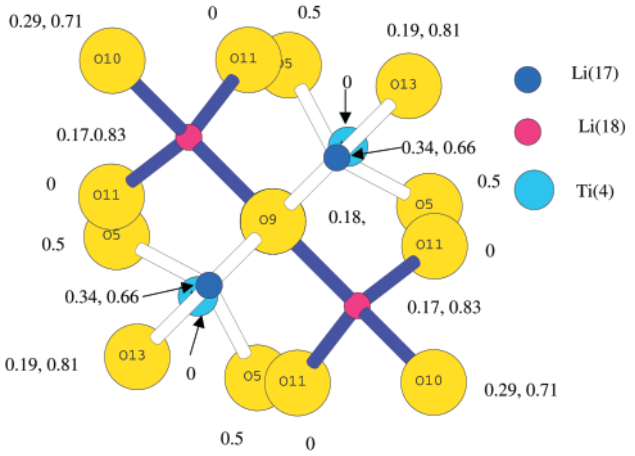

Fig. 3 Distorted zinc blende-related columns with Ti octahedrally co-ordinated in the basal plane.

column is shown in Fig. 3; Li occupies one set of tetrahedral sites to give a zinc blende arrangement, but, a twin plane exists at each unit cell face (*i.e.* $z = 0, \frac{1}{2}$) and the pattern of tetrahedral site occupancy parallel to *c* is –empty–empty–occupied–occupied–… rather than …empty–occupied –... as in zinc blende. Additionally, these distorted *ccp* cells contain Ti in sites at $z = 0$; in an undistorted structure, these sites would be two-coordinate, but because of the distortions, are octahedral, (oxygens O(11) at $z = 0$, O(13) at $z = 0.19,0.81$ and O(9) at $z = 0.18, 0.82$).

To complete the structure, it is necessary to see how the columns of perovskite-like and cation-excess, zinc blende-like structure are connected. From Figs. 1 and 2, it can be seen that adjacent columns are rotated by 45° about *c*, relative to each other. In the sections at $z = 0$ and $z = \frac{1}{2}$ (not shown), extra La(2) and La(3) atoms are located between the two types of column, whereas at $z = \frac{1}{4}, \frac{3}{4}$, all La, O atoms belong to one or other of the two column types.

The coordination numbers of the packing atoms vary, depending on their location, from a maximum of 12 for O(8) in the centres of the perovskite columns. Overall, the structure is not a continuous *cp* structure but nevertheless, the average volume of an La, O packing atom, 16.3 Å^3, is close to the lower limit found for ideal *cp* structures. Thus, within the two types of column, the packing arrangement of La, O approximates to *cp* but between the columns the structure cannot be idealised to *cp*.

Notes and references

1 A. D. Robertson, S. Garcia-Martin, A. Coats and A. R. West, *J Mater. Chem.*, 1995, **9**, 1405.
1 A. C. Larson and R. B. van Dreele, Los Alamos Laboratory Report No La-Ur-86-748, 1998.

Synthesis and structure of $[(Bu^tN)P(\mu\text{-}NBu^t)_2P(PCy)Li_2\cdot thf]_2$; an unusual cage compound containing an amido/phosphido functionalised $[(Bu^tN)P(\mu\text{-}NBu^t)_2P(PCy)]^{2-}$ dianion (Cy = C_6H_{11})

Alan Bashall,[a] Benjamin R. Elvidge,[b] Michael A. Beswick,*[b] Sara J. Kidd,[b] Mary McPartlin[a] and Dominic S. Wright*[b]

[a] *School of Chemistry, University of North London, London, UK N7 8DB*
[b] *Chemistry Department, University of Cambridge, Lensfield Road, Cambridge, UK CB2 1EW. E-mail: dsw1000@cus.cam.ac.uk*

Received (in Cambridge, UK) 2nd May 2000, Accepted 21st June 2000

The reaction of $[(Bu^tNH)P(\mu\text{-}NBu^t)_2PCl]$ (1) with CyPHLi and Bu^nLi in toluene gives $[(Bu^tN)P(\mu\text{-}NBu^t)_2P(PCy)\text{-}Li_2\cdot thf]_2$ (2), an unusual aggregate containing the first example of a phosphine-functionalised cyclodiphosphazane anion $[(Bu^tN)P(\mu\text{-}NBu^t)_2P(PCy)]^{2-}$.

In recent years there has been increasing interest in the synthesis and coordination chemistry of anionic ligand systems based on imido group 15 molecular frameworks.[1] The most extensively studied have been complexes containing $[E_2(NR)_4]^{2-}$ anions, (E = P,[2] As,[3] Sb,[4] Bi[5]), capable of coordinating a variety of metal centres using a combination of their μ-N and terminal N donor functionality.[6] Although imido frameworks of this type are comparatively robust, we found recently that the analogous phosphide systems of the heavier group 15 elements decompose at low temperatures to give cyclic $[(RP)_nE]^-$ anions (n = 3, 4; E = As–Bi) and Zintl compounds.[7] Indeed, the only group 15 phosphide which has been stable enough to isolate (< 30 °C) and structurally characterise so far is the $[Sb(PCy)_3]^{3-}$ trianion, present in the cage complex $[\{Sb(PCy)_3\}_2Li_6\cdot 6Me_2NH]$.[8] Motivated by the scarcity of stable phosphide ligands of this type, we have turned our attention to those based on phosphorus frameworks which are likely to be more stable. We report here the first example of a phosphine-functionalised cyclodiphosphazane anion present in the unusual cage complex $[(Bu^tN)P(\mu\text{-}NBu^t)_2P(PCy)Li_2\cdot thf]_2$ (**1**).

Complex **1** was prepared by the reaction of $[(Bu^tNH)P(\mu\text{-}NBu^t)_2PCl]$ (1 equiv.) with CyPHLi (1 equiv.) followed by reaction with Bu^nLi (2 equiv.),† the formation of the dianion resulting from a combination of addition of $CyPH^-$ to the framework of $[(Bu^tNH)P(\mu\text{-}NBu^t)_2PCl]$ and deprotonation with Bu^{n-} (Scheme 1).

Low-temperature X-ray crystallography‡ reveals that **1** is composed of centrosymmetric dimers, which are constructed from the association of two $[(Bu^tN)P(\mu\text{-}NBu^t)_2P(PCy)Li_2\cdot thf]$ cubane units through a central P_2Li_2 ring (Fig. 1). In addition there is a thf molecule within the lattice. The unusual manner of the association of the cubane units of **1** can be compared to related group 15 complexes containing $[E_2(NR)_4]^{2-}$ anions. Complete solvation of the Li^+ cations in $[\{E_2(NBu^t)_4\}Li_2\cdot 2thf]$ (E = P,[2a] Bi[5]) results in discrete cubane structures, whereas in $[\{E_2(NBu^t)_4\}Li_2]_2$ (E = P,[2b] As,[3] Sb[4]) the absence of Lewis base solvation results in aggregation into 'interlocked-cubane' cages. The arrangement in **1** can be regarded as representing an intermediate situation in which solvation of only one of the Li^+ cations within the cubane constituents leaves 'side-on' aggregation as the most viable method of increasing the coordination number of the unsolvated Li centre.

The presence of the CyP substituent has little effect on the P–N framework of the $[(Bu^tN)P(\mu\text{-}NBu^t)_2P(PCy)]^{2-}$ dianions of **1**, the geometry of the $[(Bu^tN)P(\mu\text{-}NBu^t)_2P]$ fragment and bond lengths involved being very similar to those found in complexes containing the related $[(Bu^tN)P(\mu\text{-}NBu^t)_2P(NBu^t)]^{2-}$ dianion.[2] In particular, the endocyclic P–N bonds (mean 1.78 Å) and endocyclic P–N–P and N–P–N angles (mean 96.9 and 83.1°, respectively) present in the planar P_2N_2 rings of **1** are similar to those found in the bis-thf solvate $[\{P_2(NBu^t)_4\}Li_2\cdot 2thf]$.[2a] This similarity suggests that the relatively short exocyclic P–P(Cy) bond in the $[(Bu^tN)P(\mu\text{-}NBu^t)_2P(PCy)]^{2-}$ dianions of **1** [P(2)–P(3) 2.171(3) Å; *cf.* single P–P *ca.* 2.21 Å and double P=P bond *ca.* 2.1 Å[9]] is largely the result of electrostatic factors (*i.e.*, stemming from the bonding of P(2) to two electronegative N

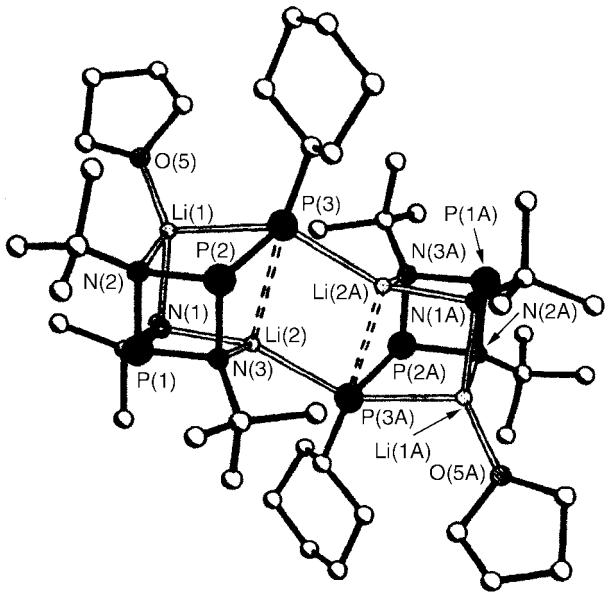

Fig. 1 Structure of dimeric molecules of **1**. H-atoms and the lattice-bound thf molecules have been omitted for clarity. Key bond lengths (Å) and angles (°); P(1)–N(1) 1.651(5), P(1)–N(2) 1.787(5), P(1)–N(3) 1.792(5), P(2)–N(2) 1.773(6), P(2)–N(3) 1.772(5), P(2)–P(3) 2.171(3), N(1)–Li(1) 2.09(1), Li(1)–O(5) 1.94(1), N(1)–Li(2) 1.98(1), N(2)–Li(1) 2.11(1), N(3)–Li(2) 2.11(1), P(3)–Li(1) 2.62(1), P(3)–Li(2) 2.88(1), P(3)–Li(2A) 2.57(1), N(1)–P(1)–N(2) 101.0(3), N(1)–P(1)–N(3) 97.9(3), N(2)–P(1)–N(3) 82.6(2), P(1)–N(2)–P(2) 97.0(3), P(1)–N(3)–P(2) 96.8(2), N(2)–P(2)–P(3) 104.1(2), N(3)–P(2)–P(3) 98.6(2), N(2)–P(2)–N(3) 83.6(2), Li(1)–N(1)–Li(2) 92.6(5), Li(1)–P(3)–Li(2) 64.4(4), N(1)–Li(1)–P(3) 102.4(5), N(1)–Li(2)–P(3) 97.1(5), Li(2)–P(3)–Li(2A) 67.6(4), P(3)–Li(2)–P(3A) 112.4(4), Li(1)–P(3)–Li(2A) 125.2(4).

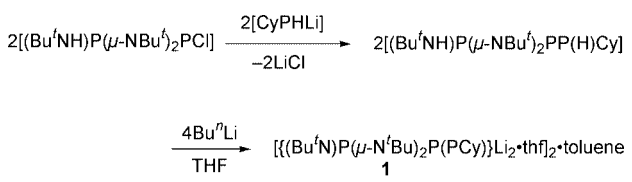

Scheme 1

DOI: 10.1039/b003468l

centres, rather than indicating the presence of any partial multiple bonding).

The coordination of the bifunctional $[(Bu^tN)P(\mu\text{-}NBu^t)_2P(PCy)]^{2-}$ ligand to the Li^+ cations in **1** inherently results in major distortion of the $[(Bu^tN)P(\mu\text{-}NBu^t)_2P(PCy)Li_2]$ cubane framework. The NLi_2P ring unit in **1** is butterfly-shaped primarily as a consequence of the relative shortness of the terminal P–N(Bu^t) bond [P(1)–N(1) 1.651(5) Å] of the ligand compared to the terminal P–P(Cy) bond. In addition, this distortion is exacerbated further by the relative shortness of the Li–N bonds [range 1.98(1)–2.11(1) Å[10]] compared to the P–Li bonds [P(3)–Li(1) 2.62(1), P(3)–Li(2) 2.88(1) Å]. Finally, it is interesting to note that the P(3)–Li(2) interaction is well outside the range found in lithium phosphide complexes (*ca.* 2.6[11]) and significantly longer than the P–Li bonds linking the cubane units [P(3A)–Li(2) 2.57(1) Å]. This observation may indicate that aggregation of the monosolvated cubane units of **1** *via* P–Li bonding, rather than the attainment of a discrete cubane structure by thf-solvation of both cations, is a consequence of the inability of the exocyclic P donor centre to coordinate both of the Li^+ cations effectively within a discrete cubane arrangement.

In summary, the first example of a phosphine-functionalised cyclodiphosphazane anion, $[(Bu^tN)P(\mu\text{-}NBu^t)_2P(PCy)]^{2-}$, has been prepared, structural studies showing that the Li salt $[(Bu^tN)P(\mu\text{-}NBu^t)_2P(PCy)Li_2{\cdot}thf]_2$ has a unique arrangement in the solid state. In view of this structural pattern and of the very different geometric demands of this anion compared to related amides, further studies of the coordination chemistry of this and other phosphides should be of interest.

We gratefully acknowledge the EPSRC (A. B., S. J. K., M. McP.) and the Leverhulme Trust (M. A. B) for financial support.

Notes and references

† *Synthesis of* **1**: the novel precursor $[(Bu^tNH)P(\mu\text{-}NBu^t)_2PCl]$ was prepared by the reaction of PCl_3 with Bu^tNH_2 (2:8 equiv.) in toluene. It was characterised by elemental analysis (C,H,N) and ^1H and ^{31}P NMR spectroscopy, and X-ray crystallography.[12] A suspension of CyPHLi (6.43 mmol) in hexane (20 ml) was added to a solution of $[(Bu^tNH)P(\mu\text{-}NBu^t)_2PCl]$ (2.0 g, 6.43 mmol) in toluene (5 ml)/hexane (20 ml) at room temperature. The white solid produced (LiCl) was removed by filtration and the orange filtrate reduced to *ca.* 5 ml under vacuum. To this was added Bu^nLi (8.6 ml, 1.50 mol dm^{-3} in hexanes, 12.9 mmol). A yellow precipitate was produced which was dissolved by the dropwise addition of thf (*ca.* 5 ml) to the suspension at reflux. Storage of the solution at 5 °C (48 h) gave small colourless cubes of **1**. Yield 1.33 g (40%). Decomp. to red solid *ca.* 180 °C. ^1H NMR ($[^2H_8]$thf, +25 °C, 400.129 MHz), 3.50 (m, *ca.* 6H, thf), 1.70 (m, *ca.* 6H, thf), *ca.* 2.1–1.0 (overlapping m, 11H, Cy), 1.13 (s, 27H, Bu^t). ^{31}P NMR ($[^2H_8]$thf, +25 °C, 161.975 Hz, rel. to 80% H_3PO_4/D_2O), 187.9 (d, J_{P-P} = 376 Hz, Cy*P*), 167.6 (s, *P*NBu^t), −10.2 (d, J_{P-P} = 376 Hz, Cy*P*). Correct analysis (C, H, N) were obtained for **1**.

‡ *Crystal data for* **1**: $C_{50}H_{104}Li_4N_6O_3P_6$, M = 1022.92, monoclinic, space group $P2_1/n$, Z = 2, a = 10.679(2), b = 21.224(8), c = 13.847(3) Å, β = 95.46(2) Å, V = 3124.0(15) Å^3, μ(Mo–Kα) = 0.211 mm^{-1}, T = 223(2) K. Data were collected on a Siemens *P*4 four circle diffractometer and corrected for absorption using Ψ scans. Of a total of 4884 reflections collected, 3836 were independent (R_{int} = 0.075). The structure was solved by direct methods and refined by full-matrix least squares on F^2.[13] Final $R1$ = 0.077 [$I > 2\sigma(I)$] and $wR2$ = 0.242 (all data). Three peaks of electron density were interpreted as a molecule of thf disordered across an inversion centre in such a way that the carbon atoms in the two components overlap. CCDC 182/1696. See http://www.rsc.org/suppdata/cc/b0/b003468l/ for crystallographic files in .cif format.

1 M. A. Beswick and D. S. Wright, *Coord. Chem. Rev.*, 1998, **176**, 373; M. A. Beswick, M. E. G. Mosquera and D. S. Wright, *J. Chem. Soc., Dalton Trans.*, 1998, 2437, and references cited therein.

2 (*a*) I. Schranz, L. Stahl and R. J. Staples, *Inorg. Chem.*, 1998, **37**, 1493; (*b*) J. K. Brask, T. Chivers, M. L. Krahn and M. Parvez, *Inorg. Chem.*, 1999, **38**, 290.

3 M. A. Beswick, E. A. Harron, A. D. Hopkins, P. R. Raithby and D. S. Wright, *J. Chem. Soc., Dalton Trans.*, 1999, 107.

4 R. A. Alton, D. Barr, A. J. Edwards, M. A. Paver, P. R. Raithby, M.-A. Rennie, C. A. Russell and D. S. Wright, *J. Chem. Soc., Chem. Commun.*, 1994, 1481.

5 D. Barr, M. A. Beswick, A. J. Edwards, J. R. Galsworthy, M. A. Paver, M.-A. Rennie, C. A. Russell, P. R. Raithby, K. L. Verhorevoort and D. S. Wright, *Inorg. Chim. Acta*, 1996, **248**, 9.

6 (*a*) D. Barr, A. J. Edwards, S. Pullen, M. A. Paver, M.-A. Rennie, P. R. Raithby and D. S. Wright, *Angew. Chem., Int. Ed. Engl.*, 1994, **33**, 1875; (*b*) M. A. Beswick, C. A. Harmer, M. A. Paver, P. R. Raithby, A. Steiner and D. S. Wright, *Inorg. Chem.*, 1997, **36**, 1740; (*c*) L. Grocholl, V. Huch, L. Stahl, R. Staples, P. Steinhart and A. Johnson, *Inorg. Chem.*, 1997, **36**, 4451; (*d*) L. Grocholl, I. Schranz, L. Stahl and R. J. Staples, *Inorg. Chem.*, 1998, **37**, 2496; (*e*) D. F. Moser, I. Schranz, M. C. Gerrety, L. Stahl and R. J. Staples, *J. Chem. Soc. Dalton Trans.*, 1999, 751; (*f*) A. Bashall, M. A. Beswick, E. A. Harron, A. D. Hopkins, S. J. Kidd, M. McPartlin, P. R. Raithby, A. Steiner and D. S. Wright, *Chem. Commun.*, 1999, 1145.

7 (*a*) M. A. Beswick, N. Choi, C. N. Harmer, A. D. Hopkins, M. McPartlin and D. S. Wright, *Science*, 1998, **281**, 1500; (*b*) M. A. Beswick, N. Choi, A. D. Hopkins, M. E. G. Mosquera, M. McPartlin, P. R. Raithby, A. Rothenberger, D. Stalke, A. E. H. Wheatley and D. S. Wright, *Chem. Commun.*, 1998, 2485; (*c*) M. A. Beswick, N. Choi, A. D. Hopkins, M. E. G. Mosquera, M. McPartlin, P. R. Raithby, A. E. H. Wheatley and D. S. Wright, *J. Chem. Soc., Dalton Trans.*, 2000, 479.

8 M. A. Beswick, J. M. Goodman, C. N. Harmer, A. D. Hopkins, M. A. Paver, P. R. Raithby, A. E. H. Wheatley and D. S. Wright, *Chem. Commun.*, 1997, 1879.

9 R. A. Jones, M. H. Seeberger and B. R. Whittlesey, *J. Am. Chem. Soc.*, 1985, **107**, 6424, and references cited therein.

10 These Li–N bonds are typical of amido lithium compounds, see: (*a*) K. Gregory; P. v. R. Schleyer and R. Snaith, *Adv. Inorg. Chem.*, 1991, **37**, 47; (*b*) R. E. Mulvey, *Chem. Rev.*, 1991, **20**, 167.

11 M. A. Beswick and D. S. Wright, *Comprehensive Organometallic Chemistry; Alkali Metals*, ed. E. W. Abel, F. G. Stone and G. Wilkinson, vol. ed. C. E. Housecroft, 1994, ch. 1, p. 1 and references cited therein.

12 The structure of $[(Bu^tNH)P(\mu\text{-}NBu^t)_2PCl]$ has a similar *cis* arrangement to that of $[\{(Me_3Si)_2N\}P(\mu\text{-}NBu^t)(\mu\text{-}NMes)PCl]$. See: G. David, E. Nieke, M. Nieger, V. von der Gönna and W. W. Schoeller, *Chem. Ber.*, 1993, **126**, 1513. The synthesis and structure of $[(Bu^tNH)P(\mu\text{-}NBu^t)_2PCl]$ will form part of a later full paper.

13 SHELXTL PC version 5.03, Siemens Analytical Instruments, Madison, WI, 1994.

ChemComm

Sol–gel entrapped TEMPO for the selective oxidation of methyl α-D-glucopyranoside†

Rosaria Ciriminna,[a] Jochanan Blum,[b] David Avnir[b] and Mario Pagliaro*[a]

[a] *Institute of Chemistry and Technology of Natural Products, CNR, via Ugo La Malfa 153, 90146 Palermo, Italy*
[b] *Institute of Chemistry, The Hebrew University of Jerusalem, Jerusalem 91904, Israel.*
E-mail: pagliaro@ictpn.pa.cnr.it

Received (in Cambridge, UK) 17th April 2000, Accepted 20th June 2000

The sol–gel entrapment of TEMPO within a silica matrix yields an efficient and recyclable catalytic system for the selective oxidation of methyl α-D-glucopyranoside (MGP) in water with NaOCl as primary oxidant, thus opening the way to the heterogeneous catalysis of the conversion of sugars into valuable uronates.

The selective oxidation of carbohydrate primary alcohols into carboxylic acids yields uronates, compounds with valuable biochemical properties.[1] Stable organic nitroxyl radicals belonging to the TEMPO family are excellent catalysts for this selective oxidation.[2] The radicals are soluble in H_2O (*ca.* 1% w/w) where, in the presence of alkaline (pH 9–10) NaOCl as primary oxidant along with a catalytic amount of bromide, they mediate the conversion of $–CH_2OH$ groups into $–COO^-$ with complete selectivity for the primary alcohol groups:

$$RCH_2OH + OH^- + 2OCl^- \xrightarrow[\text{NaBr, pH 10, 2°C}]{\text{TEMPO}} RCOO^- + 2Cl^- + 2H_2O \qquad (1)$$

A catalytic amount of bromide is added in order to increase the reaction rate upon fast formation of OBr^- that in its turn generates *in situ* the catalytic oxidant, the oxoammonium salt $TEMPO^+$.[3] In this way the important detoxifying agent D-glucuronic acid,[1] previously produced enzymatically on a small scale,[4] can now be easily obtained through the catalytic oxidation of D-methylglucose.

Apart from being clean and selective, reaction (1) is rapid and quantitative; its comparison with the heterogeneous oxidative dehydrogenation of methyl 4-*O*-methylglucose on Pt/C reveals the superiority of TEMPO mediated oxidation.[5] Of relevance to this report is also the commercial production of ascorbic acid currently prepared either through the enzymatic oxidation of the $–CH_2OH$ group in D-sorbose under cumbersome reaction conditions, or by the oxidation of sorbose primary alcohols with HNO_3.[4]

Clearly, considering the efficiency mentioned above and the commercial relevance of uronates, the immobilization of the nitroxyl radicals within a solid support would be a major advantage in the prolonged quest for heterogeneous catalysts for liquid-phase oxidations of sugars. An obvious prerequisite is that the catalytic material retains the activity of the radicals and is stable over prolonged time of use.

With these aims, several immobilization procedures have been reported in which the TEMPO moiety has been covalently linked either to organic polymers[6,7] or to a functionalized aminopropyl silica.[8,9] In all of the reported cases, the immobilization was carried out by heterogeneous reaction between a radical (or a precursor) functionalized in position 4 and a suitable function of the polymer. The catalytic organic polymers thus obtained were tested in the oxidation of organic alcohols and showed *lower* activity and stability of the radicals under solution homogeneous reactions.[6,7] On the other hand, TEMPO supported on aminopropyl-derivatized silica employed in the oxidation of various alcohols in a biphasic (H_2O–CH_2Cl_2) reaction system with NaOCl as co-oxidant, was found to be highly active, selective and recyclable.[9] However, an attempt to use this anchored TEMPO with sacrificial NaOBr for the oxidation of anomerically protected D-glucose in water, resulted in rapid loss of activity upon 3 consecutive oxidative runs.[9] Heeres *et al.* concluded that azeotropic distillation is the optimal method for the recovery of organic nitroxyl radicals in aqueous oxidations of carboyhdrates.[8b]

The *sol–gel* technology offers several advantages over the classical immobilization procedures employed in the preparation of heterogeneous catalysts.[10] Depending on the needed utilization, sol–gel materials employed in catalysis are microporous (pore sizes < 15 Å) or mesoporous (20–100 Å); very often, provided that the reagents in solution have smaller size than the average pore diameter, these materials afford superior catalytic performances compared with similar heterogeneous catalysts prepared by classical impregnation or surface derivatization methods.[11] Inorganic sol–gel supports are indeed superior in their thermal stability, inertness towards and protectability of the entrapped molecules, and in their porosity and high surface areas (several hundreds of $m^2\ g^{-1}$); moreover, the sol–gel doped materials show chromatographic properties, *i.e.* they *concentrate* the reagent at the surface enhancing (even by orders of magnitude) the chemical sensitivity and selectivity of the reactions with the dopant.[10]

Here we report that sol–gel silica organically modified with TEMPO (Scheme 1) is an effective, recyclable catalyst for the NaOBr oxidation of sugars into uronates.† The TEMPO moiety was tethered to $(CH_3O)_3Si(CH_2)_3NH_2$ by reductive amination of TEMPON (4-oxo-TEMPO). The reaction was followed by FTIR where the C=O peak at 1720 cm^{-1} decreased rapidly and the C=N peak increased at 1670 cm^{-1} showing clear evidence of CO amination. The C=N bond was thus reduced with $NaBH_3CN$ and the radical monomer homogeneously entrapped within a silica matrix by the sol–gel process, *i.e.* by hydrolysis and co-polycondensation of the radical precursor with $Si(OCH_3)_4$ in aqueous methanol.

The catalyst was then used in the oxidation of MGP to the corresponding uronic acid.† In each reaction run no other products apart from the uronate (whose content was also

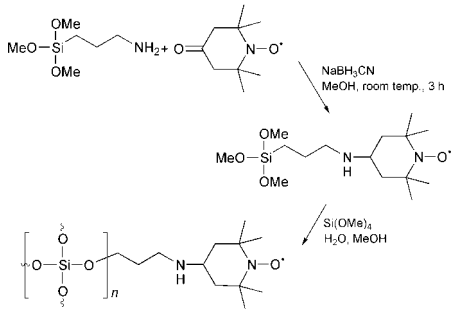

Scheme 1

† Electronic Supplementary Information (ESI) available: details of the preparation of a typical catalyst and its use in the oxidation of MGP to the corresponding uronate. See http://www.rsc.org/suppdata/cc/b0/b003096l/

DOI: 10.1039/b003096l

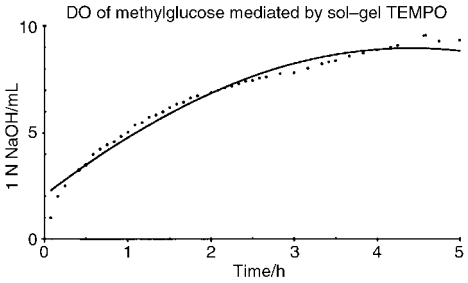

Fig. 1 The kinetics of the selective oxidation of MGP with NaOBr mediated by sol–gel entrapped TEMPO.

measured with the colorimetric test for uronic acids[12]) were detected in the reaction mixture and the catalyst retained its activity, as well as its shape and appearance, in the 4 consecutive reaction cycles in which it was tested affording at each run a high degree of oxidation (DO, *ca*. 95%); no leaching of entrapped radicals in solution was detected (with a spectroscopic limit of detection of 10 ppm). This is important since many heterogeneous oxidations can actually be promoted by catalyst leached in solution.[13] Separating the catalyst from the reaction mixture shortly (30 min) after the beginning the oxidation, we tested the mother liquor and no extra formation of uronate was observed (Fig. 1).

According to the known stability of sol–gel materials mentioned above, we observed high activity of the material and *no* modification of the EPR spectrum of the doped glass before *and* after the oxidative runs (Fig. 2). Comparing the EPR spectra of sol–gel silica TEMPO and TEMPO impregnated on commercial silica, Lev *et al.* reported that sol–gel TEMPO yields absorption peaks similar to TEMPO dissolved in H_2O, *i.e.* considerably *narrower* than those shown by TEMPO impregnated on SiO_2; since the width of EPR absorption peaks is inversely proportional to the speed of rotational motion of the molecule containing unpaired electrons (spin label), this means that the molecular environment sensed by TEMPO within sol–gel hydrophilic cages closely resembles that sensed by *free* radicals in H_2O.[14] With our organically modified silica (Ormosil), the radicals experience a situation in between these extremes, *i.e.* they are entrapped within sol–gel hydrophilic cages which resemble the aqueous medium *but* are limited in motion due to covalent linkage to the cage surface, resulting in EPR peaks of width comparable to impregnated TEMPO (Fig. 2). To explain the low activity and lack of recyclability of TEMPO linked to commercial aminopropyl silica (BioSil-NH_2),[8] one should consider that surface derivatization requires the formation of a new covalent bond through a slow *heterogeneous* reaction and leaves the anchored molecule unprotected at the pore surface; the sol–gel entrapment, on the other hand, greatly protects the radical *within* the silica cage of the final xerogel starting from an *homogeneous* solution of the dopant species in the alcoholic solution of silicon alkoxide. Furthermore, within the sol–gel cage the entrapped radical senses a hydrophilic environment similar to that of polar aqueous solutions; these cages in fact contain all types (vicinal, geminal, isolated) of silanol groups as well as water and methanol molecules and it is in this inner surface that reactions take place due to the internal porosity and accessibility of the cages (380 $m^2\ g^{-1}$ *vs.* few $m^2\ g^{-1}$ of the outer surface regions of the gel).[10,11] It may be assumed that the hydrophilic nature of the cage favours the diffusion of hydrophilic sugar molecules toward the active oxoammonium ion tethered at the surface of the cage. In fact, the origin of selectivity of sol–gel entrapped catalysts, which has also been observed in other cases,[11] has been attributed to two factors: the effect of the spatial confinement of the narrow pores, imposing a specific approach of the substrate to the catalysts *and* the participation of the intracage silanol groups in hindering free tumbling of the substrate molecule, directing specific orientational approach to the catalyst through the hydrogen bonds between the substrate and the pore–cage surface.

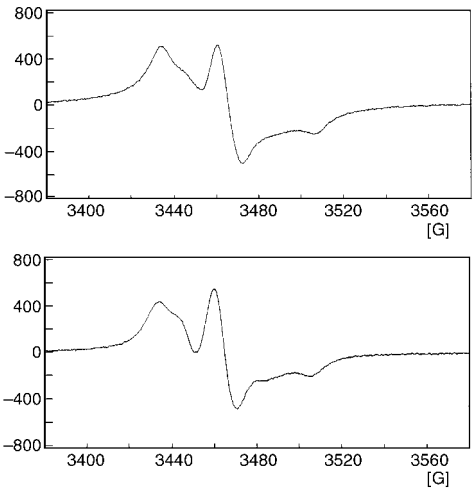

Fig. 2 The EPR spectrum of sol–gel entrapped TEMPO does not change before (a) and after (b) 4 consecutive reaction runs.

In conclusion, we found that sol–gel entrapped TEMPO is an efficient heterogeneous catalyst for the selective oxidation of D-methylglucose rapidly (turnover frequency $\sim 5\ h^{-1}$) affording high yields of the uronate and retaining its activity and selectivity upon several consecutive reaction cycles. The rates are 15 times lower than an homogeneous reaction[3] due to diffusional limitations imposed by the narrow pore network. A limitation, however, that is balanced by the advantages of the heterogenization. With the aim of practical, industrial application where continuous processes are often sought[15] it should be kept in mind that fundamental properties of the sol–gel catalytic materials (including the form: monoliths, rods, granules, powders and films, surface area, hydrophobicity, *etc*.) can be *tailored*, varying parameters such as the ratio of metal to H_2O, the amount of alcohol employed as co-solvent, the nature of alkoxide, the pH, the temperature, the drying time and other important parameters. These and other aspects have been patented.[16]

We thank Professor Mariella Brai (Institute of Medical Physics, Palermo) for the EPR measurements, and Dr. Filippo Saiano (Laboratory of Agricultural Chemistry, Palermo) for the FTIR measurements *and* for his continuous support. This work has been inspired by Arjan de Nooy's pioneering work: M. P. thanks him for sharing his intelligence with him throughout recent years. D. A. thanks the Israel Science Foundation for supporting this study.

Notes and references

1 M. Boiret and A. Marty, *J. Chem. Ed.*, 1986, **63**, 1009.
2 A. E. J. de Nooy, A. C. Besemer and H. van Bekkum, *Synthesis*, 1996, 1153.
3 A. E. J. de Nooy, A. C. Besemer and H. van Bekkum, *Tetrahedron*, 1995, **51**, 8023.
4 H. Röper, *Starch*, 1990, **42**, 342.
5 K. Li and R. F. Helm, *Carbohydr. Res.*, 1995, **273**, 249.
6 T. Miyazawa, T. Endo and M. Okawara, *J. Polym. Sci., Polym. Chem. Ed.*, 1985, **23**, 1527; T. Miyazawa, T. Endo and M. Okawara, *J. Polym. Sci., Polym. Chem. Ed.*, 1985, **23**, 2487.
7 T. Osa, U. Akiba, I. Segawa and J. M. Bobbitt, *Chem. Lett.*, 1988, 1423.
8 (*a*) A. Heeres, H. van Doren, K. F. Gotlieb and I. P. Bleeker, *Carbohydr. Res.*, 1997, **299**, 221; (*b*) A. Heeres, H. A. van Doren, K. F. Gotlieb and I. P. Bleeker, *WO 96/36621*, 1996.
9 C. T. Bolm and T. T. Frey, *Chem. Commun.*, 1999, 1795.
10 D. Avnir, *Acc. Chem. Res.*, 1995, **28**, 328.
11 J. Blum, D. Avnir and H. Schumann, *Chem. Tech.*, 1999, **29** (2), 32.
12 N. Blumenkrantz and G. Asboe-Hansen, *Anal. Biochem.*, 1973, **54**, 484.
13 R. A. Sheldon, M. Wallau, I. C. Arends and U. Schuchardt, *Acc. Chem. Res.*, 1998, **31**, 485.
14 A. Shames, O. Lev and B. Iosefzon-Kuyavskaia, *J. Non-Cryst. Solids*, 1994, **175**, 14.
15 M. Kunz and C. Recker, *Carbohydates in Europe*, 1995, **13**, 11.
16 M. Pagliaro, D. Avnir, G. Deganello and J. Blum, *WO 99/47258*, 1999.

Photocatalytic performance of TiO_2 and Fe_2O_3 immobilized on derivatized polymer films for mineralisation of pollutants

M. R. Dhananjeyan, J. Kiwi and K. Ravindranathan Thampi*

Laboratory of Photonics and Interfaces (LPI), Swiss Federal Institute of Technology (EPFL), CH-1015 Lausanne, Switzerland. E-mail: ravindranathan.thampi@epfl.ch

Received (in Oxford, UK) 17th April 2000, Accepted 15th June 2000

TiO_2, Fe_2O_3 and Fe^{3+} have been immobilized on low cost polyethylene films containing anhydride anchoring groups showed enhanced mineralisation rates for chlorophenols and Orange II, compared to previously reported immobilized catalysts with rates which are comparable to or greater than catalytic suspensions.

Photocatalysis and photo-Fenton processes are able to break down many organic pollutants totally or partially so that cheaper biological processes can be used as a second stage to achieve complete mineralisation. Since photocatalysts are often applied as suspensions, costly problems associated with catalyst leaching, settling, flocculation and the need for eventual catalyst separation by filtration during post treatment, hinders their wide scale application in industry. In systems using photo-Fenton processes, removal of Fe ions after treatment is expensive. Therefore, catalyst immobilisation related research has attracted wide attention.[1] Simple coating[2,3] of the catalyst over glass, ceramics and polymers often lead to catalyst leaching and dissolution. There are reports on buoyant TiO_2-coated glass micro-bubbles[4] and polystyrene beads made by thermal treatment.[5] Immobilized catalysts may show reduced activity. Another problem generally noticed is the chemical attack by OH· radicals on the polymer substrates.[6] Photocatalysts immobilized on Nafion films[1] are expensive.

The present study was targeted to produce stable and efficient photocatalysts on low cost polymers, which could be used over many cycles without loss of activity. Chlorophenols and azo dyes like Orange II have been selected as model pollutants. The immobilized photocatalysts are based on TiO_2, Fe_2O_3 and Fe^{3+}.

In order to bind catalyst particles on the polymer, suitable anchor groups are required on the polymer surface. In this study, a polyethylene based anhydride-modified block copolymer (30 μm), specially prepared by E.I. Dupont de Nemours & Company, was used.

To prepare the immobilized catalyst,[7] the anhydride derivatized polyethylene film is washed with water before immersing in an aqueous suspension containing 5 g L^{-1} TiO_2 (Degussa P25). The suspension was sonicated 30 min prior to use. Together with the polymer, it is then heated to 75 °C for 1 h. The film was dried at 100 °C and washed with water to remove the loosely attached TiO_2 particles. For anchoring Fe_2O_3, α-Fe_2O_3 was used as the powder precursor and for Fe^{3+}, $FeCl_3$ (Fluka) was used as the starting compound.

Photocatalytic experiments were carried out using a 125 W medium pressure mercury lamp (2.5×10^{15} photons s^{-1}; λ = 360–390 nm) when TiO_2 is used and a Hanau Suntest lamp (80 mW cm^2 total intensity; 1.6×10^{16} photons s^{-1}; λ = 350–560 nm) for experiments using Fe_2O_3 and Fe^{3+} coated layers. The short UV radiation was filtered by the Pyrex wall of the reaction vessel. The decrease in the concentration of chlorophenols and Orange II was monitored by means of UV–VIS absorption spectroscopy and Total Organic Carbon (TOC) analyser. In control experiments with light, but without catalysts, the reactions did not proceed. Merckoquant paper® was used for estimating peroxide concentration.

Illumination of chlorophenol solutions (0.5 mM) in the presence of oxygen and TiO_2 coated films, at pH 6, results in rapid mineralisation of the organic compound. Fig. 1 shows the gradual decrease of TOC value of the chlorophenol solutions: 2-chlorophenol (Fig. 1A), 4-chlorophenol (Fig. 1B) and 2,4-dichlorophenol (Fig. 1C). 95% degradation was observed within 10 h for 2-chlorophenol. For both 4-chlorophenol and 2,4-dichlorophenol this time period was only 9 h. Control experiments showed no dark reaction on TiO_2 layers. The pseudo-first-order rate constants for the total mineralization of 2-chlorophenol (2-CP), using polymer–TiO_2 and powder suspensions (75 mg L^{-1} TiO_2), are 1.5×10^{-4} and 7.5×10^{-4} s^{-1}, respectively. For 4-CP, the rate constants are 1.7×10^{-4} s^{-1} for polymer–TiO_2 and 2.3×10^{-4} s^{-1} for the suspension (75 mg L^{-1}). For 2,4-DCP, the polymer catalyst showed a rate constant of 1.2×10^{-3} s^{-1}. With a higher amount of TiO_2 (1 g L^{-1}) suspension, the pseudo-first-order rate constant is determined as 1.5×10^{-3} s^{-1} for 2,4-DCP.

It is interesting to compare the results obtained with TiO_2 suspensions containing 25, 75, 500 and 1000 mg L^{-1}, with data using polymer–TiO_2, for the same reactions. With 75 mg L^{-1} suspension, the photocatalytic activity for 2-CP and 4-CP are

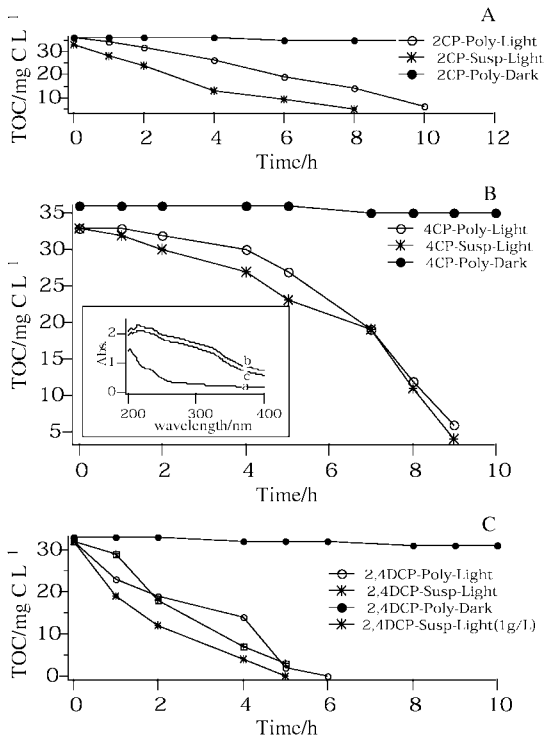

Fig. 1 Photocatalytic degradation of chlorophenols on TiO_2 coated polymer (size of sheet: 12 × 4 cm). A, [2-Chlorophenol]: 0.5 mM; poly: catalyst on polymer, susp: catalyst (75 mg L^{-1}) as a suspension. B, [4-Chlorophenol]: 0.5 mM; other descriptions as above. C, [2,4-Dichlorophenol]: 0.5 mM. The inset in Fig. 1B shows (a) the absorption spectra of polymer film, (b) TiO_2 coated film before use and (c) after six cycles.

DOI: 10.1039/b003108i

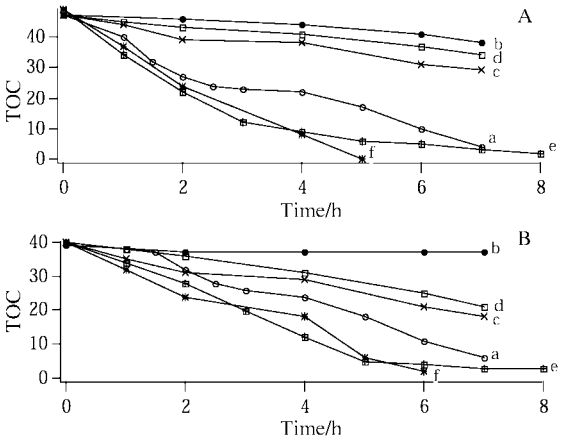

Fig. 2 Photo-Fenton degradation of 4-chlorophenol and Orange II on Fe_2O_3 polymer (size of sheet: 12 × 4 cm). A, [4-Chlorophenol]: 0.7 mM: (a): 4-CP-poly-Light; (b) Dark; $[H_2O_2]$ = 0.01 M; (c): 4-CP-susp1-Light; $[H_2O_2]$ = 0.001 M; Fe_2O_3 = 25 mg L^{-1} (d): 4-CP-susp2-Light; $[H_2O_2]$ = 0.001 M; Fe_2O_3 = 75 mg L^{-1} (e): 4-CP-susp3-Light; $[H_2O_2]$ = 0.01 M; Fe_2O_3 = 25 mg L^{-1} (f): 4-CP-susp1-Light; $[H_2O_2]$ = 0.01 M; Fe_2O_3 = 75 mg L^{-1}; poly: catalyst on polymer, susp: catalyst as a suspension. B, [Orange II] = 0.2 mM; $[H_2O_2]$ = 0.01 M. Curve (a): OrII-poly-Light; curve (b): Dark; $[H_2O_2]$ = 0.01 M, other descriptions as in Fig. 2A.

comparable to the activity of the TiO_2 layer on the catalyst. By increasing TiO_2 to 0.5–1 g L^{-1}, complete mineralisation was obtained in *ca.* 6 h, compared to 9 h recorded for the TiO_2–polymer. However the amount of TiO_2 in the polymer is only 1.5 mg (48 cm^2 sheet size), corresponding to 37 mg L^{-1}. This shows that TiO_2 layers on the derivatized polymer are twice as efficient as a photocatalyst compared to the corresponding suspensions (3 mg in 40 mL dispersion). The reaction rates as well as the total mineralisation time of 2,4-DCP are similar when data of polymer catalyst and TiO_2 (1 g L^{-1} suspension) are compared, in which case the polymer catalyst is 25 times more active than the powder suspension. Since the polymer is transparent, it will not block light from reaching the photocatalyst during illumination. Furthermore, the TiO_2 particles do not mask each other from light and in a way are far more effectively dispersed than powder suspensions. When particles are suspended in water, besides causing shadows, they tend to aggregate causing inefficient surface utilization.

The inset Fig. 1B shows the change in light absorption by the TiO_2 polymer film before and after using six illumination cycles. We did not find any TiO_2 in solution when analysed by high resolution inductively coupled plasma spectrometry. The activity of the immobilized catalyst did not decrease during six runs. This confirms that the adhesion of TiO_2 is aided due to the chemical bond formed between the TiO_2 surface and the anhydride groups on the polymer. There is no significant change in the BET surface area of the loaded (1.45 m^2 g^{-1}) and unloaded sample (1.34 m^2 g^{-1}).

The TOC values never increased during the photodegradation run, indicating that the polymer is not chemically attacked by OH· radicals. Recycling experiments were carried out six times and no decrease in catalytic activity for the film was noticed.

The pH before the reaction was 6 and it decreased to 4.2 during the reaction. This is due to the production of HCl as a reaction product. It was also found that the H_2O_2 concentration, due to the formation and consumption of H_2O_2, was steady at *ca.* 0.5 mg L^{-1} throughout the reaction. The formation of H_2O_2 proceeds due to the capture of conduction band electrons by dissolved O_2.[8] There was no need to add H_2O_2 to effect the degradation of the organic compounds.

Illumination of aqueous solutions of 0.7 mM 4-chlorophenol and 0.2 mM Orange II in the presence of Fe_2O_3 coated polymer film and H_2O_2 results in mineralisation of the above compounds at pH 3. Fig. 2 shows the degradation of 4-chlorophenol (Fig. 2A) and Orange II (Fig. 2B) on Fe_2O_3 polymer film at pH 3. The pseudo first-order rate constants for Fe_2O_3 polymer and Fe_2O_3 suspension are 4.6 × 10^{-4} and 8.7 × 10^{-4} s^{-1}, respectively.

To compare the catalyst loaded polymer and the corresponding powder suspension, four experiments with different weights of iron oxide and different concentrations of $[H_2O_2]$ were also carried out. It was found that with 25 mg L^{-1} Fe_2O_3 susension and 1 mM H_2O_2 (4CP-susp1-Light, in Fig. 2A), the degradation was slower than with the polymer catalyst indicating that the production of OH· radical is not sufficient. When the amount of iron oxide is increased three times without simultaneously increasing H_2O_2 (4CP-susp2-Light), the rate of degradation was much slower. When $[H_2O_2]$ is increased ten times, maintaining the same weight of iron oxide as 4CP-susp1-Light (4CP-susp3-Light), the rate of degradation also increased. This rate is comparable to that observed with the polymer catalyst and is also higher than 4CP-susp1-Light and 4CP-susp2-Light. In this situation, the Fe^{3+} and Fe^{2+} cycle proceeds and hence the OH· radical production is higher than in the other two cases. Here, the degradation of the compound is moderate and the activity is equal to that of the polymer catalyst. When both iron oxide and $[H_2O_2]$ are increased three times and ten times respectively (4CP-susp4-Light), the rate of degradation is found to be faster than with the polymer catalyst. This confirms that an increased production of OH· radical and increased light absorption by the particle are both necessary to attain higher activity when the catalyst is in a suspended form.

The same trend was observed for degradation of Orange II and it takes 7 h to achieve 90% degradation as shown in Fig. 2B. No Fe^{3+} or Fe^{2+} was detected in solution, using thiocyanate as a complexing agent for Fe^{3+} and phenanthroline for Fe^{2+}. There was no change in the absorption spectra of Fe_2O_3 layers before and after six experimental cycles and this confirms the stability of the loaded Fe_2O_3 polymer film. The BET surface areas of the naked polymer film and Fe_2O_3 loaded film were measured and a noticeable surface area change was observed for the loaded polymer (2.77 m^2 g^{-1}) when compared to the free polymer (1.34 m^2 g^{-1}).

Illumination of aqueous solutions of 0.7 mM 4-CP and 0.2 mM Orange II in the presence of Fe^{3+} ions, loaded polymer film and H_2O_2 results in complete mineralisation of these compounds at pH 3 and no dark degradation was observed. The results were similar to those shown in Fig. 2A and B.

For comparison between polymer catalyst and the corresponding suspensions, experiments with homogeneous $[Fe^{3+}]$ and $[H_2O_2]$ solutions were carried out. By changing the Fe^{3+} and H_2O_2 concentrations, it was concluded that the polymer loaded film requires a lower amount of Fe^{3+} and H_2O_2, when compared to the amount required in homogeneous Fenton systems.

Stable immobilized TiO_2, Fe_2O_3 and Fe^{3+} on low cost derivatized polymer films do not compromise the catalytic activity of the powders. These composite catalysts are shown to be efficient for the photodegradation of industrial pollutants like chlorophenols and an azo-dye Orange II. The immobilized catalysts were shown to be stable in acidic as well as slightly basic (pH 9) media.

Notes and references

1 J. Fernandez, J. Bandara, A. Lopez, P. Albers and J. Kiwi, *Chem. Commun.*, 1998, 1493.
2 U. Stafford, K. A. Gray and P. V. Kamat, *J. Phys. Chem.*, 1994, **98**, 6343.
3 H. Al-Ekabi and N. Serpone, *J. Phys. Chem.*, 1988, **92**, 5726.
4 J. Schwitzgebel, J. G. Ekerdt, H. Gerischer and A. Heller, *J. Phys. Chem.*, 1995, **99**, 5633.
5 M. E. Fabiyi and R. L. Skelton, *J. Photochem. Photobiol. A: Chem.*, 2000, **132**, 121.
6 B. Ranby and J. F. Rabeck, in *Photodegradation, Photo-oxidation and Photostabilization of Polymers*, J. Wiley & Sons, London, 1975, p. 290.
7 K. R. Thampi, Patent filed (EPFL).
8 K. R. Thampi, T. V. Reddy, V. Ramakrishnan and J. C. Kuriacose, *J. Indian Chem. Soc.*, 1983, **60**, 1156.

Remote asymmetric induction by using the 1,3-migration reaction of (diene)iron tricarbonyl complexes

Yoshiji Takemoto,* Kiyonori Ishii, Asami Honda, Kazuya Okamoto, Reiko Yanada and Toshiro Ibuka

Graduate School of Pharmaceutical Sciences, Kyoto University, Sakyo-ku, Kyoto 606-8501, Japan. E-mail: takemoto@pharm.kyoto-u.ac.jp

Received (in Cambridge, UK) 12th June 2000, Accepted 21st June 2000

Novel strategies for the stereoselective synthesis of molecules with remote stereogenic centers across double bonds have been developed *via* organoiron methodology allowing highly diastereoselective syntheses of 1,8- and 1,10-diol $Fe(CO)_3$ complexes using the stereospecific 1,3- and 1,5-migration of an $Fe(CO)_3$ group; this strategy could be used for stereoselective functionalization of remote terminal substituents on acyclic polyene compounds.

One of the more challenging aspects of organic synthesis is the stereoselective construction of molecules with remote (*i.e.* greater than 1,3-related) stereogenic centers with high levels of diastereo- and enantioselectivity.[1] A particularly challenging goal would be the development of a general strategy for the control of remote stereogenic centers related across double bonds of fixed configuration, because this moiety is present in many natural products, including polyene macrolide antibiotics such as filipin III.

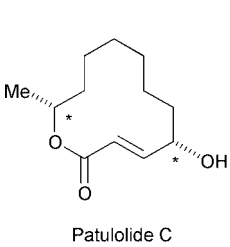

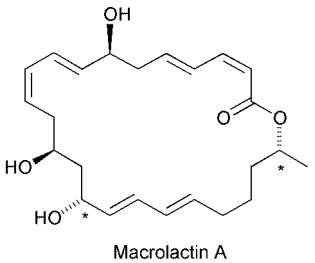

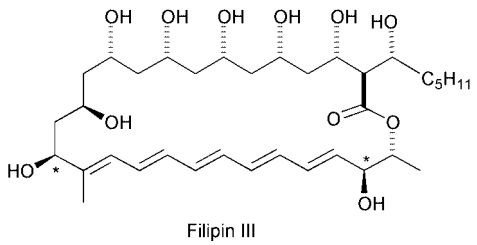

In the course of our studies on the mobility of the $Fe(CO)_3$ group on polyenes with the aim of constructing several stereogenic centers using a single chiral auxiliary,[2] we have found that the $Fe(CO)_3$ moiety of (triene)$Fe(CO)_3$ complexes shifts to the electron-deficient double bond stereospecifically on treatment with a base such as potassium bis(trimethylsilyl)-amide (KHMDS) and NaH. By taking advantage of this 1,3-migration of the $Fe(CO)_3$ group, the (polyenone)$Fe(CO)_3$ complexes **B** could be converted *via* **C** into the corresponding migrated complexes **D**, where the $Fe(CO)_3$ groups are situated in the ideal position for controlling several reactions of the ketone (Scheme 1). We herein report a novel strategy for highly diastereoselective preparation of polyene- and saturated 1,8- and 1,10-diols **E** and **F** by a combination of the 1,3- or 1,5-migration of the $Fe(CO)_3$ group and subsequent hydride reduction of the ketone, together with a formal asymmetric synthesis of epipatulolide C.

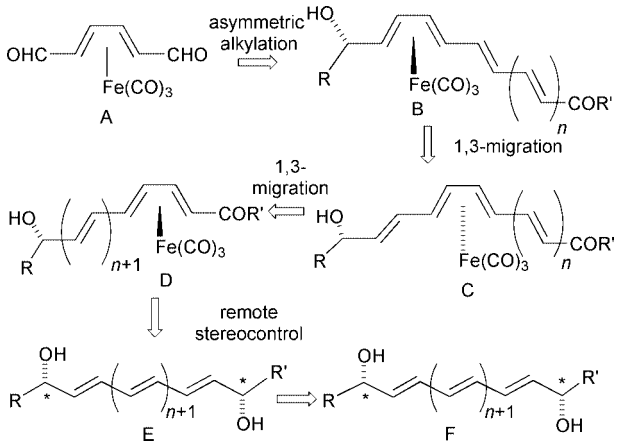

Scheme 1 Remote stereocontrol based on the 1,3-migration concept of an $Fe(CO)_3$ group.

The requisite (trienone)- and (tetraenone)$Fe(CO)_3$ complexes **2** and **8** were prepared from the chiral aldehydes **1** and **7** (Scheme 2).[3] We first examined the 1,2-reduction of the α,β-unsaturated ketone **2** *via* 1,4-asymmetric induction. In contrast to the reduction of (dienone)$Fe(CO)_3$ complex,[4] the reduction of **2** with sodium borohydride in methanol in the presence of $CeCl_3{\cdot}6H_2O$ gave a nearly equimolar ratio of the two diastereomeric trienol complexes.[5] To overcome this problem, we next

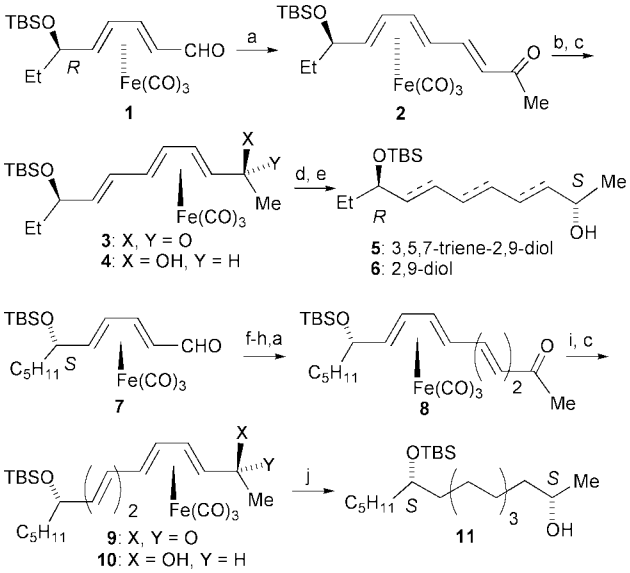

Scheme 2 *Reagents and conditions*: (a) $CH_3COCH_2P(O)(OMe)_2$, $LiOH{\cdot}H_2O$, MeOH (90% for **1**, 78% for **7**); (b) NaH, THF (81%), (c) $NaBH_4$, MeOH (91% for **3**, 72% for **8**); (d) H_2O_2, 1 M NaOH, MeOH, 0 °C (83%); (e) H_2, PtO_2, AcOEt (85%); (f) $(EtO)_2P(O)CH_2CN$, NaH, THF, 0 °C (69%); (g) DIBAL-H, −50 °C (49%); (h) n-Bu_3P, CH_2Cl_2 (71%); (i) $KN(SiMe_3)_2$, THF, 0 °C (70%); (j) H_2O_2, 1 M NaOH; H_2, PtO_2 (89%).

DOI: 10.1039/b004671j

investigated the 1,2-reduction of the 1,3-migrated complex **3**, which was easily accessible from **2** by the stereospecific 1,3-migration of the $Fe(CO)_3$ group. According to the reported procedure,[2] **2** was treated with 1.5 equiv. of NaH in THF at 0 °C to give the desired product **3** in 81% yield along with the recovered starting material (2%). The stereochemistry of **3** was deduced from the previous result, namely, that the 1,3-migration of the $Fe(CO)_3$ group proceeded with inversion of configuration. In contrast to **2**, the reduction of the migrated product **3** with $NaBH_4$ provided the alcohol **4** as the single isomer in 91% yield. The desired 3,5,7-triene-2,9-diol **5** was easily synthesized by reaction of **4** with 30% hydrogen peroxide in the presence of 1 M NaOH solution. Furthermore, subsequent hydrogenation of **5** on platinum oxide in AcOEt gave the 1,8-*anti*-diol **6** in 85% yield. To confirm the absolute stereochemistry, the diastereomerically pure alcohol **6** was converted into the corresponding (*R*)- and (*S*)-MTPA esters, respectively. As expected, the absolute stereochemistry of the C2 position was revealed to be (*R*)-configuration by comparing their ^1H NMR spectra.[6]

To extend the applicability of this method, we next examined the reduction of the (tetraenone)$Fe(CO)_3$ complex **8**, which was prepared stereoselectively from **7** in 4 steps. The key reaction in this case would be a double 1,3-migration reaction of the $Fe(CO)_3$ group (*i.e.*, 1,5-migration). Then we investigated the migration reaction of **8** with several bases. Although we could not obtain the migration product by treatment of **8** with NaH, the reaction of **8** with 0.3 equiv. of KHMDS in THF at 0 °C provided the 1,5-migration product **9** in 70% yield along with the recovered starting material (7%). In the latter case, the 1,3-migration product of the $Fe(CO)_3$ group, an intermediate of the 1,5-migration reaction, could not be observed in the crude reaction mixture. Similarly, the reduction of **9** with $NaBH_4$ in methanol gave rise to the alcohol **10** in 72% yield as a single isomer. The transformation of **10** into **11** was performed by the same reaction sequence as that of **4** to give the 1,10-*syn*-diol **11** in 89% yield. The absolute stereochemistry was also determined by the MTPA-ester method.[6] The result revealed that the 1,5-migration of the $Fe(CO)_3$ group should occur with retention of configuration as a result of a double inversion mechanism.

Finally, we applied this method to a formal asymmetric synthesis of epipatulolide C (Scheme 3).[7] By a similar 5-step sequence, the chiral aldehyde **12** was transformed into the (2*S*,9*R*)-triol derivative **13** as a single isomer. After protection and deprotection of the hydroxy groups of **13**, the resulting alcohol was oxidized, and Wittig condensation of the aldehyde so obtained and subsequent removal of the TBS group gave the unsaturated ester **14**, which had been converted into racemic epipatulolide C in three steps.

This work shows how a combination of the mobility and the stereodirecting ability of the $Fe(CO)_3$ group can be used to prepare stereoselectively compounds with remote stereogenic centers. Further applications to the construction of more remote stereogenic centers across double bonds are underway in these laboratories.

This article is dedicated to the memory of Professor Toshiro Ibuka. This work was supported in part by The Japan Health Sciences Foundation, Suzuken Memorial Foundation and Grant-in-Aid for Scientific Research (C) from the Ministry of Education, Science, Sports, and Culture, Japan.

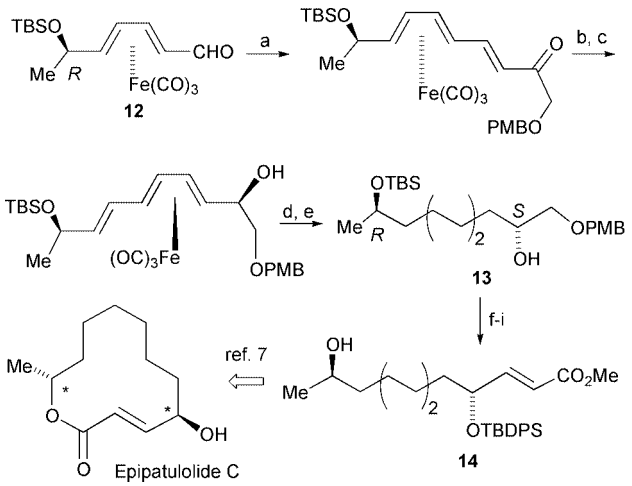

Scheme 3 *Reagents and conditions*: (a) $PMBOCH_2COCH_2P(O)(OEt)_2$, *t*-BuOH, toluene (54%); (b) KHMDS (0.1 eq.), THF, 0 °C (62%); (c) $NaBH_4$, MeOH (83%); (d) H_2O_2, NaOH; (e) H_2, PtO_2 (89%); (f) TBDPSCI, imidazole (64%), (g) DDQ (72%); (h) Swern oxidation; $Ph_3P{=}CHCO_2Me$ (69%); (i) AcOH, THF, H_2O (74%).

Notes and references

1 E. K. Dorling and E. J. Thomas, *Tetrahedron Lett.*, 1999, **40**, 471–474; Y. Tamai, T. Hattori, M. Date, S. Koike, Y. Kamikubo, M. Akiyama, K. Seino, H. Takayama, T. Oyama and S. Miyano, *J. Chem. Soc., Perkin Trans. 1*, 1999, 1685; H. J. Mitchell, A. Nelson and S. Warren, *J. Chem. Soc., Perkin Trans. 1*, 1999, 1899; M. Sugiura, Y. Yagi, S.-Y. Wei and T. Nakai, *Tetrahedron Lett.*, 1998, **39**, 4351; S. V. Ley, L. R. Cox, B. Middleton and J. M. Worrall, *Chem. Commun. (Cambridge)*, 1998, 1339; P. T. Bell, B. Dasgupta and W. A. Donaldson, *J. Organomet. Chem.*, 1997, **538**, 75; H. Fujioka, H. Kitagawa, N. Matsunaga, Y. Nagatomi and Y. Kita, *Tetrahedron Lett.*, 1996, **37**, 2245.

2 Y. Takemoto, K. Ishii, Y. Miwa, T. Taga, T. Ibuka, S. Nakao and T. Tanaka, *Tetrahedron Lett.*, 2000, **41**, 85.

3 Y. Takemoto, Y. Baba, A. Honda, S. Nakao, I. Noguchi, C. Iwata, T. Tanaka and T. Ibuka, *Tetrahedron*, 1998, **54**, 15 567; Y. Takemoto, Y. Baba, I. Noguchi and C. Iwata, *Tetrahedron Lett.*, 1996, **37**, 3345.

4 M. Franck-Neumann, P. Bissinger and P. Geoffroy, *Tetrahedron Lett.*, 1997, **38**, 4473; N. A. Clinton and C. P. Lillya, *J. Am. Chem. Soc.*, 190, **92**, 3058.

5 K. Nunn, P. Mosset, R. Gree and R. W. Saalfrank, *J. Org. Chem.*, 1992, **57**, 3359; M. Franck-Neumann, P.–J. Colson, P. Geoffroy and K. M. Taba, *Tetrahedron Lett.*, 1992, **33**, 1903.

6 I. Ohtani, T. Kusumi, Y. Kashman and H. Kakisawa, *J. Am. Chem. Soc.*, 1991, **113**, 4092.

7 E. K. Dorling, A. P. Thomas and E. J. Thomas, *Tetrahedron Lett.*, 1999, **40**, 475; F. M. C. Leemhuis, L. Thijs, B. Zwanenburg, *J. Org. Chem.*, 1993, **58**, 7170; H. Yang, H. Kuroda, M. Miyashita and H. Irie, *Chem. Pharm. Bull.*, 1992, **40**, 1616; K. Mori and T. Sakai, *Annalen*, 1988, 13.

Typeset and printed by Black Bear Press Limited, Cambridge, England

ChemComm
FEATURE ARTICLE

Catalytic enantioselective 1,3-dipolar cycloaddition reactions of nitrones

Kurt V. Gothelf and Karl Anker Jørgensen

Center for Metal Catalyzed Reactions, Department of Chemistry, Aarhus University, DK-8000 Aarhus C, Denmark. E-mail: kaj@kemi.aau.dk

Received (in Cambridge, UK) 8th June 2000, Accepted 15th June 2000
Published on the Web 11th July 2000

The rapid developments in the field of catalytic enantioselective 1,3-dipolar cycloaddition reactions of nitrones which have occurred during the last six years are reported. A series of catalysts has been applied for both the normal electron-demand and inverse electron-demand 1,3-dipolar cycloaddition reaction of nitrones with electron-deficient and electron-rich alkenes, respectively. In several cases a high degree of control of both the diastereo- and enantioselectivity has been achieved.

Introduction

After the Diels–Alder reactions, the second most important cycloaddition reaction is probably the 1,3-dipolar cycloaddition.[1] The 1,3-dipolar cycloaddition reaction of nitrones with alkenes in particular has received considerable attention in asymmetric synthesis over the past 15 years.[2,3] One of the reasons for the success of the synthetic application of nitrones is that, contrary to the majority of other 1,3-dipoles, most nitrones are stable compounds that do not require *in situ* formation. In the 1,3-dipolar cycloaddition reaction of nitrones with alkenes, up to three new contiguous chiral centers can be formed in the adduct (Scheme 1)[4,5] and the isoxazolidine formed can be

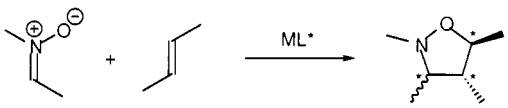

Scheme 1

transformed into numerous attractive building-block molecules for organic synthesis. The absolute majority of these 1,3-dipolar cycloaddition reactions are diastereoselective and involve chiral alkenes or nitrones.[2,3] It would, however, be highly desirable to develop a catalytic enantioselective version of this reaction. Compared to the successful development of the catalytic enantioselective Diels–Alder reaction in the late 1980s, the first examples of the catalytic enantioselective 1,3-dipolar cycloaddition reactions of nitrones did not appear until 1994.

In the early development of the catalytic enantioselective 1,3-dipolar cycloaddition reaction of nitrones with alkenes the catalysts were 'borrowed' from Diels–Alder chemistry, but in the more recent developments a series of catalysts that are optimised for the 1,3-dipolar cycloaddition reaction have been developed. A few catalysts are highly selective for both types of reaction.

In this article we wish to present to the reader an overview of this field, which has gone through rapid developments during the last six years. Several research groups have been engaged in the area and it has been attempted to include all the major contributions in which catalytic enantioselective reactions have been described. The article is divided into two major parts: (*i*) the normal electron-demand reactions and (*ii*) the inverse electron-demand reactions, which are two fundamentally different approaches to the catalytic control of the reaction. A final short part (*iii*) describing alternative catalytic approaches to the reaction is also included.

Normal electron-demand reactions

The relative FMO energies of the substrates of the 1,3-dipolar cycloaddition reaction are important for catalytic control of the reaction.[2,6,7] In order to be able to control the stereochemistry of the reaction with a sub-stoichiometric amount of a ligand–metal catalyst it is desirable that large reaction rate accelerations are obtained to assure that the reaction only takes place in the sphere of the metal and the chiral ligand. The strategy that was applied for the catalytic enhancement of the reaction rate has therefore been to alter the relative energies of the FMOs of one of the substrates using chiral Lewis acids.[6] This principle of activation can be applied to the 1,3-dipolar cycloaddition of nitrones in two different ways. The normal electron-demand involves the reaction of a nitrone with an electron-deficient alkene such as an α,β-unsaturated carbonyl compound. This reaction is primarily controlled by the interaction between $HOMO_{nitrone}$–$LUMO_{alkene}$ (Fig. 1). By the application of a Lewis acid (LA) catalyst which acts as an electron acceptor, the LUMO energy of the alkene is lowered by coordination of the α,β-unsaturated carbonyl to the Lewis acid. As a result of the decreased energy gap between the interacting FMO's a rate acceleration of the reaction is achieved.[6]

One of the problems related to the Lewis-acid activation of α,β-unsaturated carbonyl compounds for reaction with a nitrone is the competitive coordination of the nitrone and the α,β-unsaturated carbonyl compound to the Lewis acid (Scheme 2).[6] Calculations have shown that coordination of the nitrone to the Lewis acid is more feasible than a monodentate coordination of a carbonyl compound. However, this problem could be

Kurt Vesterager Gothelf (b. 1968) studied chemistry at Aarhus University, Denmark, and at Heidelberg University, Germany. He performed the two first years of his PhD studies under supervision of Professor K. B. G. Torssell and the last two under Professor K. A. Jørgensen. Following a period as a post-doctoral researcher in Professor K. A. Jørgensen's group he joined Professor M. C. Pirrung's group at Duke University. Since 1999 he has been an Assistant Professor at Aarhus University. His research interests range from asymmetric metal catalysis to studies and application of self-assembled monolayers in electron-transfer reactions.

Karl Anker Jørgensen (b. 1955) is Professor at Center for Metal Catalyzed Reactions, Department of Chemistry, Aarhus University, DK-8000 Aarhus C, Denmark. Following a PhD from Aarhus University 1984 and a post-doctoral period with R. Hoffmann, Cornell University, he joined the Aarhus University faculty. The development and understanding of metal-catalyzed reactions in organic chemistry is the main goal of his research.

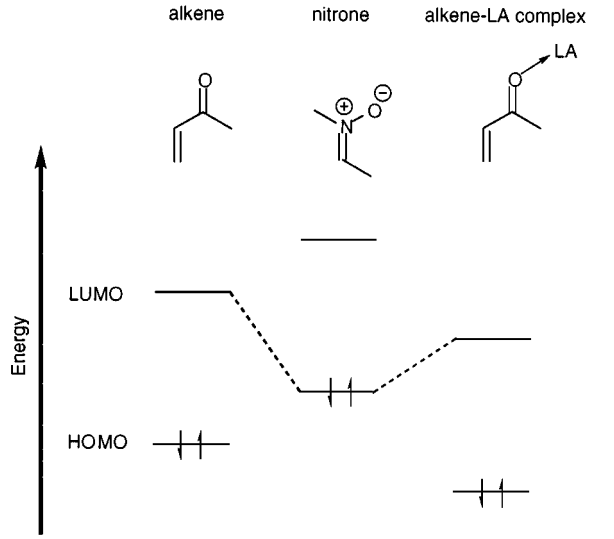

Fig. 1 The catalytic alteration of the alkene FMO's in the normal electron-demand 1,3-dipolar cycloaddition reaction.

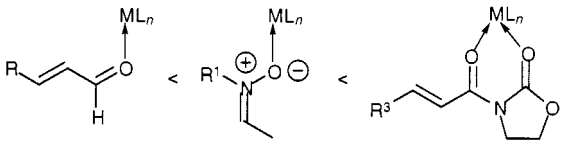

Scheme 2

circumvented by the application of alkenes such as 3-alkenoyl-oxazolidinones enabling a bidentate coordination to the Lewis acid which is favoured over the monodentate coordination.

Titanium catalysts

Several titanium(IV) complexes are efficient and reliable Lewis acid catalysts and they have been applied to numerous reactions, especially in combination with the TADDOL (α,α,α′,α′-tetraaryl-1,3-dioxolane-4,5-dimethanol) (**1**) ligands.[7–10] In the first study on normal electron-demand 1,3-dipolar cycloaddition reactions between nitrones and alkenes, which appeared in 1994, the catalytic effect of a series of chiral $TiCl_2$–TADDOLates on the reaction of nitrones **3** with alkenoyl-oxazolidinones **4** was studied (Scheme 3).[11] These substrates have turned out to be the model system of choice for most studies on Lewis-acid catalysed normal electron-demand 1,3-dipolar cycloaddition reactions of nitrones. When 10 mol% of the catalyst **2a** was applied in the reaction depicted in Scheme 3 the reaction proceeded to give a yield of up to 94%. The reaction led primarily to *exo*-**5** and in the best case an *endo*:*exo* ratio of 10:90 was obtained. The chiral information of the catalyst was transferred with a fair efficiency to the substrates as up to 60% ee of one of the isomers of *exo*-**5** was obtained.[11]

In the majority of $TiCl_2$–TADDOLate catalysed Diels–Alder and 1,3-dipolar cycloaddition reactions oxazolidinone derivatives are applied as auxiliaries for the alkenoyl moiety in order to obtain the favourable bidentate coordination of the substrate to the catalyst.[12] In a more recent study on 1,3-dipolar cycloaddition reactions the use of succinimide instead of the oxazolidinone auxiliary was introduced (Scheme 4).[13] The succinimide derivatives **6** are more reactive than **4** in the 1,3-dipolar cycloaddition reaction with nitrone **3a**. In the presence of the $TiCl_2$–TADDOLate catalyst **2a** (5 mol%), the reaction of **3a** with **6** (R = Me) gives *exo*-**7** as the only diastereomer. Additionally, the enantioselectivity of the reaction of 72% ee is also an improvement compared to the analogous reaction of the oxazolidinone derivative **4**. Similar improvements were obtained in reactions of other related nitrones.

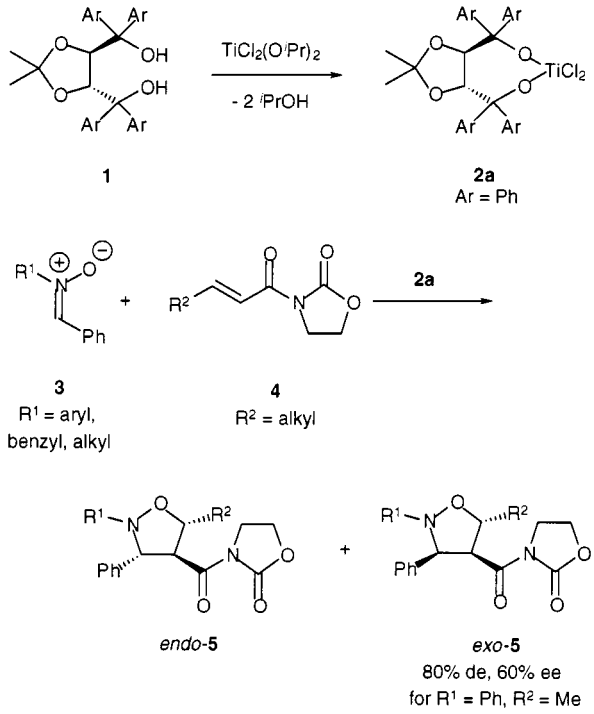

Scheme 3

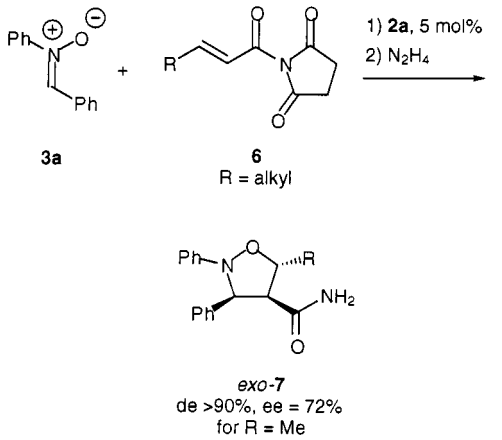

Scheme 4

In connection with the investigations of the $TiCl_2$–TADDOLate-catalysed 1,3-dipolar cycloaddition reactions between nitrones and alkenoyloxazolidinones, a complex between the chiral titanium catalyst and the alkene substrate **4c** was isolated (Scheme 5).[14] This crystalline compound **8** was characterised by X-ray crystallography and the X-ray structure showed that the oxazolidinone is coordinated to the titanium center in a bidentate fashion. The four oxygen atoms, two from the chiral ligand and two from **4c**, are located in a plane around the titanium center, while the two chloride ligands are located in the apical positions. This crystal structure is a highly valuable verification of how the mechanism of the catalytic activation is operating. To some extent, information can also be derived about how one of the faces of the alkene is shielded by the ligand leading to the enantioselective addition of the nitrone to the opposite face of the alkene. However, there are several other possible arrangements of the ligands around the titanium center and whether **8** actually represents the reactive intermediate has been the subject of some dispute.[15–18]

Based on the structure of intermediate **8**, investigations of the impact on the *endo/exo*-selectivity in the 1,3-dipolar cycloaddition reaction of changing the chloride ligands in the $TiCl_2$–TADDOLate catalyst **2a** to bulkier groups were performed.[19] In Table 1 some results of reactions between **3a** (R^1 = Ph) and **4a**

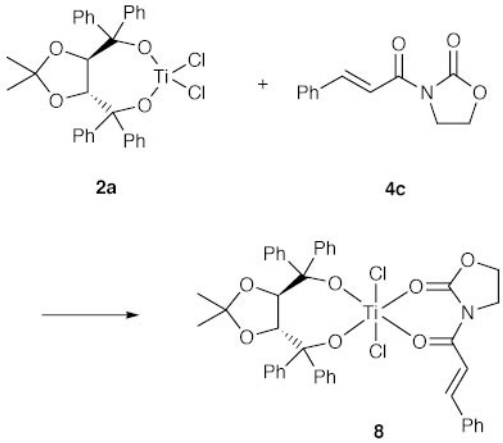

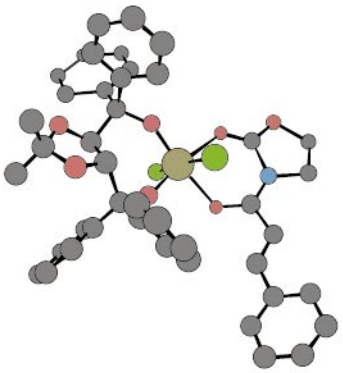

3D structure of **8**
(hydrogens are omitted for clariety)

Scheme 5

Table 1 Application of TiX_2–TADDOLate **2a–d** as catalyst for the 1,3-dipolar cycloaddition reaction between **3a** (R^1 = Ph) and **4a** (R^2 = Me) (Scheme 3)

Entry	Catalyst	Catalyst amount	Conversion (time)	*endo*:*exo*	Ee *endo* (*exo*) (%)
1	**2a**	10	98% (48)	10:90	62 (60)
2	**2b**	10	98% (20)	64:36	76 (64)
3	**2c**	10	73% (20)	79:21	0
4	**2d**	50	99% (48)	>95:<5	93

(R^2 = Me) in the presence of various TiX_2–TADDOLate catalysts are listed (see reaction in Scheme 3). By the application of **2b**, the bromide analogue to **2a**, the diastereoselectivity changes (entry 2). This reaction proceeds with a low *endo*-selectivity. Using the triflate analogue **2c**, leads to an *endo*-selective reaction (entry 3). Unfortunately, this reaction was racemic. For the reaction of **3a** and **4a** in the presence of tosylate catalyst **2d**, a high conversion is obtained (entry 4). The

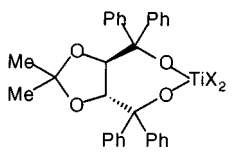

2a: X = Cl
2b: X = Br
2c: X = OTf
2d: X = OTs

endo-selectivity of this reaction is excellent, and this was the first example of a metal-catalysed 1,3-dipolar cycloaddition reaction between nitrones and alkenes proceeding with more than 90% ee.

As an extension of the successful application of **2d**, this catalyst was applied in a series of reactions (Scheme 6). For all eight reactions of nitrones **3** and alkenes **4** in which **2d** was applied as the catalyst, diastereoselectivities >90% de were

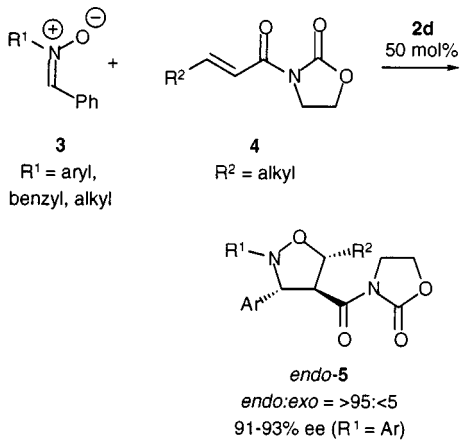

Scheme 6

observed, and most remarkably >90% ee is obtained for all reactions involving a nitrone with an aromatic R^1 substituent, whereas reactions with *N*-benzyl and *N*-alkyl nitrones led to lower enantioselectivities.[19]

The TiX_2–TADDOLate catalysed 1,3-dipolar cycloaddition reactions were extended to include an acrylate derivative.[20] In the absence of a catalyst, the reaction between nitrone **3** and acryloyloxazolidinone **4b** proceeded to give a mixture of all eight regio-, diastereo- and enantiomers (Scheme 7). However, application of $Ti(OTs)_2$-TADDOLate **2d** (10 mol%) as catalyst for the reaction of various nitrones such as **3** with alkene **4b**, led to complete regioselectivity, high *endo*-selectivity, and the *endo*-products **5** were obtained with 48–70% ee (Scheme 7).[20]

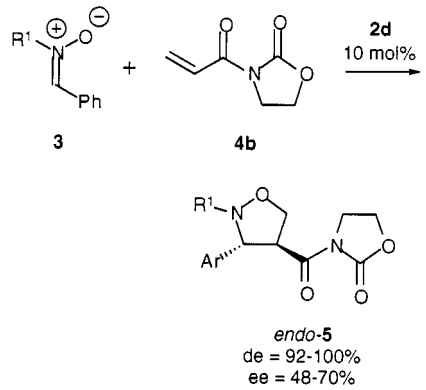

Scheme 7

Seebach *et al.*, who first developed the TADDOL ligands,[7] have also developed a number of polymer- and dendrimer-bound $TiCl_2$–TADDOLate catalysts derived from the monomeric TADDOLs.[21] Application of 10 mol% of this type of catalyst, derived from polymers and dendrimers of **9** and **10**, respectively, in the reaction between nitrone **3a** and alkene **4a** led to *endo*:*exo* ratios between 18:82 and 8:92 and up to 56% ee (Scheme 8). The selectivities are thus slightly decreased compared to similar reactions of the homogeneous catalysts. They also made a study of the relationship between the enantiomeric purity of the ligand of the homogeneous catalyst **11**, and the products obtained in both the 1,3-dipolar cycloaddition reaction between **3a** and **4a** and in the Diels–Alder reaction of **4a** with cyclopentadiene. Surprisingly, the 1,3-dipolar cycloaddition shows a linear relationship, whereas the Diels–Alder reaction shows a positive non-linear relationship. In recent work Heckel and Seebach have studied the use and reuse of $Ti(OTs)_2$–TADDOLate catalysts immobilized on porous silica gel.[22] The selectivity obtained in the 1,3-dipolar cycloaddition reaction between nitrone **3a** and **4a** catalysed by **12**, was only slightly lower compared to the corresponding homogeneous reaction.[19] The same batch of the ligand in **12** could be

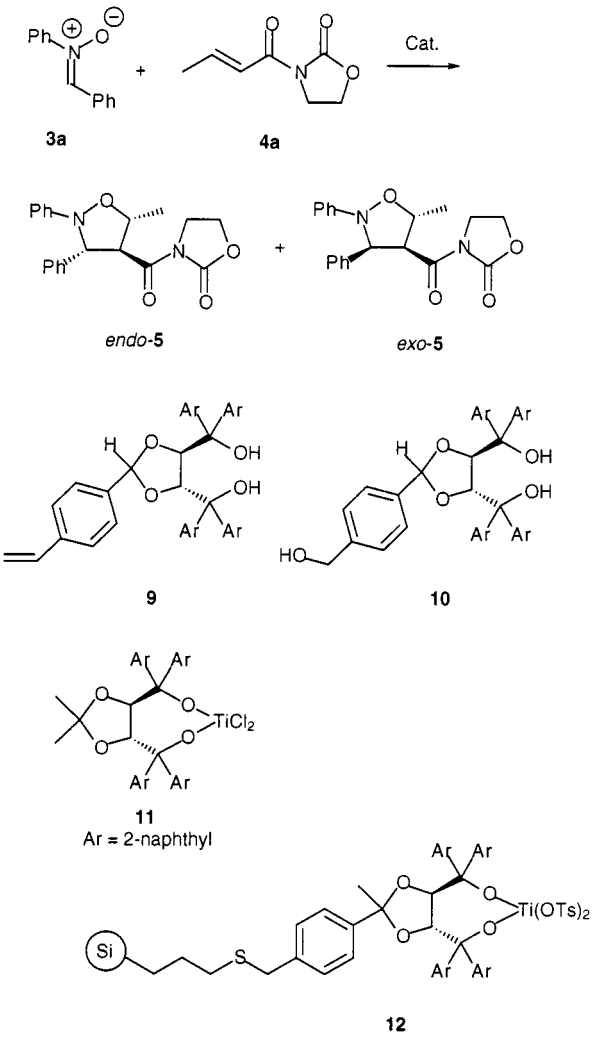

Scheme 8

used in four consecutive reactions with no significant loss of activity, when the ligand was carefully washed between the reactions.[22]

Magnesium catalysts

Prior to the first publication on chiral magnesium catalysts for 1,3-dipolar cycloaddition reactions in 1995, there had been several studies on the impact of non-chiral magnesium salts on the diastereoselectivities in cycloaddition reactions of both nitrones,[23–25] and nitrile oxides[26] with allylic alcohols.

In the first[27] and also the following[28–30] publications applying chiral magnesium catalysts, chiral bisoxazolines (BOX) were applied as the ligand for magnesium. The MgX_2–Ph-BOX catalyst **13** (X = I), proved to be a useful catalyst for the 1,3-dipolar cycloaddition between **3** and **4a**,**b** when it was activated by the addition of I_2 (Scheme 9).[27] Furthermore, the

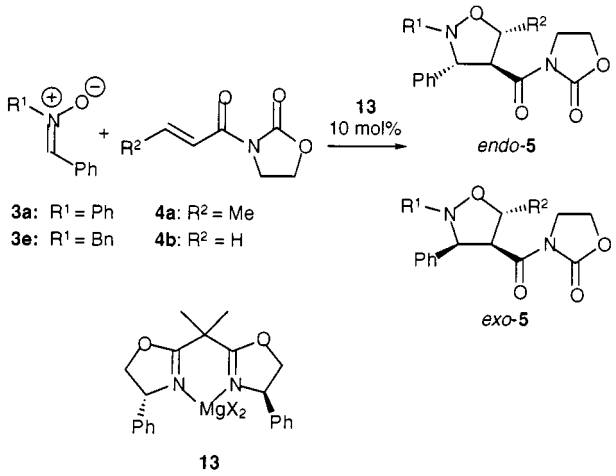

Scheme 9

reaction had to be performed in the presence of molecular sieves (MS) 4 Å. In the presence of 10 mol% of **13** (X = I) the reaction proceeded with good to high *endo*-selectivity and the *endo*-isomer was obtained in an ee of up to 82% (Scheme 9, Table 2, entry 1).

A rather unexpected discovery was made during these investigations.[28] When the 1,3-dipolar cycloaddition reaction of **3a** with **4b** catalysed by **13** (X = I) was performed in the absence of MS 4 Å a remarkable reversal of enantioselectivity was observed, as the opposite enantiomer of *endo*-**5** was obtained in up to 73% ee (Table 2, entries 1, 2). This had not been observed for enantioselective catalytic reactions before and the role of MS cannot simply be ascribed to the removal of water by the MS, since the application of MS 4 Å that were presaturated with water, also induced the reversal of enantioselectivity (Table 2, entries 3, 4). Recently, Desimoni *et al*. found that in addition to the presence of MS in the MgX_2–Ph-BOX catalysed 1,3-dipolar cycloaddition reaction shown in Scheme 9, the counter ion for the magnesium catalyst also strongly affects the absolute stereoselectivity of the reaction.[29,30] They applied MgX_2–Ph-BOX **13** (X = ClO_4, OTf) complexes and compared the results with the MgX_2–Ph-BOX **13** (X = I) catalyst. It was observed that both in the presence and absence of MS, the catalyst **13** (X = ClO_4) gave the opposite absolute configuration of the product compared to the reaction of catalyst **13** (X = I) (Table 2, entries 5, 6). For catalyst **13** (X = OTf), the reaction was racemic in the presence of MS, whereas a high enantioselectivity of 86% ee was obtained in the absence of additives. The absolute configuration of the product of the reaction catalysed by **13** (X = OTf) in the absence of MS was similar to that obtained with **13** (X = ClO_4) catalyst and opposite to that obtained with **13** (X = I) (entries 2, 6 and 8).[29]

It should also be mentioned that in relation to the investigations on MgX_2–BOX catalysts, Desimoni *et al*. also tested a $Zn(ClO_4)_2$–BOX catalyst for the 1,3-dipolar cycloaddition of a nitrone and acryloyloxazolidinone **4b** (see Scheme 9). Contrary

Table 2 Dependence of the absolute stereoselectivity on molecular sieves (MS) and counter ion in the reaction of **3a** with **4b** catalysed by 10 mol% of MgX_2–Ph-BOX catalysts **13**

Entry	MgX_2-counter ion	Additive	*endo*:*exo* (%)	Ee *endo* (%)	Absolute induction	Ref.
1	I	MS 4 Å	73:27	82	3*S*,4*R*	28
2	I	—	100:0	48	3*R*,4*S*	28
3	I	H_2O	90:10	36	3*R*,4*S*	28
4	I	MS 4 Å, H_2O	95:5	36	3*S*,4*R*	28
5	ClO_4	MS 4 Å	70:30	70	3*R*,4*S*	29,30
6	ClO_4	—	95:5	48	3*S*,4*R*	29,30
7	OTf	MS 4 Å	56:44[a]	2	—	29,30
8	OTf	—	97:3	86	3*S*,4*R*	29,30

[a] Mixture of regiomers obtained.

to the magnesium catalysts, this zinc catalyst was *exo*-selective as a 27 : 73 *endo* : *exo* ratio was obtained, with 84% ee of the *exo*-isomer.[30]

Palladium catalysts

For the activation of a substrate such as **4a** *via* coordination of the two carbonyl oxygen atoms to the metal, one should expect that a hard Lewis acid would be most suitable, since the carbonyl oxygens are hard Lewis bases. Nevertheless, Furukawa *et al*. succeeded in applying the relatively soft d^{10} palladium as the catalyst for the 1,3-dipolar cycloaddition reaction between **3** and **4a** (Scheme 10).[32,33] They applied the

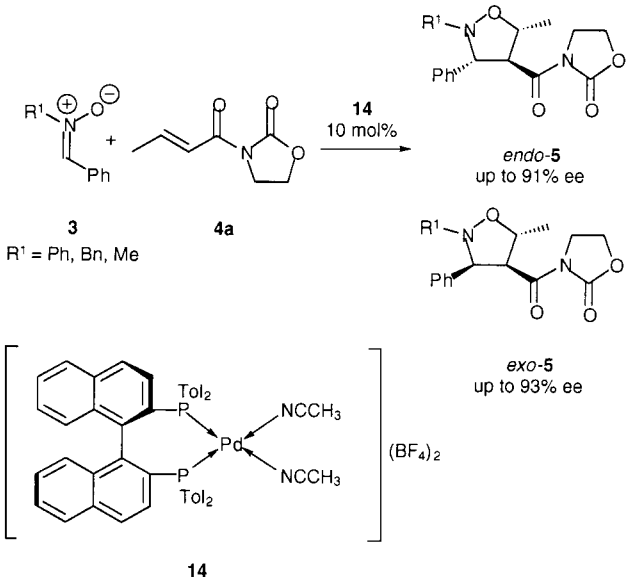

Scheme 10

dicationic Pd–BINAP **14** as the catalyst, and whereas this type of catalytic reaction is often carried out at room temperature, the reactions catalysed by **14** required heating at 40 °C in order to proceed. In most cases mixtures of *endo*-**5** and *exo*-**5** were obtained, however, high enantioselectives of up to 93% ee were obtained for reactions of some derivatives of **3**.

A model **15** for the intermediate of the reaction was proposed to account for the high selectivities obtained for some of the substrates.[33] In **15**, the two phosphorous atoms of the Tol-BINAP ligand and the two carbonyl oxygens of the crotonoyloxazolidinone are arranged in a square planar fashion around the palladium center (note that the counter ions are omitted from this model). From the model it appears that the upper *si*-face of the alkene is sterically available for the cycloaddition reaction, while the *re*-face is shielded by one of the Tol-BINAP *p*-tolyl groups.

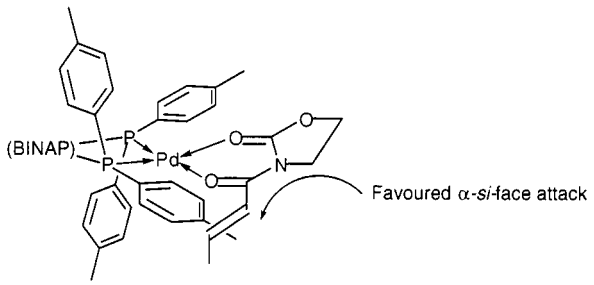

Lanthanide catalysts

In 1997 the application of two different chiral ytterbium catalysts, **16** and **17**, to the 1,3-dipolar cycloaddition reaction was reported almost simultaneously by two independent research groups.[34,35] In both reports, it was observed that the achiral $Yb(OTf)_3$ and $Sc(OTf)_3$ salts catalyse the 1,3-dipolar cycloaddition between nitrones **3** and alkenoyloxazolidinones **4** with *endo*-selectivity. In the first study 20 mol% of the $Yb(OTf)_3$–PyBOX complex **16** was applied as the catalyst for reactions of a number of derivatives of **3** and **4**. The reactions led to *endo*-selective 1,3-dipolar cycloadditions giving products with up to 73% ee (Scheme 11).[34] In the other report, Kobayashi

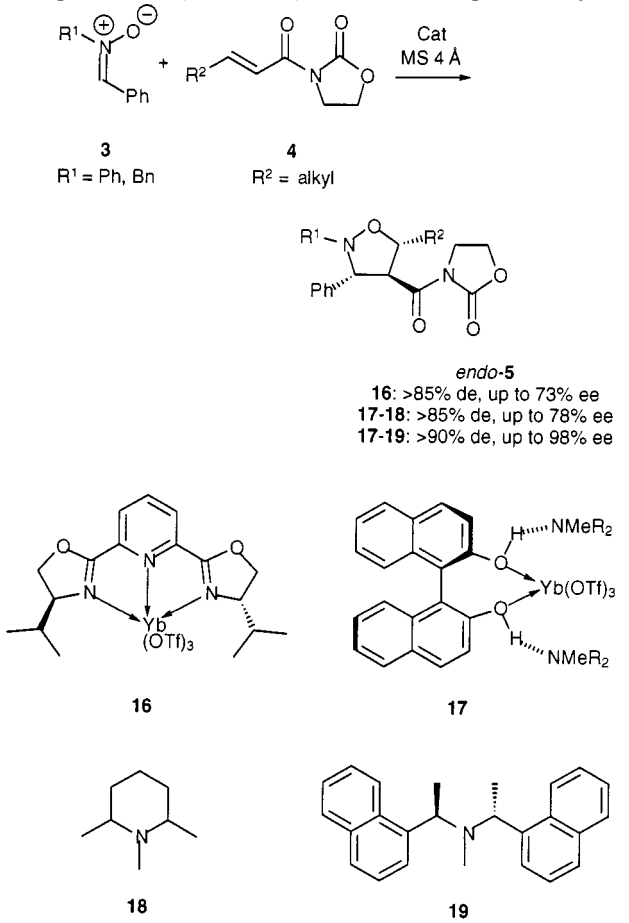

Scheme 11

et al. described a 1,3-dipolar cycloaddition catalysed by 20 mol% of the $Yb(OTf)_3$–BINOL complex **17** in the presence of the achiral tertiary amine **18**.[35] In this approach the nitrone **3** (R^1 = Bn) was formed *in situ* from the respective aldehyde and hydroxylamine. High *endo*-selectivities were observed, and for one derivative the product *endo*-**5** was obtained with 78% ee.[35] In an extension of these investigations the 1,3-dipolar cycloaddition reaction was performed in the presence of 20 mol% of the catalyst **17** and 40 mol% of the chiral amine **19**.[36] By substituting the achiral amine **18** with the chiral amine **19**, the selectivity of the reaction was improved significantly. For the reactions of some derivatives of **3** and **4**, *endo*-**5** was obtained as a single diastereomer and with up to 96% ee. Further investigation in this field by Kobayashi *et al*. led to the finding that the absolute stereoselectivity of the reaction was reversed when the reaction was performed in the absence of MS 4 Å.[37] This observation is analogous to the MgX_2–BOX catalysed reactions, where a similar incidence was observed.[28] In the reaction catalysed by **17** using **19** as the additive, *endo*-**5** (R^1 = Bn, R^2 = Me) was obtained in 96% ee in the presence of MS 4 Å. In the absence of MS 4 Å the opposite enantiomer was obtained in 50% ee. This inverse selectivity could be improved by using various *N*-oxides as a third additive.[37]

Whereas there are numerous examples of the application of the products from the diastereoselective 1,3-dipolar cycloaddition reactions in synthesis,[2,3] there are only very few examples

of the application of the products from catalytic enantioselective 1,3-dipolar cycloaddition reactions in the synthesis of potential target molecules. The reason for this may be due to the fact that most asymmetric metal-catalysed 1,3-dipolar cycloaddition reactions have been carried out on model systems that have not been optimised for further derivatisation. One exception of this is the elegant and short synthesis of a β-lactam by Kobayashi and Kawamura.[36] The isoxazolidine *endo*-**5b**, which was obtained in 96% ee from the $Yb(OTf)_3$–BINOL catalysed 1,3-dipolar cycloaddition reaction, was converted into the ester derivative **20**, quantitatively (Scheme 12). Hydrogenation over

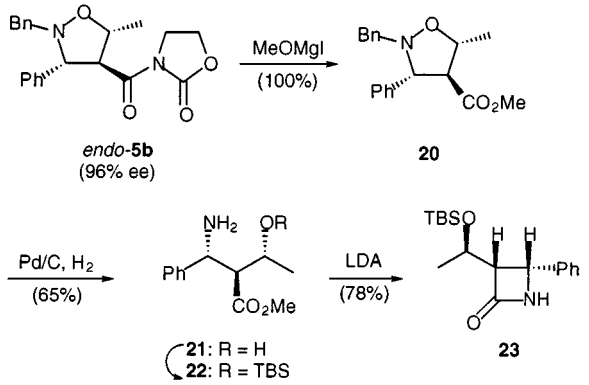

Scheme 12

palladium on carbon opens the isoxazolidine ring and cleaves the *N*-benzyl moiety to give **21**. Following a silyl protection of the hydroxy group to obtain **22**, the final ring-closure is mediated by LDA to give the β-lactam **23** in a high yield with a conserved optical purity of 96% ee.

Nickel catalysts

In 1998 Kanemasa *et al.* published the structure of dibenzofuranyl-2,2′-bisoxazoline (DBFOX) which has proved to be an excellent new ligand for a variety of Lewis acids.[38] The catalytic reactions that have been developed using this type of Lewis acid–DBFOX complex include catalytic 1,3-dipolar cycloaddition reactions of nitrones.[39] The $Ni(ClO_4)_2$–DBFOX/Ph complex **24** (Scheme 13) is a quite remarkable Lewis acid

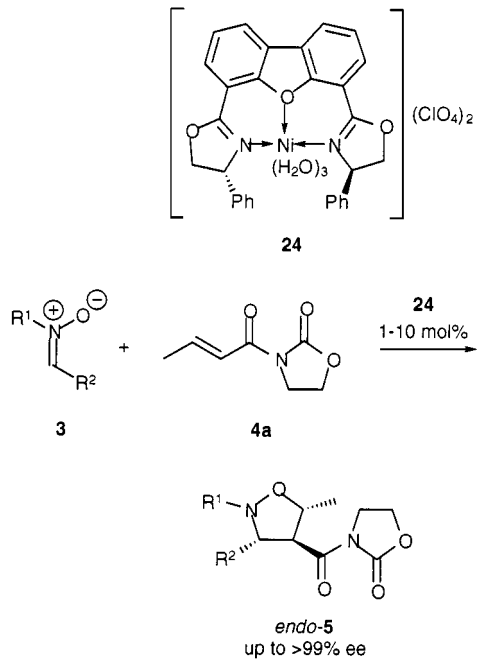

Scheme 13

catalyst as it can be formed from the aqueous $Ni(ClO_4)_2 \cdot 6H_2O$ salt and the ligand. The water can be removed by the addition of MS 4 Å. The reaction between different nitrones **3** and crotonoyloxazolidinone **4a** proceeded in the presence of 1–10 mol% of the dicationic nickel complex **24** as the catalyst. Although long reaction times were required to obtain good yields, the reactions proceeded, in most cases, with very high *endo*-selectivities, and in several cases > 99% ee of the *endo*-products **5** was obtained. So far this catalyst is undoubtedly the most selective catalyst for the normal electron-demand 1,3-dipolar cycloaddition reaction between nitrones and alkenes, especially with respect to the enantioselectivity of the reaction.[39]

The inverse electron-demand reactions

The other catalytic approach to the 1,3-dipolar cycloaddition reaction is the 'inverse electron-demand', in which the nitrone is activated for addition to an electron-rich alkene such as, for example, a vinyl ether (Fig. 2). In this scenario the $FMO's_{alkene}$

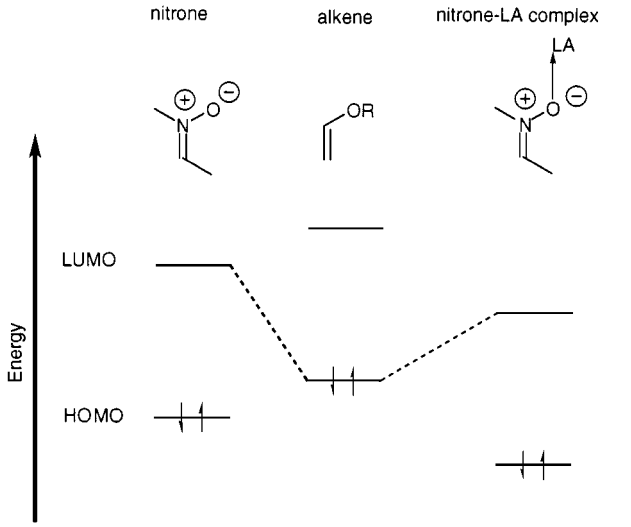

Fig. 2 The catalytic alteration of the nitrone FMO's in the inverse electron-demand 1,3-dipolar cycloaddition reaction.

have higher energies than the $FMO's_{nitrone}$ and the dominating interaction in the reaction will be $LUMO_{nitrone}$–$HOMO_{alkene}$. The nitrone can coordinate to the Lewis acid, leading to a decrease of the $LUMO_{nitrone}$ energy. The decreased energy gap between the two FMO's responsible for the dominating interaction leads to an enhanced rate of the 1,3-dipolar cycloaddition reaction of nitrones.

Boron catalysts

Scheeren *et al.* reported the first catalytic enantioselective 1,3-dipolar cycloaddition reaction of nitrones with alkenes in 1994.[40] Their approach involved *C*,*N*-diphenylnitrone **3a** and ketene acetals **25**, and the amino acid derived oxazaborolidinones **26** were applied as the catalyst (Scheme 14). This type of boron catalyst has been used successfully for asymmetric Diels–Alder reactions.[41,42] In this reaction the nitrone is activated, according to the inverse electron-demand, for a 1,3-dipolar cycloaddition with the electron-rich alkene. They found that coordination of the nitrone to the boron Lewis acid strongly accelerated the 1,3-dipolar cycloaddition reaction with ketene acetals. The reactions of **3a** with **25a**,**b** were catalysed by 20 mol% of oxazaborolidinones such as **26a**,**b**. Fair enantioselectivities were induced and **27a** was obtained with an optical purity of 74% ee, however, in a low yield. The reaction involving **25b** gave the *C*-3,*C*-4-*cis*-isomer **27b** as the only diastereomer of the product with 62% ee.

In an extension of this work Scheeren *et al.* studied a series of derivatives of *N*-tosyl-oxazaborolidinones as catalysts for the 1,3-dipolar cycloaddition reaction of **3a** with **25b**.[43] The

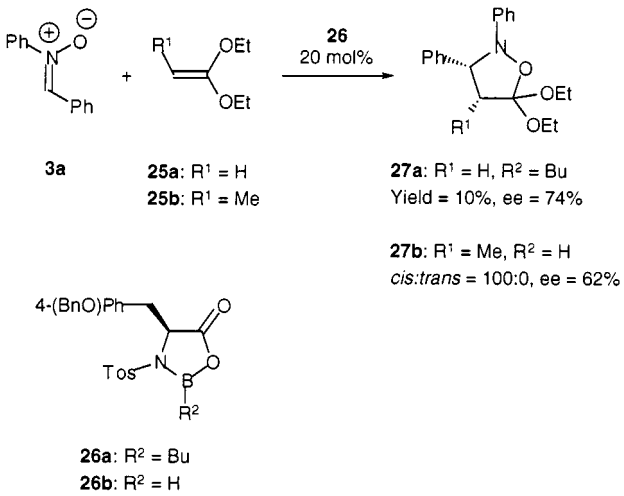

Scheme 14

addition of a co-solvent appeared to be of major importance. Catalyst **26b** was synthesized from the corresponding amino acid and BH_3·THF, hence, THF was present as a co-solvent. In this reaction (−)-**27b** was obtained with 62% ee. If the catalyst instead was synthesized from the amino acid and BH_3·SMe_2, and diphenyl ether was added, a remarkable reversal of the enantioselectivity of the reaction occurred, since (+)-**27b** was now obtained as the major isomer. Furthermore, the ee in this approach was improved to 79%. In more recent work the same research group has applied cyclic and acyclic vinyl ethers in the oxazaborolidinone catalysed 1,3-dipolar cycloaddition reaction with nitrones.[44] High diastereoselectivities were obtained, however, the highest enantioselectivity was 38% ee. In an analogous study by Meske, the impact of various oxazaborolidinone catalysts for the 1,3-dipolar cycloaddition reactions between acyclic nitrones and vinyl ethers was studied.[45] The highest enantioselectivity obtained in this work was 20% ee.

Aluminium catalysts

As for boron catalysts, the aluminium catalysts have exclusively been applied for the inverse electron-demand 1,3-dipolar cycloaddition between alkenes and nitrones. The first contribution to this field was published in 1999.[46] The initial catalytic experiments were performed using the AlMe–BINOL catalyst **29a**, that was simply synthesised by mixing the chiral BINOL ligand **28a** with $AlMe_3$ (Scheme 15). This catalyst was applied for the reaction between nitrone **3a** and vinyl ethers **30a**,**b**. A large rate enhancement was observed by using this catalyst, although, the selectivity of the reactions was rather disappointing. As part of these studies a new method for the synthesis of 3,3′-aryl substituted BINOL ligands **28b**–**f** was developed.[47] The introduction of substituents in the ligands 3,3′-position as in catalysts **29b-f** led to a remarkable improvement of the selectivities when these catalysts were applied in the reaction of **3a** with **30b** (Scheme 15). In particular, complex **29b** possessed the desired properties as the reaction performed in the presence of 20 mol% of this catalyst was completed within 45 min to give *exo*-**31b** (R^1 = Ph, R^2 = *t*-Bu) as the only observable diastereomer with 89% ee. The best results were achieved by applying the ethyl vinyl ether **30a** in the reaction instead of **30b**. The reactions between a series of nitrones **3a**–**d** with **30a** catalysed by 10 mol% of **29b** all proceeded to give the corresponding products **31** with excellent *exo*-selectivities and with enantioselectivities of 88–97% ee.[46]

A model for the mechanism of the highly enantioselective AlMe–BINOL-catalysed 1,3-dipolar cycloaddition reaction was proposed as illustrated in Scheme 16. In the first step nitrone **3a** coordinates to the catalyst **29b** to form intermediate **32**. In this intermediate, which is proposed to account for the absolute stereoselectivity of the reaction, it is apparent that one

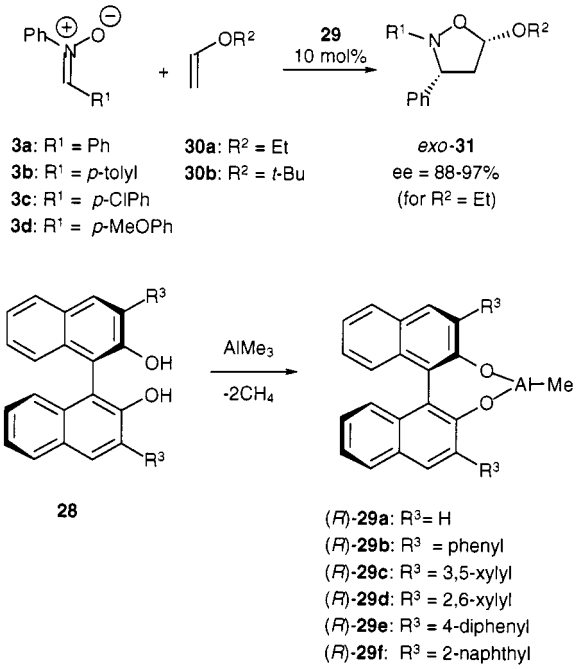

Scheme 15

of the faces of the nitrone, the *si*-face, is shielded by the ligand, whereas the *re*-face remains available for reaction with ethyl vinyl ether **30a** as shown in **33**. The high *exo*-selectivity may also be explained by the model. As appears from the step in which **30a** approaches the nitrone–catalyst complex **33**, the ethoxy moiety of **30a** is pointing away from the nitrone *N*-phenyl group which leads to formation of the *exo*-isomer of the product **31a**. The assignment of the absolute configuration of the product was in full agreement with the *re*-face selectivity proposed in this model.[46]

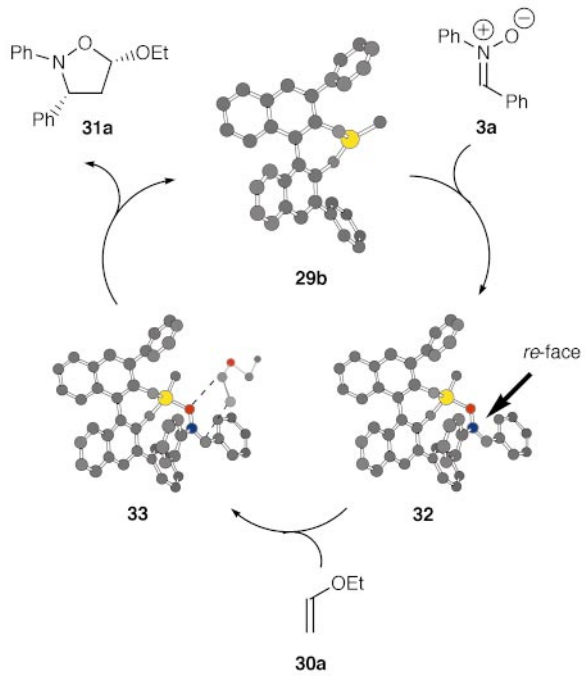

Scheme 16

Pu *et al.* have developed a new type of rigid polymer of 1,1-binaphthols.[48–50] The 3,3′-crosslinked polymeric binaphthol ligand **34** in combination with $AlMe_3$ was applied as the catalyst for the 1,3-dipolar cycloaddition (Scheme 17).[51] Very high selectivities were obtained when the aluminium catalyst of **34** (20 mol%) was applied to the 1,3-dipolar cycloaddition reaction of nitrone **3a** with alkene **30a**. The only observable

diastereomer resulting from the reactions was *exo*-**31a** (R^1 = Ph) and it was obtained with an enantioselectivity as high as 99% ee. One of the advantages of using a polymeric catalyst is the easy removal and recovery of the ligand from the reaction. Upon completion of the reaction, the catalyst was hydrolysed and the ligand precipitated by addition of methanol. After evaporation of the solvent and the excess of **30a**, the pure product *exo*-**31a** was isolated in 97% yield. Similar excellent selectivities were obtained for reactions of other nitrones.

Another important advantage of using the polymeric ligand **34** is, in addition to the easy purification of the product, that the ligand can be isolated and reused after the simple precipitation procedure. In this manner a sample of the polymeric ligand was isolated and reused in four consecutive reactions of nitrone **3a** and ethyl vinyl ether **30a**. Both yield and enantioselectivity of *exo*-**31a** showed only slight decreases after the ligand had been reused. The slight decrease was ascribed to the loss of small amounts of the ligand during the recycling procedure.[51]

The polymeric ligand's monomeric counterpart **28g** was also synthesised and applied in the 1,3-dipolar cycloaddition reaction in order to compare the properties with the polymeric ligand (Scheme 17). When **28g** in combination with $AlMe_3$ (10 mol%) was used as the catalyst for the reactions between nitrones **3a**–**c** and ethyl vinyl ether **30a**, the reactions proceeded to give the pure *exo*-**9** in yields ranging from 76–93%. The enantioselectivities of the reactions were very high at 94–99% ee, and were thus comparable to the results obtained using the polymeric ligand.

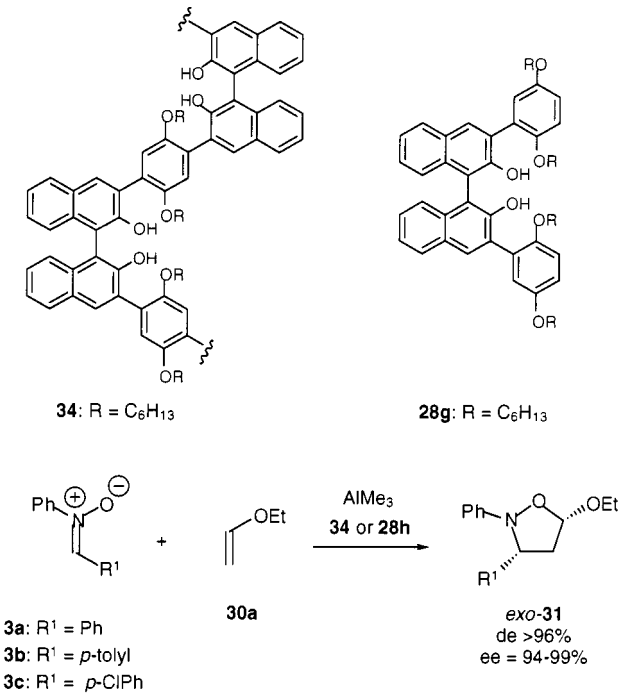

Scheme 17

Copper catalysts

In order to control the stereochemistry in the 1,3-dipolar cycloaddition reactions the bidentate glyoxylate derived nitrone **35**, chiral copper catalysts were applied.[52] For the reaction of nitrone **35**, the electron-rich ethyl vinyl ether **30a** was chosen as the dipolarophile (Scheme 18). A series of chiral catalysts was investigated for the reaction and the $Cu(OTf)_2$–*t*-Bu-BOX complex **37a** was found to be the most suitable catalyst for this reaction. In the presence of 25 mol% of **37a** the reaction proceeded to give a conversion of 98%, an *exo*:*endo* ratio of 84:16, and as the most significant result, *exo*-**36a** was obtained with 89% ee. By changing the solvent to toluene the

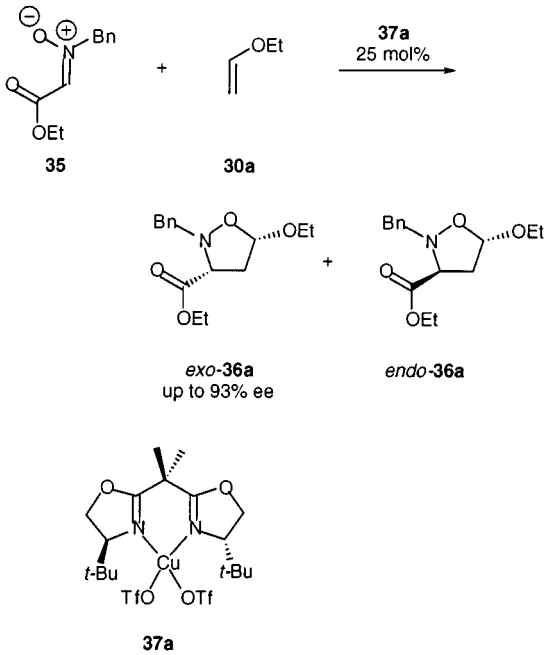

Scheme 18

diastereoselectivity of the reaction was slightly lowered, but the enantioselectivity was improved to 93% ee.[52]

In order to account for the stereoselectivity observed in this reaction a model **38** for the intermediate consisting of substrates

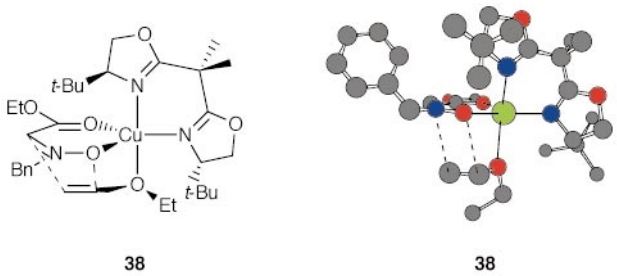

35 and ethyl vinyl ether **30a** coordinated to catalyst **37a** was proposed.[52] In the model the two triflate ligands are dissociated from copper and the ligands are arranged around the copper center as a trigonal bipyramid. It should be noted that in model **38** the oxygen atom of vinyl ether **30a** also coordinates to the metal center. However, a tetrahedral intermediate consisting of only the catalyst and the nitrone could also account for the absolute stereoselectivity of the reaction.

It should also be mentioned that Bosnich *et al.* have applied a chiral titanocene derived catalyst for the inverse electron-demand 1,3-dipolar cycloaddition reaction of nitrones with ketene acetals, however, the highest chiral induction was 14% ee.[53]

Other types of asymmetric catalysis

A different catalytic enantioselective approach was developed for the 1,3-dipolar cycloaddition reaction of nitrones with allyl alcohol (Scheme 19).[54] The zinc catalyst complex, which was used in a stoichiometric amount, was generated from allyl alcohol **39**, Et_2Zn, (*R*,*R*)-diisopropyltartrate (DIPT) and EtZnCl. Addition of the nitrone **40a** led to primarily *trans*-**41a**, which was obtained in a moderate yield, however, with a high ee of up to 95%. Application of **40b** as the nitrone in the reaction led to higher yields of **41b** (47–68%), high *trans*-selectivities and up to 93% ee. Compared to other asymmetric metal catalysed 1,3-dipolar cycloaddition reactions of nitrones, this reaction cannot be assigned as normal or inverse electron-demand. The reaction is controlled, rather than by altered FMO energies, instead by the chelation of the substrates to the catalyst

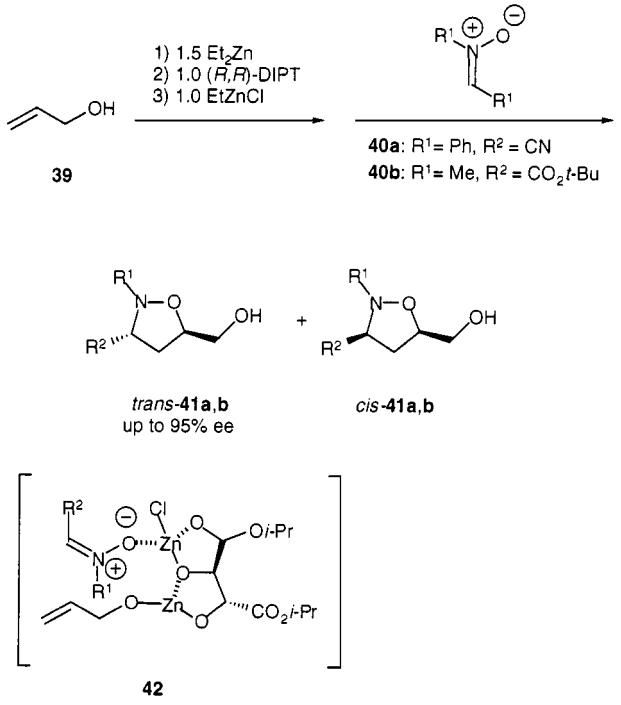

Scheme 19

leading to a favorable entropy of the proposed pseudo-intramolecular intermediate **42**.

Another quite different asymmetric copper catalysed reaction was published by Miura *et al*. in 1995.[55] The reaction of nitrone **3a** and phenylacetylene **43** is catalysed by CuI–*i*-Pr-BOX **37b** as outlined in Scheme 20. The product of this reaction is not a

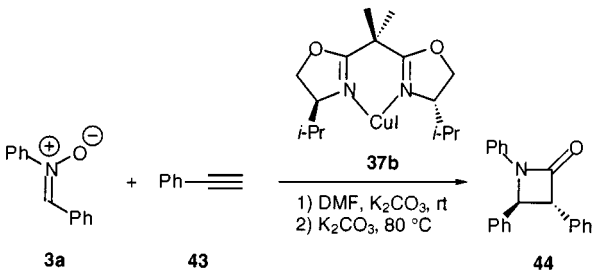

Scheme 20

1,3-dipolar cycloaddition adduct, rather it is the azetidone **44**. The reaction proceeds, however, *via* an isoxazoline intermediate and is therefore mentioned here. By using 1 equivalent of the catalyst **37b**, the *trans*-isomer **44** is obtained in 54% yield and with 68% ee. If the catalyst loading is lowered to 10 mol% CuI and 20 mol% ligand the selectivity decreases to 57% ee.

Summary

The catalytic enantioselective 1,3-dipolar cycloaddition reaction of nitrones has reached a mature stage and there are several examples of reactions that proceed with very high enantioselectivities. For the normal electron-demand 1,3-dipolar cycloaddition reaction of nitrones with electron-deficient alkenes a number of metal complexes have been applied successfully. All of these have in common that they favor a bidentate coordination of the alkenoyloxazolidinone (or succinimide) to the metal catalyst. Most of these reactions proceeded with *endo*-selectivity. The chiral $Ni(ClO_4)_2$–DBFOX/Ph has been the most selective catalyst for the *endo*-selective normal electron-demand 1,3-dipolar cycloaddition reaction so far. Application of 1–10 mol% of this catalyst induced in general very high enantioselectivities of up to 99% ee. It has been more difficult to obtain the *exo*-isomer in the above described reaction. The application of succinimide as an auxiliary for the alkene in the $TiCl_2$–TADDOLate catalysed reaction has been the only entry to a highly *exo*-selective reaction and in this case up to 72% ee of the *exo*-isomer was obtained.

Other types of catalysts had to be applied for the inverse electron-demand 1,3-dipolar cycloaddition reaction of nitrones with electron-rich alkenes. Fair enantioselectivities of up to 79% ee were obtained with oxazaborolidinone catalysts. However, the AlMe–3,3′-Ar-BINOLate complexes proved to be superior for reactions of acyclic nitrones and more than > 99% ee has been obtained in some reactions. The CuX_2–BOX catalyst was efficient for reactions of the glyoxylate derived nitrones with vinyl ethers and enantioselectivities of up to 93% ee were obtained. A few examples of different approaches to catalyst induced control of the stereoselectivity of the reaction have also been reported, however, in these examples a stoichiometric amount of the chiral catalyst was required.

The development of catalytic enantioselective 1,3-dipolar cycloaddition is probably going to continue during the next decade and there are some problems that need to be solved. One of the major drawbacks for most of the reactions is the high catalyst loadings that are required. Another challenge is to explore new substrates that are more suitable for application in synthesis. Hopefully, some of these problems will be solved, because the catalytic enantioselective 1,3-dipolar cycloaddition reaction of nitrones is a highly valuable reaction for the control of multiple stereocenters in a single reaction step.

Acknowledgements

We are indebted to The Danish National Research Foundation for financial support.

References

1 A. Padwa, *1,3-Dipolar cycloaddition chemistry*, Wiley, New York, 1984.
2 K. V. Gothelf and K. A. Jørgensen, *Chem. Rev.*, 1998, **98**, 863.
3 M. Frederickson, *Tetrahedron*, 1997, **53**, 403.
4 K. B. G. Torssell, *Nitrile Oxides, Nitrones and Nitronates in Organic Synthesis*, VCH, Weinheim, 1988.
5 J. J. Tufariello, *1,3-Dipolar cycloaddition chemistry*, ed. A. Padwa, Wiley, New York, 1984.
6 K. V. Gothelf and K. A. Jørgensen, *Acta Chem. Scand.*, 1996, **50**, 652.
7 D. Seebach, B. Weidmann and L. Wilder, *Modern Synthestic Methods*, ed. R. Scheffold, Wiley, New York, 1983.
8 K. Narasaka, N. Iwasawa, M. Inoue, T. Yamada, M. Nakashima and J. Sugimori, *J. Am. Chem. Soc.*, 1989, **111**, 5340.
9 E. J. Corey and Y. Matsumura, *Tetrahedron Lett.*, 1991, **32**, 6289.
10 R. O. Duthaler and A. Hafner, *Chem. Rev.*, 1992, **92**, 807.
11 K. V. Gothelf and K. A. Jørgensen, *J. Org. Chem.*, 1994, **59**, 5687.
12 D. A. Evans, K. T. Chapman and J. Bisaha, *J. Am. Chem. Soc.*, 1988, **110**, 1238.
13 K. B. Jensen, K. V. Gothelf, R. G. Hazell and K. A. Jørgensen, *J. Org. Chem.*, 1997, **62**, 2471.
14 K. V. Gothelf, R. G. Hazell and K. A. Jørgensen, *J. Am. Chem. Soc.*, 1995, **117**, 4435.
15 K. V. Gothelf and K. A. Jørgensen, *J. Org. Chem.*, 1995, **60**, 6847.
16 K. V. Gothelf and K. A. Jørgensen, *J. Chem. Soc., Perkin Trans. 2*, 1997, 111.
17 D. Seebach, R. Dahinden, R. E. Marti, A. K. Beck, D. A. Plattner and F. N. Kühnle, *J. Org. Chem.*, 1995, **60**, 1788.
18 C. Haase, C. R. Sarko and M. Dimare, *J. Org. Chem.*, 1995, **60**, 1777.
19 K. V. Gothelf, I. Thomsen and K. A. Jørgensen, *J. Am. Chem. Soc.*, 1996, **118**, 59.
20 K. B. Jensen, K. V. Gothelf and K. A. Jørgensen, *Helv. Chim. Acta*, 1997, **80**, 2039.
21 D. Seebach, R. E. Marti and H. W. Hintermann, *Helv. Chim. Acta*, 1996, **79**, 1710.
22 A. Heckel and D. Seebach, *Angew. Chem., Int. Ed.*, 2000, **39**, 163.
23 S. Kanemasa, T. Tsuruka and E. Wada, *Tetrahedron Lett.*, 1993, **34**, 87.
24 S. Kanemasa, T. Tsuruoka and H. Yamamoto, *Tetrahedron Lett.*, 1995, **36**, 5019.

25 S. Kanemasa and T. Tsuruoka, *Chem. Lett.*, 1995, 49.
26 S. Kanemasa, M. Nishiuchi, A. Kamimura and K. Hori, *J. Am. Chem. Soc.*, 1994, **116**, 2324.
27 K. V. Gothelf, R. G. Hazell and K. A. Jørgensen, *J. Org. Chem.*, 1996, **61**, 346.
28 K. V. Gothelf, R. G. Hazell and K. A. Jørgensen, *J. Org. Chem.*, 1998, **63**, 5483.
29 G. Desimoni, G. Faita, A. Mortoni and P. Righetti, *Tetrahedron Lett.*, 1999, **40**, 2001.
30 S. Crosignani, G. Desimoni, G. Faita, S. Filippone, A. Mortoni, P. Righetti and M. Zema, *Tetrahedron Lett.*, 1999, **40**, 7007.
31 K. V. Gothelf, R. G. Hazell and K. A. Jørgensen, *J. Org. Chem.*, 1996, **61**, 346.
32 K. Hori, H. Kodama, T. Ohta and I. Furukawa, *Tetrahedron Lett.*, 1996, **37**, 5947.
33 K. Hori, H. Kodama, T. Ohta and I. Furukawa, *J. Org. Chem.*, 1999, **64**, 5017.
34 A. I. Sanchez-Blanco, K. V. Gothelf and K. A. Jørgensen, *Tetrahedron Lett.*, 1997, **38**, 7923.
35 S. Kobayashi, R. Akiyama, M. Kawamura and H. Ishitani, *Chem. Lett.*, 1997, 1039.
36 S. Kobayashi and M. Kawamura, *J. Am. Chem. Soc.*, 1998, **120**, 5840.
37 M. Kawamura and S. Kobayashi, *Tetrahedron Lett.*, 1999, **40**, 3213.
38 S. Kanemasa, Y. Oderaotoshi, S. Sakaguchi, H. Yamamoto, J. Tanaka, E. Wada and D. P. Curran, *J. Am. Chem. Soc.*, 1998, **120**, 3074.
39 S. Kanemasa, Y. Oderaotoshi, J. Tanaka and E. Wada, *J. Am. Chem. Soc.*, 1998, **120**, 12 355.
40 J. P. G. Seerden, A. W. A. Scholte op Reimer and H. W. Scheeren, *Tetrahedron Lett.*, 1994, **35**, 4419.
41 D. Sartor, J. Saffrich and G. Helmchen, *Synlett*, 1990, 197.
42 E. J. Corey, T.-P. Loh, T. D. Roper, M. D. Azimioara and M. C. Noe, *J. Am. Chem. Soc.*, 1992, **114**, 8292.
43 J.-P. G. Seerden, M. M. M. Kuypers and H. W. Scheeren, *Tetrahedron: Asymmetry*, 1995, **6**, 1441.
44 J.-P. G. Seerden, M. M. M. Boeren and H. W. Scheeren, *Tetrahedron*, 1997, **53**, 11 843.
45 M. Meske, *J. Prakt. Chem.*, 1997, **339**, 426.
46 K. B. Simonsen, P. Bayon, R. G. Hazell, K. V. Gothelf and K. A. Jørgensen, *J. Am. Chem. Soc.*, 1999, **121**, 3845.
47 K. B. Simonsen, K. V. Gothelf and K. A. Jørgensen, *J. Org. Chem.*, 1999, **63**, 7536.
48 L. Pu, *Chem. Eur. J.*, 1999, **5**, 2227.
49 Q.-S. Hu, W.-S. Huang, D. Vitharana, X.-F. Zheng and L. Pu, *J. Am. Chem. Soc.*, 1997, **119**, 12
50 W.-S. Huang, Q.-S. Hu and L. Pu, *J. Org. Chem.*, 1998, **63**, 1364.
51 K. B. Simonsen, K. A. Jørgensen, Q.-S. Hu and L. Pu, *J. Chem. Soc., Chem. Commun.*, 1999, 811.
52 K. B. Jensen, R. G. Hazell and K. A. Jørgensen, *J. Org. Chem*, 1999, **64**, 2353.
53 W. W. Ellis, A. Gavrilova, L. Liable-sands, A. L. Rheingold and B. Bosnich, *Organometallics*, 1999, **18**, 332.
54 Y. Ukaji, K. Taniguchi, K. Sada and K. Inomata, *Chem. Lett.*, 1997, 547.
55 M. Miura, M. Enna, K. Okuro and M. Nomura, *J. Org. Chem*, 1995, **60**, 4999.

ChemComm

Self-tracking in solvent-free, low-dimensional polymer electrolyte blends with lithium salts giving high ambient DC conductivity†

Yungui Zheng, Fusiong Chia, Goran Ungar and Peter V. Wright*

Department of Engineering Materials, University of Sheffield, Sheffield, UK S1 3JD.
E-mail: p.v.wright@sheffield.ac.uk

Received (in Cambridge, UK) 24th May 2000, Accepted 26th June 2000
Published on the Web 13th July 2000

A solvent-free, low-dimensional polymer electrolyte blend is described demonstrating a novel process of 'self-tracking' along the field direction in DC polarisation between lithium electrodes and giving ambient DC and AC conductivities upto 10^{-3} S cm^{-1} with low temperature dependence of conduction.

Solvent-free polymer electrolytes have been based largely upon complexes of lithium salts in amorphous forms of poly(ethylene oxide) (PEO).[1–3] However, their application in ambient temperature batteries, requiring conductivities of *ca.* 10^{-3} S cm^{-1}, has been prohibited due to their low ambient temperature conductivities. Other amorphous systems giving conductivities between 10^{-4}–10^{-5} S cm^{-1} have been proposed.[4,5] With a view to creating low impedance pathways and inhibiting ion aggregates we have adapted the extended helical crystalline structures of PEO–alkali salt complexes[6–8] to synthesise organised low-dimensional polymer complexes[9–13] with amphiphilic polymers poly[2,5,8,11,14-pentaoxapentadecamethylene(5-alkyloxy-1,3-phenylene)] coded C*m*O5 or (**I**).

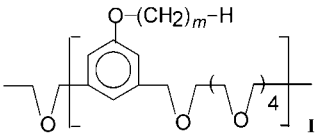

I

-[-O-(-(CH$_2$)$_4$-O-)$_x$-A-]- x = *ca.* 30 **II**

When m = 16, (C16O5), sidechains interdigitate in an hexagonal lattice layer between polyether helices into which cations are encapsulated, one per repeat unit/helical turn, in equimolar complexes denoted, *e.g.* C16O5:LiClO$_4$ (1:1). Anions lie in the interhelical spaces. (*cf.* Fig. 1) and interlamellar long spacings of 40–45 Å are observed.[9,10,11]

Here, we report enhanced ambient conduction in solvent-free LiClO$_4$ and LiClO$_4$/LiBF$_4$ complexes of C*m*O5 blended with a second copolymer of poly(tetramethylene oxide) (**II**). The *n*-alkyl side chains R in **I** are either C$_{16}$H$_{33}$ (C16O5) or a random equimolar copolymer mixture with C$_{12}$H$_{25}$ (C16C12O5). In **II** the units -A- are either -CH$_2$- (denoted **II**C1) or -CH$_2$C(=CH$_2$)CH$_2$- (denoted **II**D4). Both **I** and **II** are prepared to high molar mass ($<M_w>$ = 8 × 10^4 and 4 × 10^4 respectively) giving thin films with good mechanical properties.

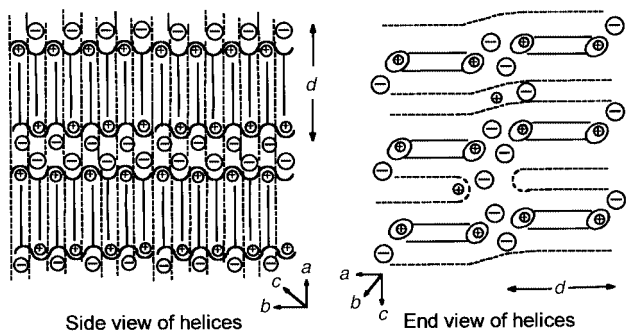

Fig. 1 Schematic molecular structure of C16O5:**II**:LiClO$_4$: Solid lines: C16O5, dashed lines: polymer **II**.

Polymers **I**[9,10] and **II** were prepared by standard Williamson condensations and complexes were prepared by mixing polymer **I** (1 mol repeating unit), polymer **II** (7 mols of (-(CH$_2$)$_4$-O-)- units) and either LiClO$_4$ (1.5 mol) or LiClO$_4$ / LiBF$_4$ (0.75/0.75) from mixed dichloromethane/acetone solvent. The heptamer segment for the stoichiometric equivalent of polymer **II** for each repeat unit of **I** is indicated by a molecular dynamics model.† The molar compositions of complexed blends are therefore denoted **I**:**II**:Li salt (1:1:1.5) where the second digit denotes the mol of heptamer segment. The schematic model (Fig. 1) and the molecular model† are consistent with small-to-wide angle X-ray analysis and with DSC which indicate that the strands of polymer **II** disrupt the alkyl sidechains of polymer **I**. Sidechain melting temperatures are reduced by *ca.* 10 °C by blending with **II**. C16O5:**II**:LiClO$_4$ melts at *ca.* 34 °C at the peak. Complexes with mixed m = 16/12 sidechains (C16C12O5) melt at *ca.* 24 °C. The pure polymers **II** melt at *ca* 20 °C.

Fig. 2 shows isothermal DC‡ conductivity *vs.* time in cells with Li electrodes (Li|**I**/**II**–LiClO$_4$|Li) for C16O5 : **II** : LiClO$_4$ (1 : 1 : 1.5) polarised with 10 mV at 30 °C, Fig. 2(*a*), and C16O5 : **II** : LiClO$_4$: LiBF$_4$ (1 : 1 : 0.75 : 0.75) polarised with 100 mV at 25 °C, Fig. 2(*b*). In a novel 'self-tracking process' the current increases stepwise over *ca.* 24 h corresponding to Li$^+$ conductivity increasing from *ca.* 10^{-6} S cm^{-1} to *ca.* 10^{-3} S cm^{-1}.

The DC data are supported by AC complex impedance measurements for C16O5:**II**:LiClO$_4$ (1:1:1.5) and C16C12O5:**II**:LiClO$_4$ (1:1:1.5) between ITO electrodes as shown in Fig. 3(*a*) and (*b*) as log σ *vs.* 1/T. From lower levels at ambient temperatures all three systems undergo similar 'transitions' on heating to *ca.* 100 °C after which ambient conductivities between 2–6 × 10^{-4} S cm^{-1} are observed. In

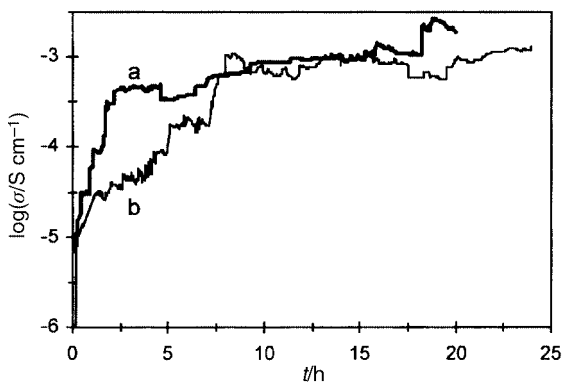

Fig. 2 DC polarisation between lithium electrodes. (*a*) C16O5:**II**D4:LiClO$_4$ (1:1:1.5), 10 mV at 30 °C, 450 μm. (*b*) C16O5:**II**C1:LiClO$_4$: LiBF$_4$ (1:1:0.75:0.75), 100 mV at 25 °C, 100 μm.

† Electronic supplementary information (ESI) available: a molecular dynamics model with coloured atoms of the C16O5:**II**:Li salt complex from Cerius[2] software. See http://www.rsc.org/suppdata/cc/b0/b004174m/

DOI: 10.1039/b004174m

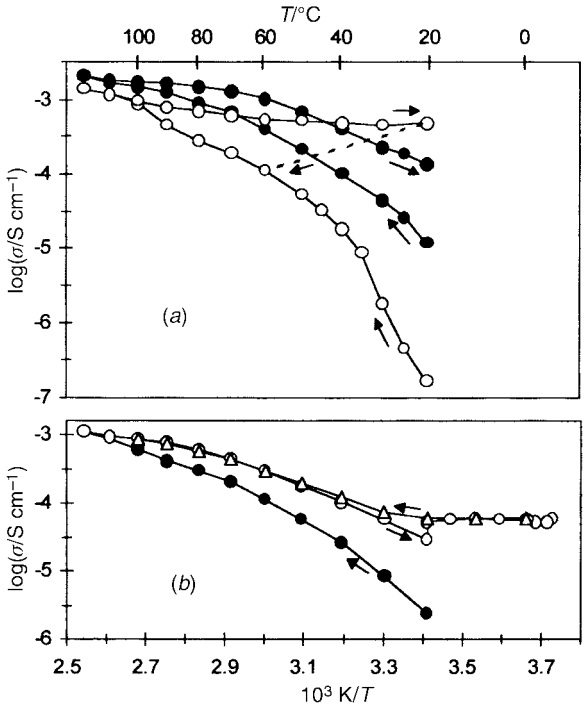

Fig. 3 Temperature dependence of AC conductivities between ITO electrodes. Arrows indicate the direction of heating. (*a*) C16O5:**II**C1:$LiClO_4$ (1:1:1.5) (—○—) and C16C12O5:**II**C1:$LiClO_4$ (1:1:2) (—●—) Cell thicknesses are 100 μm. (*b*) C16O5:**II**D4:$LiClO_4$ (1:1:1.5) Heating (—●—), cooling (—○—) and reheating (—△—). Cell thickness is 50 μm.

Fig. 3(*b*) the ambient conductivity is slightly lower at 8×10^{-5} S cm^{-1} after an isothermal increase over *ca.* 12 h at 20 °C but this level of conductivity is remarkably maintained down to −5 °C. The cooling runs of the C16O5 systems also demonstrate virtual temperature independence (temperature-independent conductivities at the level of 10^{-7}–10^{-6} S cm^{-1} have previously been observed[13] in Langmuir–Blodgett films of a variety of C16O5-Li salt complexes). However, whereas the 'cooling data' are unstable on re-heating above the sidechain melting temperature (*ca.* 35 °C), returning to the lower initial heating curve, Fig. 3(*a*), the data in Fig. 3(*b*) demonstrate that on cooling below the side chain melting endotherm (lower limit 20 °C) stable and reversible conductivities may be observed.

The possibility that Li dendrite formation has a significant influence on these and a number of other DC polarisations reproducing these results is not supported by comparisons with observed[14] dendritic growth in conventional amorphous polymer electrolyte systems. In contrast to the latter the tracking phenomenon commences almost from the outset with very low current densities (*ca.* 0.1 μA cm^{-2}) and without cycling, Furthermore, the maximum conductivities (*ca.* 10^{-3} S cm^{-1}) are reproduced over a wide range of final current densities. In Fig. 2(*b*) (100 mV and 100 μm cell thickness) the current density is 45 times greater than in Fig. 2(*a*) (10 mV and 450 μm thickness, 0.2 mA cm^{-2} maximum).

It is anticipated that polymer **II** (with the more extensive skeletal domain) will promote orientation of conducting planes *bc* in the direction normal to the electrodes when the blend is subjected to mechanical shear in the plane of the film (parallel to the electrodes). The ion current may perhaps assist such orientations by a 'melting–recrystallisation' reorganisation within the sidechain melting endotherm (20–35 °C). However, imposition of the field is expected to bring about a new steady state redistribution of ions between the channels of polymer **I** and the polymer **II** environment promoting vacancies in **I** in which ions are presumed the more mobile ($\sigma = 7 \times 10^{-7}$ S cm^{-1} for complexes of pure **II** with $LiClO_4$ at 25 °C). The relative mobilities and stabilities of ions in **I** and **II** and the identification of premelting (order–disorder) transitions which could account for the low temperature dependence of conductivity are subjects of further work.

We acknowledge financial support for this work from the Engineering and Physical Science Research Council.

Notes and references

‡ For DC measurements Li electrodes were prepared under argon from freshly-pressed Li pellets (*ca.* 2 mm diam.) in paraffin oil and cells were assembled under argon with polyethylene separators. DC and AC measurements using cellulose acetate separators were performed under vacuum using a Solartron 1287 Electrochemical Interface with a Solartron 1250 Frequency Response Analyser 1–64 kHz.

1 *Polymer Electrolyte Reviews 1*, ed. J. R. MacCallum and C. A. Vincent, Elsevier Applied Science, London, 1987.
2 *Polymer Electrolyte Reviews 2*, ed. J. R. MacCallum and C. A. Vincent, Elsevier Applied Science, London, 1989.
3 F. M. Gray, *Polymer Electrolytes*, Materials Monographs, The Royal Society of Chemistry, Cambridge, 1997.
4 C. A. Angell, C. Liu and E. Sanchez, *Nature*, 1993, **362**, 137.
5 F. Croce, C. Appetecchi, L. Persi and B. Scrosati, *Nature*, 1998, **394**, 456.
6 Y. Chatani and S. Okamura, *Polymer*, 1987, **28**, 1815.
7 P. Lightfoot, M. A. Mehta and P. G. Bruce, *Science*, 1993, **262**, 883.
8 Y. G. Andreev, P. Lightfoot and P. G. Bruce, *J. Appl. Crystallogr.*, 1997, **18**, 294.
9 F. B. Dias, J. P. Voss, S. V. Batty, P. V. Wright and G. Ungar, *Macromol. Rapid Commun.*, 1994, **15**, 961.
10 F. B. Dias, S. V. Batty, G. Ungar, J. P. Voss and P. V. Wright, *J. Chem. Soc., Faraday Trans.*, 1996, **92**, 2599.
11 P. V. Wright, Y. Zheng, D. Bhatt, T. Richardson and G. Ungar, *Polym. Int.*, 1998, **47**, 34.
12 Y. Zheng, P. V. Wright and G. Ungar, *Electrochim. Acta*, 2000, **45**, 1161.
13 Y. Zheng, A. Gibaud, N. Cowlam, T. H. Richardson, G. Ungar and P. V. Wright, *J. Mater. Chem.*, 2000, **10**, 69.
14 C. Brissot, M. Rosso, J.-N. Chazalviel and S. Lascaud, *J. Power Sources*, 1999, **81**–**82**, 925.

ChemComm

1-Ethoxyvinyl 2-furoate, an efficient acyl donor for the lipase-catalyzed enantioselective desymmetrization of prochiral 2,2-disubstituted propane-1,3-diols and meso-1,2-diols†

Shuji Akai, Tadaatsu Naka, Tetsuya Fujita, Yasushi Takebe and Yasuyuki Kita*

Graduate School of Pharmaceutical Sciences, Osaka University, Yamada-oka, Suita, Osaka 565-0871, Japan. E-mail: kita@phs.osaka-u.ac.jp

Received (in Cambridge, UK) 15th May 2000, Accepted 19th June 2000
Published on the Web 21st July 2000

A novel acyl donor, 1-ethoxyvinyl 2-furoate, was found to produce the title reactions with high enantiotopic selectivity, high reactivity and stability of the products under various conditions.

The enzymatic transesterification of alcohols with acyl donors in organic solvents has become a widely applicable protocol to provide a variety of optically active compounds.[1] However, its application to the enantioselective desymmetrization of prochiral 2,2-disubstituted propane-1,3-diols (**I**) has rarely been reported, despite the promising potential of this approach as a powerful alternative to the well-investigated chemical syntheses of compounds bearing an optically active quaternary carbon center.[2] Recently, Fadel and Arzel reported the first practical enzymatic desymmetrization of **I** using well-known acyl donors, *i.e.* vinyl acetate and isopropenyl acetate. The reactions, however, suffered from low reactivity (it usually took several days or more to consume **I**), and racemization of the products **II** *via* acyl group migration was often observed [eqn. (1)].[3] Easy racemization of the products **IV** has also been an

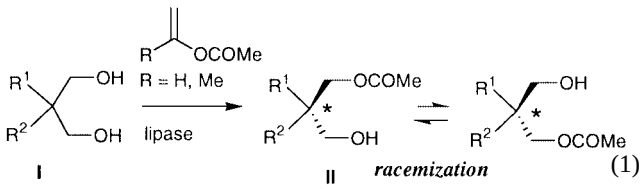

(1)

annoying problem for the desymmetrization of the *meso*-1,2-diols (**III**) [eqn. (2)].[4,5] Therefore, to solve these problems

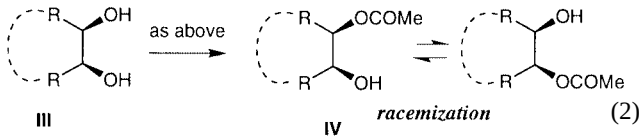

(2)

the development of an effective acyl donor which fulfills the criteria of high enantiotopic selectivity, high reactivity,[6] and production of stable products under various conditions is an urgent matter.

Very recently, we reported that 1-ethoxyvinyl acetate is similar-to-more reactive than vinyl acetate in the common enzymatic transesterifications[7] and we developed 1-ethoxyvinyl benzoate (**1a**) as an effective reagent for the desymmetrization of **I**.[8] However, this method is still unsatisfactory for sterically congested 1,3-diols in terms of the reaction time and the enantiotopic selectivity. The finding for **1a** encouraged us to find a more prominent ethoxyvinyl aromatic ester.[9] In this communication, we present 1-ethoxyvinyl 2-furoate (**1b**) as an effective reagent applicable to both diols **I** and **III**.

In the preliminary evaluation of 19 aroyl reagents **1** on the desymmetrization of the congested diol **2** under identical reaction conditions (the reaction was quenched when **2** was consumed), we observed that the 2-furoate (**1b**) was the best reagent in both reactivity and enantiotopic selectivity (Table 1, run 1). Some other reagents (**1**, Ar = *p*-tolyl, *p*-bromophenyl, 5-bromo-2-furyl, 2-thienyl) were fairly effective in producing the corresponding mono esters (75–86% ee, 46–60% isolated yields), and the rest were moderate (Ar = 2-naphthyl, *p*-

Table 1 Desymmetrization of various 1,3-diols using **1a**,**b**[a]

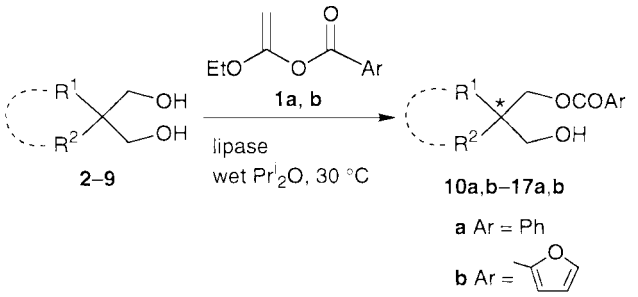

			Using **1b**			
Run	Diol	Lipase[b]		*t*/h	Ee (%)[c]	Yield (%)
1	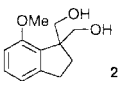 2	MY	**10b**	5	81	69
2		MY	**10b**	8[d]	90	38 (98)[e]
3	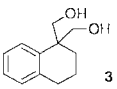 3	MY	**11b**	5	61	84
4	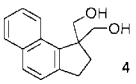 4	MY	**12b**	5	79	93
5		MY	**12b**	48[d]	91	78 (98)[e]
6	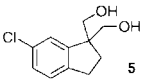 5	MY	**13b**	5	85	71
7	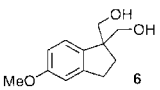 6	MY	**14b**	5	92	35
8	 7 R = Me	CRL	**15b**	5	>99	66
9	8 R = Et	CRL	**16b**	2	89	87
10	9 R = allyl	CRL	**17b**	2	82	72

[a] The reaction was run using **1b** (3.0 equiv. for runs 1–7 or 1.5 equiv. for runs 8–10) and was quenched when the diol was consumed, unless otherwise noted. Results of the similar reaction using **1a**[8]: **2**, 100 h, 71% ee, 82%; **3**, 170 h, 46% ee, 74%; **4**, 170 h, 73% ee, 53%; **5**, 100 h, 74% ee, 74%. [b] MY (from *Candida rugosa*, Meito), CRL (from *Candida rugosa*, Sigma Type VII) immobilized on Hyflo Super Cell. [c] Determined by HPLC using Daicel Chiralcel OD (hexane–PriOH). [d] Prolonged reaction. [e] In parentheses, the yield in consideration of the recovered diol is shown.

† Electronic supplementary information (ESI) available: preparation of 1-ethoxyvinyl 2-furoate. See http://www.rsc.org/suppdata/cc/b0/b003871g/

methoxyphenyl, *p*-nitrophenyl, 3-methyl-2-furyl, 3-furyl; 50–80% ee, 22–41% isolated yields) or poorly reactive (Ar = *o*-tolyl, 1-naphthyl, 1-anthryl, 1-methylpyrrol-2-yl, 4-pyridyl, 3-pyridyl, 3-quinolyl, benzofuran-2-yl, 1-methylindol-2-yl).[10] Therefore, the desymmetrization of various types of 2,2-disubstituted 1,3-diols (**3–9**) was performed using **1b** (Table 1). These results disclosed the eminent performance of **1b** as follows.

First, the reactions using **1b** were generally completed within 5 h. This is quite remarkable because all of the other aroyl donors required at least 1 day and generally more than 4 days to consume the diols. Second, the optical and the chemical yields of the products **10b**–**17b** were generally high and better than those obtained using the other aroyl reagents. Particularly, the product **15b** was obtained with > 99% ee. Third, the stability of the furoate **10b**–**17b** under acidic conditions was very much improved as noted from the following example. Thus, **16b** was inert to racemization in an acidic medium [0.1 equiv. of camphorsulfonic acid (4×10^{-4} M) in CH_2Cl_2] at room temperature after 1 d, whereas the same treatment of the corresponding benzoate resulted in gradual racemization ($t_{1/2}$ = 18 h).[8] All of these products were easily isolated by standard column chromatography on SiO_2, and the optical purity did not decrease during the chromatography.

In addition, an improvement in the optical purity of the products was observed by prolonging the reaction time beyond the complete mono acylation of the substrates due to kinetic amplification (*e.g.* runs 2 and 5). Because the only side-products, *i.e.* the diesters, were quantitatively hydrolyzed to the starting diols, this method provides products with high optical purity without any loss in chemical yield.

The furoate moiety was preserved under oxidizing conditions. Neither a decrease in optical purity nor decomposition of the furan ring was observed after treatment of **16b** (88% ee) with the Dess–Martin periodinane, and the corresponding aldehyde **18** was quantitatively obtained with 87% ee as determined using a chiral HPLC column. Further treatment of **18** with $NaClO_2$ followed by methanolysis gave the known carboxylic acid (*R*)-**20** {$[\alpha]_D^{22}$ +13.4 (*c* 0.8, $CHCl_3$), lit.[11] $[\alpha]_D^{20}$ −16.5 (*c* 1.0, $CHCl_3$) for 97% ee of the (*S*)-form}. Therefore, the absolute configuration of **16b** was determined to be *S* (Scheme 1).

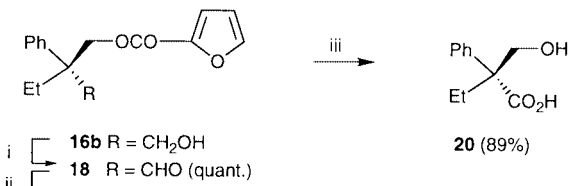

Scheme 1 *Reagents and conditions*: i, Dess–Martin periodinane, CH_2Cl_2, 0 °C → room temperature, 30 min; ii, $NaClO_2$, NaH_2PO_4, Bu^{t}OH–H_2O, room temperature, 10 min; iii, NaOMe, MeOH, 0 °C → room temperature, 1 h.

The reaction of the *meso*-1,2-diol **21** with **1b** using CHIRAZYME® L-9 (from *Mucor miehei*, Roche Diagnostics) provided the monofuroate (1*R*,2*S*)-**23** (97% ee, 77% yield) (Scheme 2). The optical purity did not change during purification by the standard column chromatography on SiO_2. Similarly, the desymmetrization of **22** gave (1*R*,2*S*)-**24** (82% ee, 55% yield).†[12,13]

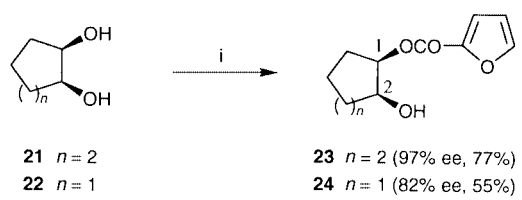

Scheme 2 *Reagents and conditions*: i, **1b** (2.5 equiv.), CHIRAZYME® L-9, Bu^{t}OMe, 45 °C, 2 d.

In conclusion, the above-mentioned procedure using **1b** features the following advantages. (1) **1b** is readily prepared from commercially available ethoxyacetylene and 2-furoic acid in high yield and may be stored in a refrigerator for more than six months. (2) The products are obtained in high optical and chemical yields. If necessary, the only side-products, diesters, can be converted to the starting diols. (3) The products are sufficiently stable under various conditions and can serve as the key synthetic intermediates for optically active compounds having a quaternary carbon center at the benzylic position. Moreover, the high reactivity and high enantiotopic selectivity of **1b** are outstanding among a large number of acyl donors and offer an interesting topic from the mechanistic point of view.

This work was supported by Grants-in-Aid for Scientific Research (No. 09557180 and 11672102) from the Ministry of Education, Science, Sports, and Culture, Japan and the Takeda Science Foundation, Japan. The Meito Sangyo Co., Ltd., Japan, and Roche Diagnostics K. K., Japan, are thanked for their generous gifts of the lipases.

Notes and references

1 For recent reviews, see: K. Faber, *Biotransformations in Organic Chemistry*, 3rd edn., Springer-Verlag, Berlin, 1997; R. D. Schmid and R. Verger, *Angew. Chem., Int. Ed.*, 1998, **37**, 1608.

2 For reviews, see: K. Fuji, *Chem. Rev.*, 1993, **93**, 2037; E. J. Corey and A. Guzman-Perez, *Angew. Chem., Int. Ed.*, 1998, **37**, 388.

3 A. Fadel and P. Arzel, *Tetrahedron: Asymmetry*, 1997, **8**, 283.

4 G. Nicolosi, A. Patti, M. Piattelli and C. Sanfilippo, *Tetrahedron: Asymmetry*, 1994, **5**, 283; G. Nicolosi, A. Patti, M. Piattelli and C. Sanfilippo, *Tetrahedron: Asymmetry*, 1995, **6**, 519.

5 The enzyme-catalyzed hydrolysis of the diacetates of **I** or **III** has also been reported to give the optically active **II** and **IV**; however, these products also suffered from racemization see, (*a*) D. H. G. Crout, V. S. B. Gaudet, K. Laumen and M. P. Schneider, *J. Chem. Soc., Chem. Commun.*, 1986, 808; (*b*) Z.-F. Xie, I. Nakamura, H. Suemune and K. Sakai, *J. Chem. Soc., Chem. Commun.*, 1988, 966; (*c*) H. Suemune, T. Harabe, Z.-F. Xie and K. Sakai, *Chem. Pharm. Bull.*, 1988, **36**, 4337.

6 Structure of the acyl moiety of an acyl donor is well-known to affect the enantioselectivity and reactivity. For a recent example, see: T. Ema, S. Maeno, Y. Takaya, T. Sakai and M. Utaka, *J. Org. Chem.*, 1996, **61**, 8610.

7 Y. Kita, T. Naka, M. Imanishi, S. Akai, Y. Takebe and M. Matsugi, *Chem. Commun.*, 1998, 1183; Y. Kita, Y. Takebe, K. Murata, T. Naka and S. Akai, *J. Org. Chem.*, 2000, **65**, 83.

8 S. Akai, T. Naka, Y. Takebe and Y. Kita, *Tetrahedron Lett.*, 1997, **38**, 4243.

9 Benzoates are generally less reactive than acetates for chemical hydrolysis and alcoholysis under both acidic and basic conditions. For an example, see: H. P. M. Fromageot, C. B. Reese and J. E. Sulston, *Tetrahedron*, 1968, **24**, 3533.

10 All these reagents were prepared according to the reported method (Y. Kita, H. Maeda, K. Omori, T. Okuno and Y. Tamura, *J. Chem. Soc., Perkin Trans. 1*, 1993, 2999) by the addition of commercial carboxylic acids to ethoxyacetylene in ⩾80% yields in most cases.

11 A. Fadel and S. Garcia-Argote, *Tetrahedron: Asymmetry*, 1996, **7**, 1159.

12 *Typical procedure for the enzymatic desymmetrization of the 1,3-diols using **1b***. Commercially available Pr$^i_2$O was distilled as usual, and 0.1% of water was added. After vigorous stirring at room temp. for 20 min, the mixture was allowed to settle. The upper layer (3.0 cm^3) was placed in a resealable test tube, to which were successively added **1b** (0.60 mmol), the 1,3-diol (0.20 mmol), and lipase MY (125 mg). The flask was sealed, and the reaction mixture was stirred at 30 °C during the time given in Table 1 and filtered through a Celite® pad. The filtrate was concentrated *in vacuo*, and the residue was purified by column chromatography on SiO_2 (hexane–EtOAc) to give the monoester and the diester. *Optical rotations of the products*: **10b**, 90% ee, $[\alpha]_D^{28}$ −37.0 (*c* 0.99, $CHCl_3$); **11b**, 61% ee, $[\alpha]_D^{23}$ +10.5 (*c* 0.95, $CHCl_3$); **12b**, 91% ee, $[\alpha]_D^{28}$ −16.5 (*c* 0.68, $CHCl_3$); **13b**, 85% ee, $[\alpha]_D^{23}$ +18.6 (*c* 1.4, $CHCl_3$); **14b**, 92% ee, $[\alpha]_D^{23}$ +30.8 (*c* 0.96, $CHCl_3$); **15b**, > 99% ee, $[\alpha]_D^{20}$ −4.9 (*c* 0.86, $CHCl_3$); **16b**, 89 ee, $[\alpha]_D^{20}$ −10.3 (*c* 0.93, $CHCl_3$); **17b**, 82 ee, $[\alpha]_D^{20}$ −19.3 (*c* 0.54, $CHCl_3$); **23**, 97% ee, $[\alpha]_D^{19}$ −3.0 (*c* 0.7, $CHCl_3$); **24**, 82% ee, $[\alpha]_D^{19}$ −1.9 (*c* 1.1, $CHCl_3$).

13 The absolute configurations of the products, (*S*)-**15b**, (*S*)-**17b**, (1*R*,2*S*)-**23** and (1*R*,2*S*)-**24**, were deduced by comparison of specific rotations of these or their derivatives with those of authentic samples. The details will be presented in a forthcoming full paper. The absolute configuration of the others (**10b**–**14b**) have not been established yet.

Intramolecular [2+2] photocycloadditions as an approach towards the bicyclo[2.1.1]hexane substructure of solanoeclepin A

Richard H. Blaauw, Jean-François Brière, Remco de Jong, Jorg C. J. Benningshof, Angeline E. van Ginkel, Floris P. J. T. Rutjes, Jan Fraanje,† Kees Goubitz,† Henk Schenk† and Henk Hiemstra*

Institute of Molecular Chemistry, Laboratories of Organic Chemistry and Crystallography, University of Amsterdam, Nieuwe Achtergracht 129, 1018 WS Amsterdam. E-mail: henkh@org.chem.uva.nl

Received (in Liverpool, UK) 9th May 2000, Accepted 20th June 2000
Published on the Web 14th July 2000

The synthesis of a tricyclic substructure of solanoeclepin A is described. The key step involves an intramolecular [2+2] photocycloaddition between a dioxinone and a tetrasubstituted bicyclic alkene providing the strained bicyclo[2.1.1]hexane moiety.

Solanoeclepin A (**1**) is the most active natural hatching agent of the potato cyst nematode.[1] Its heptacyclic structure contains all ring sizes ranging from three to seven, including a strained

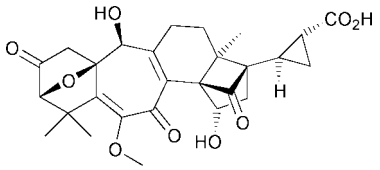

1

bicyclo[2.1.1]hexanone unit, which to the best of our knowledge is an unprecedented structural feature in natural products. The structure of **1** to a certain extent resembles that of glycinoeclepin A,[2] the hatching agent of the soybean cyst nematode. The extreme scarcity of natural material, its fascinating structure, and its potential role in the search for a benign way to control potato sickness make **1** a challenging target for total synthesis. This and the following communication[3] document our first strides towards this goal.

We have investigated intramolecular [2+2] photocycloadditions[4] between a 1,3-dioxin-4-one and variously substituted alkenes connected at C5 with a two carbon tether, to arrive at highly substituted bicyclo[2.1.1]hexanes. We wish to report herein (1) our preliminary results on these cycloadditions, which exhibit remarkably variable regioselectivities, and (2) our achievements towards the stereoselective construction of a tricyclic substructure of solanoeclepin A, containing the bicyclo[2.1.1]hexane moiety.

To investigate the viability of a photochemical approach a simple model system was selected containing the 6-methyl-1,3-dioxin-4-one moiety (see Scheme 1). This structure is known to be readily prepared and to show reliable photochemical behaviour[4] and it should eventually provide useful functionality for our total synthesis endeavour. Aldehyde **2** was prepared from commercially available *tert*-butyl acetoacetate *via* (1) alkylation with allyl bromide, (2) dioxinone formation[5] and (3) oxidative cleavage of the allyl group.[6] Subsequent alkenylation with vinylmagnesium bromide, followed by MOM protection of the allylic alcohol, afforded cyclisation precursor **3**.

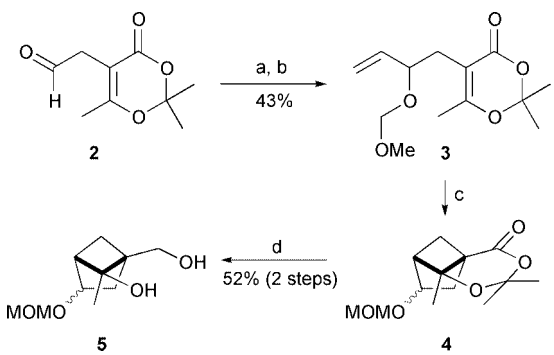

2 **3** **5** **4**

Scheme 1 *Reagents*: a, vinylmagnesium bromide, THF, −78 °C; b, MOMCl, *i*-PrNEt$_2$, CH_2Cl_2, rt; c, *hν* (300 nm), MeCN–acetone (9:1 v/v), rt; d, $LiAlH_4$, THF, rt.

Upon irradiation smooth cyclisation occurred to afford the expected bicyclo[2.1.1]hexane **4** as a 1:1 mixture of diastereoisomers. This product is in accordance with the so-called 'rule of five'.[7] A close analogue has been earlier prepared by Kaneko and co-workers.[4b] Cycloadduct **4** was found to be unstable, decomposing slowly under the reaction conditions and during the subsequent work-up. However, exhaustive reduction with lithium aluminium hydride led to stable diol **5**.

Encouraged by this result, we set out to construct a more appropriately functionalised cyclisation precursor, bearing a cyclohexenyl side chain, necessary for the construction of **1**. Chromium-mediated coupling of aldehyde **2** and vinyl triflate **6**[8] (Scheme 2), followed by oxidation of the allylic alcohol and acetalisation,[9] afforded cyclisation precursor **7**. This oxidised and protected precursor was chosen to prevent diastereomeric mixtures after the cycloaddition.

Much to our surprise, cyclisation of **7** resulted in the exclusive formation of the strained bicyclo[2.2.0]hexane **8**. This cycloadduct exhibited enhanced stability compared to **4**, even to silica gel column chromatography, allowing the complete characterisation of this molecule. Ultimate proof of the structure of **8** was obtained by performing a De Mayo fragmentation, which after esterification with diazomethane gave spiro[3.4]octane **9**.[10] The structure of one of the isomers of **9** was unambiguously secured by X-ray crystallography.

We hypothesised that this remarkable regiochemical preference could be attributed to stereoelectronic effects. In an

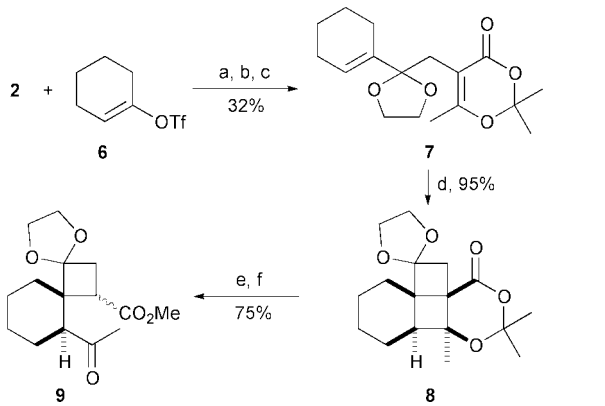

6 **7** **9** **8**

Scheme 2 *Reagents*: a, $CrCl_2$, $NiCl_2$ (cat.), DMF, rt; b, $(COCl_2)_2$, DMSO, Et_3N, CH_2Cl_2, −78 °C → rt; c, $(TMSOCH_2)_2$, TMSOTf, CH_2Cl_2, 0 °C; d, *hν* (300 nm), MeCN/acetone (9:1 v/v), rt; e, KOH, dioxane–H_2O, rt; f, CH_2N_2, MeOH, 0 °C.

DOI: 10.1039/b003755i

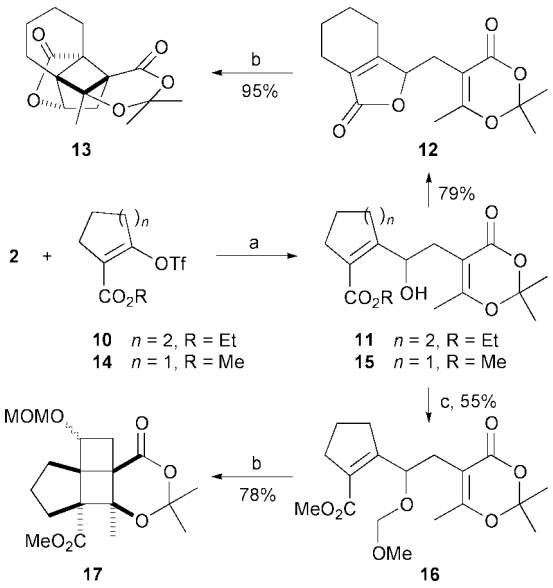

Scheme 3 *Reagents*: a, $CrCl_2$, $NiCl_2$ (cat.), DMF, 50 °C; b, hv (300 nm), MeCN–acetone (9 : 1 v/v), rt; c, MOMCl, *i*-$PrNEt_2$, CH_2Cl_2, rt.

attempt to direct the cycloaddition to the desired mode of closure, aldehyde **2** was reacted with triflate **10** bearing an additional electron-withdrawing ester substituent on the alkene (Scheme 3). Not unexpectedly,[11] the product was not the hydroxy ester **11**, but lactone **12**. Gratifyingly, subjection of this latter precursor to the irradiation conditions smoothly led to bicyclo[2.1.1]hexane **13** with complete regio- and diastereoselectivity in high yield. The cycloadduct **13** appeared unstable on a silica gel column, but was readily purified by recrystallisation (mp 177–178 °C), and its structure was confirmed by X-ray crystallography‡.

To probe the generality of this cyclisation mode we also investigated the five-membered ring triflate ester **14** as starting material. Its coupling with aldehyde **2** gave hydroxy ester **15**, which did not lactonise spontaneously nor could it be forced to do so by heating. Alcohol **15** was therefore protected as the MOM ether **16**. On irradiation of **16** under the usual conditions a *ca*. 1:1 mixture of stable stereoisomeric cycloadducts **17** was obtained containing again the bicyclo[2.2.0]hexane moiety. The diastereoisomer with the OMOM group *trans* with respect to the cyclopentane ring (mp 62–64 °C) was crystalline and allowed unambiguous structural proof by X-ray diffraction.

Thus, of the four photocyclisation precursors investigated, two (**3** and **12**) cyclise in the expected crossed mode obeying the rule of five, while the other two (**7** and **16**) cyclise in the unexpected straight mode. In view of the precedent available, **3** shows normal cyclisation behaviour. However, very little is known about tri- or tetrasubstituted alkenes in photocycloadditions with 2-carbon tethered dioxinones. It is tempting to speculate that the first C–C-bond formation by radical cyclisation to a 5- or 6-membered ring is reversible,[12] depending on the feasibility of the second, irreversible C–C-bond formation. Preliminary molecular modeling studies indicate that in the case of ester **16** initial 5-membered ring formation cannot be readily followed by a second C–C-coupling due to conformational constraints. At any rate, photochemistry once again proves to be a very powerful synthesis technique, producing in one step four contiguous quaternary carbon centres, exemplified by the formation of **13** and **17,** of which the former has the desired skeleton for our total synthesis purposes.

To examine the utility of **13** in model studies towards the natural product, it was reduced with excess lithium aluminium hydride to yield the stable tetrahydroxy compound **18** (Scheme 4). Further elaboration of **18** required a differentiation of the two primary hydroxy groups. Unfortunately, all attempts to selectively mono-protect one of the primary alcohols met with

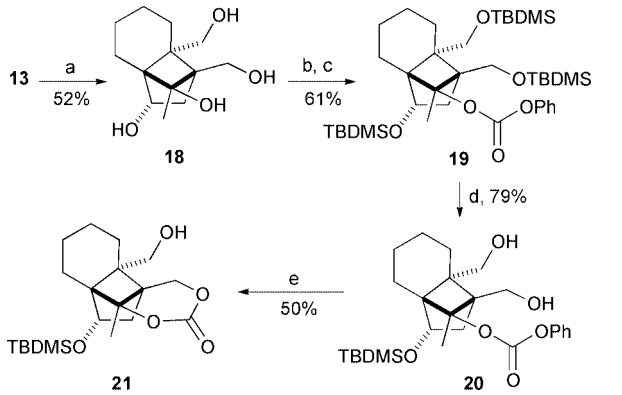

Scheme 4 *Reagents*: a, $LiAlH_4$, THF, rt; b, TBDMSOTf, 2,6-lutidine, CH_2Cl_2, 0 °C; c, KHMDS, phenyl chloroformate, THF, −78 °C; d, CSA, MeOH, 0 °C; e, NaH, THF, 0 °C.

failure. Therefore, the primary and secondary hydroxy groups were protected as their TBDMS ethers, followed by functionalisation of the tertiary alcohol with a phenyl carbonate group, affording **19**. Selective hydrolysis of the primary TBDMS ethers, yielded diol **20**. Upon treatment of this diol with sodium hydride, cyclic carbonate **21** was formed, leaving one primary hydroxy group unprotected. This compound contains appropriate substitution and stereochemistry for elaboration towards the right-hand substructure of solanoeclepin A.

These investigations are supported (in part) by the Netherlands Research Council for Chemical Sciences (CW) with financial aid from the Netherlands Technology Foundation (STW).

Notes and references

† Laboratory of Crystallography.

‡ CCDC 182/1702. See http://www.rsc.org/suppdata/cc/b0/003755i/ for crystallographic files in .cif format.

1 J. G. Mulder, P. Diepenhorst, P. Plieger, I. E. M. Brüggemann-Rotgans, PCT Int. Appl. WO 93/02,083; *Chem. Abstr.*, 1993, **118**, 185844z; H. Schenk, R. A. J. Driessen, R. de Gelder, K. Goubitz, H. Nieboer, I. E. M. Brüggemann-Rotgans, P. Diepenhorst, *Croat. Chem. Acta*, 1999, **72**, 593.

2 Structure elucidation: A. Fukuzawa, A. Furusaki, I. Mitsuhiko and T. Masamune, *J. Chem. Soc., Chem. Commun.*, 1985, 222. Total synthesis: A. Murai, N. Tanimoto, N. Sakamoto and T. Masamune, *J. Am. Chem. Soc.*, 1988, **110**, 1985; H. Watanabe and K. Mori, *J. Chem Soc., Perkin Trans. 1*, 1991, 2919; E. J. Corey and I. N. Houpis, *J. Am. Chem. Soc.*, 1990, **112**, 8997; E. J. Corey and B. Hong, *J. Am. Chem. Soc.*, 1994, **116**, 3149.

3 J. C. J. Benningshof, R. H. Blaauw, A. E. van Ginkel, F. P. J. T. Rutjes, J. Fraanje, K. Goubitz, H. Schenk and H. Hiemstra, *Chem. Commun.*, 2000, 1465.

4 (*a*) J. D. Winkler, C. Mazur Bowen and F. Liotta, *Chem. Rev.*, 1995, **95**, 2003; (*b*) M. Sato, Y. Abe, K. Takayama, K. Sekiguchi and C. Kaneko, *J. Heterocycl. Chem.*, 1991, **28**, 241; (*c*) M. T. Crimmins and T. L. Reinhold, *Org. React.*, 1993, **44**, 297.

5 M. Sato, H. Ogasawara, K. Oi and T. Kato, *Chem. Pharm. Bull.*, 1983, **31**, 1896; S. Huckin and L. Weiler, *J. Am. Chem. Soc.*, 1974, **96**, 1082.

6 E. G. Baggiolini, J. A. Iacobelli, B. M. Hennessy, A. D. Batcho, J. F. Sereno and M. R. Uskokovic, *J. Org. Chem.*, 1986, **51**, 3098.

7 R. Srinivasan and K. H. Carlough, *J. Am. Chem. Soc.*, 1967, **89**, 4932; R. S. H. Liu and G. S. Hammond, *J. Am. Chem. Soc.*, 1967, **89**, 4936.

8 K. Takai, M. Tagashira, T. Kuroda, K. Oshima, K. Utimoto and H. Nozaki, *J. Am. Chem. Soc.*, 1986, **108**, 6048.

9 T. Tsunoda, M. Suzuki and R. Noyori, *Tetrahedron Lett.*, 1980, **21**, 1357.

10 For a review, see: M. Sannigrahi, *Tetrahedron*, 1999, **55**, 9007; M. Phmakotr, T. Bunlaksananusorn and P. Tuchinda, *Tetrahedron Lett.*, 2000, **41**, 377.

11 P. Knochel and C. J. Rao, *Tetrahedron*, 1993, **49**, 29.

12 D. Andrew and A. C. Weedon, *J. Am. Chem. Soc.*, 1995, **117**, 5647.

Enantioselective synthesis of the tetracyclic left-hand substructure of solanoeclepin A

Jorg C. J. Benningshof, Richard H. Blaauw, Angeline E. van Ginkel, Floris P. J. T. Rutjes, Jan Fraanje,† Kees Goubitz,† Henk Schenk† and Henk Hiemstra*

Institute of Molecular Chemistry, Laboratories of Organic Chemistry and Crystallography, University of Amsterdam, Nieuwe Achtergracht 129, 1018 WS Amsterdam, The Netherlands. E-mail: henkh@org.chem.uva.nl

Received (in Liverpool, UK) 9th May 2000, Accepted 20th June 2000
Published on the Web 14th July 2000

The synthesis of the enantiopure left-hand substructure of solanoeclepin A is described. Key steps include a chromium-mediated coupling of an oxabicyclic aldehyde with a β-ketoester-derived enol triflate to give a lactone, and a ring-closing metathesis reaction to form the seven-membered ring.

In the preceding communication[1] we have disclosed a synthetic approach to the intricate bicyclo[2.1.1]hexane moiety of solanoeclepin A (**1**), the hatching agent of the potato cyst nematode.[2] In this paper we present the successful synthesis of the tetracyclic left-hand substructure **2** of this challenging natural product.

In our retrosynthetic analysis (Scheme 1) compound **2** was deemed accessible *via* oxidative functionalisation of diene **3**, which was thought to result from a ring-closing metathesis reaction of triene **4** as a key step. Compound **4** was expected to arise from lactone **5**, the product of a chromium-mediated[3] coupling of enol triflate **6** and aldehyde **7**. Diels–Alder product **8** has been previously reported by Mukaiyama and Iwasawa[4a] and seemed a suitable intermediate for the construction of aldehyde **7**.

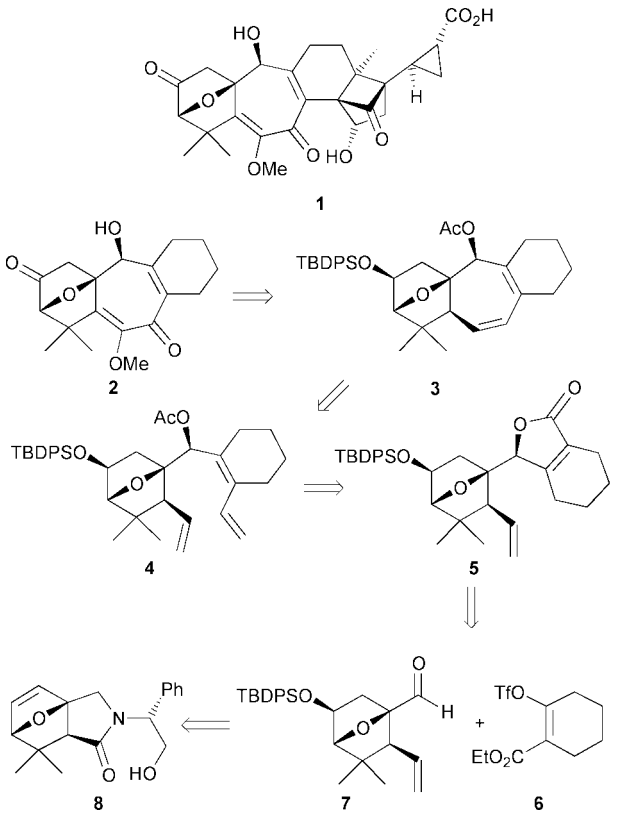

Scheme 1 Strategy for the synthesis.

The synthesis of aldehyde **7** started with the condensation of furfural with (*R*)-(−)-2-phenylglycinol and reduction of the formed imine with sodium borohydride (Scheme 2). At this point it was not possible to selectively acylate the amine. Therefore the hydroxy group was first silylated, followed by *N*-acylation and acidic work-up to give Diels–Alder precursor **9** in 87% overall yield from furfural. The intramolecular Diels–Alder reaction following the Mukaiyama protocol[4] afforded **8** in excellent diastereoselectivity (89%) on a 50 g scale. The pure diastereomer **8** was obtained after column chromatography in 69% yield.

As chemoselective hydroboration of the alkene in **8** appeared impossible in the presence of the lactam, the latter functionality was removed as follows. First, the *N*-substituent was removed *via* a non-reductive procedure to keep the 7-oxabicycloheptene moiety intact.[5] The Diels–Alder product **8** was successively treated with tosyl chloride and DBU to give an enamine, which after hydrolysis led to lactam **10** (mp 154 °C; $[\alpha]_D^{22}$ +52.4, *c* = 0.8, $CHCl_3$) in excellent yield. Lactam **10** was then *N*-nitrosated and ring-opened to a hydroxy ester,[4] which on THP-protection gave **11** in moderate yield. Highly selective hydroboration of the double bond appeared now possible with disiamylborane[6]§ to give the desired alcohol in a 92:8 regioisomeric ratio. Separation of the isomers by column chromatography and protection of the secondary hydroxy group as a silyl ether afforded **12** in a good yield. The ester function was then

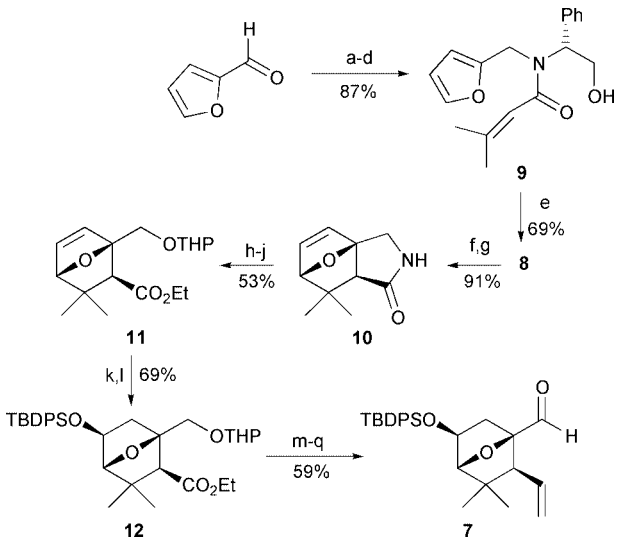

Scheme 2 *Reagents*: a, (*R*)-(−)-2-phenylglycinol, toluene, reflux; b, $NaBH_4$, *i*-PrOH; c, TMSCl, pyridine, THF; d, 3,3-dimethylacryloyl chloride then 5% HCl, H_2O; e, *n*-BuMgCl, Et_2O, −60 °C then toluene, reflux, 16 h; f, *p*-TsCl, pyridine, CH_2Cl_2; g, DBU, MeCN then 5 M HCl, H_2O; h, $NaNO_2$, AcOH, Ac_2O; i, KOH, EtOH then sat. $NaHCO_3$ (aq); j, DHP, *p*-TsOH, CH_2Cl_2; k, disiamylborane, THF then NaOH, H_2O_2; l, TDBPSCl, imidazole CH_2Cl_2; m, $LiAlH_4$, THF; n, TPAP, NMO, acetone; o, $Ph_3P{=}CH_2$, THF; p, HOAc, THF, H_2O; q, SO_3·pyridine, DMSO, Et_3N, CH_2Cl_2.

DOI: 10.1039/b003757p

transformed into a vinyl group by reduction to the alcohol, followed by TPAP[7] oxidation and Wittig olefination. After THP deprotection and oxidation,[8] aldehyde **7** was obtained.

A chromium-mediated coupling of enol triflate **6** with aldehyde **7** afforded an intermediate γ-hydroxy unsaturated ester which spontaneously lactonised to α,β-unsaturated lactone **5** and its diastereomer (Scheme 3).[3] This mixture of diastereoisomers (70:30) could be easily separated by column chromatography. The major isomer was used for the rest of the synthetic sequence and its stereochemistry was later proven to be as given in **5**.

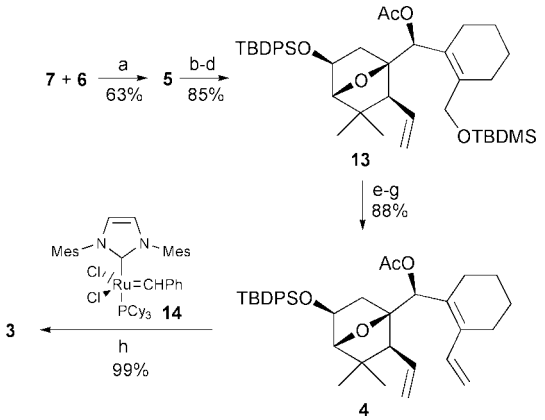

Scheme 3 *Reagents*: a, $CrCl_2$, $NiCl_2$ (cat.), DMF, 50 °C (2.3:1); b, $LiAlH_4$, Et_2O, rt; c, TBDMSCl, pyridine, CH_2Cl_2 ; d, Ac_2O, pyridine, CH_2Cl_2; e, CSA, MeOH; f, TPAP, NMO, acetone; g, $Ph_3P{=}CH_2$, THF; h, **14** (15%), toluene, reflux, 16 h.

Reduction of lactone **5** with lithium aluminium hydride resulted in a diol, which was protected with a TBDMS group on the primary hydroxy group, and an acetyl group on the secondary hydroxy group to give **13**. The primary alcohol was then selectively deprotected with CSA and subsequently oxidised with TPAP.[7] Wittig olefination of the crude aldehyde resulted in the ring-closing metathesis precursor **4**. Our first experiments to cyclise **4** were carried out with Grubbs' ruthenium benzylidene catalyst,[9] but a very slow process was observed requiring a stoichiometric amount of the catalyst for completion of the ring-closing metathesis. Gratifyingly, the use of the more stable ruthenium catalyst **14**[10] gave quantitative closure to form tetracyclic diene **3** after 16 h in refluxing toluene using only 15% of the catalyst.

With the diene **3** available we needed to functionalise the least-substituted double bond with oxygen substituents (Scheme 4). We first attempted to introduce a 1,2-diketone moiety in one step using $KMnO_4$ in Ac_2O,[11] but this reagent mixture led to complete cleavage of the C=C bond, resulting in a diacid. We then decided to introduce the 1,2-diketone *via* a milder three-step procedure. First the double bond was dihydroxylated, which was only successful by following a recent procedure of Corey and co-workers,[12] using stoichiometric osmium tetroxide activated with DMAP. Direct double oxidation of the resulting diol to the dione, using manganese dioxide, TPAP or DMSO-based reagents failed and resulted in most cases in C–C bond cleavage to give the corresponding dialdehyde. However, we then found that is was possible to selectively oxidise the allylic alcohol using 1 equiv. of Dess–Martin periodinane,[13] resulting in α-hydroxyketone **15**. Heating of **15** with cupric acetate[14] in MeOH gave the desired 1,2-diketone, which existed completely in the enol form, and was readily methylated to give methyl enol ether **16**. In the last few steps the silyl ether was cleaved and the liberated hydroxy group oxidised using a TPAP oxidation. Deprotection of the acetate group resulted in the desired **2** as a stable crystalline compound (mp 173 °C) with a high rotation ($[\alpha]_D^{24}$ +495, *c* = 0.6, $CHCl_3$). The X-ray crystal structure‡ proved its identity, including the orientation of the hydroxy function. Compound **2** has been subjected to hatching activity tests,[15] but appeared to be devoid of any activity.

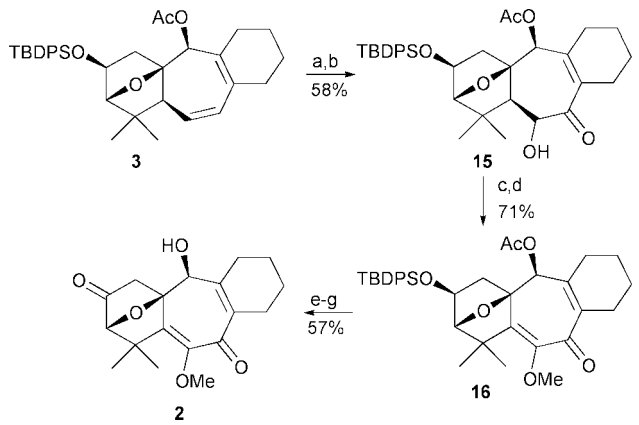

Scheme 4 *Reagents*: a, OsO_4, DMAP, *t*-BuOH–H_2O 1:1 then Na_2SO_3; b, Dess–Martin, CH_2Cl_2 (19% dialdehyde); c, $Cu(OAc)_2$, MeOH, 60 °C; d, MeI, Ag_2O, DMF; e, HF·pyridine; f, TPAP, NMO, acetone; g, K_2CO_3, MeOH.

In summary, we have completed a synthesis of the tetracyclic left-hand substructure **2** of solanoeclepin A in enantiopure form. Compound **2** appeared to be quite stable so that the reported instability of **1** can probably be ascribed to the bicyclo-[2.1.1]hexanone part of the molecule. The synthesis reported herein provides important information for the eventual synthesis of **1** itself. To this end triflate **6** needs to be replaced by a more complex molecule containing the bicyclo[2.1.1]hexane moiety. Studies in this direction will be reported in due course.

These investigations are supported (in part) by the Netherlands Research Council for Chemical Sciences (CW) with financial aid from the Netherlands Technology Foundation (STW).

Notes and references

† Laboratory of Crystallography.

‡ CCDC 182/1703. See http://www.rsc.org/suppdata/cc/b0/b003757p/ for crystallographic files in .cif format.

§ Disiamylborane = $[(CH_3)_2CHCH(CH_3)]_2BH$.

1 R. H. Blaauw, J. F. Brière, R. de Jong, J. C. J. Benningshof, A. E. van Ginkel, F. P. J. T. Rutjes, J. Fraanje, K. Goubitz, H. Schenk and H. Hiemstra, *Chem. Commun.*, 2000, 1463.
2 J. G. Mulder, P. Diepenhorst, P. Plieger and I. E. M. Brüggemann-Rotgans, PCT Int. Appl. WO 93/02,083, *Chem. Abstr.*, 1993, **118**, 185844z.
3 P. Knochel and C. J. Rao, *Tetrahedron*, 1993, **49**, 29.
4 (*a*) T. Mukaiyama and N. Iwasawa, *Chem. Lett.*, 1981, 29; (*b*) M. R. Gmünder and C. H. Eugster, *Helv. Chim. Acta*, 1990, **73**, 2190.
5 V. Nyzam, C. Belaud, F. Zammattio and J. Villiéras, *Tetrahedron: Asymmetry*, 1996, **7**, 1835; O. Fains and J. M. Vernon, *Tetrahedron Lett.*, 1997, **38**, 8265.
6 H. C. Brown, A. K. Mandal and S. U. Kulkarni, *J. Org. Chem.*, 1977, **42**, 1392.
7 For a review on TPAP oxidations, see: S. V. Ley, J. Norman, W. P. Griffith and S. P. Marsden, *Synthesis*, 1994, 639.
8 J. R. Parikh and W. E. von Doering, *J. Am. Chem. Soc.*, 1967, **89**, 5505.
9 R. H. Grubbs and S. Chang, *Tetrahedron*, 1998, **54**, 4413.
10 M. Scholl, T. M. Trnka, J. P. Morgan and R. H. Grubbs, *Tetrahedron Lett.*, 1999, **40**, 2247.
11 H. P. Jensen and K. B. Sharpless, *J. Org. Chem.*, 1974, **39**, 2314.
12 F. He, Y. Bo, J. D. Altom and E. J. Corey, *J. Am. Chem. Soc.*, 1999, **121**, 6771.
13 D. B. Dess and J. C. Martin, *J. Org. Chem.*, 1983, **48**, 4155.
14 N. L. Wendler, D. Taub and R. P. Graber, *Tetrahedron*, 1959, **7**, 173.
15 Compound **2** was tested at HLB Agricultural Research Centre, Assen, The Netherlands

ChemComm

A polymer-supported alkyl methyl sulfide as an efficient promoter of the Khand cyclisation reaction

William J. Kerr,* David M. Lindsay, Mark McLaughlin and Peter L. Pauson

Department of Pure and Applied Chemistry, University of Strathclyde, 295 Cathedral Street, Glasgow, Scotland, UK G1 1XL

Received (in Cambridge, UK) 7th June 2000, Accepted 23rd June 2000
Published on the Web 18th July 2000

A readily prepared polymer-supported alkyl methyl sulfide has been shown to be a recyclable, practically convenient, and efficient promoter of the Khand cyclisation reaction, affording good to excellent yields of cyclopentenones.

In recent years the Khand cycloaddition reaction has been developed into a highly utilisable method for generating cyclopentenone systems.[1] This cobalt carbonyl mediated annulation involving an alkyne, an alkene and carbon monoxide, was first described in 1971 and was originally conducted under thermal conditions.[2] With few exceptions, the technique of simply heating the reactants led to reaction mixtures from which the desired cyclopentenone products could only be separated in low to moderate yield after careful chromatography. Consequently, great efforts have been made to find more efficient procedures by which this valuable cycloaddition process can be carried out.[3]

Although promotion by ultrasound[4] and dry state adsorption conditions[5] have provided improvements in product yields in certain instances, it has undoubtedly been the introduction and thorough investigation of the use of amine *N*-oxides as promoters[6] that has led to the most significant advances in overall Khand reaction applicability and efficiency. More specifically, studies in our own laboratory have developed amine *N*-oxide promoted Khand techniques for use with gaseous olefins[7] and gaseous olefin equivalents,[8] and have exploited the same class of *N*-oxide promoted cyclisations within total synthesis programmes.[9] Additionally, the use of non-racemic chiral amine *N*-oxides has led to the establishment of direct asymmetric Khand cyclisation strategies.[10]

As part of an on-going optimisation of the asymmetric process, we have synthesised a novel polymer-linked amine *N*-amine *N*-oxide and shown this to be a good solid phase promoter of the Khand reaction.[11] As well as forming the basis for the construction of a potentially structurally diverse library of supported chiral amine *N*-oxides, this work also demonstrated that the widely recognised benefits associated with the technique of employing a solid phase reagent[12] could be realised within the arena of Khand cyclisation chemistry. Indeed, a major advantage offered by this resin-based *N*-oxide method is in the simplification of product isolation procedures; by routine filtration the desired cyclopentenone is removed from the (organometallic) by-products in remarkably pure form. With this knowledge, we have now gone on to further extend and widen the overall scope of this immobilised Khand reaction promoter strategy.

Sugihara has recently reported that *n*-butyl methyl sulfide was the optimum sulfide promoter of a number that were tested and provided good to excellent yields in both intra- and intermolecular Khand cyclisations.[13]† Indeed, this reaction additive is particularly notable for its ability to promote some Khand reactions which had previously failed completely or proceeded only very poorly under alternative conditions. On the other hand, we considered the use of *n*-butyl methyl sulfide to have certain drawbacks. More specifically, as a low molecular weight sulfide, the *n*-butyl methyl derivative has a very unpleasant odour and imparts a lachrymatory effect. Furthermore, it is relatively expensive and, under the developed techniques, cannot be readily recycled. Therefore, we sought to develop a reusable polymer-supported analogue of *n*-butyl methyl sulfide and examine its ability to promote the Khand annulation reaction.

To initiate this work, the supported sulfide was synthesised in a single step, using standard chemistry, from commercially available Merrified gel-type resin‡ and 4-(methylthio)butan-1-ol **1**, *via* formation of a chemically robust ether link (Scheme 1). The derivatised polymer **2** obtained was odour-free and possessed sulfide functionality which is similar to the optimum solution phase promoter. Elemental analysis and infrared spectroscopy confirmed complete displacement of all chloride atoms from the starting material and gave the expected sulfur content for the new polymer.

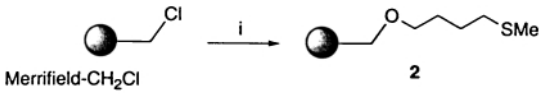

Scheme 1 *Reagents and conditions*: i, $HO(CH_2)_4SMe$ **1** (3 equiv.), NaH (6 equiv.), THF, Δ, 72 h.

Having established a simple preparation of our new solid phase reagent, we turned our attention to the study of its effectiveness as a promoter of the Khand reaction. The cyclisation of a series of alkyne substrates with norbornene was investigated and to our delight these reactions were complete in only 30 min at 83 °C in the presence of 3.5 equiv. of the supported sulfide and using 1,2-dichloroethane (1,2-DCE) as solvent.§ As shown in Table 1, very good to excellent yields of the desired cyclopentenones **3** were obtained. Furthermore, work-up of these reactions was rendered expedient by the fact that the cobalt residues produced were sequestered by the resin and merely involved filtration of the reaction mixture followed by minimal chromatographic purification. This feature of the novel promoter **2** confers a tangible practical benefit over the alternative Khand cyclisation methods.¶

In due course, using dimethylpropargyl alcohol as the alkyne substrate, we conducted several reactions using alternative alkenes. These reactions also proceeded entirely satisfactorily (Table 2); the modest yields of cyclopentenone products from the reactions of cyclopentene and 2,5-dihydrofuran reflect the lower reactivity of these olefins in Khand cyclisations.

Table 1 Solid phase sulfide promoted Khand reactions

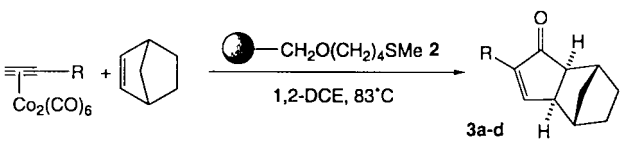

R	*t*/min	Product	Yield (%)
$Me_2(OH)C$-	30	**3a**	92
Ph-	30	**3b**	97
Me_3Si-	30	**3c**	83
t-Bu-	30	**3d**	89

DOI: 10.1039/b004568n

Table 2 Khand reactions with a selection of alkenes

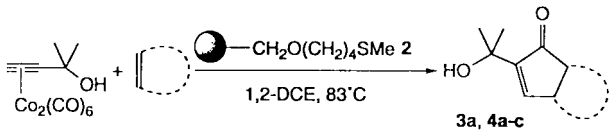

Alkene	*t*/min	Product	Yield (%)
Norbornene	30	**3a**	92
Norbornadiene	30	**4a**	91
2,5-Dihydrofuran	30	**4b**	47
Cyclopentene	90	**4c**	50

In order to further extend the substrate applicability of this new solid-phase technique, an intramolecular Khand cyclisation was examined using enyne complex **5**. This example furnished the requisite bicyclic compound **6** in 76% yield (Scheme 2).

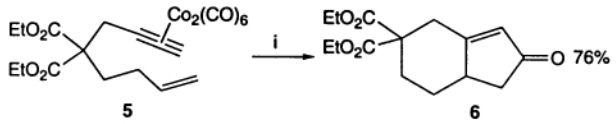

Scheme 2 *Reagents and conditions*: i, Resin **2** (3.5 equiv.), 1,2-DCE, 83 °C, 30 min.

A further important observation from this study was that, at the conclusion of all reactions the recovered polymer resin could be cleaned very easily by washing with a THF–aqueous 2 M HCl mixture. This enabled us to investigate the potential of recycling the resin. For this study the *tert*-butylacetylene–norbornene reaction was chosen. As illustrated in Table 3, the excellent yield of **3d** and short reaction time is maintained through five cycles. This aspect of the new promoter is particularly noteworthy in that, unlike our previously disclosed supported amine *N*-oxide techniques,[11] no chemical transformation is necessary for regeneration of the active solid phase promoter. Moreover, in contrast to the solution phase analogue, expense is minimised by the recyclable nature of the immobilised sulfide.

Table 3 Khand reactions using recycled resin **2**

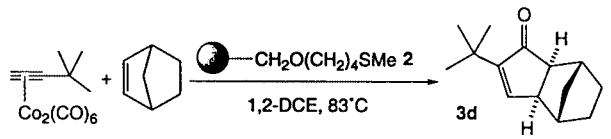

Run	1	2	3	4	5
t/min	30	30	30	30	30
Yield (%)	89	92	87	86	88

Finally, two additional *tert*-butylacetylene–norbornene cyclisations were carried out in which the quantity of the polymeric reagent used was reduced in order to determine if the 3.5 equiv. of sulfide (as established in the Sugihara solution phase studies[13] and employed throughout this work) were absolutely necessary. With 2 equiv. of resin **2** an 86% cyclisation yield was achieved, whereas 1 equiv. of **2** delivered cyclopentenone **3d** in 88% yield. Therefore, in both cases the product yield was not significantly lowered. However, it should be noted that with successive reduction in quantity of resin there was a stepwise drop in the efficiency of the cobalt residue retention.

In conclusion, a relatively cheap, commercially available gel-type resin was readily modified to afford an odourless, supported alkyl methyl sulfide. This novel solid phase reagent can be used to promote both intra- and intermolecular Khand cycloaddition reactions in a highly efficient and practical manner. Isolation of the cyclopentenone products is facilitated by the resin's ability to retain undesired cobalt residues and, furthermore, the resin can be easily and rapidly regenerated by a mildly acidic wash.

We thank the Carnegie Trust for a postgraduate scholarship (M. M.), Astra Zeneca Pharmaceuticals, Alderley Park for generous funding of our research endeavours *via* Strategic Research Funding, and the EPSRC Mass Spectrometry Service, University of Wales, Swansea, for analyses. We are also grateful to Mr Francesco Bernardis for helpful discussions.

Notes and references

† It should be noted that the promoting effect of suitably spaced methyl sulfide groups when tethered to the alkene[14] or alkyne[6d,15] was first discovered and reported by Krafft.

‡ The 1% cross-linked Merrifield resin was purchased from NovaBiochem with a chloride loading of 1.1 mmol g^{-1}.

§ Respresentative experimental procedure; To a solution of hexacarbonyl(3,3-dimethylbut-1-yne)dicobalt (34.0 mg, 0.092 mmol) and norbornene (56.0 mg, 0.596 mmol) in 1,2-DCE (2.5 ml) was added sulfide resin **2** (0.29 g, 0.29 mmol) and the mixture was stirred at 83 °C for 30 min. The solvent was drained and the resin washed with CH_2Cl_2 (10 × 2 ml) and THF (5 × 2 ml). The combined filtrates were evaporated *in vacuo* to afford a residue which was chromatographed on silica using 5% Et_2O in petrol as eluant. The product **3d** was obtained as a white crystalline solid (16.7 mg, 89%).

¶ 4-(Methylthio)butan-1-ol was also tested as a solution phase promoter using Sugihara's conditions in the *tert*-butylacetylene–norbornene reaction and provided an 89% yield of cyclopentenone **3d**. However, this additive suffers from an undesirable odour and lacks the potential to be readily recycled.

1 K. M. Brummond and J. L. Kent, *Tetrahedron*, 2000, **56**, 3263.
2 I. U. Khand, G. R. Knox, P. L. Pauson and W. E. Watts, *J. Chem. Soc., Chem. Commun.*, 1971, 36; I. U. Khand, G. R. Knox, P. L. Pauson, W. E. Watts and M. I. Foreman, *J. Chem. Soc., Perkin Trans. 1*, 1973, 977.
3 N. E. Schore, *Org. React.*, 1991, **40**, 1; Y. K. Chung, *Coord. Chem. Rev.*, 1999, **188**, 297.
4 D. C. Billington, I. M. Helps, P. L. Pauson, W. Thomson and D. Willison, *J. Organomet. Chem.*, 1988, **354**, 233.
5 W. A. Smit, A. S. Gybin, S. O. Simonyan, A. S. Shashkov, V. A. Tarasov and I. I. Ibragimov, *Izv. Akad. Nauk SSSR, Ser. Khim.*, 1985, 2650; W. A. Smit, A. S. Gybin, A. S. Shashkov, Y. T. Strychkov, L. G. Kyz'mina, G. S. Mikaelian, R. Caple and E. D. Swanson, *Tetrahedron Lett.*, 1986, **27**, 1241; S. O. Simonyan, W. A. Smit, A. S. Gybin, A. S. Shashkov, G. S. Mikaelian, V. A. Tarasov, I. I. Ibragimov, R. Caple and D. E. Froen, *Tetrahedron Lett.*, 1986, **27**, 1245; W. A. Smit, S. O. Simonyan, V. A. Tarasov, G. S. Mikaelian, I. I. Ibragimov, R. Caple, D. E. Froen and A. Kreager, *Synthesis*, 1989, 472; W. A. Smit, S. L. Kireev, O. M. Nefedov and V. A. Tarasov, *Tetrahedron Lett.*, 1989, **30**, 4021.
6 (*a*) S. Shambayati, W. E. Crowe and S. L. Schreiber, *Tetrahedron Lett.*, 1990, **31**, 5289; (*b*) N. Jeong, Y. K. Chung, B. Y. Lee, S. H. Lee and S.-E. Yoo, *Synlett*, 1991, 204; (*c*) Y. K. Chung, B. Y. Lee, N. Jeong, M. Hudecek and P. L. Pauson, *Organometallics*, 1993, **12**, 220; (*d*) M. E. Krafft, I. L. Scott, R. H. Romero, S. Feibelmann and C. E. Van Pelt, *J. Am. Chem., Soc.*, 1993, **115**, 7199.
7 A. R. Gordon, C. Johnstone and W. J. Kerr, *Synlett*, 1995, 1083.
8 W. J. Kerr, M. McLaughlin, P. L. Pauson and S. M. Robertson, *Chem. Commun.*, 1999, 2171.
9 For example, see J. G. Donkervoort, A. R. Gordon, C. Johnstone, W. J. Kerr and U. Lange, *Tetrahedron*, 1996, **52**, 7391; C. Johnstone, W. J. Kerr and U. Lange, *J. Chem. Soc., Chem. Commun.*, 1995, 457.
10 W. J. Kerr, G. G. Kirk and D. Middlemiss, *Synlett*, 1995, 1085; W. J. Kerr, D. M. Lindsay, E. M. Rankin, J. S. Scott and S. P. Watson, *Tetrahedron Lett.*, 2000, **41**, 3229; D. R. Carbery, W. J. Kerr, D. M. Lindsay, J. S. Scott and S. P. Watson, *Tetrahedron Lett.*, 2000, **41**, 3235.
11 W. J. Kerr, D. M. Lindsay and S. P. Watson, *Chem. Commun.*, 1999, 2551.
12 For reviews, see D. C. Bailey and S. H. Langer, *Chem. Rev.*, 1981, **81**, 109; A. Akelah and D. C. Sherrington, *Chem. Rev.*, 1981, **81**, 557.
13 T. Sugihara, M. Yamada, M. Yamaguchi and M. Nishizawa, *Synlett*, 1999, 771.
14 M. E. Krafft, *J. Am. Chem. Soc.*, 1988, **110**, 968; M. E. Krafft, C. A. Juliano, I. L. Scott, C. Wright and M. D. McEachin, *J. Am. Chem. Soc.*, 1991, **113**, 1693; M. E. Krafft and C. A. Juliano, *J. Org. Chem.*, 1992, **57**, 5106.
15 M. E. Krafft, I. L. Scott and R. H. Romero, *Tetrahedron Lett.*, 1992, **33**, 3829; M. E. Krafft, A. M. Wilson, O. A. Dasse, L. V. R. Bonaga, Y. Y. Cheung, Z. Fu, B. Shao and I. L. Scott, *Tetrahedron Lett.*, 1998, **39**, 5911.

ChemComm

Polymer-like complexes bridged by a fluorine substituent of the side arm in the 3′,5′-difluoro-4′-hydroxybenzyl-armed monoaza-15-crown-5 ether

Yoichi Habata,*[a] Tomomi Saeki,[a] Sadatoshi Akabori,[a] Xian X. Zhang[b] and Jerald S. Bradshaw[b]

[a] *Department of Chemistry, Faculty of Science, Toho University, Funabashi, Chiba 274-8510, Japan*
[b] *Department of Chemistry and Biochemistry, Brigham Young University, Provo, UT 84602, USA*

Received (in Cambridge) 2nd May 2000, Accepted 20th June 2000
Published on the Web 19th July 2000

3′,5′-Difluoro-4′-hydroxybenzyl-armed monoaza-15-crown-5 ethers which form fluorine-bridged polymer-like complexes with MSCN in the solid state and in solution are reported.

Recently, we reported the molecular structure of alkali metal complexes with armed-monoazacrown ethers having 3′,5′-dialkyl-4′-hydroxybenzyl groups (alkyl = Me, *i*-Pr and *t*-Bu).[1] The molecular structure of the RbSCN complexes with these ligands was systematically changed depending upon the size of the R groups at positions 3′ and 5′ in the side arm (**1** (R = Me), a polymer-like $(1:1)_n$ complex; **2** (R = *i*-Pr), a mixture of 1:1 and polymer-like $(1:1)_n$ complexes; **3** (R = *t*-Bu), a dimeric

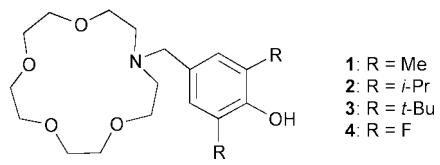

1: R = Me
2: R = *i*-Pr
3: R = *t*-Bu
4: R = F

1:1 complex). To further investigate the electronic and steric effects of the substitutents next to the phenolic OH group in the side arm on the structure of the complexes, we have prepared a new armed-azacrown ether having fluorine atoms at positions 3′ and 5′ in the side arm (**4**). Computer modeling experiments suggest that the oxygen atom of the phenolic OH group cannot bind to metal cations incorporated into the crown part of the molecule so that the ligand can form polymer-like complexes with alkali metal cations.† It was also expected that the ligand would form polymer-like complexes using the electron donating properties of fluorine atoms next to the phenolic OH group.[2] Here we report the structures of polymer-like complexes of ligand **4** which are bridged by the fluorine atoms in the side arm.

New armed-azacrown ether, **4**,‡ was prepared by the Mannich reaction of *N*-methoxymethylmonoaza-15-crown-5 ether with 2,6-difluorophenol in benzene by the method previously reported.[3] Two alkali metal thiocyanate complexes, **4-KSCN** and **4-RbSCN**, were obtained (host–guest ratio = 1:1) as single crystals.§

The structures of **4-KSCN** and **4-RbSCN** complexes have been determined by X-ray analysis.¶ As shown in Fig. 1(*a*), the K^+ ion in **4-KSCN** is eight-coordinated by four ring O atoms, the ring N atom, and the O* atom of the phenolic OH group and an F* atom in the side arm of the nearest-neighbor molecule with the S atom of SCN^- as a counter ion. The complex is a polymer-like $(1:1)_n$ complex. The K(1)–O (ring), K(1)–O(5*), K(1)–N(1), K(1)–S(1) and K(1)–F(2*) bond lengths are in the range 2.757(2)–2.792(2), 3.028(2), 2.877(2), 3.253(1) and 2.783(2) Å, respectively. The K–O and K–N bond lengths are comparable with those of the potassium complex of the lariat monoaza-15-crown-5 ethers.[4] The K–F bond length is also comparable with those of complexes including CF–K^+ contacts.[5] Fig. 1(b) shows the ORTEP view of the **4-RbSCN** complex. The Rb^+ ion is also eight-coordinated by four ring O atoms, the ring N atom, the F atom in the side arm of the nearest-neighbor molecule with the two S atoms of SCN^- as counter ions. The complex is a polymer-like $(2:2)_n$ complex which is bridged by an F atom in the side arm. Interestingly, the O atom of the phenolic OH group in the side arm is not involved in the complex formation. The Rb(1)–O (ring), Rb(1)–N(1), Rb(1)–S(1), Rb(1)–S(1*) and Rb(1)–F(2*) bond lengths are in the range 2.860(7)–2.972(8), 3.087(7), 3.412(3), 3.475(3) and 3.001(6) Å, respectively. It is important to note that the F–Rb^+ bond length in **4-RbSCN** complex is classified as a short F–Rb^+ bond length which is a rare case.[5]

To investigate the complexation ability of ligand **4** in solution, stability constants *K* and thermodynamic values (ΔH and $T\Delta S$) were measured by titration calorimetry in MeOH solution (Table 1).‖ Interestingly, the log *K* values for Na^+ (log *K* = 2.96), K^+ (log *K* = 2.95), Rb^+ (log *K* = 2.79) and Cs^+ (log *K* = 2.74) were almost equal. The log *K* values suggest that ligand **4** coordinates to the alkali metal cations not only by the crown ether moiety but also by the binding sites of the side-arm,

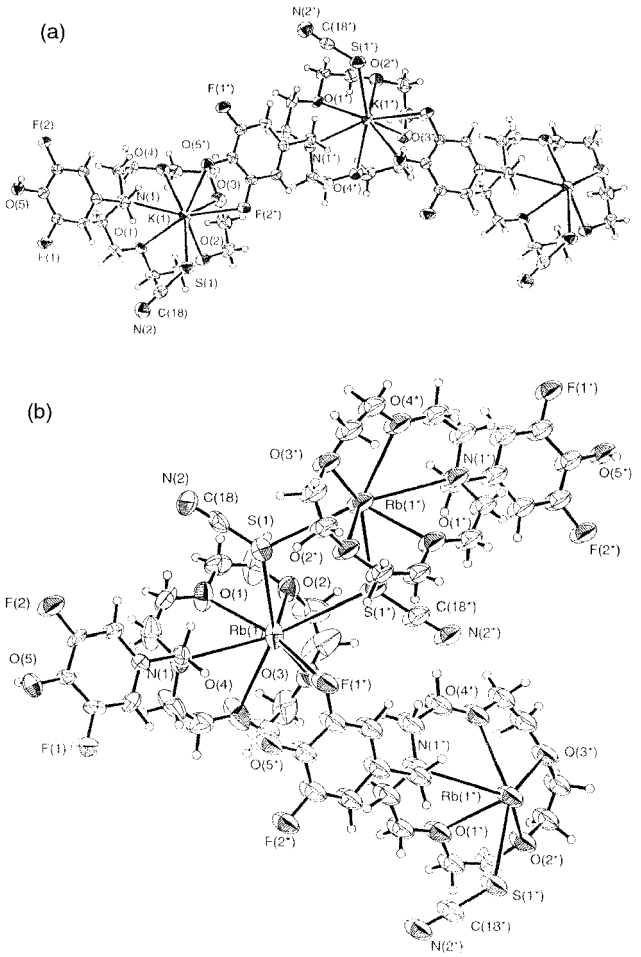

Fig. 1 The ORTEP diagrams of (a) **4-KSCN** and (b) **4-RbSCN**. Thermal ellipsoids are drawn at the 30% probability level.

DOI: 10.1039/b003451g

Table 1 Log K, ΔH(kJ mol^{-1}), and $T\Delta S$(kJ mol^{-1}) values for the 1:1 interaction of ligand **4** with metal cations in methanol solution at 25 °C

Cation	log K	ΔH	$T\Delta S$
Na^+	2.96 ±0.03	−16.5 ±0.2	−1.4
K^+	2.95 ±0.05	−23.1 ±0.7	−6.3
Rb^+	2.79 ±0.06	−17.5 ±0.4	−1.6
Cs^+	2.74 ±0.05	−8.2 ±0.4	7.4

because the log K value for Na^+ which fits to the hole size of the monoaza-15-crown-5 ether is not remarkable higher than that for the other alkali metal cations.[6] Inoue and Gokel reported that the slope (α) of the enthalpy-entropy compensation (plot of $T\Delta S$ *versus* ΔH) indicates conformational changes of host compounds on complex formation.[7] The α value was calculated as 0.923 (r^2 = 0.994) from the plot of $T\Delta S$ versus ΔH, which is close to the average (0.89) of typical armed-crown ethers, and indicates that significant conformational changes would occur when the ligand forms complexes. Therefore, the log K values and the α value support the supposition that ligand **4** forms complexes with alkali metal cations by both the crown moiety and the side arm.

Plenio and Diodone reported that the ^{19}F NMR chemical shift changes when fluorine atoms coordinate to metal cations in fluorine containing azacrown ethers and cryptands.[2] The ^{19}F NMR titration experiments were carried out in a CD_3CN solution (Table 2) to determine F atom participation from the side-arm. When 1.0 equiv. of NaSCN, KSCN and RbSCN were added to a CD_3CN solution of ligand **4**, the chemical shifts of the fluorine atoms next to the phenolic OH group shifted to a lower field by about 0.7–0.8 ppm. These values are much greater than the 0.1–0.2 ppm shifts observed with the addition of 1.0 equiv. of MSCN to a CD_3CN solution of 2,6-difluorophenol. These chemical-shift changes strongly suggest that one or both fluorine atoms along with the oxygen atom of the phenolic OH group coordinate to the alkali metal cations incorporated in the crown part of a second armed ligand to give polymer-like complexes in solution.

Table 2 MSCN Induced changes in ^{19}F NMR chemical shifts of 2,6-difluorophenol and **4**[a]

	2,6-Difluorophenol	**4**
Chemical shift[b]	−135.92	−135.90
+1.0 NaSCN	+0.12	+0.72
+1.0 KSCN	+0.19	+0.83
+1.0 RbSCN	+0.14	+0.78

[a] Titration experiments were carried out at 298 K by addition of 0.5, 0.75, 1.0, 1.5 and 2.0 equiv. of MSCN (NaSCN and KSCN: 0.001 mmol μL^{-1} in CD_3CN; RbSCN: 0.001 mmol μL^{-1} in CD_3CN–D_2O (95:5)) to 2,6-difluorophenol or ligand **4** (0.01 mmol, 0.65 mL in CD_3CN). Positive numbers show down field shifts. [b] α,α,α-Trifluorotoluene (δ −63.72) was used as an internal standard.

In conclusion, we have demonstrated that the fluorine atoms in the side arm of ligand **4** coordinate to alkali metal cations incorporated in a second ligand in the solid state and in solution. This first example for a fluorine-bridged polymer-like complex has potential for the design of new supramolecular systems. Further studies of the new armed-azacrown ethers are in progress.

Financial support from the Japan Securities Scholarship Foundation (Y. H.) is gratefully acknowledged.

Notes and references

† SPARTAN *Pro*™ (Version 1.03, Wavefunction Inc, 1999) was used as the computer-modeling software. Minimization was carried out using the *ab initio* 3-21 (G*).[8]

‡ A mixture of *N*-methoxymethylmonoaza-15-crown-5 ether (1.0 mmol) and 2,6-difluorophenol (1.0 mmol) in absolute benzene (20 ml) was refluxed under a nitrogen atmosphere for 24 h. The reaction mixture was cooled and then concentrated under reduced pressure. The residual oil was separated and purified by silica gel and then gel-permeation column chromatography to give ligand **4**: ^{1}H NMR ($CDCl_3$): δ 6.81 (d, 2H, J_{HF} = 8.0 Hz), 3.73-3.37 (m, 19H), 2.77 (t, 4H, J = 5.4 Hz); MS: EI (m/z) 362 (M^+ + 1, 100 %). Anal. Calcd. for $C_{17}H_{25}F_2NO_5{\cdot}0.75H_2O$: C, 54.46; H, 7.12; N, 3.74%. Found: C, 54.62; H, 7.48; N, 3.87%.

§ Ligand **4** (0.01 mmol) in MeCN (1 mL) was reacted with the alkali metal thiocyanate (0.01 mmol) MeOH (1 mL). After the solvent had evaporated, the crystals were recrystallized from MeCN. The crystals were dried with an Abderhalden's dryer (50 °C, 0.5 Torr). The elemental analyses of these complexes are as follows: **4**-KSCN: Anal. calcd. for $C_{17}H_{25}F_2NO_5$-KSCN: C, 47.15; H, 5.49; N, 6.11%. Found: C, 47.35; H, 5.50; N, 6.42%. **4**-RbSCN: Anal. calcd. for $C_{17}H_{25}F_2NO_5{\cdot}$RbSCN: C, 42.82; H, 4.99; N, 5.55%. Found: C, 42.72; H, 5.05; N, 5.53%.

¶ *Crystal data* for $C_{18}H_{25}N_2O_5SF_2K$, **4**-KSCN: M = 458.56, monoclinic, a = 8.564(2), b = 16.354(2)°, c = 15.510(2) Å, β = 93.81(2)°, U = 2167.6(7) Å^3, T = 295 K, space group $P2_1/n$ (no. 14), Z = 4, μ(Mo-Kα) = 3.89 cm^{-1}, 5331 reflections measured, 5152 unique (R_{int} = 0.042) which were used in all calculations. R_1 = 0.048 [$I > 2\sigma(I)$], R = 0.114 and Rw = 0.136 [all data]. Crystal data for $C_{18}H_{25}N_2O_5SF_2Rb$, **4**-RbSCN: M = 504.93, monoclinic, a = 8.875(3), b = 18.627(4), c = 13.359(3) Å, β = 93.72(2)°, U = 2203.8(10) Å^3, T = 295 K, space group $P2_1/n$ (no. 14), Z = 4, μ(Mo-Kα) = 23.84 cm^{-1}, 4294 reflections measured, 4024 unique (R_{int} = 0.062) which were used in all calculations. R_1 = 0.060 [$I > 2\sigma(I)$], R = 0.180 and Rw = 0.156 [all data]. CCDC 182/1699. See http://www.rsc.org/suppdata/cc/b0/b003451g/ for crystallographic files in .cif format. X-Ray data are available as supplementary data from BLDSC (SUPPL. NO. 57710, pp. 27) or the RSC Library. See Instructions for Authors available *via* the RSC web page (http://www.rsc.org/authors).

‖ Log K, ΔH, and $T\Delta S$ values were determined as described[9] in MeOH at 25.0 ±0.1 °C by titration calorimetry using a Tronac Model 450 calorimeter equipped with a 20 mL reaction vessel. The metal cation solutions (0.08–0.12 M) were titrated into the armed-azacrown ether solutions (1.3×10^{-3}–2.6×10^{-3} M) and the titrations were carried out to a two-fold excess of the metal cations.

1 Y. Habata and S. Akabori, *J. Chem. Soc., Dalton Trans.*, 1996, 3871; Y. Habata and S. Akabori, *Supramol. Chem.*, submitted.
2 H. Plenio and R. Diodone, *J. Am. Chem. Soc.*, 1996, **118**, 356.
3 Y. Habata, T. Saeki, S. Akabori and J. S. Bradshaw, *J. Heterocycl. Chem.*, 1999, **36**, 355.
4 R. D. Gandour, F. R. Fronczek, V. J. Gatto, C. Minganti, R. A. Schultz and G. W. Gokel, *J. Am. Chem. Soc.*, 1986, **108**, 4078.
5 H. Plenio, *Chem. Rev.*, 1997, **97**, 3363. and reference cited therein.
6 R. M. Izatt, K. Pawlak, J. S. Bradshaw and R. L. Bruening, *Chem. Rev.*, 1991, **91**, 1721.
7 *Cation Binding by Macrocycles*, eds. Y. Inoue and G. W. Gokel, Marcel Dekker, New York, 1990, p. 1 and references cited therein.
8 W. J. Pietro, M. M. Francl, W. J. Hehre, D. J. DeFrees, J. A. Pople and J. S. Binkley, *J. Am. Chem. Soc.*, 1982, **104**, 5039.
9 J. L. Oscarson, R. M. Izatt, in *Physical Methods of Chemistry*, eds. B. W. Rossiter and R. C. Baetzold, John Wiley & Sons, New York, 1992, Vol. 6, Chapter 7; R. M. Izatt, X. X. Zhang, H. Y. An, C. Y. Zhu and J. S. Bradshaw, *Inorg. Chem.*, 1994, **33**, 1007.

ChemComm

A universal approach to web-based chemistry using XML and CML

Peter Murray-Rust,[a] Henry S. Rzepa,[b] Michael Wright[b] and Stephen Zara[b]

[a] *School of Pharmaceutical Sciences, University of Nottingham, UK*
[b] *Department of Chemistry, Imperial College of Science, Technology and Medicine, London UK*

Received (in Cambridge, UK) 28th March 2000, Accepted 14th June 2000
Published on the Web 18th July 2000

We report the first fully operational system for managing complex chemical content entirely in interoperating XML-based markup languages.

The World-Wide-Web (WWW) was originally developed as a collaborative tool for scientists. In 1994 we proposed its use as a novel and widely applicable global model for expressing chemical information in an interlinked and re-usable form.[1] This model, based on HTML, has become widely used but suffers from a number of structural problems. Chemistry represents its message both *semantically* (*e.g.* as a machine-processable connection table) and graphically (*e.g. presentation* through human-readable arrows, boxes, diagrams). The existing use of HTML in chemistry emphasizes presentation, and provides no structured extension mechanisms. A presentational approach is too flexible to be reliably interpreted by machines, and cannot *validate* the integrity of the chemical *content*. Thus the chemical subscript and superscript conventions in *e.g.* $CH_4^{+\cdot}$ are only unambiguously interpretable by humans. This severely limits the re-usability of the rapidly growing amount of high-quality chemistry available on Web pages.

We therefore developed[2] our model to support both types of markup. Chemical Markup Language (CML) can carry molecules, crystallography and reactions in a formal manner. It forms the core of a comprehensive approach to publishing and communicating chemical information for both humans and machines. It uses the protocols of the WWW Consortium (W3C),[3] whose goal is to support such *interoperability* with the strategic aim of achieving a "semantic web" where automatic processing of information is possible. The core W3C approach is the *meta-language* XML (eXtensible Markup Language) which was formalised in 1998 and which encourages the creation of discipline-specific languages such as CML. The W3C have created a family of protocols supporting most aspects of managing Web-based information; the following are most relevant here: *XML Schemas* are a formal description of the language and can support arbitrary datatypes and or validate complex documents. *Scalable Vector Graphics (SVG)* provide a framework where presentation and content can be robustly combined. *XSLT (XSL stylesheets)* is a very powerful tool for transforming documents. *XML Query Language* and XLinking are under development. *XSL(FO)* provides high quality formatted output for any XML application.[3]

Much time is currently wasted on processing *legacy* unstructured and often binary documents and poor semantics leads to serious information loss. The 'plug-compatible' XML approach guarantees a document to be searchable, stylable, sortable, transformable, mergeable, transmittable and printable without extra cost. CML uses these developments and for the first time offers a universal platform- and application-independent infrastructure for chemical information. Ideally we see all future document and publishing systems being converted to XML and describe here an implementation of these concepts termed ChiMeraL.

Technical documents are often multidisciplinary and component-based and draw their components from several XML Schemas. Subdisciplines, *e.g.* MathML (for mathematics), CML, SVG, are identified within documents by discrete *namespaces*. To avoid *collision* their *tag names* are mapped onto globally unique URIs (Uniform Resource Identifier); http://www.xml-cml.org/ serves to uniquify any CML element. Components will often be glued together with XHTML (the XML version of HTML).[4] *Transformation/reformatting* through XSL stylesheets is a particularly important operation because it allows extraction of document sub-components such as molecules for *e.g.* redrawing in SVG (*vide infra*) or outputting in any desired format.

Besides transformation, various operations can be automatically performed, often without knowing the precise document structure. These include searching, whereby XML elements ('components') can be located by local or global context in a document or through content, re-use by fragmenting or combining XML documents, rendering/viewing in a browser window, high-quality printing, and data authentication services.[5]

'Chemical' information usually requires several other types of markup (text, numbers, tables, graphics, etc.). Such CML document components can come from many sources, either directly or after conversion from legacy formats. The sources include: instruments, databases, dictionaries and catalogues; hand-editing/authoring of chemical information; primary and secondary publications, and computational chemistry tools. To illustrate how the operation of transmitting, querying and processing compound chemical data within a Web browser can be combined, we have created a Web-based collection of XML tools termed ChiMeraL.[6] Its use involves five distinct stages (Fig. 1).

(1) Conventional HTML is used in conjunction with JavaScript in a browser to allow the user to select from an XML library containing CML components (Fig. 2). The library could be a server-based collection or could be generated by selective querying of a larger XML document held on an XML repository.

(2) The XML document is validated for integrity against a Schema. This is a major improvement over HTML, which has no validation for chemical or most other content. Validation can be server or browser-based.

(3) Selection of a suitable stylesheet for popular chemical editing and display programs, *e.g.* for 2D and 3D molecular co-ordinates and numerical information such as spectral/analytical data. The stylesheet is used to convert CML elements to legacy formats (*e.g.* MDL Molfile, Minnesota XYZ format, JCAMP DX format) for display using existing applets (*e.g.* JME, JMol, JSpec, Marvin, SDA), or it could be directed towards CML-compliant applets without the need for such legacy transformation. The XSL transform can again be server or browser based. The use of a stylesheet also provides the possibility of deriving new quantities from the original data such as *e.g.* aligning a range of pharmacophores or computing diverse molecular properties. The ChiMeraL demonstration (Fig. 2)† includes a range of XSL stylesheet fragments, XML example documents and a CML schema, together with utility programs which can generate CML documents.[6]

(4) The output from the stylesheet is displayed as a web page. The original CML components (*e.g.* < molecule > < /molecule >) are wrapped with suitable XHTML to allow appropriate display (Fig. 2).

(5) At this stage, the user could edit or add to the document

DOI: 10.1039/b002483j

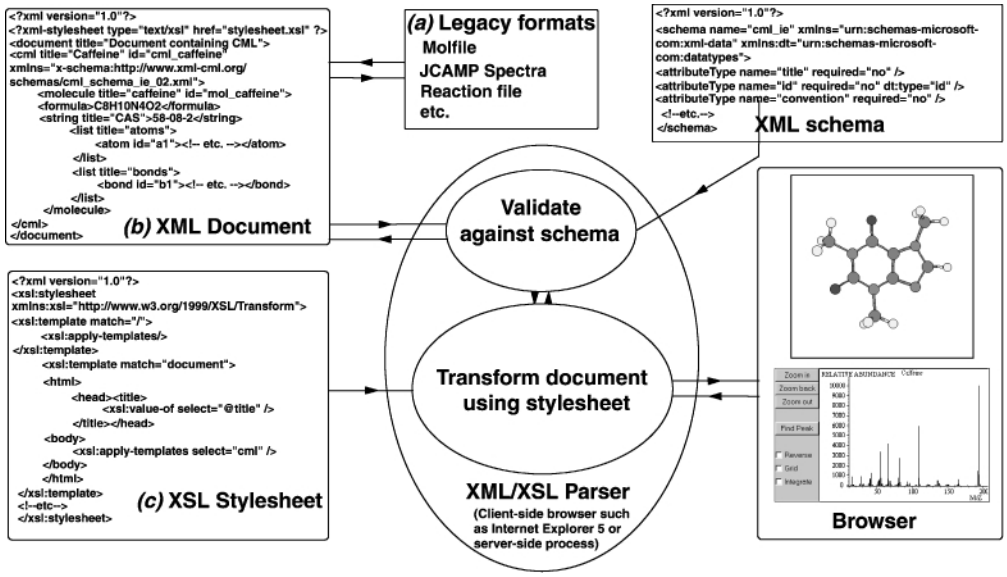

Fig. 1 Data flow between the principal components of ChiMeraL (a) The creation of a *structured document* in XML syntax from unstructured *legacy* formats (MOL, JCAMP, *etc.*). The validity of the process is checked by a CML-specific XML schema. (b) Illustrative CML document whose *root element* contains a *child molecule element*. In turn the *molecule* contains a *list* element, itself the parent of many *atom* elements (omitted for clarity); bonds are analogous. *Attributes* such as *convention* identify the usage of terms and values, while the *id* attribute identifies every element uniquely. (c) Illustrative XSL stylesheet, which transforms CML to XHTML. The *title* of the *molecule* is transformed to the XHTML document title, while the content of the *molecule* is transformed into various legacy formats (MOL, JME, *etc.*) for display by applets.

by selecting an appropriate stylesheet to invoke appropriate software tools, and with appropriate validation, create a new annotated XML document which could be returned to the original document repository. Multiple authorship of a document is possible since subsequent stylesheet transforms could *e.g.* extract either the original document, or any individual's additions to it.

Chimeral is offered as OpenSource, *i.e.* available as source code which can be used for any purpose, but especially for the development of new ideas, tools and resources in this area. XML has benefitted greatly from this movement and Chimeral uses several OpenSource components (XML tools, JMol, JSpect).[7] OpenSource is an effective means of developing high-quality robust applications very rapidly and we encourage developers to increase the volume of WWW-based collaboration in chemistry.

We have described a method for completely transparent Internet-based transfer of chemical information from creator/author to reader/user. Applications of this method might include a document such as this journal article being automatically abstracted for molecular content, and stored or used for calculations or searching. One can envisage *e.g.* laboratory robots scanning CML-based reaction schemes for starting materials and ordering them from CML-based 'dot.coms' on the WWW, and recording this in electronic notebooks. Instruments could directly output universally processable spectra and data. Databases could accept chemistry in many traditional formats and re-offer them transparently. Computational chemistry and modelling programs could be used routinely for adding information content to molecules. Finally, we note that the use of XML allows other disciplines (bioscience, pharmaceutical, materials, patents) to include semantically rich chemistry in their information.

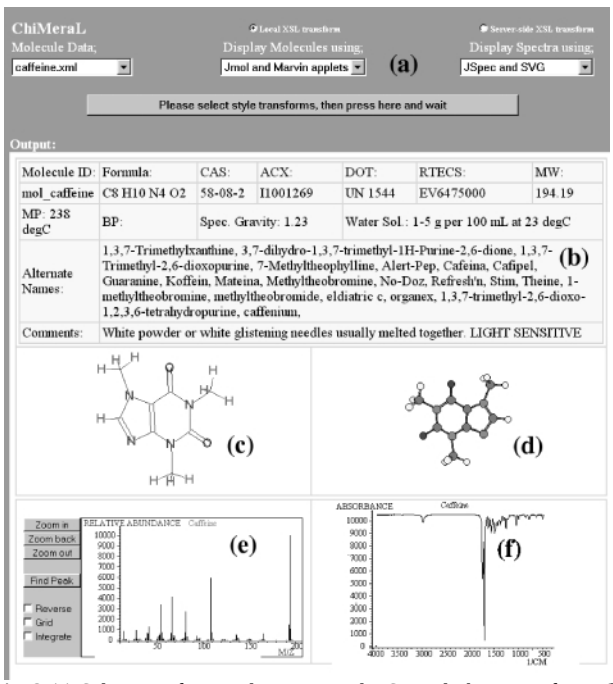

Fig. 2 (a) Selection of XML document and XSL stylesheet transform. (b) Property display using HTML table. (c) 2D Molecule display using Marvin applet. (d) 3D Molecule display using JMol applet. (e) Spectral display using JSpec applet. (f) Spectral display using SVG and Adobe plugin.

Notes and references

† This article expressed as XML is also available *via* the electronic supplementary information pages at http://www.rsc.org/suppdata/cc/b0/b002483j/

1 H. S. Rzepa, B. J. Whitaker and M. J. Winter, *J. Chem. Soc., Chem. Commun.*, 1994, 1907; O. Casher, G. Chandramohan, M. Hargreaves, C. Leach, P. Murray-Rust, R. Sayle, H. S. Rzepa and B. J. Whitaker, *J. Chem. Soc., Perkin Trans. 2*, 1995, 7; H. S. Rzepa, P. Murray-Rust and B. J. Whitaker, *Chem. Soc. Rev.*, 1997, 1; H. S. Rzepa, P. Murray-Rust and B. J. Whitaker, *J. Chem. Inf. Comput. Sci.*, 1998, **38**, 976.

2 The original concept was described in P. Murray-Rust, C. Leach and H. S. Rzepa, *Abs. Papers. Am . Chem. Soc.*, 1995, **210**, 40-COMP. For a formal description of CML version 1.0, see P. Murray-Rust and H. S. Rzepa, *J. Chem. Inf. Comput. Sci.*, 1999, **39**, 928.

3 World-Wide Web Consortium (W3C). See http://www.w3.org/

4 W3C Working draft: 'XHTML 1.0. The extensible HyperText markup language for a specification of the XHTML standard', http://www.w3.org/MarkUp/

5 W3C Working draft 'XML-Signature Syntax and Processing', http://www.w3.org/TR/xmldsig-core/

6 ChiMeraL can be viewed at http://www.ch.ic.ac.uk/chimeral/

7 V. Kiernan, *Chronicle Higher Education*, 1999, http://www.chronicle.com/free/v46/i11/11a05101.htm. See also D. Gezelter, http://www.openscience.org/

ChemComm

[26]Hexaphyrin(1.1.1.1.0.0): an all-aza isomer of rubyrin with an inverted pyrrole subunit

Jonathan L. Sessler,* Daniel Seidel, Christophe Bucher and Vincent Lynch

Department of Chemistry and Biochemistry, University of Texas at Austin, Austin, Texas 78712-1167, USA. E-mail: sessler@mail.utexas.edu

Received (in Corvallis, OR, USA) 9th May 2000, Accepted 20th June 2000
Published on the Web 19th July 2000

The synthesis, characterization and X-ray structure of an hexapyrrolic macrocycle, [26]hexaphyrin(1.1.1.1.0.0), is reported; it is characterized by a partially inverted structure.

Expanded porphyrins continue to attract attention as synthetic targets due to the fact that they often display features, such as anion binding and neutral substrate recognition, that are not seen in normal porphyrins.[1–3] Recently, a special structural feature, namely the inversion of one or two of the pyrrolic-subunits has been observed in certain expanded porphyrins. For instance, the free-base form of *meso*-tetraphenylsapphyrin exhibits such an inverted structure. Upon bis-protonation, however, this species undergoes a change in conformation adopting a 'regular' planar structure wherein all the nitrogens are pointed inward.[4,5] Similar structural features have been observed for certain heteroatom-containing *meso*-tetraphenylsapphyrins;[6–8] depending on the protonation state and the nature of the heteroatom, these latter systems can exhibit either an inverted or a planar structure. Several heterorubyrins (*e.g.* **1** with X = S or Se, respectively) have also been found to adopt bis-inverted conformations under appropriate conditions.[7] Another recent report described the isolation of a novel [26]hexaphyrin(1.1.1.1.1.1) in low yield as a side product in the Rothemund synthesis of porphyrins,[9] that exhibits a bis-inverted structure in its free-base form. In this instance, the influence of protonation has yet to be established. Interestingly, the original [26]hexaphyrin(1.1.1.1.1.1), first reported by Gossauer in 1983,[10] was found to adopt a different conformation. Rather than existing in a form wherein one or more of the pyrrolic subunits is inverted, this system, bearing substituents on the β-pyrrolic but not *meso*-carbon positions, was found to adopt a conformation wherein the two opposing *meso*-C*H* protons point inward. Upon metalation with $PdCl_2$, however, it is believed that this latter hexaphyrin, never characterized structurally, rearranges such that two of the six pyrrolic subunits point outwards.[11] The subtle nature of the conformational effects evident in hexapyrrolic macrocycles and their structural origins are currently far from understood. They thus provide an impetus for further study. In this communication we report the synthesis of the hitherto unknown hexapyrrolic macrocycle, [26]hexaphyrin(1.1.1.1.0.0) (**2**). Based on an analysis of molecular models, this particular system was expected to adopt a conformation wherein one pyrrolic subunit (only) is inverted.

The synthesis of compound **2** is summarized in Scheme 1. Briefly, it is obtained in 46% yield from the acid catalyzed condensation of a 1 : 1 mixture of the diphenyltripyrane **3**[12] with the diformylhexamethylterpyrrole **4**.[13]

[26]Hexaphyrin(1.1.1.1.0.0) (**2**) constitutes the first true isomer of rubyrin.[14] While other porphyrin analogues bearing the same combination of four *meso*-like carbon atoms and six heterocyclic subunits are known, in particular the bronzaphyrins,[15] in all cases at least one of the six pyrrolic units present in rubyrin has been replaced by a furan or a thiophene.†

Macrocycle **2** is aromatic as judged from the ^{1}H NMR (d_6-DMSO) spectra of the protonated and free-base forms, respectively. The dihydrochloride salt, $H_2\mathbf{2}^{2+}\cdot 2Cl^-$, in particular, shows a strong magnetic ring current effect. Here, upfield shifts for the inner N*H* protons are found, with resonances observed at −0.75, −0.14 and 0.05 ppm in a 1 : 2 : 2 ratio. One more upfield resonance, namely at −2 ppm is also observed. On the basis of a two-dimensional C–H correlation experiment, this signal is ascribed to a C*H* proton. Indeed, the upfield position of this resonance is considered *prima facie* evidence for the inverted nature of $H_2\mathbf{2}^{2+}\cdot 2Cl^-$.‡

The COSY spectrum of **2** shows a correlation between the peak at −2 ppm with one at 15 ppm, a signal that was found to correspond to the outer N*H* proton. The $\Delta\delta$-value of 17 ppm between these two signals provides strong support for the aromatic nature of the inverted macrocycle. Also, the C*H* protons of the *meso*-positions were found to resonate at 11.4 ppm while two doublets at 9.2 and 9.8 ppm, respectively, were found to correspond to the two outer β-pyrrole C*H* protons. Interestingly, in the ^{1}H NMR spectrum of the free-base macrocycle **2** the $\Delta\delta$-value between the β-C*H* protons of the inverted pyrrole (δ = 3.5 ppm) and the N*H* signal (δ = 9.8 ppm) of the same pyrrole is reduced to 6.3 ppm. The C*H* protons of the *meso*-positions resonate at 8.5 and the two doublets which correspond to the two outer β-pyrrole C*H* protons are shifted to 7.3 and 8 ppm, respectively. The reduced aromatic effect for the free-base form of macrocycle **2** can be rationalized in terms of a lower number of fully conjugated π-electron peripheries (*i.e.* fewer aromatic resonance structures can be drawn). It is also possible that **2** is subject to a greater distortion from planarity than $H_2\mathbf{2}^{2+}\cdot 2Cl^-$. Nevertheless, the critical point is that **2** is still considered to be inverted; the $\Delta\delta$-value between the outer and inner β-C*H* protons amounts to 5 ppm as the result of an extant but weak ring current effect.

The NOESY spectrum supports the assignment of an inverted structure to the free-base form of **2**. A correlation is found

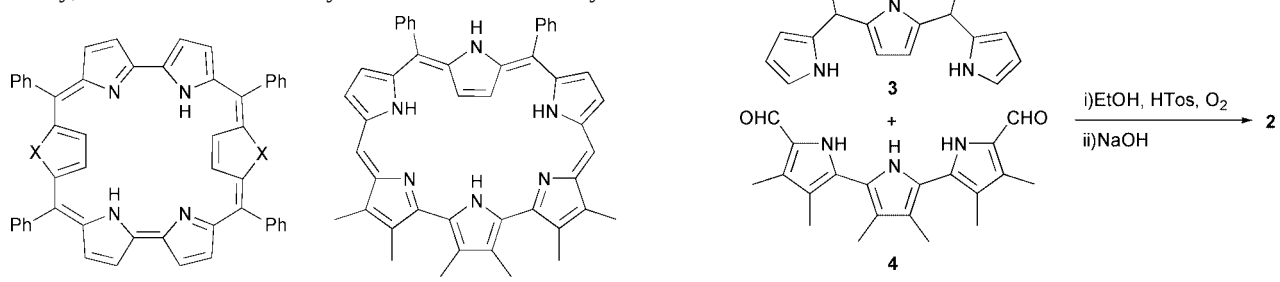

Scheme 1

DOI: 10.1039/b003777j

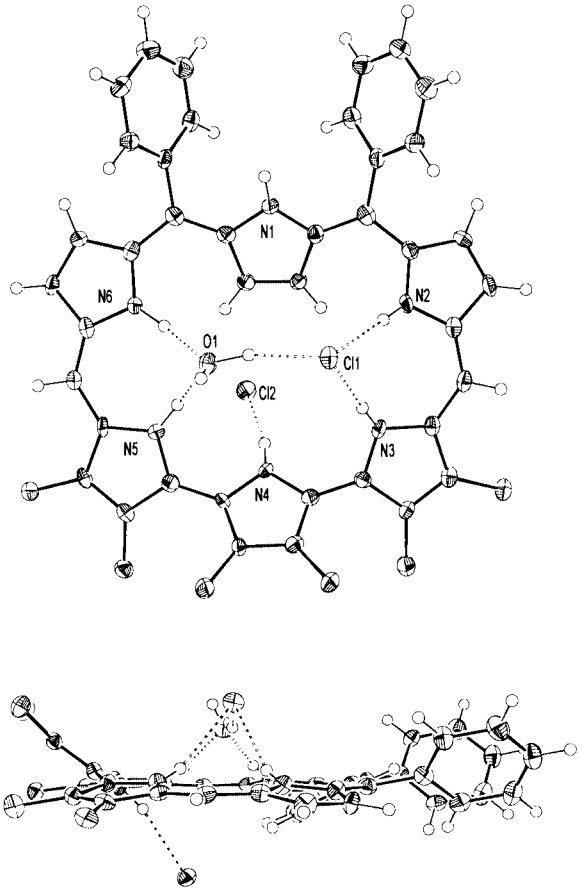

Fig. 1 Top and side views[16] of $H_2\mathbf{2}^{2+}\cdot 2Cl^-$ with a partial atom labeling scheme. Thermal ellipsoids are scaled to the 50% probability level. Hydrogen atoms shown are drawn to an arbitrary scale. Dashed lines are indicative of a hydrogen bonding interaction.

between the β-C*H* protons of the inverted pyrrole with the N*H* proton of the middle pyrrole of the terpyrrole subunit. Additionally, the outer N*H* proton clearly interacts with the *ortho-H* protons of the *meso*-phenyl substituents, findings which can only be rationalized in terms of an inverted structure. The UV-vis spectra of **2** and $H_2\mathbf{2}^{2+}\cdot 2Cl^-$ support the assumption that the free-base form of **2** is subject to a greater deviation from planarity than its bishydrochloride salt, $H_2\mathbf{2}^{2+}\cdot 2Cl^-$. In particular the extinction coefficients are found to be reduced by a factor of 2–2.5 in the case of the free-base.§

Definitive proof for the inverted nature of $H_2\mathbf{2}^{2+}\cdot 2Cl^-$ was obtained from a single crystal X-ray diffraction analysis. The resultant structure is shown in Fig. 1.¶ In addition to the two bound chloride counteranions, there is one molecule of water incorporated into the structure. Several hydrogen bonding interactions, indicated by dashed lines, are found between the pyrrolic N*H* protons and the water and the chloride anions, respectively. These might, at least to some extent, account for the partial deviation from planarity. Another hydrogen bonding interaction is found between the water and a molecule of tetrahydrofuran (not shown).¶ The middle pyrrole of the terpyrrole subunit is tilted out of the plane, minimizing the interactions between the β-methyl groups.

In summary, the approach reported here provides an easy, high-yielding access to a new class of rubyrin analogue, namely [26]hexaphyrin(1.1.1.1.0.0) (**2**). This new macrocycle differs quite dramatically from its better studied parent system. Not only is one pyrrole-unit found to be inverted in the case of **2**, this prototypical [26]hexaphyrin(1.1.1.1.0.0) is also found to be stable in both its free-base and protonated forms. Rubyrin, on the other hand, is stable only in its bisprotonated form.[14] That the middle pyrrole of the tripyrrane subunit of **2** remains inverted in both these states is interesting, especially in light of the behavior of sapphyrins. In these latter pentapyrrolic systems, the pyrrole unit may be either 'inverted' or 'normal', depending on conditions, substitution paterns and the nature of the heteroatom contained within the central heterocycle of the constituent tripyrrane-subunit. In fact, **2** can be thought of as an 'expanded sapphyrin' with the bipyrrolic subunit exchanged for a terpyrrole. In this context it is worth highlighting the fact that **2** displays a greater propensity for inversion when fully protonated than does tetraphenylsapphyrin. Indeed, this latter species is found to adopt a planar, pyrrole-in conformation when fully protonated.[4,5] These disparities underscore the richness of structural space that may be sampled through the construction of appropriately designed new expanded porphyrin systems.

This work was supported by the National Science Foundation (grant CHE-9725399 to J. L. S.).

Notes and references

† In a more systematic sense, rubyrin might be referred to as [26]hexaphyrin(1.1.0.1.1.0) while bronzaphyrin is a [26]hexaphyrin(2.0.0.2.0.0).

‡ Such behavior has been reported for N-confused porphyrins where 'inversion' is enforced.[17,18]

§ UV-vis (CH_2Cl_2) λ_{max} (nm) (ε in $mol^{-1}\cdot l^{-1}$) of **2**: 502 (61100), 531 (73400), 782 (20200); $H_2\mathbf{2}^{2+}\cdot 2Cl^-$: 533 (173000), 556 (156000), 733 (10400), 877 (30200).

¶ Crystallographic summary for $(C_{46}H_{42}N_6)^{2+}\cdot 2Cl^-\cdot 2C_4H_8O\cdot H_2O$: Crystals were grown by layering a CH_2Cl_2 solution of $H_2\mathbf{2}^{2+}\cdot 2Cl^-$ with THF. Small, very dark prisms, monoclinic, $P2_1/c$, μ = 0.189 mm^{-1}, Z = 4 in a cell of dimensions: a = 20.6415(5), b = 13.3094(4), c = 17.2658(8) Å, β = 95.591(2)°, V = 4720.8(3)Å^3, ρ_{calc} = 1.28 g cm^{-3}, $F(000)$ = 1936. A total of 8152 unique reflections were measured on a Nonius Kappa CCD using graphite monochromatized Mo-Kα radiation (λ = 0.71073Å) at −150 °C. The structure was refined on F^2 to an R_w = 0.184, with a conventional R = 0.0983 (5669 reflections with $F_o > 4[\sigma(F_o)]$), and a goodness of fit = 1.19 for 574 refined parameters using the SHELX-97 package.[19] Two molecules of THF were observed in the unit cell, one of which was severely disordered. The contribution to the data by this molecule was removed using the utility SQUEEZE, found in PLATON98.[20] CCDC 182/1704. See: http://www.rsc.org/suppdata/cc/b0/b003777j/ for crystallographic data in .cif format.

1 J. L. Sessler, A. Gebauer and S. J. Weghorn, in *Expanded Porphyrins*, ed. K. M. Kadish, K. M. Smith and R. Guilard, San Diego, 2000.
2 J. L. Sessler and S. J. Weghorn, in *Expanded, Contracted and Isomeric Porphyrins*, ed. J. E. Baldwin and P. D. Magnus, Pergamon, 1997.
3 A. Jasat and D. Dolphin, *Chem. Rev.*, 1997, **97**, 2267.
4 P. J. Chmielewski, L. Latos-Grazynski and K. Rachlewicz, *Chem. Eur. J.*, 1995, **1**, 68.
5 K. Rachlewicz, N. Sprutta, L. Latos-Grazynski, P. J. Chmielewski and L. Szterenberg, *J. Chem. Soc., Perkin Trans. 2*, 1998, 959.
6 K. Rachlewicz, N. Sprutta, P. J. Chmielewski and L. Latos-Grazynski, *J. Chem. Soc., Perkin Trans. 2*, 1998, 969.
7 S. J. Narayanan, B. Sridevi, T. K. Chandrashekar, A. Vij and R. Roy, *J. Am. Chem. Soc.*, 1999, **121**, 9053.
8 A. Srinivasan, A. V. G. Anand, S. J. Narayanan, S. K. Pushpan, M. R. Kumar, T. K. Chandrashekar, K.-i. Sugivra and Y. Sakata, *J. Org. Chem.*, 1999, **64**, 8693.
9 M. G. P. M. S. Neves, R. M. Martins, A. C. Tomé, A. J. Silvestre, A. M. S. Silva, V. Félix, M. G. B. Drew and J. A. S. Cavaleiro, *Chem. Commun.*, 1999, 385.
10 A. Gossauer, *Chimia*, 1983, **37**, 341.
11 R. Charrière, T. A. Jenny, H. Rexhausen and A. Gossauer, *Heterocycles*, 1993, **36**, 1561.
12 C. Brückner, E. D. Sternberg, R. W. Boyle and D. Dolphin, *Chem. Commun.*, 1997, 1689.
13 S. Meyer, B. Andrioletti, J. L. Sessler and V. Lynch, *J. Org. Chem.*, 1998, **63**, 6752.
14 J. L. Sessler, T. Morishima and V. Lynch, *Angew. Chem., Int. Ed. Engl.*, 1991, **30**, 977.
15 M. R. Johnson, D. C. Miller, K. Bush, J. J. Becker and J. A. Ibers, *J. Org. Chem.*, 1992, **57**, 4414.
16 L. J. Farrugia, *J. Appl. Crystallogr.*, 1997, **30**, 565.
17 H. Furuta, T. Asano and T. Ogawa, *J. Am. Chem. Soc.*, 1994, **116**, 767.
18 P. J. Chmielewski, L. Latos-Grazynski, K. Rachlewicz and T. Glowiak, *Angew. Chem., Int. Ed. Engl.*, 1994, **33**, 779.
19 G. M. Sheldrick, SHELX-97, University of Göttingen, 1997.
20 P. v. d. Sluis and A. L. Spek, *Acta Crystallogr. Sect. A*, 1990, **46**, 194.

ChemComm

Construction of a mixed valence trinuclear $Mn^{II}Mn^{III}Mn^{II}$ aggregate into a large macrocyclic ligand†

Atsushi Yoshino,[a] Tatsuya Miyagi,[a] Eiji Asato,*[a] Masahiro Mikuriya,[b] Yoshiteru Sakata,[c] Ken-ichi Sugiura,[c] Kentaro Iwasaki[d] and Shojun Hino[d]

[a] *Department of Chemistry, Biology and Marine Science, College of Science, University of the Ryukyus, Nishihara, Okinawa 903-0213, Japan. E-mail: asato@sci.u-ryukyu.ac.jp*
[b] *Department of Chemistry, School of Science, Kwansei Gakuin University, Uegahara, Nishinomiya 622-8501, Japan*
[c] *The Institute of Scientific and Industrial Research (ISIR), Osaka University, 8-1 Mihogaoka, Ibaraki, Osaka 567-0047, Japan*
[d] *Faculty of Engineering, Chiba University, Inagaku, Chiba, 263-8522, Japan*

Received (in Cambridge, UK) 2nd May 2000, Accepted 26th June 2000
Published on the Web 19th July 2000

A Schiff-base [2 + 2] macrocycle obtained by the reaction of 2,6-diformyl-4-methylphenol with 1,11-diamino-3,9-dimethyl-3,9-diazo-6-oxaundecane encapsulates three manganese ions into its cavity; EPR, UV–VIS–NIR, XPS spectroscopic data, X-ray crystallography and magnetic measurements showed that the metal ions are in a mixed valence state (II, III, II) which is rare for trimanganese systems.

Polynuclear manganese complexes are now receiving increased attention from a wide area of science, including chemistry, biology and physics. Representative target molecules fascinating synthetic inorganic chemists are tetranuclear aggregates as models of the oxygen-evolving complex (OEC) of photosystem II[1] and 'high spin Mn-clusters'[2] potentially applicable to future molecular devices. Most commonly, these complexes are synthesized utilizing self-assembling properties of manganese ions, where the metal ions are bridged by O^{2-} units and externally capped with multidentate ligands.[3] Our approach to Mn-aggregated systems has started with specially designed polynucleating macrocycles. For example, the macrocycle $(L^1)^{2-}$ functions as a tetranucleating ligand for Zn^{II},[4] but did not

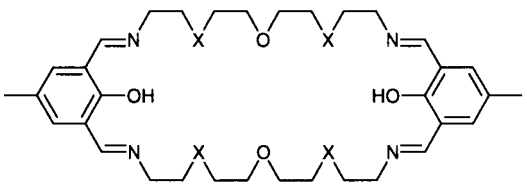

X = O : H_2L^1, X = NMe : H_2L^2

give any manganese complexes, probably owing to poor affinity of the ether oxygen towards this metal ion. Thus, we have prepared a new macrocycle H_2L^2, to enhance binding ability by substituting the ether units with tertiary amine groups. We report herein, the synthesis and characterization of a novel mixed valence $Mn^{II}Mn^{III}Mn^{II}$ trimanganese subunit formed within the macrocycle.

1,11-Diamino-3,9-dimethyl-3,9-diazo-6-oxaundecane (daud) as a precursor for H_2L^2 was prepared in a four-step synthesis with an overall yield of *ca.* 30%.† All products obtained at each step were identified by ^1H NMR spectroscopy.

The metal-templated Schiff-base condensation of 2,6-diformyl-4-methylphenol (dfmp) with the diamine in methanol was carried out in open-air using $Mn(ClO_4)_2{\cdot}6H_2O$ as the template core in the presence of triethylamine (NEt_3). The reaction using a mole ratio of dfmp:daud:Mn:NEt_3 = 2:2:4:2 gave dark-brown microcrystals formulated as $[Mn_3(L^2)(\mu\text{-}OMe)_2](ClO_4)_3$ **1**.‡ The [2 + 2] Schiff-base macrocyclization and formation of the trinuclear Mn_3 unit were supported by detection of the strongest peak in its electrospray mass spectrum (*m/z* 305.8) corresponding to the trication for an acetonitrile solution of the complex. A mixed valence state (two Mn^{II} and one Mn^{III}) expected from the formula is evident from spectroscopic data (EPR, UV–VIS-NIR and XPS). An X-band solid-state EPR spectrum of **1** at 25 °C showed two sets of overlapped six-line signals at $g \approx 2.00$ with $A \approx 0.87$ mT, suggesting the presence of two magnetically uncoupled Mn^{II} ions. The electronic spectrum of the complex in methanol showed a very broad peak centered at *ca.* 1005 nm (ε = 142 $dm^3\ mol^{-1}\ cm^{-1}$) and a shoulder at *ca.* 550 nm (ε = 280 $dm^3\ mol^{-1}\ cm^{-1}$), tentatively attributed to $^5B_{1g} \rightarrow {}^5A_{1g}$ and $^5B_{1g} \rightarrow {}^5B_{2g}$ transitions of high-spin Mn^{III} species, respectively, while no strong absorption assignable to an intervalence charge transfer was observed in the visible or near-IR region. The XPS spectrum of **1** exhibited two peaks at 641.5 and 653.3 eV, which were attributed to Mn $2p_{3/2}$ and Mn $2p_{1/2}$ core ionization potentials from each manganese. Although these values do not agree with those of Mn^{2+} or Mn^{3+} ionized states, the spectral envelope as well as the peak positions can be reproduced by superposition of corresponding spectra of $[Mn^{II}(TPP)]{\cdot}py$ and $[Mn^{III}(TPP)]Cl$ (TPP = 5,10,15,20-tetraphenylporphyrinate) with a 2:1 intensity ratio.

Recrystallization of **1** from wet methanol gave needle-like single crystals as the monohydrate (**1**·H_2O), the structure of which (Fig. 1) was determined by X-ray crystallography.§ The three manganese ions are encapsulated into the macrocycle in a bent-chain form with an angle of 129.45(6)° for Mn(1)–Mn(2)–Mn(3). Each of the two facing phenoxide moieties bridges a pair of adjacent manganese ions which are further bridged by an exogenous methoxide ion. The two terminal manganese centers, Mn(1) and Mn(3), have essentially the same coordination geometry being significantly distorted octahedral with average Mn–O,N bond distances of 2.245 and 2.230 Å, respectively, comparable with typical Mn(II)–O,N distances.[5] The central Mn(2) has an elongated octahedral geometry where its axial positions are occupied by the two phenoxide oxygen atoms [Mn(2)–O(1) 2.134(6) Å, Mn(2)–O(3) 2.137(6) Å]. These distances are significantly longer than the four basal Mn–O,N bonds [av. Mn–O,N = 1.962 Å], thus revealing a Jahn–Teller distortion expected for a high spin Mn^{III} species. Thus, we concluded that the three metal ions in the macrocycle are in a mixed valence state $Mn^{II}Mn^{III}Mn^{II}$.

The value of μ_{eff} = 9.968 μ_B at 300 K for powder sample **1** is close to the spin-only value of 9.695 μ_B expected for three spin systems of S = 5/2; S = 4/2; S = 5/2, indicating that all the

† Electronic supplementary information (ESI) available: synthetic route to diamine (daud) and ^1H NMR data for all products obtained at each step. See http://www.rsc.org/suppdata/cc/b0/b003479gl

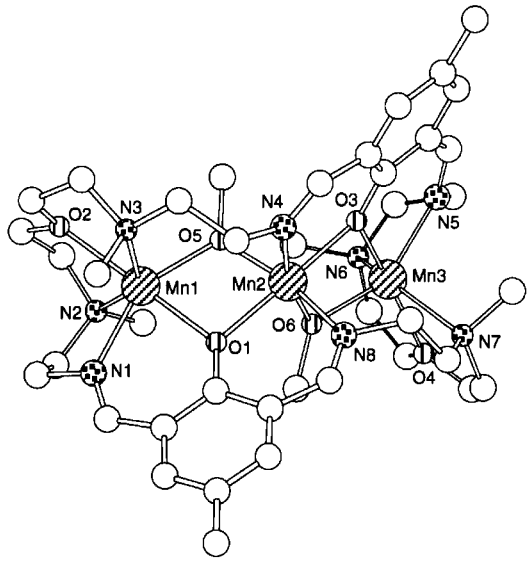

Fig. 1 Perspective view of the $[Mn_3(L^2)(\mu\text{-}OMe)_2]^{3+}$ cation; Selected distances (Å) and angles (°): Mn(1)–O(1) 2.192(6), Mn(1)–O(2) 2.217(6), Mn(1)–O(5) 2.085(5), Mn(1)–N(1) 2.178(8), Mn(1)–N(2) 2.393(8), Mn(1)–N(3) 2.403(8), Mn(2)–O(1) 2.134(6), Mn(2)–O(3) 2.137(6), Mn(2)–O(5) 1.913(5), Mn(2)–O(6) 1.899(7), Mn(2)–N(4) 2.015(7), Mn(2)–N(8) 2.022(8), Mn(3)–O(3) 2.172(6), Mn(3)–O(4) 2.200(7), Mn(3)–O(6) 2.085(7), Mn(3)–N(5) 2.16(1), Mn(3)–N(6) 2.35(1), Mn(3)–N(7) 2.41(1), Mn(1)–Mn(2) 3.235(2), Mn(2)–Mn(3) 3.218(2); Mn(1)–Mn(2)–Mn(3) 129.45(6), Mn(1)–O(1)–Mn(2) 96.8(2), Mn(1)–O(5)–Mn(2) 108.0(2), Mn(2)–O(3)–Mn(3) 96.6(2), Mn(2)–O(6)–Mn(3) 107.7(3).

metal ions are in the high-spin state. The μ_{eff} value increases with decreasing temperature up to a maximum value of 13.96 μ_B at *ca.* 6 K (Fig. 2). The drop in μ_{eff} below 6 K suggests a zero-field splitting of Mn^{II} and Mn^{III} ions or an intermolecular antiferromagnetic coupling. The magnetic data were analyzed with the Van Vleck equation including a correction term θ based on the Heisenberg model [$\mathcal{H} = -2(J_{12}S_1\cdot S_2 + J_{23}S_2\cdot S_3 + J_{13}S_1\cdot S_3)$; $S_1 = S_3 = 5/2$, $S_2 = 4/2$, $J_{12} = J_{23} = J$, $J_{13} = J'$], leading to the best-fitting parameters $g = 2.01(1)$, $J = +1.83(5)$ cm^{-1}, $J' = 0$ cm^{-1}, $\theta = -1.03(4)$ K. The result indicates that weak ferromagnetic interactions operate between the adjacent Mn^{II}–Mn^{III} pairs while interactions between the terminal ions are negligible. Structural data on oxygen-bridged $Mn^{II}Mn^{III}$ pairs showing ferromagnetic interaction remain scarce. However, observed Mn^{II}–O–Mn^{III} angles [96.8 and 108.0° for Mn(1)–Mn(2); 96.6 and 107.7° for Mn(2)–Mn(3)] are comparable to the angles (97.1 and 102.4°) reported for a mixed valence dinuclear $Mn^{II}Mn^{III}$ complex exhibiting $J = +0.89$ cm^{-1}.[6] Magnetically coupled Mn^{II} clusters with high nuclearity, *e.g.* $Mn^{II}{}_5$[7] and $Mn^{II}{}_9$,[8] often show interesting electrochemical properties. A cyclic voltammogram of **1** in methanol (1.0 mM, 0.1 M NEt_4ClO_4) indeed exhibited a quasi-reversible one-electron reduction wave at $E_{1/2} = -0.14$ V with ΔE_p = *ca.* 70 mV (glassy carbon working electrode, Pt counter electrode, Ag^+/AgCl reference electrode), which was tentatively attributed to the formation of the $Mn^{II}{}_3$ species. However, all attempts to isolate this species by chemical or electrochemical reduction were unsuccessful. Finally it should be emphasized that the metal-templated reaction in Ar atmosphere with the same stoichiometry as that for **1** yielded a yellow powder formulated as $[Mn_2(L^2)](ClO_4)_2\cdot H_2O\cdot 2MeOH$ **2**.¶

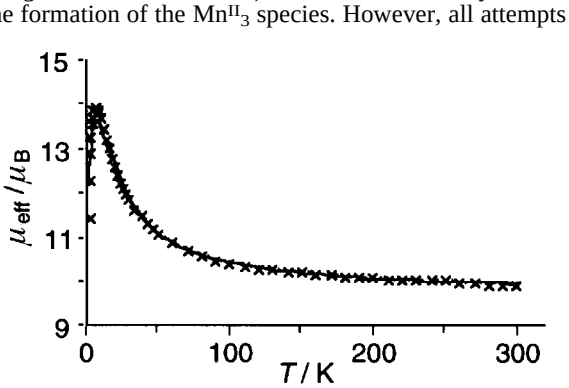

Fig. 2 Plot of μ_{eff} *vs.* *T* for a powdered sample of **1**.

In conclusion, a new Schiff-base macrocycle $(L^2)^{2-}$ obtained by the Mn-templated reaction afforded a novel $Mn^{II}Mn^{III}Mn^{II}$ complex, which is very rare[9] for mixed valence trimanganese systems in contrast to the many $Mn^{II}{}_3$[10] and $Mn^{III}Mn^{II}Mn^{III}$ [11] complexes that have been reported. In addition to EPR, UV–VIS–NIR and XPS spectroscopic evidence, the X-ray structure and the magnetic behavior finally establish that the mixed valence state is of class I type in the Robin–Day classification.[12] In principle, the macrocycle could incorporate further aggregated cores ($n > 3$), since a closely related ligand $(L^1)^{2-}$ is known to afford two types of tetrazinc complex.[4] Approaches to highly aggregated systems are now scheduled and in progress in our laboratory.

This work was supported by a Grant-in-Aid for Scientific Research on Priority Area (#11136242 'Metal-assembled Complexes' to E. A.) from the Ministry of Education, Science, Sports and Culture, Japan. We appreciate the analytical assistance provided by the Material Analysis Center of ISIR, Osaka University.

Notes and references

‡ Anal. $C_{40}H_{64}N_8O_{18}Cl_3Mn_3$. Calc.: C, 39.50; H, 5.30; N, 9.21; Cl, 8.76. Found: C, 39.26; H, 4.96; N, 9.21; Cl, 8.56%. UV-VIS [MeOH; $\lambda_{max/nm}$ (ε/dm^3 mol^{-1} cm^{-1})], 1005 (142), 550 (280), 397 (12 000), 260 (17 300)

§ *Crystal data* for $C_{40}H_{66}N_8O_{19}Cl_3Mn_3\cdot H_2O$ **1**·H_2O: M = 1234.18, orthorhombic, $a = 32.315(4)$, $b = 23.461(3)$, $c = 13.750(3)$ Å, $U = 10424(2)$ Å^3, $T = 163$ K, space group *Pbca* (no. 61), $Z = 8$, μ(Mo-Kα) = 9.49 cm^{-1}, Of the 9708 which were collected, 4140 reflections with $I > 3\sigma(I)$ were used for calculation. The structure was solved by direct methods and refined using full-matrix least-squares procedures. All hydrogen atoms were located on the calculated positions. Refinement converged with $R_1 = 0.077$ and $R_w = 0.095$ [$w = 1/\sigma^2(F_o)$].

CCDC 182/1701. See http://www.rsc.org/suppdata/cc/b0/b003479g/ for crystallographic files in .cif format.

¶ Anal. $C_{38}H_{68}N_8O_{15}Cl_2Mn_2$. Calc.: C, 44.41; H, 6.34; N, 10.36; Cl, 6.55. Found: C, 44.51; H, 6.13; N, 10.61; Cl, 6.23%.

1 V. K. Yachandra, K. Sauer and M. P. Klein, *Chem. Rev.*, 1996, **96**, 2927.
2 R. Sessoli, D. Gatteschi, A. Caneschi and M. A. Novak, *Nature*, 1993, **365**, 141; E. K. Brechin, J. Yoo, M. Nakano, J. C. Huffman, D. N. Hendrickson and G. Christou, *Chem. Commun.*, 1999, 783.
3 C. Philouze, G. Blondin, J.-J. Girerd, J. Guihem, C. Padcard and D. Lexa, *J. Am. Chem. Soc.*, 1994, **116**, 8557; D. N. Hendrickson, G. Christou, E. A. Schmitt, E. Libby, J. S. Bashkin, S. Wang, H.-L. Tsai, J. B. Vincent, P. D. W. Boyd, J. C. Huffman, K. Folting, Q. Li and W. E. Streib, *J. Am. Chem. Soc.*, 1992, **114**, 2455; E. Libby, K. Folting, J. C. Huffman and G. Christou, *J. Am. Chem. Soc.*, 1990, **112**, 5354.
4 E. Asato, H. Furutachi, T. Kawahashi and M. Mikuriya, *J. Chem. Soc., Dalton Trans.*, 1995, 3897.
5 M. Mikuriya, T. Fujii, T. Tokii and A. Kawamori, *Bull. Chem. Soc. Jpn.*, 1993, **66**, 1675.
6 J. S. Baskin, A. R. Schake, J. B. Vincent, H.-R. Chang, Q. Li, J. C. Huffman, G. Christou and D. N. Hendrickson, *J. Chem. Soc., Chem. Commun.*, 1988, 700.
7 C. J. Matthews, Z. Xu, A. K. Mandal, L. K. Thompson, K. Biradha, K. Poirier and M. J. Zaworotko, *Chem. Commun.*, 1999, 347.
8 L. Zhao, C. J. Matthews, L. K. Thompson and S. L. Heath, *Chem. Commun.*, 2000, 265.
9 T. Tanase, S. Tamakoshi, M. Doi, M. Mikuriya, H. Sakurai and S. Yano, *Inorg. Chem.*, 2000, **39**, 628.
10 R. L. Rardin, P. Poganiuch, A. Bino, D. P. Goldberg, W. B. Tolman, S. Liu and S. J. Lippard, *J. Am. Chem. Soc.*, 1992, **114**, 5240; M. J. Baldwin, J. W. Kampf and V. L. Pecoraro, *J. Chem. Soc., Chem. Commun.*, 1993, 1741.
11 D. P. Kessissoglou, M. L. Kirk, M. S. Lah, X. Li, C. Raptopoulou, W. E. Hatfield and V. L. Pecoraro, *Inorg. Chem.*, 1992, **31**, 5424.
12 M. B. Robin and P. Day, *Adv. Inorg. Chem. Radiochem.*, 1967, **10**, 247.

Preparation and structure of 3D ordered macroporous alloys by PMMA colloidal crystal templating

Hongwei Yan,[a] Christopher F. Blanford,[a] William H. Smyrl[b] and Andreas Stein*[a]

[a] *Department of Chemistry, University of Minnesota, 207 Pleasant St. SE, Minneapolis, MN 55455 USA. E-mail: stein@chem.umn.edu*

[b] *Department of Chemical Engineering and Materials Science, University of Minnesota, Minneapolis, MN 55455 USA*

Received (in Irvine, CA, USA) 18th April 2000, Accepted 20th June 2000
Published on the Web 18th July 2000

Three-dimensionally ordered macroporous (3DOM) metal alloys of Ni_xCo_{1-x} (a solid solution) and Mn_3Co_7 (an intermetallic compound) have been prepared by templated precipitation of mixed metal salts within colloidal crystals of poly(methyl methacrylate) spheres and subsequent chemical conversion of the inorganic precursors.

In the past three years, several chemical preparations of ordered macroporous materials based on colloidal crystal templating have been described. By using close-packed arrays of monodisperse spheres (polystyrene or silica) as templates, three-dimensionally ordered macroporous (3DOM) structures have been fabricated whose compositions include silica,[1–4] metal oxides,[3,5–8] simple metals,[9–11] metal chalcogenides,[12] carbon[13] and polymers.[14–17] Since the pore diameters (typically a few hundred nanometers) are comparable to optical wavelengths, 3DOM dielectric materials can be used to create photonic crystals, which exhibit interesting optical effects based on Bragg diffraction and the formation of optical stopbands.[6,18] In addition, applications including catalysis, sorption, and separations may benefit from the bicontinuous void and wall structures and from the well-defined pore sizes of these materials.

Recent theoretical and experimental studies have suggested that metals with well-ordered porous networks would also exhibit interesting photonic properties,[19] and that 3DOM metals provide relatively large surface areas which are uniformly accessible in electrochemical experiments.[9] Periodic macroporous metals have now been prepared by several methods, including hydrogen reduction of preformed macroporous oxides,[9] decomposition of templated metal oxalates in a non-oxidizing environment,[9] electroless deposition,[10] deposition of colloidal gold particles in colloidal crystals,[11] and infiltration of natural calcium carbonate skeletons with gold paint, followed by annealing.[20] All of these macroporous solids contain a single metal. However, most technological applications of metals employ alloys containing two or more elements, because with alloys it is possible to realize an extensive variety of physical properties by varying the composition of the alloy. Here we report a method of synthesizing 3DOM metal alloys, using a solid solution (Ni_xCo_{1-x}) and an intermetallic compound (Mn_3Co_7) as examples.

Colloidal crystals were prepared from uniformly sized poly(methyl methacrylate) (PMMA) spheres synthesized according to the literature[21] and close-packed by gravity sedimentation or centrifugation. To prepare a 3DOM Ni_xCo_{1-x} alloy, 0.008 mol nickel(II) acetate tetrahydrate and 0.008 mol cobalt(II) acetate tetrahydrate were dissolved in 20 mL methanol at 60 °C. After cooling to room temperature, any undissolved solid was removed by filtration and a clear precursor solution was obtained. Centimeter-scale PMMA colloidal crystals (*ca.* 8 g) were soaked in this solution for 3–5 min. Excess solution was removed from the impregnated colloidal crystals by vacuum filtration. The samples were dried in air at room temperature for 1 h. Then the dried composites were soaked in oxalic acid solution (*ca.* 3.6 g oxalic acid in 30 mL ethanol) for 2 min to form metal oxalate inside the PMMA colloidal crystals. After an additional vacuum filtration and drying step, the samples were processed at 400 °C in flowing H_2 (0.3 L min^{-1} in a 22 mm i.d. quartz tube) for 1 h (heating rate: 2 °C min^{-1}). Carbon (0.52 wt%) and hydrogen (0.19 wt%) analyses of a calcined sample confirmed that most of the PMMA template was removed by this treatment and that the metal oxalates had been fully decomposed.

Fig. 1(a) shows a typical SEM image of the template-free macroporous product. Open voids and interconnected walls form a pore structure that is ordered over a range of tens of unit cells in three dimensions. Average void diameters of 200 nm were obtained with 410 nm PMMA spheres. Some cracks can be observed, which arise mainly from the large volume shrinkage and sintering during the template removal/chemical conversion processes. X-Ray energy dispersive spectroscopy (EDS) covering one ordered colloidal crystal domain indicated a Ni : Co mol ratio in the walls of 0.69,[22] bulk elemental analysis by ICP a Ni:Co ratio of 0.86. The walls are composed of fused grains with typical sizes of 20–50 nm (determined by TEM). The average grain size based on PXRD line widths, calculated by the Scherrer equation, is 33 nm.

The PXRD pattern. [Fig. 2(a)] of the product shows a single phase cubic structure (space group *Fm*3*m*), which matches the phase determined by selected-area electron diffraction (SAED) of an ordered area in the TEM. The average calculated lattice constant is 3.529(4) Å, which is between that of Ni (3.5238 Å) and Co (3.5447 Å), suggesting that the Ni_xCo_{1-x} alloy is a solid solution.[23] The 3DOM Ni_xCo_{1-x} alloy exhibited a type II nitrogen adsorption isotherm with a BET surface area of 9.9 m^2 g^{-1}, which is attributed to the surface of fused, nonporous Ni_xCo_{1-x} nanocrystallites composing the wall structure. Owing

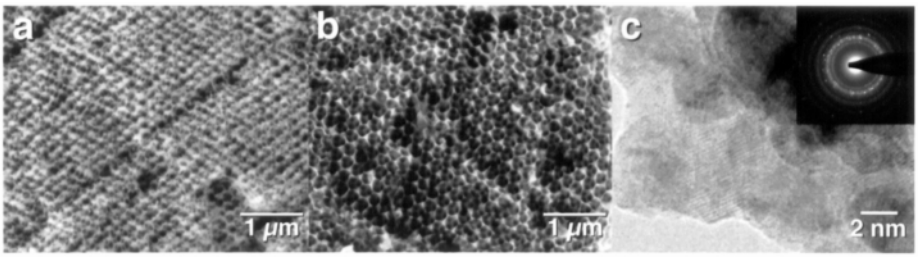

Fig. 1 Scanning electron micrographs (SEM) of (a) 3DOM Ni_xCo_{1-x} and (b) 3DOM Mn_3Co_7. (c) Transmission electron micrograph (TEM) showing a close-up view of the wall and lattice fringes of the Mn_3Co_7 grains. The inset is the SAED pattern of the ordered area including these particles.

DOI: 10.1039/b003147j

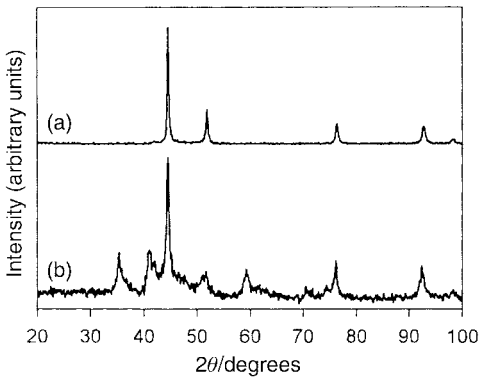

Fig. 2 Powder X-ray diffraction (PXRD) patterns of (a) 3DOM Ni_xCo_{1-x} and (b) 3DOM Mn_3Co_7.

to this large surface area, the fresh products were highly reactive, combusting upon rapid exposure to air even at room temperature. Combustion could be avoided by slow oxidation in a mixture of air (0.2 L min^{-1}) and nitrogen (1.0 L min^{-1}) for 30 min to passivate the sample surface. Passivated samples were air-stable over a period of weeks. Based on the total metals content from ICP analysis, the sample contained at most 4.8 wt% oxygen. However, no metal oxide reflections were observed in the PXRD pattern, indicating that the oxide layers were amorphous or very thin.

As another demonstration of a 3DOM alloy synthesis by the PMMA templating method, we also prepared a Mn_3Co_7 alloy from a stoichiometric mixture of manganese acetate and cobalt acetate precursors, using the same procedure as above. Mn_3Co_7 is an intermetallic compound alloy and has a crystal structure different from both Mn and Co. The PXRD pattern [Fig. 2(b)] shows reflections characteristic of the calcined Mn_3Co_7 alloy in agreement with the standard powder pattern (PDF#18-0407) and with SAED [Fig. 1(c)]. Elemental analysis of the template-free product revealed 1.79 wt% C, 0.20 wt% H and a Mn:Co mol ratio of 0.39 (expected: 0.43). The SEM [Fig. 1(b)] shows that the Mn_3Co_7 alloy has a well-ordered porous structure with average void diameters of 210 nm obtained from 290 nm diameter PMMA spheres. This more ordered structure is probably due to reduced shrinkage and smaller grain sizes [ranging from 15 to 30 nm by TEM, Fig. 1(c)], caused by slower crystal growth kinetics of Mn_3Co_7. The smaller grain size leads to a larger BET surface area of 26.4 m^2 g^{-1}.

It should be noted that the use of PMMA colloidal crystals as templates can significantly improve the periodicity and reduce the remaining carbon content of the resulting macroporous alloys/metals, relative to PS templates. The main reason for the improved performance of PMMA lies in its better thermal degradation character. PMMA decomposes by chain depolymerization, resulting in a gradual reduction in molecular weight and the production of monomer. By this mechanism, the yield of monomer can be as high as 100% in the temperature range 170–300 °C.[24] In comparison, PS degrades to *ca.* 40% of monomer in the temperature range 300–400 °C[24] and leaves a larger amount of carbon after thermal treatment of the product in a non-oxidizing atmosphere (*e.g.* in a macroporous Ni/PS sample, 39 wt% C remained after heating in nitrogen at 450 °C for 10 h, compared to 15 wt% C in a Ni/PMMA sample after 1 h of heating). As a result of the milder conditions required to remove the PMMA template, smaller framework grain sizes and larger surface areas can be obtained. An additional benefit of using PMMA over PS spheres is the better penetration of the precursor solution in the PMMA colloidal crystal owing to increased wettability. Consequently, fewer structural defects are introduced during the composite formation, if a sufficiently concentrated precursor solution is employed.[7]

The PMMA templating method can be used to synthesize 3DOM alloys containing Mn, Fe, Ni, Co and other alloy forming metals whose salt precursors are easily reducible and whose melting points exceed that of the template. Ternary or higher multicomponent alloys may also be formed. For example, we have prepared a Ni/Fe/Co 3DOM alloy by the same procedure. Besides providing a way of structuring metals on a nanometer scale and endowing them with relatively high surface areas, this technique allows one to tailor the physical properties (corrosion resistance, thermal properties, magnetic properties, *etc.*) of the 3DOM structures by changing the metallic composition of the alloy. As a result, the new class of alloys presented here may find applications as high performance catalysts, electrodes, supports and magnetic materials.

We thank 3M, Dupont, the David and Lucile Packard Foundation, the National Science Foundation (DMR-9701507 and the MRSEC Program of the NSF under Award Number DMR-9809364), and the Department of Energy (DOE/DE-FG02-93-ER14384) for support of this research.

Notes and references

1 O. D. Velev, T. A. Jede, R. F. Lobo and A. M. Lenhoff, *Nature*, 1997, **389**, 447.
2 O. D. Velev, T. A. Jede, R. F. Lobo and A. M. Lenhoff, *Chem. Mater.*, 1998, **10**, 3597.
3 B. T. Holland, C. F. Blanford, T. Do and A. Stein, *Chem. Mater.*, 1999, **11**, 795.
4 B. T. Holland, L. Abrams and A. Stein, *J. Am. Chem. Soc.*, 1999, **121**, 4308.
5 B. T. Holland, C. F. Blanford and A. Stein, *Science*, 1998, **281**, 538.
6 J. E. G. J. Wijnhoven and W. L. Vos, *Science*, 1998, **281**, 802.
7 H. Yan, C. F. Blanford, B. T. Holland, W. H. Smyrl and A. Stein, *Chem. Mater.*, 2000, **12**, 1134.
8 P. Yang, T. Deng, D. Zhao, P. Feng, D. Pine, B. F. Chmelka, G. M. Whitesides and G. D. Stucky, *Science*, 1998, **282**, 2244.
9 H. Yan, C. F. Blanford, B. T. Holland, M. Parent, W. H. Smyrl and A. Stein, *Adv. Mater.*, 1999, **11**, 1003.
10 P. Jiang, J. Cizeron, J. F. Bertone and V. L. Colvin, *J. Am. Chem. Soc.*, 1999, **121**, 7957.
11 O. D. Velev, P. M. Tessier, A. M. Lenhoff and E. W. Kaler, *Nature*, 1999, **401**, 548.
12 Y. A. Vlasov, N. Yao and D. J. Norris, *Adv. Mater.*, 1999, **11**, 165.
13 A. A. Zakhidov, R. H. Baughman, Z. Iqbal, C. Cui, I. Khayrullin, S. O. Dantas, J. Marti and V. G. Ralchenko, *Science*, 1998, **282**, 897.
14 S. H. Park and Y. Xia, *Chem. Mater.*, 1998, **10**, 1745.
15 S. H. Park and Y. Xia, *Adv. Mater.*, 1998, **10**, 1045.
16 S. A. Johnson, P. J. Ollivier and T. E. Mallouk, *Science*, 1999, **283**, 963.
17 P. Jiang, K. S. Hwang, D. M. Mittleman, J. F. Bertone and V. L. Colvin, *J. Am. Chem. Soc.*, 1999, **121**, 11 630.
18 M. S. Thijssen, R. Sprik, J. E. G. J. Wijnhoven, M. Megens, T. Narayanan, A. Lagendijk and W. L. Vos, *Phys. Rev. Lett.*, 1999, **83**, 2730.
19 D. F. Sievenpiper, M. E. Sickmiller and E. Yablonovitch, *Phys. Rev. Lett.*, 1996, **76**, 2480.
20 F. C. Meldrum and R. Seshadri, *Chem. Commun.*, 2000, 29.
21 D. Zou, S. Ma, R. Guan, M. Park, L. Sun, J. J. Aklonis and R. Salovey, *J. Polym. Sci. Part A: Polym. Chem.*, 1992, **30**, 137.
22 EDS spectra were recorded on a Hitachi S-800 FESEM operating at 15 kV and equipped with an Oxford Instrument eXL energy dispersive spectrometer with a Be window [take-off angle: 32.2°; specimen to detector distance: 40 mm; acquisition time: 120 s (live)]. Elemental ratios were determined by standardless ZAF analysis. The precision of the concentrations is lower than by ICP because of the poor counting statistics and absence of a standard.
23 T. Nishizawa and K. Ishida, in *Binary Alloy Phase Diagrams*, ed. T. B. Massalksi, Materials Park, OH, 1990.
24 J. Liggat, in *Polymer Handbook*, ed. J. Brandrup, E. H. Immergut and E. A. Grulke, New York, 1999.

Highly active iron imidazolylidene catalysts for atom transfer radical polymerization

Janis Louie and Robert H. Grubbs*

The Arnold and Mabel Beckman Laboratories of Chemical Synthesis, California Institute of Technology, Pasadena, CA 91125, USA. E-mail: rhg@cco.caltech.edu

Received (in Irvine, CA, USA) 15th May 2000, Accepted 19th June 2000
Published on the Web 19th July 2000

Iron(II) halides possessing highly donating imidazolylidene ligands were found to be remarkably active and efficient catalysts for the atom transfer radical polymerization of styrene and methyl methacrylate.

Atom transfer radical polymerization (ATRP), a method for controlling free radical polymerizations, has recently developed into a versatile tool in polymer chemistry. ATRP is a metal mediated halide exchange process that establishes a fast and dynamic equilibrium between growing (P_n•) and dormant (P_n–X) polymer chains. This equilibrium is dramatically shifted towards favoring the dormant species giving extremely low (*ca.*10^{-8} M) radical concentrations which effectively minimizes bimolecular termination. A fast halide exchange process ensures all polymer chains grow at the same rate giving excellent control over the radical polymerization. Most reports describe the use of a combination of copper(I) halides and amine ligands as ATRP catalysts.[1] However, the ability to conveniently tune catalyst reactivity has led to the emergence of other metal systems (Ru,[2] Rh,[3] Pd,[4] Ni[5,6]) since they are capable of coordinating a wide range of ligands. Recently, attention has shifted towards iron catalyzed ATRP owing to its lower cost and similar activity to their ruthenium analogs.[6]

A steady effort has been directed toward designing ligands that display improved activity in ATRP, yet are still cost effective. In copper based ATRP, replacement of bipyridine ligands with alkyl amines lowers the redox potential of the copper halide catalyst and accelerates the polymerizations.[7] A similar phenomenon was also observed in ruthenium and iron[6e] catalyzed ATRP when triphenylphosphine and bipyridine were replaced with tributylphosphine and tributylamine, respectively. Noels and coworkers reported the highly active ruthenium ring-opening metathesis polymerization (ROMP) catalyst, $Cl_2(PCy_3)_2Ru$=CHPh, was also active for ATRP.[8] Recently, a dramatic increase in the activity of ruthenium ROMP catalysts coordinated with imidazolylidenes was observed,[9] largely due to their higher Lewis-basicity. In addition to being excellent electron donating ligands that are less toxic than phosphines and amines, imidazolylidenes are attractive because they are easy to prepare and handle. These observations prompted us to explore the influence of imidazolylidenes in ATRP. Herein we report the synthesis of FeX_2L_2 [X = Cl, Br; L = 1,3-diisopropyl-4,5-dimethylimidazol-2-ylidene (Pr^iIm **3**)[10]] complexes and their use as catalysts in the ATRP of styrene and methyl methacrylate (MMA). The polymerization rates rival copper based systems and yield polymers with extremely low polydispersities.

Heating a toluene solution of FeX_2 and Pr^iIm **3** to 90 °C followed by slow cooling of the reaction mixture to room temperature afforded crystals of chloro-complex **1**† and its bromo- analog **2** in 70–85% yields [eqn. (1)]. The structure of **1**‡ was determined by X-ray crystallography and is shown in Fig. 1. To the best of our knowledge, complex **1** is the first monomeric iron halide possessing imidazolylidene ligands.[11] Complex **1** adopts a distorted tetrahedral geometry with angles in the range 102.05–115.62°. As expected the Fe–C(1) bond length (2.136 Å) in **1** is significantly shorter than Fe–P bond

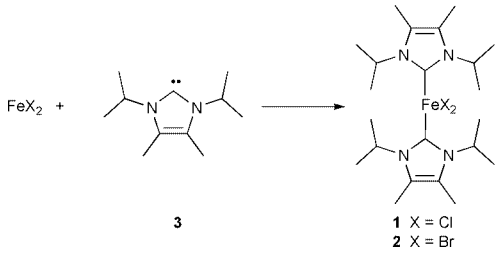

lengths [2.429 Å in $FeBr_2(PEt_3)_2$[12] and 2.639 Å in $FeCl_3(PPh_3)_2$[13]] as well as Fe–N bond lengths [2.273 Å in $FeCl_3(NMe_3)_2$[14]] in analogous iron based ATRP catalysts.

The homogeneous ATRP of styrene (100 equiv., 50% v/v toluene) initiated with 1-phenylethyl bromide (1-PEBr) and **1** was monitored at 85 °C under inert atmosphere. The semi-logarithmic plot of $\ln([M]_0/[M])$ *vs.* time was linear, with a pseudo-first order rate constant (k_{obs}) of 3.4×10^{-5} s^{-1}, and indicated that radical concentration was constant throughout the polymerization (Fig. 2). The rate of polymerization is among the highest reported for metal catalyzed ATRP in organic solvents.[15] Molecular weight (M_n, determined by gel permeation chromatography relative to polystyrene standards) increased linearly over time and agreed with theoretical weights demonstrating good control [Fig. 3(a)]. Polydispersities (M_w/M_n) were low (*ca.* 1.1) and decreased with monomer conversion [Fig. 3(b)] as expected for a controlled polymerization. In addition, determination of molecular weight by end-group analysis (M_n = 3400) of a low molecular weight polystyrene was in agreement with the targeted molecular weight (M_n = 4000). Addition of the higher oxidation metal (M^{x+1}) to polymerizations is known to lower PDIs by shifting the equilibruim towards dormant polymer chains and lowering

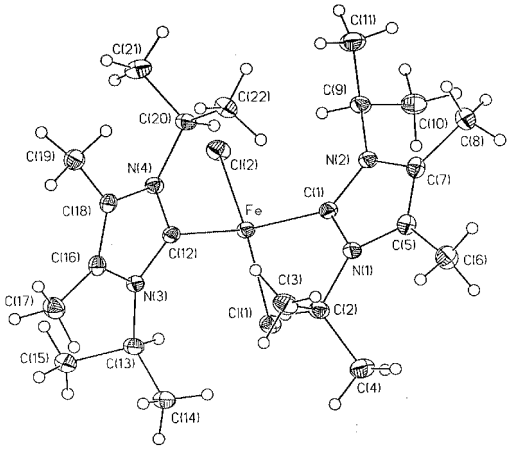

Fig. 1 Molecular structure of complex **1**. Selected bond lengths (Å) and angles (°): Fe–C(1) 2.1363(15), Fe–C1(2) 2.1298(16), Fe–Cl(1) 2.3035(4), Fe–Cl(2) 2.2976(4); C1(2)–Fe–C(1) 102.05(6), C1(2)–Fe–Cl(2) 106.85(4), C(1)–Fe–Cl(2) 114.41(4), C1(2)–Fe–Cl(1) 115.62(4), C(1)–Fe–Cl(1) 104.68(4), Cl(2)–Fe–Cl(1) 112.947(17).

DOI: 10.1039/b003957h

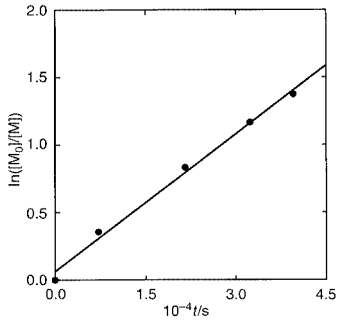

Fig. 2 First-order kinetic plot of $\ln([M]_0/[M])$ *vs.* time in the polymerization of styrene (50% v/v, toluene) at 85 °C ($[\mathbf{1}]_0$ = 44 mM, $[PEBr]_0$ = 44 mM, $[styrene]_0$ = 4.4 M).

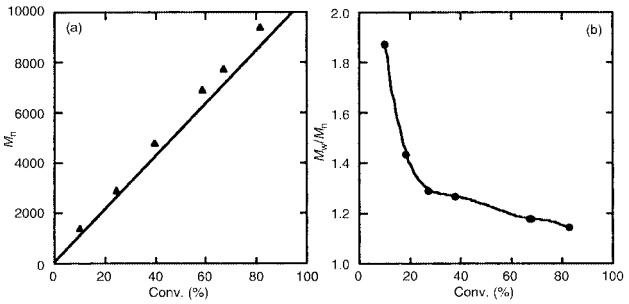

Fig. 3 Dependence of the polystyrene molecular weight (a) and polydispersity (b) on the monomer conversion at 85 °C ($[FeCl_2]_0$ = 44 mM, $[\mathbf{3}]_0$ = 90 mM, $[PEBr]_0$ = 44 mM, $[styrene]_0$ = 4.4 M).

radical concentrations. Thus, addition of 1 equiv. of $FeCl_3$ to the reaction slowed polymerization slightly (k_{obs} = 1.7 × 10^{-5} s^{-1}) but afforded polymers with lower PDIs (1.05 *vs.* 1.14). With or without additional $FeCl_3$, the PDIs of the resulting polymers rival those obtained by anionic polymerizations as well as other metal catalyzed ATRP systems.[16]

Bromo complex **2** had a higher observed rate constant (k_{obs} = 4.2 × 10^{-5} s^{-1}) than chloro complex **1** (k_{obs} = 3.4 × 10^{-5} s^{-1}) which may be related to the difference in the iron halide bond dissociation energies. A similar rate enhancement has also been observed in both copper and ruthenium based systems.[17] Although catalysts **1** and **2** are relatively simple to synthesize, iron(II) halides can be used directly in the presence of free Pr^iIm ligand **3** to generate the catalyst *in situ*. An added benefit of using Pr^iIm **3** is that it is a microcrystalline solid that is indefinitely stable under an inert atmosphere. The observed rate constant for **1** is slightly lower than when using $FeCl_2$ and Pr^iIm **3** (k_{obs} = 2.7 × 10^{-5} s^{-1}) and may be related to an induction period involving catalyst formation.

The ATRP of methyl methacrylate using complex **1,** complex **2**, and the complex formed *in situ* was also investigated. The homogeneous polymerization of MMA (100 equiv., 50% v/v benzene) was initiated with ethyl 2-bromoisobutyrate (EBIB) and monitored at 60 °C under an inert atmosphere. Results analogous to the ATRP of styrene were observed and indicated that these catalysts are also effective in controlling the polymerization of MMA. In addition, a similar trend in observed rate constants as discussed above was observed: complex **2** (k_{obs} = 1.6 × 10^{-4} s^{-1}) > complex **1** (k_{obs} = 1.2 × 10^{-4} s^{-1}) > $FeCl_2$ and Pr^iIm **3** (k_{obs} = 8.1 × 10^{-5} s^{-1}). Addition of $FeCl_3$ reduced the rate of polymerization (k_{obs} = 3.5 × 10^{-5} s^{-1}) but afforded polymers with lower PDIs (1.47 *vs.* 1.09).

Our results confirm that increased electron donacity of the ligands play an important role in the activity of ATRP catalysts. The high Lewis basicity of the imidazolylidene may lower the redox potential of the iron(II) complexes facilitating halide abstraction from dormant polymer chains. This would shift the equilibrium toward growing polymer radicals and therefore increase the rate of polymerization. Interestingly, the relatively high radical concentration does not seem to compromise the control. The increased donacity of these ligands may also stabilize the iron(III) species[18] and therefore enhance the rapid exchange of halides between dormant and active polymer chain ends.

J. L. gratefully acknowledges the National Institute of Health for a Postdoctoral Fellowship. We thank Christopher W. Bielawski for helpful discussions and crystallographers Lawrence M. Henling and Michael Day.

Notes and references

† **1**: δ_H(THF-d_8) 17.3, 6.3. IR (KBr) 2976vs, 1632s, 1551s, 1464s, 1357s, 1290w, 1239m, 1216m, 1195m, 1167w, 1137m, 1115m, 1071w, 905w, 751w, 665w, 545w. Anal. Calc. for $FeCl_2C_{22}H_{40}N_4$: C, 54.22; H, 8.27; N, 11.50. Found: C, 53.99; H, 8.28; N, 11.34%.

2: δ_H(THF-d_8) 24.8, 6.0. IR (KBr) 2987vs, 1750w, 1629s, 1557s, 1453s, 1359s, 1288w, 1237m, 1216m, 1194m, 1167w, 1137m, 1114m, 1070w, 904w, 884w, 750w, 665, 544. Anal. Calc. for $FeBr_2C_{22}H_{40}N_4$: C, 45.86; H, 7.00; N, 9.72. Found: C, 45.89; H, 7.04; N, 9.52%.

‡ *Crystal data* for $FeCl_2C_{22}H_{40}N_4$ **1**: M = 487.33, monoclinic, a = 11.2022(8), b = 14.7746(10), c = 15.1190(11) Å, U = 2502.3(3) $Å^3$, T = 93 K, space group P_1/n, Z = 4, μ(Mo-K) = 0.832 mm^{-1}, 23927 reflections collected, 5862 unique (R_{int} = 0.0521) which were used in all calculations. The final $wR(F^2)$ was 0.0607 (all data). Single crystals of $FeCl_2C_{22}H_{40}N_4$ **1** were recrystallized from benzene, mounted in inert oil and transferred to the cold gas stream of the diffractometer. The structure was solved using direct methods and refined by full-matrix least-squares on F^2.

CCDC 182/1698. See http://www.rsc.org/suppdata/cc/b0/b003957h/ for crystallographic files in .cif format.

1 T. E. Patten and K. Matyjaszewski, *Acc. Chem. Res.*, 1999, **32**, 895.
2 T. Ando, M. Kato, M. Kamigaito and M. Sawamoto, *Macromolecules*, 1996, **29**, 1070.
3 P. Lecmote, I. Draiper, P. Dubois, P. Teyssie and R. Jerome, *Macromolecules*, 1998, **31**, 542.
4 V. Percec, B. Barboiu, A. Neumann, J. C. Ronda and M. Zhao, *Macromolecules*, 1996, **29**, 3665.
5 (*a*) C. Granel, P. Dubois, R. Jerome and P. Teyssie, *Macromolecules*, 1996, **29**, 8576; (*b*) H. Uegaki, Y. Kotani, M. Kamigaito and M. Sawamoto, *Macromolecules*, 1997, **30**, 2249.
6 (*a*) M. Teodorescu, S. G. Gaynor and K. Matyjaszewski, *Macromolecules*, 2000, **33**, 2335; (*b*) T. Ando, M. Kamigaito and M. Sawamoto, *Macromolecules*, 1997, **30**, 4507; (*c*) X.-P. Chen and K.-Y. Qiu, *Chem. Commun.*, 2000, 233; (*d*) Y. Kotani, M. Kamigaito and M. Sawamoto, *Macromolecules*, 1999, **32**, 6877; (*e*) K. Matyjaszewski, M. Wei, J. Xia and N. E. McDermott, *Macromolecules*, 1997, **30**, 8161.
7 (*a*) J. Xia, S. G. Gaynor and K. Matyjaszewski, *Macromolecules*, 1998, **31**, 5958; (*b*) J. Xia and K. Matyjaszewski, *Macromolecules*, 1997, **30**, 7697.
8 F. Simal, A. Demonceau and A. F. Noels, *Angew. Chem., Int. Ed.*, 1999, **38**, 538.
9 C. W. Bielawski and R. H. Grubbs, *Angew. Chem., Int. Ed.*, 2000, in press.
10 N. Kuhn and T. Kratz, *Synthesis*, 1993, 561.
11 (*a*) The crystal structure of two iron carbonyl complexes have been reported: G. Huttner and W. Gartzke, *Chem. Ber.*, 1972, **105**, 2714; (*b*) P. B. Hitchcock, M. F. Lappert, S. A. Thomas, A. J. Thorne, A. J. Carty and N. J. Taylor, *J. Organomet. Chem.*, 1986, **315**, 27.
12 B. S. Snyder and R. H. Holm, *Inorg. Chem.*, 1988, **27**, 2339.
13 J. D. Walker and R. Poli, *Inorg. Chem.*, 1989, **28**, 1793.
14 K. R. Millington, S. R. Wade and G. R. Willey, *Inorg. Chim. Acta*, 1984, **89**, 185.
15 The rate of polymerization appears to be enhanced in aqueous systems: X.-S. Wang, R. A. Jackson and S. P. Armes, *Macromolecules*, 2000, **33**, 255.
16 T. E. Patten, J. Xia, T. Abernathy and K. Matyjaszewski, *Science*, 1996, **272**, 866.
17 (*a*) K. Matyjaszewski, D. A. Shipp, J.-L. Wang, T. Grimaud and T. E. Patten, *Macromolecules*, 1998, **31**, 6836; (*b*) T. Ando, M. Kamigaito and M. Sawamoto, *Macromolecules*, 2000, **33**, 2819.
18 It is known that many iron(III) complexes have low stabilities: K. B. Renkema, M. Ogasawara, W. E. Streib, J. C. Huffman and K. G. Caulton, *Inorg. Chim. Acta*, 1999, **317**, 226.

ChemComm

Isolation of a stable benzene oxide from a fungal biotransformation and evidence for an 'NIH shift' of the carbomethoxy group during hydroxylation of methyl benzoates

Derek R. Boyd,*[a] John T. G. Hamilton,[b] Narain D. Sharma,[a] John S. Harrison,[a] W. Colin McRoberts[b] and David B. Harper*[bc]

[a] *School of Chemistry, The Queen's University of Belfast, Belfast, UK BT9 5AG*
[b] *Department of Agriculture for Northern Ireland, Newforge Lane, Belfast, UK BT9 5PX*
[c] *School of Agriculture and Food Science, The Queen's University of Belfast, Newforge Lane, Belfast, UK BT9 5PX*

Received (in Cambridge, UK) 31st May 2000, Accepted 19th June 2000
Published on the Web 18th July 2000

Substituted methyl benzoates are biotransformed in the fungus *Phellinus ribis* by enzyme-catalysed epoxidation to yield an isolable benzene oxide and transient benzene oxides, whose presence was inferred from isomerisation to the corresponding methyl salicylates with concomitant migration of the carbomethoxy group.

Aromatic hydroxylation in eucaryotes is widely assumed to involve the monooxygenase-catalysed epoxidation of the benzene ring.[1,2] Although benzene oxides have often been proposed as intermediates in the literature,[1–4] to date none have been isolated as a metabolite. Their role as transient intermediates during aromatic hydroxylation has been inferred on the basis of hydrogen atom migration from the hydroxylation site and its retention at an adjacent carbon atom ('NIH shift').[1,2]

The 'NIH shift' was first observed during the *para*-hydroxylation of phenylalanine to yield tyrosine[5,6] **2** (Scheme 1, R = $CH_2CH(NH_2)CO_2H$, X = ^{3}H) and more than 100 examples have since been reported with ^{1}H, ^{2}H or ^{3}H atoms as the migrating species X. The detection of arene oxides of naphthalene[7] and quinoline[8] during liver microsomal hydroxylation of these arenes provided direct evidence of bicyclic arene epoxidation. By contrast, no unequivocal evidence of enzyme-catalysed benzene oxide formation from monocyclic arene substrates has been available and recently the role of transient arene oxide intermediates in the 'NIH shift' mechanism in biological systems has been questioned.[9–11] In earlier studies[12] we demonstrated that hydroxylation of ^{2}H-labelled halobenzenes **1A** (X = ^{2}H) and **1B** (X = ^{2}H) in fungi mainly occurs at the *ortho* position to yield phenols **3A** and **3B** (X = ^{2}H, Scheme 1) and proceeds *via* the 2,3- (**5A**, **5B**, X = ^{2}H) rather than the isomeric 1,2-benzene oxide (**6A**, **6B**, X = ^{2}H) which would yield phenols **7A** and **7B** (X = ^{2}H) after halogen migration.

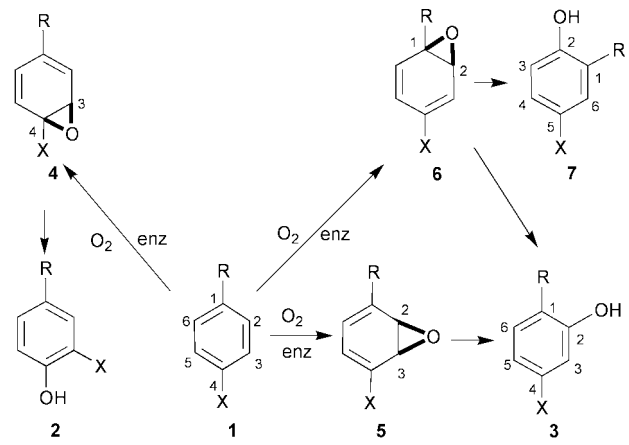

R = Cl(**A**), Br(**B**), COOMe(**C**); X = ^{1}H, ^{2}H, ^{3}H, F, Cl, Me

Scheme 1

Some substituted benzene oxides are unstable, *e.g.* the 1,2-oxide of chlorobenzene **6A** (X = ^{1}H) could not be isolated after synthesis,[12] while the 2,3-oxide **5A** and 3,4-oxide **4A** (X = ^{1}H) were found to be stable.[13] Benzene oxides have been assumed to equilibrate spontaneously with the corresponding oxepine valence tautomer by a disrotatory electrocyclic rearrangement mechanism.[1,2] However, in practice, dependent on substituent position, monosubstituted benzene oxides have been found to exist almost exclusively as either the epoxide, *e.g.* 2,3-benzene oxides **5A**–**C** rather than oxepines **8A**–**C**, or the oxepine valence tautomers *e.g.* **9C** and **10A**–**C** rather than 1,2-benzene oxides **6C** or 3,4-benzene oxides **4A**–**C**.[14] The preferred benzene oxide valence tautomers containing an electron withdrawing carboalkoxy group, *e.g.* **5C** (X = ^{1}H), and the preferred oxepine tautomers, *e.g.* **9C** and **10C** are among the most stable known compounds in this arene oxide–oxepine class.[15–17] Thus oxepine tautomer **9C** could be chemically synthesized and was isolated as a fungal metabolite.[18,19]

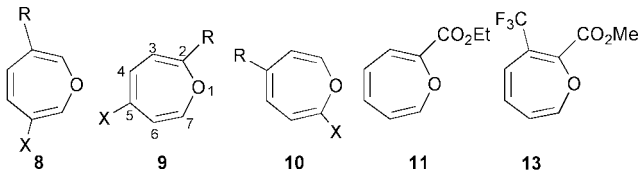

R = Cl(**A**), Br(**B**), COOMe(**C**); X = ^{1}H

The biosynthetic origin of the secondary metabolites methyl benzoate **1C** (X = ^{1}H) and methyl salicylate **3C**/**7C** (X = ^{1}H) in *Phellinus*, a widespread genus of white rot fungi, has been the subject of ongoing investigations in these laboratories. The genus is unusual in utilising CH_3Cl as a methyl donor in the biosynthesis of methyl benzoate and methyl 2-furoate.[20–23] However, the time course study of incorporation of C^2H_3 from labelled methionine (the immediate metabolic precursor of CH_3Cl) into methyl salicylate **3C**/**7C** (X = ^{1}H) by *Phellinus pomaceus* was quite different from that of methyl benzoate **1C** (X = ^{1}H). This suggests that the compound is formed by *ortho*-hydroxylation of compound **1C** (X = ^{1}H) rather than methylation of salicylic acid,[20] a conclusion consistent with the observation that isolated mycelia cannot utilize CH_3Cl in the methylation of salicylic acid.[20] A more recent study has detected carbomethoxyoxepine **9C** (X = ^{1}H) as a natural metabolite in *Phellinus tremulae*.[18] The propensity for this oxepine to rearrange *via* the postulated,[15] but undetected, benzene oxide tautomer **6C** (X = ^{1}H) with migration of the carbomethoxy group has prompted speculation[18] that it may be an intermediate in methyl salicylate biosynthesis. This hypothesis is given strong support by the results of incorporation experiments with this fungus involving administration of α-

DOI: 10.1039/b004314l

^{13}C-benzoic acid.[19] We have undertaken further biotransformation studies using *Phellinus ribis* and a range of substituted methyl benzoate substrates in the quest for the first evidence of carbomethoxy group migration *in vivo*.

P. ribis cultures were grown on 0.5% mycological peptone in shake flasks at 25 °C and the culture medium monitored for methyl esters of aromatic acids, oxepines and arene oxides by HPLC and GC/MS. As in the earlier investigations of Ayer and Cruz,[18,19] using *P. tremulae*, oxepine **9C** was detected in the medium after 12 days in addition to methyl benzoate and methyl salicylate as natural products of this fungus.[23] When cultures were supplemented after 12 days growth with 0.5 mM methyl 2,6-$^2H_2$-benzoate and examined after a further 2 days incubation, substantial incorporation of label into oxepine, 3,7-$^2H_2$-**9C** (*ca.* 70% incorporation), and methyl salicylate, 3,6-$^2H_2$-**3C** and 3-^{2}H-**7C** (*in toto* 40% incorporation) was found. GC/MS and NMR analyses of the metabolites showed that the major metabolic route involved migration of the carbomethoxy group to yield methyl salicylate **7C** (*ca.* 75% relative yield, 3-^{2}H, X = ^{1}H). A minor pathway (*ca.* 25% relative yield) involved migration and partial retention of a deuterium atom yielding methyl 3,6-$^2H_2$-salicylate **3C** (X = ^{1}H).

A series of methyl esters of monosubstitited benzoic acids were next examined as possible substrates by supplementation of the fungal growth medium as described above. Comparison of the metabolites from the methyl esters of *para*-substituted benzoic acids **1C** (X = F, Cl, Me), with authentic standard samples of the substituted methyl salicylate metabolites **7C** (X = F, Cl, Me) by GC/MS indicated that the 'NIH shift' involving migration of the carbomethoxy group had occurred during aromatic hydroxylation. Methyl esters of the corresponding *meta*-substituted benzoic acids were also examined as substrates but only the methyl *m*-fluoro- and *m*-methyl-salicylates were detected and no carbomethoxy migration was observed. Aromatic hydroxylation did not occur with the methyl esters of *ortho*-substituted benzoic acids or methyl esters of the *o*-, *m*- and *p*-trifluoromethyl benzoic acids as substrates. The only oxepine detected, other than oxepine **9C**, was oxepine **11** when ethyl benzoate was a substrate. However, GC/MS analysis of the bioextracts from metabolism of methyl 2-trifluoromethylbenzoate **12** as substrate, revealed a major bioproduct with a molecular weight identical to that of the corresponding oxepine **13.** This metabolite, purified by PLC, was obtained (*ca.* 2 mg from 300 cm^3 of culture medium) as a stable colourless liquid. ^{1}H- and ^{13}C-NMR spectra (NOE, COSY, HETCOR) of the metabolite were consistent with previously synthesised arene oxides.[13,24] It was identified as benzene oxide **14** (Scheme 2). δ_H 500 MHz, $CDCl_3$: 3.85 (s, Me), 4.23 (dd, H-2), 6.59 (ddd, H-4), 6.7 (ddd, H-3), 6.98 (dd, H-5), $J_{2,3}$ 3.7, $J_{2,4}$ = $J_{5,3}$ 1.9, $J_{3,4}$ = $J_{4,5}$ 8.6; δ_C (125 MHz, $CDCl_3$): 53.09, 61.03, 65.39, 128.02, 130.24, 130.28, 132.20, 166.55. ^{19}F-NMR, UV, IR and high resolution MS were used to confirm the identification of benzene oxide **14**.

Chemically synthesised 2,3-benzene oxides (*e.g.* **5A** and **5B** X = ^{1}H), derived from the *cis*-2,3-dihydrodiol enantiomers, were found[24] to have totally racemized *via* the oxepine tautomer in accord with predictions.[1,2] Benzene oxide **14** was similarly found to be racemic suggesting that total racemization had occurred *via* the undetected oxepine valence tautomer **13**. Addition of trifluoroacetic acid to oxide **14** resulted in aromatization to yield product **15** (Scheme 2) whose structure was confirmed by MS and NMR analysis (^{1}H-, ^{13}C-, HMBC) thus providing a further example of a carbomethoxy group migration. Interestingly phenol **15** was only detected as a trace metabolite of the methyl benzoate **12** and this appears to be a consequence of the remarkable stability of benzene oxide **14** which may be due to the presence of two strongly electron withdrawing groups, in particular the bulky CF_3 group. The location of these groups at positions C-1 and C-6 in arene oxide **14** appears to bias the equilibrium almost exclusively towards the benzene oxide valence tautomer **14**. As in other eucaryotes the enzyme is presumably a monooxygenase and attempts to isolate it are in progress.

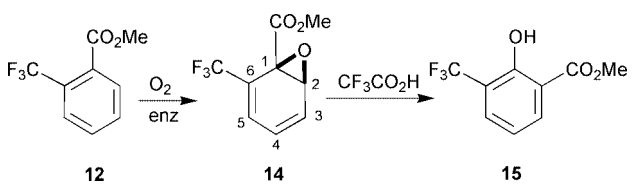

12 **14** **15**

Scheme 2

The isolation of benzene oxide **14** as a metabolite and the identification of aforesaid metabolites in cultures of *P. ribis* provide compelling evidence that *o*-hydroxylation of the methyl benzoates proceeds *via* benzene oxide intermediates. These intermediates, in turn, provide a rationale for this first report of an 'NIH shift' of the carbomethoxy group in a biological system. The apparent carboxyl group migration reported earlier[25] may in fact involve an ester intermediate.

We thank the BBSRC (N. D. S.) and European Social Fund (J. S. H.) for funding and Dr Paul J. Stevenson for helpful discussion.

Notes and references

1 D. R. Boyd and D. M. Jerina, in *Small Ring Heterocycles, Part 3, Chemistry of Heterocyclic Compounds*, vol. 42, ed. A. Hassner, Wiley, New York, 1985, p. 197.
2 D. R. Boyd and N. D. Sharma, *Chem. Soc. Rev.*, 1996, 289.
3 P. Y. Bruice, in *Organic Chemistry*, 2nd edn., Prentice-Hall, New Jersey, 1998.
4 F. A. Carey, in *Organic Chemistry*, 4th edn., McGraw Hill, Boston, 2000.
5 G. Guroff, C. A. Reifsnyder and J. W. Daly, *Biochem. Biophys. Res. Commun*, 1966, **24**, 720.
6 G. Guroff, J. W. Daly, D. M. Jerina, J. Renson, B. Witkop and S. Udenfriend, *Science*, 1967, **157**, 1524.
7 D. M. Jerina, J. W. Daly, W. Landis, B. Witkop and S. Udenfriend, *J. Am. Chem. Soc.*, 1967, **89**, 3347.
8 S. K. Agarwal, D. R. Boyd, H. P. Porter, W. B. Jennings, S. J. Grossman and D. M. Jerina, *Tetrahedron Lett.*, 1986, **26**, 4253.
9 P. F. Fitzpatrick, *J. Am. Chem. Soc.*, 1994, **116**, 1133.
10 T. Vanelli and A. D. Hooper, *Biochemistry*, 1995, **34**, 11 743.
11 S. C. Barr, N. Bowers, D. R. Boyd, N. D. Sharma, L. Hamilton, R. A. S. McMordie and H. Dalton, *J. Chem. Soc., Perkin Trans. 1*, 1998, 3443.
12 B. J. Auret, S. K. Balani, D. R. Boyd, R. M. E. Greene and G. A. Berchtold, *J. Chem. Soc., Perkin Trans. 1*, 1984, 2659.
13 H. G. Selander, D. M. Jerina, D. E. Piccolo and G. A. Berchtold, *J. Am. Chem. Soc.*, 1975, **97**, 4428.
14 D. M. Hayes, S. D. Nelson, W. A. Garland and P. A. Kollman, *J. Am. Chem. Soc.*, 1980, **102**, 1255.
15 D. R. Boyd and G. A. Berchtold, *J. Am. Chem. Soc.*, 1979, **101**, 2470.
16 B. A. Chiasson and G. A. Berchtold, *J. Org. Chem.*, 1977, **42**, 2008.
17 R. E. de Marinis, C. N. Filer, S. M. Warazkiewicz and G. A. Berchtold, *J. Am. Chem. Soc.*, 1974, **96**, 1193.
18 W. A. Ayer and E. R. Cruz, *Tetrahedron Lett.*, 1993, **34**, 1589.
19 W. A. Ayer and E. R. Cruz, *J. Nat. Prod.*, 1995, **58**, 622.
20 D. B. Harper and J. T. G. Hamilton, *J. Gen. Microbiol.*, 1988, **134**, 2831.
21 D. B. Harper, J. T. G. Hamilton, J. T. Kennedy and K. J. McNally, *Appl. Environ. Microbiol.*, 1989, **55**, 1981.
22 K. J. McNally, J. T. G. Hamilton and D. B. Harper, *J. Gen. Microbiol.*, 1990, **136**, 1509.
23 D. B. Harper, J. T. Kennedy and J. T. G. Hamilton, *Phytochemistry*, 1988, **27**, 3147.
24 D. R. Boyd, N. D. Sharma, H. Dalton and D. A. Clarke, *J. Chem. Soc., Chem. Commun.*, 1996, 45.
25 S. L. Keenan and P. J. Chapman, *J. Chem. Soc., Chem. Commun.*, 1978, 731.

Efficient planar chiral 2′-substituted 1,1′-P,N-ferrocene ligands for the asymmetric Heck reaction: control of enantioselectivity and configuration by planar chiral substituent

Wei-Ping Deng, Xue-Long Hou,* Li-Xin Dai and Xiao-Wei Dong

Laboratory of Organometallic Chemistry, Shanghai Institute of Organic Chemistry, Chinese Academy of Sciences, 354 Fenglin Lu, Shanghai 200032, China. E-mail: xlhou@pub.sioc.ac.cn

Received (in Cambridge, UK) 3rd May 2000, Accepted 20th June 2000
Published on the Web 19th July 2000

Planar chiral 1,1′P,N-2′-substituted 2′ substituted 1,1′-P,N-ferrocene derivatives were efficient ligands for the Pd-catalyzed asymmetric Heck reaction, in which 79–85% yields with high enantioselectivity (80–92%) were obtained within several hours; the enantioselectivity and the absolute configuration were controllable by changing the size of the planar chiral group and/or configuration of planar chirality.

Among palladium-catalyzed C–C bond-forming reactions, the Heck reaction enjoys considerable current popularity because of its versatility and tolerance of functionality.[1] It has only recently been exploited in the key steps of many total syntheses[2] although the first intramolecular asymmetric Heck reactions were reported, independently, by Shibasaki[3] and Overman[4] in 1989. Two years later, the intermolecular asymmetric version of the Heck reaction was reported by Hayashi,[5] with BINAP as ligand. The reaction was carried out with dihydrofuran **1** and phenyltriflate and afforded a mixture of regioisomers **2** and **3** in a 29 : 71 ratio, with the major product **3** obtained in high ee (96%) (Scheme 1).

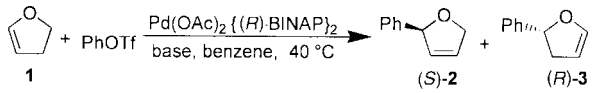

Scheme 1

In an important extension to this work, Pfalz[6] described the application of the diphenylphosphinooxazoline **4** (PHOX) ligand to arylation and alkenylation of substrate **1**. In contrast to the regioisomer problem observed by Hayashi, the phenylation of dihydrofuran **1** produced the 2,5-dihydrofuran derivative **2** in high yield (85%) and with so far the best enantioselectivity (97% ee). Although impressive results have been achieved in asymmetric inter- and intra-molecular Heck reactions with several kinds of ligands,[6–8] there are still problems for the practical use of this asymmetric reaction, such as low reaction rates (usually several days) and high catalyst loading. Therefore, it is important and challenging to develop novel highly efficient ligands.

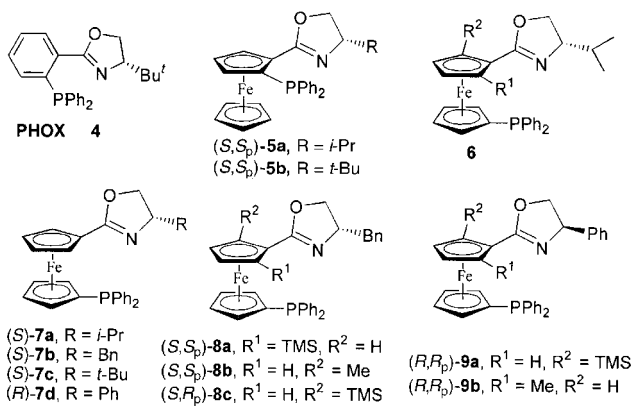

Ferrocene-based planar chiral ligands have been proven to be effective and highly reactive in many kinds of asymmetric catalytic reaction.[9] However, to the best of our knowledge, there is so far no report on their use in the asymmetric Heck reaction, except for the result of Guriy[8] that excellent enantioselectivity was observed with very low catalytic activity (14 days for a complete conversion) by using ferrocene-type ligands **5** in the phenylation of 2,2-dimethyl-2,3-dihydrofuran. Quite recently, as a part of the program aimed at the design and application of chiral ligands to asymmetric synthesis,[10] we synthesized a new kind of planar chiral 1,1′-P,N-ferrocene ligand **6**, which showed that the planar chirality is decisive in exerting control over both absolute configuration and enantiomeric excess in Pd-catalyzed allylic substitution reactions.[11] These encouraging results prompted us to extend the scope of these new structural-framework ligands to the asymmetric Heck reaction. Herein we report our initial findings on the phenylation of 2,3-dihydrofuran **1** by using palladium complexes derived from new ligands **7**, **8** and **9**, which were synthesized by our group.[11,12]

We initially tested the effectiveness of the structurally novel 1,1′-disubstituted P,N-ferrocene ligands **7**. At the same time, 1,2-disubstituted P,N-ferrocene ligands **5** were also used for this reaction in order to compare the catalytic activity of **5** and **7**. The results are summarized in Table 1.

With 3 mol% of catalyst, prepared *in situ* from $Pd(dba)_2$ and 1.5 equiv. of ligands **7a–d**, the corresponding 2,5-dihydrofurans **2** were formed as sole products (as shown by TLC), similar to the results Pfalz obtained.[6] The best enantioselectivity (76.5%) and also the highest catalyst activity (affording 80% of yield in 8 h) was observed with ligand **7b** (Table 1). Ligand **7d** showed the same catalytic activity as ligand **7b**, however, gave the lowest enantioselectivity (42.4%). It is noteworthy that 1,2-disubstituted P,N-ferrocene ligands **5a–b** had almost no catalytic activity in this reaction even with the reaction time prolonged to 24 h.[8] Usually, 1.5 equiv. of ligand were used in this reaction. However, when 1.0 or 2.0 equiv. of the ligand were used the resulting ee values and yields of reaction product were slightly lower. Next, a variety of solvents and bases were investigated and the results showed that the ee value was independent of the base used, which is in consistent with Pfaltz's results. However, the enantioselectivity with benzene as solvent was inferior to that with THF. For ligands **7b** and **7d**, the yields in asymmetric Heck reactions are good with higher reaction rates (several hours) using 3 mol% of catalyst compared with literature results[6] (2 to 3 days for a high conversion).

Considering the high reactivity of ligands **7b** and **7d**, we envisaged that the enantioselectivity and/or the configuration of the reaction product might be improved and/or inverted by introducing planar chirality into these two ligands according to our previous experience on the role of planar chirality in Pd-catalyzed allylic alkylation reactions.[11] Consequently, planar chiral ligands (S,S_p)-**8a**, (S,S_p)-**8b** and (S,R_p)-**8c**, (R,R_p)-**9a** and (R,R_p)-**9b**, containing a newly introduced Me or TMS group on the same Cp ring with oxazoline moiety, were synthesized and

DOI: 10.1039/b003530k

Table 1 Enantioselective Heck reaction of **1** and phenyltriflate with ligands **5** and **7**[a]

Entry	Ligand	Solvent	Base	Time	Yield (%)[b]	ee (%)[c] (config.)[d]
1	**7a**	THF	*i*-Pr_2NEt	8 h	46	68.1 (*R*)
2	**7b**	THF	*i*-Pr_2NEt	8 h	80	**76.5 (R)**
3	**7c**	THF	*i*-Pr_2NEt	8 h	25	64.0 (*R*)
4	**7d**	THF	*i*-Pr_2NEt	8 h	79	42.4 (*S*)
5	**5a**	THF	*i*-Pr_2NEt	24 h	Trace	n.d.
6	**5b**	THF	*i*-Pr_2NEt	24 h	Trace	n.d.
7[e]	**7b**	THF	*i*-Pr_2NEt	8 h	72	75.7
8[f]	**7b**	THF	*i*-Pr_2NEt	8 h	77	75.4
9	**7b**	THF	Proton sponge	8 h	82	76.0
10[e]	**7b**	THF	Et_3N	8 h	85	76.0
11	**7b**	Benzene	Proton sponge	8 h	71	71.0
12	**7b**	Benzene	*i*-Pr_2NEt	8 h	77	69.9

[a] The reaction was carried out under an argon atmosphere. Pd:PhOTf:**1**:base = 0.03:1.0:5.0:2.0. Reaction temperature: 60 °C. Pd:**L*** = 1:1.5 unless otherwise stated. [b] Isolated yields based on phenyltriflate. [c] Determined by chiral GC. [d] Determined by comparing the sign of optical rotation with literature data. [e] Pd:**L*** = 1:1. [f] Pd:**L*** = 1:2.

Table 2 Enantioselective Heck reaction of **1** and phenyltriflate with ligands **8** and **9**[a]

Entry	Ligand	Time	Ratio (2:3)[b]	Yield (%)[c]	ee (%)[d] (config.)[e]
1	(*S*)-**7b**	8 h	n.d.	80	76.5 (*R*)
2	(S,S_p)-**8a**	8 h	n.d.	72	83.5 (*S*)
3	(S,S_p)-**8b**	8 h	64:1	79 (82)[b]	88.5 (*R*)
4	(S,R_p)-**8c**	8 h	n.d.	75	**92.1 (*R*)**
5	(*R*)-**7d**	8 h	n.d.	79	42.4 (*S*)
6	(R,R_p)-**9a**	8 h	n.d.	75	80.2 (*R*)
7	(R,R_p)-**9b**	8 h	32:1	85 (91)[b]	88.4 (*S*)

[a] The reaction was carried out in THF in the presence of diisopropylethylamine under an argon atmosphere. PhOTf:**1**:*i*-Pr_2NEt:Pd(dba)$_2$:ligands = 1.0:5.0:2.0:0.03:0.06. Reaction temperature: 60 °C. [b] Determined by GC. [c] The isolated yields based on phenyltriflate. [d] Determined by chiral GC. [e] Configurations were assigned by comparison of the signs of optical rotation.

tested for this reaction. The results are summarized in Table 2.

A dramatic change in the enantioselectivity of the reaction was observed with (S,S_p)-**8a** containing a (S_p)-TMS planar chiral group. The enantiomeric excess of reaction product **2** changed from 76.5% with *R* configuration by using ligand **7b** to 83.5% with *S* configuration (entry 2 *vs.* entry 1 of Table 2). This exciting result encouraged us to probe the effect of the newly introduced group with opposite planar chirality, which might increase the ee value and with the same configuration of product **2** from that by using ligand **7b**. Therefore, (S,S_p)-**8b** containing a (S_p)-Me planar chiral group was synthesized and subjected to the same reaction. Just as expected, a remarkable improvement in the ee value (88.5%, *R* configuration) was observed. The same phenomenon was observed by using ligands (R,R_p)-**9a** and (R,R_p)-**9b** (compare entries 6 and 7 with entry 5). These results indicate that the effect of planar chirality on the stereochemical outcome is significant in this Heck reaction, which is inconsistent with our previous results with Pd-catalyzed asymmetric allylic alkylation.[11] Maybe the planar chirality has the same role in two different reaction systems, *i.e.* the planar chirality controls and tunes the ee value and absolute configuration of the reaction product by changing the ratio of rotamers of the axial chirality on coordinating with metal Pd due to its steric repulsion on the coordinating center.[12] If this is true, then increasing the steric bulkiness of the newly introduced planar chiral group may improve the ee value of product **2**. In fact, the ee value actually increased to 92% when ligand (S,R_p)-**8c** containing a bulky TMS group was used in this reaction. Thus, the ee value and absolute configuration of product **2** are controllable and tunable just by changing the configuration and/or size of the planar chiral group. In addition, a very small amount of regioisomer **3** (entries 3 and 7) in the reaction product was detected by GC but not observed by preparative TLC.

In conclusion, the above mentioned new kind of ligand is effective and attractive in the asymmetric Heck reaction not only because of the high reactivity and enantioselectivity but also because the absolute configuration of the reaction product can be controlled just by changing the configuration and/or size of the planar chiral group of these ligands. Further studies on the improvement of enantioselectivity *via* modifying these ligands and their application to other substrates are in progress.

Financial support from The National Natural Science Foundation of China, National Outstanding Youth Fund, Chinese Academy of Sciences, and Shanghai Committee of Science and Technology are acknowledged. We thank Dr Yong Tang for helpful and inspiring discussions.

Notes and references

1 Reviews: R. F. Heck, *Palladium Reagents in Organic Synthesis*, Academic Press, London, 1985.
2 Reviews: A. de Meijere and F. E. Meyer, *Angew. Chem., Int. Ed. Engl.*, 1994, **33**, 2379; E. Negishi, C. Coperet, S. Ma, S.-Y. Liou and F. Liu, *Chem. Rev.*, 1996, **96**, 365; M. Shibasaki, C. D. J. Boden and A. Kojima, *Tetrahedron*, 1997, **53**, 7371; M. Shibasaki and E. M. Vogl, *J. Organomet. Chem.*, 1999, **576**, 1.
3 Y. Sato, M. Sodeoka and M. Shibasaki, *J. Org. Chem.*, 1989, **54**, 4738.
4 N. E. Carpenter, D. J. Kucera and L. E. Overman, *J. Org. Chem.*, 1989, **54**, 5846.
5 F. Ozawa, A. Kubo and T. Hayashi, *J. Am. Chem. Soc.*, 1991, **113**, 1417.
6 O. Loiseleur, P. Meier and A. Pfaltz, *Angew. Chem., Int. Ed. Engl.*, 1996, **35**, 200; O. Loiseleur, M. Hayashi, M. Keenan, N. Schmees and A. Pfaltz, *J. Organomet. Chem.*, 1999, **576**, 16.
7 For recent studies on the asymmetric Heck reaction: K. K. Hii, T. D. W. Claridge and J. M. Brown, *Angew. Chem., Int. Ed. Engl.*, 1997, **36**, 984; S. Y. Cho and M. Shibaski, *Tetrahedron Lett.*, 1998, **39**, 1773; L. F. Tietze, K. Thede and F. Sannicolo, *Chem. Commun.*, 1999, 1811.
8 A. J. Hennessy, Y. M. Malone and P. J. Guiry, *Tetrahedron Lett.*, 1999, **40**, 9163.
9 Reviews: Ferrocenes, ed. A. Togni and T. Hayashi, VCH, Weinheim, 1995, and references therein.
10 S.-L. You, Y.-G. Zhou, X.-L. Hou and L.-X. Dai, *Chem. Commun.*, 1998, 2765; X. D. Du, L.-X. Dai, X.-L. Hou, L. J. Xia and M. H. Tang, *Clin. J. Chem.*, 1998, **16**, 90; X.-T. Zhou, Y.-R. Lin and L.-X. Dai, *J. Org. Chem.*, 1999, **64**, 1331; W.-P. Deng, X.-L. Hou and L.-X. Dai, *Tetrahedron: Assymetry*, 1999, **10**, 4689; L.-X. Dai, X.-L. Hou, W.-P. Deng, S.-L. You and Y. G. Zhou, *Pure Appl. Chem.*, 1999, **71**, 1401.
11 W.-P. Deng, X.-L. Hou, L.-X. Dai, Y.-H. Yu and W. Xia, *Chem. Commun.*, 2000, 285.
12 W.-P. Deng, PhD Thesis, Shanghai Institute of Organic Chemistry, Chinese Academy of Sciences, 2000.

ChemComm

Functional analysis of Phe605, a conserved aromatic amino acid in squalene–hopene cyclases†

Tsutomu Hoshino,* Masanori Kouda, Takamasa Abe and Tsutomu Sato

Department of Applied Biological Chemistry, Faculty of Agriculture and Graduate School of Science and Technology Niigata University, Ikarashi, Niigata 950-2181, Japan

Received (in Cambridge, UK) 23rd May 2000, Accepted 21st June 2000
Published on the Web 19th July 2000

Incubation of squalene with the site-directed mutant F605A of squalene–hopene cyclase from *Alicyclobacillus acidocaldarius* yielded many triterpenes consisting of the 6/6/5-fused tri-, 6/6/6/5-fused tetra-, and 6/6/6/6/5-fused pentacyclic skeletons, the function of F605 being assignable for facilitating the ring expansion and for stabilizing the hopanyl C22-cation, possibly *via* cation-π interactions.

Squalene–hopene cyclase (SHC) converts acyclic squalene into pentacyclic triterpenes, hopene **1** and hopanol **2**, with regio- and stereochemical specificity.[1] In the past few years, there have been remarkable advances in addressing both the cyclization mechanism and the catalytic sites by site-directed mutagenesis experiments.[2] The cyclization cascade is triggered by proton attack at the terminal double bond, which is supplied by D376 and/or D374.[2a] The carbocation intermediates of the initially cyclized A-ring and the bicyclic A/B-fused ring, progressively formed during the polycyclization reaction, are stabilized by the carboxylate anion of D377[2a] and by the π-electrons of F365[2b] *via* a cation-π interaction, respectively. The 6-membered C-ring (anti-Markovnikov adduct) is formed as a result of a ring expansion process from the 5-membered C-ring that has been previously formed under Markovnikov closure.[2c] This expansion may be facilitated by π-electrons of F601. The point mutation experiments targeted for W 169 and W 489 allowed us to propose the involvement of the ring expansion from the 5- to 6-membered D-ring.[2d] The bulk size at the 261 position is critical in directing the stereochemical destiny for the formation of the hopane skeleton.[2f] The question still remained unanswered as to how the last 5-membered E-ring is constructed. Phe605 is strictly conserved in all the known SHCs, but not in oxidosqualene cyclases. We describe here the enzymic products obtained by the mutant F605A and the functional analysis of Phe605.

With the cell-free homogenates from a 8L-culture of the transformed *E. coli* encoding F605A SHC, 400 mg of squalene was incubated for 14 h at optimum catalytic conditions (pH 6.0 and 50 °C). Ten new products were homogeneously purified with SiO_2 column chromatography (5% $AgNO_3$) eluting with hexane. The yields of **1**–**12** were estimated by GC to be 141, 133, 9.9, 6.6, 23.3, 11.5, 9.3, 20.4, 7.4, 0.5, 12.4, 12.6 mg, respectively, and to be 1.2 mg for the recovered squalene.

Scheme 1 shows the structures of all the isolated products, which were determined by the detailed analyses of EIMS and 2D NMR spectra. Products **3** and **4** (**3**:**4** = 1.5:1) had a 6/6/5-fused tricyclic skeleton. All the NMR data and the specific rotation of **3** and **4** were indistinguishable from those of the known podioda-8,17,21-triene and -7,17,21-triene,[3] respectively, but the stereochemistry at the 14-position has remained undetermined. These two products were formed from the common biosynthetic intermediate **13** (Scheme 2). The successive rearrangement reactions of 13βH to C14 and of the 26-Me to C13 on **13** gave the C8-cation (podiodatrienyl cation **13′**). The deprotonation of H9 or H7 afforded **3** or **4**, respectively. The cyclization reaction proceeds through intermediates **13**–**17**, as shown in Scheme 2. A ring expansion of **13** to form **14** and a further cyclization could produce **15**. Products **5**–**8** were produced *via* **15** by deprotonation reactions at different positions, rearrangement reactions of hydride and methyl, or nucleophilic attack of a water molecule. Intermediate

† Electronic supplementary information (ESI) available: EIMS spectra and NMR assignments of products **3**–**12**. See http://www.rsc.org/suppdata/cc/b0/b004129g/

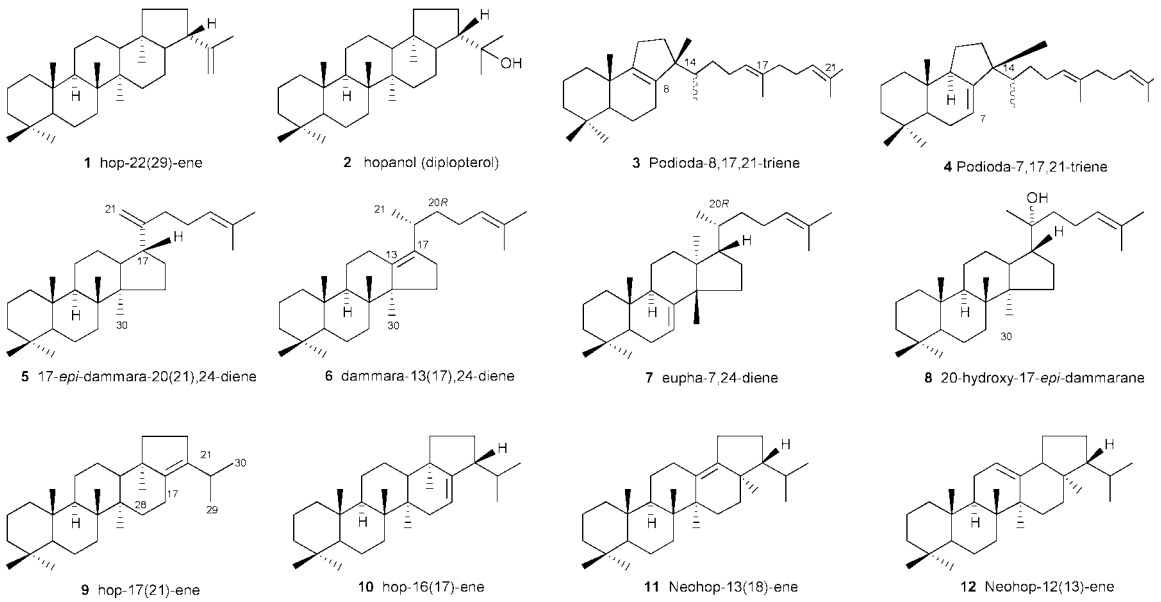

Scheme 1 Structures of the enzymic products obtained by the mutant F605A.

DOI: 10.1039/b004129g

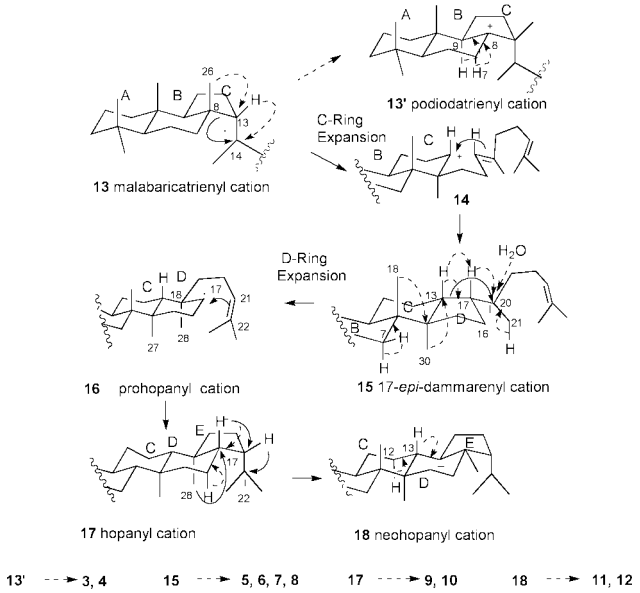

Scheme 2

15 underwent ring expansion and a further cyclization to give **16**,[2f] and **17**, respectively. **9**[2f] and **10** were produced *via* **17**. The migration of 28-Me into C17 in **17** gave **18**, which was subjected to deprotonation reactions to yield **11** and **12**. The product ratio of **2**:**1** was significantly increased by this mutation (0.9:1), compared with that of the native SHC (0.2:1). This fact strongly suggests that the perturbation occurred around the E-ring, which allowed the easy access of a water molecule to the enzyme cavity and also led to the incorrect positioning of the deprotonation site for introducing the $\Delta^{22:29}$ double bond in **1**. Therefore, a larger amount of **2** and **8** could be accumulated together with the pentacyclic **9**–**12** having different double bond positions due to the improper deprotonation reactions. The significant perturbation around the E-ring may have had a greater influence on the earlier reaction steps in forming tri- and tetracyclic ring systems to afford **3**–**8**. Many different triterpene skeletons have been found from various point mutants;[2] but the high production of podiodatrienes (**3**,**4**) and neohopanes (**11**,**12**) has not previously been reported.

To identify the function of F605, we constructed the mutants of F605Y, F605W and F605H. If F605 stabilises a carbocation intermediate through a cation–π interaction, the higher π-electron density gives the faster reaction rate.[2b] Fig. 1 shows the specific activities for the formation of **1** or of both **1** and **2** against incubation temperatures. At lower temperatures, F605Y and F605W had faster reactions than the wild-type,[4] suggesting that a cation–π interaction may be involved in the cyclization cascade.[2b] The F605Y had a bell-shape, while the F605W had a steady state in the range 45–55 °C. The cyclase activities of the mutants were somewhat sensitive to the incubation temperatures. These features may have occurred due to the decreased binding (the largest K_m of F605W[5]) and/or to the occurrence of the geometrical change around the active site region by elevating the temperature, as previously discussed for the F365Y and F365W SHCs.[2b] The mutants F605Y and F605W afforded a larger amount of **2** relative to **1** than the wild-type (Fig. 1);[4] the bulky substituents make the active site region (around the E-ring) less compact, thus the water molecule has easier access to the cavity resulting in the production of a larger amount of **2**. However, the quantities of **3**–**12** produced by the Tyr and Trp mutants were negligible, strongly suggesting that the perturbation was lower compared to that of the Ala mutant and that a cation–π interaction was still effective in the active site (Fig. 1). F605H afforded **5** in a significantly higher yield (14%) than the wild-type (1%), despite the total amount of **1** and **2** being decreased (84% of the native SHC); the His moiety would have abstracted the proton from 21-Me of **15** owing to the basic function. Thus, F605 can be situated near to 21-Me in **15**. The more favourable placement of F605 on the C17 cation (the secondary cation) in **16**, though near to the C20-cation in **15** (the tertiary cation), may facilitate the ring expansion reaction to give the energetically unfavourable **16**, as is predicted from computational studies.[6]

Tetracyclic **5**–**8** were accumulated with F605A, but never with F605Y and F605W, which definitively suggests that the π-electrons of Phe605 have a crucial role for the D-ring expansion process from **15** to **16**. A nucleophilic attack of the Δ^{21} double bond to the C17 cation in **16** yields the E-ring and the last C22 cation of **17**. The E-ring formation reaction would be further accelerated if the C22 cation could be stabilized *via* a cation–π interaction. Phe605 is not conserved in oxidosqualene cyclases. For lanosterol and cycloartenol biosyntheses, the polycyclization is quenched at the tetracyclic stage without a D-ring expansion.[1] For the syntheses of pentacyclic lupeol and β-amyrin, the ring expansion is also involved to give a common intermediate of the baccharenyl cation, but the position of the carbocation is different from that of the **16** cation.[1,2d,f] The different cyclization mechanism between eukaryotic and prokaryotic cyclases further support the proposed function of Phe605 which is conserved only in SHCs.

This work was supported by a Grant-in-Aid to T. H. (No.11660104) from the Ministry of Education, Science, Sports and Culture, Japan.

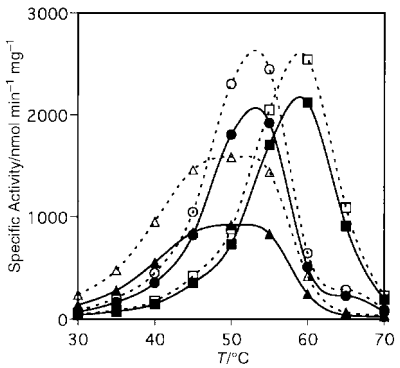

Fig. 1 Specific activities for the formation of **1** (closed symbols, solid lines) or of the both of **1** and **2** (open symbols, dotted lines) against incubation temperatures are given for the wild-type SHC (■,□), the mutants of F365Y (●,○) and F365W (▲,△). One mg of squalene was incubated with 5 μ of the homogeneously purified SHCs for 60 min at pH 6.0. The ratio of **1** to **2** can also be estimated from the difference between the solid and the dotted lines.

Notes and references

1 I. Abe, M. Rohmer and G. D. Prestwich, *Chem. Rev.*, 1993, **93**, 2189.
2 (*a*) T. Sato and T. Hoshino, *Biosci. Biotechnol. Biochem.*, 1999, **63**, 2189; (*b*) T. Hoshino and T. Sato, *Chem. Commun.*, 1999, 2205; (*c*) T. Hoshino, M. Kouda, T. Abe and S. Ohashi, *Biosci. Biotechnol. Biochem.*, 1999, **63**, 2038; (*d*) T. Sato, T. Abe and T. Hoshino, *Chem. Commun.*, 1998, 2617; (*e*) C. Füll and K. Poralla, *FEMS Microbiol. Lett.*, 2000, **18**, 221; (*f*) T. Hoshino, T. Abe and M. Kouda, *Chem. Commun.*, 2000, 441.
3 Y. Arai, M. Hirohara and H. Ageta, *Tetrahedron Lett.*, 7209, **30**, 1989.
4 On prolonged incubation for 20 h at 45 °C and pH 6.0 with equal amounts of squalene and the enzyme, the total amounts of **1** and **2** produced were almost equal for the three different SHCs. However, the product ratio of **1** to **2** was significantly altered as follows: 5.0 for the native SHC; 3.65 for the F605Y; 1.37 for the F605W (Fig. 1).
5 Kinetic data for the total amount of **1** and **2**, produced by incubating squalene at 35 or 45 °C (in parentheses) and for 60 min, were as follows: k_{cat}s; 0.25 (1.48), 0.18, 0.92 (4.52) and 1.67 (9.11) s^{-1}, and K_ms; 17.8 (18.2), 47.9, 21.1 (69.6) and 21.1 (109) μM, respectively, for the wild-type, F605A, F605Y and F605W. The more bulky substituents gave the larger K_m (looser binding) with elevating incubation temperatures, which may result in the profile of steady state in the range of 45–55 °C (Fig. 1), despite π-electron density being enhanced.[2b]
6 C. Jenson and W. L. Jorgensen, *J. Am. Chem. Soc.*, 1997, **119**, 10846.

Fabrication of novel mesoporous dimethylsiloxane-incorporated silicas

Jin Joo,[a] Taeghwan Hyeon*[a] and Jingyu Hyeon-Lee[b]

[a] *School of Chemical Engineering, Seoul National University, Seoul 151-742, Korea. E-mail: thyeon@plaza.snu.ac.kr*
[b] *Polymer Laboratory, Chemical Sector, Samsung Advanced Institute of Technology (SAIT), Taejon 305-380, Korea*

Received (in Cambridge, UK) 8th March 2000, Accepted 29th June 2000
Published on the Web 19th July 2000

Mesoporous dimethylsiloxane-incorporated silica materials are synthesized which exhibit high surface areas, regular mesopores, thick walls, high hydrophobicity and high mechanical strength.

Since the discovery of the M41S mesoporous silica materials in 1992 by Mobil researchers,[1] various mesoporous materials have been developed.[2] Several organic-group modified mesoporous silica materials have been synthesized by the *in situ* co-condensation of organosilane precursors and tetraethyl orthosilicate (TEOS) in the presence of surfactant self-assemblies.[3] Recently, several groups reported the synthesis of mesoporous organic–inorganic hybrid materials with organic groups directly incorporated into the silicate framework using bis(alkoxysilyl)-functionalized precursors. Here, we present the synthesis of mesoporous dimethylsiloxane-incorporated silica materials from the co-condensation of TEOS and diethoxydimethylsilane (DEDMS) in the presence of surfactant self-assemblies.

In the multi-component sol–gel processes it is important to control the hydrolysis and condensation rates of the precursors.[6] If the hydrolysis rates of the precursors were considerably different, phase-separated mixtures would be produced instead of homogeneous hybrid materials.[7] It is well-known that the hydrolysis rate of DEDMS is nearly zero in basic medium and that it hydrolyzes much faster in acidic medium. In consequence, we chose the so-called $S^+X^-I^+$ route (S^+: cationic surfactant, X^-: halide ion, and I^+: cationic silicate oligomer) to synthesize MCM-41 type mesoporous dimethylsiloxane-incorporated silicas.[8]

TEOS and DEDMS were partially pre-hydrolyzed separately in acidic medium by stirring for 30 minutes in an ice bath with molar ratios of 1 TEOS : 2 H_2O : 0.04 HCl and 1 DEDMS : 1 H_2O : 0.04 HCl respectively. The resulting two clear solutions were mixed with vigorous stirring and were poured into a surfactant solution at 60 °C. The resulting gel mixture had a molar composition of 1 (TEOS + DEDMS) : 0.13 octadecyltrimethylammonium bromide (OCTAB) : 5.4 HCl : 150 H_2O. The mixture was aged for 5 d with vigorous stirring at 60 °C. The surfactant was removed by refluxing in ethanol for 3 h followed by refluxing for 6 h in 5 mol% HCl in ethanol. The resulting mesoporous materials were designated as mesoporous $(CH_3)_2SiO$-*a*SiO_2 materials (*a* = the molar ratios of DEDMS and TEOS in the initial reaction mixtures, and were set to 2, 3 and 4). For comparison, pure mesoporous MCM-41 silica was synthesized according to a similar procedure using TEOS as a precursor. The elemental analytical results of these mesoporous materials revealed that most of the surfactant was successfully removed (typical elemental results in wt%: C, 7.68; H, 1.84; N, 0 for $(CH_3)_2SiO$-$4SiO_2$. C, 9.36; H, 2.41; N, 0 for $(CH_3)_2SiO$-$3SiO_2$. C, 11.11; H, 2.76; N, 0 for $(CH_3)_2SiO$-$2SiO_2$). Solid-state ^{13}C NMR also confirmed the successful removal of surfactant.

The ordered mesoporous structure of the materials was investigated by X-ray powder diffraction (XRD), transmission electron microscopy (TEM) and gas adsorption measurement. Powder X-ray diffraction patterns of mesoporous $(CH_3)_2SiO$-*a*SiO_2 materials and mesoporous silica are shown in Fig. 1. The XRD pattern of mesoporous silica [Fig. 1(*a*)] exhibited hexagonal MCM-41 pore arrangement, displaying one intense (100) reflection with d_{100} of 4.0 nm and smaller (110) and (200) reflections. On the other hand, the XRD patterns of dimethylsiloxane-incorporated silica materials shown in Fig. 1(*b*)–(*d*) revealed only a (100) reflection, demonstrating that they are less ordered in the long range than the pure silica material.

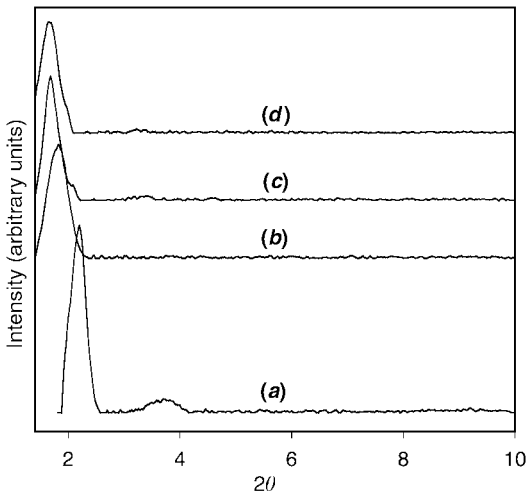

Fig. 1 X-Ray diffraction (XRD) patterns of mesoporous MCM-41 silica (trace *a*), mesoporous $(CH_3)_2SiO$-$4SiO_2$ (trace *b*), $(CH_3)_2SiO$-$3SiO_2$ (trace *c*) and $(CH_3)_2SiO$-$2SiO_2$ (trace *d*) materials. The patterns were obtained with a Rigaku D/Max-3C diffractometer equipped with a rotating anode and Cu-K_α radiation (λ = 0.15418 nm).

Table 1 shows the pore characteristics of these mesoporous materials. The BET surface areas of the dimethylsiloxane-incorporated silicas are slightly smaller than that of the pure silica material. Nitrogen adsorption/desorption isotherms of these materials exhibited type IV, which is characteristic of mesoporosity. The pore diameters of these materials were comparable to that of the pure mesoporous silica. The wall thickness was obtained by subtracting the BJH pore size from the unit cell parameter a_0 ($a_0 = 2d_{100}/\sqrt{3}$). The results revealed that the walls of these dimethylsiloxane-incorporated silicas were thicker than those of the pure silica derivative, which is very important for their future applications. A TEM image of

Table 1 Pore characteristics of mesoporous dimethylsiloxane-incorporated silicas[a]

Sample	Surface area/ $m^2\ g^{-1}$	Pore diameter/ nm	Pore volume/ $cm^3\ g^{-1}$	Wall thickness/ nm
MCM-41 SiO_2	1082	2.8	0.95	1.8
$(CH_3)_2SiO$-$4SiO_2$	1028	2.7	0.67	2.9
$(CH_3)_2SiO$-$3SiO_2$	980	2.4	0.62	3.6
$(CH_3)_2SiO$-$2SiO_2$	1029	2.3	0.73	3.8

[a] N_2 adsorption and desorption isotherms were collected on a Micromeritics ASAP2010 Gas Adsorption Analyzer after the materials were degassed at 150 °C at 30 μTorr for 5 h. The surface areas were calculated by the BET method and the pore size distributions were calculated from the adsorption branch of the nitrogen isotherm by the BJH method.

DOI: 10.1039/b001886o

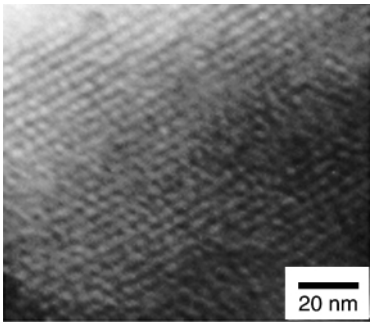

Fig. 2 Transmission electron micrograph (TEM) of mesoporous $(CH_3)_2SiO$-$4SiO_2$ material. The images were obtained with a Phillips CM-20 instrument.

the mesoporous $(CH_3)_2SiO$-$4SiO_2$ material showed a regular array of *ca*. 2.5 nm diameter holes separated by *ca*. 3 nm thick walls (Fig. 2).

One of the disadvantageous features of mesoporous silica materials for the applications is their poor mechanical stability.[9] In the present research, we have incorporated the dimethylsiloxane component into silica frameworks to increase the mechanical strength of the silica framework. The mechanical properties of these materials were evaluated by taking XRD patterns after compressing the materials. In the case of the pure silica mesoporous material, the XRD pattern after compressing at 104 MPa (15 000 psi) for 10 min showed no diffraction peak, revealing that the mesopores were completely collapsed. On the other hand, mesoporous $(CH_3)_2SiO$-$3SiO_2$ after compressing at 104 MPa exhibited a (100) reflection with slightly decreased intensity compared to the XRD pattern before the compression. The surface area and pore volume of the mesoporous material were kept nearly unchanged after compressing at 104 MPa. The results clearly demonstrated that these mesoporous dimethylsiloxane-incorporated silicas possess better mechanical stability compared to mesoporous silica materials.

The hydrophobicity of the mesoporous materials was tested by mixing with an immiscible mixture of water and methylene chloride. After shaking vigorously, the mesoporous $(CH_3)_2SiO$-$3SiO_2$ material resided exclusively in the methylene chloride layer. In contrast, the pure silica mesoporous material stayed in water layer. The same trend was observed when a mixture of diethyl ether and water was used as a partitioning medium. These results showed that these mesoporous materials are very hydrophobic. Thermogravimetric analysis (TGA) of mesoporous $(CH_3)_2SiO$-$3SiO_2$ revealed that the material decomposed around 300 °C.

The homogeneous distribution of the $(CH_3)_2Si$ moiety in the mesoporous material was investigated by FT-IR spectroscopy (Fig. 3). The successful incorporation of $(CH_3)_2Si$ groups in the silicate framework was confirmed by four peaks at *ca*. 2970, 1267, 850 and 800 cm^{-1}, which can be assigned as CH_3 asymmetric stretching, CH_3 deformation, CH_3 rocking and Si–C stretching mode, respectively. The Si–O–Si bending vibration mode was known to be sensitive to the chemical environment and was utilized as a fingerprint for the homogeneous incorporation of organic groups into the silicate framework.[10] In our samples, the Si–O–Si bending vibration mode was shifted from 467 cm^{-1} for pure silica mesoporous material to 454 cm^{-1} for $(CH_3)_2SiO$-$4SiO_2$ and $(CH_3)_2SiO$-$3SiO_2$, and 450 cm^{-1} for $(CH_3)_2SiO$-$2SiO_2$, demonstrating that the Si-$(CH_3)_2$ moieties are homogeneously distributed in the silicate framework structure.[10] The ^{13}C CP-MAS (cross polarization-magic angle spinning) NMR spectrum of mesoporous $(CH_3)_2SiO$-$3SiO_2$ material showed a single Si-$(CH_3)_2$ peak at δ −1.5. The ^{29}Si CP-MAS NMR spectrum of the material exhibited characteristic peaks attributed to $(CH_3)_2Si(OSi)_2$ (D_2 δ −15.7), $Si(OSi)_4$ (Q_4 δ −110), $(OH)Si(OSi)_3$ (Q_3 δ −103). These NMR results demonstrated that the $(CH_3)_2Si$ moiety was kept intact during the synthesis and was successfully incorporated into the silicate framework.

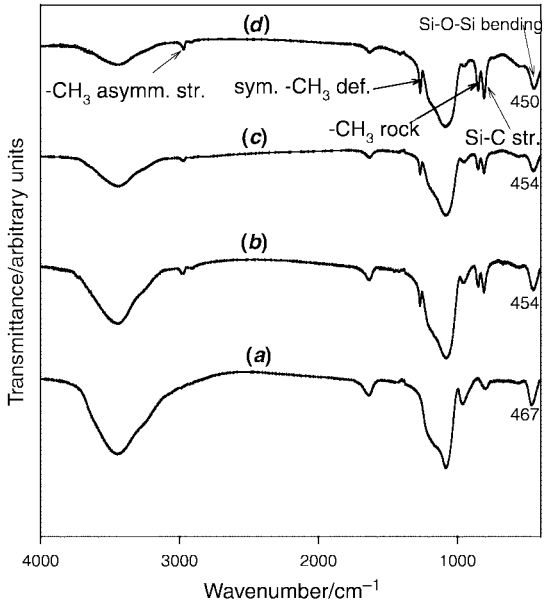

Fig. 3 FT-IR spectra of mesoporous MCM-41 silica (trace *a*), mesoporous $(CH_3)_2SiO$-$4SiO_2$ (trace *b*), $(CH_3)_2SiO$-$3SiO_2$ (trace *c*) and $(CH_3)_2SiO$-$2SiO_2$ (trace *d*) materials. The spectra were obtained with a Bomem MB-100 instrument.

These new mesoporous dimethylsiloxane-incorporated silica materials exhibit many interesting characteristics for future applications, including high surface areas, regular mesopores, thick walls, high mechanical strength and high hydrophobicity. We expect that these materials can find applications in catalysis, adsorption technology and the fabrication of low dielectric materials for ULSI (ultra large scale integration) devices.

We are grateful to the Korea Science and Engineering Foundation (Basic Research Program # 98-05-02-03-01-3) and the Brain Korea 21 Program supported by the Korean Ministry of Education for financial support. We thank the Korea Basic Science Institute for the NMR spectroscopic studies.

Notes and references

1 C. T. Kresge, M. E. Leonowicz, W. J. Roth, J. C. Vartuli and J. S. Beck, *Nature*, 1992, **359**, 710.
2 J. Y. Ying, C. P. Mehnert and M. S. Wong, *Angew. Chem., Int. Ed.*, 1999, **38**, 57; *Mesoporous Molecular Sieves 1998*, ed. L. Bonneviot, F. Béland, C. Danumah, S. Giasson and S. Kaliaguine, Elsevier, Amsterdam, 1998.
3 S. L. Burkett, S. D. Sims and S. Mann, *Chem. Commun.*, 1996, 1367; C. E. Fowler, S. L. Burkett and S. Mann, *Chem. Commun.*, 1997, 1769; K. Moller, T. Bein and R. X. Fischer, *Chem. Mater.*, 1999, **11**, 665; M. H. Lim, C. F. Blanford and A. Stein, *J. Am. Chem. Soc.*, 1997, **119**, 4090.
4 T. Asefa, M. J. MacLachian, N. Coombs and G. A. Ozin, *Nature*, 1999, **402**, 867; C. Yoshina-Ishii, T. Asefa, N. Coombs, M. J. MacLachlan and G. A. Ozin, *Chem. Commun.*, 1999, 2539.
5 S. Inagaki, S. Guan, Y. Fukushima, T. Ohsuna and O. Terasaki, *J. Am. Chem. Soc.*, 1999, **121**, 9611.
6 C. J. Brinker and G. W. Scherer, *Sol-Gel Science: The Physics and Chemistry of Sol-Gel Processing*, Academic Press, New York, 1990.
7 H. Schmidt, *J. Non-Cryst. Solids*, 1985, **73**, 681.
8 Q. Huo, D. I. Margolese, U. Ciesia, P. Feng, T. E. Gier, P. Sieger, R. Leon, P. M. Petroff, F. Schüth and G. D. Stucky, *Nature*, 1994, **368**, 317.
9 T. Tatsumi, K. A. Koyano, Y. Tanaka and S. Nakata, *Chem. Lett.*, 1997, 469.
10 Q. Deng, R. B. Moore and K. A. Mauritz, *Chem. Mater*, 1995, **7**, 2259.

Synthesis and comparative lectin-binding affinity of mannosyl-coated β-cyclodextrin-dendrimer constructs†

Isabelle Baussanne,[a] Juan M. Benito,[b] Carmen Ortiz Mellet,[b] José M. García Fernández,*[c] Ho Law[a] and Jacques Defaye*[a]

[a] *CNRS (UMR 5063) and Université Joseph Fourier-Grenoble 1, Departement de Pharmacochimie Moléculaire-Glucides, BP 138, F-38243 Meylan, France. E-mail: Jacques.Defaye@ujf-grenoble.fr*
[b] *Departamento de Química Orgánica, Facultad de Química, Universidad de Sevilla, Aptdo. 553, E-41071 Sevilla, Spain*
[c] *Instituto de Investigaciones Químicas, CSIC, Américo Vespucio s/n, Isla de la Cartuja, E-41092 Sevilla, Spain. E-mail: jogarcia@cica.es*

Received (in Liverpool, UK) 8th May 2000, Accepted 15th June 2000
Published on the Web 19th July 2000

Targeted drug delivery systems have been built from β-cyclodextrin by monoconjugation with mannosyl-coated dendritic branches following an iterative thiourea-forming convergent strategy; the multivalent adducts showed high Concanavalin A lectin binding ability and intact inclusion capabilities.

Grafting biorecognisable saccharide epitopes onto suitable molecular carriers may provide new vectors for site-specific delivery of therapeutics. Several examples of oligosaccharide-branched cyclodextrins (CDs) have been reported in recent years for this purpose, taking advantage of the known ability of CDs to include a variety of hydrophobic compounds *via* host-guest complexation.[1] The majority of such conjugates are monosubstituted derivatives at a single primary hydroxy group position of the CDs.[2] A few per-(C-6)-substituted branched-CDs have also been synthesised to comply with the need for a multivalent presentation pattern of the saccharide markers.[2a,d,3] However, although lectin-binding capacity is substantially increased when compared with the monovalent counterparts, polysubstitution at the primary face of CDs may seriously impair inclusion and complex stabilisation of potential guests. Our own results indicated approximately a 10-fold decrease in the water solubilisation power of branched β-CDs, measured for the anticancer drug Taxotère®, upon heptafunctionalisation.[2c,d]

As an attempt to combine both high biological receptor binding ability and efficient inclusion capabilities, a series of monosubstituted multivalent β-CD carriers have now been synthesised. For this purpose, we have developed an efficient preparation of dendritic wedges suitable for sequential external carbohydrate coating and covalent attachment to the β-CD core through a convergent iterative methodology that exploits the reactivity of isothiocyanate and amine functionalised mono-

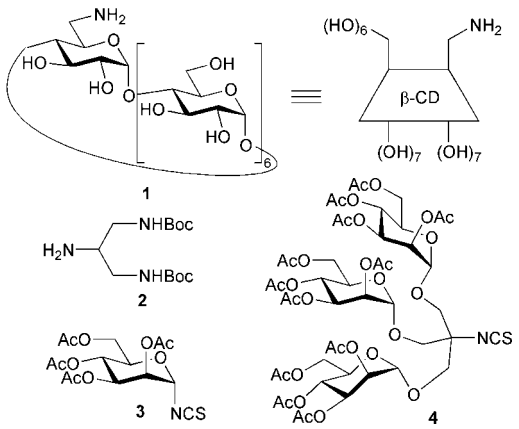

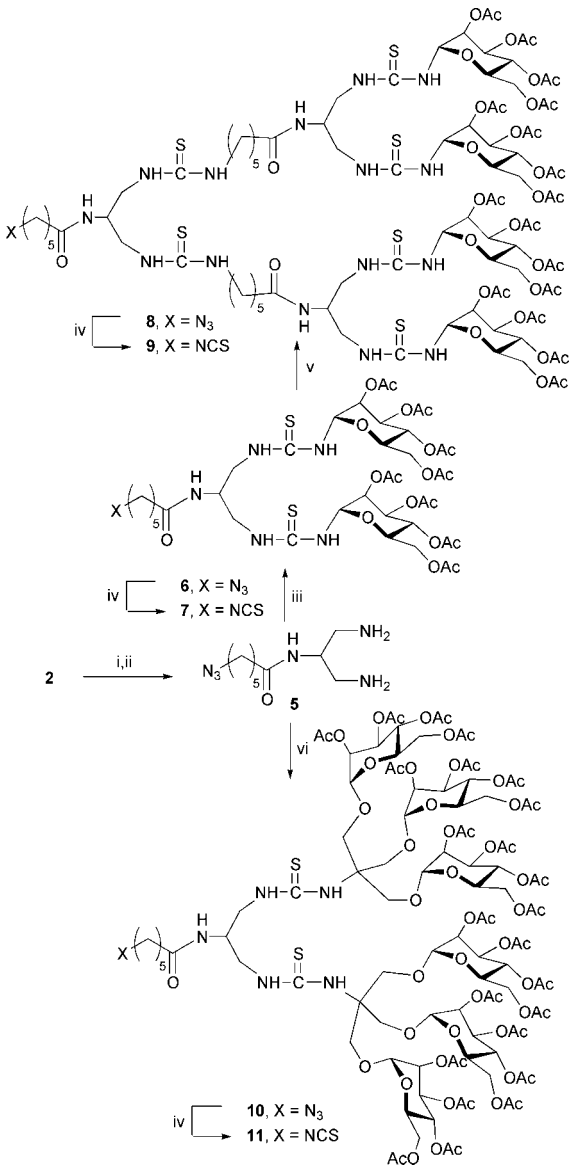

Scheme 1 *Reagents and conditions*: i, 6-azidohexanoyl chloride, 1:1 DMF–collidine, rt, 96%; ii, 1:1 TFA–water, rt, 2 h, 98%; iii, pyridine, 24 h, 87%; iv, PPh_3, CS_2, toluene, rt, 16 h, 90%; v, **7** + **5**, 1:1 water–acetone, pH 8 ($NaHCO_3$), 55%; vi, **4**, 1:1 water–acetone, pH 8 ($NaHCO_3$), 70%.

† Dedicated to Dr R. U. Lemieux, Emeritus Professor, University of Alberta (Edmonton, Canada), on the occasion of his 80th birthday.

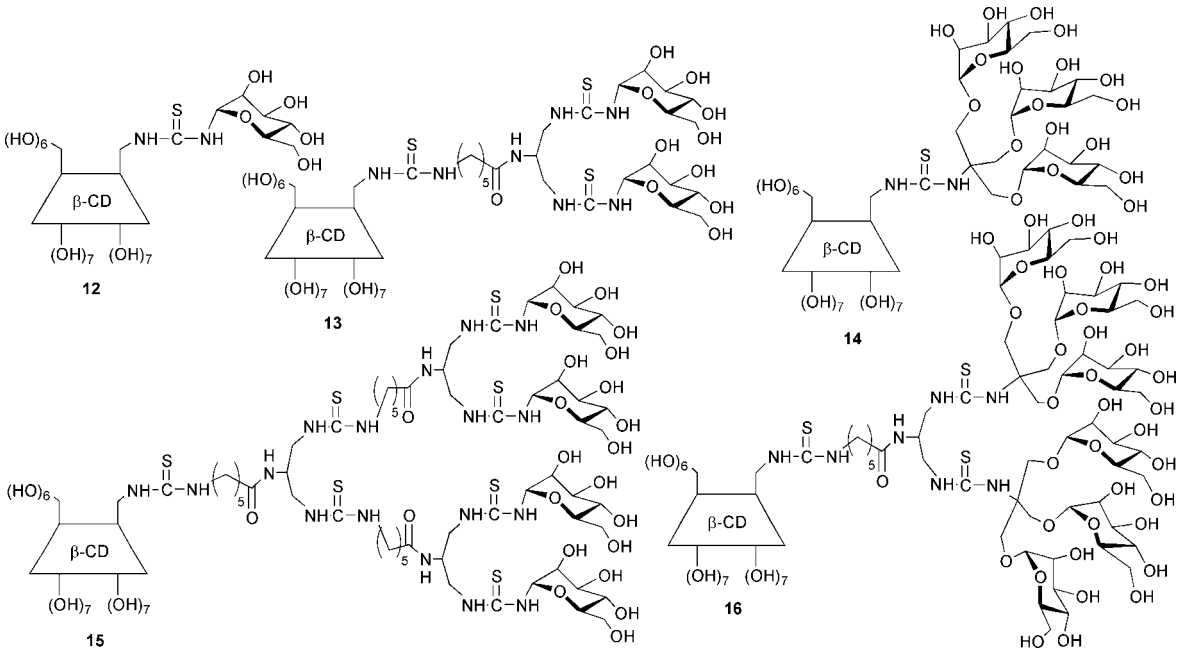

mers.[4] The key templates are 6^{I}-amino-6^{I}-deoxy-β-CD (**1**), for which an improved synthetic route has been recently elaborated,‡[5] the selectively protected 1,2,3-triaminopropane branching element **2**,[6] and the isothiocyanate functionalised α-D-mannopyranosyl derivatives **3**[4] and **4**. The latter was prepared by reaction of the known tris-α-mannopyranoside amine[7] with thiophosgene. Intercalation of a six-carbon spacer has also been considered to ensure the accessibility of the grafted bioactive components to molecular recognition events.

Mono- and trivalent mannosylated thioureido β-CDs **12** and **14** were obtained in high yield by direct coupling of **1** with **3** and **4**, respectively, followed by removal of the *O*-acetyl groups.§ Reaction of **2** with 6-azidohexanoyl chloride and further TFA-catalysed hydrolysis of the Boc N-protecting groups afforded dendron **5**, which was subsequently reacted with **3** and **4** to give the di- and hexavalent ligands **6** and **10** (Scheme 1). Aza-Wittig type isothiocyanation reaction of the terminal azido group using the triphenylphosphine–CS_2 system led to the corresponding bridging armed glycosyl clusters **7** and **11**, which were conjugated with monoamine **1** and deacetylated to yield the mannosyl labelled β-CD carriers **13** and **16**. The potential of the approach was further examined by constructing the second-generation tetravalent homologue **15** *via* nucleophilic addition of diamine **5** to the divalent isothiocyanate **7** (→**8**), isothiocyanation of the resulting adduct (→**9**), conjugation with the β-CD reagent **1** and final deacetylation.¶

Comparative protein-affinity evaluation of the mannosyl-coated thioureido β-CDs **12**–**16** towards horseradish peroxidase-labelled concanavalin A (Con A) was effected by performing the enzyme-linked lectin assay (ELLA) test.[8] The corresponding IC_{50} values for inhibition of Con A-yeast mannan binding[9] reflected the expected amplification of lectin-binding strength for the higher-valent representatives. Nonetheless, preliminary Taxotère® solubilisation experiments in water showed solubility values (*e.g.* 4.5 g L^{-1} in a 50 mM solution of **14**) that were similar to those obtained for monobranched CDs.

This research was supported by the European Comission DG XII under the FAIR programme (contract no. FAIR CT95-0300) and the DGICYT (grant no. PB 97/0747).

Notes and references

‡ A much better yield for the key precursor of **1**, namely the corresponding C-6 monotosyl derivative, was achieved by using the following procedure: To a solution of β-CD (11.35 g, 10 mmol) in water (500 mL), $CuSO_4$ (7.5 g, 30 mmol) in water (750 mL) and NaOH (10 g, 250 mmol) in water (250 mL) were successively added. After 10 min, tosyl chloride (15 g, 79 mmol) in acetonitrile (100 mL) was added dropwise within 1 h. The mixture was stirred for 4.5 h, then neutralised (1 M HCl, 50 mL), the salts were filtered off and the solution was concentrated by freeze-drying to $\frac{2}{3}$ of its original volume. The crystallised solid was washed with acetone (2 × 40 mL), ether (2 × 30 mL) and dried. After two recrystallisations from water, pure monotosyl β-CD (6.33 g, 48%) was obtained.

§ Coupling yields 45–75%. Removal of the acetyl groups was effected by a mixed transterification–saponification process (see ref. 2*d*). In the cases of compounds **12**, **13** and **15** this step was performed at 0 °C to avoid anomerization of the external mannosylthioureido subunits (see ref. 10).

¶ All new compounds gave microanalytical, mass spectral (FAB or MALDI-TOF) and ^{13}C NMR data (125.7 MHz, D_2O) in agreement with the proposed structures.

Selected data for **12**: $[\alpha]_D$ +107.1 (*c* 0.7, H_2O); ^{13}C NMR δ 182.8 (CS), 102.6–101.9 (C-1$^{I–VII}$), 82.8 (C-1′), 46.3 (C-6^{I}). For **13**: $[\alpha]_D$ +105.2 (*c* 1, H_2O); ^{13}C NMR δ 183.3 (CS), 177.3 (CO), 102.7–101.8 (C-1$^{I–VII}$), 83.0 (C-1′). For **14**: $[\alpha]_D$ +74.0 (*c* 1.1, H_2O); ^{13}C NMR δ 182.2 (CS), 102.7–102.0 (C-1$^{I–VII}$), 100.8 (C-1′) 46.8 (C-6^{I}). For **15**: $[\alpha]_D$ +54.6 (*c* 1.4, H_2O); ^{13}C NMR δ 182.5 (CS), 177.0 (CO), 102.1–101.7 (C-1$^{I–VII}$), 82.5 (C-1′). For **16**: $[\alpha]_D$ +32.0 (*c* 1.1, H_2O); ^{13}C NMR δ 182.9 (CS), 177.3 (CO), 102.1–101.9 (C-1$^{I–VII}$), 100.9 (C-1′).

1 S. A. Nepogodiev and J. F. Stoddart, in *Carbohydrate Chemistry*, ed. G.-J. Boons, Blackie Academic & Professional, London, 1998, p. 322; K. A. Connors, *Chem. Rev.*, 1997, **97**, 1325.
2 (*a*) K. Maysuda, T. Inazu, K. Haneda, M. Mizuno, T. Yamanoi, K. Hattori, K. Yamamoto and H. Kumagai, *Bioorg. Med. Chem. Lett.*, 1997, **7**, 2353; (*b*) R. Kassab, C. Felix, H. Parrot-Lopez and R. Bonaly, *Tetrahedron Lett.*, 1997, **38**, 7555; (*c*) J. M. García Fernández, C. Ortiz Mellet, S Maciejewski and J. Defaye, *Chem. Commun.*, 1996, 2741; (*d*) C. Ortiz Mellet, J. M. Benito, J. M. García Fernández, H. Law, K. Chmurski, J. Defaye, M. L. O'Sullivan and H. N. Caro, *Chem. Eur. J.*, 1998, **4**, 2523.
3 J. J. García-López, F. Santoyo-González, A. Vargas-Berenguel and J. J. Giménez-Martínez, *Chem Eur. J.*, 1999, **5**, 1775.
4 J. M. García Fernández and C. Ortiz Mellet, *Adv. Carbohydr. Chem. Biochem.*, 2000, **55**, 35.
5 J. Defaye, S. Crouzy, N. Evrard and H. Law, PCT Int. Appl. WO 99 61,483; *Chem. Abstr.*, 2000, **132**, 24077^{a}.
6 E. Benoist, A. Loussouarn, P. Remaud, J.-C. Chatal and J.-F. Gestin, *Synthesis*, 1998, 1113.
7 P. R. Ashton, E. F. Hounsell, N. Jayaraman, T. M. Nilsen, N. Spencer, J. F. Stoddart and M. Young, *J. Org. Chem.*, 1998, **63**, 3429.
8 M.-C. Shao and C. C. Q. Chin, *Methods Enzymol.*, 1994, **247**, 253.
9 Binding inhibition of horseradish peroxidase-labeled Con A to yeast mannan by mannosylated monosubstituted β-CDs (IC_{50} values): **12**, 800 μM; **13**, 780 μM; **14**, 91 μM; **15**, 110 μM; **16**, 8 μM.
10 J. M. Benito, C. Ortiz Mellet, K. Sadalapure, T. K. Lindhorst, J. Defaye and J. M. García Fernández, *Carbohydr. Res.*, 1999, **320**, 37.

A new layered niobium oxochloride cluster compound with novel framework topology†

Ekaterina V. Anokhina, Cynthia S. Day and Abdessadek Lachgar*

Department of Chemistry, Wake Forest University, Winston-Salem, NC 27109 USA. E-mail: lachgar@wfu.edu

Received (in Irvine, CA, USA) 15th March 2000, Accepted 12th May 2000
Published on the Web 19th July 2000

The asymmetric arrangement of chloride and oxide ligands around the octahedral Nb_6 cluster core and their electrostatic interaction with Ti^{3+} counterions play an important role in the formation of a novel 2D framework with cluster connectivity unprecedented in compounds containing octahedral clusters.

Low-dimensional materials containing transition metals have significant importance due to their remarkable physical properties and a wide range of applications in catalysis, ionic transport, and redox intercalation processes.[1] Thus, extensive research efforts have been spent on the design, preparation and characterization of these materials. Investigation of early transition metal cluster materials led to development of a strategy for controlling the cluster-framework dimensionality by adjusting the number of intercluster bridging ligands.[2]

Recently, we began investigating a new approach to the design and preparation of low-dimensional materials containing octahedral metal clusters. The methodology being explored is the modification of the environment of the metal core to form building blocks with well-defined anisotropic bonding preferences using a combination of ligands that create anisotropic charge distribution. In addition, a combination of counterions with large difference in their charge-to-radius ratios and, thus, different coordination preferences, is used to enhance the effects of anisotropic ligand distribution. Our systematic investigation of niobium oxochlorides containing octahedral Nb_6 clusters recently led to the preparation of the layered material $[Tl_5(Ti_2Cl_9)][(Nb_6Cl_{12}O_4)_3(Ti_3Cl_4)_2]$ which has a unique hexagonal-bronze-type cluster connectivity.[3] Here we describe a novel layered oxochloride $Cs_2Ti_3(Nb_6Cl_{12.5}O_4)_2Cl_2$ **1** in which each octahedral Nb_6 cluster is connected to three adjacent clusters through chloride ligands to form layers with graphite-type topology.[4] The factors leading to its unusual structural properties are proposed.

Compound **1** was initially obtained as black elongated rectangular plates in a reaction designed to prepare the caesium analogue of $[Tl_5(Ti_2Cl_9)][(Nb_6Cl_{12}O_4)_3(Ti_3Cl_4)_2]$ **2**. The crystals were analyzed by energy-dispersive X-ray analysis, and the crystal structure of **1** was determined by single crystal X-ray diffraction.‡ Subsequently, **1** was obtained in high yield in the reaction of stoichiometric amounts of Nb powder, Ti foil, CsCl, Nb_2O_5 and $NbCl_5$. The mixture (handled under argon atmosphere) was placed in a silica tube, sealed under vacuum, heated for 4 d at 750 °C and cooled to 500 °C in 4 d, followed by radiative cooling to room temperature. The product purity was confirmed by X-ray powder diffraction.

The main building block of the two-dimensional structure of **1** (Fig. 1) is an octahedral cluster unit $(Nb_6Cl^i_8O^i_4)Cl^a_6$,[5] in which four oxide ligands selectively occupy 'inner' positions arranged in sets of three ('triad') and one on opposite sides of the Nb_6 octahedron (Fig. 2). The ligand arrangement results in an anisotropic chiral cluster unit with symmetry close to C_2. Octahedral niobium oxochloride clusters with four oxide ligands were also encountered in **2** and in $Ti_2Nb_6Cl_{14}O_4$ **3**,[6] however in contrast to **1**, the O^i ligands in the latter oxochlorides are arranged centrosymmetrically in two sets of two, leading to a different isomer with symmetry close to C_{2h}. A cluster unit in which the oxide ligands are arranged in a 'triad' similar to that in **1**, is found in the previously reported oxochloride $ScNb_6Cl_{13}O_3$ **4** which has three oxide ligands per cluster.[7] The bond distances in the cluster in **1** are similar to those found in compounds **2**–**4** and are consistent with the presence of 14 valence electrons per cluster.[3,6–8] Each cluster shares three of its six Cl^a ligands with three adjacent clusters to form layers with topology similar to that of graphite (Fig. 3). The connectivity formula can be written as $(Nb_6Cl^i_8O^i_4)Cl^{a\text{-}a}_{3/2}Cl^a_3$. Layered frameworks based on octahedral clusters, typically, have pseudo-square topology with connectivity formula $(M_6L^i_n)L^{a\text{-}a}_{4/2}L^a_2$ (M = Zr, Nb, n = 12; M = Mo, Re, n = 8).[9] The graphite-type connectivity found here is especially surprising for cluster units with C_2 symmetry, for which one would expect an even number of bridging ligands. This could be the result of optimizing the electrostatic interactions between the ligands and Ti^{3+} ions. In the presence of highly charged counterions, the oxide and chloride ligands tend to segregate to form aggregates of oxide ions surrounded by chlorides, as illustrated by the structures of typical ternary transition metal oxochlorides such as layered MOCl (M = Ti^{3+}, Fe^{3+}, Yb^{3+})[10] and $VOCl_2$,[11] and the 1D material $NbOCl_3$.[12] In these structures, chloride ions form the surface of the layers or chains, while oxide and metal ions are

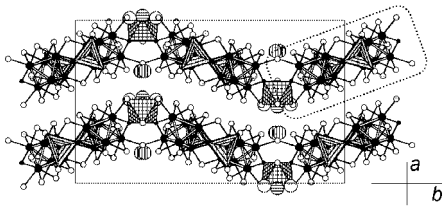

Fig. 1 A view of the crystal structure of **1** in the [001] direction. Large black, small black and small light-gray spheres represent Nb, O, and Cl, respectively. Hatched and light cross-hatched polyhedra represent $[Ti(1)Cl_2O_3]$ trigonal bipyramids and $[Ti(2)Cl_4O_2]$ octahedra, respectively. Caesium atoms are shown as large gray spheres: vertically hatched - Cs(1), horizontally hatched - Cs(2a), not hatched - Cs(2b). The dotted curve outlines the $[Ti(Nb_6Cl_{13}O_4)]$ chain running in the [001] direction.

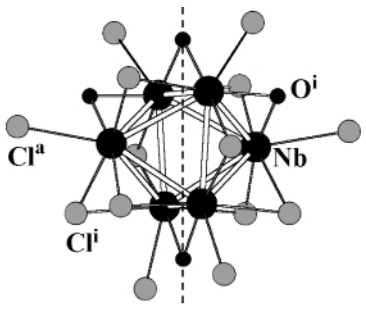

Fig. 2 The cluster unit in **1**. The dashed line shows the pseudo two-fold symmetry axis. Bond distances (Å): Nb–Nb 2.776(1)–3.028(1), Nb–Cl^i 2.430(3)–2.503(2), Nb–Cl^a 2.605(3)–2.636(2), Nb–O^i 1.963(7)–2.061(6).

† Electronic supplementary information (ESI) available: 3D interactive versions of the structure of **1**. See http://www.rsc.org/suppdata/cc/b0/b002147o/

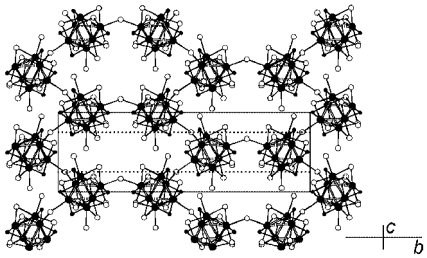

Fig. 3 A view of the graphite-type layered cluster framework in **1**; for labelling, see Fig. 1. Dotted lines represent the *a*-glide plane perpendicular to $\vec{c}$ that relates adjacent layers.

located inside. Similar ion segregation is observed in the cluster compounds **1**–**4**. The ligand arrangement in the cluster unit of **1** favors the formation of $[Ti(Nb_6Cl_{13}O_4)]$ zig-zag chains (Fig. 4) in which the clusters are connected through Ti^{3+} ions (Ti(1)) and Cl^a ligands so that oxide ligands forming the 'triads' are shielded by chlorides. Each Ti(1) connects three clusters and has a distorted trigonal-bipyramidal environment formed by three O^i and two Cl^a ligands (bond distances: $d_{Ti–Cleq}$ = 2.411(3) and 2.423(3), $d_{Ti–Oeq}$ = 1.876(6), $d_{Ti–Oax}$ = 2.035(7) and 2.037(7) Å). Bond-valence sum calculations[13] confirm the oxidation state +3 for Ti(1). The chains connect to each other through an additional titanium (Ti(2)) and Cl^a ligands to form layers, so that the remaining oxide ligands (O(4)) are shielded by chlorides (Fig. 1). This linkage type results in the wave-like geometry of the layers and novel graphite-like cluster framework topology. The titanium Ti(2) coordinates to two O^i and two Cl^a ligands, arranged in a distorted square-planar geometry. Its coordination environment is completed to octahedral or square-pyramidal by additional chloride or oxide ligands[14] (bond distances: $d_{Ti–Cl}$ = 2.36(3)–2.570(9), $d_{Ti–O}$ = 1.84(2)–2.02(1) Å). The anion segregation argument allows us to rationalize the formation of the complex 3D cluster framework and the unusual trigonal-bipyramidal coordination of scandium ions in **4** which is based on clusters with the same 'triad' of O^i ligands as that found in **1**. The clusters and the Sc^{3+} ions form chains similar to the one shown in Fig. 4, where the O(4) atoms are substituted by chlorines. These chains are connected to each other through Cl^a ligands in a tetragonal 'woodpile'-fashion to form a chiral 3D framework.

Adjacent layers in **1** are related by an *a*-glide plane perpendicular to $\vec{c}$ (Figs. 1 and 3) and interact through caesium ions that are distributed over three independent sites (Cs(1), Cs(2a), Cs(2b)) located on the layers' surface on each side of cone-shaped openings generated by six-member cluster rings (Fig. 1). The site Cs(1) is fully occupied and is coordinated by

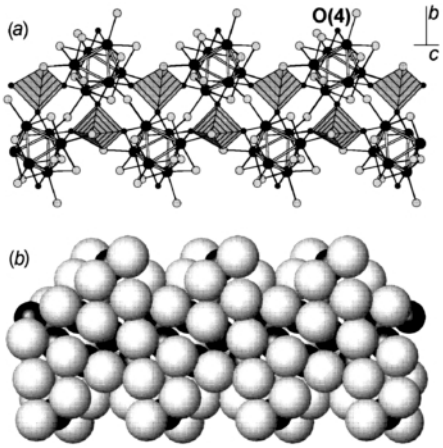

Fig. 4 (*a*) A ball-and-stick view of the $[Ti(Nb_6Cl_{13}O_4)]$ chain in **1**. For labelling, see caption to Fig. 1. (*b*) Space-filling representation of anions in the same fragment (black - O, gray - Cl).

9 chlorides within 4 Å. The Cs(2a) and Cs(2b) sites, separated by 1.29 Å, are located in the channels running between the layers in the $\vec{b}$ direction. These two sites are partially occupied (Cs(2a) 41(2)%, Cs(2b) 18.8(9)%), and are coordinated by 8 and 7 chlorines within 4 Å, respectively. The number of caesium ions per cluster was refined to 0.89(2) which agrees with the oxidation states assigned to the transition metals and the refined occupancies of Cl(14), L(15), and Cl(16) sites.

The structural properties of the new oxochloride $Cs_2Ti_3(Nb_6Cl_{12.5}O_4)_2Cl_2$ demonstrate the effectiveness of using a combination of ligands to prepare low-dimensional cluster materials. The interplay between the effects of anisotropic charge distribution around the cluster core and the trend for the anion segregation in the overall structure is conducive for the formation of diverse structural types with low-dimensional or open-framework character. These effects seem to have a greater influence on the framework dimensionality than the total number of ligands which is the primary structure-determining factor in cluster compounds with one ligand type or statistical ligand distribution.

Notes and references

‡ *Crystal data* for **1**: refined stoichiometry $Cs_{1.79(3)}Ti_3Nb_{12}Cl_{26.51(3)}O_{8.14(2)}$, orthorhombic, space group *Pnma* (No.62), a = 17.546(2), b = 29.323(3), c = 9.1556(7) Å, V = 4710.5(8) Å^3, T = 298 K, Z = 4, M = 2565.97, $\mu(Mo_{K\alpha})$ = 6.17 mm^{-1}, 7411 reflections measured, 6011 unique (R_{int} = 0.051) which were used in all calculations. Least-squares refinements were based on F^2 and converged to R_1 = 0.054, wR_2 = 0.106 ($(I > 2\sigma(I))$, R_1 = 0.101, wR_2 = 0.117 (all data). CCDC 182/1667. See http://www.rsc.org/suppdata/cc/b0/b002147o/ for crystallographic data in .cif format.

1 See for example: *Magnetic Properties of Layered Transition Metal Compounds*, ed. L. J. De Jongh, Kluwer, Dordrecht, 1990; *Physics and Chemistry of Low-Dimensional Inorganic Conductors*, ed. C. Schlenker, J. Dumas and M. Greenblatt, Plenum, New York, 1996; *Progress in Intercalation Research*, ed. W. Müller-Warmuth and R. Schöllhorn, Kluwer, Dordrecht, 1994.

2 C. Perrin, *J. Alloys Compd.*, 1997, **262**, 10; J. R. Long, L. S. McCarty and R. H. Holm, *J. Am. Chem. Soc.*, 1996, **118**, 4603 and references therein.

3 E. V. Anokhina, C. S. Day, M. W. Essig and A. Lachgar, *Angew. Chem., Int. Ed.*, 2000, **39**, 1047.

4 A framework based on $Re_6Se_{11}Cl_3$ clusters which has a graphite-type topology, but different from **1** cluster connectivity is reported in J. R. Long, A. S. Williamson and R. H. Holm, *Angew. Chem., Int. Ed. Engl.*, 1995, **34**, 226.

5 The subscripts 'i' and 'a' refer to the ligands bridging the edges of the metal octahedron ('inner' ligands), and the ligands located in the apical positions ('outer' ligands), respectively.

6 E. V. Anokhina, M. W. Essig and A. Lachgar, *Angew. Chem., Int. Ed.*, 1998, **37**, 522.

7 S. Cordier, C. Perrin and M. Sergent, *Eur. J. Solid State Inorg. Chem.*, 1994, **31**, 1049.

8 C. Perrin, S. Cordier, S. Ihmaïne and M. Sergent, *J. Alloys Compd.*, 1995, **229**, 123 and references therein.

9 R. P. Ziebarth and J. D. Corbett, *Inorg. Chem.*, 1989, **28**, 626; B. Baján and H.-J. Meyer, *Z. Allg. Anorg. Chem.*, 1997, **623**, 791; H. Schäfer, H. G. von Schnering, J. Tillack, F. Kuhnen, H. Wöhrle and H. Baumann, *Z. Allg. Anorg. Chem.*, 1967, **353**, 281; H. G. von Schnering, W. May and K. Peters, *Z. Kristallogr.*, 1993, **208**, 368; A. Perrin, L. Leduc and M. Sergent, *Eur. J. Solid State Inorg. Chem.*, 1991, **28**, 919.

10 E. M. Snegireva, S. I. Troyanov and V. B. Rybakov, *Zh. Neorg. Khim.*, 1990, **35**, 1945; M. D. Lind, *Acta Crystallogr., Sect. B*, 1970, **26**, 1058; G. Brandt and R. Diehl, *Mater. Res. Bull.*, 1974, **9**, 411.

11 H. J. Seifert and J. Uebach, *Z. Allg. Anorg. Chem.*, 1981, **479**, 32.

12 D. E. Sands, A. Zalkin and R. E. Elson, *Acta Crystallogr.*, 1959, **12**, 21.

13 I. D. Brown and D. Altermatt, *Acta Crystallogr., Sect. B*, 1985, **41**, 244.

14 The refinement of occupancies of the ligands not belonging to the clusters showed that coordination of Ti(2) is completed to octahedral by two chloride ligands (Cl(15) and Cl(14)), to square-pyramidal by one chloride ligand (Cl(16)), and to square-pyramidal by one oxide ligand ((O15)), 65(1), 21(1), and 14(2)% of the time, respectively.

ChemComm

Steady state and time-resolved IR spectroscopy of the native and unfolded states of bovine ubiquitin: protein stability and temperature-jump kinetic measurements of protein folding at low pH

Christopher S. Colley,[a] Ian P. Clark,[b] Samuel R. Griffiths-Jones,[a] Michael W. George*[a] and Mark S. Searle*[a]

[a] *Department of Chemistry, University Park Nottingham, UK NG7 2RD E-mail: mark.searle@nottingham.ac.uk and mike.george@nottingham.ac.uk*

[b] *Central Laser Facility, Rutherford Appleton Laboratory, Chilton, Didcot, Oxfordshire, UK OX11 0QX*

Received (in Cambridge, UK) 11th May 2000, Accepted 19th June 2000
Published on the Web 19th July 2000

Infrared spectroscopy has been used to characterise the folded and unfolded states of bovine ubiquitin (a small protein of 76 residues) under acidic conditions (pH ~ 1); fast time-resolved measurements of protein unfolding, initiated by a laser-induced temperature-jump of ~ 8 °C, shows rapid refolding and β-sheet secondary structure formation on a timescale of a few milliseconds.

Our understanding of the mechanism of chemical reactions has benefited greatly from time-resolved kinetic measurements to examine the order of bond breaking events and the relative strengths of covalent interactions.[1] The protein folding reaction, in which a disordered polypeptide chain can assemble into a compact 3D structure, is a highly complex process involving numerous weak co-operative non-covalent interactions.[2] Despite the complexity of the problem, many small proteins (< 100 residues) fold on a timescale of only a few milliseconds.[3] Current models suggest that folding proceeds through a hierarchical process[4] in which the lower limit to the kinetics of folding is determined by local structural events such as the formation of α-helices, β-turns and β-hairpins that nucleate the collapse and folding of the polypeptide chain.[5] Observations on the folding of these structures with submillisecond half-lives have necessitated new methods of detection.[5]

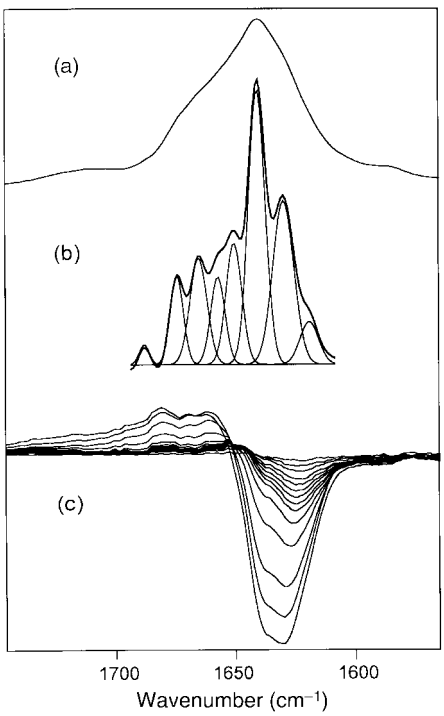

Fig. 1 (a) Conventional and (b) deconvoluted FTIR spectra of bovine ubiquitin at 25 °C pH 1.0 showing 8 principal bands.[18] (c) FTIR difference spectra, showing the change in the absorption envelope with temperature over the range 278 to 363 K. Data were collected using a Nicolet Nexus 670 FTIR spectrometer equipped with MCT detector.

Infrared spectroscopy has emerged as an important technique for studying protein structure and fast folding kinetics.[6,7] The position of the amide stretching vibration (1610–1680 cm^{-1}) has been shown to be strongly correlated with protein secondary structure because of its sensitivity to hydrogen bonding, dipole–dipole interactions and the geometry of the peptide backbone.[8,9] The possibility of detecting by IR both native, as well as transient non-native structures, on the protein folding pathway has already been demonstrated.[10] The application of vibrational spectroscopy to the study of rapid kinetic processes in chemical systems is well documented,[1] and is now being applied to biological molecules.[6,10–12] Here we examine the steady state and time-resolved folding/unfolding of a small protein by IR spectroscopy, and demonstrate rapid formation of protein secondary structure on the timescale of a few milliseconds.

We have used bovine ubiquitin (a small protein of 76 residues, free of disulfide bridges) as a model system). Ubiquitin consists of both α-helix and β-sheet, forming a highly stable, compact structure that has been shown to fold in a two-state process.[13] We have been investigating the mechanism of folding by examining the conformational propensity of protein fragments for evidence of possible nucleation sites for folding of the native structure. In particular, the N-terminal β-hairpin sequence in isolation shows evidence for a small population of native-like structure in water,[14] while hairpin analogues, with mutated β-turn sequences, have demonstrated both native and non-native conformational features.[15] The kinetics of folding of these isolated elements of secondary structure is of current interest in the context of understanding the mechanism of folding of the native protein.

Here we probe the structure of both the native and unfolded states of bovine ubiquitin, and the unfolding transition, at pD 1.0 in D_2O solution by FTIR. NMR spectra of the native protein at pH 1.0 and 7.0 are essentially identical, indicating that there are no significant changes in the structure. However, at low pH, the reduced T_m allows the thermal unfolding transition to be investigated. In Fig. 1, we illustrate conventional (a) and deconvolved (b) steady state FTIR spectra of native folded ubiquitin at 25 °C (after NH → ND exchange). Fitting the deconvolved absorption envelope enables us to identify eight principal bands which have been assigned according to literature precedent,[8–10] and on the basis of features identified in the X-ray structure.[16] The absorption profile changes significantly with temperature as the protein unfolds, resulting in a reduction of the β-sheet band at 1629 cm^{-1}. The appearance of weaker peaks in the range 1660–1680 cm^{-1} has been attributed to disordered structure or turn-type conformations.[8–10] IR difference spectra, showing the change in the absorption envelope with temperature, are shown in Fig. 1c. Monitoring thermal unfolding from the change in integrated intensity of the principal β-sheet band observed at 1629 cm^{-1} at 25 °C, demonstrates a reversible cooperative sigmoidal melting process with a T_m of ~65 °C at pH 1.0. Parallel NMR melting

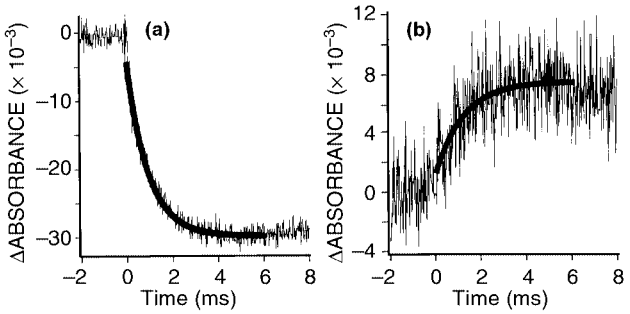

Fig. 2 Time-resolved IR spectra showing the decay/growth of the signals due to disappearance of protein secondary structure at 1635.5 cm^{-1} (a), and appearance of random coil at 1667 cm^{-1} (b) monitored as the protein unfolds following the T-jump. The line of best-fit is shown, assuming a single exponential process.

experiments under identical conditions give a very similar T_m value.

We have investigated the kinetics of folding by IR close to the mid-point of the thermal unfolding transition where the change in absorption is most temperature-sensitive. Using a 10 nanosecond-duration 1.9 μm pulse from a Raman-shifted Nd:YAG laser, we have generated effectively an instantaneous temperature-jump of ~8 °C, initiated at 67 °C. Changes in the IR spectrum, corresponding to transient perturbation of the equilibrium between folded and unfolded states, were used to measure fast folding kinetics outside the normal time-range accessible using rapid mixing techniques.[6] The transient IR spectrum obtained 4 ms after the T-jump is in good agreement with the IR difference spectrum obtained from the steady state spectra taken at 67 and 75 °C. The T-jump was calibrated from the change in absorbance of the D_2O band at 1620 cm^{-1}, providing an internal thermometer. The time-resolved change in the IR absorbance was monitored at ~1640 and ~1670 cm^{-1}, corresponding to the disappearance of bands due to ordered secondary structure, and appearance of the weak band due to random coil structure, respectively (Fig. 2). Subtraction of the solvent absorption, collected in an identical T-jump experiment in D_2O alone, reveals an exponential decay/growth curve at these wavelengths,which we are readily able to fit to a single rate process consistent with a two-state folding model (Fig. 2a, b). Despite the much lower signal-to-noise ratio at 1670 cm^{-1}, both kinetic traces yield the same observed rate constant $k_{obs} \approx 1000\ s^{-1}$. Assuming that k_{obs} is the sum of the folding and unfolding rate constants, $k_{obs} = k_F + k_U$,[5,13] and that the equilibrium constant at a given temperature is given by $K_{eq} = k_F/k_U$, then we are able to estimate a rate of folding at 75 °C (at the T_{max} of the T-jump) of ~400 s^{-1}.

We have demonstrated from equilibrium FTIR measurements of ubiquitin that the various elements of secondary structure result in a unique fingerprint. We have demonstrated that the relaxation kinetics for folding/unfolding of β-sheet structure provides a convenient handle for monitoring fast dynamic processes. Comparison with results from fluorescence and amide NH exchange experiments identified some common features.[13,17] Both methods have identified a major folding phase with a half-life of 5–10 ms at 25 °C. However, fluorescence-detected kinetics also show very rapid hydrophobic collapse (< 2 ms) within the dead-time of the stopped-flow experiment.[13] This early collapsed structure does not protect amide NHs against exchange, the latter occurring on a longer timescale (~10 ms). In the folding/unfolding studies presented in this work, we have monitored by IR spectroscopy the rapid formation of protein secondary structure with a half-life of 2–3 ms ($1/k_F$) at 75 °C. Despite the difference in folding temperature between this and earlier studies,[13,17] the rate of formation of secondary structure is in broad agreement, as far as comparisons are possible between these complementary techniques. While previous fluorescence measurements have detected very early burial of hydrophobic residues, we show that time-resolved IR, as with amide NH exchange, monitors the formation of hydrogen bonded secondary structure during a slower folding phase on the timescale of a few milliseconds.

We are grateful for access to the EPSRC-funded central Laser Facilities at the Rutherford Appleton Laboratory in Oxfordshire, and thank M. Towrie, P. Matousek and A. W. Parker for helpful discussions. We acknowledge the financial support of the EPSRC for studentships to CSC and SRG-J, and to Roche Discovery, Welwyn, UK for a CASE award to SRG-J.

Notes and references

1 See *J. Phys. Chem. A*, 2000, **18**, 104, and references therein.
2 H. Bryngelson, S. G. Sligar and P. G. Wolynes, *Proc. Natl. Acad. Sci. USA*, 1987, **84**, 7524; H. Frauenfelder, S. G. Sligar and P. G. Wolynes, *Science*, 1991, **254**, 1598.
3 P. Jennings and P. E. Wright, *Science*, 262, 892; L. L. P. Hosszu, C. J. Craven, M. J. Parker, M. Lorch, J. Spencer, A. R. Clarke and J. P. Waltho, *Nat. Struct. Biol.*, 1997, **4**, 801.
4 P. S. Kim and R. L. Baldwin, *Ann. Rev. Biochem.*, 1990, **59**, 631; R. L. Baldwin and G. D. Rose, *Trends Biochem. Sci.*, 1999, **24**, 26; R. L. Baldwin and G. D. Rose, *Trends Biochem. Sci.*, 1999, **24**, 77.
5 M. Gruebele, J. Sabelko, R. Ballew and J. Ervin, *Acc. Chem. Res.*, 1998, **31**, 699; W. Eaton, V. Munoz, P. A. Thompson, E. R. Henry and J. Hofrichter, *Acc. Chem. Res.*, 1998, **31**, 745.
6 R. B. Dyer, F. Gai, W. H. Woodruff, R. Gilmanshin and R. H. Callender, *Acc. Chem. Res.*, 1998, **31**, 707; R. H. Callender, R. B. Dyer, R. Gilmanshin, K. S. Fang and W. H. Woodruff, *Ann. Rev. Phys. Chem.*, 1998, **49**, 173; S. Williams, T. P. Causgrove, R. Gilmanshin, K. S. Fang, R. H. Callender, W. H. Woodruff and R. B. Dyer, *Biochemistry*, 1996, **35**, 691.
7 S. Krimm and J. Bandekar, *Adv. Protein Chem.*, 1986, **38**, 181; J. L. R. Arrondo, A. Muga, J. Castresana and F. M. Goni, *Prog. Biophys. Mol. Biol.*, 1993, **59**, 23; D. M. Byler and H. Suoi, *Biopolymers*, 1986, **25**, 469; J. L. R. Arrondo, F. J. Blanco, L. Serrano and F. M. Goni, *FEBS Lett.*, 1996, **384**, 35; C. S. Colley, S. R. Griffiths-Jones, M. W. George and M. S. Searle, *Chem. Commun.*, 2000, **7**, 593.
8 W. K. Surewicz, H. M. Mantsch and D. Chapman, *Biochemistry*, 1993, **32**, 389.
9 R. Chehin, I. Iloro, M. J. Marcos, E. Villar, V. L. Shnyrov and J. L. R. Arrondo, *Biochemistry*, 1999, **38**, 1525.
10 A. Troullier, D. Reinstadler, Y. Dupont, D. Naumann and V. Forge, *Nat. Struct. Biol.*, 2000, **7**, 78.
11 J. Wang and M. A. El-Sayed, *Biophys. J.*, 1999, **76**, 27.
12 I. K. Ledeev, A. S. Karnoup, M. C. Sparrow and S. A. Asher, *J. Am. Chem. Soc.*, 1999, **121**, 8074; I. K. Ledeev, A. S. Karnoup, M. C. Sparrow and S. A. Asher, *J. Am. Chem. Soc.*, 1999, **121**, 4076; Z. Chi, X. G. Chen, J. S. Hottz and S. A. Asher, *Biochemistry*, 1998, **37**, 2854; Z. Chi and S. A. Asher, *Biochemistry*, 1998, **37**, 2865.
13 S. Khorasanizadeh, I. D. Peters, T. R. Butt and H. Roder, *Biochemistry*, 1993, **32**, 7054.
14 R. Zerella, P. A. Evans, J. M. C. Ionides, L. C. Packman, B. W. Trotter, J. P. Mackay and D. H. Williams, *Protein Sci.*, 1998, **8**, 1320.
15 M. S. Searle, D. H. Williams and L. C. Packman, *Nat. Struct. Biol.*, 1995, **2**, 999; M. Jourdan, S. R. Griffiths-Jones and M. S. Searle, *Eur. J. Biochem.*, 2000, in the press.
16 S. Vijay-kumar, C. E. Bugg and W. J. Cook, *J. Mol. Biol.*, 1987, **194**, 531.
17 M. S. Briggs and H. Roder, *Proc. Natl. Acad. Sci. USA*, 1992, **89**, 2017.
18 J. K. Kauppinen, D. J. Moffat, H. H. Mantsch and D. G. Cameron, *App. Spectr.*, 1981, **35**, 271.

A highly stable copper(I)-olefin coordination polymer with strong red fluorescent emission

Jing Zhang, Ren-Gen Xiong,* Jing-Lin Zuo and Xiao-Zeng You*

Coordination Chemistry Institute, The State Key Laboratory of Coordination Chemistry, Nanjing University, 210093, Nanjing, P.R. China. E-mail: xyz@netra.nju.edu.cn

Received (in Cambridge, UK) 18th May 2000, Accepted 27th June 2000
Published on the Web 20th July 2000

Under solvothermal conditions, the reaction of 4-pyridylacrilic acid (4-hpya) and 2,2′-bipyridine (bpy) with $Cu(MeCN)_4BF_4$ gives rise to an unprecedented stable copper(I)-olefin coordination polymer $\{[(bpy)(4\text{-hpya})Cu(I)](BF_4)\}_n$ 1 which displays strong red fluorescent emission in the solid state.

Since the pioneering work of Thompson *et al.*[1] demonstrated the first stable copper(I)–olefin complexes, in which a tridentate ligand, hydrotris(3,5-dimethylpyrazol-1-yl)borate [HB(3,5-$Me_2pz)_3$], was used to stabilize the complexes, many copper(I)–olefin complexes have been reported in which bidentate ligands such as 2,2′-bipyridine(bpy) and its derivatives, di-2-pyridylamine,[2] 2,2-bipyridine[3] and 1,10-phenanthroline,[3] were used. An excellent example was shown by Doyle *et al.*[4] in which a β-diketonate was introduced to chelate the copper(I)–olefin complex. Recently, a tridentate ligand, *N*-(3-indolylethyl)-*N*,*N*′-bis(6-methyl-2-pyridylmethyl)amine (Me_2iep) and a macrocyclic ligand, *N*-[2-(1-naphthyl)ethyl]-1-aza-4,8-dithiacyclodecane, have been used to stablize copper(I)-η^2-indole[5] and copper(I)–η^2-naphthyl[5] complexes. Moreover, Hoffmann and coworkers have successfully prepared a remarkable stable (up to 108 °C) copper(I)–ethylene complex in which iminophosphanamide derivatives were used as chelating stabilizers to fix the ethylene.[6] However, it should be noted that all the above-mentioned complexes are air-sensitive and molecular in nature. More recently, Schultz and co-workers have utilized crystal engineering strategies to synthesize a unique dense monofumarate dicopper(I) metal–organic layered framework containing η^2-copper(I)–olefinic bonds.[7] They suggested that the high air stability of the copper(I)–olefin layered framework (up to 300 °C) may be due to the high concentration of bonding and exclusion of water in the lattice.

In this work we have combined the above-mentioned synthetic strategies and designed *trans*-4-pyridylacrilic acid (4-hpya) as a building block to construct a novel one-dimensional copper(I) polymer with η^2-olefin binding mode, *catena*-(2,2′-bipyridine)(*trans*-4-pyridylacrilic acid)copper(I) tetrafluoroborate $\{[bpy)(4\text{-hpya})Cu(I)](BF_4)\}_n$ **1** which, to the best of our knowledge, represents the first example of a stable copper(I)–olefin complex capable of co-existing with an organic acid (Scheme 1).

Golden yellow crystals of **1** were obtained by treating 4-hpya, bpy and $Cu(MeCN)_4(BF_4)$ under solvothermal reaction conditions.† The IR spectrum of complex **1** shows a very strong peak at 1072 cm^{-1}, indicating a typical uncoordinated BF_4^- anion. A broad peak at *ca.* 3224–3392 cm^{-1} and two peaks at 1712s and 1600m cm^{-1} suggest that the carboxylic acid group of 4-hpya in **1** is protonated.[8]

Complex **1** possesses high thermal stability, as evidenced from thermogravimetric analysis. The TGA curve of polycrystalline complex **1** showed that no weight loss occurred below *ca.* 229 °C.

The X-ray crystal analysis of complex **1**‡ revealed that Cu(I) ion in **1** is coordinated in a distorted tetrahedral geometry, which is defined by three nitrogen atoms (two from bpy and one from 4-hpya) and the C=C moiety of the olefin of 4-hpya [Fig. 1(a)]. The ligand 4-hpya acts as a neutral bidentate spacer to link two Cu(I) ions by an N atom and an olefin moiety to give rise to a 1D coordination polymer, as depicted in Fig. 1(b). The C=C bond distance [1.361(6) Å] of the coordinated olefin, is comparable to those found in $[Cu(bpy)(C_2H_4)]ClO_4$ [1.360(13)–1.346(18) Å],[3] $[Cu(phen)(C_2H_4)]\cdot ClO_4$ [1.361(22) Å],[3] $[Cu_2\{HB(3,5\text{-}Me_2pz)_3\}(C_2H_4)Cl]$ [1.347(5) Å], $[Cu(C_2H_4)$(dipyridylamine)] [1.359(7) Å],[2] $[Cu_2(O_2CCH{=}CHCO_2)]$ [1.371(14) Å][7] and $[Bu^t_2P(NSiMe_3)_2\text{-}\kappa^2N]Cu(\eta^2\text{-}C_2H_4)$ [1.362(6) Å].[6] However, it is slightly longer than those found in $[Cu\{HB(3,5\text{-}Me_2pz)_3\}(C_2H_4)]$ [1.329(9) Å][1] and $[Cu_2(cot)(hfacac)_2]$ [1.31(1)–1.33(1) Å] (cot = cycloocatatetraene, hfacac = hexafluoroacetylacetonate).[4]

Interestingly, the coordinated olefinic bond in **1** [1.361(6) Å] is longer than free ethylene [1.337(2) Å], suggesting that the coordination to copper(I) could potentially activate the olefinic bond which may be of use in catalysis.[6] The Cu–N and Cu–O bond lengths of complex **1** are normal and lie within the distances expected for Cu(I) complexes. Moreover, the Cu–C bond distances [2.058(4)–2.068(4) Å] in **1** are comparable to those found in other reported copper(I) organometallic compounds.

It is notable that in complex **1** the H atom of carboxylic acid group of 4-hpya is hydrogen-bonded to one of the fluorine atoms of BF_4^-, as shown in Fig. 1(c), while the other three fluorine atoms of BF_4^- are also weakly hydrogen-bonded to the H atoms of the pyridine ring (3.323–3.341 Å).[9] Similarly, the carbonyl oxygen is hydrogen-bonded to H atoms of pyridine ring (3.341 Å). Moreover, there are the stabilizing π–π interactions (*ca.* 3.71 Å) of adjacent strands, clearly suggesting that π–π stacking of neighboring strands plays an important role in stabilizing the copper(I)–olefin complex. Thus, overall hydrogen bonding and π–π stacking make **1** a stable 3D coordination polymer. The secondary interactions may explain why 4-hpya exists in its protonated form in complex **1**. As far as we are aware, **1** is the first example of 1D Cu(I)–olefin coordination polymer containing a protonated organic acid ligand, which is stabilized hydrogen-bonding and π–π stacking, similar to weak hydrogen bonds of the type $C\text{–}H_{aromatic}\cdots F\text{–}C$

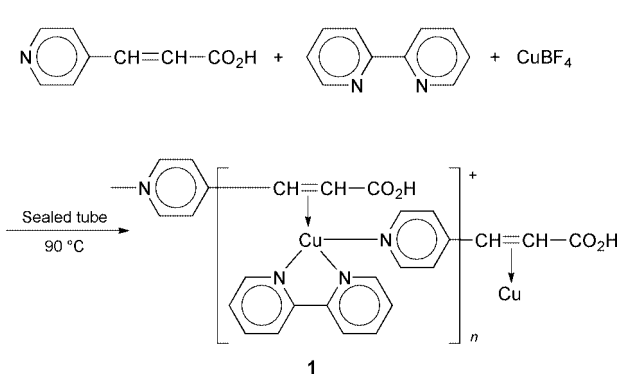

1

Scheme 1

DOI: 10.1039/b004001k

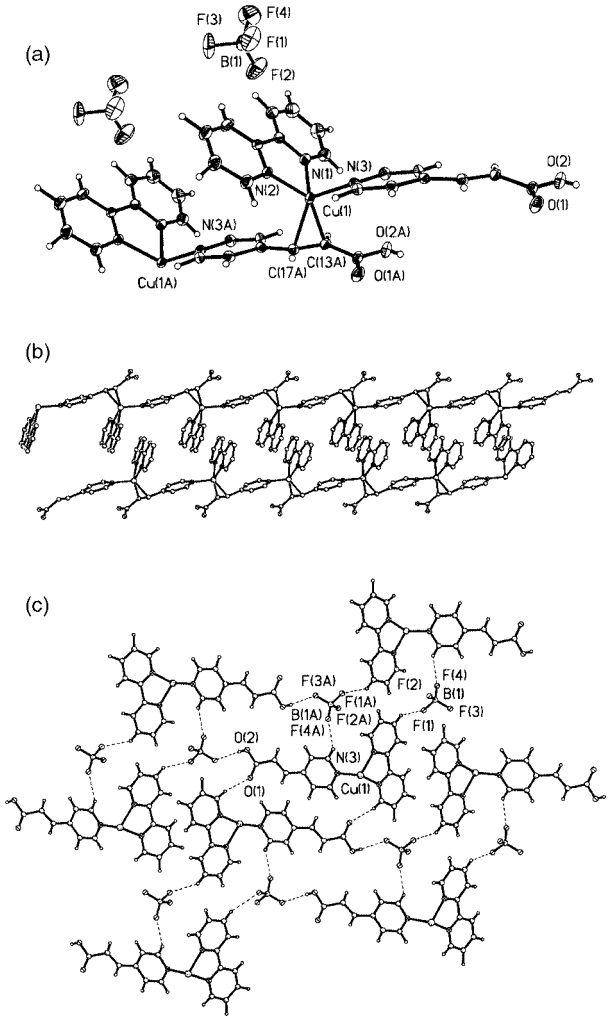

Fig. 1 (a) An ORTEP diagram of the asymmetric unit of **1** (30% ellipsoid probability). Selected bond lengths (Å) and angles (°): Cu(1)–N(1) 2.097(4), Cu(1)–N(2) 1.998(4), Cu(1)–N(3) 2.041(3), Cu(1)–C(17A) 2.068(4), Cu(1)–C(13A) 2.058(4), C(13)–C(17) 1.361(6); N(1)–Cu(1)–N(2) 80.7(14), N(3)–Cu(1)–N(1) 104.78(14), C(13)–Cu(1)–C(17) 138.52(17), N(3)–Cu(1)–C(13) 102.36(15), N(2)–Cu(1)–C(13) 142.34(16). (b) An extended 1D chain representation of **1** showing π–π stacking between adjacent strands. (c) A simplified hydrogen-bonding network representation of **1**.

in organic crystalline solids capable of stabilizing the secondary structure of biomolecules such as DNA.[9,10] Attempts to synthesize neutral $\{[bpy)(4\text{-pya})Cu(I)]\}_n$, were unsuccessful.

The diffuse-reflectance UV–VIS spectrum of **1** shows only a low-energy band at *ca.* 429 nm, which can be assigned to the metal-to-ligand charge transfer (MLCT) band.[11] The strong red emission spectrum of **1** in the solid state at room temperature is shown in Fig. 2, with a maximum at *ca.* 647 nm (λ_{exc} = 250 nm). A clearly bathochromic shift occurs in **1** relative to $[Cu_4I_4(py)]$ (λ_{emax} = 580 nm)[11] and [Cu(3,4-bpyBr] (λ_{emax} = 580 nm),[11] which is probably due to π–back-donation from the filled metal D_π orbital to the vacant antibonding π* orbital of the coordinated olefin.[1b]

In conclusion, the rational design of building blocks and the flexible combination of copper(I) in the supramolecular system provide a robust strategy for the construction of coordination polymers supported by metal–olefin bonds.

This work was supported by The Major State Basic Research Development Program (Grant No. G2000077500) and the National Natural Science Foundation of China.

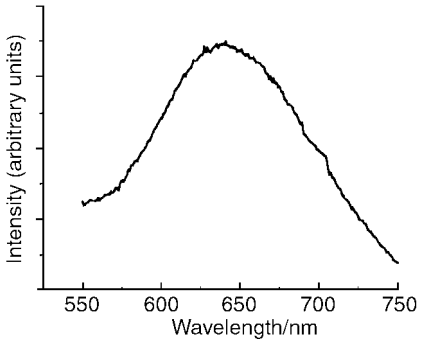

Fig. 2 Fluorescent emission spectrum of **1** in the solid state.

Notes and references

† *Compound* **1**: 1 mmol of $Cu(MeCN)_4BF_4$, 1 mmol of 2,2′-bpy and 1 mmol of 4-hpya were placed in a thick Pyrex tube (*ca.* 20 cm long). After addition of 0.1 ml of water and 2.5 ml of *n*-butanol, the tube was frozen with liquid N_2, evacuated under vaccum and sealed with a torch. The tube was then heated at 90 °C for two days to give pure golden rod crystals in 65% yield based on 4-hpya (Found: C, 47.24; H, 3.46; N, 9.65; Calc.: C, 47.44; H, 3.32; N, 9.22%). IR (KBr, cm^{-1}): 3392m, 3224m, 1712vs, 1600s, 1565w, 1441m, 1375m, 1281w, 1168s, 1072vs, 998msh, 830w, 762s, 735w and 595w.

‡ *Crystal data* for **1**: $C_{18}H_{15}BCuF_4N_3O_2$, M_r = 455.68, triclinic, space group, $P\bar{1}$, a = 7.425(2), b = 10.493(3), c = 12.177(3) Å, α = 108.12(3), β = 91.82(3), γ = 94.31(3)°, V = 905.0(4) $Å^3$, Z = 2, T = 293(2) K, D_c = 1.672 g cm^{-3}. Mo-Kα radiation (λ = 0.71073 Å), μ = 1.267 mm^{-1}, R_1 = 0.0441, wR_2 = 0.1179 for 2351 observed reflections from 3174 independent reflections, GOF = 0.976. CCDC 182/1706. See http://www.rsc.org/suppdata/cc/b0/b004001k/ for crystallographic files in .cif format.

1 (*a*) J. S. Thompson, R. L. Harlow and J. F. Whitney, *J. Am. Chem. Soc.*, 1983, **105**, 3522; (*b*) J. S. Thompson and J. F. Whitney, *J. Am. Chem. Soc.*, 1983, **105**, 5488.

2 J. S. Thompson and J. F. Whitney, *Inorg. Chem.*, 1984, **23**, 2813; J. S. Thompson and R. M. Swiatek, *Inorg. Chem.*, 1985, **24**, 110.

3 H. Masuda, N. Yamamoto, T. Taga, K. Machida, S. Kitagawa and M. Munakata, *J. Organomet. Chem.*, 1987, **322**, 121; M. Munakata, S. Kitagawa, S. Kosomo and A. N. Asahara, *Inorg. Chem.*, 1986, **25**, 2622.

4 G. Doyle, K. A. Eriksen and D. Van Engen, *Organometallics*, 1985, **4**, 830.

5 W. S. Striejewske and R. R. Conry, *Chem. Commun.*, 1998, 555; Y. Shimazaki, H. Yokoyama and O. Yamauki, *Angew. Chem., Int. Ed.*, 1999, **38**, 2401.

6 B. F. Straub, F. Eisenträger and P. Hofmann, *Chem. Commun.*, 1999, 2507.

7 D. M. Young, U. Geiser, A. J. Schultz and H. Wang, *J. Am. Chem. Soc.*, 1998, **120**, 1331.

8 T. M. Reineke, M. Edaoudi, M. Fehr, D. Kelley and O. M. Yaghi, *J. Am. Chem. Soc.*, 1999, **121**, 165.

9 V. R. Thalladi, H.-H. Weiss, D. Bläser, R. Boese, A. Nangia and G. R. Desiraju, *J. Am. Chem. Soc.*, 1998, **120**, 8702; T. A. Evans and K. R. Seddon, *Chem. Commun.*, 1997, 2024; M. L. Renak, G. P. Bartholomew, S. Wang, P. J. Ricatto, R. J. Lachicotte and G. C. Bazan, *J. Am. Chem. Soc.*, 1999, **121**, 7787.

10 N. Yoshida, H. Oshio and T. Ito, *Chem. Commun.*, 1998, 63; M. Lämsä, J. Huuskonen, K. Rissanen and J. Pursiainen, *Chem. Eur. J.*, 1998, **4**, 84; D. Ranganathan, V. Haridas, R. Gilardi and I. L. Karle, *J. Am. Chem. Soc.*, 1998, **120**, 10 793.

11 M. Hernary, J. L. Wootton, S. I. Khan and J. I. Zink, *Inorg. Chem.*, 1997, **36**, 796; C. E. A. Palmer and D. R. McMillin, *Inorg. Chem.*, 1987, **26**, 3837; M. T. Miller, P. K. Gantzel and T. B. Karpishin, *J. Am. Chem. Soc.*, 1999, **121**, 4292; K. R. Kyle, C. W. Ryu, J. A. Dibenedetto and P. C. Fordo, *J. Am. Chem. Soc.*, 1991, **113**, 2954; H. K. Fun, S. S. S. Raj, R. G. Xiong, J. L. Zuo, Z. Yu, X. L. Zhu and X. Z. You, *J. Chem. Soc., Dalton Trans.*, 1999, 1711; J. Rall, F. Stang, K. Hübler and W. Kaim, *Angew. Chem., Int. Ed.*, 1998, **37**, 2681; D. Li, H. K. Yip, C. M. Che, Z. Y. Zhou, T. C. W. Mak and S. T. Liu, *J. Chem. Soc., Dalton Trans.*, 1992, 2445.

Continuous, selective hydroformylation in supercritical carbon dioxide using an immobilised homogeneous catalyst

Nicola J. Meehan,[a] Albertus J. Sandee,[b] Joost N. H. Reek,[b] Paul C. J. Kamer,[b] Piet W. N. M. van Leeuwen*[b] and Martyn Poliakoff*[a]

[a] *School of Chemistry, University of Nottingham, Nottingham, UK NG7 2RD. E-mail: Martyn.Poliakoff@nottingham.ac.uk*

[b] *Institute of Molecular Chemistry, University of Amsterdam, Nieuwe Achtergracht 166, 1018 WV Amsterdam, The Netherlands. E-mail: pwnm@anorg.chem.uva.nl*

Received (in Liverpool, UK) 28th March 2000, Accepted 29th June 2000
Published on the Web 19th July 2000

A continuous process for the selective hydroformylation of higher olefins in supercritical carbon dioxide ($scCO_2$) is presented; the catalyst shows high selectivity and activity over several hours and no decrease in performance was observed over several days.

Hydroformylation is one of the mildest and most efficient methods of producing aldehydes and it is therefore widely applied in the petrochemical industry. The cleanest, industrially important hydroformylation process is the aqueous biphasic process, developed by Ruhrchemie/Rhône-Poulenc, affording a straightforward separation of the organic products from the catalyst.[1] The applicability of this system, however, is strictly limited to substrates which are slightly water soluble, such as propene and but-1-ene. In the industrial hydroformylation of higher olefins, the catalyst is separated by either extraction, catalyst destruction or distillation. One of the major challenges in this field is the development of a continuous hydroformylation process combining a high catalytic activity and selectivity with facile product separation, in which catalyst leaching does not occur.[2] To date, no such system has been reported; often at higher CO pressures the ligand on the metal is easily exchanged for CO molecules resulting in rhodium leaching.[3] Recently Van Leeuwen and coworkers reported a promising approach based on rhodium–diphosphine hydroformylation catalysts with a large P–Rh–P bite angle in a multiphase batch process.[4,5]

The use of $scCO_2$ is becoming increasingly important as a reaction medium in metal catalysed reactions.[6–8] The absence of a gas–liquid phase boundary and the ability of $scCO_2$ to support high concentrations of dissolved gases combined with facile product and catalyst separation makes $scCO_2$ a competitive alternative to conventional solvents. However, homogeneous catalysts often require modification in order to increase their solubility in $scCO_2$,[9–12] although unmodified[13] and even insoluble catalysts[14] have demonstrated significant activity in $scCO_2$ systems. The use of an immobilised homogeneous catalyst overcomes both solubility and catalyst recovery problems. At Nottingham, continuous processing in $scCO_2$ has been successfully applied to a wide range of hydrogenations,[15,16] Friedel–Crafts alkylations[17] and etherification reactions[18] using heterogeneous catalysts supported on polysiloxane (Deloxan®, Degussa AG). Here, we show how this technique is effectively applied in the hydroformylation reaction using an immobilised rhodium–diphosphine catalyst containing a large P–Rh–P bite angle.

The catalyst used is the rhodium complex of *N*-(3-trimethoxysilyl-*n*-propyl)-4,5-bis(diphenylphosphino)phenoxazine **A**, immobilised on silica (particle size 200–500 μm).†

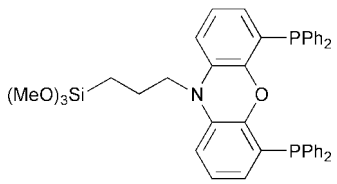

A

Typically, 1 g of ligand-modified silica was reacted with 4 mg of $Rh(acac)(CO)_2$ and then loaded into a 5 mL supercritical flow reactor.‡

The catalyst performed well in the hydroformylation of oct-1-ene with selective production of linear nonanal. The average linear to branched aldehyde ratio (l:b) was 40:1. Oct-1-ene conversions of up to 14% were obtained (Table 1, entries 5 and 7) and only a few percent of octene isomers and a trace amount (*ca.* 1%) of alcohol were observed as byproducts.

Table 1 Results from the hydroformylation of oct-1-ene, values shown are average numbers over a period of 3–6 h[a]

Entry	TOF[b]	Linear aldehyde[c] (%)	Branched aldehyde[c] (%)	Alkene isomers[c] (%)	Linear alcohol[c] (%)	Linear to branched ratio	Oct-1-ene conversion (%)
1[d]	39	96.1	2.4	1.5	0	40	3.6
2	87	92.9	3.0	3.8	0.3	32	9.4
3[e]	112	94.4	2.4	2.5	0.7	40	10.1
4[f]	117	92.6	3.8	2.5	1.0	24	10.3
5[g]	160	93.5	2.8	2.9	0.8	33	14.3
6[h]	44	90.7	4.4	3.7	1.3	21	4.1
7[i]	93	96.0	1.9	1.1	0.9	50	14.3
8[j]	96	91.3	4.1	4.3	0.3	23	4.6

[a] Ligand:Rh ratio is 10:1 and the catalysis was performed at 80 °C, 120 bar CO_2 at 0.65 L min^{-1} flow rate (at 20 °C, 1 atm), 50 bar overpressure syngas and an oct-1-ene flow rate of 0.05 mL min^{-1} (substrate:syngas = 1:10) unless otherwise stated. [b] Average turnover frequencies were calculated as mol aldehyde (mol catalyst)$^{-1}$ h^{-1}. [c] Determined by means of GC analysis using decane as an internal standard. [d] Reaction temperature is 70 °C. [e] Syngas overpressure is 25 bar (substrate:syngas = 1:5). [f] 0.3 L min^{-1} CO_2 flow rate (at 20 °C, 1 atm). [g] Reaction temperature is 90 °C. [h] 180 bar CO_2. [i] Oct-1-ene flow rate of 0.03 mL min^{-1}. [j] Oct-1-ene flow rate of 0.1 mL min^{-1}.

DOI: 10.1039/b002526g

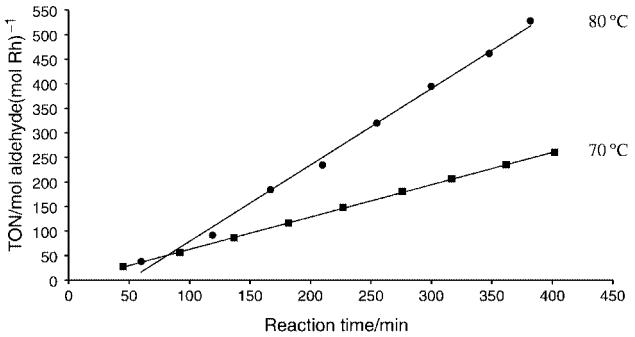

Fig. 1 Turnover number (TON) for the hydroformylation of oct-1-ene in $scCO_2$ at 70 and 80 °C.

The rate of hydroformylation is moderate (39 h^{-1}) at 70 °C with an oct-1-ene flow rate of 0.05 mL min^{-1} (Table 1, entry 1). The rate increased to 87 h^{-1} with the catalyst bed at 80 °C (Table 1, entry 2) and improved further to 112 h^{-1} on decreasing the syngas pressure from 50 to 25 bar (Table 1, entry 3). This improvement in rate is consistent with the negative order in CO pressure that is commonly observed in hydroformylation reactions.[19] A TOF of 117 h^{-1} was observed on increasing the residence time of the substrate in the reactor by decreasing the CO_2 flow rate (Table 1, entry 4). An alternative method of increasing the residence time is to increase the CO_2 pressure, however this resulted in a decrease in TOF (Table 1, entry 6). This may be explained as a higher pressure results in a higher density of CO_2 which will alter the transport properties in the reactor. The highest TOF (160 h^{-1}) was observed at 90 °C (Table 1, entry 5). Varying the oct-1-ene flow rate was found to have an effect on the l:b ratio but not on the TOF (Table 1, entries 2, 7 and 8). As the CO concentration in $scCO_2$ is relatively high, it is remarkable that the hydroformylation rate is over three times faster than the batch reaction in toluene (TOF = 35 h^{-1}) and only half the rate of the *homogeneous* analogue (TOF = 283 h^{-1}) under comparable reaction conditions (80 °C, 50 bar syngas).[5] The high rate in $scCO_2$ is probably caused by enhanced mass-transport properties and the lower viscosity of the solvent medium.[20]

It was also found that the expansion system in our apparatus facilitated the separation of the aldehyde product from the residual oct-1-ene. In our preliminary experiments, we were able to remove *ca.* 90% of oct-1-ene from the product by simply controlling the two-step depressurization of CO_2.

The catalyst appears to be very robust, as its performance is constant over at least 30 h. Fig. 1, shows a plot of the turnover number (TON) *vs.* reaction time. The TON increased linearly with time at both 70 and 80 °C. Moreover, we were able to continue using the catalyst for six non-consecutive days with no observable decrease in either activity or selectivity. Furthermore, no rhodium leaching was detected (detection limit of used technique (AES) is 0.2% of the total amount of rhodium of the catalyst). This demonstrates that the rhodium–diphosphine bond in this catalyst remains stable under hydroformylation conditions.

In conclusion, we have presented the first example of continuous selective hydroformylation of higher olefins in $scCO_2$ using an immobilised homogeneous rhodium catalyst. The process is potentially interesting in the manufacture of fine chemicals and our approach has several advantages compared to conventional homogeneously catalysed reactions. Firstly, $scCO_2$ is a clean, environmentally benign medium which can be easily separated from the organic phase. Secondly, the application of an immobilised homogeneous catalyst in the flow reactor provides a direct and quantitative separation of the products from the catalyst and avoids any solubility limitations of homogeneous catalysts. Finally, the robustness of the catalyst and absence of Rh leaching, makes this system an interesting candidate for sustainable processes.

We are grateful to Dr W. K. Gray for initiating this collaboration and thank Dr S. K. Ross for his help. We thank Thomas Swan & Co. Ltd. and the EPSRC (GR/M73644) for funding the work at Nottingham and the Innovation Oriented Research Program (IOP-katalyse) for financing the work in Amsterdam. We thank J. Elgersma for performing the Rh analyses and Dr P. A. Arnold, Dr M. Glenny, M. Guyler and K. Stanley for their assistance.

Notes and references

† *Catalyst preparation*: 100 mg (1.40×10^{-4} mol) of *N*-(3-trimethoxysilyl-*n*-propyl)-4,5-bis(diphenylphosphino)phenoxazine (Siloxantphos) was added to a suspension of 1 g silica (200–500 μm) (predried at 140 °C for several days) in 25 ml toluene and the mixture was mechanically stirred at 80 °C for 20 h. After cooling to room temperature, the liquids were removed from the residue and the silica was washed with three portions of toluene. The ligand-on-silica was dried *in vacuo* and was then suspended in a mixture of 5 mL THF and 1 mL Et_3N. The suspension was mixed for 10 min and 4 mg (1.55×10^{-5} mol) $Rh(acac)(CO)_2$ was then added. The mixture was mechanically stirred for 15 min, after which the THF was removed and the catalyst was further washed with three portions of THF. The catalyst was dried *in vacuo* and was either used directly or stored under argon at −20 °C.

‡ The substrate + internal standard, supercritical CO_2 (P_c = 73.8 bar, T_c = 31.1 °C) and CO/H_2 are brought together in a heated mixer, passed through the reactor containing catalyst, and then expanded to separate the fluid product from the process-stream. The reactor is assembled from commercially available units: $scCO_2$ pump PM101, CO/H_2 compressor CU105 and Expansion Module PE103 (all from NWA GmbH, Lörrach, Germany), a high pressure mixer (Medimix) and a Gilson 305 pump (for the organic substrate). **CAUTION**: Flow reactors have a comparatively small volume under pressure. Nevertheless, equipment with the appropriate pressure and temperature rating should always be used for high pressure experiments.

1 E. G. Kuntz, *Chemtech*, 1987, 570.
2 W. A. Herrmann and B. Cornils, *Angew. Chem., Int. Ed. Engl.*, 1997, **36**, 1048.
3 M. Beller, B. Cornils, C. D. Frohning and C. W. Kohlpainter, *J. Mol. Catal. A*, 1995, **104**, 17.
4 A. J. Sandee, V. F. S. Slagt, J. N. H. Reek, P. C. J. Kamer and P. W. N. M. van Leeuwen, *Chem. Commun.*, 1999, 1633.
5 A. J. Sandee, L. A. van der Veen, J. N. H. Reek, P. C. J. Kamer, M. Lutz, A. L. Spek and P. W. N. M. van Leeuwen, *Angew. Chem., Int. Ed.*, 1999, **38**, 3231.
6 R. Noyori, *Chem. Rev.*, 1999, **99**, 475.
7 J. A. Darr and M. Poliakoff, *Chem. Rev.*, 1999, **99**, 495.
8 B. M. Bhanage, Y. Ikushima and M. Shirai, *Chem. Commun.*, 1999, 1277.
9 S. Kainz and W. Leitner, *Catal. Lett.*, 1998, **55**, 223.
10 D. Koch and W. Leitner, *J. Am. Chem. Soc.*, 1998, **120**, 13 398.
11 D. R. Palo and C. Erkey, *Ind. Eng. Chem. Res.*, 1998, **37**, 4203.
12 D. R. Palo and C. Erkey, *Organometallics*, 2000, **19**, 81.
13 I. Bach and D. J. Cole-Hamilton, *Chem. Commun.*, 1998, 1463.
14 M. F. Sellin and David J. Cole-Hamilton, *J. Chem. Soc., Dalton Trans.*, 2000, 1681.
15 M. G. Hitzler and M. Poliakoff, *Chem. Commun.*, 1997, 1667.
16 M. G. Hitzler, F. R. Smail, S. K. Ross and M. Poliakoff, *Org. Proc. Res. Dev.*, 1998, **2**, 137.
17 M. G. Hitzler, F. R. Smail, S. K. Ross and M. Poliakoff, *Chem. Commun.*, 1998, 359.
18 W. K. Gray, F. R. Smail, M. G. Hitzler, S. K. Ross and M. Poliakoff, *J. Am. Chem. Soc.*, 1999, **121**, 10 711.
19 J. A. Moulijn, P. W. N. M. van Leeuwen and R. A. van Santen, *Catalysis: an integated approach to homogeneous, heterogeneous and industrial catalysis*, Elsevier, Amsterdam, 1993.
20 A. Baiker, *Chem. Rev.*, 1999, **99**, 453.

Trimethoxyboroxine as an 'oxygen-transfer' reagent: a non-aqueous 'sol–gel' route to alkali-free borosilicate glass

Michael A. Beckett,*[a] Martin P. Rugen-Hankey[a] and K. Sukumar Varma[b]

[a] *Department of Chemistry, University of Wales, Bangor, UK LL57 2UW. E-mail: m.a.beckett@bangor.ac.uk*
[b] *Pilkington Group Research, European Technical Centre, Lathom, Lancashire, UK L40 5UF*

Received (in Cambridge, UK) 17th April 2000, Accepted 28th June 2000
Published on the Web 19th July 2000

A synthesis of alkali-free borosilicate gel from $Si(OEt)_4$ and $(MeO)_3B_3O_3$ in non-aqueous solvents is reported; the formation of the gel proceeds *via* rapid transesterification/oxygen transfer with elimination of $B(OR)_3$; removal of volatiles from the gel, followed by drying (60 °C, 12 h) and furnacing in air (600 °C, 20 min) resulted in alkali-free borosilicate glass.

The sol–gel methodology involving hydrolysis and condensation of metal alkoxides is potentially an important low temperature route to homogeneous multicomponent oxide glass thin films and coatings.[1–3] Thus, for example, suitable coatings may be obtained by a 'dip and furnace' route without exposure to temperatures required in melt/fusion processes (> 1300 °C). The production of alkali-free borosilicate glass by sol–gel routes have generally used protic solvents and mineral acids, with the silicon source partially hydrolysed by prolonged reflux prior to addition of the boron source as either an orthoborate ester[4–8] or as boric acid.[9–10]. The susceptability of B–O–Si bonds to hydrolytic attack at boron, with subsequent leaching of borate, is a severe limitation of the aqueous sol–gel method.[9] The first synthesis of an alkali-free borosilicate gel carried out at ambient temperature in organic solvents, with exclusion of water and mineral acids and using the metaborate ester trimethoxyboroxine (TMB), has recently been reported by Varma[11] in the patent literature. Here, we report on the underlying chemistry of this new and novel 'sol–gel' route to borosilicate materials, in which the TMB functions as both a source of boron and as a non-aqueous 'oxygen transfer' reagent.

A transparent gel was obtained when TMB and tetraethoxysilane (TEOS) were dissolved in dry acetone in a 1:1 molar ratio (B:Si ratio 3:1) and left at room temperature for *ca.* 2 weeks.† We have further noted that (i) the gelation time is decreased by increasing the B:Si ratio (*e.g.* 9:1, 1 week), (ii) that gels do not form at B:Si ratios of 1:1 even after prolonged periods, and that (iii) in the absence of solvent neat TMB and TEOS (1:1) gelled within a week. The transparent gel was isolated and upon removal of all volatiles and oven-drying (60 °C) gave an opaque/glassy solid. The mass of the dried gel was *ca.* 35% of the combined masses of the added TEOS and TMB. The dried gel lost a further 30–40% of its mass upon firing to 600 °C in air and yielded a silver-grey borosilicate glass with a B:Si ratio of *ca.* 1:1.2; TGA showed that most of this mass was lost at 350–400 °C.

The solid products were characterised by elemental analysis,† IR, XRD and solid-state MAS NMR spectroscopy. Elemental analysis confirmed the presence of boron and silicon in both dried and fired samples and the mass balance of the reaction confirms that > 90% of the silicon (added as TEOS), and *ca.* 25% of the boron (added as TMB), remained in the final borosilicate glass. XRD analysis indicated that they were both non-crystalline amorphous solids. The ^{11}B MAS NMR spectrum of the furnaced glass [Fig. 1(b)] exhibited a clear residual quadrupolar 'doublet' pattern and was simulated as one signal (δ_{iso} = +14.4 ppm) indicating that the boron atoms were all in equivalent three-coordinate axially symmetrical environments

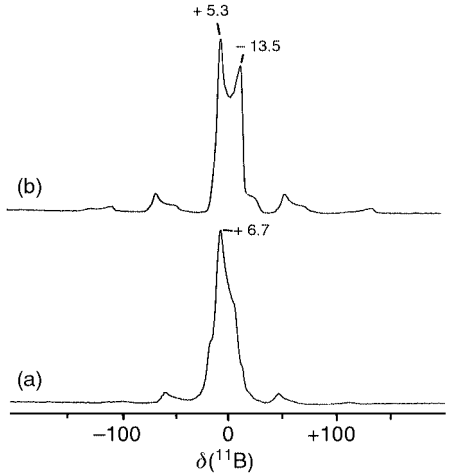

Fig. 1 Observed (96.234 MHz) MAS ^{11}B NMR spectra for (a) the dried gel and (b) the furnaced glass, spinning at 5200 and 5900 Hz, respectively. The dried gel was simulated as two signals: [δ_{iso} (ppm), rel.int, η, C_q (MHz)] 15.6, 80, 0.0, 2.38; 10.6, 20, 0.0, 1.14. The furnaced glass was simulated as a single signal: 14.4, 100, 0.0, 2.63.

and consistent with them being part of the silica network.[12–14] The dried gel gave a ^{11}B spectrum [Fig. 1(a)] simulated as an 80:20 mixture of two signals (δ_{iso} = +15.6 and +10.6 ppm), with the main species at lower field. ^{29}Si MAS NMR demonstrated that the principal species in both the dried gel and the furnaced glass was Q^4 (δ_{iso} = −109 ppm), with the furnaced glass giving an asymmetric signal which was deconvoluted as a 63:37 mixture with the lower intensity signal at δ_{iso} = −101 ppm.[14] IR spectra of both the dried and furnaced solids (Fig. 2) showed absorptions at 928 and *ca.* 670 cm^{-1} indicating that

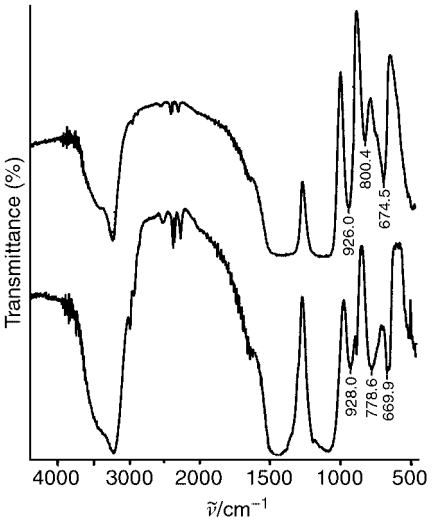

Fig. 2 FTIR spectra (KBr disc) for (a) the dried gel and (b) the furnaced glass.

DOI: 10.1039/b003047n

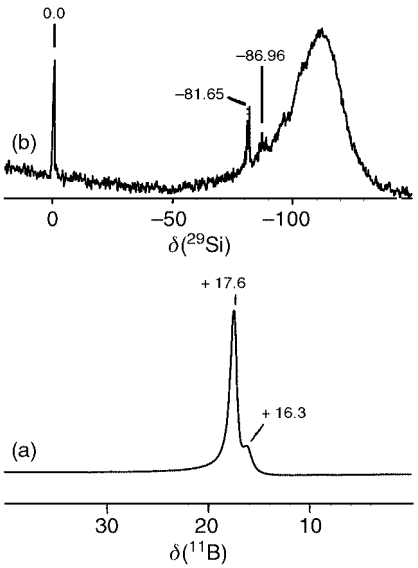

Fig. 3 Solution NMR of the sol diluted with $CDCl_3$ prior to gelling of the TMB:TEOS (1:1) reaction mixture (a) $^{11}B\{^1H\}$ spectrum (80.249 MHz) and (b) ^{29}Si spectrum (49.694 MHz) with $SiMe_4$ added as an internal standard (0.0 ppm).

both samples contain B–O–Si links.[9,15] Strong B–O (br, 1450 cm^{-1}), Si–O stretches (br,1150 cm^{-1}) and Si–O–Si (*ca.* 790 cm^{-1}) were also observed.[9,15] Heating the sample to 600 °C enhanced the relative intensity of B–O–Si bands and produced a weak shoulder (at 740 cm^{-1}) on the lower energy B–O–Si band which may indicate the formation of some B–O–B (720 cm^{-1}) upon furnacing.[15]

The volatile reaction products were investigated qualitatively by GCMS, and ^{11}B NMR and quantitatively by gravimetric boron analysis. ^{11}B NMR showed one peak (*ca.* +17.6 ppm) consistent with a trigonal boron with three oxygen substituents, and GCMS confirmed that $B(OEt)_3$ was the major species present. Gravimetric analysis showed that *ca.* 45% of boron initially added to the reaction mixture as TMB was now in the isolated volatile component.

The above observations demonstrate that orthoborate esters are produced as co-products in the gelling process and an idealised equation for the production of silica from a 2:1 B:Si stoichiometry may be written as in eqn. (1). In the preparation

$$Si(OEt)_4 + 2/3(MeO)_3B_3O_3 \rightarrow 1/n\{SiO_2\}_n + 2B(OR)_3 \ (R = Me, Et) \quad (1)$$

of the gel described above a B:Si ratio of 3:1 was used, and it was noted that gels were not formed with B:Si ratios of 1:1. The incorporation of boron in the gel, either present as B–O–Si linkages or as occluded borate, appears to be a consequence of the increased B:Si ratio. Occluded metaborate esters would disproportionate to orthoborate esters and boron oxide upon furnacing with the orthoborate esters volatilised at high temperatures.

The initial stages of the reaction (sol formation) were followed by solution ^{11}B and ^{29}Si NMR spectroscopy which show clear evidence for initial B–O–Si bond formation, and oxygen transfer and transesterification, respectively (Fig. 3). The formation of B–O–Si bonds in the sols can be seen by the appearence of a new signal in the ^{11}B spectrum at +16.3 ppm [5] in addition to that for the TMB and $B(OR)_3$ which overlap at *ca.* +17.6 ppm. ^{29}Si NMR of the sols also indicated that transesterification had occurred [Q^0 ester signals at −79.93, −80.82 and −81.65 for $Si(OMe)_2(OEt)_2$, $Si(OMe)(OEt)_3$ and TEOS[5,16]] with strong evidence for Q^1 species (centered at −87 ppm: −85.96, −86.96, −88.56 ppm) but with molecular Q^2, Q^3 and Q^4 species at *ca.* −96, −104 and −112 ppm barely discernable above the broad baseline hump due to borosilicate glass of the sample tube, and gelling sample.[5] Transesterification of orthoborates/orthosilicates has been reported in the literature but several hours at elevated temperature and acid/base catalysis were required for systems to reach equilibrium.[17] In the system described here transesterification is very rapid at room temperature and we believe this to be a consequence of the increased Lewis acidity of the metaborate ester over that of orthoborate esters.[18] It is acknowledged however, that the acetone solvent may play a non-innocent role in this reaction, by functioning as a Lewis base and as a potential catalytic proton source.

Mechanistic aspects of this unusual reaction and detailed studies of these and other multicomponent systems, including applications for the preparation of thin films by 'dip-coating' using the sols, are in progress.

We thank Dr D. Apperley (EPSRC solid-state MAS NMR service, Durham) for spectra and Pilkington plc for financial support.

Notes and references

† TMB (4.16 g; 24 mmol) and TEOS (5.0 g; 24 mmol) were disolved in dry acetone (25 cm^3) and left to stand in a dry, inert atmosphere. The transparent gel, which slowly formed over a 2 week period, was isolated as a solid (4.61 g) after removal of volatiles (25.1 g) (vacuum, RT). GCMS confirmed that $B(OEt)_3$ was the major component of the volatiles and gravimetric analysis (barium borotartrate method[19]) of a hydrolysed aliquot (1.0632 g) gave 0.9689 g of $4BaC_4H_4O_6{\cdot}Ba(BO_2)_2{\cdot}4H_2O$ (= 1.35 mmol B), and hence total B of 31.9 mmol. The gel was oven dried at 60 °C for 12 h to yield an opaque glassy solid (3.24 g) with elemental composition Si 21.7; B 10.2; C 14.3; H 3.6; (O ≈ 50.2)%. Firing a sample of the dried gel (0.51 g) to 600 °C in air for 20 min resulted in weight loss (38%) and a silvery–grey borosilicate glass (0.32 g) with elemental composition of Si 31.4 **;** B 10.1; C < 0.5; H < 0.5; (O ≈ 58.0)%.

1 H. Dislich, *Angew. Chem., Int. Ed. Engl.*, 1971, **10**, 363.
2 I. Artaki, M. Bradley, T.W. Zerda and J. Jonas, *J. Phys. Chem.*, 1985, **89**, 4399.
3 L. L. Hench and J. K. West, *Chem. Rev.*, 1990, **90**, 33.
4 N. Tohge, A. Matsuda and T. Minami, *J. Am. Ceram. Soc.*, 1987, **70**, C13.
5 A. D. Irwin, J. S. Holmgren, T. W. Zerda and J. Jonas, *J. Non-Cryst. Solids*, 1987, **89**, 191.
6 A. Kasgoz, T. Minsono and Y. Abe, *J. Non-Cryst. Solids*, 1999, **243**, 168.
7 N. Pellegri, O.D. Santus and A. Duran, *J. Sol–Gel Sci. Technol.*, 1994, **2**, 519.
8 D. M. Haaland and C. J. Brinker, *Mater. Res. Soc. Symp. Proc.*, 1984, **32**, 267.
9 C. Zha, G. R. Atkins and A. F. Masters, *J. Non-Cryst. Solids*, 1998, **242**, 63.
10 C. Zha, G. R. Atkins and A. F. Masters, *J. Sol–Gel Sci. Technol.*, 1998, **13**, 103.
11 K.S. Varma, *Int. Pat.* WO 98/42627, 1998.
12 M. A. Beckett, P. Owen and K. S. Varma, *J. Organomet. Chem.*, 1999, **588**, 107.
13 G. Engelhardt and D. Michel, *High-Resolution Solid-State NMR of Silicates and Zeolites*, Wiley, Chichester, 1987, p. 332.
14 A. D Irwin, J. S. Holmgren and J. Jonas, *J. Non-Cryst. Solids*, 1988, **101**, 249.
15 A. S. Tenney and J. Wong, *J. Chem. Phys.*, 1972, **56**, 5516.
16 J. C. Pouxviel, J. P. Boilot, J. C. Beloeil and J. Y. Lallemand, *J. Non-Cryst. Solids*, 1987, **89**, 345
17 D. F. Peppard, W. G. Brown and W. C. Johnson, *J. Am. Chem. Soc.*, 1946, **68**, 77.
18 M. A. Beckett, G. C. Strickland, J. R. Holland and K. S. Varma, *Polymer*, 1996, **37**, 4629.
19 R. S. Braman, in *Encyclopedia of Industrial Chemical Analysis*, ed. F. D. Snell and C. L. Hilton, J. Wiley and Sons, Interscience, 1968, ***7***, 384.

ChemComm

Asymmetric synthesis of indolizidine alkaloids by ring-closing–ring-opening metathesis

Huib Ovaa,[a] Roland Stragies,[b] Gijs A. van der Marel,[a] Jacques H. van Boom[a] and Siegfried Blechert*[b]

[a] *Leiden Institute of Chemistry, Gorlaeus Laboratories, P.O. Box 9502, 2300 RA Leiden, The Netherlands*
[b] *Institut für Organische Chemie, Technische Universität Berlin, Straße des 17. Juni 135, 10623 Berlin, Germany. E-mail: Blechert@chem.tu-berlin.de*

Received (in Liverpool, UK) 19th May 2000, Accepted 21st June 2000
Published on the Web 19th July 2000

Asymmetric Pd(0) catalyzed allylic amination followed by a Ru catalyzed RCM–ROM sequence converted an easily accessible racemic cyclopentenol 2 to the functionalized tetrahydropyridine 9 which can be used for the asymmetrical synthesis of indolizidine 13.

Polyhydroxylated indolizidine alkaloids are widespread in nature and possess very diverse and important physiological properties.[1] Consequently, development of general methodologies for their construction is an important challenge.

Recently we published a paper in which ruthenium catalyzed ring-rearrangement (*i.e.* sequential ring-closing–ring-opening metathesis) is described.[2] The herein reported ring-rearrangement opens the way to converting readily accessible carbocycles into stereodefined heterocycles containing highly functionalized side chains. In order to illustrate the general applicability of this reaction it was decided to synthesize (see Scheme 1) 1,2,3,5,6,8a-hexahydroindolizine-1,2-diol **A** (R=H).

Retrosynthetic analysis reveals that the target compound **A** can be attained from functionalised tetrahydropyridine **B** which, in turn, can be obtained from cyclopentenylamine **C** *via* ruthenium catalyzed ring-rearrangement. Asymmetric Pd-catalyzed allylic amination[3] of the racemic alcohol **2**, readily accessible from cyclopentadiene **1**,[4] leads to the optically pure metathesis precursor **C**.

It was expected that palladium(0) catalyzed allylic amination of a cyclopentenyl donor derived from **2** would be an appropriate way to introduce the desired nitrogen nucleophile.

We now report an asymmetric synthesis of hexahydroindolizine **13** starting from **1** using a ring-rearrangement as the key step (see Scheme 2).

In order to provide a good leaving group for the oxidative addition event of the palladium catalyzed allylic amination, alcohol **2** was converted into its corresponding methyl carbonate **3**. In the first instance a solution of optically pure **3**† in THF–triethylamine was subjected to palladium(0) catalysis, using dppb as a ligand and *o*-nitrophenylsulfonyl[5] (Ns) protected homoallylamine as the nitrogen nucleophile. Work-up and purification gave cyclopentenylamine **5** as a racemic mixture in 95% yield.

It is well established that the palladium catalyzed reaction proceeds through the symmetrical π-allyl palladium complex **4**. This indicates that the use of asymmetric ligands would open the way to the synthesis of both enantiomers of **5**. To this end ligand **6**, developed by Trost and co-workers,[6] was selected for this purpose because of its proven reliability in terms of yield and enantioselectivity. Gratifyingly, the reaction of **3** with ligand (*R*,*R*)-**6** led to the isolation of (−)-**5**‡ in good yield with > 99.5% enantiomeric excess.§

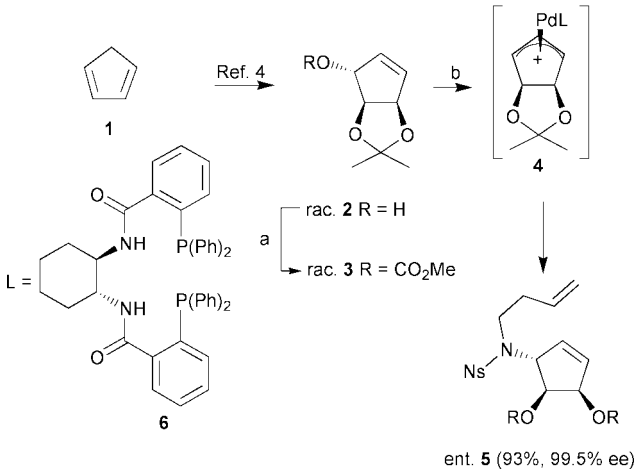

Scheme 2 *Reagents and conditions*: a $ClCO_2Me$, CH_2Cl_2, pyridine, 0 °C, 30 min, 97%; b $H_2C{=}CH(CH_2)_2NHNs$, $Pd_2dba_3{\cdot}CHCl_3$ (1 mol%), ligand **6**, Et_3N, THF, 18 h, −10 to 0 °C, 93%, 99.5% ee.

At this stage, enantiomerically pure cyclopentenylamine (−)-**5** was now subjected to ruthenium catalyzed ring-rearrangement using a catalytic amount of **8**[7] in the presence of ethylene (Scheme 3). It was established that **5** was inert under the reaction conditions, however, the corresponding TBDMS protected derivative **7** gave **9** quantitatively. It is also worth mentioning that no reaction was observed in the absence of ethylene.

It turned out that differentiation between the internal and terminal double bonds in **9** could be realized *via* regioselective dihydroxylation of the terminal double bond resulting in the corresponding diol in 80% yield as a single diastereoisomer. Periodate cleavage and *in situ* reduction of the newly generated aldehyde function gave alcohol **10**. Alcohol **10** was tosylated to provide **11**, setting the stage for an intended cyclisation–cleavage procedure. Deprotection of the Ns group was accompanied by concomitant cyclisation resulting in the 1,2,3,5,6,8a-hexahydroindolizine **12**. Removal of the TBDMS groups led to the unprotected indolizidine **13** in 87% yield based on **11**.

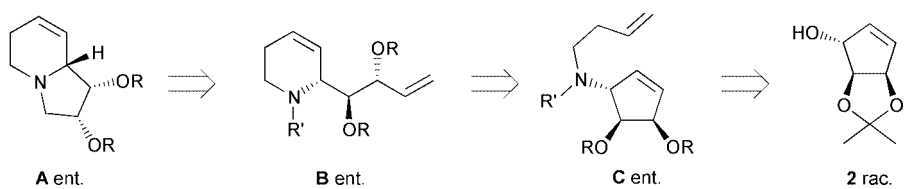

Scheme 1

DOI: 10.1039/b004106h

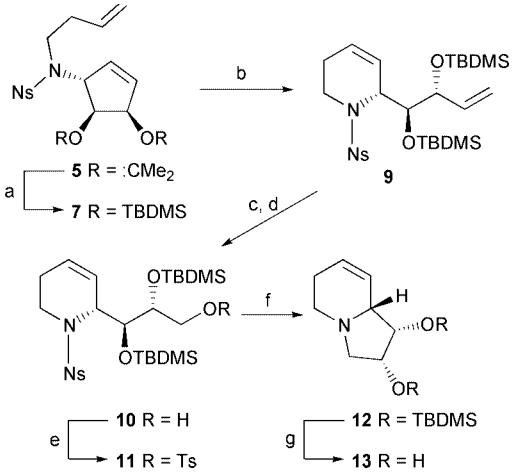

Scheme 3 *Reagents and conditions*: a, HOAc, H_2O, 80 °C, 30 min; TBDMSCl, imidazole DMF, rt, overnight, 75% (two steps); b, $Cl_2(PCy_3)_2Ru{=}CHPh$ (**8**) (4 mol%), $H_2C{=}CH_2$, CH_2Cl_2, rt, overnight, 100%; c, $K_2OsO_4{\cdot}2H_2O$ cat., NMO, acetone–H_2O, rt, 48 h, 80%; d, $NaIO_4$, MeOH/H_2O, 0 °C, 30 min, then $NaBH_4$(aq), 0 °C, 3 min, 99%; e, TsCl, pyridine, DMAP, rt, overnight, 71%; f, PhSH, $K_2C_2O_3$, DMF, 0 °C, 30 min, 100%; g, TBAF, THF, rt, overnight, 88%.

In conclusion, it has been shown that asymmetric palladium catalyzed introduction of a nitrogen nucleophile proceeds with a high degree of enantioselectivity. The resulting stereodefined platform serves as a suitable substrate for an ensuing ruthenium catalyzed ring-rearrangement leading to an azacycle carrying a highly functionalized side chain amenable to further manipulations.

This work was supported by the Council for Chemical Sciences of the Netherlands Organization for Scientific Research (CW-NWO) and the Fonds der Chemischen Industrie, Germany.

Notes and references

† Optically pure carbonate **3** was obtained from D-mannose.[8] However, it is not a requirement that **3** be optically pure.

‡ All new compounds were fully characterized by ^{1}H NMR, ^{13}C NMR, IR spectroscopy, high resolution mass spectrometry and optical rotation. Relevant data and experimental details for the compounds **5** and **9** are as follows: **5**: 1.50 g (6.94 mmol) of carbonate **3** and 2.00 g (7.80 mmol) of *N*-but-3-enyl *o*-nitrobenzenesulfonamide were dissolved in 25 mL of THF and 3 mL of Et_3N. This solution was degassed and cooled to −10 °C. 100 mg of ligand (*R*,*R*)-**6** and 50 mg of $Pd_2dba_3{\cdot}CHCl_3$ were dissolved in THF (1 mL) and stirred for one hour, after which this solution was slowly added to the reaction mixture at −10 °C. The reaction mixture was stirred for an additional 18 h at 0 °C. The solution was concentrated and purified by column chromatography (0 → 5% MeOH in CH_2Cl_2) to afford 2.54 g, 93% of (−)-**5**. ν cm^{-1}: 3078 (m), 2986 (m), 2936 (m), 1544 (s), 1372 (s), 1163 (s); δ_C (100.6 MHz, $CDCl_3$): 148.0 (Cq), 136.6 (CH), 134.1 (CH), 133.6 (CH), 133.4 (Cq), 131.6 (CH), 131.5 (CH), 130.9 (CH), 124.0 (CH), 117.4 (CH_2), 111.5 (Cq), 84.1 (CH), 83.2 (CH), 70.5, (CH), 46.2 (CH_2), 34.9 (CH_2), 27.1 (CH_3), 25.4 (CH_3); ^{1}H-NMR (400 MHz, $CDCl_3$) δ: 8.08, (m, 1H), 7.67 (m, 2H), 7.58 (m, 1H), 6.02 (ddd, *J* 7, 4, 2 Hz, 1H), 5.65 (m, 1H), 5.20 (m, 1H), 5.04 (m, 1H), 5.01 (m, 1H), 4.81 (d, *J* 1 Hz, 1H), 4.51 (d, *J* 4 Hz, 1H), 4.36 (m, 1H), 2.99 (m, 1H), 2.26 (m, 2H), 1.36 (s, 3H), 1.24 (s, 3H); HRMS: calc. for $C_{17}H_{19}N_2O_6S$ [$M^+ - CH_3$] 379.0964, found 379.09622. $[\alpha]_D^{20}$ (*c*, 1, $CHCl_3$) −33.3 °; **9**: 245 mg of **7** (0.42 mmol) were dissolved in 15 mL of CH_2Cl_2 and 20 mL of ethylene were bubbled through the solution. 14 mg (4 mol%) of catalyst **8** were added and the solution was stirred overnight. The reaction mixture was concentrated and purified by column chromatography (0 → 20% MeOtBu in hexane) to give 245 mg (100%) of **9**. IR: ν cm^{-1}: 2955 (m), 2929 (m), 2894 (w), 2857 (m), 1547 (s), 1372 (m), 1361 (m), 1171 (m); ^{13}C-NMR (126.8 MHz, $CDCl_3$) δ: 148.3 (Cq), 137.7 (CH), 134.5 (Cq), 133.3 (CH), 131.3 (CH), 130.4 (CH), 125.9 (CH), 125.6 (CH), 123.8 (CH), 116.5 (CH_2), 78.9 (CH), 76.6 (CH), 57.2 (CH), 40.2 (CH_2), 26.1 (CH_3), 22.9 (CH_2), 18.4 (Cq), 18.3 (Cq), −4.0 (CH_3), −4.4 (CH_3), −4.5 (CH_3), −4.6 (CH_3); ^{1}H-NMR (500 MHz, $CDCl_3$) δ: 7.91 (m, 1H), 7.62 (m, 2H), 7.51 (m, 1H), 5.94 (ddd, *J* 17, 10, 8 Hz, 1H), 5.77 (m, 1H), 5.67 (m, 1H), 5.22 (d, *J* 17 Hz, 1H), 5.10 (d, *J* 10 Hz), 4.50 (s, 1H), 4.35 (d, *J* 6 Hz), 3.97 (dd, *J* 14, 4 Hz, 1H), 3.87 (d, *J* 5 Hz, 1H), 3.41 (ddd, *J* 16, 10, 6 Hz), 1.82 (m, 2H), 0.91 (s, 9H), 0.89 (s, 9H), 0.09 (s, 3H), 0.08 (s, 3H), 0.06 (s, 3H), 0.04 (s, 3H); HRMS: calc. for $C_{26}H_{43}N_2O_6SSi_2$ [$M^+ - CH_3$] 567.2380, found 567.2388; $[\alpha]_D^{20}$ (*c*, 1, $CHCl_3$) +189.4°.

§ For determination of the enantiomeric excess the Ns group was replaced by a tosyl group (i, PhSH, K_2CO_3, DMF; ii, TsCl, pyridine) in order to facilitate separation of the enantiomers on a Chiralcel OD Gold column (0.5% iPrOH in hexane, 0.9 mL min^{-1}, 218 nm).

1 For a recent review article on indolizidine and quinolizidine alkaloids see: J. P. Michael, *Nat. Prod. Rep.*, 1999, **16**, 675; in *Iminosugars as Glycosidase Inhibitors*, ed. A. E. Stütz, Wiley-VCH, Weinheim, 1999, p. 1–397.

2 R. Stragies and S. Blechert, *Tetrahedron*, 1999, **55**, 8179; J. A. Adams, J. G. Ford, P. J. Stamatos and A. H. Hoveyda, *J. Org. Chem.*, 1999, **64**, 9690.

3 N. S. Sirisoma and P. M. Woster, *Tetrahedron Lett.*, 1998, **39**, 1489; B. M. Trost and D. E. Patterson, *Chem. Eur. J.*, 1999, **5**, 3279; B. M. Trost and R. C. Bunt, *J. Am. Chem. Soc.*, 1994, **116**, 4089.

4 G. Wolczunowicz, F. G. Cocu and T. Posternak, *Helv. Chim. Acta*, 1970, **53**, 2275.

5 T. Fukayama, C. Jow and M. Cheung, *Tetrahedron Lett.*, 1995, **36**, 6373.

6 For a review on asymmetric transition metal-catalyzed allylic alkylations see: B. M. Trost and D. L. Van Vranken, *Chem. Rev.*, 1996, **96**, 395.

7 P. Schwab, R. H. Grubbs and J. W. Ziller, *J. Am. Chem. Soc.*, 1996, **118**, 100.

8 H. Ovaa, J. D. C. Codée, B. Lastdrager, H. S. Overkleeft, G. A. van der Marel and J. H. van Boom, *Tetrahedron Lett.*, 1998, **39**, 7987.

ChemComm

Double aromaticity and anti-aromaticity in small carbon rings†

Sonsoles Martín-Santamaría and Henry S. Rzepa*

Department of Chemistry, Imperial College of Science, Technology and Medicine, London, UK SW7 2AY. E-mail: h.rzepa@ic.ac.uk

Received (in Cambridge, UK) 12th April 2000, Accepted 4th July 2000
Published on the Web 19th July 2000

Calculated NICS indices for C_{10} and C_{14} indicate these species are doubly aromatic and that C_{12} is doubly anti-aromatic, with the π-aromaticity dominating the σ-contribution in systems such as triplet C_{10}, C_8N_2, $C_{10}B_2$ or C_{12}^{2+} all of which have opposing aromatic/anti-aromatic character.

Recent experimental studies[1] of the electronic absorption spectra of small carbon clusters have provided evidence for the first time that the fundamentally important C_{10}–C_{14} clusters are monocyclic polyalkynes or cumulenes rather than linear species.[2] Such rings were noted[1b] as being potentially doubly aromatic, *via* both conventional p_π–p_π overlaps, and *via* the novel in-plane conjugation of $4n + 2$ π-electrons described recently by Schleyer and co-workers.[3] The latter identified [10] and [14] trannulenes (all-*trans* annulenes) as having in-plane aromaticity, on the basis of calculated nucleus independent chemical shift values at the ring centroid (NICS[4] −14.0 and −17.2 ppm respectively, *cf.* benzene, −10 ppm) and the $4n$ electron [12] trannulene as being strongly anti-aromatic (NICS +35.7 ppm). We noted that the NICS aromaticities of the C_{10}–C_{14} carbon rings have not hitherto been reported. More importantly, we considered that these small carbon rings might be suitable systems for investigating the controversial suggestion[5] that the π-electrons in benzene have a distortive tendency towards bond localisation, and that the D_{6h} symmetry of benzene itself arises purely from the σ-framework. Adding or removing two electrons to the doubly aromatic C_{10} ring could give a $4n$ count for one set of p_π–p_π electrons, and a $4n + 2$ count for the orthogonal p_π–p_π set, resulting in molecules which would be simultaneously aromatic in one dimension and anti-aromatic in another. We also speculated whether the triplet[6] and higher excited states of these species might exhibit a similar effect. Finally, our recent studies[7] suggested to us that the two orthogonal $4n + 2$ sets of p_π–p_π electrons in C_{10} might be converted to a single $4n$ set by introducing a Möbius component into the ring. Here we report our theoretical findings on these various aspects.

† Electronic supplementary information (ESI) available: computed 3D coordinates as PDB files. See http://www.rsc.org/suppdata/cc/b0/b002922j/

Initial studies† of these species were at the AM1 semi-empirical level[8] followed by B3LYP/6-31G(d) geometry optimisation[9] with no symmetry constraints of the singlet states. All the rings were characterised as planar minima *via* inspection of the Hessian matrix. Of the four valence electrons available to carbon, two contribute to conventional C–C single bonds (*e.g.* sp hybridisation) and are not considered further here. The remaining two electrons occupy orthogonal p-orbitals which for C_{10} specifically, overlap cyclically to form a set of five doubly occupied in-plane σ-molecular orbitals and a set of five out of plane π-orbitals. Each set has a characteristic benzene-like double degeneracy (E) for the highest two pairs (*e.g.* the Hückel $4n + 2$, $n = 2$ electron rule, Table 1). The calculated NICS(0)-B3LYP/6-31G(d) value at the C_{10} ring centroid (D_{5h} symmetry) of −28.9 ppm implies the molecule is indeed doubly aromatic compared to benzene itself. The C_{14} homologue showed a similar pattern of orbital occupancy and even higher aromaticity (Table 1). C_{12} differs from C_{10} in having a pair of additional p_π electrons in both the σ- and π-planes, each of which occupies a single, now non-degenerate orbital. Such $4n$ occupancy ($n = 3$) results in doubly anti-aromatic character (NICS +50.0 ppm) and a Jahn–Teller distortion towards bond localisation of the geometry (Fig. 1). The degeneracy of the π HOMO can be recovered by promoting one π electron to the π LUMO to form a triplet state, calculated to be 6.7 kcal mol^{-1} higher than singlet C_{12}. This species can be described as out-of-plane π triplet aromatic[6] but remains an in-plane σ-anti-aromatic. The overall NICS value indicates the dominance of the π aromaticity over the in-plane σ-anti-aromaticity (Table 1). Further σ–σ* electron excitation to form the quintet state of C_{12} additionally removes the in-plane σ-anti-aromaticity, increasing the overall NICS aromaticity index to −31.5 ppm.

Although reliable calculations for small carbon clusters appears to require very high levels of theory,[2] we emphasize here the relative trends in the geometries and NICS values rather than the absolute values and energies. Thus the calculated B3LYP/6-31G(d) geometries of planar C_{10}, C_{12} and C_{14} differ markedly in the degree of calculated bond alternation (Fig. 1). The doubly aromatic singlet systems show no bond alternation, doubly-antiaromatic singlet C_{12} shows strong alternation (due as we note above to a Jahn–Teller distortion) but the bonds are

Table 1 Calculated energies [kcal mol^{-1} for AM1, Hartree for B3LYP/6-31G(d)] and NICS(0) values (ppm)

Species	AM1	B3LYP/6-31G(d)	NICS(0)	Orbital occupancy[a]
C_{10}	403.8	−380.6661	−28.9	π(E), σ(E), σ(E), π(E), π, σ
B_5N_5	−57.9	−398.2935	−2.5	π(E), σ(E), π(E), σ(E), π, σ
1,6-C_8N_2	358.7	−413.9714	−16.7	σ, σ, π, π, σ, σ, π, π, σ, π, σ
C_{12}^{2+}	954.2	−456.0285	+32.4	π, σ(E), π(E), σ(E), π(E), π, σ
1,7-$C_{10}B_2$	504.7	−430.3801	−11.0	σ, π, σ, σ, π, π, σ, σ, π, π, σ
C_{12}[b]		−456.7770	−8.7	
C_{12}[c]		−456.7452	−31.5	
C_{12}	438.5	−456.7878	+50.0	π, σ, σ(E), π(E), σ(E), π(E), π, σ
C_{14}	465.1	−533.0193	−35.6	σ(E), π(E), σ(E), π(E), σ(E), π(E), π, σ
$C_{11}H_2$	350.9	−419.9766	−13.4	
$C_{13}H_2$	387.3	−496.1407	+6.8	
C_{19}	664.5	−723.2905	−11.0	

[a] Doubly occupied singly or doubly (E) degenerate orbitals arising from parallel p_π–p_π (π) and in-plane p_π–p_π (σ) overlap. [b] Triplet state. [c] Quintet state.

again symmetrised when the π-system is aromatised *via* formation of triplet state C_{12}. The additional reversal of the σ-anti-aromaticity *via* the planar σ/π doubly aromatic quintet C_{12} reveals bond relocalisation (Fig. 1), the origins of which remain to be established. These various results contrast with the proposal that π-aromaticity in benzene is bond distortive and that the symmetry is due to the σ framework alone.[5]

B_5N_5 is isoelectronic with C_{10} and also has the characteristic cumulene structure (Fig. 1) with no bond alternation and a similar orbital ordering to the carbon analogue, but a surprisingly small NICS value (Table 1) corresponding to non-aromaticity. The anomalous behaviour of B_5N_5 in a different context has been previously noted.[10] Two valence electrons added to C_{10} in the form of C_8N_2 occupy an in-plane p_π–p_π orbital, resulting in an in-plane $4n$ (n = 3) rather than $4n + 2$ occupancy. Overall, the NICS value suggests that the π $4n + 2$ aromaticity is clearly dominant over the σ $4n$ anti-aromaticity (Table 1). The reverse effect is observed with C_{12}^{2+}. This is a 12-electron ($4n$) π-antiaromatic system (NICS +32.4) associated with bond alternation, dominating a 10-electron ($4n + 2$) in-plane σ-aromatic system. A third example of this π-dominance is the isoelectronic $C_{10}B_2$ which reveals 10-electron π-aromaticity and 12-electron in-plane p_π–p_π σ-anti-aromaticity, with overall NICS aromaticity (Table 1) and only mild bond alternation (Fig. 1).

We had previously suggested[7] that replacing a two electron C=C unit in a $4n + 2$ electron annulene by a partially twisted four electron HC=C=CH unit can induce Möbius $4n$ aromaticity. Applying this analogy to replacing one four electron triple bond by this unit in C_{10} results in chiral $C_{11}H_2$, in which the in-plane p_π–p_π/σ and the out-of-plane p_π–p_π/π-systems interact to form a 20-electron Möbius $4n$ aromatic. Less effective orbital overlap reduces the NICS value compared to C_{10} and induces bond alternation (Fig. 1). Inserting the same HC=C=CH unit into the strongly anti-aromatic C_{12} to produce the 24 electron $C_{13}H_2$ reduces the anti-aromaticity substantially, but does not eliminate it (Table 1).[11] Finally, we note that two hydrogen atoms in $C_{11}H_2$ can be removed entirely by replacing them with a second carbon ring to give C_{19}, a novel form of chiral Möbius carbon (Fig. 1), again with mild NICS aromaticity indicated for each ring.

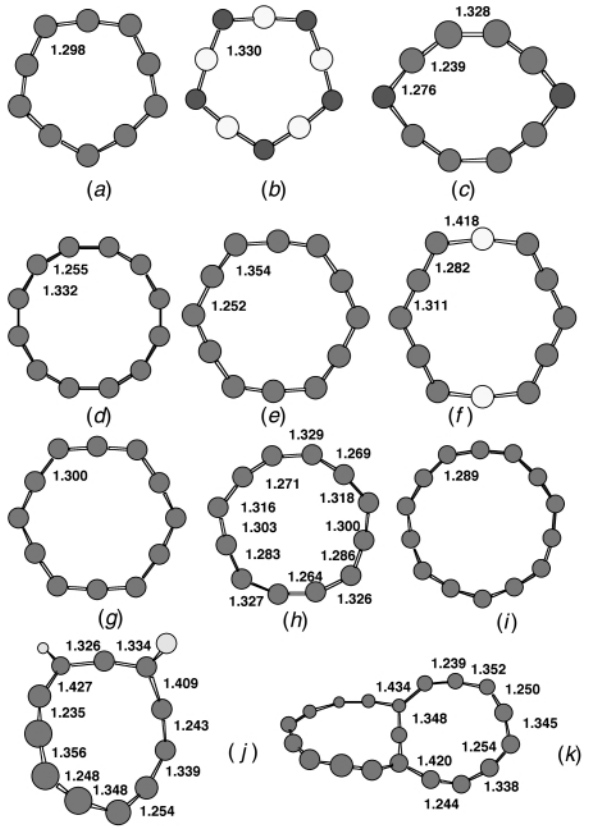

Fig. 1 B3LYP/6-31G(d) Calculated geometries (Å) for (*a*) C_{10}, (*b*) B_5N_5, (*c*) C_8N_2, (*d*) C_{12}^{2+}, (*e*) C_{12}, (*f*) $C_{10}B_2$, (*g*) triplet C_{12}, (*h*), quintet C_{12}, (*i*) C_{14}, (*j*) $C_{11}H_2$, (*k*) C_{19}.

Notes and references

1 (*a*) M. Grutter, M. Wyss, E. Riaplov, J. P. Maier, S. D. Peyerimhoff and M. Hanrath, *J. Chem. Phys.*, 1999, **111**, 7397; (*b*) M. S. Deleuze, M. G. Giuffreda, J. P. Francois and L. S. Cederbaum, *J. Chem. Phys.*, 2000, **112**, 5325.

2 A. V. Orden and R. Saykaly, *Chem. Rev.*, 1998, **98**, 2313.

3 A. A. Fokin, H. Jiao and P. v. R. Schleyer, *J. Am. Chem. Soc.*, 1998, **120**, 9364.

4 H. Jiao and P. v. R. Schleyer, *J. Phys. Org. Chem.*, 1998, **11**, 655.

5 A. Shurki and S. Shaik, *Angew. Chem., Int. Ed. Engl.*, 1997, **36**, 2205; S. Shaik, A. Shurki, D. Danovich and P. C. Hiberty, *THEOCHEM*, 1997, **398**, 155.

6 V. Gogonea, P. von R. Schleyer and P. R. Schreiner, *Angew. Chem., Int. Ed.*, 1998, **37**, 1945.

7 S. Martín-Santamaría, B. Lavan and H. S. Rzepa, *Chem. Commun.*, 2000, 1089; S. Martín-Santamaría, B. Lavan and H. S. Rzepa, *J. Chem. Soc., Perkin Trans. 2*, 2000, 1415.

8 MOPAC2000, J. J. P. Stewart, Fujitsu Limited, Tokyo, Japan, 1999.

9 Gaussian 98 (Revision A.1), M. J. Frisch, G. W. Trucks, H. B. Schlegel, G. E. Scuseria, M. A. Robb, J. R. Cheeseman, V. G. Zakrzewski, J. A. Montgomery, R. E. Stratmann, J. C. Burant, S. Dapprich, J. M. Millam, A. D. Daniels, K. N. Kudin, M. C. Strain, O. Farkas, J. Tomasi, V. Barone, M. Cossi, R. Cammi, B. Mennucci, C. Pomelli, C. Adamo, S. Clifford, J. Ochterski, G. A. Petersson, P. Y. Ayala, Q. Cui, K. Morokuma, D. K. Malick, A. D. Rabuck, K. Raghavachari, J. B. Foresman, J. Cioslowski, J. V. Ortiz, B. B. Stefanov, G. Liu, A. Liashenko, P. Piskorz, I. Komaromi, R. Gomperts, R. L. Martin, D. J. Fox, T. Keith, M. A. Al-Laham, C. Y. Peng, A. Nanayakkara, C. Gonzalez, M. Challacombe, P. M. W. Gill, B. G. Johnson, W. Chen, M. W. Wong, J. L. Andres, M. Head-Gordon, E. S. Replogle and J. A. Pople, Gaussian, Inc., Pittsburgh, PA, 1998.

10 M. S. Deleuze, M. G. Giuffreda, J. P. Francois and L. S. Cederbaum, *J. Phys. Chem. A*, 2000, **104**, 1588.

11 For a more detailed discussion of the origins of Mobius aromaticity, see: S. Martín-Santamaría and H. S. Rzepa, *J. Chem. Soc., Perkin Trans. 2*, paper B003971N, submitted for publication.

ChemComm

A hybrid network of synthetic polymer mesh and collagen sponge

Guoping Chen,*[a] Takashi Ushida[ab] and Tetsuya Tateishi[ab]

[a] *3D Tissue Engineering Group, National Institute for Advanced Interdisciplinary Research, 1-1-4 Higashi, Tsukuba, Ibaraki 305-8562, Japan. E-mail: chen@nair.go.jp*

[b] *Tissue Engineering Laboratory, Graduate School of Engineering, The University of Tokyo, Tokyo 113-8656, Japan. E-mail: ushida@ingram.t.u-tokyo.ac.jp; E-mail: tateishi@ingram.t.u-tokyo.ac.jp*

Received (in Cambridge, UK) 2nd May 2000, Accepted 27th June 2000
Published on the Web 19th July 2000

A novel hybrid network of synthetic polymer mesh and collagen sponge was prepared by forming collagen sponges with interconnected microporous structures in the interstices of the synthetic polymer mesh.

Biodegradable synthetic poly(α-hydroxy acids), such as poly(lactic acid) (PLA), poly(glycolic acid) (PGA) and their copolymer of poly(DL-lactic-co-glycolic acid) (PLGA), and collagen have been widely used for tissue engineering as temporary scaffolds to accommodate transplanted cell masses, and as materials for assisting in surgeries in clinical applications.[1–6] The synthetic polymer meshes demonstrate good biocompatibility, good mechanical properties, and are easy to handle. Their rate of degradation can also be controlled to meet the rate of new tissue formation in tissue repair. However, these synthetic polymers are relatively hydrophobic. These hydrophobic properties, together with the large mesh interstices, hinder smooth cell seeding. In contrast, collagen offers the advantage of specific cell interactions and hydrophilicity, but scaffolds constructed entirely of collagen have poor mechanical strength. Therefore, synthetic biodegradable polymers and collagen have been hybridized to combine their advantages.[7–13] In the present study, a novel hybrid biomaterial was prepared by combining synthetic biodegradable polymer mesh with collagen sponge.

The hybridization of synthetic poly(α-hydroxy acids) and collagen was achieved by forming collagen sponges between the interstices of poly(α-hydroxy acids) mesh. A Vicryl knitted mesh made of polylactin 910 (a 90 : 10 copolymer of glycolic acid and lactic acid), as shown in Fig. 1a, was immersed in a bovine collagen acidic solution (type I, pH 3.2, 0.5 wt%), and frozen at −80 °C for 12 h. It was then freeze dried under a vacuum of 0.2 Torr for 24 h to allow the formation of collagen sponge. The collagen sponge was further cross-linked by treatment with glutaraldehyde vapor saturated with 25% glutaraldehyde aqueous solution at 37 °C for 4 h. After the cross-linking, the sponge was treated with 0.1 M glycine aqueous solution to block unreacted aldehyde groups. After being washed with deionized water and freeze dried, the polymer–collagen hybrid mesh was prepared.

The hybrid mesh was coated with gold and observed by scanning electron microscopy (SEM). The SEM photomicrographs of the hybrid mesh are shown in Fig. 1. Collagen sponges with interconnected microporous structures were formed in the interstices of the synthetic polymer mesh. The polymer mesh was embedded in the collagen sponge sheet so that the fiber bundles of polymer mesh and the collagen sponges were alternately chained. The thickness of the collagen sponge sheet surrounding the polymer mesh could be manipulated by adjusting the volume of the collagen solution. A greater volume of collagen solution resulted in a thicker layer of collagen sponge. The position of the polymer mesh in the hybrid network could also be manipulated. It could be a sandwich type with the polymer mesh embedded in the middle of the collagen sponge layer, or be overlapped. The hybrid mesh could be prepared in the shape of a sheet or a cylinder by using a polymer mesh sheet or tube.

20-mM HEPES buffer-soaked hybrid mesh, polymer mesh and collagen sponge were used for static tensile mechanical tests. They were pulled to failure at a rate of 0.5 mm min^{-1}. Load–deformation curves were obtained from a chart recorder. The moduli of elasticity of the hybrid mesh, polymer mesh and collagen sponge determined from the load–deformation curves and the dimensions of each sample were 35.42 ± 1.42, 35.15 ± 1.00 and 0.02 ± 0.00 MPa, respectively. The hybrid mesh possessed almost the same mechanical property as that of the polymer mesh, much higher than that of the collagen sponge alone.

Human skin fibroblasts were subcultured in 106S serum medium supplemented with 2 (v/v)% fetal bovine serum (FBS), 10 ng mL^{-1} recombinant epidermal growth factor (rEGF), and

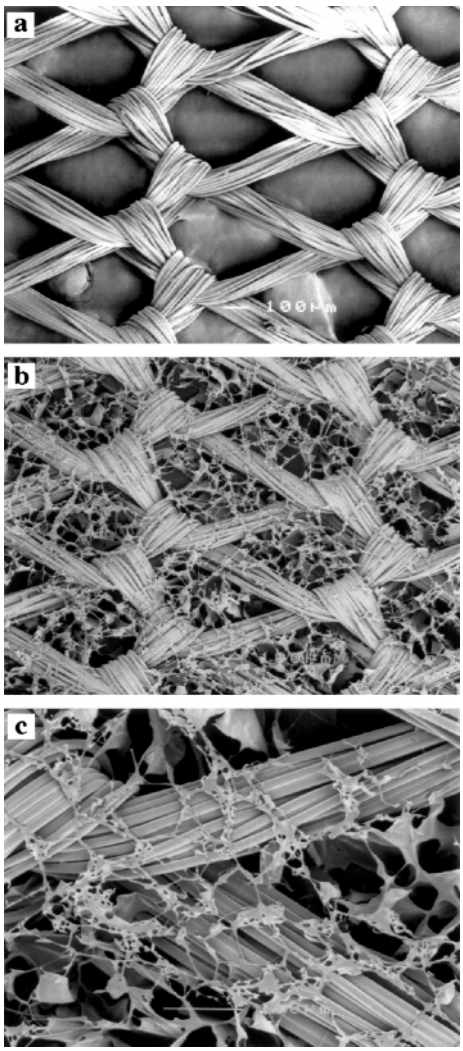

Fig. 1 SEM photomicrographs of polylactin 910 mesh (a) and its hybrid mesh with collagen at original magnification ×60 (b) and 200 (c).

DOI: 10.1039/b003508o

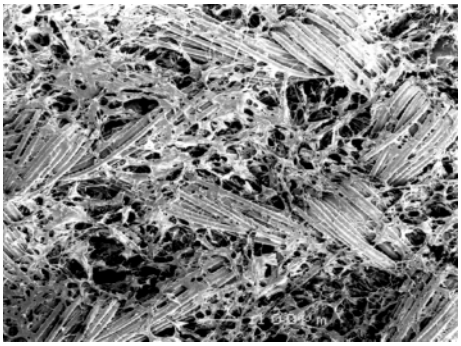

Fig. 2 SEM photomicrograph of human skin fibroblasts cultured on the hybrid mesh for 5 days at original magnification ×100.

3 ng mL^{-1} recombinant fibroblast growth factor-basic (rb-FGF). The subcultured fibroblasts were harvested and seeded on the hybrid and polymer meshes (7.64×10^4 cells/cm^2), and cultured in 106S serum medium under a 5% CO_2 atmosphere at 37 °C. The medium was replaced every 2 days. The cells adhering to the hybrid and polymer meshes after 24 h of culturing were $6.42 \pm 0.21 \times 10^4$ and $1.48 \pm 0.26 \times 10^4$ cells cm^{-2}, respectively. Many more cells adhered to the hybrid mesh than the polymer mesh. The cell morphology on the hybrid mesh was examined by SEM observation. Fig. 2 shows the appearance of the cells on the hybrid mesh after being cultured for 5 days. The fibroblasts adhered and spread well on the surfaces of the collagen sponge of the hybrid mesh after being cultured for 5 days. After 2 weeks, they proliferated to become completely connected in a layer structure. Over a longer culture period, the hybrid mesh degraded and eventually disappeared. Only cell sheet containing fibroblasts and extracellular matrices was left. These results suggest good cell interaction of the hybrid mesh.

Biodegradable synthetic poly(α-hydroxy acids) meshes have been used as temporary scaffolds for the tissue engineering of skin,[2] nerve,[9] esophagus,[10] ligament,[11] *etc*. However, the mesh interstices and their hydrophobicity hinder cell seeding. Cultured urothelial cells do not grow into a confluent layer on PGA or polyglactin mesh because of the large size of the mesh interstices.[14] To increase the cell seeding density on the PGA mesh, a method of surface hydrolysis has been used to improve the wettability of the mesh.[15] Hybridization of synthetic polymer with collagen has also been used to address these problems.[7–11] Polyglactin 910 mesh and PGA mesh have been coated with collagen solution, or embedded in collagen gels, to improve cell attachment and cell seeding. However, neither surface hydrolysis nor collagen coating changes the pore size of the interstices. The use of collagen gel produces a complete loss of pore structure. Compared to collagen gel, collagen sponge is porous enough to accommodate implanted cells, and its microporous structure facilitates cell seeding. The hybrid mesh of polylactin 910 mesh with collagen sponge exhibited a novel hybrid structure with interconnected microporous collagen sponges formed in the interstices of the synthetic polymer mesh. The polymer mesh, serving as a skeleton, reinforced the hybrid mesh and resulted in easy handling, while the collagen sponge provided the hybrid with a microporous structure and hydrophilicity, and, therefore, easy cell seeding. The hybrid mesh we developed could serve as a useful biomaterial for tissue engineering.

This work was supported in part by the New Energy and Industrial Technology Development Organization of Japan and in part by a Grant of the 'Research for the Future' Program (JSPS-RFTF96I00202) from the Japan Society for the Promotion of Science (JSPS).

Notes and references

1 R. Langer and J. P. Vacanti, *Science*, 1993, **260**, 920.
2 M. L. Cooper, J. F. Hansbrough, R. L. Spielvogel, R. Cohen, R. L. Bartel and G. Naughton, *Biomaterials*, 1991, **12**, 243.
3 A. G. Mikos, G. Sarakinos, S. M. Leite, J. P. Vacanti and R. Langer, *Biomaterials*, 1993, **14**, 323.
4 S. L. Ishaung-Riley, G. M. Crane-Kruger, M. J. Yaszemski and A. G. Mikos, *Biomaterials*, 1998, **19**, 1405.
5 P. X. Ma and R. Zhang, *J. Biomed. Mater. Res.*, 1999, **46**, 60.
6 V. Yannas and J. F. Burke, *J. Biomed. Mater. Res.*, 1980, **14**, 65.
7 M. G. Dunn, L. D. Bellincampi, A. J. Tria and J. P. Zawadsky, *J. Appl. Polym. Sci.*, 1997, **63**, 1423.
8 P. M. Kaufmann, S. Heimrath, B. S. Kim and D. J. Mooney, *Cell Transplant.*, 1997, **6**, 463.
9 T. Kiyotani, M. Teramachi, Y. Takimoto, T. Nakamura, Y. Shimizu and K. Endo, *Brain Res.*, 1996, **740**, 66.
10 M. Hirotaka, N. Ando, S. Ozawa, M. Sato, K. Hayashi and M. Kitajima, *ASAIO J.*, 1999, **45**, 502.
11 A. K. Saxena, J. Marler, M. Benvenuto, G. H. Willital and J. P. Vacanti, *Tissue Eng.*, 1999, **5**, 525.
12 G. Chen, T. Ushida and T. Tetsuya, *Adv. Mater.*, 2000, **12**, 455.
13 G. Chen, T. Ushida and T. Tetsuya, *J. Biomed. Mater. Res.*, 2000, **51**, 273.
14 S. Hakim, P. A. Merguerian and D. R. Chavez, *Urology*, 1994, **44**, 139.
15 J. Gao, L. Niklason and R. Langer, *J. Biomed. Mater. Res.*, 1998, **42**, 417.

ChemComm

Triisobutylaluminium promoted reductive rearrangement of substituted vinyl ethers to homologous alcohols

Bérengère du Roizel, Matthieu Sollogoub, Alan J. Pearce and Pierre Sinaÿ*

École Normale Supérieure, Département de Chimie, associé au CNRS, 24 rue Lhomond, 75231 Paris Cedex 05, France. E-mail: Pierre.Sinay@ens.fr

Received (in Liverpool, UK) 25th April 2000, Accepted 26th June 2000
Published on the Web 19th July 2000

Substituted vinyl ethers carrying electron-donating groups in the ether moiety undergo smooth oxygen to carbon rearrangement with triisobutylaluminium to afford chain extended alcohols.

Lewis acid promoted oxygen to carbon rearrangements of vinyl acetals have received considerable attention as synthetically useful procedures.[1] For example, we have developed efficient methodology for the preparation of carbocycles by the reductive rearrangement of carbohydrate based vinyl acetals using TIBAL (triisobutylaluminium) as the Lewis acid.[2] We recently reported[3] that unsaturated *C*-aryl glycosides (hex-5-eno-pyranosides) such as **1**, also undergo the analogous TIBAL promoted rearrangement into carbocycles, provided that the aryl moiety is sufficiently electron-donating in nature in order to stabilise the carbocationic centre of the proposed intermediate **2** (Scheme 1). It is noteworthy that **1** is however no longer a vinyl acetal but a cyclic benzyl vinyl ether. Given that the Lewis acid promoted rearrangement of acyclic vinyl acetals[4] and allyl benzyl ethers[5] has been reported, we reasoned that an acyclic variant of **1** should also undergo a Lewis acid promoted rearrangement. Therefore, as part of our evaluation of the wider scope of the TIBAL promoted reductive rearrangement, we herein report the first application of this process to the rearrangement of acyclic *non-carbohydrate* based systems.

The substituted vinyl ethers **4** were readily prepared by standard acetylation of the starting alcohols **3** and methylenation using the Tebbe reagent (Scheme 2).

The substituents were chosen in order to stabilise the proposed carbocation intermediate and therefore favour rearrangement over the known competitive hydroalumination–elimination process[3] which would afford **3**. The TIBAL promoted reductive rearrangements† of **4** proceeded smoothly (64–70%) for electron-rich aromatic derivatives **4a** and **4b**

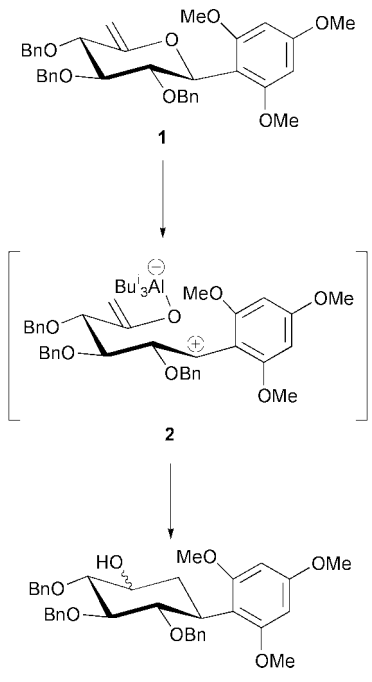

Table 1 Reaction of substituted vinyl ethers with TIBAL

Substituted vinyl ether	Product	Yield (%)
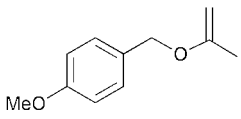 **4a**	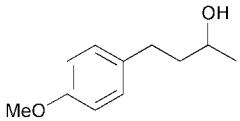 **5a**	64
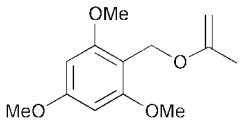 **4b**	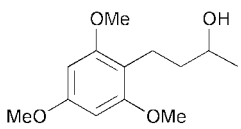 **5b**	70
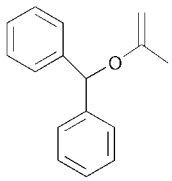 **4c**	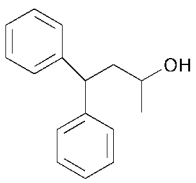 **5c**	87
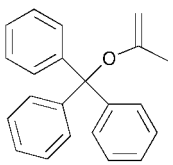 **4d**	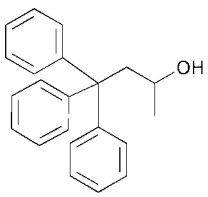 **5d**	35[a]
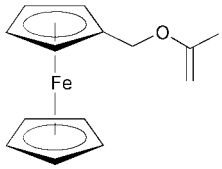 **4e**	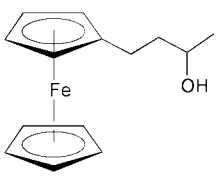 **5e**	60[a]

[a] **3d** (15%) and **3e** (10%)—the products of the competitive cleavage process *via* hydroalumination–elimination[3] were also isolated.

DOI: 10.1039/b003277h

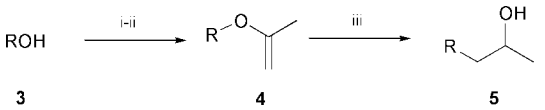

3 4 5

Scheme 2 *Reagents and conditions*: i, Ac_2O, pyridine (for **3a**,**b**); AcCl, Et_3N (for **3c**,**e**); AcBr, AcOH, NH_3, toluene (for **3d**); ii, 2.0 equiv. Tebbe reagent, 4.0 equiv. pyridine, THF, −45 °C to rt; iii, 5.0 equiv. TIBAL (1 M in toluene).†

(Table 1). The related non-reductive rearrangement of benzyl vinyl ethers has been reported as a side-reaction to Claisen rearrangements under radical[6] or forcing thermal conditions.[7] The TIBAL promoted rearrangement of diphenylmethyl isopropenyl ether (**4c**) proceeded in excellent yield. In the case of triphenylmethyl isopropenyl ether (**4d**), TIBAL rearrangement was indeed observed, although in only 35% yield, probably due to steric hindrance. Finally, the ferrocenylmethyl isopropenyl ether (**4e**) underwent smooth TIBAL promoted rearrangement to afford 4-ferrocenylbutan-3-ol (**5e**)‡ in 60% yield.

In summary, substituted vinyl ethers carrying electron-donating groups in the ether moiety undergo smooth TIBAL promoted rearrangement to afford chain extended alcohols. This approach constitutes a simple three step homologation procedure for benzylic alcohols, carrying electron-donating substituents in the aromatic nucleus and other alcohols bearing adjacent electron-donating groups and furthermore illustrates the more *general* nature of the TIBAL induced rearrangement.

We thank the European Community for a TMR Marie Curie Research Training Grant (#ERBFMBICT983225) to A. J. P.

Notes and references

† *Typical procedure*: TIBAL (1 M in toluene, 5 equiv.) was added to a stirred solution of starting material **4** in dry toluene (1 mL/100 mg), at 0 °C under argon. The cooling bath was then removed and the reaction mixture was allowed to warm to room temperature. After *ca*. 2 h (as indicated by TLC), the reaction mixture was cooled to 0 °C and distilled water was added dropwise until no further gas evolution was observed. The reaction mixture was then filtered (Celite®) and washed with EtOAc. The organic phase was then diluted with distilled water and extracted twice with EtOAc. The organic layers were then combined, dried ($MgSO_4$), filtered and the solvent was removed *in vacuo*. Purification of the residue by flash chromatography (cyclohexane–EtOAc) afforded pure **5**.

‡ *Selected data* for **5e**: δ_H(400 MHz; $CDCl_3$) 1.26 (d, 3H, *J* 6.3, CH_3), 1.57 (br s, 1H, O*H*), 1.63–1.78 (m, 2H, FnCH_2CH_2), 2.42 (ddd, 1H, *J* 14.5, 9.6 and 6.6, FnCH_aH_b), 2.51 (ddd, 1H, *J* 14.5, 9.6 and 6.2, FnCH_aH_b), 3.86 (m, 1H, C*H*OH), 4.10–4.12 (m, 4H, 4 × *H*Cp), 4.15 (5H, s, 5 × *H*Cp); δ_C(100 MHz; $CDCl_3$) 23.6 (*C*H_3), 25.7 (Fn*C*H_2), 40.4 (FnCH_2*C*H_2), 67.1 (2 × *C*Cp), 67.8 (*C*HOH), 67.8 (*C*Cp), 68.0 (*C*Cp), 68.4 (5 × *C*Cp), 88.7 (*C*CpCH_2); *m/z* (CI, NH_3) 276 (100%, M + 18); (calc. for $C_{14}H_{18}$OFe: C, 65.14; H, 7.03; found: C, 65.07; H, 7.19%).

1 Review: H. Frauenrath, *Synthesis*, 1989, 721; D. J. Dixon, S. V. Ley and E. W. Tate, *J. Chem. Soc., Perkin Trans. 1*, 1999, 2665; A. B. Smith, III, P. R. Verhoest, K. P. Minbiole and J. J. Lim, *Org. Lett.*, 1999, **1**, 909; A. B. Smith, III, K. P. Minbiole, P. R. Verhoest and T. J. Beauchamp, *Org. Lett.*, 1999, **1**, 913.

2 S. K. Das, J.-M. Mallet and P. Sinaÿ, *Angew. Chem., Int. Ed. Engl.*, 1997, **36**, 493 and see also M. Frank, R. Miethchen and H. Reinke, *Eur. J. Org. Chem.*, 1999, 1259; A. J. Pearce, M. Sollogoub, J.-M. Mallet and P. Sinaÿ, *Eur. J. Org. Chem.*, 1999, 2103; A. J. Pearce, J.-M. Mallet and P. Sinaÿ, *Heterocycles*, 2000, **52**, 819; M. Sollogoub, A. J. Pearce, A. Hérault and P. Sinaÿ, *Tetrahedron: Asymmetry*, 2000, **11**, 283; A. J. Pearce, R. Chevalier, J.-M. Mallet and P. Sinaÿ, *Eur. J. Org. Chem.*, 2000, 2203.

3 M. Sollogoub, J.-M. Mallet and P. Sinaÿ, *Angew. Chem., Int. Ed.*, 2000, **39**, 362.

4 X.-P. Gu, I. Ikeda and M. Okahara, *J. Org. Chem.*, 1988, **53**, 2737.

5 J. Wennerberg, F. Ek, A. Hansson and T. Frejd, *J. Org. Chem.*, 1999, **64**, 54; J. Wennerberg, L. Eklund, M. Polla and T. Frejd, *Chem. Commun.*, 1997, 445.

6 A. W. Burgstahler, L. K. Gibbons and I. C. Nordin, *J. Chem. Soc.*, 1963, 4986.

7 W. J. Le Noble, P. J. Crean and B. Gabrielsen, *J. Am. Chem. Soc.*, 1964, **86**, 1649.

ChemComm

Self- and hetero-recognition in the guest-controlled assembly of Pd(II)-linked cages from two different ligands

Shuichi Hiraoka,† Yasuo Kubota and Makoto Fujita*

Department of Applied Chemistry, Graduate School of Engineering, Nagoya University, CREST, Japan Science and Technology Cooperation (JST), Chikusa, Nagoya 464-8603, Japan. E-mail: mfujita@apchem.nagoya-u.ac.jp

Received (in Cambridge, UK) 30th May 2000, Accepted 27th June 2000
Published on the Web 21st July 2000

The equilibration of cage-like receptors, $M_3(L^1)_2$ + $M_3(L^2)_2$ ⇌ 2 $M_3(L^1)(L^2)$, was efficiently controlled by appropriate guest addition: large (spherical) or small (flat) guests stabilized the homoleptic cages ($M_3(L^1)_2$ or $M_3(L^2)_2$) while medium-sized guests preferred the heteroleptic cage ($M_3(L^1)(L^2)$).

A dynamic receptor library is an equilibrium mixture of several receptors from which the appropriate one is selected by an optimal guest.[1–6] It is particularly important to study the dynamic features of guest-selected receptor formation from the library because the phenomenon is closely related to biological receptor systems.[7] Herein reported is the guest-controlled assembly of Pd(II)-linked cage-like receptors from a dynamic library generated from Pd(II) complex **1** and two different tridentate ligands **2** and **3**. As shown in Scheme 1, the library contains two classes of receptors: homoleptic (**4**, **5a** and **5b**) and heteroleptic (**6**). The homoleptic receptor contains two identical ligands and, hence, is termed a 'self-recognized' receptor while the heteroleptic receptor contains two different ligands and is termed 'hetero-recognized'.[8] We show that the equilibration between the receptors is very efficiently controlled by the addition of appropriate guests which selectively stabilize their optimal receptors.

The equilibration we deal with is represented by the following equation:

$$\underset{\text{'self - recognized'}}{\mathbf{4} + \mathbf{5}} \rightleftharpoons \underset{\text{'hetero - recognized'}}{2 \bullet \mathbf{6}}$$

Self-recognition should be dominant if only **4** and/or **5** are stabilized, while hetero-recognition is favored if **6** is selectively stabilized. Note that **5a** and **5b** are structural isomers with identical composition and the equilibration between these isomers is highly controlled by guest addition, as previously reported.[6]

When Pd(II) complex **1** (10 mM) was combined with tridentate ligands **2** and **3** (3.3 mM each) in D_2O, cages **4**–**6** and uncharacterized oligomeric products were formed with a very low self/hetero ratio‡ (**4**:**5**:**6**:oligomers = 15:35:30:20 corresponding to *ca.* 6:4 self/hetero ratio; see Table 1, run 1).[9] The product ratios were estimated by ^{1}H NMR (Fig. 1). Oligomer formation became predominant at higher concentrations and exclusive when $[\mathbf{1}]_0$ > 40 mM.

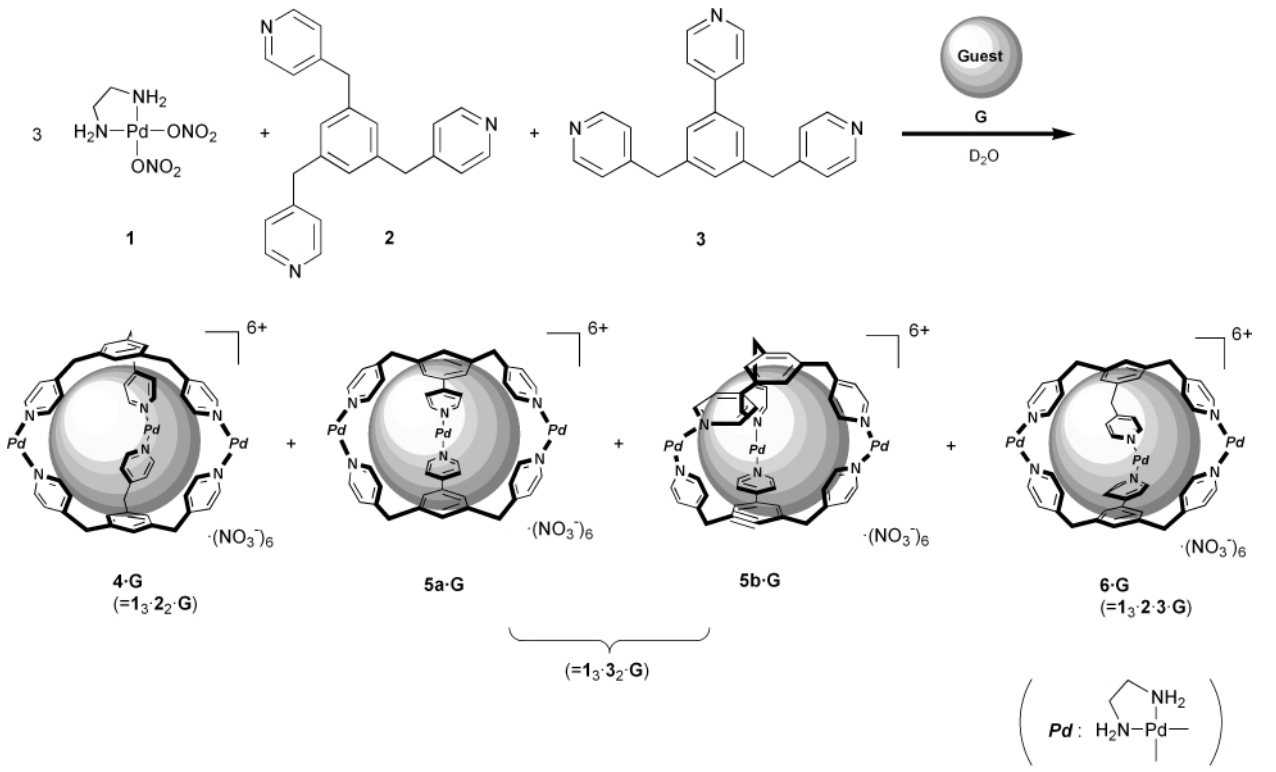

Scheme 1

DOI: 10.1039/b004271o

Table 1 Guest-selected formation of homo- and heteroleptic Pd(II)-linked receptors

Run	Guest[b]	Ratio[a] (%) **4**:**5a**:**5b**:**6**:Oligomers[c]	S/H[d]
1	None	15:0:35:30:20	6:4
2	PhCOOH	27:0:31:38:4	6:4
3	**7**	42:0:42:16:0	8:2
4	**8** + **9**	50:0:50:0:0	10:0
5	CCl_4	17:15:2:66:0	3:7
6	$CBrCl_3$	16:14:2:68:0	3:7
7	CBr_4	29:18:11:42:0	6:4
8	*c*-C_6H_{12}	19:6:13:62:0	4:6
9	*c*-C_7H_{14}	8:0:20:60:12	3:7
10	*c*-C_8H_{16}	15:0:33:34:18	6:4

[a] Determined by ^{1}H NMR ([**1**]$_0$ = 10 mM, 25 °C, D_2O). [b] Excess amounts of guests were used. [c] At 3.3 mM for each ligand, it was confirmed that only ligand **2** gives oligomeric components. Thus, the amount of the oligomers was estimated on the assumption that compound **3** does not contribute to the oligomeric fraction of complexes. [d] S/H = self/hetero ratio.

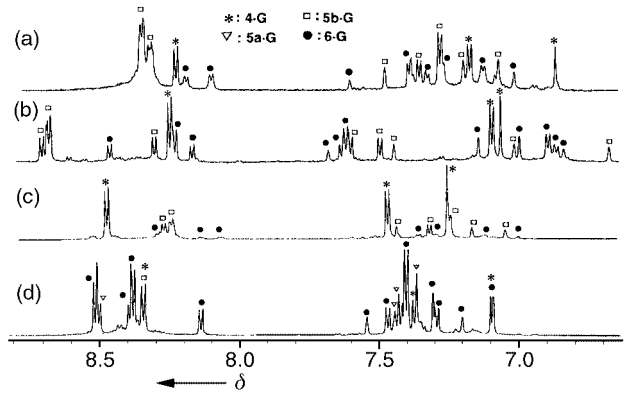

Fig. 1 ^{1}H NMR spectra (500 MHz, D_2O, aromatic region) of the mixture of complexes **4**–**6** obtained from a 3:1:1:1 mixture of **1** ([**1**]$_0$ = 10 mM), **2** ([**2**]$_0$ = 3.3 mM), **3** ([**3**]$_0$ = 3.3 mM) and various guests: (a) guest free; (b) guest = PhCOOH; (c) guest = **7**; (d) guest = $CBrCl_3$.

Upon the addition of adamantane-1-carboxylic acid (**7**), however, the oligomer formation was completely suppressed and the equilibration was significantly shifted toward the self-recognized products (**4** + **5** = 84%; run 3). The cavity size becomes larger and more spherical in the order of **5** < **6** < **4** because ligand **2** is larger than **3** by the length of a CH_2 unit. Thus the preference for the self-recognition can be ascribed to the efficient binding of the large and spherical guest by host **4**. In fact, only the signals of host **4** were downfield shifted while those of **5** and **6** were unchanged, suggesting the selective complexation of **7** and **4**.

Self-recognition should be most effective if **4** and **5** are stabilized simultaneously but not **6**. Thus, we attempted the use of two different guests adamantan-1-ol (**8**) and benzene-1,3,5-tricarboxylic acid (**9**) because the former was expected to be bound by bulky cage **4** and the latter by flat cage **5b**. When **8** and **9** were added, only self-recognized receptors **4** and **5b** were assembled exclusively as expected (**4** + **5b** = 100%; run 4). The signals of only **4** and **5b** were downfield shifted suggesting the selective formation of **4**•**8** and **5b**•**9** complexes.

In contrast, the equilibrium was markedly shifted toward hetero-recognition when $CBrCl_3$ was added as the guest: **6** was preferentially formed (68%) and the self/hetero ratio was *ca*. 3:7. This spherical and 'medium-sized' guest seems to best fit within the cavity of **6**. The formation of **6** was not exclusive because $CBrCl_3$ was also bound efficiently in the cavity of **5a**.[6] Similar spherical guests such as CCl_4 induced the preferential formation of **6** (66%) while the slightly larger CBr_4 was no longer a suitable guest for selective heteroleptic receptor formation (42%). Cyclohexane and cycloheptane were also favorable for hetero-recognition (self/hetero ratios 4:6 and 3:7, respectively), but cyclooctane, which seems too large, showed no stabilizing effects for any receptors.

Notes and references

† Present address: Department of Applied Chemistry, Kanagawa University, Kanagawa-ku, Yokohama 221-8686, Japan.

‡ Self-recognized receptors **4** and **5** have been obtained by two independent reactions: **1** + **2** → **4**;[9] **1** + **3** → **5**. Thus, from the NMR spectrum of a **4**–**6** mixture, **4** and **5** can be easily assigned. In the present reaction, the newly appeared signals, which contain the framework of both **2** and **3** in a 1:1 ratio, can be assigned as **6**. ^{1}H NMR data of **6** (from the reaction of run 6 in Table 1): ^{1}H NMR (500 MHz, D_2O, 25 °C) δ 8.51 (2H, d, *J* 6.6 Hz, PyH_α), 8.39 (4H, d, *J* 6.6 Hz, PyH_α), 8.38 (2H, d, *J* 6.6 Hz, PyH_α), 8.14 (4H, d, *J* 6.6 Hz, PyH_α), 7.54 (1H, s, Ar*H*), 7.47 (2H, d, *J* 6.8 Hz, PyH_β), 7.40 (8H, d, *J* 6.8 Hz, PyH_β), 7.31 (2H, s, Ar*H*), 7.29 (2H, d, *J* 6.8 Hz, PyH_β), 7.20 (1H, s, Ar*H*), 7.09 (2H, s, Ar*H*), 3.92–3.72 (10H, m, –CH_2–), 2.79–2.60 (12H, m, $NH_2CH_2CH_2NH_2$).

1 B. Hasenknopf, J.-M. Lehn, G. Baum and D. Fenske, *Proc. Natl. Acad. Sci. USA*, 1996, **93**, 1397; J.-M. Lehn, *Chem. Eur. J.*, 1999, **5**, 2455.

2 B. Hasenknopf, J.-M. Lehn, G. Baum, B. O. Kneisel and D. Fenske, *Angew. Chem., Int. Ed. Engl.*, 1996, **35**, 1838; B. Hasenknopf, J.-M. Lehn, N. Boumediene, A. Dupont-Gervais, A. V. Dorsserlaer, B. Kneisel and D. Fenske, *J. Am. Chem. Soc.*, 1997, **119**, 10 956.

3 S. J. Rowan and J. K. M. Sanders, *J. Chem. Soc., Perkin Trans. 1*, 1997, 1407; P. A. Brady and J. K. M. Sanders, *J. Chem. Soc., Perkin Trans. 1*, 1997, 3237.

4 M. C. Calama, P. Timmerman and D. N. Reinhoudt, *Angew. Chem., Int. Ed. Engl.*, 2000, **39**, 755; F. Cardullo, M. C. Calama, B. H. M. Snellink-Ruël, J.-L. Weidmann, A. Bielejewska, R. Fokkens, N. M. M. Nibbering, P. Timmerman and D. N. Reinhoudt, *Chem. Commun.*, 2000, 367; L. J. Prins, K. A. Jolliffe, R. Hulst, P. Timmerman and D. N. Reinhoudt, *J. Am. Chem. Soc.*, 2000, **122**, 3617.

5 J. M. Rivera, T. Martin and J. Rebek, Jr., *Science*, 1998, **279**, 1021; J. M. Rivera, T. Martin and J. Rebek, Jr., *J. Am. Chem. Soc.*, 1998, **120**, 819; F. Hof, C. Nuckolls and J. Rebek, Jr., *J. Am. Chem. Soc.*, 2000, **122**, 4251.

6 S. Hiraoka and M. Fujita, *J. Am. Chem. Soc.*, 1999, **121**, 10 239.

7 D. E. Koshland, *FEBS Lett.*, 1976, **62**, E47.

8 The terms self- and hetero-recognition have been termed in ref. 1. Also see M. Albrecht, M. Schneider and H. Rottele, *Angew. Chem., Int. Ed. Engl.*, 1999, **38**, 557.

9 Guest-induced assembly of **4** from **1** and **2**: M. Fujita, S. Nagao and K. Ogura, *J. Am. Chem. Soc.*, 195, **117**, 1649.

Li[$Cp_2Zr(C{\equiv}CPh)(\eta^2{:}1,2\text{-}PhC_2C{\equiv}CPh)$]: an anionic zirconium(II) intermediate for carbon–carbon coupling

Robert Choukroun,* Jianshe Zhao, Christian Lorber, Patrick Cassoux and Bruno Donnadieu

Equipe Précurseurs Moléculaires et Matériaux, Laboratoire de Chimie de Coordination du CNRS, 205 Route de Narbonne, 31077, Toulouse Cedex, France. E-mail: choukrou@lcc-toulouse.fr

Received (in Basel, Switzerland) 5th June 2000, Accepted 5th July 2000
Published on the Web 24th July 2000

The unexpected anionic Zr^{II} complex $[Cp_2Zr(C{\equiv}CPh)(\eta^2{:}1,2\text{-}PhC_2C{\equiv}CPh)]^-$ was isolated from $LiC{\equiv}CPh$ and Cp_2ZrCl_2 in THF, giving clear evidence for a CC coupling between two alkynyl moieties, one of them being η^2-bonded to the zirconium atom.

New prospects towards non linear optical (NLO) materials have induced, in recent years, a resurgence of interest in the chemistry of acetylenic transition metals complexes.[1] Numerous studies have focused on the CC coupling of the acetylenic moieties, which underlies the synthesis of the building block of the poly-ynes.[2] We have been interested in the reaction of vanadocene with poly-ynes.[3] An unexpected heterodimetallic complex $Cp_2V(\mu{:}\eta^2{:}\eta^4\text{-}PhC{\equiv}CC{\equiv}CPh))ZrCp_2$, containing a butadiene framework with two internal planar tetracoordinate carbons was isolated from Cp_2V and $Cp'_2Zr(C{\equiv}CPh)_2$ (Cp′ = C_5H_5, C_5H_4Me, $C_5H_4Bu^t$, $C_5H_4SiMe_3$).[4,5] The chemistry of these bis(alkynyl)metallocene precursors has previously been detailed[6–8] and their synthesis, generally in diethyl ether solvent, well described.[6] On the other hand, a CC bond forming reaction was reported by Negishi *et al.*[9] as resulting from the reaction of Cp_2ZrCl_2 with 3 equiv. of $LiC{\equiv}CPh$ in THF followed by hydrolysis affording the isomerically pure (*Z*)-1,4-diphenylbut-1-ene-3-yne. In this process, Li[$Cp_2Zr(C{\equiv}CPh)_3$] was postulated as an intermediate species.[9] The authors underline the necessity of the third equiv. of $LiC{\equiv}CPh$ to $Cp_2Zr(C{\equiv}CPh)_2$ to produce the CC coupling. More recently, the $[Zr(C{\equiv}CR)_3]^-$ anion moiety was suggested as being an intermediate species in the trimerization of *tert*-butyl acetylene to 1,3,6-tri(*tert*-butyl)fulvene.[10] We report here the X-ray structure of the intermediate anion species Li[$CpZr(C{\equiv}CPh)(\eta^2{:}1,2\text{-}PhC_2C{\equiv}CPh)$] and some aspects of its formation mechanism.

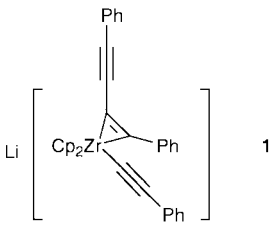

1

When the reaction of Cp_2ZrCl_2 with 2 equiv. of $LiC{\equiv}CPh$ is carried out in THF, followed by slow diffusion of pentane, the unexpected Zr^{II} lithium salt species Li[$Cp_2Zr(C{\equiv}CPh)(\eta^2{:}1,2\text{-}PhC_2C{\equiv}CPh)$] **1**,† was obtained as a red crystalline complex and fully characterized by an X-ray structure determination (Fig. 1).‡ The main feature of this structure gives clear evidence for a CC coupling between two alkynyl moieties, one of them being η^2-bonded to the zirconium atom. A titanium complex related to **1**, namely $(C_5Me_5)_2Ti(\eta^2{:}1,2\text{-}RC_2C{\equiv}CR)$] was also recently isolated by Rosenthal *et al.* by Mg reduction of $(C_5Me_5)_2TiCl_2$ in the presence of $Me_3SiC_4SiMe_3$.[11*a*] Depending on the ratio of the reactants, this reaction also affords either the tweezer Ti^{III} complex $[(C_5Me_5)_2Ti(\eta^1\text{-}C{\equiv}CSiMe_3)_2][Mg(THF)Cl)]$ (A) or $[(C_5Me_5)_2Ti((\eta^3\text{-}Me_3SiC_3{=}C(C{\equiv}CSiMe_3)SiMe_3]$[11*b*] (B). The tweezer Ti^{III} complex (A) could be described as an intermediate for the formation of complex (B).

Different crossing reactions were monitored by ^1H NMR to gain an understanding of the formation of **1**.§ When the reaction of Cp_2ZrCl_2 and 2 equiv. of $LiC{\equiv}CPh$ is carried out in THF and in the absence on sunlight, $Cp_2Zr(C{\equiv}CPh)_2$ **2** was obtained as the sole product and can be kept unchanged at least one week in the dark, whereas in presence of daylight only **1** is formed.[12] Starting from **2** and the solid lithium salt $LiC{\equiv}CPh$ in THF-d_8, complete consumption of the Li salt gives **1** nearly immediately and quantitatively in absence or in presence of daylight. We checked that in the absence of daylight no reaction occurs in C_6D_6 between **2** and $LiC{\equiv}CPh$ (1 : 1) whereas still in the absence of daylight the addition of THF-d_8 in the NMR tube, which dissolves the lithium salt, immediately generates **1**.

Complementary hydrolysis experiments on complex **1** containing the preformed CC coupling were performed to ensure that the 1,4-diphenylbut-1-en-3-yne is also formed in this case. In presence of HCl and at room temperature, hydrolysis of **1** leads to the formation of *E* and *Z* isomers of the enyne $PhCH{=}CHC{\equiv}CPh$ with a high selectivity when the reaction is carried out in toluene (toluene: *Z*:*E* = 98 : 2; THF: *Z*:*E* = 30 : 70).¶ Adding $LiC{\equiv}CBu^t$ to **2** followed by HCl hydrolysis gives *Z* enynes, namely $PhCH{=}CHC{\equiv}CBu^t$, $PhC{\equiv}CCH{=}CHBu^t$ and PhCHCHC≡CPh (roughly 30, 15, 55% respectively, characterized by GC/MS and ^1H NMR).‖ This result suggests that the first step of the reaction is the formation of the

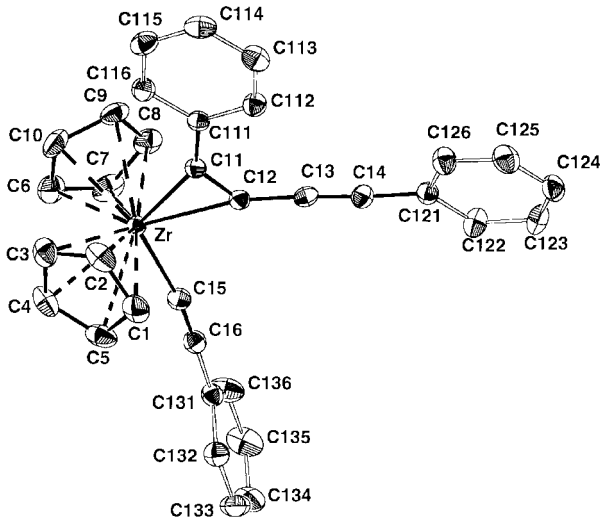

Fig. 1 Molecular structure of anionic $[\mathbf{1}]^-$ with selected bond distances (Å) and angles (°), hydrogen atoms omitted. Zr–C(11) 2.206(2), Zr–(C12) 2.342(1), Zr–C(15) 2.314(2), C(11)–C(12) 1.335(2), C(12)–C(13) 1.412(2), C(13)–C(14) 1.208(2), C(15)–C(16) 1.223(2), Zr–Cp 2.252(av.); Zr–C(11)–C(111) 147.8(1), Zr–C(15)–C(16) 171.9(1), Zr–C(12)–C(13) 127.9(1), C(12)–C(13)–C(14) 177.5(2), C(11)–Zr–C(12) 33.97(6), C(12)–Zr–C(15) 88.60(5), C(11)–Zr–C(15) 122.53(5), Zr–C(15)–C(16) 171.9(1), C(15)–C(16)–C(166) 176.3(2), Cp–Zr–Cp 129.57(av.) [Cp are the centroids of the C_5H_5 rings C(1)–C(5), C(6)–C(10)].

DOI: 10.1039/b004478o

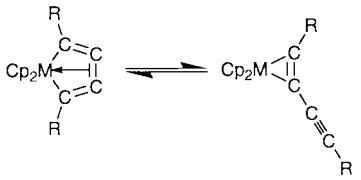

Scheme 1

$Li[Cp_2Zr(C{\equiv}CPh)_2(C{\equiv}CBu^t)]$ intermediate which could give three possible species such as $Li[Cp_2Zr(C{\equiv}CPh)(\eta^2:1,2\text{-}PhC_2C{\equiv}CBu^t)]$, $Li[Cp_2Zr(C{\equiv}CPh)(\eta^2:1,2\text{-}Bu^tC_2C{\equiv}CPh]$ and $Li[Cp_2Zr(C{\equiv}CBu^t)(\eta^2:1,2\text{-}PhC_2C{\equiv}CPh)]$, the formation of the latter being favoured by the presence of the less steric R = Ph group on the η^2 chain.**

The CC coupling between two alkynyl moieties from $Cp'_2Zr(C{\equiv}CR)_2$ ($Cp' = C_5H_5$, R = Bu^t; $Cp' = C_5Me_5$, R = Ph, $SiMe_3$) has already been demonstrated by Rosenthal *et al.*[11,13,14] This reaction occurs under *hν* irradiation or sunlight to give the zirconacyclocumulene complex $Cp'_2Zr(\eta^4:1,2,3,4\text{-}RC{=}C{=}C{=}CR)$.†† Thus $(C_5H_5)_2Zr(\eta^4:1,2,3,4\text{-}PhC{=}C{=}C{=}CPh)$ **3** should be an excellent candidate for explaining the formation of **1**. Starting from **3**, generated by *hν* daylight in THF-d_8 from **2**,[12] addition of one equiv. of LiC≡CPh gives **1**. This experiment is indicative of an equilibrium between the zirconacyclocumulene and a ($\eta^2:1,2\text{-}PhC_2C{\equiv}CPh$) containing species (Scheme 1) as already mentioned by Rosenthal *et al.*[13] Nevertheless the formation of the zirconacumulene species must be catalysed either by daylight, or by the $B(C_6F_5)_3$ borane,[15] or by the Cp_2V vanadocene for at least one day. By contrast, the formation of the ($\eta^2:1,2\text{-}PhC_2C{\equiv}CPh$) moiety in **1** is immediate in THF when adding the third LiC≡CPh equiv. to the bis(alkynyl)zirconocene complex. No catalytic reaction from **2** to **3** with LiC≡CPh as catalyst was observed by ^1H NMR.

At this stage we are not in a position to prove the involvement of LiC≡CPh in a photoassisted reaction with **2** leading to **1**. However, it is noteworthy that when the reaction is carried out in the dark, it yields only **2**. Our results clearly suggest that the alkynyl coupling reaction is induced by a third alkynyl ligand *via* the formation of the unstable 'ate' intermediate Zr^{IV} species $Li[Cp_2Zr(C{\equiv}CPh)_3]$, or an assumed tweezer Zr species $[Cp_2Zr(C{\equiv}CPh)_2][Li(C{\equiv}CPh)]$, which may subsequently rearrange to **1**.[16]

Notes and references

† *Spectroscopic data* for $C_{42}H_{41}LiO_2Zr$ **1**: M = 675.9, Calc: C, 74.55; H, 6.06. Found: C, 74.72; H, 5.86%; (40% yield based on 2 equiv. LiC≡CPh; 75% yield when the reaction is performed with 3 equiv. LiC≡CPh). IR (Nujol): ν(C≡C) 2063, 2110 cm^{-1}; ^1H NMR (C_6D_6, δ/ppm) 8.26 (pseudo triplet, 2H, *o*-Ph from the η^2-PhC_2-bonded to the zirconium atom), 7.54–6.9 (m, 13H, Ph), 5.78 (s, 10H, Cp), 3.36, 0.95 (m, 16H, THF). A ^1H NMR VTP of the complex from −80 to +80 °C does not show any change in the solution structure. Assignement of the ^{13}C NMR spectrum of **1** in THF-d_8 (δ/ppm, J(Hz)) could be tentatively done with a JMOD and 2D heteronuclear correlation technique (inverse HMQC (LR), gradient selected). $Li[Cp_2Zr(C_\alpha{\equiv}C_\beta Ph)(\eta^2\text{-}PhC_a{\equiv}C_b\text{-}C_c{\equiv}C_dPh)]$, **1**: 205.9 (s, $^3J_{CH}$ = 4 Hz, C_b), 134.9, 130.4, (s, C_a/C_α), 97.6 (s, C_c), 126.4/107.4 (t, $^3J_{CH}$ = 4–5 Hz, C_β/C_d), 142.5, 127.9, 128.3 (t, ^2J = 7–8 Hz, C_{ipso}), 130.8, 129.8, 129.0, 128.4, 128.2, 128.0, 126.1, 126.0, 125.8 (d, $^1J_{CH}$ = 158–162 Hz, Ph), 105.0 (d, $^1J_{CH}$ = 171 Hz, Cp).

‡ *Crystallographic data* for **1**: $C_{34}H_{25}LiZr{\cdot}2THF$ M = 675.95, monoclinic, space group $P2_1/c$, a = 14.986(2), b = 10.4594(8), c = 22.028(2) Å, β = 102.07(1)°, V = 3376(1) Å^3, D = 1.33 g cm^{-3}, μ = 3.61 cm^{-1}, $R(Rw)$ = 0.0272 (0.0722) for 4701 unique data and 415 parameters, G.O.F. = 1.04. Data collection were performed at *ca.* 160 K on a IPDS STOE diffractometer using graphite monochromatized Mo-Kα radiation. The structure was solved by direct methods and subsequent difference Fourier maps. CCDC 182/1708. See htpp://www.rsc.org/suppdata/cc/b0/b004478o/ for crystallographic files in .cif format.

§ A suspension of Cp_2ZrCl_2 (0.900 g, 3.08 mmol) was treated with 2 equiv. solid LiC≡CPh (0.665 g, 6.16 mmol) in benzene for 4 h and species such as Cp_2ZrCl_2, $Cp_2ZrCl(C{\equiv}CPh)$ and **2** were identified by ^1H NMR (in nearly 1:4:1 ratio respectively). After 24 h stirring and work-up, **2** was obtained as a crystalline solid (0.840 g, 64% yield). With 3 equiv. LiC≡CPh for 24 h, in the same experimental conditions, a red solution is obtained with the appearance of a paramagnetic Zr^{III} species (g = 1.997, $a(^{91}Zr)$ = 37 G, 20%) which broadens the ^1H NMR signals of the solution (the main peak observed at 5.6 ppm could not be assigned). Different experiments were conducted in THF and in absence of daylight (to avoid the formation of the zirconacyclocumulene species) between $(C_5H_4R)_2Zr(C{\equiv}CPh)_2$ (R = Me, $SiMe_3$) and LiC≡CPh. ^{13}C NMR spectroscopy shows the characteristic peak of the ($\eta^2:1,2\text{-}PhC_2C{\equiv}CPh$) moiety at 208 and 205 ppm for R = Me and $SiMe_3$, respectively which suggests the *in situ* formation of $Li[(C_5H_4R)_2Zr(C{\equiv}CPh)(\eta^2:1,2\text{-}PhC_2C{\equiv}CPh)]$ (R = Me, $SiMe_3$) (for $Cp^*_2Ti(\eta^2:1,2\text{-}Me_3SiC_2C{\equiv}CSiMe_3$[11] two peaks were observed at 227 and 205 ppm). Hydrolysis of the THF mixture with HCl gives the *Z/E* enynes (30:70).

¶ It is of note that Cp_2ZrCl_2 + 3 equiv. LiC≡CPh in toluene at room temperature for 24 h selectively affords, after hydrolysis, the *Z* isomer whereas the same reaction carried out in THF gives a mixture of *Z/E* isomers (40:60). The *Z* isomer was selectively obtained in THF when the reaction is carried out at −80 °C.[9]

‖ Hydrolysis experiments with HCl on $(C_5H_4R)_2Zr(\eta^4:1,2,3,4\text{-}PhC{=}C{=}C{=}CPh)$ (R = H, Me, $SiMe_3$) give in toluene or in THF solution nearly 100% of the *E* isomer PhCH=CH-C≡CPh, in contradiction with the described results in which the η^2 coordination is involved.

** LiC≡CBu^t was added to **2** in THF; after stirring for 4 h, the solvent was evaporated to dryness and replaced by toluene. Hydrolysis with HCl (3 equiv. in solution in diethyl ether) gives Z enynes; ^1H NMR (δ/ppm, $CDCl_3$, 250 MHz), MS: PhCH=CHC≡CBu^t: 6.55, 5.69, (d, CH=CH, J = 12 Hz), 1.32 (s, Bu^t), MS: 184; PhC≡CCH=CHBu^t: 5.87, 5.60, (d, CH=CH, J = 12 Hz), 1.26 (s, Bu^t), MS: 184; PhCH=CHC≡CPh: 6.70, 5.92, (d, CH=CH, J = 12 Hz), MS: 204. When HCl hydrolysis was performed in THF, a mixture of *Z/E* enynes was observed by GC/MS but not further characterized.

†† ^1H and $^{13}C\{^1H\}$ NMR of the reaction show complex spectra in which three main cyclopentadienyl signals can be observed at 5.76, 5.71, 5.67/105.0, 104.9, 104.7 ppm; low field quaternary carbons at 228, 225.9, 208.2, 205.9, 203, 202 ppm were also observed.

1 H. S. Nalwa and S. Miyata, *Nonlinear Optics of Organic Molecules and Polymers*, CRC Press, Boca Raton, FL, 1997.
2 (*a*) A. de Meijeire, *Top. Curr. Chem.*, 1999, **201**, 000; (*b*) F. Diederich, in *Modern Acetylene Chemistry*, ed. P. J. Stang and F. Diederich, VCH, Weinheim, 1995, p. 443; (*c*) F. Diederich and Y. Rubin, *Angew. Chem., Int. Ed. Engl.*, 1992, **31**, 1101.
3 (*a*) R. Choukroun, C. Lorber, B. Donnadieu, B. Henner, R. Frantz and C. Guerin, *Chem. Commun.*, 1999, 1099 and references therein; (*b*) R. Choukroun, B. Donnadieu, I. Malfant, S. Haubrich, R. Frantz, C. Guerin and B. Henner, *Chem. Commun.*, 1997, 2315.
4 C. Danjoy, J. Zhao, B. Donnadieu, J. P. Legros, L. Valade, R. Choukroun, A. Zwick and P. Cassoux, *Chem. Eur. J.*, 1998, **4**, 1100.
5 R. Choukroun and P. Cassoux, *Acc. Chem. Res.*, 1999, **32**, 494.
6 W. Ahlers, B. Temme, G. Erker, R. Fröhlich and T. Fox, *J. Organomet. Chem.*, 1997, **527**, 191.
7 (*a*) G. Erker, W. Frömberg, R. Mynott, B. Gabor and C. Krüger, *Angew. Chem., Int. Ed. Engl.*, 1986, **25**, 463; (*b*) G. Erker, W. Frömberg, R. Benn, R. Mynott, K. Angermund and C. Krüger, *Organometallics*, 1989, **8**, 911; (*c*) G. L. Wood, C. B. Knobler and M. F. Hawthorne, *Inorg. Chem.*, 1989, **28**, 382; (*d*) U. Rosenthal and H. Görls, *J. Organomet Chem.*, 1992, **439**, 36.
8 (*a*) G. Erker, M. Albrecht, C. Krüger, M. Nolte and S. Werner, *Organometallics*, 1993, **12**, 4979; (*b*) A. D. Jenkins, M. F. Lappert and R. C. Scrivistava, *J. Organomet. Chem.*, 1970, **23**, 165.
9 K. Takagi, C. J. Rousset and E. Negishi, *J. Am. Chem. Soc.*, 1991, **113**, 1440.
10 E. S. Johnson, G. J. Balaich, P. E. Fanwick and I. P. Rothwell, *J. Am. Chem. Soc.*, 1997, **119**, 11 086.
11 (*a*) P. M. Pellny, F. G. Kirchbauer, V. V. Burlakov, W. Baumann, A. Spannenberg and U. Rosenthal, *J. Am. Chem. Soc.*, 1999, **121**, 8313; (*b*) P. M. Pellny, F. G. Kirchbauer, V. V. Burlakov, A. Spannenberg, K. Mach and U. Rosenthal, *Chem. Commun.*, 1999, 2505 and references therein.
12 R. Choukroun, B. Donnadieu, J. Zho, P. Cassoux, C. Lepetit and B. Silvi, *Organometallics*, 2000, **10**, 1901.
13 (*a*) V. V. Burlakov, N. Peulecke, W. Baumann, A. Spannenberg, R. Kempe and U. Rosenthal, *J. Organomet. Chem.*, 1997, **536**, 293; (*b*) S. Pulst, P. Arndt, B. Heller, W. Baumann, R. Kempe and U. Rosenthal, *Angew. Chem., Int. Ed. Engl.*, 1996, **35**, 1112.
14 U. Rosenthal, A. Ohff, W. Baumann, R. Kempe, A. Tillack and V. V. Burlakov, *Angew. Chem., Int. Ed. Engl.*, 1994, **33**, 1605.
15 B. Temme, G. Erker, R. Frölich and M. Grehl, *Angew. Chem., Int. Ed. Engl.*, 1994, **33**, 1480.
16 A stable tweezer bimetallic alkynylcopper(I) titanium acetylide has been characterized. M. D. Janssen, M. Herres, L. Zsolnai, D. Grove, A. L. Spek, H. Lang and G. van Koten, *Organometallics*, 1995, **14**, 1098.

ChemComm

Synthesis, structural characterization and binding studies of a novel dinuclear gold(I) calix[4]crown acetylide complex

Vivian Wing-Wah Yam,* Kai-Leung Cheung, Li-Hua Yuan, Keith Man-Chung Wong and Kung-Kai Cheung

Department of Chemistry, The University of Hong Kong, Pokfulam Road, Hong Kong, People's Republic of China. E-mail: wwyam@hku.hk

Received (in Cambridge, UK) 3rd May 2000, Accepted 21st June 2000
Published on the Web 24th July 2000

A novel dinuclear gold(I) calix[4]crown acetylide complex, $[Au(PPh_3)]_2L$, has been synthesized and structurally characterized; binding studies of the complex revealed a high K^+/Na^+ selectivity.

During the last decade, there has been a growing interest in the study of calix[*n*]arenes,[1,2] owing to their unique molecular structure and simple one-pot preparation. Indeed, calix[4]arene has proven to be a very important building block in supramolecular chemistry.[3] The easy chemical transformability of this molecule, together with its 'tunable' molecular shape and conformation, makes calix[*n*]arene an attractive candidate for molecular design strategies and has led to an increasing number of examples in the literature. In particular the calix[4]arene is the best developed of the calix[*n*]arene family as a molecular scaffold for the synthesis of more elaborate molecules, supramolecular assemblies, sensors,[4] and receptors.[5]

The recent interest in calixcrowns, which represent a class of calixarenes functionalized with crown ether moieties on the lower rim, together with our recent efforts in the utilization of crown ether-containing metal complexes in the design of selective spectrochemical and luminescence ion probes,[6] have prompted us to extend our work to the calixcrown system. Herein are reported the synthesis, structural characterization, and binding behaviour of a novel dinuclear gold(I) calix[4]-crown acetylide complex.

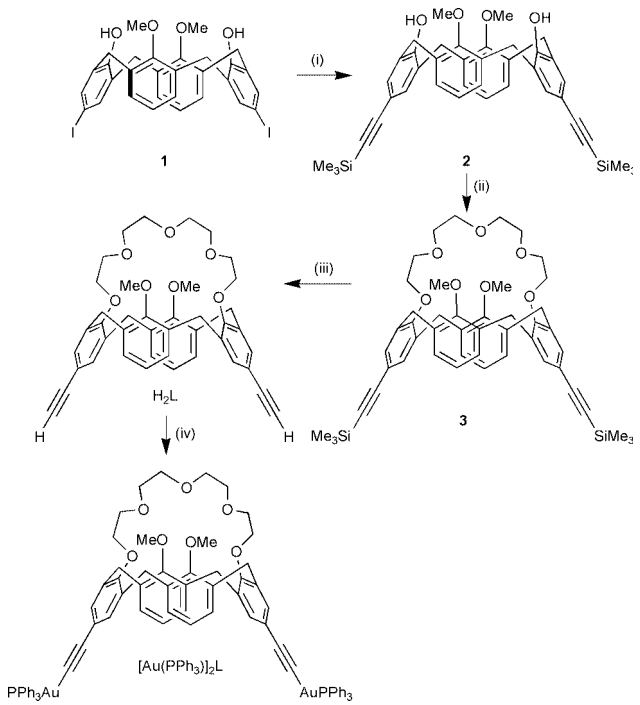

Scheme 1 *Reagents and conditions*: (i) $HC{\equiv}CSiMe_3$, Et_3N, $Pd(PPh_3)_2Cl_2$, CuI; (ii) tetraethylene glycol bis(toluene-*p*-sulfonate), Cs_2CO_3, CH_3CN; (iii) KF, DMF, 65 °C; (iv) NaOEt, $(PPh_3)AuCl$, EtOH.

The reaction of (**1**)[7] with (trimethylsilyl)acetylene in the presence of CuI, $Pd(PPh_3)_2Cl_2$ and triethylamine for 24 h at *ca.* 40 °C gave **2** in 50% yield (Scheme 1). Introduction of the polyether linkage into the lower rim was accomplished by reacting **2** with tetraethylene glycol bis(toluene-*p*-sulfonate) in the presence of Cs_2CO_3 in MeCN to give **3**, followed by deprotection of the trimethylsilyl groups by KF to give H_2L in moderate yield. Reaction of $Au(PPh_3)Cl$ with H_2L in the presence of NaOEt in EtOH afforded the desired complex, $[Au(PPh_3)]_2L$, as pale yellow crystals after subsequent recrystallisation using dichloromethane–*n*-hexane. The identities of **2**, **3**, H_2L and $[Au(PPh_3)]_2L$ have been confirmed by satisfactory elemental analyses, ^1H NMR, ^{31}P NMR, IR, and FAB-MS.† The structure of $[Au(PPh_3)]_2L$ has also been determined by X-ray crystallography.‡

Fig. 1 shows $[Au(PPh_3)]_2L$ with atomic numbering. The calix[4]crown in the gold(I) complex shows a cone conformation. Cone conformation is also known in 1,3-calixcrown compounds[8] although a 1,3-alternate conformation[9] is more commonly found. The two gold atoms adopt an essentially linear coordination geometry, with P–Au–C bond angles of

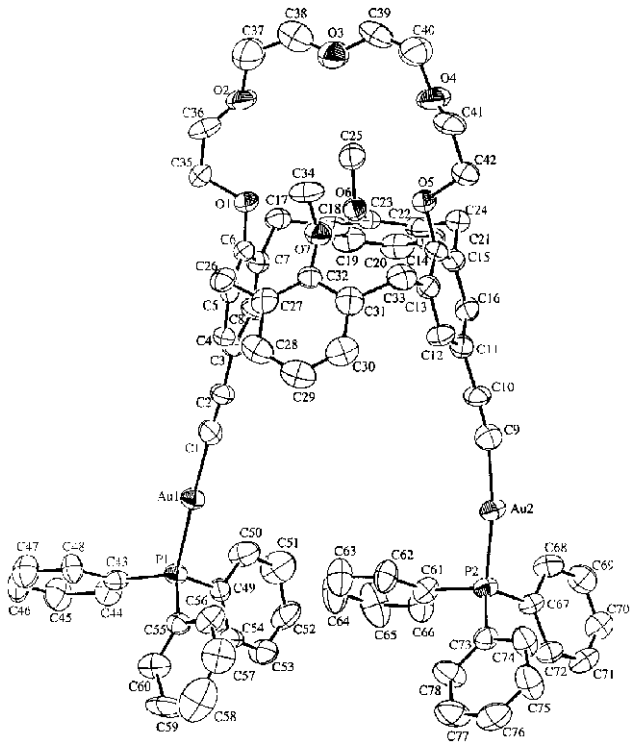

Fig. 1 Perspective drawing of $[Au(PPh_3)]_2L$ with atomic numbering. Hydrogen atoms have been omitted for clarity. Thermal ellipsoids are shown at the 40% probability level. Selected bond distances (Å) and bond angles (°): Au(1)–P(1) 2.283(3), Au(2)–P(2) 2.275(3), Au(1)–C(1) 2.04(1), Au(2)–C(9) 2.04(1), C(1)–C(2) 1.18(2), C(9)–C(10) 1.17(2); P(1)–Au(1)–C(1) 177.9(4), P(2)–Au(2)–C(9) 170.5(4), Au(1)–C(1)–C(2) 177(1), Au(2)–C(9)–C(10) 166(1).

DOI: 10.1039/b003536j

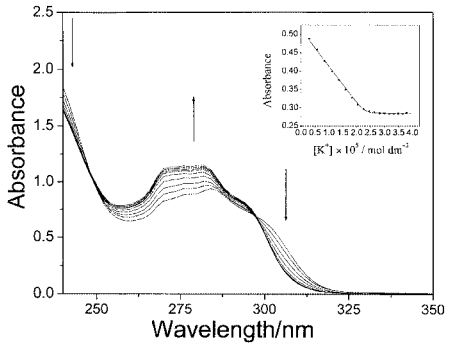

Fig. 2 UV-Vis absorption spectral changes of $[Au(PPh_3)]_2L$ (2×10^{-5} mol dm^{-3}) upon addition of various concentrations of potassium hexafluorophosphate in dichloromethane–methanol (1 : 1 v/v) containing 0.1 mol dm^{-3} tetra-*n*-butylammonium hexafluorophosphate as supporting electrolyte. The insert shows a plot of *A versus* [K^+] at 304 nm and its theoretical fit.

170.5(4) and 177.9(4)°; the slight deviation from a perfect 180° is probably a result of the steric demand of the ligands and crystal packing forces. The C≡C bond lengths of 1.18(2) and 1.17(2) Å are typical of terminal Au(I) acetylides.[10,11]

The electronic absorption spectra of $[Au(PPh_3)]_2L$ in dichloromethane–methanol (1 : 1 v/v) containing 0.1 M tetra-*n*-butylammonium hexafluorophosphate as supporting electrolyte show spectral changes upon addition of K^+ and Na^+ ions. Fig. 2 shows the UV-vis spectral traces of $[Au(PPh_3)]_2L$ upon addition of K^+ ions. Isosbestic points were observed at 244 and 298 nm which are indicative of a clean reaction. Theoretical fits of the plots of absorbance *vs.* [K^+] or [Na^+] to eqn. (1) derived for a

$$X = X_o + \frac{X_{lim} - X_o}{2C_o}[C_o + C_m + 1/K_s - [(C_o + C_m + 1/K_s)^2 - 4C_oC_m]^{\frac{1}{2}}] \quad (1)$$

1 : 1 complexation stoichiometry gave the stability constant K_s. In eqn. (1) X_o, X and X_{lim} are the initial absorbance of $[Au(PPh_3)]_2L$, the absorbance after the addition of a given amount of salt at concentration C_m, and the limiting absorbance of $[Au(PPh_3)]_2L$ in the fully complexed state, respectively; C_o is the initial concentration of $[Au(PPh_3)]_2L$ and C_m is the total salt concentration. The log K_s values of 7.24 and 2.75 were obtained for the binding of K^+ and Na^+ ions, respectively. The selective recognition of K^+ over Na^+ with a K^+/Na^+ selectivity of 3×10^5, which is higher than a related 1,3-dimethoxycalix[4]arene crown compound (K^+/Na^+ selectivity = 3×10^3),[9a] and even higher than that of the naturally occurring valinomycin,[12] may suggest that the present complex would serve as a promising candidate for application as a selective K^+ ion chemosensor.

V. W.-W. Y. acknowledges financial support from the Research Grants Council and The University of Hong Kong, K.-L. C. the receipt of a postgraduate studentship, and K. M.-C. W. the receipt of a University Post-Doctoral Fellowship, both administered by The University of Hong Kong.

Notes and references

† **2**: ^{1}H NMR (300 MHz, $CDCl_3$, 298 K, relative to Me_4Si): δ 0.15 (s, 18H, $SiMe_3$), 3.31 (d, 4H, *J* 13.2 Hz, Ar-CH_2-Ar), 3.88 (s, 6H, OCH_3), 4.15 (d, 4H, *J* 13.2 Hz, Ar-CH_2-Ar), 6.72–7.14 (m, 10H, Ar), 8.03 (s, 2H, OH); ^{13}C NMR (126 MHz, $CDCl_3$, 298 K, relative to Me_4Si): δ 30.8, 63.7, 91.7, 105.9, 113.3, 125.3, 128.0, 129.3, 132.0, 132.5, 153.0, 154.0; IR (KBr, ν/cm^{-1}): 2957, 2905s ν(C-$H_{aliphatic}$), 2150m ν(C≡C); positive FAB-MS: ion clusters at *m/z* 645 {M^+}. Elemental analyses. Found: C 73.73, H 7.16. Calcd. for $C_{40}H_{44}O_4Si_2{\cdot}\frac{1}{2}H_2O$: C 73.47, H 6.94%. **3**: ^{1}H NMR (300 MHz, $CDCl_3$, 298 K, relative to Me_4Si): δ 0.14 (s, 18H, $SiMe_3$), 3.16 (d, 4H, *J* 12.4 Hz, Ar-CH_2-Ar), 3.55–3.90 (m, 16H, OCH_2CH_2O), 4.10 (s, 6H, OCH_3), 4.37 (d, 4H, *J* 12.4 Hz, Ar-CH_2-Ar), 6.79 (s, 4H, aryl protons *ortho* to C≡C), 6.89 (t, 2H, *J* 7.3 Hz, aryl protons *para* to OCH_3), 7.09 (d, 4H, *J* 7.3 Hz, aryl protons *meta* to OCH_3); ^{13}C NMR (126 MHz, $CDCl_3$, 298 K, relative to Me_4Si): δ 31.1, 61.1, 65.8, 70.7, 70.8, 71.4, 123.0, 124.5, 128.7, 132.1, 133.5, 135.6, 156.4, 158.9. IR (KBr, ν/cm^{-1}): 2922, 2903, 2872s ν(C-$H_{aliphatic}$), 2154m ν(C≡C); positive FAB-MS: ion cluster at *m/z* 803 {M^+}, 826 {M + Na^+}. Elemental analyses. Found: C 71.63, H 7.05. Calcd. for $C_{48}H_{58}O_7Si_2$: C 71.78, H 7.28%. **H_2L**: ^{1}H NMR (300 MHz, $CDCl_3$, 298 K, relative to Me_4Si): δ 2.77 (s, 2H, C≡CH), 3.16 (d, 4H, *J* 12.6 Hz, Ar-CH_2-Ar), 3.56–3.93 (m, 16H, OCH_2CH_2O), 4.10 (s, 6H, OCH_3), 4.38 (d, 4H, *J* 12.6 Hz, Ar-CH_2-Ar), 6.76 (s, 4H, aryl protons *ortho* to C≡C), 6.88 (t, 2H, *J* 7.3 Hz, aryl protons *para* to OCH_3), 7.08 (d, 4H, *J* 7.3 Hz, aryl protons *meta* to OCH_3); ^{13}C NMR (126 MHz, $CDCl_3$, 298 K, relative to Me_4Si): δ 31.1, 61.2, 70.8, 70.9, 71.5, 73.4, 75.4, 84.32, 115.9, 123.1, 128.7, 132.1, 133.8, 156.4, 158.9; IR (KBr, ν/cm^{-1}): 3292s ν(≡CH), 2909, 2868s ν(C-$H_{aliphatic}$), 2107w ν(C≡C); positive FAB-MS: ion cluster at *m/z* 658 {M^+}, 681 {M + Na^+}. Elemental analyses. Found: C 72.86, H 6.24. Calcd. for $C_{42}H_{42}O_7{\cdot}\frac{1}{2}CH_2Cl_2$: C 72.79, H 6.18%. $[Au(PPh_3)]_2L$: ^{1}H NMR (300 MHz, $CDCl_3$, 298 K, relative to Me_4Si): δ 3.12 (d, 4H, *J* 12.6 Hz, Ar-CH_2-Ar), 3.65–4.00 (m, 16H, OCH_2CH_2O), 4.05 (s, 6H, OCH_3), 4.32 (d, 4H, *J* 12.6 Hz, Ar-CH_2-Ar), 6.55–7.10 (m, 10H, Ar), 7.25–7.58 (m, 30H, PPh_3); ^{31}P NMR (202 MHz, $CDCl_3$, 298 K, relative to 85% H_3PO_4): δ 43.5 (s, PPh_3); IR (KBr, ν/cm^{-1}): 2918, 2866s ν(C-$H_{aliphatic}$), 2099w ν(C≡C); positive FAB-MS: ion cluster at *m/z* 1597 {M + Na^+}; UV-Vis [λ/nm (ε/dm^3 mol^{-1} cm^{-1})]: CH_2Cl_2, 276 (44440), 286 (48930), 306 sh (31050), 344 (11370). Elemental analyses. Found: C 59.54, H 4.72. Calcd. for $C_{78}H_{70}O_7Au_2P_2$: C 59.47, H 4.48%.

‡ *Crystal data* for $[Au(PPh_3)]_2L$: $[C_{78}H_{70}O_7P_2Au_2.H_2O]$, M_r = 1593.30, triclinic, space group *P*1 (No. 2), *a* = 13.108(2), *b* = 15.195(2), *c* = 21.461(3) Å, α = 83.57(2), β = 76.71(2), γ = 65.43(2)°, *V* = 3782(1) $Å^3$, *Z* = 2, D_c = 1.399 g cm^{-3}, μ(Mo-Kα) = 39.80 cm^{-1}, *F*(000) = 1584, *T* = 301 K. A crystallographic asymmetric unit consists of one formula unit. Convergence for 806 variable parameters by least-squares refinement on *F* with $w = 4F_o^2/\sigma^2(F_o^2)$, where $\sigma^2(F_o^2) = [\sigma^2(I) + (0.040F_o^2)^2]$ for 7855 reflections with $I > 3\sigma(I)$ was reached at R = 0.055 and wR = 0.081 with a goodness-of-fit of 2.16. CCDC 182/1705. See http://www.rsc.org/suppdata/cc/b0/b003536j/ for crystallographic files in .cif format. X-Ray crystallographic data is available as supplementary data available from BLDSC (suppl. no. 57711, pp. 25) or the RSC library. See Instructions for Authors available *via* the RSC web page (http://www.rsc.org/authors).

1 C. D. Gutsche, *Calixarenes: Monographs in supramolecular chemistry*, The Royal Society of Chemistry, Cambridge, 1989.
2 S. Shinkai, *Tetrahedron*, 1993, **49**, 8933; V. Böhmer, *Angew. Chem., Int. Ed. Engl.*, 1995, **34**, 713.
3 P. Lhoták and S. Shinkai, *J. Synth. Org. Chem. Jpn.*, 1995, **53**, 963.
4 P. Bühlmann, E. Pretsch and E. Bakker, *Chem. Rev.*, 1998, **98**, 1593; D. Diamond and M. A. Mckervey, *Chem. Soc. Rev.*, 1996, 15.
5 R. Ungaro, A. Arduiini, A. Casnati, A. Pochini and F. Ugozzoli, *Pure Appl. Chem.*, 1996, **68**, 1213; A. F. D. de Namor, R. M. Cleverley and M. L. Zapata-Ormachea, *Chem. Rev.*, 1998, **98**, 2495.
6 V. W. W. Yam, K. M. C. Wong, V. W. M. Lee, K. K. W. Lo and K. K. Cheung, *Organometallics*, 1995, **14**, 4034; V. W. W. Yam, K. K. W. Lo and K. K. Cheung, *Inorg. Chem.*, 1995, **34**, 4013; V. W. W. Yam, V. W. M. Lee, F. Ke and K. W. M. Siu, *Inorg. Chem.*, 1997, **36**, 2124; V. W. W. Yam and V. W. M. Lee, *J. Chem. Soc., Dalton Trans.*, 1997, 3005; V. W. W. Yam, C. K. Li and C. L. Chan, *Angew. Chem., Int. Ed. Engl.*, 1998, **37**, 2857; V. W. W. Yam, Y. L. Pui, W. P. Li, K. K. W. Lo and K. K. Cheung, *J. Chem. Soc., Dalton Trans.*, 1997, 3615.
7 B. Klenke and W. Friedrichsen, *J. Chem. Soc., Perkin Trans. 1*, 1998, 3377.
8 H. Matsumoto and S. Shinkai, *Tetrahedron Lett.*, 1996, **37**, 77; T. Haino, Y. Katsutani, H. Akii and Y. Fukazawa, *Tetrahedron Lett.*, 1998, **39**, 8133; X. Chen, M. Ji, D. R. Fischer and C. M. Wai, *Inorg. Chem.*, 1999, **38**, 5449.
9 (*a*) E. Ghidini, F. Ugozzoli, R. Ungaro, S. Harkema, A. Abu El-Fadl and D. N. Reinhoudt, *J. Am. Chem. Soc.*, 1990, **112**, 6979; (*b*) R. Ungaro, A. Casnati, F. Ugozzoli, A. Pochini, J. F. Dozol, C. Hill and H. Rouquette, *Angew. Chem., Int. Ed. Engl.*, 1994, **33**, 1506; (*c*) A. Casnati, A. Pochini, R. Ungaro, F. Ugozzoli, F. Arnaud, S. Fanni, M. J. Schwing, R. J. M. Egberink, F. de Jong and D. N. Reinhoudt, *J. Am. Chem. Soc.*, 1995, **117**, 2767; (*d*) R. A. Sachleben, A. Urvoas, J. C. Bryan, T. J. Haverlock, B. P. Hay and B. A. Moyer, *Chem. Commun.*, 1999, 1751; (*e*) L. Prodi, F. Bolletta, M. Montalti, N. Zaccheroni, A. Casnati, F. Sansone and R. Ungaro, *New J. Chem.*, 2000, **24**, 155.
10 R. J. Cross and M. F. Davidson, *J. Chem. Soc., Dalton Trans.*, 1986, 411; V. W. W. Yam, S. W. K. Choi and K. K. Cheung, *J. Chem. Soc., Dalton Trans.*, 1996, 3411; V. W. W. Yam and S. W. K. Choi, *J. Chem. Soc., Dalton Trans.*, 1996, 4227.
11 J. Bourson, J. Pouget and B. Valeur, *J. Phys. Chem.*, 1993, **97**, 4552.
12 A. Casnati, A. Pochini, R. Ungaro, C. Bocchi, F. Ugozzoli and D. N. Reinhoudt, *Chem. Eur. J.*, 1996, **2**, 436.

Iron guanidinate complexes and formation of a novel dinuclear iron(II) species with a dianionic μ-η²:η² (biguanidinate) ligand

Stephen R. Foley, Glenn P. A. Yap and Darrin S. Richeson*

Department of Chemistry, University of Ottawa, Ottawa, ON, Canada K1N 6N5. E-mail: darrin@science.uottawa.ca

Received (in Irvine, CA) 2nd May 2000, Accepted 16th June 2000
Published on the Web 24th July 2000

Reaction of the lithium salt of *N*,*N*′,*N*″-triisopropylguanidinate with Fe(III) or Fe(II) halides led to isolation of the new species $[(Pr^iN)_2C(HNPr^i)]_2FeCl$ (1) and $[\mu\text{-}\eta^2\text{-}(Pr^iN)_2C(HNPr^i)]_2\{Fe[\eta^2\text{-}(Pr^iN)_2C(HNPr^i)]\}_2$ (2); attempted alkylation of 1 with 1 equiv. of a variety of reagents produced 2; the reaction of 2 with $LiCH_2SiMe_3$ resulted in a coupling reaction between the two bridging ligands to yield $[(\mu\text{-}\eta^2:\eta^2\text{-}(Pr^iN)_2C)_2NPr^i)]\{Fe[\eta^2\text{-}(PrN^i)_2C(HNPr^i)]\}_2$.

Amidinate anions are well established as versatile ligands for a variety of transition metal complexes and particularly for compounds for the early transition metals.[1,2] In contrast, the isoelectronic *N*,*N*′,*N*″-trialkylguanidinate anions have received very limited attention as ligands in organometallic and coordination chemistry (Fig. 1).[3,4] We anticipate that these species will exhibit the same flexibility in coordination properties as amidinates and that the presence of the third nitrogen center should lead to novel coordination properties. Furthermore, the added potential of generating dianionic species, by deprotonation of the second N–H function, may yield a unique, conjugated π system.

The scarcity of Fe complexes supported with anionic nitrogen-centered ligands warrants exploration of guanidinate ligands in this regard. Interestingly, the first transition metal complexes with dianionic guanidinate ligands are represented by the dinuclear iron complexes $[\mu^2\text{-}(RN)_3C][Fe(CO)_3]_2$ (R = Cy, Pr^i).[5] These species were formed by the reaction of the appropriate carbodiimide with $Fe(CO)_5$ and remain the sole examples of guanidinate anions employed in Fe chemistry.

We wish to report our initial exploration into the use of *N*,*N*′,*N*″-trisubstituted guanidinates as supporting ligands for Fe(II) and Fe(III). This necessarily requires the development of fundamental ideas regarding the introduction of these ligands into the metal coordination sphere as well as definition of the reactivity of these species.[3,4,6]

The *N*,*N*′,*N*″-tri(alkyl)guanidinatolithium $[[(RN)_2C(HNR)]Li$ (R = Pr^i, Cy) starting materials were formed by direct reaction of the guanidine with 1 equiv. of either MeLi or Bu^nLi.[4] In all cases, metathesis reactions with iron halides were carried out with freshly prepared solutions of lithium guanidinate in ether or THF (Scheme 1). Addition of 0.5 equiv. $FeCl_3$ to a solution of $[(Pr^iN)_2C(HNPr^i)]Li$ followed by recrystallization from pentane resulted in isolation of the new bis(guanidinate)iron(III) chloride complex $[(Pr^iN)_2C(HNPr^i)]_2FeCl$, **1** (Scheme 1).[7] The solid state structure of **1** revealed a monomer with two monoanionic chelating bidentate guanidinate ligands yielding planar M–N–C–N cycles as depicted in Scheme 1.[8] The coordination sphere of the metal is completed by a terminal chloride to generate a distorted pseudo-trigonal bipyramidal geometry for **1** with approximate C_2 symmetry. The average Fe–N_{ax} bond distances of 2.085(3) Å are slightly longer than the average Fe–N_{eq} distances of 2.008(3) Å. The C–N bond distances within the chelate rings (average 1.34, 1.36 Å) are consistent with partial double bond character within the NCN moiety. The central C atoms of the guanidinates, the Cl ligand and the Fe center are coplanar.

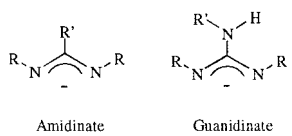

Fig. 1

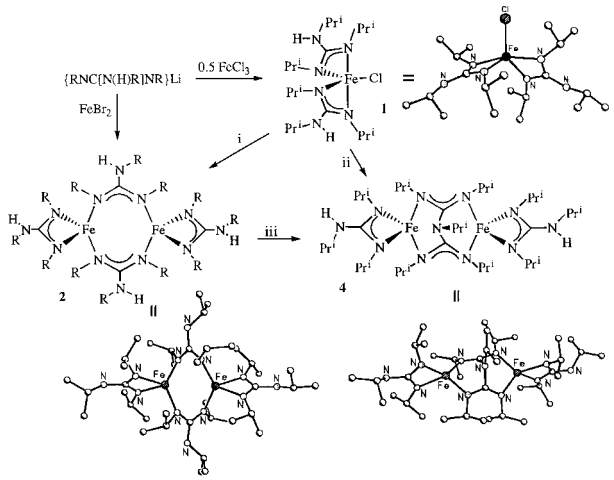

Scheme 1 Reaction scheme for the preparation of **1**, **2** and **4** and the structures of these complexes. *Reagents and conditions*: i, LiMe, $LiCH_2(SiMe_3)$, $ZnEt_2$, or BzMgCl; ii, 2 $LiCH_2(SiMe_3)$; iii, $LiCH_2(SiMe_3)$.

Attempts to exchange the chloro ligand of **1** with an alkyl group using a variety of reagents including RLi (R = Me, $CH_2(SiMe_3)$), $ZnEt_2$, and BzMgCl were examined. In all cases, reduction of the metal center from Fe(III) to Fe(II) was observed and complex **2** was isolated in 40–80% yields.[7] Single crystal X-ray analysis of this new product showed it to be a dinuclear species with two bridging guanidinate ligands and two chelating bidentate ligands with formula $Fe_2[\mu\text{-}\eta^2\text{-}(Pr^iN)_2C(HNPr^i)]_2[\eta^2\text{-}(Pr^iN)_2C(HNPr^i)]_2$ (Scheme 1).[8] Another route to the Fe(II) dinuclear species **2** was *via* direct reaction of $FeBr_2$ with 2 equiv. of $[(Pr^iN)_2C(HNPr^i)]Li$ in THF followed by recrystallization from ether. This method led to isolation of **2** in 82% yield.

The coordination sphere for each Fe center is composed of four nitrogen centers of the two different ligands. The N–Fe–N bond angles exhibit a broad range of values from 63.3 to 132.3° with an average of 106°. The Fe–N bond distances vary from 2.056(6) to 2.127(7) Å. The two chelating bidentate ligands in **2** are planar and exhibit bonding parameters reminiscent of other complexes with chelating monoanionic guanidinates such as **1**. In contrast the bridging ligands appear to be quite distorted. The central C atoms of both of these groups are planar and the four N centers deviate only slightly from planarity. The CN bond distances within the bridging groups are indicative of delocalized π-bond (av. 1.33 Å). Furthermore, the average C–N(H)Pr^i distance of 1.41 Å is consistent with a CN single bond. However, the bridging ligands coordinate to the two Fe centers with a decided twist that can be described by the dihedral angle α represented in Fig. 2. In **2** these angles are 67.2 and 70.3°.

A similarly distorted bridging ligand was observed in the case of the benzamidinate complex $Fe_2(\mu\text{-DPhBz})_2(DPhBz)_2$ (**A**).[9]

DOI: 10.1039/b003547p

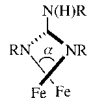

Fig. 2

In **A** the severe distortion of the bridging ligands was attributed to a weak intramolecular Fe···N interaction at a distance of 2.477(4) Å. In the case of **2** the two closest non-coordinated N atoms to the Fe centers are at distances of 2.970 and 3.007 Å. These distances are considerably further than in **A** and seem

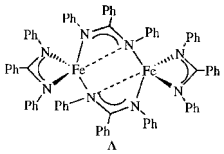

A

unlikely to be the result of an interaction between these atoms. The possibility of an Fe–Fe bond in **2** can be excluded based on the large iron–iron separation of 3.264 Å.

We have further evidence that the bonding features observed for **2** may be general for this ligand system. In a reaction scheme similar to that used in the preparation of **2**, $FeBr_2$ was reacted with 2 equiv. of $[(CyN)_2C(HNCy)]Li$ in ether to successfully generate the cyclohexyl analogue, $Fe_2[\mu\text{-}\eta^2\text{-}(CyN)_2C(HNCy)]_2[\eta^2\text{-}(CyN)_2C(HNCy)]$ **3**. The resemblance of the metrical parameters of **3** with those of **2** was confirmed through a structural analysis.[10] Complex **3** displayed a similar orientation for the bridging ligands with the dihedral angles α of 70.0 and 73.6°. In **3**, the closest non-coordinated N centers for each Fe were even further away than in **2** (*i.e.* 3.050 and 3.190 Å) and a long Fe–Fe separation (3.161 Å) ruled out a metal–metal bonding interaction.

It is worthwhile to note that for the molybdenum complex $Mo_2[\mu\text{-}\eta^2\text{-}(NPh)_2CNHPh]_4$, all four of the triaryl guanidinate ligands bridge the two metal centers resulting in the formation of a metal–metal bond and none of the bridging ligands demonstrate the distortion exhibited by complex **2**.[11]

Reaction of complex **1** with a variety of alkylating reagents led to reduction of the Fe(III) center and formation of the dinuclear structure **2**. When either **2** or **1** are allowed to react with additional $LiCH_2SiMe_3$ a reaction involving the guanidinate ligands was observed (Scheme 1). For example, reaction of **1** with 2 equiv. of $LiCH_2SiMe_3$ resulted in formation of the Fe(II) complex **4**. Examination of single crystals of **4** by X-ray diffraction provided the structure displayed in Scheme 1.[8]

The obvious result of the added lithium reagent is a coupling of the two bridging guanidinates to yield a bridging biguanidinate dianion. A likely pathway for the transformation of **2** to **4** begins with the deprotonation of one of the bridging ligands with the added lithium reagent to generate a nitrogen-centered anion. Subsequent attack of this nucleophilic center at the central carbon of the second bridging ligand and release an amido anion would generate the new dianionic ligand, $\{[(Pr^iN)_2C]_2NPr^i\}^{2-}$ observed for **4**.

Bonding parameters within the $\{[(Pr^iN)_2C]_2NPr^i\}^{2-}$ moiety are consistent with the resonance representation in Scheme 1. In particular, the π bonds within this species appear to be delocalized as depicted. Furthermore, the $C(NPr^i)_3$ carbon centers are planar (Σ = 360°) and the N atoms bonded to iron deviate only slightly from planarity (Σ = 357°). The two Fe atoms in **4** are separated by a distance of 4.945 Å.

The utility of *N*,*N*′,*N*″-trialkylguanidine ligands in the preparation of new Fe(II/III) complexes has been established. Attempts to alkylate bis(guanidinato)iron(III) chloride resulted in reduction of Fe(III) to Fe(II) and formation of dinuclear species. Complexes **1**–**4** demonstrate the versatility in coordination behavior for these ligands. Transformation of guanidinate ligands can be prompted by deprotonation and in the case of **2** led to the tetradentate biguanidinate dianion $\{[(Pr^iN)_2C]_2NPr^i\}^{2-}$. Our continuing efforts are directed toward understanding the details that dictate the formation of mono- *vs.* dianionic ligands and the intramolecular interactions exhibited by these ligands.

This work was supported by the Natural Sciences and Engineering Research Council of Canada (NSERC).

Notes and references

1 F. T. Edelmann, *Coord. Chem. Rev.*, 1994, **137**, 403; J. Barker and M. Kilner, *Coord. Chem. Rev.*, 1994, **133**, 219.

2 For recent examples see: C. Averbuj and M. S. Eisen, *J. Am. Chem. Soc.*, 1999, **121**, 8755 and references therein; J. A. R. Schmidt and J. Arnold, *Chem. Commun.*, 1999, 2149 and references therein; E. A. C. Brussee, A. Meetsma, B. Hessen and J. H. Teuben, *Organometallics*, 1998, **17**, 4090 and references therein; P. J. Stewart, A. J. Blake and P. Mountford, *Organometallics*, 1998, **17**, 3271 and references therein.

3 For some recent examples of monoanionic guanidinates as ligands see: G. R. Giesbrecht, A. Shafir and J. Arnold, *J. Chem.Soc., Dalton Trans.*, 1999, 3601; K. T. Holman, S. D. Robinson, A. Sahajpal and J. W. Steed, *J. Chem. Soc., Dalton Trans.*, 1999, 15; J. M. Decams, L. G. Hubert-Pfalzgraf and J. Vaissermann, *Polyhedron*, 1999, **18**, 2885; D. Wood, G. P. A. Yap and D. S. Richeson, *Inorg. Chem.*, 1999, **38**, 5788; M. K. T. Tin, G. P. A. Yap and D. S. Richeson, *Inorg. Chem.*, 1999, **38**, 998; M. K. T. Tin, N. Thirupathi, G. P. A. Yap and D. S. Richeson, *J. Chem. Soc., Dalton Trans.*, 1999, 2947; S. L. Aeilts, M. P. Coles, D. G. Swenson, R. F. Jordan and V. G. Young, *Organometallics*, 1998, **17**, 3265.

4 N. Thirupathi, G. P. A. Yap and D. S. Richeson, *Organometallics* 2000, **19**, 2573; N. Thirupathi, G. P. A. Yap and D. S. Richeson, *Chem. Commun.*, 1999, 2483.

5 N. J. Bremer, A. B. Cutcliffe and M. F. Farona, *Chem. Commun.*, 1970, 932.

6 Additional examples of dianionic trialkyl- and triarylguanidinate complexes can be found in: A. J. Blake, J. M. McInnes, P. Mountford, G. I. Nikonov, D. Swallow and D. J. Watkin, *J. Chem. Soc., Dalton Trans.*, 1999, 379; T. Chivers, M. Parvez and G. Schatte, *J. Organomet. Chem.*, 1998, **550**, 213; G. Rodriguez, C. K. Sperry and G. C. Bazan, *J. Mol. Catal. A*, 1998, **128**, 5; P. J. Bailey, R. O. Gould, C. N. Harmer, S. Pace, A. Steiner and D. S. Wright, *Chem. Commun.*, 1997, 1161; J. R. da S. Maia, P. A. Gazard, M. A. Kilner, S. Batsanova and J. A. K. Howard, *J. Chem. Soc., Dalton Trans.*, 1997, 4625; S. D. Robinson and A. Sahajpal, *J. Chem. Soc., Dalton Trans.*, 1997, 3349; P. J. Bailey, L. A. Mitchell and S. Parsons, *J. Chem. Soc., Dalton Trans.*, 1996, 2839; B. Dinger and W. Henderson, *Chem. Commun.*, 1996, 211; P. J. Bailey, A. J. Blake, M. Kryszczuk, S. Parsons and D. Reed, *J. Chem. Soc., Chem. Commun.*, 1995, 1647; N. J. Bremer, A. B. Cutcliffe, M. F. Farona and W. G. Kofron, *J. Chem. Soc. (A)*, 1971, 3264.

7 The paramagnetic complexes **1**–**4** have been fully characterized by IR spectroscopy, magnetic susceptibility and elemental analysis. Connectivity for all of these species have been established through single crystal X-ray diffraction studies. In all cases suitable crystals were mounted in inert oil and transferred to the cold gas stream of the diffractometer. The structures were solved using direct methods and refined by full-matrix least-squared on F^2.

8 Crystals of **1** were obtained from pentane. *Crystal data* for $C_{20}H_{44}ClFeN_6$ **1**: M = 459.91 monoclinic, a = 9.631(2), b = 14.350(2), c = 19.259(3) Å, β = 98.581(3)°, U = 2631.9(7) Å^3, T = 238 K, space group $P2_1/c$, Z = 4, μ(Mo-Kα) = 0.690 mm^{-1}, reflections measured 20672 unique 3212 [R(int) = 0.1274] which were used in all calculations. Final R indices [$I > 2\sigma(I)$] $R1$ = 0.0470, $wR2$ = 0.0995. Crystals of **2** were obtained from hexane. *Crystal data* for $C_{40}H_{88}Fe_2N_{12}(hexane)_{0.5}$ **2**: M = 892.01, triclinic, a = 10.342(2), b = 12.080(2), c = 21.651(4) Å, α = 92.435(4), β = 98.115(3), γ = 106.672(4)°, U = 2555.6(8) Å^3, T = 223 K, space group $P1$, Z = 2, μ(Mo-Kα) = 0.608 mm^{-1}, reflections measured 16200, unique 11406 [R(int) = 0.0300] which were used in all calculations. Final R indices [$I > 2\sigma(I)$] $R1$ = 0.0381, $wR2$ = 0.0883. Crystals of **4** were obtained from pentane. *Crystal data* for $C_{37}H_{79}Fe_2N_{11}$ **4**: M = 789.81, orthorhombic, a = 19.572(6), b = 12.747(4), c = 18.649(6) Å, U = 4653(3) Å^3, T = 238 K, space group $Pccn$, Z = 4, μ(Mo-Kα) = 6.59 mm^{-1}, reflections measured 29549, unique 2444 [R(int) = 0.2975] which were used in all calculations. Final R indices [$I > 2\sigma(I)$], $R1$ = 0.0488, $wR2$ = 0.1076. CCDC 182/1711. See http://www.rsc.org/suppdata/cc/b0/b003547p/ for crystallographic files in .cif format.

9 F. A. Cotton, L. M. Daniels, J. H. Matonic and C. A. Murillo, *Inorg. Chim. Acta*, 1997, **256**, 277.

10 Details for the structural analysis of **3** will be provided in a full paper.

11 P. J. Bailey, S. F. Bone, L. A. Mitchell, S. Parsons, K. J. Taylor and L. J. Yellowlees, *Inorg. Chem.*, 1997, **36**, 867; P. J. Bailey, S. F. Bone, L. A. Mitchell, S. Parsons, K. J. Taylor and L. J. Yellowlees, *Inorg. Chem.*, 1997, **36**, 5420.

ChemComm

On the rehydration of vanadyl pyrophosphate to vanadyl hydrogenphosphate hemihydrate

Gert-Ulrich Wolf, Bernd Kubias,* Britta Jacobi and Bernhard Lücke

Institut für Angewandte Chemie Berlin-Adlershof e. V., D 12489 Berlin, Germany. E-mail: b.kubias@aca-berlin.de

Received (in Cambridge, UK) 9th May 2000, Accepted 6th July 2000
Published on the Web 21st July 2000

Vanadyl pyrophosphate-based VPO catalysts for butane oxidation to maleic anhydride can be completely rehydrated in the solid phase into their vanadyl hydrogenphosphate hemihydrate precursors which again can be transformed into vanadyl pyrophosphate thus enabling a reuse of spent catalysts.

Vanadyl pyrophosphate, $(VO)_2P_2O_7$, (VPP) is well known to be the active and selective component of VPO catalysts in the partial oxidation and ammoxidation of hydrocarbons. Owing to its unique catalytic properties it plays a significant role especially in the oxidation of *n*-butane to maleic anhydride (MA).[1]

VPP is formed by dehydration of vanadyl hydrogenphosphate hemihydrate, $VOHPO_4{\cdot}0.5H_2O$, (VHP) in a topotactic reaction at temperatures above 638 K according to eqn. (1):[2]

$$2\ VOHPO_4{\cdot}0.5H_2O \rightarrow (VO)_2P_2O_7 + 2\ H_2O \qquad (1)$$

Well crystallized VPP catalysts obtained by calcination at high temperatures (*e.g.* above 900 K) or after an equilibration procedure in a chemical reactor for hundreds of hours time on stream are described to be comparatively resistent against overoxidation.[3] In this state they are insoluble in boiling water and even poorly soluble in concentrated hydrochloric acid. No rehydration reaction of VPP has been mentioned until now. Experience shows that also the presence of large amounts of water vapour in the feed and effluent gases of oxidation reactions passing through the VPP catalyst bed does not lead to any detectable hydration of VPP resulting only in a loss of phosphorus[4] and influencing recrystallization processes in the catalyst particles.[5]

Therefore, it was surprising that in a well crystallized VPP sample having been kept for some years at room temperature in a laboratory atmosphere (with a typical moisture content of 2–3% water vapour) a small amount of VHP was detected by X-ray diffraction (XRD). This observation led us to study the behaviour of VPP at higher water vapour pressure to elucidate the rehydration process of this compound and to find a new advantageous route to regenerate spent catalysts. Therefore, we studied sequences of the hydrothermal transformation of VPP into VHP and of the reconversion of these VHP samples into VPP by calcination. Furthermore, the influence of these procedures was investigated on the catalytic properties of the VPP materials obtained.

The VPP samples applied in this study were prepared as follows: the precursor VHP A1 was synthesized after stepwise addition of V_2O_5 into a hot solution of oxalic acid in dilute phosphoric acid by evaporation to dryness. The precursor VHP B1 was prepared by reaction of V_2O_5 with an ethanolic solution of oxalic acid in phosphoric acid. The P:V ratio of both VHP compounds was 1:1. The precursors were pelletized, crushed, sieved (1.25–2.5 mm) and transformed into VPP A1 and VPP B1, respectively, in a N_2 stream at 770 K for 2 h. For deactivation and 'deselectivation' a sample of VHP A1 was calcined at 923 K for 6 h and then for 5 h at 1123 K yielding VPP C1. Renewed transformations of the obtained VPP A1, VPP B1 and VPP C1 samples led to the precursor samples VHP A2, VHP B2 and VHP C2, respectively, which were calcined again as described above forming the samples VPP A2, VPP B2 and VPP C2.

The rehydration experiments were performed as follows: The VPP A,B,C samples were placed together with water in an ampoule (molar ratio VPP : H_2O = 1 : 2.5) and heated at 393–413 K for 24 h. The hydration reaction led to VHP according to eqn. (2).

$$(VO)_2P_2O_7 + 2\ H_2O \rightarrow 2\ VOHPO_4{\cdot}0.5H_2O \qquad (2)$$

This change was evident by a change of colour to blue for the VHP A samples (broad distribution of particle sizes, average particle size: 6.2 μm) and to greenish for the VHP B samples (narrow distribution of particle sizes, average particle size: 1.7 μm). Another possibility to introduce water into VPP is its reaction with water-rich vanadyl hydrogenphosphate hydrates, *e.g.* according to eqn. (3).

$$3\ (VO)_2P_2O_7 + 2\ VOHPO_4{\cdot}4H_2O \rightarrow 8\ VOHPO_4{\cdot}0.5H_2O + H_2O \qquad (3)$$

Excess water was then removed from the samples by drying of the obtained solids at 400 K.

The catalytic tests were performed in a tube reactor using 3–10 cm^3 catalyst (granules 1.25–2.5 mm) after conditioning of the fresh VPP samples for 2 h at 750 K in a butane–air mixture (1.5 vol% butane). The maximum MA yields of the VPP samples from the VPP → VHP → VPP sequences were determined at constant space velocities (GHSV = 1000 h^{-1}) adjusting a butane conversion degree of 90% by variation of the reaction temperatures. For sample VPP C1 the space velocity was reduced to 500 h^{-1} to determine the MA yields at similar temperatures relative to VPP C2.

The VPO materials were characterized using XRD, BET and chemical methods.

Fig. 1 shows diffractograms for samples in the VPP B → VHP B → VPP B transformation sequence starting with the fresh sample VHP B1. The diffractogram of VHP B2 shows typical reflections of $VOHPO_4{\cdot}0.5H_2O$,[6] *i.e.* a quantitative conversion of VPP into the VHP precursor took place. This result and the sequence of the other diffractograms in Fig. 1 reveal that the dehydration and rehydration, respectively, of VHP and VPP are reversible over a number of cycles. Preliminary experiments showed that the rates of the conversions depend on the partial pressure of H_2O, the temperature and on the properties of the solids such as their crystallinity and particle size.

The FWHM of the VPP B1–3 reflections (200) decreased from 2θ = 1.13° (VPP B1) to 2θ = 1.07° (VPP B2) and 2θ = 1.02° (VPP B3). This result was mirrored by the decrease of the FWHM of the same reflections from 2θ = 0.305 to 0.231° for the VPP A1–3 samples. Both findings are interpreted to be caused by recrystallization processes occurring especially during the hydration. Simultaneously, the specific surface areas decreased from 1.8 to 1.5, 12.2 to 11.2, 13.9 to 8.8 and 14.5 to 13.0 $m^2\ g^{-1}$ for VHP A, B and VPP A, B samples, respectively. This behaviour may also be explained by recrystallization leading to an increase in crystallite sizes. The remarkable increase in the specific surface areas in the conversion of VHP to VPP samples is interpreted in terms of particle size effects.[7]

DOI: 10.1039/b003700l

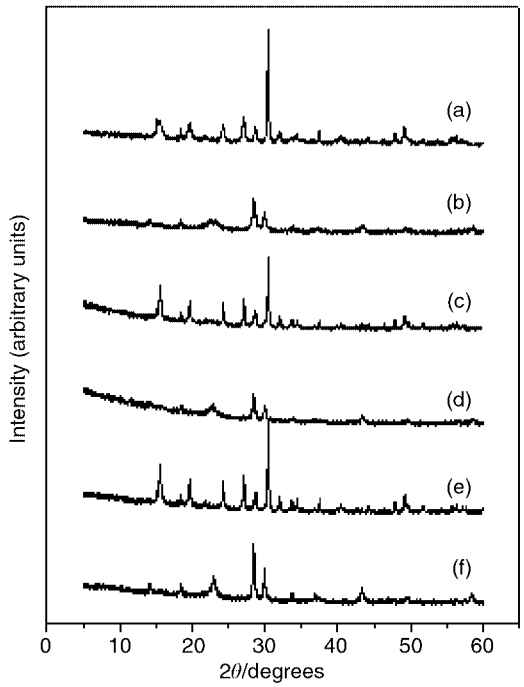

Fig. 1 Diffractograms of VHP B and VPP B samples measured during the transformation VPP B → VHP B → VPP B: (a) VHP B1, (b) VPP B1, (c) VHP B2, (d) VPP B2, (e) VHP B3, (f) VPP B3.

The fact that the colours of the different VHP samples in the sequences A1–3 and B1–3, did not change during the dehydration–rehydration transformations suggest a topotactic nature of this reaction as expected for the mild hydration conditions and the transformation rate.

The maximum MA yields of VPP A samples obtained in the course of several transformation sequences and the corresponding catalyst temperatures necessary to adjust a butane conversion degree of 90% demonstrate that the transformations can lead to both a decrease in activity and selectivity of the VPP samples: the MA yields decreased from 52 mol% MA (VPP A1) to 45 mol% MA (VPP A4 sample, obtained after the third transformation sequence) and the temperatures for 90% butane conversion increased from 690 to 707 K. This finding is interpreted to be caused by the recrystallization effect discussed above: from catalytic and EPR experiments using VPP samples of different crystallinity it is known that maximum catalytic performance requires a certain degree of disorder in the VPP lattice.[8] This is supported by recent results which showed that the catalytic performance of well crystallized VPP may be improved by tribomechanical treatment upon milling samples.[9]

Fig. 2 shows the catalytic results of the well crystallized sample VPP C1 (deactivated and 'deselectivated' by prolonged calcination at high temperatures) and of the regenerated sample VPP C2. The figure clearly shows that the transformation led to a marked increase in both the activity and the selectivity of the VPP C2 sample. This result can be explained by the increase in the low surface area from 3.2 $m^2\ g^{-1}$ of the deactivated sample to 15.9 $m^2\ g^{-1}$ of the regenerated sample and by an increase in the lattice disorder of the latter due to the transformation procedure.

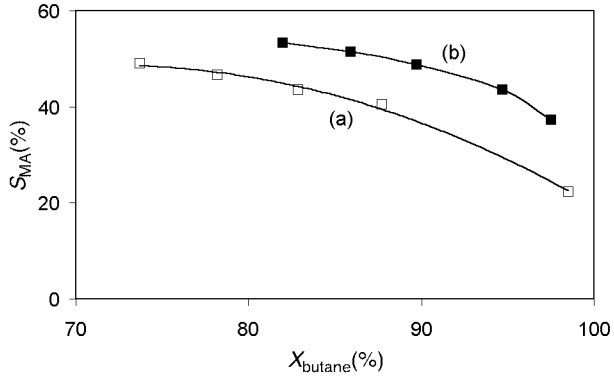

Fig. 2 MA selectivities of samples VPP C1 (a) and VPP C2 (b) as a function of the degree of conversion of butane, GHSV: 500 h^{-1} (VPP C1), 1000 h^{-1} (VPP C2), reaction temperatures: VPP C1: from 716 K ($X_{C_4H_{10}}$ = 73.7%) to 768 K ($X_{C_4H_{10}}$ = 98.5%), VPP C2: from 703 K ($X_{C_4H_{10}}$ = 82%) to 740 K ($X_{C_4H_{10}}$ = 97.5%).

The presented results illustrate that the described method is suitable for regenerating spent catalysts. Furthermore, as shown by additional experiments, it could open a way to adjust the P : V ratio in regenerated catalysts by adding the desired amount of phosphoric acid to the amount of water necessary for the transformation procedure. The new route presented here avoids chemical conversion of the spent materials by dissolution or other processes followed by separation procedures to recover the vanadium component. It could also be an alternative method of regeneration instead of treatments of catalyst beds with halide containing compounds[10] which can cause difficult technical and environmental problems.

This work was supported by the Bundesministerium für Bildung und Forschung der Bundesrepublik Deutschland (Contract No.03C30054).

Notes and references

1 *Catal. Today*, 1987, **1**, 477 (ed. B. K. Hodnett).
2 E. Bordes, J. W. Johnson and P. Courtine, *J. Solid State Chem.*, 1984, **53**, 270; C. C. Torardi and J. C. Calabrese, *Inorg. Chem.*, 1984, **23**, 1308; J. W. Johnson, D. C. Johnston, A. J. Jacobson and J. F. Brody, *J. Am. Chem. Soc.*, 1984, **106**, 8123.
3 *Catal. Today*, 1993, **16**, 1 (ed. G. Centi).
4 B. Kubias, F. Richter, H. Papp, A. Krepel and A. Kretschmer, *Stud. Surf. Sci. Catal.*, 1997, **110**, 461.
5 F. Cavani, A. Colombo, F. Giuntoli, F. Trifiro, P. Vazquez and P. Venturosi, in *Advanced Catalysts and Nanostructured Materials*, ed. W. R. Moser, Academic Press Inc., New York, 1996, p. 43.
6 M. E. Leonowicz, J. W. Johnson, J. F. Brody, H. F. Shannon and J. M. Newsam, *J. Solid State Chem.*, 1985, **56**, 370.
7 N. Duvauchelle, E. Kesteman, F. Oudet and E. Bordes, *J. Solid State Chem.*, 1998, **137**, 311.
8 A. Brückner, B. Kubias, B. Lücke and R. Stößer, *Colloids Surf. A: Physicochem. Eng. Asp.*, 1996, **115**, 179.
9 B. Kubias, M. Fait, M. Estenfelder, H.-J. Eberle, U. Steinike and M. Meisel, Recent Research Poster 054, *12th International Congress on Catalysis, Granada*, July 9–14, 2000, CD-ROM RR054.
10 R. C. Edwards, *US Pat.*, 4861738 , 29.01.88 (Amoco Corp.).

The first synthesis of both enantiomers of [α-^{2}H]phenylacetic acid in high enantiomeric excess

Kaori Matoishi,[a] Satoshi Hanzawa,[b] Hitoshi Kakidani,[a] Masumi Suzuki,[a] Takeshi Sugai[a] and Hiromichi Ohta*[a]

[a] *Department of Chemistry, Keio University, 3-14-1 Hiyoshi, Kohoku-ku, Yokohama 223-8522, Japan. E-mail: hohta@chem.keio.ac.jp*
[b] *Tokyo Research Center, Tosoh Corp., 2743-1 Hayakawa, Ayase 252-1123, Japan.*

Received (in Cambridge, UK) 17th May 2000, Accepted 30th June 2000
Published on the Web 21st July 2000

Arylmalonate decarboxylase (EC. 4. 1. 1. 76) catalysed decarboxylation followed by enantioface-differentiating protonation of [α-^{2}H]- and [α-^{1}H]phenylmalonic acid in ^1H_2O and ^2H_2O respectively, gave highly enantiomerically enriched (*R*)- and (*S*)-[α-^{2}H]phenylacetic acid in quantitative yields.

Regio- and stereospecifically [^{2}H]-labelled compounds are very useful in studying metabolic pathways and reaction mechanisms. Phenylacetic acid is the intermediary metabolite of aromatic amino acids, and also the starting material of amphetamine. For studies in this field, it will be of great use if both of the enantiomers of [α-^{2}H]phenylacetic acid **1** are available. So far, enantiomerically enriched forms of **1** have been synthesized *via* deuteriolysis of (*R*)-(−)-*N*,*N*-dimethylphenylglycine[1] and oxidative addition of optically active [α-^{2}H]benzyl halides to palladium complexes, followed by carbonyl insertion.[2] However, the products of these two methods suffer from the low enantiomeric excess (55[1], 76%[2]) and contamination of di-deuterated and non-deuterated by-products. It is practically impossible to raise the ee of the product and to separate these by-products by ordinary methods, as there are no chemical differences between the two enantiomers, and labeled and non-labeled compounds. Accordingly, high selectivity of the reaction is essential for obtaining the product in high enantiomeric excess.

Arylmalonate decarboxylase (AMDase, EC. 4. 1. 1. 76), which was found in our laboratory, catalyses decarboxylation of arylmalonate derivatives resulting in the formation of enantiomerically pure (*R*)-α-substituted phenylacetic acids (Scheme 1).[3] It is thought that enantioface-differentiating protonation to the enolate intermediate in the active site of the enzyme is the key step of this reaction. Thus, if [α-^{2}H]phenylmalonic acid was used as the substrate of this enzymatic reaction, it would give enantiomerically enriched (*R*)-[α-^{2}H]phenylacetic acid.

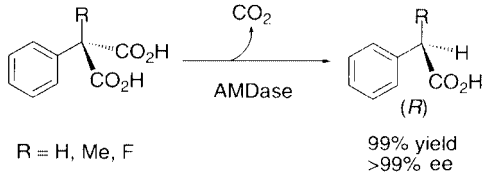

Scheme 1

[α-^{2}H]Phenylmalonic acid **2**† was prepared by deuteration of the corresponding [α-^{1}H]-diethyl ester followed by hydrolysis in ^2H_2O. The amount of non-deuterated diethyl ester was evaluated from ^{1}H-NMR to be about 3%, which was consistent with the peak intensity ratio of *m*/*z* 136 and 137 (parent ions corresponding to non- and mono-deuterated phenylacetic acids) of the enzyme-catalysed reaction product. The asymmetric decarboxylation of **2** by arylmalonate decarboxylase, which was obtained by overexpression in *E. coli* JM 109 and subsequent purification,[4] worked very well. The expected compound (*R*)-**1**‡ of over 95% ee was obtained in a quantitative yield (Scheme 2).

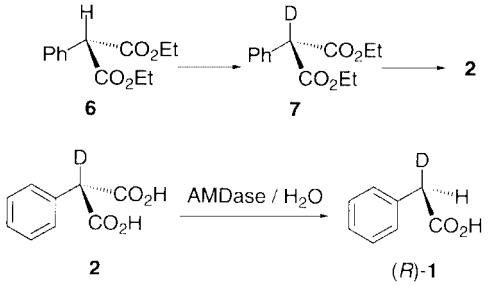

Scheme 2

In this enzyme-catalysed reaction, it is considered that the origin of the proton source can be traced back to the solvent ^1H_2O. Consequently, when the reaction is performed in ^2H_2O, then ^{2}H will be incorporated enantioselectively into the product from the same direction as that of ^{1}H in the above case. As this enzyme is purified from the culture of *E. coli*, it is obtained as a solution in ^1H_2O. When the replacement of the solvent is incomplete, it will cause the formation of non-deuterated phenylacetic acid. Thus, we tried to replace ^1H_2O with ^2H_2O. Fortunately, as this enzyme was not inactivated by repeated lyophilization, it was possible to replace the ^1H_2O of the enzyme solution by ^2H_2O *via* successive freeze-drying and addition of ^2H_2O. When substrate **3** was added to this ^2H_2O-exchanged enzyme solution, the reaction proceeded smoothly in the same manner as for ^1H_2O, although the rate of reaction was not measured accurately. As expected, (*S*)-**1**§ in over 95% ee was obtained in a quantitative yield (Scheme 3).

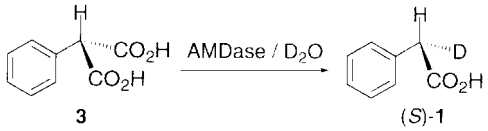

Scheme 3

The absolute configuration of the product was determined by comparison of the sign of rotation with the one reported.[2] The ee of **1** was determined by ^{1}H NMR analysis of (*R*)-α-methoxy-α-trifluoromethylphenyl acetate (MTPA ester **5**¶), which was prepared by an esterification of the corresponding alcohol obtained by the reduction of methyl ester **4** (Scheme 4). The ^{1}H NMR spectra of the benzylic protons are shown in Fig. 1. The signals of the protons in question were simplified *via* decoupling by irradiation of the adjacent methylene protons.

In conclusion, an efficient method for the asymmetric synthesis of both enantiomers of [α-^{2}H]phenylacetic acid was established *via* decarboxylation of phenylmalonate catalysed by

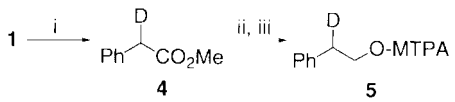

Scheme 4

DOI: 10.1039/b003941l

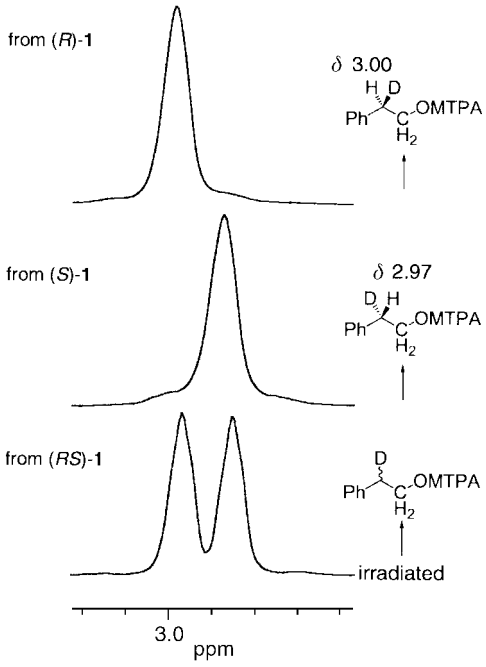

Fig. 1

arylmalonate decarboxylase. As some other analogous compounds having substituents on the aromatic ring also undergo this enzyme-catalysed reaction,[5] this procedure will be applicable to the preparation of the enantiomers of substituted [α-^{2}H]arylacetic acids.

Notes and references

† **2**: To a dispersion of NaH (12.7 mmol) in dry THF (10 ml) was added a solution of **6** (4.23 mmol) in dry THF (2 ml). The mixture was refluxed with stirring for 5 h and cooled to 0 °C. To this mixture was added D_2O (3.5 ml) and DCl (35% in D_2O, 1.4 ml). The product was extracted and purified by column chromatography on silica gel to give diethyl [α-^{2}H]phenylmalonate **7** (0.957 g, 96%). This was contaminated with **6** (3%), as judged from the signal at δ_H 4.61 [1H, s, $C_6H_5CH(CO_2CH_2CH_3)_2$]. The solution of **7** (0.747 g, 3.15 mmol) in CH_3OD (5 ml) was treated with NaOD (6.84 mmol) in D_2O (5 ml). The mixture was stirred at rt for 12 h, concentrated *in vacuo* and MeOH (15 ml) was added to the residue. The resulting precipitates were collected by suction filtration, washed with cold MeOH and ether, and then dried *in vacuo* to give the disodium salt of **2** (0.640 g, 90%) as a colorless powder. ν_{max}/cm^{-1} 3021, 1591, 1496, 1429, 1324, 1023, 910, 698; (400 MHz, D_2O) δ_H: 7.11–7.21 [m, 5H, $C_6H_5CD(CO_2Na)_2$].

‡ (*R*)-**1**: The disodium salt of **2** (0.450 g, 2.00 mmol) was added to a solution of purified arylmalonate decarboxylase (400 units) in Tris-HCl buffer (2 M, pH 8.5, 4 ml). This mixture was incubated at 35 °C for 30 min followed by acidification with 2 M HCl. The mixture was saturated with NaCl and extracted with ether. The organic layer was concentrated *in vacuo* to give (*R*)-**1** (0.279 g, quant.) as a white solid. This product was revealed to be pure by ^{1}H NMR. This was recrystallized from hexane to afford (*R*)-**1** (0.250 g, 92%) as colorless plates, mp 73.5–74.5 °C; $[\alpha]_D^{22}$ −1.1° (*c* 10.0, $CHCl_3$); ν_{max}/cm^{-1} 3033, 1700, 1412, 1263, 1224, 904, 700, 673; (400 MHz, $CDCl_3$) δ_H: 3.64 [t, 1H, *J* = 2.0 Hz, $C_6H_5CDHCO_2H$], 7.25–7.36 [m, 5H, $C_6H_5CDHCO_2H$]; MS (*m/z*, %) 92 (C_7H_6D, 100), 136 (1.2), 137 (M^+, 34.9), 138 (*M* + 1, 3.0). HRMS Found: *m/z* 137.0598. Calcd. for $C_8H_7DO_2$: 137.0586. Assuming the peak *m/z* 136 is entirely due to the presence of non-deuterated phenylacetic acid ($C_7H_8O_2$), the contamination is calculated to be about 3%. However, the peak corresponding to *M* − 1 (135) was also observed in the MS of non-deuterated phenylacetic acid. Thus the contamination of the non-deuterated compound in the enzymatic reaction product will be less than 3%.

MS of non-deuterated phenylacetic acid (*m/z*, relative intensity) 91 (C_7H_7, 100), 135 (1.2), 136 (M^+, 72), 137 (*M* + 1, 7.0), 138 (*M* + 2, 1.2).

§ (*S*)-**1**: The purified arylmalonate decarboxylase (600 units) was dissolved in a Tris-HCl buffer (2 M, pH 8.5, 5 ml) and lyophilized. The residue was dissolved in D_2O (5 ml) and incubated at 4 °C for 1 h and lyophilized again. The residue was dissolved in D_2O (5 ml) and the disodium salt of **3** (0.550 g, 2.45 mmol) was added. The mixture was incubated at 35 °C for 30 min and acidified with 2 M HCl. The mixture was saturated with NaCl and extracted with ether. The organic layer was concentrated *in vacuo* to give (*S*)-**1** (0.337 g, quant.) as a white solid. This was recrystallized from hexane to give (*S*)-**1** (0.300 g, 89%) as colorless plates, mp 74.5–75.5 °C [lit.[2] 75 °C]; $[\alpha]_D^{22}$ +1.1 (*c* 9.5, $CHCl_3$), +1.2 (*c* 25.7, $CHCl_3$) [lit.[2] for *S* enantiomer, $[\alpha]_D^{22}$ +1.5 ± 0.2 (*c* 25.7, $CHCl_3$)]; MS (*m/z*, %) 92 (C_7H_6D, 100), 136 (1.2), 137 (M^+, 34.9), 138 (*M* + 1, 3.0). HRMS Found: *m/z* 137.0566. Calcd. for $C_8H_7DO_2$: 137.0586. The IR and NMR spectra were identical with those of (*R*)-**1**. The racemic sample of **1** was prepared by the reported procedure.[6]

¶ **5** from (*R*)-**1**: (400 MHz, $CDCl_3$) δ_H: 3.00 [t, 1H, *J* = 6.3 Hz, $C_6H_5CDHCH_2OCOC(CF_3)(OCH_3)C_6H_5$], 3.47 [s, 3H, $C_6H_5CDHCH_2OCOC(CF_3)(OCH_3)C_6H_5$], 4.53 [d, 2H, *J* = 6.3 Hz, $C_6H_5CDHCH_2OCOC(CF_3)(OCH_3)C_6H_5$], 7.17–7.43 [m, 10H, $C_6H_5CDHCH_2OCOC(CF_3)(OCH_3)C_6H_5$]. **5** from (*S*)-**1**: (400 MHz, $CDCl_3$) δ_H: 2.97 [t, 1H, *J* = 7.3 Hz, $C_6H_5CDHCH_2OCOC(CF_3)(OCH_3)C_6H_5$], 3.46 [s, 3H, $C_6H_5CDHCH_2OCOC(CF_3)(OCH_3)C_6H_5$], 4.53 [d, 2H, *J* = 7.0 Hz, $C_6H_5CDHCH_2OCOC(CF_3)(OCH_3)C_6H_5$], 7.17–7.43 [m, 10H, $C_6H_5CDHCH_2OCOC(CF_3)(OCH_3)C_6H_5$].

1 H. Dahn and C. O'Murchu, *Helv. Chim. Acta*, 1970, **53**, 1379.
2 K. S. Y. Lau, P. K. Wong and J. K. Stille, *J. Am. Chem. Soc.*, 1976, **98**, 5832.
3 H. Ohta, *Bull. Chem. Soc. Jpn.*, 1997, **70**, 2895; H. Ohta, *Biocatalytic Asymmetric Decarboxylation*, ed. K. Faber, Springer-Verlag, 1999; H. Ohta and T. Sugai, *Stereoselective Biocatalysis*, ed. R. N. Patel, Marcel Dekker Inc., New York, 2000 and references cited therein.
4 Y. Fukuyama, K. Matoishi, M. Iwasaki, E. Takizawa, M. Miyazaki, H. Ohta, S. Hanzawa, H. Kakidani and T. Sugai, *Biosci. Biotechnol. Biochem.*, 1999, **63**, 1664.
5 K. Miyamoto and H. Ohta, *Biocatalysis*, 1991, **5**, 49.
6 W. Adam and O. Cueto, *J. Org. Chem.*, 1977, **42**, 38.

Diastereoselective epoxide rearrangements using lithium amide bases: first stereocontrolled synthesis of 4-deoxyconduritols

Alex Kee,[a] Peter O'Brien,*[b] Christopher D. Pilgram[b] and Simon T. Watson[b]

[a] *Aventis Pharma Ltd., Dagenham Research Centre, Rainham Road South, Dagenham, Essex UK RM10 7XS*
[b] *Department of Chemistry, University of York, Heslington, York, UK YO10 5DD. E-mail: paob1@york.ac.uk*

Received (in Cambridge, UK) 8th May 2000, Accepted 26th June 2000
Published on the Web 21st July 2000

Two novel and completely diastereoselective lithium amide-mediated rearrangements of diprotected 4,5-dihydroxycyclohexene oxides and their use in the synthesis of 4-deoxyconduritols are described.

Conduritols and structurally related cyclitols possess a range of useful biological activity (including glycosidase inhibition)[1] and the stereocontrolled synthesis of such compounds continues to attract considerable attention.[2] As part of our research programme into the synthesis of polyhydroxylated cyclohexenes using chiral bases derived from **1** and **2**, we became

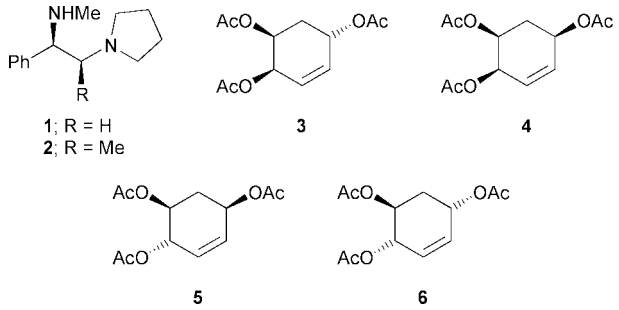

interested in the preparation of the triacetates of 4-deoxyconduritols **3**–**6**. Although the preparation of *racemic* **3**, **4** and **6** has been reported,[3–6] there exists no general, stereocontrolled method for the synthesis of 4-deoxyconduritols. Previously, we have described[7,8] the preparation of precursors to **3** and **4** in > 90% ee using the chiral base-mediated asymmetric desymmetrisation of *meso*-4,5-dihydroxycyclohexene oxides. In this paper, we describe a related but conceptually distinct lithium amide epoxide rearrangement approach to the synthesis of **5** and **6**.

In order to synthesise **5** and **6** with the required stereochemistry, we needed to study the rearrangement of *chiral* 4,5-dihydroxycyclohexene oxides like **7** using lithium amide bases (Scheme 1). Such a reaction is intrinsically different to our previously reported epoxide rearrangements: (i) the reaction is not a desymmetrisation; (ii) the reaction can proceed to give two possible *diastereomeric* allylic alcohol products (**8** and **9**) depending on the reacting conformation adopted by the epoxide (*vide infra*); (iii) any optical activity in the allylic alcohols produced must arise either from enantioenriched starting epoxide **7** or from a kinetic resolution of *racemic* **7** using a chiral base.

The rearrangement of cyclohexene oxides to allylic alcohols proceeds *via* lithium amide abstraction of a proton that is *cis* and

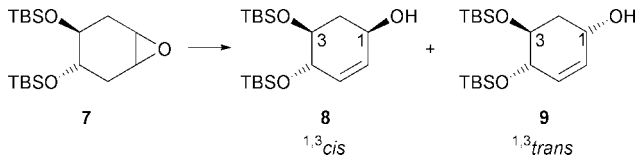

Scheme 1

pseudo-axial to the epoxide.[9] When such criteria are imposed on the two possible conformations (**A** and **B**) of **7** then it can be seen from Fig. 1 that removal of the highlighted (*cis* and pseudo-axial) proton in each conformation leads to different *diastereomers* of allylic alcohols: reaction *via* conformation **A** (diaxial silyloxy groups) generates **8** (^{1,3}*cis* stereochemistry); reaction *via* **B** (diequatorial silyloxy groups) gives **9** (^{1,3}*trans* stereochemistry). Thus, we anticipated that by controlling the reacting conformation, we would be able to synthesise allylic alcohols with either ^{1,3}*cis* or ^{1,3}*trans* relative stereochemistry. The successful implementation of this novel strategy is the subject of the present communication.

Racemic **7** was readily synthesised from cyclohexa-1,4-diene in 48% yield over three steps. The reaction of **7** with 2 equiv. of the lithium amide bases generated from *racemic* diamine **2** and diisopropylamine (Scheme 1) was studied under different conditions (Table 1). Reaction of **7** with the lithium amide base from **2** in THF, our usual solvent, generated a 32 : 68 mixture of allylic alcohols **8** and **9**† (Entry 1) which were readily separated by column chromatography. They were identified by conversion of **8** into the previously unreported 4-deoxyconduritol triacetate **5** (*vide infra*). The major product (**9**) must have arisen through reaction *via* conformation **B** (see Fig. 1).

Using *rac*-**2** and by changing the solvent to either Et_2O or cyclopentane, the coordinating ability of the solvent is reduced and only allylic alcohol **8** was formed (Entries 3 and 4). With these solvents, preferential reaction *via* conformation **A** is presumably promoted by intramolecular chelation of the silyloxy group and epoxide oxygen by the lithium cation. For

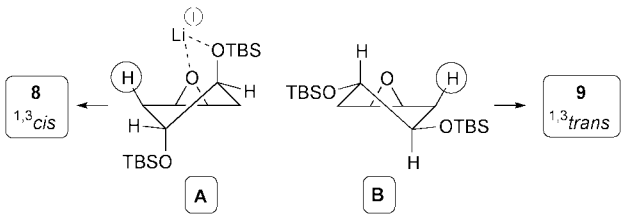

Fig. 1

Table 1 Diastereoselectivity of the lithium amide-mediated rearrangement of **7** using *rac*-**2** and LDA

Entry	Base	Solvent[a]	^{1,3}*cis* : *trans*[b]	Yield (%) of **8**[c]	Yield (%) of **9**[c]
1	**2**	THF	32 : 68	30	61
2	**2**	THF (+2 equiv. LiBr[d])	44 : 56	33	47
3	**2**	Et_2O	≥98 : 2	88	—
4	**2**	Cyclopentane	≥98 : 2	89	—
5	LDA	THF	83 : 17	82	—
6	LDA	Et_2O	95 : 5	85	—

[a] *Reaction conditions*: 2 equiv. diamine *rac*-**2** or $^{i}Pr_2NH$, 2 equiv. BuLi, solvent, 0 °C to rt over 2 h, 70 h, rt; [b] Ratio determined by ^{1}H NMR spectroscopy on the crude product mixtures; [c] Isolated yield after column chromatography; [d] Diamine was deprotonated using MeLi·LiBr rather than BuLi.

DOI: 10.1039/b003717f

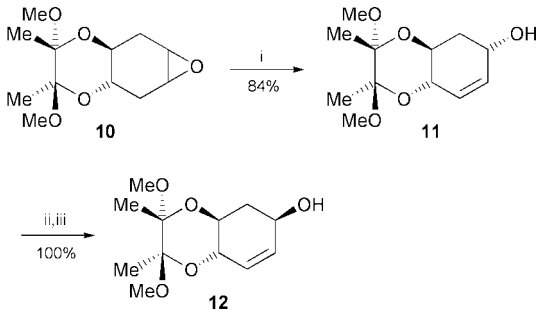

Scheme 2 *Reagents and conditions*: i, 2 equiv. *rac*-**2** + 2 equiv. BuLi, THF, 0 °C to rt over 2 h then 70 h at rt; ii, PCC, CH_2Cl_2 (100%); iii, $NaBH_4$, $CeCl_3{\cdot}7H_2O$, MeOH, 0 °C, 10 min (100%).

similar reasons, carrying out the reaction in THF with added lithium bromide led to a lowering of the ^{1,3}*trans* diastereoselectivity (Entry 2). The use of TBDPS and TES as protecting groups gave essentially the same results.

We have also investigated the use of LDA for these diastereoselective rearrangement reactions. In THF, a very good isolated yield (82%) of allylic alcohol **8** was obtained (Entry 5). The reaction must proceed preferentially *via* the chelated conformation **A** which is in stark contrast to the result obtained with diamine *rac*-**2** (Entry 1) indicating that LDA is a far better coordinator than *rac*-**2** in THF. Use of LDA in Et_2O led to a slight improvement in ^{1,3}*cis* selectivity (Entry 6) but this did not mirror the improvement in ^{1,3}*cis* selectivity observed with *rac*-**2** on moving from THF to Et_2O where none of the ^{1,3}*trans* diastereomer was observed (Entry 3).

From a synthetic viewpoint, reaction of **7** with the lithium amide derived from *rac*-**2** in cyclopentane generated **8** as the sole diastereomer which was isolated in 89% yield (Entry 4). Conversion of **8** into unknown triacetate **5**‡ was accomplished by deprotection with TBAF and subsequent acetylation (88% yield over the two steps).

Although it was possible to generate allylic alcohol **9** in 61% isolated yield (Entry 1), we wondered if it was possible to have a completely diastereoselective synthesis of an allylic alcohol with ^{1,3}*trans* stereochemistry (reaction only *via* the diequatorial conformation **B**). Thus, we used the Ley butane-2,3-diacetal protecting group[10] to lock the conformation equivalent to **B** in epoxide **10** (Scheme 2).

Racemic **10** was prepared from cyclohexa-1,4-diene in 56% yield. Reaction of **10** with the lithium amide of *rac*-**2** generated only one diastereomer of allylic alcohol in 84% yield and it was identified as the expected **11** by conversion into known[3] triacetate **6** (TFA–water deprotection followed by acetylation, 80% yield). Use of LDA produced allylic alcohol **11** in a slightly improved 89% isolated yield. In passing, we also note that it is possible to carry out a PCC oxidation–Luche reduction sequence to convert **11** into its diastereomer **12** with complete stereocontrol (axial attack of hydride in the conformationally locked intermediate enone explains the stereoselectivity). Finally, we present our preliminary findings on the kinetic resolution of **10** as a route to enantiomerically enriched allylic alcohols.[11] Reaction of *racemic* **10** with 0.7 equiv.[12] of the chiral base from (1*R*,2*S*)-**2** generated **11** in 32% yield (63% ee) and recovered *ent*-**10** in 51% yield (44% ee).

In summary, we have described two novel, completely diastereoselective and stereodivergent lithium amide-mediated epoxide rearrangement reactions (**7** → **8** and **10** → **11**). Mechanistically, our results can only be adequately explained in terms of the removal of a proton which is *cis* and pseudo-axial to the epoxide (see Fig. 1) as proposed by Rickborn and Thummel.[9] In addition, we have also reported the first example of a kinetic resolution on chiral 4,5-dihydroxycyclohexene oxides which, coupled with the oxidation–reduction sequence in Scheme 2, provides a concise approach to enantiomerically enriched 4-deoxyconduritols **5** and **6**.

We thank The University of York and Aventis Pharma Ltd for the award of a studentship (to S. T. W.) and the EPSRC for the award of a project studentship (to C. D. P.; reference GR/L 58439).

Notes and references

† All novel compounds have been fully characterised including microanalysis or HRMS.

‡ Data for novel triacetate **5**: pale yellow oil, R_F(1:1 petrol–Et_2O) 0.3; $\nu_{max}(CHCl_3)/cm^{-1}$ 1740 (C=O) and 1685; δ_H(270 MHz; $CDCl_3$) 5.85 (1H, ddd, *J* 1, 3 and 10, =CH), 5.72 [1H, ddd, *J* 2, 2 and 10 (appearing as a doublet of triplets), =CH], 5.53–5.44 (2H, m, CHOAc), 5.06 (1H, ddd, *J* 4, 7 and 12, CHOAc), 2.42 (1H, dddd, *J* 1, 4, 6 and 12, CH_AH_B), 2.07 (3H, s, Me), 2.06 (3H, s, Me), 2.05 (3H, s, Me) and 1.86 [1H, ddd, *J* 9, 12 and 12 (appearing as a triplet of doublets), CH_AH_B]; δ_C(67.5 MHz; $CDCl_3$) 170.5, 170.2, 170.1, 130.1, 127.7, 70.7, 69.7, 67.6, 32.4 and 21.0; *m/z* (CI, NH_3) 274 [100%, $(M + NH_4)^+$] and 197 (30) [Found: $(M + NH_4)^+$, 274.1288. $C_{12}H_{16}O_6$ requires *M* + H, 274.1291].

1 T. Hudlicky and M. Cebulak, *Cyclitols and Derivatives*, VCH, New York, 1993.
2 For recent examples, see: M. Honzumi, K. Hiroya, T. Taniguchi and K. Ogasawara, *J. Chem. Soc., Chem. Commun.*, 1999, 1985; K. S. Kim, J. I. Park, H. K. Moon and H. Yi, *J. Chem. Soc., Chem. Commun.*, 1998, 1945.
3 E. Salamci, H. Secen, Y. Sütbeyaz and M. Balci, *J. Org. Chem.*, 1997, **62**, 2453.
4 A. H. Haines, A. S. H. King, J. R. Knight and V.-A. Nguyen, *Tetrahedron Lett.*, 1998, **39**, 4393.
5 A. Maras, H. Secen, Y. Sütbeyaz and M. Balci, *J. Org. Chem.*, 1998, **63**, 2039.
6 N. Maezaki, N. Nagahashi, R. Yoshigami, C. Iwata and T. Tanaka, *Tetrahedron Lett.*, 1999, **40**, 3781.
7 P. O'Brien and P. Poumellec, *J. Chem. Soc., Perkin Trans. 1*, 1998, 2435.
8 S. E. de Sousa, P. O'Brien and H. C. Steffens, *Tetrahedron Lett.*, 1999, **40**, 8423.
9 B. Rickborn and R. P. Thummel, *J. Org. Chem.*, 1969, **34**, 3583; J. K. Crandall and M. Apparu, *Org. React. (N.Y.)*, 1983, **29**, 345.
10 A. Hense, S. V. Ley, H. M. I. Osborn, D. R. Owen, J.-F. Poisson, S. L. Warriner and K. E. Wesson, *J. Chem. Soc., Perkin Trans. 1*, 1997, 2023; N. L. Douglas, S. V. Ley, H. M. I. Osborn, D. R. Owen, H. W. M. Priepke and S. L. Warriner, *Synlett*, 1996, 793; J.-L. Montchamp, F. Tian, M. E. Hart and J. W. Frost, *J. Org. Chem.*, 1996, **61**, 3897.
11 For some other examples of kinetic resolutions of epoxides with chiral bases, see: K. Mori, B. G. Hazra, R. J. Pfeiffer, A. K. Gupta and B. S. Lindgren, *Tetrahedron*, 1987, **43**, 2249; M. Asami and N. Kanemaki, *Tetrahedron Lett.*, 1989, **30**, 2125.
12 Since we usually use 2 equiv. of chiral lithium amide bases for epoxide rearrangement reactions, we decided to use 0.7 equiv. of chiral base for the kinetic resolution. When 0.5 equiv. of chiral base was used, we obtained a 26% yield of allylic alcohol **11** (64% ee).

ChemComm

Preparation of an MCM-41/Nafion® composite material; a selective catalyst for α-methylstyrene dimerization

Masahiro Fujiwara,* Koji Kuraoka, Tetsuo Yazawa, Qiang Xu, Mutsuo Tanaka and Yoshie Souma

Osaka National Research Institute (AIST-MITI), 1-Midorigaoka, Ikeda, Osaka 563-8577, Japan.
E-mail: fujiwara@onri.go.jp

Received (in Cambridge, UK) 16th June 2000, Accepted 29th June 2000
Published on the Web 21st July 2000

A MCM-41/Nafion® composite prepared from tetraethoxysilane and Nafion gel solution with cetyltrimethylammonium surfactant, is a highly selective catalyst for α-methylstyrene dimerization to form the corresponding acyclic dimer.

The synthesis of mesoporous materials is one of the most important subjects in modern chemistry. MCM-41 obtained by the utilization of surfactant micelles[1] is actively studied for applications to catalysts. Recently organically modified MCM-41 materials using alkyl-substituted silane compounds have been prepared for use as catalysts and other applications.[2] On the other hand, DuPont has recently reported amorphous silica/Nafion composites which were effective solid acid catalysts.[3] It is thought that the combination of the new technology for fabricating mesoporous materials and Nafion resin creates a novel class of functional solid acid materials.[4] Here, we report the first preparation (to our knowledge) of a MCM-41/Nafion composite material and its applications as a solid acid catalyst.

The MCM-41/Nafion composite was obtained by the following procedure; 0.1 g of Nafion gel obtained from a 5% Nafion solution (Aldrich) in ethanol was dissolved in 1.5 mL of ethanol. This solution was added slowly to a mixture of tetramethylammonium hydroxide (8 mmol) and cetyltrimethylammonium bromide (4.5 mmol) in distilled water (15 mL) with vigorous stirring. Then, tetraethoxysilane (30 mmol) was added dropwise with stirring to the resulting mixture. Finally, the mixture was transferred to a Teflon beaker and crystallized in a stainless steel autoclave at 130 °C under autogeneous pressure for 24 h. The white solid obtained was washed twice with 200 mL of distilled water and dried at 60 °C. The removal of the template and acidification of the Nafion resin were performed by refluxing in concentrated sulfuric acid (3 mL) in ethanol (300 mL) for 18 h. After two further refluxes in ethanol (300 mL), the recovered solid was dried at 150 °C for 20 h.

Fig. 1 shows the XRD pattern of the MCM-41/Nafion composite obtained.† A clear peak at $2\theta = 2.15°$ was observed which was assigned to the (100) reflection of MCM-41 type materials.[1] The (110) and (200) reflections from MCM-41 appeared as broad peaks at $2\theta \approx 4.1°$. The BET surface area and pore volume were estimated at 619 $m^2\ g^{-1}$ or 0.64 $cm^3\ g^{-1}$, respectively. The diameter of the main pore type (*ca*. 90%) was 2.8 nm in accord with an organically modified MCM-41.[2] The minor pore type had a diameter of 3.8 nm and corresponded to MCM-41.[1] From the IR spectrum, it was confirmed that the template was removed because of the absence of alkyl adsorptions of the template around 2900 cm^{-1}. All these results indicate that the preparation of the MCM-41/Nafion composite was successful.

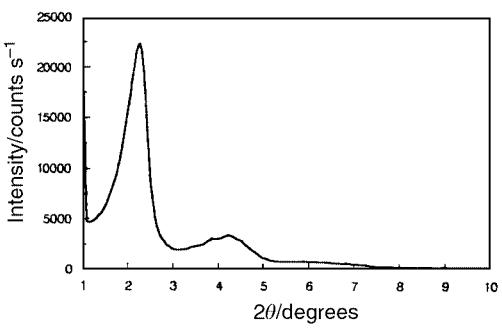

Fig. 1 X-Ray diffraction pattern of the MCM-41/Nafion composite.

This novel composite material was applied to the dimerization of α-methylstyrene (AMS) to produce the corresponding acyclic dimer, 4-methyl-2,4-diphenylpent-1-ene **1**, which is a chain transfer agent amongst other uses.[5] Although this reaction using solid sulfuric acid has been actively studied,[5] the significant side reaction to form the cyclic dimer, 1,1,3-trimethyl-3-phenylindan **3**, often results in low production of **1** (Scheme 1). The yields of the desired dimer **1** [Fig. 2(a)] and of the undesired dimer **3** [Fig. 2(b)] as a function of time are shown using the MCM-41/Nafion composite, as well as for Nafion NR-50, Nafion SAC-13 (silica/Nafion composite),[3] Amberlyst® 15 (all obtained from Aldrich) and Al-MCM-41.[6]† Although SAC-13 and Amberlyst 15 had high activity, the yields of **1** drastically decreased with time and substantial increases of the bicyclic dimer **3** were observed. For NR-50, the reaction rate was quite slow as reported[3] and **3** was formed in considerable yield even at a low conversion of AMS. On the other hand, when the MCM-41/Nafion composite was used, the yield of **1** was about 70% and scarcely decreased with reaction time. Furthermore, the formation of **3** was low even after 1000 min. This high selectivity shown by the MCM-41/Nafion composite is not simply derived from the mesoporous channel structure since **3** was obtained in high yield using Al-MCM-41 which was reported as an acid catalyst.[6] Furthermore, other types of MCM-41/Nafion composite obtained from impregnating Nafion solution to MCM-41[7] also afforded **3** in 30% yield with a lower yield of **1** (25%) after 300 min. As expected, MCM-41 itself (silica material without Nafion resin or other metals) showed no activity for this dimerization under our conditions (no conversion of AMS even after 1500 min). Thus, the MCM-41/Nafion composite prepared in this work was an excellent catalyst to produce **1** *via* the dimerization of AMS.

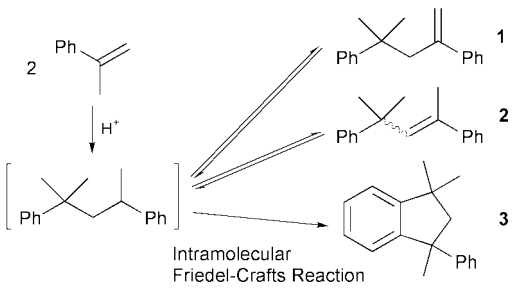

Scheme 1

The low yield of **3** for our MCM-41/Nafion composite suggests poor catalytic activity for Friedel–Crafts reactions.[8] The conversion of **1** to **3** at 60 °C scarcely proceeded with the MCM-41/Nafion composite (3% after 24 h), whereas SAC-13 considerably catalyzed this reaction (17% after 6 h and 56%

DOI: 10.1039/b004842i

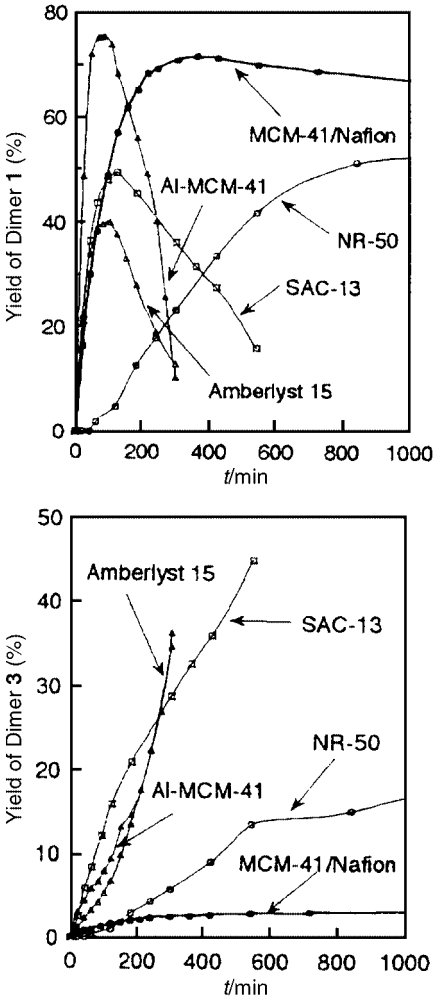

Fig. 2 Yields of **1** (a) and **3** (b) as a function of time using various catalysts.

after 24 h). The clear difference of the catalytic activity between the MCM-41/Nafion composite and SAC-13 in another Friedel–Crafts type reaction was also observed.[9] While SAC-13 catalyzed the reaction of styrene with toluene to form 1-phenyl-1-tolylethane in 27% yield with complete conversion of styrene at 70 °C for 6 h, MCM-41/Nafion composite gave only a trace of the product even after 24 h (styrene conversion: 37%). Therefore, it is thought that the low activity of the MCM-41/Nafion composite to Friedel–Crafts reaction at 60 °C results in the high selectivity towards dimer **1** from AMS. However, it is noteworthy that AMS afforded **3** in 91% yield using the MCM-41/Nafion composite at 100 °C after 3 h, and that the reaction of benzyl alcohol with toluene at 100 °C for 3 h afforded 87% of phenyltolylmethane, *cf*. trace amounts at 60 °C even after 24 h. Moreover, the competitive reaction of benzene and toluene with benzyl alcohol [eqn. (1)] at 90 °C showed a

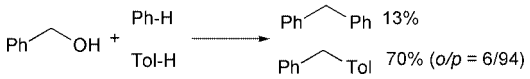

(1)

higher selectivity towards toluene (toluene/benzene = 5.4) than NR-50 (toluene/benzene = 3.6).[10] These results indicate that the catalytic properties of sulfuric acid in the MCM-41/Nafion composite are crucially influenced by the reaction temperature and the reactivity of the substrate. It is expected that some novel selective reactions can be carried out using this characteristic catalytic activity, and further studies are under investigation.

We gratefully acknowledge all the members of 'Catalysis Section' of Osaka National Research Institute, especially Dr T. Kobayashi and Dr M. Ando, for their help to the characterization study.

Notes and references

† To a solution of AMS (5 mmol) in toluene (5 mL) a solid catalyst (50 mg) was added under argon atmosphere and the resulting mixture stirred at 60 °C. Remaining AMS and all products were determined by capillary GC.

1 S. Biz and M. L. Occelli, *Catal. Rev.-Sci. Eng.*, 1998, **40**, 329.
2 M. Ganschow, M. Wark, D. Wöhrle and G. Schulz-Ekloff, *Angew. Chem., Int. Ed.*, 2000, **39**, 161; N. Igarashi, Y. Tanaka, S. Nakata and T. Tatsumi, *Chem. Lett.*, 1999, 1; A. Corma, J. L. Jordá, T. Navarro and F. Rey, *Chem. Commun.*, 1998, 1899.
3 M. A. Harmer, W. E. Farneth and Q. Sun, *Adv. Mater.*, 1998, **10**, 1255; M. A. Harmer, Q. Sun, M. J. Michalczyk and Z. Yang, *Chem. Commun.*, 1997, 1803; M. A. Harmer, W. E. Farneth and Q. Sun, *J. Am. Chem. Soc.*, 1996, **118**, 7708.
4 P. J. Evans, R. C. T. Slade, J. R. Varcoe and K. E. Young, *J. Mater. Chem.*, 1999, **9**, 3015; C. W. Jones, K. Tsuji and M. E. Davis, *Nature*, 1998, **393**, 52.
5 A. Heidekum, M. Harmer and W. F. Höldrich, *Catal. Lett.*, 1997, **47**, 243; Q. Sun, W. E. Farneth and M. A. Harmer, *J. Catal.*, 1996, **164**, 62; B. Chaudhuri and M. M. Sharma, *Ind. Eng. Chem. Res.*, 1989, **28**, 1757.
6 A. Sayari, *Chem. Mater.*, 1996, **8**, 1840.
7 J. D. Weaver, E. L. Tasset and W. E. Fry, *Catal. Today*, 1992, **14**, 195.
8 Q. Sun, M. A. Harmer and W. E. Farneth, *Ind. Eng. Chem. Res.*, 1997, **36**, 5541.
9 H. Hasegawa and T. Higashimura, *Polym. J.*, 1980, **12**, 407.
10 T. Yamato, C. Hideshima, G. K. S. Prakash and G. A. Olah, *J. Org. Chem.*, 1991, **56**, 2089.

Insertion of O_2 into a Pd(I)–Pd(I) dimer and subsequent C–O bond formation by activation of a C–H bond

Víctor Durà-Vilà, D. Michael P. Mingos, Ramón Vilar,* Andrew J. P. White and David J. Williams

Department of Chemistry, Imperial College, London, UK SW7 2AY. E-mail: r.vilar@ic.ac.uk

Received (in Cambridge, UK) 7th June 2000, Accepted 10th July 2000

The reaction between O_2 and the dimer $[Pd_2(\mu\text{-}Br)_2(PBu^t_3)_2]$ leads to the formation of the novel dimeric compound $[Pd(\mu\text{-}OCH_2\{CMe_2\}PBu^t_2)Br]_2$ by coordination of O_2 to the original palladium dimer and further formation of two C–O bonds by intramolecular activation of C–H bonds.

The study of transition metal dioxygen complexes has attracted substantial interest as these types of compounds are involved in the metabolism of O_2 in living organisms.[1,2] These bioinorganic natural systems have inspired chemists to search for synthetic analogues which can be used as industrial catalysts for the oxidation of C–H and C–C bonds.[3] It is believed that, in both the biological and synthetic systems, coordinated species such as O_2^-, O_2^{2-}, HO^-, RO^- and O^{2-} play important roles in the transfer of oxygen to the organic substrates.[4] This belief has led to extensive studies on the synthesis and reactivity of transition metal dioxygen complexes. Owing to their direct relevance to biological systems, nickel,[5] cobalt,[6] copper[7] and iron[8] mono- and bi-nuclear species have been those most extensively studied. By contrast, palladium dioxygen metals have received far less attention even though they have been implicated in various catalytic processes.[9]

During the past few years we have investigated extensively the reactivity of the dimers $[Pd_2(\mu\text{-}X)_2(PBu^t_3)_2]$ (X = Br, **1**; X = I, **2**).[10] These compounds contain two palladium(I) centres and have been demonstrated to react with a wide range of small molecules such as CO, CNR, H_2 and alkynes.[11] While studying these reactions, it was observed that dimer **1** exhibited a high reactivity towards aerial oxygen. The possibility of an oxidative addition of O_2 into this dimeric species, stimulated us to undertake a systematic study of the reaction between these dimers and oxygen. Here we report our preliminary results on the reaction of O_2 with the palladium dimer $[Pd_2(\mu\text{-}Br)_2(PBu^t_3)_2]$ (Scheme 1).

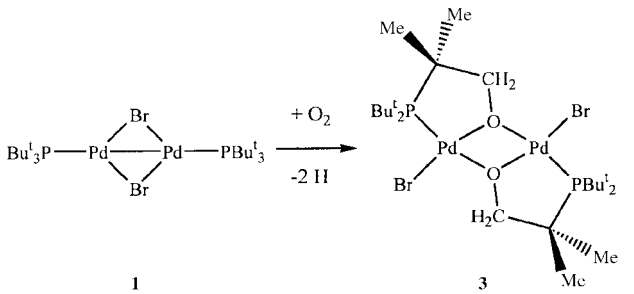

Scheme 1 The reaction between **1** and O_2 leads to the formation of a novel dimeric species in which new Pd–O and C–O bonds are formed. In this process an intramolecular C–H activation occurs.

Crystallographic evidence has demonstrated that in this reaction three transformations occur: coordination of O_2 and cleavage of an O=O bond, intramolecular activation of a C–H bond and formation of new C–O bonds.

When a solution of **1** in dry and deoxygenated benzene was reacted with aerial oxygen, the original dark green colour of the solution changed to orange after few seconds. The $^{31}P\{^1H\}$ NMR spectrum of this mixture showed a singlet at δ 108.0 (*cf.* δ 87.5 for the starting material) suggesting the presence of a single product. The solvent from this mixture was then evaporated under reduced pressure and the remaining dark orange material was analysed spectroscopically† and structurally‡ demonstrating it to be the novel dimer $[Pd(\mu\text{-}OCH_2\{CMe_2\}PBu^t_2)Br]_2$ **3** (Scheme 1). The ^1H NMR spectrum of this new compound showed three doublets in the range δ 1.4–1.7 with an integration ration of 1 : 3 : 9. The doublet integrating for 9 protons corresponds to the Bu^t groups in the PBu^t_3 while the other two doublets correspond to a CMe_2 and a CH_2 group, suggesting cyclometallation of the phosphine. This type of intramolecular rearrangement is well established for PBu^t_3 and the NMR spectra of the resulting compounds are well documented.[12] Signals at high field were not observed suggesting that O–H groups are not present in the new compound **3**. This was also verified by IR spectroscopy which did not show any O–H stretches. Elemental analyses were also consistent with the formulation of **3**.

The unambiguous nature of compound **3** was established by an X-ray crystallographic study. Single crystals were obtained by layering a benzene solution of the dimer with hexane.

This analysis‡ confirmed that **3** is the dimeric species $[Pd(\mu\text{-}OCH_2\{CMe_2\}PBu^t_2)Br]_2$ (Fig. 1) which results from the incorporation of aerial O_2 into the original complex **1**. The molecule **3** has non-crystallographic C_2 symmetry about an axis normal to, and passing through the centre of, the Pd_2O_2 ring. This central four-membered ring is folded 52° out of plane about the O··O vector; the non-bonded Pd··Pd and O··O distances are 2.911(1) and 2.566(6) Å. The two five-membered chelate rings both have envelope conformations, with Pd(1)P(1)C(1)O(1) and Pd(2)P(2)C(3)O(2) being planar to within *ca*. 0.04 and 0.08 Å, respectively, and with C(2) and C(4) lying 0.68 and 0.70 Å out of their respective planes with consequent axial/equatorial dispositions of their methyl sub-

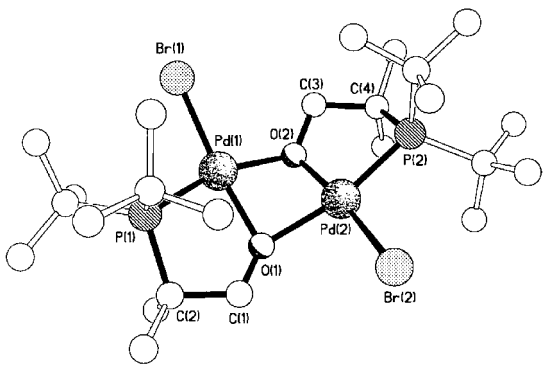

Fig. 1 The molecular structure of **3**. Selected bond lengths (Å) and angles (°): Pd(1)–O(1) 2.001(5), Pd(1)–O(2) 2.125(5), Pd(1)–P(1) 2.226(2), Pd(1)–Br(1) 2.4242(9), Pd(2)–O(1) 2.126(5), Pd(2)–O(2) 2.015(5), Pd(2)–P(2) 2.223(2), Pd(2)–Br(2) 2.4152(9), O(1)–C(1) 1.413(8), O(2)–C(3) 1.408(8), O(1)–Pd(1)–O(2) 76.9(2), O(1)–Pd(1)–P(1) 85.95(14), O(2)–Pd(2)–O(1) 76.6(2), O(2)–Pd(2)–P(2) 87.05(14), C(1)–O(1)–Pd(1) 119.1(4), C(1)–O(1)–Pd(2) 127.6(4), Pd(1)–O(1)–Pd(2) 89.7(2), C(3)–O(2)–Pd(2) 117.0(4), C(3)–O(2)–Pd(1) 127.0(5), Pd(2)–O(2)–Pd(1) 89.3(2).

DOI: 10.1039/b004537n

stituents. The geometry at each oxygen centre is distinctly pyramidal with both O(1) and O(2) lying *ca*. 0.5 Å out of the plane of their substituents. The coordination at each palladium centre is distorted square planar with *cis* angles in the range 76.9(2)–101.53(5)° and 76.6(2)–100.01(5)° at Pd(1) and Pd(2), respectively, the acute angle in each case being associated with the central Pd_2O_2 ring. The Pd–O–Pd bridges are both asymmetric, with the Pd–O bonds *trans* to bromine [2.001(5) and 2.015(5) Å] being *ca*. 0.1 Å shorter than those *trans* to phosphorus [2.125(5) and 2.126(5) Å]. These distances are comparable to those observed in the few reported examples of Pd_2O_2 rings.[13] In these literature examples the non-bonded Pd··Pd separation is in all cases longer than that we observe in **3**.

A remarkable aspect of the structure of **3** is the formation of two C–O bonds by intramolecular C–H activation of one of the Bu^t groups of each phosphine. This leads to the formation of two five-membered chelate rings, which explains the presence of the three doublets observed in the ^{1}H NMR spectrum of **3** and is also consistent with the singlet present at δ 108.0 in the ^{31}P{^{1}H} NMR spectrum.

Careful inspection of the sample from which the crystals of **3** were taken indicated the presence of very few crystals of both a different colour and morphology (the number of these crystals was negligible compared to the amount of crystals of **3**). X-Ray crystallographic analysis of one of these crystals‡ showed that the structure of this second product is the dimeric species with formula $[\overline{Pd(Bu_2^tPCMe_2CH_2}](\mu\text{-Br})]_2$ **4**. This complex is isomorphous with the already reported chloride analogue having a planar central Pd_2Br_2 ring and folded $PdPC_2$ rings (Fig. 2).[12]

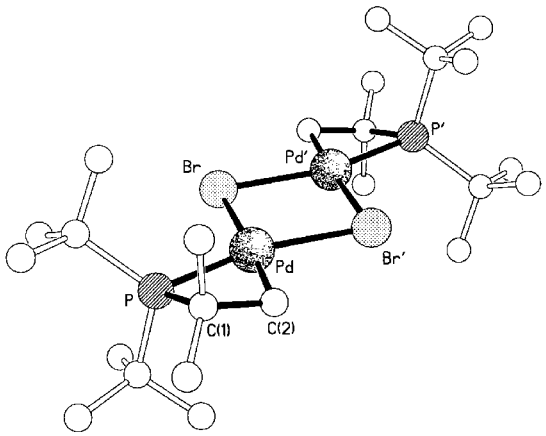

Fig. 2 The molecular structure of **4**. Selected bond lengths (Å) and angles (°): Pd–C(2) 2.048(8), Pd–P 2.215(2), Pd–Br′ 2.5497(11), Pd–Br 2.5922(12), P–Pd–C(2) 69.6(2), Br–Pd–Br′ 88.30(4), Pd–Br–Pd′ 91.70(4). There is a 25° out of plane fold about the P··C(2) vector in the $PdPC_2$ ring.

Interestingly when the oxygenation reaction was attempted with the analogous iodo-dimer $[Pd_2(\mu\text{-I})_2(PBu^t_3)_2]$, no reaction was observed. As we have reported previously, dimer **1** tends to be much more reactive than **2** towards small molecules such as CO, H_2, CNR and alkynes.[11] In the present investigation, this difference in reactivity has once again been observed.

The results presented here have demonstrated the ability of a Pd(I) dimer to react with aerial oxygen. In this process, three transformations seem to be taking place: *(i)* coordination of an O_2 molecule and cleavage on an O=O bond, *(ii)* intramolecular activation of two C–H bonds and *(iii)* formation of two new C–O bonds. To our knowledge, this is the first example of a palladium compound in which such a process has been demonstrated by crystallographic characterisation. The mechanistic aspects of this reaction are yet to be studied. For example an important question that remains to be answered is whether the two oxygen atoms come from the same O_2 molecule or from two different ones. Also important will be to establish the exact mechanism by which the reaction occurs and the fate of the two hydrogen atoms lost in the activation of the C–H bond. Experiments are currently in progress to attempt to provide answers to these questions.

Notes and references

† *Spectroscopic data* for **3**: ^{1}H-NMR (C_6D_6): δ 1.63 [9H, d, $C(CH_3)_3$], 1.58 [3H, d, $C(CH_3)_2$], 1.50 (1H, d, CH_2). ^{31}P{^{1}H} NMR {$(CD_3)_2CO$]: δ 108.0 (s). Elemental analysis. Calc. for $C_{24}H_{52}O_2P_2Br_2Pd_2$: C, 35.6; H, 6.7. Found: C, 35.9; H, 6.8%.

‡ *Crystal data*: for **3**: $C_{24}H_{52}O_2P_2Br_2Pd_2$, M = 807.2, monoclinic, space group $P2_1/c$ (no. 14), a = 15.668(1), b = 14.187(1), c = 15.099(1) Å, β = 113.44(1)°, V = 3079.1(3) Å^3, Z = 4, D_c = 1.741 g cm^{-3}, μ(Cu-Kα) = 135.8 cm^{-1}, F(000) = 1616, T = 293 K; pale orange platy rhombs, 0.37 × 0.23 × 0.05 mm, Siemens P4/PC diffractometer, graphite-monochromated Cu-Kα radiation, ω-scans, 4568 independent reflections. The structure was solved by direct methods and the non-hydrogen atoms were refined anisotropically using full-matrix least squares based on F^2 to give R_1 = 0.043, wR_2 = 0.103 for 3890 independent observed absorption corrected reflections [$|F_o| > 4\sigma(|F_o|)$, $2\theta \leq 120°$] and 290 parameters.

For **4**: $C_{24}H_{52}P_2Br_2Pd_2$, M = 775.2, monoclinic, space group $P2_1/c$ (no. 14), a = 7.788(3), b = 15.368(5), c = 13.557(3) Å, β = 105.40(2)°, V = 1564.3(8) Å^3, Z = 2 (the complex has crystallographic C_i symmetry), D_c = 1.646 g cm^{-3}, μ(Mo-Kα) = 38.2 cm^{-1}, F(000) = 776, T = 293 K; orange prisms, 0.27 × 0.13 × 0.05 mm, Siemens P4/PC diffractometer, graphite-monochromated Mo-Kα radiation, ω-scans, 2753 independent reflections. The structure was solved by direct methods and the non-hydrogen atoms were refined anisotropically using full-matrix least squares based on F^2 to give R_1 = 0.048, wR_2 = 0.089 for 1796 independent observed absorption corrected reflections [$|F_o| > 4\sigma(|F_o|)$, $2\theta \leq 50°$] and 136 parameters.

CCDC 182/1713. See http://www.rsc.org/suppdata/cc/b0/b004537n/ for crystallographic files in .cif format.

1 See the special thematic issue for Oxygen Metabolism in Bioinorganic Enzymology: *Chem. Rev.*, 1996, **96**, 2541 and references therein.

2 K. D. Karlin and Z. Tyeklar, in *Models in Inorganic Biochemistry*, G. L. Eichhorn and L. G. Marzilli, PTR Prentice Hall, Englewood Cliffs, NJ, 1994; S. Fox and K. D. Karlin, in *Active Oxygen in Biochemistry*, ed. J. S. Valentine, C. S. Foote, A. Greenberg and J. F. Liebman, Blackie Academic & Professional, London, 1995.

3 R. A. Sheldon and J. K. Kochi, *Metal-Catalyzed Oxidations of Organic Compounds*, Academic Press, New York, 1981; *Oxygen Complexes and Oxygen Activation by Transition Metals*, ed. A. E. Martell and D. T. Swayer, Plenum Press, New York, 1988.

4 See the special thematic issue for Metal–Dioxygen Complexes: *Chem. Rev.*, 1994, **94**, 567 and references therein.

5 S. Hikichi, M. Yoshizawa, Y. Sasakura, M. Akita and Y. Moro-oka, *J. Am. Chem. Soc.*, 1998, **120**, 10567.

6 S. Hikichi, H. Komatsuzaki, M. Akita and Y. Moro-oka, *J. Am. Chem. Soc.*, 1998, **120**, 4699; S. Hikichi, H. Komatsuzaki, N. Kitajima, M. Akita, M. Mukai, T. Kitagawa and Y. Moro-oka, *Inorg. Chem.*, 1997, **36**, 266.

7 N. Kitajima and Y. Moro-Oka, *Chem. Rev.*, 1994, **74**, 737 and references therein.; E. I. Solomon, F. Tuczek, D. E. Root and C. A. Brown, *Chem. Rev.*, 1994, **94**, 827 and references therein.

8 L. Que, Jr., *J. Chem. Soc. Dalton Trans.*, 1997, 3933; C. Kim, Y. Dong and L. Que, Jr., *J. Am. Chem. Soc.*, 1997, **119**, 3635.

9 For general references see: R. F. Heck, *Palladium Reagents in Organic Synthesis*, Academic Press, New York, 1990; J. Tsuji, *Palladium Reagents and Catalysis*, John Wiley & Sons, New York, 1995.

10 R. Vilar, D. M. P. Mingos and C. J. Cardin, *J. Chem. Soc., Dalton Trans.*, 1996, 4313.

11 D. M. P. Mingos and R. Vilar, *J. Organomet. Chem.*, 1998, **557**, 131; R. Vilar, S. E. Lawrence, S. Menzer, D. M. P. Mingos and D. J. Williams, *J. Chem. Soc, Dalton Trans.*, 1997, 3305; V. Durà-Vilà, D. M. P. Mingos, R. Vilar, A. White and D. J. Williams, *J. Organomet. Chem.*, 2000, **600**, 198.

12 H. C. Clark, A. B. Goel, R.G. Goel, S. Goel and W. O. Ogini, *Inorg. Chim. Acta*, 1978, **31**, L441; H. C. Clark, A. B. Goel and S. Goel, *J. Organomet. Chem.*, 1979, **166**, C29; P. E. Garrou, *Chem. Rev.*, 1981, **81**, 229.

13 G. Pieri, M. Pasquali, P. Leoni and U. Englert, *J. Organomet. Chem.*, 1995, **491**, 27; G. López, J. Ruiz, G. García, C. Vicente, J. Casabó, E. Molins and C. Miravitlles, *Inorg. Chem.*, 1991, **30**, 2605; C. Pisano, G. Consiglio, A. Sironi and M. Moret, *J. Chem. Soc., Chem. Commun.*, 1991, 421; V. V. Grushin and H. Alper, *Organometallics*, 1993, **12**, 1890; A. R. Siedle and L. H. Pignolet, *Inorg. Chem.*, 1982, **21**, 3090; A. J. Atkins, A. J. Blake and M. Schröder, *J. Chem. Soc., Chem. Commun.*, 1993, 353; M. Akita, T. Miyaji, S. Hikichi and Y. Moro-oka, *Chem. Commun.*, 1998, 1005.

ChemComm

6-*Endo-trig* and 5-*exo-trig* selective aryl radical cyclisations of *N*-(*o*-bromobenzyl) enamides

Hiroyuki Ishibashi,* Issei Kato, Yoshifumi Takeda, Momoyo Kogure and Osamu Tamura

Faculty of Pharmaceutical Sciences, Kanazawa University, Takara-machi, Kanazawa 920-0934, Japan. E-mail: isibasi@dbs.p.kanazawa-u.ac.jp

Received (in Cambridge, UK) 11th May 2000, Accepted 28th June 2000

Bu_3SnH-mediated aryl radical cyclisation of enamide 9 proceeded in a 6-*endo-trig* manner to give exclusively tetrahydroisoquinoline derivative 12, whereas enamide 10b having a (*Z*)-phenylthio group at the terminus of the *N*-vinylic bond gave exclusively the 5-*exo-trig* cyclisation product 16.

Aryl radical cyclisations are now widely used in organic synthesis for the construction of fused aromatic compounds. A 5-*exo-trig* cyclisation is generally preferred over a 6-*endo-trig* ring closure in those systems having an alkenic bond at the 5-position relative to the aryl radical centre. For example, aryl bromides **1** (X = CH_2, O or NCOR), upon treatment with Bu_3SnH in the presence of AIBN, gave almost exclusively the 5-*exo* cyclisation products **2**.[1] This was also the case for the

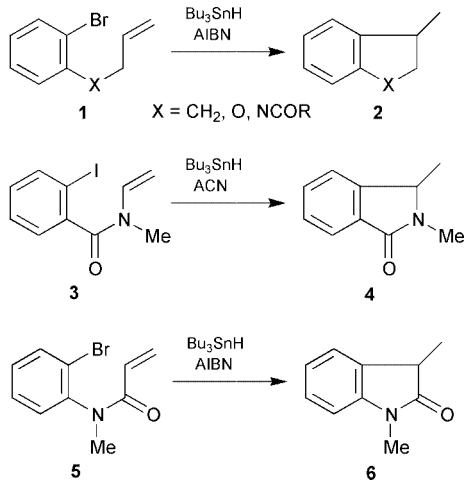

cyclisations of enamide **3** and acryloylanilide **5**, which gave only the five-membered lactams **4**[2] and **6**,[3,4] respectively. Herein we wish to report that *N*-(*o*-bromobenzyl) enamide **9** undergoes aryl radical cyclisation in a 6-*endo-trig* manner to give exclusively tetrahydroisoquinoline derivative **12**, and that the mode of cyclisation can be shifted to a 5-*exo-trig* manner by introducing a (*Z*)-phenylthio group at the terminus of the *N*-vinylic bond.

The requisite radical precursors **9**, **10a** and **10b** were prepared as shown in Scheme 1.

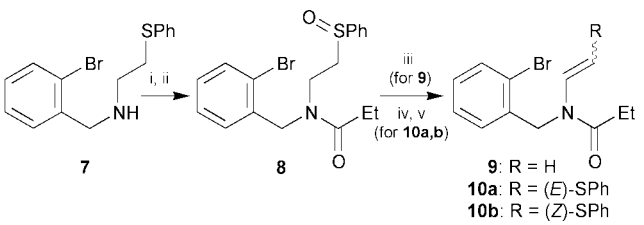

Scheme 1 *Reagents and conditions*: i, EtCOCl, Et_3N, CH_2Cl_2, rt, 90%; ii, MCPBA, CH_2Cl_2, 0 °C, 93%; iii, xylene, $NaHCO_3$, reflux, 81%; iv, $(CF_2CO)_2O$, CH_2Cl_2, rt; v, toluene, reflux, 46% for **10a**, 13% for **10b** (based on **8**).

When a mixture of Bu_3SnH (2.2 eq.) and azobis(cyclohexancarbonitrile) (ACN) (0.4 eq.) in toluene was added slowly to a boiling solution of **9** in toluene over a period of 3.5 h, the 6-*endo* cyclisation product **12**[5] was obtained in 68% yield, along with the simple reduction product **14** (16% yield) (Scheme 2). Similarly, the *N*-formyl congener **11** gave **13** and **15** in 43 and 19% yields, respectively. On the other hand, treatment of the sulfur substituted (*E*)-isomer **10a** with Bu_3SnH–ACN afforded the 5-*exo* cyclisation product **16** in 40% yield, along with dihydroisoquinoline derivative **17** in 41% yield. The corresponding (*Z*)-isomer **10b** gave **16** as a sole product in 75% yield.

The exclusive formation of the 6-*endo* cyclisation product **12** from **9** is of great interest in view of previous work on radical cyclisations of the related compounds **1**, **3** and **5**, which gave the 5-*exo* cyclisation products **2**, **4** and **6**, respectively. Formation of **4** (from **3**) and **12** (from **9**) can be rationalized by an attack of Bu_3SnH on the primary radical **18** and on the secondary radical **21**, respectively. Since enamide **3** gave no 6-*endo* cyclisation product *via* the secondary radical **19**, formation of **12** from **9** could not be explained by assuming that the nitrogen-substituted secondary radical **21** might be more stable than the primary radical **20**.

One possible explanation for the formation of **12** from **9** may involve a consecutive 5-*exo* cyclisation and neophyl-like† rearrangement of the resulting radical **20**. The possibility,

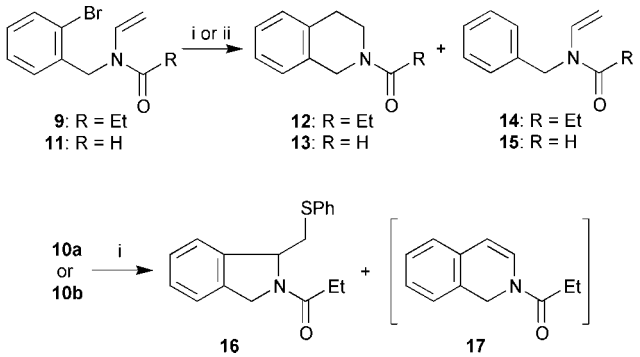

Scheme 2 *Reagents and conditions*: i, Bu_3SnH, ACN, toluene, reflux; ii, Bu_3SnH, Et_3B, toluene, rt.

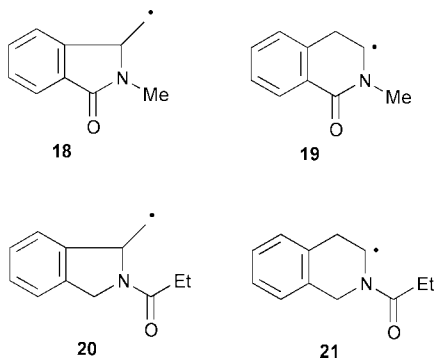

DOI: 10.1039/b003790g

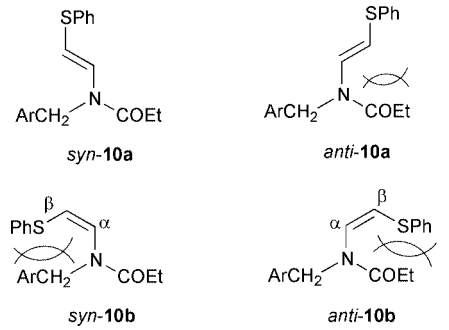

Fig. 1 Ar = *o*-BrC_6H_4.

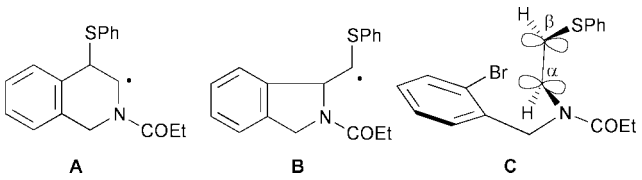

Fig. 2

however, could be ruled out by the following work to simultaneously examine the effects of various Bu_3SnH concentrations, addition times and reaction temperatures.[6] Thus, treatment of **9** with 4 eq. of Bu_3SnH (not using the slow addition technique) in the presence of triethylborane in toluene at rt for 16 h also gave the 6-*endo* cyclisation product **12** in 51% yield, along with the reduction product **14** (23%). The most plausible explanation for the results with **3** and **9**, therefore, may be derived from the consideration of the rotation of enamide.[7] Two conformers can be considered for both radical precursors, *i.e.* *syn*-**3** and *anti*-**3** for **3** and *syn*-**9** and *anti*-**9** for **9**. In the

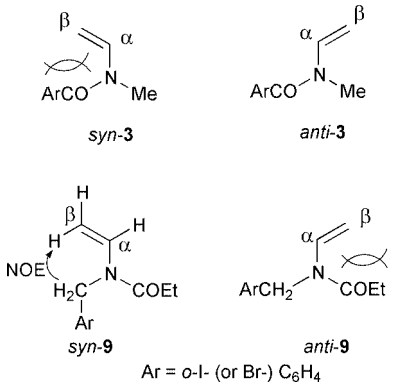

conformers *syn*-**3** and *anti*-**9**, severe steric repulsions between the aroyl (*o*-IC_6H_4CO) and C=C groups and between the acyl (EtCO) and C=C groups, respectively, are evident. The conformers *anti*-**3** and *syn*-**9** therefore predominate, and the resulting radicals attack on the more proximate C_α-position of *anti*-**3** and C_β-position of *syn*-**9**, to give the observed 5-*exo* cyclisation product **4** and the 6-*endo* cyclisation product **12**, respectively. The NOE difference spectroscopy also indicated that **9** exists only in the *syn*-**9** form.[8] Thus, irradiation of the signals due to the *N*-benzylic protons [δ 4.76 ($\frac{1}{3}$ × 2 H, s) and 4.94 ($\frac{2}{3}$ × 2 H, s)] of **9** caused an enhancement of the signals due to the C_β-proton *cis* to the nitrogen atom [δ 4.26 ($\frac{1}{3}$ H, d, *J* 15.6) and 4.29 ($\frac{2}{3}$ H, d, *J* 15.6)] and no enhancement of the signals due to the Cα-proton [δ 6.95 ($\frac{2}{3}$ H, dd, *J* 15.6 and 9.2) and 7.67 ($\frac{1}{3}$ H, dd, *J* 15.6 and 9.2)].[11] The preponderance of the *syn*-**9** conformer over *anti*-**9** seems to be independent of the size of the *N*-acyl group, since **11** having a sterically less demanding *N*-formyl group, also gave the 6-*endo* cyclisation product **13**.

For the sulfur substituted (*E*)-isomer **10a**, the two conformers *syn*-**10a** and *anti*-**10a** can be considered (Fig. 1). As in the case of *anti*-**9**, there is a severe steric repulsion between the EtCO and C=C groups in *anti*-**10a**, and the cyclisation might therefore proceed *via* the conformer *syn*-**10a** in a 6-*endo* manner to give **17** through an elimination of a benzenethiyl radical from the resulting intermediate radical **A** (Fig. 2). The major product of the reaction of **10a**, however, is the 5-*exo* cyclisation product **16**. This is probably because the sulfur atom of the intermediate radical **B** can strongly stabilise the neighboring radical centre.[9]

On the other hand, both conformers *syn*-**10b** and *anti*-**10b** for the (*Z*)-isomer **10b** have a more severe steric constraint between the *o*-$BrC_6H_4CH_2$ and SPh groups for the former and between the COEt and SPh groups for the latter (Fig. 1), and hence the C_α=C_β bond and amide nitrogen might not be conjugated in enamide **10b**.[10] If the C_α=C_β bond is almost perpendicular to the amide bond, as depicted in **C** (Fig. 2), the resulting radical can attack the more proximate C_α-position to give exclusively the observed 5-*exo* cyclisation product **16**.[11]

Notes and references

† The IUPAC name for neophyl is 2-methyl-2-phenylpropane.

1 For X = CH_2, see: A. N. Abeywickrema, A. L. J. Beckwith and S. Gerba, *J. Org. Chem.*, 1987, **52**, 4072; For X = O, see: S.-K. Chung and F.-F. Chung, *Tetrahedron Lett.*, 1979, 2473; H. Togo and O. Kikuchi, *Tetrahedron Lett.*, 1988, **29**, 4133; For X = NCOR, see: J. P. Dittami and H. Ramanathan, *Tetrahedron Lett.*, 1988, **29**, 45; Y. Özlü, D. E. Cladingboel and P. J. Parsons, *Tetrahedron*, 1994, **50**, 2183.

2 H. Ishibashi, K. Ohata, M. Niihara, T. Sato and M. Ikeda, *J. Chem. Soc., Perkin Trans. 1*, 2000, 547.

3 K. Jones, M. Thompson and C. Wright, *J. Chem. Soc., Chem. Commun.*, 1986, 115; K. Jones and J. M. D. Storey, *Tetrahedron Lett.*, 1993, **34**, 7797.

4 A limited example of 6-*endo* selective cyclisation has been reported for the palladium-mediated reaction of *N*-acryloyl-7-bromoindoline. See: J. W. Dankwardt and L. A. Flippin, *J. Org. Chem.*, 1995, **60**, 2312.

5 C. Aubert, C. Huard-Perrio and M.-C. Lasne, *J. Chem. Soc., Perkin Trans. 1*, 1997, 2837.

6 Careful examinations on the effects of varying Bu_3SnH concentration, addition time and reaction temperature, have frequently shown that 6-*endo* cyclisation products are formed by an initial 5-*exo* cyclisation followed by neophyl rearrangement. See: K. A. Parker, D. M. Spero and K. C. Inman, *Tetrahedron Lett.*, 1986, **27**, 2833; A. N. Abeywickrema, A. L. J. Beckwith and S. Gerba, *J. Org. Chem.*, 1987, **52**, 4072; K. Jones, S. A. Brunton and R. Gosain, *Tetrahedron Lett.*, 1999, **40**, 8935. See also ref. 2.

7 An initial conformation of a radical precursor has been suggested to play an important role in deciding the course of cyclisation. See: D. P. Curran and J. Tamine, *J. Org. Chem.*, 1991, **56**, 2746; O. M. Musa, J. H. Horner and M. Newcomb, *J. Org. Chem.*, 1999, **64**, 1022; D. P. Curran, W. Liu and C. H.-T. Chen, *J. Am. Chem. Soc.*, 1999, **121**, 11 012, and references cited therein.

8 It has been also suggested that the vinyl groups of *N*-alkyl-*N*-vinylcarbamates occupy *anti*-position to the alkoxycarbonyl groups. See: O. Tamura, M. Hashimoto, Y. Kobayashi, T. Katoh, K. Nakatani, M. Kamada, I. Hayakawa, T. Akiba and S. Terashima, *Tetrahedron*, 1994, **50**, 3889; T. Akiba, O. Tamura, M. Hashimoto, Y. Kobayashi, T. Katoh, K. Nakatani, M. Kamada, I. Hayakawa and S. Terashima, *Tetrahedron*, 1994, **50**, 3905.

9 For sulfur-controlled *exo* selective radical cyclisations, see: H. Ishibashi, T. Kobayashi and D. Takamasu, *Synlett*, 1999, 1286 and references cited therein.

10 This assumption was supported by IR spectral properties showing the carbonyl band for (*E*)-isomer **10a** in a higher frequency region (1680 cm^{-1}) compared to that (1660 cm^{-1}) for (*Z*)-isomer **10b**.

11 It seems that the size of the substituent on the nitrogen atom of **10a,b** does not influence the conformer population. Thus, treatment of the *N*-COBu^t congener of (*E*)-isomer **10a** also gave nearly equal amounts of 5-*exo* cyclisation product (42%) and 6-*endo* cyclisation product (37%), and the corresponding (*Z*)-isomer gave only the 5-*exo* cyclisation product in 70% yield (compare to the results with **10a**,**b**).

Pyridyl-thiazoles as a new class of ligand for metallosupramolecular chemistry: formation of double and triple helicates with Cu(II)

Craig R. Rice,*[a] Stefan Wörl,[b] John C. Jeffery,[b] Rowena L. Paul[b] and Michael D. Ward[b]

[a] *Department of Chemical and Biological Sciences, University of Huddersfield, Huddersfield, UK HD1 3DH. E-mail: c.r.rice@hud.ac.uk*

[b] *School of Chemistry, University of Bristol, Cantock's Close, Bristol, UK BS8 1TS*

Received (in Cambridge, UK) 31st May 2000, Accepted 7th June 2000

Reaction of either 1,10-phenanthroline-2-thioamide or pyridine-2-thioamide with 1,4-dibromobutane-2,3-dione affords the novel thiazole-containing polydentate ligands L^1 and L^2, respectively; these ligands form dinuclear double and triple helicate architectures, respectively, with Cu^{2+}.

Studies on the assembly of double and triple helicate complexes have been a major area of supramolecular coordination chemistry for the last 15 years. Helicate complexes have elegantly illustrated how the specific formation of architecturally complex assemblies are directed by the interplay between relatively simple parameters such as the stereoelectronic preference of the metal ion and the disposition of binding sites in the ligand.[1]

Many helicates are derived from ligands which are obviously partitioned into distinct binding sites, as exemplified by (i) the bis-catecholate ligands of Albrecht which form dinuclear triple helicates with various octahedral M(IV) ions;[2] (ii) the polybipyridyl ligands of Lehn and coworkers which form multinuclear double helicates with pseudo-tetrahedral Cu(I) and Ag(I);[3] and (iii) the bisterdentate ligands of Piguet and coworkers which afford triple helicates with nine-coordinate lanthanide(III) ions.[4] In contrast to these are the well-studied linear oligopyridines, whose partition into distinct metal-ion binding domains is controlled by the preference of the metal ion.[5] Thus, 2,2′:6′,2″:6″,2‴:6‴,2⁗:6⁗,2⁗⁗-sexipyridine (spy) splits into two terdentate domains to give dinuclear double helicates with metals such as Cd(II) which are six-coordinate, but splits into three bidentate domains to give trinuclear double helicates with metals such as Cu(I) which prefer to be pseudo-tetrahedral. Similarly 2,2′:6′2″:6″,2‴-quaterpyridine (qpy) can act as a simple tetradentate chelate in many mononuclear complexes,[6,7] or split into a '3 + 1'-dentate arrangement in octahedral $[Fe(qpy)_2]^{2+}$ in which qpy behaves as a terdentate ligand,[8] or split into a '2 + 2'-dentate arrangement in dinuclear double helicates with Cu(I) and Ag(I).[7] It is clear that the versatility of these ligands arises from their ability to adopt a wide variety of different coordination modes.

Here, we describe the preparation of a new class of ligand, containing chelating pyridyl-thiazolyl fragments, for the assembly of helicates. There are two features that make these of particular interest. Firstly, they are very simple to prepare and are readily available in far higher quantities than the analogous polypyridines; in this respect they are like the pyridyl/imine chelates of Hannon *et al.*[9] The thiazole unit is particularly easy to introduce into polydentate ligands and a number of metal complexes (but no helicates) of thiazole-based ligands have been prepared.[10] Secondly, unlike their polypyridyl analogues, these ligands naturally partition themselves into distinct binding domains because of the inability of the two adjacent thiazolyl units to chelate to the same metal: thus a substantial twist arises in the backbone of the coordinated ligand at this point.

The new ligands L^1 and L^2 are easily prepared as the bishydrobromide salts in good yield by reaction of 2 equivalents of the corresponding thioamide (2-pyridylthioamide and 1,10-phenanthroline-2-thioamide, respectively) with 1,4-dibromobutane-2,3-dione in methanol (Scheme 1).† Subsequent neutralization gives the free-base ligands. Reaction of L^1 with 2 equivalents of $Cu(PF_6)_2$ in Me_2CO gives, after precipitation in an atmosphere of ethyl acetate, a green crystalline material for which electrospray mass spectrometry and elemental analysis suggested a formula of $[Cu_2(L^1)_3](PF_6)_4$ **1**. This formulation was confirmed by X-ray crystallography, which shows two Cu(II) ions co-ordinated by three bridging ligands L^1 in a triple helical arrangement (Fig. 1).‡ Each of the Cu centres has a pseudo-octahedral coordination geometry (bite angles 77.0–79.6°, Cu–N distances 2.028–2.228 Å), formed by coordination of three thiazole-pyridyl bidentate units with each

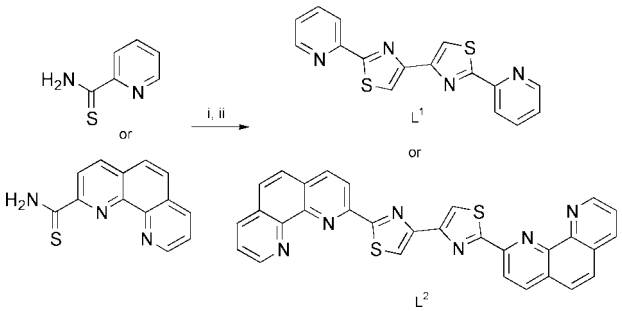

Scheme 1 *Reagents and conditions:* i, $(COCH_2Br)_2$, MeOH; ii, NH_3(aq).

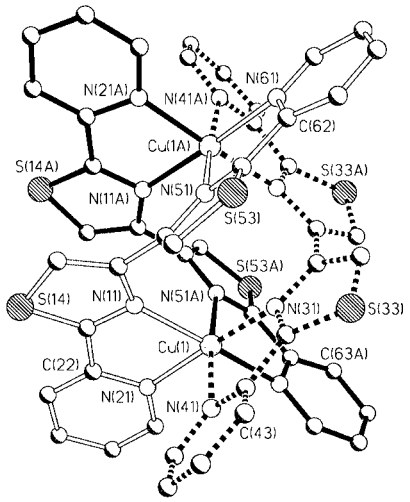

Fig. 1 Crystal structure of the complex cation of **1**·4Me_2CO. Selected bond distances (Å) and angles (°): Cu(1)–N(21) 2.028(8), Cu(1)–N(31) 2.056(7), Cu(1)–N(11) 2.187(8), Cu(1)–N(41) 2.192(8), Cu(1)–N(61A) 2.171(8), Cu(1)–N(51A) 2.219(8); N(21)–Cu(1)–N(31) 171.5(3), N(21)–Cu(1)–N(61) 96.7(3), N(31)–Cu(1)–N(61) 87.2(3), N(21)–Cu(1)–N(11) 79.2(3), N(31)–Cu(1)–N(11) 97.1(3), N(61)–Cu(1)–N(11) 175.4(3), N(21)–Cu(1)–N(41) 92.9(3), N(31)–Cu(1)–N(41) 79.1(3), N(61)–Cu(1)–N(41) 97.8(3), N(11)–Cu(1)–N(41) 84.8(3), N(21)–Cu(1)–N(51) 86.8(3), N(31)–Cu(1)–N(51) 101.4(3), N(61)–Cu(1)–N(51) 76.8(3), N(11)–Cu(1)–N(51) 100.5(3), N(41)–Cu(1)–N(51) 174.5(3).

DOI: 10.1039/b004319m

ligand twisted about the bond between the two thiazole rings. Although the coordination geometry is somewhat irregular, there is no obvious Jahn–Teller distortion axis. The structure is stabilized by extensive aromatic π-stacking interactions between overlapping, near-parallel fragments of adjacent ligand, as emphasized in the space-filling picture (Fig. 2).

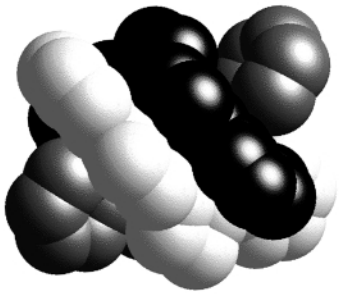

Fig. 2 Space-filling representation of the triple helicate **1**.

The formation of a triple helicate is in interesting contrast to the mononuclear complexes in which qpy acts as a simple equatorial tetradentate chelate.[6,7] In qpy this coordination mode is facilitated by the fact that each chelate ring has a bite angle appropriate for coordination to a single metal ion. In L^1, this is not the case; the two five-membered thiazolyl rings cannot chelate as the N atoms of the two five-membered rings are not sufficiently convergent, so the ligand naturally partitions into two bidentate pyridyl/thiazolyl units with a twist in the ligand backbone between them. The result is a dinuclear triple helicate instead of a simple mononuclear complex.

Reaction of L^2 with $Cu(ClO_4)_2$ in MeCN gives the double-helical complex $[Cu_2(L^2)_2](ClO_4)_4$ **2**.‡ Each of the copper centres is pseudo-octahedral, coordinated by two thiazolyl-phenanthroline tridentate units [bite angles 74.2–98.7°, Cu–N distances 1.967–2.312 Å], with each ligand again twisted about the inter-thiazole bond (Fig. 3) for the same reason as before.

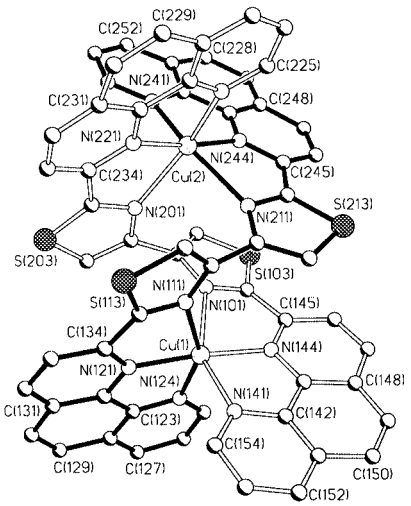

Fig. 3 Crystal structure of the complex cation of **2**·8MeCN·H_2O. Selected bond distances (Å) and angles (°): Cu(1)–N(121) 1.972(11), Cu(1)–N(144) 1.987(11), Cu(1)–N(124) 2.111(12), Cu(1)–N(141) 2.138(13), Cu(1)–N(111) 2.226(12), Cu(1)–N(101) 2.311(13); N(121)–Cu(1)–N(144) 173.9(5), N(121)–Cu(1)–N(124) 79.3(5), N(144)–Cu(1)–N(124) 95.6(5), N(121)–Cu(1)–N(141) 98.7(5), N(144)–Cu(1)–N(141) 79.2(5), N(124)–Cu(1)–N(141) 102.1(5), N(121)–Cu(1)–N(111) 76.3(5), N(144)–Cu(1)–N(111) 109.3(5), N(124)–Cu(1)–N(111) 154.1(4), N(141)–Cu(1)–N(111) 90.0(4), N(121)–Cu(1)–N(101) 108.7(5), N(144)–Cu(1)–N(101) 74.3(5), N(124)–Cu(1)–N(101) 91.1(5), N(141)–Cu(1)–N(101) 151.4(4), N(111)–Cu(1)–N(101) 88.8(4). Cu(2)–N(244) 1.965(12), Cu(2)–N(221) 1.968(12), Cu(2)–N(241) 2.129(14), Cu(2)–N(224) 2.148(11), Cu(2)–N(201) 2.258(12), Cu(2)–N(211) 2.299(13); N(244)–Cu(2)–N(221) 173.6(5), N(244)–Cu(2)–N(241) 79.5(5), N(221)–Cu(2)–N(241) 98.2(5), N(244)–Cu(2)–N(224) 96.3(5), N(221)–Cu(2)–N(224) 78.4(5), N(241)–Cu(2)–N(224) 105.3(5), N(244)–Cu(2)–N(201) 110.7(5), N(221)–Cu(2)–N(201) 75.2(5), N(241)–Cu(2)–N(201) 88.8(5), N(224)–Cu(2)–N(201) 151.6(5), N(244)–Cu(2)–N(211) 74.7(5), N(221)–Cu(2)–N(211) 108.6(5), N(241)–Cu(2)–N(211) 151.6(5), N(224)–Cu(2)–N(211) 89.3(4), N(201)–Cu(2)–N(211) 89.3(4).

In conclusion, we have demonstrated that polydentate ligands containing two central thiazolyl units are easy to prepare, and are very effective at forming double and/or triple helicates because of the way they naturally partition into two separate binding domains.[11] This method for preparing large polydentate ligands not only allows significant quantities to be produced but can also be readily extended to the preparation of a wide variety of ligands whose size, shape and functionality can be changed with ease.

We thank EPSRC for support.

Notes and references

† L^1: yield: 80%. EI mass spectrum: *m/z* 322 (75, M^+). δ_H[300 MHz, $(CD_3)_2SO$]: 8.68 (1H, d, pyridyl H), 8.26 (1H, d, pyridyl H), 8.24 (1H, s, thiazole H), 8.23 (1H, t, pyridyl H), 7.55 (1H, t, pyridyl H). Found: C, 59.5; H, 2.8; N, 16.9. $C_{16}H_{10}N_4S_2$ requires C, 59.6; H, 3.1; N, 17.4%. L^2: yield: 50%. EI mass spectrum: *m/z* 524 (80, M^+). Found: C, 60.4; H, 3.7; N, 12.8. $C_{30}H_{16}N_5S_2{\cdot}2(CH_3)_2SO$ requires C, 60.0; H, 4.1; N, 12.3%. The ^1H NMR spectrum was not obtained owing to the poor solubility of L^2 in common organic solvents. $[Cu_2(L^1)_3(PF_6)_4]$ **1** electrospray MS: *m/z* 1401 $[Cu_2(L^1)_3(PF_6)_2H_2O]$. Found: C, 33.7; H, 2.0; N, 10.0. $C_{48}H_{30}N_{12}S_6Cu_2P_4F_{24}$ requires C, 33.9; H, 1.9; N, 10.5%. $[Cu_2(L^2)_2(ClO_4)_4]$ **2**: electrospray MS: *m/z* 1473 $[Cu_2(L^2)_2(ClO_4)_3]$, 686 $[Cu_2(L^2)_2(ClO_4)_2]$. Found: C, 46.4; H, 2.1; N, 10.2. $C_{60}H_{32}N_{12}S_4Cu_2Cl_4O_{16}$ requires C, 45.8; H, 2.0; N, 10.7%.

‡ *Crystal data*: for $C_{48}H_{30}N_{12}S_6Cu_2P_4F_{24}{\cdot}4(CH_3)_2CO$ (**1**·4Me_2CO): M = 1906.5, monoclinic, space group $C2/c$, a = 13.9497(14), b = 23.133(2), c = 22.485(2) Å, β = 99.792(2) °, U = 7150.3(12) Å^3, Z = 4, D_c = 1.771 Mg m^{-3}, μ(Mo-Kα) = 0.980 mm^{-1}, F(000) = 3840, T = 173 K, 6291 independent reflections with $2\theta < 50°$. Refinement of 505 parameters with 59 restraints converged at final $R1$ = 0.0886, $wR2$ = 0.2807. The complex cation lies on a C_2 axis such that only half of it is crystallographically unique.

For $C_{60}H_{32}Cu_2Cl_4N_{12}O_{16}S_4{\cdot}8CH_3CN{\cdot}H_2O$ (**2**·8MeCN·H_2O): M = 1920.5, triclinic, space group $P1$, a = 13.4641(13), b = 15.0528(15), c = 21.859(2) Å, α = 80.685(2), β = 81.242(2), γ = 77.288(2)°, U = 4233.1(7) Å^3, Z = 2, D_c = 1.507 Mg m^{-3}, μ(Mo-Kα) = 0.806 cm^{-1}, F(000) = 1960, T = 173 K, 7887 independent reflections with $2\theta < 40°$. Refinement of 677 parameters with 8 restraints converged at final $R1$ = 0.0984, $wR2$ = 0.2884.

X-Ray measurements were made using a Bruker SMART CCD area-detector diffractometer; structure solution SHELXTL program system version 5.1, 1998. In both cases the complexes (**1** and **2**) crystallise as racemates, with equal numbers of opposite enantiomers in the achiral unit cell.

CCDC 182/1712. See http://www.rsc.org/suppdata/cc/b0/b004319m/ for crystallographic files in .cif format.

1 C. Piguet, G. Bernardinelli and G. Hopfgartner, *Chem. Rev.*, 1997, **97**, 2005.
2 M. Albrecht, *Chem. Soc. Rev.*, 1998, **27**, 281.
3 T. M. Garrett, U. Koert, J.-M. Lehn, A. Rigault, D. Meyer and J. Fischer, *J. Chem. Soc., Chem. Commun.*, 1990, 557.
4 M. Elhabiri, R. Scopelliti, J.-C. G. Bunzli and C. Piguet, *J. Am. Chem. Soc.*, 1999, **121**, 10747.
5 E. C. Constable, *Polynuclear Transition Metal Helicates*, in *Comprehensive Supramolecular Chemistry*, ed. J.-P. Sauvage, Elsevier, Oxford, 1996, vol. 9, pp. 213–252; E. C. Constable, *Prog. Inorg. Chem.*, 1994, **42**, 67.
6 E. C. Constable, S. M. Elder, J. Healy and D. A. Tocher, *J. Chem. Soc., Dalton Trans.*, 1990, 1669; C. R. Rice and K. M. Anderson, *Polyhedron*, 2000, **19**, 495.
7 E. C. Constable, S. M. Elder, M. J. Hannon, A. Martin, P. R. Raithby and D. A. Tocher, *J. Chem. Soc., Dalton Trans.*, 1996, 2423.
8 A. Bergh, P. O'D. Offenhartz, P. George and G. P. Haight, *J. Chem. Soc.*, 1964, 1533.
9 M. J. Hannon, C. L. Painting, A. Jackson, J. Hamblin and W. Errington, *Chem. Commun.*, 1997, 1807.
10 P. N. W. Baxter, J. A. Connor, W. B. Schweizer and J. D. Wallis, *J. Chem. Soc., Dalton Trans.*, 1992, 3015.
11 We have also observed identical behavior of L^1 and L^2 with Zn^{2+} ions: C. R. Rice, J. C. Jeffrey, R. L. Paul, M. D. Ward and S. Wörl, unpublished work.

ChemComm

Self expanding molecular networks

Joseph N. Grima and Kenneth E. Evans*

Department of Engineering, University of Exeter, North Park Road, Exeter, UK EX4 4QF.
E-mail: K.E.Evans@ex.ac.uk

Received (in Cambridge, UK) 31st May 2000, Accepted 5th July 2000

A series of polyphenylacetylene networks are modelled through force-field based simulations and are predicted to exhibit unusual mechanical properties, namely, negative Poisson's ratios (auxetic), a property which is explained through a simple model involving a network of connected rotating triangles.

Materials with a negative Poisson's ratio [auxetic, see methods section, eqn. (2)] exhibit the unexpected property of becoming wider when stretched and thinner when compressed.[1,2] Apart from the purely scientific importance of having such an unusual basic property, a negative Poisson's ratio gives a material many additional beneficial effects,[2,3] such as increased shear stiffness, increased plane strain fracture toughness and increased indentation resistance. Auxetics also have a natural ability to form synclastic doubly curved surfaces (*i.e.* dome shaped). This means that auxetic materials are superior to conventional counterparts in many practical applications. Unfortunately, although several auxetics have now been discovered or manufactured (*e.g.* foams,[3] microporous polymers[4] and silicates[5]), a negative Poisson's ratio is not a common feature in most everyday materials (*e.g.* the Poisson's ratio of most isotropic polycrystalline metals is approximately +0.3).

In recent years, considerable attention has been focused towards designing and synthesising molecular auxetics.[2,6] Such systems would offer the advantage over naturally occurring auxetics that they can be 'made to measure' to have a predefined set of mechanical properties.

In this communication we present a new class of molecular auxetics that have been predicted to exhibit negative Poisson's ratios.† They may be described as parallel 'graphite-like' layers each containing a planar polyphenylacetylene infinite network. These planar networks are a tessellation of a repeat unit having two equilateral molecular triangles at 60° to each other, an example of which is illustrated in Fig. 1(*a*). Homologues of the network in Fig. 1(*a*) may be produced by using longer or shorter acetylene chains. Since there is no simple way of naming these polytriangular networked systems, we shall henceforth refer to them as polytriangles-*n*-yne where *n* refers to the number of triple bonds per acetylene chain. Thus the network in Fig. 1(*a*) shall be referred to as polytriangles-2-yne.

Molecular mechanics simulations of these systems (aligned as in Fig. 1) using Cerius^2 V3.0 (Molecular Simulations Inc., San Diego, USA) have shown that the minimum energy separation between the different layers is approximately 3.6 Å, a distance which indicates the π–π interactions in between the different layers are being well represented. As illustrated in Table 1, it was observed that for $n \geqslant 2$, these polytriangles-*n*-yne networks exhibit negative Poisson's ratios (auxetic) in the Ox_2–Ox_3 plane (*i.e.* negative ν_{23} and ν_{32}) which tend to −1 as *n* increases. Furthermore, for $n \geqslant 2$, all the six Poisson's ratios were predicted to be negative. This is the first time that a material is predicted to simultaneously exhibit six negative mutually orthogonal Poisson's ratios.

In an attempt to understand the reason behind these very unusual properties, especially the very highly negative ν_{23} and ν_{32}, the minimum energy configurations at different loads in the Ox_2 and Ox_3 directions were obtained. From these minimum energy configurations, it was observed that for the larger triangles, the main type of deformation mechanism is through flexure of the acetylene chains. This flexure results in an overall

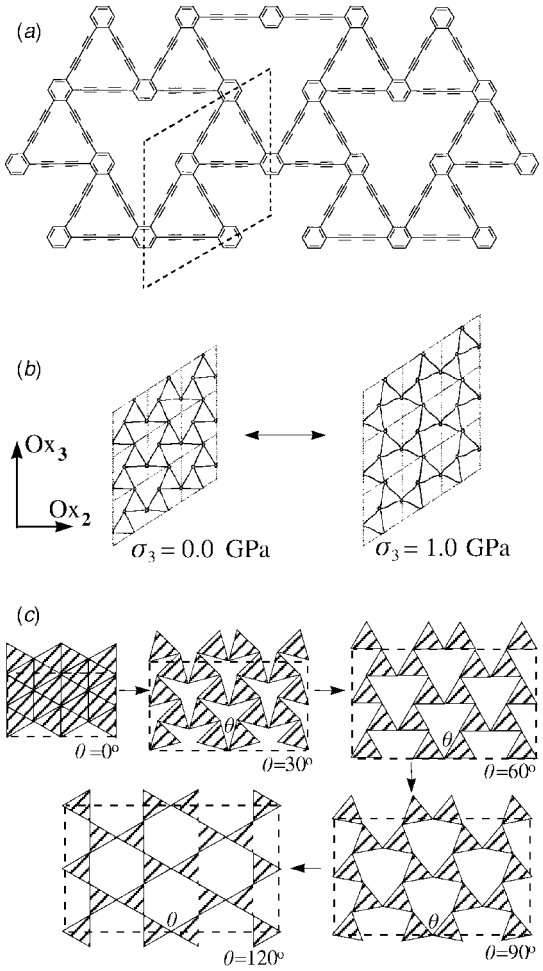

Fig. 1 (*a*) The structure of polytriangles-2-yne; (*b*) the minimum energy configurations of polytriangles-7-yne at $\sigma_3 = 0.0$ GPa and at $\sigma_3 = 1.0$ GPa; (*c*) the concept behind the design of the molecular networks: the idealised 'rotating triangles' networks. The molecular networks relate to the structure where $\theta = 60°$.

Table 1 The predicted single crystalline Poisson's ratios (ν_{ij}) of the polytriangles-*n*-yne where *n* is the number of triple bonds in the acetylene chains. The Ox_i axis are as defined in Fig. 1

n	ν_{12}	ν_{21}	ν_{31}	ν_{13}	ν_{23}	ν_{32}
1	+0.01	+0.10	+0.06	+0.01	+0.23	+0.19
2	−0.01	−0.02	−0.02	−0.01	−0.43	−0.43
3	−0.05	−0.27	−0.22	−0.04	−0.71	−0.72
4	−0.01	−0.01	−0.01	−0.01	−0.83	−0.83
5	−0.01	−0.01	−0.01	−0.01	−0.90	−0.90
6	−0.07	−0.14	−0.16	−0.08	−0.94	−0.93
7	−0.08	−0.12	−0.14	−0.09	−0.96	−0.95
8	−0.09	−0.11	−0.12	−0.10	−0.97	−0.96

DOI: 10.1039/b004305m

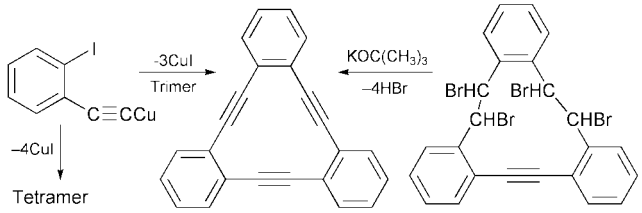

Scheme 1 The synthesis of single triangles.[11]

relative rotation of the triangles as illustrated for $n = 7$ in Fig. 1(*b*).

The possibility of achieving negative Poisson's ratios *via* rotating triangles compliments the recent predictions that a number of zeolites deform though a 'rotating squares' mechanism[7,8] and hence produce negative Poisson's ratios.[7–10] As illustrated in Fig. 1(*c*), a two dimensional structure composed of rigid hinged equilateral triangles connected together through hinges is geometrically constrained to maintain its aspect ratios and hence have in-plane Poisson's ratios of -1.[8] This simple geometric model explains why for the larger networks (*i.e.* the ones where the geometry of the triangles become more conspicuous), the Poisson's ratio tends to -1. The other four negative Poisson's ratios are probably due to a variation in the amount of interactions between the different layers.

Finally, we note that other similar two-dimensional delocalised π-systems such as graphyne and graphdiyne (*i.e.* the all-carbon fully substituted versions of polytriangles-1-yne and polytriangles-2-yne respectively) have also attracted considerable attention *vis-à-vis* their unique optical and electronic properties.[10] Unfortunately, graphyne and graphdiyne do not exhibit any auxeticity as they lack the required polytriangles geometry.[8] We also note that the synthesis of single, non-networked, equilateral molecular triangles has been known for a long time[10,11] (see Scheme 1) and that several advances have been made in the synthesis of other polyphenylacetylene networks.[10]

Thus to conclude, this work has shown the potential of these simple polyphenylacetylene networks as molecular auxetics. We hope that given the many advantages of auxetics when compared to conventional materials, these predictions will encourage further research into their chemistry so as to enable the synthesis of the first purpose-built molecular auxetic material.

J. N. G. thanks the University of Exeter for the award of a University Scholarship and the CVCP for the award of an ORS award.

Notes and references

† *Methods used:* (1) Simulation of the minimum energy configurations: Molecular mechanics simulations were carried out on an array of these networks (n = 1,2, …, 8) using the Cerius² V3.0 molecular modelling package. The polyphenylacetylene layers were aligned parallel to the Ox_2–Ox_3 planes (see Fig. 1). The energy expressions E were set up using parameters from the Dreiding force-field[12] except for the atomic charges which were calculated through the charge equilibration procedure developed by Rappé and Goddard.[13] Non-bond terms were added using the Ewald summation technique.[14] (2) Simulation of the mechanical properties:[15] The 6×6 stiffness matrix **C** (and its inverse, the compliance matrix **S**) of the minimum energy single crystalline polytriangles-*n*-yne systems were calculated from the second derivative of the potential energy function since:

$$c_{ij} = \frac{1}{V}\frac{\partial^2 E}{\partial\varepsilon_i \partial\varepsilon_j} \qquad i,j = 1,2,\ldots,6 \tag{1}$$

where E is the energy expression, V is the volume of the unit cell and ε_i are strain components. Other mechanical properties were then calculated from these matrices since, for example, the Poisson's ratios in the Ox_2–Ox_3 plane for loading in the Ox_3 direction is given by:

$$\nu_{32} = -\frac{\text{transverse strain}}{\text{axial strain}} = -\frac{\varepsilon_2}{\varepsilon_3} = -\frac{s_{32}}{s_{33}} \tag{2}$$

1 K. E. Evans, *Endeavour*, 1991, **15**, 170.
2 K. E. Evans, M. A. Nkansah, I. J. Hutchinson and S. C. Rogers, *Nature*, 1991, **353**, 124.
3 R. Lakes, *Science*, 1987, **235**, 1038.
4 B. D. Caddock and K. E. Evans, *J. Phys. D: Appl. Phys.*, 1989, **22**, 1877.
5 A. Yeganeh-Haeri, D. J. Weidner and J. B. Parise, *Science*, 1992, **257**, 650.
6 (*a*) R. H. Baughman and D. S. Galvao, *Nature*, 1993, **365**, 635; (*b*) C. B. He, P. W. Liu and A. C. Griffin, *Macromolecules*, 1998, **31**, 3145; (*c*) Z. Wu and J. S. Moore, *Angew. Chem., Int. Ed. Engl.*, 1996, **35**, 297.
7 J. N. Grima and K. E. Evans, *J. Mater. Sci. Lett.*, 2000, 19.
8 J. N. Grima, Ph.D. Thesis, University of Exeter, UK, 2000.
9 J. N. Grima, A. Alderson and K. E. Evans, *4th International Materials Conference (RSC)*, Dublin, 1999, P81.
10 U. H. F Bunz, Y. Rubin and Y. Tobe, *Chem. Soc. Rev.*, 1999, **28**, 107.
11 A. Krebs, *Cyclic Acetylenes* in *Chemistry of Acetylenes*, ed. H. G. Viehe, Marcell Dekker Inc., New York, 1969, p. 1000.
12 S. L. Mayo, B. D. Olafson and W. A. Goddard, *J. Phys. Chem.*, 1990, **94**, 8897.
13 A. K. Rappé and W. A. Goddard III, *J. Phys. Chem.*, 1991, **95**, 3358.
14 N. Karasawa and E. A. Goddard, *J. Phys. Chem.*, 1989, **93**, 7320.
15 *Cerius²* 3.0 User Guide—Property Prediction, 1997, Molecular Simulations Inc., San Diego, ch. 1, and references cited therein.

A novel one step photocatalytic synthesis of dihydropyrazine from ethylenediamine and propylene glycol†

K. V. Subba Rao,[a] B. Srinivas,[a] A. R. Prasad[b] and M. Subrahmanyam*[a]

[a] *Catalysis and Physical Chemistry Division, Indian Institute of Chemical Technology, Hyderabad-500 007, India. E-mail: subrahmanyam@iict.ap.nic.in*

[b] *Organic Chemistry Division-I, Indian Institute of Chemical Technology, Hyderabad-500 007, India*

Received (in Cambridge, UK) 16th May 2000, Accepted 7th July 2000

Dihydropyrazine (DHP), the intermediate for pyrazine, is synthesized from ethylenediamine and propylene glycol; it is assumed that the reaction proceeds by photooxidation of propylene glycol and cyclization with ethylenediamine to give dihydromethylpyrazine, which by subsequent oxidative demethylation *via* the corresponding acid, forms dihydropyrazine; molecular oxygen, light and TiO_2/zeolite promote the reaction.

In the last few years heterogeneous photocatalysis applied to synthetic chemistry has become an exciting and rapidly growing area of research. For a multistep synthesis illuminated semiconductors offer unique features. Many studies[1a–f] have reported photocatalytic organic reactions using mild experimental conditions. To date they are mostly in the categories of oxidations and oxidative cleavage, reduction, geometric and valence isomerization, substitution, condensation and polymerization. The discovery of the photo-Kolbe reaction by Kraeutler and Bard[2] using Pt/TiO_2 as a photocatalyst for the conversion of acetic acid to methane and CO_2 has attracted much attention. However, in spite of several titanium dioxide mediated reactions, examples of inducing intermolecular C–C bonding are rather limited in the literature. A recent report demonstrated that platinized TiO_2 is a successful photocatalyst in the selective *N*-cyclization of *N*ε-carbamyl-L-lysine into virtually optically pure L-pipecolinic acid.[3] Also Nishimoto *et al.*[4] showed photocatalytic intermolecular conversion of primary diamines to cyclic secondary amines in an aqueous suspension of Pt/TiO_2. In contrast to thermal processes by homogeneous and heterogeneous catalysts, these reactions proceed at ambient temperature. Furthermore, study of the photochemistry of organic molecules adsorbed on solid surfaces such as zeolites and microporous solids to conduct phototransformations has been explored.[5a–g] Combining the photocatalytic activity of TiO_2 with the utility of zeolites for photoinduced organic synthesis[9a,b]/degradation[6] has, so far, been little exploited.

Thermal catalytic processes are available for the synthesis of pyrazine and its derivatives.[7a–e] The present photocatalytic synthesis of dihydropyrazine by the cyclization of ethylenediamine and propylene glycol using TiO_2/zeolite, to the best of our knowledge, has not been reported.

In the present work zeolites HY, HZSM-5, Hβ and HM were used to support TiO_2 (Degussa P25) or ZnO (Fluka). The SiO_2/Al_2O_3 ratios of the above zeolites are 4.4, 30, 20 and 30, respectively. The preparation method for the catalysts consisted of mechanical mixing of TiO_2 or ZnO and zeolites using a low-boiling organic solvent (ethanol), evaporation of the solvent, drying at 110 °C and finally calcination at 400 °C for 6 h. Prior to the evaluation, the catalysts were activated at 300 °C for 4 h. The photocatalytic reaction was carried out in a batch type cylindrical quartz reactor of 200 ml capacity with a refluxing condensor at the top of the reactor. The slurry, which was composed of an equimolar ratio (1:1) of ethylenediamine and propylene glycol (either of the reactants in excess did not provide any better yields) and 100 mg of photocatalyst along with 20 ml of acetonitrile solvent.‡ A provision for bubbling molecular oxygen at a rate of 20 ml h^{-1} was also provided to the reactor. The reactants were stirred magnetically with simultaneous irradiation§ from a 250 W high pressure mercury lamp (Philips India) for 15 h at ambient temperature. Parallel experiments were also carried out for the synthesis of DHP using ZnO[8] and ZnO supported zeolite but lower yields were observed compared to TiO_2/zeolite catalysts. All the experimental results are shown in Table 1.

Table 1 Results obtained after 15 h of irradiation (250 W high pressure mercury lamp) over different TiO_2/zeolite combinations for the cyclization of ethylenediamine and propylene glycol[a]

Entry	Catalyst	Surface area[b]/m^2 g^{-1}	Acidity[c]/ mmol g^{-1}	Yield of DHP[d] (%)
1	2wt% TiO_2/HZSM-5	350	0.37	13.0
2	2wt% TiO_2/HY	400	0.25	13.6
3	2wt% TiO_2/Hβ	406	0.20	20.4
4	2wt% TiO_2/HM	391	0.12	2.03
5	2wt% ZnO/HZSM-5	326	0.13	8.12
6	2wt% ZnO/HY	336	0.18	8.06
7	TiO_2	50	—	—
8	ZnO	30	—	—

[a] All reactions were performed with an equimolar ratio (1:1) of ethylenediamine and propylene glycol in 20 ml of acetonitrile using 100 mg of catalyst under oxygen bubbling at room temperature. [b] Measured by the BET technique with liquid N_2 at 77 K. [c] Measured by STPD of NH_3. [d] Yields were calculated based on the recovery of propylene glycol.

At the end of the reaction, 20 ml of demineralized water was added to the reaction mixture which was centrifuged, which allowed recovery of the adsorbed substrates and products on the surface of the solid catalyst. The supernatant liquid was analyzed with a Chemito 3865 Gas Chromatography unit using a 6 ft, 10% SE-30 packed column. The products were further identified by ^{1}H NMR and mass spectrometry.

Further experiments were carried out to confirm whether the reaction is photocatalytic or non-photocatalytic and it was observed that no product was formed in the absence of molecular oxygen + irradiation + TiO_2/zeolite catalyst. Zeolite alone without TiO_2 did not yield any product. Irradiation in the presence of photocatalyst when carried out using conventional liquid acids such as HCl and solid acids such as silica gel did not yield the product.

Zeolite acidity seems to influence the reaction mechanism; the oxidation is dependent on the acidity of the reaction mixture[9a] and ethylenediamine is adsorbed preferentially relative to propylene glycol in the internal surface area of the zeolite pores. The preferential adsorption of ethylenediamine leads propylene glycol to undergo oxidation to the diketone (step 1, Scheme 1) at the oxidizing site of TiO_2. The diketone formed undergoes cyclization with ethylenediamine to give dihydromethylpyrazine (DHMP) with loss of 2 mol of water. The methyl group of dihydromethylpyrazine is oxidatively demethylated leading to dihydropyrazine (DHP) as shown in

† IICT Communication No 4561.

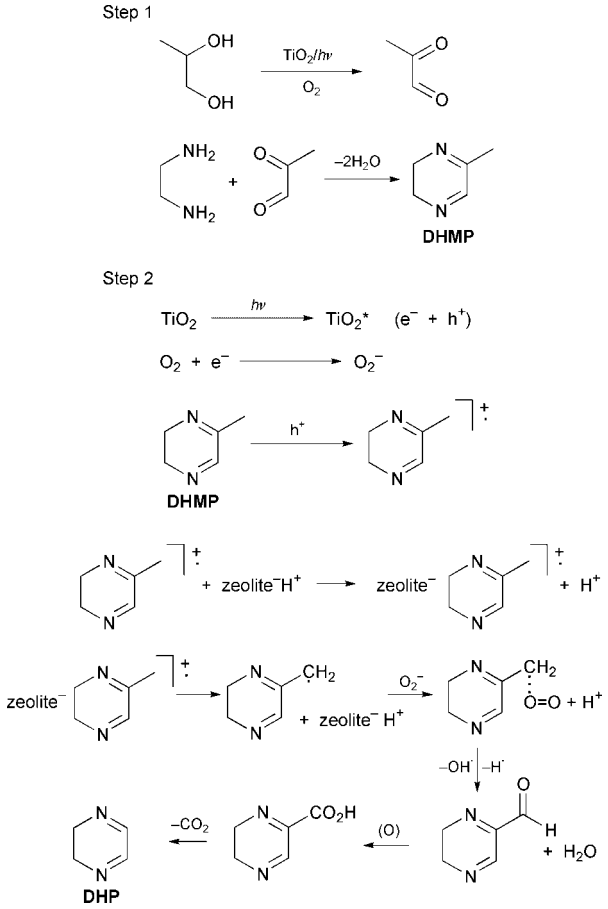

Scheme 1 Proposed reaction mechanism for the formation of DHP.

step 2 of Scheme 1. Photoexcitation of the semiconductor in step 2 would produce an electron and a hole. Oxygen serves as an electron acceptor for the conduction band electron and the dihydromethyl pyrazine supplies an electron to the photogenerated hole at the surface of the TiO_2 particle forming an adsorbed radical cation. The zeolite may assist the stability of the radical cation through proton transfer as observed by Beaune *et al*.[9b] Thus, the proposed mechanism of step 2 is enhanced by more acidic zeolites. Here, dihydropyrazine carbaldehyde undergoes further oxidation to the corresponding acid which in turn forms the dihydropyrazine after decarboxylation. The obtained dihydropyrazine was subjected to dehydrogenation[10] using a conventional method which yielded the pyrazine thereby confirming the product formation (DHP).

The reaction was then attempted with ethylene glycol instead of propylene glycol, but no cyclic product was observed. This shows that the electron donating substituent, *i.e.* the methyl group of propylene glycol, may favour the oxidation mechanism.[9c] In aerated solutions, the photogenerated electron can be trapped by adsorbed oxygen to form superoxide or other negatively charged adsorbed oxygen species.[11]

Hydrogen peroxide [eqn. (1)] thus formed by sequential

$$\begin{aligned} O_2 + e^{-} &\longrightarrow O_2^{\cdot-} \\ O_2^{\cdot-} + H^{+} &\longrightarrow HOO^{\cdot} \\ 2HOO^{\cdot} &\longrightarrow H_2O_2 + O_2 \\ H_2O_2 + O_2^{\cdot-} &\longrightarrow OH^{\cdot} + OH^{-} + O_2 \end{aligned} \qquad (1)$$

electron and proton transfer readily decomposes on illuminated TiO_2 to hydroxy radicals and oxygen. Since the recombination is inhibited by adsorbed oxygen, it is reasonable to expect that the rate of photocatalytic oxidation should be high as oxygen is continuously bubbled in a steady state. Thus the selectivity for the primary alcohol site of propylene glycol is higher in pure oxygen than in air. The secondary alcohol site is oxidized to a greater extent by the adjacent electron donating group *i.e.* methyl at the TiO_2 center. No photodegradation of compounds (formation of CO_2) was observed for lower wt% values of TiO_2 on the zeolite. The evaluation of TiO_2/zeolite catalysts in the cyclization of ethylenediamine and propylene glycol show that 2wt% TiO_2 is optimal since higher loadings lead to total oxidation.

As seen from Table 1, 2 wt% TiO_2/HZSM-5 and 2wt% TiO_2/HY show more or less the same activity and yield of dihydropyrazine. The hydrophobicity and acid site strength of zeolites influences the activity of these zeolite systems in the order Hβ > HZSM-5 = HY. This order illustrates that the cyclization is favoured by a combination of moderate hydrophobicity and acidity. However, 2wt% TiO_2/Hβ is found to be more active, leading to a high yield of dihydropyrazine which may be possibly explained by the structure of Hβ which is a combination of both HZSM-5 (channel pore system, high Si/Al ratio) and Y (12-ring pore system) zeolites.[12]

Dihydropyrazine was obtained with a yield of 20.4% over 2wt% TiO_2/Hβ during the cyclization of ethylenediamine and propylene glycol by photocatalysis *via* the proposed reaction scheme under irradiation in the presence of molecular oxygen.

One of us (K. V. S. R.) thanks the Council of Scientific and Industrial Research, New Delhi, India for the award of a Senior Research Fellowship. We thank Dr (Mrs) V. Durga Kumari for her valuable suggestions in improving the manuscript.

Notes and references

‡ MeCN is the most stable among tested solvents under photocatalytic conditions.[13]

§ Irradiation with low pressure mercury lamps was not efficient.

1 (*a*) M. A. Fox, *Acc. Chem. Res.*, 1983, **16**, 314; (*b*) M. A. Fox, *Top. Org. Electrochem.*, 1985, **4**, 177; (*c*) M. A. Fox and P. Pichat, in *Photoinduced Electron Transfer*, ed. M. A. Fox and M. Chanon, Elsevier, Amsterdam, 1988, vol. D, p. 241; (*d*) M. A. Fox, C. C. Chen, K. Park and J. N. Younathan, *Am. Chem. Soc. Symp. Ser.*, 1985, **278**, 69; (*e*) A. Mills and S. L. Hunte, *J. Photochem. Photobiol.: A*, 1997, **108**, 1; (*f*) M. A. Fox and M. T. Dulay, *Chem. Rev.*, 1983, **93**, 341.
2 B. Kraeutler and A. J. Bard, *J. Am. Chem. Soc.*, 1978, **100**, 2239.
3 B. Ohtani, E. Akoi, K. Iwai and S. Nishimoto, *J. Photosci.*, 1994, **1**, 37.
4 S. Nishimoto, B. Ohtani, T. Yoshikawa and T. Kagiya, *J. Am. Chem. Soc.*, 1983, **105**, 7180.
5 (*a*) X. Liu and J. K. Thomas, *Langmuir*, 1989, **5**, 58; (*b*) V. Ramamurthy, D. R. Corbin, N. J. Turro, Z. Zhang and M. A. Garcia-Garibay, *J. Org. Chem.*, 1991, **56**, 255; (*c*) M. A. Anderson and C. B. Grissom, *J. Am. Chem. Soc.*, 1996, **118**, 9552; (*d*) S. G. Zhang, S. Higashimoto, H. Yamashita and M. Anpo, *J. Phys. Chem.*, 1998, **102**, 5590; (*e*) R. Sadeghpoor, M. Ghandi, H. M. Najafi and F. Farzaneh, *Chem. Comm.*, 1998, 329; (*f*) C. H. Tung, H. Wang and Y. N. Ying, *J. Am. Chem. Soc.*, 1998, **120**, 5179; (*g*) Y. Xiang, S. C. Larsen and V. H. Grassian, *J. Am. Chem. Soc.*, 1999, **121**, 5063.
6 V. Durga Kumari, M. Subrahmanyam, K. V. Subba Rao and K. Tanaka, *Appl. Catal.: B.*, 2000, submitted.
7 (*a*) L. Forni and P. Pollesel, *J. Catal.*, 1991, **130**, 403; (*b*) J. G. Aston, T. E. Peterson and J. Holowchak, *J. Am. Chem. Soc.*, 1934, **56**, 153; (*c*) A. M. Gazaliev, E. P. Sim, A. Y. Matveev and A. D. Kagarlitski, *Izv. Akad. Nauk. Kaz. SSR, Ser. Khim.*, 1984, **5**, 78; (*d*) M. Subrahmanyam, A. R. Prasad, S. J. Kulkarni and A. V. Rama Rao, *Indian J. Chem. B.*, 1995, **34**, 573; (*e*) M. Subrahmanyam, S. J. Kulkarni and B. Srinivas, *Reac. Kinet. Catal. Lett.*, 1993, **49**, 455.
8 K. Hema, V. Ramakrishnan and J. C. Kuriacose, *J. Catal.*, 1981, **69**, 216.
9 (*a*) C. B. Somrani, A. Finiels, P. Geneste, P. Graffin, A. Guida, M. Klaver, J. L. Olive and A. Saeedan, *Catal. Lett.*, 1995, **33**, 395; (*b*) O. Beaune, A. Finiels, P. Geneste, P. Graffin, A. Guida, J. L. Olive and A. Saeedan, *Stud. Surf. Sci. Catal.*, 1993, **78**, 401; (*c*) O. Beaune, A. Finiels, P. Geneste, P. Graffin, J. L. Olive and A. Saeedan, *J. Chem. Soc., Chem. Commun.*, 1992, 1649.
10 P. F. Peter and R. G. Harvey, *Chem. Rev.*, 1978, **78**, 317.
11 P. Pichat, in *Organic Phototransformations in Nonhomogeneous Media*, *Am. Chem. Soc. Symp. Ser.*, 1985, **21**, 278.
12 M. M. J. Treacy and J. M. Newsam, *Nature*, 1988, **332**, 249.
13 D. D. Sackett and M. A. Fox, *J. Phys. Org. Chem.*, 1988, **103**, 1.

ChemComm

A new simple synthesis of *cis*- and *trans*-3,5-di-*tert*-butyl-3,5-diaryl-1,2,4-trithiolanes from ketones and tetraphosphorus decasulfide

Kentaro Okuma,*[a] Shinji Shibata,[a] Kosei Shioji[a] and Yoshinobu Yokomori[b]

[a] *Department of Chemistry, Faculty of Science, Fukuoka University, Jonan-ku, Fukuoka 814-0180, Japan. E-mail: kokuma@fukuoka-u.ac.jp*

[b] *Department of Applied Chemistry, National Defense Academy, Hashirimizu, Yokosuka 239-8686, Japan*

Received (in Cambridge, UK) 18th May 2000, Accepted 30th June 2000

The reaction of pivalophenones with tetraphosphorus decasulfide afforded *cis*- and *trans*-3,5-di-*tert*-butyl-3,5-diaryl-1,2,4-trithiolanes, which equilibrated to give other isomers in refluxing toluene *via* thiopivalophenones and thiopivalophenone *S*-sulfides.

1,2,4-Trithiolanes (**1**), some of which have been obtained from natural products, are well-known.[1] Methods for their synthesis include: reaction of thiobenzophenone with *o*-chloranil,[2] reaction of thiobenzophenones with 1,1-diphenylethylene sulfide,[3] reaction of thiones with Lowesson reagents,[4] reaction of dialkyl ketones with hydrogen sulfide elemental sulfur, and amines,[5] and fragmentation of 1,2,3-thiadiazoles.[6] Recently, Senning and co-workers reported that reaction of α-chlorosulfenyl disulfides with morpholine afforded the corresponding dispirotrithiolanes.[7] However, there are only a few reports on the synthesis of trithiolanes from ketones using thiation reagents although it is well known that the reaction of ketones with tetraphosphorus decasulfide (P_4S_{10}) affords the corresponding thioketones.[8] We have investigated the synthesis of trithiolanes from ketones using P_4S_{10} as a thiation reagent and report herein the isolation and X-ray crystallographic analysis of *cis*- and *trans*-**1** from P_4S_{10} and their thermal isomerization.

Treatment of 4-methylpivalophenone with P_4S_{10} in refluxing pyridine for 48 h resulted in the formation of *trans*-3,5-di-*tert*-butyl-3,5-di-*p*-tolyl-1,2,4-trithiolane (*trans*-**1a**), *cis*-3,5-di-*tert*-butyl-3,5-di-*p*-tolyl-1,2,4-trithiolane (*cis*-**1a**), and 4-methylthiopivalophenone (**2a**) in 13, 35, and 23% yields, respectively. Refluxing for 72 h resulted in the formation of *cis*-**1a** in 35 % yield along with *trans*-**1a** (24%) and **2a** (16%) (Scheme 1).

The structures *cis*-**1a** and *trans*-**1a** were confirmed by NMR and elemental analysis. Table 1 lists the ^{1}H NMR and ^{13}C NMR data for *cis*- and *trans*-**1a**. The chemical shift of the *tert*-butyl group of trans-**1a** is higher than that of *cis*-**1a**, whereas chemical shifts of the aromatic groups of trans-**1a** are lower than those of *cis*-**1a**. This observation suggests that each aromatic group of *cis*-**1a** was on the other aromatic plane whereas the *tert*-butyl group of *trans*-**1a** was on the aromatic plane.

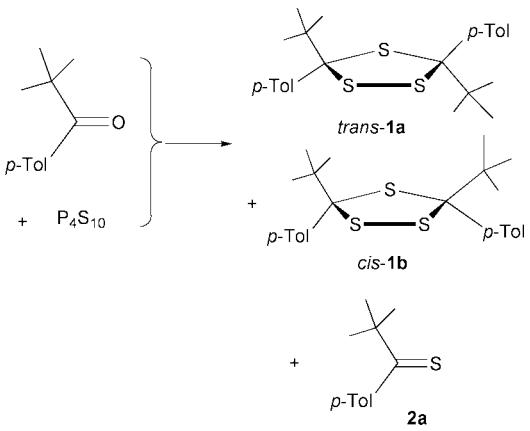

Scheme 1

Both structures were confirmed by single crystal X-ray crystallographic analysis (Fig. 1)[9]: no unusual bond lengths or angles are observed in the 1,2,4-trithiolane rings. The trithiolane rings of both products have similar conformations to other trithiolanes. The C–S bond lengths of the trithiolane rings are between 1.796 and 1.875 Å—longer than normal (1.763–1.767 Å)[6] because the trithiolane rings are compressed by bulky *tert*-butyl groups. However, the S–S bond lengths (2.027 Å for *cis*-**1a** and 2.016 Å for *trans*-**1a**) are shorter than the one reported by Senning *et al.* (2.0345 Å).[7] As suggested by their NMR spectra, the aromatic groups of *cis*-**1a** were out of plane whereas the *tert*-butyl group of *trans*-**1a** was on the aromatic plane.

Other reactions were similarly carried out. The results are shown in Table 2.

More than three decades ago, Elam and Davis reported the synthesis of dimethylthioketene dimer by the reaction of tetramethylcyclobutane-1,3-dione with tetraphosphorus decasulfide. They isolated the corresponding trithiolane as a side product (2.8%).[8] However, they did not apply the general synthesis of **1** from ketones. The reaction of pivalophenone with P_4S_{10} generally afforded thiopivalophenone in good yield.[10] The present reaction is the first practical method on the synthesis of **1** from ketones by using P_4S_{10}.

Thiocarbonyl *S*-sulfides (thiosulfines) are well-known to exhibit high reactivity such as dienophile-like behavior, for example, and can add to a variety of thiones to give **1**. 3,3,5,5-Tetraaryl-1,2,4-trithiolanes are thermally unstable and dissociate into thiocarbonyl *S*-sulfides and thiobenzophenone in refluxing chloroform.[3] Since *cis*- and *trans*-**1** were isolated, the thermal behavior of these isomers was investigated. A solution of *cis*-**1a** in deuterated toluene was heated at 110 °C for 72 h. The ^{1}H NMR spectroscopic analysis of the solution revealed that *cis*-**1a** gradually converted to *trans*-**1a** (26%), along with **2a** (44%), whereas *cis*-**1** a was recovered in 25% yield. While *trans*-**1a** also converted to *cis*-**1a**, the rate of conversion was low. After being heated at 110 °C for 72 h, 66% of *trans*-**1a** still remained, suggesting that *trans*-**1a** is more stable than the corresponding *cis*-isomer. The most straightforward explanation for the conversion of *cis*-**1a** to *trans*-**1a** involves the isomerization of *cis*-**1a** to the thiocarbonyl *S*-sulfide (**3a**) and **2a** followed by recombination *via* 1,3-dipolar cycloaddition between **3a** and **2a** (Scheme 2).

Table 1 Spectral data of *cis*- and *trans*-**1a**

	^{1}H NMR	^{13}C NMR
trans-**1a**	1.04 (s, 18H, *t*-Bu), 2.35 (s, 6H, ArMe), 7.10 (d, 4H, *J* = 8.0 Hz, Ar), 7.81 (d, 4H, *J* = 8.0 Hz, Ar)	20.93, 29.78, 40.71, 100.65, 127.11, 130.84, 136.15, 140.11
cis-**1a**	1.21 (s, 18H, *t*-Bu), 2.20 (s, 6H, ArMe), 6.81 (d, 4H, *J* = 8.2 Hz, 7.40 (d, 4H, *J* = 8.2 Hz, Ar)	20.75, 28.81, 41.96, 97.76, 126.52, 130.39, 135.74, 137.96

DOI: 10.1039/b004013o

Table 2 Reaction of ketones with tetraphosphorus decasulfide

Ketone		Conditions			Products (Yields/%)		
					Trithiolane		
R′	R″	Temp./°C	Solvent	Time/h	*cis*	*trans*	Thioketone **2**
t-Bu	*p*-Tol	110	Pyridine	24	**1a** 22	3	**2a** 52
t-Bu	*p*-Tol	110	Pyridine	96	**1b** 34	35	**2a** 28
t-Bu	Ph	110	Pyridine	48	**1b** 21	8	**2b** 30
t-Bu	*p*-$PhOC_6H_4$	110	Pyridine	48	**1c** 19	10	**2c** 35
Adamantane-2-one		110	Pyridine	48	**1d**	45	**2d** 13

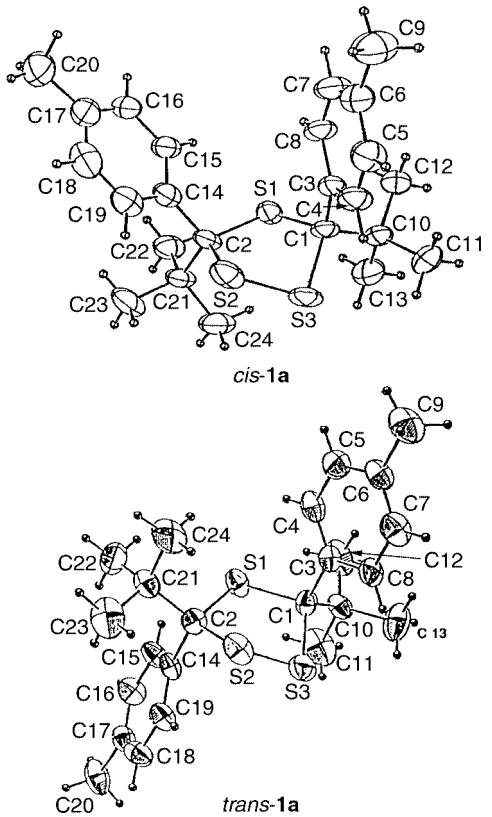

Fig. 1 X-ray crystallographic structures of *cis*- and *trans*-**1a**. Selected data for cis-**1a**. Bond lengths: C1–S1 1.864(4); C1–S3 1.841 (5); S1–C2 1.855(5); C2–S2 1.861(4); S2–S3 2.037 Å. Bond angles: C1–S1–C2 104.0(2); S3–S2–C2 99.5 (2); S2–S3–C1 94.9(2); S1–C1–S3 104.0(2); S1–C2–S2 107.1(2)°. Selected data for *trans*–**1a**. Bond lengths: C1–S1 1.870(8); C1–S3 1.796 (8); S1–C2 1.854 (8); C2–S2 1.840(8); S2–S3 2.016 (3) Å. Bond angles: C1–S1–C2 102.8(4); S3–S2–C2 96.6 (3); S2–S3–C1 95.5(3); S1–C1–S3 106.4(4); S1–C2–S2 106.5(4)°.

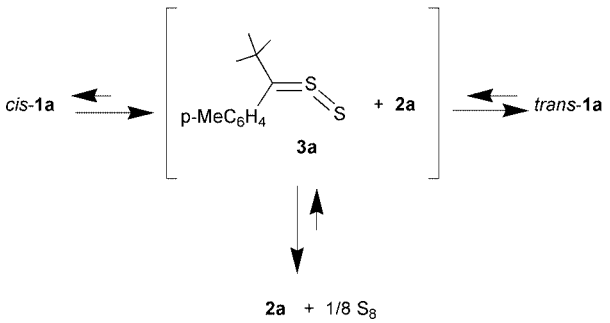

Scheme 2

When the reaction was carried out in the presence of adamantane-2-thione (2 eq.), the corresponding cycloadduct (**1e**) was obtained in 67% yield along with recovered *cis*-**1a** (15 %) and **2a** (70%) (Scheme 3).[11]

The difference in stability between *cis*- and *trans*-**1** might be attributed to the difference in their steric hindrances. As can be

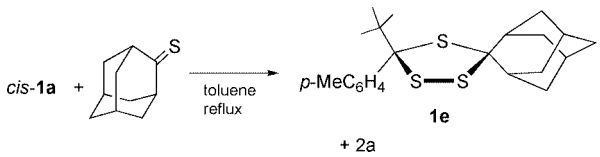

Scheme 3

seen in Figure 1, *cis*-**1a** is more crowded than the *trans* isomer. In fact, Senning *et al.* have reported that the reaction of thiosulfenyl chloride with morpholine afforded mainly the corresponding *trans*-trithiolane, suggesting that *cis*-trithiolane is generally unstable and gradually converts into the more stable *trans*-isomer.[7]

In summary, we have isolated and characterized *cis*- and *trans*-**1** by the reaction of pivalophenones with P_4S_{10}. Both isomers interconvert in refluxing toluene. The intermediate **3** was trapped by the reaction with adamantane-2-thione to afford unsymmetrical **1**.

Notes and references

1 H. W. Brinkman, H. Copier, J. J. M. de Leuw and S. B. Tjan, *J. Agric. Food Chem.*, 1972, **20**, 177; E. K. Adesogan, *J. Chem. Soc., Chem. Commun.*, 1974, 906.

2 M. M. Cambell and D. M. Evgenios, *J. Chem. Soc., Perkin 1*, 1973, 2862.

3 R. Huisgen and J. Rapp, *J. Am. Chem. Soc.*, 1987, **109**, 902; R. Huisgen and J. Rapp, *Tetrahedron*, 1997, **53**, 939.

4 A. Ishii, J. Nakayama, M.–X. Ding, N. Kotaka and M. Hoshino, *J. Org. Chem.*, 1990, **55**, 2411.

5 F. Asinger, M. Thiel and G. Lipfert, *Liebigs Ann. Chem.*, 1959, **627**, 195; F. Asinger, W. Schäfer, K. Halcour, A. Saus and H. Triem, *Angew. Chem., Int. Ed., Engl.*, 1964, **3**, 19.

6 W. Winter, H. Buehl and H. Meier, *Z. Naturforsch. B: Anorg. Chem. Org. Chem.*, 1980, **35**, 1015.

7 F. A. G. El-Essay, S. M. Yassin, I. A. El-Sakka, A. F. Khattab, I. Soetofte, J. O. Madsen and A. Senning, *J. Org. Chem.*, 1998, **63**, 9840; M. I. Hegab, F. M. E. Abdel-Megeid, F. A. Gad, S. A. Shiba, I. Soetofer, J. Moeller and A. Senning, *Acta Chem. Scand.*, 1999, **53**, 133.

8 E. U. Elam and H. E. Davis, *J. Org. Chem.*, 1967, **32**, 1562.

9 Crystal data for $C_{24}H_{32}S_3$ *cis*-**1a**: M = 416.71, a = 6.606(1), b = 10.981(3), c = 16.559(3) Å, α = 88.2(2), β = 79.16(1), γ = 76.09(2)°, T = 297 K, space group $P\bar{1}$ (No. 2), Z = 2, μ(Cu-Kα) = 29.4 cm^{-1}, 4183 reflections measured, 4036 unique (R_{int} = 0.072). 3298 reflections ($|F_o| > 3.0\sigma(F_o)$) were used in all calculations. The final R and wR were 0.090 and 0.116 respectively. Crystal data for $C_{24}H_{32}S_3$ *trans*-**1a**: M = 416.71, a = 13.987(2), b = 17.561(3), c = 9.498(3) Å, β = 79.16(1)°, T = 297 K, space group $P2_1/a$ (No. 14), Z = 4, μ = (Cu-Kα) = 29.1 cm^{-1}, 4443 reflections measured, 4126 unique (R_{int} = 0.062). 1753 reflections ($|F_o| > 3.0\sigma(F_o)$) were used in all calculations. The final R and wR were 0.078 and 0.073 respectively. Both isomers were recrystallised from methanol. The structure was solved using direct methods and refined by full-matrix least-squares on F. CCDC 182/1714.

10 N. Ramnath, V. Ramesh and V. Ramamurthy, *J. Org. Chem.*, 1983, **48**, 214.

11 Compound **1e**: mp 152.3–152.8 °C. ^{1}H NMR ($CDCl_3$) δ = 1.18 (s, 9H, *t*-Bu), 1.63–2.49 (m, 14H, Ad-H), 2.33 (s, 3H, Me), 7.07 (d, 2H, J = 4 Hz, Ar), 7.78 (d, 2H, J = 4 Hz, Ar). ^{13}C NMR ($CDCl_3$) δ = 20.90, 26.65, 29.44, 34.97, 36.53, 37.73, 38.78, 39.71, 40.20, 90.68, 98.82, 126.87, 130.52, 136.04, 139.37.

Control of crystal polymorphs by a 'latent inductor': crystallization of calcium carbonate in conjunction with *in situ* radical polymerization of sodium acrylate in aqueous solution

Kensuke Naka,* Dong-Ki Keum, Yasuyuki Tanaka and Yoshiki Chujo*

Department of Polymer Chemistry, Graduate School of Engineering, Kyoto University, Yoshida, Sakyo-ku, Kyoto, 606-8501, Japan. E-mail: ken@chujo.synchem.kyoto-u.ac.jp

Received (in Cambridge, UK) 12th June 2000, Accepted 10th July 2000

Three different crystal polymorphs of $CaCO_3$ (aragonite, vaterite and calcite) have been selectively induced by changing the time of addition of a radical initiator to a calcium carbonate solution containing sodium acrylate.

In nature, biological organisms produce polymer–inorganic hybrids. In these mineralized tissues, crystal morphology, size, polymorph, and orientation are determined by local conditions and, in particular, the presence of 'matrix' proteins or other macromolecules.[1] However, there remain many unknowns as to how the matrix affects the crystallization process, especially the initial nucleation. A final crystalline phase might arise through a multistage crystallization process.[2,3] The existence of several phases would enable organisms to control mineralization through intervention with the kinetics. By selectively interacting with the mineral at different stages during the crystal forming process, the organisms may choose to manipulate both the polymorph and the orientation of the mineral to meet specific biological requirements. Although crystallization of minerals in the presence of various additives and synthetic polymers has been investigated as a model of biomineralization,[4–6] selective interaction of synthetic additives with the minerals at different stages during the nucleation process has not been examined.

Here, we report a new concept for controlling crystal polymorphs of $CaCO_3$ by addition of a synthetic additive. The key point of our method is using a 'latent inductor' for crystal nucleation as shown in Fig. 1. The latent inductor at its inactive state does not affect nucleation and growth of the crystal. After the inactive state is transferred to an active state by a stimulus, the active inductor can induce nucleation and growth of the crystal. We used sodium acrylate as a latent inductor for this purpose and a water-soluble radical initiator was used as a stimulus. While sodium acrylate does not affect nucleation and growth of crystals[7] poly(acrylate) affects crystal morphology by inhibiting the growth of particular crystal faces.[3,8] Indeed, the precipitation of $CaCO_3$ in the presence of the sodium salt of poly(acrylic acid) (PAA) (M_n = 5100) was prevented under the nucleation conditions applied here.[6] Sodium acrylate can be transformed to poly(acrylate) by adding a radical initiator. In the present system, aqueous solutions of $CaCl_2$ and $(NH_4)_2CO_3$ were initially added to an aqueous solution of sodium acrylate and then subjected to polymerization by adding the radical initiator at 30 °C after incubation for several minutes. Crystallization of calcium carbonate with *in situ* polymerization of anionic monomers in aqueous solution has not been reported.

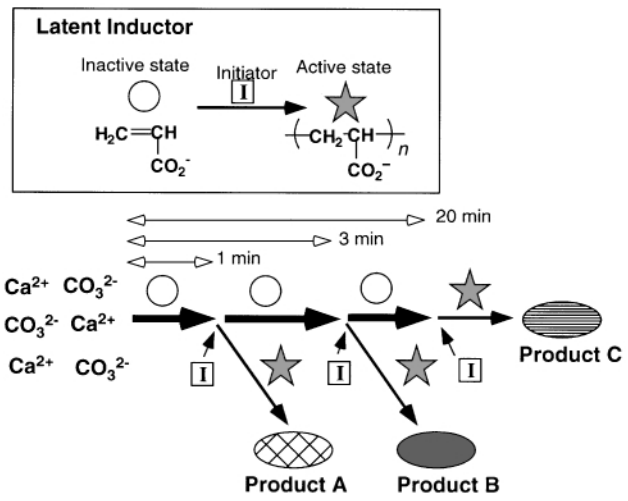

Fig. 1 Schematic depiction for the control of crystal polymorph growth by a latent inductor.

The precipitation of $CaCO_3$ was carried out under the same conditions as reported by Cölfen *et al.*[9,10] 4.95 ml of each reactant [0.1 M $CaCl_2$ and 0.1 M $(NH_4)_2CO_3$] were injected *via* syringe into 180 ml of an aqueous solution of sodium acrylate which was adjusted to pH 8.5 by NH_3(aq). The ratio of sodium acrylate to calcium ions was 0.62 : 1. After addition of the reactants was complete, an aqueous solution of $K_2S_2O_8$ as a water-soluble radical initiator was added to the reaction mixture after incubation at 30 °C for several minutes (1, 3 or 20 min). A sudden increase in the turbidity of the solution was observed after incubation for several minutes. The solutions were kept at 30 °C under N_2 for 1 day with gentle stirring. The crystalline $CaCO_3$ was collected and washed with water several times. The yields of the crystalline products obtained when the radical initiators were added to the reaction mixture after incubation for 1 min (product A), 3 min (product B) and 20 min (product C) were 33, 35 and 54%, respectively.

The crystal phases of the obtained $CaCO_3$ were characterized by FTIR analysis.[3,11,12] Product A displayed a characteristic symmetric carbonate stretching vibration at 1084 cm^{-1}, a carbonate out-of-plane bending vibration at 856 cm^{-1} and a pair of peaks at 701 and 713 cm^{-1} indicating aragonite formation. When the radical initiator was added after incubation for 3 min, product B showed several bands corresponding to a carbonate out-of-plane bending vibration. A band at 746 cm^{-1} indicated vaterite formation and bands at 877 and 713 cm^{-1} assignable to calcite were also present. The crystal phase of product C was calcite according to IR with only two bands at 877 and 713 cm^{-1} observed.

Fig. 2 shows scanning electron micrographs (SEM) of the three crystalline products. Each SEM micrograph shows different crystal modifications. The aragonite crystals (product A) were efflorescent bundles of needles [Fig. 2(a)], typical of the phase. Product B consisted of two different crystal modifications, spherical vaterite and rhombs of calcite [Fig. 2(b)]. Stable spherical vaterite crystals have already been reported in the presence of various bivalent cations,[13] double-hydrophilic block copolymers[9] and anionic PAMAM dendrimers.[6] Crystals of product C were rhombohedral [Fig. 2(c)]. The crystal phases of the obtained $CaCO_3$ samples were further confirmed by powder X-ray diffraction (XRD) analysis. The reflections of products A and C were characteristic for aragonite and calcite, respectively. The fraction of vaterite in product B

DOI: 10.1039/b004649n

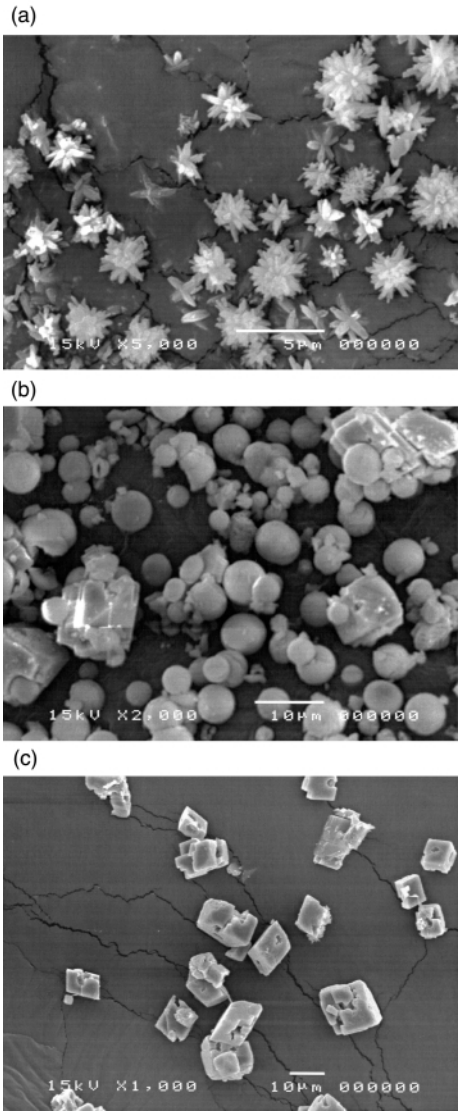

Fig. 2 Scanning electron micrographs of (a) product A, (b) product B and (c) product C.

was 63% as determined by Rao's equation.[14] These results indicate that the three different polymorphs of $CaCO_3$ were controlled simply by changing the addition time of the radical initiator to the calcium carbonate supersaturated solution containing sodium acrylate at ambient temperature. When the ratio of sodium acrylate to calcium ions was reduced to 0.37, the crystal phase obtained when the radical initiator was added after incubation for 1, 3 and 20 min was always calcite. This result suggests that the presence of the radical initiator was not the main factor for controlling the final crystal phase of $CaCO_3$.

Calcite is thermodynamically more stable than the other two crystalline modifications, aragonite and vaterite. The crystal phase of $CaCO_3$ obtained without any additives or with sodium acrylate in the absence of radical initiators was calcite under the same conditions as described above. Sodium acrylate is thus inactive for induction of metastable $CaCO_3$ crystalline phases (vaterite or aragonite). Since the crystal phase of product C was also thermodynamically stable calcite, the final crystalline phase was not affected when the polymerization of sodium acrylate was started *via* radical initiation after incubation of the reaction mixture containing calcium reactants and sodium acrylate for 20 min.

Aragonite is usually obtained at temperatures > 50 °C using a solution method of preparation.[4,11] In our present results, aragonite can be obtained at 30 °C when the radical initiator is added to the calcium ion solution with sodium acrylate after incubation for 1 min, during which time $CaCO_3$ crystal formation has not started. It is possible that aragonite is rapidly nucleated at the very beginning of the nucleation process, resulting in it being kinetically induced by the poly(acrylate). When the initiator was added to the reaction mixture after incubation for 3 min, crystals of calcite and vaterite were formed. These results indicate that the final crystalline phases are highly sensitive to the presence of the active additives at the very initial nucleation stage (first few minutes). During the phase transformation, the poly(acrylate) may kinetically and thermodynamically induce a crystal nucleation at each stage. In the absence of any additives, it is well known that vaterite transforms into stable calcite *via* a solvent-mediated process.[15] Although the crystal polymorph of product B did not change when the solution was kept for 2 days, vaterite crystals were transformed to calcite when the solution was incubated for 3 days. We speculate that the vaterite surfaces were stabilized by the resulting poly(acrylate) in aqueous solution so slowing phase transformation.

After the crystalline $CaCO_3$ was filtered off and washed with water, the combined water phase was evaporated under reduced pressure. GPC and FTIR analyses of the residue indicated the formation of poly(acrylate). Although we do not fully understand the mechanistic implication of the effect of *in situ* radical polymerization of sodium acrylate in aqueous solution for nucleation and growth of calcium carbonate, our current results have provided a new concept for controlling the crystal polymorphs of calcium carbonate. While sodium acrylate is inactive for nucleation and growth of crystals, addition of a radical initiator leads to poly(acrylate), which can influence nucleation and growth of $CaCO_3$. Sodium acrylate can be regarded as a latent active ligand for induction of crystal phases. We believe that the initial nucleation processes play an important role in controlling the final crystal modifications of $CaCO_3$ obtained. Further investigations are in progress.

We thank Dr Tetsuo Yazawa and Mr Kouji Kuraoka at Osaka National Research Institute for the SEM micrographs and XRD analysis.

Notes and references

1 L. Addadi and S. Weiner, *Proc. Natl. Acad. Sci. USA*, 1985, **82**, 4110.
2 J. R. Clarkson, T. J. Price and C. J. Adams, *J. Chem. Soc., Faraday Trans.*, 1992, **88**, 243.
3 G. Xu, N. Yao, I. A. Akasay and J. T. Groves, *J. Am. Chem. Soc.*, 1998, **120**, 11977.
4 Y. Levi, S. Albeck, A. Brack, S. Weiner and L. Addadi, *Chem. Eur. J.*, 1998, **4**, 389.
5 L. A. Gower and D. A. Tirrell, *J. Cryst. Growth*, 1998, **191**, 153.
6 K. Naka, Y. Tanaka, Y. Chujo and Y. Ito, *Chem. Commun.*, 1999, 1931.
7 H. Sugihara, K. Ono, K. Adachi, Y. Setoguchi, T. Ishihara and Y. Takita, *J. Ceram. Soc. Jpn.*, 1996, **104**, 832.
8 D. Verdoes, D. Kashichiev and G. M. van Rosmalen, *J. Crystal Growth*, 1992, **118**, 401.
9 H. Cölfen and M. Antonietti, *Langmuir*, 1998, **14**, 582.
10 M. Sedlák, M. Antonietti and H. Cölfen, *Macromol. Chem. Phys.*, 1998, **199**, 247.
11 L. Wang, I. Sondi and E. Matijević, *J. Colloid Interface Sci.*, 1999, **218**, 545.
12 D. Chakrabarty and S. Mahapatra, *J. Mater. Chem.*, 1999, **9**, 2953.
13 L. Brecevic, V. Nothing-Laslo, D. Kralj and S. Popovic, *J. Chem. Soc., Faraday Trans.*, 1996, **92**, 1017.
14 M. S. Rao, *Bull. Chem. Soc. Jpn.*, 1973, **46**, 1414.
15 D. Kralj, L. Brecevic and A. E. Nielsen, *J. Cryst. Growth*, 1990, **104**, 793.

A novel preparation of iron-doped TiO_2 nanoparticles with enhanced photocatalytic activity

Chuan-yi Wang,*[a] Detlef W. Bahnemann[a] and Jürgen K. Dohrmann[b]

[a] *Institut für Solarenergieforschung Hameln/Emmerthal (ISFH), Aussenstelle Hannover, Sokelantstr. 5, D-30165 Hannover, Germany. E-mail: isfh.bahnemann@oln.comlink.apc.org*

[b] *Freie Universität Berlin, Institut für Chemie/Physikalische und Theoretische Chemie, Takustr. 3, D-14195 Berlin, Germany. E-mail: dohrmann@chemie.fu-berlin.de*

Received (in Oxford, UK) 12th April 2000, Accepted 20th June 2000

Fe^{III}-doped TiO_2 nanoparticles prepared from organic precursors (≤2.5 atom% Fe) exhibit strongly enhanced photocatalytic activity as demonstrated by the quantum yields measured for the formation of formaldehyde by photocatalyzed oxidation of methanol in aqueous solution (Φ up to *ca.* 15%).

In recent years, considerable effort has been devoted to the study of Fe^{III}-doped titanium dioxide in order to improve the photocatalytic efficiency of TiO_2.[1–4] The generally accepted mechanism to explain this improved photocatalytic performance is the formation of shallow charge trapping sites within the TiO_2 matrix as well as on the particles' surface through the replacement of Ti^{IV} by Fe^{III} ions.[3] Thus, the undesirable recombination of electron/hole pairs generated upon ultra-bandgap irradiation can be partially prevented. In most cases such photocatalysts have been prepared by hydrolysis of a Ti-precursor in the presence of a Fe^{III}-containing aqueous solution (Scheme 1*a*). Since the reaction system is fed with the Ti and Fe precursors present as different solution phases, the Fe/Ti ratio is unavoidably changed on addition of the Ti precursor to the solution of the Fe precursor, particularly so in the initial stage of particle growth. There is little doubt that this effect influences the local distribution of iron in the particles formed and hence the photocatalytic efficiency. In view of this we have developed a novel preparation in which organic Ti and Fe precursors were employed and mixed prior to hydrolysis (Scheme 1*b*). To the best of our knowledge, such a preparation has not been reported previously.

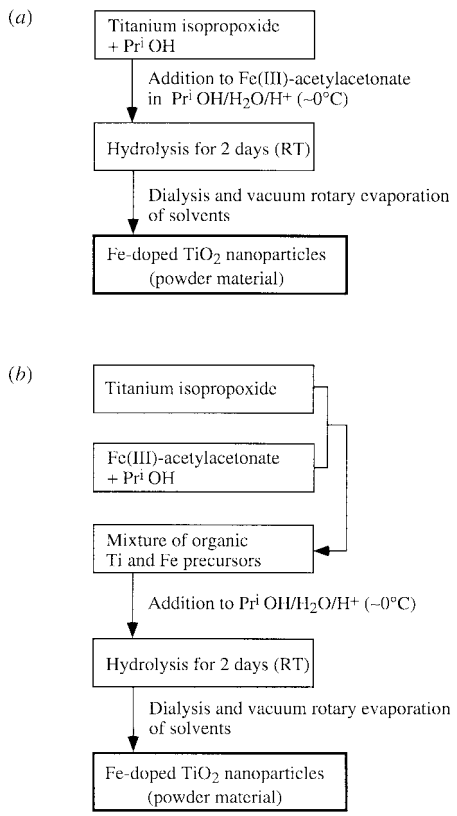

Scheme 1 Preparation of iron-doped TiO_2 nanoparticles. Previous (*a*) and present novel method (*b*).

As seen from Scheme 1*b*, the fraction of iron in the mixture and, hence, the nominal iron content of the particles can be varied as desired. As-prepared samples come as yellowish powders which can be resuspended in water, methanol or in a mixture of both solvents to obtain a colloidal suspension transparent in the visible region.

Fig. 1 shows the absorbance spectra of as-prepared samples of neat TiO_2 and of TiO_2 doped with different amounts of Fe^{III}. From Fig. 1 and by use of the procedure given by Kormann *et al.*[5] the bandgap energy, E_g, of the colloidal particles was obtained as 3.32, 3.25, 3.22 and 3.07 eV for zero, 0.25, 0.5 and 2.5 atom% iron, respectively. Clearly, E_g decreases with increasing iron content. Compared with bulk anatase TiO_2 (E_g = 3.23 eV[6]) the bandgap of the undoped TiO_2 particles (3.32 eV) is larger by *ca.* 0.1 eV. This corresponds to a mean spherical particle diameter of *ca.* 2.7 nm when the Brus equation[7] is applied.

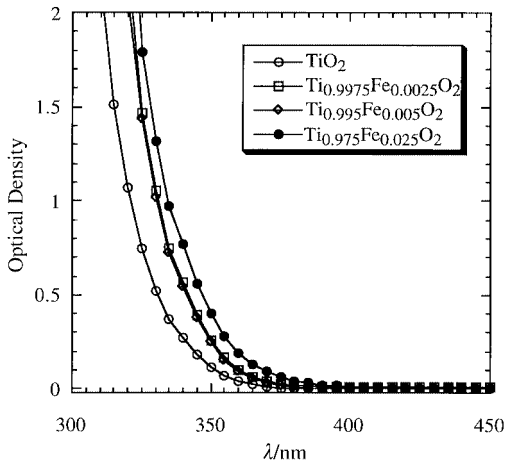

Fig. 1 Absorbance spectra of TiO_2 and iron-doped TiO_2 nanoparticles in colloidal aqueous solution (as-prepared according to Scheme 1*b*, pH ≈ 3, 1 cm cell, virtually no light scattering).

From the preparation procedures given in Scheme 1 it is expected that the distribution of iron in the TiO_2 matrix of the particles prepared by method (1*b*) is more uniform than by method (1*a*). Uniformity of doping was expected to result in enhanced photocatalytic activity. This was indeed verified by determination of the quantum yield of formaldehyde produced by photocatalytic oxidation of methanol in aerated aqueous solution[9] in the presence of the TiO_2 colloidal particles doped

DOI: 10.1039/b002988m

with iron by different methods. The photocatalytic reaction was carried out in a cylindrical cell under cw-illumination by filtered light from a xenon lamp (WG 320 + UV black filters, 60% transmission at 340 nm). The photon flux of this illumination set-up was determined by use of the Aberchrome-540 chemical actinometer.[8] The production rate of HCHO was measured by HPLC of samples taken at different time intervals[9] (total photolysis time *ca.* 30 min).

TiO_2-photocatalyzed oxidation of methanol proceeds as follows:[1,9,13]

$$TiO_2 + h\nu(\geq E_g) \xrightarrow{(fs)^1} h^+_{VB} + e^-_{CB} \quad (1)$$

$$h^+_{VB} + \equiv Ti^{IV}OH \xrightarrow{(fast)^1} \equiv Ti^{IV}OH^{\bullet +} / OH^{\bullet} \quad (2)$$

$$e^-_{CB} + \equiv Ti^{IV}OH \xrightarrow{(<100\ ps)^1} \equiv Ti^{III}OH / e^-_{tr} \quad (3)$$

$$e^-_{tr} + O_2 \xrightarrow{k_4} O_2^{\bullet -} \quad (4)$$

$$OH^{\bullet} + CH_3OH \xrightarrow{k_5} {}^{\bullet}CH_2OH + H_2O \quad (5)$$

$${}^{\bullet}CH_2OH + O_2 \xrightarrow{k_6} HCHO + HO_2^{\bullet} \quad (6)$$

$${}^{\bullet}CH_2OH + \equiv Ti^{IV}OH \xrightarrow{(fast)^{13}} HCHO + \equiv Ti^{III}OH / e^-_{tr} + H^+ \quad (7)$$

where $k_4 = 7.6 \times 10^7\ M^{-1}\ s^{-1}$ for trapped electrons,[10] $k_5 = 5 \times 10^8\ M^{-1}\ s^{-1}$ [11] and $k_6 \approx 5 \times 10^9\ M^{-1}\ s^{-1}$.[12] As detailed by Sun and Bolton[9] the quantum yield of HCHO is proportional to that of $OH^{\bullet}$ which plays a vital role in TiO_2 based photocatalytic reactions.[1,15]

Table 1 shows the values of Φ_{HCHO} determined for the TiO_2 and iron-doped TiO_2 colloidal photocatalysts prepared here by different methods. A 15 min pre-illumination of the aqueous colloidal particles was applied in the absence of CH_3OH for removal of surface flaws. Note that without pre-photolysis the concentration of HCHO was not proportional to the photolysis time but rather showed an induction-type behavior characteristic for the oxidation of residual organic material originating from the catalyst preparation. No HCHO was formed in the dark or during illumination in the absence of methanol evincing that the process was truly photocatalytic. As seen from Table 1, iron-dopant concentrations of up to 0.5 atom% increase Φ_{HCHO} dramatically. Further, Φ_{HCHO} is strongly affected by the method of photocatalyst preparation in some cases. Comparison of Φ_{HCHO} demonstrates that the novel preparation, Scheme 1*b*, is superior to that of Scheme 1*a* for the optimum dopant concentration of 0.5 atom% iron, where Φ_{HCHO} exhibits a *ca.* sixfold increase over the quantum yield measured in the presence of 2.7 nm undoped TiO_2 particles. The optimum iron-dopant concentration depends on the method of catalyst preparation (0.5 atom% for methods 1*a* and 1*b*, 0.25 atom% for the preparation from $TiCl_4$, similar to ref. 2).

Table 1 Quantum yields of formaldehyde formation by the photocatalytic oxidation of methanol in the presence of TiO_2 and iron-doped TiO_2 colloidal nanoparticles[a]

Fe/atom%	Φ_{HCHO}[b]/%	Precursor(s)	Photocatalyst preparation
0	2.3	$TiCl_4$	ref. 2
	2.8	$TiPr^iO$[c]	Scheme 1*a*
0.25	12.0	$TiCl_4 + FeCl_3$	ref. 2
	12.0	$TiPr^iO$[c] + Fe-acac[d]	Scheme 1*a*
	12.5	$TiPr^iO$ + Fe-acac	Scheme 1*b*[e]
0.50	7.2	$TiCl_4 + FeCl_3$	ref. 2
	12.7	$TiPr^iO$ + Fe-acac	Scheme 1*a*
	15.3	$TiPr^iO$ + Fe-acac	Scheme 1*b*[e]
2.50	5.2	$TiCl_4 + FeCl_3$	ref. 2
	9.2	$TiPr^iO$ + Fe-acac	Scheme 1*a*
	9.5	$TiPr^iO$ + Fe-acac	Scheme 1*b*[e]

[a] 100 mM methanol, O_2-saturated aqueous solution at pH ≈ 3, catalyst loading 0.5 g L^{-1}, reaction volume 23 mL, $I_o = 1.43 \times 10^{-6}$ Einstein L^{-1} s^{-1}, room temperature. See text for further details. [b] ±0.2. [c] Titanium tetraisopropoxide. [d] Fe^{III}-acetylacetonate. [e] Present method.

In conclusion, it has been shown that the novel preparation, Scheme 1*b*, of iron-doped TiO_2 nanoparticles yields a highly active photocatalyst for the oxidation of methanol in aqueous solution. This is tentatively attributed to conditions of particle growth more favorable than with method 1*a*. Further work on photocatalytic properties of related as-prepared materials, including structure characterization and studies by time-resolved techniques,[10,14] is under way.

Chuan-yi Wang thanks the Alexander von Humboldt-Stiftung for a research fellowship grant. Financial support from the Deutsche Forschungsgemeinschaft (grants BA 1137/3-1, BA 1137/4-1 and DO 150/7-1) is gratefully acknowledged.

Notes and references

1 M. R. Hoffmann, S. T. Martin, W. Choi and D. Bahnemann, *Chem. Rev.*, 1995, **95**, 69.
2 D. Bockelmann, M. Lindner and D. Bahnemann, in *Fine Particles Science and Technology*, ed. E. Pelizzetti, Kluwer Academic Publishers, The Netherlands, 1996, p. 675.
3 M. I. Litter and J. A. Navio, *J. Photochem. Photobiol. A: Chem.*, 1996, **98**, 171.
4 R. I. Bickley, J. S. Lees, R. J. D. Tilley, L. Palmisano and M. Schiavello, *J. Chem. Soc., Faraday Trans.*, 1992, **88**, 377.
5 C. Kormann, D. W. Bahnemann and M. R. Hoffmann, *J. Phys. Chem.*, 1988, **92**, 5196.
6 J. B. Goodenough and A. Hamnett, in *Landolt-Börnstein*, New Series, Group III, Vol. 17g, ed. O. Madelung, Springer Verlag, Berlin, Heidelberg, New York, Tokyo, 1984, p. 147.
7 L. E. Brus, *J. Phys. Chem.*, 1986, **90**, 2555.
8 H. G. Heller and J. R. Langan, *EPA Newsletter*, 1981, 71.
9 L. Sun and J. R. Bolton, *J. Phys. Chem.*, 1996, **100**, 4127.
10 D. W. Bahnemann, M. Hilgendorff and R. Memming, *J. Phys. Chem. B*, 1997, **101**, 4265.
11 G. E. Adams, J. W. Boag and B. D. Michael, *Trans. Faraday Soc.*, 1965, **61**, 1417.
12 G. E. Adams and R. L. Willson, *Trans. Faraday Soc.*, 1969, **65**, 2981.
13 R. Memming, *Top. Curr. Chem.*, 1994, **169**, 106.
14 K. Stopper and J. K. Dohrmann, *Z. Phys. Chem.*, 2000, **214**, 555.
15 P. A. Christensen, J. Eameaim and A. Hamnett, *Phys. Chem. Chem. Phys.*, 1999, **1**, 5315.

ChemComm

Template-directed stepwise post-synthesis alumination of MCM-41 mesoporous silica

Robert Mokaya

School of Chemistry, University of Nottingham, University Park, Nottingham, UK NG7 2RD.
E-mail: r.mokaya@nottingham.ac.uk

Received (in Cambridge, UK) 13th June 2000, Accepted 10th July 2000

Stepwise post-synthesis alumination of pure silica MCM-41 in which increasing proportions of the MCM-41 are aluminated depending on the amount of Al available in the synthesis gel is achieved during secondary synthesis (*i.e.* recrystallisation) of calcined pure silica MCM-41 in the presence of discrete amounts of Al.

The recent synthesis of MCM-41 type mesoporous silicas which possess well ordered pores of diameter 20–100 Å has expanded the range of heterogeneous catalysis into the mesoporous regime.[1–4] With regard to catalysis, purely siliceous mesoporous molecular sieves are of limited use owing to the absence of active sites in their matrices. Active sites may be generated *via* chemical modification involving the introduction of heteroatoms into the silica matrix.[2–4] The incorporation of Al (which gives rise to solid acid catalysts with acid sites associated with the presence of Al in framework positions) is a typical example. The introduction of Al into mesoporous silicas (*i.e.* alumination) normally takes place in a homogeneous form and results in uniform incorporation of Al with little control of its spatial distribution. Increasing the Al content in the synthesis gel generally results in a uniform increase in the amount of incorporated Al throughout the entire sample.[5] In a departure from this norm, this report describes preliminary work on the unusual stepwise post-synthesis alumination of pure silica MCM-41 in which increasing proportions of the MCM-41 are aluminated depending on the amount of Al available in the synthesis gel. This apparently step-wise alumination is achieved during secondary synthesis (recrystallisation) of calcined pure silica MCM-41 in the presence of discrete amounts of Al. Evidence from several characterisation techniques indicates that during recrystallisation, the proportion of aluminated MCM-41 increases with increase in the content of Al in the recrystallisation gel and that beyond a certain gel Si/Al ratio (determined by synthesis conditions) the whole sample is aluminated. The findings reported here suggest that it is possible to fully aluminate a portion of the pores of a pure silica MCM-41 before alumination of other pores has started, resulting in an apparently mixed-phase material. The ability to vary the spatial distribution of Al (or other heteroatoms) in such a manner may find use in the preparation of composite or multiphase materials and may open new opportunities for selective molecular engineering within the internal surface of mesoporous silicas.

We have recently shown that calcined pure silica MCM-41 is stable under normal MCM-41 synthesis conditions and that when used as the 'silica source' during secondary synthesis (*i.e.* recrystallisation) the calcined MCM-41 crystallites are preserved and act as seeds for further crystal enlargement.[6,7] This 'preservation' principle was used to prepare a series of recrystallised Al-MCM-41 samples by adding varying amounts of Al to the recrystallisation gel. The recrystallised samples were prepared as previously described[6,7] except that aluminium isopropoxide was added to the recrystallisation gel along with the calcined pure silica MCM-41 at gel Si/Al ratios in the range 5–80. In brief, tetramethylammonium hydroxide (TMAOH) and cetyltrimethylammonium bromide (CTAB) were dissolved in distilled water by stirring at 35 °C. Calcined pure silica MCM-41 and the required amount of Al (as aluminium isopropoxide) were then added to the template solution under stirring for 1 h. After further stirring for 1 h the resulting gel was aged for 20 h at room temperature and then transferred to a Teflon-lined autoclave and heated at 150 °C for 48 h. The solid product was obtained by filtration, washed with distilled water, dried in air at room temperature and calcined in air at 550 °C for 8 h. The samples were designated Al-MCM41-*x*, where *x* is the gel Si/Al ratio.

Powder X-ray diffraction (XRD) patterns of the parent pure silica MCM-41 and the aluminated samples are shown in Fig. 1. The XRD pattern of the parent Si-MCM-41 material exhibits a single (100) basal peak and several higher order peaks which is typical of a well ordered MCM-41. The XRD patterns of aluminated materials prepared at gel Si/Al ratios of 80, 40 and 20 exhibit two low angle peaks; the original 100 peak and a new peak which occurs at slightly higher 2θ values and progressively shifts to even higher values (*i.e.* lower basal spacing) as the gel Si/Al ratios reduced from 80 to 20. Furthermore the intensity of the new peak increases at the expense of the original basal peak. The position of the original peak does not however change despite the reduction in intensity (Table 1). At a gel Si/Al ratio of $\leqslant$10, the original basal peak is completely lost and only the new peak is observed. Our preliminary interpretation of the XRD results is that the new peak is due to aluminated MCM-41 which increases in proportion as the amount of Al in the recrystallisation gel increases and that at a gel Si/Al ratio close to 10, the whole sample is aluminated and therefore only the new peak is observed. The presence of the original peak for samples recrystallised at a Si/Al gel ratio of 80, 40 and 20 implies that a portion of these samples remains essentially non-aluminated and retains the characteristics of the parent Si-MCM-41 material. This interpretation is consistent with the fact that in the absence of Al (*i.e.* in all silica recrystallisation) only one peak (*i.e.* the original peak) is observed,[6] which supports our proposal that the new peak observed here is due to the presence of Al. Our interpretation of the XRD results is

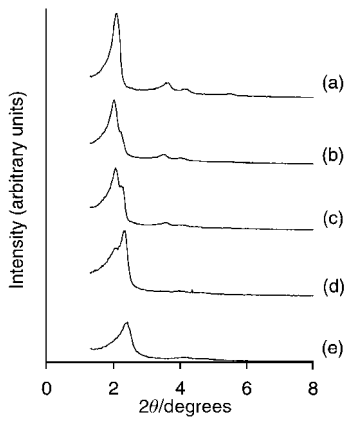

Fig. 1 Powder XRD patterns of pure silica Si-MCM-41 (a) and recrystallised Al-MCM41-80 (b), Al-MCM41-40 (c), Al-MCM41-20 (d) and Al-MCM41-10 (e) materials.

DOI: 10.1039/b004728g

Table 1 Textural properties of the studied materials

Sample	Basal (d_{100}) spacing/Å	Surface area/ $m^2\ g^{-1}$	Pore volume/ $cm^3\ g^{-1}$
Si-MCM-41	42.8	1017	0.91
Al-MCM41-80	43.2; 40.1	995	0.87
Al-MCM41-40	43.0; 39.7	922	0.78
Al-MCM41-20	42.8; 38.2	840	0.62
Al-MCM41-10	37.6	785	0.53
Al-MCM41-5	33.5	878	0.51

supported by the N_2 sorption isotherms in Fig. 2 which clearly show two capillary condensation (pore filling) steps for the 'partially' aluminated samples (Al-MCM41-80, Al-MCM41-40 and Al-MCM41-20). The first step (at lower partial pressure) is ascribed to the filling of aluminated pores and the second step to the filling of non-aluminated pores. It is noteworthy that the second pore filling step in the 'partially' aluminated samples occurs at the same partial pressure as the filling of pores in the parent Si-MCM-41. This indicates that the pore size of the channels in the parent sample remains unchanged in the 'partially' aluminated samples.

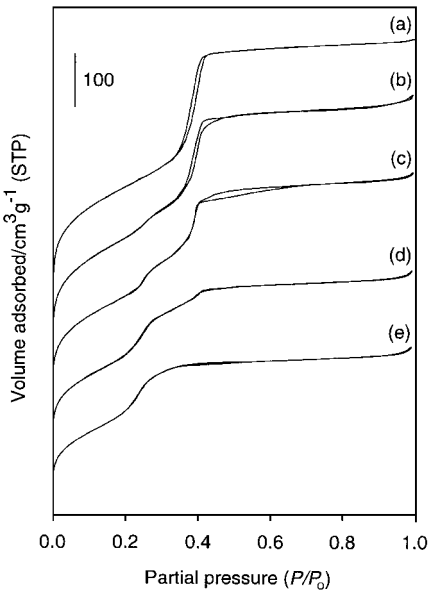

Fig. 2 Nitrogen sorption isotherms of pure silica Si-MCM-41 (a) and recrystallised Al-MCM41-80 (b), Al-MCM41-40 (c), Al-MCM41-20 (d) and Al-MCM41-10 (e) materials.

The coexistence of the two distinct pore systems within one sample implies that alumination of a portion of pores is accomplished before the start of alumination in other pores. The reduction in basal spacing and pore size (Fig. 1 and 2) and the gradual decrease in surface area and pore volume (Table 1) which accompanies the alumination is consistent with the incorporation of an aluminosilicate layer on the inner pore walls of the parent Si-MCM-41. The incorporation of Al onto the silica framework must be accompanied by charge balancing surfactant molecules since there are no inorganic ions present in the recrystallisation gel. It is likely that the strong interaction between the charge balancing surfactant molecules and the framework Al sites causes contraction of the mesoporous framework, resulting in a reduced basal spacing in the aluminated parts of the recrystallised sample. Indeed thermogravimetric analysis (TGA) of as-synthesised samples indicated the presence of strongly held surfactant molecules (associated with framework Al) whose proportion increased with the extent of alumination. Incorporation of Al onto the framework was confirmed by ^{27}Al MAS NMR of the calcined samples. More than 80% of the Al in the samples (except for Al-MCM41-5 with 65%) was found to be in tetrahedral coordination. During recrystallisation, the surfactant molecules and Al which are eventually occluded/incorporated into the recrystallised Al-MCM-41 samples must be transported into the pores of existing Si-MCM-41 particles/crystallites.[6,7] We propose that the transportation of Al into the pores is, owing to the presence of the surfactant, diffusion controlled and that the Al is therefore first incorporated into the outer region of the MCM-41 particles. Alumination then proceeds into the interior of the sample depending on the amount of Al available. If all the particles are equally accessible, then each particle is aluminated from the edges inwards until all the Al is depleted or in an aggregate of particles, the outermost particles are aluminated first while the inner particles remain untouched by the Al. In such a scenario, the proportion of aluminated MCM-41 will depend on the amount of Al available and the diffusion time. In the present study the diffusion time (*i.e.* synthesis time) was kept constant and the only variable was the amount of Al. For the partially aluminated samples, SEM with elemental analysis gave Si/Al ratios of 40.1, 28.3 and 16.9 for Al-MCM41-80, Al-MCM41-40 and Al-MCM-41-20, respectively. The implied Al content for these samples was higher than that expected from the gel Si/Al ratio which is not suprising considering that only part of the pure silica MCM-41 is aluminated. It is also evident that the Si/Al ratio approaches the expected value as the extent of alumination increases. Indeed at full alumination (gel ratio Si/Al 10 and 5) the obtained elemental composition (Si/Al = 8.8 for Al-MCM-41-10 and 5.8 for Al-MCM41-5) is very close to the expected values since the samples are essentially homogeneous with respect to spatial distribution of Al. The alumination mechanism proposed here is similar to that suggested by Anwander *et al.* for the chemisorption of trimethyaluminium into MCM-41.[8] We also note that the incorporation of Al predominantly into the outer region of MCM-41 was previously observed when Al was added to an already formed surfactant–silicate mesostructure.[9]

We have considered other scenarios that are possible during the recrystallisation; (i) the parent Si-MCM-41 can completely dissolve to generate silicate ions which then interact with the Al. This would in effect be equivalent to conventional direct mixed-gel synthesis and should yield homogeneous Al-MCM-41 materials with uniform pores and elemental compositions close to the gel Si/Al ratio irrespective of the amount of Al.[5,10] This is clearly not observed here. In any case we know that the Si-MCM-41 crystallites are stable under the recrystallisation conditions and that complete dissolution of the parent Si-MCM-41 does not occur.[6,7,11] (ii) Some silica (mainly amorphous phase) from the parent Si-MCM-41 can dissolve and interact with the Al to create a new separate Al-MCM-41 phase which coexists with the original preserved crystallites of the parent Si-MCM-41. However in such a scenario, the same amount of silica will dissolve (regardless of the recrystallisation gel Si/Al ratio) and therefore the resulting recrystallised samples should be substantially the same (irrespective of gel Si/Al ratio) with any excess Al existing as an alumina phase. This is, however, not likely since the nature of the recrystallised samples reported here is strongly dependent on the gel Si/Al ratio.

I am grateful to the EPSRC for an Advanced Fellowship.

Notes and references

1 J. Y. Ying, C. P. Mehnert and M. S. Wong, *Angew. Chem., Int. Ed.*, 1999, **38**, 56.
2 A. Corma, *Chem. Rev.*, 1997, **97**, 2373.
3 S. Biz and M. L. Occelli, *Catal. Rev.-Sci. Eng.*, 1998, **40**, 329.
4 A. Sayari, *Chem. Mater.* 1996, **8**, 1840.
5 M. T. Janicke, C. C. Landry, S. C. Christiansen, S. Birtalan, G. D. Stucky and B. F. Chmelka, *Chem. Mater.*, 1999, **11**, 1342.
6 R. Mokaya, W. Zhou and W. Jones, *Chem. Commun.*, 1999, 51.
7 R. Mokaya, W. Zhou and W. Jones, *J. Mater. Chem.*, 2000, **10**, 1139.
8 R. Anwander, C. Palm, O. Groeger and G. Engelhardt, *Organometallics*, 1998, **17**, 2027.
9 R. Ryoo, C. H. Ko and R. F. Howe, *Chem. Mater.*, 1997, **9**, 1607.
10 R. Mokaya, W. Jones, Z. Luan, M. D. Alba and J. Klinowski, *Catal. Lett.*, 1996, **37**, 113.
11 L. Huang, W. Guo, P. Deng, Z. Xue and Q. Li, *J. Phys. Chem. B*, 2000, **104**, 2817.

ChemComm

Unprecedented self-assembly of M_3L_2 trinuclear lanthanide complexes assisted by a flexible tripodal ligand containing terpyridine binding units†

Yann Bretonnière,[a] Marinella Mazzanti,*[a] Raphael Wietzke[a] and Jacques Pécaut[b]

[a] *Laboratoire de Reconnaissance Ionique et Matériaux Moléculaires, Service de Chimie Inorganique et Biologique, Département de Recherche Fondamentale sur la Matière Condensée, CEA-Grenoble, 38054 Grenoble, Cedex 09, France. E-mail: mazzanti@drfmc.ceng.cea.fr*

[b] *Laboratoire de Chimie de Coordination, Service de Chimie Inorganique et Biologique, Département de Recherche Fondamentale sur la Matière Condensée, CEA-Grenoble, 38504 Grenoble, Cedex 09, France*

Received (in Basel, Switzerland) 24th May 2000, Accepted 11th July 2000

The new dodecadentate tripodal ligand trenterpy in the presence of lanthanide triflates leads to the self assembly of homotrinuclear lanthanide complexes.

In recent years there has been a proliferation in the coordination chemistry of lanthanide(III) ions with polydentate ligands owing to their potential applications in biology, medicine and materials science.[1] However, while the assembly of oligonuclear coordination compounds is a burgeoning field,[2] only limited research has focused on the preparation of polymetallic molecular or supramolecular lanthanide-containing complexes, in spite of the interesting magnetic and luminescence properties of Ln(III) ions.[3] Moreover the creation of highly organised polymetallic architectures is crucial for the design of lanthanide-based functional devices such as light converters[2b] or MRI contrast agents,[4] with, for example, the aggregation of Gd(III) ions in trimeric centres by non-covalent pseudo-octahedral tripods leading to an increase of the relaxivity.[5] We and others have recently shown that the assembly of three neutral bidentate binding units such as phenanthroline[6] or pyridine–carboxamide[7] to [tris(2-aminoethyl)amine] (tren) through an amide linkage yields covalent tripods which form mononuclear nine-coordinate lanthanide complexes with a rigid solution structure.

Here, we report the complexation properties of the new potentially dodecadentate tripodal ligand trenterpy‡ containing three tridentate terpyridine binding units connected to a common anchor (tren) through amide linkages. 2,2′:6′,2″-Terpyridine has been widely used as a building block in metallosupramolecular chemistry[8] and the incorporation of terpyridine or tridentate terpyridine analogues in non-covalent podating ligands has led, in the presence of lanthanide ions, to the formation of mononuclear monohelical complexes[9] or to the self-assembly of dinuclear triple-helical homo- or hetero-dinuclear[10] complexes. Nevertheless the ligand trenterpy is, to our knowledge, the first example of the incorporation of terpy in a covalent tripod.

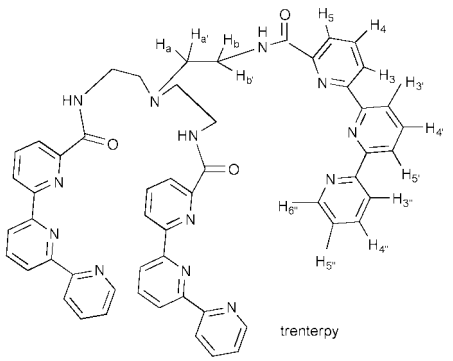

† Electronic supplementary information (ESI) available: experimental details. See http://www.rsc.org/suppdata/cc/b0/b004152l/

Here, we show that the high number of coordination sites and the likely presence of interstrand interactions in trenterpy prevent the formation of mononuclear 1:1 complexes and lead to the self-assembly of discrete homotrinuclear lanthanide complexes. Very recently Orvig and coworkers have reported another example of how the mismatch of ligand denticity and Ln(III) coordination number can be used to create polynuclear arrays.[11] While rigid C_3-symmetric ligands have often been used for the 'designed assembly' of oligonuclear compounds,[12] the work we present here is, to our knowledge, the first example of self-assembly directed by a flexible tripod.

The reaction of trenterpy with lanthanum triflate leads to the isolation, after addition of diethyl ether, of the crystalline M_3L_2 complex $[La_3(\mu_3\text{-trenterpy})_2(OTf)_4(H_2O)_2](OTf)_5$ **1**§ independently of the starting M:L stoichiometric ratio (1:1 or 3:2). Yellow crystals of **1** suitable for X-ray diffraction analyses were obtained by slow diffusion of diethyl ether in a solution of **1** in acetonitrile. The structure of the La complex is shown in Fig. 1 and an atomic numbering scheme of the asymmetric unit which contains 1.5 La ions is shown in Fig. 2. The $[La_3(\mu_3\text{-trenterpy})_2(OTf)_4(H_2O)_2]^{5+}$¶ cation lies on a twofold crystallographic axis passing through La(1) and between the capping nitrogens N(1) and N(1)A of the two ligands. Each trenterpy ligand is spread out such that each of its tetradentate carboxyterpyridine arms is coordinated to a different metal ion. Each La ion is coordinated by six terpyridine nitrogens and two amide oxygens provided by two different ligands. All La ions are ten-coordinate with two triflate oxygens binding La(1) and one water oxygen and one triflate oxygen binding the two symmetry related ions La(2) and La(2)A; the La–O distances are standard.[13] The average value of the La–N distance (2.748 Å) is longer than the average La–N bond distance found for a ten-coordinate mononuclear cationic complex of terpyridine $[La(NO_3)_2(terpy)_2]^+$ [13] (2.68 Å) but is similar to the La–N distances previously found in $[La(tbpa)(H_2O)(\eta^2\text{-}ClO_4)]^{2+}$ (2.728 Å)[14] and in $[La(edta)(H_2O)_3]^-$ (2.755 Å).[15] The geometry of the coordinated terpyridine arms is strongly distorted from planarity with the dihedral angles between two neighbouring pyridine rings ranging from 9.7 to 23.3°. Significant distortion from planarity had also been observed in the bisterpyridine La(III) complex[13] and for the complex $[Eu(terpy)_3](ClO_4)_3$[16] [dihedral angle between the two pyridine planes is: 4.8–28.6° for the La(III) complex and 12–26° for the Eu(III) complex].

The ^{1}H NMR spectrum of the trinuclear lanthanum complex in CD_3CN shows the presence of sharp signals with four resonances for the ethylene protons, one resonance for the amide proton and 10 overlapping signals for the terpyridine protons, in accord with an averaged D_3-symmetric structure on the NMR time-scale of the solution species. The ^{1}H NMR spectrum of a 1:1 solution of $La(OTf)_3$ and trenterpy in

DOI: 10.1039/b004152l

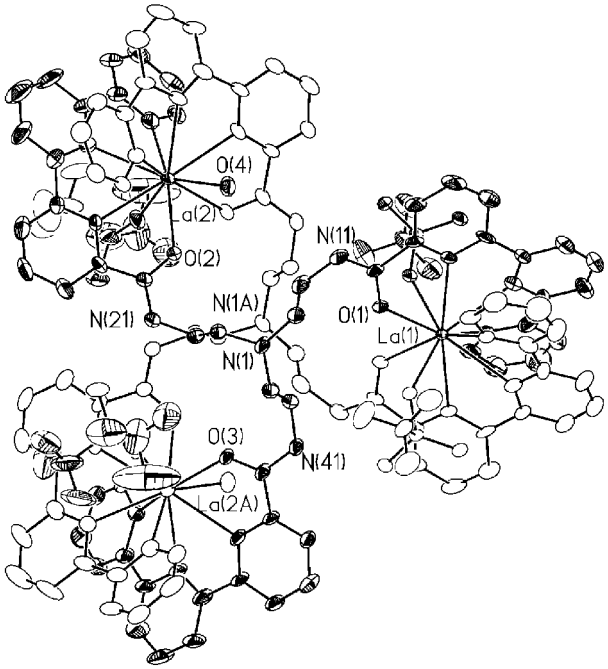

Fig. 1 Crystal structure of the $[La_3(\mu_3\text{-trenterpy})_2(OTf)_4(H_2O)_2]^{5+}$ cation in **1** with thermal ellipsoids at 30% probability. Selected bond lengths (Å): La(1)–O(1) 2.487(4), La(1)–O(11) 2.565(4), La(1)–N(14) 2.750(6), La(1)–N(12) 2.748(5), La(1)–N(13) 2.781(6), La(2)–O(2) 2.514(5), La(2)–O(3)A 2.523(5), La(2)–O(21) 2.542(5), La(2)–O(4) 2.565(5), La(2)–N(42)A 2.747(5), La(2)–N(43)A 2.717(5), La(2)–N(44)A 2.740(6), La(2)–N(22) 2.753(6), La(2)–N(23) 2.750(6), La(2)–N(24) 2.752(7) (symmetry transformations used to generate equivalent atoms A: $-x + 1$, y, $-z + 1/2$).

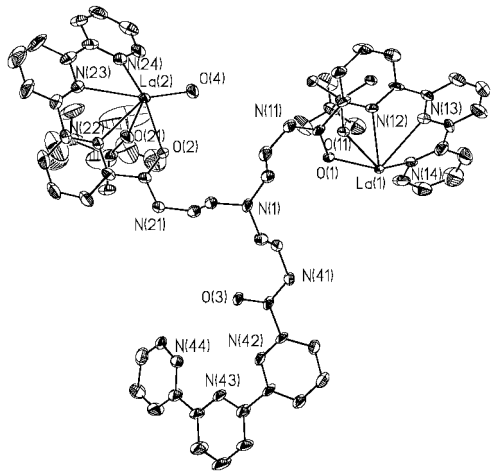

Fig. 2 Atomic numbering scheme of the $[La_3(\mu_3\text{-trenterpy})_2(OTf)_4(H_2O)_2]^{5+}$ cation in **1**. Ellipsoids are shown at the 30% probability level.

acetonitrile shows the presence of broad signals resulting from intermolecular ligand exchange. The ESMS spectra of 1:1 and 3:2 solutions of $La(OTf)_3$ and trenterpy in acetonitrile show a set of peaks which are in accord with the presence in solution of the trinuclear M_3L_2 complex. The ESMS spectrum of the 1:1 solution also shows another set of prominent peaks which were assigned to a mononuclear ML complex {$[La(trenterpy)(CF_3SO_3)_2]^+$ *m/z* 1360} and a set of minor peaks which were assigned to a dinuclear M_2L complex {$[La_2(trenterpy)(CF_3SO_3)_5]^+$ *m/z* 1945.6}. The preferential formation of the trinuclear species at different stoichiometric ratios, and its rigid solution structure indicate that **1** is the thermodynamic product of a self-assembly process. The ESMS spectra of 3:2 solutions of $Ln(OTf)_3$ (Ln = Pr, Eu, Lu) and trenterpy in acetonitrile also show the presence of peaks assigned to the M_3L_2 species. The ^{1}H NMR spectra of these solutions indicate a higher fluxionality of the solution species with respect to the La(III) complex.

In conclusion, the predisposition of three terpyridine units in a covalent tripod directs the process of self-assembly toward the formation of homotrinuclear lanthanide complexes of potential interest for the study of intramolecular metal-to-metal energy transfer. This work shows that tripodal ligands can be used to predetermine the geometric arrangement of flexible polydentate binding units containing neutral N-donors around lanthanide ions, allowing an improved control over the structure of the final polymetallic array with respect to single-stranded ligands.

This work was supported by the Commissariat à l'Energie Atomique. We thank Colette Lebrun for help in recording the mass spectra.

Notes and references

‡ The ligand trenterpy was prepared from 2,2′:6′,2″-terpyridine-6-carboxylic acid chloride and tris(2-aminoethyl)amine (tren).

§ $\delta_H(CD_3CN, 298\ K)$: 3.32 (br t, 6H, $H_{a/a'}$), 4.14 (br s, 3H, $H_{b/b'}$), 4.38 (br s, 3H, $H_{b/b'}$), 7.01 (q, 3H, $H_{5''}$), 7.80–7.84 (m, 12H), 8.02 (d, 3H), 8.05 (d, 3H), 8.13–8.17 (m, 6H), 8.23 (t, 3H), 9.55 (br s, 3H, NH). ES-MS (*m/z*): $[La_3(trenterpy)_2(CF_3SO_3)_8]^+$ (3451), $[La_3(trenterpy)_2(CF_3SO_3)_7]^{2+}$ (1653.6), $[La_3(trenterpy)_2(CF_3SO_3)_6]^{3+}$ (1052.6), $[La_3(trenterpy)_2(CF_3SO_3)_5]^{4+}$ (752.1).

¶ *Crystal data*: $[La_3(\mu_3\text{-trenterpy})_2(OTf)_4(H_2O)_2](OTf)_5{\cdot}2H_2O{\cdot}2MeCN$, $C_{121}H_{104}N_{28}O_{37}F_{27}S_9La_3$, M = 3760.59, monoclinic, space group $C2/c$, a = 19.2737(9), b = 26.4590(12), c = 30.2609(14) Å, β = 93.8740(10)°, V = 15396.7(12) Å^3, Z = 4, D_c = 1.622 g cm^{-3}, μ = 1.054 mm^{-1}. 18848 independent reflections (θ_{max} = 29.12°) were collected at 143 K. Refinement using the SHELXTL 5.05 package on all data converged at $R_1[F > 4\sigma(F)]$ = 0.0947, $wR2$ = 0.2492.

CCDC 182/1717. See http://www.rsc.org/suppdata/cc/b0/b004152l/ for crystallograpic files in .cif format.

1 D. Parker and J. A. G. Williams, *J. Chem. Soc., Dalton Trans.*, 1996, 3613.
2 (*a*) *Transition Metals in Supramolecular Chemistry*, ed. J.-P. Sauvage, John Wiley & Sons, New York, 1999; (*b*) J.-M. Lehn, *Supramolecular Chemistry—Concepts and Perspectives*, VCH, New York, 1995; (*c*) D. L. Caulder and K. N. Raymond, *J. Chem. Soc., Dalton Trans.*, 1998, 1185.
3 C. Piguet and J.-C. G. Bünzli, *Chem. Soc. Rev.*, 1999, **28**, 347; C. Piguet, *Chimia*, 1996, **50**, 144; P. Guerriero, S. Tamburini and P. A. Vigato, *Coord. Chem. Rev.*, 1995, **139**, 17.
4 P. Caravan, J. J. Ellison, T. J. McMurry and R. B. Lauffer, *Chem. Rev.*, 1999, **99**, 2293.
5 V. Comblin, D. Gilsoul, M. Hermann, V. Humblet, J. Vincent, M. Mesbahi, C. Sauvage and J. F. Desreux, *Coord. Chem. Rev.*, 1999, **185–186**, 451.
6 Y. Bretonnière, R. Wietzke, M. Mazzanti, C. Lebrun and J. Pecaut, *Inorg. Chem.*, 2000, in press.
7 F. Renaud, C. Piguet, G. Bernardinelli, J.-C. G. Bünzli and G. Hopfgartner, *J. Am. Chem. Soc.*, 1999, **121**, 9326.
8 A. M. W. C. Thompson, *Coord. Chem. Rev.*, 1997, **160**, 1; E. C. Constable, *Chem. Commun.*, 1997, 1073.
9 E. C. Constable, R. Chotalia and D. A. Tocher, *J. Chem. Soc., Chem. Commun.*, 1992, 771.
10 N. Martin, J.-C. Bünzli, V. McKee, C. Piguet and G. Hopfgartner, *Inorg. Chem.*, 1998, **37**, 577; S. Rigault, C. Piguet, G. Bernardinelli and G. Hopfgartner, *Angew. Chem., Int. Ed. Engl.*, 1998, **37**, 169.
11 I. A. Setyawati, S. Liu, S. J. Rettig and C. Orvig, *Inorg. Chem.*, 2000, **39**, 496.
12 M. Albrecht, *Angew. Chem., Int. Ed.*, 1999, **38**, 3463.
13 M. Fréchette and C. Bensimon, *Inorg. Chem.*, 1995, **34**, 3520.
14 R. Wietzke, M. Mazzanti, J.-M. Latour and J. Pecaut, *J. Chem. Soc., Dalton Trans.*, 1998, 4087.
15 J. L. Hoard, B. Lee and M. D. Lind, *J. Am. Chem. Soc.*, 1965, **87**, 1611.
16 G. H. Frost, F. A. Hart, C. Heath and M. B. Hursthouse, *Chem. Commun.*, 1969, 1421.

ChemComm

Unusual double-bond migration as a plausible key reaction in the biosynthesis of the isoprenoidal membrane lipids of methanogenic archaea†

Tadashi Eguchi,*[a] Hayato Takyo,[a] Mikio Morita,[b] Katsumi Kakinuma*[b] and Yosuke Koga[c]

[a] *Department of Chemistry and Materials Science, Tokyo Institute of Technology, O-okayama, Meguro-ku, Tokyo 152-8551, Japan. E-mail: eguchi@chem.titech.ac.jp*
[b] *Department of Chemistry, Tokyo Institute of Technology, O-okayama, Meguro-ku, Tokyo 152-8551, Japan*
[c] *Department of Chemistry, University of Occupational and Environmental Health, Yahatanishi-ku, Kitakyushu 807-8555, Japan*

Received (in Cambridge, UK) 17th May 2000, Accepted 21st June 2000

Labeling experiments of mevalonolactone-d_9 were pursued for studies of the biosynthesis of the core membrane lipids from thermophilic methanogenic archaea, which revealed that unusual double-bond migration occurred during the ultimate formation of the saturated isoprenoid chains in these particular archaea.

Archaea, which have been attracting considerable attention from both biochemical and evolutionary aspects, are distinct from bacteria and eukarya.[1] Archaeal cell membrane lipids are composed of isoprenoid-chain hydrocarbons linked to a glycerol molecule at the *sn*-2 and 3-positions by an ether linkage. The isoprenoid hydrocarbon chains of lipid molecules are frequently joined at the hydrophobic end to form a macrocyclic ring as large as 36- or 72-membered as shown in Scheme 1.[2]

The biosynthesis of these macrocyclic lipids is believed to proceed in a direct manner *via* digeranylgeranylglyceryl phosphate derived *sn*-glycerol 1-phosphate and geranylgeranyl diphosphate.[3] However, nothing is known about the mechanistic details of the final carbon–carbon bond(s) formation found in macrocyclic lipids. Described here are unanticipated observations from similar feeding experiments[4] of mevalonolactone-d_9 to thermophilic methanogens, *Methanococcus jannaschii* and *Methanobacterium thermoautotrophicum*.

The cultures of *M. jannaschii* (DSM 2661) and *M. thermoautotrophicum* JCM 10044^T (DSM 1053) were carried out as previously reported.[5,6] Mevalonolactone-d_9,[4] was aseptically and anaerobically added to the culture in a final concentration of 0.25 and 1.0 g L^{-1}, respectively. After cultivation the lipids were separately purified according to the standard procedure.[7] Repetitive chromatography afforded diphytanylglycerol, a 36-membered lipid, and a 72-membered lipid from *M. jannaschii*, and diphytanylglycerol and a 72-membered lipid from *M. thermoautotrophicum*, respectively. These core lipids were further converted to their corresponding benzoates and were first analyzed by ^{1}H NMR.

Fig. 1 shows pertinent ^{1}H NMR spectra of the benzoates of diphytanylglycerol, the 36-membered lipid, and the 72-membered lipid biosynthesized from mevalonate-d_9 from *M. jannaschii* and *M. thermoautotrophicum*. Also shown is the previously reported ^{1}H NMR spectra of perdeuterated diphytanylglycerol benzoate from *Haloarcula japonica*.[4] It was initially suggested that the signals due to the two oxymethylene groups (3.50 and 3.65 ppm, Fig. 1C and 1D) of the phytanyl chains from methanogenic archaea were significantly reduced due to the corresponding glycerol signals and the deuterium being highly incorporated, *ca.* 90%. Since the spectra of biosynthesized lipids from methanogenic archaea (Fig. 1C and 1D) are similar to that of the halophile (Fig. 1B), it seems most likely that the saturation of a geranylgeranyl group in methanogen lipids take place similarly through the addition of hydrogens in a *syn*-manner. However, closer inspection of these spectra allowed us to immediately see the different proton incorporation between methanogen and halophile, which was unexpected, including the increased signal for the methyl groups (0.85 ppm) and the appearance of signals (1.05 ppm) in methanogen lipids. The latter signals at 1.05 ppm must be

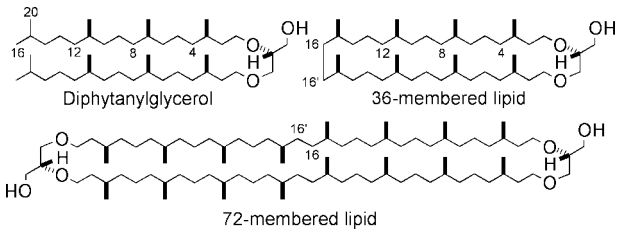

Scheme 1 Structure of core lipids of the archaeal membrane.

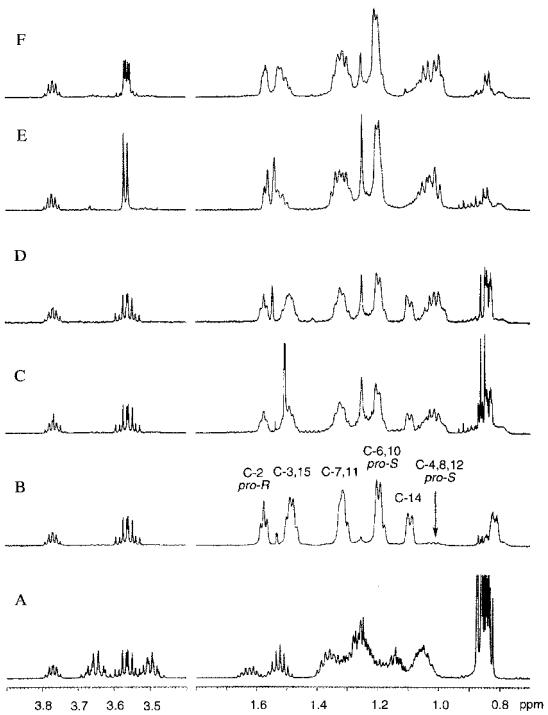

Fig. 1 Partial ^{1}H NMR spectra (500 MHz, $CDCl_3$) of (A) authentic 2,3-di-*O*-phytanyl-*sn*-glycerol benzoate, (B) multiply deuterated 2,3-di-*O*-phytanyl-*sn*-glycerol benzoate from *H. japonica* with mevalonolactone-d_9, (C) multiply deuterated 2,3-di-*O*-phytanyl-*sn*-glycerol benzoate from *M. thermoautotrophicum*, (D) multiply deuterated 2,3-di-*O*-phytanyl-*sn*-glycerol benzoate from *M. jannaschii*, (E) multiply deuterated 36-membered lipid benzoate from *M. jannaschii*, and (F) multiply deuterated 72-membered lipid benzoate from *M. jannaschii*.

† Electronic supplementary information (ESI) available: ^{1}H NMR and ^{1}H–^{1}H COSY spectra. See http://www.rsc.org/suppdata/cc/b0/b003948i/

ascribable to those of the diastereotopic protons of methylene groups at the C-4, -8 and -12 positions of phytanyl chains.[4] According to our previous assignment and the spectroscopic studies of others,[4,8] these signals were assigned to *pro-S* protons at the C-4, -8 and -12 positions. On the other hand, the signal intensities of the other positions were quite similar to those of the halophile. It now appears that the proton incorporation at these positions occurred regio- and stereospecifically in each phytanyl chain. This protonation pattern in these methanogen lipids cannot be rationalized by the well-known isomerase reaction between isopentenyl diphosphate and dimethylallyl diphosphate, because this isomerization reaction must cause stereochemical scrambling of protonation at the methylene group at the C-4, -8, and -12 positions of the phytanyl groups. Further, the increased methyl group signal at 0.85 ppm (Fig. 1C and 1D) can simply be assigned to the methyl groups at C-16 that originated from the C-2 position of mevalonate by ^{1}H–^{1}H COSY spectrum (data not shown), this was clearly verified by the reduced methyl signals of macrocyclic lipids (Fig. 1E and 1F), because the C-16 positions of macrocyclic lipids are known to originate from the C-2 position of mevalonate. Moreover, since digeranylgeranylglyceryl phosphate is known to be involved in the biosynthesis of archaeal lipids, this protonation pattern may well suggest involvement of migration of the double bonds, and this double-bond migration must occur *after* construction of the digeranylgeranylglyceryl group.

The present study now strongly suggests that the unusual double-bond migration occurred during the biosynthesis of the core lipid in the methanogenic archaea as shown in Scheme 2. Although it has not been rigorously verified, it is worth noting that the dissimilarity of the labeling patterns between methanogenic and halophilic archaea may reflect the presence and absence of macrocyclic lipids, and further, the isomerization of the double-bonds in digeranylgeranylglyceryl phosphate could be a trigger for new carbon–carbon bond(s) formation in macrocyclic lipids.

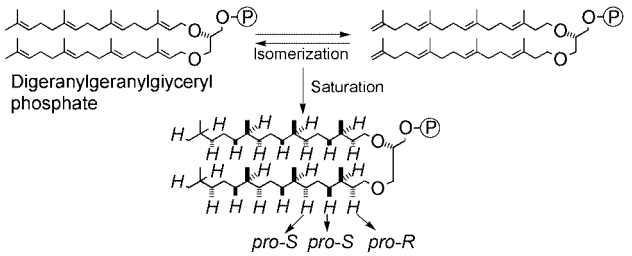

Scheme 2 Double-bond isomerization and saturation reaction in the lipid biosynthesis of methanogenic archaea.

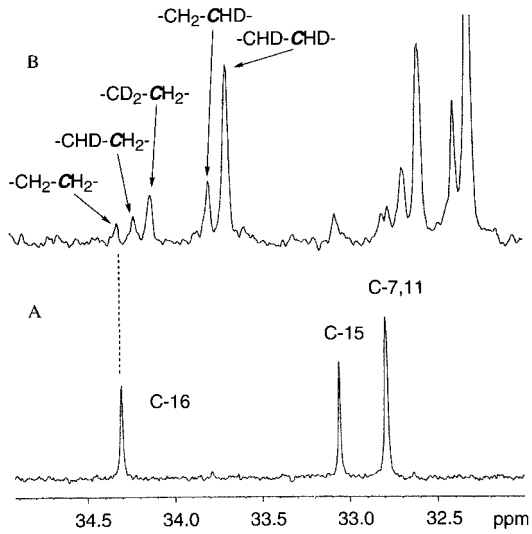

Fig. 2 Partial ^{13}C NMR spectra (125 MHz) of (A) non-labeled 72-membered lipid benzoate, and (B) multiply deuterated 72-membered lipid benzoate from *M. jannaschii* (^{1}H and ^{2}H decoupled).

Furthermore, the labeling patterns of biosynthetically deuterated 36- and 72-membered lipids were especially crucial in determining the nature of C-16, and the cyclized lipid benzoates were analyzed by ^{13}C{^{1}H,^{2}H} NMR spectroscopy. As shown in Fig. 2, the ^{13}C signals of the C-16 were observed as a cluster due to the various degrees of deuterium shift. Although the intensities of the cluster signals are low due to the isomerase reaction described above, a ^{13}C signal with two deuterium atoms retention was clearly observed at the C-16 position, which is a key feature in excluding higher oxidized states such as an aldehyde or a carboxylate as an intermediate for C–C bond formation.

These results further support the hypothesis that the isomerized intermediate having a terminal methylene functionality is a precursor. This precursor has to be ultimately saturated in the biosynthetic sequence. Saturation of isolated double bonds in various biological systems normally involves addition of a proton to generate a carbocation which is then quenched by hydride transfer from NAD(P)H. Therefore, a plausible and mechanistically simple solution to the problem of creating a new and critical C–C bond in the macrocyclic lipid biosynthesis is that the C–C bond formation occurs at the stage of the saturation step including intermolecular acid catalyzed condensation as shown in Scheme 3. While a mechanism involving a radical trigger can not be ruled out at the moment, the validity of this hypothesis is under investigation.

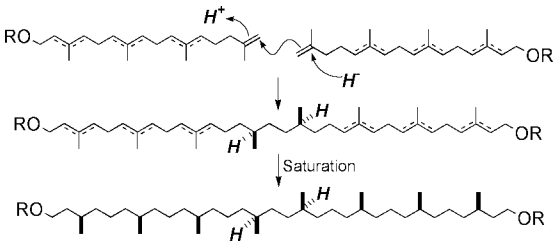

Scheme 3 Proposed mechanism of the new C–C bond forming reaction in the biosynthesis of macrocyclic lipids in methanogenic archaea.

The authors thank Ms Mami Ohga, University of Occupational and Environmental Health, for technical assistance. This work was supported by a Grant-in-Aid for Scientific Research on Priority Areas (A) from the Ministry of Education, Science, Sports, and Culture, Japan, by the 'Research for the Future' Program of The Japan Society for the Promotion of Science (JSPS-RFTF96I00302), and by Novartis Foundation (Japan) for the Promotion of Science.

Notes and references

1 C. R. Woose, *Microbiol. Rev.*, 1987, **51**, 221; C. R. Woose and M. L. Wheelis, *Proc. Natl. Acad. Sci. USA*, 1989, **87**, 4576; S. M. Barns, R. E. Fundyga, M. W. Jeffries and N. R. Pace, *Proc. Natl. Acad. Sci. USA*, 1994, **91**, 1609.

2 M. Kates, in *The Biochemistry of Archaea (Archaeobacteria)*, eds. M. Kates, D. J. Kushner, A. T. Matheson, Elsevier, Amsterdam, 1993, pp. 261; M. Kates, *Experientia*, 1993, **49**, 1027; A. Gambacorta, A. Gliozzi and M. De Rosa, *World J. Microbiol. Biotechnol.*, 1995, **11**, 115.

3 A. Chen, D. Zhang and C. D. Poulter, *J. Biol. Chem.*, 1993, **26**, 261; D. Zhang and C. D. Poulter, *J. Am. Chem. Soc.*, 1993, **115**, 1270; D. Zhang and C. D. Poulter, *J. Org. Chem.*, 1993, **58**, 3919.

4 T. Eguchi, M. Morita and K. Kakinuma, *J. Am. Chem. Soc.*, 1998, **120**, 5427.

5 W. J. Jones, J. A. Leigh, F. Mayer, C. R. Woese and R. S. Wolfe, *Arch. Microbiol.*, 1983, **136**, 254; Y. Koga, M. Akagawa-Matsushita, M. Ohga and M. Nishihara, *Syst. Appl. Microbiol.*, 1993, **16**, 342.

6 J. G. Zeikus and R. S. Wolfe, *J. Bacteriol.*, 1972, **109**, 707; N. Nishihara, H. Morii and Y. Koga, *J. Biochem.*, 1987, **101**, 997.

7 H. Morii, M. Nishihara, M. Ohga and Y. Koga, *J. Lipid Res.*, 1986, **26**, 577.

8 D. Arigoni, W. Eisenreich, C. Latzel, S. Sagner, T. Radykewicz, M. H. Zenk and A. Bacher, *Proc. Natl. Acad. Sci. USA*, 1999, **96**, 1309.

ChemComm

Chiral channels in a 3-D network of self-assembled tetranuclear copper(II) aggregates†

Alex Fragoso,[ab] Myrtil L. Kahn,[a] Alfonso Castiñeiras,[c]‡ Jean-Pascal Sutter,*[a] (the late) Olivier Kahn[a] and Roberto Cao[b]

[a] *Laboratoire des Sciences Moléculaires, Institut de Chimie de la Matière Condensée de Bordeaux, UPR-CNRS n°9048, F-33608 Pessac, France. E-mail: jpsutter@icmcb.u-bordeaux.fr*

[b] *Laboratory of Bioinorganic Chemistry, Faculty of Chemistry, Havana University, Havana 10400 Cuba*

[c] *Department of Inorganic Chemistry, Faculty of Pharmacy, University of Santiago de Compostela,15 Santiago de Compostela, Spain*

Received (in Columbia, MO, USA) 25th February 2000, Accepted 1st May 2000

A sugar-substituted ligand allowed for the synthesis of chiral Cu(II) tetranuclear aggregates which assemble *via* H-bonding in a 3D-network containing hydrophobic helical channels.

Polynuclear complexes attract much interest. They are the subject of extensive studies regarding their magnetic properties[1–4] as well as in the field of bioinorganic chemistry.[5–7] The most common strategy to obtain these complexes involves metal self-association induced by bridging ligands like alkoxyde, thiolate or carboxylate.[8–12] Alternatively, polyfunctional ligands have been used in directing construction of polynuclear architectures.[13–16] However, little attention has been paid to the construction of supramolecular networks by the association of these polynuclear entities through non-covalent interactions between their organic ligand shells. Such a supramolecular arrangement might be desirable for controlling the bulk physical properties arising from the inorganic subunits. One way to achieve the self-assembly of discrete units into a more organised network would be to take advantage of the ability of specific functional groups (*e.g.* hydroxy groups) to link the molecular unit by H-bonding.[17,18] We report here that a sugar functionalised Schiff-base may induce polymetallic aggregation. Moreover, the resulting tetranuclear complexes associate *via* H-bonding into a 3-D network.

The ligand (H_2L, Scheme 1) was synthesised in 91% yield by the condensation of salicylaldehyde and 1-amino-1-deoxy-D-sorbitol.§ The reaction of H_2L and $Cu(MeCO_2)_2$ in hot water afforded a green complex of formula $\{Cu_4L_4\}\cdot 2H_2O$¶ which it was possible to recrystallize almost quantitatively by slow diffusion of THF to a DMF solution. X-Ray structural determination revealed a molecule consisting of an inorganic core formed by four Cu(II) ions surrounded by four ligands in a head-to-tail arrangement (Fig. 1), two water molecules being associated to the molecular unit.‖ Each $\{Cu_4L_4\}$ molecule has a central core formed by an eight-membered $\{Cu_4O_4\}$ ring folded in a boat-like conformation. The phenyl rings and the polyhydroxy chains point outward from the core in an alternate disposition in all directions, giving the molecule a globular shape. The molecule is chiral, the optically pure ligand leading to the formation of a single enantiomer of the polynuclear compound. Intracluster H-bonds stabilise the structure, notably the bond formed between H(21) and O(11) with an H··O distance of 2.13 Å. The copper atoms are five-coordinate in a distorted square-pyramidal geometry and are bridged by alkoxy groups formed by the deprotonation of the sorbitol C-2 hydroxy group. The base of each pyramid consists of the imine nitrogen, the phenolate oxygen atom and the two bridging alkolate oxygen atoms. Notably, for Cu(1) the hydroxy group bound in axial position is borne by C-3 of the sorbitol chain [O(40)], while for Cu(2) it is borne by C-4 [O(21)]. Thus alternate Cu atoms are chelated by 6/5/5 and 6/5/6 ring systems.

The $\{Cu_4L_4\}$ molecules are assembled in a 3D-network by intermolecular hydrogen bonding involving the hydroxy groups of the side chains and the two water molecules located between neighbouring $\{Cu_4L_4\}$ units. This H-bonded pattern can be described as a network of supramolecular helices interconnected by H-bonds. In the *c* direction the packing generates a three-fold screw axis and parallel channels (Fig. 2). Based upon van der Waals radii, the width of the channels is 5 Å for the smaller lobes and up to 7 Å wall to wall. These channels are

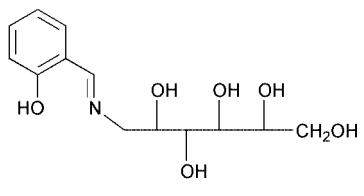

H_2L

Scheme 1

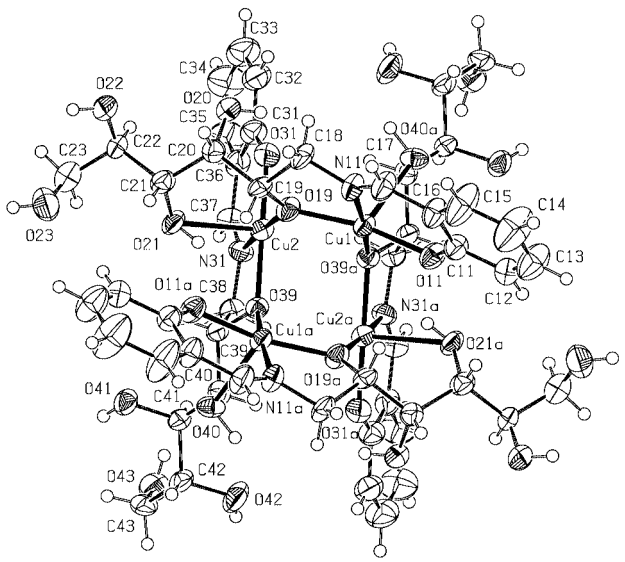

Fig. 1 Perspective view and atom labelling of the molecule $\{Cu_4L_4\}$ (ORTEP diagram, ellipsoids at 50% probability level). Selected bond length (Å) and angles (°): Cu(1)–O(11) 1.945(5), Cu(1)–O(19) 1.955(5), Cu(1)–O(39) 1.929(5), Cu(1)–O(40) 2.410(5), Cu(1)–N(11) 1.930(7), Cu(1)··Cu(2) 3.2962(15), Cu(1)··Cu(2a) 3.4462(15), Cu(1)··Cu(1a) 3.808(2), Cu(2)–O(19) 1.958(5), Cu(2)–O(21) 2.493(5), Cu(2)-O(31) 1.934(5), Cu(2)–O(39a) 1.973(5), Cu(2)–N(31) 1.945(6); Cu(1)–O(19)–Cu(2) 114.8(2), Cu(2)–O(39a)–Cu(1a) 124.1(2).

† This paper is dedicated to the memory of Professor O. Kahn who passed suddenly away on December 8, 1999.

‡ Author for enquiries relating to the crystallographic study.

DOI: 10.1039/b002360o

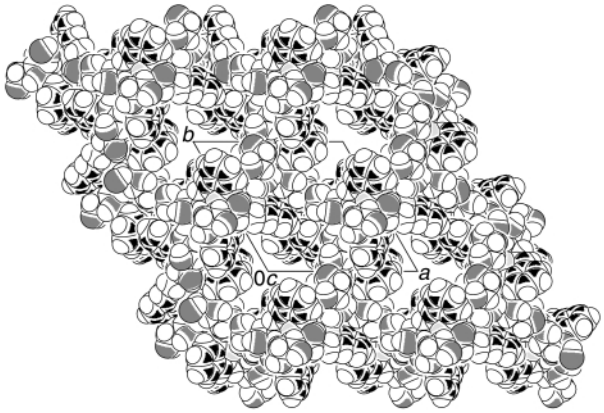

Fig. 2 CPK model view of the molecular packing along the *c* axis showing the channels (H_2O located in the channels have been omitted for clarity). H-Bonds involved in the intermolecular association (Å): OH(22)··O(42)#1 2.11, OH(40)··O(1)#3 1.99, OH(41)··O(20)#4 1.98, OH(42)··O(22)#5 2.20, OH(1B)··O(42)#4 2.45, OH(23)··H(41)#2 2.43 (Symmetry used: #1 $x - y + 1, -y + 1, -z + 2/3$; #2 $-x + 1, -x + y, -z + 1/3$; #3 $-y + 1, x - y + 1, z + 1/3$; #4 $-x + y, -x + 1, z - 1/3$; #5 $x - y, -y + 1, -z + 2/3$).

hydrophobic because the hydrogen atoms of the phenyl moieties and those in positions 2 and 3 of the sorbitol chains point towards the cavities. The X-ray structure analysis suggested that these channels are occupied by highly mobile water molecules distinct from those included in the formula $\{Cu_4L_4\}\cdot 2H_2O$.‖ However, after drying the crystalline compound *in vacuo* at room temperature, these labile water molecules are removed as found by the elemental analysis.

The magnetic interaction between the Cu(II) ions in the inorganic core was investigated, the plot of $\chi_M T$ *vs.* T being shown in Fig. 3. The observed behaviour indicates that substantial antiferromagnetic interactions among the spin carriers tend to cancel the magnetic moment of the Cu(II) cluster. It is very unlikely that they include significant intermolecular interactions, because the inorganic cores are well shielded by the organic ligands. Therefore, the magnetic data have been analysed using a model for interaction between Cu(II) ions bridged by an O-atom within the $\{Cu_4O_4\}$ ring ($H = -J(\boldsymbol{S}_1\cdot\boldsymbol{S}_2 + \boldsymbol{S}_2\cdot\boldsymbol{S}_3 + \boldsymbol{S}_3\cdot\boldsymbol{S}_4 + \boldsymbol{S}_4\cdot\boldsymbol{S}_1)$)[19] yielding an interaction parameter, $J = -87.8$ cm^{-1}.

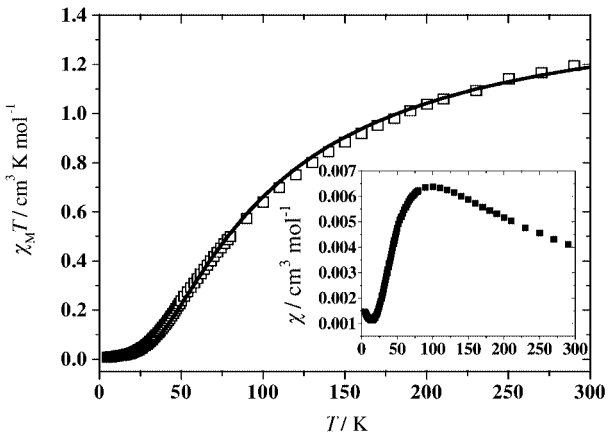

Fig. 3 Experimental (□) and calculated (—) $\chi_M T$ *vs.* T curve; χ_M *vs.* T is depicted in the insert.

The $\{Cu_4L_4\}$ compound illustrates the ability of a polyol-substituted Schiff base to induce the formation of an inorganic core. Moreover the functional groups of the ligand are able to associate the polynuclear aggregates by hydrogen bonding, so constructing a very stable network. The possibility of varying the nature of the metal ions as well as the size of the inorganic core is under investigation. The solubility of the $\{Cu_4L_4\}$ compound in hot water or alcohols suggest the possibility of trapping organic molecules in the hydrophobic cavities while still maintaining the hydrogen bond network.

A. F. is grateful for the generous financial support from the European Community ALFA Program 'Metals and Environmental Problems' (Grant C.E. 5.0273.9). A. C. thanks the Xunta de Galicia, Spain, for financial support under Project XUGA 20309B97.

Notes and references

§ H_2L:[21] salicylaldehyde (5 mmol) was added dropwise to a vigorously stirred suspension of 1-amino-1-deoxy-D-sorbitol (5 mmol) in MeOH (100 mL). The reaction mixture turned yellow and stirring was continued for 1 h. The yellow precipitate was filtered off and washed several times with MeOH followed by Et_2O and dried *in vacuo* (yield: 91%); mp 161–162 °C (decomp.). IR(KBr, cm^{-1}): 1636($\nu_{C=N}$). δ_H(200 MHz, DMSO-d_6): 3.60 (m, 6H, CH), 6.87 (m, 2H, H_{arom}), 7.37 (m, 2H, H_{arom}), 8.49 (s, 1H, HC=N). δ_C(DMSO-d_6) 61.3 (C-1), 63.4 (C-6), 70.0, 71.5, 71.7, 72.2 (C-2,3,4,5), 116.6, 118.1, 118.7, 131.6, 132.2, 161.2 (C_{arom}), 166.6 (HC=N). Anal.: Calc. for $C_{13}H_{19}O_6N$: C, 54.7; H, 6.7; N, 4.9. Found: C, 54.4; H, 6.3; N, 5.0%.

¶ $\{Cu_4L_4\}\cdot 2H_2O$: $Cu(Me_3CO_2)_2$ (0.5 mmol) in water (1 mL) was warmed to 90 °C and added with stirring to a hot solution of the ligand HL_2 (0.5 mmol). Green plate crystals of the title compound suitable for X-ray crystallography were obtained after the hot solution cooled down to room temperature. Anal. Calc. for $C_{52}H_{68}N_4O_{24}Cu_4\cdot 2H_2O$: C, 43.9; H, 5.1; N, 4.0; Cu, 17.9. Found: C, 43.6; H, 5.4; N, 4.1; Cu, 17.6%. IR(KBr, cm^{-1}): 3350s, 2927m, 1639s, 1600m, 1542m, 1471m, 1449s, 1304m, 1081m, 761m.

‖ *Crystal data* for $C_{52}H_{72}N_4O_{26}Cu_4$: M = 1423.30, trigonal, space group $P3_12_1$ (no. 152), a = 18.551(3), b = 18.551(3), c = 18.0135(16) Å, U = 5368.9(15) Å^3, T = 293 K, Z = 3, μ(Cu-Kα) = 1.54184 Å, 4227 reflections measured, 4227 unique (R_{int} = 0.0) which where used in all calculations. The final $R(F^2)$ was 0.0541. The structure was solved using direct methods and refined by full-matrix least squares on F^2. The absolute configuration was established according to published procedures.[20] Two density peaks of *ca.* 1.36 e A^3 at (−0.9163, −0.7074, −0.3644) and (−0.7885, −9601, −0.3749) were found which appear to correspond to water molecules that are highly disordered because of their great mobility in the channels. These molecules were not included in the structure refinement.

CCDC 182/1710. See http://www.rsc.org/suppdata/cc/b0/b002360o/ for crystallographic files in .cif format.

1 K. S. Murray, in *Advances in Inorganic Chemistry*, ed. A. G. Sykes, San Diego, 1995, vol. 43, pp. 261–358.
2 S. M. J. Aubin, M. W. Wemple, D. M. Adams, H.-L. Tsai, G. Christou and D. N. Hendrickson, *J. Am. Chem. Soc.*, 1996, **118**, 7746.
3 L. Thomas, F. Lionti, R. Ballou, D. Gatteschi, R. Sessoli and B. Barbara, *Nature*, 1996, **383**, 145.
4 W. Wernsdorfer and R. Sessoli, *Science*, 1999, **284**, 133.
5 F. Osterloh, Y. Sanakis, R. J. Staples, E. Münck and R. H. Holm, *Angew. Chem., Int. Ed.*, 1999, **38**, 2066.
6 D. P. Riley, *Chem. Rev.*, 1999, **99**, 2573.
7 T. N. Sorell, *Tetrahedron*, 1989, **45**, 3.
8 A. Caneschi, A. Cornia, A. C. Fabretti and D. Gatteschi, *Angew. Chem., Int. Ed.*, 1999, **38**, 1295.
9 R. Wang, Z. Zheng, T. Jin and R. J. Staples, *Angew. Chem., Int. Ed.*, 1999, **38**, 1813.
10 R. W. Saalfrank, N. Löw, B. Demleitner, D. Stalke and M. Teichert, *Chem. Eur. J.*, 1998, **4**, 1305.
11 V. Tangoulis, C. P. Raptopoulou, S. Paschalidou, E. G. Bakalbassis, S. Perlepes and A. Terzis, *Angew. Chem., Int. Ed. Engl.*, 1997, **36**, 1083.
12 S. P. Watton, P. Fuhrmann, L. E. Pence, A. Caneschi, A. Cornia, G. L. Abbati and S. J. Lippard, *Angew. Chem., Int. Ed. Engl.*, 1997, **36**, 2774.
13 J. Rojo, J.-M. Lehn, G. Baum, D. Fenske, O. Waldmann and P. Müller, *Eur. J. Inorg. Chem.*, 1999, 517.
14 B. F. Abrahams, S. J. Egan and R. Robson, *J. Am. Chem. Soc.*, 1999, **121**, 3535.
15 R. E. P. Winpenny, *Chem. Soc. Rev.*, 1998, **27**, 447.
16 A. Bino, I. Shweky, S. Cohen, E. R. Bauminger and S. J. Lippard, *Inorg. Chem.*, 1998, **37**, 5168.
17 H. Oshio, Y. Saito and T. Ito, *Angew. Chem., Int. Ed. Engl.*, 1997, **36**, 2673.
18 C. B. Aakeroy, A. M. Beatty and D. S. Leinen, *Angew. Chem., Int. Ed.*, 1999, **38**, 1815.
19 O. Kahn, *Molecular Magnetism*, VCH, Weinheim, 1993.
20 H. D. Flack, *Acta Crystallogr., Sect. A*, 1983, **39**, 876.
21 du Pont de Nemours, *US Pat.*, 2396097, 1946.

ChemComm

New linked and threaded cluster compounds

Brian F. G. Johnson,*[a] Catherine M. G. Judkins,[a] Justin M. Matters,[a] Douglas S. Shephard[a] and Simon Parsons[b]

[a] *Department of Chemistry, University of Cambridge, Lensfield Road, Cambridge, UK CB2 1EW. E-mail: bfgj1@cam.ac.uk*

[b] *Dept. of Chemistry, University of Edinburgh, West Mains Road, Edinburgh, UK EH9 3JJ*

Received (in Cambridge, UK) 25th April 2000, Accepted 3rd July 2000

The linked cluster species $[Ru_6C(CO)_{14}(\eta^6\text{-}C_6H_4C_{10}H_{20}O_6)]_2[H_3N(CH_2)_8NH_3][BF_4]_2$ 2 and the threaded derivative $[Ru_6C(CO)_{14}(\eta^6\text{-}C_6H_4C_{12}H_{24}O_8C_6H_4)][PhCH_2NH_2CH_2Ph]PF_6$ 4 have been prepared and fully characterised by single crystal X-ray analysis; these compounds are valuable precursors in the formation of nanoparticle devices.

For some time we have been investigating the potential of metal clusters to act as precursors in the formation of nanoparticle arrays for use in catalysis[1] and in the production of electronic devices.[2] A primary objective of our work has been the preparation of polymer precursors which lead to materials with cluster units bonded either within the polymer backbone [Fig. 1(a)] or as pendants, suspended from a polymeric backbone [Fig. 1(b)].

In each case clear advantages have become apparent.[3,4] Recently, we have established a route to "electron-hopping" materials which permit the production of linked nanoparticle arrays such as chains or wires. In this work we report a new and valuable route to linked and threaded clusters which has enabled us to investigate the potential of adopting such methods in the formation of polymers bearing discrete cluster units.

Several years ago we demonstrated[5] that arene clusters of the type $[(\eta^6\text{-arene})Ru_6C(CO)_{14}]$ and later $[(\mu_3\text{-arene})Ru_6C(CO)_{14}]$ could easily be prepared.[6] With this knowledge in mind, attempts were made to establish a range of derivatised arenes coordinated to cluster units. More recently, we have been able to attach benzocrown ethers to hexaruthenium clusters by direct thermolysis and this has generated our interest into the potential use of such complexes as molecular sensors.[7,8] Preliminary investigations into such applications have been conducted and the compound $[Ru_6C(CO)_{14}(\eta^6\text{-}C_{16}H_{24}O_6)]$ **1** shown to encapsulate either the NH_4^+ ion or metal ions such as K^+ and Na^+.[8]

Building on these observations, we have investigated the use of such non-covalent interactions to link two or more clusters and have developed a simple route to both linked and threaded cluster systems.

Compound **1** may be readily prepared according to the reaction sequence outlined in Scheme 1.[7] It has been fully characterised by the usual spectroscopic techniques and by single crystal X-ray analysis† (Fig. 2). The arene ring is coordinated in an η^6 fashion to a single ruthenium atom, with the average Ru–arene bond distance being 2.26 Å. In each of these cluster/crown complexes the interstitial carbon atom is displaced slightly from the centre of the cluster towards the arene ring and there is one bridging carbonyl ligand on the cluster. The oxygen atoms are tilted up at an angle to the plane of the arene ring and the undistorted cavity allows an ideal site for host–guest chemistry.

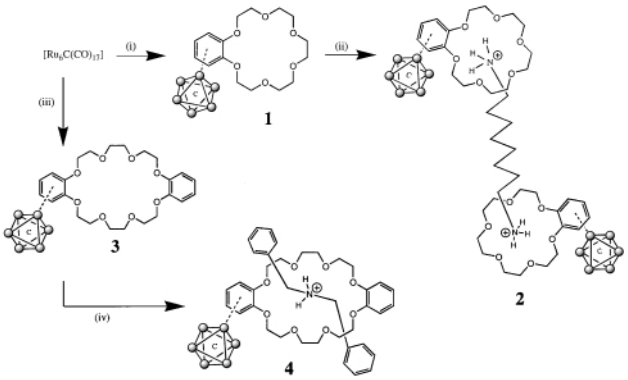

Scheme 1 Preparation of **2** and **4**: *Reagents and conditions*: (i) di-*n*-butyl ether, benzo-18-crown-6, 16 h reflux, N_2; (ii) CH_2Cl_2 + few drops MeOH, stir 24 h; (iii) di-*n*-butyl ether, dibenzo-24-crown-8, 16 h reflux, N_2; (iv) stir 24 h in CH_2Cl_2.

Treatment of **1** with the diprotonated diamine $[H_3N(CH_2)_8NH_3]^{2+}$ yields the new linked cluster system **2** (yield *ca.* 76%) in which the two quaternary ammonium units are embraced at either end by the polycyclic ether bonded to a cluster unit. This novel compound has been fully characterised by IR and NMR spectroscopy, elemental analysis and its molecular structure established by single crystal X-ray analysis. This is shown in Fig. 3, together with some relevant bond distances. As expected, the cluster units arrange themselves in a *trans*-configuration relative to the diammonium octane 'linker,' with the $-NH_3^+$ function lying *ca.* 1.3217 Å above the least squares mean plane of oxygen atoms. Two of the hydrogen atoms on each of the ammonium species interact with two of the oxygen atoms of the crown and have N–H···O bond distances of 2.970(5) and 2.967(5) Å (in each of which the N–H distances

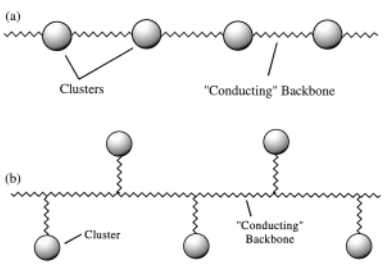

Fig. 1 (a) Polymer with cluster units within polymer backbone and (b) with cluster units as pendants.

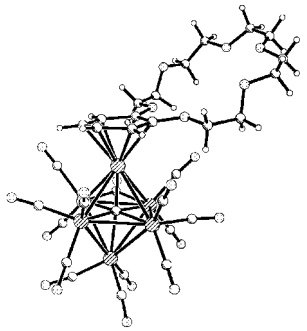

Fig. 2 Molecular structure of $[Ru_6C(CO)_{14}(\eta^6\text{-}C_6H_4C_{10}H_{20}O_6)]$ **1**.

DOI: 10.1039/b003291n

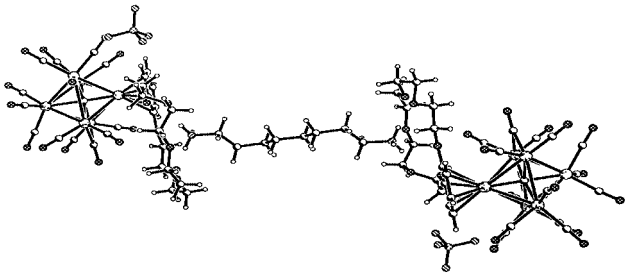

Fig. 3 Molecular structure of $[Ru_6C(CO)_{14}(\eta^6\text{-}C_6H_4C_{10}H_{20}O_6)]_2\text{-}[H_3N(CH_2)_8NH_3][BF_4]_2$ **2** Average ruthenium–arene bond length = 2.26 Å; N–O distances range from 2.952(4) to 3.231(4) Å.

are 0.91 Å). The third hydrogen of the ammonium species points in the direction of one of the oxygen atoms of the crown but is aimed above the plane and displays a long range interaction of 3.205(4) Å.

In a separate experiment, compound **3**, a relative of **1** but containing the dibenzo-24-crown-8 ligand was prepared as outlined in Scheme 1 and a crystal suitable for X-ray analysis† obtained (Fig. 4). The crown is approximately planar with the mean deviation from the plane of oxygen atoms being 0.0747 Å. The larger macrocyclic cavity size which is suitable for "threading" reactions (in which the molecules are actually threaded through the hole) to yield *pseudo*rotaxanes[9] can clearly be seen.

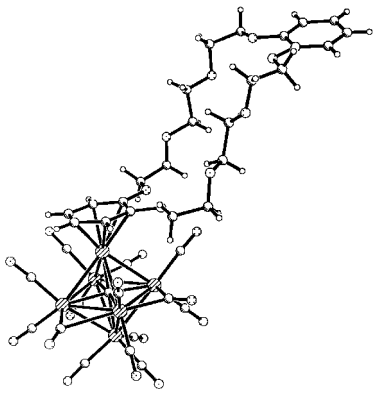

Fig. 4 Molecular structure of $[Ru_6C(CO)_{14}(\eta^6\text{-}C_6H_4C_{12}H_{24}O_8C_6H_4)]$ **3**. Average ruthenium–arene bond length = 2.26 Å.

When **3** was reacted with the protonated amine $[PhCH_2NH_2CH_2Ph]^+$ in dichloromethane, the *pseudo*rotaxane **4** was produced (yield *ca*. 70%). The amine has threaded through the macrocyclic cavity attached to the cluster to generate the classic 'bead on a string configuration.' This compound has also been fully characterised by single crystal X-ray analysis† and the molecular structure is shown in Fig. 5. In contrast to analogous organic compounds[9] in which the two arene rings of the crown ether are widely separated, the macrocycle in **4** has bent to display a π-stacking arrangement between the two arene units of the crown and one of the phenyl units of the thread. The two hydrogen atoms of the ammonium group display short range interactions with two of the oxygen atoms of the crown, with approximate distances of 2.019 and 2.131 Å. They also display longer range interactions with two further oxygen atoms of the crown (distances *ca*. 2.4–2.6 Å) and there are also several long range interactions between the hydrogen atoms of the methylene group nearest to the arene involved in the π-stack and the macrocyclic oxygen atoms.

These new materials open up a new and important route to cluster polymer precursors which, in other systems, have been shown to serve as valuable intermediates in the formation of nanoparticle materials for use in electron devices.[10]

We gratefully acknowledge Dr Neil Feeder and Dr John Davies for determining the crystal structures of **1**, **2** and **3**, the EPSRC and ICI for financial support (C. M. G. J.) and Peterhouse College, Cambridge for a research fellowship (D. S. S.).

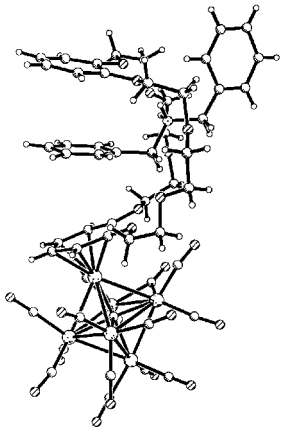

Fig. 5 Molecular structure of $[Ru_6C(CO)_{14}(\eta^6\text{-}C_6H_4C_{12}H_{24}O_8C_6H_4)]\text{-}[PhCH_2NH_2CH_2Ph]PF_6$ **4**. Distance between planes 1 and 2 = 4.105 Å, distance between planes 2 and 3 = 3.820 Å. Angle between planes 1 and 2 = 22.5°, angle between planes 2 and 3 = 8.5°. Average N···O separation = 2.9595 Å, average H···O separation = 2.075 Å.

Notes and references

† *Crystal data*: $[Ru_6C(CO)_{14}(\eta^6\text{-}C_6H_4C_{10}H_{20}O_6)]$ **1**: M = 1322.94, orthorhombic, a = 19.1672(8), b = 14.8037(6), c = 27.0061(8) Å, U = 7662.9(5) Å^3, T = 180 K, space group $Pca2_1$, Z = 8, μ(Mo-Kα) = 2.387 mm^{-1}, 30683 reflections collected, 12064 unique (R_{int} = 0.0571) which were used in all calculations. Final $R1$ (observed) was 0.0682. Single crystals of **1** were recrystallised from CH_2Cl_2–hexane. Some atoms of the crown ether moieties are not well resolved: isotropic temperature factors and extensive bond distance restraints were applied to these atoms.

$[Ru_6C(CO)_{14}(\eta^6\text{-}C_6H_4C_{10}H_{20}O_6)]_2[H_3N(CH_2)_8NH_3][BF_4]_2$ **2**: M = 2965.76, triclinic, a = 10.1350(2), b = 15.0310(4), c = 16.4410(5) Å, U = 2413.39(11) Å^3, T = 180 K, space group $P1$, Z = 1, μ(Mo-Kα) = 1.921 mm^{-1}, 29071 reflections collected, 8467 unique (R_{int} = 0.0354) which were used in all calculations. Final $R1$ (observed) was 0.0286. Single crystals of **2** were recrystallised from acetone–pentane. Some atoms of the crown are not well resolved and there is disorder over two sites. Isotropic temperature factors and bond distance restraints were applied to these atoms.

$[Ru_6C(CO)_{14}(\eta^6\text{-}C_6H_4C_{12}H_{24}O_8C_6H_4)]$ **3**: M = 1459.09, triclinic, a = 9.9611(5), b = 16.6690(10), c = 18.2217(11) Å, U = 2695.1(3) Å^3, T = 230 K, space group $P1$, Z = 2, μ(Mo-Kα) = 1.711 mm^{-1}, 16205 reflections collected, 12081 unique (R_{int} = 0.0371) which were used in all calculations. Final $R1$ (observed) was 0.0692. Single crystals of **3** were recrystallised from CH_2Cl_2–hexane. Some atoms of the crown ether moieties are not well resolved: isotropic temperature factors and extensive bond distance restraints were applied to these atoms.

$[Ru_6C(CO)_{14}(\eta^6\text{-}C_6H_4C_{12}H_{24}O_8C_6H_4)][PhCH_2NH_2CH_2Ph]PF_6$ **4**: M = 1802.34, monoclinic, a = 12.312(5), b = 9.580(7), c = 52.612(16) Å, U = 6188 (6) Å^3, T = 220 K, space group $P2_1/c$, Z = 4, μ(Mo-Kα) = 1.547 mm^{-1}, 8463 reflections collected, 7964 unique (R_{int} = 0.0445) which were used in all calculations. Final $R1$ (observed) was 0.1290.

CCDC 182/1707. See http://www.rsc.org/suppdata/cc/b0/b003291n/ for crystallographic files in .cif format.

1 R. Raja, G. Sankar, S. Hermans, D. S. Shephard, S. Bromley, J. M. Thomas and B. F. G. Johnson, *Chem. Commun.*, 1999, 1571.
2 B. F. G. Johnson, *Coord. Chem. Rev.*, 1999, **190–192**, 1269.
3 C. E. Carraher Jr., and C. U. Pittman, Jr., in *Metal Containing Polymeric Systems*, ed. J. E. Sheats, C. E. Carraher Jr., and C. U. Pittman, Jr., Plenum, New York, 1985.
4 P. Nguyen, P. Gomez-Elipe and I. Manners, *Chem. Rev.*, 1999, **99**, 1515.
5 M. P. Gomez-Sal, B. F. G. Johnson, J. Lewis, P. R. Raithby and A. H. Wright, *J. Chem. Soc., Chem Commun.*, 1985, 1682.
6 D. Braga, F. Grepioni, E. Parisini, P. J. Dyson, A. J. Blake and B. F. G. Johnson, *J. Chem. Soc., Dalton Trans.*, 1993, 2951.
7 J. M. Matters, PhD Thesis, Cambridge University, 1997.
8 D. S. Shephard, B. F. G. Johnson, J. Matters and S. Parsons, *J. Chem. Soc., Dalton Trans.*, 1998, 2289.
9 P. R. Ashton, P. J. Campbell, E. J. T. Chrystal, P. T. Glink, S. Menzer, D. Philp, N. Spencer, J. F. Stoddart, P.A. Tasker and D. J. Williams, *Angew. Chem. Int. Ed. Engl.*, 1995, **34**, 1865.
10 B. F. G. Johnson, K. M. Sanderson, D. S. Shephard, H. Ahmed, M. D. R. Thomas, L. Gladden and M. Mantle, *Chem. Commun.*, 2000, 1317.

A mixed pyridine–phenol boron complex as an organic electroluminescent material

Yanqin Li, Ya Liu, Weiming Bu, Jianhua Guo and Yue Wang*

Key Laboratory for Supramolecular Structure and Spectroscopy, Jilin University, Changchun 130023, P. R. China. E-mail: yuewang@mail.jlu.edu.cn

Received (in Cambridge, UK) 8th May 2000, Accepted 7th July 2000

A blue light emitting 1,6-bis(2-hydroxyphenyl)pyridine boron complex has been synthesized and used as an emitting material to fabricate electroluminescent devices.

The electroluminescence (EL) of Alq_3 (q = 8-hydroxyquinolinate) and its derivatives and also of other metal chelate complexes[1–14] have attracted a great deal of attention since the first light-emitting devices (LEDs) fabricated from Alq_3 were reported by Tang and VanSlyke.[1] This report describes the synthesis and EL properties of a 1,6-bis(2-hydroxyphenyl)pyridine boron complex.

The pyridine–phenol ligand dppy and its boron complex were prepared following the synthetic route shown in Scheme 1.† The dppy ligand was obtained by the reaction of 2-bromopyridine with the Grignard reagent from 2-bromoanisole in THF with [$NiCl_2$(dppe)] as catalyst at room temperature, followed by demethylation in molten pyridinium chloride.[15] The reaction of dppy with 1 equivalent of BF_3 in benzene at 60 °C resulted in the formation of (dppy)BF. An X-ray diffraction study shows that in the solid state (dppy)BF molecules exhibit intermolecular π···π interactions,‡ leading to columnar aromatic stacks as shown in Fig. 1. The average intermolecular π···π interaction distance is 3.28 Å. Our earlier report demonstrated that the higher electron mobility of tris(8-hydroxyquinolinato)-gallium is due to intermolecular π···π stacking interactions.[16] Munakata *et al*. confirmed that strong intermolecular interactions as well as intermolecular aromatic stacking could assist charge-transfer pathways.[17] We believe that the strong intermolecular π···π interactions in solid (dppy)BF are beneficial in terms of charge mobility.

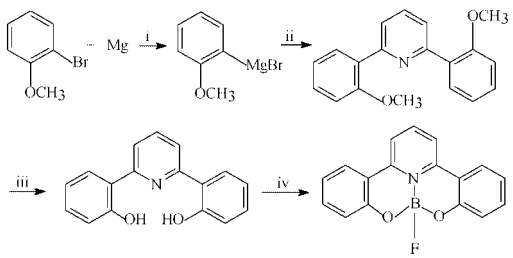

Scheme 1 Synthetic route towards dppy and (dppy)BF. *Reagents and conditions*: i, THF, 25 °C; ii, [$NiCl_2$(dppe)], 2,6-dibromopyridine, 25 °C, 12 h, 75%; iii, py·HCl, 200 °C, 3 h, 85%; iv, BF_3, benzene, 60 °C, 5 h, 70–85%.

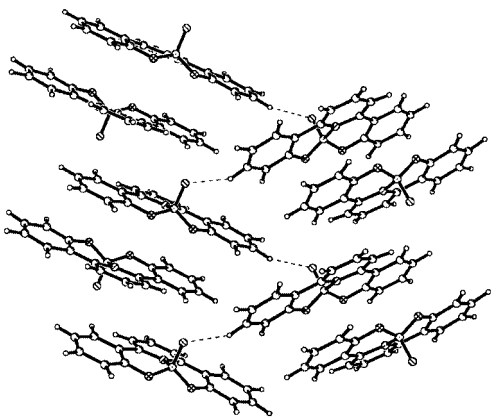

Fig. 1 Intermolecular π···π interactions in (dppy)BF.

(dppy)BF exhibits strong blue emission at *ca*. 445 nm. The PL spectra of (dppy)BF in $CHCl_3$ solution, the solid state and as an evaporated film are compared in Fig. 2 while Fig. 3 shows the PL and EL spectra of devices of structure [ITO/TPD (500 Å)/(dppy)BF (400 Å)/Al (2000 Å)].§ The EL spectrum are dramatically different from the PL spectra of pure (dppy)BF or solid TPD films, shifting to longer-wavelength (λ_{max} = 550 nm). This suggests that exciplex formation takes place at the organic solid-state interface between TPD and (dppy)BF, resulting in a yellow emission. The devices exhibit a maximum luminance (L) of 500 cd m^{-2} with an efficiency of 0.0013 lm w^{-1} and achieve a maximum efficiency of 0.01 lm W^{-1} at 18 cd m^{-2}. In order to investigate the relationship between the interface state and EL properties of boron complexes, PVK (*N*-vinylcarbazole) was employed as hole transport layer to

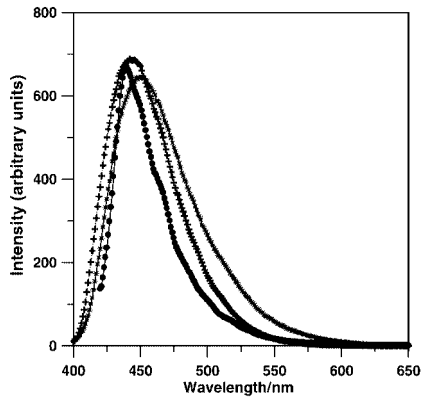

Fig. 2 The PL spectra of (dppy)BF in $CHCl_3$ (+), the solid state (●) and evaporated film (×).

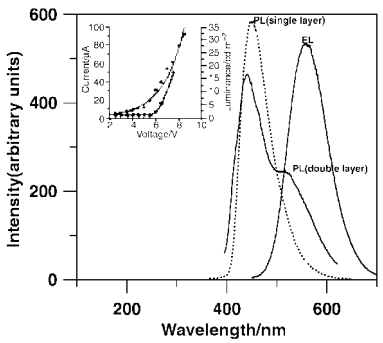

Fig. 3 EL and PL spectra for [ITO/TPD/(dppy)BF/Al] together with the PL spectrum of an evaporated single layer film of (dppy)BF; the inset shows the *I–V* (●) and *L–V* (+) characteristics for the devices.

DOI: 10.1039/b003774p

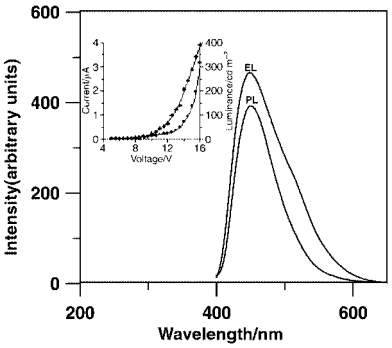

Fig. 4 The EL and PL spectra for [ITO/PVK/(dppy)BF/Al]; the inset shows the *I–V* (●) and *L–V* (+) characteristics for the devices.

fabricate emitting devices with structure [ITO/PVK (1000 Å)/(dppy)BF (500 Å)/Al (2000 Å)].§ Fig. 4 presents the EL spectrum of [ITO/PVK (1000 Å)/(dppy)BF (500 Å)/Al (2000 Å)] together with its PL spectrum. The EL spectrum exhibits a strong peak at 450 nm accompanied by a weaker shoulder at 500 nm. The above experimental results suggest that there are very little or no exciplex formation at the interface between PVK and (dppy)BF. An alternative explanation may be electroluminescence of PVK is favored by the fact that (dppy)BF acts as an electron transport material. When PVK was used as the hole transport material, the devices showed a dramatic improvement in performance. Each device exhibited a maximum luminance of 400–600 cd m^{-2} with an efficiency of 0.012 lm W^{-1} at a driving voltage of *ca*. 12.5 V and showed a maximum efficiency of 0.1 lm W^{-1} at a luminance of 26 cd m^{-2}. The devices [ITO/TPD/(dppy)BF/Al] and [ITO/PVK//(dppy)BF/Al] exhibited obviously different EL properties. Our experimental results also demonstrated that, frequently, the organic–solid interface can determine the EL properties of organic light emitting devices.[18] At present we have yet to elucidate the mechanism and further investigation is in progress.

The complexes (dppy)B(OMe) and (dppy)B(OEt) have also been synthesized and exhibited similar EL behavior as (dppy)BF. X-Ray structural studies show that there are strong intermolecular π···π interactions in the solid state of (dppy)-B(OEt) and detailed results will be reported in due course.

In conclusion, we have demonstrated that a pyridine–phenol ligand can be used as to synthesize strong blue phtoluminescent boron complexes. The pyridine–phenol boron complexes show novel electroluminescent properties. We also found that the interface state determines the EL color of the devices based on the boron complexes.

This work was supported by the National Natural Science Foundation of China (No. 597905006).

Notes and references

† Mass, ^{1}H NMR Spectroscopic and elemental analysis: dppy: EIMS: *m*/*z* 263. $\delta_H(CDCl_3$, 80 MHz) 9.41 (s 2H), 7.99–7.53 (m, 5H), 7.36–6.80 (m, 6H). Anal. Calc. for $C_{17}H_{13}NO_2$: C, 77.6; H, 4.9; N, 5.3. Found: C, 77.2; H 4.6; N, 5.6%.

(bpy)BF: EIMS: *m*/*z* 291. $\delta_H(CDCl_3$, 80 MHz) 8.20–7.72 (m, 5H), 7.57–6.88 (m, 6H). Anal.: Calc. for $C_{17}H_{11}NO_2BF$: C, 70.1; H, 3.8; N, 4.8. Found: C, 70.3; H, 3.6; N, 4.5%.

‡ *Crystal data*: (dppy)BF: $C_{17}H_{11}NO_2BF$, M_r = 291, monoclinic, space group $P2_1/c$, a = 7.5482(7), b = 7.9581, c = 22.422 Å, β = 98.227(9)°, V = 1333.0(2) Å^3, Z = 4, D_c = 1.450 g cm^{-3}, $F(000)$ = 600. Reflection data were collected on a Siemens R3 four-cicle diffractometer using graphite-monochromated Mo-Kα radiation and ω scans at room temperature, giving 3365 unique reflections. The structure was solved by direct methods (SHELXTL Version 5). All atoms were refined anisotropically using full-matrix least squares to give R_1 = 0.066 for 2340 reflections with $F > 4\sigma(F)$. CCDC 182/1716.

§ The devices of [ITO/TPD/(dppy)BF/Al] were fabricated by successive vacuum deposition of organic materials onto the ITO coated glass substrate. Then a layer of aluminum was deposited onto the layer of (dppy)BF. For devices [ITO/PVK/(dppy)BF/Al], the PVK layer was formed by spin coating a 10 mg ml^{-1} chloroform solution, and (dppy)BF was deposited on the PVK layer by thermal evaporation, followed by deposition of the aluminum cathode *in vacuo*.

1 C. W. Tang and S. A. VanSlyke, *Appl. Phys. Lett.*, 1987, **51**, 913.
2 C. W. Tang, S. A. VanSlyke and C. H. Chen, *J. Appl. Phys.*, 1989, **65**, 3610.
3 J. M. Shi and C. W. Tang, *Appl. Phys. Lett.*, 1997, **70**, 1665.
4 J. Kido and Y. Lizumi, *Appl. Phys. Lett.*, 1998, **73**, 2721.
5 Y. Hamada, T. Sano, M. Fujita, T. Fujii, Y. Nishio and K. Shibata, *Chem. Lett.*, 1993, 905.
6 Z. Shen, P. E. Burrows, V. Bulovic, S. R. Forrest and M. E. Thompson, *Science*, 1997, **276**, 2009.
7 M. A. Baldo, D. F. O'Brien, Y. You, A. Shoustikov, S. Sibley, M. E. Thompson and S. R. Forrest, *Nature*, 1998, **395**, 151.
8 Q. Wu, M. Esteghamatian, N. Hu, Z. Popovic, G. Enright, Y. Tao, M. D'Iorio and S. Wang, *Chem. Mater.*, 2000, **12**, 79.
9 Q. Wu, M. Esteghamatian, N. Hu, Z. Popovic, G. Enright, S. R. Breeze and S. Wang, *Angew. Chem., Int. Ed.*, 1999, **38**, 985.
10 X. T. Tao, H. Suzuki, T. Wada, H. Sasabe and S. Miyata, *Appl. Phys. Lett.*, 1999, **75**, 1655.
11 X. T. Tao, H. Suzuki, T. Wada, S. Miyata and H. Sasabe, *J. Am. Chem. Soc.*, 1999, **121**, 9447.
12 Y. Hamada, T. Sano, K. Shibata and K. Kuroki, *Jpn. Appl. Phys. Part 2*, 1995, **34**, L824.
13 Y. Hamada, T. Sano, M. Fujita, T. Fujii, Y. Nishio and K. Shibata, *Chem. Lett.*, 1993, 905.
14 C. H. Chen, J. Shi and C. W. Tang, *Macromol. Symp.*, 1997, **125**, 1.
15 E. M. Holligan, J. C. Jeffery, M. K. Norgett, E. Schatz and M. D. Ward, *J. Chem. Soc., Dalton Trans.*, 1992, 3345.
16 Y. Wang, W. X. Zhang, Y. Q. Li, L. Ye and G. D. Yang, *Chem. Matter.*, 1999, **11**, 530.
17 M. Munakata, L. P. Wu, T. Kuroda-Sowa, M. Maekawa, Y. Suenaga, G. L. Ning and T. Kojima, *J. Am. Chem. Soc.*, 1998, **120**, 8610.
18 K. Itano, H. Ogawa and Y. Shirota, *Appl. Phys. Lett.*, 1998, **72**, 636.

Typeset and printed by Black Bear Press Limited, Cambridge, England

ChemComm
FEATURE ARTICLE

Electronic and optical properties of conjugated group 8 metallocene derivatives

Stephen Barlow[a] and Seth R. Marder[b]

[a] *Inorganic Chemistry Laboratory, University of Oxford, South Parks Road, Oxford, UK OX1 3QR. E-mail: stephen.barlow@chem.ox.ac.uk*
[b] *Department of Chemistry and Optical Science Center, University of Arizona, Tucson, AZ 85721, USA*

Received (in Cambridge, UK) 19th June 2000, Accepted 23rd June 2000
Published on the Web 10th August 2000

Ferrocene and ruthenocene have been incorporated into a range of conjugated systems. The interaction of these metallocene donor moieties with conjugated substituents is more complex than that of organic donors; both metal-based and ligand-based orbitals of the metallocene interact with the orbitals of the π-system. Here we review the rôle of these interactions in giving rise to a variety of interesting properties including non-linear optical activity in donor–acceptor systems, mixed-valence behaviour in bis(ferrocenyl) compounds, and structural distortions in polymethines.

Introduction

While derivatives of ferrocene and, to a lesser extent, ruthenocene are one of the most widely studied classes of organometallic compounds (work on osmocene derivatives has been much more limited), a detailed understanding of the electronic structure of conjugated metallocene derivatives has only recently emerged. Here we survey some the electronic and optical properties of conjugated metallocene derivatives, illustrating how similarities in the electronic structure can be used to draw parallels between what may appear to be somewhat disparate sets of observations. We hope to highlight aspects of the structure–property relationships for metallocene derivatives which are unique and are not found in conjugated organic materials.

Steve Barlow was born and raised in Hampshire and Dorset. He obtained BA and DPhil degrees in Chemistry in 1992 and 1996 respectively, both from the University of Oxford. After postdoctoral work with Seth Marder at the California Institute of Technology, he returned to Oxford in 1998 as a temporary lecturer in the Inorganic Chemistry Laboratory and a tutorial fellow at Lady Margaret Hall. His research interests include optical, electronic and magentic properties of organometallic and unsaturated organic systems, and understanding how these properties are related to electronic structure.

Seth Marder was born and raised in New York city. He obtained his Bachelors of Science in Chemistry from Massachusetts Institute of Technology in 1981 and his Doctorate, in Chemistry, from the University of Wisconsin-Madison in 1985. After postdoctoral studies at Oxford and at the California Institute of Technology and the Jet Propulsion Laboratory, he become a Member of the Technical Staff at the Jet Propulsion Laboratory and a Member of the Beckman Institute at the California Institute of Technology. In 1998 he moved to the University of Arizona, where he is a Professor of Chemistry and Optical Science. His research interests include liquid crystals, transport phenomena, multiphoton processes in organic and organometallic materials, and labels for biological imaging.

Electronic structure of metallocenes and their conjugated derivatives

Firstly we will briefly review the electronic structure of metallocenes, and the perturbation to this structure induced by substitution with an electron-withdrawing conjugated system. The three highest filled levels of ferrocene are derived from the d_{xy}, $d_{x^2-y^2}$ (e_{2g} in staggered {D_{5d}} geometry) and the d_{z^2} (a_{1g}) orbitals (the HOMO of the neutral molecule is a_{1g}, whilst the SOMO of the cation is e_{2g}). The e_{2g} orbitals are somewhat δ-back-bonding, through interaction with combinations of the cyclopentadienyl (Cp) anion LUMOs, whilst the a_{1g} has some interaction with the metal s orbital and with the Cp rings. Nonetheless, these orbitals may be regarded as essentially metal-based. The next highest orbitals (e_{1u}) of the metallocene are principally ligand-based, possibly with some contribution from the p_x and p_y metal orbitals. The lower energy orbitals involve bonding combinations of Cp orbitals with the metal d_{yz}, d_{xz}, s and p_z orbitals and do not concern us further. The LUMO of ferrocene has symmetry e_{1g} (in D_{5d}) and is derived from an out-of-phase π interaction between the d_{xz}/d_{yz}, and Cp orbitals.

The bonding in ruthenocene (and osmocene) is qualitatively the same, but UV-photoelectron spectra reveal substantial differences in metal-based orbital energies. The first vertical ionisation potentials (IPs) for ferrocene and ruthenocene are 6.86/6.89 and 7.45 eV, respectively,[1,2] whilst the highest ligand-based levels lie at rather similar energies with e_{1u} vertical ionisations at 8.72/8.77 and 8.47/8.51 eV, respectively. Thus, ferrocene is clearly the stronger donor in an electron-transfer sense. Methylation of the cyclopentadienyl rings raises the energy of both the filled d-orbitals (the first IP of decamethylferrocene is 5.88 eV) and the highest ligand-based orbitals (lowest ligand ionisation of decamethylferrocene is 7.31 eV). For comparison, the first IPs of *N*,*N*-dimethylaniline and anisole are 7.45 and 8.42 eV, respectively,[3] indicating that these compounds are weaker electron-transfer donors than ferrocene. However, it does not necessarily follow that a stronger electron-transfer donor will lead to a greater perturbation of an attached π-conjugated system, since the detail of the electronic coupling between the donor and the π-system is also critical (*vide infra*).

When a conjugated system is attached to a metallocene the most significant perturbation is *not* to the metal-based HOMOs. Consider a ferrocene derivative with a moderately electron-withdrawing conjugated substituent, such as **1** (Fig. 1). The first IP (6.97 eV) and electrochemical oxidation potential (+25 mV *vs.* ferrocenium/ferrocene in THF) of **1** are close to those of ferrocene.[4] Similar electrochemical results have been found in related systems.[5,6] The highest *ligand* level of the metallocene

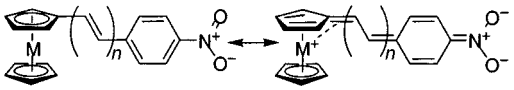

1, M = Fe, *n* = 1
2, M = Fe, *n* = 2
3, M = Ru, *n* = 1

Fig. 1 Neutral and charged resonance structures for nitrostyrene-substituted metallocenes.

(e_{1u}) shows a much greater perturbation; in **1** an ionisation is found at 8.36 eV, *i.e.* lower in energy than that e_{1u} ionisation of ferrocene, or the first ionisation of nitrostyrene. We attribute this ionisation to an orbital ('π') formed by an out-of-phase combination of one of the e_{1u} pair with the HOMO of the nitrostyrene fragment (as shown in Fig. 2).

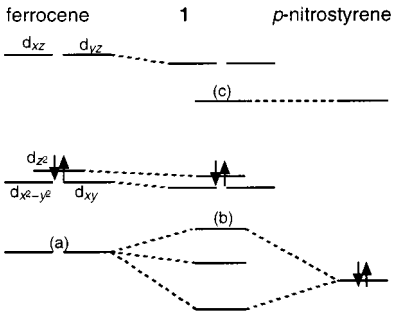

Fig. 2 Qualitative partial MO diagram showing interaction between the frontier orbitals of ferrocene and *p*-nitrostyrene fragments in **1**. The paired electrons indicate the HOMO for each compound. Orbital (a) is the highest filled Cp-based orbital of the metallocene (e_{1u} in D_{5d}), whilst (b) is the highest ligand-based orbital ('π') of **1** and (c) is the acceptor-based LUMO of **1**.

Compound **1** exhibits a molecular reduction at the same potential as *p*-nitrostyrene (−1670 mV *vs.* ferrocenium/ferrocene according to cyclic voltammetry in THF). The extended analogue **2** is reduced at −1635 mV, whilst nitrobenzene is reduced at −1730 mV. A similar chain length dependence of reduction potential was found for $[Mc(CH{=}CH)_nC_7H_6]^+$ (*n* = 0, 1, 2, 3; Mc = Fc {ferrocenyl}, Rc {ruthenocenyl}).[7] These results suggest that the LUMO is centred on the acceptor moiety, with some delocalisation onto the π-bridge (the empty d_{xz} and d_{yz} orbitals of the metallocene are at relatively high energy). An EPR study of $[\mathbf{1}]^{\bullet-}$ shows the unpaired electron to be largely localised on the nitrophenyl ring,[8] consistent with electrochemical data.

The orbital picture deduced from PES, electrochemical and EPR data above is consistent with that derived from extended-Hückel[9] and DF[4] calculations (see Fig. 3). This model can be successfully extended to other donor–acceptor metallocene derivatives (so long as the acceptor is sufficiently strong that the empty acceptor orbital lies below the metal d_{xz} and d_{yz} orbitals in energy). However, as the acceptor gets very strong it is necessary to further refine the simple model described above. Crystallographic and NMR data indicate that with electron-acceptors of moderate strength, the structure is well approximated by the neutral valence-bond picture (Fig. 1, left-hand structure). However, as the acceptor (or donor) is strengthened the zwitterionic resonance form gains in importance. This results in a reduction in the bond-length alternation (BLA) of the alkene bridge. Although there are apparently no crystallographically characterised examples of metallocene derivatives with a strong acceptor such as that in compounds **4**–**9**, the effect is manifested in NMR spectra. For example, in compound **4** (strong acceptor) the polyene protons show coupling constants of *ca.* 13 Hz over both formally double and formally single bonds, whilst in Fc″(CH = CH)$_2$CHO {Fc″ = 2,3,4,5,1′,2′,3′,3′-octamethylferrocen-1-yl, (C_5Me_4H)Fe(C_5Me_4)} (weak acceptor) coupling constants alternate between *ca.* 15 Hz across

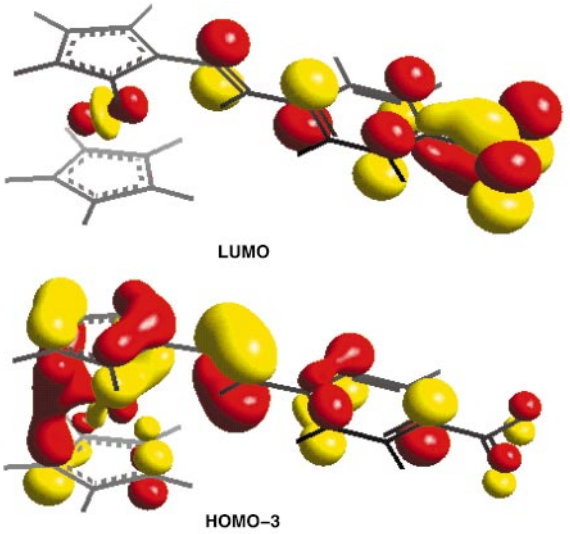

Fig. 3 The LUMO and the highest filled ligand-based π-level of **1** according to DF calculations; the three highest-filled levels are all principally metal d in character.[4]

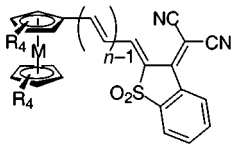

4, M = Fe, R = Me, *n* = 3
5, M = Fe, R = H, *n* = 1
6, M = Fe, R = H, *n* = 2
7, M = Fe, R = H, *n* = 3
8, M = Fe, R = H, *n* = 4
9, M = Ru, R = H, *n* = 3

formally double bonds and *ca.* 10 Hz across formally single bonds. More evidence for the increased importance of the charge-transferred resonance form in strong-acceptor compounds comes from electrochemistry: **5** is oxidised at +325 mV *vs.* ferrocenium/ferrocene in THF, suggesting a much more severe effect of the acceptor on the metal than in the nitrophenyl analogue, **1**. Moreover, the effect is strongly chain-length dependent; the potentials for **6** and **7** are +200 and +110 mV, respectively, indicating a decrease in donor–acceptor coupling as the chain length increases.[4]

A broadly similar picture is revealed by DF calculations for the bis(metallocenyl)allylium cations ([**10**]$^+$–[**14**]$^+$); here the

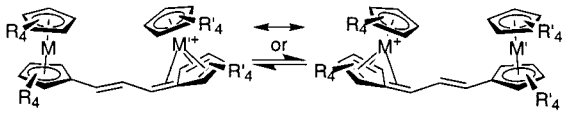

[10]$^+$, M = M′ = Fe, R = R′ = H
[11]$^+$, M = M′ = Fe, R = R′ = Me
[12]$^+$, M = M′ = Ru, R = R′ = H
[13]$^+$, M = M′ = Fe, R = H, R′ = Me
[14]$^+$, M = Fe, M′ = Ru, R = R′ = H

LUMO is the π* orbital of the unsaturated bridge (Fig. 9).[10] A similar picture of filled d-orbitals above an extended π-level presumably applies to bis(metallocenyl)polyenes, polyynes and arylenes, although, where the π-system is not particularly electron-poor, the LUMO may be the empty d_{xz}/d_{yz} orbitals rather than π*.

In many donor–acceptor systems there is little evidence to distinguish between the donor strengths of ferrocene and ruthenocene. For example, **7** and **9** are reduced at experimentally identical potential (−880 mV *vs.* ferrocenium/ferrocene in THF), indicating comparable contributions of the charge-transferred resonance form in each case (the octamethylferrocenyl group is clearly a stronger donor; the reduction potential of **4** is −960 mV).[4] However, comparison of the dipole moments of **1** (4.5×10^{-18} esu) and **3** (5.3×10^{-18} esu)[9] does suggest a slightly larger zwitterionic contribution in the ruthenium case. Systems with even stronger acceptors, such as 1,3-bis(metallocenyl)allylium cations, provide electrochemical evidence that, despite having a lower energy HOMO than ferrocene, rutheno-

cene is the stronger donor in conjugated systems. Thus, [**10**]$^+$ is reduced at −670 mV (*vs.* ferrocenium/ferrocene in THF), whilst [**12**]$^+$ is reduced at −715 mV ([**11**]$^+$ is reduced at −930 mV).[10] Crystal structures of [FcCHRc]$^+$[PF_6]$^-$ [11] and [**14**]$^+$[PF_6]$^-$ [10] show ruthenium coordination well approximated as η^6-fulvene : η^5-cyclopentadienyl, whilst the ferrocene centres are 'normal'. Thus, the superior donor properties of ruthenocene in this type of system can be attributed to the more extensive d-orbitals of ruthenium and its consequent tendency to shift towards η^6-fulvene coordination. It seems the difference in donor strength between ferrocene and ruthenocene are most evident when η^6-fulvene is an important resonance structure.

Linear and non-linear optical properties of conjugated metallocene–bridge–acceptor compounds

Much of the work on donor–acceptor conjugated metallocenes has been directed towards maximising and understanding their second-order NLO properties. Second-order NLO phenomena include frequency doubling and the linear electrooptic effect (*i.e.* electric-field-dependence of refractive index). For these properties to be observed, a non-centrosymmetric array of non-centrosymmetric molecules is required. The relevant molecular parameter is the first hyperpolarisability, β. The perturbation-theory-derived two-level model relates the static hyperpolarisability $\beta(0)$ to the characteristics of low-lying electronic excited states through eqn. (1):

$$\beta(0) \propto (\mu_{ee} - \mu_{gg})\frac{\mu_{ge}^2}{E_{ge}^2} \quad (1)$$

where μ_{ee} and μ_{gg} are excited and ground-state dipole moments respectively, μ_{ge} is the transition dipole linking ground and excited states, and E_{ge} is the energy difference between the two states.[12] The two-level model does not apply to all classes of chromophore; for example, the non-linearity of octopolar molecules, where $\mu_{ee} = \mu_{gg} = 0$, depends on three-level terms.[13] Eqn. (1) indicates that intense low-energy charge-transfer transitions should lead to large β. The prototypical chromophore is the 'push–pull' donor–(conjugated bridge)–acceptor; good examples are (*E*)-4-(methoxy)-4′-nitrostilbene **15** and (*E*)-4-(dimethylamino)-4′-nitrostilbene **16**. In analogy, ferrocene was used to replace the organic donors of **15** and **16**;

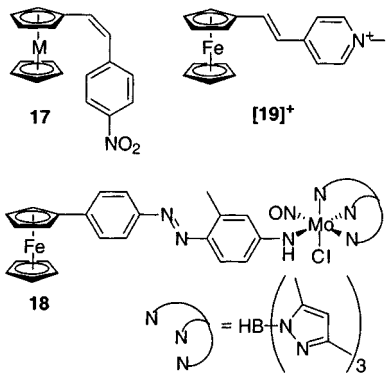

17 was found to have a powder second-harmonic generation (SHG) efficiency 62× that of urea,[14] and even larger values of 123× and 200× urea have been reported for **18**[15] and [**19**]$^+$[I]$^-$[16] respectively. Much other early work relied on powder SHG data. However, results are inherently subject to the vagaries of crystallisation; a large β chromophore will give zero SHG if it crystallises in a centrosymmetric space group. Resolved chiral chromophores have also been used;[17] these *must* crystallise in non-centrosymmetric space groups, but the molecules may still pack in such a manner that the hyperpolarisabilities of neighbouring molecules still largely cancel each other out, leading to low SHG responses. To understand relationships between molecular structure and molecular NLO properties, values of β are more useful. For non-ionic polar chromophores in solution, electric field-induced second-harmonic generation (EFISH)[18] can be used to measure $\mu\beta_\mu$, the scalar product of the permanent dipole moment (μ) and the vectorial part of the β tensor. Combined with a determination of μ, values of β_μ, the projection of the vectorial part of β onto the axis of μ, can be determined. $\mu\beta_\mu$ itself is also a figure-of-merit for the second-order NLO activity of a material where non-centrosymmetry is achieved *via* electric-field poling of a polymer matrix. Poling is carried out above the glass-transition temperature of the polymer, and the resulting polar order is 'frozen' in by cooling back below the glass transition. This means of achieving polar order is currently the most widely used approach for fabricating non-centrosymmetric materials for second-order NLO applications. More recently hyper-Raleigh scattering (HRS)[19] has also been used to measure β; the technique can be applied to ionic or octopolar chromophores, but great care must be taken to correctly account for the other non-linear optical effects which can contribute to the observed signal.

A wide variety of metallocene–donor–acceptor compounds have been synthesised; in addition to traditional organic acceptors, main group moieties,[20] transition-metal coordination complexes,[6,21–23] and organometallic groups[24–28] have been used as acceptors. The second-order NLO properties of a selection of these compounds are summarised in Table 1, along with absorption maxima.

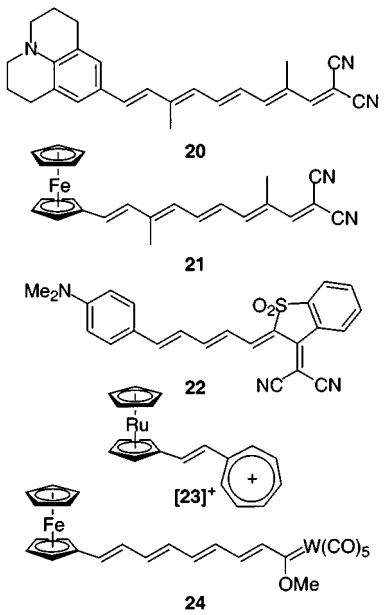

Comparison of β or $\mu\beta$ values between chromophores is complicated by the fact that eqn. (1) relates to the static (dispersion-free) hyperpolarisability. The hyperpolarisability is greater (dispersion-enhanced) if the fundamental radiation employed in the measurement, or the frequency-doubled radiation generated, is close in energy to the energy of the excited state(s) responsible for the NLO behaviour. In the case of metallocene compounds, the contributions of more than one excited state to the non-linearity means that correction for dispersion cannot be made according to the two-level model (nevertheless, estimates have been made for some compounds and are included in Table 1).

To understand the origin of the NLO properties of a class of compounds it is necessary to understand the characteristics of the excited state or states contributing to the hyperpolarisability *via* eqn. (1). The quantities in eqn. (1) can be probed by optical

Table 1 Comparison of second-order NLO properties of some metallocene and organic molecules

Compound	λ_{max}/nm	$\mu\beta/10^{-48}$ esu	$\mu\beta(0)/10^{-48}$ esu	$\beta^{a}/10^{-30}$ esu	$\beta(0)^{a}/10^{-30}$ esu	Method	Ref.
15	370	153		34		EFISH, 1.907 μm ($CHCl_3$)	29
16	430	482	363	73	55	EFISH, 1.907 μm ($CHCl_3$)	30
1	356, 496	140		31		EFISH, 1.907 μm (*p*-dioxane)	9
3	350, 390	64		12		EFISH, 1.907 μm (*p*-dioxane)	9
20	570	5 500	3220			EFISH, 1.907 μm (acetone)	31
21	458[b]	4 600	3300			EFISH, 1.907 μm (acetone)	31
5	419, 667	160		29		EFISH, 1.907 μm ($CHCl_3$)	32
7	517, 746	3 000		405		EFISH, 1.907 μm ($CHCl_3$)	32
8	552, 743	11 200				EFISH, 1.907 μm ($CHCl_3$	32
22	744	10 500	3900			EFISH, 1.907 μm (CH_2Cl_2)	33
[**23**]$^{+}$[PF_6]$^{-}$	477, 642			362[c]	105	HRS, 1.064 μm (CH_2Cl_2)	7
24	541[b]			780[d]		HRS, 1.064 μm (hexane)	28

[a] EFISH values are β_μ; HRS values are $\langle\beta\rangle$. [b] For long-chain lengths, the highest π-level may approach the metal-based HOMO in energy and the two transitions may overlap; clearly this will happen at shorter chain length for ruthenocene compounds. [c] 640 × 10^{-30} esu in $MeNO_2$. [d] 2420 × 10^{-30} esu in acetonitrile.

spectroscopy. The most striking characteristic of the metallocene compounds, in contrast to their all organic analogues, is the presence of *two* relatively low-energy bands (Fig. 4). In most of the metallocene compounds both bands show positive solvatochromism (red shifts with increasing solvent polarity), suggesting that the corresponding transitions are both associated with increases in dipole moment.[34]

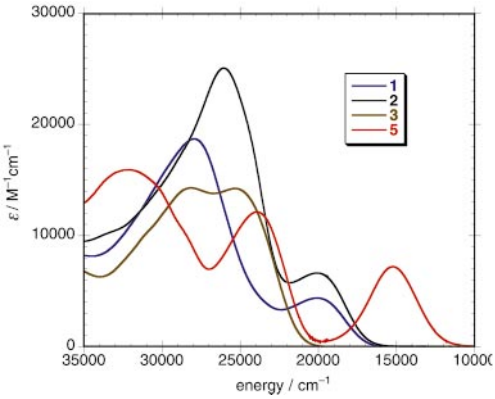

Fig. 4 UV–VIS–NIR spectra of several metallocenyl second-order NLO chromophores showing the effects on the spectra of chain length (**1** *vs*. **2**), replacing Fe with Ru (**1** *vs*. **3**), and acceptor strength (**1** *vs*. **5**).

Recently, Stark spectroscopy has been used to confirm that both transitions are indeed associated with dipole moment changes; in both **2** and **4** the lower energy (LE) band was found to have the larger $|\Delta\mu|$. Combining the observed ratio of $|\Delta\mu|$ with the transition energies and oscillator strengths, the relative contributions of the two excited states to the second-order NLO response can be estimated according to eqn. (1). In **2** the higher energy (HE) transition dominates β (63% of the two-level contributions). In the strong-acceptor compound **4** the relative importance of the two transitions is reversed (75% from LE transition).[4]

If one wishes to predict the effect of changes in molecular structure upon the optical spectrum, and hence upon the NLO behaviour, it is important to assign the two bands. We have recently suggested an assignment based on the orbital scheme described for **1** in the previous section, *i.e.* that the LE transition is metal-to-acceptor (HOMO-to-LUMO), whilst the HE transition is π-to-acceptor.[4] In contrast to previous assignments,[9,35] this model is consistent with *both* the larger $|\Delta\mu|$ of the LE transition, and with the changes in the spectra seen as the structure of the molecule is modified. The relatively high absorptivities observed for the LE band, despite poor metal–acceptor interaction, can be rationalised in terms of intensity stealing from the HE band. This intensity stealing should be most pronounced when the energy differences between the two excited states and between the ground and second excited state are minimised. This is seen experimentally; for example, the oscillator strengths of the LE and HE transitions of **1** are *ca*. 0.60 and 0.10 respectively, whilst for **5** (where the stronger acceptor leads to a smaller second excited state/ground state separation) the relevant values are 0.40 and 0.18.[36]

Many studies show the same factors used in organic chromophore design are operative in metallocene chromphores; Table 1 gives some examples of the effects of acceptor strength and chain length, as well as of changing ferrocene for ruthenocene. It should be noted, however, that in analogy with organic compounds,[37] if the donor and/or acceptor strength is increased sufficiently, a point of optimised β will be obtained, corresponding to an optimised BLA, *i.e.* optimised mixture of neutral and charge-transferred resonance forms. The data in Table 1 show that metallocene chromophores can exhibit large β and $\mu\beta$ values of similar magnitude to the best all-organic chromophores. However, metallocene derivatives with high β or $\mu\beta$ absorb at very low energies; both the energies and broadness of the absorptions are factors which would limit the utility of metallocene chromphores in devices designed for use at the telecommunications wavelengths of 1.3 and 1.55 μm. Nonetheless, films obtained by poling **1** and **2** in polymethylmethacrylate at 120 °C, showed electro-optic coefficients in excellent agreement with the values predicted from the EFISH-derived $\mu\beta$ values using an oriented gas model. The results indicate that the more three-dimensional shapes and lower oxidation potentials of ferrocene chromophores relative to traditional all-organic chromophores do not lead to any special complications.[38] Metallocene chromophores have also been covalently incorporated into a variety of polymers; the long-term orientational stability of these polymers after poling has been monitered by SHG measurements.[38–40]

We have seen that metallocene chromophores can exhibit large β and $\mu\beta$ values, but do metallocene chromophores offer any significant advantages over organic compounds for NLO applications? Comparing **1** and **15**, which have similar $\mu\beta$ and β, we find the ferrocene compound shows distinct disadvantages owing to the decreased transparency arising from its lower energy absorption band, as mentioned above. The ruthenocene analogue **3** shows superior transparency, but lower β. For the same bridge/acceptor motif, it seems that the ferrocenyl donor gives poorer β and $\mu\beta$ than *p*-dimethylaminophenyl (**1** *vs*. **16**; **7** *vs*. **22**). The LE excited state of **1** is lower in energy than the excited state of **16** (since ferrocene is a stronger electron-transfer donor), but the corresponding transition is much less intense (due to poor metal–acceptor interaction); as in **2**, the HE state is presumably the major contributor to β in **1**. In the stronger acceptor compound **7** the LE ferrocene band is much more important for β; however, it is no longer significantly lower in energy than that of its organic analogue **22**. Both **7** and

22 will show more contribution from the zwitterionic resonance form than **1** and **16**; we suggest this effect is more important for **22** (dimethylaminophenyl is a more effective donor for perturbing the electron density of a π-system than ferrocenyl), leading to larger μ and low energy absorption in the all-organic case. It is, however, possible that with even stronger acceptors, where dimethylaminophenyl compounds will have passed the point of optimal BLA, the ferrocene compound may actually give larger β.

We know of no reports of a bulk material based on a metallocene chromophore with non-linear optical properties rivalling those of the best all-organic materials. In addition, organometallic chromophores have not yet been shown to exhibit thermal[41,42] and photochemical[43] stabilities comparable to the some of the better all-organic systems; these factors are crucial to the fabrication of long-term performance devices. Thus, there is still a clear challenege to the organometallic chemist to demonstrate a specific advantage for using metallocene chromophores in second-order NLO applications.

In addition to the NLO-related studies described above, several other studies have focussed on other aspects of the spectroscopy of metallocene–(π-bridge)–acceptor compounds. Toma *et al*.[44] found the low-energy bands of (*E*)-FcCH=CHAr (Ar = aryl) were similar to those of ferrocene, with some dependence upon the Hammett coefficients of the substituent, except where Ar bore a strongly mesomerically electron-withdrawing substituent (*p*-CHO, *p*-CN, *p*-NO_2). These observations are consistent with our assignment of the spectra of **1**; presumably, in the former class of compounds the d–d transition is lowest in energy, whereas in the latter class the LUMO is acceptor-based. The complexes [(ferrocenylpyridine)$Ru(NH_3)$]$^{3+}$ could also be regarded as metallocene–donor–acceptor complexes, the LUMO here being the part-filled t_{2g}-like orbitals of Ru^{III}. The low-energy band has accordingly been assigned to a $Fe^{II} \rightarrow Ru^{III}$ transfer, and analysed to show much stronger metal–metal coupling in the [(4-FcC_5H_4N)$Ru(NH_3)$]$^{3+}$ than in [(3-FcC_5H_4N)$Ru(NH_3)$]$^{3+}$.[45] Derivatives of [**19**]$^+$ have been used as indicators in rapid screening of hydrogenation catalysis.[46]

Electronic and optical properties of bis(metallocenyl)polyenes and related compounds

In this section we consider systems where two (or more) metallocene units are linked by alkene, alkyne or arene bridges. Ferrocene systems have been attractive candidates for studying mixed-valence behaviour,[48] since ferrocene has a well-developed organic chemistry, allowing attachment to a wide variety of bridges, and since both ferrocene and the ferrocenium ion are relatively stable. When linked conjugated ferrocenes undergo one-electron oxidation, a hole is introduced into the e_{2g} d-orbitals of one of the ferrocene moieties. The lowest energy band in the UV–VIS–NIR spectra is thus a transition from the highest filled d-orbital of the Fe^{II} moiety to the partially occupied orbital of the Fe^{III} moiety. In cases where the electronic coupling, *V*, between the Fe^{II}/Fe^{III} wavefunction (Φ_A) and the Fe^{III}/Fe^{II} wavefunction (Φ_B) is small compared to the reorganisation energy, λ, the strength of this intervalence charge-transfer (IVCT) band can be analysed to afford *V* and the interaction parameter, α.[48] according to eqn. (2) where Ψ is the

$$\Psi = (1 - \alpha^2)^{0.5}\Phi_A + \alpha\Phi_B \quad (2)$$

ground state wavefunction. In bis(ferrocenyl) conjugated systems it generally seems that the assumption of small coupling is valid. The values of α and *V* in Table 2 allow one to compare the efficacies of various bridges at mediating electronic coupling. Electrochemical data are also included in Table 2; interpretation of $\Delta E_{1/2}$ data is less straightforward than that of IVCT data ($\Delta E_{1/2}$ depends on stabilising factors in the Fe^{II}/Fe^{II}, Fe^{II}/Fe^{III} and Fe^{III}/Fe^{III} species, and on through-space electrostatic effects), but the value can provide a useful rough indication of the strength of metal–metal interaction.

Both optical and electrochemical data show more interaction for alkenes than alkynes. This result is consistent with linear and non-linear optical results on analogous ferrocene–bridge–acceptors with alkene and alkyne bridges [the LE absorption of (*E*)-FcCH=CHB(mes)$_2$ {mes = 2,4,6-trimethylphenyl} is lower in energy and more intense than that of FcC≡CB(mes)$_2$ and β_μ is larger[20]] and with calculations for all-organic mixed-valence compounds.[49] Arenes are rather poor at mediating metal–metal interactions; this is consistent with the disruption of donor–acceptor coupling effected by the introduction of aromatic moieties into organic second-order NLO chromophores.[50]

Bis(ruthenocenyl) compounds have been much less studied, presumably partly due to the irreversible redox chemistry of ruthenocene itself. Recently, however, it has been found that RcCH=CHRc, and a number of substituted derivatives, undergo chemically (though not electrochemically) reversible two-electron oxidations to diamagnetic bis(η^5-cyclopentadienyl-

Table 2 Data pertaining to metal–metal interactions in some bis(ferrocenyl) systems

Compound	$\Delta E_{1/2}$[a]/mV	λ_{max} (ε_{max})[b]/nm (M^{-1} cm^{-1})	α[c]	V[d]/meV
$Fc(CMe_2)_2Fc$	80[51]	None observed	—	—
(*E*)-FcCH=CHFc	140[52]	1750 (1200)[54]	0.09	63
	170[53]	2040 (1340)[53]	0.10	61
$Fc(CH=CH)_2Fc$[e]	129[53]	1820 (1570)[53]	0.08	53
$Fc(CH=CH)_6Fc$[e]	0[53]	1800 (1600)[53]	0.03	24
FcN=NFc	235[55]	1760 (375)[54]	0.05	35
FcC≡CFc	130[56]	1560 (670)[56]	0.07	56
$Fc(C≡C)_2Fc$	100[56]	1180 (570)[54]	0.04	42
$Fc_2C=CH_2$	—	1800 (200)[55]	0.004	2.8
$Fc_2C=O$	—	1280 (62)[54]	0.002	1.9
o-$Fc_2C_6H_4$	131[e,57]	1530 (91)[e,57]	0.03	25
m-$Fc_2C_6H_4$	90[e,57]	1210 (46)[e,57]	0.013	13
p-$Fc_2C_6H_4$	104[f,57]	1340 (620)[f,57]	0.046	43
[**10**]$^+$	180[58]	—	—	—
	610[10]			
$[Fc(CH)_5Fc]^+$	140[58]	—	—	—
	610[54]			
$[Fc(CH)_{13}]^+$	40[58]	—	—	—
[**11**]$^+$	700[10]	—	—	—

[a] Separation between successive ferrocene oxidations in CH_2Cl_2. [b] Absorption maxima and maxmium absorbtivity for the IVCT band of the mono-oxidised species in CH_2Cl_2. [c] Interaction parameter and [d] electronic coupling energy derived from analysis of the IVCT band according to $V = (2.05 \times 10^{-2}/r)(\varepsilon_{max}\bar{\nu}_{max}\Delta\bar{\nu}_{1/2})^{1/2}$, where *r* is the intermetallic distance and $\Delta\bar{\nu}_{1/2}$ is the IVCT band width at half height, and $\alpha = V/\bar{\nu}_{max}$.[48] [e] In MeCN. [f] In $CHCl_3$.

ruthenium)(μ-η⁶:η⁶-pentafulvadiene) dications (Fig. 5).[60,61] These formally ligand-based oxidations can be contrasted to the metal-based oxidations of iron analogues; presumably the small differences in energy between the highest π-orbital and the

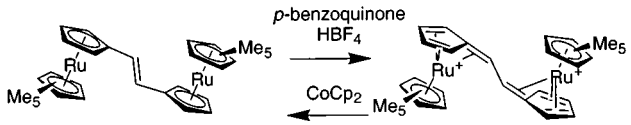

Fig. 5 Chemically reversible two-electron oxidation of a bis(ruthenocenyl) ethene.[58]

ruthenium d-orbitals is important (although di-Ru^{III} intermediates are postulated[61]), along with the greater tendency of ruthenium to adopt η⁶ coordination and to retain an 18 electron configuration. Similar two-electron oxidations involving structural rearrangemnt of a ruthenocene to η⁶-fulvene geometry, have been observed in RcC≡CRuCp(PPh$_3$)$_2$ and related compounds.[62,63] Even biruthenocene can be oxidised to the diamagnetic bis(η⁵-cyclopentadienylruthenium)(μ-η⁶:η⁶-fulvalene) dication under certain conditions.[64] In this respect, ruthenocene resembles an organic fragment more than does ferrocene. For example, the dication of *N*,*N*,*N*′,*N*′-tetramethylbenzidine has a quinoidal, and presumably diamagnetic, structure,[65] due to good mediation of N–N interaction by the π-system. By contrast, the dications of dinuclear bis(ferrocenyl) complexes typically behave as two more-or-less non-interacting spin 1/2 centres; the biferrocene dication has no significant exchange interactions between the two Fe^{III} centres.[66,67]

The metal–metal interactions possible in conjugated linked metallocenes have been exploited in poly(ferrocenylenevinylene)[68] and poly(ferrocenylenedivinylene)s;[69] when partially oxidised poly(ferrocenylenedivinylene) shows superior conductivity to similar polymers with more 'insulating' bridges.[69]

Electronic and optical properties of bis(metallocenyl)polymethines

In this class of compounds, two metallocenes are linked with an odd number of CH groups and there is an overall positive charge stabilised by contributions from (η⁶-fulvene)(η⁵-cyclopentadienyl)metal cation resonance structures. We have been studying symmetrical and unsymmetrical termethine {*n* = 3} examples with Fc, Rc and Fc″ end groups.[10,70,71] We have determined crystal structures for a number of these compounds. Whilst [**10**]$^+$[PF$_6$]$^-$ and [**11**]$^+$[PF$_6$]$^-$ showed symmetrical cations (as do a close trimetallic analogue,[72] and [FcCHFc]$^+$[BF$_4$]$^-$[73]), the crystal structure of [**12**]$^+$[PF$_6$]$^-$ showed a cation best described as a (η⁶-fulvene)(η⁵-cyclopentadienyl)ruthenium cation bridged by a vinylene moiety to a 'normal' ruthenocene, with BLA between formally single and double bonds of some 0.100(6) Å (Fig. 6). Moreover, the similarity of the IR and

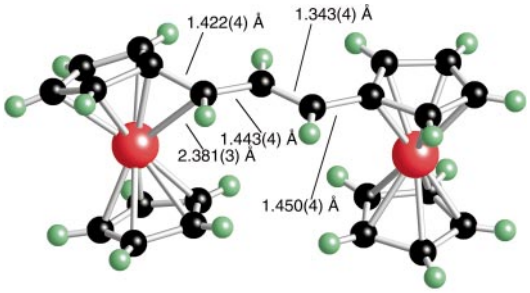

Fig. 6 The [**12**]$^+$ cation in the crystal stucture of its hexafluorophosphate salt.[10,70]

Raman spectra of [**12**]$^+$[PF$_6$]$^-$ in the solid state and in solution suggests the origin of this distortion is an intramolecular effect. The only previous report of such a distortion is that reported by Tolbert and Zhao, who showed [**25**]$^+$ to be unsymmetrical in

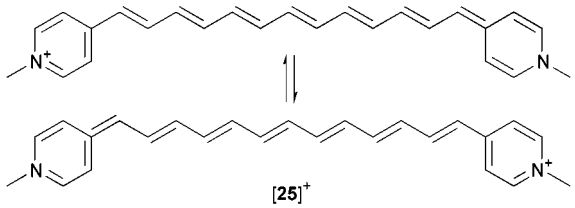

[**25**]$^+$

solution by comparing IR and UV–VIS spectra with those of lower homologues.[74,75] Such distortions afford bistable systems, which could form the basis for a switchable device, where a change in external electric field leads to a dramatic change in polarisation.

Unsymmetrical intramolecular localisation effects have been predicted to occur in long-chain (*ca*. 13 methine groups where the end group can stabilise the positive charge) all-organic polymethines,[74,76] and can be understood in analogy to the Peierls distortion,[76] or by analogy with mixed-valence chemistry.[49,74] We attribute the observation of localisation at low chain length for [**12**]$^+$ to the high reorganisation energy associated with the ruthenocene/(η⁶-fulvene)(η⁵-cyclopentadienyl)ruthenium system.

The electronic spectra of bis(metallocenyl)polymethines are strongly reminiscent of those of the metallocene donor–acceptor NLO dyes discussed earlier; *i.e.* there are two prominent transitions. Tolbert has synthesised the series [Fc(CH)$_n$Fc]$^+$[BF$_4$]$^-$ {*n* = 1, 3, 5, 9, 13}, and found the energy of the LE band to be inversely proportional to the conjugation length (N_{eff} = *n* + 6).[58] Fig. 7 shows this dependence, along

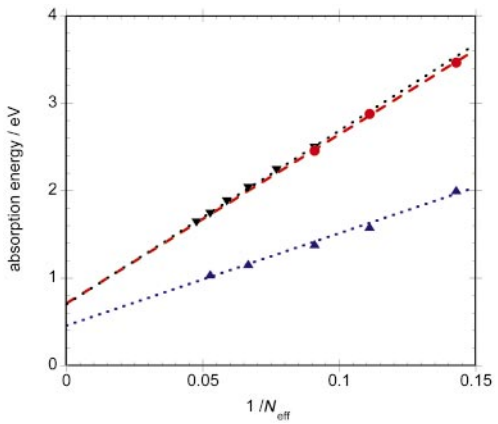

Fig. 7 Conjugation-length dependence of the absorption maxima of α,ω-bis(phenyl)polymethine cations (black; data from ref. 58), the LE (blue; data from ref. 58) and HE (red; data from refs. 10, 59 and 77) bands of α,ω-bis(ferrocenyl)polymethine cations. N_{eff} is defined as *n* + 8 for the phenyl compounds, and *n* + 6 for the ferrocenyl species.

with the stronger chain-length dependence of the HE band, which closely resembles that of the absorption of [Ph(CH)$_n$Ph]$^+$ cations. Thus, we assign the HE band as a π → π* transition. This is, of course, consistent with the assignment of the HE of metallocene–bridge–acceptor compounds as π → (acceptor), and with the orbital scheme. Assignment of the LE band as M → π* is consistent with the weaker chain-length dependence of this band, with the greater blue shift compared to that in the HE band seen on replacing iron with ruthenium (Fig. 8), with the analogous metallocene–bridge–acceptor compounds, and with the calculated orbital structure (Fig. 9). As shown in the calculated orbitals for the distorted [**12**]$^+$ cation, the highest π-level of unsymmetrical species is mainly from the cyclopentadienyl orbitals of the'normal' metallocene, whilst the π* LUMO is correspondingly displaced towards to the (η⁶-

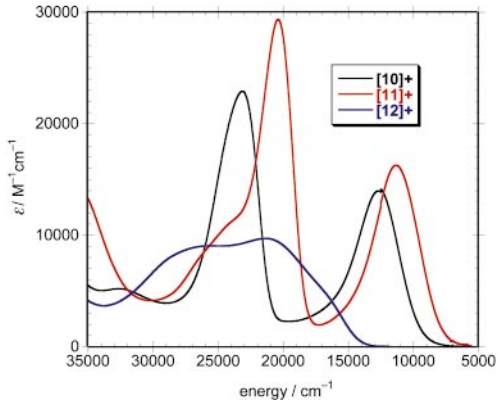

Fig. 8 UV–VIS–NIR spectra of three bis(metallocenyl)termethines, showing the effect of metallocene methylation ([**10**]$^+$ *vs.* [**11**]$^+$), and changing Fe for Ru ([**10**]$^+$ *vs.* [**12**]$^+$).

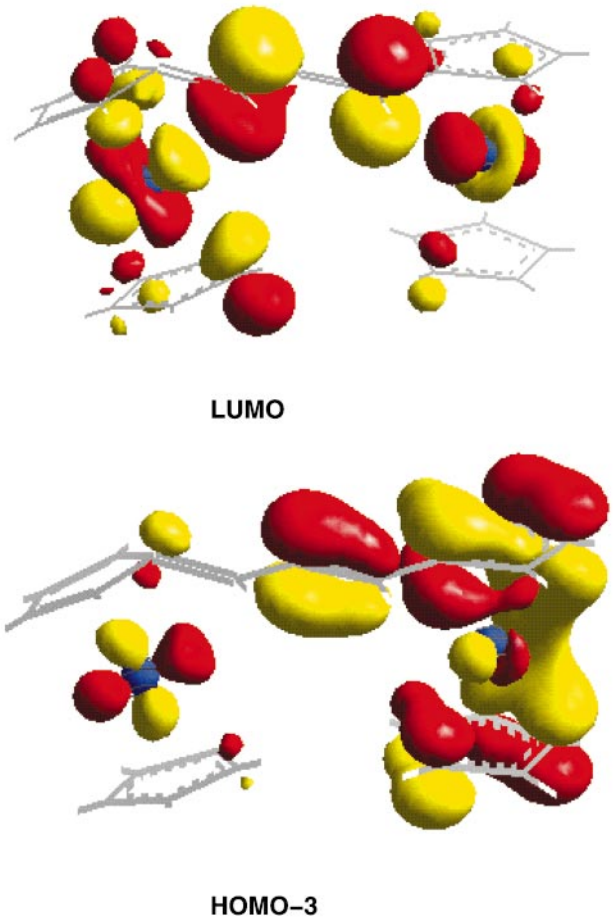

Fig. 9 The LUMO and the highest filled ligand-based π-levels of [**12**]$^+$ according to DF calculations; the three highest-filled levels are all principally metal d in character.[10]

fulvene)(η^5-cyclopentadienyl)metal end of the molecule. The HOMO is located on the 'normal' metallocene. Nevertheless, the orbitals of symmetrical and unsymmetrical bis(metallocenyl)termethines are broadly similar. The bis(metallocenyl)termethine series holds completely symmetrical species ([**10**]$^+$, [**11**]$^+$), somewhat unsymmetrical species ([**13**]$^+$, in which the octamethylferrocenyl group undergoes more distortion than the ferrocene, but the BLA is small), and fully bond-alternated structures ([**12**]$^+$, [**14**]$^+$). This variation is analogous to that found in donor–acceptor compounds, where one can tune between bond-equalised and fully bond-alternated structures through donor and acceptor strength.[37]

Summary

The work of numerous groups has demonstrated that conjugated group 8 metallocenes have a variety of interesting optical and electronic properties. Over the past several years it has become more clear that the metallocenes are different in their behaviour as π-electron donors from simple organic groups, such as those derived from anisole or aniline. In particular, a metallocene interacts with a conjugated π-system both through the cyclopentadienyl group and through the metal-based orbital. These various interactions create opportunities to control the coupling of the metal orbital with the π-system and to control the interaction between metal centres. While interesting non-linear optical and electronic properties have been reported, conjugated metallocenes have yet to find use in device applications. Perhaps, as our understanding of the electronic of this class of molecules become more complete, novel applications of these materials will be identified.

Acknowledgements

Support from the National Science Foundation (Chemistry Division), Office of Naval Research, Air Force Office of Scientific Research (AFOSR) is gratefully acknowledged. We thank our various collaborators whose names are given in the references for their contributions to the work some of which we have reviewed here. In addition, we would like to thank Jennifer Green, Joseph Perry, Laren Tolbert, Jean-Luc Brédas, Harry Gray and Mark Ratner for various stimulating discussions and many helpful comments on our work. We also thank Jennifer Green for providing Figs. 3 and 9

Notes and references

1 S. Evans, M. L. H. Green, B. Jewitt, A. F. Orchard and C. F. Pygall, *J. Chem. Soc., Faraday Trans. 2*, 1972, **68**, 1847.
2 C. Cauletti, J. C. Green, M. R. Kelly, J. Robbins and J. C. Smart, *J. Electron Spectrosc. Relat. Phenom.*, 1980, **19**, 327.
3 J. P. Maier and D. W. Turner, *J. Chem. Soc., Faraday Trans. 2*, 1973, **69**, 521.
4 S. Barlow, H. E. Bunting, C. Ringham, J. C. Green, G. U. Bublitz, S. G. Boxer, J. W. Perry and S. R. Marder, *J. Am. Chem. Soc.*, 1999, **121**, 3715.
5 B. J. Coe, C. J. Jones, J. A. McCleverty, D. Bloor and G. Cross, *J. Organomet. Chem.*, 1994, **464**, 225.
6 B. J. Coe, J.-D. Foulon, T. A. Hamor, C. J. Jones, J. A. McCleverty, D. Bloor, G. H. Cross and T. L. Axon, *J. Chem. Soc., Dalton Trans.*, 1994, 3427.
7 H. Wong, T. Meyer-Friedrichsen, T. Farrell, C. Mecker and J. Heck, *Eur. J. Inorg. Chem.*, 2000, **2000**, 631.
8 G. F. Pedulli and Z. V. Todres, *J. Organomet. Chem.*, 1992, **439**, C46.
9 J. C. Calabrese, L.-T. Cheng, J. C. Green, S. R. Marder and W. Tam, *J. Am. Chem. Soc.*, 1991, **113**, 7227.
10 S. Barlow, L. M. Henling, M. W. Day, W. P. Schaefer, J. Suter, J. C. Green, and S. R. Marder, manuscript in preparation.
11 M. Watanabe, I. Motoyama and T. Takayama, *Bull. Chem. Soc. Jpn.*, 1996, **69**, 2877.
12 J. L. Oudar and D. S. Chemla, *J. Chem. Phys.*, 1977, **66**, 2664.
13 T. Verbiest, S. Houbrechts, M. Kauranen, K. Clays and A. Persoons, *J. Mater. Chem.*, 1997, **7**, 2175 and references therein.
14 M. L. H. Green, S. R. Marder, M. E. Thompson, J. A. Bandy, D. Bloor, P. V. Kolinsky and R. J. Jones, *Nature*, 1987, **330**, 360.
15 B. J. Coe, C. J. Jones, J. A. McCleverty, D. Bloor, P. V. Kolinsky and R. J. Jones, *J. Chem. Soc., Chem. Commun.*, 1989, 1485.
16 S. R. Marder, J. W. Perry, W. P. Schaefer and B. G. Tiemann, *Organometallics*, 1991, **10**, 1896.
17 H. E. Bunting, M. L. H. Green, S. R. Marder, M. E. Thompson, D. Bloor, P. V. Kolinsky and R. J. Jones, *Polyhedron*, 1992, **11**, 1489.
18 C. G. Bethea, *Appl. Opt.*, 1975, **14**, 1447.
19 E. Hendrickx, K. Clays and A. Persoons, *Acc. Chem. Res.*, 1988, **31**, 675.
20 Z. Yuan, N. J. Taylor, Y. Sun, T. B. Marder, I. D. Williams and L.-T. Cheng, *J. Organomet. Chem.*, 1993, **449**, 27.

21 R. Loucif-Saïbi, J. A. Delaire, L. Bonazzola, G. Doisneau, G. Balavoine, T. Fillebeen-Khan, I. Ledoux and G. Puccetti, *Chem. Phys.*, 1992, **167**, 369.
22 B. J. Coe, C. J. Jones, J. A. McCleverty, D. Bloor, P. V. Kolinsky and R. J. Jones, *Polyhedron*, 1994, **13**, 2107.
23 B. J. Coe, T. A. Hamor, C. J. Jones, J. A. McCleverty, D. Bloor, G. H. Cross and T. L. Axon, *J. Chem. Soc., Dalton Trans.*, 1995, 673.
24 U. Hagenau, J. Heck, E. Hendrickx, A. Persoons, T. Schuld and H. W. H, *Inorg. Chem.*, 1996, **35**, 7863.
25 U. Behrens, H. Brussaard, U. Hagenau, J. Heck, E. Hendrickx, J. Kornich, J. G. M. van-der-Linden, A. Persoons, A. L. Spek, N. Veldman, B. Voss and H. Wong, *Chem. Eur. J.*, 1996, **2**, 98.
26 I. S. Lee, H. Seo and Y. K. Chung, *Organometallics*, 1999, **18**, 1091.
27 V. Cadierno, S. Conejero, M. P. Gamasa, J. Gimeno, I. Asselberghs, S. Houbrechts, K. Clays, A. Persoons, J. Borge and S. García-Granda, *Organometallics*, 1999, **18**, 582.
28 K. N. Jayaprakash, P. C. Ray, I. Matsuoka, M. M. Bhadbhade, V. G. Puranik, P. K. Das, H. Nishihara and A. Sarkar, *Organometallics*, 1999, **18**, 3851.
29 L.-T. Cheng, W. Tam, S. H. Stevenson, G. R. Meredith, G. Rikken and S. R. Marder, *J. Phys. Chem.*, 1991, **95**, 10 631.
30 S. R. Marder, L.-T. Cheng, B. G. Tiemann, A. C. Friedli, M. Blanchard-Desce, J. W. Perry and J. Skindhøj, *Science*, 1994, **263**, 511.
31 M. Blanchard-Desce, C. Runser, A. Fort, M. Barzoukas, J.-M. Lehn, V. Bloy and V. Alain, *Chem. Phys.*, 1995, **199**, 253.
32 V. Alain, M. Blanchard-Desce, C. T. Chen, S. R. Marder, A. Fort and M. Barzoukas, *Synth. Met.*, 1996, **81**, 133.
33 M. Ahlheim, M. Barzoukas, P. V. Bedworth, M. Blanchard-Desce, A. Fort, Z.-Y. Hu, S. R. Marder, J. W. Perry, C. Runser, M. Staehelin and B. Zysset, *Science*, 1996, **271**, 335.
34 In cationic examples (for example, see: V. Alain, A. Fort, M. Barzoukas, C. T. Chen, M. Blanchard-Desce, S. R. Marder and J. W. Perry, *Inorg. Chim. Acta*, 1996, **242**, 43) and in a few unusual neutral chromophores (P. D. Beer and H. Sikanyika, *Polyhedron*, 1990, **9**, 1091), the ground-state dipole moment is in the opposite direction from that in 'conventional' neutral chromophores. These compounds, therefore, exhibit negative solvatochromism.
35 D. R. Kanis, M. A. Ratner and T. J. Marks, *J. Am. Chem. Soc.*, 1992, **114**, 10 338.
36 V. Alain, A. Fort, M. Barzoukas, C. T. Chen, M. Blanchard-Desce, S. R. Marder and J. W. Perry, *Inorg. Chim. Acta*, 1996, **242**, 43.
37 F. Meyers, S. R. Marder, B. M. Pierce and J.-L. Brédas, *J. Am. Chem. Soc.*, 1994, **116**, 10 703.
38 M. E. Wright, E. G. Toplikar, R. F. Kubin and M. D. Seltzer, *Macromolecules*, 1992, **25**, 1838.
39 M. E. Wright and M. S. Sigman, *Macromolecules*, 1992, **25**, 6055.
40 M. E. Wright, E. G. Toplikar, H. S. Lackritz and J. T. Kerney, *Macromolecules*, 1994, **27**, 3016.
41 C. R. Moylan, R. J. Twieg, V. Y. Lee, S. A. Swanson, K. M. Betterton and R. D. Miller, *J. Am. Chem. Soc.*, 1993, **115**, 12 599.
42 T. Verbiest, D. M. Burland, M. S. Jurich, V. Y. Lee, R. D. Miller and W. Volksen, *Science*, 1995, **268**, 1604.
43 A. Galvan-Gonzalez, M. Canva, G. I. Stegeman, R. Twieg, K. P. Chan, T. C. Kowalczyk, X. Q. Zhang, H. S. Lackritz, S. Marder and S. Thayumanavan, *Optics Lett.*, 2000, 332.
44 S. Toma, A. Gáplovsky and P. Elecko, *Chem. Papers*, 1985, **39**, 115.
45 T. Y. Liu, Y. J. Chen, C.-C. Tai and K. S. Kwan, *Inorg. Chem.*, 1999, **38**, 674.
46 R. H. Crabtree, *Chem. Commun.*, 1999, 1611 and references cited therein.
47 S. Barlow and D. O'Hare, *Chem. Rev.*, 1997, **97**, 637 and references therein.
48 N. S. Hush, *Coord. Chem. Rev.*, 1985, **64**, 135.
49 S. F. Nelsen, H. Q. Tran and M. A. Nagy, *J. Am. Chem. Soc.*, 1998, **120**, 298.
50 S. R. Marder, D. N. Beratan and L.-T. Cheng, *Science*, 1991, **252**, 103.
51 H. Wadepohl, C. W. v. d. Leith, F. J. Paffen and H. Pritzkow, *Chem. Ber.*, 1995, **128**, 317.
52 B. Floris and P. Tagliatesta, *J. Chem. Res. (S)*, 1993, 42.
53 A. C. Ribou, J.-P. Launay, M. L. Sachtleben, H. Li and C. W. Spangler, *Inorg. Chem.*, 1996, **35**, 3735.
54 F. Delgado-Peña, D. R. Talham and D. O. Cowan, *J. Organomet. Chem.*, 1983, **253**, C43.
55 A. Mendiratta, S. Barlow, M. W. Day and S. R. Marder, *Organometallics*, 1999, **18**, 454.
56 C. LeVanda, K. Bechgaard and D. O. Cowan, *J. Org. Chem.*, 1976, **41**, 2700.
57 C. Patoux, C. Coudret, J.-P. Launay, C. Joachim and A. Gourdon, *Inorg. Chem.*, 1997, **36**, 5037.
58 L. M. Tolbert, X. Zhao, Y. Ding and L. A. Bottomley, *J. Am. Chem. Soc.*, 1995, **117**, 12 891.
59 S. Barlow and L. Perrins, unpublished results.
60 M. Sato, A. Kudo, Y. Kawata and H. Saitoh, *Chem. Commun.*, 1996, 25.
61 M. Sato, Y. Kawata, A. Kudo, A. Iwai, H. Saitoh and S. Ochiai, *J. Chem. Soc., Dalton Trans.*, 1998, 2215.
62 M. Sato, Y. Kawata, H. Shintate, Y. Habata, S. Akabori and K. Unoura, *Organometallics*, 1997, **16**, 1693.
63 M. Sato, A. Iwai and M. Watanabe, *Organometallics*, 1999, **18**, 3208.
64 M. Watanabe, M. Sato and T. Takayama, *Organometallics*, 1999, **18**, 5201.
65 V. Guichard, A. Bourkba, O. Poizat and G. Buntinx, *J. Phys. Chem.*, 1989, **93**, 4429.
66 D. O. Cowan, G. A. Candela and F. Kaufman, *J. Am. Chem. Soc.*, 1971, **93**, 3889.
67 W. H. Morrison, S. Krogsrud and D. N. Hendrickson, *Inorg. Chem.*, 1973, **12**, 1998.
68 M. A. Buretea and T. D. Tilley, *Organometallics*, 1997, **16**, 1507.
69 C. E. Stanton, T. R. Lee, R. H. Grubbs, N. S. Lewis, J. K. Pudelski, M. R. Callstrom, M. S. Erickson and M. L. McLaughlin, *Macromolecules*, 1995, **28**, 8713.
70 S. Barlow, L. M. Henling, M. W. Day and S. R. Marder, *Chem. Commun.*, 1999, 1567.
71 S. Barlow, M. W. Day and S. R. Marder, *Acta Crystallogr., Sect. C*, 2000, **56**, 303.
72 J. Lukasser, H. Angleitner, H. Schottenberger, H. Kopacka, M. Schweiger, B. Bildstein, K.-H. Ongania and K. Wurst, *Organometallics*, 1995, **14**, 5566.
73 M. Cais, S. Dani, F. H. Herbstein and M. Kapon, *J. Am. Chem. Soc.*, 1978, **100**, 5554.
74 L. M. Tolbert and X. Zhao, *J. Am. Chem. Soc.*, 1997, **119**, 3253.
75 Dähne and Reck have reported a more subtle asymmetry (bond-length alternation of *ca*. 0.1 Å) in the crystal structure of $[Me_2N(CH)_7NMe_2]^+[BPh_4]^-$ (L. Dähne and G. Reck, *Angew. Chem., Int. Ed. Engl.*, 1995, **34**, 690). This effect is absent with inorganic counter ions, even when, as in the $[BF_4]^-$ salt (L. Dähne, W. Grahn, P. G. Jones and A. Chrapkowski, *Z. Kristallogr.*, 1994, **209**, 54) they are unsymmetrically arranged relative to the cations and has, therefore, been attributed to polarisation of the polymethine π-system by interactions with the aromatic rings of the anion.
76 L. M. Tolbert, *Acc. Chem. Res.*, 1992, **25**, 561 and references therein.
77 V. I. Boev and A. V. Dombrovskii, *Zh. Obshch. Khim.*, 1980, **50**, 2520.

Electron transfer mechanisms of biphenyl sorption in M-ZSM-5 (M = H^+, Cu^{2+}) zeolites

Isabelle Gener, Alain Moissette and Claude Brémard*

Laboratoire de Spectrochimie Infrarouge et Raman, UMR-CNRS 8516, Bat.C5 Université des Sciences et Technologies de Lille I, 59655 Villeneuve d'Ascq, France. E-mail: claude.bremard@univ-lille1.fr

Received (in Basel, Switzerland) 17th February 2000, Accepted 4th July 2000
Published on the Web 31st July 2000

The sorption of biphenyl (BP) in dehydrated M-ZSM-5 (M = H^+, Cu^{2+}) zeolites through solid–gas exchange spontaneously causes ionisation of BP molecules; the radical cation and trapped electron disappear slowly *via* two different electron transfer mechanisms.

Spontaneous generation of long-lived organic cation radicals in porous crystalline aluminosilicates (zeolites) has been known for over three decades.[1–3] The tight fit between the radical cation and the pore size is considered to be the main factor responsible for this stabilisation and it is now accepted that the acid sites of the porous materials are related to their electron acceptor ability.[3,4] The Brönsted acid sites can impart to zeolites a dual behaviour as acid and oxidant. Earlier work has showed that persistent carbocations are formed more readily than radical cations.[5] However, the electron and proton transfer mechanisms are not yet completely understood, particularly the fate of the ejected electron.[3,4,6,7] This gap prompted this work relating to unusual biphenyl sorption behaviour in M-ZSM-5 zeolites with H^+ and Cu^{2+} as counterbalancing cations.

UV–VIS, IR, Raman, EPR spectra as well as chemical analysis of calcined zeolites $M_{m/n}(SiO_2)_{96-m}(AlO_2)_m$ (m = 3, 6; M = H^+, Na^+) (24 h, 773 K, O_2, Ar) do not exhibit any detectable impurity (Fig. 1) with X-ray diffraction patterns exhibiting the characteristics of well-crystallised ZSM-5 solids while ^{29}Si MAS NMR spectroscopy revealed the absence of abnormal defect groups. The ^{27}Al MAS NMR spectrum of hydrated H_6ZSM-5 shows only a low amount of six-coordinated non-framework Al.

Exposure under argon or helium atmosphere at room temperature of freshly dehydrated $H_m(SiO_2)_{96-m}(AlO_2)_m$ (m = 3, 6) powdered solids to dry biphenyl, turned the powder immediately from white to blue and after one week the solids turned pink. Numerous diffuse reflectance UV–VIS absorption spectra were recorded at different times, immediately after the exposure and until the reaction went to completion over one month at 330 K. The processing data for all the spectra of each sample (Fig. 2), provided evidence of three independent spectra of occluded species in H_m-ZSM-5.[8] The extracted spectrum with main bands around 380 and 666 nm reached a maximum intensity within several minutes and then decreased slowly, and was assigned to the radical cation $BP^{\cdot+}$. It should be noted that this maximum corresponds to *ca.* 10% of $BP^{\cdot+}$ with respect of the BP loading. The extracted spectrum with two prominent features at 468 and 491 nm reached maximum intensity within 20 h and then decreased slowly and was attributed straightforwardly to trapped electrons. The spectrum with two maxima at 250 (sharp) and 505 nm (broad) increased slowly with diffusion of BP in the porous void and reached a maximum within one month and was assigned to non-bonding electronic interactions of BP with protons of the Si–OH–Al framework groups. The EPR spectra recorded immediately after the exposure of H_mZSM-5 samples to BP solid exhibited the sharp features of $BP^{\cdot+}$ at 300 and 77 K. After annealing the sample at 320 K for one week, these sharp features disappeared to give a broad intense signal (77 K) corresponding to both trapped electrons and positive holes. After annealing the sample at 320 K for a month no paramagnetic species were detected. Zeolite samples with loading values from 0.2 to 1 BP per unit cell (m = 3, 6) exhibited similar behaviour.

The exposure of dehydrated $M_m(SiO_2)_{96-m}(AlO_2)_m$ (m = 3, 6, M = Li^+, Na^+, K^+, Rb^+, Cs^+) to solid BP led to no colour change and BP was found to be sorbed as an intact molecule.[9]

Photolysis at 248 nm of BP occluded in M-ZSM-5 (M = Li^+, Na^+, K^+, Rb^+, Cs^+) generated persistent UV–VIS spectra analogous to that generated spontaneously through BP sorption in $H_m(SiO_2)_{96-m}(AlO_2)_m$ without photolysis.[9] EPR spectroscopy provided evidence of paramagnetic species, namely trapped electrons and positive holes, after the disappearance of $BP^{\cdot+}$.[9] Exposure of dehydrated $M_{m/2}(SiO_2)_{96-m}(AlO_2)_m$ (m = 6, M = Zn^{2+}, Cd^{2+}) to solid BP also led to no colour change and BP was found to be sorbed without any ionisation.

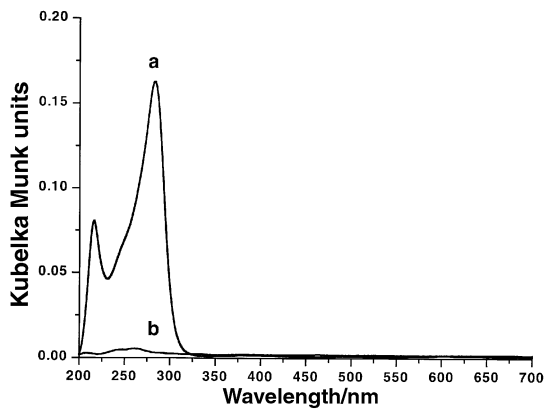

Fig. 1 Diffuse reflectance UV–VIS absorption spectra (Kubelka-Munk units) recorded (a) before thermal treatment of $(NH_4)_6$ZSM-5 zeolite $(NH_4)_6(SiO_2)_{90}(AlO_2)_6$ and (b) after thermal treatment (24 h, 773 K, O_2).

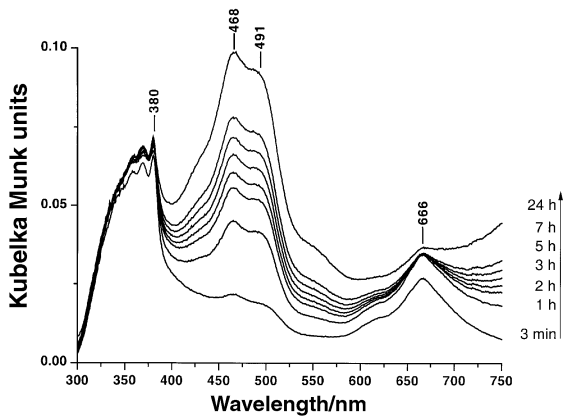

Fig. 2 Diffuse reflectance UV–VIS absorption spectra (Kubelka-Munk units) recorded during the sorption of biphenyl into H_6ZSM-5 zeolite [1BP/$H_6(SiO_2)_{90}(AlO_2)_6$]. The spectra were recorded at room temperature at different times.

DOI: 10.1039/b001307m

Exposure of $Cu_3(SiO_2)_{90}(AlO_2)_6$ after thermal treatment (24 h, 773 K, O_2) to solid BP under argon generated persistent $BP^{\cdot+}$ and trapped electrons as evidenced through data processing of the UV–VIS spectra. Surprisingly, Cu(II) does not appear to be a preferred electron trapping site.

Diffuse reflectance IR absorption spectra of dehydrated $H_m(SiO_2)_{96-m}(AlO_2)_m$ samples (m = 3, 6) exhibited two sharp OH stretching bands at 3611 and 3745 cm^{-1}. These bands were assigned to acidic (Si–OH–Al) hydroxy groups and (Si–OH) silanol groups, respectively.[10] After BP sorption was complete, the 3611 cm^{-1} band decreased in intensity and a new broad band appeared at 3300 cm^{-1}. The dehydrated $M_{m/n}$ZSM-5 (M = Li^+, Na^+, K^+, Rb^+, Cs^+, Zn^{2+}, Cd^{2+}) exchanged zeolites (24 h, 773 K, O_2) did not exhibit any intense OH stretching band at 3611 cm^{-1}. In contrast, the O_2-calcined Cu_3-ZSM-5 sample DRIFT spectrum showed an intense band at 3661 cm^{-1}.[11] It is tempting to attribute the spontaneous BP ionisation to the acidic properties of the O_2-calcined Cu_3-ZSM-5 sample. The most prominent mid-IR absorption bands (1485, 1432 cm^{-1}) of BP occluded in H_mZSM-5 do not differ from those recorded for Na_mZSM-5 (1485, 1432 cm^{-1}) or for the bulk solid (1480, 1430 cm^{-1}). ^{13}C CP-MS NMR spectra of BP occluded in H_mZSM-5 and Na_mZSM-5 were found to be very similar. Thus, in spite of the high basicity of BP (proton affinity = 814 kJ mol^{-1}), proton transfer from H-ZSM-5 to BP does not occur at room temperature.

The FT-Raman spectra (1.06 μm excitation) of occluded BP in M_mZSM-5 (M = Li^+, Na^+, K^+, Rb^+, Cs^+) were found to be similar in frequencies and relative intensities with the Raman spectrum of BP in solution. However, the relative intensities of the Raman bands of occluded BP in $M_{m/n}$ZSM-5 (M = H^+, Zn^{2+}, Cd^{2+}, Cu^{2+}) differed markedly from BP in solution and provided significant evidence of local BP symmetry lowering and electrostatic interactions between BP and the extraframework cations M^{n+}.

Spontaneous ionisation phenomena upon sorption into H_mZSM-5 has been observed for several aromatics such as biphenyl, naphthalene and anthracene which have relatively low ionisation energies (*ca.* 8 eV in the gas phase). The formation of radical cations occurs by electron detachment mediated by the combined effects of radical cation stabilisation and the electron trapping ability of the host. It should be noted that for BP, the ratio $BP^{\cdot+}$/BP is < 0.1, but for anthracene, the ionisation yield approaches unity. It appears that acid sites, either Brönsted or Lewis in nature, are necessary for this reaction to occur at room temperature. The zeolites behave both as electron acceptors to electron donor aromatics and as electron donors to electron deficient radical cations. The role of possible undetectable impurities, such as low extraframework Al content, may be ruled out, since the Na^+ exchanged ZSM-5 sample did not exhibit any spontaneous charge separation; however, the role of defect groups cannot be excluded.[6] The exact chemical nature of the electron trapping sites as well as the positive holes within the ZSM-5 zeolites is not unequivocally identified from the present spectroscopic data. Evidence for charge separation arises from electronic and EPR spectra. In addition, it is possible that the ionisation occurs at the pore openings of the zeolite microcrystals.[12] From the relationship between the zeolite Al content and the stabilisation of the charge separation, it appears that Al is directly involved in the electron trapping sites. However, the presence of nearest Si–OH–Al Brönsted sites appears to be necessary to induce the spontaneous phenomenon at room temperature since H^+–Na^+ exchange of samples with analogous Lewis sites inhibited this effect.[13] A recent model of the interaction of trapped electrons in sodalite cage sheds some light on the possible environment of the trapped electron.[14] The frame atoms for the electron can be provided by five-member ringed containing Al and bridging OH. The radical cation or the positive hole ($R^{\cdot+}$) counterbalances the negative charge in $[H(AlO_2)(SiO_2)_4$ **e**$]$ $R^{\cdot+}$. A concerted mechanism in the void space of ZSM-5 zeolites between the occluded aromatic, the proton interactions and the nearest efficient trapping site can lower the ionisation activation energy and can lead to thermally durable charge separation.

Notes and references

1 D. N. Stamires and J. Turkevich, *J. Am. Chem. Soc.*, 1964, **86**, 749.
2 F. R. Chen and J. J. Fripiat, *J. Phys. Chem.*, 1993, **97**, 5796.
3 F. L. Cozens, R. Bogdanova, M. Régimbald, H. Garcia, V. Marti and J. C. Scaino, *J. Phys. Chem. B*, 1997, **101**, 6921.
4 V. Ramamurthy, P. Lakshminarasimhan, C. P. Grey and L. J. Johnston, *Chem. Commun.*, 1998, 2411.
5 V. J. Rao, N. Prevost, V. Ramamurthy, M. Kojima and L. J. Johnston, *Chem. Commun.*, 1997, 2209.
6 J. K. Thomas, *Chem. Rev.*, 1993, **93**, 301.
7 K. B.Yoon, *Chem. Rev.*, 1993, **93**, 321.
8 W. Windig, *Chemom. Intell. Lab. Syst.*, 1994, **23**, 71.
9 I. Gener, G. Buntinx and C. Brémard, *Angew. Chem., Int. Ed.*, 1999, **182**, 278.
10 S. Kotrel, M. P. Rosynek and J. H. Lunsford, *J. Catal.*, 1999, **182**, 278.
11 J. Sárkány, *Phys. Chem. Chem. Phys.*, 1999, **1**, 5251.
12 K. K. Iu, X. Liu and J. K. Thomas, *J. Photochem. Photobiol. A: Chem.*, 1994, **79**, 103.
13 M. L. Cano, A. Corma, V. Fornes and H. Garcia, *J. Phys. Chem.*, 1995, **99**, 4241.
14 N. P. Blake and H. Metiu, *J. Chem. Phys.*, 1995, **103**, 4455.

Characterisation of a sugar epimerase enzyme involved in the biosynthesis of a vancomycin-group antibiotic

Peter N. Kirkpatrick,[a] Wendy Scaife,[a] Tina M. Hallis,[b] Hung-wen Liu,[b] Jonathan B. Spencer[a] and Dudley H. Williams*[a]

[a] *Cambridge Centre for Molecular Recognition, Department of Chemistry, Lensfield Road, Cambridge, UK CB2 1EW. E-mail: dhw1@cam.ac.uk*
[b] *Department of Chemistry, University of Minnesota, Minneapolis, Minnesota 55455, USA*

Received (in Cambridge, UK) 5th June 2000, Accepted 4th July 2000
Published on the Web 31st July 2000

An enzyme involved in the biosynthesis of the 4-*epi*-vancosamine substituents of a vancomycin group antibiotic has been expressed and its role as a TDP-4-keto-6-deoxyglucose-3,5-epimerase demonstrated.

The glycopeptide antibiotics vancomycin (**1**, Fig. 1) and teicoplanin are currently the drugs of choice for treatment of infections due to methicillin-resistant *Staphylococcus aureus*.[1] The continued rise of vancomycin-resistant bacteria has heightened the need for new therapeutic agents. Manipulation of the biosynthetic gene cluster for the glycopeptide chloroeremomycin (**2**, Fig. 1) may be a potential route to new antibiotics.[2–5] This approach will require further understanding of the biosynthetic pathway.

Chloroeremomycin consists of a crosslinked heptapeptide backbone, adorned with the unusual deoxy-sugar 4-*epi*-vancosamine (4-*e*-V) on residue 6, and the disaccharide glucosyl-4-*e*-V on residue 4. These substituents enhance antibacterial efficacy by promoting antibiotic dimerisation, which is important in the mode of action of this group of compounds.[6,7] Analysis of sequence data from the chloroeremomycin gene cluster revealed five putative proteins, ORFs 23–26 and ORF14, that had significant homologies (30–70% identity) with sugar biosynthesis enzymes in other antibiotic gene clusters, in particular those for erythromycin and daunomycin.[2,8–11] Given the ubiquitous deoxy-sugar precursor TDP-4-keto-6-deoxyglucose, homologies to enzymes identified in the biosynthetic pathways for daunosamine and mycarose allowed a probable route to 4-*e*-V to be deduced (Fig. 2).[2] This paper describes the expression of EvsA (previously referred to as ORF26) and demonstration of its role as the TDP-4-keto-6-deoxyglucose-3,5-epimerase in the 4-*e*-V biosynthetic pathway.

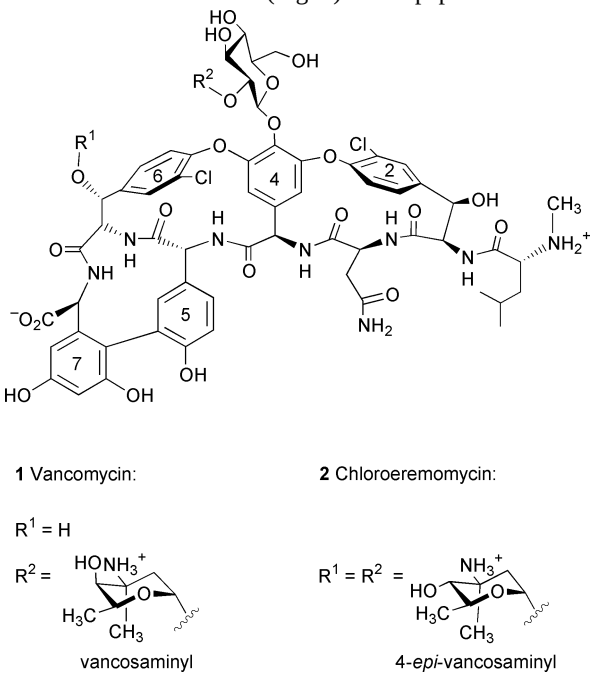

Fig. 1 Structures of vancomcyin (**1**) and chloroeremomcyin (**2**).

EvsA consists of 205 amino acids and shows strong homology (~60% identity) with putative sugar 3,5-epimerase enzymes from the gene clusters of several antibiotics containing L-sugars, including those involved in the daunosamine pathway of *S. peucetius* (DnmU) and the mycarose pathway of *S. erythraea* (EryBVII).[8–11] It is also closely related to the enzyme RmlC from the rhamnose pathway of *E. coli*, *M. tuberculosis* and *S. enterica*, which has been shown to be a TDP-4-keto-6-deoxyglucose-3,5-epimerase.[12,13] The crystal structure of RmlC from *S. enterica* has been determined and the potential active site located, but as yet the residues responsible for catalysis have not been identified.[14] All the highly conserved residues present in this region are also present in EvsA. Although epimerisation at C-3 is not required in the biosynthesis of 4-*e*-V, it seems plausible that all these enzymes have evolved from a common ancestor capable of catalysing epimerisation at both positions 3 and 5, and thus EvsA is suggested to be the first enzyme in the 4-*e*-V pathway.

In order to confirm the proposed role of EvsA, the *evs*A gene was amplified by polymerase chain reaction (PCR) and cloned into the expression vector pET28a(+) (Novagen). The resulting plasmid was used to transform *E. coli* BL21(DE3) and the cells grown at 37 °C in LB medium with induction by isopropyl β-D-thiogalactoside (IPTG, 1 mM) to produce *N*-terminal His_6-tagged EvsA. The enzyme was purified using Novagen His-Bind Quick 900 cartridges and transferred to 50 mM HEPES, pH 7.6 using Millipore centrifugal filters. The relative molecular mass of the purified protein (which gave rise to a single band on an SDS-PAGE gel) was found to be 24.52 kDa (using ESI-MS) which was in excellent agreement with that calculated from the protein sequence (24.521 kDa).

The proposed substrate for EvsA, TDP-4-keto-6-deoxyglucose, was prepared enzymatically from TDP-glucose using RmlB (also known as RfbB), the TDP-glucose-4,6-dehydratase

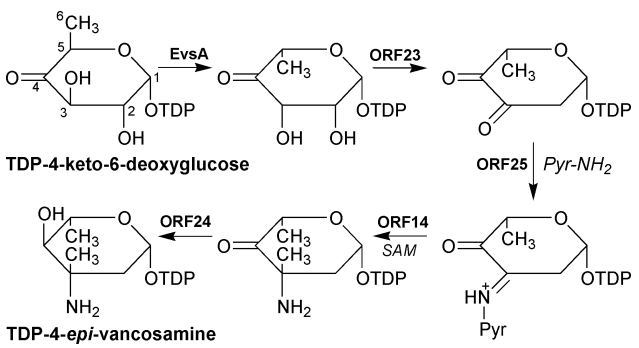

Fig. 2 Proposed route for the biosynthesis of TDP-4-*epi*-vancosamine from TDP-4-keto-6-deoxyglucose. Putative enzymes involved in each step are indicated. Cofactors thought to be required are shown in italics. Abbreviations: Pyr-NH_2, pyridoxamine-5′-phosphate; SAM, S-adenosyl-methionine.

DOI: 10.1039/b004463f

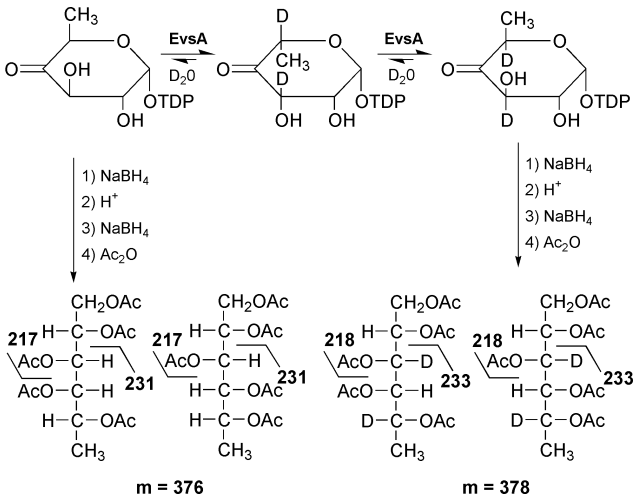

Fig. 3 The equilibrium catalysed by EvsA and the products of the subsequent derivatisation reactions (with the masses of the molecular ions and their fragments).

from the rhamnose pathway.[15] Incubation of TDP-glucose (5 mg) with RmlB (1.6 mg) at 25 °C for 3 h resulted in essentially complete conversion to TDP-4-keto-6-deoxyglucose (monitored by observing the intensity of the UV absorption band of the product at 320 nm).

The potential epimerase activity of EvsA was assayed using a technique based on that described by Stern *et al.* when investigating RmlC, the 3,5-epimerase of the rhamnose pathway.[12] This study demonstrated that incubation of the enzyme with TDP-4-keto-6-deoxyglucose in D_2O allowed for the incorporation of two deuterium atoms from the solvent at positions 3 and 5, and thus that RmlC was capable of catalysing the expected epimerisations.

Consequently, EvsA (10 μg in 50 mM HEPES, pH 7.6) was incubated with TDP-4-keto-6-deoxyglucose (10 μg) in D_2O at

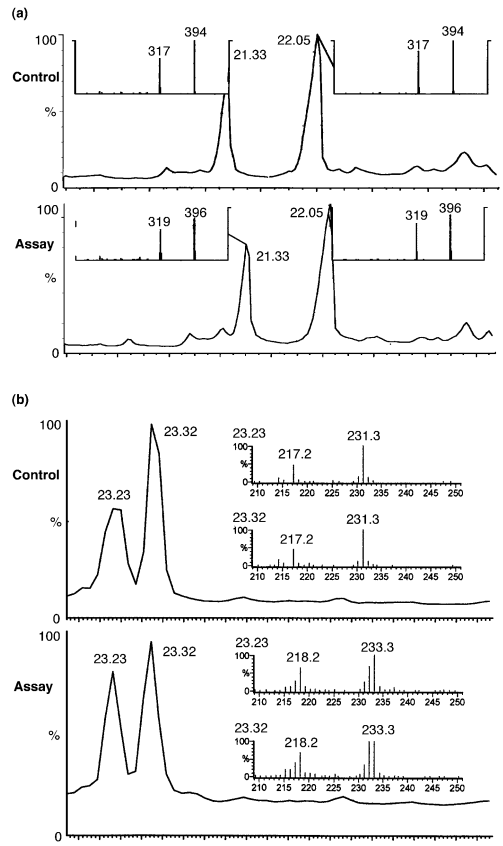

Fig. 4 GC-MS traces [(a) chemical ionisation, (b) electron impact] of the alditol acetates produced from the assay with EvsA and the control without EvsA.

37 °C for 90 min in a total volume of 100 μl. Due to $[^1H]_2O$ in the enzyme and substrate solutions, the resulting concentration of $[^2H]_2O$ was about 80%. A reaction in which protein was replaced by buffer was used as a control. The reactions were stopped by addition of EtOH and the protein removed by centrifugation. The resulting 4-keto-sugar nucleotides were then reduced with $NaBH_4$, hydrolysed with trifluoroacetic acid, reduced again, and then acetylated for analysis by GC-MS as described by Stern *et al.* (Fig. 3).[12] The alditol acetates produced were dissolved in MeOH and analysed by ammonia chemical ionisation GC-MS. The traces for the GC-MS of the EvsA and control reactions are shown in Fig. 4(*a*). Mass analysis of the two peaks revealed that the molecular ions (MNH_4^+) present in the EvsA reaction are two mass units higher (*m*/*z* 396) than those in the control reaction (*m*/*z* 394).[16] The same difference is observed in the masses of the major fragment ion, which corresponds to loss of acetic acid and ammonia. Thus two deuterium atoms have been incorporated into TDP-4-keto-6-deoxyglucose from the solvent by the action of EvsA. In order to establish the positions of incorporation, the samples were also analysed using electron impact GC-MS, which gives fragments rather than the molecular ions (Fig. 3 and Fig. 4(*b*)). No deuterium incorporation was seen in the control but incorporation at both positions 3 and 5 occurred in the presence of EvsA.[17] These results confirm that EvsA is indeed an epimerase involved in the biosynthesis of 4-*e*-V at the stage suggested (Fig. 2) and that epimerisation is catalysed at both C-5 and C-3.

We thank Samantha Barton and Oliver Choroba for valuable assistance and the BBSRC and EPSRC (P. K.) for funding. H.-w. Liu thanks the National Institutes of Health for funding.

Notes and references

1 M. Foldes, R. Monro, T. C. Sorrell, S. Shankar and M. Toohey, *J. Antimicrob. Chemother.*, 1983, **11**, 21.
2 A. M. v. Wageningen, P. N. Kirkpatrick, D. H. Williams, B. R. Harris, J. K. Kershaw, N. J. Lennard, M. Jones, S. J. Jones and P. J. Solenberg, *Chem. Biol.*, 1998, **5**, 155.
3 P. J. Solenberg, P. Matsushima, D. R. Stack, S. C. Wilkie, R. C. Thompson and R. H. Baltz, *Chem. Biol.*, 1997, **4**, 195.
4 D. P. O'Brien, P. N. Kirkpatrick, S. W. O'Brien, T. S. Staroske, T. I. Richardson, D. A. Evans, A. Hopkinson, J. B. Spencer and D. H. Williams, *Chem. Commun.*, 2000, **1**, 103.
5 O. W. Choroba, D. H. Williams and J. B. Spencer, *J. Am. Chem. Soc.*, 2000, in the press.
6 J. P. Mackay, U. Gerhard, D. A. Beauregard, M. S. Westwell, M. S. Searle and D. H. Williams, *J. Am. Chem. Soc.*, 1994, **116**, 4581.
7 J. P. Mackay, U. Gerhard, D. A. Beauregard, R. A. Maplestone and D. H. Williams, *J. Am. Chem. Soc.*, 1994, **116**, 4573.
8 S. Gaisser, G. A. Bohm, J. Cortes and P. F. Leadlay, *Mol. Gen. Genet.*, 1997, **256**, 239.
9 R. G. Summers, S. Donadio, M. J. Staver, E. WendtPienkowski, C. R. Hutchinson and L. Katz, *Microbiology*, 1997, **143**, 3251.
10 S. L. Otten, X. C. Liu, J. Ferguson and C. R. Hutchinson, *J. Bacteriol.*, 1995, **177**, 6688.
11 S. L. Otten, M. A. Gallo, K. Madduri, X. C. Liu and C. R. Hutchinson, *J. Bacteriol.*, 1997, **179**, 4446.
12 R. J. Stern, T. Y. Lee, T. J. Lee, W. Yan, M. S. Scherman, V. D. Vissa, S. K. Kim, B. L. Wanner and M. R. McNeil, *Microbiology*, 1999, **145**, 663.
13 M. Graninger, B. Nidetzky, D. E. Heinrichs, C. Whitfield and P. Messner, *J. Biol. Chem.*, 1999, **274**, 25 069.
14 M. F. Giraud, G. A. Leonard, R. A. Field, C. Berlind and J. H. Naismith, *Nat. Struct. Biol.*, 2000, **7**, 398.
15 The enzyme RmlB was originally derived from *Salmonella enterica* LT2 and was overexpressed and purified from *E. coli* HB101/pYLR1 cells in the laboratory of H.-w. Liu.
16 The presence of just two major peaks (rather than four) corresponding to the expected masses of the ammoniated molecular ions is presumably due to the previously observed equilibrium position of the reaction catalysed by 3,5-epimerases, which lies strongly on the side of the *gluco*-configuration.[12]
17 This incorporation was not total as there are ions observed at 217 and 232 in the EvsA assay. This will be in part due to the presence of some $[^1H]_2O$ in the reaction mixture, but it is also possible that reaction of the substrate was not complete.

ChemComm

Photochromic heteroaromatic thiofulgides and dimethoxybutanoic acid lactones

Matthew Badland, Alison Cleeves, Harry G. Heller,* David S. Hughes and Michael B. Hursthouse

Chemistry Department, Cardiff University, PO Box 912, Cardiff, UK CF1 3TP

Received (in Cambridge, UK) 13th March 2000, Accepted 3rd July 2000
Published on the Web 3rd August 2000

Thiofulgides 1, (X = S) cyclise on irradiation with UV light to form thermally stable photochromes 2, (X = S) that absorb at much longer wavelengths than photochromes 2, (X = O), formed from corresponding fulgides 1, (X = O), reverse reactions occur on exposure to white light; photochromic thiofulgides are prepared by reaction of fulgides with sodium hydrosulfide in hot toluene and photochromic lactones 9 and 12 are prepared by reaction of fulgides with sodium hydrosulfide in cold methanol followed by cyclisation with a carbodiimide.

Photochromic heteroaromatic thiofulgides **1**, (X = S) are of special interest because their coloured forms **2**, (X = S) have the potential to show large bathochromic shifts of their long wavelength absorption bands compared to the coloured forms **2**, (X = O) from corresponding fulgides **1**, (X = O). (The effect of replacement of oxygen by sulfur can be seen in the ultraviolet spectra of thiomaleic anhydride[2] which shows λ_{max} 230 nm compared to λ_{max} 198 nm for maleic anhydride[3].)

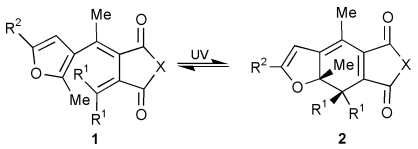

Previous attempts to synthesise photochromic heteroaromatic thiofulgides by methods used for the preparation of acetic,[4] succinic,[5] phthalic,[6] and dibenzylidenesuccinic thioanhydrides[7] were unsuccessful.

We find that (*Z*)-thiofulgides, (*Z*)-4-dicyclopropylmethylene[1-(2,5-dimethyl-3-furyl) and (2-methyl-5-phenyl-3-furyl)-ethylidene]thiosuccinic anhydrides **6a** and **6b** can be prepared

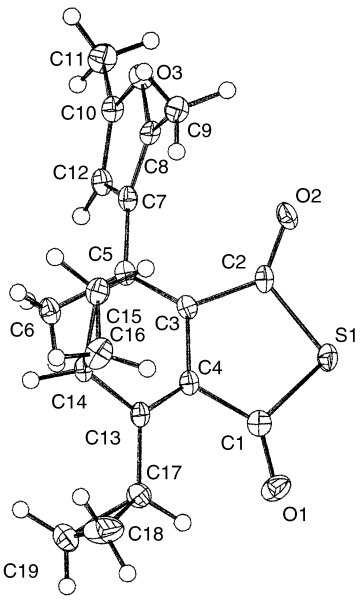

Fig. 1 The X-ray structure of (*Z*)-thiofulgide **6a**.

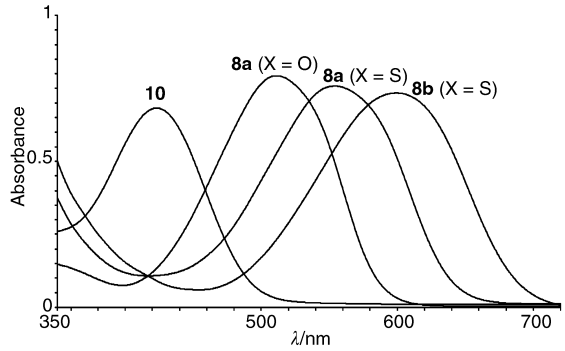

Fig. 2 The spectra of compounds **10**, **8a** (X = O), **8a** (X = S), and **8b** (X = S) (λ_{max} 424, 511, 544, and 599 nm respectively) obtained after irradiation at 366 nm of compounds **9**, **4a**, **6a** (X = S) and **6b** (X = S) (1 $\times 10^{-4}$ molar solutions in toluene) to the photostationary state, illustrating the major colour changes which can be achieved by molecular tailoring.

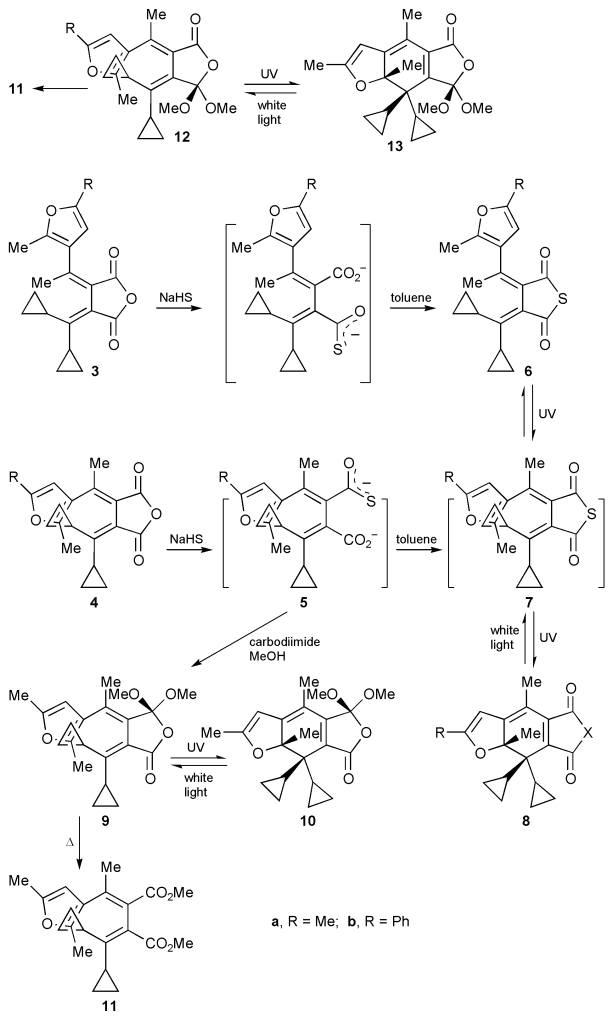

DOI: 10.1039/b002033h

by boiling (4 h) (*Z*)-fulgides **3a** and **3b** (1 g) in toluene with 2–3 eq. of yellow sodium hydrosulfide (Aldrich). They were obtained as yellow crystals, mp 133 and 147–8 °C respectively, after purification by column chromatography and crystallisation from dichloromethane and petroleum. Seven photochromic thiofulgides have been prepared in yields of *ca.* 35% by this general method. Yields depend on the quality of sodium hydrosulfide, which deteriorates with time.

The structure and stereochemistry of (*Z*)-thiofulgide **6a** was established by X-ray crystallographic analysis† (Fig. 1).

On irradiation (366 nm), (*Z*)-thiofulgides **6a** and **6b** in toluene isomerised to (*E*)-thiofulgides **7a** and **7b** which cyclised to thermally stable purple and blue photochromes **8a** (X = S) and **8b** (X = S), showing bathochromic shifts (40 and 60 nm) of the maxima of their long wavelength absorption bands compared to the red and magenta photochromes **8a** (X = O) and **8b** (X = O) (Fig. 2). On exposure to white light, photochromes **8a** (X = S) and **8b** (X = S) ring opened to pale yellow (*E*)-thiofulgides **7a** and **7b**. Quantum efficiencies for colouring ($\emptyset$c) at 366 nm for (*E*)-thiofulgides in toluene were less than for corresponding (*E*)-fulgides. $\emptyset$c for thiofulgide **1** ($R^1 = R^2$ = Me, X = S) was 9% compared to 20% for fulgide **1** ($R^1 = R^2$ = Me, X = O). Preliminary studies indicate that bleaching efficiencies and photochemical fatigue of the photochromes of thiofulgides were comparable to those of photochromes of the corresponding fulgides.

When (*E*)-fulgide **4a** was stirred with sodium hydrosulfide in MeOH at room temperature, the salt of thioacid **5** was formed which after treatment with 1-ethyl-3-(dimethylamino)propyl-carbodiimide HCl, reacted with methanol to give **9** (colourless crystals, mp 168–9 °C, 33% yield). On irradiation (366 nm), lactone **9** in toluene cyclised to the thermally stable bright intensely coloured yellow photochrome **10** which underwent the reverse reaction on exposure to white light.

(*Z*)-Fulgide **3** gave the colourless lactone **12** in 31% yield in an analogous reaction which cyclised to the pale yellow photochrome **13** on irradiation at 366 nm.

Lactones **9** and **12** were converted quantitatively into **11** on boiling with sodium hydrosulfide in MeOH, exemplifying a convenient method of preparing dimethyl esters from anhydrides. All new compounds were fully characterised.

We thank PPG Industries, Pittsburgh, USA and the Brite Euram Syladec programme for grants to MB and AC respectively and financial support for this programme, and EPSRC for support for the X-ray crystallographic work.

Notes and references

† *Crystal data for* **6a**: $C_{19}H_{20}O_3S$, M = 328.4, monoclinic, space group $P2(1)/n$, a = 10.773(2), b = 7.861(2), c = 19.492(4) Å, β = 92.42(3)°, V = 1649.2(6) Å^3, T = 150(2) K, Z = 4, D_c = 1.323 g cm^3, R_1 = 0.0686, wR_2 = 0.1179 for all 2349 data and 211 parameters. Data were recorded using a FAST TV area detector diffractometer and Mo-Kα radiation. CCDC 182/1709. See http://www.rsc.org/suppdata/cc/b0/b002033h/ for crystallographic files in .cif format.

1 H. G. Heller, *CRC Handbook of Organic Photochemistry and Photobiology*, ISBN 0-8493-8634-9, Eds. W. M. Horspool and P.-S. Song, 1995, **13**, 173.
2 H.-D. Scharf and M. Verbeek, *Angew. Chem., Int. Ed. Engl.*, 1967, **6**, 874.
3 *DMS UV Atlas of Organic Compounds*, Butterworth, London, 1968, vol. 4. Library of Congress Catalog Card Number 66-21542.
4 W. A. Bonner, *J. Am. Chem. Soc.*, 1950, **72**, 4270.
5 P. Weselsky, *Chem. Ber.*, 1869, **2**, 518; H. L. Jakobsen, E. H. Larsen and S. O. Lawesson, *Tetrahedron*, 1963, 1867.
6 A. Reissert and H. Holle, *Chem. Ber.*, 1911, **44**, 3027.
7 P. A. Davidse and J. L. M. Dillen, *Heteroatom. Chem.*, 1990, **1**, 281.

ChemComm

Chiral organolithium species: determination of the rate of cyclization and extent of racemization

Iain Coldham* and Graham P. Vennall

School of Chemistry, University of Exeter, Stocker Road, Exeter, UK EX4 4QD. E-mail: I.Coldham@exeter.ac.uk

Received (in Cambridge, UK) 6th June 2000, Accepted 10th July 2000
Published on the Web 2nd August 2000

The rate of intramolecular carbolithiation onto an unactivated alkene to give a six-membered ring has been determined and follows first order kinetics with a half life of ~ 90 min at 23 °C; this allows significant racemization using a chiral organolithium species, although good levels of optical purity are obtained with a phenylthio-substituted alkene.

The ability to use enantiomerically enriched organometallic species in asymmetric synthesis hinges on the configurational stability at the chiral centre. Since Still and Sreekumar showed that chiral organolithium species could be generated from α-alkoxyorganostannanes and reacted stereospecifically,[1] the reactions of chiral α-hetero-substituted organolithium species have been the subject of extensive studies.[2] The majority of these studies focus on the intermolecular quench, which occurs with retention, inversion or racemization of configuration. We and others have demonstrated that intramolecular (anionic) cyclization occurs with complete retention of configuration at the carbanion centre and provides enantiomerically enriched heterocyclic and carbocyclic compounds.[3–5] For example, we have found that cyclization using the α-aminoorganolithium species **1** (formed from the corresponding organostannane, 94% ee) gives (Scheme 1) the hexahydro-1*H*-pyrrolizine alkaloid (+)-pseudoheliotridane† **2**, E = H with complete diastereoselectivity and enantiospecificity.[3] Unusually, the organolithium species **1** is formed at rt, yet no racemization takes place.[6] Such cyclizations from chiral organolithium species have, so far, been restricted to the formation of five-membered rings, and must occur at rates that are significantly greater than the rate of racemization. Bailey and co-workers have determined the rate of anionic cyclization to generate a cyclopentane ring and found that $t_{1/2} \approx 5.5$ min at 23 °C.[7] We were intrigued to determine the effect of ring size on the stereochemical integrity of the chiral organolithium species. In this paper, we report the first determination of the rate of anionic cyclization to give a six-membered ring and its comparison with the rate of racemization of the chiral organolithium species.

Stannane **3** was prepared by treatment of *N*-Boc-2-tributylstannylpyrrolidine[8] with *B*-bromocatecholborane, followed by acylation with pent-4-enoyl chloride and reduction with $LiAlH_4$.[3] Transmetallation of amine **3** in hexane–Et_2O (4:1) with ^{n}BuLi (3 molar equiv. in hexanes) at rt gave the enantiomerically enriched organolithium species **4** (Scheme 2) which cyclized to give, after quenching with MeOH, the diastereomeric octahydroindolizines **5** and **6** in high yield (80–87%) and diastereoselectivity (95:5, **5**:**6**).[9] Remarkably, the use of the solvent system hexane–Et_2O–TMEDA (4:1:1, equating to 15 molar equiv. of TMEDA) completely reversed the diastereoselectivity, giving predominantly **6** (10:90, **5**:**6**).

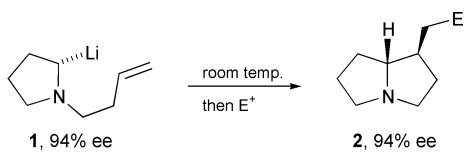

Scheme 1

In each case a small amount of proto-destannylated material **7** was formed. Intramolecular carbolithiation in hexane–Et_2O gave, after 6 h or more, **5** with 13% ee.[10] The presence of TMEDA caused complete racemization. By quenching the reaction mixture (in the absence of TMEDA) at shorter time intervals (*e.g.* 30 min), **5** and **6** (95:5) were obtained in low yield (22%) but enhanced enantiomeric excess (**5**, 62% ee). By taking aliquots of a reaction at different reaction times, it was possible to measure the rate of the cyclization. This followed first order kinetics with a rate constant, $k \approx 1.2 \times 10^{-4}$ s^{-1}, corresponding to a half-life for cyclization of approximately 90 min at 23 °C (complete transmetallation requires 20–30 min). This is significantly slower than the corresponding five-membered ring. Racemization can compete with cyclization, thereby accounting for the loss in enantiopurity. This is in stark contrast to the completely enantiospecific and diastereoselective cyclization of organolithium species **1**. The data reveal that the organolithium species **4** is racemic within approximately 30 min at rt in hexane–Et_2O and therefore the half-life for racemization of the organolithium species **4** must be less than 30 min.

In order to improve the optical purity of the indolizidine products, a method to slow the rate of racemization or to increase the rate of cyclization must be found. Alkenes substituted with an anion stabilising group have been shown to increase the rate of anionic cyclization reactions.[11] Thus the *E*- and *Z*-stannanes **8**, in which a phenylthio substituent is located at the terminus of the alkene, were prepared. The synthesis of the stannanes **8** was achieved by reductive amination.[12,13]

Stannanes **8** were treated with ^{n}BuLi in either hexane–Et_2O (4:1) or hexane–Et_2O–TMEDA (4:1:1), to give the diastereomeric cyclized products **9** and **10** (Scheme 3).‡ In the former solvent system, the organolithium species derived from stannane (*E*)-**8** gave predominantly **9** (77%, 70:30, **9**:**10**) in good ee (**9**, 75% ee; **10**, 72% ee). The organolithium species derived from the stannane *Z*-**8** cyclized to give a mixture of octahydroindolizines **9** and **10** (79%, 50:50, **9**:**10**) in slightly lower ee (**9**, 55% ee; **10**, 53% ee). In the presence of TMEDA, the organolithium species derived from stannane (*E*)- or (*Z*)-**8** cyclized to give racemic **10** exclusively in good yield (71–73%). The addition of TMEDA therefore appears to increase the rate

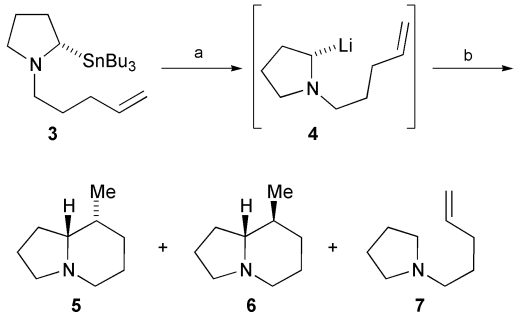

Scheme 2 *Reagents and conditions*: (a) 2.5 equiv. ^{n}BuLi, hexane–Et_2O (4:1) or hexane–Et_2O–TMEDA (4:1:1), 22 °C; (b) 6 h then MeOH, **5** and **6** (95:5, 80%), **5** (13% ee) and **7** 13%; or **5** and **6** (10:90, 76%), **6** (0% ee) and **7**, 21%.

DOI: 10.1039/b004519p

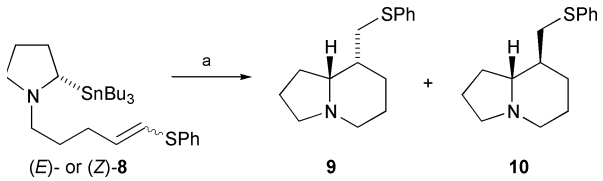

Scheme 3 *Reagents and conditions*: (a) 2.5 equiv. ^{n}BuLi, hexane–Et_2O (4:1) or hexane–Et_2O–TMEDA (4:1:1), 22 °C, 2 h then MeOH; see text for yields and selectivities.

of racemization, presumably *via* co-ordination of TMEDA to the lithium atom.[14] In the presence or absence of TMEDA, the cyclization is complete within approximately the same time as the substrate takes for complete tin–lithium exchange (≈30 min). The half-life for cyclization is therefore reduced considerably in comparison with the substrate **3**, in which no anion-stabilising phenylthio substituent is present at the terminus of the alkene.

The Leverhulme Trust is thanked for support of this work (G. P. V.). We are grateful to Zeneca Pharmaceuticals (Strategic Research Fund) and Pfizer for unrestricted grants. We acknowledge the use of the EPSRC mass spectrometry service at the University of Wales, Swansea.

Notes and references

† The IUPAC name for heliotridane is 1-methylhexahydro-1*H*-pyrrolizine.

‡ *Cyclization of the stannane E*-**8**: The stannane *E*-**8** (1.16 g, 2.16 mmol) in hexane–Et_2O (25 cm^3, 4:1) was treated with *n*-butyllithium (2.6 cm^3, 6.50 mmol, 2.5 M in hexanes) at rt. After 2 h, MeOH (2 cm^3) was added, the solvent was removed under reduced pressure and the residue was purified by column chromatography on basic alumina, eluting with light petroleum (bp 40–60 °C)–EtOAc (1:0 to 4:1) to give the amines **9** and **10** (409 mg, 77%) as a 7:3 ratio of diastereomers as an oil; ν_{max}(neat)/cm^{-1} 3020 and 2935 (C-H); δ_H(400 MHz, $CDCl_3$) 1.25–2.21 (12H, m), 2.46–2.50 (0.3H, m), 2.62 (0.3H, dd, *J* 12.2 and 8.6), 2.93–3.03 (1.7H, m), 3.05 (0.3H, dd, *J* 12.2 and 3.7), 3.19 (0.7H, dd, *J* 12.3 and 9.0), 3.32 (0.7H, dd, *J* 12.3 and 4.5), 6.98–7.04 (1H, m), 7.09–7.14 (2H, m), 7.38–7.43 (2H, m); δ_C(100 MHz, $CDCl_3$) 20.8, 21.1, 25.7, 26.3, 28.5, 29.3, 31.4, 35.4, 37.7, 41.9, 52.5, 53.8, 54.4, 54.7, 66.6, 68.3, 125.3, 125.5, 127.7, 127.8, 128.8, 138.2, 138.3 (Found: M+H 248.1468. $C_{15}H_{22}NS$ requires M + H, 248.1473); *m/z* (CI) 248 (100%, M + H), 140 (62, $C_9H_{18}N$), 138 (60, M − C_6H_5S). The enantioselectivity of the cyclization was determined by treating the mixture of amines **9** and **10** with Raney® nickel in EtOH (60 °C, 30 min, 90%) to give the amines **5** and **6**.[10]

1 W. C. Still and C. Sreekumar, *J. Am. Chem. Soc.*, 1980, **102**, 1201.
2 See, for example (*a*) P. Beak, A. Basu, D. J. Gallagher, Y. S. Park and S. Thayumanavan, *Acc. Chem. Res.*, 1996, **29**, 552; (*b*) D. Hoppe and T. Hense, *Angew. Chem., Int. Ed. Engl.*, 1997, **36**, 2282; (*c*) R. E. Gawley and Q. Zhang, *J. Org. Chem.*, 1995, **60**, 5763; (*d*) M. Schlosser and D. Limat, *J. Am. Chem. Soc.*, 1995, **117**, 12 342; (*e*) F. Hammerschmidt, A. Hanninger and H. Völlenkle, *Chem. Eur. J.*, 1997, **3**, 1728; (*f*) G. A. Weisenburger, N. C. Faibish, D. J. Pippel and P. Beak, *J. Am. Chem. Soc.*, 1999, **121**, 9522; (*g*) A. Ariffin, A. J. Blake, M. R. Ebden, W.-S. Li, N. S. Simpkins and D. N. A. Fox, *J. Chem. Soc., Perkin Trans. 1*, 1999, 2439; (*h*) N. Komine, L.-F. Wang, K. Tomooka and T. Nakai, *Tetrahedron Lett.*, 1999, **40**, 6809; (*i*) J. van Bebber, H. Ahrens, R. Fröhlich and D. Hoppe, *Chem. Eur. J.*, 1999, **5**, 1905; (*j*) B. J. Kim, Y. S. Park and P. Beak, *J. Org. Chem.*, 1999, **64**, 1705; (*k*) S. Nakamura, R. Nakagawa, Y. Watanabe and T. Toru, *Angew. Chem. Int. Ed.*, 2000, **39**, 353.
3 I. Coldham, R. Hufton and D. J. Snowden, *J. Am. Chem. Soc.*, 1996, **118**, 5322.
4 (*a*) K. Tomooka, N. Komine and T. Nakai, *Tetrahedron Lett.*, 1997, **38**, 8939; (*b*) M. J. Woltering, R. Fröhlich, B. Wibbeling and D. Hoppe, *Synlett*, 1998, 797; (*c*) C. Serino, N. Stehle, Y. S. Park, S. Florio and P. Beak, *J. Org. Chem.*, 1999, **64**, 1160; (*d*) Y. Xu, J. Choi, M. I. Calaza, S. Turner and H. Rapoport, *J. Org. Chem.*, 1999, **64**, 4069; (*e*) R. A. Bragg and J. Clayden, *Tetrahedron Lett.*, 1999, **40**, 8323; R. A. Bragg and J. Clayden, *Tetrahedron Lett.*, 1999, **40**, 8327.
5 (*a*) M. J. Woltering, R. Fröhlich and D. Hoppe, *Angew. Chem., Int. Ed. Engl.*, 1997, **36**, 1764; (*b*) K. Tomooka, N. Komine, T. Sasaki, H. Shimizu and T. Nakai, *Tetrahedron Lett.*, 1998, **39**, 9715; (*c*) M. Oestreich and D. Hoppe, *Tetrahedron Lett.*, 1999, **40**, 1881; (*d*) A. Deiters and D. Hoppe, *Angew. Chem., Int. Ed.*, 1999, **38**, 546; (*e*) M. Oestreich, R. Fröhlich and D. Hoppe, *J. Org. Chem.*, 1999, **64**, 8616; (*f*) D. Hoppe, M. J. Woltering, M. Oestreich and R. Fröhlich, *Helv. Chim. Acta*, 1999, **82**, 1860.
6 Most α-aminoorganolithium species epimerise or decompose above about −40 °C; for other chiral organolithium species with configurational stability above 0 °C, see (*a*) R. E. Gawley, Q. Zhang and S. Campagna, *J. Am. Chem. Soc.*, 1995, **117**, 11 817; (*b*) D. Hoppe, B. Kaiser, O. Stratmann and R. Fröhlich, *Angew. Chem., Int. Ed. Engl.*, 1997, **36**, 2784; (*c*) F. Marr, R. Fröhlich and D. Hoppe, *Org. Lett.*, 1999, **1**, 2081.
7 (*a*) W. F. Bailey, J. J. Patricia, V. C. DelGobbo, R. M. Jarret and P. J. Okarma, *J. Org. Chem.*, 1985, **50**, 1999; (*b*) W. F. Bailey, A. D. Khanolkar, K. Gavaskar, T. V. Ovaska, K. Rossi, Y. Thiel and K. B. Wiberg, *J. Am. Chem. Soc.*, 1991, **113**, 5720.
8 P. Beak, S. T. Kerrick, S. Wu and J. Chu, *J. Am. Chem. Soc.*, 1994, **116**, 3231.
9 For a related photochemical cyclization to racemic indolizidines, see (*a*) G. Pandey, G. D. Reddy and D. Chakrabarti, *J. Chem. Soc., Perkin Trans. 1*, 1996, 219; (*b*) S. E. Hoegy and P. S. Mariano, *Tetrahedron Lett.*, 1994, **35**, 8319.
10 The enantioselectivity of the cyclization was determined by measuring (^{1}H NMR) the relative peak areas of the methyl doublets of the free base of **6** or of the picrate salt of **5** in the presence of the Pirkle chiral solvating agent.[3]
11 (*a*) A. Krief, B. Kenda and B. Remacle, *Tetrahedron*, 1996, **52**, 7435; (*b*) W. F. Bailey and K. V. Gavaska, *Tetrahedron*, 1994, **50**, 5957; (*c*) M. P. Cooke, *J. Org. Chem.*, 1992, **57**, 1495.
12 N. J. Ashweek, I. Coldham and G. P. Vennall, *Tetrahedron Lett.*, 2000, **41**, 2235.
13 The aldehydes required for reductive amination were prepared (Swern oxidation) from their corresponding alcohols, made in the same way as R. W. Hoffmann, R. Koberstein and K. Harms, *J. Chem. Soc., Perkin Trans. 2*, 1999, 183.
14 (*a*) D. B. Collum, *Acc. Chem. Res.*, 1992, **25**, 448; (*b*) H. J. Reich, D. P. Green, M. A. Medina, W. S. Goldenberg, B. O. Gudmundsson, R. R. Dykstra and N. H. Phillips, *J. Am. Chem. Soc.*, 1998, **120**, 7201.

para-Selective nitration of halogenobenzenes using a nitrogen dioxide–oxygen–zeolite system

Keith Smith,* Saeed Almeer and Steven J. Black

Centre for Clean Chemistry, Department of Chemistry, University of Wales Swansea, Swansea, UK SA2 8PP. E-mail: K.Smith@swansea.ac.uk

Received (in Cambridge, UK) 10th May 2000, Accepted 5th July 2000
Published on the Web 2nd August 2000

The nitration of halogenobenzenes using zeolite Hβ or zeolite HY as a solid inorganic catalyst and a combination of liquid nitrogen dioxide and gaseous oxygen as the nitrating reagent leads to high yields and significant *para*-selectivities in a relatively clean process for aromatic nitration.

Electrophilic aromatic substitution reactions are of considerable importance in the production of fine chemicals. However, the traditional processes suffer a number of disadvantages, such as low selectivity towards the desired product and the requirement for large quantities of mineral or Lewis acids as activators. In turn these acids are responsible for corrosion problems within the plant and the generation of large volumes of spent reagents, which, given the current environmentally conscious climate, are increasingly unacceptable. Major efforts are therefore being made towards developing processes that can reduce the volumes of spent liquors produced. Inorganic solids can offer significant benefits for these processes by providing both effective catalysis and, in some cases, enhanced selectivity. Additionally they are easily removed from reaction mixtures and in some cases recycling is possible. For example, we have utilised zeolites to enhance the *para*-selectivity in chlorination,[1] bromination,[2] acylation[3] and methanesulfonylation[4] reactions of simple aromatic substrates.

Aromatic nitro compounds represent particularly versatile chemical feedstocks for a wide range of industrial products, such as pharmaceuticals, agrochemicals, dyestuffs and explosives. Traditionally, nitration has been performed by a mixture of nitric and sulfuric acids (mixed acid method).[5] However, the method is notoriously unselective for nitration of substituted aromatic compounds and the disposal of the spent acid reagents presents a serious environmental issue. In order to address these problems several alternative methods for aromatic nitration have been developed recently. For example, lanthanide triflates have been used to catalyse nitration with nitric acid, which avoids the use of large volumes of sulfuric acid in the process.[6] However, this provides no enhancement of selectivity. Selectivity of the nitration process can be enhanced by solid catalysts such as clays, but primarily zeolites, which can improve selectivity using alkyl nitrates,[7] acyl nitrates,[8] or even nitric acid itself.[9,10] We have reported the use of zeolite Hβ in conjunction with a mixture of acetic anhydride and nitric acid, which currently offers the best combination of yield and *para*-selectivity for nitration of simple aromatic compounds.[11] None of these methods, however, are totally devoid of disadvantages.

Another approach towards clean nitration involves the use of dinitrogen tetroxide in combination with oxygen or ozone as an oxidant.[12] The method where ozone is employed most likely involves dinitrogen pentoxide, as this is known to be a highly active nitrating agent. The method utilising oxygen is less clear cut and requires the use of tris(pentane-2,4-dionato)iron(III) ($Fe(acac)_3$) as a catalyst in an organic solvent.[13] In principle, this could lead to a highly atom-efficient process [eqn. (1)], but it is not regioselective. Therefore, we decided to study the use of dinitrogen tetroxide as a nitrating agent in the presence of zeolites, in order to determine if they were able to catalyse the process and impart *para*-selectivity.

$$4ArH + 2N_2O_4 + O_2 \xrightarrow{\text{Catalyst}} 4ArNO_2 + 2H_2O \qquad (1)$$

Zeolites have been used before in the vapour phase nitration of aromatic compounds using nitrogen dioxide. However, this process did not involve oxygen, was complicated, required a high flow rate for the carrier gas (N_2, 880 ml min^{-1}) and showed poor *para*-selectivity.[14] We now report that certain zeolites can indeed catalyse the process of nitration, as shown in eqn. (1), whilst simultaneously providing enhanced *para*-selectivity.

Initially, an attempt was made to reproduce approximately the conditions of Suzuki for nitration of chlorobenzene. Liquid N_2O_4 (approx. 10 ml) was condensed into a trap at −78 °C and was then warmed to 0 °C. $Fe(acac)_3$ (0.355 g) and chlorobenzene (10 mmol) were then added, the system was flushed with oxygen and the mixture was stirred at 0 °C for 48 h. The product thus obtained contained nitrochlorobenzenes in proportions (2-:3-:4-nitrochlorobenzene proportions of 32: < 1:67) that approximated to those reported by Suzuki, but also showed significant quantities of a product based upon nitration of acetylacetone.

We then carried out similar reactions in which various zeolites were used as catalysts instead of $Fe(acac)_3$ in an attempt to determine which zeolite, if any, would be the most applicable to *para*-selective aromatic nitration. Zeolite β and zeolite Y have three dimensional channels and large pore sizes and were selected on this basis. Mordenite, which has linear large pores, and ZSM-5, which has a medium pore size, were chosen for comparison. Additionally, variation of the cation type was undertaken, with H^+, Na^+, K^+ and NH_4^+ being used in the case of zeolite β, and H^+ and Na^+ in the case of zeolite Y. Finally, zeolite ZSM-5 was tested with two specific Si/Al ratios. Thus, the effects of pore size, channel structure, acidity, cation size and Si/Al ratio could all be assessed. A reaction in the presence of chromatographic silica was also included for comparison. The results are shown in Table 1.

As shown in Table 1, reaction occurred in the presence of all of the zeolites, and all of the reactions gave higher yields than in the absence of any catalyst. The large, three-dimensional-pore zeolites gave higher yields, comparable with those achieved with $Fe(acac)_3$ as catalyst, but the medium pore zeolites and the linear large pore zeolite gave lower yields, as did the silica. All of the zeolites demonstrated higher *para*-selectivity than that obtained with $Fe(acac)_3$, except for NH_4β. This last result may reflect the fact that this was the only zeolite not calcined (heated in air to a high temperature), since this would have caused loss of ammonia and formation of Hβ.

Mordenite and ZSM-5 gave lower *para*-selectivities as well as lower yields, which probably reflects more restricted diffusion through the pores and competition from reaction at the external surface of the solid. The selectivity was also low for the reaction in the presence of silica. The ZSM-5 sample with the higher Si/Al ratio gave a higher *para*-selectivity than that with the lower ratio, possibly because of the process of dealumination, which would have opened up the pore structure of

DOI: 10.1039/b003731l

Table 1 The effect of zeolite type on the nitration of chlorobenzene[a]

Zeolite	Si/Al	*t*/h	Conversion (%)[b]	Yield (%)[b]	Proportions[b]		
					ortho	*meta*	*para*
None[c]	—	50	6	2	39	0	61
SiO_2[c]	—	50	40	28	29	< 1	70
Hβ	25	50	100	90	14	< 1	85
Naβ	24	50	100	96	15	0	85
Kβ	24	50	97	92	21	0	79
NH_4β	25	50	76	70	30	1	69
HY	30	50	100	91	16	2	82
NaY	28	50	100	91	16	1	83
HMord.	10.5	50	36	28	27	0	73
HZSM-5	50	72	44	42	28	2	70
HZSM-5	150	72	48	32	20	< 1	79

[a] All reactions were carried out with zeolite (1.0 g), chlorobenzene (10.0 mmol), 1,2-dichloroethane (30 ml) and nitrogen dioxide (*ca.* 10 ml) at 0 °C. [b] Calculated by quantitative GC. [c] For comparison.

the zeolite, causing it somewhat to resemble the larger pore systems. However, the yield with the higher Si/Al ratio sample was less, possibly because of the lower density of effective catalytic sites. Interestingly, the nature of the cation present appeared to have a negligible effect on the reactions, the H^+, Na^+ and K^+ forms of the zeolites giving very similar results for each reaction where comparison was possible. Evidently, the process does not rely upon strong acid catalysis and does not depend significantly on cation size. Perhaps the role of the active site is merely to bring together the reagents and substrates within the confines of the pores by simple co-adsorption. Alternatively, perhaps the active site facilitates cleavage of dinitrogen tetroxide to give monomeric nitrogen dioxide, which has been suggested as the active reagent in vapour phase reactions.[15]

Zeolites Hβ and Naβ produced the greatest selectivity for *para*-chloronitrobenzene (85%) and the highest yields (90 and 96%). Therefore, zeolite Hβ was tested with a range of other substrates. The results are shown in Table 2.

Table 2 The nitration of toluene, benzene and halogenobenzenes with nitrogen dioxide and zeolite Hβ in 1,2-dichloroethane[a]

Substrate	*t*/h	Conversion (%)[b]	Yield (%)[b]	Proportions[b]		
				ortho	*meta*	*para*
Toluene	24	100	85	53	2	45
Benzene	45	55	50	—	—	—
Fluorobenzene	48	100	95	7	0	93
Chlorobenzene	48	98	95	14	< 1	85
Bromobenzene	48	> 99	94	22	< 1	77
Iodobenzene	48	99	95	37	1	62

[a] All reactions were carried out with zeolite (1.0 g), substrate (10.0 mmol), 1,2-dichloroethane (30 ml) and nitrogen dioxide (*ca.* 10 ml) at 0 °C. [b] Calculated by quantitative GC.

After 24 h toluene had been completely consumed and produced a reasonable yield of mononitrotoluenes (85%). The *para*-selectivity was fairly low, though greater than for mixed acid nitrations. The reaction with benzene was slow, being only *ca.* 50% complete after 48 h. However, all the halogenobenzenes gave good yields and reasonable *para*-selectivities. This work therefore demonstrates that zeolites β and Y, with H^+, Na^+ or K^+ cations, can be efficient inorganic catalysts for the nitration of halogenobenzenes with dinitrogen tetroxide and oxygen and produce high *para*-selectivities and yields compared to classical nitration methods.

Furthermore, this method represents a low energy and potentially clean synthesis of halonitrobenzenes using an easily recycled solvent and catalyst system. However, at this preliminary point the reactions involve a large excess of dinitrogen tetroxide, long reaction times and the use of an undesirable chlorinated solvent. Therefore, our future efforts in this area will be concentrated on minimising these factors.

The reaction of chlorobenzene illustrates the general procedure for the nitration process. In an ice-water cooling bath was placed a 100 ml round-bottom flask containing a mixture of chlorobenzene (10 mmol), zeolite (1.0 g), and 1,2-dichloroethane (30 ml). The flask was flushed with oxygen gas for 20 min at 0 °C. Liquid nitrogen dioxide (*ca.* 10 ml, *ca.* 280 mmol) was added quickly all at once to the stirred mixture, and the flask was connected to an oxygen gas balloon. After 50 h at 0 °C, the mixture was filtered through a medium porosity sintered glass funnel, and the filtrate was diluted with water. 1,2-Dichloroethane was added and the organic phase was separated and dried over magnesium sulfate. The isomer distribution was determined by gas chromatography (PU 4400) (octadecane was added as an internal standard).

Notes and references

1 K. Smith, M. Butters, W. E. Paget, D. Goubet, E. Fromentin and B. Nay, *Green Chem.*, 1999, **2**, 83.
2 K. Smith, P. He and A. Taylor, *Green Chem.*, 1999, **1**, 35.
3 K. Smith, Z. Zhenhua and P. K. G. Hodgson, *J. Mol. Catal. A*, 1998, **134**, 121.
4 K. Smith, G. M. Ewart and K. R. Randles, *J. Chem. Soc., Perkin Trans. 1*, 1997, 1085.
5 E. R. Ward, *Chem. Br.*, 1979, **15**, 297.
6 F. J. Waller, A. G. M. Barrett, D. C. Braddock and D. Ramprasad, *Chem. Commun.*, 1997, 613.
7 T. J. Kwok and K. Jayasuriya, *J. Org. Chem.*, 1994, **59**, 4939.
8 A. Cornelis, A. Gerstmans and P. Laszlo, *Chem. Lett.*, 1988, 1839.
9 K. Jayasuriya and R. Damavarapu, *US Pat. Appl.*, 5946638, 1999.
10 B. M. Choudary, M. Sateesh, M. L. Kantam, K. K. Rao, K. V. R. Prasad, K. V. Raghavan and J. A. R. P. Sarma, *Chem. Commun.*, 2000, 25.
11 K. Smith, A. Musson and G. A. DeBoos, *J. Org. Chem.*, 1998, **63**, 8448.
12 H. Suzuki and T. Mori, *J. Chem. Soc., Perkin Trans. 2*, 1994, 479.
13 H. Suzuki, S. Yonezawa, N. Nonoyama and T. Mori, *J. Chem.Soc., Perkin Trans. 1*, 1996, 2385.
14 I. Schumacher, *Eur. Pat. Appl.*, 0053031, 1981.
15 A. Germain, T. Akouz and F. Figueras, *J. Catal.*, 1994, **147**, 163; A. Germain, T. Akouz and F. Figueras, *Appl. Catal. A: Gen.*, 1996, **136**, 37.

Friedel–Crafts alkenylation of arenes using alkynes catalysed by metal trifluoromethanesulfonates

Teruhisa Tsuchimoto, Takeshi Maeda, Eiji Shirakawa* and Yusuke Kawakami

Graduate School of Materials Science, Japan Advanced Institute of Science and Technology, 1-1 Asahidai, Tatsunokuchi, Ishikawa 923-1292, Japan. E-mail: shira@jaist.ac.jp

Received (in Cambridge, UK) 9th May 2000, Accepted 3rd July 2000
Published on the Web 3rd August 2000

Metal trifluoromethanesulfonates [M(OTf)$_n$; M = Sc, Zr, In] catalyse the Friedel–Crafts alkenylation of arenes using alkynes, including internal alkynes, to give, through an alkenyl cation intermediate, 1,1-diarylalkenes in high to excellent yields.

Friedel–Crafts alkylation reactions have been extensively studied and have established a prominent historical position in organic synthesis including industrial applications.[1] In contrast, little has been known about the corresponding Friedel–Crafts alkenylation reaction with either an alkenyl halide or an alkyne. With an alkenyl halide, a substituent such as a phenylthio[2] or an aryl[3] group that stabilizes an alkenyl cation intermediate is required to attain a good yield. The reaction using an alkyne, where a C–H bond of the arene adds to the triple bond of an alkyne, is environmentally friendly without being accompanied by formation of by-products like hydrogen halide. However, the reaction often brings about the polymerization of alkynes and results in the formation of undesired side products.[1b,4] Zeolite HSZ-360 as a heterogeneous acid was found to be efficient especially for *ortho*-selective monoalkenylation of phenol, but only phenylethyne had been examined as a substrate.[5] Recently, alkenylation of arenes with trimethylsilylethyne promoted by an excess amount of $GaCl_3$ was also reported.[6] To the best of our knowledge, the Friedel–Crafts alkenylation reaction with internal alkynes has yet to be explored. We found that metal triflates [M(OTf)$_n$; M = Sc, Zr, In] are effective catalysts for the Friedel–Crafts alkenylation reaction with internal alkynes as well as terminal ones.[7]

The reaction of phenylethyne (**1a**) (0.5 mmol) with *p*-xylene (**2a**) (8.0 ml) at 85 °C for 19 h in the presence of 10 mol% of In(OTf)$_3$ proceeded smoothly to give the corresponding alkenylation product, 1-phenyl-1-(*p*-xylyl)ethene (**3a**), in 80% yield (Scheme 1). Although the reaction using Sc(OTf)$_3$[8] or Zr(OTf)$_4$ required a longer reaction time, **3a** was obtained in 92 or 53% yield, respectively. On the other hand, metal chlorides such as $ZrCl_4$ and $AlCl_3$ gave **3a** only in low yields.

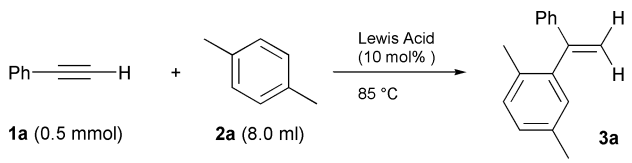

In(OTf)$_3$	Sc(OTf)$_3$[a]	Zr(OTf)$_4$	$ZrCl_4$	$AlCl_3$
80% (19 h)	92% (96 h)	53% (39 h)	1% (100 h)	6% (100 h)

[a] 0.1 ml of $MeNO_2$ was used as an additive.

Scheme 1

These results prompted us to survey the scope of the reaction. The results are summarized in Scheme 2 and Table 1. Arenes except for *p*-dimethoxybenzene were used not only as the substrates but also as solvents. Phenylethyne was successfully reacted with benzene in the presence of Sc(OTf)$_3$ to afford 1,1-diphenylethene in 73% yield (entry 2). A phenylethyne bearing an electron-donating group (–OMe) at the *para* position was also reacted with *p*-xylene using Sc(OTf)$_3$ to give **3** in 62% yield (entry 3). Although Sc(OTf)$_3$ was totally inactive for more electron-deficient alkynes than phenylethyne, In(OTf)$_3$ was effective for the reaction of phenylethyne having a *p*-Cl or *p*-CF_3 group and the products were obtained in high yields (entries 4 and 5). Internal alkynes can obviously participate in this protocol. 1-Phenylprop-1-yne satisfactorily reacted with benzene, toluene, *p*-xylene or anisole using In(OTf)$_3$ to produce the corresponding products (entries 6–11). Zr(OTf)$_4$ was especially effective for the reaction of *p*-dimethoxybenzene to furnish **3** in

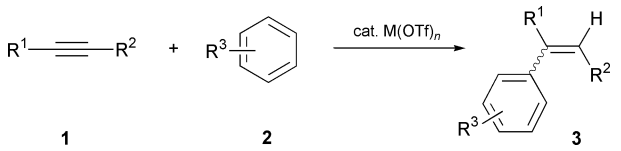

Scheme 2

Table 1 Metal triflate-catalysed Friedel–Crafts alkenylation with alkynes[a]

Entry	R^1—≡—R^2	Ar–H (ml)	Lewis Acid	Time/h	Yield (%)[b]
1	Ph—≡—H	*p*-Xylene (8)	Sc(OTf)$_3$	96	92[c]
2	Ph—≡—H	PhH (10)	Sc(OTf)$_3$	186	73[c]
3	*p*-$MeOC_6H_4$—≡—H	*p*-Xylene (8)	Sc(OTf)$_3$	10	62
4[d]	*p*-ClC_6H_4—≡—H	*p*-Xylene (8)	In(OTf)$_3$	15	73
5[d]	*p*-$CF_3C_6H_4$—≡—H	*p*-Xylene (8)	In(OTf)$_3$	50	82
6	Ph—≡—Me	PhH (4)	In(OTf)$_3$	16	63
7	Ph—≡—Me	PhMe (4)	In(OTf)$_3$	16	73[e]
8	Ph—≡—Me	*p*-Xylene (4)	In(OTf)$_3$	20	80[f]
9	Ph—≡—Me	*p*-Xylene (4)	Zr(OTf)$_4$	40	68[f]
10	Ph—≡—Me	*p*-Xylene (4)	Sc(OTf)$_3$	152	72[f]
11	Ph—≡—Me	PhOMe (4)	In(OTf)$_3$	5	72[e]
12	Ph—≡—Me	*p*-$(MeO)_2C_6H_4$[g]	Zr(OTf)$_4$	2	70[f]
13	Ph—≡—Me	PhBr (4)	In(OTf)$_3$	63	33[e]
14	Ph—≡—Me	PhCl (4)	In(OTf)$_3$	112	28[e]
15	Ph—≡—Ph	*p*-Xylene (4)	In(OTf)$_3$	70	79[f]

[a] The reaction was carried out at 85 °C using an alkyne (0.5 mmol) and an arene (4–10 ml) in the presence of 10 mol% of a Lewis acid. Nitromethane (0.1 ml) was used as an additive in entries 1, 2, 3 and 10. [b] Isolated yield based on alkyne. [c] GC yield. [d] The reaction was carried out at 130 °C. [e] The reaction gave a mixture of 6 isomers which consist of *o*-, *m*- and *p*-regioisomers including the corresponding *cis*/*trans* isomers determined by GC–MS. The isomer ratios are as follows; 30:4:3:2:31:30 (entry 7); 3.0:34.4:0.1:0.3:32.0:30.2 (entry 11); 2:29:1:1:32:35 (entry 13); 2:31:1:1:22:43 (entry 14). [f] Isomer ratios of stereoisomers were determined by GC as follows; 91:9 (entry 8); 91:9 (entry 9); 91:9 (entry 10); 90:10 (entry 12); 93:7 (entry 15). [g] The reaction was carried out with *p*-dimethoxybenzene (2.5 mmol) in chlorobenzene (4 ml) as a solvent.

DOI: 10.1039/b003702h

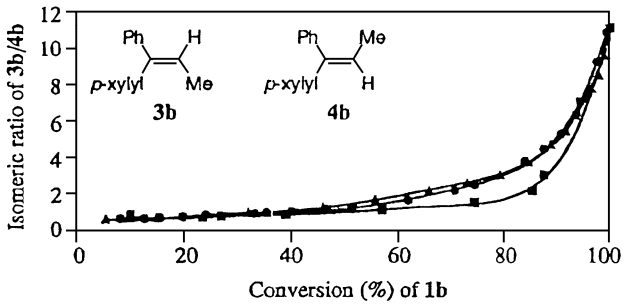

Fig. 1 Plots of isomeric ratio of **3b**:**4b** *versus* conversion (%) of **1b** for $In(OTf)_3$ (-●-), $Zr(OTf)_4$ (-■-), and $Sc(OTf)_3$ (-▲-).

70% yield, whereas $In(OTf)_3$ did not catalyse the reaction (entry 12). Treatment of halobenzenes, which can be used as a solvent in the Friedel–Crafts alkylation, with 1-phenylprop-1-yne gave the products in somewhat lower yields (entries 13 and 14). Arenes attacked these alkynes exclusively at the carbon having the aryl group. The reaction of 1,2-diphenylethyne with *p*-xylene using $In(OTf)_3$ as a catalyst also gave **3** in 79% yield (entry 15). In all cases, the triarylalkane that would be produced by the reaction of **3** and **4** with an arene was not observed.

Dependence of the isomer ratio between alkenylated products **3b** and **4b** on the conversion of 1-phenylprop-1-yne (**1b**) in the reaction with *p*-xylene is illustrated in Fig. 1.[9] Fig. 1 indicates that (1) both stereoisomers **3b** and **4b** already exist in almost a 1:1 ratio at the early stage of the reaction, and (2) there is a drastic change of the isomer ratio at the late stage of the reaction.

Two routes (path A and path B) are possible for this alkenylation reaction (Scheme 3). In path A, the attack of an arene to initially formed zwitterionic intermediate **5** from both X and Y sites affords a mixture of **7** and **8**, which are transformed by protonation to **3** and **4**, respectively. As regards path B, the activation of an alkyne by a metal triflate and the attack of an arene to the alkyne proceeds through a concerted mechanism. Therefore, an arene attacks **1b** stereoselectively from the side opposite to the metal triflate to furnish **7** and subsequent protonation of **7** gives **3** as the sole stereoisomer. The existence of both **3b** and **4b** at the early stage of the reaction

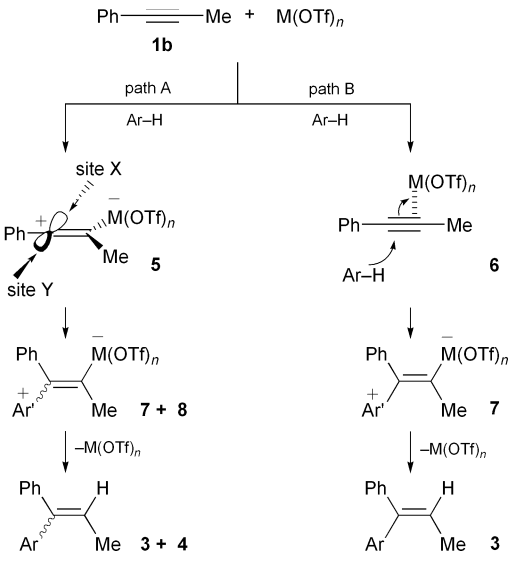

Scheme 3

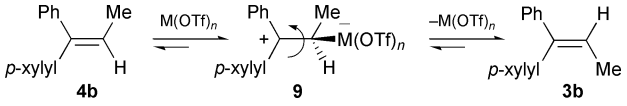

Scheme 4

strongly suggests that path A works in the reaction. The predominance of **3b** at the end of the reaction should be due to an equilibrium between **3b** and **4b** under the reaction conditions (Scheme 4). Thus, formation of alkyl cation **9** by the reaction of **4b** with a metal triflate and subsequent bond rotation followed by elimination of the metal triflate would induce the isomerization from **4b** to thermodynamically favored **3b**. Prolonged reaction time (100 h) showed no further change in the isomer ratio.

The drastic change in the isomer ratio around the point over 80% conversion of **1b**, *i.e.*, almost consumption of **1b**, may show that metal triflates prefer an alkyne rather than an alkene for complexation under the reaction conditions. Actually, in the absence of **1b**, the isomerization catalysed by 10 mol% of $In(OTf)_3$ in *p*-xylene at 85 °C was completed within 20 min to give a 91:9 ratio of **3b** and **4b** from a mixture of **3b** and **4b** in a ratio of 45:55. Such salient character of metal triflates should be ideal for the Friedel–Crafts alkenylation with alkynes to reduce the possibility of side reactions through alkyl cation **9**.

In summary, we disclose here the preliminary results on the use of some metal triflates as efficient catalysts for the Friedel–Crafts alkenylation of arenes with alkynes including internal ones. Further investigation on the reaction of alkynes with nucleophiles other than arenes is currently in progress.

Notes and references

1 For reviews of Friedel–Crafts alkylation reactions: (*a*) W. E. Bachmann, J. R. Johnson, L. F. Fieser and H. R. Snyder, *Org. React.*, 1946, **3**, 1; (*b*) G. A. Olah, *Friedel-Crafts and Related Reactions*, Wiley-Interscience, New York, 1964, *vol. II*, part 1; (*c*) R. M. Roberts and A. A. Khalaf, *Friedel-Crafts Alkylation Chemistry. A Century of Discovery*, Dekker, New York, 1984; (*d*) G. A. Olah, R. Krishshnamurit and G. K. S. Prakash, *Friedel-Crafts Alkylations* in *Comprehensive Organic Synthesis*, ed. B. M. Trost and I. Fleming, Pergamon Press, Oxford, 1991.

2 T. Takeda, F. Kanamori, H. Matsusita and T. Fujiwara, *Tetrahedron Lett.*, 1991, **32**, 6563.

3 T. Kitamura, S. Kobayashi, H. Taniguchi and Z. Rappoport, *J. Org. Chem.*, 1982, **47**, 5003.

4 For example: O. W. Cook and V. J. Chabers, *J. Am. Chem. Soc.*, 1921, **43**, 334; J. S. Reichert and J. A. Nieuwland, *J. Am. Chem. Soc.*, 1923, **45**, 3090; J. A. Reilly and J. A. Nieuwland, *J. Am. Chem. Soc.*, 1928, **50**, 2564; I. P. Tsukervanik and K. Y. Yuldashev, *J. Gen. Chem. USSR*, 1961, **31**, 790.

5 G. Sartori, F. Bigi, A. Pastorio, C. Porta, A. Arienti, R. Maggi, N. Moretti and G. Gnappi, *Tetrahedron Lett.*, 1995, **36**, 9177.

6 M. Yamaguchi, Y. Kido, A. Hayashi and M. Hirama, *Angew. Chem., Int. Ed. Engl.*, 1997, **36**, 1313; Y. Kido, S. Yoshimura, M. Yamaguchi and T. Uchimaru, *Bull. Chem. Soc. Jpn.*, 1999, **72**, 1445.

7 We have previously reported $Sc(OTf)_3$-catalysed Friedel–Crafts alkylation reactions of arenes with alcohols, aldehydes or acetals as alkylating agents: T. Tsuchimoto, K. Tobita, T. Hiyama and S. Fukuzawa, *Synlett*, 1996, 557; T. Tsuchimoto, T. Hiyama and S. Fukuzawa, *Chem. Commun.*, 1996, 2345; T. Tsuchimoto, K. Tobita, T. Hiyama and S. Fukuzawa, *J. Org. Chem.*, 1997, **62**, 6997.

8 Addition of nitromethane to make the reaction system homogeneous caused remarkable rate acceleration only in the reaction using $Sc(OTf)_3$ as a catalyst. Use of $AlCl_3$–$MeNO_2$ as a soluble Friedel–Crafts alkylation catalyst has been reported; L. Schmerling, *Ind. Eng. Chem.*, 1948, **40**, 2072; G. A. Olah, S. Kobayashi and M. Tashiro, *J. Am. Chem. Soc.*, 1972, **94**, 7448.

9 Configuration of **3b** and **4b** was determined by NOESY.

Detection of the 'invisible aluminium' and characterisation of the multiple aluminium environments in zeolite USY by high-field solid-state NMR

Colin A. Fyfe,*[a] J. L. Bretherton[a] and L. Y. Lam[b]

[a] *Department of Chemistry, University of British Columbia, 2036 Main Mall, Vancouver, British Columbia, V6T 1Z1, Canada. E-mail: fyfe@chem.ubc.ca, jerry@chem.ubc.ca*
[b] *Petrobras/Cenpes, Rio de Janeiro, Brazil.*

Received (in Irvine, CA, USA) 14th April 2000, Accepted 9th June 2000
Published on the Web 2nd August 2000

The detection of all of the aluminium present in steamed zeolite H-Y catalysts by ^{27}Al MAS NMR at high field (18.8 T, 800 MHz for ^{1}H) is reported; further, it is shown that it is possible by ^{27}Al MAS and MQMAS measurements to clearly identify four separate aluminium environments characteristic of these materials and to unambiguously assign their coordinations.

The acid form of faujasite (zeolite H-Y) is converted to a very stable material by steam treatment at elevated temperatures, producing the universally used cracking catalyst 'ultrastable-Y' (USY). Early ^{29}Si MAS NMR studies documented the increase in the framework Si/Al ratio brought about by steaming.[1–4] ^{27}Al MAS NMR indicated that six-coordinate aluminium (Al^{OCT}) is produced even during mild calcination and that substantial amounts of amorphous material can be generated by steaming,[1–8] characterised by a broad ^{27}Al resonance between those of the four-coordinate aluminium (Al^{TET}, at ≈ 60 ppm) and Al^{OCT} (at ≈ 0 ppm). The nature of the species responsible for this signal intensity has been a matter of dispute for almost twenty years. Some workers have assigned the broad signal to a second, distorted tetrahedral species.[4,5*a*,8,9] More recently, various authors have shown that the chemical shift of the intensity maximum of the broad resonance corresponded to five-coordinate aluminium (Al^{PENT}) and the broad resonance was attributed to this species.[5*b*,6,10,11] Despite considerable ongoing effort, there remains little overall agreement in the interpretation of ^{27}Al NMR data. Early studies also suffered from the problem of quantification of the ^{27}Al spectra:[3,4,7,9] Even using small pulse angles, some 30% of the aluminium known to be present could not be observed (the so-called 'invisible aluminium'). Therefore the nature of the aluminium and the related catalytic sites in USY are still poorly understood at the present time.

In the present work, we present preliminary results of an ultra-high field ^{27}Al MAS and MQMAS NMR investigation of a USY sample prepared from Na-Y by the conventional method of ammonium exchange followed by steam treatment at 600 °C, repeated twice. ^{27}Al NMR spectra were obtained at 208.43 MHz (18.8 T, 800 MHz ^{1}H) using a Varian INOVA Spectrometer. In this work we have been able to quantitatively observe all of the aluminium present and to identify four well defined aluminium environments.

The integrated intensities of the ^{27}Al single pulse MAS [Fig. 1(a) and (d)] and 90–180° spin–echo MAS NMR spectra of weighed samples were calibrated at both 104.26 MHz (9.4 T, 400 MHz for ^{1}H) and 208.43 MHz against spectra of weighed Na-Y and Na-A samples acquired under identical conditions. In line with previous work,[3,4,7,9] the data at 104.26 MHz not only fail to account for all of the aluminium present, but show considerable differences in intensity distributions between single pulse and echo experiments; the echo experiments detecting larger contributions from the broader resonances. However, there are no significant differences between the single pulse [Fig. 1(a)] and echo spectra at 18.8 T, where the integrated intensities of both spectra indicate that signal is observed from 100% of the aluminium present.

The MQMAS experiment introduced by Frydman and Harwood[12] (Fig. 2) correlates peaks in the MAS dimension (F2) to signals in the isotropic dimension (F1), with shifts in this dimension being a linear combination of isotropic chemical and

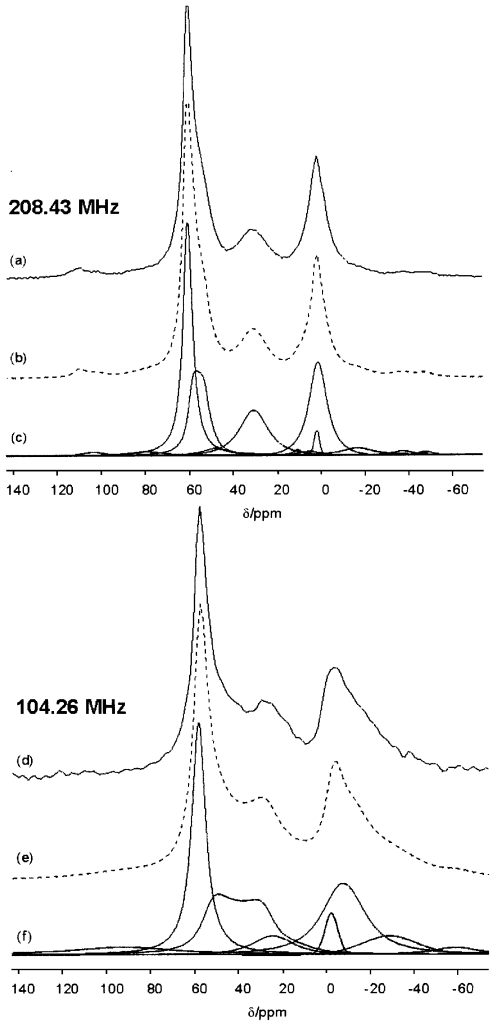

Fig. 1 (a) ^{27}Al single pulse MAS spectrum of USY at 208.43 MHz, recorded at a spinning speed of 10.2 kHz. (b) Simulation of (a). (c) Deconvolution of (b). (d) ^{27}Al single pulse MAS spectrum of USY at 104.26 MHz, recorded at a spinning speed of 9.8 kHz. (e) Simulation of (d). (f) Deconvolution of (e). Chemical shift is referenced to 1 M $Al(NO_3)_3$ aqueous solution. Spectral simulations and deconvolutions were made using 'Dmfit 98'.[15] Isotropic peaks are simulated by half-integer spin quadrupolar lineshapes (parameters given in Table 1) with superimposed exponential broadenings. Spinning sideband intensity is approximated by peaks with mixed Lorentzian and Gaussian character.

DOI: 10.1039/b003081n

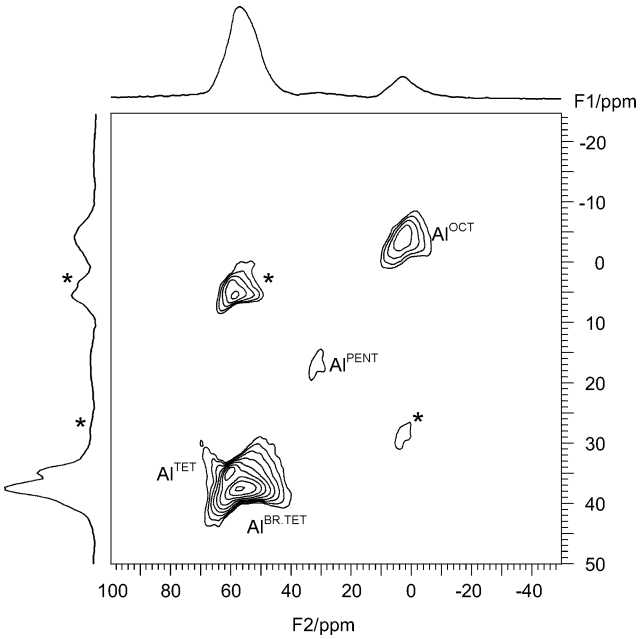

Fig. 2 ^{27}Al MQMAS spectrum of USY at 208.43 MHz, recorded at a spinning speed of 10.2 kHz. Chemical shift is referenced to 1 M $Al(NO_3)_3$ aqueous solution. Coherences were generated using a three-pulse, Rotationally Induced Adiabatic Transfer pulse sequence and selected with a 24-step phase cycle. A shearing transformation was performed after the first Fourier transform. Skyline projections along both axes are shown. * indicates spinning sidebands.

second order quadrupolar shifts. Using this technique, many of the problems caused by peak overlap in the MAS experiment are alleviated, allowing the coordinations to be clearly established.

Fig. 2 clearly shows four aluminium environments. At 61 ppm in F2 there is a sharp Al^{TET} resonance, whose F2 shift closely matches the sharp peak from the framework aluminium in Na-Y spectra. In addition there is clearly a separate and much broader $Al^{BR.TET}$ resonance with an intensity maximum at 57 ppm in F2. Upfield of the four-coordinate resonances are similarly broad Al^{PENT} and Al^{OCT} peaks, with intensity maxima in F2 at shifts typical of five- and six-coordinate aluminium species previously reported.[6,13,14]

Fig. 1(b) and (c) shows a simulation of the single pulse MAS spectrum [Fig. 1(a)] using the program 'Dmfit 98'.[15] The complete intensity profile is based on only the intensity from four peaks (and their spinning sidebands) corresponding to the signals observed in the MQMAS spectrum (Fig. 2). A small, sharp resonance in the octahedral region due to monomeric octahedral aluminium has been observed in the ^{27}Al NMR spectra of USY samples of lower Si/Al. For completeness, a similar peak is included in the simulated spectra of the sample used in this study [Fig. 1(c)], although it has no significant influence on the proportions of the different coordinations calculated to be present (Table 1).

The same parameters (Table 1) yield simulations of similar quality for the ^{27}Al MAS spectra of the same sample taken at 104.26 MHz [Fig. 1(d), (e)] and 156.38 MHz (14.4 T, 600 MHz for ^{1}H). They also reproduce the observed MQMAS isotropic (F1) shifts to within ±5 ppm at both 104.26 and 208.43 MHz, with the positions of the two tetrahedral peaks being predicted to within an accuracy of ±1 ppm. From these data it is apparent that the broad peak at ≈ 30 ppm observed in the spectrum at 104.26 MHz [Fig. 1(d)] has contributions from both broad tetrahedral and five-coordinate aluminium. Spectra at the two higher fields show that each of these account for ≈ 20% of the total spectral intensity.

Framework Si/Al ratios of the Na-Y starting material (calculated from ^{29}Si MAS NMR) and of the USY sample (calculated both by ^{29}Si NMR and IR) suggest that 33% of the aluminium remains in the USY framework following steaming.

Table 1 Summary of USY single pulse ^{27}Al MAS spectral simulation parameters[a]

	δ_{CS}[b]/ppm	Average C_Q[c]/kHz	η_Q	% of total intensity[d]
Al^{TET}	60.7	360	0.53	33
$Al^{BR.TET}$	60.4	940	0.1	21
Al^{PENT}	32.2	578	0.1[e]	20
Al^{OCT}	3.2	492	0.1[e]	26

[a] Chemical shift and quadrupolar coupling distributions are accounted for by an exponential broadening function with a chemical shift component proportional to the magnetic field strength and a quadrupolar coupling component inversely proportional to the magnetic field. [b] Isotropic chemical shift. [c] Calculated to ±3% for 208.43 MHz spectrum using spinning sideband intensities approximated by lineshapes with mixed Lorenzian and Gaussian character. [d] $C_Q = 3e^2qQ/2I(2I - 1)\hbar$. [e] The parameter η_Q has a minimal effect on the simulated MAS spectrum [Fig. 1(b)].

This is in good agreement with the intensity ratios of the simulated spectrum [Fig. 1(c)] in which 33% of the overall intensity is contained within the Al^{TET} peak (Table 1) suggesting that all of the aluminium contained within the fully intact framework could be represented by the Al^{TET} peak at 61 ppm.

In summary, this study shows that high magnetic field strengths solve the problem of the "invisible aluminium" associated with USY materials and that these quantitative ^{27}Al MAS spectra consist of intensity from four distinct aluminium environments. A complete account of this work and its extension to related systems is currently in preparation. We believe that this represents the most complete and self-consistent investigation of the aluminium species present in USY materials to date. Further investigations of the exact nature of the framework and non-framework aluminium species in these steamed zeolite systems is also being carried out.

This research was performed in the Environmental Molecular Sciences Laboratory (a national scientific user facility sponsored by the U.S. DoE Office of Biological and Environmental Research) located at the Pacific Northwest National Laboratory, operated by Battelle for the DoE. We thank Dr David Hoyt and the EMSL staff for their kind assistance and for access to their facility, without which this work would not have been possible. C. A. F. acknowledges the financial assistance of the NSERC of Canada in the form of operating and equipment grants.

Notes and references

1 J. Klinowski, J. M. Thomas, C. A. Fyfe and G. C. Gobbi, *Nature*, 1982, **296**, 533.
2 J. Scherzer, *ACS Symp. Ser.*, 1984, **284**, 160.
3 J. Klinowski, C. A. Fyfe and G. C. Gobbi, *J. Chem. Soc., Faraday Trans. 1*, 1985, **81**, 3003.
4 D. Freude, E. Brunner, H. Pfeifer, D. Prager, H.-G. Jerschkewitz, U. Lohse and G. Oehlmann, *Chem. Phys. Lett.*, 1987, **139**, 325.
5 (*a*) A. Samoson, E. Lippmaa, G. Engelhardt, U. Lohse and H.-G. Jerschkewitz, *Chem. Phys. Lett.*, 1987, **134**, 589; (*b*) G. J. Ray and A. Samoson, *Zeolites*, 1993, **13**, 410.
6 J.-P. Gilson, G. C. Edwards, A. W. Peters, K. Rajagopalan, R. F. Wormsbecher, T. G Roberie and M. P. Shatlock, *J. Chem. Soc., Chem. Commun.*, 1987, 91.
7 P. V. Shertukde, W. K. Hall, J.-M. Dereppe and G. Marcelin, *J. Catal.*, 1993, **139**, 468.
8 M. J. Remy, D. Stanica, G. Poncelet, E. J. P. Feijen, P. J. Grobet, A. J. Martens and P. A. Jacobs, *J. Phys. Chem.*, 1996, **100**, 12 440.
9 P. J. Grobet, H. Geerts, M. Tielen, J. A. Martens and P. A. Jacobs, *Stud. Surf. Sci. Catal.*, 1989, **46**, 721.
10 D. Coster, A. L. Blumenfield and J. J. Fripiat, *J. Phys. Chem.*, 1994, **98**, 6201.
11 A. L. Blumenfield and J. J. Fripiat, *Top. Catal.*, 1997, **4**, 119.
12 L. Frydman and J. S. Harwood, *J. Am. Chem. Soc.*, 1995, **117**, 5367.
13 T. E. Wood, A. R. Siedle, J. R. Hill, R. P. Skarjune and C. J. Goodbrake, *Mater. Res. Symp. Proc.*, 1990, **180**, 87.
14 D. Coster and J. J. Fripiat, *Chem. Mater.*, 1993, **5**, 1204.
15 D. Massiot, H. Thiele and A. Germanus, extended version of Bruker Winfit, *Bruker Rep.*, 1994, **140**, 43.

ChemComm

An efficient synthesis of heterocyclic *N*-oxides over molecular sieve catalysts†

M. Ramakrishna Prasad, G. Kamalakar, G. Madhavi, S. J. Kulkarni* and K. V. Raghavan

Catalysis and Physical Chemistry Division, Indian Institute of Chemical Technology, Hyderabad-500 007, India. E-mail: root@csiict.ren.nic.in

Received (in Cambridge, UK) 16th May 2000, Accepted 3rd July 2000
Published on the Web 2nd August 2000

Heterocyclic *N*-oxides have been synthesized in very high yields over redox molecular sieve catalyts in the presence of H_2O_2.

N-Oxides hold a key position in the chemistry of heterocyclics in that they offer functional group manipulation and structural modification possibilities, which are not accessible by other methods. Recently the synthesis of heterocyclic *N*-oxides using oxides of rhenium ($MeReO_3$) have been reported by Sharpless *et al.*[1,2] The catalysts/reagents used were methyltrioxyrhenium (MTO), ReO_3, Re_2O_7, $HOReO_3$,Me ReO_3. These rhenium oxide reagents are water sensitive and undergo changes in the presence of water and so cannot be reused. The compounds are often obtained by the oxidation of heterocycles with acetic acid and hydrogen peroxide[3] ($AcOH/H_2O_2$), *m*-chloroperbenzoic acid (MCPBA),[4] monoperoxyphthalic acid,[5] dioxiranes,[6] hydrogen peroxide[7] and more recently Caro's acid (H_2SO_5).[8] Dilute hydrogen peroxide is a poor oxidizing agent but an inexpensive and readily available oxidant and gives H_2O only as a by-product. Recently titanium-containing molecular sieves like TS-1, TiZSM-5 (prepared by post-synthetic modification) with MFI topologies and mesoporous materials like TiMCM-41 have been found to possess very good redox properties in catalyzing many oxidation reactions[9–12] *e.g.* olefin epoxidation, hydroxylation, oxidation of alkanes and conversion of carbonyl compounds to oximes. TiMCM-41, by virtue of its bigger pore diameter and redox property, overcomes the barrier of spatial limitation and has been used to oxidize bigger molecules like 2,6-di-*tert*-butylphenol and cinnamyl alcohol. The preparation of *N*-oxides of mono binuclear heterocycles suffers mainly from the disadvantage of very low yields of product formation in spite of using very costly and stoichiometric amounts of reagents.[13] Titanium-containing redox molecular sieves in the presence of an oxidant like H_2O_2 have the advantage of reusability, no catalyst separation problems, and no environmental disposal problems. In order to overcome problems associated with homogenous reactions, heterogeneous catalysts like molecular sieve materials were employed for the oxidation of heterocycles.

Titanium silicalite (TS-1), TiZSM-5(30) and TiMCM-41 are prepared[14,12,15] in our laboratory by the procedures reported earlier. All these catalysts were characterized using XRD and FTIR analyses and the results are in accordance with the reported literature. Oxidation of substituted pyridines and quinolines and, substituted isoquinolines have been carried out and the results are presented in Table 1. In our studies it is observed that pyridines having electron donating substituent groups such as $–CH_3$, –OH or vinyl are oxidized rapidly in a single step to yield the corresponding *N*-oxides as the exclusive oxidation product when the substrate is treated with 5% wt/wt catalyst and 2 equiv. of 30% H_2O_2. However, pyridines containing electron withdrawing substituent groups like –CN, $-NO_2$ or $–CONH_2$ take comparatively longer to reach the quantitative reaction yield of the product. It can be understood that a peroxo species like Ti(μ-O_2) oxidizes the nitrogen of the heterocycle which results in the corresponding heterocyclic *N*-oxide. TiMCM-41 was used as catalyst for the oxidation of quinolines, isoquinolines and *N*,*N*-dimethylaniline and the products were obtained in quantitative yields. The effect of varying the solvent was also studied for this reaction and the results are presented in Table 2. Methanol, acetone and acetonitrile were found to be better solvents than dichloromethane and chloroform with TS-1 as catalyst. The performance of the catalysts was also studied for 3-cyanopyridine and the results are presented in Table 3. TS-1 and TiZSM-5(30) gave better yields of the product, indicating the better redox system of the materials reported. The effect of varying the reaction temperature for the oxidation of 3-cyanopyridine was studied and the results are presented in Table 4. Methanol at a reaction temperature of 60 °C gave the optimum yield of the product.

All the starting materials and solvents were obtained commercially. A typical oxidation of a substituted pyridine was

Table 1 Oxidation of aromatic heterocycles: variation of substrate

Substrate	Yield of the product (%) (reaction time)	Substrate	Yield of the product (%) (reaction time)
2-Cyanopyridine	81.3[a] (25 h)	2-Picoline	93.0[b] (5 h)
3-Cyanopyridine	97.3[a] (25 h)	3-Picoline	96.0[b] (6 h)
4-Cyanopyridine	84.0[a] (24 h)	4-Picoline	95.0[b] (5 h)
2-Chloropyridine	91.0[a] (24 h)	*N*,*N*-Dimethylaniline	89.0[c] (7 h)
2-Carbamoylpyridine	98.0[a] (24 h)	*N*,*N*-Diethylaniline	95.0[c] (7 h)
2-Picolinic acid	91.0[a] (24 h)	*N*-Methyl-3,4-dimethoxyisoquinoline	83.3[c] (17 h)
2-Hydroxypyridine	92.0[a] (25 h)	Quinoline	34.7[c] (24 h)
2-Vinylpyridine	95.0[a] (24 h)	Isoquinoline	52.0[c] (24 h)

[a] TS-1. [b] TiZSM-5(30). [c] TiMCM-41. Products were characterized by MS, NMR and IR techniques, catalyst was washed and reused. Product was corresponding *N*-oxide.

Table 2 Oxidation of 3-cyanopyridine: variation of solvent

Solvent	Isolated yield(%) of *N*-oxide	Reaction time (h)
Acetone	85.1	25
Methanol	97.3	24
Acetonitrile	90.9	25
DCM	—	25

Reaction temp. 60 °C, substrate; oxidant ½; catalyst TS-1.

Table 3 Oxidation of 3-cyanopyridine: variation of catalyst

Catalyst	Isolated yield(%) of *N*-oxide	Reaction time (h)
TiZSM-5(30)	73.3	26
TS-1	97.3	25
TiMCM-41	53.0	25

Reaction temp. 60 °C; substrate: oxidant = ½, solvent methanol.

† Communication No. 4553.

DOI: 10.1039/b003926h

Table 4 Oxidation of 3-cyanopyridine: variation of reaction temperature

Reaction temp. °C	Isolated yield(%) of *N*-oxide	Reaction time (h)
Room temp.	22.7	23
40	38.8	24
50	52.9	24
60	97.0	25

Substrate: oxidant = $\frac{1}{2}$, solvent methanol; catalyst TS-1.

carried out as follows. A mixture of 4-cyanopyridine (10.0 g, 0.096 mol) and TS-1 (500 mg) in 40 ml of methanol as solvent was refluxed in the presence of 30% aq. H_2O_2 (19.8 ml, 0.192 mol) for 24 h. The progress of the reaction was monitored by TLC. Once the reaction was complete the catalyst was removed by filtration and the product isolated from the solvent by vacuum evaporation. The isolated product by this procedure, contained exclusively the corresponding *N*-oxide as observed from the ^{1}HNMR and mass spectra. 4-Cyanopyridine gave 9.6 g of corresponding *N*-oxide without any trace of the by-product. The products were also confirmed by mass and ^{1}H NMR techniques.

Notes and references

1 C. Copéret, H. Adolfsson, J. P. Chiang, A. K. Yudin and K. Sharpless, *J. Org. Chem.*, 1998, **63**, 1740.
2 C. Copéret, H. Adolfsson, T.-A. V. Khuong, A. K.Yudin and K. B. Sharpless, *Tetrahedron Lett.*, 1998, **39**, 761.
3 V. Boekelheide and W. J. Linn, *J. Am.Chem. Soc.*, 1954, **76**, 1286.
4 P. Albini, *Heterocyclic N-oxides*, ed. B. Raton, CRC Press, FI, 1991, p. 31.
5 P. Brougham, M. S. Cooper, D. A. Cummersoni, H.Heaney and N. Thompson, *Synthesis*, 1987, 1015.
6 R. W. Murray and R. Jeyaraman, *J. Org. Chem.*, 1985, **50**, 2847.
7 G. B. Payne, P. H. Deming and P. H. Williams, *J. Org. Chem.*, 1961, **26**, 659.
8 J. G. Robke and E. J. Behrman, *J. Chem. Soc. D*, 1971, 2867.
9 J. M. Thomas, *Nature*, 1994, **368**, 289.
10 R. A. Sheldon, *CHEM TECH*, 1991, **21**, 566.
11 A. Corma, M. Domine, J. A. Gaibam, J. L. Jorda, M. T. Navarro, F. Rey, J. P. Pariente, J. Tsui and L. T. Nemeth, *Chem. Commun.*, 1998, 2211.
12 G. Kamalakar, S. J. Kulkarni and K. V. Raghavan, *Microporous Mesoporous Mater.*, 1999, **29**, 283.
13 W. C. E. Arends, R. A. Sheldon, M. Wallau and U. Schuchardt, *Angew. Chem., Int. Ed. Engl.*, 1997, **36**, 1144.
14 B. Notari, *Stud. Surf. Sci.Catal.*, 1991, **60**, 343.
15 A. Corma, M. T. Navvarro, J. P. Pariente and F. Sanchez, *Stud. Surf. Sci. Catal.*, 1994, **84**, 69.

ChemComm

Asymmetric Diels–Alder chemistry based on a new chiral auxiliary for 1-hydroxy substituted dienes

Philip Garner,* James T. Anderson and Regis A. Turske

Department of Chemistry, Case Western Reserve University, Cleveland, Ohio 44106-7078, USA.
E-mail: ppg@po.cwru.edu

Received (in Corvallis, USA) 8th May 2000, Accepted 23rd June 2000
Published on the Web 2nd August 2000

A rationally designed chiral auxiliary for hydroxylated dienes results in stereocontrolled Diels–Alder cycloadditions under purely thermal conditions.

The Diels–Alder reaction is arguably one of the most powerful synthetic transformations in the modern organic chemist's arsenal. The stereospecific creation of 2 sigma bonds and up to 4 stereocenters in a single step allows for an unsurpassed increase in the level of molecular complexity.[1] Not surprisingly, the development of asymmetric variants of the Diels–Alder reaction to yield enantiomerically-enriched products has taken center stage. Both stoichiometric (chiral auxiliaries) and catalytic (chiral Lewis acids) approaches to asymmetric Diels–Alder reactions have been investigated. The bulk of these investigations have been concerned with chiral auxiliary modified dienophiles[2] and the development of chiral (dienophile-activating) catalysts.[3] Fewer studies have dealt with chiral auxiliary modified dienes.[4] We now disclose a new THP based chiral auxiliary system for 1-hydroxylated dienes[5] that should be of general utility for a variety of thermal Diels–Alder reactions.

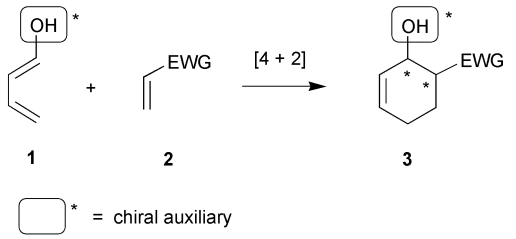

The germ for this idea came from earlier work in our laboratories which found that chiral acetaloxyalkyl radicals such as **4** were trapped preferentially on the *si*-face as a result of steric congestion by the *tert*-butyl substituent at C-6 (Fig. 1).[6] Diastereofacial bias in this TS was rationalized in terms of a radical conformation which maintained an *exo*-anomeric effect[7] and minimized steric repulsion between the acyclic side-chain and THP ring. We surmised that the same stereoelectronic control elements might be extended to the reactive *s-cis* conformation of a 1-oxygenated diene partner in a Diels–Alder reaction as well (*cf.* TS **5**). Our original design also incorporated a potential π-stacking interaction between the reactive *s-cis* diene and a properly disposed naphthalene moiety in the Diels–Alder TS. The prototype 'α-diene' **6** was synthesized along with the chromatographically separable 'β-diene' **7** from 2-naphthylisobutyraldehyde by first making the auxiliary-lactol according to ref. 6 and then incorporating it into McDougal's synthetic approach to 1-alkoxybuta-1,3-dienes.[8] α-Diene **6** was actually used as an inseparable 85:15 mixture of *E*- and *Z*-isomers, the latter being unreactive under our cycloaddition conditions.

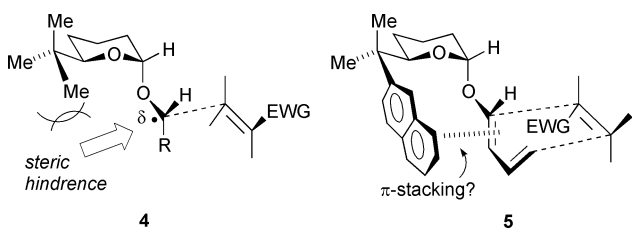

Fig. 1

Chiral dienes **6** and **7** (Fig. 2) were subjected to a battery of Diels–Alder reactions with a variety of electron-deficient dienophiles (Table 1). A number of conclusions can be drawn from these collected data. First, thermal Diels–Alder reactions proceed cleanly with these chiral dienes to give good yields of cycloadducts. As expected for the 1-alkoxy-substituted diene system, higher reaction temperatures are required with the less reactive dienophiles. The observed diastereoselectivities for reactions of the α-diene with *N*-phenyl maleimide (**6** + **8** → **9**), dimethyl maleate (**6** + **11** → **12**), and methacryaldehyde (**6** + **13** → **14**) were found to be quite high (entries 1, 3, and 4) in spite of this potential limitation. Interestingly, reaction of the β-diene with *N*-phenyl maleimide (**7** + **8** → **10**) proceeded about 5 times faster than its α counterpart but with slightly lower (and opposite!)[9] facial selectivity (entry 2). Thus, complementary stereodirection is possible starting from a single antipodal form of the auxiliary. Increasing the Diels–Alder reactivity by reducing the FMO gap between the diene HOMO and dienophile LUMO had the predicted effect of enhancing the diastereoselectivity: diene **6** reacted with the reactive quinoid dienophiles **15**[10] and **17**[11] to give the respective adducts **16** and **18** almost exclusively (entries 5 and 6).[10] On the other hand, the combination of a less sterically encumbered acetylenic dienophile **19** and higher reaction temperatures resulted in a somewhat lower facial selectivity (entry 7).[12]

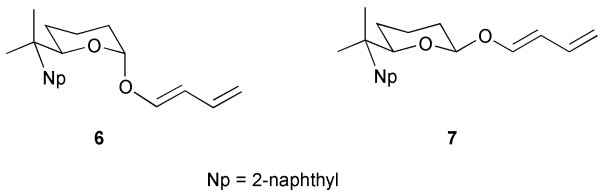

Fig. 2

Chiral dienes such as **6** offer the advantages of high and predictable facial selectivity without the need for Lewis acid activation along with the option of recovering the auxiliary while leaving the synthetically versatile cyclohexen-3-ol substructure intact. The ability to control the diastereoselectivity to the extent shown in purely thermal Diels–Alder reactions (some conducted at temperatures above 100 °C!) is quite remarkable. Although the goal of these initial studies was hypothesis validation, further optimization of the auxiliary design as well as an improved diene synthesis (*via* cross-coupling methodology as described in reference 5*g*) can certainly be envisioned. The incorporation of these chiral auxiliaries into more reactive dienes (for example, a Danishefsky-like system) is also possible. These preliminary results auger well for the further development of this asymmetric Diels–Alder variant as well as

Table 1 Auxiliary-controlled Diels–Alder reactions

Entry	Diene	Dienophile (equiv.)	Reaction conditions	Major product	Yield (%)	Ds
1	**6**	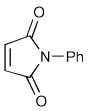 **8** (1.5)	PhH, 80 °C (sealed tube) 12 h	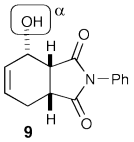 **9**	76	9/1
2	**7**	**8** (1.5)	PhH, 80 °C (sealed tube) 2.5 h	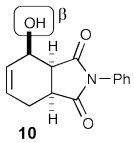 **10**	75	6/1
3	**6**	 **11** (3.0)	PhMe, 130 °C (sealed tube) 1 d	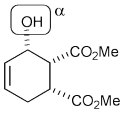 **12**	72	9/1
4	**6**	 **13** (5.0)	PhMe, 115 °C (sealed tube) 3 d	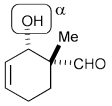 **14**	67	9/1
5	**6**	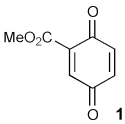 **15** (0.4)	PhH, 0 °C → RT 1 h	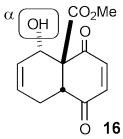 **16**	87	>20/1
6	**6**	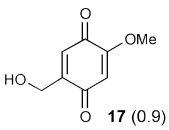 **17** (0.9)	MeOH reflux 14 h	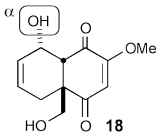 **18**	73	>19/1
7	**6**	 **19** (7.0)	PhH, 80 °C (sealed tube) 3 d	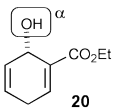 **20**	86	4/1

the application of THP-based auxiliaries to other important synthetic transformations.

This work was supported by the National Science Foundation under Grant No. CHE-9616632.

Notes and references

1 For discussion of this point as well as some classic synthetic applications of the Diels–Alder reaction, see: E. J. Corey and X.-M. Cheng, *The Logic of Chemical Synthesis*, John Wiley & Sons, New York, 1989.

2 G. Sarakinos and E. J. Corey, *Org. Lett.*, 1999, **1**, 1741, and references cited therein.

3 Examples of asymmetric Diels−Alder catalysis: (*a*) D. A. Evans, S. J. Miller, T. Lectka and P. von Matt, *J. Am. Chem. Soc.*, 1999, **121**, 7559; (*b*) A. K. Gosh and H. Matsuda, *Org. Lett.*, 1999, **1**, 2157.

4 For a recent review of chiral heterosubstituted buta-1,3-dienes, see: J. Barluenga, A. Suárez-Sobrino and L. A. López, *Aldrichimica Acta*, 1999, **32**, 4.

5 (*a*) S. David and J. Eustache, *J. Chem. Soc., Perkin Trans. 1*, 1979, 2521; (*b*) B. A. Trost, D. O'Krongly and J. L. Belletire, *J. Am. Chem. Soc.*, 1980, **102**, 7595; (*c*) M. Bednarski and S. Danishefsky, *J. Am. Chem. Soc.*, 1986, **108**, 7060; (*d*) A. Lubineau and Y. Queneau, *J. Org. Chem.*, 1987, **52**, 1001; (*e*) R. C. Gupta, D. S. Larsen, R. J. Stoodley, A. M. Z. Slawin and D. J. Williams, *J. Chem. Soc., Perkin Trans. 1*, 1989, 739; (*f*) R. Tripathy, P. J. Carroll and E. R. Thornton, *J. Am. Chem. Soc.*, 1991, **113**, 7630; (*g*) M. Virgili, M. A. Pericàs, A. Moyano and A. Riera, *Tetrahedron*, 1997, **53**, 13 427.

6 P. Garner and J. T. Anderson, *Tetrahedron Lett.*, 1997, **38**, 6647.

7 R. U. Lemieux, A. A. Pavia, J. C. Martin and K. A. Watanabe, *Can. J. Chem.*, 1969, **47**, 4427.

8 P. G. McDougal and J. G. Rico, *J. Org. Chem.*, 1987, **52**, 4817.

9 This selectivity reversal was ascertained by comparing the optical rotations of the corresponding alcohols derived from cycloadducts **9** and **10** by exposure to PPTS–MeOH. These conversions were very clean and, in both cases, the auxiliary was recovered in high yield as a mixture of anomeric methyl pyranosides. We note that the absolute sense of asymmetric induction with **7** is in accord with Stoodley's TS model for Diels–Alder additions to β-glucosylated dienes (reference 5*e*).

10 White and co-workers used a related Diels–Alder reaction in their synthesis of (±)-euonyminol: J. D. White, N. S. Cutshall, T.-S. Kim and H. Shin, *J. Am. Chem. Soc.*, 1995, **117**, 9780.

11 Danishefsky and co-workers used this dienophile in a racemic approach to vernolepin: S. Danishefsky, P. Shida and K. J. Kato, *J. Org. Chem.*, 1976, **41**, 1081.

12 An analogous Diels–Alder reaction was used by Trost and co-workers in their recent synthesis of (±)-valienamine: B. M. Trost, L. S. Chupak and T. Lübbers, *J. Am. Chem. Soc.*, 1998, **120**, 1732.

An immunochemical approach for the determination of trace amounts of enantiomeric impurities†

Oliver Hofstetter,*[ab] Heike Hofstetter,[b] Meir Wilchek,[b] Volker Schurig[c] and Bernard S. Green*[d]

[a] *Department of Chemistry and Biochemistry, Northern Illinois University, DeKalb, Illinois 60115, USA. E-mail: ohofst@niu.edu*
[b] *Department of Biological Chemistry, The Weizmann Institute of Science, 76100 Rehovot, Israel*
[c] *Institut für Organische Chemie, Universität Tübingen, Auf der Morgenstelle 18, 72076 Tübingen, Germany*
[d] *Department of Pharmaceutical Chemistry, School of Pharmacy, The Hebrew University of Jerusalem, PO Box 12065, 91120 Jerusalem, Israel. E-mail: csgreen@md2.huji.ac.il*

Received (in Cambridge, UK) 8th June 2000, Accepted 11th July 2000
Published on the Web 2nd August 2000

The application of stereoselective antibodies in an enzyme immunoassay enables the quantitative determination of enantiomeric impurities beyond the outer limits of currently available methods; thus, using an antibody raised against a derivative of D-phenylalanine, the D-enantiomer of the free amino acid can be detected in a 100 000 fold excess of the L-enantiomer (ee 99.998%).

The determination of low ees is exceedingly important in wide-ranging chemical studies, such as, asymmetric synthesis,[1] dating of material of biological origin,[2] and the analysis of material of extraterrestrial origin.[3] In experiments where the ee may be very low, *e.g.*, those based upon non-conservation of parity,[4] ultra-sensitive assays are essential. The increasing understanding of the stereoselectivity of drug actions is causing regulatory agencies to define guidelines for the development of stereoisomeric drugs and to demand the specification of their stereochemical purity.[5] In some cases, even minor enantiomeric impurities may cause severe pharmacological and toxicological side effects.[6] Commonly used methods for the determination of enantiopurity include polarimetry, NMR spectroscopy and chromatography, which may allow detection of 0.1% enantiomeric impurity (99.8% ee).[7] More sensitive analytical tools are desirable, and may be vital for health safety, with regard to the production and investigation of therapeutic or nutritional chiral compounds. Improved techniques require the development of highly selective chiral hosts that specifically bind to one enantiomer present in a large excess of the opposite enantiomer. Stereoselective interaction between enantiomers and biological macromolecules such as antibodies, enzymes and receptor proteins is well known and has found various applications in stereochemistry.[8] Recently, we have shown that enantiomeric impurities can be determined by a chiral immunosensor utilizing the exquisite stereoselectivity of antibodies.[9] Here, we demonstrate the determination of enantiomeric impurities at an unprecedented level of detectability using an enzyme immunoassay.

Stereoselective antibodies sensitive to the chiral center of α-amino acids[10] were used to detect D-phenylalanine in non-racemic mixtures by a competitive enzyme-linked immunosorbent assay (ELISA, Fig. 1).[11] Rabbit antibodies, raised against a conjugate, prepared by diazotization of *p*-amino-D-phenylalanine and coupling to the protein keyhole limpet hemocyanin (KLH), stereoselectively bind to D-phenylalanine, but not to L-phenylalanine (Fig. 2). Typical sigmoidal inhibition curves were obtained with D-phenylalanine diluted in phosphate buffered saline (PBS) in the concentration range between 0.01 μM and 500 μM, while no inhibition was observed using L-phenylalanine even at much higher concentrations (up to 50 mM). Antibody binding to D-phenylalanine in the presence of a large excess of L-phenylalanine was shown using the D-enantiomer diluted in a solution of 10 mM L-enantiomer in PBS (Fig. 2). The inhibition curves obtained with D-phenylalanine in the presence and absence of L-phenylalanine are virtually identical, indicating that the stereoselective interaction between the antibody and D-phenylalanine is not affected by the presence of the L-enantiomer. As seen in Fig. 2, D-phenylalanine concentrations as low as 0.1 μM can be detected in the presence of 10 mM L-phenylalanine. This is equivalent to one part of D-phenylalanine in 100 000 parts of L-phenylalanine, corresponding to an ee of 99.998%. The limit of detection is dependent primarily on the affinity of the antibody and the sensitivity of the assay.

The suitability of this antibody for the quantitative determination of enantiomeric impurities was demonstrated in com-

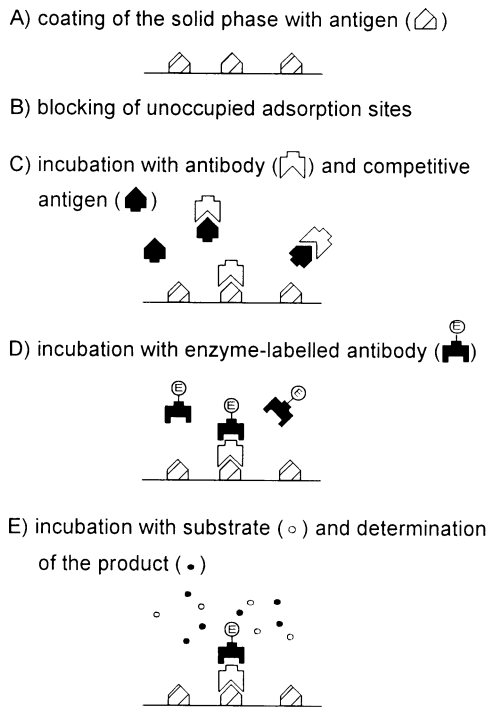

Fig. 1 Schematic depiction of the competitive ELISA procedure.[11] The antigen, in this case *p*-amino-D-phenylalanine, is bound to the wells of a polystyrene microtiter plate (A). After blocking of unoccupied adsorption sites on the plastic surface (B), antibody specific to D-amino acids is added to the wells along with the test sample (competitive antigen) (C). Enzyme-labelled antibody specific for the first antibody is added (D), and a chromogenic enzyme substrate is dispensed (E). The colored product which indicates the amount of the first antibody bound to the solid-phase immobilized antigen is determined photometrically. Between steps A–E, excess reagents are removed by washing.

† This paper is dedicated to Prof. Guenter Wulff on the occasion of his 65th birthday.

DOI: 10.1039/b004587j

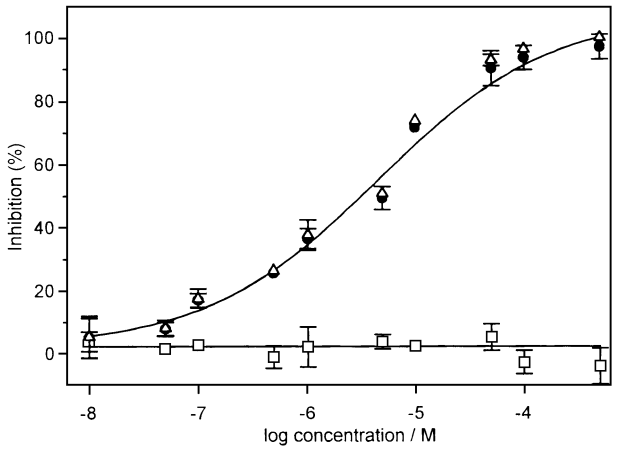

Fig. 2 Inhibition of antibody binding to solid-phase immobilized *p*-amino-D-phenylalanine by increasing concentrations of D-phenylalanine (■); by D-phenylalanine in the presence of 10 mM L-phenylalanine (△); by L-phenylalanine (□). Absorbance values were converted to % inhibition by: % inhibition = $(1 - (A/A_0)) \times 100$; A represents values in the presence of competitor, while A_0 is the absorbance without competitor. Here and in Fig. 3 error bars indicate standard deviations of triple determinations (missing error bars are obscured by the symbols).

petitive assays employing non-racemic mixtures of phenylalanine. Enantiomeric impurities of 0.1% and 0.01% were simulated by the addition of D-phenylalanine (2 μl of a 100 mM stock solution in PBS) to L-phenylalanine (1998 μl and 19 998 μl, respectively, of a 100 mM stock solution in PBS). Fig. 3 shows the inhibition curves obtained with these mixtures. The concentrations of total phenylalanine necessary to cause 50% inhibition of binding (I_{50}) were determined to be 3.12 ± 0.25 mM and 29.12 ± 2.26 mM, respectively. These results are in good accord with the I_{50} value of 3.1 ± 0.3 μM obtained from the calibration curve using enantiomerically pure D-phenylalanine in PBS (Fig. 2), and indicate that, within the accuracy of the method, the test mixtures indeed contain one part D-enantiomer in 1000 parts and 10 000 parts, respectively, of the L-enantiomer.

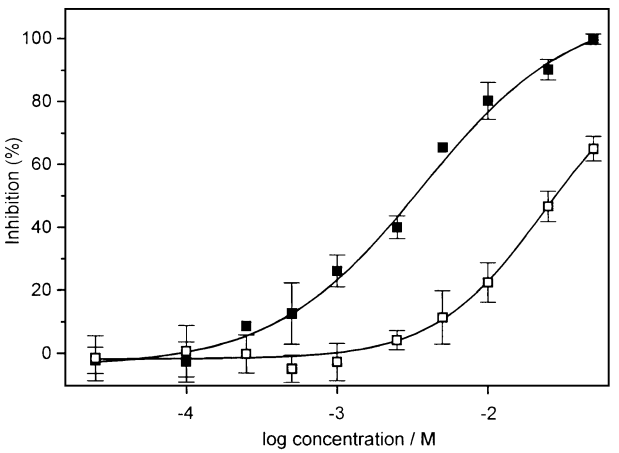

Fig. 3 Inhibition of antibody binding to solid-phase immobilized *p*-amino-D-phenylalanine by increasing concentrations of test mixtures containing 1 part of D-phenylalanine in 1000 parts of L-phenylalanine (■), and 1 part of D-phenylalanine in 10 000 parts of L-phenylalanine (□).

We have demonstrated the value of stereoselective antibodies for the detection of trace enantiomeric impurities and the determination of ee for the α-amino acid phenylalanine. Stereoselective antibodies have been raised for a variety of purposes, including the measurement of degree of racemization.[12] Enzymes have been used to determine enantiopurity[13] but their use is confined to natural substrates and suitable analogs, and is restricted by the number of appropriate enzymes. In contrast, antibodies can be raised against virtually any compound of interest[14] and can be selected and engineered according to one's needs.[15] Their use is routine and they are suitable for automated assays. Thus, the use of antibodies for the determination of enantiomeric impurities at extremely low levels may be extended to other compounds. This approach should be particularly valuable in chemical or pharmaceutical studies where the highest enantiopurity is essential.

We thank the G.I.F., the German-Israeli Foundation for Scientific Research and Development, for financial support, D. Then for technical assistance, and Prof. J. Gal for comments.

Notes and references

1 B. L. Feringa and R. A. van Delden, *Angew. Chem., Int. Ed.*, 1999, **38**, 3418.
2 J. L. Bada, in *Chemistry and Biochemistry of the Amino Acids*, ed. G. C. Barrett, Chapman and Hall, London, 1985, p. 399; A. Maroudas, M. T. Bayliss, N. Uchitel-Kaushansky, R. Schneiderman and E. Gilav, *Arch. Biochem. Biophys.*, 1998, **350**, 61.
3 J. R. Cronin and S. Pizzarello, *Science*, 1997, **275**, 951; M. H. Engel and S. A. Macko, *Nature*, 1997, **389**, 265.
4 S. F. Mason, in *Circular Dichroism. Principles and Applications*, ed. K. Nakanishi, N. Berova and R. W. Woody, VCH Publishers, New York, 1994, p. 39.
5 FDA, *Chirality*, 1992, **4**, 338.
6 M. Eichelbaum and A. S. Gross, *Adv. Drug Res.*, 1996, **28**, 2.
7 V. Schurig, *Methoden Org. Chem. (Houben-Weyl) 4th ed.*, 1995, **Vol. E21a**, p. 147.
8 E. L. Eliel and S. H. Wilen, *Stereochemistry of Organic Compounds*, Wiley, New York, 1996, pp. 201, 257, 273, 409.
9 O. Hofstetter, H. Hofstetter, M. Wilchek, V. Schurig and B. S. Green, *Nature Biotechnol.*, 1999, **17**, 371.
10 O. Hofstetter, H. Hofstetter, V. Schurig, M. Wilchek and B. S. Green, *J. Am. Chem. Soc.*, 1998, **120**, 3251.
11 O. Hofstetter, H. Hofstetter, D. Then, V. Schurig and B. S. Green, *J. Immunol. Methods*, 1997, **210**, 89.
12 C. E. Cook, in *Drug Stereochemistry: Analytical Methods and Pharmacology*, ed. I. W. Wainer and D. E. Drayer, Marcel Dekker, New York, 1988, p. 45; K. L. Rominger, A. Mentrup and M. Stiasni, *Arzneim. Forsch./Drug Res.*, 1990, **40**, 887; A. Huhtikangas, T. Lehtola, R. Virtanen and P. Peura, *Finn. Chem. Lett.*, 1982, 63.
13 J. P. Greenstein and M. Winitz, *Chemistry of the Amino Acids*, vol. 2, Wiley, New York, 1961, p. 1738; H. Scannone, D. Wellner and A. Novogrodsky, *Biochemistry*, 1964, **3**, 1742.
14 K. Landsteiner, *The Specificity of Serological Reactions*, Dover Publications, New York, 1962; D. Pressman and A. Grossberg, *The Structural Basis of Antibody Specificity*, Benjamin, New York, 1968, p. 30.
15 *Antibody Engineering, A Practical Approach*, ed. J. McCafferty, H. Hoogenboom and D. Chiswell, IRP Press, Oxford, 1996.

The fullerene cross-dimer C_{130}: synthesis and properties

Koichi Komatsu,* Koichi Fujiwara and Yasujiro Murata

Institute for Chemical Research, Kyoto University, Uji, Kyoto 611-0011, Japan. E-mail: komatsu@scl.kyoto-u.ac.jp

Received (in Cambridge, UK) 9th May 2000, Accepted 30th June 2000
Published on the Web 2nd August 2000

The fullerene C_{60}–C_{70} cross-dimer C_{130} was synthesized by the mechanochemical solid-state reaction using a high-speed vibration milling technique, and was characterized by UV-vis and ^{13}C NMR spectroscopy as well as electrochemical methods.

The multiple [2 + 2] cycloadditions of C_{60} molecules afford the all-carbon C_{60} polymers by photo-irradiation[1] or high-pressure/high-temperature treatment of C_{60}.[2] However, it is rather difficult to control these reactions to give selectively the dimers and/or trimers. In contrast, it was demonstrated in our previous work that the fullerene dimer C_{120}[3] and trimer C_{180}[4] were successfully produced by the mechanochemical solid-state reaction using a high-speed vibration milling (HSVM) technique. So far there has been no report concerning the oligomerization of C_{70}.† In this paper we report the formation of a C_{60}–C_{70} cross-dimer, C_{130}, by the use of the solid-state HSVM reaction in the presence of 4-aminopyridine which proved to be an effective catalyst for the synthesis of C_{120}[3] and C_{180}.[4]

The reaction was conducted by placing C_{60} (23 mg, 0.032 mmol) and C_{70} (27 mg, 0.032 mmol) in a mixing capsule made of stainless steel, together with 4-aminopyridine (6.5 mg, 0.069 mmol) and a mixing ball, and treating them by HSVM for 30 min. The mixture was examined by HPLC on a Buckyprep column eluted with toluene. Although most of the mixture was found to be the starting materials, the formation of a small amount of what was possibly C_{130} was observed with a retention time of 24 min (HPLC peak area, 1.5%) in addition to C_{120} at 14.5 min (6%), unchanged C_{60} at 7.5 min (46%), and C_{70} at 12 min (44%).

The portion with an HPLC peak at the retention time of 24 min on a Buckyprep column was isolated by the use of a 5PBB column eluted with *o*-dichlorobenzene (ODCB). The analytical HPLC on a Buckyprep column showed that this is composed of a single isomer, and this was confirmed by the ^{13}C NMR spectrum (*vide infra*). The isolated fraction was found to undergo slow dissociation into C_{60} and C_{70} under room light with a half life of about 2 days, suggesting that this peak actually corresponds to C_{130}, which is the [2 + 2] cycloaddition product of C_{60} and C_{70}. The isolated yield of C_{130} was 3.0% (1.5 mg).

After treating this fraction with NaCN in ODCB–*N*,*N*-dimethylformamide, atmospheric pressure chemical ionization mass spectroscopy operated in the negative ion mode exhibited peaks at *m*/*z* 1586 and 1613 corresponding to the mono- and biscyanated C_{130}, *i.e.* $C_{130}(CN)^-$ and $C_{130}H(CN)_2^-$, respectively, thus proving the presence of C_{130} in this fraction.

The UV-vis spectrum‡ of C_{130} has the characteristic absorptions for C_{120} and also for the 1,2-dihydro[70]fullerene[5] as shown in Fig. 1. The ^{13}C NMR spectrum† of C_{130} (Fig. 2) clearly exhibits four signals for sp^3 carbons at 78.03, 75.75 (C_{60} carbons), 69.96, and 68.90 ppm (C_{70} carbons) and partially overlapped > 52 signals for the sp^2 carbons at 156.42–131.93 ppm, which corresponds to a structure with C_{60} and C_{70} connected by a shared cyclobutane ring with C_s symmetry. From these results, the most plausible structure of C_{130} is the one with a C_{60} cage attached at a 6–6 bond to a C_{70} cage at a 1,2-junction bond in a [2 + 2] fashion (Fig. 3). In fact, this isomer has been predicted to be more stable than the 3,4-isomer, in which the C_{70} cage is connected at the 3,4-junction bond.[6]

The redox behavior of C_{130} was examined by cyclic voltammetry and differential pulse voltammetry to give the voltammograms shown in Fig. 4. The curve with a dotted line is the voltammogram of a 1:1 mixture of C_{60} and C_{70}. It is clearly seen that the first reduction occurs at the same potential as the reduction potential of both C_{60} and C_{70}. The following three reduction waves are also identical to those of C_{60} and C_{70}. Therefore, it is quite likely that, as in the case of the C_{60} dimer,[3]

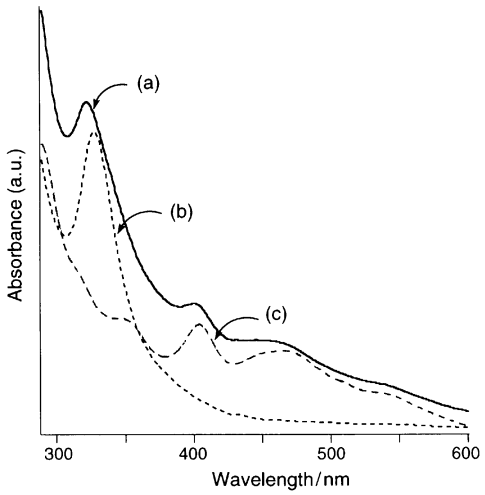

Fig. 1 UV-vis spectra of (a) C_{130} and (b) C_{120} in ODCB and (c) 1,2-H_2C_{70} in toluene–hexane (3:2).

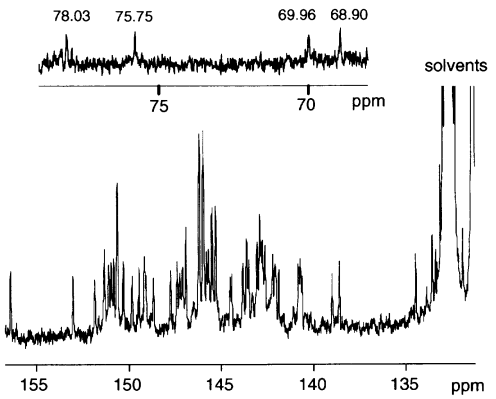

Fig. 2 ^{13}C NMR spectrum of C_{130} (100 MHz, ODCB–C_6D_6 (5:1)).

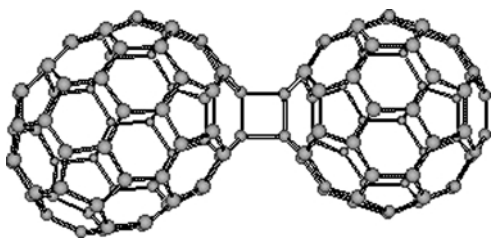

Fig. 3 PM3 calculated structure of C_{130}.

DOI: 10.1039/b003719m

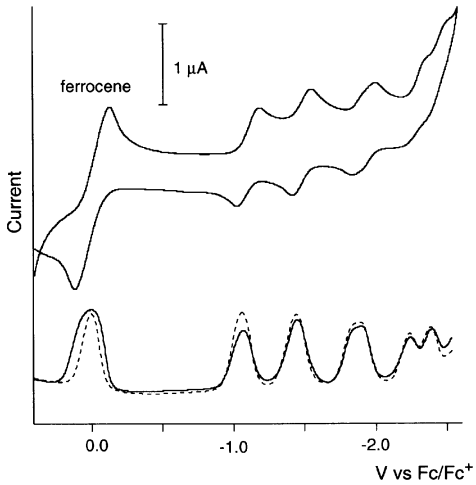

Fig. 4 Cyclic voltammogram (upper) and differential pulse voltammogram (lower) for C_{130} (a solid line) and a 1:1 mixture of C_{60} and C_{70} (a dotted line) measured in ODCB with 0.1 M $Bu_4N^+BF_4^-$: scan rate, 0.02 V s^{-1}.

the central intercage bonds are weak and are readily cleaved off to give radical anions of C_{60} and C_{70} upon obtaining extra negative charge.

Finally an attempt was made to dimerize C_{70} under the solid-state reaction conditions used to dimerize C_{60}, but absolutely no indication for such dimerization was observed. It is known that the most reactive 6–6 junction bond in a C_{70} molecule is the one at the '1,2' position.[7] The possibility of this bond in each C_{70} molecule encountering another is geometrically much lower than in the case of C_{60}, and this would be the reason for the poor reactivity of C_{70} towards dimerization.

The present work was supported by Japan Society for the Promotion of Science (RFTF97R11601). K. F. thanks JSPS Research Fellowship for Young Scientists.

Notes and references

† **Note added in proof:**
A report has appeared on the high-pressure dimerization of C_{70}: S. Lebedkin, W. E. Hull, A. Soldatov, B. Renker and M. M. Kappes, *J. Phys. Chem. B*, 2000, **104**, 4101.

‡ λ_{max} (ODCB)/nm 323, 400, 462sh, 538sh; δ_C (100 MHz, ODCB-d_4) 156.42, 153.03, 151.85, 151.33, 151.10, 150.95, 150.82, 150.63, 150.30, 149.82, 149.45, 149.15, 149.08, 148.67, 147.74, 147.39, 147.25, 147.10. 146.92, 146.18, 145.97, 145.79, 145.69, 145.48, 145.30, 144.52, 144.44, 143.82, 143.63, 143.51, 143.07, 143.05, 143.00, 142.90, 142.83, 142.76, 142.63, 142.21, 142.10, 142.06, 142.03, 141.88, 140.83, 140.77, 140.70, 140.62, 138.99, 138.60, 134.47, 133.57, 133.15, 131.93, 78.03, 75.75, 69.96, and 68.90.

1 A. M. Rao, P. Zhou, K.-A. Wang, G. T. Hager, J. M. Holden, Y. Wang, W.-T. Lee, X.-X. Bi, P. C. Eklund, D. S. Cornett, M. A. Duncan and I. J. Amster, *Science*, 1993, **259**, 955; Y. Wang, J. M. Holden, X.-X. Bi and P. C. Eklund, *Chem. Phys. Lett.*, 1994, **217**, 413; Y.-P. Sun, B. Ma, C. E. Bunker and B. Liu, *J. Am. Chem. Soc.*, 1995, **117**, 12 705.

2 H. Yamawaki, M. Yoshida, Y. Kakudate, S. Usuba, H. Yokoi, S. Fujiwara, K. Aoki, R. Ruoff, R. Malhotra and D. Lorents, *J. Phys. Chem.*, 1993, **97**, 11 161; Y. Iwasa, T. Arima, R. M. Fleming, T. Siegrist, O. Zhou, R. C. Haddon, L. J. Rothberg, K. B. Lyons, H. L. Carter Jr., A. F. Hebard, R. Tycko, G. Dabbagh, J. J. Krajewski, G. A. Thomas and T. Yagi, *Science*, 1994, **264**, 1570; M. Núñez-Regueiro, L. Marques, J.-L. Hodeau, O. Béthoux and M. Perroux, *Phys. Rev. Lett.*, 1995, **74**, 278; C. Goze, F. Rachdi, L. Hajji, M. Núñez-Regueiro, L. Marques, J.-L. Hodeau and M. Mehring, *Phys. Rev. B*, 1996, **54**, R3676; P.-A. Persson, U. Edlund, P. Jacobsson, D. Johnels, A. Soldatov and B. Sundqvist, *Chem. Phys. Lett.*, 1996, **258**, 540.

3 G.-W. Wang, K. Komatsu, Y. Murata and M. Shiro, *Nature*, 1997, **387**, 583; K. Komatsu, G.-W. Wang, Y. Murata, T. Tanaka, K. Fujiwara, K. Yamamoto and M. Saunders, *J. Org. Chem.*, 1998, **63**, 9358.

4 K. Komatsu, K. Fujiwara and Y. Murata, *Chem. Lett.*, in press.

5 C. C. Henderson, C. M. Rohlfing, K. T. Gillen and P. A. Cahill, *Science*, 1994, **264**, 397.

6 P. W. Fowler, D. Mitchell, R. Taylor and G. Seifert, *J. Chem. Soc., Perkin Trans. 2*, 1997, 1901.

7 C. Thilgen, A. Herrmann and F. Diederich, *Angew. Chem., Int. Ed. Engl.*, 1997, **36**, 2269.

The use of hydrazones for efficient mannich type coupling with aldehydes and secondary amines

Valérie Atlan, Hugues Bienaymé, Laurent El Kaim* and Adinath Majee

Laboratoire Chimie et Procédés, Ecole Nationale Supérieure de Techniques Avancées, 32 Bd Victor, 75015 Paris, France. E-mail: elkaim@ensta.fr

Received (in Cambridge, UK) 6th April 2000, Accepted 4th July 2000
Published on the Web 3rd August 2000

The Mannich reaction of hydrazones originally limited to the coupling of hydrazones with formaldehyde has been extended to a large variety of aldehydes through appropriate selection of experimental conditions; in conjunction with the Japp–Klingmann reaction, this process provides an efficient synthetic tool for the formation of carbon–carbon bonds.

The Mannich reaction is one of the most widely used reactions for the formation of carbon–carbon bonds. In its initial form, it implied the addition of aldehydes to ketones in the presence of amines.[1] The scope of the Mannich reaction was then extended to the addition of different carbon nucleophiles such as nitro compounds.[2] The ease of deprotonation of monosubstituted hydrazones **1** under basic conditions is dependent upon the attached substituents. The resulting salt can be viewed as an aza-substituted carbanion and as such may interact in a Mannich reaction leading to carbon–carbon bond formation (Scheme 1). Indeed in 1957, Keil and Ried[3] reported such behavior but their study revealed only modest synthetic potential as moderate to good yields were only obtained with formaldehyde; furthermore the hydrazones needed an electron withdrawing group (R^1) tethered to the carbonyl function. The potential of this reaction has led us to perform a more extensive study and we were delighted to find that different experimental conditions and the appropriate selection of the amine permit the condensation of hydrazones **1** with many different aldehydes **2** (Table 1, Scheme 1) giving the new aminohydrazones **4** in good yields. Most noteworthy are the good yields obtained with several aliphatic aldehydes possessing α-hydrogens. For the latter, competing aldol type reactions usually preclude their efficient use in Mannich reactions.[4] The first indication of success probably came from the choice of *N*-benzylpiperazine as the amine partner in this reaction. A net increase in yield is observed in going from aliphatic amine to morpholine and finally to *N*-benzylpiperazine. The reaction is best performed in a concentrated toluene solution (2 M) at 80 °C with nearly equimolar amounts of aldehyde (1.1 eq.) and amine (1.1 eq.).

The main drawback of this reaction is, as observed by Reid and Keil,[3] the need for an electron withdrawing group tethered to the hydrazone functionality. This limitation on the starting hydrazones is however deeply counter-balanced by their easy access *via* the Japp–Klingmann reaction between β-ketoacids and diazonium salts (Scheme 2).

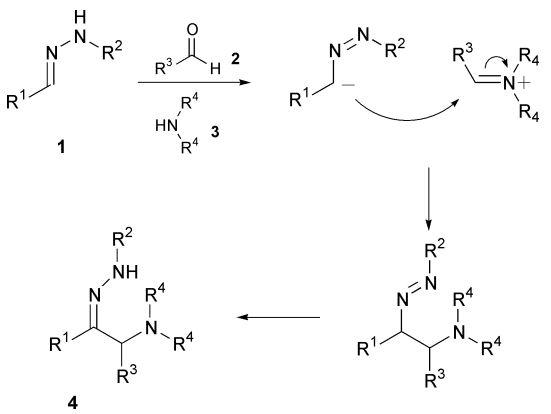

Scheme 1

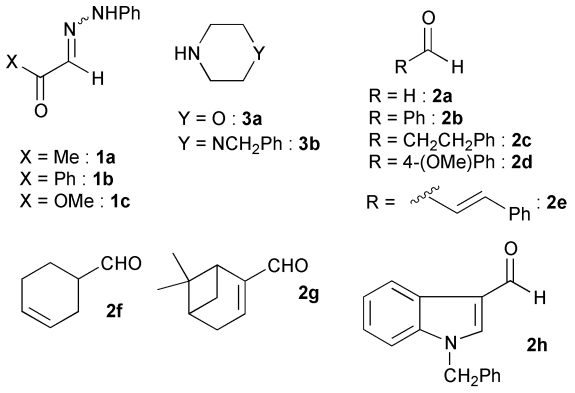

	X	Y	R
4a	Me	O	H
4b	Me	NCH_2Ph	H
4c	Me	O	Ph
4d	Me	NCH_2Ph	Ph
4e	Me	O	$(CH_2)_2Ph$
4f	Me	NCH_2Ph	CH=CHPh
4g	Ph	NCH_2Ph	H
4h	OMe	O	Ph
4i	OMe	O	$(CH_2)_2Ph$
4j	OMe	NCH_2Ph	4-(OMe)Ph

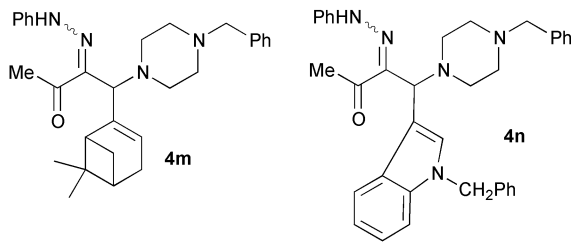

Since the use of *N*-benzylpiperazine leads to good yields of product, a clean way to displace this group becomes crucial for the synthetic potential of this reaction. The chemistry of azoalkenes brings us a possible answer to this problem: treatment of hydrazone **4g** in various alcohols with two equivalents of 1,2-dibromoethane under reflux generates the new ether **5** probably *via* an azoalkene trapping by the alcohol (Scheme 3); hydrazone **4b** behaves similarly. This substitution process needs an alcohol with a rather high boiling point (at

DOI: 10.1039/b002750m

Table 1 Mannich reaction of hydrazones **4**

Hydrazone	Aldehyde	Amine	Product[a]	Time	Yield (%)
1a	**2a**	**3a**	**4a**	0.5 h[b]	60
1a	**2a**	**3b**	**4b**	1 h[b]	96
1a	**2b**	**3a**	**4c**	14 h[c]	58
1a	**2b**	**3b**	**4d**	5 h[c]	76
1a	**2c**	**3a**	**4e**	2 h[c]	73
1a	**2e**	**3b**	**4f**	3 h[c]	74
1b	**2a**	**3b**	**4g**	2.5 h[b]	92
1c	**2b**	**3a**	**4h**	6 h[c]	50
1c	**2c**	**3a**	**4i**	6 h[c]	30
1c	**2d**	**3b**	**4j**	8 h[c]	46
1a	**2f**	**3b**	**4k**	3.5 h[c]	79
1b	**2f**	**3b**	**4l**	9 h[c]	65
1a	**2g**	**3b**	**4m**	10 h[c]	35
1a	**2h**	**3b**	**4n**	8 h[d]	72

[a] The NMR spectra (C13, DEPT-135) of all products show that the Mannich condensations have taken place at carbon and not at the nitrogen of the ambident system. [b] Addition of 1.1 eq. aldehyde, 1.1 eq. amine to a 3 M solution of hydrazone in refluxing ethanol. [c] Addition of 1.1 eq. aldehyde, 1.1 eq. amine to a 2 M solution of hydrazone in toluene at 80 °C. [d] Addition of 1.1 eq. aldehyde, 1.1 eq. amine to a 2 M solution of hydrazone in refluxing toluene.

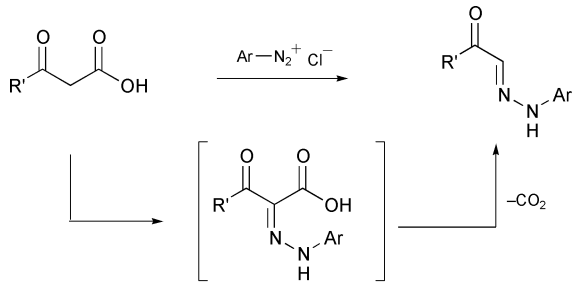

Scheme 2

least 100 °C) as no reaction is observed in MeOH or EtOH. The use of 1,2-dibromoethane seems to be important for elimination of the piperazine unit; MeI reacts cleanly with hydrazone **4b** in ethanol giving a salt that does not react in refluxing EtOH or

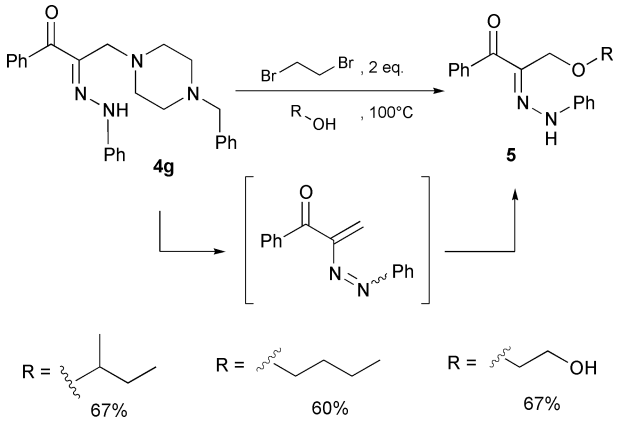

Scheme 3

reacts sluggishly in higher boiling alcohols (the regiochemistry of the alkylation step could be invoked to explain these results).

This 1,2-dibromoethane assisted elimination procedure further emphasises the potential of the preceding Mannich reaction as many fruitful applications of transient azoalkenes (cycloadditions to give various heterocycles, Michael additions, *etc*.) have been reported in the literature[5] and could be applied to the Mannich addition products. These features and the selectivity of the 1,2-dibromoethane alkylation are currently being studied in our research group and will be reported soon.

We thank Rhône-Poulenc Industrialisation for financial support.

Notes and references

1 E. F. Kleinman, in *Comprehensive Organic Synthesis*, ed. B. M. Trost, Pergamon Press, 1991, **2**, 893 and references cited therein.
2 K. L. Yamada, M. Shibasaki, S. J. Harwood and H. Gröger, *Angew. Chem., Int. Ed.*, 1999, **38**, 3504.
3 G. Keil and W. Ried, *Liebigs Ann. Chem.*, 1957, **605**, 167.
4 The use of enolisable aldehyde often requires preliminary formation of iminium derivatives, see: D. Seebach, C. Betschart and M. Schiess, *Helv. Chem. Acta*, 1984, **67**, 1593.
5 O. A. Attanasi and P. Filippone, *Synlett*, 1997, 1128.

Intramolecular borylation reaction catalyzed by Lewis acid: preparation of 1*H*-2,1-benzazaborole derivatives

Alexander M. Genaev,[a] Sandor M. Nagy,*[b] Georgii E. Salnikov[a] and Vyacheslav G. Shubin[a]

[a] *Novosibirsk Institute of Organic Chemistry, Siberian Division of Russian Academy of Sciences, Novosibirsk 630090, Russia*

[b] *Equistar Chemicals, L.P., Equistar Technology Center, 11530 Northlake Drive, Cincinnati, Ohio, USA*

Received (in Corvallis, USA) 17th May 2000, Accepted 6th July 2000
Published on the Web 3rd August 2000

It has been found that 1*H*-2,1-benzazaboroles can be prepared by the interaction of substituted benzylaminochloroboranes with Al_2Cl_6 in CH_2Cl_2 at 0 °C, the ^{13}C NMR spectroscopy data obtained being in favour of an electrophilic substitution mechanism involving formation of cationic complexes as reactive intermediates.

The π-delocalized anions accessible through deprotonation of 1*H*-2,1-benzazaboroles (**1**) are isoelectronic with indenyl anions (Scheme 1), making them attractive precursors for single site olefin polymerization catalysts based on heterocyclic analogues of metallocenes[1] (*cf.* ref. 2).

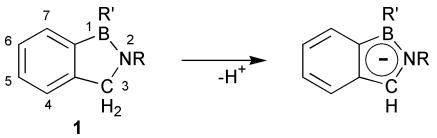

Scheme 1

The two well known approaches towards benzazaborole derivatives involve intramolecular condensation of *o*-(aminomethyl)benzene boronic acids[3] (Scheme 2) and intramolecular cyclization of benzylaminoboranes[4] (Scheme 3). The first method is applicable for preparation of derivatives with B–OH or B–O–B fragments only, while the second route requires high process temperatures and is not applicable to compounds in which there is no B–H bond.

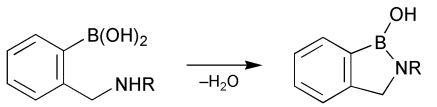

Scheme 2

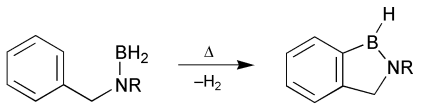

Scheme 3

As part of our program to develop synthetically attractive approaches towards precursors for heterocyclic analogues of cyclopentadienyl ligands, we studied the utility of Lewis acid catalysed borylation reactions for the preparation of benzoborazoles **1**. To the best of our knowledge there have been no data on their preparation by this reaction, the closest related data being those of M. J. S. Dewar on the $AlCl_3$ catalysed preparation of (10*R*)-9-aza-10-boraphenanthrene and related heteroaromatics at high temperature and without solvent[5] (Scheme 4).

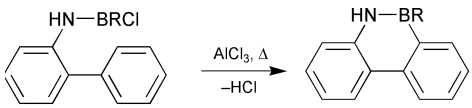

Scheme 4

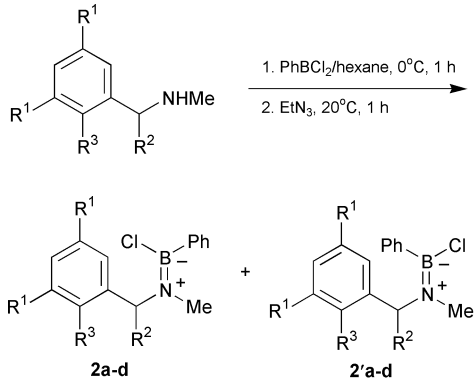

Scheme 5

The starting materials, halogen substituted aminoboranes **2a**–**d**,† have been prepared by the procedures analogous to those described in refs. 6 and 7 (Scheme 5). There are two sets of signals in the ^1H and ^{13}C NMR spectra of each of these compounds indicating the presence of mixtures of *cis*- and *trans*-isomers, obviously due to partially double bond character of the B–N bond‡ (*cf.* ref. 6).

Aminoboranes **2a** and **2b**, when treated with $AlCl_3$ under Dewar's conditions[5] (without solvent, 150 °C) yielded polymeric products only.

It has been found that the interaction of compounds **2b** and **2c** with equimolar amounts of Al_2Cl_6 in CH_2Cl_2 at 0 °C results in formation of the target products, **3b** and **3c**, respectively, the yields being 75% (Scheme 6).§ In contrast, the compounds **2a** and **2d** do not react at 0 °C, while at rt they give multicomponent mixtures of unidentified products.

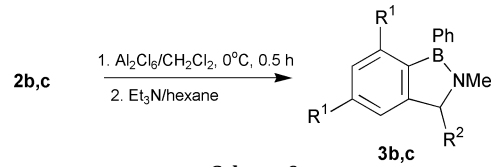

Scheme 6

The mechanism of the cyclization reaction has been studied by NMR using **2b** as starting material, CD_2Cl_2 solvent and Al_2Br_6 as a Lewis acid which is more soluble in this solvent than Al_2Cl_6.¶ These experiments indicate that upon the interaction of **2b** with Al_2Br_6 at −90 °C a mixture of **4** and **5** is formed, their ratio being approximately 1:1 (Scheme 7).‖ When the temperature rises to 0 °C, the structure **4** transforms entirely into **5**.

The results reported here suggest that intramolecular electrophilic borylation is a viable approach toward 1*H*-2,1-benzaza-

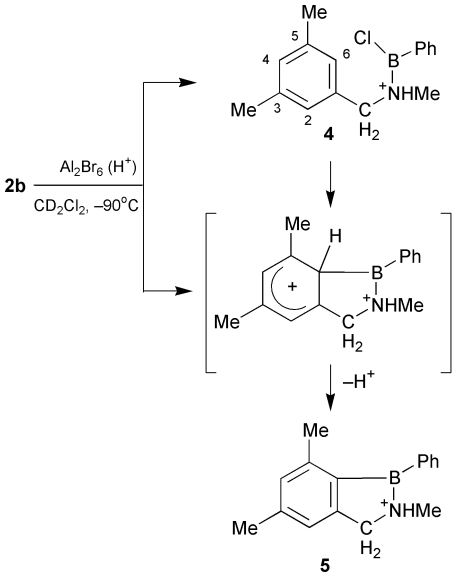

Scheme 7

boroles, starting from readily available and inexpensive chemicals.

Notes and references

† Satisfactory spectral data have been obtained for all the new compounds. The signals of the carbon atoms bearing B-centred fragments were not observed in the ^{13}C NMR spectra.

‡ For example, the mixture of **2b** and **2b′** (approx. 1 : 1, numeration as for structure **4**): ^1H NMR (CD_2Cl_2) δ 2.35 (s, 6H, 3- and 5-CH_3), 2.37 (s, 6H, 3- and 5-CH_3), 2.99 (s, 3H, N–CH_3), 2.65 (s, 3H, N–CH_3), 4.59 (s, 2H, N–CH_2), 4.40 (s, 2H, N–CH_2), 6.99 (s, 1H, H^4), 6.96 (s, 1H, H^4), 7.01 (s, 2H, H^2 and H^6), 6.88 (s, 2H, H^2 and H^6), 7.3–7.8 (m, 10H, Ph); ^{13}C NMR (CD_2Cl_2) δ 21.28 (q, 2C), 21.30 (q, 2C), 38.0 (q), 37.3 (q), 56.0 (t), 56.4 (t), 125.7 (d, 2C), 125.0 (d, 2C), 127.9 (d, 2C), 127.8 (d, 2C), 129.07 (d), 129.10 (d), 129.28 (d), 129.32 (d), 133.1 (d, 2C), 132.5 (d, 2C), 138.12 (s), 138.14 (s), 138.3 (s, 2C), 138.4 (s, 2C).

§ Preparation of **3b**. Chloroaminoborane **2b** (2 mmol) was added to the suspension of Al_2Cl_6 (2 mmol) in 5 mL of CH_2Cl_2 at 0 °C whilst stirring in an argon atmosphere. The dark-red solution formed after stirring for 0.5 h was added dropwise to the solution of 1 mL NEt_3 in 30 mL of hexane at 0 °C. The reaction mixture was allowed to warm to rt, decanted and evaporated. The residue was extracted with 5 mL of hexane, the solution was filtered and evaporated. ^1H NMR (CD_2Cl_2) δ 2.32 (s, 3H, 5- or 7-CH_3), 2.49 (s, 3H, 7- or 5-CH_3), 3.13 (s, 3H, N–CH_3), 4.36 (s, 2H, CH_2), 7.00 (m, 1H, H^4 or H^6), 7.18 (m, 1H, H^6 or H^4), 7.6–7.7 (m, 5H, Ph); ^{13}C NMR (CD_2Cl_2) δ 21.3 (q), 21.6 (q), 34.4 (q), 60.5 (t), 119.9 (d), 127.7 (d, 2C), 127.8 (d), 129.0 (d), 132.6 (d, 2C), 138.7 (s), 141.4 (s), 151.7 (s); ^{11}B NMR (CD_2Cl_2) δ 40.4; MS 235 (M^+). Analogous procedure was used for the preparation of **3c**. ^1H NMR (CD_2Cl_2) δ 3.14 (s, 3H, N–CH_3), 5.44 (s, 1H, CH), 7.28–7.34 (m, 1H), 7.36–7.42 (m, 1H), 7.42–7.55 (m, 5H), 7.60–7.66 (m, 1H), 7.66–7.72 (m, 2H), 7.94–7.99 (m, 1H), 8.00–8.06 (m, 2H); ^{13}C NMR (CD_2Cl_2) δ 32.6 (q), 74.9 (d), 122.9 (d), 126.8 (d), 127.8 (d, 2C), 127.9 (d), 128.2 (d, 2C), 129.00 (d, 2C), 129.03 (d), 129.1 (d), 130.7 (d), 133.9 (d, 2C), 140.4 (s), 155.7 (s); ^{11}B NMR (CD_2Cl_2) δ 40.4; MS 283 (M^+).

¶ Taking into account that $AlCl_3$ used in the preparative experiments obviously contains some proton donating impurities ($AlCl_2OH$ and the like) we did not use 'extra dry' Al_2Br_6 in mechanistic experiments.

‖ Structure **4**: ^1H NMR (−15 °C, CD_2Cl_2) δ 2.25 (s, 6H, 3- and 5-CH_3), 3.45 (d, J_{HNCH} 5 Hz, 3H, N–CH_3), 4.69 and 4.73 (m, J_{HCH} 13, J_{HNCH} 8 and 4 Hz, 2H, N–CH_2), 7.04 (br s, 1H, N–H), 7.00 (s, 1H, H^4), 7.08 (s, 2H, H^2 and H^6), 7.5–8.0 (m, 5H, Ph); ^{13}C NMR (−42 °C, CD_2Cl_2) δ 20.8 (q, 2C), 39.6 (q), 60.5 (t), 126.7 (s), 127.6 (d, 2C), 129.1 (d, 2C), 132.6 (d), 137.0 (d, 2C), 138.8 (d), 139.9 (s, 2C). Structure **5**: ^1H NMR (−15 °C, CD_2Cl_2) δ 2.53 (s, 3H, 5- or 7-CH_3), 2.60 (s, 3H, 7- or 5-CH_3), 3.11 (d, J_{HNCH} 6 Hz, 3H, N–CH_3), 4.55 (dd, J_{HCH} 16, J_{HNCH} 2 Hz, 1H, N–CH_2), 5.32 (dd, J_{HCH} 16 Hz, J_{HNCH} 6 Hz, 1H, N–CH_2), 6.80 (br s, N–H), 7.28 (s, 1H, H^4 or H^6), 7.29 (s, 1H, H^6 or H^4), 7.5–8.0 (m, 5H, Ph); ^{13}C NMR (−42 °C, CD_2Cl_2) δ 22.3 (q), 22.5 (q), 40.9 (q), 60.4 (t), 121.5 (d), 128.7 (d, 2C), 132.5 (d), 133.8 (d), 134.5 (d, 2C), 148.7 (s), 151.6 (s), 154.1 (s).

1 S. Nagy, R. Krishnamurti and B. P. Etherton, WO 96/34021, (*Chem. Abstr.*, 1996, **126**, 19432j).
2 G. Schmid, S. Amirkhalili, U. Höhner, D. Kampmann and R. Boese, *Chem. Ber.*, 1982, **115**, 3830.
3 P. T. Hawkins and A. U. Blackham, *J. Org. Chem.*, 1967, **32**, 597 and references cited therein; H. E. Dunn, J. C. Catlin and H. R. Snyder, *J. Org. Chem.*, 1968, **33**, 4483; M. Lauer and G. Wulff, *J. Organomet. Chem.*, 1983, **256**, 1.
4 R. Köster, K. Iwasaki, S. Hattori and Y. Marita, *Ann.*, 1968, **720**, 23; R. Köster and K. Iwasaki, *Advan. Chem. Ser.*, 1964, **42**, 148 (*Chem. Abstr.*, 1964, **60**, 10 705).
5 M. J. S. Dewar, V. P. Kubba and R. Pettit, *J. Chem. Soc.*, 1958, 3073; M. J. S. Dewar and V. P. Kubba, *Tetrahedron*, 1959, **7**, 213; M. J. S. Dewar and W. H. Poesche, *J. Org. Chem.*, 1964, **29**, 1757.
6 D. Imbery, A. Jaeschke and H. Friebolin, *Org. Magn. Reson.*, 1970, **2**, 3271.
7 P. Kölle and H. Nöth, *Chem. Ber.*, 1986, **119**, 313.

ChemComm

Synthesis and crystal structure of an unprecedented bismuth porphyrin containing ester pendant arms

Lydie Michaudet, Philippe Richard and Bernard Boitrel*

Université de Bourgogne/LSEO, UMR-CNRS 5632, 6, boulevard Gabriel, 21000 Dijon, France.
E-mail: bboitrel@satie.u-bourgogne.fr

Received (in Cambridge, UK) 1st June 2000, Accepted 11th July 2000
Published on the Web 3rd August 2000

An easily prepared porphyrin with pendant arms is shown to form a stable complex with bismuth(III) ion; the complex is eight coordinate with a square antiprismatic coordination geometry; the solid-state structure exhibits the formation of a dimer assembled *via* mutual coordination of a terminal ester group.

The chemistry of bismuth has been somewhat neglected until recently when bismuth complexes have become of interest in the treatment of gastric ulcers[1] and cancer therapy.[2] In this context, the coordination of bismuth with several types of ligands has been developed in the last ten years. The synthesis of bismuth(III) complexes with nitrogen-donor macrocycles[3,4] has been investigated and it appears that the bismuth(III) ion has a high affinity for these ligands. The promising interest of ^{212}Bi as an α-emitter for radioimmunotherapy has induced studies concerning the complexation[5,6] of this ion with polyaminoacid ligands derived from diethylenetriaminepentaacetic acid, in these types of complexes, the metal exhibits a coordination with carboxylate groups and nitrogen atoms. This background about the coordination of the Bi(III) ion has led us to consider with a new point of view our studies with porphyrins acting as ligands. The literature concerning the metallation of porphyrin with bismuth salts is not very widespread.[7,8] In a recent publication,[9] we have described the structure of (OEP)Bi(SO_3CF_3) as a dimer with a seven coordination geometry in which the bismuth lies 1.07 Å from the plane formed by the four nitrogen of the porphyrin. To quote Brechbiel,[10] 'An important ligand property that increases metal complex stability is preorganization, the tendency of the free ligand to assume the conformation necessary for metal ion complexation'.[11] On the basis of this particular structural feature, we have designed porphyrins with pendant arms as potentially oxygen-atom donors. It is worth noting that in our case, and in contrast with tetraazamacrocycles such as DOTA, the four pickets are not coplanar with the four-nitrogen macrocycle but pre-oriented in a perpendicular direction, as a result of their grafting to *ortho* positions of the meso phenyl ring. Ligand $4ESH_2$ **1**† (the free-base analogue of **2**) was synthesized by reaction of *meso*(tetra-*o*-aminophenyl)porphyrin (atropisomer αααα, TAPP)[12] with ethylsuccinyl chloride (Scheme 1) and isolated in high yield (93%). The Bi(III) complex was prepared under mild conditions with metallation occurring in pyridine at 50 °C during 2 h. The yield of the reaction was almost quantitative (85%) and no demetallation was observed during the purification of the product. Indeed, in contrast to unfunctionalized porphyrins such as (OEP)Bi(SO_3CF_3), chromatography of coumpound **2** does not afford any free base analogue. Crystals‡ suitable for X-ray study were obtained by a slow diffusion of H_2O–MeOH onto a saturated THF solution of **2**. The ORTEP[13] plot of the X-ray structure is shown in Fig. 1. As depicted in Fig. 2, the Bi(III) is eight coordinate with an approximate square antiprismatic geometry. The four nitrogen atoms of the macrocycle form a square, the other distorted square being formed by four oxygen atoms described as follows: two oxygen atoms of the nitrate anion, the oxygen atom of a water molecule and a carbonyl oxygen atom of the terminal ester group belonging to an arm attached to a

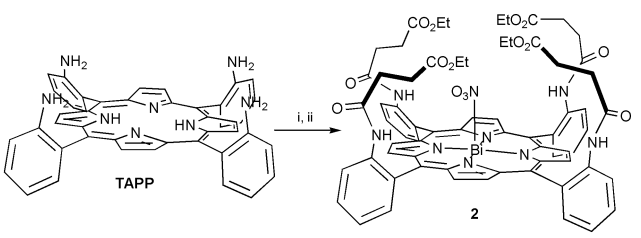

Scheme 1 *Reagents and conditions*: i, $ClCO(CH_2)_2CO_2Et$, NEt_3, THF; ii, pyridine, $Bi(NO_3)_3{\cdot}5H_2O$, 50 °C.

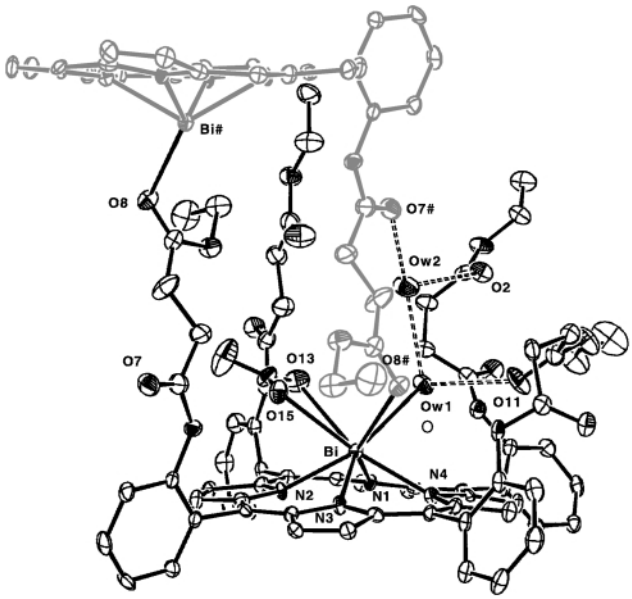

Fig. 1 ORTEP view of the Bi(III) complex (4ES)Bi(NO_3) **2**. For clarity, only the relevant part of one symmetrically related molecule forming the dimer is shown (shaded); the labeling # refers to the symmetrical related molecule.

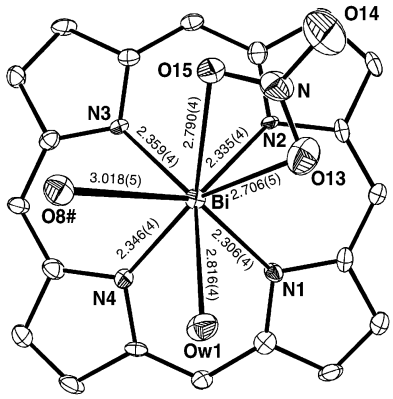

Fig. 2 Polyhedron coordination view of the bismuth in (4ES)Bi(NO_3) **2**.

DOI: 10.1039/b004394j

symmetrically related macrocycle, thus forming a centrosymmetric dimer in the solid state (Fig. 1). The Bi atom lies 1.125 Å above the N_4 plane and the mean Bi–N bond length is 2.34(2) Å, similar to those observed in (OEP)Bi(SO_3CF_3)[9] which also adopts a centrosymmetric dimeric form [ΔN_4 = 1.07 Å and < Bi–N > = 2.31(1) Å]. The Bi–O bond lengths [2.706(5) and 2.789(4) Å] are larger than the sum of their ionic radii (1.13 + 1.40 = 2.53 Å)[14] for the bonds with the nitrate anion O13 and O15, respectively), 2.816(5) Å with the oxygen of the water molecule (Ow1) and 3.018(5) Å with the oxygen atom of the carbonyl group (O8#). This later value is large but, to the best of our knowledge, this type of bond between a Bi atom and an ethoxycarbonyl group is unprecedented, however such a large distance is observed in the (OEP)Bi(SO_3CF_3) dimer[9] where a Bi–O distance of 2.98(2) Å was found between the Bi atom and a triflate oxygen atom. A second water molecule (Ow2) is present in the cage and as shown in Fig. 1, both water molecules are engaged in an intra- and inter-molecular hydrogen bond net, contributing to the stability of the dimer. One arm of the molecule does not participate in any interaction and thus exhibits a regular conformation. As reported above, one arm participates to the coordination sphere of the Bi atom, belonging to the second molecule of the dimer, and the two remaining arms involved in the hydrogen bond net with Ow1 and Ow2, adopt folded conformations.

As it is of interest to know if this particular structure is also plausible in solution, the complex **2** has been studied by NMR spectroscopy. A previous variable temperature ^{1}H NMR study[8] has been made on the compound [Bi(TTP)]NO_3 investigating the aromatic protons of the tolyl groups. The slow rotation of aryl groups of this complex induced broadened signals at room temperature, whereas at low temperature the signal of the tolyl protons were split. In our complex, at 300 K, the methylene protons of the ester groups appear at δ 3.37 as a broad singlet whereas at 290 K, these protons become magnetically non-equivalent, as two singlets at δ 3.31 and 3.39, the same observation being made for the methyl group. It is of note that a 1 : 3 intensity ratio is observed instead of the 1 : 2 : 1 expected. When the temperature decreases, we can clearly see that the pendant arm of the porphyrin is not in the same magnetic environment as the three others, as shown by the integration of the signal. The same temperature dependence is observed for the aromatic protons of the phenyl rings, with the exception of the apparent triplet at δ 7.90 ppm.[15] These observations suggest an unsymmetrical geometry around the Bi(III) ion involving one arm of the porphyrin, which is plausible with the radiocrystallographic structure of 4ESBi(NO_3) **2**. However, the geometry of the molecule is not exactly the same in solution as in the solid state. It seems that the dimer is broken in solution. Indeed, the protons of the pendant arm if bonded to the bismuth *via* the carbonyl, would be strongly upfield shifted because of their localization in the anisotropic current of the porphyrin. As all the aliphatic protons are normally shifted between 0.5 and 3.5 ppm, the ^{1}H NMR spectrum is in accord with a monomer complex in which one of the 'picket' groups is able to interact with the metal.

In conclusion, this new bismuth(III) porphyrin demonstrates that the metal can be stabilized by the presence of a suitable coordination sphere, and particularly by oxygen-donor groups. Indeed, in the reported complex, even if the ethoxycarbonyl groups are not ideal in stabilizing the complex, their spatial arrangement seem to be sufficient to increase the rate of metallation and the stability of the complex. Work is now in progress to characterize corresponding analogues with carboxylate picket groups and to study their coordination around Bi(III).

Notes and references

† *Selected data* for 4ESH$_2$ **1**: yield 93%. Anal. Calc. for $C_{68}H_{66}N_8O_{12}\cdot CH_3OH$: C, 67.97; H, 5.79; N, 9.19. Found: C, 68.25; H, 5.44; N, 9.33%. MS (FAB): *m/z* 1187.8 [$(M+H)^+$, 100%]. UV–VIS (CH_2Cl_2): λ_{max}/nm (log ε/dm^3 mol^{-1} cm^{-1}): 419 (5.52), 514 (4.3), 546 (3.76), 588 (3.83), 643 (3.58). δ_H(500 MHz, $CDCl_3$, 323 K): 8.86 (s, 8H, β-pyr), 8.59 (d, *J* 7.09 Hz, 4H, arom.), 8.00 (d, *J* 5.75 Hz, 4H, arom), 7.86 (t, *J* 7.58 Hz, 4H, arom), 7.55 (t, *J* 7.21 Hz, 4H, arom), 7.19 (s, 4H, –NHCO), 3.47 (br s, 8H, C*H*$_2$CH$_3$); 2.18 (t, *J* 6.72 Hz, 8H, CH_2CH_2), 1.65 (br s, 8H, CH_2CH_2), 0.82 (br s, 12H, CH_2CH_3), −2.59 (s, 2H). For (4ES)Bi(NO_3) **2**: yield 85%. Anal. Calc. for $C_{68}H_{64}BiN_9O_{15}\cdot 2H_2O$: C, 54.73; H, 4.59; N, 8.45. Found: C, 55.16; H, 4.47; N, 8.27%. MS (FAB): *m/z* 1393.8 [$(M - NO_3)^+$, 100%]. UV–VIS (CH_2Cl_2): λ_{max}/nm(log ε/dm^3 mol^{-1} cm^{-1}): 354 (4.62), 472 (5.25), 598 (3.99), 644 (3.92). δ_H(500 MHz, $CDCl_3$, 300 K): 9.24 (s, 8H, β-pyr), 8.68 (br s, 4H, arom), 8.22 (br s, 3H, –NHCO), 8.13 (br s, 1H, –NHCO), 7.89 (m, 4H, arom); 7.90 (t, *J* 7.7 Hz, 4H, arom); 7.56 (br s, 4H, arom), 3.46 (br s, 2H, C*H*$_2$CH$_3$), 3.32 (br s, 6H, C*H*$_2$CH$_3$), 2.04 (br s, 8H, CH_2CH_2), 1.92 (br s, 8H, CH_2CH_2), 0.96 (br s, 3H, CH_2CH_3); 0.87 (s, 9H, CH_2CH_3).

‡ *Crystal data*: $C_{68}H_{64}BiN_9O_{15}\cdot 2H_2O$, *M* = 1492.3, triclinic, space group $P\bar{1}$, *a* = 14.3980(4), *b* = 14.9790(4), *c* = 16.5670(4) Å, α = 116.205(1), β = 97.2490(11), γ = 92.6720(12)°, *V* = 3159.02(14) Å^3, *Z* = 2, D_c = 1.569 g cm^{-3}, *F*(000) = 1516. Data were collected at 110 K on a Nonius Kappa CCD diffractometer with Mo-Kα radiation (λ = 0.7173 Å). The structure was solved by the mean of a Patterson search program[16] and refined by full-matrix least squares on F^2 (14 332 unique reflections, 1054 parameters). The anisotropic refinement led to final residuals *wR*2 = 0.101 for all data and *R1* = 0.055 for 10 533 intensities with $I > 2\sigma(I)$, and GOF = 1.028. The largest $\Delta(\rho)$ residual densities are 1.36 and −1.69 e Å^{-3}.

CCDC 182/1715. See http://www.rsc.org/suppdata/cc/b0/b004394j/ for crystallographic files in .cif format.

1 G. F. Baxter, *Chem. Ber.*, 1992, **28**, 445.
2 R. W. Kozak, T. A. Waldmann, R. W. Atcher and O. A. Gansow, *Trends Biotechnol.*, 1985, **4**, 259.
3 R. D. Hancock, I. Cukrowski, J. Baloyi and J. Mashishi, *J. Chem. Soc., Dalton Trans.*, 1993, 2895.
4 R. Luckay, J. H. Reibenspie and R. D. Hancock, *J. Chem. Soc., Chem. Commun.*, 1995, 2365; R. Luckay, I. Cukrowski, J. Mashishi, J. H. Reibenspies, A. H. Bond, R. D. Rogers and R. D. Hancock, *J. Chem. Soc., Dalton Trans.*, 1997, 901.
5 M. W. Brechbiel and O. A. Gansow, *J. Chem. Soc., Perkin Trans. 1*, 1992, 1173.
6 R. B. Huneke, C. G. Pippin, R. A. Squire, M. W. Brechbiel, O. A. Gansow and M. Strand, *Cancer Res.*, 1992, **52**, 5818.
7 J. W. Buchler and K. L. Lay, *Inorg. Nucl. Chem. Lett.*, 1974, **10**, 297.
8 T. Barbour, W. J. Belcher, P. J. Brothers, C. E. F. Rickard and D. C. Ware, *Inorg. Chem.*, 1992, **31**, 746.
9 L. Michaudet, D. Fasseur, R. Guilard, Z. Ou, K. M. Kadish, S. Dahoui and C. Lecomte, *J. Porphyrins Phtalocyanines*, 2000, **4**, 261.
10 M. W. Brechbiel, O. A. Gansow, C. G. Pippin, R. D. Rogers and R. P. Planalp, *Inorg. Chem.*, 1996, **35**, 6343.
11 R. D. Hancock and A. E. Martell, *Chem. Rev.*, 1989, **89**, 1875.
12 J. P. Collman, R. R. Gagne, C. A. Reed, T. R. Halbert, G. Lang and W. T. Robinson, *J. Am. Chem. Soc.*, 1975, **97**, 1427.
13 L. J. Farrugia, *J. Appl. Crystallogr.*, 1997, **30**, 565.
14 R. D. Shannon, *Acta Crystallogr., Sect. A*, 1976, **A32**, 751.
15 P. Permutter, M. Rose and P. Shenan, *Tetrahedron Lett.*, 1988, **29**, 1427; B. Boitrel, E. Camilleri, Y. Fleche, A. Lecas and E. Rose, *Tetrahedron Lett.*, 1989, **30**, 2923.
16 Programs for Crystal Structure Analysis (Release 97-2). G. M. Sheldrick, Institüt für Anorganische Chemie der Universität, Tammanstrasse 4, D-3400 Göttingen, Germany, 1998.

ChemComm

Breakdown of the hydrogen bond strength–length analogy: a revision

Mark Mascal,* Christopher E. Marjo and Alexander J. Blake

Department of Chemistry, University of Nottingham, Nottingham, UK NG7 2RD.
E-mail: mark.mascal@nottingham.ac.uk

Received (in Columbia, MO, USA) 10th March 2000, Accepted 16th June 2000
Published on the Web 3rd August 2000

A recent study which addressed the nature of the association between hydrogenoxalate anions in the solid state came to the conclusion that short OH···O contacts between these species did not constitute an attractive interaction, but one which simply minimized inter-anion repulsion; in the light of new crystallographic evidence and a solution study, some issues raised in this work need to be re-evaluated.

It was recently put forward that an interaction which had the physical appearance of a short, charge-assisted hydrogen bond was, in fact, not a hydrogen bond. The case of the hydrogenoxalate anion **1** was examined in detail by Braga *et al.*[1] using

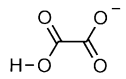

1

computational methods, where the conclusion was reached that charge delocalization over the whole species meant that no attractive force of interaction could be present between these anions, despite the fact that they organize into chains in the solid state connected through close, interanionic OH···O contacts. This then led to the reassignment of these contacts as the 'least repulsive' orientation of the two species, rather than a bond. This, finally, was cited as a breakdown of the widely accepted length–strength inverse analogy of hydrogen bonding, since, despite its shortness, the H-bond was not strong, indeed not even a bond but a repulsive interaction held in place by a stronger cation–anion network.

One problem with the above assertions is contextual. To be sure, in a vacuum and in the absence of counterions, the isolated OH···O interaction is not sufficient to keep the interanionic complex associated.[2] Under such circumstances, as was claimed, the relationship could not be characterized as 'bonding', since energy would be required to maintain it, rather than dissociate it. This view, however, does not take into account that the association of any two species consists of a combination of interaction energies, the totality of which must result in a net force of attraction. In salts of **1**, four primary interactions are present: (+)–(−), (+)–(+), (−)–(−) and OH···O. These interactions can be modeled and evaluated individually, but the report in question isolated two of the interactions and compared them to each other, *i.e.* (−)–(−) to OH···O, found the former dominant, and came to the conclusion the latter was therefore not enthalpically favorable.[1]

Perhaps the most significant feature of this work was however the remarkable and counterintuitive finding that the absence of positive regions in the molecular electrostatic potential map calculated for **1** indicated that, 'irrespective of the relative orientation, two $HC_2O_4^-$ anions repel each other electrostatically.'[1] This suggested that, under *no* circumstances could the OH···O interaction in question ever be considered 'bonding'.

We first confronted this issue by doing a study of the behavior of soluble salts of **1** in chloroform solution by ^{1}H NMR spectroscopy. We chose as counter ion the large, non-coordinating tetrapropylammonium cation. Systematic variation of the concentration [Pr_4N^+**1**$^-$] produced a classic H-bonding isotherm for the acidic proton in the NMR (Fig. 1), to which a curve could be fit modeled either on linear oligomers or on a combination of cyclic H-bonded dimers plus linear oligomers to give association constants K_a = 294 or 226, respectively.[3] Parallel control studies of acetic acid and the tetrapropylammonium acetate–acetic acid (1 : 1) complex under the same experimental conditions gave association constants for these species of 89 and 861, respectively, the latter value reflecting the charge-assisted nature of the bond.[4] No noteworthy change in chemical shift for the protons of the counterion was observed in any case. If acetic acid and its acetate complex can be taken as reasonable models for the hydrogen bonding between hydrogenoxalates, the **1**···**1** association can not be accounted for by cyclic dimers alone, but requires a substantial contribution from charge-assisted linear interactions. Clearly, however, the repulsion term (−)–(−) leads to less effective hydrogen bonding in **1**···**1** than for AcO^-···HOAc, although its influence is greatly diminished relative to vacuum by the dynamic charge-screening effects of the solvent and counterions.

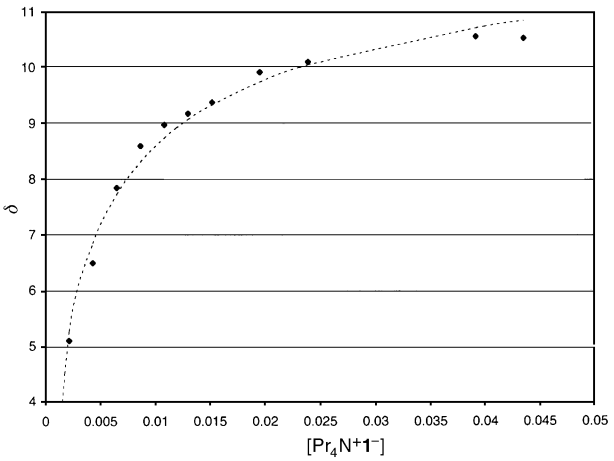

Fig. 1 Plot of the variation in chemical shift of the acidic proton in [Pr_4N^+**1**$^-$] with increasing concentration; (●) experimental, (----) best fit curve.

Our second approach to examining the nature of the OH···O interactions in **1** was crystallographic. If it is indeed the case that this interaction is actually repulsive, despite the very short O···O contact distance of 2.52 Å in potassium hydrogenoxalate (the example used in ref. 1), then distancing the cationic centers from hydrogenoxalate chain would be likely to disrupt this 'explosive' motif. In any case, the tremendous electrostatic compression which would be experienced by two *repulsive* functions (O^- and OH) being forced into such close proximity should be relaxed as less effective cations lose influence over the anions. We chose to test this concept by preparing the tetramethyl- and tetraethyl-ammonium hydrogenoxalate salts and determining their X-ray crystal structures.† Although the tetrapropylammonium salt is also a solid, X-ray quality crystals could not be not obtained, and the higher alkylammonium hydrogenoxalates are oils. As shown in Fig. 2, the hydrogen bonded chain is preserved in the Me_4N^+ and Et_4N^+ salts, thus no

DOI: 10.1039/b002361m

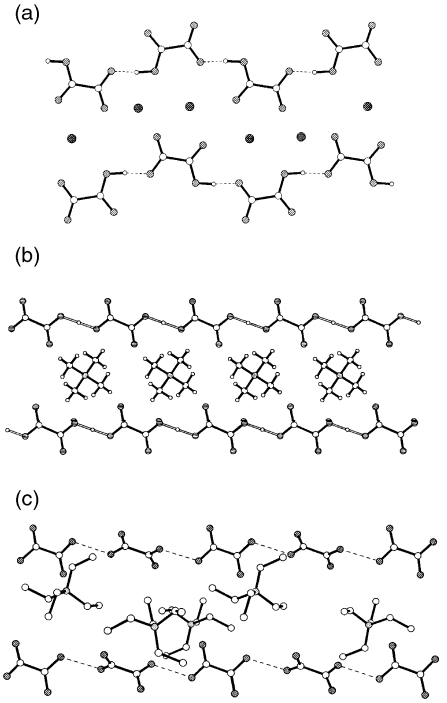

Fig. 2 (*a*) X-Ray crystal structure of [K$^+$**1**$^-$] (ref. 5). (*b*) X-Ray crystal structure of [Me$_4$N$^+$**1**$^-$]. The hydrogen bond appears to be symmetric with the hydrogen atom located equidistant between two oxygen atoms. Note, however, that it is not always possible to distinguish between an ordered H atom on a symmetry element from two disordered H atoms close to that symmetry element. Although the electron density contour maps gave no sign of disorder, the assignment of this hydrogen as an ordered atom in the center of the H-bond is not conclusive. (*c*) X-Ray crystal structure of [Et$_4$N$^+$**1**$^-$].

disruption of the motif occurs. Furthermore, the O···O distances in both the Me$_4$N$^+$ (2.476 Å) and Et$_4$N$^+$ (2.485 Å) derivatives are actually shorter than for the K$^+$ salt (2.518 Å),[5] even though the separation between the charged center of these cations and the H-bonded chain is considerably greater than for the K$^+$ ion.

In conclusion, if no hydrogen bonding were possible between hydrogenoxalate anions, as suggested,[1] we would expect no **1**···**1** interaction in solution; we would anticipate the lengthening of the OH···O contact and the eventual disruption of the chain motif in the solid as more weakly coordinating counterions are used; and in any case, very short O···O distances, typically diagnostic of strong or very strong hydrogen bonds,[6] would not be expected. In fact, all of the experimental observations suggest the contrary, *i.e.* a case is clearly made for hydrogen bonding between hydrogenoxalates in solution, and the O···O distances actually decrease in the solid state on association with more diffuse cations.

Indeed, one must consider the overall picture of **1**···**1** and its counterions in terms of a balance of interactions, two 'associative' [(+)–(−), and OH···O] and two dissociative [(+)–(+), (−)–(−)], with the net effect, both in solution and the solid state, being the assembly of hydrogenoxalate anions into aggregates of some description, depending on the medium. The assertion that a breakdown in the H-bonding length–strength analogy has been observed (based on the hypothesis that interanionic OH···O contacts are not hydrogen bonds) must herewith be revised: although no direct measurement of the quality of these interactions has been made, the experimental evidence supports their characterization as hydrogen bonds, and there is at present no argument to suggest that the length–strength analogy should not apply in this or related cases.

We also note that in the course of this study, Steiner[7] produced statistical evidence that the O–H and H···O distances in $^-$[O–H]···O$^-$ hydrogen bonds were consistent with those in undisputed hydrogen bonded systems, as well as citing the key example of dimethylammonium hydrogenoxalate, whose counterions do not bridge the hydrogenoxalates and thus can not be responsible for the assembly of the '*pseudo*-hydrogen bonded' chain, as implied by Braga *et al.* for [K$^+$**1**].[1] We feel our spectroscopic and crystallographic studies are complementary with the results of Steiner, and that the weight of experimental evidence now strongly implies that the computational model of the electron density in **1** used by Braga *et al.* is not an ideal representation, since it does not predict the observed association.

We thank the Leverhulme Trust for a Research Grant (C. E. M.) and the RSC for a Journals Grant For International Authors (M. M.). Dario Braga, Juan J. Novoa and Fabrizia Grepioni are thanked for discussions concerning this work on a number of occasions.

Notes and references

† *Crystal data:* for [Me$_4$N$^+$**1**$^-$]: $C_4H_{12}N^+C_2HO_4^-$, M = 163.17, monoclinic, a = 8.386(2), b = 5.700(2), c = 9.456(2) Å, β = 103.81(3)°, U = 438.9(2) Å^3, T = 220(2) K, space group $P2/n$ (alt. $P2/c$, no. 13), Z = 2, D_c = 1.235 g cm^{-3}, μ(Mo-Kα) = 0.103 mm^{-1}, 867 unique reflections (R_{int} 0.019) measured and used in all calculations. Final R_1 [752 $F \geqslant 4\sigma(F)$] = 0.0420 and wR (all F^2) was 0.120. Data collection at temperatures below 220 K was impossible due to the presence of a phase change.

For [Et$_4$N$^+$**1**$^-$]: $C_8H_{20}N^+C_2HO_4^-$, M = 219.28, monoclinic, a = 14.291(6), b = 10.933(7), c = 15.38(2) Å, β = 90.99(11)°, U = 2403(4) Å^3, T = 220(2) K, space group $P2_1/c$ (no. 14), Z = 8, D_c = 1.212 cm^{-3}, μ(Mo-Kα) = 0.092 mm^{-1}, 3133 unique reflections measured and used in all calculations. Final R_1 [1959 $F \geqslant 4\sigma(F)$] = 0.152 and wR(all F^2) was 0.422. The structure contains extensive disorder affecting all four methylene groups in one of the cations. One of the oxalate anions is less seriously affected, with disorder in both oxygen atoms of one CO_2^- terminus. There is a major [0.854(10)] component to the methylene disorder but the anion disorder is 50:50 within estimated standard uncertainties.

CCDC 182/1718. See http://www.rsc.org/suppdata/cc/b0/b002361m/ for crystallograpic files in .cif format.

1 D. Braga, F. Grepioni and J. J. Novoa, *Chem. Commun.*, 1998, 1959; see also: D. Braga, F. Grepioni, E. Tagliavini, J. J. Novoa and F. Mota, *New. J. Chem.*, 1998, 755.

2 The measured hydrogen bond enthalpy in KHC_2O_4 is 51.4 kJ mol^{-1} (M. S. Rozenberg, *Spectrochim. Acta, Part A*, 1996, **52**, 1559), whereas the simple point charge model $q_aq_b/4\pi\varepsilon\varepsilon_0 r$ gives a value of 270 kJ mol^{-1} for the interanionic repulsion in vacuum.

3 A least-squares fitting procedure was used to obtain K_a from the expression for the calculated chemical shift values. An expression for hydrogenoxalate where equilibria between a cyclic dimer, linear dimer, linear trimer and linear tetramer are taken into account is:

$$\delta_{calc} = \delta_{dimer}\frac{2K_d[O\times H]^2}{[O\times H]_i} + \delta_{end}\frac{\Sigma_n K_a^{n-1}[O\times H]^n}{[O\times H]_i} + \delta_{complex}\frac{\Sigma_n (n-1)K_a^{n-1}[O\times H]^n}{[O\times H]_i}$$

where K_d is the association constant for the cyclic dimer and is given the value 89 as determined for acetic acid in deuterochloroform under strictly anhydrous conditions, and δ_{dimer} is the associated chemical shift for this dimer. K_a is the association constant for the equilibria between monomeric **1** and the **1**···**1** linear dimer and each n-mer up to n = 4. The values of δ_{end} and $\delta_{complex}$ represent the chemical shifts of the non-associated protons at the end of the chain and the hydrogen bonded protons present in these oligomers, respectively. The value $[OxH]_i$ is the total concentration of hydrogenoxalate and [OxH] is the concentration of non-hydrogen bonded hydrogenoxalate present at equilibrium. The equilibria present in the (Pr$_4$N$^+$AcO$^-$)(AcOH) system can be modeled on a similar expression.

4 The K_a value for acetic acid dimerization in chloroform is consistent with those in the same concentration range as determined by IR spectroscopy: G. M. Barrow and E. A. Yerger, *J. Am. Chem. Soc.*, 1954, **76**, 5248.

5 F. H. Moore and L. F. Power, *Inorg. Nucl. Chem. Lett.*, 1971, **7**, 873.

6 P. Gilli, V. Bertolasi, V. Ferretti and G. Gilli, *J. Am. Chem. Soc.*, 1994, **116**, 909.

7 T. Steiner, *Chem. Commun.*, 1999, 2299.

Lowering the operating temperature of selective oxidation catalysts

Stanislaw Golunski*[a] and Andrew Walker[b]

[a] *Johnson Matthey Technology Centre, Blount's Court, Sonning Common, Reading, UK RG4 9NH. E-mail: golunse@matthey.com*

[b] *Autocatalyst Technical Centre, Johnson Matthey, Orchard Road, Royston, Hertfordshire, UK SG8 5HE*

Received (in Cambridge, UK) 23rd June 2000, Accepted 11th July 2000
Published on the Web 3rd August 2000

By incorporating palladium into oxidative dehydrogenation catalysts, a key step in the usual Mars–van Krevelen redox cycle has been by-passed, resulting in a decrease in operating temperature of around 200 °C.

In the partial oxidation of hydrocarbons by gas-phase oxygen, the desired reaction (*i.e.* oxidative dehydrogenation, oxygen insertion, or ammoxidation) has to compete with total combustion. In general, chemisorbed oxygen will react with adsorbed hydrocarbons to generate waste products, unless it can first form lattice oxide ions—the species implicated in selective partial oxidation.[1] By definition, therefore, metals usually catalyse total combustion, while metal oxides have the potential to generate added-value products. This potential is realised when hydrocarbon molecules are adsorbed near available oxide ions, which in turn can be replenished as soon as they are consumed in the selective reaction.

The parent materials used in this study, iron(III) oxide and bismuth molybdate, both belong to a category of catalysts that function by a cyclic redox mechanism, first described by Mars and van Krevelen.[2] In this cycle, the mobility of oxygen through the lattice is crucial to the overall process of replenishing oxide ions close to the hydrocarbon adsorption sites. Since the mobility of lattice oxygen is strongly dependent on temperature, it can become rate limiting when the operating temperature is lowered.[3] Eventually, a threshold is reached (usually at about 300 °C), below which the mobility is so low that the oxide has negligible catalytic activity. However, we have been able to induce partial oxidation activity at operating temperatures within the range 100–200 °C and even lower, by incorporating palladium into Fe_2O_3 and Bi_2MoO_6. This dramatic reduction in temperature is brought about by a change in the prevailing reaction mechanism.

The method by which Pd is introduced into the metal oxide is critical to inducing low temperature activity. We have found that controlled precipitation is the optimum route, resulting in reproducible catalysts that do not require any special activation procedures. The incorporation of Pd into iron(III) oxide (Pd–Fe–O) and bismuth molybdate (Pd–Bi–Mo–O) is described in detail in a family of patent filings.[4]

XPS of freshly dried precipitate of Pd–Fe–O (as used in activity tests) showed Pd in the +2 state (Pd $3d_{5/2}$ E_b = 337.3 eV) and Fe in the +3 state (Fe $2p_{3/2}$, E_b = 710.6 eV). XRD revealed the material to be amorphous, which was also the case when the precipitation was carried out in the absence of Pd.

As bismuth molybdate catalysts require calcination in order to form the active binary phases,[5] our precipitate of Pd–Bi–Mo–O was also subjected to the same thermal treatment, before characterisation and testing. XRD of the calcined Pd–Bi–Mo–O showed it to be a mixture of α-bismuth molybdate (monoclinic $Bi_2Mo_3O_{12}$) and β-bismuth molybdate (monoclinic $Bi_2Mo_2O_9$), with no evidence of a crystalline Pd-phase. Without Pd, the bismuth molybdate catalyst was also a mixture of two allotropes, but these were the β- and γ-(orthorhombic Bi_2MoO_6) forms.

In common with other metal oxides, conventional catalysts derived from iron oxide are not active for butene oxidation below 300 °C.[6] However, when fresh samples of Pd–Fe–O made by coprecipitation were exposed to a feed of 14% but-1-ene in air at 100 °C, there was a delay (2–10 min, depending on Pd content) and then reaction began. Starting temperatures as low as 80 °C (for a catalyst containing 4% Pd by mass) and 60 °C (10% Pd) were recorded. In order to assess whether this low temperature activity was due to a synergy between the palladium and iron oxide phases or was primarily a result of the preparative method, we also tested palladium oxide and iron oxide prepared by essentially the same precipitation method. Neither showed any activity at such low temperatures. However, some reduction in operating temperature could be induced by impregnating Fe_2O_3 with Pd (4% by mass). This material was capable of achieving 50% butene conversion with 35% selectivity to butadiene at a feed temperature of 200 °C, but showed no activity below 150 °C.

Initial butadiene yield of the coprecipitated Pd–Fe–O catalysts was poor (*ca.* 10%), and their sensitivity to the butene/air feed ratio was high. During the first few hours on line, the yield improved and the sensitivity declined, before stabilising. For example, after 5 h on line, 4%Pd–Fe–O converted 50% of the hydrocarbon in a 20% butene/air feed with 70% butadiene selectivity; after the same time in a 14% butene/air feed, it converted 55% with 60% selectivity. The on-line improvement in yield appeared to be closely related to the blocking of non-selective (combustion and isomerisation) sites by carbon. As shown in Table 1, the catalysts could be 'regenerated' by heat treatment in flowing air (550 °C), during which the retained carbon was displaced as CO_2.

Pd–Bi–Mo–O required a higher operating temperature and a leaner hydrocarbon feed (12.5% butene/air) than Pd–Fe–O. After no activity was observed at 150 °C, the bed temperature was raised to 200 °C, whereupon reaction began as soon as the gas feed was introduced. The initial conversion of butene was 55%, with 45% selectivity to butadiene. Again, the performance improved with time, before stabilising after 30 min at 60% conversion and 60% butadiene selectivity. By contrast, unmodified bismuth molybdate showed only short-term activity under the same conditions (Fig. 1). Its temperature had to be raised to 350 °C before activity could be sustained (80% conversion; 70% selectivity). The fact that the selectivity of Pd–Bi–Mo–O (at 200 °C) was not as high as that of the unmodified bismuth molybdate (at 350 °C) may reflect the change in phase composition caused by the presence of Pd.

Both Pd–Fe–O and Pd–Bi–Mo–O are derived from catalysts that conform to a redox mechanism, in which the movement of

Table 1 Oxidation of butene over 4%Pd–Fe–O as function of catalyst condition[a]

		Selectivity (%)			
Catalyst condition	Conversion/ (%)	CO_2	*trans*-But-2-ene	*cis*-But-2-ene	Butadiene
Fresh	65	45	14	12	15
Aged on line	54	36	3	2	59
Regenerated	70	42	13	11	21

[a] Feed: 14% butene/air; contact time: 0.6 s; feed temperature: 100 °C.

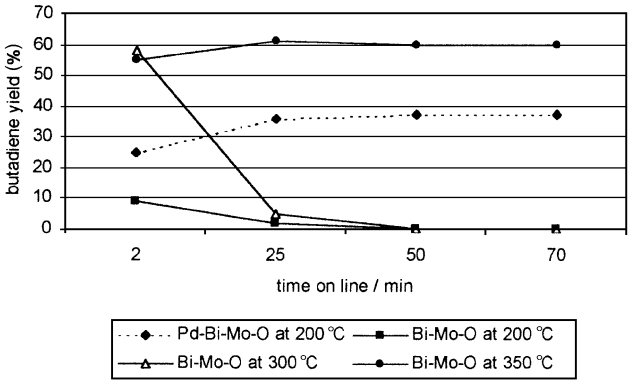

Fig. 1 Yield of butadiene as a function of time, over unmodified and Pd-modified bismuth molybdate, at operating temperatures of between 200 and 350 °C (feed: 12.5% butene/air; contact time: 0.6 s).

lattice oxygen is a key step in the selective partial oxidation of hydrocarbons.[7] The performance (preferred feed-composition; product distribution; activity/selectivity correlation) of the Pd-containing materials is similar to that of the unmodified catalysts, except in terms of operating temperature. Our working model, therefore, is one in which the same alkene adsorption sites are present in both forms, but the role of Pd is to supply selective oxygen at lower temperatures, by-passing the need for transport through the lattice.

A TAP study of the initial steps in the butene to butadiene reaction over 4%Pd–Fe–O, compared to a conventional α-Fe_2O_3 catalyst, provides support for this model.[8] Even at 150 °C, unmodified Fe_2O_3 is capable of converting butene/O_2 to butadiene, but only for a short time. At this temperature, it only forms butadiene, while it is consuming O_2. Although the same applies to Pd–Fe–O, it continues to consume O_2 indefinitely. The presence of the Pd enables the catalyst to activate gas-phase oxygen into selective species at low temperatures, leading to sustainable oxidative dehydrogenation under conditions where Fe_2O_3 does not usually function.[6] This mechanistic short cut enables low-temperature activity to be achieved by redox catalysts in which oxygen mobility would normally be the limiting factor. It cannot, however, overcome some of the other factors (such as product desorption) that can prevent low-temperature activity—as we have found to be the case for the conversion of propene to acrolein over Pd–Fe–O and Pd–Bi–Mo–O.

During the past thirty years, there have been a number of reported examples of heterogeneously catalysed oxidation reactions at unexpectedly low temperatures. In most cases, the reaction has been the total oxidation of a simple molecule.[9–13] Furthermore, these instances of low-temperature activity have appeared to be isolated and exceptional effects, associated with very specific compositions, preparations or interactions. We believe that our studies of Pd-incorporation into metal oxides illustrate a more general phenomenon that can allow the normal activity of a redox catalyst to be achieved at temperatures much lower than previously expected. Indeed, the Pd–Fe–O family of catalysts is particularly versatile, exhibiting catalytic activity at exceptionally low temperatures for CO oxidation[14] and the water–gas shift reaction,[4] as well as for the partial oxidation of hydrocarbons described here. For each reaction, the minimum operating temperature is about 250 °C below that observed for unmodified iron(III) oxide.

Notes and references

1 V. D. Sokolovskii, *Catal. Rev.-Sci. Eng.*, 1990, **32**, 1.
2 P. Mars and D. W. van Krevelen, *Chem. Eng. Sci. Special Suppl.*, 1954, **3**, 41.
3 J. M. Libre, Y. Barbaux, B. Grzybowska, P. Conflant and J. P. Bonnelle, *Appl. Catal.*, 1983, **6**, 325.
4 S. E. Golunski, J. M. Gascoyne, A. Fulford and J. W. Jenkins, *US Pat.*, 5877377, 1999.
5 Ph. A. Batist, J. F. H. Bouwens and G. C. A. Schuit, *J. Catal.*, 1972, **25**, 1.
6 M. Zhang, R. Lan, J. Liu, X. Chen and W. Zhou, *J. Chem. Soc., Faraday Trans.*, 1992, **88**, 637.
7 C. F. Cullis and D. J. Hucknall, in *Catalysis*, ed. G. C. Bond and G. Webb, Royal Society of Chemistry, London, 1982, p. 273.
8 S. E. Golunski and A. P. Walker, in preparation.
9 M. I. Brittan, H. Bliss and C. A. Walker, *AIChE. J.*, 1970, **16**, 305.
10 M. Haruta, H. Kageyama, N. Kamijo, T. Kobayashi and F. Delannay, in *Successful Design of Catalysts*, ed. T. Inui, Elsevier, Amsterdam, 1988, p. 33.
11 S. D. Gardner, G. B. Hoflund, B. T. Upchurch, D. R. Schryer, E. J. Kielin and J. Schryer, *J. Catal.*, 1991, **129**, 114.
12 S. E. Golunski, H. A. Hatcher, R. R. Rajaram and T. J. Truex, *Appl. Catal. B: Environ.*, 1995,**5**, 367.
13 G. C. Bond and D. T. Thompson, *Catal. Rev.—Sci. Eng.*, 1999, **41**, 319.
14 S. E. Golunski, M. I. Petch and A. P. Walker, in preparation.

Carborane–fullerene hybrids as a seemingly attractive–attractive dyad with high hyperpolarizability†

Mouad Lamrani,[a] Ryo Hamasaki,[a] Masaya Mitsuishi,[b] Tokuji Miyashita[b] and Yoshinori Yamamoto*[a]

[a] *Department of Chemistry, Graduate School of Science, Tohoku University, Sendai 980-8578, Japan. E-mail: yoshi@yamamoto1.chem.tohoku.ac.jp*

[b] *Institute for Chemical Reaction Science, Tohoku University, Katahira 2-2-1, Aoba-ku, Sendai 980-8577, Japan*

Received (in Cambridge, UK) 16th May 2000, Accepted 28th June 2000
Published on the Web 3rd August 2000

A combination between seemingly attractive carboranes and fullerene through an ethynyl π-system (compounds 1a–c) gives unexpectedly high β-values, thereby providing a guideline that in certain cases a seemingly A–A system becomes a promising complementary combination for obtaining high hyperpolarizability; the β values of 1a, 1b and 1c were 346, 483, and 1189 × 10^{-30} esu, respectively.

Quadratic nonlinear optical (NLO) materials have increasingly attracted attention owing to their direct application in the development of efficient optical telecommunication networks lacking electrical-to-optical, and *vice versa*, signal conversion.[1] Such application requires thermally robust materials with highly nonlinear optical (NLO) response (first hyperpolarizability β). The use of organic materials may offer significant advantages over conventional inorganic crystals. Typical organic NLO compounds include Donor (D) and Acceptor (A) moieties bridged by a π-conjugated linker. Until now, most efforts to obtain better hyperpolarizability (β) have been directed to finding both the right combination of D and A species and the right length of the conjugated bridge between D and A.[2] It has been known for many years that *closo*-carboranes are *electron deficient boron clusters* having highly polarizable σ-aromatic character.[3] Previously carboranes (A) containing certain donor (D) groups were synthesized, but their hyperpolarizable properties were not satisfactory.[4] More recently it has been recognized that fullerenes are *electron attracting carbon clusters* having highly delocalizable π-electrons.[5] Actually, fullerenes (A) containing electron donor (D) moieties have been reported,[6] but there are no NLO studies on those compounds at all, to the best of our knowledge. It occurred to us that carborane–fullerene dyads bridged by an appropriate linker might exhibit an interesting NLO response, in spite of the fact that both groups are electron attracting clusters, since both clusters have highly polarizable electrons. We wish to report that a combination between seemingly attractive carboranes and fullerene through an ethynyl π-system (compounds **1a**–**c**) gives unexpectedly high β-values, thereby providing a guideline that in certain cases a seemingly A–A system becomes a promising complementary combination for obtaining high hyperpolarizability.

The synthetic procedure for **1a** is shown in Scheme 1 (see ESI.†) The *meta*- and *para*-carborane analogues, **1b** and **1c**, were prepared in a similar manner.[7]

For clarity, the cyclic voltammetries of only **1a** and C_{60} are shown in Fig. 1 (see ESI†). Those of the phenylethynyl analogue **7** are similar. The redox potentials of **1a**–**c**, **6**, **7** and C_{60} are summarized in Table 1. Only E_1^{red}/E_2^{ox} values are shown for simplicity, although three quasireversible reduction–oxidation peaks were observed. The one-electron reduction of the non-charged molecules **1** (E_1^{red}) and the one-electron oxidation to **1** (E_1^{ox}) are more important than the further

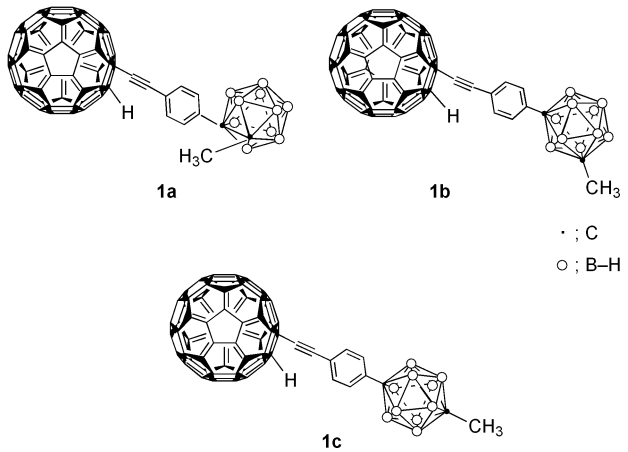

reductions of the charged molecules (E_2^{red} and E_3^{red}) and the oxidations to the charged molecules (E_2^{ox} and E_3^{ox}), when we discuss the electrochemical property of the C_{60} end group. The three quasireversible reduction peaks of **1a** are similar to those found for C_{60}, **6** and **7** under the same experimental conditions. One additional irreversible oxidation wave at −187 mV (E^{ox}) most probably corresponds to the oxidation peak of the conjugated spacer fragment, since authentic samples of **6** and **7** also exhibited similar peaks at −122.5 and −286 mV, respectively. The three reduction potentials of **1a** were remarkably shifted to more negative values in comparison with those of the parent C_{60}, presumably due both to the saturation of a double bond of C_{60} and the electron donating character of the ethynylphenyl group. Consequently, it is clear that the C_{60} framework of **1a** behaves as an A group.

Similar observations were made for the *meta*- and *para*-derivatives **1b** and **1c**. An important question was whether the

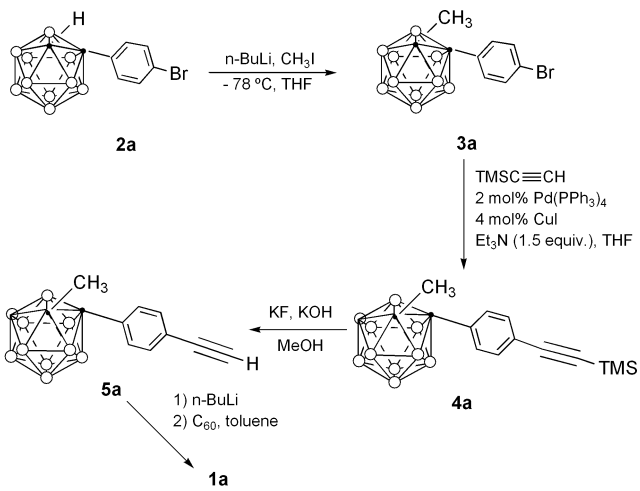

Scheme 1

† See http://www.rsc.org/suppdata/cc/b0/b003931o/ for electronic supplementary information (ESI): a detailed procedure of Scheme 1, Fig. 1 and 2, absorption spectra of **1**, **5**, **6**, **7** and C_{60}, and fluorescence spectrum of **1a**.

DOI: 10.1039/b003931o

Table 1 Results of cyclic voltammetries and β values

Compd.	E_1^{red}/E_1^{ox} (mV)[a,b]	E^{ox} (mV)[a,c]	β (× 10^{-30} esu)
1a	−1242/−552	−187	346
1b	−1210/−581	−79	483
1c	−1193/−615	−170	1189
C_{60}	−1103/−631	—	0
6	−1262/−590	−123	87
7	−1086/−752	−286	139
5a	—[d]	—[d]	7
5b	—[d]	—[d]	28
5c	—[d]	—[d]	48

[a] Potentials in mV *vs.* ferrocene/ferrocenium measured in *o*-dichlorobenzene (see Fig. 1) (see ESI†). [b] Among three quasireversible redox peaks, only the first peaks E_1^{red}/E_1^{ox} are shown and the other peaks are shown in the ESI†. [c] Irreversible oxidation peak most probably due to the ethynyl spacer units. [d] The compound did not exhibit electroactivities within the potential range we investigated.

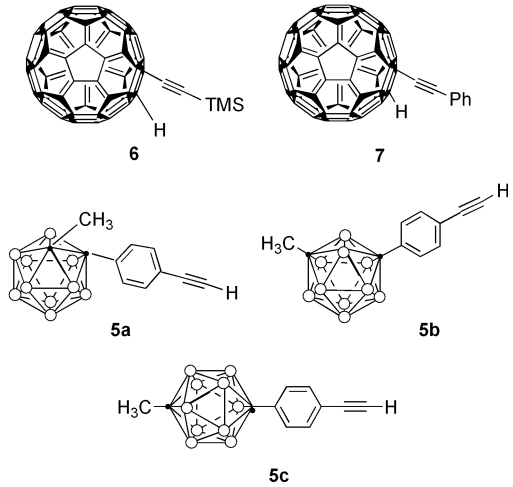

carborane framework acted as a donor or (as usual) an attractor. We synthesized the reference compounds **5a–c** in order to help clarify this point, but those compounds did not exhibit electroactivities within the potential range we investigated. The E^{ox} value of **7** was −286 mV, which was the most negative value among those observed in Table 1, indicating that the electron density of the ethynyl group of **7** was higher than that of **1a–c**. Accordingly, we assume at present that the carborane end group acts as an attractor, as well established previously.[8]

Absorption spectra of **1a–c**/$CHCl_3$ in the UV-vis range showed two large absorption bands at 258 and 328 nm; **1a**, λ_{max} 258 (log ε 5.10), 328 (4.77); **1b**, 258 (5.05), 328 (4.58); **1c**, 258 (5.32), 328 nm (4.71). Absorption spectra of **5a–c** in $CHCl_3$ showed absorption bands at 260 (log $\varepsilon \approx$ 4.66–4.49) and 283 nm (3.83–4.36), and those of C_{60} in $CHCl_3$ showed two strong bands at 259 (4.85) and 329 nm (4.28). These data in addition to those for **6** and **7**[9] clearly indicate that the two strong bands of **1a–c** are due to the phenylethynyl–C_{60} chromophore and the influence of the carborane groups to the UV absorption is very small (see ESI†). Very weak absorption bands between 400–440 nm (log $e \approx$ 4.00–3.50) were observed for **1b** and **1c**, which were presumably due to a forbidden transition (see ESI†). In $CHCl_3$ solution of **1a–c**, no absorption was observed after 450 nm, although C_{60} itself, **6** and **7** in cyclohexane exhibited very weak absorption bands between 470–700 nm with log ε 2.3–3.2.[9]

The fluorescence spectra of **1a–c** in $CHCl_3$ following excitation at 258 and 328 nm showed broad band emission in the range 350–390 nm, which was attributed to Raman scattering of the $CHCl_3$ (see ESI†). Fullerene fluorescence is usually observed around 700 nm; this was in general measured in cyclohexane.[10] We attempted to dissolve **1a–c** in cyclohexane, THF and CH_3CN, but they were soluble only in $CHCl_3$. The emission spectra of **6** and **7** in $CHCl_3$ also exhibited Raman scattering of $CHCl_3$. In conclusion, no significant spectroscopic absorption or/and emission was observed for the $CHCl_3$ solution of **1a–c** (10^{-6} M) in the range of the double frequency value 532 nm, allowing us to get the necessary measurements to deduce the β coefficients of **1a–c**.[11]

The quadratic dependence of the second-harmonic signal intensity to the harmonic intensity for **1a**, for example, is demonstrated in Fig. 2 (see ESI†). The laser wavelength of 1064 nm was used. The molar absorption coefficients (ε) of **1a–c** at 532 nm were below *ca.* 1000 $dm^3\ mol^{-1}\ cm^{-1}$, so that the influence of resonance effects were very small.[12] The β values of **1a–c** were 346, 483 and 1189 × 10^{-30} esu, respectively (Table 1). It should be noted especially that *the para-derivative* ***1c*** *exhibited a large* β *value*. As expected, the β value of C_{60} itself was zero under the same experimental conditions owing to its centrosymmetric structure. For comparison, the β values of **6** and **7**, which are typical D–A systems, were measured: the β of **6** was 87 × 10^{-30} and that of **7** 139 × 10^{-30} esu. The β-values of **5a–c** were 7, 28 and 48 × 10^{-30} esu, respectively. It is clear that the reference compounds exhibit ordinary level of β-values, although the values of **6** and **7** (~100 × 10^{-30} esu) are still higher than that for a standard *para*-nitroaniline, which showed 23 × 10^{-30} esu under the same experimental conditions. By attaching the carboranes, the β value increased up to 1189 × 10^{-30} esu confirming the strong electronic polarizable influence of the boron clusters.

Very high hyperpolarizability of **1c**, which constitutes the first example of its kind, is quite fascinating since it has often been surmised[13] that, by forming charge-transfer complexes with appropriate donors, the center of symmetry of C_{60} is broken. In our case the hybride **1** do not form any charged complex but present high β values. Further investigation on boron–carbon cluster hybrids is being pursued actively in our laboratories.

Notes and references

1 P. N. Prasad and D. J. Williams, *Nonlinear Optical Effects in Molecules and Polymers*, Wiley, New York, 1991; P. Prasad, *Nonlinear Optical Properties of Organic Materials*, Plenum, New York, 1991.
2 For example: S. R. Marder, C. B. Gorman, B. G. Tiemann and L.-T. Cheng, *J. Am. Chem. Soc.*, 1993, **115**, 3006; S. R. Marder, D. N. Beratan and L.-T. Cheng, *Science*, 1991, **252**, 103.
3 D. M. Murphy, D. M. P. Mingos, J. L. Haggitt, H. R. Powell, S. A. Westcott, T. B. Marder, N. J. Taylor and D. R. Kanis, *J. Mater. Chem.*, 1993, **3**(2), 139.
4 D. M. Murphy, J. M. Forward and D. M. P. Mingos, *J. Mater. Chem.*, 1993, **3**, 67.
5 N. Martin, L. Sanchez, B. Illescas and I. Perez, *Chem. Rev.*, 1998, **98**, 2527.
6 D. R. Kanis, M. A. Ratner and T. J. Marks, *Chem. Rev.*, 1994, **94**, 195.
7 Compound **2a** was obtained following the slightly modified preparative route reported in R. Could, M. A. Fox, W. R. Gill, P. L. Herbertson, J. A. H. Macbride and K. Wade, *J. Organomet. Chem.*, 1993, 19.
8 For a recent example on the strong electron-withdrawing nature of *closo*-carboranes, see Y. Endo and Y. Taoda, *Tetrahedron Lett.*, 1999, **40**, 9073. One referee posed a question concerning the electron-withdrawing character of the carborane groups of **1a–c**: whether the observed E^{ox} values of the phenylethynyl groups should be similar to those for **5a–c** if the carborane groups act as electron-withdrawing groups. However, the CVs of **5a–c** did not show any signals in the voltammograms. A possible explanation might be that C_{60} is a very strong EWG group, but that the carboranes are weaker EWG moieties.
9 K. Komatsu, Y. Murata, N. Takimoto, S. Mori, N. Sugita and T. S. M. Wan, *J. Org. Chem.*, 1994, **59**, 6101.
10 J. Catalán and J. Elguero, *J. Am. Chem. Soc.*, 1993, **115**, 9249.
11 The measurements to deduce the β coefficients of **1a–c**, **5a–c**, **6**, **7** and C_{60} were carried out in $CHCl_3$ with 10^{-6} M substrates.
12 In general, when log ε is greater than 4, resonance effect is discussed.
13 Y. Wang and L.-T. Cheng, *J. Phys. Chem.*, 1992, **96**, 530.

Huge enhancement of the quadratic nonlinear optical susceptibility in push–pull chromophores based on bridged dithienylethylene spacers

Jean-Manuel Raimundo,[a] Philippe Blanchard,[a] Isabelle Ledoux-Rak,[b] Rolland Hierle,[b] Laurent Michaux[a] and Jean Roncali*[a]

[a] *Ingénierie Moléculaire et Matériaux Organiques, CNRS UMR 6501, Université d'Angers, 2 Bd Lavoisier, 49045 Angers Cedex, France. E-mail: jean.roncali@univ-angers.fr*

[b] *Laboratoire de Photonique Quantique et Moléculaire, Ecole Normale Supérieure, 61 av. du Président Wilson, 94235 Cachan, France*

Received (in Cambridge, UK) 1st March 2000, Accepted 11th July 2000
Published on the Web 4th August 2000

Replacement of the open chain dithienylethylene π-conjugating spacer by its bridged analog in push–pull NLO-phores produces a dramatic increase of the quadratic hyperpolarisability.

Chromophores for 2nd order nonlinear optics consist of electron-donor and electron-acceptor groups interacting through a π-conjugating spacer.[1] Whereas the optimization of the donor[2] and acceptor[3] groups has led to considerable progress in the synthesis of stable and efficient systems, the relationship between the structure of the conjugating spacer and 2nd order nonlinearity are less clearly understood. Push–pull polyenes can reach huge nonlinearities,[2a,4] but their practical use might be limited by stability problems.

As shown in recent work, thiophene-based spacers lead to stable NLO-phores with second order hyperpolarisabilities sometimes exceeding $10\,000 \times 10^{-48}$ esu.[2b–d,3] These high performances can be related to the moderate resonance energy of thiophene which allows a better π-electron delocalization than *e.g.* benzene-containing spacers.

It has been shown that the static hyperpolarizability is correlated with the ground state polarization which is in turn reflected by bond length alternation (BLA).[5] Optimal β values, predicted for BLA intermediate between those for unsubstituted polyenes (~0.10 Å) and the cyanine limit (0.00 Å), have been approached by selecting appropriate combinations of donor and acceptor groups in order to tune the balance between the neutral and charge-separated limiting resonance forms.[4,5]

Previous theoretical and experimental work has shown that the covalent bridging of dithienylethylene (DTE) results in a 0.40 eV decrease of the HOMO–LUMO gap due to a reduction of BLA.[6] On this basis, replacement of DTE by a bridged analog with inherently reduced BLA, can be expected to improve the quadratic hyperpolarizability of the derived push–pull chromophores. In this context, we report here preliminary results on two series of NLO-phores derived from open chain (**1c**–**e**) and bridged (**2**,**3**) DTE spacers, used in conjunction with *N*,*N*-dialkylaniline donors, and various acceptors.

All NLO-phores have been prepared according to the general procedure shown in Scheme 1. DTE **1f** and its bridged analog **2f**[6c] were converted into aldehydes **1g** and **2g** by Vilsmeier formylation. Wittig olefination of **1g** and **2g** with phosphonium iodides bearing the *N*,*N*-dialkylaniline group led to compounds **1h**–**3h** as a mixture of *E* and *Z* isomers. After separation of the *Z*-isomer, a second formylation led to aldehydes **1i**–**3i** and the target molecules were obtained by Knoevenagel condensation between **1i**, **2i** and **3i** and various acceptors with active methylene groups. All final compounds have been fully characterized by ^{1}H and ^{13}C NMR, mass spectroscopy and elemental analysis.

Table 1 lists the UV-vis absorption maxima (λ_{max}), second order nonlinear hyperpolarizabilities ($\beta\mu$), and decomposition temperatures (*T*d) of the NLO-phores. Comparison of the data for the open chain and bridged compounds containing similar donor–acceptor pairs shows that the bridging of the spacer produces a considerable red shift of λ_{max}, (up to 100 nm between **1d** and **2d**), indicating an enhancement of the effective conjugation. Preliminary tests on **1e** and **2d** gave anomalously low μβ values which were attributed to the poor solubility of the

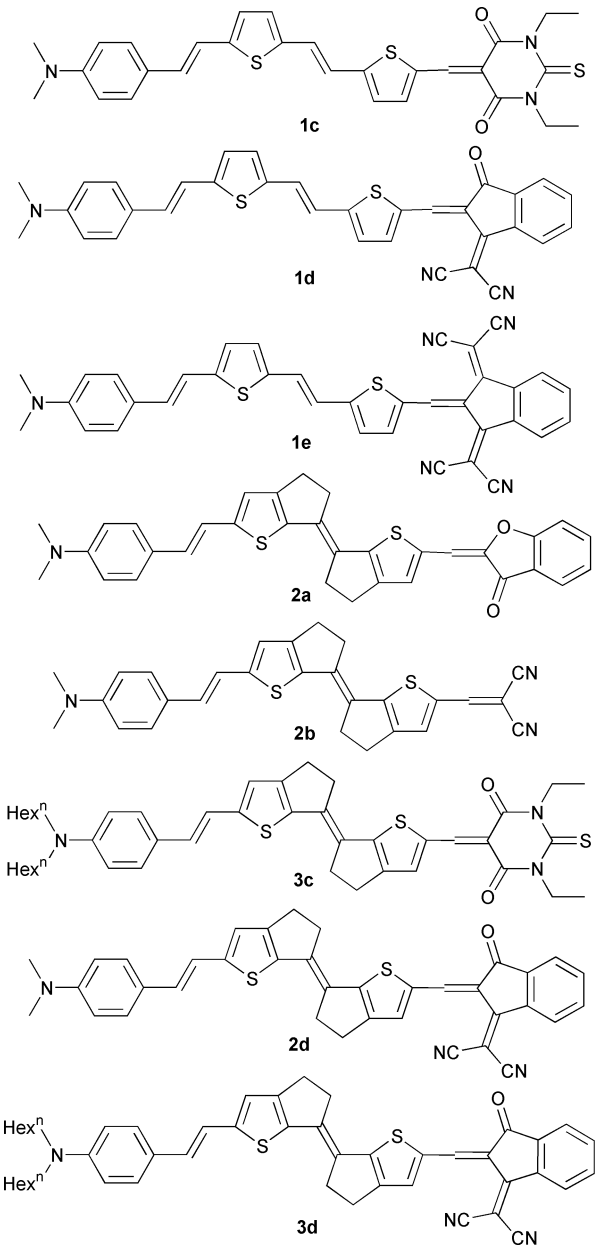

DOI: 10.1039/b001700k

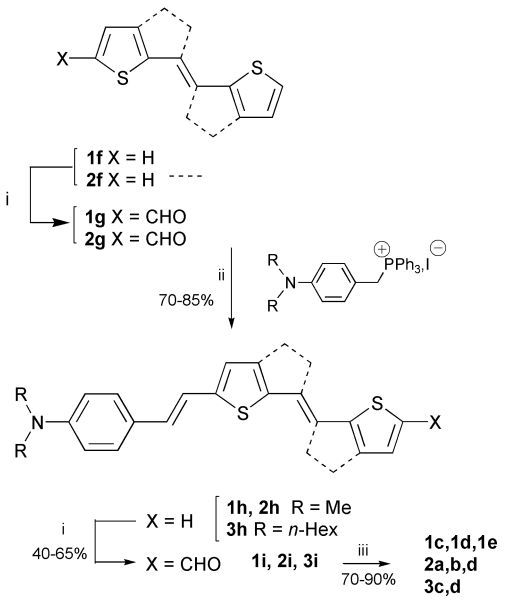

Scheme 1 *Reagents and conditions* (i) $POCl_3$/DMF; (ii) *t*-BuOK/MeCN-THF; (iii) **2b**, malononitrile, $Et_3N/CHCl_3$, rflx 12 h; **2a**, coumaranone, $Al_2O_3/CHCl_3$, room temp, 48 h; **1c**, **3**, thiobarbituric acid, Ac_2O, rflx 2 h; **1d**, **2d**, **3d**, dicyanovinylindan-3-one, EtOH rflx 10 h; Ac_2O, 60 °C 1 h; **1e**, bisdicyanovinylindane, Ac_2O, rflx 1 h.

Table 1 Absorption maxima, quadratic hyperpolarisabilities and decomposition temperatures of chromophores **1**–**3**

Compound	λ_{max}/nm[a]	$\mu\beta/10^{-48}$ esu[b]	*T*d/°C[c]
1c	606	2720 (1450)	235
1d	656	7100 (3300)	256
1e	720	Nd	250
2a	592	2500 (1500)	300
2b	614	3100 (1600)	308
3c	682	10400 (4400)	235
2d	756	Nd	258
3d	768	19400 (5680)	245

[a] In CH_2Cl_2. [b] Measured in $CHCl_3$ at 1.9 μm by EFISH, values in parentheses represent the zero-frequency hyperpolarizability product $\mu\beta_0$. [c] Determined by differential scanning calorimetry at a rate of 10 °C min^{-1}.

compounds. This problem was resolved by replacing methyl by hexyl groups in compounds **3c** and **3d**.

Comparison of the data for the two series of compounds shows that, for a given acceptor, the bridging of the DTE spacer produces a huge enhancement of μβ which increases from 2720 to 10 400 × 10^{-48} esu for the **1c**/**3c** pair, while for the **1d**/**3d** one, μβ increases by a factor of three and reaches a value of 19 400 × 10^{-48} esu. To the best of our knowledge, this value is the largest ever reported for a NLO-phore based on an heteroaromatic spacer.

Improved thermal stability has already been reported for NLO-phores based on configuration-locked olefinic spacers,[7] or for bridged dithienyl hexatrienes.[8] While the various acceptor groups used here make it difficult to evaluate the specific effect of the spacer on the stability, the similarity of the Td values for open chain and bridged compounds bearing the same acceptor *e.g.* **1d** and **2d** suggests that, in that case, the stability is limited by that of the acceptor. Further support for this hypothesis is provided by the identical *T*d values (235 °C) found for **3c**, **1c** and its analog containing the more stable diphenylamino substituted thiophene donor.[2d] On the other hand, the high Td values for **2a** and **2b** (⩾ 300 °C) definitively show that thermally stable chromophores can be synthesized from bridged DTE spacers.

Notes and references

1 (*a*) L. R. Dalton, A. W. Harper, R. Ghosn, W. H. Steier, M. Ziari, H. Fetterman, Y. Shi, R. V. Mustacich, A. K.-Y. Jen and K. J. Shea, *Chem. Mater.*, 1995, **7**, 1060; (*b*) T. J. Marks and M. A. Ratner, *Angew. Chem., Int. Ed. Engl.*, 1995, **34**, 155.

2 (*a*) S. R. Marder, L.-T. Cheng, B. G. Tiemann, A. C. Friedli, M. Blanchard-Desce, J. W. Perry and J. Skindhøj, *Science*, 1994, **263**, 511; (*b*) A. K.-Y. Jen, V. P. Rao, K. J. Drost, K. Y. Wong and M. P. Cava, *J. Chem. Soc., Chem. Commun.*, 1994, 2057; (*c*) V. P. Rao, Y. M. Cai and A. K.-Y. Jen, *J. Chem. Soc., Chem. Commun.*, 1994, 1689; (*d*) A. K.-Y. Jen, Y. Cai, P. V. Bedworth and S. R. Marder, *Adv. Mater.*, 1997, **9**, 132.

3 (*a*) V. P. Rao, A. K.-Y. Jen, K. Y. Wong and K. J. Drost, *J. Chem. Soc., Chem. Commun.*, 1993, 1118; (*b*) S. Gilmour, R. A. Montgomery, S. R. Marder, L.-T. Cheng, A. K.-Y. Jen, Y. Cai, J. W. Perry and L. R. Dalton, *Chem. Mater.*, 1994, **6**, 1603; (*c*) P. Boldt, G. Bourhill, C. Bräuchle, Y. Jim, R. Kammler, C. Müller, J. Rase and J. Wichern, *Chem. Commun.*, 1996, 793; (*d*) X. Wu, J. Wu, Y. Liu and A. K.-Y. Jen, *J. Am. Chem. Soc.*, 1999, **121**, 472; (*e*) X. Wu, J. Wu, Y. Liu and A. K.-Y. Jen, *Chem. Commun.*, 1999, 2391.

4 M. Blanchard-Desce, V. Alain, P. V. Bedworth, S. R. Marder, A. Fort, C. Runser, M. Barzoukas, M. S. Lebus and R. Wortmann, *Chem. Eur. J.*, 1997, **3**, 1091.

5 S. R. Marder, C. B. Gorman, F. Meyers, J. W. Perry, G. Bourhill, J.-L. Brédas and B. M. Pierce, *Science*, 1994, **265**, 632.

6 (*a*) J. Roncali, C. Thobie-Gautier, E. Elandaloussi and P. Frère, *J. Chem. Soc., Chem. Commun.*, 1994, 2249; (*b*) H. Brisset, P. Blanchard, B. Illien, A. Riou and J. Roncali, *Chem. Commun.*, 1997, 569; (*c*) P. Blanchard, H. Brisset, A. Riou and J. Roncali, *J. Org. Chem.*, 1997, **62**, 2401.

7 (*a*) I. Cabrera, O. Althoff, H. T. Man and H. N. Yoon, *Adv. Mater.*, 1994, **6**, 43; (*b*) C.-F. Shu, W.-J. Tsai and A. K.-Y. Jen, *Tetrahedron Lett.*, 1996, **39**, 7055.

8 P. Blanchard, H. Brisset, R. Hierle, A. Riou and J. Roncali, *J. Org. Chem.*, 1998, **63**, 8310.

ChemComm

Diels–Alder chemistry of 2-cyanoalk-2-enones. A convenient general approach to angularly substituted polycyclic systems

Jia-Liang Zhu,[a] Kak-Shan Shia[b] and Hsing-Jang Liu*[ab]

[a] *Department of Chemistry, University of Alberta, Edmonton, Alberta, Canada, T6G 2G2*
[b] *Department of Chemistry, National Tsing Hua University, Hsinchu, Taiwan 30013, Republic of China. E-mail: hjliu@mx.nthu.edu.tw*

Received (in Cambridge, UK) 31st May 2000, Accepted 30th June 2000
Published on the Web 4th August 2000

Under zinc chloride catalysis, a number of 2-cyanoalk-2-enones representing various ring sizes were found to undergo facile cycloaddition with several selected conjugated dienes; sequential treatment of the adducts with lithium naphthalenide and an alkylating agent resulted in the direct replacement of the angular cyano group with an alkyl group, providing easy access to angularly substituted polycyclic systems.

The Diels–Alder reaction has long played an important role in synthetic organic chemistry. One of the most important features of its application is to build fused polycyclic skeletons, a process requiring only a straightforward addition of a cyclic dienophile to an appropriately substituted buta-1,3-diene. However, early investigations have demonstrated that under thermal conditions, the cycloaddition of dienes to cyclic dienophiles, such as cyclohex-2-enone is a poor process, often resulting in low yields of products.[1] Over the years, there have been extensive studies directed towards the enhancement of the dienophilicity of cycloalkenones, resulting in the development of two general solutions. One makes use of Lewis acid catalysis and the other involves the incorporation of an additional electron-withdrawing group to the dienophilic carbon–carbon double bond. In l977, we showed that the introduction of a methoxycarbonyl group to C-2 of 4,4-dimethylcyclohexa-2,5-dien-1-one vastly improved the Diels–Alder reactivity of an otherwise poor dienophile.[2] This strategy proved to be useful for the activation of the dienophilic double bond in systems where the conjugated enone functionality could not undergo enolization towards the C-4 carbon and has been successfully applied in facilitating the total synthesis of various polycyclic natural products.[3] This strategy, however, was found to be less effective when the cycloalk-2-enone contains an enolizable hydrogen at C-4, as the placement of an ester group onto the C-2 carbon makes the compound extremely labile. For instance, although 2-methoxycarbonylcyclohex-2-enone can be applied as a dienophile,[4] the efficiency of its Diels–Alder reaction is much lower than that of its 4,4-dimethyl derivative because of the poor stability associated with the former compound. Another drawback of using an ester as an activating group is the multi-step operation required for its subsequent conversion to an alkyl group, which is often necessary in natural product synthesis. In continuation of our investigations on the activation of cycloalk-2-enones as dienophiles, we have observed that the placement of a cyano group at C-2 induces a high degree of enhancement of the dienophilicity of the parent molecule. Interestingly, the enolizable 2-cyanocyclohex-2-enones, unlike the corresponding 2-alkoxycarbonyl compounds, are rather stable.† Also the cyano group in the adducts can be directly replaced by an alkyl group *via* a reductive alkylation process.

Four 2-cyanocycloalk-2-enones **1**–**4** representing various ring sizes were examined. Compound **4** was readily prepared from 2-methylcyclooctanone *via* a four-step synthetic sequence (Scheme 1), involving formylation,[6] isoxazole formation and its subsequent rearrangement,[7] and phenylselenenylation–oxidative elimination.[8] Compounds **1**–**3** were easily accessible by

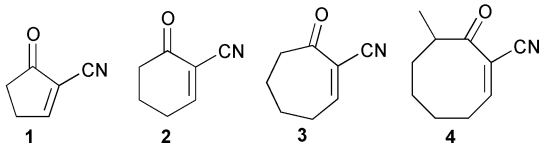

Thorpe–Ziegler condensation of the corresponding alkanedinitriles followed by phenylselenenylation–oxidative elimination. In sharp contrast to the instability associated with the corresponding 2-alkoxycarbonylcycloalk-2-enones, cyano compounds **1**–**4**‡ were shown to be rather stable and could be distilled, chromatographed and stored at 0 °C over a long period of time without apparent decomposition. Under Lewis acid catalysis, zinc chloride in particular, the Diels–Alder reaction of these compounds occurred readily at room temperature with a variety of dienes to give adducts in high yields.§ As shown in Table 1, which summarizes the results obtained for the present studies, the regioselectivity strictly follows the general rules governing the Diels–Alder reaction; 1-substituted and 2-substituted buta-1,3-dienes gave *ortho*- and *para*-adducts, respectively. In terms of stereochemistry, all of the reactions, where applicable (Entries 3, 6 and 7), gave the *endo*-to-ketone addition products. Interestingly, the addition of 2-cyano-8-methylcyclooct-2-enone (**4**) to two selected dienes (Entries 6 and 7) occurred with a complete face-selectivity from what appears to be the sterically less hindered face to give adducts **10** and **11**, respectively.

The cyano group present in each of the adducts could be readily replaced by a proton or an alkyl group *via* reductive removal of the cyano group using lithium naphthalenide (LN) followed by trapping of the ensuing enolate ion with a proton source or an appropriate electrophile.[9] As an example, treatment of adduct **6** with a stock solution of LN (6 eq.) in THF[10] at −25 °C for 30 min resulted in the reductive elimination of the cyano group. Protonation of the enolate thus formed with MeOH gave ketone **12** (80% yield), whereas treatment with allyl bromide (20 °C, 20 h) gave the angularly substituted ketone **13** (75% yield). The reductive alkylation process is apparently general and highly stereoselective. In all of the cases examined (Table 2), only the *cis*-fused alkylation product was observed.

In conclusion, 2-cyanoalk-2-enones, which are surprisingly stable, have proved to be useful dienophiles. Their Diels–Alder reaction coupled with the ease of replacement of the cyano

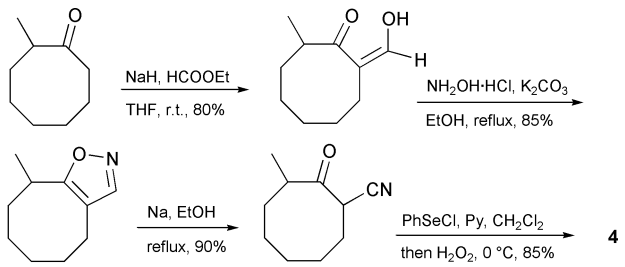

Scheme 1

DOI: 10.1039/b004297h

Table 1 Diels–Alder reactions of 2-cyanocycloalk-2-enones

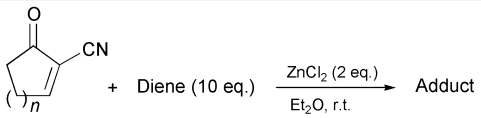

Entry	Dienophile	Diene	Time/h	Product(s)	Yield (%)
1	**1**		28	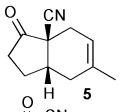 **5**	80
2	**2**		24	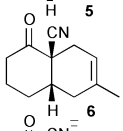 **6**	85
3	**2**		24	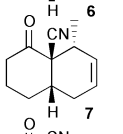 **7**	75
4	**2**		18	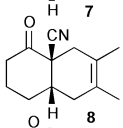 **8**	90
5	**3**		40	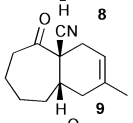 **9**	75
6	**4**		26	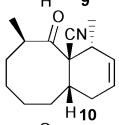 **10**	78
7	**4**	 OTBDMS	16	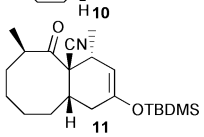 OTBDMS **11**	70

group with an alkyl group provides convenient access to various angularly substituted, *cis*-fused bicyclic systems. This newly developed process is expected to have broad synthetic utility, particularly towards polycyclic natural products of structural complexity. For instance, the complete carbon framework of neolemnane (**14**)[11]¶ could be rapidly constructed by two simple operations. Addition of cyano enone **4** to 2-*tert*-butyldimethylsilyloxypenta-1,3-diene (Table 1, Entry 7) gave adduct **11**. Sequential treatment of **11** with LN and methyl iodide (Table 2, Entry 11) completed the carbon skeleton of neolemnane (**14**). Modification of the existing functionalities to effect the total synthesis of **14** is under active investigation.

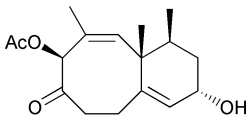

14

We are grateful to the Natural Sciences and Engineering Research Council of Canada and the National Science Council of the Republic of China for financial support.

Notes and references

† The same observation has been made previously by Fleming *et al.*[5]
‡ For an alternative synthetic approach to compounds **2** and **3**, see ref. 5.
§ Satisfactory spectral and elemental or HRMS analytical data were obtained for all new compounds. The structure of several compounds was further confirmed by X-ray crystallography.
¶ The IUPAC name for neolemnane is 2-hydroxy-4,4a,6-trimethyl-8-oxo-2,3,4,4a,7,8,9,10-octahydrobenzocyloocten-7-yl acetate.

1 P. D. Bartlett and G. F. Woods, *J. Am. Chem. Soc.*, 1940, **62**, 2933; M. D. Soffer, G. E. Gunnay, O. Korman and M. B. Adams, *Tetrahedron Lett.*, 1963, 389; M. D. Soffer and G. E. Gunnay, *Tetrahedron Lett.*, 1965, 3567.
2 H. J. Liu and E. N. C. Browne, *Tetrahedron Lett.*, 1977, 2919.
3 H. J. Liu, G. Ulibarri and L. A. K. Nelson, *J. Chem. Soc., Chem. Commun.*, 1990, 1419; H. J. Liu, W. L. Yeh and S. Y. Chew, *Tetrahedron Lett.*, 1993, **34**, 4435; H. J. Liu, K. S. Shia, Y. Han, D. Sun and Y. Wang, *Can. J. Chem.*, 1997, **75**, 646; H. J. Liu and K. S. Shia, *Tetrahedron*, 1998, **54**, 13 449.
4 H. J. Liu and T. K. Ngooi, *Can. J. Chem.*, 1984, **62**, 2676.
5 F. F. Fleming, A. Huang, V. A. Sharief and Y. Pu, *J. Org. Chem.*, 1999, **64**, 2830.
6 M. Kim, R. S. Gross, H. Sevestre, N. K. Dunlap and D. S. Watt, *J. Org. Chem.*, 1988, **53**, 93.
7 S. Takagi and H. Yasuda, *Yakugaku Zasshi*, 1959, **79**, 467.
8 D. Liotta, R. P. Barnum, G. Zima, C. Bayer and H. S. Kezar III, *J. Org. Chem.*, 1981, **46**, 2920.
9 H. J. Liu, J. L. Zhu and K. S. Shia, *Tetrahedron Lett.*, 1998, **39**, 4183.
10 H. J. Liu, J. Yip and K. S. Shia, *Tetrahedron Lett.*, 1997, **38**, 2253.
11 R. R. Izac, W. Fenical, B. Tagle and J. Clardy, *Tetrahedron*, 1981, **37**, 2569.

Table 2 Reductive decyanation and alkylation of the Diels–Alder adducts

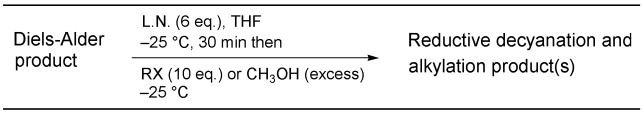

Entry	Adduct	RX or CH_3OH	Time/h	Product(s)	Yield (%)
1	**5**	benzyl bromide	12	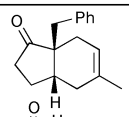	60
2	**6**	CH_3OH	0.5	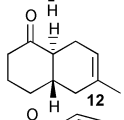 **12**	80
3	**6**	allyl bromide	20	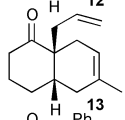 **13**	75
4	**6**	benzyl bromide	40[a]	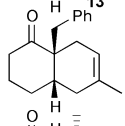	65
5	**7**	CH_3OH	0.5	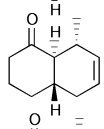	80
6	**7**	CH_3I	12	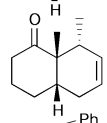	70
7	**7**	benzyl bromide	12	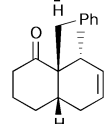	80
8	**8**	allyl bromide	12	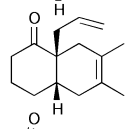	70
9	**9**	CH_3I	13	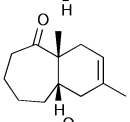	80
10	**10**	CH_3I	14	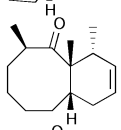	70
11	**11**	CH_3I	14	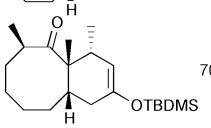 OTBDMS	70

[a] This alkylation was carried out at 20 °C.

$C_{60}F_2$ exists!

Olga V. Boltalina,[a] Andrei Yu. Lukonin,[a] Joan M. Street[b] and Roger Taylor[c]*

[a] *Chemistry Department, Moscow State University, Moscow 119899, Russia*
[b] *Chemistry Department, The University, Southampton, UK SO17 1BJ*
[c] *The Chemistry Laboratory, CPES School, University of Sussex, Brighton, UK BN1 9QJ. E-mail: R.Taylor@sussex.ac.uk*

Received (in Cambridge, UK) 5th June 2000, Accepted 11th July 2000
Published on the Web 4th August 2000

From the fluorination of [60]fullerene with K_2PtF_6 at 470 °C under *ca.* 0.01 bar we have isolated (HPLC) 1,2-F_2C_{60}, the structure of which is confirmed by ^{13}C NMR and a single ^{19}F NMR line at −148.3 ppm.

As synthons, halogenofullerenes containing very few halogen atoms are desirable, but thus far they have been unattainable. Both chlorination and bromination involve a radical cascade process which necessitates, for steric reasons, contiguous *para* (1,4) halogenation. This is terminated by *ortho* (1,2) halogenation only as a necessity for the formation of a non-radical product such as $C_{60}X_6$ (X = Br, Cl)[1,2] or $C_{70}Cl_{10}$.[3] The adjacency of the bulky halogens creates instability, and these are preferentially lost for example either in subsequent reactions[4,5] or through rearrangement *e.g.* the conversion of $C_{60}Br_6$ to $C_{60}Br_8$ on standing.[1] In $C_{60}Br_8$ (and also in $C_{60}Br_{24}$)[6] all of the bromines are in either a 1,4- or a 1,3-relationship. Thus no 1,2-dibromo- or 1,2-dichlorofullerene has been either isolated or inferred from subsequent substitutions.

By contrast, the lack of steric hindrance in fluorination permits 1,2-addition which results in contiguous activation of adjacent double bonds (through increased bond localisation). The ensuing halogenation cascade tends to cease only when a product is obtained of enhanced aromaticity (such as $C_{60}F_{18}$ or $C_{60}F_{36}$)[7,8] *i.e.* containing delocalised benzenoid rings.

Characterisation of bromo- and chlorofullerenes is rendered difficult by their instability towards mass spectrometry, which becomes greater the fewer halogens that are present; so far, only a FAB spectrum of $C_{60}Cl_{24}$ has been obtained.[9] Fluorofullerenes are more stable towards mass spectrometry and the existence of $C_{60}F_n$ (n = 18, 36 or 48)[8–10] shows that fluorines can be attached to adjacent carbon atoms without introducing undue strain. Nevertheless, as with the other halogenofullerenes noted above, *the stability decreases the fewer the number of attached fluorines*, seen for example by the appearance of lower fluorinated species (through fragmentation) in the EI mass spectrum of $C_{60}F_{18}$.[8] In fluorination by fluorine gas, the EI mass spectrum showed a continuous spectrum of derivatives from $C_{60}F_2$ up to *ca.* $C_{60}F_{42}$ (and numerous oxygenated derivatives).[11–13] However, it was unclear if the lower fluorinated species were compounds or merely fragmentation ions.

We now report the successful isolation and characterisation of $C_{60}F_2$.

[60]Fullerene (240 mg) was fluorinated with K_2PtF_6 (575 mg) and a toluene solution of the product (280 mg after prepurification by sublimation) was filtered with precautions to minimise interaction with atmospheric moisture, all as described previously.[14] HPLC separation of the product was carried out using a 10 mm × 250 mm Cosmosil Buckyprep column with elution by toluene at 4.7 ml min^{-1}. This yielded mainly $C_{60}F_{18}$[8] (elution time 37 min) together with a large number of other components, most of which are ethers. A fraction (*ca.* 1.5 mg) which eluted at 10.5 min (*cf.* 7 min for [60]fullerene) was shown by the mass spectrum (Fig. 1) to contain $C_{60}F_2$ (758 amu). The spectrum also gave peaks at 858 [$C_{60}(CF_3)_2$], 840 ($C_{60}C_2F_5H$), and 790 amu ($C_{60}CF_3H$). [Formation of CF_3 radicals by fragmentation is well-known to accompany fluorination of [60]fullerene,[13,15] and is especially marked when using K_2PtF_6; the radicals then attack other [60]fullerene molecules.] The mass spectrum is however very misleading (as the ^{13}C and ^{19}F spectra show) because it *greatly* underestimates the concentration of $C_{60}F_2$ in the sample due to fragmentation (as described above), and which is severe at this fluorination level. This is shown (Fig. 1) by the peak at 720 amu being 960 × the intensity of the 758 amu peak, *yet no [60]fullerene was present in the sample*. The same effect was evident in the spectra of $C_{60}F_nO$, (n = 8,6,4) which due to increasing fragmentation with lower addend level, showed increased amount of [60]fullerene relative to the parent ion, along this series.[14]

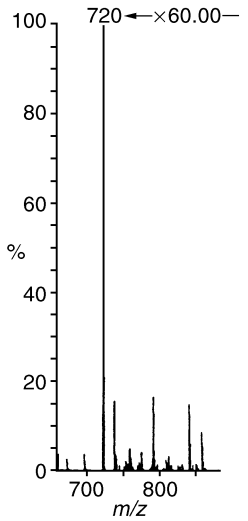

Fig. 1 EI mass spectrum (70 eV) for $C_{60}F_2$.

The IR spectrum (KBr, Fig. 2) shows two sharp peaks at 1070 and 1035 cm^{-1} in the C–F stretching region, and also sharp bands at 770, 724, 648, 594, 527 and 500 cm^{-1}. The very simple spectrum is consistent with a highly symmetrical structure, and the strong band at 527 cm^{-1} is characteristic of unaddended [60]fullerene,[16] which the present structure closely resembles.

The ^{19}F NMR spectrum (Fig. 3, 338.9 MHz, $CDCl_3$) showed a singlet at −148.3 ppm together with two very small peaks at −67.9 and −69.7 ppm, which are typical of CF_3-containing [60]fullerenes. The peak area intensities indicate that these derivatives constitute *ca.* 6% of the total fluorinated fullerene present, which further emphasises the misleading nature of the EI mass spectrum (see above).

This singlet thus falls in the range obtained for fluorinated [60]fullerenes, *e.g.* −(132–158) for $C_{60}F_{18}$ and −(130–166) ppm for $C_{60}F_{36}$. 1,2-Isomers of [60]fullerene are more stable than 1,4-isomers, since the latter contain a destabilising double bond in a pentagon and are obtained only when the addend is large. Thus due to the difference in addend size, methylation gives a mixture of 1,2- and 1,4-dimethyl derivatives, whereas benzylation gives 1,4-addition.[17] Since fluorine is smaller than

DOI: 10.1039/b004467i

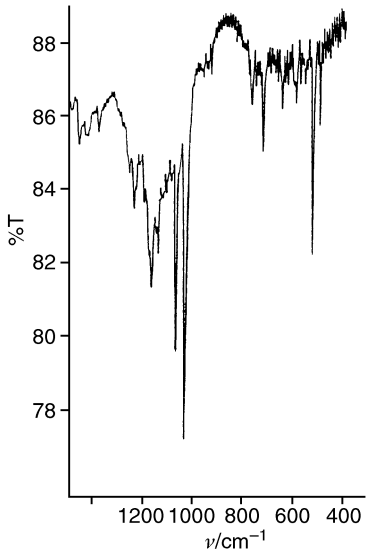

Fig. 2 IR spectrum (KBr) for $C_{60}F_2$.

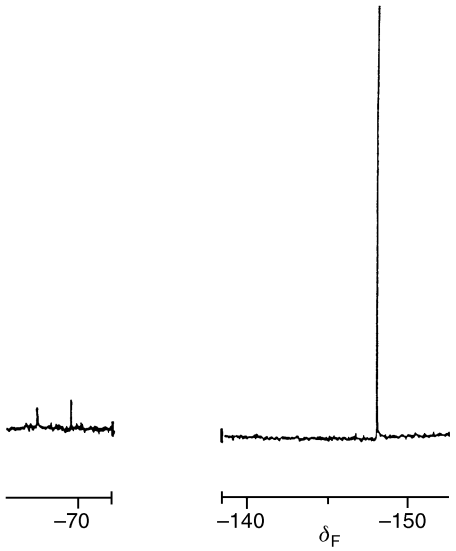

Fig. 3 ^{19}F NMR spectrum (338.9 MHz) for $C_{60}F_2$.

carbon, there is no advantage, either thermodynamic or kinetic, in forming the 1,4-isomer.

The location of the ^{19}F NMR peak is also consistent with a 1,2- rather than the 1,4-isomer. In the latter, each sp^3-hybridised carbon bearing the fluorine is surrounded by *three* sp^2-hybridised carbons (which are more electron withdrawing than sp^3), whereas there are only *two* in the 1,2-isomer. This differential effect is clearly seen in the $C_{60}F_{18}$ peak positions which are −132, −140 (av.) and −158 ppm for C–F bonds having 2, 1, and 0 sp^2 neighbours,[9] or in *T* $C_{60}F_{36}$ where they are −138 (av.) and −155 ppm for C–F bonds having 1 and 0 sp^2 neighbours.[18] Thus for the 1,4-isomer the peak would be expected to appear more downfield, the above data suggesting a value of −(120–130) ppm.

Final proof that we have isolated the 1,2-isomer comes from the ^{13}C NMR spectrum (Fig. 4). Obtaining such spectra for F-containing compounds requires F-decoupling which is unavailable, nevertheless for $C_{60}F_{18}$ we obtained a spectrum showing singlets for γ-carbons (and those more remote) relative to the

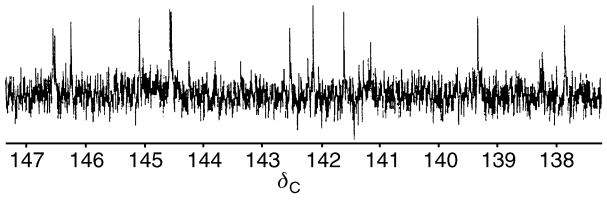

Fig. 4 ^{13}C NMR spectrum for $C_{60}F_2$.

(F)C_α carbons. Whereas 1,4-F_2C_{60} (C_s symmetry) requires in the sp^2 region (29–3) = (26 × 2 C lines, 1,2-F_2C_{60} (C_{2v} symmetry) requires 3 × 2 C and (13 − 1) = 12 × 4 C lines. Our spectrum (which required 90 h acquisition time) shows 12 × 2 C lines at 146.54, 146.50, 146.24, 145.08, 145.01, 144.54 (two coincident), 142.53, 142.23, 142.14, 141.62, 139.32, 137.85. Lines of 2 C intensity appeared at 141.16 and 138.35. Other lower intensity lines at δ_C 144.23, 143.79, 143.36, 141.29 and 141.20 were barely above background and may not be real. The compound is thus fully confirmed as the 1,2-isomer. No peak is seen in the sp^3 region due to coupling with fluorine.

In early work with F_2-fluorinated [60]fullerene, treatment of the crude product with either acetone or THF gave a product showing a single ^{19}F NMR line at *ca.* −150.5 ppm, and two sharp IR bands at 1067 and 1035 cm^{-1}; a single line NMR was also obtained by treatment of $C_{60}F_{48}$ with diethyl ether.[10] We conjectured that this line could be due to $C_{60}F_{60}$,[11] but later work showed this to be unlikely.[19] Since both the NMR line and especially the IR peaks for $C_{60}F_2$ are remarkably similar to those described above, $C_{60}F_2$ could conceivably be the species responsible in the earlier work. However, the availability now of a defined HPLC retention time for $C_{60}F_2$ means that repetition of the earlier work and separation of the products may provide an answer. We plan to undertake this work.

We thank the Royal Society for a Joint Project grant, NATO for additional support, and Dr Anthony Avent for the ^{13}C NMR spectrum.

Notes and references

1 P. R. Birkett, P. B. Hitchcock, H. W. Kroto, R. Taylor and D. R. M. Walton, *Nature*, 1992, **357**, 479.
2 P. R. Birkett, A. G. Avent, A. D. Darwich, H. W. Kroto, R. Taylor and D. R. M. Walton, *J. Chem. Soc., Chem. Commun.*, 1993, 1230.
3 P. R. Birkett, A. G. Avent, A. D. Darwich, H. W. Kroto, R. Taylor and D. R. M. Walton, *J. Chem. Soc., Chem. Commun.*, 1995, 683.
4 A. G. Avent, P. R. Birkett, J. D. Crane, A. D. Darwich, G. J. Langley, H. W. Kroto, R. Taylor and D. R. M. Walton, *J. Chem. Soc., Chem. Commun.*, 1994, 1463.
5 P. R. Birkett, A. G. Avent, A. D. Darwich, H. W. Kroto, R. Taylor and D. R. M. Walton, *Tetrahedron*, 1996, **52**, 5235.
6 F. N. Tebbe, R. L. Harlow, D. B. Chase, D. L. Thorn, G. C. Campbell, J. C. Calabrese, N. Herron, R. J. Young and E. Wasserman, *Science*, 1992, **256**, 822.
7 O. V. Boltalina, A. Ya. Borschevskii, L. V. Sidorov, J. M. Street and R. Taylor, *Chem. Commun.*, 1996, 529.
8 A. Adamson, E. G. Hope, J. H. Holloway and R. Taylor, *Fullerene Science and Technology*, 1997, **5**, 629.
9 O. V. Boltalina, V. Yu. Markov, R. Taylor and M. P. Waugh, *Chem. Commun.*, 1996, 2549.
10 A. A. Gakh, A. A. Tuinman, J. L. Adcock, R. A. Sachleben and R. A. Compton, *J. Am. Chem. Soc.*, 1994, **116**, 819; O. V. Boltalina, L. N. Sidorov, V. F. Bagryantsev, V. A. Seredenko, A. S. Zapolskii and R. Taylor, *J. Chem. Soc., Perkin Trans. 2*, 1996, 2275.
11 J. H. Holloway, E. G. Hope, R. Taylor, G. J. Langley, A. G. Avent, T. J. Dennis, J. P. Hare, H. W. Kroto and D. R. M. Walton, *J. Chem. Soc., Chem. Commun.*, 1991, 966.
12 R. Taylor, G. J. Langley, J. H. Holloway, E. G. Hope, A. K. Brisdon, H. W. Kroto and D. R. M. Walton, *J. Chem. Soc., Perkin Trans. 2*, 1995, 181.
13 R. Taylor, G. J. Langley, J. H. Holloway, E. G. Hope, H. W. Kroto and D. R. M. Walton, *J. Chem. Soc., Chem. Commun.*, 1993, 875.
14 O. V. Boltalina, A. Yu. Lukonin, A. G. Avent, J. M. Street and R. Taylor, *J. Chem. Soc., Perkin Trans. 2*, 2000, 683.
15 A. A. Tuinman, P. Mukherjee, J. L. Adcock, R. L. Hettich and R. N. Compton, *J. Phys. Chem.*, 1992, **96**, 7584.
16 J. P. Hare, T. J. Dennis, H. W. Kroto, R. Taylor, A. W. Allaf, S. Balm and D. R. M. Walton, *J. Chem. Soc., Chem. Commun.*, 1991, 412.
17 For references and Schlegel diagrams see pp. 75–76 in R. Taylor, '*Lecture Notes on Fullerene Chemistry: A Handbook for Chemists*', Imperial College Press, 1999.
18 O. V. Boltalina, M. Bühl, A. Khong, M. Saunders, J. M. Street and R. Taylor, *J. Chem. Soc., Perkin Trans 2*, 1999, 1475.
19 H. Selig, K. Kniaz, G. B. M. Vaughan, J. E. Fischer and A. B. Smith, *Macromol. Symp.*, 1994, **82**, 89; K. Kniaz, J. E. Fischer, H. Selig, G. B. M. Vaughan, W. J. Romanov, D. M. Cox, S. K. Chowdhury, J. P. McCauley, R. M. Strongin and A. B. Smith, *J. Am. Chem. Soc.*, 1993, **115**, 6060.

ChemComm

Homogeneously catalyzed, chelate assisted hydrogenolysis of an amine C–N bond

Mark Gandelman and David Milstein*

Department of Organic Chemistry, The Weizmann Institute of Science, Rehovot, Israel, 76100

Received (in Cambridge, UK) 15th June 2000, Accepted 12th July 2000
Published on the Web 4th August 2000

Reaction of $[RhCl(COE)_2]_2$ with an excess of the aromatic aminophosphine 1-(diethylaminomethyl)-3-(di-*tert*-butylphosphinomethyl)-2,4,6-trimethylbenzene (2) in dioxane under mild H_2 pressure results in selective catalytic activation of an unstrained C–N single bond.

The design of homogeneous processes for selective activation and catalytic functionalization of strong single bonds by transition metal complexes is a highly desirable goal.[1] The catalytic C–N bond activation is of considerable current interest, as it is a key step in hydrodenitrogenation (HDN)—an important part of the hydrotreating process whereby crude oil or coal-derived liquids are upgraded to fuels.[2] Relatively few clear examples of metal-complex promoted C–N cleavage of amines are known, most of them being stoichiometric.[3–6] Catalytic reactions of this type are scarce.[7] We report here a remarkable example of *homogeneous catalytic* hydrogenolysis of an unstrained sp^3 C–N bond. This chelate-assisted rhodium catalyzed process occurs under homogeneous reaction conditions and is highly selective.

We have recently reported that the PCP-based ligand **1** undergoes selective catalytic C–C bond activation by Rh under H_2 pressure at 180 °C (Scheme 1).[8]

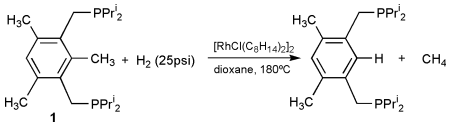

Scheme 1

In order to extend the scope of this process to other systems, we tried this reaction with the PCN-based ligand **2**. As we have recently shown, the stoichiometric reaction of **2** with $[RhCl(COE)_2]_2$ (COE = cyclooctene) results in exclusive C–C activation of the Ar–CH_3 bond situated in between the phosphine and amine 'arms'.[9] Surprisingly, when the reaction is performed in a catalytic manner C–N rather than C–C bond activation takes place. Thus, reaction of $[RhCl(COE)_2]_2$ with 10 eq. of **2** under mild H_2 pressure (25 psi) in dioxane at 160 °C for 24 h leads to quantitative formation of the hydrodenitrogenated phosphine **3** and diethylamine (Scheme 2, 10 turnovers based on Rh and 100% yield). The catalysis can be continued by adding more of substrate **2**, demonstrating that the catalyst remains active. The yield was lower when larger quantities of **2** were used. 13 turnovers (93%) were observed when 15 eq. of compound **2** were reacted, and 21 turnovers (47% yield) for 45 eq. of the starting material.

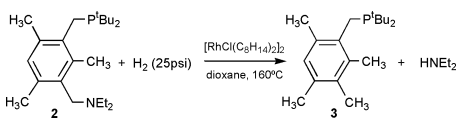

Scheme 2

The product diethylamine was identified and quantified by GC-MS and GC analysis, respectively. It was also detected by ^{1}H-NMR, when the reaction was performed in dioxane-d_8. The phosphine **3** was isolated by evaporation of diethylamine and subsequent extraction of the residue with pentane and was fully characterized by $^{31}P\{^1H\}$, ^{1}H, $^{13}C\{^1H\}$, ^{13}C-DEPT NMR and MS techniques. The structure of **3** was confirmed by comparison with an authentic sample, which was independently prepared by phosphination of bromomethylisodurene.† Formation of **3** is highly selective, no other organic products being catalytically formed (*vide infra*). Control experiments showed that substrate **2** does not undergo catalytic C–N activation under the reaction conditions in the absence of Rh or H_2.

A postulated catalytic cycle is presented in Scheme 3. Initially, selective insertion of Rh(I) into the aryl-CH_3 bond resulting in complex **4** most probably takes place. As reported, the stoichiometric reaction of **2** with $[RhCl(COE)_2]_2$ leads to **4**.[9] Subsequently, **4** reacts with H_2 to yield the hydrido chloride complex **5** and CH_4. Indeed, when the reaction was performed with a small excess of **2** (5–7 eq.), a stoichiometric amount of **5** was detected by NMR spectroscopy. Also, a stoichiometric amount of CH_4 (based on Rh) was regularly observed by GC analysis in the catalytic reaction. Compound **5** and CH_4 were independently obtained by the reaction of **4** with H_2 (25 psi) at 80 °C for 3 d. The products were analyzed by $^{31}P\{^1H\}$, ^{1}H, $^{13}C\{1H\}$, ^{13}C-DEPT NMR‡ and by GC. This reaction may proceed through a Rh(V) intermediate or *via* σ-bond metathesis. Complex **5** is part of the catalytic cycle and can also be used as catalyst under the same reaction conditions.

The exchange of the amine 'arm' of **5** by the phosphine moiety of **2** most probably proceeds *via* intermediates **A** and **B**. Replacement of a pincer-type amino ligand of Ru(II) by a phosphine analog was reported recently.[10] The exchange of the phosphine group in **5** by the amine 'arm' of **2** is impeded, since an amine is, in general, a poorer ligand for low valent late transition metals than a phosphine.[11] At this stage, most probably, C–N bond activation and hydrogenolysis by the unsaturated Rh center takes place, giving the phosphine-coordinated product **C** and diethylamine. Following replacement of **3** by the amine 'arm', **5** is regenerated, this process being assisted by the generation of two stable five-membered chelating rings. The liberated **3** most probably competes with **2**, slowing down the catalytic process as its concentration increases.

An alternative mechanism involving phosphine displacement by the amine group in **B** can be excluded, as we have observed that Ar-CH_3 bond activation occurs immediately even under very mild conditions, when both P and N ligands are coordinated.[12]

In summary, catalytic hydrogenolysis of an unstrained C–N bond has been presented. The phosphinoamine mixed system **3** undergoes selective stoichiometric C–C and catalytic C–N bond activation by Rh. In addition to the general interest in catalytic C–N activation, the reactivity of pincer-type complexes is the focus of much current research.[13]

DOI: 10.1039/b004820h

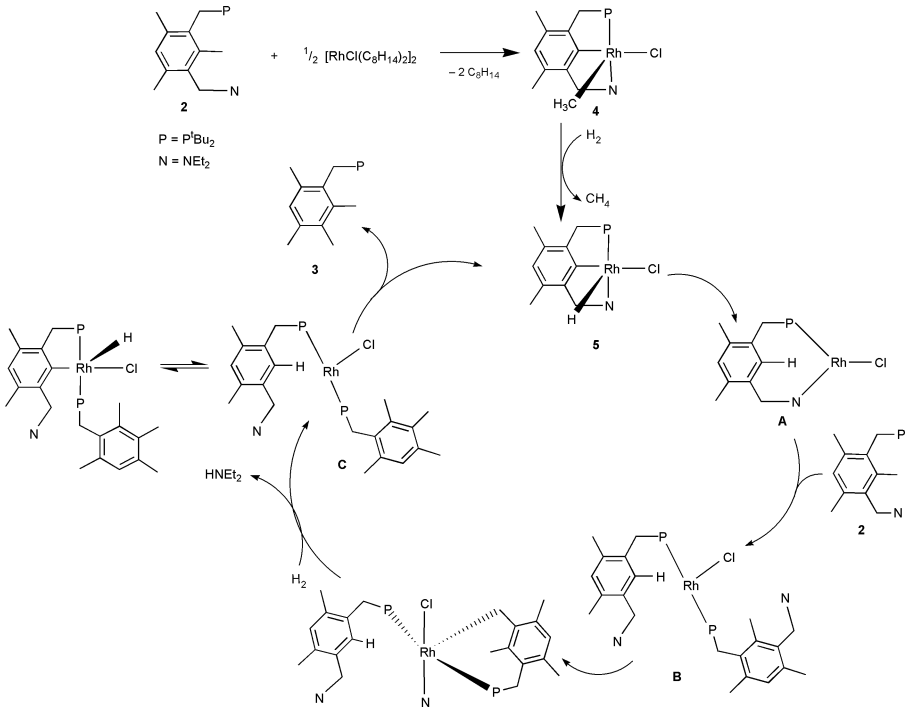

Scheme 3

Notes and references

† *Independent synthesis of 1-(di-tert-butylphosphinomethyl)-2,3,4,6-tetramethylbenzene* (**3**). 1-Bromomethyl-2,3,4,6-tetramethylbenzene was prepared by bromomethylation of isodurene (1,2,3,5-tetramethylbenzene) according to a literature procedure.[14] The resulting bromomethylisodurene (2 g, 8.81 mmol) and di-*tert*-butylphosphine[15] (1.29 g, 8.81 mmol) in acetone (20 ml) were heated under reflux with stirring for 2 h.[16] The mixture was cooled to rt, the white precipitate that formed was filtered off and washed with hexane to remove unreacted starting material. The obtained phosphonium salt was dissolved in water and treated with a 10-fold excess (based on starting bromide) of sodium carbonate. The organic product was extracted with ether (3 × 20 ml). The ether fractions were combined, and the solvent was evaporated, giving the clean phosphine **3** in 86% yield (2.21 g). Selected NMR data for **3**: ^{31}P{^{1}H} NMR ($CDCl_3$): 26.86 (s); δ_H($CDCl_3$): 6.82 (s, 1H, Ar-*H*), 2.91 (d, J_{PH} = 1.9 Hz, 2H, Ar-CH_2-P), 2.49 (s, 3H, Ar-CH_3), 2.47 (s, 3H, Ar-CH_3), 2.13 (s, 3H, Ar-CH_3), 2.03 (s, 3H, Ar-CH_3), 1.10 (d, J_{PH} = 10.3 Hz, 18H, 2 P-C(CH_3)$_3$; δ_H($CDCl_3$): 32.05 (d, J_{PC} = 26.4 Hz, 2 (CH$_3$)$_3$*C*-P), 29.71 (d, J_{PC} = 13.4 Hz, 2 (*C*H$_3$)$_3$C-P), 24.15 (d, J_{PC} = 29.5 Hz, Ar-*C*H$_2$-P), 21.89 (d, J_{PC} = 6.8 Hz, Ar-*C*H$_3$), 20.38 (s, Ar-*C*H$_3$), 18.17 (d, J_{PC} = 10.9 Hz, Ar-*C*H$_3$), 15.87 (s, Ar-*C*H$_3$). (Assignment of ^{13}C {^{1}H} NMR signals was confirmed by ^{13}C DEPT.)

‡ *Spectral data for* **5**. δ_P(benzene-d_6): 95.39 (dd, J_{RhP} = 147.3, J_{HP} = 21.8 Hz); δ_H(benzene-d_6): 6.55 (s, 1H, Ar), 3.84 (br d, J_{HH} = 15.9 Hz, 1H, Ar-CH_2-N), 3.50 (br d, J_{HH} = 15.9 Hz, 1H, Ar-CH_2-N), 3.46 (m, 1H, Ar-CH_2-P), 2.94 (m, 1H, Ar-CH_2-P), 2.68 (m, 1H, CH$_3$-CH_2-N), 2.52 (m, 1H, CH$_3$-CH_2-N), 2.17 (s, 3H, Ar-CH_3), 2.03 (s, 3H, Ar-CH_3), 1.35 (d, J_{PH} = 13.0 Hz, 9H, (CH_3)$_3$C-P), 1.21 (d, J_{PH} = 13.6 Hz, 9H, (CH_3)$_3$C-P), 1.19 (t, J_{HH} = 7.4 Hz, 3H, CH_3-CH$_2$-N), 0.83 (t, J_{HH} = 7.3 Hz, 3H, CH_3-CH$_2$-N), −26.83 (dd, J_{PH} = 23.2, J_{RhH} = 54.7 Hz, 1H, Rh-H); δ_C(benzene-d$_6$): 163.61 (dd, J_{RhC} = 33.8, $J_{PC,cis}$ = 4.8 Hz, C$_{ipso}$, Rh-Ar), 145.81 (s, Ar), 144.47 (dd, J_{PC} = 10.9, J_{RhC} = 3.4 Hz, Ar), 130.79 (dd, J_{PC} = 16.1, J_{RhC} = 1.9 Hz, Ar), 130.03 (s, Ar), 126.65 (s, Ar), 63.39 (s, Ar-*C*H$_2$-N), 54.84 (s, CH$_3$-*C*H$_2$-N), 54.32 (s, CH$_3$-*C*H$_2$-N), 32.28 (dd, J_{PC} = 26.4, J_{RhC} = 3.5 Hz, Ar-*C*H$_2$-P), 29.22 (d, J_{PC} = 3.3 Hz, (CH$_3$)$_3$C-P), 28.77 (d, J_{PC} = 3.2 Hz, (CH$_3$)$_3$C-P), 20.71 (s, CH$_3$-Ar), 19.65 (s, CH$_3$-Ar), 12.38 (s, *C*H$_3$-CH$_2$-N), 11.61 (s, *C*H$_3$-CH$_2$-N). (Assignment of ^{13}C {^{1}H} NMR signals was confirmed by ^{13}C DEPT.)

1 For some reviews regarding bond activation see: R. H. Crabtree, *Chem. Rev.*, 1985, **85**, 245; W. A Herrmann and B. Cornils, *Angew. Chem., Int. Ed. Engl.*, 1997, **36**, 1048; G. C. Saunders, *Angew. Chem., Int. Ed. Engl.*, 1996, **35**, 2615; J. Burdeniuc, B. Jedlicak and R. H. Crabtree, *Chem. Ber./Recl*, 1997, **130**, 145; J. L. Kiplinger, T. G. Richmond and C. E. Osterberg, *Chem. Rev.*, 1994, 373; P. Steenwinkel, R. A. Gossage and G. van Koten, *Chem. Eur. J.*, 1998, **4**, 759; B. Rybtchinski and D. Milstein, *Angew. Chem. Int. Ed.*, 1999, **38**, 870; M. Murakami and Y. Ito, in *Topics in Organometallic Chemistry*, ed. S. Murai, Springer–Verlag, Berlin, Heidelberg, 1999, vol. 3, p. 97.

2 T. C. Ho, *Catal. Rev. Sci. Eng.*, 1988, **30**, 117; D. M. A. Radhi, G. Palyi and L. Marko, *J. Mol. Catal.*, 1983, **22**, 195; R. M. Laine, *Catal. Rev. Sci. Eng.*, 1983, **25**, 459; Y. T. Shah and D. C. Cronauer, *Catal. Rev. Sci. Eng.*, 1979, **20**, 209; S. I. Murahashi and T. Watanable, *J. Am. Chem. Soc.*, 1979, **101**, 7429.

3 J. B. Bonanno, T. P. Henry, D. R. Neithamer, P. T. Wolczanski and E. B. Lobkovsky, *J. Am. Chem. Soc.*, 1996, **118**, 5132.

4 S. D. Gray, K. J. Weller, M. A. Bruck, P. M. Briggs and D. E. Wigley, *J. Am. Chem. Soc.*, 1995, **117**, 10 678.

5 S. Calet, F. Urso and H. Alper, *J. Am. Chem. Soc.*, 1989, **111**, 931; L. M. Atagi, D. E. Over, D. R. McAlister and J. M. Mayer, *J. Am. Chem. Soc.*, 1991, **113**, 870; M. D. Wang and H. Alper, *J. Am. Chem. Soc.*, 1992, **114**, 7018; G. Proulx and R. G. Bergman, *J. Am. Chem. Soc.*, 1994, **116**, 7953.

6 S. I. Ikeda, N. Chatani and S. Murai, *Organometallics*, 1992, **11**, 3494; J. R. Hagadorn and J. Arnold, *Organometallics*, 1994, **13**, 4670; Y. Imada and H. Alper, *J. Org. Chem.*, 1996, **61**, 6766; K. Hiraki, T. Matsunaga and H. Kawano, *Organometallics*, 1994, **13**, 1878; M. Cattenot, J. L. Portefaix, J. Afonso, M. Breysse, M. Lacroix and G. Perot, *J. Catal.*, 1998, **173**, 366; M.-C. Rodriguez, F. Lambert and I. Morgenstern-Badarau, *Inorg. Chem.*, 1997, **36**, 3525; S. Bhattacharyya, D. Ghosh, A. Endo, K. Shimizu, T. J. R. Weakley and M. Chaudhury, *J. Chem. Soc., Dalton Trans.*, 1999, 3859.

7 R. M. Laine, D. W. Thomas and L. W. Cary, *J. Am. Chem. Soc.*, 1982, **104**, 1763; Y. Shvo and R. M. Laine, *Chem. Commun.*, 1980, 753; Y. Shvo, M. Abed, Y. Blum and R. M. Laine, *Isr. J. Chem.*, 1986, 267.

8 Sh.-Y. Liou, M. E. van der Boom and D. Milstein, *Chem. Commun.*, 1998, 687.

9 M. Gandelman, A. Vigalok, L. J. W. Shimon and D. Milstein, *Organometallics*, 1997, **16**, 3981.

10 P. Dani, T. Karlen, R. A. Gossage, W. J. J. Smeets, A. L. Spek and G. van Koten, *J. Am. Chem. Soc.*, 1997, **119**, 11 317.

11 For coordination of nitrogen *vs*. phosphorus ligands, see: A. Togni and L. Venanzi, *Angew. Chem., Int. Ed. Engl.*, 1994, **33**, 497.

12 M. Gandelman, A. Vigalok, L. Konstantinovski and D. Milstein, unpublished results.

13 For some recent examples, see: P. Steenwinkel, H. Kooijman, W. J. J. Smeets, A. L. Spek, D. M. Grove and G. van Koten, *Organometallics*, 1998, **17**, 5411; D. E. Bergbreiter, P. L. Osburn and Y.-S. Liu, *J. Am. Chem. Soc.*, 1999, **121**, 9531; A. Vigalok and D. Milstein, *Organometallics*, 2000, **19**, 2061; A. Vigalok and D. Milstein, *Organometallics*, 2000, **19**, 2341.

14 A. W. van der Made and R. H. van der Made, *J. Org. Chem.*, 1993, **58**, 1262.

15 For the synthesis of di-*tert*-butylphosphine, see: H. Hoffmann and P. Schellenbeck, *Chem. Ber.*, 1966, **99**, 1134.

16 Phosphination: C. J. Moulton and B. L. Shaw, *J. Chem. Soc., Dalton Trans.*, 1976, 1020.

ChemComm

Highly efficient enantioselective synthesis of optically active dihydropyrones by chiral titanium(IV) (5,5′,6,6′,7,7′,8,8′-octahydro-1,1′-bi-2-naphthol) complexes

Bin Wang, Xiaoming Feng,* Xin Cui, Hui Liu and Yaozhong Jiang*

Chengdu Institute of Organic Chemistry, Chinese Academy of Sciences, Chengdu 610041, China.
E-mail: ulas@cioc.ac.cn

Received (in Cambridge, UK) 15th June 2000, Accepted 13th July 2000
Published on the Web 4th August 2000

The asymmetric hetero-Diels–Alder reaction of Danishefsky's diene and an aldehyde catalyzed by 20 mol% chiral H_8-BINOL–Ti(IV) affords the corresponding 2-substitutent-2,3-dihydro-4*H*-pyran-4-one with ees of up to 99% under mild reaction conditions.

The formal hetero-Diels–Alder reaction between 1-methoxy-3-(trimethylsilyloxy)buta-1,3-diene and aldehydes provides useful access to dihydropyrones, a class of compounds with extensive utility in organic synthesis.[1] Asymmetric catalysis of this reaction has been previously reported by a number of investigators.[2] Corey *et al.* found that the tryptophan-derived oxazaborolidine catalyst gave good yields and moderate enantioselectivities for the reaction of Danishefsky's diene with representative aldehydes.[2a] Keck *et al.* reported that catalysts generated using 2 : 1 BINOL–Ti(O-i-Pr)$_4$ in the presence of 4 Å

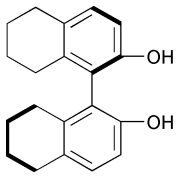

(*R*)-H_8-BINOL

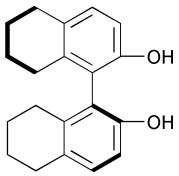

(*S*)-H_8-BINOL

MS and 0.0003 equiv. of CF_3CO_2H led to dihydropyrones in Et_2O with good to excellent ee.[2b] Jacobsen and co-workers developed some chiral (Salen)Cr(III) catalysts which afforded cycloadducts with good enantioselectivity.[2c] However, progress in the area of asymmetric hetero-Diels–Alder reactions has been limited. A catalyst that can be used with a wide range of substrates will be pursued.

5,5′,6,6′,7,7′,8,8′-octahydro-1,1′-bi-2-naphthol (H_8-BINOL) is a new atropisomeric diol ligand, which possesses a unique structure compared to conventional BINOLs.[3] Chan *et al.* reported its outstanding asymmetric induction ability in the asymmetric alkylation of aromatic aldehydes with triethylaluminium.[4] Herein, we wish to describe that chiral H_8-BINOL–Ti(O-i-Pr)$_4$ complexes are more effective catalysts than BINOL–Ti(O-i-Pr)$_4$ and others for the asymmetric hetero-Diels–Alder reactions.

Our studies started with benzaldehyde as a test substrate. A H_8-BINOL–Ti(O-i-Pr)$_4$–4 Å MS system was found to be the most promising catalyst for this reaction. In toluene solvent and at 0 °C, benzaldehyde gave (*R*)-2-phenyl-2,3-dihydro-4*H*-pyran-4-one in 92% isolated yield with 97% ee (Table 1, entry 1). Further studies showed that several parameters were important for both the reactivity and enantioselectivity of the cycloaddition reaction. The best results were obtained when 1.1 equiv. of (*R*)-H_8-BINOL were used per Ti. A solvent study showed that toluene provided the best overall results.[5] The yield and enantioselectivity were also found to be dependent on temperature. When the reaction was carried out below 0 °C, dihydropyrone was obtained in lower conversion and enantioselectivity. The optimal temperature ranged between 0 and 14 °C depending on the aldehydes used. At rt, high yield (92%) and enantioselectivity (93% ee) were also obtained (Table 1, entry 3). It should be noted that the ee of 93% was particularly high at rt, since most precedent catalytic asymmetric hetero-Diels–Alder reactions require a rather low temperature (−78 to −30 °C) to attain a good level of enantioselectivity. The amount of the catalyst was also revealed to be an important parameter for the attainment of high enantioselectivity. When the amount of catalyst was reduced to 10 mol%, the enantioselectivity of the reaction was decreased considerably (Table 1, entries 1 and 2).

Encouraged by the result obtained for benzaldehyde (Table 1, entry 1), we investigated a number of other aldehydes to probe their behavior under the current catalyst conditions. As shown in Table 1, the aromatic, heteroaromatic, conjugated and aliphatic aldehydes afforded the corresponding product in moderate to high isolated yield with quite high ee. A comparison of the experimental results (Table 1, entries 1, 4–11) revealed the effect on enantioselectivity by *ortho*-substitutents on benzaldehyde. This was probably due to the

Table 1 Asymmetric hetero-Diels–Alder reactions of diene and aldehydes

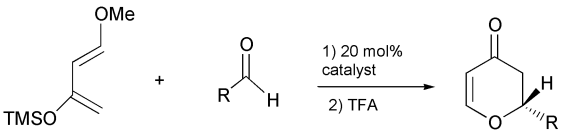

(predominant enantiomer with (*R*)-H_8-BINOL)

Entry[a]	R	Temp/°C	Time/h	Yield (%)[b]	% ee[c]
1	Ph	0	24	92	97[d]
2[e]	Ph	0	12	75	73[d]
3	Ph	23–25	6	92	93[d]
4	*p*-$MeOC_6H_4$	0	24	52	>99
5	*p*-MeC_6H_4	0	24	60	99
6	*p*-FC_6H_4	0	24	54	98
7	*p*-NCC_6H_4	0	24	64	94
8	*m*-MeC_6H_4	0	24	81	99
9	*m*-ClC_6H_4	0	24	81	94
10	*o*-$MeOC_6H_4$	0	48	54	90[f]
11	*o*-ClC_6H_4	0	24	71	90
12	Furyl	0	30	78	96[g]
13	2-Py	0	24	55	92[f]
14	(*E*)-CH_3CH=CH	12–14	92	35	98
15	(*E*)-PhCH=CH	0	30	80	98[g]
16	n-C_8H_{17}	12–14	92	76	94

[a] All reactions were carried out using 20 mol% of catalyst as detail in the experimental procedure,[6] unless otherwise mentioned. [b] All yields are isolated yields. Satisfactory spectral data (^{1}H NMR, ^{13}C NMR, IR) and C, H, N combustion analyses were obtained for the new compounds. [c] In all cases ee was determined by HPLC using a chiral column (chiracel OD), unless otherwise mentioned. [d] Determined by GC using a chiral column (Cyclodex-β). Absolute configurations were *R*, which were determined by comparison of optical rotations with literature values.[2c,e] The reactions were carried out using 10 mol% of catalyst as detail in the experimental procedure.[7] [f] Determined by HPLC using a chiral column (chiracel AD). [g] Absolute configurations were *R*, which were determined by comparison of optical rotations with literature values.[2c]

DOI: 10.1039/b004813p

strong steric hindrance effect of the *ortho*-substitutents, which weakened the coordination of the aldehyde and consequently lowered the enantioselectivity of reaction. These results are consistent with Chan *et al's* report about asymmetric alkylation of aromatic aldehydes with triethylaluminium.[4] The precise structure of the catalyst is not clear at present. An investigation of the mechanism is underway.

In conclusion, we have developed a new, highly efficient method for the synthesis of chiral 2-substitutent-2,3-dihydro-4*H*-pyran-4-one from aldehydes and Danishefsky's diene using chiral H_8-BINOL-Ti(IV).[3] High levels of enantioselectivity in the synthesis of 2-substitutent-2,3-dihydro-4*H*-pyran-4-one with wide substrate generality were obtained according to this reaction.

We are grateful for the financial support from the National Science Foundation of China (No. 29832020).

Notes and references

1 For reviews, see: (*a*) S. J. Danishefsky, *Chemtracts*, 1989, 273; (*b*) S. J. Danishefsky and M. P. De Ninno, *Angew. Chem., Int. Ed. Engl.*, 1987, **26**, 15; (*c*) S. J. Danishefsky, *Aldrichimica Acta*, 1986, **19**, 59; for application in total synthesis (*d*) J. D. Rainier, S. P. Allwein and J. M. Cox, *Org. Lett.*, 2000, **2**, 231.

2 (*a*) E. J. Corey, C. L. Cywin and T. D. Roper, *Tetrahedron Lett.*, 1992, **33**, 6907; (*b*) G. E. Keck, X. Y. Li and D. Krishnamurthy, *J. Org. Chem.*, 1995, **60**, 5998; (*c*) S. E. Schaus, J. Brånalt and E. N. Jacobsen, *J. Org. Chem.*, 1998, **63**, 403; (*d*) Q. Z. Gao, T. Maruyama, M. Mouri and H. Yamamoto, *J. Org. Chem.*, 1992, **57**, 1951; (*e*) K. Mikami, O. Kotera, Y. Motoyama and H. Sakaguchi, *Synlett*, 1995, 975; (*f*) T. Hanamoto, H. Furuno, Y. Sugimoto and J. Inanaga, *Synlett*, 1997, 79; (*g*) K. Maruoka, T. Itoh, T. Shirasaka and H. Yamamoto, *J. Am. Chem. Soc.*, 1988, **110**, 310; (*h*) A. Togni, *Organometallics*, 1990, **9**, 3106; (*i*) A. K. Ghosh, P. Mathivanan, J. Cappiello and K. Krishnan, *Tetrahedron: Asymmetry*, 1996, **7**, 2165; (*j*) S. Matsukawa and K. Mikami, *Tetrahedron: Asymmetry*, 1997, **8**, 815; (*k*) A. K. Ghosh, P. Mathivanan and J. Cappiello, *Tetrahedron Lett.*, 1997, **38**, 2427; (*l*) H. Furuno, T. Hanamoto, Y. Sugimoto and J. Inanaga, *Org. Lett.*, 2000, **2**, 49.

3 D. J. Cram, R. C. Helgeson, S. C. Peacock, L. J. Kaplan, L. A. Domeier, P. Moreau, K. Koga, J. M. Mayer, Y. Chao, M. G. Siegel, D. H. Hoffman and G. D. Y. Sogah, *J. Org. Chem.*, 1978, **43**, 1930.

4 A. S. C. Chan, F. Y. Zhang and C. W. Yip, *J. Am. Chem. Soc.*, 1997, **119**, 4080.

5 A series of solvents was screened including toluene, TBME, CH_2Cl_2, DMF, Et_2O and THF.

6 A typical experimental procedure is given for the synthesis of (*R*)-2-phenyl-2,3-dihydro-4*H*-pyran-4-one: a mixture of (*R*)-H_8-BINOL (16.2 mg, 0.055 mmol), 1 M Ti(O-i-Pr)$_4$ in CH_2Cl_2 (50 μl, 0.05 mmol), and activated powdered 4 Å molecular sieves (120 mg) in toluene (1 ml) was heated at 35 °C for 1 h. The yellow mixture was cooled to rt, and benzaldehyde (26 μl, 0.25 mmol) was added. The mixture was stirred for 10 min and cooled to 0 °C. Danishefsky's diene (60 μl, 0.30 mmol) was added. The mixture was stirred at 0 °C for 24 h, then it was treated with 5 drops of TFA. After the mixture was stirred for 15 min at 0 °C, saturated $NaHCO_3$ (1.5 ml) was added, the mixture was then stirred for 10 min and filtered through a plug of Celite. The organic layer was separated, and the aqueous layer was extracted with ether (5 × 3 ml), the combined organic layers were dried over Na_2SO_4 and concentrated. The crude residue was purified by flash chromatography (petroleum ether–ethyl acetate, 4 : 1) to yield (*R*)-2-phenyl-2,3-dihydro-4*H*-pyran-4-one (40 mg, 0.23 mmol, 92% yield) as a clear oil. The isolated material was determined to be in 97% ee by chiral GC analysis (cyclodex-β, 159 °C, 20 min, isothermal, t_S(minor) = 14.43 min, t_R(major) = 14.66 min).

7 1-Methoxy-3-(trimethylsilyloxy)buta-1,3-diene was purchased from Lancaster with 95% content.

Novel diphosphite derived from D-*gluco*-furanose provides high regio- and enantioselectivity in Rh-catalysed hydroformylation of vinyl arenes

Montserrat Diéguez,*[a] Oscar Pàmies,[a] Aurora Ruiz,[a] Sergio Castillón[b] and Carmen Claver[a]

[a] *Departament de Química Física i Inorgànica, Universitat Rovira i Virgili, Pl. Imperial Tarraco 1, 43005 Tarragona, Spain. E-mail: dieguez@quimica.urv.es*

[b] *Departament de Química Analítica i Orgànica, Universitat Rovira i Virgili, Pl. Imperial Tarraco 1, 43005 Tarragona, Spain*

Received (in Cambridge, UK) 15th June 2000, Accepted 14th July 2000
Published on the Web 4th August 2000

Both high enantioselectivity (91%) and high regioselectivity (98.8%) are achieved under mild reaction conditions in the Rh-catalysed hydroformylation of vinyl arenes with a new chiral diphosphite ligand derived from the readily available D-(+)-glucose.

Asymmetric hydroformylation has attracted much attention as a potential tool for preparing enantiomerically pure aldehydes. These are important as precursors for synthesising biologically active compounds, biodegradable polymers and liquid crystals.[1] In the last ten years, several studies have reported a remarkable improvement in the rhodium-catalysed asymmetric hydroformylation based on the use of diphosphite[2] or phosphine–phosphite[3] (Binaphos) ligands. At the moment, Binaphos is the only ligand with a wide scope in asymmetric hydroformylation, although its difficult preparation limits its application. Furthermore, its regioselectivy in 2-phenylpropanal is not completely satisfactory even under carefully optimised conditions.[3] More recently, perfluoroalkyl substituents at the aryl group of the Binaphos increased the regioselectivity, in the best case up to 96%, but high pressures and an excess of ligand were still needed for good enantioselectivities.[4] In this context, much research still needs to be done to find ligands that are readily available and provide both good regio- and enantioselectivities in asymmetric hydroformylation.

In the last few decades carbohydrates have been widely used in asymmetric synthesis.[5] Nevertheless their full potential in providing chiral ligands has scarcely been exploited[6] despite the accessibility and low cost of the carbohydrate synthons. In previous work on diphosphite ligands with a furanose backbone moderate results (up to 60% ee) in asymmetric hydroformylation of styrene have been reported.[7] Since these ligands had a phosphorus moiety bonded to a nonstereogenic center (C-5), we tested whether further modifying the ligand would improve enantioselectivities. With this purpose and following from our interest in using carbohydrates as a chiral source for preparing ligands,[7b,8] we designed a new diphosphite ligand **4** which was easily prepared from D-(+)-glucose. This ligand has the two phosphite moieties bonded to two stereogenic centers (C-3 and C-5) and has proven to be highly enantioselective and regioselective in the asymmetric hydroformylation of vinylarenes (Scheme 1).

Diphosphite **4**[9] was synthesised in 3 steps from 1,2-*O*-isopropylidene-3-*O*-acetyl-α-D-glucofuranose **5** as shown in Scheme 2. Diol **5** is easily prepared from D-(+)-glucose on a large scale by previously described highly effective methods.[10] Tosylation of **5** produced a good yield of the expected 5-tosyl derivative (88%).[11] Treatment with NaOMe at rt followed by reduction with lithium aluminium hydride produced crystalline 6-deoxy-1,2-*O*-isopropylidene-α-D-glucofuranose **7** in 92% yield.[12]

Reacting diol **7** with two equiv. of 3,3′-di-*tert*-butyl-5,5′-dimethoxy-1,1′-biphenyl-2,2′-diyl phosphorochloridite[13] *in situ* formed in the presence of pyridine produced the desired diphosphite **4** in good overall yield.

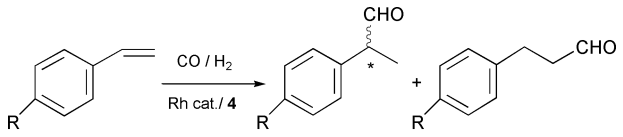

1 a R = H; **b** R = F; **c** R = OMe (*R*)-**2**/(*S*)-**2** **3**

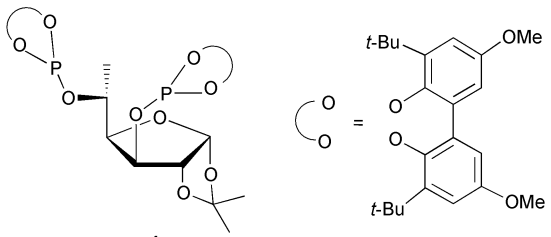

4

Scheme 1

Ligand **4** was used in the rhodium-catalysed asymmetric hydroformylation of styrene and other vinylarenes.[14] Results are given in Table 1. In no cases were hydrogenated or polymerised products observed.

Varying the ligand-to-rhodium ratio shows that it is not necessary to have excess ligand to obtain good regio- and enantioselectivities (entries 1–2). This contrasts with Rh–Binaphos systems, for which a large excess of ligand is needed.[3,4] Moreover, activities were best at low P_{CO}–P_{H2} ratios

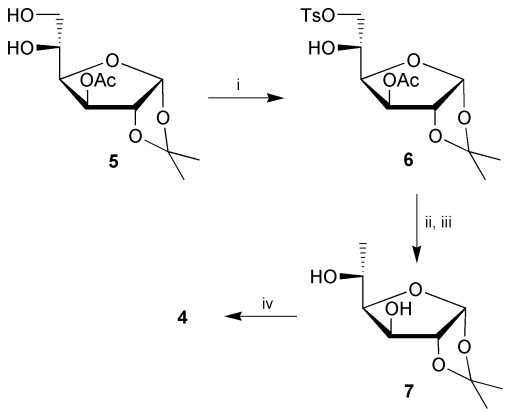

5 **6** **4** **7**

Scheme 2 Synthesis of ligand **4**: (i) TsCl, pyridine, CH_2Cl_2, 16h, −20 to 25 °C, 88%; (ii) NaOMe, CH_2Cl_2, 1 h, 25°C, quantitative; (iii) $LiAlH_4$, THF, 60 °C, 92%; (iv) phosphorochloridite, pyridine, toluene, 100 °C, 71%.

DOI: 10.1039/b004799f

Table 1 Asymmetric hydroformylation catalysed by [Rh(acac)$(CO)_2$]/**4**[a]

Entry	Substrate	P_{CO}–P_{H2}	T/°C	TOF[b]	%Conv (time/h)[c]	%Regio[d]	%Ee[e]
1	**1a**	1	40	98	98 (10)	97.8	78 (*S*)
2[f]	**1a**	1	40	97	96 (10)	97.7	78 (*S*)
3	**1a**	0.5	40	174	100 (6)	97.9	78 (*S*)
4	**1a**	0.5	20	18	83 (48)	98.6	90 (*S*)
5	**1b**	0.5	20	17	80 (48)	98.8	89 (+)
6	**1c**	0.5	20	16	81 (48)	98.6	91 (−)

[a] Reaction conditions: P = 10 bar, styrene (13 mmol), [Rh(acac)$(CO)_2$] (0.013 mmol), toluene (15 mL), PP/Rh = 1.1. [b] TOF in mol styrene × Rh^{-1} × h^{-1} determined after 1 h reaction time by GC. [c] % Conversion of styrene measured by GC. [d] % Regioselectivity defined as **2**/(**2** + **3**). [e] % Ee measured by GC. [f] PP/Rh = 2.

(entry 3). This is in line with detailed kinetic studies on rhodium-catalysed hydroformylation with bulky phosphites reported by van Leeuwen *et al.*, who showed that the rate-determining step is the oxidative addition of H_2 to the acyl–rhodium complex.[15] Comparing entries 1 and 3 also shows that regio- and enantioselectivities are not affected by varying the partial pressure of CO. A remarkable increase in enantioselectivities (up to 91%, entries 4–6) combined with excellent regioselectivities (up to 98.8%) were found by lowering the reaction temperature. There were no changes in the enantioselectivities over time, which indicates that no decomposition of the catalyst took place.

Results were similar when **4** was used in the asymmetric hydroformylation of the substituted vinylarenes **1b** and **1c**. The presence of different substituents in the *para* position does not seem to affect the conversion or the regio- and enantioselectivities of the hydroformylation.

In conclusion, a novel chiral diphosphite **4**, derived from readily available D-(+)-glucose, is a highly efficient ligand for the asymmetric rhodium-catalysed hydroformylation of vinyl arenes under mild reaction conditions and without an excess of ligand. The combination of excellent regio- and enantioselectivities (up to 98.8 and 91% respectively) in simple unoptimised reactions and the low cost of the ligand make this catalyst system attractive for further investigation of its potential use for the industrial preparation of biologically active compounds in asymmetric hydroformylation. Studies of the scope and mechanistic aspects of the catalytic process are currently in progress.

We thank the Spanish Ministerio de Educación y Cultura and the Generalitat de Catalunya (CIRIT) for their financial support (PB97-0407-CO5-01).

Notes and references

1 (*a*) M. Beller, B. Cornils, C. D. Frohning and V. W. Kohlpainter, *J. Mol. Catal.*, 1995, **104**, 17; (*b*) F. Agboussou, J. F. Carpentier, A. Mortreux, *Chem. Rev.*, 1995, **95**, 2485.

2 (*a*) J. E. Babin and G. T. Whiteker, WO 93/03839, US 911, 518, 1992; (*b*) G. J. H. Buisman, L. A. van deer Veen, A. Klootwijk, W. G. J. de Lange, P. C. J. Kamer, P. W. N. M. van Leeuwen and D. Vogt, *Organometallics*, 1997, **16**, 2929.

3 K. Nozaki, N. Sakai, T. Nanno, T. Higashijima, S. Mano, T. Horiuchi and H. Takaya, *J. Am. Chem. Soc.*, 1997, **119**, 4413.

4 G. Franciò and W. Leitner, *Chem. Commun.*, 1999, 1663.

5 (*a*) S. Hanessian in *Total Synthesis of Natural Products: The "Chiron" Approach*, Pergamon Press, vol. 3, London 1983; (*b*) J. S. Penne in *Chiral Auxiliaries and Ligands in Asymmetric Synthesis*, John Wiley & Sons, New York, 1995.

6 (*a*) H. U. Blaser, *Chem. Rev.*, 1992, **92**, 935; (*b*) H. Brunner and W. Zettlmeier in *Handbook of Enantioselective Catalysis*, VCH, Weinheim, 1993; (c) T. V. RajanBabu and T. A. Ayers, *Tetrahedron Lett.*, 1994, **35**, 4295; (*d*) M. T. Reetz and T. Neugebauer, *Angew. Chem., Int. Ed.*, 1999, **38**, 179; (*e*) T. V. RajanBabu, B. Radetich, K. K. You, T. A. Ayers, A. L. Casalnuovo and J. C. Calebrese, *J. Org. Chem.*, 1999, **64**, 3429 and references cited therein; (*f*) K. Yonehara, T. Hashizume, K. Mori, K. Ohe and S. Uemura, *Chem. Commun.*, 1999, 415

7 (*a*) G. J. H. Buisman, M. E. Martin, E. J. Vos, A. Klootwijk, P. C. J. Kamer and P. W. N. M. van Leeuwen, *Tetrahedron: Asymmetry*, 1995, **6**, 719; (*b*) O. Pàmies, G. Net, A. Ruiz and C. Claver, *Tetrahedron: Asymmetry*, 2000, **11**, 1097.

8 (*a*) O. Pàmies, G. Net, A. Ruiz, C. Bó, J. M. Poblet and C. Claver, *J. Organomet. Chem.*, 1999, **586**, 125; (*b*) O. Pàmies, M. Diéguez, G. Net, A. Ruiz and C. Claver, *J. Chem. Soc., Dalton Trans.*, 1999, 3439; (*c*) O. Pàmies, G. Net, A. Ruiz and C. Claver, *Tetrahedron: Asymmetry*, 1999, **10**, 2007; (*d*) O. Pàmies, M. Diéguez, G. Net, A. Ruiz and C. Claver, *Organometallics*, 2000, **19**, 1488; (*e*) O. Pàmies, G. Net, A. Ruiz and C. Claver, *Eur. J. Inorg. Chem.*, in the press.

9 *Selected data for* **4**: δ_P (CD_2Cl_2, 233 K) 144.6 (d, 1P, J_{P-P} = 30.9 Hz), 145.1 (d, 1P, J_{P-P} = 30.9 Hz).

10 O. T. Schmidt in *Methods in Carbohydrate Chemistry*, eds. R. L. Whistler and M. L. Wolfrom, Academic Press, New York, 1963, Vol. II.

11 Compound **6** was preprared by a minor modification of the procedure described in M. Nakjima and S. Takahashi, *Agric. Biol. Chem.*, 1967, **31**, 1079.

12 J. Hiebl and E. Zbiral, *Monatsh. Chem.*, 1990, **121**, 691.

13 3,3′-di-*tert*-butyl-5,5′-dimethoxy-1,1′-biphenyl-2,2′-diyl phosphorochloridite is easily prepared in one step from the corresponding biphenol as described in (*a*) G. J. H. Buisman, P. C. J. Kamer and P. W. N. M. van Leeuwen, *Tetrahedron: Asymmetry*, 1993, **4**, 1625. The corresponding biphenol is easily prepared on large scale in the same way as the related 4,4′,6,6′-tetra-*tert*-butyl-2,2′-biphenol described in (*b*) T. Jongsma, M. Fossen and P. W. N. M. van Leeuwen, *J. Mol. Catal.*, 1993, **83**, 17.

14 The standard hydroformylation procedure is described in ref. 8*d*.

15 A. van Rooy, E. N. Orij, P. C. J. Kamer and P. W. N. M. van Leeuwen, *Organometallics*, 1995, **14**, 34.

Synthesis of zeolites P1 and SUZ-4 through a synergy of organic *N,N,N,N′,N′,N′*-hexaethylpentanediammonium and inorganic cations†

Woon Chang Paik,[a] Chae-Ho Shin[b] and Suk Bong Hong*[a]

[a] *Department of Chemical Technology, Taejon National University of Technology, Taejon 300-717, Korea. E-mail: sbhong@hyunam.tnut.ac.kr*

[b] *Department of Chemical Engineering, Chungbuk National University, Chungbuk 361-763, Korea*

Received (in Cambridge, UK) 18th May 2000, Accepted 11th July 2000
Published on the Web 4th August 2000

Zeolites P1 and SUZ-4 with enhanced Si/Al ratios (*ca.* 4.9 and 8.2) compared to previously reported isostructural materials have been synthesized in the presence of *N,N,N,N′,N′,N′*-hexaethylpentanediammonium together with Na^+ and K^+ ions, respectively.

The use of the doubly charged cation *N,N,N,N′,N′,N′*-hexaethylpentanediammonium (Et_6-diquat-5) as an organic structure-directing agent (SDA) in the synthesis of zeolites was first attempted by Valyocsik and Page in 1986.[1] It has been shown that this diquarternary cation can direct the crystallization of ZSM-57 (MFS topology) with the intersecting 10- and 8-ring channel system when used together with Na^+ ions.[2] Very recently, we have studied zeolite synthesis related to the use of a series of diquarternary cations with different chain lengths and found that the type and amount of alkali metal cations added to the synthesis mixture may play a major role in determining the phase selectivity of the crystallization.[3]

Zeolite P1 is the synthetic analogue of the GIS-type zeolites and contains a two-dimensional pore system with two intersecting 8-ring channels.[4] On the other hand, SUZ-4,[5,6] a new zeolite closely related to ferrierite and ZSM-57, has been considered to have a topology that corresponds to the hypothetical model 5b described by Gramlich-Meier.[7] To our knowledge, the only organic SDA leading to the successful SUZ-4 formation is the tetraethylammonium cation.[8] Here, we report for the first time, the synthesis of zeolites P1 and SUZ-4 from sodium- and potassium-containing aluminosilicate gels in the presence of Et_6-diquat-5, a new organic SDA for these structure-types of materials.

In a typical synthesis of zeolite P1, 0.48 g of $Al(NO_3)_3{\cdot}9H_2O$ (98%, Junsei) and 2.20 g of NaOH (50% aqueous solution, Aldrich) were dissolved into 22.01 g of H_2O. To this clear solution, 5.63 g of colloidal silica (Ludox AS-40, DuPont) and 2.48 g of Et_6-diquat-5 dibromide prepared according to the procedure described elsewhere[1] were added. The oxide composition of the resulting gel was $4.5Et_6$-diquat-5 : $11.0Na_2O$: 1.0-Al_2O_3 : $30SiO_2$: $1200H_2O$. For the crystallization of SUZ-4, NaOH was replaced by an equivalent amount of KOH (45% aqueous solution, Aldrich) under the conditions described above. After stirring at room temperature for 1 day, the final synthesis mixture was transferred to Teflon-lined 45 mL autoclaves and heated at 160 °C under slow rotation (60 rpm) for 8 days. The white solid products were recovered by filtration, washed repeatedly water, and then dried overnight at room temperature.

Fig. 1 shows the typical powder X-ray diffraction patterns (Rigaku Miniflex, Cu-Ka radiation) of P1 and SUZ-4 prepared here. Comparison of the patterns in Fig. 1 with those in the literature[6,9] reveals that both materials are highly crystalline and no reflections other than those from the corresponding zeolites are observed. This can be further supported by the N_2 adsorption data (Micromeritics ASAP 2410) of P1 and SUZ-4 calcined at 500 °C for 6 h to remove the occluded organic species, from which the BET surface areas of 124 and 370 $m^2\ g^{-1}$ were derived, respectively. SEM photographs (JEOL JSM-6300) show that zeolite P1 appears as agglomerates of small (1.5–2.0 μm), heavily overlapped cuboids, while SUZ-4 consists of needle-like crystals that are *ca.* 1 μm in length and 0.2 μm in diameter. On the other hand, it can be seen from the ^{13}C-^1H CP/MAS NMR spectra (Fig. SI 1, ESI†) of as-synthesized P1 and SUZ-4 that both samples exhibit three main resonances around δ 54, 21 and 8, which can be assigned to the methylene carbons bonded to the nitrogen, the methylene carbons in the pentyl chain and the methyl carbons in the ethyl groups of Et_6-diquat-5, respectively. This indicates that the organic SDA remains intact upon its occlusion in the P1 and SUZ-4 pores. A combination of elemental and thermal analyses reveals, within experimental error, that as-synthesized P1 and SUZ-4 zeolites have the chemical compositions (Et_6-diquat-5)$_{0.6}Na_{1.8}Al_{2.7}$-$Si_{13.3}O_{32}{\cdot}2.0H_2O$ and (Et_6-diquat-5)$_{1.2}K_{2.0}Al_{3.9}Si_{32.1}$-$O_{72}{\cdot}4.8H_2O$, respectively. Thus, there is a small but non-negligible dissimilarity between the amount of Al and the sum of Et_6-diquat-5 and alkali metal cations for the unit cell formula of each material. This suggests that a portion of the organic occluded is present in either bromide or hydroxide form to act as a space-filling species. Also, it should be noted that the Si/Al ratios (4.9 and 8.2) of P1 and SUZ-4 zeolites prepared here are higher than those of previously known isostructural materials. The Si/Al ratios for all the natural and synthetic GIS-type zeolites reported so far are always in the range 1.0–3.2,[4,10] while SUZ-4 materials are known to have a narrow Si/Al ratio range of 6.2–7.1.[5,6,8] The enhanced Si/Al ratios of our P1 and SUZ-4 zeolites can be rationalized by considering that the length (*ca.* 15 Å) of the Et_6-diquat-5 used as an organic SDA here is much larger than that of the already known SDAs (*e.g.* tetramethylammonium and tetraethylammonium cations) for these materials.

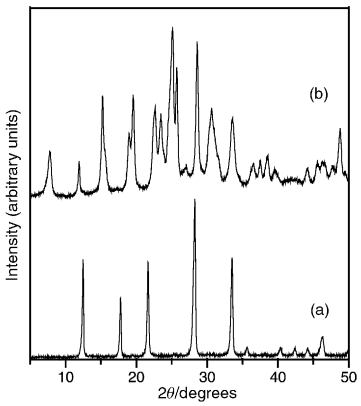

Fig. 1 Powder X-ray diffraction patterns of as-synthesized (a) P1 and (b) SUZ-4. Rigaku Miniflex diffractometer, Cu-Ka radiation, 0.02° 2θ step size and 0.50 s count time.

† Electronic supplementary information (ESI) available: Fig. SI 1 and 2 (^{13}C–^1H CP/MAS and ^{27}Al NMR Spectra for P1 and SUZ-4). See http://www.rsc.org/suppdata/cc/b0/b004004p/

DOI: 10.1039/b004004p

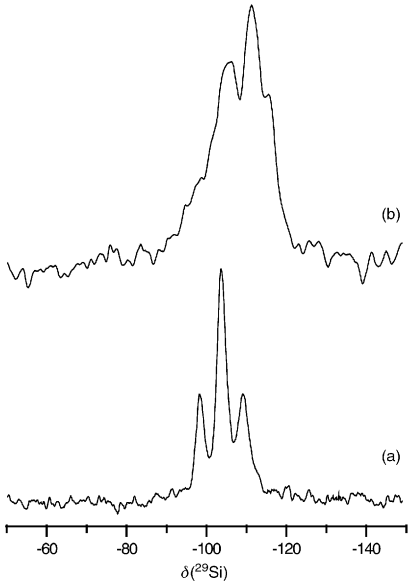

Fig. 2 ^{29}Si MAS NMR spectra of as-synthesized (a) P1 and (b) SUZ-4 zeolites. Spectra recorded on a Bruker DSX 400 at 12 kHz spinning rate, 60 s recycle delay, 79.459 MHz, π/5 rad, 2 μs pulse length, 1200 scans.

The ^{27}Al MAS NMR measurements (Bruker DSX 400, 13.0 kHz spinning rate) show that as synthesized P1 and SUZ-4 exhibit only one line at δ 58.2 and 52.7, respectively, typical of tetrahedral Al sites in zeolites (Fig. SI 2, ESI†). The ^{29}Si MAS NMR spectra of these phases are shown in Fig. 2. The spectrum of zeolite P1 is characterized by three ^{9}Si resonances at δ −109.8, −104.1 and −98.6, assigned to Si(*n*Al) species with *n* = 0, 1 and 2, respectively. Deconvolution of this spectrum allowed us to calculate a Si/Al ratio of 4.5 for our P1 that is in good agreement with the value determined from elemental analysis. On the other hand, the ^{29}Si MAS NMR spectrum of SUZ-4 shows three main resonances at −115.1, −111.3 and −106.8. We note here that the high-field resonance has not been clearly found in the reported spectrum of an SUZ-4 material with Si/Al = 6.4.[9] This again confirms the enhanced Si/Al ratio of SUZ-4 prepared here, although the existence of multiple T-sites in the proposed framework of SUZ-4 makes it impossible to determine accurately the framework Si/Al ratio from its ^{29}Si MAS NMR spectrum at this time. Further details on the physicochemical properties of our P1 and SUZ-4 will be given elsewhere.[11]

The overall synthetic results of this study reveal that the crystallization conditions and the oxide composition of synthesis mixtures yielding pure P1 or SUZ-4 in the presence of Et_6-diquat-5 are restricted within narrow limits, which is quite similar to the trend found in the synthesis of ZSM-57 using the same organic SDA.[3] When trying to reproduce the synthesis of zeolite P1 under static conditions, for example, the synthesis mixture remains amorphous even after heating at 160 °C for 2 weeks. By contrast, a MOR zeolite is the phase that crystallizes from the synthesis mixture with Si/Al = 20 under stirring in conditions described above. Thus, it appears that the structure-directing ability of the organic Et_6-diquat-5 itself is not strong enough to govern the crystallization of P1 and SUZ-4. This suggests that the synergy of alkali metal cations and a particular organic Et_6-diquat-5 may be a critical factor affecting the phase selectivity of the crystallization, although the exact role of alkali cations in the Et_6-diquat-5-mediated synthesis of P1, SUZ-4, and ZSM-57 remains to be elucidated. In order to follow a more rigorous study on this issue, extensive investigations of the host–guest interactions in these zeolites are currently underway in our laboratory.

We acknowledge the financial support of the Korea Energy Management Corporation R&D Management Center for Energy and Resources and the Korea Science and Engineering Foundation through the Advanced Materials Research Center for a Better Environment at Taejon National University of Technology.

Notes and references

1 E. W. Valyocsik and N. M. Page, *Eur. Pat. Appl.*, 174121A2, 1986.
2 J. L. Schlenker, J. B. Higgins and E. W. Valyocsik, *Zeolites*, 1990, **10**, 293.
3 S.-H. Lee, D.-K. Lee, C.-H. Shin, W. M. Lee and S. B. Hong, *J. Catal.*, in press.
4 R. Szostak, *Handbook of Molecular Sieves*, Van Nostrand Reinhold, New York, 1992.
5 S. I. Barri, *US Pat.*, 5118483, 1992.
6 S. L. Lawton, J. M. Bennett, J. L. Schlenker and M. K. Rubin, *J. Chem. Soc., Chem. Commun.*, 1993, 894.
7 R. Gramlich-Meier, *Z. Kristallogr.*, 1986, **177**, 237.
8 M. A. Asensi, M. A. Camblor and A. Martinez, *Microporous Mesoporous Mater.*, 1999, **28**, 427.
9 M. M. J. Treacy, J. B. Higgins and R. von Ballmoos, *Collection of Simulated XRD Patterns for Zeolites*, Elsevier, London, 1996.
10 Ch. Baerlocher and W. M. Meier, *J. Helv. Chim. Acta*, 1970, **53**, 1285.
11 W. C. Paik, C.-H. Shin and S. B. Hong, manuscript in preparation.

ChemComm

A neutral dicopper(III) bis(μ-oxo) complex from a copper(I) ethylene iminophosphanamide and O_2†

Bernd F. Straub, Frank Rominger and Peter Hofmann*

Organisch-Chemisches Institut der Universität Heidelberg, Im Neuenheimer Feld 270, D-69120 Heidelberg, Germany. E-mail: ph@phindigo.oci.uni-heidelberg.de

Received (in Cambridge, UK) 24th May 2000, Accepted 14th July 2000
Published on the Web 4th August 2000

The copper(I) ethylene complex [$Bu^t_2P(NSiMe_3)_2$-κ^2N]Cu(η^2-C_2H_4) reacts with O_2, yielding an uncharged dinuclear copper(III) bis(μ-oxo) species, which has been fully characterized, *e.g.* by single-crystal X-ray diffraction.

Tyrosinase, the longest known monooxygenase, activates dioxygen for transforming phenols to catechols and quinones.[1] Similar to hemocyanin, the oxygen transport protein of invertebrates, tyrosinase contains a dinuclear copper site, where each copper atom is coordinated by three histidine imidazole ligands.[2] A great number of model complexes have been synthesized to realize different coordination modes of dioxygen in dinuclear copper complexes and to understand their reactivity.[3] Amine, pyridine, imidazole and pyrazole derivatives have been utilized as ligands. The coordination number at copper, the steric demand of ligands as well as counter ions, temperature and solvent have been varied in order to correlate ligand features with spectroscopic, structural, kinetic and thermodynamic data of the resulting (μ-η^2:η^2)peroxo,[3,4] μ-1,2-peroxo[5] and bis(μ-oxo)[6] dicopper complexes. Despite intense research directed towards ligand effects in copper dioxygen chemistry, neither extremely electron-rich and basic ligands nor four-membered chelate systems have been investigated.

We have introduced the anionic iminophosphanamide ligand $[Bu^t_2P(NSiMe_3)_2]^-$ into copper(I) coordination chemistry.[7] Its basicity is many orders of magnitude higher than that of any ligand used in copper dioxygen chemistry so far. In addition, the small N–Cu–N bite angle of the neutral d^{10} fragment [Bu^t_2P(N-$SiMe_3)_2$-κ^2N]Cu of *ca.* 78° leads to increased Lewis acidity of the copper center, provides better back-bonding capability and stabilizes the copper(III) oxidation state.[7,8]

The copper(I) ethylene complex **1**[7] is oxidized by O_2, yielding a brown crystalline precipitate of bis(μ-oxo) complex **2** (Scheme1).‡ The reaction is irreversible; no ethylene complex **1** could be detected upon addition of C_2H_4 to a solution of **2**.

The low solubility of **2** in various solvents is in contrast to the extremely high solubility of the precursor complex **1**. A 444 nm absorption maximum of **2** is characteristic for a bis(μ-oxo) dicopper chromophore.[3,6] Formation of a butterfly (μ-η^2:η^2)peroxo dicopper(II) complex, which also would show an absorption band at 420–490 nm,[9] is hampered by the bulky trimethylsilyl groups (*viz.* Fig. 1) and so far an out-of-plane distortion could only be enforced by linkers between the ligand units. Even in concentrated solutions, no absorption bands at 340–370 nm 500–600 nm, indicative of the presence of a (μ-η^2:η^2)peroxo complex, could be observed. Thus, a nearly thermoneutral equilibrium of **2** with its (μ-η^2:η^2)peroxo isomer, as reported for some dicationic analogues,[3,6a] can be ruled out.[3,4] $^{29}Si\{^1H\}$ and $^{31}P\{^1H\}$ NMR spectra of **2** at room temperature are in accordance with a diamagnetic low-spin d^8-ML_4 copper(III) species. The respective low-field shifts, unprecedented among all other derivatives synthesized so far, indicate a distinct net charge transfer from the [Bu^t_2P-$(NSiMe_3)_2$-κ^2N]Cu fragment to the oxygen atoms.[7,10] An antiferromagnetically coupled bis(μ-hydroxo) dicopper(II) complex is ruled out for **2** by IR spectroscopy and LT-FAB[11] mass spectrometry, which reveals stepwise fragmentation of the bis(μ-oxo) complex **2**.† At ambient temperature, complex **2** decomposes within minutes in solution and within days in the solid state. This decomposition occurs independently of the solvent (pentane, toluene or $CDCl_3$), leading to a copper(II) species (λ_{max} = 640 nm, $\varepsilon \approx 10^2$ M^{-1} cm^{-1}), which possibly results from an intramolecular process. The product remains unidentified so far.

The solid-state structure of **2** reveals a perfectly planar bis(μ-oxo) dicopper unit (Fig. 1).§ Compound **2** represents the first neutral bis(μ-oxo) dicopper complex, that has been structurally characterized; all other bis(μ-oxo) dicopper complexes are dicationic.[3,6] The Cu–Cu distance of 2.906(1) Å has no precedent and is distinctly longer than Cu–Cu distances reported for bis(μ-oxo) dicopper cores so far.[6] The O–O

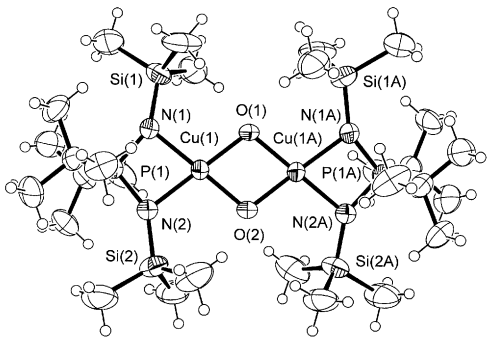

Fig. 1 ORTEP diagram of the solid state structure of **2**.‡ Distances and bond lengths (Å): O(1)–O(2) 2.338(6), Cu(1)–Cu(1A) 2.906(1), Cu(1)–N(1) 1.976(4), Cu(1)–N(2) 1.980(4), Cu(1)–O(1) 1.865(3), Cu(1)–O(2) 1.864(3), P(1)–N(1) 1.607(4), P(1)–N(2) 1.605(4), Si(1)–N(1) 1.726(4), Si(2)–N(2) 1.723(4). Bond angles (°): P(1)–N(1)–Si(1) 148.2(3), P(1)–N(2)–Si(2) 148.0(3), N(1)–P(1)–N(2) 100.7(2), P(1)–N(1)–Cu(1) 91.0(2), P(1)–N(2)–Cu(1) 90.9(2), N(1)–Cu(1)–N(1A) 77.4(2), O(1)–Cu(1)–O(2) 77.6(2), Cu(1)–O(1)–Cu(1A) 102.3(2), Cu(1)–O(2)–Cu(1A) 102.4(2). Dihedral angles (°): Cu(1)–O(1)–Cu(1A)–O(2) 0.0, N(1)–Cu(1)–O(1)–O(2) −173.7(1), N(2)–Cu(1)–O(2)–O(1) −175.2(1).

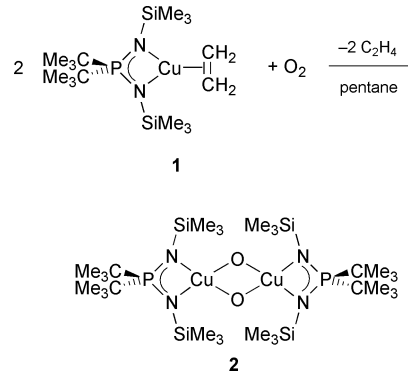

Scheme 1

† Dedicated to Professor R. Neidlein on the occasion of his 70th birthday.

DOI: 10.1039/b004173o

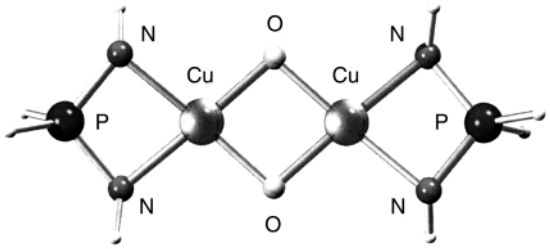

Fig. 2 Ball-and-stick plot of the model complex $[\{H_2P(NH)_2\text{-}\kappa^2N\}_2Cu_2(\mu\text{-}O)_2]$ **3** [B3LYP/6–311+G(2d,p), NIMAG = 0].§ Distances and bond lengths (Å): O–O 2.330, Cu–Cu 2.739, Cu–N 1.969, Cu–O 1.798, P–N 1.613. Bond angles (°): N–P–N 99.55, P–N–Cu 91.52, N–Cu–N 77.41, O–Cu–O 80.77, Cu–O–Cu 99.23. Dihedral angles (°): Cu–O–Cu′–O′ 0.0, N–Cu–O–O′ 174.2. NBO charges: Cu +1.40, O –0.93, N –1.32, P +1.55.

distance of 2.338(6) Å is unexceptional.[6] The Cu–N bond lengths of 1.980(4) and 1.976(4) Å underline the presence of copper(III), consistent with all spectroscopic data even in the absence of K-edge X-ray absorption investigations.[12] The minimally elongated Si–N bonds compared to ethylene complex **1** can be attributed to the reduced negative partial charge of the nitrogen atoms in **2**. For the first time, the neutral species **2** offers an opportunity to compare theoretical and experimental geometries without Coulomb repulsion artifacts, which are a problem for calculations of gas-phase dications.

Full B3LYP 6-311+G(2d,p) geometry optimization of the simplified model complex $[\{H_2P(NH)_2\text{-}\kappa^2N\}_2Cu_2(\mu\text{-}O)_2]$ **3** accurately reproduces the PN_2Cu geometry.¶ The Cu_2O_2 core is similar to that of the dicationic bis(μ-oxo) dicopper(III) complexes,[3,6] however, the calculation underestimates the Cu–O bond length by 0.066 Å and the Cu–Cu distance by 0.167 Å compared to the solid-state structure of **2** (Fig. 2).

From CASSCF and DFT calculations as well as from orbital arguments for the dicationic model $[\{(H_3N)_3Cu\}_2(\mu\text{-}O)_2]^{2+}$, Tolman and coworkers have rationalized that the energy surface for elongating the Cu_2O_2 core of bis(μ-oxo) copper complexes in the Cu–Cu direction, with concomitant decrease of the O–O distance, is flat.[13] This is corroborated by a single-point calculation for model **3** with the experimental Cu_2O_2 geometry of **2**, leading to an increase in energy of only 19.4 kJ mol^{-1}. Thus steric interactions in the solid-state structure of real system **2** and the need for a still higher level of theory may explain the discrepancy between the Cu_2O_2 cores of the computed model **3** and of **2**. By contrast, accurate $[(H_3N)_6Cu_2O_2]^{2+}$ geometries were obtained even with modest basis sets.[13] However, such studies on dications may benefit from a mutual cancellation of errors due to an underestimation of bond lengths by small basis sets§ and bond enlargement by repulsive Coulomb forces, respectively.

Related to the well documented small isomerization barrier between dicationic bis(μ-oxo) copper(III) and (μ-η^2:η^2)peroxo copper(II) complexes,[3,6a] a relative stabilization of the bis(μ-oxo) core in **2** can be expected from the electronic stabilization of high copper oxidation states by the iminophosphanamide ligand and the lack of intramolecular Coulomb repulsion, which would favor the peroxo isomer.[11] We expect compound **2** to allow further interesting model studies.

Notes and references

‡ *Synthesis* of **2**: 421 mg of ethylene complex **1**[7] (1.02 mmol) are dissolved in 50 ml of pentane in a Schlenk tube under an argon atmosphere. The Schlenk tube is sealed with a $CaCl_2$ drying tube, the solution is heated to reflux and subsequently cooled to −25 °C. Upon cooling, atmospheric dioxygen is automatically drawn into the Schlenk tube through the $CaCl_2$ drying tube. Dark brown crystals grow from the brown solution. After 20 h, the mother liquor is removed, the crystals are washed with pentane and dried at 10^{-3} mbar. 295 mg (0.37 mmol, 72%) of **2** are isolated; 87–88 °C color change to green, mp 126 °C (decomp.); IR (KBr/cm^{-1}): ν/cm^{-1} 2951m, 2901m, 1478w, 1396w, 1363w, 1248m, 1149m, 1115s, 845s, 756m, 691m, 633m; UV (pentane, $c \approx 0.4$ mM): λ_{max}/nm 256 (≈ 315 sh), 444 (ε 10^4 M^{-1} cm^{-1}); ^{1}H NMR (268 K, toluene-d_8, 300.13 MHz): δ 1.11 [d, $^3J_{PH}$ 14.5 Hz, $C(CH_3)_3$, 36H], 0.45 [s + sat, $^1J_{CH}$ 117 Hz, $Si(CH_3)_3$; 36H]; ^{13}C{^{1}H} NMR (298 K, C_6D_6, 75.47 MHz): δ 27.30 [d, $^2J_{PC}$ 2 Hz, $C(CH_3)_3$], 5.38 [d, $^3J_{PC}$ 2 Hz, $Si(CH_3)_3$], $C(CH_3)_3$ not found because of low solubility and too rapid decomposition of **2** at room temperature; ^{29}Si{^{1}H} NMR (DEPT) (298 K, $CDCl_3$, 99.36 MHz): δ −4.3 (d + sat, $^2J_{PSi}$ 7 Hz); ^{31}P{^{1}H} NMR (268 K, toluene-d_8, 121.50 MHz): δ 82.6 (s + sat, $^2J_{PSi}$ 7 Hz); LT-FAB[11] (toluene) (%): *m/z* 798.3 (63) [M^+], 781.3 (73) [M − OH^-], 768.3 (85) [$M^+ - CH_2O$], 767.3 (80) [M − CH_3O^-], 711.2 (35) [M^+ − Bu^t − CH_2O], 631.3 (100) [$(LH)_2Cu^+$ + H − $SiMe_3$], 305.3 (88) [LH^+ − Me], correct isotopic pattern; Anal. $C_{28}H_{72}N_4Cu_2P_2Si_4$; calc: C, 42.13; H, 9.09; N, 7.02; P, 7.76; found: C, 42.51; H 9.05; N, 7.07; P, 7.64%.

§ Single crystals suitable for X-ray diffraction analysis were obtained by slow oxidation of **1** in a pentane solution at −25 °C with trace amounts of dioxygen in argon. Higher temperatures or air as oxidant only led to microcrystalline material. Data were collected on a Bruker SMART CCD instrument[14,15] *Crystal data* for **2**: $C_{28}H_{72}Cu_2N_4O_2P_2Si_4$, M = 798.28, monoclinic, space group $C2/c$ μ = 1.186 mm^{-1}, $R1$ = 0.058, $wR2$ = 0.140 (observed reflections), a = 28.4009(7), b = 11.2930(3), c = 16.9370(5) Å, β = 126.604(1)°, V = 4360.9(2) Å^3, T = 200(2) K, Z = 4, half a molecule per asymmetric unit, 21976 reflections measured 4991 independent (R_{int} = 0.0629). CCDC 182/1720. See http://www.rsc.org/suppdata/cc/b0/b004173o/ for crystallographic files in .cif format.

¶ For the DFT calculations, the empirically parametrized B3LYP[16] method within the Gaussian 98 (Revision A.5) package[17] was used. Restricted and unrestricted energy calculations of singlet **3** yield identical energies (−4338.1224 E_h), an unrestricted single point calculation of triplet **3** leads to an energy 105.4 kJ mol^{-1} above the singlet [B3LYP 6-31G(d): 102.2 kJ mol^{-1}]. Cu–Cu distance of **3**: B3LYP 6-31G(d): 2.685 Å; B3LYP 3-21G: 2.649 Å. NBO Version 3.1, E. D. Glendening, A. E. Reed, J. E. Carpenter and F. Weinhold.

1 H. S. Mason, W. L. Fowlks and E. Peterson, *J. Am. Chem. Soc.*, 1955, **77**, 2914.
2 E. I. Solomon, M. J. Baldwin and M. D. Lowery, *Chem. Rev.*, 1992, **92**, 521; K. A. Magnus, H. Ton-That and J. A. Carpenter, *Chem. Rev.*, 1994, **94**, 727; E. I. Solomon, U. M. Sundaram and T. E. Machonkin, *Chem. Rev.*, 1996, **96**, 2563.
3 P. L. Holland and W. B. Tolman, *Coord. Chem. Rev.*, 1999, **190**–**192**, 855.
4 N. Kitajima, K. Fujisawa, C. Fujimoto, Y. Moro-oka, S. Hashimoto, T. Kitagawa, K. Toriumi, K. Tatsumi and A. Nakamura, *J. Am. Chem. Soc.*, 1992, **114**, 1277.
5 N. J. Blackburn, R. W. Strange, A. Farooq, M. S. Haka and K. D. Karlin, *J. Am. Chem. Soc.*, 1988, **110**, 4263; P. Comba, P. Hilfenhaus and K. D. Karlin, *Inorg. Chem.*, 1997, **36**, 2309.
6 (*a*) J. A. Halfen, S. Mahapatra, E. C. Wilkinson, S. Kaderli, V. G. Young Jr., L. Que Jr. and W. B. Tolman, *Science*, 1996, **271**, 1397; (*b*) S. Mahapatra, J. A. Halfen, E. C. Wilkinson, G. Pan, X. Wang, V. G. Young Jr., C. J. Cramer, L. Que Jr. and W. B. Tolman, *J. Am. Chem. Soc.*, 1996, **118**, 11 555; (*c*) S. Mahapatra, V. G. Young Jr., S. Kaderli, A. D. Zuberbühler and W. B. Tolman, *Angew. Chem., Int. Ed. Engl.*, 1997, **36**, 130; (*d*) W. B. Tolman, *Acc. Chem. Res.*, 1997, **30**, 227; (*e*) V. Mahadevan, Z. Hou, A. P. Cole, D. E. Root, T. K. Lal, E. I. Solomon and T. D. P. Stack, *J. Am. Chem. Soc.*, 1997, **119**, 11 996; (*f*) H. Hayashi, S. Fujinami, S. Nagatomo, S. Ogo, M. Suzuki, A. Uehara, Y. Watanabe and T. Kitagawa, *J. Am. Chem. Soc.*, 2000, **122**, 2124.
7 B. F. Straub, F. Eisenträger and P. Hofmann, *Chem. Commun.*, 1999, 2507.
8 P. Hofmann, H. Heiß and G. Müller, *Z. Naturforsch. Teil B*, 1987, **42**, 395.
9 E. Pidcock, H. V. Obias, M. Abe, H.-C.Liang, K. D. Karlin and E. I. Solomon, *J. Am. Chem. Soc.*, 1999, **121**, 1299.
10 B. F. Straub, F. Rominger and P. Hofmann, *Organometallics*, accepted; B. F. Straub, F. Rominger and P. Hofmann, in preparation.
11 J. H. Gross, *Rapid Commun. Mass Spectrom.*, 1998, **12**, 1833.
12 J. L. Dubois, P. Mukherjee, T. D. P. Stack, B. Hedman, E. I. Solomon and K. O. Hodgson, *J. Am. Chem. Soc.*, 2000, **122**, 5787.
13 C. J. Cramer, B. A. Smith and W. B. Tolman, *J. Am. Chem. Soc.*, 1996, **118**, 11 283.
14 SHELXTL V5.10; G. M. Sheldrick, Bruker Analytical X-ray-Division, Madison, WI, 1997.
15 SADABS; G. M. Sheldrick, 1996, unpublished work, based on the method described in R. H. Blessing, *Acta Crystallogr., Sect. A*, 1995, **51**, 33.
16 A. D. Becke, *J. Chem. Phys.*, 1983, **98**, 5648; C. Lee, W. Yang and R. G. Parr, *Phys. Rev. B*, 1988, **37**, 785; S. H. Volko, L. Wilk and M. Nusair, *Can. J. Phys.*, 1980, **58**, 1200.
17 Gaussian 98; Gaussian, Inc., Pittsburgh PA, 1998.

Electrochemical preparation of macroporous polypyrrole films with regular arrays of interconnected spherical voids

Takayuki Sumida, Yuji Wada, Takayuki Kitamura and Shozo Yanagida*

Material and Life Science, Graduate School of Engineering, Osaka University, Suita, Osaka 565-0871, Japan. E-mail: yanagida@chem.eng.osaka-u.ac.jp

Received (in Cambridge, UK) 25th April 2000, Accepted 14th July 2000
Published on the Web 4th August 2000

Polypyrrole films possessing regular macropores interconnected through size-controlled holes have been prepared by electrochemical oxidation in the presence of ordered arrays of silica spheres as templates.

Ordered porous ceramics, metals and polymers have attracted much attention currently because of their applications in catalysis, separation films, porous electrodes and photonic crystals. For synthesis of these materials, useful methods using emulsions[1] or colloidal crystals, which are comprised of submicron-sized monodisperse lateces[2–8] or silica particles,[9–12] as templates have been successfully developed. The advantages of the template-directed methods are mainly due to their size tunability and the simple procedure involving impregnation of the interstitial channels of templates with the desired precursors, reactions and subsequent removal of the templates.

Thus obtained macroporous materials generally possess two types of characteristic void closely related to the applications mentioned above. One is a macropore that is well controlled by the size of the particles that constitute the templates. The other is a smaller hole, which forms at each contact point between the nearest neighbor particles of templates and three-dimensionally connects each macropore. The size of these holes as well as the macropores strongly influence the mass transportation in the bulk of the porous materials. Therefore, the size control of these holes is the critical issue in the fields that require easy access to the high internal surface area of the materials and designed diffusion pathways. However, its control is more difficult than that of the macropores. This is because their size is sensitive to the degree of filling of the channels of the original templates which depends on the viscosity and concentration of precursors and shrinkage of materials when the precursors react. Consequently, there have been only a few reports in which the control of the interconnecting hole size has been achieved through changing the viscosity of the precursor which depends on temperature,[11] repetitions of the filling process[3] or sintering of templates to give larger contact areas between original particles.[9,10]

Recently, electrodeposition has been applied to colloidal template-directed synthesis toward complete impregnation of interstitial channels with group II–VI semiconductors.[13] The electrochemical technique should be an effective route not only for complete filling but also for governing the growth and volumes of materials being deposited in the complex channels *via* parameters such as potential and current that are easy to vary and monitor.

Here we describe the size control of the small interconnecting holes as well as the macropores in template-directed electrochemical synthesis of macroporous polypyrrole. This new material should be of practical value for electrochemical capacitor and battery material applications.

According to a convective self-assembly technique by Jiang *et al.*[14] which relies on capillary forces, we prepared silica colloidal crystals supported on F-doped SnO_2 coated glasses (OTE). An OTE was dipped into ethanol containing monodisperse silica spheres with a mean diameter of 238 nm. Because rapid ethanol evaporation led to poor uniformity of the thickness of the colloidal crystals, the OTE dipped into silica/ethanol dispersion was covered by a 200 mL beaker to slow the evaporation rate. After ethanol was evaporated for 5 days, opalescent colloidal crystals of 3.0 μm average thickness were deposited on the conducting surface. These colloidal crystals used as templates were hydrothermally treated at 473 K for 3 h at a heating rate of 2 K min^{-1} leading to slight necking between silica particles which mechanically stabilizes the templates.[9,10] The necking also resulted in a shrinkage of *ca.* 2% of the thickness compared to the as-grown crystals. Finally, the templates were washed with ethanol several times and kept in a vacuum desiccator until use. The electropolymerization was potentiostatically performed using 0.1 M pyrrole and 0.1 M $LiClO_4$ in acetonitrile solutions with a BAS 100W apparatus (Bioanalytical Systems, Inc.). The counter electrode was Pt wire and the reference electrode was Ag/Ag^+. After electropolymerization of pyrrole, the templates were dissolved by immersing in 20% HF aqueous solutions for 48 h. The polypyrrole films which were peeled off from the OTE were washed with deionized water and characterized by SEM (Hitachi S-800) without the requirement for deposition of metal because of the conductivity of polypyrrole.

Fig. 1 shows chronoamperometric responses of pyrrole polymerization at applied potentials of 0.55, 0.75 and 0.85 V *vs.* Ag/Ag^+. Transition points (marked by the arrows), where the current rapidly increased were observed and shifted toward shorter times at higher potentials. Similar transition points have been observed in template synthesis using membranes with topologically simple cylindrical pores.[15] These rapidly increased currents were suggested to be mainly caused by a rapid increase of the electrochemical reaction area when the growing surface of materials reached the membrane/bulk solution interface. In our case, the surfaces of the colloidal crystals were almost fully covered with cauliflower-like polypyrrole at

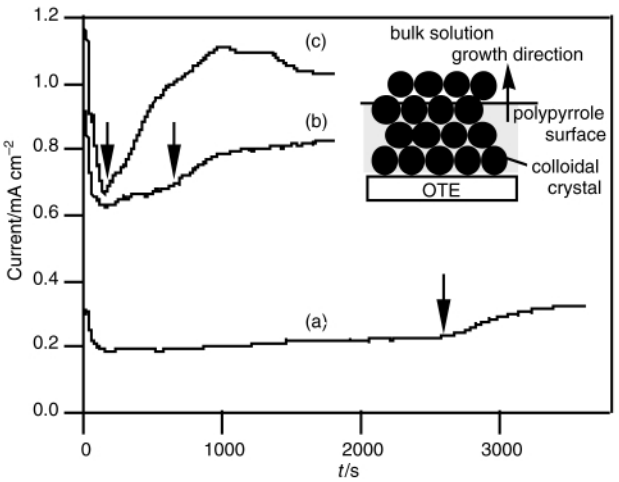

Fig. 1 Chronoamperometric responses of pyrrole electropolymerization in channels of silica colloidal crystals by applying (a) 0.55 V, (b) 0.75 V and (c) 0.85 V. The inset shows a schematic represetation of colloidal crystals and the growth direction of polypyrrole.

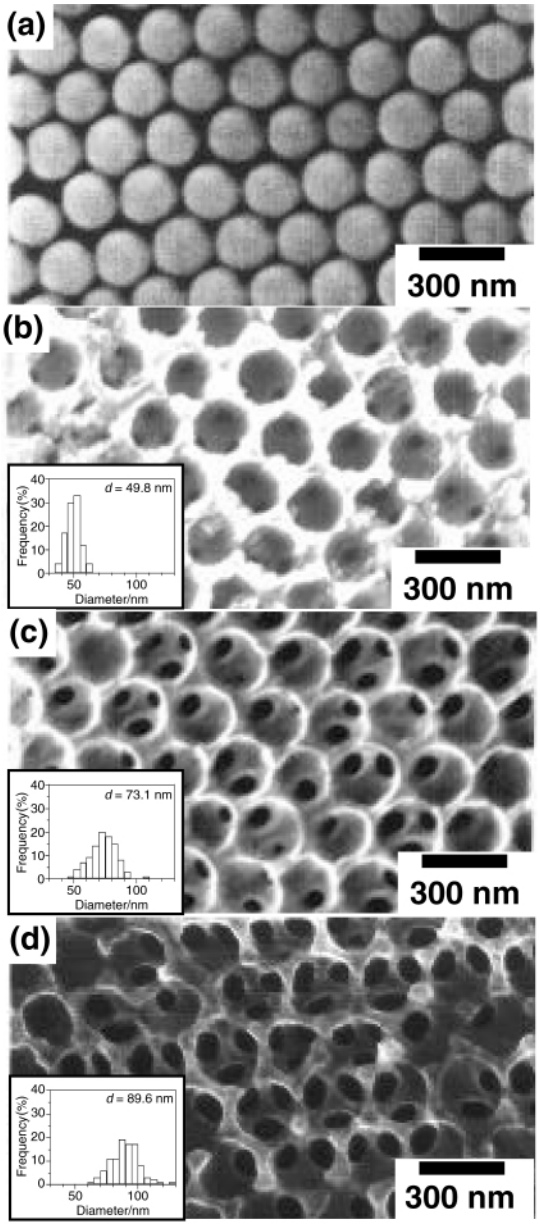

Fig. 2 SEM imges of (a) the original templates and the macroporous polypyrrole films prepared by applying (b) 0.55 V, (c) 0.75 V and (d) 0.85 V. The insets show the hole size distributions corresponding to each SEM image. The size distributions were determined by counting more than 200 holes.

deposition times beyond the transition points (data not shown). Hence, in the present colloidal template synthesis, the transition points are considered to appear according to a similar phenomenon as above. These transition points also should enable us to avoid covering the pores of the top surface of the films with excess polypyrrole.

Fig. 2 shows typical SEM images of the original templates and the macroporous polypyrrole prepared at various potential with electropolymerization stopped before each transition point. Fig. 2(b), (c) and (d) demonstrate that the polypyrrole films had honeycomb macroporous structures mirroring the ordered channels of the original templates [Fig. 2(a)] and smaller holes inside each macropore were clearly observed. As shown in the insets of Fig. 2, their average size increased with increasing polymerization potential from 49.8(5.68) to 73.1(10.6) to 89.6(11.2) nm (esds in parentheses) at 0.55, 0.75 and 0.85 V. These results demonstrated that simple potential change should allow the hole size to be controlled. At 0.55, 0.75 and 0.85 V, the center-to-center distances between the macropores were smaller by 0.1, 0.2 and 3% than the diameters of the original silica spheres, respectively. Taking into account the low shrinkage, the hole size is likely determined rather by incomplete filling during the electropolymerization process than by shrinkage of polypyrrole. The charges passed at each transition time were 0.8, 0.6 and 0.2 C at 0.55, 0.75 V and 0.85 V, respectively implying that smaller quantities of polypyrrole were deposited within the channels at higher potentials, which would decrease the degree of filling.

In conclusion, we have electrochemically prepared macroporous polypyrrole films using colloidal templates. Furthermore, we found that their smaller hole size could be controlled by changing the polymerization potentials. Preliminary experiments showed that this electrochemical control of the hole size can be extended to other templates with different diameters of silica spheres. More detailed mechanisms of the variation of the hole size and the growth of materials in three-dimensionally complex channels are under investigation by experiments with other conducting polymers and metals.

The present study was supported in part by the Japan Society for the Promotion of Science as part of the ‘Reserch for the Future Program’ and also by a Grant-in-Aid for Scientific Reserch from the Ministry of Education, Science, Sports and Culture of Japan.

Notes and references

1 A. Irnhof and D. J. Pine, *Nature*, 1997, **389**, 948.
2 O. D. Velev, T. A. Jede, R. F. Lobo and A. M. Lenhoff, *Nature*, 1997, **389**, 447.
3 J. E. G. J. Wijnhoven and W. L. Vos, *Science*, 1998, **281**, 802.
4 B. T. Holland, C. F. Blanford and A. Stein, *Science*, 1998, **281**, 538.
5 M. Antonietti, B. Berton, C. Göltner and H.-P. Hentze, *Adv. Mater.*, 1998, **10**, 154.
6 S. H. Park and Y. Xia, *Chem. Mater.*, 1998, **10**, 1745.
7 G. Subramanian, V. N. Manoharan, J. D. Thorne and D. J. Pine, *Adv. Mater.*, 1999, **11**, 1261.
8 G. Subramania, K. Constant, R. Biswas, M. M. Sigalas and K. Ho, *Appl. Phys. Lett.*, 1999, **74**, 3933.
9 A. A. Whidov, R. H. Baughman, Z. lqbal, C. Cui, I. Khayrullin, S. O. Dantas, J. Marti and V. G. Ralchenko, *Science*, 1998, **282**, 897.
10 Y. A. V1asov, N. Yao and D. J. Norris, *Adv. Mater.*, 1999, **11**, 165.
11 P. Jiang, K. S. Hwang, D. M. Mittleman, J. F. Bertone and V. L. Colvin, *J. Am. Chem. Soc.*, 1999, **121**, 11 630.
12 S. A. Johnson, P. J. Ollivier and T. E. Mallouk, *Science*, 1999, **283**, 963.
13 P. V. Braun and P. Wiltzius, *Nature*, 1999, **402**, 603.
14 P. Jiang, J. F. Bertone, K. S. Hwang and V. L. Colvin, *Chem. Mater.*, 1999, **11**, 2132.
15 C. Schönenberger, B. M. I. van der Zande, L. G. J. Fokkink, M. Henny, C. Schmid, M. Krüger, A. Bachtold, R. Huber, H. Birk and U. Staufer, *J. Phys. Chem. B*, 1997, **101**, 5497.

Peptides with nucleobase moieties as a stabilizing factor for a two-stranded α-helix

Sachiko Matsumura,[a] Akihiko Ueno[a] and Hisakazu Mihara*[ab]

[a] *Department of Bioengineering, Graduate School of Bioscience and Biotechnology, Tokyo Institute of Technology, Nagatsuta, Yokohama 226-8501, Japan. E-mail: hmihara@bio.titech.ac.jp*

[b] *Form and Function, PRESTO, Japan Science and Technology Corporation, Tokyo Institute of Technology, Nagatsuta, Yokohama 226-8501, Japan*

Received (in Cambridge, UK) 31st May 2000, Accepted 20th July 2000
Published on the Web 9th August 2000

The designed α-helical coiled-coil peptides, which contain nucleobase moieties at the amino acid side chains, were found to take a stable α-helical form owing to the base-pair interaction.

α-Helical coiled-coil, found in many natural proteins, is one of the well-studied motifs aiming to understand protein sequence–structure relationships,[1] and also to develop novel proteins with functional properties by *de novo* protein design.[2] The initial studies have focused on the usage of hydrophobic and electrostatic interactions between amino acid side chains to assemble α-helical peptide chains.[3] In this study we, for the first time, provide another example utilizing hydrogen bonds between nucleobases at amino acid side chains to form an α-helical coiled-coil. In nature, DNA and RNA take advantage of hydrogen bonds in their structures and functions. Sequence-complementarity of antiparallel strands and high-fidelity information transfer including transcription, translation, and replication are performed owing to the nucleobase-molecular complementarity through hydrogen bonds. Thus, peptides equipped with the nucleobase-molecular complementarity should gain new useful characters in their structure and function. In order to explore the applicability of nucleobase-complementarity in a peptide structure, we have introduced nucleobase amino acids (NBAs)[4] in a two-stranded α-helix with the coiled-coil motif (Fig. 1), and examined the effects on the peptide secondary structure.

We designed an antiparallel, two-stranded coiled coil QQ as a basic framework, based on the peptide designed by Zhou *et al*.[5] QQ consists of two amphiphilic α-helices, each containing a two-heptad repeat unit with the amino acid sequence $A_cL_dQ_eK_fQ_gL_aA_b$. In the design of the peptide, Leu residues at the a and d positions are expected to form a hydrophobic face, which drives coiled-coil formation through its burial in the interface. Gln residues are selected at the e and g positions to prevent induction of inter- or intrahelical electrostatic interactions. To produce a disulfide-bridged coiled-coil in an antiparallel fashion, the sequence Cys-Gly-Gly- is added to the N-terminus of one helix, and the sequence -Gly-Gly-Cys is placed at the C-terminus of the other helix. Since the Cα-Cβ vectors of amino acid at the g and g′ positions are pointed toward each other in antiparallel coiled-coils in the wheel diagram (Fig. 1c), NBAs were incorporated at the g and g′ heptad positions instead of Gln. Thereby, we expected the specific interaction between thymine NBA (T_{NBA}) and adenine NBA (A_{NBA}) in the two-stranded α-helix. We designed three peptides with T–A pair(s) at the g and g′ heptad positions; TA-1 has the pair apart from the disulfide-bridged end, TA-2 has the pair near the disulfide linker, and TA-1·2 contains pairs at both positions (Fig. 1).

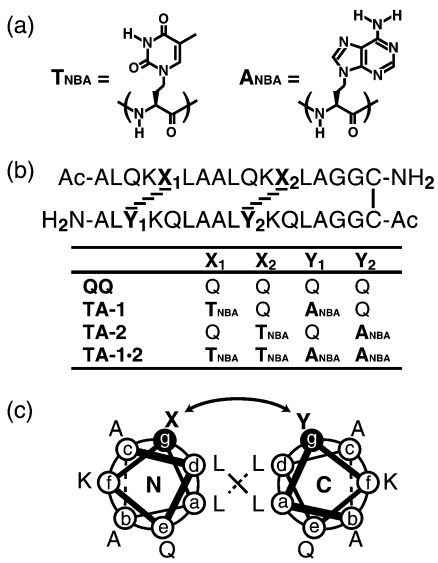

	X_1	X_2	Y_1	Y_2
QQ	Q	Q	Q	Q
TA-1	T_{NBA}	Q	A_{NBA}	Q
TA-2	Q	T_{NBA}	Q	A_{NBA}
TA-1·2	T_{NBA}	T_{NBA}	A_{NBA}	A_{NBA}

Fig. 1 (a) Structures of nucleobase amino acids (NBAs); (b) amino acid sequences; (c) helix wheel drawing of the designed peptides.

The designed peptides were synthesized manually by the solid-phase method using the Fmoc-strategy.[6] To introduce A_{NBA} and T_{NBA} to the Fmoc chemistry protocols, *N*-Fmoc-*L*-α-amino-γ-(6-*N*-benzyloxycarbonyl)adenine butanoic acid [Fmoc-A_{NBA}(Z)-OH] and *N*-Fmoc-L-α-amino-γ-thymine butanoic acid [Fmoc-T_{NBA}-OH] were prepared according to literature methods with some modifications.[7] All peptides were acetylated at the N-terminus and amidated at the C-terminus to avoid unfavorable helix–dipole interactions. To build an antiparallel heterodimer, an asymmetric disulfide bond formation between two peptides was performed *via* activation of the thiol function of one peptide by pyridinesulfenylation, and the reaction with the second peptide with the free thiol.[8] The peptides were purified by reversed-phase HPLC, and identified by matrix-assisted laser desorption time-of-flight mass spectrometry and amino acid analysis.[9] The concentrations of the peptides were determined by quantitative amino acid analysis using valine as an internal standard.

The circular dichroism (CD) spectra of the designed peptides in a buffer (pH 7.4) at 25 °C are shown in Fig. 2. All peptides showed spectra characteristic of an α-helical conformation with negative maxima near 208 and 222 nm and a positive maximum at 195 nm. The ratio of the molar ellipticities at 222 and 208 nm, $[\theta]_{222}/[\theta]_{208}$, was reduced in a solution containing trifluoroethanol, known as a solvent enhancing an α-helix form but isolating a helix-dimer, indicating two-stranded α-helical formation in the buffer. The $[\theta]_{222}$ values of TA-1 and TA-2, both having a T–A pair, were −20500 and −22100 deg cm^2 dmol^{-1}, respectively, showing their higher helical contents than the content of QQ ($[\theta]_{222}$ = −15100 deg cm^2 dmol^{-1}). Furthermore, TA-1·2 having two T–A pairs showed a higher α-helicity ($[\theta]_{222}$ = −23800 deg cm^2 dmol^{-1}) than TA-1 and TA-2. We assumed that this helix-inducing effect was not the result of the peptide aggregation, judged from the concentration independence of the $[\theta]_{222}$ values of designed peptides (ranging

DOI: 10.1039/b004318o

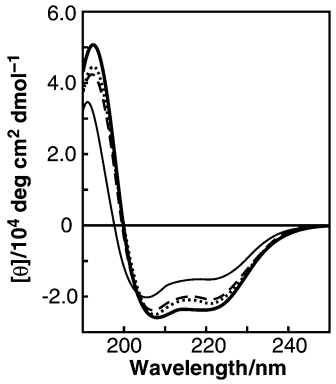

Fig. 2 CD spectra for the designed peptides in 2.0×10^{-2} mol dm^{-3} Tris·HCl buffer (pH 7.4) at 25 °C. [Peptide] = 1.0×10^{-5} mol dm^{-3}. QQ, (——); TA-1, (– – –); TA-2, (-----); TA-1·2, (▬).

from 7.5×10^{-7} to 1.0×10^{-4} mol dm^{-3}). The addition of an excess amount of exogenous adenine reduced the α-helical contents in the cases of peptides possessing T–A pair(s) ($\Delta[\theta]_{222}$ = 6500 deg cm^2 dmol^{-1} in TA-1·2), whereas no change occurred in the case of QQ.[10] This demonstration implied that the added interaction between A and T increases the α-helical content.

Denaturation studies were carried out to determine the stabilities of the peptides. With increasing temperature of the peptide solution, the bimodal spectra were gradually converted into those of a random conformation, indicating the decrease of the fraction of α-helix structure. The presence of an isodichroic point at *ca*. 202 nm was consistent with the helix-coil transition. From the temperature dependence of $[\theta]_{222}$ shown in Fig. 3, it was apparent that the thermal stabilities of the nucleobase-containing species, especially TA-1·2, were noticeably increased as compared to the stability of QQ. Furthermore, the guanidine hydrochloride (GuHCl) denaturation study also provided the observation of the stabilizing effect in nucleobase-containing peptides (Table 1). The incorporation of one T–A pair in the two-stranded α-helix (TA-1 and TA-2) made peptides with a higher stability than QQ, and the additional incorporation (TA-1·2) afforded further stability to the peptide. TA-2 is slightly more stable than TA-1, which is consistent with the α-helicity. An explanation may be the difference of the position of a T–A pair (Fig. 1). In TA-2 the pair was located near the disulfide-linker so that T and A might configure to interact at g–g′ positions, whereas in TA-1 the pair was at the end leading to fluctuation of T and A. Moreover, the effect of nucleobase-incorporation on the helix stability was not additive. The incorporation of one T–A pair into QQ increased ΔGu^{H_2O} by 0.56 (TA-1) and 0.90 kcal mol^{-1} (TA-2), whereas two T–A pairs increased greatly by 1.88 kcal mol^{-1}.

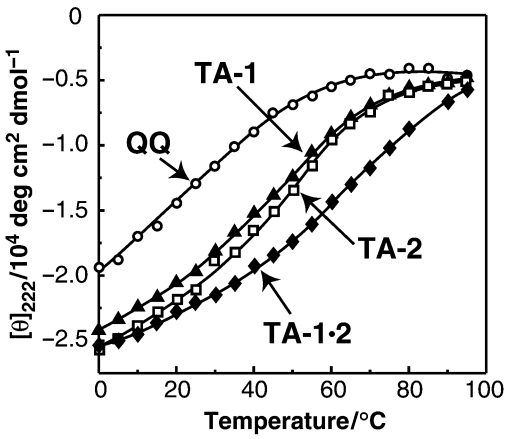

Fig. 3 Temperature dependence of the CD signal at 222 nm for QQ, TA-1, TA-2, and TA-1·2 in 2.0×10^{-2} mol dm^{-3} Tris·HCl buffer (pH 7.4).

Table 1 Stabilities of the designed peptides estimated by GuHCl denaturation

Peptide	QQ	TA-1	TA-2	TA-1·2
ΔGu^{H_2O}[a]/kcal mol^{-1}	0.74	1.30	1.64	2.62
$\Delta\Delta Gu^{H_2O}$[a]/kcal mol^{-1}	0	0.56	0.90	1.88
$[GuHCl]_{1/2}$[b]/mol dm^{-3}	1.7	2.0	2.3	3.2
$\Delta[GuHCl]_{1/2}$[b]/mol dm^{-3}	0	0.3	0.6	1.5

[a] ΔGu^{H_2O} is the free energy of unfolding in the absence of GuHCl at 25 °C, estimated according to the equation: $\Delta Gu = \Delta Gu^{H_2O} - m[GuHCl]$, where m is the slope term. ΔGu is calculated from the equation: $\Delta Gu = -RT\ln[(1 - fn)/fn]$.[11] [b] The $[GuHCl]_{1/2}$ values represent the concentration of GuHCl at which 50% of the peptide is unfolded.

We also examined the peptides having two T–T pairs (TT-1·2) or two A–A pairs (AA-1·2) at the g–g′ positions in the two-stranded α-helix. However, these mismatch pairs did not significantly improve the α-helical form unlike T–A pairs (TT-1·2, $[\theta]_{222}$ = −17800; AA-1·2, $[\theta]_{222}$ = −18100 deg cm^2 dmol^{-1}). These results strongly suggest that the specific interaction between the T–A pair is important in promoting the α-helical formation. In such a case of the specific pair(s), T and A in the two-α-helix might orient and interact in the appropriate fashion. One possible interaction might be base stacking (hydrophobic interaction), and another might be hydrogen-bonding. The former does not contribute greatly to the helix formation, because the α-helical content of AA-1·2, containing two A–A mismatch pairs, is not as large as that of TA-1 or TA-2. In respect to the latter interaction, the pH dependence of $[\theta]_{222}$ revealed that T–A-containing peptides took a higher helical form under neutral conditions than under acidic or basic conditions. The protonation of nucleobases had an influence on the interaction between T and A, suggesting a large contribution of the hydrogen-bonding interaction. Although detailed inspection is necessary to answer how these bases interact and induce the helical structure, the specific interaction, including the hydrogen-bonds, were successful at stabilizing two-stranded α-helix structures.

In conclusion, peptides containing NBAs at the g–g′ positions in the coiled-coil structure were synthesized, and the incorporated A–T nucleobase pairs were found to make an effective contribution to the formation of stable α-helical structures. The base-pair interaction can be utilized as a new tool for designing secondary or tertiary peptide structure, and also applied to development of novel functions based on the complementarity.

Notes and references

1 P. B. Harbury, T. Zhang, P. S. Kim and T. Alber, *Science*, 1993, **262**, 1401.
2 C. Micklatcher and J. Chmielewski, *Curr. Opin. Chem. Biol.*, 1999, **3**, 724.
3 N. E. Zhou, C. M. Kay and R. S. Hodges, *J. Mol. Biol.*, 1994, **237**, 500.
4 T. Takahashi, K. Hamasaki, I. Kumagai, A. Ueno and H. Mihara, *Chem. Commun.*, 2000, 349.
5 N. E. Zhou, C. M. Kay and R. S. Hodges, *Protein Eng.*, 1994, **7**, 1365.
6 W. C. Chan and P. D. White, in *Fmoc Solid Phase Peptide Synthesis: A Practical Approach*, ed. W. C. Chan and P. D. White, Oxford University Press Inc., New York, 2000, p. 41.
7 A. Lenzi, G. Reginato and M. Taddei, *Tetrahedron Lett.*, 1995, **36**, 1713; P. Ciapetti, F. Soccolini and M. Taddei, *Tetrahedron*, 1997, **53**, 1167.
8 S. Futaki and K. Kitagawa, *Tetrahedron*, 1997, **53**, 7479.
9 QQ, *m/z* 3563.9 [$(M + H)^+$] (calc. = 3563.8); TA-1, *m/z* 3734.7 [$(M + H)^+$] (calc. = 3735.0); TA-2, *m/z* 3736.1 [$(M + H)^+$] (calc. = 3735.0); TA-1·2, *m/z* 3904.8 [$(M + H)^+$] (calc. = 3906.4).
10 [Peptide] = 7.0–9.0 × 10^{-6} mol dm^{-3}, [Adenine] = 1.0 × 10^{-3} mol dm^{-3}.
11 M. M. Santoro and D. W. Bolen, *Biochemistry*, 1988, **27**, 8063.

ChemComm

Highly selective anodic monofluorination of 4-arylthio-1,3-dioxolan-2-ones: a marked solvent effect on product selectivity

Hideki Ishii, Norihisa Yamada and Toshio Fuchigami*

Department of Electronic Chemistry, Tokyo Institute of Technology, Nagatsuta, Midori-ku, Yokohama 226-8502, Japan

Received (in Cambridge, UK) 12th June 2000, Accepted 17th July 2000
Published on the Web 8th August 2000

This is the first example of a solvent effect on fluorinated product selectivity; anodic fluorination of 4-arylthio-1,3-dioxolan-2-ones in CH_2Cl_2 containing a fluoride supporting electrolyte using an undivided cell provided the fluorodesulfurization product, 4-fluoro-1,3-dioxolan-2-one preferentially while anodic fluorination in DME resulted in α-fluorination, without desulfurization, selectively.

Fluorinated ethylene carbonates seem to be promising organic electrolytic solvents or additives for rechargeable Li batteries since introduction of fluorine atom(s) into ethylene carbonate is expected to increase its electrochemical stability and decrease its melting point. We have studied selective anodic fluorination of various organic compounds.[1,2] The selective anodic fluorination has many advantages since the fluorination can be carried out in one step under safe conditions and the use of hazardous reagents is not required. So far, limited examples of selective anodic fluorination of oxygen-containing heterocycles have been reported.[3] With these facts in mind, we have attempted anodic fluorination of ethylene carbonates having an arylthio group **1** using various supporting fluoride salts and solvents.

At first, we investigated anodic fluorination of 4-phenylthio derivative **1a** under various conditions. Constant current electrolysis was carried out at platinum plate electrodes in an undivided cell at rt until **1a** was completely consumed. The results are summarized in Table 1.

As shown in Table 1, anodic fluorodesulfurization of **1a** proceeded selectively in $Et_4NF{\cdot}4HF$–CH_2Cl_2 and $Et_3N{\cdot}5HF$–CH_2Cl_2 to provide monofluorinated product **2**[4] in moderate to good yields (runs 3 and 5). In sharp contrast, α-fluorination of **1a** took place preferentially in $Et_4NF{\cdot}4HF$–DME to give **3a**[5] (run 4). In this case, difluorinated products such as **4** (Scheme 2) were not formed. This can be explained in terms of the oxidation potential of **3a** (E_p^{ox}: 2.2 V *vs.* SCE) being 0.3 V higher than that of **1a** (E_p^{ox}: 1.9 V *vs.* SCE).

Table 1 Anodic fluorination of 4-arylthio-1,3-dioxolan-2-ones

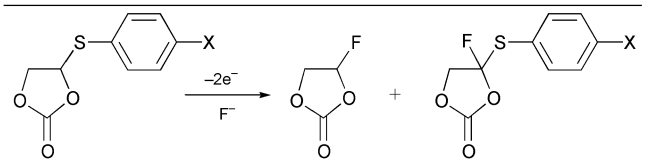

1a : X = H
1b : X = Cl
2 **3**

Run	Substrate **1**	Supporting electrolyte	Solvent	Electricity/ F mol^{-1}	Yield (%)[a] **2**	**3**
1	**1a**	$Et_4NF{\cdot}3HF$	CH_2Cl_2	3.1	29	16
2	**1a**	$Et_4NF{\cdot}3HF$	DME	7.2	5	40
3	**1a**	$Et_4NF{\cdot}4HF$	CH_2Cl_2	5.2	53	Trace
4	**1a**	$Et_4NF{\cdot}4HF$	DME	3.4	28	54
5	**1a**	$Et_4NF{\cdot}5HF$	CH_2Cl_2	5.5	67	Trace
6	**1b**	$Et_4NF{\cdot}4HF$	DME	3.1	20	80
7	**1b**	$Et_4NF{\cdot}5HF$	CH_2Cl_2	4.2	96	0

[a] Determined by ^{19}F-NMR spectroscopy.

Next, we extended this anodic fluorination to the 4-(4-chlorophenylthio) derivative **1b**. Similarly, the use of $Et_3N{\cdot}5HF$–CH_2Cl_2 provided **2** exclusively in almost quantitative yield (run 7) while the use of $Et_4NF{\cdot}4HF$–DME afforded **3b**[6] selectively in good yield (run 6). Thus, it was found that electrolytic conditions, particularly electrolytic solvents, greatly affected the fluorinated product selectivity. Such marked product selectivity depending on electrolytic solvents has not been previously reported for anodic fluorination.

In order to clarify the solvent effects, we investigated anodic fluorination of **1b** in a mixed solvent of DME and CH_2Cl_2 containing $Et_4NF{\cdot}4HF$. As shown in Fig. 1, the product ratio of **2** to **3b** increased with an increase in the ratio of CH_2Cl_2 to DME. Notably, addition of only 25% CH_2Cl_2 to DME caused a dramatic change in the product ratio and **2** was mainly formed in *ca.* 60% yield.

This interesting phenomenon can be explained as follows. The fluorination can be rationalised by postulating a radical cation intermediate **A** as shown in Scheme 1.

CH_2Cl_2 has a poor ability to solvate carbocations, therefore, **A** seems to be unstable in CH_2Cl_2. Consequently it is reasonable to assume that desulfurization followed by fluorination mainly takes place prior to α-fluorination of **A**.[7] On the other hand, DME is known to strongly coordinate cations.[8] Therefore, DME should stabilize the intermediate **A** and DME also enhances the fluoride ion nucleophilicity.[9] Then, the deprotonation of **A** with fluoride ions takes place prior to desulfurization followed by further oxidation to generate cation **B** and this cation reacts with a fluoride ion to provide the α-fluorinated product.

Furthermore, we examined anodic fluorodesulfurization of **3a**. As shown in Scheme 2, anodic fluorodesulfurization of **3a** in $Et_4NF{\cdot}4HF$–CH_2Cl_2 and $Et_3N{\cdot}5HF$–CH_2Cl_2 proceeded to give desired difluorinated product **4**[10] in reasonable yield. However, anodic fluorodesulfurization of **3a** did not take place at all in $Et_4NF{\cdot}4HF$–DME and **3a** was almost recovered.

Finally, we also examined chemical fluorination of **1a**. However, treatment of **1a** with various *N*-fluoropyridinium

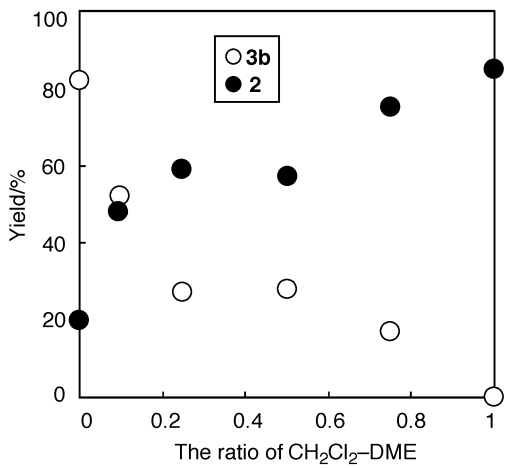

Fig. 1 Dependence of yield of **2** and **3b** on the ratio of CH_2Cl_2 to DME.

DOI: 10.1039/b004652n

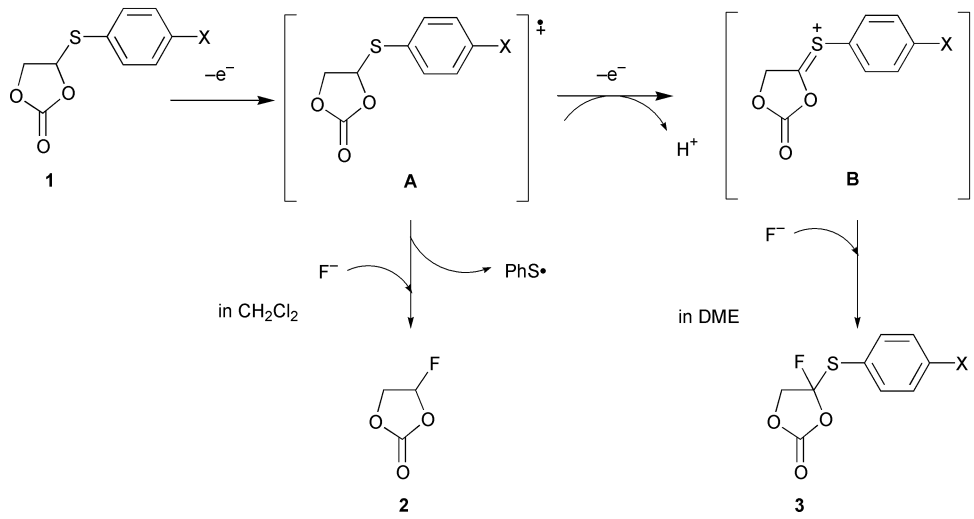

Scheme 1

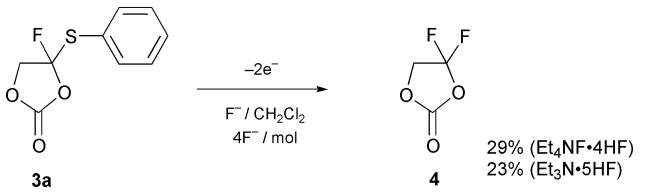

Scheme 2

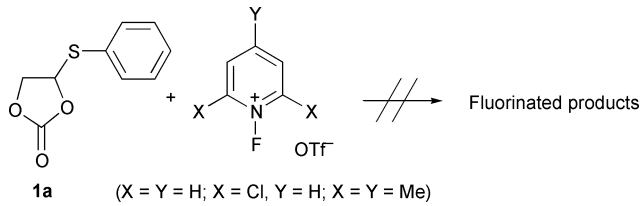

Scheme 3

triflates in CH_2Cl_2 resulted in the formation of none of the desired fluorinated products, as shown in Scheme 3. Therefore, electrochemical fluorination is more advantageous than conventional chemical methods for such heterocyclic sulfides.

In summary, we have developed a novel synthesis of fluorinated ethylene carbonates using anodic fluorination and we also found a unique marked solvent effect on fluorinated product selectivity.

We thank the Kato Foundation and the Ministry of Education, Science, Sports and Culture of Japan for Financial support (Grant-in-Aid for Scientific Research, No. 12555252).

Notes and references

1 (*a*) T. Fuchigami and K. M. Dawood, *J. Org. Chem.*, 1999, **64**, 138; (*b*) S. Higashiya, A. Narizuka, A. Konno, K. Momota and T. Fuchigami, *J. Org. Chem.*, 1999, **64**, 133.

2 (*a*) T. Fuchigami, *Advances in Electron-Transfer Chemistry*, vol. 6, ed. P. S. Mariano, JAI Press, CT, 1999, p. 41; (*b*) T. Fuchigami, S. Higashiya, Y. Hou and K. M. Dawood, *Rev. Heteroatom. Chem.*, 1999, **19**, 67.

3 (*a*) Y. Hou, S. Higashiya and T. Fuchigami, *J. Org. Chem.*, 1999, **64**, 3346; (*b*) G. P. Gambaretto, M. Napoli, C. Franccaro and L. Conte, *J. Fluorine Chem.*, 1982, **19**, 427; (*c*) J. H. Meurs and W. Eilenberg, *Tetrahedron*, 1991, **47**, 705.

4 *4-Fluoro-1,3-dioxolan-2-one* (**2**): colorless cubes: mp 19.0–20.0 °C; ^{1}H-NMR ($CDCl_3$, 270 MHz) δ 6.31 (ddd, J = 64, 1.3, 4.0 Hz, 1H), 4.70–4.49 (m, 2H); ^{13}C-NMR ($CDCl_3$, 67.8 MHz) δ 152.65, 104.98 (d, J = 237 Hz), 70.67 (d, J = 28 Hz); ^{19}F-NMR ($CDCl_3$, 254 MHz) δ −44.42 (ddd, J = 64, 34, 21 Hz); MS (*m/z*) 106 (M^+), 62 ($M - CO_2$); Anal. calc. for $C_3H_3FO_3$: C, 33.98; H, 2.85; F, 17.91; O, 45.26. Found C, 33.73; H, 2.91; F, 17.72%.

5 *4-Fluoro-4-phenylthio-1,3-dioxolan-2-one* (**3a**): colorless oil; ^{1}H-NMR ($CDCl_3$, 270 MHz) δ 7.66–7.62 (m, 2H), 7.50–7.39 (m, 3H), 4.63 (dd, J = 16.8, 10.9 Hz, 1H), 4.47 (dd, J = 26.4, 10.9 Hz, 1H); ^{13}C-NMR ($CDCl_3$, 67.8 MHz) δ 150.64, 136.21, 130.89, 129.70, 125.03, 119.54 (d, J = 270 Hz), 73.88 (d, J = 31 Hz); ^{19}F-NMR ($CDCl_3$, 254 MHz) δ 0.54 (dd, J = 27, 17 Hz); MS (*m/z*) 214 (M^+); HRMS calc. for $C_9H_7FO_3S$: 214.0100. Found: 214.0133.

6 *4-Fluoro-4-(p-chlorophenylthio)-1,3-dioxolan-2-one* (**3b**): colorless needles; mp 60.0–61.0 °C; ^{1}H-NMR ($CDCl_3$, 270 MHz) δ 7.60–7.57 (m, 2H), 7.43–7.40 (m, 2H), 4.66 (dd, J = 16.8, 10.9 Hz, 1H), 4.47 (dd, J = 26.4, 10.9 Hz, 1H); ^{13}C-NMR ($CDCl_3$, 67.8 MHz) δ 150.40, 137.72, 137.43, 129.96, 123.34, 119.21 (d, J = 271 Hz), 73.83 (d, J = 31 Hz); ^{19}F-NMR ($CDCl_3$, 254 MHz) δ 0.93(dd, J = 27, 17 Hz); MS (*m/z*) 250 (M^+); HRMS calc. for $C_9H_6ClFO_3S$: 247.9710. Found: 247.9720.

7 In this reaction, the formation of diphenyl disulfide was detected by MS and ^{1}H-NMR.

8 S. E. Hill, D. Feller and E. D. Glendening, *J. Phys. Chem. A*, 1998, **93**, 159.

9 (*a*) K. M. Dawood, S. Higashiya, Y. Hou and T. Fuchigami, *J. Fluorine Chem.*, 1999, **93**, 159; (*b*) Y. Hou and T. Fuchigami, *Electrochem. Commun.*, 1999, **1**, 445.

10 *4,4-Difluoro-1,3-dioxolan-2-one* (**4**): ^{1}H-NMR ($CDCl_3$, 270 MHz) δ 4.72 (t, J = 11 Hz, 2H); ^{19}F-NMR ($CDCl_3$, 254 MHz) δ 3.90 (t, J = 12 Hz); MS (*m/z*) 124 (M^+); HRMS calc. for $C_3H_2F_2O_3$: 123.9972. Found: 123.9939.

ChemComm

High yield olefination of a wide scope of aryl chlorides catalyzed by the phosphinito palladium PCP pincer complex: [PdCl{$C_6H_3(OPPr^i_2)_2$-2,6}]

David Morales-Morales, Rocío Redón, Cathleen Yung and Craig M. Jensen*

Department of Chemistry, University of Hawaii, Honolulu, Hawaii 96822, USA.
E-mail: jensen@gold.chem.hawaii.edu

Received (in Irvine, CA, USA) 30th May 2000, Accepted 12th July 2000
Published on the Web 9th August 2000

[PdCl{$C_6H_3(OPPr^i_2)_2$-2,6}] efficiently catalyzes the olefination of a broad scope of aryl chlorides; as a result of the high thermal stability of the catalyst, the coupled products are obtained in excellent and in many cases nearly quantitative yields.

The formation of vinylic C–C bonds from the palladium catalyzed coupling of aryl bromides, iodides and triflates with alkenes (the Heck reaction) is one of the "true power tools of contemporary organic synthesis".[1] However, the industrial application of the reaction has been very limited owing to the instability of the palladium catalysts and the high cost of the aryl starting materials. Recently a great deal of progress has been made toward overcoming these limitations.[2–9] In a pioneering study, Milstein and coworkers found that the olefination of relatively inexpensive aryl chlorides is catalyzed by [$Pd(OAc)_2$] in the presence of 1,3-bis(diisopropylphosphino)propane.[2] Higher turnovers and yields have recently been achieved with activated aryl chlorides using palladacycle,[3] carbene–palladium[4] and palladium–phosphite[5] catalysts. It has also been discovered that the activity of more traditional Heck coupling systems is enhanced by the addition of [PPh_4]Cl[6] or PBu^t_3[7] such that the chloro substrates can be utilized in the reaction. Notably, Littke and Fu found that in the presence of PBu^t_3, $Pd_2(dba)_3$ catalyzes the olefination of a broad scope of aryl chlorides.[7]

A key feature of several of these systems is the stabilization of the active catalysts by either ligand chelation or steric shielding of the metal center. Both of these stabilizing effects can be realized with mixed donor polydentate ligands. This combination has been used to good advantage in catalytic aliphatic dehydrogenation reactions by iridium PCP pincer complexes, [$IrH_2\{C_6H_3(CH_2PR_2)_2$-2,6}]. The pincer ligand confers high stability on the complexes at the temperatures required for oxidative additions of aliphatic C–H bonds.[10] Similarly, the palladium PCP pincer complexes, [Pd{O-C(O)CF_3}{$C_6H_3(CH_2PPr^i_2)_2$-2,6}], [Pd{OC(O)CF_3}{C_6CH_2-1-$(CH_2PR_2)_2$-2,6-$(CH_2)_2$-3,5-H-4}] (R = Pr^i, Bu^t) have been found to be an extraordinarily active catalyst for the Heck couplings with iodo- and bromo-arenes.[11] However, the phosphino pincer complexes were found to be almost inactive with chloroarenes. Beller[5] and Zapf van Leeuwen and coworkers[9] have recently reported cases in which the catalytic activity of palladium complexes are remarkably enhanced upon substitution of phosphine ligands by alternative phosphorus ligands containing electron withdrawing groups.[5,9] We have found that unlike 1,3-bis(phos*phino*)benzenes, 1,3-bis(phos*phinito*)benzene, can be conveniently prepared in 95% yield from the reaction of inexpensive precursors.[12] It was therefore of interest to examine the activity of the phosphinito palladium complex, [PdCl{$C_6H_3(OPPr^i_2)_2$-2,6}] **1**, as a catalyst for Heck couplings of aryl chlorides. We report here that **1** is an efficient catalyst for this reaction, giving olefinated products in excellent, and in many cases nearly quantitative yields.

The results of our studies of the catalytic activity of **1** are presented in Table 1. In order to optimize the efficiency of the catalytic system, we initially examined the coupling of

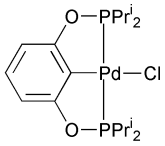

1

chlorobenzene and styrene by **1** under a variety of reaction conditions† and analyzed the product mixtures through gas chromatography. Unlike most previously reported systems for Heck couplings of aryl chlorides, additional cocatalyst such as excess LiBr,[3] PBu^t_3,[7] [NBu_4][Br][3–5] or [PPh_4]Cl,[6] are not required to achieve high catalytic activity. We found that > 99% isolated yield of *trans*-stilbene is obtained when the reaction is carried in dioxane solvent and caesium acetate is used as base. Employing this same combination of reagents in a preparative scale experiment, we were able to isolate the coupled product in nearly quantitative yield. At 120 °C, a reaction time of 5 days is required to achieve this high conversion. We found, however, that the catalyst can withstand prolonged heating to 180 °C and thus the request reaction time can be reduced to 24 h.

The reactivities of a variety of aryl chlorides were examined under the optimized conditions and uniformly showed > 99% selective for the *trans* configured product. The system is also one of the few reported systems to show high reactivity with electron-rich[2,7] and sterically hindered[7] aryl chlorides. The practical utility of this catalytic system was probed by carrying out preparative scale couplings of 4-chloroacetophenone and 4-chloroanisole with styrene. We obtained the corresponding *E*-

Table 1 Heck couplings of aryl chlorides with styrene using **2** as catalyst. Experiments conducted with 0.67 mol% catalyst and 1.1 equivalents of base in dioxane solution except where noted

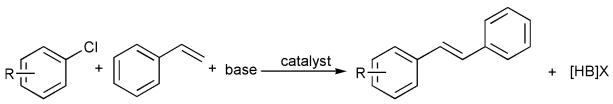

Entry	Aryl chloride	Base	Yield[a] (%)	Yield[b] (%)
1	H	CsOAc	> 99	> 99
2	H	CsOAc		4.4[c]
3	H	CsOAc		2.0[d]
4	H	Cs_2CO_3		95
5	H	Na_2CO_3		87
6	H	KOAc		40
7	H	CsOH		31
8	H	$EtNPr^i_2$		3.0
9	4-MeC(O)	CsOAc	> 99	> 99
10	4-MeO	CsOAc	86	88
11	4-HC(O)	CsOAc	81	82
12	2-Me	CsOAc	83	85

[a] Yields obtained at 120 °C. [b] Yields obtained by GC analysis are based on chlorobenzene. In all experiments only the *trans* configured product was detected. [c] DMF solution. [d] Dimethylacetamide solution.

DOI: 10.1039/b004412l

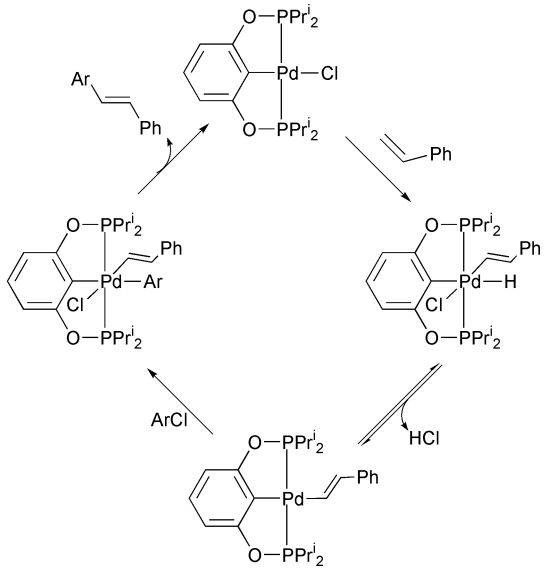

Scheme 1 Proposed mechanism for the catalytic olefination of aryl chlorides by [PdCl{C_6H_3($OPPr^i_2$)$_2$-2,6}].

stilbenes in > 95% and 85% isolated yields respectively. To our knowledge, these yields are the highest that have been achieved to date for the Heck coupling of these aryl chlorides with styrene.

In order to verify that the high catalytic activity of **1** requires the presence of phosphinito rather than a phosphino PCP ligand, we examined the catalytic activity of, [PdCl{C_6H_3($CH_2PPr^i_2$)$_2$-2,6}] **2**† under the conditions that were optimized for **1**. The chloro complex **2**, like [Pd{OC(O)CF_3}{C_6H_3($CH_2PPr^i_2$)$_2$-2,6}],[11] showed only a very low level of activity with aryl chlorides.

It has been suggested that Heck couplings catalyzed by PCP complexes proceed through Pd(II) and Pd(IV) rather than Pd(0) and Pd(II) intermediates.[11,13] Additionally, it seems unlikely that catalytic sequence in our system could be initiated by the oxidative addition of aryl chlorides to **1** as the resulting 18-electron complex would not be expected to undergo further reaction. We therefore conclude that the mechanism of the catalytic olefination of aryl chlorides by **1** is fundamentally different from those commonly considered for palladium catalyzed Heck couplings[1c] and operates through a mechanism like that seen in Scheme 1. Our suggestion is that the catalytic process is initiated by the oxidative addition of a vinyl C–H bond of the alkene reactant. This hypothesis is supported by the recent observation that the reaction of the palladium PCP pincer complex, with tributylstannyl furan results in the substitution of the triflate by an η^1-vinyl ligand.[14] Also the deuterium labeling studies of the reaction of *tert*-butylethylene with the related PCP pincer complex, [IrH_2{C_6H_3-($CH_2PBu^t_2$)$_2$}-2,6] have shown that activation of vinyl C–H bonds at the metal center occurs rapidly at room temperature.[15] The Pd(IV) intermediate resulting from the vinyl C–H oxidative addition would be expected to undergo a reductive elimination of HCl. It is well established that reductive elimination is promoted by decreasing ligand donor strengths.[16] Thus the finding that the phosphinito PCP complex has markedly higher activity than its phosphino analog suggests that this step is rate determining. The catalytic cycle is completed by oxidative addition of the aryl chloride followed by reductive elimination of the coupled product. Similar mechanistic considerations may explain the extraordinary high catalytic activities that Beller and Zapf[5] and van Leeuwen and coworkers[9] have observed respectively for palladium phosphite and phosphorus amidite complexes.

In summary, the relatively inexpensive, phosphinito PCP pincer complex **1** catalyzes the high yield olefination of broad scope of aryl chlorides. It should be noted, that while most of the reactions reported here were expedited by heating to 180 °C, high yields of coupled products can be obtained at longer times at temperatures as low as 120 °C. Thus it should be possible to apply this catalytic system to the synthesis of commercially important, structurally complex fine chemicals containing thermally sensitive groups.

This work was supported by the U.S. Department of Energy Hydrogen Program.

Notes and references

† *General procedure* for the olefination of aryl chlorides. Under an atmosphere of nitrogen, a solution of 0.924 mmol of aryl chloride, 1.83 mmol of olefin, 3.0 mg of **2** (0.0062 mmol) and 202 mg (0.924 mmol) of diethylene glycol di-*n*-butyl ether (internal standard) in 1.0 mL of dioxane, was introduced into a Schlenk tube containing a magnetic stir bar and charged with 1.01 mmol of base. The tube was sealed and fully immersed in a 180 (120) °C silicon oil bath. After 24 (120) h, the reaction mixture was cooled to room temperature and, the organic phase analyzed by gas chromatography (GC/FID, GC–MS). For quantitative analysis a gas chromatograph GC HP 5980A with flame ionization detector (FID), and a HP-1 capillary column (25.0 m) from Hewlett Packard was used.

1 (*a*) K. C Nicolaou and E. J. Sorensen, *Classics in Total Synthesis*, VCH, Weinheim, 1996. Reviews: (*b*) R. F. Heck, *Comprehensive Organic Synthesis*, eds. B. M. Trost and I. Flemming, Pergamon Press, Oxford, 1991, vol. 4, ch. 3.4, p. 833; (*c*) A. de Meijere and F. E. Meyer, *Angew. Chem., Int. Ed. Engl.*, 1994, **33**, 2379; (*d*) W. Cabri and I. Caudiani, *Acc. Chem. Res.*, 1995, **28**, 2; (*e*) T. Jeffery, *Adv. Met. Org. Chem.*, 1996, **5**, 153; (*f*) S. Brase and A. de Meijere, *Metal Catalyzed Cross-Coupling Reactions*, eds. P. J. Stang and F. Diederich, Wiley, New York, 1998, ch. 3.

2 Y. Ben-David, M. Portnoy, M. Gozin and D. Milstein, *Organometallics*, 1992, **11**, 1995; M. Portnoy, Y. Ben-David and D. Milstein, *Organometallics*, 1993, **12**, 4734.

3 W. A. Herrmann, C. Brossmer, K. Öfele, C. Reisinger, T. Priermeier, M. Beller and H. Fischer, *Angew. Chem., Int. Ed. Engl.*, 1995, **34**, 1844; W. A. Herrmann, C. Brossmer, C. Reisinger, T. H. Riermeier, K. Öfele and M. Beller, *Chem. Eur. J.*, 1997, **3**, 1357.

4 W. A. Herrmann, M. Elison, J. Fischer, C. Köcher and G. R. J. Artus, *Angew. Chem., Int. Ed. Engl.*, 1995, **34**, 2371.

5 M. Beller and A. Zapf, *Synlett.*, 1998, 792.

6 M. T. Reetz, G. Lohmer and R. Schwickardi, *Angew. Chem., Int. Ed.*, 1998, **37**, 481.

7 A. F. Littke and G. C. Fu, *J. Org. Chem.*, 1999, **64**, 10.

8 K. H. Shaughnessy and J. F. Hartwig, *J. Am. Chem. Soc.*, 1999, **121**, 2123.

9 G. F. P. Van Strijdonck, M. D. K. Boele, P. C. J. Kamer, J. G. de Vries and P. W. N. M. van Leeuwen, *Eur. J. Inorg. Chem.*, 1999, 1073.

10 M. Gupta, C. Hagen, W. C. Kaska, R. Flesher and C. M. Jensen, *Chem. Commun.*, 1996, 2083; M. Gupta, W. C. Kaska, R. E. Cramer and C. M. Jensen, *J. Am. Chem. Soc.*, 1997, **119**, 840; M. Gupta, W. C. Kaska and C. M. Jensen, *Chem. Commun.*, 1997, 2083; W-W. Xu, G. Rossini, M. Gupta, C. M. Jensen, W. C. Kaska, K. Krough-Jespersen and A. S. Goldman, *Chem. Commun.*, 1997, 2273; F. Liu, E. B. Pak, B. Singh, C. M. Jensen and A. S. Goldman, *J. Am. Chem. Soc.*, 1999, **121**, 4086; C. M. Jensen, *Chem. Commun.*, 1999, 2443.

11 M. Ohff, A. Ohff, M. E. van der Boom and D. Milstein, *J. Am. Chem. Soc.*, 1997, **119**, 11687.

12 D. Morales-Morales, C. Grause, K. Kasaoka, R. Redón, R. E. Cramer and C. M. Jensen, *Inorg. Chim. Acta.*, 2000, **300–302**, 958.

13 B. L. Shaw and S. D. Perera, *Chem. Commun.*, 1998, 1863.

14 W. A. Cotter, L. Barbour, K. L. McNamara, R. Hechter and R. J. Lachicotte, *J. Am. Chem. Soc.*, 1998, **120**, 11016.

15 D. W. Lee, W. C. Kaska and C. M. Jensen, *Organometallics*, 1998, **17**, 1.

16 G. O. Spessard and G. L. Miessler, *Organometallic Chemistry*, Prentice-Hall, Upper Saddle River, New Jersey, 1997, p. 178.

ChemComm

A novel method for the synthesis of ZSM-5 zeolite membranes on a porous alumina tube: the role of a dry-gel barrier in pores

Hongbin Zhao,[a] Tetsuro Jin,[b] Koji Kuraoka[b] and Tetsuo Yazawa*[b]

[a] *New Energy and Industrial Technology Development Organization, 1-8-31 Midorigaoka, Ikeda City, Osaka 563-8577, Japan*

[b] *Department of Optical Materials, Osaka National Research Institute, 1-8-31 Midorigaoka, Ikeda City, Osaka 563-8577, Japan. E-mail: yazawa@onri.go.jp*

Received (in Cambridge, UK) 19th June 2000, Accepted 14th July 2000
Published on the Web 8th August 2000

An aluminosilicate gel barrier as a zeolite precursor is first incorporated in the pores of an alumina support tube and then subjected to hydrothermal crystallization, leading to ZSM-5 zeolite membranes with high compactness at the molecular level.

The potential industrial applications of zeolite membranes in continuous separation and reaction–separation processes on the basis of molecular sieving have recently motivated many attempts and efforts in zeolite membrane preparation. The last ten years have witnessed significant progress in the demonstration of the potential of zeolite membranes to separate hydrocarbon gas mixtures and organic/aqueous mixtures using MFI and A type zeolite membranes.[1,2] *In situ* hydrothermal crystallization in solution or the vapor phase is mainly applied in zeolite membrane synthesis.[3–5] However, presently good quality zeolite membranes are obtained in plate form rather than in tube form though the latter is preferable for industrial applications owing to its large volume/area ratio. It appears to be difficult to adapt a synthesis method applied to plate-form zeolite membranes for tubular zeolite membranes since the membrane quality is sensitive to the geometry of a substrate (plate *vs*. tube) and the manner of contacting a substrate with a zeolite synthesis mixture. Therefore, synthesis of tubular zeolite membranes is still a subject of importance and remains to be addressed.

We note in the literature[6–10] that the separation performance of zeolite membranes is strongly related to the degree that zeolite crystallites are incorporated in the pores of the substrate during hydrothermal crystallization. In addition, in view of the methodology for zeolite membrane preparation it seems that plugging pores of a substrate with inter-grown zeolite crystals is easier to achieve than growing a continuous defect-free zeolite layer on top of a substrate. Therefore, based on the concept of pore plugging, we anticipated developing a novel synthesis method for tubular zeolite membranes.

Here we outline such a method by the synthesis of ZSM-5 zeolite membranes using a tubular substrate. Our synthetic strategy was to incorporate a highly dense aluminosilicate gel barrier in the substrate pores followed by hydrothermal crystallization. The method can generate a compact zeolite barrier and appears to be reproducible.

In our synthesis, a commercial porous alumina tube of 10 mm outside diameter and 7 mm inside diameter and *ca*. 50 mm length was employed as the substrate. The tube has a multilayer structure with a 0.1 μm porous outer layer. One end of the tube was sealed and the other end was connected with a dense alumina tube *via* a high-temperature glaze. The synthesis procedure consisted of two sequential processes. The first was to incorporate an aluminosilicate gel barrier in the outer layer pores by the urea technique. The substrate was first impregnated *in vacuo* with an alcohol-based solution containing $Si(OEt)_4$, $Al(NO_3)_3$, $CO(NH_2)_2$, H_2O (EtOH as balance). The impregnated substrate was dried at *ca*. 50 °C to such an extent that all the solution was sucked by and further concentrated in the outer layer pores by capillary action. The sample was then placed in a closed glass vessel at 90 °C. Thus, precipitation of $Si(OEt)_4$ and $Al(NO_3)_3$ occurred exclusively in the pores by homogeneous alkalinization from decomposition of $CO(NH_2)_2$ [$CO(NH_2)_2 + 3H_2O \rightarrow 2OH^- + 2NH_4^+ + CO_2$]. The above steps were repeated until the N_2 gas flow of the sample was below 10^{-9} mol m^{-2} s^{-1} Pa^{-1} at room temperature. The second process was to convert the aluminosilciate gel barrier to a desired zeolite barrier by hydrothermal treatment. The modified substrate tube was filled with $Si(OPr)_4$ (bp 225 °C) and then placed into a solution of composition $0.005NaAlO_2 : 0.55TPABr : 0.42NaOH : 100H_2O$ in a Teflon vessel. In this arrangement, a reactive interface at the incorporated gel barrier was developed between the two separate liquids. Thus, during hydrothermal treatment, hydrolysis of $Si(OPr)_4$ supplied an additional silica source to the crystallization front while the gel barrier was being converted to zeolitic materials. Hydrothermal treatment was performed in a stainless steel autoclave at 190 °C for 10 days. When the hydrothermal treatment was complete, the sample was thoroughly washed with H_2O and dried at 50 °C overnight and then carefully calcined at 400 °C for 12 h to remove the TPA occluded within the zeolite channels.

In each synthesis experiment, the membranes were shown by XRD to be highly crystalline, pure zeolite ZSM-5. Fig. 1 shows SEM micrographs of the cross-section of a representative ZSM-5 zeolite membrane. From the micrographs, the following two points can be made. (a) As seen in Fig. 1A, the substrate outer layer displays an SEM contrast comparable to those of the ZSM-5 zeolite films indicating that some zeolitic materials were formed from the aluminosilicate gel barrier incorporated in the pores. (b) It was observed that 10 and 100 μm ZSM-5 zeolite films grew on the inner and outer surface, respectively (Fig. 1B and C). These films showed significant morphological differences. The crystals of the inner zeolite film were essentially parallelepipeds of size *ca*. 30 μm and well intergrown. In contrast, those of the outer zeolite film were coffin-shaped and much larger being *ca*. 80 μm along the *c*-axis. It was also observed that few non-zeolitic pathways existed in both the inner and outer zeolite film, which act as defects for gas separation.

A dead-end method was applied for gas permeation measurements with pure He, N_2, CO_2, *n*-butane and isobutane. The permeation measurements were performed at room temperature with the permeation side set at an atmospheric pressure. The gas flow rates were measured with a mass flow meter. The flow rates were plotted *vs*. the kinetic diameters of gas molecules in Fig. 2. As seen, the permeance of all the gases showed a good correlation with their kinetic diameters except for *n*-butane and isobutane. Noble's group reported that an MFI zeolite membrane on a 5 nm γ–alumina tubular substrate showed a *n*-butane/isobutane perm-selectivity of 3–20 and a *n*-butane permeance of

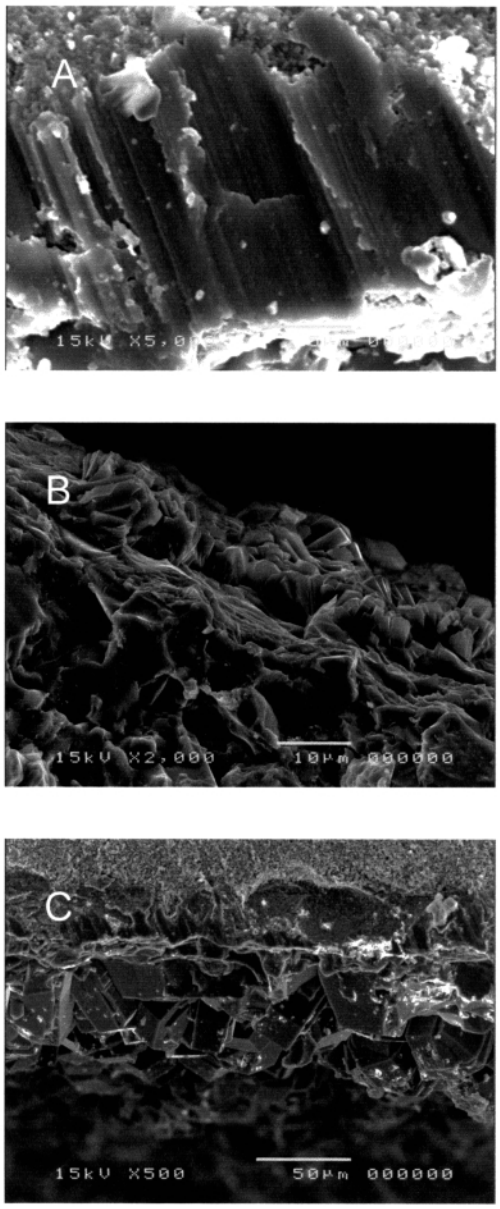

Fig. 1 SEM micrographs of a cross-section of the ZSM-5 zeolite membrane: (a) the 0.1 μm porous outer layer, (b) the inner layer and (c) the outer layer.

ca. 10^{-9} mol m^{-2} s^{-1} Pa^{-1}. The ZSM-5 zeolite membrane in the present study showed a comparable permeance although it exhibited no *n*-butane/isobutane perm-selectivity.

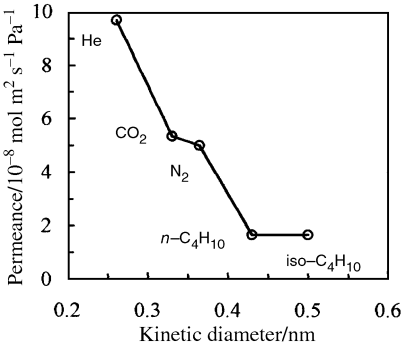

Fig. 2 Permeance of pure gases through the ZSM-5 zeolite membrane *vs*. their kinetic diameters.

Accordingly, a highly compact zeolite barrier with few defects has been formed within and on the substrate. Further, on the basis of SEM observations, zeolite barriers, mainly that in the pores, led to a significant contribution to gas separation. The reason for the formation of defects could be that the reactive interface has insufficient additional aluminosilicate at the crystallization front during crystallization and contracting of the gel barrier, or/and the gel barrier was partially dissolved during hydrothermal treatment.

In summary, the present study has explored a new route for the preparation of tubular zeolite membranes. The resulting ZSM-5 zeolite membrane shows the potential of the novel preparation method. However, improvement of the membrane integrity with regard to separation performance is underway by studying the process kinetics of the preparation method.

Notes and references

1 T. Bein, *Chem. Mater.*, 1996, **8**, 1636.
2 A. Tavolaro and E. Drioli, *Adv. Mater.*, 1999, **11**, 975.
3 K. Jansen and T. Maschmeyer, *Top. Catal.*, 1999, **9**, 113.
4 M. Tsapatsis, G. Xomeritakis, H. Hillhouse, S. Nair, V. Nikolakis, G. Bonilla and Z. Lai, *CATTECH*, 1999, **3**, 148.
5 M. Matsukata and E. Kikuchi, *Bull. Chem. Soc. Jpn.*, 1997, **70**, 2341.
6 M. Jia, B. Chen, R. Noble and J. Falconer, *J. Membr. Sci.*, 1994, **90**, 1.
7 J. Coronas, J. Falconer and R. Noble, *AIChE J.*, 1997, **43**, 1797.
8 V. Tuan, J. Falconer and R. Noble, *Ind. Eng. Chem. Res.*, 1999, **38**, 3635.
9 H.-S. Oh, M.-H. Kim and H.-K. Rhee, *Stud. Surf. Sci. Catal.*, 1997, **105**, 2217.
10 Y. Ando, M. Kato, Y. Kamei, Y. Kirano, S. Yamada and H. Taguchi, *Proc. 5th Int. Conf. Inorg. Membr*, 1998, 1016.

A novel acetated 54-member crown-shaped polyoxomolybdate with unprecedented structural features: $Na_{26}[\{Na(H_2O)_2\}_6(\{\mu_3\text{-}OH)_4Mo^V_{20}Mo^{VI}_{34}O_{164}(\mu_2\text{-}CH_3COO)_4\}]\cdot\approx 120H_2O$

Wenbin Yang, Canzhong Lu,* Xiang Lin and Honghui Zhuang

The State Key Laboratory of Structural Chemistry, Fujian Institute of Research on the Structure of Matter, The Chinese Academy of Sciences, Fuzhou, Fujian, 350002 P.R. China. E-mail: czlu@ms.fjirsm.ac.cn

Received (in Cambridge, UK) 20th June 2000, Accepted 20th July 2000
Published on the Web 9th August 2000

The EPR silent acetated 54-member crown-shaped polyoxomolybdate $Na_{26}[\{Na(H_2O)_2\}_6(\{\mu_3\text{-}OH)_4Mo^V_{20}Mo^{VI}_{34}O_{164}(\mu_2\text{-}CH_3COO)_4\}]\cdot\approx 120H_2O$ (1), constructed from two different but related building blocks in a new mode, is synthesized in high yield by reducing an acidified aqueous solution of $Na_2MoO_4\cdot 2H_2O$ and $CH_3COONa\cdot 3H_2O$.

Ever since interest was sparked by the biological activity of the sodium cryptate $[NaW_{21}Sb_9O_{86}]^{18-}$, a species that has been subsequently applied as HAP23 in AIDS therapy,[1,2] there has been an enormous growth in the area of inorganic 'host–guest' polyoxometalates, partly motivated by their potential applications in catalysis, biology, medicine and materials science.[3,4] Generally, the guests are linked to the *endo* oxygen atoms of the host shells *via* valence bonds or intermolecular interactions such as hydrogen bonding.[5–7] One among many examples is that the N_3^- or NO_3^- anion is encapsulated within an approximately spherical $\{H_{12}V_{18}O_{44}\}^{n-}$ polyoxovanadate 'host' cage.[8]

Octamolybdates exhibit various structural patterns in the solid-state and these isomers can interconvert with each other by 'bond-making/breaking' in solution.[9,10] Although a number of corresponding oxide-based composite solid-state materials were synthesized in the presence of structure-directing organic ligands such as diamines, few nanometered polyoxomolybdates constructed from these octamolybdates have been reported. We report here the synthesis and characterization of a novel acetated 54-member crown-shaped polyoxomolybdate, which contains unprecedented building blocks, and exhibits interesting structural features.

$$Na_{26}[\{Na(H_2O)_2\}_6(\{(\mu_3\text{-}OH)_4Mo^V_{20}Mo^{VI}_{34}O_{164}\text{-}(\mu_2\text{-}CH_3COO)_4\}]\cdot\approx 120H_2O \quad (1)$$

Compound **1** was synthesized in high yield by reducing an acidified aqueous solution of Na_2MoO_4,† and characterized by elemental analysis, cerimetric titration (to determine the number of Mo^V), thermogravimetric analysis (to determine the amount of crystallized water), bond valence sum (BVS) calculations[11,12] (to determine the number and the positions of OH groups, as well as the number of Mo^V centers), spectroscopic methods (IR, Raman and UV–VIS)‡ and single-crystal X-ray structure analysis.§

The structure of **1** consists of a discrete 54-member crown-shaped $[\{Na(H_2O)_2\}_6(\{\mu_3\text{-}OH)_4Mo^V_{20}Mo^{VI}_{34}O_{164}(\mu_2\text{-}CH_3COO)_4\}]^{26-}$ **1a** nanoanion (containing four bridging acetate groups and six encapsulated seven-coordinated sodium cations as 'guests'), and 26 Na^+ cations. As shown in Figs. 1 and 2, two different but related building blocks have been found in **1a**. The first building block is the centrosymmetric octamolybdate $\{Mo_8O_{28}\}$ ($\equiv[Mo^V_2Mo^{VI}_6O_{28}]^{10-}$) moiety, which consists of eight distorted edge-shared molybdenum–oxygen octahedra. The structure of this centrosymmetric octamolybdate is very similar to other reported octamolybdate anions, which can be described as $[Mo_8O_{26}(X)_2]^{2n-4}$, for example, $[(HO)_2Mo_8O_{26}]^{6-}$, where *n* is the normal charge of coordinated base X.[12–14] However, in addition to long interblock distances existing within this octamolybdate unit, rather short metal–metal bonds are also found between two neighboring $\{Mo_8O_{28}\}$ units (Mo(7)–Mo(27), 2.58216(18), Mo(19)–Mo(20), 2.5985(16) Å). To the best of our knowledge, such short Mo–Mo distances have rarely been observed in other polyoxomolybdates, particularly in nano-size systems. The second feature is the unprecedented asymmetric $\{Mo_9O_{30}(X)_2\}$ ($\equiv[(\mu_3\text{-}OH)_2Mo^V_4Mo^{VI}_5\text{-}O_{28}(CH_3COO)_2]^{10-}$) unit, which is constructed by nine molybdenum atoms (four Mo^V and five Mo^{VI} centers). Each molybdenum is coordinated by six oxygen atoms in distorted octahedral arrangement with one short Mo=O bond for Mo^V and two for Mo^{VI}. Again, long Mo–Mo distances (around 3.21 Å) and short Mo–Mo bonds (shorter than 2.6 Å) are also formed within the new $\{Mo_9O_{30}(X)_2\}$ unit. In summary, each crown-shaped anion **1a** contains ten short Mo–Mo bonds and eight long interblock Mo–Mo distances, which are listed in the caption to Fig. 1.

The two building blocks are connected to each other into a spiral $[(HO)_4Mo^V_{16}Mo^{VI}_{34}\text{-}O_{160}(CH_3COO)_4]^{44-}$ ring, in which the linkage between the two neighboring $\{Mo_8O_{28}\}$ units is edge-shared, while that between $\{Mo_8O_{28}\}$ and $\{Mo_9O_{30}(X)_2\}$ is corner-shared (Fig. 2). Four additional $\{Mo_1\}$ ($\equiv[Mo^VO]^{3+}$) groups, which cap the linking Mo atoms between $\{Mo_8O_{28}\}$ and $\{Mo_9O_{30}(X)_2\}$ units, are bridged by four acetate ligands to complete the crown-shaped 'host' nanoanion. Six seven-coordinated Na^+ cations with (distorted) pentagonal-

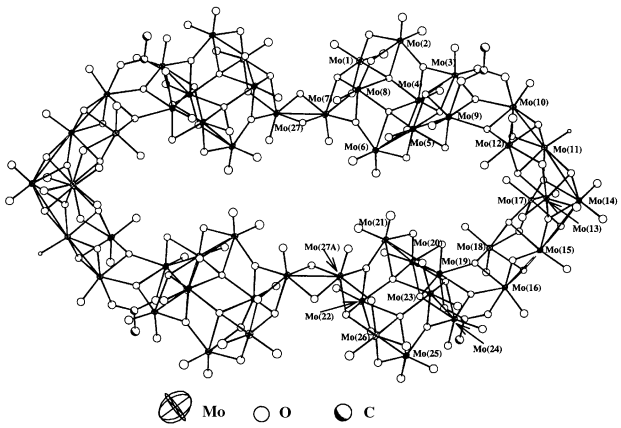

Fig. 1 (*a*) Perspective drawing of **1a** constructed by two different building blocks: $\{Mo_8O_{28}\}$ ($\equiv[Mo^V_2Mo^{VI}_6O_{28}]^{10-}$) and novel unprecedented $\{Mo_9O_{30}(X)_2\}$ ($\equiv[(\mu_3\text{-}OH)_2Mo^V_4Mo^{VI}_5O_{28}[(CH_3COO)_{2/2}]_2]^{10-}$) moieties. According to BVS calculations, the following molybdenum centers are Mo^V: Mo(5), Mo(7), Mo(9), Mo(10), Mo(11), Mo(15), Mo(16), Mo(19), Mo(20) and Mo(27). Selected Mo–Mo distances: Mo(5)–Mo(9) 2.5974(18), Mo(5)–Mo(6) 3.2146(18), Mo(7)–Mo(27) 2.5816(18), Mo(10)–Mo(11) 2.5962(17), Mo(11)–Mo(14) 3.2185(17), Mo(14)–Mo(15) 3.2143(18), Mo(15)–Mo(16) 2.5933(18), Mo(19)–Mo(20) 2.5985(16), Mo(20)–Mo(21) 3.2096(17) Å.

DOI: 10.1039/b004948o

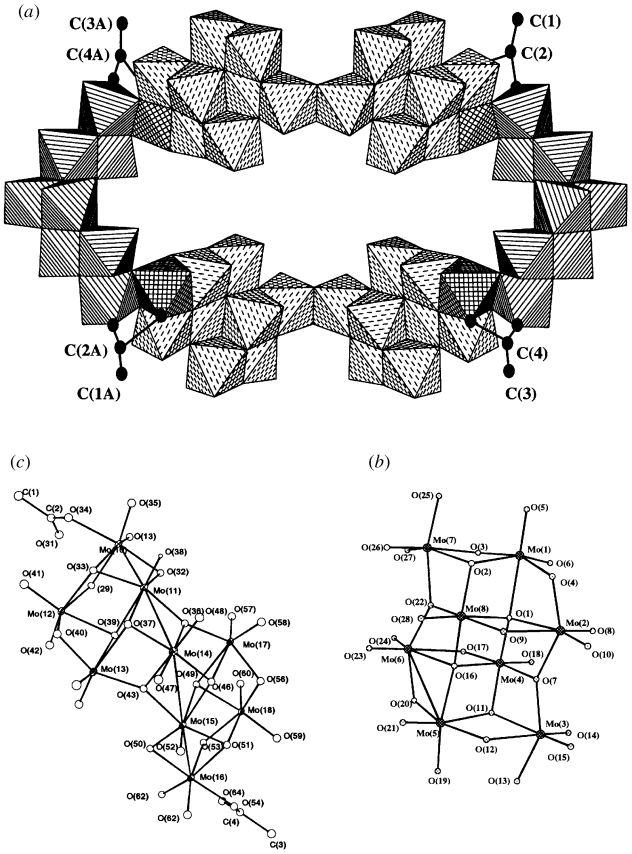

Fig. 2 (*a*) Polyhedral representation of **1a** (all encapsulated Na^+ cations are deleted for clarity). The linkage between two neighboring $\{Mo_8O_{28}\}$ moieties (having a pattern of dashed lines) is edge-shared, while that between $\{Mo_8O_{28}\}$ and $\{Mo_9O_{30}(X)_2\}$ units (marked with parallel lines) are corner-shared. $\{Mo^{V}O\}^{3+}$ units are cross-hatched; (*b*) the $\{Mo_8O_{28}\}$ unit in **1a**; (*c*) the $\{Mo_9O_{30}(X)_2\}$ (X=CH_3COO) moiety in **1a**.

bipyramid environments are held inside the 'host' nanoanion by linking to five *endo* oxygen atoms with Na–O distances of 2.264–3.010 Å. These encapsulated Na^+ cations are located near Mo atoms (Na(1)–Mo(10), 3.691, Na(2)–Mo(16), 3.697, and Na(3)–Mo(6), 3.989 Å), and may play an important template role in the formation of the crown-shaped anion **1a**.

The silent EPR spectrum of compound **1** indicates that the unpaired electrons of the two neighboring Mo^{V} atoms are completely coupled, which is consistent with structural analysis. The IR spectrum of **1** exhibits strong bands at 962 (s), 947 (s) and 901 (s) attributed to ν(Mo=O), and a series of characteristic bands for bridging acetate groups in the range 1550–1200 cm^{-1}.

The positions of OH^- and Mo^{V} sites are assigned on the basis of the *s* values, in which *s* is the bond strength derived from the expression $s = (R/1.882)^{-6.0}$ (R = Mo–O distances).[11] According to this procedure, the O(39), O(39A), O(49) and O(49A) ascribed to OH^- sites, have *s* values (0.9875–0.9927) are significant smaller than that of the others (1.5707–2.0930) which are normal for the O^{2-} sites.

In summary, a novel 54-member crown-shaped polyoxomolybdate has been synthesized and characterized crystallographically. It seems that there exists various building blocks in solution, and it is possible to link those building blocks to a variety of crown-shaped polyoxomolybdates. This has been confirmed recently by our preliminary experiments.

We thank the Chinese Academy of Sciences, the State Education Ministry and the State Personnel Ministry for financial support.

Notes and references

† *Synthesis of* **1**: to a solution of $Na_2MoO_4{\cdot}2H_2O$ (40 mmol, 9.68 g) and $CH_3COONa{\cdot}3H_2O$ (50 mmol) in H_2O (55 ml) acidified by 8.5 ml of 17% HCl (pH = 4.15), $NH_2NH_2{\cdot}2HCl$ (4.8 mmol, 0.5 g) was added under continuous stirring for 5 min. The resulting reaction mixture was then kept at room temperature in a wide-necked Erlenmeyer-flask for ten days (color changed from green to dark brown). Black–red columnar crystals of **1** were filtrated from the mother liquor, washed with cooled propan-2-ol, and finally dried in air (4.95 g, yield 59.54%). Anal. calcd. for $C_8H_{280}Mo_{54}Na_{32}O_{308}$: Mo, 46.16, Na, 6.56, C, 0.86, H, 2.51. Found: Mo, 46.62, Na, 6.59 (atomic absorption method), C, 0.79, H, 2.71% (determination was carried out on EA1110 (CHNS-0 CE instruments). Cerimetric titration was carried out to determine the number of Mo^{V} ($\sim 20 \pm 2$ electrons), which is consistent with the results of BVS calculations.

‡ Characteristic IR bands for **1** (KBr pellet, ν/cm^{-1}): 1630 (s, $\delta(H_2O)$), 1541 (s-m, ν_{as}(COO)), 1444 (m, ν_s(COO)), 962 (s), 947 (s), 901 (s) (ν(Mo=O)), 862(s), 721 (s), 727 (s), 494 (m): Characteristic FT-Raman bands (λ_e = 1064 nm, ν/cm^{-1}): 969 (vs), 940 (s), 927 (m), 912 (w) (ν(Mo=O)), 875 (w), 796 (w), 472 (m), 352 (m), 323 (m), 281 (m). Characteristic UV/VIS bands (λ/nm): 308.00 ($\varepsilon = 6.71 \times 10^4$ M^{-1} cm^{-1}) and 209.50 ($\varepsilon = 3.59 \times 10^5$ M^{-1} cm^{-1}).

§ *Crystal data*: $C_8H_{280}Mo_{54}Na_{32}O_{308}$, 11222.76, triclinic, $P\bar{1}$, a = 17.6814(6), b = 19.8620(7), c = 23.4663(8) Å, α = 90.0210(10), β = 102.6740(10), γ = 100.41°, V = 7902.0(5) $Å^3$ and Z = 1. The diffraction data were collected on a Simens SMART CCD diffractometer with graphite monochromated Mo-Kα radiation (λ = 0.71073 Å) at room temperature. A total of 41201 reflections (0.89 to 25.02°) were collected, of which 27539 independent reflections [R(int) = 0.0507] were used. The coordinates of molybdenum atoms were determined by direct methods, and the remaining non-hydrogen atoms were located and refined by a usual procedure of a combination of the difference Fourier synthesis and least-squares technique. All molybdenum atoms and partial other non-hydrogen atoms were refined with anisotropic thermal parameters giving rise to convergence with R_1 = 0.0718 and wR_2 = 0.1969 ($I > 2(I)$). CCDC182/1725. See http://www.rsc.org/suppdata/cc/b0/b004948o/ for crystallographic files in .cif format.

1 J. Fischer, L. Ricard and R. Weiss, *J. Am. Chem. Soc.*, 1976, **98**, 3050.
2 V. W. Day, *Nature*, 1991, **352**, 115.
3 A comprehensive review on the present studies of the field of polyoxometalates has been given in *Chem. Rev.*, 1998, **98**, P1-387.
4 A. Müller, H. Reuter and S. Dillinger, *Angew. Chem., Int. Ed. Engl.*, 1995, **34**, 2328.
5 V. W. Day, W. G. Klemperer and O. M. Yahi, *J. Am. Chem. Soc.*, 1989, **119**, 5959.
6 A. Müller, K. Hovemeier and R. Rohlfing, *Angew. Chem., Int. Ed. Engl.*, 1992, **31**, 1192.
7 Y.-N. Zhao, G.-S. Zhao, W. Liu, Y.-C. Zou and W.-Q. Pang, *Chem. Commun.*, 1999, 2219.
8 A. Müller, E. Krickemeyer, M. Penk, R. Holfing, A. Armatage and H. Bögge, *Angew. Chem., Int. Ed. Engl.*, 1991, **30**, 1674.
9 P. J. Hagrman, D. Hagrman and J. Zubieta, *Angew. Chem., Int. Ed.*, 1999, **98**, 2638.
10 R.-M. Xi, B. Wang, K. Isobe, T. Nishioka, K. Toriumi and Y. Ozawa, *Inorg. Chem.*, 1994, **33**, 833.
11 J. C. J. Bart and V. Ragaini, Proceedings of the Climax 3rd International Conference on the Chemistry and Uses of Molybdenum, ed. H. F. Barry and P. C. H. Mitchell, Climax Molybdenum Co. Ann Arbor, MI, USA, 1979.
12 E. M. McCarron III, J. F. Whitney and D. B. Chase, *Inorg. Chem.*, 1984, **23**, 3275.
13 R. D. Adams, *J. Chem. Soc., Chem. Commun.*, 1979, 256.
14 E. M. McCarron III and R. L. Harlow, *J. Am. Chem. Soc.*, 1983, **105**, 6179.

A new reagent for duplex DNA detection

Peter G. Sammes,* Louise Shek and David Watmore

Department of Chemistry, School of Physics and Chemistry, University of Surrey, Guildford, Surrey, UK GU2 7XH. E-mail: p.sammes@surrey.ac.uk

Received (in Cambridge, UK) 17th May 2000, Accepted 19th July 2000
Published on the Web 9th August 2000

The phenanthridinium-linked terbium complex [4Tb.5] serves as a novel probe for DNA duplexes.

In recent work[1] we have demonstrated a cooperative procedure for the detection of DNA sequences. In this procedure, the phenanthridinium group of the sensitiser **1** intercalates in the locality of the duplex DNA formed between a probe DNA strand, to which is attached an EDTA complexing group **2**, for a europium ion, and a target sequence of DNA. Under appropriate conditions, the sensitiser **1** can also bind to the europium complex of **2** to form a 1 : 1 : 1 complex [**2Eu.1**][2] that,

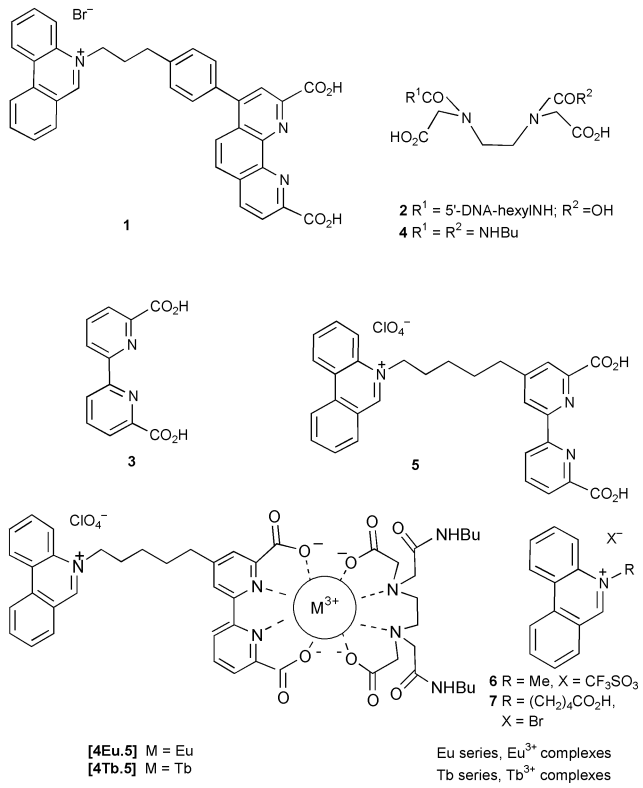

when irradiated, exhibits a strong luminescence signal from the europium ion. The system thus signals the presence of a target strand of DNA since, in its absence, the complex dissociates and only a very weak signal is observed.

In attempting to develop a two-colour signalling system suitable for discriminating between normal and point mutated target DNA strands, a sensitiser system was required that would work for both europium and a second luminescent lanthanide ion, such as terbium. Thus, for example, a 'normal' DNA sequence could be matched by a europium probe (red emission) and a mutated sequence by the corresponding terbium probe (green emission). The phenanthroline sensitiser, such as **1**, was not suitable for use with terbium, presumably because terbium requires a higher energy triplet sensitiser than europium.[3]

Examination of several alternative systems revealed that the 2,2′-dipyridyl-6,6′-dicarboxylic acid system, **3** is suitable, giving excitation of both europium and terbium chelated with EDTA bisbutylamide **4**, as complexes [**4Eu.3**] and [**4Tb.3**] respectively, although the optimal excitation wavelength with this system was shorter (λ_{ex} = *ca.* 320 nm) compared to that possible with the phenanthroline sensitiser **1** (λ_{ex} = 340 nm). In addition, luminescence intensities were temperature dependent and measurements were therefore conducted within a narrow ambient range (around 23 °C).

The dipyridyl dicarboxylic acid unit was then incorporated into the probe **5**.† Examination of the properties of this probe revealed that the complex with the Eu^{3+}·EDTA bisbutylamide, chelate [**4Eu.5**] exhibited a strong luminescence signal on irradiation at 318 nm (Table 1). However, on standing, the intensity of the luminescence dropped with time. After exploring several possible explanations for this fading of the signal it was discovered that the effect could be countered by the addition of a surfactant, such as the cationic CTAB (cetyl trimethylammonium bromide), whereupon a stable signal was observed. Independent experiments showed that the complex [**4Eu.5**] has a strong tendency to adhere to the surface of the cuvette, thus removing it from solution.

The corresponding Tb^{3+} complex, [**4Tb.5**], only exhibited a very weak signal (Table 1), which was not enhanced by the addition of CTAB. This inefficiency with the terbium complex is in contrast with the behaviour of the simpler complexes described above, *e.g.* [**4Tb.3**], and is ascribed to an intramolecular quenching process from the attached phenanthridinium group. Since only the terbium complex was affected but not the europium complex, this quenching process was not of the sensitising dipyridyl species, common to both systems, but of the excited lanthanide ion.

It is known[4] that the triplet level of the phenanthridinium group (*ca.* 21 300 cm^{-1}) is near in energy to that of the excited $^5D_4$ state of the terbium ion (*ca.* 20 500 cm^{-1}) and is capable of quenching the latter. In order to confirm this triplet quenching mechanism an experiment involving the intermolecular quenching of the terbium complex [**4Tb.3**] with the phenanthridinium salts **6** and **7** was carried out. The results followed Stern–Volmer plots (Fig. 1). Of note was the observation that the carboxylic acid derivative **7** was a less efficient quencher than the *N*-methyl salt **6**. Presumably, electrostatic effects play a part

Table 1 Luminescence signals for various chelates

Ln^{3+}	Complex	I_{max}[a]	Notes
Eu^{3+}	[**4Eu.3**]	500	
Tb^{3+}	[**4Tb.3**]	350	
Eu^{3+}	[**4Eu.5**]	170[b]	
Eu^{3+}	[**4Eu.5**]	150	calf thymus DNA added[c]
Tb^{3+}	[**4Tb.5**]	1	
Tb^{3+}	[**4Tb.5**]	300	calf thymus DNA added[c]
Tb^{3+}	[**4Tb.5**]	210	SDS added[d]

[a] I_{max} in arbitrary units. Measurements all with same instrument settings using a PE LS50B spectrofluorimeter; slit widths 10 nm; delay time 0.1 ms; gate time 1.0 s. Measurements at 23 °C, pH 7.5 in buffer; complex concentrations at 1×10^{-6} mol dm^{-3}. For Eu^{3+} I_{max} for the band at *ca.* 614 nm was measured; for Tb^{3+} I_{max} for the emission at *ca.* 545 nm was measured. [b] Initial intensity in the absence of CTAB. [c] Intensity measured at a ratio of DNA base pair : complex of > 10 : 1. [d] Intensity measured at a concentration of SDS of 2×10^{-4} mol dm^{-3}.

DOI: 10.1039/b003970p

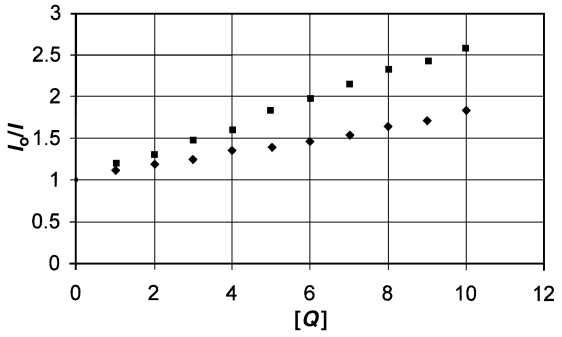

Fig. 1 Stern–Volmer plots: Tb^{3+} signal at λ_{em} = 545 nm, delay time 0.1 ms; [**4Tb.3**] at 1×10^{-6} mol dm^{-3}, buffered at pH 7.5 at 23 °C; ◆ addition of **6** as quencher; ■ addition of **7** as quencher; no degassing. [Q] in molar equivalents of quencher to complex.

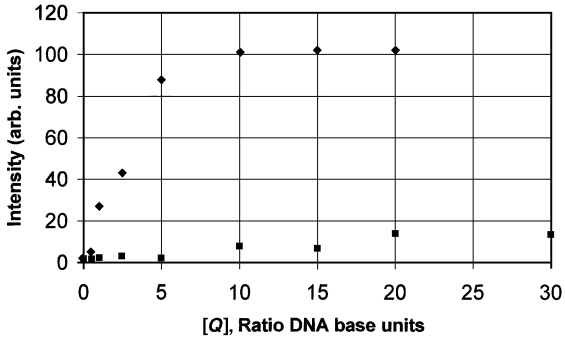

Fig. 2 Enhancement of Tb^{3+} signal at λ_{em} = 545 nm, delay time 0.1 ms; [**4Tb.5**] at 1×10^{-6} mol dm^{-3}, buffered at pH 7.5 at 23 °C; ◆ addition of calf thymus duplex DNA; ■ addition of synthetic 15-mer DNA single strand oligomer. [Q] in molar DNA base equivalents to the probe.

and the latter, net positively charged species, can approach the net negatively charged complex [**4Tb.3**] more easily than the former, which is net neutral under the quenching conditions utilised.

The possible involvement of oxygen, as a known quenching agent for the excited phenanthridinium species[5] was also examined but deoxygenation of the system by a number of freeze–thaw cycles had little effect on the overall levels of emission from the europium [**4Eu.5**] complex, whilst, as anticipated there was a small increase for the terbium [**4Tb.5**] complex. This indicates that, although the *N*-substituted phenanthridinium species can act as a sensitiser for the terbium ions, under our conditions the dominant sensitiser is the dipyridyl chromophore, the phenanthridinium ion acting as a net triplet energy sink.

Triplet quenching requires close contact of the interacting species in order to operate. Quenching would not be expected to occur if the terbium ion could be held apart from the phenanthridinium unit. Since the phenanthridinium ion has a propensity to intercalate with duplex DNA,[6] it was of interest to test whether or not quenching was observed in the presence of such DNA. Thus to a solution of the terbium complex [**4Tb.5**] in HEPES buffer, was added a solution of duplex DNA (calf thymus); the onset of the terbium signal appeared within seconds and approached a maximum at DNA base to complex concentration ratios > 10 : 1 (Fig. 2). Thus intercalation of the phenanthridinium group is sufficient to prevent its intramolecular approach to the complexed terbium ion. In contrast, the luminescent properties of the corresponding europium complex, [**4Eu.5**] were only slightly altered by the addition of calf thymus DNA, a slight reduction in the europium emission being observed. In both cases no substantial changes in the patterns of lanthanide emissions were observed upon the addition of the DNA.

Further experiments have shown that these effects could be reproduced using synthetic DNA hybrids. Addition of the complex [**4Tb.5**] to single stranded DNA showed only a small increase in the terbium signal (Fig. 2).

The triggering of the terbium signal thus serves as a useful 'switch' for the detection of duplex DNA in solution and complements the behaviour of the dipyridophenazine–ruthenium complexes described by Barton *et al.*[7]

Since we believe the onset of the terbium signal was caused by a physical barrier to approach of the phenanthridinium ion to the chelated terbium species and hence quenching, we subsequently tried use of the anionic surfactant, SDS (sodium dodecyl sulfate). No effect was observed at low concentrations but at molar equivalents > 10 : 1 SDS: [**4Tb.5**] a typical terbium emission signal appeared, reaching a maximum at molar concentrations > 100 : 1. We ascribe this to a micellar effect, the phenanthridinium group being surrounded by SDS molecules as micellation occurs thus effectively restricting approach by these groups to the hydrophilic and net anionic, dipyridyl lanthanide segment of the complex. Thus the complex [**4Tb.5**] can also act as a probe for anionic micellation.

We thank the EPSRC and the BBSRC for support of this work.

Notes and references

† All new compounds were characterised with supporting microanalytical and/or accurate mass measurements.

1 J. Coates, P. G. Sammes, G. Yahioglu, R. M. West and A. J. Garman, *J. Chem. Soc., Chem. Commun.*, 1994, 2311; J. Coates, P. G. Sammes and R. M. West, *J. Chem. Soc., Chem. Commun.*, 1995, 1107.
2 J. Coates, P. G. Sammes and R. M. West, *J. Chem. Soc., Perkin Trans. 2*, 1996, 1277; J. Coates, P. G. Sammes and R. M. West, *J. Chem. Soc., Perkin Trans. 2*, 1996, 1283.
3 E. Soini and T. Lövgren, *CRC Crit. Rev. Anal. Chem.*, 1987, **18**, 105; *Handbook on the Physics and Chemistry of Rare Earths*, ed. K. Schneider and L. Eyring, North-Holland, Amsterdam, 1979.
4 D. Parker, P. K. Senanayake and J. A. G. Williams, *J. Chem. Soc., Perkin Trans. 2*, 1998, 2129.
5 D. Parker and J. A. G. Williams, *Chem. Commun.*, 1998, 245.
6 H. W. Zimmerman, *Angew. Chem., Int. Ed. Engl.*, 1986, **25**, 115.
7 J. K. Barton and Y. Jenkins, *J. Am. Chem. Soc.*, 1992, **114**, 8736; J. K. Barton and R. M. Hartshorn, *J. Am. Chem. Soc.*,1992, **114**, 5919.

Electronic properties of metal nanorods probed by surface-enhanced Raman spectroscopy

Jian-Lin Yao,[a] Xin Xu,[a] De-Yin Wu,[a] Yong Xie,[a] Bin Ren,[a] Zhong-Qun Tian*[a] Gu-Ping Pan,[b] Dong-Mei Sun[b] and Kuan-Hong Xue*[b]

[a] *State Key Laboratory for Physical Chemistry of Solid Surfaces and Institute of Physical Chemistry, Xiamen University, Xiamen 361005, China. E-mail: zqtian@xmu.edu.cn*
[b] *Department of Chemistry, Nanjing Normal University, Nanjing 210097, China*

Received (in Cambridge, UK) 5th April 2000, Accepted 21st July 2000
Published on the Web 9th August 2000

Applying the probe molecule strategy, surface-enhanced Raman spectroscopy has been used, for the first time, as a diagnostic tool of the electronic properties of metal nanorods; the vibrational frequency of the probe molecule SCN^- at Cu nanorods is shown to critically depend on the nanorod's diameter in the range from 50 to 15 nm; the upshifting of the Fermi level with a decrease of the nanorod's diameter is interpreted based on the change of cohesive energy owing to the high ratio of surface to bulk atoms.

Metal nano-rods (-wires) have aroused tremendous interest recently because of their novel properties and potential applications in a wide variety of fields.[1–5] So far many techniques have been employed to characterize the novel optical, electronic and magnetic properties of such materials.[2–5] UV–VIS absorption and fluorescence spectroscopies are two of the most widely used methods.[3–5] Raman spectroscopy has, however, only been applied to characterize semiconductor nanowires and carbon nanotubes.[6–9] Important and meaningful information can be obtained in these cases, as some forbidden Raman modes in the bulk materials become Raman active.[6,7] Raman spectroscopic study on metal nanowires can only detect the mechanical vibration bands (also denoted inelastic Mie scattering or acoustic modes) located in the extremely low frequency region (typically 2–10 cm^{-1}).[10] Consequently, an alternative way has to be established to study metal nano-wires (-rods) with Raman spectroscopy.

It is well known that for a molecule which interacts strongly with a surface, its vibrational band frequency and shape are very sensitive to the electronic property, the chemical environment and the morphology of the surface. Hence Raman spectroscopy has long been used to analyze the atomic structures and the electronic properties of surfaces indirectly through assessing carefully the spectral changes of the adsorbate, the so called probe molecule.[11] On that account, it is of great interest to diagnose the electronic structures of metal nanorods *via* the vibrational spectrum of a probe molecule. In the present work, surface-enhanced Raman spectroscopy (SERS) has been used because of its extremely high sensitivity in characterizing the surface species on metals. In order to examine the changes in the electronic properties of nanorods by analysis of the spectral changes of the probe molecule, a typical SERS system of SCN^-/Cu was employed in the present study. SERS measurements were performed on a confocal microprobe Raman system (LabRam I).[12]

The arrays of Cu nanorods were fabricated using anodic aluminum oxide (AAO) templates as described in ref. 13. By controlling the electrochemical conditions during AAO formation and/or metal deposition processes, one can prepare nanorod arrays with different diameters from *ca.* 15 to 70 nm. As the SERS intensity depends critically on the nanorods' length exposed at the surface,[14] the length was varied between several tens to several thousands of nanometers, which was controlled by chemically etching off the AAO template to the desired extent in an aqueous solution of phosphoric acid or sodium hydroxide. SERS intensities from these ordered nanorod arrays are higher than those from the electrochemically or chemically roughened electrodes even with the best surface preparation.[14]

Fig. 1 shows the wavenumber–diameter profile of SCN^- adsorbed at Cu nanorod arrays with lengths of *ca.* 100 nm but with variation of the diameter from 15 to 70 nm. The vibrational frequency of ν_{CN} is shown to critically depend on the nanorods' diameter when the diameter is < 50 nm. It is essential to compare this interesting vibrational property to that of a normal Cu electrode in the same solution. The wavenumber–potential profile of SCN^- adsorbed at an electrochemically roughened Cu electrode is also displayed in Fig. 1. The wavenumber shows a linear downshift as the applied electrode potential is made more negative, showing a similar trend to the size effect of decreasing the diameters of the metal nanorods. It can be seen that the effect on the wavenumber upon changing the diameter from 50 to 15 nm is equivalent to that of decreasing the applied potential by *ca.* 200 mV. Similar results have also been obtained from Au and Ag nanorods. Therefore, it is of importance to reveal the reason for the wavenumber–size dependence of the metal nanorods.

The Fermi energy level is well known as one of the most important parameters, with which to characterize a metal. The Fermi level determines many of the gross electronic properties that could consequently influence the intermolecular bonding and the relevant vibrational frequency of an adsorbate. The more negative the applied electrode potential, the more upshifted the Fermi level, and so the greater tendency to supply electrons from the electrode to the adsorbate. This leads to a down-shift of ν_{CN} as found for SCN^-/Ag.[15] It is well known that if a bulk metal is cut into very small pieces whose characteristic size is about or smaller than the electron mean free path, many physical properties will be changed substantially.[1,2] At present, we think the surface effect and small

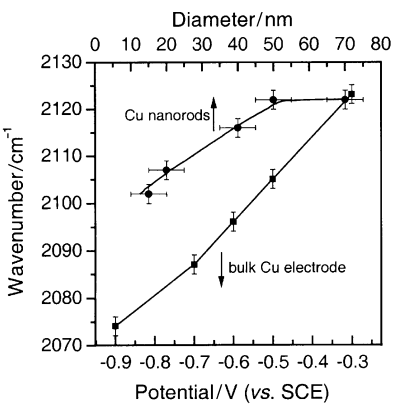

Fig. 1 The wavenumber–diameter profile of SCN^- adsorbed at Cu nanorod arrays and the wavenumber–potential profile of SCN^- adsorbed at a bulk Cu electrode.

DOI: 10.1039/b002717k

size effect may play an important role on the considerable change of the Fermi energy.

The Fermi level of a metal nanorod can be estimated in a simple way by considering free electrons confined to a cylindrical rod of length l and radius r. The energy level in atomic units is given by:

$$E = \frac{n^2\pi^2}{l^2} + \frac{C_m^2}{r^2} \qquad n = 1, 2, 3, \ldots; m = 0, \pm 2, \ldots$$

where C_m is a parameter determined by the Bessel function. This equation indicates, at least qualitatively, that the Fermi level of a metal nanorod would increase as the diameter decreases. Since the present study on the Cu nanorods was performed in electrolyte solution, the electrode potential should be calculated under open circuit conditions, where E_{op} corresponds to the Fermi level of a metal nanorod (M_{solid}) in solution. In general, several factors affect the value of E_{op}. These are (i) sublimation of a solid metal, (ii) ionization of a gaseous metal atom, (iii) hydration of a gaseous ion, (iv) hydration of n gaseous electrons; which could be best considered in a Born–Haber type of cycle (Scheme 1).

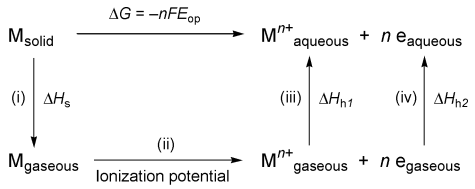

Scheme 1

For a set of nanorods of the same metal with different diameters, the energy changes for processes of (ii)–(iv) are all the same. Therefore, the differences of the electrode potential E_{op} of a set of nanorods should depend only on the differences of the sublimation energies, ΔH_s. The value of ΔH_s is related directly to the cohesive energy, which is determined by the metal–metal bonding. It is reasonable to assume that the metal–metal bonds are the same in the bulk phase for all the nanorods studied here. However, one has to consider the fact that a surface atom possesses a lower coordinate number as compared to a bulk atom. This implies that the change of the cohesive energy might depend substantially on the ratio of the surface atoms to bulk atoms for nanorods of different size. Based on this, we have carried out the relevant calculations on the potential difference ΔE of a set of nanorods with respect to the bulk electrode potential. Fig. 2 shows the dependence of the potential difference on the diameter ($d = 2r$) of the Cu nanorods. It is clearly seen that the potential difference significantly depends on the nanorod's diameter when the diameter is < 50 nm, and small nanorods show a larger potential difference, indicating an up-shift of the Fermi level. This trend is in general agreement with our experimental results. If we consider the additional influence of the sublayer atoms, the calculated values are even closer to the experimental data. Although more sophistical theoretical investigation on this aspect is required, it has shown that Raman spectroscopy can be developed into a diagnostic tool for measuring the electronic properties of metal nanorods by applying the probe molecule strategy.

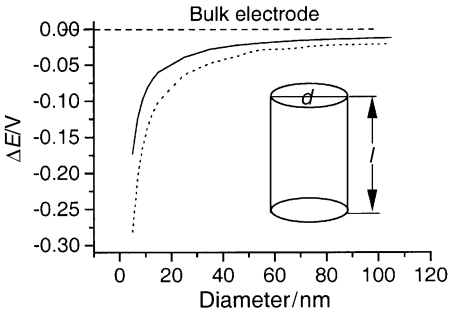

Fig. 2 Dependence with diameter of the difference potential of Cu nanorods ($l \approx 100$ nm) with respect to the bulk Cu electrode after consideration of the surface effect (—) and surface and subsurface effect (····), see text.

We gratefully acknowledge the financial support from the Natural Science Foundation of China and the Ministry of Education of China. We also sincerely thank D. M. Huang for stimulating discussion.

Notes and references

1 C. R. Martin, *Science*, 1994, **266**, 1961.
2 J. C. Hulteen and C. R. Martin, in *Nanoparticles and Nanostructured Films*, ed. J. H. Fendler, Wiley-VCH, Weinheim, 1998, ch. 10.
3 S. Link, M. B. Mohamed and M. A. Elsayed, *J. Phys. Chem. B*, 1999, **103**, 3073.
4 C. K. Preston and M. Moskovits, *J. Phys. Chem.*, 1988, **92**, 2957.
5 N. A. F. Al-Rawashdeh, M. L. Sandrock, C. J. Seudling and C. A. Foss, *J. Phys. Chem. B*, 1998, **102**, 361.
6 D. Routkevitch, T. L. Haslett, L. Ryan, T. Bigioni, C. Douketis and M. Moskovits, *Chem. Phys.*, 1996, **210**, 343.
7 B. B. Li, D. P. Yu and S. L. Zhang, *Phys. Rev. B*, 1999, **59**, 1645.
8 A. M. Rao, P. C. Eklund, S. Bandow, A. Thess and R. E. Smalley, *Nature*, 1997, **388**, 257.
9 H. Hiura, T. W. Ebbesen, K. Tanigaki and H. Takahashi, *Chem. Phys. Lett.*, 1993, **202**, 509.
10 D. A. Weitz, T. J. Gramila, A. Z. Genack and J. I. Gersten, *Phys. Rev. Lett.*, 1980, **45**, 355.
11 V. M. Browne, S. G. Fox and P. Hollins, *Catal. Today*, 1991, **9**, 1.
12 Z. Q. Tian, B. Ren and B. W. Mao, *J. Phys. Chem. B*, 1997, **101**, 1338.
13 S. Shingubara, O. Okino, Y. Sayama, H. Sakaue and T. Tanahagi, *Jpn. J. Appl. Phys.*, 1997 **36**, 7791.
14 J. L. Yao, K. H. Xue, B. Ren and Z. Q. Tian, to be submitted.
15 Z. Q. Tian, W. H. Li, Z. H. Qiao, W. F. Lin and Z. W. Tian, *Russian J. Electrochem.*, 1995, **31**, 1014.

ChemComm

Alcohol induced stereospecific P–C bond cleavage to afford Ru–phenyl derivatives containing three different types of stereogenicity: novel and unprecedented complexes of P(OH)(OR)Ph

Tilmann J. Geldbach, Daniela Drago and Paul S. Pregosin*

Laboratory of Inorganic Chemistry, ETHZ, Universitätstr. 6, CH-8092 Zurich, Switzerland.
E-mail: pregosin@inorg.chem.ethz.ch

Received (in Basel, Switzerland) 31st May 2000, Accepted 19th July 2000
Published on the Web 10th August 2000

Alcohol induced stereospecific P–C bond cleavage in a Ru–P(OH)Ph_2 fragment affords new chiral-Binap and MeO-Biphep based complexes containing three different forms of stereogenicity: ligand atropisomerism plus stereogenic Ru and P atoms; these represent the first reported transition metal complexes of the ligands P(OH)(OR)Ph.

The atropisomeric chelating phosphines, Binap **1** and MeO-Biphep **2** are well known to be excellent chiral auxiliaries

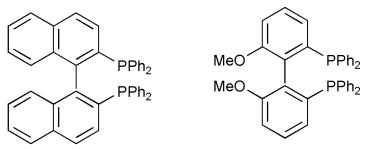

1 **2**

though there is relatively little known with respect to their Ru-organometallic chemistry.[1–5]

It is now known[6,7] that both of these bidentate ligands are capable of acting as six-electron donors to Ru(II), in that one of the biaryl double bonds, immediately adjacent to one of the two P-donors, can complex the metal, *e.g.* **3** and **4**.

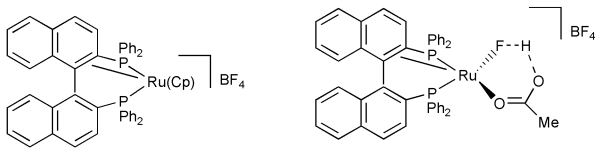

3 **4**

Once the proximate double bond complexes to Ru(II), it is relatively easy to cleave a P–C bond,[7] with the metal attaining an 18e configuration by sliding from the η^2 mode to the η^6 arene form, *e.g.* complex **6** of eqn. (1).

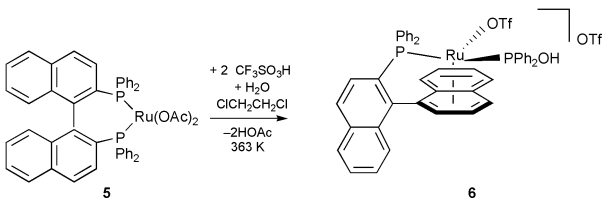

5 **6** (1)

We report here an extension of the chemistry of eqn. (1) in which compound **6** reacts with aliphatic alcohols to afford the Ru–phenyl products, **7** [eqn. (2)]. These arise from a stereospecific P–C bond splitting and P–O bond making reaction of the P(OH)Ph_2 ligand to afford P(OH)(OR)Ph complexes.

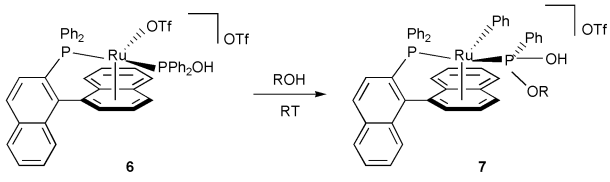

6 **7** (2)

a, R = Me, **b** R = Et, **c** R = Pr^i

The Binap complexes **7** and the MeO-Biphep analogues **8** have been prepared using MeOH, EtOH and Pr^{i}OH, by simply stirring the starting materials **6** in the appropriate alcohol[8] [eqn. (2)] The new phenyl complexes **7** and **8** are unique in that (a) they are produced in only *one* diastereomeric form, *i.e.* the phenyl migration and P–O bond formation are specific, (b) they contain *three* different forms of stereogenicity: atropisomerism, from the biaryl moiety,[9] a chiral transition metal and the newly formed stereogenic P atom and (c) these are the first reported transition metal complexes of the ligands P(OH)(OR)Ph. We know of only one example in which a marginally related species arises through P–C bond protonation, *i.e.* a Mo–P(OH)PhMe moiety can be formed by protonation of one of the two P–C phenyl bonds of a $PMePh_2$.[10] In this chemistry the $PMePh_2$ is complexed as an η^6-arene and not as a tertiary phosphine.

In solution the formation of **7a** from **6** is conveniently followed by ^{31}P NMR spectroscopy in that the disappearance of the signal for the complexed P(OH)Ph_2 ligand of **6**, δ = 114.5, is accompanied by the appearance of a new signal for the Ru–P(OH)(OMe)Ph moiety at δ = 144.7. The presence of the new P(OR) fragment was confirmed by a ^{31}P–^{1}H-correlation, *e.g.* see Fig. 1 for the ethanol analogue **7b**. This NMR spectrum shows cross-peaks for the P(OH), at high frequency, and the two non-equivalent (diastereotopic) methylene protons as multiplets (one of which is almost completely covered by the OCH_2 of the solvent, THF-d_8) all correlated to the new ^{31}P signal at δ 142.4. In addition cross-peaks are observed from the *ortho* (intense) and *meta* (weaker) P–phenyl aromatic protons. The *ipso* ^{13}C resonance of the new η^1 phenyl ligand is found at δ 150.3.

The solid-state structure of the Binap Pr^{i}OH analog **7c**, was determined by X-ray diffraction methods (Fig. 2).[12] The immediate coordination sphere consists of the two phosphorus atoms, the π-arene and the η^1-phenyl ligand. Whereas four of the Ru–C(arene) separations are normal,[11] the remaining two distances, from the bridgehead carbons C2 and C3, are quite long (see **9**) and suggest little or no bonding to the metal. Selected bond lengths and bond angles are given in the caption to Fig. 2.[13]

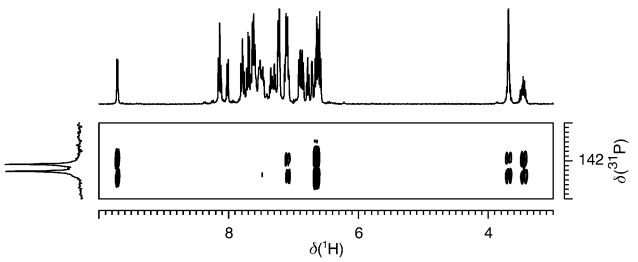

Fig. 1 Slice through the ^{31}P–^{1}H correlation (δ 142.4) showing the cross-peaks arising from the hydroxy P(OH), at high frequency, and the two non-equivalent methylene protons of the EtO moiety as multiplets (one of which is almost completely covered by the OCH_2 of the solvent, THF-d_8). There are also cross-peaks from the *ortho* and *meta* protons of the remaining P–phenyl ring.

DOI: 10.1039/b004385k

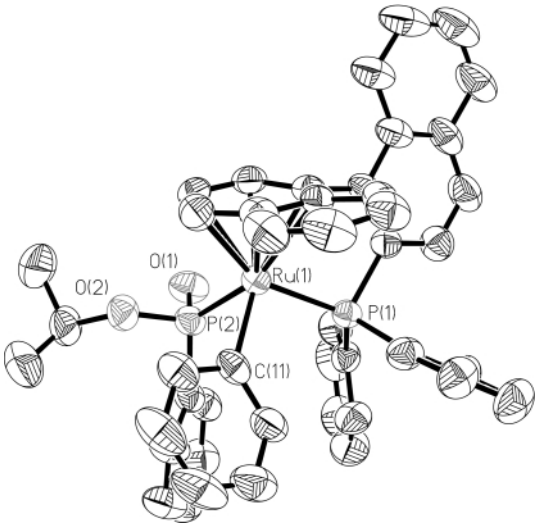

Fig 2 ORTEP view of the cation of **7c**. Selected bond lengths (Å) and angles (°): Ru–C(11), 2.105(6), Ru–P1 2.3074(16), Ru–P2 2.2507(16), Ru–C1 2.221(6), Ru–C2 2.430(5), Ru–C3 2.411(6), Ru–C4 2.275(6), Ru–C5 2.258(6), Ru–C6 2.268(6), C11–Ru–P1 97.14(18), C11–Ru–P2 81.30(16), P1–Ru–P2 98.09(6).

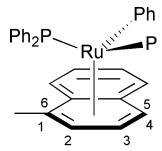

fragment **9**
Ru-C2 2.433(7) Å, Ru-C3 2.419(8) Å

Complexes **7** and **8** are relatively reactive and offer unique opportunities for studying the stereospecificity of subsequent reactions. Details of this chemistry are in preparation.

P. S. P. thanks the Swiss National Science Foundation, and the ETH Zurich for financial support. We also thank Johnson Matthey for the loan of $RuCl_3$ and F. Hoffmann La Roche, Basel, for MeO-Biphep ligands.

Notes and references

1 R. Noyori, *Asymmetric Catalysis in Organic Synthesis*, John Wiley and Sons, Inc. 1994; H. Kumobayashi, *Rec. Trav. Chim. Pays-Bas*, 1996, **115**, 201.

2 R. Schmid, E. A. Broger, M. Cereghetti, Y. Crameri, J. Foricher, M. Lalonde, R. K. Mueller, M. Scalone, G. Schoettel and U. Zutter, *Pure Appl. Chem.*, 1996, **68**, 131; Y. Crameri, J. Foricher, U. Hengartner, C. Jenny, F. Kienzle, H. Ramuz, M. Scalone, M. Schlageter, R. Schmid and S. Wang, *Chimia*, 1997, **51**, 303.

3 J. Wiles and S. H. Bergens, *Organometallics*, 1999, **18**, 3709; J. Wiles and S. H. Bergens, *Organometallics*, 1998, **17**, 2228.

4 A. Mezzetti, A. Tschumper and G. Consiglio, *J. Chem. Soc., Dalton Trans.*, 1995, 49.

5 J. Wiles and S. H. Bergens, *J. Am. Chem. Soc.*, 1997, **119**, 2940.

6 D. D. Pathak, H. Adams, N. A. Bailey, P. J. King and C. White, *J. Organomet. Chem.*, 1994, **479**, 237.

7 N. Feiken, P. S. Pregosin and G. Trabesinger, *Organometallics*, 1997, **16**, 5756; N. Feiken, P. S. Pregosin, G. Trabesinger and M. Scalone, *Organometallics*, 1997, **16**, 537; C. den Reijer, M. Woerle and P. S. Pregosin, *Organometallics*, 2000, **19**, 309.

8 Binap complex **6** (54 mg, 0.052 mmol) was dissolved in 12 ml MeOH and the solution stirred at room temperature for 30 min. The solvent was removed *in vacuo* and the remaining residue washed three times with diethyl ether. Product **7a** is obtained as an orange–yellow solid. Yield: 46 mg (96%). ^{1}H NMR (d^8-thf, 400 MHz): δ 9.64 (d, $^2J_{PH}$ 8.1 Hz, 1H, OH), 8.15 (d, $^3J_{HH}$ 7.5 Hz, 1H), 8.13 (d, $^3J_{HH}$ 8.1 Hz, 1H), 8.02 (d, $^3J_{HH}$ 8.53 Hz, 1H). 7.86 (d, $^3J_{HH}$ 8.4 Hz, 1H), 7.77 (m, 1H), 7.73 (t, $^3J_{HH}$ 7.7 Hz, 1H), 7.69 (m, 1H), 7.67 (m, 1H), 7.64 (m, 1H), 7.63 (m, 2H), 7.55 (m, 2H), 7.37 (m, 1H), 7.35 (m, 2H), 7.28 (d, $^3J_{HH}$ 7.6 Hz), 7.24 (t, $^3J_{HH}$ 7.8 Hz, 1H), 7.15 (m, 2H), 7,11 (m, 2H), 6.90 (m, 2H), 6.89 (d, $^3J_{HH}$ 5.5 Hz, 1H), 6.79 (t, $^3J_{HH}$ 7.1 Hz, 1H), 6.75 (m, 1H), 6.71 (m, 2H), 6.62 (m, 2H), 6.60 (d, $^3J_{HH}$ 7.9 Hz), 3.68 (d, $^3J_{PH}$ 11.9 Hz, 3H, CH_3). ^{13}C NMR (d^8-thf, 100 MHz): δ 150.3, 148.5, 147.3 (d, $^2J_{CP}$ 5.1 Hz), 140.9, 137.9, 135.6 (d, $^2J_{CP}$ 11.0 Hz), 134.8, 134.7, 133.9, 131.4, 131.0, 130.9, 130.8 (d, $^3J_{CP}$ 10.6 Hz), 130.6, 130.5, 129.4, 129.0, 128.6, 128.5, 127.9 (d, $^2J_{CP}$ 10.1 Hz), 127.7, 126.6, 126.1, 123.1, 117.8, 116.2, 106.8, 101.1 (d, $^3J_{CP}$ 5.4 Hz), 93.5, 91.6 (d, $^3J_{CP}$ 9.1 Hz), 53.6 (d, $^2J_{CP}$ 13.0 Hz). ^{19}F NMR (d^8-thf, 282 MHz): δ −78.17. ^{31}P NMR (d^8-thf, 162 MHz): δ 144.7 (d, $^2J_{PP}$ 61.2 Hz), 60.3 (d, $^2J_{PP}$ 61.2 Hz). MS (FAB): 773.0 (M^+), 695.0 (M^+ − Ph), 539.0 [M^+ − PPh(OH)(OMe) − Ph; 100%]. Elemental analysis: $C_{46}H_{37}F_3O_5P_2RuS{\cdot}H_2O$. Calc.: C, 58.78; H, 4.19. Found: C, 58.66; H, 4.78%.

9 Only one diastereomer is observed starting from optically pure (*R*)-MeO-Biphep. Interestingly the same diastereomer is observed starting from racemic MeO-Biphep (based on ^{31}P NMR results). This implies that a mixture containing *e.g.*, (*R*,*S*,*R*) and (*S*,*R*,*S*) [or (*R*,*R*,*R* and (*S*,*S*,*S*)] is present.

10 R. H. Morris, J. F. Sawer, C. T. Schweitzer and A. Sella, *Organometallics*, 1989, **8**, 2099.

11 A. G. Orpen, L. Brammer, F. H. Allen, O. Kennard, D. G. Watson and R. Taylor, *J. Chem. Soc., Dalton Trans.*, 1989, S1.

12 *Crystal data* for **7c**: $C_{60}H_{41}F_3O_5P_2RuS$, M = 1094.00, monoclinic, space group $P2_1/n$, a = 11.415(2), b = 35.057(5), c = 13.524(2) Å, β = 100.54°, V = 5320.7(14) Å^3, Z = 4, D_c = 1.381 Mg m^{-3}, μ = 0.453 mm^{-1}, F(000) = 2232, Crystal size = 0.54 × 0.40 × 0.32 mm. Data were collected on a Siemens SMART platform diffractometer equipped with a CCD detector using graphite monochromated Mo-Kα radiation (λ = 0.71069 Å). Total number of reflections was 33233 of which 10942 were independent. The structure was solved by direct methods and refined on F^2, $R1$ = 0.0772, $wR2$ = 0.1751. The CF_3SO_3 molecule is disordered and was refined as a rigid group. Further, two molecules of disordered benzene solvent were found and refined in two different orientations. CCDC 182/1723.

13 There is no doubt as to the structure of the molecule; however, owing to disorder in several molecules of benzene, which co-crystallise, and some disorder in the triflate anion, the *R* factor is rather large. This does not interfere with a reasonable determination of the various Ru–(ligand atom) bond lengths.

The synthesis and characterization of an efficient green electroluminescent conjugated polymer: poly[2,7-bis(4-hexylthienyl)-9,9-dihexylfluorene]

Jian Pei,[a] Wang-Lin Yu,[a] Wei Huang[a]* and Alan J. Heeger[b]

[a] *Institute of Materials Research and Engineering, National University of Singapore, 3 Research Link, Singapore 117602, Republic of Singapore. E-mail: wei.huang@imre.org.sg*

[b] *Institute for Polymers and Organic Solids, University of California at Santa Barbara, CA 93106-5090, USA*

Received (in Cambridge, UK) 9th June 2000, Accepted 19th July 2000
Published on the Web 9th August 2000

A novel soluble electroluminescent (EL) material, poly[(4-hexylthiophene-2,5-diyl)(9,9-dihexyl-9*H*-fluoren-2,7-ylene)(4-hexylthiophene-2,5-diyl)] (PHTDHFHT), with high absolute photoluminescence (PL) quantum efficiency (32 ± 3%) compared with other polythiophene derivatives, was synthesized and a green EL is observed.

During the past decade, design and synthesis of novel conjugated polymers as low-cost materials with high potential for electronic and optoelectronic applications have received considerable attention.[1–3] The development of novel highly efficient materials that emit primary color lights is particularly attractive due to the requirement for full-color displays. Among conjugated polymers, polythiophene (PT) and its processable derivatives are an important class of representatives as electrically conductive and optoelectronic materials because of their high electrical conductivity and environmental and thermal stability in both neutral and doped states, as well as their interesting electronic and optical properties.[4–6] However, the low PL quantum efficiency of PTs in solid films, typically 1–3%, has limited the application of PTs in polymer light-emitting diodes (PLEDs).[7] In our previous reports, a significant increase in PL efficiency of PTs by modifying the backbone structure with phenylene groups was demonstrated.[8,9] Recent progress made in our group demonstrates that 9,9-disubstituted polyfluorene copolymers with arylene groups, such as a phenylene ring, may exhibit relatively high PL and EL efficiencies as well as good EL performances.[10,11] Here we present a novel conjugated polymer, PHTDHFHT, in which thiophene moieties are introduced into the backbone of poly(9,9-dihexyl-9*H*-fluoren-2,7-ylene) in place of phenylene units. The resultant polymer emits green PL and EL with high quantum efficiencies.

The synthetic approach towards PHTDHFHT is outlined in Scheme 1. Compound **2** is synthesized through the coupling reaction between thienylzinc chloride and 2,7-dibromo-9,9-dihexylfluorene catalyzed by $Pd(PPh_3)_4$ in a high yield (89%). The bromination of compound **2** with NBS produces monomer **3**, 2,7-bis(5-bromo-4-hexylthienyl)-9,9-dihexyl-9*H*-fluorene. The polymer, PHTDHFHT, was obtained through a nickel-catalyzed reductive polymerization. Usually the preparation of PFs and PTs can also employ direct oxidative polymerization using ferric chloride as an oxidant. It was found that residual iron in the polymers was difficult to remove completely, which could affect the performance of devices.[12] Metal-catalyzed coupling reactions of dihalo compounds in place of the oxidative polymerization by ferric chloride was employed in our synthesis. The reductive polymerization also avoids irregular coupling or branching that easily happens in conventional electrochemical and oxidative polymerization. After careful purification,† the polymer was obtained as a light-yellow solid in a yield of 60%.

PHTDHFHT is highly soluble in common organic solvents, *e.g.*, THF, toluene, xylene, and $CHCl_3$. Uniform and transparent films on substrates, such as ITO-coated glasses and microslides, can be obtained by spin-casting the solutions. The molecular structure and purity of the polymer are verified by ^1H and ^{13}C NMR, FT-IR, and elemental analysis.‡ The molecular weights of the polymer determined by gel permeation chromatography (GPC) against the polystyrene standards in THF are M_w = 2.1 × 10^4, M_n = 1.3 × 10^4 (polydispersity, 1.67). Thermal gravimetry analyses (TGA) (heating at 10 °C min^{-1} in nitrogen) indicate that the polymer is stable up to 300 °C. Differential scanning calorimetry (DSC) reveals an exothermic phase transition around 70 °C, which is higher than those of our previously reported poly[bi(thienyl)phenylene] derivatives.

The absorption and photoluminescence (PL) spectra of the polymer as film (spun-cast from a solution in xylene at the concentration of 30 mg ml^{-1}) on microslides are shown in Fig. 1. The absorption onsets at 490 nm and gives a broad spectrum with the maximum at 396 nm. From the onset wavelength, the optical band gap of the polymer can be estimated to be 2.53 eV. The film emits intensive green light when it is exposed to UV light. The PL spectrum exhibits a peak at 493 nm with a shoulder at 515 nm, corresponding to green emission (CIE: x = 0.24, y = 0.51). The absolute PL quantum yield of the neat polymer film was measured to be 32 ± 3% in an integrated sphere at rt in air using an argon ion laser line of 358 nm as the excitation source according to the procedure described by Greenham *et al.*[13] The PL efficiency is quite high compared with conventional PTs, and is also higher than those of our previously reported polythiophene derivatives modified by the phenylene group in their backbones, although it is still lower than those measured from 9,9-disubstituted polyfluorenes which are highly efficient blue light-emitting polymers.[14] The photochemical stability of PHTDHFHT is also high. The fluorescence intensity of the thin film shows negligible degradation in 5 h under irradiation of UV light (367 nm) in air. This is similar to other polyfluorene and polythiophene

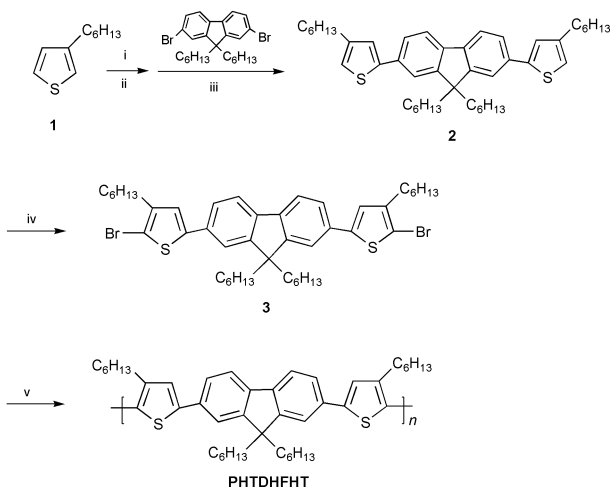

Scheme 1 *Reagents and conditions*: i, LDA, THF, −78 °C, 2 h; ii, $ZnCl_2$, THF, −78 °C, 2 h; iii, $Pd(PPh_3)_4$, THF, reflux, 20 h; iv, NBS, $CHCl_3$–AcOH, 10 h; v, $NiCl_2$, Zn, PPh_3, 2,2′-dipyridyl, DMAC, 20 h.

DOI: 10.1039/b004614k

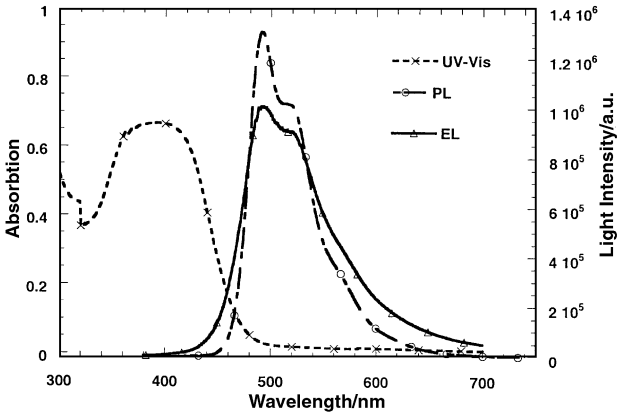

Fig. 1 UV-visible absorption (film), photoluminescence (film), and electroluminescence spectra of PHTDHFHT.

derivatives. These results indicate that PHTDHFHT is an efficient and stable green emissive material.

Cyclic voltammetry (CV) was performed on a thin polymer film of PHTDHFHT coated onto a glassy carbon disc electrode in a 0.1 mol L^{-1} tetrabutylammonium hexylfluorophosphate (*n*-Bu_4NPF_6) solution in acetonitrile by using platinum wire as a counter electrode and a silver wire as a quasi-reference electrode. All the experiments were performed in a glove-box under an argon atmosphere at rt. As shown in Fig. 2, in the anodic scan, the oxidation started at about 0.90 V and gave a sharp oxidation peak at 1.21 V. The re-reduction peak appeared at 1.15 V. On sweeping the polymer cathodically, the reduction (*n*-doping) began at −1.60 V and then the cathodic current increased quickly and produced a cathodic peak at −1.81 V, and a corresponding re-oxidation peak occurred at −1.75. The oxidation and reduction reactions are reversible. The clear redox behavior and the good doping reversibility prove that the polymer may be a good candidate of EL materials for applications in polymer light emitting diodes and polymer light-emitting electrochemical cells (LECs).[15] The electrochemically measured band gap is 2.5 V, which agrees well with the HOMO–LUMO energy gap of 2.53 eV as determined from the absorption onset. The HOMO and LUMO energy levels of this polymer were estimated from the oxidation and reduction onset potentials to be −5.30 and −2.85 eV, respectively.

The fabrication of LED devices was carried out in a glove box under a nitrogen atmosphere. The thickness of the PHTDHFHT film was about 100 nm and the thickness of the calcium electrode, which was thermally evaporated onto the polymer film under 10^{-6} Torr, as about 200 nm. First, the single devices

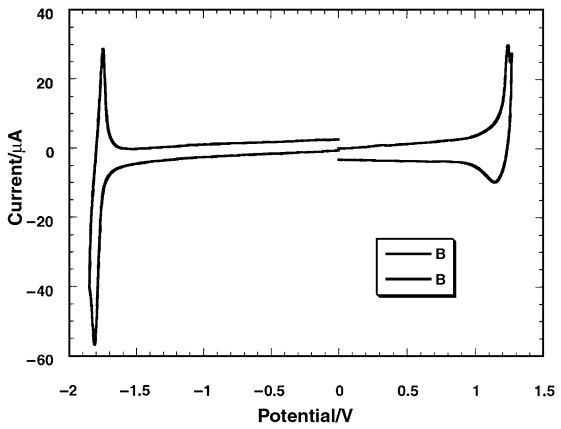

Fig. 2 Cyclic voltammograms of PHTDHFHT recorded in a solution of TBAPF6 (0.1 M) in acetonitrile at rt.

with the configuration ITO–PHTDHFHT–Ca were fabricated. In forward bias, the single-layer devices turned on at about 20 V for current and emitted green light at about 21 V. Considering the energy barrier for hole injection at the anode, double-layer devices with the configuration ITO–PVK–PHTDHFHT–Ca were also fabricated. By employing a PVK layer (90 nm) between the ITO and the polymer film the turn-on voltage for light output was reduced to about 8 V, and the maximum external quantum efficiency was increased from 0.05 to 0.6%. It indicates that PVK as hole-transporting layer can reduce the turn-on voltage of the devices and improve their efficiency.

In conclusion, a novel poly(fluorene-*co*-bithiophene) conjugated polymer, PHTDHFHT, was prepared through metal-catalyzed coupling polymerization in place of ferric chloride oxidative reaction. This polymer shows good thermal stability and photostability. Efficient green PL and EL are demonstrated with the polymer.

Notes and references

† The polymer was precipitated from the reaction mixture by pouring it into MeOH. The precipitate was washed with MeOH and was then re-dissolved in THF. The THF solution was vigorously stirred together with the 50% aqueous solution of hydrazine monohydrate (v:v 1:1) at rt for 24 h. The THF solution was separated and filtered. The solution was then poured into MeOH to precipitate the polymer. The polymer was collected by filtration and was washed with MeOH. Finally, the polymer was washed with acetone in a Soxhlet apparatus for 24 h and then dried under vacuum at rt.

‡ *Selected data* for the monomer (compound **3**): δ_H($CDCl_3$, 200 MHz, ppm) 7.64–7.68 (2H, d, J = 7.93 Hz, Ar-H), 7.45–7.64 (4H, m, Ar-H), 7.06 (2H, s, Th-H), 2.56–2.63 (4H, t, J = 7.2 Hz, CH_2), 1.96–2.04 (4H, m, CH_2), 1.61–1.65 (4H, m, CH_2), 1.25–1.35 (14H, m, CH_2), 1.00–1.10 (10H, m, CH_2), 0.89–0.95 (6H, m, CH_3), 0.76–0.85 (6H, m, CH_3); EI-MS (*m/z*): 824, 822, 820 (M^+); for PHTDHFHT: δ_H($CDCl_3$, 200 MHz, ppm): 7.58–7.74 (6H, m, Ar-H), 7.31 (2H, s, Th-H), 2.59–2.65 (4H, t, J = 7.2 Hz, CH_2), 2.00–2.11 (4H, m, CH_2), 1.61–1.75 (4H, m, CH_2), 1.21–1.42 (12H, m, CH_2), 1.00–1.20 (12H, m, CH_2), 0.82–0.95 (6H, m, CH_3), 0.74–0.81 (6H, m, CH_3); δ_c($CDCl_3$, 50 MHz, ppm): 151.69, 144.40, 143.53, 140.29, 133.08, 128.03, 124.53, 124.48, 120.07, 119.60, 55.31, 31.68, 31.48, 30.78, 29.68, 29.21, 23.78, 23.72, 22.60, 14.10, 14.01. Anal. Calc. For $C_{45}H_{60}S_2$: C, 81.26; H, 9.09; S, 9.64. Found: C, 81.44; H, 9.16; S, 9.47%.

1 R. H. Friend, R. W. Gymer, A. B. Holmes, J. H. Burroughes, R. N. Marks, C. Taliani, D. D. C. Bradley, D. A. Dos Santos, J. L. Brédas, M. Lögdlund and W. R. Salaneck, *Nature*, 1999, **397**, 121.
2 A. Kraft, A. C. Grimsdale and A. B. Holmes, *Angew. Chem., Int. Ed.*, 1998, **37**, 402.
3 A. J. Heeger, *Solid State Commun.*, 1998, **107**, 673.
4 R. D. McCullough, *Adv. Mater.*, 1998, **10**, 93.
5 M. Berggren, O. Inganäs, G. Gustafsson, J. Rasmusson, M. R. Andersson, T. Hjertberg and O. Wennerström, *Nature*, 1994, **372**, 444.
6 M. R. Andersson, M. Berggren, O. Inganäs, G. Gustafsson, J. C. Gustafsson-Carlberg, D. Selse, T. Hjertberg and O. Wennerström, *Macromolecules*, 1995, **28**, 7525.
7 O. Inganäs, T. Granlund, M. Theander, M. Berggren, M. R. Andersson, A. Ruseckas and V. Sundström, *Opt. Mater. N. Y.*, 1998, **9**, 104.
8 J. Pei, W.-L. Yu, W. Huang and A. J. Heeger, *Synth. Met.*, 1999, **105**, 43.
9 J. Pei, W.-L. Yu, W. Huang and A. J. Heeger, *Macromolecules*, 2000, **33**, 2462.
10 W.-L. Yu, J. Pei, Y. Cao, W. Huang and A. J. Heeger, *Chem. Commun.*, 1999, 1837.
11 W.-L. Yu, Y. Cao, J. Pei, W. Huang and A. J. Heeger, *Appl. Phys. Lett.*, 1999, **75**, 3270.
12 F. Chen, P. G. Mehta, L. Takiff and R. D. McCullough, *J. Mater. Chem.*, 1996, **6**, 1763.
13 N. C. Greenham, I. D. W. Samuel, G. R. Hayes, R. T. Philips, Y. A. R. R. Kessener, S. C. Moratti, A. B. Holmes and R. H. Friend, *Chem. Phys. Lett.*, 1995, **241**, 89.
14 Q. Pei and Y. Yang, *J. Am. Chem. Soc.*, 1996, **118**, 7416.
15 D. M. Leeuw, M. M. J. Simenon, A. R. Brown and R. E. F. Einerhand, *Synth. Met.*, 1997, **87**, 53.

Degradation of an antitumour bicyclic hexapeptide RA-VII into cycloisodityrosines

Yukio Hitotsuyanagi,[a] Tomoyo Hasuda,[a] Yuji Matsumoto,[a] Kentaro Yamaguchi,[b] Hideji Itokawa[a] and Koichi Takeya*[a]

[a] *Tokyo University of Pharmacy and Life Science, 1432-1 Horinouchi, Hachioji, Tokyo 192-0392, Japan. E-mail: takeyak@ps.toyaku.ac.jp*
[b] *Chemical Analysis Center, Chiba University, Yayoi-cho, Inage-ku, Chiba 263-8522, Japan*

Received (in Cambridge, UK) 5th June 2000, Accepted 17th July 2000
Published on the Web 9th August 2000

Degradation of an antitumour bicyclic hexapeptide, RA-VII 1, produced protected cycloisodityrosines in an efficient manner through bis(thioamide) intermediate 6.

RA-VII **1**[1] and bouvardin (NSC 259968) **2**[2] are a class of peptides originating from Rubiaceous plants. They show potent antitumour activity, and their mode of action is considered to be inhibition of protein synthesis through interaction with eukaryotic 80 S ribosomes.[3] While the cycloisodityrosine moiety is proposed to be the pharmacophore for this type of peptide,[4] the role of the 18-membered ring moiety for the activity is still an outstanding issue. Although several approaches towards the synthesis of cycloisodityrosines have been reported,[5–7] their multi-step synthesis inevitably requires construction of a strained diphenyl ether linkage, which is not easily accessible, using unusual amino acids. Also, the easily epimerisable properties of cycloisodityrosines[6d–f,7b] hamper ready access to the cycloisodityrosine unit needed for the synthesis of 18-membered ring modified analogues. We report herein an alternative practical approach towards cycloisodityrosines from RA-VII **1** which is the most abundant congener of RAs obtained from commercially available Rubiae Radix.[8]

To obtain cycloisodityrosines from peptide **1**, selective cleavage of the peptide bonds at specific positions was required. Previously, we reported that when RA-VII **1** was treated with 2,4-bis(methylthio)-1,3,2λ^5,4λ^5-dithiadiphosphetane-2,4-dithione **3** at rt, [Tyr-3-Ψ(CS-NH)-Ala-4; Tyr-6-Ψ(CS-NH)-D-Ala-1]RA-VII **4**, with accompanying monothioamides and other bis(thioamides), was obtained in 38% yield.[9] We deemed that bis(thioamide) **4** would be a suitable substrate for such degradation. Although some enhancement of the yield (~50%) of **4** has been made by modifying the reaction conditions, we found that when [*N*-methyl-Ala-2]RA-VII **5**, which is readily prepared from peptide **1** in 97% yield,[10] was thionated using the same reagent, bis(thioamide) **6** possessing thioamide bonds at the same positions as **4** was produced in 91% yield (Scheme 1). Compound **6** was converted into bis(imidothioate) **7** using

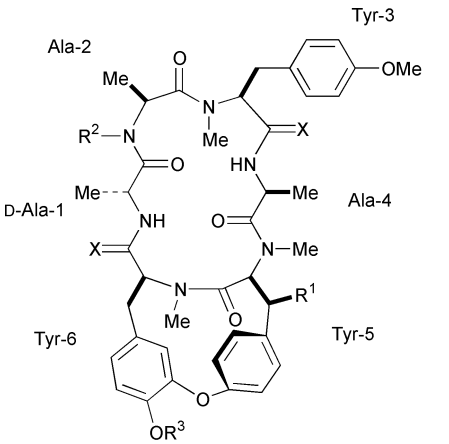

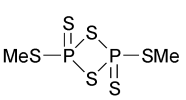

3

Scheme 1 *Reagents and conditions*: i, **3**, dioxane, rt, 4 d, 91%.

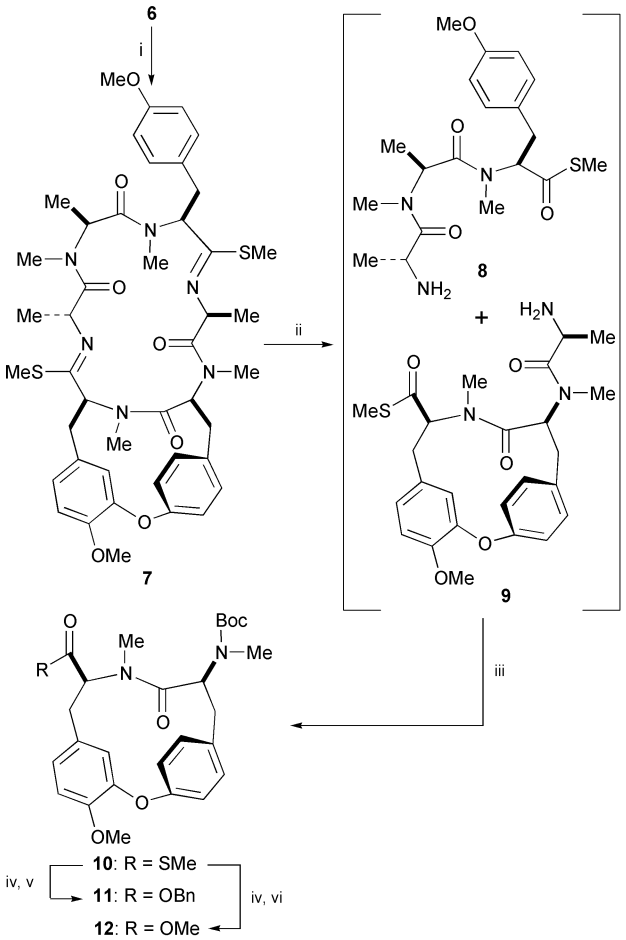

Scheme 2 *Reagents and conditions*: i, MeI, K_2CO_3, acetone, rt, 6 h; ii, 6 M HCl, MeCN, rt, 2 h; neutralised with 1 M K_2CO_3; iii, phenyl isothiocyanate, rt, 2 h; 6 M HCl, MeCN, rt, 5 h; neutralised with 1 M K_2CO_3; Boc_2O, rt, 4 h, 78% from **6**; iv, LiOH, H_2O_2, THF–H_2O, 0 °C, 20 min; v, benzyl alcohol, DEAD, Ph_3P, THF, 0 °C, 2 h, 90% from **10**; vi, (trimethylsily)diazomethane, MeCN–MeOH, rt, 3 h, 97% from **10**.

DOI: 10.1039/b004459h

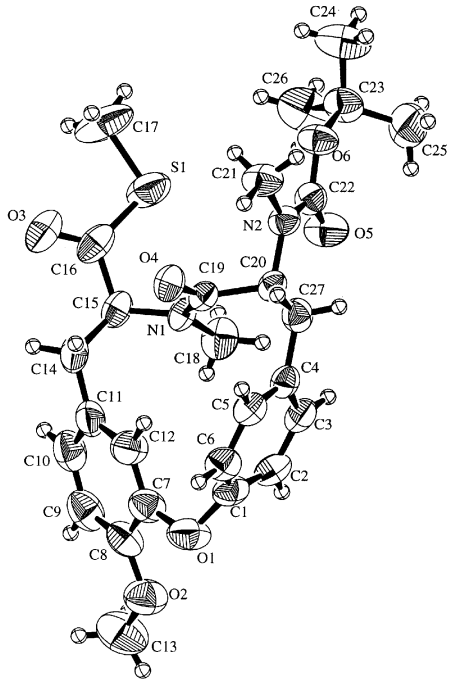

Fig. 1 The crystal structure of compound **10**.

iodomethane and potassium carbonate, and successive treatment with 6 M HCl in acetonitrile resulted in the cleavage of two imidothioate linkages to produce a mixture of two tripeptide segments **8** and **9** (Scheme 2). This mixture, without separation, was then subjected to Edman degradation, and *N*-protection using di-*tert*-butyl dicarbonate afforded cycloisodityrosine thioester **10** in 78% yield from bis(thioamide) **6**.† The structure of compound **10** was confirmed by X-ray crystallography (Fig. 1).‡ Compound **10** was converted into benzyl ester **11** and known methyl ester **12**[6f,7b] in yields of 90 and 97%, respectively.§ The spectroscopic data of **12** were in good agreement with those of **12** previously reported. The chemical conversion described here proceeds in an efficient manner; the overall yields of cycloisodityrosines **11** and **12** from RA-VII **1** were 62 and 67%, respectively. We are currently engaged in the design and synthesis of 18-membered ring modified analogues of RA-VII using **11** and **12**, and the results will be disclosed in due course.

Notes and references

† This key transformation (**6** → **10**) was most effectively carried out on a 0.15–0.2 mmol scale.

‡ *Crystal data* for **10**: $C_{27}H_{34}N_2O_6S$, M = 514.64, 0.30 × 0.10 × 0.40 mm, monoclinic, $P2_1$ (no. 4), a = 6.359(3), b = 21.465(5), c = 9.991(2) Å, β = 92.68(2)°, V = 1362.2(7) Å^3, T = 298(1) K, Z = 2, μ(Cu-Kα) = 14.09 cm^{-1}, 5470 reflections measured, 2494 unique reflections (R_{int} = 0.015), R = 0.036, Rw = 0.031. The structure was solved by direct methods and expanded using Fourier techniques. CCDC 182/1722. See http://www.rsc.org/suppdata/cc/b0/b004459h/ for crystallographic files in .cif format.

§ Compound **11**: $[\alpha]_D^{18}$ –202 (*c* 0.10, $CHCl_3$); compound **12**: $[\alpha]_D^{18}$ −198 (*c* 0.18, $CHCl_3$).

1 H. Itokawa, K. Takeya, Y. Hitotsuyanagi and H. Morita, in *The Alkaloids*, ed. G. A. Cordell, Academic Press, New York, 1997, vol. 49, p. 301.

2 (*a*) S. D. Jolad, J. J. Hoffmann, S. J. Torrance, R. M. Wiedhopf, J. R. Cole, S. K. Arora, R. B. Bates, R. L. Gargiulo and G. R. Kriek, *J. Am. Chem. Soc.*, 1977, **99**, 8040; (*b*) R. B. Bates, J. R. Cole, J. J. Hoffmann, G. R. Kriek, G. S. Linz and S. J. Torrance, *J. Am. Chem. Soc.*, 1983, **105**, 1343.

3 (*a*) M. Zalacaín, E. Zaera, D. Vázquez and A. Jiménez, *FEBS Lett.*, 1982, **148**, 95; (*b*) B. V. Sirdeshpande and P. L. Toogood, *Bioorg. Chem.*, 1995, **23**, 460.

4 D. L. Boger, J. B. Myers, D. Yohannes, P. A. Kitos, O. Suntornwat and J. C. Kitos, *Bioorg. Med. Chem. Lett.*, 1991, **1**, 313.

5 (*a*) T. Inaba, I. Umezawa, M. Yuasa, T. Inoue, S. Mihashi, H. Itokawa and K. Ogura, *J. Org. Chem.*, 1987, **52**, 2957; (*b*) T. Inoue, T. Inaba, I. Umezawa, M. Yuasa, H. Itokawa, K. Ogura, K. Komatsu, H. Hara and O. Hoshino, *Chem. Pharm. Bull.*, 1995, **43**, 1325.

6 (*a*) D. L. Boger and D. Yohannes, *J. Am. Chem. Soc.*, 1991, **113**, 1427; (*b*) D. L. Boger, D. Yohannes, J. Zhou and M. A. Patane, *J. Am. Chem. Soc.*, 1993, **115**, 3420; (*c*) D. L. Boger and J. Zhou, *J. Am. Chem. Soc.*, 1995, **117**, 7364; (*d*) D. L. Boger, J. Zhou, R. M. Borzilleri and S. Nukui, *Bioorg. Med. Chem. Lett.*, 1996, **6**, 1089; (*e*) D. L. Boger and J. Zhou, *J. Org. Chem.*, 1996, **61**, 3938; (*f*) D. L. Boger, J. Zhou, R. M. Borzilleri, S. Nukui and S. L. Castle, *J. Org. Chem.*, 1997, **62**, 2054.

7 (*a*) R. Beugelmans, A. Bigot, M. Bois-Choussy and J. Zhu, *J. Org. Chem.*, 1996, **61**, 771; (*b*) A. Bigot, R. Beugelmans and J. Zhu, *Tetrahedron*, 1997, **53**, 10753; (*c*) A. Bigot, M. E. T. H. Dau and J. Zhu, *J. Org. Chem.*, 1999, **64**, 6283.

8 (*a*) H. Itokawa, K. Takeya, N. Mori, T. Hamanaka, T. Sonobe and K. Mihara, *Chem. Pharm. Bull.*, 1984, **32**, 284; (*b*) H. Itokawa, K. Takeya, N. Mori, T. Sonobe, S. Mihashi and T. Hamanaka, *Chem. Pharm. Bull.*, 1986, **34**, 3762.

9 Y. Hitotsuyanagi, Y. Matsumoto, S. Sasaki, J. Suzuki, K. Takeya, K. Yamaguchi and H. Itokawa, *J. Chem. Soc., Perkin Trans. 1*, 1996, 1749.

10 Y. Hitotsuyanagi, J. Suzuki, K. Takeya and H. Itokawa, *Bioorg. Med. Chem. Lett.*, 1994, **4**, 1633.

ChemComm

Methylation of (2-methylethanethiol-bis-3,5-dimethylpyrazolyl)methane zinc complexes and coordination of the resulting thioether: relevance to zinc-containing alkyl transfer enzymes

Brian S. Hammes and Carl J. Carrano*

Department of Chemistry and Biochemistry, Southwest Texas State University, San Marcos, TX 78666, USA. E-mail: cc05@swt.edu

Received (in Irvine, CA, USA) 26th May 2000, Accepted 12th July 2000
Published on the Web 9th August 2000

Methylation of the coordinated thiolate in pseudotetrahedral Zn complexes of the form [(L3S)ZnX] by a variety of alkylating agents appears to occur *via* a nondissociative route and the resulting thioether can remain coordinated to the metal center as it does in zinc dependent alkyl transfer enzymes such as the DNA repair protein, Ada, from *Escherichia coli.*

The role of zinc metalloproteins in enzymatic alkyl group transfer is an emerging area of bioinorganic chemistry.[1] Examples of such enzymes include the DNA repair protein Ada from *E. coli*, the cobalamin dependent and independent methionine synthases, farnasyl transferase, and others.[2–6] In all of these proteins the zinc ion is in a thiol rich coordination environment with multiple cysteine residues as ligands. Zinc in the Ada protein, for example, is surrounded by four such cysteine residues (designated a CCCC site) although systems in which one or two of the cysteine residues have been replaced by histidines (CCHC and CCHH) are also known.[2–6] Interestingly, these same motifs also characterize the non-enzymatic zinc-finger proteins.[1]

A major question, which has been addressed by several model compound studies, has been: what is the role of the zinc in modulating the reactivity of cysteine residues toward methyl group transfer? In seminal mechanistic work, Wilker and Lippard have shown that in reactions of $Zn(SPh)_4^{2-}$ and its derivatives with trimethylphosphate as the methyl donor, methyl group transfer from the model substrate did not require the presence of zinc.[7] Thiolate anions were actually more readily alkylated although no transfer was seen when thiols were the acceptors. Methylation also occurred in the presence of $Zn(SPh)_4^{2-}$ but since all of its reactivity could be attributed to dissociated thiolate anion, doubts existed regarding the reactivity of a true zinc bound thiolate. More recently however, both we and Vahrenkamp and associates, have presented evidence for a nondissociative mechanism in the alkylation of [(L)ZnSR] (where L is a trispyrazolylborate or other scorpionate ligand) complexes by a variety of methylating agents.[8,9] Evidence has been accumulating that zinc-bound thiolates are in fact the active nucleophiles in the enzymatic reactions as well.[10]

One aspect of the enzymatic reactions not mimicked in any model system studied thus far is the fact that in many of the former, the thioether produced in the alkyl transfer remains coordinated to the zinc. Thioether coordination has been unequivocally demonstrated for the Ada protein and spectroscopic evidence consistent with this has been presented in several other cases as well.[11–13] In all of the model studies conducted to date the thioether has never been found in the zinc coordination sphere after alkylation.[7–9] This observation has prompted Vahrenkamp to propose that the apparently very poor donor capabilities of the thioether group toward zinc may contribute significantly to the overall reactivity in these systems.[9] Using a new N_2S heteroscorpionate ligand that is isostructural and isoelectronic with the well known N_3 trispyrazolylborates, we report here a system where a zinc-bound thiolate appears to be the active nucleophile[8b] and the thioether resulting from methyl group transfer reaction remains in the coordination sphere of the zinc in the absence of superior anionic ligands.

The ligand L3SH is prepared in reasonable yield using the same approach used to prepare previous members of this family.[8a] Thus bis(3,5-dimethylpyrazolyl)ketone reacts with 2-methyldithioisobutyraldehyde as a melt at 80 °C in the presence of $CoCl_2$ as a catalyst. The thio-protected intermediate, L3SSMe, was cleanly reduced with $LiAlH_4$ to yield the desired product. Pseudotetrahedral zinc complexes such as [(L3S)ZnI] **1**, or [(L3S)ZnOAc] **2**, were readily prepared by either direct reaction of deprotonated $(L3S)^-$ (methoxide ion) with the appropriate zinc salt or protonation of the $[(L3S)ZnCH_3]$ derivative with HX. Methylation of the coordinated thiolate in these complexes was achieved using methyl iodide, trimethyloxonium tetrafloroborate, or *p*-nitrobenzene sulfonic acid methyl ester as methyl donors.

Reaction of **1** with an equivalent of methyl iodide in dichloromethane yields the complex $[(L3SCH_3)ZnI_2]$, **3**, where the thioether is uncoordinated as has been previously found in related systems. Reasoning that the neutral thioether could not compete with the anionic iodide ion released in the methylation reaction, we removed one iodide by treatment of **3** with an equivalent of $AgBF_4$. Isolation of the product after filtration of precipitated AgI yielded the pseudotetrahedral complex **4**, $[(L3SCH_3)ZnI][BF_4]$ where the thioether is now bound to the zinc (Fig. 1).† These transformations are summarized in Scheme 1. The same reaction sequence starting with **2** leads to $[(L3SCH_3)ZnOAc][BF_4]$ which in the solid state dimerizes to the acetato bridged complex **5**, $[(L3SCH_3)Zn(\mu\text{-}OAc)_2(\mu\text{-}OH)Zn(L3SCH_3)][BF_4]$ containing octahedral zinc with coordinated thioethers (Fig. 2).† These reactions show clearly,

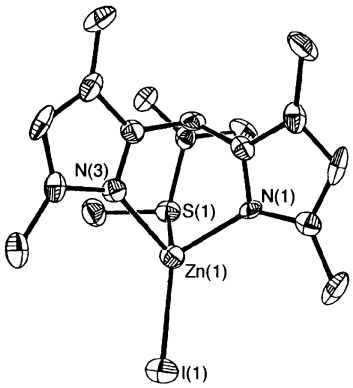

Fig. 1 Thermal ellipsoid diagram of $[(L3SCH_3)ZnI]^+$. The ellipsoids are drawn at the 30% probability level and hydrogens are removed for clarity. Selected bond distances (Å) and angles (°): Zn(1)–N(1) = 2.03(2); Zn(1)–N(3) = 2.03(2); Zn(1)–S(1) = 2.388(6); Zn(1)–I(1) = 2.471(3); N(1)–Zn(1)–N(3) = 94.2(7); N(1)–Zn(1)–S(1) = 90.6(5); N(1)–Zn(1)–I(1) = 122.4(5); N(3)–Zn(1)–S(1) = 89.9(5); N(3)–Zn(1)–I(1) = 124.3(5); S(1)–Zn(1)–I(1) = 125.8(2).

DOI: 10.1039/b004338i

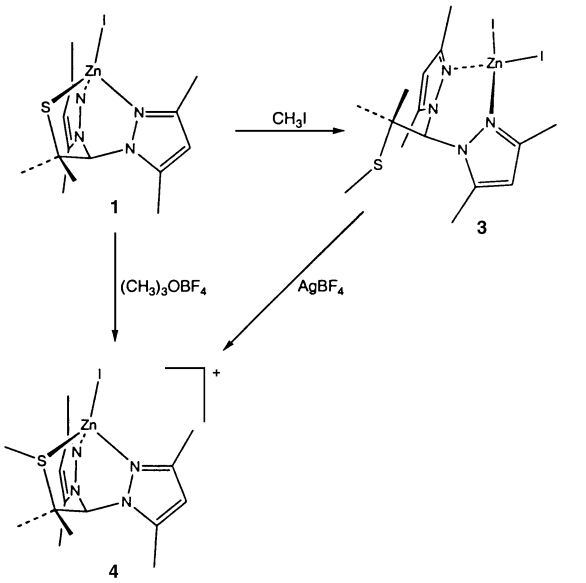

Scheme 1

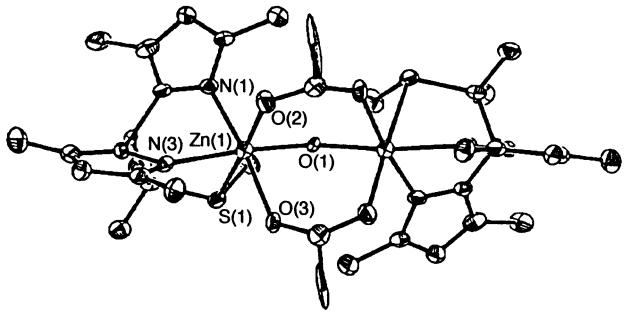

Fig. 2 Thermal ellipsoid diagram of $[(L3SCH_3)Zn(\mu\text{-}OAc)_2(\mu\text{-}OH)Zn(L3SCH_3)]^+$. The ellipsoids are drawn at the 30% probability level and hydrogens are removed for clarity. Selected bond distances (Å) and angles (°): Zn(1)–N(1) = 2.174(9); Zn(1)–N(3) = 2.118(9); Zn(1)–S(1) = 2.619(3); Zn(1)–O(1) = 1.979(4); Zn(1)–O(2) = 2.157(7); Zn(1)–O(3) = 2.078(8); N(1)–Zn(1)–N(3) = 85.1(3); N(1)–Zn(1)–O(1) = 96.0(3); N(1)–Zn(1)–O(2) = 173.5(3); N(1)–Zn(1)–O(3) = 93.5(3); N(1)–Zn(1)–S(1) = 82.6(2); N(3)–Zn(1)–O(1) = 173.0(3); N(3)–Zn(1)–O(2) = 90.0(3); N(3)–Zn(1)–O(3) = 92.0(3); N(3)–Zn(1)–S(1) = 87.9(2); O(1)–Zn(1)–O(2) = 88.3(3); O(1)–Zn(1)–O(3) = 94.9(3); O(1)–Zn(1)–S(1) = 85.3(2); O(2)–Zn(1)–O(3) = 91.0(3); O(2)–Zn(1)–S(1) = 92.9(2); O(3)–Zn(1)–S(1) = 176.2(2).

that in the absence of superior anionic ligands such as iodide, neutral thioethers can bind to a zinc center in either a tetrahedral or octahedral geometry.

Although coordinated thioether complexes could be prepared by removal of iodide by treatment with silver salts, the question remained, would a thioether formed by methylation of a zinc-bound thiolate remain coordinated without the addition of outside intervention? Trimethyloxonium tetrafloroborate and *p*-nitrobenzenesulfonic acid methyl ester are methyl donors used extensively to modify cysteine residues in proteins and are expected to produce only the weakly coordinating CH_3OCH_3 or *p*-nitrobenzene sulfonate as byproducts. Reaction of [(L3S)ZnX] where X = I^- or OAc^- with either of the above gave the expected $[(L3SCH_3)ZnX]^+$ directly as determined by NMR and electrospray-MS.‡ Thus the system reported herein mimics the known chemistry of the relevant zinc enzymes such as Ada.

Although the chelate effect is clearly important helping the thioethers produced here remain coordinated, it is not decisive. Thus while complexes of zinc with coordinated thioethers incorporated into anionic ligands are known,[14–16] numerous neutral chelates containing thioethers have been examined and invariably the thioethers are uncoordinated.[17–21] Thus we can envision zinc enzymes of this type being divided into two groups: the first where the sulfur to be methylated is part of the protein backbone *i.e.* one of the cysteine donors in the zinc coordination sphere as in the Ada protein. Under these conditions the resulting thioether can be expected to remain coordinated to the zinc due the macromolecular chelate effect. In the case where the thiol to be methylated represents an exogenous substrate, as in the cobalamin independent methionine synthases, the resulting neutral monodentate coordinated thioether is expected to be easily displaced by other ligands such as water (hydroxide). Such a process would yield free product and zinc enzyme with an open coordination site ready to repeat the catalytic cycle.

Notes and references

† *Crystal data* for **4**: $C_{15}H_{24}BF_4IN_4SZn$, M = 571.52, a = 9.754(2), b = 19.761(4), c = 22.977(4) Å, V = 4429(2) Å^3, orthorhombic, space group *Pbca*, Z = 8, T = 293(2) K, final $R1$ = 0.0795, $wR2$ = 0.1888, GOF (on F^2) = 1.047. For **5**: $C_{17}H_{27}B_{0.5}F_2N_4O_{2.5}SZn$, M = 468.26, a = b = 17.674(5), c = 15.531(3) Å, β = 120°, V = 4202(2) Å^3, trigonal, space group $P3_221$, Z = 6, T = 198(2) K, final $R1$ = 0.0799, $wR2$ = 0.2317, GOF (on F^2) = 1.067. CCDC 182/1726. See http://www.rsc.org/suppdata/cc/b0/b004338i/ for crystallographic files in .cif format

‡ In the case where X = OAc with *p*-nitrobenzenesulfonate as a counterion we can isolate solid monomeric **6** whose dimerization to $[(L3SCH_3)Zn(\mu\text{-}OAc)_2(\mu\text{-}OH)Zn(L3SCH_3)]^+$ is greatly suppressed *vis á vis* that of the BF_4^- salt.

1 W. N. Lipscomb and N. Straeter, *Chem. Rev.*, 1996, **96**, 2375.
2 E. C. Friedberg, G. C. Walker and W. Siede, *DNA Repair and Mutagenesis*, ASM Press, Washington, DC, USA, 1995.
3 E. C. Friedberg, *BioEssays*, 1994, **16**, 645.
4 K. Peariso, C. W. Goulding, S. Huang, R. G. Matthews and J. E. Penner-Hahn, *J. Am. Chem. Soc.*, 1998, **120**, 8410.
5 Z. S. Zhou, K. Peariso, J. E. Penner-Hahn and R. G. Matthews, *Biochemistry*, 1999, **38**, 15 915.
6 H. W. Park, S. R. Boduluri, J. F. Moomaw, P. J. Casey and L. S. Beese, *Science*, 1997, **275**, 1800.
7 J. J. Wilker and S. J. Lippard, *Inorg. Chem.*, 1997, **36**, 969.
8 (*a*) B. S. Hammes and C. J. Carrano, *Inorg. Chem.*, 1999, **38**, 3562; (*b*) B. S. Hammes, C. R. Warthen and C. J. Carrano, *J. Biol. Inorg. Chem.*, 2000, submitted.
9 U. Brand, M. Rombach and H. Vahrenkamp, *Chem. Commun.*, 1998, 2717.
10 C. Huang, K. E. Hightower and C. A. Fierke, *Biochemistry*, 2000, **39**, 2593.
11 L. C. Meyers, T. D. Cushing, G. Wagner and G. L. Verdine, *Biochemistry*, 1993, **32**, 14 089.
12 T. Ohkubo, H. Sakashita, T. Sakuma, M. Kainosho, M. Sekiguchi and K. Morikawa, *J. Am. Chem. Soc.*, 1994, **116**, 6035.
13 C. Huang, P. J. Casey and C. A. Fierke, *J. Biol. Chem.*, 1997, **272**, 20.
14 S. Chiou, P. Ge, C. G. Riordan, L. M. Liable-Sands and A. L. Rheingold, *Chem. Commun.*, 1999, 159.
15 P. Ghosh and G. Parkin, *Chem. Commun.*, 1998, 413.
16 D. C. Goodman, T. Tuntulani, P. J. Farmer, M. Y. Darensbourg and J. H. Reibenspies, *Angew. Chem., Int. Ed. Engl.*, 1993, **32**, 116.
17 P. Ghosh, M. Wood, J. B. Bonanno, T. Hascall and G. Parkin, *Polyhedron*, 1999, **18**, 1107.
18 P. C. Roehm and J. M. Berg, *J. Am. Chem. Soc.*, 1998, **120**, 13 083.
19 R. Gregorzik and H. Vahrenkamp, *Chem. Ber.*, 1994, **127**, 1857.
20 C. J. Matthews, W. Clegg, S. L. Heath, N. C. Martin, M. N. Hill and J. C. Lockhart, *Inorg. Chem.*, 1998, **37**, 199.
21 C. A. Grapperhaus, T. Tuntulani, J. H. Reibenspies and M. Y. Darensbourg, *Inorg. Chem.*, 1998, **37**, 4052.

Ambident σ- and π-donor ability of a neutral 10π-aromatic phosphoniobenzophospholide†

Dietrich Gudat,* Stefan Häp, Laszlo Szarvas and Martin Nieger

Institut für Anorganische Chemie der Universität Bonn, Gerhard-Domagk-Str. 1, 53121 Bonn, Germany. E-mail: dgudat@uni-bonn.de

Received (in Cambridge, UK) 27th June 2000, Accepted 18th July 2000
Published on the Web 9th August 2000

1-Triphenylphosphoniobenzo[*c*]phospholide 2 which is accessible *via* $NaBH_4$ reduction of 1,3-bis(triphenylphosphonio)benzophospholide 1 displays an ambident coordination ability similar to a phosphinine; this is shown by its reactions with (cyclooctene)$Cr(CO)_5$ and (naphthalene)$Cr(CO)_3$ which gave (σ(*P*)-2)$Cr(CO)_5$ and (η⁵-2)$Cr(CO)_3$, the first π-complex of a 10π-aromatic phosphorus heterocycle with a d-block metal.

Phosphinines **I** and phospholides **II** are aromatic phosphorus heterocycles whose use as ligands in transition metal complexes receives substantial current interest,[1] in particular in connection with possible applications in catalysis.[2] As compared to their organic analogues, *viz.* arenes and cyclopentadienides, **I**, **II** are more versatile ligands which may bind to metals not only *via* the π-electron system (η⁵/η⁶-coordination) but also *via* the phosphorus lone-pair (σ(*P*)-coordination), or a combination of both.[1] For phosphinines, formation of σ(*P*)-complexes in which the ligand displays σ-donor/π-acceptor-properties similar as a phosphane or phosphite is generally more favourable with metals in low oxidation states, although complexes with η⁶-coordinated phosphinines are also accessible for various metal centres.[1] Phospholides prefer, in contrast, π-coordination and the vast majority of complexes feature η⁵-bound ligands; pure σ(*P*)-phospholide complexes are known,[3] but remain rare.

We have recently established that cationic 1,3-bis-triphenylphosphonio-benzophospholide **1** binds to various transition metals in a σ(*P*)- or μ_2(*P*)-coordination mode.[4,5] The donor ability of the π-electron system in **1** was found to be inferior to that of the phosphorus lone-pair, and on the whole the structural features of the complexes resembled more closely those of topologically related phosphinine complexes rather than genuine phospholide complexes.[4] These findings suggested that the reduction of π-nucleophilicity and enhancement of π-electrophilicity induced by the phosphonio groups is of pivotal importance for the complexation regioselectivity and lead us to conclude that mono-phosphonio-substituted benzophospholides might display a balanced ligand behaviour with prospects for both σ(*P*)- and π-coordination, similar to the case of phosphinines. Here, we report on the synthesis and coordination studies of the phosphonio-benzophospholide **2** which lead to the isolation and structural characterisation of the first π-complex of a 10π-aromatic phosphaarene with a d-block transition metal.[6]

During our studies of reductive fragmentation reactions of the cation **1**[7] we discovered that **1**[Cl] reacts selectively with excess $NaBH_4$ *via* cleavage of PPh_3 to form neutral species **2** (Scheme 1). The latter was isolated in satisfactory yield after recrystallisation from THF–isopropyl alcohol and its constitution established by analytical and spectroscopic data.† Interestingly, the first UV–VIS absorption band of **2** [λ_{max} (CH_2Cl_2) = 352 nm] which is attributable to a π–π* transition of the benzophospholide chromophore occurs at nearly the same wavelength as for **1** [λ_{max} (CH_2Cl_2) = 354 nm[5]], thus indicating similar frontier orbital gaps in both molecules. As the effect of the positive charge in **1** should shift all orbitals to more negative energies,[8] neutral **2** is thus expected to behave as a better π-donor but less effective π-acceptor than **1**.

To survey the coordination behaviour of **2**, we explored reactions with equimolar amounts of [(cyclooctene)$Cr(CO)_5$] and [(naphthalene)$Cr(CO)_3$], respectively. Both reactions proceeded according to an ^{31}P NMR spectroscopic assay with quantitative formation of a single phosphorus containing species. The products were isolated after precipitation with hexane and recrystallisation from toluene, and their nature as the complexes **3**, **4** was established by microanalytical and spectroscopic data and single crystal X-ray diffraction studies.[9]

Complex **3** displays a moderate negative coordination shift for the endocyclic phosphorus atom [δ^{coord} = δ(ligand) − δ(complex) = −29] while coordination shifts for the benzophospholide carbon atoms are insignificant (δ^{coord} < ± 3) and the proton at C3 is slightly deshielded (δ^{coord} = 0.3). All these features are characteristic for complexes featuring σ(*P*)-coordinated low valent phosphorus species.[1] The carbonyl region of the IR spectrum of **3** displays the expected pattern of a $M(CO)_5$ moiety with the band at highest energy (ν = 2064 cm^{-1}) appearing at slightly lower wavenumbers than in [$(Ph_3P)Cr(CO)_5$] ($\tilde{\nu}$ = 2070 cm^{-1}) or the phosphinine complex [σ-(2,4,6-triphenylphosphinine)$Cr(CO)_5$] **5** ($\tilde{\nu}$ = 2071 cm^{-1} [10]). Although comparison of this vibrational frequency in $LM(CO)_5$ complexes has been used to relate the π-acceptor qualities of L,[2] a more common and quantitative approach is provided by evaluation of Tolman's electronic parameter χ which can be obtained from vibrational spectra of $LNi(CO)_3$ complexes.[11] We have therefore recorded IR spectral data of the $Ni(CO)_3$ complex of **2** (prepared *in situ* from equimolar amounts of **2** and $Ni(CO)_4$) and determined a value of χ = 13 indicating that the π-acceptor ability of **2** should match that of PPh_3 (χ = 13[11]) but is lower than that of $P(OMe)_3$ (χ = 23[11]) or 2,4,6-triphenylphosphinine (χ = 23[2]).

The ^1H, ^{13}C and ^{31}P NMR spectra of complex **4** reveal large negative coordination shifts for the endocyclic phosphorus (δ^{coord} = −158), the hydrogen at C3 (δ^{coord} = −2.6) and the carbon atoms in the five membered ring (δ^{coord} = −17 to −24) whereas the remaining nuclei in the benzophospholide unit exhibit similar chemical shifts as in free **2**. Altogether, these

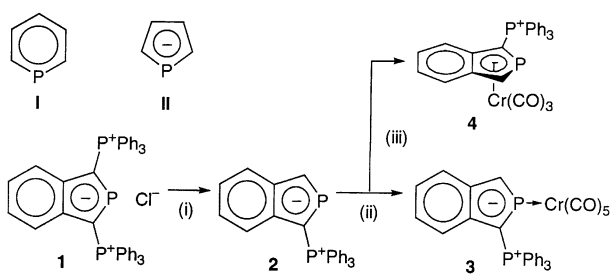

Scheme 1 *Reagents and conditions*: i, excess $NaBH_4$, THF, 24 h, r.t.; ii, 1 equiv. [(cyclooctene)$Cr(CO)_5$], THF, 6 h, r.t.; iii, 1 equiv. [(naphthalene)$Cr(CO)_3$], THF, 6 h, r.t.

† Electronic supplementary information (ESI) available: analytical and spectroscopic data for **2**-**4**. See http://www.rsc.org/suppdata/cc/b0/b005130f/

DOI: 10.1039/b005130f

data indicate π-coordination of **2** *via* the five-membered ring which has likewise been observed for indenyl complexes such as $[(\eta^5\text{-indenyl})Cr(CO)_3]^-$ **6**.[12] The carbonyl stretching vibrations in the IR spectrum of **4** ($\tilde{\nu}$ = 1925, 1835, 1826 cm^{-1}) appear at higher wavenumbers than in both **6** ($\tilde{\nu}$ = 1895, 1791 cm^{-1} [12] and $[\eta^5\text{-}(C_5H_4PPh_3)Cr(CO)_3]$ **7** ($\tilde{\nu}$ = 1900, 1805, 1785 cm^{-1} [13]), indicating that the amount of π-electron density transferred to the metal is lower for **2** than for the carbocyclic ligands $C_9H_7^-$ and $C_5H_4PPh_3$, respectively.

The results of the X-ray structure analysis of complex **3** [Fig. 1(a)] confirms the presence of a σ(*P*)-coordinated benzophospholide ligand with a planar annulated ring system. Unlike as in known complexes of σ(*P*)-coordinated phospholides,[3] the metal-bound phosphorus atom lacks any evidence for pyramidalisation (sum of bond angles 360°). The exocyclic P–C bond [P2–C2 1.744(1) Å] is similar as in complexes of **1** (1.75 ± 1 Å[4]) whereas of the endocyclic P–C distances the one to the protonated carbon atom is shortened [P1–C9 1.691(2) Å] and the other lengthened [P1–C2 1.767(2) Å]. The P1–Cr1 bond [2.376(5) Å] matches that in the phosphinine complex **5** [2.372(15) Å[4]]. The Cr–C distances in **3** [$Cr–C_{trans}$ 1.862(4) Å, $Cr–C_{cis}$ 1.895–1.912, av. 1.902 Å] are generally longer than those in **5** [$Cr–C_{trans}$ 1.822(12) Å, $Cr–C_{cis}$ 1.825–1.865, av. 1.843 Å[10]]. Although interpretation of these data in terms of electronic effects is difficult in view of sterically induced distortions in both structures, the more pronounced shortening of the *trans*-relative to the *cis*-Cr–C bonds in **3** agrees with a lower π-acceptor ability of **2** as compared to 2,4,6-$Ph_3H_2C_5P$ which was predicted on grounds of the spectroscopic data.

The molecular structure of **4** [Fig. 1(b)] displays a three-legged piano-stool geometry with the coordinated five membered ring featuring a flat twist conformation. The Cr–C distances range between 2.229(2) and 2.341(3) Å with the closest distances observed for the carbons atoms C2, C9 adjacent to P1 which are presumably the centres of highest π-electron density,[8] and the Cr–P distance amounts to 2.407(4) Å. The distances between the metal and the carbonyl C-atoms [1.806(3)–1.837(3) Å] and the centroid of the phospholide ring [1.874(3) Å], respectively, compare well with the corresponding values of $[\eta^5\text{-}(C_5H_4PPh_3)Cr(CO)_3]$ **7** (Cr–CO 1.77–1.83, Cr–Cent. 1.862 Å[13]) and [(η⁶-2,4,6-triphenylphosphinine)$Cr(CO)_3$] (Cr–CO 1.80–1.82, Cr–Cent. 1.686 Å[14]). The exocyclic P2–C2 bond in **4** [1.755(3) Å] is similar than in **3** but the endocyclic P–C [1.744(2), 1.805(2) Å] and adjacent C–C bonds [1.426(3), 1.460(3) Å] are lengthened as expected for a π-complex. The extent of this lengthening is somewhat more pronounced for the P–C than for the C–C bonds which agrees with the finding that the largest coefficients in the frontier orbitals of benzo[*c*]phospholides are found at the phosphorus and the two adjacent carbon atoms.[8]

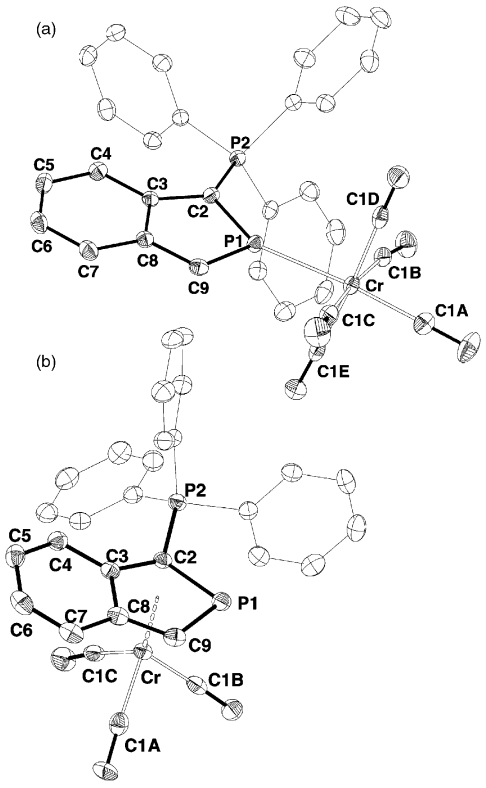

Fig. 1 Molecular structures of **3** (a) and **4** (b). Thermal ellipsoids are drawn at 50% probability level, and H atoms have been omitted for clarity. Selected bond lengths (Å); for **3**, Cr–P1 2.3760(5), P1–C9 1.6910(17), C9–C8 1.414(2), C–C7 1.422(2), C7–C6 1.370(3), C6–C5 1.398(3), C5–C4 1.379(2), C4–C3 1.417(2), C3–C8 1.430(2), C3–C2 1.456(2), C2–P1 1.7670(18), C2–P2 1.7438(17), Cr1–C1D 1.9030(19), Cr–C1B 1.912(2), Cr–C1E 1.8953(19), Cr–C1A 1.862(2). For **4**: P1–C9 1.744(4), C9–C8 1.426(0), C8–C7 1.429(3), C7–C6 1.354(0), C6–C5 1.418(1), C5–C4 1.367(3), C4–C3 1.419(0), C3–C8 1.436(1), C3–C2 1.460(2), C2–P1 1.805(0), C2–P2 1.755(3), Cr–C1A 1.826(2), Cr–C1B 1.806(1), Cr–C1C 1.837(1).

Preliminary studies indicate that analogous complexes as **3**, **4** are likewise accessible with molybdenum and tungsten. In conclusion, our reported findings strongly suggest that the electron withdrawing effect of the PPh_3 group induces a balanced coordination behaviour which enables the benzophospholide **2** to act both as a phosphine-like σ-donor/π-acceptor ligand in σ(*P*)-complexes and a phosphaarene like ligand in π-complexes. A similar switching between different coordination modes was previously known for phosphinines,[1] but scarcely for phospholide type species. Further exploration of this feature as well as the possible exploitation of the chiral nature of **4** are currently under investigation and may possibly add new facets to the coordination chemistry of phospholide ligands.

We thank the Fonds der Chemischen Industrie and Deutsche Forschungsgemeinschaft for financial support.

Notes and references

1 F. Mathey, *Coord. Chem. Rev.*, 1994, **137**, 1; P. Le Floch and F. Mathey, *Coord. Chem. Rev.*, 1998, **179**–**180**, 771; K. B. Dillon, F. Mathey and J. F. Nixon, *Phosphorus: The Carbon Copy*, John Wiley, Chichester, 1998 and references therein.

2 B. Breit, *Chem. Commun.*, 1996, 2071; B. Breit, *J. Mol. Catal. A*, 1999, **143**, 143.

3 F. Mercier, L. Ricard and F. Mathey, *Organometallics*, 1993, **12**, 98.

4 D. Gudat, M. Nieger and M. Schrott, *Chem. Ber.*, 1995, **128**, 259; D. Gudat, M. Schrott and M. Nieger, *J. Chem. Soc., Chem. Commun.*, 1995, 1541; D. Gudat, M. Schrott, V. Bajorat, M. Nieger, S. Kotila, R. Fleischer and D. Stalke, *Chem. Ber.*, 1996, **129**, 337; D. Gudat, A. W. Holderberg, N. Korber, M. Nieger and M. Schrott, *Z. Naturforsch. Teil B*, 1999, **54**, 1244.

5 D. Gudat, *Coord. Chem. Rev.*, 1997, **173**, 71.

6 π-Complexes of a benzo[*b*]phospholide with Li^+ and Sm^{2+} have been described, see: E. Niecke, M. Nieger and P. Wenderoth, *Angew. Chem.*, 1994, **106**, 362; *Angew. Chem., Int. Ed. Engl.*, 1994, **33**, 353; F. Nief and L. Ricard, *J. Organomet. Chem.*, 1994, **464**, 149.

7 D. Gudat, V. Bajorat, S. Häp, M. Nieger and G. Schröder, *Eur. J. Inorg. Chem.*, 1999, 1169.

8 D. Gudat, V. Bajorat and M. Nieger, *Bull. Chim. Soc. Fr.*, 1995, **132**, 280.

9 *Crystal data*: for **3**: $C_{31}H_{20}CrO_5P_2$, M = 586.4, triclinic, space group $P\bar{1}$, (no. 2), a = 10.2695(4), b = 11.0128(4), c = 13.7391(4) Å, α = 111.151(2), β = 93.476(2), γ = 110.126(2)°, U = 1330.03(8) Å^3, Z = 2, D_c = 1.46 g cm^{-3}, μ(Mo-Kα) = 0.59 mm^{-1}, 18922 reflections measured, 6253 unique which were used in all calculations, $wR2(F^2)$ = 0.084 (all data), $R1$ = 0.035 [$I > 2\sigma(I)$]. For **4**: $C_{29}H_{20}CrO_3P_2$, M = 530.4, monoclinic, space group $P2_1/n$ (no. 14), a = 8.5429(4), b = 13.2026(9), c = 21.3056(14) Å, β = 97.658(4)°, U = 2381.6(3) Å^3, Z = 4, D_c = 1.48 g cm^{-3}, μ(Mo-Kα) = 0.65 mm^{-1}, 21481 reflections measured, 4163 unique which were used in all calculations, $wR2(F^2)$ = 0.082 (all data), $R1$ = 0.036 [$I > 2\sigma(I)$]. CCDC 182/1721. See http://www.rsc.org/suppdata/cc/b0/b005130f/ for crystallographic files in .cif format.

10 J. Deberitz and H. Nöth, *J. Organomet. Chem.*, 1973, **49**, 453; H. Vahrenkamp and H. Nöth, *Chem. Ber.*, 1973, **106**, 2227.

11 C. A. Tolman, *Chem. Rev.*, 1977, **77**, 313.

12 A. Ceccon, A. Gambero, F. Gottardi, S. Santi and A. Venzo, *J. Organomet. Chem.*, 1991, **412**, 85.

13 J. C. Kotz and D. G. Pedrotty, *J. Organomet. Chem.*, 1970, **22**, 425.

14 J. Deberitz and H. Nöth, *Chem. Ber.*, 1970, **103**, 2541; H. Vahrenkamp and H. Nöth, *Chem. Ber.*, 1972, **105**, 1148.

A novel fluorescent chemosensor exhibiting exciplex emission. An example of an elementary molecular machine driven by pH and by light

Andrea Bencini,*[a] Antonio Bianchi,*[a] Carlos Lodeiro,[b] Andrea Masotti,[a] A. Jorge Parola,[b] Fernando Pina,*[b] J. Seixas de Melo[c] and Barbara Valtancoli[a]

[a] *Department of Chemistry, University of Florence, Via Maragliano 75/77, 50144 Florence, Italy. E-mail: bianchi@chim1.unifi.it*
[b] *Departamento de Química, Centro de Química-Fina e Biotecnologia, Faculdade de Ciências e Tecnologia, Universidade Nova de Lisboa, Quinta da Torre 2825 Monte de Caparica, Portugal. E-mail: fjp@dq.fct.unl.pt*
[c] *Departamento de Química, Universidade de Coimbra, 3049 Coimbra, Portugal. E-mail: sseixas@ci.uc.pt*

Received (in Cambridge, UK) 6th June 2000, Accepted 21st July 2000
Published on the Web 9th August 2000

Coordination/detachment of a pendent functionality in the Zn(II) complex with a macrocyclic ligand L gives rise to on/off switching of exciplex emission, defining an elementary molecular machine whose movements are driven by both pH and light.

Chemical systems capable of performing controlled movements at the molecular level are a topic of great interest. In particular great attention is paid to molecular systems whose movements can be controlled by external inputs (pH, temperature, light, redox potential, metal ions).[1–6]

In the present work we describe a Zn(II) complex behaving as an elementary molecular machine driven by pH and light. The mechanical function of this machine consists in the movement of a ligand moiety determined by pH-controlled coordination–detachment of a donor atom leading to the formation of an exciplex emitter. The ligand used, **L**, was obtained by reaction

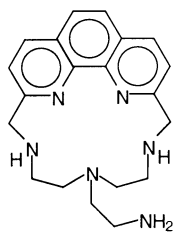

1

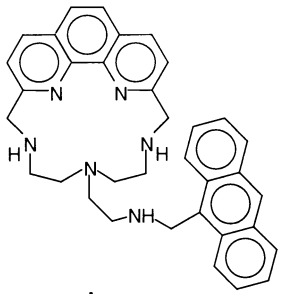

L

of anthracene-9-carbaldehyde (EtOH, room temperature, 48 h) with the macrocyclic precursor **1**, followed by reduction *in situ* of the resulting imine with $NaBH_4$, according to a reported procedure.[7] **1** was synthesized by condensation of 2,9-bis-(bromomethyl)-1,10-phenanthroline with tris(2-tosylaminoethyl)amine by using the Richman and Atkins procedure.[8]

The absorption spectrum of the free ligand presents the characteristic band of the anthracene moiety (λ_{max} = 352 nm), and is only slightly dependent on the pH. The most intense absorption band occurs at 252 nm, a region where both the first singlet of phenanthroline, and the second singlet of anthracene absorb. However, the fluorescence emission exciting at 352 or 252 nm is the same, as expected from the Kasha–Vavilov's rule.[9]

The most interesting feature of the fluorescence emission concerns its dramatic dependence on the protonation state of the compound.† A total quenching of the emission is observed for the species **L**, $H\mathbf{L}^+$ and $H_2\mathbf{L}^{2+}$, while the $H_3\mathbf{L}^{3+}$ form exhibits an intense emission. As observed for many other similar molecules possessing the anthracene fluorophore attached to a polyamine chain, the quenching effect can be explained by an electron transfer process from unprotonated amine groups to the excited anthracene.[10,11] On the other hand protonation of amines rises their oxidation potential to > 2.5 V changing the photoinduced electron transfer reaction from exoergonic to endoergonic, thus precluding the quenching effect.[12] ^{1}H NMR titrations performed at different pH values showed that in $H_3\mathbf{L}^{3+}$ all three benzylic nitrogens are protonated. Only the N2 amine remains unprotonated, although, according to the emission spectra, this would not be an efficient site for photo-induced electron transfer quenching, probably because of involvement in hydrogen bonding to adjacent protonated nitrogens. The species $H_2\mathbf{L}^{2+}$, $H\mathbf{L}^+$ and **L** have two, three and four unprotonated nitrogens, respectively, accounting for the observed quenching effect.

Potentiometric measurements performed in water–MeCN (1 : 1, v/v) solutions, containing Zn(II) and **L** in 1 : 1 molar ratios, showed the formation of stable complexes ($[Zn\mathbf{L}]^{2+}$, $[ZnH\mathbf{L}]^{3+}$, $[ZnH_2\mathbf{L}]^{4+}$, $[Zn\mathbf{L}(OH)]^+$, $[Zn\mathbf{L}(OH)_2]$) over the entire pH region investigated.† The formation of these Zn(II) complexes has also been followed by recording ^{1}H NMR spectra at different pH values, indicating that deprotonation of $[ZnH_2\mathbf{L}]^{4+}$ to form $[ZnH\mathbf{L}]^{3+}$ (pH 3–5) takes place at the amine nitrogen of the pendant arm. At the same time, remarkable shifts for the signals of anthracene and phenanthroline protons evidence the formation of a π-stacking interaction between the two aromatic moieties in the $[ZnH\mathbf{L}]^{3+}$ complex. In other words, metal coordination by the deprotonated amine group of the pendant arm enables the two aromatic moieties to interact *via* π-stacking. Such stacking interaction is maintained in the $[Zn\mathbf{L}]^{2+}$ and $[Zn\mathbf{L}(OH)]^+$ species, as shown by the fact that the spectra do not bear significant changes at neutral or slightly alkaline pH. By contrast, NMR data obtained in very alkaline media (pH 10–13), where $[Zn\mathbf{L}(OH)_2]^{2+}$ is formed, suggest that binding of the second OH^- ion causes the detachment of the amine group of the pendant arm and consequent loss of the π-stacking interaction.

Like many other Zn(II) complexes bearing polyamine chains attached to a fluorophore, the fluorescence emission spectra of the Zn(II) complexes with **L** (λ_{max} = 418 nm) are quite similar to those of the protonated ligand (Fig. 1). This is explained by the fact that coordination of Zn(II) to the amine groups (like protonation) precludes the electron transfer quenching effect.[10–12] On this basis, the quenching effect occurs only at pH values that permit the existence of nitrogens which are neither attached to the metal nor protonated (Fig. 1). This clearly occurs for all the complexes species except $[ZnH_2\mathbf{L}]^{4+}$ which still exhibits an intense emission with a maximum at 418 nm. The most intersting feature of this system, however, is the formation of a non-structured and red shifted emission band (Fig. 1), occurring for all metal complexes with the exception of $[Zn\mathbf{L}OH)_2]$. The excitation spectrum at pH = 6.4, collected at 418 nm is coincident with the absorption spectrum. However the excitation spectrum collected at 600 nm is slightly red shifted, as expected from a ground state association. This exciplex type emission can thus be ascribed to an intramolecular

DOI: 10.1039/b004506n

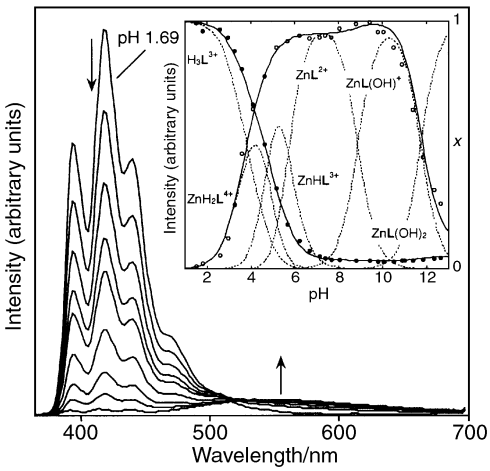

Fig. 1 Fluorescence emission spectra of the Zn(II)–**L** (1 : 1) system in 0.15 M NaCl MeCN–H_2O (1 : 1, v.v) at different pH values: 1.69; 3.73; 4.4; 4.87; 5.1; 5.57; 6.05; 6.55, 10.37 (λ_{exc} = 352 nm). Inset: fluorimetric titration of the same system: (●) emission followed at 418 nm, (○) exciplex emission followed at 600 nm. Species distribution curves (inset) represent mol fractions.

π-stacking complex in the excited state, involving phenanthroline and anthracene. As described above, the π-stacking complex is already formed in the ground state for the species $[ZnH\mathbf{L}]^{3+}$, $[Zn\mathbf{L}]^{2+}$ and $[Zn\mathbf{L}(OH)]^{+}$, but not for $[ZnH_2\mathbf{L}]^{4+}$ and $[Zn\mathbf{L}(OH)_2]$. As a consequence, for $[ZnH_2\mathbf{L}]^{4+}$ the π-stacking complex must be formed during the excited state lifetime. The π stacking complex in the ground state and the *exciplex* emission from the excited state can be explained as a consequence of coordination of the nitrogen of the pendent arm to the metal, since this leads to a geometry where phenanthroline and anthracene are forced to stay close to each other in a sandwich-like mode. This structure is maintained upon coordination of a single OH^- ion to the metal, probably because the binding occurs at the opposite side of the pendent arm, while the exciplex emission, as well as the π-stacking complex, disappear at more basic pH values, in agreement with the detachment of the amine nitrogen of the pendent arm caused by coordination of the second OH^- ion.

Time-resolved fluorescence measurements collected at 419 and 550 nm reveal that, independently of the pH value considered, the decays are always fitted with sums of two or three exponentials. The fluorescence decay of the parent compound, 9-(methylaminomethyl)anthracene, measured at pH = 2 is however single exponential with a lifetime of 10.5 ns. Within the pH range studied (1.6–12.0), two lifetimes with values of 2–2.9 and 5.2–10.5 ns are observed. For lower pH values the contribution of the shorter lifetime is largely predominant at 419 nm (99%), but not so much at 550 nm (70%). As the pH increases the contribution of the second lifetime increases with a concomitant decrease of the shorter component. A third lifetime, attributed to the emissive exciplex species of 21–25 ns, begins to appear at pH = 5. For pH = 8.7 the contribution of this new species is predominant at λ_{em} = 550 nm (45% of the overall decay) but almost negligible at λ_{em} = 419 nm. This means that the back reaction from the exciplex to the monomer(s) is almost non-existent. Although always present for pH > 5, the emission contribution of the exciplex seems to reach a maximum at pH *ca.* 8, slowly decreasing at higher pH values.

We interpret the existence of the two first lifetimes to the presence of two opened structures (monomers) in equilibrium, one clearly ascribable to the free $[H_3\mathbf{L}]^{3+}$ species and the other probably to the $[ZnH_2\mathbf{L}]^{4+}$ complex. In conjunction with steady-state data it is clear that these two monomer species emit in the same region and can only be distinguished by time-resolved fluorescence. In cases where exciplex emission occurs, no negative pre-exponential, *i.e.* a rise-time, is observed as a result of two factors: the first is related to previous findings that

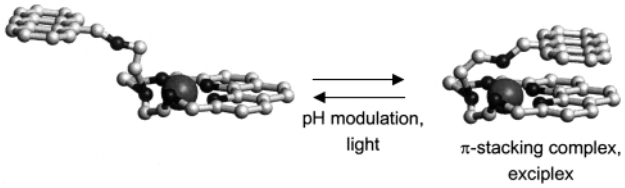

Fig. 2 Modulated formation of the π-stacking complex (exciplex).

a pre-formed exciplex is already present in the ground-state, and the second is a consequence of the fact that the fluorescence emission of the monomer(s) extends to the emission region where the exciplex emits.

The system here reported exhibits a significant advantage, in comparison with other similar compounds, because coordination of the pendent arm to the metal can be easily monitored by the appearance of the *exciplex* emission. The system defines an elementary molecular machine whose movements are driven by pH, and also by light around pH 4 (Fig. 2). Additionally, it can operate in acidic media switching from the species $H_3\mathbf{L}^{3+}$ to $[ZnH_2\mathbf{L}]^{4+}$ or in alkaline media between $[Zn\mathbf{L}(OH)]^{+}$ and $[Zn\mathbf{L}(OH)_2]$.

Interestingly the exciplex emission occurs not only in MeCN–water mixtures but also in pure water, in contrast with other exciplexes or excimers reported in literature which are only stable in non-polar solvents.[9]

Financial support from MURST (Italy), COFIN project, and FCT-MCT, project 32442/99 (Portugal) are gratefully acknowledged.

Notes and references

† Ligand protonation and Zn(II) complexation constants were determined by potentiometric titration performed in 0.10 mol dm^{-3} NMe_4Cl water–MeCN (1 : 1, v/v) solutions at 298.1 ± 0.1 K. Calculated values are: log K_L^{HL} = 9.0(1), log $K_{HL}^{H_2L}$ = 8.3(1), log $K_{H_2L}^{H_3L}$ = 6.1(2), log K_M^{ML} = 14.0(1), log K_{ML}^{MHL} = 5.8(1), log $K_{MHL}^{MH_2L}$ = 4.6(1), log K_{ML}^{MLOH} = 6.1(1), log $K_{MLOH}^{ML(OH)_2}$ = 4.3(1) (K_A^{AB} = [AB]/[A][B]).

1 V. Balzani, A. Credi, F. M. Raymo and J. F. Stoddart, *Angew. Chem., Int. Ed.*, 2000, in press; P. R. Ashton, R. Ballardini, V. Balzani, S. E. Boyd, A. Credi, M. T. Gandolfi, M. Gómez-López, Sayeedha Iqbal, D. Philp, J. A. Preece, L. Prodi, H. G. Ricketts, J. F. Stoddart, M. S. Tolley, M. Ventin, A. J. P. White and D. J. Williams, *Chem. Eur. J.*, 1997, **3**, 152; R. A. Bissell, E. Córdova, A. E. Kaifer and J. F. Stoddart, *Nature*, 1994, **369**, 133; R. Ballardini, V. Balzani, M. T. Gandolfi, L. Prodi, M. Venturi, D. P. Philp, H. G. Ricketts and F. Stoddart, *Angew. Chem., Int. Ed. Engl.*, 1993, **32**, 1301; V. Balzani, M. Gómez-López and J. F. Stoddart, *Acc. Chem. Res.*, 1988, **31**, 405; S. Nishizawa, M. Watanabe, T. Uchida and N. Teramae, *J. Chem. Soc., Perkin Trans. 2*, 1999, 141.

2 M. W. Hosseini and J.-M. Lehn, *J. Am. Chem. Soc.*, 1982, **104**, 3525.

3 T. R. Kelly, H. De Silva and R. A. Silva, *Nature*, 1999, 150; N. Koumura, R. W. J. Zijlstra, R. A. van Delden, N. Harada and B. L. Feringa, *Nature*, 1999, **397**, 152.

4 L. Fabbrizzi, M. Licchelli, P. Pallavicini and A. Perotti, *Inorg. Chem.*, 1996, **35**, 1733; R. Bergonzi, L. Fabbrizzi, M. Lichelli and C. Mangano, *Coord. Chem. Rev.*, 1998, **170**, 31; L. Fabbrizzi, F. Gatti, P. Pallavicini and E. Zambarbieri, *Chem. Eur. J.*, 1999, **5**, 682.

5 E. Kimura and T. Koike, *Chem. Commun.*, 1998, 1495 and references therein; E. Kimura, *Top. Curr. Chem.*, 1985, **128**, 113.

6 B. König, M. Pelka, H. Zieg, T. Ritter, H. Bouas-Laurent, R. Bonneau and J. P. Desvergne, *J. Am. Chem. Soc.*, 1999, **121**, 1681.

7 G. De Santis, L. Fabbrizzi, M. Licchelli, A. Poggi and A. Taglietti, *Angew. Chem., Int. Ed. Engl.*, 1996, **35**, 202.

8 J. E. Richman and T. J. Atkins, *J. Am. Chem. Soc.*, 1974, **96**, 2268.

9 A. Gilbert and J. Baggott, *Essentials of Molecular Photochemistry*, Blackwell Scientific Publications, Oxford, 1991.

10 A. W. Czarnik, *Acc. Chem. Res.*, 1994, **27**, 302; A. W. Czarnik, *Fluorescent Chemosensors for Ion and Molecule Recognition*, American Chemical Society, Washington DC, 1992.

11 M. A. Bernardo, F. Pina, B. Escuder, E. Garcia-España, M. L. Godino-Salido, J. Latorre, S. V. Luis, J. A. Ramirez and C. Soriano, *J. Chem. Soc., Dalton Trans.*, 1999, 915.

12 R. A. Bissel, A. P. de Silva, H. Q. N. Gunaratne, P. L. M. Lynch, G. E. M. Maguire and K. R. A. S. Sandanayake, *Chem. Soc. Rev.*, 1992, 187.

Photochromic cross-linked copolymer containing thermally stable fluorescing 2-indolylfulgimide

Yongchao Liang, A. S. Dvornikov and P. M. Rentzepis*

Department of Chemistry, University of California, Irvine, CA 92697, USA. E-mail: pmrentze@uni.edu

Received (in Irvine, CA, USA) 20th March 2000, Accepted 30th June 2000
Published on the Web 10th August 2000

A new photochromic cross-linked copolymer composed of PMMA and fluorescing 2-indolylfulgimide is synthesized which can be converted photochemically into two forms which are found to be thermally stable; the spectroscopic properties and quantum yields of photochemistry and fluorescence are also measured.

The increasing fast developments in new technologies associated with optoelectronics, waveguides, molecular switches, optical computer memories among others, require the design and synthesis of novel materials with properties which satisfy the specific needs of each new device.[1] Organic photochromic materials have attracted significant attention, in recent years, because of their potential application to optical devices, and in particular to switches and 3D optical storage.[2] One of the most promising classes of photochromic materials are fulgides because they possess excellent fatigue resistance and thermal stability in both isomeric forms.[3]

In previous papers we have reported the synthesis, photochromic and spectroscopic properties of several new thermally stable fluorescing photochromic 2-indolylfulgides and fulgimides which may be potential materials for use as media in rewritable 3D optical memory devices.[4–6] Here we describe the synthesis and properties of a new fluorescing photochromic 2-indolylfulgimide which is attached to methyl methacrylate monomer, to form a cross-linked photochromic fluorescing polymer.

Photochromic molecules must be uniformly dispersed in a polymer matrix at relatively high concentration to be suitable for use in optical devices. The photochromic materials which have been used in 3D optical memory devices, based on two-photon absorption, require concentrations of 10^{-1} M and higher in order to record a sufficient number of bits of information.[2] The photochromic cross-linked copolymer described here is formed by attaching the photochromic molecule to the polymer chain by copolymerization with the corresponding monomer. We were able to copolymerize the methyl methacrylate monomer and the photochromic 2-indolylfulgimide (*E*-**8**), which we synthesized, to form an optically clear photochromic cross-linked copolymer.

Fulgimide *E*-**8** was readily prepared by the process shown in Scheme 1. Commercially available 3-methylindole (**1**) was converted to **2** by reacting it with vinyl benzyl chloride in potassium hydroxide DMSO solution (78% yield). Product **2** was then converted to **3** using the Vilsmeier-Haack formylation reaction (42% yield).[7] Diethyl isopropylidenesuccinate (**6**) was prepared by Stobbe condensation (86% yield).[8] Stobbe condensation of indole-2-carbaldehyde (**3**) with diethyl isopropylidenesuccinate (**6**) followed by hydrolysis and intramolecular acid anhydride formation yields 2-indolylfulgide (*E*-**7** and *Z*-**7**) with 23% yield from **3** to **7**, where *E*-**7** was separated as the main product. Fulgimide *E*-**8** was synthesized from *E*-**7** by Lewis acid and hexamethyldisilazane-promoted one pot reaction (42% yield).[9,10]

The fulgimide *E*-**8** was subsequently dissolved in methyl methacrylate and the initiator (AIBN) was added forming a homogenous mixture. This mixture was transferred to a glass cell and sealed under vacuum. After 24 h of polymerization, at 50 °C, a rigid optically clear polymer was formed. The structure of this copolymer was determined by immersing it into 1,2-dichloroethane solvent for one month, in which both PMMA and fulgimide *E*-**8** are very soluble. We found, as expected, for cross-linked copolymers, that this immersed material was not dissolved, at all, in 1,2-dichloroethane. This indicates, strongly, that this material is a cross-linked copolymer of MMA and *E*-**8**. After the solid, nondissolved polymer was removed from the solution, the absorption spectra of the remaining phase were measured. The spectra showed that not

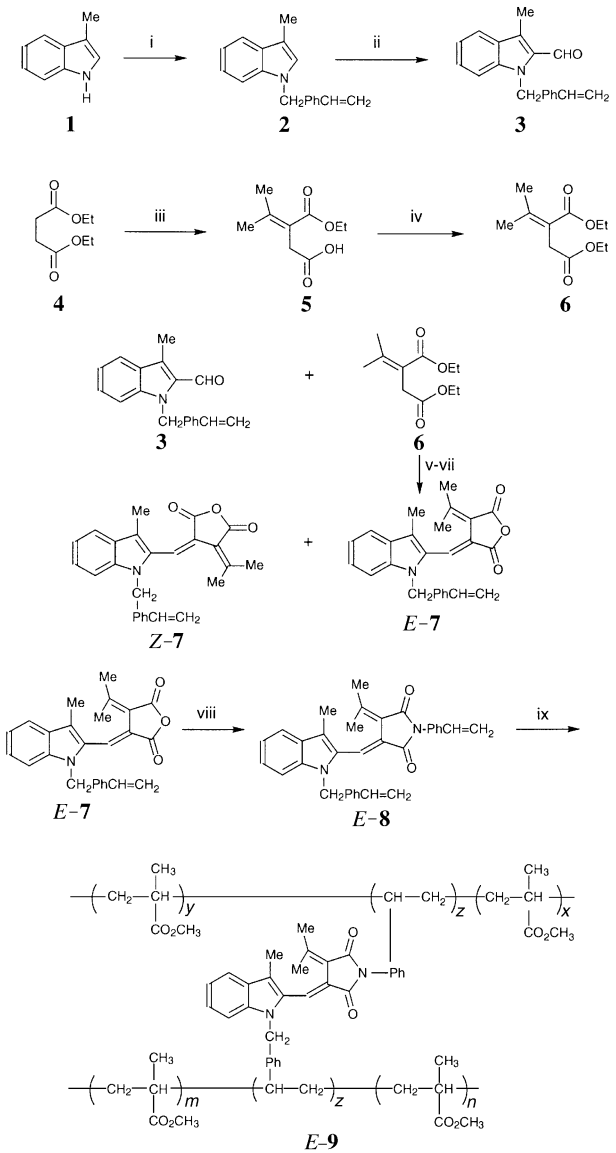

Scheme 1 *Reagents and conditions*: i, KOH, DMSO, 4-vinyl benzyl chloride, 0 °C to r.t., 78%; ii, $POCl_3$, DMF, 0 °C to r.t., 42%; iii, acetone, Bu^{t}OK, Bu^{t}OH, then HCl; iv, EtOH, H_2SO_4, 86% (from **4** to **6**); v, NaH, benzene; vi, KOH, EtOH, then HCl; vii, DCC, THF, 23% (from **3** to **7**); viii, 4-vinylaniline, HMDS, $ZnCl_2$, benzene, 43%; ix, MMA, AIBN, 50 °C.

DOI: 10.1039/b002335n

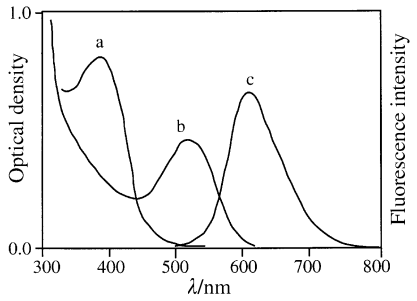

Fig. 1 Absorption and fluorescence spectra of cross-linked copolymer *E*-**9**. (*a*) absorption spectrum of the *E* form; (*b*) and (*c*) absorption and fluorescence spectra of the *C* form.

even traces of fulgimide *E*-**8** were present in the solution and only the spectrum of 1,2-dichloroethane solvent was recorded. To the best of our knowledge, this is the first cross-linked photochromic fulgimide copolymer ever synthesized.

The copolymer was found to possess photochromism, *i.e.* can be reversibly colored and bleached by irradiation with light of the appropriate wavelength. In addition the colored form (*C*) also fluoresces when excited with visible light which is rather seldom found in fulgimides. This is, also, the first time that a copolymer of this class has been observed. Fig. 1 shows the absorption spectra of the copolymer in its colorless and colored forms and the fluorescence spectrum of the colored form. The colored form was photoinduced by irradiating the copolymer with 400 nm light. When irradiated with visible light, λ = 530 nm, the colored form can be easily bleached back to the original colorless form, as shown in Scheme 2. The quantum efficiency of the coloration and bleaching processes were measured to be 0.13 and 0.17 respectively. These numbers are the same as the quantum efficiencies measured for pure *E*-**8** in ethyl acetate solution. We thought, previously, that in rigid cross-linked copolymer matrices, where the moieties of the fulgimide molecule are attached to the polymer chains, the efficiency of *E*–*Z* isomerization would be decreased, because of stereo constrains. In addition we had expected that because the *E*–*Z* isomerization competes with the ring-closure reaction, the cyclization reaction yield will increase. However, our data show that in a copolymer composed of fulgimide *E*-**8** and methyl methacrylate the efficiency of cyclization yield does not change. This suggests that the *E*–*Z* isomerization be not significantly reduced compared to the solution, probably due to segment rotation of the polymer chain.

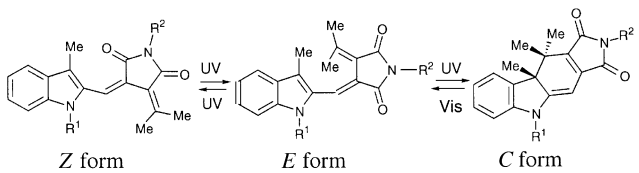

Scheme 2

The colored form of the fulgimide–MMA copolymer emits red fluorescence when promoted to its first excited state. The fluorescence spectra observed are similar to the colored forms of the pure fulgimides in solution. To confirm that the recorded fluorescence is due to the colored forms of the organic photochrome rather than any impurities or other species, we measured the excitation spectra and fluorescence emission spectra intensity change as a function of bleaching/coloration cycles. The data show that the fluorescence intensity and the excitation spectra of the colored from decrease proportionally with the decrease of the absorption of the fulgimide colored form. When the material was completely bleached, *i.e.* the absorption band of the *C* form disappeared no fluorescence was detected. When the fluorescence spectrum appeared again, its intensity increased with the same rate as the rate of growth of the *C* form concentration. The fluorescence quantum yield of the colored form was found to be 5%. The method that we have used to measure the quantum efficiencies of these forms has been described previously by us.[5]

This work was supported in part by the United States Air Force, Rome Laboratory, under contract number F 30603-97-C-0029.

Notes and references

1 R. Piyaket, I. Cokgor, F. B. McCormick, S. Esener, A. S. Dvornikov and P. M. Rentzepis, *Opt. Lett.*, 1996, **21**, 1032.
2 A. S. Dvornikov and P. M. Rentzepis, *Advances in Chemistry Series 240*, ed. Robert R. Birge, ACS, Washington DC, 1994, ch. 7, pp. 161–177.
3 H. G. Heller, in *CRC Handbook of Organic Photochemistry and Photobiology*, ed. W. M. Horpool and P. S. Song, CRC Press, FL, 1995, p. 174.
4 Y. C. Liang, A. S. Dvornikov and P. M. Rentzepis, *Res. Chem. Intermed.*, 1998, **24**, 905.
5 Y. C. Liang, A. S. Dvornkov and P. M. Rentzepis, *J. Photochem. Photobiol. A: Chem.*, 1999, **125**, 79.
6 Y. C. Liang, A. S. Dvornikov and P. M. Rentzepis, *Tetrahedron Lett.*, 1999, **40**, 8067.
7 C. Bastianelli, C. Cipiciani and G. Giulietti, *J. Heterocycl. Chem.*, 1981, **18**, 1275.
8 C. G. Overberger and C. W. Roberts, *J. Am. Chem. Soc.*, 1949, **71**, 3618.
9 P. Y. Reddr, S. Konodo, T. Toru and Y. Ueno, *J. Org. Chem.*, 1997, **62**, 2652.
10 *E*-**8**: mp: 149.5–150.5 °C, ^{1}H NMR (500 MHz, $CDCl_3$ TMS) δ 1.17 (s, 3H), 1.96 (s, 3H), 2.50 (s, 3H), 5.21 (d, J = 10.9 Hz, H), 5.31 (d, J = 10.9 Hz, H), 5.41 (m, 2H); 5.68 (d, J = 17.6 Hz, H), 5.79 (d, J = 17.6 Hz, H), 6.63 (dd, J = 17.6, 10.9 Hz, H), 6.74 (dd, J = 17.6, 10.9 Hz, H), 7.02 (d, J = 8.15 Hz, H), 7.16–7.71 (m, 10H); ^{13}C NMR (500 MHz, $CDCl_3$, TMS) δ 11.7, 22.8, 27.2, 47.3, 109.6, 114.1, 114.9, 119.9, 124.0, 126.5, 126.7, 126.8, 136.0, 136.2, 137.4, 154.5, 167.5, 168.3; HRMS (CI) m/z calcd for $C_{34}H_{30}N_2O_2$ 498.2307 (M^+), found 498.2317; Anal. Calcd for $C_{34}H_{30}N_2O_2$: C, 81.90; H, 6.06; N, 5.62. Found: C, 81.73; H, 6.04; N, 5.60%.

ChemComm

Asymmetric synthesis of febrifugine and isofebrifugine using yeast reduction

Yasuo Takeuchi,* Kumiko Azuma, Kentaro Takakura, Hitoshi Abe and Takashi Harayama

Faculty of Pharmaceutical Sciences, Okayama University, Tsushima-naka 1-1-1, Okayama 700-8530, Japan. E-mail: take@pharm.okayama-u.ac.jp

Received (in Cambridge, UK) 22nd June 2000, Accepted 21st July 2000
Published on the Web 11th August 2000

The antimalarial agents febrifugine ((+)-1) and isofebrifugine ((+)-2) were asymmetrically synthesized from chiral piperidin-3-ol ((+)-4), which was prepared by the reductive dynamic optical resolution of the 3-piperidone derivatives ((±)-3) using baker's yeast.

Febrifugine ((+)-**1**) is an antimalarial agent that was isolated from *Dichroa febrifuga* and *Hydrangea umbellata* along with isofebrifugine ((+)-**2**).[1a–c] The plane structure[2a] of (+)-**1** and (+)-**2** was first proposed in 1950. Subsequently, the relative[2b] and absolute[2c] structures were proposed on the basis of Baker's synthetic work.[3a–c] The relative configuration[2d] of (+)-**1** was corrected in 1973 and then the absolute structures[2e,f] of (+)-**1** and (+)-**2** were corrected in 1999 (Fig. 1). We previously synthesized the racemates of (+)-**1** and (+)-**2** *via* the unusual Claisen rearrangement and highly diastereoselective reduction.[4a,b] In this paper, we describe the asymmetric synthesis of (+)-**1** and (+)-**2** based on our synthetic method.

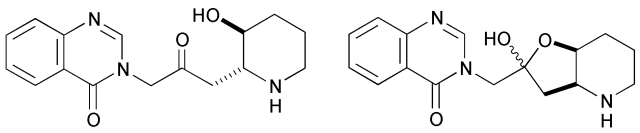

Fig. 1 Structures of febrifugine and isofebrifugine

As a key asymmetric reaction, we selected the yeast reduction of 3-piperidone derivatives ((±)-**3**)[4a,b] protected by a benzyloxycarbonyl (*Z*) group (Scheme 1). The reaction of (±)-**3** with baker's yeast and sucrose in EtOH and water at rt for 24 h afforded chiral piperidin-3-ol ((±)-**4**), for which the ^{1}H-NMR data agreed with reported values[4b] for (±)**4**, in high yield (40%) and enantiomeric purity (98% ee).[5] The remaining piperidone ((−)-**3**, 34%) also had high enantiomeric purity (90% ee). Since epimerization of (−)-**3** with K_2CO_3 for 4 h gave (±)-**3** in 67% yield, we could be sure of the possibility of reductive dynamic optical resolution. Epimerization that maintained the reductive activity of the yeast was examined under a variety of concentrations of K_2CO_3 and EtOH in water. Stirring a mixture of (±)-**3**, baker's yeast, sucrose, and K_2CO_3 in EtOH and water at rt for 90 h afforded (+)-**4** in 62% yield (97% ee) along with (−)-**3** in 14% yield (14% ee).[6]

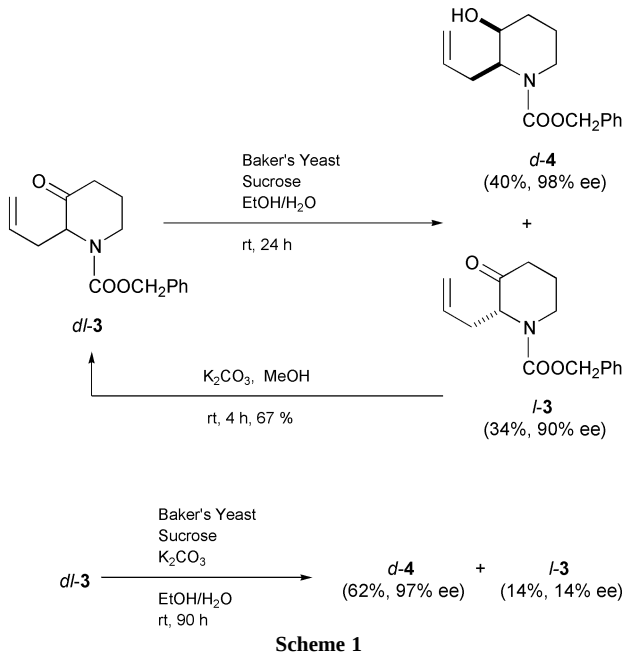

Scheme 1

Isofebrifugine ((+)-**2**) was prepared by improving our previous method (Scheme 2). The intramolecular bromoetherification of (+)-**4** using NBS afforded octahydrofuro[3,2-*b*]-pyridine (**5**) in 87% yield. The HPLC data indicated that this was a 3:1 mixture of the diastereomeric isomers. To improve the yield and reproductivity of preparing *Z*-protected isofebrifugine (**7**) from **5**, we designed a 2-methoxy derivative **6**. The new intermediate **6** could be prepared by a 2-step reaction in high yield (90%) as a 4 : 1 mixture of the diastereomeric isomers. The steps were dehydrobromination using potassium *tert*-butoxide and bromoetherification using NBS and MeOH. Deacetalization of **6** followed by a coupling reaction with 4(3*H*)-quinazolinone afforded **7** in 69% yield. The hydrogenolysis of **7** gave isofebrifugine ((+)-**2**) in 62% yield as a crystalline solid. The melting point,[1b] ^{1}H-NMR data,[7a,b] and optical rotation[1b] for (+)-**2** agreed with reported values for the natural product.[8] It was clear that the yeast reduction of (±)-**3** followed the Prelog rule[9] with high enantio- and diastereoselectivity to give (+)-**4** having the absolute configuration of 2*S*,3*S*.

In our previous method for synthesizing (±)-febrifugine ((±)-**1**), the large differences[4b] in the melting point and solubility of (±)-**1** and (±)-**2** played a convenient role for the isolation of (±)-**1**. However, we could not isolate pure (+)-**1** by refluxing (+)-**2** in EtOH. Although it is known that isomerization of the congeners of (+)-**2** run under the reversible Michael reactions,[7a,10] there are no reports of (+)-**2** itself. We examined the isomerization of (+)-**2** to (+)-**1** in various solvents, including toluene, DMF, pyridine, EtOH, water, and 10% HCl aq. Heating (+)-**2** at 80 °C for 30 min in water resulted in the largest ratio (2 : 1) of (+)-**1** to (+)-**2** among these solvents. On the other hand, the epimerization of (+)-**2** in 10% HCl aq. was not observed under the same conditions. Based on these results, we isolated pure (+)-**1**[11] as the hydrochloride salt and its physicochemical

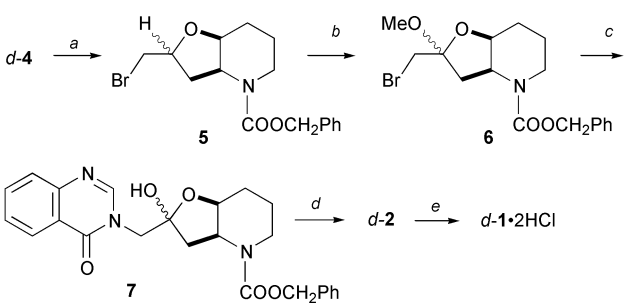

Scheme 2 *Reagents and conditions*: *a*, NBS, MeCN, rt, 0.5 h, 87%; *b*, (i) ^{t}BuOK, THF, 0 °C, 0.5 h; (ii) NBS, MeOH, rt, 1 h, 90%; *c*, (i) H^+, MeCN, rt, 1 h; (ii) 4(3*H*)-quinazolinone, K_2CO_3, DMF, rt, 2 h, 69%; *d*, H_2, 20%-Pd(OH)$_2$/C, MeOH, rt, 3.5 h, 62%; *e*, (i) H_2O, 80 °C, 15 min; (ii) H^+, 73%.

DOI: 10.1039/b005028h

properties[1c] and spectral data[7a,b] were identical with those reported for the natural product.

We were able to prepare febrifugine ((+)-**1**) in 15.2% yield and 6 isolated steps from (±)-**3** without using compounds that were very expensive, toxic, or dangerous. We think that our method is widely applicable to the synthesis of the derivatives needed to study the structure–activity relationship of febrifugine.

We are grateful to the SC-NMR Laboratory of Okayama University for the use of the facilities.

Notes and references

1 (*a*) J. B. Koepfli, J. F. Mead and J. A. Brockman Jr., *J. Am. Chem. Soc.*, 1947, **69**, 1836; (*b*) J. B. Koepfli, J. F. Mead and J. A. Brockman Jr., *J. Am. Chem. Soc.*, 1947, **69**, 1048; (*c*) F. Ablondi, S. Gordon, J. Morton II and J. H. Williams, *J. Org. Chem.*, 1952, **17**, 14.

2 (*a*) J. B. Koepfli, J. A. Brockman and J. Moffat, *J. Am. Chem. Soc.*, 1950, **72**, 3323; (*b*) B. R. Baker, F. J. McEvoy, R. E. Schaub, J. P. Joseph and J. H. Williams, *J. Org. Chem.*, 1953, **18**, 178; (*c*) R. K. Hill and A. G. Edwards, *Chem. Ind.*, 1962, 858; (*d*) D. F. Barringer, G. Berkelhammer and R. S. Wayne, *J. Org. Chem.*, 1973, **38**, 1937; (*e*) S. Kobayashi, M. Ueno, R. Suzuki and H. Ishitani, *Tetrahedron Lett.*, 1999, **40**, 2175; (*f*) S. Kobayashi, M. Ueno, R. Suzuki, H. Ishitani, H.-S. Kim and Y. Wataya, *J. Org. Chem.*, 1999, **64**, 6833.

3 (*a*) B. R. Baker, R. E. Schaub, F. J. McEvoy and J. H. Williams, *J. Org. Chem.*, 1952, **17**, 132; (*b*) B. R. Baker, F. J. McEvoy, R. E. Schaub, J. P. Joseph and J. H. Williams, *J. Org. Chem.*, 1953, **18**, 153; (*c*) B. R. Baker and F. J. McEvoy, *J. Org. Chem.*, 1955, **20**, 136.

4 (*a*) Y. Takeuchi, H. Abe and T. Harayama, *Chem. Pharm. Bull.*, 1999, **47**, 905; (*b*) Y. Takeuchi, M. Hattori, H. Abe and T. Harayama, *Synthesis*, 1999, 1814.

5 **Yeast Reduction (Method A)**; A mixture of (±)-**3** (3.00 g), baker's yeast (30 g), and sucrose (30 g) in EtOH (30 ml) and water (300 ml) was stirred at rt for 24 h. AcOEt (900 ml) was added to the mixture and stirred at rt for 10 min. The AcOEt layer separated by centrifugation (×1000 *g*, 10 min) was dried, filtered, and concentrated. MeCN was added to the residue and the precipitates were filtered through a membrane filter (0.5 μm). The filtrate was concentrated and the residue was subjected to column chromatography (silica gel). The first eluant (AcOEt–hexane, 1:7) gave (−)-**3** (1.02 g, 90% ee based on HPLC with a chiral column) as a colorless oil, $[\alpha]_D^{29}$ −45.5 (*c* 1.00, EtOH). HPLC conditions: column, Chiralcel OJ (Daicel); column temperature, rt; eluant, hexane–IPA, 37:3; flow rate = 1.5 ml min^{-1}; wavelength, 254 nm; t_R = 8.54 and 11.17 min. The second eluant (AcOEt–hexane, 1:3) gave (+)-**4** (1.20 g, 98% ee based on HPLC with a chiral column) as a viscous colorless oil. HPLC conditions: column, Chiralcel OJ (Daicel); column temperature, rt; eluent, hexane–IPA, 37:3; flow rate = 1.5 ml min^{-1}; wavelength, 254 nm; t_R = 6.43 and 7.51 min.

6 **Yeast Reduction (Method B)**; A mixture of (±)-**3** (1.00 g), K_2CO_3 (1.00 g), baker's yeast (10 g), and sucrose (30 g) in EtOH (30 ml) and water (300 ml) was stirred at rt for 90 h. The reaction mixture was treated in the same way as described above. The eluant (AcOEt–hexane, 1:7) gave (−)-**3** (0.14 g, 14% ee based on HPLC with a chiral column) as a colorless oil. The second eluant (AcOEt–hexane, 1:3) gave (+)-**4** (0.62 g, 97% ee based on HPLC with a chiral column) as a viscous colorless oil, $[\alpha]_D^{24}$ +76.2 (*c* 1.00, EtOH).

7 (*a*) S. Uesato, Y. Kuroda, M. Kato, Y. Fujiwara, Y. Hase and T. Fujita, *Chem. Pharm. Bull*, 1998, **46**, 1; (*b*) K. Murata, F. Takano, S. Fushiya and Y. Oshima, *J. Nat. Prod.*, 1998, **61**, 729.

8 **Isofebrifugine**; mp 130–131 °C (lit.[1b] 129–130 °C). $[\alpha]_D^{22}$ +124.3 (*c* 0.50, $CHCl_3$) {lit.[1b] $[\alpha]_D^{25}$ +131 (*c* 0.35, $CHCl_3$)}. The ^1H NMR spectrum agreed with that reported in the literature.[7a,b]

9 V. Prelog, *Pure Appl. Chem.*, 1964, **9**, 119.

10 D. F. Barringer, G. Berkelhammer, S. D. Carter, L. Goldman and A. E Lanzilotti, *J. Org. Chem.*, 1973, **38**, 1933.

11 **Febrifugine dihydrochloride**; Isofebrifugine ((+)-**2**, 0.34 g) in water (10 ml) was heated at 80 °C for 15 min. To the mixture, 10% HCl aq. (2 ml) was added and the solvent was evaporated off. The residue was washed with hot EtOH to give almost pure febrifugine dihydrochloride ((+)-**1**•2HCl, 0.31 g, 73%), which was recrystallized from a mixture of EtOH and water (9:1), mp 218–219 °C (decomp.) (lit.[1c] 223–225 °C (decomp.)). $[\alpha]_D^{29}$ +13.3 (*c* 1.01, H_2O) {lit.[1c] $[\alpha]_D^{31}$ +12.8 (*c* 0.85, H_2O)}. The ^1H NMR spectrum of free base ((+)-**1**) agreed with that reported in the literature.[7a,b]

ChemComm

Synthesis, morphology and optoelectronic properties of tris[(*N*-ethylcarbazolyl)(3′,5′-hexyloxybenzoyl)methane](phenanthroline)-europium†

Matthew R. Robinson,[ab] Marie B. O'Regan[c] and Guillermo C. Bazan*[abd]

[a] *Department of Materials Engineering, University of California, Santa Barbara CA 93106, USA*
[b] *Institute for Polymers and Organic Solids, University of California, Santa Barbara, CA 93106, USA*
[c] *UNIAX Corporation, 6780 Cortona Drive, Santa Barbara, CA 93117, USA*
[d] *Department of Chemistry, University of California, Santa Barbara, CA 93106 USA. E-mail: bazan@chem.ucsb.edu*

Received (in Irvine, CA, USA) 8th June 2000, Accepted 12th July 2000

The complex tris[1(*N*- ethylcarbazolyl)(3′,5′-hexyloxybenzoyl)methane](phenanthroline)europium 1 incorporates a phenanthroline ligand for electron transport and a carbazole fragment in the diketonate ligand for hole transport; furthermore, the six hexyloxy groups prevent crystallization and allow for the formation of transparent clear films directly from solution; the photoluminescence from films of 1 is nearly monochromatic, characteristic of the europium ion and proceeds with an efficiency of 50(3)%; light emitting diodes(LEDs) were fabricated using the simplest possible device architecture comprising an anode (ITO), a layer of 1 and a cathode (Ca); a second LED configuration with a PVK layer on top of the ITO was also investigated; the performance of the two types of devices is discussed.

Europium tris(β-diketonate) complexes are finding innovative applications as the electroluminescent layer in molecular light emitting diodes (LEDs).[1] Since the emission from these complexes stems from transitions between f levels that are well protected from environmental perturbations by the filled $5s^2$ and $5d^{10}$ orbitals, the resulting emission bands (585 nm, $^5D_0 \rightarrow {}^7F_1$ and 617 nm $^5D_0 \rightarrow {}^7F_2$) are nearly monochromatic.[2] Color purity of this type is required for full color displays. Pure red, green and blue light can be obtained by the use of filters, albeit with a decrease in light output.[3]

Typically, LEDs using lanthanide-based materials are fabricated by vacuum deposition of the complex onto a suitable charge injection layer. To optimize charge balance, the best devices take advantage of a multilayer architecture.[4] We recently reported polymeric light-emitting diodes that emit pure red light with a 3.5 nm linewidth by making use of energy transfer from poly[2-(6′-cyano-6″-methylheptyloxy)-1,4-pheneylene] (CN-PPP) to europium complexes with β-diketonate and phenanthroline ligands.[5] In this approach, a film containing the polymer and the complex can be cast directly from solution thereby facilitating fabrication. Efficient excitation transfer from CN-PPP results in complete quenching of the broad emission of the polymer and pure red Eu-based emission.

It occurred to us that it should be possible to design a ligand for europium that contained structural features for optimizing charge transport across the bulk and that gave the complex topological attributes which would discourage crystallization. The latter requirement was incorporated so as to obtain stable glasses and uniform optical quality thin films directly from solution. As our target, we chose the complex tris[(*N*-ethylcarbazolyl)(3′,5′-hexyloxybenzoyl)methane](phenanthroline)europium **1** (Scheme 1). The phenanthroline ligand was included since it is thought to enhance the electron transport of the material.[6] A carbazole fragment was appended to the diketonate ligand with the intention of improving hole transport.[7] Finally the hexyloxy groups were introduced to prevent crystallization and to increase solubility in common organic solvents.

As shown in Scheme 1, the diketonate ligand is prepared by Claisen condensation of 3-acetyl-9-ethylcarbazole[8] and hexyl-3,5-hexyloxybenzoate in the presence of NaH. After refluxing in dimethoxyethane for 24 h, followed by acetic work-up and purification by chromatography, (*N*-ethylcarbazolyl)(3,5-hexyloxybenzoyl)methane is obtained in 24% yield. The europium complex **1** is prepared by taking advantage of well established protocols.[9] Deprotonation of three equivalents of (*N*-ethylcarbazolyl)(3,5-hexyloxybenzoyl)methane with an excess of NaOH, followed by treatment with $EuCl_3(H_2O)_6$ and finally phenanthroline affords **1** in 50% yield. Purification can be accomplished by precipitation from concentrated acetone solutions.

Compound **1** is a pale yellow powder, which by differential scanning calorimetry (DSC) shows a glass transition temperature at 65 °C. Powder diffraction experiments show no evidence of crystalline regions. The morphological properties of compound **1** make it possible to spin-cast clear transparent films directly from solution.

Fig. 1 shows the absorption and photoluminescence spectra of a thin film of **1**. The absorption onset at *ca.* 458 nm corresponds to a HOMO–LUMO energy difference of 2.71 eV. This value is also observed in the spectrum of the sodium salt of the diketonate ligand. Light absorption is therefore controlled by the ligand framework. The sharp emission at 612 nm is characteristic of the europium ion within a tris(β-diketonate)-phenanthroline environment. Therefore, the triplet level of the ligand is sufficiently high to allow energy transfer to the ion.[10] Use of an integrating sphere revealed that the solid state photoluminescence efficiency from films of **1** is 50(3)%. These measurements were made using the 351 nm line from an argon laser (intensity of 2.5 mW cm^{-2}), an integrating sphere, a high pass filter that blocks the laser line, and a silicon diode.[11]

The resistance to crystallization and exceptionally low self quenching of **1** prompted us to examine its electroluminescent properties. Two types of LED structures were fabricated.[12] In

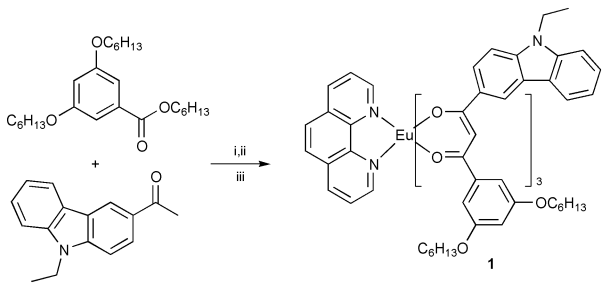

Scheme 1 *Reagents and conditions*: i, NaH/dimethoxyethane; ii, NaOH, $EuCl_3(H_2O)_6$, ethanol; iii, phenanthroline, toluene.

† Complete details for the synthesis of **1** (PDF). The material is available free of charge *via* the Internet at http://pubs.acs.org.

DOI: 10.1039/b004739m

the first device, a film of **1** (600 Å) was spin-cast directly onto the indium tin oxide (ITO) anode. The spin-casting solution was 1 wt% in toluene and was filtered through a 5 micron Nylon filter. The layer of **1** was subsequently dried under vacuum at ambient temperature for *ca.* 1 h. The calcium cathode layer was deposited as described previously and subsequently overcoated with aluminium.[12] This device has only a single layer and only one molecular component between the electrodes; *i.e.* the simplest architecture possible.

Fig. 2 shows the current–voltage curve of the single-layer device. Light emitted from this device is identical to the PL spectrum shown in Fig. 1. The turn-on voltage for current and luminance, is observed at *ca.* 5.3 V (8.8 mV $Å^{-1}$) and is similar in magnitude to many polymer LEDs and lower than many multilayer organic LEDs (OLEDs) prepared by sublimation. These characteristics demonstrate that the ligand design was successful in facilitating electron and hole injection and transport into and across the europium layer. At 15 mA cm^{-2}, the light output is 9 cd m^{-2} with an external EL quantum efficiency of 0.08%.

A second device architecture was fabricated in an effort to improve the device efficiency, and to gain insight into the mechanism of europium electroluminescence. In this archetecture, a layer of polyvinylcarbazole (PVK) (30 nm) was first spin-cast from a 2% solution of PVK in 1,1,2,2-tetrachloroethane on top of the ITO-glass substrate and, after drying at 60 °C for 1 h, a 700 Å layer of **1** was spin-cast as before. The cathode layer is the same as in type 1. Only emission from Eu was observed, *i.e.* identical to Fig. 1. Fig. 3 shows the current–voltage relationship for this device. Compared to the single layer device, the turn-on voltage is higher, *ca.* 8.7V (8.75 mV $Å^{-1}$), owing to the extra thickness introduced by the PVK layer; but both devices operate at equivalent field strengths. The device efficiency was improved considerably (50 cd m^{-2} at 15 mA cm^{-2})[13] with an external quantum efficiency of 0.3%. It is thought that the PVK layer acts both as a hole injection and an electron blocking layer[14] facilitating more balanced carrier injection from the anode and cathode.

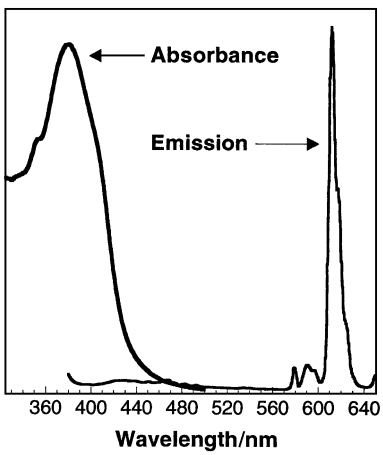

Fig. 1 Absorption and emission spectra of a thin film of **1**.

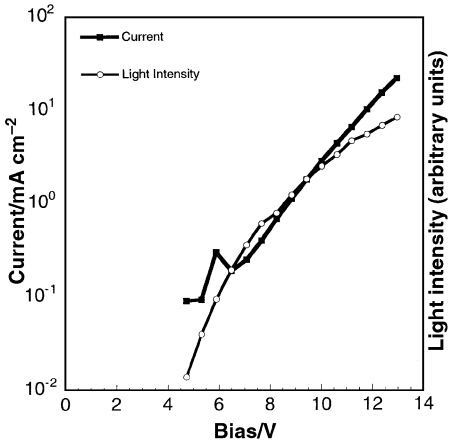

Fig. 2 Current–voltage curve of the device with configuration ITO/**1**/Ca.

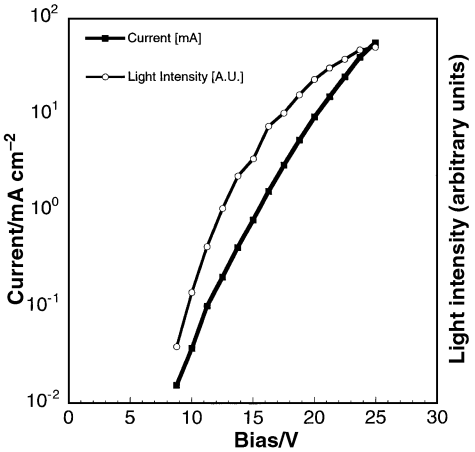

Fig. 3 Current–voltage curve of the device with configuration ITO/PVK/**1**/Ca.

In summary, it is possible to introduce structural attributes to the ligand framework of an europium complex that allow its use as the electroluminescent layer in a single component LED. The key design components include the use of hole and electron transport fragments, together with aliphatic sidegroups that lead to a stable amorphous phase. The film forming properties of **1** play an important role in device fabrication.

We thank Dr Vojislav Srdanov and Dr Troy Bergstedt for helpful discussions. This work was supported in part by the MRL Program of the NSF under Award No. DMR 96-32716 and the AFOSR under Contract No. FQ8671-9901244 STTR-TX.

Notes and references

1 (*a*) J. Kido, K. Nagai and Y. Okamoto, *J. Alloys. Compds.*, 1993, **192**, 30; (*b*) J. Kido, H. Hayase, K. Hongawa, K. Nagai and K. Okuyama, *Appl. Phys. Lett.*, 1994, **65**, 2124; (*c*) A. Edwards, C. Claude, I. Sokolik, T. Y. Chu, Y. Okamoto and R. Dorsinvill, *J. Appl. Phys.*, 1997, **82**, 1841; (*d*) K. Okada, M. Uekawa, Y.-F. Wang, T.-M. Chen and T. Nakaya, *Chem. Lett.*, 1998, 801.

2 A. P. B. Sinha, in *Spectroscopy in Inorganic Systems*, ed. C. N. R. Rao and J. R. Ferraro, Academic Press, New York, vol. 2, 1971; *Lasers and Excited States of Rare Earths*, R. Reisfeld and C. K. Jorgensen, North Holland, New York, 1978.

3 J. Kido, M. Kimura and K. Nagai, *Science*, 1995, **267**, 1332.

4 R. A. Campos, I. P. Kovalev, Y. Guo, N. Wakili and T. Skotheim, *J. Appl. Phys.*, 1996, **80**, 7144.

5 M. D. McGehee, T. Bergstedt, C. Zhang, A. P. Saab, M. B. O'Regan, G. C. Bazan, V. I. Srdanov and A. J. Heeger, *Adv. Mater.*, 1999, **11**, 1349.

6 J. Kido, W. Ineda, M. Kimura and K. Nagai, *Jpn. J. Appl. Phys.*, 1996, **35**, L394.

7 L. Liu, W. Li, Z. Hong, J. Peng, X. Liu, C. Liang, Z. Liu, J. Yu and D. Zhao, *Synth. Met.*, 1997, **91**, 267.

8 N. P. Buu-Hoi and R. Royer, *Recl. Trav. Chim.*, 1947, **66**, 533.

9 L. R. Melby, N. J. Rose, E. Abramson and J. C. Caris, *J. Am. Chem. Soc.*, 1964, **86**, 5117.

10 G. A. Crosby, R. E. Whan and R. M. Alire, *J. Chem. Phys.*, 1961, **34**, 743.

11 N. C. Greenham, I. D. W. Samuel, G. R. Hayes, R. T. Phillips, Y. A. R. R. Kessener, S. C. Moratti, A. B. Holmes and R. H. Friend, *Chem. Phys. Lett.*, 1995, **241**, 89; J. C. de Mello, H. F. Wittmann and R. H. Friend, *Adv. Mater.*, 1997, **9**, 230.

12 Y. Yang, Q. Pei and A. J. Heeger, *J. Appl. Phys.*, 1996, **79**, 934.

13 Under these conditions the efficiency may be expressed as 0.33 cd A^{-1}. For comparison, trilayer devices containing a mixture of tris(1,3-diphenylpropane-1,3-dionato)(monophenanthroline)europium with PBD have been reported to exhibit efficiencies of 1.7 cd A^{-1} at 2.2 mA cm^{-2} and 0.16 cd A^{-1} at 290 mA cm^{-2}. See ref. 1(*b*).

14 I. D. Parker, Q. Pei and M. Marrocco, *Appl. Phys. Lett.*, 1994, **65**, 1272.

ChemComm

Nickel bromide as a hydrogen transfer catalyst

Matthew D. Le Page and Brian R. James*

Department of Chemistry, University of British Columbia, Vancouver, British Columbia, Canada V6T 1Z1

Received (in Corvallis, OR, USA) 30th June 2000, Accepted 21st July 2000

Catalysed transfer hydrogenation of a range of organics is achieved using $NiBr_2$ in alkaline ^{i}PrOH

During our studies on $NiX_2(PPh_{3-n}py_n)_2$ complexes (X = halogen, py = 2-pyridyl, n = 1–3), some of which are water-soluble,[1] a report appeared on the use of a $NiCl_2(PPh_3)_2$–NaOH–^{i}PrOH system for transfer hydrogenation of ketones and aldehydes.[2] Our Ni(II) pyridylphosphines, under corresponding conditions, were of comparable activity, but some 'blank tests' soon revealed that $NiCl_2{\cdot}6H_2O$ had similar activity, while anhydrous $NiBr_2$ or $NiI_2{\cdot}6H_2O$ had much higher activity. For example, 90% conversion of cyclohexanone to cyclohexanol was attained after 1 h of refluxing in an alkaline ^{i}PrOH solution containing $NiBr_2$, whereas conversions of only 14 and 24%, respectively, were achieved with $NiCl_2(PPh_3)_2$ and $NiBr_2(PPh_3)_2$, under comparable conditions (0.4 mM Ni, 35 mM NaOH, 100 mM ketone in 3.0 cm^3 ^{i}PrOH). More optimised reaction conditions for a practical scale synthesis (5 mM $NiBr_2$, 0.5 M NaOH, 1.5 M cyclohexanone) resulted in 100% conversion after 30 min refluxing. The use of $CoBr_2$ and CoI_2 under corresponding conditions resulted in conversions of ~60%. The simplicity of the system using commercially available $NiBr_2$ makes it attractive for laboratory hydrogenations without the need for H_2, especially as it is applicable to a wide range of organic substrates (see below). A further advantage is that the system operates under aerobic conditions, while the often used platinum metal, phosphine-containing complexes are usually air-sensitive in solution.[3]

$$\text{substrate (A)} + {}^i\text{PrOH} \xrightarrow[\text{reflux}]{NiBr_2,\ NaOH} A(H)_2 + \text{acetone} \qquad (1)$$

The $NiBr_2$–NaOH–^{i}PrOH system† (eqn. 1) can be effective for catalytic hydrogen transfer of saturated ketones, aldehydes, alk-1-enes, cyclohex-2-en-1-one, nitrobenzene and 4-nitrobenzaldehyde (Table 1). For cyclohexanone, butan-2-one and oct-1-ene, the conversion activity is generally comparable with, or greater than, that reported by others for transfer hydrogenation using more 'exotic' catalysts.[2–6] The extremely efficient hydrogenation of a terminal olefin such as oct-1-ene using ^{i}PrOH is unusual; more commonly, 'hydrogenated aromatics' like 1,2-dihydronaphthalene and indoline have been used as hydrogen donors with either homogeneous or heterogeneous-based platinum metal systems,[6] but the systems are much less efficient than the $NiBr_2$ system. Internal olefins and cod are not hydrogenated; of note, the system effects selective hydrogenation of oct-1-ene in a 1 : 1 mixture with (*t*) oct-2-ene, but at a lower rate (27% conversion in 0.5 h) than with oct-1-ene alone. With α,β-unsaturated ketones, cyclohex-2-en-1-one is converted initially to cyclohexanone but this saturated ketone is subsequently reduced at a rate comparable to the rate of appearance of the cyclohexanol; *e.g.* after 0.5 h, there is 40% reduction of the enone to equal amounts of the saturated ketone and alcohol, while after 48 h there is 73% conversion of enone to essentially just cyclohexanol (Table 1)—no cyclohexen-1-ol is detected. The non-reduction of but-3-en-2-one may be due to its coordination to the Ni as a chelate, which could block coordination of the propoxide (the usually postulated steps for a homogeneously catalysed process are: propoxide coordination, hydride abstraction, and transfer to coordinated substrate[3,7]). Nitrobenzene is reduced selectively to aniline, but the conversion is only ~20% after 48 h, and there is a significant 'base-only' contribution (Table 1); correspondingly, 4-nitrobenzaldehyde undergoes Ni-promoted hydrogenation (38% in 24 h), but non-selectively to mainly the nitrobenzyl alcohol and smaller amounts of aminobenzyl alcohol and the aminobenzaldehyde.

Of interest, although the use of base co-catalysts for metal complex catalysed hydrogen transfer is common,[2–4,7–11] data on the 'base-only' systems are rarely reported.[8,9] In the strongly basic medium employed in our work, acetophenone and heptan-1-al are effectively reduced to the respective alcohols even in the absence of the $NiBr_2$ (Table 1). The basic conditions used preclude reduction of pentane-2,4-dione and hexane-2,5-dione because these were converted, respectively, to sodium acetylacetonate and a self-condensation product (probably 5-methylundec-5-ene-2,7,10-trione); in a related manner, benzaldehyde undergoes the Cannizzaro reaction to yield the alcohol and sodium benzoate. Nitriles were not reduced and, to our knowledge, there are no reports on transfer hydrogenation of nitriles.

The $NiBr_2$ system appears to be homogeneous, at least for cyclohexanone. For all the substrate systems, the initially light-coloured solutions gradually darken through yellow to orange with reaction time but, after filtration through a 0.22 μm pore, the orange filtrate showed no loss of activity, for example, for

Table 1 $NiBr_2$ catalysed transfer hydrogenation of organics[a]

Substrate	% Conversion (time, h)	% Conversion (time, h)[b]	Product(s)
Cyclohexanone	99.9 (0.5)	29.1 (0.5)	Cyclohexanol
Acetophenone	60.1 (4), 99.4 (24)	65.4 (4), 98.8 (24)	1-Phenylethanol
Butan-2-one	55.2 (2), 97.2 (24)	8.4 (2), 18.5 (24)	Butan-2-ol
Pentan-2-one	31.0 (24), 99.9 (48)	12.2 (24), 27.8 (48)	Pentan-2-ol
Oct-1-ene	99.9 (0.5)	0.0 (0.5)	*n*-Octane
Cyclohex-2-en-1-one	73.0 (48)[c]	20.0 (48)[d]	Cyclohexanone Cyclohexanol
Heptan-1-al	92.2 (4)	83.0 (4)	Heptan-1-ol
Nitrobenzene	14.1 (0.5), 19.2 (48)	4.0 (0.5), 14.0 (48)	Aniline
4-Nitrobenzaldehyde	38.0 (24)[e]	12.5 (24)[f]	ABA, NBA, AB[e]

[a] In 24 h, no conversion for: (*t*) oct-2-ene, but-3-en-2-one, pentane-2,4-dione, hexane-2,5-dione, 2-propionic acid, MeCN, PhCN and benzene, and < 5% for cyclooctene and cod. [b] In presence of base only, no $NiBr_2$. [c] 2% ketone, 71% alcohol. [d] 4% ketone, 16% alcohol. [e] 10.5% 4-aminobenzyl alcohol (ABA), 21.9% 4-nitrobenzyl alcohol (NBA), 5.6% 4-aminobenzaldehyde (AB). [f] 3.6% ABA, 7.4% NBA, 1.5% AB.

DOI: 10.1039/b005338o

cyclohexanone hydrogenation; also the addition of Hg(0), an inhibitor for colloidal activity,[12] to a 'fresh' system gave only a 7% decrease in conversion (*cf*. Table 1). Further, the solid inorganic residue obtained after a hydrogenation of cyclohexanone was re-used three more times for repeat conversions, when only slow deactivation of the catalyst was noted: 1st run, 99.9% conversion after 0.5 h; 2nd, 95% (3 h); 3rd, 92% (7 h); 4th, 63% (3 h).

Of interest, addition of up to 4 equiv. of PPh_3 to the $NiBr_2$ system has no effect on the rate of hydrogenation of cyclohexanone, and also $NiBr_2(PPh_3)_2$ is unstable in the alkaline medium (with dissociation of the phosphine), implying that in the earlier work on the $NiCl_2(PPh_3)_2$ system[2] the precursor catalyst may be simply $NiCl_2$.

We thank the NSERC of Canada for financial support.

Notes and references

† A glass vessel (35 mL) equipped with a Teflon-coated magnetic stirrer was charged in air with $NiBr_2$, NaOH and ^{i}PrOH, and the mixture heated at 95 °C to yield a pale-green solution. After this was cooled to rt, the vessel was fitted with a condenser and charged with substrate; the mixture was then refluxed, and samples were withdrawn for GC and NMR analysis (Table 1). The $NiBr_2$: NaOH : substrate ratios were 1 : 85 : 250 in all cases, with [$NiBr_2$] between 1–6 mM.

1 I. R. Baird, M. B. Smith and B. R. James, *Inorg. Chim. Acta*, 1995, **235**, 291.

2 S. Iyer and J. P. Varghese, *J. Chem. Soc., Chem. Commun.*, 1995, 465.

3 G. Zassinovich, G. Mestroni and S. Gladiali, *Chem. Rev.*, 1992, **92**, 1051.

4 K. Jothimony and S. Vancheesan, *J. Mol. Catal.*, 1989, **52**, 301.

5 M. Shibagaki, K. Takahashi and H. Matsushita, *Bull. Chem. Soc. Jpn.*, 1988, **61**, 3283.

6 T. Nishiguchi, H. Imai, H. Hirose and K. Fukuzumi, *J. Catal.*, 1976, **41**, 249; U. Gessner and A. Heesing, *Chem. Ber.*, 1985, **118**, 2593.

7 P. Kvintovics, B. R. James and B. Heil, *J. Chem. Soc., Chem. Commun.*, 1986, 1810, and references cited therein.

8 R. Chowdhury and J. Backväll, *J. Chem. Soc., Chem. Commun.*, 1991, 1063.

9 A. Mezzetti and G. Consiglio, *J. Chem. Soc., Chem. Commun.*, 1991, 1675.

10 R. Sariego, M. Martinez, I. Carkovic, R. Contreras and S. A. Moya, *J. Mol. Catal.*, 1989, **51**, 67.

11 Y. Sasson and J. Blum, *J. Org. Chem.*, 1975, **40**, 1887, and references cited therein; R. Spogliarich, J. Kaspar and M. Graziani, *J. Catal.*, 1985, **94**, 292; H. W. Krause and A. K. Bhatnagar, *J. Organomet. Chem.*, 1986, **302**, 265; S. Gladiali, G. Chelucci, G. Chessa, G. Delogu and F. Soccolini, *J. Organomet. Chem.*, 1987, **327**, C15; R. Marcec, Z. Raza and V. Šunjic, *J. Mol. Catal.*, 1991, **69**, 25; F. A. Jalón, A. Otero, A. Rodríguez and M. Perez-Manrique, *J. Organomet. Chem.*, 1996, **508**, 69; K. Püntener, L. Schwink and P. Knochel, *Tetrahedron Lett.*, 1996, **37**, 8165; T. Sammakia and E. L. Strangeland, *J. Org. Chem.*, 1997, **62**, 6104; Y. T. Jiang, Q. Z. Jiang, G. X. Zhu and X. M. Zhang, *Tetrahedron Lett.*, 1997, **38**, 215; T. T. Upadhya, S. P. Katdare, D. P. Sabde, V. Ramaswamy and A. Sudalai, *J. Chem. Soc., Chem. Commun.*, 1997, 1119; K. Matsumuru, S. Hashiguchi, I. Ikariya and R. Noyori, *J. Am. Chem. Soc.*, 1997, **119**, 8738; K. Haack, S. Hashiguchi, A. Fujii, T. Ikariua and R. Noyori, *Angew. Chem., Int. Ed. Engl.*, 1997, **36**, 285; P. Barbaro, C. Bianchini and A. Togni, *Organometallics*, 1997, **16**, 3004, and references cited therein; C. de Bellefon and N. Tanchoux, *Tetrahedron: Asymmetry*, 1998, **9**, 3677.

12 D. R. Anton and R. H. Crabtree, *Organometallics*, 1983, **2**, 855.

ChemComm

A new phthalocyanine derivative having peripheral 2-thienyl substituents

Tsuyoshi Muto, Tetsuji Temma, Mutsumi Kimura, Kenji Hanabusa and Hirofusa Shirai*

Department of Functional Polymer Science, Faculty of Textile Science and Technology, Shinshu University, Ueda, Nagano 386-8567, Japan. E-mail: hshirai@giptc.shinshu-u.ac.jp

Received (in Cambridge, UK) 9th June 2000, Accepted 24th July 2000

A phthalocyanine derivative having eight 2-thienyl substituents at the β-position was synthesized and electrochemical oxidation of the phthalocyanine gave an insoluble polymer film on the electrode surface.

π-Conjugated polymers such as polythiophenes or polyphenylenes have been the subject of intensive studies.[1] Due to the high stability of the polymers, they are readily characterized by chemical or physical methods, making them good candidates for electronic or photonic devices. Polythiophenes are the type most frequently investigated because they are easily obtained from chemical reactions[2] or electrochemical couplings of thiophene derivatives,[3] and the monomers or precursors are readily derived by conventional synthetic methods from thiophene.[4] Recently, several groups reported the design of novel conducting polymer architectures which alternatively contain functional moieties and αα′-coupled oligothiophene moieties.[5] The wide range of these studies contributed towards the application of the polymers as organic semiconductors, sensory materials or electrocatalysts.[6] Our current interest in this class of materials is motivated by the property of the attractive characteristics, endowed by functional molecules embedded in the polymer backbone, for the development of electronic devices. Phthalocyanines or phthalocyanine metal complexes are known to have a diversity of functions such as electrocatalysts or organic electronic devices.[7] Therefore, introduction of phthalocyanine moieties to the new polymer architectures imparts a variety of functions to the polymers. In this communication we demonstrate the synthesis, photo- and electrochemical properties of a new phthalocyanine (pc) derivative which has thiophene moieties as substituents, and the electrochemical construction of a pc-based polymer film deposited on the electrode surface.

The synthetic route to **1** used 4,5-dibromophthalonitrile[8] as starting material which was converted into 4,5-di-2-thienylphthalonitrile with thiophene-2-boronic acid[9] in the presence of $Pd(0)(PPh_3)_4$ under basic conditions (Scheme 1). Refluxing of 4,5-di-2-thienylphthalonitrile with NaOMe in MeOH gave 5,6-di-2-thienyl-2,3-dihydro-1,3-diiminoisoindole, and the reaction of this compound in *N*,*N*-dimethylaminoethanol at 140 °C gave **1** as a dark-green solid. Analytically pure **1** was obtained by column chromatography of the crude product on silica gel by eluting with CH_2Cl_2–*n*-hexane (2/1 v/v). This new pc derivative **1** was characterized by ^1H NMR and MALDI-TOF mass spectrometry.†

The pc derivative **1** was soluble in common organic solvents such as CH_2Cl_2, $CHCl_3$, THF and DMF but not in hexane, toluene or acetonitrile. The shape of absorption and emission spectra of **1** in $CHCl_3$ were similar to that of tetrakis(*tert*-butyl)phthalocyanine (^{t}Bupc) except for a broad absorption around 430 nm and a weak, structureless emission peak centered around 500 nm. The position of both absorption and emission bands of **1** were red-shifted about 20 nm from that of the corresponding ^{t}Bupc. These results obtained from the photophysical measurements are consistent with the presence of electronic interaction between the pc ring and 2-thienyl substituents in a molecule of **1** at their ground and excited states.

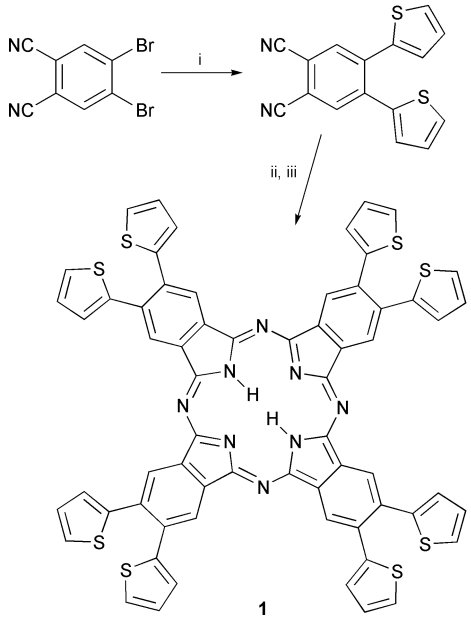

Scheme 1 (i) Thiophene-2-boronic acid, $Pd(0)(PPh)_4$, toluene, THF, EtOH, 2 M Na_2CO_3 aq., reflux under N_2, 18 h, 62%; (ii) NaOMe, MeOH, reflux under NH_3 gas, 5 h, 95%; (iii) *N*,*N*-dimethylaminoethanol, reflux under N_2, 36 h, 32%.

The pc derivative **1** was oxidatively polymerized when the potential of the electrode was swept between 0.0 and +1.1 V *vs.* Ag/Ag^+ at a scan rate of 100 mV s^{-1}. [Working electrode, indium/tin oxide coated glass (ITO) electrode; Counter electrode, Pt wire; Reference electrode, Ag/Ag^+; Solvent, 0.1 M tetra-*n*-butylammonium hexafluorophosphate ($TBAPF_6$)–CH_2Cl_2]. An anodic polymerization trace of **1** is shown in Fig. 1. The first oxidative scan is characterized by monomer

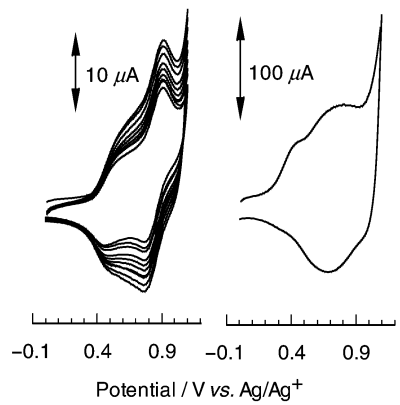

Fig. 1 Trace of oxidative scan of **1** ([**1**] = 2×10^{-4} M) in 0.1 M $TBAPF_6$–CH_2Cl_2 with ITO glass electrode (left) and cyclic voltammogram of poly(**1**) film deposited on ITO glass electrode in 0.1 M $TBAPF_6$–CH_3CN (right). Conditions: 0.1 V s^{-1}, Pt wire counter electrode; Ag/Ag^+ reference electrode.

DOI: 10.1039/b004694i

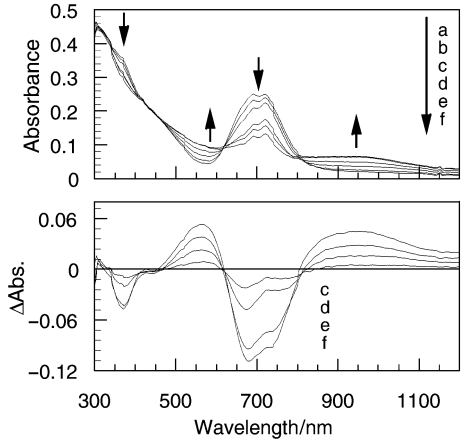

Fig. 2 *In situ* UV-Vis-NIR absorption spectra of poly(**1**) on ITO electrode upon applied potential (top): (a) 0.0 V *vs*. Ag/Ag^+; (b) +0.3 V; (c) +0.5 V; (d) +0.6 V; (e) +0.7 V; (f) + 0.8 V. Difference spectra obtained from the data of the *in situ* spectra (bottom). The neutral-point spectrum (V = 0.0 V) was used as the reference.

oxidation at +0.60 and +0.90 V followed by associated reduction at +0.45 and +0.75 V in the return process. The first oxidation wave observed in the oxidative trace of **1** is attributed to the oxidation of free-base pc[10] and the second could be attributed to the oxidation of 2-thienyl substituents at the β-position. In subsequent potential sweeps, an oxidation wave grows in around +0.70 V. Applied potential cycling results in further increased electroactivity of the electrode, indicative of insoluble polymer deposition on the electrode surface.[5] The cyclic voltammogram (CV) of the electrochemical deposited polymer (poly(**1**)) in monomer-free 0.1 M $TBAPF_6$–CH_3CN is shown in Fig. 1. The CV is characterized by the appearance of an oxidation wave at +0.4 V and a redox couple at +0.70 V. The observed difference between the redox potentials of monomer **1** and poly(**1**) is in agreement with the difference in π-conjugation length elongated in the polymerization and oxidation processes.

The *in situ* electronic absorption measurement of poly(**1**) film deposited on the ITO electrode recorded at various doping levels shows that the transition around 360 nm and pc Q-band absorption (λ_{max} = 634, 662, 692, 724 nm) decreases continuously as doping proceeds while two new absorption bands appear around 560 and 950 nm (Fig. 2). In the absorption of poly(**1**) film at high doping levels, the new lower energy π–π* transition[11] around 950 nm was promoted and grew as shown in Fig. 2. The optoelectrochemical behavior observed in our system is assigned to formation of oxidized states of poly(**1**) and the effective conjugation paths include a pc ring system and αα′-bithienyl bridges have been formed. The position of the lower energy π–π* absorption maximum is close to that reported for cation radicals of oligothiophenes, but the shape of the band is broader than that of oligothiophene cation radicals.[12] From these observations, we assume that poly(**1**) in the oxidized state has intermediary effective conjugation length of oxidized oligothiphenes and oxidized polythiophenes.

In conclusion, we have synthesized a new pc derivative **1** and constructed a π-conjugated polymer film by electrochemical oxidation of **1**. The π-conjugation length of the polymer was switched between pc-like and oligothiophene-like by application of the appropriate voltage. Since this switching is accompanied by a color change at the applied potential between 0 and +0.8 V *vs*. Ag/Ag^+, the polymer has potential electrochromic material applications.[11]

This work was supported by a Grant-in-Aid for COE Research 'Advanced Fiber/Textile Science and Technology' (No. 10CE2003) and Scientific Research (No. 11450366) from the Ministry of Education, Science, Sports, Culture of Japan.

Notes and references

† *Selected data* for **1**: (400 MHz, $CDCl_3$, 298 K, TMS): δ_H = 6.96 (br, 8H), 7.04 (br, 8H), 7.36 (br, 8H), 8.12 (br, 8H); MALDI-TOF spectrum *m/z* calcd. for ($C_{64}H_{34}N_8S_8$) 1171.5, found 1172.6. UV/Vis (in CH_2Cl_2): λ_{max} (log ε) = 724 (5.018), 692 (5.033), 662 (4.782), 634 (4.585), 364 (4.865).

1 (*a*) *Handbook of Conducting Polymers*, 2nd edn., ed. T. A. Skotheim, R. L. Elsenbaumer and J. R. Reynolds, Marcel Dekker, New York, 1998; (*b*) M. E. Lyons, in *Electroactive Polymer Electrochemistry*, ed. M. E. Lyons, Plenum, New York, 1994 vol. 1.
2 R. D. McCullough, *Adv. Mater.*, 1998, **10**, 93.
3 J. Roncali, *Chem. Rev.*, 1992, **92**, 711.
4 P. Bäuerle, in *Electronic Materials: The Oligomer Approach*, ed. K. Müllen and G. Wegner, Wiley-VCH, Weinheim, 1998.
5 (*a*) S. S. Zhu, P. J. Carroll and T. M. Swager, *J. Am. Chem. Soc.*, 1996, **118**, 8713; (*b*) R. P. Kingsborough and T. M. Swager, *Adv. Mater.*, 1998, **10**, 1100; (*c*) R. P. Kingsborough and T. M. Swager, *J. Am. Chem. Soc.*, 1999, **121**, 8825; (*d*) H. Segawa, F.-P. Wu, N. Nakayama, H. Maruyama, S. Sagisaka, N. Higuchi, M. Fujitsuka and T. Shimidzu, *Synth. Met.*, 1995, **71**, 2151; (*e*) J. L. Reddinger and J. R. Reynolds, *Macromolecules*, 1997, **20**, 673; (*f*) M. O. Wolf and M. S. Wrighton, *Adv. Mater.*, 1994, **6**, 1526.
6 R. P. Kingsborough and T. M. Swager, *Prog. Inorg. Chem.*, 1999, **48**, 123.
7 N. B. McKeown, *Phthalocyanine Materials: Synthesis, Structure and Function*, Cambridge University Press, Cambridge, 1998.
8 C. C. Leznoff, Z. Li, H. Isago, A. M. D'ascanio and D. S. Terekhov, *J. Porphyrins Phthalocyanines*, 1999, **3**, 406.
9 S. Gronowitz and D. Peters, *Heterocycles*, 1990, **30**, 645.
10 E. Ough, T. Nyokong, K. A. M. Creber and M. J. Stillman, *Inorg. Chem.*, 1988, **27**, 2724.
11 (*a*) T.-C. Chung, J. H. Kaufman, A. J. Heeger and F. Wudl, *Phys. Rev. B*, 1984, **30**, 702; (*b*) A. O. Patil, A. J. Heeger and F. Wudl, *Chem. Rev.*, 1988, **88**, 183.
12 (*a*) M. G. Hill, J. F. Penneau, B. Zinger, K. R. Mann and L. L. Miller, *Chem. Mater.*, 1992, **4**, 1106; (*b*) P. Bäuerle, U. Segelbacher, A. Maier and M. Mehring, *J. Am. Chem. Soc.*, 1993, **115**, 10 217; (*c*) D. D. Graf, R. G. Duan, J. P. Campbell, L. L. Miller and K. M. Mann, *J. Am. Chem. Soc.*, 1997, **119**, 5888.

ChemComm

Superior ion-exchanged ZSM-5 catalysts for selective catalytic oxidation of ammonia to nitrogen

Richard Q. Long and Ralph T. Yang*

Department of Chemical Engineering, University of Michigan, Ann Arbor, MI 48109-2136, USA. E-mail: yang@umich.edu

Received (in Cambridge, UK) 20th June 2000, Accepted 21st July 2000

Fe-ZSM-5 showed the best catalytic performance (nearly 100% N_2 yield) and resistance to water vapor for selective catalytic oxidation of NH_3 to N_2 at a high gas hourly space velocity (2.3×10^5 h^{-1}) among transition-metal (Cr, Mn, Fe, Co, Ni and Cu) ion-exchanged ZSM-5 catalysts.

The removal of ammonia from waste streams is becoming an increasingly important issue due to environmental reasons. Many chemical processes use reactants containing ammonia or produce ammonia as a by-product. They are all plagued with the ammonia slip problem. Selective catalytic oxidation (SCO) of ammonia to nitrogen is potentially an ideal technology for removing ammonia from oxygen-containing waste gases and consequently it is of increasing interest in recent years.[1–12] The SCO process could also be applied to the selective catalytic reduction (SCR) of NO by ammonia where ammonia slip has been a serious problem,[2] as well as to the combustion of biomass-derived gases for removing the NH_3 impurity.[3-5]

Early results[1] on ammonia oxidation showed that noble metals (*e.g.* Pt and Pd) were active for oxidation of NH_3 to NO and N_2O, while transition metal oxides such as V_2O_5 could selectively convert NH_3 to N_2, but were much less active than the noble metals. Li and Armor[2] reported that Pt, Rh and Pd exchanged to ZSM-5 or supported on Al_2O_3 showed good SCO performance in a wet stream, which were more active than V_2O_5/TiO_2 and Co-ZSM-5. More recently, Burch and Southward found that 12-tungstophosphoric acid[4] and Ni, Fe and Mn oxides supported on γ-Al_2O_3[5] were active for the reaction. A number of other catalysts were also investigated, such as $CuMoO_4$,[6] CuO/Al_2O_3,[7,8] Cu, Co and Ni oxides doped on SiO_2,[9] Cu–Mn/TiO_2,[10] V_2O_5/TiO_2, CuO/TiO_2 and Cu-ZSM-5,[11] as well as V_2O_5, MoO_3 and WO_3 on various supports.[12] They all exhited activities for N_2 formation under different conditions. However, the aforementioned work was normally performed at low space velocities ($< 10^5$ h^{-1}) and in the absence of H_2O or SO_2. Here, we report a series of transition metal (*i.e.* Cr, Mn, Fe, Co, Ni and Cu) ion-exchanged ZSM-5 samples that have excellent catalytic performance (both activity and product selectivity) for the SCO reaction at a high space velocity. The effects of H_2O and/or SO_2 are also studied.

Transition metal ion-exchanged ZSM-5 samples were prepared using the conventional ion exchange procedure. NH_4-ZSM-5 (Si/Al $\approx$ 10) was obtained from Alsi-Penta Zeolithe Gmbh (Germany). In each experiment, 2 g NH_4-ZSM-5 was added to 200 ml of 0.05 M $Cr(MeCO_2)_3$, $Mn(MeCO_2)_2$, $FeCl_2$, $Co(MeCO_2)_2$, $Ni(MeCO_2)_2$ or $Cu(MeCO_2)_2$ solution with constant stirring at room temperature. After 24 h, the particles were filtered off and washed with deionized water. Pd-ZSM-5 was prepared by exchanging NH_4-ZSM-5 with 100 ml 0.015 M $Pd(NO_3)_2$ solution at room temperature for 24 h.[2] The obtained samples were first dried at 120 °C in air for 12 h, then calcined at 500 °C for 6 h. H-ZSM-5 was prepared by calcining NH_4-ZSM-5 at 500 °C for 3 h. The metal contents measured by neutron activation analysis in the Cr, Mn, Fe, Co, Ni, Cu and Pd ion-exchanged ZSM-5 samples were 0,13, 1.03, 1.59, 1.24, 0.85, 4.35 and 5.51% by weight, respectively.

The SCO performance tests were carried out in a fixed-bed quartz reactor described elsewhere.[13] The typical reaction conditions were as follows: 0.1 g (0.13 ml) catalyst, 1000 ppm NH_3, 2% O_2, 500 ppm SO_2 (when used), 4% water vapor (when used) and balance He. The total flow rate was 500 ml min^{-1} (ambient conditions) and thus a high gas hourly space velocity (GHSV = 2.3×10^5 h^{-1}) was obtained. Premixed gases (1.05% NH_3 in He and 0.99% SO_2 in He) were supplied by Matheson. Water vapor was generated by passing He through a heated gas-wash bottle containing deionized water. The tubings of the reactor system were heat traced with heating tapes to prevent formation and deposition of ammonium sulfate/hydrogensulfate. A magnetic deflection type mass spectrometer (AERO VAC™, Vacuum Technology Inc.) was used to monitor continuously the effluent gas from the reactor. The concentrations of unreacted NH_3 and formed NO_x (NO + NO_2) were also continually monitored by a chemiluminescent NO/NO_x analyzer (Thermo Electro Corporation, Model 10), where a high temperature converter oxidized NH_3 to NO_x by the reaction $NH_3 + O_2 \rightarrow NO_x + H_2O$.

The catalytic performances of different ion-exchanged ZSM-5 catalysts are summarized in Table 1. H-ZSM-5 showed a good activity for NH_3 oxidation at 350–450 °C, with 62–74% selectivity for N_2 and 23–37% selectivity for NO. N_2 selectivity increased slightly with temperature. It is noted that a moderate

Table 1 Catalytic performance of ion-exchanged ZSM-5 catalysts[a]

Catalyst	*T*/°C	NH_3 conv. (%)	Selectivity (%)			N_2 yield (%)
			N_2	N_2O	NO	
Empty tube	350	23	51	1	48	12
	400	37	43	2	55	16
	450	55	35	1	64	19
H-ZSM-5	350	52	74	3	23	38
	400	80	73	2	25	58
	450	88	62	1	37	55
Cr-ZSM-5	350	72	75	2	23	54
	400	83	77	2	21	64
	450	96	94	1	5	90
Mn-ZSM-5	350	68	77	3	20	52
	400	81	47	4	49	38
	450	82	40	3	57	33
Fe-ZSM-5	350	63	92	0	8	58
	400	95	98	0	2	93
	450	99	100	0	0	99
Co-ZSM-5	350	58	73	4	23	42
	400	61	59	1	40	36
	450	70	49	0	51	34
Ni-ZSM-5	350	39	69	4	27	27
	400	51	62	2	36	32
	450	63	60	0	40	38
Cu-ZSM-5	350	48	95	2	3	46
	400	95	98	1	1	93
	450	97	100	0	0	97
Pd-ZSM-5	300	80	73	19	8	58
	350	92	73	17	10	67
	400	90	63	18	19	57

[a] *Reaction conditions*: 0.1 g catalyst, [NH_3] = 1000 ppm, [O_2] = 2%, He = balance, total flow rate = 500 ml min^{-1} and GHSV = 2.3×10^5 h^{-1}.

DOI: 10.1039/b004957n

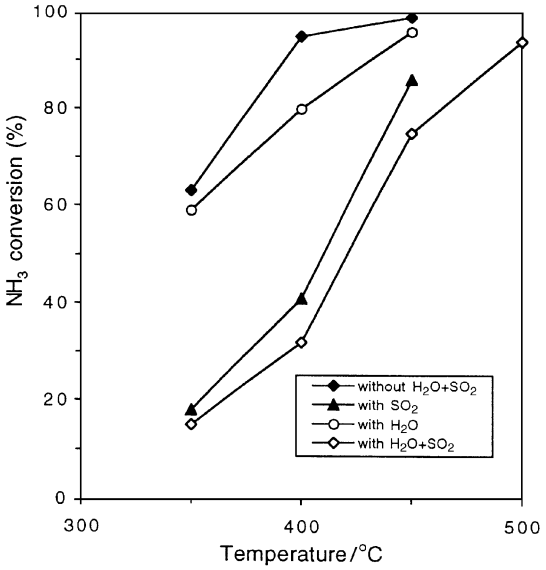

Fig. 1 Effect of H_2O and SO_2 on NH_3 conversion for Fe-ZSM-5. *Reaction conditions*: 0.1 g catalyst, $[NH_3]$ = 1000 ppm, $[O_2]$ = 2%, 500 ppm SO_2 (when used), 4% water vapor (when used), He = balance, total flow rate = 500 ml min^{-1} and GHSV = 2.3×10^5 h^{-1}.

activity was also observed on the empty reactor under the same conditions, resulting from homogeneous NH_3 oxidation, but the major product was NO (Table 1). When transition metal ions were exchanged to ZSM-5, Cr-ZSM-5, Fe-ZSM-5 and Cu-ZSM-5 showed very high activities for oxidation of NH_3 to N_2. Only small amounts of N_2O and NO were produced by Fe-ZSM-5 and Cu-ZSM-5 catalysts. Both NH_3 oxidation activity and N_2 selectivity increased with temperature. Near 100% N_2 yield was obtained on Fe-ZSM-5 at 450 °C. In comparison, a lower activity was observed on Mn-ZSM-5, Co-ZSM-5 and Ni-ZSM-5, with large amounts of NO formation. These results suggest that metal cations in the ZSM-5 play an important role in the SCO of NH_3 to N_2. Pd-ZSM-5, a good SCO catalyst reported by Li and Armor,[2] also showed high NH_3 conversions under our reaction conditions, *i.e.* a higher space velocity (2.3×10^5 h^{-1} *vs.* 4.6×10^4 h^{-1} in ref. 2), but the selectivity for N_2 was lower than that on Fe-ZSM-5 and Cu-ZSM-5. The maximum N_2 yield on the above catalysts increased in the sequence of Co-ZSM-5 ≈ Ni-ZSM-5 < Mn-ZSM-5 < H-ZSM-5 < Pd-ZSM-5 < Cr-ZSM-5 < Cu-ZSM-5 < Fe-ZSM-5. This rank order is similar to the previous results obtained on the metal ion-exchanged Y zeolites, except for Fe.[1] The nitrogen balance was above 95% in this work.

It is known that the waste streams usually contain water vapor and small amounts of SO_2. We further studied the effects of H_2O and SO_2 on the catalytic performance of Cr-ZSM-5, Fe-ZSM-5 and Cu-ZSM-5. For Cr-ZSM-5, when 500 ppm SO_2 and/or 4% H_2O were added to the reactants, NH_3 conversion decreased significantly. Only 50% NH_3 conversion was obtained at 450 °C in the presence of both H_2O and SO_2. Comparatively, NH_3 conversion was decreased only slightly by H_2O on Fe-ZSM-5 (Fig. 1). SO_2 and $H_2O + SO_2$ decreased NH_3 conversion at 350–450 °C, but the decrease was less significant at high temperatures. For example, 94% NH_3 conversion could be obtained at 500 °C. H_2O and SO_2 also inhibited NH_3 conversion over Cu-ZSM-5. Only 65% NH_3 conversion was observed at 450 °C in the presence of H_2O and SO_2. Increasing the temperature to 500 °C resulted in 73% NH_3 conversion. N_2 was the dominant product for NH_3 oxidation in the presence of H_2O and/or SO_2.

The above results indicate that Fe, Cu and Cr ion-exchanged ZSM-5 are very active for selective catalytic oxidation of NH_3 to N_2. Our previous results showed that, although iron cations were exchanged with NH_4-ZSM-5 as Fe^{2+}, most iron cations in the Fe-ZSM-5 are present as Fe^{3+} ions after calcination, leaving only a small amount of Fe^{2+}.[14] An equilibration between Fe^{2+} and Fe^{3+} exists in the Fe-ZSM-5. It has also been reported that both Cu^+ and Cu^{2+} ions are present in Cu-ZSM-5[15] and the ratio of Cu^+/Cu^{2+} depends on the Cu content and the preparation procedure. The variable valence of metal cations in these two catalysts may be beneficial to oxygen adsorption and activation. Therefore, a high activity for the SCO reaction is expected. Relatively lower activities were observed on Mn, Co, and Ni ion-exchanged ZSM-5. This may be attributed to their stabilized valence in zeolites,[1] which is not favorable for oxygen activation. H_2O and SO_2 have strong negative effects on NH_3 conversion for Cr-ZSM-5 and Cu-ZSM-5, whereas H_2O decreased NH_3 conversion slightly for Fe-ZSM-5. Although SO_2 decreased NH_3 conversion at low temperatures for Fe-ZSM-5, a high NH_3 conversion (94%) was obtained at 500 °C in the presence of H_2O and SO_2 at such a high space velocity (GHSV = 2.3×10^5 h^{-1}). Fe-ZSM-5 may be suitable as a practical catalyst for oxidation of NH_3 to N_2 in a wet stream. In addition, the effects of the ammonia concentration on activity and other Fe-exchanged zeolites were also studied for the SCO reaction. The initial results showed that NH_3 conversion over Fe-ZSM-5 increased with a decrease in NH_3 concentration. For example, 99% NH_3 conversion was obtained at 350 °C when the NH_3 concentration was decreased to 10 ppm (*vs.* 63% at 1000 ppm). Also, the SCO performance was found to follow the trend Fe-ZSM-5 ≈ Fe-mordenite ≈ Fe-clinoptilolite > Fe-Y ≈ Fe-beta > Fe-ferrierite ≈ Fe-chabazite. More details will be presented in a future paper. Moreover, Fe-ZSM-5 is also a good catalyst for the selective catalytic reduction (SCR) of NO with ammonia.[13] In the SCR reaction, the reactions of NH_3 with NO/O_2 and that with O_2 are known as two competitive reactions. A decrease in reactivity of NH_3 with O_2 by $H_2O + SO_2$ will be beneficial to NO reduction, which has indeed been observed in our previous results that $H_2O + SO_2$ increased the SCR activity at high temperatures on Fe-ZSM-5.[13]

We gratefully acknowledge Dr Ramsay Chang of EPRI for discussions.

Notes and references

1 N. I. II'chenko, *Russ. Chem. Rev.*, 1976, **45**, 1119.
2 Y. Li and J. N. Armor, *Appl. Catal. B*, 1997, **13**, 131.
3 E. M. Johansson and S. G. Järås, *Catal. Today*, 1999, **47**, 359.
4 R. Burch and B. W. L. Southward, *Chem. Commun.*, 1999, 1475.
5 M. Amblard, R. Burch and B. W. L. Southward, *Appl. Catal. B*, 1999, **22**, L59.
6 H. S. Gandhi and M. Shelef, *J. Catal.*, 1975, **40**, 312.
7 L. Gang, J. van Grondelle, B. G. Anderson and R. A. van Santen, *J. Catal.*, 1999, **186**, 100.
8 T. Curtin, F. O'Regan, C. Deconinck, N. Knuttle and B. K. Hodnett, *Catal. Today*, 2000, **55**, 189.
9 F. Dannevang, *US Pat.*, 5 587 134, 1996.
10 A. Wollner and F. Lange, *Appl. Catal. A*, 1993, **94**, 181.
11 N. N. Sazonova, A. V. Simakov, T. A. Nikoro, G. B. Barannik, V. F. Lyakhova, V. I. Zheivot, Z. R. Ismagilov and H. Veringa, *React. Kinet. Catal. Lett.*, 1996, **57**, 71.
12 M. de Boer, H. M. Huisman, R. J. M. Mos, R. G. Leliveld, A. J. Vandillen and J. W. Geus, *Catal. Today*, 1993, **17**, 189.
13 R. Q. Long and R. T. Yang, *J. Catal.*, 1999, **188**, 332.
14 R. Q. Long and R. T. Yang, *J. Catal.*, in press.
15 C. Torre-Abreu, M. F. Ribeiro, C. Henriques and G. Delahay, *Appl. Catal. B*, 1997, **12**, 249.

ChemComm

First oxidative cyclization of 1,3-bis(trimethylsilyloxy)buta-1,3-dienes

Peter Langer* and Valentin Köhler

Institut für Organische Chemie der Georg-August-Universität Göttingen, Tammannstrasse 2, 37077 Göttingen, Germany. E-mail: planger@uni-goettingen.de

Received (in Cambridge, UK) 1st June 2000, Accepted 26th July 2000

The first oxidative cyclizations of 1,3-bis(trimethylsilyloxy)-buta-1,3-dienes, electroneutral 1,3-dicarbonyl dianion synthons, result in regioselective formation of functionalized 1,4-dihydroquinones.

The development of new, preparatively useful single-electron-transfer (SET) reactions is of considerable current interest. Although SET-oxidations of monoanions have been extensively studied,[1] little is known about dianion oxidations.[2] Herein, we wish to report, to the best of our knowledge, the first oxidative cyclizations of 1,3-bis(trimethylsilyloxy)buta-1,3-dienes which represent electroneutral 1,3-dicarbonyl dianion synthons.[3] This methodology provides a direct, mild and regioselective synthesis of 2,3-acceptor-substituted 1,4-dihydroquinones which can be regarded as products of a formal oxidative cyclization of 1,3-dicarbonyl dianions.[4] These products, which have been previously prepared by multi-step syntheses under drastic conditions,[5] represent useful intermediates in organic synthesis. 2,3-Acceptor-substituted 1,4-dihydroquinones are present in a variety of polyketide-derived natural products, such as *dericamycin A* and the related *fredericamycin A*,[5a] or prominent enediynes, such as *calicheamicin*, *esperamicin*, *neocarzinostatin* chromophore or *dynemicin A*.[6a] Simple 1,4-dihydroquinone-2,3-dicarbonyl derivatives have proven biologically active against murine tumors.[6b]

Oxidation of the dianion[7,8] of ethyl acetoacetate with iodine or bromine in the presence of catalytic amounts of copper(I) chloride has been reported to afford the open-chain dimerization product **2** rather than a cyclization product (Scheme 1).[9] The use of 1,2-dibromoethane, $CuCl_2$ and $Cu(OTf)_2$ as the oxidizing agents resulted in formation of complex mixtures. The main problem associated with the oxidative cyclization of dianions is the fact that, due to electrostatic repulsion, dimerization of the radical anionic intermediates is slow and many side-reactions, such as deprotonation of the solvent (THF), can occur.

Our concept to overcome these problems was to study the oxidative dimerization of 1,3-bis(trimethylsilyloxy)buta-1,3-dienes **3**.[10] Slow addition of an acetonitrile solution of CAN to an acetonitrile solution of $NaHCO_3$ and diene **3a**[3c] resulted in formation of the ester-substituted 1,4-dihydroquinone **4a**, however, in only low yield. Much to our satisfaction, employment of an inverse addition protocol resulted in an increase of the yield. Optimal yields (up to 56%) were obtained when an acetonitrile solution of **3a** (2 eq.) was slowly added to a solution of CAN (6 eq.) and $NaHCO_3$ (12 eq.) at −45 °C.†

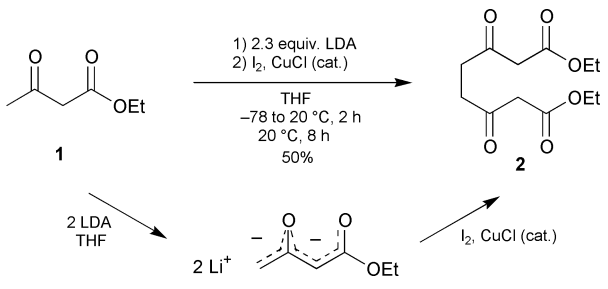

Scheme 1

Formation of **4a** can be explained by the following working hypothesis (Scheme 2): SET-oxidation of **3a** affords the radical-cation **A**. Formation of a ceric enolate, supported by the chelating nature of the two oxygen atoms, can not be excluded.[11] Cleavage of the Si–O bond and $NaHCO_3$-assisted extrusion of a silyl-cation results in formation of radical **B** which subsequently attacks the terminal carbon atom of a second molecule of **3a** to give intermediate **C**. Radical **B** should be more stable than the isomeric, cross-conjugated radical **B′**. Oxidation and extrusion of the second silyl group affords intermediate **D**. Oxidation of the latter and extrusion of the third silyl group results in formation of intermediate **E**. Cyclization, oxidation and extrusion of the fourth silyl group affords intermediate **F** which is subsequently oxidized to give the final product **4a**.

The 'head–head' regioselectivity may be rationalized by considering that attack at the γ-position of radical **B** leads to the most stabilized carbonyl conjugated α-silyloxy radical **C**. Radical **C** is probably formed through a transition state less

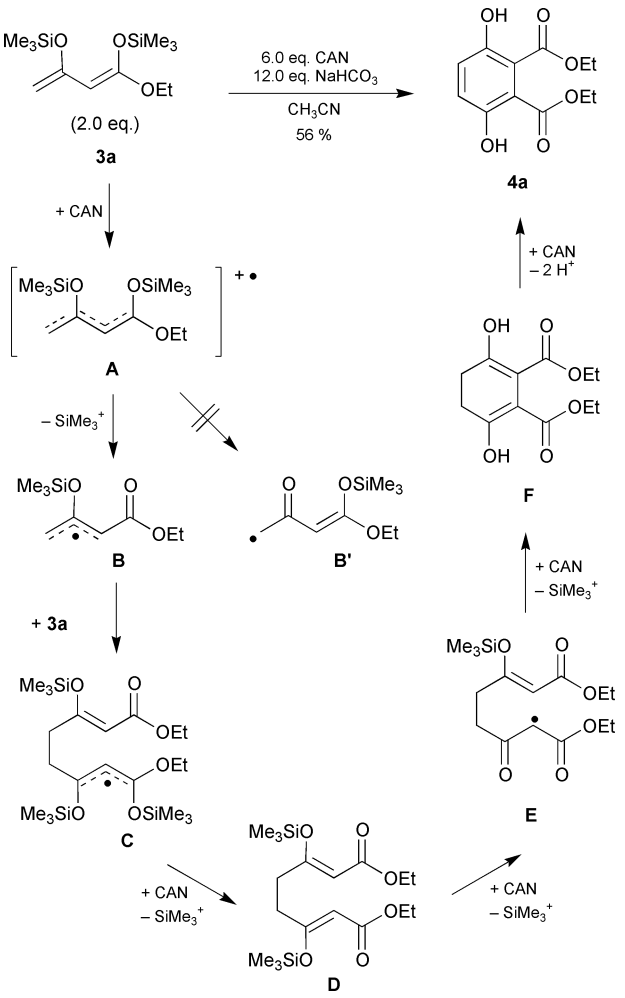

Scheme 2

DOI: 10.1039/b004387g

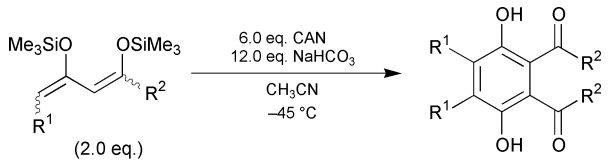

Scheme 3

Table 1 Oxidative cyclization of 1,3-bis(trimethylsilyloxy)buta-1,3-dienes **3**

4	R^1	R^2	yield (%)[a]
a	H	OEt	56
b	H	OMe	55
c	H	O(*i*-Pr)	52
d	H	$O(CH_2)_2OMe$	54
e	H	O(*i*-Bu)	54
f	H	O(*t*-Bu)	26
g	H	OCH_2Ph	41
h	H	Me	28
i	Me	OMe	38
j	Et	OEt	41
k	OMe	OMe	29
l	CO_2Me	Me	18

[a] Isolated yields.

energetic than that leading to the respective unconjugated α-silyloxy radical (by attack of the central carbon atom of intermediate **B** onto **3a**), assuming the addition step possesses a substantial product-like character. This suggestion is supported by the regioselectivity observed for the alkoxy radical catalyzed auto-oxidation of 1,4-dienes.[12] It is noteworthy, that the open-chain dimer **2** was isolated as a side-product in low yield. This result supports the assumption that bis-silyl enol ether **D** represents an intermediate of the reaction.

In order to study the preparative scope of our new cyclization reaction, the substituents of the 1,3-bis(trimethylsilyloxy)buta-1,3-dienes were systematically varied (Table 1). Oxidation of the dienes derived from ethyl-, methyl-, iso-propyl-, methoxy-ethyl-, iso-butyl-, *tert*-butyl- and benzyl acetoacetate afforded the corresponding ester-substituted 1,4-dihydroquinones **4a**–**g** with very good regioselectivities. Dimerization of the diene derived from acetylacetone afforded 2,3-diacetyl-1,4-dihydroquinone (**4h**). Oxidation of the 1,3-bis(trimethylsilyloxy)buta-1,3-dienes derived from methyl 3-oxopentanoate and ethyl 3-oxohexanoate afforded the 1,4-dihydroquinones **4i**–**j** containing two ester groups at carbons C-2 and C-3 and two alkyl groups at carbons C-5 and C-6. Oxidation of the 1,3-bis-(trimethylsilyloxy)buta-1,3-diene derived from methyl 4-methoxyacetoacetate resulted in formation of the highly functionalized 1,4-dihydroquinone **4k**. Reaction of the diene derived from methyl 3,5-dioxohexanoate afforded the highly functionalized 1,4-dihydroquinone **4l**.

In summary, we have developed the first oxidative cyclizations of 1,3-bis(trimethylsilyloxy)buta-1,3-dienes which represent electroneutral 1,3-dicarbonyl dianion synthons. Currently, we are studying the mechanism and preparative scope of the new transformation.

P. L. thanks Professor A. de Meijere for his support. Financial support from the *Fonds der Chemischen Industrie* (Liebig scholarship and funds for P. L.) and from the *Deutsche Forschungsgemeinschaft* is gratefully acknowledged.

Notes and references

† *Preparation of 1,4-dihydroquinone* **4a**. To a thoroughly degassed CH_3CN solution (25 ml) of $NaHCO_3$ (15.3 mmol, 12 eq., 1.29 g) and CAN (7.65 mmol, 6 eq., 4.20 g) was slowly added a CH_3CN solution (2 ml) of 1,3-bis(trimethylsilyloxy)buta-1,3-diene **3a** (2.55 mmol, 2 eq., 0.7 g) at −45 °C. The temperature of the reaction mixture was allowed to rise to 20 °C during 2 h. After stirring for 1 h at 20 °C a saturated aqueous solution of brine was added, the organic layer was separated and the aqueous layer was repeatedly extracted with ether. The combined organic extracts were dried ($MgSO_4$), filtered and the solvent of the filtrate was removed *in vacuo*. The residue was purified by column chromatography (silica gel, ether–petrol ether = 1:1; ($CDCl_3$, 250 MHz) δ_H 1.34 (t, 6 H, J = 7, CH_3), 4.34 (q, 4 H, J = 7, OCH_2), 7.07 (s, 2 H, CH), 8.85 (s, 2 H, OH; ($CDCl_3$, 62.5 MHz) δ_C 13.98, 62.01, 112.66, 123.83, 152.29, 168.98; MS (70 eV) 254 (22, M^+), 208 (40), 180 (100), 162 (58); *Anal*. calcd. for $C_{12}H_{14}O_6$: C, 56.69; H, 5.55. Found: C, 56.42; H, 5.68. All compounds were characterized by spectroscopic methods and gave correct elemental analyses and/or high resolution mass spectra.

1 (*a*) T. Linker and M. Schmittel, *'Radikale und Radikalionen in der Organischen Synthese'*, Wiley-VCH, Weinheim, New York, 1998; (*b*) R. D. Guthrie, in *'Studies in Organic Chemistry*, **5**, *Comprehesive Carbanion Chemistry*, Part A', eds. E. Buncel and T. Durst, Elsevier/North-Holland, New York, 1980, ch. 5, p. 197.
2 For the oxidative cyclization of dianions, see: (*a*) R. B. Bates, F. A. Camou, V. V. Kane, P. K. Mishra, K. Suvannachut and J. J. White, *J. Org. Chem.*, 1989, **54**, 311; (*b*) M. A. Fox and C.-C. Chen, *J. Chem. Soc., Chem. Commun.*, 1985, 23; (*c*) O. Witt, H. Mauser, T. Friedl, D. Wilhelm and T. Clark, *J. Org. Chem.*, 1998, **63**, 959; for other oxidations of dianions, see: (*d*) R. B. Bates and T. J. Siahaan, *J. Org. Chem.*, 1986, **51**, 1432; (*e*) R. B. Bates and C. A. Ogle, *J. Org. Chem.*, 1982, **47**, 3949; (*f*) J. J. Bahl, R. B. Bates, W. A. Beavers and N. S. Mills, *J. Org. Chem.*, 1976, **41**, 1620.
3 We and others consider dienes **3** as dianion synthons knowing that they represent electroneutral bis-silyl enol ethers. From a preparative viewpoint, 1,3-dicarbonyl dianions and dienes **3** show the same regioselectivity in reactions with electrophiles: (*a*) P. Brownbridge, T.-H. Chan, M. A. Brook and G. J. Kang, *Can. J. Chem.*, 1983, **61**, 688; (*b*) T.-H. Chan and P. Brownbridge, *J. Am. Chem. Soc.*, 1980, **102**, 3534; (*c*) G. A. Molander and K. O. Cameron, *J. Am. Chem. Soc.*, 1993, **115**, 830.
4 For the oxidative dimerization of malonic esters to give acceptor-substituted alkenes, see: T. Linker and U. Linker, *Angew. Chem.*, 2000, **112**, 934; *Angew. Chem., Int. Ed.*, 2000, **39**, 902.
5 (*a*) T. R. Kelly, S. H. Bell, N. Ohashi and R. J. Armstrong-Chong, *J. Am. Chem. Soc.*, 1988, **110**, 6471; (*b*) M. F. Ansell, B. W. Nash and D. A. Wilson, *J. Chem. Soc.*, 1963, 3028; (*c*) J. Thiele and J. Meisenheimer, *Chem. Ber.*, 1900, **33**, 675.
6 (*a*) A. G. Myers, N. J. Tom, M. E. Fraley, S. B. Cohen and D. J. Madar, *J. Am. Chem. Soc.*, 1988, **110**, 6471 and references cited therein; (*b*) E. M. Newman, A. J. Lin and A. C. Sartorelli, *J. Med. Chem.*, 1980, **23**, 627.
7 For 1,3-dicarbonyl dianions, see: (*a*) L. Weiler, *J. Am. Chem. Soc.*, 1970, **92**, 6702; (*b*) D. Seebach and V. Ehrig, *Angew. Chem.*, 1974, **86**, 446; *Angew. Chem., Int. Ed. Engl.*, 1974, **13**, 401.
8 For recent cyclization reactions of 1,3-dicarbonyl dianion synthons with 1,2-dielectrophiles, see: (*a*) P. Langer and M. Stoll, *Angew. Chem.*, 1999, **111**, 1919; *Angew. Chem., Int. Ed.*, 1999, **38**, 1803; (*b*) P. Langer, T. Schneider and M. Stoll, *Chem. Eur. J.*, 2000, in the press; (*c*) P. Langer and E. Holtz, *Angew. Chem.*, 2000, in the press; (*d*) P. Langer and T. Eckardt, *Angew. Chem.*, 2000, accepted; (*e*) P. Langer and T. Krummel, *Chem. Commun.*, 2000, 967.
9 K. G. Hampton and J. J. Christie, *J. Org. Chem.*, 1975, **40**, 3887.
10 For CAN promoted oxidations of silyl enol ethers, see: (*a*) E. Baciocchi, A. Casu and R. Ruzziconi, *Tetrahedron Lett.*, 1989, 3707; (*b*) A. B. Paolobelli, D. Latini and R. Ruzziconi, *Tetrahedron Lett.*, 1993, 721; a $TiCl_4$ mediated oxidative dimerization of a bis-silyl enol ether to give an open-chain product has been previously noted: see reference 3*a*.
11 For the spectroscopic detection of radical cations of titanium enolates, enols and silyl enol ethers, see: (*a*) M. Schmittel, G. Gescheidt and M. Röck, *Angew. Chem.*, 1994, **106**, 2056; *Angew. Chem., Int. Ed. Engl.*, 1994, **33**, 1961; (*b*) M. Schmittel, M. Keller and A. Burghart, *J. Chem. Soc., Perkin Trans. 2*, 1995, 2327; (*c*) M. Schmittel and R. Söllner, *Angew. Chem.*, 1996, **108**, 2248; *Angew. Chem., Int. Ed. Engl.*, 1996, **35**, 2107.
12 (*a*) E. N. Frankel, R. F. Garwood, J. R. Vinson and B. C. L. Weedon, *J. Chem. Soc., Perkin Trans. 1*, 1982, 2707; (*b*) N. A. Porter, *Acc. Chem. Res.*, 1986, **19**, 262.

ChemComm

Entropy–enthalpy compensation and anticompensation: solvation and ligand binding

Otto Exner

Institute of Organic Chemistry and Biochemistry, Academy of Sciences of the Czech Republic, 16610 Praha 6, Czech Republic. Fax: +420 2 3111733

Received (in Cambridge, UK) 6th April 2000, Accepted 21st July 2000

Plots of $\Delta H°$ *versus* $T\Delta S°$ are misleading and can suggest an apparent linear relationship (compensation) with a slope near to unity when $\Delta S°$ has been obtained from experimental $\Delta G°$ and $\Delta H°$; recently reported relationships with a slope of -1 in the fields of enzyme complexes and hydration processes are still more misleading and have arisen only by deliberately selecting the input data.

Linear dependences between enthalpy and entropy in a series of related reactions (isokinetic relationship) have been observed in various fields and have been the subject of many theoretical considerations.[1,2] However, a regression or plot according to eqn. (1) presents non-trivial statistical problems. Neglecting these often leads to results[2,3] which are totally at variance with the original experimental data.[4]

$$\delta\Delta H = \beta\delta\Delta S \quad (1)$$

In the notation used here, the symbol δ is the difference between a given reaction and the reaction used as reference and Δ is the difference between the products and reactants as usual. Both ΔH and ΔS may refer either to thermodynamics ($\Delta H°$ and $\Delta S°$) or to kinetics ($\Delta H^{\ddagger}$ and $\Delta S^{\ddagger}$). The slope β has dimension of temperature (isokinetic temperature). The problems and their solution depend on how ΔH and ΔS have been obtained.[1,5] When the original experimental quantities are $\Delta H°$ (obtained for instance by calorimetry) and $\Delta G°$ (from equilibrium measurements),[6] a plot according to eqn. (1) may yield a slope β near to the experimental temperature. One speaks about compensation[2,4] since the contributions of $\Delta H°$ and of $\Delta S°$ to the resulting $\Delta G°$ are opposite. In a formal modification, eqn. (1a), the dimensionless slope (β/T) is near to unity.

$$\delta\Delta H = (\beta/T)\, T\, \delta\Delta S \quad (1a)$$

However, dependence with this slope means only that ΔG is nearly constant, a plot according to eqn. (1) or (1a) expresses in fact the dependence of ΔH on itself. A plot of ΔH *vs.* ΔG was recommended in these cases.[7]

In a recent communication,[8] plots of $\delta\Delta H°$ *versus* $T\delta\Delta S°$ according to eqn. (1a) were reported for two series of reactions. In both, a regression line of a slope near to -1 was found. The conclusions were drawn[8] that (a) there is a linear relation between enthalpy and entropy in both sets and (b) that a compensation of enthalpy and entropy[2,4] is not a general feature since the present case is just an example of anti-compensation. The purpose of the present work is to prove that these conclusions are not right: (a) any plot of ΔH *versus* ΔS cannot be recommended when these two variables are *a priori* dependent by the procedure of their estimation and (b) the slope (β/T) equal to -1 is not a result of any natural law but has arisen by an arbitrary choice of data.

The first example, complex formation of various peptides with an enzyme, was thoroughly investigated[9,10] by thermometric titration.[11] In this method, one obtains $\Delta G°$ and $\Delta H°$ simultaneously from a non-linear regression.[12] One can assume with a good approximation that their estimates are not intercorrelated, *i.e.* not statistically dependent from the procedure of their calculation.[12] Fig. 1(a) shows all data from one experimental study,[9] concerning seven compounds at five temperatures. No dependence is evident: $\Delta H°$ are more variable than $\Delta G°$ and depend rather more on temperature, still more strongly than on the reactant. In any case, it is evident that the choice of data into the correlation,[8] eqn.(1a), was arbitrary. One has always withdrawn two data and plotted their difference. Four such pairs are shown by arrows in Fig. 1(a). Their position is suitable to obtain the slope $\beta/T = -1$ in eqn. (1a) but other points would yield different slopes. For instance, it would be sufficient to choose the same pair of compounds as in the uppermost example in Fig. 1(a) (points ○→△) but at a different temperature (dashed arrow): instead of -1 a slope of +0.61 would be obtained in eqn. (1a).

The picture changes when one goes from the plot $\Delta H°/\Delta G°$ to the plot $\Delta H°/T\Delta S°$ [Fig. 1(b)]. Plots of this type may be misleading[5,7] when $\Delta G°$ is almost constant, since they express mainly the dependence of $\Delta H°$ on itself. This is also the case in Fig. 1(b). The apparent correlation coefficient $R = 0.975$ expresses only this dependence. The slope $b = \beta/T$ is not significantly different from unity. In terms of eqn. (1), this means that the isokinetic temperature β is equal to the experimental temperature T. This was commonly assumed[1] as a proof that the isokinetic relationship is only apparent, although it is not a deciding proof in all cases.[14] In the paper under criticism,[8] the picture represented by Fig. 1(b) was not accepted as an (apparent or actual) dependence with unity slope but several particular pairs of points were taken off, yielding an opposite slope of -1. As shown already in Fig. 1(a), selection of these points was arbitrary if not biased, and there is no physical reason for choosing just these points. The whole procedure[8] of treating eqn. (1) is unique. The operator δ means commonly comparison with a reference object, reaction, or substrate but this reference is always common for all objects. Introducing this operator means shifting the origin of coordinates and has no effect on the statistics. In ref. 8, a particular

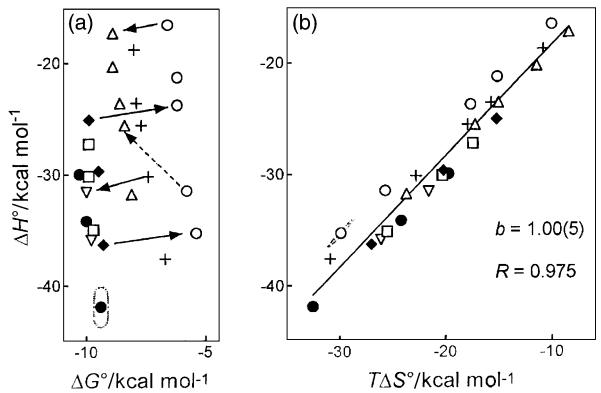

Fig. 1 (a) Experimental (ref. 9) enthalpy $\Delta H°$ *versus* Gibbs energy $\Delta G°$ of binding in a series of peptides with ribonuclease S: (○) peptide M13A, (△) M13ANB, (▽) M13V, (□) M13I, (◆) M13L, (●) S15, (+) M13F. The arrows show the pairs of peptides selected in ref. 1; the broken arrow is an alternative possibility. (b) Plot of $\Delta H°$ *versus* $T\Delta S°$ for the same set of data. The experimental uncertainty is shown as an ellipse corresponding to $\pm 3\sigma$ at one point in each graph.

DOI: 10.1039/b002758h

reference object is chosen in each case: one does not deal with the objects but with the arbitrarily selected pairs of objects.

The conclusion for this set of data is that there is no relationship between experimental[9] $\Delta G°$ and $\Delta H°$. The values of $\Delta H°$ are strongly dependent on temperature and it seems that their experimental uncertainty was somewhat underestimated.[9] When one chooses arbitrarily two compounds, one can observe various slopes, even the reported[8] value of -1.

The second case[8] concerns hydration enthalpies $\Delta H°_h$ and Gibbs energies $\Delta G°_h$ of simple organic compounds and is different in character. The two quantities have been obtained from independent experiments. From some 160 compounds listed in a review,[15] 33 pairs were selected,[8] again rather arbitrarily: some compounds were even chosen several times. In all pairs the first compound is simpler, the second may be considered as its derivative or analogue. However, the relation is not always evident. In Fig. 2(a) only these selected[8] compounds are shown. In the whole set, there is no stochastic dependence of $\Delta H°_h$ and $\Delta G°_h$ but relationships are evident when one divides the compounds into classes; most evident is a group of O- and N-derivatives with large negative values of both $\Delta H°_h$ and $\Delta G°_h$. Pairs of compounds compared were selected intentionally to obtain an increase in the two quantities in a ratio approximately $\delta\Delta G°_h/\delta\Delta H°_h = 2$; two such pairs are shown in Fig. 2(a) by arrows. Some of these choices were quite artificial and certain alternatives seem more natural (broken arrows) which would not produce the desired result. For instance, one cannot understand why cyclohexane should be compared with toluene (arrow ⊙→□) instead of with benzene (broken arrow ⊙→□) or cyclopropane with but-1-yne (arrow ⊙→▽) and not with prop-1-ene (broken arrow ⊙→△). When the plot is transformed into a plot $\Delta H°_h/T\Delta S°_h$ [Fig. 2(b)], the groups of compounds are represented by approximate linear relationships which can be considered as a dependence of $\Delta H°_h$ on itself (slope near to +1). Arbitrary pairs of near points can be selected in this graph, giving a slope -1, similarly one can select pairs with any other slope.

The conclusion concerning the hydration process is that there is a stochastic, not a linear dependence between $\Delta H°_h$ and $\Delta G°_h$: compounds can be divided into groups, in which greater negative values belong particularly to hydrophilic compounds. Values of $\Delta G°_h$ within each subset are nearly constant while $\Delta H°_h$ are more sensitive to small structural changes. For a given pair of compounds, any arbitrary slope can be found.

Examples analyzed here confirm the previous statement[1,4,5] that the plots of $\Delta H°$ *versus* $T\Delta S°$ are misleading and can suggest an apparent dependence without a physical meaning when $\Delta S°$ was obtained from $\Delta H°$ and $\Delta G°$. Still more misleading may be comparing only pairs of reactions.[8] Then even a slope of -1 can be obtained for selected pairs. Nevertheless, anti-compensation with a negative slope, not exactly -1, exists and was detected in kinetics by exact statistical methods.[14]

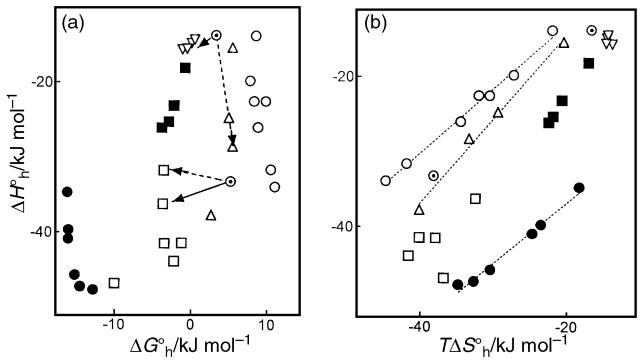

Fig. 2 (a) Experimental (ref. 15) hydration enthalpy $\Delta H°_h$ *versus* hydration Gibbs energy $\Delta G°_h$: (○) alkanes, (⊙) cycloalkanes, (△) alkenes, (▽) alkynes, (□) aromatic hydrocarbons, (■) monohalogenomethanes, (●) oxygen and nitrogen derivatives. The arrows show some of the pairs selected in ref. 8, broken arrows indicate physically more justified choices. (b) The plot of $\Delta H°_h$ *versus* $T\Delta S°_h$ for the same set of data. Dotted lines are regression lines for some subgroups.

This work has been supported by the grant 203/99/1454 of the Grant Agency of the Czech Republic.

Notes and references

1 O. Exner, *Prog. Phys. Org. Chem.*, 1973, **10**, 411; W. Linert, *Chem. Soc. Rev.*, 1994, **23**, 429.

2 For instance: J. E. Leffler, *J. Org. Chem.*, 1955, **20**, 1202; R. Lumry and S. Rajender, *Biopolymers*, 1970, **9**, 1125; R. F. Brown, *J. Org. Chem.*, 1962, **27**, 3015; P. Beltrame and M. Simonetta, *Gazz. Chim. Ital.*, 1959, **89**, 495; A. K. Galwey, *Adv. Catal*, 1977, **26**, 247.

3 For instance: L. M. Gnanados and D. Kalaivani, *J. Org. Chem.*, 1985, **50**, 1178; S. S. Kim., S. Y. Choi and C. H. Kang, *J. Am. Chem. Soc.*, 1985, **107**, 4234; T. Asano, T. Okada, S. Shinkai, K. Shigematsu, Y. Kusano and O. Manabe, *J. Am. Chem. Soc.*, 1981, **103**, 5161; V. Dorovska-Taran, R. Momtcheva, N. Gulubova and K. Martinek, *Biochim. Biophys. Acta*, 1982, **702**, 37; E. M. Y. Quinga and G. D. Mendenhall, *J. Org. Chem.*, 1985, **50**, 2836; V. Palm and S. Kaasik, *Org. React. (Tartu)*, 1996, **30**, 73.

4 O. Exner, *Collect. Czech. Chem. Commun.*, 1964, **29**, 1094; S. Wold, *Chem. Scr.*, 1972, **2**, 145; W. Linert, *J. Chem. Inf. Comput. Sci.*, 1992, **32**, 321; R. R. Krug, W. G. Hunter and R. A. Grieger, *J. Phys. Chem.*, 1976, **80**, 2335.

5 O. Exner, *J. Phys. Org. Chem.*, 1997, **10**, 797.

6 An alternative when ΔH and ΔS have been obtained simultaneously from the temperature dependence of k or K is still more misleading from the point of view of statistics but correct statistical procedures have been elaborated: O. Exner, *Collect. Czech. Chem. Commun.*, 1972, **37**, 1425; O. Exner and V. Beránek, *Collect. Czech. Chem. Commun.*, 1973, **38**, 781; R. R. Krug, W. G. Hunter and R. A. Grieger, *J. Phys. Chem.*, 1976, **80**, 2341; V. I. Shimulis, *Kinet. Katal.*, 1983, **24**, 715. The two alternatives were distinguished and presented on examples in ref. 5.

7 O. Exner, *Collect. Czech. Chem. Commun.*, 1973, **38**, 799.

8 E. Gallicchio, M. M. Kubo and R. M. Levy, *J. Am. Chem. Soc.*, 1998, **120**, 4526.

9 R. Varadarajan, P. R. Connelly, J. M. Sturtevant and F. M. Richards, *Biochemistry*, 1992, **31**, 1421.

10 P. S. Charifson, L. M. Shewchuk, W. Rocque, C. W. Hummel, S. R. Jordan, C. Mohr, G. J. Pacofsky, M. R. Peel, M. Rodriguez, D. D. Sternbach and T. G. Consler, *Biochemistry*, 1997, **36**, 6283.

11 J. J. Christensen, J. Ruckman, D. J. Eatough and R. M. Izatt, *Thermochim. Acta*, 1972, **3**, 203; D. J. Eatough, J. J. Christensen and R. M. Izatt, *Thermochim. Acta*, 1972, **3**, 219.

12 Estimates of $\Delta G°$ and $\Delta H°$ from a common set of data can be considered as nearly independent. Two cases were analyzed in detail, ref. 13: in one $\Delta G°$ and $\Delta H°$ were independent, in the other the greater estimate of $\Delta G°$ was weakly correlated with greater $\Delta H°$.

13 R. Karlsson and L. Kullberg, *Chem. Scr.*, 1976, **9**, 54.

14 O. Exner, *Collect. Czech. Chem. Commun.*, 1975, **40**, 2762.

15 S. Cabani, P. Gianni, V. Mollica and L. Lepori, *J. Solution Chem.*, 1981, **10**, 563.

Cycloaddition reaction of *tert*-butyl isocyanate and a tellurium diimide dimer: extended helical structure of the ureato telluroxide $\{[OC(\mu\text{-}NBu^t)_2TeO]_2(thf)\}_\infty$

Gabriele Schatte, Tristram Chivers,* Cory Jaska and Nicole Sandblom

Department of Chemistry, University of Calgary, Calgary, Alberta, Canada T2N 1N4. E-mail: chivers@ucalgary.ca

Received (in Irvine, CA, USA) 22nd May 2000, Accepted 20th July 2000
Published on the Web 11th August 2000

The reaction of $Bu^tNTe(\mu\text{-}NBu^t)_2TeNBu^t$ with Bu^tNCO in a 1:4 molar ratio in thf produces *N,N′*-bis(*tert*-butyl)ureato telluroxide dimers $[OC(\mu\text{-}NBu^t)_2TeO]_2$, which form an extended helical network *via* weak >C=O···Te interactions.

Reactions of transition-metal imido compounds with heteroallenes have been investigated extensively.[1] The M=NR linkage reacts with isocyanates RNCO *via* cycloaddition of the N=C double bond to give *N,N′*-ureato complexes which, in some cases, can be isolated.[2] The *N,N′*-ureato ligand may also be generated by interaction of oxo complexes of Ru or Os with Bu^tNCO, presumably through the formation of an M=NR intermediate.[3] *N,O*-ureato complexes have been implicated in reactions of isocyanates with some transition-metal complexes, but none of the products of C=O cycloaddition to the M = NR bond have been isolated.[4–6] Iminophosphoranes Ph_3P=NR normally react with isocyanates by an Aza-Wittig process to generate carbodiimides and Ph_3PO.[7] By contrast, sulfur diimides, *e.g.* Bu^tN=S=NBu^t undergo exchange reactions with certain isocyanates RNCO (R = R′SO_2, R′CO or Ar) to form Bu^tNCO and Bu^tNSNR.[8] In the context of this divergent behaviour, we have investigated the reactions of the tellurium(IV) diimide dimer $Bu^tNTe(\mu\text{-}NBu^t)_2TeNBu^t$ **1**, which contains two highly reactive terminal Te=NBu^t groups,[9] with isocyanates. We describe here, the facile reaction between **1** and Bu^tNCO, which yields the *N,N′*-ureato telluroxide **3** *via* the corresponding ureato tellurium imide **2** (Scheme 1). In the solid state **3** forms an extended helical network *via* weak >C=O···Te interactions.

Treatment of the dimer **1** with 2 equiv. of Bu^tNCO in toluene at 23 °C produces an extremely moisture-sensitive yellow solid, which was identified as the *N,N′*-ureato tellurium(IV) imide $O{=}C(\mu\text{-}NBu^t)_2Te{=}NBu^t$ **2** on the basis of CHN analysis, IR and NMR spectroscopic data.† The ^1H NMR spectrum of **2** in C_6D_6 exhibits two singlets at δ 1.46 and 1.35 in the intensity ratio 1:2. An IR absorption attributed to the CO stretch is observed at 1653 cm^{-1}, and the carbonyl carbon appears in the $^{13}C\{^1H\}$ NMR spectrum at δ 160.7. Hydrolysis of **2** by atmospheric moisture produces *N,N′*-bis(*tert*-butyl)urea $OC[N(H)Bu^t]_2$ (δ_H 1.24 in d_8-thf). Complex **2** can be viewed as the product of the cycloaddition reaction of the monomeric tellurium(IV) diimide $Bu^tN{=}Te{=}NBu^t$ and Bu^tNCO. By contrast, the reaction of **1** with Bu^tNCS (1:2 molar ratio) in *n*-hexane at 65 °C produces the cyclic tellurium(II) imide $[Te(NBu^t)]_3$[9a] (95% yield) and no cycloaddition intermediate could be isolated.

When a solution of **1** in *n*-hexane is added to a solution of Bu^tNCO in thf (1:4 molar ratio) a white solid identified by X-ray crystallography‡ as $\{[OC(\mu\text{-}NBu^t)_2TeO]_2(thf)\}_\infty$ (**3**·thf)$_\infty$ is obtained in essentially quantitative yield.† The carbodiimide Bu^tN=C=NBu^t was detected as a by-product of this reaction by ^1H NMR (δ_H 1.17). This observation implies that an unstable tellurium(IV) complex involving both *N,N′* and *N,O*-bound ureato ligands is an intermediate in the formation of **3**. As indicated in Fig. 1 the asymmetric unit in **3** is *N,N′*-bis(*tert*-butyl)ureato telluroxide [*d*(Te=O) = 1.9040(17) Å] which, in common with other telluroxides, dimerizes *via* O→Te [2.0723(18) Å] interactions, *cf.* *d*(TeO) = 1.885(7) and 2.170(7) Å in metal complexes of the related dimer $[Bu^tNTe(\mu\text{-}NBu^t)_2(\mu\text{-}O)]_2$.[10] The ureato ligands in **3** adopt a *cis* arrangement with respect to the Te_2O_2 ring which is essentially planar (torsion angle −2.6°). The CNTeN rings are slightly puckered (torsion angle −7.2°). In the parent urea $OC(NHBu^t)_2$[11] and in ureato complexes of Ru and Os[3] the NCN unit is symmetrical [|*d*(CN)| = 1.352 and 1.380 Å, respectively]. By contrast, the CN bonds in **3** are unsymmetrical [*d*(CN) = 1.345(4) and 1.420(3) Å] as are the TeN bonds [*d*(TeN) = 2.034(2) and 2.087(2) Å]. The C=O bond length is 1.227(3) Å, *cf.* 1.252(3) Å in $OC(NHBu^t)_2$[11] and 1.22–1.26 Å in ureato complexes of Ru[3], Os[3] and W.[12] Complex **3** is readily hydrolyzed by traces of moisture to give the urea $OC[N(H)Bu^t]_2$ and TeO_2.

The presence of a two-fold screw axis (2_1) at the centre and corners of the unit cell and a four-fold (4_1) axis at the mid-points of the cell axes results in two different channels parallel to the *ab* plane involving weak >C=O···Te contacts [3.020(2) Å, *cf.* sum of van der Waals radii for Te and O = 3.58 Å][13] as depicted in Fig. 2. The first type involves a lantern-shaped arrangement of four dimers. Two disordered thf molecules located in the middle of the lantern also engage in weak Te···O interactions [2.961(6) Å]. The second type of >C=O···Te interaction involves only one Te atom of four dimeric units and gives rise

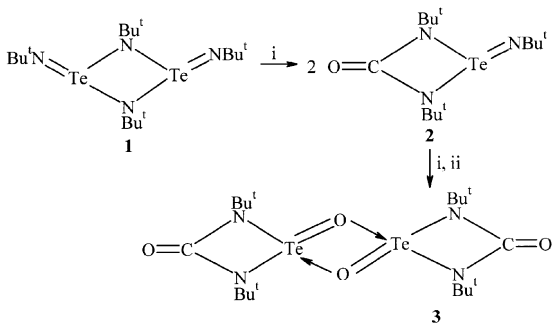

Scheme 1 *Reagents and conditions*: i, +2Bu^tNCO; ii, −2Bu^tNCNBu^t.

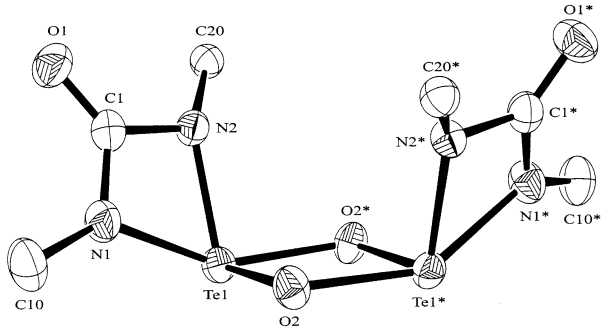

Fig. 1 The structure of $[OC(\mu\text{-}NBu^t)_2TeO]_2$ **3** with the atomic numbering scheme. Thermal ellipsoids are drawn at the 50% probability level. Selected bond angles (°): Te(1)–O(2)–Te(1)* 102.84(8), O(2)–Te(1)–O(2)* 77.10(8), O(2)–Te(1)–N(2) 104.52(9), O(2)*–Te(1)–N(2) 92.08(8), O(2)–Te(1)–N(1) 88.71(9), O(2)*–Te(1)–N(1) 148.18(9), N(1)–Te(1)–N(2) 63.88(9), Te(1)–N(1)–C(1) 95.79(17), Te(1)–N(2)–C(1) 95.76(17), N(1)–C(1)–N(2) 104.0(2). Symmetry transformation used to generate equivalent atoms marked with an asterisk: *y*, *x*, −*z*.

DOI: 10.1039/b004137h

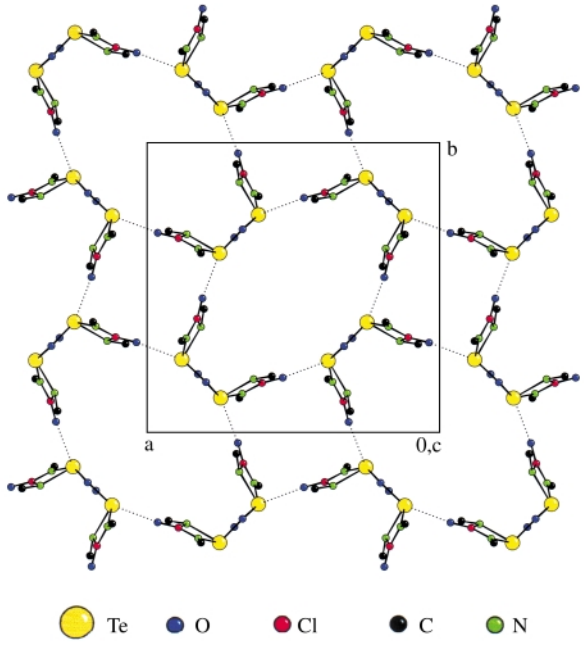

Fig. 2 Unit cell of $\{[OC(\mu\text{-}NBu^t)_2TeO]_2(thf)\}_\infty$ viewed down the *c*-axis. Disordered thf molecules are omitted.

to a square-shaped arrangement. In both of these structural motifs one of the >C=O···Te interactions links dimeric units in adjacent planes of the unit cell to give a helical arrangement, which is apparent when viewed down the *c* axis. The Te···Te distance in both cases is 12.4867(8) Å, *i.e.* the length of the *c* axis. Although weak intermolecular E···Te (E = O, N, S) interactions are a well known feature of tellurium complexes,[14] an extended network involving carbonyl–tellurium contacts is unique.

In summary, the presence of *two* Te=NBu^t linkages in **1** presents a unique opportunity for the study of double cycloadditions with heteroallenes. The reaction of **1** with Bu^{t}NCO generates a *N,N′*-ureato ligand *and* converts a tellurium imide (TeNBu^t) to a telluroxide (TeO) linkage, presumably *via* an unstable *N,O*-ureato complex. Thus it combines features of the reactions of both transition-metal imides and iminophosphoranes with isocyanates.

We thank the NSERC (Canada) for financial support, Dr R. MacDonald (University of Alberta) for assistance with the data collection, and Dr M. Parvez for helpful discussions of the disorder problem.

Notes and references

† *Experimental procedure*: all manipulations were performed under an inert atmosphere of dry argon using standard Schlenk techniques. All solvents were dried prior to use.

2: a colourless solution of Bu^{t}NCO (0.120 mL, 1.112 mmol) in toluene (10 mL) was added to an orange solution of **1**[9c] (0.30 g, 0.556 mmol) in toluene (5 mL) at room temperature. The addition of a small amount of Bu^{t}NCNBu^t prevents the formation of **3**. A yellow precipitate of **2** was formed after 3 min. The pale orange solution was stirred for 2 h, cooled to −10 °C and then the supernatant was decanted *via* cannula. The solid product was washed with cold *n*-pentane (3 mL) to give **2** (0.185 g, 0.501 mmol, 45%) as a yellow solid. ^{1}H NMR (400.13 MHz, C_6D_6, 25 °C) δ 1.46 (9 H), 1.35 (18 H). ^{13}C NMR (100.62 MHz, C_6D_6, 25 °C) δ 160.70 (CO), 64.17 [$C(CH_3)_3$], 54.83 [$C(CH_3)_3$], 34.69 [$C(CH_3)_3$], 31.86 [$C(CH_3)_3$]. ^{125}Te NMR (126.20 MHz, C_6D_6, 25 °C) δ 1225. IR:1653 [ν(CO)] cm^{-1}.

3: an orange solution of **1** (0.30 g, 0.556 mmol) in *n*-hexane (10 mL) was added to a colourless solution of Bu^{t}NCO (0.257 mL, 2.223 mmol) in thf (10 mL) at 23 °C. The pale yellow solution was stirred for 1.5 h and then volatile materials were removed under vacuum and **3**·2 thf (0.423 g, 0.549 mmol, 99%) was obtained as a white solid. Colourless crystals of **3**·thf suitable for X-ray diffraction were obtained after two days at 23 °C by layering an orange–red solution of **3** in *n*-hexane (3 mL) over a solution of Bu^{t}NCO in thf (3 mL). ^{1}H NMR (400.13 MHz, C_6D_6, 25 °C) δ 3.55 (thf), 1.45 (Bu^t, 18H), 1.41 (thf). ^{13}C NMR (100.62 MHz, C_6D_6, 25 °C) δ 160.39 (CO), 68.15 (thf), 54.97 [$C(CH_3)_3$], 31.27 [$C(CH_3)_3$], 26.15 (thf). ^{125}Te NMR (126.20 MHz, C_6D_6, 25 °C) δ 1090. IR: 1669 [ν(CO)], 663 [ν(TeO)] cm^{-1}.

‡ *Crystal data* for $(\mathbf{3}\cdot thf)_\infty$: $C_{22}H_{44}N_4O_5Te_2$, M = 699.81, tetragonal, space group $P4_12_12$ (no. 92), a = b = 15.5941(7), c = 12.4867(8) Å, V = 3036.5(3) Å^3, Z = 4, D_c = 1.531 g cm^{-3}, μ(Mo-Kα) = 19.55 cm^{-1}. Crystal dimensions 0.26 × 0.23 × 0.15 mm. Data were collected on a Bruker AXS P4/RA/SMART 1000 CCD diffractometer with graphite-monochromated Mo-Ka radiation using ϕ and ω scans. The structure was solved using direct methods (SIR-97) and refined by full-matrix least squares on F^2 (SHELXL-97). The thf molecule was disordered around the two-fold screw axis with partial occupancy factors of 0.5. Of the 2593 unique reflections 2410 had $I \geqslant 2.00\sigma(I)$. The final agreement factors were R_1 = 0.0164 and wR_2 = 0.041.

CCDC 182/1728. See http://www.rsc.org/suppdata/cc/b0/b004137h/ for crystallographic files in .cif format.

1 For reviews, see: D. E. Wigley, *Prog. Inorg. Chem.*, 1994, **42**, 239; P. Mountford, *Chem. Commun.*, 1997, 2127.
2 For some recent examples, see: R. I. Michelman, R. A. Andersen and R. G. Bergman, *J. Am. Chem. Soc.*, 1991, **113**, 5100; M. Jolly, J. P. Mitchell and V. C. Gibson, *J. Chem. Soc., Dalton Trans.*, 1992, 1329; P. Legzdins, E. C. Phillips, S. J. Rettig, J. Trotter, J. E. Veltheer and V. C. Lee, *Organometallics*, 1992, **11**, 3104; A. J. Blake, P. Mountford, G. I. Nikonov and D. Swallow, *Chem. Commun.*, 1996, 1835.
3 W.-H. Leung, G. Wilkinson, B. Hussain-Bates and M. B. Hursthouse, *J. Chem. Soc., Dalton Trans.*, 1991, 2791.
4 P. J. Walsh, F. J. Hollander and R. G. Bergman, *Organometallics*, 1993, **12**, 3705.
5 K. R. Birdwhistell, T. Boucher, M. Ensminger, S. Harris, M. Johnson and S. Toporek, *Organometallics*, 1993, **12**, 1023.
6 J. L. Thorman, I. A. Guzzi, V. G. Young Jr. and L. K. Woo, *Inorg. Chem.*, 1999, **38**, 3814.
7 A. W. Johnson, *Ylides and Imides of Phosphorus*, John Wiley & Sons Ltd., N.Y., 1993, pp. 429–430.
8 R. Appel and M. Montenarh, *Chem. Ber.*, 1976, **109**, 2437; H. W. Roesky and G. Sidiropoulos, *Chem. Ber.*, 1978, **111**, 3460.
9 (*a*) T. Chivers, X. Gao and M. Parvez, *J. Am. Chem. Soc.*, 1995, **115**, 2359; (*b*) T. Chivers, X. Gao and M. Parvez, *Angew. Chem., Int. Ed. Engl.*, 1995, **34**, 2549; (*c*) T. Chivers, G. D. Enright, N. Sandblom, G. Schatte and M. Parvez, *Inorg. Chem*, 1999, **38**, 5431.
10 T. Chivers, M. Parvez and G. Schatte, *Inorg. Chem.*, 1999, **38**, 5171.
11 T. Chivers, A. Downard and G. P. A. Yap, unpublished work.
12 H.-W. Lam, G. Wilkinson, B. Hussain-Bates and M. B. Hursthouse, *J. Chem. Soc., Dalton Trans.*, 1993, 781.
13 N. W. Alcock, *Adv. Inorg. Chem. Radiochem.*, 1972, **15**, 1.
14 For examples, see: E = O: R. O. Day and R. R. Holmes, *Inorg. Chem.*, 1981, **20**, 3071; E = N: R. E. Allan, H. Gornitzka, J. Kärcher, M. A. Paver, M.-A. Rennie, C. A. Russell, P. R. Raithby, D. Stalke, A. Steiner and D. S. Wright, *J. Chem. Soc., Dalton Trans.*, 1996, 1727; E = S: A. Silvestru, I. Haiduc, K. H. Ebert, H. J. Breunig and D. B. Sowerby, *J. Organomet. Chem.*, 1994, **482**, 253.

Syntheses of complexes containing the novel 1,2,3-azadiphosphole and 1,2,5-azadiphosphole ring systems: crystal and molecular structure of $[Ir(\eta^5\text{-}C_5Me_5)(\eta^4\text{-}(Bu^tCPNBu^tPCBu^t)]$

F. Geoffrey N. Cloke,*[a] Peter B. Hitchcock,[a] John F. Nixon,*[a] Udo Schiemann,[b] Rainer Streubel*[b] and D. James Wilson[a]

[a] *School of Chemistry, Physics and Environmental Science, University of Sussex, Brighton, Sussex, UK BN1 9QJ*
[b] *Institut für Anorganische und Analytische Chemie der Technischen Universität Braunschweig, Postfach 3329, D-38106 Braunschweig, Germany. E-mail: r.streubel@tu-bs.de*

Received (in Cambridge, UK) 13th June 2000, Accepted 21st July 2000

The first examples of complexes containing the novel 1,2,5-azadiphosphole and 1,2,3-azadiphosphole ring systems are presented, together with the molecular structure of $[Ir(\eta^5\text{-}C_5Me_5)(\eta^4\text{-}(Bu^tCPNBu^tPCBu^t)]$ as established by a single crystal X-ray diffraction study.

Transition metal-promoted syntheses of unsaturated P-heterocycles has received considerable attention in recent years in the quest for sophisticated ligands containing sp^2- and/or sp^3-hybridised phosphorus atoms in heterocyclic rings.[1] Tungsten complexes of 2*H*-1,2-azaphosphole,[2] 2*H*-1,3,2-diazaphosphole[3] and 2*H*-1,4,2-diazaphosphole[3,4] rings can be obtained using the dual precursor potential of 2*H*-azaphosphirene complexes *via* intermediate terminal phosphanediyl and nitrilium phosphane-ylide complexes, the former giving rise to 3- and 4-membered and the latter to 5-membered P-heterocycles. The planar, aromatic 1,2,4-azadiphosphole ring systems, $P_2C_2Bu^t_2NR$[5] (R = Pr^i, Et, Ph, Tol, Pr^n, Cy, Bu^tCH_2) on the otherhand, have recently been reported *via* coupling reactions involving the phospha-alkyne, $PCBu^t$, with the imido fragment of $[TiCl_2(NR)(py)_3]$ (R = Pr^i, Et, Ph, Tol) or $[VCl_3(NR)]$ (R = Pr^i, Pr^n, Cy, Bu^tCH_2) complexes.[5] We now describe the syntheses of complexes containing the previously unknown 1,2,3-azadiphosphole and 1,2,5-azadiphosphole ring systems; we also provide first evidence for 1,2,4-azadiphosphole complexes.

Extending our three-component reaction concept[3] towards phospha-alkynes, we have now observed that 2*H*-azaphosphirene complex **1**[6] react with 1-piperidinonitrile (2 equiv.) and an excess of Bu^tCP[7] **2a** or 1-AdCP[8] **2b** (Ad = adamantyl) in toluene at elevated temperature to give the 1,2,3-azadiphosphole complexes **3a**,**b** and 1,2,4-azadiphosphole complexes **4a**,**b**. Based on observations made earlier, *cf.* ref. 3 we assume that a transiently formed *C*-1-piperidino-substituted nitrilium phosphane-ylide complex react with the phospha-alkynes in [4 + 2] cycloaddition reactions to yield the two regioisomers, which were formed in ratios of 8:1 (**3a**:**4a**) and 3:1 (**3b**:**4b**) respectively. Unfortunately, even using low-temperature column chromatography, only complex **3b** could be separated by extraction and subsequent crystallisation (Scheme 1).

Bergman and co-workers,[9] synthesised the monomeric imido complex $[Ir(\eta^5\text{-}C_5Me_5)(NBu^t)]$ from $[\{Ir(\eta^5\text{-}C_5Me_5)Cl_2\}_2]$ and 4 equiv. of $LiNHBu^t$ in THF and described its cycloaddition reaction with dimethyl acetylenedicarboxylate to afford the structurally characterised compound $[Ir(\eta^5\text{-}C_5Me_5)\{NBu^t\text{-}(MeO_2CCCCO_2Me)_2\}]$, which contains an η^4-coordinated pyrrole ring. Since phospha-alkynes, PCR, are known to behave very like alkynes,[1] we have extended this type of cyclisation reaction and find that $[Ir(\eta^5\text{-}C_5Me_5)(NBu^t)]$ **5** on treatment with an excess of $PCBu^t$ **2a** in toluene at ambient temperature afforded the η^4-ligated 1,2,5-azadiphosphole ring complex **6**.¶

The E.I. mass spectra† exhibited the molecular ions of **3b** and **6**, which are consistent with the proposed formulations. The molecular structures of **3b** and **6** were deduced by NMR spectroscopy‡ (^{13}C, ^{31}P) (*vide infra*) and confirmed by a single crystal X-ray diffraction study§ in the case of **6** (Fig. 1). The $^{31}P\{^1H\}$ NMR spectra of complexes **3** and **4** displayed the expected AB-type spectra with low-field resonances for the two-coordinated phosphorus centers and with typical magnitudes of phosphorus–phosphorus coupling constants (for **3** *ca.* 294 Hz; for **4** *ca.* 34 Hz). Additionally, complex **3b** shows signals in its $^{13}C\{^1H\}$ NMR spectrum at δ 180.3 (m) and 196.5 (dd, $^1J_{(PC)}$ 61.1 Hz, $^2J_{(PC)}$ 9.7, *C*=P), which were readily assigned to the imino- and the phosphaalkene-carbon atoms respectively. The $^{31}P\{^1H\}$ NMR spectrum of **6** displayed a singlet (δ 0.26) implying a symmetrical environment for the two P atoms. The three signals (δ 1.92, 1.48, 1.07) observed in the ^1H NMR spectrum were readily assigned to C_5Me_5, $PCBu^t$ and NBu^t respectively. Further insight into the structure of this molecule was gained from the $^{13}C\{^1H\}$ NMR spectrum which showed two pseudo triples (δ 34.7 $^3J_{(PC)}$ 6.51 Hz, 28.7 $^3J_{(PC)}$ 7.28 Hz) in an intensity ratio of 2:1 which were assigned to the methyl resonances of the two sets of non-equivalent *tert*-butyl groups, thereby establishing the connectivity of both phosphorus nuclei with nitrogen.

The molecular structure of complex **6** which was confirmed by a single crystal X-ray analysis of crystals grown from a saturated pentane solution (−50 °C), is shown in Fig. 1 together

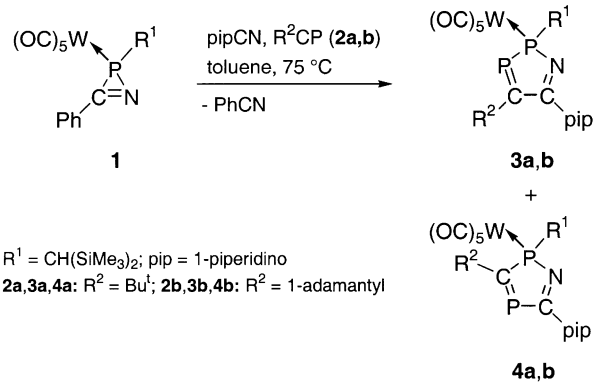

Scheme 1 Reaction of complex **1** with 1-piperidinonitrile and phospha-alkynes **2a**,**b**§

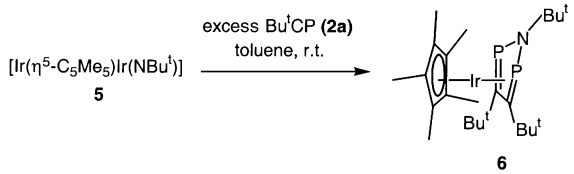

Scheme 2 Reaction of $[Ir(\eta^5\text{-}C_5Me_5)(NBu^t)]$ **5** with the phospha-alkyne $PCBu^t$ **2a**.¶

DOI: 10.1039/b004692m

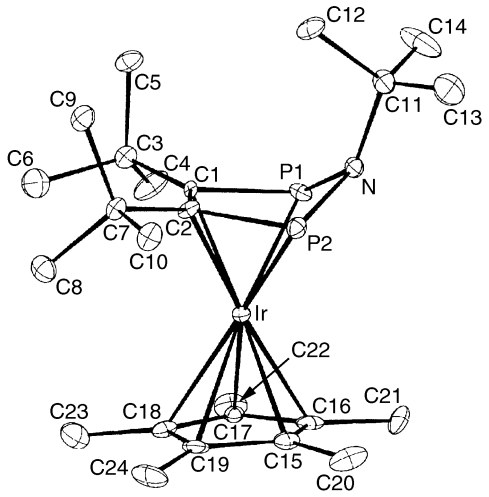

Fig. 1 Molecular structure of [Ir(η^5-C_5Me_5)(η^4-(Bu^{t}CPNBu^{t}PCBu^t)] **6**. Selected distances (Å) and angles (°): P(1)–C(1) 1.846(7), C(2)–P(2) 1.837(11), P(1)–N 1.718(7), P(2)–N 1.733(6), C(2)–C(1) 1.427(12), Ir–C(2) 2.161(11), Ir–C(1) 2.173(5), Ir–P(2) 2.333(2), Ir–P(1) 2.338(3), C(18)–C(19) 1.433(14) Å. N–P(2)–C(2) 101.3(4), N–P(1)–C(1) 101.2(3), P(1)–N–P(2) 98.9(3), C(2)–C(1)–P(1) 108.8(5), C(1)–C(2)–P(2) 109.1(7), P(2)–N–C(11) 121.8(4), P(2)–C(2)–C(7) 118.6(7), C(1)–C(2)–C(7) 132.0(8)°. Hydrogen atoms are omitted for clarity. Displacement ellipsoids are shown at the 50% probability level.

with principal bond lengths and angles. The IrC_5Me_5 fragment is η^4-ligated to the 1,2,5-azadiphosphole ring resulting in the nitrogen atom becoming pyramidalised and it lies out of the plane formed by P(2)–C(2)–C(1)–P(1), (dihedral angle between P(2)–C(2)–C(1)–P(1) and P(1)–N–P(2), 44.2(3)°). The longer Ir–P(1)/Ir–P(2) (av. 2.335 Å) bond lengths compared with Ir–C(2)/Ir–C(1) (av. 2.167 Å) causes the P(2)–C(2)–C(1)–P(1) fragment to tilt away from the plane of the C_5Me_5 ring (dihedral angle between P(1)–C(1)–C(2)–P(2) and C(15)–C(16)–C(17)–C(18)–C(19), 7.7°). The C(1)–C(2) bond distance (1.427(12) Å) lies within the range expected for η^4-bonded systems, whereas the P(1)–C(1) and P(2)–C(2) distances (1.846(7), 1.837(11) Å) are considerably longer than anticipated for P=C double bonds. This is the first structurally characterised metal complex containing a 1,2,5-azadiphosphole derivative.

It is interesting to note that Regitz and co-workers[10] recently proposed, on the basis of $^{31}P\{^1H\}$ NMR spectroscopic data, the possible intermediacy of a 1,2,5-azadiphosphole ring system in the metal-mediated formation of azatetraquadricyclanes from phosphaalkynes. Complex **1**, which has a formal electron count of 18e, was found to be remarkably stable and column chromatography (silica gel, pentane) in air resulted in only very slight decomposition of the sample (1% loss), likewise attempts to displace the heterocycle from iridium by carbonylation of the metal centre proved unsuccessful.

R. S. and U. S. are grateful to the Deutsche Forschungsgemeinschaft and the Fonds der Chemischen Industrie for financial support. F. G. N. C., J. F. N. and D. J. W. thank the EPSRC for their continuing support for phospha-organometallic chemistry.

Notes and references

† Satisfactory elemental analysis were obtained for complexes **3b** and **6**. NMR data were recorded in [$^2H_6$]benzene solutions (295 K) at 75.5 MHz (^{13}C) and 81.0 (^{31}P), using TMS and 85% H_3PO_4 as standard references; *J*/Hz. *Selected spectroscopic data for* **3**, **4** *and* **6**. $^{31}P\{^1H\}$ NMR: **3a**: δ 340.4 (d, $^1J_{(PP)}$ 297.1), 91.2 (d, $^1J_{(PP)}$ 297.1, $^1J_{(PW)}$ 211.0). **4a**: δ 234.1 (d, $^2J_{(PP)}$ 34.2), 107.6 (d, $^2J_{(PP)}$ 34.2). **3b**: δ 341.8 (d, $^1J_{(PP)}$ 296.2), 93.3 (d, $^1J_{(PP)}$ 296.2, $^1J_{(PW)}$ 209.5). **4b**: δ 232.9 (d, $^2J_{(PP)}$ 34.8), 105.8 (d, $^2J_{(PP)}$ 34.8). **3b**: $^{13}C\{^1H\}$ NMR: δ 2.7 [m_c, br, ($SiCH_3$)], 21.7 [m_c, (*C*H($SiCH_3$)$_2$)], 23.9 [s, $NCH_2CH_2CH_2$], 25.9 [s, NCH_2CH_2], 29.4 [s, Ad *C*3/*C*5/*C*7], 36.7 [s, Ada *C*4/*C*6/*C*10], 42.9 [dd, $J_{(PC)}$ 10.1, $J_{(PC)}$ 11.8, Ad *C*1], 44.0 [d, $^3J_{(PC)}$ 14.3, Ad *C*2/*C*8/*C*9], 54.7 [s, NCH_2], 180.3 [m_c, *C*=N], 196.5 [dd, $^1J_{(PC)}$ 61.1, $^2J_{(PC)}$ 9.7, *C*=P], 197.3 [dd, $J_{(PC)}$ 3.5, $J_{(PC)}$ 4.5, *cis*-CO], 198.6 [d, $J_{(PC)}$ 19.4 Hz, *trans*-CO]. EI-MS (pos.-CI, NH_3) *m/z* (%): 802 (80) $[M]^+$. **6**: $^{31}P\{^1H\}$ NMR: δ 0.26. $^{13}C\{^1H\}$ NMR: δ 11.5 [$C_5(CH_3)_5$], 28.7 [t, NC(CH_3)$_3$, $^3J_{(PC)}$ 7.28], 34.7 [*pseudo*-t, PCC(CH_3)$_3$, $^3J_{(PC)}$ 6.51 Hz], 36.2 [*pseudo*-t, PC*C*(CH_3)$_3$, $^2J_{(PC)}$ 8.21], 95.2 [m, PCC], 94.0 [$C_5(CH_3)_5$]. EI-MS *m/z* (%): 559 (30) $[M]^+$.

‡ *Crystal data* for **6**: $C_{24}H_{42}IrNP_2$, M = 598.73, orthorhombic, space group $Pna2_1$ (no. 33), a = 20.067(2), b = 14.271(3), c = 8.775(5) Å, U = 2513(2) Å^3, Z = 4, D_c = 1.58 Mg m^{-3}, crystal dimensions 0.2 × 0.2 × 0.2 mm, F(000) = 1200, T = 173(2) K, Mo-Kα radiation, λ = 0.71073 Å. Data were collected on an Enraf-Nonius CAD4 diffractometer and of the total 4635 reflections measured 2151 having $I > 2\sigma(I)$ were used in the calculations. The final indices ($I > 2\sigma(I)$) were $R1$ = 0.022, $wR2$ = 0.049. CCDC 182/1727. See http://www.rsc.org/suppdata/cc/b0/b004692m/ for crystallographic files in .cif format.

§ *Experimental*: to a solution of 2.15 g (3.5 mmol) 2*H*-azaphosphirene complex **1** in 20 ml toluene was added 0.6 mL (5 mmol) 1-piperidinonitrile and 1.4 g (14 mmol) Bu^{t}CP or 2.5 g (14 mmol) 1-AdaCP. The solutions were heated with stirring at 75–80 °C for 3 h and the volatiles removed *in vacuo* (0.1 mbar). In the case of **3b**, the crude product was separated by extraction of the brown residue with light petroleum (60:40) and crystallised from *n*-pentane/toluene at −20 °C; yield 2.13 g, 19%.

¶ *Experimental*: to a stirred solution of [Ir(η^5-C_5Me_5)(NBu^t)] (0.370 g, 0.9 mmol) in toluene (30 ml) was added dropwise, PCBu^t (0.232 g, 2.3 mmol) and the resulting black solution was allowed to stir for 24 h. The solvent was removed *in vacuo* and the residue sublimed (180 °C, 10^{-5} mbar) yielding a white waxy solid (yield 0.205 g, 40%). Crystals suitable for X-ray analysis were grown from a slowly cooled and concentrated pentane solution (−48 °C).

1 K. B. Dillon, F. Mathey and J. F. Nixon, *Phosphorus: The Carbon Copy*, John Wiley, Chichester, 1998.
2 R. Streubel, H. Wilkens, A. Ostrowski, C. Neumann, F. Ruthe and P. G. Jones, *Angew. Chem., Int. Ed. Engl.*, 1997, **36**, 1492.
3 H. Wilkens, F. Ruthe, P. G. Jones and R. Streubel, *Eur. Chem. J.*, 1998, **4**, 1542.
4 R. Streubel, H. Wilkens, F. Ruthe and P. G. Jones, *Chem. Commun.*, 1999, 2127.
5 F. G. N. Cloke, P. B. Hitchcock, J. F. Nixon, D. J. Wilson, F. Tabellion, U. Fishbeck, F. Preuss, M. Regitz and L. Nyulaszi, *Chem. Commun.*, 1999, 2363.
6 R. Streubel, A. Ostrowski, S. Priemer, U. Rohde, J. Jeske and P. G. Jones, *Eur. J. Inorg. Chem.*, 1998, 257.
7 G. Becker, G. Gresser and W. Uhl, *Z. Naturforsch., Teil B*, 1981, **36**, 11.
8 T. Allspach, M. Regitz, G. Becker and W. Becker, *Synthesis*, 1986, 31.
9 D. S. Glueck, J. Wu, F. J. Hollander and R. G. Bergman, *J. Am. Chem. Soc.*, 1991, **113**, 2041.
10 F. Tabellion, A. Nachbauer, S. Leininger, C. Peters, F. Preuss and M. Regitz, *Angew. Chem., Int. Ed.*, 1998, **76**, 1223.

ChemComm

Non-ionic surfactant assembly of ordered, very large pore molecular sieve silicas from water soluble silicates

Seong-Su Kim, Thomas R. Pauly and Thomas J. Pinnavaia*

Department of Chemistry and Center for Fundamental Materials Research, Michigan State University, East Lansing, Michigan 48824, USA. E-mail: pinnavai@cem.msu.edu

Received (in Irvine, CA, USA) 4th April 2000, Accepted 26th June 2000

Very large pore hexagonal and cellular foam-like molecular sieve silicas with well cross-linked framework walls (denoted MSU-H and MSU-F, respectively), have been prepared from soluble silicate precursors under neutral pH conditions.

The supramolecular assembly of periodically ordered mesoporous molecular sieves, such as hexagonal MCM-41, is normally accomplished through an electrostatically mediated pathway involving ionic surfactants assemblies (S^+ or S^-) and inorganic reagents (I^+ or I^-).[1,2] Electrostatic assembly also is involved in the preparation of exceptionally large pore mesostructured silicas such as hexagonal SBA-15 and mesostructured cellular foams (MCF) in the presence of non-ionic surfactants (N^0) derived from triblock co-polymers of propylene and ethylene oxides.[3] These materials are assembled under strongly acidic conditions to allow for counter ion mediated interactions of the type $(N^0H^+)(X^-I^+)$, where X^- is the counter anion and I^+ is the protonated silicic acid derived from a silicon alkoxide reagent. Although the very large pore sizes (50 to 300 Å diameter) are attractive features for applications in large molecule reactions and separations, the high cost of silicon alkoxides and the strong acid reaction conditions, which can limit framework cross-linking and structural stability, are undesirable features of the preparative chemistry.

Mesoporous silica molecular sieves with wormhole framework structures, such as the MSU-X family of materials,[4] are also assembled from neutral surfactants and cost-intensive silicon alkoxides. In an effort to replace the costly alkoxides with sodium silicate, Guth and co-workers[5] reported the preparation of disordered mesostructures from sodium silicate solutions in the presence of a non-ionic surfactant. The complete removal of the surfactant by calcination at 600 °C, however, led to either the extensive restructuring of the silica framework or to the formation of a completely amorphous material. More recently, we achieved the high-yield synthesis of stable wormhole molecular sieve silicas from low-cost, water-soluble silicate precursors and non-ionic surfactants at near neutral pH.[6] In the present work we demonstrate that it is also possible to assemble from sodium silicate *highly ordered* mesoporous silica molecular sieves with very large framework pore structures analogous to both hexagonal SBA-15 and MCF, which we denote MSU-H and MSU-F, respectively.

In a typical synthesis the surfactant and an amount of acid equivalent to the hydroxide content of the sodium silicate solution (*e.g.* 27% SiO_2, 14% NaOH) were mixed at ambient temperature and then added to the sodium silicate to form a reactive silica in the presence of the structure directing surfactant. This allows for the assembly of the framework under neutral pH conditions. The assembly process for the preparation of a hexagonal mesostructure was carried out at molar ratios of H_2O/Si = 230 and N^0/Si = 0.008–0.017 and at a desired temperature for a period of 10–20 h. The surfactant was then removed from the washed, air-dried products either by solvent extraction with hot ethanol or by calcination in air at 600 °C.

Fig. 1 illustrates the powder X-ray diffraction patterns of as-synthesized and calcined (600 °C) forms of hexagonal MSU-H silica as prepared from Pluronic P123 ($EO_{20}PO_{70}EO_{20}$) as the surfactant at a synthesis temperature of 60 °C. The as-synthesized and calcined products exhibit resolved *hkl* reflections consistent with two-dimensional hexagonal symmetry and unit cell dimensions of 130 and 119 Å, respectively. We may conclude that MSU-H mesostructures are isostructural with SBA-15. However, the two classes of as-made silicates are readily distinguishable on the basis of framework connectivity. The ^{29}Si NMR spectra of as-synthesized MSU-H (not shown) typically exhibit three resonances corresponding to the Q^2 (93 ppm), Q^3 (100 ppm) and Q^4 (109 ppm) connectivities of the SiO_4 tetrahedra. The ratio of fully condensed (Q^4) silica sites to incompletely condensed Q^3 and Q^2 sites is 4.5, considerably higher than the value of 1.28 reported[3a] for conventional SBA-15. The neutral pH conditions of the present assembly pathway allow for a much higher degree of framework crosslinking, presumably, because there is little or no charge present on the silica framework walls under these conditions.

Further evidence for the hexagonal mesostructure of MSU-H silica is provided by the transmission electron micrograph (TEM) images shown in Fig. 2. In comparison to conventional SBA-15, which has a particle size in the micron range, MSU-H shows smaller particle sizes in the range 300–500 nm [Fig. 2(a)]. Fig. 2(b) unmistakably shows the highly ordered hexagonal arrays of mesopores and equidistant parallel lines related to the hexagonal repeat between tubules. Also evident are the small hexagonal domain sizes within the small particles.

Fig. 3 illustrates the N_2 adsorption–desorption isotherms and BJH pore size distribution plot (insert) calculated from the adsorption branch of the N_2 isotherms for calcined MSU-H. A typical, type IV adsorption isotherm with an irreversible H1 hysteresis loop is observed as expected for a large pore material.[7] The step-like uptake of N_2 in the range 0.7–0.9 P/P_0 corresponds to capillary condensation within framework pores with a BJH diameter of 98 Å. The pore volume is 1.24 $cm^3\ g^{-1}$, the BET surface area is 625 $m^2\ g^{-1}$ for this calcined MSU-H.

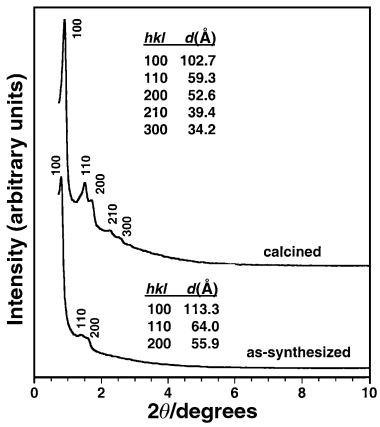

Fig. 1 XRD patterns of as-synthesized and calcined (600 °C) forms of a MSU-H silica molecular sieve assembled from sodium silicate and Pluronic P123 ($EO_{20}PO_{70}EO_{20}$) under neutral pH conditions at 60 °C.

DOI: 10.1039/b002856h

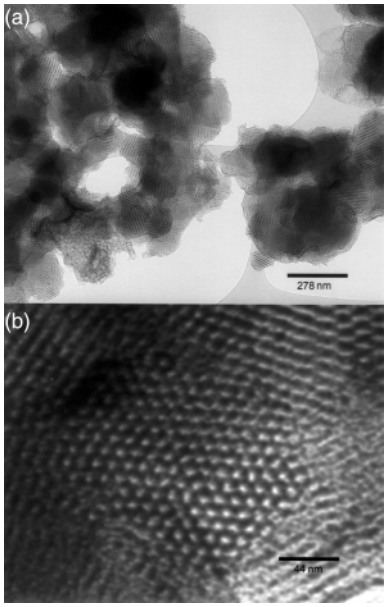

Fig. 2 TEM images of the calcined MSU-H silica: (a) low and (b) high magnification.

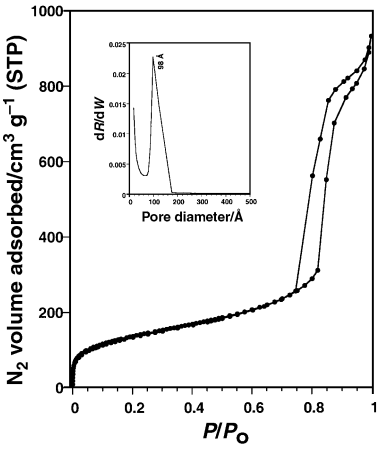

Fig. 3 N_2 adsorption–desorption isotherms for the calcined MSU-H silica molecular sieve. The insert provides the BJH pore size distribution calculated from the adsorption branch of the N_2 isotherm.

MSU-H silicas with (100) X-ray spacings in the range 99–108 Å and pore sizes between 82 and 110 Å have been synthesized with Pluronic P123 surfactant simply by varying the N^0/silica ratio or the synthesis temperature. More significantly, the addition of 1,3,5-trimethylbenzene (TMB) to expand the pore size of MSU-H leads instead to mesostructured cellular foams (denoted MSU-F) that are composed of large, uniform spherical cells, as shown in Fig. 4. This material has an average pore size of 225 Å, a BET surface area of 759 $m^2\ g^{-1}$, and a mesopore volume of 1.87 $cm^3\ g^{-1}$, very much like conventional MCF silicas[3b] formed from acidic TEOS mixtures in the presence of P123 and TMB (Fig. 5). The formation of a TMB/P123 microemulsion and the assembly of silica around the microemulsion droplets explain the phase transition from MSU-H to MSU-F.

The same chemistry described above for the preparation of MSU-H and MSU-F also applies to other non-ionic polyethylene oxide surfactants. For instance, molecular sieve silicas with two-dimensional hexagonal symmetry and BJH pore sizes of 32–53 Å, BET surface areas of 492–745 $m^2\ g^{-1}$ and pore volumes of 0.31–0.70 $cm^3\ g^{-1}$ were assembled from water-soluble silicate precursors using Brij 76 as the non-ionic surfactant at temperatures in the range 25–60 °C. Thus, the new assembly pathway reported here is general, as well as being especially suitable for the assembly of stable analogs of silica

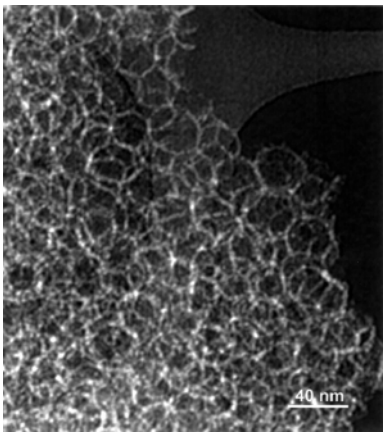

Fig. 4 TEM image of the calcined MSU-F silica formed from sodium silicate, TMB and Pluronic P123 under neutral pH conditions at 60 °C.

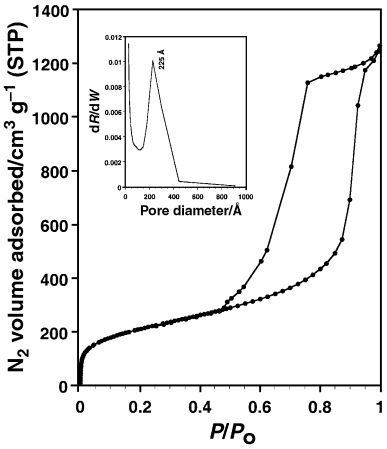

Fig. 5 N_2 adsorption–desorption isotherms for the calcined MSU-F silica. The insert provides the BJH pore size distribution calculated from the adsorption branch of the N_2 isotherm.

mesostructures with the largest of known framework pore sizes. The generality of the assembly pathway, together with the use of low-cost sodium silicate as the silica source, are attractive features for use in the commercial production of mesostructured silicas with framework pore sizes over the entire range from 20 to > 225 Å.

Note added in proof: The synthesis of SBA mesostructures from sodium metasilicate and non-ionic block copolymers as structure directing agents under strong acid conditions has recently been reported: J. M. Kim and G. D. Stucky, *Chem. Commun.*, 2000, 1159.

The support of this research by NSF-CRG grant CHE-9903706 is gratefully acknowledged.

Notes and references

1 C. T. Kresge, M. E. Leonowicz, W. J. Roth, J. C. Vartuli and J. S. Beck, *Nature*, 1992, **359**, 710.
2 Q. Huo, D. I. Margolese, U. Ciesla, D. G. Demuth, P. Feng, T. E. Gier, P. Sieger, A. Firouzi, B. F. Chemlka, F. Schüth and G. D. Stucky, *Chem. Mater.*, 1994, **6**, 1176; Q. Huo, D. I. Margolese and G. D. Stucky, *Chem. Mater.*, 1996, **8**, 1147.
3 (*a*) D. Zhao, Q. Huo, J. Feng, B. F. Chmelka and G. D. Stucky, *J. Am. Chem. Soc.*, 1998, **120**, 6024; (*b*) P. Schmidt-Winkel, W. W. Lukens, Jr., D. Zhao, P. Yang, B. F. Chmelka and G. D. Stucky, *J. Am. Chem. Soc.*, 1999, **121**, 254.
4 S. A. Bagshaw, E. Prouzet and T. J. Pinnavaia, *Science*, 1995, **267**, 865.
5 L. Sierra, B. Lopez, J. Gil and J.-L. Guth, *Adv. Mater.*, 1999, **11**, 307; L. Sierra and J.-L. Guth, *Microporous Mesoporous Mater.*, 1999, **27**, 243.
6 S.-S. Kim, T. R. Pauly and T. J. Pinnavaia, *Chem. Commun.*, 2000, 835.
7 K. S. W. Sing, D. H. Everett, R. A. W. Haul, L. Moscow, R. A. Pierotti, J. Rouquerol and T. Siemieniewska, *Pure Appl. Chem.*, 1985, **57**, 603

Rationally designed improvement of the bis(phospholano)ethane ligand for asymmetric hydrogenation leads to a reappraisal of the factors governing the enantioselectivity of Duphos catalysts

Elena Fernandez,[a] Amy Gillon,[b] Katie Heslop,[b] Emily Horwood,[b] David J. Hyett,[b] A. Guy Orpen*[b] and Paul G. Pringle*[b]

[a] *Universitat Rovira i Virgili, Departament de Química Física Inorgànica, Plaça Imperial Tàrraco, 1, Tarragona, Spain*

[b] *School of Chemistry, University of Bristol, Cantocks Close, Bristol, UK. E-mail: paul.pringle@bristol.ac.uk*

Received (in Cambridge, UK) 13th April 2000, Accepted 18th July 2000

Enhancement of enantioselectivity in hydrogenations catalysed by δ *vs.* λ rhodium chelate complexes of *trans*-1,2-bis(phospholano)cyclopentanes cannot be rationalised using the current quadrant model for Duphos ligands and therefore a new consistent model is suggested.

Diphosphines containing the 2,5-dialkylphospholane moiety (*e.g. R,R*-Duphos, *R,R*-bpe) are currently the most efficient

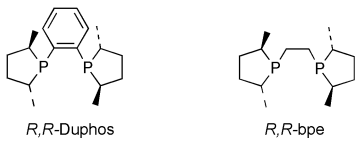

ancillary ligands for the asymmetric hydrogenation of many alkenes;[1–4] several of these catalytic processes are of commercial interest.[4] The enantioselectivity is a sensitive function of the ligand backbone.[1–7] For example, for the hydrogenations shown in eqns. (1) and (2), the enantioselectivity increases with

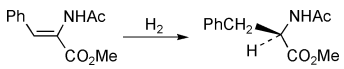

(1)

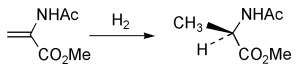

(2)

increasing rigidity of the ligand backbone. Here, we show an example of how the enantioselectivity for the bis(phospholane)-ethane complex **1** can be improved by rational design of the ligand backbone; our results challenge the currently accepted explanations for the selectivity of Duphos ligands.

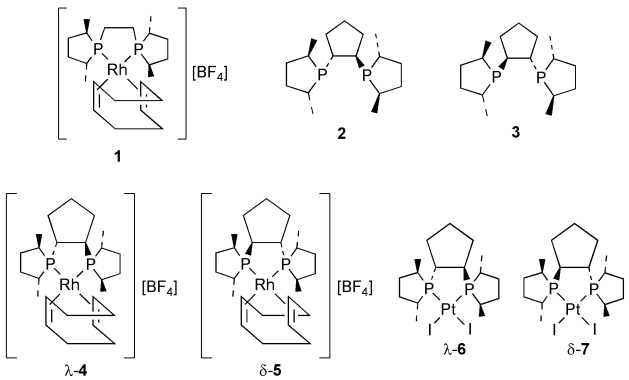

The chelate ring of the *R,R*-bpe complex **1** is flexible and an interconverting mixture of diastereomeric λ and δ chelate conformers would be anticipated [eqn. (3)]. It was predicted that

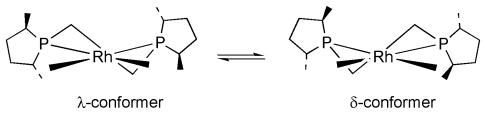

(3)

the λ conformer of **1** would give the higher enantioselectivity (see below)[3] and we reasoned that this hypothesis could be tested by comparing the optical yields obtained with **2** and **3**, the two diastereoisomers of *trans*-1,2-bis(*R,R*-phospholano)cyclopentane since **2** would give exclusively a λ-conformer chelate complex and **3** would give a δ-conformer.

The new ligands **2** and **3** were prepared from resolved *trans*-1,2-diphosphinocyclopentane[8] and the 1,4-diol cyclic sulfate[1] as shown in eqn. (4) for **2**. The rhodium(I) chelate complexes λ-

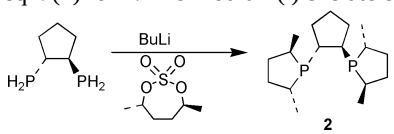

(4)

4 and δ-**5** have been synthesised and fully characterised but we have been unable to obtain crystals suitable for X-ray crystallography. However the crystal structures of the diiodoplatinum(II) complexes of **2** and **3**, λ-**6** and δ-**7** have been determined (Figs. 1 and 2).† These confirm the assignment of the chelate conformations. The bond lengths and angles around platinum in λ-**6** and δ-**7** are not substantially different (lengths differ by 0.01–0.02 Å and angles by 1–2°).[11] The principal effect of the change in backbone stereochemistry seems to be in the orientation of the phospholane rings. Changing the MP_2C_2 chelate conformation from λ to δ leads to a rotation about the M–P bond of *ca*. 30°, as measured by I–Pt–P–C torsions (see Figs. 1 and 2). As a consequence, the methyl groups are closer to the other ligands in the metal coordination plane (here iodine) in λ-**6** (I···CH_3 3.70 Å) than in δ-**7** (I···CH_3 4.11, 4.20 Å). Conversely the axial hydrogen atoms adjacent to the phosphorus are closer to the iodo ligands in δ-**7** (I···H 3.07, 3.00 Å) than

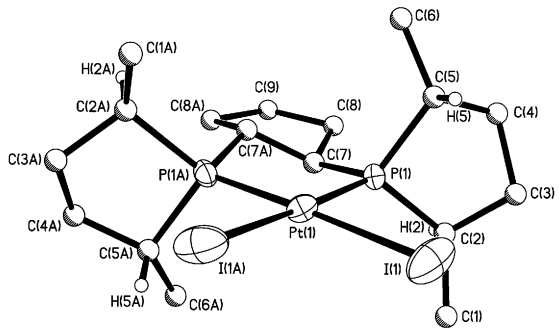

Fig. 1 Molecular structure and numbering scheme for λ-**6**. All but phospholane tertiary hydrogen atoms have been omitted for clarity. Important molecular dimensions: bond lengths (Å) Pt(1)–P(1) 2.237(2), Pt(1)–I(1) 2.6453(8); bond angle (°) P(1)–Pt(1)–P(1A) 88.25(10); torsion angles (°) I(1)–Pt(1)–P(1)–C(2) 46.5(2), I(1)–Pt(1)–P(1)–C(5) −69.2(2).

DOI: 10.1039/b002994g

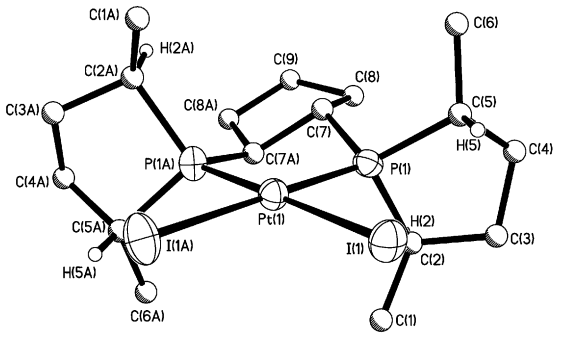

Fig. 2 Molecular structure and numbering scheme for δ-**7**. All but phospholane tertiary hydrogen atoms have been omitted for clarity. Important molecular dimensions include: bond lengths (Å) Pt(1)–P(1) 2.248(2), Pt(1)–P(1A) 2.258(2), Pt(1)–I(1) 2.6533(9), Pt(1)–I(1A) 2.6690(8); bond angle (°) P(1)–Pt(1)–P(1A) 86.44(9); torsion angles (°) I(1)–Pt(1)–P(1)–C(2) 78.4(2), I(1)–Pt(1)–P(1)–C(5) −38.3(2), I(1A)–Pt(1)–P(1A)–C(2A) 70.6(2), I(1A)–Pt(1)–P(1A)–C(5A) −47.5(2).

in λ-**6** (I···H 3.37 Å). The PC_4 rings in *R*-phospholanes have δ-conformations and so in δ-**7** the conformations are δδδ for the PC_4, PtP_2C_2 and PC_4 rings, respectively, while in λ-**6** these rings show δλδ conformations.

The results of the hydrogenations shown in eqns. (1) and (2) catalysed by the rhodium catalysts λ-**4**, δ-**5** and **1** are shown in Table 1. It is clear that the optical yields obtained with λ-**4** are inferior to **1** and those for δ-**5** are superior to **1**. The unequivocal conclusion is that the δ-chelate gives *higher* enantioselectivities than the λ-chelate, *i.e.* δ-**5** is the *matched* diastereomeric catalyst.[6] Since this is the opposite of what was predicted,[3] we decided to re-examine the basis of the current heuristic model for Duphos catalysts.[12]

Table 1 Optical yields for the hydrogenations of methyl-(*Z*)-2-acetamidocinnamate [eqn. (1)] and methyl-2-acetamidoacrylate [eqn. (2)][a]

Catalyst	Methyl-(*Z*)-2-acetamidocinnamate	Methyl-2-acetamidoacrylate
λ-**4**	77 (*R*)	73 (*R*)
1[b]	85 (*R*)	91 (*R*)
δ-**5**	98 (*R*)	95 (*R*)

[a] *Experimental conditions*: solvent MeOH, 2 atm H_2, 20–25 °C, 0.05–0.1% Rh catalyst, reaction time, 1–16 h. Conversions and enantiomeric excesses were determined by GC using a Hewlett-Packard 5800 A with a L-Chirasil-Val column. [b] Results from ref. 3.

In the stereochemical model of refs. 3, 6 and 12, it is assumed that the alkyl substituents of the phospholanes block the diagonal of quadrants shown in Fig. 3(a) for bis(*R*-phospholane) chelates. In turn this implies that the favoured, major, adduct diastereoisomer is that in which the enamide substrate is bound through its *si* face (see ref. 12 for explicit confirmation of this view).

Seminal mechanistic work[9] revealed that the major enantiomer formed in asymmetric hydrogenation by rhodium complexes of 'traditional' chiral diphosphines such as chiraphos was derived from the minor diastereoisomer of the prochiral alkene complex. Burk and coworkers showed[10] that, when the hydrogenation shown in eqn. (1) is catalysed by [Rh(*S*,*S*-Duphos)(cod)]$^+$, the major product enantiomer (having *S*-configuration) is derived, in Halpern-like manner, from the minor diastereoisomer of the substrate complex (which therefore must be *re*-face bound). Indeed they were able to confirm this assignment of adduct stereochemistry by NMR experiments and by analogy with iridium chemistry. By implication, for *R*,*R*-phospholanes, as here, the minor adduct is *si*-face bound (and the *R*-configuration product results from its Halpern-type hydrogenation). This directly contradicts the standard quadrant model prediction noted above.

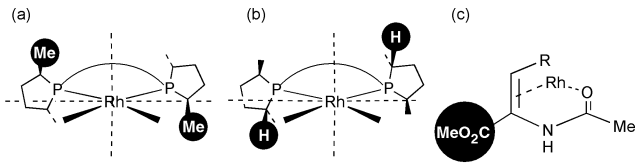

Fig. 3 (a) Quadrants that are reportedly[3,6,12] blocked by the methyl substituents in Rh(*R*,*R*-bpe) chelate; (b) quadrants that are proposed to be blocked by the axial hydrogens in a Rh(*R*,*R*-bpe) chelate; (c) *si*-face binding of substrate alkenes.

In λ-**6** the phospholane methyl groups are closer to the metal coordination plane than in δ-**7** and therefore would be expected to present more steric interaction at the sites where the alkene substrates would bind. However in δ-**7** (whose analogue δ-**5** is the more stereoselective catalyst) the axial hydrogen atoms are closer to the substrate binding site. This leads us to suggest an alternative stereochemical model for these phospholane ligands: it is the *axial* hydrogens rather than the equatorial methyls that offer the critical, diastereofacially-discriminating steric interactions with a prochiral substrate. The corollary of this suggestion is that the diagonal of blocked quadrants [Fig. 3(b)] is orthogonal to that currently accepted. The new quadrant diagram predicts (in accord with ref. 10) that the *less* stable (minor) diastereoisomer is formed when the substrate is *si*-face bound, Fig. 3c. A Halpern-type hydrogenation mechanism would then lead to the observed *R*-configuration of the product, again in accord with the results reported in ref. 10.

Hydrogenation of very bulky enamides (*e.g.* H_2C=CBu^{t}N-HAc) catalysed by *R*,*R*-Duphos complexes leads to a product of *S*-configuration. While this inversion of stereochemistry poses problems for any quadrant model, we note that it is possible that extreme bulk of the α-substituent may render the concentration of the minor adduct diastereoisomer effectively zero, thereby leading to no product from that pathway regardless of the rate of hydrogenation of the major (only) species.

Note added in proof: The quadrant models discussed in this paper implicitly assume that crowding in the plane of the metal–diphosphine moiety is important in enantioselection. A recent report (I. D. Gridnev, N. Higashi, K. Asakura and T. Imamoto, *J. Am. Chem. Soc.*, 2000, **122**, 7183) suggests that octahedral *cis*-dihydride species are critical.

We would like to thank Dr Guy Lloyd-Jones for useful discussions, EPSRC and Albright and Wilson for a CASE studentship (to E. L. H.), Acciones Integradas for a travel grant and Johnson-Matthey for a loan of precious metals.

Notes and references

† *Crystal structure analyses*: λ-**6**: $C_{17}H_{32}P_2I_2Pt$, M = 747.26, trigonal, space group $P3_221$ (no. 154), a = 12.699(3), c = 11.995(2) Å, U = 1675.1(5) Å^3, Z = 3, μ = 9.186 mm^{-1}, T = 173 K, 2589 unique data, $R1$ = 0.0343. Molecules of λ-**6** lie at sites of exact crystallographic C_2 symmetry and show signs of some disorder in the cyclopentane ring [leading to artificial flattening of the ring at C(9)]. δ-**7**: $C_{17}H_{32}P_2I_2Pt$, M = 747.26, monoclinic, space group $P2_1$ (no. 4), a = 8.3470(19), b = 13.844(4), c = 10.3968(19) Å, β = 111.574(11)°, U = 1117.2(4) Å^3, Z = 2, μ = 9.183 mm^{-1}, T = 173K, 5096 unique data, $R1$ = 0.0361.

CCDC 182/1724. See http://www.rsc.org/suppdata/cc/b0/b002994g/ for crystallographic files in .cif format.

1 M. J. Burk, *J. Am. Chem. Soc.*, 1991, **113**, 8518.
2 M. J. Burk, J. E. Feaster and R. L. Harlow, *Organometallics*, 1990, **9**, 2653.
3 M. J. Burk, J. E. Feaster, W. A. Nugent and R. L. Harlow, *J. Am. Chem Soc.*, 1993, **115**, 125.
4 M. J. Burk, M. F. Gross, T. G. P. Harper, C. S. Kalberg, J. R. Lee and J. P. Martinez, *Pure Appl. Chem.*, 1996, **68**, 37.
5 M. J. Burk and M. F. Gross, *Tetrahedron Lett.*, 1994, **35**, 9363.
6 M. J. Burk, A. Pizzano, J. A. Martín, L. M. Liable-Sands and A. L. Rheingold, *Organometallics*, 2000, **19**, 250.
7 M. J. Burk, J. E. Feaster and R. L. Harlow, *Tetrahedron: Asymmetry*, 1991, **2**, 569.
8 C. Eckert, L. Dahlenburg and A. Wolski, *Z. Naturforsch., Teil B.*, 1995, **50**, 1004.
9 W. S. Knowles, *Acc. Chem. Res.*, 1983, **16**, 106; C. Landis and J. Halpern, *J. Am. Chem. Soc.*, 1987, **109**, 1746 and references therein.
10 S. K. Armstrong, J. M. Brown and M. J. Burk, *Tetrahedron Lett.*, 1993, **34**, 879.
11 A. Martín and A. G. Orpen, *J. Am. Chem. Soc.*, 1996, **118**, 1464.
12 M. J. Burk, *Acc. Chem. Res.*, 2000, **33**, 363.

Rapid solid-state transformation of tetrahedral $[AlH_4]^-$ into octahedral $[AlH_6]^{3-}$ in lithium aluminohydride

Viktor P. Balema,[a] Kevin W. Dennis[a] and Vitalij K. Pecharsky*[ab]

[a] *Ames Laboratory, Iowa State University, Ames, IA 50011-3020, USA*
[b] *Department of Materials Science and Engineering, Iowa State University, Ames, IA 50011, USA. E-mail: vitkp@ameslab.gov*

Received (in Irvine, CA, USA) 22nd May 2000, Accepted 20th July 2000

Polycrystalline $LiAlH_4$ transforms into polycrystalline Li_3AlH_6 and Al during short time (5 min) ball-milling with 3 mol% $TiCl_4$ at room temperature; solid-state rearrangement of tetrahedral $[AlH_4]^-$ into octahedral $[AlH_6]^{3-}$ at ambient conditions was previously unknown; this transformation does not occur during ball-milling of pure $LiAlH_4$ or in the presence of 3 mol% $TiCl_4$ without mechanochemical treatment.

High capacity solid-state storage of hydrogen is becoming increasingly important as fuel cell power plants approach broad use in automotive and electrical utility applications. Overall hydrogen content of two alkali metal aluminohydrides, $LiAlH_4$ and $NaAlH_4$ (10.5 and 7.3 wt% H_2, respectively), is amongst the highest for about 70 known complex hydrides[1] reviving recent interest to them as potential ultra-high capacity hydrogen storage solids.[2–6] Temperature induced transformation of lithium aluminohydride ($LiAlH_4$) into lithium hexahydroaluminate (Li_3AlH_6) has been known for almost three decades.[7] However, the processes occurring in pure $LiAlH_4$ during its thermal decomposition were understood only recently.[8,9] According to results obtained by Bastide *et al.*[8] and Dymova *et al.*,[9] $LiAlH_4$ is quite stable in the solid state below its melting temperature but rapidly transforms in the melt, where rearrangement of the tetrahedral $[AlH_4]^-$ ion into the octahedral $[AlH_6]^{3-}$ ion[10,11] is easily achieved. The stability of the solid $LiAlH_4$ is, therefore, attributed to kinetic restrictions of the solid-state transformation process in the alumohydride anion rather than to thermodynamic reasons (ΔG of the reaction $LiAlH_4 = 1/3Li_3AlH_6 + 2/3Al + H_2$ is -27 kJ mol^{-1}).[12] Recently, a significant reduction of the decomposition temperatures of alkali metal aluminium hydrides doped with transition metal derivatives has been reported.[3–6] It is, however, unclear, whether transition metal dopants reduce melting points of complex aluminium hydrides or act as catalysts of solid-state transformations near the respective melting temperatures.

Here we report on the first observation of the rapid solid-state transformation of lithium aluminohydride into lithium hexahydroaluminate in the presence of a catalytic amount of titanium tetrachloride ($TiCl_4$) during mechanochemical activation at ambient conditions.† A reaction mixture containing 97 mol% $LiAlH_4$ and 3 mol% $TiCl_4$ was ball-milled in a Spex mill under helium for 5 min and then investigated using X-ray powder diffraction (XRD), differential thermal (DTA) and gas-volumetric analyses. According to XRD data, $LiAlH_4$ was completely transformed during the short mechanochemical treatment with a catalytic quantity of $TiCl_4$. Only Bragg peaks corresponding to the crystalline Li_3AlH_6,[13a] Al and LiCl are seen in the X-ray powder diffraction pattern of the reaction mixture (Fig. 1). The DTA trace of the reaction mixture in the temperature range between 380 and 500 K contains one broad endothermic peak between approximately 395 and 485 K with a minimum at 445 K (inset in Fig. 2). The endothermic process occurs at lower temperatures when compared to that observed in the pure mechanochemically prepared Li_3AlH_6[13a] (*ca.* 480–535 K, minimum at 505 K). This lowering of the hydrogen release temperature is, however, in good agreement with previously reported data on reduction of decomposition temperature of transition metal-doped alkali metal aluminohydrides.[3–5] The gas-volumetric analysis of the reaction mixture between 295 and 675 K in vacuum revealed a slow one-step hydrogen evolution at 395 ± 5 K (Fig. 2), *i.e.* at the onset temperature of the endothermic effect observed in the DTA experiment. The amount of released hydrogen, 2.08 wt%, agrees well with the decomposition of Li_3AlH_6 [eqn. (1)], which was formed according to eqn. (2) (the theoretical hydrogen content in the mixture is 2.1 wt%). The intensities of Bragg peaks (Fig. 1) are in quantitative agreement with the amounts of reaction products. Eqn. (2) summarizes transformations of $LiAlH_4$ and $TiCl_4$ during ball-milling [eqns. (3) and (4)]:

$$2Li_3AlH_6 = 6LiH + Al + 3H_2 \uparrow \quad (1)$$

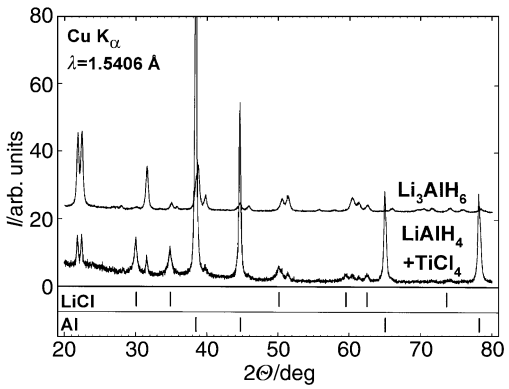

Fig. 1 The X-ray powder diffraction pattern of the reaction mixture obtained during 5 min ball-milling of 97 mol% $LiAlH_4$ and 3 mol% $TiCl_4$ compared with the X-ray powder diffraction pattern of Li_3AlH_6 prepared mechanochemically.[13] Vertical bars at the bottom of the chart indicate positions of Bragg peaks of pure LiCl and Al.

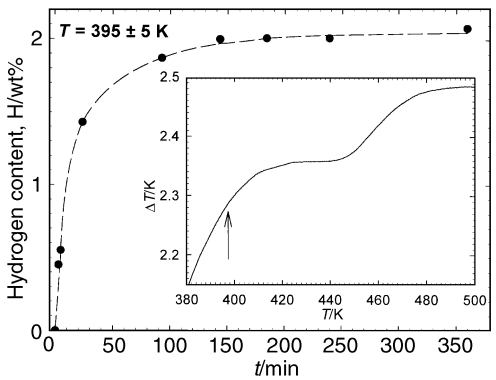

Fig. 2 The results of gas-volumetric analysis at 395 ± 5 K of the reaction mixture obtained during 5 min ball-milling of 97 mol% $LiAlH_4$ with 3 mol% $TiCl_4$. The inset shows the DTA trace of the same reaction mixture. The vertical arrow on the inset indicates the onset of the endothermic process.

DOI: 10.1039/b004144k

$$0.97LiAlH_4 + 0.03TiCl_4 = 0.283Li_3AlH_6 + 0.12LiCl + 0.687Al + 0.03[Ti] + 1.091H_2 \uparrow \quad (2)$$

$$4LiAlH_4 + TiCl_4 = 4LiCl + 4Al + [Ti] + 2H_2 \uparrow \quad (3)$$

$$3LiAlH_4 + [Ti] = Li_3AlH_6 + 2Al + [Ti] + 3H_2 \uparrow \quad (4)$$

The formation of lithium chloride, aluminium and a Ti-containing micro-crystalline phase with unknown composition during 5 min ball-milling of lithium aluminohydride and titanium tetrachloride was confirmed by mechanochemical treatment of stoichiometric amounts (4 : 1) of $LiAlH_4$ and $TiCl_4$ [eqn. (3)].[13b] No Bragg peaks corresponding to either $LiAlH_4$ or Li_3AlH_6 were detected from XRD data. Furthermore, the gas-volumetric analysis of the obtained reaction mixture [eqn. (3)] did not reveal observable hydrogen gas evolution up to 925 K.

To verify that the titanium catalyzed solid state transformation of $LiAlH_4$ into Li_3AlH_6 proceeds only during mechanochemical activation, the mixture containing 97 mol% of lithium aluminohydride and 3 mol% of titanium tetrachloride was thoroughly ground in a mortar under helium for 10 min. Although slight changes of the reaction mixture color from grayish-white to gray were observed, XRD did not indicate the formation of detectable amounts (*i.e.* 5 vol% or more) of Li_3AlH_6 during grinding. Weak Bragg peaks corresponding to polycrystalline LiCl and Al were found in the X-ray diffraction pattern of the reaction mixture after grinding, and therefore, the observed color changes were likely associated with the reduction of $TiCl_4$ by $LiAlH_4$ according to eqn. (3). Furthermore, our experiments with pure $LiAlH_4$ revealed that this complex hydride is stable during ball-milling without $TiCl_4$ for up to 35 h.

Currently, several different models describing the observed rapid solid-state rearrangement of $LiAlH_4$ (*i.e.* tetrahedral $[AlH_4]^-$ ion) into Li_3AlH_6 (*i.e.* octahedral $[AlH_6]^{3-}$ ion) in the presence of $TiCl_4$ during mechanochemical treatment at ambient conditions are being considered. One of the most likely mechanisms explaining the catalytic effect of $TiCl_4$ can be its reduction to a highly reactive nanocrystalline or amorphous titanium phase [eqn. (3)], which subsequently mechanically alloys into the crystal lattice of $LiAlH_4$. The following destabilization of the host crystal lattice caused by the presence of titanium leads to the formation of metastable 'melt-like' hydride phases, where the rearrangement of the tetrahedral $[AlH_4]^-$ ion into the octahedral $[AlH_6]^{3-}$ ion becomes kinetically possible. Although the nature of intermediate phase(s) is presently unclear, it is feasible that they are similar to the metastable high-pressure γ-$LiAlH_4$ with hexa-coordinated $[AlH_6]^{3-}$ ion,[10,15] and their formation becomes possible due to mechanically induced strain in the presence of titanium catalyst.

The Ames Laboratory is operated for the U.S. Department of Energy (DOE) by Iowa State University under contract No.W-7405-ENG-82. Different aspects of this work were supported by the Office of Basic Energy Sciences, Materials Sciences Division of the U.S. DOE and Iowa State University Carver Trust Grant.

Notes and references

† All experiments described in this communication were carried out in a glove box in a purified helium atmosphere and in a hardened-steel vial sealed under helium. The X-ray diffraction experiments were performed under helium in a sample holder covered by X-ray transparent polymer film. The differential thermal analysis was carried out in an argon atmosphere at ambient pressure using commercially available equipment. The heating rate during DTA measurements was 10 K min^{-1}. The gas-volumetric experiments were performed using a standard Sievert's type apparatus.

1 K. Yvon, *Chimia*, 1998, **52**, 613.
2 G. Sandrock, in *Hydrogen Energy Systems*, ed. Y. Yürüm, Kluwer Academic Publishers, Dordrecht and Boston, 1995, p. 135.
3 B. Bogdanovic and M. J. Schwickardi, *J. Alloys Compd.*, 1997, **253**, 1.
4 R. A. Zidan, S. Takara, A. G. Hee and C. M. Jensen, *J. Alloys Compd.*, 1999, **285**, 119.
5 C. M. Jensen, R. A. Zidan, N. Mariels, A. G. Hee and C. Hagen, *Int. J. Hydrogen Energy*, 1999, **24**, 461.
6 K. J. Gross, S. Guthrie, S. Takara and G. Thomas, *J. Alloys Compd.*, 2000, **297**, 270.
7 J. A. Dilts and E. C. Ashby, *Inorg. Chem.*, 1972, **11**, 1230.
8 J. P. Bastide, B. M. Bonnetot, J. M. Letoffe and P. Claudy, *Mater. Res. Bull.*, 1985, **20**, 999.
9 T. N. Dymova, V. N. Konoplev, D. P. Aleksandrov, A. S. Sizareva and T. A. Silina, *Russ. J. Coord. Chem.*, 1995, **21**, 165.
10 J. C. Bureau, J. P. Bastide, P. Claudy, J. M. Letoffe and Z. Amri, *J. Less-Common Met.*, 1987, **22**, 185.
11 J. C. Bureau, Z. Amri, P. Claudy, J. M. Letoffe, B. Balland and P. Gonnard, *Mater. Res. Bull.*, 1989, **24**, 551.
12 T. N. Dymova, D. P. Aleksandrov, V. N. Konoplev, T. A. Silina and A. S. Sizareva, *Russ. J. Coord. Chem.*, 1994, **20**, 263.
13 (*a*) Solvent free Li_3AlH_6 was prepared by ball-milling of 0.80 g (0.1 mol) LiH and 1.90 g (0.05 mol) $LiAlH_4$ in a helium atmosphere for 5 h. *Crystal data*: for Li_3AlH_6 monoclinic, space group $P2_1/c$, a = 5.667(1), b = 8.107(2), c = 7.917(2) Å, β = 92.17(1)°, V = 363.5(2) Å^3, M = 53.8, Z = 4, T = 298 K . The obtained lattice parameters are in excellent agreement with the previously reported data[14] for conventionally prepared Li_3AlH_6; (*b*) ball-milling of stoichiometric amounts of $LiAlH_4$ and $TiCl_4$ was carried out in a Spex mill in a hardened-steel vial sealed under helium. According to XRD, the reaction mixture contains polycrystalline LiCl, Al and an unidentified intermetallic $Ti_{1-x}Al_x$ phase.
14 J. P. Bastide, B. Bonnetot, J. M. Letoffe and P. Claudy, *Stud. Inorg. Chem. (Solid State Chem.)*, 1983, **3**, 785.
15 J. P. Bastide, J. C. Bureau, J. M. Letoffe and P. Claudy, *Mater. Res. Bull.*, 1987, **22**, 185.

Dealkylation of a 1,2-bis(benzylthio)benzene derivative: generation of benzodithiete or its equivalent *via* a dithia dication†

Kenji Kobayashi,* Emiko Koyama, Mariko Goto, Chikako Noda and Naomichi Furukawa*‡

Department of Chemistry, University of Tsukuba, Tsukuba, Ibaraki 305-8571, Japan.
E-mail: kenjinor@staff.chem.tsukuba.ac.jp

Received (in Cambridge, UK) 20th June 2000, Accepted 21st July 2000

The reaction of 1,2-bis(4-methylbenzylthio)benzene *s*-oxide with triflic anhydride in CH_3CN–CH_2Cl_2 in the presence of alkynes affords 1,4-benzodithiin derivatives and *N*-(4-methylbenzyl)acetamide after quenching with H_2O; this suggests the generation of benzodithiete or its equivalent.

The development of new methodologies for the generation of reactive species is an important goal in organic chemistry. Benzodithiete **5** is a highly reactive transient species, which occurs in thermolysis[1–3] and photolysis[4–6] of appropriate precursors, and is trapped by alkynes to form 1,4-benzodithiin derivatives.[7,8] Benzodithiete **5** is estimated to be 17 kcal mol^{-1} more stable than *o*-dithiobenzoquinone by calculations at the MP2 level[9] and decomposed at more than −90 °C.[1] σ-Bonded dithia dications have attracted considerable attention in heteroatom chemistry from the viewpoint of structural interests.[10] The strained dication of 1,4-dithiane reacts with alkynes to give dithiabicyclo[2.2.2]octene derivatives.[11] Recently, we have demonstrated the facile dealkylation of dithia dications with a flexible conformation to afford thiasulfonium salts;[12] in particular, the dithia dication obtained from the reaction of 2,2′-bis(benzylthio)biphenyl *s*-oxide with triflic anhydride (Tf_2O) is decomposed even at −20 °C to afford biphenyl disulfide and a benzyl cation.[13] Herein we report the reactions of 1,2-bis(4-methylbenzylthio)benzene mono-*s*-oxide **1** with Tf_2O in the presence of alkynes **2** and alkenes **3**, which produce 1,4-benzodithiins **6** and 2,3-dihydro-1,4-benzodithins **7**, respectively. The key reaction for the generation of benzodithiete **5** or its equivalent is based on the dealkylation of **1** *via* a dithia dication **4** (Scheme 1).

The substrate **1** was prepared by the reaction of benzene-1,2-dithiol with 4-methylbenzyl chloride in the presence of KOH (86% yield) followed by the oxidation of the resulting bissulfide with MCPBA (73% yield).

The reaction of **1** with triflic anhydride (Tf_2O) was monitored by ^{1}H NMR spectroscopy. When 1 eq. of Tf_2O was added to a solution of **1** in CD_3CN-CD_2Cl_2 (v/v 1:1) at −75 °C, **1** immediately disappeared and a sole peak due to the *N*-benzyl–acetonitrile adduct appeared at δ 5.21 in the region of benzyl groups.[13] This result indicates that both benzyl groups of **1** are completely eliminated at −60 °C within a minute, although we have no direct evidence for the generation of dithia dication **4** and benzodithiete **5**. After warming up to rt, the reaction mixture gave a white precipitate. Treatment of the supernatant with H_2O afforded *N*-(4-methylbenzyl)acetamide (57% yield), and treatment of the white precipitate with $NaBH_4$ in THF followed by addition of iodomethane gave 1,2-bis(methylthio)-benzene (42% yield).

In order to elucidate the generation of benzodithiete **5** indirectly, the reaction of **1** with Tf_2O was carried out in the presence of alkynes **2** as a trapping reagent (Scheme 2).§¶ After complete dealkylation of **1** with Tf_2O in CH_3CN–CH_2Cl_2 (v/v 1:1) at −60 °C, **2** was added to the reaction mixture. From diarylacetylenes **2a**–**c**, 2,3-diaryl-1,4-benzodithiins **6a**–**c** were obtained in 44, 64, and 20% respective yields, and from arylacetylenes **2d**–**e**, 2-aryl-1,4-benzodithiins **6d**–**e** were produced in 18 and 21% respective yields. Thus, the formation of **6** strongly suggests the generation of **5** or its equivalent in the course of the reaction of **1** with Tf_2O. Diarylacetylenes serve as a more effective trapping reagent of **5** than arylacetylenes. However, dimethyl acetylenedicarboxylate[2,5] did not give 2,3-bis(methoxycarbonyl)-1,4-benzodithiin, although *N*-(4-methylbenzyl)acetamide and 1,2-bis(methylthio)benzene were obtained in 59 and 20% yields, respectively, after as treatment mentioned above. This result implies that a concerted mechanism may not be involved in the reaction of **5** or its equivalent with alkynes.

The reaction of **1** with Tf_2O in the presence of alkenes **3** was also conducted under the same conditions (Scheme 3).§¶ The stereochemistry of the product reflects the reaction mechanism. *trans*-Stilbene (*trans*-**3a**) gave *trans*-2,3-diphenyl-2,3-dihydro-1,4-benzodithiine (*trans*-**7a**) (29% yield), whereas *cis*-stilbene (*cis*)-**3a**) afforded a mixture of *trans*-**7a** (17% yield) and (*cis*)-**7a** (10% yield). The formation of two stereoisomers (*trans*)- and

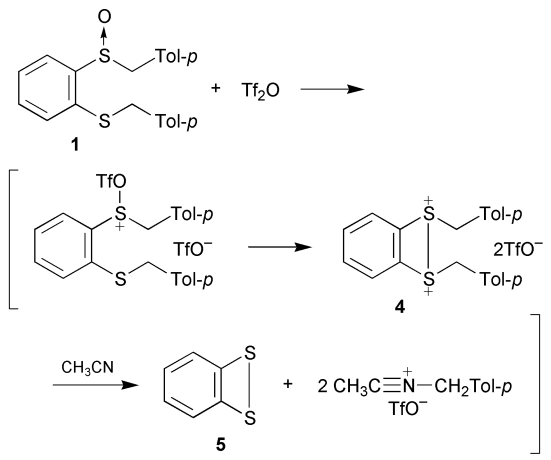

Tf_2O = $(CF_3SO_2)_2O$, Tol-*p* = C_6H_4Me-*p*

Scheme 1

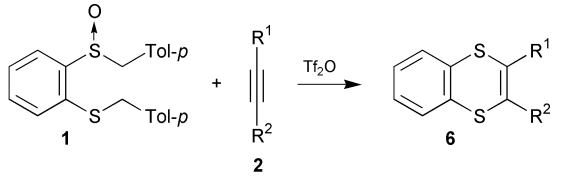

2a: $R^1 = R^2 = C_6H_5$ **6a** (44%)
2b: $R^1 = R^2 = C_6H_4Me$-*p* **6b** (64%)
2c: $R^1 = R^2 = C_6H_4OMe$-*p* **6c** (20%)
2d: $R^1 = C_6H_5$, R^2 = H **6d** (18%)
2e: $R^1 = C_6H_4Me$-*p*, R^2 = H **6e** (21%)

Scheme 2

† Electronic supplementary information (ESI) available: spectral data of compounds. See http://www.rsc.org/suppdata/cc/b0/b004940i/

DOI: 10.1039/b004940i

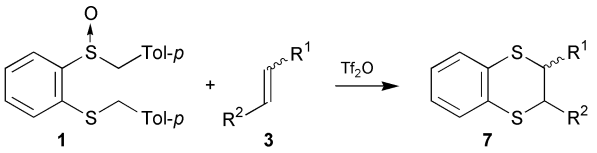

(*trans*)-**3a**: $R^1 = R^2 = C_6H_5$ — (*trans*)-**7a** (29%)

(*cis*)-**3a**: $R^1 = R^2 = C_6H_5$ — (*trans*)-**7a** (17%), (*cis*)-**7a** (10%)

(*trans*)-**3b**: $R^1 = C_6H_5$, $R^2 = CO_2Et$ — (*trans*)-**7b** (19%)

3c: $R^1 = C_6H_4Me$-*p*, $R^2 = H$ — **7c** (32%)

Scheme 3

(*cis*)-**7a**) from *cis*-**3a**, but not from (*trans*)-**3a**, suggests a stepwise addition mechanism of benzodithiete **5** or its equivalent to carbon–carbon multiple bonds such as an Ad_E path. Ethyl (*E*)-cinnamate (*trans*-**3b**) and 4-methylstyrene **3c** gave the corresponding (*trans*)-**7b** and **7c** in 19 and 32% yields, respectively.

The redox behavior of 1,4-benzodithiin derivatives has been studied extensively from the viewpoint of cationic π-conjugated systems.[7,14] Cyclic voltammetry of 1,4-benzodithiins **6** in CH_3CN with Bu_4NClO_4 (0.1 M) at rt showed two oxidation waves, where, in all cases, the first ones are reversible and the second ones are irreversible. The redox potentials of **6a**–**e** obtained here are summarized in Table 1. The first half-wave potentials are in the range of $E^1_{1/2}$ = +0.93– +1.02 V and the second oxidation potentials are in the range of E^2_{pa} = +1.26– +1.53 V *vs*. Fc/Fc$^+$. The first oxidation potentials of 1,4-benzodithiin derivatives are heightened with increasing the number of aromatic groups at the 2- and 3-positions owing to a π-conjugative effect: unsubstituted 1,4-benzodithiin[15] < **6d** (**6e**) < **6a** (**6b**). The oxidation potentials are lowered as the electron-donating ability of a substituent at the *para*-position of the aromatic ring is increased: **6a** > **6b** > **6c**. A good linear relationship between the first half-wave potentials and their σ_p^+ values was obtained with ρ = 0.12 and a correlation coefficient r = 0.98.

In conclusion, we have demonstrated the generation of benzodithiete **5** or its equivalent through the facile dealkylation of a 1,2-bis(benzylthio)benzene derivative **1** *via* a dithia dication **4**. The present study opens the way to the synthetic application of dithia dications.

This work was supported in part by grants-in-aid from the Ministry of Education, Science, Sports and Culture, Japan (No. 11440186) and University of Tsukuba (TARA project fund).

Table 1 Redox potentials of 1,4-benzodithiin derivatives **6**[a]

Compound	E^1_{pa} [b]	$E^1_{1/2}$ [b]	E^2_{pa} [b]
6a	1.06	1.02	1.52
6b	1.04	1.00	1.47
6c	0.96	0.93	1.26
6d	1.03	1.00	1.53
6e	0.99	0.96	1.53

[a] In CH_3CN with Bu_4NClO_4 (0.1 M) at rt. [b] V *vs*. Fc/Fc$^+$; scan rate, 0.1 V s^{-1}.

Notes and references

‡ Present address: Foundation for Advancement of International Science, 586-9 Akatsuka-Ushigahuchi, Tsukuba, Ibaraki 305-0062, Japan.

§ To a solution of **1** in CH_3CN–CH_2Cl_2 (v/v 1:1) at −60 °C under Ar were added 1 eq. of Tf_2O and, after about 30 s, 2 eq. of **2** or **3**. The mixture was stirred at −60 °C for 10 min and then at rt for 1 h, and quenched with aqueous $NaHCO_3$. Extraction with CH_2Cl_2 followed by purification with silica gel chromatography gave 1,4-benzodithiin derivatives **6** from **2** or 2,3-dihydro-1,4-benzodithiin derivatives **7** from **3** and *N*-(4-methylbenzyl)-acetamide in modest yields.

¶ Representative data for **6b**: wax; ^{1}H NMR (270 MHz, $CDCl_3$) δ 2.26 (s, 6H), 6.96 (d, J = 7.8 Hz, 4H), 7.07 (d, J = 7.8 Hz, 4H), 7.25 (dd, J = 3.5 and 5.7 Hz, 2H), 7.46 (dd, J = 3.5 and 5.7 Hz, 2H); ^{13}C NMR (67.8 MHz, $CDCl_3$) δ 21.2, 127.6, 127.9, 128.8, 129.6, 133.8, 135.5, 136.1, 137.5; EI-MS *m*/*z* 346 (M^+); Calc. for $C_{22}H_{18}S_2$: C, 76.26; H, 5.24. Found: C, 76.02; H, 5.49%. For *trans*-**7a**: mp 120–121 °C; ^{1}H NMR (270 MHz, $CDCl_3$) δ 4.67 (s, 2H), 7.10 (dd, J = 3.8 and 5.9 Hz, 2H), 7.14–7.19 (m, 10H), 7.33 (dd, J = 3.8 and 5.9 Hz, 2H); ^{13}C NMR (67.8 MHz, $CDCl_3$) δ 54.6, 125.4, 127.8, 128.0, 128.1, 128.4, 134.2, 138.3; EI-MS *m*/*z* 320 (M^+); Calc. for $C_{20}H_{16}S_2$: C, 74.96; H, 5.03. Found: C, 74.84; H, 5.19%.

1 M. Breitenstein, R. Schulz and A. Schweig, *J. Org. Chem.*, 1982, **47**, 1979.
2 J. Nakayama, H. Fukushima, R. Hashimoto and H. Hoshino, *J. Chem. Soc., Chem. Commun.*, 1982, 612.
3 H. Bock and P. Rittmeyer, *Phosph. Sulf.*, 1988, **35**, 291.
4 R. B. Boar, D. W. Hawkins, J. F. McGhie, S. C. Misra, D. H. R. Barton, M. F. C. Ladd and D. C. Povey, *J. Chem. Soc., Chem. Commun.*, 1975, 756.
5 P. de Mayo, A. C. Weedon and G. S. K. Wong, *J. Org. Chem.*, 1979, **44**, 1977.
6 E. Fanghänel, R. Herrmann, J. Bierwisch, H. Hartung, U. Baumeister, G. Maier and H. P. Reisenauer, *J. Prakt. Chem.*, 1994, **336**, 444.
7 G. Klar, in *Methods of Organic Chemistry*, ed. E. Schaumann, Thieme, Stuttgart, 1997, vol. E9a, pp 250–407.
8 J. H. Verheijen and H. Kloosterziel, *Synthesis*, 1975, 451; B. L. Chenard, R. L. Harlow, A. L. Johnson and S. A. Vladuchick, *J. Am. Chem. Soc.*, 1985, **107**, 3871; A. Padwa, D. J. Austin, M. Ishida, C. L. Muller, S. S. Murphree and P. E. Yeske, *J. Org. Chem.*, 1992, **57**, 1161.
9 M. Mann and J. Fabian, *Int. J. Quantum Chem.*, 1996, **60**, 859.
10 N. Furukawa, *Bull. Chem. Soc. Jpn.*, 1997, **70**, 2571 and references cited therein.
11 V. G. Nenajdenko, N. E. Shevchenko and E. S. Balenkova, *J. Org. Chem.*, 1998, **63**, 2168.
12 H. Shima, R. Kobayashi, T. Nabeshima and N. Furukawa, *Tetrahedron Lett.*, 1996, **37**, 667.
13 H. Shima, R. Kobayashi and N. Furukawa, unpublished results.
14 T. Nishinaga, A. Wakamiya and K. Komatsu, *Chem. Commun.*, 1999, 777.
15 W. Schroth, R. Borsdorf, R. Herzschuh and J. Seidler, *Z. Chem.*, 1970, **10**, 147.

ChemComm

Preparation and functionalization of hydride terminated porous germanium†

Hee Cheul Choi and Jillian M. Buriak*

Department of Chemistry, 1393 Brown Laboratories, Purdue University, West Lafayette, IN 47907-1393, USA. E-mail: buriak@purdue.edu

Received (in Irvine, CA, USA) 17th May 2000, Accepted 20th July 2000

Porous germanium (PG) is prepared by a novel bipolar electrochemical etching (BEE) technique; scanning electron microscopy (SEM) clearly reveals formation of a porous layer up to a few microns thick that is Ge–H_x terminated as indicated by FTIR spectroscopy; the hydride terminated PG material is quite resistant to oxidation, even under thermal conditions, but can be induced to undergo hydrogermylation reactions with alkenes and alkynes.

Porous semiconducting materials are a topic of intense interest because of their unique electronic,[1] optoelectronic,[2] and morphological[3] properties, and biocompatibility[4] characteristics. Up to now, the vast majority of research efforts have concentrated on porous silicon, although other materials such as porous GaAs, InP, SiC, Si_xGe_{1-x}, GaP, and GaN,[5] have also been investigated to a lesser extent. The unusual light emitting properties of porous silicon through photo-, electrochemi- and chemi-luminescence routes are a result of the highly complex nanoscale architecture. Embedded nanocrystallites and nanowires of silicon within the porous silicon matrix exhibit quantum confinement effects, and thus the material acts very differently from the bulk parent. There is a surprising dearth of knowledge about porous silicon's congener, porous germanium (PG), and thus any potentially important properties intrinsic to this material remain unknown. There are two published procedures[6,7] for preparation of PG involving an anodic etch with aqueous HF electrolytes, but in our hands yield an oxidized surface instead of hydride terminated germanium surface. Little morphological investigation and no chemical reactivity studies have been carried out on the reported PG surfaces prepared in this manner.[8,9] Here, we describe the formation of highly ordered PG with a nanoscale architecture, as determined from plan and cross-sectional views of the porous layer by scanning electron microscopy (SEM), utilizing a novel and reproducible etching technique, termed *bipolar* electrochemical etching (BEE), with an HCl-based etchant. Through transmission FTIR studies of the PG, we have determined that the surface is Ge–H_x terminated, and can undergo surface hydrogermylation reactions with alkynes and alkenes, yielding alkenyl and alkyl terminated interfaces respectively. Light emission upon UV irradiation is also observed at 77 K in air.

The porous germanium (PG) was prepared from polished single crystalline Ge(100) wafers, either n- or p-doped, using an ethanoic HCl solution (1 : 1.8 of 48% HCl : EtOH v/v) in air. A wide variety of conditions were examined, but only a bipolar electrochemical etching (BEE) procedure produced the desired results.‡ BEE was carried out in a homemade Teflon etching cell, identical to that used to prepare porous silicon.[10] Initially, the germanium surface is anodized at 350 mA cm^{-2} for 5 min, followed by cathodization for 1 min with a negative bias, at the same current density, as outlined in Fig. 1. Longer cathodization leads to surface damage due to electropolishing. Upon anodization, the surface turns visibly gray, and is believed to be composed of surface hydroxide or surface chloride, as suggested by the lack of Ge–H_x vibrations in the transmission FTIR spectrum and literature precedent.[11] Scanning electron microscopy indicates formation of a *ca*. 700 nm thick amorphous layer after 2 min anodization, which fully dissolves after 5 min, leaving no observable film on the surface of the bulk germanium within the resolution of the instrument (10 nm). Germanium oxide is soluble in aqueous solution, and thus appears to be formed transiently before dissolution under these conditions. The subsequent cathodization step is critical for formation of the porous layer and hydride termination. Presumably, the weak Ge–Ge bonds are protonated under the cathodic potential[11] which eventually leads to GeH_4 production, and dissolution of the bulk germanium, resulting in hydride termination and pore formation[12] (Fig. 1). Formation of thin porous layers on silicon has been reported under cathodic conditions.[13] Without the prior anodic step, only hydrogen evolution from the cathodic germanium electrode occurs. The PG layer shows false colors due to Fabry–Perot fringes, resulting from constructive and destructive interference of the reflected white light from the top and bottom of the thin porous layer, as is observed with thin porous silicon layers.[14,15]

Scanning electron microscopy (SEM) clearly reveals PG in both cross-sectional and plan views (Fig. 2) for both n- and p-type wafers. The porous layer of a PG sample prepared from n^+ Ge is *ca*. 15 μm thick (Figs. 2(*a*) and (*b*)), and features down to the resolution of the instrument, *ca*. 10 nm, can be discerned.

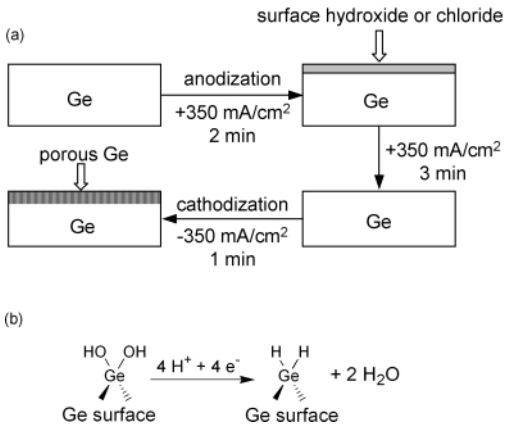

Fig. 1 (*a*) Schematic representation of the bipolar electrochemical etching (BEE) of Ge(100) wafers. (*b*) Surface electrochemical conversion of oxidized Ge(100) surfaces to hydride-terminated Ge(100) under cathodic bias in an acidic medium.[12]

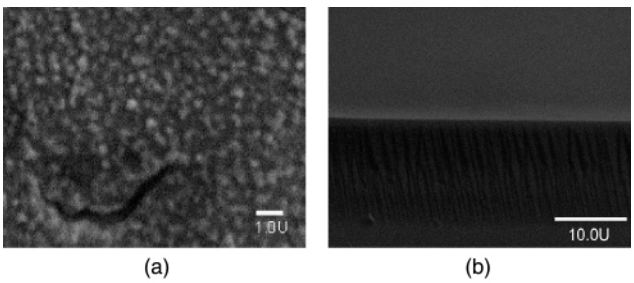

Fig. 2 Plan (*a*) and cross-sectional (*b*) views of n^+ type derived PG.

† Electronic supplementary information (ESI) available: FTIR thermal stability measurements and SEM images. See http://www.rsc.org/suppdata/cc/b0/b004011h/

The pores are tilted by 9° from the surface normal due to the 9° miscut of the starting wafers. The thickness of the porous layer can vary somewhat across an etched surface (1–15 μm), most likely due to heterogeneities in the electrical field during the etch as a result of the simplicity of our set-up. PG prepared from p-type Ge shows similar features, and is *ca.* 1.5 μm thick (Figs. 2(*c*) and (*d*)). Higher magnification of the surface layer in plan view of either n- or p-type samples reveals a highly porous top layer in the center of the 0.3 cm^2 etched area (Fig. 2(*a*) and (SI5†)), which progressively becomes populated by crystallites with an average size of 500 nm towards the edge.†

FTIR analysis of PG reveals a broad ν(Ge–H_x) vibration with features at 2044 cm^{-1} and 2015 cm^{-1}, as shown in Fig. 3(*a*), which appear at slightly lower energies than gas phase $Me_{4-x}GeH_x$.[16] Oxygen back-bonded Ge–H_x vibrations, expected at higher energies[11] are not observed. Because of the surface roughness and broad Ge–H_x stretching region, it is expected that the surface is terminated with mono-, di- and trihydrides, like porous silicon.[17] In order to definitively prove the formation of the Ge–H bonds, a deuterated surface (Ge–D_x) was made by same etching technique using deuterated ethanol and DCl solution. The resulting Ge–D_x stretching mode appears at 1455 cm^{-1}, as expected, with a very weak Ge–H_x band observed at 2020 cm^{-1} (Fig. 3(*b*)). The thermal stability of the hydride termination is surprising and is described in the ESI†.

In order to determine whether the hydride terminated PG surface could be functionalized, hydrogermylation of alkynes was examined. Refluxing a PG sample in a 20% 1-dodecene solution in mesitylene (v/v) for 2 h resulted in incorporation of surface-bound dodecyl moieties[18] (Fig. 3(*c*)). Application of other known reaction conditions for formation of Si–C bonds on porous and flat silicon to PG were unsuccessful, including Lewis acid[19] mediated hydrogermylation, and Ge–Ge bond attack with Grignard reagents.[20] The crystalline PG structure may be more sensitive to Lewis acids and nucleophilic attack under these conditions. In any case, the surface of PG may be tailored through thermally induced hydrogermylation reactions.

Homogeneous red photoluminescence is observed by eye across the entire PG surface at 77 K in a darkened room upon illumination with 365 nm irradiation, but is considerably weaker than that observed from porous silicon; the weak light emission, unfortunately, fell below the optical detection limit of our CCD set-up, and thus a λ_{max} could not be collected. Samples etched only anodically, as opposed to the bipolar etching procedure, on the other hand, emit yellow-white photoluminescence under 254 nm UV illumination at 77 K. Since there are no observable Ge–H_x bonds formed after anodization by FTIR, nor a porous layer by SEM, the source of the photoluminescence is believed to arise from germanium oxide layers, as opposed to germanium nanoparticles. This supposition is supported by the fact that all emission is eliminated after washing the sample with 25% aqueous HF, while the Ge–H_x terminated samples are unaffected. We propose that the weak red light emission observed from Ge–H_x terminated PG arises from Ge nanoparticles, whilst that from the anodically etched samples results from oxide.

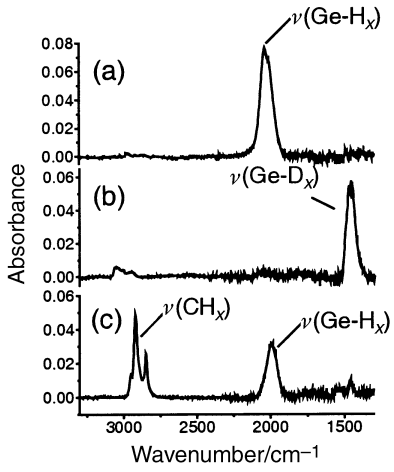

Fig. 3 FTIR spectrum of PG: (*a*) etched by BEE using ethanoic HCl, (*b*) using deuterated ethanol and DCl, and (*c*) thermally hydrogermylated using 1-dodecene.

To summarize, we report a new and highly reproducible etching procedure to produce hydride-terminated porous germanium. Through a bipolar HCl etch, porous layers up to 15 microns thick can be prepared and subsequently functionalized with alkyl monolayers through a thermally induced hydrogermylation reaction. Detailed mechanistic studies are presently underway in our laboratories to further elucidate the complex etching process. Optimization of the etching procedures through a better understanding of the PG formation process should permit us to improve the light emission from this material.

Notes and references

‡ *Experimental*: electrochemical etching of Ge was conducted using highly P doped (100) n-type (0.004–0.020 Ω cm) or Ga doped p-type (7–23 Ω cm) Ge wafers in a homemade Teflon etching cell equipped with an aluminium tongue in contact with the Ge wafer, and a Pt loop wire as a counter electrode, and ethanoic HCl (1 : 1.8 of 48% HCl : EtOH v/v) as the etchant/electrolyte. A Princeton Instruments 273 potentiostat was utilized as the current source. 350 mA cm^{-2} current density was applied for 5 min during anodization of n-type Ge followed by cathodization with the same current density. Light illumination was applied during cathodization for the p-type PG to harness the photocurrent, allowing for this high current density to pass. Thermal hydrogermylation of the PG was performed in a Schlenk flask with 20% 1-dodecyne in mesitylene solvent under nitrogen atmosphere, and was refluxed at 250 °C for 2 h. After completion of the reaction, the sample was washed with CH_2Cl_2, THF, ethanol and pentane, then dried under N_2 stream. All FTIR spectra were taken with a Nicolet Nexus FTIR spectrometer 670 equipped with a MCT detector cooled with liquid nitrogen. SEM images were taken using a JEOL JSM-35CF scanning electron microscope at an accelerating voltage of 10 kV.

1 M. V. Wolkin, J. Jorne, P. M. Fauchet, G. Allan and C. Delerue, *Phys. Rev. Lett.*, 1999, **82**, 197.
2 L. T. Canham, T. I. Cox, A. Loni and A. J. Simons, *Appl. Surf. Sci.*, 1996, **102**, 436.
3 A. G. Cullis, L. T. Canham and P. D. J. Calcott, *J. Appl. Phys.*, 1997, **82**, 909.
4 J. Wei, J. M. Buriak and G. Siuzdak, *Nature*, 1999, **399**, 243.
5 (*a*) P. Schmuki, D. J. Lockwood, H. J. Labbe and J. W. Fraser, *Appl. Phys. Lett.*, 1996, **69**, 1620; (*b*) T. Takizawa, S. Arai and M. Nakahara, *Jpn. J. Appl. Phys. 2*, 1994, **33**, L643; (*c*) A. G. Cullis, L. T. Canham and P. D. J. Calcott, *J. Appl. Phys.*, 1997, **82**, 909; (*d*) J. N. Chazalviel, R. B. Wehrspohn and F. Ozanam, *Mater. Sci. Eng. B*, 2000, **69**, 1.
6 S. Miyazaki, K. Sakamoto, K. Shiba and M. Hirose, *Thin Solid Films*, 1995, **255**, 99.
7 S. Bayliss, Q. Zhang and P. Harris, *Appl. Surf. Sci.*, 1996, **102**, 390.
8 S. Bayliss, L. Buckberry, P. Harris and C. Rousseau, *Thin Solid Films*, 1997, **297**, 308.
9 S. S. Chang and R. E. Hummel, *J. Lumin.*, 2000, **86**, 33.
10 E. J. Lee, T. W. Bitner, J. S. Ha, M. J. Shane and M. J. Sailor, *J. Am. Chem. Soc.*, 1996, **118**, 5375.
11 F. Maroun, F. Ozanam and J.-N. Chazalviel, *J. Phys. Chem. B*, 1999, **103**, 5280.
12 E. A. Efimov and I. G. Erusalimchik, *Electrochemistry of Germanium and Silicon*, Sigma Press, Washington D.C., 1963.
13 S. P. Zimin, M. N. Preobrazhenskii and D. S. Zimin, *Tech. Phys. Lett.*, 2000, **26**, 12.
14 A. Janshoff, K. P. S. Dancil, C. Steinem, D. P. Greiner, V. S. Y. Lin, C. Gurtner, K. Motesharei and M. J. Sailor, *J. Am. Chem. Soc.*, 1998, **120**, 12108.
15 K. P. S. Dancil, D. P. Greiner and M. J. Sailor, *J. Am. Chem. Soc.*, 1999, **121**, 7925.
16 D. F. Van De Vondel and G. P. Van der Kelen, *Bull. Soc. Chim. Belg.*, 1965, **74**, 453.
17 P. Gupta, A. C. Dillon, A. S. Bracker and S. M. George, *Surf. Sci.*, 1991, **245**, 360.
18 A. B. Sieval, V. Vleeming, H. Zuilhof and E. J. R. Südholter, *Langmuir*, 1999, **15**, 8288.
19 F. Glocking, *The Chemistry of Germanium*, Academic Press, New York, 1969, p. 85.
20 J. L. He, Z. H. Lu, S. A. Mitchell and D. D. M. Wayner, *J. Am. Chem. Soc.*, 1998, **120**, 2660.
21 K. Choi and J. M. Buriak, *Langmuir*, 2000, in press.

ChemComm

Electrochemical deposition of macroporous platinum, palladium and cobalt films using polystyrene latex sphere templates

Philip N. Bartlett,* Peter R. Birkin and Mohamed A. Ghanem

Chemistry Department, University of Southampton, Highfield, Southampton, UK SO17 1BJ.
E-mail: P.N.Bartlett@soton.ac.uk

Received (in Cambridge, UK) 1st June 2000, Accepted 27th July 2000

Highly ordered macroporous films of platinum, palladium and cobalt with regular arrays of spherical pores with diameters of 0.40, 0.70 or 1 μm are prepared by electrochemical deposition into the interstitial spaces of a template formed by polystyrene latex spheres self-assembled on gold electrodes; after deposition of platinum, palladium or cobalt, the polystyrene spheres are fully removed by washing in toluene to leave a highly periodic, hexagonal close packed, interconnected network of monodisperse spherical pores within the metal film, the size of which is determined by the diameter of the polystyrene latex particles used to prepare the template.

The production of materials with micron and submicron scale structure in two and three dimensions is of importance in a range of applications, such as photonic materials,[1,2] high density magnetic data storage devices,[3] microchip reactors[4] and biosensors.[5] Several new templating techniques are being developed to achieve such macroporous solids with highly ordered structure and high surface area.[6–11] Highly ordered three-dimensional macroporous oxides with pore diameters of a few hundred nanometers have recently been prepared by the chemical hydrolysis of the corresponding metal alkoxide in the interstitial spaces of close packed arrays of polystyrene latex spheres as the template.[12–14] Macroporous titanium dioxide photonic crystals synthesised by a similar procedure have been shown to exhibit photonic band gaps.[15,16] In related studies other authors have described the synthesis of three-dimensional microporous films of semiconducting cadmium selenium (CdSe) by electrochemical deposition in the interstitial spaces in a close packed array of polystyrene latex spheres assembled on an indium tin oxide substrate surface.[17] Van Duyne *et al.*[18,19] have reported using monolayers or bilayers of polystyrene latex particles as masks for the deposition by evaporation of two-dimensional arrays of isolated silver nanoparticles on an insulating substrate.

Here we report the preparation of highly ordered macroporous metal films with pores of predetermined sizes. The preparation of the structured macroporous films was carried out by the electrochemical reduction of $[PtCl_6]^{2-}$, $[PdCl_4]^{2-}$, or $[Co(Ac)_2]$ complex ions in aqueous solution within the interstitial spaces of a close packed polystyrene latex sphere template, self-assembled on a gold surface. The thickness of the resulting films can be many multiples of the diameter of the polystyrene latex spheres used to prepare the template and is readily controlled by the amount of charge passed during deposition of the metal film.†

Most recently Xu *et al.* have described the electrochemical deposition of nanoscale Ni and Au meshes through templates made from close-packed silica sphere arrays (opal).[20] Although the two approaches give similar metal meshes there are several important differences between the method described in our work over that of Xu *et al.* First, the polystyrene latex particles we use are commercially available in a range of sizes; second, our close-packed templates can be prepared by evaporation in 2 d rather than by sedimentation over a period of several months; third, there is no need to sinter the template; fourth, the metal deposition is achieved in a few minutes rather than over 36 h; fifth, the template can be removed by dissolving the polystyrene in toluene rather than requiring the use of HF.

Scanning electron micrographs of cobalt films prepared by electrochemical deposition of cobalt at −0.90 V *vs.* SCE through a template formed from 0.40 and 1.0 μm diameter polystyrene latex spheres are shown in Figs. 1(*a*) and 1(*b*) respectively. The quantities of charge passed were −0.80 and −1.15 C cm^{-2} respectively. These values were chosen in order to grow films whose thickness corresponded to the radius of the template particles used in each case. Fig. 1(*a*) shows that the cobalt film made using the 0.40 μm polystyrene latex sphere template has a highly ordered two dimensional hexagonal network of monodisperse submicron voids each with a hemispherical shape. In the most ordered regions, the pores have a diameter of 380 ± 10 nm (n = 10) and pore to pore centre separation of 450 ± 10 nm (n = 30) The cobalt films made by using the larger, 1.00 μm, polystyrene latex spheres [Fig. 1(*b*)] have a pore diameter of 980 ± 10 nm (n = 10), however, this film shows less two-dimensional order. We attribute this to the fact that the larger latex spheres take a longer time to assemble into a highly ordered structure.[21]

Fig. 1(*c*) shows a scanning electron micrograph of a platinum film deposited into a template formed from 0.70 μm polystyrene latex spheres at a deposition potential of 0.10 V *vs.* SCE (total charge passed −1.20 C cm^{-2}). The image shows that the electrochemically deposited platinum film consists of a highly

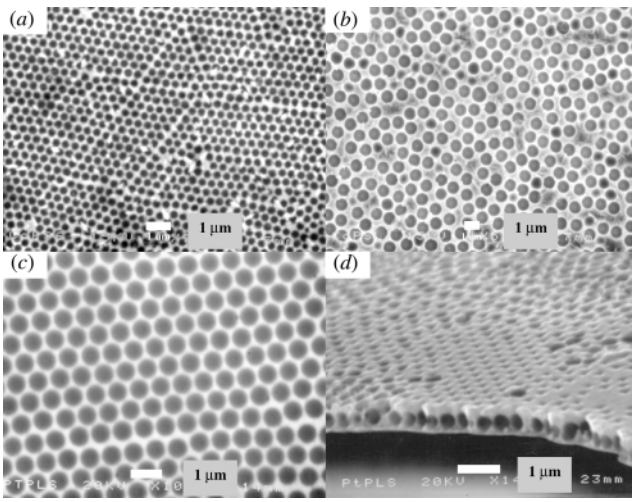

Fig. 1 Scanning electron micrographs of macroporous platinum and cobalt films electrochemically deposited, at 0.10 and −0.90 V *vs.* SCE respectively, through templates formed using polystyrene latex spheres pre-assembled on gold electrode surfaces. (*a*) Cobalt film, deposition charge −0.85 C cm^{-2}, polystyrene latex sphere diameter 0.40 μm; (*b*) cobalt film, deposition charge −1.15 C cm^{-2}, polystyrene latex sphere diameter 1.0 μm; (*c*) platinum film, deposition charge −1.20 C cm^{-2}, polystyrene latex sphere diameter 0.70 μm; (*d*) cross-sectional image of a platinum film, deposition charge −1.00 C cm^{-2}, polystyrene latex sphere diameter 0.40 μm.

DOI: 10.1039/b004398m

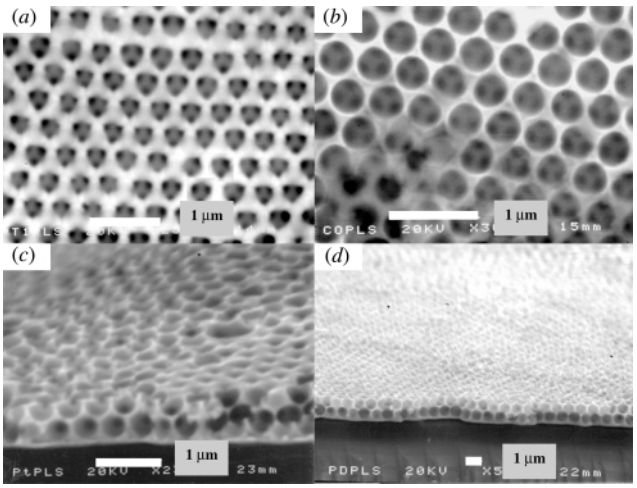

Fig. 2 Scanning electron micrographs of macroporous films of platinum, palladium and cobalt electrochemically deposited, at potentials of 0.10, 0.25 and −0.90 V *vs*. SCE respectively, through templates formed using polystyrene latex spheres pre-assembled on gold electrode surfaces. (*a*) Platinum film, deposition charge −2.00 C cm^{-2}, polystyrene latex sphere diameter 0.40 μm; (*b*) cobalt film, deposition charge −1.40 C cm^{-2}, polystyrene latex sphere diameter 0.40 μm; (*c*) cross-sectional image of a platinum film, deposition charge −1.50 C cm^{-2}, polystyrene latex sphere diameter 0.40 μm; (*d*) palladium film, deposition charge −1.15 C cm^{-2}, polystyrene latex sphere diameter 0.70 μm.

periodic hexagonal array of monodisperse pores. The pore to pore centre separation in this case was 770 ± 10 nm (n = 30). Fig. 1(*d*) shows a cross sectional image of a platinum film prepared by deposition of −1.00 C cm^{-2} through a template of 0.40 μm polystyrene latex spheres. The formation of a monolayer of spherical pores embedded in the platinum film (which in this case was grown to a thickness of approximately 0.4 μm) can be clearly seen.

Figs. 2(*a*) and 2(*b*) show scanning electron micrographs of thicker films of platinum and cobalt where sufficient charge has been passed to deposit films several multiples of the polystyrene latex sphere diameter in thickness. The micrographs show that the spherical pores left in the platinum or cobalt films after removal of the polystyrene latex spheres are arranged in a well ordered three dimensional hexagonal close packed structure. In addition, the connections between the spherical voids within the film, formed where the polystyrene latex spheres in one layer were in contact with those in the underlayer, can be seen as the three dark areas within each pore. In Fig. 2(*a*) the mouths of the pores have a rounded triangular shape. This appears to be a regular feature of films which are grown to a thickness corresponding to about (n + $\frac{3}{4}$) layers of spheres, where n = 0, 1, 2, …. Figs. 2(*c*) and 2(*d*) show cross-sectional images of platinum and palladium films prepared using templates formed from 0.40 and 0.70 μm polystyrene latex spheres. These micrographs also demonstrate the formation of three dimensional macroporous films with thickness of 1.5 or 2.0 times the pore diameters for the platinum and palladium films respectively. The spherical voids have a diameter determined by the diameter of the polystyrene latex spheres used for the template and are arranged as part of an hexagonal lattice, again indicating that the polystyrene latex particles were arranged in three-dimensional hexagonal close packed structure. This was also confirmed by scanning electron micrographs of the templates themselves before the deposition of the metal (not shown).

Our studies have shown that self-assembled layers of polystyrene latex particles formed on gold surfaces by slow evaporation of water from the latex suspension can be used as templates through which to electrochemically deposit metal films. In the resulting metal/polystyrene composite the polystyrene spheres are in contact and can be dissolved out of the metal to leave a regular array of interconnected spherical voids. The size of these voids is determined by the size of the polystyrene latex particles used. Since polystyrene latex particles of tightly controlled size distribution are readily commercially available in sizes from 0.05 to 90 μm the size of the voids can be readily controlled. Control over the quantity of charge passed in the electrochemical deposition of the film allows control over the final film thickness. Thus this method represents a simple route to the production of ordered macroporous films of metals, metal alloys, and polymers with potentially interesting and useful photonic, catalytic, magnetic, or other properties.

We thank the Embassy of the Arab Republic of Egypt, Educational and Cultural Bureau, London for their support of Mohamed A. Ghanem. We also thank Alastair Clark for assistance in obtaining the SEM images and manufacture of the gold substrates.

Notes and references

† *Experimental:* Cobalt acetate [$Co(Ac)_2{\cdot}4H_2O$, 99.5%] and potassium acetate (KAc, 99.4%) were obtained from Fluka. Hexachloroplatinic acid and diammonium tetrachloropalladate were obtained from Aldrich (purity 99.99%). 0.5 wt% suspensions of 0.40 and 1.00 μm diameter polystyrene latex spheres in water were obtained from Agar Scientific, 2.5 wt% suspensions of 0.70 μm diameter polystyrene latex spheres in water were obtained from Alfa Asear. The working electrodes were prepared by evaporating 10 nm of a chromium adhesion layer followed by 200 nm of gold onto thin glass microscope slides. A large area platinum gauze was used as the counter electrode and home made saturated calomel (SCE) as the reference electrode. Before use, the gold working electrodes were sonicated in propanol for 1 h and then rinsed with deionised water. A volume of *ca*. 0.3 cm^3 of the suspension of polystyrene latex spheres diluted with water to 0.5 wt% was spread over *ca*. 1 cm^2 area of the gold electrode and allowed to dry slowly over 2 d in a controlled humidity chamber. The working electrode, together with the adherent, dry, polystyrene latex bead template, was dipped in to the appropriate electrolyte solution to deposit the metal film. The deposition solutions were either 50 mmol dm^{-3} H_2PtCl_6, 40 mol dm^{-3} $(NH_4)_2PdCl_4$, or 0.1 mol dm^{-3} $Co(Ac)_2$ with 0.1 mol dm^{-3} KAc. The deposition was carried out potentiostatically at potentials of 0.10, 0.25 or −0.90 V *vs*. SCE for the electrochemical deposition of platinum, palladium, or cobalt. After deposition the polystyrene latex spheres were dissolved out of the metal films by soaking in toluene for 24 h.

1 S. Y. Lin, E. Chow, V. Hietala and J. D. Joannopoulos, *Science*, 1998, **282**, 274.
2 O. Painter, R. K. Lee, A. Scherer, A. Yariv, J. D. O'Brien, P. D. Dapkus and I. Kim, *Science*, 1999, **284**, 1819.
3 C. Haginoya, M. Ishibashi and K. Koike, *Appl. Phys. Lett.*, 1997, **71**, 2934.
4 H. Gau, S. Herminghaus, P. Lenz and R. Lipowsky, *Science*, 1999, **283**, 46.
5 O. D. Velev and E. W. Kaler, *Langmuir*, 1999, **15**, 3693.
6 A. Corma, Q. B. Kan, M. T. Navarro, J. Perez Pariente and F. Rey, *Chem. Mater.*, 1997, **9**, 2123.
7 D. Zhao, J. Feng, Q. Huo, N. Melosh and G. D. Stucky, *Science*, 1998, **279**, 548.
8 M. Antonietti, B. Berton, C. Göltner and H. P. Hentze, *Adv. Mater.*, 1998, **10**, 154.
9 A. Imhof and D. J. Pine, *Nature*, 1997, **389**, 948.
10 A. Imhof and D. J. Pine, *Adv. Mater.*, 1998, **10**, 697.
11 M. Campbell, D. N. Sharp, M. T. Haerrison, R. G. Denning and A. J. Tuberfield, *Nature*, 2000, **404**, 53.
12 B. T. Holland, C. F. Blandford and A. Stein, *Science*, 1998, **281**, 538.
13 B. T. Holland, C. F. Blandford, D. Thang and A. Stein, *Chem. Mater.*,1999, **11**, 795.
14 Z. Zhong, Y. Yin, B. Gates and Y. Xia, *Adv. Mater.*, 2000, **12**, 206.
15 J. E. Wijnhoven and W. L. Vos, *Science*, 1998, **281**, 802.
16 G. Subramania, K. Constant, R. Biswas, M. M. Sigalas and K. M. Ho, *Appl. Phys. Lett.*, 1999, **74**, 3933.
17 P. V. Braun and P. Wiltziuz, *Nature*, 1999, **402**, 603.
18 T. R. Jensen, G. C. Schatz and R. P. Van Duyne, *J. Phys. Chem. B*, 1999, **103**, 2394.
19 J. C. Hulteen, D. A. Treichel, M. T. Smith, M. L. Duval, T. R. Jensen and R. P. Van Duyne, *J. Phys. Chem. B*, 1999, **103**, 3854.
20 L. Xu, W. L. Zhou, C. Frommen, R. H. Baughman, A. A. Zakhidov, L. Malkinski, J.-Q. Wang and J. B. Wiley, *Chem. Commun.*, 2000, 997.
21 N. D. Denkove, O. D. Velve, P. A. Kralchevaky, I. B. Ivanov, H. Yoshimura and K. Nagayama, *Langmuir*, 1992, **8**, 3183.

ChemComm

Electrochemical synthesis of ammonia at atmospheric pressure and low temperature in a solid polymer electrolyte cell

V. Kordali, G. Kyriacou* and Ch. Lambrou

Department of Chemical Engineering, Aristotle University of Thessaloniki, Thessaloniki 54006, Greece. E-mail: kyriakou@vergina.eng.auth.gr

Received (in Cambridge, UK) 19th June 2000, Accepted 24th July 2000

The heterogeneous electrocatalytic synthesis of ammonia from nitrogen and water is carried out at Ru cathodes, using a Solid Polymer Electrolyte Cell (SPE), at atmospheric pressure and low temperature; the reduction rate increases with increase of temperature up to 100 °C, while with the increase of the negative potential a maximum is observed at −1.02 V *vs.* Ag/AgCl and gradually decreases in the hydrogen discharge region.

Industrially the synthesis of ammonia takes place by passing N_2 and H_2 over Fe or Ru surfaces at about 430–480 °C and 100 atm.[1] The synthesis of ammonia over these catalysts at ambient temperatures is a very difficult process because of the high energy barrier for the breaking of the N≡N bond which is about 1000 kJ mol^{-1} at 25 °C.

Numerous efforts have been reported so far on the conversion of nitrogen to ammonia at room temperature and atmospheric pressure using, photocatalytic,[2,3] electrochemical[4–11] or catalytic methods.[12] Recently, Marnellos and Stoukides studied the electrochemical synthesis of ammonia at Pd cathodes using a solid proton conductor at 570 °C and atmospheric pressure and pointed out that the thermodynamic demand for high pressure can be compensated by the use of an electrochemical reactor.[13] However, the operation temperature of that cell is high and ammonia undergoes decomposition at this temperature. The high electrical resistance of the electrolyte is an additional disadvantage of this method. The present study deals with the electrochemical synthesis of ammonia in a Solid Polymer Electrolyte (SPE) cell on Ru cathodes at atmospheric pressure and low temperature from nitrogen and water.

The reduction of nitrogen (99.999%) was performed in a two-compartment cell, as shown in Fig. 1. The cell was placed in a thermostated bath. Ruthenium was electrochemically deposited on a carbon felt (Electrosynthesis Corporation) from a 0.05 M $RuCl_3$ solution using a constant current of 25 mA cm^{-2} for 60 min. Consequently, it was washed with water to remove the chloride ions and it was finally placed into the electrolytic cell in contact with the Nafion membrane, where it was dried by a nitrogen stream for 24 h. The Nafion membrane was pretreated by heating in H_2O_2 5% solution at 80 °C for 1 h and in ultrapure water for another 1 h. The apparent surface area of the cathode was 2.35 cm^2. A 2 M KOH solution in ultra pure water was used as electrolyte in all experiments. The anode was in contact with the KOH solution (10 cm^3) and the anodic reaction was the oxygen evolution. A saturated Ag/AgCl electrode was used as a reference.

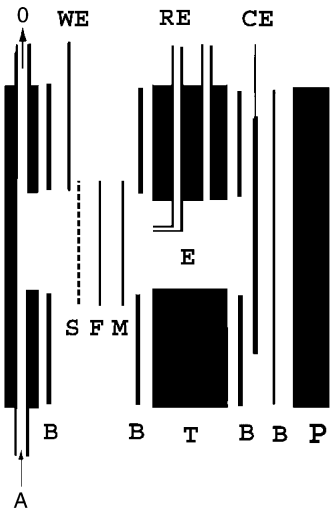

Fig. 1 Exploded view of the electrolysis cell: (A) gas inlet, (O) gas outlet, (T) polytetrafluoroethylene plate, (B) silicone gasket, (M) Nafion membrane, (F) carbon felt, (S) stainless steel screen 150 mesh, (E) electrolyte chamber, (P) stainless steel plate, (WE) working electrode, (RE) reference electrode, (CE) Pt anode.

A nitrogen steam with a constant flow rate withdrew the gaseous products from the cell. The NH_3, which was produced, was stripped by a 15 ml of 0.1 M H_3BO_3 solution. Ammonia was determined by Ion Chromatography using a CS15 column (Dionex Corp.) and a Dionex 4500i Chromatograph, as well as colorimetrically by using the phenate method.[14] Experiments have been conducted for the possible presence of hydrazine colorimetrically at 458 nm using the *p*-dimethylaminobenzaldehyde method.[15] Ammonia was the only product detected in the electrochemical reduction of nitrogen at 90 °C and at potential of −1.10 V, using ruthenium as cathode. Two control experiments were performed at 90 °C and for 24 h, in order to verify that the detected ammonia was a product of nitrogen reduction (i) Nitrogen gas was introduced into the cell at open-circuit (I = 0). (ii) Inert gas (Ar) was introduced into both compartments of the cell for 4 h, so that the air trapped within the carbon felt would be expelled. The flow of argon was continued and then a potential of −1.10 V was applied for 24 h. In both cases no ammonia was detected.

At all potential values examined, the amount of the produced ammonia is in an almost linear relationship with time, which confirms that ammonia was produced by an electrochemical reaction. The rate of ammonia formation remained constant even when the electrolysis was continued for another 100 h at a potential of −1.10 V. This implies that the electrode is not deactivated with time. Given this fact, the same electrode was used for all experiments.

The standard potential for the N_2 reduction to NH_3, as calculated from the Nernst equation, was found to be −0.67 V *vs.* NHE or −0.88 V *vs.* Ag/AgCl. The calculations were performed assuming that P_{N_2} = 0.99 atm. P_{NH_3} = 0.01 atm and pH = 14. The reduction of nitrogen in our experiments on Ru began at −0.96 V; a value which is slightly higher (0.08 V) than that anticipated from the thermodynamic calculations. The rate of ammonia formation, as is shown in Fig. 2, was increased with the negative potential until −1.02 V, where a maximum value was displayed and afterwards it was decreased. A similar behaviour was reported by Sclafani *et al.*,[11] in the electrochemical reduction of nitrogen at iron cathodes in the region of hydrogen discharge, which was attributed to the competitive adsorption of nitrogen and hydrogen species on the electrode surface. An explanation similar to this might be proposed for the observed behaviour at our ruthenium electrode.

DOI: 10.1039/b004885m

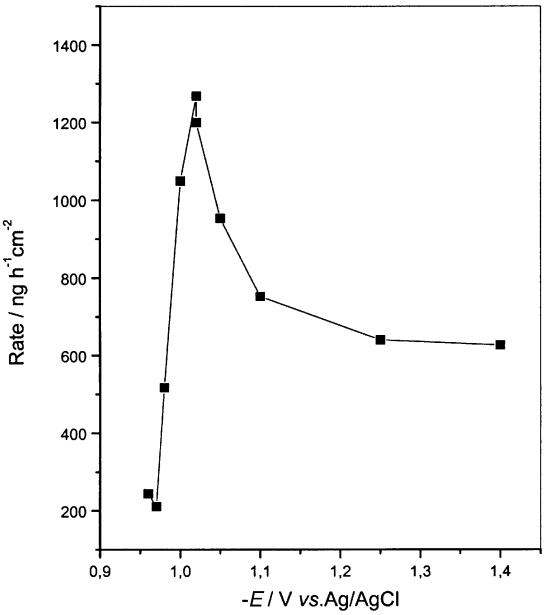

Fig. 2 The rate of formation of ammonia against negative cathodic potential, at 90 °C and an electrolysis time of 24 h.

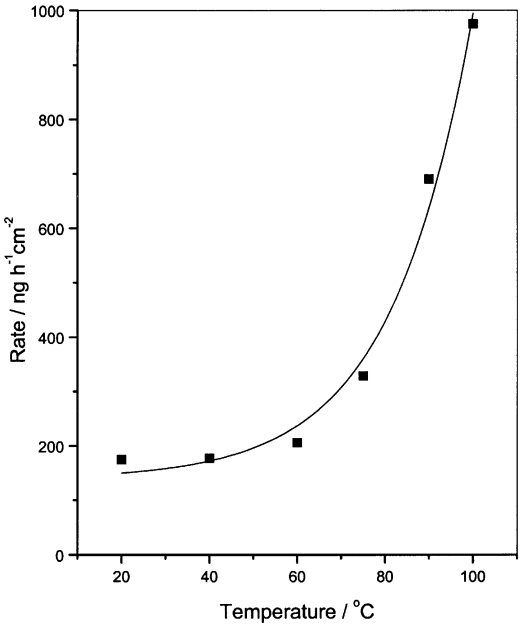

Fig. 3 Rate of formation of ammonia against temperature at −1.10 V and at an electrolysis time of 24 h.

Table 1 Rate and CE of ammonia formation at the Ru cathode at various experimental conditions

Potential/V	N_2 flow rate/ cm^3 min^{-1}	T/°C	Current[a]/mA	CE(%)	Rate of NH_3/μg h^{-1} cm^{-2}
−1.02	1	90	6.1	0.24	1.30
−1.02	10	90	5.8	0.23	1.20
−1.02	15	90	6.8	0.20	1.25
−0.96	25	90	0.3	0.92	0.25
−1.10	25	90	16.2	0.17	0.90
−1.10	25	20	8.2	0.28	0.21

[a] Average current.

The rate and the current efficiency (CE) of the process, as shown in Table 1, were quite low and in the best case they reached about 1.3 μg h^{-1} cm^{-2} at −1.02 V and 0.92% at −0.96 V respectively. This rate is about fifty times lower than that previously reported at 570 °C.[13]

Experiments were also conducted at −1.02 V and 90 °C and at various flow rates of 1, 10 and 15 cm^3 min^{-1}. Within the experimental error, no measurable effect was observed in the (CE) and at the rate of the reaction. This indicates that diffusion was not the rate determining step. Furthermore, the chemical yield (CY) of the reaction was 0.003% when the flow rate of nitrogen was 1 cm^3 min^{-1} and it was about inversely proportional to the flow rate of nitrogen. The chemical yield (CY) of the reaction can be increased with a different planning of the cell so that the retention time of N_2 will be increased. The rate displayed an exponential growth with temperature in accordance to the Arrhenius equation, as is shown in Fig. 3, and it was about 5 times higher at 100 than that at 20 °C. A corresponding increase of the reduction rate with temperature was previously observed in the reduction of nitrogen with hydrogen on Ru catalyst at ambient temperature.[12]

These results are in agreement with the recent work of Rod *et al.*,[16] who showed that it could be possible to produce ammonia at ambient temperature on Ru from nitrogen and hydrogen *via* a dissociative mechanism, by using density functional theory (DFT) calculations. Furthermore, the fact that hydrazine was not detected in any of our experiments, suggests the ammonia was produced *via* a dissociative mechanism, in a similar way to that in the gas phase.[17,18]

Examination of the crystal structure of the electrode (after electrolysis) by XRD indicated that the main reflections (101) and (100) of Ru had a ratio 100:10. It is known that the ammonia synthesis reaction is extremely structure sensitive and that the energy barrier for the dissociation of nitrogen depends strongly on the particle size and the crystal structure of Ru.[16,19] The Ru, which was used in our experiments, had planes with different activities and this fact led to the decrease of the number of active catalytic sites and therefore to a low reaction rate. Moreover, the competitive adsorption of hydrogen to that of nitrogen and the low number of sites, where a contact N_2/Ru/membane exists, are two additional reasons.

This is the first report regarding ammonia production at atmospheric pressure and low temperature. The main problems that exist at the present are the low rate of ammonia formation and the hydrogen evolution at the cathode. Further work to optimize these factors is in progress.

We are grateful to Professor M. Stoukides for his helpful suggestions concerning this work.

Notes and references

1 F. M. Herman, D. F. Othmer, C. G. Overberger and G. T. Seaborg, *Encyclopedia of Chemical Technology*, Wiley and Sons, New York, 1978, vol. 2, p. 494.
2 G. N. Schrauzer and T. D. Guth, *J. Am. Chem. Soc.*, 1977, **99**, 7189.
3 M. M. Taqui Khan, R. C. Bhardwaj and C. Bhardwaj, *Angew. Chem., Int. Ed. Engl.*, 1988, **27**, 923.
4 E. E. van Tamelen and D. A. Seeley, *J. Am. Chem. Soc.*, 1969, **91**, 5194.
5 M. E. Vol'pin, *J. Organomet. Chem.*, 1980, **200**, 319.
6 J. Y. Becker, S. Avraham and B. Posin, *J. Electroanal. Chem.*, 1987, **230**, 143.
7 J. Y. Becker and B. Posin, *J. Electroanal. Chem.*, 1988, **250**, 385.
8 J. Y. Becker and S. Avraham, *J. Electroanal. Chem.*, 1990, **280**, 119.
9 C. J. Pickett, K. S. Ryder and J. Talarmin, *J. Chem. Soc., Dalton Trans.*, 1986, 1453.
10 C. J. Pickett and J. Talarmin, *Nature*, 1985, **317**, 652.
11 A. Sclafani, V. Augugliaro and M. Schiavello, *J. Electrochem. Soc.*, 1983, **130**, 734.
12 K. Aika, *Angew. Chem., Int. Ed. Engl.*, 1986, **25**, 558.
13 G. Marnellos and M. Stoukides, *Science*, 1998, **282**, 95.
14 L. S. Clesceri, A. E. Greenberg and R. Trussell Rhodes, *Standard Methods for the Examination of Water and Wastewater*, American Public Health Association, Washington, 1989, pp. 120–121.
15 G. W. Watt and J. D. Chrisp, *Anal. Chem.*, 1952, **24**, 2006.
16 T. H. Rod, A. Logadottir and J. K. Nørskov, *J. Chem. Phys.*, 2000, **112**, 5343.
17 O. Hinrichsen, F. Rosowski, A. Hornung, M. Mihler and G. Ertl, *J. Catal.*, 1997, **165**, 33.
18 W. Liu and T. T. Tsong, *Surf. Sci.*, 1986, **165**, L26.
19 S. Dahl, A. Logadottir, R. C. Egeberg, J. H. Larsen, J. Chorkendorff, E. Tornqvist and J. K. Nørskov, *Phys. Rev. Lett.*, 1999, **83**, 1814.

ChemComm

Direct formation of 1-vinyl-1*H*-isochromene derivatives *via* a palladium-catalysed coupling reaction

Roger Mutter, Eva M. Martin de la Neva† and Martin Wills*

Department of Chemistry, University of Warwick, Coventry, UK CV4 7AL. E-mail: m.wills@warwick.ac.uk

Received (in Liverpool, UK) 6th July 2000, Accepted 26th July 2000

The palladium-catalysed reaction of the *tert*-butyldimethylsilyl ether of a 3-(*o*-bromophenyl)allylic alcohol with a methyl ketone leads directly to a 1-vinyl-1*H*-isochromene *via* a tandem ketone arylation–allylic cyclisation reaction.

As a part of a wider project concerned with the synthesis of biologically active molecules, we wished to prepare 1-vinyl-1*H*-isochromenes **1**. We felt that we could achieve this end in two stages. The first stage (for the example shown in Scheme 1) would require the coupling reaction of an appropriate aryl

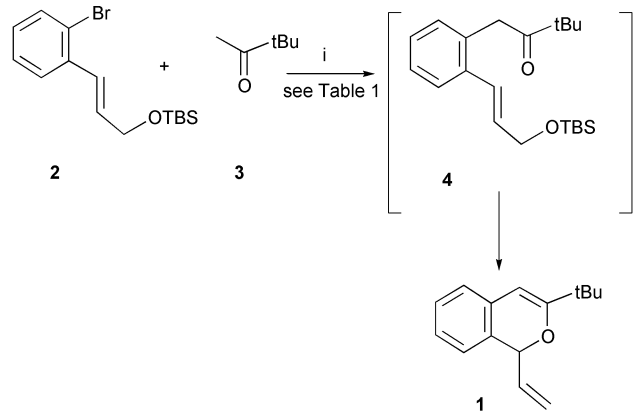

Scheme 1 Intramolecular cyclisation reaction to form 1-vinyl-1*H*-isochromenes. *Reagents and conditions*: (i) ligand, base, solvent, $[Pd_2(dba)_3]$, 85 °C (See Table 1).

bromide **2** with a ketone **3** to give **4**.[1] The second stage would involve replacement of the TBS with an acetyl group and subsequent cyclisation of the ketone enolate onto the allylic system. For the first step, we were confident that a palladium-catalysed ketone arylation reaction would be effective. The reason for the choice of a non-activating silyl group in **2** was simply to prevent the allylic substitution from outpacing the aryl coupling at the high reaction temperatures required (> 80 °C). Allylic acetates, for example, are known to react with ketones under palladium-catalysed reactions at rt.[2]

We first examined the coupling of the *tert*-butyldimethylsilyl-protected allylic alcohol substrate **2** with pinacolone (Scheme 1). Starting material **2** was prepared from readily available 2-bromobenzaldehyde in three steps in 90% overall yield following a literature procedure to the alcohol which was then silyated.[3] Initial attempts to couple **2** to pinacolone following the procedure of Hartwig *et al*.[1] (NaO*t*-Bu, Pd/DPPF, toluene, 100 °C) led mainly to the debrominated cinnamyl ether **5**; no coupling product was observed. Investigation of several

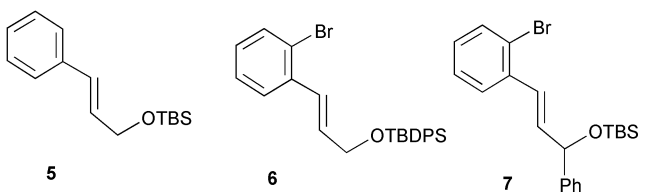

bases (NaO*t*-Bu, Na_2CO_3, Cs_2CO_3 LHMDS) gave none of the expected product **4**. In the case of LiHMDS, however, the 1*H*-isochromene **1**‡ was formed as the major product. Subsequent optimisation of this tandem arylation–allylic substitution reaction improved the yield of this product to 71%.§ As far as we are aware, this represents the first observation of such a tandem enolate arylation–allylic cyclisation reaction. Notable in this process is the involvement of a silyloxy leaving group, which would normally not be considered to be a suitable group for allylic activation. Presumably this reacts because of the high reaction temperature. Related intramolecular reactions of β-keto ester enolates and diketones have been reported to form five-membered rings in palladium-catalysed intramolecular cyclisations.[4]

During this work it appeared that a lithium base and a co-ordinating solvent must be employed to make the reaction work. Trost has reported a similar requirement for a lithium base in an allylic alkylation reaction.[2d] A series of phosphine ligands and ketones were also investigated (Table 1) and it was found that a

Table 1 Palladium-catalysed ketone arylation–allylic cyclisation reactions

Aryl bromide	Ketone	Solvent	Ligand	Product	Yield (%)
2	**3**	Toluene/THF	dppf	**1**	67
2	**3**	Dioxane/THF	dppf	**1**	71
2	**3**	Toluene	dppf	—	0
6	**3**	Toluene/THF	dppf	**1**	54
7	**3**	Toluene/THF	dppf	—	0
2	**3**	Dioxane	L-S-ESPHOS	**1**	15[a]
2	**3**	Toluene/THF	$(o\text{-Tol})_3P$	**1**	61
2	**3**	Toluene/THF	$(t\text{-Bu})_3P$	**1**	27[b]
2	Acetophenone	Toluene/THF	dppf	**8**	28
2	Propiophenone	Toluene/THF	dppf	**9**	36[c]

[a] Side-products: **4**; 21%, **5**: 6% [b] Side-products; **4**: 30%, **5**: 6%. [c] Side-product; **10** 6%.

substantial amount of the intermediate **4** could be isolated when either tri-*tert*-butylphosphine or the bis(diazaphospholidine) ligand semi-ESPHOS[5] were used. This intermediate, **4**, was then exposed to the reaction conditions in the absence of palladium and ligands. No cyclisation occurred after several hours, indicating that the cyclisation step was also palladium catalysed. Tri-*o*-tolylphosphine also proved to be a good ligand for isochromene formation. The isolation of **4** from certain experiments suggests that it may be possible to 'tune' the reaction conditions towards the formation of either cyclic or acyclic products. We are currently investigating this issue.

Changing the protecting group on the bromide in **2** from TBS- to the TBDPS- (*i.e.* **6**) did not effect the tandem reaction. Substitution at the allylic ether carbon with a phenyl group (*i.e.* **7**) led to an unreactive substrate. Aromatic ketones such as acetophenone and propiophenone also proved compatible with the reaction conditions. In each case the desired cyclic products **8** and **9** respectively were formed, although the non-optimised yields were low to moderate in both cases. In the case of propiophenone a small amount (6%) of non-cyclised material **10** was also formed.

We wished to confirm that the choice of a trialkylsilyloxy-allylic substrate was essential for a successful reaction. This was achieved through the attempted reaction of acetate **11** with both

DOI: 10.1039/b005519k

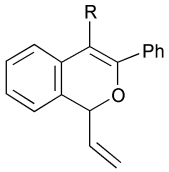

8 R = H
9 R = Me

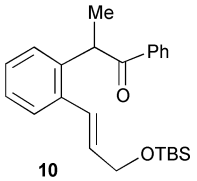

10

pinacolone and acetophenone under our reaction conditions for cyclisation. In the former case the result was a complex mixture, in the latter case the deacetylated alcohol was the major product of the reaction, together with a small amount of ketone **12**. The latter result serves to confirm the ability of the silyloxy group to delay the allylic reaction conveniently until after the arylation process has been completed.

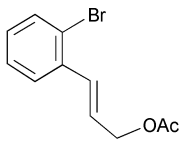

11

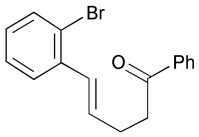

12

In conclusion, we have demonstrated that, through the careful choice of ether protecting group, a tandem enolate-arylation–allylic cyclisation process may be 'fine-tuned' in order for the steps to take place in a desired order. The overall result is a convenient and rapid synthesis of vinyl-1*H*-isochromenes, which represent valuable synthetic building blocks for further reactions. The results of our studies on these products, together with further details of the coupling–cyclisation process, will be reported in full in due course.

We thank the CVCP for an Overseas Research Studentship (ORS) award (to R. M.) and Professor D. Games, Dr J. Ballantine and Dr B. Stein of the EPSRC Mass Spectrometry Service at Swansea for carrying out analyses of certain compounds.

Notes and references

† Visitor from University of Salamanca, Summer 1999. Current address: Departamento de Quimica Organica, Facultad de Quimica, Plaza de los Caidos 1-5, 37008-Salamanca, Spain.

‡ *Characterisation data* for 1-vinyl-3-*tert*-butyl-1*H*-isochromene 1. ν_{max}(NaCl)/cm^{-1} 2954, 1638, 1085, 914, 750; δ_H(300 MHz, $CDCl_3$) 1.16 (9H, s, C(C*H*$_3$)$_3$), 5.16 (1H, dt, *J* 17.1 and 1.3, CH=C*H*$_2$), 5.23 (1H, dt, *J* 10.4 and 1.3, CH=C*H*$_2$), 5.46 (1H, d, *J* 6.6, ArC*H*(OR)CH=CH$_2$), 5.67 (1H, s, ArC*H*=C(OR)), 6.15 (1H, ddd, *J* 17.1, 10.4 and 6.6, CH(OR)C*H*=CH$_2$), 6.90–7.30 (4H, m, Ar*H*); δ_C(75 MHz, $CDCl_3$) 28.3, 35.5, 79.3, 97.7, 118.2, 123.8, 124.9, 126.2, 128.5, 129.4, 132.0, 136.7, 164.2; *m/z* (EI) 214 [M]$^+$, 187, 129 (Found: [M]$^+$, 214.136173. $C_{15}H_{18}O$ requires *m/z*, 214.135765).

§ General experimental procedure for the synthesis of 1-vinyl-3-*tert*-butyl-1*H*-isochromene 1. To a solution of LiHMDS (1 M in THF, 3 eq.) was slowly added a solution of the pinacolone (2 eq.) in solvent at 5 °C. A solution of $Pd_2(dba)_3$ (5% mol) and ligand (10% mol) in solvent was added at room temperature, followed by a solution of *tert*-butyldimethyl [3-(2-bromophenyl)allyloxy]silane **2** (1 eq.). The reaction mixture was heated to 100 °C overnight, allowed to cool and then quenched with 1 M HCl solution at room temperature. The mixture was twice extracted with dichloromethane and the combined organic layers were dried and the solvent was evaporated under reduced pressure yielding the crude product. The crude product was purified by flash chromatography.

1 (*a*) M. Palucki and S. L. Buchwald, *J. Am. Chem. Soc.*, 1997, **119**, 11 108; (*b*) B. C. Hamann and J. F. Hartwig, *J. Am. Chem. Soc.*, 1997, **119**, 12 382; (*c*) J. Ahman, J. P. Wolfe, M. V. Troutman, M. Palucki and S. L. Buchwald, *J. Am. Chem. Soc.*, 1998, **120**, 1918; (*d*) M. Kawatsura and J. F. Hartwig, *J. Am. Chem. Soc.*, 1999, **121**, 1473; (*e*) T. Satoh, Y. Kametani, Y. Terao, M. Miura and M. Nomura, *Tetrahedron Lett.*, 1999, **40**, 5345; (*f*) H. Muratake and M. Natsume, *Tetrahedron Lett.*, 1997, **38**, 7581.

2 (*a*) J. C. Fiaud and J. L. Malleron, *J. Chem. Soc., Chem. Commun.*, 1981, 1159; (*b*) E.-I. Negishi, H. Matsushita, S. Chatterjee and R. A. John, *J. Org. Chem.*, 1982, **47**, 3190; (*c*) B. M. Trost, R. Radinov and E. M. Grenzer, *J. Am. Chem. Soc.*, 1997, **119**, 7879; (*d*) B. M. Trost and G. M. Schroeder, *J. Am. Chem. Soc.*, 1999, **121**, 6759; (*e*) B. M. Trost and X. Ariza, *J. Am. Chem. Soc.*, 1999, **121**, 10 727; (*f*) Y. Inoue, M. Tofofuku, M. Taguchi, S.-I. Okada and H. Hashimoto, *Bull. Chem. Soc. Jpn.*, 1986, **59**, 885.

3 M. L. Hammond, R. A. Zambias, M. N. Chang, N. P. Jensen, J. McDonald, K. Thompson, D. A. Boulton, I. E. Kopka, K. M. Hand, E. E. Opas, S. Luell, T. Bach, P. Davies, D. E. MacIntyre, R. J. Bonney and J. L. Humes, *J. Med. Chem.*, 1990, **33**, 908.

4 (*a*) T. Hayashi, M. Yamane and A. Ohno, *J. Org. Chem.*, 1997, **62**, 204; (*b*) B. M. Trost, *Angew. Chem., Int. Ed. Engl.*, 1989, **28**, 1173.

5 M. Wills and S. W. Breeden, *J. Org. Chem.*, 1999, **64**, 9735.

ChemComm

Room temperature formation of rhodium nanoparticles on TiO_2[110] *via* MetalOrganic Chemical-Vapour Deposition (MOCVD) of $[Rh(CO)_2Cl]_2$

Mark A. Newton,*[a] Roger A. Bennett,*[b] Rupert D. Smith,[b] Michael Bowker[b] and John Evans[a]

[a] *Department of Chemistry, University of Southampton, Highfield, Southampton, UK SO17 1BJ. E-mail: m.a.newton@soton.ac.uk*

[b] *Centre for Surface Science and Catalysis, Department of Chemistry, University of Reading, Whiteknights Park, Reading, UK RG6 6AD. E-mail: r.a.bennett@reading.ac.uk*

Received (in Cambridge, UK) 11th May 2000, Accepted 25th July 2000

Room temperature adsorption of $[Rh(CO)_2Cl]_2$ on TiO_2[110] is investigated using Scanning Tunnelling Microscopy (STM) which reveals the formation of nanoparticles that coexist with the mono-disperse $Rh(CO)_2Cl$ species; the spatial distribution of these particles indicates that nanoparticle formation occurs principally at step edges.

Since the determination of the existence of mono-disperse $Rh^I(CO)_2$ species on supported Rh systems[1] a wealth of research has been directed at quantifying the role played by this species in Rh based catalysts, particularly with regards to NO_x removal processes.[2–9] CO may also oxidatively disrupt small metallic Rh clusters forming $Rh^I(CO)_2$.[10–13] A complete understanding of the behaviour of supported Rh systems must therefore include a detailed knowledge of how this species behaves under a variety of conditions.

Model supported $Rh^I(CO)_2$ systems can be created *via* two routes. Firstly, catalysts may be prepared from $RhCl_3$ which, after calcination and reduction, may be redispersed using CO to give an adsorbed layer of $Rh(CO)_2$ species.[1,7,14] Typically, however, this method is only viable for Rh loadings of < 2.5 wt%. A second approach is to use a volatile Rh organometallic which may be adsorbed to a prepared oxide surface to yield a $Rh(CO)_2$ adlayer directly.[15–17] As the $Rh^I(CO)_2$ is immediately present it has the perceived advantage of accessing higher Rh loadings whilst still producing a truly mono-disperse adlayer. The use of MetalOrganic Chemical-Vapour Deposition (MOCVD) of Rh organometallics has found particular favour in surface science studies of the chemistry of $Rh^I(CO)_2$ species[17] adsorbed on single crystal oxide surfaces. In these cases involatile inorganic salts, such as $RhCl_3$ may not be used, and the larger Rh clusters formed by Metal Vapour Deposition (MVD) may not be re-dispersed to yield a mono-disperse $Rh^I(CO)_2$ adlayer.[17]

Previous studies concerning the adsorption of $[Rh(CO)_2Cl]_2$ on both high area and [110] oriented single crystal rutile, have indicated that the dissociative adsorption of this species results in a uniform $Rh^I(CO)_2Cl$ adlayer.[15–17] However, there has been no determination of the local structures that result from the adsorption as no LEED structures[17] have been observed. Evidence for a molecular orientation with Rh–C–O bonds aligned in the $< 1\bar{1}0 >$ azimuth has however been demonstrated by Fourier Transform Reflection Absorption Infrared Spectroscopy.[18] We have therefore employed Scanning Tunnelling Microscopy (STM) to determine how the adsorbed $Rh^I(CO)_2Cl$ species interact with the surface and each other.

Experiments were carried out in a UHV chamber equipped with LEED/Auger, and variable temperature STM facilities.[19] The preparation of the rutile TiO_2[110](1 × 1)[20] surface, and the purification of the organometallic sample[17] have been described previously. Rh dosing was controlled *via* a fine leak valve and a line of sight tube doser permitting *in situ* STM measurements whilst the surface is being exposed the organometallic vapour. Unfortunately adsorption of carbonyl along the length of the tube precludes a sharp transition between 'on' and 'off' so considerable exposure of the surface continues after shutting the valve. All STM measurements were carried out with a positive sample bias and therefore unoccupied electronic states are imaged.

Fig. 1(*a*) shows a (97 × 97 Å) STM image of a freshly deposited $Rh(CO)_2Cl$ adlayer. The layer consists of elements showing some low level of local order. The average area per individual unit in Fig 1(*a*) is 40–50 Å^2 which places the coverage at *ca.* 0.2 ML where 1 ML is equivalent to the density of Ti in the surface (0.1 Ti Å^{-2}). Comparison of images taken before and after dosing indicate the features reside preferentially near the centre of the dark rows imaged on the clean TiO_2; *i.e.* on the rows of bridging oxygen. Lack of resolution precludes determination of the lateral position along the row.

Fig. 1(*b*) shows an area (198 × 198 Å) of the same adlayer *ca.* 40 minutes after initial deposition. The features now show a distinct ordering with the appearance of rows on the surface running in two rotationally related domains at ±42 ± 3° to the principal crystallographic directions. The apparent density of the species has increased within this more ordered adlayer and each feature now occupies 25–30 Å^2 corresponding to *ca.* 0.35–0.4 ML. This increased density is due to continued exposure from the dosing tube as mentioned above, and represents a saturation coverage of $Rh(CO)_2Cl$. Given the tunnelling conditions used (above), the size and density of the small features observed in Figs. 1(*a*) and (*b*), we associate these with the $4d_{x^2-y^2}$) orbital of individual, square planar coordinated Rh^I atoms. We believe that the Cl is intimately associated with the $Rh(CO)_2$ and not adsorbed as a separate species. Cl adsorbed upon TiO_2[110][21] appears as an anomalously large (*ca.* 6–8 Å diameter), immobile bright feature in STM: the features we observe do not show such character.

The adlayer in Fig 1(*b*) does show a LEED pattern. However, it is destroyed within *ca.* 2 seconds exposure to the LEED electron beam; the details of this structure will be discussed in a future communication. Also visible in Fig. 1(*b*) are two new

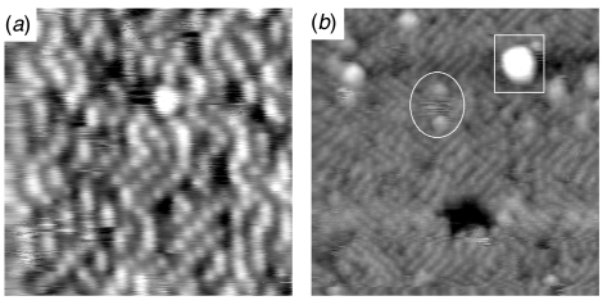

Fig. 1 (*a*) STM image (97 × 97 Å, 1 V, 0.3 nA) of a freshly prepared adlayer derived from room temperature adsorption of $[Rh(CO)_2Cl]_2$ to the TiO_2[110](1 × 1) surface approximately 3 minutes after dosing. (*b*) STM image (198 × 198 Å, 1 V, 0.3 nA) of the adlayer shown in Fig. 1(*a*) approximately 40 minutes after dosing. A large discrete particle is marked by the rectangle while an oval marks two of the smaller, less distinct, particles.

DOI: 10.1039/b003782f

types of feature: the first comprises small, indistinct particles with an apparent height slightly greater than the $Rh(CO)_2Cl$ adlayer; the second comprises discrete larger particles.

Fig. 2 shows a large area scan (998 × 998 Å) of the surface approximately 150 minutes after deposition. The large particles shown in Fig. 1(*b*) are found all over the surface preferentially residing at step edges of the underlying rutile. The particles co-exist with the $Rh(CO)_2Cl$ adlayer. Taking the width of the step region to be that of the largest particle we find large particle formation in the step region to be 5 times more probable than on the terrace on an area for area basis. This indicates that a regio-specific formation of Rh nanoparticles occurs alongside the production of domains of $Rh^I(CO)_2Cl$. Smaller particles are also observed but do not show a distribution that favours the step edges. This particulate formation is not an artefact due to the presence of the tip; moving the tip to new areas of the surface yields similar images.

Fig. 3 shows the particle size distributions derived from Fig. 2 in terms of particle heights, areas, volumes and perimeters. The distributions show two clear groups; a multitude of small particles, and long tail of large particles. An analysis of the height and volume data for the larger particles indicates that they contain up to a few hundred atoms at maximum. The total volume of these particles is *ca*. 435000 Å^3 giving an effective coverage of *ca*. 0.3 ML Rh in particulate form (assuming a bulk Rh lattice constant). It should also be noted, however, that

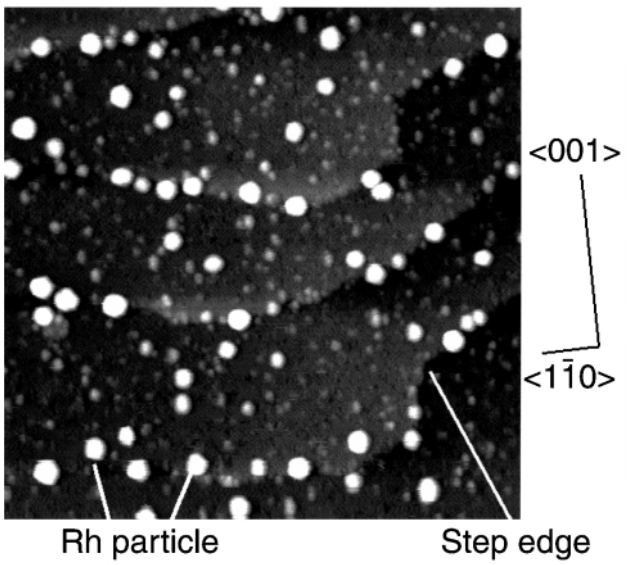

Fig. 2 Large area STM image (998 × 998 Å, 1 V, 0.1 nA) taken *ca*. 150 minutes after Rh deposition.

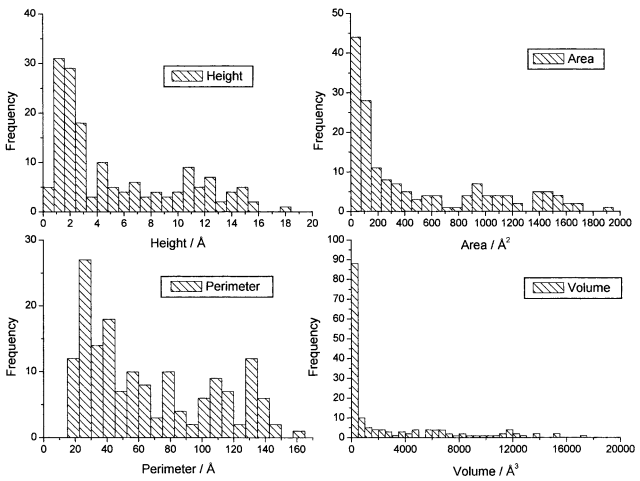

Fig. 3 Particle size distribution functions for Fig. 2. Area and perimeter are derived directly from the particles projected shape onto the surface, while volume and height are calculated from the apparent height and therefore may be influenced by electronic effects.

preliminary analysis of the scaling relationships of the measured parameters of Fig. 2 (*i.e.* volume, area, height *versus* perimeter) indicates that the particles have a well-defined shape despite the apparent lack of clear facets.

The spatial distribution of these particles is distinct from similar Rh particles grown *via* MVD which are reported to show no preferential decoration of step edges.[22] The reasons for this are as yet unclear, but this most probably relates to the need to activate the decomposition of the carbonyl in MOCVD, *versus* the surface diffusion limited growth in MVD.

In summary, and in contrast to a number of previous investigations,[15–17] we have shown that room temperature MOCVD of $[Rh(CO)_2Cl]_2$ does not necessarily lead to a uniform mono-disperse $Rh(CO)_2Cl$ adlayer. Adsorption of this species may initially result in formation of such a layer but this configuration is only metastable even at room temperature. Room temperature adsorption of $[Rh(CO)_2Cl]_2$ on vacuum reduced TiO_2[110] can result in the formation of Rh nano-particles that are distinct from similar sized particles grown *via* MVD, and that may coexist with an ordered layer of $Rh^I(CO)_2Cl$ species. The spatial distribution of these particles indicates that step edges on the rutile surface act as enhanced sites for nucleation of particulate Rh *via* the decomposition of the $Rh(CO)_2Cl$ species. Terraces show a much lower rate of particle formation. We have therefore demonstrated a previously unknown chemistry of TiO_2[110] step edges that produces the nanoparticles. Further, our results indicate that, in systems such as this, the time-scale of interrogation must be considered due to the possibility of changes in the phase of the adsorbed metal species.

We thank the EPSRC for post-doctoral funding to M. A. N. and R. A. B., and the EPSRC/Johnson Matthey PLC for funding a CASE award to R. D. S. We also thank A. J. Ramirez-Cuesta for development of the particle analysis software.

Notes and references

1 A. C. Yang and C. W. Garland, *J. Phys. Chem.*, 1957, **61**, 1504.
2 H. Arai and H. Tominanga, *J. Catal.*, 1976, **43**, 131.
3 G. Srinvas, S. S. C. Chuang and S. Debnath, *J. Catal.*, 1994, **148**, 748.
4 E. A. Hyde and R. Rudham, *J. Chem. Soc., Faraday Trans.*, 1984, **80**, 531.
5 R. Krishnamurthy and S. S. C. Chuang, *J. Phys. Chem.*, 1995, **99**, 16 727.
6 S. H. Oh and C. Eickel, *J. Catal.*, 1991, **128**, 526.
7 K. Almusaiteer, S. S. C. Chuang and C. D. Tan, *J Catal.*, 2000, **189**, 247.
8 T. Chafik, D. I. Kondarides and X. E. Verykios, *J. Catal.*, 2000, **190**, 446; D. I. Kondarides, T. Chafik and X. E. Verykios, *J. Catal.*, 2000, **191**, 147.
9 H. F. T. Van't Blik, J. B. A. D. van Zon, T. Huizinga, J. C. Vis, D. C. Koningsberger and R. Prins, *J Phys. Chem.*, 1983, **87**, 2264.
10 S. S. C. Chuang and C. D. Tan, *J. Catal.*, 1988, **173**, 95.
11 P. Johnston and R. W. Joyner, *J. Chem. Soc., Faraday Trans.*, 1993, **89**, 863.
12 P. Johnston, R. W. Joyner, P. D. A. Pudney, E. S. Shpiro and B. P. Williams, *Faraday Discuss. Chem. Soc.*, 1990, **89**, 144.
13 F. Solymosi, T. Bansagi and E. Novak, *J. Catal.*, 1988, **112**, 183.
14 For example: J. T. Yates, T. M. Duncan, S. D. Worley and R. W. J. Vaughan, *J. Chem. Phys.*, 1979, **71**, 1219.
15 M. P. Keyes and K. L. Watters, *J. Catal.*, 1986, **100**, 44; *J. Catal.*, 1988, **100**, 96.
16 B. G. Frederick, G. Apai and T. N. Rhodin, *J. Am. Chem. Soc.*, 1987, **109**, 4797.
17 J. Evans, B. E. Hayden, F. Mosselmans and A. Murray, *J. Am. Chem. Soc.*, 1992, **114**, 6912; J. Evans, B. E. Hayden, F. Mosselmans and A. Murray, *Surf. Sci.*, 1994, **301**, 61.
18 B. E. Hayden, A. King and M. A. Newton, *Chem. Phys. Lett.*, 1997, **269**, 485.
19 M. Bowker, S. Poulston, R. A. Bennett, P. Stone, A. H. Jones, S. Haq and P. Hollins, *J. Mol. Catal. A: Chemical*, 1998, **131**, 185.
20 R. A. Bennett, P. Stone and M. Bowker, *Faraday Discuss.*, 1999, **114**, 267.
21 U. Diebold, W. Hebenstreit, G. Leonardi, M. Schmid and P. Varga, *Phys. Rev. Lett.*, 1998, **81**, 405.
22 A. Berkó, G. Ménesi and F. Solymosi, *Surf. Sci.*, 1997, **372**, 202.

ChemComm

Michael addition of *N*-bonded enolato ligands to acrylonitrile in iron and ruthenium complexes†

Masafumi Hirano, Sayori Kiyota, Masataka Imoto and Sanshiro Komiya*

Department of Applied Chemistry, Tokyo University of Agriculture and Technology, 2-24-16 Nakacho, Koganei, Tokyo 184-8588, Japan. E-mail: komiya@cc.tuat.ac.jp

Received (in Cambridge, UK) 22nd May 2000, Accepted 26th July 2000

Treatment of the *N*-bonded enolatoiron(II) complex [M(H)(NCCHCO$_2$R)(L)$_2$] [1a, M = Fe, R = Me, L = depe {1,2-bis(diethylphosphino)ethane}; 1b, M = Fe, R = Et, L = depe; 2, M = Ru, L = dppe] with acrylonitrile results in mono-Michael addition to give [M(H)-{NCC(C$_2$H$_4$CN)CO$_2$R}(L)$_2$], which is found to be an active intermediate for the catalytic double-Michael reaction of cyanoacetate with acrylonitrile.

Transition-metal enolates have attracted considerable attention as key compounds in chemo-, regio- and stereospecific C–C bond forming reactions under neutral and mild conditions.[1] We previously reported the isolation of zwitterionic *N*-bonded enolate complexes of ruthenium[2] and rhenium[3] as active intermediates in catalytic Michael and Knöevenagel reactions. In these catalyses enhanced nucleophilicity of the enolato moiety by the zwitterionic structure was considered to be responsible for the driving force of the chemoselective C–C bond formations. Here we report the isolation of the mono-Michael adducts of the enolato-iron and -ruthenium complexes to acrylonitrile as active intermediates for the Michael reaction. The role of these adducts in the catalytic double-Michael reaction of cyanoacetate with acrylonitrile is also described.

The enolatoiron(II) complexes [Fe(H)(NCCHCO$_2$R)-(depe)$_2$]† (**1a**, R = Me; **1b**, R = Et) were newly prepared by the oxidative addition of cyanoacetate to a dinitrogen complex of iron(0) [Fe(N$_2$)(depe)$_2$][4] in 81 and 90% yields, respectively [eqn. (1)].

$$[Fe(N_2)(depe)_2] \xrightarrow{+\ NCCH_2CO_2R} [Fe(H)(NCCHCO_2R)(depe)_2] \quad (1)$$

1a R = Me
b R = Et

The molecular structure of **1b**[5] revealed that the structure of the enolato ligand is similar to those in other isolated enolato-ruthenium(II)[2] and -rhenium(I)[3] complexes, showing its delocalised zwitterionic character as suggested by the planarity of the O(1)–C(3)–C(2)–C(1) linkage [dihedral angle = 177.4(5)°] and linear structure of Fe(1)–N(1)–C(1)–C(2) [bond angles Fe–N(1)–C(1) = 173.3(4)°, N(1)–C(1)–C(2) = 178.6(5)°].

The ^{1}H and ^{31}P{^{1}H} NMR spectra of **1a** and **1b** indicate the presence of two isomers due to (*E*)- and (*Z*)-enolato ligands as observed for *N*-bonded ruthenium[2] and rhenium[3] enolates. The major : minor ratio for **1a** and **1b** at 23 °C was estimated as 4 : 1 and 3 : 1, respectively.

Treatment of **1b** with an equimolar amount of acrylonitrile in benzene in the absence of ethyl cyanoacetate at room temperature resulted in mono-Michael addition to the enolato ligand giving *trans*-[Fe(H){NCC(C$_2$H$_4$CN)CO$_2$Et}(depe)$_2$] (**3**) in 44% yield (Scheme 1).[6] The ^{1}H and ^{31}P{^{1}H} NMR spectra of **3** indicate the presence of two isomers (major : minor = 3 : 1 at 24 °C), probably due to (*E*)- and (*Z*)-isomerism of the enolato ligand. The ^{31}P{^{1}H} NMR spectrum of the major species shows two singlets at δ 84.3(s) and 89.4(s) and the ^{1}H NMR spectrum shows two quintets at δ − 25.70 and −25.61, suggesting that the hydrido and enolato ligands are *trans* to each other and all phosphorus atoms located in an equatorial plane. Methylene protons of the cyanoethyl group in **3** were observed as two multiplets at δ 2.4 (m, 2 H) and 2.5 (m, 2 H), as confirmed by COSY and homo-decoupling experiments.

We also carried out the reaction of the analogous enolato-ruthenium complex *trans*-[Ru(H)(NCCHCO$_2$Et)(dppe)$_2$][2a] (**2**) with acrylonitrile giving *trans*-[Ru(H){NCC(C$_2$H$_4$CN)-CO$_2$Et}(dppe)$_2$] (**4**) in quantitative yield.[7] The NMR spectra of **4** also show the presence of two isomers in 1 : 1 ratio, where the cyanoethyl group appears as a couple of A$_2$B$_2$ patterns at δ 1.84 (t, 2 H, J = 6 Hz) and 2.43 (t, 2 H, J = 6 Hz), and δ 2.28 (t, 2 H, J = 6 Hz) and 2.50 (t, 2 H, J = 6 Hz) in the same intensities.

The formation of these adducts **3** and **4** was further confirmed by the following chemical reactions. Acidolysis of **3** and **4** by excess dry HCl released the mono-Michael product NCCH(C$_2$H$_4$CN)CO$_2$Et in 48% and quantitative yields, respectively [eqn. (2)].

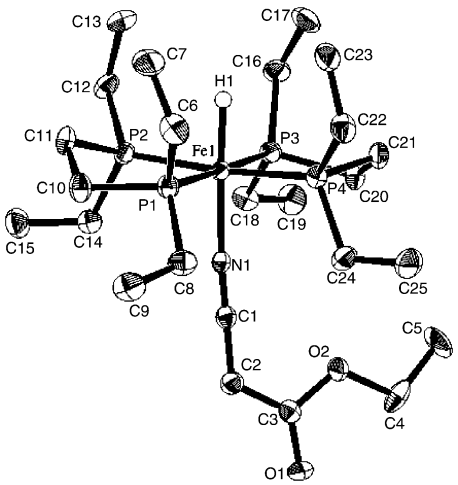

Fig. 1 Molecular structure of [Fe(H)(NCCHCO$_2$Et)(depe)$_2$] (**1b**). All hydrogen atoms except hydride and incorporated solvents are omitted for clarity. Ellipsoids represent 50% probability.

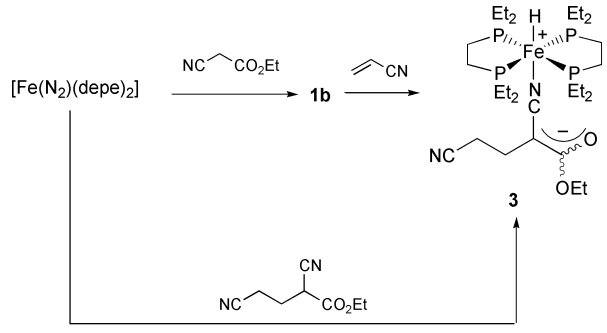

Scheme 1

† Electronic supplementary information (ESI) available: physical and spectroscopic data for **1a** and **1b**. See http://www.rsc.org/suppdata/cc/b0/b004099l/

DOI: 10.1039/b004099l

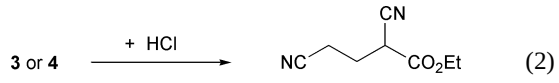

(2)

Reactions of $NCCH(C_2H_4CN)CO_2Et$[8] with $[Fe(N_2)(depe)_2]$ and with [Ru(cod)(cot)]/dppe also gave **3** and **4** in 61 and 62% yields, respectively [eqns. (3) and (4)].

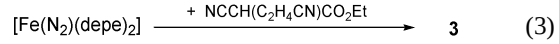

(3)

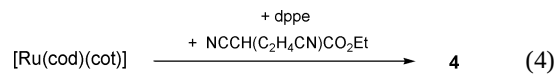

(4)

It is interesting to note that treatment of **3** (or **4**) with excess of either acrylonitrile or ethyl cyanoacetate resulted in no reaction, even at 50 °C, whilst the **3** (or **4**) catalysed double-Michael reaction of ethyl cyanoacetate with acrylonitrile exclusively gave ethyl 2,2-bis(cyanoethyl)cyanoacetate. Both enolate complexes **1b** and the mono-Michael adduct **3** (1.0 mol%) smoothly catalysed this double-Michael addition at room temperature for 36 h in 88 and 79% yields, respectively.[9] Similarly, complexes **2** and **4** also catalysed this reaction in 88 and 75% yields, respectively, under the same conditions.

By taking into account these facts, the possible reaction mechanism for the double-Michael reaction is illustrated in Scheme 2.

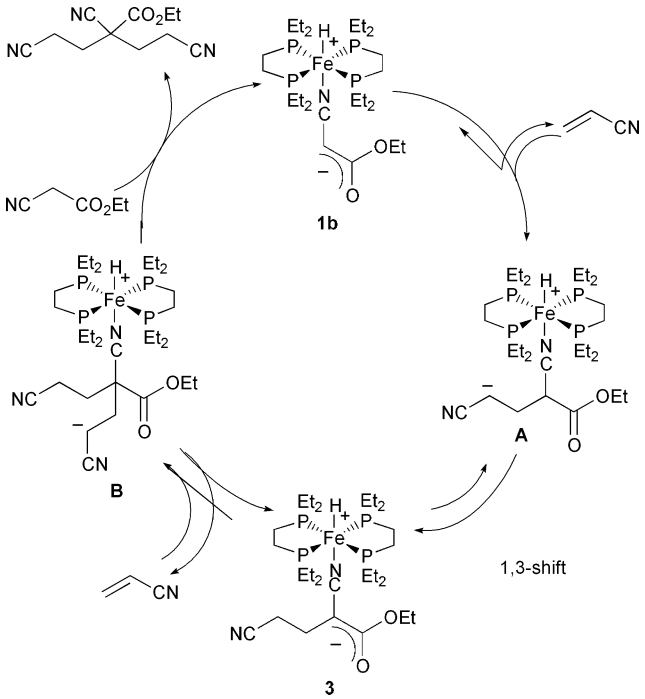

Scheme 2

The *N*-bonded enolate complex **1b** is nucleophilic enough to react with acrylonitrile to give **A**. The intermediate **A** rapidly converts to **3** by 1,3-proton migration. This process is probably driven by the high acidity of the methine proton in **A** and thermodynamic stability of the resulting oxo-π-allyl structure in **3**. This system exclusively affords the double-Michael product regardless of the amount of Michael acceptor and no trace of signals due to the mono-Michael product were detected by NMR. Thus, the direct formation of **1b** from **3** is negligible. Whereas compound **3** catalyses the double-Michael reaction, it remained unreacted with acrylonitrile or ethyl cyanoacetate. This fact suggests that the protonolysis of intermediate **B** took place by ethyl cyanoacetate to reproduce **1b**. When the isotopic labeled $FeD(NCCDCO_2Et)(depe)_2$ (**1b**-d_2) (45 atom% D for Fe–D) was employed in this reaction, the deuteride ligand in **1b**-d_2 remained intact during the catalytic Michael reaction of ethyl cyanoacetate with acrylonitrile (41 atom% D for Fe–D after TON = 3). This is good evidence for this double-Michael product being released from the catalyst, not by reductive elimination, but by protonation.

We are grateful to Proposal-based New Industry Creative Type Technology R&D Promotion Program from NEDO of Japan and the Ministry of Education, Science, Sports and Culture, Japan for financial support.

Notes and references

1 (*a*) S.-I. Murahashi and H. Takaya, *Acc. Chem. Res.*, 2000, **33**, 225; (*b*) S. G. Alvalez, S. Hasegawa, M. Hirano and S. Komiya, *Tetrahedron Lett.*, 1998, **39**, 5209; (*c*) R. Kuwano, H. Miyazaki and Y. Ito, *Chem. Commun.*, 1998, 71; (*d*) H. Bricout, J.-F. Carpentier and A. Mortreux, *Chem. Commun.*, 1997, 1393; (*e*) E. Gômez-Bengoa, J. M. Cuerva, C. Mateo and A. M. Echavarren, *J. Am. Chem. Soc.*, 1996, **118**, 8553; (*f*) H. Sasai, S. Arai and M. Shibasaki, *J. Org. Chem.*, 1994, **59**, 2661; (*g*) D. A. Evans, J. L. Duffy and M. J. Dart, *Tetrahedron Lett.*, 1994, **35**, 8537; (*h*) Y. Lin, X. Zhu and M. Xiang, *J. Organomet. Chem.*, 1993, **448**, 215; (*i*) P. Veya, C. Floriani, A. Chiesi-Villa and C. Rizzoli, *Organometallics*, 1993, **12**, 4892, 4899; (*j*) T. Naota, H. Taki, M. Mizuno and S.-I. Murahashi, *J. Am. Chem. Soc.*, 1989, **111**, 5954; (*k*) G. A. Slough, R. G. Bergman and C. H. Heathcock, *J. Am. Chem. Soc.*, 1989, **111**, 938 and references cited therein.

2 (*a*) M. Hirano, A. Takenaka, Y. Mizuho, M. Hiraoka and S. Komiya, *J. Chem. Soc., Dalton Trans.*, 1999, 3209; (*b*) S.-I. Murahashi, T. Naota, H. Taki, M. Mizuno, H. Takaya, S. Komiya, Y. Mizuho, N. Oyasato, M. Hiraoka, M. Hirano and A. Fukuoka, *J. Am. Chem. Soc.*, 1995, **117**, 12436; (*c*) Y. Mizuho, N. Kasuga and S. Komiya, *Chem. Lett.*, 1991, 2127.

3 (*a*) M. Hirano, M. Hirai, Y. Ito, T. Tsurumaki, A. Baba, A. Fukuoka and S. Komiya, *J. Organomet. Chem.*, 1998, **569**, 3; (*b*) M. Hirano, Y. Ito, M. Hirai, A. Fukuoka and S. Komiya, *Chem. Lett.*, 1993, 2057.

4 (*a*) T. Morikita, M. Hirano, A. Sasaki and S. Komiya, *Inorg. Chim. Acta*, 1999, **291**, 341; (*b*) M. Hirano, M. Akita, T. Morikita, H. Kubo, A. Fukuoka and S. Komiya, *J. Chem. Soc., Dalton Trans.*, 1997, 3453; (*c*) M. Hirano, M. Akita, K. Tani, K. Kumagai, N. C. Kasuga, A. Fukuoka and S. Komiya, *Organometallics*, 1997, 4206; (*d*) S. Komiya, M. Akita, N. Kasuga, M. Hirano and A. Fukuoka, *J. Chem. Soc., Chem. Commun.*, 1994, 1115; (*e*) S. Komiya, M. Akita, A. Yoza, N. Kasuga, A. Fukuoka and Y. Kai, 1993, 787.

5 *Crystal data* for **1b**·Et_2O·H_2O: $C_{29}H_{67}FeNO_4P_4$ monoclinic, *C*2/*c* (No. 15), *a* = 32.31(2), *b* = 13.63(1), *c* = 17.54(1) Å, β = 111.68(4)°, *V* = 7179(8) Å^3, *Z* = 8, *T* = −160.0 °C, D_{calc} = 1.246 g cm^{-3}, Total reflections = 6421, Unique reflection = 6302, F_{000} = 2928.00, μ = 6.30 cm^{-1}, $R(R_w)$ = 0.054 (0.098). Goodness of Fit Indicator = 1.03. The hydride in **1b** was found in the differential Fourier map and was refined isotropically. CCDC 182/1729. See http://www.rsc.org/suppdata/cc/b0/b004099l/ for crystallographic files in .cif format.

6 *Spectroscopic data* for **3**: major isomer: ^{1}H NMR (300.4 MHz, C_6D_6): δ −25.70 (qnt, *J* = 46.5 Hz, 1 H, Fe-*H*), 0.75 (br, 12 H, PCH_2CH_3), 0.98 (sext, *J* = 7.2 Hz, 4 H, PCH_2CH_3), 1.00 (sext, *J* = 7.2 Hz, 4 H, PCH_2CH_3), 1.08 (br, 12 H, PCH_2CH_3), 1.27 (t, *J* = 7.5 Hz, 3 H, OCH_2CH_3), 1.59 (sext, *J* = 7.7 Hz, 4 H, PCH_2CH_3), 1.61 (sext, *J* = 8.1 Hz, 4 H, PCH_2CH_3), 2.06 (sext, *J* = 8.1 Hz, 2 H, PC_2H_4P), 2.09 (sext, *J* = 7.7 Hz, 2 H, PC_2H_4P), 2.4 (m, 2 H, C_2H_4CN), 2.5 (m, 2 H, C_2H_4CN), 4.39 (q, *J* = 6.9 Hz, 2 H, OCH_2CH_3); ^{31}P{^{1}H} NMR (121.6 MHz, C_6D_6): δ 89.2; Minor isomer: ^{1}H NMR (300.4 MHz, C_6D_6); δ −25.61 (qnt, *J* = 46.8 Hz, 1 H, Fe-*H*), 4.26 (q, *J* = 6.3 Hz, 2 H, OCH_2CH_3); ^{31}P{^{1}H} NMR (121.6 MHz, C_6D_6): δ 89.4; IR (KBr, ν/cm^{-1}): 2162 (νN≡C), 1831 (νFe–H), 1608 (νC=O); Anal. Calcd for $C_{28}H_{58}FeN_2O_2P_4$: C, 53.00; H, 9.21; N, 4.41%. Found: 53.75; H, 9.58; N, 5.56%.

7 *Spectroscopic data* for **4**: compound **4** is insoluble in most of organic solvents such as methanol or dmso. However, the initial stage of the reaction in an NMR tube afforded the following NMR spectra: isomer A; ^{1}H NMR (300.4 MHz, C_6D_6): δ −16.44 (qnt, *J* = 19.6 Hz, 1 H, Ru-*H*), 1.44 (t, *J* = 7 Hz, 3 H, OCH_2CH_3), 1.84 (t, *J* = 6 Hz, 2 H, C_2H_4CN), 1.9–2.1 (br, 4 H, PC_2H_4P), 2.43 (t, *J* = 6 Hz, 2 H, C_2H_4CN), 2.5 (br, 2 H, PC_2H_4P), 2.8 (br, 2 H, C_2H_4CN), 4.58 (q, *J* = 6 Hz, 2 H, OCH_2CH_3), 6.8 (m, 12 H, *Ph*), 7.0 (m, 12 H, *Ph*), 7.1 (m, 8 H, *Ph*), 7.4 (m, 8 H, *Ph*); ^{31}P{^{1}H} (121.6 MHz, C_6D_6): δ 58.9 or 62.3 (s); isomer B: ^{1}H NMR (300.4 MHz, C_6D_6): δ −16.29 (qnt, *J* = 18.3 Hz, 1 H, Ru-*H*), 1.46 (t, *J* = 6 Hz, 3 H, OCH_2CH_3), 2.28 (t, 2 H, *J* = 6 Hz, C_2H_4CN), 2.50 (t, 2 H, *J* = 6 Hz, C_2H_4CN), 4.6 (q, *J* = 6 Hz, 2 H, OCH_2CH_3); ^{31}P{^{1}H} (121.6 MHz, C_6D_6): δ 62.3 or 58.9 (s); IR (KBr, ν/cm^{-1}): 2165 (νN≡C), 1933 (νRu–H), 1621 (νC=O).

8 E. E. van Tamelen and E. E. Smissman, *J. Am. Chem. Soc.*, 1953, **75**, 2031.

9 *Conditions*: [ethyl cyanoacetate] = 0.81 M, [acrylonitrile] = 1.6 M, [catalyst] = 0.0081 M, solvent = thf (2.0 cm^3), temp. = r.t., time = 36 h.

Oxidation of [(cyclic triamine)(1,5-cyclooctadiene)iridium]$^+$ cations by hydrogen peroxide forms metallaoxetanes

Thomas C. Flood,*[a] Masanori Iimura,[a] Jeremy M. Perotti,[a] Arnold L. Rheingold[b] and Thomas E. Concolino[b]

[a] *Department of Chemistry, University of Southern California, Los Angeles, CA 90089-0744, USA. E-mail: flood@chem1.usc.edu*

[b] *Department of Chemistry and Biochemistry, University of Delaware, Newark, DE 19716-2522, USA*

Received (in Irvine, CA, USA) 8th March 2000, Accepted 20th July 2000

Iridaoxetane 3 formed by oxidation of 1 with aqueous H_2O_2 is isolated and characterized, providing a rare example of formation of a metallaoxetane by direct oxidation of a metal–alkene complex.

Metallaoxetanes (1-metalla-2-oxacyclobutanes) have been invoked over the years as key intermediates in certain transition metal-mediated oxygen atom transfer reactions to olefins.[1,2] A number of metallaoxetanes of transition metals have been prepared by indirect methods,[3] but to our knowledge there is no example of isolation, or even spectroscopic detection, of a metallaoxetane from a catalytically oxidizing medium. Thus, their intermediacy has been the subject of much speculation and some debate over the past two decades.[2]

We are aware of only two reports of direct stoichiometric oxygenation of coordinated alkenes that result in formation of characterizable metallaoxetanes.[4,5] One of these is the recent elegant work of Gal and coworkers[5] on oxidation of olefins bonded to rhodium(I) bearing *fac*-coordinating triaza and tetraaza ligands. For example, $[(N_4)Rh(C_2H_4)]^+$ [N_4 = *N*,*N*,*N*-tris(2-pyridylmethyl)amine] and H_2O_2 gave a rhodaoxetane which was isolated and an X-ray crystal structure determination was completed.

Over the last several years we have been developing the synthetic organometallic chemistry of CnIr- and Cn*Ir-containing molecules,† and we have observed that Ir^{III} in these 'hard' coordination environments binds olefins very strongly. We decided to check the reactions of $[(Cn^*/Cn)Ir(cod)]^+$ (**1**/**2**) and $[(Cn^*/Cn)Ir(C_2H_4)_2]^+$ with H_2O_2 and other oxidants. Perhaps iridaoxetane 'intermediates' would be stable enough to detect or isolate before rearrangement to some other species. Ideally, the chemistry of iridium might depart substantially from that reported of rhodium.

[Cn*Ir(cod)]OTf **1** is obtained in up to 86% yield as a light yellow precipitate from reaction of Cn* with $[(cod)IrCl]_2$ in THF in the presence of NaOTf. Off-white [CnIr(cod)]OTf **2** is similarly prepared in up to 73% yield. [Cn*Ir(cod)]Cl can also be isolated in the absence of NaOTf, but the yield is very variable because of formation of a byproduct of stoichiometry $Cn^*Ir_2(cod)_2Cl_2$ and indeterminate structure. Both **1** and **2** are stable in the absence of air in DMSO, methanol or THF for days at 60 °C.

Treatment of **1** with an excess of aqueous H_2O_2 in methanol (Scheme 1), followed by precipitation with diethyl ether results in isolation of a pale-yellow solid. Various 1-D and 2-D NMR techniques were used to assign it iridaoxetane structure **3**.[6] The ^{13}C NMR spectrum contains 17 unique carbons, comprising of 3 CH_3, 10 CH_2 and 4 CH groups (DEPT). Despite considerable effort, X-ray quality crystals of **3** were not obtained.

After 2 days at 20 °C, a sample of **3** in MeOH-d_4 in a sealed NMR tube was unchanged. After 6 h at 60 °C, a new species, **5**, began to form, and after 24 h at 60 °C the conversion was quantitative. Since **5** is chiral (17 unique carbons) it cannot be the iridium analogue of the achiral rhodium product[5] $[Cn^*Rh(oxabicyclononadiyl)]^+$. Rearrangement of **3** was repeated on a synthetic scale in THF. Removal of solvent after

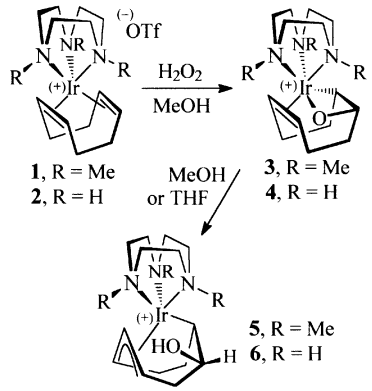

Scheme 1

16 h at reflux gave a beige powder for which DEPT NMR showed 3 CH_3, 9 CH_2 and 5 CH carbons. A ^1H–^{13}C correlation NMR experiment was consistent with the assignment of Ir(III) hydroxycyclooctenediyl species **5**.[7]

$[CnIr(cod)]^+$ **2** was also treated with aqueous H_2O_2 under conditions similar to those for **1**, but iridaoxetane **4** was not observed. Instead, the reaction proceeded directly to yield Ir(III)–hydroxycyclooctenediyl **6** in almost quantitative yield (Scheme 1). The structure was assigned by ^1H and ^{13}C 1-D and 2-D NMR. An X-ray diffraction study of a single crystal of **6** grown from THF–pentane confirms its structure (Fig. 1).[8] As expected, the hydroxy group is *endo* with respect to the iridium center, consistent with its origin in **4**. Formation of iridaoxetane intermediate **4** was established by low temperature NMR spectroscopy. A slight excess of aqueous H_2O_2 was added to **2** in MeOH-d_4 in an NMR tube immersed in liquid nitrogen. Reaction progress was monitored by NMR as the sample warmed. No change was seen below −20 °C, but at −10 °C formation of **4** was observed. After 10 min at −10 °C the resonances of iridaoxetane **4** had begun to be replaced by those of **6**, and conversion of **4** to **6** was rapid at 0 °C. Several attempts to isolate iridaoxetane **4** at low temperature were unsuccessful.

Complexes **1** and **2** were treated with other oxidants like pyridine *N*-oxide, iodosobenzene, and O_2 in aprotic solvents ($MeNO_2$, THF and CH_2Cl_2), all of which gave no reaction. *tert*-Butyl hydroperoxide and **2** generated **6**, but more slowly than H_2O_2. Dioxygen in methanol did form **3**, but the yield was much reduced and there was substantial decomposition during the reaction. We suspect that in the case of O_2 protic solvent is required to allow destructive oxidation of **1** and concomitant formation of H_2O_2 which then effects the usual oxidation of residual **1**. Treatment of $[CnIr(C_2H_4)_2]^+$ with H_2O_2 or Bu^tOOH in methanol or THF gave uncharacterizable mixtures, and its oxidation was not pursued further.

Overall, the oxidation of **2** to **4** is qualitatively faster than that of **1** to **3**, and clearly the rearrangement of **4** to **6** is much faster than **3** to **5**. The reason(s) for the faster reactions of **2** and **4** are not obvious. Since we would have expected the presumably

DOI: 10.1039/b002079f

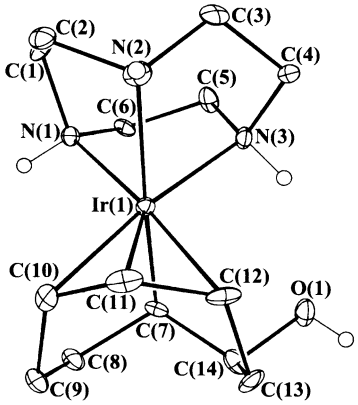

Fig. 1 Thermal ellipsoid plot (30% probability) of the cation of **6**. The OTf counter ion and hydrogen atoms, except H(1)–H(4) which were located, have been omitted for clarity. Selected bond lengths (Å) and angles (°): Ir(1)–N(1) 2.158(7), Ir(1)–N(2) 2.198(8), Ir(1)–N(3) 2.140(7), Ir(1)–C(7) 2.096(9), Ir(1)–C(10) 2.164(8), Ir(1)–C(11) 2.081(8), Ir(1)–C(12) 2.157(8); N(1)–Ir(1)–N(2) 80.0(3), N(2)–Ir(1)–N(3) 79.7(3), N(1)–Ir(1)–N(3) 79.4(3), N(1)–Ir(1)–C(12) 175.2(3), N(2)–Ir(1)–C(7) 171.5(3), N(3)–Ir(1)–C(10) 172.9(3), C(7)–Ir(1)–C(10) 81.3(4), C(7)–Ir(1)–C(12) 82.4(4).

more electron rich **1** to oxidize faster, steric differences may be the more likely explanation. Although we were not able to obtain X-ray quality crystals of either **3** or **4**, from the X-ray crystal structures of [CnIr(H)$_2$(η^2-cyclooctene)]OTf and [Cn*Ir(H)$_2$(η^2-cyclooctene)]Cl we have observed average Ir–N distances of 2.15 and 2.20 Å, respectively, so the methyl groups have only a small effect on the Ir–N distances. Thus, the *N*-methyl groups cause considerably more crowding around the equator of the complex than the N–H groups. It may be that the methyl groups restrict conformational mobility of the oxidized ligand in **3** relative to that in **4** leading to a larger barrier for the rearrangement. Similarly, the slower oxidation of **1** compared to **2** may result form steric hindrance to attack by peroxide on the metal or on the coordinated alkene.

It is interesting that in the three cases where metallaoxetane species have been isolated from oxidation of coordinated olefins, the complexes contain ancillary ligands which coordinate to the metal *via* the relatively non-polarizable atoms oxygen and nitrogen. There is too little information as yet to conclude if this observation is significant.

This work was funded by the US National Science Foundation.

Notes and references

† Abbreviations used in this paper: Cn = 1,4,7-triazacyclononane, Cn* = 1,4,7-trimethyl-1,4,7-triazacyclononane.

1 K. B. Sharpless, A. Y. Teranishi and J. E. Backvall, *J. Am. Chem. Soc.*, 1977, **99**, 3120.
2 K. A. Jorgensen and B. Schiott, *Chem. Rev.*, 1990, **90**, 1483.
3 D. P. Klein, J. C. Hayes and R. G. Bergman, *J. Am. Chem. Soc.*, 1988, **110**, 3704; D. P. Klein and R. G. Bergman, *J. Am. Chem. Soc.*, 1989, **111**, 3079; A. A. Zlota, F. Frolow and D. Milstein, *J. Am. Chem. Soc.*, 1990, **112**, 6411; M. J. Calhorda, A. M. Galvao, C. Unaleroglu, A. A. Zlota, F. Frolow and D. Milstein, *Organometallics*, 1993, **12**, 3316; J. C. Hartwig, R. G. Bergman and R. A. Andersen, *Organometallics*, 1991, **10**, 3344; J. C. Hartwig, R. G. Bergman and R. A. Andersen, *J. Am. Chem. Soc.*, 1990, **112**, 3234.
4 V. W. Day, W. G. Klemperer, S. P. Lockledge and D. J. Main, *J. Am. Chem. Soc.*, 1990, **112**, 2033.
5 B. de Bruin, M. J. Boerakker, J. J. J. M. Donners, B. E. C. Christiaans, P. P. J. Schlebos, R. de Gelder, J. M. M. Smits, A. L. Spek and A. W. Gal, *Angew. Chem., Int. Ed. Engl.*, 1997, **36**, 2064; B. de Bruin, Ph.D. Thesis, Katholieke Universiteit Nijmegen, The Netherlands, 1999.
6 Data for **3**: ^{1}H NMR (DMSO-d_6, 500 MHz): δ 0.78–2.47 (complex, 8H, cod), 2.41 (m, 1H, IrCH), 2.83–3.40 (complex, 12H, NCH_2), 2.68 (s, 3H, NCH_3), 2.95 (s, 6H, NCH_3), 5.17 (pseudo-d, 2H, –CH=), 5.56 (t, 1H, IrOCH). ^{13}C{^{1}H} NMR (DMSO-d_6, 126 MHz) δ 0.88 (IrCH), 19.67, 24.52, 26.95, 34.17 (cod CH_2), 47.49, 49.12, 55.78 (NCH_3), 58.45, 58.60, 61.09, 61.63, 62.58, 64.13 (NCH_2), 78.34, 85.30 (cod −CH=), 88.04 (IrOCH). Anal. Calc. for $C_{18}H_{33}N_3O_4F_3IrS•H_2O$: C, 33.02; H, 5.39; N, 6.42. Found: C, 32.75; H, 5.25; N, 6.38%.
7 Recently, the rhodium analogue of **5** has been reported; B. de Bruin, J. A. Brands, J. J. J. M. Donners, M. P. J. Donners, R. de Gelder, J. M. M. Smits, A. W. Gal and A. L. Spek, *Chem. Eur. J.*, 1999, **5**, 2921.
8 *Crystallographic characterization* of **6**: $C_{15}H_{27}F_3IrN_3O_4S$, M = 594.66, monoclinic, space group $P2_1/c$, a = 9.6533(3), b = 11.5159(4), c = 16.8150(4) Å, β = 98.6347(13)°, V = 848.09(16) Å^3, Z = 4, T = 173(2) K, D_c = 2.137 g cm^{-3}, μ = 73.95 cm^{-1}, $R(F^2)$ = 0.0453, $wR(F^2)$ = 0.1078 for 4191 observed independent reflections. DIFABS absorption corrections were applied to the data set. All non-hydrogen atoms were refined with anisotropic displacement coefficients. The hydrogen atoms bonded to the nitrogen atoms of the Cn ligand and the hydrogen atom of the hydroxy group were located from a difference map and allowed to refine. All other hydrogen atoms were treated as idealized contributions. CCDC 182/1731.

Newly discovered non-isoprenoid glycerol dialkyl glycerol tetraether lipids in sediments

Jaap S. Sinninghe Damsté,*[a] Ellen C. Hopmans,[a] Richard D. Pancost,[a] Stefan Schouten[a] and Jan A. J. Geenevasen[b]

[a] *Netherlands Institute for Sea Research (NIOZ), Department of Marine Biogeochemistry and Toxicology, PO Box 59, 1790 AB Den Burg, Texel, The Netherlands. E-mail: damste@nioz.nl*

[b] *University of Amsterdam, Faculty of Chemistry, Organic Chemistry Unit, Nieuwe Achtergracht 129, 1018 WS Amsterdam, The Netherlands*

Received (in Liverpool, UK) 6th June 2000, Accepted 3rd August 2000

Newly discovered non-isoprenoid dialkyl diglycerol tetraethers containing 13,16-di- or 5,13,16-trimethyloctacosanyl moieties have been identified in peats and coastal marine and lake sediments by HPLC–MS and high-field NMR spectroscopy.

Hyperthermophilic archaea thrive at temperatures > 60 °C and their ecological occurrence is, therefore, restricted to extreme environments such as waters near volcanic areas.[1] To meet the requirements posed by these hostile environments,[2] the membranes of these archaea (the third kingdom of life) are predominantly composed of isoprenoid glycerol dialkyl glycerol tetraethers (GDGTs),[3] which are mainly comprised of acyclic (**1**)† or cyclic biphytane core lipids. Recently we reported a new technique for the direct analysis of intact GDGTs in extracts of archaeal cell material and sediments using high performance liquid chromatography–atmospheric pressure chemical ionization mass spectrometry.[4] Initial results indicated that GDGTs are widespread in low temperature environments, in contrast to the previous belief that GDGTs are restricted to hyperthermophilic archaea. Using this technique we also encountered unidentified GDGTs in extracts of peats. Here we report the identification of these abundant GDGTs as unprecedented, non-isoprenoid GDGTs.

The total ion current chromatogram of the HPLC–MS analysis revealed unknown components in the peat extracts, which possessed $[M + H]^+$ ions of 1050, 1036 and 1022 in order of increasing elution time (Fig. 1). Characteristic losses of $[M+H]^+$-18 and $[M+H]^+$-74 corresponding to loss of water and of a glycerol moiety (as $C_3H_6O_2$)[4] suggested these components to be GDGTs. Cleavage of ether bonds[5] with HI and subsequent reduction of the formed iodides with $LiAlH_4$, performed on a fraction of an extract of the Holocene Bargerveen peat (SE Drenthe, the Netherlands) containing these newly discovered GDGTs, produced two dominant branched hydrocarbons. The first eluting hydrocarbon was identified as 13,16-dimethyloctacosane by GC–MS analysis and co-elution with an authentic standard.[6] The second eluting isomer is a C_{31} alkane; its mass spectral characteristics indicate also a C_{28} linear alkyl chain with methyl branching at C-13, C-16 and C-5. Its relative retention time is consistent with this structure; the experimental Kovats index of 2912 compares favourably with the one calculated[7] (RI = 2914). The iodides formed upon HI treatment were also treated with $NaSCH_3$,[5] resulting in the formation of the α,ω-diSMe derivatives of the C_{30} and C_{31} branched alkanes. This established the number and positions by which these

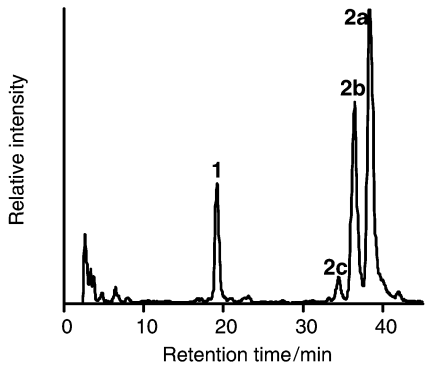

Fig. 1 Total ion current chromatogram of an extract of the Bargerveen peat revealing the abundance of GDGTs **1** and **2a**–**c**.

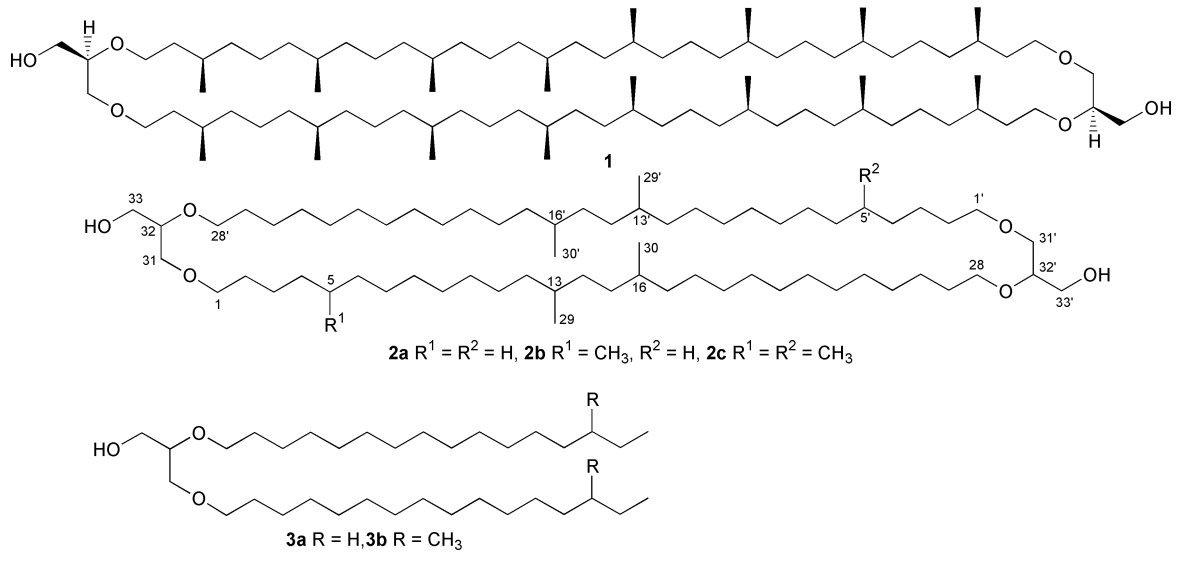

DOI: 10.1039/b004517i

skeletons are ether-bound. These data suggest that the new GDGTs comprise diether-linked di- or trimethyl branched C_{28} linear chains (**2a**–**c**), which fits with the determined molecular weights and indicates elemental compositions of $C_{66+n}H_{132+2n}O_6$ (n = 0–2).

These structural assignments were confirmed by high field ^{1}H and ^{13}C NMR‡ of GDGTs **2a** and **2b**, which were isolated from the peat extract by HPLC on a semi-preparative NH_2 Econosphere 10 × 250 mm column (Alltech) eluted with a linear gradient from 1 to 2% propanol in hexane in 55 min, yielding 1.6 and 1.1 mg per component, respectively. Both the ^{1}H and ^{13}C NMR gave substantial evidence for the presence of ether-bound glycerol units in **2a** and **2b**. The ^{13}C shifts of the carbon atoms of the glycerol moieties and the ether-bound CH_2 units of the alkyl moieties are in good agreement with those reported for GDGT **1**[3b] and commercially available 1,2-dihexadecylglycerol (**3a**). The remaining signals in the ^{13}C spectrum of **2a**, apart from a large suite of secondary C-atoms, indicated only 4 equivalent primary and 4 equivalent tertiary C-atoms, consistent with the proposed structure. The ^{13}C spectrum of **2b** is somewhat more complicated due to the additional methyl group in one of the branched alkyl chains. The shifts of the C-atoms around this additional methyl group are in good agreement with the proposed position for branching. A TOCSY experiment with **2b** indicated that the additional methyl group is present in the *O*-bound alkyl chain attached at the C-1 position of the glycerol moiety through a correlation between H-1 and the protons of the methyl group at C-5.

We have thus established a new type of GDGT not composed of isoprenoid but of branched alkyl core lipids. The new tetraethers all consist of a 64-membered ring with 6–8 stereocentres. Although the newly discovered GDGTs have been isolated from peat, they also occur in lake and coastal marine sediments. Their close structural similarity to **1** suggests that **2a**–**c** are also core membrane lipids, although they have not yet been identified in organisms. Branched dialkyl glycerol diethers (*e.g.* **3b**) have been reported in a thermophilic bacterium[8] and it may be that the GDGTs **2** represent 'dimers' of such lipids, in the same way as **1** is a dimer of the isoprenoid dialkyl glycerol ether, *sn*-2,3-diphytanylglycerol diether. This suggests that bacteria are more likely producers of these membrane lipids than archaea.

We would like to thank Dr P. Albrecht (University of Strasbourg) for his kind donation of a GC sample of the authentic standard of 13,16-dimethyloctacosane, Mr C. Erkelens (University of Leiden) for access to the 600 MHz NMR spectrometer, and Dr B. van Geel (University of Amsterdam) for peat samples. We acknowledge the Dutch Organisation for Scientific Research (NWO-ALW; grant number 809.33.001) for funding.

Notes and references

† Antiparallel arrangement of glycerol units is indicated and assumed for **2** but it has been shown for **1** that the parallel arrangement occurs in approximately equal amounts.[9]

‡ NMR data for **2a** and **2b** at 600 MHz for ^{1}H in $CDCl_3$, COSY, TOCSY, HMBC: δ 3.71 (2H, m, H-33, 33′), 3.62 (4H, m, H-28, 28′, H′-33, 33′), 3.52 (6H, m, H′-28, 28′, H-31, 32, 31′, 32′), 3.49 (2H, m, H′-31, 31′), 3.43 (4H, m, H-1, 1′), 2.17 (2H, OH), 1.58 (4H, m, H-27, 27′), 1.56 (4H, m, H-2, 2′), 1.39 (1H, m, H-5, **2b**), 1.33 (4H, m, H-13, 16, 13′, 16′), 1.10 (~16H, m, H-12, 14, 15, 17, 12′, 14′, 15′, 17′ and 4 and 6 for **2b**), 0.845 (3H, d, J = 7 Hz, H-34, **2b**), 0.84 (12H, d, J = 7 Hz, H-29, 29′, 30, 30′). ^{13}C (125 MHz), APT: δ 78.38 (C-32, 32′), 71.78 (C-1, 1′), 71.10 (C-31, 31′), 70.41 (C-28, 28′), 63.06 (C-33, 33′), 37.14 (C-12, 17, 12′, 17′), 36.94, 36.77 (C-4, 6, **2b**), 34.35 (C-14, 15, 14′, 15′), 33.04 (C-13, 16, 13′, 16′), 32.66 (C-5, **2b**), 30.04, 29.96 (C-2, 10, 19, 27, 2′, 10′, 19′, 27′; C-8, **2b**), ~29.7 (all other C's), 29.39 (C-25, 4′, 25′; C-4, **2a**), 27.03 (C-11, 18, 11′, 18′; C-7, **2b**), 26.06 (C-26, 3′, 26′; C-3, **2a**), 22.65 (C-3, **2b**), 19.79 (C-29, 30, 29′, 30′), 19.75 (CH_3 at C-5, **2b**).

1 K. O. Stetter, in *Extremophiles: Microbial life in extreme environments*, ed. K. Horikoshi and W. D. Grant, Wiley Series in Ecological and Applied Microbiology, Wiley-Liss, New York, 1998, pp. 1–24.
2 J. C. M. van den Vossenberg, A. J. M. Driessen and W. N. Konings, *Extremophiles*, 1998, **2**, 163.
3 (*a*) Y. Koga, M. Nishihara, H. Morii and M. Akagawa-Matsushita, *Microbiol. Rev.*, 1993, **57**, 164; (*b*) M. DeRosa and A. Gambacorta, *Prog. Lipid Res.*, 1988, **27**, 153.
4 E. C. Hopmans, S. Schouten, R. D. Pancost, M. J. T. van der Meer and J. S. Sinninghe Damsté, *Rap. Comm. Mass. Spectrom.*, 2000, **14**, 585.
5 S. Schouten, M. J. L. Hoefs, M. P. Koopmans, H.-J. Bosch and J. S. Sinninghe Damsté, *Org. Geochem.*, 1996, **29**, 1305.
6 B. Chappe, W. Michaelis and P. Albrecht, in *Advances in Organic Geochemistry 1979*, ed. A. G. Douglas and J. R. Maxwell, Pergamon, Oxford, 1980, pp. 265-274.
7 Y. V. Kissin, G. P. Feulmer and W. B. Wayne, *J. Chrom. Sci.*, 1986, **24**, 164.
8 T. A. Langworthy, G. Holzer, J. G. Zeikus and T. G. Tornabene, *System. Appl. Microbiol.*, 1983, **4**, 1.
9 O. Gräther and D. Arigoni, *J. Chem. Soc., Chem. Commun.*, 1995, 405.

Anion controlled 2D assembly of a La–Cu cation array and its unusual magnetic properties

Qin-De Liu,[a] Jun-Ran Li,*[a] Song Gao,*[a] Bao-Qing Ma,[a] Qing-Zhong Zhou,[a] Kai-Bei Yu[b] and Hui Liu[a]

[a] *State Key Laboratory of Rare Earth Materials Chemistry and Applications & PKU-HKU Joint Laboratory on Rare Earth Materials and Bioinorganic Chemistry, College of Chemistry and Molecular Engineering, Peking University, Beijing 100871, China. E-mail: gaosong@pku.edu.cn*

[b] *Chengdu Center for Analysis and Measurement, Academia Sinica, Chengdu 610041, China*

Received (in Cambridge, UK) 25th April 2000, Accepted 27th July 2000

A novel 2D La–Cu heteronuclear coordination polymer, formed by the synergetic effect of Cl^- and ClO_4^-, possesses an irregular triangular lattice of copper ions, and shows unusual magnetic relaxation properties.

Ladder-like 2D copper arrays have attracted much attention in the last fifteen years owing to the key role of Cu–O layers in high temperature superconductors.[1] Meanwhile, the structure and magnetic behavior of many square-planar molecular compounds have been studied extensively, especially for the A_2CuX_4 series.[2,3] On the other hand, geometrically frustrated two-dimensional systems with triangular or kagome lattices have attracted continued interest both theoretically and experimentally.[4] However, genuine 2D copper molecular materials containing such lattices are surprisingly scarce. $Cu_2(OH)_3X$ may be a unique example of a triangular lattice, which shows a coexistence of long range ordering and spin glass-like behavior.[5] In 1998, we reported the 2D 4f–3d coordination polymers $Ln_2M_3(EDTA)_3(H_2O)_{11}\cdot 12H_2O$ (M = Co, Mn), in which the connection of the M ions led to a kagome lattice.[6] In continuation of this work, nitrilotriacetic acid (H_3NTA) was used as a multidentate bridging ligand, and two types of inorganic anions were introduced, which led to a novel 2D La–Cu assembly formulated as $[LaCuCl(NTA)(H_2O)_6]ClO_4\cdot H_2O$ **1**, in which the copper connections afforded an irregular triangular lattice. From the view point of synthetic chemistry, the template effect of inorganic anions has been well documented in the formation of some cluster compounds, for example, Cl^- for $[Eu_{15}Cl(\mu_3\text{-}Tyr)_{10}(\mu_3\text{-}OH)_{20}(\mu_2\text{-}H_2O)_5(OH)_{12}(H_2O)_8](ClO_4)_2\cdot 56H_2O$, μ_{12}-ClO_4^- in $[Ln_6Cu_{12}(OH)_{24}(H_2O)_{18}(pyb)_{12}ClO_4](ClO_4)_{17}\cdot nH_2O$ (pyb = pyridine betaine) (Ln = Nd, Sm, Gd and Y) and O^{2-} in $[Ln_6O(OH)_8(H_2O)_{24}](ClO_4)_8\cdot 6H_2O$.[7] In contrast, as monodentate ligands and counter ions, both Cl^- and ClO_4^- play a crucial role in the formation of compound **1**.

A mixture of $Cu(OH)_2$ (3 mmol) and H_3NTA (3 mmol) was dissolved in 30 ml H_2O, then $La(ClO_4)_3$ (1.5 mmol) and $LaCl_3$ (1.5 mmol) were added under vigorous stirring. The pH of the solution was adjusted carefully to 5.0. After being filtered, the solution was concentrated to 15 ml and left at room temperature. Blue rectangular crystals of **1** were deposited in *ca*. 40% yield after two weeks.†

X-Ray crystallography‡ has established that complex **1** adopts a two-dimensional honeycomb-like layer with nine-coordinate lanthanum and five-coordinate copper ions located at the apexes of each hexagon. As shown in Fig. 1(a), the NTA ligand coordinates to Cu in a tetradentate manner through three oxygen atoms (O1, O3, O5) of three different carboxyl groups and a nitrogen atom (N), forming three five-membered rings. The fifth coordination site of Cu is occupied by a chloride ion (Cl1). The remaining three carboxyl oxygen atoms (O2, O4, O6) of the NTA coordinate to three different adjacent lanthanum ions forming three *anti–anti* carboxylic bridges between Cu and La ions. For La, three oxygen atoms from three different NTA ligands (O2, O4A, O6B) occupy three coordination sites of La with three similar angles (O2–La–O4A 76.0°, O2–La–O6B 81.6° and O4A–La–O6B 78.5°). The remaining six coordination sites of La are taken up by six water molecules (O7–O12). The complex can be regarded as a polymer in which CuCl(NTA) units are linked to each other by $La(H_2O)_6$ bridges from three different directions, forming a two-dimensional metal-apex honeycomb [Fig. 1(b)], very different from the honeycomb of $[Ln_2M_3]$ found in $Ln_2(ox)[Cu(pba)]_3[Cu(H_2O)_5]\cdot 20H_2O$ [Ln = La–Gd, pba = 1,3-propylenebis(ox-

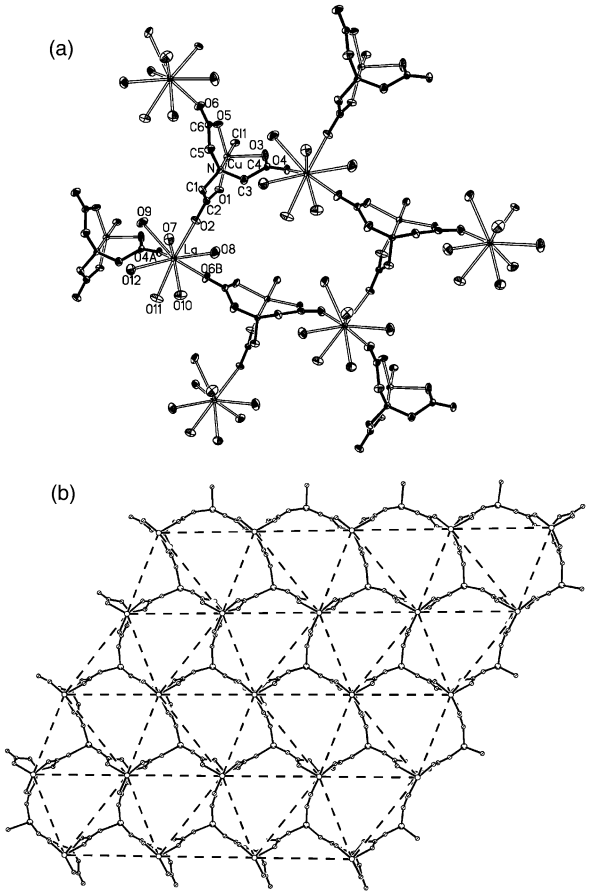

Fig. 1 (a) An ORTEP drawing of **1** showing the connections between La^{3+} and Cu^{2+}. Hydrogen atoms are omitted for clarity. Selected interatomic distances (Å) and angles (°): La–O6 2.466(5), La–O4 2.501(5), La–O2 2.541(6), La–O7 2.545(6), La–O10 2.566(6), La–O11 2.568(6), La–O8 2.579(6), La–O12 2.604(7), La–O9 2.622(6), Cu–O1 1.969(4), Cu–O5 1.988(5), Cu–N 2.010(6), Cu–Cl1 2.218(2), Cu–O3 2.222(5); O4A–La–O6B 78.47(19), O2–La–O6B 81.6(2), O2–La–O4A 75.97(19), O1–Cu–O5 151.9(2), O1–Cu–N 84.3(2), O5–Cu–N 85.1(2), O1–Cu–Cl1 95.90(17), O5–Cu–Cl1 95.13(16), N–Cu–Cl1 178.97(18), O1–Cu–O3 110.0(2), O5–Cu–O3 93.9(2), N–Cu–O3 81.2(2). (b) Viewed along the *c* axis (*ab* plane) showing the honeycomb structure and the irregular triangular lattice formed by copper ions (dashed lines).

DOI: 10.1039/b003293j

amato)][8] and $Ln_2M_3(edta)_3(H_2O)_{11}\cdot 12H_2O$,[6] where M ions occupy the center position of edges of hexagons. The intralayer La···Cu distances (6.34, 6.35 and 6.43 Å) are nearly equal but the distortion of the hexagon leads to neighboring intralayer Cu···Cu distances of 8.57, 9.30 and 10.11 Å, respectively; accordingly the connection of closest neighboring copper ions affords an irregular triangular lattice. It is also noted that the closest interlayer Cu···Cu separations are 7.44, 8.56 and 9.16 Å, comparable with those in the layer. In this sense, **1** is not an ideal 2D compound.

Experiments using only $La(ClO_4)_3$ or $LaCl_3$ did not give rise to this La–Cu complex, suggesting that both Cl^- and ClO_4^- have a synergetic effect in forming this heteronuclear complex. Compared with the Ln_{15} cluster which contains a central Cl^- ion as a template and ClO_4^- ions as counter ions,[7a] the Cl^- in complex **1** does not act as a template, but directly coordinates to Cu, and formation of **1** was impossible without Cl^-. The role of ClO_4^- as a counter ion in complex **1** may lie in it occupying the holes of the honeycomb and stabilizing the lattice. Since the volume of Cl^- is much smaller than that of ClO_4^-, the lattice might be destabilized if the counter ion is changed from ClO_4^- to Cl^-. These facts suggest that the formation of **1** is controlled by both Cl^- and ClO_4^-. Presumably, Cl^- and ClO_4^- could be replaced by other anions similar to them. For example, Cl^- may be replaced by Br^-, I^-, CN^-, OCN^- or even SCN^- , and ClO_4^- may be replaced by PF_6^-, BF_4^-, NO_3^- *etc.* The use of larger organic anions to explore the possibility of obtaining well separated 2D triangular compounds as well as replacement of La^{3+} by other lanthanide ions to yield chain complexes, will be reported elsewhere.

Preliminary magnetic investigations were made for **1**. The temperature dependence of the magnetic susceptibility in the temperature range 2–200 K at an applied field of 10 kOe is shown in Fig. 2(a). The value of $\chi_M T$ is 0.4 $cm^3\ mol^{-1}$ K at 200 K and increases very slowly to a maximum of 0.47 $cm^3\ mol^{-1}$ K between 13 and 6 K, then decreases upon further cooling. The data could not be fitted well using the Lines' model for a quadratic layer Heisenberg antiferromagnet,[9] but fitting the data to the Curie–Weiss law gave C = 0.398 $cm^3\ mol^{-1}$ K and θ = 2.6 K, indicative of weak ferromagnetic behavior. This might be considered as the result of frustration in the 2D triangular array of copper ions. If so, spin glass behavior should be expected for the geometrically frustrated system as for $Cu_2(OH)_3X$.[5b] However, zero field ac measurements did not give any peaks for either real χ' or imaginary χ'' as shown in Fig. 2(b) probably owing to weak coupling between Cu ions in **1** at zero field as a result of the large Cu···Cu separations. When a dc field (10 kOe) was applied, the antiferromagnetic (AF) interactions among Cu ions (including inter-layer) will be enhanced, and accordingly the frustration due to the AF interaction of triangularly arranged Cu ions may result in the very unusual magnetic relaxation shown in Fig. 2(b).[10] Peaks for χ' and χ'' are observed in the dc field, and are strongly frequency dependent. If we calculate the value of relative variation of peak temperature (T_p) per decade of frequency, $\varphi = \Delta T_p/[T_p\Delta(\log f)] = 1.2$, which is rather large and distinctly different from the behavior of normal spin glasses ($\varphi < 0.1$).[11] Further investigation on the mechanism of the unusual magnetic relaxation is under way.

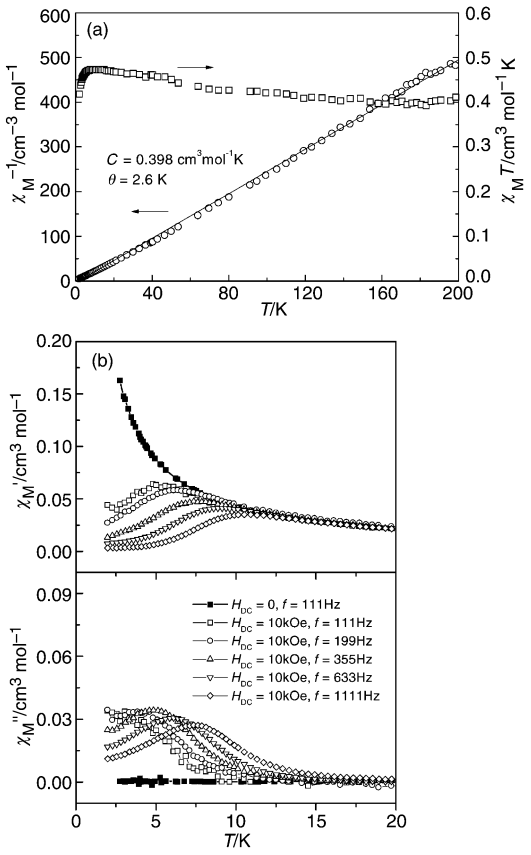

Fig. 2 (a) Temperature dependence of the dc susceptibility of **1** measured at a field of 10 kOe. (b) Temperature dependence of the ac susceptibility of **1** measured at zero dc bias field and at 10 kOe for different ac frequencies (top: real χ', bottom: imaginary χ'').

This work is supported by the National Natural Science Foundation of China (No. 29771001, 29831010), National Key Project for Fundamental Research (G1998061306), the Excellent Young Teachers Fund of MOE, P.R.C.

Notes and references

† *Elemental analysis* for **1**: Calc. C, 11.06; H, 3.09; N, 2.15. Found: C, 11.18; H, 2.94; N, 1.95%.

‡ *Crystal data*: $C_6H_{20}Cl_2CuLaNO_{17}$, M = 651.58, orthorhombic, space group $Pca2_1$, a = 15.975(2), b = 9.2980(10), c = 12.726(2) Å, V = 1890.3(4) Å^3, Z = 4, D_c = 2.290 Mg m^{-3}, μ = 3.722 mm^{-1}, $F(000)$ = 1276, GOF = 1.040. The final R_1 and wR_2 are 0.0273 and 0.0698, respectively, for 275 parameters and 1948 relections [$I > 2\sigma(I)$]. CCDC 182/1730. See http://www.rsc.org/suppdata/cc/b0/b003293j/ for crystallographic files in .cif format.

1 H. Mayaffre, P. Auban-Senzier, M. Nardone, D. Jérome, D. Poilblanc, C. Bourbonnais, U. Ammerahl, G. Dhalenne and A. Revcolevschi, *Science*, 1998, **279**, 345; S. Maekawa, *Science*, 1996, **273**, 1515 and references therein.

2 For example: L. Deakin, A. M. Arif and J. S. Miller, *Inorg. Chem.*, 1999, **38**, 5072; I. G. de Muro, F. A. Mautner, M. Insausti, L. Lezama, M. I. Arriortua and T. Rojo, *Inorg. Chem.*, 1998, **37**, 3243; J. Darriet, M. S. Haddad, E. N. Duesler and D. N. Hendrickson, *Inorg. Chem.*, 1979, **18**, 2679.

3 For example: G. S. Long, M. Wei and R. D. Willett, *Inorg. Chem.*, 1997, **36**, 3102; R. Willett, H. Place and M. Middleton, *J. Am. Chem. Soc.*, 1988, **110**, 8639; C. P. Landee, K. E. Halvorson and R. D. Willett, *J. Appl. Phys.*, 1987, **61**, 3295.

4 For example: G. Aeppli and P. Chandra, *Science*, 1997, **275**, 177; W. H. Zheng, R. H. McKenzie and R. R. P. Singh, *Phys. Rev. B*, 1999, **59**, 14 367; H. F. Pen, J. van den Brink, D. I. Khomskii and G. A. Sawatzky, *Phys. Rev. Lett.*, 1997, **78**, 1323; M. Benakli, H. Zheng and M. Gabay, *Phys. Rev. B*, 1997, **55**, 278; S. Maruti and L. W. ter Haar, *J. Appl. Phys.*, 1994, **75**, 5949; C. M. Wynn, A. S. Albrecht, C. P. Landee, C. Navas and M. M. Turnbull, *Mol. Cryst. Liq. Cryst.*, 1995, **274**, 1; A. S. Wills and A. Harrison, *J. Chem. Soc., Faraday Trans.*, 1996, **92**, 2161; A. Harrison, A. S. Wills and C. Ritter, *Physica B*, 1997, **241**, 722; S. J. Clarke, A. J. Fowkes, A. Harrison, R. M. Ibberson and M. J. Rosseinsky, *Chem. Mater.*, 1998, **10**, 372.

5 (*a*) M. A. Girtu, C. M. Wynn, W. Fujita, K. Awaga and A. J. Epstein, *J. Appl. Phys.*, 1998, **83**, 7378; (*b*) W. Fujita, K. Awaga and T. Yokoyama, *Inorg. Chem.*, 1997, **36**, 196.

6 T. Yi, S. Gao and B. G. Li, *Polyhedron*, 1998, **17**, 2243.

7 (*a*) R. Y. Wang, Z. P. Zheng, T. J. Jin and R. J. Staples, *Angew. Chem., Int. Ed.*, 1999, **38**, 1813; (*b*) X. M. Chen, S. M. J. Aubin, Y. L. Wu, Y. S. Yang, T. C. W. Mak and D. N. Hendrickson, *J. Am. Chem. Soc.*, 1995, **117**, 9600; (*c*) D. S. Zhang, B. Q. Ma, T. Z. Jin, S. Gao, C. H. Yan and T. C. W. Mak, *New J. Chem.*, 2000, **24**, 61.

8 O. Guillou, O. Kahn and R. L. Oushoorn, *Inorg. Chim. Acta*, 1992, **198**–**200**, 119.

9 M. E. Lines, *J. Phys. Chem. Solids*, 1970, **31**, 101.

10 S. Gao, G. Su, T. Yi and B. Q. Ma, *Phys. Rev. B*, submitted.

11 J. A. Mydosh, *Spin Glasses: An Experimental Introduction*, Taylor and Francis, London, 1993.

Anion recognition through hydrogen bonding: a simple, yet highly sensitive, luminescent metal-complex receptor

Shih-Sheng Sun and Alistair J. Lees*

Department of Chemistry, State University of New York at Binghamton, Binghamton, New York 13902-6016, USA. E-mail: alees@binghamton.edu

Received (in Irvine, CA, USA) 5th June 2000, Accepted 26th July 2000

A new luminescent rhenium(I) polypyridyl-based receptor for a variety of inorganic anions has been designed and synthesized and this artificial receptor shows high affinities for halides, cyanide and acetate anions with binding constants as high as 10^4–10^5 M^{-1} and a detection limit as low as 10^{-8} M in CH_2Cl_2 solution.

The design and synthesis of efficient artificial receptors for selective binding of biologically or environmentally important anionic species is an emerging field with many applications.[1,2] A variety of synthetic receptors have been designed and studied for their binding strength and selectivity toward different anions. These have included Lewis acids,[1] protonated polyammonium macrocycles,[1] pyrroles,[3] guanidiniums,[4] metalloreceptors[1] and amides.[1] However, many of these receptors have very elaborate structures that typically require multiple synthetic steps with relatively low overall yields which make it impractical to prepare them on a large scale. There are only a few structurally simple receptors exhibiting both sensitivity and selectivity. [5]

Nature provides many examples of proteins utilizing hydrogen bonding for binding substrates. The incorporation of luminescent chromophores into the receptor which are sensitive to interactions between the receptor and analytes has gained considerable attention due to their high sensitivity and detection limit.[6] Although there have been several literature reports concerning luminescence-based anion detection,[6,7] the highly sensitive luminescence-based halide and cyanide sensory systems are much rarer.[7] Thus, we embarked on designing a very simple and easily prepared luminescent metal complex integrated with an amide moiety functioning as a hydrogen bonding site. We report herein, the synthesis and binding properties of this highly sensitive and selective luminescent anion receptor, $[\{(Bu^t_2bpy)Re(CO)_3\}_2(\mu\text{-}L)](PF_6)_2$ **1**, (Bu^t_2bpy = 4,4′-di-*tert*-butylbipyridine).

The synthesis of L and complex **1** is shown in Scheme 1. The bridging ligand **2** was prepared in 56% yield from 2 equivalents of 4-aminopyridine and 2,6-pyridinedicarbonyl dichloride. Subsequent reaction of **2** and 2 equivalents of $[MeCN)(Bu^t_2bpy)Re(CO)_3](PF_6)$[8] in refluxing THF, followed by recrystallization from CH_2Cl_2–pentane, afforded a bright yellow crystalline solid **1**† in 81% yield.

The N–H protons of complex **1** exhibit a chemical shift δ 10.59 in $CDCl_3$. The very downfield chemical shift indicates the presence of strong intramolecular hydrogen bonding between the N–H protons and nitrogen in the central pyridine. This results in ligand **2** having an approximate right angle geometry[9,10] and the converged structure of complex **1** renders it as an effective anion receptor through hydrogen bonding. In deoxygenated CH_2Cl_2 solution, complex **1** exhibited intense absorption bands in the near UV to visible spectral region (λ_{max} = 254, 281 and 380 nm, ε_{max} = 63600, 61500 and 7700 M^{-1} cm^{-1}, respectively) and a very strong luminescence at 536 nm with quantum yield of 0.37 and lifetime of 0.48 μs.

Addition of different halides or inorganic polyatomic anions (as tetrabutylammonium salts) into a 1×10^{-5} M solution of complex **1** was observed to cause different degrees of quenching of the luminescence intensities.‡ The N–H protons in ^1H NMR spectra all showed significant downfield shifts (> 1.5 ppm), indicating the strong hydrogen bonding formation between the amide protons of complex **1** and the anions. Fig. 1

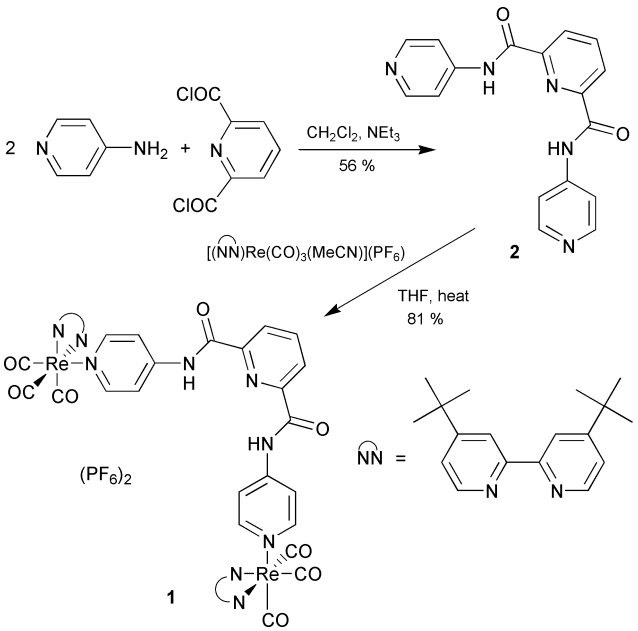

Scheme 1

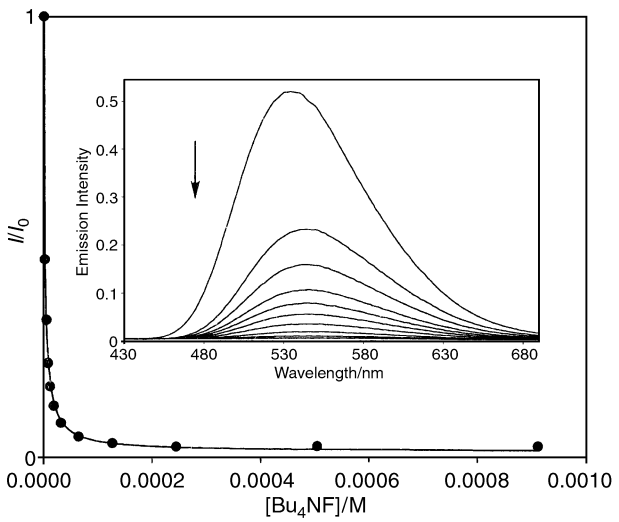

Fig. 1 Titration curve of the addition of F^- anion (as tetrabutylammonium salt). The inset shows the change of the emission intensity of complex **1** in CH_2Cl_2 solution upon addition of F^- anion. Excitation wavelength is 360 nm.

DOI: 10.1039/b004541l

Table 1 Binding constants K_b determined by luminescence titration in CH_2Cl_2 at 298 K

Anion	K_b/M^{-1}
CN^-	8.80×10^5
F^-	3.82×10^5
Cl^-	3.99×10^4
Br^-	3.90×10^4
I^-	1.49×10^5
OAc^-	3.41×10^4
$H_2PO_4^-$	1.47×10^2
NO_3^-	63.4
ClO_4^-	8.4

shows a typical titration curve for the luminescence intensity upon addition of F^- to a CH_2Cl_2 solution of **1**.§ The curve was determined to fit well to a 1 : 1 binding isotherm.[11] Concomitant with the quenching, the luminescence wavelength slightly red-shifted from 536 to 546 nm. Table 1 summarizes the binding constants measured for complex **1** toward different anions. Clearly, this molecule shows strong binding affinity toward halides, cyanide or acetate anions, only moderate binding affinity toward dihydrogen phosphate and very weak binding affinity to nitrate or perchlorate anions.

The overall order determined for binding affinity is: $CN^- > F^- > I^- > Cl^- \approx Br^- \approx OAc^- >> H_2PO_4^- > NO_3^- > ClO_4^-$. This finding is significant as it is not common for charged receptors to exhibit such outstanding selectivity for anion species.[12] In fact, the combination of interactions involving electrostatic force, hydrogen bonding strength and steric effects all apparently influence the binding affinities toward anions in complex **1**. Importantly, the sensitivity of complex **1** is so high that the emission intensity can be effectively quenched by as much as 10% even in the presence of only 10^{-8} M cyanide or fluoride anions.

The origin of the emission quenching upon addition of anions is not certain at this stage. The red shift of the emission band, however, indicates that the emission quenching is associated with a change in the energy of the excited state and, thus, the enhancement of nonradiative decay.

In summary, complex **1** represents a simple and easy to prepare luminescent anion sensory system. The strong binding affinity and high selectivity of complex **1** for certain anions also may make it a promising candidate for many other different applications besides sensors, such as homogeneous catalysis[13] and membrane transport.[14] Currently, we are working on anion binding studies in H-bonding competitive solvents such as MeCN as well as modifying the dipyridyl ligands so that the receptors will be soluble in aqueous solvents. These results are expected to be intriguing given the fact that most biologically and environmentally important anions are only soluble in aqueous environments.

We are grateful to the U. S. Department of Energy (Grant DE-FG02-89ER14039) for support of this research.

Notes and references

† IR ($\nu_{C\equiv O}$, CH_2Cl_2): 2032, 1928. δ_H (300 MHz, $CDCl_3$): 10.59 (s, 2 H, NH), 8.91 (d, 4 H, J_{HH} 5.9 Hz, $H^{6,6'}$-Bu$^t_2$bpy), 8.34 (d, 2 H, J_{HH} 7.7 Hz, H_m-py), 8.28 (s, 4 H, $H^{3,3'}$-Bu$^t_2$bpy), 8.04 (t, 1 H, J_{HH} 7.6 Hz, H_p-py), 7.93 (d, 4 H, J_{HH} 6.4 Hz, H_α-py), 7.81 (d, 4 H, J_{HH} 6.6 Hz, H_β-py), 7.67 (d, 4 H, J_{HH} 7.1 Hz, $H^{5,5'}$-Bu$^t_2$bpy), 1.46 (s, 36 H, CH_3). δ_C(360 MHz, $CDCl_3$): 196.3, 192.0, 166.3, 162.7, 155.8, 152.6, 152.1, 148.0, 147.7, 139.7, 126.6, 126.4, 122.0, 117.1, 36.3, 30.3. ES-MS: *m/z* 1540.2 (calc. *m/z* 1541.6 for $[M - PF_6^-]^+$) and 698.6 (calc. 698.3 for $[M - 2PF_6^-]^{2+}$). Anal. Calc for $C_{59}H_{61}N_9O_8Re_2P_2F_{12}$: C, 42.02; H, 3.65; N, 7.47. Found: C, 41.80; H, 3.62; N, 7.26%.

‡ The binding studies were conducted in air-equilibrated CH_2Cl_2 solution. We found the emission intensities were *ca.* 10% lower than those in deoxygenated CH_2Cl_2 solutions. However, the resultant I/I_0 and fitted binding constants toward different anions did not change upon deaeration.

§ Luminescence titrations were carried out by adding CH_2Cl_2 solutions of anions to complex **1** in CH_2Cl_2. Emission spectra were collected on a SLM 48000S spectrophotometer. Fitting was carried out using eqn. (1), as described by Connors (see ref. 11).

$$I/I_0 = (1 + (k_f/k_s)K_b[L])/(1 + K_b[L]) \quad (1)$$

Here, I and I_0 represent the emission intensity and k_f and k_s are the proportionality constants for the bound complex and free complex **1**, respectively, and K_b is the binding constant.

1 P. D. Beer and D. K. Smith, *Prog. Inorg. Chem.*, 1997, **46**, 1 and references therein.
2 F. P. Schmidtchen and M. Berger, *Chem. Rev.*, 1997, **97**, 1609.
3 P. A. Gale, J. L. Sessler, V. Král and V. Lynch, *J. Am. Chem. Soc.*, 1996, **118**, 5140.
4 E. F. Scott, V. Arman, S. Kincaid and A. D. Hamilton, *J. Am. Chem. Soc.*, 1993, **115**, 369.
5 K. Kavallieratos, S. R. de Gala and R. H. Crabtree, *J. Am. Chem. Soc.*, 1997, **119**, 2325.
6 A. P. de Silva, H. Q. N. Gunaratne, T. Gunnlaugsson, A. J. M. Huxley, C. P. McCoy, J. T. Rademacher and T. E. Rice, *Chem. Rev.*, 1997, **97**, 1515 and references therein.
7 C. R. Cooper, N. Spencer and T. D. James, *Chem. Commun.*, 1998, 1365; C. B. Black, B. Andrioletti, A. C. Try, C. Ruiperez and J. L. Sessler, *J. Am. Chem. Soc.*, 1999, **121**, 10438.
8 J. V. Caspar and T. J. Meyer, *J. Phys. Chem.*, 1983, **87**, 952.
9 A. P. Bisson, V. M. Lynch, M.-K. C. Monahan and E. V. Anslyn, *Angew. Chem., Int. Ed. Engl.*, 1997, **36**, 2340.
10 C. A. Hunter and L. D. Sarson, *Angew. Chem., Int. Ed. Engl.*, 1994, **33**, 2313; K.-S. Jeong, Y. L. Cho, J. U. Song, H.-Y. Chang and M.-G. Choi, *J. Am. Chem. Soc.*, 1998, **120**, 10982.
11 K. A. Connors, *Binding Constants*, John Wiley & Sons, New York, 1st edn., 1987.
12 D. E. Kaufmann and A. Otten, *Angew. Chem., Int. Ed. Engl.*, 1994, **33**, 1832.
13 D. A. Bell and E. V. Anslyn, *Comprehensive Supramolecular Chemistry*, ed. J. L. Atwood, J. E. D. Davies, D. D. MacNicol, F. Vogtle and J.-M. Lehn, Pergamon, Oxford, 1996, vol. 2, ch. 14 and references therein; P. Tecilla, S.-K. Chang and A. D. Hamilton, *J. Am. Chem. Soc.*, 1990, **112**, 9586; K. Kavallieratos and R. H. Crabtree, *Chem. Commun.*, 1999, 2109.
14 F. de Jong and H. C. Visser, *Comprehensive Supramolecular Chemistry*, ed. J. L. Atwood, J. E. D. Davies, D. D. MacNicol, F. Vogtle and J.-M. Lehn, Pergamon, Oxford, 1996, vol. 10, ch. 2 and references therein; L. A. J. Chrisstoffels, F. de Jong and D. N. Reinhoudt, *Chem. Eur. J*, 2000, **6**, 1376.

ChemComm

Synthesis and ligand substitution reactions of a homoleptic acetonitrile dipalladium(I) complex†

Tetsuro Murahashi,* Tomoki Nagai, Taketoshi Okuno, Teruo Matsutani and Hideo Kurosawa*

Department of Applied Chemistry, Faculty of Engineering, Osaka University, Suita, Osaka 565-0871, Japan

Received (in Cambridge, UK) 13th June 2000, Accepted 25th July 2000

The first homoleptic nitrile dipalladium(I) complex $[Pd_2(CH_3CN)_6][BF_4]_2$ is prepared; the CH_3CN ligand undergoes facile displacement by phosphine or bidentate nitrogen ligands while the Pd–Pd bond remains intact.

Homoleptic transition metal complexes containing weakly coordinated ligands have long been recognized as versatile sources of active catalysts or inorganic functional materials.[1] For example, the combination of an electrophilic Pd(II) complex $[Pd(CH_3CN)_4][BF_4]_2$ **1**[2] and appropriate auxiliary ligands has been frequently used as a pre-catalyst for olefin oligomerization, aromatic substitution, Wacker type oxidation, or alkyne hydroamination reaction.[3] While the corresponding homoleptic di- or multi-nuclear complexes of weakly coordinated ligands are relatively rare, several acetonitrile complexes of Mo≡Mo,[4] Tc≡Tc,[5] Re≡Re,[6] and Rh–Rh[7] have been prepared. Here, we report the first synthesis and reactivity of homoleptic acetonitrile dipalladium complex $[Pd_2(CH_3CN)_6][BF_4]_2$ **2**.

When **1** was treated with 0.5 equiv. of $Pd_2(dba)_3$ at room temperature in dry CH_3CN–CH_2Cl_2, the solution turned reddish-orange. Pouring this solution into Et_2O afforded an orange powder of **2** in 90% isolated yield [eqn. (1)].‡ Elemental

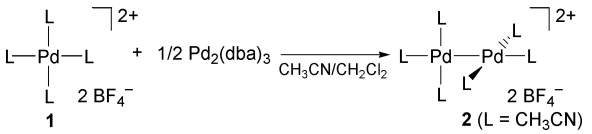

(1)

analysis supported the composition of **2**. UV–VIS spectra of **2** showed a σ–σ* transition at λ_{max} = 436 nm (ε = 1095 M^{-1} cm^{-1}). The homoleptic complex **2** was soluble in CD_3CN or CD_3OD. In CD_3OD, the coordinated acetonitrile protons appeared at δ 2.55, although gradual decomposition occurred with the formation of Pd black. When **2** was dissolved in H_2O, decomposition occurred within 10 min although it has been known that rather stable mononuclear aqua complexes are formed from **1** in H_2O.[3h] It should be mentioned that further addition of 0.5 equiv. of $Pd_2(dba)_3$ to **2** in CH_3CN–CH_2Cl_2 at room temperature resulted in decomposition instead of the desired formation of Pd_3 complexes such as $[Pd_3(CH_3CN)_8]^{2+}$.[8]

The dipalladium complex **2** underwent facile ligand-substitution reaction with the Pd–Pd bond remaining *intact* under moderate conditions. For example, addition of 2 equiv. of PPh_3 to **2** in CD_3CN afforded bisphosphine dipalladium complex $[Pd_2(CH_3CN)_4(PPh_3)_2][BF_4]_2$ **3**[9] quantitatively [eqn. (2)]. The reaction of **2** with >2 equiv. of PPh_3 afforded several

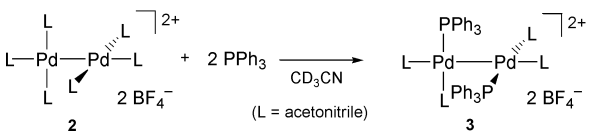

(2)

† Electronic supplementary information (ESI) available: NMR spectroscopic data and elemental analysis for **6** and **7**. See http://www.rsc.org/suppdata/cc/b0/b004726k/

unidentified species. On the other hand, controlled addition of an equimolar amount of PPh_3 to a CH_2Cl_2 solution of **2** afforded monophosphine complex $[Pd_2(CH_3CN)_5(PPh_3)][BF_4]_2$ **4** which was detectable by ^{31}P NMR spectroscopy (δ 19.3). The position of PPh_3 ligand in **4** is suggested to be *cis* to the Pd–Pd bond by considering the relative *trans*-influence of PPh_3, CH_3CN and [Pd] ligands.[9] Further addition of PPh_3 (1 equiv.) afforded **3** quantitatively. The reaction of **2** with 2 equiv. of bidentate phosphine, dppm (diphenylphosphinomethane), in CD_3CN afforded a known complex $[Pd_2(dppm)_2(CH_3CN)_2][BF_4]_2$ **5**[10] quantitatively [eqn. (3)]. The reaction of **2** with 2 equiv. of

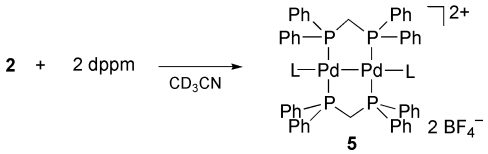

(3)

1,10-phenanthroline (phen) afforded $[Pd_2(phen)_2(CH_3CN)_2][BF_4]_2$ **6** [eqn. (4)].[11] ^1H NMR signals including non-

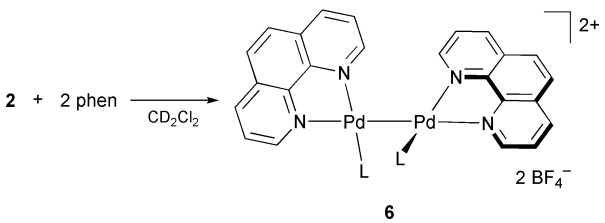

(4)

equivalent H^5 and $H^{5'}$ resonances showing H^5–$H^{5'}$ coupling (J 8.64 Hz). The coordination of CH_3CN in solution was confirmed by observation of a methyl resonance at δ 2.56. The reaction of **2** with *N*,*N*-ethylenebis(benzaldiimine) (diimine) afforded $[Pd_2(diimine)_2(CH_3CN)_2][BF_4]_2$ **7** [eqn. (5)].

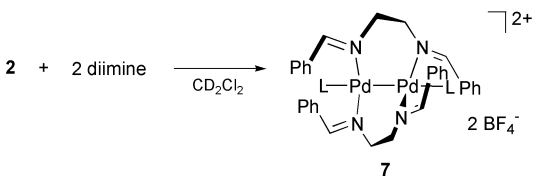

(5)

The observation of only one aldimine proton and carbon resonances suggests that the diimine ligands bridge over the Pd–Pd bond unlike phen in **6**. The ethylene proton resonances appearing as an AA′BB′ pattern suggest a chiral structure of **7** in solution arising from the non-planar Pd_2N_4 group.

Finally, to test the utility of the homoleptic acetonitrile dipalladium complex **2** as a 'naked' $[Pd–Pd]^{2+}$ building block of palladium clusters, we examined the preparation of palladium sandwich chains. Thus, the Pd_4 complex $[Pd_4(\mu\text{-}\eta^3:\eta^2:\eta^2:\eta^3\text{-}1,8\text{-diphenylocta-1,3,5,7-tetraene})_2][BF_4]_2$ **8**[12] was prepared

DOI: 10.1039/b004726k

(76% after recrystallization) [eqn. (6)] without formation of any

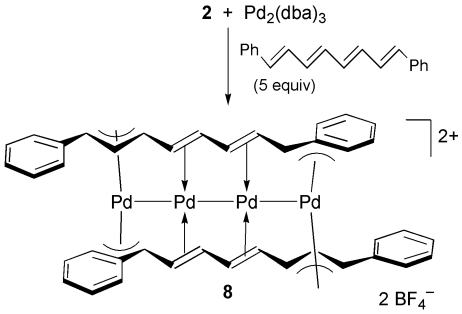

(6)

palladium black which was formed in considerable amounts in the previous method from **1**, 1.5 equiv. of $Pd_2(dba)_3$ and tetraene.

In summary, we have prepared the first homoleptic nitrile dipalladium(I) complex **2**. The nitrile ligands in **2** were proven to be substitutionally labile with the Pd–Pd bond remaining intact. Applications of **2** to catalysis as well as being a potential versatile building block towards palladium clusters are now under investigation.

Notes and references

‡ To a solution of $[Pd(CH_3CN)_4][BF_4]_2$ (1.00 g, 2.25 mmol) in CH_3CN (50 mL) was added $Pd_2(dba)_3{\cdot}CHCl_3$ (1.17 g, 1.13 mmol) and CH_2Cl_2 (50 mL). The mixture was stirred for 1 h at room temperature. The reaction mixture was filtered and poured into dry Et_2O to give an orange precipitate. After washing with Et_2O several times, **2** was obtained in 90% yield (1.28 g, 2.02 mmol). IR (Nujol): $\nu_{C\equiv N}$ 2331, 2307, 2282 cm^{-1}. Anal. Calc. (Found) for $Pd_2C_{12}H_{18}N_6B_2F_8$: C, 22.78 (22.65); H, 2.87 (2.92); N, 13.28 (13.03%).

1 *Synthetic Coordination Chemistry: Principles and Practice*, ed. J. A. Davies, C. M. Hockensmith, V. Y. Kukushkin and Y. N. Kukushkin, World Scientific Publishing, 1996, Ch. 4; for recent examples, W. E. Buschmann and J. S. Miller, *Chem. Eur. J.*, 1998, **4**, 1731.

2 B. B. Wayland and R. F. Schramm, *Inorg. Chem.*, 1965, **4**, 427; R. F. Schramm and B. B. Wayland, *Chem. Commun.*, 1968, 898; R. R. Thomas and A. Sen, *Inorg. Synth.*, 1990, **28**, 63.

3 For selected examples: (*a*) B. M. Trost, S. A. Godleski and J. P. Genêt, *J. Am. Chem. Soc.*, 1978, **78**, 3930; (*b*) A. Sen and T.-W. Lai, *J. Am. Chem. Soc.*, 1981, **103**, 4627; (*c*) B. M. Trost and J. M. D. Fortunak, *Organometallics*, 1982, **1**, 7; (*d*) A. Sen and T.-W. Lai, *Organometallics*, 1982, **1**, 415. (*e*) T.-W. Lai and A. Sen, *Organometallics*, 1984, **3**, 866; (*f*) L. S. Hegedus, T. A. Mulhern and H. Asada, *J. Am. Chem. Soc.*, 1986, **108**, 6224; (*g*) A. Sen, *Acc. Chem. Res.*, 1988, **21**, 421; (*h*) A. Sen, T.-W. Lai and R. R. Thomas, *J. Organomet. Chem.*, 1988, **358**, 567; (*i*) Z. Jiang and A. Sen, *J. Am. Chem. Soc.*, 1990, **112**, 9655; (*j*) Z. Jiang and A. Sen, *Organometallics*, 1993, **12**, 1406; (*k*) S. Oi, K. Kashiwagi and Y. Inoue, *Tetrahedron Lett.*, 1998, **39**, 6253; (*l*) Y. Uozumi, K. Kato and T. Hayashi, *J. Org. Chem.*, 1998, **63**, 5071.

4 F. A. Cotton and K. J. Wiesinger, *Inorg. Chem.*, 1991, **30**, 871; F. A. Cotton, J. L. Eglin and K. J. Wiesinger, *Inorg. Chim. Acta.*, 1992, **195**, 11.

5 J. C. Bryan, F. A. Cotton, L. M. Daniels, S. C. Haefner and A. P. Sattelberger, *Inorg. Chem.*, 1995, **34**, 1875.

6 S. N. Bernstein and K. R. Dunbar, *Angew. Chem., Int. Ed. Engl.*, 1992, **31**, 1360.

7 K. R. Dunbar, *J. Am. Chem. Soc.*, 1988, **110**, 8247; K. R. Dunbar and L. E. Pence, *Inorg. Synth.*, 1992, **29**, 182; M. E. Prater, L. E. Pence, R. Clérac, G. M. Finniss, C. Campana, P. Auban-Senzier, D. Jérome, E. Canadell and K. R. Dunbar, *J. Am. Chem. Soc.*, 1999, **121**, 8005.

8 Homoleptic isocyanide di- and tri-palladium complex has been previously synthesized; D. J. Doonan, A. L Balch, S. Z. Goldberg, R. Eisenberg and J. S. Miller, *J. Am. Chem. Soc.*, 1975, **97**, 1961; J. R. Boehm, D. J. Doonan and A. L. Balch, *J. Am. Chem. Soc.*, 1976, **98**, 4845; A. L. Balch, J. R. Borhm, H. Hope and M. M. Olmstead, *J. Am. Chem. Soc.*, 1976, **98**, 7431.

9 T. Murahashi, T. Otani, E. Mochizuki, Y. Kai, H. Kurosawa and S. Sakaki, *J. Am. Chem. Soc.*, 1998, **120**, 4563.

10 A. Miedaner and D. L. Du Bois, *Inorg. Chem.*, 1988, **27**, 2479.

11 The analogous isocyanide dipalladium complexes containing bidentate nitrogen ligands have been prepared: T. Tanase, H. Ukaji and Y. Yamamoto, *J. Chem. Soc., Dalton Trans.*, 1996, 3059.

12 T. Murahashi, E. Mochizuki, Y. Kai and H. Kurosawa, *J. Am. Chem. Soc.*, 1999, **121**, 10 660.

A rearrangement-based approach to secondary difluorophosphonates

Afshan H. Butt, Jonathan M. Percy* and Neil S. Spencer

School of Chemistry, University of Birmingham, Edgbaston, Birmingham, UK B15 2TT

Received (in Liverpool, UK) 26th June 2000, Accepted 27th July 2000

[3,3]-Claisen rearrangements allowed the conversion of a readily available allylic difluorophosphonate to nucleic acid and inositol phosphate-related products *via* epoxide cyclisation or ring closing metathesis respectively.

Secondary hydroxy groups undergo phosphorylation in many of the key molecules of Nature. Inositols undergo phosphorylation and dephosphorylation events that are critical in intracellular signalling pathways while a phosphodiester linkage between primary 5′-hydroxy and secondary 3′-hydroxy groups provides the critical structural backbone of the nucleic acids. Oxygen atom replacement by a CF_2 centre has been used extensively as a mimetic strategy, replacing a scissile O–P bond with a non-scissile C–P bond, in the quest for enzyme inhibitors and molecular probes. A relatively limited range of target types has been synthesised; one of our major interests lies in expanding the range of species accessible using convenient methodology and starting materials. In this communication, we wish to show how a rearrangement-based route affords butyrolactone derivatives **1** (related to building blocks for nucleic acid analogues[1,2]) and cyclohexenone derivatives **2** (related to deoxyinositol phosphate analogues[3]). The approach complements our earlier conjugate addition[4,5] and cycloaddition[6] chemistry which was based upon chlorodifluoromethane as a feedstock.

Known alcohol **3** was prepared according to a modification of the published method[7] and protected as the THP ether **4**. Coupling under the Shibuya–Yokomatsu[8] conditions afforded a good yield of **5** which was deprotected smoothly to afford **6** (Scheme 1). Rearrangement under Johnson–Claisen conditions[9] was uneventful and alkenoate **7** could be isolated and purified rigorously. Overall, this sequence is synthetically equivalent to the selective addition at C_β of a difluoromethylphosphonate anion equivalent to an alkyl α,β,γ,δ-unsaturated dienoate.

To learn about the behaviour of the educt, dihydroxylation of **7** was attempted under a range of conditions, none of which were found to be satisfactory. Though starting material could be converted completely, apparently in a highly stereoselective manner, we were never able to isolate more than 11% of lactone **1**† formed *via* diol **8** (the configuration was inferred from that of **1**). The ^{19}F NMR spectrum of the crude product appeared to be that of a single diastereoisomer (as a racemic modification); the single product was identified as the 5-ring lactone **1** (by gradient HMBC) of *cis*-stereochemistry (by GOESY spectroscopy),

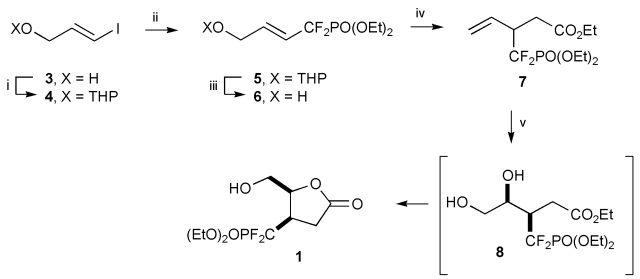

Scheme 1 *Reagents and conditions*: i, dihydropyran, Amberlyst-15, dry hexane, 86%; ii, $BrZnCF_2PO(OEt)_2$, CuBr, DMF, 96%; iii, MeOH, Amberlyst-15, hexane, 82%; iv, triethyl orthoacetate, propionic acid, hydroquinone, 140 °C, 86%; v, 10% OsO_4, 2.0 NMO, acetone–water (2 : 1), rt, 11%.

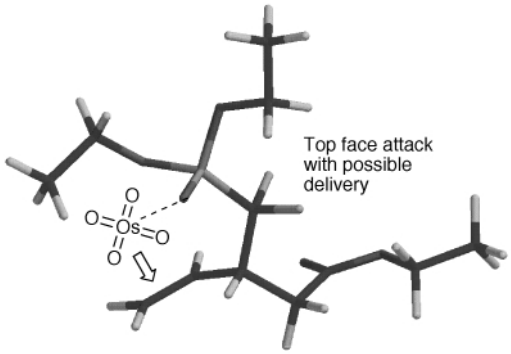

Fig. 1 Possible attack trajectory to explain the formation of lactone **1**.

which showed a strong transfer of magnetisation from H-3 to H-4. Attack from the face occupied by the bulky (diethoxyphosphoryl)difluoromethyl group (Fig. 1) appears to have led to the observed product, suggesting a possible role for the phosphoryl P=O oxygen atom in delivering the reagent.[10]

We then tried to reverse the stereochemical relationship and obtain the *trans*-lactone by forming epoxide **9b** which would undergo nucleophilic ring-opening under acid catalysis, either intramolecularly with the ester carbonyl, or intermolecularly by traces of water in the medium (followed by cyclisation) to form the *trans*-lactone (Scheme 2).

Both reactions would involve a single inversion of configuration at the epoxide stereogenic centre. Epoxidation was very slow indeed under MCPBA or methyl trioxorhenium[11] conditions but the *in situ* dioxirane method of Yang[12] proved most effective and both epoxides **9a** and **9b** were obtained as an inseparable mixture in good (91%, **9a**:**9b** 1:2) yield.

However, treatment with Amberlyst-15 in dry dichloromethane[13] (Scheme 3) resulted in the isolation of only *cis*-lactone **1** in good (78%) yield.

A lower facial selectivity for oxidation with the smaller dioxirane reagent (which cannot coordinate to the phosphoryl oxygen either) was no surprise, but the convergence of the epoxides was unexpected. One epoxide (we believe **9a**) reacted considerably more quickly than the other and we were able to recover the less reactive species as a pure compound by careful ^{19}F NMR monitoring of the consumption of **9a**. The stereochemical convergence may involve neighbouring group participation by the phosphoryl oxygen in a double inversion mechanism *via* **10**; effectively, the all *cis*-epoxide **9b** must be opened with overall retention at the secondary carbon for the *cis*-lactone to form. Interestingly, an NMR sample of the less reactive epoxide in untreated $CDCl_3$ was converted to **1** and a trace of **11** upon standing. Neighbouring group participation by *thio*phosphoryl oxygen has been exploited to control glycosylation stereochemistry[14] but we are not aware of examples of a phosphoryl group exerting such an influence. Further under-

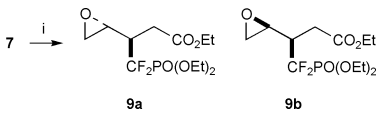

Scheme 2 *Reagents and conditions*: i, CF_3COCH_3, Oxone, $NaHCO_3$, Na_2EDTA, MeCN, H_2O, 91%.

DOI: 10.1039/b005110l

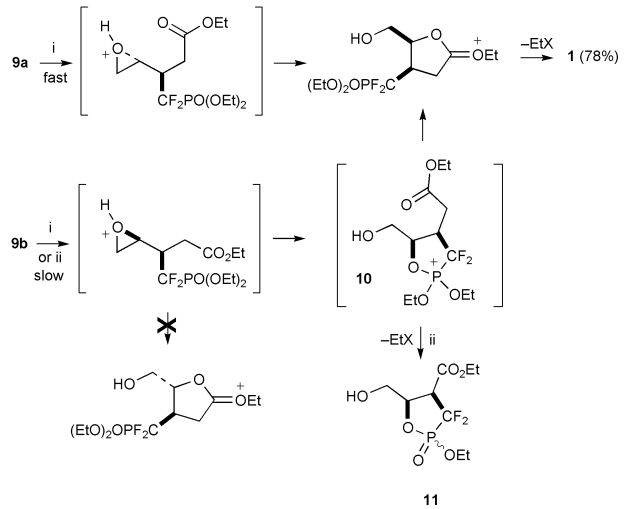

Scheme 3 *Reagents and conditions*: i, Amberlyst-15, dry DCM, rt; ii, $CDCl_3$, rt, 18 h.

standing of this process is sought currently, but clearly the direct cyclisation of **9b** *via* nucleophilic attack involving the ester carbonyl group is highly unfavourable.[15]

A change of tactics allowed access to an attractively functionalised cyclohexenone (Scheme 4); vinylation of **3** protected the hydroxy group as **12** for the Shibuya–Yokomatsu coupling allowing Dauben–Dietsche rearrangement[16] to proceed affording enal **14**.

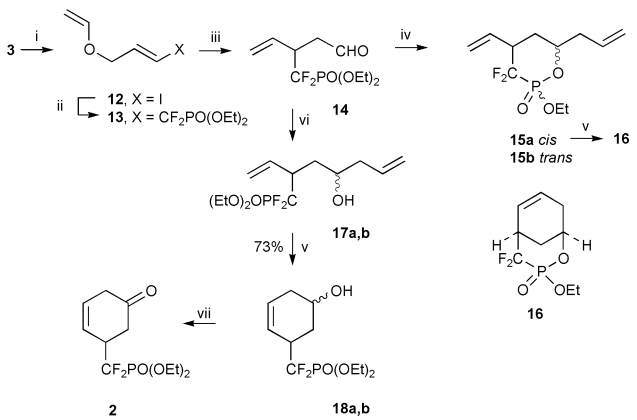

Scheme 4 *Reagents and conditions*: i, ethyl vinyl ether, $Hg(OAc)_2$, reflux, 70%; ii, $BrZnCF_2PO(OEt)_2$, CuBr, DMF, 84%; iii, 140 °C, xylene, 75%; iv, allylmagnesium bromide, ethyl ether, 60% (1:1 ratio); v, Grubbs' catalyst, DCM, reflux, 48 h; vi, allyltrimethylsilane, $BF_3{\cdot}OEt_2$, DCM, rt, 83% (7:2 ratio); vii, PDC, DCM, rt.

Allylation under Grignard conditions afforded a pair (in a 1:1 ratio) of diastereoisomeric phosphodiesters **15a** and **15b**; slow (48 h) RCM under standard Grubbs' conditions[17] then closed the *cis* congener to yield **16** (64% by NMR) leaving the *trans* isomer **15b** unchanged. We inferred that cyclisation with loss of ethanol had occurred after Grignard addition. Boron trifluoride-catalysed (Sakurai) allylation with allyltrimethylsilane[18] afforded homoallyl alcohols **17a** and **17b** in a 7:2 ratio (unassigned) then RCM afforded a 7:2 mixture of cyclohexenols **18a** and **18b** which were converged by oxidation to **2**‡ with PDC. Enone **2** contains a pattern of functional groups from which four contiguous hydroxylated positions could be developed and we will explore its chemistry further.

The appeal of this strategy lies in the possibility of asymmetric catalysis of the [3,3] rearrangement controlling the absolute configuration of the mimetic-bearing carbon atom and the potential for a high degree of subsequent stereocontrol on the cyclohexene template. The products of this study are under evaluation as components for novel nucleoside and inositol phosphate analogues as we learn more about the steric and electronic effects of the mimetic group.

The authors wish to thank the Engineering and Physical Sciences Research Council of Great Britain for support (Quota Award to A. H. B).

Notes and references

† *Selected data* for **1**: ν_{max} (film)/cm^{-1} 3434br s, 1786s; δ_H($CDCl_3$, 300 MHz) 4.88–4.79 (m, 1H), 4.32–4.20 (m, 4H), 3.95 (dd, 1H, $^2J_{H\text{-}H}$ 12.5, $^3J_{H\text{-}H}$ 2.2), 3.65 (dd, 1H, $^2J_{H\text{-}H}$ 12.5, $^3J_{H\text{-}H}$ 2.6), 3.5 (br s, 1H, OH), 3.44–3.20 (m, 2H), 2.85 (dd, 1H, $^2J_{H\text{-}H}$ 18.8, $^3J_{H\text{-}H}$ 9.2), 2.77 (dd, 1H, $^2J_{H\text{-}H}$ 18.4, $^3J_{H\text{-}H}$ 7.0), 1.38 (t, 6H, $^3J_{H\text{-}H}$ 7.0); ^{13}C δ_C($CDCl_3$, 75 MHz) 175.2 (s), 119.4 (td, $^1J_{C\text{-}F}$ 263.4, $^1J_{C\text{-}P}$ 214.8), 78.8 (q, $^3J_{C\text{-}F=C\text{-}P}$ 4.5), 65.4 (d, $^2J_{C\text{-}P}$ 6.8), 65.2 (d, $^2J_{C\text{-}P}$ 6.8), 63.4 (s), 40.3 (td, $^2J_{C\text{-}F}$ 20.9, $^2J_{C\text{-}P}$ 15.3), 29.1 (td, $^3J_{C\text{-}F}$ 5.1, $^3J_{C\text{-}P}$ 2.3), 16.4 (d, $^3J_{C\text{-}P}$ 5.7); δ_F($CDCl_3$, 282 MHz) −116.8 (ddd, $^2J_{F\text{-}F}$ 342.1, $^2J_{F\text{-}P}$ 105.5, $^3J_{F\text{-}H}$ 16.5). −117.99 (ddd, $^2J_{F\text{-}F}$ 343.3, $^2J_{F\text{-}P}$ 104.3, $^3J_{F\text{-}H}$ 17.8); δ_P($CDCl_3$, 121 MHz) 5.6 (t, $^2J_{P\text{-}F}$ 103.9 Hz); *m/z* (ES) 325 (M + Na, 100) HRMS calc. for $C_{10}H_{17}O_6F_2NaP$ 325.0629, found 325.0632. Anal. Calcd for $C_{10}H_{17}O_6F_2P$: C, 39.74, H, 5.70; found: C, 39.55, H, 5.45%.

‡ *Selected data* for **2**: ν_{max} (film)/cm^{-1} 2987m, 1725s, 1684m; δ_H($CDCl_3$, 300 MHz) 6.10–5.89 (m, 2H), 4.25–4.10 (m, 4H), 3.39–3.19 (m, 1H), 2.89 (d, 1H, $^2J_{H\text{-}H}$ 22.4), 2.77 (d, 1H, $^2J_{H\text{-}H}$ 22.6), 2.71 (dd, 1H, $^2J_{H\text{-}H}$ 14.7, $^3J_{H\text{-}H}$ 6.6), 2.55 (dd, 1H, $^2J_{H\text{-}H}$ 15.1, $^3J_{H\text{-}H}$ 6.3), 1.28 (t, 6H, $^3J_{H\text{-}H}$ 6.3); δ_C($CDCl_3$, 75 MHz) 206.5 (s), 128.7 (s), 122.2–122.0 (m), 120.4 (td, $^1J_{C\text{-}F}$ 264.5, $^1J_{C\text{-}P}$ 211.9), 64.7 (t, $^3J_{C\text{-}F}$ 7.4), 41.9 (td, $^2J_{C\text{-}F}$ 21.5, $^2J_{C\text{-}P}$ 15.8), 39.1 (s), 37.5 (q, $^3J_{CF=CP}$ 5.1), 16.3 (d, $^3J_{C\text{-}P}$ 5.7); δ_F($CDCl_3$, 282 MHz) −114.1 (ddd, $^2J_{F\text{-}F}$ 300.1, $^2J_{F\text{-}P}$ 105.5, $^3J_{F\text{-}H}$ 15.3), −115.8 (ddd, $^2J_{F\text{-}F}$ 300.1, $^2J_{F\text{-}P}$ 109.8, $^3J_{F\text{-}H}$ 17.8); δ_P($CDCl_3$, 121 MHz) 6.0 (t, $^2J_{F\text{-}P}$ 106.8); *m/z* (ES) 305 (M + Na, 100); HRMS calc. for $C_{11}H_{17}O_4F_2P$ 305.0730, found 305.0722.

1 T. Yokomatsu, Y. Hayakawa, K. Suemune, T. Kihara, S. Soeda, H. Shimeno and S. Shibuya, *Bioorg. Med. Chem. Lett.*, 1999, **9**, 2833.
2 J. Matulic-Adamic, P. Haeberli and N. Usman, *J. Org. Chem.*, 1995, **60**, 2563.
3 A. S. Campbell and G. R. J. Thatcher, *Tetrahedron Lett.*, 1991, **32**, 2207.
4 K. Blades, A. H. Butt, G. S. Cockerill, H. J. Easterfield, T. P. Lequeux and J. M. Percy, *J. Chem. Soc., Perkin Trans. 1*, 1999, 3609.
5 K. Blades, D. Lapôtre and J. M. Percy, *Tetrahedron Lett.*, 1997, **38**, 5895.
6 K. Blades and J. M. Percy, *Tetrahedron Lett.*, 1998, **39**, 9085.
7 M. Abarbi, J. Parran, J. Cintrat and A. Duchene, *Synthesis*, 1995, 82; I. Marek, C. Mayer and J.-F. Normant, *Org. Synth.*, 1996, **74**, 194.
8 T. Yokomatsu, K. Suemune, T. Murano and S. Shibuya, *J. Org. Chem.*, 1996, **61**, 7207.
9 We used the following procedure; R. Bao, S. Valverde and B. Herradon, *Synlett*, 1992, 217.
10 D. A. Evans, G. C. Fu and A. H. Hoveyda, *Chem. Rev.*, 1993, **93**, 1307.
11 C. Copéret, H. Adolfsson and K. B. Sharpless, *Chem. Commun.*, 1999, 1565.
12 D. Yang, M.-K. Wong and Y.-C. Yip, *J. Org. Chem.*, 1995, **60**, 3887.
13 The reaction was based upon the cyclisation reported by J. Cardellac, C. Estopa, J. Font, M. Moreno-Mañas, R. M. Ortuño, F. Sanchez-Ferrado, S. Valle and L. Vilamajo, *Tetrahedron*, 1982, **28**, 2377.
14 T. Yokomatsu, T. Sada, T. Shimizu and S. Shibuya, *Tetrahedron Lett.*, 1998, **39**, 6299.
15 Iodolactonisation according to Ito *et al*. (H. Ito, A. Saito and T. Taguchi, *Tetrahedron Asymm.*, 1998, **9**, 1979; I_2, MeCN, rt, 18 h) of **7** afforded exclusively the *cis*-iodolactone **19** (68%, stereochemistry assigned by

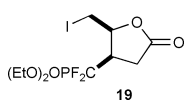

GOESY); this process must follow a trajectory similar to that of the closure of **9a** to **1**.
16 W. G. Dauben and T. J. Dietsche, *J. Org. Chem.*, 1972, **37**, 1212.
17 For a review, see R. H. Grubbs and S. Chang, *Tetrahedron*, 1998, **54**, 4413.
18 A. Bottoni, A. L. Costa, D. DiTommaso, I. Rossi and E. Tagliavini, *J. Am. Chem. Soc.*, 1997, **119**, 12 131.

ChemComm

Electrochemical reduction of oxygen on mesoporous platinum microelectrodes

Peter R. Birkin,* Joanne M. Elliott and Yvonne E. Watson

Department of Chemistry, University of Southampton, Southampton, UK SO17 1BJ. E-mail: prb2@soton.ac.uk

Received (in Cambridge, UK) 5th June 2000, Accepted 11th July 2000

The electrochemical reduction of oxygen is studied using electrochemically deposited mesoporous platinum microelectrodes, which exhibit efficient mass transfer of material to the electrode surface and accelerated reduction kinetics when compared to polished microelectrodes.

The reduction of molecular oxygen at the surface of an electrode is of considerable importance to many fields of research. Specific areas of interest include the quantitative analysis of oxygen concentration, the monitoring of enzymatic reactions and the conversion of chemical to electrical energy within a fuel cell. The mechanism for the reduction of molecular oxygen is known to be complex and dependent on the substrate employed.[1] In particular, two groups of substrates can be identified, those reducing oxygen to hydrogen peroxide through a 2 electron pathway[2,3] and those reducing oxygen to water through a 4 electron pathway.[4] In many instances it is desirable that the 4-electron pathway be selected. As an example, the reduction of molecular oxygen within a fuel cell is commonly achieved by a platinum-loaded high surface area cathode.[5] This choice is governed by platinum's superior catalytic activity. However, the performance of the platinum cathode is still limited at high potentials due to the formation of adsorbed species on the surface of the platinum metal.[1,6,7] These species inhibit oxygen reduction and reduce the operating potential of the electrode to around 0.8 V *vs.* RHE instead of the theoretical performance 1.229 V *vs.* RHE.[6,8] This limitation imposes a significant loss in the overall performance of the fuel cell, which has as yet to be fully addressed. It is reported here, for the first time, that Pt mesoporous modified microelectrodes have significantly altered oxygen reduction kinetics when compared to polished platinum microelectrodes of the same dimensions within the same solution.

Attard *et al.* first reported the use of a 'true liquid crystal templating technique' for the synthesis of mesoporous platinum powders (H_I-Pt) *via* the reduction of hexachloroplatinic acid (HCPA).[9]

Attard *et al.* also showed that it was possible to electrochemically produce mesoporous electrode materials and modified electrodes with a variety of nanostructures, for example, either hexagonal (H_I-ePt) or cubic (V_I-ePt) and that the dimensions of the mesoporosity could be finely tuned by varying the deposition conditions.[10–13]

Here we report the results of a study where the thickness of the mesoporous deposit is increased by controlling the deposition charge density. The results presented here are representative of a larger number of H_I-ePt modified microelectrodes studied. The subsequent effect on the mass transfer characteristics of the microelectrodes and electroreduction of molecular oxygen are now reported.

Electrodeposition was performed on a number of polished 25 μm diameter Pt microelectrodes sealed in glass. The platinum metal was deposited potentiostatically at a potential of −0.1 V *vs.* SCE from a template solution described previously.[10,12] Monitoring the charge passed during the deposition process enabled the amount of platinum metal deposited to be controlled. The control of the deposition conditions and charge enables the characteristics of the deposit to be chosen. Cyclic voltammograms of the H_I-ePt modified microelectrodes in 2 mol dm^{-3} sulfuric acid were performed and showed polycrystalline Pt characteristics as shown previously.[10,12] These voltammograms demonstrated that as the charge density is increased the surface area of the microelectrodes increases as expected. The voltammograms can be used to gain an estimate of the effective surface area of the Pt deposit by analysis of hydrogen UPD onto the surface.[10,13] Table 1 gives a summary of the effective surface roughness, R_f, of the deposit as a function of deposition charge within the template mixture. It can be seen that the surface area of the metal deposit scales approximately linearly with the charge density of the deposition process.

Microelectrodes were chosen for this project due to their unique properties which are related to their size.[14] Clearly as the electrodeposition proceeds the geometric characteristics could be altered by the H_I-ePt deposited. In order to test this we cycled the microelectrodes in a solution containing a suitable redox species. Fig. 1 shows the voltammetry of a series of microelectrodes within a solution containing $[Fe(CN)_6]^{3-}$ [16] and demonstrates that as the electrodeposition charge density was increased in the range 0 to 37.9 C cm^{-2} the reduction current for the redox species also increased. This indicates that the geometric area of the 25 μm Pt microelectrode has been effectively enlarged by the modification procedure. Further evidence for this change in geometric area is shown by the SEM image of one of the H_I-ePt modified microelectrodes (see insert in Fig. 1). This image shows that the deposit has spread over the surface of the glass insulator effectively increasing the geometric surface area. The SEM image also shows that the deposit is largely uniform and attached rigidly to the substrate surface. It is possible to calibrate the geometric surface area of the modified electrodes by comparing the average steady state current at −0.1 V *vs.* SCE for the electroreduction of $[Fe(CN)_6]^{3-}$ at a polished 25 μm Pt microelectrode and comparing this with the signal recorded with the H_I-ePt

Table 1 Measured parameters for the 25 μm diameter Pt microelectrodes investigated

Electrode	Deposition charge/μC	Real surface area/10^{-3} cm^2	R_f[a]	Effective diameter[a]/μm	$E_{1/2}$ O_2/mV[b]	n_{app}[c]
Polished (A)	—	0.01242	2.53	25	−422	2.36
H_I-ePt (B)	31	1.38	281	25.8	−219	3.82
H_I-ePt (C)	93	3.57	727	31.8	*ca.* −222	3.95
H_I-ePt (D)	186	5.69	1160	36.5	*ca.* −231	4.4

[a] R_f calculated by dividing the real surface area by the geometric area prior to modification. [b] vs. Hg/Hg_2SO_4. [c] The apparent number of electrons involved in the reduction of molecular oxygen, n_{app} was calculated from the current recorded at a potential of −0.5 V *vs.* Hg/Hg_2SO_4 for the H_I-ePt microelectrodes and −0.7 V *vs.* Hg/Hg_2SO_4 for the polished microelectrode (see Fig. 2).

DOI: 10.1039/b004468g

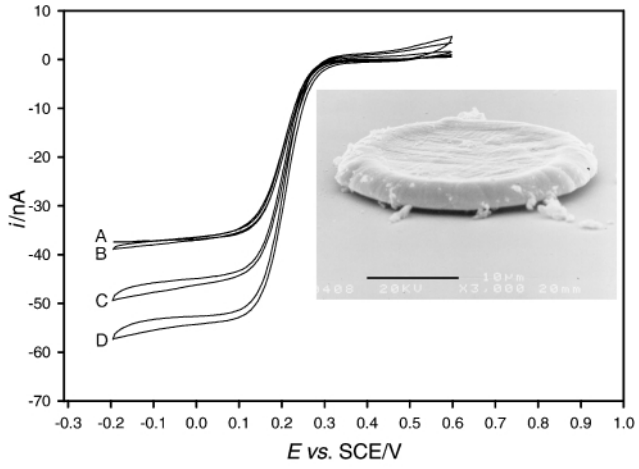

Fig. 1 Plot showing cyclic voltammograms recorded for a series of 25 μm Pt microelectrodes recorded at 2 mV s^{-1} in a solution containing 10 mmol dm^{-3} $K_3[Fe(CN)_6]$ in $Sr(NO_3)_2$ at 25 °C under anaerobic conditions; A, B, C, D as in Table 1. The insert in the figure shows a SEM image of the 93 μC H_I-ePt modified microelectrode recorded after the experiments were performed. The scale bar on the SEM represents 10 μm.

modified microelectrodes. This calibration shows that the effective geometric diameter changes in the range 25–37 μm for the thinnest and thickest film respectively. The actual values are shown in Table 1.

Turning to the activity of the H_I-ePt modified microelectrodes for oxygen electroreduction, a series of voltammograms were recorded in air-saturated pH 7 phosphate buffer. Fig. 2 shows the voltammetry recorded at 2 mV s^{-1} between +0.1 and −0.7 V *vs.* Hg/Hg_2SO_4. For comparison the electroreduction of oxygen under the same conditions on a polished 25 μm Pt microelectrode is included. A marked difference between the polished microelectrode and the H_I-ePt can clearly be seen. First, the plateau current for the H_I-ePt modified microelectrodes is consistently higher than at the polished microelectrode. It is possible to calculate the effective number of electrons involved in the reduction of oxygen on the polished Pt microelectrode as *ca.* 2 assuming an oxygen concentration[17] of 0.24 mmol dm^{-3} and a value for the diffusion coefficient of oxygen, *D*,[18] of 2.29×10^{-5} cm^2 s^{-1}. This is unusual for Pt, as normally the mechanism for electroreduction of molecular oxygen is stated as a 4 electron process. However, under the conditions employed in this study a consistent value of 2.36 electrons was obtained. The reason for this change is unclear but it is known that adsorption of ions[1,19,20] and high rates of mass transfer[18] can force the number of apparent electrons to fall below 4. Nevertheless the reduction

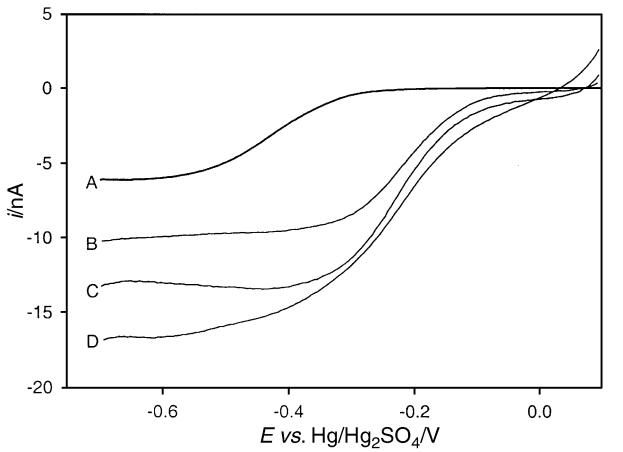

Fig. 2 Plot showing voltammograms recorded for a series of 25 μm Pt microelectrodes recorded at 2 mV s^{-1} in 0.2 mol dm^{-3} pH 7 phosphate at 25 °C under aerobic conditions; A, B, C, D as in Table 1.

of molecular oxygen on the H_I-ePt modified microelectrodes was associated with an increase in the plateau current to a value close to 4 electrons. Fig. 2 also shows that as the surface area of the deposit increased, the voltammogram became less well defined. This leads to some difficulty in accurately measuring the apparent number of electrons involved in the reaction for the thicker films studied. This distortion was attributed to the rising background signal associated with surface reactions on the increasingly large Pt surface. The anodic current supports the distortion, presumably due to oxide formation, above 0.0 V *vs.* Hg/Hg_2SO_4 for the larger surface area microelectrodes. Cyclic voltammograms (not shown) in the absence of oxygen also support these findings. Second, the reduction of molecular oxygen at the H_I-ePt proceeds at a considerably more positive potential *ca.* −219 mV *vs.* Hg/Hg_2SO_4 for the 31 μC H_I-ePt modified microelectrode compared to *ca.* −422 mV *vs.* Hg/Hg_2SO_4 for the polished microelectrode. However, increasing the surface area of the deposit further by increasing the deposition charge did not significantly shift the reduction wave to more positive potentials. In these cases the inhibition of oxygen reduction by adsorbed species is presumably still the predominant factor and increasing the surface area further has no beneficial kinetic effect. However, the increase in apparent number of electrons involved in the reaction and the improved kinetics of oxygen reduction, point to these materials being of potential use in either analytical chemistry or fuel cell technology. It is important to remember that these materials are electrodeposited onto the surface and as such are adherent and mechanically robust. Additionally the current densities, due to the unique mass transfer characteristics of microelectrodes, are of the order of 1.95 mA cm^{-2} for a catalyst loading calculated to be 1.29 mg cm^{-2} at 25 °C under stagnant conditions. This calculation assumed a maximum deposition efficiency of *ca.* 43%.[12]

Notes and references

1 M. R. Tarasevich, A. Sadkowski and E. Yeager, *Comprehensive Treatise of Electrochemistry*, ed. Conway *et al.*, Plenum, New York, vol. 7, 1983.
2 H. S. Wroblowa, Y. C. Pan and G. Razumney, *J. Electroanal. Chem.*, 1976, **69**, 195.
3 R. W. Zurilla, R. K. Sen and E. Yeager, *J. Electrochem. Soc.*, 1978, **125**, 1103.
4 A. Damjanovic, M. A. Greenshaw and J. O'M. Bockris, *J. Electrochem. Soc.*, 1967, **114**, 1107.
5 M. S. Wilson and S. Gottesfeld, *J. Appl. Electrochem.*, 1992, **22**, 1.
6 L. D. Burke, J. K. Casey, J. A. Morrissey and J. F. O'Sullivan, *J. Appl. Electrochem.*, 1994, **24**, 30.
7 V. L. Lukyanycheva, A. V. Yuzhenina, B. J. Lentsner, L. L. Knots, N. A. Shumilova and V. S. Bagotskii, *Sov. Electrochem.*, 1971, **7**, 1240.
8 *Handbook of Chemistry and Physics*, ed. D. L. Lide, CRC Press, London, 1994.
9 G. S. Attard, J. M. Corker, C. G. Göltner, S. Henke and R. H. Templer, *Angew. Chem., Int. Ed. Engl.*, 1997, **36**, 1315.
10 G. S. Attard, P. N. Bartlett, N. R. B. Coleman, J. M. Elliott, J. R. Owen and J. H. Wang, *Science*, 1997, **278**, 838.
11 G. S. Attard, N. R. B. Coleman and J. M. Elliott, *Stud. Surf. Sci. Catal.*, 1998, **117**, 89.
12 J. M. Elliott, G. S. Attard, P. N. Bartlett, N. R. B. Coleman, D. A. S. Merckel and J. R. Owen, *Chem. Mater.*, 1999, **11**, 3602.
13 J. M. Elliott, P. R. Birkin, P. N. Bartlett and G. S. Attard, *Langmuir*, 1999, **15**, 7411.
14 R. M. Wightman and D. O. Wipf, *Electroanal. Chem.*, 1989, **15**, 267.
15 D. Pletcher, *Microelectrodes: Theory and Application*, ed. M. I. Montenegro, M. A. Queirós and J. L. Daschbach, Kluwer Academic Publishers, Dordrecht, 1990, sect. 1.
16 C. Beriet and D. Plecther, *J. Electroanal. Chem.*, 1993, **361**, 93.
17 Calculated from the figures given in reference 18.
18 D. Pletcher and S. Sotiropoulos, *J. Electroanal. Chem.*, 1993, **356**, 109.
19 V. S. Vilinskaya and M. R. Tarasevich, *Sov. Electrochem.*, 1973, **9**, 1123.
20 L. I. Antropov, C. G. Vrzhosek, M. R. Tarasevich and M. A. Marinich, *Sov. Electrochem.*, 1972, **8**, 147.

ChemComm

Scandium(III) triflate immobilised in ionic liquids: a novel and recyclable catalytic system for Friedel–Crafts alkylation of aromatic compounds with alkenes

Choong Eui Song,*[a] Woo Ho Shim,[b] Eun Joo Roh[a] and Jung Hoon Choi*[b]

[a] *Life Sciences Division, Korea Institute of Science and Technology, PO Box 131, Cheongryang, Seoul, 130-650, Korea. E-mail: s1673@kistmail.kist.re.kr*

[b] *Department of Chemistry, Hanyang University, Seoul, 133-791, Korea*

Received (in Cambridge, UK) 3rd July 2000, Accepted 28th July 2000

Scandium(III) triflate catalysed Friedel–Crafts alkylation of aromatic compounds with alkenes proceeded readily in the hydrophobic ionic liquid solvents based on 1,3-dialkylimidazolium salts with easy catalyst/solvent recycling, whereas these reactions did not occur in common organic solvents, water or hydrophilic ionic liquids at all.

The Friedel–Crafts alkylation of aromatic compounds with alkenes is of great synthetic significance in view of laboratory synthesis and particularly industrial production.[1] For example, a number of important industrial processes for ethylbenzene, cumene and linear alkylbenzenes, *etc*. are based on this reaction. In general, this type of reaction is catalysed by $AlCl_3$, H_2SO_4, HF and other acid catalysts. However, a common problem, particularly in industrial processes, is that catalysts cannot be reused after the usual aqueous work-up.

Recently, considerable attention has been focused on the catalytic use of rare earth(III) (RE) salts, especially, RE(III) trifluoromethanesulfonates [$RE(OTf)_3$] as water-tolerant and recyclable Lewis acid catalysts in carbon–carbon bond forming reactions.[2] The RE(III) compound-catalysed Friedel–Crafts alkylations of aromatic compounds using alcohols, mesylates, halides, aldehydes, acetals, *etc*. as alkylating agents have also been reported.[3] However, to the best of our knowledge, there has been no previous report on the use of $RE(OTf)_3$ for the Friedel–Crafts alkylation of aromatics using alkenes as alkylating agents.

We disclose here our preliminary results on the Friedel–Crafts alkylation of aromatics with alkenes using a novel and recyclable catalytic system, $Sc(OTf)_3$ immobilised in air and moisture-stable rt ionic liquids.[4]

To examine the catalytic effect of lanthanide trifluoromethanesulfonates, we first carried out the alkylation of benzene with hex-1-ene in the presence of 20 mol% of $Sc(OTf)_3$ in various organic solvents (none, CH_2Cl_2, acetonitrile, nitromethane and nitrobenzene) or H_2O at 20 °C for 12 h. However, in all cases neither alkylation nor olefin isomerisation took place at all (Table 1, entries 1–6). It is therefore not surprising that there has been no report on the use of $RE(OTf)_3$ for the Friedel–Crafts alkylation of aromatics using alkenes as alkylating agents so far.

Very interestingly, however, when the same reaction was carried out in air and moisture-stable rt ionic liquids consisting of 1,3-dialkylimidazolium cations and their counter anions **2**,[5] [emim][X] ([emim]$^+$ = 1-ethyl-3-methylimidazolium cation; X = SbF_6 (**2a**), BF_4 (**2b**), OTf (**2c**)), [bmim][X] ([bmim]$^+$ = 1-butyl-3-methylimidazolium cation; X = PF_6 (**2d**), SbF_6 (**2e**), BF_4 (**2f**)and OTf (**2g**)), [pmim][PF_6] ([hmim]$^+$ = 1-pentyl-3-methylimidazolium cation; **2h**) and [hmim][PF_6] ([hmim]$^+$ = 1-hexyl-3-methylimidazolium cation; **2i**), we obtained quite satisfactory results in some cases. In this reaction, the catalytic activity of $Sc(OTf)_3$ was strongly influenced by the nature of the anion [X].

When the hydrophobic ionic liquids such as the [emim][SbF_6] (**2a**), [bmim][PF_6] (**2d**), [bmim][SbF_6] (**2e**),

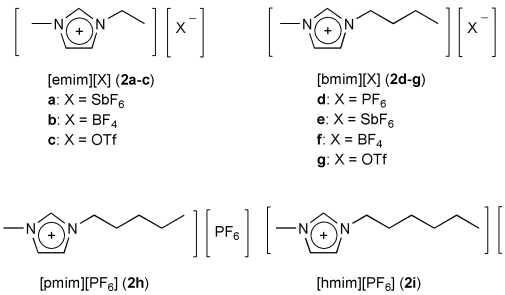

[pmim][PF_6] (**2h**) or [hmim][PF_6] (**2i**) were used, the desired alkylated products were obtained quantitatively, although $Sc(OTf)_3$ is only slightly soluble and thus exists as a suspended form in these ionic solvents (Table 1, entries 7, 10, 11, 14 and 15).† It is noteworthy here that the rearrangement of alkene takes place prior to the ring substitution, which indicates that the carbonium ion is formed first. Polarity of these ionic solvents leads to the stabilisation of the polar cationic intermediate. In sharp contrast to these results, in the hydrophilic ionic liquids, [emim][BF_4] (**2b**), [emim][OTf] (**2c**), [bmim][BF_4] (**2f**) or [bmim][OTf] (**2g**), the catalyst was highly soluble and thus totally immobilised in these ionic liquids, but the reaction did not occur at all (Table 1, entries 8, 9, 12 and 13). Thus, we next

Table 1 Friedel–Crafts alkylation of benzene with hex-1-ene in the presence of 20 mol% of $Sc(OTf)_3$ in various solvents[a]

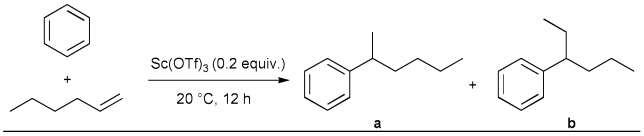

Entry	Solvent	Conversion[b] (%) of hex-1-ene	Yield[b] (%) of monoalkylated product (**a**:**b**)
1	None	0	0
2	CH_2Cl_2	0	0
3	CH_3CN	0	0
4	CH_3NO_2	0	0
5	$PhNO_2$	0	0
6	H_2O	0	0
7	[emim][SbF_6] (**2a**)	>99	96 (1.5:1)
8	[emim][BF_4] (**2b**)	0	0
9	[emim][OTf] (**2c**)	0	0
10	[bmim][PF_6] (**2d**)	>99	96 (2:1)
11	[bmim][SbF_6] (**2e**)	~99	93 (1.5:1)
12	[bmim][BF_4] (**2f**)	0	0
13	[bmim][OTf] (**2g**)	0	0
14	[pmim][PF_6] (**2h**)	>99	95 (1.6:1)
15	[hmim][PF_6] (**2i**)	>99	95 (2:1)

[a] Reaction conditions: hex-1-ene (1 mmol), benzene (2 mL), $Sc(OTf)_3$ (0.2 mmol), solvent (1 mL), 20 °C, 12 h. [b] Conversions and yields based on hex-1-ene were determined by the internal standard method in GC.

DOI: 10.1039/b005335j

Table 2 $Sc(OTf)_3$ catalysed Friedel–Crafts alkylation of benzene with various alkenes in the ionic liquid **2e**[a]

Entry	Aromatic compound	Alkene	Product	Conversion[b] (%) of alkene	Yield[b] (%) of monoalkylated product
1	Benzene	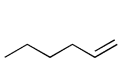	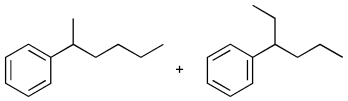	>99	93[c]
2	Benzene		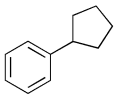	>99	84
3	Benzene		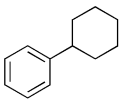	>99	90
4[d]	Benzene		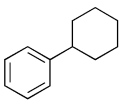	>99	92
5[e]	Benzene		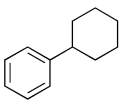	>99	92
6	Benzene		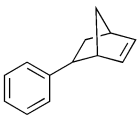	>99	65
7	Phenol		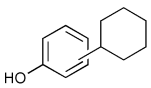	>99	93[f]
8	Anisole		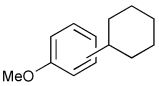	>99	85[g]

[a] Reaction conditions: alkene (1 mmol), benzene (2 mL), $Sc(OTf)_3$ (0.2 mmol for entries 1–6 and 0.1 mmol for entries 7–8), the ionic liquid **2e** (1 mL), 20 °C, 12 h. [b] Conversions and yields based on alkene were determined using the internal standard method in GC. [c] **a**:**b** = 1.5:1. [d] Reaction was carried out with the ionic liquid **2e** containing $Sc(OTf)_3$ recovered from the reaction in entry 3. [e] Reaction was carried out with the ionic liquid **2e** containing $Sc(OTf)_3$ recovered from the reaction in entry 4. [f] The ratio of *ortho* to *para* product is *ca.* 2.5:1. [g] The ratio of *ortho* to *para* product is *ca.* 1.8:1.

examined Friedel–Crafts alkylation of other substrates only using the ionic liquid **2e**. As shown in Table 2, in all cases the reaction proceeded smoothly to furnish the corresponding alkylation products in quantitative yields. Moreover, the ionic liquid phase containing $Sc(OTf)_3$ was almost quantitatively recovered by simple decantation of the organic layer (the upper phase) after reaction. Second and third reactions of benzene with cyclohexene using the recovered ionic liquid **2e** containing catalyst afforded quantitative yield of cyclohexylbenzene (Table 2, entries 4 and 5).

In a typical reaction, the alkene and aromatic compound are added to the ionic liquid **2e** containing 20 mol% of $Sc(OTf)_3$ directly. Two phases are formed and the mixture is stirred at 20 °C for 12 h. The organic layer is separated to leave the ionic liquid phase containing the catalyst which can be reused.

In summary, Friedel–Crafts alkylation of aromatic compounds with alkenes using the novel reusable catalytic system, $Sc(OTf)_3$-ionic liquid, has been developed. The simple procedures, easy recovery and reuse of this novel catalytic system are expected to contribute to development of benign and waste-free chemical processes for Friedel–Crafts alkylation of aromatics with alkenes.

Notes and references

† $Y(OTf)_3$ (16%), $Ho(OTf)_3$ (16%), $Tm(OTf)_3$ (11%), $Lu(OTf)_3$ (64%) also catalysed the reaction of benzene with cyclohexene in the ionic liquid **2e**. However, the yields of the cyclohexylbenzene were significantly inferior to that with $Sc(OTf)_3$. All other lanthanide(III) triflates were inactive under the same reaction conditions. These results can be ascribed to the stronger Lewis acidity of $Sc(OTf)_3$ than that of lanthanide analogues.

1 For reviews of Friedel–Crafts alkylation reactions, see: G. A. Olah, *Friedel–Crafts and Related Reactions*, Wiley-Interscience, New York, 1964, vol. II, part 1; R. M. Roberts and A. A. Khalaf, *Friedel–Crafts Alkylation Chemistry A Century of Discovery*, Dekker, New York, 1984; G. A. Olah, R. Krishnamurit and G. K. S. Prakash, *Friedel–Crafts Alkylations in Comprehensive Organic Synthesis*, ed. B. M. Trost and I. Fleming, Pergamon Press, Oxford, 1991.

2 For reviews, see: S. Kobayashi, *Synlett*, 1994, 689; R. W. Marshman, *Aldrichimica Acta*, 1995, **28**, 77; S. Kobayashi, *J. Synth. Org. Chem. Jpn.*, 1995, **53**, 370.

3 N. Mine, Y. Fujiwara and H. Taniguchi, *Chem. Lett.*, 1986, 357; T. Tsuchimoto, T. Hiyama and S. Fukuzawa, *Synlett*, 1996, 557; T. Tsuchimoto, T. Hiyama and S. Fukuzawa, *Chem. Commun.*, 1996, 2345; T. Tsuchimoto, K. Tobita, T. Hiyama and S. Fukuzawa, *J. Org. Chem.*, 1997, **62**, 6997; H. Kotsuki, T. Oshisi and M. Inoue, *Synlett*, 1998, 255.

4 Reviews for ionic liquids: T. Welton, *Chem. Rev.*, 1999, **99**, 2071; K. R. Seddon, *J. Chem. Tech. Biotechnol.*, 1997, **68**, 351; K. R. Seddon, ionic liquid database, QUB School of Chemistry homepage, http://www.ch.qub.ac.uk; Y. Chauvin and H. Olivier, *CHEMTECH*, 1995, 26.

5 Preparation of ionic liquids: For BF_4 and PF_6 salts (**2b**, **2d**, **2f**, **2h** and **2i**): P. A. Z. Suarez, J. E. L. Dullius, S. Einloft, R. F. de Souza and J. Dupont, *Polyhedron*, 1996, **15**, 1217; The synthesis of the SbF_6 salts (**2a**, **2e**) was similar to that of BF_4 and PF_6 salts with the exception that $NaSbF_6$ was used in place of $NaBF_4$ or $NaPF_6$; For the triflates (**2c**, **2g**): P. Bonhôte, A.-P. Dias, N. Papageorgiou, K. Kalyanasundaram and M. Grätzel, *Inorg. Chem.*, 1996, **35**, 1168. All ionic liquids used in this paper were pre-dried under reduced pressure (0.5 mmHg) at 50 °C for 24 h.

Typeset and printed by Black Bear Press Limited, Cambridge, England

ChemComm
FEATURE ARTICLE

Light-harvesting dendrimers

Alex Adronov and Jean M. J. Fréchet*

Department of Chemistry, University of California, Berkeley, CA 94720-1460, USA.
E-mail: frechet@cchem.berkeley.edu

Received (in Cambridge, UK) 25th July 2000, Accepted 31st July 2000
First published as an Advance Article on the web 31st August 2000

Natural photosynthetic systems collect sunlight using a vast array of light-harvesting chromophores that channel the absorbed energy to a single reaction center. Recently, it has been realized that dendritic macromolecules can exhibit similar properties, though on a more modest scale. The preparation of dendritic structures and assemblies composed of numerous light-collecting chromophores that transfer their energy to a single energy 'sink' at the core has been achieved in a number of diverse and creative ways. These novel structures are being used as model systems in light-emitting diodes, signal amplifiers, fluorescent sensors, frequency converters, and other photonic devices.

Introduction

It has been estimated that the average yearly incidence of solar radiation at the earth's surface amounts to several orders of magnitude more energy than is consumed by its population.[1] Clearly, harnessing this energy is an important endeavor that will reduce our dependence on fossil fuels. Indeed, our own existence depends on light-harvesting by the plethora of photosynthetic organisms in the biosphere. These organisms have evolved intricate and extremely efficient mechanisms for the transduction of light into chemical energy in the form of ATP.[2] If we are to utilize sunlight in a similar fashion, it is not unreasonable to borrow some design concepts from structures that have evolved over billions of years.

To date, the most studied of all photosynthetic systems is probably that of purple bacteria.[3] The high resolution X-ray crystal structure of the photosynthetic unit (PSU) reveals a central reaction center (RC) that is surrounded by light-harvesting (LH) complexes (Fig. 1).[4] The LH1 complex is composed of a ring-shaped assembly of chlorophyll and carotenoid moieties embedded in a protein matrix that immediately surrounds the RC. Similar ring-shaped assemblies, somewhat further removed from the RC, make up the LH2 and LH3 complexes.[3] The role of these chlorophyll-containing assemblies is that of an antenna, absorbing photons that strike the relatively large surface area that they cover. Remarkably, the energy of any photon that strikes any of the several hundred chlorophylls within the extensive LH system is transferred to the RC with unit efficiency.[3]

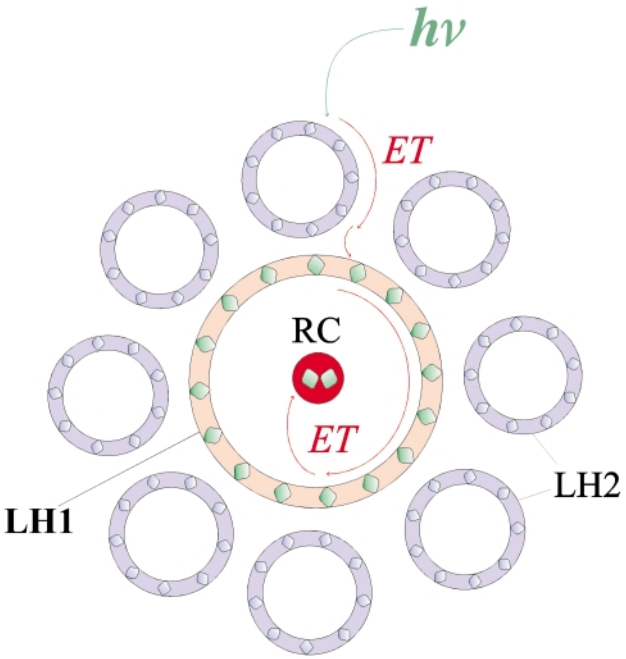

Fig. 1 Schematic representation of bacterial light-harvesting complexes (LH1 and LH2), showing the different protein-embedded light-absorbing porphyrins arranged in circles around the reaction center (RC). The path of energy transfer (ET) is indicated by arrows.

Dendrimers are perfectly branched synthetic macromolecules having numerous chain ends all emanating from a single core.[5–8] Their synthesis, first reported in 1985 by the groups of Tomalia[9] and Newkome,[10] involves a divergent iterative coupling and activation protocol[9–12] that results in the formation of concentric layers of building blocks terminated by a large number of reactive moieties. The convergent synthesis we introduced later[13] provides for growth through a single focal point, an approach that affords even better control over both the dendrimer backbone structure and the placement of functional groups within it. Overall, the accurate positioning of chromophores can be achieved, locating them at the core, focal point, periphery, or even at each branching point of the dendritic structure (Fig. 2). This schematic diagram of a dendrimer is reminiscent of the architecture of natural light-harvesting complexes, where antenna molecules surround the central RC. Although the appropriate placement of chromophores is

Alex Adronov was born in Kaunas, Lithuania in 1973 and moved to Windsor, Ontario, Canada in 1980 with his family. He received a BSc degree in Biological Chemistry from McMaster University in 1996. Currently, he is pursuing a PhD at the University of California, Berkeley, under the supervision of Professor Jean M. J. Fréchet.

Jean M. J. Fréchet obtained his first degree at the Institut de Chimie et Physique Industrielles (now CPE) in Lyon, France, and PhD degrees from the College of Environmental Sciences and Forestry and Syracuse University. Following academic appointments at the University of Ottawa (1973–86) and Cornell University (1987–96), he joined the Department of Chemistry at the University of California, Berkeley. J. Fréchet received both the American Chemical Society awards in Polymer Chemistry and in Applied Polymer Science; in 2000 he was elected a Fellow of the American Academy of Arts and Sciences, a member of the National Academy of Engineering, and a member of the National Academy of Science.

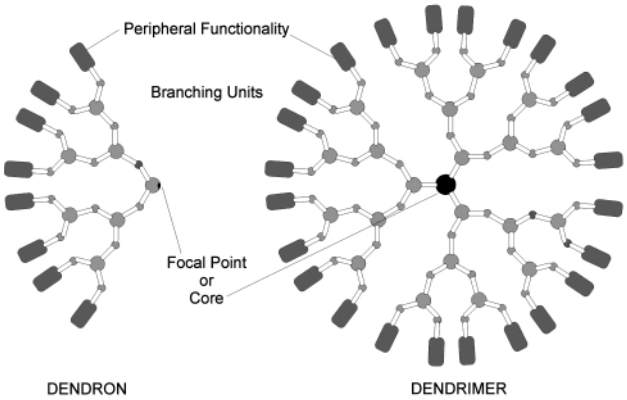

Fig. 2 Schematic diagram of the structure of a dendron and a dendrimer, highlighting the focal point or core (black) surrounded by rings of branching units (gray circles) and end-groups (rectangles).

important, judicious choices must be made both for the selection of the chromophores themselves, and for the design of each successive layer in order to maximize favorable energy transfer interactions.

Over the past several decades, there has been much work done on a number of synthetic light-harvesting complexes in which energy transfer is demonstrated. After a brief introduction to energy transfer, this article will focus on the more recent dendrimer-based light-harvesting structures.

Energy transfer and the choice of chromophores

In a bichromophoric system where one chromophore (the energy donor, D) is in its excited state and the other (the energy acceptor, A) is in its ground state, energy transfer can occur such that the donor returns to its ground state simultaneously with the promotion of the acceptor to its excited state (Fig. 3).[14] This

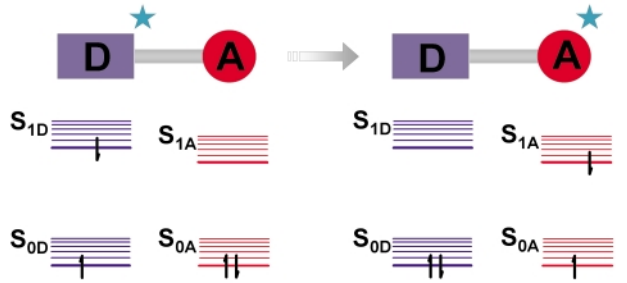

Fig. 3 The process of energy transfer involves the migration of excitation energy from an excited-state donor (D) to a nearby ground-state acceptor (A).

transfer can occur by either a through-bond[15] (Dexter) or through-space[16,17] (Förster) mechanism. In the former, an electron exchange occurs from the S_1 state of the donor to the S_1 state of the acceptor, with a simultaneous exchange of an S_0 electron from acceptor to donor (Fig. 3). This electron exchange requires strong D–A orbital overlap and is therefore a short-range (< 10 Å) interaction that diminishes exponentially with distance.[14] The rate constant for this process is described by eqn. (1):

$$k_{ET} = KJ\exp(-2R_{DA}/L) \quad (1)$$

where K is related to the specific orbital interactions, J is the spectral overlap integral (see below) normalized for the extinction coefficient of the acceptor, and R_{DA} is the donor–acceptor separation relative to their van der Waals radii, L.[14]

In contrast, the Förster mechanism does not require electron exchange and is rather a through-space dipole–dipole interaction.[18] In this case, D–A orbital overlap is not necessary, allowing the chromophores to be separated by a relatively large distance (10–100 Å). The Förster energy transfer rate constant is described by eqn. (2):

$$k_{ET} = \frac{9000(\ln 10)\kappa^2\phi_D J}{128\pi^5 n^4 N\tau_D R_{DA}^6} \quad (2)$$

where κ^2 is the orientation factor (related to the relative orientation of the donor and acceptor transition dipole moments), ϕ_D is the donor quantum yield in the absence of the acceptor, J is the overlap integral, n is the index of refraction of the solvent, N is Avogadro's number, τ_D is the donor lifetime in the absence of the acceptor, and R_{DA} is the inter-chromophoric distance in cm. The overlap integral J ($cm^6\ mol^{-1}$) is given by eqn. (3):

$$J = \int f_D(\nu)\varepsilon_A(\nu)\nu^{-4}d\nu \quad (3)$$

where $f_D(\nu)$ is the fluorescence intensity of the donor, $\varepsilon_A(\nu)$ is the molar extinction coefficient of the acceptor, and the integral is calculated over the whole spectrum with respect to the frequency expressed in wavenumbers. This integral represents the overlap between the donor emission spectrum and the acceptor absorption spectrum, and is closely related to the probability of energy transfer from the donor to the acceptor.

Unlike the Dexter interaction, where normalization of J diminishes its significance, Förster energy transfer is greatly influenced by this parameter.[14] In addition, the transition dipole moments of the interacting chromophores play a large role in the energy transfer efficiency of the through-space mechanism.[18] Hence, the bridging moiety plays a crucial role in Dexter energy transfer, where rigidity and conjugation are the key parameters, whereas the properties of the chromophores themselves (transition dipole moments and spectral overlap of donor emission and acceptor absorption) as well as the interchromophoric distance play the more important role in Förster energy transfer.

Within dendritic structures, practically all of the above parameters can be controlled and varied. Chromophore functionalization of the dendrimer can involve only the core and the end-groups, or it can involve the entire dendrimer backbone. The rigidity, conjugation, size, and polarity of the dendritic backbone all depend on the type of branched monomer that is utilized. Hence, the choice of the monomer will affect the overall properties and the energy transfer mechanism of the dendritic system. As the dendrimer generation increases, two competing factors become prevalent (Fig. 4). The number of

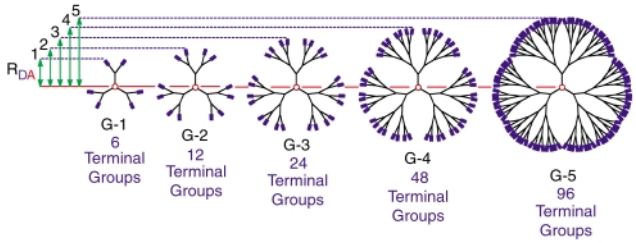

Fig. 4 As dendrimer generation increases, the number of terminal groups doubles, but the distance between the terminal groups (energy donors) and the core (energy acceptor) also increases.

monomer units, closely reflected by the number of end-groups surrounding the core, doubles with each successive generation, and the distance between the core and the end-groups increases. If each branching point or end-group acts as a chromophore, then increasing the generation allows for the harvesting of increasing amounts of light by the molecule. However, at a certain dendrimer generation, or size, it is expected that R_{DA} will become too large to sustain efficient energy transfer. It is thus necessary to reach a balance between the light-harvesting capacity of the dendritic shell, and the energy transfer efficiency to the core.

In the following paragraphs, some key examples of light-harvesting dendrimers will be highlighted.

Chromophoric dendrimer backbones and the role of an energy gradient

The initial reports of multichromophoric dendrimers undergoing intramolecular energy transfer were published by Balzani and coworkers in 1992.[19,20] Their 'complexes as metals/complexes as ligands' strategy provided a means of selectively incorporating different metal and ligand combinations into these low-generation dendrimers. Ru and Os were the metals of choice in this work owing to the ideal luminescence and redox properties of their polypyridine complexes.[20,21] The schematic representation of these molecules (Fig. 5) indicates the presence

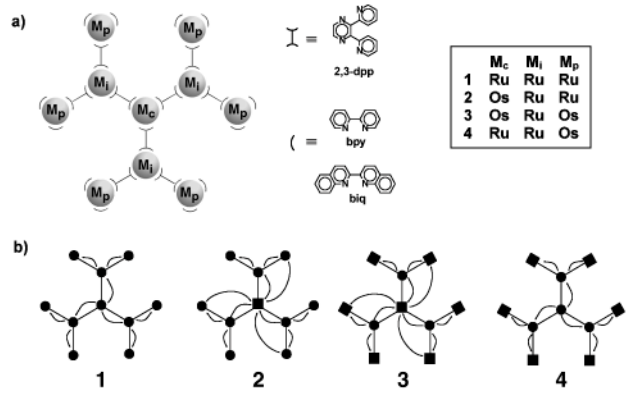

	M_c	M_i	M_p
1	Ru	Ru	Ru
2	Os	Ru	Ru
3	Os	Ru	Os
4	Ru	Ru	Os

Fig. 5 (a) Schematic representation of metallodendrimers having branching ligands and different combinations and positions of Ru and Os metals. (b) Direction of energy transfer (indicated by arrows) in the different structures depicted in (a). ● = Ru, ■ = Os.

of three distinct metal-binding positions: a single core site; three intermediate sites; and six peripheral sites. In addition, it is well known that the oxidation potential of the metal ion in these polypyridyl complexes can depend on the nature of the coordinated ligands.[21] Hence, bandgap energies of the metal complexes located at the different sites (core, intermediate, and peripheral) within the dendrimer are controlled by both the nature of the metal (Ru complexes have larger bandgap energies than the corresponding Os complexes) and the nature of the surrounding ligands. Balzani and coworkers showed that metal complex bandgap energies depend on the ligands in the order dpp > biq > bpy.[22] Indeed, it was found that energy transfer in the all-Ru compounds (**1**) occurred from the internal higher energy units (dpp ligands) to the external lower energy units having bpy or biq ligands.[20] In the heterometallic complexes, energy migration predominantly occurred from the Ru-containing units to the Os-containing units. Hence, controlled energy migration from the internal units to the external units could be achieved by complexes **1** and **4**. Conversely, energy migration from the dendrimer periphery to the core was more difficult to achieve owing to the lower energy of the outermost complexes *vs*. the intermediate ones [Fig. 5(b)].

In all of these structures, energy transfer is dominated by the Dexter electron exchange mechanism,[20,23] which precludes long-range interactions between the periphery and the core. Indeed, in the third-generation structure having an Os core, it was again shown that energy migrates from the intermediate higher bandgap units to the lower bandgap units at either the periphery or the core.[24,25] Although the concept of intramolecular energy transfer within dendritic structures was clearly illustrated by these initial reports, the structures synthesized did not ideally function as photosynthetic mimics, where numerous peripheral light-harvesting chromophores channel absorbed energy in a unidirectional manner to a single, central, energy acceptor complex.

Efficient, unidirectional energy transfer from a dendritic framework to a single core chromophore was first reported in elegant work by Xu and Moore.[26] The robust, high-yielding synthesis of their phenylacetylene dendrimers allowed for the preparation of high-generation (G-*n*) molecules, up to G-6.[27,28] These cross-conjugated structures (Fig. 6) exhibit strong UV

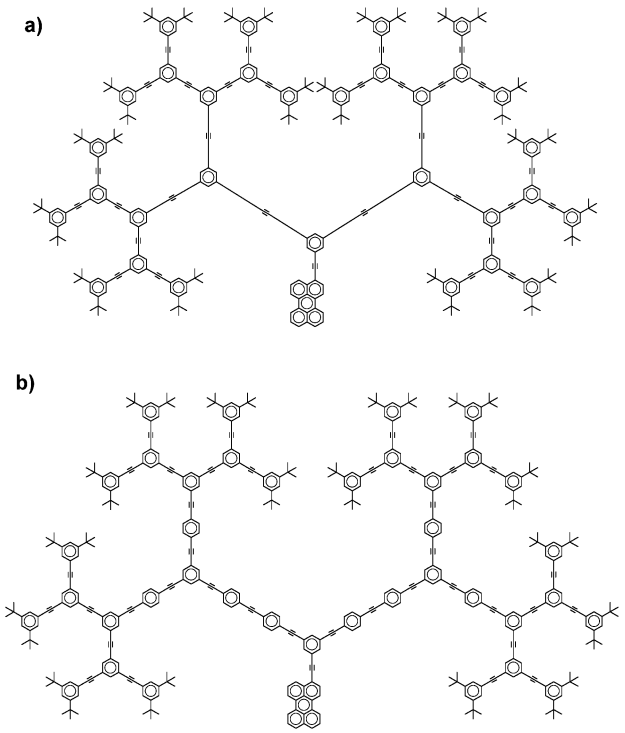

Fig. 6 Chemical structure of perylene-functionalized phenylacetylene dendrimers without (a) and with (b) an energy gradient.

absorption features in the 250–350 nm range that double in magnitude with increasing generation.[29] Additionally, it was found that these dendrimers act as luminescent chromophores that have an emission in the 350–450 nm range. By functionalizing the core of these structures with the lower bandgap perylene chromophore, the authors introduced an energy 'sink' into the system. Hence, the phenylacetylene monomer units act as the peripheral energy donors, and the perylene acts as the central energy acceptor. Excitation of the dendrimer backbone at 312 nm resulted in emission emanating solely from the perylene dye (450–600 nm), with nearly complete quenching of the dendrimer emission.[29]

Further, the versatile synthetic scheme allowed for the synthesis of dendrimers having a directional energy gradient, with the bandgap energy of each branch decreasing owing to increasing conjugation length [Fig. 6(b)].[30,31] Interestingly, it was found that this energy gradient dramatically increases (by two orders of magnitude) the energy transfer rate constant within the dendrimer.[29] Hence, the directional energy transfer from periphery to core must be greatly facilitated by the built-in energy gradient. Indeed, theoretical work by Klafter and coworkers afforded the same conclusion, suggesting that 'random walk' energy transfer from periphery to core, as in the former structures, is much less productive than the directional multi-step process.[32–34] These structures represent the first examples of effective photosynthetic mimics, and the latter molecules remain the *only* example of built-in multi-step energy gradients within dendritic macromolecules. However, the mechanism of energy transfer in these systems was difficult to ascertain. Owing to the cross-conjugated dendrimer backbone, orbital overlap contributions to the energy transfer cannot be ruled out. In addition, spectral overlap between donor emission and acceptor absorption is not very large in this case, and would

preclude the Förster mechanism alone from producing in the high energy transfer efficiencies that were observed.

Poly(benzyl ether) dendrimers and the 'antenna effect'

Several years ago our group studied the encapsulation of lanthanide ions (Ln^{3+}) by dendritic ligands in the context of a possible application for optical signal amplification. The impetus for this project originated from the self-quenching of fluorescence by lanthanide ions, such as erbium, when they are clustered together in the solid state. This self-quenching limits their effectiveness as signal amplifiers for optical fiber communications, since the poor solubility of Ln^{3+} ions in substrates such as silica leads to the formation of ion clusters.[35,36] Encapsulation of individual Er^{3+} and Tb^{3+} ions within a dendritic shell (Fig. 7) was expected to lead to their

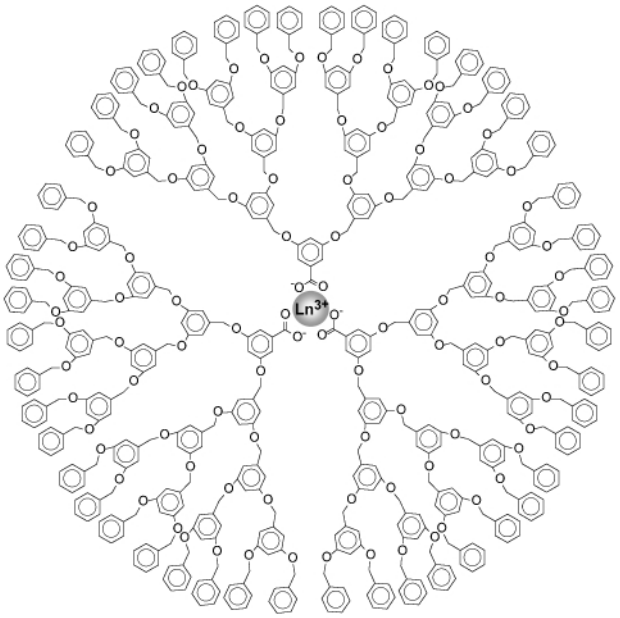

Fig. 7 Structure of a lanthanide-cored poly(benzyl ether) dendrimer.

site-isolation, thereby increasing interchromophoric distance and decreasing the self-quenching effect. Indeed, this site-isolation was realized by self-assembly of suitably functionalized carboxylate-cored dendrons around the lanthanide ion, and the resulting assemblies possessed all the characteristics desired for use in signal amplification. During the course of photophysical studies on these ionically bound supramolecular assemblies, it was found that irradiation at wavelengths where the dendrimer backbone absorbed (280–290 nm) resulted in strong luminescence from the lanthanide core.[37,38] Apparently, energy absorbed by the peripheral dendrimer shell was efficiently transferred to the luminescent Ln^{3+} at the focal point by a mechanism postulated to be of the Förster type. At these wavelengths, energy transfer to Tb^{3+} was found to be more efficient than in the case of Er^{3+}, likely due to the better overlap of dendrimer emission with Tb^{3+} absorption. This channeling of excitation energy from a dendrimer shell to a single core unit was termed the 'antenna effect'. Interestingly, it was also found that this energy transfer phenomenon was critically dependent on the substitution pattern within the dendritic shell. When the isomeric dendrons having 2,5- rather than 3,5-substitution at the focal aromatic ring were utilized, the energy transfer interaction practically disappeared.

Several other research groups have observed similar antenna effects while utilizing different luminescent cores. Jiang and Aida reported that singlet energy transfer could be observed from the same Fréchet-type poly(benzyl ether) dendrons to a core porphyrin ring (Fig. 8).[39] A variety of structures, differing

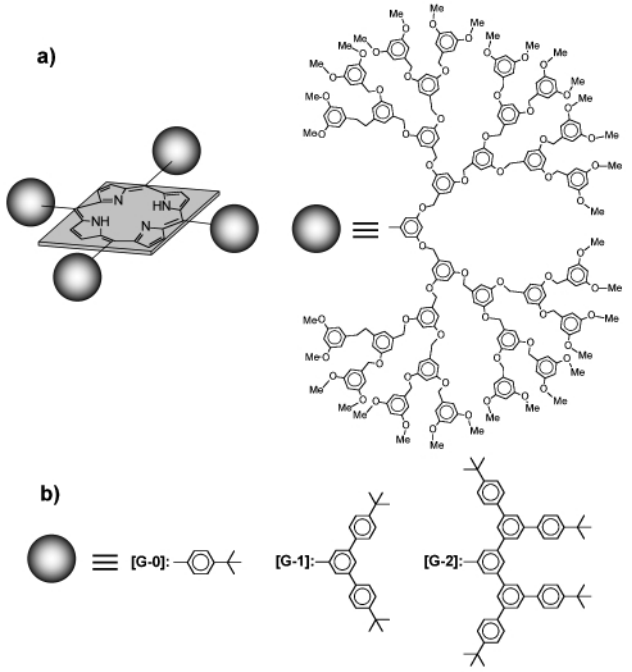

Fig. 8 Schematic representation of porphyrins encapsulated by (a) poly(benzyl ether) dendrimers, and (b) 1,3,5-phenylene-based dendrimers.

in the number of dendrons attached to the central porphyrin, as well as in the generation number of the dendrons, were prepared and studied. A small amount of overlap between the fluorescence spectrum of the dendrons and the Soret absorption of the porphyrin allows for some degree of energy transfer to occur. Indeed, excitation of the tetra-substituted dendritic porphyrin at 280 nm (dendrimer absorption) resulted in quenching of the dendrimer emission (310 nm), with most of the light being emitted by the porphyrin core (600–750 nm). The energy transfer efficiency in both the G-4 and G-5 analogs was calculated to be approximately 80%. However, if the porphyrin was only partially substituted, with one, two, or three G-5 dendrons instead of four, the energy transfer efficiency dropped dramatically, to 10, 20 and 32%, respectively. Similar phenomena were also observed when G-4 dendrons were used. Temperature-dependent effects indicated that increased flexibility and conformational freedom were responsible for the decreased energy transfer efficiency. Only the highly crowded molecule having four G-5 dendrons retained a constant level of energy transfer, even at high temperatures. It was also postulated that cooperativity between dendrons is necessary for efficient energy transfer, and this cooperativity appeared to decrease with increasing conformational mobility.

A slight variation of this work was recently published by Kimura *et al*., who synthesized low-generation (G-1 and G-2) 1,3,5-phenylene-based dendritic porphyrins [Fig. 8(b)].[40] Interestingly, the authors found that energy transfer between the dendrimer and the porphyrin was highly efficient at low generations. This seemingly contradictory result may be rationalized by the fact that the energy transfer mechanism may be different in these cross-conjugated molecules than for the dendrimers of Aida and coworkers.[39] Additionally, the authors point out that the spectral overlap between the emission of the dendrons and the absorption of the porphyrin core is larger in this case, which may also have a significant effect on the energy transfer efficiency.

In a more recent publication, Aida and coworkers reported the encapsulation of a poly(phenyleneethynylene) rigid-rod polymer by a poly(benzyl ether) Fréchet-type dendrimer shell.[41] The dendritic shell was again effective as both a steric 'bumper' preventing polymer chains from aggregating, and as a light-harvesting antenna. The authors showed that upon direct

excitation of the polymer backbone, the fluorescence quantum yield remained constant over a wide concentration range only if a large enough dendrimer envelope, composed of G-4 dendrons or higher, was utilized. Additionally, excitation of the dendritic shell at 278 nm resulted in complete quenching of dendrimer emission, and a high fluorescence intensity emanating from the conjugated polymer. It was found that this sensitized polymer fluorescence was greatly enhanced over the emission resulting from direct excitation of the polymer at 425 nm, again illustrating the dendrimer 'antenna effect'. Owing to the importance of such conjugated polymers in organic light-emitting diode (OLED) technology, these findings could have a significant impact on the future of LED devices.

In a separate report, Jiang and Aida have demonstrated an unusual acceleration of the *cis–trans* isomerization within an azobenzene moiety at the core of G-4 and G-5 poly(benzyl ether) dendrimers.[42] This acceleration was observed under low-flux IR irradiation of a stretching vibrational band of the aromatic rings at 1597 cm^{-1}. Interestingly, irradiation at different IR frequencies, such as 2500 or 1155 cm^{-1} resulted in no apparent acceleration above the thermal rate. Additionally, when low-generation dendrimers were utilized, the acceleration was not apparent. Any change in substitution, such as in the mono-dendritic analog (Fig. 9), also eliminated the acceleration.

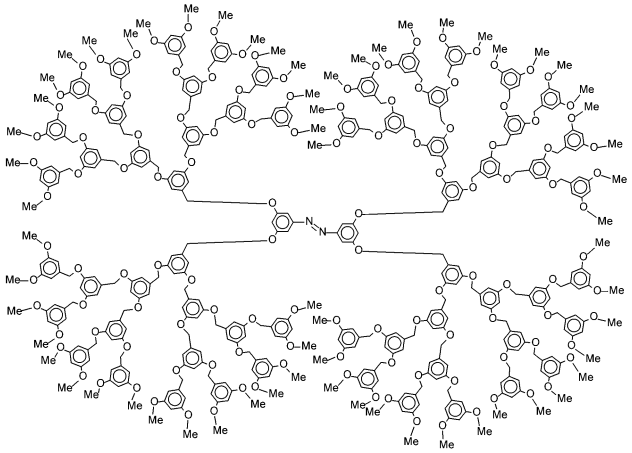

Fig. 9 Structure of a G-5 azobenzene-cored dendrimer.

This latter point is not surprising in light of our own work on encapsulated lanthanide ions (*vide supra*) in which the critical dependence of energy transfer on the substitution pattern of the focal aromatic ring was demonstrated. However, UV irradiation of the dendrons at 280 nm did result in a similar acceleration. In order to rationalize these observations, the authors proposed that the dendritic shell not only insulates the azobenzene core from collisional energy dissipation, but also acts as a photon-harvesting antenna. By comparison with thermally induced accelerations at 60 °C and by determining the dependence of the isomerization rate constant on the applied photon flux, it was found that the energy required for the observed rate acceleration required the simultaneous delivery of the energy of 4.9 IR photons to the azobenzene core. This calculation is consistent with the observed requirement of high-generation dendrons, since the simultaneous absorption of multiple photons from such weak photon sources could only be plausible in extremely large molecules.

Using a different approach, Stewart and Fox[43] utilized the known photoinduced electron transfer interaction between aryl chromophores (naphthyl or pyrenyl) and tertiary amines.[44] Since it is well known that excited states of aryl chromophores are quenched by electron donating amines, it was postulated that excitation of the periphery of dendrimers having naphthyl or pyrenyl groups at their chain ends and an amine at the core, would lead to intramolecular electron transfer through the dendrimer backbone (Fig. 10). Indeed, fluorescence quenching

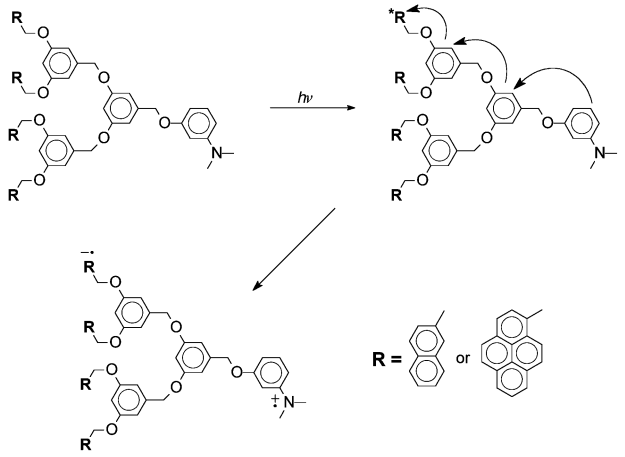

Fig. 10 Illustration of the electron transfer process occurring through the dendrimer backbone as a result of photoexcitation of the peripheral acceptor chromophores.

of the peripheral chromophores by the amine core was observed, but only in small dendrons (G-1 and G-2). At higher generations, the quenching efficiency decreased dramatically, probably as a result of the increased distance between periphery and core.

Dendrimer-independent energy transfer

In order to create a more versatile system in which the energy transfer between peripheral chromophores and core was not affected by the dendrimer backbone itself, we have designed dendrimers with photochemically silent building blocks. Since the energy transfer process with such structures requires a highly efficient through-space interaction between chromophores located at their focal point and periphery, chromophore selection must meet certain requirements.[45] Specifically, the chromophores should be suitable for Förster energy transfer, with a large spectral overlap between donor emission and acceptor absorption, high transition dipole moments, high extinction coefficients, and high quantum yields of fluorescence.[14] In addition to these photophysical requirements, the chosen chromophores should (i) be soluble in organic solvents—this is particularly important for the peripheral donor chromophores, since the solubility properties of dendrimers are known to be highly sensitive to the nature of the surface groups—and (ii) contain a functional 'handle' through which attachment to the dendritic structure could be achieved.

Amino-functionalized Coumarin-2 and acid-functionalized Coumarin-343 were selected as the donor and the acceptor, respectively (Fig. 11). The solubility of these chromophores was adequate for the preparation of dendrimers up to generation four using an AB_2 building block with orthogonal functionalities (Fig. 11).[46] The photophysical properties of these molecules were studied by steady-state and time-resolved absorption and emission spectroscopy.[47] Initially, steady-state data was collected for model compounds containing either the donor chromophores or the acceptor, but not both. These models showed that the large spectral overlap between donor emission and acceptor absorption is preserved after coupling of the chromophores to the dendritic architecture (Fig. 12). Additionally, exclusive excitation of either the donor or the acceptor was found to be possible, simplifying the analysis of fluorescence data for energy transfer calculations.

The steady-state absorption characteristics of the fully-labeled dendrimers showed the expected doubling of donor absorption as a function of dendrimer generation, indicating that no deleterious ground-state aggregation phenomena were occurring in this system [Fig. 13(a)]. The acceptor absorption was shown to remain relatively constant at each generation, with only slight solvatochromic shifts being evident due to the

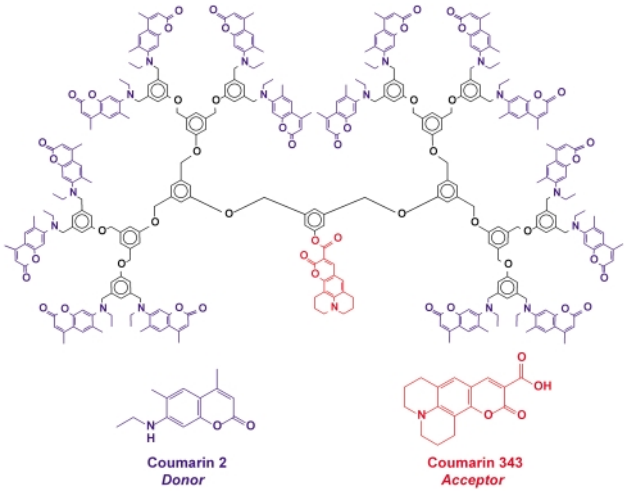

Fig. 11 Chemical structure of the Coumarin-2 donor, Coumarin-343 acceptor, and the fully chromophore-functionalized G-4 dendrimer.

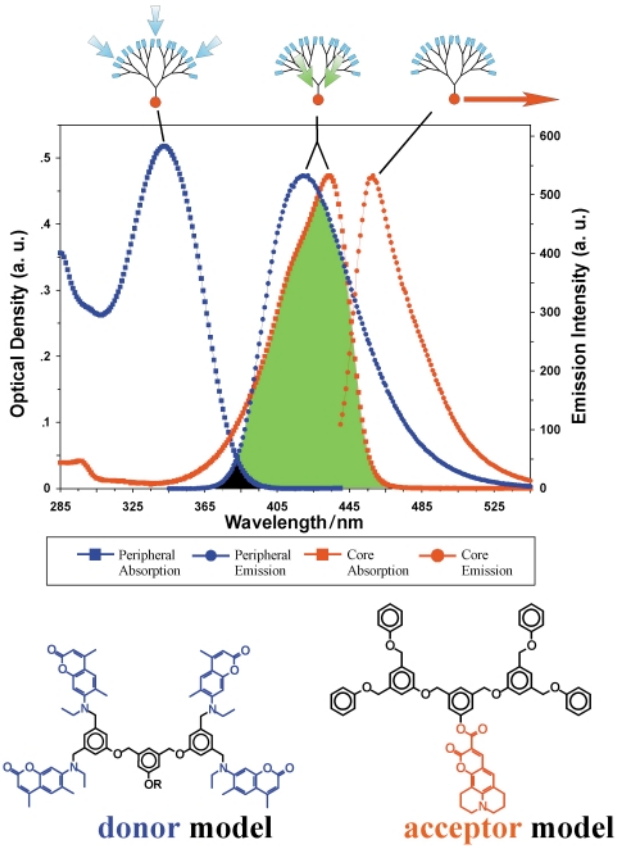

Fig. 12 Structures and spectral properties of donor and acceptor model compounds, indicating the strong overlap between donor emission and acceptor absorption.

increasing influence of the polar dendrimer shell around the focal chromophore. Upon irradiation of the donor absorption band, strong fluorescence was observed exclusively from the acceptor chromophore. The complete quenching of the donor chromophores attests to the highly efficient energy transfer occurring in these molecules. Additionally, a comparison of the emission intensity from sensitized acceptor excitation (λ_{ex} = 343 nm) to that from direct acceptor excitation (λ_{ex} = 440 nm) could be made [Fig. 13(b)]. It was found that in dendrimer generations beyond G-2, the emission intensity from sensitized excitation was greatly enhanced [Fig. 13(b), dotted curve], confirming that energy transfer efficiency is extremely high in these molecules. Time-resolved experiments indicated that energy migration from the periphery to the core occurred on extremely fast, sub-picosecond timescales. Using single-photon

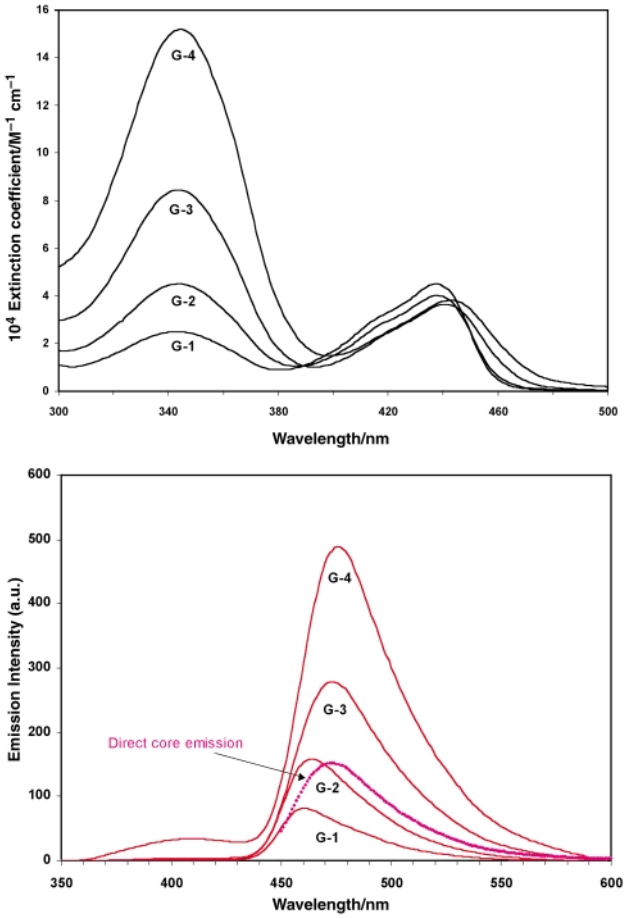

Fig. 13 UV–VIS absorption (top) and fluorescence emission (bottom) properties of the Coumarin-functionalized G-1 to G-4 series of dendrimers.

counting, it was not possible to resolve the rise-time of the core excitation upon irradiation of the periphery. Although these preliminary studies indicate that the Förster mechanism is the dominant energy transfer pathway, exact values for energy transfer rate constants must be ascertained before this claim can be fully substantiated. Further spectroscopic experiments with much faster time resolution will enable accurate measurements of the energy transfer rate constants and their quantitative comparison with theoretical calculations from Förster theory and molecular modeling.

Interesting insight into the relative rates of energy transfer *vs.* nonradiative relaxation of Coumarin-2 was provided by a study of the energy transfer dependence on solvent composition. When G-1 and G-2 donor model dendrons were dissolved in methanol (higher generation dendrimers were not soluble), it was found that the Coumarin-2 emission was completely quenched (Fig. 14). This was likely due to hydrogen bonding of the solvent with the tertiary amine lone pair, precluding optimal alignment of this lone pair orbital with the aromatic system of the chromophore. However, upon coupling of the acceptor chromophore to the focal point of these dendrons, excitation of the donors resulted in strong emission from the core. This indicates that, although fast nonradiative decay processes can compete with the nanosecond-scale donor fluorescence, the energy transfer process is much faster and still results in energy localization on the acceptor dye. The acceptor fluorescence is not quenched by the hydrogen bonding solvent presumably because the amine lone pair orbital is kept in conjugation by the two cyclohexyl rings (Fig. 11).

More recent work has shown that replacement of the Coumarin-343 acceptor by other chromophores can result in efficient energy transfer, as long as the absorption spectrum retains good overlap with the donor emission.[48] Oligothiophene

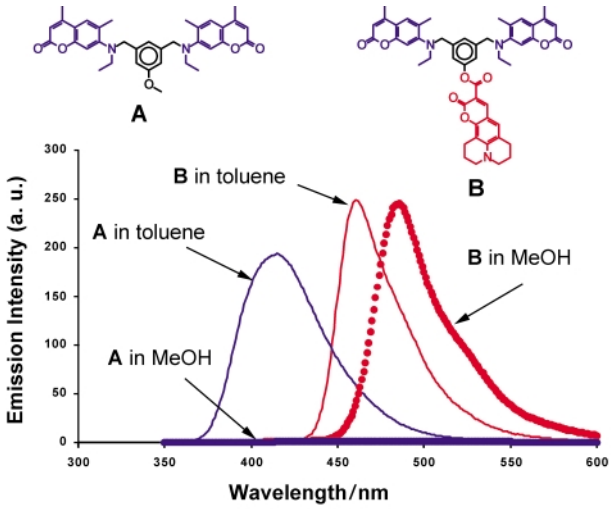

Fig. 14 Emission spectra of G-1 dendrons without (A) and with (B) the core acceptor chromophore in toluene (solid line) and methanol (dotted line).

chromophores proved ideal for this purpose, since it is possible to tune their absorption and emission properties by changing the degree of oligomerization. Two different oligothiophenes—a pentamer linked through its terminal ring, and a heptamer linked through its central ring—were chosen owing to their favorable absorption properties. Dendrimers up to the third generation were prepared, and it was shown that energy transfer was quantitative in all cases. Again, the emission intensity of the oligothiophenes, which have relatively low quantum yields of fluorescence (Φ_f = 0.15), was greatly enhanced by sensitized excitation upon irradiation of the peripheral light-harvesting antenna. This phenomenon may prove useful in the emission enhancement of photonic devices in which it is necessary to utilize components that have low fluorescence quantum yields. Interestingly, the oligothiophenes in this study had emission spectra that were strongly red-shifted from the emission of Coumarin-343. Hence, by simply changing the core functionality of the dendrimer, it is possible to tune the emission wavelengths across almost the entire visible spectrum, while irradiating at a single wavelength [Fig. 15(b)]. Molecules with this feature serve as ideal probes for experiments requiring simultaneous excitation and detection of several different targets, such as in the area of fluorescent conjugates for biological molecules.

Dendrimer-based light-emitting diodes

The findings made with the dendrimer antennas can be extended to the design of single-layer multichromophoric light-emitting diodes. The dendritic framework provides for both the energy transfer interaction and the site-isolation of different chromophores, enabling them to fluoresce simultaneously.[49–51] Separate emission from each dye is difficult to achieve in classical solid-state devices owing to intermolecular energy transfer to the chromophore with the smallest bandgap. By isolating the different chromophores within a dendritic shell, it should be possible to diminish or even eliminate this energy transfer in their mixture, and enable emission from each individual dye. Dendrimers peripherally-functionalized with hole-transporting triarylamines and core-functionalized with two different fluorescent chromophores were synthesized separately, and incorporated as a mixture into a single-layer light-emitting device (Fig. 16). These structures allowed the excitation energy to be changed from applied light to an applied voltage across two electrodes. Based on the solution work outlined above, the chosen fluorescent chromophores were Coumarin-343 and a pentathiophene, since their absorption bands overlap well with the emission band of the peripheral triarylamine. Our preliminary studies[49–51] indicate that it is possible to observe

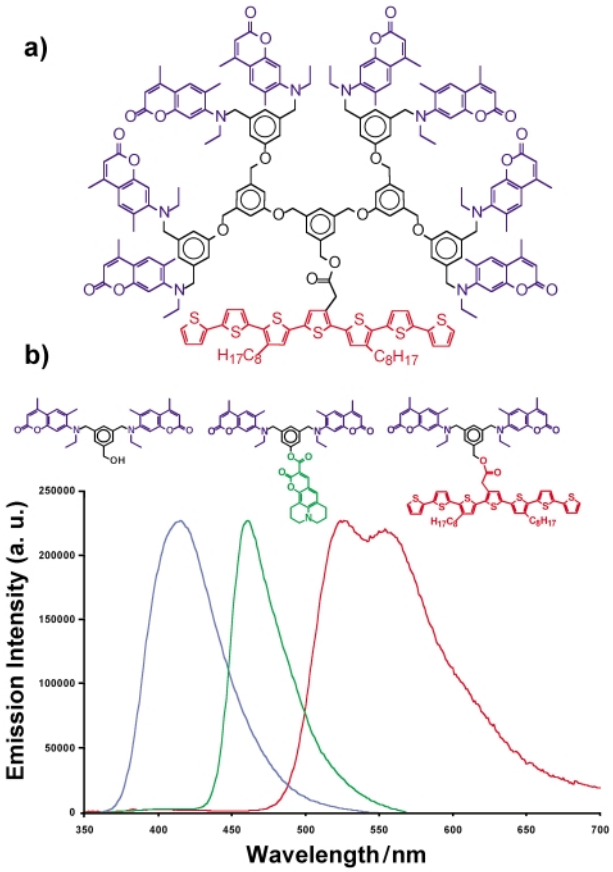

Fig. 15 (a) Structure of the G-3 heptathiophene (T-7) core-functionalized dendrimer. (b) Normalized emission spectra of G-1 dendrons having different moieties at the core: (i) no core chromophore; (ii) Coumarin-343; (iii) heptathiophene.

simultaneous emission from both chromophores when they are encapsulated in a dendrimer. In contrast, the light produced by mixtures of the free dyes originates solely from the lower bandgap oligothiophene.[49–51]

Dendrimer-based organic LEDs have also been reported by Moore and coworkers.[52] In this example, phenylacetylene dendrimers were prepared with peripheral triphenylamine groups for hole transport, and a core 9,10-bis(phenylethynyl)-anthracene as the light emitter. Unfortunately, thin films of these molecules exhibited only modest electroluminescence (EL) intensities. Solid-state aggregation of the rigid dendrimers and self-quenching by the low Stokes shift anthracene chromophores were the likely causes of diminished EL.

Light-harvesting in self-assembled monolayers

To further simplify the antenna concept without recourse to the tedious preparation of multichromophoric dendrimers, we studied the self-assembly of harvesting antennas and emitting components on silicon surfaces. Small Coumarin-2 functionalized donor dendrons and the Coumarin-343 acceptor chromophore (Fig. 17) were therefore functionalized with triethoxysilane moieties, which could then be adsorbed onto a silicon wafer to form self-assembled monolayers (SAMs).[53] The self-assembly process enables the use of a variety of donor–acceptor ratios by adjusting the adsorbate ratios in solution prior to SAM assembly. The photophysical properties of the monolayers were determined using front-face fluorescence techniques. As expected, variations in the donor–acceptor ratio on the surface had a large effect on the efficiency of energy transfer. Fig. 18(a) illustrates the normalized emission spectra from mixed monolayers of **6** and **8** having a 2:1 and a 3:1 ratio.[53] The larger average donor–acceptor distance obtained with a 3:1 ratio leads to a broader emission spectrum with contributions from both

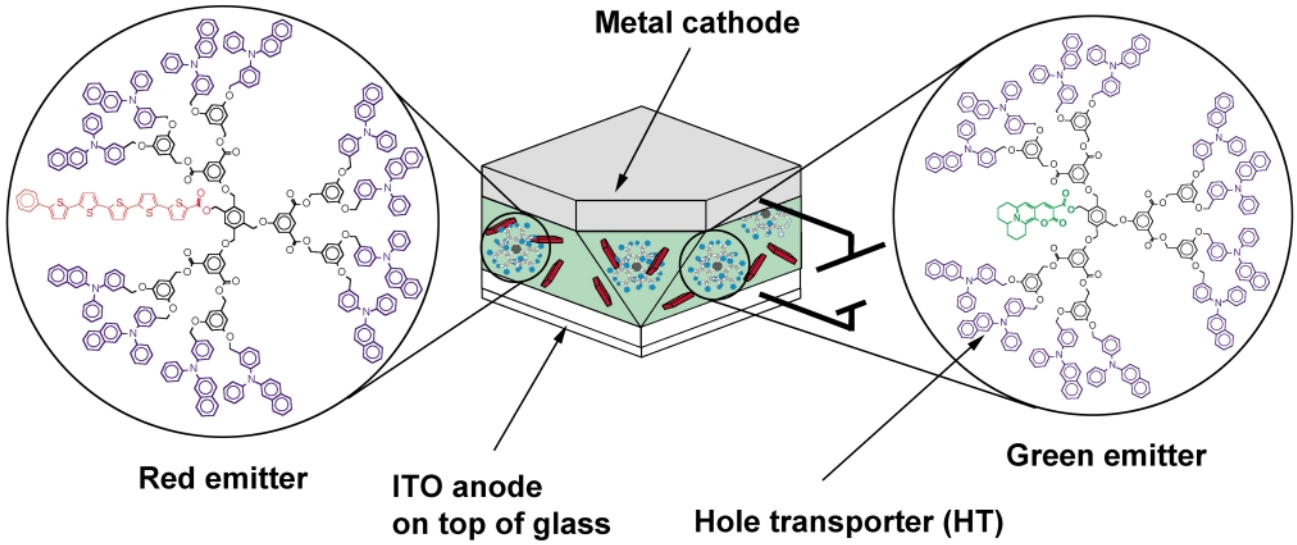

Fig. 16 Schematic diagram of an LED device incorporating hole-transporting dendrimers with pentathiophene (red emitter) and Coumarin-343 (green emitter) cores.

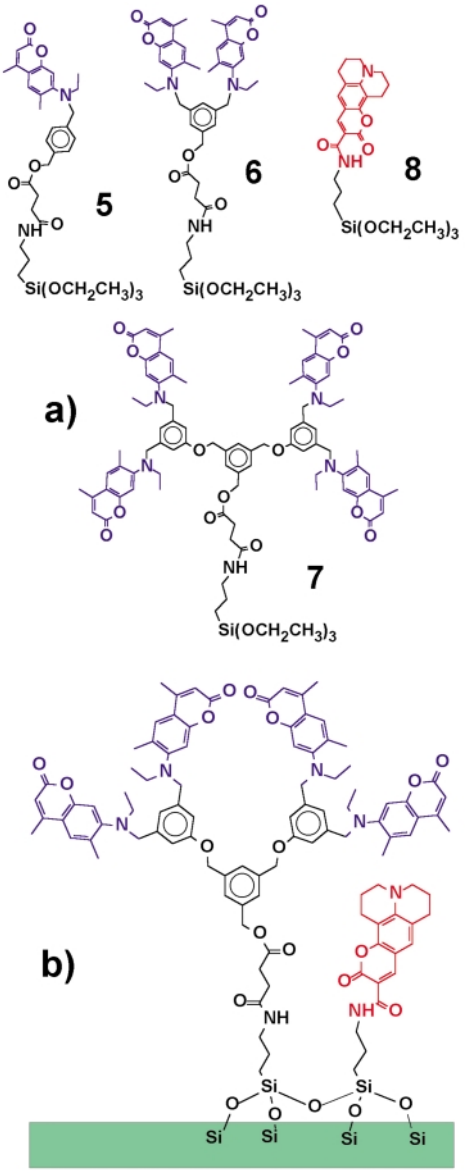

Fig. 17 (a) Structures of the triethoxysilane-functionalized donor and acceptor adsorbates. (b) Schematic representation of a mixed SAM of separate G-2 donor dendron and the Coumarin-343 acceptor on a silicon surface.

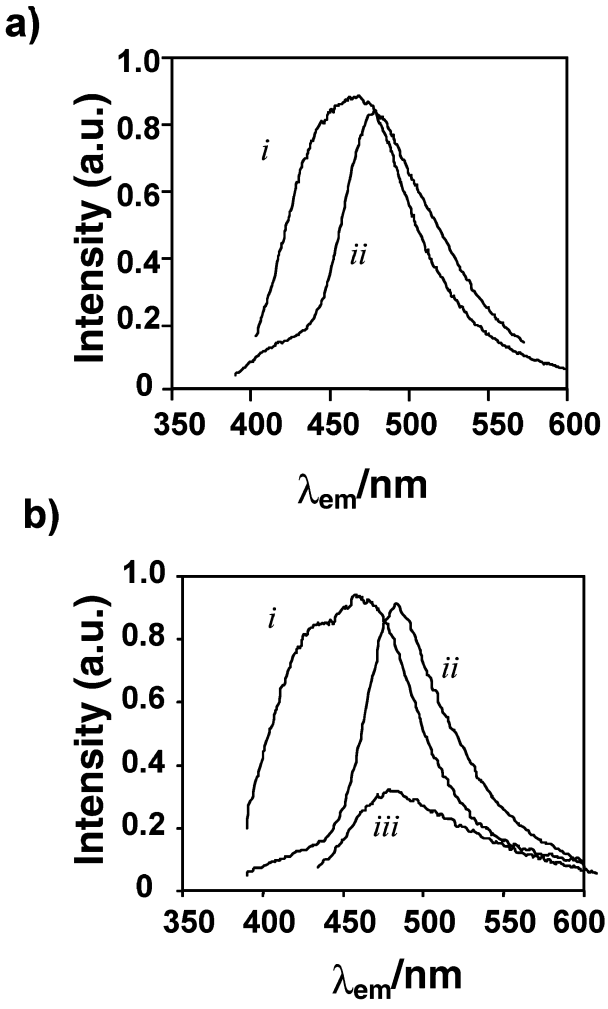

Fig. 18 (a) Normalized emission spectra from mixed monolayers of **6** and **8** having a 3:1 (i) and a 2:1 (ii) ratio. (b) Normalized emission spectra from mixed monolayers of a 4:1 ratio of adsorbates **5** and **8** (i), and a 1:1 ratio of adsorbates **7** and **8** (ii). Emission due to direct excitation of the acceptor at 420 nm is also illustrated (iii).

donor and acceptor as a result of inefficient energy transfer. In contrast, the emission spectrum of a SAM prepared with a 2:1 ratio of **6** to **8** is narrow, resulting purely from Coumarin-343 emission as energy transfer is highly efficient.

The importance of the dendritic character of donor chromophore **7** was confirmed in experiments involving adsorbate **5**

with its single Coumarin-2. The use of a 4 : 1 ratio of **5** to **8**, equivalent to the 1 : 1 ratio of **7** to **8**, led to incomplete energy transfer [Fig. 18(b)]. This illustrates the importance of the average inter-adsorbate distance in the energy transfer process as the dendritic nature of **7** facilitates the productive assembly of chromophores in the monolayer. Amplification of acceptor emission by sensitized excitation was clearly illustrated as the light output from the acceptor chromophore is significantly higher when it results from donor excitation at 350 nm than from its direct excitation at 420 nm.

Energy transfer in self-assembled dendritic structures of a different sort have recently been reported by Meijer and coworkers.[54] Poly(propylene imine) dendrimers were surface-modified with oligo(*p*-phenylene vinylene) (OPV) units affording amphiphilic structures that function as hosts capable of extracting water-soluble guests into the organic phase. Since the OPV-surface units are fluorescent, with an emission maximum at 492 nm when excited at 420 nm, it was speculated that energy transfer to a suitable chromophoric guest could occur. Using Sulforhodamine B as the energy-accepting guest (Fig. 19),

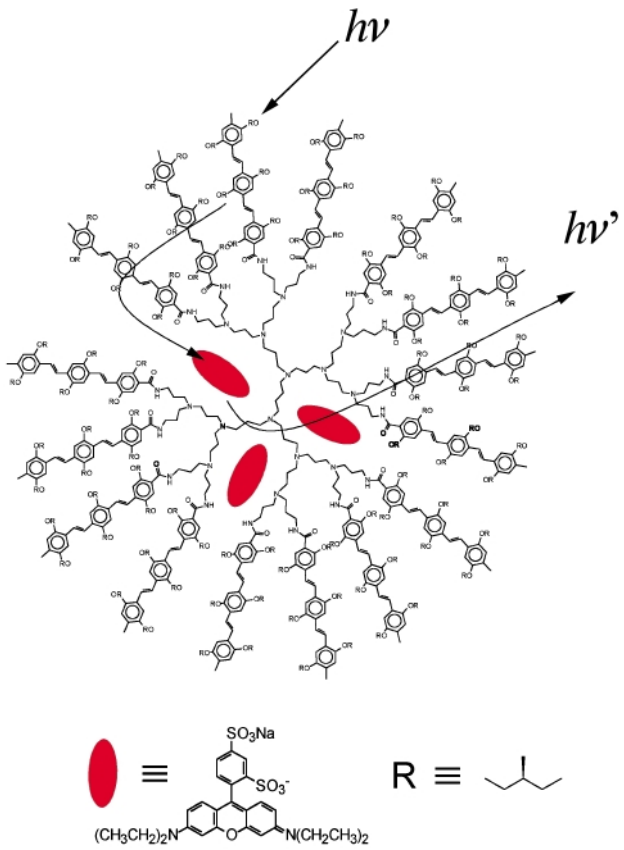

Fig. 19 Schematic representation of energy transfer from the peripheral OPV units to the encapsulated Sulforhodamine B guest within poly(propylene imine) dendrimers.

energy transfer was indeed observed with an efficiency of roughly 40% at maximal loading. This efficiency is significantly lower than achieved with dendrimers in which donor and acceptor are covalently linked, but this may be due, at least in part, to the poor overlap between donor emission and acceptor absorption.

Conclusions and outlook

In analogy to the natural photosynthetic systems, dendrimers, with their numerous branching units and chain ends uniformly surrounding a single core unit, seem ideally suited to function as light-harvesting structures. The examples illustrated in this article give testimony to our ability, through chemical manipulation, to create effective—if still very simple—mimics of natural photosystems. It is possible to vary the structural units in order to affect the physical properties of these molecules, while still maintaining a well defined, monodisperse macromolecule. Although it is unlikely that the current generation of light-harvesting dendrimers will be utilized in any but the most specialized applications owing to the somewhat tedious and expensive nature of their synthesis, they will prove to be effective model systems that will impact sensor technology, light-emitting diodes, fluorescent labeling of biological molecules, as well as a variety of photonic devices. It should be noted however that new routes to dendrimers[55] and less precise but nevertheless useful hyperbranched polymers[56] and dendritic hybrids are being developed, and some of these have already been applied to easily accessed multichromophoric systems.[57,58] In addition, it is envisioned that future work in this field will advance toward more complex mimics of natural photosynthetic systems, in which the energy absorbed at the dendrimer periphery will be employed to catalyze a chemical reaction. Nature utilizes the sun's energy to enable an electron transfer within the reaction complex, which eventually leads to the production of biologically important molecules such as ATP. Clearly, synthetic antennas have a long way to go as they aim to reach similar goals. The stakes of this research are high, as the development of novel synthetic photocatalysts and more efficient photovoltaic cells, such as the Grätzel cells,[59,60] would expand our ability to better utilize the sun's energy and decrease our dependency on fossil fuels.

Acknowledgements

Financial support of our research by the National Science Foundation (NSF-DMR 9816166) and the AFOSR-MURI and ARO-MURI programs is gratefully acknowledged. The authors also thank Sylvain Gilat for his contributions to this work, and Stefan Hecht for stimulating discussions and technical assistance.

Notes and references

1 J. A. Merrigan, *Prospects for Solar Energy Conversion by Photovoltaics*, MIT Press, Cambridge, 1975.
2 A. L. Lehninger, D. L. Nelson and M. M. Cox, *Principles of Biochemistry*, Worth Publishers Inc., New York, 1993.
3 X. Hu, A. Damjanovic, T. Ritz and K. Schulten, *Proc. Natl. Acad. Sci. U.S.A.*, 1998, **95**, 5935.
4 G. McDermott, S. M. Prince, A. A. Freer, A. M. Hawthornthwaite-Lawless, M. Z. Papiz, R. J. Cogdell and N. W. Isaacs, *Nature*, 1995, **374**, 517.
5 D. A. Tomalia, A. M. Naylor and W. A. Goddard III, *Angew. Chem., Int. Ed. Engl.*, 1990, **29**, 138.
6 J. M. J. Fréchet, *Science*, 1994, **263**, 1710.
7 J. M. J. Fréchet and C. J. Hawker, in *Comprehensive Polymer Science, 2nd Suppl.*, ed. S. L. Aggarwal and S. Russo, Pergamon Press, Oxford, 1996, p. 140.
8 G. R. Newkome, C. N. Moorefield and F. Vögtle, *Dendritic Molecules: Concepts, Syntheses, Perspectives*, VCH, New York, 1996.
9 D. A. Tomalia, H. Baker, J. R. Dewald, M. Hall, G. Kallos, S. Martin, J. Roeck, J. Ryder and P. Smith, *Polym. J.*, 1985, **17**, 117.
10 G. R. Newkome, Z.-Q. Yao, G. R. Baker and V. K. Gupta, *J. Org. Chem.*, 1985, **50**, 2003.
11 C. Wörner and R. Mülhaupt, *Angew. Chem., Int. Ed. Engl.*, 1993, **32**, 1306.
12 E. M. M. de Brabander-van den Berg and E. W. Meijer, *Angew. Chem., Int. Ed. Engl.*, 1993, **32**, 1308.
13 C. J. Hawker and J. M. J. Fréchet, *J. Am. Chem. Soc.*, 1990, **112**, 7638.
14 N. J. Turro, *Modern Molecular Photochemistry*, University Science Books, Sausalito, 1991.
15 D. L. Dexter, *J. Chem. Phys.*, 1953, **21**, 836.
16 T. Förster, *Ann. Phys.*, 1948, **2**, 55.
17 T. Förster, *Z. Naturforsch.*, 1949, **4**, 321.
18 B. Wieb Van Der Meer, G. Coker III and S.-Y. Simon chen, *Resonance Energy Transfer, Theory and Data*, VCH, Weinheim, 1994.
19 S. Campagna, G. Denti, S. Serroni, M. Ciano, A. Juris and V. Balzani, *Inorg. Chem.*, 1992, **31**, 2982.
20 G. Denti, S. Campagna, S. Serroni, M. Ciano and V. Balzani, *J. Am. Chem. Soc.*, 1992, **114**, 2944.

21 A. Juris, V. Balzani, F. Barigelletti, S. Campagna, P. Belser and A. von Zelewsky, *Coord. Chem. Rev.*, 1988, **84**, 85.
22 V. Balzani, S. Campagna, G. Denti, A. Juris, S. Serroni and M. Venturi, *Acc. Chem. Res.*, 1998, **31**, 26.
23 P. Belser, A. von Zelewsky, M. Frank, C. Seel, M. Frank, F. Vögtle, L. De Cola, F. Barigelletti and V. Balzani, *J. Am. Chem. Soc.*, 1993, **115**, 4076.
24 S. Campagna, G. Denti, S. Serroni, A. Juris, M. Venturi, V. Ricevuto and V. Balzani, *Chem. Eur. J.*, 1995, **1**, 211.
25 S. Serroni, A. Juris, M. Venturi, S. Campagna, I. R. Resino, G. Denti, A. Credi and V. Balzani, *J. Mater. Chem.*, 1997, **7**, 1227.
26 Z. Xu and J. S. Moore, *Acta Polym.*, 1994, **45**, 83.
27 Z. Xu and J. S. Moore, *Angew. Chem., Int. Ed. Engl.*, 1993, **32**, 246.
28 Z. Xu and J. S. Moore, *Angew. Chem., Int. Ed. Engl.*, 1993, **32**, 1354.
29 C. Devadoss, P. Bharathi and J. S. Moore, *J. Am. Chem. Soc.*, 1996, **118**, 9635.
30 M. R. Shortreed, S. F. Swallen, Z.-Y. Shi, W. Tan, Z. Xu, C. Devadoss, J. S. Moore and R. Kopelman, *J. Phys. Chem. B*, 1997, **101**, 6318.
31 S. F. Swallen, Z.-Y. Shi, W. Tan, Z. Xu, J. S. Moore and R. Kopelman, *J. Lumin.*, 1998, **76–77**, 193.
32 A. Bar-Haim, J. Klafter and R. Kopelman, *J. Am. Chem. Soc.*, 1997, **119**, 6197.
33 A. Bar-Haim and J. Klafter, *J. Phys. Chem. B*, 1998, **102**, 1662.
34 A. Bar-Haim and J. Klafter, *J. Lumin.*, 1998, **76–77**, 197.
35 W. J. Miniscalco, *J. Lightwave Technol.*, 1991, **9**, 234.
36 E. Desurvire, *Erbium-Doped Fiber Amplifiers: Principles and Applications*, John Wiley & Sons, New York, 1994.
37 M. Kawa and J. M. J. Fréchet, *Chem. Mater.*, 1998, **10**, 286.
38 M. Kawa and J. M. J. Fréchet, *Thin Solid Films*, 1998, **331**, 259.
39 D.-L. Jiang and T. Aida, *J. Am. Chem. Soc.*, 1998, **120**, 10 895.
40 M. Kimura, T. Shiba, T. Muto, K. Shirai and H. Hanabusa, *Marcromolecules*, 1999, **32**, 8237.
41 T. Sato, D.-L. Jiang and T. Aida, *J. Am. Chem. Soc.*, 1999, **121**, 10 658.
42 D.-L. Jiang and T. Aida, *Nature*, 1997, **388**, 454; T. Aida, D.-L. Jiang, E. Yashima and Y. Okamoto, *Thin Solid Films*, 1998, **331**, 254.
43 G. M. Stewart and M. A. Fox, *J. Am. Chem. Soc.*, 1996, **118**, 4354.
44 M. A. Fox, *Photoinduced Electron Transfer*, Elsevier, Amsterdam, 1988.
45 S. L. Gilat, A. Adronov and J. M. J. Fréchet, *Angew. Chem., Int. Ed.*, 1999, **38**, 1422.
46 S. L. Gilat, A. Adronov and J. M. J. Fréchet, *J. Org. Chem.*, 1999, **64**, 7474.
47 A. Adronov, S. L. Gilat, J. M. J. Fréchet, K. Ohta, F. V. R. Neuwahl and G. R. Fleming, *J. Am. Chem. Soc.*, 2000, **122**, 1175.
48 A. Adronov, P. R. L. Malenfant and J. M. J. Fréchet, *Chem. Mater.*, 2000, **12**, 1463.
49 A. W. Freeman, J. M. J. Fréchet, S. C. Koene and M. E. Thompson, *Polym. Prepr.*, 1999, **40**, 1246.
50 S. C. Koene, A. W. Freeman, K. A. Killeen, J. M. J. Fréchet and M. E. Thompson, *Polym. Mater. Sci. Eng.*, 1999, **80**, 238.
51 A. W. Freeman, S. C. Koene, P. R. L. Malenfant, M. E. Thompson and J. M. J. Fréchet, 2000, submitted.
52 P.-W. Wang, Y.-J. Liu, C. Devadoss, P. Bharathi and J. S. Moore, *Adv. Mater.*, 1996, **8**, 237.
53 L. A. J. Chrisstoffels, A. Adronov and J. M. J. Fréchet, *Angew. Chem., Int. Ed.*, 2000, **39**, 2163.
54 A. P. H. J. Schenning, E. Peeters and E. W. Meijer, *J. Am. Chem. Soc.*, 2000, **122**, 4489.
55 H. Ihre, A. Hult, I. Gitsov and J. M. J. Fréchet, *Macromolecules*, 1998, **31**, 4061.
56 H. T. Chang and J. M. J. Fréchet, *J. Am. Chem. Soc.*, 1999, **121**, 2313.
57 S. Hecht, T. Emrick and J. M. J. Fréchet, *Chem. Commun.*, 2000, 313.
58 S. Hecht, H. Ihre and J. M. J. Fréchet, *J. Am. Chem. Soc.*, 1999, **121**, 9239.
59 B. O'Reagan and M. Grätzel, *Nature*, 1991, **335**, 737.
60 A. Hagfeldt and M. Grätzel, *Acc. Chem. Res.*, 2000, **33**, 269.

Simultaneous atom transfer and nitroxide mediated controlled free radical polymerization of styrene†

Michael R. Korn*[a] and Michel R. Gagné*[b]

[a] *Department of Chemistry, Southwest Texas State University, San Marcos, TX 78666, USA. E-mail: mk15@swt.edu*
[b] *Department of Chemistry, University of North Carolina at Chapel Hill, Chapel Hill, NC 27599-3290, USA. E-mail: mgagne@unc.edu*

Received (in Corvallis, OR, USA) 22nd May 2000, Accepted 24th July 2000
First published as an Advance Article on the web 21st August 2000

Equimolar mixtures of NMRP and ATRP initiators lead to polystyrene that is unimodal by GPC; the mechanism of action most consistent with the data suggests that under the reaction conditions, TEMPO and Cl end groups scramble rapidly relative to the propagation rate, and result in a single type of polymer chain.

Recent developments in controlled free radical polymerizations of vinyl monomers mediated by either Cu complexes (atom transfer radical polymerization, ATRP) or by TEMPO-derivatives (nitroxide mediated radical polymerizations, NMRP) have stimulated much research as they yield homopolymers and block copolymers with predictable MWs along with narrow polydispersities.[1]

While ATRP and NMRP are almost always used separately, we wondered whether the ATRP and NMRP initiators could each be used as the end groups on a single polymer chain. Critical to the success of this idea is whether the ATRP and NMRP end groups show crossover reactivity. If no crossover occurs, then the end groups of a one-pot mixed ATRP–NMRP initiator system should operate independently and grow polymers of different molecular weights if the rates of polymerization are different. If ATRP and NMRP end groups do exchange, however, then the structure of the resulting polymers will be sensitive to the relative rates of exchange and propagation.

To first address the issue of end group reactivity, four initiators (**1**–**4**) were used to synthesize polystyrene (PS): the monofunctional ATRP initiators benzyl chloride **1** and 4-(pyren-1-yl)butyl 3-chloromethylbenzoate **3**,[2] the monofunctional NMRP initiator 2-phenyl-2-(2,2,6,6-tetramethylpiperidin-1-yloxy)ethyl benzoate **2** and the symmetrical difunctional NMRP initiator bisphenol A bis[2-phenyl-2-(2,2,6,6-tetramethylpiperidin-1-yloxy)ethyl carbonate] **4**.

Polymerization conditions were chosen where both ATRP and NMRP mechanisms should be able to function, and were not varied during the study. Reaction solutions were first degassed with three freeze–pump–thaw cycles, and the polymerizations run at 135 °C under nitrogen (4 h), with equimolar amounts of initiator, CuCl, hexamethyltriethylenetetramine (N_4)[3] and acetic anhydride.[4] The results are listed in Table 1.

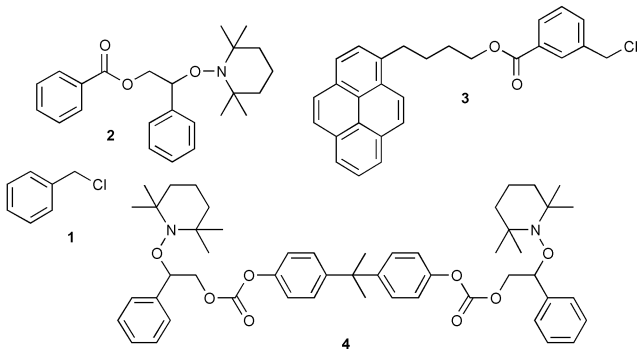

Prototypical ATRP and NMRP initiators were first tested separately as control reactions. Under exclusive ATRP conditions monofunctional initiator **1** (benzyl chloride) gave **PS-1a** (M_n = 36 000 g mol^{-1}, 70% conversion) and PDI of 1.89 (Table 1, entry **1a**). Polymerization of styrene using **1** under the modified ATRP–NMRP conditions (addition of acetic anhydride) also yielded PS with a broad MWM_n (distributions (MWD) PDI = 2) and polydispersity index, of 62 000 g mol^{-1} (42% conversion) (Table 1, entry **PS-1b**). Unlike typical ATRP conditions where the catalyst is a greenish colour, the modified reaction solution is deep blue.[5] Both experiments show that for **1**, the ATRP mechanism does not effectively control the polymerization under these conditions, and autopolymerization likely dominates. Polymerization of **3** under ATRP conditions is fast (100% conversion) and yields **PS-3** with a M_n of 28 000 g mol^{-1}, significantly closer to the theoretical M_n of 21 000 g mol^{-1}. The GPC chromatograms at 254 and 350 nm are both unimodal; the 350 nm trace is slightly shifted towards lower MW as expected for a chromophoric endgroup.[6] Polymerization of styrene with NMRP initiator **2** under exclusive NMRP conditions (no CuCl–N_4) was slow (14% conversion) and resulted in low molecular weight **PS-2** (M_n = 4600 g mol^{-1},

† The IUPAC name for a nitroxide is aminoxyl.

Table 1 MWD of PS obtained using modified NMRP–ATRP conditions

Entry	Initiator(s)	Reaction	$M_{n,\,calc.}$[a]/ g mol^{-1}	$M_{n,\,exp.}$ GPC[b]/ g mol^{-1}	PDI	Conversion[c] (%)
PS-1a	**1**	ATRP[d]	21 000	36 000	1.89	69
PS-1b	**1**	ATRP/Ac_2O[e]	21 000	62 000	1.97	42
PS-2	**2**	NMRP[d]	21 000	4 600	1.32	14
PS-3	**3**	ATRP[d]	21 000	28 000	1.52	100
PS-4	**1,2**	NMRP–ATRP[f]	10 500	9 000	1.29	50
PS-5	**2,3**	NMRP–ATRP[f]	10 500	9 000	1.46	60
PS-6	**3,4**	NMRP–ATRP[f]	10 500	18 500	1.42	73
PS-7	**PS-6**	Hydrolysis[g]	n/a	15 000	1.25	n/a

[a] Based on ratio of moles of initiation sites and styrene for 100% initiation and 100% conversion. [b] Based on PS standards, THF, UV (254 nm) detector. [c] Based on isolated yield. [d] 200 equiv. of styrene. [e] Ac_2O equimolar to **1**. [f] 100 equiv. of styrene. [g] In KOH–dioxane, 80 °C overnight, followed by acidification (HCl) and precipitation into MeOH–water.

DOI: 10.1039/b004157m

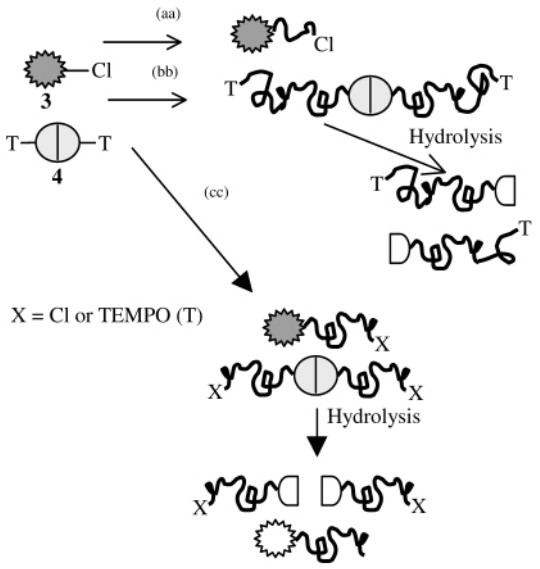

Scheme 1 Scenarios (aa)–(cc) for the polymerisation of styrene in a one-pot mixture of ATRP and NMRP initiators **3** and **4**.

PDI = 1.32), which if extrapolated to 100% conversion results in M_n of 29 000 g mol^{-1}. Combining monofunctional ATRP and NMRP initiators **1** and **2**, respectively, together (one pot), obtains **PS-4** that was *monomodal* by GPC (M_n = 9000 g mol^{-1}, PDI = 1.29, 50% conversion). The monomodal distribution has several mechanistic interpretations: either (a) **1** or **2** initiates and propagates; or (b) **1** and **2** each initiate, but they propagate independently and at the same rate; or (c) the chlorine atom and nitroxide radicals exchange rapidly between end groups relative to propagation, *i.e*. the end groups don't remain unique.

To test for scenario (a) and to determine if the ATRP initiator led to polymer, UV-tagged **3** was employed together with **2**. The resulting polymer **PS-5** again was unimodal by GPC (M_n = 9000 g mol^{-1}, PDI = 1.46, 60% conversion), similar to **PS-4**. Most significantly, GPC traces recorded at 254 and 320 nm were superimposable and confirmed that initiation of at least the benzyl chloride functionality occurs in the mixture.

To similarly test if the NMRP initiator led to polymer, 0.5 equiv. of the difunctional initiator **4** was employed with one equiv. of **3**. This experiment allows three scenarios to be distinguished (see Scheme 1): (aa) if only **3** initiates and propagates, then a monomodal GPC trace with overlapping 254/350 nm GPC absorbances would result; (bb) if only compound **4** initiates and propagates, then no GPC trace would be observed at 350 nm and hydrolysis of the carbonate linkage would cut the resulting PS in half; (cc) if both types initiate and the end groups exchange more rapidly than propagation occurs, then a bimodal GPC trace would result with the low MW peak being UV-active at 350 nm. Hydrolysis of the carbonate linkage should halve the MW of the peak that doesn't absorb at 350 nm and return to an overlapping 254/350 nm GPC chromatogram.

This combination of **4** and **3** yielded **PS-6** (M_n = 18 500 g mol^{-1}, maximum peak at 30 000 g mol^{-1}, and PDI = 1.42, 73% conversion) that was *bimodal* at 254 nm and *unimodal* at 350 nm (Fig. 1). The 350 nm UV-active peak at M_n ~ 15 000 g mol^{-1} confirms that **3** has initiated and propagated in the presence of **4**, consistent with the experiment in entry **3**. A separate peak at ~ 30 000 g mol^{-1} in the 254 nm trace confirms that **4** also initiates and propagates in the presence of **3**. Since both initiators lead to polymer, these data eliminate scenarios (aa) and (bb) where only a single initiator leads to polymer.

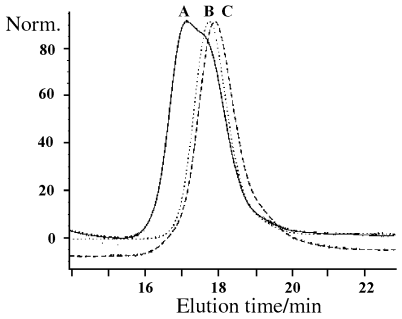

Fig. 1 GPC chromatogram of **PS-6** at 254 nm (A), 350 nm (B), and of **PS-7** at 254 nm (C).

Hydrolysis of **PS-6** yields **PS-7** that is *unimodal* at 254 nm (M_n = 15 000 g mol^{-1}, PDI = 1.25), and is now superimposable with the 350 nm GPC trace of **PS-5** (Fig. 1). Since all three PS blocks have the same MW, these data indicate that either the two propagation mechanisms form polymer at the same rate [*cf.* scenario (b)], or some process permutes the end groups rapidly enough to have a single propagation rate constant describe chain growth [scenario (c)].

From the productivity and MWD of the resulting PS as compared to the controls, it is clear that the modified reaction conditions affect both the ATRP and NMRP processes and most reasonably point to a common propagation mechanism for each of the two initiators in the reaction. For this to occur, Cl and nitroxide end groups must exchange rapidly relative to propagation. Crossover experiments in NMRP processes show that nitroxide end groups freely permute between growing polymer chains *via* indiscriminate nitroxide–radical recombinations,[7] and presumably do so in the present experiments as well. By homolysing the benzyl chloride end group, the ATRP mechanism similarly generates benzyl radicals and the opportunity to redeposit the Cl$^{\bullet}$ onto a nitroxide derived free radical. Thus, Cu^{I} amine complexes might reasonably catalyse the exchange between Cl and nitroxide end groups, and provide a mechanism for the global exchange of end groups.

In summary, the data presented herein indicate that under our reaction conditions, the NMRP and ATRP mechanisms do not operate independently and end group crossover occurs. Consequently, both initiators lead to polymers that grow at a common rate. However, the data don't distinguish if ATRP, NMRP, or both mechanisms are responsible for chain growth.

We thank the UNC Chapel Hill Curriculum in Applied Sciences, UNC Research Council, DuPont, 3M, and the Camille Dreyfus Foundation for partial support, and Ms Wendy Y. Mills for providing a sample of **4**.

Notes and references

1 *Controlled Radical Polymerization*, ed. K. Matyjaszewski, ACS Symp. Ser. 685, American Chemical Society, Washington DC, 1998; D. Benoit, V. Chaplinski, R. Braslau and C. J. Hawker, *J. Am. Chem. Soc.*, 1999, **121**, 3904.
2 For preparation, see: M. R. Korn, J. D. Lennon, III, G. L. Glish and M. R. Gagné, *Macromolecules*, 1999, **32**, 5149.
3 J. Xia and K. Matyjaszewski, *Macromolecules*, 1997, **30**, 7697.
4 E. Malstroem, R. D. Miller and C. J. Hawker, *Tetrahedron*, 1997, **53**, 15 225.
5 M. Wei, J. Xia, S. G. Gaynor and K. Matyjaszewski, *Polym. Prepr.*, 1997, **38**, 685.
6 Y. Zhu, B. A. Howell and D. B. Priddy, *Polym. Prepr.*, 1997, **38**, 97.
7 C. J. Hawker, G. G. Barclay and J. Dao, *J. Am. Chem. Soc.*, 1996, **118**, 11 467.

ChemComm

Oriented growth of MCM-22 zeolite films

Mojie Cheng,* Dali Tan and Xinhe Bao

State Key Laboratory of Catalysis, Dalian Institute of Chemical Physics, Chinese Academy of Sciences, Dalian 116023, China. E-mail: mjcheng@ms.dicp.ac.cn

Received (in Cambridge, UK) 31st May 2000, Accepted 27th July 2000
First published as an Advance Article on the web 21st August 2000

MCM-22 zeolite films have been grown with layers vertical to the substrate under hydrothermal synthesis conditions, and characterized by X-ray diffraction and scanning electron microscopy.

In situ synthesis of zeolites and molecular sieves on various supports is of significant importance in utilizing the well defined intracrystalline pores for membrane separation, membrane catalysis and molecular sensing. A variety of zeolites and molecular sieves, *e.g.* ZSM-5 or silicalite-1,[1,2] zeolite A[3,4] and UTD-1,[5] have been grown into films and membranes. Most zeolite films and membranes are obtained with random crystal orientation, and better performances are expected for an oriented zeolite film or membrane.[6,7] Particularly for zeolites with one- or two-dimensional pore systems, the accessibility of zeolite pores in a film depends on crystal orientation. Zeolite MCM-22, which is a good catalyst in a variety of reactions,[8,9,11] has an unusual layered structure and dual two-dimensional pore systems.[10] Here we report the oriented growth of MCM-22 films under static hydrothermal synthesis conditions.

The synthesis mixture was prepared using silica sol (25wt% SiO_2), sodium aluminate, hexamethyleneimine (HMI), sodium hydroxide and deionized water. 0.8 g sodium hydroxide and 1.7 g sodium aluminate was dissolved in 135 g deionized water, then 10.3 g HMI and 50.2 g silica sol were added with stirring. The molar composition of the resultent mixture was $13.5Na_2O:5Al_2O_3:100SiO_2:4500H_2O:50HMI$. After stirring for 1 h at 303 K, the mixture was transferred into a Teflon-lined autoclave, and a glass plate was immersed vertically in the mixture. Crystallization was carried out at 423 K for 96 h. The powder product and the glass plate were separated, washed with deionized water, and then dried at 353 K. Calcination was carried out at 813 K for 10 h with a temperature ramping rate of 2 K min^{-1}. The products were characterized by X-ray diffraction (XRD) and scanning electron microscopy (SEM).

The XRD pattern of the as-synthesized powder sample [Fig. 1(a)], characterized by both sharp and broad peaks, agrees well with that of the as-synthesized MCM-22 sample, and the XRD pattern of the calcined powder sample [Fig. 1(b)], with only sharp peaks, is consistent with that of MCM-22.[12] Although the detailed structure of as-synthesized MCM-22 is unclear, it is clear that as-synthesized MCM-22 and the MCM-22 sample have the same *a*-parameter, but the *c*-parameter of MCM-22 is smaller than that of as-synthesized MCM-22. As-synthesized MCM-22 exhibits two separated XRD peaks at 2θ 6.5 and 7.2° for (002) and (100), respectively, whereas the two reflections overlap into one peak in MCM-22. Compared with the XRD patterns of as-synthesized MCM-22 and MCM-22 powder samples, no other phases except for as-synthesized MCM-22 and MCM-22 are present in the as-synthesized and calcined films [Fig. 1(c) and (d)]. The broad and sharp peaks of the as-synthesized film are unambiguously from as-synthesized MCM-22, and the sharp peaks of the calcined film are from MCM-22. The as-synthesized MCM-22 film gives an intense peak for (100) but very weak peaks for (001), (002), (101) and (102), which indicates that the MCM-22 crystals are grown with a preferred orientation. As the layers of MCM-22 are linked together along the [001] direction, the MCM-22 layers in the film are vertical to the substrate.

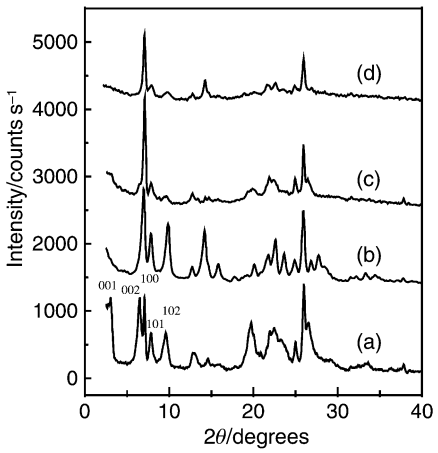

Fig. 1 XRD patterns of the as-synthesized MCM-22 powder (a), MCM-22 powder (b), as-synthesized MCM-22 film (c) and MCM-22 film (d).

SEM micrographs of MCM-22 crystals and the MCM-22 film are depicted in Fig. 2. MCM-22 crystals show stacked-thin-disk morphology. Most particles are aggregates of MCM-22 crystals intergrown in the [001] direction as illustrated in Fig. 2B. Sometimes intergrowth also occurs in the [100] direction. The MCM-22 film shows continuous intergrowth of MCM-22 crystals. The aligned-thin-sheet surface morphology, similar to that of MCM-22 crystals, further demonstrates that the MCM-22 layers are vertical to the substrate. The film has some cracks along the layer direction. Because as-synthesized MCM-22 lacks interlayer linkages and the *c*-parameter is larger than that of MCM-22, the formation of these cracks is ascribed to the contraction of the *c*-parameter during calcination. A cross-section micrograph (Fig. 2D) shows that the film has a thickness of *ca.* 5 μm. Only a monolayer of MCM-22 crystals is grown on the substrate and these crystals are largely normal to the substrate.

The formation of oriented zeolite films and membranes is closely related to the nucleation and crystal growth of zeolites. It has been demonstrated that completely oriented LTA-type zeolite films can be prepared by the intergrowth of oriented seed crystals.[6] Oriented zeolite films and membranes, *e.g.* of MFI-type[13,14] and AFI-type,[15] have also been prepared by direct hydrothermal syntheses. Zeolite crystals tend to orient with the largest crystal faces parallel to the smooth substrate, whereas crystal growth is preferred in the direction with the largest crystal growth rate vertical to the substrate. For thin disks, MCM-22 crystals would laterally lie on the smooth substrate. Thus, the vertical growth of MCM-22 film is not due to the orientation of the MCM-22 crystals. The high growth rate of the MCM-22 layer structure, indicated from the thin-disk-like crystal morphology, appears to be responsible for the vertical growth.

For MCM-22, shape-selective reactions occur in the channels and supercages, whereas the surface active sites can reduce the selectivity.[11] The low outer surface area vertically oriented MCM-22 film, for which the two pore systems are easily

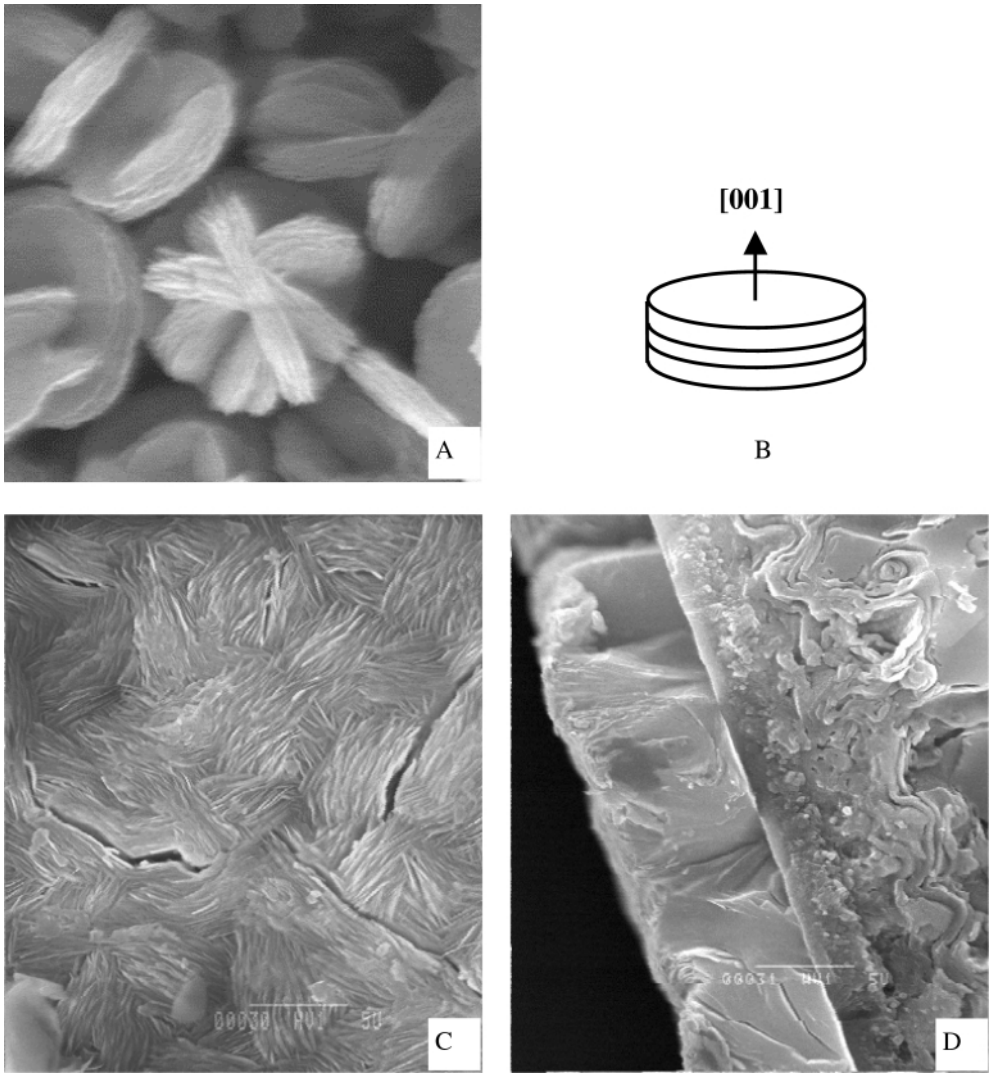

Fig. 2 SEM micrograph of the MCM-22 powder sample (A), the schematic intergrowth of MCM-22 crystals (B), and SEM photographs of the surface (C) and cross section (D) of the oriented MCM-22 film.

accessible to reactants may be a highly selective catalyst for some reactions.

Notes and references

1 J. G. Tsikoyiannis and W. O Haag, *Zeolites*, 1992, **12**, 126.
2 Y. Yan, M. E. Davis and G. R. Gavalas, *Ind. Eng. Chem. Res.*, 1995, **34**, 1652.
3 G. J. Myatt, P. M. Budd, C. Price and S. W. Carr, *J. Mater. Chem.*, 1992, **2**, 1103.
4 M. C. Lovallo and M. Tsapatsis, *Chem. Mater.*, 1997, **9**, 1705.
5 K. J. Balkus Jr., T. Munoz Jr. and M. E. Gimon-Kinsel, *Chem. Mater.*, 1998, **10**, 464.
6 T. Ban, T. Ohwaki, Y. Ohya and Y. Takahashi, *Angew. Chem., Int. Ed.*, 1999, **38**, 3324.
7 A. Gouzinis and M. Tsapatsis, *Chem. Mater.*, 1998, **10**, 2497.
8 A. Corma, C. Corell, F. Flopis, A. Martínez and J. Pérez-Pariente, *Appl. Catal.*, 1994, **115**, 121.
9 A. Corma and J. Martínez-Triguero, *J. Catal.*, 1997, **165**, 102.
10 M. E. Leonowicz, J. A. Lawton, S. L. Lawton and M. K. Rubin, *Science*, 1994, **264**, 1910.
11 P. Wu, T. Komatsu and T. Yashima, *Microporous Macroporous Mater.*, 1998, **22**, 343.
12 S. L. Lawton, A. S. Fung, G. J. Kennedy, L. B. Alemany, C. D. Chang, G. H. Hatzikos, D. N. Lissy, M. K. Rubin, H.-K. C. Timken, S. Steuernagel and D. E. Woessner, *J. Phys. Chem.*, 1996, **100**, 3788.
13 J. C. Jansen and G. M. van Rosmalen, *J. Cryst. Growth*, 1993, **128**, 1150.
14 M. Cheng, L. Lin, W. Yang, Y. Yang, Y. Xu and X. Li, *Stud. Surf. Sci. Catal.*, 1997, **105**, 2233.
15 S. Feng and T. Bein, *Nature*, 1994, **368**, 834; S. Feng and T. Bein, *Science*, 1994, **265**, 1839.

ChemComm

Unconventional layered mesophase-like TGBA phase in non-chiral α-(4′-propoxyphenylbenzyl-4-ylthio)-ω-(4′-butoxyphenybenzyl-4-ylthio)perfluorohexane

Xiaotun Yang and Shinichi Yano*

Department of Chemistry, Faculty of Engineering, Gifu University, Yanagido 1-1, Gifu 501-1193, Japan. E-mail: yano@apchem.gifu-u.ac.jp

Received (in Cambridge, UK) 1st June 2000, Accepted 1st August 2000
First published as an Advance Article on the web 22nd August 2000

Existence of a stable unconventional mesophase-like twist grain boundary smectic A (TGBA) phase was found in a wide temperature range for non-chiral α-(4′-propoxyphenylbenzyl-4-ylthio)-ω-(4′-butoxyphenylbenzyl-4-ylthio)-perfluorohexane (3BF6B4), which may be a consequence of the boomerang shape of the molecules.

Recently the generation and structure of TGB (twist grain boundary) phases have been investigated by several researchers[1–4] because of their unique packing structure. TGBA and TGBC phases can be regarded as smectic A and C variants composed of small SmA or SmC domains, respectively. The layer planes of the domains are arranged helically to form a macroscopic helical structure. Since the discovery of TGBA phases in (*R*)- or (*S*)-1-methylheptyl-4′-{[(4″-alkoxyphenyl)-propioloyl]oxy}biphenyl-4-carboxylate by Goodby *et al.*,[4] several liquid crystalline (LC) compounds exhibiting TGB phases have been reported, but, up to now, only chiral LC compounds were found to generate TGB phases, to our knowledge, with the chiral moiety causing a frustration of smectic ordering, so resulting in the helical ordering of the smectic domains. In this work, we have found unconventional layered mesophase-like TGBA (hereafter, simply denoted TGBA) phase in non-chiral α-(4′-propoxyphenylbenzyl-4-ylthio)-ω-(4′-butoxyphenylbenzyl-4-ylthio)perfluorohexane (3BF6B4, Fig. 1),† which is stabilized over a wide temperature range.

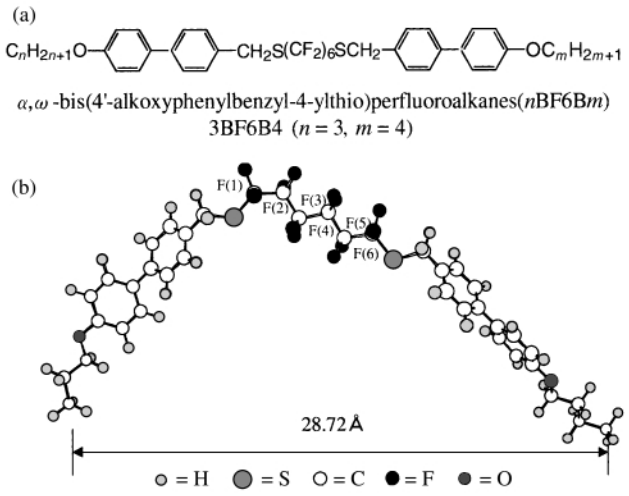

Fig. 1 Chemical structure of *n*BF*x*B*m* compounds (a) and the molecular model of 3BF6B4 obtained by PM3 calculation, where $–CF_2(1)–CF_2(2)–$ and $–CF_2(5)–CF_2(6)–$ bonds are in *gauche* and *trans* conformation, respectively (b).

Fig. 2(c) shows DSC curves of 3BF6B4.‡ For the first heating, the 3BF6B4 crystallites (Cr phase) melt to a TGBA state at 78.4 °C which changes into the isotropic liquid (I) phase at 99.4 °C. It is noted that the TGBA phase exists in the wide

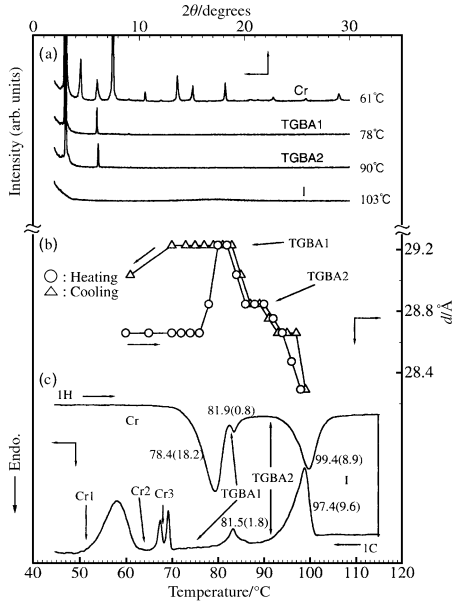

Fig. 2 X-Ray diffraction patterns of 3BF6B4 (a) and the temperature dependence of the spacing *d* (b) and DSC thermograms of 3BF6B4 (c). 1H: 1st heating, 1C: 1st cooling; Cr: crystalline state, I: isotropic phase. These figures in (c) denote the phase transition temperatures (°C) and enthalpy changes (kJ mol^{-1}).

temperature range from 78.4 to 99.4 °C. The identification of the TGBA phase was made from texture observations; Fig. 3 shows a cylindrical domain (CC) texture when the two glass plates are untreated [Fig. 3(a)] and a spiral filament texture when the two plates are rubbed parallel to the plane [Fig. 3(b)], this result indicating that the mesophase is a TGBA phase.[6] Moreover, we find an endothermic peak near 81.9 °C on heating of the DSC curve of Fig. 2(c), suggesting the presence of two TGBA phases, TGBA1 below 81.9 °C and TGBA2 above 81.9 °C; the TGBA textures of Fig. 3 were observed over the temperature range exhibiting the TGBA 1 and 2 phases and did not show any change between TGBA1 and TGBA2, hence it is believed that both phases essentially belong to the TGBA state. In Fig. 2(a), the X-ray scattering intensity (*I*) is plotted *vs.* the scattering angle (2θ) for 3BF6B4, as a function of temperature.‡ In the crystalline state (61 °C), the *I vs.* 2θ curve shows several sharp peaks, but only three peaks are seen at *ca.* 3.0, 6.0 and 9.0° for TGBA1 (78 °C) and at *ca.* 3.1, 6.1 and 9.2° for TGBA2 (90 °C). These three peaks are attributable to reflections from SmA layers of thickness 29.23 and 28.85 Å, respectively. A conformational structure was calculated for 3BF6B4, using PM3 (parametric method). As shown in Fig. 1(b), assuming a *gauche* conformation for $–CF_2(1)–CF_2(2)–$ a *trans* conformation for $–CF_2(5)–CF_2(6)–$, and a *trans* conformation for all the other bonds, the molecule is boomerang-shaped and the molecular length is estimated as 28.72 Å.[7] When the $–CF_2(1)–CF_2(2)–$ and $–CF_2(5)–CF_2(6)–$ bonds are in *trans* and *gauche*

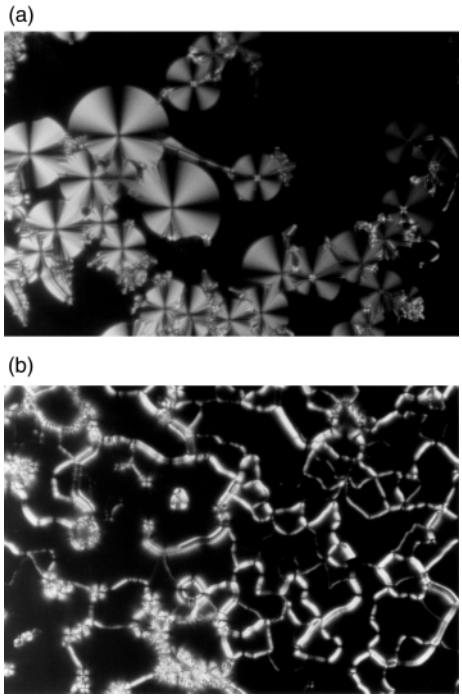

Fig. 3 The cylindrical domain (CC) texture of the TGBA phase at 92.5 °C (a) and spiral filament texture of the TGBA phase at 93.7 °C (b) in 3BF6B4 under a polarized microscope (magnification ×100).

conformation, respectively, the molecular length is estimated as 28.43 Å. Both molecular lengths are well consistent with the layer thickness obtained from the X-ray data.[8] From these results, both TGBA1 and TGBA2 phases can be tentatively concluded to be TGBA phases consisting of SmA domains. In Fig. 2(b), the spacing (*d*) is plotted *vs.* temperature. On heating, the value of *d* changes from 28.66 to 29.23 Å near the Cr–TGBA1 phase transition temperature, and suddenly decreases to 29.04 Å near the TGBA1–TGBA2 transition temperature, and rapidly decreases approaching the TGBA2–isotropic liquid (I) phase transition temperature. The decrease of *d* in the TGBA2 phase with increasing temperature may be caused by either the packing of 3BF6B4 molecules in the SmA layer being disturbed or the packing of the long molecular axes of 3BF6B4 molecules at a tilt angle to the layer normal (TGBC). At present, we infer that the former packings may be responsible for the appearance of TGBA2, since the texture of TGBA2 is similar to that in TGBA1.

In conclusion, this work has revealed the existence of a TGBA phase in non-chiral 3BF6B4, as a consequence of its boomerang-molecular shape, reminiscent of the generation of ferroelectricity in banana-shaped molecules.[9]

We are investigating the phase transition behaviors of *n*BF6B*m* homologues (Fig. 1), and at present, find the existence of TGBA phases in 3BF6B3, 3BF6B4 and 3BF6B5. Further studies will be published elsewhere in the near future.

Notes and references

† *Synthesis* of 3BF6B4: 4-*n*-propoxyphenylbenzylthioalcohol[5] (0.5 g, 0.002 mol) and 4-*n*-butoxyphenylbenzylthio (0.53 g, 0.002 mol) in THF (50 ml) was added to a soution of NaH (0.186 g, 0.0048 mol) in THF (30 ml) under N_2, to give a muddy white mixture. Dodecafluoro-1,6-diiodohexane (1.3 g, 0.0024 mol) was added dropwise to this mixture which was stirred at room temperature for 10 h. The crude product was obtained by evaporation to dryness after extraction into diethyl ether. The product was purified by column chromatography [silica gel, benzene–hexane (1 : 2.5)] and further by recrystallization from ethanol, giving 3BF6B4 (white powder, yield:18%). ^{1}H NMR (400 MHz, $CDCl_3$): δ 0.99 (3H, t, CH_3, *J* 7.6), 1.06 (3H, t, CH_3, *J* 7.6), 1.26 (2H, m, CH_2), 1.82 (4H, m, CH_2), 3.97 (2H, t, CH_2, *J* 6.6), 4.01 (2H, t, CH_2, *J* 6.3), 4.21 (4H, s, CH_2), 6.97 (4H, d, Ph-H, *J* 8.8), 7.39 (4H, d, Ph-H, *J* 8.3), 7.50 (4H, d, Ph-H, *J* 8.8), 7.53 (4H, d, Ph-H, *J* 8.3); 19F NMR (400 MHz, $CDCl_3$): δ 68.28, 35.99, 34.52.

‡ Phase transition parameters were measured by differential scanning calorimetry (Seiko Denshi DSC-210, SSC-5000) at a scanning rate of 5 K min^{-1}. The texture of the mesophase was observed by use of a polarizing microscope (NIKON OPTIPHOT-POL) equipped with a Mettler FP-82 hot stage. Wide-angle X-ray diffraction measurements were performed as a function of temperature with a Rigaku, Rinto 200 diffractometer equipped with a home-made cell using Cu-Kα radiation (40 kV, 30 mA), where the scattering intensities detected with a scintillation counter incorporating a pulse-height analyser.

1 C. C. Huang, D. S. Lin, J. W. Goodby, M. A. Waugh, S. M. Stein and E. Chin, *Phys. Rev. A*, 1989, **40**, 4153.
2 L. Navailles, H. T. Nguyen, P. Barois, C. Destrade and N. Isaert, *Liq. Cryst.*, 1990, **15**, 479.
3 S. R. Renn and T. C. Lubensky, *Phys. Rev. A*, 1988, **38**, 2132; S. R. Renn, *Phys. Rev. A*, 1992, **45**, 953.
4 J. W. Goodby, M. A. Waugh, E. Chin, R. Pindak and J. S. Patel, *J. Am. Chem. Soc.*, 1989, **111**, 8119; G. Strajer, R. Pindak, M. A. Waugh and J. W. Goodby, *Phys. Rev. Lett.*, 1990, **64**, 1545.
5 K. Abe, X. T. Yang, R. Kato and S. Yano, *Liq. Cryst.*, 2000, **27**, 839.
6 A. C. Ribeiro, H. T. Nguyen, Y. Galerne and D. Guillon, *Liq. Cryst.*, 2000, **27**, 27.
7 T. Sato and S. Yano, *Mol. Cryst. Liq. Cryst.*, 1987, **144**, 179; In this work, the crystal structure of cholesteryl δ-monohydrofluoropentanoate was determined by X-ray diffraction studies. The $–CF_2(\alpha)–CF_2(\beta)–$ bond in the pentanoate is found to be in a *gauche* transformation, similar to the present assumption.
8 The molecular lengths for *gauche*, *gauche* and *trans*, *trans* conformations, are estimated to be 33.86 or 22.69, and 37.12 Å, respectively, which differ from the observed layer.
9 T. Niori, T. Sekine, J. Watanabe, T. Furukawa and H. Takezoe, *J. Mater. Chem.*, 1996, **6**, 1231.

Unexpected regiochemistry of a tethered bismethano[60]fullerene

Glenn A. Burley,[a] Paul A. Keller,*[a] Stephen G. Pyne*[a] and Graham E. Ball[b]

[a] *Department of Chemistry, University of Wollongong, Wollongong, New South Wales, 2522, Australia. E-mail: Stephen_Pyne@uow.edu.au; Paul_Keller@uow.edu.au*
[b] *NMR Spectroscopy Unit, University of New South Wales, Sydney, New South Wales, 2052, Australia*

Received (in Cambridge, UK) 27th June 2000, Accepted 1st August 2000
First published as an Advance Article on the web 22nd August 2000

The structure of a novel tethered fullerene bis-adduct, of unexpected regiochemistry, has been unequivocally assigned using INADEQUATE 2D NMR experiments.

The regioselective, multifunctionalization of C_{60} is a continuing challenge in fullerene chemistry.[1] Bis- and tris-additions to fullerenes can generally be made regioselective through the use of tethered systems.[2] It is not clear, however, if the regiochemical outcome of tethered reactions is solely dependent upon the nature of the tether, or the stereoelectronic requirements of the reactive addend, or the mechanism of addition or some combination of these factors. An additional challenge for studies in this area is the development of methods for the unequivocal assignment of the structure of bis-tethered fullerene adducts. Earlier structural assignments of multiple adducts have relied on comparative methods (^{13}C NMR symmetry elements and UV-vis spectroscopy).[2e,3] However, as the production of higher order fullerene adducts increases, these methods will become less reliable, due to the decreasing symmetry of products and the lack of definitive structures for comparison. We report here the structure of a novel tethered fullerene bis-adduct of unexpected regiochemistry and the unequivocal assignment of its structure using INADEQUATE 2D NMR experiments.[4]

Earlier work has shown that tethered bis-malonate esters undergo regioselective bis-cyclopropanation reactions with C_{60} under Bingel conditions.[2e] For example, the *meta*-substituted bis-tethered system **2** gave exclusively the *cis*-**2** regioisomer as determined by UV-vis spectroscopy and from its symmetry, determined by 1D ^{13}C NMR spectroscopy. Interestingly, the *ortho*-isomer of **2** also gives a *cis*-**2** adduct, while the corresponding *para*-isomer gives predominantly the *trans*-**4** adduct. In contrast, we have found that treatment of C_{60} with the corresponding *meta*-substituted bis-imino-glycine tethered system **1** gives, under similar reaction conditions,[5] two regioisomeric adducts **3** and **4**[6] in a ratio of 80 : 20 from ^{1}H NMR analysis (Scheme 1). Compound **3** was obtained pure in 28% yield after separation by column chromatography and recrystallization. The ^{1}H NMR of **3** showed resonances for the two pairs of diastereotopic methylenes at δ 5.06 and 5.71 (AB q, J_{AB} 11.2 Hz), consistent with a tethered fullerene structure. Furthermore, the MALDI-TOF spectrum of **3** showed a characteristic parent molecular ion at *m/z* 1297. The UV-vis spectrum of **3** showed bands in the 400–800 nm region that suggested a *trans*-**4** structure but this conclusion was not definitive due to the lack of good reference compounds. Unequivocal evidence for the structure of **3** came from ^{13}C NMR and INADEQUATE experiments.[7]

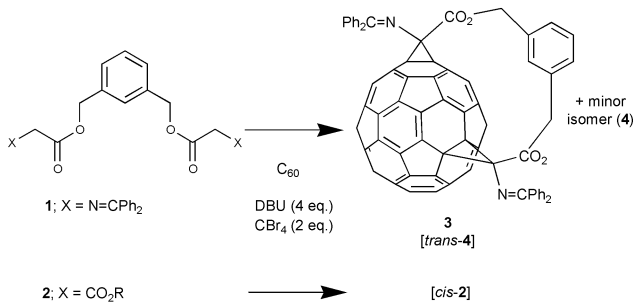

Scheme 1

^{13}C NMR spectroscopy revealed 31 peaks associated with the fulleryl carbons in **3**. The resonance at δ 150.56 was shown to arise from the fortuitous overlap of one full-intensity peak and one half-intensity peak. Hence **3** has 32 unique fullerene carbons, four of which give half-intensity peaks (labelled as grey circles in Fig. 1), indicative of a dimethanofullerene with C_S symmetry. To distinguish between the 3 possible structural isomers, *cis*-**1**, *cis*-**2** and *trans*-**4**, INADEQUATE experiments were performed on a 10% ^{13}C enriched sample of **3**.[8,9]

The above three possible isomers would be expected to show 2, 1 and 3 bond separations respectively, between a fulleryl sp^3 hybridized carbon and its nearest carbon on the plane of symmetry (*i.e.* half-intensity peak). These experiments revealed a 3-bond connectivity (shown as grey lines in Fig. 1) between C1 (sp^3 carbon) and C19 (half-intensity peak) providing unequivocal evidence for its *trans*-**4** structure. Starting from C19, correlations were observed to the other half-intensity peak (C20) with a relatively large coupling constant ($^1J_{CC}$ = 66.8 Hz) typical for 6,6 ring fusion carbons and one to C5 with a smaller $^1J_{CC}$ (57.2 Hz) typical for 6,5 ring fusion carbons.[4] C5 showed correlations to C6 ($^1J_{CC}$ = 73.1 Hz) and C4 ($^1J_{CC}$ = 53.2 Hz), consistent with their 6,6 and 5,6 ring fusion positions, as well as to C19. C6 showed a correlation to the sp^3 carbon C1, unequivocally confirming the position of the cyclopropane ring to the plane of symmetry. Further corroborative evidence for this structure was the observation that C4 showed only 2 correlations (to C3 and C5) consistent with the magnetic

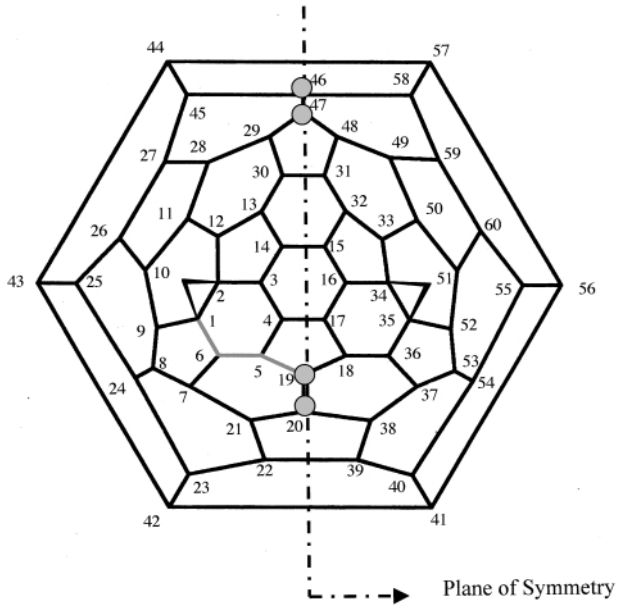

Fig. 1 Schlegel diagram of **3** (tether not shown) with carbons that lie on the plane of symmetry shown as grey circles.

DOI: 10.1039/b005157h

Table 1 Chemical shifts (δ), peak assignments, and carbon–carbon coupling constants ($^1J_{CC}$) for the [60]fullerene cage of **3** (^{13}C-enriched)[7]

Carbon Number	δ (ppm)	(Carbon number) $^1J_{C-C}$/Hz
1,35	81.37	(2),[b] (6) 44.5, (9) 44.5
2,34	81.25	(1),[b] (3) 40.8, (12) 41.2
3,16	145.73	(2) 40.8, (4) 69.9, (14) 58.8
4,17	129.04	(3) 69.9, (5) 53.2
5,18	136.24	(4) 53.2, (6) 73.1, (19) 57.2
6,[a]36	150.56	(1) 44.5, (5) 73.1, (7) 56.8
7,37	146.49	(6) 56.8, (8),[b] (21) 67.2
8,53	146.4	(7),[b] (9) 56.0, (24) 67.2
9,52	149.6	(1) 44.5, (8) 56.0, (10) 72.3
10,51	147.13	(9) 72.3, (11) 53.0, (26) 56.8
11,50	136.24	(10) 53.0, (12) 71.1, (28) 57.2
12,33	146.55	(11) 71.1, (13) 56.4, (2) 41.2
13,32	145.28	(12) 56.4, (14) 54.4, (30) 68.0
14,15	143.52	(13) 54.4, (15) 58.8
19[c]	142.21	(5) 57.2, (20) 66.8
20[c]	148.68	(19) 66.8, (21) 56.4
21,38	139.39	(7) 67.2, (20) 56.4, (22) 56.8
22,39[b]	141.11	(21) 56.8, (23)[b]
23,40[b]	141.28	(22),[b] (24),[b] (42) 56.4
24,54	140.89	(8) 67.2, (23),[b] (25) 56.4,
25,55	141.29	(24) 56.4, (26) 68.3, (43) 55.6
26,60	143.39	(10) 56.8, (25) 68.3, (27) 55.2
27,59	148.31	(26) 55.2, (28) 55.2, (44/45) 68.3
28,59	140.31	(11) 57.2, (27) 55.2, (29) 68.0
29,48	145.28	(28) 68.0, (30) 56.4, (47) 54.4
30,31	138.72	(29) 56.4, (13) 68.0
42,41	141.82	(23),[b] (43) 54.8
43,56	145.54	(25) 55.6, (42) 54.8, (44/45)[b]
44,57	145.46	(11),[b] (45)[b]
45,58	145.46	(27) 68.3, (44),[b] (46) 56.0
46[ac]	150.56	(45) 56.0, (47) 68.0
47[c]	145.73	(46) 68.0, (29) 57.2

[a] Denotes peak has two resonances, one full-intensity and one half-intensity. [b] Denotes coupling is not first order; peak positioning is consistent with structure model. [c] Denotes half-intensity peaks.

equivalence of C4 and C17 due to their positions relative to the plane of symmetry.

Using the above methods we have assigned all carbons in **3** and obtained information about the relative bond lengths from the measurement of $^1J_{CC}$ values (Table 1). These measured values were consistent with the radialene structure of **3**.

The regiochemical difference between our tethered reaction and that of **2** with C_{60} clearly demonstrates that much has yet to be understood about tethered fullerene reactions before generalizations on regiochemical outcomes can be made. These differences in regiochemistry may indicate that these reactions proceed *via* different mechanisms and experiments are in progress to help understand these differences.[10]

We thank the Australian Research Council for financial support and for a PhD scholarship to G. A. B.

Notes and references

1 F. Diederich and R. Kessinger, *Acc. Chem. Res.*, 1999, **32**, 537; A. Hirsch, Fullerenes and Related Structures, *Topics in Current Chemistry*, vol. 199, Springer-Verlag, Berlin, 1999, pp. 1–65.

2 (*a*) L. Isaacs, R. F. Haldimann and F. Diederich, *Angew. Chem., Int. Ed. Engl.*, 1994, **33**, 2339; (*b*) L. Isaacs, F. Diederich and R. F. Haldimann, *Helv. Chim. Acta*, 1997, **80**, 317; (*c*) F. Cardullo, P. Seiler, L. Isaacs, J. F. Nierengarten, R. F. Haldimann, F. Diederich, T. Mordasinidenti, W. Thiel, C. Boudon, J. P. Gisselbrecht and M. Gross, *Helv. Chim. Acta*, 1997, **80**, 343; (*d*) J. F. Nierengarten, A. Herrmann, R. R. Tykwinski, M. Ruttimann, F. Diederich, C. Boudon, J. P. Gisselbrecht and M. Gross, *Helv. Chim. Acta*, 1997, **80**, 293; (*e*) J. F. Nierengarten, T. Habicher, P. Kessinger, F. Cardullo, F. Diederich, V. Gramlich, J. P. Gisselbrecht, C. Boudon and M. Gross, *Helv. Chim. Acta*, 1997, **80**, 2238; (*f*) H. Isobe, H. Tokuyama, M. Sawamura and E. Nakamura, *J. Org. Chem.*, 1997, **62**, 5034; (*g*) M. Taki, S. Sugita, Y. Nakamura, E. Kasashima, E. Yashima, Y. Okamoto and J. Nishimura, *J. Am. Chem. Soc.*, 1997, **119**, 926; (*h*) T. Ishi-I, K. Nakashima, S. Shinkai and A. Ikeda, *J. Org. Chem.*, 1999, **64**, 984; (*i*) T. Ishi-I, R. Iguchi and S. Shinkai, *Tetrahedron*, 1999, **55**, 3883; (*j*) J. P. Bourgeois, P. Seiler, M. Fibbioli, E. Pretsch, F. Diederich and L. Echegoyen, *Helv. Chim. Acta*, 1999, **82**, 1572; (*k*) G. Rapenne, J. Crassous, A. Collet, L. Echegoyen and F. Diederich, *Chem. Commun.*, 1999, 1121.

3 F. Djojo, A. Herzog, I. Lamparth, F. Hampel and A. Hirsch, *Chem. Eur. J.*, 1996, **2**, 1537.

4 J. M. Hawkins, A. Meyer and R. Nunlist, *J. Am. Chem. Soc.*, 1991, **113**, 7770; J. M. Hawkins, T. A. Lewis, U. R. Nunlist, G. E. Ball, T. W. Ebbeson and K. Tanigaki, *J. Am. Chem. Soc.*, 1992, **114**, 7954.

5 G. A. Burley, P. A. Keller, S. G. Pyne and G. E. Ball, *Chem. Commun.*, 1998, 2539.

6 The minor isomer **4** was obtained pure in 12% yield and has C_2 symmetry from ^{13}C NMR analysis which showed no half-intensity peaks and 30 sp^2 resonances. The possible structures for this molecule therefore are, *cis*-**3**, *trans*-**3** or *trans*-**2**. The *trans* isomers seem unlikely from PM3 calculations, leaving *cis*-**3** as the most likely structure.

7 The INADEQUATE experiment was performed on a Bruker DMX 600 spectrometer fitted with a Bruker TXI-XYZ ^{1}H/^{13}C/^{15}N probe. The sample (*ca*. 16 mg) was dissolved in CS_2–$CDCl_3$ 6:4 (*ca*. 250 μl) in a Shigemi tube and the spectrum was recorded at 288 K. A standard pure phase (States-TPPI) double quantum spectrum with power-gated proton decoupling was employed. A spectral width of 13020.8 Hz was used in both dimensions resulting in deliberate folding in f_1 which does not cause any ambiguity of peak assignments. 2048 × 8192 total points were collected in t_1 and t_2 respectively. A recycle delay of 9 s and 16 scans per increment were employed. The 90° pulse length was 11.6 μs.

8 ^{13}C enriched (10%) C_{60} purchased from Mer Fullerenes, Arizona.

9 To a solution of [60]fullerene, CBr_4 (0.54 g, 1.42 mmol) and **1** (0.47 g, 0.810 mmol) in PhCl (200 mL) was added DBU (0.43 g, 0.675 mmol), at room temperature and the solution was stirred for 2 h. The crude material was filtered through a short plug of silica, eluting first with toluene (to retrieve unreacted [60]fullerene) and then with CH_2Cl_2 (DCM). Column chromatography eluting with (90:10; DCM–light petroleum) and recrystallised from DCM–Et_2O provided **3** (0.245 g, 28%) and **4** (0.093 g, 12%). Data for **3**: λ (DCM)/nm (ε/dm^3 mol^{-1} cm^{-1}): 420 (15000), 630 (250), 690 (150). δ_H($CDCl_3$, 400 MHz): 5.06 (d, *J* 11.2), 5.71 (d, *J* 11.2), 7.07 (t, *J* 7.6), 7.14 (s), 7.30 (t, *J* 7.6), 7.40 (t, *J* 7.2), 7.46 (t, *J* 7.2), 7.55 (t, *J* 7.2), 7.92 (d, *J* 8.4), 8.04 (d, *J* 8.4). δ_C($CDCl_3$, 100 MHz): 68.04, 81.47, 81.80, 97.06, 127.93, 128.04, 128.32, 129.36, 129.60, 136.42, 137.66, 138.92, 139.61, 140.60, 140.94, 141.27, 141.33, 141.39, 141.54, 142.10, 142.48 (*ipso*), 143.64, 143.92, 145.63, 145.68, 145.75, 145.80 (1C), 145.98, 146.03 (1C), 146.65, 146.75, 146.82, 147.40, 148.62, 148.99 (1C), 149.89, 150.88 (two peaks, one full-intensity and one half-intensity), 160.71, 161.25. MALDI-TOF *m/z* (-ve ion mode, 9-nitroanthracene): 1296 (M-H), 720 (C_{60}^-). Data for **4**: λ (DCM)/nm (ε/dm^3 mol^{-1} cm^{-1}): 320 (19000), 430 (sh, 1700), 450 (sh, 1400), 640 (280), 695 (190). δ_H($CDCl_3$, 400 MHz): 5.31 (d, *J* 11.2), 5.41 (d, *J* 11.2), 6.95 (s), 7.23 (t, *J* 7.6), 7.37 (dd, *J* 7.2, 1.6), 7.50 (dd, 7.6, *J* 1.2), 7.62 (t, *J* 8.4), 8.17 d, *J* 7.6), 8.21 (d, *J* 7.6). δ_C($CDCl_3$, 100 MHz): 68.46, 81.83, 82.38, 96.02, 128.32, 128.56, 129.64, 129.94, 131.37, 134.55, 134.77, 138.49, 139.24, 140.71, 141.02, 141.20, 141.84, 143.36, 143.46, 143.98, 144.06, 144.11, 144.30, 144.42, 144.70, 144.92, 145.00, 145.92, 147.28, 147.38, 147.51, 147.80, 148.55, 148.86, 149.01, 149.21, 150.93, 153.44, 154.37, 161.03, 161.14. MALDI-TOF *m/z* (−ve ion mode, 9-nitroanthracene): 1296 (M-H), 720 (C_{60}^-).

10 PM3 calculations indicated little difference in heats of formation between **3** and its *cis*-**2** isomer.

ChemComm

Solid-state NMR evidence for the presence of two crystallographically distinct tetrahedral sites in zeolite merlinoite†

Suk Bong Hong,*[a] Duk-Young Han,[b] Oc Hee Han[c] and In-Sik Nam[d]

[a] *Department of Chemical Technology, Taejon National University of Technology, Taejon 300-717, Korea. E-mail: sbhong@hyunam.tnut.ac.kr*
[b] *Korea Basic Science Institute, Seoul Branch, Seoul 136-701, Korea*
[c] *Korea Basic Science Institute, Headquarters, Taejon 305-333, Korea*
[d] *Department of Chemical Engineering, School of Environmental Engineering, Pohang University of Science and Technology (POSTECH), Pohang 790-784, Korea*

Received (in Cambridge, UK) 13th June 2000, Accepted 31st July 2000
First published as an Advance Article on the web 22nd August 2000

Two crystallographically distinct tetrahedral sites in zeolite merlinoite are identified by ^{29}Si MAS NMR and 2D ^{27}Al quadrupole nutation NMR spectroscopies.

Since the initial work of Lippmaa and Engelhardt in 1981,[1] the use of multi-nuclear solid-state NMR techniques in the characterization of zeolites and related materials has provided many new insights into the structure and chemistry of this important class of microporous solids, particularly in the short-range order. For instance, ^{29}Si MAS NMR can detect the relative populations of five distinct Si environments, *i.e.* $Si(OSi)_n(OAl)_{4-n}$ with n = 0–4.[2] When all tetrahedral atoms (T-atoms) in the zeolite framework are crystallographically equivalent with avoidance of Al–O–Al linkages, therefore, the quantitative framework Si/Al ratio can be easily calculated from the ^{29}Si resonance intensities. However, many of the already known zeolite structures contain two or more crystallographically distinct T-sites characterized by different T–O–T and O–T–O bond angles and T–O bond lengths. This allows the Si atoms situated in these sites to exhibit different ^{29}Si chemical shifts, even for the same $Si(OSi)_n(OAl)_{4-n}$ environments, making it difficult to accurately determine the framework Si/Al ratio from the spectra. When structurally distinct lines overlap heavily with one another, in particular, it is not possible to directly deconvolute the ^{29}Si NMR spectra.

Merlinoite (MER topology) is a small-pore, low-silica zeolite that is rarely found in nature.[3] Amongst the early zeolite discoveries, in addition, zeolites W and K-M are known to be synthetic counterparts of MER zeolite.[4,5] The structure of this zeolite is characterized by a three-dimensional pore system consisting of intersecting 8-ring channels.[6] To date, there are three reported ^{29}Si MAS NMR spectra of MER-type zeolites prepared *via* different synthetic routes.[7–9] In all cases, the interpretation and assignment of the spectra have been made based on the implicit assumption that only one crystallographically distinct T-site exists in the zeolite framework. A recurring question is the fact that the Si/Al ratios calculated from the ^{29}Si NMR spectra are not in reasonable agreement with those determined from elemental analysis. This implies that each line in the ^{29}Si MAS NMR spectra of MER zeolites previously reported may be misunderstood. Here we present the ^{29}Si MAS NMR and 2D ^{27}Al quadrupole nutation NMR results showing that two crystallographically distinct T-sites are present in the framework of MER-type zeolites.

An MER zeolite with Si/Al = 1.8 was prepared by heating an aluminosilicate gel with the oxide composition of $1.2Na_2O \cdot 4.8K_2O \cdot 1.0Al_2O_3 \cdot 10SiO_2 \cdot 150H_2O$ at 100 °C for 18 d. The powder XRD of MER zeolite prepared here reveals that the solid is a highly crystalline MER zeolite and no reflections other than those from MER are observed.[10] This pattern was indexed as orthorhombic with unit-cell dimensions of a = 14.13(1), b = 14.24(2) and c = 10.10(1) Å. A combination of elemental and thermal analyses of the as-synthesized Al-MER sample gives a unit cell composition of $K_{11.1}Na_{0.3}Al_{11.4}Si_{20.6}O_{64} \cdot 17.8H_2O$. The ^{27}Al MAS NMR spectrum of this zeolite exhibits only one line at 58.5 typical of tetrahedral Al sites in zeolites.

Fig. 1 shows the ^{29}Si MAS NMR spectrum of our MER zeolite together with the simulated spectrum and its deconvoluted components. Five well-resolved ^{29}Si lines at −85.1, −89.4, −94.0, −98.7 and −103.2 ppm are observed. The general feature of this spectrum is very similar to the case of zeolite structures having only one T-site such as LTA and FAU zeolites with high Al contents. As seen in Fig. 1, however, curve deconvolution reveals that there is an additional low-intensity shoulder around −108 ppm, reflecting the presence of more than one crystallographically distinct T-site in the framework of MER zeolite. This clearly shows that the ^{29}Si NMR spectra for Al-MER zeolites cannot be interpreted following the manner that the individual lines are implicitly regarded as single Si environments, which has been repeatedly employed in the literature.[7–9] Actually, an attempt to deconvolute the ^{29}Si NMR spectrum of our Al-MER material by assigning the first five lines to $Si(OSi)_n(OAl)_{4-n}$ species with n = 0–4 and by ignoring the presence of the high-field line, due to its low intensity, gave a $(Si/Al)_{NMR}$ value of 2.3 that is fairly larger than the bulk Si/Al

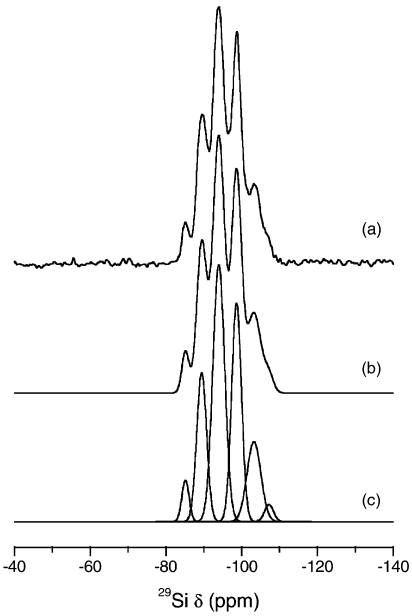

Fig. 1 ^{29}Si MAS NMR spectra of MER zeolite prepared: (*a*) experimental, (*b*) simulated and (*c*) deconvoluted components. Spectrum recorded on a Bruker DSX 400 at 12 kHz spinning rate, 60 s recycle delay, 79.459 MHz, 2.0 μs pulse length (π/5 rad), 1200 scans.

† Electronic supplementary information (ESI) available: powder XRD and ^{27}Al MAS NMR spectrum of the MFR zeolite. See http://www.rsc.org/suppdata/cc/b0/b004748l/

Table 1 Chemical shifts, intensities, and assignments of the ^{29}Si NMR resonances in MER zeolite prepared here

Chemical shift (ppm from TMS)	Relative intensity (%)	Assignment	Average T–O–T angle[11]	
			Si_I–O–T	Si_{II}–O–T
−85.1	3.6	$Si_I(OAl)_4$	142.1	
−89.4	17.8	$Si_I(OSi)(OAl)_3$ + $Si_{II}(OAl)_4$	140.3	148.8
−94.0	37.1	$Si_I(OSi)_2(OAl)_2$ + $Si_{II}(OSi)(OAl)_3$	139.0	147.2
−98.7	26.1	$Si_I(OSi)_3(OAl)$ + $Si_{II}(OSi)_2(OAl)_2$	137.8	145.7
−103.2	13.5	$Si_I(OSi)_4$ + $Si_{II}(OSi)_3(OAl)$	136.4	144.0
−107.5	1.9	$Si_{II}(OSi)_4$		142.1

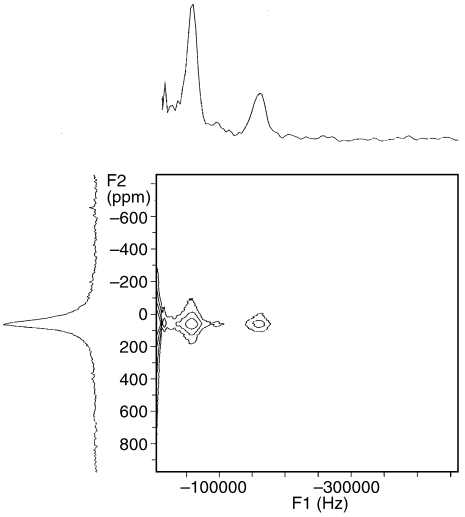

Fig. 2 1D and 2D ^{27}Al quadrupole nutation spectra of MER zeolite recorded on a Varian Unity Inova 200 with an ω_{rf} of 53 kHz. 512 data points were collected in the t_1 dimension in increments of 0.25 μs.

ratio (1.8) from chemical analysis. Although the topological symmetry for the MER framework was initially found to be the tetragonal subgroup *I*4/*mmm*, on the other hand, it has recently been shown that a better refinement is achieved from the orthorhombic subgroup *Immm*.[8,9] In this space group two crystallographically distinct sites T_1 and T_2 with 1 : 1 distribution exist in the unit cell. Considering that the average shift difference in the six ^{29}Si lines of Fig. 1 is 4.5 ppm, the shift effect due to site non-equivalence in the MER framework may be comparable in magnitude to the effect of Al substitution in the first tetrahedral coordination sphere of Si (*ca*. 5 ppm). If such is the case, structurally distinct lines should be superimposed upon one another and a deceptively simple spectrum could be observed as that in Fig. 1(a). A list of the positions, relative intensities, and assignments of the six deconvoluted components of the spectrum is given in Table 1, together with the average Si–O–T angles calculated using the relationship of Ramdas and Kinowski[11] for every resolved Si site. Based on the assignment in Table 1 and assuming a random Al distribution over the two T-sites with avoidance of Al–O–Al linkages, the Si/Al ratio derived from the intensities of the deconvoluted components of 1.9 was calculated to be very close to that from elemental analysis. This result supports the validity of our ^{29}Si NMR interpretation for MER-type zeolites based on the presence of two different T sites in this type of zeolites, which can be further evidenced by the fact that the average Si–O–T angle (142.6°) in our MER zeolite calculated from ^{29}Si MAS NMR data in Table 1 is in good agreement with the value (143.5°) in an MER zeolite with Si/Al = 2.1 from powder XRD Rietveld refinement.[8]

To obtain more firm evidence for the speculation given above, the static ^{27}Al quadrupole nutation NMR spectra[12] for MER zeolite prepared here have been measured with a radio-frequency field (ω_{rf}) of *ca*. 53 kHz, which was previously determined with an $Al(H_2O)_6^{3+}$ solution. Like the MAS spectrum, the 1D ^{27}Al static NMR spectrum exhibits one single line at 58 ppm with the full width at half-maximum of about 4 kHz. As seen in Fig. 2, however, the 2D nutation NMR spectrum consists of two distinct lines at 57 and 162 kHz along the axis F_1. Thus, the two lines corresponding to tetrahedral environments for Al atoms, which overlap in the ordinary MAS NMR spectrum, are further resolved by 2D quadrupole nutation. This reveals the presence of two different quadrupolar environments for framework Al atoms in the MER framework. The line at 57 kHz, which is similar to ω_{rf}, has a negligible quadrupolar interaction and can be attributed to framework Al atom at the site of spherical symmetry.[12] By contrast, the line at 162 kHz, which is about 3 times larger than ω_{rf}, has a quadrupole coupling constant (C_Q) of ≥ 12 MHz. Thus, it can be assgined to the Al site that is severely distorted from spherical symmetry. This clearly shows that the second Al site is crystallographically different from the first Al site. We believe that the asymmetric parameter (η) of the second Al site must be close to unity, since only one sharp peak is observed in the MAS and static ^{27}Al NMR spectra without any trace of a broad second order quadrupole powder pattern with several singularities typical for site with $C_Q \geqslant 12$ MHz and $\eta < 1$.[13] In parallel with the ^{29}Si MAS NMR evidence, in conclusion, it is clear that two crystallographically distinct T-sites are present in the framework of MER-type zeolites.

The results shown here clearly deomonstrate that if the Si/Al ratios calculated from the ^{29}Si MAS NMR spectra for zeolites, especially for novel materials, do not match well with those from elemental analysis, one must use caution in the interpertation of the spectra obtained. This is because we cannot rule out the possibility that structurally distinct lines are superimposed upon one another, yielding the deceptively simple spectra. In addition, the overall results of this study show that the ^{27}Al quadrupole nutation NMR technique can be very useful for determining the presence of crystallographically different T-sites in the zeolite framework, which is difficult to ascertain by other analytical methods.

We acknowledge the financial support of the Korea Science and Engineering Foundation through the Advanced Materials Research Center for a Better Environment at Taejon National University of Technology.

Notes and references

1 E. Lippmaa, M. Magi, A. Somoson, M. Tarmak and G. Engelhardt, *J. Am. Chem. Soc.*, 1981, **103**, 4992.
2 G. Engelhardt and D. Michel, *High-Resolution Solid-State NMR of Silicates and Zeolites*, John Wiley & Sons, New York, 1987.
3 E. Passaglia, D. Pongiluppi and R. Rinaldi, *N. Jb. Miner. Mh.*, 1977, 355.
4 R. M. Barrer and J. W. Baynham, *J. Chem. Soc.*, 1956, 2882.
5 J. D. Sherman, *ACS Symp. Ser.*, 1977, **40**, 30.
6 W. M. Meier, D. H. Olson and Ch. Baerlocher, *Atlas of Zeolite Structure Types*, Elsevier, London, 4th edn., 1996.
7 A. A. Belhekar, A. J. Chandwadkar and S. G. Hedge, *Zeolites*, 1995, **15**, 535.
8 A. Bieniok, K. Bornholdt, U. Brendel and W. H. Baur, *J. Mater. Chem.*, 1996, **6**, 271.
9 P. A. Barrett, S. Valencia and M. A. Camblor, *J. Mater. Chem.*, 1998, **8**, 2263.
10 M. M. J. Treacy, J. B. Higgins and R. von Ballmoos, *Collection of Simulated XRD Patterns for Zeolites*, Elsevier, New York, 1996.
11 S. Ramdas and J. Klinowski, *Nature*, 1984, **308**, 521.
12 A. P. M. Kentgens, J. J. M. Lemmens, F. M. M. Geurts and W. S. Veeman, *J. Magn. Reson.*, 1987, **71**, 62.
13 J. F. Baugher, P. C. Taylor, T. Oja and P. J. Bray, *J. Chem. Phys.*, 1968, **50**, 4914.

ChemComm

Conformational control in the SuperQuat chiral auxiliary 5,5-dimethyl-4-*iso*-propyloxazolidin-2-one induces the *iso*-propyl group to mimic a *tert*-butyl group

Steven D. Bull, Stephen G. Davies,* Min-Suk Key, Rebecca L. Nicholson and Edward D. Savory

The Dyson Perrins Laboratory, University of Oxford, South Parks Road, Oxford, UK OX1 3QY.
E-mail: steve.davies@chem.ox.ac.uk

Received (in Liverpool, UK) 3rd July 2000, Accepted 1st August 2000
First published as an Advance Article on the web 22nd August 2000

^{1}H NMR nOe spectroscopic studies reveal that conformational control in the enolates of *N*-acyl-5,5-dimethyl-4-*iso*-propyloxazolidin-2-ones ensures that the stereodirecting effect of its 4-*iso*-propyl-5,5-dimethyl functional group affords superior levels of facial selectivity normally associated with enolates derived from *N*-acyl-4-*tert*-butyloxazolidin-2-ones.

The versatile oxazolidin-2-one based chiral auxiliary methodology first developed by Evans *et al.* has been widely used for the asymmetric synthesis of homochiral α-substituted carboxylic acids.[1] L-Valine derived 4-*iso*-propyloxazolidin-2-one **1a** is normally employed to control the asymmetric alkylation of enolates derived from the corresponding *N*-acyloxazolidin-2-ones, however it is known that the *tert*-leucine derived 4-*tert*-butyloxazolidin-2-one **1b** affords superior diastereoselectivities for this class of enolate alkylation. Thus, while methylation of the enolate of (*S*)-*N*-butyryl-4-*iso*-propyloxazolidin-2-one **2a** affords (4*S*,2′*S*)-**3a** in 82% de, methylation of the corresponding (*S*)-*N*-butyryl-4-*tert*-butyloxazolidin-2-one **2b** affords (4*S*,2′*S*)-**3b** in 97% de (Scheme 1).[2] However, the parent non-proteinogenic α-amino acid (*S*)-*tert*-leucine, from which **1b** is derived, is prohibitively expensive.[3]

We have recently reported on the development of a new family of SuperQuat 5,5-dimethyl-4-alkyloxazolidin-2-ones for asymmetric synthesis which fully address the troublesome endocyclic cleavage pathway associated with alkaline hydrolysis of *N*-acyloxazolidin-2-ones.[4] Whilst the primary function of the C(5)-*gem*-dimethyl group within *N*-acyl-5,5-dimethyl-4-alkyloxazolidin-2-ones is to completely suppress the endocyclic cleavage pathway, it was proposed on the basis of molecular modelling calculations (Fig. 1)[4] that the presence of this functionality might also serve a secondary function by enhancing the observed diastereofacial selectivity during enolate alkylation.[5,6]

As a consequence of this conformational preference, it was predicted that the facial selectivity observed for alkylation of 5,5-dimethyl-4-*iso*-propyl enolate **5c** would be significantly higher than that observed for alkylation of the corresponding enolate **5a** derived from 4-*iso*-propyloxazolidin-2-one **1a**. It follows therefore in terms of enolate alkylation that the *iso*-propyl group of the SuperQuat oxazolidin-2-ones mimics a *tert*-butyl group. In order to investigate this hypothesis, competitive enolate alkylations were carried out on the three enolates **5a**–**c** under identical conditions, *via* deprotonation of the corresponding *N*-acyloxazolidin-2-ones **4a**–**c** in THF at −78 °C, followed by warming to 0 °C, and addition of 1.1 equiv. MeI. These studies revealed that the diastereoselectivity for alkylation of enolate **5a** {(92% (4*S*,2′*S*)-**6a**: 8% (4*S*,2′*R*)-**7a**); 84% de} was significantly lower than that observed for both enolate **5b** {(98.5% (4*S*,2′*S*)-**6b**: 1.5% (4*S*,2′*R*)-**7b**); 97% de} and enolate **5c** {(97% (4*S*,2′*S*)-**6c**: 3% (4*S*,2′*R*)-**7c**); 94% de} (Scheme 2). These enolate alkylation reactions were then repeated under more precisely controlled conditions by carrying out the enolate methylation reactions on a 1:1 mixture of (*S*)-4-*iso*-propyl enolate **5a** and (*S*)-5,5-dimethyl-4-*iso*-propyl enolate **5c**, and a 1:1 mixture of (*S*)-4-*tert*-butyl enolate **5b** and enolate **5c**, in the same reaction vessel. These direct comparison studies reveal an identical trend to the separate enolate studies affording diastereoselectivities for (*S*)-4-*tert*-butyl enolate **5b** (97% de) > (*S*)-5,5-dimethyl-4-*iso*-propyl enolate **5c** (94% de) > (*S*)-4-*iso*-

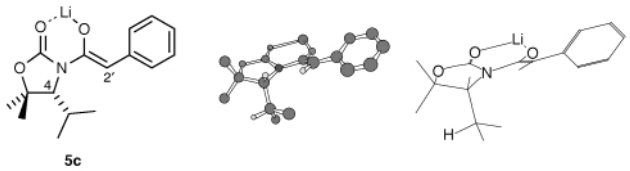

Fig. 1 Energy minimisation of SuperQuat enolate **5c** using MOPAC with an MM2 force field.

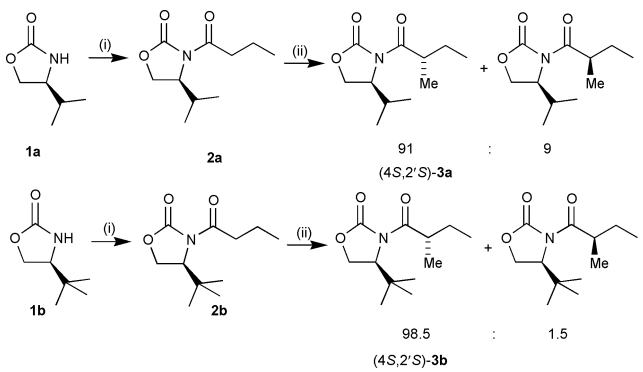

Scheme 1 *Reagents and conditions:* (i) *n*-BuLi, butyryl chloride, THF, −78 °C; (ii) LDA, MeI, THF, −30 °C.

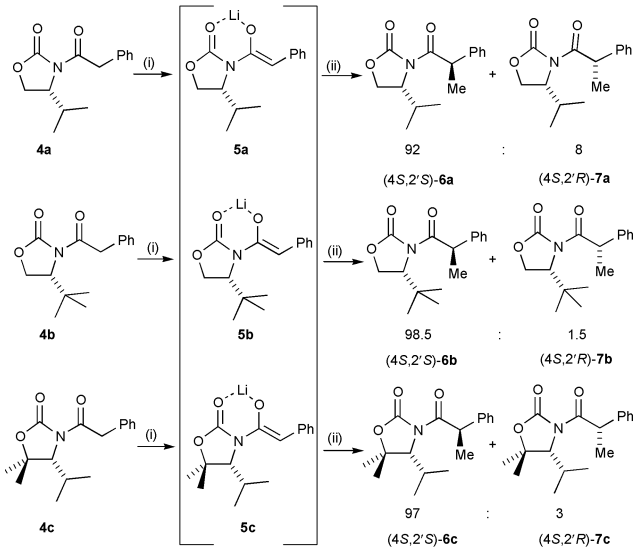

Scheme 2 *Reagents and conditions:* (i) LHMDS, THF, −78 to 0 °C; (ii) 1.1 equiv. MeI.

propyl enolate **5a** (84% de). The diastereoselectivities for all of the enolate alkylation reactions investigated were calculated from integration of the resonances corresponding to both the major (4*S*,2′*S*)-diastereoisomers **6a**–**c** and minor (4*S*,2′*R*)-diastereoisomers **7a**–**c** in the ^{1}H NMR spectrum of each crude reaction mixture. Authentic pure samples of both the major (4*S*,2′*S*)-diastereoisomers **6a**–**c** and minor (4*S*,2′*R*)-diastereoisomers **7a**–**c** were obtained *via* chromatographic purification of the three pairs of diastereoisomers **6a**–**c** and **7a**–**c** obtained from *N*-acylation of the lithium anions of each of the parent oxazolidin-2-ones with racemic 2-phenylpropanoyl chloride, and fully characterised.

Having clearly demonstrated that methylation of the 5,5-dimethyl-4-*iso*-propyl enolate **5c** with MeI at 0 °C occurred in higher de than methylation of the corresponding 4-*iso*-propyl enolate **5a**, ^{1}H nOe NMR spectroscopic analysis on the enolates **5a** and **5c** was carried out in order to probe directly their conformation in solution. Enolates **5a** and **5c** were generated *via* treatment of **4a** and **4c** with 1 equiv. of LHMDS at −78 °C in d_8-THF, followed by warming the resulting solution to 0 °C. The ^{1}H NMR spectra of both **5a** and **5c** were entirely consistent with the proposed (*Z*)-enolate structures since enolate **5a** showed a singlet resonance at δ 4.58, while enolate **5c** exhibited a singlet resonance at δ 4.68, corresponding to the C(2′) vinylic proton of the enolate functionality in each case. Examination of the resonances corresponding to the *iso*-propyl C*H*(Me)$_2$ protons in the ^{1}H NMR spectrum of enolates **5a** and **5c** revealed small vicinal coupling constants of 3.2 and 2.3 Hz respectively between the *iso*-propyl C*H*(Me)$_2$ proton and the oxazolidin-2-one H(4) proton. This is consistent with both enolates **5a** and **5c** adopting conformations in which the C*H*(Me)$_2$ protons of their *iso*-propyl groups lie approximately syn- or anti-periplanar to the C(4)–C(5) bond of the oxazolidin-2-one ring, with both methyl groups of their *iso*-propyl units directed either towards, or away from the attached enolate fragment. Qualitative ^{1}H nOe NMR spectroscopic analysis of the 4-*iso*-propyl enolate **5a** in d_8-THF at 0 °C revealed a strong enhancement between the C(2′) vinylic proton of the enolate fragment and the oxazolidin-2-one *iso*-propyl C*H*(Me)$_2$ proton, with no nOe enhancement with either of the *iso*-propyl CH(C*H*$_3$)$_2$ groups. Further strong nOe enhancements were observed between the *pro*-(*S*) H(5) proton and both of the *iso*-propyl CH(C*H*$_3$)$_2$ methyl groups. These nOe enhancements are consistent with a major enolate conformer **5a** in which both of the *iso*-propyl methyl groups are directed away from the attached enolate fragment (Fig. 2). In contrast, qualitative ^{1}H nOe NMR spectroscopic analysis of enolate **5c** revealed both a medium and small enhancement between the C(2′) vinylic proton of the enolate fragment and each of the methyl groups of the *iso*-propyl CH(C*H*$_3$)$_2$ group. A further strong nOe enhancement was observed between the C*H*(Me)$_2$ proton and one of the C(5)-*gem*-dimethyl groups. These nOe enhancements are consistent with the proposed model for 5,5-dimethyl-4-*iso*-propyl enolate **5c** in which the major conformer in solution has both methyl groups of the stereocontrolling *iso*-propyl group directed towards the attached enolate fragment (Fig. 3). Importantly, both samples of enolates **5a** and **5c** in d_8-THF at 0 °C used in these ^{1}H NMR

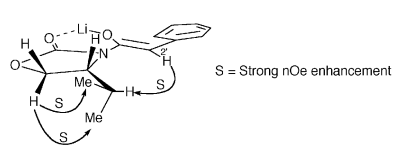

Fig. 2 nOe study on Evans' enolate **5a**. Other nOe enhancements omitted for clarity.

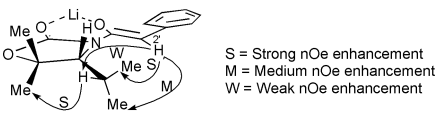

Fig. 3 nOe study on SuperQuat enolate **5c**. Other nOe enhancements omitted for clarity.

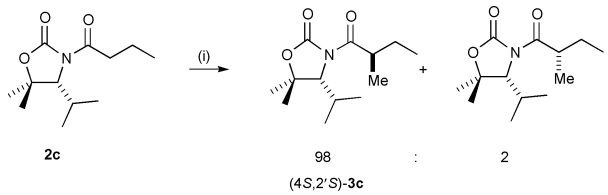

Scheme 3 *Reagents and conditions:* (i) LDA, MeI, THF, −30 °C.

studies were shown to be stable over the period of the experiment *via* subsequent treatment of both solutions of enolates **5a** and **5c** with MeI to afford the major diastereoisomers **6a** and **6c** with diastereoselectivites identical to those obtained previously.

In order to confirm the enhanced facial selectivity observed for alkylation of *N*-acyl-5,5-dimethyl-4-*iso*-propyl enolates, methylation of the enolate of *N*-butyryl-5,5-dimethyl-4-*iso*-propyloxazolidin-2-one **2c** was carried out under the original conditions described by Evans *et al.* for *N*-butyryloxazolidin-2-ones **2a** and **2b**. Thus, methylation of the enolate of **2c** gave the major diastereoisomer (4*S*,2′*S*)-**3c** in 96% de (Scheme 3), which is significantly higher than that obtained for methylation of the enolate of *N*-butyryl-4-*iso*-propyloxazolidin-2-one **3a** of 82% de, and compares favourably with that observed for methylation of the enolate of *N*-butyryl-4-*tert*-butyryloxazolidin-2-one **3b** of 97% de.

In conclusion, ^{1}H NMR nOe spectroscopic studies confirm that the superior enolate alkylation diastereoselectivities observed for (*S*)-5,5-dimethyl-4-*iso*-propyl enolate **5c** over (*S*)-4-*iso*-propyl enolate **5a** is a result of steric interactions between the C(5)-*gem*-dimethyl and the *iso*-propyl group of **5c** which direct both methyl groups of the *iso*-propyl stereocontrolling group towards the enolate fragment. We believe that the strategy outlined above of employing adjacent *gem*-dimethyl groups to control the conformation of an *iso*-propyl group such that it mimics a *tert*-butyl group is a general one, and we are currently investigating the development of a wide range of novel ligands and auxiliaries containing this structural motif, which is easily prepared from valine, as replacements for the corresponding *tert*-leucine derived analogues.[7]

We thank Dr Barbara Odell for her technical assistance with the qualitative ^{1}H nOe NMR spectroscopic studies on enolates **5a** and **5c**.

Notes and references

1 D. A. Evans, *Aldrichim. Acta*, 1982, **15**, 23; D. A. Evans, in *Asymmetric Synthesis*, ed. J. D. Morrison, 1984, vol. 3, Academic Press, New York; D. A. Evans, T. C. Britton and J. A. Ellman, *Tetrahedron Lett.*, 1987, **28**, 6141.

2 D. A. Evans, K. T. Chapman, D. T. Hung and A. T. Kawaguchi, *Angew. Chem., Int. Ed. Engl.*, 1987, **26**, 1184.

3 L-*tert*-Leucine is commercially available at £16.50 per gram while the corresponding D enantiomer is £101.60 per gram from Aldrich Chemical Company.

4 Energy minimisation on enolate **5c** was carried out using MOPAC with a MM2 forcefield calculation.

5 S. G. Davies and H. J. Sanganee, *Tetrahedron: Asymmetry*, 1995, **6**, 671; S. D. Bull, S. G. Davies, S. Jones, M. E. C. Polywka, R. S. Prasad and H. J. Sanganee, *Synlett*, 1998, 519; S. D. Bull, S. G. Davies, S. Jones and H. J. Sanganee, *J. Chem. Soc., Perkin Trans 1*, 1999, 387; S. G. Davies, H. J. Sanganee and P. Szolcsanyi, *Tetrahedron*, 1999, **55**, 3337.

6 Similar arguments have been proposed to explain the high facial selectivity observed for a 2,2-dimethyloxazolidine derived chiral auxiliary in controlling (a) the [3 + 2] cycloaddition of dipolarophiles with alkenes, K. Onimura and S. Kanemasa, *Tetrahedron*, 1992, **48**, 8631; (b) the [4 + 2] cycloaddition of dienes with singlet oxygen, W. Adam, M. Güthlein, E.-M. Peters, K. Peters and T. Wirth, *J. Am. Chem. Soc.*, 1998, **120**, 4091; (c) and a 5,5-diphenyloxazolidin-2-one for enolate alkylations, T. Hintermann and D. Seebach, *Helv. Chim. Acta*, 1998, **81**, 2093.

7 For a review on the use of the advantages of employing homochiral *tert*-leucine in asymmetric synthesis see A. S. Bommarius, M. Schwarm, K. Stingl, M. Kottenhahn, K. Huthmacher and K. Drauz, *Tetrahedron: Asymmetry*, 1995, **12**, 2851.

ChemComm

The first asymmetric Suzuki cross-coupling reaction

Andrew N. Cammidge* and Karen V. L. Crépy

School of Chemical Sciences, University of East Anglia, Norwich, UK NR4 7TJ

Received (in Cambridge, UK) 6th June 2000, Accepted 27th July 2000
First published as an Advance Article on the web 22nd August 2000

The first asymmetric coupling reactions between aryl halides and aryl boronates (Suzuki coupling) are described to give binaphthalene derivatives in up to 85% ee.

Restricted rotation around the aryl–aryl bond in biaryls can lead to the phenomenon of atropisomerism (sometimes called helical chirality). Chiral binaphthalenes constitute an important class of such atropisomeric compounds, not least because they are amongst the most useful chiral ligands and auxiliaries employed in asymmetric synthesis.[1] Transition metal-catalysed cross-coupling between organometallic species and aryl halides (for example) is a powerful synthetic tool and represents one of the most straightforward methods for aryl–aryl carbon–carbon bond formation.

A small number of asymmetric biaryl syntheses have been reported. High selectivity has been achieved in the asymmetric synthesis of 2,2′-dimethyl-1,1′-binaphthalene **9** using chiral auxiliaries (chiral oxazoline[2,3] or a chiral leaving group[4]) or using chiral catalysts.[5] However, variable results have been reported depending on the nature of the catalyst used (*e.g.* Ni or Pd) and in all cases a Grignard reagent is used as the organometallic component.

Here we report the first examples of an *asymmetric* Suzuki coupling protocol for the construction of binaphthalenes.[6] The Suzuki coupling reaction has many inherent advantages over related Ni- and Pd-catalysed couplings and has found widespread application in the synthesis of simple and complex biaryls. The main advantage is its tolerance of a broad range of functional groups and its non-toxic by-products.[7] The organometallic partner in the Suzuki coupling (an organoboronic acid derivative) is thermally stable, inert to air and water (which allows its handling without special precautions) and unreactive to many of the electrophilic functional groups which cannot be employed (unprotected) in conjunction with Grignard reagents.

In our investigation of the asymmetric Suzuki reaction, we chose the synthesis of substituted binaphthalenes to allow comparison with previously reported methods (Scheme 1). Naphthyl halide starting materials **1**–**4** were obtained commercially or synthesised following standard procedures.[8] Boronic acid **5** was synthesised by converting the corresponding naphthyl bromide **3** into its Grignard reagent,[9] quenching with trimethylborate and aqueous acidic work-up. Boronic acid **5** was also converted to boronate esters **6** and **7** by treatment with pinacol and ethylene glycol respectively (Dean–Stark trap).

It is well known that use of sterically congested coupling partners can lead to poor yields in Suzuki reactions.[7,10] Racemic coupling was therefore first performed to optimise the reaction conditions (base–solvent combinations, heterogeneous *vs*. homogeneous conditions, boronic acid *vs*. boronate esters *etc*.) and selected results are summarised in Table 1. Both homogeneous and heterogeneous conditions were established to allow isolation of binaphthalenes **8** and **9** in acceptable yields. Optimum conditions typically involved treating aryl halides **1**–**4** with 1.1–2 mol eq. of boronic acid **5** or boronate esters **6**, **7** in the presence of 3 mol% $PdCl_2$/6 mol% PPh_3[11] and 1.5–2 mol eq. of base at elevated temperatures.[12] Competing deboronation was observed when the sterically congested boronic acids were reacted with hindered aryl halides and coupling was only observed in these cases when boronate esters were used. As expected, reactions with 1-iodonaphthalenes proved faster and led to greater yields than those reactions employing 1-bromonaphthalenes, especially with the combination $Ba(OH)_2$–DME–H_2O[12a] (Table 1, entries 1 and 4).

Our best conditions were then extended to investigation of the asymmetric Suzuki reaction using chiral ligands. Diamine ligands (*e.g.* **11**) gave racemic products but selectivity was

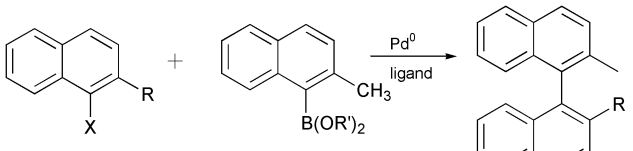

1 X = Br, R = H
2 X = I, R = H
3 X = Br, R = CH_3
4 X = I, R = CH_3

5 R' = H,H
6 R' = -$C(CH_3)_2$-$C(CH_3)_2$-
7 R' = -CH_2CH_2-

8 R = H
9 R = CH_3

Scheme 1 Binaphthalene synthesis *via* Suzuki coupling.

Table 1 Results from racemic Suzuki coupling

Entry	Halide	Boronic acid derivative	Product	Base/solvent[a]	Yield % (conversion[d])
1	**1**	**5**	**8**	$Ba(OH)_2$–DME–H_2O	44
2	**1**	**5**	**8**	CsF–DME	72
3	**2**	**5**	**8**	$Ba(OH)_2$–tol–EtOH–H_2O	(> 98)
4	**2**	**5**	**8**	$Ba(OH)_2$–DME–H_2O	61
5	**2**	**5**	**8**	$Ba(OH)_2$–DME–H_2O[b]	(> 98)
6	**2**	**5**	**8**	CsF–DME	74
7	**2**	**5**	**8**	NaOH–DME	36
8	**2**	**6**	**8**	CsF–DME[c]	(> 98)
9	**3**	**5**	**9**	Na_2CO_3–DME–H_2O	(trace[e])
10	**3**	**5**	**9**	$Ba(OH)_2$–DME–H_2O	(trace[e])
11	**4**	**5**	**9**	$Ba(OH)_2$–DME–H_2O	(trace[e])
12	**4**	**5**	**9**	CsF–DME	(trace[e])
13	**4**	**6**	**9**	CsF–DME[c]	36
14	**4**	**7**	**9**	CsF–DME[c]	69

[a] Reaction time 17–19 h. [b] Carried out at 50 °C for 5 h and with 2 eq. of boronic acid. [c] Reaction time 3–6 d. [d] Determined by ^{1}H-NMR. The only side product observed was from deboronation. [e] The product from deboronation was observed.

DOI: 10.1039/b004513f

Table 2 Results from asymmetric Suzuki coupling.

Entry	Halide	Boronate	Ligand[a]	Product	Base	Solvent	Time, h	ee[b] %, (yield[c] %)
1	**2**	**5**	**13**	R-(−)-**8**	$Ba(OH)_2$	DME–H_2O	19	63 (44)
2	**2**	**5**	**13**	R-(−)-**8**	CsF	DME	19	55 (44)
3	**2**	**5**	**13**	R-(−)-**8**	$Ba(OH)_2$	Toluene–EtOH–H_2O	19	52 (45)
4	**2**	**5**	**10**	S-(+)-**8**	$Ba(OH)_2$	DME–H_2O	19	25 (55)
5	**2**	**5**	**10**	S-(+)-**8**	CsF	DME	19	21 (43)
6	**2**	**5**	**10**	S-(+)-**8**	$Ba(OH)_2$	Toluene–EtOH–H_2O	19	8 (47)
7	**2**	**5**	**12**	R-(−)-**8**	$Ba(OH)_2$	DME–H_2O	19	14 (74)
8	**2**	**5**	**14**	S-(+)-**8**	$Ba(OH)_2$	DME–H_2O	19	4 (73)
9	**2**	**5**	**11**	**8**	$Ba(OH)_2$	DME–H_2O	19	0 (9)
10	**4**	**7**	**13**	R-(−)-**9**	CsF	DME	6 days	85 (50)
11	**4**	**7**	**14**	S-(+)-**9**	CsF	DME	9 days	17 (13)
12	**4**	**7**	**10**	S-(+)-**9**	CsF	DME	5 days	14 (21)
13	**4**	**6**	**10**	R-(−)-**9**	CsF	DME	4 days	10 (17)

[a] Carried out with 1.1–2 eq. of boronic acid derivative in refluxing solvent using 3 mol% $PdCl_2$/6 mol% monophosphine chiral ligand or 3 mol% $PdCl_2$/3 mol% bidentate chiral ligand. [b] ee's were determined by optical rotation measurements[5b,13]. [c] Products isolated by column chromatography. To avoid fractionation, recrystallisation was not performed.

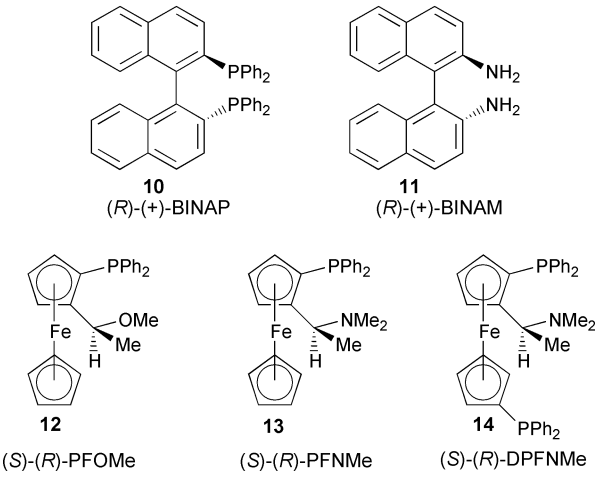

observed when phosphine ligands were employed. BINAP **10** led to modest ee's of 8–25% (summarised results are reported in Table 2). Furthermore, use of different boronate esters led to different selectivity (use of bulky pinacol ester **6** gave the opposite enantiomer to that observed when the boronic acid **5** or ethylene glycol ester **7** was employed (Table 2, entries 5, 12 and 13)) implying kinetic control. Highest selectivity was observed when a mono-phosphine ligand was employed. Diastereomeric ferrocene **12**, which has diphenyl phosphine and ether ligands gave disappointing ee's when **2** and **5** were coupled (**12** was found to be far superior to binaphthalene ligands in asymmetric couplings employing Grignard reagents[5b]). The related ligand **13**, in which a tertiary amine replaces the methoxide of **12**, was found to lead to the highest selectivity. With this ligand 2-methyl-1-1′-binaphthalene **8** could be synthesised in yields of 44–55% and ee's of 52–63%. The dimethyl derivative **9** gave the highest observed ee (85%) when boronate ester **7** was employed.

Our results obtained for the asymmetric Suzuki coupling can be compared to the nickel- and palladium-catalysed couplings of Grignard reagents with naphthyl halides. In the nickel-catalysed reaction, ligand **12** gives the highest ee and coupling reactions using **13** were ineffective. The selectivity in this reaction was suggested to arise through complexation of the magnesium ion of the Grignard reagent to the oxygen (methoxide) of the chiral ligand resulting in stereoselective delivery of the organometallic and kinetic control. Such complexation is not possible with a naphthylboronate so the observed low ee is perhaps not surprising. The high ee obtained with tertiary amine phosphine ligand **13** suggests that pre-complexation is arising between nitrogen and boron prior to transmetallation. Use of a bidentate phosphine ligand (**14**) resulted in a decrease in the observed selectivity which is similar to the results obtained with Grignard reagents.[5]

In summary, we have performed the first series of asymmetric Suzuki cross-coupling reactions to prepare chiral binaphthalenes with ee's up to 85%. The reaction permits the use of functional groups which are incompatible with Grignard reagents (the organometallic component used in all previously reported syntheses). The extension of this methodology to other biaryl systems is ongoing in our laboratories.

Support for this work from the School of Chemical Sciences (UEA) is gratefully acknowledged (K. V. L. C.).

Notes and references

1 L. Pu, *Chem. Rev.*, 1998, **98**, 2405.
2 A. I. Meyers and K. A. Lutomski, *J. Am. Chem. Soc.*, 1982, **104**, 879.
3 J. M. Wilson and D. J. Cram, *J. Am. Chem. Soc.*, 1982, **104**, 881.
4 J. M. Wilson and D. J. Cram, *J. Org. Chem.*, 1984, **49**, 4930.
5 (*a*) K. Tamao, H. Yamamoto, H. Matsumoto, N. Miyake, T. Hayashi and M. Kumuda, *Tetrahedron Lett.*, 1977, **16**, 1389; (*b*) T. Hayashi, K. Hayashizaki, T. Kiyoi and Y. Ito, *J. Am. Chem. Soc.*, 1988, **110**, 8153; (*c*) T. Frejd and T. Klingstedt, *Acta Chem. Scand.*, 1989, **43**, 670.
6 A small number of asymmetric palladium catalysed desymmetrisation reactions based on aryl–aryl coupling have been reported; (*a*) M. Uemura, H. Nishimura and T. Hayashi, *J. Organomet. Chem.*, 1994, **473**, 129; (*b*) T. Hayashi, S. Niizuma, T. Kamikawa, N. Suzuki and Y. Uozumi, *J. Am. Chem. Soc.*, 1995, **117**, 9101.
7 N. Miyaura and A. Suzuki, *Chem. Rev.*, 1995, **95**, 2457.
8 (*a*) A. N. Cammidge, K. V. Crépy and M. Fugier, *Synth. Commun.*, 1997, **27**, 4159; (*b*) A.-S. Carlstrom and T. Frejd, *J. Org. Chem.*, 1991, **56**, 1289; (*c*) N. G. Andersen, S. P. Maddaford and B. A. Keay, *J. Org. Chem.*, 1996, **61**, 9556.
9 S. Miyano, S. Okada, T. Suzuki, S. Handa and H. Hashimoto, *Bull. Chem. Soc. Jpn.*, 1986, **59**, 2044.
10 W. J. Thompson and J. Gaudino, *J. Org. Chem.*, 1984, **49**, 5237.
11 (*a*) D. F. O'Keefe, M. C. Dannock and S. M. Marcuccio, *Tetrahedron Lett.*, 1992, **33**, 6679; (*b*) J. Lindley, *Tetrahedron*, 1984, **40**, 1433.
12 (*a*) T. Watanabe, N. Miyaura and A. Suzuki, *Synlett*, 1992, 207; (*b*) J. W. Benbow and B. L. Martinez, *Tetrahedron Lett.*, 1996, **37**, 8829.
13 D. D. Fitts, M. Siegel and K. Mislow, *J. Am. Chem. Soc.*, 1958, **80**, 480.

ChemComm

Ultra fast and efficient synthesis of Ti-ITQ-7 and positive catalytic implications

Avelino Corma,* Ma José Díaz-Cabañas,[a] Marcelo E. Domine and Fernando Rey

Instituto de Tecnología Química, UPV-CSIC, Universidad Politécnica de Valencia, Avda. de los Naranjos, s/n, 46022 Valencia, Spain. E-mail: acorma@itq.upv.es

Received (in Oxford, UK) 24th May 2000, Accepted 27th July 2000
First published as an Advance Article on the web 22nd August 2000

Incorporation of germanium into a zeolite framework allows the synthesis of Ti-Ge-ITQ-7 without seeding in < 12 h, instead of 12 days when seeding or > 40 days without seeding for the Ge-free ITQ-7; the synthesis reported also increases the efficiency of Ti incorporation and allows the preparation of almost nanocrystaline Ti-ITQ-7 materials with a corresponding beneficial effect on the final catalytic activity.

The synthesis of zeolite containing framework transition metals has opened new catalytic possibilities for the use of such materials in the synthesis of chemicals and fine chemicals.[1] This is especially true for Ti zeolites, Ti-silicalite and Ti-beta being good examples of stable materials which can catalyse epoxidation of olefins, oxidation of alcohols, hydroxylation of phenol and sulfoxidation of sulfurs containing species among other reactions.[2] The potential applications of Ti-zeolites have been extended to bulkier reactants by the synthesis of mesoporous Ti-MCM-41[3,4] and delaminated Ti-zeolite ITQ-6.[5] The interest in Ti-zeolites is still high, but while the incorporation of Ti has been attempted in numerous structures very limited success has been observed. Indeed, isomorphic substitution of Ti in the framework of zeolites has been shown to occur in very few cases,[6–8] and in others[9] the introduction of Ti in the synthesis gel not only fails to lead to its incorporation in the final structure, but in many cases the presence of Ti slows down, or even prevents growth of the desired structure. This has also been the case in a recent publication on the synthesis of Ti-ITQ-7,[10] a zeolite with a three-directional system of large pore channels. When the synthesis was attempted in the absence of seeds and using a Si/Ti ratio of 30 in the synthesis gel, the crystallisation did not proceed to completion and stopped when the crystallinity reached *ca*. 30%. On the other hand, in the presence of seeds it was found that Ti-ITQ-7 grows much more slowly than the analogous pure silica zeolite; furthermore the efficiency in the incorporation of Ti is low and, also lower than that found for Ti-beta zeolite. These results seem to indicate that the presence of Ti slows the nucleation of ITQ-7 and can also severely affect the zeolite growth. We have carried out a theoretical study using *ab initio* methods with periodic systems on the effect of the incorporation of Ge in the framework of zeolites *viz-à-viz* the stabilisation of the Ti atoms in the framework structure.[11] It was found that substitution of Si atoms by Ge close to the Ti sites results in a stabilisation of the system owing to the additional framework flexibility provided by the less rigid GeO_4 units, similar to that occurring during the direct synthesis of Al-Ge-ITQ-7 catalysts.[12]

On this basis, we have attempted the synthesis of Ti-ITQ-7 by introducing Ge in the synthesis gel. Thus, a sample of Ti-Ge-ITQ-7 was synthesised in the following manner: 0.63 g of GeO_2 were dissolved in 34.31 g of a 0.97 M aqueous solution of 1,3,3-trimethyl-6-azoniumtricyclo[3.2.1.4^{6,6}]dodecane hydroxide (SDAOH). Then, 0.61 g of tetraethylorthotitanate and 12.61 g of tetraethylorthosilicate (TEOS) were hydrolysed in the above solution, and the reaction mixture was stirred until complete elimination of ethanol and water, to reach the desired gel composition. Finally, 1.38 g HF (48.1 wt%) were added and the mixture was transferred to a Teflon-lined stainless steel autoclave and left to crystallise under static conditions at 150 °C. An analogous synthesis was carried out without adding Ge to the synthesis gel. Different crystallisation times were considered in order to obtain the kinetic curves for the crystallisation of the zeolite (Fig. 1). The final compositions of the gels were: 0.90 SiO_2:0.10 GeO_2:*x* TiO_2:0.50 SDAOH:0.50 HF:3 H_2O and SiO_2:0.05 TiO_2:0.50 SDAOH:0.50 HF:3 H_2O, for the Ge and the Ge-free synthesis, respectively. The solids were recovered by filtration, and after exhaustive washing with distilled water, were dried at 100 °C, overnight. In all the syntheses, the yields of the solids recovered, in terms of oxides, were > 90% with respect to the initial gel composition.

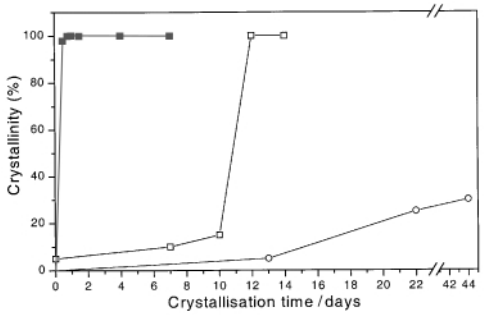

Fig. 1 Crystallization curves for the synthesis of Ti-Ge-ITQ-7 (■) and Ti-ITQ-7 with (□) and without seeds (○).

The XRD pattern (Fig. 2) of the Ti-Ge-ITQ-7 zeolite (sample D) shows a shift of the diffraction peaks to higher *d*-values when compared to the analogous Ti-ITQ-7 material (sample A) (*i.e.* without Ge and having a similar T^{IV}/Ti ratio in its composition) which indicates that the unit cell volume expands upon Ge incorporation in the zeolitic ITQ-7 framework. This result can be taken as unambiguous proof of the effective isomorphous substitution of Si by Ge in the Ti-Ge-ITQ-7 material.

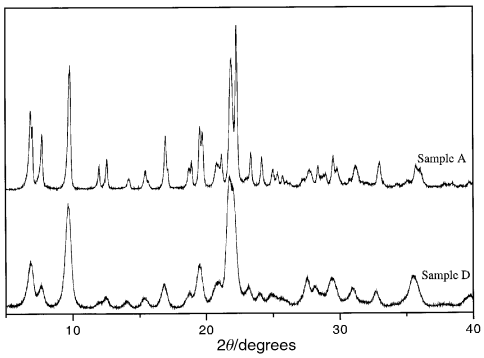

Fig. 2 XRD patterns of as-made samples: (a) Ti-ITQ-7 (sample A) and (b) Ti-Ge-ITQ-7 (sample D).

It was found (see Fig. 1) that when Ge is introduced on the synthesis gel, Ti-Ge-ITQ-7 is fully crystallised, even in the absence of seeds, in only 12 h (crystallinity measured in terms of the peak area between 2θ = 20.15 and 23.65° and referred to a sample arbitrarily assigned a value of 100%). Moreover, the nucleation period is strongly reduced with respect to the Ge-free

DOI: 10.1039/b004203j

Table 1 Efficiency for Ti incorporation as a function of gel composition

Sample	Si/Ge	F source	% TiO_2[a] (gel)	% TO_2 (solid)[b] SiO_2	GeO_2	TiO_2	% Ti incorporated
A[c]	∞	HF	6.64	98.86	—	1.14	17.2
B	10	HF	2.46	87.35	12.05	0.60	24.4
C	10	HF	5.01	85.67	12.93	1.40	28.0
D[c]	10	NH_4F	2.46	86.78	11.97	1.25	50.8
E	10	HF	0	87.65	12.35	0	—

[a] % TiO_2 calculated as: $TiO_2 \times 100/(SiO_2 + GeO_2 + TiO_2)$. [b] Measured by atomic absorption; % SiO_2 is calculated as difference. [c] Samples used for catalytic activity testing.

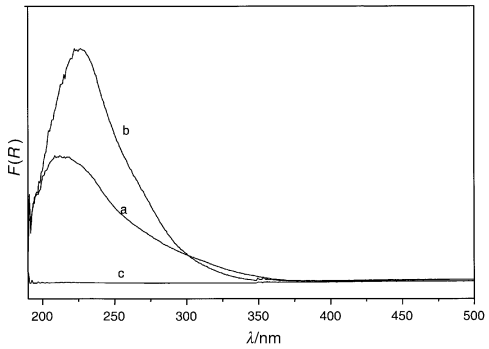

Fig. 3 Diffuse reflectance UV–VIS absorption spectra of calcined samples: (a) Ti-ITQ-7 (sample A), (b) Ti-Ge-ITQ-7 (sample D) and (c) Ge-ITQ-7 (sample E).

synthesis even if seeds were added to the synthesis gel. These facts, important in themselves, are even more impressive by considering that the efficiency of Ti incorporation is higher in the presence of Ge (Table 1), and more specifically when NH_4F is used instead of HF. In this case, the efficiency of the Ti incorporation is close to that found for Ti-beta zeolite. The high incorporation of Ti in the zeolite framework can be inferred from the UV–VIS band appearing at 220 nm (Fig. 3) which is much more intense than that of the Ge-free Ti-ITQ-7 synthesised by the previously reported procedure.[10] The higher intensity of the band is not due to the presence of Ge, since Ti-free Ge-ITQ-7 does not absorb in this region of the UV-visible spectrum (Fig. 3). Furthermore, anatase is not detected in the sample synthesised in the presence of Ge, either by UV–VIS (Fig. 3) or by Raman spectroscopy. By contrast some anatase formation was observed for Ge-free Ti-ITQ-7 samples[10] having similar Ti content as Ti-Ge-ITQ-7 catalysts described here.

The more efficient incorporation of Ti in the synthesis with Ge has an impact on the catalytic activity for the epoxidation of a linear olefin (*n*-octene) which can diffuse easily in the pores of ITQ-7 structure. The results presented in Table 2 show that a higher activity is observed for the Ti-Ge-ITQ-7 sample (D).

It is important to point out that the fast nucleation rate obtained in the presence of Ge produces much larger number of nuclei, giving Ti-Ge-ITQ-7 samples with a much smaller crystallite size (< 0.1 μm) than ITQ-7 synthesised by the previous method (1–2 μm).[9] This has important catalytic implications when reacting molecules diffuse slowly. Under these circumstances, a zeolite with smaller crystallite size is preferred in order to increase the number of Ti sites that can be reached by the reactants. We have proven this here by carrying out the epoxidation of dodec-1-ene with two Ti-ITQ-7 samples with different crystallite sizes. As seen before,[13,14] for Ti-silicalite and Ti-beta zeolites, a decrease in conversion occurs from oct-1-ene to dodec-1-ene owing to a decrease in the diffusion rate upon increasing the length of the hydrocarbon chain; this is also seen for Ti-ITQ-7. The results presented in Table 2 clearly show the increased activity of the smaller crystallites of Ti-Ge-ITQ-7 which results in a five fold increase in the turnover number with respect to the conventional Ti-ITQ-7 material.

Table 2 Catalytic activity of Ti-ITQ-7 for olefin epoxidation[a]

Olefin	Sample	X_{olefin}[b]	Selectivity to epoxide (%)	Selectivity to H_2O_2 (%)	TON[c]
Oct-1-ene	Ti-ITQ-7 (A)	14.9	98	55	27
	Ti-Ge-ITQ-7 (D)	25.9	100	52	41
Dodec-1-ene[d]	Ti-ITQ-7 (A)	0.8	100	17	3
	Ti-Ge-ITQ-7 (D)	4.8	100	43	16

[a] *Reaction conditions*: 16.5 mmol olefin; 11.8 g acetonitrile; 4.5 mmol H_2O_2 (slowly added); 200 mg of catalyst; 333 K, 3.5 h. [b] Conversion of olefin (mol% referred to the maximum possible). [c] TON = mol olefin converted/mol Ti. [d] 100 mg of catalyst.

In conclusion, we have found that it is possible to strongly increase the rate of nucleation and/or crystallisation of Ti-ITQ-7, to increase the efficiency of Ti incorporation in the framework and to produce an almost nanocrystalline zeolite, by introducing Ge to the ITQ-7 zeolite framework. All this has a clear beneficial effect on the catalytic activity of the resultant Ti-Ge-ITQ-7. It is remarkable that by a rigorous theoretical study, it was possible to predict that the incorporation of Ge should facilitate the synthesis of Ti-zeolites, as established here for Ti-ITQ-7.

We acknowledge financial support from the CICYT of Spain (Project MAT97-1016-C02-01).

Notes and references

1 R. A. Sheldon, *J. Mol. Catal. A: Chem.*, 1996, **107**, 75.
2 B. Notari, *Adv. Catal.*, 1996, **41**, 253.
3 A. Corma, M. T. Navarro and J. Pérez-Pariente, *J. Chem. Soc., Chem. Commun.*, 1994, 47
4 K. A. Koyano and T. Tatsumi, *Microporous Mater.*, 1997, **10**, 259.
5 A. Corma, U. Díaz, M. E. Domine and V. Fornés, *Chem. Commun.*, 2000, 137.
6 C. B. Dartt, C. B. Khouw, H. X. Li and M. E. Davis, *Microporous Mater.*, 1994, **2**, 425.
7 B. Sulikowski, *Heterog. Chem. Rev.*, 1996, **3**, 203.
8 G. Bellusi and M. S. Rigutto, *Stud. Surf. Sci. Catal.*, 1994, **85**, 177.
9 M. J. Díaz Cabañas, Ph.D. Thesis, Universidad Politécnica de Valencia, 1999.
10 M. J. Díaz-Cabañas, M. A. Camblor and L. Villaescusa, *Chem. Commun.*, 2000, 761.
11 C. M. Zicovich-Wilson and A. Corma, *J. Phys. Chem. B*, 2000, **104**, 4134.
12 A. Corma, M. J. Días-Cabañas and V. Fornés, *Angew. Chem., Int. Ed.*, 2000, **39**, 2346.
13 M. G. Clerici and P. Ingallina, *J. Catal.*, 1993, **140**, 71.
14 A. Corma, P. Esteve, A. Martínez and S. Valencia, *J. Catal.*, 1995, **152**, 18.

ChemComm

Amphiphilic α-alkoxyalkyl hydroperoxide (α-AHP): a new oxidising reagent in aqueous media

Araki Masuyama,* Kazuyuki Fukuoka, Masanori Wakita and Masatomo Nojima

Department of Materials Chemistry, Faculty of Engineering, Osaka University, Suita, Osaka 565-0871, Japan. E-mail: toratora@ap.chem.eng.osaka-u.ac.jp

Received (in Cambridge, UK) 6th July 2000, Accepted 1st August 2000
First published as an Advance Article on the web 22nd August 2000

Effective oxidation of benzyl sulfide to the corresponding sulfoxide in water was achieved by using amphiphilic α-alkoxyalkyl hydroperoxide (α-AHP) in the presence of a catalytic amount of $MoO_2(acac)_2$ under mild conditions.

Exploration of organic reactions in aqueous media is now becoming important from the standpoint of environmentally benign processes.[1] One of the major problems in these reactions, however, is the poor solubility of most organic substrates in water. The application of micellar or vesicular systems made from amphiphilic molecules to organic reactions in water is an effective device to overcome this substantial problem.[2] For example, Jaeger *et al*. have studied in detail the rate and/or regioselectivities of certain reactions, such as monohalogenation of alkyl phenyl ethers or Diels–Alder reactions, in specially designed micellar or vesicular systems.[3] Kobayashi *et al.* have developed Lewis acid–surfactant combined catalysts and have applied micellar systems made from these functional surfactants to aldol or Mannich-type reactions.[4] A number of other papers concerning organic reactions in aqueous micellar systems have been published over the past decade.[5]

For oxidation reactions in aqueous media, commercially available 30–60% hydrogen peroxide has been used as an oxidising reagent because its oxygen efficiency is excellent and water is a resultant side product.[6] *tert*-Butyl hydroperoxide (TBHP) is another choice of reagent in aqueous media.[7] Because these hydroperoxides are potentially hazardous compounds, however, they must be handled with special care. With this in mind, we developed a unique amphiphilic α-alkoxyalkyl hydroperoxide (α-AHP) to act both as a micellar-forming reagent to solubilise organic substrates and as an oxidising reagent. The compounds designed for this work could be easily prepared by ozonation of α-olefins in the presence of oligo(ethylene glycol)s† (Scheme 1).

Fundamental surface-active properties of **1** were as follows: T_{cp} (cloud point at 1 wt%) = 40 °C; cmc = 3.1×10^{-3} mol dm^{-3}; γ_{cmc} (the surface tension at cmc, as an indication of the effectiveness of adsorption at the air/water interface)[8] = 30 mN m^{-1}; pC_{20} (the efficiency of adsorption)[8] = 3.7.‡ This cloud point means that **1** is soluble in water at rt and forms micelles at any concentration above its cmc. Compound **2** was additionally synthesised as a reference because it was freely soluble in water but showed no surface-active properties.

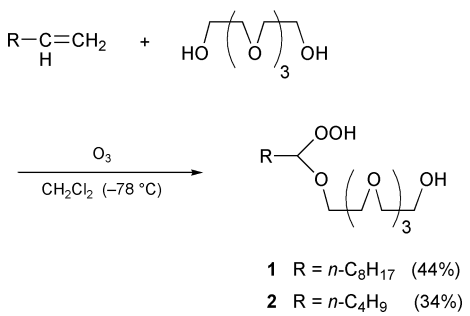

1 R = *n*-C_8H_{17} (44%)
2 R = *n*-C_4H_9 (34%)

Scheme 1

Differential thermal analyses (DTA/TG) of **1** and **2** were carried out.§ Both compounds were stable up to about 100 °C but gradually decomposed above that temperature. These results indicate that this type of α-AHP is moderately thermostable. Although careful treatment is still required, the α-AHP is easier to handle than TBHP. The ^{1}H and ^{13}C NMR spectra of a 5 wt% D_2O solution of **1** did not change at all after the solution was kept at 60 °C for 24 h.

Oxidation of benzyl sulfide was chosen to determine the effectiveness of α-AHP as an oxidising reagent in aqueous media. The reaction was run at rt and the reaction products were directly monitored by HPLC.¶ The oxidation reaction in each system was carried out at least three times to confirm its reproducibility. The results are summarised in Table 1 along with data for the same reaction conducted in dichloromethane.

It was confirmed that **1** certainly acted as an oxidising reagent in the presence of $MoO_2(acac)_2$ catalyst[9] under homogeneous conditions in dichloromethane (entry 8). In an aqueous system, too, **1** could oxidise water-insoluble benzyl sulfide very effectively (entries 1 and 2). The reaction proceeded cleanly. In no cases, were any compounds other than unreacted substrate, unreacted α-AHP, benzyl sulfoxide, (benzyl sulfone), alkyl aldehyde and tetra(ethylene glycol) detected in the reaction mixture after 24 h. Aldehyde and tetra(ethylene glycol) were fragements derived from the corresponding α-AHP through the oxidation reaction. Addition of a catalytic amount of $MoO_2(acac)_2$ to the aqueous micellar system promoted the reaction. In the presence of excess α-AHP, however, benzyl sulfone as well as benzyl sulfoxide was formed in quantity (entry 4). In contrast to the $MoO_2(acac)_2$ system, addition of $VO(acac)_2$[9] caused no acceleration of the reaction in aqueous media (entries 5 and 6). The conversion of the substrate was only 16% when **2** was employed as an oxidising reagent (entry 7). Compound **2** is water-soluble but does not form micelles in water. Evidently, a

Table 1 Oxidation of benzyl sulfide with α-AHP **1** or compound **2** at room temperature[a]

Entry	Oxidant/ mmol dm^{-3}	System[b]	Metal-catalyst[c]	Conversion (%)	Molar ratio sulfoxide : sulfone
1	**1** (10)	A	None	52	100 : 0
2	**1** (20)	A	None	89	100 : 0
3	**1** (10)	A	$MoO_2(acac)_2$	72	100 : 0
4	**1** (20)	A	$MoO_2(acac)_2$	100	80 : 20
5	**1** (10)	A	$VO(acac)_2$	52	100 : 0
6	**1** (20)	A	$VO(acac)_2$	88	100 : 0
7	**2** (10)	A	$MoO_2(acac)_2$	16	100 : 0
8	**1** (10)	B	$MoO_2(acac)_2$	90	80 : 20

[a] In 10 mmol dm^{-3} benzyl sulfide dispersion (or solution) of water (or dichloromethane) (0.01 dm^3) containing 10 or 20 mmol dm^{-3} of oxidant, at rt for 24 h. [b] A: in water and B: in dichloromethane. [c] Three mol% toward benzyl sulfide.

DOI: 10.1039/b005414n

key feature of success in promotion of this oxidation in water is the formation of micelles.

When the concentration of **1** in water was 10 mmol dm^{-3}, the maximum conversion was only 72% (entry 3). It is surmised that the oxygen atom transfer from **1** to benzyle sulfide results in the formation of the corresponding hemiacetal, which in turn is easily decomposed into non-surface-active nonanal and tetra(ethylene glycol). Because the cmc of **1** is 3.1 mmol dm^{-3}, most of the micelles will disappear at the final stage of the reaction. This results in the loss of effective solubilisation of substrate in the system. The appearance of insoluble solids in the reaction system was actually observed after 18 h with the naked eye. However, when using excess **1** (20 mmol dm^{-3}) micelles were still present after 24 h, so that the conversion of substrate in each system was higher than in the corresponding system containing 10 mmol dm^{-3} of **1**.

The precise mechanism of these micellar oxidation systems has not yet been established, but it seems reasonable to surmise that benzyl sulfide solubilised within the α-AHP micelles will be oxidised effectively by hydroperoxy groups of α-AHP, which will exist in the vicinity of the solubilised site.

In summary, effective oxidation of benzyl sufide to the corresponding sulfoxide (and sulfone) in water has been achieved by using micellar α-AHP **1** in the presence of a catalytic amount of $MoO_2(acac)_2$ under very mild conditions. Studies on the preparation of a series of α-AHPs and their application to other oxidation reactions in these micellar systems are now in progress.

This work was supported by a Grant-in-Aid for Scientific Research on Basic Research Area (12650835) from the Ministry of Education, Science, Culture and Sports of Japan.

Notes and references

† Over a solution of 1-alkene (10 mmol) and tetra(ethylene glycol) (80 mmol) in dichloromethane (0.04 dm^3) was passed a slow stream of ozone (1.2 equiv.) at −78 °C. Then, the mixture was poured into aqueous $NaHCO_3$ and was extracted with ether. After evaporation of the solvent, the crude products were separated by column chromatography on silica gel. Elution with ether–methanol (95 : 5, v/v) gave the target α-AHP as an oil. *Selected data* for compound **1** (R = *n*-C_8H_{17}), δ_H(270 MHz; $CDCl_3$) 0.88 (t, 3H), 1.15–1.45 (m, 12H), 1.60–1.85 (m, 2H), 3.1 (s, 1H), 3.52–3.90 (m, 16H), 4.84 (t, 1H), 10.66 (s, 1H); δ_C(67.5 MHz) 13.98, 22.53, 24.71, 29.07, 29.23, 29.32, 31.05, 31.71, 61.49, 65.12, 69.95, 70.02, 70.19, 70.42, 70.92, 72.38, 107.00 (Calc. for $C_{17}H_{36}O_7$: C, 57.93; H, 10.30. Found: C, 58.12; H, 10.09%). For compound **2** (R = *n*-C_4H_9), similar NMR data were recorded (Calc. for $C_{13}H_{28}O_7$: C, 52.69; H, 9.52. Found: C, 52.39; H, 9.37%).

‡ Cmc, γ_{cmc} and pC_{20} values were obtained from a surface tension *vs.* concentration (on a log scale) curve measured by the Wilhelmy method (Kyowa CBVP-A3 model; platinum plate) at 20 °C.

§ DTA/TG measurements were performed in a stream of nitrogen at 2 °C min^{-1} of programming rate (Seiko DTA/TG30 model).

¶ Oxidation of benzyl sulfide in aqueous systems was conducted as follows: to a stirred aqueous solution of α-AHP (0.01 dm^3, 10 or 20 mmol dm^{-3}) in a 0.05 dm^3 sample vial equipped with a magnetic bar and a septum were added benzyl sulfide (0.1 mmol) and metal catalyst (3 mol%). The reaction mixture was stirred in dark at rt for 24 h. Then, acetonitrile (0.015 dm^3) was poured into the mixture and bromobenzene as an internal standard was added to the solution. The resultant solution was injected directly into the HPLC apparatus equipped with a TSKgel ODS-80Ts column (eluate: water–acetonitrile = 2/3, flow rate: 8×10^{-4} dm^3 min^{-1}). From the comparison with authentic samples, formation of nonanal (in the case of α-AHP **1**) or pentanal (in the case of compound **2**), and tetra(ethylene glycol) was confirmed in the reaction mixture.

1 C.-J. Li and T.-K. Chan, *Organic Reactions in Aqueous Media*, John Wiley & Sons, New York, 1997; *Organic Synthesis in Water*, ed. P. A. Grieco, Blackie Academic & Professional, London, 1998.
2 J. H. Fendler and E. J. Fendler, *Catalysis in Micellar and Macromolecular Systems*, Academic Press, London, 1975.
3 D. A. Jaeger, M. W. Clennan and J. Jamrozik, *J. Am. Chem. Soc.*, 1990, **112**, 1171; D. A. Jaeger and J. Wang, *J. Org. Chem.*, 1993, **58**, 6745; D. A. Jaeger, D. Su, A. Zahar, B. Piknova and S. B. Hall, *J. Am. Chem. Soc.*, 2000, **122**, 2749.
4 S. Kobayashi, T. Wakabayashi, S. Nagayama and H. Oyamada, *Tetrahedron Lett.*, 1997, **38**, 4559; S. Kobayashi and T. Wakabayashi, *Tetrahedron Lett.*, 1998, **39**, 5389; S. Kobayashi, *Eur. J. Org. Chem.*, 1999, **3**, 15; K. Manabe, Y. Mori and S. Kobayashi, *Tetrahedron*, 1999, **55**, 11 203; K. Manabe and S. Kobayashi, *Chem. Commun.*, 2000, 669.
5 I. Grassert, E. Paetzold and G. Oehme, *Tetrahedron*, 1993, **49**, 6605; G. Cerichelli, L. Luchetti, G. Mancini and G. Savelli, *Tetrahedron*, 1995, **51**, 10 281; Y. Zhang and W. Wu, *Tetrahedron: Assymetry*, 1997, **8**, 2723; M. J. Diego-Castro and H. C. Hailes, *Chem. Commun.*, 1998, 1549; S. Otto, J. B. F. N. Engberts and J. C. T. Kwak, *J. Am. Chem. Soc.*, 1998, **120**, 9517; J. Schulz, A. Roucoux and H. Patin, *Chem. Commun.*, 2000, 535.
6 K. Sato, M. Aoki, J. Takagi, K. Zimmermann and R. Noyori, *Bull. Chem. Soc. Jpn.*, 1999, **72**, 2287; C. W. Jones, *Applications of Hydrogen Hydroperoxide and Derivatives*, RSC, Cambridge, 1999.
7 M. Hudlicky, *Oxidations in Organic Chemistry*, ACS Monograph 186, Washington, D.C., 1990, p. 9; *Handbook of Reagents for Organic Synthesis, Oxidizing and Reducing Agents*, ed. S. D. Burke and R. L. Danheiser, John Wiley & Sons, Chichester, 1999, pp. 61–68.
8 M. J. Rosen, *Surfactants and Interfacial Phenomena*, 2nd edn., John Wiley & Sons, New York, 1989, ch. 2, 3 and 5.
9 R. A. Sheldon and J. K. Kochi, *Metal-Catalyzed Oxidations of Organic Compounds*, Academic Press, New York, 1981, ch. 1, 3 and 13.

The first thermally-stable singly oxo-bridged dinuclear Ni(III) complex

Bappaditya Bag,[a] Nijhuma Mondal,[a] Georgina Rosair[b] and Samiran Mitra*[a]

[a] *Department of Chemistry, Jadavpur University, Calcutta, 700032 India. E-mail: pkbose@cal.vsnl.net.in*
[b] *Department of Chemistry, Heriot-Watt University, Edinburgh, UK EH14 4AS. E-mail: g.m.rosair@hw.ac.uk*

Received (in Cambridge, UK) 24th May 2000, Accepted 1st August 2000
First published as an Advance Article on the web 24th August 2000

A new thermally stable oxo-bridged dinuclear nickel(III) complex has been synthesised and its crystal structure showed two nickel(III) ions with distorted square pyramidal coordination geometry.

Complexes of Ni(III) are very significant for their participation in the catalytic action of hydrogenases.[1] Generally Ni(III) complexes are obtained by electrochemical oxidation of the corresponding Ni(II) species.[2] Although many homo- and hetero-metallic oxo-bridged complexes have been reported,[3,4] there are a limited number of high valent metal oxo-species that have been extensively characterised. Recently, structures of doubly oxo bridged dinuclear nickel(III) complexes were published.[5,6] However, both these species are thermally unstable. Usually M–O–M type complexes, where M has a d^n electronic configuration with $n > 5$, are unstable due to the presence of electrons in the higher level antibonding orbitals.[7]

We have synthesised and structurally characterised the stable oxo-bridged nickel(III) complex $[Ni(salen)]_2O$ **1**. The present

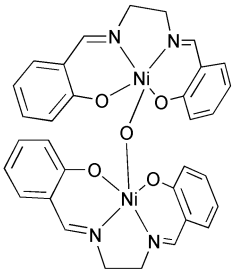

1

work provides the elemental analysis, X-ray structure analysis and magnetic studies of the complex and the results show that the two nickel ions in 3+ oxidation state are joined together by a bridging oxo group to form the dinuclear unit (Fig. 1).

The [Ni(salen)] complex was synthesised as reported earlier.[8] Pure oxygen gas was allowed to pass through a methanolic solution of [Ni(salen)], containing a few drops of NEt_3. On standing overnight, deep red crystals were obtained from the solution (yield 17%).† The crystals were thoroughly washed and air dried and one single crystal was selected for X-ray crystal structure analysis.‡

A perspective view of the molecule is shown in Fig. 1. As in most oxo-bridged complexes,[9] the Ni–O–Ni linkage is not linear [146.32(16)°]. Both the nickel(III) ions are five coordinate with distorted square pyramidal geometry. However, calculation of the geometrical factor τ shows that the degree of distortion in the two nickel centres is different [τ for Ni(1) is 0.15, for Ni(2), 0.33]. However the apical Ni–O(5) distance is 1.790(2) Å for both Ni centres.

The Ni–O distances are shorter here than in the doubly-bridged species [1.870(8), 1.841(7) Å]. The Ni–O distances found in closely related aqua species[6] are longer, typically by 0.1 Å and in the bridging hydroxo species,[5] longer still, by 0.2 Å.

The mean Ni–O and Ni–N salen distances are substantially longer [1.929(15) and 2.115(9) Å, respectively] than those

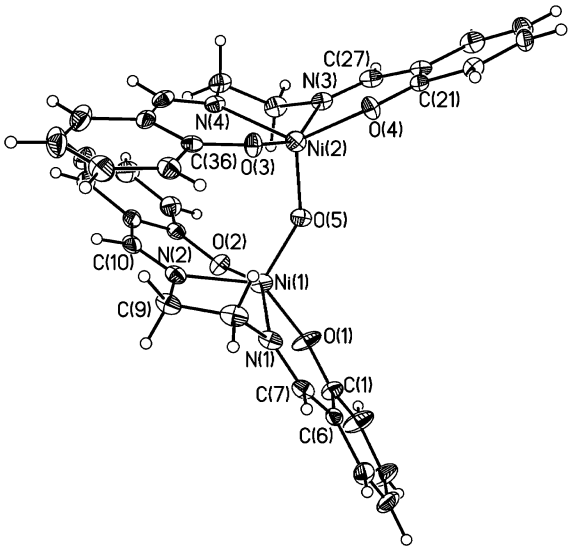

Fig. 1 Perspective view of **1** with displacement ellipsoids drawn at the 50% probability level. Selected distances (Å) and angles (°): Ni(2)–O(5) 1.790(2), Ni(2)–O(4) 1.918(2), Ni(2)–N(3) 2.108(3), Ni(2)–O(3) 1.949(2), Ni(2)–N(4) 2.116(3), Ni(1)–O(1) 1.912(2), Ni(1)–O(2) 1.938(2), Ni(1)–N(2) 2.130(3), Ni(1)–O(5) 1.790(2), Ni(1)–N(1) 2.108(3); O(2)–Ni(1)–O(1) 148.46(11), O(1)–Ni(1)–N(2) 139.37(12), Ni(1)–O(5)–Ni(2) 146.32(16).

found in a survey on Ni(II) salen species using the Cambridge Structural Database[10] where the mean Ni–N distance was found to be 1.858(32) Å and the mean Ni–O distance 1.849(15) Å. The standard deviations quoted are those of the population.

The thermally stable complex decomposed at 41 °C. The solid reflectance electronic spectrum of the complex exhibited two intense absorption bands at 390 and 320 nm which are assigned as salen-based bands, but there are no characteristic absorption bands due to d–d transitions of the nickel ions. The IR spectrum shows bands at 882 and 430 cm^{-1} assigned as ν_{as}(NiONi) and δ(NiONi) respectively and there is no characteristic band for ν(OH). An electrochemical study of the complex shows a reversible process ($E_{1/2}$ = 1.05 V *vs.* SCE in methanol). The spectroscopic and CV results strongly support an oxo-bridged Ni(III) complex with square pyramidal geometry. The presence of strong donating groups in the Schiff base ligand stabilises the nickel ion in the higher oxidation state.

The observed room temperature magnetic moment value for **1** is 6.16 μ_B, fairly close to the expected value of 5.5 μ_B for two high spin d^7 ions.

Financial assistance from UGC, CSIR and DST, New Delhi is gratefully acknowledged. We also acknowledge the use of the EPSRCs Chemical Database Service at Daresbury.

Notes and references

† *Analytical results* for **1**. Found C, 57.9; H, 4.3; N, 8.3. calc. for $C_{32}H_{28}N_4Ni_2O_5$: C, 57.7; H, 4.2; N, 8.4%.

‡ *Crystal data* for **1**, $C_{32}H_{28}N_4Ni_2O_5$, M_w = 666, triclinic, space group $P\bar{1}$, a = 10.7370(14), b = 10.8370(14), c = 13.7620(14) Å, α = 67.040(11), β = 85.710(10), γ = 73.110(11)°, V = 1409.5(2) Å^3, Z = 2, D_c = 1.569

Mg m^{-3}, μ = 1.386 mm^{-1}, T = 160(2) K, Crystal size 0.28 × 0.48 × 0.30 mm, 4820 independent reflections 4820 (R_{int} = 0.0323), R_1 = 0.0443, wR_2 = 0.1296. A single crystal was mounted with vacuum grease on a glass fibre and transferred to a Bruker AXS P4 diffractometer[11] and data were measured at 160 K, using an Oxford Cryosystems Cryostream. Solution and refinement were performed using the SHELXTL[12] suite of programs.

CCDC 182/1733. See http://www.rsc.org/suppdata/cc/b0/b004165n/ for crystallographic files in .cif format.

1 M. A. Halcrow and G. Christou, *Chem. Rev.*, 1994, **94**, 2421; *The Bioinorganic Chemistry of Nickel*, ed. J. R. Lancaster, VCH, New York, 1988.
2 B. de Castro, C. Freire and E. Pereira, *J. Chem. Soc., Dalton Trans.*, 1994, 571.
3 J. E. Davies and B. M. Gatehouse, *Acta Crystallogr., Sect. B*, 1973, **29**, 1934; F. Corazza, C. Floriani and M. Zehnder, *J. Chem. Soc., Dalton. Trans.*, 1987, 709.
4 B. G. Gafford, R. A. Holwerda, H. J. Schugar and J. A. Potenza, *Inorg. Chem.*, 1988, **27**, 1126; J. A. Gilbert, D. S. Eggleston, W. R. Murphy, D. A. Geselowitz, S. W. Gersten, D. J. Hodgson and T. J. Meyer, *J. Am. Chem. Soc.*, 1985, **107**, 3855.
5 S. Hikichi, M. Yoshizawa, Y. Sasakura, M. Akita and Y. Moro-oka, *J. Am. Chem. Soc.*, 1998, **120**, 10 567.
6 K. Shiren, S. Ogo, S. Fujinami, H. Hayashi, M. Suzuki, A. Uehara, Y. Watanabe and Y. Moro-oka, *J. Am. Chem. Soc.*, 2000, **122**, 254.
7 K. Tatsumi and R. Hoffmann, *J. Am. Chem. Soc.*, 1981, **103**, 3328.
8 A. G. Manfredotti and C. Guastini, *Acta Crystallogr. Sect. C*, 1983, **39**, 863.
9 B. O. West, *Polyhedron*, 1989, **8**, 219 and references therein.
10 The United Kingdom Chemical Database Service, D. A. Fletcher, R. F. McMeeking and D. Parkin, *J. Chem. Inf. Comput. Sci.*, 1996, **36**, 746.
11 XSCANS, Data collection and reduction program, Version 2.2, Bruker AXS, Madison, WI, 1994.
12 G. M. Sheldrick, Structure determination and refinement programs, Version 5.1. Bruker AXS, Madison, WI, 1999.

ChemComm

Complexes containing the heptadentate cogwheel C_7Me_7: synthesis and structural characterization of heptamethylcycloheptatrienyl (CHT*) tungsten complexes

Matthias Tamm,*[a] Bernd Dreßel,[a] Roland Fröhlich[b] and Klaus Bergander[b]

[a] *Anorganisch-Chemisches Institut, Westfälische Wilhelms-Universität, Wilhelm-Klemm-Straße 8, D-48149 Münster, Germany. E-mail: mtamm@uni-muenster.de*

[b] *Organisch-Chemisches Institut, Westfälische Wilhelms-Universität, Corrensstraße 40, D-48149 Münster, Germany*

Received (in Cambridge, UK) 21st June 2000, Accepted 2nd August 2000
First published as an Advance Article on the web 22nd August 2000

The first heptamethylcycloheptatrienyl (CHT*) complexes $[(\eta^5\text{-}C_7Me_7)W(CO)_3(NCR)][BF_4]$ (R = Me, Et) and $[(\eta^5\text{-}C_7Me_7)W(CO)_3I]$ have been prepared from $[(C_7Me_7)BF_4]$.

In contrast to complexes with sterically demanding peralkylated or perarylated cyclopentadienyl (η-C_5R_5) and arene (η-C_6R_6) groups (R ≠ H),[1] the corresponding cycloheptatrienyl complexes, (η-C_7R_7)M, are unknown despite the fact that the aromatic cycloheptatrienyl cations $C_7Me_7^+$ and $C_7Ph_7^+$ have been known for decades.[2,3] The molecular structures of $C_7Me_7^+$ and $C_7Ph_7^+$, however, have been determined only recently and represent the first structurally characterized cycloheptatrienyl cations with seven substituents to date.[4,5] Attempts to coordinate transition metals to the central seven-membered ring of these persubstituted π-perimeters have not been succesful so far.[6]

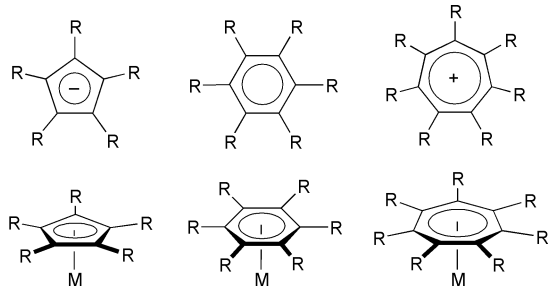

In continuation of our work on transition metal complexes with novel cycloheptatrienyl ligands,[7] we became interested in the synthesis of salts containing the heptamethylcycloheptatrienyl cation, $C_7Me_7^+$, and in the use of these compounds as ligands in organotransition metal chemistry. Thus, we have recently reported an improved protocol for the synthesis of heptamethylcycloheptatriene, C_7Me_7H, from hexamethylbenzene together with the synthesis and structural characterization of $[(C_7Me_7)BF_4]$ **1**,[4] which revealed a non-planar, boat-like geometry of the seven-membered ring owing to steric congestion caused by the seven methyl substituents. Consequently, we had stated that this strong distortion might impede applications of the C_7Me_7 ligand to the synthesis of organometallic derivatives. In the meantime, however, we have observed that coordination of this sterically demanding cation to transition metal centers is surprisingly easy, and with this contribution, we present the first transition metal complexes containing this molecular cogwheel.

The reaction of tropylium salts with complexes of the type *fac*-$[M(CO)_3(NCR)_3]$ (M = Mo, W; R = Me, Et) can result in the formation of cationic cycloheptatrienyl complexes $[(\eta^7\text{-}C_7R_7)M(CO)_3]^+$ by substitution of the three nitrile ligands,[8,9] *e.g.* 1,2,4,6-tetramethylcycloheptatrienyl hexafluorophosphate gives $[(\eta^7\text{-}1,2,4,6\text{-}C_7Me_4H_3)W(CO)_3][PF_6]$ upon treatment with *fac*-$[W(CO)_3(NCEt)_3]$ in the presence of a catalytic amount of ferricenium ion. This cationic tungsten complex reacts further with halides to form neutrally charged complexes $[(\eta^7\text{-}1,2,4,6\text{-}C_7Me_4H_3)W(CO)_2X]$ (X = Br, I),[9] which agrees with the reactivity observed for related cationic molybdenum and tungsten tricarbonyl complexes.[8,10]

In view of the observations described above, the reaction of $[(C_7Me_7)BF_4]$ **1** with *fac*-$[W(CO)_3(NCEt)_3]$ appeared to be a promising method for the preparation of the first CHT* complex (CHT* = C_7Me_7).[11] Hence, a thf–dichloromethane solution of **1** was treated with an equimolar amount of the nitrile complex in the presence of a catalytic quantity of $[Cp_2Fe][PF_6]$. After stirring for 2 h and evaporation of the solvents, the intermediate product (presumably **2b**, *vide infra*) was redissolved in acetone, and a large excess of sodium iodide was added (Scheme 1). Surpringly, no CO evolution could be observed, which is inconsistent with the formation of a complex $[(\eta^7\text{-}C_7Me_7)W(CO)_2I]$, which we had expected arguing from analogy with the 1,2,4,6-tetramethylcycloheptatrienyl system (*vide supra*). Instead, a stable, purple–red crystalline solid could easily be separated by column chromatography, of which the spectroscopic characterization indicated a C_7Me_7 ring not coordinated in a symmetric η^7-fashion. Its ^{1}H NMR spectrum exhibits four different resonances for the methyl protons in a 6:6:6:3 ratio. Consistently, in the ^{13}C NMR spectrum the methyl and the ring carbon atoms give rise to four resonances each, in addition to two signals for the carbonyl carbon atoms.† These results together with the observation of three carbonyl stretching frequencies in the IR spectrum suggest the formation of $[(\eta^5\text{-}C_7Me_7)W(CO)_3I]$ **3**, in which the C_7Me_7 ligand is only η^5-coordinated (Scheme 1).

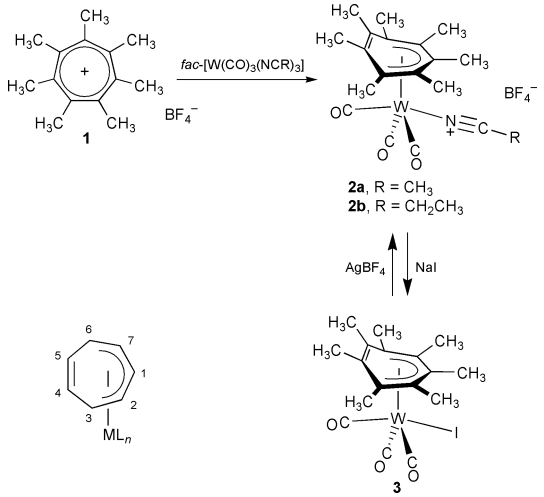

Scheme 1

In order unambiguously to confirm this conclusion, the molecular structure of **3** was established by X-ray diffraction analysis.‡ The asymmetric unit contains two independent, almost identical molecules, and the structure of molecule A is

shown in Fig. 1. The complex is almost C_s symmetric with the pseudo mirror plane including I, W, C1, C15 and O1. The η^5-coordinated ring is strongly distorted from planarity and rather adopts a boat conformation with its uncoordinated part strongly bending back from the rest of the molecule.[12] Furthermore, the distance between the two uncoordinated carbon atoms [C4A–C5A 1.312(10) Å, C4B–C5B 1.310(10) Å] clearly corresponds to a C(sp^2)–C(sp^2) double bond, and hence the solid state structure of **3** is best described as a pentadienyl complex as shown in Scheme 1. In fact, the structural features compare well with those of other complexes containing 'true' pentadienyl ('open Cp')[13] or related cycloheptadienyl ligands.[14]

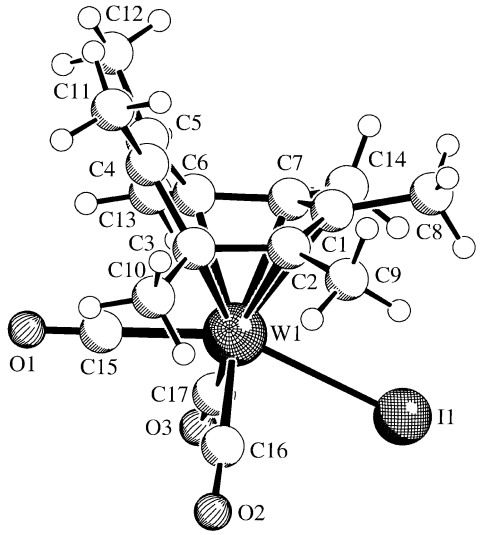

Fig. 1 Molecular structure of **3**. Selected bond lengths (Å) and angles (°): molecule A [molecule B] C1–C2 1,447(9) [1.428(9)], C1–C7 1.427(10) [1.432(10)], C2–C3 1.429(9) [1.451(9)], C3–C4 1.497(9) [1.503(9)], C4–C5 1.312(10) [1.310(10)], C5–C6 1.506(9) [1.496(9)], C6–C7 1.440(10) [1.442(9)], W1–I1 2.8425(6) [2.8659(5)], W1–C1 2.440(7) [2.425(6)], W1–C2 2.308(7) [2.303(7)], W1–C3 2.332(7) [2.335(6)], W1–C6 2.346(6) [2.329(6)], W–C7 2.323(6) [2.292(6)], W1–C15 2.008(10) [1.984(8)], W1–C16 1.988(8) [1.991(9)], W1–C17 2.000(8) [1.995(7)]; C15–W1–I1 153.2(2) [154.2(2)], C16–W1–C17 93.1(3) [93.7(3)].

Nevertheless, this η^5-bonding mode is quite unique for a cycloheptatrienyl ligand,[15] and only very few examples have been reported in the older literature[16] in addition to proposed intermediates containing an η^5-cycloheptatrienyl ring.[17] In contrast, the η^7–η^3 hapticity interconversion in cycloheptatrienyl complexes has been studied in great detail.[18] It appears that the constrained geometry of the uncoordinated heptamethylcycloheptatrienyl cation[4] accounts for the unusual reactivity observed here as the C_7Me_7 ring tries to retain its boat conformation.

In order to prove the intermediacy of **2b** in the formation of **3** from **1**, the iodine in **3** was removed by treatment of **3** with [$AgBF_4$] in acetonitrile solution. The IR and NMR spectroscopic characterization of the red crystalline compound reveals that the η^5-bound cycloheptatrienyl complex **2a** must have formed.† Even after one week in CD_2Cl_2 solution, the NMR spectrum gave no indication for a η^5–η^7 hapticity interconversion by intramolecular substitution of the coordinated acetonitrile by the pendent double bond. Thus, a η^7-C_7Me_7 complex still remains elusive.

With this contribution, we have demonstrated that η^5-bound heptamethylcycloheptatrienyl complexes are surprisingly stable and easy to prepare. These are very promising candidates for further reactions, *e.g.* for the preparation of bimetallic complexes[19] by specifically utilizing the pendant double bond for the coordination of an additional metal center. Future work in this area will also elucidate the possibility to prepare (η^7-C_7Me_7)M complexes which can be expected to be very reactive due to the permethylated ligand being in an 'entatic' state.

Notes and references

† *Spectroscopic data* for **2a** and **3**; all resonances have been unambiguously assigned by two-dimensional NMR spectroscopy (COSY experiments); for the numbering, see Scheme 1.

2a: IR (CH_2Cl_2): $\tilde{\nu}$ 2042, 2000, 1954 cm^{-1} (CO). δ_H(600 MHz, CD_2Cl_2): 2.71 (s, 3H, CH_3CN), 2.46 (s, 3H, 1-CH_3), 2.41 (s, 6H, 2,7-CH_3), 2.40 (s, 6H, 3,6-CH_3), 1.46 (s, 6H, 4,5-CH_3). δ_C(150 MHz, CD_2Cl_2): 212.7 (2 × Mo–CO), 211.7 (1 × Mo–CO), 137.0 (C-4,5), 134.0 (C-1), 132.4 (CN), 110.8 (C-2,7), 102.9 (C-3,6), 27.1 (3,6-CH_3), 20.6 (2,7-CH_3 + 1-CH_3), 17.4 (4,5-CH_3), 4.7 (CH_3CN).

3: IR (CH_2Cl_2): $\tilde{\nu}$ 2018, 1976, 1930 cm^{-1} (CO). δ_H(600 MHz, CD_2Cl_2): 2.74 (s, 3H, 1-CH_3), 2.25 (s, 6H, 3,6-CH_3), 2.16 (s, 6H, 2,7-CH_3), 1.41 (s, 6H, 4,5-CH_3). δ_C(150 MHz, CD_2Cl_2): 213.8 (1 × Mo–CO), 209.3 (2 × Mo–CO), 135.1 (C-4,5), 131.4 (C-1), 106.0 (C-2,7), 97.0 (C-3,6), 26.5 (3,6-CH_3), 22.0 (2,7-CH_3), 21.0 (1-CH_3), 17.3 (4,5-CH_3).

‡ *Crystal data* for $C_{17}H_{21}IO_3W$ **3**: M = 584.09, a = 7.515(1), b = 29.376(1), c = 16.328(1) Å, β = 90.13(1)°, V = 3604.6(5) Å^3, μ = 81.31 cm^{-1}, Z = 8, monoclinic, space group $P2_1/n$ (no. 14), T = 198 K, 28135 reflections collected (±h, ±k, ±l), 8237 independent (R_{int} = 0.087) and 5361 observed reflections [$I \geqslant 2\sigma(I)$], R = 0.044, wR^2 = 0.064, two chemically identical molecules with different conformation in the asymmetric unit. CCDC 182/1735.

1 *Comprehensive Organometallic Chemistry*, ed. G. Wilkinson, F. G. A. Stone and E. W. Abel, Pergamon Press, Oxford, 1982; *Comprehensive Organometallic Chemistry II*, ed. E. W. Abel, F. G. A. Stone and G. Wilkinson, Chapman and Hall, Oxford, 1995.
2 K. Takeuchi, Y. Yokomichi and K. Okamoto, *Chem. Lett.*, 1977, 1177.
3 M. A. Battiste, *J. Am. Chem. Soc.*, 1961, **83**, 4101.
4 M. Tamm, B. Dreßel and R. Fröhlich, *J. Org. Chem.*, in press.
5 S. Brydges, J. F. Britten, L. C. F. Chao, H. K. Gupta and M. J. McGlinchey, *Chem. Eur. J.*, 1998, **4**, 1201.
6 L. C. F. Chao, H. K. Gupta, D. W. Hughes, J. F. Britten, S. S. Rigby, A. D. Bain and M. J. McGlinchey, *Organometallics*, 1995, **14**, 1139; H. K. Gupta, S. Brydges and M. J. McGlinchey, *Organometallics*, 1999, **18**, 115.
7 M. Tamm, T. Bannenberg, K. Baum, R. Fröhlich, T. Steiner, T. Meyer-Friedrichsen and J. Heck, *Eur. J. Inorg. Chem.*, 2000, 1161.
8 A. Roberts and M. W. Whiteley, *J. Organomet. Chem.*, 1993, **458**, 131.
9 E. Schwed, H.-U. Hund, H. W. Bosch and H. Berke, *Helv. Chim. Acta*, 1991, **74**, 189.
10 M. L. H. Green and D. K. P. Ng, *J. Chem. Soc., Dalton Trans.*, 1993, 17.
11 On the analogy of Cp* = C_5Me_5, we propose the name CHT* for the heptamethylcycloheptatrienyl system.
12 The bend angles between the planes containing C3–C6 and C1, C2, C3, C6, C7 are 60.3(3)° (molecule A) and 60.9(3)° (molecule B).
13 R. D. Ernst, *Chem. Rev.*, 1988, **88**, 1255; M. S. Kralik, A. L. Rheingold, J. P. Hutchinson, J. W. Freeman and R. D. Ernst, *Organometallics*, 1996, **15**, 551.
14 C. Wang and J. B. Sheridan, *Organometallics*, 1994, **13**, 3639; R. L. Beddoes, J. R. Hincliffe and M. W. Whiteley, *J. Chem. Soc., Dalton Trans.*, 1993, 501; J. R. Hincliffe and M. W. Whiteley, *J. Organomet. Chem.*, 1991, **402**, C50; A. Salzer and H. Werner, *Z. Anorg. Chem.*, 1975, **418**, 88; A. Salzer and H. Werner, *J. Organomet. Chem.*, 1975, **87**, 101.
15 M. L. H. Green and D. K. P. Ng, *Chem. Rev.*, 1995, **95**, 439.
16 [(η^5-C_7H_7)(η^5-C_7H_9)Fe] and [(η^5-C_7H_7)(η^5-C_7H_9)Ru] have been obtained in very low yield from cycloheptatriene by ligand metal co-condensation or by a reductive method: J. R. Blackborow, K. Hildenbrand, E. Koerner von Gustorf, A. Scrivanti, C. R. Eady and D. Ehnholt, *J. Chem. Soc., Chem. Commun.*, 1976, 16; H. Schmid and M. L. Ziegler, *Chem. Ber.*, 1976, **109**, 125.
17 P. Powell, L. J. Russell and E. Styles, *J. Organomet. Chem.*, 1978. **149**, C1; R. H. Hooker and A. J. Rest, *J. Organomet. Chem.*, 1982, **234**, C23.
18 See, for example: R. L. Beddoes, Z. I. Hussain, A. Roberts, C. R. Barraclough and M. W. Whiteley, *J. Chem. Soc., Dalton Trans.*, 1996, 3629 and references therein.
19 For two recent recent publications, see: H. Wadepohl, W. Galm and H. Pritzkow, *Organometallics*, 1996, **15**, 570; M. Airoldi, G. Deganello, G. Gennaro, M. Moret and A. Sironi, *Organometallics*, 1993, **12**, 3964.

ChemComm

Synthesis and characterization of dehydrothieno[18]annulenes

Abhijit Sarkar and Michael M. Haley*

Department of Chemistry and Materials Science Institute, University of Oregon, Eugene, OR 97403-1253, USA. E-mail: haley@oregon.uoregon.edu

Received (in Corvallis, USA) 20th June 2000, Accepted 2nd August 2000
First published as an Advance Article on the web 25th August 2000

Use of a palladium/copper alkyne cross-coupling strategy provides access to three tris(thiophene-fused) dodecadehydro[18]annulenes, including examples of both highly symmetrical C_{3h} and unsymmetrical C_s structures.

We have been investigating dehydrobenzoannulenes with the aim of exploring diverse properties such as liquid crystalline behavior, solid state polymerization, and nonlinear optical activity.[1] Specifically, diacetylenic dehydrobenzoannulenes (DBAs) and related phenylacetylene macrocycles[2] have been shown to be useful precursors for a variety of carbon-rich polymeric systems, such as ladder polymers,[3] molecular tubes[4] and novel allotropes of carbon.[5] Recently, we described a simple yet versatile methodology for the preparation of site-specifically functionalized DBAs.[6] By applying a stepwise synthetic route, we were able to introduce donor and/or acceptor functional groups on the phenyl rings in a discrete manner, thereby permitting a detailed structure–property relationship study of this class of macrocycles and thus making advances toward molecular engineering.[7] In the course of further refining the design for our target annulenes, we planned to introduce thiophene rings in place of the phenyl moieties in the DBA skeleton. The choice of thiophene in our annulenes was inspired by factors such as the chemical and electrochemical polymerizability of thiophene, environmental stability of macrocycles containing thiophene, the ability to form two-dimensional π-systems useful for electronics and photonics, and interaction among the individual macrocycles due to the lone pairs present in the sulfur of thiophene rings.[8] Herein we report the preparation of three diacetylenic dehydrothieno[18]annulenes (**1**–**3**, DTAs), including the synthesis of **2** and **3** which possess unsymmetrical topologies.

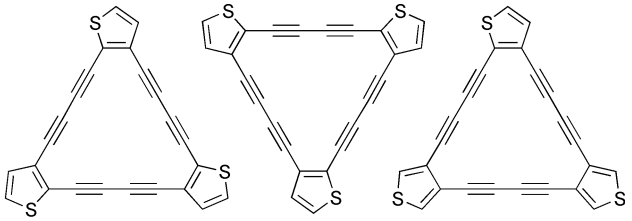

1 **2** **3**

Compounds **1**–**3** represent three of the seven possible regioisomers resulting from thiophene fusion to the [18]annulene core.[9] Other routes to thienoannulenes have relied on metal-mediated intermolecular couplings.[10] By virtue of the structure of the starting materials, only C_{nh}- and D_{nh}-symmetric macrocycles are produced. In order to probe the structure–property relationships among the various structural isomers, it is necessary to introduce the thiophene moieties in a stepwise manner to produce DTAs possessing lower symmetries (C_s), *i.e.* **2** and **3**.[11]

The synthesis of **1**, which illustrates the stepwise technique for DTA assembly, was accomplished as shown in Scheme 1. Sequential Sonogashira cross-coupling of 2-bromo-3-iodothiophene (**4**)[12] with 1-(trimethylsilyl)buta-1,3-diyne and (triisopropylsilyl)ethyne, respectively, gave triyne **5** in 31% yield. *In situ* protiodesilylation of **5** followed by Pd-catalyzed coupling[13] with an equimolar amount 3-bromo-2-iodothiophene[12] furnished bis-thiophene **6** as the major product in 40% yield. Attachment of triyne **7**, obtained in a reaction sequence similar to regioisomeric triyne **5** starting instead with 3-bromo-2-iodothiophene, provided the α,ω-bis-protected polyyne **8**. Removal of the TIPS groups with Bu_4NF in THF–EtOH and subsequent cyclization using CuCl–$Cu(OAc)_2$ in pyridine afforded **1**† in 50% yield. In an analogous manner, **2**† was prepared from **4** and two equivalents of triyne **5**, **3**† from **4** and two equivalents of the 3,4-regioisomeric triyne.[11]

In **1** and **2**, the thiophene moieties are fused at the 2,3-positions to the [18]annulene core, the sole difference between the macrocycles being the reversal of one thiophene ring. Therefore, the overall π-conjugation of **2** is expected to be similar to that of **1**. In **3**, two of the thiophene rings are fused to the macrocycle through the 3,4-positions. The C3–C4 bond in a thiophene ring is known to have less double bond character than the C2–C3 bond.[14] As a consequence, the overall conjugation of annulene **3** is expected to be lower than that in **1** or **2**. These arguments are supported by the electronic absorption spectra for

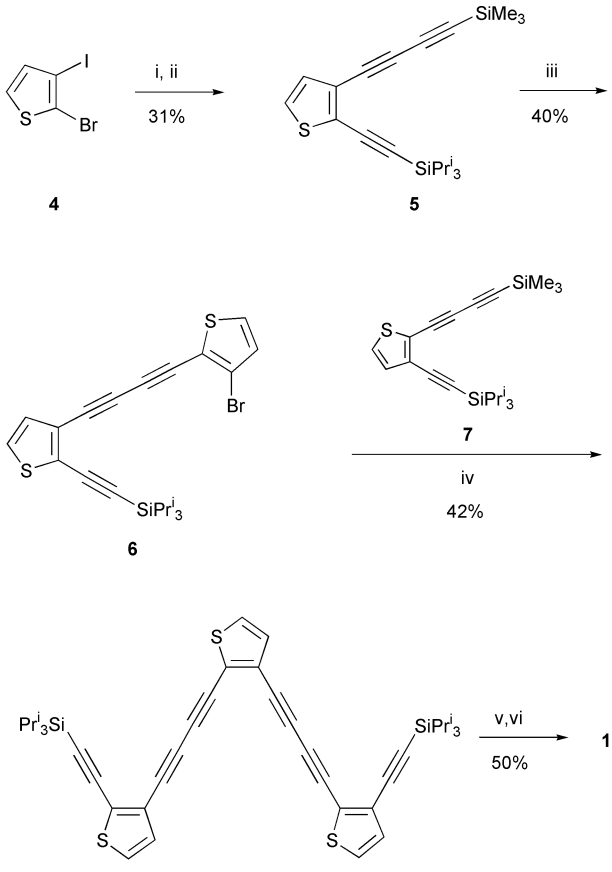

Scheme 1 *Reagents and conditions*: i, 1-(trimethylsilyl)buta-1,3-diyne, $PdCl_2(PPh_3)_2$, CuI, Et_3N, rt; ii, (triisopropylsilyl)ethyne, $PdCl_2(PPh_3)_2$, CuI, Et_3N, 120 °C; iii, 3-bromo-2-iodothiophene, aq. KOH, $PdCl_2(PPh_3)_2$, CuI, Et_3N, 60 °C; iv, **7**, aq. KOH, $PdCl_2(PPh_3)_2$, CuI, Et_3N, 60 °C; v, Bu_4NF, EtOH, rt; vi, CuCl, $Cu(OAc)_2$, pyridine, O_2, 60 °C.

DOI: 10.1039/b004962j

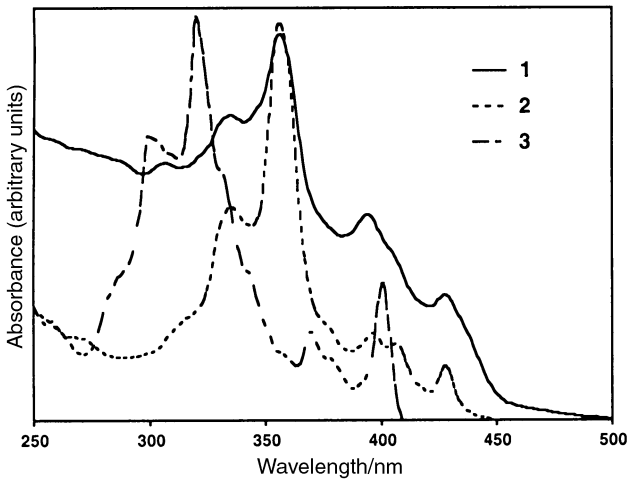

Fig. 1 Electronic absorption spectra for **1**–**3**.

1–**3** (Fig. 1). Quite expectedly, the spectra for **1** and **2** are essentially identical. Both molecules have λ_{max} at 428 nm; however, λ_{max} for **3** (401 nm) is significantly blue-shifted compared to **1** and **2**, thus indicating a lesser overall conjugation in **3**, as discussed above.

The thermal properties of **1**–**3** were studied using DSC and TGA scans. The macrocycles do not melt upon heating; instead, when heated above 150 °C, they are transformed into shiny black solids that are completely insoluble in common organic solvents. For example, DSC analysis of **1** showed a sharp exotherm at 168 °C. The TGA scan for **1** showed almost no weight loss ($< 5\%$) at the temperature range corresponding to the DSC exotherm. Therefore, the exotherm is most likely attributable to a polymerization reaction occurring in the solid state. Investigations to probe the polymerization reaction and the resultant products are in progress.

In summary, we have developed a versatile route for the synthesis of dehydrothieno[18]annulenes, including both symmetrically and unsymmetrically fused systems. A detailed structure–property relationship study of this class of macrocycles is currently underway.

We thank the National Science Foundation and the Camille and Henry Dreyfus Foundation for support of this work.

Notes and references

† *Selected spectral data*. **1**: $\delta_H(CDCl_3$, 299.96 MHz) 7.08 (d, *J* 6, 3H), 6.97 (d, *J* 6, 3H); ν_{max}(KBr)/cm^{-1} 3109, 2198, 2139, 1640, 722; *m/z* (MALDI-TOF): calcd. 390.50, found 390.47. **2**: $\delta_H(CDCl_3$, 299.96 MHz) 7.44–7.40 (m, 3H), 7.36–7.34 (m, 3H); ν_{max}(KBr)/cm^{-1} 3109, 2198, 2139, 1640, 728; *m/z* (MALDI-TOF): calcd. 390.50, found 390.68. **3**: $\delta_H(CDCl_3)$ 7.61–7.57 (m, 4H), 7.24 (d, *J* 6, 1H), 7.08 (d, *J* 6, 1H); ν_{max}(KBr)/cm^{-1} 3110, 2198, 2146, 1654, 725; *m/z* (MALDI-TOF): calcd. 390.50, found 390.53.

1 M. M. Haley, *Synlett*, 1998, 557.
2 M. M. Haley, J. J. Pak and S. C. Brand, *Topics in Current Chemistry (Carbon-Rich Compounds II)*, ed. A. de Meijere, Springer-Verlag, Berlin, 1999, vol. 201, p. 81.
3 Q. Zhou, P. J. Carroll and T. M. Swager, *J. Org. Chem.*, 1994, **59**, 1294.
4 K. P. Baldwin, A. J. Matzger, D. A. Scheiman, C. A. Tessier, K. P. C. Vollhardt and W. J. Youngs, *Synlett*, 1995, 1215.
5 R. Boese, A. J. Matzger and K. P. C. Vollhardt, *J. Am. Chem. Soc.*, 1997, **119**, 2052; Y. Tobe, N. Nakagawa, K. Naemura, T. Wakabayashi, T. Shida and Y. Achiba, *J. Am. Chem. Soc.*, 1998, **120**, 4544.
6 J. J. Pak, T. J. R. Weakley and M. M. Haley, *J. Am. Chem. Soc.*, 1999, **121**, 8182.
7 H. S. Nalwa, T. Watanabe and S. Miyata, *Nonlinear Optics of Organic Molecules and Polymers*, ed. H. S. Nalwa and S. Miyata, CRC Press, New York, 1997, p. 99, and references cited therein.
8 J. Roncali, *Chem. Rev.*, 1992, **92**, 711; A. K. Jen, V. P. Rao, K. Y. Wong and K. J. Drost, *J. Chem. Soc., Chem. Commun.*, 1993, 90; R. Zamboni, R. Danieli, G. Ruini and C. Taliani, *Opt. Lett.*, 1989, **14**, 1321.
9 Seven possible regioisomers: C_{3h} (1 possible, *e.g.* **1**), D_{3h} (1 possible), C_{2v} (2 possible), C_s (3 possible, *e.g.* **2** and **3**).
10 D. Solooki, J. D. Bradshaw, C. A. Tessier and W. J. Youngs, *Organometallics*, 1994, **13**, 451; D. Zhang, C. A. Tessier and W. J. Youngs, *Chem. Mater.*, 1999, **11**, 3050; M. J. Marsella, I. T. Kim and F. Tham, *J. Am. Chem. Soc.*, 2000, **122**, 974.
11 The synthesis of the remaining four isomers as well as a detailed comparison of the physical properties of all seven will be detailed in a full report; A. Sarkar and M. M. Haley, work in progress.
12 S. Gronowitz and B. Holm, *Acta Chem. Scand., Ser. B*, 1976, **30**, 423.
13 M. M. Haley, M. L. Bell, J. J. English, C. A. Johnson and T. J. R. Weakley, *J. Am. Chem. Soc.*, 1997, **119**, 2956.
14 F. Fringuelli, G. Marino and A. Taticchi, *J. Chem. Soc., Perkin Trans. 2*, 1974, 1215.

ChemComm

Diastereoselective synthesis of tetrahydrofuran-containing fragments by the permanganate oxidation of 1,5,9-trienes

Richard C. D. Brown,* Robert M. Hughes, John Keily and Anne Kenney

Department of Chemistry, University of Southampton, Highfield, Southampton, UK SO17 1BJ. E-mail: rcb1@soton.ac.uk

Received (in Cambridge, UK) 31st May 2000, Accepted 4th August 2000
First published as an Advance Article on the web 25th August 2000

The permanganate oxidation of several readily accessible 1,5,9-trienes occurs regioselectively to provide very short diastereoselective routes to substituted octahydro-2,2′-bifuranyl systems.

Substituted tetrahydrofurans constitute important structural and functional sub-units of a variety of biologically active natural products including the polyether antibiotics and annonaceous acetogenins.[1,2] An attractive approach to the synthesis of *cis*-2,5-disubstituted tetrahydrofurans is the permanganate-promoted oxidative cyclisation of 1,5-dienes,[3–5] and there have been several elegant applications of oxidative cyclisation in the synthesis of polyether antibiotic fragments.[4,6,7] Unfortunately, modest yields and the non-availability of suitably functionalised isomerically pure 1,5-dienes have restricted more widespread application of oxidative cyclisation in natural product synthesis. Other metal oxo species have also been reported to effect oxidative cyclisation of 1,5-dienes,[8,9] although no overall advantage over the permanganate-promoted process is evident. Herein we report short diastereoselective syntheses of *cis*-2,5-disubstituted tetrahydrofuran-containing fragments that are suitably functionalised to permit further elaboration.

By exploiting the different reactivity of different types of olefin, regioselective oxidative cyclisation of certain 1,5,9-trienes can be achieved to provide rapid access to useful tetrahydrofuran building blocks. For example, oxidation of methyl (*E*,*E*)-farnesoate (**2**), obtained in 2 steps from (*E*,*E*)-farnesol (**1**),[10] by potassium permanganate in buffered aqueous acetone provides lactol **3** as an approximately 6:1 mixture of epimers (Scheme 1).[11] The formation of **3** can be explained by kinetically controlled attack at the C=C bond of the α,β-unsaturated ester,[12] leading to an intermediate hypomanganate diester **5**, which underwent extremely rapid oxidation to a manganate diester and cyclisation in line with the mechanism proposed by Baldwin (Scheme 2).[13] Independent oxidation of the remaining double bond present in **6** by permanganate afforded the observed product **3**. Lead tetraacetate cleavage of the vicinal diol completed the synthesis of the lactone **4** in an overall yield of 23% and in 4 steps from a commercial starting material.

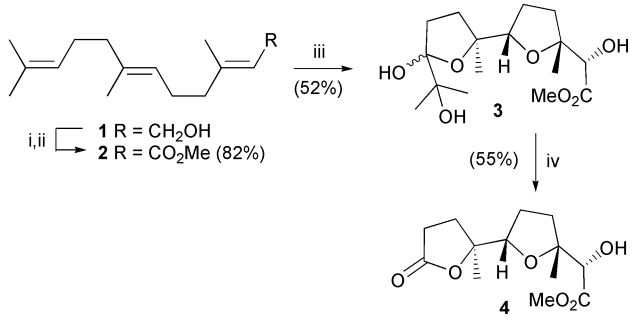

Scheme 1 *Reagents and conditions*: i, MnO_2, hexane; ii, MnO_4, KCN, AcOH, MeOH; iii, $KMnO_4$, AcOH, acetone, acetate buffer (pH 6.5); iv, $Pb(OAc)_4$, Na_2CO_3, CH_2Cl_2.

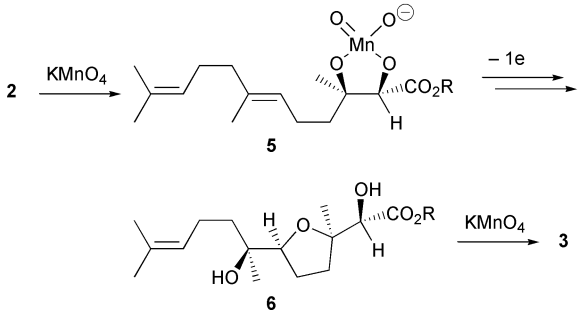

Scheme 2

The scope of the triene oxidation is increased by the availability of other double bond isomers of ethyl farnesoate, which can be prepared conveniently using methodology developed by Weiler.[14] For example, the dianion of ethyl acetoacetate was alkylated with neryl chloride (**7**) to afford β-ketoester **8** (Scheme 3), which underwent stereoselective conversion to the corresponding (*Z*)-enolphosphate. Treatment of the enolphosphate with lithium dimethylcuprate† gave the desired triene **9** as a single isomer‡ in good overall yield. Permanganate oxidation of ethyl (2*E*,6*Z*)-farnesoate (**9**) under the usual conditions provided an epimeric mixture of lactols, which was cleanly converted to a single diastereomeric lactone **10** upon brief exposure to lead tetraacetate. In principle, all four possible diastereoisomers of lactones **4** and **10** could be prepared from geraniol or nerol using this approach.[15]

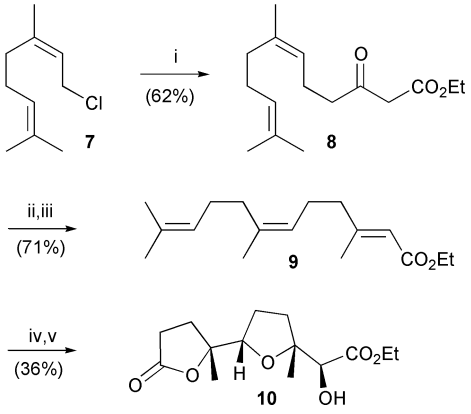

Scheme 3 *Reagents and conditions*: i, ethyl acetoacetate, NaH (1 eq.), n-BuLi (1 eq.); ii, LiHMDS, $(EtO)_2POCl$; iii, Me_2CuLi, Et_2O; iv, $KMnO_4$, AcOH, acetone, phosphate buffer (pH 6.2); v, $Pb(OAc)_4$, Na_2CO_3, CH_2Cl_2.

Our interest in the synthesis of annonaceous acetogenins such as Asiminenin A led us to consider use of the triene oxidation to generate a suitable lactone precursor **12** (Scheme 4). The requisite triene **11** was synthesised following a route described by Hoye.[16] Oxidation of **11** with potassium permanganate afforded an apparently complex mixture of products, from which compounds **13** (9%), **14** (23%) and unexpectedly **12**

DOI: 10.1039/b004307i

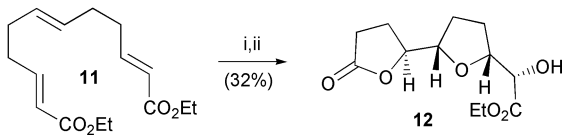

Scheme 4 *Reagents and conditions*: i, $KMnO_4$, AcOH, phosphate buffer (pH 6.2), acetone; ii, $NaIO_4$, acetone, H_2O.

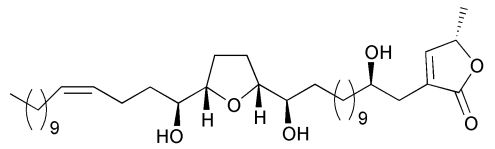

Asiminenin A

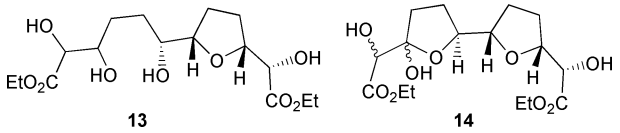

(10%) were identified. Rigorous assignment of the proton NMR spectra of the major component **14** was complicated by the presence of a number of isomers. Further indirect evidence for the structure of **14** came from its oxidative cleavage to yield the desired lactone **12** using sodium metaperiodate. Alternatively, the crude reaction mixture obtained from the permanganate oxidation of **11** could be treated with sodium metaperiodate to afford the lactone **12** in 32% yield over the two steps. The *cis*-relationship of the side chains on the tetrahydrofuran ring was confirmed by means of NOE experiments.

In summary, we have presented a very short diastereoselective synthesis of potentially useful tetrahydrofuran-containing fragments from readily accessible 1,5,9-trienes. The use of a chiral auxiliary in the oxidative cyclisations would provide the corresponding optically enriched tetrahydrofurans.[6,7] Future work will focus on the application of the oxidative cyclisation in the synthesis of the annonaceous acetogenin natural products and synthetic ionophores.

We wish to thank the Royal Society for a University Research Fellowship (R. C. D. B.), the EPSRC for MRes and PhD studentships (A. K. and J. K.), Pfizer Ltd. for a consumables grant and Mrs Joan Street and Mr Neil Wells for performing NMR experiments. We also wish to acknowledge the use of the EPSRC's Chemical Database Service at Daresbury.[17]

Notes and references

† We found it essential that methyllithium in ether was used in this reaction. On one occasion when a THF solution of methyllithium containing cumene was used a mixture of the desired product and the reduced *E*-disubstituted olefin was obtained (ratio of 5:1 estimated from the 300 MHz ^{1}H NMR spectrum).

‡ Only one isomer was observed in the 300 MHz ^{1}H NMR spectrum of **9**.

1 C. J. Dutton, B. J. Banks and C. B. Cooper, *Nat. Prod. Rep.*, 1995, 165.
2 L. Zeng, Q. Ye, N. H. Oberlies, G. Shi, Z.-M. Gu, K. He and J. L. McLaughlin, *Nat. Prod. Rep.*, 1996, 275.
3 E. Klein and W. Rojahn, *Tetrahedron*, 1979, **21**, 2353.
4 C. Spino and L. Weiler, *Tetrahedron Lett.*, 1987, **28**, 731.
5 D. M. Walba and P. D. Edwards, *Tetrahedron Lett.*, 1980, **21**, 3531.
6 P. J. Kocienski, R. C. D. Brown, A. Pommier, M. Procter and B. Schmidt, *J. Chem. Soc., Perkin Trans. 1*, 1998, 9.
7 D. M. Walba, C. A. Przybyla and C. B. J. Walker, *J. Am. Chem. Soc.*, 1990, **112**, 5624.
8 M. de Champdore, M. Lasalvia and V. Piccialli, *Tetrahedron Lett.*, 1998, **39**, 9781.
9 P. H. J. Carlsen, T. Katsuki, V. S. Martin and K. B. Sharpless, *J. Org. Chem.*, 1981, **46**, 3937.
10 E. J. Corey, N. W. Gilman and B. E. Ganem, *J. Am. Chem. Soc.*, 1968, **90**, 5616.
11 The stereochemical assignment of one of the epimers was unambiguously determined by X-ray crystallography: M. E. Light and M. B. Hursthouse, personal communication.
12 The accelerating effect of electron withdrawing groups on the permanganate oxidation is known: D. G. Lee, K. C. Brown and H. Karaman, *Can. J. Chem.*, 1986, **64**, 1054.
13 J. E. Baldwin, M. J. Crossley and E.-M. M. Lehtonen, *J. Chem. Soc. Chem. Commun.*, 1979, 918.
14 M. Alderdice, C. Spino and L. Weiler, *Tetrahedron Lett.*, 1984, **25**, 1643.
15 Recently a closely related strategy has been reported by others: Y. Shao, J. T. Eummer and R. A. Gibbs, *Org. Lett.*, 1999, **1**, 627.
16 T. R. Hoye and J. C. Suhadolnik, *Tetrahedron*, 1986, **42**, 2855.
17 D. A. Fletcher, R. F. McMeeking and D. Parkin, *J. Chem. Inf. Comput. Sci.*, 1996, **36**, 746.

ChemComm

Short cuts toward forskolin synthesis: a pentacyclic approach†

Massoumé Leclaire,*[a] Raymond Levet,[a] Franck Ferreira,[a] Paul-Henri Ducrot[b], Jean-Yves Lallemand[a] and Louis Ricard[c]

[a] *Laboratoire DCSO, École Polytechnique, 91128 Palaiseau Cedex, France. E-mail: leclaire@poly.polytechnique.fr*
[b] *Unité de Phytopharmacie et Médiateurs Chimiques, INRA, Route de Saint-Cyr, 78026 Versailles Cedex, France*
[c] *Laboratoire DCPH, École Polytechnique, 91128 Palaiseau Cedex, France*

Received (in Cambridge, UK) 6th June 2000, Accepted 11th July 2000
First published as an Advance Article on the web 25th August 2000

A practical synthetic route for the preparation of forskolin intermediate 20 is described. Previously reported lactone 3 was converted to 20 through intermediate 16. The main feature of this work lies in the formation and the cleavage of a tetracyclic intermediate for the stereochemical control in the formation of the tricyclic core of forskolin.

Forskolin **1**,[1] a labdane diterpene isolated from the roots of the Indian plant *Coleus forskolii*, has emerged as a highly attractive target for total[2] and partial[3] synthetic investigations. Besides the challenging structure of this natural product, its biological and therapeutic potential, mainly in the cardiovascular area,[4] has encouraged the efforts of numerous synthetic chemistry groups all over the world.

However, despite the diversity of the synthetic schemes used in the early steps of these studies, most of them have emphasized the so called 'Ziegler intermediate', **2** (Scheme 1), as the most versatile synthon for further synthetic strategies aimed at the formation of the tetrahydropyran ring of the target molecule.[5]

In preceding work, we designed several synthetic approaches toward the fully functionalized decalinic system of forskolin (A/B bicycle). Our approaches were mainly based either on the use of pericyclic reactions[6] or on the transformation of lactone **3**,[7] available in enantiomeric pure form.[8] This later methodology led to a highly efficient synthesis of the 'Ziegler intermediate'.[9]

The main original feature of this synthesis relies on the stereochemical control of the ring junction of the bicycle A/B through the formation, in the earlier steps of the synthetic scheme, of an intramolecular ketal **4** of the carbonyl group at C-11. This ketal links C-11 to C-1 and C-5 through an oxygen atom (Scheme 1). A base induced rearrangement of the tetracyclic system of **4** with fragmentation of the tetrahydrofuran ring produced the α-hydroxyketone **5** with complete stereocontrol of the asymetric centers C-1, C-5, C-9 and C-10 under thermodynamic conditions.

In order to design a more straightforward route to forskolin, we have investigated the possibility of formation of the tetrahydropyran ring C of **1** in an early stage of the synthesis, through introduction of the three missing carbon atoms as an allyl residue at the beginning of the synthetic sequence.

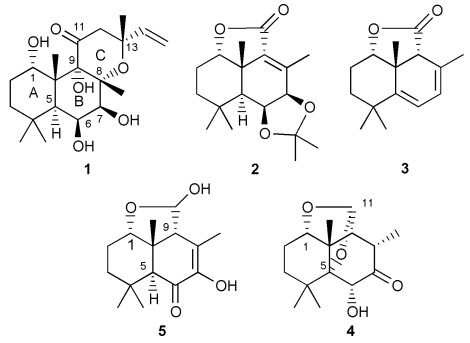

Scheme 1

Lactone **3** was first submitted to the previously described regioselective epoxidation procedure (MCPBA, CH_2Cl_2, 92%) to produce known epoxide **6**.[9a] Then the Grignard addition of allylmagnesium bromide stereoselectively produced hemiketal **7**, having the three required carbons. Hemiketal **7** was in turn converted into tetracyclic ketal **8** upon treatment with silica gel under sonication (Scheme 2, 86% from **6**) using our previously reported strategy.[9]

Epoxidation of both double bonds was then performed in a one-pot procedure using an excess of peracid; diepoxide **9a**,**b** was obtained in 76% yield (MCPBA, 4 eq., CH_2Cl_2, rt) as a mixture (1:1) of epimers at C-13. Then, reduction of **9** by lithium aluminium hydride led in high yield to the reductive opening of the more reactive 13,14-epoxide, while the basicity of the reaction conditions allowed a Payne-like rearrangement of the 8-hydroxy-6,7-epoxide and gave 6α-alcohol **10a**,**b**.

The key step in this sequence of reactions was the acid catalyzed formation of the tetrahydropyran ring C of the target molecule (camphorsulfonic acid, CH_2Cl_2, −10 °C, 90%), which resulted in a stereoselective inversion of the configuration at C-8 (Scheme 2), leading to the pentacyclic diols **11a**† and **11b** which can be separated by careful chromatography. The following steps were thus performed on both epimers separately. The two equatorial hydroxy groups at C-6 and C-7 were easily differentiated according to their steric hindrance: etherification with one eq. of chlorotriethylsilane (imidazole, DMF, 95%) yielded the formation of the mono-silyl ether at C-7 **12a** and **12b**. Then, **13a** and **13b** were synthesized through oxidation with Dess–Martin's periodinane (CH_2Cl_2, rt). Thereafter, extensive experimental investigations using various reaction conditions allowed the emergence of samarium(II) iodide as the best reducing agent to perform the desired cleavage of the C–O bond at C-5, thus leading to the formation of hemiketals **14a** and **14b** in 70% yield [5 eq. SmI_2, THF–MeOH (50:1) 13 mM, −90 °C, hydrolysis and extraction performed at pH 7.4, phosphate buffer].

At this stage of the synthesis, the synthetic aim was to reduce the carbonyl group at C-6 and to cleave the C-11 carbonyl ketal in order to complete the functional elaboration of ring C of forskolin.

Treatment with hydrofluoric acid in acetonitrile of isomer **14a** cleanly gave the expected free alcohol **15** while isomer **14b**, under similar conditions, produced enol ether **16** in quantitative yield.

Taking advantage of this unexpected dehydration, we completed this approach by reduction of the carbonyl at C-6 ($LiAlH_4$, Et_2O, −65 °C, 85%) to give **17** with the correct diol configurations (Scheme 3). Thereafter, treatment of enol ether **17** with phenylselanyl chloride at low temperature resulted in addition of the phenylselenenyl group at C-12,[10] without cleaving the enol ether. This reaction was assumed to proceed through a two step procedure, consisting of the electrophilic addition of the phenylselanyl moiety, followed by hydrochloric acid elimination. Then, oxidation of the selenium and elimination of the resulting selenoxide under basic conditions led to the formation of the desired dehydro-γ-pyrone **20**.[11] Compound **20** is also the result of a two step reaction, involving hydroxide

DOI: 10.1039/b004515m

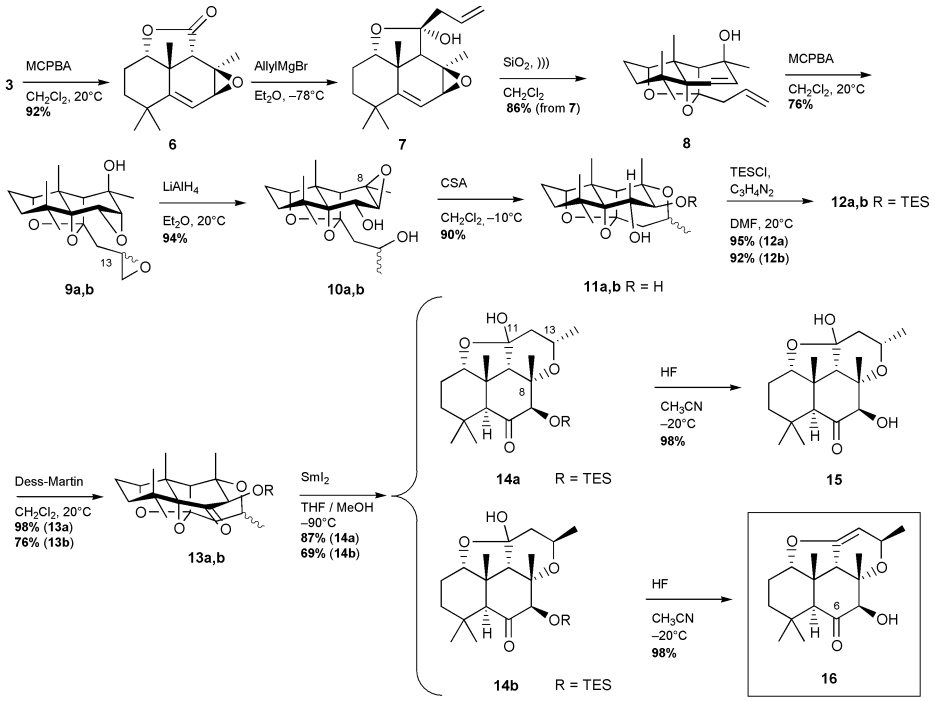

Scheme 2

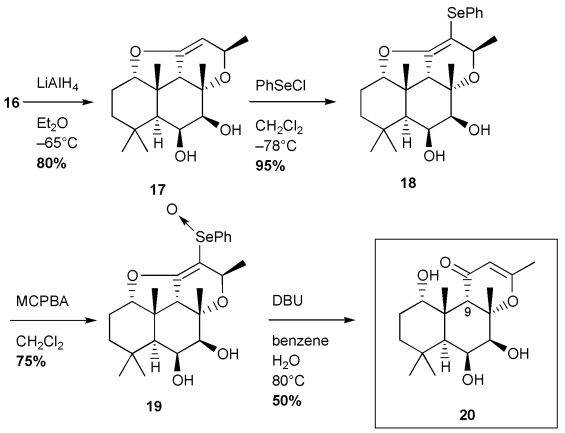

Scheme 3

addition to the activated enol followed by phenylselenenic acid elimination.

In summary, we have developed a practical, stereoselective synthetic route to analogs of 9-deoxyforskolin and forskolin **1**, taking account of the previous reports dedicated to the introduction of the vinyl group at C-13 as a cuprate,[2c] and of the hydroxy group at C-9.[12]

Notes and references

† CCDC 182/1719. See http://www.rsc.org/suppdata/cc/b0/b004515m/ for crystallographic files in .cif format.

1 S. Bath, B. S. Bajawa, H. Dornauer, N. J. de Souza and H. W. Fehlhaber, *Tetrahedron Lett.*, 1977, **18**, 1669; J. Sen, A. K. Sharma, N. P. Sahu and S. B. Mahato, *Phytochemistry*, 1993, **34**, 1309.

2 (*a*) F. E. Ziegler, B. H. Jaynes and M. T. Saindane, *J. Am. Chem. Soc.*, 1987, **109**, 8115; (*b*) E. J. Corey and P. Da Silva Jardine, *Tetrahedron Lett.*, 1989, **30**, 7297; (*c*) F. E. Ziegler and B. H. Jaynes, *Tetrahedron Lett.*, 1988, **29**, 2031; (*d*) S. Hashimoto, S. Sakata, M. Sonegawa and S. Ikegami, *J. Am. Chem. Soc.*, 1988, **110**, 3670, (*e*) B. Delpech, D. Calvo and R. Lett, *Tetrahedron Lett.*, 1996, **37**, 1019.

3 C. Anies, A. Pancrazi, J.-Y. Lallemand and T. Prangé, *Bull. Soc. Chim. Fr.*, 1997, **134**, 203; J. Pan, I. Hanna and J.-Y. Lallemand, *Bull. Soc. Chim. Fr.*, 1994, **131**, 665; I. Hanna and P. Wlodyka, *J. Org. Chem.*, 1997, **62**, 6985; A. P. Kozikowski, S. H. Jung and J. P. Springer, *J. Chem. Soc., Chem. Commun.*, 1988, **3**, 167; J. H. Hutchinson, G. Pattenden and P. L. Myers, *Tetrahedron Lett.*, 1987, **28**, 1313; Hsing-Jang Liu and Xiao Shang, *Heterocycles*, 1997, **44**, 143; S. Nagashima and K. Kanematsu, *Tetrahedron: Asymmetry*, 1990, **1**, 743; S. Bick, S. Zimmermann, H. Meuer, W. S. Sheldrick and P. Welzel, *Tetrahedron*, 1993, **49**, 2457; E. R. Koft, A. S. Kotnis and T. A. Broadbent, *Tetrahedron Lett.*, 1987, **28**, 2799; H. Venkataraman and J. K. Cha, *J. Org. Chem.*, 1989, **54**, 2505.

4 W. Kramer, J. Thormann, M. Kindler and M. Schlepper, *Arzneim.-Forsch.*, 1987, **37**, 364; E. Lindner and H. Metzger, *Arzneim.-Forsch.*, 1983, **33**, 1436; A. Hara, H. Yokoyama and Y. Abiko, *Arzneim.-Forsch.*, 1995, **45**, 1257; N. Ogawa and H. Ono, *J. Pharm. Pharmacol.*, 1988, **40**, 207; Y. Khandelwal, K. Rajeshwari, R. Rajagopalan, L. Swamy and A. N. Dohadwalla, *J. Med. Chem.*, 1988, **31**, 1872.

5 G. Jordine, S. Bick, U. Moeller, P. Welzel, B. Daucher and G. Maas, *Tetrahedron*, 1994, **50**, 139.

6 M. Leclaire, S. Bathnagar and J.-Y. Lallemand, *Bull. Soc. Chim. Fr.*, 1993, **130**, 310; M. Leclaire and J.-Y. Lallemand, *Tetrahedron Lett.*, 1989, **30**, 6331; M. Leclaire, P. Jean, L. Ricard and J.-Y. Lallemand, *Synth. Commun.*, 1998, **28**, 4371.

7 M. Leclaire, R. Levet and J.-Y. Lallemand, *Synth. Commun.*, 1993, **23**, 1923.

8 J.-Y. Lallemand, M. Leclaire, R. Levet and G. Aranda, *Tetrahedron: Asymmetry*, 1993, **4**, 1775.

9 (*a*) M. Leclaire, R. Levet, F. Pericaud, L. Ricard and J. Y. Lallemand, *Tetrahedron*, 1996, **52**, 7703; (*b*) M. Leclaire, F. Pericaud and J. Y. Lallemand, *J. Chem. Soc., Chem. Commun.*, 1995, **13**, 1333.

10 K. C. Nicolaou, R. L. Magolda and W. J. Sipio, *Synthesis*, 1979, 982.

11 (400 MHz, $CDCl_3$) δ_H(ppm): 5.08 (br s, H-12), 4.46 (br s, H-7), 4.12 (br t, 4 Hz, H-1β), 3.53 (d, 4 Hz, H-6), 2.50 (s, H-9), 2.03 (m, 2H, H-2), 1.61 (s, 3H), 1.46 (s, 3H), 1.33 (s, 3H), 1.19 (s, 3H), 1.05 (s, 3H). CIMS, (NH_3): 342 (M + NH_4^+), 325 (MH^+).

12 N. J. Hrib, *Tetrahedron Lett.*, 1987, **28**, 19; S. R. Nadkarni, P. N. Akut, B. N. Ganguli, Y. Khandelwal, N. J. De Souza and R. H. Rupp, *Tetrahedron Lett.*, 1986, **27**, 5265.

Chiral amine–silyl triflate complex mediated asymmetric intramolecular Michael–aldol reaction *via* a novel enantioselective enol silylation process

Kiyosei Takasu,* Keiko Misawa, Masami Yamada, Yoshiyuki Furuta, Takahiko Taniguchi and Masataka Ihara*

Department of Organic Chemistry, Graduate School of Pharmaceutical Sciences, Tohoku University, Aobayama, Sendai 980-1578, Japan. E-mail: mihara@mail.pharm.tohoku.ac.jp

Received (in Cambridge, UK) 31st May 2000, Accepted 1st August 2000
First published as an Advance Article on the web 25th August 2000

An asymmetric intramolecular Michael–aldol reaction of a C_s symmetric ketone using chiral amine and silyl triflate is described as a new methodology of chiral induction; nonracemic tricyclic cyclobutanes were obtained from a 4-substituted cyclohexanone in high yields with moderate enantioselectivities in one step.

Carbon–carbon bond-forming reactions are among the most fundamental and important methodologies in organic transformations, and many of them have been focused and elaborated to give asymmetric products. Recently, the asymmetric C–C bond formations induced by the desymmetrization of C_s symmetric compounds have emerged as a powerful strategy for asymmetric synthesis.[1] For example, an asymmetric deprotonation of the prochiral ketones, followed by C–C bond formation (alkylation, aldol reaction, Michael reaction, *etc.*), can afford useful chiral intermediates.[2,3] Simpkins and Koga have elaborated the excellent desymmetrization process of C_s symmetric ketones by the use of chiral lithium amide bases to give enantiomerically enriched enolate equivalents with excellent enantioselectivities.[2–4]

We have established the intramolecular Michael–aldol reaction as a new and efficient methodology to build polycyclic cyclobutanes.[5] The reaction of a C_s symmetric substrate, such as **2**, could form two bonds and five stereogenic centers with high stereoselectivity in a single operation. However, the use of lithium amides resulted in the termination of the reaction at the mono-Michael addition stage.[5b] The cascade reaction proceeded only under silyl triflate–amine, silyl iodide–hexamethyldisilazane (HMDS), or boron triflate–HMDS conditions. Simchen has shown that enol silylation using triethylamine in the presence of TMSOTf proceeds through the coordination of silyl ammonium complex **1** to carbonyl oxygen followed by deprotonation and silylation (Scheme 1).[6] Based on this mechanism, a chiral amine reagent in the presence of silyl triflate could be envisaged to effect an asymmetric induction in the Michael–aldol reaction. We herein report an enantioselective intramolecular Michael–aldol reaction of a prochiral substrate *via* asymmetric enol silylation as a new method of chiral induction.

We first examined suitable conditions for the intramolecular Michael–aldol reaction of **2** (Scheme 2). It was observed that more than 3 equiv. of amine and silyl triflate at temperatures higher than −30 °C were required for the production of **3** in high yield, whereas the use of 1.2 equiv. of the reagents gave the enol ether **4** quantitatively at −78 °C. The Michael–aldol reaction was typically performed as follows. To a solution of **2**

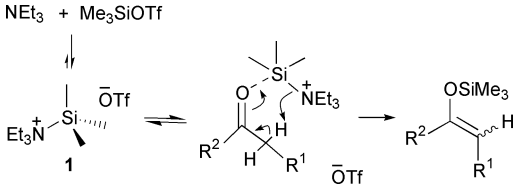

Scheme 1

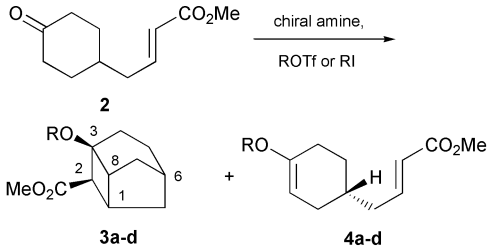

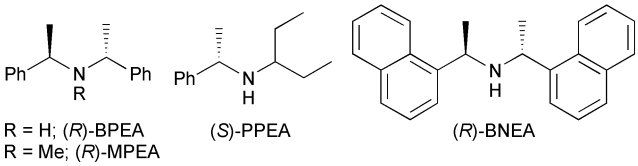

Scheme 2

(0.26 mmol) in CH_2Cl_2 was added chiral amine (0.83 mmol) at room temperature. This solution was then cooled to −78 °C and silyl triflate (0.78 mol, −78 °C) was added dropwise. The whole was stirred for several hours at −78 °C, and further stirring was continued at −30 °C or at rt.[7] After the usual work up, the product **3** was purified by column chromatography (silica gel). The enantiomeric excess of **3** was determined, after its transformation into **5**, by HPLC analysis using a chiral column.[8] The asymmetric reaction using a variety of silyl Lewis acids with bis[(*R*)-1-phenylethyl]amine (BPEA) was investigated (Table 1). The reaction with TMSOTf afforded (−)-**3a** with 23% ee (run 1). Although no significant improvement was observed in the reaction with TMSI instead of triflate (run 2), the enantioselectivities were increased by the use of bulky silyl triflates such as TESOTf and TBDMSOTf (runs 3 and 4). However, the reaction with the bulkier triflate, TIPSOTf, furnished no Michael–aldol adduct **3d** but only the silyl enol ether **4d** (run 5). On the basis of the above observation, the following studies were carried out using TBDMSOTf as the silyl Lewis acid.

Results using various chiral amines under standard conditions are shown in Table 2. With bis[(*R*)-1-(1-naphthyl)ethyl]-

Table 1 Effect of silyl Lewis acids to the Michael–aldol reaction of **2** in the presence of (*R*)-BPEA[a]

Run	Reagent	Product	Yield (%)	ee (%)[b]	Yield of **4** (%)
1	TMSOTf	(−)-**3a**	58	23	6
2	TMSI	(−)-**3a**	39	24	Not isolated
3	TESOTf	(−)-**3b**	31	28	46
4	TBDMSOTf	(−)-**3c**	89	31	Trace
5	TIPSOTf	**3d**	0	—	73

[a] Reactions were carried out at −78 to −30 °C. [b] All enantiomeric excesses were determined, after transformation into **5**, through chiral HPLC analysis using a Chiracel OJ column.

DOI: 10.1039/b004320f

Table 2 Asymmetric Michael–aldol reactions using chiral amine and TBDMSOTf

			Yield (%)		ee (%)	
	Chiral amine	Temp./°C	**3c**	**4c**	**3c**[a]	**4c**[b,c]
1	(*R*)-BPEA	−78 to rt	85	14	32	nd
2	(*R*)-MPEA	−78 to rt	82	11	7	nd
3	(*S*)-PPEA	−78 to rt	87	8	8[d]	nd
4	(*R*)-BNEA	−78 to rt	88	12	36	35
5	(−)-sparteine	−78 to rt	77	9	8	nd
6	(*R*)-BPEA	rt	75	8	12	nd
7	(*R*)-BPEA	−78	0	88	—	31
8	(*R*)-BPEA	−90 to rt	85	13	42	nd

[a] All enantiomeric excesses were determined, after transformation into **5**, through chiral HPLC analysis using a Chiralcel OJ column. [b] Ees were determined in the same manner as **3c**, after conversion into (−)-**3c** by the treatment of (−)-**4c** with TBDMSOTf in the presence of NEt_3 at rt. [c] 'nd' means 'not determined'. [d] (+)-**3c** was obtained.

amine (BNEA) as chiral amine, (−)-**3c** and (−)-**4c** were obtained in 88 and 12% yield with 36 and 35% ee, respectively (run 4). Reactions in the presence of other amines, such as *N*-methylbis[(*R*)-1-phenylethyl]amine (MPEA), 3-pentyl-(*S*)-1-phenylethylamine (PPEA)[3a] and (−)-sparteine, afforded less than 10% ee of **3c** (runs 2, 3 and 5). The effect of temperature was as expected; higher enantioselectivities were observed at lower temperature (see runs 1, 6 and 8). The reaction, carried out at −90 °C to rt, resulted in 42% ee of **3c** (run 8). Note, quenching the reaction at −78 °C produced only the silyl enol ether **4c** having 31% ee (run 7).

The absolute configuration of (−)-**3c** was determined by circular dichroism of bicyclo[3.2.1]octanone **6** (24% ee; $[\theta]$ = +708, λ = 296 nm), which was obtained by treatment of (−)-**3c** (24% ee) with hydrogen fluoride–pyridine complex. The application of the octant rule[9] suggested (*R*)-configuration at the asterisked carbon of **6**. Accordingly, (−)-**3c** has a (1*S*,2*R*,3*S*,6*R*,8*R*)-tricyclo[4.2.1.0^{3,8}]nonane structure.

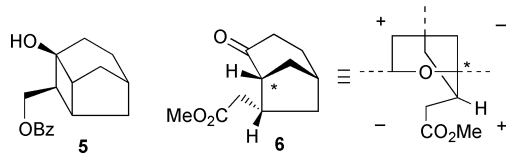

Some possibilities can be considered for the asymmetric induction of the above reaction. One is the desymmetrization of C_s symmetric substrate **1** by means of enantioselective enol silylation. Another possibility is that kinetic resolution is involved in the Michael–aldol reaction of silyl enol ether **4**. However the latter induction process could be ruled out by the observation that the treatment of isolated racemic **4c** with TBDMSOTf in the presence of (*R*)-BPEA at −78 °C to rt furnished only the racemate of **3c**. Hence, the asymmetric induction of the reaction occurs in the enol silylation step. To our knowledge this is the first demonstration of asymmetric enol silylation without the use of amide base.[10] The asymmetric intramolecular Michael–aldol reaction subsequently proceeds under the same conditions. It is worth noting that we have demonstrated the direct asymmetric C–C bond-forming reaction of a C_s ketone in a single operation, omitting the isolation of an enolate equivalent, to give a nonracemic tricyclo-[4.2.1.0^{3,8}]nonane compound. Further studies on the development and the application of this asymmetric process are in progress.

This work was partly supported by a Grants-in-Aid for Research on Priority Areas (Nos. 11119206 and 11147202) from the Ministry of Education, Science, Sports and Culture, Japan.

Notes and references

1 For reviews, see: H.-J. Gais, in *Houben–Weyl, Stereoselective Synthesis*, ed. G. Helmchen, R. W. Hoffmann, J. Mulzer and E. Schaumann, Thieme, Stuttgart, 1996, vol. 1, pp. 589–644; R. S. Ward, *Chem. Soc. Rev.*, 1990, **19**, 1.

2 For a review, see: P. O'Brien, *J. Chem. Soc., Perkin Trans. 1*, 1998, 1439.

3 (*a*) H. Izawa, R. Shirai, H. Kawasaki, H.-D. Kim and K. Koga, *Tetrahedron Lett.*, 1989, **30**, 7221; (*b*) J. E. Krops and S. M. Weinreb, *Chem. Commun.*, 1998, 2357.

4 For reviews, see: N. S. Simpkins, *Tetrahedron: Asymmetry*, 1991, **2**, 1; K. Koga and M. Shindo, *J. Synth. Org. Chem. Jpn.*, 1995, **53**, 1021.

5 (*a*) M. Ihara, M. Ohnishi, M. Takano, K. Makita, N. Taniguchi and K. Fukumoto, *J. Am. Chem. Soc.*, 1992, **114**, 4408; (*b*) M. Ihara, T. Taniguchi, K. Makita, M. Takano, M. Ohnishi, N. Taniguchi, K. Fukumoto and C. Kabuto, *J. Am. Chem. Soc.*, 1993, **115**, 8107; (*c*) M. Ihara, T. Taniguchi, M. Yamada, Y. Tokunaga and K. Fukumoto, *Tetrahedron Lett.*, 1995, **36**, 8071; (*d*) K. Takasu, M. Ueno and M. Ihara, *Tetrahedron Lett.*, 2000, **41**, 2145.

6 H. Emde, A. Götz, K. Hofmann and G. Simchen, *Liebigs Ann. Chem.*, 1981, 1643.

7 We found that **4a** was racemized at temperatures higher than −30 °C under the Michael–aldol conditions, but **4b**–**c** were not racemized even at room temperature. Consequently, the asymmetric Michael–aldol reaction with TMSX had to be carried out at −78 to −30 °C.

8 **5** was obtained from **3** in 3 steps. That is, the reduction of **3** by DIBAL-H, followed by desilylation and acylation with benzoyl chloride, gave the benzoate **5**.

9 The determination of the absolute configuration of some substituted bicyclo[3.2.1]octan-2-ones by means of circular dichroism was reported, see: W. Klyne, *Tetrahedron*, 1961, **13**, 29.

10 A few methodologies for asymmetric enolization without amide bases were reported. For asymmetric enol borination; D. E. Ward and W.-L. Lu, *J. Am. Chem. Soc.*, 1998, **120**, 1098. For asymmetric enol esterification; A. J. Carnell, J. Barkley and A. Singh, *Tetrahedron Lett.*, 1997, **38**, 7781.

ChemComm

Construction of α-helical peptide dendrimers conjugated with multi-metalloporphyrins: photoinduced electron transfer on dendrimer architecture

Muneyoshi Sakamoto, Akihiko Ueno and Hisakazu Mihara*

Department of Bioengineering, Graduate School of Bioscience and Biotechnology, Tokyo Institute of Technology, Nagatsuta, Yokohama 226-8501, Japan. E-mail: hmihara@bio.titech.ac.jp

Received (in Cambridge, UK) 11th May 2000, Accepted 31st July 2000
First published as an Advance Article on the web 25th August 2000

Noncovalent assembly of Zn^{II}–mesoporphyrin IX was accomplished by coordination to α-helical peptides (4–64 segments) based on polyamideamine dendrimer; the electron transfer functions were expressed more effectively with the growth of the dendrimer generation.

Assemblies of peptides or functional groups perform a significant role in nature, displaying highly efficient functions including energy transfer and electron transfer. For example, in photosynthetic bacteria, light-harvesting complexes (LH),[1] in which many bacteriochlorophylls are assembled and oriented with α-helix peptides, absorb light energy, and delocalize and transfer the energy to the reaction center where charge separation occurs. The development of an artificial system with native-like properties but without the complexity of the natural components, has been attempted using *de novo* designed peptides.[2,3] On the other hand, dendrimers have also attracted much attention in the field of polymer chemistry.[4–8] Some dendrimers have been investigated for electron transfer[6] and energy transfer[7] functions because of their morphological similarities to LH. Using dendrimers as templates in the *de novo* design proteins, the peptide assembly conditions and functionalization may be controlled precisely. In this study, designed amphiphilic α-helix peptides (4, 8, 16, 32 and 64 segments) were introduced at the end groups of polyamideamine dendrimers (PAMAMs)[4] (Fig. 1). Zn^{II}–Mesoporphyrin (Zn-MP) was coordinated between the 2α-helix peptides[3] to accomplish a multi-Zn-MP array so that electron transfer properties were expressed more effectively with the growth of the dendrimer generation.

Synthesis of peptide dendrimers was performed by a domain ligation strategy.[8] The 20-residual peptide (R-HL4) was designed to take an amphiphilic α-helical structure, which was stabilized by four sets of Glu–Lys salt bridges. As an axial ligand of metalloporphyrin, His was introduced to deploy a porphyrin parallel to the helix axis. Four Leu residues per α-helix were arranged to construct a hydrophobic pocket as a porphyrin-binding site.[3] Cys was used at the N-terminus of the peptide to ligate to the outer termini of the template dendrimer through the thioether linkage. Arg was introduced at the C-terminus of the peptide to form an electrostatic field at the outer shell of the peptide dendrimers. R-HL4 was synthesized by the solid-phase method using Fmoc-strategy and purified with reversed-phase (RP) HPLC. The peptide was identified by matrix assisted laser desorption ionization time-of-flight mass spectrometry (MALDI-TOFMS).[9] To conjugate the peptide with PAMAM [Starburst Dendrimer, G0, G1, G2, G3 and G4, from Aldrich], the chloroacetyl group was introduced at each amino terminal group of PAMAM, by treatment with *N*-ethoxycarbonyl-2-ethoxy-1,2-dihydroquinoline[10] and chloroacetic acid in MeOH. Perchloroacetylated (*n*-ClAc) PAMAMs were purified by size exclusion chromatography (SEC, Sephadex LH-60–MeOH) and RP-HPLC, and identified by MALDI-TOFMS.[11] R-HL4 and *n*-ClAc-PAMAM were combined by the ligation reaction[12] between the thiol side chain of Cys in R-HL4 and the chloroacetyl group of *n*-ClAc-PAMAM. The peptide dendrimers, *n*-(R-HL4)PAMAMs, were purified by SEC (Sephadex G-50–30% AcOH) and RP-HPLC, and identified by MALDI-TOFMS[13] or ultracentrifugation.[14]

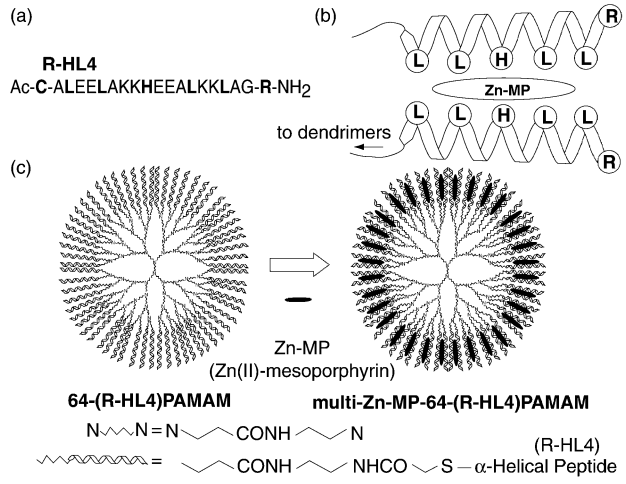

Fig. 1 Structure of the peptide dendrimers, (a) amino acid sequence of R-HL4; (b) schematic illustration of Zn-MP coordination to 2α-helix; and (c) 64-(R-HL4)PAMAM and multi-Zn-MP-64-(R-HL4)PAMAM.

Circular dichroism (CD) study revealed that *n*-(R-HL4)PAMAM, (*n* = 4, 8, 16, 32 and 64) showed a typical α-helical pattern in pH 7.4 buffer. The α-helicity[15] of the peptides in the dendrimers was estimated as *ca*. 50% (Table 1), indicating that *n*-(R-HL4)PAMAMs with different extents of dendrimer generation have similar α-helical properties. UV-Vis titration[3] of Zn-MP with *n*-(R-HL4)PAMAM showed an increase of the Soret band at 415 nm and decrease of the band at 403 nm of Zn-MP. The binding constant (K_a) was determined from the absorbance change at 415 nm using an equation assuming the 1/*n* (2α-helix in peptide dendrimer–Zn-MP) complexation (Table 1). The *n* values were found to be close to 1.0, indicating that Zn-MP bound to the peptide dendrimers almost equivalently per 2α-helix. The K_a values indicated that Zn-MP bound to the peptide dendrimers efficiently, and binding affinities to peptide dendrimers were almost identical. *n*-(R-HL4)PAMAM conjugated with multi-Zn-MP showed a strong induced CD

Table 1 Ellipticity at 222 nm and α-helicity of peptide dendrimers, and binding constant K_a and *n* value for peptide dendrimers with Zn-MP

n-(R-HL4) PAMAM	$[\theta]_{222}/10^4$ deg cm^2 dmol^{-1}	α-Helicity (%)	$K_a/10^5$ dm^3 mol^{-1}	*n* value
n = 4	−1.68	53	3.2	1.01
n = 8	−1.67	53	1.7	0.84
n = 16	−1.51	48	1.5	0.93
n = 32	−1.45	46	1.8	0.98
n = 64	−1.45	46	2.1	0.99

Ellipticity [θ] at 222 nm and α-helicity were estimated from the CD spectra. [*n*-(R-HL4)PAMAM] = 1.0×10^{-5} mol dm^{-3} (per 2α-helix), in 2.0×10^{-2} mol dm^{-3} Tris·HCl buffer (pH 7.4) at 25 °C. The binding constant K_a and *n* value were estimated by UV-Vis spectra titration, in pH 7.4 buffer at 25 °C. [Zn-MP] = 5.0×10^{-6} mol dm^{-3}.

DOI: 10.1039/b003786i

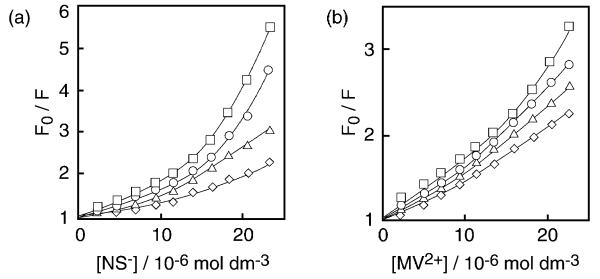

Fig. 2 Stern–Volmer plot for fluorescence quenching of Zn-MP (2.5×10^{-7} mol dm^{-3}) conjugated with *n*-(R-HL4)PAMAM (7.5×10^{-7} mol·dm^{-3} per 2α-helix) by quenchers. λ_{ex} = 415 nm, λ_{em} = 582 nm, in the buffer (pH. 7.4) at 25 °C. Electron acceptors = (a); NS^-, (b); MV^{2+}: □; *n* = 64, ○; *n* = 32, △; *n* = 16, ◇; *n* = 8 and 4.

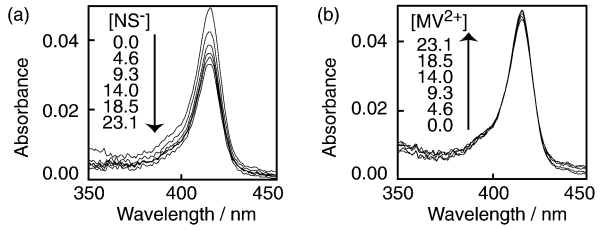

Fig. 3 UV-Vis spectra of Zn-MP (2.5×10^{-7} mol dm^{-3}) conjugated with 64-(R-HL4)PAMAM (7.5×10^{-7} mol dm^{-3} per 2α-helix) with increasing concentration (0, 4.6, 9.3, 14.0, 18.5, 23.1 $\times 10^{-6}$ mol dm^{-3}) of electron acceptors, (a); NS^-, (b); MV^{2+} in the buffer (pH. 7.4) at 25 °C.

peak at the Soret region,[16] suggesting that Zn-MP was coordinated in a regulated manner. In addition, the α-helicity was not changed by the binding with Zn-MP.

To examine electron transfer properties of multi-Zn-MP-conjugated *n*-(R-HL4)PAMAM, fluorescence quenching studies were performed by the addition of a negatively charged electron acceptor, naphthalene sulfonate[6] (NS^-), and a positively charged methylviologen[6] (MV^{2+}). Upon excitation at the Soret band, multi-Zn-MP–*n*-(R-HL4)PAMAM emitted fluorescence at 582 and 630 nm, which was quenched by the addition of NS^-. The Stern–Volmer plots (Fig. 2a) showed that the quenching occurred more strongly with increase in dendrimer generation. In each generation, the concentrations of 2α-helix and Zn-MP were constant. This result indicates that the positive charges of Arg residues were assembled more densely on the surface of the peptide dendrimer with the growth of each generation so that the negative charged NS^- was bound more effectively by the electrostatic force. Consequently, quenching was amplified with the growth of generation. On the other hand, when positively charged MV^{2+} was employed, the fluorescence quenching (Fig. 2b) was also observed to increase with the growth of the peptide dendrimer, although the charge repulsion became stronger with the generation growth. It was suggested that the quenching mechanism of MV^{2+} was different from that of NS^-. To examine these mechanisms, UV-Vis spectra on the addition of NS^- and MV^{2+} were measured (Fig. 3). In the case of NS^-, the Soret band decreased, supporting electrostatic binding between multi-Zn-MP–*n*-(R-HL4)PAMAM and NS^- in the ground state. By contrast, UV-Vis spectra were little changed by the addition of MV^{2+}, indicating that MV^{2+} does not have a strong influence on the ground state of Zn-MP. Table 2 shows the fluorescence lifetimes of multi-Zn-MP–*n*-(R-HL4)PAMAM. With the growth of generation, a percentage of the long-lived component (2.3–2.6 ns) increased. In 32- and 64-(R-HL4)PAMAM, the short-lived component (1.7–1.8 ns) disappeared. In the presence of NS^-, the fluorescence lifetime of multi-Zn-MP–64-(R-HL4)PAMAM was not changed (2.3 ns). This result supports the idea that NS^- causes electron transfer by a static mechanism.[17] By contrast, addition of MV^{2+} caused the fluorescence lifetime to be extremely shortened (0.5 ns, 88%). These results indicated that the electron was transferred mainly by a dynamic mechanism.[17]

Table 2 Fluorescence lifetime of multi-Zn-MP–*n*-(R-HL4)PAMAM

n-(R-HL4) PAMAM	Electron acceptors	τ_1/ns	A_1 (%)	τ_2/ns	A_2 (%)
n = 4	—	1.8	74.7	2.6	25.3
n = 8	—	1.8	73.8	2.6	26.2
n = 16	—	1.7	47.8	2.3	52.2
n = 32	—	—	—	2.4	100.0
n = 64	—	—	—	2.3	100.0
n = 64	NS^-	—	—	2.3	100.0
n = 64	MV^{2+}	0.5	88.0	2.3	12.0

Fluorescence lifetime was measured using Zn-MP (2.5×10^{-7} mol dm^{-3}) conjugated with *n*-(R-HL4)PAMAM (7.5×10^{-7} mol dm^{-3} per 2α-helix) at 25 °C. λ_{ex} = 415 nm, λ_{em} = 570–650 nm, electron acceptors, [NS^-] = [MV^{2+}] = 2.0×10^{-5} mol dm^{-3}. Decay profiles were analyzed by the double exponential equation, $I_f(t) = A_1\exp(t/\tau_1) + A_2\exp(t/\tau_2)$.

In conclusion, noncovalent Zn-MP assembly was accomplished by coordination to novel peptide dendrimers, and the electron transfer function was expressed more effectively with the growth of dendrimer generation. Dynamic quenching with viologen can be applied to the catalytic reactions. The nanoscale assembly of a system combining *de novo* designed peptides with dendrimers will be utilized in artificial photosynthesis.

We are grateful to Dr K. Aoi, Nagoya University, for valuable discussions on dendrimers, Dr F. Arisaka, Tokyo Institute of Technology, for ultracentrifugation analyses and Dr S. Sakamoto, Tokyo Institute of Technology, for valuable discussions on the *de novo* design.

Notes and references

1 G. McDermott, S. M. Prince, A. A. Freer, A. M. Hawthornthwaite-Lawless, M. Z. Papiz, R. J. Cogdell and N. W. Isaacs, *Nature*, 1995, **374**, 517.
2 F. Rabanal, W. F. DeGrado and P. L. Dutton, *J. Am. Chem. Soc.*, 1996, **118**, 473; H. K. Rau and W. Haehnel, *J. Am. Chem. Soc.*, 1998, **120**, 468.
3 S. Sakamoto, I. Obataya, A. Ueno and H. Mihara, *J. Chem. Soc., Perkin Trans. 2.*, 1999, 2059; I. Obataya, S. Sakamoto, A. Ueno and H. Mihara, *Protein Peptide Lett.*, 1999, **6**, 141.
4 D. A. Tomalia, A. M. Naylor and W. A. Goddard III, *Angew. Chem., Int. Ed. Engl.*, 1990, **29**, 138.
5 J. F. G. A. Jansen, E. M. M. Branander-van den Berg and E. W. Meijer, *Science*, 1994, **266**, 1226; K. Aoi, K. Itoh and M. Okada, *Macromolecules*, 1995, **28**, 5391.
6 R. Sadamoto, N. Tomioka and T. Aida, *J. Am. Chem. Soc.*, 1996, **118**, 3978.
7 V. Balzani, S. Campagna, G. Denti, A. Juris, S. Serroni and M. Venturi, *Acc. Chem. Res.*, 1998, **31**, 26.
8 C. Rao and J. P. Tam, *J. Am. Chem. Soc.*, 1994, **116**, 6975.
9 MALDI-TOFMS result of R-HL4; 2281.6[(M + H)$^+$] (calc. 2279.7).
10 E. Gross and J. Meienhofer, *The Peptide*, Academic Press, New York, 1979, vol. 1, 289.
11 MALDI-TOFMS data of *n*-(ClAc)PAMAM, *n* = 4; 823.6[(M + H)$^+$] (calc. 823.6): *n* = 8; 2065.7[(M + Na)$^+$] (calc. 2064.7): *n* = 16; 4483.0[(M + H)$^+$] (calc. 4480.9): *n* = 32; 9355.3[(M + H)$^+$] (calc. 9357.4): *n* = 64; 19130.6[(M + Na)$^+$] (calc. 19133.7).
12 S. Futaki, M. Aoki, M. Fukuda, F. Kondo, M. Niwa, K. Kitagawa and Y. Nakaya, *Tetrahedron Lett.*, 1997, **38**, 7071.
13 MALDI-TOFMS data of *n*-(R-HL4) PAMAM (*n* = 4, 8), *n* = 4; 9791.6 [(M + H)$^+$] (calc. 9792.9): *n* = 8; 19900.9[(M + H)$^+$] (calc. 19895.6).
14 *n*-(R-HL4)PAMAMs (*n* > 8) were identified by ultracentrifugation since it was difficult to estimate by MALDI-TOFMS, *n* = 8; found 19900 ± 2100 (calc. 19896): *n* = 16; found 37500 ± 2300 (calc. 40356): *n* = 32; found 84800 ± 7700 (calc. 81108): *n* = 64; found 155100 ± 5700 (calc. 162612).
15 J. M. Scholtz, H. Qian, E. J. York, J. M. Stewart and R. L. Baldwin, *Biopolymers*, 1991, **31**, 1463.
16 CD data at the Soret region of multi-Zn-MP-*n*-(R-HL4)PAMAMs, $[\theta]_{mp}/10^4$ deg cm^2 dmol^{-1} (λ/nm), *n* = 4; +10.3 (413), −9.2 (423): *n* = 8; +7.9 (414), −0.2 (423): *n* = 16; +8.4 (413): *n* = 32, +7.6 (413), −0.2 (423): *n* = 64; +9.7 (413), −0.3 (423).
17 Q. Zhou and T. M. Swager, *J. Am. Chem. Soc.*, 1995, **117**, 12 593.

Cr(salen) catalysed asymmetric ring opening reactions of epoxides in room temperature ionic liquids

Choong Eui Song,*[a] Chun Rim Oh,[ab] Eun Joo Roh[a] and Dong Joon Choo[b]

[a] *Life Sciences Division, Korea Institute of Science and Technology, PO Box 131, Cheongryang, Seoul, 130-650, Korea. E-mail: s1673@kistmail.kist.re.kr*

[b] *College of Liberal Arts and Sciences, Kyunghee University, Hoigi 1, Dongdaemun, Seoul, 130-701, Korea*

Received (in Cambridge, UK) 12th June 2000, Accepted 31st July 2000
First published as an Advance Article on the web 25th August 2000

Cr(salen) catalysed asymmetric ring opening reactions of epoxides with $TMSN_3$ proceed readily in the room temperature ionic liquid 1-butyl-3-methylimidazolium salts ([bmim][X]) with easy catalyst/solvent recycling.

Optically pure β-amino alcohols are important structural elements in many biologically active molecules as well as the starting point in the design of many chiral ligands. Among many other methods, asymmetric ring opening reactions (ARO)[1] of epoxides with $TMSN_3$ catalysed by Cr(salen) complex **1** has been recognised as an attractive approach to the synthesis of optically pure β-amino alcohols.[2] Especially, the Cr(salen) catalyst exhibits indefinite stability under catalytic conditions which allows for its repeated recycling. Jacobsen reported that this reaction can be run without solvents and the catalyst can be recycled a number of times without loss of activity and enantioselectivity.[2a] However, this catalyst recycling procedure involves the potentially hazardous distillation of the neat liquid azides, which may prove a limitation for large scale applications.

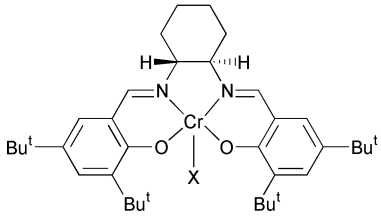

(*R*,*R*)-**1a**; X = Cl
(*R*,*R*)-**1b**; X = N_3

For catalyst recycling,[3] homogeneous chiral catalysts can be immobilised either by anchoring the catalyst on a solid support[3a] or by use of a two-phase system.[3b] All of these approaches are interesting but usually require additional modification of the catalyst. Moreover, such approaches frequently lead to partial loss of activity and/or enantioselectivity. Recently, a new approach has been adopted for catalyst separation and recycling in a few types of catalytic reaction involving the use of ionic liquids,[4] *i.e.* a salt mixture with a melting point below ambient temperature. Air and moisture stable room temperature ionic liquids consisting of 1,3-dialkylimidazolium cations and their counter anions, in particular, have attracted growing interest in the last few years.[5] In these solvents, catalysts having polar or ionic character can be immobilised and thus the ionic solutions containing the catalyst can be easily separated from reagents and products. For example, we reported recently a practical method for recycling a chiral Mn(salen) epoxidation catalyst by using this type of ionic liquid.[5g]

Herein we report a new and highly practical recycling procedure of Cr(salen) catalyst involving the use of air and moisture stable ionic liquids based on 1-butyl-3-methylimidazolium [bmim] salts **2a**–**d**.[6]

To compare the effect of ionic liquids on both reactivity and enantioselectivity, we first examined the asymmetric ring opening reactions of cyclopentene oxide with $TMSN_3$ which were carried out in the presence of 3 mol% of (*R*,*R*)-**1a** in four

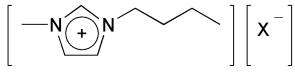

[bmim][X] (**2**); X = PF_6 (**2a**)
SbF_6 (**2b**)
BF_4 (**2c**)
OTf (**2d**)

different ionic liquids, [bmim][X] **2** {X = PF_6 (**2a**),[6a] SbF_6 (**2b**),[6b] BF_4 (**2c**)[6a] and OTf (**2d**)[6c]} at 20 °C. After completion of the reaction, hexane (15 mL in 2 mmol scale experiment) was added and the reaction mixture stirred for 10 min. The hexane phase (upper phase) was then separated from the ionic liquid phase containing the Cr(salen) complex (*R*,*R*)-**1b**[7] by simple decantation and analysed by chiral GC to determine ee values.† After removing the hexane under reduced pressure, methanol and camphorsulfonic acid were added to the residue, and the mixture was allowed to stir at room temperature for 30 min. The methanol was evaporated off and the residue was purified by column chromatography on silica gel with ethyl acetate–hexane to afford the pure azido alcohol.

As shown in Table 1 (entries 1–4), both reactivity and enantioselectivity were strongly influenced by the nature of the anion [X]. When the hydrophobic ionic liquid [bmim][PF_6] **2a** was used, the desired azido silyl ether was obtained with the same degree of yield and enantiomeric excess (94% ee) as those[2a] obtained under homogeneous conditions reported by Jacobsen *et al*. (Table 1, entry 1). Using the other hydrophobic ionic liquid [bmim][SbF_6] (**2b**), the reaction was run with similar conversion, although in slightly lower ee (Table 1, entry 2). In sharp contrast to these results, in the hydrophilic ionic liquids, [bmim][BF_4] (**2c**) or [bmim][OTf] (**2d**), the reaction hardly occurred (Table 1, entries 3 and 4). In the case of using the BF_4 salt (**2c**), only a 5% yield of product was obtained in nearly racemic form (3% ee). More dramatically, in the OTf salt **2d** the reaction did not proceed at all. Although this counter ion

Table 1 Enantioselective ring opening of *meso* epoxides in ionic liquids **2a–d**[a]

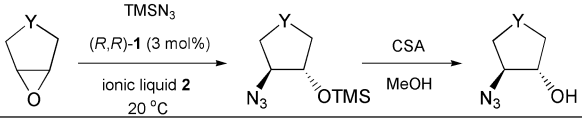

Entry	Substrate (Y)	Ionic liquid **2**	*t*/h	Yield[b] (%)	% ee[c]
1	CH_2	**a**	28	76	94
2	CH_2	**b**	28	75	87
3	CH_2	**c**	28	5	3
4	CH_2	**d**	28	trace	—
5	$(CH_2)_2$	**a**	18	86	85
6	O	**a**	18	74	97

[a] All reactions were run on 2 mmol scale of epoxide at 20 °C using 3 mol% of (*R*,*R*)-**1** in 1 mL of ionic liquid **2**. [b] Isolated yield of azido alcohol. [c] All ee's correspond to those of azido silyl ether and were determined by chiral GC: see footnote†.

effect can not be explained easily, it is apparent that the different hydrophobic character of **2** depending on the anion plays a decisive role in this reaction. Thus, we examined the ARO of other epoxides in the hydrophobic ionic liquid **2a**. All the yields and enantiomeric excesses were quite comparable to those[2a] obtained under homogeneous conditions (Table 1, entries 5 and 6). Although, as mentioned above, excellent results were achieved using the ionic liquid **2a**, the catalyst existed in a suspended form in the ionic liquid **2a** when hexane was added to the reaction mixture after reaction. On the other hand, although the reaction hardly occurred in the ionic liquids **2c** and **2d**, the catalyst was immobilised more efficiently in these solvents after reaction than in **2a**, and thus formed a clear red–brown solution phase, which can make its separation from the hexane phase more easy. We expected that a system combining the hydrophobic and hydrophilic ionic liquids might provide beneficial effects on the catalyst immobilisation. As we expected, in the mixture of **2a** and **2d** with a volume ratio of 5:1, the reaction proceeded with comparable yield and enantiomeric excess to those[2a] obtained under homogeneous conditions (Table 2, entry 1). Moreover, the catalyst could be much better immobilised in this mixture after reaction than in the ionic liquid **2a** alone, and thus the ionic liquid phase containing the catalyst was almost quantitatively recovered from the hexane phase.[8] The recovered ionic liquid phase containing the catalyst was reused several times without any loss of activity and enantioselectivity even after the fifth use (Table 2).

Table 2 Enantioselective ring opening of cyclopentene oxide with catalyst recycling using a mixture of ionic liquids **2a** and **2d**[a]

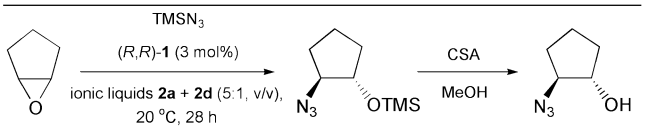

Entry	Recycle no.	Yield (%)	%ee
1	0	68	94
2	1	72	93
3	2	85	93
4	3	75	94
5	4	76	93

[a] All reactions were run on 2 mmol of epoxide at 20 °C using 3 mol% of (*R*,*R*)-**1** in 1.2 mL of the ionic liquid mixture (1 mL of **2a** and 0.2 mL of **2d**).

In summary, we have developed a new and highly practical recycling procedure of Cr(salen) catalyst by using the air and moisture stable ionic liquids **2**. This procedure does not include hazardous work-up stages such as distillation of the azide product, and moreover, provides not only simple recycling of catalyst but also the additional advantage that the catalyst can be used without any modification of the structure. The catalytic activity and enantioselectivity were strongly dependent on the nature of the anion [X] in the ionic liquids [bmim][X] **2**. Detailed studies for the optimisation of this process and the extension of this methodology to other ARO's are currently in progress.

This research was supported by a grant from the Korea Institute of Science and Technology.

Notes and references

† The ee values of products were determined by chiral GC: for 1-azido-2-(trimethylsiloxy)cyclopentane: Chrompak Chiralsil-dex CB, 95 °C isothermal, 25.1 min (1*R*,2*R*), 27.3 min (1*S*,2*S*). For 1-azido-2-(trimethylsiloxy)-cyclohexane; Chrompak Chiralsil-dex CB, 110 °C isothermal, 24.3 min (1*R*,2*R*), 27.1 min (1*S*,2*S*). For 3-azido-4-(trimethylsiloxy)tetrahydrofuran; Chrompak Chiralsil-dex CB, 75 °C for 10 min, then 2 °C min^{-1}, 34.4 min (3*R*,4*S*), 35.2 min (3*S*,4*R*).

1 E. N. Jacobsen and M. H. Wu, *Ring Opening of Epoxides and Related Reactions*, in *Comprehensive Asymmetric Catalysis III*, ed. E. N. Jacobsen, A. Pfaltz and H. Yamamoto, Springer-Verlag, Berlin-Heidelberg-New York, 1999, p. 1309.

2 (*a*) L. E. Martínez, J. L. Leighton, D. H. Carsten and E. N. Jacobsen, *J. Am. Chem. Soc.*, 1995, **117**, 5897; (*b*) J. F. Larrow, S. E. Schaus and E. N. Jacobsen, *J. Am. Chem. Soc.*, 1996, **118**, 7420; (*c*) H. Lebel and E. N. Jacobsen, *J. Org. Chem.*, 1998, **63**, 9624; (*d*) S. E. Schaus, J. F. Larrow and E. N. Jacobsen, *J. Org. Chem.*, 1997, **62**, 4197; (*e*) M. H. Wu and E. N. Jacobsen, *Tetrahedron Lett.*, 1997, **38**, 1693; (*f*) J. L. Leighton and E. N. Jacobsen, *J. Org. Chem.*, 1996, **61**, 389; (*g*) L. E. Martínez, W. A. Nugent and E. N. Jacobsen, *J. Org. Chem.*, 1996, **61**, 7963.

3 (*a*) B. Pugin and H.-U. Blaser, *Catalyst Immobilization: Solid Supports*, in *Comprehensive Asymmetric Catalysis III*, ed. E. N. Jacobsen, A. Pfaltz and H. Yamamoto, Springer-Verlag, Berlin-Heidelberg-New York, 1999, p. 1367; (*b*) G. Oehme, *Catalyst Immobilization: Two-Phase System*, in *Comprehensive Asymmetric Catalysis III*, ed. E. N. Jacobsen, A. Pfaltz and H. Yamamoto, Springer-Verlag, Berlin-Heidelberg-New York, 1999, p. 1377.

4 (*a*) T. Welton, *Chem. Rev.*, 1999, **99**, 2071; (*b*) K. R. Seddon, *J. Chem. Tech. Biotechnol.*, 1997, **68**, 351; (*c*) Y. Chauvin and H. Olivier, *CHEMTECH*, 1995, 26.

5 (*a*) A. Stark, B. L. MacLean and R. D. Singer, *J. Chem. Soc., Dalton Trans.*, 1999, 63; (*b*) T. Fischer, A. Sethi, T. Welton and J. Woolf, *Tetrahedron Lett.*, 1999, **40**, 793; (*c*) B. Ellis, W. Keim and P. Wasserscheid, *Chem. Commun.*, 1999, 337; (*d*) W. A. Herrmann and V. P. W. Bohm, *J. Organomet. Chem.*, 1999, **572**, 141; (*e*) W. Keim, D. Vogt, H. Waffenschmidt and P. Wasserscheid, *J. Catal.*, 1999, **186**, 481; (*f*) W. Chen, L. Xu, C. Chatterton and J. Xiao, *Chem. Commun.*, 1999, 1247; (*g*) C. E. Song and E. J. Roh, *Chem. Commun.*, 2000, 843.

6 Preparation of ionic liquids: (*a*) For **2a** and **2c**: P. A. Z. Suarez, J. E. L. Dullius, S. Einloft, R. F. de Souza and J. Dupont, *Polyhedron*, 1996, **15**, 1217; (*b*) The synthesis of **2b** was similar to that of **2a** and **2c** with the exception that $NaSbF_6$ was used in place of $NaPF_6$ or $NaBF_4$; (*c*) For **2d**: P. Bonhôte, A.-P. Dias, N. Papageorgiou, K. Kalyanasundaram and M. Grätzel, *Inorg. Chem.*, 1996, **35**, 1168. All ionic liquids used in this paper were pre-dried under reduced pressure (0.5 mmHg) at 50 °C for 24 h.

7 The recovered catalyst displayed a strong IR absorbance at 2058 cm^{-1}; see ref. 2(*a*).

8 The Cr(salen) catalyst **1** is slightly soluble in hexane. However, in this case, the amount of catalyst dissolved in the hexane phase is negligible.

ChemComm

Syntheses of the novel cage compounds $P_3Se_3C_3Bu^t_3$ and $P_3Se_4C_3Bu^t_3$ and an unusual insertion reaction of $[PtCl_2(PMe_3)]$ into the Se–Se bond of the latter to give the six-coordinate Pt(IV) complex $[PtCl_2(PMe_3)P_3Se_4C_3Bu^t_3]$

Peter B. Hitchcock, John F. Nixon* and Nurgün Sakarya

School of Chemistry, Physics and Environmental Science, University of Sussex, Brighton, Sussex, UK BN1 9QJ. E-mail: J.Nixon@sussex.ac.uk

Received (in Cambridge, UK) 26th June 2000, Accepted 2nd August 2000
First published as an Advance Article on the web 29th August 2000

The novel cage compounds $P_3Se_3C_3Bu^t_3$ and $P_3Se_4C_3Bu^t_3$ are formed (together with the 1,2,4-selenadiphosphole $P_2SeC_2Bu^t_2$) from the reaction of the phosphaalkyne Bu^tCP with selenium; the $[PtCl_2(PMe_3)]$ fragment undergoes an unusual insertion reaction into the Se–Se bond of $P_3Se_4C_3Bu^t_3$.

There is current interest in the chemistry of (i) low-coordinate phosphorus compounds, (ii) phospholes containing additional heteroatoms and (iii) novel phosphorus containing cage compounds.[1–14] Regitz and coworkers have recently described[15] the facile, high-yield, synthesis of the previously known[8,9] 1,2,4-selenadiphosphole $P_2SeC_2Bu^t_2$ **1** by treatment of selenium with

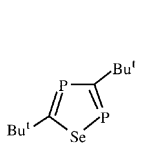

1

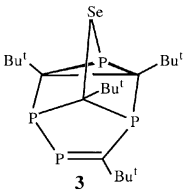

3

the phosphaalkyne Bu^tCP **2** in the presence of NEt_3. The ready [2 + 2 + 2] cycloaddition reaction of **1** with two further mol of **2** to yield the tetracyclic cage compound $P_4SeC_4Bu^t_4$ **3**, prompts us to describe the syntheses and structural characterisation of

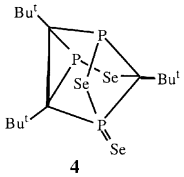

4

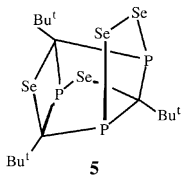

5

two new cages $P_3Se_3C_3Bu^t_3$ **4** and $P_3Se_4C_3Bu^t_3$ **5**, both also derived from **1**. We also report an unusual oxidation of a Pt(II) complex to a Pt(IV) complex *via* insertion of the Pt(II) into the Se–Se bond of **5**.

Treatment of a suspension of a slight excess of selenium in toluene with **2** for 4 days at 75 °C, afforded **1** as the expected main product, which was removed by sublimation. The residue was chromatographed (Florisil/hexane) to give colourless crystals of $P_3Se_3C_3Bu^t_3$ **4** (5.3%) and red crystals of $P_3Se_4C_3Bu^t_3$ **5** (7%). ^1H, ^{31}P and ^{77}Se NMR data for **4** and **5** were entirely consistent with the proposed structures,† which were also confirmed by single crystal X-ray diffraction studies. The molecular structures of **4**‡ and **5**‡ are shown in Fig. 1 and 2. Both cages are most likely to have been derived from a common intermediate **6**, which would be formed *via* the initial [4 + 2] cycloaddition reaction of **1** with **2**.

Thus **4** probably arises from (i) insertion of Se, still present in the reaction mixture, into the weak P–P bond (resulting from the intramolecular [2 + 2] cycloaddition cage-formation step) of the intermediate **6** and (ii) a second exocyclic Se addition to one of these phosphorus atoms. Likewise, in an analogous way, the more symmetrical cage compound **5** would result from insertion of Se_2 into the P–P bond, as well as a separate single Se atom insertion into the C–C bond of the initially formed strained three-membered CPC ring. Compound **5** is noteworthy because

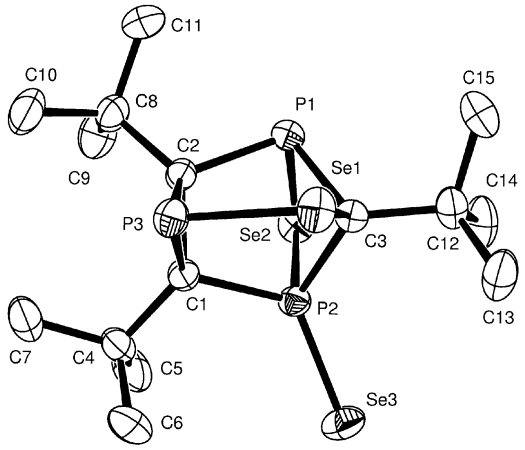

Fig. 1 Molecular structure of **4**. Selected bond lengths (Å) and angles (°): Se(1)–C(3) 1.980(2), Se(1)–P(3) 2.2392(8), Se(2)–P(2) 2.2707(7), Se(2)–P(1) 2.3023(7), Se(3)–P(2) 2.0862(7), P(1)–C(3) 1.890(3), P(1)–C(2) 1.892(3), P(2)–C(3) 1.839(3), P(2)–C(1) 1.886(3), P(3)–C(1) 1.857(2), P(3)–C(2) 1.858(3); C(3)–Se(1)–P(3) 91.61(8), P(2)–Se(2)–P(1) 70.81(2), C(3)–P(1)–C(1) 95.24(12), C(3)–P(1)–Se(2) 87.22(8), C(2)–P(1)–Se(2) 94.31(8), C(3)–P(1)–P(2) 43.96(8), C(2)–P(1)–P(2) 71.83(8), Se(2)–P(1)–P(2) 54.04(2), C(3)–P(2)–C(1) 98.22(11), C(3)–P(2)–Se(3) 20.49(9).

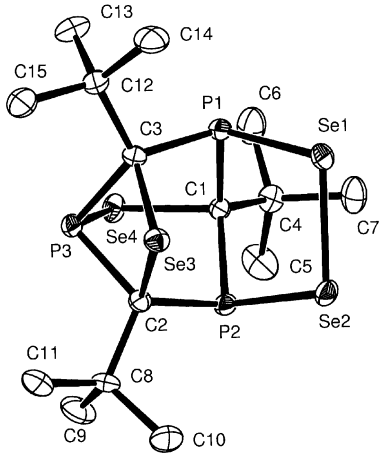

Fig. 2 Molecular structure of **5**. Selected bond lengths (Å) and angles (°): Se(1)–P(1) 2.2260(13), Se(1)–Se(2) 2.3966(9), Se(2)–P(2) 2.2267(14), Se(4)–P(3) 2.2445(14), Se(4)–C(1) 2.016(4), Se(3)–C(2) 1.998(4), Se(3)–C(3) 1.997(4), P(1)–C(1) 1.874(4), P(1)–C(3) 1.900(4), P(2)–C(1) 1.885(4), P(2)–C(2) 1.890(4): P(3)–C(2) 1.862(4), P(3)–C(3) 1.867(4); P(1)–Se(1)–Se(2) 99.32(4), P(2)–Se(2)–Se(1) 99.16(4), C(3)–Se(3)–C(2) 79.51(17), C(1)–Se(4)–P(3) 89.22(13), C(1)–P(1)–C(3) 101.13(19), C(1)–P(1)–Se(1) 102.37(13).

DOI: 10.1039/b005123n

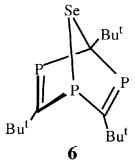

6

although homonuclear S–S bonds are common in monocyclic $(RP)_xS_y$ systems, analogous Se–Se bonded compounds are rare.[16]

Interestingly, the cage compound **5** undergoes an unexpected reaction with $[PtCl_2(PMe_3)]_2$. It was anticipated that simple η^1-coordination would occur, *via* either the P or Se lone pair electrons, however the platinum(II) fragment also unexpectedly inserts into the Se(1)–Se(2) bond of **5** as well as undergoing ligation to Se(3) of the four-membered P(3)C(3)Se(3)C(2) ring, to afford the novel deep-red Pt(IV) complex $[PtCl_2(PMe_3)P_3Se_4C_3Bu^t_3]$ **7** (55.8%).§

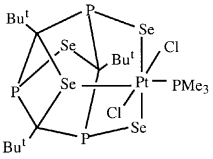

7

The latter was fully structurally characterised by a single crystal X-ray diffraction study‡ and its molecular structure is shown in Fig. 3.

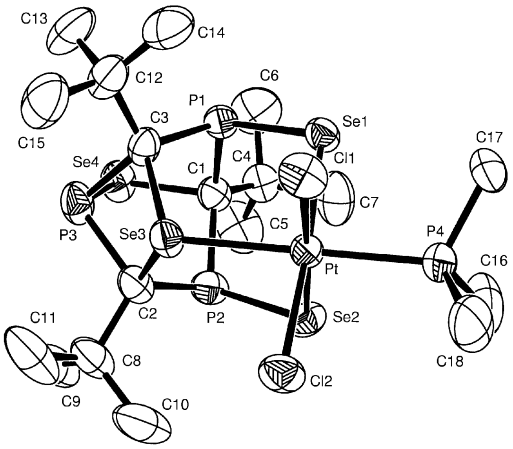

Fig. 3 Molecular structure of **7**. Selected bond lengths (Å) and angles (°): Pt–P(4) 2.3103(13), Pt–Cl(1) 2.4120(14), Pt–Cl(2) 2.4241(12), Pt–Se(2) 2.4434(6), Pt–Se(1) 2.4493(5), Pt–Se(3) 2.4679(5), Se(1)–P(1) 2.2266(13), Se(2)–P(2) 2.2175(14), Se(4)–P(3) 2.2301(16), Se(4)–C(1) 2.007(5), Se(3)–C(2) 2.026(5), Se(3)–C(3) 2.030(5), P(1)–C(1) 1.869(5), P(1)–C(3) 1.869(5), P(2)–C(1) 1.885(5), P(2)–C(2) 1.872(6): P(3)–C(2) 1.890(6), P(3)–C(3) 1.889(5); P(4)–Pt–Cl(1) 88.03(5), P(4)–Pt–Cl(2) 92.33(5), Cl(1)–Pt–Cl(2) 89.28(5), P(1)–Pt–Se(2) 93.57(4).

We thank the Turkish government for a research grant (for N. S.) and the British Council for financial support for part of this work.

Notes and references

† *NMR data*: for **4**: $^{31}P\{^1H\}$ NMR (121.49 MHz, $CDCl_3$): δ 80.7 [P(2), dd, $^2J(^{31}P^{31}P)$ 53.3, $^1J(^{31}P^{77}Se)$ 208.4, $^2J(^{31}P^{31}P)$ 53.3 Hz], 21.5 [P(3), d, $^1J(^{31}P^{77}Se)$ 170.4, $^2J(^{31}P^{31}P)$ 51.3 Hz], −54.2 [P(1), d, $^1J(^{31}P^{77}Se)$ 203.0, $^2J(^{31}P^{77}Se)$ 48.1 Hz]. For **5**: ^1H NMR (toluene-d_8): δ 0.80 (s, 18H, ^{t}Bu), 0.97 (s, 9H, ^{t}Bu). $^{31}P\{^1H\}$ NMR (121.49 MHz, $CDCl_3$): δ 74.5 [P(1) and P(2), d, $^2J(^{31}P^{31}P)$ 7.2, $^1J(^{31}P^{77}Se)$ 317.4, $^2J(^{31}P^{77}Se)$ 0.4, 14.0 Hz], −36.0 [P(3), t, $^1J(^{31}P^{77}Se)$ 177.8, $^2J(^{31}P^{77}Se)$ 42.1, $^2J(^{31}P^{77}Se)$ 14.5 Hz]. $^{77}Se\{^1H\}$ NMR: δ 256.5 [Se(4), dt, $^1J(^{31}P^{77}Se)$ 177.8, $^2J(^{31}P^{77}Se)$ 23.2 Hz], 514.3 [Se(3), d, $^2J(^{31}P^{77}Se)$ 52.5], 67.6 [Se(1) and Se(2), m, $^1J(^{31}P^{77}Se)$ 317.4, $^2J(^{31}P^{77}Se)$ 40.3, $^2J(^{31}P^{77}Se)$ 15.4 Hz].

‡ *Crystal data*: **4** $C_{15}H_{27}P_3Se_3$, M = 537.16, monoclinic, space group $P2_1/n$ (no. 14), a = 10.7751(3), b = 16.2798(7), c = 11.6992(3) Å, β = 102.264(2)°, U = 2005.4(1) Å^3, Z = 4, D_c = 1.78 Mg m^{-3}, crystal dimensions 0.2 × 0.1 × 0.1 mm, $F(000)$ = 1056, T = 293(2) K, Mo-Kα radiation, λ = 0.71073 Å. Data collection Kappa CCD, 16312 reflections collected, 5787 independent (R_{int} = 0.0498), $R1$ = 0.038, $wR2$ = 0.083 for 4569 reflections with $I > 2\sigma(I)$, $R1$ = 0.055, $wR2$ = 0.090 for all data.

5: $C_{15}H_{27}P_3Se_4$, M = 16.12, triclinic, space group $P\bar{1}$ (no. 2), a = 9.902(2), b = 10.340(4), c = 12.760(4) Å, α = 69.17, β = 71.11(2), γ = 61.57°, U = 1054.6(6) Å^3, Z = 2, D_c = 1.94 Mg m^{-3}, crystal dimensions 0.35 × 0.20 × 0.20 mm, $F(000)$ = 596, T = 173(2) K, Mo-Kα radiation, λ = 0.71073 Å. Data collection CAD4. Of the total 5081 independent reflections measured, the final indices for 3999 reflections with $I > 2\sigma(I)$ were $R1$ = 0.037, $wR2$ = 0.076 and $R1$ = 0.057, $wR2$ = 0.088 for all data.

7: $C_{18}H_{36}Cl_2P_4PtSe_4$, M = 958.18, rhombohedral, space group $R\bar{3}$ (no. 148), a = 34.5455(6), c = 16.7221(2) Å, U = 17282.4(5) Å^3, Z = 18, D_c = 1.66 Mg m^{-3}, crystal dimensions 0.2 × 0.1 × 0.1 mm, $F(000)$ = 8136, T = 293(2) K, Mo-Kα radiation, λ = 0.71073 Å. Data collection Kappa CCD, 41518 reflections collected, 10989 independent (R_{int} 0.0553), $R1$ = 0.039, $wR2$ = 0.083 for 7872 reflections with $I > 2\sigma(I)$, $R1$ = 0.069, $wR2$ = 0.095 for all data.

CCDC 182/1736. See http://www.rsc.org/suppdata/cc/b0/b005123n/ for crystallograhic files in .cif format.

§ NMR data for **7**: $^{31}P\{^1H\}$ NMR (121.49 MHz, $CDCl_3$): δ 62.7 [P(1) and P(2), m, $^2J(^{31}P^{31}P)$ 14.9, $^1J(^{31}P^{77}Se)$ 330.5, $^2J(^{31}P^{31}P)$ 6.0 Hz]; 35.4 [P(3), m, $^2J(^{31}P^{31}P)$ 13.1, $^2J(^{31}P^{31}P)$ 6.0 Hz], −8.1 [P(4), m, $^1J(^{31}P^{195}Pt)$ 2221, $^2J(^{31}P^{31}P)$ 14.9, $^2J(^{31}P^{31}P)$ 5.9 Hz]. $^{195}Pt\{^1H\}$ NMR: δ −3630.4 [$^1J(^{31}P^{195}Pt)$ 2209 Hz].

1 K. B. Dillon, F. Mathey and J. F. Nixon, *Phosphorus: The Carbon Copy*, John Wiley and Sons, Chichester, 1998, pp. 1–366 and references therein.
2 *Carbocyclic and Heterocyclic (P, As, N) Cage Compounds and their Building Blocks: Synthesis, Structure, Mechanism and Theory*, ed. K. K. Laali and B. Halton, JAI Press Inc., Stamford, CT, 1999.
3 A. Mack and M. Regitz, *Chem. Ber.*, 1997, **130**, 823.
4 V. Caliman, P. B. Hitchcock and J. F. Nixon, *J. Chem. Soc., Chem. Commun.*, 1995, 1661.
5 P. B. Hitchcock, J. F. Nixon and N. Sakarya, *Chem. Commun.*, 1996, 2751.
6 V. Caliman, P. B. Hitchcock and J. F. Nixon, *J. Organomet. Chem.*, 1997, **536**, 273.
7 V. Caliman, P. B. Hitchcock, J. F. Nixon, L. Nyulászi and N. Sakarya, *Chem. Commun.*, 1997, 1305.
8 V. Caliman, P. B. Hitchcock, J. F. Nixon and N. Sakarya, *Bull. Soc. Chim. Belg.*, 1996, **105**, 675.
9 M. Regitz and S. Krill, *Phosphorus, Sulfur Silicon Relat. Elem.*, 1996, **115**, 99.
10 V. Caliman, P. B. Hitchcock and J. F. Nixon, *Heteroatom Chem.*, 1998, **9**, 1.
11 F. G. N. Cloke, P. B. Hitchcock, P. Hunnable, J. F. Nixon, L. Nyulászi, E. Niecke and V. Thelen, *Angew. Chem., Int. Ed.*, 1998, **37**, 1083.
12 V. Caliman, P. B. Hitchcock and J. F. Nixon, *Chem. Commun.*, 1998, 1537.
13 M. D. Francis, D. E. Hibbs, P. B. Hitchcock, M. B. Hursthouse, C. Jones, T. Mackewitz, J. F. Nixon, L. Nyulászi, M. Regitz and N. Sakarya, *J. Organomet. Chem.*, 1999, **580**, 156.
14 F. G. N. Cloke, P. B. Hitchcock, J. F. Nixon, D. J. Wilson, F. Tabellion, U. Fishbeck, F. Preuss, M. Regitz and L. Nyulászi, *Chem. Commun.*, 1999, 2363.
15 S. M. F. Asmus, U. Bergstrasser and M. Regitz, *Synthesis*, 1999, 1642.
16 P. Lonnecke and R. Blachnik, *Phosphorus, Sulfur Silicon Relat. Elem.*, 1997, **131**, 191 and references therein.

ChemComm

Excited state interactions in phenol/olefin bichromophoric compounds: direct detection of an intramolecular exciplex

Francisco Galindo, M. Consuelo Jiménez, Miguel A. Miranda* and Rosa Tormos

Departamento de Química-Instituto de Tecnología Química UPV-CSIC, Universidad Politécnica de Valencia, Camino de Vera s/n, Apdo 22012, 46071 Valencia, Spain. E-mail: mmiranda@qim.upv.es

Received (in Liverpool, UK) 22nd June 2000, Accepted 2nd August 2000
First published as an Advance Article on the web 29th August 2000

The emission from an intramolecular exciplex detected in *trans*-4-methoxy-2-(3-phenyl-2-propenyl)phenol (1) is the first direct evidence for the excited state interchromophoric interaction in phenol–styrene systems.

Bichromophoric compounds have attracted considerable interest as models for the understanding of energy or electron transfer processes. They have also found application for mimicking some biological processes (*i.e.* photosynthesis) and for the development of new materials such as photoconducting polymers.[1]

trans-2-Cinnamylphenols are bichromophoric compounds containing phenol and styrene subunits connected by a methylene spacer. Upon the introduction of suitable substituents, these simple systems allow the reproduction at will of a wide range of intramolecular proton, electron or energy transfer processes.[2]

Previously, the photochemical reactivity of *trans*-2-cinnamylphenols and their relatively low fluorescence quantum yields, as compared with models containing the isolated chromophores, has been attributed to an intramolecular interaction in the excited state between the two chromophores.[3] However, no direct evidence has been provided in support of such interaction. In the present work, direct detection of an intramolecular exciplex has been achieved in the case of *trans*-4-methoxy-2-(3-phenyl-2-propenyl)phenol (**1**), by measuring the emission spectra in acetonitrile. To our knowledge, this is the first case of an intramolecular exciplex involving a phenol chromophore.

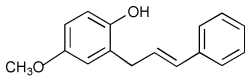

1

The emission properties of **1** are summarized in Table 1, together with those measured under the same conditions for the isolated 4-methoxyphenol chromophore. Thus, the fluorescence spectra of **1** in hexane displayed a single band with λ_{max} = 320 nm, clearly attributable to emission from the lowest lying phenolic singlet (compare trace B, Fig. 1a with trace A, Fig. 1b). The same result was obtained by exciting either at 250 nm (styrene) or at 290 nm (phenol), clearly due to efficient energy transfer between the excited singlets of both chromophores (Fig. 1c). By contrast, a completely different behaviour was observed in the more polar solvent acetonitrile. The most remarkable result was the presence of a much longer wavelength band centered at 420 nm and the concomitant disappearance of the phenolic emission at 320 nm (see Fig. 1b). This new band is clearly attributable to a charge-transfer

Table 1 Photophysical data of **1** and the reference compound 4-methoxyphenol in hexane and acetonitrile at room temperature[a]

Compound	Solvent	$\lambda_{emission}$/nm	ϕ_F	τ_F(ns)
1	Hexane	320	0.056	1.0
	Acetonitrile	420	0.051	5.1
4-Methoxyphenol	Hexane	320	0.143	1.9
	Acetonitrile	320	0.141	2.1

[a] $\lambda_{excitation}$ = 290 nm.

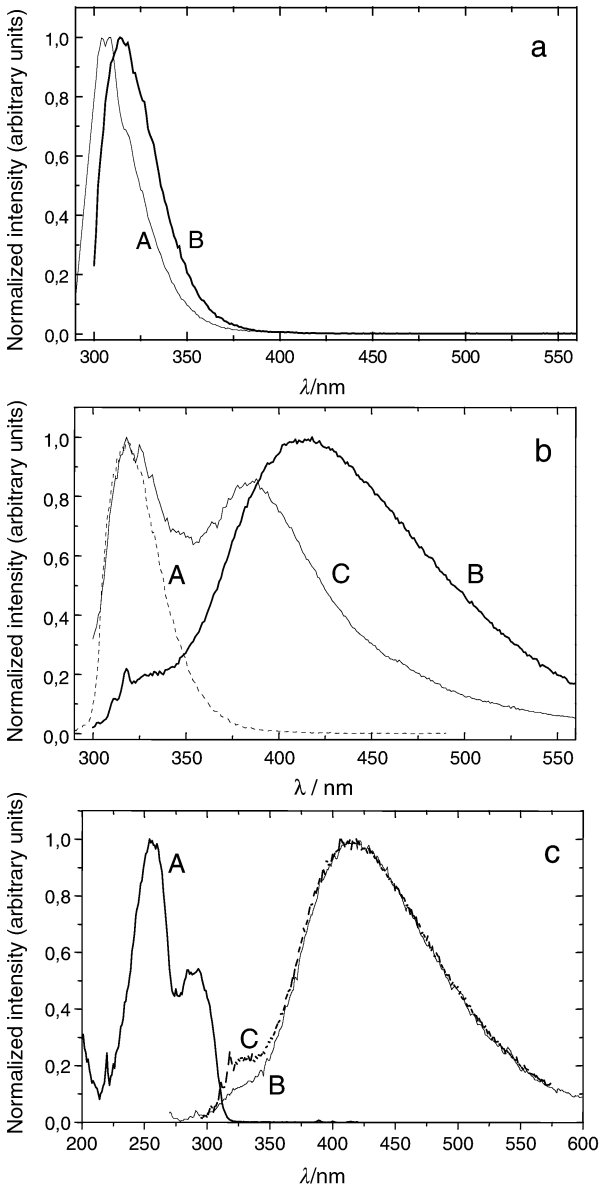

Fig. 1 Fluorescence spectra of: (a) the isolated β-methylstyrene (trace A) and 4-methoxyphenol (trace B); (b) **1** in hexane (trace A), in acetonitrile (trace B) and in a 9 : 1 dichloromethane–acetonitrile mixture (trace C); (c) **1** in acetonitrile; excitation spectrum (trace A), emission upon excitation at 250 nm (trace B) and emission upon excitation at 290 nm (trace C).

DOI: 10.1039/b005026l

exciplex, whose formation would be exergonic according to the Rehm–Weller eqn (1)[4]

$$\Delta G_f \text{ (kcal mol}^{-1}) = 23.06\,(E_{D/D^{+\cdot}} - E_{A/A^{-\cdot}}) - E^* \quad (1)$$

where $E_{D/D^{+\cdot}}$ and $E_{A/A^{-\cdot}}$ are the redox potentials of the donor and acceptor moieties, and E^* is the singlet energy of the phenolic chromophore. Using the excitation energy determined from the intersection between normalized excitation and emission spectra, together with the reported literature values for the redox potentials,[5] the resulting Gibbs free energy associated with exciplex formation would be *ca.* −25 kcal mol^{-1}. The emission spectra were also obtained for solutions of **1** in solvents of intermediate polarity and in a variety of solvent mixtures. For instance, using CH_2Cl_2–CH_3CN (9:1, v:v), both the monomer and the exciplex bands were observed (see trace C, Fig. 1b). As expected for a charge-transfer exciplex, the position of the longer wavelength band showed a clear dependence on the solvent polarity (see Fig. 2 for the Lippert–Mataga plot with the data obtained in pure solvents).[6]

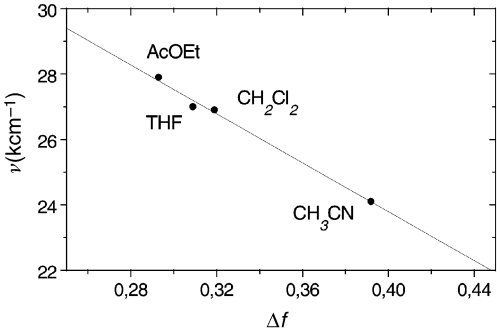

Fig. 2 Solvent polarity dependence of the exciplex emission maxima for **1**. Solvent parameter Δf has been calculated as follows: $\Delta f = (\varepsilon - 1)/(2\varepsilon + 1) - (n^2 - 1)/(4n^2 + 2)$ where ε is the dielectric constant and n is the refraction index of the solvent.

The quantum yield of emission at 420 nm was 0.05, and the lifetime was relatively long (5.1 ns), as compared with the monomer under the same conditions (1.0 ns). The exciplex was quenched by oxygen (k_q = 4.2 × 10^{10} M^{-1} s^{-1}) and by tetrabutylammonium hydrogensulfate (k_q = 3.3 × 10^9 M^{-1} s^{-1}). The Stern–Volmer plot for quenching by the ammonium salt is shown in Fig. 3. Similar salt effects have been observed for other exciplexes; they have been attributed to dissociation into radical ions, with the concomitant decrease of fluorescence.[7]

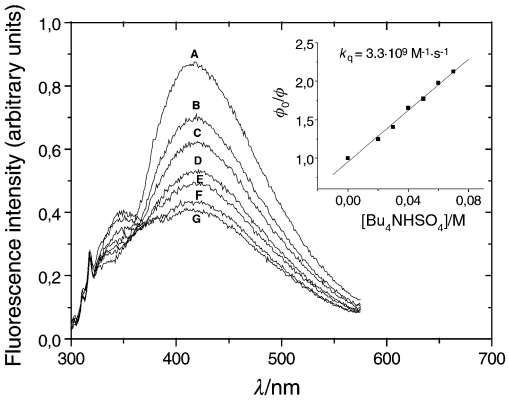

Fig. 3 Quenching of the exciplex fluorescence for **1** by [Bu_4NHSO_4] at different molar concentrations: curve A) 0.0 M; B) 0.02 M, C) 0.03 M, D) 0.04 M, E) 0.05 M, F) 0.06 M, G) 0.07 M.

All the above data were obtained using 5 × 10^{-5} M solutions of **1**. To check whether the corresponding intermolecular exciplex is also observable, equimolar mixtures of 4-methoxyphenol and β-methylstyrene in acetonitrile (5 × 10^{-5} M each) were studied. The emission spectra consisted of the bands assignable to the isolated chromophores (either phenolic maximum at 320 nm, upon excitation at 290 nm, or styrenic maximum at 310 nm when exciting at 250 nm). However, using much higher concentrations of the partners (0.1 M), the exciplex emission at *ca*. 440 nm was clearly observable.

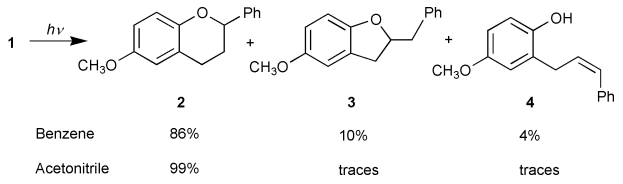

Scheme 1

After determining the photophysical properties of **1**, its preparative photochemistry was also investigated. Irradiation of **1** for 1 h in acetonitrile and benzene, with the Pyrex-filtered light of a medium pressure Hg lamp resulted in the almost complete (>95%) consumption of the starting material, accompanied by formation of the six-membered ring compound **2** as the major photoproduct. Minor amounts of the *cis*-isomer **4** and the five-membered ring product **3** were also obtained in benzene. These results are summarized in Scheme 1.

As the formation of six-membered ring product **2** is considered to be an indication for the involvement of intramolecular excited state electron transfer,[2] detection of a charge-transfer exciplex is compatible with the preparative photochemistry of **1**.

In summary, the intramolecular excited state interaction between phenol and styrene has been directly observed for the first time as an exciplex emission. This strongly supports the previous mechanistic proposals to explain the photochemistry of bichromophoric cinnamylphenols. Although such interaction is reported here for a single compound (**1**), preliminary data in hand show that other analogues with electron donating substituents at the phenolic ring [such as 4-methyl, 4,6-dimethyl- and 4,6-di-*tert*-butyl-2-(3-phenyl-2-propenyl)phenol] exhibit similar photophysical and photochemical properties.

Financial support by the DGICYT (PB 97-0339) is gratefully acknowledged. M. C. J. thanks the European Commision for a grant (MCFI-1999-00101). F. G. thanks Ministerio de Educación y Cultura for a grant.

Notes and references

1 S. Speiser, *Chem. Rev.*, 1996, **96**, 1953; V. Balzani and F. Scandola, *Supramolecular Photochemistry*, Ellis Horwood Limited, Chichester, 1991; D. Gravel, S. Gauthier, F. Brisse, S. Raymond, M. D'Amboise, P. Messier, B. Zelent and G. Durocher, *Can. J. Chem.*, 1990, **68**, 908; E. Cotsaris, J. W. Verhoeven and N. S. Hush, *J. Am. Chem. Soc.*, 1987, **109**, 3258.

2 M. C. Jiménez, F. Márquez, M. A. Miranda and R. Tormos, *J. Org. Chem.*, 1994, **59**, 197; M. C. Jiménez, P. Leal, M. A. Miranda and R. Tormos, *J. Org. Chem.*, 1995, **60**, 3243; M. C. Jiménez, M. A. Miranda and R. Tormos, *Tetrahedron*, 1997, **53**, 14 729; M. C. Jiménez, M. A. Miranda and R. Tormos, *J. Org. Chem.*, 1998, **63**, 1323; M. C. Jiménez, P. Leal, M. A. Miranda, J. C. Scaiano and R. Tormos, *Tetrahedron*, 1998, **54**, 4337.

3 M. T. Bosch-Montalvá, L. R. Domingo, M. C. Jiménez, M. A. Miranda and R. Tormos, *J. Chem. Soc., Perkin Trans. 2*, 1998, 2175.

4 A. Weller, *Z. Phys. Chem.*, 1982, **133**, 93.

5 E_{ox} for 4-methoxyphenol is +0.406 V *vs*. SCE and E_{red} of β-methylstyrene is −2.54 V *vs* SCE as reported in *Technique of Electroorganic Synthesis*, ed. N. L. Weinberg, part 2, John Wiley & Sons, New York, 1975.

6 N. Mataga, *Adv. Chem. Phys.*, 1999, **107**, 431; *The Exciplex*, ed. M. Gordon and W. R. Ware, Academic Press, New York, 1975.

7 B.-W. Zhang, Y. Cao, J.-W. Bai and J.-R. Chen, *J. Photochem. Photobiol., A: Chem.*, 1997, **106**, 169.

ChemComm

Mesostructured iron sulfides

Jianquan Li and Linda F. Nazar*

Department of Chemistry, University of Waterloo, Waterloo, Ontario, Canada N21 3G1. E-mail: lfnazar@uwaterloo.ca

Received (in Bloomington, IN, USA) 6th July 1999, Revised manuscript received 1st May 2000, Accepted 14th June 2000
First published as an Advance Article on the web 29th August 2000

The synthesis and characterization of the first mesostructured iron sulfides are reported: the first is a disordered hexagonal structure prepared *via* a neutral template route; the other, formed using an ionic template, is a relatively ordered phase which represents the first hexagonal mesostructured transition metal sulfide.

Since the first synthesis of mesoporous silicates, much activity has focussed on self-assembled inorganic/surfactant composites[1–5] due to their potential applications as catalysts and absorbents. The best known member of this family, MCM-41, possesses a hexagonal array of channels while the atomic arrangement in the channel walls is disordered. Following this, many different types of surfactants have been used to prepare numerous mesostructured oxides, primarily in the silicate family. A liquid crystal templating mechanism[1] and a self-assembly process involving electrostatic interaction between the inorganic ions in solution and the charged surfactant head group[2,3] were proposed for the mechanism of formation. Using a neutral template, formation of a mesoporous silicate containing a disordered arrangement of channels was explained on the basis of hydrogen bonding and self-assembly between neutral primary amine micelles and neutral inorganic precursors.[4] Neutral surfactants have also been used to prepare mesoporous transition metal oxides with a high specific surface area.[5]

Compared with oxygen, sulfur has a far richer coordination chemistry due to its low-lying d orbitals. The lack of thermodynamic stability of sulfides in the presence of oxygen has made synthesis of mesostructured sulfides more difficult, however, and hence only a few have been reported. These include primarily the main group family, namely mesolamellar and pseudo-hexagonal phases of Group IV (Sn,[6] Ge[7]), and Group II (Cd,[8] Zn[9]). As metal sulfides are generally semiconductors, while many metal oxides are insulators, open-framework metal sulfides may be potentially useful for different applications. Iron sulfides are particularly interesting since they play an important role in life's beginning.[10] The catalytic formation of complex organic molecules from simple precursors is considered to take place on the surface of iron monosulfide or pyrite as a result of redox reactions between FeS and FeS_2.[11] Furthermore, bulk iron(II) and iron(III) sulfides have shown potential applications as cathodes,[12] high refractive index materials[13] and catalysts for coal liquefaction.[14] Herein we report the first mesostructured phases based on iron sulfides, prepared *via* different routes.

Mesostructured iron(II) sulfide [denoted DDA-FeS-M (DDA = dodecylamine)] was formed in the system dodecylamine–iron(II) sulfate–sodium sulfide–ethanol–H_2O at room temperature. Use of the two solvent system improved the solubility of dodecylamine. Fig. 1(*a*) shows the resulting XRD pattern: One peak is evident with a *d*-spacing of 33.8 Å, similar to the value observed for HMS.[4] The presence of a single broad peak is considered an indication of randomly ordered pores.[4,15] A very broad, low intensity line at about 20° (2θ), similar to that of MCM-41 and HMS-type materials, also observed in the XRD pattern, suggests that the inorganic wall is amorphous as expected.[1–4,15] We have found that DDA-FeS-M is formed at an optimum H_2O/ethanol ratio of 7.7: at lower ratios the material is not formed at all. An unknown impurity phase was found in the product when the ethanol was increased, or the amount of iron sulfate and sodium sulfide was increased in the reactant mixture. The impurity phase therefore is minimized under slightly acidic conditions.

The presence of DDA in the material was confirmed by thermal gravimetric analysis (TGA). The TGA curve (under N_2) shows an initial weight loss of about 3.6% below 135 °C due to the desorption of water. Weight loss (48.7%) above this temperature corresponds to the loss of organic material and also some sulfur species. The corresponding differential thermal analysis (DTA) curve in air shows two exothermic peaks at low temperature attributable to reaction with oxygen that result in a weight gain of about 4.4 wt%, evident from the TGA trace. Two exothermic peaks between 250 and 500 °C correspond to combustion of the surfactant. The total weight loss corresponding to the loss of surfactant and transformation from iron(II) sulfide to iron(III) oxide is about 61.5%, translating into an empirical composition of $FeS(DDA)_{0.6}{\cdot}0.4H_2O$. This material displayed a very disordered structure in its TEM image, similar to HMS.[4]

Employment of an ionic surfactant hexadecyltrimethylammonium hydroxide/chloride as a structure-directing agent,

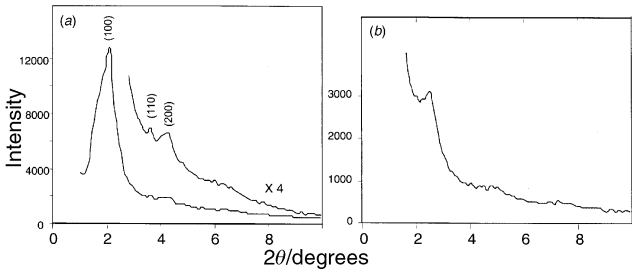

Fig. 1 (*a*) Powder X-ray diffraction patterns (Siemens D-500; Cu-Kα radiation) of DDA-FeS-M; (*b*) XRD pattern of C_{16}TMA-Fe_2S_3-M. Inset shows scale expansion of the 3–10° 2θ range showing the weak 110 and 200 reflections. Values for the experimental and calculated *d*-spacings, respectively for the hexagonal unit cell where a = 48.4 Å are (100), 41.92, 41.89 Å; (110), 24.25, 24.19 Å; (200), 20.59, 20.94 Å.

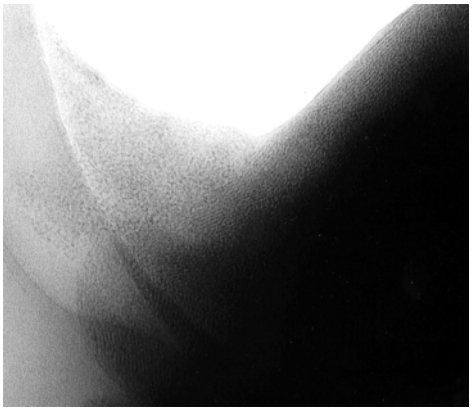

Fig. 2 Transmission electron micrograph image (Phillips, CM20, 200 keV) of mesostructured C_{16}TMA-Fe_2S_3-M (1 cm = 74 nm).

Table 1 Influence of reaction composition on the formation of $C_{16}TMA$-Fe_2S_3-M

Sample No.	Molar ratio Fe_2S_3/CTMA	H_2O/CTMA	$(NH_4)_2S$/CTMA	Crystallization time/h	Products
f	0.50	100	0.0	23	Fe_2O_3
g	0.50	150	0.0	12	$C_{16}TMA$-Fe_2S_3-M + Fe_2O_3
h	0.50	200	0.0	23	Fe_2O_3 + FeS_2
i	0.50	150	0.5	15	$C_{16}TMA$-Fe_2S_3-M
j	0.75	150	0.5	8.5	$C_{16}TMA$-Fe_2S_3-M
k	1.00	150	0.5	8.5	$C_{16}TMA$-Fe_2S_3-M
l	0.50	150	0.5 S[a]	24	$C_{16}TMA$-Fe_2S_3-M + Fe_2O_3

[a] Elemental sulfur was used in place of $(NH_4)_2S$

and an amorphous iron(III) sulfide,[16] as iron and sulfur sources yielded $C_{16}TMA$-Fe_2S_3-M after hydrothermal synthesis at 110 °C for 16 h. Fig. 1(*b*) shows the resultant XRD pattern in which three reflections are observed, consistent with diffraction from a poorly ordered hexagonal phase with a = 48.4 Å. Moreover, a broad peak at $2\theta \approx 20°$ is also evident in the XRD pattern, which indicates the inorganic wall is amorphous as previously described. The TEM image (Fig. 2) is in accord with the XRD pattern, in that a poorly organized phase is evident with no long range order apparent. The material is clearly not lamellar, however. The instability of the material in the beam precludes any further detailed TEM study.

Table 1 shows the influence of reaction composition on the products. The molar ratio of $H_2O/C_{16}TMA$ plays a key role in the formation of $C_{16}TMA$-Fe_2S_3-M, as it influences the basicity of the reactant mixture. For example, Fe_2O_3 was formed when the basicity was higher in the reactant mixture, while a mixture of Fe_2O_3 and FeS_2 was obtained when the basicity was lower. Our experiments also show that the addition of a small amount of ammonium sulfide in the reactant mixture can effectively prevent the formation of iron(III) oxide and result in formation of pure $C_{16}TMA$-Fe_2S_3-M. Addition of elemental sulfur cannot inhibit the formation of iron(III) oxide under the same conditions, however. Bulk chemical analysis results indicate that S/Fe molar ratio is about 1.5, with a C/N ratio close to 20.[17] This indicates that the inorganic component is amorphous iron(III) sulfide, and suggests the aliphatic surfactant chains remain intact during the formation of $C_{16}TMA$-Fe_2S_3-M.

Confirmation of the presence of intact surfactant was obtained by FT-IR. The spectrum of $C_{16}TMA$-Fe_2S_3-M shows several absorption bands, which may be assigned to occluded $[C_{16}H_{33}N(CH_3)_3]^+$ at: 2960(sh), $\nu_{as}(CH_3)$; 2920, $\nu_{as}(CH_3)$; 2850, $\nu_{as}(CH_2)$; 1467, $\delta_s(CH_2)$.[7a,18] The absorption band at 334 cm^{-1} is assigned to Fe–S.[19] The bands at about 3400 and 1635 cm^{-1} are due to water adsorbed in the pores of the material. Thermal gravimetric analysis confirms that surfactant is present in the material. The TGA curve under N_2 showed that physisorbed water was removed at about 40 °C, corresponding to a weight loss of 3.1%. The DTA curve in air revealed an exothermic peak at 85 °C and a corresponding weight gain in the TGA of 7.8%, assigned to an oxidation reaction. Subsequent weight loss between 150 and 700 °C, arising from the loss of H_2O and combustion of the surfactant was 71.3% corresponding to a composition of $C_{16}TMA$-Fe_2S_3-M as $0.8C_{16}TMA{\cdot}Fe_2S_3{\cdot}0.4H_2O$. The surfactant/inorganic element ratio of about 1/2 is in accord with previous reports for MCM-41 obtained at higher synthesis pH (CTMA/SiO_2 molar ratio = 0.44).[20] and mesoporous tin(IV) sulfide ($0.5\ C_{16}TMA{\cdot}SnS_2{\cdot}0.75\ H_2O$).[21] Similar to bulk iron(III) sulfide,[22] $C_{16}TMA$-Fe_2S_3-M is very unstable towards oxidation and therefore attempts to remove the surfactant were not successful.

Two probe electrical conductivity measurements indicated that whereas amorphous Fe_2S_3 is a poor semiconductor ($\sigma = 5.4 \times 10^{-8}$ S cm^{-1}), as-synthesized $C_{16}TMA$-Fe_2S_3-M is an insulator. This is probably the result of the large surfactant content and poor electronic transport along the confined dimensions of the amorphous wall. Other factors which would contribute to low conductivity include the possibility of incomplete polycondensation in the inorganic component which would lead to defects, and grain boundary effects.

In summary, two different synthetic routes provide new mesostructured iron sulfide phases, including the first hexagonal transition metal sulfide phase. Their lack of thermodynamic stability with respect to oxygen inhibits ready removal of the surfactant. Controlled oxidation of this material may provide a facile route to a hitherto unknown mesostructured or mesoporous iron oxide.

We gratefully acknowledge the financial support of the NSERC (Canada) through the Research Grants Program. Professor Jim Corbett (Physics, University of Waterloo) and Dr Jessie Zhou are thanked for their help in obtaining the TEM image.

Notes and references

1 C. T. Kresge, M. E. Leonowicz, W. J. Roth, J. C. Vartuli and J. S. Beck, *Nature*, 1992, **359**, 710.
2 Q. Huo, D. I. Margolese, U. Ciesla, D. G. Demuth, P. Feng, T. E. Gier, P. Sieger, A. Firouzi, B. F. Chmelka, F. Schüth and G. D. Stucky, *Chem. Mater.*, 1994, **6**, 1176.
3 G. D. Stucky, Q. Huo, A. Firouzi, B. F. Chmelka, S. Schacht, I. G. Voigt-Martin and F. Schüth, *Stud. Surf. Sci. Catal.*, 1997, **150A**, 3.
4 P. T. Tanev and T. J. Pinnavaia, *Science*, 1995, **269**, 865.
5 D. M. Antonelli, A. Nakahira and J. Y. Ying, *Inorg. Chem.*, 1996, **35**, 3126.
6 (*a*) J. Li, L. Delmotte and H. Kessler, *J. Chem. Soc., Faraday Trans.*, 1997, **93**, 665; (*b*) J. Li, L. Delmotte and H. Kessler, *Chem. Commun.*, 1996, 1023; (*c*) G. A. Ozin, *Supramol. Chem.*, 1995, **6**, 125; T. Jiang and G. A. Ozin, *J. Mater. Chem.*, 1997, **7**, 2213.
7 (*a*) M. Froba and N. Oberender, *Chem. Commun.*, 1997, 1729; (*b*) M. J. Maclachlan, N. Coombs and G. A. Ozin, *Nature*, 1999, **397**, 681.
8 P. V. Braun, P. Osenar and S. I. Stupp, *Nature*, 1996, **380**, 325.
9 J. Li, H. Kessler, M. Soulard, L. Khouchaf and M.-H. Tuilier, *Adv. Mater.*, 1998, **10**, 946.
10 M. Kaschke and M. J. Russell, *Origins Life Envol. Biosphere*, 1994, **24**, 43.
11 (*a*) G. Wächtershäuser, *Appl. Microbiol.*, 1994, **10**, 207; (*b*) G. Wächtershäuser, *Microbiol. Rev.*, 1988, **52**, 452.
12 G. L. Henriksen and D. R. Vissers, *J. Power Sources*, 1994, **51**, 115.
13 T. Kyprianidou-Leodidou, H.-J. Althaus and Y. Wyser, *J. Mater. Res.*, 1997, **12**, 2198.
14 Z. Y. Lin, J. W. Zondlo and D. B. Dadyburjor, *Energy Fuels*, 1995, **5**, 673.
15 F. Vaudry, S. Khodabandeh and M. E. Davis, *Chem. Mater.*, 1996, **8**, 1451.
16 A. H. Stiller and B. J. McCormick, *J. Am. Chem. Soc.*, 1978, **100**, 2553.
17 Elemental analysis results, experimental (calcd.) for $[C_{19}H_{42}N]_{0.8}Fe_2S_3{\cdot}2H_2O$: Fe, 22.41 (21.3); S, 18.26 (18.29). C, 34.74 (34.76); N, 2.04 (2.13); H: 7.13 (8.3)%. Percentage water loss by TGA: 67.7%; calculated from above, 69.6%.
18 K. Endo, Y. Sugahara and K. Kuroda, *Bull. Chem. Soc. Jpn.*, 1994, **67**, 3352.
19 T. Baird, K. C. Campbell, P. J. Holliman, R. Hoyle, D. Stirling and B. P. Williams, *J. Chem. Soc., Faraday Trans.*, 1996, **92**, 445.
20 A. C. Voegtlin, A. Matijasic, J. Patarin, C. Sauerland, Y. Grillet and L. Huve, *Microporous Mater.*, 1997, **10**, 137.
21 J. Li, Ph.D. Thesis, Univ. Haute Alsace, 1997.
22 A. H. Stiller, B. J. McCormick, P. Russell and P. A. Montano, *J. Am. Chem. Soc.*, 1978, **100**, 2553.

Syntheses and structural characterization of novel luminescent heteronuclear rhenium(I)–zinc(II) and –cadmium(II) chalcogenolate complexes†

Vivian Wing-Wah Yam,* Yung-Lin Pui, Keith Man-Chung Wong and Kung-Kai Cheung

Department of Chemistry, The University of Hong Kong, Pokfulam Road, Hong Kong SAR, People's Republic of China. E-mail: wwyam@hku.hk

Received (in Cambridge, UK) 26th June 2000, Accepted 4th August 2000

Novel heteronuclear rhenium(I)–zinc(II) and –cadmium(II) complexes with chalcogenolate ligands have been synthesized and shown to exhibit rich luminescence properties; the X-ray crystal structures of [{(bpy)Re(CO)$_3$(μ-SC$_6$H$_4$Me-*p*)}$_2$Zn(bpy)](PF$_6$)$_2$ (2) and [{(bpy)Re(CO)$_3$(μ-SC$_6$H$_4$Me-*p*)}$_2$Cd(bpy)$_2$](PF$_6$)$_2$ (4) have been determined.

There has been a growing interest in luminescence studies of transition metal complexes, particularly with the increasing attention on the design of functional materials with unique properties.[1,2] The most widely studied and well-documented systems are those of the d^6 metal polypyridines[1–3] and very recently, the d^8 and d^{10} metal complexes.[4,5] Recently, a series of mono- and di-nuclear rhenium(I) diimine complexes with chalcogenolate ligands have been reported by us to show rich luminescence behaviour.[6] It is believed that extension of this work to heterometallic complex formation by using mononuclear rhenium(I) chalcogenolates as metalloligands, would give rise to a novel series of luminescent mixed-metal rhenium(I) complexes. In view of the known luminescence properties of zinc(II) and cadmium(II) thiolate systems[7] and our continuing interest in luminescent d^{10} metal complexes,[5] a series of trinuclear mixed-metal rhenium(I)–zinc(II) and –cadmium(II) chalcogenolate complexes have been synthesized and their luminescence behaviour studied. It is also envisaged that the attachment of zinc and cadmium moieties to the rhenium chalcogenolate would serve as an efficient method to perturb the excited state properties of the complexes. The X-ray crystal structures of [{(bpy)Re(CO)$_3$(μ-SC$_6$H$_4$Me-*p*)}$_2$Zn(bpy)](PF$_6$)$_2$ and [{(bpy)Re(CO)$_3$(μ-SC$_6$H$_4$Me-*p*)}$_2$Cd(bpy)$_2$](PF$_6$)$_2$ have been determined.‡

Reaction of [(bpy)Re(CO)$_3$(SC$_6$H$_4$R)][6b] with a mixture of Zn(NO$_3$)$_2$·6H$_2$O and 2,2′-bipyridine in a molar ratio of 2 : 1 : 1 in methanol under an inert atmosphere of nitrogen, followed by metathesis with NH$_4$PF$_6$ and subsequent recrystallization from MeCN–Et$_2$O, afforded [{(bpy)Re(CO)$_3$(μ-SC$_6$H$_4$R)}$_2$Zn(bpy)](PF$_6$)$_2$ (R = H **1**, Me-*p* **2**). Similar reactions of [(N–N)Re(CO)$_3$(μ-EC$_6$H$_4$R)] with Cd(NO$_3$)$_2$·4H$_2$O and 2,2′-bipyridine in a molar ratio of 2:1:2 gave [{(N–N)Re(CO)$_3$(μ-EC$_6$H$_4$R)}$_2$Cd(bpy)$_2$](PF$_6$)$_2$ (N–N = bpy, E = S, R = H **3**, Me-*p* **4**; N–N = bpy, E = Se, R = H **5**; N–N = Bu$^t_2$bpy, E = S, R = Me-*p* **6**). All the complexes have been characterized by ^{1}H NMR spectroscopy and positive ESI-MS and gave satisfactory elemental analyses.†

Fig. 1 and 2 show perspective drawings of the complex cations of **2** and **4** with atomic numbering, respectively. In **2**, the two Re centres adopt a distorted octahedral geometry with a S(1)–Re(1)–N(1) angle of 81.6(2)° and a S(2)–Re(2)–N(5) angle of 85.7(2)°. The zinc centre adopts a distorted tetrahedral geometry with a S(1)–Zn(1)–S(2) angle of 110.45(9)°. The angles Re(1)–S(1)–Zn(1) and Re(2)–S(2)–Zn(1) are 114.01(10) and 112.17(10)°, respectively. The average Re–S and Zn–S bond lengths are 2.523(2) and 2.285(8) Å, respectively, which are comparable to those observed in other related rhenium(I)[6,8] and zinc(II) thiolate complexes.[7c,9] In **4**, the two Re and the Cd centres adopt a distorted octahedral geometry with a S(1)–Re(1)–N(1) angle of 88.0(1)°, a S(1)–Cd(1)–S(1*) angle of 100.89(8)° and a Re(1)–S(1)–Cd(1) angle of 150.49(7)°. The average Re–S and Cd–S bond lengths are 2.523(2) and 2.713(2) Å, respectively, which are comparable to those found in related rhenium(I)[6,8] and cadmium(II) thiolate complexes.[7f,9,10]

The electronic absorption spectra of complexes **1**–**6** show absorption bands at *ca.* 350–380 nm with absorption shoulders at *ca.* 450–520 nm in MeCN. The photophysical data of the

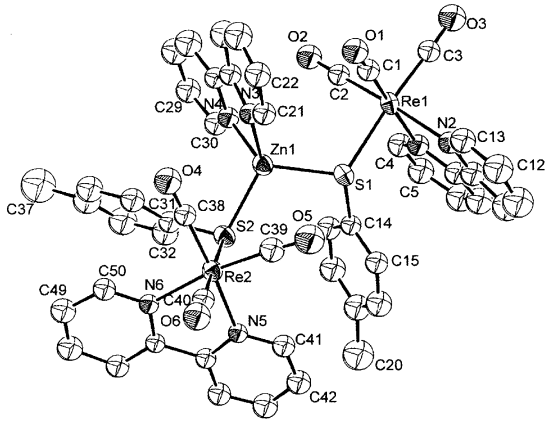

Fig. 1 Perspective drawing of the complex cation of **2** with the atomic numbering scheme. Selected bond distances (Å) and bond angles (°): Re(1)–S(1) 2.519(2), Re(2)–S(2) 2.527(2), Zn(1)–S(1) 2.284(2), Zn(1)–S(2) 2.287(3); S(1)–Zn(1)–S(2) 110.45(9), Re(1)–S(1)–Zn(1) 114.01(10), Re(2)–S(2)–Zn(1) 112.17(10).

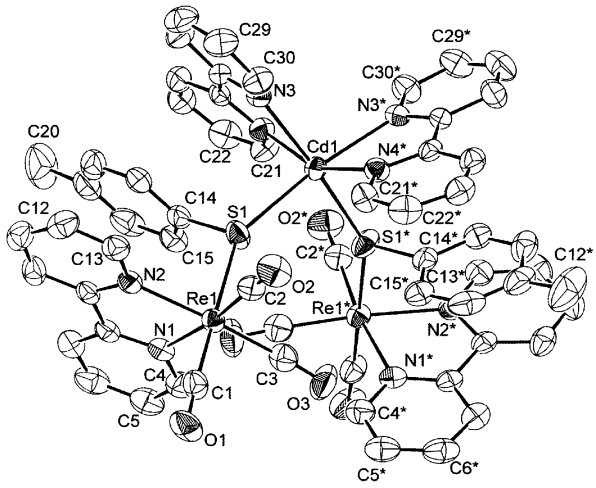

Fig. 2 Perspective drawing of the complex cation of **4** with the atomic numbering scheme. Selected bond distances (Å) and bond angles (°): Re(1)–S(1) 2.523(2), Cd(1)–S(1) 2.713(2); S(1)–Re(1)–N(1) 88.0(1), S(1)–Cd(1)–S(1*) 100.89(8), Re(1)–S(1)–Cd(1) 150.49(7).

† Electronic supplementary information (ESI) available: characterization for complexes **1**–**6** and experimental crystallographic details for **2**. See http://www.rsc.org/suppdata/cc/b0/b005092j/

Table 1 Photophysical data for complexes **1**–**6**[a]

Complex	Medium (T/K)	λ_{abs}/nm (ε/dm^3 mol^{-1} cm^{-1})	λ_{em}/nm (τ_o/μs)[c]
1	MeCN (298)	247 (76 610), 296 (54 620), 308 (52 840), 354(sh) (9590), 480(sh) (1080)	567 [597]
	Solid (298)		536(0.58) [539]
	Glass (77)[b]		525(sh), 593 [617]
2	MeCN (298)	247 (75 240), 296 (47 150), 308 (46 080), 368(sh) (8780), 488(sh) (1410)	588 [607]
	Solid (298)		550(0.51) [552]
	Glass (77)[b]		525(sh), 596 [608]
3	MeCN (298)	246 (97 600), 296 (70 600), 308 (61 510), 355 (9380), 485(sh) (920)	548 [565 (sh)]
	Solid (298)		559(0.69) [560]
	Glass (77)[b]		548 [570]
4	MeCN (298)	246 (95 480), 295 (64 780), 308 (55 240), 364 (7160), 494(sh) (1300)	553(0.12) [564 (sh)]
	Solid (298)		600(0.53) [600]
	Glass (77)[b]		560 [565]
5	MeCN (298)	248 (79 010), 297 (57 390), 308 (52 090), 368 (9000), 502(sh) (1320)	557(0.11) [560(sh)]
	Solid (298)		562(0.49) [560]
	Glass (77)[b]		554 [562]
6	MeCN (298)	246 (89 080), 295 (62 460), 306 (54 500), 356 (8200), 475(sh) (1240)	532(0.16) [590(sh)]
	Solid (298)		555(0.45) [556]
	Glass (77)[b]		540 [564]

[a] Absorption and emission wavelengths are reported to ±2 nm. [b] Ethanol–methanol (4:1 v/v) glass. [c] Excitation wavelength at 355 nm. Values in square brackets are λ_{em} with excitation wavelength at 450 nm.

complexes are summarized in Table 1. The former is tentatively assigned as $p_\pi(SR^-) \rightarrow \pi^*(\alpha,\alpha'$-diimine on Re^{I} or Zn^{II} or Cd^{II}) LLCT transitions as similar spectral assignments have been suggested in related zinc(II),[7a–c] cadmium(II)[7a,7f] and rhenium(I) systems,[6] while the latter is assigned as a $d_\pi(Re) \rightarrow \pi^*(\alpha,\alpha'$-diimine on Re) MLCT transition. Similar assignments have also been made in related Re(I) α,α'-diimine systems.[1–3,6] These have been further supported by the observation of an energy dependence on the nature of the chalcogenolate and the diimine ligands. The lower LLCT absorption energies in **2** compared to **1** and in **4** compared to **3** are in accordance with the presence of the more electron rich 4-methylthiophenolate ligand relative to thiophenolate. In view of the almost identical absorption patterns and energies for the Re^{I}–Zn^{II}–Re^{I} and Re^{I}–Cd^{II}–Re^{I} analogues, it is reasonable to assume that the transitions are dominated by the LLCT and MLCT transitions of the rhenium(I) diimine thiolate core, with minor contributions due to the zinc and cadmium moieties.

Upon excitation of complexes **1**–**6** at 350–450 nm, emission bands at *ca*. 520–630 nm were observed in the solid state, in 77 K glasses and in fluid solutions (Table 1). The close resemblance of the emission energies to those reported for the related dinuclear $[\{(N–N)Re(CO)_3\}_2(\mu\text{-}SR)]^+$ complexes[6a] is suggestive of a similar ^{3}MLCT $[d_\pi(Re) \rightarrow \pi^*(\alpha,\alpha'$-diimine)] emissive origin. Upon monitoring the emission at *ca*. 560–625 nm, bands at *ca*. 450–500 nm were observed in the excitation spectra, in regions close to the MLCT absorption. However, the broadness of the band as well as the dependence of the emission energy on the excitation wavelength may be suggestive of a dual luminescence. It is likely that the higher energy emission shoulder is derived from an ^{3}IL(diimine)/^{3}LLCT origin while the low-energy emission is dominated by a ^{3}MLCT origin. Similar to the trend observed in electronic absorption studies, the lower emission energy of **2** compared to **1** and **4** compared to **3** in the solid state, is in line with the electron donating ability of the substitutents on the thiophenolate ligand, giving rise to higher $d_\pi(Re)$ and/or $p_\pi(SR^-)$ orbital energies. The higher emission energy of **6** relative to that of **4** is also in line with a ^{3}MLCT origin, probably with some mixing of ^{3}LLCT $[p_\pi(ER^-) \rightarrow \pi^*(\alpha,\alpha'$-diimine)] character, since the presence of electron rich *tert*-butyl substituents on Bu$^t_2$bpy would raise the $\pi^*(\alpha,\alpha'$-diimine) orbital energy relative to that of bpy.

V. W.-W. Y. acknowledges financial support from The Research Grants Council and The University of Hong Kong, Y.-L. P. the receipt of a postgraduate studentship, and K. M.-C. W the receipt of a University Postdoctoral Fellowship, both of which are administered by The University of Hong Kong.

Notes and references

‡ *Crystal data*: for **2**: $[(C_{50}H_{38}N_6O_6S_2ZnRe_2)^{2+}\ 2PF_6^-]$; M_r = 1610.73, triclinic, space group $P\bar{1}$ (no. 2), a = 12.107(5), b = 12.348(5), c = 20.271(4) Å, α = 74.30(2), β = 85.20(2), γ = 79.10(2)°, U = 2863(3) Å^3, Z = 2, D_c = 1.868 g cm^{-3}, μ(Mo-Kα) = 48.55 cm^{-1}, F(000) = 1556, T = 301 K. 10397 reflections were measured, 9885 were unique (R_{int} = 0.054). 6087 reflections were considered observed and used in the structural analysis. $w = 4F_o^2/\sigma^2(F_o^2)$, where $\sigma^2(F_o^2) = [\sigma^2(I) + (0.030F_o^2)^2]$ for 6087 reflections was reached at R = 0.035 and wR = 0.043 with a goodness-of-fit of 1.34. For **4**: $[(C_{60}H_{46}N_8O_6S_2CdRe_2)^{2+}2PF_6^-]$; M_r = 1813.95, monoclinic, space group $P2/n$ (no. 13), a = 13.691(2), b = 15.663(3), c = 15.551(3) Å, β = 106.34(2)°, U = 3200(1) Å^3, Z = 2, D_c = 1.882 g cm^{-3}, μ(Mo-Kα) = 43.12 cm^{-1}, F(000) = 1756, T = 301 K. 6102 unique reflections were obtained from a total of 27436 measured reflections (R_{int} = 0.080). 4914 reflections were considered observed and used in the structural analysis. $w = 4F_o^2/\sigma^2(F_o^2)$, where $\sigma^2(F_o^2) = [\sigma^2(I) + (0.036F_o^2)^2]$ for 4914 reflections was reached at R = 0.038 and wR = 0.056 with a goodness-of-fit of 1.27.

CCDC 182/1738. See http://www.rsc.org/suppdata/cc/b0/b005092j/ for crystallographic files in .cif format/

1 K. Kalyanasundaram, *Photochemistry in Microheterogeneous Systems*, Academic Press, New York, 1987; V. Balzani and F. Scandola, *Supramolecular Photochemistry*, Ellis Horwood Chichester, UK, 1991; F. Vögtle, *Supramolecular Chemistry*, Wiley, Chichester, 1993.

2 K. Kalyanasundaram, *Photochemistry of Polypyridine and Polyphyrin Complexes*, Academic Press, London, 1992; O. Horváth and K. L. Stevenson, *Charge Transfer Photochemistry of Coordination Compounds*, VCH, New York, 1993.

3 M. S. Wrighton and D. L. Morse, *J. Am. Chem. Soc.*, 1974, **96**, 998; J. V. Caspar, B. P. Sullivan and T. J. Meyer, *Inorg. Chem.*, 1984, **23**, 2104; A. Juris, S. Campagna, I. Ibied, J. M. Lehn and R. Ziessel, *Inorg. Chem.*, 1988, **27**, 4007; L. A. Sacksteder, A. P. Zipp, E. A. Brown, J. Streich, J. N. Demas and B. A. DeGraff, *Inorg. Chem.*, 1990, **29**, 4335; V. W. W. Yam, V. C. Y. Lau and K. K. Cheung, *J. Chem. Soc., Chem. Commun.*, 1995, 259; V. W. W. Yam, V. C. Y. Lau and K. K. Cheung, *Organometallics*, 1996, **15**, 1740.

4 A. P. Zipp, *Coord. Chem. Rev.*, 1988, **84**, 47; D. M. Roundhill, H. B. Gray and C. M. Che, *Acc. Chem. Res.*, 1989, **22**, 55; C. Kutal, *Coord. Chem. Rev.*, 1990, **99**, 213; P. C. Ford and A. Vogler, *Acc. Chem. Res.*, 1993, **26**, 220; H. Schmidbaur, *Chem. Soc. Rev.*, 1995, 391; P. Pyykkö, *Chem. Rev.*, 1997, **97**, 597.

5 V. W. W. Yam, *J. Photochem. Photobiol. A*, 1997, **106**, 75; V. W. W. Yam and K. K. W. Lo, *Comments Inorg. Chem.*, 1997, **19**, 209; V. W. W. Yam, K. K. W. Lo, W. K. M. Fung and C. R. Wang, *Coord. Chem. Rev.*, 1998, **171**, 17; V. W. W. Yam and K. K. W. Lo, *Chem. Soc. Rev.*, 1999, **28**, 323.

6 (*a*) V. W. W. Yam, K. M. C. Wong and K. K. Cheung, *Organometallics*, 1997, **16**, 1729; (*b*) V. W. W. Yam, K. M. C. Wong and K. K. Cheung, unpublished work.

7 (*a*) G. A. Crosby, R. G. Highland and K. A. Truesdell, *Coord. Chem. Rev.*, 1985, **64**, 41; (*b*) R. G. Highland, J. G. Brummer and G. A. Crosby, *J. Phys. Chem.*, 1986, **90**, 1593; (*c*) K. J. Jordan, W. F. Wacholtz and G. A. Crosby, *Inorg. Chem.*, 1991, **30**, 4588; (*d*) T. Türk, U. Resch, M. A. Fox and A. Vogler, *Inorg. Chem.*, 1992, **31**, 1854; (*e*) T. Türk, A. Vogler and M. A. Fox, *Adv. Chem. Ser.*, 1993, 233; (*f*) V. W. W. Yam, Y. L. Pui and K. K. Cheung, *New J. Chem.*, 1999, **23**, 1163.

8 E. W. Abel, W. Harrision, R. A. N. Mclean, W. C. Marsh and J. Trotter, *J. Chem. Soc., Chem. Commun.*, 1970, 1531.

9 A. D. Watson, C. P. Rao, J. R. Dorfman and R. H. Holm, *Inorg. Chem.*, 1985, **24**, 2820.

10 J. G. Brennan, T. Siegrist, P. J. Carroll, S. M. Stuczynsku, L. E. Brus and M. L. Stuczynsku, *J. Am. Chem. Soc.*, 1989, **111**, 4141.

ChemComm

Synthesis of mesoporous TiO_2 with a crystalline framework

Yinghong Yue and Zi Gao*

Department of Chemistry, Fudan University, Shanghai 200433, P.R. China. E-mail: zigao@fudan.edu.cn

Received (in Cambridge, UK) 23rd May 2000, Accepted 2nd August 2000
First published as an Advance Article on the web 29th August 2000

A thermally stable mesoporous TiO_2 with a crystalline framework and ordered large pores is synthesized using a block copolymer as a structure-directing agent through an N^0I^0 assembly pathway, followed by a hydrothermal process.

The synthesis of mesoporous silica with a high surface area and uniform cylindrical mesopores, which was designated as M41S, was first demonstrated in 1992.[1] Since then, the use of surfactants and amphiphilic block copolymers to organize mesoporous structures has been extended to the preparation of non-silica mesoporous metal oxides. Mesoporous MnO_2,[2] Al_2O_3,[3,4] TiO_2,[4,5] Nb_2O_5,[4,6] Ta_2O_5,[4,6] ZrO_2[4,7] and SnO_2[4,8] have been synthezied over the past few years. Among them, mesoporous TiO_2 is most attractive due to its excellent performance in photocatalytic reactions.[9] It is well known that the effectiveness of titania as a photocatalyst is very sensitive to its crystal phase, particle size and crystallinity, and the mesoporous TiO_2 prepared using phosphate surfactants has low photocatalytic activity because the amorphous titania channel walls afford low quantum yield for photocatalytic reactions.[10] Calcination of the as-synthesized mesoporous TiO_2 at high temperature is essential for the crystallization of titania in the channel wall.[4] However, damage to the integrity of the mesoporous structure will take place upon calcination at high temperature, thus only mesoporous TiO_2 with amorphous or semicrystallized channel walls have been reported till now. Here we present the first example of mesoporous TiO_2 with crystalline framework, prepared through an N^0I^0 assembly pathway using a triblock copolymer as a structure-directing agent and followed by a hydrothermal process.

The mesoporous titania with crystalline framework was prepared as follows: a calculated amount of titanium ethoxide $Ti(OC_2H_5)_4$ was dissolved in an ethanol solution containing triblock poly(ethylene oxide)–poly(propylene oxide)–poly(ethylene oxide) ($EO_{20}PO_{70}EO_{20}$, Aldrich) and a very small amount of $CeCl_3$ which acts as a stabilizer in the syntheses.[11] After stirring for 1 h at ambient temperature, a water–ethanol mixture containing a 20% molar fraction of water was added dropwise. The molar composition of the reaction mixture was: 0.05 Ce^{3+} : 1.0 TEOT : 0.02 $EO_{20}PO_{70}EO_{20}$: 4.0 H_2O : 15.5 C_2H_5OH. The mixture was stirred at ambient temperature for another 48 h. In the hydrothermal process, a large amount of water was added to the resulting solution until the H_2O/TiO_2 molar ratio = 90. Then, the mother liquor containing the precipitate was transferred to a stainless steel autoclave, and heated at 80–180 °C for 24 h. The product obtained was filtered off, washed with distilled water, dried at 100 °C, and finally calcined in air at 350 °C or 500 °C for 4 h. The samples studied are denoted as TiO_2-*x*-*y*, where *x* and *y* represent the temperatures of hydrothermal aging and calcination, respectively. A mesoporous TiO_2 sample untreated hydrothermally was also prepared for comparison.

Fig. 1 shows the results of wide-angle X-ray diffraction studies performed on a Rigaku D/MAX-IIA diffractometer using Cu-Kα radiation of the hydrothermally treated mesoporous titania before and after calcination. No clear diffraction peaks are observed for as-synthesized mesoporous TiO_2 without hydrothermal treatment before calcination. After calcination weak and broad peaks, which can be indexed as the (101), (004), (200), (105) and (204) reflections of anatase crystalline phase, appear on the pattern, showing that the channel walls are semicrystallized and some anatase nanocrystallites are formed and embedded in the amorphous titania channel walls. In contrast, sharp diffraction peaks of anatase appear on the XRD patterns of samples hydrothermally treated at 80–180 °C even before calcination and the intensity of the peaks increases little after calcination, indicating that the channel walls of the mesoporous oxides can be successfully crystallized at the low hydrothermal treatment temperatures. The crystals in the TiO_2-120-350 and TiO_2-180-350 samples are estimated to be of size 10 and 15 nm, respectively, by applying the Scherrer formula on the (101) diffraction peaks. The degree of crystallization and the anatase crystal size increase as the hydrothermal treatment temperature is increased from 80 to 180 °C. A brookite peak at 31° (2θ) appears for samples treated at 180 °C. Calcination up to 500 °C does not have significant effects on the diffraction patterns of the samples, showing that the anatase crystal phase is retained at this temperature and no phase transformation has occurred.

Thermogravimetric experiments of the hydrothermally treated samples carried out in flowing air on a Rigaku Thermoflex instrument indicate that there are three endothermic processes in the TG/DTG/DTA curves at 20–120 °C, 120–320 °C and 320–420°C, corresponding to the release of adsorbed water, block copolymer and structural water, respectively. Therefore, the block copolymer template in this type of mesoporous TiO_2 samples can be completely removed upon calcination in air at 350 °C.

Transmission electron micrographs of the TiO_2-120-350 sample recorded on a Philips CM 200 FEG Microscope (Fig. 2) shows that the pore channel walls are not totally continuous and the mesostructure is spotted with a few micro-domains of less ordered worm-like pore symmetry. Selected-area electron diffraction patterns (Fig. 2 inset) recorded on the same sample

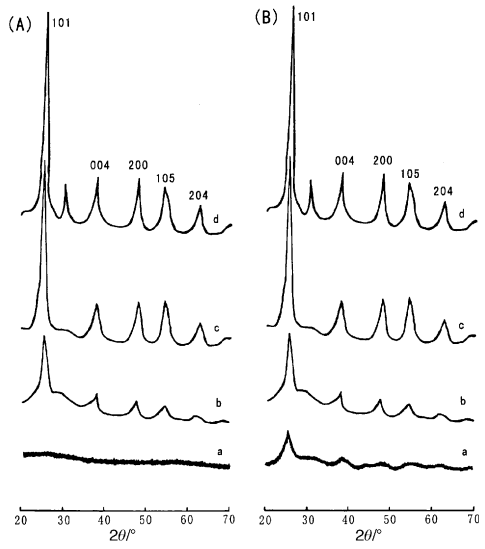

Fig. 1 XRD patterns of mesoporous TiO_2 before (A) and after (B) calcination. (a) TiO_2; (b) TiO_2-80-350; (c) TiO_2-120-350; (d) TiO_2-180-350.

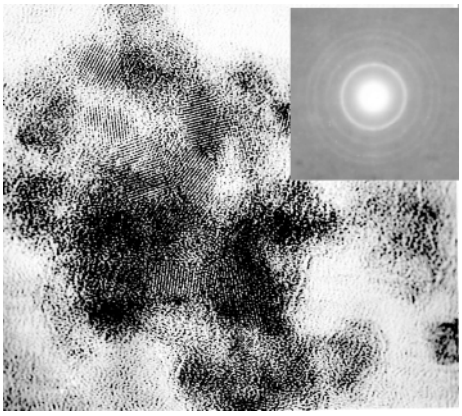

Fig. 2 TEM image and selected-area electron diffraction pattern (inset) of the TiO_2-120-350 sample

confirm that the channel walls are comprised of nanocrystalline anatase displaying characteristic diffuse electron diffraction rings.

Fig. 3 illustrates the N_2 adsorption/desorption isotherms of the TiO_2-120-350 sample measured using a Micromeritics ASAP 2000 system. A large H1-type hysteresis loop at high relative pressure is observed, which is related to the capillary condensation associated with large pore channels. BJH analysis of the desorption isotherm is shown in Fig. 3 (inset). The narrow gaussian pore size distribution curve implies that the material has very regular pore channels in the mesoporous region. The textural properties of all the hydrothermally treated samples are listed in Table 1 along with the data of the untreated samples. The pore size and volume of the hydrothermally treated samples are significantly greater than those of the untreated sample, whereas their specific surface areas are slightly lowered. The dramatic increase in pore size of the samples shows that the mesoporous TiO_2 could be restructured under hydrothermal treatment in the presence of the block copolymer template. The

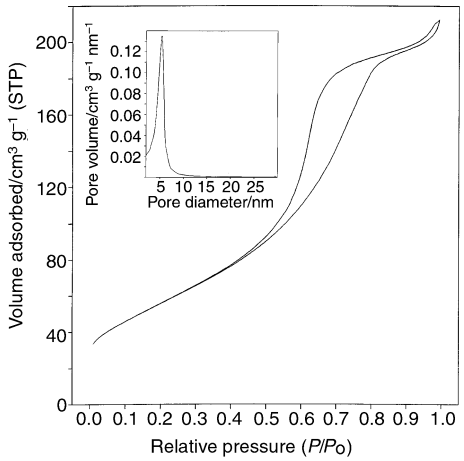

Fig. 3 N_2 adsorption/desorption isotherm and BJH pore size distribution plot (inset) of the TiO_2-120-350 sample at 77 K.

Table 1 Textural properties of mesoporous TiO_2 samples

Sample	Aging temperature/ °C	Calcination temperature/ °C	BET surface area/m^2 g^{-1}	Pore diameter/ nm	Pore volume/ cm^3 g^{-1}
TiO_2-80-350	80	350	201	4.4	0.271
TiO_2-80-500	80	500	150	5.2	0.249
TiO_2-120-350	120	350	204	5.5	0.315
TiO_2-120-500	120	500	157	6.2	0.302
TiO_2-180-350	180	350	159	7.0	0.366
TiO_2-180-500	180	500	134	8.0	0.336
TiO_2	none	350	242	2.2	0.156
TiO_2	none	500	191	2.0	0.130

pore sizes of TiO_2-180-350 and TiO_2-180-500 reach 7.0 and 8.0 nm, respectively, which are the largest reported for mesoporous titania until now.[4] The mesoporous TiO_2 materials with crystalline framework retain their structural integrity and mesoporosity when calcined at 500 °C.

This work shows that mesoporous TiO_2 materials with anatase crystalline framework can be successfully prepared using a templating procedure followed by hydrothermal treatment and calcination. Amorphous titania in the channel walls of the mesoporous structure is crystallized at low hydrothermal temperature without sacrificing porosity and pore regularity, and the template is removed at a relatively low calcination temperature to ensure the materials against structure degradation. The crystalline framework, high specific surface area, large pore size and high thermal stability of these new materials are expected to afford better activity toward photocatalytic reactions, in particular those concerned with bulky molecules and high space velocity.

This work was supported by the Major State Basic Research Development Program (Grant No. 2000077500) and the Foundation for University Key Teacher by the Ministry of Education.

Notes and references

1 C. T. Kresge, M. E. Leonowicz, W. J. Roth, J. C. Vartuli and J. S. Breck, *Nature*, 1992, **359**, 710.
2 Z. Tian, W. Tong, J. Wang, N. Duan, V. V. Krishnan and S. L. Suib, *Science*, 1997, **276**, 926.
3 S. A. Bagshaw and T. J. Pinnavaia, *Angew. Chem., Int. Ed. Engl.*, 1996, **35**, 1102.
4 P. Yang, D. Zhao, D. I. Margolese, B. F. Chmelka and D. G. Stucky, *Chem. Mater.*, 1999, **11**, 2813.
5 D. M. Antonelli and J. Y. Ying, *Angew. Chem., Int. Ed. Engl.*, 1995, **34**, 2014.
6 D. M. Antonelli and J. Y. Ying, *Chem. Mater.*, 1996, **8**, 874.
7 J. A. Knowles and M. J. Hudson, *J. Chem. Soc., Chem. Commun.*, 1995, 2083.
8 K. G. Severin, T. M. AbdelFattah and T. J. Pinnavaia, *Chem. Commun.*, 1998, 1471
9 Z. B. Zhang, C. C. Wang, R. Zakaria and J. Y. Ying, *J. Phys. Chem. B*, 1998, **102**, 10871.
10 V. F. Stone and R. J. Davis, *Chem. Mater.*, 1998, **10**, 1468.
11 W. Zhang and T. J. Pinnavaia, *Chem. Commun.*, 1998, 1185.

ChemComm

Synthesis of the mixed lithium–magnesium, mixed amide (*R,R/S,S*)-[{LiMg(TMP)[$CH_2Si(Me)_2N(SiMe_3)$]}$_2$]: a conformationally-locked structure of five fused rings inducing two stereogenic nitrogen centres

Lorna Barr, Alan R. Kennedy, Jonathan G. MacLellan, Jennifer H. Moir, Robert E. Mulvey* and Philip J. A. Rodger

Department of Pure and Applied Chemistry, University of Strathclyde, Glasgow, UK G1 1XL. E-mail: r.e.mulvey@strath.ac.uk

Received (in Cambridge, UK) 31st May 2000, Accepted 2nd August 2000

Reaction of the magnesium amide $Mg(TMP)_2$ with the lithium amide LiHMDS is accompanied by an unexpected, sterically-promoted hydrogen transfer/amine elimination process, to yield the novel title compound which is the first such heterometallic composition to contain a heteroleptic amide ligand set.

Lithium amide compounds have been long-standing friends to the synthetic chemist, especially sterically encumbered types which find widespread use in regio-, stereo- and enantioselective deprotonation applications.[1] By comparison, magnesium amides are much more recent acquaintances, but they too are beginning to make an impression as specialist reagents,[2] most notably in the asymmetric arena.[3] While these mainstream homonuclear compounds have been commanding most attention, the effect of pairing a lithium (or another alkali metal) amide with a magnesium amide, in the same molecular package,[4] is also under scrutiny. Could this mixing promote a useful synergy, giving rise a new chemistry and novel structures, not known or not possible with the conventional homonuclear compounds? Studies directed towards answering this intriguing question are still at a preliminary stage; however, initial signs appear promising. For example, the idea of 'inverse crown ether' complexes was conceived from this heterobimetallic approach. These are eight-membered $(MNMgN)^{2+}$ rings (M = Li, Na or K)[5] which act as polymetallic hosts to oxygen-based O^{2-} or $(O_2)^{2-}$ dianions. Larger twelve-membered $(NaNMgNNaN)_2^{2+}$ or twenty four-membered $(KNMgN)_6^{2+}$ variants,[6,7] which function as single or multiple traps for larger arene-based anions, have also been introduced. In all of these mixed-metal macrocycles there is only one type of amido bridge, belonging to either 1,1,1,3,3,3-hexamethyldisilazide (HMDS) or 2,2,6,6-tetramethylpiperidide (TMP) ligands. Similarly, the few other mixed lithium–magnesium amides in the literature are also homoamido in composition. Therefore we set out to prepare the first mixed lithium–magnesium, mixed amide compound. As reported herein, while this aim has been achieved through the synthesis of [{LiMg(TMP)[$CH_2Si(Me)_2N(SiMe_3)$]}$_2$], **1**, which contains both TMP and HMDS ligands, surprisingly it is not an inverse crown ether and furthermore it is accompanied by an unexpected deprotonation of one of the Me groups attached to Si in the latter ligand. Interest is heightened by the fact that the molecular structure is chiral, as determined by X-ray crystallographic studies on representative crystals of **1**. This stereochemical outcome can be explained by an intramolecular hydrogen transfer, promoted by the sterically crowded, conformationally locked heteronuclear structure expected to form initially on mixing the component homonuclear amides.

We first observed **1** on attempting to prepare the homonuclear amides *in situ* by adding, in order, Bu^nLi (5 mmol) in hexane, HMDS(H) (5 mmol), Bu_2Mg (5 mmol) in heptane, and TMP(H) (10 mmol). The reaction mixture was subsequently heated to reflux for 90 min. A mutually coupled pair of doublets (^2J, 13.1 Hz) in the negative region of the ^{1}H NMR spectrum of a C_6D_6 solution of the product,† alerted us to the presence of the metal bound CHH′ group (a point later verified by X-ray crystallography). This surprising finding prompted us to try an alternative direct approach, preparing and isolating $Mg(TMP)_2$ (as an oil)[8] and LiHMDS (as a crystalline solid)[9] separately (to ensure all butyl anions had been consumed, a point confirmed by NMR studies), before adding them together in a 1:1 stoichiometry in hydrocarbon solution. Stirred and gently warmed for a few min but not heated to reflux, this solution also afforded pale yellow crystals of **1**.† Absolute yields could not be determined due to the high solubility of **1** which makes the low temperature filtration/isolation procedure problematical; however, in one attempt 30% was collected, though the true yield was considerably greater.

The molecular structure of **1** (Fig. 1)‡ is dimeric, composed of dinuclear (LiNMgN) monomeric fragments with pendant Me_2SiCH_2 arms which bind 'intramolecularly' through the methylene C atom to the Mg centre. Dimerisation is effected *via* 'intermolecular' bonds from the methylene C atom to the Mg centre of the other monomeric fragment. The Mg centres occupy distorted tetrahedral [80.80(10)–128.62(11)°] environments made up of two C and two N atoms. Formally occupying bent [104.3(2)°] geometries between two N atoms, each Li centre finds electronic relief through agostic interactions with one TMP [Li(1)···C(12), 2.565(6) Å; Li(2)···C(24), 2.585(6) Å] and one HMDS-Me group [Li(1)···C(4), 2.359(6) Å; Li(2)···C(28), 2.332(6) Å]. 'Intramolecular' Mg–C bonds are marginally longer than their 'intermolecular' counterparts (mean lengths, 2.320 and 2.258 Å, respectively). The $(MgC)_2$ ring they make, which represents the central component of a fivefold system of fused four-membered rings, is puckered

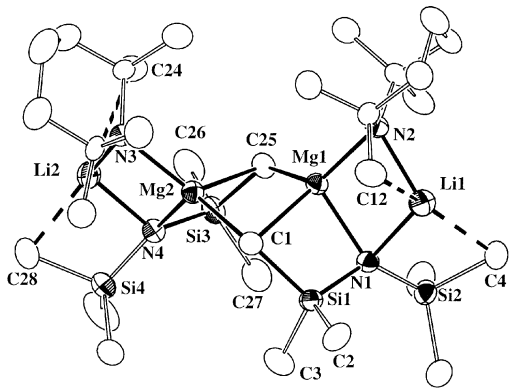

Fig. 1 Molecular structure of **1** showing agostic contacts as dashed lines. Hydrogen atoms are omitted for clarity. Selected dimensions (Å and °): Mg1–C1 2.319(3), Mg1–C25 2.252(3), Mg2–C1 2.264(3), Mg2–C25 2.321(4), Li1–N1 2.009(6), Li1–N2 1.990(6), Li2–N3 1.989(6), Li2–N4 2.012(6), Si1–N1 1.726(3), Si1–C1 1.875(3), Si3–N4 1.730(3), Si3–C25 1.877(3), Mg1–N4–Si1 92.0(1), N1–Si1–C1 105.4(1), Mg1–C1–Mg2 76.0(1), Mg1–C25–Mg2 76.2(1), Mg2–N4–Si3 91.9(1), N4–Si3–C25 105.4(1).

DOI: 10.1039/b004317f

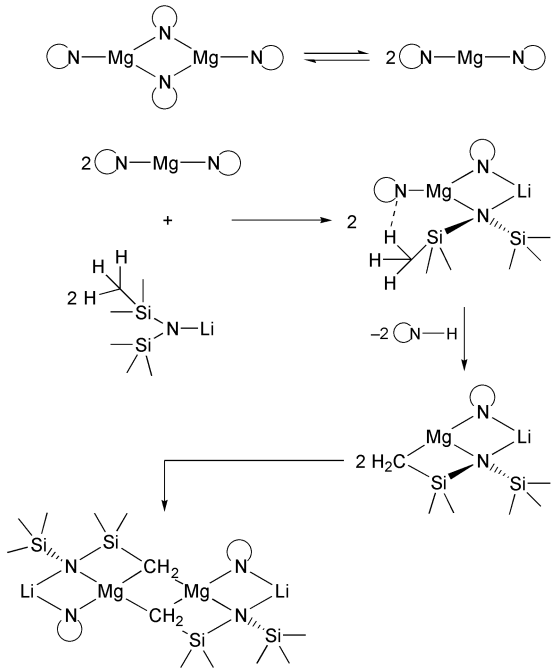

Scheme 1 Note that the stereochemistry shown here is idealized and not representative of that in **1**

(RMS deviation from planarity, 0.2138 Å). In contrast, the dinuclear (LiNMgN) rings at opposite ends of the structure are essentially planar. Mean Mg–N and Li–N bond lengths (2.104 and 2.000 Å, respectively) lie in the usual range for bonds of this type with the same connectivity. Also essentially planar, two (MgNSiC) rings complete the structure.

The most interesting aspect of the structure is the chiral nature of the HMDS N atoms N(1) and N(4). Each binds to one Li and one Mg centre, and to one $SiMe_3$ and one $SiMe_2CH_2$ group. Only the enantiomeric *R,R* and *S,S* pair has been observed. The *R,S* diastereoisomer has not been detected. Based on knowledge of related magnesium and mixed lithium–magnesium amide structures, it is possible to construct a structural pathway (Scheme 1) to rationalise the formation of **1**. Though not yet confirmed crystallographically, the structure of $Mg(TMP)_2$ is almost certainly either a monomer or a loosely-associated dimer. These two structural types co-exist in solutions of $Mg(HMDS)_2$,[10] so it is likely that solutions of $Mg(TMP)_2$ would contain an even more significant preponderance of monomer given the greater steric bulk of TMP. In the first step of the pathway, it is envisioned that a $Mg(TMP)_2$ monomer would approach a molecule of LiHMDS (formally a trimer in the solid state, but here shown as a monomer for simplicity). This should result in a heteronuclear arrangement, akin to that known for $LiMg(HMDS)_3$,[5a] but more sterically crowded and with a mixed TMP-HMDS bridge. A close contact between a C–H bond on the bridging $Me(SiMe_2)N$ group and the N atom of the terminal TMP ligand could then trigger hydrogen transfer and subsequent loss of TMPH. Concomitantly, a new Mg–C bond and fixed stereogenic N centre are formed. Relief of steric crowding around the Mg centre then allows dimerisation to proceed in the final step, thus increasing the coordination number of the Mg centre from 3 to 4. It is pertinent to note that no analogous pathway is possible in a homonuclear LiHMDS–LiTMP system, as from valency considerations no terminal TMP ligand would be available for subsequent displacement.

Though rare, it is known that certain transition metal (Ti,[11] V,[12] Zr[13]) HMDS-containing complexes can for steric reasons lose a hydrogen atom to generate $CH_2Si(Me)_2NSiMe_3$ ligands through direct metallation with a strong base (Bu^nLi, LiHMDS, NaHMDS), but these reactions afford only achiral products. A more interesting analogy is provided by a mixed Sb–Ga *geminal* organodimetallic complex[14] in which a $(2\text{-}C_5H_4N)C(SiMe_3)_2$ ligand is converted to $(2\text{-}C_5H_4N)C(SiMe_3)Si(Me)_2CH_2$ with generation of a new stereogenic C centre. Thermally induced *via* an intramolecular MeH elimination (*cf.*, the amine elimination here), this deprotonation is facilitated by a Me–Ga bond (*cf.*, the R_2N–Mg bond here) within the cyclic precursor.

Finally, given that **1** retains a bulky amide ligand within a conformationally-locked ring structure, as well as a bifunctional C, N-alkide, amide ligand, it will be of interest to ascertain whether it and similar heterometallic complexes have a future as companion reagents to the conventional homometallic bases and nucleophiles.

We thank Drs D. R. Armstrong and K. W. Henderson for many useful discussions and the EPSRC service at the University of Southampton for the X-ray crystallographic study.

Notes and references

† NMR data for **1** revealed an unusual asymmetrical pattern for the TMP ligand which we attribute to a fixed, rigid environment. δ_H (400.13 MHz, C_6D_6) –0.75 (d, 2 H, C*H*H′), –0.40 (d, 2 H, CH*H*′), 0.19 (s, 18 H, Si*Me*$_3$), 0.39 (s, 6 H, Si*Me*Me′), 0.61 (s, 6 H, SiMe*Me*′), 0.65/0.78/1.53 (m, 8 H, *β-CH*$_2$, TMP), 1.12 (s, 6 H, *Me*-TMP), 1.28 (s, 6 H, *Me*′-TMP), 1.46 (s, 12 H, *2Me*″-TMP), 1.53/1.82 (m, 4 H, *γ-CH*$_2$, TMP); δ_C (100.61 MHz, C_6D_6) 5.03 (Si*Me*$_3$), 6.11 (*C*HH′), 9.20 (Si*Me*Me′), 9.89 (SiMe*Me*′), 19.81 (*γ-C*, TMP), 32.21/34.93/38.19/38.98 (4*Me*-TMP), 43.62 (*β-C*, TMP), 52.24/52.62 (*α-C*, TMP). Assignments were verified by COSY, DEPT and ^{1}H, ^{13}C HMQC experiments. Crystals of **1** start to decompose at 146 °C and finally melt at 164–166 °C.

‡ *Crystal data* for **1**: $C_{30}H_{70}Li_2Mg_2N_4Si_4$, M = 661.76, orthorhombic, space group *Pna*2$_1$, a = 11.6682(2), b = 16.8825(4), c = 20.9980(4) Å, V = 4136.3(2) Å^3, Z = 4, λ = 0.71073 Å, μ = 0.197 mm^{-1}, T = 150 K, R = 0.0504 for 6153 reflections with $I > 2\sigma(I)$, R_w = 0.1181 for 9097 unique reflections. 30186 reflections measured (R_{int} = 7.86%) to a $2\theta_{max}$ of 54.96°. Refinement on F^2 with SHELXL gave a final maximum residual electron density of 0.318 e Å^{-3}. CCDC 182/1734. See http://www.rsc.org/suppdata/cc/b0/b004317f/ for crystallographic files in .cif format.

1 (*a*) C. H. Heathcock, in *Comprehensive Carbanion Chemistry*, ed. E. Buncel and T. Durst, Elsevier, New York, 1980, vol. B, ch. 4; (*b*) D. A. Evans, in *Asymmetric Synthesis*, ed. J. D. Morrison, Academic Press, New York, 1983, vol. 3, ch. 1.

2 J. F. Allan, K. W. Henderson and A. R. Kennedy, *Chem. Commun.*, 1999, 1325.

3 K. W. Henderson, W. J. Kerr and J. H. Moir, *Chem. Commun.*, 2000, 479.

4 W. Clegg, K. W. Henderson, R. E. Mulvey and P. A. O'Neil, *J. Chem. Soc., Chem. Commun.*, 1994, 769.

5 (*a*) A. R. Kennedy, R. E. Mulvey and R. B. Rowlings, *J. Am. Chem. Soc.*, 1998, **120**, 7816; (*b*) A. R. Kennedy, R. E. Mulvey and R. B. Rowlings, *Angew. Chem.*, 1998, **110**, 3321; *Angew. Chem., Int. Ed.*, 1998, **37**, 3180; (*c*) A. R. Kennedy, R. E. Mulvey, C. L. Raston, B. A. Roberts and R. B. Rowlings, *Chem. Commun.*, 1999, 353.

6 D. R. Armstrong, A. R. Kennedy, R. E. Mulvey and R. B. Rowlings, *Angew. Chem.*, 1999, **111**, 231; D. R. Armstrong, A. R. Kennedy, R. E. Mulvey and R. B. Rowlings, *Angew. Chem., Chem., Int. Ed.*, 1999, **38**, 131.

7 P. C. Andrews, A. R. Kennedy, R. E. Mulvey, C. L. Raston, B. A. Roberts and R. B. Rowlings, *Angew. Chem.*, 2000, **112**, 2036; P. C. Andrews, A. R. Kennedy, R. E. Mulvey, C. L. Raston, B. A. Roberts and R. B. Rowlings, *Angew. Chem., Int. Ed.*, 2000, **39**, 1960.

8 P. E. Eaton, C.-H. Lee and Y. Xiong, *J. Am. Chem. Soc.*, 1989, **111**, 8016.

9 R. D. Rogers, J. L. Atwood and R. Grüning, *J. Organomet. Chem.*, 1978, **157**, 229.

10 L. M. Engelhardt, B. S. Jolly, P. C. Junk, C. L. Raston, B. W. Skelton and A. H. White, *Aust. J. Chem.*, 1986, **39**, 1337.

11 (*a*) C. R. Bennett and D. C. Bradley, *J. Chem. Soc., Chem. Commun.*, 1974, 29; (*b*) M. A. Putzer, B. Neumüller and K. Dehnicke, *Z. Anorg. Allg. Chem.*, 1998, **624**, 1087.

12 P. Berno, R. Minhas, S. Hao and S. Gambarotta, *Organometallics*, 1994, **13**, 1052.

13 S. J. Simpson and R. A. Andersen, *Inorg. Chem.*, 1981, **20**, 3627.

14 P. C. Andrews and P. J. Nichols, *Organometallics*, 2000, **19**, 1277.

'Inverse crown ether' complexes extended to group 12 through the syntheses of $[Na_2Zn_2(HMDS)_4(O)]$ and $[\{K_2Zn_2(HMDS)_4(O_2)_x(O)_y\}_\infty]$

Glenn C. Forbes,[a] Alan R. Kennedy,*[a] Robert E. Mulvey,*[a] René B. Rowlings,[a] William Clegg,[b] Stephen T. Liddle[b] and Chick C. Wilson[c]

[a] *Department of Pure and Applied Chemistry, University of Strathclyde, Glasgow, UK G1 1XL. E-mail: a.r.kennedy@strath.ac.uk*
[b] *Department of Chemistry, University of Newcastle, Newcastle upon Tyne, UK NE1 7RU*
[c] *Rutherford Appleton Laboratory, ISIS Facility, Chilton, Oxon, UK OX11 0QX*

Received (in Cambridge, UK) 29th June 2000, Accepted 9th August 2000

The first sodium–zinc and potassium–zinc members of the inverse crown ether family, an emerging class of heterometallic macrocyclic amides previously limited to alkali metal–magnesium combinations, have been synthesised and crystallographically characterised.

The use of sterically hindered lithium amide bases, such as LDA, as selective deprotonating agents is widespread throughout organic chemistry.[1] Although these and other homometallic amides have been extensively studied, the possibility of fine-tuning the reactivity profiles of lithium amides by introducing a second metal centre has only recently been explored and has resulted in the characterisation of new structural types. We have described the formation of a new form of heterometallic macrocyclic amide, the inverse crown ether, which can be subdivided into two types. The first group consists of eight-membered $[MgNMN]_2$ rings (M = Li, N = HMDS or TMP;† M = Na or K, N = HMDS) which balance their 2+ charge by acting as oxygen scavengers and encapsulating oxide or peroxide dianions.[2–4] The second group consists of larger twelve-membered, $[NaNMgNNaN]_2$, and twenty-four-membered, $[MgNKN]_6$, rings (N = TMP) which encapsulate one dideprotonated or six monodeprotonated arene molecules, respectively, derived from the solvents used during the reaction.[5] This previous work encompasses a range of M^+ metals, of amide ligands and of guest anions, only the Mg^{2+} centre has remained constant. Substituting metals outside the s-block for magnesium would open new avenues for exploration. One intriguing possibility is that of performing redox chemistry on the guest anions by taking advantage of the range of easily accessible oxidation states displayed by many d-block metals. As a first step towards such compounds we sought to form mixed group 1 metal/zinc analogues. Zinc was chosen for these initial investigations owing to its similar size to magnesium, for its readiness to assume a trigonal-planar coordination geometry and for its stability in the +2 oxidation state, all of which fit the design criteria for inverse crown ether formation. As reported herein, this aim has been realised through the synthesis and crystallographic characterisation of the first sodium–zinc, $[Na_2Zn_2(HMDS)_4(O)]$ **1**, and potassium–zinc, $[\{K_2Zn_2(HMDS)_4(O_2)_x(O)_y\}_\infty]$ **2**, inverse crown ether complexes.

The magnesium containing macrocycles were formed on reacting mixtures of alkyl metal reagents with the appropriate amine;[2–4] however, following the same synthetic procedure with dimethylzinc and *n*-butyllithium did not give the expected macrocyclic product (Scheme 1). Instead one methyl group was retained and $[\{Li(\mu\text{-}HMDS)_2ZnMe\}_\infty]$ **3a**, was the only product isolated, forming in 39% yield as long, colourless needle crystals. The molecular structure of **3a**‡ was found to be based on planar four-membered ZnNLiN rings (Fig. 1) with the methyl group occupying a third (terminal) coordination site on Zn. The molecule has crystallographically imposed two-fold symmetry with Zn, Li and C1 lying on a rotation axis. The

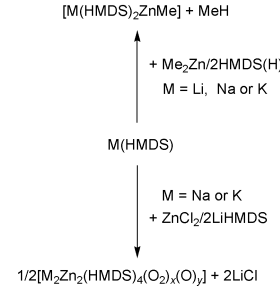

Scheme 1

coordinatively unsaturated (with respect to N) Li attains a higher coordination number by forming a short, linear, intermolecular bridging contact with a neighbouring methyl group (Li···C1 2.435(12) Å, Zn–C1···Li 180°) thus giving rise to a relatively insoluble and structurally robust (*vide infra*) polymer. This is in marked contrast to $[Li(\mu\text{-}HMDS)_2Mg(HMDS)]^2$ **4**, where lithium attains a tetrahedral geometry by forming two intramolecular Li···C contacts [of length 2.294(10) and 2.320(9) Å] with methyl groups from the HMDS ligands. Despite the methyl group being shared between the two metal centres the Zn–C1 distance in **3a** of 1.957(7) Å is similar to those in comparable, but molecularly discrete, compounds.[6] The linear, CH_3 face-capping[7] nature of the methyl to lithium interaction in **1a** is unusual and contrasts strongly with the bent motifs found both in **4** and in other mixed Zn/Li species.[8]

Varying the reaction conditions by including a 4 h reflux or by initially preparing a separate '$Zn(HMDS)_2$' solution from $ZnMe_2$ and amine prior to addition of Li(HMDS) failed to dislodge the second methyl group and produced only **3a** as identified by ^{1}H NMR spectral data [C_5D_5N, δ 0.58 (s 12H, $SiMe_3$), −0.05 (s 1H, Me)]. Repeating the reaction with Bu^nNa or Bu^nK in place of Bu^nLi gave the equivalent sodium and potassium compounds, **3b** and **3c**, respectively, as assigned by comparison of their NMR spectra. To circumvent the retention of the methyl group, $Zn(HMDS)_2$ was prepared by a literature method[9] from $ZnCl_2$ and 2 equivalents of Li(HMDS), and subsequently purified by filtration and vacuum distillation. The pure zinc amide was then added to Na(HMDS) (in a 1 : 1 molar

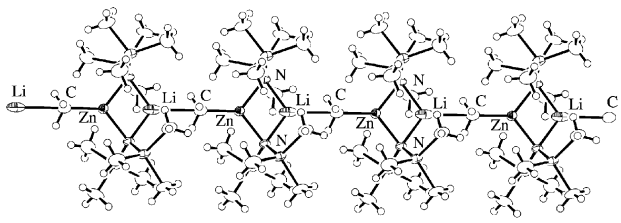

Fig. 1 Polymeric structure of **3a**. Selected geometric parameters (Å,°): Li–N 1.959(7); N–Zn–N* 102.0(2), C–Zn–N 129.0(1), Zn–N–Li 76.1(3), N–Li–C** 127.1(2), N–Li–N* 105.7(5). * = 1 − *x*, *y*, 1.5 − *z*, ** = *x*, 1 + *y*, *z*.

DOI: 10.1039/b005233g

ratio) in an arene solvent (which had previously had dry oxygen bubbled through it) and heated to reflux for 2 h. On cooling to room temperature, large colourless crystals were formed. These were found to be the desired product **1**.‡ Note that when 12-crown-4 is present during this reaction only the zincate $[Na(12\text{-crown-}4)_2][Zn(HMDS)_3]$ is obtained.[10] Repeating our reaction using K(HMDS) in place of Na(HMDS) gave crystals of peroxide rich **2** ($x = 0.82$, $y = 0.18$, for the crystal examined by X-ray diffraction). **2** is the first organoamido-group 12 metal peroxide to be crystallographically characterised, although relevant zinc oxides are known.[11] Compounds **1** and **2** are isomorphous with each other and with their magnesium containing analogues, **1a**[3] and **2a**.[4] Each consists of a near planar octagonal ring containing alternate metal and nitrogen centres (Figs. 2 and 3). Like metal atoms occupy transannular positions and all of them form a third attachment to the central oxide or peroxide guest. The Zn–N distances in **1** and **2** are essentially identical within each compound [mean 1.984(2) and 1.963(1) Å, respectively] and are shorter than that found for **3a** (2.010 Å), seemingly in line with the increasing electronegativity of the group 1 metal. Each Na or K atom forms one short and one long bond to an amide [Na–N 2.541(3), 2.597(2), K–N 2.797(1, 2.838(1) Å] and, unlike the smaller zinc atoms, are displaced both away from the centre of the ring and from the plane of the ring. This leaves both sodium and, more especially, potassium in relatively unfavoured low coordination states and with all their formal bonds on the same side of the coordination sphere. **2** compensates for this by forming short $K\cdots CH_3(SiMe_2)$ contacts. Each potassium forms one intermolecular contact [K··C 3.324(2) Å, K··C–Si 155.6(1)°], to give the linear polymer shown in Fig. 3, as well as several intramolecular contacts [range 3.309(2)–3.362(2) Å]. Note that, in contrast to **2a**, the intermolecular contact is no longer the shortest. It is of interest that the Na compounds display similar carbon contact distances but that these are normally disregarded due to the smaller size of Na. Preliminary results from a single crystal neutron diffraction study of **1** gave longer Na··H distances than those obtained from X-ray diffraction, which reinforces this view. Although the Zn–N distances are systematically 0.07–0.08 Å shorter than the Mg–N distances in **1a** and **2a**, the remaining ring bond lengths and angles are similar, giving essentially isostructural species and hence further encouragement for the future synthesis of larger heterometallic zinc macrocycles of the $[NaNZnNNaN]_2$ and $[KNZnN]_6$ types.

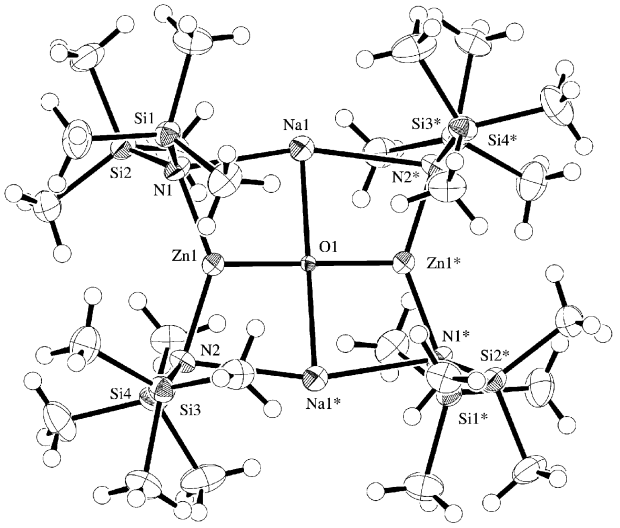

Fig. 2 Molecular structure of **1**. Selected geometric parameters (Å,°): Na1–O1 2.265(2), Zn1–N1 1.986(2), Zn1–N2 1.983(2), Zn1–O1 1.873(1); N1–Na1–N2* 158.96(8), N1–Zn1–N2 141.58(9), Na1–N1–Zn1 78.72(8), Na1*–N2–Zn1 79.78(8). * = $-x$, $-y$, $-z$.

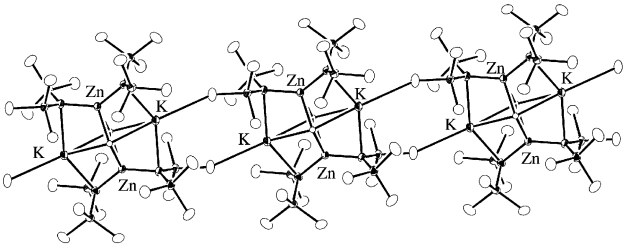

Fig. 3 Extended structure of **2** with H-atoms and the minor disorder component omitted for clarity. Selected geometric parameters (Å,°): Zn–N1 1.961(1), Zn–N2 1.965(1), O–O* 1.579(4), N1–K–N2* 143.75(3), N1–Zn–N2 135.32(4), K–N1–Zn 83.07(4), K*–N2–Zn 84.14(4). * = 1 + x, 1 + y, 1 + z.

We thank the EPSRC for a grant (award no. GR/M78113) to fund G. C. F. and R. B. R., for partial funding for a diffractometer (W. C.) and also for a beamtime award (R. B. 11126) at the Rutherford Appleton Laboratory.

Notes and references

† TMP(H) = 2,2,6,6-tetramethylpiperidine; HMDS(H) = 1,1,1,3,3,3-hexamethyldisilazane.

Reported yields are for the first crystalline crop of materials obtained and have not been optimised. **1**: yield 40%, mp 172–173 °C; satisfactory C, H, N, Na, Zn analyses; δ_H(400 MHz, C_6D_6), 0.31 (s). δ_C(100.61 MHz, C_6D_6) 7.09. **2**: yield 18%, mp 165–166 °C; satisfactory C, H, N, K, Zn analyses. δ_H(400 MHz, C_6D_6), 0.30 (s), 0.29 (s) ratio 4:1, tentatively assigned to peroxo and oxo species respectively; δ_C(100.61 MHz, C_6D_6) δ 7.01. **3a**: yield 39%; satisfactory C, H, N, Li, Zn analyses; δ_H(400 MHz, C_5D_5N), 0.58 (s, 12H, $SiMe_3$), −0.05 (s, 1H, Me). **3b**: yield 14%. δ_H (400 MHz, C_6D_6), δ 0.21 (s, 12H, $SiMe_3$), −0.10 (s, 1H, Me). **3c**: yield 12%, δ_H(400 MHz, C_6D_6), 0.24 (s, 12H, $SiMe_3$), −0.48 (s, 1H, Me).

‡ *Crystal data*: **3a**: $C_{13}H_{39}LiN_2Si_4Zn$, M = 408.13, monoclinic, $C2/c$, a = 17.040(10), b = 6.840(8), c = 21.558(10) Å, β = 108.47(4)°, U = 2383(3) Å^3, Z = 4, λ = 0.71069 Å, μ = 1.228 mm^{-1}, T = 123 K, R = 0.0593 for 2047 observed reflections with $I > 2\sigma(I)$, *wR2* = 0.1441 for 2442 unique reflections (4689 measured, R_{int} = 0.0654).

1: $C_{24}H_{72}N_4Na_2OSi_8Zn_2$, M = 834.30, triclinic, $P\bar{1}$, a = 10.711(6), b = 12.810(6), c = 8.970(4) Å, α = 108.96(3), β = 99.77(4), γ = 96.13(4)°, U = 1129.6(9) Å^3, Z = 1, λ = 0.71069 Å, μ = 1.316 mm^{-1}, T = 183 K, R = 0.0546 for 5530 observed reflections, *wR2* = 0.1305 for 6590 unique reflections (6914 measured, R_{int} = 0.0134).

2: $C_{24}H_{72}K_2N_4O_{1.82}Si_8Zn_2$, M = 879.64, triclinic, $P\bar{1}$, a = 8.9898(4), b = 10.9763(5), c = 12.9529(6) Å, α = 97.322(2), β = 108.154(2), γ = 101.162(2)°, U = 1167.11(10) Å^3, Z = 1, λ = 0.71073 Å, μ = 1.436 mm^{-1}, T = 160 K, R = 0.0188 for 4753 observed reflections, *wR2* = 0.0549 for 5263 unique reflections (10058 measured, R_{int} = 0.0112). All structures solved and refined on F^2 using programs of the SHELX family (G. M. Sheldrick, University of Göttingen, Göttingen, Germany).

CCDC 182/1740. See http://www.rsc.org/suppdata/cc/b0/b005233g/ for crystallographic files in .cif format.

1 C. H. Heathcock, in *Comprehensive Carbanion Chemistry*, ed. E. Buncel and T. Durst, Elsevier, New York, 1980, vol. B, ch. 4.
2 A. R. Kennedy, R. E. Mulvey and R. B. Rowlings, *J. Am. Chem. Soc.*, 1998, **120**, 7816.
3 A. R. Kennedy, R. E. Mulvey and R. B. Rowlings, *Angew. Chem.*, 1998, **110**, 3321; A. R. Kennedy, R. E. Mulvey and R. B. Rowlings, *Angew. Chem., Int. Ed.*, 1998, **37**, 3180.
4 A. R. Kennedy, R. E. Mulvey, C. L. Raston, B. A. Roberts and R. B. Rowlings, *Chem. Commun.*, 1999, 353.
5 D. R. Armstrong, A. R. Kennedy, R. E. Mulvey and R. B. Rowlings, *Angew. Chem*, 1999, **111**, 231; D. R. Armstrong, A. R. Kennedy, R. E. Mulvey and R. B. Rowlings, *Angew. Chem., Int. Ed.*, 1999, **38**, 131; P. C. Andrews, A. R. Kennedy, R. E. Mulvey, C. L. Raston, B. A. Roberts and R. B. Rowlings, *Angew. Chem.*, 2000, **112**, 2036; P. C. Andrews, A. R. Kennedy, R. E. Mulvey, C. L. Raston, B. A. Roberts and R. B. Rowlings, *Angew. Chem., Int. Ed.*, 2000, **39**, 1960.
6 N. A. Bell, H. M. M. Shearer and C. B. Spencer, *Acta Crystallogr., Sect. C*, 1983, **39**, 1182.
7 K. W. Klinkhammer, *Chem. Eur. J.*, 1997, **3**, 1418.
8 E. Weiss and R. Wolfrum, *Chem. Ber.*, 1968, **101**, 35; M. Westerhausen, B. Rademacher and W. Schwarz, *Z. Naturforsch., Teil B*, 1994, **49**, 199.
9 H. Bürger, W. Sawodny and U. Wannagat, *J. Organomet. Chem.*, 1965, **3**, 113.
10 M. A. Putzer, B. Neumüller and K. Dehnicke, *Z. Anorg. Allg. Chem.*, 1997, **623**, 539.
11 See, for example: M. Azad Malik, P. O'Brien, M. Motevalli and A. C. Jones, *Inorg. Chem.*, 1997, **36**, 5076.

ChemComm

Molecular amplification in a dynamic combinatorial library using non-covalent interactions

Ricardo L. E. Furlan, Graham R. L. Cousins and Jeremy K. M. Sanders*

Cambridge Centre for Molecular Recognition, University Chemical Laboratory, Lensfield Road, Cambridge, UK CB2 1EW. E-mail: jkms@cam.ac.uk

Received (in Cambridge, UK) 31st July 2000, Accepted 4th August 2000
First published as an Advance Article on the web 29th August 2000

A trace component within a dynamic combinatorial library of pseudo-peptide hydrazones has been dramatically amplified in a reversible manner through recognition by [18]crown-6.

Dynamic combinatorial libraries (DCLs) have attracted great interest because of their potential for the identification of new catalysts, enzyme inhibitors and host–guest systems.[1] Their successful implementation will hinge on our ability to effect control over the library composition using non-covalent interactions with a template: because of the dynamic equilibria established in a DCL, the stabilisation of any given member by molecular recognition will lead to its amplification by virtue of the Le Chatelier principle. In principle, even species which are present in only trace quantities should be able to be amplified, but since our original proposal of thermodynamic templating of 'living' mixtures in 1996,[2] only small changes in the product distribution of covalent DCLs induced by templates have been reported.[3,4] We now report that recognition by [18]crown-6 leads to dramatic amplification of a trace component within a pseudo-peptide DCL; we also show that this amplification is controllable and reversible.

Our group initially showed that DCLs generated by methoxide-catalysed transesterification of steroidal macrocycles can be influenced by the presence of NaI,[3b] but more recently we have sought to generate libraries using chemistry which offers exchange under milder conditions more suitable for supramolecular recognition such as transimination[5,6] and palladium-catalysed allyl transesterification.[7] A DCL of pseudo-peptide hydrazones can be prepared in chloroform from monomer **1** (5 mM) using TFA as catalyst (Scheme 1).[5a] Analysis of the library using ESI-MS† revealed the presence of 10 macrocyclic compounds ranging from dimer to undecamer. These major macrocyclic products must interconvert *via* at least 10 linear hydrazide species which are present in the DCL but at concentrations too low for detection by HPLC or ESI-MS. HPLC analysis of the library after 24 h showed as major products the dimer **2**, trimer **3**, tetramer **4**, pentamer **5** and higher cyclic oligomers (Fig. 1a). The products were identified using LC-MS.‡

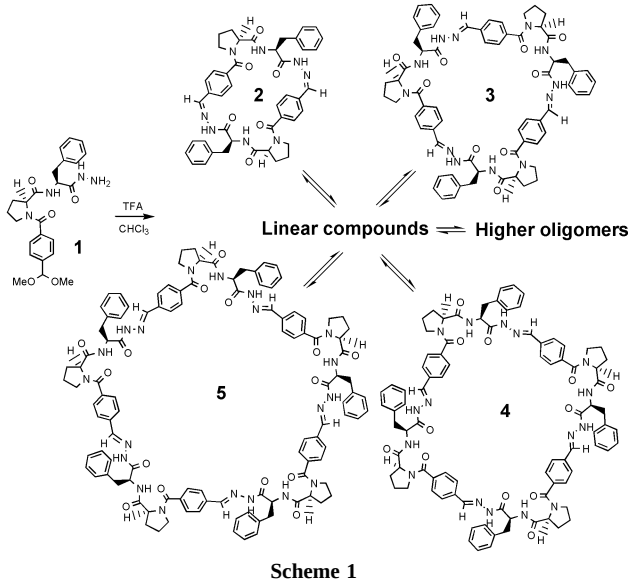

Scheme 1

Unlike the cyclic members, the linear species present in the DCL contain a free hydrazide functionality, which under the acidic conditions used is likely to be protonated. As the affinity of [18]crown-6 for primary alkylammonium[8] and hydrazinium[9] ions is well known, similar behaviour could be expected for the closely related protonated hydrazides present in our system. Introduction of 4 eq. of [18]crown-6 to the reaction mixture shifted the equilibrium by formation of a hydrazide–crown ether complex. HPLC analysis showed a decrease in the concentration of the larger macrocycles and the presence of a new peak corresponding to **6** with a retention time of 3 min (Fig. 1b). At equilibrium, **6**, previously present in an undetectable amount, was the major component of the library (67%).§ As a control experiment, the library was prepared in the presence of [18]crown-6 by treating a solution of **1** and the crown ether with TFA, and the same distribution of products was achieved.

Compound **6** cannot be isolated as it reacts with itself to form hydrazones, but its UV spectrum was recorded using the diode array facility of the HPLC; it does not show the characteristic 288 nm absorption of the cyclic aromatic hydrazones but a band at 257 nm is observed which corresponds well with the spectrum of the model aldehyde **7**.¶ The ESI mass spectrum of the reaction mixture (Fig. 2) was dominated by a major peak at 673.4 corresponding to the **6**·[18]crown-6·H^+ complex, accompanied by small peaks for **6**H^+(409.4), cyclic dimer **2**H^+(781.6) and trimer **3**H^+(1171.7), as well as the complex of the protonated linear dimer **8** with [18]crown-6 (1063.5).

As the DCL contains a complex network of equilibria, it is important to show that kinetic traps have not been introduced

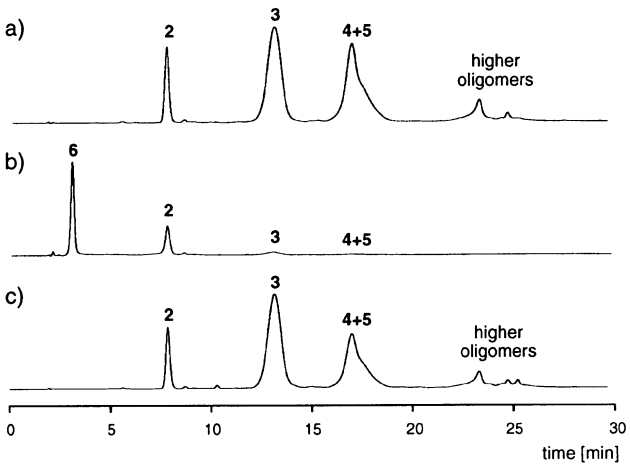

Fig. 1 (a) Chromatogram of the DCL at 24 h, (b) chromatogram of the DCL after addition of 18-crown-6, (c) chromatogram of the DCL showing the regeneration of the cyclic products by addition of 3 eq. of KBr with respect to the amount of [18]crown-6.

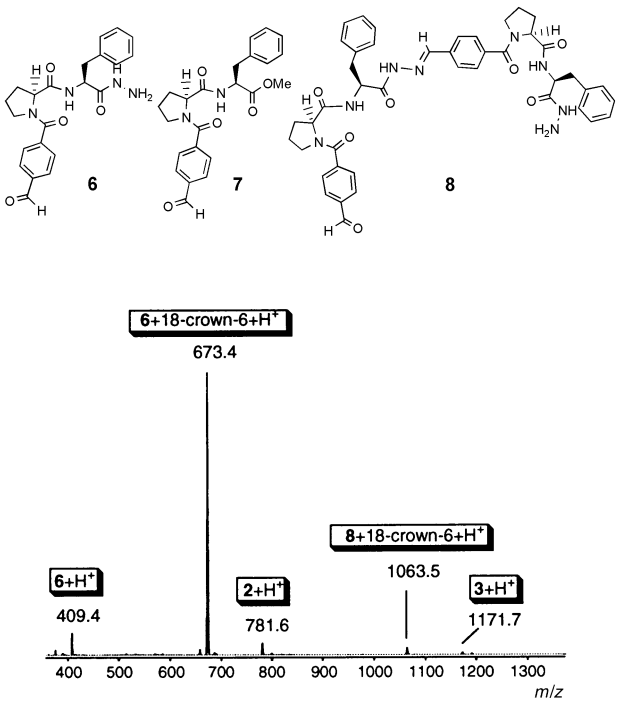

Fig. 2 ESI-MS of the library in presence of 4 eq. of [18]crown-6.

into the system. When KBr was added as a competitive guest that strongly interacts specifically with the crown ether, the original cyclic products were regenerated (Fig. 1c). In a control experiment, the same amount of KBr was added to the library in the absence of crown ether and no change in the composition was observed over 2 days.

Any variation in the strength or extent of hydrazide–crown ether binding should result in a corresponding change in the library composition. When the amount of added [18]crown-6 was varied in the range 0.4–5.0 eq., the proportion of peptide material present as **6** similarly ranged from 20–74%. When different crown ethers were introduced to the library the observed response from the system was related to the size of the ring. Within the series of unsubstituted crown ethers the amount of **6** increases with the size of the crown ether up to [18]crown-6; and in the series of the dibenzo crown ethers, the yield of **6** decreased with crown ethers larger than dibenzo [18]crown-6 (Fig. 3). These results are likely to be related to the affinity of the protonated hydrazide for the crown ethers. It is well known that [18]crown-6 possess the right size and shape to bind primary ammonium cations through three-point hydrogen bonds.[10]

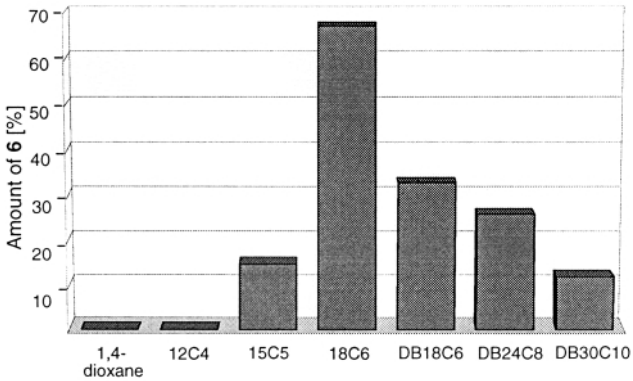

Fig. 3 Amount of **6** in the library when 4 eq. of differents crown ethers were added. 12C4 = [12]crown-4; 15C5 = [15]crown-5; 18C6 = [18]crown-6; DB18C6 = dibenzo [18]crown-6; DB24C8 = dibenzo [24]crown-8; DB30C10 = dibenzo [30]crown-10.

In summary, we have demonstrated that non-covalent interactions between a protonated hydrazide and [18]crown-6 can be used to generate a strong response from a hydrazone-based DCL. The response consists in the amplification of a member previously present in trace amounts to become the major constituent. That increase in concentration is achieved through the preferential consumption of all the unselected cyclic products. The amplification can be reversed by adding a competitive guest that specifically interacts with the crown ether, leading to the regeneration of the original macrocyclic products. To the best of our knowledge, this is the first example of a very substantial amplification in a covalent DCL.

The interaction between protonated hydrazide and crown ether can also be regarded as a *non-covalent* protection of the hydrazide, competing efficiently with the reaction between the hydrazide and an aldehyde to form new *covalent* bonds. Further exploration of the concept of non-covalent protection is under investigation in our laboratory.

We thank S. Otto and J.-C. Meillon for helpful discussions, and the BBSRC, the Ethyl Corporation, Fundacion Antorchas and Consejo Nacional de Investigaciones Cientificas y Tecnicas (Argentina) for financial support.

Notes and references

† Electrospray mass spectra were recorded on a Micromass Quattro-LC triple quadrupole apparatus fitted with a z-spray electrospray source. The electrospray source was heated to 100 °C and the sampling cone voltage was 65 V. Samples were introduced into the mass spectrometer source with an LC pump (Shimadzu LC-9A LC pump) at a rate of 4 μL min^{-1} of MeCN–H_2O (1:1).

‡ HPLC analysis was carried out using a Hewlett-Packard 1050 instrument, coupled to a HP 1050 DAD; data were analysed using HP ChemStation. LC-MS was carried out using an identical HPLC system containing a solvent splitter which diverted 1% of the eluant to a Micromass Platform MS operating in simultaneous positive and negative electrospray modes with a cone voltage of 30 V. The UV and MS data sets were analysed using a MassLynx software suite. Reverse phase HPLC separations were carried out using a 15 cm × 4.6 mm i.d. 3 μM particle size, Supelco ABZ+ C16 alkylamide column using acetonitrile and water gradients.

§ As the extinction coefficient of the new compound is different from that of a hydrazone, its concentration was indirectly determined by the absolute loss of signal intensity belonging to the macrocycles. Loss of hydrazone intensity was directly related to the increase in the signal due to the peak at 3 min.

¶ Aldehyde **7** was prepared from carboxybenzaldehyde dimethoxy acetal, Cbz-proline and phenylalanine methyl ester using standard peptide chemistry. Removal of the dimethoxy acetal was achieved with TFA.

1 J.-M. Lehn, *Chem. Eur. J.*, 1999, **5**, 2455; B. Klekota and B. J. Miller, *Trends Biotechnol.*, 1999, **17**, 205; G. R. L. Cousins, S.-A. Poulsen and J. K. M. Sanders, *Curr. Opin. Chem. Biol.*, 2000, **4**, 270.
2 P. A. Brady, R. P. Bonar-Law, S. J. Rowan, C. J. Suckling and J. K. M. Sanders, *Chem. Commun.*, 1996, 319; S. J. Rowan, P. A. Brady and J. K. M. Sanders, *Angew. Chem., Int. Ed. Engl.*, 1996, **35**, 2143.
3 (*a*) I. Huc and J.-M Lehn, *Proc. Natl. Acad. Sci. USA*, 1997, **94**, 2106; (*b*) P. A. Brady and J. K. M. Sanders, *J. Chem. Soc., Perkin Trans. 1*, 1997, 3237; (*c*) O. Ramstrom and J.-M Lehn, *CHEMBIOCHEM*, 2000, **1**, 41.
4 For a large template-controlled change in the composition of a non-covalent DCL see M. C. Calama, P. Timmerman and D. N. Reinhoudt, *Angew. Chem., Int. Ed.*, 2000, **39**, 755.
5 (*a*) G. R. L. Cousins, S. A. Poulsen and J. K. M. Sanders, *Chem. Commun.*, 1999, 1575; (*b*) M. G. Simpson, S. P. Watson, N. Feeder, J. E. Davies and J. K. M. Sanders, *Org. Lett.*, 2000, **2**, 1435.
6 For the clinical potential of this concept see D. Rideout, *Cancer Investigation*, 1994, **12**, 189.
7 G. Kaiser and J. K. M. Sanders, *Chem. Commun.*, 2000, 1763, following paper in this issue, DOI: 10.1039/b006151o.
8 I. Goldberg, *Inclusion Compounds*, ed. J. L. Atwood, J. E. D. Davies and D. D. MacNicol, Academic Press, London, 1984, vol. 2, p. 269.
9 K. N. Trueblood, C. B. Knobler, D. S. Lawrence and R. V. Stevens, *J. Am. Chem. Soc.*, 1982, **104**, 1355.
10 J. S. Bradshaw, R. M. Izatt, A. V. Bordunov, C. Y. Zhu and J. K. Hathaway, *Comprehensive Supramolecular Chemistry*, ed. J. L. Atwood, J. E. D. Davies, D. D. MacNicol and F. Vogtle, Elsevier Science Ltd., 1996, vol. 1, p. 76.

ChemComm

Synthesis under reversible conditions of cyclic porphyrin dimers using palladium-catalysed allyl transesterification

Guido Kaiser and Jeremy K. M. Sanders*

Cambridge Centre for Molecular Recognition, University Chemical Laboratory, Lensfield Road, Cambridge, UK CB2 1EW. E-mail: jkms@cam.ac.uk

Received (in Cambridge, UK) 31st July 2000, Accepted 4th August 2000
First published as an Advance Article on the web 29th August 2000

Cyclic zinc-porphyrin dimers have been synthesised using reversible π-allyl palladium chemistry in the presence of bidentate pyridyl ligand templates.

Reversible covalent chemistry has the potential to be useful in the creation of diverse dynamic combinatorial libraries (DCLs)[1,2] and in the synthesis of specific supramolecular structures such as macrocycles and catenanes.[3] Examples of reversible reactions used to date include imine, hydrazone and disulfide exchange, olefin metathesis and metal–ligand interactions. However, there is always the need to expand the repertoire of available reactions and conditions. Here we report what we believe to be the first supramolecular application of π-allyl palladium-catalysed chemistry: furthermore, we demonstrate the use of a template to amplify an otherwise inaccessible synthetic target molecule from a complex mixture of interconverting oligomers.

We chose to apply π-allyl palladium chemistry to the synthesis of cyclic porphyrin dimers which might help our understanding of structure–activity relationships in the acceleration of a hetero Diels–Alder reaction.[4] Previously, such dimers have been prepared by intramolecular oxidative coupling of a linear porphyrin diester species (Fig. 1, route a)[4,5] since all attempts by our group to cyclise a linear dimer by irreversible esterification reactions (Fig. 1, route b) have failed; inevitably, these failures are unpublished. The attraction of route (b) using reversible π-allyl palladium chemistry is that, provided the product is thermodynamically accessible, its formation should be favoured by stabilisation through supramolecular complexation with an appropriate template. This is conceptually the inverse of the host-accelerated Diels–Alder reaction since the small guest is used to template the formation of the large host.

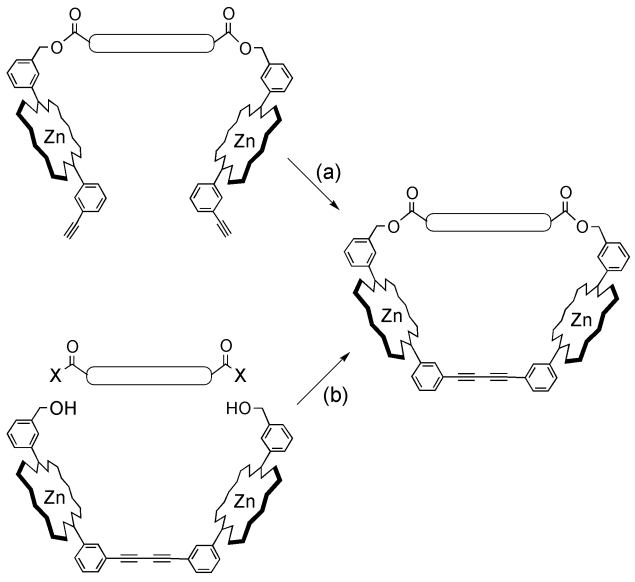

Fig. 1 Synthetic routes to capped porphyrin dimers.

It is well known that π-allyl palladium complexes generally undergo reversible reactions (Scheme 1),[6] and Amatore and Jutand *et al.* have recently confirmed the reversibility of the reaction between allyl esters and palladium(0).[7] Carboxylates and phenolates represent an ideal class of functional groups for isoenergetic exchange *via* reversible π-allyl palladium chemistry since they can act as both nucleophiles and leaving groups. In order to confirm the feasibility of using allyl esters as substrates, a simple model system based on cinnamyl esters was set up (Scheme 1, R = phenyl and *o*-tolyl; $R^1 = CH_3$, R^2 = Et). Complete exchange of the ester groups was observed after 6 h at 50 °C: all 4 possible permutations were present in equal amounts independently of which starting combination was employed. The reaction conditions appeared to be mild enough to be employed in the capping reaction of linear porphyrin dimers. The scientific challenge was therefore to devise a system where, for the first time, a linear porphyrin dimer would undergo a multi-step ring-closing transesterification reaction catalysed by palladium(0).

The linear porphyrin dimer **1** (Scheme 2) was synthesised according to previously published procedures:[5] the asymmetric porphyrin synthesis was carried out in 25% yield, followed by a Glaser–Hay coupling of the deprotected porphyrin monomers to give the linear dimer (60% yield). The simple dipyridyl **2** was chosen as the template, its role being kinetically to preorganise the linear porphyrin dimer by restricting rotation about the butadiyne axis, or thermodynamically to favour capped dimers over linears.

For the initial exchange experiments, alkyl diacids were expected to be sufficiently flexible and nucleophilic, in contrast to aryl acids which are more rigid and less nucleophilic. In the first instance, succinic acid was chosen. To aid structural analysis of the cyclic porphyrin dimer by NMR methods, labelled 1,4-^{13}C succinic acid was used.† In a typical experiment the linear porphyrin dimer **1** (20 mg, 1 eq.) and the template **2** (1 eq.) were dissolved in chloroform (2 ml), succinic acid (8 eq.), triethylamine (40 eq.) and tetrakis(triphenylphosphine)palladium(0) (0.1 eq.) were added and the solution was stirred at 55 °C under an inert atmosphere for 6 h. The mixture was demetallated using trifluoroacetic acid to remove the template and then remetallated using zinc acetate. The different porphyrin fractions were separated by preparative thin layer chromatography and dissolved in a fixed amount of solvent. Quantitative analysis of the product fractions was carried out by UV–Vis spectroscopy, based on the assumption that the molar extinction coefficients of the linear and cyclic dimers were similar. The relative absorbance of the products was measured and values are given in arbitrary absorbance units. Due to the

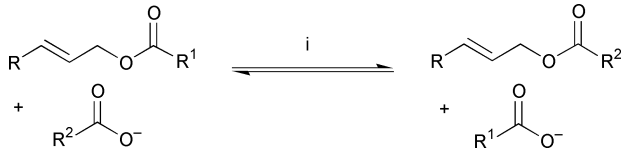

Scheme 1 *Reagents and conditions*: i, concentration of cinnamyl esters 10 mM, $Pd(PPh_3)_4$ (0.1 eq.), R^1CO_2H (< 0.1 eq.), Et_3N, $CHCl_3$, 50 °C, 6 h.

DOI: 10.1039/b006151o

small quantities of the fractions, accurate determination of the weights of the product was not possible.

In the absence of the template only traces of the capped dimer could be isolated (0.009 au—absorbance unit; less than 2% yield). However, in the templated experiments the isolated yield of pure **3** increased 6-fold to approximately 10% (0.055 au). The structure of the ring-closed dimer was confirmed by HMBC-NMR showing a cross-peak for the single enriched ^{13}C signal (δ = 172.4 ppm) with the allylic CH_2 protons (δ = 4.63 ppm). This significant and reproducible increase in the yield confirms the templating effect of the bidentate ligand and represents the first thermodynamic capping of a linear porphyrin dimer using reversible π-allyl palladium chemistry. To test the generality of the reaction, and to illustrate the feasibility of utilising libraries of capping groups at a later stage, cyclic dimers containing glutaric and 1,3-phenylenediacetic acid as capping groups were also prepared in comparable yields. In addition to NMR characterisation, MALDI-TOF mass spectrometry was used to distinguish between linear and cyclic species.

The control experiments without template and those in the presence of pyridine (2 eq.) gave the same results. Pyridine is a monodentate equivalent of the template **2**, *i.e.* the pyridine units are not covalently linked as for the bidentate template. This result confirms that the dipyridyl compound **2** templates the formation of the cyclic dimer by stabilising it and that the pyridyl functionality of the template does not influence the outcome of the transesterification. The large binding constants of template **2** to the linear and cyclic dimers, 3×10^6 and 2×10^7 M^{-1} respectively, are consistent with the observed templating effect.[8] However, the relatively small increase in the binding constant upon cyclization highlights the flexibility of the host and rationalises the low yield of **3**, *i.e.* the equilibrium is shifted only slightly from oligomeric species towards the formation of **3**.‡

It was possible to identify mono- and disubstituted linear dimers as intermediates of the reaction by MALDI-TOF and ^1H NMR. However, the relative quantities of all intermediates could not be estimated accurately due to the low solubility of oligomers and disubstituted linear dimers with two free carboxylic acid groups.§ It should be noted that the solubility of the mixture was not problematic during the reaction itself as the triethylamine salts of all intermediates are soluble in chloroform.

In summary, we have shown the synthesis under reversible conditions of three cyclic porphyrin dimers using palladium-catalysed transesterification. The reaction was templated by a bidentate pyridyl ligand which improved the yield of the cyclic product 6-fold. To our best knowledge, this is the first supramolecular application of reversible π-allyl palladium chemistry; it is also one of the most effective examples yet reported of amplification of a specific product from an exchanging library of components.

We thank the BBSRC, AstraZeneca and the Cambridge European Trust for financial support and Dr Y.-F. Ng for recording some of the NMR spectra.

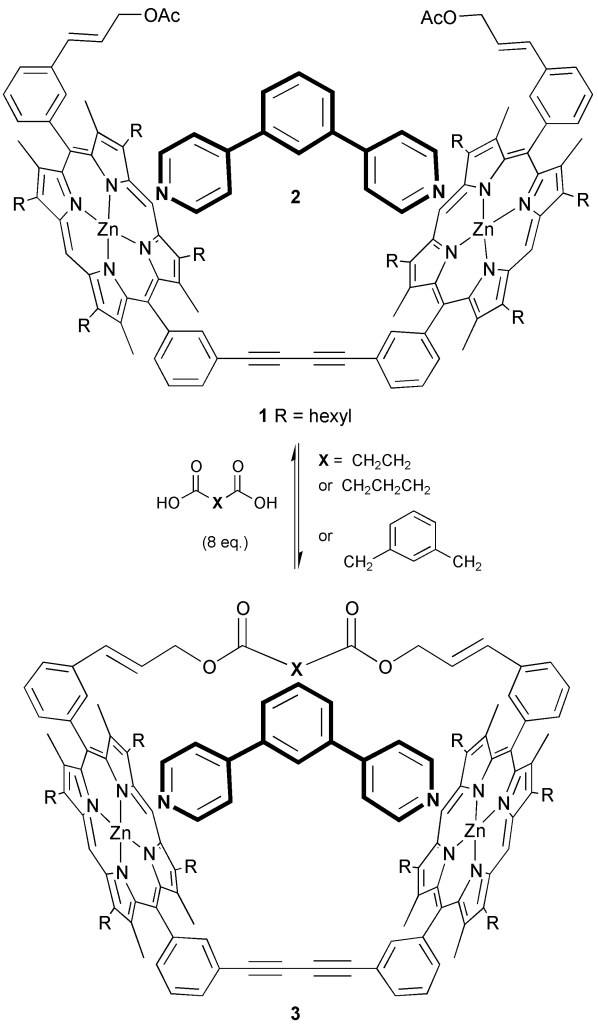

Scheme 2 *Reagents and conditions*: concentration of porphyrin dimer 5 mM, $Pd(PPh_3)_4$ (0.1 eq.), Et_3N, $CHCl_3$, 55 °C, 6 h.

Notes and references

† The molecular weights of linear dimer and unlabelled succinic capped dimer differ by only 2 a.m.u., precluding the use of MALDI-TOF mass spectrometry.

‡ This point is also apparent in the uniformity of yield from the three different capping acids of very different geometry.

§ The overall amount of isolated porphyrinic material was measured by UV–Vis spectroscopy and marked differences between the templated and non-templated reactions were observed. The overall recovery of soluble porphyrinic material was considerably lower for the non-templated reaction (0.1 au compared with 0.2 au for the templated reaction). This result implies that the template suppresses the formation of insoluble oligomers in addition to promoting the formation of cyclic product. The decrease in total oligomer formation is greater than the increase in cyclic dimer formation, suggesting that these are two separate effects, *i.e.* the dipyridyl compound **2** is a positive template for the cyclic dimer formation and a negative template for the oligomer formation.

1 For reviews covering this area see: G. R. L. Cousins, S.-A. Poulsen and J. K. M. Sanders, *Curr. Opin. Chem. Biol.*, 2000, **4**, 270; J.-M. Lehn, *Chem. Eur. J.*, 1999, **5**, 2455; B. Klekota and B. L. Miller, *Trends Biotechnol.*, 1999, **17**, 205.

2 For more recent examples see: R. L. E. Furlan, G. R. L. Cousins and J. K. M. Sanders, *Chem Commun.*, 2000, 1761, previous paper in this issue (DOI: 10.1039/b006149m); M. G. Simpson, S. P. Watson, N. Feeder, J. E. Davies and J. K. M. Sanders, *Org. Lett.*, 2000, **2**, 1435; O. Ramström and J.-M. Lehn, *CHEMBIOCHEM*, 2000, **1**, 41.

3 D. G. Hamilton, N. Feeder, S. J. Teat and J. K. M. Sanders, *New J. Chem.*, 1998, **22**, 1019; T. J. Kidd, D. A. Leigh and A. J. Wilson, *J. Am. Chem. Soc.*, 1999, **121**, 1599.

4 M. Nakash, Z. Clyde-Watson, N. Feeder, J. E. Davies, S. J. Teat and J. K. M. Sanders, *J. Am. Chem. Soc.*, 2000, **122**, 5286; M. Nakash and J. K. M. Sanders, *J. Org. Chem.*, in the press.

5 L. J. Twyman and J. K. M. Sanders, *Tetrahedron Lett.*, 1999, **40**, 6681.

6 J. Tsuji, *Palladium Reagents and Catalysts*, John Wiley & Sons, Chichester, 1995.

7 C. Amatore, A. Jutand, G. Meyer and L. Mottier, *Chem. Eur. J.*, 1999, **5**, 466.

8 The binding constants were measured in dry $CHCl_3$ at 25 °C with host and guest concentrations of 10^{-5} M and 10^{-4} M respectively. The data were analysed using the commercial program Specfit.

Palladium catalyzed intramolecular nucleophilic addition of allylic species, generated from allene, to aryl aldehydes and ketones

Xinjie Gai,[a] Ronald Grigg,*[a] Simon Collard[b] and Jayne E. Muir[b]

[a] *Molecular Innovation, Diversity and Automated Synthesis (MIDAS) Centre, School of Chemistry, Leeds University, Leeds UK LS2 9JT. E-mail: R.Grigg@chem.leeds.ac.uk*

[b] *Johnson Matthey, Precious Metal Division, Royston, Hertfordshire, UK SG8 5HE*

Received (in Cambridge, UK) 17th July 2000, Accepted 27th July 2000
First published as an Advance Article on the web 29th August 2000

2-Haloaryl aldehydes and ketones react with allene (1 atm) in the presence of 2 mol% of a non-phosphine cyclopalladated catalyst to afford cyclopentenols and cyclohexenols *via* nucleophilic cyclisation of intermediate π-allylpalladium species. A possible mechanism for this unusual reactivity is suggested.

One of the major features of palladium catalysed processes is their tolerance of a wide range of functional groups. However, the versatility of palladium catalysts would be considerably enhanced if they incorporated, in a predictable way, reaction with functional groups heretofore immune to palladium catalysts. Arguably the most important 'immune' functional group is the carbonyl group. We[1,2] and others[3] have recently reported bimetallic Pd/In catalysis that permits both inter- and intramolecular allylation of carbonyl groups. Others have reported intramolecular vinylation and arylation of carbonyl groups[4] or nitriles[5] *via* undefined nucleophilic palladium species. In addition palladium(II)-catalysed aldol reactions have been reported.[6]

Allylation of carbonyl compounds is well known for the nucleophilic allyl derivatives of main group metals[7] whereas π-allylpalladium(II) species are usually electrophilic.[8] In order to explore the desired unusual reactivity of π-allylpalladium(II) species we elected to utilize a novel non-phosphine-containing palladacycle **3**[9] as catalyst and allene as the source of the π-allyl species (Scheme 1).

2-Iodo- and 2-bromobenzaldehyde **1a** and **1b** were found to react with allene (1 atm) in DMF at 80 °C over 18 h in the presence of 2 mol% **3** and Cs_2CO_3 (2 mol eq.) to afford the desired benzocyclopentenol **2a** (Table 1, entry 1). The iodoaldehyde **1a** was more reactive than bromoaldehyde **1b**. The reaction proved to be general for a range of substrates, **1b**–**1f** furnishing both 5-membered, **2a**–**2d**, and 6-membered, **2e**, **2f**, products. Arylalkyl ketones (Table 1, entry 2) and diaryl ketones (Table 1, entries 3,4) reacted to give the expected products with formation of 5-membered products proving more efficient than formation of 6-membered products for the limited examples surveyed thus far. 2-(2-Bromophenyl)indane-1, 3-dione **1f** gave **2f** (Table 1, entry 6), the product of dehydration of the expected cyclohexenol. The processes described herein occur under significantly milder conditions than the other reported examples of nucleophilic Pd^{II} species. Evidence to hand thus far[9] suggests that palladacycle **3** functions *via* controlled release of Pd^0 nanoparticles[11] and that Scheme 1 involves Pd^0/Pd^{II} rather than Pd^{II}/Pd^{IV}.[12]

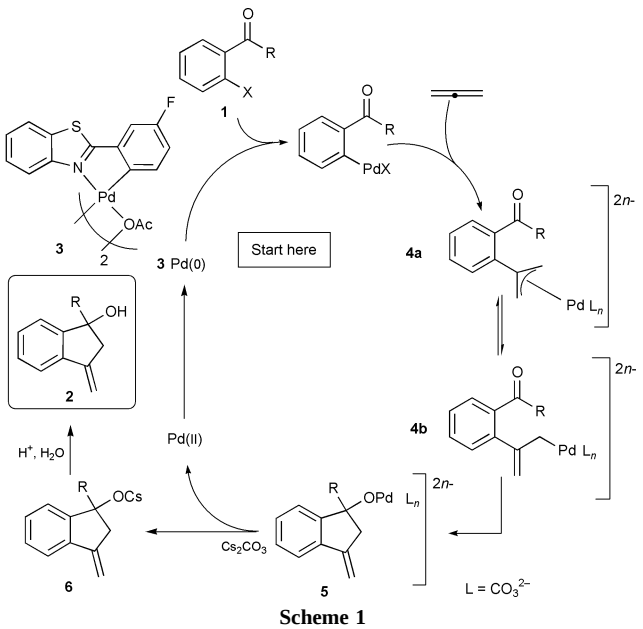

Scheme 1

Cs_2CO_3 was the superior base of those (Cs_2CO_3, K_2CO_3, KOAc) tested. Possible mechanisms for the processes described herein and those reported previously[3–5] must account for the fact that only intramolecular processes forming 5- and 6-membered rings have been observed. A possible rationalization is shown in Scheme 1.

The key features of Scheme 1 are that coordination of the carbonate anions to Pd^{II} produces anionic η^3- and η^1-species **4a** and **4b**. The η^1-species **4b** is then postulated to undergo bond shift as depicted in **8** or **9**. The ability of carbonate to function as a mono- or hemilabile bidentate ligand might also be a factor. A common problem to both Scheme 1 and the previously reported nucleophilic vinyl and aryl palladium(II) species[4,5] is the mechanism by which Pd^{II} is reduced to Pd^0 to allow catalyst recycling. It is instructive that the reactions reported herein and the related work[4,5] all employ DMF as solvent. It is clear that DMF from certain sources contains formate impurities,[13] or that such impurities may be generated *in situ*, and these then react with Pd^{II} to produce HPdX which is then converted by base to Pd^0. In Yamamoto's examples, addition of 5 mol eq. of a primary alcohol is necessary. Although the role of the primary alcohol is not entirely clear it is not, apparently, active as a reductant for Pd^{II} to Pd^0.

The potentially bidentate CO_3^{2-} anion might be expected to be more effective in generating a carbon nucleophile perhaps *via* trace amounts of allyl anion **9** whose effective molarity[14] would be high, which would account for the failure to observe the analogous intermolecular reactions.

It seems likely that anionic Pd^{II} species may be important in the nucleophilic processes reported herein and those reported previously by Yamamoto.[4] Larock's nitrile–alkyne examples[5] do not employ inorganic bases but polyhalo anionic Pd^{II} species would appear to play a role in these phosphine free cases employing R_4NCl[14]. Although anionic Pd^{II} species have been detected in Heck reactions[14] they were not catalytically active in this reaction.

A further interesting and unresolved feature in many instances of Pd^0 nanoparticle catalysis is whether the catalytic processes occur on the surface of the nanoparticle at edges and/or vertices or in homogeneous solution by substrate leaching of the Pd^0.

DOI: 10.1039/b005740l

Table 1 Generation and intramolecular capture of allylic species from **1a–j** and allene catalysed by **3**[a]

Entry	Substrates	Temp[b]/°C	Time/h	Products	Yield[c] %
1	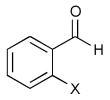 **1a**	80	18	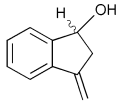 **2a**	90(95[d])
2	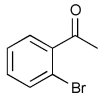 **1b**	90	18	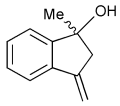 **2b**	70(90[d])
3	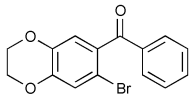 **1c**	88	21	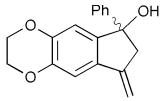 **2c**	70(75[d])
4	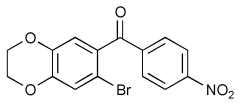 **1d**	88	18	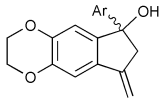 **2d**	81
5	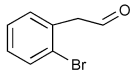 **1e**	80	18	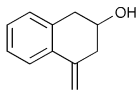 **2e**	34
6	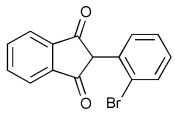 **1f**	90	23	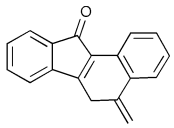 **2f**	45

[a] Reactions carried out in DMF employing 2 mol% catalyst and Cs_2CO_3 (2 mol eq.). [b] Oil bath temperature. [c] Isolated yield. [d] Conversion calculated by ^{1}H-NMR.

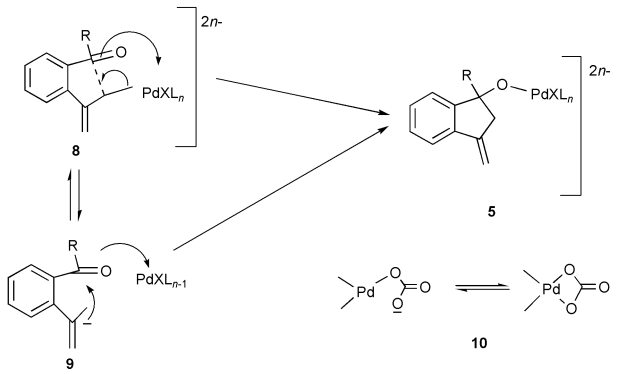

Further studies of these and related processes are underway.

We thank the ORS and Tetley and Lupton for scholarships (to X. G.) and Johnson Matthey and Leeds University for support.

Notes and references

1 U. Anwar, R. Grigg, M. Rasparini, V. Savic and V. Sridharan, *Chem. Commun.*, 2000, 645.
2 U. Anwar, R. Grigg and V. Sridharan, *Chem. Commun.*, 2000, 933.
3 S. Araki, T. Kamei, T. Hirashita, H. Yamamura and M. Kawai, *Org. Lett.*, 2000, **2**, 847.
4 L. G. Quan, V. Gevorgyan and Y. Yamamoto, *J. Am. Chem. Soc.*, 1999, **121**, 3545; L. G. Quan, V. Gevorgyan and Y. Yamamoto, *Tetrahedron Lett.*, 1999, **40**, 4089; L. G. Quan, M. Lamrani and Y. Yamamoto, *J. Am. Chem. Soc.*, 2000, **122**, 4827.
5 R. C. Larock, Q. Tian and A. A. Pletnev, *J. Am. Chem. Soc.*, 1999, **121**, 3238.
6 H. Groger, E. M. Vogl and M. Shibasaki, *Chem. Eur. J.*, 1998, **4**, 1137; M. Sodeoka, R. Tokunoh, F. Miyazaki, E. Hagiwara and M. Shibasaki, *Synlett*, 1997, 463; M. Sodeoka, K. Othrai and M. Shibasaki, *J. Org. Chem.*, 1995, **60**, 2649.
7 For leading references see: S. Steurer and J. Podlech, *Eur. J. Org. Chem.*, 1999, 1551.
8 J. Tsuji, *Palladium Reagents and Catalysts*, Wiley, 1995, Ch. 4, p. 292 *et seq*.
9 X. Gai, R. Grigg, M. I. Ramzan, V. Sriharan, S. Collard and J. E. Muir, *Chem. Commun.*, in the press.
10 D. G. Blackmond, J. S. Bradley, J. Le Bars and M. Specht, *Langmuir*, 1999, **15**, 7621; M. Reetz and E. Westermann, *Angew. Chem., Int. Ed.*, 2000, **39**, 165.
11 B. L. Shaw, *New J. Chem.*, 1998, 77.
12 V. Calo, R. D. Sole, A. Nacci, E. Schingaro and F. Scordari, *Eur. J. Org. Chem.*, 2000, 869.
13 A. J. Kirby, *Adv. Phys. Org. Chem.*, 1980, **17**, 183.
14 C. Amatore and A. Jutand, *Acc. Chem. Res.*, 2000, **33**, 314.

ChemComm

Paclitaxel synthetic studies. A Diels–Alder approach to the A-ring†

Santiago Carballares,[a] Donald Craig,*[a] Charlotte A. L. Lane,[a] A. Roderick MacKenzie,[b] William P. Mitchell[a] and Anthony Wood[b]

[a] *Centre for Chemical Synthesis, Department of Chemistry, Imperial College of Science, Technology and Medicine, London, UK SW7 2AY. E-mail: d.craig@ic.ac.uk*
[b] *Pfizer Central Research, Sandwich, Kent, UK CT13 9NJ*

Received 11th July 2000, Accepted 4th August 2000
First published as an Advance Article on the web 29th August 2000

Highly substituted cyclohexenes corresponding to the A-ring of the anti-cancer diterpene natural product paclitaxel are synthesised using a Diels–Alder reaction and decarboxylative elimination as the key steps.

The paclitaxel family of molecules, exemplified by the parent paclitaxel (Taxol®) **1**[1] has commanded the attention of a significant number of organic chemistry research teams worldwide.[2] The strategies we are pursuing for the assembly of paclitaxel involve late-stage formation of the eight-membered B-ring by the joining together of C-9 and C-8 using radical- or carbocation-mediated cyclisation of a substrate **2**; in one of the approaches we intend to form the C-ring in the same step using a Lewis acid-induced carbocation-mediated cascade process starting from **3** in which the C-3–C-4 bond is formed as well. Both these sequences require a pre-formed A-ring fragment such as **5**, and this Communication reports the synthesis of key precursor **4** (Scheme 1).

In our synthetic plan for **4** we were keen to incorporate the required C-13 oxygenation directly using the Diels–Alder reaction rather than introducing it later by oxidation of C-13.[2a] This choice posed a strategic problem concerning Diels–Alder regiochemistry, in that [4+2] cycloaddition of **6** and a simple alkyne-containing dienophile such as a but-2-ynoate ester was likely to give a cycloadduct **7** bearing a C-12 rather than a C-11 ester substituent. Therefore it was decided to use citraconic anhydride as the dienophile,[3] since it was anticipated that the regiochemical orientation of the Diels–Alder reaction would be controlled by steric repulsion between the fully-substituted

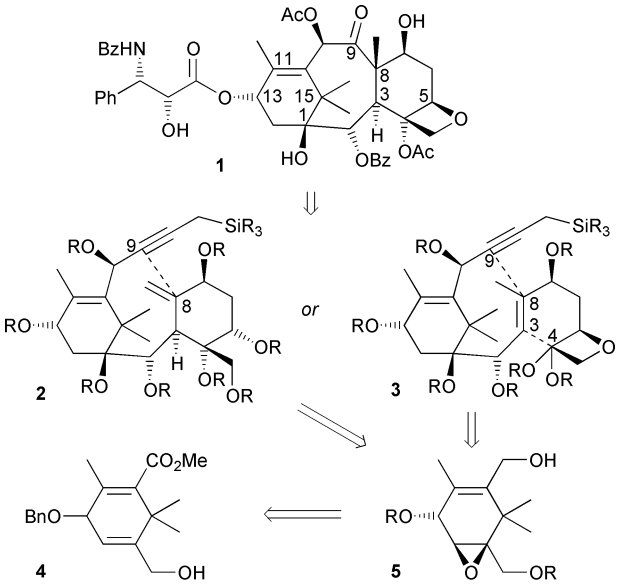

Scheme 1

† Experimental details for **4**, **13**, **16**, **17**, **19**–**21** are available as supplementary data. For direct electronic access see http://www.rsc.org/suppdata/cc/b0/b005533f/

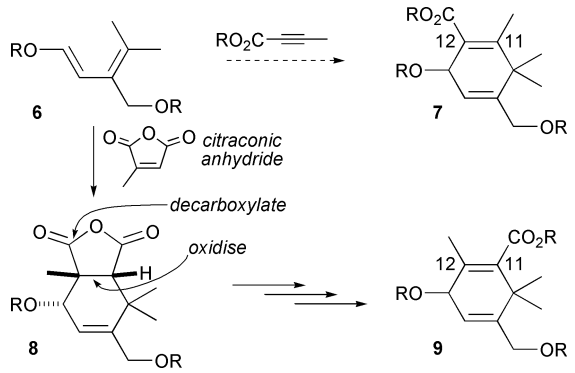

Scheme 2

diene and dienophile termini; subsequent selective decarboxylation and oxidation of adduct **8** would deliver the required C-11–C-12 unsaturation, as in **9** (Scheme 2).

The required diene was synthesised using the Julia procedure for the olefination step.‡ Thus, mono-protection of diol **10**[4] followed by oxidation using TPAP–NMO[5] gave enal **11**. Combination of **11** with the lithio-anion of benzyloxy(phenylsulfonyl)methane[6] and *in situ* trapping with benzoyl chloride gave a mixture of esters, which was exposed to samarium(II) iodide[7] to provide the required differentially protected diene **12**. Diels–Alder reaction of **12** with citraconic anhydride gave cycloadduct **13** as a single regio- and stereoisomer in 63% yield based on **12** (Scheme 3). The *endo* stereochemistry of **13** was inferred from the analogous reaction of **12** with maleic anhydride,[3] which had given a crystalline product amenable to X-ray structure determination.

With Diels–Alder adduct **13** in hand it was necessary to differentiate between the anhydride carbonyl groups. Treatment of **13** with dimethylamine gave an unstable§ half-amide as a

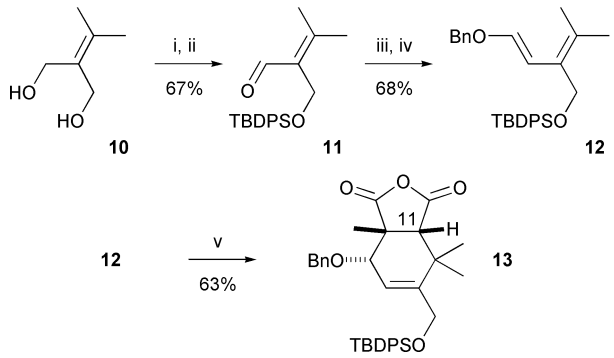

Scheme 3 *Reagents and conditions*: i, NaH (1.01 eq.), THF (0.07 M), rt, 1 h, then TBDPSCl (1 eq.), rt, 15 h; ii, TPAP (2.4 mol%), NMO (1.6 eq.), powdered 4 Å mol sieves, CH_2Cl_2 (0.5 M), rt, 1 h; iii, $BnOCH_2SO_2Ph$ (1 eq.), LDA (1 eq.), THF (0.1 M), −78 °C, 10 min, then add **11**, −78 °C, 10 min, then add BzCl (1 eq.), −78 °C→rt, 45 min; iv, SmI_2 (5 eq.), DMPU (15 eq.), THF, (0.1 M), rt, 1 h; v, citraconic anhydride (2 eq.), PhMe (3.3 M), 150 °C, 24 h.

DOI: 10.1039/b005533f

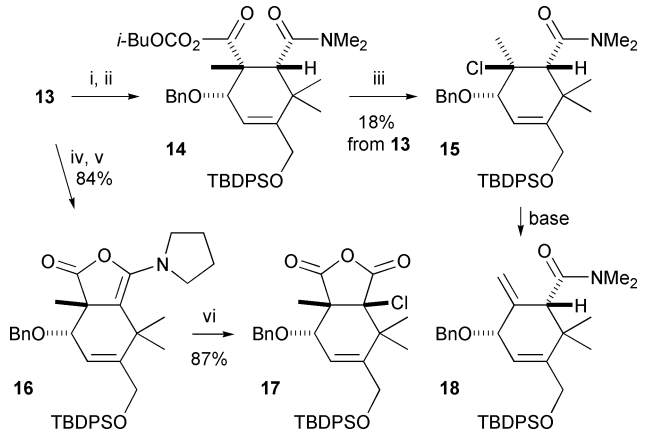

Scheme 4 *Reagents and conditions*: i, Me_2NH (5 eq.), THF (0.5 M), rt, 16 h; ii, *i*-BuOCOCl (1.1 eq.), Et_3N (1.1 eq.), CH_2Cl_2 (0.1 M), −15 °C→rt; iii, 2-mercaptopyridine *N*-oxide (1 eq.), Et_3N (1.1 eq.), CCl_3 (0.03 M), 80 °C, 2 h; iv, pyrrolidine (5 eq.), THF (0.5 M), rt, 2 h; v, *i*-BuOCOCl (1.1 eq.), Et_3N (2.5 eq.), CH_2Cl_2 (0.2 M), rt, 1 h; vi, NCS (1 eq.), Et_3N (2 eq.), H_2O (5 eq.), THF (0.1 M), rt, 2 h.

single regioisomer,¶ which was converted into the mixed anhydride **14** by addition of isobutyl chloroformate. Treatment of **14** with *N*–hydroxy-2-thiopyridone in CCl_4 under reflux[8] gave in low yield the product **15** of decarboxylation–chlorination. The stereochemistry of **15** was presumed on the basis of expected attack by CCl_4 on the less hindered face of the intermediate radical.‖ All attempts to effect base-mediated elimination of the elements of HCl from **15** resulted in the formation of the β,γ-unsaturated isomer **18**. In a modified approach, treatment of cycloadduct **13** with pyrrolidine gave a half-amide adduct which was considerably more stable than the dimethylamine-derived analogue. Surprisingly, subsequent exposure of this adduct to the mixed anhydride-forming conditions resulted in cyclodehydration, giving the cyclic *O*-acylketaminal **16** in virtually quantitative yield.** The desired oxidation at C-11 was now effected by treatment of **16** with NCS–aqueous THF, giving α-chloro anhydride **17** in high yield (Scheme 4). The difference in behaviour of the dimethylamino and pyrrolidino analogues under the carbonic anhydride-forming conditions is striking; the apparent greater nucleophilicity of the amide oxygen in the latter is consistent with greater delocalisation of the amide nitrogen lone pair into the carbonyl group, which in turn inhibits the reverse reaction during ring-opening of **13** with the secondary amine nucleophile.

The final part of the synthesis involved decarboxylation and introduction of the double bond, and again this depended on initial regioselective ring-opening to give a β-chloro carboxylic acid. In the event, treatment of **17** with a large excess of pyrrolidine gave amide **19** as a single regioisomer (Scheme 5). Interestingly, **19** existed in $CDCl_3$ and d_6-DMSO solutions as mixtures of rotamers. In similar fashion, treatment of **17** with benzyltrimethylammonium methoxide in large excess gave methyl ester **4**. Mechanistically, the presumed initial ring-opened half-amide and -ester either might form β-lactone intermediates which subsequently lose CO_2,[9] or might spontaneously undergo β-elimination with concerted loss of CO_2 and chloride ion.[10] Amide **19** was converted in high yield by desilylation and esterification into the 3,5-dinitrobenzoate **20**, which yielded crystals suitable for X-ray diffraction analysis. Similar treatment of **4** gave the crystalline ester **21**.††

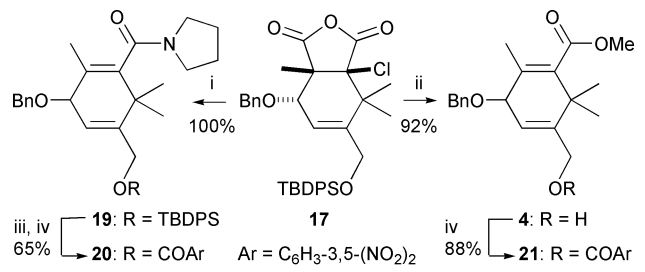

Scheme 5 *Reagents and conditions*: i, pyrrolidine (50 eq.), DMSO–DMPU (5:3; 0.14 M), rt , 2 h; ii, $BnMe_3N^+OMe^-$ (50 eq.), MeCN–DMPU (0.14 M), rt, 27 h; iii, TBAF (1.1 eq.), THF (0.2 M), rt, 15 min; iv, ArCOCl (1.1 eq.), Et_3N (1.5 eq.), DMAP (0.2 eq.), CH_2Cl_2 (0.2 M), rt.

In summary, we have demonstrated that a highly substituted cyclohexa-1,4-diene may be accessed using a sequential Diels–Alder–decarboxylative olefination approach to introduce the C-11–C-12 unsaturation present in the paclitaxel A-ring. Ongoing studies in our laboratory seek to identify a direct [4+2] cycloaddition entry to **17**, and to develop ways of making the cycloaddition enantioselective. The results of these and related studies will be reported in due course.

We thank the EPSRC and Pfizer Central Research (CASE Studentships to C. A. L. L. and W. P. M.) and the Spanish Ministerio de Educacion y Ciencia (Studentship to S. C.) for financial support of this research.

Notes and references

‡ All yields reported herein refer to isolated, pure materials which had ^1H and ^{13}C NMR, IR and high-resolution MS characteristics in accord with the proposed structures.

§ The half-amide had a half-life in $CDCl_3$ of approximately 14 h.

¶ Treatment of this half-amide with ethyl chloroformate gave a mixed anhydride which was reduced using sodium borohydride to give a γ-lactone. The appearance of both lactone -CH_2- protons as simple doublets confirmed the absence of a vicinal proton, and therefore the complete regioselectivity of ring-opening of **13**.

‖ This assumption was later confirmed by single-crystal X-ray diffraction analysis of the product of one-pot epoxidation–debenzylation mediated by dimethyldioxirane.

** For other examples of cyclic ketaminal formation, see: A. E. Baydar and G. V. Boyd, *J. Chem. Soc., Perkin Trans. 1*, 1978, 1360; I. Tapia, V. Alcázar, J. R. Morán and M. Grande, *Bull. Chem. Soc. Jpn.*, 1990, **63**, 2408.

†† We thank Professor David Williams and Dr Andrew White of this Department for these determinations.

1 Isolation: W. C. Wani, H. L. Taylor, M. E. Wall, P. Coggon and A. T. McPhail, *J. Am. Chem. Soc.*, 1971, **93**, 2325.

2 Total synthesis: (*a*) K. C. Nicolaou, H. Ueno, J.-J. Liu, P. G. Nantermet, Z. Yang, J. Rebaud, K. Paulvannan and R. Chadha, *J. Am. Chem. Soc.*, 1995, **117**, 653, and preceding papers; (*b*) R. A. Holton, H. B. Kim, C. Somoza, F. Liang, R. J. Biediger, P. D. Boatman, M. Shindo, C. C. Smith, S. C. Kim, H. Nadizadeh, Y. Suzuki, C. L. Tao, P. Vu, S. H. Tang, P. S. Zhang, K. K. Murthi, L. N. Gentile and J. H. Liu, *J. Am. Chem. Soc.*, 1994, **116**, 1599, and preceding paper; (*c*) J. J. Masters, J. T. Link, L. B. Snyder, W. B. Young and S. J. Danishefsky, *Angew. Chem., Int. Ed. Engl.*, 1995, **34**, 1723; (*d*) P. A. Wender, N. F. Badham, S. P. Conway, P. E. Floreancig, T. E. Glass, J. B. Houze, N. E. Krauss, D. S. Lee, D. G. Marquess, P. L. McGrane, W. Meng, M. G. Natchus, A. J. Shuker, J. C. Sutton and R. E. Taylor, *J. Am. Chem. Soc.*, 1997, **119**, 2757; (*e*) K. Morihira, R. Hara, S. Kawahara, T. Nishimori, N. Nakamura, H. Kusama and I. Kuwajima, *J. Am. Chem. Soc.*, 1998, **118**, 12980; (*f*) T. Mukaiyama, I. Shiina, H. Iwadare, M. Saitoh, T. Nishimura, N. Ohkawa, H. Sakoh, K. Nishimura, Y. Tani, M. Hasegawa, K. Yamada and K. Saitoh, *Chem. Eur. J.*, 1999, **5**, 121.

3 Maleic anhydride reacted quantitatively with **12**, giving only the *endo* cycloadduct: C. A. L. Lane, PhD Thesis, University of London, 1997. For the related Diels–Alder reaction of citraconic anhydride with (*E*)-1-ethoxy-4-methylpenta-1,3-diene, see: F. Kienzle, I. Mergelsberg, J. Stadlwieser and W. Arnold, *Helv. Chim. Acta*, 1985, **68**, 1133.

4 J. A. Marshall and T. M. Warne, *J. Org. Chem.*, 1971, **36**, 178; R. Gleiter, R. Merger and B. Nuber, *J. Am. Chem. Soc.*, 1992, **114**, 8921.

5 S. V. Ley, J. Norman, W. P. Griffith and S. P. Marsden, *Synthesis*, 1994, 639.

6 H. Finch, A. M. M. Mjalli, J. G. Montana, S. M. Roberts and R. J. K. Taylor, *Tetrahedron*, 1990, **46**, 4925.

7 G. E. Keck, K. A. Savin and M. A. Weglarz, *J. Org. Chem.*, 1995, **60**, 3194.

8 D. H. R. Barton, D. Crich, Y. Hervé, P. Potier and J. Thierry, *Tetrahedron*, 1985, **41**, 4347.

9 For a review of β-lactone chemistry, see: A. Pommier and J.-M. Pons, *Synthesis*, 1993, 441.

10 For analogous olefin-forming reactions from β-haloesters, see: J. L. Belletire and D. R. Walley, *Tetrahedron Lett.*, 1983, **24**, 1475.

ChemComm

Synthesis and structure of a tris imido phosphonate anion; the missing link in imido analogues of phosphorus oxoanions

Lisa T. Burke,[a] Eva Hevia-Freire,[a] Rebecca Holland,[a] John C. Jeffery,[a] Angela P. Leedham,[a] Christopher A. Russell,*[a] Alexander Steiner[b] and Anette Zagorski[a]

[a] *School of Chemistry, University of Bristol, Cantock's Close, Bristol, UK BS8 1TS. E-mail: Chris.Russell@bristol.ac.uk*

[b] *Department of Chemistry, University of Liverpool, Crown Street, Liverpool, UK L69 7ZD*

Received (in Cambridge, UK) 25th May 2000, Accepted 4th August 2000
First published as an Advance Article on the web 31st August 2000

The reaction of PCl_3 with 3 equivalents of 2-methoxyaniline in THF/NEt_3, followed by metallation with Bu^{n}Li (2 equivalents) yields a complex $[Li_2P(H)(NR)_3]_2$ 1 (R = 2-methoxyphenyl), whose tris imido phosphonate anion is the imido analogue of the phosphite anion, $[HPO_3]^{2-}$.

The chemistry of main group imido complexes is relatively underdeveloped compared to the vast body of knowledge that has been accumulated on the related imido transition metal species.[1] Recently this imbalance has started to be redressed with the discovery of a diverse series of anionic imido complexes of the main group elements.[2–6] Our own interest in this area has focused on the study of imido analogues of phosphorus oxoanions. Recent studies on related P–N systems have revealed the beginnings of a family of these compounds. Alkali metal salts of the bis(imino)phosphinate anion, $[R_2P(NR')_2]^-$ have been prepared.[2] Niecke *et al.* have reported several structures that are imido analogues of kinetically unstable phosphorus oxoanions. This group described the planar tris(imino)metaphosphate anion, $[P(NR)_3]^-$ and the $[P(NR)_2]^-$ anion, isoelectronic with the kinetically unstable $[PO_3]^-$ and $[PO_2]^-$ anions respectively, but more importantly isoelectronic with the corresponding nitrate $[NO_3]^-$ and nitrite $[NO_2]^-$ anions.[3,4] Recently, we succeeded in synthesising the complex $[Li(THF)_4][(THF)_2Li(\mu\text{-}NR)_2P(\mu\text{-}NR)_2Li(THF)_2]$ from the reaction of P_2I_4 with 1-aminonaphthalene (1:4 equivalents) in THF/NEt_3, followed by metallation with Bu^{n}Li (4 equivalents). The $[P(NR)_4]^{3-}$ trianion of this complex is isoelectronic with the orthophosphate anion, $[PO_4]^{3-}$.[5] Related phosphorus–nitrogen complexes have recently found extensive uses as ligands to a range of metals, some of which have found application as polyolefin catalysts. This work has been reported and reviewed in several recent articles.[6]

Herein, we report the synthesis and structure of the imido analogue of the phosphite anion, $[HPO_3]^{2-}$. Reaction of PCl_3 with 3 equivalents of 2-methoxyaniline in THF/NEt_3, followed by addition of Bu^{n}Li (2 equivalents) and subsequent crystallisation from toluene gives $[Li_2P(H)(NR)_3]_2$ **1** (R = 2-methoxyphenyl.†

A low-temperature single-crystal X-ray diffraction study was performed on complex **1**.‡ The complex has an ion-contacted dimeric structure with a crystallographically imposed centre of symmetry wherein two $[HP(NR)_3]^{2-}$ anions sandwich four lithium cations. The $[HP(NR)_3]^{2-}$ dianion is formally the imido analogue of the phosphite dianion, $[HPO_3]^{2-}$.[7] The crystal structure of **1** is illustrated in Fig. 1.

Each of the phosphorus centres has a distorted tetrahedral geometry, being coordinated to three imido nitrogen atoms and one hydrogen atom. The phosphorus atoms are bound approximately equally to each imido nitrogen atom [with P–N distances ranging from 1.613(2) to 1.630(2) Å]. The shorter bond distances in **1** compared to those in the related imido analogue of the orthophosphate anion, $[P(NR)_4]^{3-}$ [1.645(4) Å][5] is perhaps due to the enhanced double bond character in **1** where formally, one P=N bond and two P–N bonds form a resonance hybrid, whereas in $[P(NR)_4]^{3-}$ the ratio is one P=N bond to three P–N bonds.

Within the core of **1** there are two distinct lithium environments. In one domain the lithium centre is complexed by one imido nitrogen centre from each $[HP(NR)_3]^{2-}$ unit and is additionally complexed by two methoxy sidearms of the corresponding methoxyanilido groups. The second lithium environment has the lithium centre complexed by two imido nitrogen atoms from one $[HP(NR)_3]^{2-}$ unit but by only one imido centre from the other $[HP(NR)_3]^{2-}$ unit. The methoxy sidearm of the latter unit completes the distorted tetrahedral geometries about these lithium centres.

The P–H proton could not be unequivocally located from the electron difference map, but its presence could be discerned from the ^{1}H and ^{31}P NMR spectra and from solution IR spectroscopy. Hence, the ^{1}H spectra in benzene-d_6, in addition to confirming the presence of 2-methoxyanilido ligands, show a

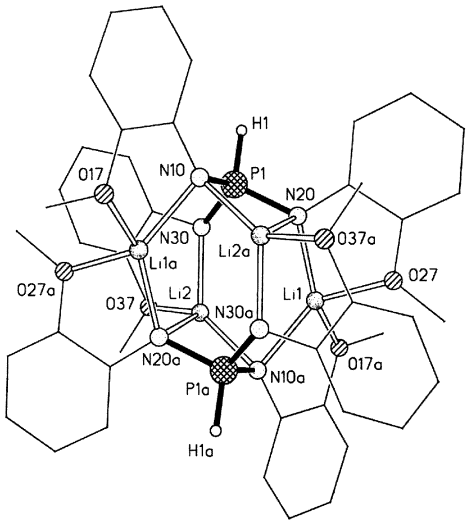

Fig. 1 The crystal structure of **1**. All hydrogen atoms (except P–H hydrogen atoms) have been omitted for clarity. Selected bond lengths (Å) and angles (°): P(1)–N(30) 1.613(2), P(1)–N(20) 1.6194(14), P(1)–N(10) 1.630(2), Li(1)–N(20) 1.991(3), Li(1)–N(10a) 2.063(3), Li(2)–N(30) 1.972(3), Li(2)–N(10a) 2.050(3), Li(2)–N(20a) 2.337(4), Li(1)–O(27) 1.945(3), Li(1)–O(17a) 1.981(3), Li(2)–O(37) 1.925(3), N(30)–P(1)–N(20) 104.60(7), N(30)–P(1)–N(10) 112.77(7), N(20)–P(1)–N(10) 108.91(8), O(27)–Li(1)–O(37a) 99.5(2), O(27)–Li(1)–N(20) 82.68(13), O(17a)–Li(1)–N(20) 141.3(2), O(27)–Li(1)–N(10a) 134.7(2), O(17a)–Li(1)–N(10a) 80.71(12), N(20)–Li(1)–N(10a) 124.6(2), O(37)–Li(2)–N(30) 84.65(13), O(37)–Li(2)–N(10a) 142.0(2), N(30)–Li(2)–N(10a) 130.0(2), O(37)–Li(2)–N(20a) 116.1(2), N(30)–Li(2)–N(20a) 105.74(14), N(10a)–Li(2)–N(20a) 73.78(11), C(11)–N(10)–P(1) 128.33(12), C(11)–N(10)–Li(2a) 124.45(14), P(1)–N(10)–Li(2a) 92.64(11), C(11)–N(10)–Li(1a) 108.32(14), P(1)–N(10)–Li(1a) 109.98(12), Li(2a)–N(10)–Li(1a) 84.54(13), C(21)–N(20)–P(1) 122.86(12), C(21)–N(20)–Li(1) 111.49(14), P(1)–N(20)–Li(1) 125.64(12), C(21)–N(20)–Li(2a) 93.95(12), P(1)–N(20)–Li(2a) 83.05(10), Li(1)–N(20)–Li(2a) 94.68(13), C(31)–N(30)–P(1) 122.67(12), C(31)–N(30)–Li(2) 107.44(14), P(1)–N(30)–Li(2) 122.74(12).

DOI: 10.1039/b004192k

doublet at δ 9.07 with a coupling constant of 436 Hz, consistent with the $^1J_{PH}$ coupling frequencies observed in related systems.[8] The corresponding doublet can be observed in the ^{31}P NMR spectra at δ 0.28. This bond can also be observed by IR spectroscopy with a band at 2266 cm^{-1} in THF solution being attributed to the P–H stretching frequency.

Although we have so far been unable to unequivocally identify the intermediates in the steps leading to complex **1**, it seems reasonable to postulate that the $[HP(NR)_3]^{2-}$ anion of **1** has resulted from a proton exchange from an amido centre to the phosphorus centre in addition to metallation of the remaining amido protons. Similar proton transfer from N to P in iminophosphoranes, R_2P–N(H)R′ has shown that the P–H tautomer is stabilised by both electron withdrawing amide groups (R′) and by bulky substituents on the P and N centres (R and R′).[9] Hence, N to P proton transfer accompanying metallation in the postulated $P\{N(H)R\}_3$ intermediate from the first step of our reaction system would yield complex **1**. It is interesting to note that phosphites (or rather phosphorous acid) can be produced by a similar route, *i.e.* hydrolysis of PCl_3.[10]

We gratefully acknowledge the EPSRC (J. C. J., A. S.), The Royal Society (University Research Fellowship for C. A. R.), The Nuffield Foundation (L. T. B., C. A. R.) and the European Union (Socrates award to E. H.-F.) for financial support. We also thank Professor W. Siebert (Heidelberg) for an Erasmus exchange student (A. Z.).

Notes and references

† *Preparation* of **1**: to an ice-cooled stirred solution of PCl_3 (0.17 ml, 2 mmol) in THF (15 ml) and NEt_3 (4 ml, 28.7 mmol) was added 2-methoxyaniline (0.68 ml, 6 mmol). A white solid was observed in a yellow solution. After stirring for 3 h, the reaction was filtered (porosity 3 sinter with Celite) to give a yellow solution. To this was added Bu^{n}Li (2.5 ml, 1.6 mol l^{-1}, 4 mmol) which caused the solution to turn browny yellow followed by the precipitation of a white solid after *ca.* 1 min. The solvent was removed *in vacuo* and the solid was redissolved with toluene (8 ml). Storage for 24 h at −30 °C yields colourless cubic blocks of **1**. Yield 0.836 g (51%).

No melting or decomposition up to 280 °C; IR (THF solution) ν/cm^{-1} = 2266 (P–H stretch); ^{1}H NMR (+25 °C, 300 MHz, benzene-d_6): δ 9.07 (d, 2H, P–H, $^1J_{PH}$ 436 Hz), 7.25–6.30 (collection of m, 24H, –$NC_6H_4OCH_3$), 2.80 (s, 18H, –$NC_6H_4OCH_3$); ^{31}P NMR (+25 °C, 121.55 MHz, benzene-d_6): δ 0.28 (d, $^1J_{PH}$ 436 Hz). Anal. Calc. C, 61.6; H, 5.4; N, 10.3; P, 7.6. Found: C, 61.2; H, 5.4; N, 10.2; P, 7.5%.

‡ *Crystal data* for **1**: $C_{21}H_{22}Li_2N_3O_3P$, M = 409.27, orthorhombic, space group *Pbca*, a = 16.026(5), b = 11.410(2), c = 22.560(5) Å, U = 4125(2) Å^3, Z = 8, D_c = 1.318 Mg m^{-3}, T = 173(2) K, μ(Mo-Kα) = 0.160 mm^{-1}, 24588 reflections measured, 4710 unique (R_{int} = 0.0508) which were used in all calculations. Data were collected on a Bruker SMART CCD area-detector diffractometer[11] using a crystal mounted on a glass fibre in a rapidly cooled perfluoropolyether.[12] The structure was solved by direct methods and refined by least squares on F^2 values for all reflections. Absorption corrections were applied, based on multiple and symmetry equivalent measurements.[13] Final $R1$ = 0.0402 [$I > 2\sigma(I)$] and $wR2$ = 0.1042 (all data).[14]

CCDC 182/1739. See http://www.rsc.org/suppdata/cc/b0/b004192k/ for crystallographic files in .cif format.

1 D. E. Wigley, *Prog. Inorg. Chem.*, 1994, **42**, 239.
2 A. Steiner and D. Stalke, *Inorg. Chem.*, 1993, **32**, 1977.
3 E. Niecke, M. Frost, M. Nieger, V. von der Gönna, A. Ruban and W. W. Schoeller, *Angew. Chem.*, 1994, **106**, 2170; *Angew. Chem., Int. Ed. Engl.*, 1994, **33**, 2111.
4 R. Detsch, E. Niecke, M. Nieger and W. W. Schoeller, *Chem. Ber.*, 1992, **125**, 1119.
5 P. R. Raithby, C. A. Russell, A. Steiner and D. S. Wright, *Angew. Chem.*, 1997, **109**, 670; *Angew. Chem., Int. Ed. Engl.*, 1997, **36**, 649.
6 M. Witt and H. W. Roesky, *Chem. Rev.*, 1994, **94**, 1163; K. Dehnicke, M. Krieger and W. Massa, *Coord. Chem. Rev.*, 1999, **182**, 19; K. Aparna, M. Ferguson and R. G. Cavell, *J. Am. Chem. Soc.*, 2000, **122**, 726 and references therein.
7 D. R. Powell, S. K. Smith, T. C. Farrar and F. K. Ross, *Acta Crystallogr., Sect. C*, 1994, **50**, 342.
8 A. Schmidpeter, J. Ebeling, H. Stary and C. Weingand, *Z. Anorg. Allg. Chem.*, 1972, **394**, 171.
9 P. V. Sudhakar and K. Lammertsma, *J. Am. Chem. Soc.*, 1991, **113**, 1899; D. Gonbeau, G. Pfister-Guillouzo, M. Mazieres and M. Sanchez, *Can. J. Chem.*, 1985, **63**, 3242; A. Schmidpeter and J. Ebeling, *Angew. Chem.*, 1968, **80**, 197; *Angew. Chem., Int. Ed. Engl.*, 1968, **7**, 209; A. Schmidpeter and H. Rossknecht, *Angew. Chem.*, 1969, **81**, 572; *Angew. Chem., Int. Ed. Engl.*, 1969, **8**, 614; G. Schick, A. Loew, M. Nieger, K. Airola and E. Niecke, *Chem. Ber.*, 1996, **129**, 911; H. Binder and R. Fischer, *Chem. Ber.*, 1974, **107**, 205; H. R. O'Neal and R. H. Neilson, *Inorg. Chem.*, 1984, **23**, 1372; N. Burford, J. A. C. Clyburne, S. Mason and J. F. Richardson, *Inorg. Chem.*, 1993, **32**, 4988; A. Schmidpeter and H. Rossknecht, *Z. Naturforsch., Teil B*, 1971, **26**, 81.
10 J. Novosad, in *Encyclopedia of Inorganic Chemistry*, John Wiley and Sons, Chichester, 1994, vol. 6, p. 3169.
11 SMART diffractometer control software, Siemens Analytical X-ray Instruments Inc., Madison, WI, 1994.
12 T. Kottke and D. Stalke, *J. Appl. Crystallogr.*, 1993, **26**, 615.
13 SADABS absorption correction software, Siemens Analytical X-ray Instruments Inc., Madison, WI, 1994.
14 G. M. Sheldrick, SHELXTL, Madison, WI, 1995.

ChemComm

Asymmetric synthesis of 2-substituted 5-, 6- and 7-membered nitrogen heterocycles by oxime addition ring-closing metathesis

James C. A. Hunt, Pierre Laurent and Christopher J. Moody*

School of Chemistry, University of Exeter, Stocker Road, Exeter, UK EX4 4QD

Received (in Liverpool, UK) 30th June 2000, Accepted 24th July 2000
First published as an Advance Article on the web 30th August 2000

Ring closing metathesis reactions of the dienes 6 and 9 leads to the nitrogen heterocycles 7 and 10, respectively, one of which 10c was converted into (*R*)-(−)-coniine.

The development of methods for the asymmetric synthesis of pyrrolidines and piperidines remains an area of current interest due to the presence of such saturated heterocyclic rings in a large number of biologically important compounds.[1] One possible approach to the synthesis of nitrogen heterocycles involves the ring-closing olefin metathesis (RCM) reaction. The RCM reaction is a powerful synthetic method and, with the development of practical and reliable catalysts by Grubbs and others,[2,3] has been widely used in a number of syntheses in the recent past,[4,5] including examples of nitrogen heterocycles.[6–14] In continuation of our interest in the asymmetric synthesis of saturated nitrogen heterocycles,[15] we decided to investigate the combination of the highly diastereoselective addition reactions of *O*-(1-phenylbutyl) aldoximes with the RCM reaction as a new route to this class of heterocycle. This combination of oxime addition–RCM is shown in outline in Scheme 1, and our preliminary results are described herein.

As outlined in Scheme 1, the substrates for the RCM reactions are the dienes **3**, accessible either by the addition of an alkene containing organometallic reagent to the aldoxime ether **1**, or by organometallic addition to an aldoxime **2** derived from an unsaturated aldehyde, followed in both cases by *N*-allylation of the resulting hydroxylamine. Both approaches were successful and a number of dienes **6** were prepared by the highly diastereoselective addition of organolithium reagents to the *O*-(1-phenylbutyl) oximes of cinnamaldehyde or allylmagnesium bromide to the oximes of butyraldehyde or benzaldehyde,[16,17] followed by reaction with allyl bromide in the presence of potassium carbonate (Table 1). The RCM reaction was carried out by heating the dienes **6** in dichloromethane in the presence of Grubbs' catalyst, and gave the required 5- and 6-membered rings **7** in modest to excellent yield (Table 1).

Although the above results indicate that basic or nucleophilic nitrogen atoms are tolerated in the RCM reaction of the hydroxylamine derived substrates, we also investigated the diene substrates **9** in which the nitrogen is rendered non-basic by protection as its benzyloxycarbonyl (Z) derivative. Thus a range of carbamates **8**, prepared as previously described,[16,17] or as indicated in Table 2, was converted into the corresponding *N*-allyl derivatives **9** by reaction with allyl bromide in the presence of sodium hydride. In the case of **8b**, these conditions caused migration of the double bond, and therefore the allyl group was introduced using the palladium catalysed reaction of allyl methyl carbonate.[18] Again the RCM reaction proceeded smoothly and gave the 5- and 6-membered nitrogen heterocycles **10a**–**10d** in good to excellent yield, with the yield of the 7-membered ring **10e** being slightly lower (Table 2).

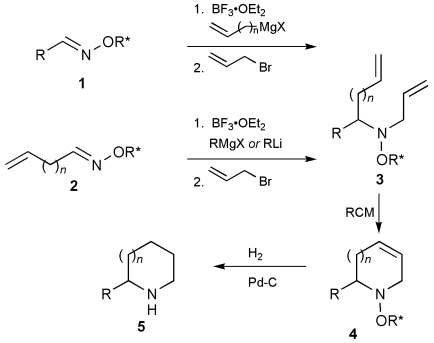

Scheme 1 (R* = 1-phenylbutyl).

Table 1

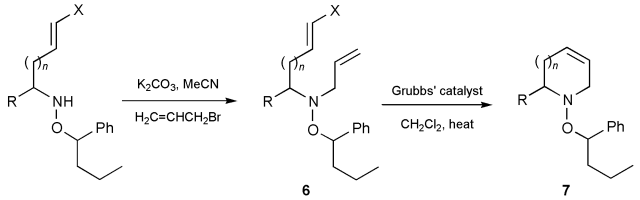

(E)-Oxime[a]	Organometallic Addition	Yield (%) (de (%))	R	X	*n*	Diene	Yield (%)	Heterocycle (configuration at C-2)	Yield (%)
(*R*)-PhCH=CHCH=NOR*	MeLi[b]	[c](>95)	Me	Ph	0	**6a**	72[c]	**7a** (*R*)	87
(*R*)-PhCH=CHCH=NOR*	*n*-BuLi[b]	[c](>95)	*n*-Bu	Ph	0	**6b**	66[c]	**7b** (*R*)	78
(*S*)-PhCH=CHCH=NOR*	*i*-BuLi[d]	95 (88)	*i*-Bu	Ph	0	**6c**	83	**7c** (*S*)	74
(*R*)-PhCH=CHCH=NOR*	PhLi[b]	62 (>95)	Ph	Ph	0	**6d**	52	**7d** (*S*)	51
(*S*)-*n*-PrCH=NOR*	H_2C=$CHCH_2MgBr$	[c](87)	*n*-Pr	H	1	**6e**	39[c]	**7e** (*R*)	90
(*S*)-PhCH=NOR*	H_2C=$CHCH_2MgBr$[e]	[c](94)	Ph	H	1	**6f**	71[c]	**7f** (*S*)	62

[a] R* = 1-phenylbutyl; configuration as indicated. [b] This addition reaction reported in ref 15. [c] Yield over 2 steps. [d] The addition to the (*R*)-enantiomer of the oxime reported in ref 15. [e] The addition to the (*R*)-enantiomer of the oxime reported in ref 16.

DOI: 10.1039/b005353h

Table 2

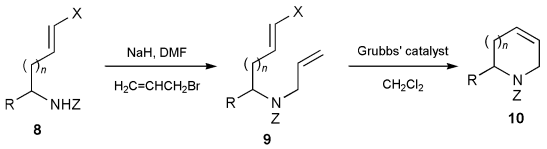

Carbamate	Configuration (ee (%))	R	X	*n*	*N*-Allyl carbamate	Yield (%)	Heterocycle (configuration at C-2)	Yield (%)
8a[a]	*S* (89[b])	Me	Ph	0	**9a**	74	**10a** (*S*)	84
8b[c]	*R* (>95[d])	Ph	Ph	0	**9b**	63[e]	**10b** (*R*)	93
8c[f]	*R* (90)	*n*-Pr	H	1	**9c**	90	**10c** (*R*)	88
8d[g]	*S* (98)	4-MeO-C_6H_4	H	1	**9d**	97	**10d** (*S*)	91
8e[h]	*R* (90)	Ph	H	2	**9e**	90	**10e** (*R*)	65

[a] The preparation of the (*R*)-enantiomer is described in ref 15. [b] Enantiomeric excess (ee) of the *N*-allyl derivative **9a** not **8a**. [c] The preparation of the (*S*)-enantiomer is described in ref 15. [d] Refers to the diastereomeric excess (de) of the immediate precursor to **8b**. [e] Allylation using allyl bromide/base caused double bond migration; prepared using allyl methyl carbonate/Pd(0); see text. [f] Prepared by addition of allylmagnesium bromide to the oxime ether (Table 1), followed by cleavage of the N–O bond, and reaction with benzyl chloroformate. [g] Prepared as described in ref 16. [h] Prepared by addition of phenyllithium to the oxime ether, followed by cleavage of the N–O bond, and reaction with benzyl chloroformate.

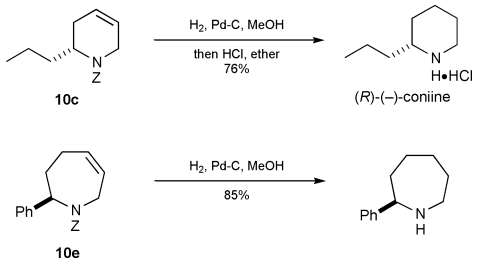

Scheme 2

Finally two of the heterocycles prepared by the RCM reaction were converted into known compounds for confirmation of structure and configuration. Thus the 6- and 7-membered Z-protected compounds **10c** and **10e** were hydrogenated over palladium-on-charcoal to give (*R*)-(−)-coniine and the known 2-phenylazepane[19] respectively (Scheme 2).

We thank the EPSRC for support of this work.

Notes and references

1 For a review, see: A. Mitchinson and A. Nadin, *J. Chem. Soc., Perkin Trans. 1*, 1999, 2553 and earlier reviews in this series.
2 R. H. Grubbs, S. J. Miller and G. C. Fu, *Acc. Chem. Res.*, 1995, **28**, 446.
3 R. H. Grubbs and S. Chang, *Tetrahedron*, 1998, **54**, 4413.
4 S. K. Armstrong, *J. Chem. Soc., Perkin Trans. 1*, 1998, 371.
5 D. L. Wright, *Curr. Org. Chem.*, 1999, **3**, 211.
6 S. N. Osipov, C. Bruneau, M. Picquet, A. F. Kolomiets and P. H. Dixneuf, *Chem. Commun.*, 1998, 2053.
7 A. J. Phillips and A. D. Abell, *Aldrichimica Acta*, 1999, **32**, 75.
8 A. Fürstner and L. Ackermann, *Chem. Commun.*, 1999, 95.
9 E. Jo, Y. Na and S. Chang, *Tetrahedron Lett.*, 1999, **40**, 5581.
10 P. Evans, R. Grigg and M. Monteith, *Tetrahedron Lett.*, 1999, **40**, 5247.
11 A. Fürstner and O. R. Thiel, *J. Org. Chem.*, 2000, **65**, 1738.
12 A. J. Souers and J. A. Ellman, *J. Org. Chem.*, 2000, **65**, 1222.
13 A. Fürstner, O. R. Thiel, L. Ackermann, H. J. Schanz and S. P. Nolan, *J. Org. Chem.*, 2000, **65**, 2204.
14 K. Tjen, S. S. Kinderman, H. E. Schoemaker, H. Hiemstra and F. Rutjes, *Chem. Commun.*, 2000, 699.
15 C. J. Moody, A. P. Lightfoot and P. T. Gallagher, *J. Org. Chem.*, 1997, **62**, 746.
16 C. J. Moody, P. T. Gallagher, A. P. Lightfoot and A. M. Z. Slawin, *J. Org. Chem.*, 1999, **64**, 4419.
17 J. C. A. Hunt, C. Lloyd, C. J. Moody, A. M. Z. Slawin and A. K. Takle, *J. Chem. Soc., Perkin Trans. 1*, 1999, 3443.
18 F. L. Zumpe and U. Kazmaier, *Synthesis*, 1999, 1785.
19 C. A. Willoughby and S. L. Buchwald, *J. Am. Chem. Soc.*, 1994, **116**, 8952.

ChemComm

Best design of heterogenized β-aminoalcohols for improvement of enantioselective addition of diethylzinc to benzaldehyde

Sébastien Abramson, Monique Laspéras,* Anne Galarneau, Delphine Desplantier-Giscard and Daniel Brunel

Laboratoire de Matériaux Catalytiques et Catalyse en Chimie Organique, UMR 5618 - CNRS - Ecole Nationale Supérieure de Chimie de Montpellier, 8, rue de l'Ecole Normale, 34296 Montpellier Cedex 5, France. E-mail: lasperas@cit.enscm.fr; Fax: +33 4 67 14 43 49

Received (in Cambridge, UK) 10th July 2000, Accepted 4th August 2000
First published as an Advance Article on the web 4th September 2000

Covalent immobilization of (1*R*,2*S*)-(−)-ephedrine, used as a model molecule of β-aminoalcohols, on the surface of MCM-41-type mesoporous aluminosilicates, performed by a new sol–gel method, leads to chiral auxiliaries which show greatly enhanced rates and ee's compared to those reported up to now in the enantioselective addition of diethylzinc to benzaldehyde.

Increasing interest has been devoted to the design of heterogeneous asymmetric catalysts.[1] One major method involves heterogenization of homogeneous catalysts by their immobilization on organic polymers or inorganic supports.[2] However, the efficiency of the catalysts of the heterogenized catalysts is different compared with their homogeneous counterparts. This is the case for chiral β-aminoalcohols used in the enantioselective addition of dialkylzincs to aldehydes[3] in C–C bond forming reactions. The efficiency of such catalysts depends mainly on the native of the support. Since the pioneering work of Frechet[4] who used polymer-bound chiral aminoalcohols, various authors have described such immobilization on organic polymers.[5,6] Ee's are high, and only slightly lower than those obtained in homogeneous conditions but rates are notably lower. On the other hand, immobilization on mineral surfaces has attracted little attention. Our first results using (−)-ephedrine supported on MCM-41-type mesoporous silicas[7] were in good agreement with precedent results of Soai *et al.*[8] using silica gel or alumina supported (−)-ephedrine. Lower rates, selectivities and enantioselectivities were obtained compared with homogeneous catalysis. Investigations involving changes in the pore size,[9] the composition[10] of the support, end-capping of the surface[9] and the dilution of the catalytic sites[9,10] failed to improve the ee's significantly. These results indicate significant activity of the naked surface towards the formation of racemic alcohols.

The aim of this work was to decrease the negative effects of the uncovered mineral surface by increasing the coverage by organics on the inner surface of the pores.[11] In this work, the synthesis of high surface densities of chloropropyl groups covalently grafted on mesoporous micelle templated aluminosilicates (Al-MTS) of various initial pore diameters is performed. The hybrid inorganic–organic materials resulting from halogen substitution by (−)-ephedrine are applied in the enantioselective addition of diethylzinc to benzaldehyde.

Two mesoporous aluminosilicates of the same composition (Si/Al = 27) and 3.6 (Al-MTS **1**, S = 833 m^2 g^{-1}, V = 0.76 mL g^{-1})[12] and 8.3 nm (Al-MTS **2**, S = 822 m^2 g^{-1}, V = 1.71 mL g^{-1})[13] mean initial pore diameter were used as supports, respectively. In order to remove the template, the as-synthesized solids were activated before surface modification at 550 °C for 12 h under a flow of synthetic air. Up to now, covalent anchorages have been performed in anhydrous conditions, by silylation (method **a**) with 3-chloropropyltrimethoxysilane (CPTMS) (Al-MTS-Cl **1a**) followed by the nucleophilic substitution of chlorine by the basic amino group of (−)-ephedrine (Al-MTS-Cl-E **1a**). Alternatively, grafting of the coupling CPTMS agent by the sol–gel method[11,14] (method **b**, Al-MTS-Cl **1b**, Al-MTS-Cl **2b**) and reaction with (−)-ephedrine leads to new hybrid materials (Al-MTS-Cl-E **1b**, Al-MTS-Cl-E **2b**) (Scheme 1).

Loadings of grafted chloroalkylsiloxanes (Al-MTS-Cl **1a**, **1b**, **2b**) or ephedrine moieties (Al-MTS-Cl-E **1a**, **1b**, **2b**) have been calculated from elemental and thermogravimetric analyses. They depend mainly on the grafting method used, the sol–gel method **b** leading to notably higher amounts of organics on the surface.

Textural properties are recorded in Table 1. Method **a** leads to conservation of the mesoporosity after modification by organics. As shown previously[7,9,10] textures are maintained after grafting of halogens and substitution by (−)-ephedrine. However, a decrease in the residual mesoporous volume is observed. In the case of method **b**, the porosity of hybrids Al-MTS-Cl **1b** and Al-MTS-Cl-E **1b** becomes a microporosity. Increasing the initial pore diameter allows high residual mesoporous volumes to be obtained even after immobilization of a high density of organic functions by method **b** (Al-MTS-Cl **2b**, Al-MTS-Cl-E **2b**, Table 1).

Enantioselective addition of diethylzinc to benzaldehyde conducted in the presence of these solid chiral auxiliaries leads to the formation of (*R*)- or (*S*)-1-phenylpropan-1-ol (Scheme 2). All experiments were performed at 0 °C using the same weight of solid chiral auxiliary (0.29 g) and 2.3 eq. of Et_2Zn to benzaldehyde.[9,10] Results are shown in Table 2.

Such chiral auxiliaries are efficient in the enantioselective transfer of an ethyl group to benzaldehyde. The best results are obtained using (−)-ephedrine anchored on the Al-MTS **2** support (entry 11) and it is worth noting that ee and activity are close to those obtained in homogeneous catalysis (entries 2 and 3). On the other hand, efficiency depends on the synthetic method and on the initial pore diameter of the support. The

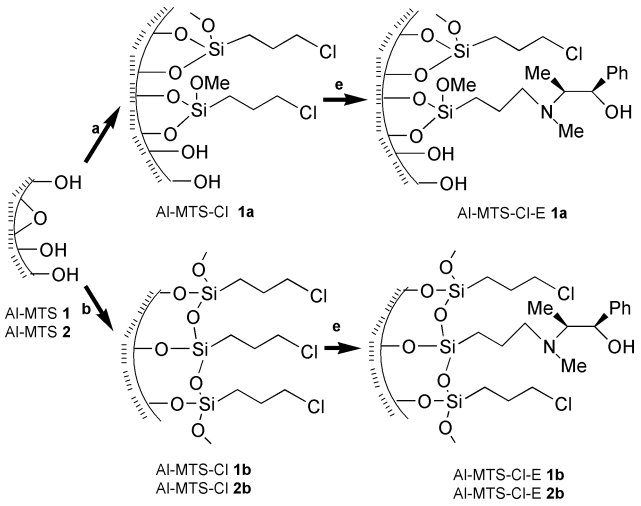

Scheme 1 *Reagents and conditions*: **a**, CPTMS, toluene, anhydrous conditions, −130 °C, 4 h; **b**, CPTMS, toluene, H_2O, NH_4F–*p*TsOH, −60 °C, 6 h; **c**, (1*R*,2*S*)-(−)-ephedrine, Xylene, −140 °C, 6 h.

DOI: 10.1039/b005518m

Table 1 Characterization of hybrid inorganic–organic mesoporous aluminosilicates

Materials	Cl loading[a]/ mmol g^{-1}	N loading[a]/ mmol g^{-1}	Cl density[b]/ 10^6 mol/m^{-2}	S^c_{BET}/ m^2 g^{-1}	V^c_{mp}/ mL g^{-1}	Mean pore diameter[c]/nm
Al-MTS-Cl **1a**	2.1	—	2.3	756	0.42	2.2
Al-MTS-Cl-E **1a**	0.8	1.3		689	0.30	1.7
Al-MTS-Cl **1b**	4.4	—	—		0.21[d]	
Al-MTS-Cl-E **1b**	2.5	1.9			0.07[d]	
Al-MTS-Cl **2b**	4.3	—	7.7	559	0.77	5.5
Al-MTS-Cl-E **2b**	2.4	1.9		440	0.62	5.5

[a] Loadings are calculated relatively to the weight of dry initial silica content. [b] Densities are expressed by the ratio of the loading to the surface area of the naked support. [c] N_2 adsorption and desorption isotherms were collected on a Micromeritics ASAP 2000 apparatus at 77 K, after outgassing samples at 423 K for 8 h. Mean pore diameters are calculated by the $4V_{mp}/S_{BET}$ ratio. [d] BET equation used for the determination of surface area is inoperative.

Table 2 Alkylation of benzaldehyde with diethylzinc

Entry	Materials	(−)-Ephedrine (mol%)[a]	k^b_{obs}/h^{-1}	Selectivity[c] (%)	Ee[d] (%)
1	Without catalyst	—	$1.2\ 10^{-2}$	51	0
2	(−)-Ephedrine	8.5	0.53	98	65
3	(−)-*N*-Propylnorephedrine	8.5	0.68	98	76
4	Al-MTS **1**	—	0.17	84	0
5	Al-MTS-Cl **1a**	—	0.11	82	0
6	Al-MTS-Cl-E **1a**	13.6	0.17	93	47
7	Al-MTS-Cl **1b**	—	0.05	84	0
8	Al-MTS-Cl-E **1b**	15.4	0.11	94	54
9	Al-MTS **2**	—	0.26	87	0
10	Al-MTS-Cl **2b**	—	0.07	86	0
11	Al-MTS-Cl-E **2b**	16.8	0.55	98	64

[a] The number of catalytic sites is calculated relative to the total weight of hybrid material. [b] Fitting of BA (%) *versus* time (h) by an exponential regression leads to k_{obs} (h^{-1}). [c] % selectivity = 100 ([*R*] + [*S*])/([*R*] + [*S*] + [$PhCH_2OH$]). [d] (%) Ee = 100 ([*R*] − [*S*])/[*R*] + [*S*].

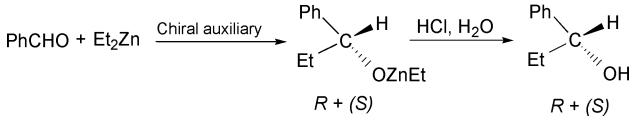

Scheme 2

inorganic surface of the support catalyzes the racemic alkyl transfer (entries 4 and 9) as shown by comparison with the uncatalyzed reaction (Table 2, entry 1) and the activity increases with the mesoporous volume (Table 1). Coverage of the surface by chloropropyl moieties leads to a decrease in the activity whatever the support (entries 4, 5 and 7 for Al-MTS **1**, entries 9 and 10 for Al-MTS **2**). The higher the coverage is, the lower the activity of the mineral surface. Solids derived from Al-MTS **1** show a slight increase in activity after modification by (−)-ephedrine; the activity of the high density solid (entry 8) is lower than that of the low density auxiliary (entry 6). Taking into account the low residual volume of the high density Al-MTS-Cl-E **1b**, we believe that accessibility to the catalytic sites is limited by diffusional constraints and that the reaction mainly proceeds on the external surface and at the pore opening. An increase in the mean pore diameter of the support allows the synthesis of high density hybrids with conservation of available mesoporous volumes. Hence, Al-MTS-Cl-E **2b** shows the highest activity obtained up to now, concomitant with good enantioselectivity related to the organic coverage of the mineral surface. It can be assumed that the catalytic sites located on the inner surface of the pores are active in the reaction. Bae *et al.*[15] reported recently the use of new chiral heterogeneous catalysts based on mesoporous silica, either MCM-41 or SBA-15 based catalysts. They attempted to improve ee's by using a more selective ligand than (−)-ephedrine and by addition of butyllithium as an extra metal reagent. It is worth noting that ee's were improved only in the latter case using a lithium salt in place of zinc alcoholate as the catalyst. Our approach based on the comprehension of the various effects led to the synthesis of the first inorganic–organic hybrid chiral auxiliaries, the efficiency of which can be compared with that obtained in homogeneous catalysis. Moreover, these catalysts may be reused three times without loss of enantioselectivity. In summary, two factors determine the design of new inorganic–organic chiral auxiliaries effective in C–C bond formation: firstly, the coverage of the surface by organics in order to suppress the activity towards the racemic reaction and secondly, the accessibility to the catalytic sites by using inorganic supports with large mesopore diameters.

The authors are grateful to F. Di Renzo, F. Fajula and P. Moreau for fruitful discussions.

References

1 J. M. Thomas, T. Maschmeyer, B. F. G. Johnson and D. S. Shepard, *J. Mol. Catal. A Chem.*, 1999, **141**, 139.
2 B. Pugin and H.-U. Blaser, in *Comprehensive Asymmetric Catalysis*, ed. E. N. Jacobsen, A. Pfaltz and H. Yamamoto, Springer-Verlag, Berlin, 1999, **vol. 3**, p. 1368.
3 R. Noyori and N. Kitamura, *Angew. Chem., Int. Ed. Engl.*, 1991, **30**, 49.
4 S. Itsuno and J. M. J. Fréchet, *J. Org. Chem.*, 1987, **52**, 4140.
5 K. Soai, S. Niwa and M. Watanabe, *J. Org. Chem.*, 1988, **53**, 927; M. Watanabe and K. Soai, *J. Chem. Soc., Perkin Trans 1*, 1994, 837.
6 D. W. L. Sung, P. Hodge and P. W. Stratford, *J. Chem. Soc., Perkin Trans. 1*, 1999, 1463.
7 M. Laspéras, N. Bellocq, D. Brunel and P. Moreau, *Tetrahedron: Asymmetry*, 1998, **9**, 3053.
8 K. Soai, M. Watanabe and A. Yamamoto, *J. Org. Chem.*, 1990, **55**, 4832.
9 N. Bellocq, S. Abramson, M. Laspéras, D. Brunel and P. Moreau, *Tetrahedron: Asymmetry*, 1999, **10**, 3229.
10 S. Abramson, N. Bellocq and M. Laspéras, *Top. Catal.*, in the press.
11 A. Galarneau, T. Martin, V. Izard, V. Hulea, A. Blanc, S. Abramson, F. Di Renzo, F. Fajula and D. Brunel, unpublished results.
12 F. Di Renzo, B. Chiche, F. Fajula, S. Viale and E. Garrone, *Stud. Surf. Sci. Catal.*, 1996, **101**, 851.
13 F. Di Renzo, A. Galarneau, D. Desplantier-Giscard, L. Mastrantuono, F. Testa and F. Fajula, *Sci. Technol.*, 1999, **81**, 587.
14 W. M. Van Rhijn, D. E. De Vos, B. F. Sels, W. D. Bossaert and P. Jacobs, *Chem. Commun.*, 1998, 317.
15 S. J. Bae, S.- W. Kim, T. Hyeon and B. M. Kim, *Chem. Commun.*, 2000, 31.

ChemComm

Synthesis, X-ray structure and NMR data of 12-amino-15-phenyl-2,5,8-trioxa-13-azabicyclo[9.2.2]pentadeca-1(14),12-diene-11,14-dicarbonitrile†

Luís Fuentes,*[a] M. Jesús Lorenzo,[a] Mikhail Galakhov,[a] Avelino Martín,[b] César Márquez[a] and Pilar Gómez-Sal[b]

[a] *Department of Organic Chemistry, University of Alcalá, Ctra. Madrid-Barcelona, Km. 33.6, 28871-Alcalá de Henares, Madrid, Spain. E-mail: luis.fuentes@alcala.es*

[b] *Department of Inorganic Chemistry, University of Alcalá, Ctra. Madrid-Barcelona, Km. 33.6, 28871-Alcalá de Henares, Madrid, Spain*

Received (in Cambridge, UK) 5th June 2000, Accepted 20th July 2000
First published as an Advance Article on the web 4th September 2000

Synthesis of unprecedented *oxygen-bridged* [*n*](2,5)pyridinophane dihydro-analogues

The development of new methods which allow the synthesis of [*n*]pyridinophanes and their dihydro-analogues is a major focus in supramolecular chemistry due to the many roles played by cyclophanes in biology and new technologies.[1] Pyridinophanes and their dihydro-analogues constituted the first examples of NADH models[2,3] capable of mimicking the diastereo-differentiating course of hydride exchange at pyridine dinucleotides under enzymatic conditions. In this way the asymmetric reduction of carbonyl substrates by optically active NADH model compounds has received wide attention.[3,4] Recently, crown ether annelated tetrathiafulvalenes were described as attractive components for sensor technology[5–7] and in some of these cases[6] pyridinophanes incorporating the tetrathiafulvalene (TTF) moiety have been studied as metal cations sensors.

In 1968 Gerlach and Huber[8] synthesized the first [*n*](2,5)pyridinophanes, *carbon-bridged* compounds, some *sulfur-bridged* [*n*](2,5)pyridinophanes were constructed and described as Vitamin B_6,[9] pyridoxal[10] and pyridoxamine[11] analogues; however, no synthetic procedure was reported to afford [*n*](2,5)pyridinophanes in which some methylene groups of the bridge were replaced by oxygen.

The synthesis of nearly all [*n*](2,5)pyridinophanes known has previously been accomplished using different synthetic strategies: (i) *via* the construction of the pyridine ring as happens in the acid-catalyzed cyclization of bis(β-aminovinyl)diketones[8] or (ii) by building the *ansa-chain* around the pyridine ring as in the thermal 1,6-Hofmann elimination from an intimate mixture of (4-methylbenzyl)trimethylammonium hydroxide and (5-methyl-2-picolinyl)trimethylammonium hydroxide.[12] *Sulfur-bridged* [*n*](2,5)pyridinophanes have been obtained through the Vögtle method by the condensation of dithiols with dihalogenopyridine compounds.[13]

Herein we present an unprecedented method for synthesis of dihydro-analogues of *oxygen-bridged* [*n*](2,5)pyridinophanes by a C–C bond formation between the pyridine ring and the ω-position of a chain. As a preliminary result we report here the synthesis and structural studies of the *oxygen-bridged* [9](2,5)pyridinophane‡ dihydro-analogues **5**.

Cyclic voltammetric data on the mercury cathode of the 2-amino-6-methoxy-4-phenylpyridine-3,5-dicarbonitrile[14] showed two peaks in the cathodic region at −1.88 and −2.20 V (*vs*. Ag/Ag^+),§ which make this compound susceptible to reduction by amalgam (Na·Hg).[15] On the basis of this behavior, we have developed a molecular system containing a latent nucleophilic pyridine ring moiety, switched on by electrochemical reduction, and an electrophilic center moiety linked by oxyethylene bridges. Pyridine derivative **4**, also having two reduction peaks at −1.88 and −2.20 V (*vs*. Ag/Ag^+),§ was chosen as a molecular model of this system. We have carried out its synthesis in multistep processes from pyridine **1**[16] as depicted in Scheme 1, *via* the substitution of the phenylthio group by triethylene glycol to afford **2** and followed by tosylation to **3** which could be converted in good yield to chloride **4**.

The synthesis of the *oxygen-bridged* [9](2,5)pyridinophane dihydro-analogues **5** was accomplished with an amalgam (Na·Hg) reduction of **4** in *N*,*N*-dimethylformamide under argon and required two eq. of Na per mol of **4**. The structure of **5** was well established by NMR spectroscopy,¶ X-ray diffraction study‖ and elemental analysis.

The structure of **5** can be clearly seen in the X-ray crystal structure (Fig. 1). Noteworthy structural features are the *trans* stereochemistry between the phenyl group on C15 and the *ansa-chain* bonding to the C11 atom, the very short distance C12–N20 (1.330 (4) Å) and sp^2 hybridization of N20.

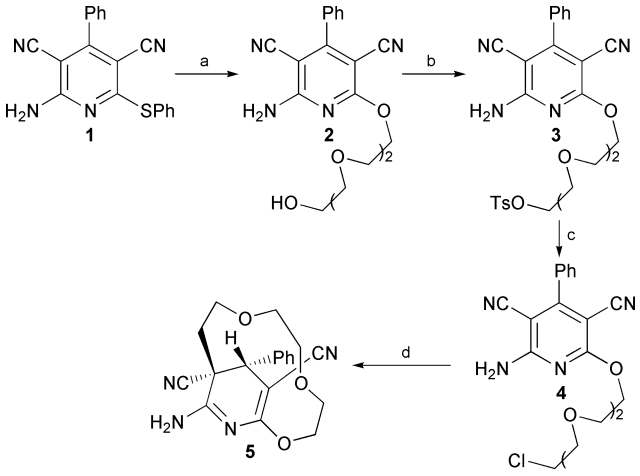

Scheme 1 *Reagents and conditions*: (*a*) Under argon atmosphere, NaH (9 eq.), triethylene glycol (18 eq.), **1** (3 eq.), DMF, rt, 48 h, then poured on water, the precipitate was chromatographed (silica gel, CH_2Cl_2–EtOH, 25 : 1), 70%; (*b*) Under argon atmosphere, triethylamine (3.3 eq.), **2** (3 eq.) in dry CH_2Cl_2 (25 ml), 30 min, then toluene-*p*-sulfonyl chloride (3.3 eq.) in dry CH_2Cl_2 (10 ml) was added dropwise, rt, 12 h, then was neutralized with HCl (10%), solvent was removed *in vacuo* and the residue was chromatographed (silica gel, CH_2Cl_2–hexane, 25 : 1), 70%; (*c*) **3** (2 eq.), LiCl (8 eq.), dry MeOH (50 ml), reflux 4 d, purified by column chromatography (silica gel, CH_2Cl_2), 60%; (*d*) Under argon atmosphere, **4** (2 eq.), dry DMF (4 ml), amalgam (Na·Hg) (0.97% w.w. Na = 92 mg = 4 eq.), 0 °C, 24 h, then the solution was separated and evaporated to dryness and the residue was purified by column chromatography (neutral aluminium oxide, CH_2Cl_2–hexane, 20 : 1), 40%.

† Electronic supplementary information (ESI) available: 2D-J resolved ^1H spectra, 2D-COSY ^1H–^1H–^{13}C spectra of **5**. See http://www.rsc.org/suppdata/cc/b0/b004474l/

DOI: 10.1039/b004474l

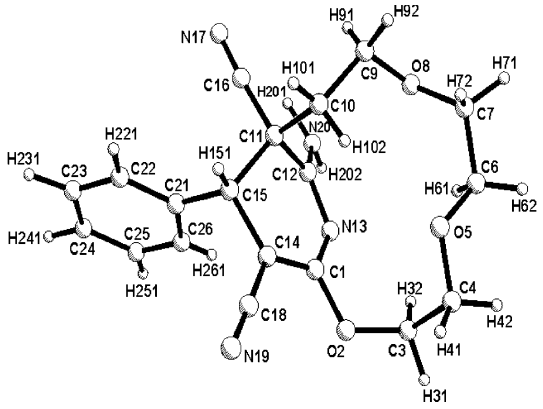

Fig. 1 View of the molecular structure of compound **5**. Selected bond lengths [Å] and angles [°]: C(1)–C(14) 1.343(5), C(1)–O(2) 1.352(4), C(1)–N(13) 1.369(4), C(11)–C(12) 1.524(5), C(11)–C(15) 1.564(4), C(12)–N(13) 1.298(4), C(12)–N(20) 1.330(4), C(14)–C(18) 1.411(5), C(14)–C(15) 1.523(4), C(15)–C(21) 1.517(4), N(13)–C(12)–N(20) 119.0(3), N(20)–C(12)–C(11) 119.0(3).

The ^{1}H NMR of **5**¶ shows two multiplets for the Ph ring, one singlet for the C15-H resonance and the three expected ABCD spin systems with typical values of SSCC for CH_2CH_2 groups of *ansa*-moiety, which were assigned by using the ^{1}H *J*-resolved, 2D-COSY ^{1}H–^{1}H and 2D-COSY ^{1}H–^{13}C spectra.† The observation of two unequivalent protons for the NH_2 group at δ = 8.5 and 7.8 ppm is due to very slow rotation around the C_{12}–N bond.

This work was supported by DGICYT (grant SAF96-1704).

Notes and references

‡ The IUPAC name for [9](2,5)pyridinophane is 12-azabicyclo[9.2.2]pentadeca-11,13,14-triene.

§ *Measurement of reduction potential.* The reduction potentials of the 2-amino-3,5-dicyano-6-methoxypyridine and **4**, were measured by means of cyclic voltammetry at 25 °C and at the scan rate of 0.2 V s^{-1} using a mercury cathode as the working electrode and Ag/AgCl as the reference electrode.

¶ *Selected data* for **5**: mp. 265–266 °C (from ethyl acetate–hexane, 15 : 1); ν_{max}(KBr)/cm^{-1} 3420, 3352, 2900, 2220 (*weak*), 2186, 1630, 1548, 1450, 1366, 1314, 1150, 1130, 702; δ_H(500 MHz, DMSO-d_6, 25 °C) 8.49 (1H, s, NH_2), 7.79 (1H, s, NH_2), 7.34 (3H, m, *meta*- and *para*-Ph), 7.15 (2H, m, *ortho*- Ph), 5.12 and 3.81 ($C3H_2$), 3.70 and 3.47 ($C4H_2$), 3.50, 3.27, 3.74 and 3.39 ($C6H_2C7H_2$), 3.76 and 3.64 ($C9H_2$), 2.77 and 2.02 ($C10H_2$), 3.82 (1H, s, C15H); δ_C(125 MHz, DMSO-d_6, 25 °C) 166.54 (m, C1), 62.59 (t, $^1J_{C\text{-}H}$ = 145.8 Hz, C3), 70.40 (t, $^1J_{C\text{-}H}$ = 140.8 Hz, C4), 70.41 and 71.94 (two t, $^1J_{C\text{-}H}$ = 140.8, 140.8 Hz, C6, C7), 67.89 (t, $^1J_{C\text{-}H}$ = 140.8 Hz, C9), 35.69 (t, $^1J_{C\text{-}H}$ = 134.6 Hz, C10), 44.25 (m, C11), 160.58 (tm, $^2J_{C\text{-}H}$ = 6.66 Hz, C12), 61.52 (d, $^2J_{C\text{-}H}$ = 6.2 Hz, C14), 46.05 (d, $^1J_{C\text{-}H}$ = 138.7 Hz, C15), 117.82 (dd, $^3J_{C\text{-}H}$ = 9.46, 3.05 Hz, C16), 119.67 (d, $^3J_{C\text{-}H}$ = 4.90 Hz, C18), 137.73, 127.96, 127.66 and 127.58 (*ipso*-, *meta*-, *ortho*-, *para*- of Ph ring); MS (CI) *m*/*z* 353 [M + H$^+$]; Anal. calc. for $C_{19}H_{20}N_4O_3$, C, 64.77, H, 5.68, N, 15.91. Found C, 64.95, H, 5.52, N, 16.15%.

‖ Crystals of **5**, suitable for X-ray crystallography grown from ethyl acetate. Crystal data of **5**. $C_{19}H_{20}N_4O_3$, M_t = 352.39, triclinic, space group $P\bar{1}$, a = 9.377(1), b = 9.409(1), c = 11.909(1) Å, α = 68.17(2), β = 84.5(1), γ = 60.62(2)°, V = 845.0(1)Å^3, T = 293 K, Z = 2, μ($Mo_{K\alpha}$) = 0.096 mm^{-1}; 3225 measured reflections, 2976 were independent; $R1$ = 0.056 and $wR2$ = 0.118 (for 1623 reflections with $F > 4\sigma(F)$).

CCDC 182/1757.

1 (*a*) E. Vögtle, in *Cyclophane Chemistry*, Wiley, Chichester, 1993; (*b*) F. Diederich, in *Cyclophanes. Monographs in Supramolecular Chemistry*, ed. J. F. Stoddart, The Royal Society of Chemistry, London, 1991.
2 F. Rob, H. J. Van Ramesdonk, W. Van Gerresheim, P. Bosma, J. J. Scheele and J. W. Verhoeven, *J. Am. Chem. Soc.*, 1984, **106**, 3826.
3 S. Shinkay, in *Enzyme Chemistry-Impact and Applications*, 2nd ed., ed. C. J. Suckling, Chapman and Hall, London, 1990.
4 R. M. Kellogg, *Angew. Chem., Int. Ed. Engl.*, 1984, **23**, 782.
5 T. K. Hansen, T. Jorgensen, P. C. Stein and J. Becher, *J. Org. Chem.*, 1992, **57**, 6403.
6 T. K. Hansen, T. Jorgensen, F. Jensen, P. H. Thygesen, K. Christiansen, M. B. Hursthouse, M. E. Harman, M. A. Malik, B. Girmay, A. E. Underhill, M. Begtrup, J. D. Kilburn, K. Belmore, P. Roepstorff and J. Becher, *J. Org. Chem.*, 1993, **58**, 1359.
7 K. B. Simonsen, N. Svenstrup, J. Lau, N. Thorup and J. Becher, *Angew. Chem., Int. Ed. Engl.*, 1999, **38**, 1417.
8 H. Gerlach and E. Huber, *Helv. Chim. Acta.*, 1968, **51**, 2027.
9 T. Komatsu, M. Ando, F. Sugawara and H. Kuzuhara, *Tennos Yuki Kagobutsu Toronkai*, 22nd, 1979, Japan, p. 627.
10 H. Kuzuhara, M. Iwata and S. Emoto, *J. Am. Chem. Soc.*, 1977, **99**, 4173.
11 M. Ando and H. Kuzuhara, *Bull. Chem. Soc. Jpn.*, 1989, **62**, 244.
12 J. Bruhin and W. Henny, *Chimia*, 1972, **26**, 420.
13 (*a*) F. Vögtle, *Chem. Ber.*, 1969, **102**, 1784; (*b*) R. H. Mitchell and V. Boekelheide, *Tetrahedron Lett.*, 1969, 2013.
14 L. Fuentes, Mª. J. Lorenzo, C. Márquez and M. Galakhov, *J. Heterocycl. Chem.*, 1999, **36**, 481.
15 L. Horner and K. Dickerhof, *Chem. Ber.*, 1983, **116**, 1615.
16 S. Kambe, K. Saito, A. Sakurai and H. Midorikawa, *Synthesis*, 1981, 531.

ChemComm

Reactions of allylpalladium(II) complexes with free radicals

Simon J. Reid, Neil T. Freeman and Michael C. Baird*

Department of Chemistry, Queen's University, Kingston, ON, Canada K7L 3N6. E-mail: bairdmc@chem.queensu.ca

Received (in Irvine, CA, USA) 4th April 2000, Accepted 7th July 2000
First published as an Advance Article on the web 4th September 2000

Allylpalladium(II) compounds react readily in benzene with free phenyl and trityl radicals, generated from the thermal decomposition of phenylazotriphenylmethane, and with free cyclohexyl radicals, generated from the photolysis of (cyclohexyl)(pyridine)cobaloxime; the reactions appear to involve initial attack of the radicals at palladium, followed by secondary processes which convert the coordinated allyl ligands preferentially to terminal rather than internal alkenes.

Free radicals have been invoked as reactive intermediates in a wide variety of reactions involving organotransition metal compounds, *e.g.* oxidative addition reactions,[1a] SmI_2 induced coupling of organic halides with carbonyl compounds,[1b] reduction of organic halides by complexes of chromium(II),[1c] and hydrogenation and hydrometallation of aromatic alkenes[1d] and conjugated dienes.[1e] Recent years have also seen increasing interest in free radicals as *reactants* with unsaturated organic ligands, *e.g.* with coordinated aromatic,[2a] allylic,[2b] carbenoid[2c] and alkenyne[2d] ligands although there is as yet no general understanding of the reactions of free radicals with coordinated ligands. We have therefore undertaken an investigation of reactions of a variety of free radicals with allylic palladium(II) compounds of the types $[(\eta^3\text{-allyl})PdCl]_2$, $(\eta^3\text{-allyl})PdCl(PPh_3)$ and $[(\eta^3\text{-allyl})Pd(PPh_3)_2]Cl$, the latter being of interest because the enhanced susceptibility of the allyl groups in these types of compounds to nucleophilic attack has proven very useful in synthetic organic methodology.[3]

Our initial studies have utilized triphenylmethyl (trityl) and phenyl radicals, derived *via* the thermal decomposition of phenylazotriphenylmethane ($PhN{=}NCPh_3$, PAT),[4] and cyclohexyl radicals, generated from visible light photolysis of (cyclohexyl)(pyridine)cobaloxime [*c*-$C_6H_{11}Co(DMG)_2(py)$].[5] Both procedures generate free radicals in good yields and under relatively mild conditions, and molar ratios of radical source to palladium of 2–3 : 1 ensured that reactions of the palladium substrates proceeded to completion.

Reaction of $[(\eta^3\text{-}C_3H_5)PdCl]_2$ with PAT in benzene or benzene-d_6 at 60 °C resulted in the formation of palladium metal, 3-phenylprop-1-ene, 1-phenylprop-1-ene, chlorotriphenylmethane (in high yield by GC) and a small amount of 4,4,4-triphenylbut-1-ene but no chlorobenzene. By monitoring the reaction products as a function of time, it was found that 3-phenylprop-1-ene was formed initially in *ca*. 90% yield (NMR) and that 1-phenylprop-1-ene was formed by subsequent isomerization of the kinetic product. Control experiments showed that this isomerization reaction is catalyzed by palladium metal, and thus the primary reaction involves the formation of 3-phenylprop-1-ene, $PhCH_2CH{=}CH_2$.

In contrast, the analogous reactions of $[(\eta^3\text{-}C_3H_5)PdCl]_2$ in the presence of either 1 or 2 equivalents of PPh_3 per palladium were found to produce 4,4,4-triphenylbut-1-ene (> 90% yield by NMR) and $[PdPh(\mu\text{-}Cl)(PPh_3)]_2$[6a] or *trans*-$PdPhCl(PPh_3)_2$,[6b,c] respectively. In addition, the reaction of $[(\eta^3\text{-2-methylallyl})PdCl]_2$ with PAT in the presence of PPh_3 produced *trans*-2-methyl-4,4,4-triphenylbut-1-ene and $PdPhCl(PPh_3)_2$, while the reaction of $[(\eta^3\text{-allyl})Pt(PPh_3)_2]^+Cl^-$ produced 4,4,4-triphenylbut-1-ene and *trans*-$PtPhCl(PPh_3)_2$.[6d]

Assuming a similar first step in all of these reactions, the results may be rationalized on the basis of initial attack of phenyl radical on palladium. In the absence of triphenylphosphine, it seems likely that initial phenyl radical coupling with the palladium to form a palladium(III) intermediate is followed by reductive coupling of the phenyl group with a terminal carbon atom of the allyl ligand to give an intermediate chloropalladium(I) complex [eqn. (1)]. In possibly a concerted

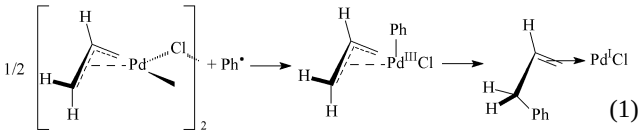

(1)

process, the chlorine atom is abstracted from the intermediate by free trityl radical to form chlorotriphenylmethane, palladium metal and free 3-phenylbut-1-ene.

Initial abstraction of a chlorine atom from $[(\eta^3\text{-}C_3H_5)PdCl]_2$ by trityl radical can presumably be ruled out since no chlorobenzene was formed. Although one might anticipate that the initially formed trityl radical could react with $[(\eta^3\text{-}C_3H_5)PdCl]_2$ before significant amounts of the intrinsically more reactive phenyl radical are formed, in fact the relative rates of formation of the two radicals are very similar[4d] and pre-empting of any reactive site by the trityl radical seems unlikely. On the other hand, with analogous triphenylphosphine-containing phenylpalladium(III) intermediates such as $[(\eta^3\text{-}C_3H_5)Pd^{III}(Ph)Cl(PPh_3)]$ or $[(\eta^3\text{-}C_3H_5)Pd^{III}(Ph)(PPh_3)_2]^+$, steric hindrance by the bulky phosphine ligands may prevent attack on the coordinated chlorine atoms by the bulky trityl radical. Instead, the latter apparently couples in these cases with the sterically less congested allyl ligand to form 4,4,4-triphenylbut-1-ene, again possibly *via* a concerted process but not, presumably, *via* initial trityl radical attack as there is no obvious reason why at least *some* phenyl radical involvement to give 3-phenylprop-1-ene would not occur. Interestingly, in a control experiment, it was found that trityl radical, added as the corresponding dimer with which it is in equilibrium,[7] does react with $[(\eta^3\text{-}C_3H_5)PdCl]_2$ in the presence of PPh_3, the trityl and allyl groups combining to form exclusively 4,4,4-triphenylbut-1-ene. On the other hand, the formation of 4,4,4-triphenylbut-1-ene apparently does not involve trityl coupling with free allyl radicals as no hexa-1,5-diene, the product of allyl free radical coupling,[8] was formed.

In contrast to the above, photolysis of *c*-$C_6H_{11}Co(DMG)_2(py)$ with visible light in the presence of $[(\eta^3\text{-}C_3H_5)PdCl]_2$ (PPh_3 : Pd ratios 1 : 1, 2 : 1) in benzene or benzene-d_6 at 25 °C did not give 3-cyclohexylprop-1-ene and/or cyclohexyl–palladium complexes, but rather propene, cyclohexene and palladium(0) species. Similar reactions of $[(\eta^3\text{-1-methylallyl})PdCl]_2$, $[(\eta^3\text{-2-methylallyl})PdCl]_2$ and $[(\eta^3\text{-2-phenylallyl})PdCl]_2$ (PPh_3 : Pd ratios 1 : 1) resulted in the exclusive formation of but-1-ene, isobutene and 2-phenylprop-1-ene respectively, while reaction of $[(\eta^3\text{-1-phenylallyl})PdCl]_2$ (PPh_3 : Pd ratio 1 : 1) resulted in the formation of a mixture of 3-phenylprop-1-ene and 1-phenylprop-1-ene at 25 °C but only 3-phenylprop-1-ene at 5 °C if the PPh_3:Pd ratio were 2:1. The reaction of $[(\eta^3\text{-}C_3H_5)PdCl]_2$ with *c*-$C_6H_{11}Co(DMG)_2(py)$ gave propene and palladium metal while reaction of $[(\eta^3\text{-1-phenylallyl})PdCl]_2$ gave 1-phenylprop-1-ene and palladium metal; as above, isomerization of a terminal alkene kinetic product to internal alkene may be catalyzed by palladium metal. Control

DOI: 10.1039/b002851g

experiments showed that the allyl–palladium compounds are stable under the above conditions in the absence of *c*-$C_6H_{11}Co(DMG)_2(py)$.

Assuming a mechanism analogous to the above and considering the nature of the products, these reactions probably involve initial attack of the cyclohexyl radical at the metal to form a cyclohexyl–Pd(III) species, followed by β-hydrogen elimination of cyclohexene to form a hydrido–allylpalladium(III) complex [eqn. (2)]. Subsequent reductive elimination of propene could

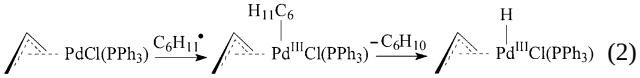

(2)

result in the palladium(I) species $PdCl(PPh_3)$, which could undergo a second attack by a cyclohexyl radical to form the palladium(II) cyclohexyl compound $PdCl(C_6H_{11})(PPh_3)$, which could also undergo β-hydrogen elimination of cyclohexene to give the hydride $PdHCl(PPh_3)$.

Although cyclohexene is anticipated as a byproduct in these reactions, it is expected to be formed in any case as a product of the photolysis of *c*-$C_6H_{11}Co(DMG)_2(py)$[5] and we therefore cannot take its formation as evidence for the postulated mechanism. While neither the putative hydride $PdHCl(PPh_3)$ nor its dimer appear to have been reported, the ^1H NMR spectrum of a reaction mixture in benzene-d_6 exhibited a resonance at δ –13, indicative of a palladium hydride. This *same* resonance is also observed in reactions involving $[(\eta^3\text{-1-methylallyl})PdCl]_2$, $[(\eta^3\text{-2-methylallyl})PdCl]_2$, $[(\eta^3\text{-1-phenylallyl})PdCl]_2$ and $[(\eta^3\text{-2-phenylallyl})PdCl]_2$, consistent with the general mechanism proposed. Also consistent is an observation that the reaction of $[(\eta^3\text{-allyl})Pt(PPh_3)_2]Cl$ with $C_6H_{11}Co(DMG)_2(py)$ gives comparable amounts of propene and *trans*-$PtHCl(PPh_3)_2$, identified by comparison of its hydride resonance (δ −15.2) with that of an authentic sample,[9] in addition to cyclohexene.

Seemingly anomalous, however, is the exclusive formation of but-1-ene in the reaction of $[(\eta^3\text{-1-methylallyl})PdCl]_2$ and of 3-phenylprop-1-ene in the reaction of $[(\eta^3\text{-1-phenylallyl})PdCl]_2$. While these products are consistent with the reductive elimination step implied above, reductive elimination of alkenes from allylpalladium(II) hydrido complexes normally results in the formation of the thermodynamically preferred internal alkenes.[3b] Thus the fact that the reactions discussed here give solely terminal alkenes is perhaps evidence that the reactions do indeed involve allylpalladium(III) hydrido species, although it is not readily obvious why formation of the terminal alkenes should become kinetically preferred. A better understanding of these processes must await further labelling and stereochemical studies which are underway.

Although the mechanisms are as yet uncertain, the reactions lead in all cases to preferential conversion of the allylic ligands to terminal alkenes. Since compounds of the type $[(\eta^3\text{-1-}RC_3H_4)PdCl]_2$ (R = alkyl, aryl) are readily prepared from, *e.g.* alkenes $RCH{=}CHCH_3$[3a] and allylic acetates $RCH{=}CHCH_2OAc$,[3a] the chemistry involving hydrogen transfer from the cyclohexyl radical would seem in effect to provide a route for both the isomerization of the alkene or the hydrogenolysis of the allylic acetate, *via* η^3-allylpalladium compounds, to terminal alkenes $RCH_2CH{=}CH_2$. Both types of reactions have potential utility, as we note that hydrogenolysis of allylpalladium complexes by hydride sources normally results in the formation of internal alkenes unless the source is formate ion.[10]

We thank the Natural Sciences and Engineering Research Council and the Government of Ontario for financial support.

Notes and references

1 (*a*) J. K. Stille, in *The Chemistry of the Metal–Carbon Bond*, ed. F. R. Hartley and S. Patai, Wiley and Sons, Chichester, 1985, vol. 2, ch. 9; (*b*) A. Krief and A. M. Laval, *Chem. Rev.*, 1999, **99**, 745; (*c*) R. Sustmann and R. Altevogt, *Tetrahedron Lett.*, 1981, 5167; (*d*) R. M. Bullock and E. G. Samsel, *J. Am. Chem. Soc.*, 1990, **112**, 6886; (*e*) T. A. Shackleton, S. C. Mackie, S. B. Fergusson, L. J. Johnston and M. C. Baird, *Organometallics*, 1990, **9**, 2248.

2 (*a*) H.-G. Schmalz, S. Siegel and A. Schwarz, *Tetrahedron Lett.*, 1996, **37**, 2947; (*b*) C. A. G. Carter, R. McDonald and J. M. Stryker, *Organometallics*, 1999, **18**, 820; (*c*) C. A. Merlic and D. Xu, *J. Am. Chem. Soc.*, 1991, **113**, 9855; (*d*) G. G. Melikyan, O. Vostrowsky, W. Bauer, H. J. Bestmann, M. Khan and K. M. Nicholas, *J. Org. Chem.*, 1994, **59**, 222.

3 (*a*) S. A. Godleski, in *Comprehensive Organic Synthesis*, ed. B. M. Trost, Pergamon Press, Oxford, 1991, vol. 4, p. 585; (*b*) F. Guibe, *Tetrahedron*, 1998, **54**, 2967.

4 (*a*) S. G. Cohen and C. H. Wang, *J. Am. Chem. Soc.*, 1953, **75**, 5504; (*b*) R. R. Bridger and G. A. Russell, *J. Am. Chem. Soc.*, 1963, **85**, 3754; (*c*) R. G. Kryger, J. P. Lorand, R. R. Stevens and N. R. Herron, *J. Am. Chem. Soc.*, 1977, **99**, 7589; (*d*) R. C. Neuman and G. D. Lockyer, *J. Am. Chem. Soc.*, 1983, **105**, 3982; (*e*) J. E. Leffler, *An Introduction to Free Radicals*, John Wiley & Sons, Inc., New York, 1993, pp. 148–150; (*f*) J. E. Leffler, *An Introduction to Free Radicals*, John Wiley & Sons, Inc., New York, 1993, p. 183.

5 B. P. Branchaud, M. S. Meier and M. N. Maedzadeh, *J. Org. Chem.*, 1987, **52**, 212; B. P. Branchaud and Y. L. Choi, *J. Org. Chem.*, 1988, **53**, 4638; B. Giese, J. Hartung, J. He, O. Hüter and A. Koch, *Angew. Chem., Int. Ed. Engl.*, 1989, **28**, 325.

6 (*a*) V. V. Grushin, *Organometallics*, 2000, **19**, 1888; (*b*) D. R. Coulson, *Chem. Commun.*, 1968, 1530; (*c*) A. Mentes, R. R. W. Kemmit, G. Fawcett and D. R. Russel, *Polyhedron*, 1999, **18**, 1141; (*d*) C. Eaborn, K. J. O'Dell and A. Pidcock, *J. Chem. Soc., Dalton Trans.*, 1978, 357.

7 T. H. Colle, P. S. Glaspie and E. S. Lewis, *J. Org. Chem.*, 1978, **43**, 2722; H. Lankamp, W. T. Nauta and C. MacLean, *Tetrahedron Lett.*, 1968, 249.

8 G. Carturan, M. Biasiolo, S. Danielle, G. A. Mazzochin and P. Ugo, *Inorg. Chim. Acta*, 1986, **119**, 19.

9 W. McFarlane, *J. Chem. Soc., Dalton Trans.*, 1974, 324.

10 J. Tsuji and T. Mandai, *Synthesis*, 1996, 1.

Asymmetric synthesis of tetrahydrofurans and tetrahydropyrans with competitive [1,2]-phenylsulfanyl (PhS) migrations (I): thermodynamic control

David House,[a] Fraser Kerr[b] and Stuart Warren*[a]

[a] *University Chemical Laboratory, Lensfield Road, Cambridge, UK CB2 1EW. E-mail: sw134@cam.ac.uk*
[b] *AstraZeneca R&D Södertälje, Process R&D, S-151 85 Södertälje, Sweden*

Received (in Cambridge, UK) 3rd July 2000, Accepted 2nd August 2000
First published as an Advance Article on the web 4th September 2000

Triols were prepared in enantiomerically enriched form by a short route that included a Sharpless asymmetric dihydroxylation; treatment of these triols with toluene *p*-sulfonic acid gave THFs as thermodynamic products.

Previously, we have reported the outcome of competitive cyclisations between two primary hydroxy groups at the end of separate or branched side chains (**1** and **2**, Fig. 1).[1,2] We then wished to investigate cyclisations of 2,4,5-triols (bearing a phenylsulfanyl group at C-1) with primary and secondary hydroxy groups in the same side-chain (Scheme 1). In each case two modes of cyclisation are possible: route (**A**) would result in tetrahydropyran (THP) formation, route (**B**) in tetrahydrofuran (THF) formation.

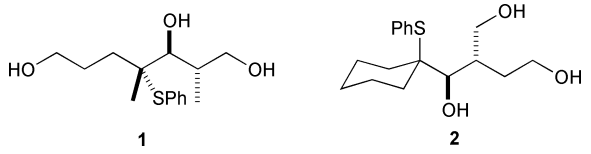

Fig. 1

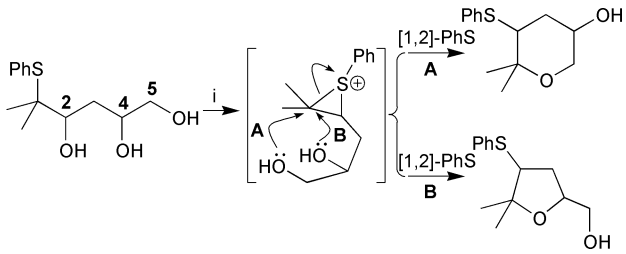

Scheme 1 *Reagents*: i, TsOH, CH_2Cl_2.

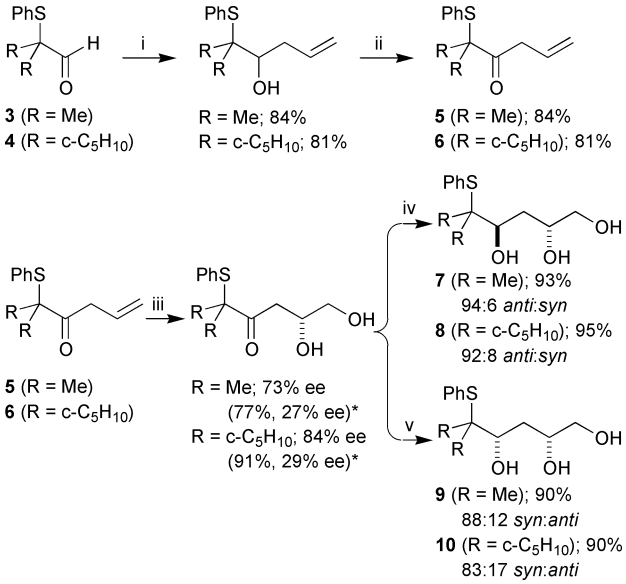

Scheme 2 *Reagents*: i, CH_2=$CHCH_2MgBr$, Et_2O, rt; ii, PCC, CH_2Cl_2, rt; iii, $K_2OsO_2(OH)_4$, $(DHQD)_2PYR$, K_2CO_3, $K_3Fe(CN)_6$, Bu^tOH–H_2O, 0 °C; iv, Me_4N^+ $BH(OAc)_3^-$, AcOH-MeCN, −20 °C, 7 days; v, Et_2BOMe, THF–MeOH, −78 °C then $NaBH_4$. * Yields and enantiomeric excesses in parentheses denote those obtained using AD-mix-β at 25 °C.

Two sets of diastereomeric triols were prepared for this study with different migration origins; for one pair (**7** and **9**) *gem*-dimethyl substitution was used and for the other (**8** and **10**) a cyclohexane ring was used (Scheme 2). The triols were readily synthesised starting from the aldehydes **3** and **4**. Grignard addition followed by oxidation gave the homoallylic ketones **5** and **6**. The asymmetric dihydroxylation reaction[3] gave optimum enantiomeric excess (73–84%) when Sharpless' PYR ligand was used.[4] Finally a 1,3-diastereocontrolled reduction gave either the 2,4-*anti*[5] (**7** and **8**) or 2,4-*syn*[6] diastereoisomers (**9** and **10**) of each triol.

Initially these compounds were subjected to our standard conditions for rearrangement: a 5 min reflux with 5 mol% toluene *p*-sulfonic acid in dichloromethane. To our initial disappointment, triol **8** gave a 50:50 mixture of THF **11** and THP **12** (Scheme 3).[7] Previously we have shown that these reaction are under thermodynamic control,[8,9] so resubmitting this mixture to the reaction conditions, or taking a fresh sample of the triol **8**, and heating to reflux in dichloromethane for 48 h led to the complete conversion into the spirocyclic THF **11** Scheme 3). Similarly the *syn*-triol **10** gave an initial product

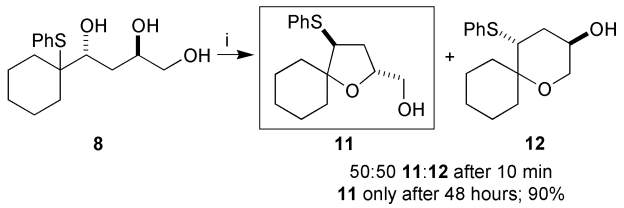

Scheme 3 *Reagents*: i, TsOH, CH_2Cl_2, 40 °C.

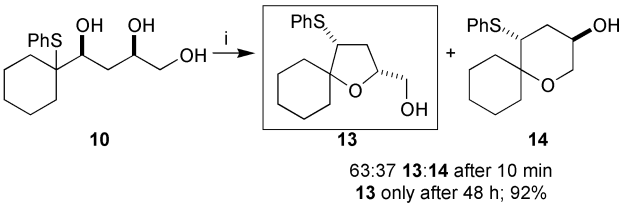

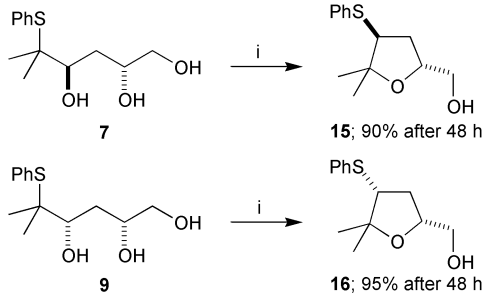

Scheme 4 *Reagents*: i, TsOH, CH_2Cl_2, 40 °C.

DOI: 10.1039/b005342m

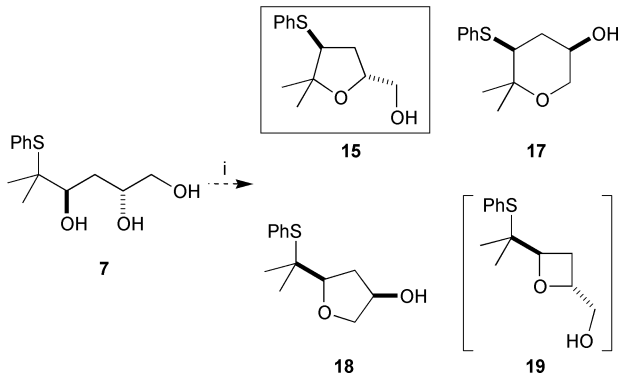

Scheme 5 *Reagents*: i, TsOH, $CDCl_3$.

distribution of 63 : 37 THF **13** : THP **14**, but after a prolonged reflux (48 h) gave only THF **13** (Scheme 4). These results were followed by rearrangement of the structurally related triols **7** and **9**. Again, short reaction times led to THF–THP mixtures, but a longer reaction time (48 h) led to THFs **15** and **16** (Scheme 4).

In contrast to other systems we have studied,[1,2] ring-size has become more important than the relative stereochemistry. A 2,4-*syn* THF is preferred to the alternative 2,4-*anti* THP, where one of the two substituents would enter an axial environment. More interestingly though, the 2,4-*anti* THF is preferred to the 2,4-*syn* THP, where both groups could now be equatorial. We presume in this case that the factor governing the cyclisation outcome (the degree of substitution being equal for both rings) is the *gem*-disubstituted migration origin. In the THP one of the C–C bonds is forced to be axial; presumably the 1,3-diaxial interactions are too severe and the flatter THF ring is preferred.

The rearrangement of triol **7** was followed by 400 MHz ^{1}H NMR spectroscopy. By recording spectra at regular intervals it was possible to watch the initial formation of the heterocycles **15**, **17** and **18** and the subsequent equilibration of the mixture to the THF **15** (Scheme 5). Interestingly, the unrearranged[10] THF **18** was observed as a metastable product but none of the oxetane **19**, which would also be formed by attack on the less substituted end of the episulfonium ion, was detected.

In summary we have demonstrated further evidence that [1,2]-PhS rearrangements are under thermodynamic control and that for a simple class of triols **7**–**10** the most stable products are the THFs **11, 13, 15** and **16**. We believe that in this case the difference in product stability can be attributed to the *gem*-disubstituted migration origin. In other cases we have investigated[1,2] the relative stability of products may be dependent on ring-size, stereochemistry or a thermodynamic Thorpe–Ingold effect.

We thank the EPSRC and AstraZeneca for a grant to D. H.

Notes and references

1 S. McIntyre, F. H. Sansbury and S. Warren, *Tetrahedron Lett.*, 1991, **32**, 5409.
2 F. H. Sansbury and S. Warren, *Tetrahedron Lett.*, 1992, **33**, 539.
3 H. C. Kolb, M. S. VanNieuwenhze and K. B. Sharpless, *Chem. Rev.*, 1994, **94**, 2483.
4 G. A. Crispino, K.-S. Jeong, H. C. Kolb, Z.-M. Wang, D. Xu and K. B. Sharpless, *J. Org. Chem.*, 1993, **58**, 3785.
5 D. A. Evans, K. T. Chapman and E. M. Carreira, *J. Am. Chem. Soc.*, 1988, **110**, 3560.
6 K. M. Chen, G. E. Hardtmann, K. Prasad, O. Repič and M. J. Shapiro, *Tetrahedron Lett.*, 1987, **28**, 155.
7 The two types of heterocycle are readily distinguished by ^{1}H NMR spectroscopy: the hydrogen atom adjacent to the PhS group has a characteristic chemical shift in the range $3.0 < \delta_H < 3.5$ ppm. For the THPs this signal appears as a double doublet: for the THFs it is normally a triplet, or at least a double doublet with very similar coupling constants. Integration of these proton resonances provided an accurate means of assessing product ratios.
8 L. Djakovitch, J. Eames, R. V. H. Jones, S. McIntyre and S. Warren, *Tetrahedron Lett.*, 1995, **36**, 1723.
9 J. Eames, N. Kuhnert, F. H. Sansbury and S. Warren, *Synlett*, 1999, **8**, 1211.
10 By 'unrearranged' we mean a product in which the phenylsulfanyl group remains bound to the same carbon as it was before the cyclisation, *i.e.* a product that has not undergone a [1,2]-PhS rearrangement.

ChemComm

Asymmetric synthesis of tetrahydrofurans and tetrahydropyrans with competitive [1,2]-phenylsulfanyl (PhS) migration (II): synthesis of protected tetrahydropyrans

David J. Fox,[a] David House,[a] Fraser Kerr[b] and Stuart Warren*[a]

[a] *University Chemical Laboratory, Lensfield Road, Cambridge, UK CB2 1EW. E-mail: sw134@cam.ac.uk*
[b] *AstraZeneca R&D Södertälje, Process R&D, S-151 85 Södertälje, Sweden*

Received (in Cambridge, UK) 3rd July 2000, Accepted 2nd August 2000
First published as an Advance Article on the web 4th September 2000

Enantiomerically enriched triols were treated with trimethylorthoacetate and pyridinium toluene *p*-sulfonate to give a mixture of unrearranged THF and rearranged THP; treatment of the product mixture with toluene *p*-sulfonic acid equilibrated the mixture to the THP.

In the preceeding article[1] we reported the preparation of enantiomerically enriched triols (*e.g.* **1**) and their conversion to the thermodynamic tetrahydrofuran (THF) products (*e.g.* **2**) (Scheme 1). In this publication we disclose details of how the same cyclisation precursors can be converted to the complementary tetrahydropyran (THP) products (*e.g.* **3**).

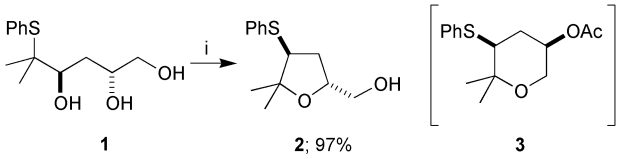

Scheme 1 *Reagents*: i, TsOH, CH_2Cl_2.

An obvious approach to the THPs would be an orthogonal protecting group strategy, which would leave the secondary hydroxy nucleophile protected and the primary hydroxy unprotected and available for cyclisation. Alternatively, we envisaged a situation where it would be possible to protect the secondary hydroxy nucleophile and simultaneously activate the other secondary hydroxy group to nucleophilic displacement. By using an orthoester in the appropriate conditions an exchange could be set up between a 5- and a 6-membered orthoester (Scheme 2). So long as the 5-membered orthoester was inert under these reaction conditions it would be possible to trigger the episulfonium ion formation and protect the secondary hydroxy group as its acetate.

Pyridinium *p*-toluenesulfonate (PPTS) (pK_a ~ 5.5) was chosen as the acid catalyst for this reaction because orthoesters exchange under general acid catalysis,[2] but we did not expect such a weak acid to promote direct formation of the episulfonium ion. Hence triol **1** was treated with 1 eq. of trimethylorthoacetate with PPTS as the acid catalyst. In the first instance the product was the orthoester **4** which is formed by exchange of all three molecules of MeOH (Scheme 3). However, with longer

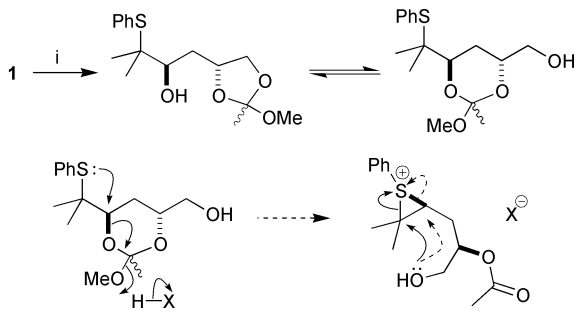

Scheme 2 *Reagents*: i, $(MeO)_3CMe$, $C_5H_6N^+$ TsO^-, CH_2Cl_2.

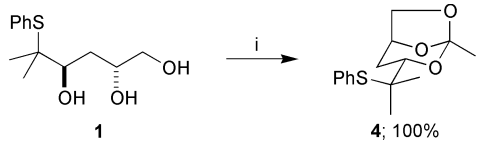

Scheme 3 *Reagents*: i, $(MeO)_3CMe$, $C_5H_6N^+$ TsO^-, CH_2Cl_2, rt, 2 min.

reaction times we obtained none of this orthoester but two heterocyclic products. The two heterocycles were the unrearranged[3] THF **5** and the rearranged[3] THP **3**: both products derive from cyclisation of the primary hydroxy nucleophile, but to different ends of the episulfonium ion intermediate (Schemes 2 and 4).

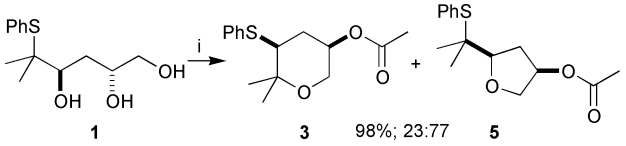

Scheme 4 *Reagents*: i, $(MeO)_3CMe$, $C_5H_6N^+$ TsO^-, CH_2Cl_2, rt, 24 h.

This result is important in the context of our research programme because it constitutes the first example of cyclisation on to the less substituted end of an episulfonium ion (where the alternative cyclisation would not give a 7-membered ring).[4] This raised the question of whether these reactions were therefore under kinetic control. (We have previously shown that cyclisations catalysed by toluene *p*-sulfonic acid are under thermodynamic control.[5,6]) To address this question we performed three control experiments. First we took a sample of the triol and treated it with PPTS, without adding trimethylorthoacetate, and showed that no reaction occurred. Secondly the 77:23 THF **5**: THP **3** mixture isolated from the cyclisation

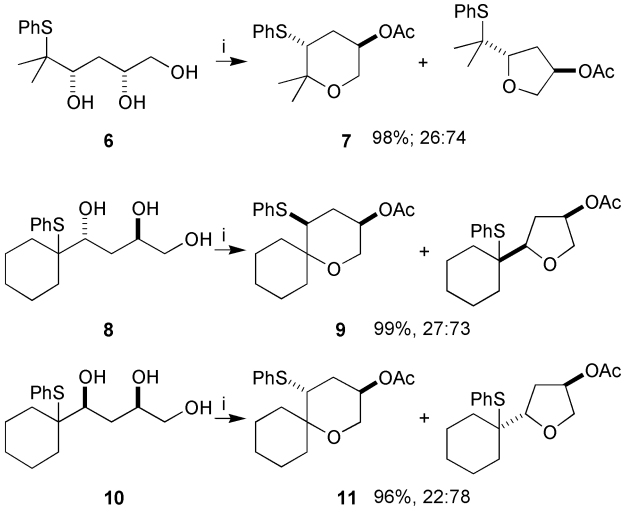

Scheme 5 *Reagents*: i, $(MeO)_3CMe$, $C_5H_6N^+$ TsO^-, CH_2Cl_2, rt, 24 h.

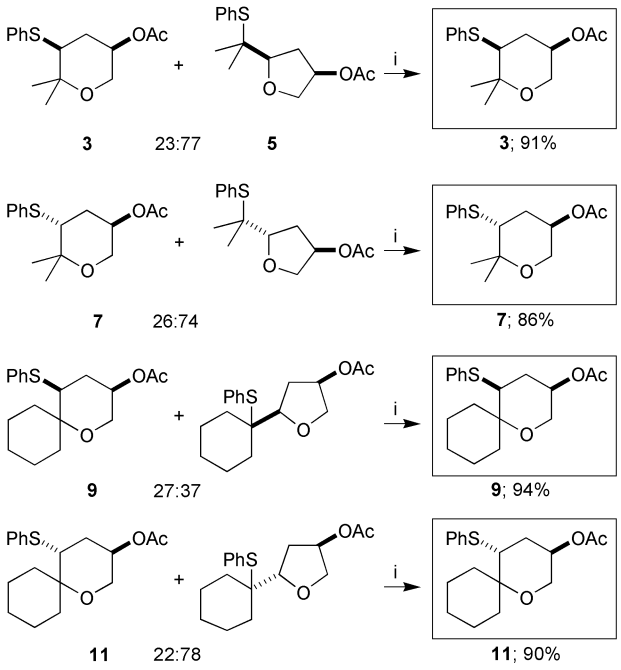

Scheme 6 *Reagents*: i, TsOH, CH_2Cl_2, 40 °C, 24 h.

reaction was resubmitted to the PPTS acid catalyst: no equilibration of the mixture occurred. Finally we confirmed the second experiment by showing that a pure sample of the unrearranged THF **5** was not converted to the THP **3** by PPTS. At this point we could conclude this orthoester-promoted cyclisation is in fact under kinetic control.

Following the reaction of triol **1**, we also cyclised triols **6** (the diastereoisomer of **1**), **8** and **10** under the same conditions and observed in each case that the unrearranged THF was the major product (Scheme 5). For the case of the 2,4-*syn* triols **6** and **10** none of the bicyclic orthoester intermediate could be isolated.

In order to exploit this interesting mechanistic observation synthetically we reasoned that treatment of the THF–THP mixtures with a strong acid, toluene *p*-sulfonic acid, should lead to equilibration of the mixture to the rearranged THPs. Indeed

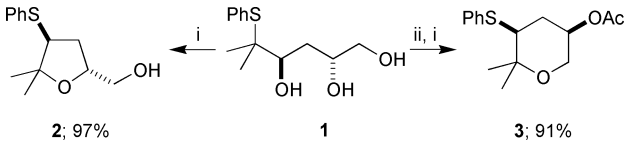

Scheme 7 *Reagents*: i, TsOH, CH_2Cl_2; ii, $(MeO)_3CMe$, $C_5H_6N^+$ TsO^-.

this was observed in all four cases; complete equilibration occurred to give the THPs **3**, **7**, **9** and **11**, protected as their acetates (Scheme 6). Hence this two-step synthetic procedure can give the THP products (which are complementary to the THF products of the one-step toluene *p*-sulfonic acid cyclisation) without the need for any purification of the intervening mixture.

In summary, we have demonstrated a rapid approach to enantiomerically enriched THPs or THFs from a common triol precursor depending on the choice of reagent (Scheme 7). For THF synthesis the episulfonium ion is formed directly, under specific acid catalysis. Use of the orthoester route promotes episulfonium ion formation under general acid catalysis and results in THP–THF mixtures that can be equilibrated to THP.

We thank the EPSRC and AstraZeneca for a grant to DH and Martin Christlieb, David Hodgson and Adam Nelson for useful discussions.

Notes and references

1 D. House, F. Kerr and S. Warren, *Chem. Commun.*, 2000, 1779 (preceding article DOI: 10.1039/b005342m).
2 M. Ahmad, R. G. Bergstrom, M. J. Cashen, Y. Chiang, A. J. Kresge, R. A. McClelland and M. F. Powell, *J. Am. Chem. Soc.*, 1979, **101**, 2669; for a detailed review, see: E. H. Cordes and H. G. Bull, *Chem. Rev.*, 1974, **74**, 581.
3 We use the terms ‘rearranged’ and ‘unrearranged’ to designate cyclisation products that have been formed either with or without [1,2]-PhS rearrangement respectively.
4 J. Eames, D. J. Fox, F. H. Sansbury and S. Warren, *J. Chem. Soc., Perkin Trans. 1*, 1999, 2771.
5 L. Djakovitch, J. Eames, R. V. H. Jones, S. McIntyre and S. Warren, *Tetrahedron Lett.*, 1995, **36**, 1723.
6 J. Eames, N. Kuhnert, F. H. Sansbury and S. Warren, *Synlett*, 1999, **8**, 1211.

Scope and limitation of the [1,2]-phenylsulfanyl (PhS) migration in the asymmetric synthesis of tetrahydrofurans and tetrahydropyrans from common triol precursors

David House,[a] Fraser Kerr[b] and Stuart Warren*[a]

[a] *University Chemical Laboratory, Lensfield Road, Cambridge, UK CB2 1EW. E-mail: sw134@cam.ac.uk*
[b] *AstraZeneca R&D Södertälje, Process R&D, S-151 85 Södertälje, Sweden*

Received (in Cambridge, UK) 3rd July 2000, Accepted 2nd August 2000
First published as an Advance Article on the web 4th September 2000

Triols containing three secondary hydroxy groups were reacted with either (i) toluene *p*-sulfonic acid or (ii) trimethylorthoacetate–pyridinium toluene *p*-sulfonate followed by toluene *p*-sulfonic acid.

In the previous two articles[1,2] we demonstrated how enantiomerically enriched triols (*e.g.* **2**) could be converted in a single step to THFs (*e.g.* **1**) (thermodynamic control) or in two steps to THPs (*e.g.* **3**) (kinetic control–equilibration sequence) (Scheme 1). The subject of the final communication in this series is our attempts to assess the generality of these reactions, particularly by replacement of the primary hydroxy in **2** with a secondary alcohol.

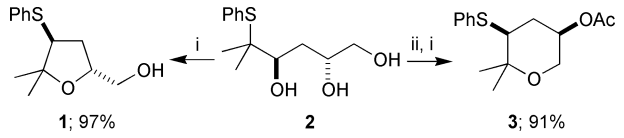

Scheme 1 *Reagents*: i, TsOH, CH_2Cl_2, 40 °C; ii, $(MeO)_3CMe$, $C_5H_6N^+$ TsO^-, CH_2Cl_2, rt.

Triols **7** and **8** were prepared by essentially the same method as used previously,[1] *i.e.* by Sharpless asymmetric dihydroxylation[3] of the styrene **6** and diastereoselective reduction of the β-hydroxyketones (Scheme 2).[4,5] Styrene **5** was derived from the homoallylic alcohol **4** by a Heck reaction with iodobenzene. The remaining triols **10**–**13** were prepared by an aldol reaction[6] of the lactic acid derived aldehyde **9**, followed by stereocontrolled reduction (Scheme 3). We were able to prepare all diastereoisomers of the triol target molecules since the aldol route gave poor diastereoselectivity and necessitated a difficult separation of the aldol products by preparative HPLC.

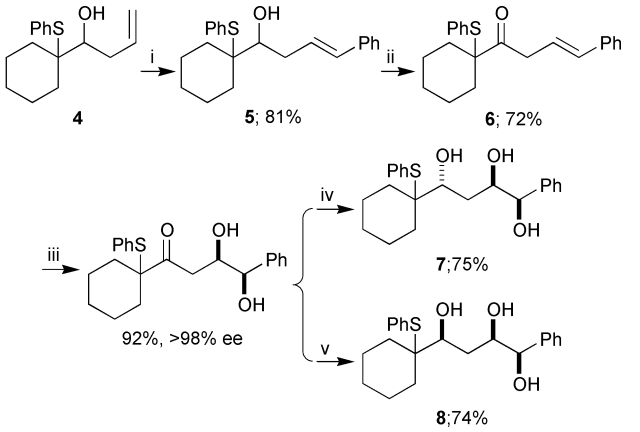

Scheme 2 *Reagents*: i, PhI, 5 mol% $Pd(OAc)_2$, 10 mol% Ph_3P, Et_3N, MeCN, 80 °C, 24 h; ii, PDC, CH_2Cl_2, rt; iii, AD-mix-β, $MeSO_2NH_2$, Bu^tOH–H_2O, rt; iv, Me_4N^+ $BH(OAc)_3^-$, AcOH–MeCN, −20 °C, 7 days; v, Et_2BOMe, THF–MeOH, −78 °C then $NaBH_4$.

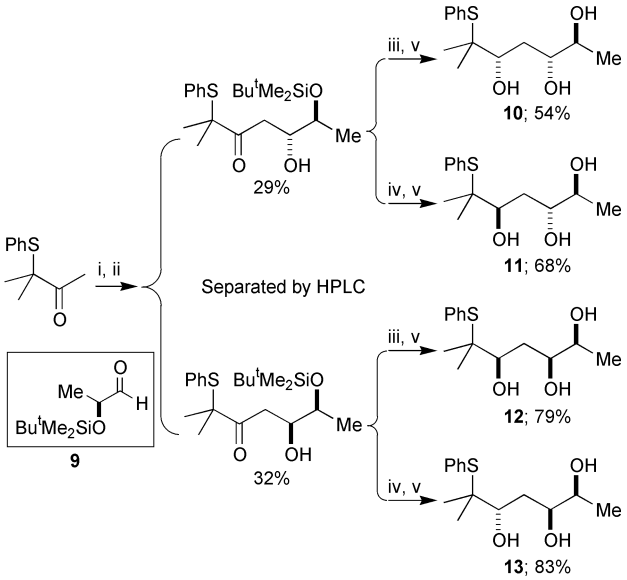

Scheme 3 *Reagents*: i, LDA, THF, −78 °C; ii, aldehyde **9**; iii, Et_2BOMe, THF–MeOH, −78 °C then $NaBH_4$; iv, Me_4N^+ $BH(OAc)_3^-$, AcOH–MeCN, −20 °C, 7 days; v, $Bu^n_4N^+$ F^-, THF, rt.

The toluene *p*-sulfonic acid catalysed cyclisations are under thermodynamic control and so we used long reaction times to ensure equilibrium was established. The triols in the lactic acid series (*i.e.* triols **10**–**13**) all rearranged to give the THFs (**14**–**17**, respectively) as the major product (Scheme 4). We were particularly interested to establish the outcome of rearranging the ^{2,4}*anti*,^{4,5}*anti* triol **11**, since the THP **18** derived from this triol would have the maximum number of equatorial substituents (Fig. 1). Despite this 'favourable' arrangement of substituents in the THP product, the THF was still the major

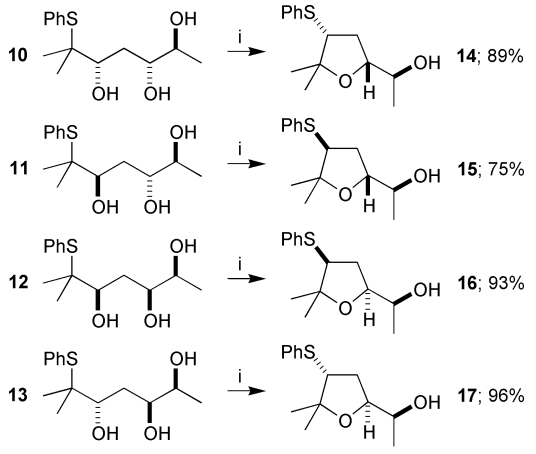

Scheme 4 *Reagents*: i, TsOH, CH_2Cl_2, 40 °C.

DOI: 10.1039/b005336h

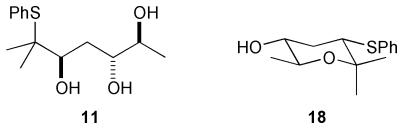

Fig. 1

product, though THP **18** did account for 17% of the equilibrium.

The rearrangement of the triols **7** and **8** required careful handling (presumably due to the benzylic hydroxy group). The ^{2,4}*anti*,^{4,5}*syn* triol **7** rearranged exclusively to THF **19** after being heated to reflux in dichloromethane for 24 h (Scheme 5). The ^{2,4}*syn*,^{4,5}*syn* triol **8**, however, had to be rearranged at rt (3 days) to avoid decomposition. Again, the THF **20** was the only isolated product.

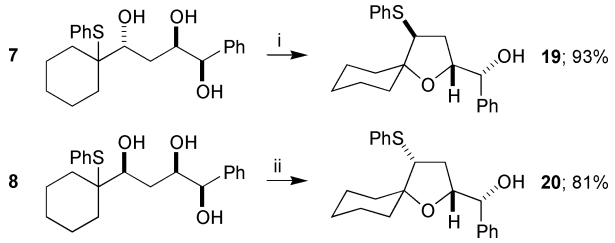

Scheme 5 *Reagents*: i, TsOH, CH_2Cl_2, 40 °C; ii, TsOH, CH_2Cl_2, rt.

The products of the kinetically controlled orthoester rearrangement reported in the preceding communication[2] were equilibrated with toluene *p*-sulfonic acid in dichloromethane with the aim of converting the unrearranged[7] THFs to THPs.

Reactions of the triols in the lactic acid series turned out to be very substrate dependent. Rearrangement of the ^{2,4}*syn*,^{4,5}*anti* triol **10** under kinetic conditions gave the unrearranged THF **22** as the major product (Scheme 6). Equilibration with toluene *p*-sulfonic acid gave only a 74:26 mixture of the rearranged THP **21** and unrearranged THF **22**. The inference here could be that it is unfavourable for the sulfur to occupy an axial position, indeed sufficiently unfavourable that it can partly overcome the driving force for 'downhill' migration.[8] The ^{2,4}*anti*,^{4,5}*anti*-triol **11** behaved quite differently; after equilibration of an initial THF–THP mixture the only product identified was the THP **23**, with methyl, acetoxy and phenylsulfanyl groups all occupying equatorial positions (Scheme 6). The ^{2,4}*syn*,^{4,5}*syn*-triol **12** gave,

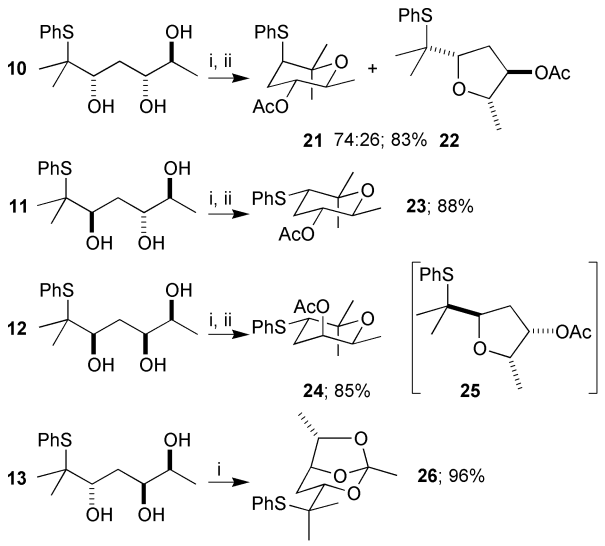

Scheme 6 *Reagents*: i, $(MeO)_3CMe$, $C_5H_6N^+$ TsO^-, CH_2Cl_2, rt; ii, TsOH, CH_2Cl_2, 40 °C.

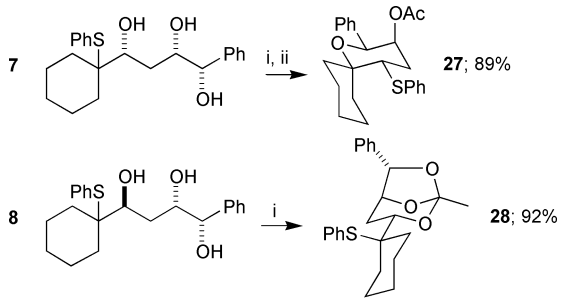

Scheme 7 *Reagents*: i, $(MeO)_3CMe$, $C_5H_6N^+$ TsO^-, CH_2Cl_2, rt; ii, TsOH, CH_2Cl_2, rt.

after the two-step reaction sequence, the THP **24** with an axial acetate (the alternative THF **25** contains an unfavourable 2,3-*syn* relationship) (Scheme 6). Finally, in this series of compounds, the ^{2,4}*anti*,^{4,5}*syn*-triol **13** gave a single product after treatment with trimethylorthoacetate and PPTS: the bicyclic orthoester **26**. Attempts to repeat the reaction at higher temperatures, or with longer reaction times, led only to decomposition products that were not characterised. It is interesting to note the stabilising effect of an *exo*-methyl group on these compounds. When triol **11** (with 2,4-*anti* stereochemistry) was reacted with the same reagent system no bicyclic orthoester intermediate was observed; presumably an *endo*-methyl group here destabilises the orthoester intermediate (if the corresponding orthoester forms at all).

The triols **7** and **8,** each containing a benzylic hydroxy group, behaved similarly to their analogues in the lactic acid series. Triol **7** was converted into the THP **27**, bearing an axial acetate, and triol **8** gave only the bicyclic orthoester **28**, which was not successfully transformed into the target heterocycles (Scheme 7).

In summary, we have demonstrated that for the general class of triols under investigation THFs are formed as thermodynamic products when toluene *p*-sulfonic acid is used as the catalyst. This is attributed to the 1,3-diaxial interactions which exist in the THPs when one of the C–C bonds of the tertiary migration origin is forced to enter an axial environment. The orthoester reaction was shown to be general apart from triols with ^{2,4}*anti*,^{4,5}*syn* stereochemistry in which case the intermediate bicyclic orthoester is overstabilised by a 6-*exo* substituent. The subsequent equilibration of the product mixture gives THPs as exclusive products in all cases except for triol precursors with ^{2,4}*syn*,^{4,5}*anti* stereochemistry.

We thank the EPSRC and AstraZeneca for a grant to D. H.

Notes and references

1 D. House, F. Kerr and S. Warren, *Chem. Commun.*, 2000, 1779 (DOI: 10.1039/b005342m).
2 D. J. Fox, D. House, F. Kerr and S. Warren, *Chem. Commun.*, 2000, 1781 (DOI: 10.1039/b005341o).
3 H. C. Kolb, M. S. VanNieuwenhze and K. B. Sharpless, *Chem. Rev.*, 1994, **94**, 2483.
4 K.-M. Chen, G. E. Hardtmann, K. Prasad, O. Repič and M. J. Shapiro, *Tetrahedron Lett.*, 1987, **28**, 155.
5 D. A. Evans, K. T. Chapman and E. M. Carreira, *J. Am. Chem. Soc.*, 1988, **110**, 3560.
6 E. P. Lodge and C. H. Heathcock, *J. Am. Chem. Soc.*, 1987, **109**, 3353.
7 By 'unrearranged' we mean a product in which the phenylsulfanyl group remains bound to the same carbon as it was before the cyclisation, *i.e.* a product that has not undergone a [1,2]-PhS rearrangement.
8 By 'downhill' we refer to the phenylsulfanyl group undergoing a [1,2] shift from a more substituted to a less substituted carbon atom. Sulfanyl groups generally only move 'downhill'; in exceptional cases they may undergo 'flat' migration, *i.e.* from one secondary centre to another. For more details see: D. J. Fox, D. House and S. Warren, *Angew. Chem., Int. Ed. Engl.*, manuscript in preparation.

An unexpected valence bond isomerization to the heteroaromatic ring system: [1,2,3]triazolo[4,5-*d*]pyridazine

Péter Kövér,[a] György Hajós,*[a] Zsuzsanna Riedl,[a] László Párkányi[a] and Gert Kollenz[b]

[a] *Institute of Chemistry, Chemical Research Center, Hungarian Academy of Sciences, H-1525 Budapest, PO Box 17, Hungary. E-mail: ghajos@cric.chemres.hu*

[b] *Institute of Organic Chemistry, University of Graz, Heinrichstr. 28, A-8020 Graz, Austria.*

Received (in Liverpool, UK) 12th June 2000, Accepted 7th August 2000
First published as an Advance Article on the web 4th September 2000

The arylazo substituted salt 2 when treated with a base underwent a valence bond isomerization to yield a derivative of the heteroaromatic ring system, [1,2,3]triazolo[4,5-*d*]pyridazine (4).

Recently we have elaborated an easy synthetic pathway to some tricyclic zwitterionic fused pyridazo[1,2,4]triazines[1] (*e.g.* **1**) and have shown that these compounds readily undergo cycloadditions as well as Michael additions.[2] As a continuation of these studies the reactivity of the new zwitterions towards diazonium salts seemed of particular interest.

When the zwitterion **1** was treated with aryldiazonium salts at rt, the change of colour from green to bright red indicated that an azo coupling had taken place. Work-up of the reaction mixture led to the isolation of the stable brilliant red crystalline fluoroborate salt **2**.[3] This salt when treated with a base was converted into the neutral azo compound which decomposed upon storage at rt and a yellow component, as shown by tlc, appeared gradually. This decomposition could be accelerated by heating the suspension of **2** in toluene for a few minutes: a yellow crystalline substance was then formed in good yield. For the structure of this yellow compound the *peri* fused **3** was first anticipated. This could be easily rationalized by assuming attachment to the negatively and positively polarized nitrogen atoms (1,5-dipolar cyclization or 'pseudo-electrocyclization'[4]). Upon observation of some further transformations, however, this conclusion seemed ambiguous and structure **4** (*i.e.* a product of a possible thermal electrocycloreversion of **3**) had to be considered.[5] The ring closure (which might proceed *via* the intermediate *peri*-fused tetracycle **3**, or could also be formed from **2** in one single step) seems to represent a special case of a ring closure to [1,2,3]triazole starting from an azo compound.[6]

Comparison of the heats of formation of **3** (208.0 kcal mol^{-1}) and **4** (164.2 kcal mol^{-1}), calculated for a derivative unsubstituted at the triazole ring by the semiempirical PM3 method,[7] also revealed that the ring-opened form **4** is energetically more favourable (by 44 kcal mol^{-1}). A final decision on this structural problem was provided by an X-ray analysis of the product obtained from **2b** which showed that the isolated compound has in fact the ring-opened structure **4b**, as shown in Fig. 1.

The X-ray analytical data revealed that the bond distances and angles are normal.[8] The endocyclic bond angle at N2 is 116.2(2)°, at N1 and N3 102.5(2) and 102.7(2)°. The bond distances N1–N2 and N2–N3 are 1.336(2) and 1.345(2) Å, shorter than N5–N6 (1.364(2) Å).

The whole molecule is basically planar, with the exception of the pyridine moiety which is perpendicular to the mean molecular plane. A characteristic feature of the crystal packing is the infinite stacking with strong π ring interactions. The centroids of the nirophenyl ring at (*x*,*y*,*z*) and the pyridazine ring at (1 + *x*,*y*,*z*) are 3.52 Å apart (the dihedral angle is 0.81°).[9]

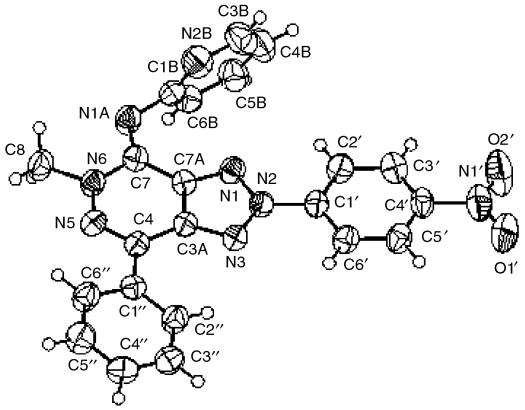

Fig. 1 A molecular diagram[9] of **4b** with the numbering of atoms. Anisotropic displacement parameters represent 50% probabilities.

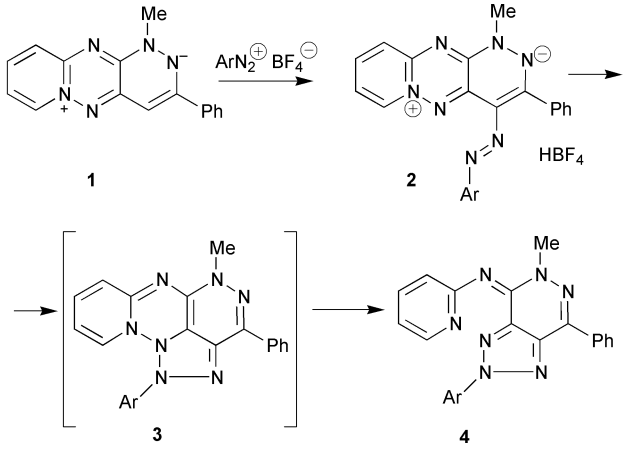

Scheme 1 (a) Ar = 4-ClC_6H_4–, (b) Ar = 4-$NO_2C_6H_4$–, (c) Ar = 4-$CH_3OC_6H_4$–.

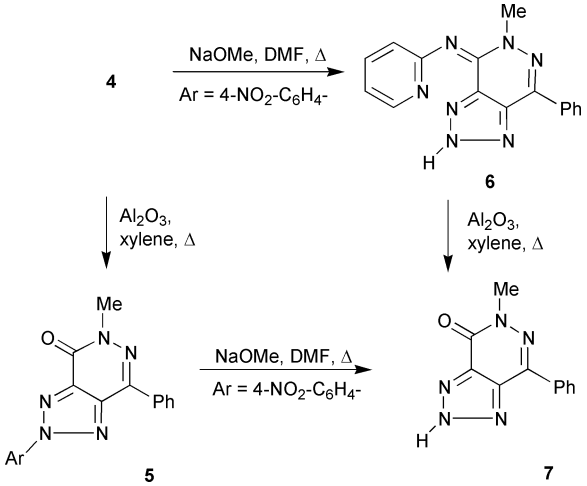

Scheme 2

DOI: 10.1039/b004775i

The Schiff base side-chain of **4** easily underwent hydrolysis in the presence of alumina at higher temperature (*i.e.* in boiling xylene) and gave rise to the triazolopyridazinone **5**,[10] a derivative of the heteroaromatic [1,2,3]triazolo[4,5-*d*]pyridazine ring system (saturated[11] and unsaturated derivatives[12,13] of this ring skeleton have been described elsewhere).

The 4-nitrophenyl substituted compounds (*i.e.* **4b** and **5b**) proved to be suitable for transformations to the derivatives containing an unsubstituted triazole moiety. Thus, these compounds when treated with sodium methylate in DMF underwent an *ipso* substitution and afforded the dearylated products **6**[14] and **7**.[15]

Our results reveal that this observed valence bond isomerization provides an easy access to a hitherto unexplored area of triazolopyridazines.

The financial support of OTKA 22111 and 26476, as well as of Aktion Austria/Hungary, Proj. 34OeU9, is gratefully acknowledged.

Notes and references

1 Zs. Juhász-Riedl, Gy. Hajós, E. Gács-Baitz, G. Kollenz and A. Messmer, *Chem. Ber.*, 1990, **123**, 1415; Zs. Riedl, Gy. Hajós, G. Kollenz and A. Messmer, *Chem. Ber.*, 1994, **127**, 1799.

2 Zs. Riedl, Gy. Hajós, A. Messmer, A. Rockenbauer, L. Korecz, G. Kollenz, W. Fabian, K. Peters and E. M. Peters, *Chem. Commun.*, 1997, 757.

3 **2a**: mp 228–230 °C (95 %); **2b**: mp 269–271 °C (67%); **2c**: 234–236 °C (95%). *Selected spectroscopic data for* **2b**: ^{1}H NMR (400 MHz, DMSO-d_6): δ 3.8 (3H, s, 1-Me), 7.2–7.9 (7H, m, Ar), 8.1–8.25 (5H, m, Ph), 9.4 (1H, d, J = 7 Hz, 7-H), 13.0 (1H, s, 2-NH).

4 W. M. F. Fabian, V. A. Bakulev and O. Kappe, *J. Org. Chem.*, 1998, **63**, 5801.

5 **4a**: mp 225–227 °C (74%); **4b**: mp 269–271 °C (67%); **4c**: 226–228 °C (70%). *Selected spectroscopic data for* **4b**: ^{1}H NMR (400 MHz, $CDCl_3$): δ 4.07 (3H, s, 5-Me), 7.01 (1H, m, J = 8, 1, 1 Hz, 3′-Py), 7.13 (1H, m, J = 7, 5, 1 Hz, 5′-Py), 7.47 (1H, m, Ph), 7.53 (2H, m, Ph), 7.74 (1H, m, J = 7, 8, 2 Hz, 4′-Py), 8.05 (2H, m, Ar), 8.32 (2H, m, Ph), 8.34 (2H, m, Ar), 8.47 (1H, m, J = 5, 2 , 1 Hz, 6′-Py); ^{13}C NMR ($CDCl_3$): δ 42.1, 116.6, 118.6, 120.5, 125.1, 127.1, 128.6, 129.6, 133.1, 135.1, 137.8, 138.57, 141.8, 142.9, 144.6, 147.6, 148.7, 162.4; MS, M_{calcd}: 424.1396, M_{found}: 424.1390 ± 5 ppm.

6 R. N. Butler, A. M. Evans, A. M. Gillan, J. P. James, E. M. NcNeela, D. Cunningham and I. McArdle, *J. Chem. Soc., Perkin Trans. 1*, 1990, 2537.

7 J. J. P. Stewart, *J. Comput. Chem.*, 1989, **10**, 209.

8 *Crystal data for* **4b**: $C_{22}H_{16}N_8O_2$, M = 424.43, monoclinic, a = 6.163(1), b = 17.243(4), c = 18.471(1) Å, β = 92.00(1)°, U = 1961.7(6) Å^3, T = 293(2) K, space group $P2_1/c$ (No. 14), Z = 4, μ(Mo-Kα) = 0.099 mm^{-1}, 4175 reflections measured, 3713 unique (R_{int} = 0.0206) which were used in all calculations. The final *wR*2 was 0.1036 (all data).

9 G. M. Sheldrick, (1997) SHELXL-97 Program for Crystal Structure Refinement, University of Göttingen, Germany; *International Tables for X-ray Crystallography Vol C*, ed. A. J. C. Wilson, Kluwer Academic Publisher, Dordrecht, 1992; A. L. Spek, *Acta Cryst.*, **A46**, 1990, C-3.

10 *Selected spectroscopic data for* **5b** : yellow crystals, mp 262–264 °C (86%); ^{1}H NMR (400 MHz, DMSO-d_6): δ 3.87 (3H, s, Me), 7.56–7.64 (3H, m, Ph), 8.34 (2H, m, Ar), 8.52 (2H, m, Ar), 8.58 (2H, m, Ph); Calc. for: $C_{17}H_{12}N_6O_3$, C, 58.62; H, 3.45; N, 24.14. Found: C, 58.56; H, 3.51; N, 24.06%.

11 G. E. Mertzanos, J. Stephanidou-Stephanatou, C. A. Tsoleridis and N. E. Alexandrou, *Tetrahedron Lett.*, 1992, **33**, 4499.

12 S. F. Martin and R. N. Castle, *J. Heterocycl. Chem.*, 1969, **6**, 93.

13 M. Yanai, T. Kinoshita, S. Takeda, M. Mori, H. Sadaki and H. Watanabe, *Chem. Pharm. Bull.*, 1970, **18**, 1685.

14 *Selected spectroscopic data for* **6**: Pale yellow crystals, mp 260 °C (70%); ^{1}H NMR (400 MHz**,** DMSO-d_6): δ 4.18 (3H, s, 5-Me), 7.15 (1H, m, J = 7, 5, 1 Hz, 5′-Py), 7.4 (1H, m, J = 8, 1, 1 Hz, 3′-Py), 7.55–7.6 (3H, m, Ph), 7.99 (1H, m, J = 8, 7, 2 Hz, 4′-Py), 8.21 (1H, m, J = 5, 2, 1 Hz, 6′-Py), 8.65 (2H, m, Ph), 14.6 (1H, b, 5-NH); MS, M_{calcd}: 303.1232, M_{found}: 303.1233 ± 5 ppm.

15 *Selected spectroscopic data for* **7**: white crystals, mp 245–246 °C (70%); ^{1}H NMR (400 MHz, DMSO-d_6): δ 3.82 (3H, s, 5-Me), 7.5–7.6 (3H, m, Ph), 8.3 (2H, m, Ph); MS, M_{calcd}: 227.0807, M_{found}: 227.0808 ± 5 ppm.

Temperature effect on the epoxidation of olefins by an iron(III) porphyrin complex and *tert*-alkyl hydroperoxides

Wonwoo Nam,* So-Young Oh, Mi Hee Lim, Mee-Hwa Choi, So-Yeop Han and Gil-Ja Jhon

Department of Chemistry and Division of Molecular Life Sciences, Ewha Womans University, Seoul 120-750, Korea. E-mail: wwnam@mm.ewha.ac.kr

Received (in Cambridge, UK) 27th June 2000, Accepted 11th August 2000
First published as an Advance Article on the web 4th September 2000

An electron-deficient iron porphyrin complex catalyzes the epoxidation of olefins by *tert*-alkyl hydroperoxides *via radical-free* oxidation reactions in aprotic solvent; the epoxidation reactions were markedly influenced by reaction temperature and high yields of epoxide products were obtained with retention of stereospecificity at low temperature.

The reactions of iron(III) complexes of porphyrin and non-porphyrin ligands with alkyl hydroperoxides have been extensively studied as biomimetic models for heme- and non-heme-containing enzymes.[1] It has been shown in a number of reports that oxidation of hydrocarbons by iron(III) porphyrin complexes and *tert*-alkyl hydroperoxides proceeds *via* O–O bond homolysis (*i.e. free* alkoxyl radical chemistry) in aprotic solvents.[1–3] In addition, Ingold and coworkers evidenced, using 2-methyl-1-phenyl-2-propyl hydroperoxide (MPPH) as a mechanistic probe to distinguish between *free* alkoxyl radical chemistry and *radical-free* chemistry, that O–O bond homolysis is a predominant pathway in non-porphyrin iron complex-catalyzed oxidation of hydrocarbons by *tert*-alkyl hydroperoxides.[1,4] Despite intensive study for the last two decades, it has rarely been observed that simple iron complexes of porphyrin and non-porphyrin ligands are able to catalyze the oxidation of hydrocarbons by alkyl hydroperoxides *via radical-free* chemistry in aprotic solvents.[5,6]† Since we found recently that a highly electron-deficient iron(III) porphyrin complex, $Fe(TF_4TMAP)(CF_3SO_3)_5$ [TF_4TMAP = *meso*-tetrakis(2,3,5,6-tetrafluoro-*N*,*N*,*N*-trimethyl-4-aniliniumyl)porphinato dianion], catalyzes the epoxidation and hydroxylation of hydrocarbons by H_2O_2 *via* radical-free oxidation reactions,[7] we attempted the epoxidation of olefins with the iron porphyrin complex and *tert*-alkyl hydroperoxides such as *tert*-butyl hydroperoxide (Bu^tOOH) and MPPH. Here we report that the epoxidation reactions were markedly influenced by reaction temperature and high yields of epoxide products with retention of stereospecificity were obtained at low temperature.

The catalytic epoxidation of cyclohexene by Bu^tOOH was carried out in the presence of $Fe(TF_4TMAP)^{5+}$ at various reaction temperatures under argon atmosphere in MeCN. As detailed in Table 1, the formation of cyclohexene oxide, cyclohexenol and *tert*-butyl cyclohexenyl peroxide (*c*-$C_6H_{11}OOBu^t$) was observed at room temperature, indicating that the cyclohexene oxidation proceeds *via* free alkoxyl radical chemistry (*i.e.* O–O bond homolysis of Bu^tOOH).[1,8] Interestingly, we found that the product distribution varied depending on reaction temperature. As the reaction temperature was lowered, the yields of cyclohexene oxide increased, while those of allylic oxidation products (*i.e.* cyclohexenol and *c*-$C_6H_{11}OOBu^t$) diminished (Table 1). These results indicate that the reaction of iron(III) porphyrin complex with Bu^tOOH is sensitive to reaction temperature and that two-electron epoxidation becomes a major pathway in the cyclohexene epoxidation at low temperature [Scheme 1(A), pathway A]. Further evidence that the epoxidation of olefins by $Fe(TF_4TMAP)^{5+}$ and Bu^tOOH at low temperature occurs *via* radical-free chemistry was obtained by analyzing products obtained in *cis*-stilbene epoxidation. *cis*-Stilbene was predominantly oxidized to *cis*-stilbene oxide [eqn. (1)],‡ demonstrating that the $Bu^tOO\cdot$ radical was not involved as an epoxidizing agent in the epoxidation reactions.[2,8]

The temperature effect on the reaction of $Fe(TF_4TMAP)^{5+}$ with alkyl hydroperoxides in MeCN was also observed when MPPH was used as an oxidant (Table 1). Only a small amount

Table 1 Epoxidation of cyclohexene by $Fe(TF_4TMAP)^{5+}$ and *tert*-alkyl hydroperoxides at various reaction temperatures in MeCN and in MeOH–CH_2Cl_2[a,b]

		Yields (%) of products formed in Bu^tOOH reactions[c,d]				Yields (%) of products formed in MPPH reactions[c]				
	T/°C	*t*/h	Cyclohexene oxide	Cyclohexenol	*c*-$C_6H_{11}OOBu^t$	*t*/h	Cyclohexene oxide	MPPOH	$PhCH_2OH$	PhCHO
MeCN	20	2	20 ± 3	29 ± 3	12 ± 5	2	7 ± 1	20 ± 3	63 ± 6	8 ± 4
	10	2	31 ± 3	22 ± 3	8 ± 4	2	12 ± 2	23 ± 3	47 ± 5	8 ± 3
	0	4	45 ± 4	18 ± 3	5 ± 3	4	17 ± 3	29 ± 3	33 ± 4	8 ± 2
	−10	4	52 ± 4	14 ± 2	< 2	4	32 ± 3	44 ± 4	27 ± 3	6 ± 2
	−20	4	70 ± 4	9 ± 2	< 2	5	38 ± 3	46 ± 5	18 ± 3	12 ± 4
	−30	4	74 ± 4	7 ± 2	0	6	46 ± 4	55 ± 6	12 ± 3	12 ± 4
MeOH–CH_2Cl_2[e]	20	2	59 ± 3	8 ± 2	Trace[f]	2	36 ± 2	47 ± 3	30 ± 3	Trace[f]
	10	2	70 ± 5	5 ± 1	Trace[f]	2	42 ± 3	45 ± 3	20 ± 2	Trace[f]
	0	4	68 ± 5	4 ± 2	Trace[f]	4	57 ± 4	62 ± 4	13 ± 2	Trace[f]
	−10	4	76 ± 5	< 2	Trace[f]	4	63 ± 5	69 ± 5	< 4	Trace[f]
	−20	4	75 ± 5	< 2	Trace[f]	5	68 ± 5	79 ± 6	< 4	Trace[f]

[a] MPPH[4] and *tert*-butyl cyclohexenyl peroxide (*c*-$C_6H_{11}OOBu^t$)[11] were prepared according to literature procedures. All reactions were run at least in triplicate, and the data represent the average of these reactions. [b] In a typical reaction, oxidant (2×10^{-2} mmol diluted in 80 μL of MeCN) was added to a reaction solution containing $Fe(TF_4TMAP)(CF_3SO_3)_5$ (1×10^{-3} mmol) and cyclohexene (0.3 mmol) in 0.3 mL MeCN at the given temperature under an inert atmosphere. After the reaction mixture was stirred for the given time, the reaction solution was directly analyzed by GC or GC–MS with known authentic sample. [c] Yields were based on oxidants added. [d] < 5% of cyclohexenone was formed in all of the reactions. [e] Since methanolysis of cyclohexene oxide took place under the reaction conditions, the yields of cyclohexene oxide were determined by summing the amounts of cyclohexene oxide and 2-methoxycyclohexanol.[12] [f] < 2% based on oxidant added was formed.

DOI: 10.1039/b005162o

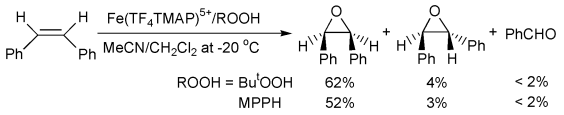

(1)

of cyclohexene oxide was formed and $PhCH_2OH$ was the major product derived from MPPH decomposition at room temperature. This result demonstrates that the reaction of $Fe(TF_4TMAP)^{5+}$ with MPPH occurs *via* O–O bond homolysis [Scheme 1(B), pathway A].[4] As the reaction temperature was lowered, the formation of cyclohexene oxide and $PhCH_2CMe_2OH$ (MPPOH) products increased, indicating that two-electron epoxidation takes place in the reaction of $Fe(TF_4TMAP)^{5+}$ and MPPH at low temperature [Scheme 1(B), pathway B]. When the epoxidation of *cis*-stilbene by $Fe(TF_4TMAP)^{5+}$ and MPPH was performed at low temperature, *cis*-stilbene oxide was obtained as a major product [eqn. (1)].‡ Also, MPPOH was the predominant product of MPPH decomposition (70% based on MPPH used). These results demonstrate unambiguously that the epoxidation of olefins by MPPH at low temperature occurs *via* radical-free chemistry.

Since it is known that methanol is a better solvent for iron porphyrin complex-catalyzed epoxidation of olefins by hydroperoxides,[5] the epoxidation of cyclohexene by Bu^tOOH and MPPH was carried out in a solvent mixture of MeOH and CH_2Cl_2 (3:1). As shown in Table 1, the yields of cyclohexene oxide formed in MeOH–CH_2Cl_2 were higher than those obtained in MeCN. In addition, as observed in the MeCN reactions, the oxide yields in the MPPH reactions increased as the reaction temperature was lowered. Interestingly, *ca.* 80% of MPPH was converted to MPPOH below −20 °C, and, to the best of our knowledge, this is the highest MPPOH formation in iron complex-mediated O–O bond cleavage of MPPH.[4]

We then studied ^{18}O-labeled water experiments in the epoxidation of cyclohexene by Bu^tOOH and MPPH,[9] in order to understand the source of oxygen atoms in cyclohexenol and benzyl alcohol products formed in the reactions of Bu^tOOH and MPPH, respectively.[4b,10] When the epoxidation reactions were carried out in the presence of $H_2{}^{18}O$ at room temperature,§ the percentages of ^{18}O incorporated from the labeled water into cyclohexenol and benzyl alcohol were 21 ± 2 and 14 ± 2%, respectively. The observation that some of the oxygen in the alcohol products came from $H_2{}^{18}O$ demonstrates unambiguously that cyclohexenyl and benzyl radicals were trapped by the $(TF_4TMAP)Fe^{IV}$–OH intermediate [pathway B in Scheme 1(A) and pathway D in Scheme 1(B)].[4b,9,10] The different and relatively small amounts of ^{18}O-incorporation into the cyclohexenol and benzyl alcohol products are ascribed to the fact that the oxygen exchange between the iron(IV)–OH intermediate and labeled water [pathway C in Scheme 1(A) and pathway E in Scheme 1(B)] is competing with the C–O bond-forming step between the intermediate and alkyl radicals [pathway B in Scheme 1(A) and pathway D in Scheme 1(B)].[3,9b]

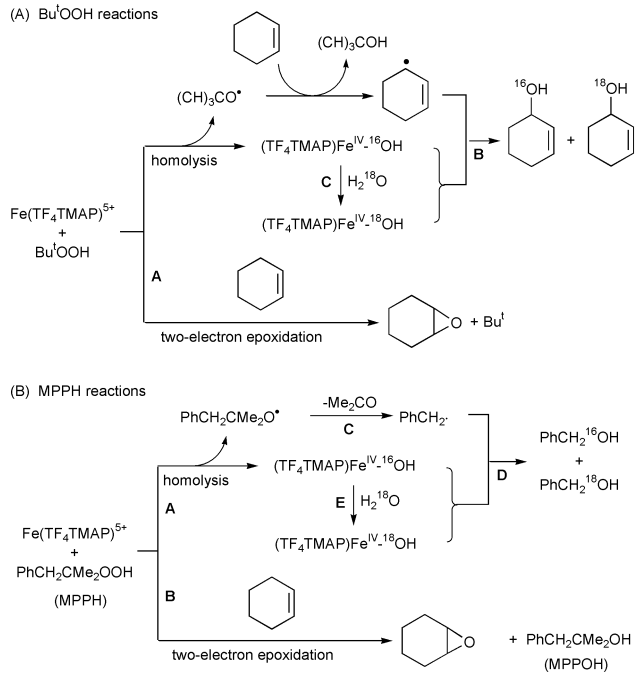

Scheme 1

In conclusion, we have shown here that high yields of oxide products were formed *via* a *radical-free* mechanism in the epoxidation of olefins by *tert*-alkyl hydroperoxides at low temperature. The oxide yields were found to depend significantly on reaction temperature. In addition, it has been demonstrated unambiguously that alcohol products such as cyclohexenol and benzyl alcohol were formed by the trapping of alkyl radicals by $(TF_4TMAP)Fe^{IV}$–OH species. Future studies will focus on attempts to understand the temperature effect on the mechanism of hydroperoxide O–O bond activation by iron porphyrin complexes and to use the alkyl hydroperoxides in biomimetic alkane hydroxylation reactions.

This research was supported by KOSEF (1999-2-122-002-4 for W. N. and 981-0304-022-1 for G. J.), KRF (KRF-99-042-D00068), the MOST through the Women's University Research Fund, Brain Korea 21 Project.

Notes and references

† Traylor *et al.* reported that epoxidation of olefins by electron-deficient iron(III) porphyrin complexes and Bu^tOOH gives high yields of oxide products in protic solvents (*i.e.* MeOH).[5] We have shown that the reactions of water-soluble iron(III) porphyrins with *tert*-alkyl hydroperoxides epoxidize olefins to give the corresponding oxide products in aqueous solution.[6]

‡ *Reaction conditions*: oxidant (2×10^{-2} mmol, diluted in 80 μL of MeCN) was added to a reaction solution containing $Fe(TF_4TMAP)^{5+}$ (3×10^{-3} mmol) and *cis*-stilbene (0.3 mmol) in a solvent mixture (1 mL) of MeCN and CH_2Cl_2 (1:1) at −20 °C. After stirring for 4 h, the reaction solution was directly analyzed by HPLC.

§ ^{18}O-labeled water experiments with Bu^tOOH and MPPH were performed at 20 °C under the same reaction conditions as described in footnote a of Table 1 except that $H_2{}^{18}O$ (25 μL, 95% ^{18}O enriched) was present in the reaction media. The ^{16}O and ^{18}O compositions in cyclohexenol and benzyl alcohol were determined by the relative abundances of mass peaks at *m*/*z* 83 and 85 for cyclohexenol and at *m*/*z* 108 and 110 for benzyl alcohol.

1 K. U. Ingold and P. A. MacFaul, in *Biomimetic Oxidations Catalyzed by Transition Metal Complexes*, ed. B. Meunier, Imperial College Press, London, 2000, pp. 45–89.
2 F. Minisci, F. Fontana, S. Araneo, F. Recupero and L. Zhao, *Synlett*, 1996, 119; F. Minisci, F. Fontana, S. Araneo, F. Recupero, S. Banfi and S. Quici, *J. Am. Chem. Soc.*, 1995, **117**, 226; G.-X. He and T. C. Bruice, *J. Am. Chem. Soc.*, 1991, **113**, 2747.
3 Y. M. Goh and W. Nam, *Inorg. Chem.*, 1999, **38**, 914.
4 (*a*) P. A. MacFaul, D. D. M. Wayner and K. U. Ingold, *Acc. Chem. Res.*, 1998, **31**, 159; (*b*) P. A. MacFaul, K. U. Ingold, D. D. M. Wayner and L. Que Jr., *J. Am. Chem. Soc.*, 1997, **119**, 10 594.
5 T. G. Traylor, C. Kim, W.-P. Fann and C. L. Perrin, *Tetrahedron*, 1998, **54**, 7977 and refs. therein.
6 W. Nam, H. J. Choi, H. J. Han, S. H. Cho, H. J. Lee and S.-Y. Han, *Chem. Commun.*, 1999, 387.
7 W. Nam, Y. M. Goh, Y. J. Lee, M. H. Lim and C. Kim, *Inorg. Chem.*, 1999, **38**, 3238; Y. J. Lee, Y. M. Goh, S.-Y. Han, C. Kim and W. Nam, *Chem. Lett.*, 1998, 837.
8 R. A. Sheldon and J. K. Kochi, *Metal Catalyzed Oxidations of Organic Compounds*, Academic Press, New York, 1981.
9 (*a*) J. Bernadou and B. Meunier, *Chem. Commun.*, 1998, 2167; (*b*) K. A. Lee and W. Nam, *J. Am. Chem. Soc.*, 1997, **119**, 1916.
10 S. J. Lange, H. Miyake and L. Que, Jr., *J. Am. Chem. Soc.*, 1999, **121**, 6330.
11 T. W. Campbell and G. M. Coppinger, *J. Am. Chem. Soc.*, 1951, **73**, 1788.
12 G. H. Posner and D. Z. Rogers, *J. Am. Chem.Soc.*, 1977, **99**, 8208.

One-pot conversion of citronellal into isopulegol epoxide on mesoporous titanium silicate

Matteo Guidotti,*[a] Giuliano Moretti,[b] Rinaldo Psaro[a] and Nicoletta Ravasio[a]

[a] *Centro CNR "CSSCMTBSO", Dipartimento di Chimica Inorganica, Metallorganica e Analitica, via Venezian 21, 20133 Milano, Italy. Fax: +39-02-2362748; E-mail: labcat@csmtbo.mi.cnr.it*
[b] *Centro CNR "SACSO", Dipartimento di Chimica, p.le Aldo Moro 5, 00185 Roma, Italy*

Received (in Liverpool, UK) 26th April 2000, Accepted 4th August 2000
First published as an Advance Article on the web 4th September 2000

Citronellal was converted into isopulegol epoxide in a one-pot two-step reaction achieving a 68% global yield on Ti-MCM-41 and designing a two-solvent catalytic system.

The push of environmental concerns makes bifunctional catalysts the object of growing interest as the tool to reduce the number of steps in a fine chemistry synthesis process.

In a programme aimed at the substitution of homogeneous with heterogeneous Lewis acids in organic synthesis, some of us reported that citronellal **1** (Scheme 1) can be easily cyclized to isopulegol **2** in the presence of acidic mixed oxides.[1] Likewise, we recently reported the epoxidation activity of Ti-containing MCM-41 materials, which easily transform **2** into isopulegol epoxide **3** using *tert*-butylhydroperoxide (TBHP).[2] The high selectivity observed in this reaction, together with the growing interest in isopulegol and related terpenic compounds for uses other than those for the flavour and cosmetic industry (*e.g.* isopulegol derivatives have been claimed to possess a high bactericidal and fungicidal activity[3] and a long-lasting insect repellent action[4]), prompted us to investigate the possibility of obtaining isopulegol epoxide **3** directly from citronellal **1** on the same catalyst.

Preliminary experiments, carried out starting from **1** in the presence of either in-framework or extra-framework Ti-containing MCM-41's, showed that Ti-MCM-41, obtained by grafting an organotitanium precursor onto the MCM-41 surface, leads to better catalytic features than other in-framework Ti-containing solids. This behaviour is also consistent with high conversion values recorded on this mesoporous material, when the epoxidation step is carried out separately (Table 1; tests 5 and 6).

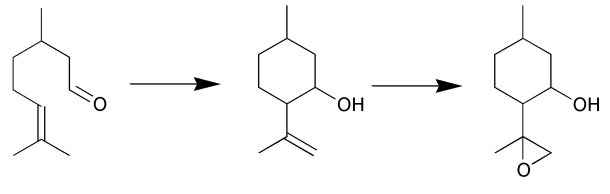

1 **2** **3**

Scheme 1

As in other examples, where an epoxidation reaction is coupled to an acid-catalysed one,[5] the choice of the solvent is not trivial. In fact, while the cyclization reaction is easily carried out in apolar hydrocarbons, *i.e*. n-heptane or toluene (tests 1 and 2), the best results in the epoxidation reactions are achieved in aprotic polar solvents, *i.e.* acetonitrile or ethylacetate, which are bad solvents for the first-step reaction (tests 3 and 4). Therefore, the use of a unique solvent throughout the two-step reaction appeared to be hardly feasible. Moreover, to avoid the oxidation of the non-reacted citronellal **1** by TBHP, it is advisable to add the oxidant after the complete conversion of **1** into **2**. In fact, whenever TBHP is added at the beginning of the cyclization step, a plethora of products is registered, among which is menthone. So, during the first 6 h of reaction the intramolecular cyclization was performed in apolar hydrocarbon. After that time an equal volume of polar solvent was added together with the required TBHP aliquot.

Ti-MCM-41 has been prepared in the following way: MCM-41 was synthesized according to procedures developed by Mobil researchers.[6] Titanium was grafted onto the MCM-41 surface using titanocene dichloride as precursor following the procedure described by Maschmeyer *et al.*[7] Details about the preparation of the samples are reported in ref. 2. The Ti content, determined by ICP-atomic emission spectroscopy, of the Ti-MCM-41 sample was 1.88 wt.%. The specific surface area (BET), the total pore volume and the effective mean pore diameter of the solid were 860 m^2g^{-1}, 0.52 cm^3g^{-1} and 2.3 nm, respectively. The mesoporous solid was pretreated by heating at 773 K for 1 h in air. The catalytic reactions were carried out in a glass batch reactor at 363 K under anhydrous nitrogen using acetonitrile and toluene or n-heptane and ethyl acetate as solvents, anhydrous TBHP as oxidant (oxidant : substrate molar ratio = 1.1) and 15 wt.% catalyst with respect to the substrate citronellal **1**. The solvent : citronellal volume ratio is 25. The samples taken during the 24 h reaction were analysed by gas chromatography (FID detector; mesitylene as internal standard). The products were identified by GC-MS and NMR spectroscopy.

It is worth noting that pure MCM-41 (without titanium) was completely inactive, while some amorphous silica is able to catalyse the cyclization reaction.[1,8] This confirms that the Ti-

Table 1 Catalytic tests on Ti-MCM-41 (1.88% Ti)

Test no.	$Solv_1$[a]	$Solv_2$[b]	$Conv_1$[c] (%)	Sel_1[d] (%)	$Conv_2$[e] (%)	Sel_2[f] (%)
1	$PhCH_3$	$PhCH_3$	> 98	> 98	9	—[g]
2	n-C_7H_{16}	n-C_7H_{16}	> 98	> 98	5	—[g]
3	CH_3CN	—	47	90	—[h]	—[h]
4	AcOEt	—	74	95	—[h]	—[h]
5	—	CH_3CN	—[h]	—[h]	73[i]	80[i]
6	—	AcOEt	—[h]	—[h]	78[i]	41[i]
7	$PhCH_3$	$PhCH_3$ + CH_3CN	> 98	> 98	76	90
8	n-C_7H_{16}	n-C_7H_{16} + AcOEt	> 98	> 98	58	75

[a] Cyclisation: 5 ml solvent; 15 wt.% catalyst; 358 K under reflux; 6 h. [b] Epoxidation: 5 + 5 ml solvent; 15 wt.% catalyst; TBHP:isopulegol molar ratio = 1.1; 358 K under reflux; 18 h. [c] Conversion based on consumption of **1**. [d] Selectivity to **2**. [e] Conversion based on consumption of **2**. [f] Selectivity to **3**. [g] Under detection limit. [h] Step not run. [i] From Ref. 2.

DOI: 10.1039/b003397i

free mesoporous material is lacking in acidic sites and also that the presence of titanium(IV) in a siliceous matrix gives rise by itself to a material containing both redox and acidic properties.[9] Besides, the introduction of trivalent metal ion, although widely used in bifunctional catalysts,[10,11] appears to be redundant. The use of a MCM-41 sample containing both titanium (1.91 wt.% grafted from titanocene) and aluminium (0.59 wt.% inserted by isomorphous substitution for Si) did not lead to a remarkable improvement in catalytic features: the Al insertion shortens the first-step reaction time (cyclization is complete after 2 h), leaving the second-step reaction time and selectivity (74% conversion of **2** and 88% selectivity to **3** after 18 h in toluene + acetonitrile) practically unaffected.

Both toluene and n-heptane exhibit a complete and selective conversion of **1** into **2** within 6 h and this is consistent with the results obtained on amorphous mixed-oxide TiO_2–SiO_2.[1] The reaction time is rather longer, but is necessary to avoid the presence of unreacted citronellal in the second step.

In the epoxidation step, as in the tests on other terpenic unsaturated alcohols,[2] acetonitrile (test 7) showed better performances than ethyl acetate (test 8). This behaviour might be attributed to the weakly basic character of acetonitrile that inhibits the formation of acid-catalysed secondary products from isopulegol epoxide **3**.[12] The main by-product formed in the second-step reaction is isopulegone, *i.e.* 5-methyl-2-(1-methylethenyl)cyclohexanone.

With the purpose of obtaining a deeper insight about the heterogeneity of the system,[13] the reaction mixture was carefully filtered at *ca*. 50% conversion (2 h reaction) in the second step. Testing the colourless filtered solution for further reaction, no activity of the liquid mixture was observed. From this behaviour, the observed catalyst is presumably heterogeneous. Because of the intrinsic low chemical and mechanical stability of MCM-41-based materials,[14] work is in progress to verify whether or not the catalyst is stable and recyclable.

In summary, the best result for the one-pot conversion of citronellal into isopulegol epoxide with a *ca*. 68% global yield was achieved on Ti-MCM-41 as follows. Toluene was used as the solvent for the 6 h long cyclization step during which all the citronellal **1** was completely and selectively converted into isopulegol **2**. Then, after the addition of TBHP and acetonitrile, over the following 18 h isopulegol **2** was epoxidised to **3** with a 76% conversion and a 90% selectivity (test 7).

In this reaction, employing Ti-MCM-41 obviates the use of homogeneous catalysts in both steps, namely zinc halides in the first and transition metal complexes or peroxy acids in the second, thereby limiting the waste production to the work-up phase, when the TBHP in excess has to be quenched. Such bifunctional behaviour is to be attributed to the high dispersion of Ti^{IV} onto the surface of the mesoporous solid, which brings acidity into the silica matrix and causes the excellent activity in the epoxidation step.

The authors gratefully acknowledge the CNR-MURST for financial support through the 'Program Chemistry Law 95/95-I year'.

Notes and references

1 N. Ravasio, M. Antenori, F. Babudri and M. Gargano, *Stud. Surf. Sci. Catal.*, 1997, **108**, 625.
2 C. Berlini, M. Guidotti, G. Moretti, R. Psaro and N. Ravasio, *Catal. Today*, 2000, **60**, 219.
3 P. Kalck, R. Naigre and S. Sirol, *Fr. Pat.* 2,721,926, 1996.
4 S. Okura, A. Amano, T. Yamamoto and H. Ota, *Jpn. Pat.* 10 36,201, 1998.
5 M. van Klaveren and R. A. Sheldon in: *3rd World Congress on Oxidation Catalysis*, ed. R. K. Grasselli, S. T. Oyama, A. M. Gaffney and J. E. Lyons, Elsevier, 1997, p. 567
6 J. S. Beck, J. C. Vartuli, W. J. Roth, M. E. Leonowicz, C. T. Kresge, K. D. Schmitt, C. T.-W. Chu, D. H. Olson, E. W. Sheppard, S. B. McCullen, J. B. Higgins and J. L. Schlenker, *J. Am. Chem. Soc.*, 1992, **114**, 10 834.
7 T. Maschmeyer, F. Rey, G. Sankar and J. M. Thomas, *Nature*, 1995, **378**, 159; R. D. Oldroyd, G. Sankar, J. M. Thomas and D. Özkaya, *J. Phys. Chem. B*, 1998, **102**, 1849.
8 P. J. Kropp, G. W. Breton, S. L. Craig, S. D. Crawford, W. F. Durland, J. E. Jones and J. S. Raleigh, *J. Org. Chem.*, 1995, **60**, 4146.
9 J. C. van der Waal, P. Lin, M. S. Rigutto and H. van Bekkum, *Stud. Surf. Sci. Catal.*, 1997, **105**, 1093; A. Bhaumik and T. Tatsumi, *J. Catal.*, 1999, **182**, 349.
10 D. Trong On, M. P. Kapoor, P. N. Joshi, L. Bonneviot and S. Kaliaguine, *Catal. Lett.*, 1997, **44**, 171.
11 A. Corma, M. Iglesias and F. Sànchez, *J. Chem. Soc., Chem. Commun.*, 1995, 1635.
12 A. Corma, P. Esteve and A. Martìnez, *J. Catal.*, 1996, **161**, 11.
13 R. A. Sheldon, M. Wallau, I. W. C. E. Arends and U. Schuchardt, *Acc. Chem. Res.*, 1998, **31**, 485.
14 N. Igarashi, Y. Tanaka, S.-I. Nakata and T. Tatsumi, *Chem. Lett.*, 1999, 1.

ChemComm

Generation of metalloenamines by carbon–carbon bond formation: ring opening reactions of 2-methyleneaziridines with organometallic reagents

Jerome F. Hayes,[a] Michael Shipman*[b] and Heather Twin[b]

[a] *SmithKline Beecham Pharmaceuticals, Old Powder Mills, Tonbridge, Kent, UK TN11 9AN*
[b] *School of Chemistry, University of Exeter, Exeter, Devon, UK EX4 4QD. E-mail: M.Shipman@exeter.ac.uk*

Received (in Liverpool, UK) 7th July 2000, Accepted 31st July 2000
First published as an Advance Article on the web 4th September 2000

Ring opening of 2-methyleneaziridines with Grignard reagents in the presence of CuI yields metalloenamines in a regiospecific fashion which can be further reacted with electrophiles to produce functionalised ketones *via* a one-pot process.

Following their introduction independently by Stork[1] and by Wittig,[2] metalloenamines (metallated imines) have become established as one of the best methods of forming carbon–carbon bonds at the α-carbon atom of aldehydes and ketones.[3] Metalloenamines are known to be extremely reactive and undergo clean *C*-alkylation reactions with a wide range of electrophiles including primary and secondary alkyl halides, aldehydes, ketones, nitriles, epoxides and oxetanes. Consequently, alkylation reactions of these carbanions are widely used in organic synthesis. Metalloenamines are traditionally made by deprotonation of the corresponding imine using a strong base such as EtMgBr or LDA. One limitation with this method stems from the fact that regiochemical control in the enolisation process is not always possible when imines derived from unsymmetrical ketones are used, resulting in mixtures of alkylated products being formed.[4] Few alternative methods for the generation of metalloenamines have been developed, with the only notable contributions being made by Wender.[5] We imagined that ring opening of 2-methyleneaziridines with organometallic reagents might provide an alternative entry into metalloenamines, as depicted in Scheme 1. We felt that this conceptually new approach to metalloenamines might offer two significant advantages over the traditional route to such species by way of imine enolisation. Firstly, the overall transformation would result in the formation of two new carbon–carbon bonds and thus could be considered as an efficient and potentially highly flexible three-component coupling reaction. Secondly, the ring opening of the aziridine might be expected to provide the metalloenamine as a single regioisomer, circumventing problems associated with regioselectivity in the deprotonation of unsymmetrical imines. Here, we describe our preliminary results regarding the ring opening reactions of 2-methyleneaziridines with organometallic reagents and demonstrate their potential as metalloenamine precursors.

At the outset of this study, no ring opening reactions of methyleneaziridines using carbon based nucleophiles had been reported.[6,7] Initially, we chose to investigate the ring opening reactions of methyleneaziridine (±)-**1** (R = CHMePh) as it is very easy to prepare on a multigram scale.[8] Since Ganem has shown that simple *N*-alkylated aziridines can be ring opened with Gilman-type cuprates in the presence of boron trifluoride ethereate,[9] we anticipated that these conditions might effect ring opening of 2-methyleneaziridines. Gratifyingly, treatment of

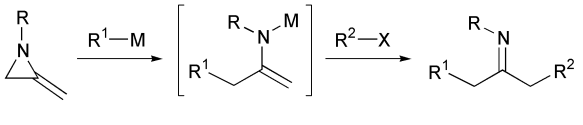

where M = metal, X = leaving group

Scheme 1

methyleneaziridine **1** (R = CHMePh) with Bu_2CuLi (1.5 equiv.) and $BF_3{\cdot}OEt_2$ (1.5 equiv.) in THF (−78 → 0 °C) and subsequent hydrolysis with aqueous acid furnished heptan-2-one in 40% isolated yield after distillation. Further studies determined that this ring opening reaction can be accomplished more conveniently using BuMgCl in the presence of $BF_3{\cdot}OEt_2$ and a catalytic amount of CuI (Table 1, entry 1). The modest isolated yield observed for the formation of heptan-2-one is due to its volatility, as the chemical conversion is excellent as judged by GC analysis using an internal standard. The copper catalysed ring opening of methyleneaziridines with Grignard reagents appears general and we have used it to make a variety of methyl ketones **2** in moderate to good yields (Table 1).† Importantly, in control experiments, we have determined that at low temperatures, both CuI and the Lewis acid are essential for rapid ring opening to occur.

Our initial attempts to alkylate the presumed metalloenamine intermediate produced by ring opening of methyleneaziridine **1** (R = CHMePh) with BuMgCl, CuI and $BF_3{\cdot}OEt_2$ were entirely unsuccessful. Introduction of an electrophile such as BnCl into the vessel prior to aqueous hydrolysis did not result in the formation of any further alkylated products. Control experiments using a metalloenamine made by the traditional method of imine deprotonation using EtMgCl revealed that the presence of $BF_3{\cdot}OEt_2$ in the reaction mixture completely suppresses alkylation reactions of the metalloenamine. To overcome this problem, we sought conditions to effect the ring opening of 2-methyleneaziridines with organometallic reagents in the absence of an added Lewis acid. After further experimentation, we determined that the ring opening could be achieved using Grignard reagents in the presence of CuI (20 mol%) by warming the mixture to room temperature and stirring for an extended period (24 h) prior to introduction of the electrophile. Using these conditions, treatment of methyleneaziridine **1** (R = CHMePh) with BuMgCl then BnCl yielded alkylated ketone **4** in 78% isolated yield after imine hydrolysis and silica gel

Table 1

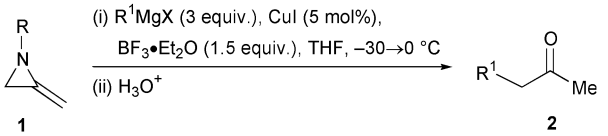

1 **2**

Entry	R	R^1	Yield[a] (%)
1	CHMePh	$(CH_2)_3CH_3$	56 (90)[b]
2	CHMePh	$(CH_2)_7CH_3$	81
3	CHMePh	Ph	65
4	CHMePh	CH_2Ph	69
5	CHMePh	Cyclohexyl	50
6	CHMePh	C_6H_4OMe	60
7	CHMePh	$(CH_2)_6CH{=}CH_2$	88
8	Cyclohexyl	$(CH_2)_7CH_3$	85

[a] Refers to yield of purified product after work-up and purification by silica gel chromatography. [b] GC yield determined using nonane as internal standard.

DOI: 10.1039/b005623p

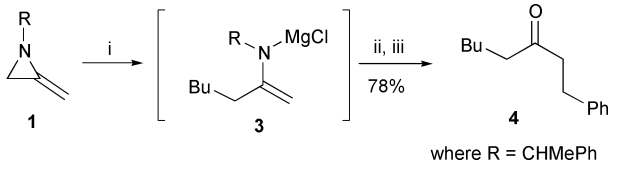

Scheme 2 *Reagents and conditions*: (i) BuMgCl (3.0 equiv.), CuI (20 mol%), THF, −30 °C → rt, 24 h; (ii) BnCl (1.5 equiv.), 40 °C; (iii) 10% HCl, 50 °C, 2 h.

chromatography (Scheme 2).‡ Significantly, the formation of metalloenamine **3** is highly regiospecific, and no trace of 3-benzylheptan-2-one could be detected in the crude reaction mixture.§

We have extended the scope of this method of metalloenamine generation to other Grignard reagents and electrophiles (Table 2).† Moderate to good yields of products are obtained in all cases and the method provides a flexible and efficient approach to functionalised ketones. The only notable limitation with this chemistry is the requirement to use excess Grignard reagent (3 equiv.) to drive the reaction to completion. Currently, we are searching for more active copper catalysts in an effort to address this problem. Future work will also be aimed at extending the scope of this method and to applying it in natural product synthesis.

Table 2

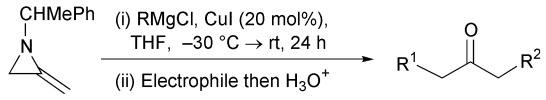

Grignard[a]	Electrophile	R^1	R^2	Yield[b] (%)
BuMgCl	BnCl[c]	Bu	Bn	78
OctylMgCl	$H_2C{=}CHCH_2Br$	Octyl	$H_2C{=}CHCH_2$	80
OctylMgCl	$H_2C{=}CHCH_2CH_2OTs$	Octyl	$H_2C{=}CHCH_2CH_2$	67
BuMgCl	4-$MeC_6H_4CH_2Cl$	Bu	4-$MeC_6H_4CH_2$	75
BnMgCl	4-$MeC_6H_4CH_2Cl$	Bn	4-$MeC_6H_4CH_2$	80
BuMgCl	$TBDMSO(CH_2)_3Br$	Bu	$TBDMSO(CH_2)_3$	58

[a] All reactions performed with 3 equiv. of Grignard reagent and 2 equiv. of electrophile unless otherwise stated. [b] Refers to yield of purified product after work-up and purification by silica gel chromatography. [c] Performed using 1.5 equiv. of electrophile.

We are grateful to the EPSRC and SmithKline Beecham Pharmaceuticals for their generous financial support of this work. We are indebted to Julie Ince and David Ennis for their assistance at the early stages of this project. We thank the EPSRC National Mass Spectrometry Centre for performing some of the mass spectral measurements and the EPSRC Chemical Database Service at Daresbury.[10]

Notes and references

† All new compounds were fully characterised using standard spectroscopic and analytical methods.

‡ *Typical procedure:* CuI (48 mg, 0.252 mmol) in a round-bottomed flask was heated under vacuum then purged with nitrogen (3 cycles performed). Freshly distilled THF (4 ml) was added and the mixture cooled to −30 °C whereupon BuMgCl (2.0 M in THF, 1.89 ml, 3.78 mmol) was added. After stirring for 10 min, *N*-(1-phenylethyl)-2-methyleneaziridine (200 mg, 1.26 mmol) in THF (2 ml) was added. The reaction mixture was allowed to warm up to room temperature and stirred for 24 h. The flask was then cooled to 0 °C and BnCl (218 μl, 1.89 mmol) added dropwise. A reflux condenser was fitted and the reaction mixture heated at 40 °C for 2 h then allowed to cool to room temperature and stirred overnight. Finally, 10% aq. HCl (3 ml) was added, and the mixture heated at 50 °C for 2 h (for all other entries in Table 2, imine hydrolysis was effected using 1 M AcOH–hexane at rt). Upon cooling, solid NaCl was added and the mixture extracted with Et_2O. The combined organic layers were washed with 0.5 M aq. HCl (2 × 15 ml), saturated NH_4Cl (2 × 20 ml), saturated $NaHCO_3$ (2 × 20 ml) and brine (2 × 20 ml). The organic layer was dried ($MgSO_4$) and the solvent removed *in vacuo*. Column chromatography on silica gel (2.5% EtOAc in hexane) gave 1-phenyloctan-3-one (201 mg, 78%) as a yellow oil. ν_{max} (thin film) 2947, 2931, 2856, 1713, 1450 cm^{-1}; δ_H (400 MHz, $CDCl_3$) 7.30–7.17 (5H, m, Ph), 2.89 (2H, m), 2.72 (2H, m), 2.37 (2H, t, *J* 7.6), 1.56 (2H, m), 1.30–1.21 (4H, m), 0.88 (3H, t, *J* 7.2); δ_C (100.9 MHz, $CDCl_3$) 210.5 (s), 141.2 (s), 128.5 (d), 128.3 (d), 126.1 (d), 44.3 (t), 43.0 (t), 31.4 (t), 29.8 (t), 23.5 (t), 22.5 (t), 13.9 (q); Observed 204.1519; $C_{14}H_{20}O$ requires 204.1514.

§ By comparison with an authentic sample of 3-benzylheptan-2-one using gas chromatography and ^1H NMR spectroscopy.

1 G. Stork and S. R. Dowd, *J. Am. Chem. Soc.*, 1963, **85**, 2178.
2 G. Wittig, H. D. Frommeld and P. Suchanek, *Angew. Chem., Int. Ed. Engl.*, 1963, **2**, 683.
3 For reviews, see (*a*) P. W. Hickmott, *Tetrahedron*, 1982, **38**, 3363; (*b*) J. K. Whitesell and M. A. Whitesell, *Synthesis*, 1983, 517.
4 For a detailed discussion on the factors that effect regiochemical control in the deprotonation of unsymmetrical imines, see A. Hosomi, Y. Araki and H. Sakurai, *J. Am. Chem. Soc.*, 1982, **104**, 2081.
5 (*a*) P. A. Wender and J. M. Schaus, *J. Org. Chem.*, 1978, **43**, 782; (*b*) P. A. Wender and M. A. Eissenstat, *J. Am. Chem. Soc.*, 1978, **100**, 292.
6 For a leading reference on ring opening reactions of methyleneaziridines, see D. S. Ennis, J. Ince, S. Rahman and M. Shipman, *J. Chem. Soc., Perkin Trans. 1*, 2000, 2047.
7 It has been postulated that the decomposition of 3-lithio-1-*tert*-butyl-2-methyleneaziridine involves ring opening of 1-*tert*-butyl-2-methyleneaziridine by this organolithium species, see H. Quast and C. A. Weise Vélez, *Angew. Chem., Int. Ed. Engl.*, 1974, **13**, 342.
8 J. Ince, T. M. Ross, M. Shipman, A. M. Z. Slawin and D. S. Ennis, *Tetrahedron*, 1996, **52**, 7037.
9 M. J. Eis and B. Ganem, *Tetrahedron Lett.*, 1985, **26**, 1153.
10 D. A. Fletcher, R. F. McMeeking and D. Parkin, *J. Chem. Inf. Comput. Sci.*, 1996, **36**, 746.

ChemComm

Organoimido-polyoxometalates as polymer pendants†

Aaron R. Moore, Haidoo Kwen, Alicia M. Beatty and Eric A. Maatta*

Department of Chemistry, Kansas State University, Manhattan, Kansas 66506-3701 USA. E-mail: eam@ksu.edu

Received (in Irvine, CA, USA) 20th June 2000, Accepted 2nd August 2000

The *p*-styrenyl substituent borne by the organoimido ligand in the Lindqvist derivative $[NBu_4]_2[Mo_6O_{18}(NC_6H_4CH{=}CH_2)]$ 1 allows the polyoxometalate complex to be introduced as a pendant group in polystyrene compositions *via* conventional free radical-induced copolymerization.

Research involving polyoxometalates[1]—the multimetallic oxo-anions formed by Mo, W, V and, to a lesser extent, Nb and Ta—continues to increase in scope and pace, driven by the goal of harnessing these species' remarkable and versatile attributes for catalytic, medical and imaging applications, and for use in magnetic and photo- and electro-chromic materials.[2] In their solid state applications, polyoxometalates generally are employed as components embedded heterogeneously within various matrices, rather than as covalently bound integral elements.[3] The covalent incorporation of polyoxometalates into conventional polymeric systems therefore may provide additional opportunities for their technological development.

There are few examples of polymers bearing covalently attached polyoxometalate species. Knoth[4] has described the 'all-inorganic' polymer $[(OC)_3CoGe_2W_{11}SiO_{40}^{5-}]_n$. Difunctional polyoxotungstates $[(RSiOSiR)W_{11}SiO_{39}]^{4-}$ have been homo-polymerized by Judeinstein[5] and incorporated into siloxane compositions by Katsoulis and Keryk.[6] Very recently, Mayer, Thouvenot *et al.*[7] have reported well characterized acrylamide and methacrylate networks cross-linked by the polyoxometalates $[\gamma\text{-}SiW_{10}O_{36}(RSiO)_4]^{4-}$ or $[\gamma\text{-}SiW_{10}O_{36}(RSiOSiR)]^{4-}$ [R = $C_3H_6OC(O)C(Me){=}CH_2$]. Here, we describe a different approach to organic polymers bearing polyoxometalate pendants, involving co-polymerization of the styrylimido ligand in the Lindqvist derivative $[NBu_4]_2[Mo_6O_{18}(NC_6H_4CH{=}CH_2)]$ **1**.

Reaction of $[NBu_4]_2[Mo_6O_{19}]$ with $Ph_3P{=}NC_6H_4CH{=}CH_2$ in pyridine solution at 90 °C produces $Ph_3P{=}O$ and the red styrylimido-hexamolybdate complex **1** in high yield (Scheme 1).‡ To our knowledge, **1** represents the first example of a styrylimido complex.[8] In MeCN solution, cyclic voltammetry of **1** reveals a one-electron reduction at $E_{1/2}$ = − 886 mV (*vs.* Ag/Ag^+); this value is more negative than that of the $[Mo_6O_{19}]^{2-}$ parent ($E_{1/2}$ = −707 mV) and is typical of other monosubstituted $[Mo_6O_{18}(NR)]^{2-}$ systems.[9] **1** is soluble in polar organic solvents such as 1,2-dichloroethane and its solutions display good hydrolytic stability: the deliberate addition of H_2O (*ca.* 15 equiv.) to a CD_3CN solution of **1** produced no detecable amount of 4-vinylaniline after 4 d at 25 °C as monitored by ^1H NMR spectroscopy.

Crystals of **1** were grown by diffusion of Et_2O vapor into an acetonitrile solution, and the molecular structure was determined by X-ray crystallography (Fig. 1).§ The styrylimido ligand occupies a terminal position on the hexamolybdate cage and its metrical parameters [Mo(1)–N(1) 1.728(7) Å, Mo(1)–N(1)–C(1) 159.9(7)°] indicate substantial [Mo≡NR] triple bond character. Along the Mo(1)–O(1)–Mo(5) axis, the central O(1) atom is substantially nearer to the imido-bearing Mo(1) site [2.223(5) Å] than to the *trans* oxo site Mo(5) [2.353(5) Å].

Co-polymerization of **1** (0.50 g, 0.34 mmol) and 4-methylstyrene (0.16 g, 1.34 mmol) initiated by AIBN [2,2′-azobis(2-methylpropionitrile), 0.010 g, 0.061 mmol] was conducted in 1,2-dichloroethane (5 mL) at 60 °C for 48 h, and led to the separation of an oily brown insoluble residue (0.435 g) from the brown solution. Dissolution of this residue in acetonitrile (10 mL), filtration to remove a small amount of gummy material, and evaporation to dryness afforded a green–brown solid **2**. In the IR spectrum of **2**, no bands were observed in the vinylic ν(C=C) region, and the presence of an imido-substituted hexamolybdate was confirmed by its characteristic 'doublet' pattern in the $\nu(Mo{-}O_t)$ stretching region [975(sh), 952s cm^{-1}]. The ^1H NMR spectrum of **2** taken in CD_3CN revealed features consistent with the formation of the expected co-polymer of **1** and 4-methylstyrene: the vinylic resonances of both precursors had disappeared; a pair of broadened aryl resonances were observed centered at δ *ca.* 7.0 and 6.5; a broad signal at δ 2.3 was assignable as the CH_3 resonance of the 4-methyl styrene component; the resonances of the $[NBu_4]^+$ cations were observed as virtually unbroadened signals in their characteristic regions; and broadened resonances assignable as the methine and methylene units of the polymer backbone were observed in the range δ 1.8–1.5 overlapped with the resonances of the interior CH_2 groups of the $[NBu_4]^+$ cations. A comparison of the relative intensities due to the aryl groups, the α-CH_2 groups of the $[NBu_4]^+$ cations, and the styrenic CH_3 group suggested a

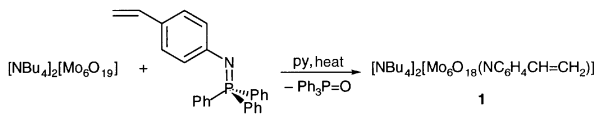

Scheme 1 Synthesis of styrylimido-hexamolybdate complex **1**.

† Electronic supplementary information (ESI) available: colour version of Fig. 2. See http://www.rsc.org/suppdata/cc/b0/b005022i/

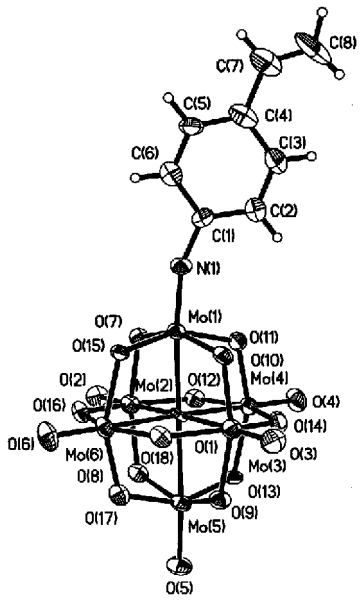

Fig. 1 ORTEP representation and labelling scheme for the $[Mo_6O_{18}(NC_6H_4CH{=}CH_2)]$ dianion within **1**. Selected bond lengths (Å) and angles (°): Mo(1)–N(1) 1.728(7), N(1)–C(1) 1.388(12), Mo(1)–O(1) 2.223(5), Mo(1)–O(7) 1.897(5), Mo(1)–O(10) 1.994(6), Mo(1)–O(11) 1.996(6), Mo(1)–O(15) 1.887(5), Mo(5)–O(1) 2.353(5), Mo(5)–O(5) 1.689(6), Mo(5)–O(8) 1.966(6), Mo(5)–O(9) 1.864(6), Mo(5)–O(13) 1.867(5), Mo(5)–O(17) 1.971(6); Mo(1)–N(1)–C(1) 159.9(7).

DOI: 10.1039/b005022i

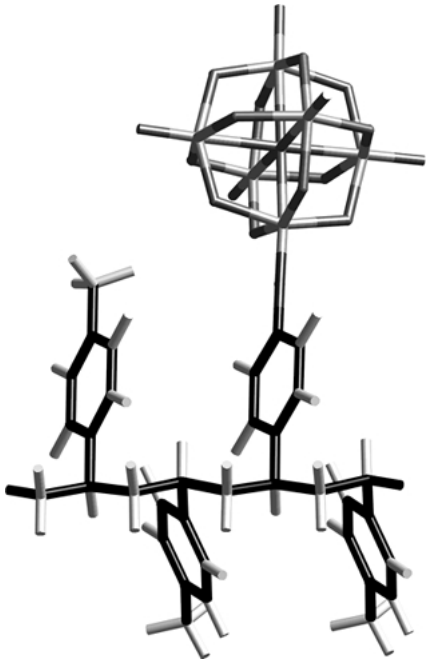

Fig. 2 Idealized representation of a segment within **2** (cations omitted for clarity). Colour version is shown as ESI†.

composition for **2** of nearly three 4-methyl styrene units per unit of **1**, as indicated in Fig. 2. Elemental analysis of **2** is consistent with this formulation. Molecular weight determinations of **2** are in progress.[10]

This work demonstrates that the styrylimido ligand can be employed as a reactive site capable of delivering its metal complex into a conventional polymeric environment. Similar methodology should be broadly applicable to the synthesis of other new classes of hybrid inorganic/organic polymers which incorporate covalently attached organoimido-metal complexes as exploitable backbone substituents. Further characterization of the properties of **2** is underway, as are studies on a variety of other polymerizable organoimido systems.

We are grateful to the United States Department of Energy, Office of Basic Energy Sciences, for support of this work.

Notes and references

‡ *Experimental procedure* for **1**: under an N_2 atmosphere, $[NBu_4]_2[Mo_6O_{19}]$ (6.54 g, 4.79 mmol) and $Ph_3P{=}NC_6H_4CH{=}CH_2$ (2.73 g, 7.19 mmol) were added to 20 mL pyridine and the mixture stirred for 5 d at 90 °C. After cooling to room temperature, the solution was filtered and solvent was removed under vacuum. The residue was washed successively with Et_2O (50 mL) and benzene (3 × 75 mL) and dried *in vacuo* to afford red–orange solid **1** (6.30 g, 89.7%). Anal. Calc. for $C_{40}H_{79}Mo_6N_3O_{18}$: C, 32.78; H, 5.43; N, 2.87. Found: C, 32.97; H, 5.55; N, 3.02%. $\delta_H(CD_3CN, 296\ K)$: 7.49, 7.47, 7.21, 7.19 (AA′BB′ 'quartet', 4H, C_6H_4), 6.77 (m, 1H, CH), 5.79 (d, 1H, $=CH_2$ *cis*, ^3J 17.2 Hz), 5.26 (d, 1H, $=CH_2$ *trans*, ^3J 10.8 Hz), 3.08 (m, NCH_2, 16 H), 1.60 (m, CH_2, 16 H), 1.35 (m, CH_2, 16 H), 0.97 (t, CH_3, 24 H). IR (Nujol, cm^{-1}): ν(C=C) 1605 w; ν(Mo≡O), 975(sh), 952s. UV–VIS [MeCN; λ/nm (ε/M^{-1} cm^{-1})]: 272 (64200), 366 (50400).

§ *Crystal data* for $C_{40}H_{79}Mo_6N_3O_{18}$ **1**: orange–red crystals, M_w = 1465.70, monoclinic, space group $P2_1/n$, a = 17.316(2), b = 15.6017(17), c = 20.774(2) Å, β = 105.098(9)°, V = 5418.6(11) Å^3, Z = 4, D_c = 1.797 g cm^{-3}. Of the 8303 reflections collected [T = 173(2) K, $2\theta_{max}$ = 47°], 8001 were unique (R_{int} = 0.0422) and 6784 were observed [$I > 2\sigma(I)$]. Full-matrix least squares refinement on F^2 converged with R_1 = 0.0450 and wR_2 = 0.1268. CCDC 182/1742. See http://www.rsc.org/suppdata/cc/b0/b005022i/ for crystallographic files in .cif format.

1 M. T. Pope, *Heteropoly and Isopoly Oxometalates*, Springer-Verlag, New York, 1983; M. T. Pope and A. Müller, *Angew. Chem., Int. Ed. Engl.*, 1991, **30**, 34; *Polyoxometalates: From Platonic Solids to Anti-Retroviral Activity*, ed. M. T. Pope and A, Müller, Kluwer Academic Publishers, Dordrecht, The Netherlands, 1994.

2 *Chem. Rev.*, 1998, **98**, 1 (thematic issue on polyoxometalates: C. L. Hill, guest editor).

3 D. E. Katsoulis, *Chem. Rev.*, 1998, **98**, 359.

4 W. E. Knoth, *J. Am. Chem. Soc.*, 1979, **101**, 2211.

5 P. Judeinstein, *Chem. Mater.*, 1992, **4**, 4.

6 D. E. Katsoulis and J. R. Keryk, *Mat. Res. Soc. Symp. Proc.*, 1996, **435**, 589.

7 C. R. Mayer, V. Cabuil, T. Lalot and R. Thouvenot, *Angew. Chem., Int. Ed.*, 1999, **38**, 3672; C. R. Mayer, R. Thouvenot and T. Lalot, *Chem. Mater.*, 2000, **12**, 257.

8 D. E. Wigley, *Prog. Inorg. Chem.*, 1994, **42**, 239.

9 J. B. Strong, G. P. A. Yap, R. Ostrander, L. M. Liable-Sands, A. L. Rheingold, R. Thouvenot, P. Gouzerh and E. A. Maatta, *J. Am. Chem. Soc.*, 2000, **122**, 639.

10 A composition for **2** incorporating an average of 2.7 (4-methylstyrene) units for each unit of **1** has the empirical formula $C_{64.3}H_{106}N_3Mo_6O_{18}$ and requires: C, 43.27; H, 5.99; N, 2.35. Found for **2**: C, 43.10; H, 6.08; N, 2.90%.

ChemComm

Highly *Z*-selective synthesis of α,β-unsaturated amides with the Peterson reaction between α-silylamides and aldehydes†

Satoshi Kojima,* Hiroki Inai, Tsugihiko Hidaka and Katsuo Ohkata

Department of Chemistry, Graduate School of Science, Hiroshima University, Kagamiyama, Higashi-Hiroshima 739-8526, Japan. E-mail: skojima@sci.hiroshima-u.ac.jp

Received (in Cambridge, UK) 2nd June 2000, Accepted 3rd August 2000
First published as an Advance Article on the web 4th September 2000

The Peterson reaction of triphenylsilylacetamide Ph_3Si-CH_2CONBn_2 with aromatic aldehydes and certain aliphatic aldehydes proceeded to give the corresponding *α,β*-unsaturated amide with high *Z* selectivity (up to *Z*:*E* = > 97 : < 3).

Geometry-defined olefins serve as good building blocks in organic synthesis. Of particular utility are olefins bearing electron-withdrawing groups, such as the ester group, since not only are these groups viable of further functionalization, but they also activate the olefin moiety for reactions such as Michael addition and pericyclic reactions. While it is rather facile to obtain disubstituted *E*-olefins bearing an electron-withdrawing group with high selectivity from aldehydes, only a few methods are available for moderate to highly selective preparation of the thermodynamically less stable *Z*-olefins, and so far they have been limited to the ester,[1–5] the cyano,[6,7] and the recently reported methyl ketone group.[8] For disubstituted *Z*-olefins bearing an amide group, it would be desirable to have a direct method of preparation from an aldehyde, especially for multifunctional carbonyl compounds. Peterson olefination with reagents bearing a trimethylsilyl (TMS) group has been widely utilized as a useful complementary reaction to that of Wittig type.[9] However, for disubstituted olefins with electron-withdrawing groups, the selectivity observed for this reaction is generally low (even for *E*-olefins) compared with its phosphorus counterpart. Previous amide formation with Peterson reagents bearing the TMS group is no exception.[10] Thus, based upon the notion that a more bulky and more electronegative silyl group would shift the selectivity towards the *Z*-olefin, we examined a reagent bearing the triphenylsilyl group, which had previously proved to be effective in combination with the cyano group.[6] In accordance with expectations, we have realized the first highly *Z*-selective preparation of α,β-unsaturated amides. Herein we describe our results.

The Peterson reagents **1a**,**b** examined for the reactions were prepared by treating the lithium enolate of *N*,*N*-dibenzylacetamide with Ph_3SiCl or Me_3SiCl, regioselectively giving the *C*-silylated products in moderate yield.[10,11] The results of using the triphenylsilyl reagent **1a** are given in Table 1. Since a countercation effect is usually observed for the analogous Horner–Wadsworth–Emmons (HWE) reaction, the examination of various metal-containing bases was first carried out in the reaction with benzaldehyde. The effect of the countercation proved to be quite significant as the ratio of *Z*-amide increased from 54 : 46 with *n*-BuLi to 80 : 20 with NaHMDS, and an exclusive > 97 : < 3 with KHMDS‡ (entry 1). In the case of *n*-BuLi, the reaction temperature was gradually raised from −78 to 0 °C in order to effect reaction. More common bases such as NaH and *t*-BuOK were found to be unsuitable. The reaction of **1a** and 3-phenylpropionaldehyde with KHMDS as base (entry 8) was also found to be *Z*-selective, although not quite as high as with benzaldehyde. In seeking a possible improvement in selectivity, an examination of solvents was carried out. However, neither a decrease (ether, 74 : 26, 15%) or increase (THF–HMPA mixture, 71 : 29, 64%) in polarity proved fruitful. Lowering of the reaction temperature to −95 °C led to a slight increase in selectivity to 94:6 but with a lower yield of 58%.

Table 1 Peterson reaction of $Ph_3SiCH_2CONBn_2$ (**1a**) with various aldehydes[a]

Entry	R	*Z*:*E*[b]	Yield (%)[c]
1	Ph	> 97 : < 3	88
2	*p*-$MeOC_6H_4$	> 97 : < 3	87
3	*o*-$MeOC_6H_4$	81 : 19	72
4	*p*-ClC_6H_4	88 : 12	91
5	2-Furyl	91 : 9	92
6	2-Pyridyl	59 : 41	47
7	(*E*)-PhCH = CH	81 : 19	99
8	$PhCH_2CH_2$	91 : 9	77
9	*c*-Hexyl	83 : 17	82

[a] All reactions were carried out in THF at −78 °C with KHMDS as base. [b] Determined by 500 MHz ^{1}H NMR measurement of crude mixture. [c] Combined isolated yield of *E* and *Z* olefins.

Under the standard conditions of using THF and KHMDS at −78 °C, other aldehydes were examined.§ For 4-substituted benzaldehyde derivatives, a drop-off in selectivity was observed with the electronegative Cl substituent (entry 4), but remained high with the electron-donating MeO group (entry 2). Although sterically hindered 2-substituted aromatic aldehydes are usually more *Z*-selective than their 4-substituted counterparts in HWE reactions, with the MeO group the Peterson reaction here gave lower selectivity (entry 3). With heterocyclic aldehydes, the highly electronegative pyridylaldehyde showed very low selectivity (entry 6), whereas that of furfural was highly *Z*-selective (entry 5). The conjugated *E*-cinnamaldehyde also furnished the *Z*-product as the predominant isomer (entry 7).

As for other aliphatic aldehydes, whereas α-branched 2-phenylpropionaldehyde did not react, the same α-branched cyclohexanecarboxyaldehyde did, giving the *Z*-olefin as the major product (entry 9). This indicates that with readily enolizable aldehydes, enolization is favoured over the olefination reaction. Apparently due to steric factors, pivalaldehyde was unreactive.

The 4-substituent effect observed with KHMDS as base was more profound upon using *n*-BuLi as base, with the *Z*-selectivity decreasing with increasing electron-withdrawing ability; from 69 : 31 with *p*-$MeOC_6H_4CHO$ to 54 : 46 with benzaldehyde and 43 : 57 with *p*-ClC_6H_4CHO.

The efficacy of the triphenylsilyl group was confirmed by making comparisons with reactions of trimethylsilyl reagent **1b**

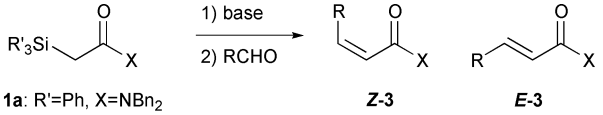

1a: R'=Ph, X=NBn_2
1b: R'=Me, X=NBn_2
2: R'=Ph, X=OEt

***Z*-3** ***E*-3**

Scheme 1

† Electronic supplementary information (ESI) available: synthesis and characterisation data for **1a**,**b** and **3a**–**i**. See http://www.rsc.org/suppdata/cc/b0/b004416o/

DOI: 10.1039/b004416o

Table 2 Comparison between differently substituted reagents **1a**, **b**, and **2**[a]

Entry	Reagent	R	$Z:E$[b]	Yield (%)[c]
1	$Ph_3SiCH_2CONBn_2$	Ph	> 97 : < 3	88
2	$Me_3SiCH_2CONBn_2$	Ph	27 : 73	63
3	$Ph_3SiCH_2CO_2Et$	Ph	71 : 29	82
4	$Ph_3SiCH_2CONBn_2$	$PhCH_2CH_2$	91 : 9	77
5	$Me_3SiCH_2CONBn_2$	$PhCH_2CH_2$	—	0
6	$Ph_3SiCH_2CO_2Et$	$PhCH_2CH_2$	77 : 23	78

[a] All reactions were carried out in THF at −78 °C with KHMDS as base. [b] Determined by 500 MHz ^{1}H NMR measurement of crude mixture. [c] Combined isolated yield of *E* and *Z* olefins.

using KHMDS as base, as shown in Table 2.[10] The reaction of **1b** with benzaldehyde resulted in a complete turnaround in selectivity, favouring *E*-olefin formation (entry 2) while that with 3-phenylpropionaldehyde gave no olefin product (entry 5). The effectiveness of the amide group for high *Z*-selectivity was exhibited by comparing corresponding reactions of an ester analogue **2**. The reaction of ethyl triphenylsilylacetate with benzaldehyde (entry 3) and 3-phenylpropionaldehyde (entry 6) with KHMDS as base gave the corresponding electron-deficient olefin as $Z:E$ = 71 : 29 and 77 : 23 mixtures, respectively, which are clearly inferior ratios compared with those of corresponding amide reactions (entries 1, 4). Thus, we have the general trend in which the larger the electron-donating ability of the group directly attached to the carbonyl group in both the aldehyde and the silyl reagent, the higher the *Z*-selectivity tends to be. Considering these electronic effects, the results we have obtained here fit in well with the generally accepted mechanism which involves an intermediate formed by rearrangement of the silyl group from a carbon to an oxygen atom, preceding olefin formation.[12]

In summary, we have developed a highly geometry-selective method of preparing *Z*-unsaturated amides based upon the Peterson reaction. Further examination of substituent effects are underway.

Notes and references

‡ Olefin geometries were determined by the coupling constants and chemical shifts of the olefinic protons, and were verified by NOE experiments for representative products.

§ The general procedure for the Peterson reaction is given as follows as the example of the reaction of benzaldehyde. To a solution of **1a** (206 mg, 0.415 mmol) in THF (4 mL) cooled to −78 °C was added KHMDS (0.5 M in toluene, 0.98 mL, 0.49 mmol). After stirring for 30 min at 0 °C, the solution was recooled to −78 °C. To this solution was added benzaldehyde (39.0 mg, 0.368 mmol) in THF (2.5 mL), and stirring was continued for 3 h. Water was then added to quench the solution, and extraction was carried out with ether. After the usual workup and chromatographic purification by preparative TLC (SiO_2; hexane : ethyl acetate = 5 : 1), (*Z*)-*N*,*N*-dibenzylcinnamamide (106 mg) was obtained as a viscous oil in 88% yield.

1 M. Larcheveque and A. Debal, *J. Chem. Soc., Chem. Commun.*, 1981, 877–878.
2 W. C. Still and C. Gennari, *Tetrahedron Lett.*, 1983, **24**, 4405–4408.
3 K. Ando, *Tetrahedron Lett.*, 1995, **36**, 4105–4108; K. Ando, *J. Org. Chem.*, 1997, **62**, 1934–1939; K. Ando, *J. Org. Chem.*, 1998, **63**, 8411–8416; K. Ando, *J. Org. Chem.*, 1999, **64**, 8406–8408.
4 S. Kojima, R. Takagi and K.-y. Akiba, *J. Am. Chem. Soc.*, 1997, **119**, 5970–5971.
5 K. Kokin, J. Motoyoshiya, S. Hayashi and H. Aoyama, *Synth. Commun.*, 1997, **27**, 2387–2392.
6 Y. Yamakado, M. Ishiguro, N. Ikeda and H. Yamamoto, *J. Am. Chem. Soc.*, 1981, **103**, 5568–5570.
7 T. Y. Zhang, J. C. O'Toole and J. M. Dunigan, *Tetrahedron Lett.*, 1998, **39**, 1461–1464.
8 W. Yu, M. Su and Z. Jin, *Tetrahedron Lett.*, 1998, **40**, 6725–6728.
9 For reviews on the Peterson reaction: D. J. Ager, *Synthesis*, 1984, 384–398; D. J. Ager, *Org. React.*, 1990, **38**, 1–223.
10 For the use of $Me_3SiCH_2CONMe_2$ with LDA see: R. P. Woodbury and M. W. Rathke, *J. Org. Chem.*, 1978, **43**, 1947–1949.
11 For the regioselectivity of silylation see: M. W. Rathke and D. F. Sullivan, *Synth. Commun.*, 1973, **3**, 67–72; P. F. Hudrlik, D. Peterson and D. Chou, *Synth. Commun.*, 1975, **5**, 359–365; G. L. Larson and L. M. Fuentes, *J. Am. Chem. Soc.*, 1981, **103**, 2418–2419.
12 K. Yamamoto, Y. Tomo and S. Suzuki, *Tetrahedron Lett.*, 1980, **21**, 2861–2864.

ChemComm

Non-covalent immobilization of homogeneous cationic chiral rhodium–phosphine catalysts on silica surfaces†

Francis M. de Rege,[a] David K. Morita,[a] Kevin C. Ott,[a] William Tumas[a] and Richard D. Broene*[b]

[a] *Chemistry Division, Los Alamos National Laboratory, Los Alamos, NM, USA*
[b] *Department of Chemistry, Bowdoin College, Brunswick, ME, USA. E-mail: rbroene@bowdoin.edu*

Received (in Oxford, UK) 25th April 2000, Accepted 10th August 2000
First published as an Advance Article on the web 4th September 2000

Non-covalent immobilization of [(*R*,*R*)-Me-(DuPHOS)Rh-(COD)]OTf by interaction of the triflate counter ion with surface silanols of silica supports leads to an active, stable, enantioselective, asymmetric hydrogenation catalyst.

We have found that cationic rhodium complexes containing chiral bidentate phosphines can be non-covalently immobilized on silica surfaces. This method, which should be general for ionic catalysts, enables the 'heterogenization' of readily available enantioselective catalysts, and avoids the tedious and often difficult task of ligand modification involved in numerous previously described covalent approaches for the immobilization of homogeneous catalysts on solid supports. We demonstrate this concept through the immobilization of [(*R*,*R*)-Me-(DuPHOS)Rh(COD)]$^+$ trifluoromethane sulfonate [Me-DuPHOS = 1,2-bis(2,5-dimethylphosphacyclopentyl)ethane] on mesoporous MCM-41 and silica gel which leads to a recyclable, non-leaching asymmetric hydrogenation catalyst with activity and selectivity equal to or greater than the homogeneous reaction. We also provide chemical and spectroscopic evidence for the mechanism of immobilization of these catalysts on silica surfaces.

The goal of heterogenization of homogeneous catalysts is to combine the superior activity and selectivity offered by homogeneous catalysts with the ease of separation and recycling of heterogeneous catalysts.[1–3] To date, the main approach for immobilizing homogeneous catalysts on solid supports involves covalent attachment of functionalized ligands or ligand–metal complexes which typically requires multistep syntheses.[4,5] Recently, hydrogen bonding between a sulfonated ligand and surface silanols has been demonstrated to lead to the immobilization of an achiral rhodium hydrogenation catalyst.[6] This approach requires the sulfonation of aryl phosphines, which, while possible, also requires multistep syntheses for chiral phosphine ligands.

Our studies focused on mesoporous silica, such as MCM-41, as a solid support due to the large, tailorable and well defined pore structure, high surface area and high area density of surface silanols found in this class of silicas.[3,7] Orange solutions of [(*R*,*R*)-Me-(DuPHOS)Rh(COD)]OTf **1**[8] (OTf = trifluoromethanesulfonate, triflate) in CH_2Cl_2 rapidly decolorized upon addition of MCM-41[9] and stirring. The powder X-ray diffraction pattern of the isolated orange powder (**2**) remains unchanged from the unfunctionalized MCM-41. Quantitative loading of the organometallic complex was demonstrated by thermal gravimetric analysis which showed 5.26% weight loss (calc. 5.29 wt%) and elemental analysis which gave 1.03 wt% Rh (calc. 0.96 wt%). The BET surface area was found to decrease from 953 $m^2\ g^{-1}$ in the unfunctionalized MCM-41 to 854 $m^2\ g^{-1}$ for composite **2** with a corresponding decrease in mesopore volume from 1.003 to 0.840 $cm^3\ g^{-1}$; this is consistent with partial mesopore filling by the organometallic catalyst.[10] While this work was in progress, Augustine and Tanielyan demonstrated that cationic rhodium complexes could be sorbed onto heteropolyacids to yield recyclable catalysts.[11a]

^{31}P and ^{19}F NMR spectra of the free and bound complexes (**1** and **2**) suggest that it is the triflate counter ion that interacts strongly with the support in **2**. The ^{31}P NMR spectrum (unlocked) of a slurry of **2** in CH_2Cl_2 shows a doublet at δ_P 76.6 (J_{RhP} 147 Hz) which is considerably broader [$\nu_{1/2}$ 130 Hz, Fig. 1(b)] than that for the free complex **1** in solution [$\nu_{1/2}$ 30 Hz, Fig. 1(a)]. The corresponding ^{19}F NMR spectra are shown in Fig. 2. The sharp singlet ($\nu_{1/2}$ 50 Hz) for the homogenous system [Fig. 2(a)] is broadened considerably ($\nu_{1/2}$ 575 Hz) in the spectrum of a slurry of **2**. The line broadening seen in both the ^{19}F and the ^{31}P NMR spectra of **2** is consistent with restricted mobility of the organometallic complex within MCM-41, as would be expected for a heterogenized molecule.[12]

The counter anion is very important for the successful immobilization of the catalyst onto MCM-41. Whereas the triflate DuPhos–Rh complex **1** was effectively immobilized, the analogous complex with the lipophilic BAr_F anion {BAr_F = $B[C_6H_3(CF_3)_2\text{-}3,5]_4$[13]} [(*R*,*R*)-Me-(DuPHOS)Rh(COD)]$^+$ BAr_F^- **3**, does not 'load' onto the support; solutions of **3** in CH_2Cl_2 remained orange upon addition of MCM-41. Indeed, addition of $NaBAr_F$ to a slurry of **2** in solvent caused the solvent to take on the characteristic orange color and ^{31}P NMR spectrum [$\nu_{1/2}$ 35 Hz, Fig. 1(c)] of dissolved [(*R*,*R*)-Me-(DuPHOS)Rh(COD)]$^+$, indicating release of the Rh cation from the support. The ^{19}F spectrum of the triflate ion, however, remains broad and unchanged [Fig. 2(c)] indicating the triflate is still immobilized on the support. The lack of immobilization of **3** onto the support, and the lack of exchange of bound triflate for BAr_F^- implies that triflate is strongly bound to the support and interacts with and binds the [(*R*,*R*)-Me-(DuPHOS)Rh-(COD)]$^+$ fragment to the MCM-41, a role BAr_F^- does not fulfill.[14] The mechanism of triflate binding is likely hydrogen bonding, similar to that demonstrated by Bianchini's group in the immobilization of an achiral sulfonated phosphine–rhodium

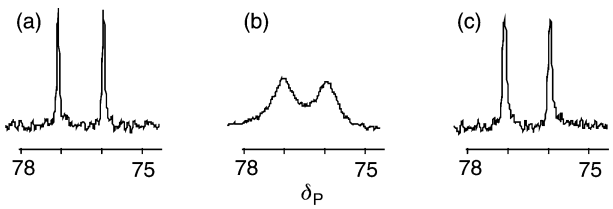

Fig. 1 ^{31}P NMR of (a) **1** in CH_2Cl_2, (b) **1** after addition of MCM-41 and (c) **2** with added $NaBAr_F$.

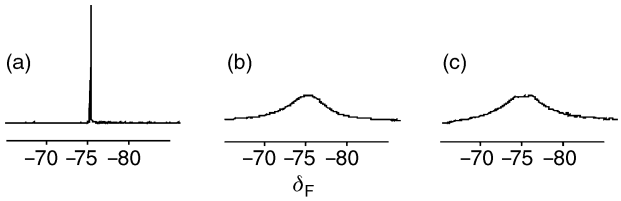

Fig. 2 ^{19}F NMR of (a) **1** in CH_2Cl_2, (b) **1** after addition of MCM-41 and (c) **2** with added $NaBAr_F$.

† Electronic supplementary information (ESI) available: experimental details. See http://www.rsc.org/suppdata/cc/b0/b003354p/

Table 1 Hydrogenation results (*conditions*: 20 mL hexane, 8 psi H_2 and room temp. except where noted. Reaction time: **A** 30 min; **B**,**C**, 16 h)

Substrate	Support	Solvent	Temp	Anion	Conv. (%)	Ee (%)
A	MCM-41	Hexane	R.T.	OTf	> 99	99
A	None	Hexane	R.T.	OTf	> 99	87
A	None	MeOH	R.T.	OTf	> 99	> 99
B	MCM-41	Hexane	R.T.	OTf	> 99	98
B	None	Hexane	R.T. (50 psi)	BAr_F[a]	92	93
B	None	MeOH	R.T. (90 psi)	OTf	> 99	96.2
C	MCM-41	Hexane	R.T.	OTf	> 99	98
C	None	Hexane	R.T. (40 psi)	BAr_F[a]	26	85
C	None	MeOH	R.T. (90 psi)	OTf	99	96

[a] The lipophilic BAr_F^- anion is more soluble than OTf^- and provided more consistent results than the OTf salt. See also ref. 13.

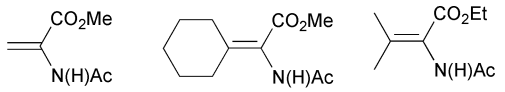

Fig. 3 Substrates utilized for catalytic hydrogenation studies.

complex to silica by hydrogen bonding.[6] Unfortunately, because of the low level of loading of the highly active catalyst (see below), we could not confirm the presence of hydrogen bonding using IR spectroscopy. Further work on other catalyst systems is underway. Other evidence that surface hydroxy groups may be involved in immobilization was found on studies of MCM-41 supports that were pretreated with trimethylsilyl chloride to protect the hydroxy groups. These supports were much less effective in immobilizing complex **1** (1.9 *vs*. 6.7 wt% based on Rh). We have found that other silica supports such as commercial silica gel, which are known to contain fewer surface silanols,[3] also led to significantly lower loadings of **1**.

The immobilized complex **2** was found to exhibit high catalytic activity, selectivity and recoverability for the hydrogenation of three prochiral α-enamide esters, used as test substrates. Hydrogenation of enamide **A** (Fig. 3) in hexane using **2** led to complete conversion with high enantioselectivity. As shown in Table 1, the immobilized catalyst **2** led to higher activity and selectivity than the homogeneous catalyst in hexane for the β,β-disubstituted substrates **B** and **C**,[15] and rivals the enantioselectivity reported in MeOH.[15] For example, **B** was hydrogenated with 98% ee with **2** as the catalyst in hexane while the optimized reaction with unsupported **3** gave 96% ee in MeOH and 93% ee in hexane.[15] Even more striking, the conversions for enamide **C** were significantly higher using the immobilized catalysts rather than the homogeneous analog in hexane, where conversion was only 26% (85% ee) with unsupported **3** in hexane after 22 h at 40 psi, while the reaction with **2** was complete (98% ee) after 16 h at 8 psi. Few reports[11] of such a positive influence on activity and selectivity for heterogenized catalysts exist. Other silica supports, including commercial silica gels, can be used to immobilize **1**; however, decreased loading (and therefore activity) was observed.

The recyclability of the immobilized catalyst was demonstrated using standard procedures. After completion of the initial hydrogenation of enamide **A**, the reaction mixture was filtered and the filtrate was tested for activity by adding more enamide; no further conversion was observed indicating the absence of highly active soluble catalyst leaching from the support. In a second set of recycling experiments, the materials were reacted under standard conditions for 30 min and the contents were then decanted leaving solid **1** in a small amount of solvent.[16] The bottle was recharged, and the reaction repeated four times, with the final run differing in that the catalyst was stored in hydrogen-free hexane for 16 h prior to the final reaction. Under these conditions, the catalyst remains active with no loss of conversion or enantioselectivity.

This work clearly shows that a chiral cationic rhodium catalyst can be simply and efficiently sorbed onto silicas without any ligand modification, a method that in principle could be applied to a wide variety of cationic catalysts. The surface-bound triflate counter ion immobilizes the cationic Rh complex onto the surface of the MCM-41 and the surface-sorbed complex is recyclable and stable to leaching from the surface in non-polar solvents. The results show that binding [(*R*,*R*)-Me-(DuPHOS)Rh]OTf to an MCM-41 surface has a beneficial effect on enantioselectivity and activity in the hydrogenation of prochiral enamides when compared to the homogeneous catalyst.

This work was carried out with Laboratory Directed Research and Development funds at Los Alamos National Laboratory, operated by the University of California for the U.S. Department of Energy under contract W-7405-ENG-36. R. D. B thanks the National Science Foundation (CAREER Award). We thank J. Rau, N. Clark, G. Brown and C. Hijar (all LANL) for materials synthesis and characterization.

Notes and references

1 H.-U. Blaser and B. Pugin, in *Supported Reagents and Catalysts in Chemistry*, ed. B. K. Hodnett, A. P. Kybett, J. H. Clark and K. Smith, RSC, Cambridge, 1998, vol. 216, p. 101.
2 B. Pugin, *J. Mol. Catal. A*, 1996, **107**, 273; D. Brunel, N. Bellocq, P. Sutra, A. Cauvel, M. Lasperas, P. Moreau, F. Di Renzo, A. Galarneau and F. Fajula, *Coord. Chem. Rev.*, 1998, **178**, 1085; A. Sayari and P. Liu, *Microporous Mater.*, 1997, **12**, 149; K. Moller and T. Bein, *Chem. Mater.*, 1998, **10**, 2950.
3 J. Y. Ying, C. P. Mehnert and M. S. Wong, *Angew. Chem., Int. Ed.*, 1999, **38**, 56.
4 R. H. Grubbs and L. C. Kroll, *J. Am. Chem. Soc.*, 1971, **93**, 3062; S. C. Bourque, F. Maltais, W.-J. Xiao, O. Tardif, H. Alper, P. Arya and L. E. Manzer, *J. Am. Chem. Soc.*, 1999, **121**, 3035.
5 S.-G. Shyu, S.-W. Cheng and D.-L. Tzou, *Chem. Commun.*, 1999, 2337; H. Yang, H. Gao and R. J. Angelici, *Organometallics*, 2000, **19**, 622.
6 C. Bianchini, D. G. Burnaby, J. Evans, P. Frediani, A. Meli, W. Oberhauser, R. Psaro, L. Sordelli and F. Vizza, *J. Am. Chem. Soc.*, 1999, **121**, 5961.
7 C.-Y. Chen, H.-X. Li and M. E. Davis, *Microporous Mater.*, 1993, **2**, 17; J. H. Clark and D. J. Macquarrie, *Chem. Commun.*, 1998, 853.
8 M. J. Burk, J. E. Feaster, W. A. Nugent and R. L. Harlow, *J. Am. Chem. Soc.*, 1993, **115**, 10 125.
9 The MCM-41 was synthesized by a previously published procedure.[3] A summary of experimental details is provided as ESI†.
10 M. Kruk, M. Jaroniec and A. Sayari, *J. Phys. Chem. B.*, 1997, **101**, 583; S.-S. Kim, W. Zhang and T. J. Pinnavaia, *Catal. Lett.*, 1997, **43**, 149; C. Liu, Y. Shan, X. Yang, X. Ye and Y. Wu, *J. Catal.*, 1997, **168**, 35; C. P. Mehnert and J. Y. Ying, *Chem. Commun.*, 1997, 22; R. Anwander and R. Roesky, *J. Chem. Soc., Dalton Trans.*, 1997, 137; R. Burch, N. Cruise, D. Gleeson and S. C. Tsang, *Chem. Commun.*, 1996, 951.
11 R. Augustine and S. Tanielyan, *Chem. Commun.*, 1999, 1257; A. Corma, M. Iglesias, C. del Pino and F. Sanchez, *J. Chem. Soc., Chem. Commun.*, 1991, 1253.
12 K. D. Behringer and J. Blümel, *Z. Naturforsch., Teil B*, 1995, **50**, 1723.
13 M. Brookhart, B. Grant and A. F. Volpe, *Organometallics*, 1992, **11**, 3920.
14 Triflate is known to be a hydrogen bond acceptor, while BAr_F^- cannot bond in this fashion: S. Spange, A. Reuter and W. Linert, *Langmuir*, 1998, **14**, 3479; O. Kristiansson and M. Schuisky, *Acta. Chem. Scand.*, 1997, **51**, 270.
15 M. J. Burk, M. F. Gross and J. P. Martinez, *J. Am. Chem. Soc.*, 1995, **117**, 9375.
16 We found that if all the solvent is removed, after two recycles the activity starts to decrease. Examination of the catalyst reveals that the catalyst becomes fouled with the product of the hydrogenation.

ChemComm

Six-coordinate aluminium phosphinate

Y. Wang, S. Parkin and D. Atwood*

Department of Chemistry, University of Kentucky, Lexington, KY 40506-0055, USA. E-mail: datwood@pop.uky.edu

Received (in Cambridge, UK) 31st May 2000, Accepted 14th July 2000

Unique models of solid state aluminophosphate materials containing, for the first time, six-coordinate aluminium atoms, may be achieved in chelated phosphinate derivatives; the degree of aggregation of these species, specifically the remarkable transition from a dimeric molecule to a polymeric material, depends on just one methylene unit; thus, [(Bu$^t_4$salpen)Al{O_2P(H)Ph}]$_2$ 1 is dimeric while [(Bu$^t_4$salen)-Al{O_2P(H)Ph}]$_\infty$ 2, with one fewer methylene unit in the connection between the two nitrogens, is a polymeric material with the polymers aligned to form pores containing thf molecules.

Nanoporous or open-framework[1] group 13 phosphate materials have far-ranging applications in catalysis,[2] separations and many other areas.[3] There are a limited number of naturally occurring aluminophosphates (turquoise is one example). However, synthetic chemistry has dramatically expanded this class of compounds and is providing new[4,5] and unique[6] materials with a wide range of new applications.[7] In these materials the aluminium atom is often six-coordinate. Thus far, molecular models of these materials have contained four-coordinate aluminium,[8–11] while none have six-coordinate atoms found in many materials.[12,13] The present work demonstrates that six-coordinate aluminium may be achieved in chelated phosphinate derivatives, and that the degree of aggregation of these species, the transition from a dimeric molecule to a polymeric material, is dependent on just one methylene unit. Thus, [(Bu$^t_4$salpen)Al{O_2P(H)Ph}]$_2$ **1** is dimeric while [(Bu$^t_4$salen)Al{O_2P(H)Ph}]$_\infty$ **2** is a polymeric material.

The compounds are prepared by combining the chelated group 13 reagent with the phosphinic acid (Scheme 1).[14] Use of (Bu$^t_4$salpen)AlMe in this reaction leads to the dimeric compound [(Bu$^t_4$salpen)Al{O_2P(H)Ph}]$_2$ **1**. The dimeric nature of **1** is supported by the spectroscopic data and verified by a crystal structure (Fig. 1).[15] In the structure the aluminium atom is in an octahedral environment. The Al–O(ligand) distances, *ca.* 1.83 Å, are marginally shorter than the Al–O–P distances, *ca.* 1.93 Å. There are no known solid-state materials based on phosphinates [O_2P(H)R] but these bond distances are similar to that observed in an aluminium phenylphosphonate (O_3PR)[4] with Al–O distances in the range 1.786(6)–1.951(6) Å. By comparison, these distances are just slightly shorter in derivatives containing four-coordinate aluminium such as [$Me_2AlO_2P(OBu^t)_2$]$_2$ (Al–O ≈ 1.77 Å).[12] Aggregation of **1** is expected based upon previously reported compounds, including [$Me_2Al(O_2PPh_2)$]$_2$, first reported by Coates in 1964,[16] which are most commonly dimeric with four-coordinate aluminium atoms. Although the bonding within compound **1** is not unusual the compound still serves to demonstrate that molecular phosphinates of six-coordinate aluminium can be obtained.

Compound **2** differs from **1** in having one less methylene (CH_2) unit in the ligand 'backbone'. Surprisingly, this leads to a dramatic change in the structure of the resulting compound. Thus, [(Bu$^t_4$salen)Al{O_2P(H)Ph}]$_\infty$ **2**, is found to consist of polymeric chains of –[(Bu$^t_4$salen)Al(OP{(H)Ph}O]– units (Fig. 2). The –[O–Al–O–P]– backbone is not linear but curved at the O–P–O junctions with an angle of 119.1(3)°. The same angle in **1** is 116.81(8)°. The Al–O distances are also similar. Adjacent ligand Bu^t groups are arranged in a staggered configuration to reduce steric contacts. The effect of this arrangement is to make the polymers appear as columns in the packing diagram (Fig. 3). These columns are arranged so that the Bu^t groups point inwards towards channels containing thf molecules. In this manner the structure of **2** is similar to the structure of other inorganic phosphate solid state materials.[17] It is likely that many other materials like this should be accessible when using ligands that coordinate in a linear manner.

This work was supported by the National Science Foundation NSF-CAREER award (CHE 9625376) and the donors of the Petroleum Research Fund (Grant 31901-AC3), administered by the American Chemical Society. NMR instruments used in this research were obtained with funds from the CRIF program of the National Science Foundation (CHE 997841) and from the

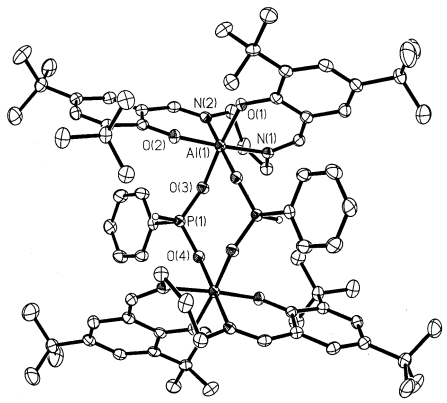

Fig. 1 ORTEP view of [(Bu$^t_4$salpen)Al{O_2P(H)Ph}]$_2$ **1**. Selected bond distances (Å) and angles (°): Al(1)–O(1) 1.830(2), Al(1)–O(2), 1.830(2), Al(1)–O(3) 1.917(2), Al(1)–O(4)′ 1.900(2), Al(1)–N(1) 2.052(2), Al(1)–N(2) 2.034(2), P(1)–O(3) 1.507(2), P(1)–O(4) 1.507(2), P(1)–C(34) 1.801(2), P(1)–H(1) 1.30; O(1)–Al–O(3) 174.68(7), N(1)–Al(1)–O(2) 174.07(7), N(2)–Al(1)–O(4)′ 174.87(7), O(3)–Al(1)–O(4)′ 90.19(7), O(3)–P(1)–O(4) 116.81(8).

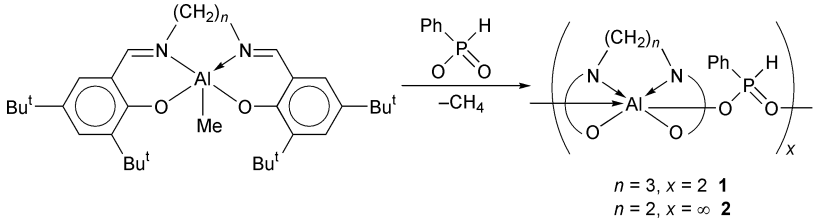

n = 3, *x* = 2 **1**
n = 2, *x* = ∞ **2**

Scheme 1 Syntheses of [(Bu$^t_4$salpen)Al{O_2P(H)Ph}]$_2$ **1** and [(Bu$^t_4$salen)Al{O_2P(H)Ph}]$_\infty$ **2**.

DOI: 10.1039/b004342g

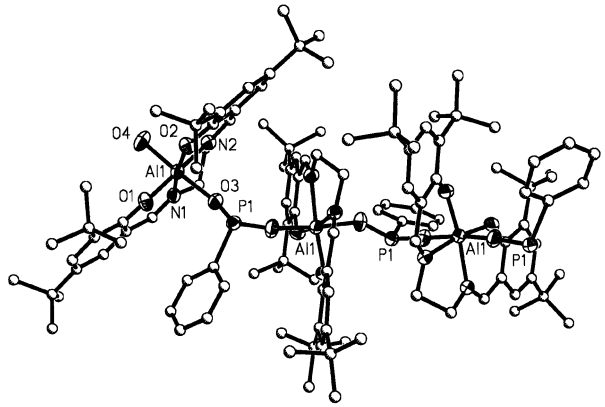

Fig. 2 ORTEP view (partial) of [(Bu$^t_4$salen)Al{O_2P(H)Ph}]$_\infty$ **2**. Selected bond distances (Å) and angles (°): Al(1)–O(1) 1.818(2), Al(1)–O(2) 1.817(2), Al(1)–O(3) 1.907(2), Al(1)–O(4)′ 1.890(2), Al(1)–N(1) 2.007(2), Al(1)–N(2) 2.008(2), P(1)–O(3) 1.435(2), P(1)–O(4) 1.476(2), P(1)–C(34) 1.788(2); O(3)–Al(1)–O(4) 174.80(7), N(1)–Al(1)–O(2) 169.72(7), N(2)–Al(1)–O(1) 170.51(7), O(3)–P(1)–O(4) 114.40(8). The P–H hydrogens were not found crystallographically owing to a disorder of the P atoms across two positions.

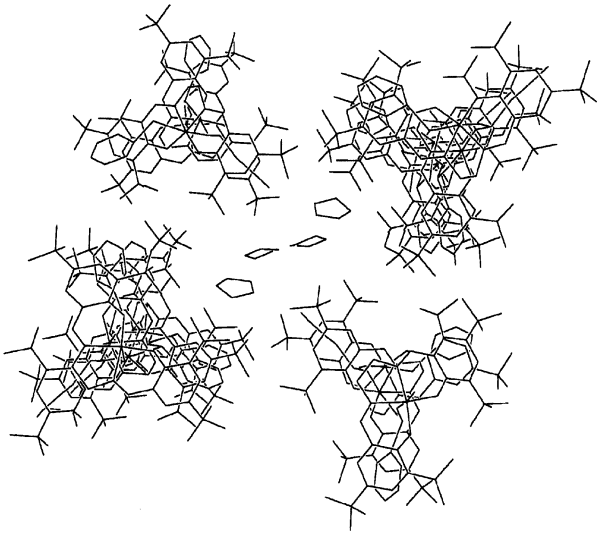

Fig. 3 Packing diagram of [(Bu$^t_4$salen)Al{O_2P(H)Ph}]$_\infty$ **2** showing the columnar arrangement of the polymers and the pores containing thf molecules.

Research Challenge Trust Fund of the University of Kentucky.

Notes and references

1 A. K. Cheatham, G. Ferey and T. Loiseau, *Angew. Chem., Int. Ed.*, 1999, **38**, 3268.

2 J. Hartmann, *Chem. Rev.*, 1999, **99**, 635.

3 For a brief overview of this area, see: T. J. Pinnavaia, in *Materials Chemistry: An Emerging Discipline*, ed. L. V. Interrante, L. A. Casper and A. B. Ellis, *Adv. Chem. Ser.*, 245, ACS, Washington DC, 1995, ch. 11.

4 A. Cabeza, M. A. G. Aranda, S. Bruque, D. M. Poojary, A. Clearfield and J. Sanz, *Inorg. Chem.*, 1998, **37**, 4168.

5 K. O. Kongshaug, H. Fjellvag and K. P. Lillerud, *Microporous Mesoporous Mater.*, 1999, **32**, 17.

6 M. E. Davis, C. Saldarriaga, C. Montes, J. Garces and C. Crowder, *Nature*, 1988, **331**, 698.

7 R. Raja, G. Sankar and J. M. Thomas, *J. Am. Chem. Soc.*, 1999, **121**, 11926.

8 M. G. Walawalkar, R. Murugavel, H. W. Roesky and H. G. Schmidt, *Inorg. Chem.*, 1997, **36**, 4202.

9 M. R. Mason, *J. Cluster Sci.*, 1998, **9**, 1.

10 Y. Yang, M. G. Walawalkar, J. Pinkas, H. W. Roesky and H.-G. Schmidt, *Angew. Chem., Int. Ed.*, 1998, **37**, 96.

11 J. Pinkas, D. Chakraborty, Y. Yang, R. Murugavel, M. Noltemeyer and H. W. Roesky, *Organometallics*, 1999, **18**, 523.

12 S. Dick, G. Grossmann, G. Ohms and T. Zeiske, *Z., Naturforsch., Teil B*, 1997, **52**, 1439; S. Dick, G. Grossmann, G. Ohms and T. Zeiske, *Z., Naturforsch., Teil B*, 1997, **52**, 1447.

13 One unusual five-coordinate phosphonate molecule is described in: C. G. Lugmair, T. D. Tilley and A. L. Rheingold, *Chem. Mater.*, 1999, **11**, 1615.

14 [(Bu$^t_4$salpen)AlO_2P(H)Ph]$_2$ **1**: to a stirring solution of (Bu$^t_4$salpen)-AlMe (0.500 g, 0.91 mmol) in THF (40 mL) was added a solution of phenylphosphinic acid (0.129 g, 0.91 mmol) in 20 mL of THF at −78 °C. After 3 h of stirring, the THF was removed under vacuum yielding a yellow solid which was dissolved in CH_2Cl_2 (20 mL) and allowed to stand for several days at room temperature during which time yellow crystals formed. Yield: 0.340 g (55.3%); mp > 400 °C. ^{1}H NMR ($CDCl_3$, 200 MHz): δ 1.06 [s, 36H, C(CH_3)$_3$], 1.31 [s, 36H, C(CH_3)$_3$], 2.14(m, 4H, $CH_2CH_2CH_2$), 3.25, 3.49 (m, 8H, NCH_2), 7.25 (d, $^1J_{PH}$ 556 Hz, 2H, P*H*), 6.61, 6.96, 7.20, 7.42 (m, 18H, Ph*H*), 7.91 (s, 4H, PhC*H*). ^{31}P{^{1}H} NMR ($CDCl_3$, 80.9 MHz): δ 7.24 (s). IR(KBr; ν/cm^{-1}): 3053m, 2956s, 2902s, 2867s, 2402w, 2362w, 2157w, 1632s, 1548s, 1536s, 1475s, 1462s, 1440s, 1416s, 1386s, 1360s, 1341m, 1327s, 1277m, 1259s, 1234s, 1207s, 1172s, 1140s, 1087m, 1071s, 974s, 841m, 787m, 750m. MS(EI, positive): *m/z* 1346.5 (82.4%, Dimer$^+$), 672.0 (91.2%, M$^+$). [Bu$^t_4$salen)AlO_2P(H)Ph]$_\infty$ **2**: to a stirring solution of (Bu$^t_4$salen)AlMe (0.540 g, 1.01 mmol) in THF (40 mL) was added a solution of phenylphosphinic acid (0.144 g, 1.01 mmol) in 20 mL of THF at −78 °C. After 3 h of stirring, the solution was allowed to stand at ambient temperature overnight to yield clear yellow crystals. Yield: 0.380 g (56.4%); mp: the color of the crystal became darker at 340 °C and the crystal melted at 361–362 °C. ^{1}H NMR ($CDCl_3$, 200 MHz): δ 1.19 [s, 18H, C(CH_3)$_3$], 1.28 [s, 18H, C(CH_3)$_3$], 3.05(br, 4H, NCH_2), 6.66 (d, $^1J_{PH}$ 552 Hz, 1H, P*H*), 6.51, 6.70, 6.92, 7.43 (m, 9H, Ph*H*), 7.28 (s, 2H, PhC*H*). ^{31}P{^{1}H} NMR ($CDCl_3$, 80.9 MHz): δ 7.08 (s). IR(KBr; ν/cm^{-1}): 3054w, 2954s, 2905m, 2867m, 2385w, 1656s, 1548m, 1536m, 1477m, 1462m, 144(s, 1416m, 1390m, 1335m, 1197s, 1171s, 1141m, 1080m, 970m, 875m, 770m, 760m, 610m. MS(EI, positive): *m/z* 1317.7 (41%, Dimer$^+$), 658.3 (100%, M$^+$).

15 *Crystal data*: **1**·4CH_2Cl_2: $C_{82}H_{116}Al_2Cl_8N_4O_8P_2$, M = 1685.29, triclinic, space group $P\bar{1}$ a = 9.337(1), b = 16.245(2), c = 16.297(2) Å, α = 66.95(1), β = 73.91(1), γ = 78.89(1)°, V = 2175.6(4) Å^3, T = 173(1) K, Z = 1, (Mo-Kα) D_c = 1.286 g cm^{-3}, 15256 reflections measured, 7657 unique (R_{int} = 0.0312) which were used in all calculations, final R values were 0.0425 [$F > 4\sigma(F)$] and 0.0632 (all data). **2**·thf: $C_{142}H_{209.5}Al_3N_6O_{19}P_3$, M = 2478.51, monoclinic, space group $P2_1/c$, a = 16.650(1), b = 27.518(2), c = 31.149(2) Å, β = 92.28(1)°, V = 14260(2) Å^3, T = 173(1) K, Z = 4, (Mo-Kα) D_c = 1.154 g cm^{-3}, 18627 reflections measured, 36396 unique (R_{int} = 0.0393) which were used in all calculations, final R values were 0.0765 [$F > 4\sigma(F)$] and 0.1059 (all data). CCDC 182/1741. See http://www.rsc.org./suppdata/cc/b0/b004342g/ for crystallographic files in .cif format.

16 G. E. Coates, *J. Chem. Soc.*, 1964, 1295.

17 S. Dick, G. Grossmann, G. Ohms and T. Zeiske, *Z. Naturforsch., Teil B*, 1997, **52**, 1439.

Molecular architecture *via* coordination: quasi-octahedral macrocycles of rhodium and iridium bearing a pentamethylcyclopentadienyl group

Hajime Suzuki,[a] Nobuo Tajima,[b] Kazuyuki Tatsumi[b] and Yasuhiro Yamamoto*[a]

[a] *Department of Chemistry, Faculty of Science, Toho University, Miyama, Funabashi, Chiba 274-8510 Japan. E-mail: yamamoto@chem.sci.toho-u.ac.jp*

[b] *Research Center for Materials Science and Department of Chemistry, Graduate School of Science, Nagoya University, Furo-cho, Chkusa-ku, Nagoya 454-8602 Japan. E-mail: i45100a@nucc.cc.nagoya-u.ac.jp*

Received (in Cambridge, UK) 27th April 2000, Accepted 9th August 2000

Reactions of $[Cp^*MCl_2]_2$ (M = Rh, Ir) with bidentate ligand (L = pyrazine; L′ = diisocyanide) gave $[Cp^*MCl_2(L \text{ or } L')]_2$, which were converted into tetranuclear complexes $[Cp^*_2M_2Cl_2(L)(L')]_2(OTf)_4$ containing different ligands on treatment with Ag(OTf).

Metal-containing supramolecules and coordination polymers have attracted interest in recent years since there are many promising metal fragments which can be used for construction of novel supramolecular materials.[1] In particular, square planar complexes of platinum and palladium are attractive as building blocks which occupy vertices. For example, diphosphine and diamine derivatives as ligands in metallic building blocks have been used extensively by many groups.[2] We are interested in supramolecular complexes, based on quasi-octahedral geometries, bearing arene and cyclopentadienyl groups and their derivatives, since new types of supramolecular series would be developed by introduction of these organic moieties. Octahedral building blocks can be applied to form cubic or ladder-shaped structures. As our first report of this study, we report here, the stepwise assembly of tetranuclear rhodium and iridium supramolecules bearing pentamethylcyclopentadienyl and binary ligands. Complexes constructed here are novel because they contain 2-D architectures with two different ligand 'edges', *i.e.* molecular rectangles. Self-assembled supramolecules bearing pentamethylcyclopentadienyl groups, to our knowledge, have been reported only by Rauchfuss and coworkers;[3,4] $[Cp_4Cp^*_4Co_4Rh_4(CN)_{12}]^{4+}$, $[Cp^*_7Rh_7(CN)_{12}]^{2+}$ and $[Cp^*_7Rh_3Ir_4(CN)_{12}]^{2+}$ ($Cp^* = C_5Me_5$).

When bis[dicloro(pentamethylcyclopentadienyl)iridium] **1** was treated with 1,4-diisocyano-2,5-dimethylbenzene (**a**) or 1,4-diisocyano-2,3,4,5-tetramethylbenzene (**b**) in a 1:1 molar ratio at room temperature (Scheme 1), yellow crystals, formulated as $[Cp^*IrCl_2]_2[CN–R–NC]$ (**3a**: R = 2,5-$Me_2C_6H_2$; **3b**: R = 2,3,5,6-Me_4C_6) by FAB mass spectrometry, were formed in high yields.† Their IR spectra showed a strong band at *ca.* 2140 cm^{-1} owing to terminal isocyanide groups. In the ^1H NMR spectra two singlet resonances due to the Cp* and Me protons appeared at δ *ca.* 1.86 and 2.40. These spectroscopic data suggested dimeric structures for **3a** and **3b**, where the Ir centers are connected by a μ-diisocyanide ligand. X-Ray crystal analysis of **3a** confirmed the dimeric structure.‡ The Ir–C(11) and average Ir–Cl bond lengths are 1.96 and 2.401 Å, respectively, and the two Ir atoms are separated by 11.6 Å. The analogous rhodium compound $[Cp^*RhCl_2]_2$[μ-1,4-$(NC)_2$-2,3,5,6-Me_4C_6] **4b**, was prepared as orange crystals in 80% yield by the reaction of $[Cp^*RhCl_2]_2$ **2** with **b**.†

Treatment of **1** or **2** with pyrazine (**c**) also generated dinuclear complexes, $[(Cp^*MCl_2)_2(\mu\text{-}C_4H_4N_2)]$ (**5c**, M = Ir; **6c**, M = Rh), according to FAB mass spectrometry.† In the ^1H NMR spectra in dmso-d_6, two singlets appeared at δ *ca.* 1.62 and 8.65, due to the Cp* and pyrazine protons, respectively. When **6c** was reacted with AgOTf (Tf = CF_3SO_2) in a 1:2 ratio in CH_2Cl_2–MeCN at room temperature, reddish orange crystals of $[(Cp^*RhCl)_4(pyz)_2](OTf)_4$ **8c** (pyz = pyrazine) were produced,

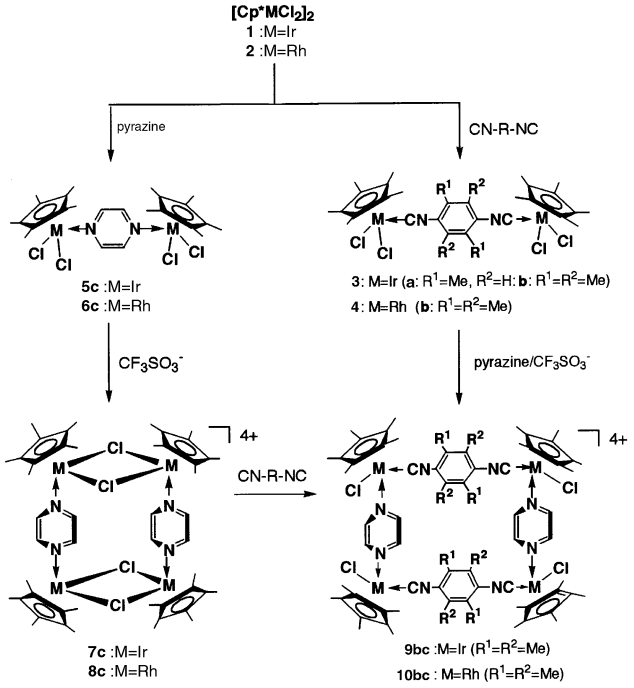

Scheme 1 Reactions of $[Cp^*MCl_2]_2$ (**1**: R = Ir and **2**: M = Rh) with pyrazine or isocyanides.

and FAB mass spectrometry showed a peak at *m/z* 1254 ($[M + 1]^+$).† The ^1H NMR spectrum consists of two characteristic singlets at δ 1.61 and 8.65 in a 60:8 intensity ratio, suggesting a symmetric tetranuclear structure. Indeed, X-ray crystallographic analysis revealed that the complex cation has a rectangular structure bridged by four Cl atoms and pyrazine molecule with Rh···Rh separations of 3.68 and 7.02 Å (Fig. 1).‡ The crystal contains MeOH as crystal solvent. Both Rh(1)Rh(2)Cl(1)Cl(2) and pyrazine least-squares planes are perpendicular to the Rh(1)Rh*(1)Rh(2)Rh*(2) plane. The average Rh–N bond length is 2.413 Å. A tetranuclear iridium complex **7c** was obtained from **5c** and AgOTf in a similar manner to the rhodium analog.† The ^1H NMR spectrum showed two types of resonances for each of the Cp* and pyrazine ligands; at δ 1.58 and 1.74 for the former and at δ 8.84 and 8.97 for the latter, suggesting the presence of configurational isomers.

When μ-chloro-bridged complex **7c** was treated with 2 equiv. of **b**, the Cl bridges were replaced by **b** to produce yellow crystals formulated as $[(Cp^*IrCl)_4(pyz)_2\{1,4\text{-}(NC)_2\text{-}2,3,5,6\text{-}Me_4C_6\}_2](OTf)_4$ **9bc**.† This complex can also be obtained from the reaction between **3b** and pyrazine in the presence of Ag(OTf). In the IR spectrum, the CN band appeared at 2176 cm^{-1} while the ^1H NMR spectrum showed three singlets at δ 1.94, 2.42 and 8.65 in a 30:12:4 intensity ratio, due to Cp*, isocyanide and pyrazine protons, respectively. In addition, the

DOI: 10.1039/b003416i

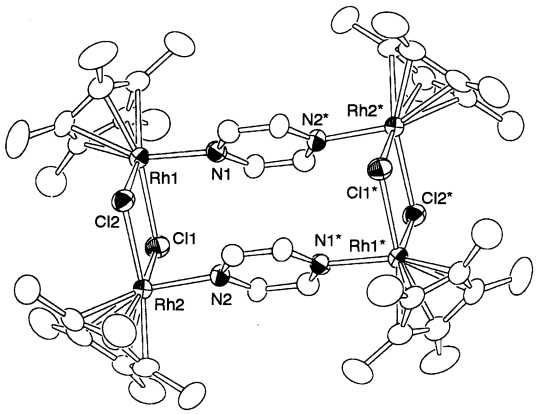

Fig. 1 Molecular structure of $[(Cp^*_4Rh_4Cl_4)(\mu\text{-}Cl)_4(\mu\text{-}pyz)_2](CF_3SO_3)_4$ **8c** (CF_3SO_3 anions omitted for clarity). Selected bond lengths (Å) and angles (°): Rh(1)–Cl(1) 2.466(3), Rh(1)–Cl(2) 2.467(2), Rh(1)–N(1) 2.133(7), Rh(2)–Cl(2) 2.474(3), Rh(2)–Cl(2) 2.459(2), Rh(2)–N(2) 2.153(8); Cl(1)–Rh(1)–Cl(2) 83.50(8), Cl(1)–Rh(1)–N(1) 88.0(2), Cl(2)–Rh(1)–N(1) 87.8(2), Cl(1)–Rh(2)–Cl(2) 83.47(8), Cl(1)–Rh(2)–N(2) 88.5(2), Cl(2)–Rh(2)–N(2) 88.5(2).

structure was determined by single crystal X-ray analysis (Fig. 2).‡ An asymmetric unit of the crystal of **9bc** consists of two halves of the molecules, each having a crystallographically imposed inversion center in the middle of the Ir···Ir* vector. Each iridium atom is surrounded by isocyanide, pyrazine, Cl and Cp*. The complex has a tetranuclear rectanglar structure with Ir···Ir* lengths of 6.986(1), 7.9145(9), 11.6459(9) and 11.668(1) Å. The dihedral angles between the Ir_4 plane and pyrazine are 49.44, 48.82° and those between Ir_4 plane and phenyl rings are 83.55, 83.58° and 75.75, 75.95°. The average Ir–C and Ir–Cl bond lengths are 1.97 and 2.388 Å, similar to

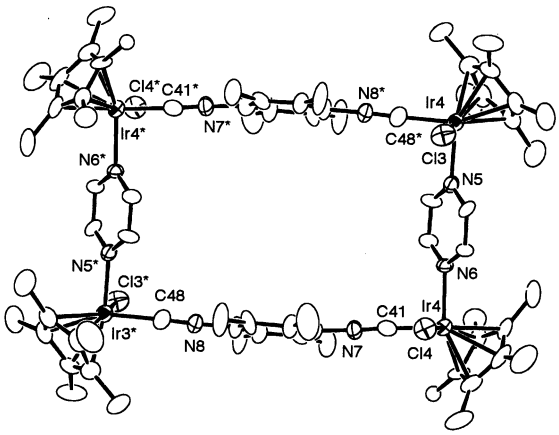

Fig. 2 Molecular structure of $[(Cp^*_4Ir_4Cl_4)\{\mu\text{-}1,4\text{-}(NC)_2\text{-}2,3,5,6\text{-}Me_4C_6\}_2(\mu\text{-}pyz)_2](CF_3SO_3)_4$ **9bc** (CF_3SO_3 anions omitted for clarity). Selected bond lengths (Å) and angles (°): Ir(1)–Cl(1) 2.379(5), Ir(1)–N(1) 2.12(1), Ir(1)–C(12) 1.92(2), C(12)–N(4) 1.18(2), Ir(2)–Cl(2) 2.368(5), Ir(2)–N(2) 2.11(1), Ir(2)–C(5) 1.96(2), C(5)–N(3) 1.14(2), Ir(3)–Cl(3) 2.408(5), Ir(3)–N(5) 2.11(1), Ir(3)–C(48) 1.98, C(48)–N(8) 1.14(2), Ir(4)–Cl(4) 2.395(4), Ir(4)–N(6) 2.12(1), Ir(4)–C(41) 1.98(2), C(41)–N(7) 1.13(2); Cl(1)–Ir(1)–N(1) 87.5(4), Cl(1)–Ir(1)–C(12) 86.7(6), N(1)–Ir(1)–C(12) 87.2(6), Cl(2)–Ir(2)–N(2) 86.5(4), Cl(2)–Ir(2)–C(5) 87.7(5), N(2)–Ir(2)–C(5) 90.8(6), Cl(3)–Ir(3)–N(5) 86.0(4), Cl(3)–Ir(3)–C(48) 88.8(5), N(5)–Ir(3)–C(48) 90.5(6), Cl(4)–Ir(4)–N(6) 86.0(4), Cl(4)–Ir(4)–C(41) 87.8(5), N(6)–Ir(4)–C(41) 93.2(6).

those of **3a**. The average Ir–N bond length of 2.12 Å is somewhat shorter than that of **8c**. A rhodium analog **10bc** was obtained in 45% yield from the direct reaction of **4b** with pyrazine in the presence of AgOTf.†

Studies on the self-assembly of cubic or ladder-shaped complexes by this synthetic methodology and the use of molecular materials are now in progress.

Notes and references

† Satisfactory analytical data were obtained for new complexes: **3a** (yellow, 75%): IR(Nujol): 2137 cm^{-1}. $\delta_H(CDCl_3)$: 1.86 (s, Cp*, 30H), 2.42 (s, Me, 6H), 7.29 (s, Ph, 2H). Calc. for $C_{30}H_{38}N_2Cl_4Ir_2$: C, 37.81; H, 4.02; N, 2.94. Found: C, 37.26; H, 4.04; N, 2.97%. **3b** (orange, 86%): FAB mass: *m/z* 981 (M + 1). IR(Nujol): 2150 cm^{-1}. $\delta_H(CDCl_3)$: 1.86 (s, Cp*, 30H), 2.39 (s, Me, 12H). Calc. for $C_{32}H_{42}N_2Cl_4Ir_2$: C, 39.18; H, 4.32; N, 2.86. Found: C, 38.67; H, 4.26; N, 2.95%. **4b** (orange, 73%): FAB mass: *m/z* 802 (M). IR(Nujol): 2176 cm^{-1}. $\delta_H(CDCl_3)$: 1.83 (s, Cp*, 30H), 2.40 (s, Me, 12H). Calc. for $C_{32}H_{42}N_2Cl_4Rh_2$: C, 47.90; H, 5.28; N, 3.49. Found: C, 48.26; H, 5.46; N, 4.24%.

5c (yellow, 83%): δ_H(dmso-d_6): 1.62 (s, Cp*, 60H), 8.65 (s, pyz, 8H). Calc. for $C_{24}H_{34}N_2Cl_4Ir_2$: C, 32.88; H, 3.91; N, 3.20. Found: C, 32.51; H, 3.81; N, 3.27%. **6c** (orange, 82%): δ_H(dmso-d_6): 1.61 (s, Cp*, 30H), 8.66 (s, pyz, 4H). Calc. for $C_{24}H_{34}N_2Cl_4Rh_2H_2O$: C, 40.25; H, 5.07; N, 3.91. Found: C, 40.29; H, 4.84; N, 4.04%. **7c** (yellow, 64%): δ_H(dmso-d_6): 1.58 (s, Cp*, 30H), 1.74 (s, Cp*, 30H), 2.05 (s, pyz, 12H), 8.84 (s, pyz, 4H), 8.97 (s, pyz, 4H). Calc. for $C_{60}H_{80}N_8Cl_4F_{12}O_{12}S_4Ir_4$: C, 30.43; H, 3.23; N, 4.73. Found: C, 30.24; H, 3.48; N, 4.59%. **8c** (reddish orange, 67%): δ_H(dmso-d_6): 1.61 (s, Cp*, 60H), 8.65 (s, pyz, 8H). Calc. for $C_{52}H_{68}N_4Cl_4F_{12}O_{12}S_4Rh_2$: C, 33.75; H, 3.70; N, 3.03. Found: C, 33.55; H, 3.67; N, 3.19%.

9bc (yellow, 65%): IR(Nujol): 2176 cm^{-1} (N≡C). δ_H(dmso-d_6): 1.94 (s, Cp*, 60H), 2.42 (s, Me, 24H), 8.66 (s, pyz, 8H). Calc. for $C_{76}H_{92}N_8Cl_4F_{12}O_{12}S_4Ir_4$: C, 34.78; H, 3.53; N, 4.27. Found: C, 34.87; H, 3.71; N, 4.61%.

10bc (orange, 49%): IR (nujol): 2186 cm^{-1} (N≡C). δ_H(dmso-d_6): 1.88 (s, Cp*, 60H), 2.43 (s, Me, 24H), 8.65 (s, pyz, 8H). Calc. for $C_{76}H_{92}N_8Cl_{10}F_{12}O_{12}S_4Rh_4$: C, 38.35; H, 3.99; N, 4.53. Found: C, 38.30; H, 4.39; N, 4.20%.

‡ *Crystal data*: for **3a**: $C_{30}H_{38}N_2Cl_4Ir_2$, M = 952.9, monoclinic, space group $P2_1/n$ (no. 14), a = 7.54(1), b = 16.571(7), c = 12.800(7) Å, β = 95.69(7)°, V = 1590(2) Å^3, D_c = 1.989 g cm^{-3} (Z = 2) at 27 °C, μ = 87.4 cm^{-1}; $R1$ = 0.041 and R_w = 0.111.

For **8c**: $C_{54}H_{76}N_4O_{14}S_4F_{12}Cl_4Rh_4$, M = 1914.9, monoclinic, space group $P2_1/n$ (no. 14), a = 13.245(7), b = 20.417(6), c = 14.419(4) Å, β = 108.31(2)°, V = 3701(1) Å^3, D_c = 1.718 g cm^{-3} (Z = 2) at 28 °C, μ = 12.20 cm^{-1}; $R1$ = 0.050 and R_w = 0.100.

For **9bc**: $C_{78}H_{98}N_8Cl_4F_{12}O_{14}S_4Ir_4$, M = 2638.6, triclinic, space group $P\bar{1}$ (no. 2), a = 13.1339(9), b = 16.203(1), c = 26.309(2) Å, α = 73.953(2), β = 87.9327(7), γ = 81.7369(6)°, V = 5324.7(6) Å^3, D_c = 1.646 g cm^{-3} (Z = 2) at −90 °C, μ = 52.1 cm^{-1}; $R1$ = 0.086 and R_w = 0.089.

CCDC 182/1743. See http://www.rsc.org/suppdata/cc/b0/b003416i/ for crystallographic files in .cif format.

1 R. Robson, B. F. Abrahams, S. R. Batten, R. W. Gable, B. F. Hoskins and J. Liu, in *Supramolecular Architecture*, ed. T. Bein, ACS Symp. Ser. 499, American Chemical Society, Washington, DC, 1992, p. 256; *Comprehensive Supramolcular Chemistry*, ed. J.-M. Lehn, Pergamon Press, Oxford, 1995; P. L. Stang and B. Olenyuk, *Acc. Chem. Res.*, 1997, **30**, 502; M. Fujita and K. Ogura, *Coord. Chem. Rev.*, 1996, **148**, 249.

2 A. Mayr and J. Guo, *Inorg. Chem.*, 1999, **38**, 921; J. A. Whiteforld, P. J. Stang and S. D. Huang, *Inorg. Chem.*, 1998, **37**, 5795; J. Manna, C. J. Kuehl, J. A. Whiteford, P. J. Stang, D. C. Muddiman, S. A. Hofstadler and R. D. Smith, *J. Am. Chem. Soc.*, 1997, **119**, 11 611; P. J. Stang, J. Fan and B. Olenyuk, *Chem. Commun.*, 1997, 1455.

3 K. K. Klausmeyer, T. B. Rauchfuss and S. R. Wilson, *Angew. Chem., Int. Ed.*, 1998, **37**, 1694.

4 S. M. Contakes, K. K. Klausmeyer, R. M. Milberg, S. R. Wilson and T. B. Rauchfuss, *Organometallics*, 1998, **17**, 3633.

ChemComm

Lithium atom exchange in solid *tert*-butyllithium

Glenn H. Penner* and Y. C. Phillis Chang

Department of Chemistry and Biochemistry, University of Guelph, Guelph, Ontario, Canada N1G 2W1. E-mail: gpenner@uoguelph.ca

Received (in Irvine, CA, USA) 11th April 2000, Accepted 2nd May 2000
First published as an Advance Article on the web 4th September 2000

Lithium-7 NMR spectral lineshapes and T_1 measurements show that the lithium atoms in the solid tetrameric form of *tert*-butyllithium are rapidly exchanging between the apical sites of a tetrahedron with activation energies of 23.8 ± 0.2 and 23.0 ± 0.6 kJ mol^{-1}, above and below a phase transition (310 ± 3 K), respectively.

Inter- and intra-molecular exchange in organolithium oligomers in solution is well documented.[1] An example of intramolecular exchange is the scrambling of the *tert*-butyl groups within the lithium-6 labelled[Bu^{t}Li]$_4$ tetramer **1** in cyclopentane solution.[2]

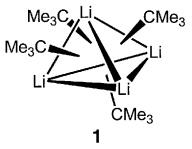

1

In this case the coupling $^1J(^{13}C^6Li)$ is observed between the α-carbon and all four ^{6}Li nuclei above 268 K. Below 251 K the exchange has stopped and coupling to only three ^{6}Li nuclei is observed. It has been shown that solid *tert*-butyllithium also exists as a tetramer.[3] These observations leads one to question whether a similar exchange process might occur in the solid state. Evidence for this comes from an early investigation of the ^{7}Li nuclear quadrupolar coupling constants (QCC) in solid methyllithium and ethyllithium where Lucken determined maximum values that were only a few kHz.[4] These values are unusually small and are much smaller than our calculated values for the [MeLi]$_4$ and [Bu^{t}Li]$_4$ tetramers.[5] Therefore it is expected that some kind of motional averaging might be responsible for the rather small QCC at ambient temperatures.

The ^{7}Li spectra of solid **1**, at various temperatures, are shown in Fig. 1.† At room temperature (293 K) we also observe a lineshape consistent with a ^{7}Li QCC of < 5 kHz. If an intramolecular exchange process is occurring, one should be able to observe changes in the spectral lineshapes as the temperature is reduced. This is indeed what happens between 200 and 150 K. Below 150 K the lineshape does not change and is consistent with a ^{7}Li QCC of 100 ± 3 kHz. The higher temperature lineshape shows that the quadrupolar interaction is nearly averaged to zero owing to either isotropic or pseudo-isotropic motion of the lithium atoms. Since the X-ray structure (at 180 K) shows lithium atoms occupying well defined sites located at the apices of a tetrahedron, pseudo-isotropic motion, *i.e.* exchange between tetrahedral sites, is the most likely averaging process. The lineshape changes indicate that the exchange rate is on the order of 10^5 s^{-1} in the temperature range 150–200 K, is $> 10^5$ s^{-1} above 200 K and $< 10^5$ s^{-1} below 150 K. In contrast the ^{1}H lineshape (not shown) changes very little in this temperature range. The relative temperature independence of the ^{1}H lineshape indicates that the *tert*-butyl groups are not exchanging, although rapid internal rotation of the methyl groups (about the C_α–C_β bonds) and the *tert*-butyl groups is expected to average the linewidth at these temperatures.

Another method for following molecular dynamics by NMR spectroscopy is through measurement of the spin–lattice relaxation time T_1. Fig. 2 shows a plot of the ^{7}Li T_1 as a function of temperature. It is quite clear that there is a well defined break in the T_1 curve at *ca.* 310 ± 3 K. We attribute this to a solid–solid phase transition. Above and below the phase transition temperature, the T_1 values are on the fast and slow motional side of the T_1 minimum, respectively. It would be informative to be able to discuss the lithium exchange process in terms of an exchange rate, *k*. This is possible if the spin–lattice relaxation rate can be described in terms of a single motional correlation time, τ_c, employing the commonly used BPP spectral density. Then the relaxation rate for a quadrupolar nucleus is given by eqn. (1)

$$R_1 = \frac{1}{T_1} = \frac{3\pi^2}{50}\frac{2I+3}{I^2(2I-1)}\chi^2\left[\frac{\tau_c}{1+(\omega_0\tau_c)^2}+\frac{4\tau_c}{1+(2\omega_0\tau_c)^2}\right] \quad (1)$$

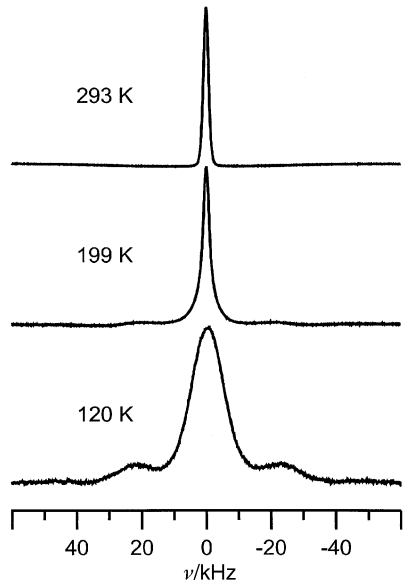

Fig. 1 The ^{7}Li spectra of solid *tert*-butyllithium at several temperatures.

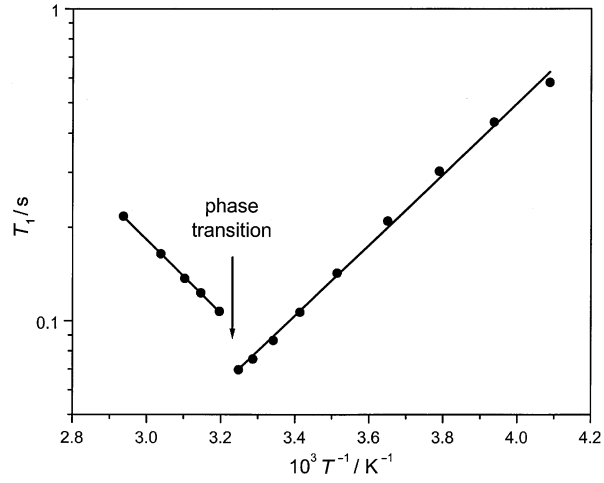

Fig. 2 Temperature dependence of the ^{7}Li T_1 for solid *tert*-butyllithium at a spectrometer frequency of 77.7 MHz.

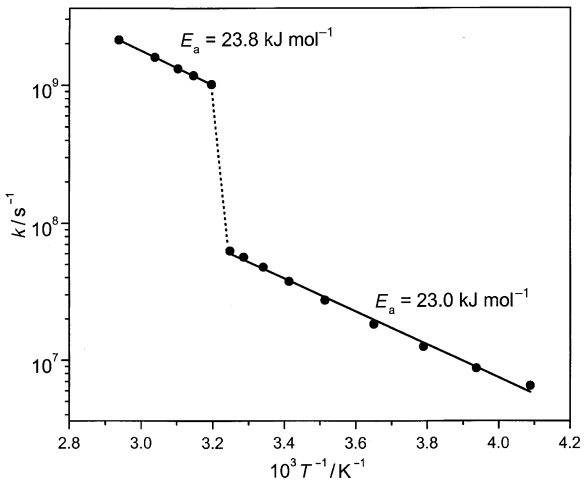

Fig. 3 Temperature dependence of the rate for lithium atom exchange in solid *tert*-butyllithium.

where I is the nuclear spin, χ is the nuclear QCC and ω_0 is the spectrometer (Larmor) frequency (in rad s^{-1}). If I, χ and ω_0 are known, τ_c values can be obtained from the T_1 measurements. The second assumption is that the lithium atoms are undergoing a 4-site exchange between equivalent tetrahedral sites. In that case the exchange rate is given as $k = 1/4\tau_c$.

Fig. 3 shows the temperature dependence of the lithium atom exchange rate. At the phase transition the rate changes by a factor of 16. The activation parameters for the exchange process are $E_a = 23.8 \pm 0.1$ kJ mol^{-1} and $k_\infty = 9.58 \pm 0.05 \times 10^{12}$ s^{-1} for the high temperature phase and $E_a = 23.0 \pm 0.6$ kJ mol^{-1} and $k_\infty = 4.85 \pm 0.33 \times 10^{11}$ s^{-1} for the low temperature phase. This analysis indicates that at 25 °C the lithium atoms in solid *tert*-butyllithium are exchanging at a rate of 8.5×10^8 s^{-1}!

Phase transitions are usually accompanied by changes in crystal and/or molecular structure. It would be of interest to compare a crystallographic study above 310 K with the earlier work at 180 K.[3]

Our calculated value of the ^{7}Li QCC for tetrameric **1** is 150 kHz.‡ This is larger than the observed value but does not take into account that the X-ray structure gives unrealistically short C–H bond lengths. Intermolecular effects are also not taken into account in this calculation. Details of our calculations and measurements of Li QCC values and chemical shift anisotropies in organolithium compounds will be published elsewhere.[5]

We are grateful to the Natural Sciences and Engineering Research Council (NSERC) of Canada for financial support. We are particularly indebted to Prof. Marcel Schlaf for the use of his inert atmosphere box and for help with sample preparation.

Notes and references

† Solid **1** was obtained by stripping the solvent from a 1.5 M pentane solution of *tert*-butyllithium (Aldrich) inside an inert atmosphere box under argon. About 1 g of the white powder was packed into a small airtight 10 mm o.d. container. A separate sample was prepared for magic angle spinning experiments (^{13}C, ^{6}Li and ^{7}Li) which showed that the solid sample was pure. In particular, the ^{6}Li MAS spectrum, which gave excellent signal-to-noise and a linewidth of only 0.09 ppm, showed a single small impurity peak (2.1% of total peak intensity). The non-spinning ^{7}Li spectra were obtained at a frequency of 77.7 MHz with a Bruker ASX-200 spectrometer using a single channel wideline probe. Single pulse experiments using 3 μs pulses and relaxation delays of 10 s were employed. Quadrupolar echo experiments at the lowest temperature were identical to the single pulse experiments. The T_1 experiments employed the inversion recovery pulse sequence, π–t_d–$\pi/2$ with 8 t_d values for each T_1 determination. The magnetization curves as a function of delay time showed mono-exponential decay.

‡ We performed a DFT calculation using the B3LYP functional and a 6-31G** basis set. We have found that this combination gives QCC values in good agreement with experiment. The crystal structure geometry of a single [Bu^{t}Li]$_4$ tetramer was used. Calculations were done with the Gaussian 98 software package.[6]

1 For example, see: G. Fraenkel, W. E. Beckenbaugh and P. P. Yang, *J. Am. Chem. Soc.*, 1976, **98**, 6878; M. Witanowski and J. D. Roberts, *J. Am. Chem. Soc.*, 1966, **88**, 737; J. L. Wardell, *Comprehensive Organometallic Chemistry*, ed. G. Wilkinson, F. G. A. Stone and E. W. Abel, Pergamon, Oxford, 1982, vol. 1, pp. 43–120.
2 R. D. Thomas, M. T. Clarke, R. M. Jensen and T. C. Young, *Organometallics*, 1986, **5**, 1851.
3 T. Kottke and D. Stalke, *Angew. Chem., Int. Ed. Engl.*, 1993, **32**, 580.
4 E. C. Lucken, *Chem. Phys. Lett.*, 1965, **4**, 252.
5 G. H. Penner and Y. C. P. Chang, unpublished work.
6 Gaussian 98, Revision A.3, M. J. Frisch, G. W. Trucks, H. B. Schlegel, G. E. Scuseria, M. A. Robb, J. R. Cheeseman, V. G. Zakrzewski, J. A. Montgomery Jr., R. E. Stratmann, J. C. Burant, S. Dapprich, J. M. Millam, A. D. Daniels, K. N. Kudin, M. C. Strain, O. Farkas, J. Tomasi, V. Barone, M. Cossi, R. Cammi, B. Mennucci, C. Pomelli, C. Adamo, S. Clifford, J. Ochterski, G. A. Petersson, P. Y. Ayala, Q. Cui, K. Morokuma, D. K. Malick, A. D. Rabuck, K. Raghavachari, J. B. Foresman, J. Cioslowski, J. V. Ortiz, B. B. Stefanov, G. Liu, A. Liashenko, P. Piskorz, I. Komaromi, R. Gomperts, R. L. Martin, D. J. Fox, T. Keith, M. A. Al-Laham, C. Y. Peng, A. Nanayakkara, C. Gonzalez, M. Challacombe, P. M. W. Gill, B. Johnson, W. Chen, M. W. Wong, J. L. Andres, C. Gonzalez, M. Head-Gordon, E. S. Replogle and J. A. Pople, Gaussian, Inc., Pittsburgh PA, 1998.

A new route to dilithio boraamidinates: formation and X-ray structures of the dimeric and trimeric clusters $\{Li_2[RB(NBu^t)_2]\}_x$ (R = Bu^n, x = 2 and R = Me, x = 3)

Justin K. Brask, Tristram Chivers* and Gabriele Schatte

Department of Chemistry, University of Calgary, 2500 University Dr. NW, Calgary, Alberta, Canada T2N 1N4. E-mail: chivers@ucalgary.ca

Received (in Cambridge, UK) 20th July 2000, Accepted 18th August 2000

The dilithio boraamidinate complexes $\{Li_2[RB(NBu^t)_2]\}_x$ (R = Bu^n, x = 2 and R = Me, x = 3), prepared unexpectedly by treating $B[N(H)Bu^t]_3$ with 3 equiv. LiR, represent the first structurally characterized s-block metal derivatives of the boraamidinate ion.

Amidinate ions $[RC(NR')(NR'')]^-$ **1** have been investigated extensively as ligands for both transition metal and main group element centers.[1] In the presence of Lewis bases, *e.g.* THF or HMPA, the lithium derivatives of these important reagents form dimeric step-shaped structures.[2,3] This structural motif is also evident in the lithio ligands of the lithium oxide complex $\{Li[Bu^nC(NBu^t)_2]\}_4{\cdot}Li_2O$.[4] By contrast, the isoelectronic boraamidinate ions $[RB(NR')(NR'')]^{2-}$ **2** have received little attention. The reagent $\{Li_2[PhB(NBu^t)_2]\}_n$, prepared by dilithiation of $PhB[N(H)Bu^t]_2$, has been used in metathetical reactions to generate several main group derivatives, *e.g.* $[PhB(\mu\text{-}NBu^t)_2]_2Te$[5] and $[PhB(\mu\text{-}NBu^t)_2Pb]_2$,[6] and the transition-metal derivative $[PhB(\mu\text{-}NBu^t)_2]_2Ti$.[7] The X-ray structures of these complexes were reported, but s-block metal derivatives of **2** have not been structurally characterized. We describe here

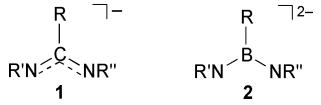

1 **2**

the unexpected formation and X-ray structures of dimeric and trimeric dilithio boraamidinates $\{Li_2[RB(NBu^t)_2]\}_x$ (**3**: R = Bu^n, x = 2; **4a**: R = Me, x = 3) from the reaction of $B[N(H)Bu^t]_3$ with LiR (R = Bu^n or Me, respectively).

Treatment of the trisaminoborane $B[N(H)Bu^t]_3$ with 3 equiv. $LiBu^n$ in *n*-hexane gives a 1:2 mixture of the dimer $\{Li_2[Bu^nB(NBu^t)_2]\}_2$ **3** and $LiN(H)Bu^t$ [eqn. (1)]. Complex **3** is the first product to crystallize from *n*-hexane at 0 °C and it can be isolated in 71% yield free from $LiN(H)Bu^t$.† The ^1H NMR spectrum of **3** in C_6D_6 consists of a single Bu^t resonance at δ 1.25 as well as resonances corresponding to a Bu^n group (Bu^n:Bu^t ≈ 1:2). The ^7Li and ^{11}B NMR spectra each exhibit single resonances at δ −0.63 and 36.6 ppm, respectively.

$$3\ LiR + B[N(H)Bu^t]_3 \rightarrow {}^1/_x\{Li_2[RB(NBu^t)_2]\}_x + LiN(H)Bu^t + 2\ RH$$

3: R = Bu^n, x = 2
4a: R = Me, x = 3
4b: R = Me, x = 2 (1)

X-Ray structure analysis revealed a 10-atom $Li_4B_2N_4$ cluster core for **3** (Fig. 1),‡ isostructural with the $Li_4Si_2N_4$ framework in $\{Li_2[(Me)_2Si(NBu^t)_2]\}_2$.[8] Although no crystallographic symmetry is imposed on the molecule, **3** displays near D_{2d} symmetry with the S_4-axis parallel to the B(1)–B(2) vector. This structure is consistent with the solution NMR data. The B–N distances for **3** [mean 1.458(4) Å, range 1.451(4)–1.464(4) Å] are similar to those found in $[PhB(\mu\text{-}NBu^t)_2]_2Ti$ [mean 1.464(10) Å, range 1.453(9)–1.475(10) Å],[7] while the Li–N distances [mean 2.037(6) Å, range 2.009(6)–2.091(5) Å] fall in the range for those of $\{Li_2[(Me)_2Si(NBu^t)_2]\}_2$ [mean 2.075(7) Å, range 2.003(6)–2.129(6) Å].[8] The distortion of the central Li_4N_4 cube along the S_4-axis [Li–N–Li: mean 75.42(20)°, range 68.30(18)–88.3(2)°; N–Li–N: mean 97.15(30)°, range 70.99(18)–110.8(2)°; Li(2)–N(1)–Li(1)–N(2) 46.16(18)°, Li(4)–N(4)–Li(3)–N(3) = 46.22(18)°] is attributed to the rigidity of the boraamidinate ions **2** (R = Bu^n, R′ = R″ = Bu^t). The geometry at the three-coordinate boron atoms of these dianions is essentially planar [Σ B(1) = Σ B(2) = 359.9(3)°]. The agostic C(–H)···Li contacts in **3** (mean 2.41 Å) are considerably shorter than those reported for the cluster complex $\{Li_3[Sb(NBu^t)_3]\}_2$ (mean 2.65 Å),[9] but longer than those observed for $\{Li_2[(Me)_2Si(NBu^t)_2]\}_2$ (mean 2.34 Å).[8]

The formation of **3** requires cleavage of a B–N bond in favor of a B–C bond. In effect, the added $LiBu^n$ functions as a base to deprotonate two $N(H)Bu^t$ groups per $B[N(H)Bu^t]_3$ molecule and as a nucleophile to displace the third $N(H)Bu^t$ group in the form of $LiN(H)Bu^t$. A similar displacement was observed in the reaction of $[(THF)_2Li]_2[Nb(NMes)_3(NHMes)]$ with 1 equiv. $LiBu^n$ to produce the alkyl complex $[(THF)_2Li]_2[Bu^nNb(NMes)_3]$ and LiN(H)Mes in a 1:1 molar ratio.[10] In order to gauge the versatility of this novel methodology for preparing dilithio boraamidinates, $B[N(H)Bu^t]_3$ was treated with 3 equiv. LiMe in diethyl ether. After removal of $LiN(H)Bu^t$, recrystallization of the product mixture from *n*-pentane gave $\{Li_2[MeB(NBu^t)_2]\}_3$ **4a** in 28% yield [eqn. (1)].†

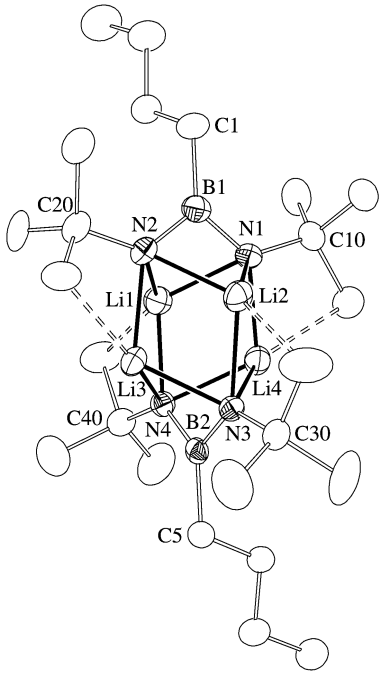

Fig. 1 Molecular structure of $\{Li_2[Bu^nB(NBu^t)_2]\}_2$ **3** (40% probability ellipsoids). For clarity, H atoms are omitted and only one orientation of the disordered Bu^t group centered at C(20) is shown. Relevant bond distances and bond angles are provided in the text.

DOI: 10.1039/b005852l

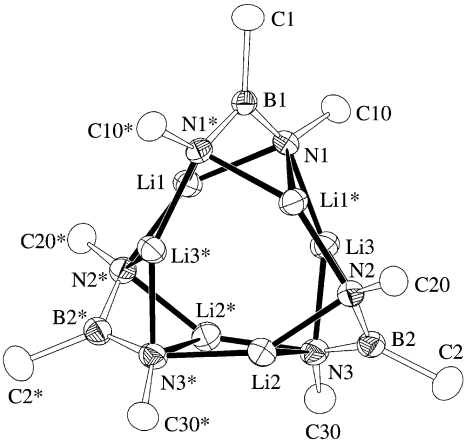

Fig. 2 Molecular structure of $\{Li_2[MeB(NBu^t)_2]\}_3$ **4a** (40% probability ellipsoids). For clarity, H atoms are omitted and only the α-carbon atoms of the Bu^t groups are shown. Starred atoms are related by the symmetry transformation: $-x+1, y, -z+{}^1/_2$. Selected bond distances (Å) and angles (°): B(1)–N(1) 1.452(3), B(1)–C(1) 1.604(4), B(2)–N(2) 1.456(3), B(2)–N(3) 1.451(3), B(2)–C(2) 1.608(3), Li–N [mean 2.051(4), range 2.001(4)–2.100(4)]; N(1)–B(1)–N(1*) 110.0(2), N(1)–B(1)–C(1) 125.02(12), N(2)–B(2)–N(3) 110.51(19), N(2)–B(2)–C(2) 124.4(2), N(3)–B(2)–C(2) 125.0(2).

The ^{1}H NMR spectrum of **4a** in C_6D_6 shows Bu^t and Me resonances at δ 1.29 and 0.85 in a 2 : 1 ratio, respectively. Single resonances are observed at δ −0.86 and 35.5 in the ^{7}Li and ^{11}B NMR spectra, respectively. A more soluble product, tentatively identified as the dimer $\{Li_2[MeB(NBu^t)_2]\}_2$ **4b**, was characterized by ^{1}H, ^{7}Li and ^{11}B NMR spectra.† The molar ratio of **4a**:**4b** was *ca.* 1:3 based on the integrated intensities of the resonances in the ^{1}H NMR spectrum of the mixture.

X-Ray structure analysis of **4a** disclosed a novel trimeric arrangement based on a severely distorted $Li_6(NBu^t)_6$ hexagonal prism, for which alternate Li_2N_2 rings are *N*,*N*′-capped by a BMe unit (Fig. 2).‡ The resulting 15-atom $Li_6B_3N_6$ core provides the first example of a tricapped hexagonal prismatic cluster. Although only a C_2-axis is imposed on the molecule crystallographically [through C(1), B(1) and the centre of the Li(2)N(3)Li(2*)N(3*) ring], **4a** displays near D_3 symmetry. The capped Li_2N_2 rings in **4a** deviate greatly from planarity [Li(1*)–N(1)–Li(1)–N(1*) = 44.99(16)°, Li(3)–N(2)–Li(2)–N(3) 45.14(13)°] as compared with their non-capped counterparts [Li(2*)–N(3)–Li(2)–N(3*) 10.9(2)°, Li(1*)–N(1)–Li(3)–N(2) −11.60(16)°], demonstrating the dominance of the dianion **2** in structure formation, *cf.* structural direction by the trianions $[Sb(NR)_3]^{3-}$.[11]

The reaction of readily accessible trisaminoboranes, $B[N(H)R]_3$ (R = alkyl or aryl),[12] with the appropriate organolithium reagent is a potentially versatile method for generating dianionic ligands **2** with variable steric requirements. Unlike the lithiation of bisaminoboranes $RB[N(H)R']_2$,[7] this new route to dilithio boraamidinates does not require the preparation of $RBCl_2$ reagents.

We thank Dr R. McDonald (University of Alberta) for assistance with the X-ray data collection for **3** and **4a** and NSERC (Canada) for financial support.

Notes and references

† *Synthesis*: **3**: a 2.5 M solution of LiBu^n in hexanes (2.49 mL, 6.33 mmol) was added slowly to a solution of $B[N(H)Bu^t]_3$[12] (0.48 g, 2.11 mmol) in *n*-hexane (30 mL) at 23 °C and the mixture was stirred for 2.5 h. Concentration (*ca.* 3 mL), by removal of solvent *in vacuo*, and subsequent cooling (0 °C for 1 h) of the resulting solution yielded colorless blocks of **3** (0.33 g, 0.74 mmol, 71%); mp 109–110 °C. Anal. Calc. for $BC_{12}H_{27}Li_2N_2$: C, 64.33; H, 12.15; N, 12.50. Found: C, 63.80; H, 11.64; N, 12.65%. ^{1}H NMR (C_6D_6, 23 °C): δ 1.68 [m, 4 H, $CH_2(CH_2)_2CH_3$], 1.35 [m, 2 H, $CH_2(CH_2)_2CH_3$], 1.25 (s, 18 H, Bu^t), 1.11 [t, 3 H, $CH_2(CH_2)_2CH_3$]. ^{7}Li NMR (C_6D_6, 23 °C): δ −0.63 (s). ^{11}B NMR (C_6D_6, 23 °C): δ 36.6 (s). A 1 mL aliquot of the initial *n*-hexane reaction mixture was pumped to dryness *in vacuo* and taken up in C_6D_6. The ^{1}H and ^{7}Li NMR spectra indicated the presence of **3** and LiN(H)Bu^t [^{1}H NMR: δ 1.36 (s, Bu^t), *cf.* lit.:[13] 1.37, ^{7}Li NMR: δ 0.14 (s)] in a 1:2 molar ratio [eqn. (1)].

4a: a 1.4 M solution of LiMe in diethyl ether (4.52 mL, 6.33 mmol) was added slowly to a solution of $B[N(H)Bu^t]_3$[12] (0.48 g, 2.11 mmol) in diethyl ether (30 mL) at 23 °C and the mixture was stirred for 2.5 h. The resulting cloudy reaction mixture was filtered to remove LiN(H)Bu^t [^{1}H and ^{7}Li NMR (*vide supra*)] and subsequently pumped to dryness by removal of solvent *in vacuo*. The white powder obtained was redissolved in *n*-pentane (5 mL) and the solution was cooled (−20 °C for 4 days), yielding colorless blocks of **4a** (0.11 g, 0.20 mmol, 28%); mp 124–125 °C (decomp.). Anal. Calc. for $BC_9H_{21}Li_2N_2$: C, 59.40; H, 11.63; N, 15.39. Found: C, 58.76; H, 11.21; N, 14.68%. ^{1}H NMR (C_6D_6, 23 °C): δ 1.29 (s, 18 H, Bu^t), 0.85 (s, 3 H, Me). ^{7}Li NMR (C_6D_6, 23 °C): δ −0.86 (s). ^{11}B NMR (C_6D_6, 23 °C): δ 35.5 (br).

The white powder, prior to the recrystallization step, contains a second product **4b**: ^{1}H NMR (C_6D_6, 23 °C): δ 1.20 (s, 18 H, Bu^t), 0.81 (s, 3 H, Me). ^{7}Li NMR (C_6D_6, 23 °C): δ −0.69 (s). ^{11}B NMR (C_6D_6, 23 °C): δ 35.5 (br). The CHN analyses for the mixture of **4a** and **4b** were consistent with the empirical formula $Li_2[MeB(NBu^t)_2]$.

‡ *Crystal data*: for **3**: $C_{24}H_{54}B_2Li_4N_4$, M = 448.09, monoclinic, a = 12.671(5), b = 17.562(5), c = 14.026(5) Å, β = 98.825(5)°, V = 3084.2(9) Å^3, T = 193(2) K, space group $P2_1/n$ [a non-standard setting of $P2_1/c$ (no. 14)], Z = 4, μ(Mo-Kα) = 0.053 mm^{-1}, D_c = 0.965 g cm^{-3}, 9679 reflections measured, 5898 unique (R_{int} = 0.0791), 2277 observed [$I > 2\sigma(I)$]. The final R_1 and $wR_2(F^2)$ were 0.0641 [$I > 2\sigma(I)$] and 0.1678 (all data), respectively.

For **4a**: $C_{27}H_{63}B_3Li_6N_6$, M = 545.90, monoclinic, a = 17.3587(13), b = 12.0750(8), c = 19.2718(14) Å, β = 116.0730(14)°, V = 3628.4(4) Å^3, T = 193(2) K, space group $C2/c$ (no. 15), Z = 4, μ(Mo-K$_\alpha$) = 0.055 mm^{-1}, D_c = 0.999 g cm^{-3}, 10 572 reflections measured, 3104 unique (R_{int} = 0.0388), 2302 observed [$I > 2\sigma(I)$]. The final R_1 and $wR_2(F^2)$ were 0.0611 [$I > 2\sigma(I)$] and 0.1775 (all data), respectively.

CCDC 182/1749. See http://www.rsc.org/suppdata/cc/b0/b005852l/ for crystallographic files in .cif format.

1 F. T. Edelmann, *Coord. Chem. Rev.*, 1994, **137**, 403; J. Barker and M. Kilner, *Coord. Chem. Rev.*, 1994, **133**, 219.
2 D. Stalke, M. Wedler and F. T. Edelmann, *J. Organomet. Chem.*, 1992, **431**, C1.
3 J. Barker, D. Barr, N. D. R. Barnett, W. Clegg, I. Cragg-Hine, M. G. Davidson, R. P. Davies, S. M. Hodgson, J. A. K. Howard, M. Kilner, C. W. Lehmann, I. Lopez-Solera, R. E. Mulvey, P. R. Raithby and R. Snaith, *J. Chem. Soc., Dalton Trans.*, 1997, 951.
4 T. Chivers, A. Downard and M. Parvez, *Inorg. Chem.*, 1999, **38**, 4347; T. Chivers, A. Downard and G. P. A. Yap, *J. Chem. Soc., Dalton Trans.*, 1998, 2603.
5 H.-J. Koch, H. W. Roesky, S. Besser and R. Herbst-Irmer, *Chem. Ber.*, 1993, **126**, 571.
6 A. Heine, D. Fest, D. Stalke, C. D. Habben, A. Meller and G. M. Sheldrick, *J. Chem. Soc., Chem. Commun.*, 1990, 742.
7 D. Fest, C. D. Habben, A. Meller, G. M. Sheldrick, D. Stalke and F. Pauer, *Chem. Ber.*, 1990, **123**, 703.
8 D. J. Brauer, H. Bürger and G. R. Liewald, *J. Organomet. Chem.*, 1986, **308**, 119.
9 M. A. Beswick, N. Choi, C. N. Harmer, A. D. Hopkins, M. McPartlin, M. A. Paver, P. R. Raithby, A. Steiner, M. Tombul and D. S. Wright, *Inorg. Chem.*, 1998, **37**, 2177.
10 D. P. Smith, K. D. Allen, M. D. Carducci and D. E. Wigley, *Inorg. Chem.*, 1992, **31**, 1319.
11 M. A. Beswick, M. E. G. Mosquera and D. S. Wright, *J. Chem. Soc., Dalton Trans.*, 1998, 2437.
12 D. W. Aubrey and M. F. Lappert, *J. Chem. Soc.*, 1959, 2927.
13 N. D. R. Barnett, W. Clegg, L. Horsburgh, D. M. Lindsay, Q.-Y. Liu, F. M. Mackenzie, R. E. Mulvey and P. G. Williard, *Chem. Commun.*, 1996, 2321.

By-product formation causes leaching of Ti from the redox molecular sieve TS-1

Lucinda Davies,[a] Paul McMorn,[a] Donald Bethell,[b] Philip C. Bulman Page,[c] Frank King,[d] Frederick E. Hancock[d] and Graham J. Hutchings*[a]

[a] *Department of Chemistry, Cardiff University, PO Box 912, Cardiff, UK CF10 3TB. E-mail: hutch@cf.ac.uk*
[b] *Department of Chemistry,University of Liverpool, Liverpool, UK L69 3BX*
[c] *Department of Chemistry, University of Loughborough, Loughborough, UK LE11 3TU*
[d] *Synetix, PO Box 1, Billingham, UK TS23 1LB*

Received (in Cambridge, UK) 14th May 2000, Accepted 14th August 2000

Triols, formed as by-products from the titanium silicalite (TS-1) catalysed epoxidation of allylic alcohols, can cause leaching of Ti from the microporous framework.

The titanium(IV) silicalite known as TS-1 has been considered by many to be a unique redox molecular sieve since its discovery by Enichem researchers.[1,2] TS-1 has been shown to be an active heterogeneous catalyst for the epoxidation of alkenes[3] and allylic alcohols.[4] Two features are responsible for the uniqueness of TS-1. First, incorporation of Ti into the microporous silicate framework increases the hydrophobicity[5] and enables H_2O_2 to be used as an oxidant. Other redox molecular sieves are ineffective with H_2O_2 and require more active oxygen sources, *e.g. tert*-butyl hydroperoxide.[6] Secondly, TS-1 is considered very stable under the reaction conditions and to date, loss of Ti from the framework of TS-1 has not been studied in detail. These features have been emphasised recently by Sheldon *et al.*,[7] who also stress that most papers pay scant attention to the loss of framework transition metal ions from redox molecular sieves. Recently, it has been shown that other redox molecular sieves containing Cr and V leach these metal cations into solution during reaction, and therefore act as reservoirs for active homogeneous catalysts.[8,9] If leaching is common for transition metals incorporated into microporous frameworks, then it is surprising that this should not be the case for Ti in TS-1. We have now studied the stability of TS-1 with respect to loss of Ti during reaction and we demonstrate that by-product formation unfortunately can lead to the loss of Ti from titanium(IV) silicalite.

TS-1 (2.4 wt% Ti) was prepared according to the following method, which has been used in many previous studies. Titanium butoxide (3.4 g Aldrich) was added dropwise to tetraethyl orthosilicate (62.5 g Merck) and the resulting mixture stirred for 30 min. Tetrapropylammonium hydroxide (40 wt% in H_2O, 76.3 g Alfa) was added dropwise with stirring. The resulting mixture was then heated at 60 °C for 2 h to evaporate ethanol produced by the hydrolysis/condensation reactions between the silicon and titanium reagents. Water was then added to the synthesis gel to return the volume of the gel to that prior to the evaporation step. The gel was mixed thoroughly and autoclaved under autogeneous pressure at 175 °C for 48 h. The resulting solids were filtered off, washed and dried at 100 °C for 4 h. The materials were calcined at 550 °C in air for 16 h prior to use. The material was characterised by X-ray diffraction, scanning electron microscopy, FTIR and reflectance laser Raman spectroscopy. The data were found to be in agreement with literature data and the crystallites of TS-1 were found to be uniform, rhombohedral and 0.2 μm in diameter. The sample of TS-1 was used as a catalyst for the hydroxylation of phenol with H_2O_2 at 70 °C. After 75 min, the products formed were 49% catechol and 50% hydroquinone; this is in agreement with previous literature studies[10] confirming the quality of the TS-1.

The TS-1 was also shown to be an effective catalyst for the epoxidation of allylic alcohols [Fig. 1(a) and (b)]. In a typical reaction, crotyl alcohol (0.1 mol) was reacted with aqueous

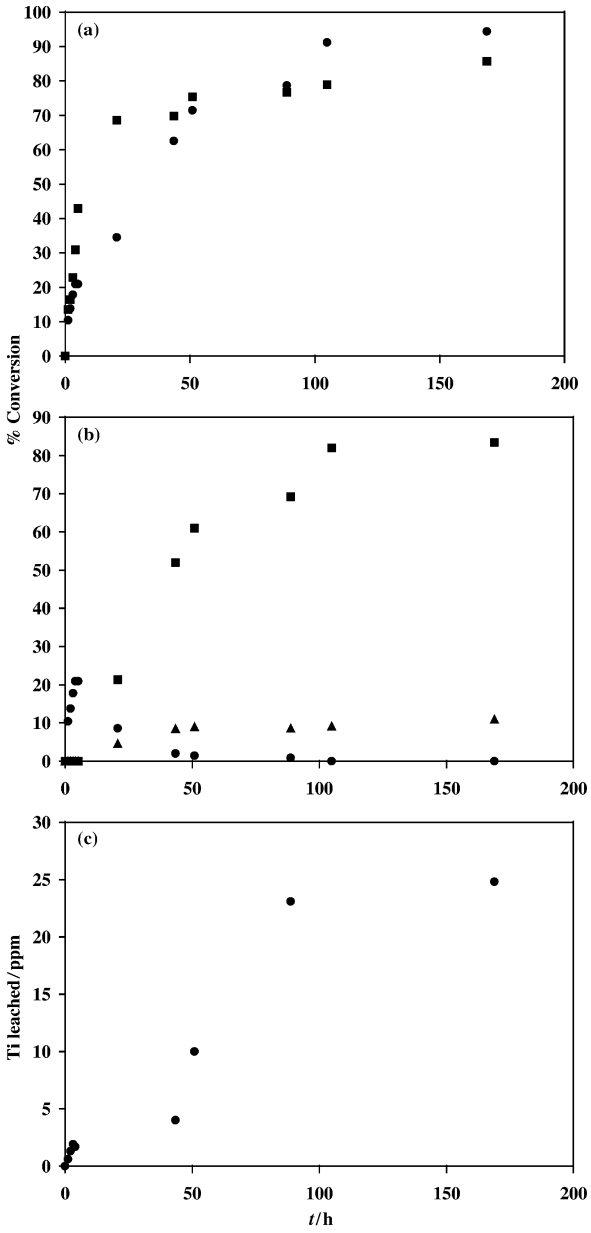

Fig. 1 Reaction of crotyl alcohol with H_2O_2 at 50 °C with TS-1 in methanol. (a) Conversion: (●) crotyl alcohol, (■) H_2O_2; (b) reaction products: (●) epoxide, (▲) ether diols, (■) triol; (c) Ti leaching.

DOI: 10.1039/b002055i

H_2O_2 (30% vol, 0.11 mol) at 50 °C with TS-1 (0.1 g) in methanol (10 ml) in a stirred flask fitted with a reflux condenser. Samples were withdrawn at various time intervals and the products analysed by GC using dimethyl sulfone as an internal standard. Samples were also filtered hot through a heated sinter funnel which contained a bed of Celite to remove small particles of zeolite. Blank experiments confirmed that this method was effective in removing any particulate Ti-containing material and, furthermore, that any titanium observed in solution did not originate from the Celite. The solutions were then analysed by ICPMS to determine the Ti content [Fig. 1(c)]. Initially, TS-1 is active and selective for the formation of the oxirane product and, at this stage, no Ti leaching is observed. However, in a sequential reaction the oxirane ring opens by nucleophilic attack by the solvent to form the triol (reaction with water) or ether diols (reaction with methanol). At this time, Ti is observed to leach from TS-1 and the pH of the reaction mixture decreases. These results clearly demonstrate that the structural integrity of TS-1 is not maintained in the presence of the secondary reaction products formed under typical reaction conditions.

In a further set of experiments, TS-1 (crystallisation period 2 d) was slurried with a range of reagents at 50 °C for 35 h. No Ti leaching was observed with hydrogen peroxide in methanol (30% by vol, < 3 ppm Ti), crotyl alcohol (< 0.3 ppm Ti), butane-2,3-diol (< 2 ppm Ti) or hydrochloric acid (1 M, < 0.7 ppm Ti). Several further experiments were conducted with glycerol as a model triol. No Ti leaching was observed with glycerol and hydrochloric acid (< 2 ppm Ti), or glycerol together with hydrochloric acid and methanol (< 1.3 ppm Ti). However, when TS-1 was slurried with glycerol and hydrogen peroxide using methanol as solvent, extensive leaching of Ti was observed (3571 ppm Ti) corresponding to removal of 16% of the Ti from TS-1. These model experiments confirm that the necessary condition for Ti-leaching from TS-1 is the combined presence of a triol together with hydrogen peroxide, and hence for the successful operation of TS-1 as a truly heterogeneous catalyst the formation of triols must be avoided.

It is interesting to comment on the mechanism by which Ti is removed from the framework of TS-1. Detailed UV–VIS spectroscopy[11] has shown that TS-1 contains four-coordinate Ti^{4+} in the absence of water. When TS-1 is suspended in water or water–H_2O_2 mixtures, the Ti^{4+} species becomes six co-ordinate, retaining three Ti–O–Si bonds, which are considered to anchor the Ti firmly within the microporous framework. The solvent molecules, in our case methanol, could be expected to displace one or more of the water molecules. We suggest that, when this site is exposed to triols, further Ti–O–Si bonds are broken and this leads to the irreversible loss of Ti from the structure (Fig. 2). Since triol by-product formation can be commonly observed in TS-1 catalysed reactions, we suggest that Ti leaching from TS-1 is probably more common than has previously been considered. It is also interesting to determine if the Ti that is leached during the catalytic reaction originates from the surface of the TS-1 crystallites. To determine if this is so, a further experiment was carried out in which the non-calcined TS-1 was silanised according to the method of Beck *et al.*[12] using trimethylsilyl chloride and hexamethyldisiloxane. As the non-calcined TS-1 retains the template within the intra-crystalline pores, this procedure effectively silanises just the exterior surface. On subsequent calcination (550 °C, 4 h), the template is removed and TS-1 crystallites covered on the external surface with silica are formed. Using this material as a catalyst for crotyl alcohol oxidation did not result in any significant leaching of Ti, yet the catalytic performance was essentially the same as that observed for the non-silanised sample [Fig. 1(a), (b)]. These data indicate that it is Ti located on the external surface of the TS-1 crystallites that is preferentially leached by the by-product triol.

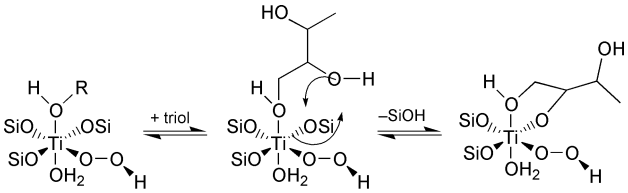

Fig. 2 Interaction of triols with the active site of TS-1.

We would like to thank Synetix, EPSRC, and the DTI/Link programme on asymmetric catalysis for financial support and the Department of Earth Sciences, Cardiff University for ICPMS results.

Notes and references

1 M. Taramasso, G. Perego and B. Notari, *US Pat.*, 4 410 510, 1983.
2 M. Taramasso, G. Manara, V. Fattore and B. Notari, *US Pat.*, 4 666 692, 1986.
3 M. G. Clerici and P. Ingallina, *J. Catal.*, 1993, **140**, 71.
4 G. J. Hutchings, D. F. Lee and A. R. Minihan, *Catal. Lett.*, 1995, **33**, 369.
5 J. Weitkamp, S. Ernest, E. Roland and G. F. Thiele, *Stud. Surf. Sci. Catal.*, 1997, **105**, 763.
6 M. A. Camblor, M. Constantini, A. Corma, L. Gilbert, P. Esteve, A. Martinez and S. Valencia, *Chem. Commun.*, 1996, 1339.
7 R. A. Sheldon, m. Wallau, I. W. C. E. Ahrens and U. Schuchardt, *Acc. Chem. Res.*, 1998, **31**, 485.
8 H. E. B. Lempers and R. A. Sheldon, *Appl. Catal.*, 1996, **143**, 137.
9 W. I. Caravalho, P. B. Varaldo, M. Wallau and U. Schuchardt, *Zeolites*, 1997, **18**, 408.
10 J. A. Martens, P. Buskeni, P. A. Jacobs, A. van der Pol, J. H. C. van Hoof, C. Ferrini, H. W. Kouwenhoven, P. J. Kooyman and H. van Bekkum, *Appl. Catal. A*, 1993, **99**, 71.
11 A. Zecchina, S. Bordiga, C. Lamberti, G. Ricchiardi, D. Scarano, G. Petrini, G. Leofanti and M. Mantegazza, *Catal. Today*, 1996, **32**, 97.
12 J. S. Beck, J. C. Vartulli, W. J. Roth, M. E. Leonwicz, C. T. Kresge, K. D. Schmitt, C. T. W. Chu, D. H. Olson, E. W. Shepheard, S. B. McCullen, J. G. Higgins and J. L. Schenter, *J. Am. Chem. Soc.*, 1992, **114**, 10 834.

Cr(NAr)(O)(NPr$^i_2$)(Ar): a strongly-bent monoimido complex resulting from nitrosyl ligand cleavage

Eric W. Jandciu, Peter Legzdins,* W. Stephen McNeil, Brian O. Patrick and Kevin M. Smith†

Department of Chemistry, University of British Columbia, 2036 Main Mall, Vancouver, BC, Canada, V6T 1Z1. E-mail: legzdins@chem.ubc.ca

Received (in Irvine, CA, USA) 26th May 2000, Accepted 31st July 2000

The molecular structure of Cr(NAr)(O)(NPr$^i_2$)(Ar) (Ar = 2-MeC$_6$H$_4$) is analysed by X-ray crystallographic and density functional theoretical techniques.

Tetrahedral imido complexes of the Group 6 metals are in the vanguard of applied organometallic chemistry.[1–4] In d^0 M(NR)(E)X$_2$ complexes (E = O, NR, CHR; X = OR, NR$_2$, CH$_2$R), the competition among the π-donor ligands for available metal orbitals is a critical component of their overall reactivity.[5] Here, we report the molecular structure of Cr(NAr)(O)(Ar)(NPr$^i_2$) (Ar = 2-MeC$_6$H$_4$), which contains a strongly-bent imido ligand.[6] Density functional theory (DFT) calculations have been employed to help analyse the π-bonding conflicts that underpin the experimentally observed geometry.

We recently reported that the alkylation of Cr(NO)(NPr$^i_2$)(O$_2$CPh)$_2$ with R$_2$Mg•*x*(dioxane) reagents yields unsaturated diamagnetic Cr(II) alkyl complexes (Scheme 1).[7] The structures of Cr(NO)(NPr$^i_2$)(CH$_2$SiMe$_3$)$_2$ and Cr(NO)(NPr$^i_2$)(CH$_2$Ph)$_2$ were confirmed by X-ray crystallography, and fluxional processes involving the amido and benzyl ligands were established by variable-temperature ^{1}H NMR spectroscopy.[7] However, the product resulting from treatment of Cr(NO)(NPr$^i_2$)(O$_2$CPh)$_2$ with Ar$_2$Mg•*x*(dioxane) has an anomalously sharp ^{1}H NMR spectrum with no indication of amido rotation. When the structure of this product was determined by X-ray crystallography, it was established that the original assignment as Cr(NO)(NPr$^i_2$)Ar$_2$ was incorrect; the complex is in fact Cr(NAr)(O)(NPr$^i_2$)(Ar) **1** (Fig. 1, Table 1).

The most remarkable feature of the structure of **1**[8] is the strikingly non-linear Cr1–N1–C1 angle of 146.2(3)°. The NAr ligand lies in the O–Cr–N(imido) plane, with the aryl substituent bent toward the oxo group. The Cr–N(amido) bond length, and the amido group planarity (sum of angles at N2 = 359.8°) and alignment are indicative of a Cr–N(amido) π-bonding interaction.[5] Similarly, the Cr–O bond length is consistent with maximum oxo-to-chromium π-donation. The O–Cr–N angles between the oxo and both the amido and imido groups are larger than the typical tetrahedral angle. The structure of complex **1** exhibits disorder in the Cr-bound aryl ligand. This ligand occupies two distinct orientations, in equal proportions, related by a roughly 180° rotation about the Cr–C8 bond. Each disordered fragment was modelled using rigid phenyl groups with isotropic thermal parameters.

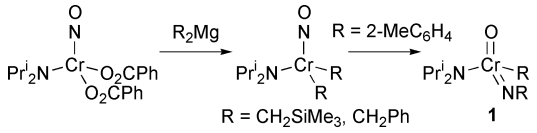

Scheme 1 Alkylation of Cr(NO)(NPr$^i_2$)(O$_2$CPh)$_2$.

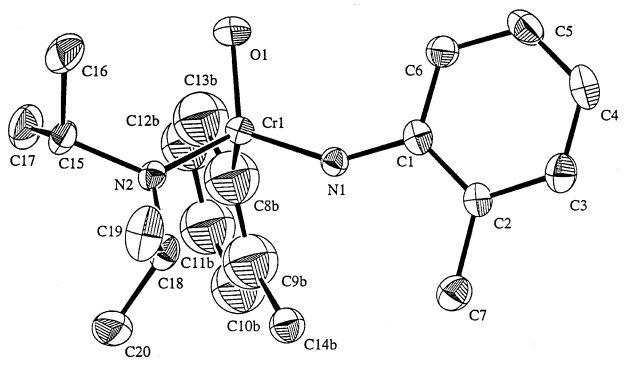

Fig. 1 Crystallographic structure of complex **1**.

Table 1 Comparison of experimental (**1**)[a] and calculated (**2**) bond lengths (Å) and angles (°) of Cr(NR)(O)(NR′$_2$)(R)[b]

Parameter	**1**	**2**
Cr–N1	1.670(2)	1.626
Cr–N2	1.801(3)	1.797
Cr–O	1.589(3)	1.592
Cr–C8a	2.103(6)	2.011
Cr–C8b	2.025(5)	
Cr–N1–C1	146.2(3)	149.0
O–Cr–N1	115.3(2)	115.2
O–Cr–N2	115.5(1)	115.4
O–Cr–C8a	112.6(2)	103.0
O–Cr–C8b	99.9(2)	
N1–Cr–N2	109.9(1)	110.8
N1–Cr–C8a	99.3(2)	101.8
N1–Cr–C8b	107.9(2)	
N2–Cr–C8a	102.3(2)	109.1
N2–Cr–C8b	107.9(2)	

[a] Parameters to C8 in **1** represent the two distinct orientations of the disordered aryl group. [b] **1**: R = 2-MeC$_6$H$_4$, R′ = Pr^i; **2**: R = R′ = Me.

DFT calculations[9] were performed on Cr(NMe)(O)(NMe$_2$)(Me) **2** to investigate the origin and relative importance of the imido angle in this unusual structure.[10] While the simplified model compound lacks the steric bulk present in **1**, the DFT-optimised geometry faithfully reproduces the pertinent structural features determined by X-ray crystallography (Fig. 2, Table 1). The Cr–N(imido)–C angle is calculated to be 149.0°, confirming that this distortion is electronic rather than steric in origin. Remarkably good agreement is attained for the Cr–O and Cr–N(amido) bond lengths and the O–Cr–N bond angles, which match the structural determination within experimental error. The parameters involving the Cr–C bond show poorer agreement, surely due to the disorder exhibited by the aryl group. Interestingly, the DFT-optimised structure has Cr–N(imido)

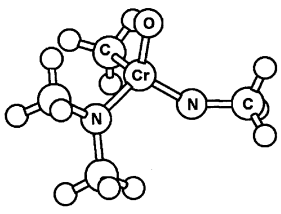

Fig. 2 Calculated structure of complex **2**.

† Permanent address: Department of Chemistry, University of Prince Edward Island, 550 University Avenue, Charlottetown, PEI, Canada, C1A 4P3.

DOI: 10.1039/b004340k

and N(imido)–C distances that are markedly shorter and longer, respectively, than the corresponding experimental bond lengths. This discrepancy may be due to the delocalisation of electron density from the N atom to the aromatic substituent, an electronic redistribution that is unavailable to the NMe ligand of the computational model.

Complex **1** is the most strongly-bent chromium imido complex observed to date, as confirmed by a search of the Cambridge Structural Database (October 1999 release), and is the *only* example of a chromium *mono*imido compound with a Cr–N–C angle $< 165°$.[11] While $Cr(NR)_2X_2$ compounds exhibit a wide range of Cr–N–C angles (typically 155 to 175°), none approaches the degree of bending observed in **1** unless the two imido groups are joined in a strained chelate ring.[3b] The evident π-donation of the NPr^i_2 group is not responsible for the Cr–N–Ar bending, in that amido π-bonding in the related $Cr(NR)_2(NHR)Cl$ complexes fails to disrupt the Cr–imido interaction.[12,13] The geometry of **1** is therefore attributed to the competition between the oxo and imido groups for available d_π orbitals.[14]

A series of single-point calculations were performed to see what variation of the overall energy of **2** would result from variation of the imido Cr–N–C angle. As shown in Fig. 3, this is a remarkably soft deformation mode, requiring < 18 kJ mol^{-1} to make the imido ligand perfectly linear. The relative ease of imido bending/straightening has been established theoretically,[15] spectroscopically[16] and structurally.[17]

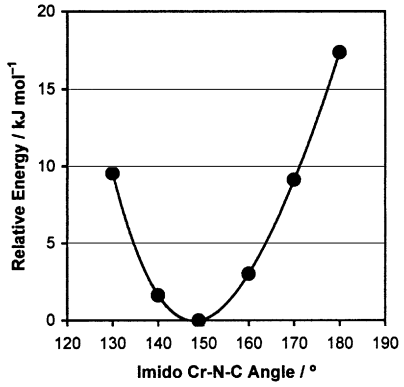

Fig. 3 Energy change with imido ligand angle in **2**.

As indicated in Scheme 1, $Cr(NO)(NPr^i_2)Ar_2$ is presumably an intermediate in the formation of complex **1**, though our attempts to trap or observe the diaryl precursor have thus far been unsuccessful. The relative instability of the putative diaryl compound with respect to nitrosyl bond cleavage may be related to the propensity of aryl (in contrast to alkyl) groups to undergo migration reactions to M=E linkages.[20] The cleavage of nitrosyl ligands is still relatively rare, but several examples of this reactivity are now known for unsaturated Group 6 complexes.[21] The transformation of R–Cr–NO to RN=Cr=O provides access to rare chromium d^0 monoimido species,[22] a potentially useful synthetic alternative to the chromyl chloride-derived $Cr(NR)_2X_2$ compounds that dominate Cr(VI) imido research.[12]

As established by DFT calculation, the strongly-bent imido angle of **1** clearly has an electronic origin, which we attribute to oxo–imido π-conflict, and which stands in contrast to the range of angles found in related bisimido structures. The calculations further reveal the soft nature of the distortion, in accord with experimentally determined examples of facile imido bending in Group 6 $M(NR)(E)X_2$ complexes. Given the influence of imido geometry on the reactivity of such complexes,[23] we feel the effect of these π-conflicts on imido-bending energy surfaces has been underappreciated. Further synthetic and theoretical studies to explore this phenomenon will undoubtedly aid in the rational design of catalysts for ROMP,[1] RCM[2] and olefin polymerisation[3] chemistries.

Notes and references

1 M. R. Buchmeiser, *Chem. Rev.*, 2000, **100**, 1565.
2 G. S. Weatherhead, J. G. Ford, E. J. Alexanian, R. R. Schrock and A. H. Hoveyda, *J. Am. Chem. Soc.*, 2000, **122**, 1828.
3 (*a*) M. P. Coles, C. I. Dalby, V. C. Gibson, I. R. Little, E. L. Marshall, M. H. Ribera da Costa and S. Mastroianni, *J. Organomet. Chem.*, 1999, **591**, 78; (*b*) U. Siemeling, L. Kölling, A. Stammler, H.-G. Stammler, E. Kaminski and G. Fink, *Chem. Commun.*, 2000, 1177.
4 M. P. Coles, V. C. Gibson, W. Clegg, M. R. J. Elsegood and P. A. Porrelli, *Chem. Commun.*, 1996, 1963.
5 V. C. Gibson, *J. Chem. Soc., Dalton Trans.*, 1994, 1607.
6 (*a*) W. A. Nugent and J. M. Mayer, *Metal–Ligand Multiple Bonds*, Wiley-Interscience, New York, 1988; (*b*) D. E. Wigley, *Prog. Inorg. Chem.*, 1994, **42**, 239; (*c*) T. R. Cundari, *Chem. Rev.*, 2000, **100**, 807.
7 E. W. Jandciu, J. Kuzelka, P. Legzdins, S. J. Rettig and K. M. Smith, *Organometallics*, 1999, **18**, 1994.
8 *Crystal data*: $C_{20}H_{28}N_2OCr$, M = 364.45, monoclinic, a = 14.822(1), b = 7.7784(6), c = 17.655(1) Å, β = 107.730(2)°, U = 1938.7(2) Å^3, T = 173 K, space group $P2_1/a$ (no. 14), Z = 4, μ(Mo-Kα) = 5.98 cm^{-1}, 14569 reflections measured, 3650 unique (R_{int} = 0.074) used in calculations. Final $wR(F^2)$ was 0.133 (all data). CCDC 182/1737. See http://www.rsc.org/suppdata/cc/b0/b004340k/ for crystallographic files in .cif format.
9 *Computational details*: Calculations were carried out in Gaussian 98 with geometries optimised without constraint at the B3LYP/LANL2DZ level of theory, using standard basis sets. The energies of non-optimal imido angles were determined as single-point calculations, leaving the rest of the geometry unchanged. M. J. Frisch *et. al.*, Gaussian 98, Revision A.7. Gaussian Inc., Pittsburgh PA, 1998.
10 For previous calculations on Cr imido complexes, including $Cr(NH)(O)Cl_2$ at the HF level, see: T. R. Cundari, *J. Am. Chem. Soc.*, 1992, **114**, 7879.
11 There is one structurally characterized bent *silyl*imido chromium complex (Cr–N–Si = 144°), the dimer $[Cr(O)(NSiMe_3)(py)]_2(\mu\text{-}OSiMe_3)_2$: H.-W. Lam, G. Wilkinson, B. Hussain-Bates and M. B. Hursthouse, *J. Chem. Soc., Dalton Trans.*, 1993, 1477.
12 K. C. Chew, W. Clegg, M. P. Coles, M. R. J. Elsegood, V. C. Gibson, A. J. P. White and D. J. Williams, *J. Chem. Soc., Dalton Trans.*, 1999, 2633.
13 M. P. Coles, C. I. Dalby, V. C. Gibson, W. Clegg and M. R. J. Elsegood, *Polyhedron*, 1995, **14**, 2455.
14 M. Jolly, J. P. Mitchell and V. C. Gibson, *J. Chem. Soc., Dalton Trans.*, 1992, 1329.
15 D. W. H. Rankin, H. E. Robertson, A. A. Danopoulos, P. D. Lyne, D. M. P. Mingos and G. Wilkinson, *J. Chem. Soc., Dalton Trans.*, 1994, 1563; K. A. Jørgensen, *Inorg. Chem.*, 1993, **32**, 1521.
16 D. C. Bradley, S. R. Hodge, J. D. Runnacles, M. Hughes, J. Mason and R. L. Richards, *J. Chem. Soc., Dalton Trans.*, 1992, 1663.
17 There exist cases where two independent imido compounds in the same unit cell exhibit highly disparate M–N–C angles, suggesting that such near-linear imido groups are susceptible to perturbation from intermolecular packing forces.[18] These angles are equally sensitive to *ortho* substitution; the classic structure of $Mo(NPh)_2(S_2CNEt_2)_2$ displays one linear and one bent imido ligand,[19a] while $Mo(NAr')_2(S_2CNEt_2)_2$ (Ar′ = 2,6-$Pr^i_2C_6H_3$) possesses two linear imido groups.[19b]
18 A. A. Danopoulos, G. Wilkinson, T. K. N. Sweet and M. B. Hursthourse, *J. Chem. Soc., Dalton Trans.*, 1995, 2111; A. Bell, W. Clegg, P. W. Dyer, M. R. J. Elsegood, V. C. Gibson and E. L. Marshall, *J. Chem. Soc., Chem. Commun.*, 1994, 2247.
19 (*a*) B. L. Haymore, E. A. Maatta and R. A. D. Wentworth, *J. Am. Chem. Soc.*, 1979, **101**, 2063; (*b*) T. A. Coffey, G. D. Forster, G. Hogarth and A. Sella, *Polyhedron*, 1993, **12**, 2741.
20 See ref. 6(*a*), p. 246.
21 P. Legzdins and M. A. Young, *Comments Inorg. Chem.*, 1995, **17**, 239.
22 N. Meijboom, C. J. Schaverien and A. G. Orpen, *Organometallics*, 1990, **9**, 774.
23 R. R. Schrock, *Polyhedron*, 1995, **14**, 3177.

ChemComm

Preparation, characterization and condensation of novel metal chalcogenide/MCM-41 complexes

Collin Kowalchuk, John F. Corrigan* and Yining Huang*

Department of Chemistry, The University of Western Ontario, London, Ontario, Canada N6A 5B7. E-mail: corrigan@uwo.ca

Received (in Irvine, CA, USA) 16th March 2000, Accepted 2nd August 2000

Hexagonally ordered mesoporous MCM-41 with 3 nm pores has been impregnated with the metal chalcogenolate $Cu_6(TePh)_6(PPh_2Et)_5$ 1: the analysis and condensation of this material is a step toward the synthesis of semiconducting nanowires.

The ability of mesoporous materials to act as hosts for quantum structures has been the focus of numerous research efforts as exemplified with reports on the absorption and subsequent polymerization of analine,[1] the encapsulation of semiconducting Ge filaments,[2] the preparation of ferrocenophane polymer[3] and the fabrication of nanostructured Pt clusters and wires.[4]

The independent development of the chemistry of mesoporous materials and metal chalcogenide clusters over the past decade have seen dramatic growth.[5–7] The union of these two fields, the encapsulation of metal chalcogenide clusters and their subsequent condensation into size limited semiconductor particles, should provide novel one-directional nanostructures.

The copper–chalcogenolate cluster $Cu_6(TePh)_6(PPh_2Et)_5$ **1** can be accessed in high yields *via* the reaction of CuCl and $Te(Ph)SiMe_3$ with an excess of the phosphine PPh_2Et.[8] Cluster **1**, like many metal–tellurolate complexes[9] undergoes a series of condensation reactions *via* the photochemical elimination of $TePh_2$. For **1**, this yields the cluster $[Cu_{50}(TePh)_{20}Te_{17}(PEtPh_2)_8]^{4-}$.[8] Our efforts in this area are to exploit these facile condensation processes within the channels of nanoporous MCM-41. Pure silica MCM-41, prepared with cetyltrimethylammonium bromide, has a pore size easily large enough to accommodate clusters such as **1**.[10]

The synthesis of **1**/MCM-41† was achieved using sublimation techniques under an inert atmosphere. During impregnation, maintaining an inert atmosphere is extremely important since at these elevated temperatures rapid cluster decomposition is otherwise observed. However, after loading, these materials are stable under atmospheric conditions for an extended period of time.

TGA data provide important information about the loading features. Characteristic decomposition curves of **1** and **1**/MCM-41 are shown in Fig. 1. For pure **1** [Fig. 1(a)] a single decomposition is observed, produced by two distinct endothermic steps obtained by DTA. This decrease in mass results from the loss of 3 equivalents of $TePh_2$ and 5 equivalents of PPh_2Et per cluster molecule as determined by TGA and subsequent GC–MS analysis. The observed 70.5% weight loss is close to the calculated loss of 71.5%. Since no strong interaction between the outer surface of the host and copper cluster is expected, the thermal decomposition of **1** adsorbed onto the MCM-41 exterior surface should be very similar to that observed for pure **1**. The TGA of a sample **I** of MCM-41 combined with **1** (70 °C, 10^{-3} Torr) [Fig. 1(b)] displays a weight loss at low temperature (onset = 150 °C) due to **1** adsorbed on the external surface. A 150 °C onset decomposition temperature is consistently observed for externally adsorbed **1** on MCM-41 and is identical to that observed for pure **1**. The high temperature (250 °C) weight loss can thus be attributed to cluster loaded inside the MCM-41 channels. The TGA results indicate some impregnation at 70 °C (10^{-3} Torr), with cluster **1** being only partially loaded inside of MCM-41. In contrast, a sample of **1**/MCM-41 complex **II** prepared by heating at 110 °C (10^{-3} Torr) [Fig. 1(c)] displays only one, high temperature decomposition suggesting complete loading of **1** inside of the MCM-41 host.

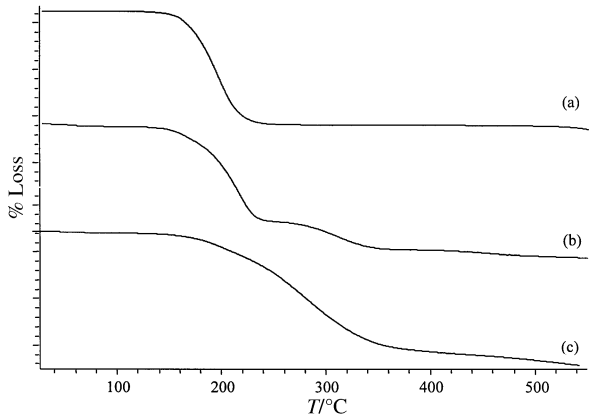

Fig. 1 TGA decomposition in the range 25–550 °C at a heating rate of 10 °C min^{-1}: (a) pure **1**; (b) **1**/MCM-41 treated at 70 °C at 10^{-3} Torr (sample **I**); (c) **1**/MCM-41 treated at 110 °C at 10^{-3} Torr (sample **II**).

The actual weight percent loading may be calculated from these curves. It is observed that loading is virtually time independent. Factors such as temperature and **1**/MCM-41 ratio affect the loading percent if loading is carried out for a minimum time of 12 h. For mechanical mixing under atmospheric conditions, a maximum of 5% loading is observed and can be attributed to a small quantity of cluster blocking the entrance to the pores. At 70 °C the loading increases to 11%. An increase in temperature leads to higher loading with a maximum of 34% achieved at 110 °C.

Nitrogen adsorption studies confirm that **1** is indeed loaded into the channels of MCM-41. The adsorption curve for pure MCM-41 [Fig. 2(a)] with a type IV isotherm and distinct capillary condensation characteristic of MCM-41 has a BET surface area of 1126 $m^2\ g^{-1}$. The BET surface area decreases to 272 $m^2\ g^{-1}$ for **II** [Fig. 2(b)]. No significant lattice contraction

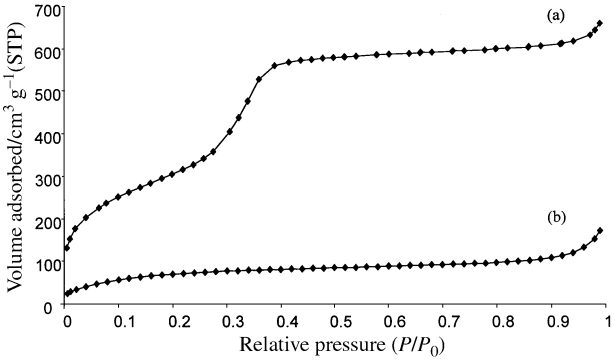

Fig. 2 Nitrogen adsorption curves: (a) MCM-41; (b) **1**/MCM-41 treated at 110 °C at 10^{-3} Torr (sample **II**).

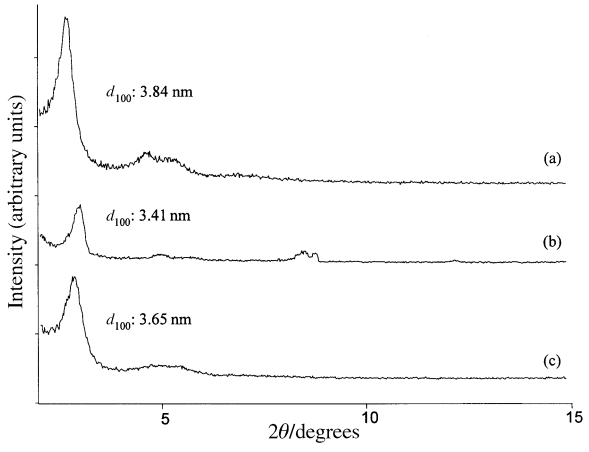

Fig. 3 PXRD patterns in the range 2θ = 2–15° (intensities normalized to the d_{100} reflection intensity of calcined MCM-41): (a) pure MCM-41; (b) **1**/MCM-41 treated at 70 °C at 10^{-3} Torr (sample **I**); (c) **1**/MCM-41 treated at 110 °C at 10^{-3} Torr (sample **II**).

was observed by powder X-ray diffraction (PXRD) and thus we conclude that this decrease in surface area is a result of the loaded cluster. The inflection point of the loaded sample becomes less sharp and shifts to lower relative pressure. This shift indicates the presence of smaller mesopores due to the impregnation of **1**. However the mesoporous structure is maintained as indicated by the overall shape of the isotherms and from PXRD.

The powder pattern of samples of MCM-41 has a characteristic diffraction pattern (h_{100}, h_{110}, h_{200}) with a calculated d_{100} of 4.4 nm.[10] The partial impregnation of **1** into MCM-41 [Fig. 3(b)] gives rise to diffraction patterns for host and guest species, with reflections of **1** due to crystallites of the cluster adsorbed on the external surface of MCM-41. With **II**, only the diffraction pattern of MCM-41 is observed [Fig. 3(c)]. We therefore conclude that the structural integrity of MCM-41 is maintained during impregnation and the clusters are dispersed within the channels with no long range ordering. A decrease in the intensity of the d_{100} diffraction and a smaller *d*-spacing are observed in both loaded samples **I** and **II**. The loading of **1** into the pores of MCM-41 causes a decrease in the mean electron density of silicate walls compared to the pores, thus decreasing the d_{100} diffraction.[11] The smaller *d*-spacing in Fig. 3(b) and (c) suggests the loading process slightly decreases the size of the pore walls.

The IR spectrum of **1**/MCM-41 in the ν(CH) stretching region suggests that cluster integrity is maintained during impregnation as the number of ν(CH) bands and their position of **II** are virtually identical to those for **1**. CP MAS ^{31}P NMR spectra of **II** display only a single peak at −11.8 ppm in close agreement with the observed solution shift (−10.4 ppm)[8] of the free cluster, as expected when the cluster is 'diluted' in the solid framework.

The photolysis of **1** and the **1**/MCM-41 complex provides evidence of cluster condensation, in agreement with its developed solution chemistry.[8] The UV–VIS spectra of non-photolysed **1**/MCM-41 in hexane show two distinct maxima at 210 and 249 nm.

Since **1** has low solubility in hexane, a slurry of **II** was prepared and the suspension was photolysed.‡ A darkening of the sample and a red shift is observed for both **1** and **II**. The observed red shift in the UV–VIS spectra suggests cluster condensation, as previously observed.[12] Increasing the irradiation time increases the red shift for both samples and yields a new absorbance at 440 nm for irradiated **1**. No further change is observed after 10 h of irradiation. Although identical condensation as that observed in solution, which results in the formation of $[Cu_{50}(TePh)_{20}Te_{17}(PEtPh_2)_8]^{4-}$, from **1** inside the pores of MCM-41 is unlikely, a condensation process is nonetheless occurring. Thermally activated condensation of **1** inside the pores of MCM-41 is also possible with complete loss of $TePh_2$ and PPh_2Et moieties with only copper telluride remaining as characterized by PXRD. We are currently perusing the characterization of the condensed materials and the general applicability of this method to metal chalcogenolate complexes.

We thank The University of Western Ontario, NSERC Canada and the Canada Foundation for Innovation for financial support. Dr L. Mercier (Laurentian University) is thanked for the nitrogen adsorption studies.

Notes and references

† 0.1 g of calcined MCM-41 was dehydrated at 130 °C under dynamic vacuum (10^{-3} Torr) for 3 h. Homogeneous samples of cluster:MCM-41 (weight ratios 1:4, 1:2) were prepared by mechanical mixing under atmospheric conditions producing a yellow microcrystalline powder. These samples were then heated at 70 or 110 °C under a static vacuum (10^{-3} Torr) for a minimum of 12 h.

‡ *Preparation* of UV–VIS samples: 0.05 g samples of **1** and **1**/MCM-41 (**II**) were charged in quartz UV cells with glass-distilled hexane and a stir bar to prepare a suspension. The samples were irradiated at room temperature with a low-pressure Hg lamp ($\lambda > 254$ nm).

1 C. Wu and T. Bein, *Chem. Mater.*, 1994, **6**, 1109.
2 R. Leon, D. Magolese, G. Stucky and P. M. Petroff, *Phys. Rev. B*, 1995, **52**, 2285.
3 M. J. MacLachlan, P. Aroca, N. Coombs, I. Manners and G. A. Ozin, *Adv. Mater.*, 1998, **10**, 144.
4 M. Sasaki, M. Osada, N. Sugimoto, S. Inagaki, Y. Fukushima, A. Fukuoka and M. Ichikawa, *Microporous Mesoporous Mater.*, 1998, **21**, 597.
5 J. Y. Ying, C. P. Mehnert and M. S. Wong, *Angew. Chem., Int. Ed.*, 1999, **38**, 56.
6 L. C. Roof and J. W. Kolis, *Chem. Rev.*, 1993, **93**, 1037.
7 I. Dance and K. Fisher, *Prog. Inorg. Chem.*, 1994, **41**, 637.
8 J. F. Corrigan and D. Fenske, *Angew. Chem., Int. Ed. Engl.*, 1997, **36**, 1981.
9 J. Arnold, *Prog. Inorg. Chem.*, 1995, **43**, 353.
10 J. S. Beck, J. C. Vartuli, W. J. Roth, M. E. Leonowicz, C. T. Kresge, K. D. Schmitt, C. T.-W. Chu, D. H. Olson, E. W. Sheppard, S. B. McCullen, J. B. Higgens and J. L. Schlenker, *J. Am. Chem. Soc.*, 1992, **114**, 10 834.
11 B. Marler, U. Oberhagemann, S. Vortmann and H. Gies, *Microporous Mater.*, 1996, **6**, 375.
12 Y. M. Tricot and J. H. Fendler, *J. Phys. Chem.*, 1986, **90**, 3369.

Oxygen atom transfer from $Re^{V}O$ to tertiary diphosphines: spacer length and chemical differentiation of products

Sibaprasad Bhattacharyya, Indranil Chakraborty, Bimal Kumar Dirghangi and Animesh Chakravorty*

Department of Inorganic Chemistry, Indian Association for the Cultivation of Science, Calcutta 700 032, India. E-mail: icac@mahendra.iacs.res.in

Received (in Cambridge, UK) 7th June 2000, Accepted 16th August 2000

The reaction of *mer*-[ReL(O)Cl_3], [L = 2-(*p*-chlorophenylazo)-1-methylimidazole] with $Ph_2P(CH_2)_nPPh_2$ (abbreviated P*n*P) affords [ReL(OP1P)Cl_3] 2a, [ReL(OP1PO)Cl_3] 4 and [ReL(OP2P)Cl_3] 2b, [Cl_3LRe(OP2PO)ReLCl_3] 5, all having *mer* geometry; unlike 2b which is stable in solution, 2a spontaneously isomerizes to *fac*-[ReL(P1PO)Cl_3] *via* an associative pathway; the origin of the observed differentiation (2a *vs.* 2b and 4 *vs.* 5) is scrutinized in terms of structures and reaction models.

Tertiary phosphines are model oxygen atom acceptors from oxo moieties such as $Re^{V}O$.[1,2] Chelation by the π-acidic azoimidazole L as in **1**, facilitates the transfer process.[3] This work

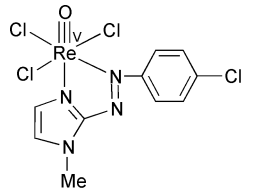

1 *mer*-[ReL(O)Cl_3]

2a *mer*-[Re^{III}L(OP1P)Cl_3]
2b *mer*-[Re^{III}L(OP2P)Cl_3]
3 *fac*-[Re^{III}L(P1PO)Cl_3]
4 *mer*-[Re^{III}L(OP1PO)Cl_3]
5 *mer*-[Cl_3LRe^{III}(OP2PO)$Re^{III}LCl_3$]

concerns the species **2**–**5** formed from **1** and $Ph_2P(CH_2)_nPPh_2$ (abbreviated P*n*P, *n* = 1, 2)[4] directly or *via* subsequent transformations. The differentiation referred to in the title relates to the pairs **2a, 2b** and **4, 5** in which the length of the spacer –$(CH_2)_n$– varies.

With P*n*P in excess, stereoretentive one-atom transfer [eqn. (1)] afforded† **2a** and **2b** (Fig. 1).‡ Both are stable in the solid state and **2b** is also stable in solution. In contrast, **2a** undergoes spontaneous linkage-*cum*-geometrical isomerization [eqn. (2)] in solution furnishing† **3** (Fig. 2).‡

$$R{\equiv}O + PnP \rightarrow Re{-}OPnP \quad (1)$$

$$Re{-}OP1P \rightarrow Re{-}P1PO \quad (2)$$

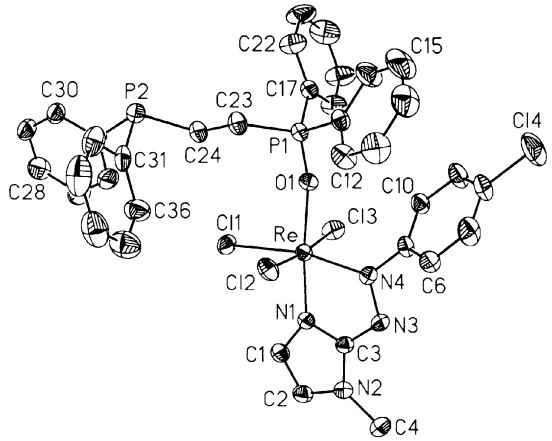

Fig. 1 Perspective view of *mer*-[Re^{III}L(OP2P)Cl_3] **2b**. Selected bond distances (Å) and angles (°): Re–N(1) 2.000(6), Re–N(4) 2.002(7), Re–O(1) 2.048(5), Re–Cl(3) 2.355(2), Re–Cl(2) 2.372(2), Re–Cl(1) 2.375(2); N(1)–Re–O(1) 173.9(2), Cl(3)–Re–Cl(2) 174.67(8), N(4)–Re–Cl(1) 166.9(2), P(1)–O(1)–Re 164.0(4).

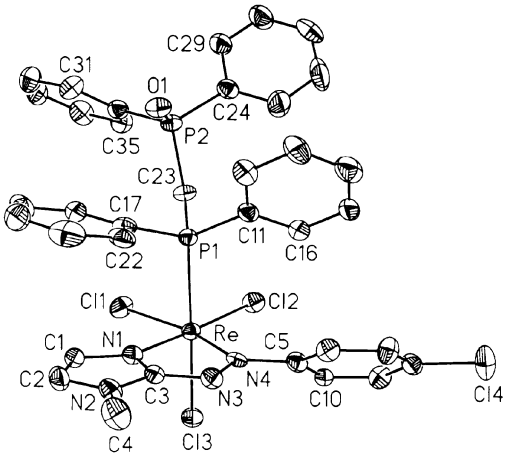

Fig. 2 Perspective view of *fac*-[Re^{III}L(P1PO)Cl_3] **3**. Selected bond distances (Å) and angles (°): Re–N(1) 2.050(8), Re–N(4) 2.055(8), Re–Cl(2) 2.351(3), Re–Cl(1) 2.372(3), Re–Cl(3) 2.401(3), Re–P(1) 2.476(3); N(1)–Re–Cl(2) 176.7(2), N(4)–Re–Cl(1) 162.9(2), Cl(3)–Re–P(1) 174.9(1).

The reaction follows§ the rate law of eqn. (3). Variable temperature rate constants (10^3 *k*/min^{-1}: 308 K, 5.30; 313 K, 7.78; 318 K, 10.06; 323 K, 12.75) correspond to the activation parameters $\Delta H^{\ddagger}$ 12.3 kcal mol^{-1} and $\Delta S^{\ddagger}$ −38.2 cal K^{-1} mol^{-1}. The reaction is thus intramolecular and strongly associative in nature.

$$\mathbf{2a} \xrightarrow{k} \mathbf{3} : \text{rate} = k[\mathbf{2a}] \quad (3)$$

Oxygen atom transfer to the pendent phosphine function of **2** occurs† upon reacting it with an excess of **1** [eqn. (4) and (5)]. While **2a** furnishes **4** (Fig. 3),‡ **2b** yields insoluble **5** in which both the phosphine oxide functions are coordinated, the metal atoms presumably having *mer* geometry.[5]

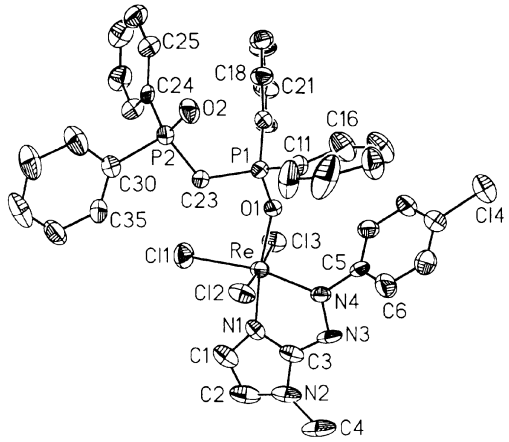

Fig. 3 Perspective view of *mer*-[Re^{III}L(OP1PO)Cl_3] **4**. Selected bond distances (Å) and angles (°): Re–N(4) 1.985(10), Re–N(1) 1.993(11), Re–O(1) 2.033(7), Re–Cl(3) 2.356(4), Re–Cl(2) 2.370(4), Re–Cl(1) 2.377(4), P(1)–O(1) 1.523(8), P(2)–O(2) 1.459(8); N(1)–Re–O(1) 172.7(4), Cl(3)–Re–Cl(2) 174.4(1), N(4)–Re–Cl(1) 168.0(3), P(1)–O(1)–Re 147.5(5).

DOI: 10.1039/b004565i

$$\text{Re–OP1P} + \text{Re}\equiv\text{O} \rightarrow \text{Re–OP1PO} \quad (4)$$

$$\text{Re–OP2P} + \text{Re}\equiv\text{O} \rightarrow \text{Re–OP2PO–Re} \quad (5)$$

The remarkable double isomerization of **2a** can be rationalized. **2a** did not afford single crystals but the structure of **4** provides a credible geometrical model in which the pendent P(1)C(23)P(2) fragment is positioned near the Cl(1)Cl(2)O(1) face. A simple rotation around the P(1)–C(23) bond brings the P(2) atom to within 2.6 Å of the face as in **6** which is a plausible

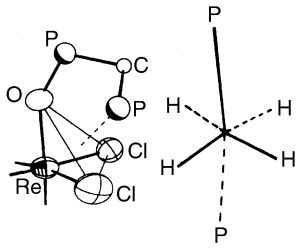

6 **7**

model for the associative transition state of the reaction. The attack by P(2) can progress *via* edge displacement[6] of a chloride ligand with concomitant Re–OP(1) bond cleavage leading to **3**, [eqn. (6)]. The *fac* geometry of **3** is sustained by concerted

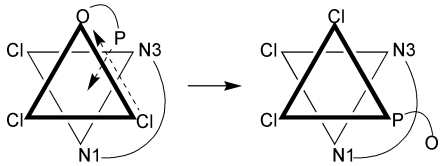

2a **3** (6)

Re–L and Re–P back-bonding as in *fac*-[ReL(PPh$_3$)Cl$_3$].[3] In **2b** the PCH_2CH_2P fragment has the *anti* conformation **7**. The potentially reactive *gauche* conformation is not accessible due to the bulk of PPh_2, and accordingly **2b** fails to isomerize.

The conformation **7** is, however, ideally suited for sustaining binucleation as in **5**.[5] On the other hand only the dangling phosphine oxide function is preserved in **4** as a vestige of transient binucleation. The environment of the O(2) atom in **4** is crowded [O(2)···P(1) 3.57 Å, O(2)···C(11) 3.55 Å] and model building has confirmed that the $n = 1$ analog of **5** is not sterically viable.

In summary, there is a strong chemical differentiation between the $n = 1$ and 2 products formed in both one-atom (**2a**, **2b**) and two-atom (**4**, **5**) transfer from **1** to P*n*P. The applicability of the observed structural and dynamical features to other systems is under scrutiny.

We thank the Indian National Science Academy, the Department of Science and Technology and the Council of Scientific and Industrial Research for financial support. Affiliation with the Jawaharlal Nehru Centre for Advanced Scientific Research, Bangalore, India, is acknowledged.

Notes and references

† **2a** was prepared from P1P (0.6 mmol) and **1** (0.2 mmol) in CH_2Cl_2 solution followed by rapid solvent removal, washing with hexane and drying; **2b** was similarly prepared; **3** was made by leaving **2a** in C_6H_6 for 8 h and **4** was prepared from **2a** (0.1 mmol) and **1** (0.2 mmol) in C_6H_6; for each, purification was carried out by chromatography on a silica gel column using C_6H_6–MeCN mixtures as eluents. Reaction of **2b** (0.1 mmol) and **1** (0.1 mmol) in C_6H_6 afforded insoluble **5**. The yields in all cases were in the range 75–85% and satisfactory elemental analyses were obtained for all. *Selected spectral data*: UV–VIS (C_6H_6): λ_{max}/nm (ε/dm^3 mol^{-1} cm^{-1}): **2a**, 660(610), 454(5680), 355(7570); **2b**, 658(450), 460(3550), 348(4970); **3**, 660(840), 468(5530), 362(9510); **4**, 655(510), 450(5230), 358(6910). IR (KBr, cm^{-1}): **2a**, 300, 310 (Re–Cl), 1120 (O–P), 1330 (N=N); **2b**, 310, 320 (Re–Cl), 1120 (O–P), 1330 (N=N); **3**, 310, 320 (Re–Cl), 1190 (P–O), 1325 (N=N); **4**, 310, 320 (Re–Cl), 1120 (O–P), 1200 (P–O), 1335 (N=N); **5**, 300, 320 (Re–Cl), 1120 (O–P), 1335 (N=N).

‡ *Crystal data* for **2b**·1.5C_6H_6: $C_{45}H_{42}Cl_4N_4OP_2Re$, M = 1044.77, triclinic, space group $P\bar{1}$, a = 11.957(4), b = 12.383(3), c = 17.046(6) Å, α = 88.36(2), β = 74.21(2), γ = 84.10(2)°, U = 2415.8(12) Å^3, Z = 2, T = 293 K, μ(Mo-Kα) = 2.84 mm^{-1}, 7237 reflections measured, 7109 unique, 5904 observed [$I > 2\sigma(I)$], $R1$ = 0.0467, $wR2$ = 0.1273; **3**·1.5C_6H_6: $C_{44}H_{40}Cl_4N_4OP_2Re$, M = 1030.74, triclinic, space group $P\bar{1}$, a = 10.110(6), b = 10.668(5), c = 20.760(7) Å, α = 89.47(3), β = 80.08(4), γ = 81.41(4)°, U = 2181(2) Å^3, Z = 2, T = 293 K, μ(Mo-Kα) = 3.143 mm^{-1}, 6515 reflections measured, 6424 unique, 5198 observed [$I > 2\sigma(I)$], $R1$ = 0.0542, $wR2$ = 0.1279; **4**: $C_{35}H_{31}Cl_4N_4O_2P_2Re$, M = 929.58, monoclinic, space group $C2/c$, a = 35.353(11), b = 12.730(6), c = 16.840(7) Å, β = 104.68(3)°, U = 7332(5) Å^3, Z = 8, T = 293 K, μ(Mo-Kα) = 3.73 mm^{-1}, 5705 reflections measured, 5422 unique, 3386 observed [$I > 2\sigma(I)$], $R1$ = 0.0585, $wR2$ = 0.1060. CCDC 182/1746. See http://www.rsc.org/suppdata/cc/b0/b004565i/ for crystallographic files in .cif format.

§ UV–VIS spectra of thermostatted isomerizing benzene solutions of **2a** displayed well defined isosbestic points at 482, 422 and 307 nm. The rate was followed at 360 nm. The first order rate constants were obtained from the slope of linear plot of $-\ln(A_\infty - A_t)$ *vs.* time t where A_t is the absorbance at time t and A_∞ is the absorbance at the completion of reaction (after 24 h).

1 S. Banerjee, S. Bhattacharyya, B. K. Dirghangi, M. Menon and A. Chakravorty, *Inorg. Chem.*, 2000, **39**, 6; B. K. Dirghangi, M. Menon, A. Pramanik and A. Chakravorty, *Inorg. Chem.*, 1997, **36**, 1095; S. B. Seymore and S. N. Brown, *Inorg. Chem.*, 2000, **39**, 325; R. R. Conry and J. M. Mayer, *Inorg. Chem.*, 1990, **29**, 4862; R. Rossi, A. Duatti, L. Magon, V. Casellato, R. Graziani and L. Toniolo, *J. Chem. Soc., Dalton Trans.*, 1982, 1949; J. F. Rowbottom and G. Wilkinson, *J. Chem. Soc., Dalton Trans.*, 1972, 826.

2 J. R. Dilworth, D. V. Griffiths, S. J. Parrott and Y. Zheng, *J. Chem. Soc., Dalton Trans.*, 1997, 2931; X. L. R. Fontaine, E. H. Fowles, T. P. Layzell, B. L. Shaw and M. Thornton-Pett, *J. Chem. Soc., Dalton Trans.*, 1991, 1519; X.-L. Luo and R. H. Crabtree, *J. Am. Chem. Soc.*, 1990, **112**, 4813.

3 I. Chakraborty, S. Bhattacharyya, S. Banerjee, B. K. Dirghangi and A. Chakravorty, *J. Chem. Soc., Dalton Trans.*, 1999, 3744.

4 The n = 1–3 cases have been examined but only n = 1, 2 are reported here as n = 2, 3 constitute a similar pair.

5 The similarly prepared binuclear complex [Cl_3L′Re(OP2PO)ReL′Cl_3], where L′ is the Schiff base of pyridine-2-carbaldehyde and *p*-toluidine has been structurally characterized. It is centrosymmetric with the PCH_2CH_2P fragment having *anti* and the metals having *mer* geometry. S. Bhattacharyya, I. Chakraborty, B. K. Dirghangi and A. Chakravorty, unpublished work.

6 N. Serpone and D. G. Bickley, *Prog. Inorg. Chem.*, 1972, **17**, 391.

The first D–π–A octupolar cryptand molecule to exhibit bulk non-linearity

Pritam Mukhopadhyay,[a] Parimal K. Bharadwaj,*[a] G. Savitha,[a] Anu Krishnan[b] and Puspendu K. Das*[b]

[a] *Department of Chemistry, Indian Institute of Technology, Kanpur, 208016, India. E-mail: pkb@iitk.ac.in*
[b] *Department of Inorganic and Physical Chemistry, Indian Institute of Science, Bangalore, 560012, India*

Received (in Cambridge, UK) 12th June 2000, Accepted 8th August 2000

The cryptand derivative has H-bond mediated trigonal network structure that leads to octupolar bulk nonlinearity

Optically nonlinear organic materials are of paramount importance for applications in optical signal processing and telecommunications.[1] We present here a new strategy for obtaining molecules with bulk optical nonlinearity by derivatizing a cryptand with three D–π–A units related by a 3-fold rotational symmetry. Thus, compound **1** (Scheme 1) is engineered with the ultimate aim of a trigonal network necessary for bulk octupolar nonlinearity. The classical molecular requirements for second-order nonlinear optical (NLO) effects have led to the development of strongly conjugated materials asymmetrized by interacting donor and acceptor groups.[2] Even though these molecules exhibit large hyperpolarizabilty, major drawbacks arise due to their anisotropic dipolar character, *e.g.* a high tendency towards unfavorable aggregation, difficult non-centrosymmetric crystallization, and small off-diagonal tensor components. To alleviate such problems, isotropic molecules with attached octupolar nonlinearities have been proposed, on the basis of group-theoretical and quantum-mechanical calculations.[3] Solution-phase studies by Hyper-Rayleigh Scattering (HRS) technique on crystal violet and tris(4-methoxyphenyl)cyclopropenylium bromide as octupoles have been reported.[4] However, assembly of octupolar molecules into an acentric bulk presents an arduous task. To-date, only 2,4,6-triamino-1,3,5-trinitrobenzene (TATB) (3 × urea),[5] substituted triazenes (0.1 × urea)[6] and cyclohexane-1,3,5-triamide derivative (0.06 × urea),[7] are the only octupolar organic materials reported to exhibit bulk NLO properties.

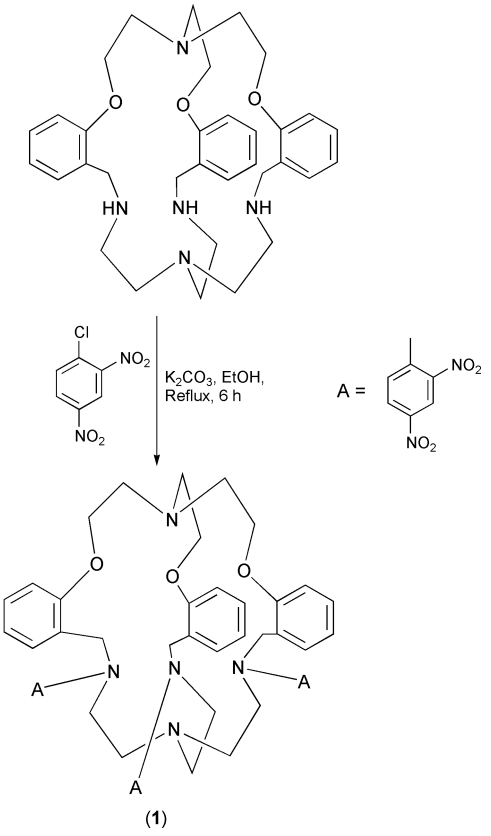

(1)

Scheme 1 Synthetic scheme for compound **1**.

No cryptand-based octupolar molecule having bulk NLO properties has been reported in the literature although cryptands are an important class of molecules having a 3-D cavity with proven recognition properties through supramolecular interactions.[8] Our principal motivation to use the cryptand as a central core stems from the following three assets: (i) a 3-fold rotational symmetry passing through the two bridgehead nitrogen atoms of the cryptand molecule, (ii) three phenyl rings as rigid segments would favor ordered structures and (iii) three easily functionalizable secondary nitrogen atoms would assist in grafting acceptor molecules of choice. We have chosen 2,4-dinitrobenzene as it has been shown to have adequate electronic asymmetry in methyl 2-(2,4-dinitroanilino)propanoate (MAP).[9] Besides, the nitro substitution at the *ortho* position would provide a more rounded-off shape to the molecules (Scheme 1), which would ease their packing in the crystal lattice.

Compound **1** was synthesized (Scheme 1) by refluxing the cryptand[10] with 3 equiv. of 2,4-dinitrochlorobenzene and anhydrous K_2CO_3 for 6 h in dry EtOH under N_2. The yellow–orange tri-substituted product was isolated in 92% yield.

Single crystals suitable for X-ray diffraction were grown by slow evaporation from pyridine solution. The compound afforded very large triangular crystals (~ 5 mm each side) in just two days. It crystallizes† in the desired non-centrosymmetric trigonal space group *P*3, containing three strands in the asymmetric unit. The C_3 symmetry generates the donor–acceptor substituted cryptand molecules **A**, **B** and **C** with the symmetry axis passing through the bridgehead nitrogens which also coincides with the triad axes of the lattice. Supramolecular assembly of these C_3 symmetric cryptand molecules generates an octupolar trigonal network. The molecules **A**, **B** and **C** vary considerably in their conformation. Three different forms of intramolecular forces are operational in the D–π–A substituted cryptand molecule: (i) aromatic π-stacking between the phenyl ring of one strand with the dinitro-substituted ring of the symmetry related strand in an edge-to-face fashion with a distance of 3.923 Å, (ii) CH···π interaction within the same strand of the molecule with a distance of 3.355 Å, and (iii) CH···O hydrogen bonding between the carbon atom of the benzylic amino group and the oxygen atom of the *ortho*-nitro group with a distance of 2.92 Å (Fig. 1).

The intermolecular interactions leading to the trigonal network structure involve each phenyl ring of the cryptand **B** stacked face-to-face[11] (3.328 Å) with a dinitrobenzene moiety of cryptand **C** while at the same time interacting with a phenyl ring of cryptand **C** in edge-to-face (3.585 Å) manner (Fig. 2). The intermolecular interactions also involve anti-parallel stacking of the dinitro-substituted rings of neighboring cryptands at a distance that ranges between 4.425–4.665 Å and that attenuates the bulk non-linear efficiency of **1** to some extent.

We performed Kurtz powder second-harmonic generation (SHG) measurements[12] on compound **1**. The non-centrosymmetric nature was confirmed by a visible SHG powder signal at

DOI: 10.1039/b004679p

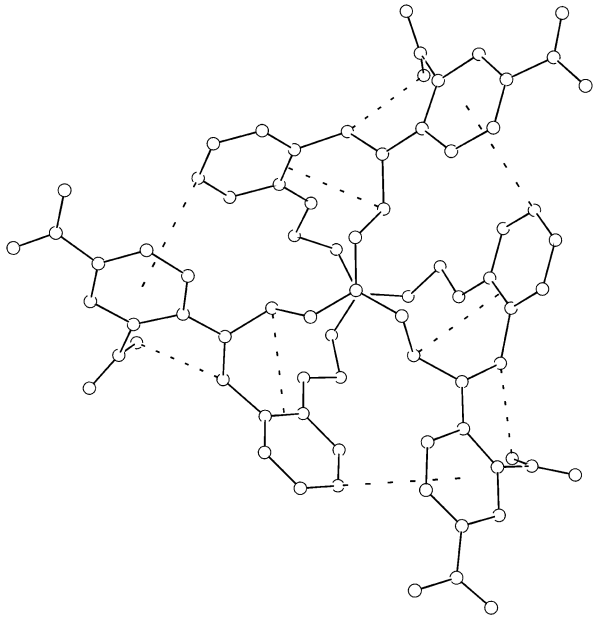

Fig. 1 A perspective view of one cryptand molecule showing the intramolecular H-bonding interactions.

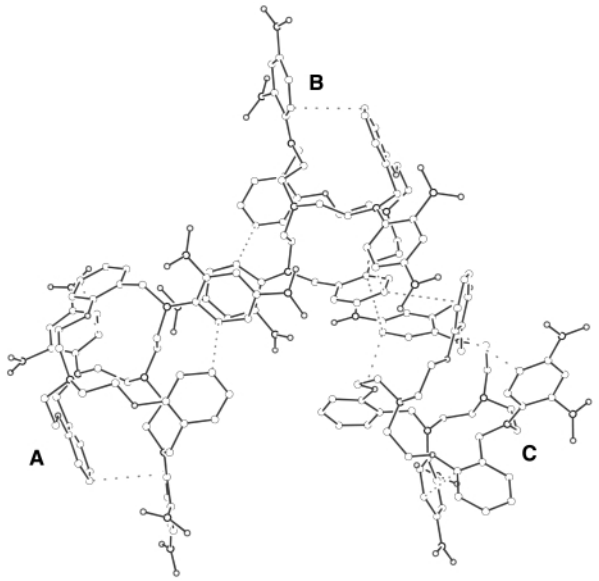

Fig. 2 A perspective view of **A**, **B** and **C** cryptand molecules showing both intra- and intermolecular H-bonding interactions.

1.064 μm of the order of 0.6 × urea and represents the first cryptand-based NLO-active bulk molecule. The non-linear $\sqrt{<\beta^2>}$ coefficient of **1** was determined by HRS technique[13] at 1.064 μm in $CHCl_3$ and gave a value of 16×10^{-30} esu. The corresponding $\sqrt{<\beta^2>}(0)$ static value was found to be 11×10^{-30} esu, which is comparable[6] to that of the classical dipolar PNA molecule under the same measurement conditions. Although powder efficiency of compound **1** is modest, it has a good transparency at the visible region of the spectrum (λ_{max} ~ 370 nm in $CHCl_3$). Most strikingly, compound **1** by virtue of its strong intermolecular interactions has a mp of 215 °C, which is the highest among all of the nitroaniline-based compounds reported[14] to have bulk NLO properties. This will make it potentially useful for further device applications. Furthermore, this work presents ample scope for modulating the NLO property through recognition of different metal ions in the cavity of the cryptand as well as by functionalizing the three amino groups with stronger acceptor units.

This work was supported by the Department of Science and Technology, New Delhi, India (Grant No. SP/S1/F-08/96 to P. K. B.).

Notes and references

† *Crystal data for* **1**: $C_{51}H_{51}N_{11}O_{15}$, M = 1137.133, trigonal, space group $P3$, a = 16.63(5), b = 16.62(9), c = 16.01(3) Å, V = 3829(9) Å^3, Z = 3, T = 293 K, λ = 0.71073 Å, μ = 0.11 mm^{-1}, 3753 independent reflections, R = 0.045, wR_2 = 0.103. Satisfactory elemental analyses (C, H, N) were obtained for **1**.

CCDC 182/1747. See http://www.rsc.org/suppdata/cc/b0/b004679p/ for crystallographic files in .cif format.

1 J. Zyss, *Molecular Nonlinear Optics: Materials, Physics and Devices*, Academic Press, New York, 1993.
2 M. Barzoukas, M. Blanchard-Desce, D. Josse, J.-M. Lehn and J. Zyss, *Chem. Phys.*, 1989, **133**, 323.
3 J. Zyss, *Nonlinear Opt.*, 1991, **1**, 3; J. Zyss and I. Ledoux, *Chem. Rev.*, 1994, **94**, 77.
4 T. Verbiest, K. Clays, C. Samyn, J. Wolff, D. Reinhoudt and A. Persoons, *J. Am. Chem. Soc.*, 1994, **116**, 9320.
5 I. Ledoux, J. Zyss, J. S. Siegel, J. Brienne and J.-M. Lehn, *Chem. Phys. Lett.*, 1990 **172**, 440.
6 V. R. Thalladi, S. Brasselet, H.-C. Weiss, D. Blaser, A. K. Katz, H. L. Carrell, R. Boese, J. Zyss, A. Nangia and G. R. Desiraju, *J. Am. Chem. Soc.*, 1998, **120**, 2563; V. R. Thalladi, R. Boese, S. Brasselet, I. Ledoux, J. Zyss, R. K. R. Jetti and G. R. Desiraju, *Chem. Commun.*, 1999, 1639.
7 E. Fan, J. Yang, S. J. Geib, T. C. Stoner, M. D. Hopkins and A. D. Hamilton, *J. Chem. Soc., Chem. Commun.*, 1995, 1251.
8 J.–M. Lehn, *Supramolecular Chemistry—Concepts and Perspectives*, VCH, Weinheim, 1995.
9 J. L. Oudar and R. Hierle, *J. Appl. Phys.*, 1997, **48**, 2699.
10 P. Ghosh, P. K. Bharadwaj, J. Ray and S. Ghosh, *J. Am. Chem. Soc.*, 1997, **119**, 11 903.
11 C. A. Hunter, *Chem. Soc. Rev.*, 1994, **23**,101.
12 S. K. Kurtz, *J. Appl. Phys.*, 1968, **39**, 3798.
13 K. Clays and A. Persoons, *Phys. Rev. Lett.*, 1991, **66**, 2980.
14 J. Zyss, *Molecular Nonlinear Optics: Materials, Physics and Devices*, Academic Press, New York, 1993, p. 210.

Hydrothermal synthesis and crystal structures of two bimetallic chain-like and cluster complexes $[\{Co(phen)_2\}_2V_6O_{17}]_n$ and $[\{Cu(phen)_2\}_4V_{10}O_{29}]\cdot 6H_2O$†

Xian-Ming Zhang, Ming-Liang Tong and Xiao-Ming Chen*‡

State Key Laboratory of Ultrafast Laser Spectroscopy and School of Chemistry & Chemical Engineering, Zhongshan University, Guangzhou, 510275, P.R. China

Received (in Cambridge, UK) 20th July 2000, Accepted 15th August 2000

Two complexes, $[\{Co(phen)_2\}_2V_6O_{17}]_n$ 1 and $[\{Cu(phen)_2\}_4V_{10}O_{29}]\cdot 6H_2O$ 2, have been hydrothermally synthesized; X-ray crystallography shows that 1 consists of one-dimensional stepped chains built up from covalently linked $\{V_6O_{17}\}_n^{4n-}$ chains and $[Co(phen)_2]^{2+}$ fragments while 2 is composed of a discrete $V_{10}O_{29}^{8-}$ cluster covalently attached to four $[Cu(phen)_2]^{2+}$ fragments.

There has been extensive interest in organic–inorganic hybrid vanadium oxides and polyvanadate clusters owing to their structural diversity and potential application in catalysis and material science.[1–5] An important advance in organic–inorganic vanadium oxides has recently been the study of solid state coordination chemistry, which is characterized by transition metal complexes or fragments covalently bonded to metal oxide framework or polyanion clusters. A variety of vanadium solid state complexes including discrete clusters, infinite chains and layer structures have been prepared by hydrothermal methods.[6–12] However, in terms of discrete organic–inorganic bimetallic clusters formulated as $[(ZnL_2)V_4O_{12}]$ [L = 2,2′-bipyridine (bpy) or 1,10-phenanthroline (phen)],[6] the vanadium clusters are limited to $V_4O_{12}^{4-}$, and in the metavanadate chain-like compounds formulated as $[(CuL_m)V_2O_6]_n$ (L = NH_3, ethylenediamine, bpy, diethylenetriamine; m = 1, 2) the vanadium oxide chains are limited to $\{V_2O_6\}_n^{2n-}$.[7–9] Herein, we report two interesting solid state vanadium(v) complexes $[\{Co(phen)_2\}_2V_6O_{17}]_n$ **1** and $[\{Cu(phen)_2\}_4V_{10}O_{29}]\cdot 6H_2O$ **2**, where the tetranuclear $V_4O_{12}^{4-}$ and dinuclear $V_2O_7^{4-}$ building units are unprecedentedly linked together by sharing oxygen atoms.

Complex **1** was synthesised as brown blocks in 80% yield based on vanadium by a hydrothermal method. A mixture of V_2O_5, $Co(OAc)_2\cdot 4H_2O$, phen and water in a molar ratio of 1:1:2:1100 was stirred for 20 min in air, before being transferred and sealed in a 23 cm^3 Teflon-lined reactor, which was heated to 140 °C and held at this temperature for 72 h. Complex **2** was synthesised as blue blocks in 40% yield under similar conditions to **1** using $Cu(OAc)_2\cdot 2H_2O$ in place of $Co(OAc)_2\cdot 4H_2O$. Both **1** and **2** are insoluble in water and common organic solvents. The IR spectra§ of **1** and **2** exhibit characteristic bands for both V=O and phen. Thermogravimetric analysis shows a weight loss of *ca*. 50% for **1** in the range 300–550 °C corresponding to the loss of phen. A weight loss of *ca*. 4% for **2** in the range 120–150 °C corresponds to removal of the lattice water molecules while a further weight loss of *ca*. 51% occurs in the range 300–550 °C consistent with the loss of phen.

The crystal structure of **1**¶ shows the presence of an unprecedented one-dimensional stepped chain constructed from $\{V_6O_{17}\}_n^{4n-}$ chains with $[Co(phen)_2]^{2+}$ fragments covalently attached *via* oxygen atoms, as shown in Fig. 1. The anionic chain in **1** is composed of alternate tetranuclear $V_4O_{12}^{4-}$ and dinuclear $V_2O_7^{4-}$ building units, which are linked by sharing oxygen atoms. All vanadium sites show VO_4 tetrahedral geometry, each of which has a terminal vanadyl (V=O) group and shares three corners with CoN_4O_2 octahedra and/or VO_4 tetrahedra. There are three crystallographically independent vanadium atoms in the anionic chain; V(1) and V(2) share oxygen atoms with one CoN_4O_2 octahedron and two VO_4 tetrahedra while V(3) only shares oxygen atoms with three VO_4 tetrahedra. The Co(II) atom, which is in a slightly distorted octahedral geometry, is ligated by two phen ligands, with the $[Co(phen)_2]^{2+}$ fragments further covalently bonded to the anionic chain through atoms O(1) and O(2) and their symmetry equivalents. Such a linking gives rise to three eight-membered rings, CoV_3O_4, V_4O_4 and CoV_3O_4, in chair-like configuration similar to that found in $[Cu(phen)MoO_4]$.[5] Although the empirical formula of **1** is similar to that of $[\{Zn(bpy)_2\}_2V_6O_{17}]$,[6] its architecture is different from the latter in which each VO_4 tetrahedron shares three corners with adjacent VO_4 tetrahedra forming layers rather than chains.

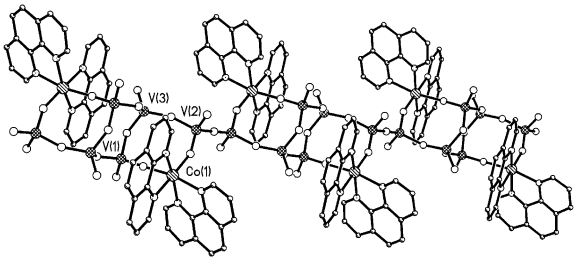

Fig. 1 Perspective view of the stepped chain of **1**.

The structure of **2** features a discrete tetradecanuclear heterometallic cluster built up from $V_{10}O_{29}^{8-}$ clusters and four $[Cu(phen)_2]^{2+}$ fragments (Fig. 2). The Cu(II) atoms, which are in a distorted square-pyramidal geometry, are attached to the vanadium cluster *via* O(6) and O(11) and their symmetry equivalents. In contrast to **1**, while the anionic vanadium cluster

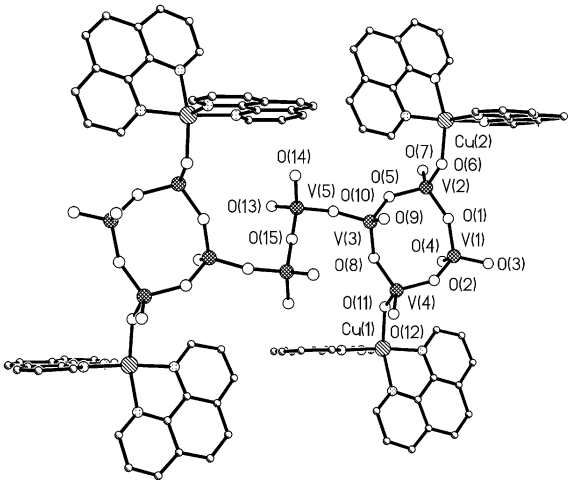

Fig. 2 Perspective view of the molecular structure of **2**.

† Electronic supplementary information (ESI) available: Fig. 1S–3S; three-dimensional supramolecular arrays for **1** and **2**. See http://www.rsc.org/suppdata/cc/b0/b005880g/

‡ Correspondence should be directed to School of Chemistry & Chemical Engineering. E-mail: cescxm@zsu.edu.cn

also consists of corner-sharing VO_4 tetrahedra, all VO_4 tetrahedra in **2** have one [V(2)–V(4)] or two [V(1) and V(5)] terminal oxygen atom(s). The $V(1)O_4$ tetrahedron has two terminal oxygen atoms, which may be directly responsible for the formation of the cluster rather than a chain. Similarly to the anion in **1**, the $V_{10}O_{29}^{8-}$ cluster consists of a dinuclear $V_2O_7^{4-}$ and two tetranuclear $V_4O_{12}^{4-}$ fragments linked by sharing oxygen atoms. Although the $V_{10}O_{28}^{6-}$ cluster is common in solution and a chiral $V_{10}O_{22}$ cluster[13] has recently been synthesised, the $V_{10}O_{29}^{8-}$ cluster found in **2** has not been reported before. In addition, the coordination mode of V_4O_{12} fragments in both **1** and **2** is unprecedented, in contrast to all documented and proposed coordination modes of the $V_4O_{12}^{4-}$ cluster, in which each heterometallic atom is attached to two or four oxygen atoms of the $V_4O_{12}^{4-}$ cluster.[6]

It is of note that π–π stacking interaction between interchain or intermolecular phen groups plays a significant role in stabilisation of the structures of **1** and **2**. Adjacent phen groups in **1** or **2** are generally parallel and separated by 3.1–3.5 Å, which indicates strong π–π stacking interactions.[14] Therefore, the heterometallic stepped chains of **1** and discrete tetradecanuclear heterometallic clusters of **2** are further extended into interesting three-dimensional supramolecular arrays *via* π–π stacking interactions of phen groups (see Fig. 1S, 2S and 3S in ESI†). It should also be noted that while **1** and **2** were prepared under the same conditions, their structures differ significantly. This may originate from the nature of heterometallic atoms employed. Co(II) tends to adopt octahedral geometry whereas Cu(II) favours a square-planar or square-pyramidal geometry owing to the strong Jahn–Teller effect. Meanwhile, the steric effect of phen appears to play an important role in the formation of the unique structures of **1** and **2**. The large steric hindrance of phen prevents the formation of heterometallic layered structures.

This work was supported by the National Natural Science Foundation of China (No. 29971033, 29625102).

Notes and references

§ Anal. Calc. for $C_{48}H_{32}N_8O_{17}V_6Co_2$ **1**: C, 40.70; H, 2.28; N, 7.91%. Found: C, 40.58; H, 2.32; N, 7.96. Calc. for $C_{96}H_{76}N_{16}O_{35}V_{10}Cu_4$ **2**: C, 41.52; H, 2.76; N, 8.07. Found: C, 41.38; H, 2.64; N, 8.02%. IR (KBr, cm^{-1}) for **1**: 3356m, 3058w, 1931w, 1607m, 1582m, 1513m, 1421s, 1141m, 1103w, 968s, 891s, 834s, 664s; for **2**: 3431m, 3046w, 1980w, 1607w, 1581m, 1517m, 1427s, 1143m, 968s, 941s, 913m, 787s, 624s.

¶ *Crystal data*: for **1**: triclinic, space group $P\bar{1}$, M_r = 1416.32, a = 10.216(7), b = 11.732(6), c = 11.788(7) Å, α = 82.76(1), β = 72.70(1), γ = 75.57(1)°, V = 1264(1) Å^3, Z = 1, D_c = 1.860 g cm^{-3}. Data collection was performed at 293 K on a Siemens R3m diffractometer (Mo-Kα, λ = 0.71073 Å). Lorentz-polarization and absorption corrections were applied. The structures were solved with direct methods (SHELXS-97) and refined by full-matrix least-squares (SHELXL-97), giving a final R_1 value of 0.0671 for 368 parameters and 3279 unique reflections with $I \geqslant 2\sigma(I)$ and wR_2 of 0.1916 for all 4973 reflections.

For **2**: monoclinic, space group $P2_1/n$, M_r = 2777.29, a = 14.726(3), b = 14.612(3), c = 25.310(5) Å, β = 105.81(3)°, V = 5240(2) Å^3, Z = 2, D_c = 1.760 g cm^{-3} Data collection was performed at 293 K on a Bruker CCD diffractometer (Mo-Kα, λ = 0.71073 Å), giving a final R value of 0.0522 for 755 parameters and 8042 unique reflections with $I \geqslant 2\sigma(I)$ and wR_2 of 0.1547 for all 15179 reflections. All other conditions were the same as for **1**. CCDC 182/1745. See http://www.rsc.org/suppdata/cc/b0/b005880g/ for crystallographic files in .cif format.

1 T. Chirayil, P. Y. Zavalij and M. S. Whittingham, *Chem. Mater.*, 1998, **10**, 2629.
2 Louis C. W. Baker and D. C. Glick, *Chem. Rev.*, 1998, **98**, 3; P. Gouzerh and A. Proust, *Chem. Rev.*, 1998, **98**, 77.
3 G. Centi, F. Trifiro, J. R. Ebner and V. M. Franchetti, *Chem. Rev.*, 1988, **88**, 55.
4 J. M. Tarascon, E. Wang, F. K. Shokoohi, W. R. McKinnon and S. Colson, *J. Electrochem. Soc.*, 1991, **138**, 2859.
5 P. J. Hagrman, D. Hagrman and J. Zubieta, *Angew. Chem., Int. Ed.*, 1999, **38**, 2638; A. K. Cheetham, G. Férey and T. Loiseau, *Angew. Chem., Int. Ed.*, 1999, **38**, 3268.
6 Y. Zhang, P. J. Zapf, L. M. Meyer, R. C. Haushalter and J. Zubieta, *Inorg. Chem.*, 1997, **36**, 2159.
7 S. Aschwanden, H. W. Schmalle, A. Reller and H. R. Oswald, *Mater. Res. Bull.*, 1993, **28**, 45.
8 J. R. D. DeBord, Y. Zhang, R. C. Aushalter, J. Zubieta and C. J. O'Connor, *J. Solid State Chem.*, 1996, **122**, 251.
9 L.-M. Zheng, J.-S. Zhao, K.-H. Lii, L.-Y. Zhang, Y. Liu and X.-Q. Xin, *J. Chem. Soc., Dalton Trans.*, 1999, 939.
10 Y. Zhang, J. R. D. DeBord, C. J. O'Connor, R. C. Haushalter, A. Clearfield and J. Zubieta, *Angew. Chem., Int. Ed. Engl.*, 1996, **35**, 989.
11 L.-R. Zhang, Z. Shi, G.-Y. Yang, X.-M. Chen and S.-H. Feng, *J. Chem. Soc., Dalton Trans.*, 2000, 275.
12 Z. Shi, L.-R. Zhang, G.-S. Zhu, G.-Y. Yang, J. Hua, H. Ding and S.-H. Feng, *Chem. Mater.*, 1999, **11**, 3565.
13 K. Oyaizu and E. Tsuchida, *J. Am. Chem. Soc.*, 1998, **120**, 237.
14 S. B. Ferguson, E. M. Sanford, E. M. Seward and F. Diederich, *J. Am. Chem. Soc.*, 1991, **113**, 5410.

ChemComm

Selective oxygen capture in lithium zincate chemistry: the syntheses and solid-state structures of (μ-O)Zn_4[N(2-C_5H_4N)Bz]$_6$ and Bu^t(μ$_3$-O)Li_3(μ$_6$-O)Zn_3[N(2-C_5H_4N)Me]$_6$ (Bz = benzyl)

Robert P. Davies, David J. Linton, Ronald Snaith† and Andrew E. H. Wheatley*

Department of Chemistry, University of Cambridge, Lensfield Road, Cambridge, UK CB2 1EW. E-mail: aehw2@cam.ac.uk

Received (in Cambridge) 29th June 2000, Accepted 17th August 2000

Sequential reaction of $ZnMe_2$ with the (2-pyridyl)amines HN(2-C_5H_4N)R (R = Bz = benzyl 1, Me 2), Bu^tLi and oxygen affords species which demonstrate oxo-encapsulation {(μ$_4$-O)Zn_4[N(2-C_5H_4N)Bz]$_6$ 3}, and both encapsulation and insertion into a C–Li bond {Bu^t(μ$_3$-O)Li_3(μ$_6$-O)Zn_3[N(2-C_5H_4N)Me]$_6$ 4}; in the solid-state 4 has a new type of *fac*-isomeric (μ$_6$-O)$M_3M'_3$ octahedral core.

Current interest in the properties of lithium containing heterobimetallic species derives from their ability to effect organic transformations whose selectivity differs from those afforded by homometallic organolithium compounds. Hence, whereas organolithium reagents perform 1,2-addition across α,β-unsaturated ketones,[1] it has been reported lately that in the presence of group 13 Lewis acids 1,4-addition is preferred,[2] with the formation of a lithium aluminate recently being implicated in this process.[3] Also of use in such conjugate additions,[4] lithium organozincates find extensive employment in synthetic chemistry.[5] In spite of this utility, lithium zincate structural chemistry is not well understood, and of the few known structures two classes dominate. Ion-separated species are favoured by the presence of strongly coordinating Lewis bases[6] whereas in their absence ion-associated [Li(μ$_2$-C)$_2$]$_n$Zn (n = 1, 2)[7] motifs prevail. In the light of advances in the controlled oxygenation of heterobimetallic compounds[8] we report here on the incorporation of oxygen by mixed Li–Zn systems and detail the variable reactivity towards oxygen of the products afforded by sequentially treating (2-pyridyl)amines with organozinc and organolithium reagents (Scheme 1).

The reaction of a non-donor solution of HN(2-C_5H_4N)R (R = Bz = benzyl **1**) with $ZnMe_2$ and Bu^tLi was followed by treatment with air (pre-dried over P_2O_5) until the evolution of fumes subsided. Storage of the resultant solution afforded two crystalline compounds.‡ The characterisation of both species was made possible by their mechanical separation, with ^{1}H NMR spectroscopy verifying that one of these products was Bu^tOLi. The remaining compound was shown by X-ray crystallography§ to be the trigonal pyramidal complex (μ$_4$-O)Zn_4[N(2-C_5H_4N)Bz]$_6$ **3** [Fig. 1(a)] for which formulation there is a toluene molecule in the lattice. Of the two types of Zn centre in this species, three describe the pyramid base [Zn1A···Zn1B 3.130(2) Å] each non-bonding edge of which is spanned by a [N(2-C_5H_4N)Bz]$^-$ ligand [Zn–N(2-C_5H_4N) 2.069(7) Å, Zn–NBz 1.984(7) Å]. The final metal centre (Zn2) occupies the C_{3v} cluster apex and is stabilised by the pyridyl N-centres of the remaining three organic residues [Zn2–N(2-C_5H_4N) 2.045(7) Å], each of which spans one non-bonding Zn1···Zn2 [3.089(2) Å] pyramid edge [Zn1–NBz 2.002(7) Å]. At the core of the C_{3v} cluster is a nearly tetrahedral O^{2-} centre (mean Zn–O 1.903 Å, mean Zn–O–Zn 108.9°). It is noteworthy that previous examples of oxo-encapsulation by Zn_4-tetrahedra have resulted from the deliberate introduction of water[9,10] or

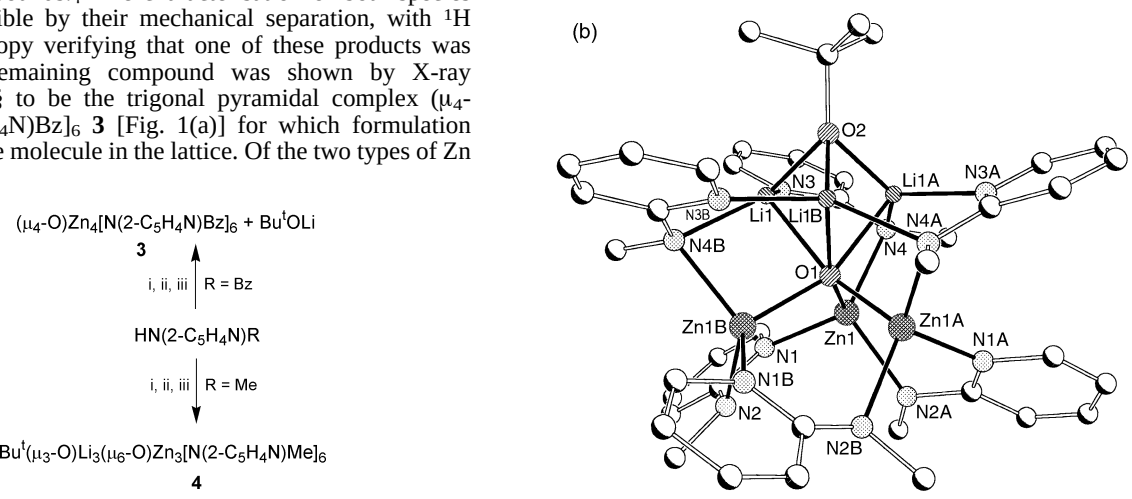

Scheme 1 *Reagents and conditions*: i, $ZnMe_2$; ii, Bu^tLi; iii, O_2.

Fig. 1 (a) Molecular structure of **3**; hydrogen atoms and lattice toluene molecule omitted and only the *ipso*-C of Ph shown. (b) Molecular structure of **4**; hydrogen atoms and lattice thf molecule omitted.

† Deceased.

carbon dioxide[11] whereas **3** is afforded by exposure to oxygen.

Significant structural modification was observed in the product of the analogous reaction for which R was the less sterically demanding Me group (**2**), this process affording **4**.‡ X-Ray crystallography§ reveals **4** to be the unique distorted octahedral oxo-encapuslation complex $Bu^t(\mu_3\text{-}O)Li_3(\mu_6\text{-}O)Zn_3[N(2\text{-}C_5H_4N)Me]_6$ [Fig. 1(b)] for which formulation there is one thf molecule in the lattice. That the Li_3 face is μ_3-capped by an OBu^t group points to an oxygen atom having inserted into a Li–C(Bu^t) bond [Li–O2 1.849(14) Å, Li–O2–Li 83.7(7)°].[12] The three lithium centres are less strongly bonded to the encapsulated μ_6-O centre [Li–O1 2.074(13) Å, Li–O1–Li 73.0(6)°] which in turn interacts with the three Zn centres [Zn–O1 1.944(4) Å, Zn–O1–Zn 101.4(3)°]. The result—a molecular *fac*-isomeric $(\mu_6\text{-}O)M_3M'_3$ octahedron—has not been seen before. Instead, existing examples of molecular μ_6-O heterobimetallic octahedra have either (MM'_5)[13] or $(M_2M'_4)$[14] formulations. The only previous report of a lithium containing heterobimetallic μ_6-O octahedral complex is that of $[RuH(SiHPh_2)(CO)X_2]_2{\cdot}[Li_2Ru_4OCl_8X_4]$ (X = PBu^t_2Me), which has a *trans*-isomeric $(\mu_6\text{-}O)Li_2Ru_4$ core;[15] all other examples of lithium containing μ_6-O octahedra have been homometallic.[16] The coordination spheres of both Li and Zn centres in **4** are completed by $[N(2\text{-}C_5H_4N)Me]^-$ ligands. Three of these residues span the 3.007(2) Å Zn···Zn non-bonding distances in the lower tier of the cluster [Zn–N1 2.038(7) Å, Zn–N2 2.050(7) Å]. The remaining organic residues circumscribe the non-bonding Li_3 [Li···Li 2.47(2) Å] upper tier but are orientated such that their N-pyridyl centres are precisely in the Li_3 plane while their NMe-groups span non-bonding heterobimetallic [Li···Zn 2.75(1) Å] octahedron edges [Zn1–N4 2.065(7) Å]. The sp^2-orbital on their deprotonated N-centres almost bisects the Li–N(Me)–Zn bond angle [N3–C11–N4–M torsional angles = 42.8° (M = Li1A), 45.4° (M = Zn1)] with the consequent mismatch in orientation of the NMe-centred lone-pairs with the Li^+ ions in the upper tier probably being responsible for the respective Li–N(2-C_5H_4N) and Li–NMe bond lengths of 2.071(14) and 2.160(13) Å. This variability in ligand coordination contrasts with the uniformly μ_2- or μ_3-bridging modes adopted by ligand heteroatoms in previously reported μ_6-O molecular heterobimetallic octahedra.[14]

Compounds **3** and **4** both incorporate six-membered MO-M′NCN rings by virtue of $[N(2\text{-}C_5H_4N)R]^-$ coordination [M = M′ = Zn (**3**); both M = M′ = Zn/Li and M = Li, M′ = Zn (**4**)]. Further, both species show almost identical $Zn_3[N(2\text{-}C_5H_4N)R]_3$ basal tiers [Fig. 1(a) and (b)], whilst the remaining three amide ligands exhibit significant variability between **3** and **4**. The orientation which they adopt in **3** results in their pyridyl N-centres bonding only to Zn2 which they render approximately tetrahedral, their deprotonated N-centres bonding only to Zn1. Conversely, in **4** the upper tier ligands are orientated such that the pyridyl N-centres lie in the Li_3 plane with the concomitant stabilisation of adjacent Li centres (by NMe groups) being accompanied by bridging to basal Zn atoms. Thus, **3** and **4** can be viewed as empirically incorporating a $\{(\mu_3\text{-}O)Zn_3[N(2\text{-}C_5H_4N)R]_6\}^{2-}$ ligand which is capable of acting either as a heptadentate donor to a C_{3v} cation [$(Bu^tOLi_3)^{2+}$ in **4**] or as a tetradentate donor to an R_3 cation (Zn^{2+} in **3**) by virtue of flexibility in the orientations demonstrated by the upper tier of $[N(2\text{-}C_5H_4N)R]^-$ ligands.

Attempts to elucidate the structural characteristics of the precursors to **3** and **4** are ongoing, as are studies into the nature of the competition between oxo-insertion (*cf.* the Bu^tO fragment in **4**) and oxo-encapsulation [*cf.* **3** and the $(\mu_6\text{-}O)Li_3Zn_3$ fragment in **4**]. Finally, the integrity of the $\{(\mu_3\text{-}O)Zn_3[(2\text{-}C_5H_4N)NR]_6\}^{2-}$ ligand is being investigated (by attempting to effect substitution reactions, *e.g.* the conversion of **4** to **3** by reaction with $ZnCl_2$).

We thank the UK EPSRC (D. J. L.) for a Studentship and St. Catharine's (R. P. D.) and Gonville & Caius (A. E. H. W.) Colleges for Research Fellowships.

Notes and references

‡ **3**: $ZnMe_2$ (0.5 ml, 1 mmol, 2 M in toluene) was added to a stirred −78 °C solution of 2-(benzylamino)pyridine (0.18 g, 1 mmol) in toluene (5 ml). After 30 min the mixture was warmed to −40 °C and Bu^tLi (0.59 ml, 1 mmol, 1.7 M in pentane) was added. Treatment of the room-temperature mixture with (P_2O_5) dry air (until observable reaction ceased after *ca.* 1 min) was followed by reflux and by storage at ambient temperature for 24 h whereupon needles of Bu^tOLi (by ^1H NMR) and blocks of **3** formed. Mechanical separation allowed the characterisation of **3**. Yield 42% (by **1** consumed), mp 140 °C (decomp.). Found: C, 64.96; H, 5.16; N, 11.34. Calc. for $C_{79}H_{74}N_{12}OZn_4$: C 64.53, H 5.04,N 11.44%. δ_H(500 MHz, CD_3CN), 7.40–6.46 (m, 20H, Ar + *Ph*Me), 4.56 (s, 4H, CH_2), 2.33 (s, 1H, Ph*Me*). **4**: $ZnMe_2$ (0.5 ml, 1 mmol, 2 M in toluene) was added to a stirred −78 °C solution of 2-(methylamino)pyridine (0.11 g, 1 mmol) in hexane (1 ml). After 30 min Bu^tLi (0.59 ml, 1 mmol, 1.7 M in pentane) was added. Treatment of the room-temperature mixture with (P_2O_5) dry air (until observable reaction ceased after *ca.* 1 min) and the addition of thf (0.08 ml) was followed by storage at room temperature for 1 week whereupon blocks of **4** formed. Yield 32% (by **2** consumed), mp >300 °C. Found: C, 50.68; H, 6.48; N, 12.64. Calc. for $C_{44}H_{59}Li_3N_{12}O_3Zn_3$: C, 51.69; H, 6.45; N, 13.45%. δ_H(500 MHz, [$^2H_8$]thf), 8.00–6.01 (m, 24H, Ar), 3.65 (m, 4H, thf), 2.81 (s, 9H, NMe), 2.53 (br m, 9H, NMe), 1.80 (m, 4H, thf), 1.12 (s, 9H, Bu^t).

§ *Crystal data*: for **3**: $C_{79}H_{74}N_{12}OZn_4$; M = 1468.98, cubic, space group $Ia3$, a = 30.8060(7) Å, U = 29235.2(12) Å^3, Z = 16, D_c = 1.335 g cm^{-3}, Mo-Kα (λ = 0.71073 Å), μ = 1.350 mm^{-1}, T = 180(2) K. 8240 reflections (4297 unique, θ < 25.02°, R_{int} = 0.0886), data were collected. Refinement on F^2 values of all data gave $wR2$ = 0.1987, conventional R = 0.0849 on F values of all reflections with $F^2 > 2\sigma(F^2)$, 276 parameters. Residual electron density within ±1.45 e Å^{-3}.

4: $C_{11}H_{14.75}Li_{0.75}N_3O_{0.75}Zn_{0.75}$; M = 255.24, cubic, space group $P2_13$, a = 16.694(10) Å, U = 4882.0(10) Å^3, Z = 4, D_c = 1.389 g cm^{-3}, Mo-Kα (λ = 0.71073 Å), μ = 1.513 mm^{-1}, T = 180(2) K. 20356 reflections (2128 unique, θ < 22.44°, R_{int} = 0.0744), data collected. Refinement on F^2 values of all data gave $wR2$ = 0.2093, conventional R = 0.0744 on F values of all reflections with $F^2 > 2\sigma(F^2)$, 205 parameters. Residual electron density within ±1.02 e Å^{-3}.

CCDC 182/1748. See http://www.rsc.org/suppdata/cc/b0/b005238h/ for crystallographic files in .cif format.

1 M. T. Reetz, *Angew. Chem., Int. Ed. Engl.*, 1984, **23**, 556.
2 K. Maruoka, T. Itoh, M. Sakurai, K. Nonoshita and H. Yamamoto, *J. Am. Chem. Soc.*, 1988, **110**, 3588.
3 W. Clegg, E. Lamb, S. T. Liddle, R. Snaith and A. E. H. Wheatley, *J. Organomet. Chem.*, 1999, **573**, 305.
4 H. B. Mekelburger and C. S. Wilcox, *Comprehensive Organic Synthesis*, ed. B. M. Trost and I. Fleming, Pergamon, Oxford, 1991, vol. 2, p. 124.
5 M. Uchiyama, M. Kameda, O. Mishima, N. Yokoyama, M. Koike, Y. Kondo and T. Sakamoto, *J. Am. Chem. Soc.*, 1998, **120**, 4934.
6 M. Westerhausen, M. Wieneke, W. Ponikwar, H. Nöth and W. Schwarz, *Organometallics*, 1998, **17**, 1438.
7 E. Rijnberg, J. T. B. H. Jastrzebski, J. Boersma, H. Kooijman, G. van Koten, N. Veldman and A. L. Spek, *Organometallics*, 1997, **16**, 2239.
8 R. E. Mulvey, *Chem. Soc. Rev.*, 1998, **27**, 339; A. R. Kennedy, R. E. Mulvey, C. L. Raston, B. A. Roberts and R. B. Rowlings, *Chem. Commun.*, 1999, 353; R. P. Davies, D. J. Linton, R. Snaith and A. E. H. Wheatley, *Chem. Commun.*, 2000, 193.
9 For C_{2v} see, for example: F. A. Cotton, L. M. Daniels, L. R. Falvello, J. H. Matonic, C. A. Murillo, X. Wang and H. Zhou, *Inorg. Chim. Acta*, 1997, **266**, 91.
10 For C_{3v} see: C.-F. Lee, K.-F. Chin, S.-M. Peng and C.-M. Che, *J. Chem. Soc., Dalton Trans.*, 1993, 467.
11 A. Belforte, F. Calderazzo, U. Englert and J. Strähle, *Inorg. Chem.*, 1991, **30**, 3778.
12 J. L. Wardell, *Comprehensive Organometallic Chemistry*, ed. G. Wilkinson, F. G. A. Stone and E. W. Abel, Pergamon, Oxford, 1982, vol. 1, pp. 46–47.
13 T. M. Che, V. W. Day, L. C. Francesconi, M. F. Fredrich, W. G. Klemperer and W. Shum, *Inorg. Chem.*, 1985, **24**, 4055.
14 M. Veith, E.-C. Yu and V. Huch, *Chem. Eur. J.*, 1995, **1**, 26; P. Miele, G. Foulon and N. Hovnanian, *Inorg. Chim. Acta*, 1997, **255**, 289; J. L. Jolas, S. Hoppe and K. H. Whitmire, *Inorg. Chem.*, 1997, **36**, 3335; W. J. Evans, M. A. Ansari and J. W. Ziller, *Inorg. Chem.*, 1999, **38**, 1160.
15 R. H. Heyn, J. C. Huffman and K. G. Caulton, *New J. Chem.*, 1993, **17**, 797.
16 J. F. K. Müller, M. Neuburger and B. Spingler, *Angew. Chem., Int. Ed.*, 1999, **38**, 3549.

Typeset and printed by Black Bear Press Limited, Cambridge, England

The IMOMM method opens the way for the accurate calculation of "real" transition metal complexes

Feliu Maseras

Unitat de Química Física, Edifici C.n, Universitat Autònoma de Barcelona, 08193 Bellaterra, Catalonia, Spain. E-mail: feliu@klingon.uab.es

Received (in Cambridge, UK) 1st August 2000, Accepted 16th August 2000
First published as an Advance Article on the web 4th September 2000

The Integrated Molecular Orbital Molecular Mechanics (IMOMM) method is spearheading the entry of hybrid quantum mechanics/molecular mechanics (QM/MM) approaches in computational transition metal chemistry. The high ratio between quality of results and computer cost offered by these methods allows the introduction, for the first time, of the full experimental complexes, in accurate calculations. Several chemically relevant topics in this way become available to theoretical consideration. This article reviews a few representative examples of these applications.

Introduction

Computational chemistry has made huge progress in recent decades.[1] It has gone from the qualitative explanation of chemical trends to the accurate calculation of physical properties. This evolution has been made possible in good part because of the ever-increasing power of computers and because of the development of new methods. Progress has been even more dramatic in the field of computational transition metal chemistry.[2,3] The relatively cheap Hartree–Fock methods, which are sufficiently precise for a good deal of organic chemistry, providing at least a reasonable starting point into the properties and reactivity of small organic molecules, are usually too inaccurate for transition metal chemistry. Transition metal compounds often require the introduction of correlation energy and relativistic effects for a qualitatively acceptable description. Methods including these features have not been readily available for systems of large size until the last decade.

There is nevertheless still a new dimension to be gained in computational transition metal chemistry, namely the full introduction of the complete ligands. Most of the calculations have traditionally made use of model ligands, with only the atoms directly attached to the metal being described as such. Typical examples of this practice would be the replacement of any phosphine by PH_3, or of any cyclopentadienyl derivative by C_5H_5. This approach has been successful because it provides a reasonable description of the metal–ligand bonding. However, there are a number of chemical features that depend on the specific nature of the ligand, and cannot be reproduced by these simplified models.

A very promising method for the introduction of the real ligands in theoretical calculations is the use of hybrid quantum mechanics/molecular mechanics (QM/MM) methods. In these methods, the system is divided in different regions, each of them with a different computational description, as shown for a particular example in Fig. 1. In this way, the interactions related to the bulk of the ligands, mostly of steric nature, can be appropriately treated with the much more affordable molecular mechanics approach. A complementary approach, the use of pure molecular mechanics, requires the development of a specific force field for each compound, or family of compounds, that are to be studied, and will not be discussed here.[5]

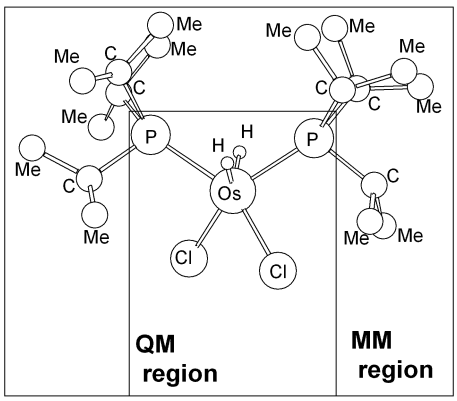

Fig. 1 Separation in QM and MM regions for an IMOMM calculation on $[OsCl_2H_2(PPr^i_3)_2]$.[4]

There are a variety of QM/MM methods proposed in the chemical literature, each with its particular methodological flavor.[6] This article will concentrate almost exclusively on the applications of one of them, Integrated Molecular Orbital Molecular Mechanics (IMOMM),[7] and of its derived forms.[8–10] This method has been so far the most widely applied to transition metal chemistry, mostly because of its robustness and simplicity. Precise descriptions of the method, and of its practical implementations can be found elsewhere.[7,11] Some aspects, like the mathematical treatment of the hydrogen bonds capping the dangling bonds in the QM region, which define the nature of different QM/MM methods, are still the subject of eventual improvement, but discussion of these aspects is outside the scope of this article,

There are nevertheless two characteristics of the IMOMM scheme that merit mention here because of their relevance in the

Feliu Maseras was born in 1962 in Martorelles, Catalonia. He studied at the Universitat Autònoma de Barcelona, where he obtained his B.Sc. in 1985 and his Ph.D. in 1991. He then spent two years as a postdoctoral fellow with Keiji Morokuma at the Institute for Molecular Science in Okazaki, Japan. After a two-year position as a CNRS Associate Researcher in the group of Odile Eisenstein in Montpellier, France, he took the position of Associate Professor at the Universitat Autònoma de Barcelona in 1998. His current research interests involve the development and application of theoretical methods to transition metal compounds, with special focus on the use of hybrid methods combining quantum mechanics and molecular mechanics for modeling species of experimental interest.

DOI: 10.1039/b006249i

interpretation and analysis of results. The first of these is that IMOMM is a full multistep method,[11] where the optimal geometry corresponds neither to the optimal QM arrangement nor to the optimal MM arrangement, but to the optimal, in a mathematical sense, compromise between both. The second defining characteristic of the IMOMM approach is that atoms in the MM region do not have a direct effect on the QM wavefunction, except through the distortions they induce in the geometry. Because of this, it can be stated that the IMOMM scheme introduces only the steric effects of the atoms in the MM region. On one hand, this supposes the introduction of an error, because the eventually important electronic contributions of these atoms are left out. On the other hand, this allows a straightforward separation between electronic and steric effects. The natural solution to the problem of electronic effects within the IMOMM scheme is the expansion of the QM region, which must include all electronic effects that are significant to the problem under study. As will be seen in the following sections, this can be used in some cases for the performance of computational experiments. Other QM/MM methods[6] introduce part of the electronic effects through the use of point charges. An alternative approach, available within the ONIOM scheme,[8] is the use of different quality QM descriptions for different regions of the systems.

A final methodological comment concerns the fact that the quality of IMOMM results, like that of any other QM/MM approach, depends critically on the appropriateness of the respective QM and MM methods to describe the interactions within the respective regions. Because of this, the quality of an IMOMM calculation is usually described in the form IMOMM(QM-method:MM-method), where the labels in parentheses describe the methods used in each of the two regions.

After this introduction, the current article focuses on a few selected applications of the IMOMM and related QM/MM methods to transition metal chemistry. The presentation does not intend to be exhaustive, but to be sufficiently general to show the possibilities of these methods to a general audience.

Structural studies

The most obvious feature of the application of hybrid QM/MM methods to transition metal chemistry is the possibility of introducing steric effects, and because of that a significant part of the published hybrid QM/MM calculations has been devoted to the analysis of how steric effects alter geometries and relative energies of transition metal complexes.

A representative study of how IMOMM calculations can be used in the identification of steric effects is provided by the joint experimental and theoretical study[12] on [Ir(biph)X(QR_3)$_2$] (biph = biphenyl-1,2-diyl; X = Cl, I; Q = P, As). These five-coordinate complexes have a distorted trigonal bipyramidal structure, as shown in Fig. 2. The phosphines (or arsines)

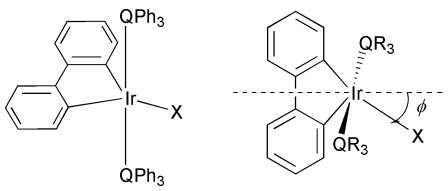

Fig. 2 Geometrical distortion of the equatorial X ligand in trigonal bipyramidal [Ir(biph)X(QR_3)$_2$] complexes.[12]

occupy the axial sites, and the halide and the chelating biph ligands are in the equatorial sites. A most intriguing feature of these compounds is the deviation that the halide presents from the symmetric arrangement between the two coordinating carbons of biph, a deviation characterized by values of φ (Fig. 2) different from zero. Previously reported calculations at the extended Hückel level suggested an electronic origin for the deviation. However, pure Becke3LYP calculations on the [Ir(biph)Cl(PH_3)$_2$] model system produced a symmetrical structure (φ = 0), making an electronic origin for the distortion unlikely.

The steric origin of the distortion was proved by IMOMM(Becke3LYP:MM3) calculations on the real system [Ir(biph)Cl(PPh_3)$_2$], which yielded a distortion angle φ of 11.4° (to be compared with the experimental value of 10.1°). The steric origin of the distortion shown by the hybrid QM/MM calculation was further confirmed by new experiments. In one of them, PPh_3 was replaced by $AsPh_3$, and in the other Cl was replaced by I. The logic behind these tests was that the modification of the size of the ligands should affect the importance of the steric effects, and therefore the value of the distortion angle. Values were merely indicative for [Ir(biph)Cl($AsPh_3$)$_2$] because of the presence of two different conformations of the arsine in the crystal structure, but clear for [Ir(biph)I(PPh_3)$_2$]. In this latter case the experimental value for the angle φ was 17.2°, 7.1° larger than for the parent compound, a trend reproduced by the corresponding IMOMM calculation. Therefore, the steric origin of the distortion from the electronically preferred symmetry was fully confirmed. Comparison of IMOMM and X-ray structures has allowed the characterization of steric effects also in [$ReH_5(PR_3)_2(SiR_3)_2$],[13] [$OsCl_2H_2(Pr^i_3)_2$],[4] and [Pd(P–N)($SiCl_3$)$_2$] (P–N = chiral chelating ligand).[14]

The application of hybrid QM/MM methods to structural problems is not restricted to the reproduction of crystal structures. A second block of structural studies has been centered in the evaluation of steric effects on the relative stabilities of two possible isomers. This type of work is well exemplified by the work on $Ru(CO)_2(PR_3)_3$,[15] where the study was centered in the comparison between the two isomers, *cis* and *trans*, as shown in Fig. 3. Both isomers have a trigonal

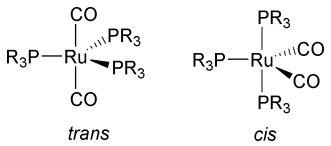

Fig. 3 The two isomers observed experimentally for $Ru(CO)_2(PR_3)_2$ complexes.[15]

bipyramidal geometry, and they are labeled following the arrangement of the two carbonyl ligands. The two forms have been observed experimentally[15,16] with different phosphine ligands PR_3. In particular, when PR_3 = PEt_3, the *cis* isomer is the species present in the crystal, with a C–Ru–C bond angle of 133.6°. When PR_3 = PPr^i_2Me, two independent molecules are present in the crystal, one of them of showing *trans* configuration (C–Ru–C 173.6°) and the other *cis* configuration (C–Ru–C 146.7°). IMOMM(MP2:MM3) calculations were carried out on these complexes using $Ru(CO)_2(PH_3)_3$ for the QM part. Both isomers, *cis* and *trans*, were found to be local minima for each complex. The computed C–Ru–C bond angles showed a clear separation between *trans* (178.2, 173.3°) and *cis* (136.7, 145.6°) forms, in good agreement with experimental data.

The most relevant part of this study was, however, comparison of the relative energies. For $Ru(CO)_2(PEt_3)_3$, the *cis* isomer, the only form existing in the crystal, was computed to be more stable than the *trans* isomer by 3.0 kcal mol^{-1}. The relationship between the two isomers is reversed for $Ru(CO)_2(Pr^i_2Me)_3$, the *trans* species being more stable by 2.8 kcal mol^{-1}. Electronic effects, represented by the QM energy, always favor the *cis* isomer, which has the two π-acceptor carbonyl ligands in equatorial positions. Steric effects, represented by the MM part, however, favor the *trans* isomer, with the three bulky phosphine ligands in equatorial positions. The

difference is that while electronic effects are similar for both PEt_3 and Pr^i_2Me, steric effects are significantly larger for the latter. As a result, the presence of the larger phosphine can invert the electronic preference for the *cis* isomer and make the *trans* isomer the most stable.

A similar IMOMM(Becke3LYP:MM3) study was carried out on $[MoO_2Cl_2(N–N)_2]$ (N–N = chelating ligand) complexes.[17] The nature of the adduct between $[OsHCl(CO)(PBu^t_2Me)_2]$ and $(CF_3)_2CHOH$ could also be clarified with the help of IMOMM(Becke3LYP:MM3) calculations.[18]

A final structural application of the IMOMM method to transition metal chemistry that will be analyzed in some more detail concerns the characterization of agostic interactions. An agostic interaction is the intramolecular interaction that takes place within one complex between the metal center and a C–H bond of one of the ligands.[19] Following their initial characterization, agostic interactions have been found to be very common in transition metal chemistry. They involve a three-center, two-electron bonding similar to that observed in main group Lewis acids such as diborane, and can also be viewed as an arrested state of the oxidative addition process of the C–H bond that would lead to the cyclometalated product. It follows that, from a molecular orbital point of view, the agostic interaction requires an empty orbital in the metal center, which must thus be unsaturated.

The steric repulsion associated with the presence of bulky ligands destabilizes high coordination numbers, also favoring unsaturated compounds. The coincidence of bulky ligands and agostic interactions in a number of complexes was therefore attributed mostly to its common association to unsaturated compounds. Recent hybrid QM/MM calculations have nevertheless proved a much more intimate relationship between steric influence and agostic interactions.[20–22]

A first proof of this relationship was obtained from the study, both experimental and theoretical, of the $Ir(H)_2(PBu^t)_2Ph)_2^+$ system (Fig. 4).[20] NMR and X-ray data showed the existence of

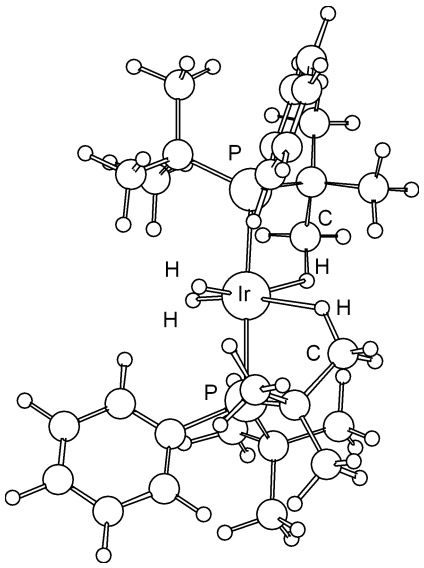

Fig. 4 IMOMM(Becke3LYP:MM3) optimized structure of $Ir(H)_2(PBu^t_2Ph)_2^+$.[20]

two agostic interactions in this complex, characterized geometrically by Ir–P–C angles of 97.0 and 99.0° (to be compared with Ir–P–C non-agostic angles of *ca.* 115°). Pure Becke3LYP calculations on $Ir(H)_2(PEtH_2)_2^+$ showed no agostic interactions at all (Ir–P–C angle of 118.4°). In contrast, IMOMM(Becke3LYP:MM3) calculations on the real complex using the same model for the QM part properly identified the agostic interactions (Ir–P–C angle of 101.7°). This result reveals two important consequences. The first is that the failure of the pure QM calculations on the model system means that the agostic interaction is intimately associated to the presence of the real ligands. The second consequence is that the success of the corresponding IMOMM calculation proves that the role of the ancillary substituents is steric in nature, and that the electronic contribution is at best minor.

While these first calculations on $Ir(H)_2(PBu^t_2Ph)_2^+$ clearly illustrated the importance of the introduction of the full ligand in the formation of the agostic interaction, they did not allow separation of the electronic and steric contributions to the steric distortion. This was accomplished within a systematic study of the steric influence on agostic interactions on a homologous series of Ir(III) complexes of general formula $Ir(H)_2(PR_3)_3^+$.[21] These complexes differ from that discussed above, with the presence of an extra phosphine, leading therefore to only one empty site in the coordination sphere, and one potential agostic interaction. In particular, the results for $Ir(H)_2(PCy_2Ph)_3^+$ are discussed. For this system, two different sets of partitioning of atoms between the QM and MM domains were applied in the IMOMM calculation (Fig. 5). In model I, all atoms not directly

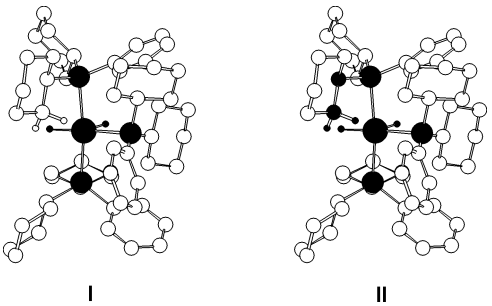

Fig. 5 The two different models used in IMOMM calculations on $Ir(H)_2(PR_3)_3^+$.[21] Atoms in the QM region are depicted in black.

bound to the metal were calculated at the MM level, the QM part being therefore $Ir(H)_2(PH_3)_3^+$. In model II, the QM part of the phosphine included the chain agostically distorted, the QM part thus being $Ir(H)_2(PEtH_2)_3^+$. The essential difference between each model is in the description of the potentially agostic C–H bond.

The geometry of $Ir(H)_2(PCy_2Ph)_3^+$ was fully optimized at four different computational levels, defined by the two different partitions and the use of MP2 and Becke3LYP methods for the QM part. Since IMOMM(MP2:MM3) led to slightly more accurate values, only these results will be discussed here. The IMOMM(MP2/I:MM3) calculation gave results essentially in agreement with the X-ray determined structure, with the largest discrepancy being in the value of 105.6° for the agostic Ir–P–C angle. This was larger than the experimental X-ray value of 100.9°, but already smaller than the computed average Ir–P–C value at this phosphorus center of 109.9°. This result is relevant because it proves that the bulk of the ligands alone is able to push one of the C–H bonds of the cyclohexyl group into the proximity of the metal atom even without any agostic orbital interaction. Use of the more elaborate model IMOMM(MP2/II:MM3), with the C–H bond in the QM part, led to results even closer to the X-ray values. The Ir–P–C bond angle improved to 99.8°, only 1.1° from the experimental value. This change proves that there is also an orbital contribution to the agostic interaction. The ability to determine the consequence of only one type of interaction is a strength of the hybrid method, which allows the execution of "computational experiments".

The accuracy of the hybrid QM/MM method in the characterization of this type of complex further proved by the calculation[21] on the isoelectronic $Ir(H)_2(PPr^i_2Ph)_3^+$ complex, with smaller phosphines, which is observed experimentally as non-agostic. This behavior is correctly reproduced by the IMOMM(MP2:MM3) calculation, which finds Ir–P–C bond angles of 115.7°. The successful application of the IMOMM method to the description of agostic interactions is not limited to late transition metals such as iridium, as proved by an

experimental and theoretical study[22] on $Tp^*Nb(Cl)(CHMe_2)$-(PhC≡CMe).

Homogeneous catalysis

The past two decades have witnessed the development of enantioselective catalysis both as a discipline and a production methodology in response to the increasing demand for enantiopure compounds for the pharmaceutical industry and the raising of environmental concerns.[23] Frequently, the key species in the catalytic cycle involves a metal atom chelated by a polyfunctional organic molecule. The role of the metal center is essential in offering neighbouring sites for coordination of the substrate and reagent molecules, and in providing a low energy pathway for their reaction. The selectivity of the reaction is however decided by the interactions involving enantiotopic groups in the polyfunctional organic ligand and the substrate, which give rise to energetically well differentiated diastereomeric transition states.

Homogeneous catalysis presents therefore two characteristics that make it especially appealing for hybrid QM/MM methods: the requirement of a high-level QM description for the metal center and its immediate environment, and the need to include in the calculation a large system that can only be introduced through an MM description. As a result, some of the more fruitful applications of the IMOMM method have been in the field of homogeneous catalysis.

Mechanisms for these processes are often complicated, and the interactions involved in enantioselectivity are often subtle. Because of this, and for the sake of the brevity of the article, the discussion will be concentrated on one of the reactions studied with the IMOMM method, the dihydroxylation of olefins by osmium tetroxide, with a brief mention made to other processes.

The osmium tetroxide-catalyzed dihydroxylation of olefins is a highly efficient method for the enantioselective introduction of chiral centers in organic substrates.[24] The reaction goes through an osmate ester intermediate containing a five-membered ring, and the stereoselectivity is decided in the formation of this intermediate after the initial interaction between catalyst and substrate. The mechanism for this part of the reaction has been the subject of intense discussion, and there seems to be finally an emerging consensus on the so-called [3 + 2] mechanism. A substantial role in the formation of this consensus has been provided by theoretical evidence from pure QM calculations on the $OsO_4(NH_3)$ + $H_2C{=}CH_2$ model system.[25]

Despite its relevance for the determination of the mechanism, calculations with the $OsO_4(NH_3)$ model cannot provide any explanation on the enantioselectivity of the reaction, because this property is related to the nature of the substituents in the NR_3 group, which are usually very bulky, as shown in the example presented in Fig. 6. A first preliminary IMOMM

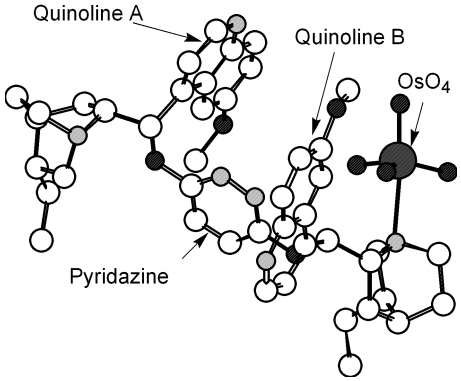

Fig. 6 Schematic presentation of the $(DHQD)_2PYDZ{\cdot}OsO_4$ catalyst.

study[26] on the subject consisted of the geometry optimization of the only two models of the catalyst where X-ray structures are available, namely $[OsO_4$(quinuclidine)] and [OsO_4\{(dimethylcarbamoyl)dihydroquinidine\}], and results showed an acceptable agreement with the experimental geometries.

The reaction of the catalyst with the olefin has been analyzed theoretically in detail in the case of the $(DHQD)_2PYDZ{\cdot}OsO_4$ [$(DHQD)_2PYDZ$ = 3,6-bis(dihydroquinidine)pyridazine] + $H_2C{=}CHPh$ system with the IMOMM(Becke3LYP:MM3) method using an $OsO_4(NH_3)$ + $H_2C{=}CH_2$ model for the QM part.[27,28] A first study[27] was concerned with the reaction profile of the formation of the osmate ester from the separated reactants. A likely reaction path leading to the experimentally observed *R* isomer was characterized though the location of the separate reactants, an intermediate, a transition state, and the product. Their relative energies, with respect to the reactants, were 0.0, −9.7, −3.3 and −34.3 kcal mol^{-1}, respectively. The geometries of both transition state and product were very similar to those obtained by pure QM calculations on the model system.[25] This proved the validity of the studies on the model system for the late stages of the reaction. The IMOMM study revealed nevertheless the presence of an intermediate that had not been located in the model system. The existence of this intermediate, shown in Fig. 7, is intimately associated to the

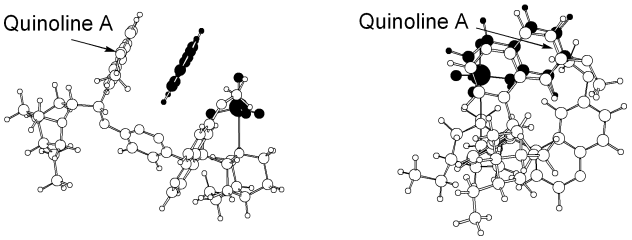

Fig. 7 IMOMM(Becke3LYP:MM3)-optimized[27] structure of the intermediate in the dihydroxylation of styrene catalyzed by $(DHQD)_2PYDZ{\cdot}OsO_4$.

interaction between the substrate and the bulky NR_3 ligand. The styrene substrate is sandwiched by two methoxyquinoline walls, with the parallel arrangement of the aromatic rings producing an attractive interaction. This interaction between substrate and catalyst has important implications on the reaction mechanism, because it is likely to be affected by the orientation of the catalyst. This point was clarified by the second study that is discussed below.

The second IMOMM(Becke3LYP:MM3) study[28] on the reaction of $(DHQD)_2PYDZ{\cdot}OsO_4$ with styrene was specifically focused on the origin of the enantioselectivity of the reaction. Because the selectivity is defined by the initial approach of the substrate to the catalyst, a number of possible pathways must be analyzed. There are twelve such paths, defined by the three possible regions (A, B and C) of approach of the substrate to the catalyst and the four possible orientations (I, II, III and IV) of the phenyl ring of the substrate within each region, as shown in Fig. 8. Each of these twelve possible pathways was theoretically

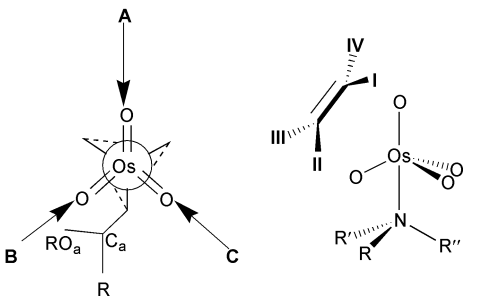

Fig. 8 Definition of the twelve possible reaction pathways in the reaction of $H_2C{=}CHPh$ with $(DHQD)_2PYDZ{\cdot}OsO_4$.

characterized through the location of the corresponding transition state, with its associated energy. The lowest energy saddle point, therefore the most likely transition state for the reaction, was B–I, followed closely by B–III and B–IV, 0.1 and 2.7 kcal mol^{-1} higher in energy. The next saddle point in energy,

A–IV, lies 4.7 kcal mol^{-1} above B–I. The fact that the three lowest energy saddle points correspond to region B, which is not the least sterically hindered (Fig. 8), is a clear indication that the non-bonding interactions between catalyst and substrate are of an attractive nature, in agreement with the existence of an intermediate.

The preference for paths B–I and B–III has an immediate consequence on the enantioselectivity of the reaction, because both lead to the *R* product. This is in excellent agreement with experimental data, that give a high enantiomeric excess of *R* product. In fact, all paths of type I and III go to the *R* product, while paths of type II and IV lead to the *S* product. The *S* product, which is a minor product of the reaction, must therefore come from path B–IV. Agreement with experiment reaches even to the value of the enantiomeric excess. If the ratio of products follows a Maxwell–Boltzmann distribution based on the internal energies of the transition states at 0 K, the theoretically computed enantiomeric excess would be 99%, close to the experimental value of 96%.

Application of hybrid QM/MM methods to the study of this reaction is not limited to the identification of the transition states and the reproduction of experimental data. It leads also to the analysis of the effect of the different regions of the catalyst on this enantioselectivity. The energy difference between the transition states, which is concentrated in the MM part of the calculation, can be further decomposed on a term by term basis. Grouping of the atoms in the regions of the catalyst according to the labels in Fig. 6 proves that the most decisive part in the selectivity (with a weight of *ca.* 50% of the interaction) is played by quinoline A, with significant, but smaller, contributions from quinoline B and pyridazine, and a very minor contribution from the OsO_4 unit.

The homogeneous catalysis process that has been the subject of more hybrid QM/MM calculations to date is however not dihydroxylation but olefin polymerization. This process had been traditionally carried out through heterogeneous catalysis, but several efficient homogeneous processes have gained importance in recent years.[29,30] Two major types of homogeneous catalysts are being used in this reaction, and both have been the subject of intense study through the IMOMM method. The most studied catalysts[31–33] have been those most recently developed, consisting of late transition metal complexes containing diimine ligands.[30] A typical QM/MM partition for these studies is shown in Fig. 9. The approach of the entering

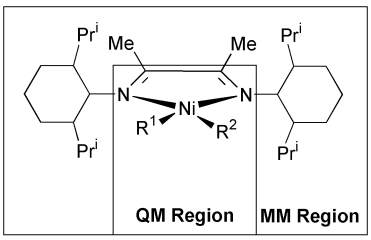

Fig. 9 Usual QM/MM partition applied in IMOMM calculations on the mechanism of olefin polymerization catalyzed by late transition metals.

monomer to the chain decides the general arrangement of the resulting polymer and, consequently, its physical properties. Calculations prove conclusively that this approach is controlled by the interactions of both fragments with the bulky substituents in the diimine group. It is worth mentioning that results of similar quality have been obtained in the application to related systems of different QM/MM combinations like IMOMM-(Becke3LYP:MM3),[31] IMOMM(BP:Amber)[32] and IMOMM(BP:CHARMM).[33] Apart from these studies on late-transition metal complexes, more traditional catalysts derived from bis-cyclopentadienyl complexes of early transition metals[29] have also been the subject of a number of IMOMM calculations.[34,35] All these calculations confirm that the tacticity and the chain length of the polymer are decided by steric interactions between substrate and catalyst. Both characteristics of the polymer depend on the relative values of the energy barriers for the insertion, branching and termination reactions. The values obtained for these processes from IMOMM calculations are in good agreement with experiment, and in an opposite order to that obtained in pure QM calculations on model systems.

A different catalytic process where hybrid QM/MM methods have made a recent entry is the enantioselective addition of diethylzinc to benzaldehyde promoted by chiral ligands.[36,37] Here, the RHF description is sufficient for the QM region, and the use of either UFF or MM3 descriptions in the MM region has provided satisfactory results. The IMOMM method has also been applied to the analysis of steric effects of bulky phosphine ligands on the mechanism of some particular reactions, such as the oxidative addition of hydrogen to $[Pt(PR_3)_2]$,[38] and the transformation of vinylidene to acetylene in the coordination sphere of $[RhCl(PPr^i_3)_2(C{=}CH_2)]$ complexes.[39]

Bioinorganic chemistry, heterogeneous catalysis, *etc*

The IMOMM method has found the most successful of its applications within transition metal chemistry in the two major fields described in the previous sections, where it is by far the most widely applied method. This notwithstanding, IMOMM and its modifications have also been applied to other areas of transition metal chemistry where other more elaborate QM/MM schemes have a well established tradition.

Biochemistry is probably the field where hybrid QM/MM schemes have found most of their applications. Proteins and nucleic acids have very large numbers of atoms, complicated folded structures, and both their structure and reactivities are heavily affected by the presence of water solvent molecules. The interaction with solvent molecules, which polarize the solute, is critical for a proper description of these systems, which consequently must introduce explicit polarization terms on the QM region.[6] Schemes like the original implementation of IMOMM,[7] where no polarization from the MM region is introduced in the QM region, are not adequate to the study of solvation problems, although the related ONIOM approach,[8] with a semiempirical description instead of MM should be appropriate.

The case of bioinorganic chemistry is however slightly different. There are a number of enzymes and proteins containing transition metals at their active center, with many atoms directly involved, and requiring the use of high level computational methods. The IMOMM method can be applied in this context to understand the properties of the active center, isolated from the rest of the protein. The analysis will be valid as far as the properties of the system are well reproduced in the isolated system, in a reasoning quite similar to that justifying experimental studies on biomimetic complexes. The performance of this approach can be seen in the example of IMOMM studies on complexes containing the heme group.

The heme group, constituted by an iron center and a porphyrin ring, occupies a prominent position in biochemistry as the active center of several relevant proteins and enzymes.[40] Although today computers allow calculation of the full heme group, the size of the system puts it at the limits of computer capacity, and hampers the performance of reactivity studies or very high level calibrations. An interesting alternative is the description of part of the porphyrin ring with an MM method.

The QM/MM partition used in the IMOMM calculations discussed here is presented in Fig. 10. In the QM part of the calculation the heme group is represented by $[Fe\{NH(CH)_3NH\}_2]$. The validity of the introduction of a QM/MM partition within the aromatic porphyrin ring is more arguable than in other topics previously discussed where the partition was across a single σ bond. One must however realize the fact that the four nitrogen donor atoms of the porphyrin are part of a large aromatic ring which has two different types of

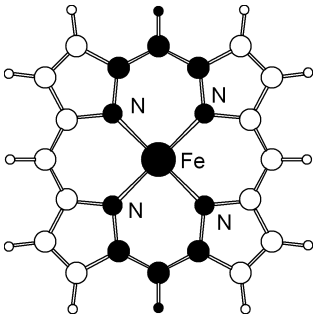

Fig. 10 QM/MM partition applied to the IMOMM calculation of iron porphyrin complexes. The QM atoms are depicted in black.

effects. One of those is the possibility that the aromatic ring has of acting as an electronic reservoir where occupied and empty orbitals are relatively close. This property is poorly reproduced in these IMOMM calculations. However, the other effect, the existence of a quite rigid framework, which precludes strong distortions out of planarity, is accurately described by the IMOMM calculation.

There was therefore a question on the reliability of this QM/MM modelization. This question was answered by a systematic set of calibrations,[41] where the results of the IMOMM calculation were compared with full *ab initio* and experimental data. Three different systems were analyzed, the four-coordinate [Fe(P)] (P = porphyrin) triplet system, the five-coordinate [Fe(P)(Im)] (Im = imidazole) quintet system, and the six-coordinate [Fe(P)(Im)(O_2)] singlet system. Computed IMOMM(Becke3LYP:MM3) geometries were always in reasonable agreement with those obtained from pure Becke3LYP calculations on the full systems, and with experimental X-ray crystal structure data on related species. The test was extended to the energy cost of the out of plane displacement of the iron atom. This factor, which ought to be ruled almost exclusively by electronic effects, *i.e.*, by the binding of the Fe center to the N atoms of the porphyrin ring, was examined with both pure Becke3LYP and IMOMM(Becke3LYP:MM3) calculations on the three different systems. The agreement of the values computed with both methods was good, with discrepancies smaller than 2 kcal mol^{-1} for displacements as large as 0.3 Å and as costly as 15 kcal mol^{-1}. Furthermore, the differences between the three different chemical systems were also well described, with the energy cost of a displacement of 0.3 Å being *ca.* 10 kcal mol^{-1} for the four-coordinate system, *ca.* 5 kcal mol^{-1} for the five-coordinate system and *ca.* 15 kcal mol^{-1} for the six-coordinate system. This QM/MM modeling of the heme group has been applied to the IMOMM(Becke3LYP:MM3) study[42] of the structural properties of [Fe(T_{piv}PP){1-Me(Im)}(O_2)], where T_{piv} is 5,10,15,20-tetrakis(α,α,α,α-*o*-pivalamidophenyl)porphyrin, a so-called picket-fence porphyrin.

A different example of application of IMOMM to bioinorganic problems is provided by the study of the catalytic mechanism of galactose oxidase.[43] In this case, the IMOMM method was used to introduce a backbone link between two residues attached to the copper center, a tyrosine and a histidine. The existence of the backbone is shown to affect the chemical nature of some reaction intermediates, but to have little effect on the overall energetics of the reaction.

Another field where QM/MM methods have been applied for a number of years is heterogeneous catalysis.[44,45] The simulation of a solid surface is much more affordable if one can describe at least part of it with an MM description. Some QM/MM methods have been specifically designed to deal with these chemical situations, and they have been applied with success to the case of zeolites.[44] Some success has also been obtained[46] in the application of IMOMM(Becke3LYP:MM3) calculations to the study of Cu atom deposition on SiO_2 surface defects. An IMOMM method that has been specifically designed for application to heterogeneous catalysis is the so-called SIMOMM (Surface IMOMM) method.[10] This method has been successfully applied to the description of the structure of the Si(001) surface[47] and to the cycloaddition reaction of cyclohexa-1,3-diene on this surface.[48] In this latter case, it has been shown that the presence of the bulk solid allows the possibility of a [2+2] reaction mechanism that was not available in gas phase studies on model reaction sites.

Concluding remarks

This article has shown how the IMOMM method, proposed only as recently as 1995, has already produced a significant amount of valuable theoretical contributions in transition metal chemistry. Its success has been logically concentrated in areas where the calculation of simplified models could not account for the experimental complexity, as in homogeneous catalysis and in structural issues associated with steric effects. Work in the area is nevertheless far from finished. There are many processes in transition metal chemistry where the bulk of the ligands seems crucial that have not as yet been tackled from a theoretical point of view. One must also expect developments from the methodological point of view. IMOMM is in fact a particular case of the more general ONIOM scheme,[8] which goes beyond the strict field of QM/MM methods by allowing the use of different QM descriptions, an approach that also has a role in transition metal chemistry.[49] Other developments in QM/MM methods will also find applications sooner or later to transition metal chemistry. In summary, the application of IMOMM and of other hybrid QM/MM methods to this field of chemistry looks very promising, and a sharp increase in the number of applications must be expected in forecoming years.

Acknowledgment

Profs. Keiji Morokuma (Emory), Odile Eisenstein (Montpellier) and Agustí Lledós (Barcelona) are thanked for helpful discussions throughout the years. Thanks must also be extended to the long list of graduate students and visitors in our group during recent years. Financial support from the Spanish DGES (Project No. PB98-0916-CO2-01) and DURSI (Generalitat de Catalunya) is acknowledged.

Notes and references

1 *The Encyclopedia of Computational Chemistry*, ed. P. v. R. Schleyer, N. L. Allinger, T. Clark, J. Gasteiger, P. A. Kollman, H. F. Schaefer and P. R. Schreiner, Wiley, New York, 1998.
2 E. R. Davidson, *Chem. Rev.*, 2000, **100**, 351.
3 *Computational Organometallic Chemistry*, ed. T. R. Cundari, Marcel Dekker, New York, 2000.
4 F. Maseras and O. Eisenstein, *New J. Chem.*, 1998, **22**, 5.
5 P.-O. Norrby, *J. Mol. Struct. (THEOCHEM)*, 2000, **506**, 9.
6 A. Warshel and M. Levitt, *J. Mol. Biol.*, 1976, **103**, 227; U. C. Singh and P. A. Kollman, *J. Comput. Chem.*, 1986, **7**, 718; M. H. Field, P. A. Bash and M. Karplus, *J. Comput. Chem.*, 1990, **11**, 700; J. Gao, *Acc. Chem. Res.*, 1996, **29**, 298; I. Tuñón, M. T. C. Martins-Costa, C. Millot, M. F. Ruiz-López and J.-L. Rivail, *J. Comput. Chem.*, 1996, **17**, 19; G. Monard and K. M. Merz, *Acc. Chem. Res.*, 1999, **32**, 904; Y. Zhang, H. Liu and W. Yang, *J. Chem. Phys.*, 2000, **112**, 3483.
7 F. Maseras and K. Morokuma, *J. Comput. Chem.*, 1995, **16**, 1170.
8 S. Humbel, S. Sieber and K. Morokuma, *J. Chem. Phys.*, 1996, **105**, 1959; S. Dapprich, I. Komáromi, K. S. Byun, K. Morokuma and M. J. Frisch, *J. Mol. Struct. (THEOCHEM)*, 1999, **461**, 1.
9 T. K. Woo, L. Cavallo and T. Ziegler, *Theor. Chem. Acc.*, 1997, **119**, 6177.
10 J. R. Shoemaker, L. W. Burggraf and M. S. Gordon, *J. Phys. Chem. A*, 1999, **103**, 3245.
11 F. Maseras, *Top. Organomet. Chem.*, 1999, **4**, 165.
12 G. Ujaque, F. Maseras, O. Eisenstein, L. Liable-Sands, A. L. Rheingold, W. Yao and R. H. Crabtree, *New J. Chem.*, 1998, **22**, 1493.
13 G. Barea, F. Maseras, Y. Jean and A. Lledós, *Inorg. Chem.*, 1996, **35**, 6401.
14 T. K. Woo, G. Pioda, U. Rothlisberger and A. Togni, *Organometallics*, 2000, **19**, 2144.

15 M. Ogasawara, F. Maseras, N. Gallego-Planas, K. Kawamura, K. Ito, K. Toyota, W. E. Streib, S. Komiya, O. Eisenstein and K. G. Caulton, *Organometallics*, 1997, **16**, 1979.
16 M. Ogasawara, F. Maseras, N. Gallego-Planas, W. E. Streib, O. Eisenstein and K. G. Caulton, *Inorg. Chem.*, 1996, **35**, 7468.
17 G. Barea, A. Lledós, F. Maseras and Y. Jean, *Inorg. Chem.*, 1998, **37**, 3321.
18 D. V. Yandulov, K. G. Caulton, N. V. Belkova, E. S. Shubina, L. M. Epstein, D. V. Khoroshun, D. G. Musaev and K. Morokuma, *J. Am. Chem. Soc.*, 1998, **120**, 12553.
19 M. Brookhart and M. L. H. Green, *J. Organomet. Chem.*, 1983, **250**, 395.
20 G. Ujaque, A. C. Cooper, F. Maseras, O. Eisenstein and K. G. Caulton, *J. Am. Chem. Soc.*, 1998, **120**, 361.
21 A. C. Cooper, E. Clot, J. C. Huffman, W. E. Streib, F. Maseras, O. Eisenstein and K. G. Caulton, *J. Am. Chem. Soc.*, 1999, **121**, 97.
22 J. Jaffart, R. Mathieu, M. Etienne, J. E. McGrady, O. Eisenstein and F. Maseras, *Chem. Commun.*, 1998, 2011.
23 *Comprehensive Asymmetric Catalysis*, ed. E. N. Jacobsen, A. Pfaltz and H. Yamamoto, Springer, Berlin, 1999.
24 H. C. Kolb, M. S. VanNieuwnhze and K. B. Sharpless, *Chem. Rev.*, 1994, **94**, 2483.
25 S. Dapprich, G. Ujaque, F. Maseras, A. Lledós, D. G. Musaev and K. Morokuma, *J. Am. Chem. Soc.*, 1996, **118**, 11660; U. Pidun, C. Boehme and G. Frenking, *Angew. Chem., Int. Ed. Engl.*, 1996, **35**, 2817.
26 G. Ujaque, F. Maseras and A. Lledós, *Theor. Chim. Acta*, 1996, **94**, 67.
27 G. Ujaque, F. Maseras and A. Lledós, *J. Org. Chem.*, 1997, **62**, 7892.
28 G. Ujaque, F. Maseras and A. Lledós, *J. Am. Chem. Soc.*, 1999, **121**, 1317.
29 H. H. Brintzinger, D. Fischer, R. Müllhaupt, B. Rieger and R. M. Waymouth, *Angew. Chem., Int. Ed. Engl.*, 1995, **34**, 1143.
30 L. K. Johnson, C. M. Killian and M. Brookhart, *J. Am. Chem. Soc.*, 1995, **117**, 6414.
31 R. D. J. Froese, D. G. Musaev and K. Morokuma, *J. Am. Chem. Soc.*, 1998, **120**, 1581; D. G. Musaev, R. D. J. Froese and K. Morokuma, *Organometallics*, 1998, **17**, 1850.
32 L. Deng, T. K. Woo, L. Cavallo, P. M. Margl and T. Ziegler, *J. Am. Chem. Soc.*, 1997, **119**, 6177; L. Deng, P. Margl and T. Ziegler, *J. Am. Chem. Soc.*, 1999, **121**, 6479; M. S. W. Chan, L. Deng and T. Ziegler, *Organometallics*, 2000, **19**, 2741; T. K. Woo, P. E. Blöchl and T. Ziegler, *J. Phys. Chem. A*, 2000, **104**, 121.
33 G. Milano, G. Guerra, C. Pellecchia and L. Cavallo, *Organometallics*, 2000, **19**, 1343.
34 G. Guerra, P. Longo, P. Corradini and L. Cavallo, *J. Am. Chem. Soc.*, 1999, **121**, 8651.
35 G. Moscardi, F. Piemontesi and L. Resconi, *Organometallics*, 1999, **18**, 5264.
36 B. Goldfuss, M. Steigelmann, S. I. Khan and K. N. Houk, *J. Org. Chem.*, 2000, **65**, 77.
37 J. Vàzquez, M. A. Pericàs, F. Maseras and A. Lledós, submitted to *J. Org. Chem.*
38 T. Matsubara, F. Maseras, N. Koga and K. Morokuma, *J. Phys. Chem.*, 1996, **100**, 2753.
39 Y. Wakatsuki, N. Koga, H. Werner and K. Morokuma, *J. Am. Chem. Soc.*, 1997, **119**, 360.
40 L. Stryer, *Biochemistry*, Freeman, New York, 1995.
41 J.-D. Maréchal, G. Barea, F. Maseras, A. Lledós, L. Mouawad and D. Perahia, *J. Comput. Chem.*, 2000, **21**, 282.
42 F. Maseras, *New J. Chem.*, 1998, **22**, 327.
43 F. Himo, L. A. Eriksson, F. Maseras and P. E. M. Siegbahn, *J. Am. Chem. Soc.*, 2000, **122**, 8031.
44 U. Eichler, C. M. Kölmel and J. Sauer, *J. Comput. Chem.*, 1996, **18**, 463.
45 A. H. de Vries, P. Sherwood, S. J. Collins, A. M. Rigby, M. Rigutto and G. J. Kramer, *J. Phys. Chem. B*, 1999, **103**, 6133.
46 N. Lopez, G. Pacchioni, F. Maseras and F. Illas, *Chem. Phys. Lett.*, 1998, **294**, 611.
47 J. R. Shoemaker, L. W. Burggraf and M. S. Gordon, *J. Chem. Phys.*, 2000, **112**, 2994.
48 C. H. Choi and M. S. Gordon, *J. Am. Chem. Soc.*, 1999, **121**, 11 311.
49 A. Sundermann, O. Uzan, D. Milstein and J. M. L. Martin, *J. Am. Chem. Soc.*, 2000, **122**, 7095.

β-Glycosidase inhibitors mimicking the pyranoside boat conformation

Edwige Lorthiois, Muthuppalaniappan Meyyappan and Andrea Vasella*

Laboratorium für Organische Chemie, ETH-Zentrum, Universitätstrasse 16, CH-8092 Zürich, Switzerland. E-mail: vasella@sugar.org.chem.ethz.ch

Received (in Cambridge, UK) 17th July 2000, Accepted 14th August 2000
First published as an Advance Article on the web 11th September 2000

Polyhydroxylated isoquinuclidines mimicking the boat conformation of pyranosides are strong and selective inhibitors of a retaining β-mannosidase.

According to the principle of stereoelectronic control,[1] heterolytic cleavage of an acetal C–O bond requires an antiperiplanar orientation of a doubly occupied, non-bonding orbital. This antiperiplanar lone pair hypothesis (ALPH) means that hydrolysis of β-D-pyranosides involves a conformational change of the tetrahydropyran ring from a chair to a twist-boat or boat resulting in a pseudoaxial orientation of the aglycon (Fig. 1).[2] A

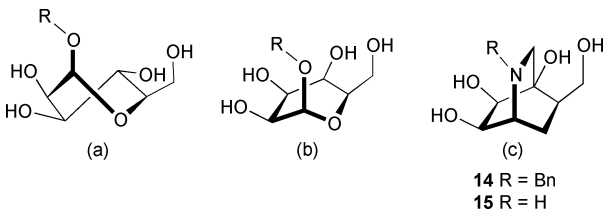

Fig. 1 Skew boat ($^1S_3$, a) and boat ($^{1,4}B$, b) conformers of a β-D-mannopyranoside and isoquinuclidines **14** and **15**.

similar conformational change is required for nucleophilic assistance of the cleavage according to an intermediate S_N1/S_N2 mechanism. The relevance of ALPH for enzymic glycoside cleavage has met with strong scepticism,[2c] but crystal structures of three *endo*-glycosidases in complex with substrate analogues show a skew boat or a flattened boat conformation of the tetrahydropyran ring.[3] A skew boat or boat-like conformer with a pseudoaxial (elongated) C(1)–O bond may conceivably be closer to the transition state of an enzymic β-glycoside cleavage than a reactive intermediate of an oxycarbenium cation type. If so, inhibitors mimicking the boat-like conformation of a glycoside, the proper location of the 'glycosidic heteroatom' (*i.e.* the heteroatom attached to C(1) of the glycoside), and the correct orientation of its lone pairs may possess a more strongly pronounced character as transition state analogues than inhibitors mimicking the cationic reactive intermediate. Inhibitors mimicking the shape of an oxycarbenium cation appear indeed to be only partial transition state analogues.[4] Since the conformational change from a chair to a twist-boat or boat should be induced by all β-glycosidases, we wanted to synthesize and evaluate a mimic of such a conformer of a glycoside that is cleaved by an *exo*-glycosidase. The cyclohexane ring of **14** and **15** (Fig. 1) mimics the tetrahydropyran ring of a β-mannoside in a $^{1,4}B$ conformation; it is substituted by a pseudoaxial amino group that should allow lateral protonation.[5] Only one[6] of the known bicyclic glycosidase inhibitors[7] mimicks a tetrahydropran ring in a ($^{2,5}B$) boat conformation. It has been designed in another conceptual context, and was not tested against β-mannosidases; it is a poor inhibitor of other glycosidases.

The isoquinuclidines **14** and **15** were synthesised in 14 and 15 steps and in 6.6 and 5.4% overall yields, respectively, from 3-hydroxypyridone *via* the known tosylate **1**[8] as shown in Scheme 1. Notable features are the diastereoselective high yielding Michael addition and aldolisation of **2** to **4**, the epimerisation and hydrolysis (dealkylation?) of the ester **6** to **7a**, and the two step reduction of **11a** *via* **12** to **13**.†

Both **14**‡ (K_i = 0.17 μM; IC_{50} = 0.69 μM)§ and **15**¶ (K_i = 20 μM; IC_{50} = 29.4 μM) inhibit snail β-mannosidase competitively, as determined from a Lineweaver–Burk plot, **14** being about 120 times stronger than **15**. Jack bean α-mannosidase is inhibited *ca.* 10^4 times more weakly by **14** (IC_{50} = 9.6 mM) than snail β-mannosidase and about 700 times more weakly by **15** (IC_{50} = 20 mM). Both **14** (IC_{50} > 5.0 mM) and **15** (IC_{50} = 4.3 mM) are poor inhibitors of β-glucosidase from *Caldocellum saccharolyticum*. The value of IC_{50} for β-mannosidase dropped from 4.08 to 0.69 μM for **14** and from 183 to 29.4 μM for **15** as the preincubation was prolonged from 10

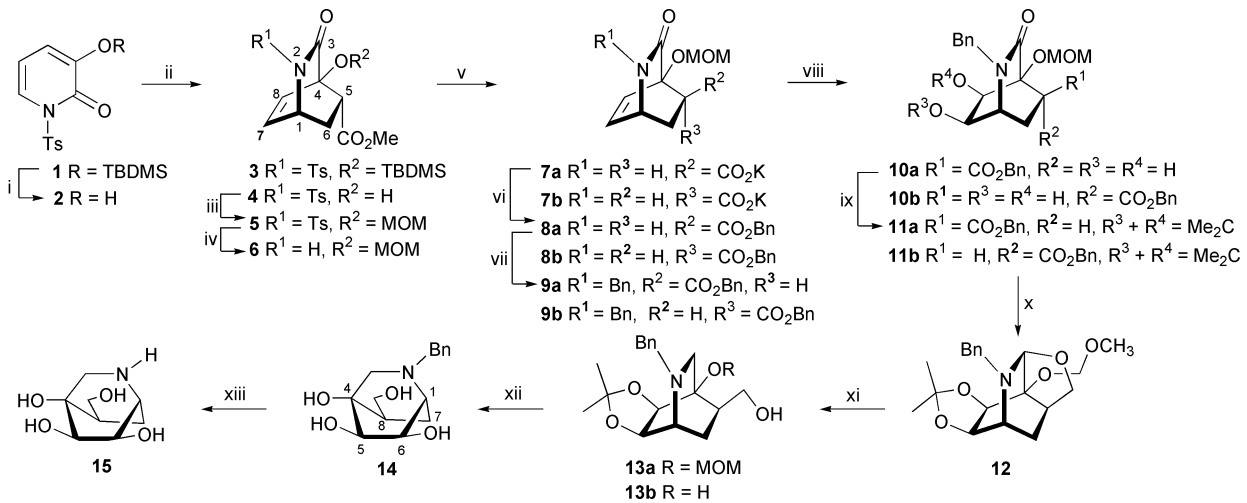

Scheme 1 *Reagents and conditions*: i, $BF_3{\cdot}Et_2O$, CH_2Cl_2, 98%; ii, CH_2=CH–CO_2Me, Et_3N, 92% from **2**; iii, $CH_2(OMe)_2$, P_2O_5, $CHCl_3$, 88%; iv, Na–$C_{10}H_8$, DME, −78 °C, 88% from **5**; v, K_2CO_3, MeOH, Δ; vi, BnBr, $NaHCO_3$, DMF, **8a**/**8b** 80:20 (49% from **6**), **9a**/**9b** 80:20 (18% from **6**); vii, NaH, BnBr, DMF, 89%; viii, OsO_4, acetone–H_2O, 89%; ix, $Me_2C(OMe)_2$, acetone, CSA, 94%; x, THF, Δ, **12** (57%), **13a** (17%), **13b** (8%); xi, $LiAlH_4$, dioxane, Δ, **13a** (67%); xii, TFA, H_2O, Δ, 84%; xiii, H_2/$Pd(OH)_2$/C, conc. HCl, MeOH/H_2O, 82%.

DOI: 10.1039/b005578f

min to 2 h. The inhibition by **14** and **15**, as represented by $1/IC_{50}$, shows a linear dependence on pH, revealing inhibition by the free amines rather than by the ammonium salts. The inhibition is *ca.* 4–6 times stronger at pH 5.6 than at pH 4.5 and again *ca*. 4–6 times weaker at pH 3.6.‖

Since **15** (pK_{HA} = 8.4) is a stronger base than **14** (pK_{HA} = 7.5), one expects **14** to be a stronger inhibitor than **15** at pH 4.5 by a factor of about 10. That **14** is 120 times stronger than **15** evidences a hydrophobic interaction of the benzyl group of **14** with the aglycon binding site. Such interactions are well precedented.[10,11]

The pH dependence of the inhibition by **14** and **15** evidences the essential interaction with the catalytic acid, and confirms its flexibility.[12] In contrast to the inhibition by the azole type inhibitors,[4,13–15] that is characterised by a cooperative interaction of the inhibitor with the catalytic acid and the catalytic nucleophile[2b] the interaction of **14** and **15** with the catalytic nucleophile appears to play at best a minor role. The inhibitory activity of **14** and **15** is in agreement with the postulate that a conformational change of the pyranose ring precedes or accompanies the enzymatic cleavage of β-glycosides.

Notes and references

† The esters **9a** and **9b** were isolated in yields of 41 and 10% from **5**. Selected ^{1}H-NMR data for **8a**: 4.00 (ddt, *J* = 5.6, 3.4, 2.1, H-C(1)), 2.93 (dd, *J* ≈ 10.5, 4.9, H-C(5)), 1.95 (ddd, *J* = 12.5, 5.0, 3.4, H_{exo}-C(6)), 1.79 (ddd, *J* = 12.5, 10.6, 2.2, H_{endo}-C(6)); selected ^{1}H-NMR data for **8b**: 4.05 (ddt, *J* ≈ 5.3, 3.6, 1.4, H-C(1)), 3.06 (ddd, *J* = 10.0, 5.1, 0.9, H-C(5)), 2.09 (ddd, *J* = 12.8, 10.0, 3.7, H_{exo}-C(6)), 1.56 (ddd, *J* = 12.5, 5.0, 1.6, H_{endo}-C(6)). The *exo* configuration of the diols **10** (*exo* refers to the face *syn* to the C(1)–N bond) was assigned on the basis that $J_{1,6}$ = 2.1 Hz (**10a** and **10b**) is smaller than $J_{1,7exo}$ = 3.6 (**10a**) and 4.4 Hz (**10b**) and closer to $J_{1,7endo}$ = 2.0 (**10a**) and 1.7 Hz (**10b**).[8] An attempt to reduce **11a** to **13** in one step was not successful.

‡ Data for **14**: R_f (AcOEt–MeOH 5:1), 0.40; δ_H(300 MHz, CD_3OD): 7.40–7.13 (m, arom. H), 3.88 (dd, *J* = 12.1, 6.5, CH_2OH), 3.85 (dd, *J* = 8.4, 2.1, irrad. at 2.66 → d, *J* = 8.4, H-C(6), 3.81, 3.72 (2d, *J* = 13.1, N-CH_2Ph), 3.65 (dd, *J* = 10.6, 6.5, CH_2OH), 3.60 (dd, *J* = 8.4, 1.3, H-C(5)); 2.89 (dd, *J* ≈ 9.5, 1.8, H_b-C(3)), 2.66 (br q, *J* ≈ 2.6, H-C(1)), 2.47 (dd, *J* ≈ 9.6, 1.6, irrad. at 2.89 → d, *J* = 4.4, H_a-C(3)), 1.84–1.61 (m, irrad. at 2.66 → change, irrad. at 2.89 → change, H_{exo}-C(7), H-C(8)), 1.59 (ddd, *J* ≈ 13.7, 10.6, 2.8, irrad. at 2.66 → change, H_{endo}-C(7)); δ_C(75 MHz, CD_3OD): 140.54 (s), 130.22 (d), 129.60 (d); 128.38 (arom. C); 73. 56 (s, C(4)); 73.45 (d, C(6)); 70.33 (d, C(5)); 63.81 (t, CH_2OH), 61.29 (t, N-CH_2Ph), 56.82 (d, C(1)), 51.32 (t, C(3)), 40.14 (d, C(8)), 24.89 (d, C(7)); ESI–MS: 280 ([*M* + 1]$^+$), 302 ([*M* + Na]$^+$). Anal. calc. for $C_{15}H_{21}NO_4{\cdot}0.5H_2O$: C 62.48, H 7.69, N 4.86%. Found: C 62.24, H 7.47, N 4.83%.

§ Snail β-mannosidase: at 25 °C and pH 4.5; jack bean α-mannosidase: at 37 °C and pH 4.5; β-glucosidase from *Caldocellum saccharolyticum*: at 55 °C and pH 6.8.

¶ Data for **15**: R_f (AcOEt–MeOH 5:1): 0.40; δ_H(300 MHz, D_2O): 3.99 (dd, *J* ≈ 8.6, 2.1, irrad. at 2.75 → d, *J* = 8.7, H-C(6)), 3.85 (dd, *J* = 10.9, 5.3, irrad. at 1.85 → d, *J* = 10.6, CH_b–C(8)), 3.73 (dd, *J* ≈ 8.6, 1.8, irrad. at 2.65→ d, *J* = 8.7, irrad. at 3.99 → t, *J* = 1.9, H–C(5)), 3.62 (dd, *J* ≈ 11.1, 8.0, irrad. at 1.85 → d, *J* = 10.6, –CH_a–C(8)), 2.88, br. dd, *J* ≈ 11.2, 2.0, irrad. at 1.85 → d, *J* = 11.2, irrad. at 2.65 → d, *J* ≈ 5.0, H_a–C(3)), 2.75 (br q, *J* ≈ 2.4, irrad. at 1.52 → br. t, *J* ≈ 2.5, irrad. at 1.85 → t, *J* = 2.2, irrad. at 3.99 → change, H–C(1)); 2.65 (dd, *J* ≈ 11.4, 1.8, H_b–C(3)), 1.76–1.95 (m, irrad. at 1.52 → change, irrad. at 2.75 → change, H_{endo}–C(7), H–C(8)), 1.52 (dd, *J* = 7.8, 3.4, irrad. at 1.85 → d, *J* = 2.5, irrad. at 2.75 → d, *J* = 7.8, H_{exo}–C(7)). δ_C(75 MHz, D_2O): 73.49 (d, C(6)), 73.35 (s, C(4)), 70.24 (d, C(5)), 65.00 (t, *C*H_2–C(8)), 41.58 (t, C(3)), 40.53 (d, C(1)), 29.01 (t, C(7)); MALDI-MS: 190 (100, [*M* + 1]$^+$), 212 (10, [*M* + Na]$^+$). Anal. calc. for $C_8H_{15}NO_4{\cdot}0.5\ H_2O$: C 48.48, H 8.14, N 7.07%. Found: C 48.28, H 7.91, N 6.77%.

‖ The enzyme loses *ca*. 50% activity at pH 5.5 and *ca*. 10% at pH 3.5.[9]

1 (*a*) C. L. Perrin, R. E. Engler and D. B. Young, *J. Am. Chem. Soc.*, 2000, **122**, 4877; (*b*) A. J. Kirby, *The Anomeric Effect and Related Stereoelectronic Effects at Oxygen*, Springer–Verlag, Berlin, 1983; (*c*) P. Deslongchamps, *Stereoelectronic Effects in Organic Chemistry*, Pergamon Press, Oxford, 1983.

2 Recent reviews on glycosidase mechanisms: (*a*) D. L. Zechel and S. G. Withers, *Acc. Chem. Res.*, 2000, **33**, 11; (*b*) T. D. Heightman and A. T. Vasella, *Angew. Chem., Int. Ed.*, 1999, **38**, 750; (*c*) G. Davies, M. L. Sinnott and S. G. Withers, in *Comprehensive Biochemical Catalysis*, ed. M. Sinnott, Academic Press, London, 1998, 1, p. 119 and references cited there.

3 (*a*) G. J. Davies, L. Mackenzie, A. Varrot, M. Dauter, A. M. Brzozowski, M. Schülein and S. G. Withers, *Biochemistry*, 1998, **37**, 11 707; (*b*) I. Tews, A. Perrakis, A. Oppenheim, Z. Dauter, K. S. Wilson and C. E. Vorgias, *Nat. Struct. Biol.*, 1996, **3**, 638; (*c*) G. Sulzenbacher, H. Driguez, B. Henrissat, M. Schülein and G. Davies, *Biochemistry*, 1996, **35**, 15280.

4 P. Ermert, A. Vasella, M. Weber, K. Rupitz and S. G. Withers, *Carbohydr. Res.*, 1993, **250**, 113.

5 T. D. Heightman, M. Locatelli and A. Vasella, *Helv. Chim. Acta*, 1996, **79**, 2190.

6 K. S. E. Tanaka and A. J. Bennet, *Can. J. Chem.*, 1998, **76**, 431.

7 (*a*) K. H. Smelt, Y. Bleriot, K. Biggadike, S. Lynn, A. L. Lane, D. J. Watkin and G. W. J. Fleet, *Tetrahedron Lett.*, 1999, **40**, 3255; (*b*) K. H. Smelt, A. J. Harrison, K. Biggadike, M. Müller, K. Prout, D. J. Watkin and G. W. J. Fleet, *Tetrahedron Lett.*, 1999, **40**, 3259; (*c*) A. Stütz, *Iminosugars as Glycosidase Inhibitors: Nojirimycin and Beyond*, Wiley–VCH, Weinheim, 1999.

8 G. H. Posner, V. Vinader and K. Afarinkia, *J. Org. Chem.*, 1992, **57**, 4088.

9 B. V. McCleary, *Carbohydr. Res.*, 1983, **111**, 297.

10 (*a*) A. Blaser and J.-L. Reymond, *Org. Lett.*, 2000, **2**, 1733; (*b*) A. M. Davis and S. J. Teague, *Angew. Chem., Int. Ed.*, 1999, **38**, 737.

11 N. Panday, Y. Canac and A. Vasella, *Helv. Chim. Acta*, 2000, **83**, 58.

12 S. L. Lawson, W. W. Wakarchuk and S. G. Withers, *Biochemistry*, 1997, **36**, 2257.

13 N. Panday and A. Vasella, *Synthesis*, 1999, 1459.

14 K. Tatsuta, Y. Ikeda and S. Miura, *J. Antibiot.*, 1996, **49**, 836.

15 K. Tatsuta, S. Miura, S. Ohta and H. Gunji, *J. Antibiot.*, 1995, **48**, 286.

Nanomolar scale nitric oxide generation from self-assembled monolayer modified gold electrodes

Yongchun Hou, Yongsheng Chen, Nabil A. Amro, Kapila Wadu-Mesthrige, Peter R. Andreana, Gang-yu Liu and Peng G. Wang*

Department of Chemistry, Wayne State University, Detroit, MI 48202, USA. E-mail: pwang@chem.wayne.edu

Received (in Corvallis, OR, USA) 23rd May 2000, Accepted 7th August 2000
First published as an Advance Article on the web 11th September 2000

A SAM-modified gold electrode has been developed for the first time for quantitative NO generation of a nanomolar amount that is proportional to the surface area of the electrode.

Nitric oxide, a relatively unstable, potentially toxic gas, has been implicated in a wide variety of physiological and pathological processes.[1–4] Considering the numerous functions of NO in the human body, controlled delivery of a quantitative amount of NO to specific sites is most critical for biomedical applications of NO donor compounds.[5,6] On the other hand, extensive research on a variety of self-assembled monolayers (SAMs) on different metal electrodes has resulted in many biomedical applications during the past decade.[7–11] In our efforts to develop quantitative and site-specific NO donating compounds, we explored the possibility of using the self-assembled monolayer of an NO donor to achieve controlled NO release. Here we report the development of a novel SAM moiety **6** by attaching a thiol tail to the NO donor molecule and allowing it to self-assemble onto the surface of a thin gold electrode (Scheme 1). Upon applying an electric potential, the electrode achieves quantitative NO release on a nanomolar scale.

N-Nitroso-*N*-oxido-*p*-thiomethylbenzenamine ammonium salt **5** was synthesized according to Scheme 1. 4-Nitrobenzyl bromide (**1**) was reacted with potassium thioacetate to give compound **2**. Subsequent zinc reduction of the nitro group, nitrosation with isobutyl nitrite, and finally neutralization and spontaneous deacetylation afforded **5**.† Although compound **5** slowly decomposes at rt, successful preparation of the SAM gold electrode of compound **5** was achieved at −4 °C, leading to the formation of **6**. According to Lawless and others who have illustrated the oxidative electrochemical release of NO from cupferron‡ and its derivatives,[12,13] a similar mechanism is proposed to account for NO generation from the SAM donor **6** (Scheme 2). Upon applying an electric potential, **6** undergoes a one-electron electrochemical oxidation to form presumably the highly unstable free radical intermediate **7**, which spontaneously decomposes to release NO and form the nitroso SAM **8** as well.

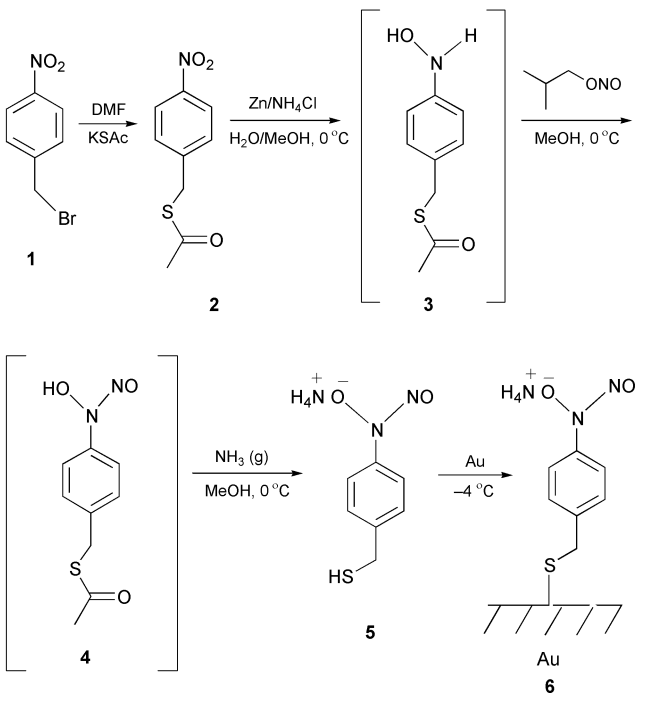

Scheme 1 Synthesis of NO donor **5** and preparation of SAM **6**.

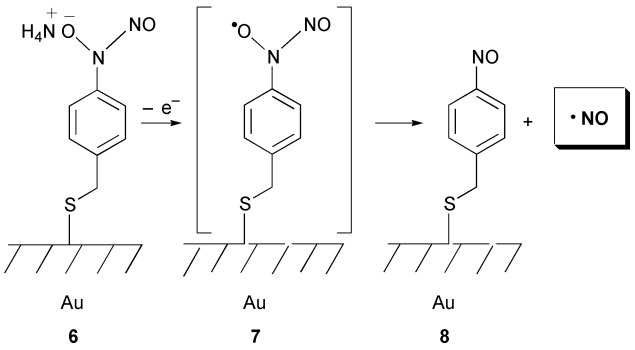

Scheme 2 Proposed NO releasing mechanism from the SAM modified gold electrodes.

An Osteryoung square wave voltammetry (OSWV) technique was employed to characterize the donor SAM **6**. Typical OSWV responses using a BAS-100B electroanalyzer were shown in Fig. 1. From 0 to 800 mV, the donor SAM modified gold electrode exhibited a single peak at a potential of 270 mV

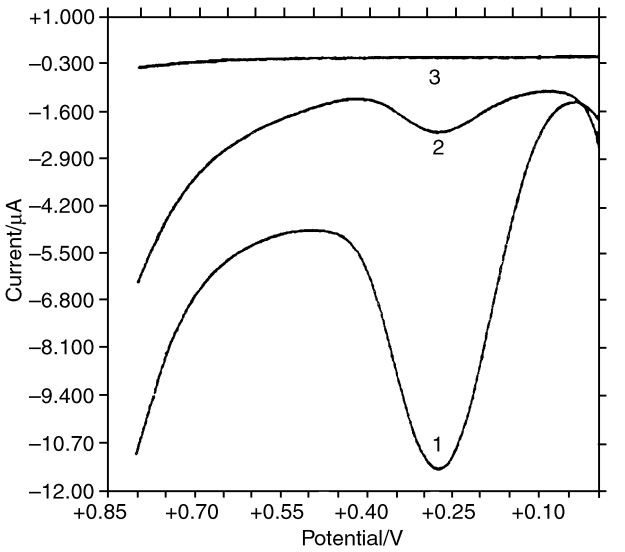

Fig. 1 Typical OSWV responses of SAM functionalized gold electrodes. Curve 1: first scan; curve 2: second scan; and curve 3: a 'real' background obtained after multiple scans.

DOI: 10.1039/b004159i

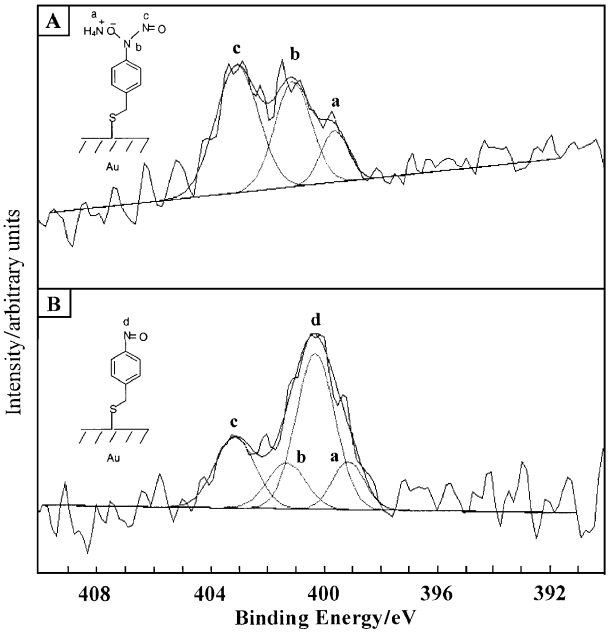

Fig. 2 XPS spectra of the SAM covered gold electrode prior to (A) and after (B) the electrolysis.

corresponding to an irreversible oxidation process (curve 1). A second continuous scan resulted in a lowered peak current (curve 2), indicating a reduced quantity of the donor compound **5** on the surface of the electrode. Upon multiple scans, the peak eventually disappeared and a 'real' background curve was obtained (curve 3), which represented the formation of **8**.

X-ray photoelectron spectroscopy (XPS) has proven to be a useful technique in characterizing SAM-functionalized metal surfaces by determining the oxidation state of nitrogen within SAM electrodes.[14] XPS specta in Fig. 2A are the results of three peaks that correspond to nitrogen atoms[15,16] in three different chemical environments in donor SAM **6** (binding energy of 399.66, 401.21 and 403.14 eV for $N_{1S}^{1/2}$, respectively). After electrolysis, the overall spectra changed with the appearance of a new peak with lower binding energy. The new spectrum (Fig. 2B) is best fitted for $N_{1S}^{1/2}$ peaks at binding energy of 399.33, 400.44, 401.38 and 403.22 eV, respectively. The new peak at 400.44 eV corresponds to the $N_{1S}^{1/2}$ intensity of the nitroso group in SAM **8**, which is consistent with the oxidation of the bulky terminal group in SAM **6**.

To directly monitor the generation of NO from the SAM functionalized gold electrode, a commercially available NO detector probe was inserted into the electrolysis cell through a bypass to the vicinity of a gold electrode at a fixed position. Due to the actual detection limit of the NO detector probe (~ 2 nM), the gold bead working electrode was replaced with a larger gold plate electrode (Au (111)) in order to generate a significant amount of NO for detection. NO generation was monitored simultaneously during a quantitative electrolysis process while the solution was vigorously stirred. The amount of NO released was determined by subtracting the highest point on the current plateau from the background current and converting the result into the corresponding quantities of NO using a standard calibration curve. It was shown that the amount of NO generated increased with the electrode potential during a bulk electrolysis process; however, no linear relationship appeared between the amount of NO released and the electrolysis potential.[13] Next, we carried out the electrolysis with various sizes of gold electrodes all having the same square geometry. Interestingly, a linear relationship between the amount of NO generated and the area of the electrode was established (Fig. 3),§ which indicates that controlled NO release could be achieved by selecting an appropriately sized surface area of the gold electrode.

In summary, this work demonstrates the principle and initial design of a gold electrode functionalized by a self-assembled

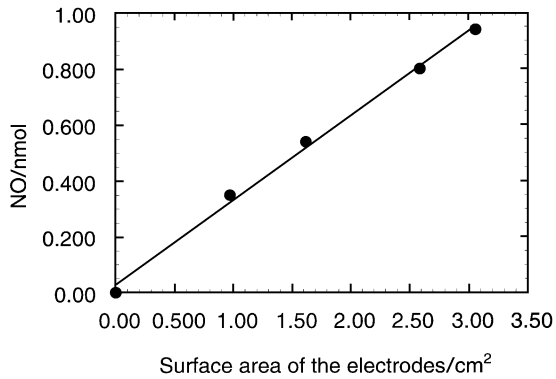

Fig. 3 A linear relationship between the amount of NO released and the surface area of the gold electrodes.

monolayer of NO donor compound. Upon electrolysis, such an electrode quantitatively generates NO at a nanomolar scale and the amount of NO produced can be controlled by changing the surface area of the gold electrode. It is thus envisioned that this type of electrode can be developed into practical NO generating micro electrode arrays for a variety of biochemical applications where a small but quantitative amount of NO can be targeted at specific sites.

This work was supported by research grants from the NIH (GM 54074) and the American Heart Association, FL Affiliate (9701760). P. G. Wang and Y.-C. Hou thank Professor Luis Echegoyen for useful discussions at the University of Miami where the ideas regarding this work were initiated.

Notes and references

† *Selected data* for **5**: δ_H(500 MHz, CD_3OD) 3.62 (s, 2H), 7.29 (d, J = 8.5 Hz, 2H), 7.53 (d, J = 9.0 Hz, 2H); δ_C(125 MHz, CD_3OD) 27.2, 119.2, 128.2, 136.8, 144.5; UV/Vis (MeOH): λ_{max} (ε) = 299 nm (11,000); Anal. calcd. for $C_7H_{11}N_3O_2S_1$: C, 41.78; H, 5.51; N, 20.88; S, 15.93. Found: C, 41.82; H, 5.48; N, 20.80; S, 15.87%.

‡ The IUPAC name for cupferron is *N*-nitroso-*N*-phenylhydroxylamine ammonium salt.

§ Out of several sets of NO generation data, the single best one was chosen for the plot.

1 S. Moncada, R. M. J. Palmer and E. A. Higgs, *Pharmacol. Rev.*, 1991, **43**, 109.
2 J. S. Beckman, in *Nitric Oxide: Principles and Actions*, ed. J. Jr. Lancaster, Academic Press, San Diego, 1996, p. 1.
3 M. Feelish and J. S. Stamler, in *Methods in Nitric Oxide Research*, eds. M. Feelish and J. S. Stamler, John Wiley & Sons, New York, 1996, p. 71.
4 J. M. Fukuto, in *Nitric Oxide: Biochemistry, Molecular Biology, and Therapeutic Implications*, eds. L. Ignarro and F. Murad, Academic Press, New York, 1995, p. 1.
5 Y.-C. Hou, A. Janczuk and P. G. Wang, *Curr. Pharm. Des.*, 1999, **5**, 417.
6 L. K. Keefer, *CHEMTECH*, 1998, **28**, 30.
7 J. Aizenberg, A. J. Black and G. M. Whitesides, *Nature*, 1998, **394**, 868.
8 C. M. Ruan, F. Yang, C. H. Lei and J. Q. Deng, *Anal. Chem.*, 1998, **70**, 1721.
9 G. E. Poirier, *Chem. Rev.*, 1997, **97**, 1117.
10 L. Jian, A. Glidle, A. Griffith, C. J. McNeil and J. M. Cooper, *Bioelectrochem. Bioenerg.*, 1997, **42**, 15.
11 A. J. Guiomar, S. D. Evans and J. T. Guthrie, *Supramol. Sci.*, 1997, **4**, 279.
12 J. G. Lawless and M. D. Hawley, *Anal. Chem.*, 1968, **40**, 948.
13 A. D. McGill, Y. Yang, J. Wang, L. Echegoyen and P. G. Wang, in *Methods in Enzymology*, ed. L. Packer, Academic Press, New York, 1999, **301**, 235.
14 T. Ishida, N. Nishida, S. Tsuneda, M. Hara, H. Sasabe and W. Knoll, *Jpn. J. Appl. Phys.*, 1996, **35**, L1710.
15 G. Beamson and D. Briggs, in *High Resolution XPS of Organic Polymers: The Scienta ESCA300 Database*, John Wiley & Sons, New York, 1992, p. 182.
16 C. D. Wagner, W. M. Riggs, L. E. Davis, J. F. Moulder and G. E. Muilenberg, in *Handbook of X-ray Photoelectron Spectroscopy*, Perkin–Elmer Corporation, Minnesota, 1979, p. 40.

DFT exploration of structural and magnetic properties of [*n*]annulene ring carbomers

Cyril Godard, Christine Lepetit and Remi Chauvin*

Laboratoire de Chimie de Coordination, UPR 8241 CNRS, 205 Route de Narbonne, 31077 Toulouse cedex 4 France. E-mail: chauvin@lcc-toulouse.fr

Received (in Cambridge, UK) 25th July 2000, Accepted 15th August 2000
First published as an Advance Article on the web 11th September 2000

DFT calculations of structural and magnetic properties of the ring carbomers of [*n*]annulenic species (*n* = 3–6), show that the aromatic *vs.* antiaromatic character of [*n*]annulenic species is qualitatively preserved by the carbomerisation process.

The constitutive, practical, and aesthetical importance of the carbon element in molecular chemistry[1] can be doubled with a formal function to expand the size of Dreiding (or ball-and-stick) models of molecules independently from other structural features. Indeed, by inserting an $(sp\text{-}C)_2$ unit into each bond of a Lewis structure, one constructs a so-called 'carbomer' structure of the former which has approximately a three-fold expanded size, and yet preserves the connectivity, the symmetry, the shape and π-electron resonance properties of its antecedent (Scheme 1).[2]

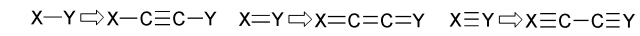

Scheme 1 Basic process in the definition of carbomers.

The general question to be addressed is whether the preservation/transformation of such essential characteristics of the chemical model entails preservation/transposition of physicochemical properties. The addition of two π-electron pairs per connection in the carbomerisation process makes a carbomer molecule *a priori* more reactive than the parent molecule. In order to correct this additive bond energy scheme and restore some stability in future synthetic targets, one here considers possible aromatic carbomer molecules: these molecules might simply be the carbomers of known aromatic molecules. This would allow us to test the way aromaticity, an intensively long debated concept,[3] is transposed by the carbomerisation process. In an exploratory study, we now consider the 'ring carbomers' of [*n*]annulenic species.[4]

Lewis structures of the ring carbomers ***n*b** of the lowest classical [*n*]annulenic molecules and ions ***n*a** (*n* = 3–6) are depicted in Scheme 2.[5] According to the simple VSEPR model, the structures should be planar and more or less symmetrical, depending on the electron delocalisation. Although none of these molecules are experimentally known,[6] substituted derivatives of the ring carbomer of benzene **6b** have been described.[7] In particular, the D_{6h} symmetry of the ring of the hexaphenyl derivative has been established by X-ray crystallography.[8] Since geometry optimisation of **6b** at the B3PW91/6-31G** level reproduced the experimental symmetry and bond lengths, this method was used for calculating the structures of all carbomers ***n*b** (Fig. 1).

As anticipated from the application of the basic Hückel rule to the sole π_z-electron systems,[9] the singlet $4m + 2$ π_z electron structures ***n*b** (*n* = 6, 5, 3) and the triplet $4m$ π_z-electron structure ***n*bT** (*n* = 4), exhibit D_{nh} symmetry just as their respective parent molecules ***n*a**. Likewise, the singlet $4m$ = 12 π_z-electron structure **4bS** possesses a lower D_{2h} symmetry just as its parent singlet cyclopentadiene **4aS** (Table 1). These results prove that structural aromaticity (resp. structural antiaromaticity) of a [*n*]annulenic species ***n*a** is preserved in its ring carbomer ***n*b**. Moreover, the application of the Hückel rule, early established for [*n*]annulenic molecules, is thus valid for their ring carbomers on the basis of a π_z electron count. The specific presence of in-plane π_{xy} electrons does not have a qualitative influence on the structural aromaticity of [*n*]annulene ring carbomers.

According to Katritsky's factor analysis, the aromaticity concept is two dimensional.[10] Whereas structural aromaticity (D_{nh} symmetry) can be regarded as a measure of the cyclic delocalisation of σ electrons,[11] magnetic aromaticity (ring current) is a measure of the cyclic delocalisation of the π electrons.[12] The Nucleus Independent Chemical Shift (NICS), propounded by Schleyer in 1996, proves to be a universal magnetic aromaticity measure revealing the existence of an overall diatropic ring current when negative, and an overall paratropic ring current when positive.[13] The NICS values of the optimised structures ***n*b** (*n* = 3–6) have been calculated at the ring center, at the B3LYP/6-31+G* level within the framework of GIAO formalism.[14] The data are compared with the NICS values of corresponding [*n*]annulenic species (Table 1):[15] ring

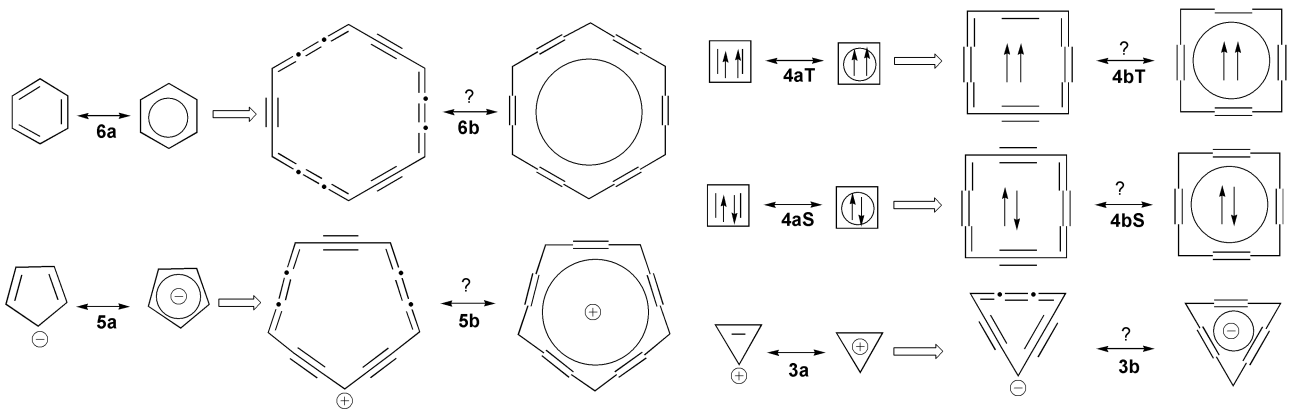

Scheme 2 [*n*]annulenic species and their ring carbomers.

Table 1 Comparative DFT-computed structural and magnetic data of [*n*]annulenic structures ***na*** and their ring carbomers ***nb***

No	Geometry[a]	sp–sp	sp–sp²	sp–sp²–sp	sp²–sp–sp	NICS[b]	No	Geometry[a]	sp²–sp²	NICS[b]
6b	D_{6h}	1.239	1.369	122.6°	178.7°	−17.9	**6a**	D_{6h}	1.394	−8.0
5b	D_{5h}	1.238	1.369	118.5°	174.8°	−16.9	**5a**	D_{5h}	1.419	−12.5
4bT	D_{4h}	1.241	1.378	115.2°	167.4°	−15.8	**4aT**	D_{4h}	1.437	−2.0
4bS	D_{2h}	1.267,1.218	1.334, 1.428	115.2°	167.3°	53.0	**4aS**	D_{2h}	1.572, 1.334	28.2
3b	D_{3h}	1,253	1.391	109.7°	155.1°	−22.3	**3a**	D_{3h}	1.365	−22.4

[a] Optimised geometries at the B3PW91/6-31G** level. Bond lengths are in Å units. [b] In ppm units. NICS were calculated at the centroids of the rings within the framework of the GIAO formalism at the B3LYP/6-31+G* level from the B3PW91/6-31G** optimised geometries.

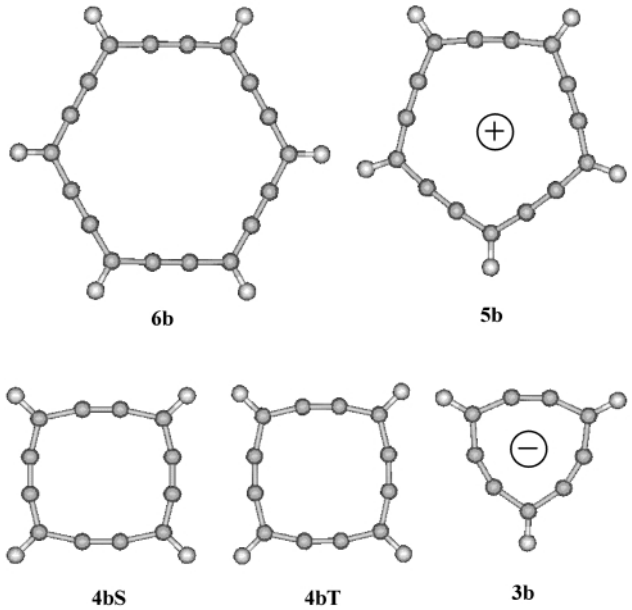

Fig. 1 Optimised geometries of ring carbomers ***nb*** at the B3PW91-6-31G** level.

carbomers ***nb*** have the same NICS sign as their respective parent [*n*]annulenes ***na***. This shows that magnetic aromaticity is qualitatively preserved in the carbomerisation process. The high positive NICS value of singlet 12-π_z electron **4bS** must be emphasised: it is the signature of a rather strong paratropic ring current, as in singlet cyclobutadiene.

In order to bring out the specific influence of the out-of-plane π_z system *versus* that of the in-plane π_{xy} system in the ring carbomer structures ***nb***, the π_{xy} in-plane system is formally isolated in the corresponding [*n*]pericyclynes. For example, the ring center NICS value of [5]pericyclyne **7** (Scheme 3) in its optimised geometry has been calculated. The weak value found (NICS(**7**) = +0.6 ppm, at the HF/6-31+G* level) confirms the absence of homoaromaticity in **7** claimed by Schleyer *et al.*[16] The ring geometry of **7** is $\boldsymbol{D}_{5h}$ (with d(C≡C) = 1.208 and d(C–C) = 1.466 Å), similar to that of **5b**. Therefore, by

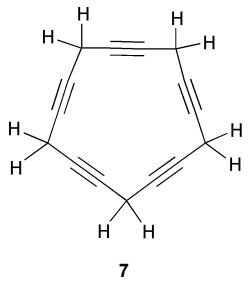

7

Scheme 3 [5]pericyclyne, assumed to have a π_{xy} system similar to that of **5b**.

resorting to the additive scheme NICS ≈ NICS(σ) + NICS(π_z) + NICS(π_{xy}),[17] it can be approximated that **7** and **5b** have similar NICS(σ) and NICS(π_{xy}) contributions: the high NICS value of **5b** is thus merely due to the NICS(π_z) component, while the in-plane π_{xy} system plays a minor role.

As for [*n*]annulenes, structural and magnetic aromaticity criteria correlate perfectly well together and with the Hückel rule applied to the sole π_z-electron system of [*n*]annulene ring carbomers. In conclusion, the preservation of aromaticity *vs.* antiaromaticity character during the carbomerisation process is clearly illustrated. This result encourages further efforts in the carbomeric comparison of physicochemical properties. In particular the transposition of energetic aromatic criteria going from ***na*** to ***nb*** will be reported shortly.[18]

The authors are grateful to Dr Guy Lavigne for encouraging discussions. We also wish to thank the Centre National de la Recherche Scientifique and the Ministère de l'Enseignement Supérieur de la Recherche et de la Technologie for financial support and IDRIS for computing facilities.

Notes and references

1 *Topics in Current Chemistry*, ed. A. de Meijere, 1998, **196**, and 1999, **201**.
2 R. Chauvin, *Tetrahedron Lett.*, 1995, **36**, 397.
3 V. E. Minkin, M. N. Glukhovtsev and B. Y. A. Simkin, *Aromaticity and Antiaromaticity. Electronic and Structural Aspects*, Wiley, New York, 1994.
4 Since substituents generally exert a weak influence on the aromaticity of the benzene ring, peripheral C–H bonds are not required to undergo C_2-insertion. Therefore, in a preliminary study, the VSEPR symmetry of the Dreiding structures is preserved, but not the exact shape.
5 In order to satisfy the Hückel rule for **5b** and **6b**, one decides to define the carbomer of a charged species as the everywhere C_2-inserted structure with an opposite whole charge. In the case of non-covalent neutral structures, this is formally equivalent to a reversal of the charge separation.
6 R. Chauvin, *Tetrahedron Lett.*, 1995, **36**, 401.
7 Y. Kuwatani, N. Watanabe and I. Ueda, *Tetrahedron Lett.*, 1995, **36**, 119.
8 R. Suzuki, H. Tsukuda, N. Watanabe, Y. Kuwatani and I. Ueda, *Tetrahedron*, 1998, **54**, 2477.
9 The *z* axis is taken perpendicular to the main plane of the structure.
10 A. R. Katritsky, P. Barczynski, G. Musumarra, D. Pisano and M. Szafran, *J. Am. Chem. Soc.*, 1989, **111**, 7.
11 S. S. Shaik, P. C. Hiberty, J.-M. Lefour and G. Ohanessian, *J. Am. Chem. Soc.*, 1987, **109**, 363.
12 P. Lazzeretti, *Prog. Nucl. Magn. Reson. Spectrosc.*, 2000, **36**, 1.
13 P. v. R. Schleyer, C. Maerker, A. Dransfeld, H. Jiao and N. J. R. v. E. Hommes, *J. Am. Chem. Soc.*, 1996, **118**, 6317.
14 K. Wolinski, J. F. Hinton and P. Pulay, *J. Am. Chem. Soc.*, 1990, **112**, 8251; J. R. Cheeseman, G. W. Trucks, T. A. Keith and M. J. Frisch, *J. Chem. Phys.*, 1996, **104**, 5497.
15 V. Gogonea, P. v. R. Schleyer and P. R. Schreiner, *Angew. Chem., Int. Ed.*, 1998, **37**, 1945.
16 H. Jiao, N. R. J. v. E. Hommes, P. v. R. Schleyer and A. de Meijere, *J. Org. Chem.*, 1996, **61**, 2826.
17 P. v. R. Schleyer, H. Jiao, N. J. R. v. E. Hommes, V. G. Malkin and O. L. Malkina, *J. Am. Chem. Soc.*, 1997, **119**, 12669.
18 C. Lepetit, C. Godard and R. Chauvin, submitted for publication.

ChemComm

Solid-phase synthesis of novel achiral hydantoin- and isoxazoline-substituted dispirocyclobutanoids†

Kyung-Ho Park and Mark J. Kurth*

Department of Chemistry, University of California, One Shields Avenue, Davis, CA 95616 USA

Received (in Corvallis, OR, USA) 18th May 2000, Accepted 31st July 2000
First published as an Advance Article on the web 11th September 2000

A synthesis of novel achiral hydantoin- and isoxazoline-substituted dispirocyclobutanoids from solid-phase synthesis has been achieved. The facial and selective Boc-NH-mediated hydrogen-bond delivery of the nitrile oxide afforded 6 as the major compound.

In the field of drug discovery, considerable effort has been applied to the synthesis of hydantoin derivatives[1] using both solution- and solid-phase organic synthesis techniques. Many of the hydantoins reported to date are either racemic or diastereomeric mixtures. For example, we have synthesized a number of hydantoins.[1i–l]

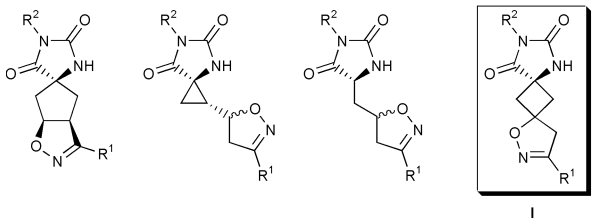

I

The need to further diversify these compounds, together with recent reports regarding the biological activities of spirohydantoins[2] and spiroisoxazolines,[3] led us to explore development of a solid-phase synthetic strategy for the construction of hydantoin- and isoxazoline-containing heterocycle **I** with its central cyclobutane core. In this dispiro [4.1.4.1] system, the target molecule itself is achiral and thus avoids the formation of racemic mixtures—an important synthetic consideration when designing a potential drug scaffold.

Our solid-phase approach to **I** began with the coupling of Boc-protected amino acid **1**[4] with hydroxymethyl substituted polystyrene (1.1 mmol OH gram^{-1}) in the presence of 1,3-diisopropylcarbodiimide (DIC). A solid-phase 1,3-dipolar cycloaddition reaction[5] of the alkene moiety in **2** with a Mukaiyama-generated nitrile oxide[6] delivered resin **3**. Deprotection of the Boc moiety (TFA–CH_2Cl_2) and neutralization (Et_3N) of the resin delivered amino ester **4**. Treatment of this intermediate with isocyanates gave the urea ester intermediate **5** which released the achiral dispirohydantoins **6** and **7** by treatment with Et_3N (Scheme 1, Table 1). In previous studies,[1i–j] we discovered that urea-NH in cyclopentenyl amino acids can be a very effective stereocontrol element in solid-phase intermolecular nitrile oxide 1,3-dipolar cycloaddition reactions. With **2** now in hand, we were positioned to probe whether the Boc-NH moiety here would mediate similar stereoselectivity.

Indeed, the *exo*-methylenecyclobutane system realized some diastereoselectivity such that the H-bond directed product (*i.e.* **6**) was obtained with ≈3:1 selectivity relative to the non-H-bond directed product (*i.e.* **7**). X-ray crystallographic analysis of **6c**‡ (Fig. 1) verified the relative stereochemistries of **6**/**7**. This solid-phase stereoselectivity is in accord with our preliminary solution-phase studies where the ethyl ester equivalent of **2** (R^1 = C_6H_5–) undergoes 1,3-dipolar cycloaddition giving the ethyl ester equivalent of **3** with ≈3:1 stereoselectivity. Moreover, the solution-phase parallels of **2** → **3** → **4** → **5** → **6** (R^1 = C_6H_5–; R^2 = $C_6H_5CH_2$–) proceed in 52% overall yield (64, 89, 96, and 95%, respectively), while the solid-phase overall yield of **6** + **7** from hydroxymethyl substituted polystyrene (*i.e.* one additional step; **1** → **2**) is 45–56%. Thus, while solution- and solid-phase yields are comparable, the solid-phase protocol reported here enjoys the typical advantages of bead-based chemistry[7] and it allows for the easy manipulation of diastereomer mixtures with only end-product (*i.e.* **6** and **7**) separation.

Typical procedure for solid-phase synthesis of dispirohydantoins. A solution of DMAP (20 mg, 0.16 mmol) in DMF–CH_2Cl_2 (1 mL–4 mL) was prepared. Boc-protected amino acid **1** (0.37 g, 1.65 mmol) and DIC (0.21 g, 1.65 mmol) were dissolved in DMF–CH_2Cl_2 (1–4 mL) and this solution was added to the flask which contained the hydroxymethyl substituted polystyrene (0.5 g, 0.55 mmol, 1.1 mmol OH gram^{-1}). Finally the DMAP solution was added and the reaction mixture was stirred overnight at ambient temperature. The resin was washed with DMF, CH_2Cl_2, and ether, and dried to give the resin **2**. Resin **2** was swollen in THF (15 mL) and nitropropane (0.15 g, 1.65 mmol), phenylisocyanate (0.39 g, 3.3 mmol), and Et_3N (15 mg) were added. The reaction mixture was stirred at 60 °C overnight, then washed with DMF, CH_2Cl_2, and ether. This 1,3-dipolar cycloaddition step was repeated a second time. Drying *in vacuo* gave the resin **3** (R^1 = Et) which was treated

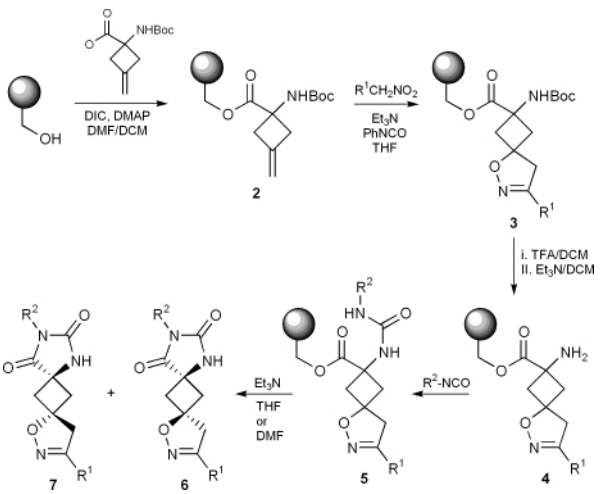

Scheme 1

Table 1 Dispirocyclobutanoids (**6**/**7**) from solid-phase synthesis

Compound	R^1	R^2	% Yield[a]
6a	C_6H_5CO–	C_6H_5–	40
7a	C_6H_5CO–	C_6H_5–	16
6b	Et–	$C_6H_5CH_2$–[b]	36
7b	Et–	$C_6H_5CH_2$–[b]	11
6c	C_6H_5CO–	^{n}Bu–[b]	35
7c	C_6H_5CO–	^{n}Bu–[b]	10
6d	Et–	C_6H_5–	39
7d	Et–	C_6H_5–	15

[a] Overall yield from hydroxymethyl substituted polystyrene. [b] Cyclo-elimination was achieved using DMF.

DOI: 10.1039/b004033i

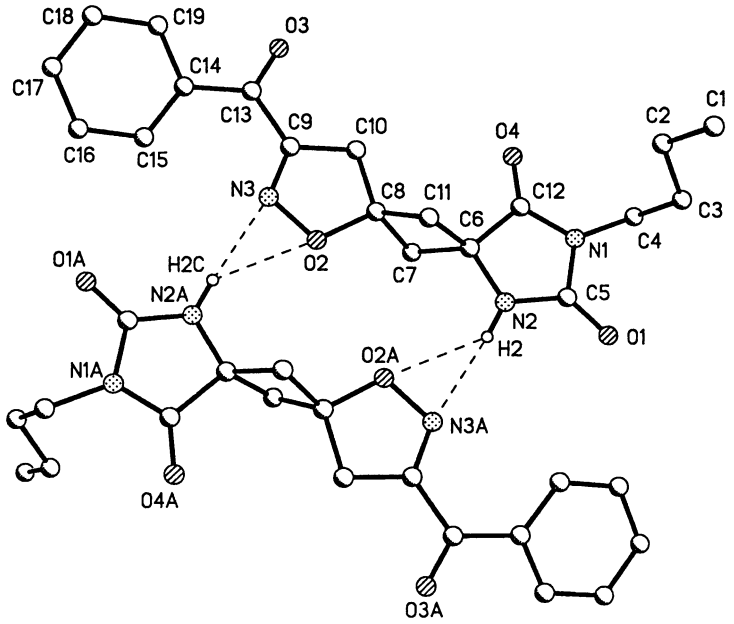

Fig. 1

with 50% TFA–CH_2Cl_2 (20 mL) at ambient temperature for 1 h. The resin was washed with DMF and CH_2Cl_2, followed by treatment with 10% Et_3N in CH_2Cl_2 (20 mL) for 1 h. The resulting resin was washed with DMF, CH_2Cl_2, and ether, and dried under vacuum to give resin-bound **4** with its free amine functional group. Resin **4** was treated with benzyl isocyanate (0.22 g, 1.65 mmol) in THF overnight at ambient temperature. The resin was washed with THF, DMF, and CH_2Cl_2 to afford the urea **5** (R^1 = Et–, R^2 = $C_6H_5CH_2$–). This resin was treated with Et_3N (0.33 g, 3.3 mmol) in DMF (20 mL) at 110 °C for 30 h to release the achiral dispirohydantoins as a mixture (**6b**:**7b** = 3:1), which was finally separated by column chromatography (ethyl acetate–hexane = 1:4) to give **6b** (62 mg, 0.2 mmol, 36% overall yield§) and **7b** (20 mg, 0.06 mmol, 11% overall yield§). **6b**: Mp 157 °C; FTIR (KBr) 3259, 2939, 1760, 1723, 1450 cm^{-1}; δ_H (300 MHz, $CDCl_3$) 7.37–7.23 (m, 5H), 7.11 (s, 1H), 4.62 (s, 2H), 3.32 (s, 2H), 2.95 (d, 2H, J = 13.8 Hz), 2.78 (d, 2H, J = 13.8 Hz), 2.34 (q, 2H, J = 7.4 Hz), 1.15 (t, 3H, J = 7.4 Hz); δ_C (75 MHz, $CDCl_3$) 176.8, 161.4, 155.7, 135.9, 128.6, 128.4, 127.8, 77.6, 53.4, 47.9, 46.6, 42.1, 21.3, 10.6; Anal. Calcd for $C_{17}H_{19}N_3O_3$: C, 65.16; H, 6.11; N, 13.41. Found: C, 65.11; H, 6.08; N, 13.27%. **7b**: Mp 194 °C; FTIR (KBr) 3196, 2934, 1778, 1714, 1431 cm^{-1}; δ_H (300 MHz, $CDCl_3$) 8.21 (s, 1H), 7.32–7.25 (m, 5H), 4.63 (s, 2H), 3.26–3.23 (m, 4H), 2.42–2.34 (m, 4H), 1.16 (t, 3H, J = 7.5 Hz); δ_C (75 MHz, $CDCl_3$) 174.2, 160.4, 158.0, 135.8, 128.6, 128.3, 128.0, 79.0, 54.8, 48.1, 46.6, 42.4, 21.4, 10.8; Anal. Calcd for $C_{17}H_{19}N_3O_3$: C, 65.16; H, 6.11; N, 13.41. Found: C, 65.36; H, 6.17; N, 13.41%.

In summary, we have developed a synthetic strategy for the preparation of novel heterocycles of generalized structure **I** from solid-phase. The work reported here secures this stage in a program aimed at the structural diversification of hydantoin- and isoxazoline-based pharmacophores. Combinatorial library production employing this general and expedient synthetic solid-phase methodology and subsequent biological evaluation are underway.

Notes and references

† We thank the National Science Foundation for financial support of this research and the National Science Foundation CRIF program (CHE-9808183) for Varian Inova 400 MHz and Mercury 300 MHz NMR instrument purchases.

‡ *Crystal data*: for **6c** $C_{19}H_{21}N_3O_4$, colorless plate, M = 355.39, triclinic, space group $P1$, a = 6.1496(7) Å, α = 93.194(2)°, b = 96315(11) Å, β = 92.728(2)°, c = 15.2827(10) Å, γ = 106.031(2)°, U = 866.77(15) $Å^3$, Z = 2, D_c = 1.362 Mg m^{-3}, μ = 0.097 mm^{-1}, R = 0.0515, wR = 0.1206, GOF = 1.008, T = 89(2) K, $F(000)$ = 376, 4328 independent reflections were collected on a Bruker SMART 1000 (λ = 0.71073 Å).

§ The optimized solid-phase overall yield of **6b** + **7b** is 47% which translates to ≈86% yield per step from **1**.

1 (*a*) B. A. Dressman, L. A. Spangle and S. W. Kaldor, *Tetrahedron Lett.*, 1996, **37**, 937; (*b*) S. Hanessian and R. Y. Yang, *Tetrahedron Lett.*, 1996, **37**, 5835; (*c*) J. Matthews and R. A. Rivero, *J. Org. Chem.*, 1997, **62**, 6090; (*d*) X. Xiao, K. Ngu, C. Chao and D. V. Patel, *J. Org. Chem.*, 1997, **62**, 6968; (*e*) J. Stadlweiser, E. P. Ellmerer-Muller, A. Taco, N. Maslouh and W. Bannwarth, *Angew. Chem. Int. Ed.*, 1998, **37**, 1402; (*f*) L. J. Wilson, M. Li and D. E. Portlock, *Tetrahedron Lett.*, 1998, **39**, 5135; (*g*) A. Nefzi, C. Dooley, J. M. Ostresh and R. A. Houghten, *Bioorg. Med. Chem. Lett.*, 1998, **8**, 2273; (*h*) A. Boeijen, J. A. W. Kruijtzer and R. M. J. Liskamp, *Bioorg. Med. Chem. Lett.*, 1998, **8**, 2375; (*i*) K.-H. Park, M. M. Olmstead and M. J. Kurth, *J. Org. Chem.*, 1998, **63**, 113; (*j*) K.-H. Park, M. M. Olmstead and M. J. Kurth, *J. Org. Chem.*, 1998, **63**, 6579; (*k*) K.-H. Park, E. Abbate, S. Najdi, M. M. Olmstead and M. J. Kurth, *Chem. Commun.*, 1998, 1679; (*l*) K.-H. Park and M. J. Kurth, *Tetrahedron Lett.*, 1999, **40**, 5841.

2 (*a*) T. W. Brandstetter, Y. Kim, J. C. Son, H. M. Taylor, P. M. de Q. Lilley, D. J. Watkin, L. N. Johnson, N. G. Oikonomakos and G. W. J. Fleet, *Tetrahedron Lett.*, 1995, **36**, 2149; (*b*) H. Haruyama, T. Takayama, T. Kinoshita, M. Kondo, M. Nakajima and T. Haneishi, *J. Chem. Soc., Perkin Trans. 1*, 1991, 1637; (*c*) S. Mio, H. Sano, M. Shindou, T. Honma and S. Sugai, *Agric. Biol. Chem.*, 1991, **43**, 133.

3 (*a*) J. Wityak, T. M. Sielecki, D. J. Pinto, G. Emmett, J. Y. Sze, J. Liu, A. E. Tobin, S. Wang, B. Jiang, P. Ma, S. A. Mousa, R. R. Welxler and R. E. Olson, *J. Med. Chem.*, 1997, **40**, 50; (*b*) P. Ciminiello, C. Dell'Aversano, E. Fattorusso, S. Magno and M. Pansini, *J. Nat. Prod.*, 1999, **62**, 590.

4 K.-H. Park and M. J. Kurth, *J. Org. Chem.*, 2000, **65**, in the press.

5 *1,3-Dipolar Cycloaddition Chemistry*, ed. A. Padwa, Wiley; New York, 1984, Vol. 1 and 2.

6 For reviews of nitrile oxide–isoxazoline methodology, see (*a*) D. P. Curran, *Advances in Cycladdition*, 1988, **1**, 129; (*b*) K. B. G. Torssel, *Nitrile Oxides, Nitrones and Nitronates in Organic Synthesis*, VCH Publishers, Weinheim, 1988.

7 M. J. Kurth, *Chimia*, 1996, **50**, 261.

ChemComm

Palladium-catalysed cyclotrimerisation reactions of polycyclic alkenes under the Stille and Grigg coupling conditions

Antonio Paulon, Sergio Cossu, Ottorino De Lucchi* and Cristiano Zonta

Dipartimento di Chimica, Università Ca' Foscari di Venezia, Dorsoduro 2137, I-30123 Venezia, Italy

Received (in Cambridge, UK) 12th May 2000, Accepted 16th August 2000
First published as an Advance Article on the web 11th September 2000

Preformed or *in situ* generated polycyclic bromostannylalkenes react under palladium catalysis under Stille or Grigg reaction conditions to afford cyclotrimerised adducts *via* a three-fold carbon–carbon coupling reaction.

Due to their unusual electronic features, the class of molecules composed by trisannelated benzenes of polycyclic structures has attracted considerable interest in the past few years.[1] These molecules also have a peculiar cup-shaped structure that makes them suitable for use in molecular recognition as the component host.[2] Here we present a new and effective method of preparation of benzoannellated cyclotrimers which is based on the Stille coupling reaction.†[3] The cyclotrimerisation is accomplished by placing the metal center (the stannyl residue) and the leaving group (the bromine atom) (Scheme 1) at the two ends of the olefinic substrate.

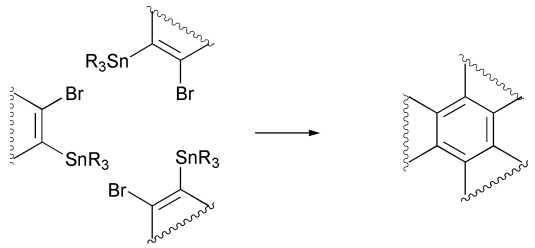

Scheme 1

Bromostannylbenzonorborna-2,5-dienes‡ **1,2** were prepared by bromine–tin exchange from the dibromo derivative **3** or by LDA treatment of the bromobenzonorborna-2,5-diene **4** followed by quenching with trimethyltin chloride.[4] When **1** was heated at 70 °C for 24 h in DMF in the presence of palladium(II) acetate (10% mol eq.), triphenylphosphine (20% mol eq.) and LiCl a 4:1 mixture of *anti* and *syn* trimers **5** was obtained in 38% yield (Scheme 2). No detectable formation of dimers, as previously noticed in the reaction with copper nitrate, was observed.[4] Yields and *anti* to *syn* ratio are affected by temperature, solvent or by the changes to the other reaction conditions.

For example, the same reaction carried out in toluene at 120 °C affords, after 24 h, a 3:1 mixture of *anti* and *syn* isomers **5** in 30% yield. By comparison, in refluxing THF, the system is unreactive even after 94 h. The effect of co-catalysts has been considered. LiCl,[5] a well known Stille coupling activator, does not significally improve the yields of the reaction.

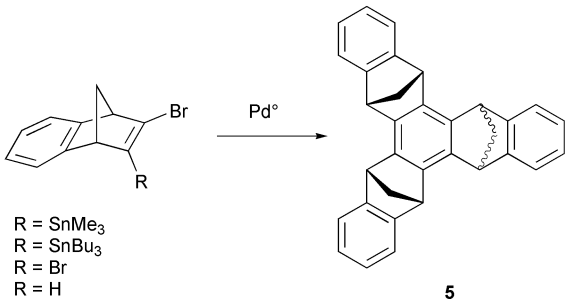

Scheme 2

Relevantly, the bromotributyltin derivative **2** treated with palladium(II) acetate (7% mol eq.) and triphenylphosphine (14% mol eq.) at 110 °C for 24 h in toluene leads to trimer **5** as only the *anti* isomer in 58% yield.

The toxic nature of tin compounds, which is especially crucial for the trimethyl derivative as well as the handling and storage of quantities of bromostannylalkenes, prompted us to test the feasability of the *in situ* reaction under the methodology developed by Grigg.[6] Accordingly, by heating a mixture of dibromobenzonorborna-2,5-diene **3**, palladium(II) acetate (10% mol eq.), triphenylphosphine (20% mol eq.) and hexamethylditin in refluxing toluene, cyclotrimer **5** is obtained in comparable yields with the Stille method (50%). In this case, however, only the *anti* isomer is formed. Remarkably the reaction can be achieved in much higher yields by using hexabutylditin, which besides being less toxic,[7] is less expensive than the methyl derivative. The latter reaction conditions, using hexabutylditin in place of hexamethylditin, gave **5** quantitatively, and were considered as the most convenient conditions for the desired transformation and were applied to other substrates for the determination of the scope of the method.§ All of the dibromoderivatives **6**–**8** afforded the respective trimer *anti*-**9**, *anti*-**10** and **11** in almost quantitative yields.¶[8]

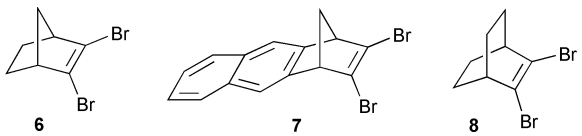

The mechanism by which trimers are formed could be attractively envisaged as a 'head to tail' coupling amongst the tin and bromine termini of the double bonds. If this in indeed the case the cyclotrimerisation reaction of racemic **1** either preformed under the Stille reaction conditions or generated *in situ* with the Grigg method, should always afford a statistical 3:1 ratio of the *anti* and *syn* product.[1b] The formation of the *anti* product only suggests that the reaction occurs with the coupling of both antipods, while that derived from the coupling of the homochiral enantiomers does not form because of steric hindrance.[1b] Alternatively, the reaction may occur *via* an acetylene intermediate stabilised by complexation with palladium. However, no further data regarding the mechanism are available so far.

In conclusion we have reported the Stille reaction applied to an unusual bifunctional substrate that leads to a useful application and developed a method that, especially in the optimised Grigg variant, competes with the best method so far available for the cyclotrimerisation of polyclic alkenes both in terms of yields and safety.

This work was supported by MURST (Rome) within the National Project 'Stereoselezione in Chimica Organica. Metodologie e Applicazioni'.

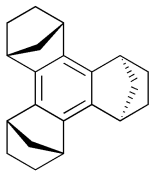

anti-**9**

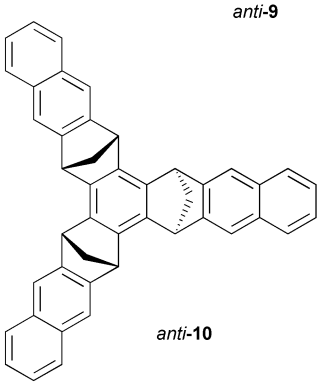

anti-**10**

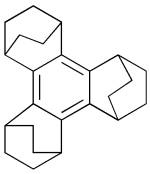

11

Notes and references

† As reported in ref. 1*a*, 2-bromo-3-trimethyltinnorborna-2,5-diene does not undergo cyclotrimerisation under Stille-coupling conditions. The reason for this failure is assumed to be Pd complexation to the double bond between carbons 5 and 6 in this substrate.

‡ The IUPAC name for benzonorborna-2,5-diene is tricyclo[6.2.1.$0^{2,7}$]undeca-2,4,6,9-tetraene.

§ A mixture of 2,3-dibromobenzonorborna-2,5-diene (0.34 mmol), $Pd(OAc)_2$ (0.04 mmol), PPh_3 (0.08 mmol) and hexabutylditin (0.51 mmol) in dry toluene (3 mL) in a screw capped pyrex test tube was purged with argon, sealed and heated at reflux for 24 h. After cooling to rt, water (20 mL) was added and extracted with diethyl ether (3 × 30 mL), washed with brine, dried ($MgSO_4$) and concentrated at reduced pressure. The residue was purified by flash chromatography through a short silica gel column eluting with a hexane–dichloromethane gradient.

¶ It should be pointed out that the cyclotrimerisation reaction carried out on the boron derivative under Suzuki type reaction conditions afforded only a very moderate yield of cyclotrimer.

1 (*a*) C. Zonta, S. Cossu and O. De Lucchi, *Eur. J. Org. Chem.*, 2000, 1965; (*b*) C. Zonta, S. Cossu, P. Peluso and O. De Lucchi, *Tetrahedron Lett.*, 1999, **40**, 8185; (*c*) R. Rathore, S. V. Lindeman, A. S. Kumar and J. K. Kochi, *J. Am. Chem. Soc.*, 1998, **120**, 6012; (*d*) R. Durr, O. De Lucchi, S. Cossu and V. Lucchini, *J. Chem. Soc., Chem. Commun.*, 1996, 2447; (*e*) F. Cardullo, D. Giuffrida, F. H. Kohnke, F. M. Raymo, J. F. Stoddart and D. J. Williams, *Angew. Chem., Int. Ed. Engl.*, 1996, **35**, 339; (*f*) N. L. Franck, K. K. Baldridge and J. S. Siegel, *J. Am. Chem. Soc.*, 1995, **117**, 2102; (*g*) K. Komatsu, S. Aonuma, Y. Jinbu, R. Tsuji, C. Hirosawa and K. Takeuchi, *J. Org. Chem.*, 1991, **56**, 195; (*h*) S. B. Singh and H. Hart, *J. Org. Chem.*, 1990, **55**, 3412; (*i*) P. G. Gassman and I. Gennick, *J. Am. Chem. Soc.*, 1980, **102**, 6863.

2 J. C. Ma and D. A. Dougherty, *Chem. Rev.*, 1997, **97**, 1303; R. Rathore, S. V. Lindeman and J. K. Kochi, *J. Am. Chem. Soc.*, 1997, **119**, 9393. General Reviews on supramolecular chemistry: C. A. Hunter, *Chem. Soc. Rev.*, 1994, 101; J.-M. Lehn, *Supramolecular Chemistry*, VCH, Weinheim, 1995; F. Diederich, *Cyclophanes*, The Royal Society of Chemistry, Cambridge, 1994; F. Vogtle, *Supramolekulare Chemie*, Teubner, Stuttgart, 1989.

3 S. P. Stanforth, *Tetrahedron*, 1998, **54**, 263; V. Farina, V. Krishnamurthy and W. J. Scott, *Org. React.*, 1997, **50**, 1; J. K. Stille, *Angew. Chem., Int. Ed. Engl.*, 1986, **25**, 508.

4 R. Durr, S. Cossu, V. Lucchini and O. De Lucchi, *Angew. Chem., Int. Ed. Engl.*, 1997, **36**, 2805; S. Cossu, O. De Lucchi, V. Lucchini, G. Valle, M. Balci, A. Dastan and B. Demirci, *Tetrahedron Lett.*, 1997, **38**, 5319.

5 M. Fujita, H. Oka and K. Ogura, *Tetrahedron Lett.*, 1995, **36**, 5247; W. J. Scott and J. E. McMurry, *Acc. Chem. Res.*, 1988, **21**, 47.

6 R. Grigg, A. Teasdale and V. Sridharan, *Tetrahedron Lett.*, 1991, **32**, 3859.

7 M. Bragadin and D. Marton, *J. Inorg. Biochem.*, 1997, 76.

8 For **9**: see ref. 1*i*. For **10**: see ref. 1*a*. For **11**: see ref. 1*g*.

A novel synthetic route to peralkylated carborane anions, 1-H-$CB_9Me_9^-$ and 1-H-$CB_{11}R_{11}^-$ (R = Me, Et)

Chi-Wing Tsang and Zuowei Xie*

Department of Chemistry, The Chinese University of Hong Kong, Shatin, New Territories, Hong Kong, China. E-mail: zxie@cuhk.edu.hk

Received (in Cambridge, UK) 13th June 2000, Accepted 22nd August 2000
First published as an Advance Article on the web 11th September 2000

Treatment of carborane anions with excess RBr (R = Me, Et) in a sealed Pyrex tube at 200 °C gives peralkylated carborane anions in quantitative yields, which represents the most convenient and the most economic method so far reported in the literature for the preparation of peralkylcarborane anions.

As a class of the robust and weakly coordinating anions, carborane anions have found many applications in catalysis, metathesis, and oxidation chemistry as well as in stabilizing highly reactive cations.[1] Many derivatives of carborane anions have recently been reported; among these, the polymethylated species have received much attention.[2–7] Two main methods have been developed for the transformation of B–H or B–I vertices to B–C ones; they include palladium-catalyzed alkylation of B–I vertices of iodocarboranes with Grignard reagents,[2–5] and electrophilic substitution of B–H vertices by strong methylating reagents such as methyl triflate or trimethylaluminium/MeI.[6,7] These methods often involve complicated workup procedures, and sometimes a mixture of products, which lead to a lower yield. We report herein a very facile synthesis of peralkylated carborane anions.

Treatment of $[Me_3NH][1\text{-H-}CB_9H_9]$ or $[Me_3NH][1\text{-R-}CB_{11}H_{11}]$ with excess MeBr in a sealed Pyrex tube at 200 °C for 5 days gives permethylated products $[Me_3NH][1\text{-H-}CB_9Me_9]$ (**1**) or $[Me_3NH][1\text{-R-}CB_{11}Me_{11}]$ [R = H (**2**), CH_3 (**3**)] in almost quantitative yields.† The first perethylated carborane anion, $[Me_3NH][1\text{-H-}CB_{11}Et_{11}]$ (**4**), can also be prepared quantitatively in the same manner by using EtBr as a reagent [eqn. (1)].

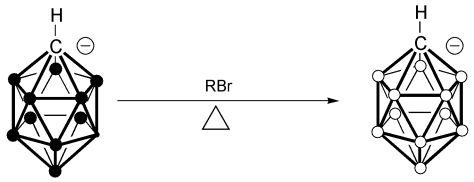

(1)

No organic solvent is involved and no workup procedures are needed. After the reaction is complete, the Pyrex tube is opened and excess RBr is immediately evaporated leaving a pure product. These compounds have been fully characterized by ^1H, ^{13}C and ^{11}B NMR, MS and IR spectroscopy. The complete conversion of B–H vertices into B–R (R = Me, Et) vertices is indicated by the absence of the characteristic B–H absorption (*ca.* 2600 cm^{-1}) in the IR spectra and identical proton-coupled and proton-decoupled ^{11}B NMR spectra. The formation of the B–C bonds is also reflected in the broadening and upfield shifted carbon chemical shifts in their ^{13}C NMR spectra due to the close proximity of carbon nuclei to both ^{11}B and ^{10}B nuclei.[3,8]

Reaction of $[Me_3NH][1\text{-H-}CB_{11}H_{11}]$ with excess ^{i}PrBr under the same or more rigorous reaction conditions, however, affords a mixture of polyalkylated carboranes $[Me_3NH][1\text{-H-}CB_{11}H_{11-n}{}^i Pr_n]$ (n = 4–7) on the basis of MS analyses. The reasons for that are probably due to the steric effects of the isopropyl groups. It is noteworthy that no brown Br_2 is produced and only HBr gas is detected in the above-mentioned reactions. If the permethylation is carried out in a $(MeO)_3P(O)$ solution or the perethylation is performed in a $(EtO)_3P(O)$ solution, both the reaction temperature and reaction time are reduced.[9]

In contrast, reaction of $[Me_3NH][1\text{-H-}CB_{11}H_{11}]$ with excess MeI, under the same reaction condition, yields a mixture of products $[Me_3NH][1\text{-H-}CB_{11}Me_{11-n}I_n]$ (n = 3–5) on the basis of MS analyses, along with the formation of HI and purple I_2. These results indicate that MeI may undergo both heterolytic and homolytic reactions generating Me^+, $Me^{\cdot}$, I^- and $I^{\cdot}$. Coupling of $I^{\cdot}$ yields purple I_2. Both Me^+ and I_2 are electrophiles, which react with carborane to form a mixture of $[1\text{-H-}CB_{11}Me_{11-n}I_n]^-$.

In summary, a very facile and economic method has been developed for the first time for the synthesis of permethylated and perethylated carborane anions. Applications of this novel methodology to other carborane and borane molecules are under investigation.

We thank the Research Grants Council of the Hong Kong Special Administration Region (Project No. CUHK 4210/99P) for financial support.

Notes and references

† *Preparation* of **4***: Method A*. A thick-walled Pyrex tube was charged with $[Me_3NH][1\text{-H-}CB_{11}H_{11}]$ (0.10 g, 0.49 mmol) and ethyl bromide (0.5 mL, 6.70 mmol) at 0 °C. This tube was then cooled with liquid N_2, sealed under vacuum and placed in a furnace. The temperature of the furnace was gradually increased to 160 °C, and this temperature was maintained for 2 days. The temperature was then slowly raised to 220 °C, and this temperature was maintained for 3 days. The tube was opened and excess ethyl bromide was evaporated, leaving a pale yellow solid. The ^{11}B NMR showed that it is a pure compound. This pale yellow solid can be further recrystallized from a water/acetone solution to give **4** as a white crystalline solid (0.23 g, 92%). ^1H NMR (acetone-d_6): δ 2.96 [s, $(CH_3)_3NH$], 0.96 [br s, B-CH_2CH_3], 0.87 [br s, B-CH_2CH_3]; ^{13}C NMR (acetone-d_6): δ 45.48 [$(CH_3)_3NH$], 12.24 [s, B-CH_2CH_3(2–6)], 10.95 [s, B-CH_2CH_3(7–12)], 6.94 [br, B-CH_2CH_3(2–12)]; ^{11}B NMR (acetone-d_6): δ 2.95 (s, 1B), −4.05 (s, 5B), −7.78 (s, 5B); IR (cm^{-1}, KBr): ν 2953 (s), 2908 (s), 2874 (s), 1457 (m), 1156 (m), 1034 (w), 956 (m), 521(s); Negative-ion MALDI MS, *m/z* (isotopic abundance): calcd. for $[1\text{-H-}CB_{11}(CH_2CH_3)_{11}]^-$ 449(34), 450(70), 451(100), 452(90), 453(45); found 449(32), 450(67), 451(100), 452(91), 453(43).

Method B. A thick-walled Pyrex tube was charged with $[Me_3NH][1\text{-H-}CB_{11}H_{11}]$ (0.10 g, 0.49 mmol), ethyl bromide (0.5 mL, 6.70 mmol), and triethylphosphate (1.5 mL, 8.83 mmol) at 0 °C. This tube was then cooled with liquid N_2, sealed under vacuum and placed in a furnace. The temperature of the furnace was gradually increased to 180 °C, and this temperature was maintained for 3 days. The tube was opened and excess ethyl bromide was evaporated. The residue was dissolved in hot water and the precipitate formed was immediately filtered off. This solid was washed with CH_2Cl_2 and then hexane to give a white crystalline solid (0.21 g, 84%) that was identified as **4** by spectroscopic data.

Compounds **1**–**3** were prepared as white crystalline solids in the same manner in > 95% yield.

Spectroscopic data for **1**: ^1H NMR (acetone-d_6): δ 2.90 [s, $(CH_3)_3NH$], −0.29 [br s, B-CH_3(2–5)], −0.55 [br s, B-CH_3(6–10)]; ^{13}C NMR (acetone-

d_6): δ 52.62 [cage C], 45.00 [$(CH_3)_3NH$], −4.10 [br, CH_3(2–10)]; ^{11}B NMR (acetone-d_6): δ 37.04 (s, 1B), −4.19 (s, 4B), −8.24 (s, 4B); IR (cm^{-1}, KBr): ν 2919 (br s), 2863 (m), 1623 (m), 1456 (m), 1384 (s), 1093 (s), 1032 (s), 804 (w); these data are identical with those reported in the literature.[5]

Spectroscopic data for **2**: ^{1}H NMR (acetone-d_6): δ 3.08 [s, $(CH_3)_3NH$], −0.21 [s, B-CH_3(2–6)], −0.44 [s, B-CH_3(7–12)]; ^{13}C-NMR (acetone-d_6): δ 60.49 [cage C], 45.00 [$(CH_3)_3NH$], −3.05 [v br, B-CH_3(2–12)]; ^{11}B NMR (acetone-d_6): δ 4.24 (s, 1B), −3.91 (s, 5B), −7.36 (s, 5B); IR (cm^{-1}, KBr): ν 2927 (s), 2896 (s), 2831 (s), 1476 (m), 1458 (m), 1303 (m), 1226 (m), 1050 (s), 523 (m); Negative-ion MALDI MS, *m/z* (isotopic abundance): calcd. for [1-H-$CB_{11}(CH_3)_{11}$]$^-$ 294(12), 295(36), 296(74), 297(100), 298(87), 299(38), 300(24); found 294(28), 295(61), 296(91), 297(100), 298(92), 299(57), 300(23).

Spectroscopic data for **3**: ^{1}H NMR (acetone-d_6): δ 3.16 [s, $(CH_3)_3NH$], 0.80 [s, C-CH_3], −0.19 [s, B-CH_3(2–6)], −0.29 [s, B-CH_3(7–12)]; ^{13}C NMR (acetone-d_6): δ 45.00 [$(CH_3)_3NH$], 14.30 [C-CH_3], −2.67 [v br, B-CH_3(2–12)]; ^{11}B NMR (acetone-d_6): δ 0.53 (s, 1B), −8.86 (s, 5B), −10.85 (s, 5B); IR (cm^{-1}, KBr): ν 2953 (s), 2913 (s), 2848 (m), 1640 (w), 1476 (m), 980 (s), 937 (s), 774 (s), 512 (vs); these data are identical with those reported in the literature.[6]

1 C. A. Reed, *Acc. Chem. Res.*, 1998, **31**, 133; C. A. Reed, *Acc. Chem. Res.*, 1998, **31**, 325; S. H. Strauss, *Chem. Rev.*, 1993, **93**, 927.

2 J. Li, C. M. Logan and N. Jones Jr., *Inorg. Chem.*, 1991, **30**, 4866.

3 Z. Zheng, W. Jiang, A. A. Zinn, C. B. Knobler and M. F. Hawthorne, *Inorg. Chem.*, 1995, **34**, 2095; W. Jiang, C. B. Knobler, C. E. Curtis, M. D. Mortimer and M. F. Hawthorne, *Inorg. Chem.*, 1995, **34**, 3491; T. Peymann, C. B. Knobler and M. F. Hawthorne, *Inorg. Chem.*, 1998, **37**, 1544; M. D. Mortimer, C. B. Knobler and M. F. Hawthorne, *Inorg. Chem.*, 1996, **35**, 5750.

4 B. Grüner, Z. Janousek, B. T. King, J. N. Woodford, C. H. Wang, V. Vsetecka and J. Michl, *J. Am. Chem. Soc.*, 1999, **121**, 3122.

5 C.-W. Tsang, Q. Yang, E. T.-P. Sze, T. C. W. Mak, D. T. W. Chan and Z. Xie, *Inorg. Chem.*, 2000, **39**, 3582.

6 B. T. King, Z. Janousek, B. Grüner, M. Trammel, B. C. Noll and J. Michl, *J. Am. Chem. Soc.*, 1996, **118**, 3313; B. T. King, B. C. Noll, A. J. McKinley and J. Michl, *J. Am. Chem. Soc.*, 1996, **118**, 10902.

7 W. Jiang, C. B. Knobler, M. D. Mortimer and M. F. Hawthorne, *Angew. Chem., Int. Ed. Engl.*, 1995, **34**, 1332; W. Jiang, C. B. Knobler and M. F. Hawthorne, *Angew. Chem., Int. Ed. Engl.*, 1996, **35**, 2536; A. Herzog, A. Maderna, G. N. Harakas, C. B. Knobler and M. F. Hawthorne, *Chem. Eur. J.*, 1999, **5**, 1212; T. Peymann, C. B. Knobler and M. F. Hawthorne, *J. Am. Chem. Soc.*, 1999, **121**, 5601; T. Peymann, C. B. Knobler and M. F. Hawthorne, *Chem. Commun.*, 1999, 2039.

8 R. K. Harris and B. E. Mann, *NMR and the Periodic Table*, Academic Press, London, 1978, p. 195.

9 Reaction of HBr with $(RO)_3P(O)$ gives RBr and $(HO)_3P(O)$, see: D. E. Pearson, M. G. Frazer, V. S. Frazer and L. C. Washburn, *Synthesis*, 1976, 621.

The characterisation and reactivity of $(\eta^5\text{-}C_5H_5)M(CO)_3(Xe)$ (M = Nb or Ta) in solution at room temperature

David C. Grills, Gavin I. Childs and Michael W. George*

School of Chemistry, University of Nottingham, University Park, Nottingham, UK NG7 2RD.
E-mail: Mike.George@nottingham.ac.uk

Received (in Cambridge, UK) 16th June 2000, Accepted 4th August 2000
First published as an Advance Article on the web 11th September 2000

Employing fast time-resolved infrared (TRIR) spectroscopy we have characterised $CpM(CO)_3(Xe)$ (M = Nb or Ta) at room temperature in supercritical Xe solution; $CpM(CO)_3(Xe)$ were found to exhibit a similar reactivity with CO to the corresponding alkane complexes, $CpM(CO)_3$(*n*-heptane) and we report a trend in reactivity of the early transition metal Xe complexes.

Organometallic noble gas complexes have a long history. More than 20 years ago Perutz and Turner used matrix isolation to show that photolysis of $M(CO)_6$ (M = Cr, Mo or W) in low temperature (12 K) matrices generated $M(CO)_5L$ (L = Ar, Kr, Xe or CH_4).[1] Matrix isolation has subsequently been used to characterise a wide range of organometallic noble gas complexes.[2–6] Although matrix isolation is a powerful technique for the characterisation of unstable species at low temperature, it does not provide any kinetic information quantifying the reactivity of these species at room temperature.

Organometallic noble gas complexes have been observed in solution. Simpson *et al*. characterised $Cr(CO)_5(Xe)$ in liquefied Xe (lXe) at −98 °C using conventional FTIR spectroscopy following UV photolysis of $Cr(CO)_6$.[7] Weiller extended this work, detecting $M(CO)_5L$ (M = Cr or W; L = Kr or Xe) in liquefied noble gas solution at low temperature using rapid-scan FTIR spectroscopy.[8] A similar approach was used to detect Cp*Rh(CO)L (L = Kr or Xe).[9–12] Organometallic noble gas complexes have also been observed in the gas phase at room temperature[13] and theoretical studies have predicted Au–Xe bond dissociation energies (BDEs) up to 127 kJ mol^{-1}.[14]

We have recently shown that organometallic noble gas complexes can be observed in fluid solution at room temperature following irradiation of transition metal carbonyls in supercritical fluids. Using fast TRIR spectroscopy we characterised $M(CO)_5L$ [M = Cr, Mo or W; L = Ar (W only), Kr or Xe][15] and $(\eta^5\text{-}C_5R_5)M(CO)_2L$ [M = Mn or Re; R = H, Me or Et (Mn only); L = Kr or Xe].[16,17] The reactivity of these complexes increases in the order Xe < Kr < Ar and Re ≤ W < Mo ≈ Cr ≈ Mn.

The comparison of reactivity between organometallic noble gas and alkane complexes is important. We reported $CpRe(CO)_2$(*n*-heptane) as being the longest lived alkane complex at room temperature[16] and this proved significant since Ball and Geftakis were subsequently able to characterise $CpRe(CO)_2$(cyclopentane) at low temperature using NMR spectroscopy.[18] $CpRe(CO)_2(Xe)$ was only twice as reactive towards CO in scXe compared to $CpRe(CO)_2$(*n*-heptane) in *n*-heptane solution.[16] Here, we investigate the photochemistry of the Group V complexes, $CpM(CO)_4$ (M = Nb or Ta) in supercritical Xe at room temperature, and report a trend in reactivity for the early transition metal noble gas complexes.

Fig. 1(a) shows the TRIR spectrum† obtained 80 ns following 355 nm excitation of $CpNb(CO)_4$ in scXe (1940 psi, 25 °C) in the presence of CO (100 psi). The parent *ν*(CO) IR absorptions at 2041 and 1936 cm^{-1} are bleached and new bands are produced at 1986 and 1885 cm^{-1} which can be assigned to $CpNb(CO)_3(Xe)$ by comparison with previous matrix isolation results[19] and the TRIR spectrum of the analogous *n*-heptane complex.[20] A similar experiment was performed with $CpTa(CO)_4$ dissolved in scXe (2070 psi, 25 °C) in the presence of CO (100 psi). The parent bands at 2037 and 1929 cm^{-1} were bleached and new absorptions at 1983, 1879(sh) and 1873 cm^{-1} were produced, which can be assigned to $CpTa(CO)_3(Xe)$ [Fig. 1(b)]. In the presence of CO, the formation of $CpNb(CO)_3(Xe)$ and $CpTa(CO)_3(Xe)$ in scXe is completely reversible with no observable secondary photoproducts. This reversibility is demonstrated more clearly in Fig. 2, which shows the relevant TRIR kinetic decay traces. Fig. 2 also shows that the decay of $CpNb(CO)_3(Xe)$ and $CpTa(CO)_3(Xe)$ in scXe depends linearly on CO concentration and from these plots we estimate the second order rate constants for the reaction of $CpNb(CO)_3(Xe)$ with CO [k_{CO} = 5.7 (± 0.6) × 10^6 dm^3 mol^{-1} s^{-1}] and for $CpTa(CO)_3(Xe)$ with CO [k_{CO} = 4.9 (± 0.5) × 10^6 dm^3 mol^{-1} s^{-1}] in scXe. $CpNb(CO)_3(Xe)$ and $CpTa(CO)_3(Xe)$ have similar reactivities towards CO in scXe compared to the analogous alkane complexes, $CpNb(CO)_2$(*n*-heptane) and $CpTa(CO)_3$(*n*-heptane) in *n*-heptane solution (Table 1).

The reactivities of early transition metal noble gas and alkane complexes show several trends. Thus far we have found that for a given metal/ligand combination the reactivity of organometallic noble gas complexes towards CO is very similar (≈× 2–3) to the reactivity of the corresponding alkane (*n*-heptane) complex.[15–17,21] In our previous studies we have found that the alkane complexes decrease in reactivity on moving down the Periodic Table and on moving from Group V to Group VII. The results reported here further demonstrate the similarity of the reactivity of early transition metal organometallic xenon complexes to that of their corresponding alkane complexes (Table 1). Preliminary results‡ obtained with $CpV(CO)_4$

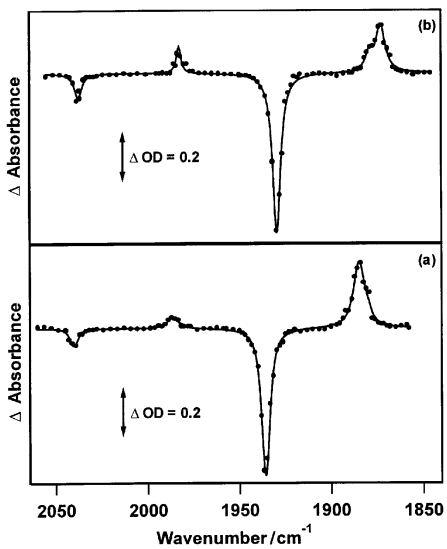

Fig. 1 (a) TRIR spectrum recorded 80 ns after 355 nm photolysis of $CpNb(CO)_4$ in scXe (1940 psi, 25 °C) in the presence of CO (100 psi). (b) TRIR spectrum recorded 150 ns after 355 nm photolysis of $CpTa(CO)_4$ in scXe (2070 psi, 25 °C) in the presence of CO (100 psi).

DOI: 10.1039/b004843g

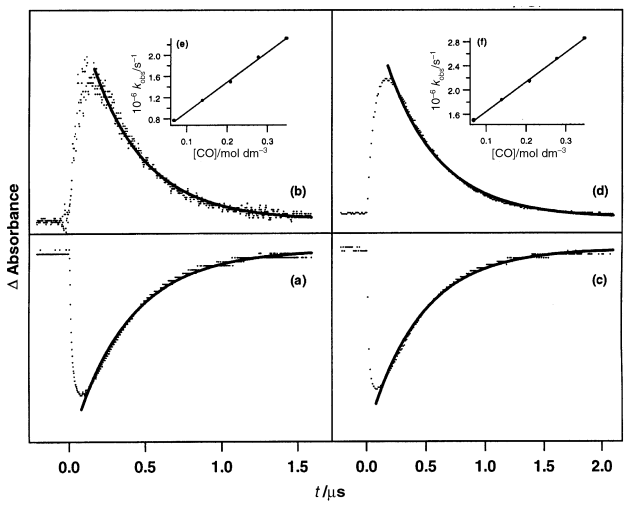

Fig. 2 TRIR kinetic traces corresponding to (a) $CpNb(CO)_4$ (1936.4 cm^{-1}), (b) $CpNb(CO)_3(Xe)$ (1883.9 cm^{-1}), (c) $CpTa(CO)_4$ (1929.7 cm^{-1}) and (d) $CpTa(CO)_3(Xe)$ (1875.3 cm^{-1}) obtained from the experiments shown in Fig. 1. Plots of observed decay rates of (e) $CpNb(CO)_3(Xe)$ and (f) $CpTa(CO)_3(Xe)$ *vs.* CO concentration in scXe.

Table 1 Second order rate constants, k_{CO} ($dm^3\ mol^{-1}\ s^{-1}$), for the reaction of early transition metal–xenon and –*n*-heptane complexes with CO in scXe and *n*-heptane solution, respectively, at 298 K

V	VI	VII
$CpV(CO)_3(Xe)$	$Cr(CO)_5(Xe)$[d]	$CpMn(CO)_2(Xe)$[f]
—	8.4×10^6	1.6×10^6
$CpV(CO)_3(hep)$[a,b]	$Cr(CO)_5(hep)$[e]	$CpMn(CO)_2(hep)$[f]
1.3×10^8	9.3×10^6	8.1×10^5
$CpNb(CO)_3(Xe)$	$Mo(CO)_5(Xe)$[d]	
5.7×10^6	1.1×10^7	—
$CpNb(CO)_3(hep)$[c]	$Mo(CO)_5(hep)$[e]	
4.5×10^6	7.8×10^6	—
$CpTa(CO)_3(Xe)$	$W(CO)_5(Xe)$[d]	$CpRe(CO)_2(Xe)$[g]
4.9×10^6	2.0×10^6	4.8×10^3
$CpTa(CO)_3(hep)$[c]	$W(CO)_5(hep)$[e]	$CpRe(CO)_2(hep)$[g]
2.0×10^6	1.8×10^6	2.0×10^3

[a] hep = *n*-heptane. [b] Ref. 20. [c] Ref. 23. [d] Ref. 15. [e] Ref. 24. [f] Ref. 17. [g] Ref. 16.

suggest that $CpV(CO)_3(Xe)$ also fits into this trend. The similarity between the reactivity of alkane and noble gas complexes towards CO is surprising since for a given metal/ligand system the BDE for a metal–xenon bond is expected to be significantly less than that of the corresponding metal–heptane bond. For example, the W–Xe BDE in $W(CO)_5(Xe)$ (34.3 kJ mol^{-1}) determined from gas phase studies[13] is significantly less than the W–heptane BDE in $W(CO)_5$(*n*-heptane) (62.8 kJ mol^{-1}) estimated from photoacoustic calorimetry measurements.[22] Detailed kinetic studies on Group VII xenon and alkane complexes[17,21] suggested that the early transition metal xenon complexes react with CO in scXe by a different mechanism than the early transition metal *n*-heptane complexes in *n*-heptane.

In conclusion, there is a general decrease in reactivity of the early transition metal xenon complexes, similar to that observed for the analogous alkane complexes, upon moving down the Periodic Table and on moving from Group V to Group VII, resulting in $CpRe(CO)_2(Xe)$ being the least reactive transition metal xenon complex reported so far. It is therefore hoped that the similar reactivity of $CpRe(CO)_2$(*n*-heptane) and $CpRe(CO)_2(Xe)$ will make the characterisation of an organometallic xenon complex by low temperature NMR a realistic possibility. There is clearly still much to learn about organometallic alkane and noble gas complexes and it is likely that TRIR spectroscopy will prove increasingly useful for this purpose.

Notes and references

† The TRIR experiments used a cw IR diode laser to monitor temporal changes in IR absorbance following 355 nm excitation by a Nd:YAG laser (Quanta-Ray GCR-12S, 7 ns pulse). IR spectra were built up on a 'point-by-point' basis by repeating this measurement at different IR frequencies. See: M. W. George and J. J. Turner, *Analyst*, 1994, **119**, 551 for further details.

‡ Initial TRIR kinetic decay studies on $CpV(CO)_3(Xe)$ in scXe show that $CpV(CO)_3(Xe)$ and $CpV(CO)_3$(*n*-heptane) have a similar reactivity towards CO. However we have not been able to obtain, to our satisfaction, a linear behaviour of the rate of decay of $CpV(CO)_3(Xe)$ with respect to CO concentration in scXe.

1 R. N. Perutz and J. J. Turner, *J. Am. Chem. Soc.*, 1975, **97**, 4791.
2 M. Poliakoff and J. J. Turner, *J. Chem. Soc., Dalton Trans.*, 1974, 2276.
3 S. A. Fairhurst, J. R. Morton, R. N. Perutz and K. F. Preston, *Organometallics*, 1984, **3**, 1389.
4 M. Brookhart, W. Chandler, R. J. Kessler, Y. Liu, N. J. Pienta, C. C. Santini, C. Hall, R. N. Perutz and J. A. Timney, *J. Am. Chem. Soc.*, 1992, **114**, 3802.
5 R. J. Mawby, R. N. Perutz and M. K. Whittlesey, *Organometallics*, 1995, **14**, 3268.
6 M. K. Whittlesey, R. N. Perutz, I. G. Virrels and M. W. George, *Organometallics*, 1997, **16**, 268.
7 M. B. Simpson, M. Poliakoff, J. J. Turner, W. B. Maier II. and J. G. McLaughlin, *J. Chem. Soc., Chem. Commun.*, 1983, 1355.
8 B. H. Weiller, *J. Am. Chem. Soc.*, 1992, **114**, 10 910.
9 B. H. Weiller, E. P. Wasserman, R. G. Bergman, C. B. Moore and G. C. Pimentel, *J. Am. Chem. Soc.*, 1989, **111**, 8288.
10 R. H. Schultz, A. A. Bengali, M. J. Tauber, B. H. Weiller, E. P. Wasserman, K. R. Kyle, C. B. Moore and R. G. Bergman, *J. Am. Chem. Soc.*, 1994, **116**, 7369.
11 A. A. Bengali, R. H. Schultz, C. B. Moore and R. G. Bergman, *J. Am. Chem. Soc.*, 1994, **116**, 9585.
12 B. H. Weiller, E. P. Wasserman, C. B. Moore and R. G. Bergman, *J. Am. Chem. Soc.*, 1993, **115**, 4326.
13 J. R. Wells and E. Weitz, *J. Am. Chem. Soc.*, 1992, **114**, 2783.
14 D. Schröder, H. Schwarz, J. Hrusák and P. Pyykkö, *Inorg. Chem.*, 1998, **37**, 624.
15 X. Z. Sun, M. W. George, S. G. Kazarian, S. M. Nikiforov and M. Poliakoff, *J. Am. Chem. Soc.*, 1996, **118**, 10 525.
16 X. Z. Sun, D. C. Grills, S. M. Nikiforov, M. Poliakoff and M. W. George, *J. Am. Chem. Soc.*, 1997, **119**, 7521.
17 D. C. Grills, X.-Z. Sun, G. I. Childs and M. W. George, *J. Phys. Chem. A*, 2000, **104**, 4300.
18 S. Geftakis and G. E. Ball, *J. Am. Chem. Soc.*, 1998, **120**, 9953.
19 T. E. Bitterwolf, S. Gallagher, J. T. Bays, B. Scallorn, A. L. Rheingold, I. A. Guzei, L. LiableSands and J. C. Linehan, *J. Organomet. Chem.*, 1998, **557**, 77.
20 M. W. George, M. T. Haward, P. A. Hamley, C. Hughes, F. P. A. Johnson, V. K. Popov and M. Poliakoff, *J. Am. Chem. Soc.*, 1993, **115**, 2286.
21 G. I. Childs, C. S. Colley, J. Dyer, D. C. Grills, X.-Z. Sun, J. Yang and M. W. George, *J. Chem. Soc., Dalton Trans.*, 2000, 1901.
22 D. P. Burney and T. J. Burkey, *Abstr. Pap. Am. Chem. Soc.*, 1994, **207**, 19.
23 The previously reported values of k_{CO} were slightly higher than these (see ref. 20). The earlier values were calculated by measuring k_{obs} at only one concentration of CO and using the relationship, $k_{obs} = k_{CO}[CO] + k_{Ar}$ to obtain k_{CO}, where k_{Ar} is the observed rate constant in the absence of added CO. We have repeated the determination of these values by using a more accurate method in which k_{obs} is measured at a series of CO concentrations and k_{CO} is obtained from the slope of the resulting plot.
24 C. J. Breheny, J. M. Kelly, C. Long, S. O'Keeffe, M. T. Pryce, G. Russell and M. M. Walsh, *Organometallics*, 1998, **17**, 3690.

Flexible QM/MM modelling embraces alternative mechanisms for lactate dehydrogenase

Vicent Moliner[a] and Ian H. Williams*[b]

[a] *Departament de Ciències Experimentals, Universitat Jaume I, Box 224, 12080 Castellón, Spain*
[b] *Department of Chemistry, University of Bath, Bath, UK BA2 7AY. E-mail: i.h.williams@bath.ac.uk*

Received (in Cambridge, UK) 10th July 2000, Accepted 21st August 2000
First published as an Advance Article on the web 11th September 2000

A flexible AM1/CHARMM treatment finds two distinct mechanistic pathways across the megadimensional energy hypersurface computed for lactate dehydrogenase catalysed reduction of pyruvate to lactate: these differ in the timing of the hydride transfer and proton transfer components of the reaction.

Current applications of hybrid quantum-mechanical/molecular-mechanical (QM/MM) approaches to modelling of enzyme reactivity commonly neglect flexibility in very large systems. Two recent independent studies of lactate dehydrogenase (LDH) catalysed interconversion of pyruvate and lactate, using similar QM/MM methods, yielded very different transition structures (TSs) and mechanisms.[1,2] We now report the simultaneous existence of two distinct mechanistic pathways across the megadimensional energy hypersurface for this system, and suggest that both earlier studies failed to explore its topography to a sufficient extent. To determine which mechanism is preferred will require use not only of a theoretical method giving reliable energies but also of statistical averaging over many configurations. Our finding is significant because it shows that a rigid approach to modelling of any complex system may easily miss an important feature of reaction mechanism.

The chemical step of the LDH cataysed reaction involves hydride transfer (HT) from the dihydronicotinamide ring of NADH to the carbonyl C atom of pyruvate and proton transfer (PT) to the carbonyl O atom of pyruvate from a protonated histidine residue (Fig. 1). The relative timing of the HT and PT is a matter of some interest in mechanistic enzymology. Ranganathan and Gready[2] (RG) found a mechanism (HT,PT) in which HT preceded PT in a stepwise manner, contrasting with the usual chemical and enzymatic arguments for HT processes and their own results from supermolecule calculations,[3] but in accord both with the assumption of an earlier empirical valence-bond study[4] and with the results of a later QM/MM study of the analogous malate dehydrogenase.[5] On the other hand, we (MTW) found a family of TSs (with differing relative dispositions of active site residues) corresponding to a concerted mechanism (PT/HT) with PT considerably more advanced than HT.[1]

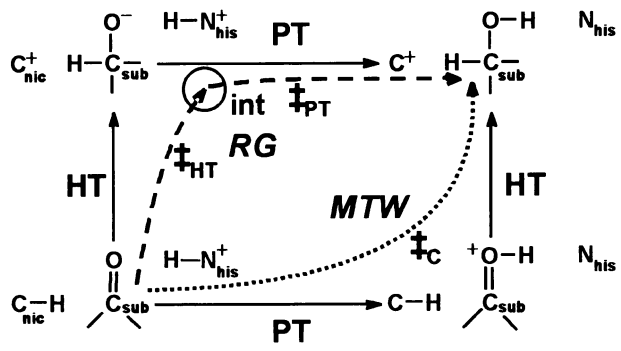

Fig. 1 Reaction map for LDH catalyzed reduction of pyruvate reactant (bottom left) to lactate product (top right); 'his' is histidine-195, 'nic' is nicotinamide, and 'sub' is substrate.

The RG and MTW studies both used the AM1 method[6] for the QM region. RG used the AMBER[7] MM method for the entire dogfish LDH sub-unit ternary complex, but with a relatively small number of atoms allowed to move. In contrast MTW used the CHARMM[8] force field for a truncated (1900 atom) *B. stearothermophilus* LDH but with a very large number of mobile atoms. The first important result of our recent studies is that these and other differences of detail (*e.g.* nature and location of QM/MM link atoms and QM/MM electronic coupling) are not primarily responsible for the different mechanisms found previously. We have now used a large-QM/full-MM model which includes all atoms (~5600) of the monomeric *B. stearothermophilus* LDH subunit,[9] plus NADH, pyruvate, and water molecules within a 20 Å radius ball of water centred on His-195.[10] All atoms were free to move in the optimisations and TS searches. A larger QM region (52 AM1atoms) containing also the ribose moiety was employed, as shown in Fig. 2. Schmidt and Gready have recently asserted that AM1 is likely to be adequate for modelling conformational preferences in QM/MM calculations for the LDH catalyzed reaction.[11]

Approximate saddle points were located by grid searches using constrained ABNR minimization of the CHARMM24b2[12] QM/MM energy.[13] TS refinement in GRACE[1b] employed an explicit hessian for the QM 'core' (Fig. 2) while the MM enzyme 'environment' was continually relaxed to a r.m.s. gradient < 10^{-3} kcal mol^{-1} Å^{-1}. TS optimisation in the core was continued until no element of the gradient vector of the entire system (core plus environment) was larger than 10^{-2} kcal mol^{-1} Å^{-1}. To characterise each saddle point, its hessian was recomputed for a total of 147 atoms (QM core + six amino acid residues in the active-site region) by central finite-differencing of the gradient vector: the single negative eigenvalue of the resultant hessian corresponded to the transition vector. The intrinsic reaction coordinate (IRC) was computed in both directions from each saddle point to confirm each as being the expected TS; energy minimisations from a point along each IRC path yielded structures for the reactant,

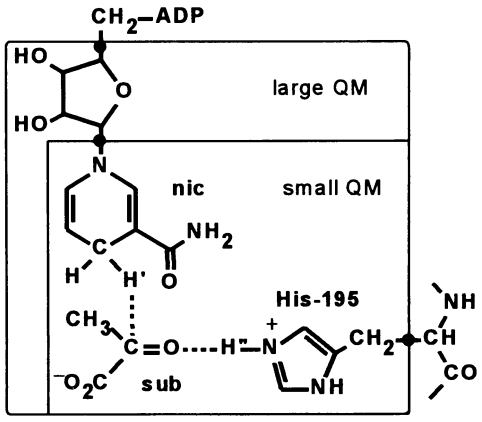

Fig. 2 Large and small QM regions in QM/MM models for LDH; link atoms are indicated as '●'.

DOI: 10.1039/b005549m

Table 1 Selected bond lengths (Å) and energies (kcal mol^{-1}) for AM1/CHARMM large-QM/full-MM optimized structures on the reaction map for LDH catalyzed reduction of pyruvate

	$C_{nic}\cdots H'$	$H'\cdots C_{pyr}$	$O_{pyr}\cdots H''$	$H''\cdots N_{his}$	E_{total}	$E_{QM} + E_{QM/MM}$
reactant	1.130	2.550	2.043	0.998	−12225.1	−514.0
$\ddagger_C$	1.286	1.458	0.996	1.892	−12173.5	−462.7
$\ddagger_{HT}$	1.730	1.234	1.981	1.017	−12155.9	−481.1
int	2.766	1.144	1.700	1.054	−12191.0	−511.4
$\ddagger_{PT}$	2.773	1.140	1.565	1.091	−12183.7	−500.0
product	2.561	1.110	0.978	2.517	−12243.7	−577.5

intermediate, and product. Table 1 contains optimised bond lengths for the HT and PT components of LDH catalysed pyruvate reduction and energies for minima and TSs.

The second important result of this study is that we find reaction paths and TSs for *both* the stepwise HT,PT and the concerted PT/HT mechanisms for both the present large-QM/full-MM model and (results not shown here) small-QM/truncated-MM and small-QM/full-MM models. There is no fundamental disagreement between the MTW and RG results: the apparent discrepancy arose simply because different parts of the hypersurface had been explored in each of the earlier studies. Subtle but significant differences in many coordinates other than just HT and PT dictate whether a particular geometry for the QM region lies within that part of the overall hypersurface belonging to the HT,PT mechanism or else in that different part corresponding to the PT/HT mechanism. It is as if the hypersurface contains a watershed separating two distinct drainage basins: depending upon how a gentle breeze may gust at the crucial moment, a raindrop falling on the Andes watershed may flow to either the Atlantic or the Pacific. So it is with geometry optimisation in a very large and flexible system: two computational runs may start at very similar structures in the core region but be subtly influenced by small differences in their environments to follow separate courses to very different final structures. However, owing to the particular bias provided by the environment, optimisations initiated within the same basin may all tend to converge to the same mechanistic result, despite scanning of the key parameters within the core over adequate ranges of values. A difference in some detail of the QM/MM treatment may of itself generate only a trivial difference in energy for an initial structure but, as a consequence of small differences in the gradient and second derivatives, may cause an optimisation (or TS search) to proceed towards a significantly different stationary point.

The obvious question is which mechanism is preferred: HT,PT or PT/HT? Unfortunately, and perhaps surprisingly, there is no easy answer.[14] The order of the total energies ($E_{QM} + E_{QM/MM} + E_{MM}$) for the three TSs is $\ddagger_{HT} > \ddagger_C > \ddagger_{PT}$. This would suggest that the concerted PT/HT mechanism is preferred over the stepwise HT,PT mechanism, for which HT is the rate-determining step. If, however, only the energy of the QM core within the electrostatic environment of the MM atoms is considered ($E_{QM} + E_{QM/MM}$), then for both models the order of energies of the three TSs is $\ddagger_C > \ddagger_{HT} > \ddagger_{PT}$, favouring the HT,PT mechanism. If no MM atoms are allowed to move in the TS search, then $E_{MM} = 0$ and $E_{total} = E_{QM} + E_{QM/MM}$. However, as flexibility in the MM region is introduced, and the number of atoms contributing to E_{MM} is increased from zero to several thousand, it seems that the mechanistic preference changes. We are unable yet to make a definitive statement as to which mechanism is preferred, but are currently performing *ab initio* QM/MM calculations for this system with a view to obtaining more reliable energetics. We would also like to be able to describe the specific physical interactions within the MM region that favour each of the two mechanisms. Visual inspection of the two structures reveals no obvious significant differences, and as yet the origin of the change in E_{MM} responsible for the mechanistic shift eludes characterisation; we hope to report upon this important point in a full paper. It should be noted that, even for our smallest model, there are several thousand degrees of freedom in the MM region and the critical energetic difference is likely to be the sum of a large number of very small contributions.

Finally, our refined stationary points are not unique. The multiple minima issue has its counterpart for TSs: there exist multiple local saddle points differing in the conformation of the environment. Accurate determination of transition state properties will require statistical averaging over many configurations, each one individually being a transition structure.[1b] Free-energy calculations must not only sample representative configurations along an assumed *in vacuo* reaction path but also must consider the possibility of alternative mechanistic pathways.

We are grateful to the British Council/Acciones Integradas for a collaborative award and HEFCE/EPSRC JREI and Universitat Jaume I for provision of computer time.

Notes and references

1 (*a*) V. Moliner, A. J. Turner and I. H. Williams, *Chem. Commun.*, 1997, 1271; (*b*) A. J. Turner, V. Moliner and I. H. Williams, *Phys. Chem. Chem. Phys.*, 1999, **1**, 1323.
2 S. Ranganathan and J. E. Gready, *J. Phys. Chem. B*, 1997, **101**, 5614.
3 S. Ranganathan and J. E. Gready, *J. Chem. Soc., Faraday Trans.*, 1994, **90**, 2047.
4 A. Yadav, R. M. Jackson, J. J. Holbrook and A. Warshel, *J. Am. Chem. Soc.*, 1991, **113**, 4800.
5 M. A. Cunningham, L. L. Ho, D. T. Nguyen, R. E. Gillilan and P. A. Bash, *Biochemistry*, 1997, **36**, 4800.
6 M. J. S. Dewar, E. G. Zoebisch, E. F. Healy and J. J. P. Stewart, *J. Am. Chem. Soc.*, 1985, **107**, 3902.
7 S. J. Weiner, P. A. Kollman, D. T. Nguyen and D. A. Case, *J. Comput. Chem.*, 1986, **7**, 230.
8 J. J. Pavelites, J. Gao, P. A. Bash and A. D. Mackerell, *J. Comput. Chem.*, 1997, **18**, 221; A. D. MacKerell, D. Bashford, M. Bellott, R. L. Dunbrack, J. D. Evanseck, M. J. Field, S. Fischer, J. Gao, H. Guo, S. Ha, D. Joseph-McCarthy, L. Kuchnir, K. Kuczera, F. T. K. Lau, C. Mattos, S. Michnick, T. Ngo, D. T. Nguyen, B. Prodhom, W. E. Reiher, B. Roux, M. Schlenkrich, J. C. Smith, R. Stote, J. Straub, M. Watanabe, J. Wiorkiewicz-Kuczera, D. Yin and M. Karplus, *J. Phys. Chem. B*, 1998, **102**, 3586.
9 D. B. Wigley, S. J. Gamblin, S. P. Turkenburg, E. J. Dodson, K. Piontek, H. Muirhead and J. J. Holbrook, *J. Mol. Biol.*, 1992, **223**, 317.
10 T. R. Dafforn, I. G. Badcoe, R. B. Sessions, A. S. El Hawrani and J. J. Holbrook, *Proteins: Struct. Funct. Genet.*, 1997, **29**, 228.
11 R. K. Schmidt and J. E. Gready, *Theochem*, 2000, **498**, 101.
12 B. R. Brooks, R. E. Bruccoleri, B. D. Olafson, D. J. States, S. Swaminathan and M. Karplus, *J. Comput. Chem.*, 1983, **4**, 187; CHARMM24b2, M. Karplus, Harvard University, 1996.
13 M. J. Field, P. A. Bash and M. Karplus, *J. Comput. Chem.*, 1990, **11**, 700.
14 S. J. Titmuss, P. L. Cummins, A. A. Bliznyuk, A. P. Rendell and J. E. Gready, *Chem. Phys. Lett.*, 2000, **320**, 169.

ChemComm

Amavadine as a catalyst for the peroxidative halogenation, hydroxylation and oxygenation of alkanes and benzene

Patrícia M. Reis, José Armando L. Silva, João J. R. Fraústo da Silva* and Armando J. L. Pombeiro*

Centro de Química Estrutural, Complexo I, Instituto Superior Técnico, Av. Rovisco Pais, 1049-001 Lisboa, Portugal. E-mail: pcd1950@popsrv.ist.utl.pt; pombeiro@popsrv.ist.utl.pt

Received (in Cambridge, UK) 10th July 2000, Accepted 31st July 2000
First published as an Advance Article on the web 14th September 2000

Synthetic amavadine models, $[V(HIDPA)_2]^{2-}$ and $[V(HIDA)_2]^{2-}$ [where HIDPA and HIDA stand for the basic forms of 2,2′-(hydroxyimino)dipropionic and 2,2′-(hydroxyimino)diacetic acid, respectively], exhibit haloperoxidase- or peroxidase-type activities, and act as catalysts for the selective peroxidative monohalogenation, hydroxylation or oxo-functionalization of alkanes or aromatic compounds such as benzene and mesitylene at room temperature.

The roles of vanadium in biology have been the object of current and growing interest[1] from both biological and chemical perspectives. In particular, the biological role of amavadine, the natural bare octacoordinated vanadium(IV) complex $[V(HIDPA)_2]^{2-}$, [$HIDPA^{3-}$ = basic form of (*S*,*S*)-2,2′-(hydroxyimino)dipropionic acid][2] present in some *Amanita* fungi, is still an intriguing matter, although circumstantial evidence has started to emerge suggesting[3] that it can act either as a peroxidase which catalyses the oxidation of particular thiols to disulfide products, or as a catalase by promoting the decomposition of H_2O_2. Vanadium(V) haloperoxidases which have been found mainly in some brown and red marine algae have also raised much interest and their structures and functions have been investigated,[1] inorganic biomimetic reagents proposed and other vanadium complexes applied[4–6] to the peroxidative oxidation of alkenes and aromatic hydrocarbons. However, alkanes have been much less studied[6b,c,7] and only very rarely has a catalytic activity of vanadium been recognized for such reactions.

We now report that saturated (*e.g.* cyclohexane or cyclooctane) and aromatic (benzene or mesitylene) hydrocarbons can be oxidized catalytically, at room temperature, by a system composed of synthetic amavadine models and H_2O_2 in acidic medium, to give halo-, hydroxo- or oxo-functionalized compounds, thus suggesting a potential wider biological role for naturally occurring amavadine than that considered so far and demonstrating the capacity of a biogenic vanadium complex, much simpler than an enzyme, to catalyse, in mild conditions, the functionalization of alkanes, a challenging problem[8] in modern chemistry. Moreover, this complex constitutes, to our knowledge, the first reported vanadium catalyst for the peroxidative halogenation of alkanes.

In effect, we have observed that $Ca[V(HIDPA)_2]$ (the Ca^{2+} salt of synthetic amavadine) **a** or its model $Ca[V(HIDA)_2]$

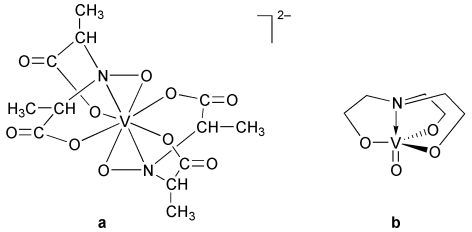

a **b**

[HIDA = basic form of 2,2′-(hydroxyimino)diacetic acid], in a two-phase water–NCMe system also containing H_2O_2, KBr and HNO_3 (in high excess relative to the vanadium compound), catalyse at room temperature the peroxidative bromination of saturated and aromatic hydrocarbons, as shown in Tables 1 and 2 for typical experiments with cyclohexane and benzene to give bromocyclohexane and bromobenzene, respectively, according to the overall reaction (1). Catalytic chlorination (using KCl instead of KBr) also occurred for benzene and, in all the cases, only the mono-halogenated products were selectively obtained.

$$RH + Br^- + H_2O_2 + H^+ \xrightarrow{\text{Amavadine}} RBr + 2H_2O \quad (1)$$

The activity of the system increases with the amounts of H_2O_2 and of the acid, but beyond a limit (*e.g. ca.* 150 molar ratio for H_2O_2, relatively to vanadium, for the case of the bromination of cyclohexane) no further increase is observed and the activity can even decrease. Values of the turnover number (TON) are given in Tables 1 and 2 for typical essays (6 h reaction time) and indicate that both vanadium complexes have a comparable

Table 1 Amavadine catalysed peroxidative bromination,[a] hydroxylation[b] and oxygenation[b] of cyclohexane

			Turnover number (TON)[d]		
V complex	H_2O_2 : V[c]	HNO_3 : V[c]			
Bromination:					
$Ca[V(HIDPA)_2]$	175	3610	10	—	—
$Ca[V(HIDA)_2]$	175	50	0	—	—
	175	290	2	—	—
	175	580	5	—	—
	175	1155	6	—	—
	175	2890	17	—	—
	175	3610	15	—	—
$[VO\{N(CH_2CH_2O)_3\}]$	175	2890	9	—	—
Hydroxylation and oxygenation:					
$Ca[V(HIDPA)_2]$	220	72	—	18	4
	440	72	—	32	4
	880	72	—	32	—
	440	144	—	30	3
$Ca[V(HIDA)_2]$	110	72	—	11	4
	220	72	—	33	7
	440	72	—	33	4
	880	72	—	25	4
	220	36	—	25	6
	220	144	—	21	6
	440	0	—	3	0.7
	440	144	—	42	8
	440	290	—	37	10
	440	580	—	26	8
$[VO\{N(CH_2CH_2O)_3\}]$	440	72	—	46	7

[a] Two-phase liquid system: V complex (0.010 mmol), cyclohexane (5 mmol), KBr (2.5 mmol), H_2O (2.5 cm^3), NCMe (2.5 cm^3), H_2O_2 and HNO_3 (amounts given in the Table), 20 °C, 6 h. [b] V complex (0.010 mmol), cyclohexane (5 mmol), NCMe (2.5 cm^3), H_2O_2 and HNO_3 (amounts given in the Table). [c] Molar ratio relative to the V complex. [d] Moles of product per mole of V complex [corrected for blanks (for an high excess of acid in the absence of V complex, the halogenated product is detected in lower yield)], determined by GLC or GC-MS, using an internal standard, after separation from the vanadium and ionic species. The molar yields (%) relative to the substrate (*i.e.* moles of product per 100 moles of substrate) are given by 0.2 × TON.

DOI: 10.1039/b005513l

Table 2 Amavadine catalysed peroxidative bromination and hydroxylation of benzene[a]

V complex	H_2O_2:V	HNO_3:V	Turnover number (TON) BrC_6H_5	PhOH
Bromination:				
$Ca[V(HIDPA)_2]$	175	5050	9	—
$Ca[V(HIDA)_2]$	175	3610	10	—
	175	5050	11	—
$[VO\{N(CH_2CH_2O)_3\}]$	175	3610	9	—
Hydroxylation:				
$Ca[V(HIDPA)_2]$	440	72	—	6
$Ca[V(HIDA)_2]$	440	72	—	16
$[VO\{N(CH_2CH_2O)_3\}]$	440	72	—	8

[a] See footnotes to Table 1.

activity. Hence, *e.g.* TON *ca.* 10–15 for the molar ratios H_2O_2:V = 175 and HNO_3:V = 3610.

No activity was found for the free (hydroxyimino)dicarboxylic acids H_3·HIDPA or H_3·HIDA and the active species has the metal in the 5+ oxidation state (the starting blue V^{IV} complexes are oxidized by H_2O_2 to the corresponding red V^V forms, as observed by the immediate colour change of the reaction solution on addition of the peroxide). The presence of vanadium in the 5+ oxidation state has also been demonstrated in the vanadium-dependent bromoperoxidases and the formation of peroxo–vanadium complexes as active intermediate species has been proposed.[1a,b] In our system, the hydroxyimine(1−) groups, η^2-(O–N<), of the $HIDPA^{3-}$ or $HIDA^{3-}$ ligands that bind to the metal are isoelectronic with peroxide(2−) and therefore the oxidized complexes relate to bis(peroxo)-vanadium(V) species. Nevertheless, the presence of H_2O_2 is required for the detection of activity and the vanadium-promoted Br^- oxidation by H_2O_2 (to HOBr or a derivative thereof) occurs in the aqueous phase and the halogenation of the organic substrate in the organic phase (NCMe). The vanadium complexes are soluble in both solvents and the peroxidative halogenation occurs smoothly even without addition of a phase-transfer agent.

Apart from behaving as catalysts for the halo-functionalization of alkanes and aromatics, as shown above, synthetic amavadine and its model can also catalyse, at room temperature, the hydroxylation (reactions 2) and/or oxo-functionalization of these types of substrates. The reactions occur in homogeneous conditions (single-phase system), by treatment of an acetonitrile solution of the vanadium complex, in the presence of H_2O_2 and HNO_3, with the substrate (Tables 1 and 2).

$$RH + H_2O_2 \xrightarrow{\text{Amavadine}} ROH + H_2O \qquad (2)$$

The system does not require so high an acidic medium as for bromination, and the activity towards oxygenation of cyclohexane to cyclohexanol and cyclohexanone, which is already detected without added acid (overall TON = 4, 6 h reaction time), reaches a maximum (overall TON *ca.* 50 in the $[V(HIDA)_2]^{2-}$ system) for an acid:vanadium molar ratio of *ca.* 140 (for H_2O_2:V = 440). The alcohol is always the main product, but the ketone also forms. The selectivity is dependent on the experimental conditions, in particular the amounts of H_2O_2 and HNO_3, and *e.g.* for the above conditions, the obtained cyclohexanol/cyclohexanone molar ratio is 5.3, whereas a value of 9.2 is reached for HNO_3:V = 72 (also for H_2O_2:V = 440).

The selective oxidation to the alcohol, although less extensive, occurs for benzene (that forms exclusively phenol, TON = 16 or 6 for the corresponding $[V(HIDA)_2]^{2-}$ or $[V(HIDPA)_2]^{2-}$ systems), whereas mesitylene (1,3,5-trimethylbenzene) is oxidized to the aldehyde (3,5-dimethylbenzaldehyde) (TON = 13 or 7, respectively) rather than to the alcohol.

Attempts to characterize active intermediate vanadium species are under way, as well as the extension of the work to other substrates and to other amavadine models and related complexes. In particular, we have also observed catalytic activity towards the above reactions for various vanadium(V) complexes with other polydentate ligands with N,3O-donor atom sets such as triethanolaminate, *e.g.* $[VO\{N(CH_2CH_2O)_3\}]$ **b** (see Tables 1 and 2), aminocarboxylates, *etc.*

To the best of our knowledge, this study provides the first examples of vanadium catalysts for the peroxidative halogenation of alkanes, at room temperature. It might be expected that natural amavadine showed similar properties, *i.e.* the possibility to act as a haloperoxidase or a peroxidase, catalysing the peroxidative halogenation, hydroxylation and/or oxygenation of organic substrates, but we note that, since for the halogenation reactions the pH was very low, the results cannot be directly extrapolated to biological conditions. Curiously, the vanadium-dependent haloperoxidases, which probably developed later, since vanadium is in the oxidation state 5+, catalyse halogenation reactions at pH 5–6 to give products that appear to have defensive roles. On the basis of electrochemical studies[3] we have suggested that amavadine, which, as stated, is a simple complex, not an enzyme, may act as a kind of primitive peroxidase (towards thiols) or as a catalase (if substrates other than H_2O_2 are not present), behaving also as a protective agent against external microbial pathogens or host body damage. Halogenation of alkanes and aromatics which, as shown in this work, occur in the laboratory at room temperature but very low pH for the particular substrates studied, is unlikely to occur *in vivo* with the substrates studied but may eventually be viable in less extreme (even physiological) pH conditions for other more favourable substrates.

This work has been partially supported by the Fundação para a Ciência e a Tecnologia and the PRAXIS XXI programme, Portugal.

Notes and references

1 (*a*) *Vanadium Compounds*, ed. A. S. Tracey and D. C. Crans, ACS Symposium Series no. 711, ACS, Washington, 1998; (*b*) *Metal Ions in Biological Systems*, ed. H. Siegel and A. Siegel, Marcel Dekker Inc., New York, vol. 31, 1995; (*c*) *The Biological Chemistry of the Elements*, ed. J. J. R. Fraústo da Silva and R. J. P. Williams, Clarendon Press, Oxford, 1993.

2 (*a*) M. A. A. F. C. T. Carrondo, M. T. L. S. Duarte, J. C. Pessoa, J. A. L. Silva, J. J. R. Fraústo da Silva, M. C. T. A. Vaz and L. Vilas-Boas, *J. Chem. Soc., Chem. Commun.*, 1988, 1158; (*b*) R. E. Berry, E. M. Armstrong, R. L. Beddoes, D. Collison, S. N. Ertok, M. Helliwell and C. D. Garner, *Angew. Chem., Int. Ed.*, 1999, **38**, 795; (*c*) E. Bayer, E. Koch and G. Anderegg, *Angew. Chem., Int. Ed. Engl.*, 1987, **26**, 545.

3 (*a*) C. M. M. Matoso, A. J. L. Pombeiro, J. J. R. Fraústo da Silva, M. F. C. Guedes da Silva, J. A. L. Silva,, J. L. Baptista-Ferreira and F. Pinho-Almeida, in ref. 1(*a*), ch. 18, pp. 241–247; (*b*) M. F. C. Guedes da Silva, J. A. L. Silva, J. J. R. Fraústo da Silva, A. J. L. Pombeiro, C. Amatore and J.-N. Verpeaux, *J. Am. Chem. Soc.*, 1996, **118**, 7568.

4 (*a*) A. Butler, M. J. Clague and G. E. Meister, *Chem. Rev.*, 1994, **94**, 625; (*b*) D. Rehder, *Coord. Chem. Rev.*, 1999, **182**, 297.

5 (*a*) B. Sels, D. De Vos, M. Buntinx, F. Pierard, A. Kirsch-De Mesmaeker and P. Jacobs, *Nature*, 1999, **400**, 855; (*b*) J. V. Walker, M. Morey, H. Carlsson, A. Davidson, G. D. Stucky and A. Butler, *J. Am. Chem. Soc.*, 1997, **119**, 6921; (*c*) B. J. Hamstra, G. J. Colpas and V. L. Pecoraro, *Inorg. Chem.*, 1998, **37**, 949; (*d*) C. V. Dinesh, R. Kumar, B. Pandey and P. Kumar, *J. Chem. Soc., Chem. Commun.*, 1995, 611.

6 (*a*) A. E. Gekhman, I. P. Stolarov, N. I. Moiseeva, V. L. Rubaijlo, M. N. Vargaftik and I. I. Moiseev, *Inorg. Chim. Acta*, 1998, **275–276**, 453; (*b*) G. B. Shul'pin, D. Attanasio and L. Suber, *J. Catal.*, 1993, **142**, 147; (*c*) H. Mimoun, L. Saussine, E. Daire, M. Postel, J. Fischer and R. Weiss, *J. Am. Chem. Soc.*, 1983, **105**, 3101.

7 (*a*) I. I. Moiseev, A. E. Gekhman and D. I. Shishkin, *New J. Chem.*, 1989, **13**, 683; (*b*) P. R. H. P. Rao, A. V. Ramaswany and P. Ratnasamy, *J. Catal.*, 1993, **141**, 604; (*c*) P. R. H. P. Rao and A. V. Ramaswany, *J. Chem. Soc., Chem. Commun.*, 1992, 1245.

8 (*a*) *Catalytic Activation and Functionalisation of Light Alkanes*, ed. E. G. Derouane, J. Haber, F. Lemos, F. Ramôa Ribeiro and M. Guinet, NATO ASI Series, vol. 44, Kluwer Academic Publ., Dordrecht, The Netherlands, 1998; (*b*) A. E. Shilov and G. B. Shul'pin, *Chem. Rev.*, 1997, **97**, 2879.

Electrochemical characterization of monolayers of a biotinylated polythiophene: towards the development of polymeric biosensors

Lievin Kumpumbu-Kalemba and Mario Leclerc*

Département de Chimie, Centre de Recherche en Sciences et Ingénierie des Macromolécules, Université Laval, Quebec City, Qc Canada,G1K 7P4. E-mail: mario.leclerc@chm.ulaval.ca

Received (in Columbia, MI, USA) 7th December 1999, Accepted 14th August 2000
First published as an Advance Article on the web 13th September 2000

Ultrathin films of an electrostatically-modified biotinylated polythiophene have shown interesting electrochemical properties which lead to the detection of femtomoles of the protein avidin in aqueous electrolytes.

Conjugated polymers (polyanilines, polythiophenes, polypyrroles, poly(phenylene vinylene)s, polyfluorenes, *etc.*) and related oligomers have become an important class of organic materials due to their unusual electrical and optical properties which lend themselves to the development of various devices in the areas of micro-electronics, electro-optics, photonics, sensors, genomics, *etc.*[1–7] In this respect, functionalized polythiophenes have been the subject of many investigations since some of them combine good processability and environmental stability with an ability to detect, transduce, and amplify various physical or chemical information into an electrical or optical signal.[5–7] These novel organic materials may serve in integrated sensory devices where the optical or electrical signal will not require any external tagging procedures but would come directly from the responsive polymeric supports. In order to achieve these goals, simple, specific, highly sensitive, and miniaturized polymeric devices must also be developed.

Along these lines, we have recently reported the easy preparation of electroactive thin films of functionalized polythiophenes through electrostatic interactions.[8] The deposition of ultrathin films (even monolayers) could be very important for solid-state biosensors since it is believed that the interaction between large biochemical molecules and the binding sites present within the electroactive materials will mainly occur at the interface. In the present study, we have electrochemically characterized the stability and the sensitivity of such simple polymeric assemblies for the future development of microarrays of polymeric sensors.

Following previously reported procedures,[8] ultrathin films of 50% pre-neutralized poly(2-(4-methyl-3-thienyloxy)ethanesulfonic acid) (PMTOES) have been easily transfered onto aminosilane-treated ITO electrodes.† Depending upon the nature of the side chains, various functionalized polythiophenes can be obtained but in the course of the present study, only biotinylated polythiophenes will be analyzed (see Fig. 1). As shown in Fig. 2, these electroactive ultrathin films have been characterized in an aqueous electrolyte (pH = 6–7) and have revealed a clear and reversible redox (related to a doping/undoping electrochemical process) process around 0.4 V *vs.* SCE. This quasi-reversible redox process occurs at a much lower potential than that previously reported in an organic electrolyte.[8] This could be related to the hydrophilic nature of the polymeric salt which allows very efficient wetting of the polymer in aqueous solutions. The good electrochemical activity of this polythiophene derivative in water opens the door to electrochemical detection in real biological systems. Various sizes (1 to 100 mm^2) of electrodes have been analyzed and a good correlation has been obtained between the surface of the electrode and the integrated charge exchanged during the redox process. On average the oxidative charge obtained by integration of the 0.44 V peak is 0.24 μC mm^{-2}. The number of electrons exchanged per repeat unit is difficult to assess but, on the basis of previous studies on electroactive polythiophenes,[9,10] it is reasonable to assume an exchange of one electron per three repeat units (*i.e.* a doping level of 33%). This rough estimate corresponds to a molecular density of 22 Å^2 per repeat unit. This value is in good agreement with recent results (21–23 Å^2) obtained with self-assembled polythiophene monolayers.[11]

The electrochemical responses of these biotinylated electrodes have been investigated upon addition of the protein avidin. This protein is built from four identical subunits (for a total M.W. = 68 000) and has a strong affinity for biotin.[12] This strong affinity between avidin and biotin is related to an exceptionally high binding constant of 10^{15} M^{-1}, which

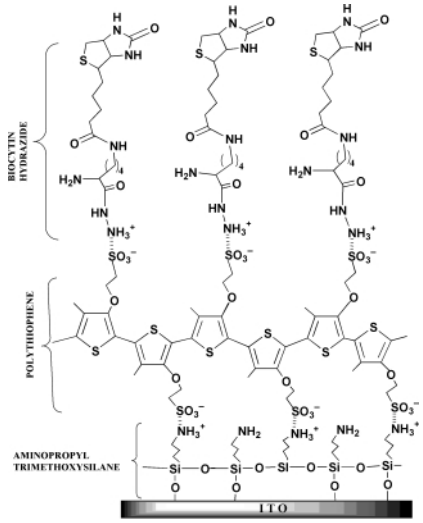

Fig. 1 Schematic and idealistic description of a biotinylated polythiophene electrode.

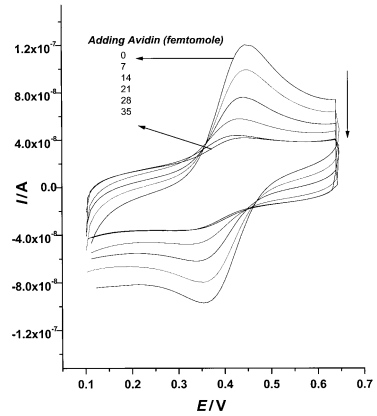

Fig. 2 Cyclic voltammogram of a 1 mm^2 biotinalyted polythiophene electrode in a 0.1 M KCl aqueous solution upon addition of aliquots of avidin, at room temperature. Scan rate of 20 mV s^{-1} *vs.* SCE.

DOI: 10.1039/a909744i

corresponds to a binding energy of 20 kcal mol^{-1}. For these reasons, the biotin/avidin couple has been extensively used in different types of biosensors[8,12–19] and is utilized here as a model compound for the future design of various types of sensors based on functionalized polythiophenes.

Interestingly a 1 mm^2 biotin-functionalized polythiophene electrode shows a clear modification of its cyclic voltammogram‡ (a decrease of the electrochemical activity) upon addition of as low as 7×10^{-15} mole of avidin in the aqueous electrolyte (Fig. 2 and 3). Saturation is almost obtained at 3.5×10^{-14} mole of avidin. Modified electrodes of area 1 cm^2 have shown similar electrochemical effects upon addition of aliquots of avidin but at concentrations multiplied by a factor of 100 (which corresponds to their surface ratio). A similar decrease of the electrochemical activity has been observed in nucleobase-functionalized polythiophenes[20] and could be explained by a decrease of the interfacial electron-transfer rates between the polymer and the electrode, due to the binding of the protein.[21] In other words, the bound avidin may shield the electroactive polymer and therefore affect the electronic exchanges between the electrode, the polymer and the electrolyte. First experiments on similar biotinylated electrodes in acetonitrile have revealed an increase of the redox potential[8] which had been explained by a twisting of the backbone upon complexation, but this mechanism does not seem to be dominant in aqueous electrolytes. Another explanation could be a release of the polymer from the electrode upon avidin binding. A similar mechanism was recently proposed for fluorescent conjugated polyelectrolytes.[22] It is clear that covalently-attached polythiophene derivatives would shed some light on the mechanism involved in the detection and these new polythiophene derivatives are currently being developed in our laboratory. It is also interesting to note that polythiophene-modified electrodes without biotin moieties (50% pre-neutralization of the sulfonic acid polymer with sodium hydroxide) do not show any significant modification of their electrochemical properties. These results also give clear evidence of the electrochemical and mechanical stability of such polymeric electrodes. Indeed, although these polythiophene derivatives are soluble in water, it seems that the multiple electrostatic interactions along the backbone are strong enough to avoid any significant release of the ultrathin polymeric film when immersed in aqueous electrolytes, the electrochemical activity being reproducible even after hours of immersion in the electrolyte.

From Fig. 3, it is also possible to assume that about 24% of the thiophene units are affected by the presence of 7×10^{-15} mole of avidin and that could mean that one avidin molecule affects about 250 repeat units. This amplification factor is similar to that calculated from biochromic measurements.[8] It is believed that the present amplification factor is more or less related to the difference in size between the protein avidin and one repeat thiophene unit. Indeed, as mentioned above, it is possible to determine that one thiophene unit occupies a surface of 22 $Å^2$, and from this amplification factor of 250 that could indicate that avidin occupies a surface of roughly 55 nm^2. These dimensions are in the same range as those determined by X-ray analyses for a parent protein (streptavidin, M.W. = 60 000 with dimensions of $4.5 \times 4.5 \times 5.8$ nm).[13]

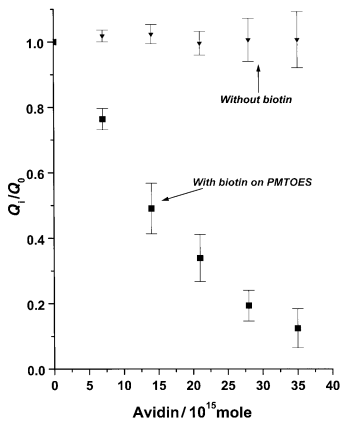

Fig. 3 Relative electroactivity (integrated charge exchanged during the oxidative 0.44 V peak) upon addition of avidin for a monolayer made of a 0.5:1 complex between sodium hydroxide and poly(2-(4-methyl-3-thienyloxy)ethanesulfonic acid) (▼) and a monolayer made of a 0.5:1 complex between biocytin hydrazide and poly(2-(4-methyl-3-thienyloxy)ethanesulfonic acid) (■).

In conclusion, this simple methodology, based on non-covalent interactions between water-soluble amine-bearing molecules and partially neutralized poly(2-(4-methyl-3-thienyloxy)ethanesulfonic acid), has allowed the efficient preparation of stable, highly sensitive, functionalized polythiophene electrodes and constitutes a promising platform for the future development of novel electrochemical biosensor arrays.

Notes and references

† Poly(2-(4-methyl-3-thienyloxy)ethanesulfonic acid) (PMTOES) was prepared following procedures described in previous publications.[8,23] 3-Aminopropyltrimethoxysilane (Aldrich), biocytin hydrazide and avidin (Pierce) were used as received. Amino-functionalized silanized ITO electrodes were prepared following well established procedures.[8,24,25] The electrostatic transfer of 50% pre-neutralized (performed with biocytin hydrazide or sodium hydroxide) poly(2-(4-methyl-3-thienyloxy)ethanesulfonic acid) was carried out by dipping the glass slides into 0.01–0.001 M aqueous solutions of the resulting polymer.

‡ Cyclic voltammograms were obtained with a Solartron 1287 potentiostat/galvanostat driven by Corrview software. The integrated charges during redox processes have been digitally calculated using this software. Satured calomel electrode (SCE) and a platinum plate were used as reference and auxiliary electrodes, respectively. Electrochemical measurements were performed at 20 mV s^{-1} in a 0.1 M KCl aqueous solution. All cyclic voltammograms shown in the present figures are the third ones in a series of three electrochemical cycles. Addition of aliquots of aqueous solutions of avidin were carried out directly in the electrolyte near the biotinylated electrodes. All reported electrochemical data are the averaged responses of five different electrodes.

1 *Handbook of Conducting Polymers*, ed.T. Skotheim, J. R. Reynolds and R. L. Elsenbaumer, Marcel Dekker, New York, 1988, 2nd edn.
2 W. J. Feast, J. Tsibouklis, K. L. Pouwer, L. Groenendaal and E. W. Meijer, *Polymer*, 1996, **37**, 5017.
3 *Conjugated Polymers*, ed. J. L. Brédas and R. Silbey, Kluwer Academic Publishers, Dordrecht, The Netherlands, 1991.
4 S. J. Higgins, *Chem. Soc. Rev.*, 1997, **26**, 247.
5 (*a*) M. Leclerc and K. Faid, *Adv. Mater.*, 1997, **9**, 1087; (*b*) M. Leclerc, *Adv. Mater.*, 1999, **11**, 1491.
6 R. D. McCullough, *Adv. Mater.*, 1998, **10**, 93.
7 T. M. Swager, *Acc. Chem. Res.*, 1998, **31**, 201.
8 K. Faid and M. Leclerc, *J. Am. Chem. Soc.*, 1998, **120**, 5274.
9 G. Tourillon, *Polythiophene and Its Derivatives*, in *Handbook of Conducting Polymers*, ed. T. A. Skotheim, Marcel Dekker, NY, 1986, p. 293.
10 M. Dietrich and J. Heinze, *Synth. Met.*, 1991, **41**–**43**, 503.
11 S. Inaoka and D. M. Collard, *Langmuir*, 1999, **15**, 3752.
12 M. Ahlers, W. Muller, A. Reichert, H. Ringsdorf and J. Venzmer, *Angew. Chem., Int. Ed. Engl.*, 1990, **29**, 1209.
13 L. Haussling, W. Knoll, H. Ringsdorf, F. J. Schmitt and J. Yang, *Makromol. Chem., Macromol. Symp.*, 1991, **46**, 145.
14 S. A. Sundberg, R. W. Barrett, M. Pirrung, A. L. Lu, B. Kiangsoontra and C. P. Holmes, *J. Am. Chem. Soc.*, 1995, **117**, 12 050.
15 K. Faid and M. Leclerc, *Chem. Commun.*, 1996, 2761.
16 L. M. Torres-Rodriguez, A. Roget, M. Billon, T. Livache and G. Bidan, *Chem. Commun.*, 1998, 1993.
17 J. Mack, D. Leipert, A. Badia, W. Knoll and G. Jung, *Adv. Mater.*, 1999, **11**, 809.
18 S. Cosnier, *Biosens. Bioelectr.*, 1999, **14**, 443.
19 M. Dequaire, C. Degrand and B. Limoges, *J. Am. Chem. Soc.*, 1999, **121**, 6946.
20 P. Bäuerle and A. Emge, *Adv. Mater.*, 1998, **10**, 324.
21 F. Garnier, H. K. Youssoufi, P. Srivastava and A. Yassar, *J. Am. Chem. Soc.*, 1994, **116**, 8813.
22 L. Chen, D. W. McBranch, H. L. Wang, R. Helgeson, F. Wudl and D. G. Whitten, *Proc. Natl. Acad. Sci. USA*, 1999, **96**, 12 287.
23 M. Chayer, K. Faid and M. Leclerc, *Chem. Mater.*, 1997, **9**, 2902.
24 G. Decher, *Science*, 1997, **277**, 1232.
25 M. Ferreira and M. F. Rubner, *Macromolecules*, 1995, **28**, 7107.

ChemComm

Intramolecular carbometalation of functionalized terminal alkynes *via* low-valent titanium complexes

Natalia Morlender-Vais, Nicka Solodovnikova and Ilan Marek*

Department of Chemistry and Institute of Catalysis Science and Technology, Technion-Israel Institute of Technology, Technion City, Haifa 32 000 Israel. E-mail: chilanm@tx.technion.ac.il

Received (in Cambridge, UK) 20th June 2000, Accepted 20th July 2000
First published as an Advance Article on the web 14th September 2000

Treatment of δ- and γ-functionalized monosubstituted alkynes with diisopropoxy(η²-propene)titanium induces an intramolecular cyclisation to afford the 4- and 5-membered cycloalkanols in good overall yields.

Various disubstituted alkynes react with diisopropoxy(η²-propene)titanium **1**, readily generated by the reaction of $Ti(OiPr)_4$ with 2 eq. of iPrMgX (Sato's reagent), to give the corresponding titanacyclopropene derivatives as described in Scheme 1, path A.[1] However, as terminal alkynes failed to participate in the present reaction[1] (path B *vs.* path A), we have recently used the fact that a metalated alkyne can behave like a disubstituted alkyne to prepare the first titano–titanacyclopropene in good overall yield (Scheme 1, path C).[2]

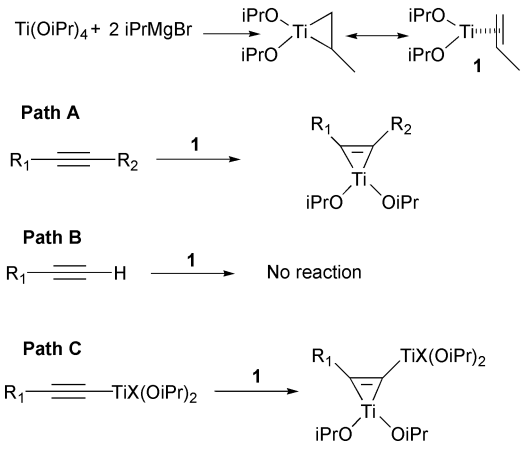

Scheme 1

On the other hand, when **1** is opposed to an *unactivated* olefin, the ligand exchange is not efficient and therefore the desired olefin–titanium complex **2** is not formed (Scheme 2, path A). Only activated olefins undergo this exchange as styrene,[3] conjugated dienes,[4] vinyl silane[5] or stannane.[6] However, the presence of an electrophile in the carbon skeleton (Scheme 2, path B) promotes this reaction since an intramolecular nucleophilic acyl substitution[7] reaction occurs in a second step to give the cyclopropanolate derivative[8] (known as the Kulinkovitch reaction).[9]

As part of our studies on the use of early transition metal complexes such as **1** for the carbometalation of unactivated alkynes,[10] we anticipated by analogy with the results described in Scheme 2 that the facile intramolecular nucleophilic acyl substitution reaction of a functionalized *terminal* alkyne (known to be totally unreactive,[1,11] Scheme 1, path B) might act as a driving force for shifting the equilibrium.[7] In this case, a transient monosubstituted titanacyclopropene will be formed as intermediate before the carbocyclisation reaction. Indeed, treatment of dec-9-yn-5-one **4** (n = 2) with a stoichiometric amount of $Ti(OiPr)_4$ and 2 eq. of iPrMgX at −78 °C leads to the cyclic product **8**, after hydrolysis, in 78% isolated yield (Scheme 3).

In order to probe the existence of a remaining carbon–titanium bond in the molecule, iodine was added at the end of the reaction. The vinyl iodide **10** (n = 2) was isolated in 67% yield as single isomer (the stereochemistry was determined by NOE). Interestingly, this reaction can be applied to the formation of more strained carbocycles such as 4-membered ring derivatives in a very easy and straightforward manner (**3**, n = 1, Scheme 3). Here again, the non-isolated terminal titanacyclopropene **5** (n = 1) reacts intramolecularly with the ketone to give the organometallic derivative **6** (n = 1). Hydrolysis of the reaction mixture leads to the *exo*-methylenecyclobutanol **7** in 50% isolated yield whereas the iodinolysis gives only the *Z*-isomer of the vinyl iodide **9** in good chemical yield.[12]

Although the reaction mechanism described in Scheme 3 seems plausible, we have not been able to isolate even in very small amounts the transient titanacyclopropene derivative **5**. So, we have also considered an alternative mechanistic pathway for the formation of **6**. Indeed, it is known that early transition metal

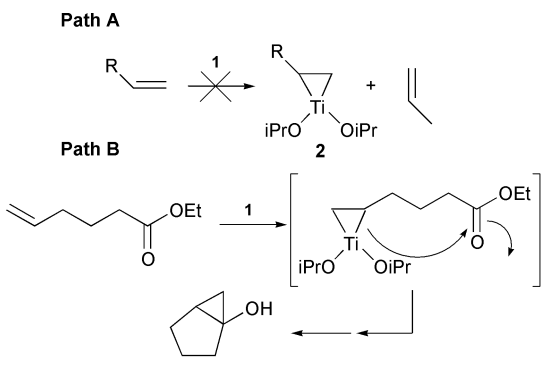

Scheme 2

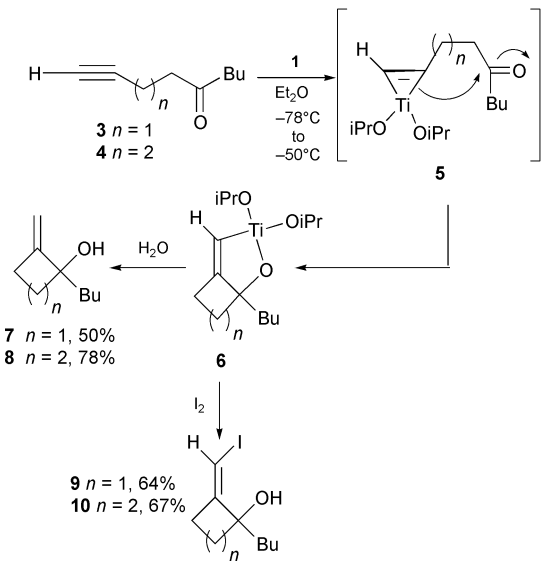

Scheme 3

DOI: 10.1039/b005027j

complexes can form some η^2-ketone complexes, **11**, (metalla-oxiranes)[13] which can further insert into an alkyne moiety to give the same oxatitanacyclopentene derivatives **6**. This mechanism was already reported for the reaction of δ-ynones with $[(C_5H_5)_2Ti(PMe_3)_2]$ to form 3-bis(cyclopentadienyl)-2-oxa-3-titanabicyclo[3.3.0]oct-4-ene in good overall yield.[14] Although the intramolecular addition to a substituted alkyne to form the unsaturated oxatitanacycle worked well, here again the reaction on a terminal alkyne gives a low isolated yield (35%) of the cyclic product after hydrolysis, as described in Scheme 4.

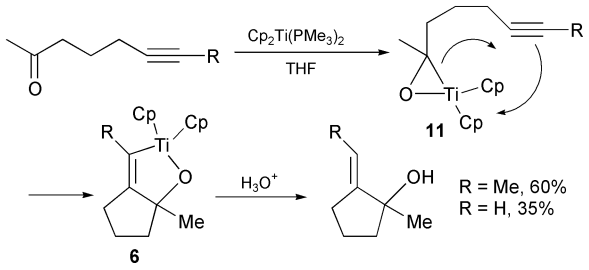

Scheme 4

So, in order to check if the first step of the reaction of **1** with **3** or **4** was a reaction at the alkynyl (Scheme 3) or at the carbonyl centers (Scheme 4), we decided to investigate the behavior of **1** with cyclohexanone as described in Scheme 5.

Treatment of 1 eq. of $Ti(OiPr)_4$ with 2 eq. of iPrMgX in the presence of 1 eq. of cyclohexanone leads to two products, **12** and **13**, in a respectively 5 to 1 ratio and in quantitative yields. The major product **12** results from the reaction of diisopropoxy(η^2-propene)titanium **1** with the carbonyl moiety which can further react with iodine to give **14** whereas **13** is formed from the direct attack of the Grignard reagent on the cyclohexanone.[15] No trace of cyclohexanol was detected after hydrolysis in the crude reaction mixture which clearly indicates that the reaction does not proceed through the oxametallacycle

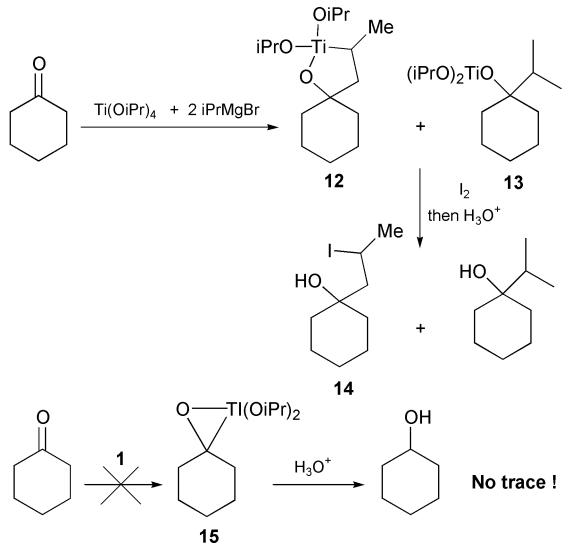

Scheme 5

15. Thus, although **5** cannot be isolated, it is present as the first intermediate in the reaction before the nucleophilic attack on the carbonyl moiety occurs as described originally in Scheme 3.

In conclusion, the synthesis of *exo*-methylene-cyclopentane and -cyclobutane has been achieved in a one-pot sequence from readily available starting material with diisopropoxy(η^2-propene)titanium. The mechanism of this reaction has been investigated and is composed by a carbometalation reaction of the monosubstituted-unactivated alkyne followed by intramolecular nucleophilic acyl substitution.

I. M. is a Ygal Alon fellow. This research was supported in part by The Israel Science Foundation founded by The Academy of Sciences and Humanities (No. 060-471) and by the fund for the promotion of research at the Technion. Acknowledgement is also made to the donors of The Petroleum Research Fund, administered by the ACS, for partial support of this research (PRF#33747-AC1).

Notes and references

1 K. Harada, H. Urabe and F. Sato, *Tetrahedron Lett.*, 1995, **36**, 3203.
2 C. Averbuj, J. Kaftanov and I. Marek, *Synlett*, 1999, 1939.
3 O. G. Kulinkovitch, A. I. Savchenko, S. V. Sviridov and D. A. Vasilevski, *Mendeleev Commun.*, 1993, 230.
4 C. M. Williams, V. Chaplinski, P. R. Schreiner and A. de Meijere, *Tetrahedron Lett.*, 1998, **39**, 7695.
5 R. Mizojiri, H. Urabe and F. Sato, *Tetrahedron Lett.*, 1999, **40**, 2557.
6 K. L. Lee, S. I. Kim and J. K. Cha, *J. Org. Chem.*, 1998, **63**, 9135.
7 For pertinent references on the intramolecular nucleophilic acyl substitution, see: S. Okamoto, A. Kasatkin, P. K. Zubaidha and F. Sato, *J. Am. Chem. Soc.*, 1996, **118**, 2208.
8 A. Kasatkin and F. Sato, *Tetrahedron Lett.*, 1995, **36**, 6079; A. Kasatkin, K. Kobayashi, S. Okamoto and F. Sato, *Tetrahedron Lett.*, 1996, **37**, 1849; R. Mizojiri, H. Urabe and F. Sato, *Angew. Chem., Int. Ed.*, 1998, **37**, 2666.
9 O. G. Kulinkovich, S. V. Sviridov, T. S. Vasilevski and T. S. Pritskaya, *Zh. Org. Khim.*, 1989, **25**, 2245; O. G. Kulinkovich and T. S. Pritskaya, *J. Org. Chem. USSR (Engl. Transl.)*, 1990, **25**, 2027; O. G. Kulinkovitch, S. V. Sviridov and D. A. Vasilevski, *Synthesis*, 1991, 234; J. Lee, J. D. Ha and J. K. Cha, *J. Am. Chem. Soc.*, 1997, **119**, 8127; J. Lee and J. K. Cha, *J. Org. Chem.*, 1997, **62**, 1584; S. Y. Cho, J. Lee, R. K. Lammi and J. K. Cha, *J. Org. Chem.*, 1997, **62**, 8235; V. Chaplinski and A. de Meijere, *Angew. Chem., Int. Ed. Engl.*, 1995, **34**, 2545; V. Chaplinski, H. Winsel, M. Kordes and A. de Meijere, *Synlett*, 1997, 111; C. M. Williams and A. de Meijere, *J. Chem. Soc., Perkin Trans. 1*, 1998, 3699.
10 I. Marek and J. F. Normant, *Carbometalation reactions* in *Metal-catalyzed Cross-coupling Reactions*, ed. F. Diederich and P. J. Stang, Wiley-VCH, 1998, 271.
11 E.-I. Negishi, S. J. Holmes, J. M. Tour, J. A. Miller, F. E. Cederbaum, D. R. Swanson and T. Takahashi, *J. Am. Chem. Soc.*, 1989, **111**, 3336.
12 The synthesis of a 6-membered ring was also performed successfully but for unknown reasons, the expected product was not stable during the purification by chromatography.
13 G. Erker and F. Rosenfeldt, *J. Organomet. Chem.*, 1982, **224**, 29; R. M. Waymouth, K. R. Clauser and R. H. Grubbs, *J. Am. Chem. Soc.*, 1986, **108**, 6385; G. Fachinetti, C. Birani, C. Floriani, A. Chiesi-Villa and C. Guastini, *J. Am. Chem. Soc.*, 1978, **100**, 1921; E.-I. Negishi and T. Takahashi, *Bull. Chem. Soc. Jpn.*, 1998, **71**, 755.
14 D. F. Hewlett and R. J. Whitby, *J. Chem. Soc., Chem. Commun.*, 1990, 1684.
15 The fact that iPrMgX reacts faster with $Ti(OiPr)_4$ than with a ketone has been successfully used for the synthesis of functionalized alkynyl titanium derivatives: N. Morlender-Vais, J. Kaftanov and I. Marek, *Synthesis*, 2000, 917.

ChemComm

Enantioselective conjugate addition of thiols to enones and enals catalyzed by chiral *N*-oxide–cadmium complex

Makoto Saito, Makoto Nakajima* and Shunichi Hashimoto

Graduate School of Pharmaceutical Sciences, Hokkaido University, Sapporo 060-0812, Japan.
E-mail: nakajima@pharm.hokudai.ac.jp

Received (in Cambridge, UK) 28h July 2000, Accepted 14th August 2000
First published as an Advance Article on the web 14th September 2000

A novel method of enantioselective conjugate addition of thiols to enones and enals produces sulfides with enantioselectivities up to 78% ee, employing a cadmium complex of (*S*)-3,3′-dimethyl-2,2′-biquinoline *N*,*N*′-dioxide 1 as a catalyst.

The development of enantioselective reactions requires the design of chiral ligands. Many recent studies have focused on the development of novel chiral ligands for use in metal-catalyzed reactions. Although *N*-oxide is a functional group possessing a unique electron-donating property, allowing it to form complexes with a variety of metals,[1] few attempts have been made to employ *N*-oxides as chiral ligands.[2,3] We recently reported an enantioselective allylation of aldehydes with allyltrichlorosilanes utilizing a chiral *N*,*N*′-dioxide **1** as a

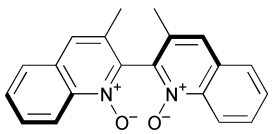

1

catalyst, exploiting the electron-donating property of the *N*-oxide.[3c] Here, we describe an enantioselective conjugate addition of thiols to enones and enals catalyzed by a chiral *N*-oxide–cadmium complex.

Several chiral amine-catalyzed reactions have received considerable attention[4] since the first report on the enantioselective conjugate addition of thiols catalyzed by cinchona alkaloid.[4a] Due to their high efficacy, catalysis of enantioselective conjugate addition by lithium thiolate complexes of amino bisether,[5] heterobimetallic complexes,[6] and nickel oxazoline complexes[7] are of particular interest.

Recently, we described the optical resolution of **1** through the hydrogen-bonding of **1** and optically active binaphthol.[3a] We then hypothesized that thiophenol forms a hydrogen-bonding complex with **1**, controlling the nucleophilicity and steric accessibility of thiophenol to electron-deficient olefins in its enantioselective conjugate addition. We initially tested this hypothesis using 10 mol% of **1** as a catalyst in the conjugate addition of thiophenol to cyclohex-2-en-1-one in DCM. The reaction produced a significant yield of the corresponding sulfide, although the enantioselectivity was quite low (35%, 12% ee).

To enhance the reactivity and enantioselectivity, we used 10 mol% metal salt as an additive expected to coordinate with carbonyl oxygen. Among the various metal salts surveyed, addition of CdI_2 yielded the corresponding sulfide in high chemical quantity with moderate enantioselectivity (93%, 57% ee). Enantioselectivity increased up to 78% when the reaction was performed in toluene, whereas polar solvents decreased enantioselectivity substantially (THF: 99%, 0% ee; acetonitrile: 97%, 33% ee). Stoichiometric studies revealed that equimolar amounts of **1** and CdI_2 are sufficient for optimum enantioselectivity. The reaction was promoted by CdI_2 in the absence of *N*-oxide to produce the sulfide in 96% yield. These results suggest that a 1:1 complex of **1** and CdI_2[8] functions catalytically in this enantioselective addition. This is the first example of an enantioselective reaction utilizing a cadmium compound,[9] exhibiting a distinctive binding to *N*-oxide.

Table 1 summarizes the conjugate addition of various thiols to cyclic enones under optimized conditions.† Slight modifications of the substrate strongly influenced enantioselectivity. Cyclohept-2-en-1-one (entry 2) gave an enantioselectivity comparable to that of cyclohex-2-en-1-one (entry 3), while cyclopent-2-en-1-one (entry 1) demonstrated low selectivity. It is surprising that the reaction of 4-methylthiophenol (entry 5) gave low selectivity compared to that of thiophenol (entry 3).

Although acyclic conjugate ketones were unsuccessful (chalcone: 30%, 10% ee), the reaction of acyclic conjugate aldehydes gives the corresponding sulfides in high chemical yields with enantioselectivities up to 70% ee after conversion to the corresponding alcohol (Table 2). The mildness of the reaction conditions allows the enantioselective conjugate addition of thiols to enals, a reaction never previously reported due to the lability of aldehydes.

To determine the reaction mechanism, we investigated several additives to the reaction of cyclohex-2-en-1-one and thiophenol in toluene. Addition of cyclohexanone (1.0 eq.) influenced neither chemical yield nor enantioselectivity (92%, 74% ee) of the reaction. The addition of cyclohexene (1.0 eq.), however, dramatically reduced enantioselectivity (92%, 45% ee). These results suggest the importance of the coordination of the cadmium complex to the carbon–carbon double bond, though the detail is not clear.

We have demonstrated the effectiveness of a chiral *N*-oxide–cadmium iodide complex as a catalyst for enantioselective conjugate addition of thiols to cyclic enones and enals. The present reaction provides the first example of utilizing a cadmium complex in an enantioselective reaction. Mechanistic studies and the design of chiral *N*-oxides, currently in progress, will further enhance enantioselectivity.

Table 1 Enantioselective conjugate addition of thiols to enones catalyzed by CdI_2–**1** complex

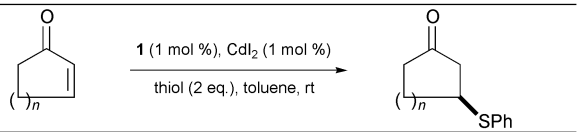

Entry	*n*	Thiol	Time/h	Yield (%)	Ee (%)[a]	Confgn[b]	$[\alpha]_D^{24}$[c]
1	1	PhSH	4	94	21	—	+1.8
2	3	PhSH	24	68	61	—	−27.2
3	2	PhSH	6	96	78	*S*	−68.7
4	2	4-$MeOC_6H_4SH$	6	88	58	*S*	−43.2
5	2	4-MeC_6H_4SH	12	40	29	*S*	−23.7
6	2	$PhCH_2SH$	12	48	40	*S*	−43.1

[a] Determined by HPLC analysis employing Daicel Chiralpak AD or AS. [b] Configuration assignment by comparison to literature[4b] values of optical rotations. [c] *c* 1, $CHCl_3$.

DOI: 10.1039/b005994n

Table 2 Enantioselective conjugate addition of thiophenol to enals catalyzed by CdI_2–**1** complex

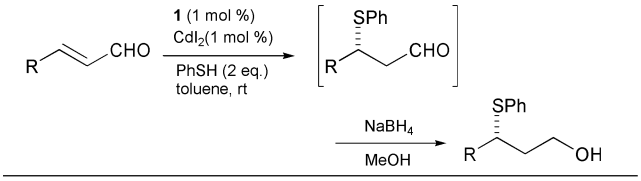

Entry	R	Time/h	Yield (%)	Ee (%)[a]	Confgn	$[\alpha]_D^{23}$[b]
1	Me	12	89	69	*S*[c]	+24.9
2	Et	12	91	70	*S*[d]	+14.0
3	^{i}Pr	24	80	63	*S*[d]	+24.8
4	$PhCH_2$	24	76	52	*S*[d]	+5.2[e]

[a] Determined by HPLC analysis employing a Daicel Chiralcel OD. [b] *c* 1, $CHCl_3$. [c] Configuration assignment by comparison to literature[5a] values of optical rotations. [d] Configuration assignment by analogy. [e] *c* 1, benzene.

This work was partly supported by a Grant-in-Aid for Scientific Research from the Ministry of Education, Science, Sports and Culture of Japan and Otsuka Chemical Award in Synthetic Organic Chemistry, Japan. The authors thank the Japan Society for the Promotion of Science for Research Fellowships for Young Scientists (to M. S.).

Notes and references

† The conjugate addition of thiol to enone was performed as follows: Thiophenol (220 mg, 2.0 mmol) in toluene (1 mL) was added to a stirred solution of cyclohex-2-en-1-one (96 mg, 1.0 mmol), *N*-oxide **1** (3.2 mg, 10 μmol) and CdI_2 (3.6 mg, 10 μmol) in toluene (7 mL) and stirred for 6 h at rt. The reaction mixture was diluted in toluene and successively washed with aq. NaOH and brine. The solvent was evaporated and the residue was chromatographed on a silica gel column (eluent, toluene–AcOEt, 100 : 1) to afford 3-phenylthiocyclohexanone (198 mg, 96%) as an oil. *N*-Oxide **1** was recovered by elution with 10% EtOH in DCM without a loss of optical purity. The ee of the product was determined by chiral HPLC (Daicel Chiralpak AD, hexane–Pr^{i}OH, 9 : 1, 1.0 mL min^{-1}, t_R (*S*), 8.5 min; (*R*), 10.0 min).

1 For a review on amine *N*-oxide complexes, see: N. M. Karayannis, L. L. Pytlewski and C. M. Mikulski, *Coord. Chem. Rev.*, 1973, **11**, 93.
2 (*a*) M. B. Diana, M. Marchetti and G. Melloni, *Tetrahedron: Asymmetry*, 1995, **6**, 1175; (*b*) I. A. O'Neil, C. D. Turner and S. B. Kalindjian, *Synlett*, 1997, 777; (*c*) G. Dyker, B. Hölzer and G. Henkel, *Tetrahedron: Asymmetry*, 1999, **10**, 3297; (*d*) K. Miura and T. Katsuki, *Synlett*, 1999, 783.
3 (*a*) M. Nakajima, Y. Sasaki, M. Shiro and S. Hashimoto, *Tetrahedron: Asymmetry*, 1997, **8**, 341; (*b*) M. Nakajima, Y. Sasaki, H. Iwamoto and S. Hashimoto, *Tetrahedron Lett.*, 1998, **39**, 87; (*c*) M. Nakajima, M. Saito, M. Shiro and S. Hashimoto, *J. Am. Chem. Soc.*, 1998, **120**, 6419; (*d*) M. Nakajima, M. Saito and S. Hashimoto, *Chem. Pharm. Bull.*, 2000, **48**, 306.
4 (*a*) R. Helder, R. Arends, W. Bolt, H. Hiemstra and H. Wynberg, *Tetrahedron Lett.*, 1977, **25**, 2181; (*b*) H. Hiemstra and H. Wynberg, *J. Am. Chem. Soc.*, 1981, **103**, 417; (*c*) J. Gawronski, K. Gawronska and H. Wynberg, *J. Chem. Soc., Chem. Commun.*, 1981, 307; (*d*) N. Kobayashi and K. Iwai, *J. Am. Chem. Soc.*, 1978, **100**, 7071; (*e*) N. Kobayashi, *Polym. J.*, 1981, **16**, 205; (*f*) T. Mukaiyama, A. Ikegawa and K. Suzuki, *Chem. Lett.*, 1981, 165; (*g*) K. Suzuki, A. Ikegawa and T. Mukaiyama, *Bull. Chem. Soc. Jpn.*, 1982, **55**, 3277; (*h*) H. Yamashita and T. Mukaiyama, *Chem. Lett.*, 1985, 363; (*i*) A. Kumar, R. V. Salunkhe, R. A. Rane and S. Y. Dike, *J. Chem. Soc., Chem. Commun.*, 1991, 485.
5 (*a*) K. Nishimura, M. Ono, Y. Nagaoka and K. Tomioka, *J. Am. Chem. Soc.*, 1997, **119**, 12 974; (*b*) K. Tomioka, M. Okuda, K. Nishimura, S. Manabe, M. Kanai, Y. Nagaoka and K. Koga, *Tetrahedron Lett.*, 1998, **39**, 2141.
6 (*a*) G. Manickam and G. Sundararajan, *Tetrahedron: Asymmetry*, 1997, **13**, 2271; (*b*) E. Emori, T. Arai, H. Sasai and M. Shibasaki, *J. Am. Chem. Soc.*, 1998, **120**, 4043.
7 S. Kanemasa, Y. Oderaotoshi and E. Wada, *J. Am. Chem. Soc.*, 1999, **121**, 8675.
8 Pyridine *N*-oxide is known to form a complex with CdI_2. See: M. Nieuwenhuyzen, W. T. Robinson and C. J. Wilkins, *Polyhedron*, 1991, **10**, 2111.
9 For the application of CdI_2 as a catalyst, see: (*a*) D. Prajapati and J. S. Sandhu, *J. Chem. Soc., Perkin Trans. 1*, 1993, 739; (*b*) B. Baruah, A. Boruah, D. Prajapati and J. S. Sandhu, *Tetrahedron Lett.*, 1997, **38**, 1449; (*c*) D. D. Laskar, D. Prajapati and J. S. Sandhu, *Chem. Lett.*, 1999, 1283.

ChemComm

Polypyrazolylborate copper(I) complexes as catalysts of the homogeneous and heterogeneous styrene epoxidation reaction

M. Mar Díaz-Requejo, Tomás R. Belderraín and Pedro J. Pérez*

Departamento de Química y Ciencia de Materiales, Universidad de Huelva Carretera de Palos de la Frontera, s/n, E-21819-Huelva, Spain. E-mail: perez@uhu.es

Received (in Liverpool, UK) 12th June 2000, Accepted 8th August 2000
First published as an Advance Article on the web 13th September 2000

The complexes BpCu (1) and Tp*Cu (2) catalyse the transformation of styrene into styrene oxide using Oxone as the oxidising agent; the use of silica gel-supported 1 or 2 as heterogeneous catalysts affords similar results, using water as the sole solvent.

Copper complexes have been extensively used as catalysts in metal-induced carbene transfer reactions to olefins to give cyclopropanes.[1] Their use in olefin aziridination reactions has also been frequently reported in the last decade.[1] By contrast, very few chemical systems based on this element are known to promote the oxidation of an olefin into the corresponding epoxide:[2–7] most of them have been developed with cyclic or strained olefins (thus avoiding undesired, side-reactions), and their catalytic capabilities are not as yet comparable to those of well-known catalysts based on manganese–salen or iron–porphyrin complexes.[8] For example, Cu(II) salicylaldehyde derivatives have been reported in the epoxidation of alkenes with molecular oxygen and 2-methylpropanal, the yields being found in the 22–40% range.[3] Murahashi and co-workers have reported the use of copper salts for a similar transformation, but in this case the yields were considerably higher (80–90%).[5] Cu(TPP) and Cu(cyclam)$^{2+}$ have also been used[2] in the epoxidation of cyclohexene with oxygen and aldehydes, with low to moderate yield, although the participation of metal-oxo intermediates in the epoxide formation pathway could not be established. In the last few years, we have focused our attention on the use of polypyrazolylborate[9] copper(I) complexes as catalysts for olefin cyclopropanation and aziridination reactions under homogeneous conditions,[10,11] and we have also developed their immobilization by supporting the catalyst precursors on silica gel, thus achieving the heterogenisation of the homogeneous system.[12] We have now studied the use of the complexes BpCu (**1**) and Tp*Cu (**2**) (Bp = dihydridobispyrazolylborate; Tp* = hydrotris(3,5-dimethylpyrazolyl)borate) as the catalyst precursors in the epoxidation reaction under both

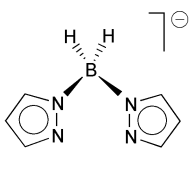

$H_2B(pz)_2$, Bp

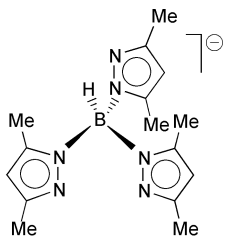

$HB(pz^*)_3$, Tp*

homogeneous and heterogeneous conditions, and we have discovered that these Cu(I) complexes also display catalytic activity towards this transformation. Complex **1** was reported by Bruce as a 14-electron compound.[13] Although its solid state structure is unknown, molecular weight studies revealed the existence of discrete BpCu units in solution. Complex **2** was reported by Ibers and co-workers:[14] its solid state structure was determined by X-ray as a dimeric compound $[Tp^*Cu]_2$, but in solution the mononuclear species Tp*Cu prevailed. Thus, both complexes **1** and **2** seem to display monomeric structures when dissolved.

The addition of an aqueous solution of potassium peroxymonosulfate (Oxone = $2KHSO_5{\cdot}KHSO_4{\cdot}K_2SO_4$) neutralised

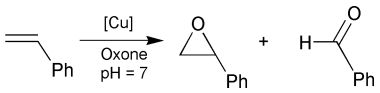

(1)

with $NaHCO_3$, to an acetonitrile solution containing the styrene and the catalyst precursors BpCu or Tp*Cu led to the conversion of the olefin into a mixture of mainly styrene oxide and benzaldehyde (eqn. 1, Table 1)†. The overall yield, based on oxidant, was nearly 70% for BpCu and 60% for Tp*Cu, of which at least 85–90% corresponded to styrene oxide (60 and 50% respectively, based on oxidant). Other minor products, including benzoic acid, accounted for *ca.* 5%. These conversion rates are clearly an improvement over most of those obtained with the copper-based epoxidation systems known to date.[2–5] In addition, no phase-transfer catalyst has been added to the biphasic reaction mixture, unlike the common procedure employed in related systems.[15]

The formation of benzaldehyde in metal-induced olefin oxidation was reported by Groves *et al.*[16] with an iron–porphyrin complex as catalyst. However, it is worth mentioning that control experiments have also shown the formation of benzaldehyde when reacting styrene oxide and Oxone in the absence of the copper complexes, as well as the oxidation of benzaldehyde to benzoic acid under the same conditions. This is in agreement with recent results from Corma and co-workers with Ti-zeolites as epoxidation catalysts,[17] in which benzoic acid and benzaldehyde were obtained along with the major product, the styrene oxide. Obviously, we have also checked the reaction between the olefin and Oxone in the absence of copper complexes but under otherwise identical reaction conditions: no epoxide nor any other oxidation products were observed.

As mentioned above, we have already reported the immobilization of complexes **1** and **2** in silica gel as well as their use as heterogeneous catalysts for the olefin cyclopropanation reaction.[12] Now, we have found that they also catalyse the styrene oxidation, using Oxone as the oxidant, to give a mixture of styrene oxide, 1-phenylethanediol, benzaldehyde and ben-

Table 1 Epoxidation of styrene catalysed by complexes **1** and **2**

Catalyst	Styrene oxide[a]	PhCHO[a]	Yield[b] (%)
BpCu	> 85	< 5	70
Tp*Cu	> 90	< 5	60

[a] Quantified after 18 h by GC, mol% of the products. [b] Based on oxidant.

DOI: 10.1039/b004806m

zoic acid, eqn. (2). Water is the sole solvent in this case. Table 2 displays the results of these heterogeneous experiments

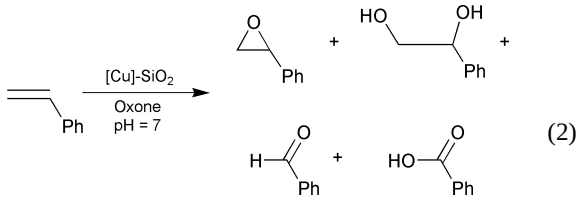

(2)

(average of three cycles with the same reused catalyst). The yields, based on oxidant, are similar to those observed in the homogeneous case, although the reaction is faster in the former. The unique difference seems to be the appearance of the epoxide-opening product, the diol. This must be a consequence of the acidic nature of the solid support, the silica gel, since this transformation is usually acid-catalysed.[18] The epoxide and the diol account for 70–85% of the products (Table 2), very close to the 90% value obtained with the soluble catalysts. It is important to point out that the immobilisation of the catalyst does not seem to significantly alter the catalytic capabilities of this system, *i.e.*, it provides an excellent route to accomplish one of the permanent goals in catalysis: to heterogenise an homogeneous system without loss of the activity and/or selectivity of the latter, in order to achieve the well-known advantages of the heterogeneous system.

In conclusion, we have discovered that copper(I) complexes containing polypyrazolylborate ligands present catalytic activity towards the epoxidation reaction, as they did with the olefin cyclopropanation and aziridination reactions. These complexes can operate under both homogeneous and heterogeneous conditions, with no significant differences when moving from the former to the latter, thus achieving the well-known advantages of the recycling and reuse of the catalyst in the heterogeneous system. Moreover, the parallels between the epoxidation and the carbene and nitrene transfer reactions are reinforced since the same metal complexes assure those three catalytic conversions. Mechanistic, comparative studies for the three reactions are currently underway in this laboratory.

We thank the Universidad de Huelva (Plan Propio de Investigación) and the Ministerio de Educación y Ciencia (PB98-0958) for financial support. M. M. D.-R. also thanks the Junta de Andalucía for a research studentship. The Instituto de Investigaciones Químicas (CSIC-La Cartuja, Sevilla) is also thanked for the use of their NMR facilities.

Table 2 Epoxidation of styrene catalysed by complexes **1** and **2** supported on silica gel

Catalyst	Styrene oxide[a]	1-phenyl-ethanediol[a]	PhCHO[a]	PhCOOH[a]	Yield[b]
BpCu	28	38	22	11	57
Tp*Cu	17	70	3	10	68

[a] Quantified after 6 h by GC, mol% of the products. Average of three cycles. [b] Based on oxidant.

Notes and references

† *Homogeneous catalytic experiment*: 0.05 mmol of the catalyst (**1** or **2**) was dissolved in 10 mL of acetonitrile and styrene (2 mmol) was added. An aqueous solution of Oxone (0.5 mmol, 1 mmol of $KHSO_5$, 10 mL H_2O) with three equiv. of sodium bicarbonate (1.5 mmol) was prepared and added to the catalyst-containing solution. The mixture turned greenish, and was stirred for 18 h. The products were quantified by GC, using acetophenone as an internal standard (added at the end of the reaction, immediately before quantification). The products were identified by NMR from experiments carried out in deuterated solvents, and by comparison with pure samples. The results are shown in Table 1.

Heterogeneous catalytic experiment: the copper complexes were supported as reported in ref. 12. One gram of silica-gel containing BpCu (0.02 mmol) or alternatively Tp*Cu (0.04 mmol) was suspended in 20 mL of H_2O along with 2 mmol of styrene. Neutralised Oxone (prepared as above) was added, and the mixture was stirred for 8 h. The solid was filtered off, and reused twice in an identical manner. Table 2 displays the average results of the three cycles.

1 M. P. Doyle, M. A. McKervey and T. Ye, *Modern Catalytic Methods for Organic Synthesis with Diazo Compounds*, John Wiley & Sons, New York, 1998.
2 G. Das, R. Shukla, S. Mandal, R. Singh and P. K. Bharadwaj, *Inorg. Chem.*, 1997, **36**, 323.
3 W. Nam, H. J. Kim, S. H. Kim, R. Y. N. Ho and J. S. Valentine, *Inorg. Chem.*, 1996, **35**, 1045.
4 G. Rousselet, C. Chassagnard, P. Capdevielle and M. Mauny, *Tetrahedron Lett.*, 1996, **47**, 8497.
5 S.-I. Murahashi, Y. Oda, T. Naota and N. Komiya, *J. Chem. Soc., Chem. Commun.*, 1993, 139.
6 C. C. Franklin, R. B. VanAtta, A. F. Tai and J. S. Valentine, *J. Am. Chem. Soc.*, 1984, **106**, 814.
7 M. B. Andrus and B. W. Poehlein, *Tetrahedron Lett.*, 2000, **41**, 1013.
8 E. N. Jacobsen, *Catalytic Asymmetric Synthesis*, ed. I. Ojima, VCH Publishers, New York, 1993; J. P. Collman, Z. Wang, A. Straumanis and M. Quelquejeu, *J. Am. Chem. Soc.*, 1999, **121**, 460.
9 S. Trofimenko, *Scorpionates, The Coordination Chemistry of Polypyrazolylborate Ligands*, Imperial College Press, 1999.
10 P. J. Pérez, M. Brookhart and J. L. Templeton, *Organometallics*, 1993, **12**, 261.
11 M. M. Díaz-Requejo, M. C. Nicasio and P. J. Pérez, *Organometallics*, 1998, **17**, 3051.
12 M. M. Díaz-Requejo, T. R Belderrain, M. C. Nicasio and P. J. Pérez, *Organometallics*, 2000, **19**, 285.
13 M. I. Bruce and J. D. Walsh, *Aust. J. Chem.*, 1979, **32**, 2753.
14 C. Mealli, C. S. Arcus, J. L. Wilkinson, T. J. Marks and J. A. Ibers, *J. Am. Chem. Soc.*, 1975, **98**, 711.
15 Y. Golberg and H. Alper, *Applied Homogeneous Catalysis with Organometallic Compounds*, ed. B. Cornils and W. A. Herrman, VCH Publishers, Weinheim, 2000.
16 J. T. Groves, Z. Groos and M. K. Stern, *Inorg. Chem.*, 1994, **33**, 5065.
17 A. Sanjuan, M. Alvaro, A. Corma and H. García, *Chem. Commun.*, 1999, 1641.
18 J. March, *Advanced Organic Chemistry*, Wiley Interscience, 4th edn., New York, 1992.

A mutually perpendicular phthalocyanine pentamer obtained by a one-step reaction

Nagao Kobayashi* and Atsuya Muranaka

Department of Chemistry, Graduate School of Science, Tohoku University, Sendai 980-8578, Japan. E-mail: nagaok@mail.cc.tohoku.ac.jp

Received (in Cambridge, UK) 26th July 2000, Accepted 14th August 2000
First published as an Advance Article on the web 14th September 2000

A phthalocyanine pentamer consisting of mutually orthogonal Pc units has been prepared by a one-step reaction using oxo(phthalocyaninato)titanium(IV) and 2,3,9,10,16,17,23,24-octahydroxyphthalocyanine and characterized by mass, electronic absorption and magnetic circular dichroism spectroscopy and gel-permeation chromatography.

In contrast with the porphyrins, it is difficult to control steric interactions with the phthalocyanines (Pcs). Accordingly, most reported poly-Pc structures are limited to a few well-known types: one dimensional stacked μ-oxo SiPcs, liquid crystalline Pcs, cofacial rare earth sandwich Pcs, and planar dimers.[1] In addition, controlling the relative orientation of Pc units in Pc multimers is much more difficult than for porphyrins, since Pcs are generally obtained by template reactions and many peripheral substitution patterns are conceivable.[1] In this communication we report the first example of a Pc pentamer, in which four peripheral Pc units are covalently bound, and orthogonal to, a central Pc, **$H_2Ti_4Pc_5$** (Scheme 1).

In synthesizing **$H_2Ti_4Pc_5$**, we utilized the reactivity of the axial oxygen in TiOPc, which is readily displaced by *ortho*-phenolic OH groups, with the elimination of water, to produce two ether linkages.[2] Thus, an excess of tetra-*tert*-butyl TiOPc, obtained by a literature procedure,[3] was reacted with 2,3,9,10,16,17,23,24-octahydroxy H_2Pc[4] in dichloromethane at rt for several days (Scheme 1),[2b] and the mixture was imposed on a gel permeation column (Bio-beads SX-1, Bio-Rad), using the same solvent as eluent. The first green fraction was collected. Although this portion did not give a clear NMR spectrum due to poor solubility, satisfactory elemental analyses were obtained. Time-of-flight mass spectrometry showed *m/z* = 3774, which corresponds to the structure of **$H_2Ti_4Pc_5$** (calcd. for $C_{224}H_{202}N_{40}O_8Ti_4$ = 3773.46), together with cluster of peaks at *ca. m/z* = 2977, 2207, and 1495 (Fig. 1).[5] The difference between each peak corresponds to *ca.* one Pc unit. Since this mass spectrum could also be obtained from a mixture of compounds consisting of two to five Pc units, the elution time of **$H_2Ti_4Pc_5$** in gel-permeation chromatography was compared

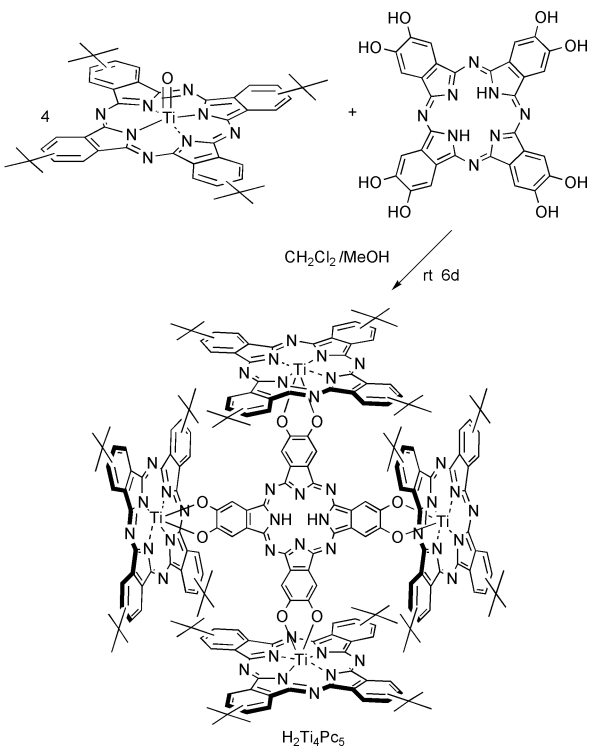

Scheme 1

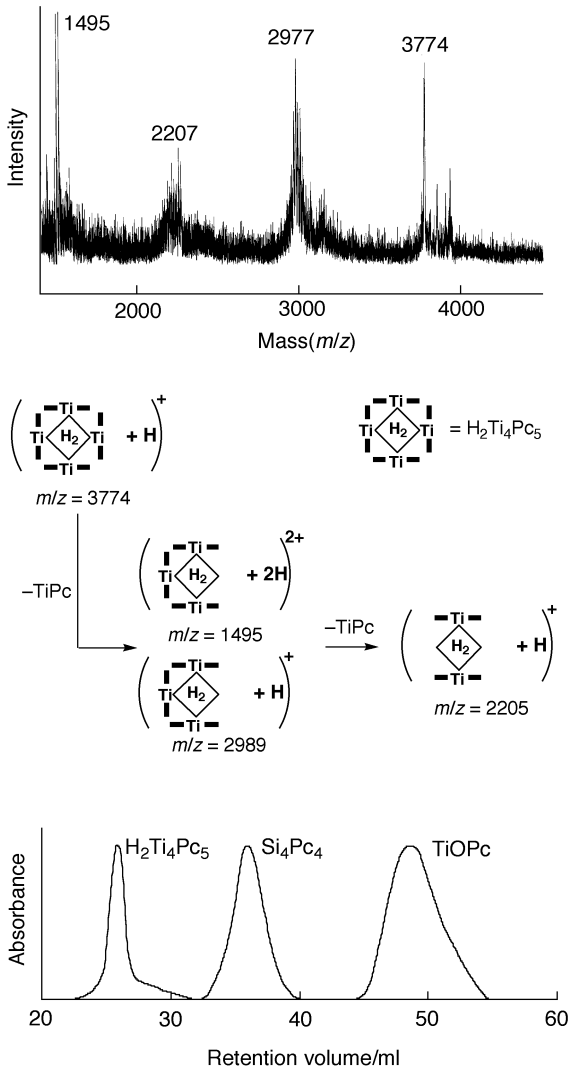

Fig. 1 MALDI-TOF Mass spectrum (top) of **$H_2Ti_4Pc_5$** and its anticipated fragment ions (middle) and gel-permeation chromatograms of **$H_2Ti_4Pc_5$**, Si4Pc4 and TiOPc (bottom). For mass measurements, dithranol (1,8,9-anthracenetriol) was used as a matrix. Chromatograms were obtained separately but superimposed.

DOI: 10.1039/b005969m

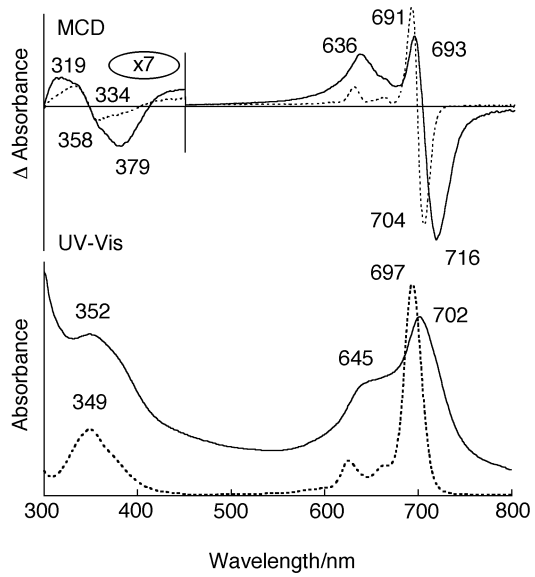

Fig. 2 Electronic absorption (bottom) and MCD (top) spectra of $\mathbf{H_2Ti_4Pc_5}$ (solid lines) and *tert*-butylated TiOPc (dotted lines) in dichloromethane.

with those of tetra-*tert*-butylated TiOPc and μ-oxo tetramer[6] of tetra-*tert*-butylated SiPc (*i.e.* Si_4Pc_4). $\mathbf{H_2Ti_4Pc_5}$ showed a single sharp peak, confirming the presence of a single compound. In addition, the shorter elution time of $\mathbf{H_2Ti_4Pc_5}$ (elution speed in column = 1.59 cm min^{-1}) indicated that $\mathbf{H_2Ti_4Pc_5}$ (Mw = 3773.89) is volumetrically larger than Si_4Pc_4 (Mw = 3142.21) (elution speed in column = 1.14 cm min^{-1}), in agreement with the proposed structure. The mass spectroscopy and gel-permeation chromatography results clearly indicate the formation of a pentamer, corresponding to $\mathbf{H_2Ti_4Pc_5}$. Although we have been unable to obtain crystals suitable for X-ray diffraction, an arrangement in which all Pc units are mutually orthogonal seems most likely, since only the Ti=O functionality can react with hydroxy groups of the octahydroxy H_2Pc to form the pentamer.

Fig. 2 shows electronic absorption and magnetic circular dichroism (MCD) spectra of tetra-*tert*-butylated TiOPc monomer and $\mathbf{H_2Ti_4Pc_5}$. Compared with the spectra of the monomer, those of $\mathbf{H_2Ti_4Pc_5}$ are shifted slightly to the red and broader. Excitonic interactions among mutually orthogonal chromophores are anticipated to be small.[7] However, our calculations[8] on the basis of an excitonic theory[7a] predict Q band transitions for $\mathbf{H_2Ti_4Pc_5}$ at 657, 689, 699 and 707 nm, and thus explain the broad and structureless Q band (the band at 689 nm corresponds to both in-plane and out-of-plane transitions and others are all in-plane transitions).

In conclusion, we have synthesized the first example of a well-defined mutually perpendicular phthalocyanine pentamer.

Notes and references

1 *Phthalocyanines—Properties and Applications*, ed. C. C. Leznoff and A. B. P. Lever, VCH, Weinheim, New York, 1989, 1992, 1993 and 1996, vols. 1–4; *Phthalocyanines—Chemistry and Functions*, ed. H. Shirai and N. Kobayashi, IPC, Tokyo, 1997; N. B. McKeown, *Phthalocyanine Materials—Synthesis, Structure and Function*, Cambridge University Press, 1998.

2 (*a*) V. L. Goedken, G. Dessy, C. Ercolani, V. Fares and L. Gastaldi, *Inorg. Chem.*, 1985, **24**, 991; (*b*) N. Kobayashi, A. Muranaka and K. Ishii, *Inorg. Chem.*, 2000, **39**, 2256.

3 J. Yao, H. Yonehara and C. Pac, *Bull. Chem. Soc. Jpn.*, 1995, **68**, 1001.

4 J. F. Van del Pol, E. Neeleman, J. C. van Miltenburg, J. W. Zwickker, R. J. M. Nolte and W. Drenth, *Macromolecules*, 1990, **23**, 155.

5 The Ti=O stretching vibration, seen in the IR spectrum of TiOPc at 972 cm^{-1}, was absent in $\mathbf{H_2Ti_4Pc_5}$.

6 Si_4Pc_4 was prepared by refluxing a toluene solution of tetra-*tert*-butylated SiPc in the presence of $CaCl_2$ and subsequent purification using gel-permeation columns of Bio-beads SX-1 (Bio-rad). It gave a parent ion peak at expected *m/z* = 3142 in the mass spectrum using MALDI-TOF technique, and satisfactory elemental analytical data.

7 (*a*) M. Kasha, H. R. Rawls and M. A. Bayoumi, *Pure Appl. Chem.*, 1965, **11**, 371; (*b*) The pseudo *A* term type Q band MCD spectra of the pentamer indeed suggests that the interaction of each constituting unit is not large M. J. Stillman and T. Nyokong, in *Phthalocyanines—Properties and Applications*, ed. C. C. Leznoff and A. B. P. Lever, VCH, Weinheim, New York, 1989, Chapter 3.

8 N. Kobayashi and A. Muranaka, details will be published in a full paper. If the central Pc unit in $\mathbf{H_2Ti_4Pc_5}$ contains TiO in its center, the Q transitions are anticipated at 689 (out-of plane), 683 and 711 (in-plane) nm.

A one-pot synthesis of *N*-alkylaminobenzenes from nitroaromatics: reduction followed by reductive amination using $B_{10}H_{14}$

Jong Woo Bae, Young Jin Cho, Seung Hwan Lee, Choon-Ock Maing Yoon and Cheol Min Yoon*

Department of Life Science & Biotechnology, Graduate School of Biotechnology, Korea University, Seoul, South Korea. E-mail: cmyoon@tiger.korea.ac.kr; Fax: +82-2-3290-3433

Received (in Corvallis, OR, USA) 27th June 2000, Accepted 27th July 2000
First published as an Advance Article on the web 14th September 2000

_N_-Alkylaminobenzenes were prepared in a simple and efficient one-pot synthesis by reduction of nitrobenzenes followed by reductive amination with decaborane ($B_{10}H_{14}$) in the presence of 10% Pd/C.

Consecutive reactions[1] have received much attention because they give complex molecules efficiently from simple starting materials. In the first step of these reactions, the functional group necessary for the following transformation is formed. An ideal place for such consecutive reactions is in one-pot synthesis, in which all these processes occur consecutively by successive addition of reagents, without isolation of intermediates. Well known examples of one-pot processes are multicomponent condensations[2] and palladium-catalyzed reactions,[3] which are known to be useful owing to mild reaction conditions and stability against other functional groups.

Aromatic amines are important intermediates for dyes and agricultural and pharmaceutical chemicals. One popular method for the preparation of these amines is the reduction of nitroaromatics using various reagents and conditions.[4,5] One of the methods for the synthesis of secondary amines is the reductive amination of primary amines with carbonyls using a variety of reducing reagents.[6]

In the course of our work using decaborane as a mild and stable reducing agent,[7] we found that the reduction of

Table 1 Synthesis of *N*-alkylaminobenzenes

Entry	Nitroaromatics (**1**)	Carbonyls (**2**)[a]	Time/h	Product (**3**)[b]	Yield[c] (%)
1	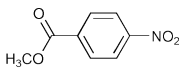	Butan-2-one	0.5 (*ca.* 40 °C) 2 (rt)	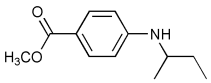	93
2	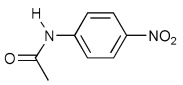	Butan-2-one	0.5 (*ca.* 40 °C) 2 (rt)	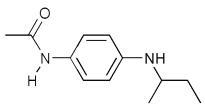	91
3	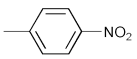	Butan-2-one	1.5 (*ca.* 40 °C) 2 (rt)	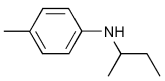	92
4	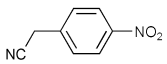	Butan-2-one	2.5 (*ca.* 40 °C) 2 (rt)	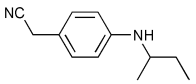	88
5	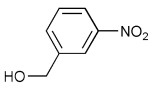	Butan-2-one	3 (*ca.* 40 °C) 2 (rt)	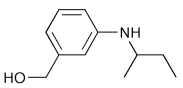	89
6	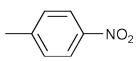	Ethyl acetoacetate	1.5 (*ca.* 40 °C) 2 (rt)	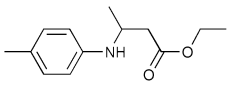	92
7	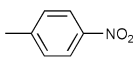	2-Hydroxyacetophenone	1.5 (*ca.* 40 °C) 10 (rt)	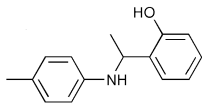	84
8	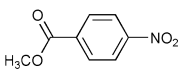	Propanal	0.5 (reflux) 2 (rt)	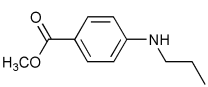	91
9	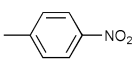	4-Hydroxybenzaldehyde	1.5 (reflux) 2 (rt)	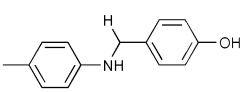	90

[a] 1.1 equiv. of carbonyls (of nitroaromatics) was used in all cases. [b] All products are known compounds and gave spectra (GC-MS, ^{1}H NMR, IR) consistent with the assigned structures. [c] Isolated yields.

DOI: 10.1039/b005194m

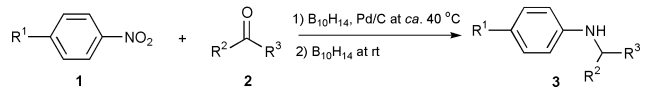

Scheme 1

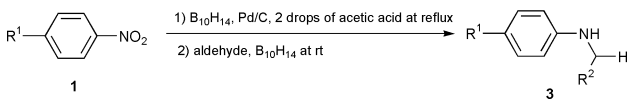

Scheme 2

nitroaromatics using a decaborane–Pd/C system followed by reductive amination with carbonyls using decaborane gave a one-pot synthesis of *N*-alkylaminoaromatics in high isolated yield. To the best of our knowledge, this is the first example of a one-pot preparation of *N*-alkylaminoaromatics from nitroaromatics.

Decaborane was added in two batches in all of the examples.[8] 30 mol% of decaborane ($B_{10}H_{14}$) was added for the reduction of the nitro group in the first batch, and 20 or 30 mol%[9] was used for reductive amination in the second batch. When a ketone was used for the reductive amination (entries 1–7, Table 1), it was added to the reaction solution at the beginning of the reaction (Scheme 1). The reactions proceeded smoothly at 40 °C without addition of acetic acid. However, when aldehydes were used (entries 8 and 9, Table 1), they were added after the completion[10] of the nitro-group reduction to prevent reductive etherification[11] (Scheme 2). Under these conditions, the reactions were complete in several hours and gave the corresponding secondary amines chemoselectively and in high yields. Other functional groups such as esters (entries 1, 6 and 8), amides (entry 2), nitriles (entry 4) and hydroxy groups (entry 5) were intact under the reaction conditions.†

In conclusion, nitroaromatics were converted into *N*-alkylaminoaromatics in a single-pot synthesis using decaborane as a reducing agent in the presence of Pd/C in methanol. The reaction is efficient and chemoselective. Investigations of the scope of this one-pot synthesis are currently underway.

The authors wish to acknowledge the financial support of the Korea Research Foundation made in 2000.

Notes and references

† *Representative experimental procedures*: *Ketone (entry 3)*. To a solution of 4-nitrotoluene (50 mg, 0.364 mmol) in methanol (5 ml) was added butan-2-one (28.9 mg, 0.401 mmol), decaborane (13.4 mg, 0.109 mmol) and 10% Pd/C (15 mg). The resulting solution was stirred at *ca.* 40 °C under nitrogen for 1.5 h. The mixture was then cooled to rt and decaborane (8.9 mg, 0.073 mmol) was added to the mixture. The resulting solution was stirred at rt under nitrogen for 2 h. The mixture was concentrated under reduced pressure, chromatographed on a short pad of silica gel using a solution of ethyl acetate and *n*-hexane (1 : 8) and concentrated to give the product amine as a pale pink syrup. *Aldehyde (entry 8)*. To a solution of methyl 4-nitrobenzoate (50 mg, 0.276 mmol) in methanol (5 ml) was added two drops of acetic acid, decaborane (10 mg, 0.083 mmol) and 10% Pd/C (15 mg). The resulting solution was heated to reflux under nitrogen for 0.5 h and the mixture was cooled to rt. Propanal (17 mg, 0.303 mmol) and decaborane (6.7 mg, 0.052 mmol) were then added to the reaction mixture. The solution was stirred at rt under nitrogen for 2 h. The mixture was concentrated under reduced pressure, chromatographed on a short pad of silica gel using a solution of ethyl acetate and *n*-hexane (1 : 8), and concentrated to give the amine as a white solid.

1 L. F. Tietze and U. Beifuss, *Angew. Chem., Int. Ed. Engl.*, 1993, **32**, 131; L. F. Tietze, *Chem. Rev.*, 1996, **96**, 115.
2 *Multicomponent Reactions in Organic Chemistry*, I. Ugi, A. Domling and W. Horl, *Endeavour*, 1994, **18**, 115.
3 S. Brase and A. de Meijere, in *Metal-catalyzed Cross-coupling Reactions*, ed. F. Diederich and P. J. Stang, Wiley-VCH, Weinheim, 1998, p. 99; A. de Meijere and F. E. Meyer, *Angew. Chem., Int. Ed. Engl.*, 1994, **33**, 2379; T. J. J. Muller, M. Ansorge and S. Aktah, *Angew. Chem., Int. Ed.*, 2000, **39**, 1253.
4 G. Mestoni, A. Camus and G. Zassinovich, in *Aspects of Homogeneous Catalysis*, ed. R. Ugo, Reidel, Dordrecht, 1981, Vol. 4, pp. 71–80.
5 G. Sauve and V. S. Rao, *Comprehensive Organic Functional Group Transformations*, ed. A. R. Katritzky, O. Meth-Cohn and C. W. Rees, Pergamon Press, Oxford, 1995, Vol. 2, pp. 737–817.
6 W. S. Emerson, *Org. React.*, 1948, **4**, 174; M. V. Klyuev and M. L. Khidekel, *Russ. Chem. Rev.*, 1980, **49**, 14; R. Hutchins and N. R. Natale, *Org. Prep. Proced. Int.*, 1979, **11**, 201; M. D. Bomann, I. C. Guch and M. DiMare, *J. Org. Chem.*, 1995, **60**, 5995; N. M. Yoon, E. G. Kim, H. S. Son and J. Choi, *Synth. Commun.*, 1993, **23**, 1595; J. Brussee, R. A. T. M. van Benthem, C. G. Kruse and A. van der Gen, *Tetrahedron: Asymmetry*, 1990, **1**, 163; A. F. Abdel-Magid, K. G. Carson, B. D. Harris, C. A. Maryanoff and R. D. Shah, *J. Org. Chem.*, 1996, **61**, 3849; B. C. Ranu, A. Majee and A. Sakar, *J. Org. Chem.*, 1998, **63**, 370.
7 J. W. Bae, S. H. Lee, Y. J. Cho and C. M. Yoon, *J. Chem. Soc., Perkin 1*, 2000, 145.
8 The addition of 50 or 60 mol% decaborane in one batch at the beginning of the reaction resulted in incomplete reaction.
9 In some cases (entries 1, 2 and 7), the reductive amination was slow with 20 mol% of decaborane. In these instances, 30 mol% of decaborane was added.
10 The completion of the reduction of the nitro group was followed by TLC using a solution of ethyl acetate and *n*-hexane (1 : 4).
11 S. H. Lee, Y. J. Park and C. M. Yoon, *Tetrahedron Lett.*, 1999, **40**, 6049.

ChemComm

First tether-directed regioselective bis-functionalisation of C_{70}: effects of cation complexation on the redox properties of diastereoisomeric fullerene crown ether conjugates

Maurice J. van Eis,[a] Robert J. Alvarado,[b] Luis Echegoyen,*[b] Paul Seiler[a] and François Diederich*[a]

[a] *Laboratorium für Organische Chemie, ETH-Zentrum, Universitätstrasse 16, CH-8092 Zürich, Switzerland. E-mail: diederich@org.chem.ethz.ch*

[b] *Department of Chemistry, University of Miami, Coral Gables, FL 33124, USA*

Received (in Cambridge, UK) 28th July 2000, Accepted 14th August 2000
First published as an Advance Article on the web

The covalently templated bis-functionalisation of C_{70}, employing a dibenzo-18-crown-6 tether, proceeds with complete regiospecificity and provides a bis-addition pattern which is disfavoured in sequential transformations.

Tether-directed remote functionalisation has proven to be a powerful tool for obtaining regiochemical control in multiple additions to buckminsterfullerene, C_{60}.[1–4] However, up until now, this approach had not been applicable to C_{70} or other higher fullerenes.

Double *Bingel* cyclopropanation of C_{70}[5] occurs on opposing hemispheres at the most curved α-type[6] 6–6 bonds (bonds at the junction between two six-membered rings) emanating from the two polar pentagons through which the C_5 symmetry axis of the higher fullerene passes. In a *Newman*-type projection looking down the C_5 axis onto the two polar pentagons, the two addends adopt a twelve, two and five o'clock geometrical relationship, respectively. Accordingly, the kinetically controlled *Bingel* bis-cyclopropanation with achiral dialkyl malonates provides three constitutional isomers, two of which (two and five o'clock) are pairs of enantiomers, in a ratio of 2.8:6.8:1.0, respectively (twelve, two and five o'clock orientation of the addends). Similar addition patterns were also obtained in other bis-functionalisation reactions, with the two o'clock geometric relationship being highly favored in each case.[7–10] Here we report the application of the tether-directed remote functionalisation to prepare C_{70} bis-adducts (±)-**1a** and (±)-**1b** with complete regioselectivity, featuring the kinetically disfavoured five o'clock addition pattern.

C_{70} was reacted with dibenzo-18-crown-6- (DB18C6) linked bis-malonate **2**[11] under modified *Bingel*-conditions (I_2, DBU, toluene) in the presence of KPF_6 (10 eq.), which was added as a template to rigidify the tether by complexation (Scheme 1). This afforded the two products (±)-**1a** and (±)-**1b** in a 56:44 ratio with an overall yield of 41%. Both compounds were separated by column chromatography (Silica-*H*; toluene–ethyl acetate (1:1)) and fully characterised (^{1}H and ^{13}C NMR, high-resolution MALDI-TOF-MS, IR and UV/Vis). Transesterfication of the crude product mixture of (±)-**1a** and (±)-**1b** (Cs_2CO_3, THF–EtOH (1:1)) afforded only one single C_2-symmetrical bis-adduct (±)-**3**. The spectroscopic data (^{1}H and ^{13}C NMR) revealed its identity with the C_{70} bis-adduct featuring diethyl malonate addends at the two polar C(1)–C(2) and C(67)–C(68) bonds (five o'clock addition pattern), which had previously been obtained by sequential double *Bingel* addition.[5,6b] This leads to the remarkable conclusion that reaction of C_{70} with **2** proceeds with complete regioselectivity to give the normally kinetically least favoured regioisomer. Surprisingly, the absence of KPF_6 in the *Bingel* macrocyclisation did not affect the regioselectivity at all, although the diastereoisomeric ratio changed slightly, providing (±)-**1a** and (±)-**1b** as the only products in a ratio of 37:63 with a substantial higher yield of 68%.

The presence of the inherently chiral five o'clock addition pattern and the *out–out* orientation of the EtOOC groups in

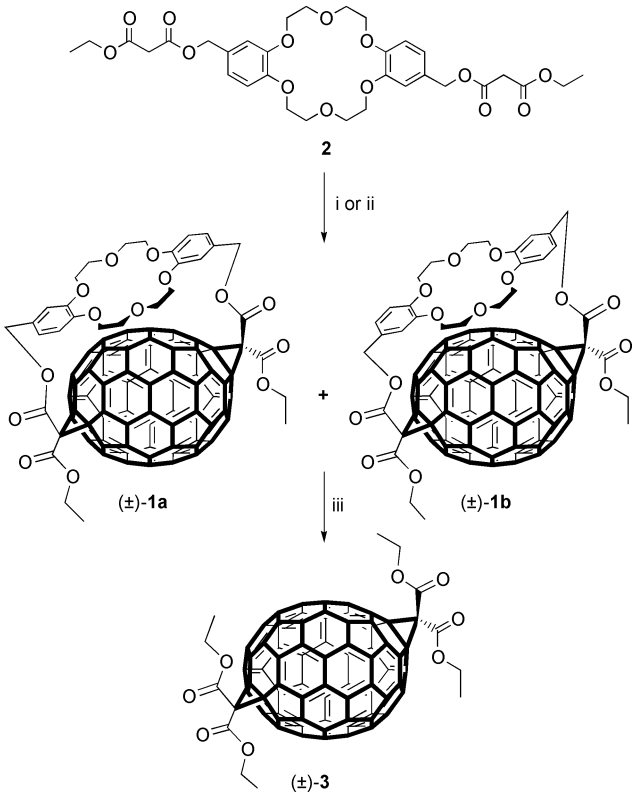

Scheme 1 *Reagents and conditions*: i, C_{70}, I_2, DBU, KPF_6 (10 equiv.), toluene, rt, 23% ((±)-**1a**), 18% ((±)-**1b**); ii, C_{70}, I_2, DBU, toluene, rt, 25% ((±)-**1a**), 43% ((±)-**1b**); iii, Cs_2CO_3, THF–MeOH (1:1), rt, 2 h.

(±)-**1a** was unequivocally established by X-ray crystallography (Fig. 1).† The fullerene core in this first crystal structure of a cyclopropanated C_{70} derivative has a spheroidal shape with a distance of 8.03 Å along the principal axis. As a consequence of cyclopropanation, the carbon atoms C(1), C(2), C(67) and C(68) are pulled out of the C_{70}-surface leading to a slightly longer distance along the main axis than observed for the complex (η^2-C_{70})Ir(CO)Cl(PPh_3)$_2$ (7.90 Å).[14] Distances from the carbon atoms at the equator to the center of the sphere range from 3.52–3.56 Å with a mean value of 3.54 Å. The bond lengths between the bridgehead atoms C(1)–C(2) and C(67)–C(68) of 1.605(9) and 1.596(10) Å, respectively, are strongly elongated compared to the analogous bonds reported for several η^2-transition metal C_{70}-complexes (1.512–1.523 Å).[8] However, they are similar to the lengths of the corresponding bonds reported for a *trans*-1 bis-cyclopropanated C_{60} crown ether conjugate (1.606–1.610 Å),[11b] and a Diels–Alder mono-adduct of C_{70} (1.603 Å).[15] Most geometrical features of **1a** are comparable to those of the latter Diels–Alder adduct.

The crown ether moiety exists in a conformation different from the four conformations reported so far in the literature for

DOI: 10.1039/b006066f

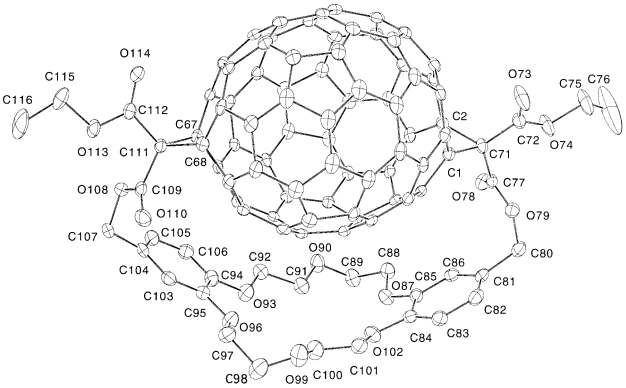

Fig. 1 Molecular structure of (±)-**1a** in the crystal. Atomic displacement parameters obtained at 233 K are drawn at the 30% probability level.

uncomplexed DB18C6.[16] In order to bridge the fullerene poles, it adopts an 'umbrella shaped' geometry with a distorted C_2-symmetry. The approximate dihedral angle between the two aromatic planes is about 124°. This is comparable to the value reported for DB18C6 complexes (128–102°),[11b,16b,c] but considerably larger than for uncomplexed C_{2v}-symmetrical DB18C6 (98.8°).[16c] Several close contacts between the DB18C6 tether and the fullerene surface are observed.

The structure of the other isomer ((±)-**1b**) was deduced from MM2-calculations,[17] which indicated that the *in–out* and *in–in* isomers are not feasible because of their much higher steric energy. Thus, (±)-**1a**, and (±)-**1b** are diastereoisomeric pairs of enantiomers, differing only in the orientation of the DB18C6 tether as a result of planar chirality.

To determine the effects of cation complexation on the redox properties of (±)-**1a** and (±)-**1b**, cyclic voltammetric (CV) studies were performed in toluene–MeCN (4 : 1) in the absence and presence of KPF_6 and $NaBF_4$ (Table 1). Based on the ΔE_{pp} values and the cathodic : anodic current ratio, the first reduction waves of (±)-**1a** and (±)-**1b** are electrochemically and chemically reversible. However, the second reduction is chemically irreversible as judged by an additional oxidation wave observed on the reverse scan. Consequently, ion binding effects were monitored only for the first reduction. Similar to the behavior of the previously reported C_{60}–DB18C6 conjugate,[11b] addition of sub-stoichiometric amounts of Na^+ ions to the solution of (±)-**1a** causes the appearance of a new poorly resolved, yet clearly discernible redox wave which is anodically shifted by 70 mV relative to that for the free compound.[11] This new redox couple, assigned to the cation complex, grows at the expense of the one for the uncomplexed species as the concentration of Na^+ ions increases. This was firmly established by the observation of isopotential points on both the forward and reverse scans. Addition of one eq. of Na^+ ions causes the redox wave of the free compound to disappear completely, and further addition causes no further observable changes in the voltammetry. This behavior implies strong complexation between the crown ether conjugate and one Na^+ ion.[18] The anodic shift must be attributed to the electrostatic effect of the Na^+ ion which is bound to the DB18C6 ionophore in close proximity to the fullerene surface. The behavior with K^+ ions was very similar (Table 1), and the same was observed for (±)-**1b** with either cation.

Table 1 Redox potentials (*vs.* ferrocene–ferricinium couple) of (±)-**1a** and (±)-**1b** in absence and presence of alkali metal cations[a]

	E_1/V	E_2/V	+ KPF_6[b] E_1/V	+ $NaBF_4$[c] E_1/V
(±)-**1a**	−1.13 (67)	−1.57[d]	−1.05 (65)	−1.06 (68)
(±)-**1b**	−1.14 (68)	−1.58[d]	−1.07 (68)	−1.06 (67)

[a] Measurements were performed under Ar in toluene–MeCN (4:2) containing 0.1 M Bu_4NPF_6 as the supporting electrolyte, using a concentration of 0.3 mM for (±)-**1a** and 0.2 mM for (±)-**1b**. Glassy carbon working electrode. Non-aqueous Ag/Ag^+ reference electrode Pt wire counter electrode. The scan rate was 100 mV s^{-1}. Values in parentheses are the ΔE_{pp} in mV. [b] 1.0 eq. of KPF_6. [c] 1.0 eq. of $NaBF_4$. [d] Cathodic peak potential.

This work was supported by the Swiss National Science Foundation and the US National Science Foundation (CHE-9816503). M. J. v. E. is grateful for a TALENT stipend of the Netherlands Organisation for Scientific Research (NWO). R. J. A. is grateful to Dr Lourdes Echegoyen for her help and advice.

Notes and references

† *Crystal data*: **1a**: $C_{102}H_{36}O_{14}\cdot 6CHCl_3$, M_r = 2201.52, monoclinic space group $P2_1/n$ (no. 14), Z = 4, a = 14.395(4), b = 33.405(9), c = 19.277(6) Å, β = 108.67(2)°, V = 8782(4) Å^3, T = 233 K. A semi-empirical absorption correction, based on psi-scans was applied to the data (T(max) = 0.99, T(min) = 0.78). The structure was solved by direct methods (SIR92)[12] and refined by full-matrix least-squares analysis (SHELXL-97),[13] using an isotropic extinction correction, and $w = 1/[\sigma^2(F_o^2) + (0.115P)^2 + 43.34P]$, where $P = (F_o^2 + 2F_c^2)/3$. It consists of one ordered molecule of (±)-**1a** and six slightly disordered $CHCl_3$ molecules. All heavy atoms were refined anisotropically (H-atoms isotropically, whereby H-positions are based on stereochemical considerations). Final $R(F)$ = 0.077, $wR(F^2)$ = 0.205 for 1262 parameters, and 7220 reflections with $I > 2\sigma(I)$ and $2.6 < \theta < 53.0°$ (corresponding R-values based on all 9732 reflections are 0.105 and 0.234, respectively). CCDC 182/1756. See http://www.rsc.org/suppdata/cc/b0/b006066f/ for the crystallographic file in .cif format.

1 (*a*) L. Isaacs, R. F. Haldimann and F. Diederich, *Angew. Chem., Int. Ed. Engl.*, 1994, **33**, 2339; (*b*) F. Diederich and R. Kessinger, *Acc. Chem. Res.*, 1999, **32**, 537.
2 E. Nakamura, H. Isobe, H. Tokuyama and M. Sawamura, *Chem. Commun.*, 1996, 1747.
3 M. Taki, S. Sugita, Y. Nakamura, E. Kasashima, E. Yashima, Y. Okamoto and J. Nishimura, *J. Am. Chem. Soc.*, 1997, **119**, 926.
4 F. Diederich and M. Gómez-López, *Chem. Soc. Rev.*, 1999, **28**, 263.
5 C. Bingel and H. Schiffer, *Liebigs Ann. Chem.*, 1995, 1551.
6 (*a*) A. Herrmann, M. Rüttimann, C. Thilgen and F. Diederich, *Helv. Chim. Acta*, 1995, **78**, 1673; (*b*) A. Herrmann, M. W. Rüttimann, T. Gibtner, C. Thilgen, F. Diederich, T. Mordasini and W. Thiel, *Helv. Chim. Acta*, 1999, **82**, 261.
7 X. Zhang and C. S. Foote, *J. Am. Chem. Soc.*, 1995, **117**, 4271.
8 (*a*) A. L. Balch, J. W. Lee and M. M. Olmstead, *Angew. Chem., Int. Ed. Engl.*, 1992, **31**, 1356; (*b*) A. L. Balch, L. Hao and M. M. Olmstead, *Angew. Chem., Int. Ed. Engl.*, 1996, **35**, 188.
9 H. P. Spielmann, G.-W. Wang, M. S. Meier and B. R. Weedon, *J. Org. Chem.*, 1998, **63**, 9865.
10 C. Thilgen and F. Diederich, *Top. Curr. Chem.*, 1998, **199**, 135.
11 (*a*) J.-P. Bourgeois, L. Echegoyen, M. Fibbioli, E. Pretsch and F. Diederich, *Angew. Chem., Int. Ed.*, 1998, **37**, 2118; (*b*) J.-P. Bourgeois, P. Seiler, M. Fibbioli, E. Pretsch, F. Diederich and L. Echegoyen, *Helv. Chim. Acta*, 1999, **82**, 1572.
12 A. Altomare, G. Cascarano, C. Giacovazzo, A. Guagliardi, M. C. Burla, G. Polidori and M. Camalli, *J. Appl. Crystallogr.*, 1994, **27**, 435.
13 G. M. Sheldrick, *SHELXL-97 Program for the Refinement of Crystal Structures*, University of Göttingen, Germany, 1997.
14 A. L. Balch, V. J. Catalano, J. W. Lee, M. M. Olmstead and S. R. Parkin, *J. Am. Chem. Soc.*, 1991, **113**, 8953.
15 P. Seiler, A. Herrmann and F. Diederich, *Helv. Chim. Acta*, 1995, **78**, 344.
16 (*a*) D. Bright and M. R. Truter, *J. Chem. Soc. B*, 1970, 1544; (*b*) P. Dapporto, P. Paoli, I. Matijasic and L. Tusek-Bozic, *Inorg. Chim. Acta*, 1996, **252**, 383; (*c*) P. Dapporto, P. Paoli, I. Matijasic and L. Tusek-Bozic, *Inorg. Chim. Acta*, 1998, **282**, 76.
17 *Program CS Chem3D Pro*, Version 5.0, CambridgeSoft Corporation, Cambridge, 1995.
18 S. R. Miller, D. A. Gustowski, Z. Chen, G. W. Gokel, L. Echegoyen and A. E. Kaifer, *Anal. Chem.*, 1988, **60**, 2021.

ChemComm

Microwave discharge-assisted catalytic conversion of NO to N_2

Junwang Tang, Tao Zhang,* Dongbai Liang, Changhai Xu, Xiaoying Sun and Liwu Lin

State Key Laboratory of Catalysis, Dalian Institute of Chemical Physics, Chinese Academy of Sciences, Dalian 116023, China. E-mail: taozhang@ms.dicp.ac.cn

Received (in Cambridge, UK) 2nd May 2000, Accepted 14th August 2000
First published as an Advance Article on the web 15th September 2000

By coupling microwave discharge with an Fe/HZSM-5 catalyst, novel effects have been observed for the conversion of NO to N_2 in the presence of excess oxygen with high efficiency.

The reduction of NO has been investigated for many years. Especially in the past decade, it has attracted much attention.[1] Recently, with the progress of advanced techniques, many papers have described the application of new methods in different branches of chemistry.[2] Among these techniques, microwave dielectric heating is a convenient and effective way of bringing about chemical reactions in the field of catalysis.[3] The use of microwave heating to stimulate catalytic reactions has provided some remarkable results,[4–6] Bond *et al*. and Wan and co-workers have investigated the effect of microwave heating on many catalytic reactions.[7] The reduction of NO by CH_4 by a microwave heating technique has also been reported by this laboratory.[8] Here, we report on a new process for the removal of NO by coupling the microwave discharge (not microwave heating) with the selective catalytic reduction (SCR) reaction by CH_4. We designate this kind of process as catalysis assisted by microwave discharge (CAMD).

A Fe/HZSM-5 catalyst was employed to demonstrate the effect of the CAMD of NO–CH_4. The Fe/HZSM-5 was prepared by impregnating HZSM-5 (SiO_2/Al_2O_3 = 25) in an aqueous $Fe(NO_3)_3$ solution (Fe in the catalyst was 10 wt%); all catalysts prepared were of 1.25–1.60 mm granule size. The flow rate of the feed, which consisted of 2000 ppm NO, 1600 ppm CH_4 and 2.0% O_2 (helium as a balance gas), was 60 ml min^{-1} (GHSV = 3600 h^{-1}).

A special quartz tubular reactor (i.d. 10 mm) was aligned vertically at the center of the microwave cavity. The catalyst bed was supported on a fused quartz frit of medium porosity. The gas composition was determined by an on-line NO_x-analyser and gas chromatograph (GC-8800 type, with 13X and PQ columns).

In this work, Fe/HZSM-5 was used not only as a catalyst, but also as a discharge igniter, by which discharge was achieved without any electrode at atmospheric pressure: after the microwaves were induced in the reactor, red discharge with weak sounds was observed among the catalyst granules.

Results obtained over the Fe/HZSM-5 in a conventional reaction mode (CRM) are presented in Table 1. From these data, it is apparent that the Fe/HZSM-5 was almost inactive for the reduction of NO with CH_4 in excess O_2 in the CRM. When CH_4 was wholly consumed, the conversion of NO to N_2 did not exceed 5%, which is almost in accordance with the results of Chen *et al*.[9] The results indicate that the activity of the Fe/HZSM-5 catalyst for CH_4–NO reaction is very low in the presence of excess O_2 in the CRM.

Results obtained over Fe/HZSM-5 in the CAMD process are presented in Table 2. It can be seen from these results that the conversion of NO to N_2 is increased to 44.5% in the presence of excess O_2, while at the same time the CH_4 consumption is 50.5%.

In order to confirm the enhancement of the catalytic activity by the microwave discharge, another microwave discharge experiment without any catalyst was conducted and the results are also given in Table 2. In this experiment, the average conversion of NO to N_2 was 18.2%. It can be noted that even the sum of the conversion of NO to N_2 in the microwave discharge mode without any catalyst and that in the CRM were still lower than that of NO to N_2 *via* CAMD.

From the above results it can be seen that, regardless of temperature, the Fe/HZSM-5 catalyst is inactive in the CRM for the CH_4–NO reaction (Table 1). However, when in the microwave discharge mode the conversion of NO to N_2 on Fe/HZSM-5 increases from *ca*. 5 to 44%. Apparently the catalytic activity of the Fe/HZSM-5 is enhanced remarkably by the microwave discharge. This increase in catalytic activity cannot be readily explained by an increase in reaction temperature, suggesting that microwave discharge can cause non-Arrhenius effects.

As we know, in the CRM all reactants gain energy by thermal conduction. In fact, the reaction of CH_4 with O_2 proceeds more rapidly than the reaction of CH_4 with NO at high temperatures so that a large portion of CH_4 is consumed by O_2, resulting in the restraint of the reaction rate for CH_4 with NO. Therefore, the conversion of NO to N_2 in the presence of excess O_2 is both very low and independent of temperature in the CRM. On the other hand, in the microwave discharge mode a high frequency electromagnetic field is formed easily in the reactor, and since the molecules in the gas phase are transparent to the electromagnetic field no interaction will take place between the electromagnetic field and the gaseous molecules. Our temperature-programmed desorption (TPD) experiments on Fe/HZSM-5 indicated that supported Fe_2O_3 is a good material for the adsorption of NO_x, which agrees well with the report of Otto and Shelef.[10] Moreover, it is known that the high frequency

Table 1 Activity of Fe/HZSM-5 catalyst in the conventional reaction mode[a]

T/°C	NO conversion (%)	CH_4 conversion (%)
300	0.7	2.0
400	4.5	4.5
500	5.0	7.3
600	4.4	9.0
650	3.0	27.3
700	3.3	81.3
740	2.1	100.0

[a] *Reaction conditions*: 2000 ppm NO, 1600 ppm CH_4, 2% O_2, balance He; total flow rate 60 ml min^{-1} (GHSV = 3600 h^{-1}).

Table 2 Performance of the system with Fe/HZSM-5 catalyst and without a catalyst in the microwave discharge mode[a]

Catalyst	Microwave power/W	NO conversion (%)	CH_4 conversion (%)
Fe/HZSM-5	43–54	40.0	37.1
	54–65	42.0	47.3
	65–76	44.5	50.5
No catalyst	54–65	18.0	70.2
	65–76	18.4	74.1

[a] *Reaction conditions*: 2000 ppm NO, 1600 ppm CH_4, 2% O_2, balance He; total flow rate 60 ml min^{-1} (GHSV = 3600 h^{-1}).

DOI: 10.1039/b003499l

electromagnetic field is beneficial for the activation of polar molecules. So, it is speculated that the NO_x adsorbed on the Fe/HZSM-5 but not the O_2 in the gas phase, can be activated effectively by the high frequency electromagnetic field. This speculation agrees with the results of our previous paper.[8] Then again, microwave discharge can produce many active electrons with higher energy and higher temperature, and by the action of these electrons plenty of radicals, especially CH_x, can be produced. However, the average temperature of the gas feed is still very low in the microwave discharge mode, which is beneficial for lowering the energy consumption greatly and hence retarding the reaction of CH_4 with O_2. Under the same circumstances, the reaction between the activated NO_x adsorbed on the catalyst and the CH_x radicals is easily accelerated by the Fe/HZSM-5 catalyst so that the conversion of NO to N_2 can be enhanced greatly *via* CAMD on the Fe/HZSM-5. Although the mechanism of CAMD is not yet clear, it is likely that the reaction pathways in the CMR are different from those in the CAMD, and this may be the reason why the activity of the Fe/HZSM-5 catalyst varies significantly under the two modes.

In conclusion, the Fe/HZSM-5 catalyst exhibits a rather remarkable catalytic performance in the SCR of NO by CH_4 in the CAMD process, indicating that CAMD has a beneficial effect on the activation of reacting molecules.

The authors thank Professor Can Li, the director of State Key Laboratory of Catalysis, Dalian Institute of Chemical Physics, CAS, for helpful discussions.

Notes and references

1 A. Fritz and V. Pitchon, *Appl. Catal., B*, 1997, **13**, 1.
2 L. Seyfried, F. Garin, G. Maire, J. M. Thiebaut and G. Roussy, *J. Catal.*, 1986, **99**, 499.
3 C. S. Cundy, *Collect. Czech. Chem. Commun.*, 1998, **63**, 1700.
4 L. F. Nazar, G. A. Ozin, F. Hugues, J. Godber and D. Rancourt, *Angew. Chem., Int. Ed. Engl.*, 1983, **22**, 624.
5 Y. F. Chang, A. Sanjurjo, J. G. McCarty, G. Krishnan, B. Woods and E. Wachsman, *Catal. Lett.*, 1999, **57**, 187.
6 S. Ringler, P. Girard, G. Maire, S. Hilaire, G. Roussy and F. Garin, *Appl. Catal., B*, 1999, **20**, 219.
7 G. Bond, R. B. Moyes and D. A. Whan, *Meas. Sci. Technol.*, 1991, **2**, 571; G. Bond, R. B. Moyes and D. A. Whan, *Catal. Today*, 1993, **17**, 427; T. R. J. Dinesen, M. Y. Tse, M. C. Depew and J. K. S. Wan, *Res. Chem. Intermed.*, 1991, **15**, 113; G. Bamwenda, M. C. Depew and J. K. S. Wan, *Res. Chem. Intermed.*, 1993, **19**, 553.
8 X. Wang, T. Zhang, C. Xu, X. Sun, D. Liang and L. Lin, *Chem. Commun.*, 2000, **4**, 279.
9 H. Y. Chen, T. Voskaboinikov and W. M. H. Sachtler, *J. Catal.*, 1998, **180**, 173.
10 K. Otto and M. Shelef, *J. Catal.*, 1970, **18**, 184.

ChemComm

Design, synthesis and structural investigation of a 1-D directional coordination network based on the self-assembly of an unsymmetrical mono-tridentate ligand and cobalt cation

Abdelaziz Jouaiti, Mir Wais Hosseini* and André De Cian

Laboratoire de Chimie de Coordination Organique, Université Louis Pasteur, F-67000 Strasbourg, France, UMR CNRS 7513

Received (in Cambridge, UK) 27th July 2000, Accepted 24th August 2000
First published as an Advance Article on the web

Using an *exo* ligand containing a pyridine unit as a monodentate coordination site and a PyS_2 moiety as a tridentate coordination pole, a directional 1-D coordination network has been obtained in the presence of $CoCl_2$ under self-assembly conditions; a single-crystal X-ray study revealed that in the crystalline phase the 1-D networks are packed in a centrosymmetric fashion.

The formation of coordination networks based on *exo* ligands (ligands with coordination sites outwardly oriented) and metal cations are currently attracting much attention.[1] The formation of such networks may take place in the crystalline phase through self-assembly processes based on the reversible coordination of metal cations by *exo* ligands. The iterative binding process leads to the assembling cores acting as structural nodes of the network. The dimensionality of coordination networks (1-, 2- or 3-D) is defined by the number of translations (1, 2 or 3) operating on the assembling core. The dimensionality depends, on one hand, on the topological and coordination features of the organic *exo* ligand and, on the other hand, on the stereochemical requirements of the metal. Although the majority of reported coordination networks are formed using bis-monodentate *exo* ligands based on 4,4′-bipyridine,[2] examples of coordination networks based on bis-bidentate[3,4] or tetrakis-monodentate[5,6] ligands have also been reported. However, dealing with bis-tridentate *exo* ligands, only a few structurally characterised networks have been published.[7–9]

At present, let us consider the formation of 1-D coordination networks based on a single translation of an assembling core. For such a network, owing to the fact that exploitation of directional physical properties requires vectorial arrangements of the building blocks, the control of directionality remains a challenging issue.

The design of ligands for the formation of 1-D networks using metals with linear coordination geometry is trivial and may only be based on bis-monodentate systems (one may use homo-L(*n*,*m*) and hetero-L(*n*,*m*) notation to design the *exo* ligand L composed of two coordination poles each containing *n* and *m* coordination sites of the same (homo) or different (hetero) nature: thus, bis-monodentate ligands may be described as homo- or hetero-L(1,1) and bis-bidentate ligands as homo- or hetero-L(2,2) *etc*.). For metal cations requiring four coordination sites arranged either in square planar or in tetrahedral coordination geometry, two different types of *exo* ligands based on either bis-bidentate (homo- or hetero-L(2,2)) or a combination of mono ($n = 1$) and tridentate ($m = 3$) (hetero-L(1,3) may be envisaged. For metal cations with octahedral coordination geometry, if all six coordination positions are taken into account, 1-D networks may be obtained using bis-tridentate *exo* ligands (homo- or hetero-L(3,3)). However, in the latter case, further design of the assembling core may be based on the use of four coordination positions located at the square planar base of the octahedron. In such a design the two axial positions would be occupied by two ligands acting as terminal coordinators and thus not participating in the formation of the network. Again, for such a strategy, one may use either homo- or hetero-L(2,2) or hetero-L(1,3) ligands. Whereas for symmetrical ligands of the homo-L(2,2) type no directional network may be formed, with hetero-L(2,2) or hetero-L(1,3) ligands the formation of directional 1-D networks may be envisaged.

In the present contribution we report the design and synthesis of a new hetero-L(1,3) *exo* ligand **1** and its self assembly in the crystalline phase into a 1-D directional network in the presence of $CoCl_2$.

The strategy that was followed for the design of 1-D directional networks was based on the self-assembly of the neutral hetero-L(1,3) *exo* ligand **1** and octahedral $CoCl_2$ complex. The design of **1** (Scheme 1) is based on a combination of two different coordination poles, one composed of a monodentate pyridine derivative and the other on a pyridine unit bearing at the 2 and 6 positions CH_2SCH_3 thioether fragments leading thus to a tridentate PyS_2 coordination system. The ethynyl spacer was chosen to interconnect the two coordination poles through the pyridine units at the 4 positions. The ethynyl spacer appeared as an interesting bridge since it should allow avoidance of possible steric effects which may alter the packing of 1-D networks in the solid state and based on its ability to permit possible electronic communication between the two pyridine rings.

The starting material for the synthesis of **1** was chelidamic acid **2**. Upon treatment of the latter with PBr_5 followed by EtOH, compound **3** was obtained in 61% yield.[10] The latter was reduced to **4** in 62% yield using $NaBH_4$ in dry EtOH.[11] Although the preparation of compound **5** from the diol **4** was reported using PBr_3,[11] it was found that bromination of **4** using 33% HBr/AcOH at 125 °C for 5 h was much more efficient and produced compound **5** in 89% yield. Treatment for 48 h at r.t. of **5** by NaSMe (2 eq.) in dry THF afforded **6** in 60% yield. The synthesis of the ligand **1** was achieved by coupling the bromopyridine derivative **6** with 4-ethynylpyridine **7** in the presence of $Pd(OAc)_2$ and Ph_3P in Et_3N under reflux for 48 h. The pure compound **1** was obtained in 94% yield as a colourless viscous oil after chromatography (SiO_2, CH_2Cl_2/MeOH 0–1%).

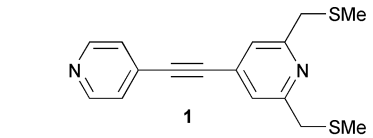

1

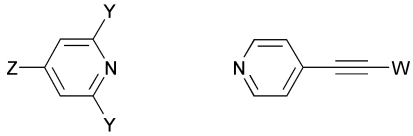

2 Y = CO_2H, Z = OH
3 Y = CO_2Et, Z = Br
4 Y = CH_2OH, Z = Br
5 Y = CH_2Br, Z = Br
6 Y = CH_2SMe, Z = Br

7 W = H
8 W = $C(CH_3)_2OH$

Scheme 1

DOI: 10.1039/b006099m

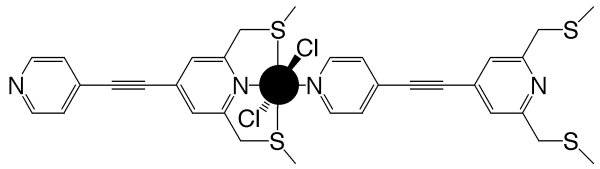

Fig. 1 Representation of the assembling core based on the coordination of $CoCl_2$ complex by two consecutive ligands **1** which by translation leads to the directional 1-D network.

Compound **7** was obtained in two steps upon treatment at r.t. of 4-bromopyridine hydrochloride by 2-methyl-3-butyn-2-ol in the presence of $(PPh_3)_2PdCl_2$ and CuI in diethylamine affording compound **8** and the removal of the protecting group by treatment under reflux with NaOH in toluene.[12]

Upon slow diffusion at r.t. of a MeOH solution containing $CoCl_2{\cdot}6H_2O$ (8 mg, 6.1 mmol) into a CH_2Cl_2 solution of compound **1** (8 mg, 3.3 mmol), purple crystals were obtained after three weeks. A single-crystal X-ray study† showed the following relevant features: the crystal (orthorhombic) was composed of **1**, $CoCl_2$ and MeOH molecules. As expected, a directional 1-D neutral network based on the interconnection of $CoCl_2$ units by the ligand **1** is observed. The assembling core is a distorted octahedral Co(II) complex for which the coordination sphere is composed of two Cl^- anions, two nitrogen and two sulfur atoms. The two Cl^- anions are located at axial positions with a Co–Cl distance of 2.425 Å and a Cl–Co–Cl angle of 178.8°. The square base of the octahedron is composed of one pyridine and one NS_2 coordination set belonging to the tridentate moiety of the ligand with Co–N and Co–S distances of 2.118 Å and 2.490 Å respectively. Whereas the ClCoS angle varies from 85° to 95°, the ClCoN angle is *ca.* 90° and the NCoN angle is 180.0°. Dealing with the ligand **1**, the two pyridine units are almost untilted and the CC triple bond distance is 1.207 Å (Fig. 1).

Owing to the unsymmetrical nature of the ligand **1** and, thus, the assembling core, upon a single translation a 1-D directional coordination network is indeed obtained. In the crystalline phase, in principle, a directional 1-D network may either be packed in centrosymmetric (Fig. 2a) or non-centrosymmetric modes (Fig. 2b). In the case reported here, the directional networks are positioned in a parallel fashion but oriented in opposite directions, thus generating centres of symmetry. Consequently, the overall system is non-directional (Fig. 3). This centrosymmetric packing may be due to cancellation of dipolar moments.

In conclusion, the unsymmetrical ligand **1** based on two different coordination poles was shown to form a directional 1-D coordination network in the presence of $CoCl_2$ demonstrating the viability of the approach. The network was structurally characterised by X-ray diffraction methods on single crystals.

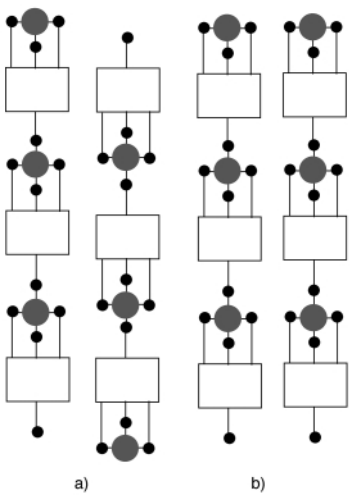

Fig. 2 Schematic representation of consecutive directional 1-D networks leading to symmetrical (a) or unsymmetrical (b) packing.

Fig. 3 A portion of the X-ray structure of the directional 1-D network showing the packing of consecutive networks in 'head to tail' fashion. H atoms and solvent molecules are not presented for clarity. For distances and angles see text.

However, the 1-D networks were packed parallel to each other with opposite orientation of linear arrays. The possibility of controlling the unsymmetrical packing of such 1-D coordination networks is currently under exploration using chiral analogues of the ligand **1**.

We thank the CNRS and the Institut Universitaire de France (IUF) for financial support.

Notes and references

† *Crystal data* for **1**: (purple, 173 K), $C_{16}H_{16}Cl_2CoN_2S_2{\cdot}2CH_3OH$, M = 494.37, orthorhombic, a = 13.3874(4), b = 13.9184(7), c = 12.0950(7) Å, U = 2253.7(3) Å^3, Z = 4, space group *Pbcn*, D_c = 1.46 g cm^{-3}, Nonius Kappa CCD, Mo-Kα, μ = 1.199 mm^{-1}, 1739 data with $I > 3\sigma(I)$, R = 0.036, Rw = 0.075. The structural determination was achieved using the Nonius OpenMolenN package.[13] CCDC 182/1762. See http://www.rsc.org/suppdata/cc/b0/b006099m/ for crystallographic files in .cif format.

1 R. Robson, in *Comprehensive Supramolecular Chemistry Vol. 6*, ed. D. D. Macnicol, F. Toda and R. Bishop, Pergamon, Oxford, 1996, p. 733; S. R. Batten and R. Robson, *Angew. Chem., Int. Ed.*, 1998, **37**, 1460.

2 M. Fujita, in *Comprehensive Supramolecular Chemistry, Vol. 9*, ed. J. P. Sauvage and M. W. Hosseini, Pergamon, Oxford, 1996, p. 253; O. M. Yaghi, H. Li, C. Davis, D. Richardson and T. L. Groy, *Acc. Chem. Res.*, 1998, **31**, 474; T. L. Hennigar, D. C. MacQuarrie, P. Losier, R. D. Rogers and M. J. Zaworotko, *Angew. Chem., Int. Ed. Engl.*, 1997, **36**, 972; J. Blake, N. R. Champness, S. S. M. Chung, W.-S. Li and M. Schröder, *Chem. Commun.*, 1997, 1675; M. A. Withersby, A. J. Blake, N. R. Champness, P. Hubberstey, W.-S. Li and M. Schröder, *Chem. Commun.*, 1997, 2327.

3 U. Velten and M. Rehahn, *Chem. Commun.*, 1996, 2639.

4 C. Kaes, M. W. Hosseini, C. E. F. Rickard, B. W. Skelton and A. White, *Angew. Chem., Int. Ed.*, 1998, **37**, 920.

5 G. Mislin, E. Graf, M. W. Hosseini, A. De Cian, N. Kyritsakas and J. Fischer, *Chem. Commun.*, 1998, 2545.

6 C. Klein, E. Graf, M. W. Hosseini, A. De Cian and J. Fischer, *Chem. Commun.*, 2000, 239.

7 E. C. Constable and A. M. W. Cargill Thompson, *J. Chem. Soc., Dalton Trans.*, 1992, 3467; E. C. Constable, A. J. Edwards, D. Philips and P. R. Raithby, *Supramol. Chem.*, 1995, **5**, 93.

8 S. J. Loeb and G. K. H. Shimizu, *Chem. Commun.*, 1993, 1395; M. Ferigo, P. Bonhôte, W. Marty and H. Stoeckli-Evans, *J. Chem. Soc., Dalton Trans.*, 1994, 1549; A. Neels, B. Mathez Neels and H. Stoeckli-Evans, *Inorg. Chem.*, 1997, **36**, 3402.

9 M. Loï, E. Graf, M. W. Hosseini, A. De Cian and J. Fischer, *Chem. Commun.*, 1999, 603; M. Loï, M. W. Hosseini, A. Jouaiti, A. De Cian and J. Fischer, *Eur. J. Inorg. Chem.*, 1999, 1981.

10 H. Takalo and J. Kankare, *Acta Chem. Scand., Ser. B*, 1987, **41**, 219.

11 H. Takalo, P. Pasanen and J. Kankare, *Acta Chem. Scand. Ser. B*, 1988, **42**, 373.

12 L. della Ciana and A. Haim, *J. Heterocycl. Chem.*, 1984, **21**, 607.

13 OpenMolenN, Interactive Structure Solution, Nonius B.V., Delft, The Netherlands, 1997.

ChemComm

Proton-controlled photoisomerization: rhenium(I) tricarbonyl bipyridine linked to amine or azacrown ether groups by a styryl pyridine bridging ligand†

Jared D. Lewis, Robin N. Perutz and John N. Moore*

Department of Chemistry, The University of York, Heslington, York UK YO10 5DD. E-mail: jnm2@york.ac.uk

Received (in Cambridge, UK) 20th July 2000, Accepted 25th August 2000
First published as an Advance Article on the web 15th September 2000

Complexes in which *fac*-(bpy)Re(CO)$_3$ is linked by a styryl pyridine to an amine or an azacrown ether show no photoreaction in acetonitrile in the absence of acid, but they photoisomerize readily at the stilbene-like bridging ligand when the terminal amine or azacrown ether group is protonated because an intramolecular energy-transfer mechanism becomes available.

There is widespread interest in the design of molecular photodevices whose properties change on the addition of specific analytes.[1] Devices range from sensors where the analyte turns the emission on or off, to switches where the analyte controls the occurrence or route of a photochemical reaction. Photoinduced intramolecular electron or energy transfer often underlies the mechanism by which the sensing or switching effect occurs. Here we describe a molecular design in which protonation controls a photochemical switching reaction which is driven by intramolecular energy transfer.

We report two new complexes which combine three functional groups: (bpy)Re(CO)$_3$ is linked by a stilbene-like bridging ligand to either an *N*,*N*-diethylamine (**1**) or an aza-

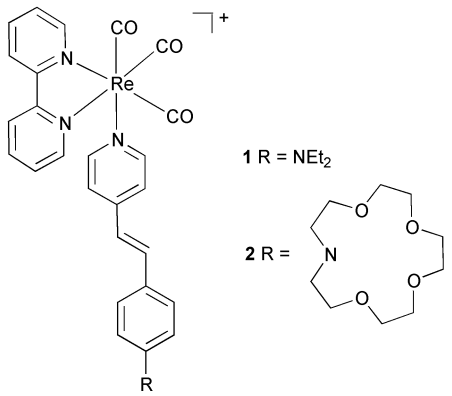

15-crown-5 ether (**2**) group.‡ The (bpy)Re(CO)$_3$ chromophore is being used increasingly within molecular sensors and switches because it is luminescent, and its photophysics can be controlled by intramolecular electron and energy transfer.[2] Stilbene has been used as the basis for molecular photoswitches because its well-studied *trans–cis* photoisomerization reaction can be driven by excitation directly to the excited singlet state or indirectly by energy transfer to form the excited triplet state.[3] Crown ethers are attractive as receptors for analytes within many photodevices because cation binding at the crown generally modifies the absorption and emission properties of the attached group, and can control its photochemistry.[1] We report new complexes that combine all three of these groups in a photoswitchable device: photoisomerization at the styryl group is the switch, and proton binding at the amine or azacrown N-heteroatom controls the effect.

† Electronic supplementary information (ESI) available: UV/vis absorption spectra of **2**. See http://www.rsc.org/suppdata/cc/b0/b005889k/

The UV/vis absorption spectrum of *trans*-**1** in acetonitrile (Fig. 1) comprises an intense, solvatochromic band at 435 nm and weaker features at 240–350 nm. The 435 nm band is assigned to an intraligand charge-transfer (ILCT) transition localised on the py-DEAS ligand,§ in which charge is transferred from the amine N-atom donor to the pyridyl N-atom acceptor, and the weaker features at *ca.* 300 nm and *ca.* 250 nm are assigned to $\pi \rightarrow \pi^*$ transitions localised on the bpy and py-DEAS ligands, respectively. The $d\pi(Re) \rightarrow \pi^*(bpy)$ metal-to-ligand charge-transfer (MLCT) transition of (bpy)Re(CO)$_3$ complexes typically gives an absorption band at *ca.* 380 nm (absorption coefficient, $\varepsilon \approx 3500$ dm^3 mol^{-1} cm^{-1}), and excitation into this band gives MLCT emission at *ca.* 600 nm which is moderately intense in ambient temperature solution (emission quantum yield, $\Phi_{em} \approx 10^{-2}$).[4] The MLCT absorption band of *trans*-**1** underlies the intense ILCT feature (Fig. 1); excitation at 380 nm, or at any wavelength in the range 300–500 nm, resulted only in very weak MLCT emission, with $\Phi_{em} < 6 \times 10^{-4}$.

Addition of HCl to a solution of *trans*-**1** in acetonitrile resulted in a blue-shift of the ILCT absorption band to *ca.* 320 nm (Fig. 1): this change is attributed to the production of *trans*-**1**-H$^+$, in which protonation at the amine N-atom inhibits charge transfer and raises the energy of the ILCT state. Protonation would not be expected to cause a significant shift in the MLCT absorption band, which is revealed on the long-wavelength edge of the shifted ILCT feature. Excitation of *trans*-**1**-H$^+$ in the range 300–450 nm resulted in one extremely weak emission band at *ca.* 400 nm (excitation peak at *ca.* 330 nm) which is assigned to ILCT emission, and another slightly more intense band at 590 nm ($\Phi_{em} = 1 \times 10^{-3}$) which is assigned to MLCT emission. Excitation spectra recorded on monitoring the emission at ⩾590 nm were found to mirror the expected MLCT absorption profile (excitation peak at *ca.* 355 nm). Only MLCT emission was observed on excitation at >400 nm, confirming that irradiation at >400 nm excites *trans*-**1**-H$^+$ exclusively to the MLCT state.

Prolonged irradiation¶ of *trans*-**1** in acetonitrile at any wavelength in the range 350–450 nm, exciting to either ILCT or MLCT states, resulted in no change in the UV/vis absorption spectrum, indicating that there is no significant photoreaction.‖

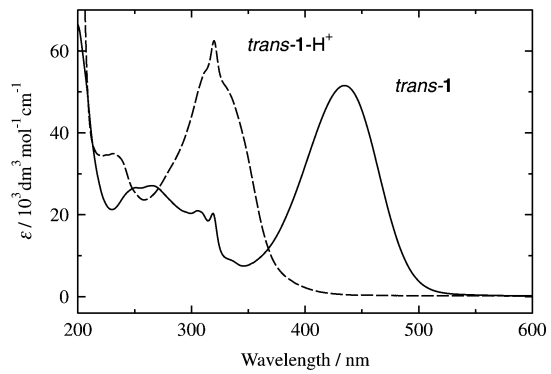

Fig. 1 UV/vis absorption spectrum of *trans*-**1** (2×10^{-5} mol dm^{-3}) in CH_3CN (—) and in CH_3CN on addition of excess HCl (---).

DOI: 10.1039/b005889k

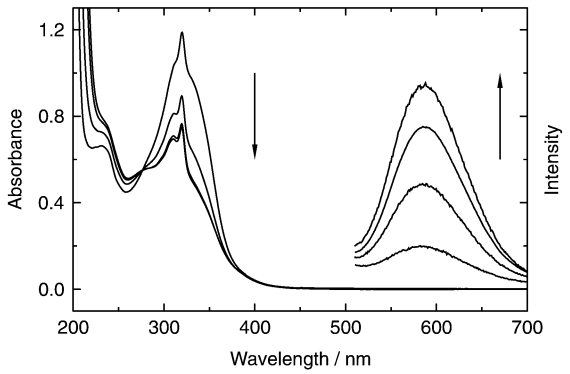

Fig. 2 UV/vis absorption spectra obtained from a solution of *trans*-**1** in CH_3CN (2×10^{-5} mol dm^{-3}), with excess HCl added, after arc-lamp irradiation at 406.7 nm (*ca.* 3 mW) for 0, 30, 120, and 180 min, along with corresponding emission spectra obtained on excitation at 380 nm; no distinct emission features were observed at < 500 nm following irradiation.

By contrast, irradiation of *trans*-**1**-H^+ at wavelengths in the range 400–430 nm, exciting exclusively to the MLCT state, resulted in pronounced changes in the absorption spectrum, and in a significant increase in the MLCT emission intensity (Fig. 2). The changes in the absorption spectrum of **1**-H^+ are consistent with *trans–cis* photoisomerization at the styryl –C=C– bond.[5] This interpretation was confirmed by ^1H NMR, which showed the production of new vinylic proton resonances characteristic of the *cis*-isomer;** integration of the *cis*- and *trans*-isomer peaks showed that the photostationary state reached on irradiation of *trans*-**1**-H^+ at 406.7 nm consisted of a *ca.* 50 : 50 *cis* : *trans* mixture. These results demonstrate that the photoisomerization of *trans*-**1** in acetonitrile is controlled by protonation.

The MLCT excited state of $(bpy)Re(CO)_3$ complexes typically decays back to the ground state in *ca.* 0.1 μs, by radiative and non-radiative routes, giving moderately intense MLCT emission in ambient temperature solution.[4] The extremely weak emission and the absence of any photochemical reaction for *trans*-**1** indicate that an additional non-radiative decay route that regenerates the ground state is available from the MLCT state of this complex. For complexes in which $(bpy)Re(CO)_3$ is linked to a dialkylamine by a saturated spacer, intramolecular electron transfer from the amine group to the Re centre in the MLCT state can result in the rapid (< 1 ns) formation of a charge-separated ligand-to-ligand charge-transfer (LLCT) state which decays non-radiatively back to the ground state.[2,6] Our observations are consistent with this mechanism for the decay of the MLCT state of *trans*-**1**.

The moderately weak emission observed from *trans*-**1**-H^+ indicates that, like *trans*-**1**, an additional non-radiative decay route is available from the MLCT state in comparison with typical $(bpy)Re(CO)_3$ complexes. The results of the irradiation experiments show that the mechanism is dependent on protonation, and that *trans–cis* photoisomerization occurs only for the protonated form, *trans*-**1**-H^+. Recent studies of complexes in which $(bpy)Re(CO)_3$ is attached to stilbene-like ligands have shown that the MLCT state can decay by intramolecular energy transfer to form a triplet excited state of stilbene from which *trans–cis* isomerization occurs.[7] We attribute the photoisomerization of *trans*-**1**-H^+ to this mechanism:

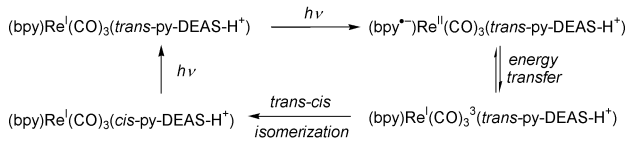

The increase in MLCT emission on irradiation (Fig. 2) can be attributed to the loss of this intramolecular energy-transfer decay route on isomerization to *cis*-**1**-H^+ because the energy of the styryl-centred triplet excited state is raised in the *cis*-isomer;[7] $\Phi_{em} \approx 10^{-2}$ is estimated for *cis*-**1**-H^+. The significant increase in the MLCT emission intensity on isomerization serves as an effective 'signal' that photoswitching has occurred.

The experiments described above for the diethylamino derivative **1** have been repeated for the azacrown ether derivative **2** (see ESI†). The spectra of these two complexes, and of the free styryl ligands, are similar under all of the conditions studied. As for *trans*-**1**, photoisomerization in acetonitrile was observed only on protonation at the azacrown to form *trans*-**2**-H^+.

In addition to describing these complexes as proton-controlled photoswitches, they can also be described as two-input photoionic signal-processing devices:[8] the presence of both protons (ionic input) and visible light (photonic input) is required to give a photonic output change, observed as an increase in the emission intensity.

In summary, we have demonstrated that protonation can be used to control the *trans–cis* photoisomerization reaction of a complex in which $(bpy)Re(CO)_3$ is linked by a stilbene-like bridging ligand to an amine or an azacrown ether. The effectiveness of this approach for the azacrown ether complex provides an opportunity to explore the use of cations within the crown to control the photoisomerization reaction, and such experiments are in progress.

Notes and references

‡ $(bpy)Re(CO)_3Cl$ was stirred with an excess of CF_3SO_3H at room temperature for 1 h to yield $(bpy)Re(CO)_3(CF_3SO_3)$, which was refluxed overnight in THF under N_2 with < 1 equiv of the appropriate styryl ligand, 4-(4-diethylaminostyryl)pyridine (py-DEAS) or 4-(4-aza-15-crown-5-styryl)pyridine (py-AZAS) (see ref. 9 for synthetic method for styryl ligands). The product was metathesized with NH_4PF_6 to yield $[(bpy)Re(CO)_3(py\text{-}DEAS)]PF_6$ (**1**) or $[(bpy)Re(CO)_3(py\text{-}AZAS)]PF_6$ (**2**), respectively. The complexes were purified by repeated recrystallization and column chromatography (5% MeOH–CH_2Cl_2 eluting on silica), and were characterized by IR, ES-MS and ^1H NMR, which showed that the *trans*-isomers were formed exclusively.

§ The absorption spectrum of the free *trans*-py-DEAS ligand in acetonitrile has a similar profile to that of *trans*-**1**, with an intense, solvatochromic absorption band at 375 nm and a weaker band at 250 nm.

¶ Samples were irradiated in a sealed 1 cm pathlength cell with the output from either a krypton ion laser (350.6 or 406.7 nm; 50 mW) or a xenon-arc lamp (monochromated to 5 nm bandpass; 1–3 mW).

‖ No changes were observed in the absorption spectrum of *trans*-**1** following arc-lamp irradiation at 406 nm (3 mW) for 180 min; these conditions are identical to those illustrated for *trans*-**1**-H^+ in Fig. 2 except the absorbance at 406 nm was 0.7 for *trans*-**1** (*versus* 0.03 for *trans*-**1**-H^+).

** The ^1H NMR spectrum showed vinylic proton resonances assigned to *trans*-**1**-H^+ (δ 6.95, 7.28; $J_{H\text{-}H}$ = 16 Hz) before irradiation, and to both *cis*-**1**-H^+ (δ 6.35, 6.70; $J_{H\text{-}H}$ = 12 Hz) and *trans*-**1**-H^+ after irradiation.

1 A. P. de Silva, H. Q. N. Gunaratne, T. Gunnlaugsson, A. J. M. Huxley, C. P. McCoy, J. T. Rademacher and T. E. Rice, *Chem. Rev.*, 1997, **97**, 1515.

2 K. S. Schanze, D. B. MacQueen, T. A. Perkins and L. A. Cabana, *Coord. Chem. Rev.*, 1993, **122**, 63.

3 H. Görner and H. J. Kuhn, in *Advances in Photochemistry*, ed. D. C. Neckers, D. H. Volman and G. von Bünau, John Wiley & Sons, New York, 1995, vol. 19, p. 1.

4 K. Kalyanasundaram, *J. Chem. Soc., Faraday Trans.*, 1986, **82**, 2401; L. A. Sacksteder, A. P. Zipp, E. A. Brown, J. Streich, J. N. Demas and B. A. DeGraff, *Inorg. Chem.*, 1990, **29**, 4335.

5 H. Mrozek, H. Nikol, A. Vogler and F. Vögtle, *J. Photochem. Photobiol. A: Chem.*, 1994, **84**, 227.

6 K. S. Schanze and D. B. MacQueen, *J. Am. Chem. Soc.*, 1991, **113**, 6108.

7 V. W. W. Yam, V. C. Y. Lau and K. K. Cheung, *J. Chem. Soc., Chem. Commun.*, 1995, 259; V. W. W. Yam, V. C. Y. Lau and L. X. Wu, *J. Chem. Soc., Dalton Trans.*, 1998, 1461; K. S. Schanze, L. A. Lucia, M. Cooper, K. A. Walters, H. F. Ji and O. Sabina, *J. Phys. Chem.*, 1998, **102**, 5577; S. S. Sun, E. Robson, N. Dunwoody, A. S. Silva, I. M. Brinn and A. J. Lees, *Chem. Commun.*, 2000, 201.

8 A. P. de Silva, H. Q. N. Gunaratne and C. P. McCoy, *Nature*, 1993, **364**, 42.

9 A. Juris, S. Campagna, I. Bidd, J.-M. Lehn and R. Ziessel, *Inorg. Chem.*, 1988, **27**, 4007.

On the reductive amination of aldehydes and ketones catalyzed by homogeneous Rh(I) complexes

Vitali I. Tararov,[a,b] Renat Kadyrov,[a,c] Thomas H. Riermeier[c] and Armin Börner*[a]

[a] *Institut für Organische Katalyseforschung an der Universität Rostock e.V., Buchbinderstr. 5/6, D-18055 Rostock, Germany. E-mail: armin.boerner@ifok.uni-rostock.de*

[b] *A. N. Nesmeyanov Institute of Organoelement Compounds, Russian Academy of Sciences, Vavilova 28, 117813 Moscow, Russian Federation*

[c] *Aventis Research & Technologies GmbH Industriepark Höchst, G 830, D-65926 Frankfurt/Main, Germany*

Received (in Cambridge, UK) 18th July 2000, Accepted 15th August 2000
First published as an Advance Article on the web 15th September 2000

The homogeneously catalyzed reductive amination of aldehydes and ketones under smooth conditions is reported, showing for the first time, that Rh(I) catalysts based on chelating diphosphines and diphosphinites can be advantageously employed for this reaction, even for the production of chiral amino acid derivatives.

One-stage (or direct) reductive amination of aldehydes and ketones with amines affording higher alkylated amines is an interesting target in modern organic chemistry with great synthetic potential for application in academia and industry. Hitherto several chemical reducing agents, in particular borohydrides, have been shown to be valuable for this reaction giving rise to the alkylated amines in good yield.[1] However, from the ecological point of view and taking into account the demand for atom economy, more promising is the use of molecular hydrogen as a reducing agent. Indeed it was shown that reductive amination with hydrogen can be mediated by heterogeneous platinum, palladium, nickel or ruthenium metal catalysts.[2] Several amines have been prepared by this methodology even on an industrial scale.

Interestingly, only a few preliminary studies on the homogeneous version of this reaction can be found in the literature in spite of the tremendous progress which homogeneous catalysis has seen over the last decades.[3] For example, typical hydroformylation catalysts such as rhodium and cobalt carbonyls were tested, but were found to require rather severe reaction conditions (100–300 atm H_2, 100–200 °C).[4] The selectivity and efficiency of some glyoxyme Rh and Co complexes were studied in the reductive amination of cyclohexanone with ammonia.[5] A related cyanocobalt catalyst afforded only moderate yields of product amines.[6] More noteworthy is the unique reaction of a sterically hindered aniline with methoxyacetone in the presence of a chiral Ir–diphosphine catalyst.[7] Tandem hydroformylation–amination reactions (hydroaminomethylation) also contain a reductive amination step, however the range of products is limited owing to the use of olefins as starting material.[8]

Recently, we reported that cationic rhodium(I) complexes [Rh(dppb)(cod)]BF_4 **1** [dppb = 1,4-bis(diphenylphosphino)butane, cod = cycloocta-1,5-diene] and [Rh(dpoe)(cod)]BF_4 **2** [dpoe = 1,2-bis(diphenylphosphinito)ethane] are highly efficient precatalysts in the hydrogenation of imines[9] and enamines[10] under mild conditions (room temperature, 1–50 bar H_2 pressure). Usually these substrates are considered to be intermediates in some direct reductive amination reactions.[11]

Herein we demonstrate that complexes **1** and **2** are also useful for reductive amination (Scheme 1). For this reaction, besides the activity of the catalyst the selectivity for the formation of the desired amine is important. The production of the relevant alcohol by the competitive reduction of the carbonyl compound should be minimized.

Our results obtained with selected aldehydes and piperidine as the amine are listed in Table 1. Conversion with respect to the

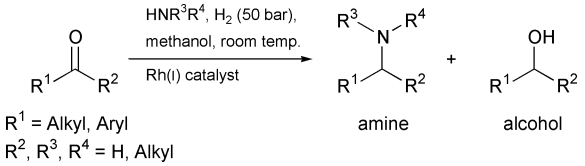

Scheme 1 Reductive amination of aldehydes and ketones with Rh(I) catalysts.

starting carbonyl compound and selectivity in terms of produced amine/alcohol ratio in the final reaction mixtures were determined by ^{1}H NMR spectroscopy. As shown, cationic precatalysts **1** and **2** are efficient for reductive amination. It is of note that in all trials the desired amine and the corresponding alcohol were exclusively formed. Both complexes were more effective and selective than Wilkinson's complex $Rh(PPh_3)_3Cl$ (run 1, *cf.* runs 3 and 6; run 9, *cf.* runs 11 and 14). Also the hydroformylation precatalyst $Rh(PPh_3)_2(CO)Cl$ (run 10), frequently applied in hydroaminomethylation,[8] is inferior. Similar behavior was observed for the *in situ* prepared neutral complex $[Rh(dppb)Cl]_2$ (run 2). Although the conversion measured after 20 h was similar to that for precatalyst **1** the hydrogen uptake proceeded significantly more slowly.

Increasing concentrations of the amine had no pronounced effect on the selectivity, this applying for PhCHO (runs 3 and 4) as well as for PhCHMeCHO (runs 11 and 12) as substrate when precatalyst **1** was used. Application of precatalyst **2** in the

Table 1 Reductive amination of aldehydes with piperidine as the amine[a]

Run	Catalyst	Molar ratio piperidine/ aldehyde	Conv. aldehyde (%)[b]	Ratio produced amine/ alcohol
PhCHO				
1	$Rh(PPh_3)_3Cl$	1:1	94	0.1
2	$[Rh(dppb)Cl]_2$	1:1	>99	1.0
3	**1**	1:1	>99	1.5
4	**1**	2:1	>99	1.5
5	**1**[c]	1:1	>99	1.3
6	**2**	1:1	>99	1.8
7	**2**	2:1	>99	1.2
8	**2**[c]	1:1	>99	1.4
PhCHMeCHO				
9	$Rh(PPh_3)_3Cl$	1:1	70	0.4
10	$Rh(PPh_3)_2(CO)Cl$	1:1	4	n.d.
11	**1**	1:1	>99	1.7
12	**1**	2:1	>99	1.9
13	**1**[c]	1:1	>99	4.8
14	**2**	1:1	>99	6.1
15	**2**[c]	1:1	>99	3.2

[a] *Reaction conditions*: 5 mmol aldehyde, 0.2 mol% precatalyst, 10 ml MeOH, 50 bar initial pressure of H_2, room temp. [b] Measured after 20 h. [c] $TsOH{\cdot}xH_2O$ added ($TsOH{\cdot}xH_2O$/Rh = 20).

DOI: 10.1039/b005777k

reductive amination of benzaldehyde led to a slight decrease in selectivity (runs 6 and 7). The absence of a significant dependence of the selectivity on the amine concentration is noteworthy. Obviously, the rate limiting step in the overall process is the reduction of the corresponding intermediates but not their formation. This assumption is also confirmed by the fact that preliminary heating of a mixture of PhCHO and piperidine in methanol had no effect on the selectivity.

It is interesting that both precatalysts exhibited approximately the same selectivity with PhCHO as carbonyl component (runs 3 and 6) while the selectivity observed in the reductive amination of PhCHMeCHO with **1** as a precatalyst was lower than with **2** (runs 11 and 14).

The effect of $TsOH{\cdot}xH_2O$ as additive is less clear. Thus, this additive slightly diminished the selectivity of precatalysts **1** and **2** in the reaction of benzaldehyde with piperidine (runs 3/5, 6/8). However, in the reaction with PhCHMeCHO the effect of the additive was dependent upon the precatalyst used (runs 11/13, 14/15). In general, in the presence of $TsOH{\cdot}xH_2O$, the rate of the hydrogen uptake was lowered.

We next investigated the reductive amination of aldehydes with a two-fold excess of piperidine as a function of the substitution pattern of the aldehyde using precatalyst **1** (Table 2). In the series of substituted benzaldehydes (runs 1–5) the beneficial effect of electron-withdrawing groups upon the selectivity is evident. The presence of a methyl group in an *ortho* position exhibited no steric effect on the selectivity (run 3). Unfortunately, NO_2- and CN-groups did not survive under the reaction conditions. An alkyl substituent α to the carbonyl group strongly affected the selectivity of amination (runs 6–8). The highest selectivity was observed with *n*-octanal (run 8).

Table 2 Comparison of the selectivity and the rate of amination of various aldehydes with piperidine using [Rh(dppb)(cod)]BF_4 **1** as a precatalyst[a]

Run	Aldehyde	Ratio produced amine/alcohol[b]
1	4-HOC_6H_4CHO	0.8
2	4-$MeOC_6H_4CHO$	0.9
3	2-MeC_6H_4CHO	1.0
4	PhCHO	1.5
5	4-ClC_6H_4CHO	1.9
6	PhCHMeCHO	1.9
7	EtCHMeCHO	2.4
8	*n*-$C_7H_{15}CHO$	12.0

[a] For reaction conditions see Table 1. [b] After 20 h full conversion was observed in all reactions.

The results of reductive amination of PhCHO with various amines are summarized in Table 3. In general, good correlation between the selectivity of the reaction and the basicity of the amine was observed (runs 1–4). Apparently, steric effects can exert a strong influence. Thus, with 2-methylpiperidine as substrate, which has approximately the same basicity as piperidine but is sterically more hindered, only traces of the desired amine were formed (run 5).

Table 3 Comparison of reductive amination of PhCHO with various amines employing [Rh(dppb)(cod)]BF_4 **1** as a precatalyst[a]

Run	Amine	pK_a (amine)	Ratio produced amine/alcohol[b]
1	Pyrrolidine	11.27	2.30
2	Piperidine	11.02	1.50
3	Me_2NH	10.73	0.43
4	Et_2NH	10.49	0.07
5	2-Methylpiperidine	10.99	< 0.05

[a] *Reaction conditions*: 5 mmol aldehyde, 10 mmol amine, for other conditions see Table 1. [b] After 20 h full conversion was observed in all reactions.

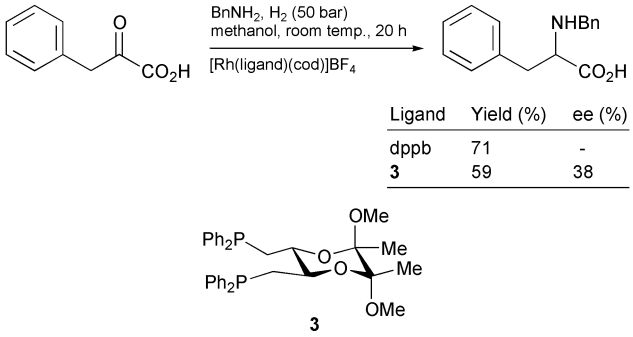

Scheme 2 Preparation of racemic and enantiomerically enriched *N*-benzylphenylalanine.

In contrast to the reductive amination of PhCHO with piperidine, the reaction with $PhCH_2NH_2$ using precatalyst **1** was slow. After 20 h only 39% conversion was observed. However the high observed amine/alcohol ratio of 11 is remarkable.

Unexpectedly, reductive alkylation with α-keto acid derivatives afforded good yields of the desired amino acids. Thus, the industrially relevant reductive amination of $PhCH_2COCOH$ with benzyl amine gave *N*-benzylphenylalanine in a yield of 71% (Scheme 2). The product precipitated from the reaction mixture and the analytically pure compound could simply be isolated by filtration and subsequent washing with ethanol. In a preliminary investigation the reaction was also run with a catalyst bearing the chiral diphosphine **3**.[12] (*R*)-*N*-Benzylphenylalanine was obtained in 59% isolated yield and 38% ee.

In conclusion, Rh(I) complexes represent efficient homogeneous catalysts for reductive amination of aldehydes and ketones. The successful employment of chelating phosphorus ligands for this reaction opens up a broad field of modifications, whereby asymmetric reductive amination is one of the most challenging goals.

Financial support from Aventis Research & Technologies GmbH (Frankfurt, Germany) and the Fonds der Chemischen Industrie is gratefully acknowledged.

Notes and references

1 A. F. Abdel-Magid, K. G. Carson, B. D. Harris, C. A. Maryanoff and R. D. Shah, *J. Org. Chem.*, 1996, **61**, 3849 and references therein; D. Dubé and A. A. Scholt, *Tetrahedron Lett.*, 1999, **40**, 2295; I. Saxena, R. Borah and J. C. Sharma, *J. Chem. Soc., Perkin Trans. 1*, 2000, 503.
2 P. N. Rylander, *Catalytic Hydrogenation in Organic Synthesis*, Academic Press, New York, 1979, p. 165; P. N. Rylander, *Catalytic Hydrogenation over Platinum Metals*, Academic Press, New York, 1967, p. 292.
3 *Applied Homogenous Catalysis with Organometallic Compounds*, ed. B. Cornils and W. A. Herrmann, VCH, Weinheim, 1996, vol. 1 and 2; *Transition Metals for Organic Synthesis*, ed. M. Beller and C. Bolm, Wiley-VCH, Weinheim, 1998, vol. 1 and 2.
4 L. Markó and J. Bakos, *J. Organomet. Chem.*, 1974, **81**, 411.
5 M. V. Klyuev and M. L. Khidekel, *Transition Met. Chem.*, 1980, **5**, 134.
6 M. Murakami and J.-W. Kang, *Bull. Chem. Soc. Jpn.*, 1963, **36**, 763.
7 H.-U. Blaser, H.-P. Buser, H.-P. Jalett, B. Pugin and F. Spindler, *Synlett*, 1999, 867.
8 P. Eilbracht, L. Bärfacker, C. Buss, C. Hollmann, B. E. Kitsos-Rzychon, C. L. Kranemann, T. Rische and R. Roggenbuck and A. Schmidt, *Chem. Rev.*, 1999, **99**, 3329.
9 V. I. Tararov, R. Kadyrov, T. H. Riermeier, J. Holz and A. Börner, *Tetrahedron: Asymmetry*, 1999, **10**, 4009.
10 V. I. Tararov, R. Kadyrov, T. H. Riermeier, J. Holz and A. Börner, *Tetrahedron Lett.*, 2000, **41**, 2351.
11 W. S. Emerson, *Org. React.*, 1948, **4**, 174; K. A. Schellenberg, *J. Org. Chem.*, 1963, **28**, 3259.
12 U. Berens, D. Leckel and S. C. Oepen, *J. Org. Chem.*, 1995, **60**, 8294.

Retraction

New highly active chiral phosphapalladacycle catalysts. First isolation and characterization of a Pd(IV) intermediate

Jean Michel Brunel, Marie-Hélène Hirlemann, Andreas Heumann and Gérard Buono

Chem. Commun., 2000, 1869 (DOI: 10.1039/b005521m). ***Retraction published 16 May 2002***

We, the named authors, hereby wholly retract this Chemical Communication.

Signed: Gérard Buono, Jean Michel Brunel, Marie-Hélène Hirlemann and Andreas Heumann, Marseille, France, May 2002.

Retraction endorsed by Sarah Thomas, Managing Editor.

New highly active chiral phosphapalladacycle catalysts. First isolation and characterization of a Pd(IV) intermediate†

Jean Michel Brunel, Marie-Hélène Hirlemann, Andreas Heumann and Gérard Buono*

UMR CNRS 6516, Faculté de St Jérôme, ENSSPICAM, Av. Escadrille Normandie Niemen, 13397 Marseille, Cedex 20, France. E-mail: buono@spi-chim.u-3mrs.fr

Received (in Liverpool, UK) 6th July 2000, Accepted 14th August 2000
First published as an Advance Article on the web 18th September 2000

The synthesis and characterization of a new active P*-active phosphapalladacycle and its successful use in the asymmetric hydroarylation of norbornene with turnover numbers (TONs) of up to 10^{10} is described.

C–C coupling reactions using numerous transition metals are of fundamental interest in modern synthetic chemistry.[1] Thus, the arylation and vinylation of olefins catalyzed by Pd complexes (Heck reaction) has been extensively studied to achieve industrial scale technical application during the last decade.[2] In this area, Herrmann *et al.* discovered in 1995 highly efficient palladacycle catalysts in Heck and related reactions of aryl halides with catalyst turnover numbers (TONs)[3] up to 500 000.[4,5] On the other hand, because of the excellent control of regio- and stereo-selectivity in Heck reactions, intra- and inter-molecular asymmetric variations were developed.[6] Nevertheless, all of the results reported in the literature suffer from insufficient catalyst turnover frequencies (TOF < 10 h^{-1} and TON < 100) and are limited in the use of aryl triflates and aryl iodides as arylating agents.[7] Thus, few syntheses of chiral palladacycle catalysts have been envisioned and all these attempts failed.[8] To our knowledge, only Dunina *et al.* have successfully reported the synthesis of an optically active P*-chiral phosphapalladacycle *via* resolution of diastereomeric (*S*)-prolinate derivatives of the racemic dimer.[9] In the context of our studies, we have recently described the potentialities of oxaza- and diazaphospholidine ligands in various catalytic enantioselective reactions[10] as well as the synthesis of a new class of highly efficient new phosphapalladacycle catalysts for hydroarylation of norbornene with TON levels > 10^{10}.[14] Here, we report the synthesis and use of a new chiral phosphapalladacycle catalyst, as well as the isolation of an intermediate palladium complex involved in the hydroarylation of norbornene.

The synthesis of the chiral *o*-tolyldiazaphospholidine ligand **3** was readily achieved in 89% yield by an exchange reaction in refluxing toluene from bis(dimethylamino)(*o*-tolyl)phosphine **1** and (*S*)-anilinomethylpyrrolidine **2** (readily obtained from L-glutamic acid) [eqn. (1)].[15] The structure of this ligand was

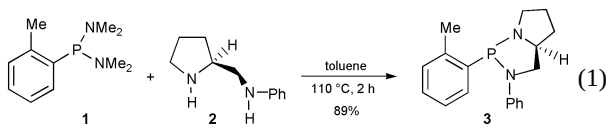

unambiguously established by ^{1}H, ^{13}C, ^{31}P NMR spectroscopy and also by X-ray structure analysis (Fig. SI 1, ESI†).[16]

Treatment of palladium(II) acetate with ligand **3** in refluxing toluene afforded the expected phosphapalladacycle complex **4** in 75% yield as a thermally, air and moisture stable yellow solid [eqn. (2)]. The structure of this cyclometallated compound,

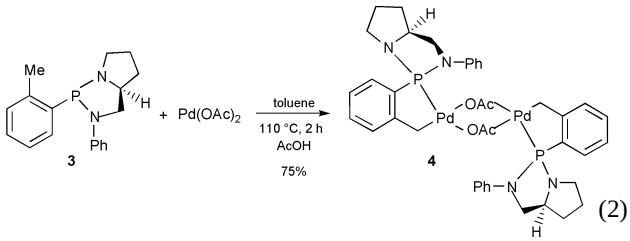

resulting from simple C–H activation of *ortho*-methyl group in the aryl phosphine part, was established by NMR spectroscopy and elemental analysis. However, all attempts to crystallize this phosphapalladacycle complex have so far failed. This phosphapalladacycle catalyst mediates arylation of norbornene under reductive conditions (NEt_3/HCO_2H) [eqn. (3)] and the reactions

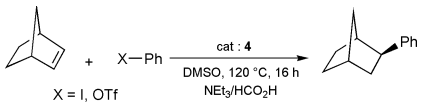

of phenyl triflate or iodobenzene with norbornene affording the corresponding *exo*-phenylnorbornane were investigated (ESI†).[17,18] Table 1 summarizes the results.

As already observed using achiral catalysts, an extraordinary high activity of complex **4** was observed at 120 °C in DMSO.[14] Consequently, exceptional turnover numbers up to 1.96×10^8 mol product (mol Pd)$^{-1}$ and yields of 98% were achieved (Table 1, entries 1–4). In addition, turnover frequencies up to 1.6×10^7 mol product (mol Pd h)$^{-1}$ were encountered. To our knowledge, these values are the highest TOF reported to date for palladium catalysis involving chiral palladacycle complexes. On the other hand, whatever the experimental conditions, low enantiomeric excesses (ee) up to 25% using phenyl triflate as arylating agent were observed (Table 1, entry 5). Nevertheless, these results constitute the first example of the use of an active chiral P*-phosphapalladacycle catalyst in an enantioselective hydroarylation reaction.

In the course of our investigations on the mechanism (Scheme 1) of this reaction,[19] we were able to isolate an intermediate Pd(IV) complex **5** which was fully characterized by X-ray structure analysis (Fig. 1).[16,20] Isolation of this inter-

Table 1 Catalytic hydroarylation of norbornene using palladacycle **4**

Entry	Ar–X	Catalyst **4** (mol% Pd)	Conv. (%)[a]	Yield (%)[b]	TON	Ee (%)[c]
1	Ph–I	0.5	100	99	1.9×10^2	14
2	Ph–I	5×10^{-6}	100	98	1.9×10^7	4
3	Ph–I	5×10^{-7}	100	98	1.96×10^8	2
4	Ph–I	5×10^{-9}	100	84	1.68×10^{10}	2
5	Ph–OTf	0.5	100	99	1.9×10^2	25
6	Ph–OTf	5×10^{-4}	100	99	1.98×10^5	14

[a] Conversion determined by GC. [b] Isolated yield. [c] Enantiomeric excess determined by GC on a fused silica gel column (25 m × 0.25 mm) coated with 10% heptakis(2,3,6-tri-*O*-methyl)-β-cyclodextrin at 100 °C, t_R(−) 39.30 min; t_R (+) 40.58 min.

† Electronic supplementary information (ESI) available: Fig. SI 1 (structure of **3**, with labelling scheme), physical and spectroscopic data for **3**, and general information for norbornene hydroarylation. See http://www.rsc.org/suppdata/cc/b0/b005521m/

DOI: 10.1039/b005521m

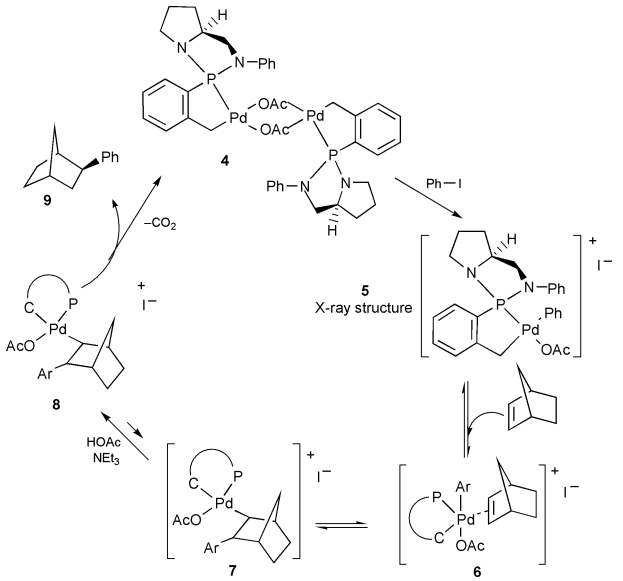

Scheme 1

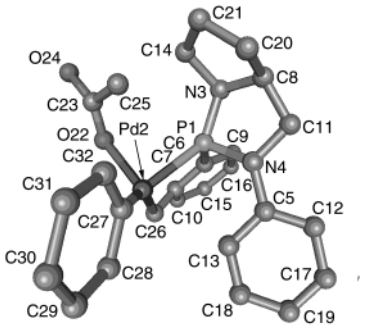

Fig. 1 X-Ray structure of **5**, with labeling scheme (for clarity the iodine ion has been omitted). Selected bond distances (Å) and angles (°): P1–Pd2 2.321(3), Pd2–O22 2.1810(1), Pd2–C27 1.221(2), Pd2–C26 2.195(3), C23–O22 1.212(4), P1–N3 1.662(4), P1–N4 1.662(3), P1–C6 1.790(2); Pd2–C27–O22, 115.2(1), P1–Pd2–N3 140.8(1), P1–Pd2–N4 105.7(2), P1–N3–N4 94.5(2), P1–N4–C5 122.1(2), P1–N4–C11 111.4(3), P1–N4–C5 122.1(3), Pd2–C26–C7 132.2(1), Pd2–C26–O22 84.0(1), P1–N3–C14 117.4(4), P1–N3–N4 94.5(3), Pd2–P1–C27 138.4(2), Pd2–P1–C26 86.6(1).

mediate suggests a mechanism for the Heck reaction involving Pd^{II}–Pd^{IV} species and suggests that the first step of the catalytic cycle is oxidative addition of a haloarene to a palladium(II) compound to form a palladium(IV) species. In the next step, an alkene molecule is coordinated and inserts into the Pd–Ar bond. The insertion process occurs *via* a four-centered transition state which requires a planar assembly of the alkene and Pd–Ar bond. Hence, insertion proceeds in a *syn* manner to generate a σ-alkylpalladium complex. The formate anion reacts subsequently with the intermediate **7** producing the norbornyl palladium formate **8** from which *exo*-phenylnorbornane **9** is generated through decarboxylation and Pd(II) deinsertion.

In conclusion, we have described the synthesis of a new active P*-chiral phosphapalladacycle and its successful use in the asymmetric hydroarylation of norbornene, with TON up to 10^{10}. On the other hand, although the enantiomeric excesses are low (up to 25% ee) they constitute, to our knowledge, the first results in asymmetric catalysis using a chiral phosphapalladacycle catalyst. Further studies relating to structural modification of the chiral ligand are now underway and will be reported in due course.

Notes and references

1 A. de Meijere and F. E. Meyer, *Angew. Chem.*, 1994, **106**, 2473; A. de Meijere and F. E. Meyer, *Angew. Chem., Int. Ed. Engl.*, 1994, **33**, 2379; W. Cabri and I. Candiani, *Acc. Chem. Res.*, 1995, **28**, 2; K. C. Nicolaou and E. J. Sorensen, *Classics in Total Synthesis*, VCH, Weinheim, 1996; G. Poli, G. Giambastiani and A. Heumann, *Tetrahedron*, 2000, **56**, 5959.

2 W. A. Herrmann, *Catalytic Carbon–Carbon Coupling by Palladium Complexes : Heck Reactions in Applied Homogeneous Catalysis with Metal Complexes*, eds. B. Cornils, VCH, Weinheim, 1996; V. V. Grushin and H. Alper, *Chem. Rev.*, 1994, **94**, 1047; R. F. Heck, *Palladium Reagents in Organic Synthesis*, Academic Press, London, 1985; J. Tsuji, *Palladium Reagents, Innovation in Organic Synthesis*, Wiley, Chichester, 1995; M. Beller and C. Bolm, *Transition Metals for Organic Synthesis*, VCH, Weinheim, 1998.

3 TON: turnover number [mol product (mol Pd)$^{-1}$]; TOF: turnover frequency [mol product (mol Pd h)$^{-1}$].

4 W. A. Herrmann, C. Brossmer, C. P. Reisinger, T. H. Riermeier, K. Ofele and M. Beller, *Chem. Eur. J.*, 1997, **3**, 1357; M. Beller, H. Fisher, W. A. Herrmann, K. Öfele and C. Brossmer, *Angew. Chem.*, 1995, **107**, 1992.

5 It is noteworthy that Milstein and coworkers have also reported the successful use of phosphapalladacycles as catalysts for the Heck reaction: Y. Ben-David, M. Portnoy, M. Gozin and D. Milstein, *Organometallics*, 1992, **11**, 1995.

6 M. Shibaski, C. D. J. Boden and A. Kojima, *Tetrahedron*, 1997, **53**, 7371; O. Loiseleur, M. Hayashi, N. Schmees and A. Pfaltz, *Synthesis*, 1997, 1338; L. E. Overman and D. J. Poon, *Angew. Chem., Int. Ed.*, 1997, **36**, 518.

7 It is noteworthy that for aryl iodides a stoichiometric amount of silver salts is necessary to obtain good yields and high enantiomeric excesses. See: T. Sakamoto, Y. Kond and H. Yamanaka, *Tetrahedron Lett.*, 1992, **33**, 6845; C. Larock, W. H. Gong and B. E. Baker, *Tetrahedron Lett.*, 1989, **30**, 2603; T. Sato, S. Nukui, M. Sodeoka and M. Shibasaki, *Tetrahedron*, 1994, **50**, 371.

8 M. Beller, T. H. Riermeier, S. Haber, H. J. Kleiner and W. A. Herrmann, *Chem. Ber.*, 1996, **129**, 1259.

9 V. V. Dunina, O. N. Gorunova, L. G. Kuz'mina, M. V. Livantsov and Y. K. Grishin, *Tetrahedron Asymmetry*, 1999, **10**, 3951.

10 In recent years, we have studied and developed the potentialities of oxazaphospholidine and diazaphospholidine ligands in various catalytic reactions. Some of these systems in which the phosphorus atom is substituted concommitantly with 2 nitrogen and one oxygen atoms or one aromatic carbon atom proved to be excellent mediators for, *inter alia*, highly selective allylic substitution,[11] copper-catalyzed Diels–Alder[12] or asymmetric cyclopropanation reactions.[13]

11 T. Constantieux, J. M. Brunel, A. Labande and G. Buono, *Synlett*, 1998, 49; G. Muchow, J. M. Brunel, M. Maffei, O. Pardigon and G. Buono, *Tetrahedron*, 1998, **54**, 10435; J. M. Brunel, T. Constantieux and G. Buono, *J. Org. Chem.*, 1999, **64**, 8940.

12 J. M. Brunel, B. Del Campo and G. Buono, *Tetrahedron Lett.*, 1998, **39**, 9663.

13 J. M. Brunel, O. Legrand, S. Reymond and G. Buono, *J. Am. Chem. Soc.*, 1999, **121**, 5807.

14 J. M. Brunel, A. Heumann and G. Buono, *Angew. Chem., Int. Ed.*, 2000, **39**, 1946.

15 Ligand **3** was purified by distillation and was obtained as a white air and moisture stable solid in 89% yield on cooling; bp 130 °C (10 Pa); mp 138 °C.

16 *Crystal data*: for **3**: colourless cubic monocrystal, $C_{18}H_{20}N_2P$ (M = 295.35) obtained by recrystallization from ethyl acetate, approximate dimensions 0.2 × 0.2 × 0.2 mm, monoclinic, space group $P2_1$, a = 8.2642(5), b = 8.0347(4), c = 12.4008(8) Å, Z = 2, D_c = 1.22 g cm^{-3}, T = 248 K, Cu-Kα radiation, R = 0.045. For **5**: yellow plate monocrystal, $C_{26}H_{28}IN_2O_2PPd$ (M = 664.81) obtained by recrystallization from ethyl acetate, approximate dimensions 0.3 × 0.4 × 0.5 mm, orthorhombic, space group $P2,2,2$, a = 9.1514(2), b = 10.8405(4), c = 15.8227(6) Å, Z = 4 , D_c = 1.25 g cm^{-3}, T = 298 K, Cu-Kα radiation, R = 0.044. CCDC 182/1744. See http://www.rsc.org/suppdata/cc/b0/b005521m/ for crystallographic files in .cif format.

17 No other isomer was formed, nor was disubstitution observed.

18 *General information*, for the hydroarylation of norbornene see ESI†.

19 For some references on mechanistic aspects, see: B. L. Shaw, S. D. Perera and E. A. Staley, *Chem. Commun.*, 1998, 1361; B. L. Shaw and S. D. Perera, *Chem. Commun.*, 1998, 1863.

20 It is noteworthy that the P, C and O atoms around the Pd center adopt a distorted tetrahedral arrangement with bond angles between 84.0 and 138.4°. The complexation of Pd occurs with retention of configuration at the P atom. The shortness of the P–N3 bond (1.662 *cf.* 1.701 Å in the free phosphine **3**) and of the P–N4 bond (1.662 *cf.* 1.73 Å) may be assigned to negative hyperconjugation due to electron donation from π_N to σ^*_{P-Pd} orbitals. See: D. G. Gilheany, *Chem. Rev.*, 1994, **94**, 1339.

Carbon nanofiber supported palladium catalyst for liquid-phase reactions. An active and selective catalyst for hydrogenation of C=C bonds

C. Pham-Huu,[a] N. Keller,[a] L. J. Charbonniere,[b] R. Ziessel[b] and M. J. Ledoux*[a]

[a] *Laboratoire de Chimie des Matériaux Catalytiques, ECPM-ULP, UMR 7504 CNRS, 25, rue Becquerel, 67087 Strasbourg Cedex 02, France. E-mail: ledoux@cournot.u-strasbg.fr*

[b] *Laboratoire de Chimie, d'Electronique et de Photonique Moléculaire, ECPM-ULP, UPRES-A 7008 CNRS, 25, rue Becquerel, 67087 Strasbourg Cedex 02, France*

Received (in Oxford, UK) 30th June 2000, Accepted 21st August 2000
First published as an Advance Article on the web 18th September 2000

Carbon nanofibers with a mean diameter of about 50 nm were successfully used as support for a palladium catalyst in the liquid phase selective hydrogenation of the C=C bond in an α,β-unsaturated molecule: a less critical problem of mass-transfer limitation led to the obtention of a highly active and chemo-selective catalyst compared to a commercial high surface area activated charcoal supported palladium catalyst.

Since their discovery at the beginning of the last decade,[1] carbon nanotubes and nanofibers seemed to be promising candidates for use as catalyst supports for heterogeneous catalytic reactions.[2–4] Such materials were expected to be efficient in liquid phase media due to their high external surfaces which can allow a significant decrease in critical mass transfer limitations,[5,6] also leading to an increase in the rate and the selectivity of the reactions.[7–10]

The aim of the present communication is to report the preparation of a highly dispersed palladium catalyst supported on carbon nanofibers, which is active and chemo-selective in the liquid phase hydrogenation of the C=C bond of cinnamaldehyde, at atmospheric pressure. The reaction rate and the product distribution are compared with those obtained on a commercially available activated charcoal supported palladium catalyst under the same reaction conditions.

The carbon nanofibers (CNF) were synthesized by a gas phase catalytic decomposition of a mixture of ethane and hydrogen over a high surface area alumina supported nickel catalyst at 650 °C. This nickel catalyst was prepared by incipient wetness impregnation of an alumina support with an aqueous solution of nickel nitrate containing 20 vol% of glycerol as viscous agent. After synthesis and sonication the carbon nanofibers were subsequently purified by acid treatment at 80 °C for 2 h in order to dissolve any residual nickel catalyst that they might have contained. The carbon nanofibers had a mean diameter of around 50 nm and lengths up to several micrometers and they were built with graphene planes in a herringbone pattern, sometimes connected in the middle of the fiber, forming a closed angle of about 75°. The distance between the planes was found to be 0.34 ± 0.01 nm.

The palladium deposition (5 wt%) onto the support was achieved by incipient wetness impregnation with an aqueous solution of palladium nitrate. The solid was dried overnight at 110 °C and subsequently reduced under flowing hydrogen at 350 °C for 2 h. Transmission Electron Microscopy (TEM) images evidenced the high and homogeneous dispersion of spheroidal palladium metal particles, with a narrow particle size distribution centered at around 3–5 nm diameter (Fig. 1). This homogeneous dispersion was attributed to a relatively strong metal-support interaction between the metal salt precursor and the graphite edges of the carbon nanofibers, increasing the resistance to the growth of the palladium particle. A similar observation has also been reported by Baker and co-workers[2–4] for graphite nanofibers supported on a nickel catalyst. However the distribution profile of the metal particles was relatively broad, ranging in size from 1.5 to 43.5 nm, with an average size of the metal particles of *ca.* 7–10 nm.

The hydrogenation of cinnamaldehyde was carried out at atmospheric pressure and low temperature, *i.e.* < 100 °C, with bubbling hydrogen. For the test, 10 ml of cinnamaldehyde (Athos, > 99.95 vol%) were dissolved in 40 ml of dioxane (RP, > 99.95 vol%). The catalyst (loading 1.05×10^{-3} g Pd) was added to the liquid under vigorous stirring (400 rpm) and subsequently, the reaction temperature was increased from rt to 80 °C, under continuous hydrogen bubbling through the liquid phase. The cinnamaldehyde concentration and the product distribution were followed by gas chromatography analysis (PONA capillary column equipped with a FID detector) of microsamples periodically withdrawn, and diluted with dioxane.

The catalytic results obtained over the Pd supported on carbon nanofibers and the commercial catalyst (Aldrich), are reported in Figs. 2 and 3. The superiority in terms of reaction rate of the nanofiber based catalyst was clear when the slopes of disappearance of CALD were compared. This performance was quite surprising as the literature reports that a relatively low surface area (45 m^2 g^{-1} instead of 900 m^2 g^{-1} for the

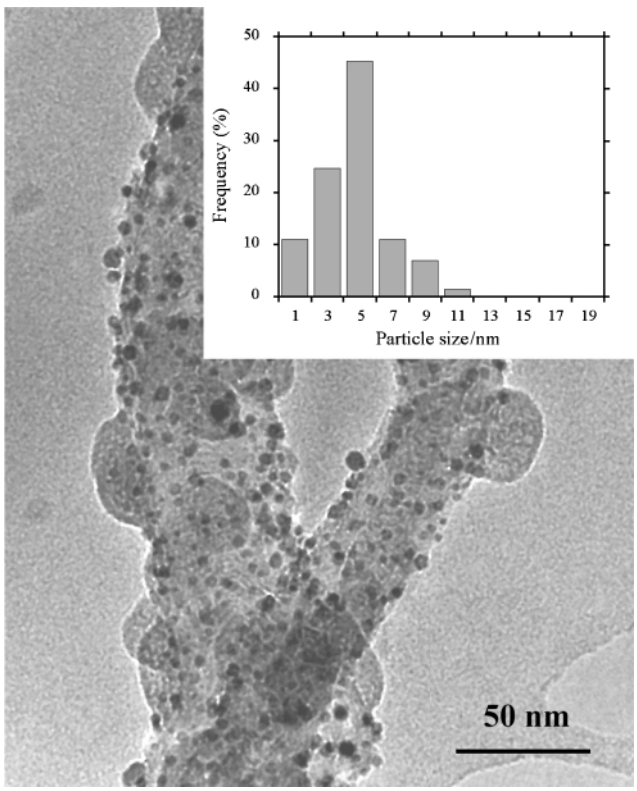

Fig. 1 A Transmisson Electron Microscopy image of the carbon nanofibers supported palladium catalyst and the particle distribution.

DOI: 10.1039/b005306f

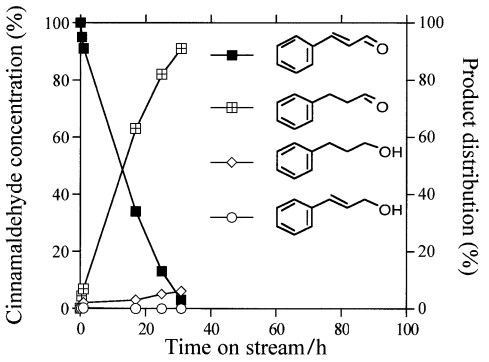

Fig. 2 Cinnamaldehyde conversion and product distribution as a function of time on stream obtained at 80 °C over the carbon nanofibers supported palladium catalyst. Cinnamaldehyde = CALD, cinnamyl alcohol = CALH, hydrocinnamaldehyde = HCALD and 3-phenylpropanol = PP.

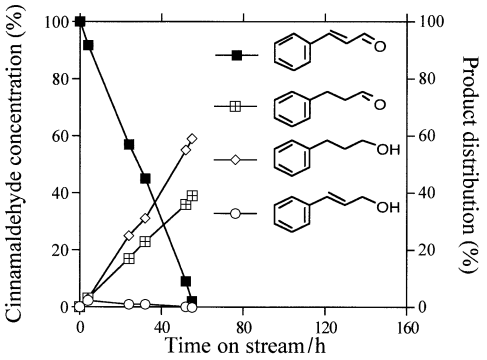

Fig. 3 Cinnamaldehyde conversion and product distribution as a function of time on stream obtained at 80 °C over the commercial activated charcoal supported palladium catalyst.

commercial catalyst) creates a major drawback for such an application.[4,11–13] Such behaviour is comparable to the results reported by Baker *et al.* over graphite nanofiber and alumina supported nickel catalysts.[4] This high catalytic activity was attributed to the high external surface area (high surface-to-volume ratio) of the carbon nanofibers compared to the charcoal grains (grains size *ca.* 50–100 μm) which improves the mass transfer during the reaction. In addition, the presence of a large amount of micropores (> 60% of the total surface area) in the commercial catalyst can be at the origin of diffusion phenomena, slowing down the apparent rate of the reaction. The total absence of microporosity in the nanofibers avoided such a drawback.

It is worth noting that only hydrocinnamaldehyde (HCALD) was detected and only trace amounts of C=O hydrogenated products (CALH or PP) were found over the carbon nanofiber catalyst, thus demonstrating a high selectivity for the C=C bond hydrogenation (98%), while a mixture of dihydrocinnamaldehyde (HCALD), cinnamyl alcohol (CALH) and 3-phenylpropanol (PP) was observed on the commercial catalyst (Fig. 3) and for related catalysts.[14–17] This could be explained both by the presence of microporosity and by some residual acidity on the activated charcoal surface which could favour the hydrogenation of the C=O bond in a consecutive reaction pathway.[4,14]

In conclusion, carbon nanofibers (mean diameter at *ca.* 50 nm) can be efficiently used as a catalyst support, for liquid phase reactions. The high external surface area of the catalyst inhibits the mass transfer limitation of the reactant to the active sites and leads to the obtention of an active and chemo-selective catalyst. Such performances can open routes for the design of new catalysts for liquid phase heterogeneous catalysis, and particularly for enantioselective allylic substitutions or ketone reductions.

Notes and references

1 S. Iijima, *Nature*, 1991, **354**, 56.
2 A. Chambers, T. Nemes, N. M. Rodriguez and R. T. K. Baker, *J. Phys. Chem. B*, 1998, **102**, 2251.
3 C. Park and R. T. K. Baker, *J. Phys. Chem. B*, 1998, **102**, 5168.
4 F. Salman, C. Park and R. T. K. Baker, *Catal. Today*, 1999, **53**, 385.
5 J. M. Planeix, N. Coustel, B. Coq, V. Brotons and P. M. Ajayan, *J. Am. Chem. Soc.*, 1994, **116**, 7935.
6 J. W. Geus, A. J. van Dillen and M. S. Hoogenraad, *Mat. Res. Soc. Symp. Proc.*, 1995, **368**, 87.
7 P. N. Rylander, *Catalytic Hydrogenation in Organic Syntheses*, Academic Press, New York, 1979, pp. 1.
8 J. M. Smith, *Chemical Engineering Kinetics*, 3rd Edn., McGraw-Hill, New York, 1981, pp. 450.
9 R. J. Madon and M. Boudart, *Ind. Eng. Chem. Fundam.*, 1982, **21**, 438.
10 S. Sato, R. Takahashi, T. Sodesawa, F. Nozaki, X.-Z. Jin, S. Suzuki and T. Nakayama, *J. Catal.*, 2000, **191**, 261.
11 N. M. Rodriguez, *J. Mater. Res.*, 1993, **8**, 3233.
12 N. M. Rodriguez, A. Chambers and R. T. K. Baker, *Langmuir*, 1995, **11**, 3862.
13 M.-S. Kim, N. M. Rodriguez and R. T. K. Baker, *Mat. Res. Soc. Symp. Proc.*, 1995, **368**, 99.
14 L. Zhang, J. M. Winterbottom, A. P. Boyes and S. Raymahasang, *J. Chem. Technol. Biotechnol.*, 1998, **72**, 264.
15 B. Liu, L. Lu, T. Cai and K. Iwatani, *Appl. Catal. A: General*, 1999, **180**, 105.
16 K.-C. Tin, N.-B. Wong, R.-X. Li, Y.-Z. Li, J.-Y. Hu and X.-J. Li, *J. Mol. Cat. A: Chemical*, 1999, **137**, 121.
17 Y. Zhang, S. Liao, Y. Xu and D. Yu, *Appl. Catal. A: General*, 2000, **192**, 274.

ChemComm

Growth of ultrafine zeolite Y crystals on metakaolin microspheres

Mingcan Xu, Mojie Cheng and Xinhe Bao*

State Key Laboratory of Catalysis, Dalian Institute of Chemical Physics, Chinese Academy of Sciences, Dalian 116023, P.R. China. E-mail: xhbao@ms.dicp.ac.cn

Received (in Cambridge, UK) 18th July 2000, Accepted 17th August 2000
First published as an Advance Article on the web 18th September 2000

Ultrafine zeolite Y crystals (*ca.* 100–200 nm) have been successfully grown on metakaolin microspheres (< 100 μm) for which good hydrothermal stability was observed; products were characterized by powder X-ray diffraction, scanning electronic microscopy and transmission electronic microscopy.

Zeolite Y is the most widely used catalyst in petroleum cracking and reforming processes.[1] In order to increase the yield of diesel oil in FCC (fluid catalytic cracking), improve the catalytic selectivity and reduce coke formation,[2,3] fine and even ultrafine zeolite Y crystals are desirable. Although ultrafine zeolite Y crystals have been synthesized in the laboratory,[4,5] there are still two key problems remaining. One is the difficulty of production in large quantities for industry since separation of ultrafine crystals by centrifugation is not viable on such a scale. The other drawback of such crystals is their low hydrothermal stability.[5,6] *in situ* Crystallization of ultrafine zeolite Y on supports may solve these problems. In an early report zeolite Y was crystallized on shaped kaolin pellets.[7] Here, we report a method to grow ultrafine zeolite Y crystals on metakaolin microspheres. At the same time, better hydrothermal stability of the ultrafine crystals was observed after growth on the support.

The synthesis was performed under hydrothermal conditions. Initially, a clear aqueous solution with composition (molar ratio) of 16 : 16 : 283 : 1 (SiO_2 : Na_2O : H_2O : Al_2O_3) was prepared upon addition of NaOH, $Al_2(SO_4)_3 \cdot 18H_2O$ and deionized water to silica sol (30%). This solution was aged for 3 days at room temperature. Uniform metakaolin microspheres (GSS600) of *ca.* 40–100 μm diameter were prepared by flotation with deionized water from kaolin microspheres (GSS), and then calcined at 600 °C for 3 h. 2.8 g sodium citrate was then added to the above aged solution and stirred for 2 h until dissolution was complete. Then, 6 g GSS600 was added under strong stirring. After 6 h, aqueous sulfuric acid was added dropwise with agitation leading to a gel mixture with final composition (molar ratio) 1 : 16 : 7.8 : 400 (Al_2O_3 : SiO_2 : Na_2O : H_2O) excluding the kaolin microspheres. Finally the mixture was maintained at 100 °C for 10 h. Two products were separated by flotation, which were filtered off and washed. One product (KYAOLIN) consisted of spherical particles with a similar diameter as the kaolin microspheres while the other product (NNY) was a fine white powder. Both were dried at 120 °C.

The powder X-ray diffraction (XRD) pattern [Fig. 1(a)] of NNY is typical for zeolite Y, and no peaks from any other crystalline substances were present. Clearly NNY consists of zeolite Y crystals that did not grow on the metakaolin microspheres. This result suggests that zeolite Y is the only crystalline product present in this synthesis system. Fig. 1(b) shows the XRD pattern of GSS600; besides peaks attributed to mica and quartz impurities, only a broad background, characteristic of amorphous material, was observed. Kaolin-type clay is essentially an aggregation of book-shaped units of the clay mineral kaolinite.[8] Upon calcination at 600 °C GSS600 transformed into metakaolin[9] and all the kaolinite peaks disappeared. Fig. 1(c) shows the XRD pattern of KYAOLIN, which reveals a clear XRD pattern of zeolite Y above the background of the metakaolin microspheres (GSS600); no other crystalline peaks were identified. The above analysis of the XRD patterns undoubtedly indicates that zeolite Y crystals were synthesized on the metakaolin microspheres.

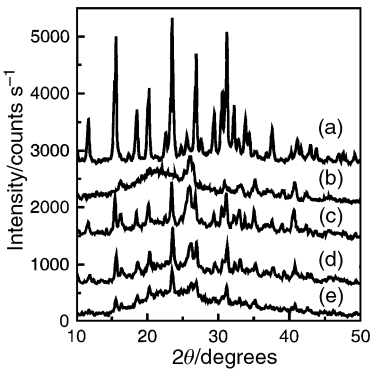

Fig. 1 XRD patterns of NNY (a), GSS600 (b), KYAOLIN (c), hydrothermally treated KYAOLIN (HKYAOLIN) (d) and hydrothermally treated NNY (HNNY) (e) obtained on a Rigaku D/MAX-γb diffractometer using Cu-Kα radiation.

On the surface of GSS600 [Fig. 2(a)], only irregular flakes can been seen. In comparison to GSS600, scanning electronic microscopy (SEM) of KYAOLIN [Fig. 2(b)] revealed many closely packed cubic crystals on the surface of the metakaolin microspheres. Fig. 3 shows a transmission electronic microscopy (TEM) image of a KYAOLIN section. The region shown

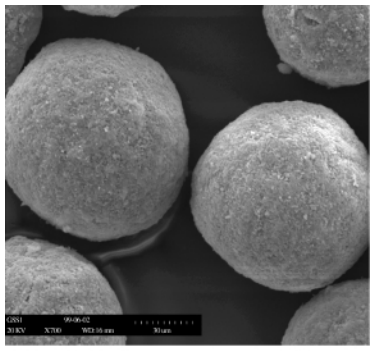

(a)

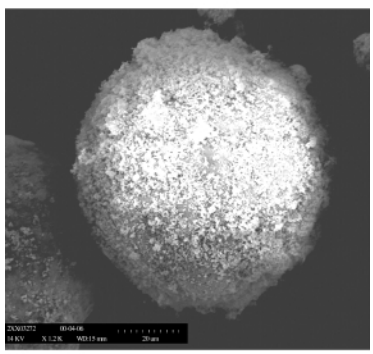

(b)

Fig. 2 SEM image of GSS600 (a) and KYAOLIN (b) obtained on a S3200N (HITACHI) scanning electronic microscope.

DOI: 10.1039/b005787h

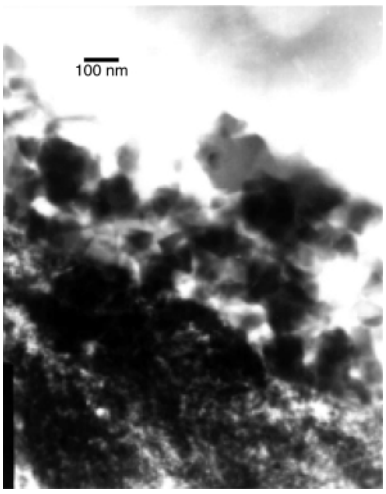

Fig. 3 TEM picture of a section (40–70 nm thickness) of KYAOLIN obtained on a JEM-2000EX, 100 kV instrument.

is part of a metakaolin microsphere section and was found to be homogeneous. A layer of cubic crystals, distinctly different from the metakaolin microspheres, were spread along the surface of the metakaolin microspheres. It is also observed that the crystals with sizes in the range 100–200 nm grow out of the metakaolin microspheres. The electronic microscope images and the XRD patterns unequivocally show that ultrafine zeolite Y crystals are grown on metakaolin microspheres.

HKYAOLIN [Fig. 1(d)] and HNNY [Fig. 1(e)] are, respectively, the products KYAOLIN and NNY treated with 100% water vapour at 650 °C for 2 h. In the XRD pattern of HKYAOLIN, clear peaks from the zeolite Y crystals are still present. Compared with KYAOLIN [Fig. 1(c)], the corresponding peaks from zeolite Y crystals in HKYAOLIN are somewhat broadened and reduced in intensity. This indicates that the crystalline structure of zeolite Y crystals grown on metakaolin microspheres are degraded to some extent during the hydrothermal treatment. As seen in Fig. 1(e), the intensities of peaks from zeolite Y crystals in HNNY are much weaker than those of the product NNY [Fig. 1(a)], and some amorphous substance was evident, *i.e.* during the hydrothermal treatment, the crystalline structure of the zeolite Y crystals is largely destroyed and changed into amorphous materials. The difference in decrease of the relative intensity of the HKYAOLIN and HNNY demonstrates that the hydrothermal stability of the ultrafine zeolite crystals is improved after growth on the metakaolin microspheres. The reasons for this improved hydrothermal stability upon growth on metakaolin spheres are, as yet, unclear, and require further investigation.

All the information obtained from XRD patterns, SEM and TEM images demonstrates that ultrafine zeolite Y crystals have been successfully grown on metakaolin microspheres and that they show good hydrothermal stability. The ultrafine zeolite Y crystals grown on metakaolin microspheres may have potential use in FCC processes.

Notes and references

1 M. Estermann, L. B. MicCusker, C. Baerlocher, A. Merrouche and H. Kessler, *Nature*, 1991, **352**, 320.
2 L. Zhang, Z. Li and Y. Xu, *Petroleum Process Petrochem.*, 1995, **26**, 38.
3 *Method of Analysis for Fluid Cracking Catalysts*, Grace and Co., Division Chemicals, Baltimore, MD, 1980.
4 B. J. Schoeman, J. Sterte and J. E. Otterstedt, *Zeolites*, 1994, **14**, 110.
5 S. Mintova and V. Valtchev, *Stud. Surf. Sci. Catal.*, 1991, **125**, 141.
6 K. Rajagopalan, A. W. Peters and G. C. Edwards, *Appl. Catal.*, 1986, **23**, 69.
7 L. L. Taggart and G. L. Ribaud, *US Pat.*, 3 119 659, 1964.
8 *The New Encyclopaedia Britannica*, 15th edn., vol. 4, p. 700.
9 D. W. Breck, *Zeolite Molecular Sieves: Structure, Chemistry and Use*, Wiley, New York, 1994, p. 313.

Low-temperature hydrogen production using electrically activated catalysts

Bijan Miremadi,[a] Tapesh Yadav,*[a] Jun Z. Zhang[b] and John L. Falconer*[b]

[a] *Nanomaterials Research Corporation, 2620 Trade Center Avenue, Longmont, CO 80503, USA. E-mail: tapesh@nrcorp.com*

[b] *Department of Chemical Engineering, University of Colorado, Boulder, CO 80309-0424, USA. E-mail: john.falconer@colorado.edu*

Received (in Irvine, CA, USA) 11th May 2000, Accepted 2nd August 2000
First published as an Advance Article on the web 18th September 2000

Electrical current was flowed through indium oxide/tin oxide nanoparticles to create highly active catalysts for selective oxidation of methanol to H_2 and CO_2 with low concentrations of CO.

A new type of catalyst and catalyst activation procedure is presented for selective oxidation of methanol to H_2 and CO_2 at low temperatures. This catalyst is of interest as a way to use liquid methanol as a source of H_2 for fuel cells.[1–3] The catalyst was activated by passing electrical current through it while gas phase reactions took place.[4] The catalyst consists of a mixture of 90% In_2O_3 and 10% SnO_2 and will be referred to as indium tin oxide (ITO).

To prepare the catalyst, a mixed chloride was precipitated from an aqueous solution by adding NH_3(aq). The precipitate was filtered off, washed, and then calcined at 723 K. A mixture of 75% ITO (BET surface area 15.7 $m^2\ g^{-1}$) and 25% Al_2O_3 (surface area 61.7 $m^2\ g^{-1}$) nanoparticles was formed by milling the two powders together. The nanoparticles were deposited from a suspension onto porous (0.2–0.3 mm pores) honeycomb Al_2O_3 structures (3.8 × 1.3 × 0.6 cm). The two ends of the honeycomb were coated with a conductive paste, before the catalyst was deposited, so that electrical connections could be made. The honeycomb was placed in a circuit with a constant-current dc power supply. The deposited catalyst was reduced in 5–20% H_2 at 575 K; this lowered the resistance and changed the catalyst color to light blue. A chromel–alumel thermocouple (0.2 mm diameter) was inserted into a honeycomb pore near the center to record the temperature during reaction. The product and feed streams were analyzed by gas chromatography. The mass balances were checked by calculating the H/C and O/C atomic ratios for the products. Typical average deviation from the feed ratios were 5% for the H/C ratio and 9% for the O/C ratio.

Results presented here were obtained on several honeycomb structures. Methanol oxidation was carried out in three ways.

(1) The catalyst temperature was raised by thermally heating it with a small ceramic heating element directly attached to the honeycomb. No current passed through the catalyst.
(2) Electric current was passed through the catalyst, and ohmic heating raised the catalyst temperature.
(3) After the catalyst was used for reaction with the electrical current, the current was decreased to zero. The catalyst temperature was then increased using the attached ceramic heating element.

Fig. 1 shows the methanol conversion and selectivity for H_2 formation as a function of temperature during oxidation over an ITO catalyst honeycomb for the first two types of experiments. The selectivity for H_2 was defined as the molar ratio: $H_2/(H_2 + H_2O + CH_2O)$. These experiments used a 20% O_2/80% He gas feed and a $MeOH/O_2$ feed ratio of 1.3. When the reduced catalyst was heated by the ceramic heater alone, the reaction products were only detected above 473 K, and the same rates and selectivities were obtained when raising or lowering the temperature. The main products were H_2, CO_2, and H_2O. As the temperature increased, the rate of H_2 formation and the selectivity to H_2 both increased.

As shown in Fig. 1, the catalyst was much more active at a given temperature when an electrical current was passed through it.[4] At 373 K, methanol conversion was > 5%, and by 473 K, methanol conversion was 80%. The H_2 selectivity increased with temperature as the conversion increased, so that the rate of H_2 formation increased dramatically above 425 K. The H_2 production rate was higher at all temperatures with electrical current through the catalyst than for the thermally heated catalyst. At 525 K, the rate of H_2 production was 50 times higher than seen with thermal heating. As with thermal heating, H_2, CO_2 and H_2O were the main products. Only slightly more than 1% of the products were CO at 532 K, and a much smaller percentage were CH_2O. The percentage of H_2 in the reactor effluent at 500 K was 17.5% on a wet basis; the current was 0.15 A and the voltage was 95 V dc.

A turnover frequency (TOF, the number of molecules reacting per surface site per second) was estimated using the BET surface area of the ITO powder. At 450 K, where the conversion was *ca.* 50%, the TOF was 0.15 s^{-1}. Since the reaction was run for 30–60 min or longer at each temperature, this TOF shows that each site reacted with a large number of methanol molecules without deactivation.

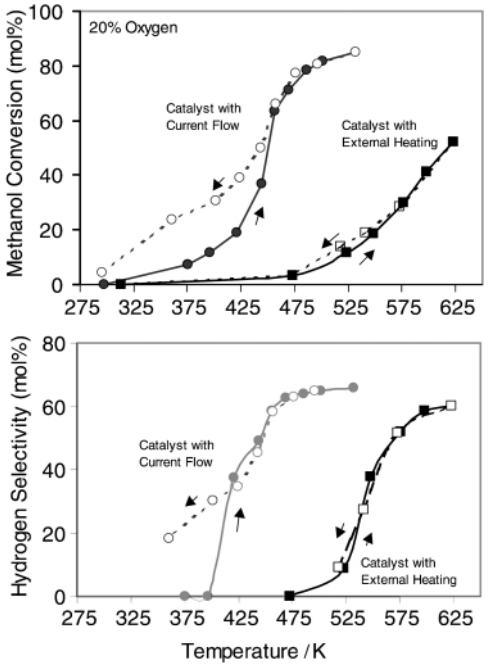

Fig. 1 (a) Percent methanol conversion and (b) selectivity [$H_2/(H_2 + H_2O + CH_2O)$] for H_2 formation *vs.* temperature for oxidation of methanol on an indium oxide/tin oxide catalyst. The results for thermal heating were obtained as the catalyst temperature was increased (—, ■) and decreased (-----, □). The results when an electrical current flowed through the catalyst were obtained as the current (and temperature) was increased (—, ●) and decreased (-----, ○).

DOI: 10.1039/b003920i

After the catalyst temperature had reached 525 K, the current was decreased in increments, and steady state measurements were made at several temperatures. Interestingly, the catalyst was more active at a given temperature during these measurements than when the current increased. That is, after the catalyst was exposed to the reaction mixture at 525 K with electrical current, it was more active at lower temperatures.

When 60% O_2/40% He was used as the gas feed instead of 20% O_2/80% He, the selectivity to H_2 was lower. After the catalyst had been exposed to the reaction mixture at 625 K with the electrical current, it was active for methanol oxidation even at 360 K with the current turned off. The percentage of H_2 in the reactor effluent was 12% on a wet basis with zero power. The reaction was reproducible and stable for at least 48 h, suggesting that this is not a transient artifact. When the electrically activated catalyst was heated thermally, it was much more active than when the original catalyst was heated thermally. Moreover, as shown in Fig. 2, the methanol conversion at low temperatures was higher for the activated catalyst (heated thermally) than for the catalyst with current flow. The selectivity to H_2 formation (Fig. 2) was higher at all temperatures after the catalyst had been activated by electrical current.

The products from electrically activated ITO catalysts were predominantly H_2, H_2O and CO_2. On 1% Pd/ZnO, Cubeiro and Fierro[5] reported selective oxidation of methanol to H_2 and CO_2 at 503–543 K, though more than 20% of their product was CO. On $Cu_{40}Zn_{55}Al_5$ catalysts, Alejo *et al.*[6] reported selective H_2 formation and low CO formation for MeOH oxidation near 500 K, but the O_2/MeOH feed ratio was only 0.06, so conversions were 20% or lower.

Previous studies have used electrical current to activate heterogeneous catalysts, but the present process is quite different. In the previous studies, a voltage applied across a solid electrolyte caused reversible increases in catalytic activity and dramatic changes in selectivity of metals supported on the electrolyte. These results have been explained using the non-Faradaic electrochemical modification of catalytic activity (NEMCA) effect.[7] For oxidation reactions, the rate increased by up to a factor of about 100 when an electrical current was applied. For most systems, NEMCA was attributed to electrochemically controlled back spillover of oxygen from a solid electrolyte such as yttrium-stabilized zirconia, and the rate enhancement depended dramatically whether the voltage was positive or negative. When the current was turned off, the NEMCA effect disappeared. The mechanism on the ITO catalyst appears to be quite different from the NEMCA effect for several reasons: (1) reversing the electrical leads to the catalyst did not change the reaction kinetics or selectivity, (2) when the current was shut off, the ITO catalyst was still active, and (3) reaction takes place on the ITO semiconductor oxide deposited on a porous insulating substrate and not on a metal deposited onto a solid ion conducting electrolyte.

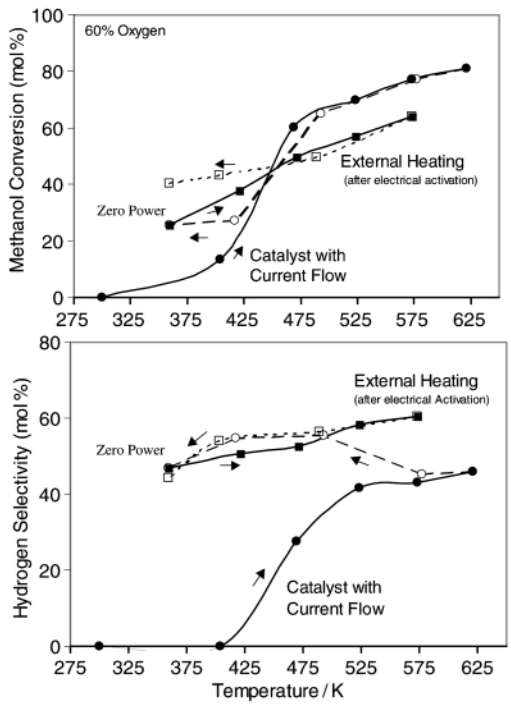

Fig. 2 (a) Percentage methanol conversion and (b) selectivity [$H_2/(H_2 + H_2O + CH_2O)$] for H_2 formation *vs.* temperature for oxidation of methanol in 60% O_2 on an indium oxide/tin oxide catalyst. The results were obtained when the current through the catalyst was increased (—, ●) and decreased (-----, ○). The point where the power was turned off is indicated. After the current was shut off, the catalyst temperature was raised thermally (—, ■) and then decreased again (-----, ○).

X-Ray photoelectron spectroscopy analysis was carried out on samples before and after reduction and after electrical activation in the methanol/air mixture. A reduced sample that was reacted in the methanol/air mixture at elevated temperature was also analyzed. A Physical Electronics Quantum 2000-1 system was used with electron and ion guns for charge neutralization. The reduced sample and the electrically activated sample had surface compositions that were 85–90% In and 10–15% Sn, and the sample reacted without electrical activation was 95% In. The bulk composition of the catalyst was 90% In, so surface enrichment does not appear to be responsible for the enhanced activity of the electrically activated catalyst. Small binding energy shifts (0.6 eV) toward more reduced states were observed for the indium peak on two out of three locations on the electrically activated catalyst, but the peak shifts could not be unambiguously assigned. Thus, the electrically activated catalyst may be reduced more than the H_2 pretreated catalyst.

The enhanced rate on the electrically activated catalyst could perhaps be due to reaction on local regions of the catalyst that were hotter than the temperature measured by the thermocouple. While we did not observe any hot spots on the visible external surfaces of the catalyst, such hot spots may exist internally. Alternatively, at contact points of the catalytic particles, the grain boundaries may be hot because of the ohmic heating. Given the nanostructured form of the catalysts, these microscopic hot spots may be localized. As shown in Fig. 1, the temperature to obtain 50% conversion is 200 K lower for the catalyst with current flow. If only a fraction of the catalyst is at a higher temperature than the average, then the temperature difference would have to be more than 200 K to yield the same conversion as when the entire catalyst was 200 K hotter. Since the ITO catalyst is expected to be a good thermal conductor (*e.g.* SnO_2 has a thermal conductivity similar to graphite) such large temperature differences over the short distances between particle contact points seems unlikely. Moreover, localized heating cannot explain why the conversion and selectivity are lower on raising the current than on lowering the current. Nor would localized heating explain why the catalyst was active when the current was off after electrical activation.

More extensive studies are necessary to determine the reasons for the enhanced activity, low carbon monoxide concentration in product gas, and other unusual effects observed when current is passed through the catalyst. The method of using electrical current to activate heterogeneous catalysts may be broadly useful to many other chemical reactions. In preliminary studies we have observed electrically activated ITO to catalyze methane reforming and the remediation of toluene and acetone.

Notes and references

1 R. F. Service, *Science*, 1999, **285**, 682.
2 R. Alpert, *Sci. Am.*, 1999, **281**, 74.
3 http://www.fuelcells.org/; http://www.e-sources.com/fuelcell.html
4 B. Miremadi and T. Yadav, *US Pat. Appl.* 09/165 439, 1998 Nanomaterials Research Corp.
5 M. L. Cubeiro and J. L. G. Fierro, *Appl. Catal. A: Gen.*, 1998, **168**, 307.
6 L. Alejo, R. Lago, M. A. Pena and J. L. G. Fierro, *Appl. Catal. A: Gen.*, 1997, **162**, 281.
7 C. G. Vayenas and S. Bebelis, *Catal. Today*, 1999, **51**, 581.

ChemComm

Cyclopalladated imine catalysts in Heck arylation: search for the catalytic species†

Mathias Nowotny,* Ulf Hanefeld, Henk van Koningsveld and Thomas Maschmeyer

Laboratory for Applied Organic Chemistry and Catalysis, TU Delft, Julianalaan 136, 2628BL Delft, The Netherlands. E-mail: nowotny@tnw.tudelft.nl

Received (in Cambridge, UK) 6th June 2000, Accepted 22nd August 2000
First published as an Advance Article on the web 18th September 2000

The application of the new cyclopalladated imine complexes of the Milstein-type 1d, 2a and 2b and the immobilised derivative 2c in the Heck reaction has provided evidence that these complexes are unstable and the active species is metallic palladium.

The palladium-catalysed reaction of organic halides with alkenes (the Heck reaction, Scheme 1) is a well-established method for carbon–carbon bond formation.[1] The reaction is usually carried out homogeneously in the presence of phosphine ligands and a base.

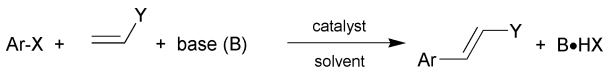

Scheme 1 The Heck reaction.

The need for relatively large amounts of catalyst and the early precipitation of palladium black are severe limitations that have so far prevented widespread industrial application of the Heck reaction. However, thermally robust cyclopalladated complexes offer a way to overcome these stability limitations. Specifically, in addition to the numerous examples that are based on palladated phosphines,[2] the cyclopalladated imine complexes **1a–c** were recently described.[3] Contrary to the ubiquitous application of palladium phosphine complexes as catalysts for the Heck reaction, the use of nitrogen-based catalysts is still very rare. However, these cyclopalladated imines form thermally and air-stable catalysts with high activities (turnover numbers {TON} $> 10^6$ were achieved).

In order to improve the recyclability, and thereby the applicability, of these highly active cyclopalladated imine catalysts, we attempted to immobilise one of these complexes. Among the numerous attempts to immobilise Pd catalysts on various supports,[4] there is only one example of an immobilisation *via* nitrogen-based tethers.[5] To avoid problems arising from the dimeric nature of catalysts **1a–c**, we utilised $Pd(hfac)_2$ instead of $Pd(OAc)_2$ as the source of Pd(II). The monomeric nature of cyclopalladated phosphine complexes bearing acac and hfac counterions has been reported.[2d] To guarantee comparability of results, we also synthesised the homogeneous model complexes **1d**, **2a** and **2b**. All these new palladacycles have been fully characterised.† Additionally, the monomeric nature of **2b** was verified by X-ray analysis (Fig. 1).‡

Utilising commercially available aminomethyl-functionalised polystyrene beads (AMPS, Fluka 81553), the catalyst **2c** was readily prepared in two steps (Scheme 2). A catalyst loading of 0.544 mmol g^{-1} was determined by XRF analysis. The characteristic imine C = N stretch vibration of 1661 cm^{-1} in the IR spectrum for the imine-functionalised support shifted to 1636 cm^{-1} in **2c**. The latter value is in good agreement with that of the homogeneous analogue **2b**.

The catalytic behaviour of the new palladacycles **1d** and **2a–c** was studied in the coupling reaction of iodobenzene with styrene in *N*-methylpyrrolidinone (NMP). *n*-Pr_3N was employed as the base in all experiments. In accordance with the results for **1a–c**, all experiments were performed in air. A

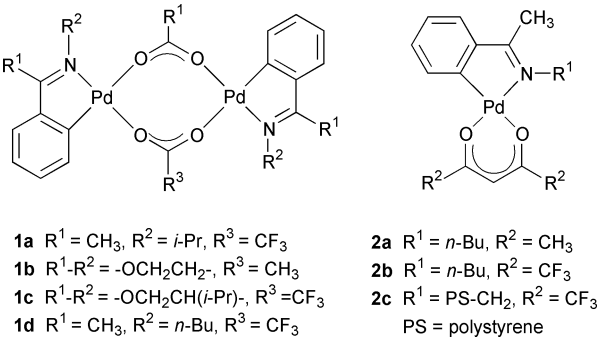

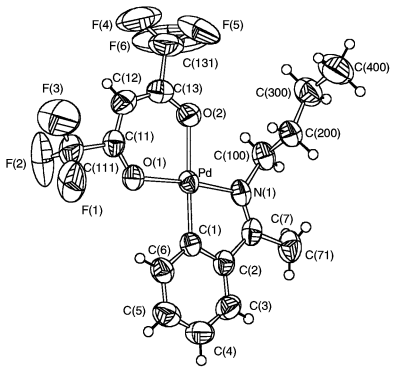

Fig. 1 The molecular structure of **2b**. Relevant bond distances (Å) and angles (°): Pd–C(1) 1.9461(30), Pd–N(1) 1.9788(43), Pd–O(1) 2.0159(46), Pd–O(2) 2.1106(23), N(1)–C(7) 1.2776(42), C(1)–C(2) 1.3808(44), C(2)–C(7) 1.4630(49); N(1)–Pd–C(1) 80.73(13), N(1)–Pd–O(2) 95.68(11), O(1)–Pd–O(2) 89.82(10), O(1)–Pd–C(1) 93.64(12).

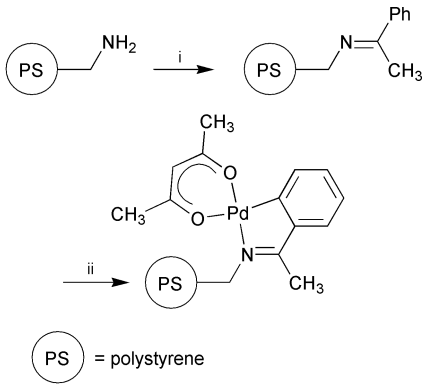

Scheme 2 *Reagents and conditions:* i, acetophenone (1.1 equiv.), cat. TsOH, toluene, 112 °C, 16 h; ii, $Pd(hfac)_2$ (0.75 equiv.), C_6H_6, 68 °C, 12 h.

† Electronic supplementary information (ESI) available: selected spectroscopic data for **1d**, **2a** and **2b**. See http://www.rsc.org/suppdata/cc/b0/b004503k/

DOI: 10.1039/b004502k

Table 1 Results of the Heck reaction catalysed by imine catalysts **1d** and **2a–c**[a]

Entry	Catalyst/mmol	Run	*T*/°C	*t*/h	Yield (%)[b]	TON
1	**2a** (3.2×10^{-3})	1	100	14	100	1562
2	**2b** (3.2×10^{-3})	1	100	12	100	1562
3	**1d** (3.2×10^{-3})	1	100	12	100	1562
4	**2b** (5×10^{-5})	1	140	120	91	91000
5	**2c** (3.2×10^{-4})	1	140	11	100	15625
6	**2c** (2.8×10^{-4})[c]	2[d]	140	20	95	17006
7	**2c** (4.0×10^{-5})	2[e]	140	40	0	0
8	**2c** (3.2×10^{-3})	1	100	13	100	1562
9	**2c** (4.5×10^{-4})[c]	2[d]	100	120	100	11108
10	**2c** (2.7×10^{-3})	2[e]	100	13	100	1852
11	**2c** (1.9×10^{-3})[c]	3[d]	100	18	100	2630
12	**2c** (8.0×10^{-4})	3[e]	100	40	0	0

[a] Amounts: PhI, 5 mmol; styrene, 6 mmol; *n*-Pr_3N, 7 mmol; NMP, 5 ml; mesitylene (int. standard), 0.25 ml. [b] Stilbene, *trans*/*cis* = 6.8–7.4; determined by GC. [c] Determined by AAS analysis. [d] Filtrate of previous run. [e] Recovered **2c** from previous run.

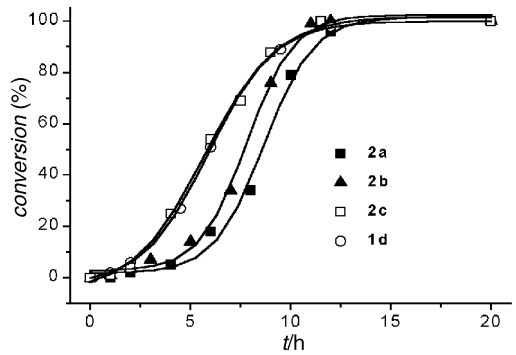

Fig. 2 Plot of conversion *versus* time for the Heck reaction of iodobenzene with styrene for the cyclopalladated catalysts **1d**, **2a–c** at 100 °C.

control experiment under N_2 with otherwise identical conditions showed no difference in catalyst activity. All catalysts were active under the employed conditions and pure stilbene (*trans*/*cis* = 6.8–7.4) was obtained (Table 1).

The immobilised catalyst **2c** showed a level of activity in the first run that is comparable to that of the three homogeneous analogues **1d**, **2a** and **2b** (Table 1, entries 1–3, 8). An increase of the reaction temperature from 100 to 140 °C led, as expected, to a rise of several orders of magnitude in TON (entry 2 *cf.* 4). An intriguing feature, which is exhibited by all the new catalysts in their first catalytic runs, is the presence of an induction period of about one hour (Fig. 2). Hence, the catalytically active species is not identical with the originally employed palladacycle, but is only formed during the course of the reaction. The gradual increase of the reaction rate after the initial induction period is indicative of a steady increase of catalyst concentration over the course of the reaction. Further evidence about the nature of the catalytically active species arises from the observation that the immobilised catalyst **2c**, recovered by filtration from an initial catalytic run at 140 °C (Table 1, entry 5), proved to be completely inactive in a consecutive run (entry 7). Instead, the filtrate of the initial run exhibited an undiminished level of activity upon addition of another equivalent of substrates and base (entry 6). Furthermore, the filtrate catalyses the Heck coupling without the occurrence of an induction period (Fig. 3). Therefore the catalytically active species has to be soluble. The imine ligand of the immobilised palladacycle in **2c** cannot be removed from the polystyrene support due to the firm C–C linkage. Hence, the catalytically active species must be formed under loss of this ligand. The liberation of the catalytic species from **2c** is slowed sufficiently at 100 °C to allow some of the catalyst precursor to remain on the support after the first run. Therefore some activity is maintained for a second, but not a third run. Accordingly, the

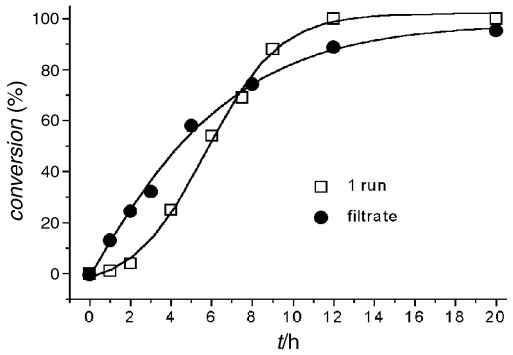

Fig. 3 Plot of conversion *versus* time for the Heck reaction of iodobenzene with styrene for **2c** in the first catalytic run at 100 °C and for the filtrate of the former after addition of a second equivalent of substrates and amine base.

filtrates of both the first and second runs exhibit high levels of activity (entry 8–12).

Contrary to the claim of high thermal stability of the cyclopalladated imine complexes **1a–c**, the catalyst precursors **2a–c** and especially **1d** proved to be thermally labile to such an extent that even moderate heating during the synthesis of these palladacycles caused precipitation of some palladium black. The particularly high lability of **1d** corresponds well with the relatively short induction period found in catalytic runs employing this complex (Fig. 2). The expected rapid decomposition of the palladacycles under the conditions of the Heck reaction was proven by the fact that heating **1d** in NMP to 140 °C for 2 h in the absence of substrates and amine base caused complete degradation under formation of Pd black. In accordance with recent observations by Reetz, who detected catalytically active, $R_4N^+X^-$-stabilised Pd colloids in comparable phosphine-free systems after a similar induction period,[6] we assume that finely divided palladium particles are also the true source of catalytic activity in our system. The stabilising role of $R_4N^+X^-$ may in our system be adopted by the *n*-$Pr_3NH^+I^-$ that is formed in the course of the catalytic cycle. The high activity of the examined cyclopalladated imine catalysts may be ascribed to the formation of Pd(0) nanoparticles in a particularly active form under the applied conditions.

M. N. gratefully acknowledges a Senior Research Fellowship from TU Delft. U. H. would like to thank the Koninklijke Nederlandse Akademie van Wetenschappen for a fellowship.

Notes and references

‡ *Crystal data* for **2b**: $C_{17}H_{17}F_6NO_2Pd$, M = 484.74 , triclinic , space group $P\bar{1}$ a = 8.314(6), b = 9.565(5), c = 12.293(4) Å, α = 77.57(7), β = 87.72(4), γ = 79.55(14)°, U = 938.8(10) Å^3, λ = 0.71073 Å, Z = 2, D_c = 1.725 Mg m^{-3}, T = 293 ± 2 K, μ(Mo-Kα) = 1.057 mm^{-1}, θ_{max} = 30.26°. Structure solved by Patterson technique. Full matrix least squares refinement on F to final R = 0.059 (R_w = 0.037) for all 5559 reflections and to R = 0.037 (R_w = 0.037) for the 4486 reflections with $F > 2.5\sigma(F)$. CCDC 182/1754. See http://www.rsc.org/suppdata/cc/b0/b004502k/ for crystallographic files in .cif format.

1 For a recent review see: A. de Meijere and F. E. Meyer, *Angew. Chem., Int. Ed. Engl.*, 1994, **33**, 2379; W. Cabri and I. Candiani, *Acc. Chem. Res.*, 1995, **28**, 2.

2 (*a*) W. A. Herrmann, C. Brossmer, C.-P. Reisinger, T. H. Riermeier, K. Öfele and M. Beller, *Chem. Eur. J.*, 1997, **3**, 1357; (*b*) M. Ohff, A. Ohff, M. E. van der Boom and D. Milstein, *J. Am. Chem. Soc.*, 1997, **119**, 11 687; (*c*) M. Beller and T. H. Riermeyer, *Eur. J. Inorg. Chem.*, 1998, **1**, 29; (*d*) B. L. Shaw, S. D. Perera and E. A. Staley, *Chem. Commun.*, 1998, 1361; (*e*) D. A. Albisson, R. B. Bedford and P. N. Scully, *Tetrahedron Lett.*, 1998, **39**, 9793; (*f*) F. Miyazaki, K. Yamaguchi and M. Shibasaki, *Tetrahedron Lett.*, 1999, **40**, 7379.

3 M. Ohff, A. Ohff and D. Milstein, *Chem. Commun.*, 1999, 357.

4 F. Zhao, B. M. Bhanage, M. Shirai and M. Arai, *Chem. Eur. J.*, 2000, **6**, 843, and references therein.

5 Z. Zhuangyu, P. Yi, H. Honwen and K. Tsi-Yu, *Synthesis*, 1991, 539.

6 M. T. Reetz and E. Westermann, *Angew. Chem., Int. Ed.*, 2000, **39**, 165.

Development of a new force field for open shell ions: application to modelling of $LaMnO_3$

Scott M. Woodley,*[a] C. Richard A. Catlow,[a] Julian D. Gale[b] and Peter D. Battle[c]

[a] *Davy-Faraday Research Laboratory, The Royal Institution of Great Britain, 21 Albemarle Street, London, UK W1X 4BS. E-mail: smw@ri.ac.uk*

[b] *Department of Chemistry, Imperial College of Science, Technology and Medicine, South Kensington, London, UK SW7 2AY*

[c] *Inorganic Chemistry Laboratory, University of Oxford, South Parks Road, Oxford UK OX1 3QR*

Received (in Cambridge, UK) 18th July 2000, Accepted 25th August 2000
First published as an Advance Article on the web 18th September 2000

A new type of force-field, based on the angular overlap model, has been developed in order to model compounds containing 'non-spherical' ions; the model has been successfully applied to $LaMnO_3$, with the Mn–O bond distances within the distorted MnO_6 octahedra and the lattice parameters being reproduced to within 0.33% of those determined experimentally.

There have been many successes over the last thirty years in the modelling of oxides using simple interatomic potentials based on the ionic model, particularly when ion polarisability is accounted for *via* the shell model.[1–3] Such calculations have typically used potentials comprising a Buckingham term to describe the short-range interaction between two ions along with the Coulomb term (evaluated *via* an Ewald sum) for the long-range interaction. Although potential parameters may be derived theoretically, particularly from fitting to *ab initio* energy surfaces, most have been obtained by empirical fitting to experimental data including structural and physical properties. However, the Coulomb and Buckingham potentials are purely radial, and consequently can only accurately model structures that contain spherical ions, representing a major limitation on the applicability of these methods to transition metal oxides. In order to extend the scope of structural modelling to include topical materials that contain 'non-spherical' (especially Jahn–Teller) ions, for example, manganates and cuprates which require accurate Mn^{3+}–O^{2-} and Cu^{2+}–O^{2-} potentials, we have developed a new short range potential. In this communication, we show that we are now able to model $LaMnO_3$, which contains the Jahn–Teller Mn^{3+}: $3d^4$ cation, which will clearly enable predictive computational chemistry to be applied to the area of colossal magnetoresistance (CMR) research. We expect the same basic method to be applicable in the case of Cu^{2+}: $3d^9$, and thus in the area of high T_c superconductivity.

The driving force for the distortions of the coordination sphere of Mn^{3+} and Cu^{2+} is associated with the Jahn–Teller effect, which removes a degeneracy in the electronic energies. In order to model the irregular coordination geometry associated with these 'non-spherical' ions, we chose to add a contribution to the lattice energy that corresponds to this energy-level splitting. Adding a ligand field stabilisation energy, and implementing numerical gradients, has previously proved[4] successful in the framework of molecular mechanics as applied to gas phase coordination complexes. Our model implements an adaptation of the angular overlap model (AOM).[5] The resulting parameterised interatomic energy term, E_{LF}, and its analytical gradients have been incorporated within the General Utility Lattice Program (GULP),[6,7] which is widely used for modelling ionic solids. One significant feature of our approach was to change the AOM formalism in order to introduce rotational invariance into the model, which is essential for application to energy minimisation studies. Thus, the GULP code creates a 5×5 overlap matrix for each transition metal ion,

$$H_{dd'} = \sum_{\text{ligands}} Ae^{-r/\rho}\Gamma_d\Gamma_{d'} \quad (1)$$

by taking the products of the angular contributions to the overlap integrals, Γ_d,[8] between the transition metal ion d-orbital and the orbitals of any surrounding ligand. A and ρ, which will subsequently be denoted with the subscript LF, are parameters that depend upon the transition metal and the ligand. From the eigenvalues of $H_{dd'}$, we can compute the approximate energy level diagram that results when the orbitals of the surrounding ligands overlap the d-orbitals of the transition metal ion *via* a σ-bonding interaction. In this way, we can calculate E_{LF}, for each transition metal ion, which is simply a weighted sum over these energy levels (eigenvalues). The second important modification of the AOM is the inclusion of an exponential distance dependence, rather than just inclusion of the nearest neighbour ions, such that a ligand that is further away makes a smaller contribution to E_{LF}. Moreover, the use of the exponential provides a way to decrease cut-off discontinuities and removes the need to specify which ligands belong to the first coordination sphere.

The mixing of the orbitals lowers the populated 'ligand' energy levels, creating a more stable environment. To conserve energy, the sum of the energy levels of the d-orbitals must increase. Because we do not explicitly consider the 'ligand' energy levels, the stabilising energy E_{LF} is calculated by summing up the energy levels of the unoccupied d-orbitals; thus, if there are 10 d-electrons there are no unoccupied states and no stabilisation energy. To avoid singularities (for example, when one or two electrons occupy d-orbitals that are three-fold degenerate) we have also allowed partial occupancies (or a non-zero probability that an electron can populate a higher energy state) through the use of a Fermi function. The Fermi energy, E_f, defined to be that which gives the required number of d-electrons, can only be expressed implicitly, and so it is calculated by an iterative method. Because we treat spin-up and spin-down separately, there are two Fermi energies, and E_{LF} for each transition metal ion is therefore a double summation over the weighted energy levels. The 'electronic temperature' of the Fermi function is fixed at room temperature in the present work.

Table 1 Buckingham parameters (B) for the interaction between the cations and the oxygen shells, O_s^{2-}, and the new force field parameters (LF) obtained for the Jahn–Teller interaction between the Mn^{3+} ion and the surrounding oxygen cores, O_c^{2-}. A cut-off radius of 10 Å was used for the cation–anion short-range potentials

	i	A_i/eV	ρ_i/Å
La^{3+}–O_s^{2-}	B	4317.17	0.2987
Mn^{3+}–O_s^{2-}	B	1265.17	0.3176
Mn^{3+}–O_c^{2-}	LF	8.98	0.3300

DOI: 10.1039/b005802p

Table 2 Structural data of $LaMnO_3$ within the *Pnma* space group

	Calculated (this work)			Observed (ref. 10)			Calculated (ref. 2)		
	a/Å	*b*/Å	*c*/Å	*a*/Å	*b*/Å	*c*/Å	*a*/Å	*b*/Å	*c*/Å
Unit cell parameters	5.7483	7.7199	5.5298	5.743	7.695	5.537	5.553	7.818	5.528
Fractional co-ordinates	*x*	*y*	*z*	*x*	*y*	*z*	*x*	*y*	*z*
La^{3+}	0.5457	0.2500	0.0044	0.550	0.250	0.009	0.521	0.250	0.002
Mn^{3+}	0.0000	0.0000	0.0000	0.000	0.000	0.000	0.000	0.000	0.000
O^{2-}	0.9782	0.2500	0.9333	0.989	0.250	0.929	0.981	0.250	0.938
O^{2-}	0.6889	0.5344	0.7787	0.691	0.539	0.775	0.716	0.532	0.785

Table 3 The three unique Mn–O bond distances within the MnO_6 octahedron and two unique tilt angles of the MnO_6 octahedra within $LaMnO_3$ together with the electronic data of the Mn^{3+} ion

	Calculated			Observed (ref. 10)			Calculated (ref. 2)		
Mn–O/Å	1.9038	1.9689	2.1830	1.901	1.965	2.189	1.987	1.992	1.995
Mn–O–Mn/°	154.71	157.18		154.46	156.61		158.68	159.28	
Calculated energy levels/eV	0.001			0.001		0.001	0.440		0.696
Calculated occupations/e	1.000			1.000		1.000	0.993		0.007

To test the applicability of this new approach, we have parameterised a potential model including the AOM description for $LaMnO_3$. This material, which shows a substantial Jahn–Teller distortion of the MnO_6 octahedron, is of importance both for its relevance to CMR and for its use as the cathode material in solid oxide fuel cells. The total lattice energy is the sum of E_{LF} and the energy created by the two-body potential:

$$V = \frac{qq'}{r} + Ae^{-r/\rho} - \frac{C}{r^6} \quad (2)$$

where the first term represents the Coulomb interactions. The remaining terms constitute the Buckingham potential representing the anion–anion and cation–anion short-range interactions. We choose to use formal ionic charges for q and q', although the charge on the transition metal ion may not be quite as high,[9] as this leads to greater transferability. The potential parameters, A_B, ρ_B and C_B, together with A_{LF} and ρ_{LF} used in the formulation of the angular overlap model, may be derived using standard empirical fitting techniques.[6]

Our strategy was to perform a 'relaxed fit', whereby we minimise the square of the differences between the observed[10] and calculated lattice parameters and ionic positions. Initially only the Mn^{3+}–O^{2-} Buckingham parameter A_B was refined whilst we tested a range of trial parameter values (A_{LF} and ρ_{LF}) for our new force field. In these preliminary calculations we used an equivalent exponential dependence for both the Buckingham and 'AOM' interaction between Mn^{3+} and the surrounding O^{2-} ions (*i.e.* $\rho_B = \rho_{LF}$) and the Buckingham parameters for the La^{3+}–O^{2-} interaction were held at the values determined previously.[1] To help find suitable potential parameters, the data used in the least squares fit included the Mn–O bond distances within the MnO_6 octahedron. Once our calculated Mn–O bond distances were reasonable, we refined the cation–anion parameters A_B and ρ_B along with A_{LF} and ρ_{LF}, again using a relaxed fit but with the calculated structure constrained within the experimentally determined *Pnma* space group. To increase the transferability of our potential parameters, we used the O^{2-}–O^{2-} Buckingham parameters[1] that were previously refined to be consistent with a range of binary and ternary oxides.

In Table 1 we report the potential parameters obtained for the best fit to the structural properties of $LaMnO_3$. The structural parameters of $LaMnO_3$ obtained using our new force field are presented in Tables 2 and 3, along with those calculated from previously published force field parameters[2] and the observed values.[10] As shown in Table 3, after minimising the lattice energy, our calculated Mn–O bond distances within the distorted MnO_6 octahedron are within 0.006 Å of those observed, and the tilt of these octahedra is within 0.6° of that observed. Comparison with the bond lengths obtained when the previously published Buckingham potential parameters[2] were used to model $LaMnO_3$ shows quite clearly that that the Mn^{3+} ion cannot be represented as a spherical ion and emphasises the progress made in the present study.

In Table 3, we also present the energy levels and their respective occupancies. With an 'electronic' temperature within the Fermi function set to that of room temperature, we note that there is a small probability (0.007) of an electron being in the highest energy level. The splitting of these energy levels is of the correct order of magnitude (although possibly too small) compared to typical orbital splittings for first row transition metals with weak field ligands, although no constraint was placed on these energies during fitting. As expected, the energies of the three non-bonding t_{2g} orbitals do not change whereas there is a Jahn–Teller splitting ($\sim$0.25 eV) of the anti-bonding e_g energy levels.

To summarise, we have shown that we can model Jahn–Teller distortions within $LaMnO_3$, the parent compound of the manganese perovskites that display CMR. This is the first time that a code primarily based on the inter-atomic potentials has been able to reproduce the Jahn–Teller distortion within this material. Furthermore, we have subsequently shown that our potential parameters are transferable, in that they have been used to reproduce the structure of Mn_2O_3 (with the calculated lattice parameters coming within 0.4% of the experimental value). The basic strategy described above increases the range of compounds that can be modelled using computationally inexpensive methods to include some of the most technologically important inorganic compounds studied in the last twenty years.

We thank EPSRC for financial support (grant GR/K85216).

Notes and references

1 T. S. Bush, J. D. Gale, C. R. A. Catlow and P. D. Battle, *J. Mater. Chem.*, 1994, **4**, 831.
2 M. Cherry, M. S. Islam and C. R. A. Catlow, *J. Solid State Chem.*, 1995, **118**, 125.
3 S. M. Woodley, P. D. Battle, J. D. Gale and C. R. A. Catlow, *Phys. Chem. Chem. Phys.*, 1999, **1**, 2535.
4 V. J. Burton, R. J. Deeth, C. M. Kemp and P. J. Gilbert, *J. Am. Chem. Soc.*, 1995, **117**, 8407.
5 M. Gerloch, J. H. Harding and R. G. Woolley, *Struct. Bonding*, 1981, **46**, 1.
6 J. D. Gale, *Philos. Mag. B*, 1996, **73**, 3.
7 J. D. Gale, *J. Chem. Soc., Faraday Trans.*, 1997, **93**, 629.
8 A. J. Bridgeman and M. Gerloch, *Prog. Inorg. Chem.*, 1997, **45**, 179.
9 W. C. Mackrodt and E. A. Williamson, *Ber. Bunsen-Ges. Phys. Chem.*, 1997, **101**, 1215.
10 J. B. A. A. Elemans, B. van Laar, K. R. van der Veen and B. O. Loopstra, *J. Solid State Chem.*, 1971, **3**, 238.

ChemComm

Selective ammoxidation of isobutane on a crystalline $SbRe_2O_6$ catalyst

Haichao Liu, Takafumi Shido and Yasuhiro Iwasawa*

Department of Chemistry, Graduate School of Science, The University of Tokyo, Hongo-7-3-1, Bunkyo-ku, Tokyo 113-0033, Japan. E-mail: Iwasawa@chem.s.u-tokyo.ac.jp

Received (in Cambridge, UK) 20th July 2000, Accepted 31st August 2000
First published as an Advance Article on the web 18th September 2000

The catalytic ammoxidation of isobutane to methacrylonitrile at 673 K proceeds on a new class of Re mixed-oxide $SbRe_2O_6$ with alternate $(Re_2O_6)^{3-}$ and $(SbO)^+$ layers, where ammonia is prerequisite for the C–H bond scission of isobutane.

Much attention has been devoted to selective ammoxidation of light alkanes from both fundamental and industrial interests. To date, a large number of multicomponent metal-oxide catalysts containing V, Mo, *etc*. have been explored to develop efficient catalytic systems for selective ammoxidation. However, owing to the inertness of light alkanes, very few catalysts have showed good performances that are comparable to those for the corresponding alkenes.[1–4] There is thus a clear need to develop new catalytic materials for the selective ammoxidation of light alkanes. Except for the oxidation of methanol and ethanol, compared with V, Mo and W there are limited uses of Re as a key element in selective ammoxidation/oxidation, in spite of Re having similar redox properties to those of V, Mo and W oxides.[5–7] Here, we report a first Re mixed-oxide catalyst (crystalline $SbRe_2O_6$) active for the selective ammoxidation of isobutane (i-C_4H_{10}) to methacrylonitrile (MAN) at 673 K, where NH_3 not only stabilizes the catalyst but also promotes the C–H bond scission of i-C_4H_{10}.

$SbOReO_4{\cdot}2H_2O$, $SbRe_2O_6$ and $Sb_4Re_2O_{13}$ were synthesized in the similar way to that reported previously.[6–12] The specific surface areas of the three samples were approximately 1 $m^2\ g^{-1}$. For comparison, Sb_2O_3-supported Re_2O_7 catalyst (Re_2O_7/Sb_2O_3; 10 wt% Re) was prepared by an impregnation method using an aqueous solution of NH_4ReO_4.[9] A coprecipitated $SbRe_2O_x$ catalyst (copr.$SbRe_2O_x$) was also prepared by a coprecipitation method using an ethanol solution of $ReCl_3$ and $SbCl_3$, followed by washing with water to eliminate the residual Cl ions from the sample. Ammoxidation reactions were carried out in a continuous-flow, fixed-bed reactor at 673 K under the conditions of 10% i-C_4H_{10}, 15% NH_3 and 25% O_2 balanced with He and a gas-hourly-space-velocity (GHSV) of 5000 h^{-1} at atmospheric pressure. Prior to each run, the catalysts (typically 0.3 g) were pretreated at 673 K under He for 1 h. The reactants and products were analyzed by two on-line gas chromatographs with Unibeads C, Gaskuropack 54 and VZ-10 columns. The conversion of NH_3 to N_2 and NO_x was < 10% under the present reaction conditions.

Table 1 presents the conversions, reaction rates and selectivities of the i-C_4H_{10} ammoxidation on the various Re–Sb–O catalysts and bulk ReO_x and SbO_x at 673 K. $SbOReO_4{\cdot}2H_2O$, $Sb_4Re_2O_{13}$ and Sb oxides such as Sb_2O_3 and Sb_2O_4 showed no activity. Bulk Re_2O_7 was active solely for i-C_4H_{10} combustion to CO_2. Bulk ReO_3 and ReO_2 produced MAN, but the selectivities were lower than 10% and the main product was CO_2. Re_2O_7/Sb_2O_3 or mechanically mixed $Re_2O_7{\cdot}Sb_2O_3$ samples showed almost no activity for the i-C_4H_{10} ammoxidation either. Copr.$SbRe_2O_x$ produced i-C_4H_8 (20.6% selectivity), but no formation of MAN was observed. Isobutane combustion was dominant also with this catalyst. Only the $SbRe_2O_6$ among these samples was active for the ammoxidation of i-C_4H_{10} to MAN. The selectivities to MAN and to the sum of MAN + i-C_4H_8 at the steady-state conversion of 4.4% were 44.9 and 84.3%, respectively. A decrease in the GHSV from 5000 to 2500 h^{-1} increased the conversion to 7.5% while keeping good selectivities to MAN and to MAN + i-C_4H_8, as shown in parentheses in Table 1.

The active $SbRe_2O_6$ compound consists of connected, alternate octahedral $(Re_2O_6)^{3-}$ and $(SbO)^+$ layers and grows as thin plate-like crystals preferably exposing the (100) plane.[12] The square basal (100) faces of $SbRe_2O_6$ crystals remained unchanged before and after the ammoxidation at 673 K as imaged by scanning electron microscopy. Further, neither change nor modification of the surface composition and crystallinity were observed by means of X-ray diffraction, X-ray photoelectron spectroscopy (XPS) and *in-situ* micro confocal laser Raman spectroscopy. The results indicate that the crystalline $SbRe_2O_6$ works as a promising catalyst for the ammoxidation. The fresh $SbOReO_4{\cdot}2H_2O$ and $Sb_4Re_2O_{13}$ possess Re^{7+} species, but the Re species were reduced to two valent states (possibly Re^{6+} and Re^{4+}) which exhibit XPS binding energies of 42.3 and 44.7 eV, and 45.1 and 47.5 eV for Re $4f_{7/2}$ and Re $4f_{5/2}$, respectively (compared to C 1s = 284.6 eV) under the ammoxidation conditions. These binding energies are similar to those for the $SbRe_2O_6$ surface after ammoxidation at 673 K. Thus, the difference in the catalytic performances of the crystalline Re–Sb–O catalysts may not be

Table 1 Isobutane ammoxidation on different Re–Sb–O catalysts and bulk ReO_x and SbO_x at 673 K

	Conversion (%)	Reaction rate/ μmol g-cat^{-1} h^{-1}	Selectivity (%)				
			MAN + i-C_4H_8	MAN	i-C_4H_8	CH_3CN	CO_2
$SbRe_2O_6$	4.4 (7.5)[a]	785.6 (669.5)[a]	84.3 (82.6)[a]	44.9 (44.2)[a]	39.4 (38.4)[a]	4.7 (5.6)[a]	10.2 (11.4)[a]
$SbOReO_4{\cdot}2H_2O$	0	0	—	—	—	—	—
$Sb_4Re_2O_{13}$	0	0	—	—	—	—	—
mix.$Re_2O_7{\cdot}Sb_2O_3$	0.5	89.3	trace	0	trace	0	~100
copr.$SbRe_2O_x$	0.4	71.4	20.6	0	20.6	0	79.4
Re_2O_7/Sb_2O_3	0.1	17.8	0	0	0	0	100
Re_2O_7	11.6	2071.3	0	0	0	0	100
ReO_3	2.1	374.9	31.5	7.7	23.8	25.7	42.6
ReO_2	5.6	999.9	31.0	9.1	21.9	32.1	36.4
Sb_2O_3	0	0	—	—	—	—	—
Sb_2O_4	0	0	—	—	—	—	—

[a] The data listed in parentheses were obtained at a GHSV of 2500 h^{-1}.

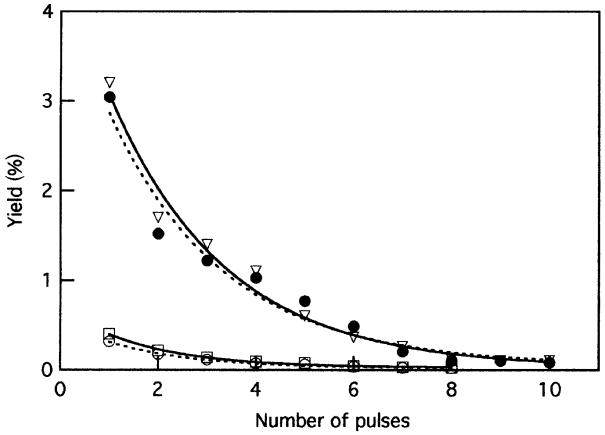

Fig. 1 Yields of MAN (∇, □) and i-C_4H_8 (●, ○) as a function of the number of pulses of i-C_4H_{10} alone (□, ○) and an i-C_4H_{10}–O_2 mixture (∇, ●) on an NH_3-preadsorbed $SbRe_2O_6$ catalyst at 673 K.

due to the difference in their surface Re oxidation states, but to the difference in their surface structures. This is entirely different from the finding in the selective oxidation of i-C_4H_{10} (773 K) and i-C_4H_8 (673 K) to methacrolein (MAL) that the activities of the three crystalline Re–Sb–O compounds are ascribed to a cooperation between Re_2O_7 and $Sb_4Re_2O_{13}$, both being formed by decomposition of the compounds under the oxidation conditions.[8–10] It is also different from the feature observed in the ammoxidation of i-C_4H_8 where the three Re–Sb–O compounds are more or less active at 673 K.[13]

It is to be noted that $SbRe_2O_6$ was inactive for i-C_4H_{10} selective oxidation as well as for the total oxidation at 673 K in the absence of NH_3, whereas it exhibited a good performance for i-C_4H_{10} ammoxidation at 673 K (Table 1). These results may indicate a promoting effect of NH_3 on the C–H activation in i-C_4H_{10}. To examine the role of NH_3, a series of pulse experiments were conducted on $SbRe_2O_6$ at 673 K in Fig. 1. No products were produced by pulsing i-C_4H_{10} alone or an i-C_4H_{10}–O_2 mixture on to the $SbRe_2O_6$ catalyst, which indicates that no C–H bond breaking in i-C_4H_{10} molecules occurs on the catalyst. However, when the catalyst was pretreated with an NH_3 pulse (the catalyst surface was saturated with NH_x), i-C_4H_{10} was converted to MAN and i-C_4H_8. The promotion effect of NH_3 pretreatment on the formation of MAN and i-C_4H_8 was more remarkable with the i-C_4H_{10}–O_2 pulse reaction as shown in Fig. 1. The formation of MAN and i-C_4H_8 decreased with the number of the i-C_4H_{10}–O_2 pulses. The pulse experiments show that adsorbed NH_x species are incorporated to the ammoxidation of i-C_4H_{10} to form MAN. These results demonstrate that NH_3 not only behaves as a reactant but also plays a crucial role in enhancing and/or generating the activity of $SbRe_2O_6$ for the dehydrogenation (C–H bond breaking) of i-C_4H_{10} to i-C_4H_8. Upon pulsing NH_3 on $SbRe_2O_6$, N_2 and H_2O were produced indicating the reaction of NH_3 with the lattice oxygen atoms of $SbRe_2O_6$ to form oxygen vacancies that may also be responsible for the C–H bond breaking. To our knowledge, $SbRe_2O_6$ is the first case where NH_3 changes an inactive catalyst to an active one for light alkane activation, although promoting effects of NH_3 have been documented.[14,15] Further study is necessary for depicting a detailed mechanism of the promoting effect of NH_3 on the $SbRe_2O_6$ selective catalysis.

In conclusion, a new class of Re mixed-oxide $SbRe_2O_6$ catalyzes the selective ammoxidation of i-C_4H_{10} to MAN. The activity of $SbRe_2O_6$ may be relevant partly to its specific crystal structure. The presence of ammonia is considered to be prerequisite, not only for maintaining the stable crystal structure of $SbRe_2O_6$, but also for promoting $SbRe_2O_6$ activity for C–H bond breaking in i-C_4H_{10} under the ammoxidation conditions.

This work has been supported by Core Research for Evolutional Science and Technology (CREST) of the Japan Science and Technology Corporation (JST). The authors acknowledge Professor H. Imoto, Utsunomiya University, for his helpful discussion on the preparation and structure of $SbRe_2O_6$.

Notes and references

1 R. K. Grasselli, *Catal. Today*, 1999, **49**, 141.
2 S. Albonetti, F. Cavani and F. Trifiro, *Catal. Rev.-Sci. Eng.*, 1996, **38**, 413.
3 C. J. Pereira, *Science*, 1999, **285**, 670.
4 T. Inoue, S. T. Oyama, H. Imoto, K. Asakura and Y. Iwasawa, *Appl. Catal., A*, 2000, **191**, 131.
5 J.-M. Jehng, H. Hu, X. Gao and I. E. Wachs, *Catal. Today*, 1996, **28**, 335.
6 W. T. A. Harrison, A. V. P. Mcmanus, A. P. Kaminsky and A. K. Cheetham, *Chem. Mater.*, 1993, **5**, 1631.
7 Y. Yuan, H. Liu, H. Imoto, T. Shido and Y. Iwasawa, *Chem. Lett.*, 2000, 674.
8 H. Liu, E. M. Gaigneaux, H. Imoto, T. Shido and Y. Iwasawa, *J. Phys. Chem. B*, 2000, **104**, 2033.
9 E. M. Gaigneaux, H. Liu, H. Imoto, T. Shido and Y. Iwasawa, *Top. Catal.*, 2000, **11**–**12**, 185.
10 H. Liu, E. M. Gaigneaux, H. Imoto, T. Shido and Y. Iwasawa, *Appl. Catal. A: General.*, 2000, **202**, 251.
11 H. Watanabe and H. Imoto, *Inorg. Chem.*, 1997, **36**, 4610.
12 H. Watanabe, H. Imoto and H. Tanaka, *J. Solid State Chem.*, 1998, **138**, 245.
13 H. Liu, H. Imoto, T. Shido and Y. Iwasawa, submitted for publication.
14 V. D. Sokolovskii, A. A. Davydov and O. Yu. Ovsitser, *Catal. Rev.-Sci. Eng.*, 1995, **37**, 425.
15 G. Centi and S. Perathoner, *Catal. Rev.-Sci. Eng.*, 1998, **40**, 175.

ChemComm

A novel intramolecular defluorinative cyclization approach to the synthesis of difluoromethylated quinazolic acid derivatives

Jian Hao, Hironari Ohkura, Hideki Amii and Kenji Uneyama*

Department of Applied Chemistry, Faculty of Engineering, Okayama University, Tsushimanaka 3-1-1, Okayama 700-8530, Japan. E-mail: uneyamak@cc.okayama-u.ac.jp

Received (in Cambridge, UK) 11th July 2000, Accepted 25th August 2000
First published as an Advance Article on the web 18th September 2000

***tert*-Butyl 2-(difluoromethyl)-3-benzyl-6-methoxy-3,4-dihydro-4-quinazoline-4-carboxylic ester (4) and its related 6-substituted esters, precursors of a new type of cyclic amino acid, were synthesized *via* intramolecular defluorinative cyclization under basic conditions.**

The recent achievement of the synthesis of fluorinated isoserines[1] *via* Wittig rearrangement of **1** to **2** in Scheme 1, engaged us in exploration on the synthesis of other new heteroatom-substituted amino acids and their derivatives which are expected to be candidates for biologically important inhibitors.[2] Here, we report the discovery of a novel defluorinative cyclization (**3** → **4**) leading to the synthesis of difluoromethylated quinazolic derivatives.

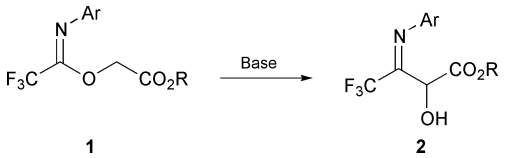

1 **2**

Scheme 1

Difluoromethylated amino acids are known to be important members of the family of fluorinated amino acids.[3] Introduction of difluoromethyl groups into nonfluorinated amino acids[4] or the synthesis of difluoromethyl-substituted amino acids from suitable fluorinated building blocks[5] is a great challenge in synthetic organofluorine chemistry. Selective defluorination from a trifluoromethyl moiety has been widely employed for promising construction of difluoromethylene moiety due to easy availability of trifluoromethyl compounds.[6] The present discovery of defluorinative cyclization of trifluoromethyl-substituted iminoamines **3**[7] provides a novel and efficient approach to the new *N*-heterocyclic *tert*-butyl 2-(difluoromethyl)-3-benzyl-6-methoxy-3,4-dihydro-4-quinazoline-4-carboxylic ester **4**[8] and the related 6-substituted esters (Scheme 2, Table 1), which is otherwise difficult.

The ester **3** was treated with LTMP (1.3 eq.) in THF at −60 °C for 10 min or *n*-BuLi (1.2 eq.) at 0 °C, and then the temperature was raised to 20 °C. The mixture was stirred for several hours (monitored by TLC) or 1 h, respectively.

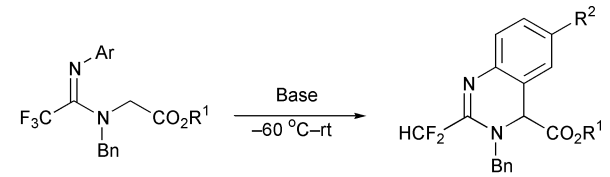

3 **4**

Ar = 4-MeO-C_6H_4, 4-CH_3-C_6H_4, 3,4-Cl_2-C_6H_3, C_6H_5, Naphthyl

R^1 = *t*-Bu, Me; R^2 = OMe, Me, H.

Base = LTMP or *n*-BuLi LTMP = Lithium tetramethylpiperidide

Scheme 2

A sterically hindered base (LTMP) provided better yield (63%) of **4a** than LDA (47%). In the 3,4-dichloro-substituted iminoamine (entry 7 in Table 1), *n*-BuLi was found to be more useful than LTMP. Both electron-withdrawing and -donating substituents on the aromatic ring affected the formation of **4**. The 2,6-dimethylphenyl compound (entry 9) afforded no corresponding cyclized compound **4** and the starting substrate was recovered.

The quinazolic esters (**4a**–**f**) obtained in the reaction are liquids and their structures were elucidated by spectroscopic and elemental analyses, along with X-ray crystallographic structural analysis of its methyl ester (**4g**),[9] which are colorless needle crystals. Existence of both CHF_2 group and a 1,2,4-trisubstituted benzene ring in **4a** (entry 1 in Table 1, Ar = *p*-methoxyphenyl, R^1 = *t*-Bu) was rationalized by the observation of a doublet at δ = 45.8 ppm (J_{HF} = 53.6 Hz) in ^{19}F NMR (C_6F_6 as an internal standard) and a triplet at δ = 6.33 ppm (J_{HF} = 53.6 Hz) in ^{1}H NMR, and three sets of aromatic protons [δ = 6.52 (d, J = 2.8 Hz), 6.74 (dd, J = 8.7 Hz, 2.8 Hz), and 7.11 ppm (d, J = 8.7 Hz)], respectively.

A mechanism of this reaction is tentatively proposed as shown in Scheme 3.

No Stevens-type rearrangement[9] products **8** were observed although Wittig-type rearrangement is known in fluorinated imino ethers (**1** → **2**).[1] The generation of carbanions **5** by LTMP at lower temperature (−60 °C) was confirmed by the quantitative formation of deuterated product **6** on treating with D_2O. Intramolecular nucleophilic attack of the carbanion onto the imino carbon followed by nucleophilic ring opening of the aziridine type intermediate (**7** → **9**) and simultaneous defluorination would lead to the formation of the quinazoline intermediate **9**, which undergoes base-catalyzed proton migration to the quinazolic products **4**. The rate-determining intramolecular nucleophilic attack *via* intermediate **7** would make the equilibrium (**5** ⇄ **7**) proceed in the forward direction. Thus, the sterically hindered 2,6-dimethyl compound (Table 1, entry 9) was recovered entirely though an α-proton of the carboalkoxy group of **3** (Ar = 2,6-dimethylphenyl) was deuterated by quenching the reaction mixture with D_2O at −60 °C. The preference of path A over path B would arise from the poorer leaving ability of *N*-benzyl anion (Scheme 3) than alkoxide anion in Wittig rearrangement (**1** → **2**).

The authors are grateful to the Ministry of Education, Science, Sports, and Culture of Japan for the financial support

Table 1 Yield of **4** in the base-catalyzed rearrangement of **3**

Entry	Ar	R^1	Base (eq.)	Yield of **4** (%)
1	4-$MeOC_6H_4$	*t*-Bu	LTMP (1.3)	**4a** (63)
2	4-$CH_3C_6H_4$	*t*-Bu	*n*-BuLi (1.2)	**4b** (58)
3	C_6H_5	*t*-Bu	*n*-BuLi (1.2)	**4c** (54)
4	1-Naphthyl	*t*-Bu	LTMP (1.3)	**4d** (80)
5	1-Naphthyl	Me	LTMP (1.3)	**4e** (67)
6	3,4-$Cl_2C_6H_3$	*t*-Bu	LTMP (1.3)	**4f** (78)
7	3,4-$Cl_2C_6H_3$	*t*-Bu	*n*-BuLi (1.2)	**4f** (91)
8	3,4-$Cl_2C_6H_3$	Me	LTMP (1.3)	**4g** (29)
9	2,6-$(CH_3)_2C_6H_3$	*t*-Bu	LTMP (1.3)	Recovery of **3**

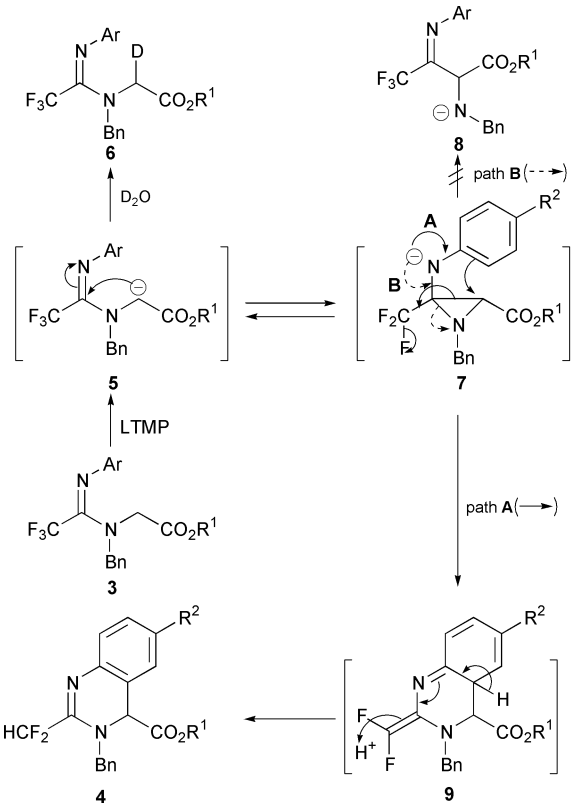

Scheme 3

(No 12450356) and the SC-NMR Laboratory of Okayama University for ^{19}F NMR analysis and VBL for X-ray analysis.

Notes and references

1 K. Uneyama, J. Hao and H. Amii, *Tetrahedron Lett.*, 1998, **39**, 4079.

2 (*a*) K. L. Kirk and R. Filler, *Recent Advances in the Biomedicinal Chemistry of Fluorine-containing Compounds*, in *Biochemical Frontiers of Fluorine Chemistry*, ed. I. Ojima, J. R. McCarthy and J. T. Welch, ACS Symposium series, Washington, D.C., 1996; (*b*) J. Kollonitsch, in *Biomedicinal Aspects of Fluorine Chemistry*, ed. R. Filler and Y. Kobayashi, Kodansha & Elsevier, 1982, pp. 93–122; (*c*) J. Kollonitsch, L. M. Perkins, A. A. Patchett, G. A. Doldouras, S. Marburg, D. E. Duggan, A. L. Maycock and S. D. Aster, *Nature*, 1978, **274**, 906: (*d*) E. A. Wang and C. Walsh, *Biochemistry*, 1981, **20**, 7539.

3 (*a*) J. T. Welch and S. Eswarakrishnan, *Fluorine in Bioorganic Chemistry*, John Wiley & Sons, 1994, pp 7–65; (*b*) V. P. Kukhar and V. A. Soloshonok, *Fluorine-containing Amino Acids, Synthesis and Properties*, John Wiley & Sons, 1994.

4 T. Tsushima, S. Ishihara and Y. Fujita, *Tetrahedron Lett.*, 1990, **31**, 3017.

5 (*a*) O. Kitagawa, A. Hashimoto, Y. Kobayashi and T. Taguchi, *Chem. Lett.*, 1990, 1307; (*b*) J. E. Baldwin, G. P. Lynch and C. J. Schofield, *J. Chem. Soc., Chem. Commun.*, 1991, 736; (*c*) B. P. Hast and J. K. Coward, *Tetrahedron Lett.*, 1993, **34**, 4917; (*d*) K. S. Kim and L. Qian, *Tetrahedron Lett.*, 1993, **34**, 7195; (*e*) T. Tsukamoto, T. Kitazume, J. J. Mcguiro and J. K. Coward, *J. Med. Chem.*, 1996, **39**, 66.

6 (*a*) J. M. Percy, *Building Block Approaches to Aliphatic Organofluorine Compounds* in *Topics in Current Chemistry 193*, ed. R. D. Chambers, Springer-Verlag, 1997; (*b*) P. Cavel, M. P. Legar-lambert, C. Biran, F. Serein-Spirau, M. Bordeau, N. Roques and H. Marzouk, *Synthesis*, 1999, 829; (*c*) K. Uneyama, G. Mizutani, K. Maeda and T. Kato, *J. Org. Chem.*, 1999, **64**, 6717; (*d*) H. Amii, T. Kobayashi, Y. Hatamoto and K. Uneyama, *Chem. Commun.*, 1999, 1323.

7 The esters **3** were readily prepared by the reaction of *N*-benzyl glycinates with trifluoroacetimidoyl chlorides[11] in good to excellent yields.

8 The 3,4-dihydroquinazoline skeleton has been mostly constructed by intramolecular condensation of iminoesters of *o*-aminobenzylamines; (*a*) A. R. Katritzky, G. Zhang and J. Jiang, *J. Org. Chem.*, 1995, **60**, 7625; (*b*) M. L. El Efrit, B. Hajjem, H. Zantour and B. Baccar, *Synth. Commun.*, 1996, **26**, 3167.

9 $C_{18}H_{14}O_2N_2F_2Cl_2$, M = 399.38, Z = 2, D_{calc} = 1.46, triclinic, a = 8.788(6), b = 13.147(7), c = 8.763(4) Å, α = 96.347(2), β = 113.782(4), γ = 78.837(2)°, U = 908.300 Å^3, T = 288 K, space group $P\bar{1}$ (no. 2), Z = 2, μ(Mo-Kα) = 3.91 cm^{-1}, 2549 reflections measured. The final R was 0.062, R_w was 0.090. CCDC 182/1766. See http://www.rsc.org/suppdata/cc/b0/b005611l/ for crystallographic files in .cif format.

10 (*a*) B. P. Mundy and M. G. Ellerd, in *Name Reactions and Reagents in Organic Synthesis*, Wiley, New York, 1988, pp 202–203; (*b*) T. Thomson and T. S. Stevens, *J. Chem. Soc.*. 1932, 55; (*c*) I. Coldham, M. L. Middleton and P. L. Taylor, *J. Chem. Soc., Perkin Trans. 1*, 1998, 2817; (*d*) I. E. Marko, *Comp. Org. Syn.*, 1991, **3**, 913.

11 K. Tamura, H. Mizukami, K. Maeda, H. Watanabe and K. Uneyama, *J. Org. Chem.*, 1993, **58**, 32.

Synthesis of quinolines *via* ruthenium-catalysed amine exchange reaction between anilines and trialkylamines

Chan Sik Cho, Byoung Ho Oh, Joon Seok Kim, Tae-Jeong Kim and Sang Chul Shim*

Department of Industrial Chemistry, College of Engineering, Kyungpook National University, Taegu 702-701, Korea. E-mail: scshim@kyungpook.ac.kr

Received (in Cambridge, UK) 24th July 2000, Accepted 25th August 2000
First published as an Advance Article on the web 18th September 2000

Anilines react with an array of trialkylamines in the presence of a catalytic amount of $RuCl_3{\cdot}nH_2O$ and bis(diphenylphosphino)methane together with $SnCl_2{\cdot}2H_2O$ and hex-1-ene as hydrogen acceptor in dioxane at 180 °C to afford the corresponding 2,3-disubstituted quinolines in moderate to good yields.

It is well-known that the quinoline skeleton plays an important role as an intermediate for the design of antimalarial compounds. The structural core of quinolines has generally been synthesised by various conventional named routes such as Skraup, Döbner-von Miller, Conrad-Limpach, Friedlaender and Pfitzinger syntheses. In conjunction with the conventional syntheses, transition metal-catalysed versions utilising various substrates have also been attempted because of facility, efficiency and convenience for the formation of quinolines.[1–4] We recently developed and reported a novel ruthenium-catalysed synthetic approach for the formation of indoles[5] and quinolines[6] *via* a mechanistic amine exchange reaction between primary aromatic amines and functionalised aliphatic amines.[7] However, except for the aforementioned indoles and quinolines, a clear-cut example for the synthesis of N-heterocyclic compounds using the amine exchange reaction seems as yet to be limited to palladium-catalysed synthesis of pyrimidines and imidazoles.[7d] In the course of our continuing studies on ruthenium-catalysed synthesis of N-heterocyclic compounds using the amine exchange reaction, we now report another ruthenium-catalysed synthesis of quinolines from an array of primary aromatic amines and trialkylamines *via* an amine exchange reaction.

The results of several attempted ruthenium-catalysed cyclisations between aniline (**1**) and tripropylamine (**2**) are summarised in Table 1 (Scheme 1). Treatment of **1** with **2** in dioxane in the presence of a catalytic amount of $RuCl_3{\cdot}nH_2O$ (8 mol% based on **2**) and dppm (12 mol% based on **2**) together with $SnCl_2{\cdot}2H_2O$ and hex-1-ene as hydrogen acceptor at 180 °C for 20 h afforded 2-ethyl-3-methylquinoline (**3**) in 63% yield along with *N*-propylaniline (**4**) (28%). This reaction condition was eventually revealed to be the best for obtaining **3** (run 1). The absence of both $SnCl_2{\cdot}2H_2O$ and hex-1-ene stopped the reaction almost completely, but **4** was produced in a considerable yield by an alkyl group transfer between **1** and **2** (run 2). The addition of either $SnCl_2{\cdot}2H_2O$ or hex-1-ene was effective for the formation of quinoline **3** compared with the results in the absence of both $SnCl_2{\cdot}2H_2O$ and hex-1-ene (runs 3,4). Thus, the coexistence of $SnCl_2{\cdot}2H_2O$ and hex-1-ene was essential for the effective formation of **3**. Other hydrogen acceptors such as cyclohexene, hex-1-yne, acetone, and nitrobenzene were almost ineffective for the formation of **3** (runs 5–8).

Table 1 Ruthenium-catalysed reaction of **1** with **2** under various conditions[a]

Run	Hydrogen acceptor	Additive	GLC yield (%)[b] **3**	**4**
1	Hex-1-ene	$SnCl_2{\cdot}2H_2O$	63 (49)[c]	28
2	—	—	1	62
3	—	$SnCl_2{\cdot}2H_2O$	48	27
4	Hex-1-ene	—	14	41
5	Cyclohexene	$SnCl_2{\cdot}2H_2O$	40	20
6	Hex-1-yne	$SnCl_2{\cdot}2H_2O$	6	9
7	Acetone	$SnCl_2{\cdot}2H_2O$	16	11
8	Nitrobenzene	$SnCl_2{\cdot}2H_2O$	9	2

[a] All reactions were carried out with **1** (6 mmol), **2** (1 mmol), $RuCl_3{\cdot}nH_2O$ (0.08 mmol), dppm (0.12 mmol), $SnCl_2{\cdot}2H_2$ (1 mmol), and hydrogen acceptor (10 mmol) in dioxane (10 ml) at 180 °C for 20 h. [b] Based on **2**. [c] Isolated yield.

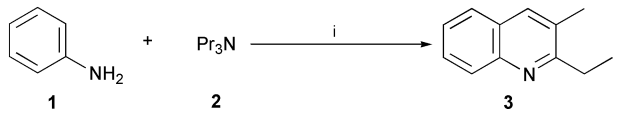

1 2 3

Scheme 1 *Reagents and conditions*: i, $RuCl_3{\cdot}nH_2O$, dppm, dioxane, 180 °C, 20 h.

From the heteroannulation between an array of anilines and trialkylamines under the described controlled reaction conditions above, the corresponding quinolines were also formed in good yields, and several representative results are summarised in Table 2.† The quinoline yield was not decisively affected by the position of the substituent on aniline. With chloroaniline having electron-withdrawing Cl substituent, the product yield

Table 2 Ruthenium-catalysed synthesis of quinolines from anilines and trialkylamines[a]

Anilines	Trialkylamines	Quinolines	Yield (%)[b]
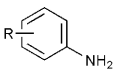		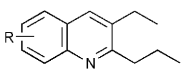	
R = H	Bu_3N	R = H	51
R = 4-Me	Bu_3N	R = 6-Me	52
R = 3-Me	Bu_3N	R = 7-Me	67
R = 2-Me	Bu_3N	R = 8-Me	47
R = 4-OMe	Bu_3N	R = 6-OMe	46
R = 4-Cl	Bu_3N	R = 6-Cl	21
R = 4-Bu	Bu_3N	R = 6-Bu	77
R = 4-*s*-Bu	Bu_3N	R = 6-*s*-Bu	75
R = 3,5-Me	Bu_3N	R = 5,7-Me	76
R = 4-Me	$[(CH_3)_2CH(CH_2)_2]_3N$	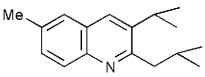	45
		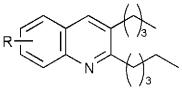	
R = 4-Me	$[CH_3(CH_2)_5]_3N$	R = 6-Me	86
R = 4-*s*-Bu	$[CH_3(CH_2)_5]_3N$	R = 6-*s*-Bu	66
R = 4-Me	$[CH_3(CH_2)_7]_3N$	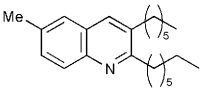	81

[a] All reactions were carried out with aniline (6 mmol), trialkylamine (1 mmol), $RuCl_3{\bullet}nH_2O$ (0.08 mmol), dppm (0.12 mmol), $SnCl_2{\bullet}sH_2O$ (1 mmol), and hex-1-ene (10 mmol) in dioxane (10 ml) at 180 °C for 20 h. [b] Isolated yield based on trialkylamine.

DOI: 10.1039/b005966h

was lower than that when anilines having electron-donating character were used. However, compared with the cases of anilines having electron-donating character, much more *N*-alkylaniline was produced. This result indicates that the reaction proceeds competitively between heteroannulation and *N*-alkylation and the electronic nature of the substituent on aniline determines relative rate. In the case of *m*-toluidine, the quinolines were obtained as a regioisomeric mixture, favoring predominantly the formation of the 7-substituted isomer.

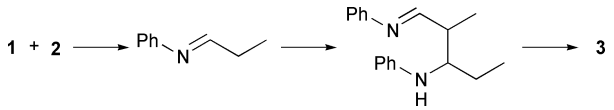

Scheme 2

Although the details of the present reaction including the role of $SnCl_2{\cdot}2H_2O$ are not fully understood, the initial formation of imines by amine exchange reaction between anilines and trialkylamines seems to be a crucial step. Subsequent steps seem to be followed by the known Schiff-base dimerisation[8] and ruthenium-mediated heteroannulation (Scheme 2).[3c] However, one plausible role of $SnCl_2{\cdot}2H_2O$, as a ruthenium–tin complex formed by the insertion of tin(II) chloride into the ruthenium–chloride bond of $RuCl_3{\cdot}nH_2O$, seems to accelerate the initial amine exchange reaction between anilines and trialkylamines.[9] This can be rationalised by the result of Table 1 (runs 1–4). The statistical sum of **3** and **4** reveals the extent of amine exchange reaction between **1** and **2**.[10] Apparently, as shown in Table 1, the alkyl group transfer was effective for the reaction in the presence of $SnCl_2{\cdot}2H_2O$ (runs 1,3) as compared with the reaction in the absence of $SnCl_2{\cdot}2H_2O$ (runs 2,4).

In summary, we have demonstrated that quinolines can be synthesised by reaction of an array of anilines with easily available trialkylamines in the presence of a ruthenium catalyst. The present heteroannulation is a novel synthetic approach leading to quinolines *via* an amine exchange reaction.

This work was supported by Korea Science & Engineering Foundation (KRF-97-05-01-05-01-3) and grant of Post-Doc. (C. S. C.) Program from Kyungpook National University (1999).

Notes and references

† *General experimental procedure*: a mixture of aniline (6 mmol), trialkylamine (1 mmol), $RuCl_3{\cdot}nH_2O$ (0.08 mmol), dppm (0.12 mmol), hex-1-ene (10 mmol) and $SnCl_2{\cdot}2H_2O$ (1 mmol) in dioxane (10 ml) was placed in a pressure vessel. After the system was flushed with argon, the mixture was stirred at 180 °C for 20 h. The reaction mixture was passed through a short silica gel column ($CHCl_3$), poured into brine, extracted with $CHCl_3$ and dried over anhydrous Na_2SO_4. Removal of the solvent left an oil which was separated by column chromatography (silica gel, ethyl acetate–hexane mixture) to give quinolines.

1 For palladium-catalysed versions, see: N. A. Cortese, C. B. Ziegler, B. J. Hrnjez and R. F. Heck, *J. Org. Chem.*, 1978, **43**, 2952; L. S. Hegedus, G. F. Allen, J. J. Bozell and E. L. Waterman, *J. Am. Chem. Soc.*, 1978, **100**, 5800; R. C. Larock and S. Babu, *Tetrahedron Lett.*, 1987, **28**, 5291; R. C. Larock and M.-Y. Kuo, *Tetrahedron Lett.*, 1991, **32**, 569; N. G. Kundu, J. S. Mahanty, P. Das and B. Das, *Tetrahedron Lett.*, 1993, **34**, 1625; A. Arcadi, S. Cacchi, G. Fabrizi, F. Manna and P. Pace, *Synlett*, 1998, 446; S. Cacchi, G. Fabrizi and F. Marinelli, *Synlett*, 1999, 401.

2 For rhodium-catalysed versions, see: S. E. Diamond, A. Szalkiewicz and F. Mares, *J. Am. Chem. Soc.*, 1979, **101**, 490; Y. Watanabe, M. Yamamoto, S. C. Shim, T. Mitsudo and Y. Takegami, *Chem. Lett.*, 1979, 1025; Y. Watanabe, N. Suzuki, S. C. Shim, M. Yamamoto, T. Mitsudo and Y. Takegami, *Chem. Lett.*, 1980, 429; Y. Watanabe, S. C. Shim and T. Mitsudo, *Bull. Chem. Soc. Jpn.*, 1981, **54**, 3460; W. J. Boyle and F. Mares, *Organometallics*, 1982, **1**, 1003; Y. Watanabe, N. Suzuki, Y. Tsuji, S. C. Shim and T. Mitsudo, *Bull. Chem. Soc. Jpn.*, 1982, **55**, 1116.

3 For ruthenium-catalysed versions, see: (*a*) Y. Watanabe, Y. Tsuji and N. Suzuki, *Chem. Lett.*, 1981, 1067; (*b*) Y. Watanabe, Y. Tsuji and Y. Ohsugi, *Tetrahedron Lett.*, 1981, **22**, 2667; (*c*) Y. Watanabe, Y. Tsuji and Y. Ohsugi and J. Shida, *Bull. Chem. Soc. Jpn.*, 1983, **56**, 2452; (*d*) Y. Watanabe, Y. Tsuji and J. Shida, *Bull. Chem. Soc.*, 1984, **57**, 435; (*e*) Y. Tsuji, H. Nishimura, K.-T. Huh and Y. Watanabe, *J. Organomet. Chem.*, 1985, **286**, C44; (*f*) Y. Tsuji, K.-T. Huh and Y. Watanabe, *J. Org. Chem.*, 1987, **59**, 1673.

4 For iron-catalysed version, see: Y. Watanabe, K. Takatsuki, S. C. Shim, T. Mitsudo and Y. Takegami, *Bull. Chem. Soc. Jpn.*, 1978, **51**, 3397.

5 C. S. Cho, H. K. Lim, S. C. Shim, T. J. Kim and H.-J. Choi, *Chem. Commun.*, 1998, 995; C. S. Cho, J. H. Kim and S. C. Shim, *Tetrahedron Lett.*, 2000, **41**, 1811.

6 C. S. Cho, B. H. Oh and S. C. Shim, *Tetrahedron Lett.*, 1999, **40**, 1499; C. S. Cho, B. H. Oh and S. C. Shim, *J. Heterocycl. Chem.*, 1999, **36**, 1175.

7 For transition metal-catalysed amine exchange reactions, see: (*a*) N. Yoshimura, I. Moritani, T. Shimamura and S.-I. Murahashi, *J. Am. Chem. Soc.*, 1973, **95**, 3038; (*b*) S.-I. Murahashi, T. Hirano and T. Yano, *J. Am. Chem. Soc.*, 1978, **100**, 348; (*c*) Y. Shvo and R. M. Laine, *J. Chem. Soc., Chem. Commun.*, 1980, 753; (*d*) S.-I. Murahashi, K. Kondo and T. Hakata, *Tetrahedron Lett.*, 1982, **23**, 229; (*e*) S.-I. Murahashi, N. Yoshimura, T. Tsumiyama and T. Kojima, *J. Am. Chem. Soc.*, 1983, **105**, 5002.

8 M. S. Kharasch, I. Richlin and F. R. Mayo, *J. Am. Chem. Soc.*, 1940, **62**, 494.

9 For transition metal–tin chemistry, see: M. S. Holt, W. L. Wilson and J. H. Nelson, *Chem. Rev.*, 1989, **89**, 11.

10 One equiv. of **3** corresponds to two equiv. of imine since **3** is formed *via* a dimerisation of imine. The amount of **4** is equal to that of imine since **4** is produced by the hydrogenation of imine under catalysis.

ChemComm

The nucleophilic 5-*endo-trig* cyclization of *gem*-difluoroolefins with homoallylic functional groups: syntheses of ring-fluorinated dihydroheteroaromatics

Junji Ichikawa,*[a] Masaki Fujiwara,[a] Yukinori Wada,[a] Tatsuo Okauchi[b] and Toru Minami*[b]

[a] *Department of Chemistry, Graduate School of Science, The University of Tokyo, Hongo, Bunkyo-ku, Tokyo 113-0033, Japan. E-mail: junji@chem.s.u-tokyo.ac.jp; Fax: +81-3-5841-4345; Phone: +81-3-5841-4345*

[b] *Department of Applied Chemistry, Kyushu Institute of Technology, Sensui-cho, Tobata, Kitakyushu 804-8550, Japan*

Received (in Cambridge, UK) 21st June 2000, Accepted 15th August 2000
First published as an Advance Article on the web 18th September 2000

gem-Difluoroolefins bearing homoallylic tosylamido, hydroxy, or mercapto groups undergo intramolecular nucleophilic substitution of the nitrogen, oxygen, or sulfur with loss of fluorine *via* a 5-*endo-trig* process, leading to 2-fluoro-2-pyrrolines, 5-fluoro-2,3-dihydrofurans, or -thiophenes in high yields.

5-*endo-trig* cyclization has long been considered to be a geometrically disfavored process in accord with Baldwin's rules.[1] Efficient examples of the cyclization, however, have been recently devised in radical-initiated[2] and electrophile-driven[3] ring closures. In contrast with these two types of 5-*endo-trig* cyclizations, the corresponding nucleophile-driven ring closure has still rarely been observed in synthetic chemistry.[4,5]

gem-Difluoroolefins possess remarkable reactivity toward nucleophilic substitution for their fluorine atoms *via* addition–elimination processes.[6] As one of its applications, we have recently disclosed that β,β-difluorostyrenes bearing *ortho*-nitrogen, oxygen, or sulfur heteroatoms readily undergo nucleophilic 5-*endo-trig* cyclization to provide ring-fluorinated heteroaromatics: 2-fluorinated indoles, benzo[*b*]furans, and benzo[*b*]thiophenes.[5] Such unique reactivity of *gem*-difluoroolefins is exerted presumably due to (i) the highly polarized C–C double bond (significant single bond character implied by ^{13}C NMR: *ca.* 150 and 90 ppm for CF_2=C), which would allow initial 5-membered ring formation, and (ii) the successive elimination of fluoride ion suppressing the reverse ring opening. In this ring-forming reaction the substrates had a benzene ring as an sp^2-carbon linker between the nucleophilic functional group and the difluoroolefin part.

In order to broaden the scope of this nucleophilic 5-*endo-trig* cyclization and rule out the possibility of an 6π-electrocyclization mechanism, we investigated the reaction of *gem*-difluoroolefins **1**–**3** bearing an *N*-, *O*-, or *S*-functional group which was linked by two sp^3 carbons to the olefinic carbon. Herein we report a facile synthesis of selectively ring-fluorinated pyrroline **5**, dihydrofuran **4**, and dihydrothiophene **6** (Scheme 1), which are difficult to access despite the potential uses of ring-fluorinated heterocycles as components of agrochemicals, pharmaceuticals, and dyestuffs.[7]

gem-Difluoroolefin substrates were designed to bear a nucleophilic nitrogen, oxygen, or sulfur atom at the homoallylic position suitable for substitution in a 5-*endo-trig* fashion. To introduce a functional group (HY) at the *gem*-difluoro-homoallylic position, we tried the regioselective hydroboration of 1,1-difluoro-1,3-dienes **7**, which were readily prepared from 2,2,2-trifluoroethyl toluene-*p*-sulfonate and vinyl halides in a one-pot operation according to our method.[8] The electron-rich, non-fluorinated double bond in **7** might be more reactive toward borane reagents. Treatment of difluorodienes **7** with 9-borabicyclo[3.3.1]nonane (9-BBN) under reflux in THF selectively promoted hydroboration as expected to generate difluorohomoallylboranes, and successive treatment with alkaline aqueous hydrogen peroxide gave *gem*-difluorohomoallyl alcohols **1a**–**c** in good yields (Scheme 2). The corresponding nitrogen- and sulfur-containing substrates **2a**–**e**, **3a**,**b** were easily obtained from **1** as shown in Scheme 2.

The cyclization of homoallyl alcohols **1a**,**b** was attempted by treatment with 1.2 eq. of NaH in several solvents. While the use DMPU or NMP gave no cyclized products, DMF, DMA, or DMSO successfully promoted the 5-*endo-trig* cyclization to afford 5-fluoro-2,3-dihydrofurans **4a**,**b** in good yields (Table 1, Entries 1,2).[9]† KH was less effective than NaH, and high-dilution conditions ([**1a**] = 0.03 mol L^{-1}) raised the yield by 10% compared to the case of [**1a**] = 0.2 mol L^{-1}.

Moreover, we examined the 5-*endo-trig* cyclization of the substrates with *N*-nucleophiles under similar conditions. Whereas *N*-unsubstituted and *N*-butylhomoallylamines **2c**,**d** did not cyclize, the *N*-phenyl substrate **2e** afforded 4-methyl-1-phenyl-3-(3-phenylpropyl)-2-pyrrolidone **8** *via* hydrolysis of

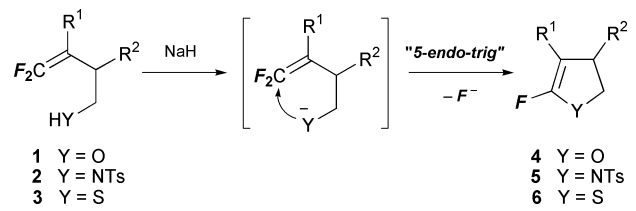

Scheme 1 Nucleophilic 5-*endo-trig* cyclization of *gem*-difluoroolefins **1**–**3**.

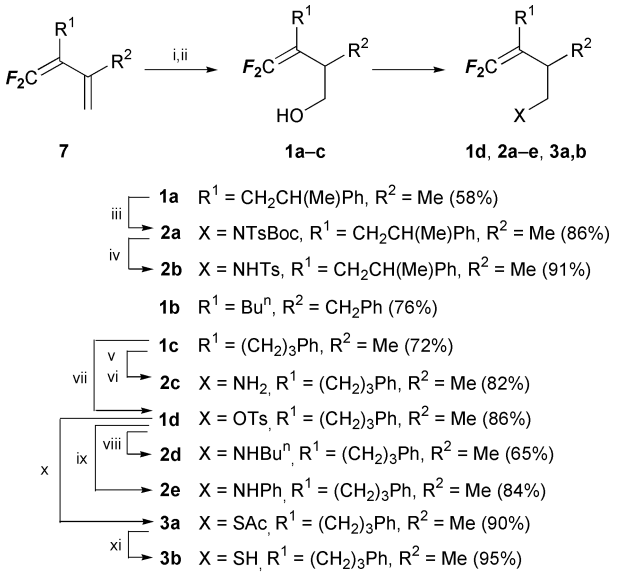

Scheme 2 Preparation of *gem*-difluoroolefins **1**–**3**. *Reagents and conditions*: i, 9-BBN (1.1–1.4 eq.), THF, reflux, 6–7 h; ii, aq.H_2O_2, aq. NaOH, 0 °C, 2 h; iii, BocNHTs (1 eq.), PPh_3 (1 eq.), $EtO_2CN{=}NCO_2Et$ (1 eq.), THF, rt, 2 h; iv, CF_3CO_2H (15 eq.), CH_2Cl_2, rt, 2 h; v, phthalimide (1 eq.), PPh_3 (1 eq.), $EtO_2CN{=}NCO_2Et$ (1 eq.), THF, rt, 2 h; vi, $NH_2NH_2{\bullet}H_2O$ (2 eq.), EtOH, reflux, 2 h; vii, TsCl (1 eq.), Py, rt, 8 h; viii, Bu^nNH_2 (26 eq.), reflux, 6 h; ix, $PhNH_2$ (26 eq.), reflux, 6 h; x, AcSNa (1 eq.), DMF, 70 °C, 3 h; xi, K_2CO_3 (1 eq.), MeOH, 0 °C, 1 h.

DOI: 10.1039/b004978f

Table 1 Synthesis of ring-fluorinated dihydroheteroaromatics **4**–**6**[a]

Entry	YH	R^1	R^2	Substrate	Base (eq.)	Time	Product	Yield (%)[b]
1	OH	$CH_2CH(Me)Ph$	Me	**1a**[c]	NaH (1.2)	7 h	**4a**[c]	67
2	OH	Bu^n	CH_2Ph	**1b**	NaH (1.2)	11 h	**4b**	62
3	PhNH	$(CH_2)_3Ph$	Me	**2e**	NaH (1.1)	24 h	**8**	62
4	TsNH	$CH_2CH(Me)Ph$	Me	**2b**[c]	NaH (1.1)	4 d	**5**[c]	80
5	SH	$(CH_2)_3Ph$	Me	**3b**	NaH (1.1)	4 h	**6**	76
6	SC(O)Me	$(CH_2)_3Ph$	Me	**3a**	NaOMe (1.0)	8 h	**6**	69

[a] The reaction was conducted in DMF at 90 °C. [Substrate] = 0.02–0.03 mol L^{-1}. [b] Isolated yield. [c] 1:1 Diastereomer mixture.

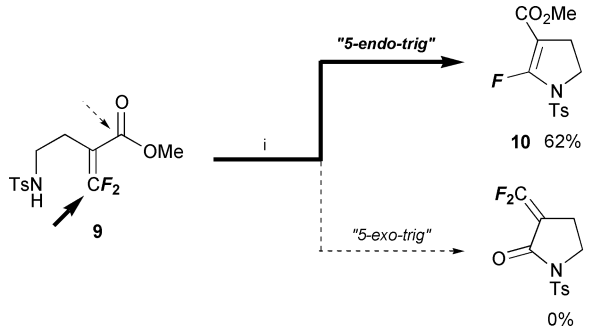

Scheme 3 Competitive cyclization: 5-*endo-trig vs*. 5-*exo-trig Reagents and conditions*: i, NaH (1.1 eq.), DMF, 100 °C, 0.3 h.

the expected 2-fluoropyrroline (Entry 3). The *N*-4,4-difluorobut-3-enyltoluene-*p*-sulfonamide **2b** underwent the desired ring closure to give 2-fluorinated pyrroline **5** in 80% yield (Entry 4).[10]‡

As a further example of the cyclization, the intramolecular substitution of sulfur nucleophiles (which Baldwin's rules allow for the normally disfavored 5-*endo-trig* process) was also examined.[1b] The reaction of **3b** under similar conditions to those for **1** and **2** provided 5-fluorinated dihydrothiophene **6** in 76% yield (Entry 5).[11] In addition, treatment of thioacetic *S*-acid ester **3a** with sodium methoxide allowed the cyclization *via in situ* generated thiolate to give **6** (Entry 6).§

In order to demonstrate the favored nature of 5-*endo-trig* cyclization in *gem*-difluoroolefins, we tried the competitive reaction between 5-*endo-trig* and 5-*exo-trig* processes. The β,β-difluoro-α,β-unsaturated ester **9** bearing a 2-toluene-*p*-sulfonamidoethyl group was designed as a substrate which could undergo the Michael reaction and the transacylation *via* 5-*endo-trig* and 5-*exo-trig* processes, respectively. Compound **9** was prepared by the S_N2' reaction of methyl 2-(trifluoromethyl)propenoate[12] with benzyloxymethylcopper[13] and successive deprotection of the benzyl group, followed by the introduction of an NHTs group according to the same procedure for **2b**. On treatment of **9** with NaH in DMF, the 5-*endo-trig* cyclization proceeded to lead exclusively to the 2-fluorinated pyrroline derivative **10** as shown in Scheme 3.¶‖

In conclusion, normally 'disfavored' 5-*endo-trig* ring closures are successfully achieved in the intramolecular addition–elimination reaction of *gem*-difluoroolefins bearing nucleophilic heteroatoms linked by two sp^3 carbons to the vinylic carbon as well as two sp^2 carbons.[5] Thus, *gem*-difluorohomoallylamine, alcohol, and thiol derivatives open a new way to the syntheses of selectively ring-fluorinated heterocyclic compounds.

We gratefully acknowledge the financial support for this research by a grant from Central Glass Co., Ltd. to J. I. We also thank F-Tech, Inc. for a generous gift of 2-(trifluoromethyl)propenoic acid.

Notes and references

† **4b**: δ_F (471 MHz, $CDCl_3$–C_6F_6) 42.4 (1F, s).
‡ **5**: δ_F (471 MHz, $CDCl_3$–C_6F_6) 36.2 (0.5F, s), 36.6 (0.5F, s).
§ **6**: δ_F (471 MHz, $CDCl_3$–C_6F_6) 35.7 (1F, br s).
¶ The fluorine-free analogue, dimethyl 4-methyleneglutamate was reported to cyclize to 5-methoxycarbonyl-3-methylene-2-pyrrolidone *via* 5-*exo-trig* pathway without formation of the 5-*endo-trig* product.[1b,14]
‖ **10**: δ_F (471 MHz, $CDCl_3$–C_6F_6) 61.8 (1F, t, J_{FH} = 4.8 Hz).

1 (*a*) J. E. Baldwin, *J. Chem. Soc., Chem. Commun.*, 1976, 734; (*b*) J. E. Baldwin, J. Cutting, W. Dupont, L. Kruse, L. Silberman and R. C. Thomas, *J. Chem. Soc., Chem. Commun.*, 1976, 736; (*c*) J. E. Baldwin, R. C. Thomas, L. I. Kruse and L. Silberman, *J. Org. Chem.*, 1977, **42**, 3846.
2 For recent reports, see: A. J. Clark, C. P. Dell, J. M. Ellard, N. A. Hunt and J. P. McDonaph, *Tetrahedron Lett.*, 1999, **40**, 8619; D. T. Davies, N. Kapur and A. F. Parsons, *Tetrahedron Lett.*, 1999, **40**, 8615 and references cited therein; H. Ishibashi, A. Toyao and Y. Takeda, *Synlett*, 1999, 1468 and references cited therein; S. Bogen, M. Gulea, L. Fensterbank and M. Malacria, *J. Org. Chem.*, 1999, **60**, 4920 and references cited therein; J. Cassayre and S. Z. Zard, *Synlett*, 1999, 501; M. Ikeda, M. Hamada, T. Yamashita, K. Matsui, T. Sato and H. Ishibashi, *J. Chem. Soc., Perkin Trans. 1*, 1999, 1949; A. Kittaka, T. Asakura, T. Kuze, H. Tanaka, N. Yamada, K. T. Nakamura and T. Miyasaka, *J. Org. Chem.*, 1999, **64**, 7081; Y. Nonami, J. Baran, J. Sosnicki, H. Mayr, A. Masuyama and M. Nojima, *J. Org. Chem.*, 1999, **64**, 4060; C. Chatgilialoglu, T. Gimisis and G. P. Spada, *Chem. Eur. J.*, 1999, **5**, 2866; J. Gao and J. Rusling, *J. Org. Chem.*, 1998, **63**, 218.
3 For recent reports, see: A. D. Jones, D. W. Knight, A. L. Redfern and J. Gilmore, *Tetrahedron Lett.*, 1999, **40**, 3267 and references cited therein; S. B. Bedford, K. E. Bell, F. Bennett, C. J. Hayes, D. W. Knight and D. E. Shaw, *J. Chem. Soc., Perkin Trans. 1*, 1999, 2143 and references cited therein; F. Bravo, M. Kassou and S. Castillón, *Tetrahedron Lett.*, 1999, **40**, 1187.
4 D. Craig, N. J. Ikin, N. Mathews and A. M. Smith, *Tetrahedron*, 1999, **55**, 13471 and references cited therein. For the 5-*endo-trig* process onto a π-allylpalladium system, see: S. Thorimbert and M. Malacria, *Tetrahedron Lett.*, 1998, **39**, 9659. For the *ab initio* calculation on the cyclization of 4,4-difluorobut-3-en-1-ol, see: T. Yamazaki, S. Hiraoka, J. Sakamoto and T. Kitazume, *J. Phys. Chem. A*, 1999, **103**, 6820; T. Yamazaki, S. Hiraoka, J. Sakamoto and T. Kitazume, *J. Fluorine Chem.*, 2000, **101**, 309.
5 J. Ichikawa, Y. Wada, T. Okauchi and T. Minami, *Chem. Commun.*, 1997, 1537.
6 L. G. Sprague, K. B. Baucom, S. F. Sellers and R. A. DuBoisson, in *Chemistry of Organic Fluorine Compounds II*, ed. M. Hudlicky and A. E. Pavlath, ACS Monograph 187, American Chemical Society, Washington, DC, 1995, p. 729.
7 M. J. Silvester, *Adv. Heterocyclic Chem.*, 1994, **59**, 1; L. G. Sprague, K. B. Baucom, S. F. Sellers and R. A. DuBoisson, *Aldrichim. Acta*, 1991, **24**, 31; *Organofluorine Chemistry, Principles and Commercial Applications*, ed. R. E. Banks, B. E. Smart and J. C. Tatlow, Plenum Press, New York, 1994.
8 J. Ichikawa, C. Ikeura and T. Minami, *Synlett*, 1992, 739.
9 For the synthesis of fluorofurans, see: A. K. Forrest and P. J. O'Hanlon, *Tetrahedron Lett.*, 1995, **36**, 2117; K. Burger and B. Helmreich, *J. Chem. Soc., Chem. Commun.*, 1992, 348; H. L. Sham and D. A. Betebenner, *J. Chem. Soc., Chem. Commun.*, 1991, 1134.
10 For the synthesis of fluoropyrroles, see: M. S. Novikov, A. F. Khlebnikov, E. S. Sidorina and R. R. Kostikov, *J. Fluorine Chem.*, 1998, **90**, 117 and references cited therein.
11 For the synthesis of fluorothiophenes, see: D. F. Andrés, E. G. Laurent and B. S. Marquet, *Tetrahedron Lett.*, 1997, **38**, 1049 and references cited therein.
12 T. Kitazume and T. Ohnogi, *Synthesis*, 1988, 615; T. Fuchikami, Y. Shibata and Y. Suzuki, *Tetrahedron Lett.*, 1986, **27**, 3173.
13 D. K. Hutchinson and P. L. Fuchs, *J. Am. Chem. Soc.*, 1987, **109**, 4930.
14 For examples where *N*-substituents played an important role, see: B. Tarnchompoo, C. Thebtaranonth and Y. Thebtaranonth, *Tetrahedron Lett.*, 1987, **28**, 6675; A. Padwa and B. H. Norman, *J. Org. Chem.*, 1990, **55**, 4801.

ChemComm

A novel method for the synthesis of high performance silicalite membranes

Xiao Lin, Hidetoshi Kita and Ken-ichi Okamoto

Department of Advanced Materials Science and Engineering, Faculty of Engineering, Yamaguchi University, Ube, Yamaguchi 755-8611, Japan. E-mail: okamotok@po.cc.yamaguchi-u.ac.jp; Fax: +81-836-85-9601

Received (in Cambridge, UK) 28th June 2000, Accepted 25th August 2000
First published as an Advance Article on the web 18th September 2000

Silicalite membranes have been successfully synthesized onto mullite tubular supports by *in-situ* hydrothermal synthesis for only 8 h of crystallization, and showed high ethanol permselectivity for pervaporation of ethanol/water mixtures.

Zeolite membranes have strong potential applications for gas separation, pervaporation, and membrane reactors, especially MFI (silicalite and ZSM-5) membranes. On the other hand, less attention has been paid to pervaporation separation through zeolite membranes, even though zeolite A membranes are commercialized on a large scale by Mitsui Engineering Co. Ltd, in cooperation with Yamaguchi University, for dehydration of organic liquids. Silicalite membranes with hydrophobic properties exhibit preferentially selective permeation of organic components in contrast to zeolite A membranes. In 1994, Sano *et al.*[1] first reported that a separation factor of about 60 for ethanol (EtOH)/water mixtures was obtained for their silicalite membrane formed on a stainless steel disk with a crystal layer thickness of 400–500 μm, and further improved the separation factor up to 120 for 144 h crystallization in 1998.[2] They also prepared silicalite membranes on alumina disks, but their selectivity of 19 was much lower compared with that on the stainless steel support. Later, several groups tried to synthesize MFI membranes on tubular supports and made some progress. For example, separation factors of 11–44 were achieved.[3–5] However, the pervaporation performance of these membranes reported in the literature is still not good enough for industrial applications. Furthermore, various strategies have been successfully developed for the production of good quality zeolite membranes on various porous supports,[6–9] especially on flat discs. Considering practical applications, preparation of reproducible and high performance MFI zeolite membranes on cheaper porous tubular supports on a large scale, in which the cost greatly reduces, is still a challenge. In this paper, we report a simple and effective method to synthesize high performance silicalite membranes on mullite tubular supports for the shortest hydrothermal synthesis time among all the published papers.

A clear solution for the synthesis of silicalite membranes was prepared by mixing and stirring tetraethyl orthosilicate (TEOS, Aldrich), tetrapropylammonium hydroxide (TPAOH) and water at room temperature for 1 h. The resultant molar composition is SiO_2:0.17TPAOH:120H_2O. In such a Na-free medium, less gelation would affect the crystal growth onto the surface of a seeded support. A mullite porous tube with a pore size of 1 μm was chosen as the support because it is much cheaper than pure α-Al_2O_3 tubes, especially at pore sizes of less than 1 μm. Before *in-situ* hydrothermal synthesis, mullite tubes were simply rubbed with a slurry of H-ZSM-5 (Si/Al = ∞, Tosho Comp.). This seeding method was first used for the synthesis of zeolite A membranes by Kita *et al.*[10] which has been identified as an effective and reproducible seeding method.[11,12] The seeded support was vertically immersed in the synthesis solution. Crystallization was carried out at 175 °C or 185 °C for 8 h. After crystallization, the sample was taken out, washed carefully with hot distilled water, dried at 100 °C for several hours, and then calcined at 400 °C for 20–40 h at a heating rate of 1 °C min^{-1}.

The SEM surface view of the mullite support shown in Fig. 1 clearly indicates that the morphology is quite different from that of pure α-Al_2O_3. After hydrothermal treatment for 8 h at 175 °C, a well inter-grown silicalite crystal layer with a thickness of about 10 μm was formed on the seeded support, as shown in Fig. 2.

The pervaporation (PV) tests for EtOH/water mixtures were carried out at 60 °C. The effective membrane area was about 10 cm^2. The permeation side was kept under vacuum. The flux was calculated by weighing the condensed permeate. The separation factor was determined as $\alpha_{A/B} = (Y_A/Y_B)/(X_A/X_B)$, where X_A, X_B, Y_A, and Y_B denote the mass fractions of components A and B in the feed and permeate sides. The pervaporation results for the silicalite membranes synthesized at 175 °C and 185 °C for 8 h are listed in Table 1. Table 1 clearly shows that the pervaporation performance of our silicalite membranes was significantly improved compared with the previous results and also the membranes were prepared in a

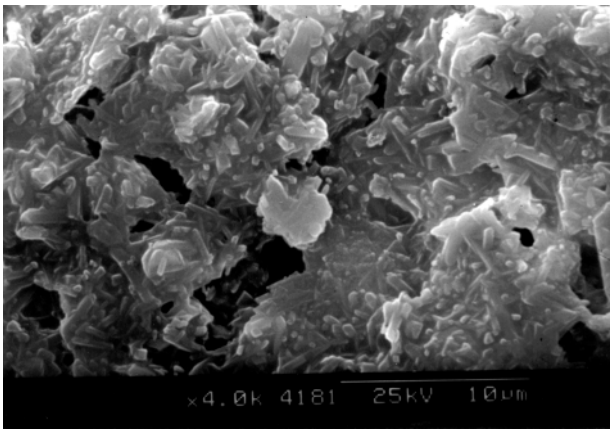

Fig. 1 SEM view of the surface of the mullite tube.

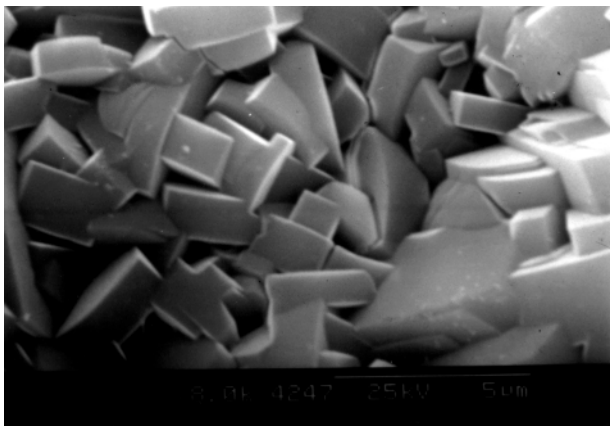

Fig. 2 SEM view of the surface of the silicalite membrane synthesized at 175 °C for 8 h.

DOI: 10.1039/b005180m

Table 1 Pervaporation performance through the silicalite membranes for EtOH/H_2O mixtures at 60 °C

Member No	Synthesis conditions		EtOH/H_2O (10 wt% EtOH)	
	T/°C	t/h	Flux/kg m^{-2} h^{-1}	Separation factor
Si-1	175	8	2.34	56
Si-2	175	8	2.55	72
Si-3	185	8	1.67	65
Si-4	185	8	1.58	64

highly reproducible manner. This suggests that silicalite membranes with both high flux and high separation factors can be prepared under suitable synthesis conditions, which has strong potential applications in the preferential separation of organic compounds from aqueous solutions. A systematic investigation of membrane preparation and membrane performance, including gas and vapor permeation, is under way.

This work was supported by the Proposal-based New Industry Creative Type Technology R&D Promotion Program (98Ec-04-002) from the New Energy and Industrial Technology Development Organization (NEDO) of Japan.

Notes and references

1 T. Sano, H. Yanagishita, Y. Kiyozumi, F. Mizukami and K. Haraya, *J. Membr. Sci.*, 1994, **95**, 221.
2 H. Matsuda, H. Yanagishita, D. Kitamoto, T. Nakane, K. Haraya, N. Koura and T. Sano, *Membrane*, 1998, **23**, 259 (in Japanese).
3 Q. Liu, R. D. Noble, J. L. Falconer and H. H. Funke, *J. Membr. Sci.*, 1996, **117**, 163.
4 H. Kita, *Proceedings of International Workshop on Zeolitic Membranes and Films, Gifu, Japan*, 1998, p. 43.
5 M. Kondo, T. Nakane, H. Yanagishita, T. Sano, H. Kita and K. Okamoto, *Proceedings of 5th International Conference on Inorganic Membranes, Nagoya, Japan*, 1998, p. 528.
6 W. J. Bakker, F. Kapteijn, J. Poppe and J. A. Moulijn, *J. Membr. Sci.*, 1996, **117**, 57.
7 Z. A. P. Vroon, K. Keizer, M. J. Gilde, H. Verweij and A. J. Burggraaf, *J. Membr. Sci.*, 1996, **113**, 293.
8 V. A. Tuan, J. L. Falconer and R. D. Noble, *Ind. Eng. Chem. Res.*, 1999, **38**, 3635.
9 G. Xomeritakis, A. Gouzinis, S. Nair, T. Okubo, M. He, R. M. Overney and M. Tsapatsis, *Chem. Eng. Sci.*, 1999, **54**, 3521.
10 H. Kita, K. Horii, Y. Ohtoshi and K. Okamoto, *J. Mater. Sci. Lett.*, 1995, **14**, 206.
11 H. Kita, T. Inoue, H. Asamura, K. Tanaka and K. Okamoto, *Chem. Commun.*, 1997, 45.
12 M. Kondo, M. Komori, H. Kita and K. Okamoto, *J. Membr. Sci.*, 1997, **133**, 133.

Insertion of extra-framework Al into the framework of mesoporous MCM-41 aluminosilicates

Robert Mokaya

School of Chemistry, University of Nottingham, University Park, Nottingham, UK NG7 2RD. E-mail: r.mokaya@nottingham.ac.uk

Received (in Cambridge, UK) 3rd July 2000, Accepted 25th August 2000
First published as an Advance Article on the web 18th September 2000

Virtually all octahedrally coordinated (extra-framework) Al in calcined Al-grafted MCM-41 materials can be inserted into (tetrahedral) framework positions upon treatment with an aqueous solution of NH_4OH; the insertion of Al into the framework is accompanied by an increase in (Brønsted) acidity and ion exchange capacity.

The recent synthesis of structurally well ordered mesoporous molecular sieves with uniform pores[1] has generated considerable research interest in the preparation and use of heteroatom containing mesoporous silicas as heterogeneous catalysts.[1,2] The incorporation of Al into mesoporous silicas is of particular interest as it gives rise to materials with solid acid and cation exchange properties. The acid and ion exchange sites are primarily associated with the presence of tetrahedrally coordinated Al in framework positions within the silica matrix. Al may be introduced into mesoporous silicas by direct synthesis[4,5] or by post-synthesis grafting methods.[6–8] Both methods, however tend to result in (calcined) materials with a significant proportion of extra-framework (octahedrally coordinated) Al.[4–8] It is desirable, with respect to acid catalysis and ion exchange properties, to maximise the proportion of Al in framework (tetrahedral) positions. So far no method has been described for modifying the siting of Al in calcined mesoporous aluminosilicates so as to maximise the amount (or proportion) of Al in framework positions. Reinsertion of extra-framework Al (EFAL) into framework positions has been previously described for dealuminated Y zeolites *via* hydrothermal treatment of the zeolite in an aqueous solution of KOH.[9] However, such treatment is not feasible for mesoporous aluminosilicates because it is too severe. The relatively fragile mesoporous frameworks would readily dissolve in the highly basic (pH = 13.5) KOH solution. Here we report a method *via* which virtually all octahedrally coordinated (extra-framework) Al in calcined Al-grafted MCM-41 materials can be inserted into (tetrahedral) framework positions. The method, which involves treatment of the mesoporous aluminosilicates with an aqueous solution of NH_4OH (pH $\approx$ 11.1), can be performed either at room temperature (30 °C) or at a range of temperatures up to 80 °C. NH_4OH was chosen due to the well known stability of Al-grafted MCM-41 materials at pH = 11,[10] and also because NH_4^+ is potentially an acid generating cation (and therefore no further ion exchange would be required to maintain Brønsted acidity). Our findings show that insertion of EFAL into the framework increases the proportion of tetrahedrally coordinated Al and is accompanied by an increase in acidity and ion exchange capacity. Although the Al insertion method described here is generally applicable to any mesoporous aluminosilicates, this preliminary report concentrates on Al-grafted materials because they offer distinct advantages over directly synthesised materials with respect to accessibility to active (Al) sites, structural ordering and stability.[6–8,10–13]

The purely siliceous MCM-41 from which the Al-grafted materials were derived was prepared using normal procedures. The Al-grafted materials were prepared *via* two methods.[13] In the first method, 2.0 g of pure silica MCM-41 were dispersed in 50 ml dry hexane and added to 150 ml dry hexane containing the appropriate amount of aluminium isopropoxide to give a grafting gel Si/Al ratio of 5. The resulting mixture was stirred for 10 min and allowed to react at room temperature for 30 h. The obtained powder was filtered off, washed with dry hexane, dried at room temperature and calcined at 550 °C for 4 h. The resulting material with a bulk Si/Al ratio of 4.6 was designated CAP5.[13] In the second method, pure silica MCM-41 was added to a 50 ml solution of 0.48 mol l^{-1} (w.r.t. Al) aluminium chlorhydrol at 80 °C and stirred for 2 h (at 80 °C). The resulting solid was otained by filtration and thoroughly washed with distilled water (until free of Cl^- ions), dried at room temperature and calcined in air at 550 °C for 4 h. To increase the amount of Al, the 'graft–wash–calcine' cycle was repeated once. The resulting material, designated CAH5, had a bulk Si/Al ratio of 4.7.[13] The calcined Al-grafted samples were then stirred in 1 M NH_4OH at a solution to solid ratio of 100 ml g^{-1}. At 30 °C, four 'stir–wash–dry' cycles were performed with each stirring lasting for 2 h. At 80 °C, the stirring was performed only once for 16 h. In both cases the NH_4OH-treated samples were thoroughly washed with distilled water and dried at 150 °C.

Fig. 1 shows the ^{27}Al MAS NMR spectra of CAP5 and CAH5 before and after treatment with NH_4OH. The untreated samples contain both tetrahedrally coordinated (δ 53) framework Al and octahedrally coordinated (δ 0) extra-framework Al. The proportion of tetrahedrally coordinated Al, calculated from the NMR spectra, is approximately 61% and 55% for CAP5 and CAH5 respectively. For both samples the proportion of tetrahedral Al increases significantly after treatment with NH_4OH. Indeed, after treatment with NH_4OH at 30 °C, virtually all (> 95%) of the Al is in tetrahedral coordination (Fig. 1b, e). Treatment in NH_4OH at 80 °C for 16 h appears to be slightly less effective in inserting the EFAL into framework positions probably due to its severity which affects structural integrity (see later). It is clear from Fig. 1 that the nature and environment of the Al in CAP5 and CAH5 is transformed by the relatively mild treatments in NH_4OH. Elemental analysis of the NH_4OH-

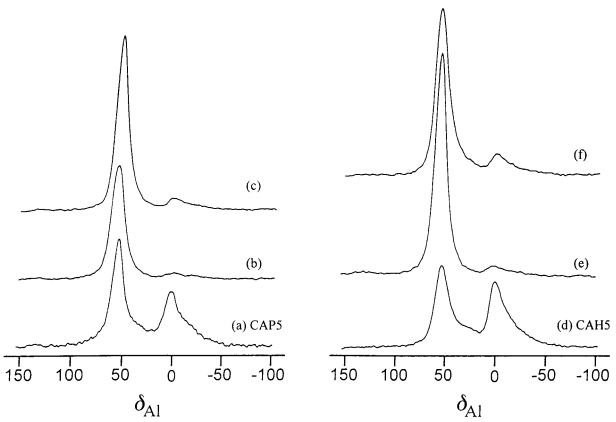

Fig. 1 ^{27}Al MAS NMR spectra of Al-grafted materials before and after treatment with NH_4OH; (a) CAP5, (b) CAP5 treated at 30 °C, (c) CAP5 treated at 80 °C, (d) CAH5, (e) CAH5 treated at 30 °C and (f) CAH5 treated at 80 °C.

DOI: 10.1039/b005316n

Table 1 Elemental composition, textural properties and acidity of the studied materials

Sample	Si/Al	Surface area/ $m^2\ g^{-1}$	Pore volume/ $cm^3\ g^{-1}$	Acidity/mmol $H^+\ g^{-1}$
CAP5	4.6	791	0.74	0.81
30 °C[a]	4.9	728	0.67	1.15
80 °C[a]	4.8	428	0.45	1.09
CAH5	4.7	740	0.52	0.95
30 °C[b]	4.9	620	0.55	1.16
80 °C[b]	4.3	490	0.36	1.11

[a] CAP5 treated with NH_4OH at the temperature shown. [b] CAH5 treated with NH_4OH at the temperature shown.

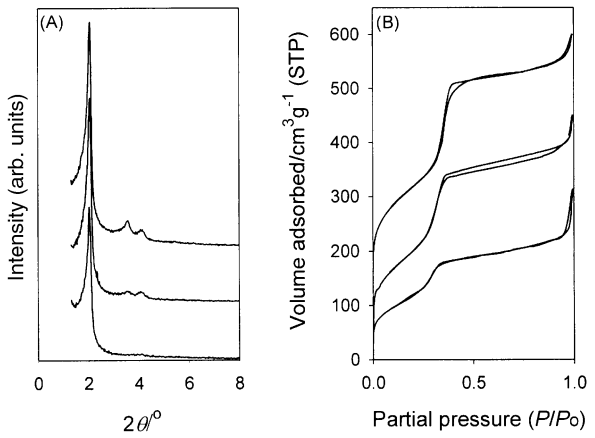

Fig. 2 Powder XRD patterns (A) and nitrogen sorption isotherms (B) of CAP5 before and after treatment with NH_4OH; CAP5 (top), CAP5 treated at 30 °C (middle) and CAP5 treated at 80 °C (bottom).

treated samples was performed in order to find out whether any preferential leaching of Si or Al occurred during the treatments. The Si/Al ratios of the NH_4OH-treated samples are given in Table 1. In all cases the elemental composition remained unchanged, *i.e.*, all the Si and Al was retained during NH_4OH treatment. This indicates that the increase in the tetrahedral/octahedral Al ratio observed from the MAS NMR spectra was due to insertion of EFAl into the framework rather than preferential dissolution of octahedral Al.

The acid contents of the Al-grafted samples and their NH_4OH-treated analogues are given in Table 1. The acid content was determined using thermally programmed desorption of cyclohexylamine.[13] Prior to analysis, the base (cyclohexylamine) containing samples were heated at 80 °C for 2 h. The acidity data indicate that an increase in the proportion of tetrahedral Al following NH_4OH treatment is accompanied by an increase in acid content. The increase is particularly remarkable for CAP5. Since the elemental composition remained unchanged (*i.e.* the amount of Al per gram of sample remained the same), the only explanation for the increased acidity is insertion of EFAL into acid generating framework sites. The insertion of EFAL into the framework is expected to specifically increase the proportion of Brønsted acid sites. Indeed, using FTIR spectroscopy of adsorbed pyridine (see ref. 17 for details) we observed a significant increase in the Brønsted acid content of NH_4OH-treated samples. For example, after evacuation at 100 °C,[14] the Brønsted acid content of CAH5 increased from 34 to 72 μmol g^{-1} and the Brønsted/Lewis acid ratio increased from 0.27 to 0.58. The same trend was observed after evacuation at 200 and 300 °C.[14] Furthermore, a preliminary check on ion exchange properties indicated that NH_4OH-treated samples exhibit substantially higher cation exchange capacities compared to the untreated samples; M^+/Al ratios of the Al-grafted materials (obtained following ion exchange) increased from *ca*. 0.4 to as high as 0.9 after treatment with NH_4OH at 30 °C. We were also able to observe Brønsted acid bridging OH groups in the FTIR spectra of NH_4OH-treated samples. These observations clearly point to the insertion of EFAL into framework positions rather than the formation of a separate alumina phase in which the Al is tetrahedrally coordinated.

The XRD patterns and sorption isotherms (obtained using a Coulter SA3100 Sorptometer after evacuating overnight at 200 °C) for CAP5 and its NH_4OH-treated analogues are shown in Fig. 2A. The insertion of Al into the framework (especially at 30 °C) does not appear to be detrimental to the structural ordering. CAP5 treated at 30 °C exhibits an XRD pattern and sorption isotherm comparable to that of the parent material. We note that CAP5 treated at 30 °C is very well ordered for an MCM-41 material with such a low (*ca*. 4.9) framework Si/Al ratio. Treatment at 80 °C results in rather more structural degradation; however, the resulting material still retains some hexagonal ordering and mesopore uniformity. The greater structural degradation for the 80 °C treated CAP5 may be the cause of the slightly less efficient insertion of Al into the framework observed from the MAS NMR spectra in Fig. 1. Table 1 shows the textural properties for the Al-grafted materials and their NH_4OH treated analogues. In general Al insertion results in a decrease in the surface area and pore volume. The decrease is modest at 30 °C but greater for materials treated at 80 °C. Note, however, that the effects of 80 °C NH_4OH treatment are reported here as an upper limit (with respect to severity of the treatment) and to show the versatility of the insertion method.

The mechanism for Al insertion most likely involves the dissolution of EFAL and the formation of aluminate ions that are inserted into the framework.[9] This is possible due to the amorphous nature of the pore walls and the presence of silanols (which may act as anchoring sites) on the pore wall surfaces. The pH of the basic solution used is important; a strongly basic solution dissolves both the EFAL and the mesoporous framework while a mildly basic solution does not dissolve the EFAL and is therefore not effective in Al insertion. Indeed when the strongly basic KOH solution (pH = 13.5) was used, the Al-grafted materials were destroyed. On the other hand, Al-grafted materials treated with KNO_3 (pH ≈ 8.8) remained virtually unchanged; neither structural ordering nor Al siting was affected. It appears therefore that NH_4OH (pH ≈ 11.1) is just right with respect to both the dissolution (and insertion) of EFAL into the framework and the preservation of structural integrity of the mesoporous framework. At the moment we have no evidence that the nature of the cation affects the insertion process.

The author is grateful to the EPSRC for an Advanced Fellowship. The assistance of Dr Y. Khimyak with NMR measurements is gratefully acknowledged.

Notes and references

1 C. T. Kresge, M. E. Leonowicz, W. J. Roth, J. C. Vartuli and J. S. Beck, *Nature*, 1992, **359**, 710.
2 A. Corma, *Chem. Rev.*, 1997, **97**, 2373.
3 S. Biz and M. L. Occelli, *Catal. Rev., Sci. Eng.*, 1998, **40**, 329.
4 A. Corma, V. Fornés, M. T. Navarro and J. Pérez-Pariente, *J. Catal.*, 1994, **148**, 569.
5 R. Mokaya, W. Jones, Z. Luan, M. D. Alba and J. Klinowski, *Catal. Lett.*, 1996, **37**, 113.
6 R. Mokaya and W. Jones, *Chem. Commun.*, 1997, 2185.
7 R. Ryoo, S. Jun, J. M. Kim and M. J. Kim, *Chem. Commun.*, 1997, 2225.
8 R. Mokaya and W. Jones, *J. Mater. Chem.*, 1999, **9**, 555.
9 X. Liu, J. Klinowski and J. M. Thomas, *J. Chem. Soc., Chem. Commun.*, 1986, 582; H. Hamdan, B. Sulikowski and J. Klinowski, *J. Phys. Chem.*, 1989, **93**, 350.
10 S. C. Shen and S. Kawi, *Chem. Lett.*, 1999, 1293.
11 R. Mokaya and W. Jones, *Phys. Chem. Chem. Phys.*, 1999, **1**, 207.
12 R. Mokaya and W. Jones, *Chem. Commun.*, 1998, 1839.
13 R. Mokaya, *Angew. Chem., Int. Ed.*, 1999, **38**, 2930.
14 R. Mokaya and W. Jones, *J. Catal.*, 1997, **172**, 211.

Synthesis of FER type zeolite with tetrahydrofuran as the template

Guo-qing Guo,[ab] Yao-jun Sun[c] and Ying-cai Long[a]*

[a] *Chemistry Department of Fudan University, Shanghai 200433, P.R. China. E-mail: yclong@fudan.edu.cn*
[b] *Institute of Beijng Yanshan Petrochemical Corporation, Beijing 102500, P.R. China*
[c] *Center of Analysis and Measurement of Fudan University, Shanghai 200433, P.R. China*

Received (in Cambridge, UK) 6th July 2000, Accepted 29th August 2000
First published as an Advance Article on the web 18th September 2000

FER (ferrierite) zeolite was hydrothermally crystallized in a gel system of sodium aluminosilicate with tetrahydrofuran (THF), a nitrogen-free organic compound, as the template; characterization by using TG/DTG/DTA and ^{13}C MAS NMR shows that THF is incorporated in the pores of the as-synthesized FER zeolite.

FER type zeolite is an aluminosilicate molecular sieve with medium pore openings. It has a variety of uses in catalytic processes, such as hydrocarbon cracking and isomerization. In particular, in recent years it has been found that FER zeolite possesses excellent shape selectivity for the isomerization of n-butene to isobutene. The latter is a raw material for manufacturing MTBE (methyl *tert*-butyl ether), an additive in lead-free gasoline.[1] What is more, it can be used as a catalyst for skeletal isomerization of n-olefins to iso-olefins.[2] Thus, the development of a novel method to synthesize FER zeolite in a cheap way will be a decisive step for the commercialization of these industrial processes.

FER zeolite can be prepared in an inorganic reactant system in the presence of Na^+ and K^+ simultaneously. However, the reaction temperature is usually high.[3] It is difficult to exchange K^+ in the zeolite synthesized from this system, leading to limited applications as catalysts and adsorbents. FER type zeolite was firstly synthesized by using an organic compound as the structure-directing reagent (template) in 1977.[4] Up to now more than 30 organic compounds have been employed as templates,[5] most of which are nitrogen-containing organic compounds, and some of which are large organic molecules, such as bis[*N*-methylpyridyl]ethylinium.[6]

Quite a lot of efforts have been made to synthesize various zeolites using oxygen-containing organic compounds. It is known that three types of organic compounds have been used as the templates: (1) ethers, such as 15-crown-5 and 16-crown-6;[7] (2) alkyl oxide compounds, such as trioxane and poly(ethylene oxides);[8] and (3) alcohols, such as ethanol and butan-1-ol.[9] Zeolites FAU, EMT, MAZ, MFI, TON, *etc*., have been synthesized in the presence of the above templates. One method was disclosed that FER zeolite can be prepared by using 2,4-diketones as the organic templates.[10] In this paper a novel process of using THF as the template[11] for the synthesis of FER zeolite is reported.

The process of synthesizing FER zeolite was as follows: 24.44 g of silica sol (SiO_2 = 25.07%, Na_2O = 0.27%, Qingdao Ocean Chemical Plant) was mixed with 6.94 g aqueous solution of aluminium sulfate (Al_2O_3 = 7.49%, H_2O = 74.9%, Shanghai Xinxing Material Corp.) to form a mixture in a plastic vessel. Then 1.69 g of NaOH and 13.25 g of deionized water were added to the mixture. A homogeneous gel of the reactant was formed after 3.71 g of THF (analytical grade, Shanghai Chemical Reagent Corp.) were added into the mixture with vigorous stirring. The molar composition of the reactant gel was $0.5THF:0.215Na_2O:SiO_2:0.05Al_2O_3:20H_2O$. The gel was sealed into a 30 ml stainless steel Teflon lined autoclave, and hydrothermally crystallized in an oven at 200 °C for 8–12 days under static conditions. The spontaneously crystallized product was washed with distilled water, filtered and then dried at 120 °C. A reactant with the same molar composition but without THF remained amorphous for a long time under the same conditions.

The XRD pattern (Cu-Kα radiation, Rigaku D-MAX/II A) indicates that the as-synthesized product is highly crystalline FER type zeolite without any impurity phase (Fig. 1). The cell composition of the as-synthesized FER zeolite is $Na_{3.42}[Al_{3.59}Si_{32.41}O_{72}]\cdot 1.05THF\cdot 6.19H_2O$ as determined by chemical analysis. The SEM photo (Shimadzu S-520) shows that the morphology of the zeolite is agglomerate with a shape like a spindle (Fig. 2).

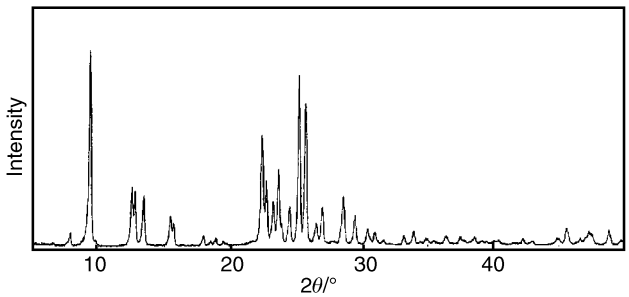

Fig. 1 XRD pattern of FER type zeolite synthesized in the reactant system with THF as the template.

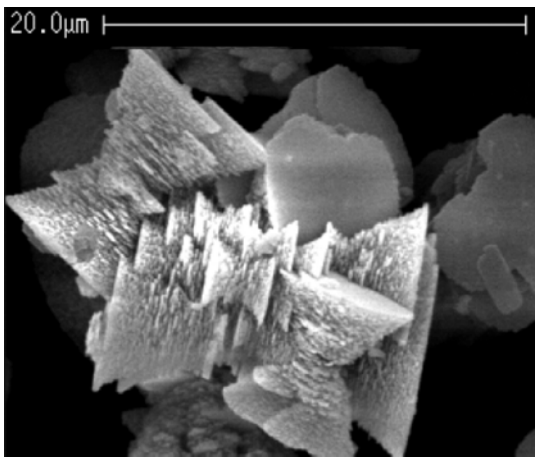

Fig. 2 SEM photograph of FER type zeolite synthesized in the reactant system with THF as the template.

The TG/DTG/DTA curves (PCT-10A thermal analyzer with a flow of air of 70 ml min^{-1} at a rate of 5 °C min^{-1} from room temperature to 600 °C) are displayed in Fig. 3. The weight loss below 350 °C is attributed to the loss of water incorporated into the pores of the as-synthesized FER zeolite. The weight loss in the temperature range of 350–550 °C is attributed to the loss of THF. The content of THF in the zeolite calculated from the weight loss is 3.12 wt.%. The maximum temperature in the DTG curve is 393 °C, and an obviously endothermal effect followed by an exothermal one are observed at 415 and 431 °C

respectively in the DTA curve (Fig. 3), indicating the escape of THF from the zeolite and the subsequent oxidation in air. This implies that THF is incorporated in the pores of the as-synthesized FER zeolite.

Fig. 4 shows the ^{13}C CP and HPDEC MAS NMR spectra (recorded at room temperature with a Bruker MSL-300 spectrometer, ^{13}C resonance frequency 78.468 MHz, rotor spun at 4.0 KHz, radiofrequency field 50 kHz, recycle time 2 s with an accumulation number of 2000–6000, contact time 2 ms for CP spectrum, decoupling power 50 kHz for HPDEC spectrum, adamantane was used as a second reference). Two peaks are observed in both the CP NMR and HPDEC ^{13}C NMR spectra of the as-synthesized FER zeolite compared with that of THF in the liquid phase. The chemical shifts of C_1 (-C-C_1-C_1-C-) and C_2 (-C_2-O-) are 23.99 and 66.09 ppm respectively for the THF molecules in the liquid state. In comparison, the chemical shifts of C_1 and C_2 in the CP spectrum move to 26.55 and 69.67 ppm respectively for the THF molecules trapped in the as-synthesized FER zeolite. The obvious shift to lower field is caused by

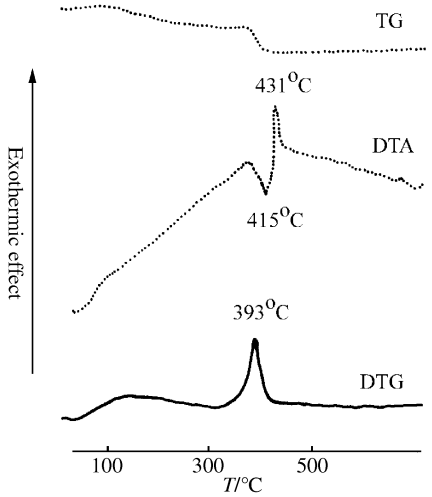

Fig. 3 TG/DTG/DTA curves of as-synthesized FER type zeolite in a flow of air.

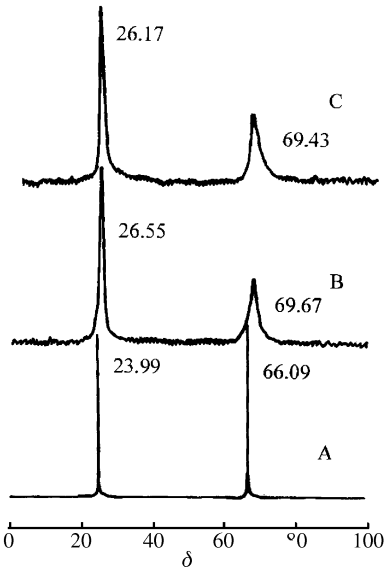

Fig. 4 ^{13}C MAS NMR spectra of THF (A) in liquid state, (B) CP spectrum of as-synthesized FER zeolite, (C) HPDEC spectrum of as-synthesized FER zeolite.

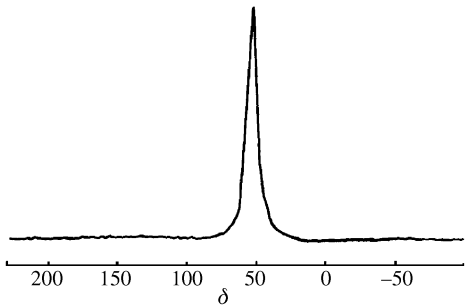

Fig. 5 ^{27}Al MAS NMR spectrum of FER type zeolite synthesized in the reactant system with THF as the template.

electronic deshielding effects of the framework oxygen atoms in the small cage formed by intersection of the 8-ring (0.48 × 0.34 nm) and 6-ring channels in the cell of FER zeolite. The deduction is consistent with our earlier observation of TMEDA (tetramethylethylenediamine) trapped in the cages of several as-synthesized zeolites, such as MTN, MON and FER.[12]

Fig. 5 shows ^{27}Al MAS NMR (resonance frequency 78.205 MHz, rotor spun at 3.5 kHz, frequency field 27.8 kHz, recycle time 500 ms, $AlCl_3(H_2O)_6$ as reference. The peak at 53 ppm in the ^{27}Al MAS NMR spectrum of the as-synthesized FER zeolite corresponds to tetrahedrally coordinated framework aluminium, indicating that the framework of the FER zeolite discussed herein does not include non-framework aluminium.

The nitrogen adsorption isotherm was measured (at 77.35 K using a Micromeritics ASAP 2000 instrument) on the sample of FER zeolite calcined to remove THF and treated by ion-exchange. The adsorption isotherm of N_2 belongs to the Langmuir type. The microporous volume was 0.15 ml g^{-1} calculated from the adsorption isotherm, which is consistent with the value determined for the FER zeolite synthesized by using TMEDA as the templete.[13]

This work was supported by the Doctoral Fund of the State Ministry of Education and the Institute of Beijing Yanshan Petrochemical Corporation.

Notes and references

1 R. E. Morris, S. J. Weigel, N. J. Henson, L. M. Janicke, B. F. Chmelka and A. K. Cheetham, *J. Am. Chem. Soc.*, 1994, **116**, 11 849.
2 R. J. Pellet, C. L. O'Yang, J. Hazen, A. E. Hadowanetz and J. E. Browne, *US Patent*, 5 523 510, 1996.
3 J. Arika, H. Miyazaki, K. Igawa and K. Itabashi, *US Patent*, 4 650 654, 1987.
4 C. J. Plank, E. R. Rosinski and M. K. Bubin, *US Patent*, 4 6016 245, 1977.
5 G.-q. Guo and Y.-c. Long, *Adv. Chem. Ind. (in Chinese)*, in press.
6 E. W. Volyocsik, *US Patent*, 4 584 286, 1986.
7 C.-n. Wu and K.-j. Chao, *J. Chem. Soc., Faraday Trans.*, 1995, **91**(1), 167.
8 A. Matijasic and J. Patarin, *Microporous Mesoporous Mater.*, 1999, **29**(3), 405.
9 T. Santo, A. Suzuki, S. Fukuya, F. Matsuoka, Z. B. Wang, K. Soga and Y. Kohtoku, *Proceedings of the 12th International Zeolite Conference, Baltimore, 1998*, ed. M. M. J. Treacy, B. K. Marcus, M. E. Bisher and J. B. Higgins, Materials Research Society, Warrendale, PA, USA, 1999, p. 2041.
10 J. A. Kaduk, *US Patent*, 4 323 481, 1982.
11 Y.-c. Long and G.-q. Guo, *Chin. Pat., Application*, No. 00111893,2000.
12 Y.-j. Sun, T.-l. Wu, L.-p. Wang, L. Fei and Y.-c. Long, *Proceedings of the 9th International Zeolite Conference, Montreal, 1992*, ed. R. Von Ballmoos, J. B. Higgins and M. M. J. Treacy, Butterworth-Heinemann, Stoneham, MA, 1993, p. 497.
13 Y.-c. Long, M.-h. Ma, Y.-j. Sun and H.-w. Jiang, *J. Inclusion Phenom. Macrocycl. Chem.*, 2000, **37**(3), 365.

Diphenylphosphinophenolate: a ligand for the palladium-catalysed silylation of aryl halides activating simultaneously both palladium and silicon

Eiji Shirakawa,*[a] Takuya Kurahashi,[b] Hiroto Yoshida[b] and Tamejiro Hiyama*[b]

[a] *Graduate School of Materials Science, Japan Advanced Institute of Science and Technology, Asahidai, Tatsunokuchi, Ishikawa 923-1292, Japan. E-mail: shira@jaist.ac.jp*

[b] *Department of Material Chemistry, Graduate School of Engineering, Kyoto University, Sakyo-ku, Kyoto, 606-8501, Japan. E-mail: thiyama@NPC05.kuic.kyoto-u.ac.jp*

Received (in Cambridge, UK) 31st July 2000, Accepted 25th August 2000
First published as an Advance Article on the web 18th September 2000

Diphenylphosphinophenolate was found to be an effective ligand for the palladium-catalysed silylation of aryl halides, activating not only palladium but also silicon of a disilane, where aryl bromides and iodides having such substituents as methyl, methoxy, amino, ethoxycarbonyl, trifluoromethyl, formyl or phenyl are applicable to the reaction with hexamethyldisilane to give the corresponding trimethylsilylarenes.

The transition metal-catalysed silylation of aryl halides with disilanes should be one of the most straightforward and economical ways to arylsilanes,[1,2] which are versatile synthetic precursors especially for the palladium-catalysed cross-coupling reaction with organic electrophiles.[3] Although there have been many reports on the palladium-catalysed silylation using triphenylphosphine as a ligand,[1] the reaction requires drastic conditions to obtain arylsilanes in acceptable yields. Low reaction rate is ascribed to the low reactivity of a disilane toward a Pd(II) complex that is generated by oxidative addition of an aryl halide to a Pd(0) complex. In order to accelerate the rate-determining transmetalation step, two routes are possible in terms of electronic balance: one is to make the palladium(II) more electron-deficient and the other is to increase the electron density of the nucleophile. Ligands play significant roles for the former but not for the latter.

We envisaged that a phosphine having a phenolate group should not only serve as a bidentate ligand for palladium but also activate directly an incoming silyl nucleophile. Thus, in the palladium-catalysed silylation of aryl halides with disilanes, we considered that the phenolate anion in the ligand could coordinate to the silicon atom of a disilane and enhance its nucleophilicity in the transmetalation step in the catalytic cycle that we assumed to be working (Scheme 1). Here we report that a palladium complex coordinated by 2-(diphenylphosphino)-phenolate (PO)[4] efficiently catalyses the silylation of aryl halides using hexamethyldisilane.

We first compared the PO ligand in efficiency with other phosphines in the palladium-catalysed reaction of bromobenzene (**6a**) with hexamethyldisilane (**7**) (Scheme 2). Thus, **6a** (1.0 mol) was treated with **7** (1.1 mol) in the presence of a 1 : 2

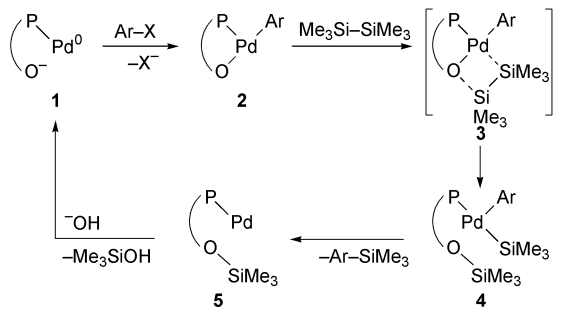

The oxygen atom may coordinate on palladium in complex **1**, **4** and **5**.

Scheme 1

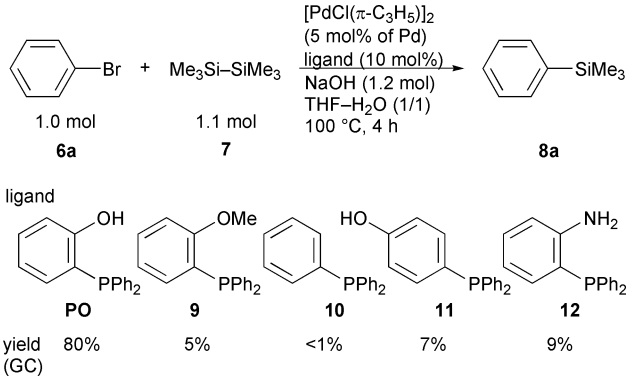

Scheme 2

mixture of $[PdCl(\pi\text{-}C_3H_5)]_2$–PO (5 mol% of Pd) and sodium hydroxide (1.2 mol) in a 1 : 1 mixture of THF and H_2O at 100 °C for 4 h to give trimethylsilylbenzene (**8a**) in 80% yield. Reduction of the amount of sodium hydroxide (0.1 mol, 9%; 0 mol, 0%), masking the hydroxy group of PO as **9**, or use of triphenylphosphine (**10**) in lieu of PO decisively reduced the yield, implying the significance of the phenolate moiety, whereas inefficiency of *p*-hydroxy derivative **11** revealed the importance of the *o*-phenolate anionic functionality. Aminophosphine **12** also was ineffective. These results clearly demonstrate that the catalytic cycle depicted in Scheme 1 is working smoothly with the Pd–PO catalyst.

The applicability of the catalytic system was proved by trimethylsilylation of various aryl bromides and iodides (Scheme 3 and Table 1). Trimethylsilylbenzene and 4-trimethylsilyltoluene were obtained in high yields from bromobenzene and 4-bromotoluene, respectively (Table 1, entries 1 and 2). Although an electron-donating substituent like methoxy or amino on the aryl bromide decreased the yield, as was the case with a triphenylphosphine ligand,[1a] use of a 1 : 1 mixture of toluene and H_2O as the solvent in combination with 10 mol% tetrabutylammonium bromide afforded the corresponding arylsilanes in yields over 90% (entries 3–6). The toluene/H_2O/Bu_4NBr system was effective also for the silylation of an aryl bromide having an ester moiety, preventing ester hydrolysis during the reaction (entries 7 and 8). Other aryl bromides with various substituents gave the corresponding arylsilanes in good yields (entries 9–12). Dibromo- or tribromobenzene also reacted smoothly to give bis(trimethylsilyl)- or tris(trimethylsilyl)benzene, respectively (entries 13 and 14). Aryl iodides also were found to be good substrates for this silylation reaction (entries 15–17). This is noteworthy, as iodobenzene is recorded not to react at all with a Pd–Ph_3P catalyst, the low efficiency of

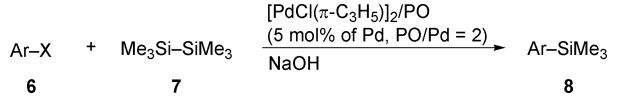

Scheme 3

DOI: 10.1039/b006165o

Table 1 Palladium-catalysed silylation of aryl halides with hexamethyldisilane

Entry	Aryl halide **6**	Conditions[a]	Amount of **8** (mol)	Yield[b] (%)
1[c]	PhBr	A	1.1	88
2	4-MeC_6H_4Br	A	2.5	82
3	4-$MeOC_6H_4Br$	A	2.5	73
4	4-$MeOC_6H_4Br$	B	2.5	91
5	4-$NH_2C_6H_4Br$	A	2.5	50
6	4-$NH_2C_6H_4Br$	B	2.5	92
7	4-$EtOCOC_6H_4Br$	A	2.5	23
8	4-$EtOCOC_6H_4Br$	B	2.5	87
9	4-$CF_3C_6H_4Br$	A	2.5	70
10	4-$HCOC_6H_4Br$	A	1.1	65
11	4-PhC_6H_4Br	A	2.5	80
12	2-NaphthBr	A	2.5	64
13	$C_6H_4Br_2$-1,4	A	5.0	81
14	$C_6H_3Br_3$-1,3,5	A	7.5	81
15	PhI	A[c]	1.1	83
16	4-$MeOC_6H_4I$	A	2.5	76
17	4-$CF_3C_6H_4I$	A	2.5	70

[a] The reaction was carried out at 100 °C for 24 h using an aryl halide (0.40 mmol), hexamethyldisilane and sodium hydroxide (0.48 mmol) in the presence of $[PdCl(\pi\text{-}C_3H_5)]_2$ (0.01 mmol) and PO (0.04 mmol). A: THF(1 ml)–H_2O(1 ml); B: tetrabutylammonium bromide(0.04 mmol), toluene(1 ml)–H_2O(1 ml). [b] Isolated yields based on aryl halide are given. [c] The reaction was completed in 10 h.

the catalyst being attributed to the inertness of the oxidative adduct $PhPdI(Ph_3P)_2$.[1a,5] In our case the oxidative adduct **2** lacks a halide ligand which explains the results that the Pd–PO catalyst is free from the influence of the kind of halide.

In conclusion, we have demonstrated that a palladium catalyst coordinated by phosphinophenolate is efficient for the silylation of aryl halides using hexamethyldisilane. The protocol using a ligand that activates a transition metal and an incoming nucleophile simultaneously should be applicable to various transition metal-catalysed reactions. Studies on the details of the mechanism as well as application of the protocol are in progress in our laboratories.

Notes and references

1 (*a*) H. Matsumoto, S. Nagashima, K. Yoshihiro and Y. Nagai, *J. Organomet. Chem.*, 1975, **85**, C1; (*b*) D. Azarian, S. S. Dua, C. Eaborn and D. R. M. Walton, *J. Organomet. Chem.*, 1976, **117**, C55; (*c*) H. Matsumoto, K. Yoshihiro, S. Nagashima, H. Watanabe and Y. Nagai, *J. Organomet. Chem.*, 1977, **128**, 409; (*d*) C. Eaborn, R. W. Griffiths and A. Pidcock, *J. Organomet. Chem.*, 1982, **225**, 331; (*e*) Y. Hatanaka and T. Hiyama, *Tetrahedron Lett.*, 1987, **28**, 4715.

2 The palladium-catalysed decarbonylative silylation of arenecarbonyl halides also affords arylsilanes: (*a*) J. D. Rich, *J. Am. Chem. Soc.*, 1989, **111**, 5886; (*b*) J. D. Rich and T. E. Krafft, *Organometallics*, 1990, **9**, 2040; (*c*) T. E. Krafft, J. D. Rich and P. J. McDermott, *J. Org. Chem.*, 1990, **55**, 5430.

3 T. Hiyama, in *Metal-catalyzed Cross-coupling Reactions*, ed. F. Diederich and P. J. Stang, Wiley-VCH, Weinheim, 1998, ch. 10, pp. 421–453 and references therein.

4 Although there have been many reports on PO as a ligand for various transition metals, no report appeared concerning direct activation of a reaction partner for the transition metal. For Pd–PO complexes, see: H. D. Empsall, B. L. Shaw and B. L. Turtle, *J. Chem. Soc., Dalton Trans.*, 1976, 1500.

5 Aryl iodides react with **7** in the presence of $Pd(PPh_3)_4$ and TASF $(Et_2N)_3S^+F_2Si^-Me_3$, see ref. 1(*e*).

A novel nonacoordinate bridging selenido ligand in a tricapped trigonal-prismatic geometry. X-Ray structure of $Cu_{11}(\mu_9\text{-}Se)(\mu_3\text{-}Br)_3[Se_2P(OPr^i)_2]_6$

C. W. Liu,*[a] Chiu-Mine Hung,[a] Hsiu-Chih Chen,[a] Ju-Chung Wang,[b] Tai-Chiun Keng[b] and Kermin Guo[b]

[a] *Department of Chemistry, Chung Yuan Christian University, Chung-Li, Taiwan 320, R. O. C. E-mail: chenwei@mbox.cycu.edu.tw*

[b] *Department of Chemistry, Soochow University, Taipei, Taiwan, 111, R. O. C.*

Received (in Cambridge, UK) 4th July 2000, Accepted 22nd August 2000
First published as an Advance Article on the web

The first nonacoordinate bridging selenido ligand in a tricapped trigonal prismatic geometry, $Cu_{11}(\mu_9\text{-}Se)(\mu_3\text{-}Br)_3[Se_2P(OPr^i)_2]_6$, is prepared along with closed-shell ion-centered Cu^I_8 cubes, $Cu_8(\mu_8\text{-}Se)[Se_2P(OPr^i)_2]_6$ and $Cu_8(\mu_8\text{-}Br)[Se_2P(OPr^i)_2]_6(PF_6)$, from the reaction of $NH_4Se_2P(OPr^i)_2$, $Cu(CH_3CN)_4PF_6$, and Bu_4NBr in CH_2Br_2 at 0 °C.

One of the most commonly observed coordination geometries for a central atom which is surrounded by nine outer or ligand atoms is a tricapped trigonal prism.[1] Notable examples are lanthanide complexes,[2] $[ReH_9]^{2-}$ and its derivatives.[3] To the best of our knowledge this geometry has never been observed in any main group elements, though a main-group element in the cavity of a monocapped square antiprism is known in a couple of metal carbonyls.[4]

Molecular cubic clusters encapsulating main-group elements are particularly interesting from the general point of view of bonding.[5] To date two types of main-group element-centered transitional metal cubic clusters which include face-capped and edge-capped cubes have been characterized. While $Ni_8(\mu_8\text{-}As)(\mu_4\text{-}As)_6(PPh_3)_8$ is the only face-capped cube,[6] several edge-capped Cu^I_8 cubes centered by S^{2-},[7] Cl^- and Br^- [8] are known for dithiophosphate ligands. An unusual sulfide-centered, edge-capped mixed-metal cube, $[Mn_4Cu_4S(SPr^i)_{12}]^{2-}$, which is defined by two interpenetrating copper and manganese tetrahedra, is also accessible by reaction of $[Mn_2(SPr^i)_6]^{2-}$ with CuCl.[9] With the dialkyl diselenophosphate ligands (dsep), we uncovered the first selenide-centered edge-capped Cu^I_8 cubes.[10] Subsequently an exceptional co-crystallization with clusters, $Ag_8(\mu_8\text{-}Se)[Se_2P(OR)_2]_6$ and $Ag_6[Se_2P(OR)_2]_6$, superimposing on a trigonal lattice, was observed.[11] To extend our research efforts in centered cubic cluster synthesis, we focus on the halide ion and uncovered, besides selenide-centered Cu^I_8 cubes, **1**, a halide-centered Cu^I_8 cube, **3**, and a remarkable, undecanuclear copper cluster containing a selenide ion in the center of a pentacapped trigonal prism, $Cu_{11}(\mu_9\text{-}Se)(\mu_3\text{-}X)_3[Se_2P(OPr^i)_2]_6$, **2**. Cluster **2** is a novel example possessing not only a 3,3,4,4,4-pentacapped trigonal prismatic copper framework but also a nonacoordinate bridging selenido ligand in a tricapped trigonal prismatic geometry.

At least three clusters are produced from the reaction of $NH_4Se_2P(OPr^i)_2$ (1.2 g, 3.69 mmol), $Cu(CH_3CN)_4PF_6$ (0.917 g, 2.46 mmol) and Bu_4NBr (0.793 g, 2.46 mmol) in CH_2Br_2 (50 mL) at 0 °C for 24 hours. Both yellow clusters **1** and **2** dissolved in n-hexane are separated by column chromatography (eluent: ethyl acetate/hexane = 3/4) whereas the cationic species **3** is insoluble.† The formulation of **2** was confirmed by elemental analyses, positive FAB mass spectroscopy, ^1H and ^{31}P NMR spectroscopy. In the positive FAB mass spectrum of **2**, three major peaks which correspond to the intact molecule, an intact molecule with the loss of a bromide ion, $\{Cu_{11}(\mu_9\text{-}Se)(\mu_3\text{-}Br)_2[Se_2P(OPr^i)_2]_6\}^+$, and an intact molecule with the loss of a dsep ligand, $\{Cu_{11}(\mu_9\text{-}Se)(\mu_3\text{-}Br)_3[Se_2P(OPr^i)_2]_5\}^+$, respectively, were identified. These observed peaks are in agreement with the results of their respective, simulated isotopic patterns.

X-Ray analysis‡ of **2** reveals a $Cu_{11}Se$ core, stabilized by three bromide and six dsep ligands. The central core adopts a slightly distorted, fivefold capped trigonal prismatic copper framework, with an encapsulated selenium ion. Shown in Fig. 1 is the $SeCu_{11}$ core which displays an idealized D_{3h} symmetry. Both Cu(1) and Cu(2), each capping the triangular face of the prism, are located on the pseudo-three-fold axis, as is the encapsulated selenium ion Se(01). The Cu–Se(01) bond distances are noteworthy. Whereas two on the C_3 axis, 3.480 and 3.574 Å, are extremely long, the rest are in the range 2.519(2)–2.748(2) Å and are within the limits reported by Fenske and coworkers.[12] Consequently a novel nonacoordinate bridging selenido ligand in a tricapped trigonal primastic geometry is revealed in the title compound. The edges of the trigonal prism are in the range 3.431–3.588 Å while the heights (Cu7–Cu8, Cu6–Cu9, and Cu10–Cu11) are on average 3.103(2) Å. There exist a total of nine Cu_4 butterflies where the wing-tip positions are represented by five capping copper atoms with each edge and height of the trigonal prism being the hinges. Those Cu_4 butterflies comprising a copper atom on the C_3 axis are each connected by a dsep ligand having a tetrametallic

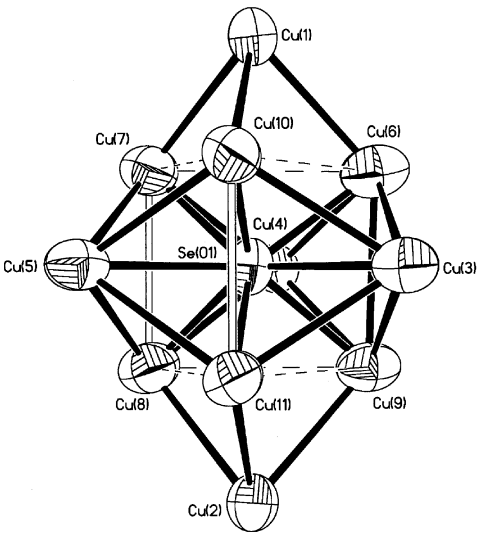

Fig. 1 The $Cu_{11}Se$ core in **2**. Selected bond lengths [Å]: Se(01)–Cu(3) 2.748(2), Se(01)–Cu(4) 2.739(2), Se(01)–Cu(5) 2.736(2), Se(01)–Cu(6) 2.568(2), Se(01)–Cu(7) 2.576(2), Se(01)–Cu(8) 2.580(2), Se(01)–Cu(9) 2.519(2), Se(01)–Cu(10) 2.551(2), Se(01)–Cu(11) 2.552(2), Cu(1)–Cu(10) 2.804(2), Cu(1)–Cu(7) 2.851(2), Cu(1)–Cu(6) 2.869(2), Cu(2)–Cu(9) 2.787(2), Cu(2)–Cu(8) 2.842(2), Cu(2)–Cu(11) 2.861(2), Cu(3)–Cu(9) 2.883(2), Cu(3)–Cu(6) 2.886(2), Cu(3)–Cu(11) 2.919(2), Cu(3)–Cu(10) 2.925(2), Cu(4)–Cu(6) 2.860(2), Cu(4)–Cu(9) 2.877(2), Cu(4)–Cu(7) 2.936(2), Cu(4)–Cu(8) 2.970(2), Cu(5)–Cu(10) 2.897(2), Cu(5)–Cu(7) 2.916(2), Cu(5)–Cu(8) 2.932(2), Cu(5)–Cu(11) 2.947(2), Cu(6)–Cu(9) 3.052(2), Cu(7)–Cu(8) 3.134(2), Cu(10)–Cu(11) 3.124(2).

DOI: 10.1039/b005366j

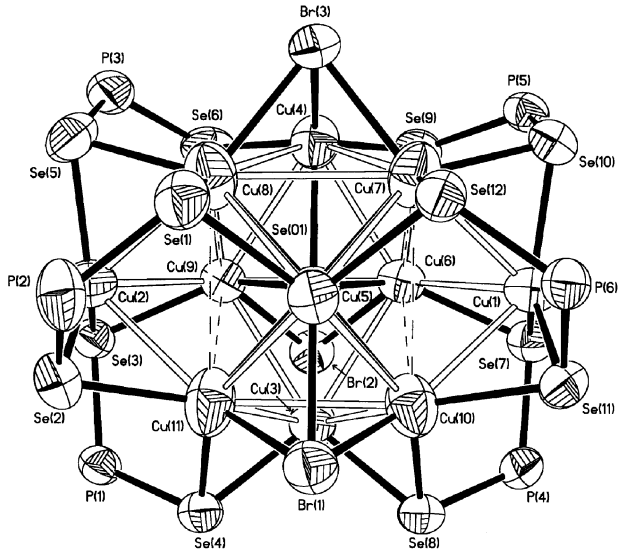

Fig. 2 The thermal ellipsoid drawing (50% probability) of **2**. The isopropoxy groups have been omitted for clarity. Selected bond lengths [Å]: Br(1)–Cu(5) 2.452(2), Br(1)–Cu(10) 2.565(2), Br(1)–Cu(11) 2.627(2), Br(2)–Cu(3) 2.451(2), Br(2)–Cu(6) 2.564(2), Br(2)–Cu(9) 2.622(2), Br(3)–Cu(4) 2.453(2), Br(3)–Cu(7) 2.539(2), Br(3)–Cu(8) 2.595(2), Cu–Se 2.350(2)–2.502(2).

tetraconnective (μ_2,μ_2)[13] coordination pattern (Fig. 2) The remaining three, where hinge positions are the heights of the prism, are each occupied by a triply bridging bromide atom over an alternating set of three of the six triangular faces. The Cu–Br bond distances are on average 2.541(2) Å. Two distinct coordination environments around copper atoms of the cluster are observed: two on the C_3 axis are coordinated by three selenium atoms of three different dsep ligands and the rest are surrounded by three selenium atoms and one bromine atom. Overall, owing to the existence of three, alternating triply bridging bromides, the D_{3h} symmetry depicted in Fig. 1 has been lowered to C_{3h}.

Compound **3** forms colorless crystals in the monoclinic space group *C*2/*c* and reveals a bromide-centered Cu^I_8 cube of which each edge of the cube is bridged by a selenium atom of the dsep ligand (Fig. 3). The averaged Cu–Cu bond length of 3.179(4) Å is about 0.25 Å longer than the corresponding Cu–Cu distance in the selenide-centered Cu^I_8 cube.[10] The averaged Cu–Br distance of 2.754(1) Å is comparable with those previously

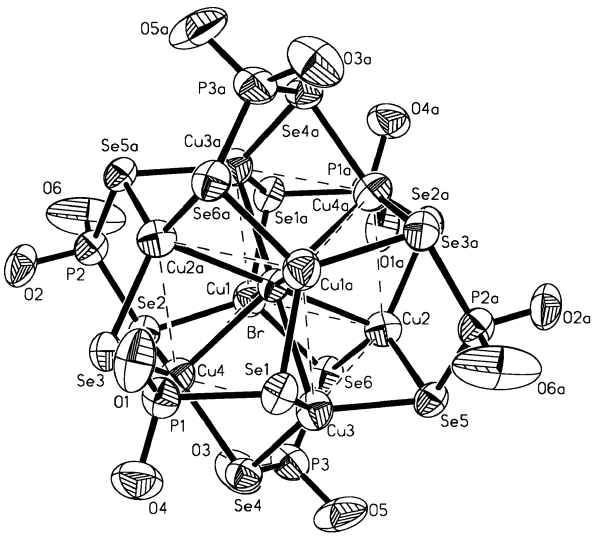

Fig. 3 The thermal ellipsoid drawing (50% probability) of the cation in **3**. The isopropyl groups have been omitted for clarity. Selected bond lengths [Å]: Cu–Se 2.374(1)–2.399(1), Cu–Br 2.732(1)–2.771(1), Se–P 2.169(3)–2.185(2).

reported in $[Cu_8(\mu_8\text{-}Br)(S_2P(OPr^i)_2)_6][PF_6]$[8] and significantly longer than those in **2**.

In summary, the first selenium atom surrounded by nine copper atoms in a tricapped trigonal prismatic geometry is identified along with a halide-centered Cu^I_8 cube containing dsep ligands during the preparation of closed-shell ion-centered cubic clusters. The silver analogues of **2** and **3** have been characterized structurally and details will be reported soon. This research was supported by the National Science Council of Taiwan (NSC 89-2113-M-033-004).

Notes and references

† *Characterization* of **2**: ^{1}H NMR ($CDCl_3$) δ 1.34 (d, J = 6 Hz, 36H, CH_3), 1.37 (d, J = 6 Hz, 36H, CH_3), 4.75 (m, 6H, CH), 5.17 (m, 6H, CH); ^{31}P{^{1}H} NMR ($CDCl_3$), δ 74.8 (J_{SeP} 647, 668 Hz); positive ion FAB-MS: *m/z*: 2859.4 $(M)^+$, 2779.3 $(M - Br)^+$, 2552.1 $(M - dsep)^+$. Anal. calcd. for $C_{36}H_{84}O_{12}P_6Se_{13}Br_3Cu_{11}\cdot 1/2C_6H_{14}$: C, 16.13; H, 3.13; found: C, 16.15; H, 3.25%; **3**: ^{1}H NMR ($CDCl_3$) δ 1.41 (d, J = 6 Hz, 72H, CH_3), 4.81 (m, 12H, CH); ^{31}P{^{1}H} NMR ($CDCl_3$), δ 68.2 (J_{SeP} 648 Hz); positive ion FAB-MS: *m/z*: 2430.5 $(M)^+$. Anal. calcd. for $C_{36}H_{84}F_6O_{12}P_7Se_{12}BrCu_8$: C, 16.79; H, 3.29; found: C, 16.75 ; H, 3.20%.

‡ *Crystal data* for **2**: $C_{36}H_{84}O_{12}P_6Se_{13}Br_3Cu_{11}$, M = 2860.00, triclinic, $P\bar{1}$, a = 15.2820(8), b = 15.5376(8), c = 20.4796 (11) Å, α = 93.011(1), β = 106.941(1), γ = 108.216(1)°, V = 4363.1(4) Å^3, T = 298(2) K, Z = 2, μ(Mo-Kα) = 9.568 mm^{-1}, 20983 reflections measured, 14482 unique [R(int) = 0.0398] which were used in the calculations. The final $R1$ = 0.0639, $wR2$ = 0.1397 and for all data $R1$ = 0.0851, $wR2$ = 0.1535.

3: $C_{36}H_{84}F_6O_{12}P_7Se_{12}BrCu_8$, M = 2575.57, monoclinic, *C*2/*c*, a = 24.345(5), b = 13.151(3), c = 24.991(5) Å, β = 91.34(3)°, V = 7999(3) Å^3, T = 293(2) K, Z = 4, μ(Mo-Kα) = 8.241 mm^{-1}, 11231 reflections measured, 6703 unique [R(int) = 0.0356] which were used in the calculations. The final $R1$ = 0.0502, $wR2$ = 0.1096 and for all data $R1$ = 0.0647, $wR2$ = 0.1189.

CCDC 182/1763. See http://www.rsc.org/suppdata/cc/b0/b005366j/ for crystallographic files in .cif format.

1 F. A. Cotton and G. Wilkinson, *Advanced Inorganic Chemistry*, 5th edn., John Wiley & Sons, Chichester, 1988.

2 J. P. White, H. Deng, E. P. Boyd, J. Gallucci and S. G. Shore, *Inorg. Chem.*, 1994, **33**, 1685; R. Baggio, M. T. Garland and M. Perce, *Inorg. Chem.*, 1997, **36**, 950; N. Martin, J. C. G. Bunzli, V. Mckee, C. Piguet and G. Hopfgartner, *Inorg. Chem.*, 1998, **37**, 577; D. F. Mullica, J. M. Farmer and J. A. Kautz, *Inorg. Chem. Commun.*, 1999, **2**, 73; M. C. Favas and D. L. Kepert, *Prog. Inorg. Chem.*, 1981, **28**, 309, and references therein.

3 S. C. Abrahams, A. P. Ginsberg and K. Knox, *Inorg. Chem.*, 1964, **3**, 558; D. Baudry, M. Ephritikhine and H. Felkin, *J. Organomet. Chem.*, 1982, **224**, 363; X.-L. Luo, D. Baudry, P. Boydell, P. Charpin, M. Nierlich, M. Ephritikhine and R. H. Crabtree, *Inorg. Chem.*, 1990, **29**, 1511.

4 $[Rh_9(P)(CO)_{21}]^{2-}$: J. L. Vidal, W. E. Walker, R. L. Pruett and R. C. Schoening, *Inorg. Chem.*, 1979, **18**, 129; $[Co_9(Si)(CO)_{21}]^{2-}$: K. M. Mackay, B. K. Nicholson, W. T. Robinson and A. W. Sims, *J. Chem. Soc., Chem. Commun.*, 1984, 1276.

5 R. A. Wheeler, *J. Am. Chem. Soc.*, 1990, **112**, 8737; E. Furet, A. L. Beuze, J.-F. Halet and J.-Y. Saillard, *J. Am. Chem. Soc.*, 1995, **117**, 4936; B. Zouchoune, F. Ogliaro, J.-F. Halet, J.-Y. Saillard, J. R. Eveland and K. H. Whitmire, *Inorg. Chem.*, 1998, **37**, 865; R. Gautier, F. Ogliaro, J.-F. Halet, J.-Y. Saillard and E. J. Baerends, *Eur. J. Inorg. Chem.*, 1999, 1161.

6 K. Vogt, Ph.D. Dissertation, University of Karlsruhe, Germany, 1994.

7 C. W. Liu, R. T. Stubbs, R. J. Staples and J. P. Fackler, Jr., *J. Am. Chem. Soc.*, 1995, **117**, 9778; Z. X. Huang, S. F. Lu, J. Q. Huang, D. M. Wu and J. L. Huang, *J. Struct. Chem.*, 1991, **10**, 213.

8 J. P. Fackler, Jr., R. J. Staples, C. W. Liu, R. T. Stubbs, C. Lopez and J. T. Pitts, *Pure Appl. Chem.*, 1998, **70**, 839.

9 H.-O. Stephan, M. G. Kanatzidis and G. Henkel, *Angew. Chem., Int. Ed. Engl.*, 1996, **35**, 2135.

10 C. W. Liu, H.-C. Chen, J.-C. Wang and T.-C. Kang, *Chem. Commun.*, 1998, 1831.

11 C. W. Liu, I.-J. Shang, J.-C. Wang and T.-C. Keng, *Chem. Commun.*, 1999, 995.

12 N.-Y. Zhu and D. Fenske, *J. Chem. Soc., Dalton Trans.*, 1999, 1067; M. Semmelmann, D. Fenske and J. F. Corrigan, *J. Chem. Soc., Dalton Trans.*, 1998, 2541; A. Deveson, S. Dehnen and D. Fenske, *J. Chem. Soc., Dalton Trans.*, 1997, 4491.

13 I. Haiduc, D. B. Snowerby and S.-F. Lu, *Polyhedron*, 1995, **14**, 3389.

Thermotropic liquid-crystalline folic acid derivatives: supramolecular discotic and smectic aggregation†

Kiyoshi Kanie,[a] Takayasu Yasuda,[a] Seiji Ujiie[b] and Takashi Kato*[a]

[a] *Department of Chemistry and Biotechnology, Graduate School of Engineering, The University of Tokyo, Hongo, Bunkyo-ku, Tokyo 113-8656, Japan. E-mail: kato@chiral.t.u-tokyo.ac.jp*
[b] *Department of Material Science, Shimane University, Matsue, Shimane 690-8504, Japan*

Received (in Cambridge, UK) 15th June 2000, Accepted 29th August 2000
First published as an Advance Article on the web 18th September 2000

Thermotropic discotic and smectic liquid crystallinity can be induced for folic acid derivatives having octadecyl and undecyl substituents in wide temperatures ranges, respectively; the addition of sodium triflate to smectic liquid-crystalline folic acid leads to a change of the assembled structures from smectic to columnar phases.

Nanoscale molecular architectures formed by non-covalent interactions have been intensively studied because highly functional molecular materials can be obtained by self-organization processes.[1–4] For liquid-crystalline (LC) materials, the utilization of the molecular interactions such as hydrogen bonding has been shown to be quite useful.[4] The control of the patterns and the reversible self-assembling nature of hydrogen-bonded liquid crystals would lead to the preparation of a novel dynamically functional material. Our intention is to use self-organization behavior of biomolecules, which in many cases show lyotropic behavior, for the formation of new thermotropic LC materials.

In the present study, we have focused on the pterin ring of folic acid. Thermotropic LC folic acids have not yet been developed although the lyotropic mesomorphism through discotic tetramer formation of sodium folate in aqueous solution has been reported.[5] The induction of the thermotropic liquid crystallinity of this molecule may lead to the development of dynamically functional anisotropic systems.

We succeeded in inducing thermotropic liquid crystallinity for folic acid derivatives **1a–c** by incorporating 2-(3,4-dialkyloxyphenyl)ethyl groups into the glutamic acid moiety. Compound **1c** exhibited columnar mesophases, while smectic phases were seen for compounds **1a** and **1b** containing shorter alkyl chains.‡ The phase transition behavior of **1a–c** is summarized in Table 1.§

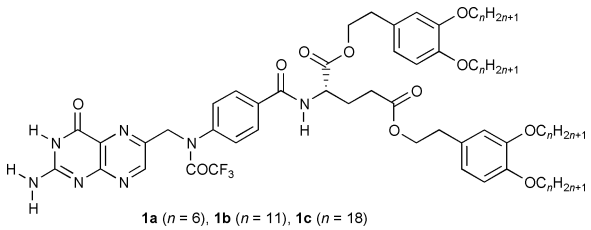

1a (n = 6), **1b** (n = 11), **1c** (n = 18)

X-Ray diffraction measurements showed that **1c** exhibited ordered and disordered discotic hexagonal columnar (D_{ho} and D_{hd}) phases (D_{ho} phase at 25 °C: d_{100} = 50.5, d_{110} = 29.2, d_{200} = 25.3, and the distance between disks = 4.1 Å; D_{hd} phase at 100 °C: d_{100} = 50.6, d_{110} = 29.2, and d_{200} = 25.3 Å). Only one sharp peak (small angle) and a broad halo were observed for the smectic phases of **1a** and **1b**. The layer spacings for **1a** and **1b** were 37.6 and 41.2 Å at 25 °C, respectively. It is noteworthy that the phase behavior of **1** was greatly dependent on the length of the alkyl chains. The textures observed for these compounds supported the difference of the phase structures.[6] The formation of the smectic and discotic phases can be attributed to the ribbon- and disk-like aggregation of pterin rings of **1**, respectively, as shown in Fig. 1.[7,8] The IR spectra of **1b** and **1c** also indicated the existence of the two types of the hydrogen-bonded structures.¶ The layer structure for **1a** and **1b** should be induced by the ribbon-like aggregation of the pterin ring (Fig. 1A).[7] In contrast, the induction of the discotic hexagonal columnar phase of **1c** was based on the disk-like aggregation of the pterin ring of **1c** (Fig. 1B).[8] For **1c**, the disordered alkyl chains can be closely packed in the discotic arrangement. The difference of these aggregated structures was due to the dynamic nature of the hydrogen bonding.

Table 1 Phase transition temperatures of **1**[a]

Compound	Phase transition temp./°C						
1a (n = 6)					S	238	Iso
1b (n = 11)			Cr	−13	S	240	Iso
1c (n = 18)	D_{ho}	62	D_{hd}	207	M	223	Iso

[a] Cr: crystalline; S: smectic; D_{ho}: ordered discotic hexagonal columnar; D_{hd}: disordered discotic hexagonal columnar; M: mesomorphic with low viscosity; Iso: isotropic.

The formation of columnar molecular assemblies has been a recent topic for the development of functional materials.[9,10] We were able to change the LC phase of **1b** from smectic to columnar by the addition of sodium triflate (NaOTf). The isotropization temperatures and the mesomorphic temperature

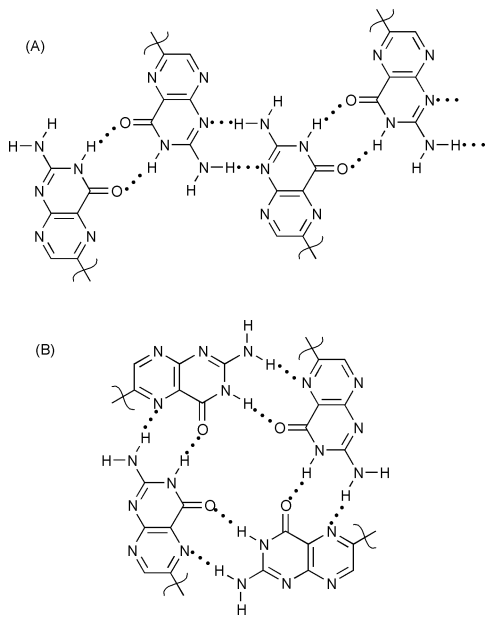

Fig. 1 Hydrogen-bonded self-assembled structures of the pterin rings of folic acid. (A) Linear ribbon-like aggregation style, (B) cyclic disk-like aggregation style.

† Electronic supplementary information (ESI) available: synthesis details and IR data. See http://www.rsc.org/suppdata/cc/b0/b004815l/

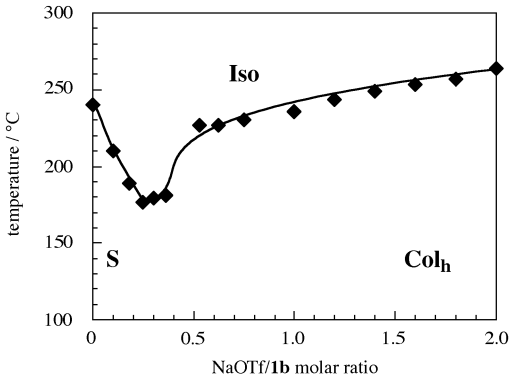

Fig. 2 Isotropization temperatures of the complexes of NaOTf and **1b**.

ranges of the resulting mixtures of **1b** and NaOTf on heating are summarized in Fig. 2.

The temperatures decrease drastically with the increase of the molar ratio of NaOTf to **1b** from 0 to 0.3. Further addition of NaOTf results in the increase of the clearing points. Fan-like textures characteristic of a hexagonal columnar phase (Col_h) were observed for the mixtures in the ratio of NaOTf to **1b** from 0.5 to 2.0. The addition of more than 2.5 mol of NaOTf led to the phase separation of the sodium salt from the mixture. The X-ray diffraction pattern of an equimolar complex of NaOTf and **1b** at 200 °C showed a sharp inner peak at 45.2 Å (d_{100}), small peaks at 26.0 and 22.6 Å (d_{110} and d_{200}, respectively), and a diffuse halo at 4.1 Å, which confirmed the formation of a disordered Col_h phase.

This phase transition behavior of the complexes can be explained as follows. The initial decrease of the temperatures was caused by the co-existence of hydrogen-bonded forms A and B (Fig. 1) in the smectic order. Further addition of NaOTf resulted in the formation of discotic aggregates leading to the induction of a hexagonal columnar order by ion–dipole interaction through sodium salts and the carbonyl oxygen of the pterin rings. These aggregates were further stabilized by the increase of the ion–dipole interactions. The formation of columnar phases by the complexation of covalently bonded cyclic molecules with metal salts has been reported.[11] However, to our knowledge, there has been no example of liquid crystals changing from smectic to columnar phases due to the change of hydrogen-bonding patterns by the effect of metals.

In summary, we have prepared, for the first time, thermotropic LC folic acid derivatives. In particular, for compound **1b**, the smectic phase can be changed to hexagonal columnar phases by the ion–dipole interactions. We are further exploring nanostructures formed by hydrogen-bonded aggregation of folic acid derivatives.

This work was financially supported by the Shiseido Fund for Science and Technology and by the Ministry of Education, Science, Sports, and Culture (Grant-in-Aid No. 12650864).

Notes and references

‡ Compound **1b** was prepared by amidation[12] of N^{10}-trifluoroacetylpteroic acid with bis[2-(3,4-diundecyloxyphenyl)ethyl] L-glutamate (**2b**) resulting in a yield of 40% as a pale yellow waxy oil. R_f = 0.40 (CH_2Cl_2/ethanol/benzene = 13/1/1); ^{1}H NMR (400 MHz, $CDCl_3$) δ 8.81 (s, 1 H), 7.87 (d, J = 8 Hz, 2 H), 7.42 (d, J = 8 Hz, 2 H), 6.81–6.69 (m, 6 H), 5.16 (s, 2 H), 4.77–4.72 (m, 1 H), 4.36–4.21 (m, 4 H), 3.99–3.93 (m, 8 H), 2.88 (t, J = 7 Hz, 2 H), 2.83 (t, J = 7 Hz, 2 H), 2.47–2.35 (m, 2 H), 2.26–2.20 (m, 1 H), 2.11–2.04 (m, 1 H), 1.80–1.76 (m, 8 H), 1.43–1.24 (m, 64 H), 0.86 (t, J = 7 Hz, 12 H); Maldi-TOF MAS (matrix, IAA): *m/z* 1427.65. Experimental details for the preparation of **2b** as well as **1b** are summarized in the ESI.†

§ A differential scanning calorimetric apparatus (Mettler DSC 30) and a polarizing microscope (Olympus BH2) equipped with a Mettler FP82HT hot stage were used for characterization of **1**. X-Ray diffraction measurements were carried out on a Rigaku X-ray Rad 2B system with a heating stage using Ni-filtered Cu-Kα radiation. IR spectra were recorded on a JASCO FT/IR-8900μ at room temperature using a thin pellet of KBr as the substrate.

¶ Similar patterns were observed for the N–H stretching band of **1a** and **1b** in IR spectra (3351 and 3341 cm^{-1}, respectively), whereas the peaks were split to 3304 and 3251 cm^{-1} for **1c**. See ESI† for the IR spectra.

1 J.-H. Fuhrhop and J. Köning, *Membranes and Molecular Assembles: The Synkinetic Approach*, The Royal Society of Chemistry, Cambridge, 1994; J.-M. Lehn, *Supramolecular Chemistry*, VCH, Weinheim, 1995.
2 Molecular Self-Assembly Organic Versus Inorganic Approaches, *Structure and Bonding, Vol. 96*, ed. M. Fujita, Springer, Berlin, 2000.
3 S. D. Hudson, H.-T. Jung, V. Percec, W.-D. Cho, G. Johansson, G. Ungar and V. S. K. Balagurusamy, *Science*, 1997, **278**, 449; V. Percec, G. Johansson, G. Ungar and J. Zhou, *J. Am. Chem. Soc.*, 1996, **118**, 9855.
4 T. Kato, in *Handbook of Liquid Crystals, Vol. 2B*. ed. D. Demus, J. W. Goodby, G. W. Gray, H. W. Spiess and V. Vill, Wiley-VCH, Weinheim, 1998, p. 969; C. M. Paleos and D. Tsiourvas, *Angew. Chem., Int. Ed. Engl.*, 1995, **34**, 1696; T. Kato, *Struct. Bonding*, 2000, **96**, 95; T. Kato and J. M. J. Fréchet, *Macromol. Symp.*, 1995, **98**, 311; N. Zimmerman, J. S. Moore and S. C. Zimmerman, *Chem. Ind.*, 1998, 604.
5 F. Ciuchi, G. D. Nicola, H. Franz, G. Gottarelli, P. Mariani, M. G. P. Bossi and G. P. Spada, *J. Am. Chem. Soc.*, 1994, **116**, 7064.
6 G. W. Gray and J. W. Goodby, *Smectic Liquid Crystals*, Leonard Hill, Glasgow, 1984.
7 The layered self-organized structures of guanine bases were reported, see: K. Araki, M. Abe, A. Ishizaki and T. Ohya, *Chem. Lett.*, 1995, 359; G. Gottarelli, S. Masiero, E. Mezzina, S. Pieraccini, G. P. Spada and P. Mariani, *Liq. Cryst.*, 1999, **26**, 965.
8 The cyclic tetramer formation of guanosine derivatives by complexation with alkaline metals was reported, see: G. Gottarelli, S. Masiero and G. P. Spada, *J. Chem. Soc., Chem. Commun.*, 1995, 2555.
9 D. Guillon, *Struct. Bonding*, 1999, **95**, 41; R. Kleppinger, C. P. Lillya and C. Yang, *Angew. Chem., Int. Ed. Engl.*, 1995, **34**, 1637; M. Suárez, J.-M. Lehn, S. C. Zimmerman, A. Skoulios and B. Heinrich, *J. Am. Chem. Soc.*, 1998, **120**, 9526; D. Goldmann, D. Janietz, R. Festag, C. Schmidt and J. H. Wendorff, *Liq. Cryst.*, 1996, **21**, 619.
10 The tetramer formation of guanine base was applied for ionophore formation and enantioselective extraction of amino acid derivatives, see: S. Tirumala and J. T. Davis, *J. Am. Chem. Soc.*, 1997, **119**, 2769; V. Andrisano, G. Gottarelli, S. Masiero, E. H. Heijne, S. Pieraccini and G. P. Spada, *Angew. Chem., Int. Ed.*, 1999, **38**, 2386.
11 See, for example: A. Liebmann, C. Mertesdorf, T. Plesnivy, H. Ringsdorf and J. H. Wendorff, *Angew. Chem., Int. Ed. Engl.*, 1991, **30**, 1375; V. Percec, D. Tomazos, J. Heck, H. Blackwell and G. Ungar, *J. Chem. Soc., Perkin Trans. 2*, 1994, 31.
12 H. A. Godwin, I. H. Rosenberg, C. R. Ferenz, P. M. Jacobs and J. Meienhofer, *J. Biol. Chem.*, 1972, **247**, 2266.

Unexpected synthesis of (bis(diphenylphosphinoyl)ethane)·2(2,2-dihydroperoxypropane) 1 : 2 adduct: a new route to stable organic dihydroperoxides

Claudio Pettinari,*[a] Fabio Marchetti,[a] Augusto Cingolani,[a] Andrei Drozdov[b] and Sergei Troyanov†[b]

[a] *Dipartimento di Scienze Chimiche, Università degli Studi, via S. Agostino 1, 62032 Camerino, Italy. E-mail: pettinar@camserv.unicam.it*

[b] *Moscow State University, Chemistry Department, Vorobjevy Gory, 119899, Moscow, Russia. E-mail: troyanov@thermo.chem.msu.ru*

Received (in Liverpool, UK) 27th June 2000, Accepted 22nd August 2000
First published as an Advance Article on the web

By reaction of hydrogen peroxide and bis(diphenylphosphino)ethane in acetone, the 1 : 2 adduct (bis(diphenylphosphinoyl)ethane)·2(2,2-dihydroperoxypropane) ($dppeO_2$)·2[$Me_2C(OOH)_2$], stabilized by H-bonding between $Me_2C(OOH)_2$ and $dppeO_2$, was rapidly obtained in high yields in the presence of R_2SnCl_2 (R = Me or Bu^n).

Organic peroxides derived from acetone and hydrogen peroxide have been extensively studied.[1–5] The products identified to date in aqueous acetone–hydrogen peroxide solutions are 2-hydroxy-2-hydroperoxy propane **1**,[3] 2,2-dihydroperoxypropane **2**,[1,2] α,α′-bis(hydroperoxy)diisopropyl peroxide **3**[1,2] and 1,1,4,4,7,7-hexamethyl-1,4,7-cyclononatriperoxane **4**.[1,2,5]

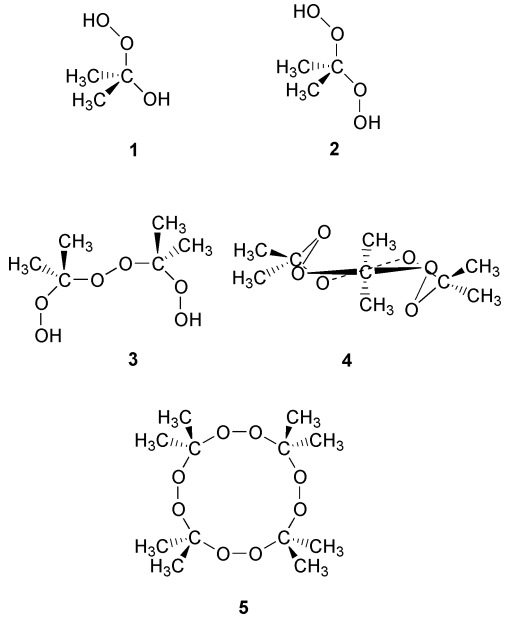

Very recently a tetrameric species [1,1,4,4,7,7,9,9-octamethyl-1,4,7,9-tetraundecotetraperoxane) **5** has been isolated from an acetone–H_2O_2 solution containing $SnCl_4$·$5H_2O$ or $SnCl_2$·$2H_2O$. It has been hypothesized that tin(IV) salts catalyze the oxidation of acetone by hydrogen peroxide to tetrameric acetone peroxide at room temperature.[6] All the species **1**–**5** readily decompose. The structures of **1**–**3** and **5** have been hypothesized only on the basis of spectroscopic IR and NMR data, whereas the crystal structure of **4** was determined some years ago.[5] During our studies[7] on the interaction between tin(IV) acceptors and diphosphinoyl donors in acetone, using hydrogen peroxide as oxidizing agent for organic phosphines, we observed the formation of the crystalline adduct ($dppeO_2$)·2[$Me_2C(OOH)_2$] **6**.[8] Whereas the free 2,2-dihydroperoxypropane **2** decomposes rapidly due to its fast transformation into the more stable cyclic peroxo compounds **4** or **5**, **6** is very stable under the same conditions in both solid and solution states. The stabilization of dihydroperoxide **2** in the crystals of **6** can be explained by formation of H-bonds between the hydrogen atoms of $Me_2C(OOH)_2$ and the oxygen atoms of $dppeO_2$, which in this case acts as hydrogen acceptor. The energy of the hydrogen bond most likely prevents the oligomerization of the peroxide into the usual trimeric or tetrameric forms. The adduct **6** has a molecular structure[9] with two molecules of dihydroperoxide H-bonded to $dppeO_2$ (Fig. 1). The O–O distances in the peroxide (mean value 1.461 Å) are close to those in hydrogen peroxide (1.453 Å).[10] The bis(diphenylphosphinoyl)ethane molecule is stabilized in a staggered conformation. Each oxygen atom of $dppeO_2$ forms two H-bonds with a dihydroperoxide molecule (O(3)–H(3)···O(1) 2.758(2) Å, ∠O(3)–H(3)–O(1) 170(3)°; O(5)–H(5)···O(1) 2.824(3) Å, ∠O(5)–H(5)–O(1) 169(3)°).

When the reaction between dppe and H_2O_2–acetone was carried out in the absence of R_2SnCl_2 (R = Me or Bu^n) acceptors, compound **6** was obtained in only 40% yield after 10 days, whereas in the presence of tin acceptors the yield was much higher (90%) after only 24 h. This result is in accordance

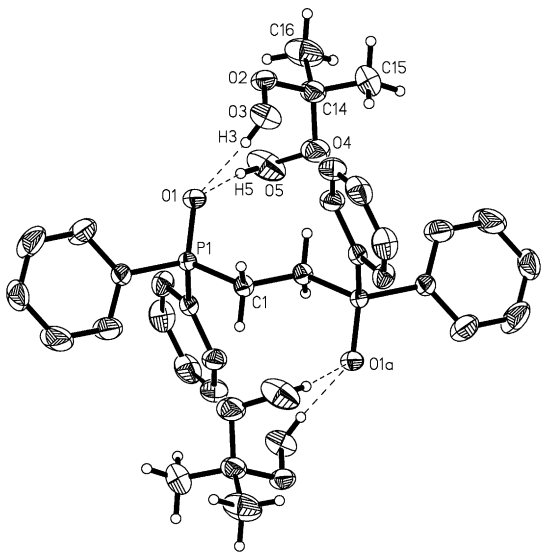

Fig. 1 Molecular structure of ($dppeO_2$)·2[$Me_2C(OOH)_2$] **6**. Selected bond distances (Å) and angles: P(1)–O(1) 1.511(1), P(1)–C(1) 1.805(2), P(1)–C(2) 1.795(2), P(1)–C(8) 1.812(2), C(14)–O(2) 1.425(3), O(2)–O(3) 1.464(2), C(14)–O(4) 1.428(2), O(4)–O(5) 1.457(3); ∠O(2)–C(14)–O(4) 110.2(2)°.

DOI: 10.1039/b005221n

with the recent work[6] on the oxidation of acetone by H_2O_2 catalysed by tin(IV) and tin(II) compounds.

When the reaction between dppe and H_2O_2–acetone was carried out in the presence of Ph_2SnCl_2, the derivative $Ph_2SnCl_2(dppeO_2)$[11] precipitated from the reaction mixture and no trace of **6** was detected after 48 h.

When **6** was reacted with Ph_2SnCl_2, the derivatives $Ph_2SnCl_2(dppeO_2)$,[11] **3** and **4** are afforded. In fact Ph_2SnCl_2 is a stronger Lewis acid than dialkyltin(IV) dihalides and it is able to substitute the dihydroperoxide in **6**, yielding the well known stable adduct $Ph_2SnCl_2(dppeO_2)$.[11] On the other hand, when R_2SnBr_2 (R = Me or Bu^n) were employed, **6** was obtained in 90% yields after 6 h. The substitution of chloride groups with the less electronegative bromide in diorganotins seems to accelerate the formation of **6**, in accordance with the weaker acceptor power of the corresponding Lewis acid.

Finally, when dppm, dppp (1,3-bis(diphenylphosphino)propane) or triphenylphosphine were employed, no dihydroperoxide adducts such as **6** were obtained, thus indicating that the methylene chain between the $–P(O)Ph_2$ units can be an important steric factor.

In summary, oxidized diphosphine ligand $dppeO_2$ is able to stabilize 2,2-dihydroperoxide formed by interaction of acetone with H_2O_2 and prevent cyclo-oligomerization. The formation of adduct **6** can be accelerated by R_2SnCl_2 (R = Me or Bu^n). Studies on the possibility of obtaining different dihydroperoxides by starting from different ketones, on the ability of other tin(IV) salts to catalyse the reaction between H_2O_2 and acetone, and finally on the importance of the diphosphine chain for the obtainment of compounds as **6**, are actually in progress.

This work was supported by Universities of Camerino and Moscow.

Notes and references

† Correspondence author for X-ray structure.

1 A. Rieche, *Angew. Chem.*, 1958, **70**, 251.
2 N. A. Milas and A. Golubovic, *J. Am. Chem. Soc.*, 1959, **81**, 6461.
3 M. C. V. Sauer and J. O. Edwards, *J. Phys. Chem.*, 1971, **75**, 3004.
4 M. C. V. Sauer and J. O. Edwards, *J. Phys. Chem.*, 1972, **76**, 1283.
5 P. Groth, *Acta Chem. Scand.*, 1969, **23**, 1311.
6 H. Jiang, G. Chu, H. Gong and G. Qiao, *J. Chem. Res. (S)*, 1999, 288.
7 C. Pettinari, F. Marchetti, A. Cingolani, R. Pettinari, A. Drozdov and S. Troyanov, *Inorg. Chim Acta*, submitted.
8 *[Bis(diphenylphosphineoxo)ethane·2(2,2-dihydroperoxypropane)]* (**1**): Me_2SnCl_2 (0.219 g, 1.0 mmol) and dppe (0.398 g, 1.0 mmol) were dissolved in 30 ml acetone. To the colorless solution, 5 ml 10% H_2O_2 was added. The clear solution was stirred for 24 h, and then kept at 4 °C overnight. A colorless precipitate formed which has been identified as ($dppeO_2$)·2(2,2-dihydroperoxypropane). It was recrystallized from acetone. Yield 90%. Mp 146 °C dec. Found, %: C 59.70; H 6.30; calc. for $C_{32}H_{40}O_{10}P_2$: C 59.44; H 6.24. IR (nujol, cm^{-1}): 3384br ν(O–H···O), 1704s δ(O-H···O), 1175sh, 1158s, 1148vs, 1120s ν(P=O). ^{1}H NMR ($CDCl_3$) δ 1.49s (12H, CH_3), 2.61t (4H, PCH_2CH_2P), 7.5m (10H, $P–C_6H_5$), 7.8m (10H, $P–C_6H_5$), 10.7br (4H, OH).
9 *Crystal data* for **1**: $C_{32}H_{40}O_{10}P_2$, M = 646.58 g cm^{-3}. IPDS(Stoe) Mo-Kα, T 180 K, orthorhombic, space group *Pbca*, a = 15.447(3), b = 10.989(2), c = 19.907(4) Å, Z = 4, μ = 12.07 cm^{-1}, 3414 measured and 2081 independent reflections, no absorption corrections, hydrogen atoms of dppe were placed in the calculated positions, R_1 = 0.0362, wR_2 = 0.0861 with 2777 reflections and 210 parameters (SHELXL-93). CCDC reference number 182/1765. See http://www.rsc.org/suppdata/b005221n/ for crystallographic files in .cif format.
10 N. N. Greenwood and A. Earnshaw, *Chemistry of the Elements*, Pergamon Press, 1985, p. 720.
11 P. G. Harrison, N. W. Sharpe, C. Pelizzi, G. Pelizzi and P. Tarasconi, *J. Chem. Soc., Dalton Trans.*, 1983, 921.

ChemComm

Photocatalytic water oxidation by Nafion-stabilized iridium oxide colloids

Michikazu Hara and Thomas E. Mallouk*

Department of Chemistry, The Pennsylvania University, University Park, PA 16802, USA.
E-mail: tom@chem.psu.edu

Received (in Columbia, MO, USA) 20th April 2000, Accepted 29th August 2000
First published as an Advance Article on the web 18th September 2000

A photosystem composed of colloidal $IrO_2 \cdot xH_2O$ stabilized by soluble Nafion, tris(2,2′-bipyridyl)ruthenium(II), and persulfate efficiently oxidizes water to oxygen under visible light.

Much effort has been applied to the development of photosystems for visible light cleavage of water into H_2 and O_2.[1–3] Although the reaction is thermodynamically possible with light of wavelength ⩽1000 nm, efficient water photolysis has not yet been reported. One of the key components of such photolysis systems is the catalyst that converts water into O_2.[4–8] As a four-electron redox process, the evolution of O_2 from water is more difficult than kinetically simpler processes, such as H_2 evolution. Recently, we have reported photocatalytic oxidation of water by a buffered $[Ru(bpy)_3]^{2+}$–colloidal $IrO_2 \cdot xH_2O$ system that uses $S_2O_8^{2-}$ as a sacrificial electron acceptor.[9] In this case, the quantum efficiency for O_2 evolution under optimized conditions is about 50%, and the turnover number with respect to the photosensitizer exceeds 200. The turnover rate is very fast compared with that of other $[Ru(bpy)_3]^{2+}$–catalyst–$S_2O_8^{2-}$ systems, but is still too slow to be coupled with a non-sacrificial hydrogen evolving system[10] for overall water photolysis.

Colloidal catalysts in these photosystems are stabilized by coordinating reagents such as citrate ions and polyethylene glycol. The colloid is negatively charged, and adsorbed cationic sensitizers take part in the water oxidation cycle. Interestingly, there is little or no activity at concentrations below that required to saturate the colloid with sensitizer molecules.[9] This suggests that colloidal catalysts stabilized by polyanions might exhibit a higher activity for O_2 evolution than conventional catalysts. In this paper, we report O_2 evolution from a $[Ru(bpy)_3]^{2+}$–Nafion-stabilized $IrO_2 \cdot xH_2O$–$S_2O_8^{2-}$ photosystem. Very stable colloids form in solutions containing soluble Nafion, and the $[Ru(bpy)_3]^{2+}$ photosystem incorporating these catalytic colloids has an appreciably higher quantum efficiency for water oxidation than conventional systems at moderate to high light intensity.

Nafion-stabilized and citrate-stabilized $IrO_2 \cdot xH_2O$ colloids (Nafion/IrO_2 and citrate/IrO_2) were compared as O_2 evolution catalysts. Citrate/IrO_2 was available from our earlier study, in which hexachloroiridate ions ($IrCl_6^{2-}$) were hydrolyzed in a citrate solution at pH 7.[9] Nafion/IrO_2 was prepared similarly in the presence of soluble Nafion perfluorinated ion-exchange resin.[11] The deep blue colloidal solution was stable over a period of three months. The UV–VIS spectrum of the solution had a broad absorption band in the range of 500–700 nm, signaling the formation of colloidal $IrO_2 \cdot xH_2O$,[7] which is apparently stabilized by interaction with the sulfonate groups of Nafion. A TEM image of Nafion/IrO_2 (0.05 g Nafion/0.030 g K_2IrCl_6) is shown in Fig. 1. Primary particles less than 10 nm in diameter form small aggregates that have diameters of 20–30 nm. The grouping of these aggregates into the micron-size patch shown in Fig. 1 is probably an artifact of TEM sample preparation, since the colloidal solutions are not turbid. Citrate/IrO_2 makes similar colloids, except that larger primary particles (10–15 nm) are observed.[9]

The photolysis reactions were carried out in 5 mL aqueous solutions containing $[Ru(bpy)_3]Cl_2 \cdot 6H_2O$, colloidal IrO_2, $Na_2S_2O_8$, Na_2SO_4 and Na_2SiF_6–$NaHCO_3$ buffer in a Pyrex test tube reactor. The concentrations of $Na_2S_2O_8$, Na_2SO_4 and Na_2SiF_6–$NaHCO_3$ buffer were 1.0×10^{-2}, 5.0×10^{-2} and 2.2×10^{-2}–2.8×10^{-2} M, respectively, and the constantly stirred solutions were irradiated with a Xe lamp of 300 W, equipped with a 450 ± 20 nm interference filter. Except as noted, the intensity of visible light reaching the solution was 18 mW cm^{-2}. The solutions were buffered at pH 5.4–5.7 during photolysis. The details are described elsewhere.[9]

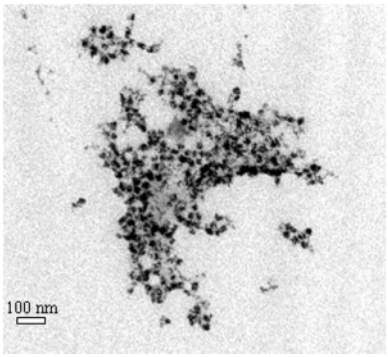

Fig. 1 TEM image of Nafion-stabilized IrO_2 colloid (prepared from 0.05 g Nafion/0.030 g K_2IrCl_6).

Fig. 2 shows the dependence of the sensitizer turnover number and initial O_2 evolution rate on concentration of the sensitizer for $[Ru(bpy)_3]$–Nafion/IrO_2 ([Ir] = 1.0×10^{-4} M) and $[Ru(bpy)_3]$–citrate/IrO_2 ([Ir] = 6.2×10^{-5} M). Nafion/IrO_2 colloids prepared from 0.05 g Nafion/0.030 g K_2IrCl_6 were used for these reactions. The rate of O_2 evolution plotted in this figure is that observed in the early stages of the reaction (5–10

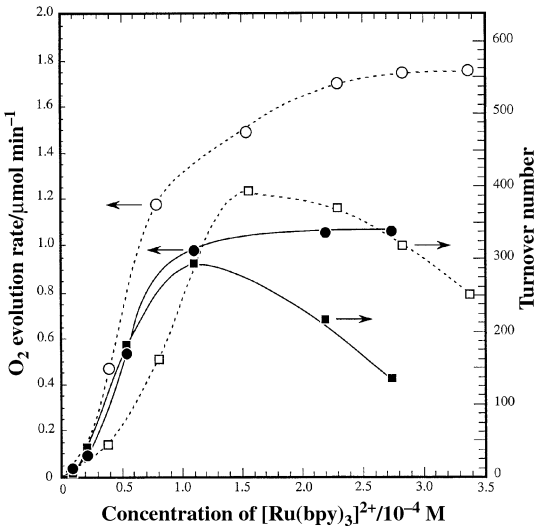

Fig. 2 Dependence of the initial rate of O_2 evolution and turnover number on the concentration of $[Ru(bpy)_3]^{2+}$. For $[Ru(bpy)_3]^{2+}$–Nafion/IrO_2–persulfate, initial rate of O_2 evolution (○), turnover number (□); $[Ru(bpy)_3]^{2+}$–citrate/IrO_2–persulfate, initial rate of O_2 evolution (●), turnover number (■). Nafion/IrO_2: [Ir] = 1.0×10^{-4} M; citrate/IrO_2: [Ir] = 6.2×10^{-5} M.

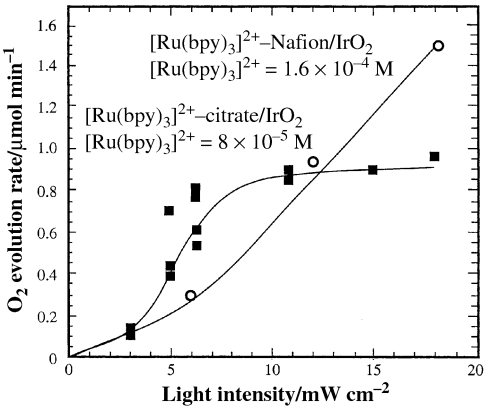

Fig. 3 Light intensity dependence of the initial rate of oxygen evolution for $[Ru(bpy)_3]^{2+}$–Nafion/IrO_2 and $[Ru(bpy)_3^{2+}$–citrate/IrO_2.

min) before significant decomposition of the sensitizer occurs. Each photosystem showed the highest O_2 evolution rate at the colloid concentration used in these experiments. Further addition of colloid to either system decreased both the turnover number and the O_2 evolution rate, because at high concentration the colloidal catalyst begins to quench the MLCT excited state of the sensitizer oxidatively.[6] In both systems, the turnover number reaches a maximum and the rate of O_2 evolution reaches a plateau at high sensitizer concentration. Beyond (1.1–1.5) $\times$ 10^{-4} M, the background decomposition rate of $[Ru(bpy)_3]^{3+}$ exceeds the rate of O_2 evolution and the turnover number decreases.[9] At high light intensity, $[Ru(bpy)_3]^{2+}$–Nafion/IrO_2 surpassed $[Ru(bpy)_3]^{2+}$–citrate/IrO_2 in the rate of O_2 evolution at all concentrations, and the difference in rate increased with increasing sensitizer concentration. The turnover number of the former system also exceeded that of the latter at high concentration. The highest quantum efficiencies for O_2 evolution, ϕO_2, with Nafion/IrO_2 and citrate/IrO_2 catalysts were 73% (2.8 $\times$ 10^{-4} M sensitizer) and 45% ($\geq$2.2 $\times$ 10^{-4} M), respectively.[12] The rate of O_2 evolution in the Nafion/IrO_2 system is light-limited up to the highest light intensity used (18 mW cm^{-2}), whereas that of citrate/IrO_2 is catalyst-limited above about 10 mW cm^{-2} (Fig. 3). This indicates that the turnover rate of the former catalyst is approximately twice that of the latter.

The effects of ionic strength and pH on the time course of O_2 evolution were determined by changing the concentration of buffer and ratio of Na_2SiF_6 to $NaHCO_3$. With buffer concentrations in the range (3.5–5.7) $\times$ 10^{-2} M, there was no noticeable effect of concentration on the time course of O_2 evolution. At lower concentrations, both the rate and turnover number decreased, but in this case the final pH was <4, so the loss in activity can be attributed to the failure of the dilute buffer to maintain the optimum pH (4–6). At initial pH >6.5 the rate also decreases, because the driving force for O_2 evolution decreases. An essentially identical pH dependence has been previously noted by Harriman and coworkers.[6–8]

Interestingly, both initial rate curves in Fig. 2 saturate in the manner of an adsorption isotherm, suggesting that O_2 evolution from these catalysts only occurs when sensitizer molecules are adsorbed on to the colloid.[9] In particular, the rate plot for citrate-stabilized IrO_2 resembles a Langmuir adsorption isotherm.[9] This behavior has also been observed in the $[Ru(bpy)_3]^{2+}$–colloidal RuO_2 system.[6] In contrast, the rate–concentration curve of $[Ru(bpy)_3]^{2+}$–Nafion/IrO_2 has a different shape, and appears to be the sum of two different kinds of isotherms. The turnover plot also peaks at higher $[Ru(bpy)_3]^{2+}$ concentration in this case. We tentatively attribute this behavior to the adsorption of more than a single monolayer of sensitizer on the Nafion polyanion-stabilized colloid.

In summary, colloidal IrO_2 can be stabilized using soluble Nafion, which promotes the photocatalytic oxidation of water through adsorption of sensitizer cations. Very high quantum yields and turnover numbers were achieved under optimized conditions. The high activity of these polyanion-stabilized colloids suggests that further rate enhancement may be possible using structured polyanion/polycation films or other organized assemblies. These possibilities are currently under investigation.

This work was supported by the Division of Chemical Sciences, Office of Basic Energy Sciences, Department of Energy, under contract DE-FG02-93ER14374. We thank Dr Rosemary Walsh and the Electron Microscope Facility for the Life Sciences in the Biotechnology Institute at Pennsylvania State University for the use of the transmission electron microscope.

Notes and references

1 K. Domen, *Catal. Today*, 1998, **44**, 17.
2 O. Khaselev and J. A. Turner, *Science*, 1998, **280**, 425.
3 A. Kudo, H. Kato and S. Nakagawa, *J. Phys. Chem. B*, 2000, **104**, 571; H. G. Kim, D. W. Hwang, J. Kim, Y. G. Kim and J. S. Lee, *Chem. Commun.*, 1999, 1077.
4 J. Kiwi and M. Grätzel, *Nature*, 1979, **285**, 657.
5 J. Kiwi and M. Grätzel, *J. Am. Chem. Soc.*, 1979, **101**, 7214.
6 A. Harriman, M. Richoux, P. A. Christensen, S. Moseri and P. Neta, *J. Chem. Soc., Faraday Trans. 1*, 1987, **83**, 3001.
7 A. Harriman, J. M. Thomas and G. R. Millward, *New J. Chem.*, 1987, **11**, 757.
8 A. Harriman, I. J. Pickering, J. M. Thomas and P. A. Christensen, *J. Chem. Soc., Faraday Trans. 1*, 1988, **84**, 2795.
9 M. Hara, C. C. Waraksa, J. T. Lean, B. A. Lewis and T. E. Mallouk, *J. Phys. Chem. A*, 2000, **104**, 5275.
10 G. B. Saupe, W. Kim, R. H. Schmehl and T. E. Mallouk, *J. Phys. Chem. B*, 1997, **101**, 2508.
11 20 g Nafion–aliphatic alcohols–water solution (Aldrich, Nafion 5 wt%) was added to 300 mL deionized water. The solution was heated to 70–80 °C on a hot-plate until the total volume was reduced to 50 mL, and was then diluted to 300 mL. This procedure was repeated three times to remove aliphatic alcohols from the solution. The total volume of the final solution was adjusted to 100 mL. 0.030 g K_2IrCl_6 (6.2 $\times$ 10^{-5} mol) was added to 50 mL aqueous solutions containing 0.01–0.25 g dissolved Nafion, which were prepared from the Nafion stock solution described above. The resulting red-brown solution was adjusted to pH 5.0 with 0.25 M NaOH and was heated to 95 °C on the hot-plate with constant stirring. If less than 0.01 g dissolved Nafion was added, or if the pH was above 7, solid IrO_2 precipitated upon heating. After heating for 1 h, the deep blue solution was cooled to room temperature and NaOH solution was added to adjust the pH to the initial value. The solution was transferred to a round bottom flask with a reflux condenser and was kept at 95 °C for 2 h with O_2 bubbling through the solution. The pH was then adjusted to 5.0 with NaOH solution, and the solution was stirred with 10 mL of DOWEX 2X8-50 anion exchange resin to remove excess Nafion. After 30 min, the DOWEX resin was removed by filtration, and the final solution was diluted to 100 mL.
12 Quantum efficiencies (ϕO_2) were calculated using the following equation,[8] in which ϕO_2 (%) = $(2RO_2/I) \times 100$, where RO_2 and I represent the O_2 evolution rate (molecules min^{-1}) and the rate of absorption of incident photons (photons min^{-1}), respectively. The factor of two arises because two photons produce one O_2 molecule when persulfate is used as the sacrificial electron acceptor.

Amine guest size and hydrogen-bonding influence the structures of *p-tert*-butylcalix[4]arene inclusions†

Eric B. Brouwer, Kostantin A. Udachin, Gary D. Enright and John A. Ripmeester*

Steacie Institute for Molecular Sciences, National Research Council, Ottawa, Ontario, Canada K1A 0R6. E-mail: jar@ned1.sims.nrc.ca

Received (in Columbia, MO, USA) 4th February 2000, Accepted 24th July 2000
First published as an Advance Article on the web

A novel structure involving a 2(*p-tert*-butylcalix[4]arene)·3.5(1,4-butanediamine) inclusion compound shows amine sites both *exo* and *endo* to the cavity, with the amine hydrogen-bonding to itself as well as to the host hydroxyl groups; for bulky amines with large pK_a values, steric factors are more important than basicity, and the formation of a 1:1, high-symmetry host–guest structure is preferred over a low-symmetry hydrogen-bonded structure.

The upper and lower rims of the *p-tert*-butylcalix[4]arene **1** basket-shaped cavity have been extensively derivatised in order to tailor supramolecular behaviour,[1] and almost all modifications at the lower (OH-bonded) rim have been covalent. We report the modification of the cavity's lower rim *via* H-bonding with amines, giving a non-covalent elaboration of the calixarene in the solid state. A delicate balance between amine size and basicity in forming H-bonded structures is observed. The molecular structure changes upon the induction of dynamics or guest loss for at least one of the amine guests in the 2(*p-tert*-butylcalix[4]arene)·3.5(1,4-butanediamine) compound **2**.

In general, interactions between amines and calixarenes in solution depend on the steric nature of the amine. If not too bulky the amine can abstract a proton from a calixarene hydroxyl group *via* a proton-transfer mechanism, forming an ion pair in which the guest occupies the host cavity in an *endo* arrangement.[2] Bulkier amines appear to interact with the host so that the amine is outside (*exo*) the host cavity.[3] Thermodynamic and conductance measurements of alkylamines and **1** in solution indicate H-bonding or ion-pair interactions between calixarene and amine.[4] A theoretical study of amine salts of the anion of **1** shows the preference for amine *endo* and *exo* positions to be solvent-dependent.[5] Amine interaction with the calix phenolic hydroxyl group forms the basis of sensors that change colour upon molecular recognition.[6]

Structures of several calixarene–amine complexes show that the amine interacts with the calixarene phenol in both *endo* and *exo* positions,[7] and structures of calixarenes with alkyl ammonium cations indicate cation inclusions, but no interactions between the guest and the H-bonded OH groups of the host.[8]

Solid-state ^{13}C NMR spectra of **1**·guest inclusion compounds provide a rapid means to determine symmetry elements.[9] An inclusion compound in which the host molecule has an axis of 4-fold symmetry gives a single resonance for each chemically distinct carbon of the *p-tert*-butylphenol repeat unit.[10] Lowering the symmetry element increases the multiplicity of each carbon resonance, as the four repeat units are no longer equivalent symmetrically. The ^{13}C CP-MAS NMR spectrum of **2** [Fig. 1(a)] indicates that the structure has very few, if any, symmetry elements. In particular, the δ 135–160 region shows the signals from the H1 and H4 aromatic carbons of the host. Whereas a high-symmetry structure gives only two host signals in this region, and three in the aliphatic region (δ 22–48),[9] the present spectrum shows 14 resolved lines over the region δ 135–160 and 11 lines (host and guest) in the aliphatic region. Peaks at 39.8 and 42.2 ppm arise from guest methylene carbons attached to the amine nitrogen, and are broadened due to coupling to the ^{14}N quadrupole or because of dynamic effects. The extent to which the aromatic carbon signals are spread out, the multiplicity, and the signal intensity distribution all contrast to the comparable features seen for nitrobenzene inclusion in the same host.[11] Clearly, the structure of **2** shows low symmetry, and is distinct from other low-symmetry structures such as **1**·nitrobenzene.

The existence of a significantly distorted host cavity is confirmed by the X-ray diffraction structure.‡ The asymmetric unit contains two crystallographically inequivalent host molecules, each without any element of symmetry. Each host molecule has two ordered and two disordered Bu^t groups: the *C*-host has the disordered groups positioned *cis* and the *T*-host has the disordered groups positioned *trans*. Unlike other structures of **1**, there is no clear correlation between the disorder in the host Bu^t groups and the disorder in the guest. The two Bu^t groups in the *C*-host are disordered over two positions each, while those in the *T*-host are disordered over two and four positions. There are 3.5 molecules of 1,4-butanediamine in the asymmetric unit (which contains two host molecules). Each *C*- and *T*-cavity contains one *endo* guest molecule, and that in the *T*-cavity is disordered over two positions. There are two, fully occupied *exo* guest sites outside the host cavities; one is on the inversion centre thus giving the fractional stoichiometry.

The structure possesses two independent groupings of H-bonded guests, one a finite trimer and the other an infinite chain. The trimer involves the *endo* guest of the *C*-host cavity (Fig. 2). This fully ordered guest adopts a curled ⊂-conformation in which the guest is H-bonded to itself ($d_{N–N}$ 2.72 Å), to one hydroxyl group of a *T*-host ($d_{N–O}$ 2.80 Å), and an amine group of the *exo* guest on the inversion centre ($d_{N–N}$ 2.77 Å). The *exo* amine group also interacts weakly with a second hydroxyl group of the same *T*-host ($d_{N–O}$ 3.3 Å); this hydroxyl group is

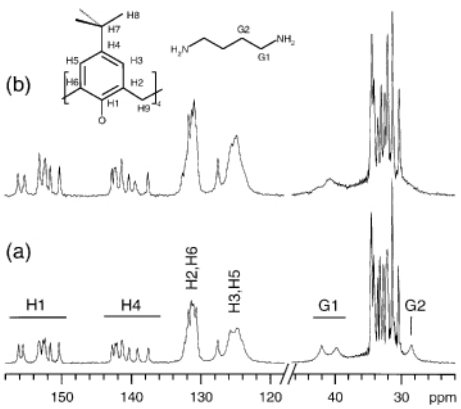

Fig. 1 Partial 75.48 MHz ^{13}C-{^{1}H} CP-MAS spectra: (a) **2**, (b) **2** after stirring in *n*-hexane. The aromatic host carbons are assigned; the aliphatic host carbons (H7, H8, H9) occur in the δ 27–36 region. Experimental details: 5.3 kHz spinning speed, 1600 transients, 3.4 μs 90° pulse, 50 kHz ^{1}H-decoupling field, 3.5 ms contact time, 1.5 s recycle delay, 40 kHz spectral width, 4 K data points collected and zero-filled to 16 K points.

† Issued as NRCC No. 43850. E. B. B. and J. A. R. thank NSERC for partial support of this work.

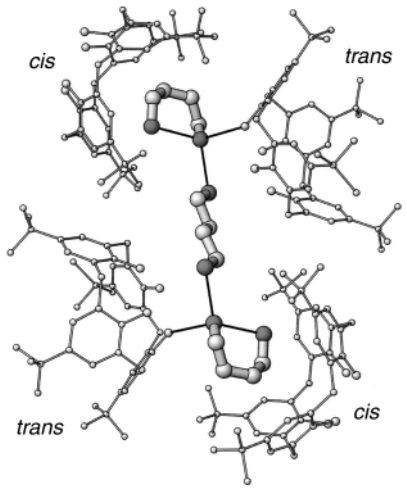

Fig. 2 Geometry of **2** indicating the finite hydrogen-bonding trimer involving the *endo* amine guest in the *C*-host cavity and the *exo* amine on the inversion centre.

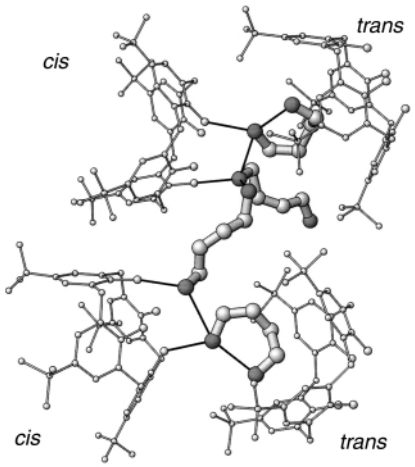

Fig. 3 Geometry of **2** indicating the infinite hydrogen-bonding chain involving the *endo* amine guest in the *T*-host cavity and the *exo* amine in the general position.

located *trans* to the first H-bonded hydroxyl group. The infinite chain involves the *endo* guest of the *T*-host cavity (Fig. 3); this guest is disordered over two positions. It is similarly curled and H-bonds to itself ($d_{N–N}$ 2.77 Å), to one hydroxyl group of a *C*-host ($d_{N–O}$ 3.01 Å), and an amine group of the second *exo* guest ($d_{N–N}$ 2.70 Å). This second *exo* guest further H-bonds with a symmetrically equivalent *exo* guest ($d_{N–N}$ 2.70 Å) and two adjacent hydroxyl groups of the *C*-host ($d_{N–O}$ 2.70 Å, $d_{N–O}$ 2.70 Å).

Hydrogen-bond formation is expected to depend primarily on the acidity of the host hydroxyl group (pK_a = 19.33 in benzonitrile)[4] and the amine basicity. Several amines have been used to form inclusion compounds of **1**, and the solid-state ^{13}C NMR spectra indicate the presence or absence of H-bonded structures.§ While amines with pK_a > 9 appear to favour H-bonded structures, the *sec*- and *tert*-butylamine compounds indicate that the amine basicity does not appear to direct the symmetry of the resultant structures, which show NMR spectra of the high-symmetry 1 : 1 host–guest inclusions.[9] Inclusion and orientation of these two guests in the host cavity are dominated by steric factors. It is intriguing to consider an amine guest in which the basicity and steric factors are so closely balanced that slight changes in conditions (*P*, *T*) cause the structural motifs in the inclusion compound to switch.

Finally, we report preliminary findings on the structural modifications of compound **2** that result from stirring in *n*-hexane.¶ The ^{13}C NMR spectrum in [Fig. 1(b)] shows a single guest amine G1 carbon signal (δ 41.0) whereas in **2**, there were two signals (δ 39.8 and 42.2). This feature indicates that *n*-hexane induces dynamic changes in the guest that may result from exchange of two rigid G1 carbons and/or loss of one of the guests from the lattice. Changes in the aromatic host carbon signals, though subtle, are well enough defined as slight differences in chemical shifts and intensities. Both NMR observations indicate that the structural modifications lie primarily with the guest, and that the affected guest likely occupies an interstitial or *exo* site, due to its longer intermolecular hydrogen bonds relative to the *endo* guests.

Notes and references

‡ *Crystal data* for **2**: $2(C_{44}H_{56}O_4)\cdot3.5(C_4H_{12}N_2)$, M = 1606.38, monoclinic, space group $P2_1/c$, a = 19.8406(12), b = 39.310(2), c = 13.3090(8) Å, β = 108.1070(10)°, V = 9866.2(10) Å^3, T = 173 K, Z = 4, D_c = 1.081 g cm^{-3}, μ(Mo-Kα) = 0.068 mm^{-1}, 85570 reflections measured, 16869 unique (R_{int} = 0.0735), R = 0.0755, R_w = 0.1573 [data $I > 2\sigma(I)$]. Disordered Bu^t groups were refined anisotropically over two (and the *T*-host, four) sites with occupancy ratios ranging from 80 : 20 to 50 : 50. Disordered *endo* 1,4-butanediamine molecules were refined anisotropically over two sites with 50% occupancy. Single crystals of **2** crystallise from 1,4-butanediamine at 70 °C. The structure was solved using direct methods and refined by full-matrix least squares on F^2 using SHELXTL.[12] CCDC 182/1769. See http://www.rsc.org/suppdata/cc/b0/b001274m/ for crystallographic files in .cif format.

§ **1**·amine compounds without host–guest hydrogen bonding: aniline (pK_a = 4.63), pyridine (5.25),[13] *sec*-butylamine (10.56), *tert*-butylamine (10.68); with host–guest hydrogen bonding: ammonia (9.25), benzylamine (9.33), 2-aminoethanol (9.50), 1,4-butanediamine (10.80, 9.35), 1-cyclohexylethylamine. H-bonded structures indicated by low-symmetry ^{13}C CP-MAS NMR spectra; pK_a values taken from CRC Handbook, CRC Press, Inc., Boca Raton, FL, 79th edn., 1998–99, pp. 8–46.

¶ 100 mg of **2** was added to *n*-hexane (3 mL) and stirred overnight at room temperature. Both **1**[4] and **2** have low solubility in *n*-hexane. The ^{13}C NMR spectrum indicates that no **1**·*n*-hexane compound is formed.[9]

1 C. D. Gutsche, *Calixarenes Revisited*, Royal Society of Chemistry, Cambridge, UK, 1998.
2 L. J. Bauer and C. D. Gutsche, *J. Am. Chem. Soc.*, 1985, **107**, 6063; C. D. Gutsche, M. Iqbal and A. Alam, *J. Am. Chem. Soc.*, 1987, **109**, 4314.
3 G. Görmar, K. Seiffarth, M. Schulz and C. L. Chachimbombo, *J. Prakt. Chem.*, 1991, **333**, 475.
4 A. F. Danil de Namor, M. T. Garrido Pardo, D. A. Pacheco Tanaka, F. J. Sueros Velarde, J. D. Cárdenas García, M. C. Cabaleiro and J. M. A. Al-Rawi, *J. Chem. Soc., Faraday Trans.*, 1993, **89**, 2727; A. F. Danil de Namor, J. Wang, I. Gomez Orellana, F. J. Sueros Velarde and D. A. Pacheco Tanaka, *J. Inclusion Phenom. Mol. Recognit. Chem.*, 1994, **19**, 371; A. F. Danil de Namor, R. M. Cleverley and M. L. Zapata-Ormachea, *Chem. Rev.*, 1998, **98**, 2495.
5 F. Fraternali and G. Wipff, *J. Inclusion Phenom. Mol. Recognit. Chem.*, 1997, **28**, 63.
6 Y. E. Jung, B. M. Song and S.-K. Chang, *J. Chem. Soc., Perkin Trans. 2*, 1995, 2031; T. Grady, S. J. Harris, M. R. Smith, D. Diamond and P. Hailey, *Anal. Chem.*, 1996, **68**, 3775; Y. Kubo, *Synlett*, 1999, 161; I. Mohammed-Ziegler, M. Kubinyi, A. Grofcsik, A. Grün and I. Bitter, *J. Mol. Struct.*, 1999, **480–481**, 289.
7 G. D. Andreetti, F. Ugozzoli, Y. Nakamoto and S.-I. Ishida, *J. Inclusion Phenom. Mol. Recognit. Chem.*, 1991, **10**, 241; M. Czugler, S. Tisza and G. Speier, *J. Inclusion Phenom. Mol. Recognit. Chem.*, 1991, **11**, 323; C. Bavoux and M. Perrin, *J. Inclusion Phenom. Mol. Recognit. Chem.*, 1992, **14**, 247.
8 J. M. Harrowfield, M. I. Ogden, W. R. Richmond, B. W. Skelton and A. H. White, *J. Chem. Soc., Perkin Trans. 2*, 1993, 2183; J. M. Harrowfield, W. R. Richmond, A. N. Sobolev and A. H. White, *J. Chem. Soc., Perkin Trans. 2*, 1994, 5.
9 E. B. Brouwer, J. A. Ripmeester and G. D. Enright, *J. Inclusion Phenom. Mol. Recognit. Chem.*, 1996, **24**, 1.
10 T. Komoto, I. Ando, Y. Nakamoto and S. Ishida, *J. Chem. Soc., Chem. Commun.*, 1988, 135; G. A. Facey, R. H. Dubois, M. Zakrzewski, C. I. Ratcliffe, J. L. Atwood and J. A. Ripmeester, *Supramol. Chem.*, 1993, **1**, 199.
11 E. B. Brouwer, G. D. Enright and J. A. Ripmeester, *Supramol. Chem.*, 1996, **7**, 7; E. B. Brouwer, G. D. Enright and J. A. Ripmeester, *J. Am. Chem. Soc.*, 1997, **119**, 5404.
12 G. M. Sheldrick, *Acta Crystallogr. Sect. A*, 1990, **46**, 467; G. M. Sheldrick, *Acta Crystallogr. Sect. A*, 1993, **49**, C467.
13 E. B. Brouwer, G. D. Enright, C. I. Ratcliffe, G. A. Facey and J. A. Ripmeester, *J. Phys. Chem. B*, 1999, **103**, 10 604.

ChemComm

A new general method for selective β-polynitration of porphyrins; preparation and redox properties of Zn-porphyrins bearing one through to eight β-nitro substituents and X-ray structure of the first Zn β-pernitro porphyrin†

Magali Palacio,[a] Virginie Mansuy-Mouries,[a] Guillaume Loire,[a] Karine Le Barch-Ozette,[a] Philippe Leduc,[a] Kathleen M. Barkigia,[b] Jack Fajer,[b] Pierrette Battioni[a] and Daniel Mansuy*[a]

[a] *UMR 8601, Université Paris V, 45 Rue des Saints-Pères, 75270 Paris Cedex 06, France. E-mail: daniel.mansuy@biomedicale.univ.paris5.fr*

[b] *Department of Applied Science, Brookhaven National Laboratory, Upton, New York 11973-5000, USA*

Received (in Basel, Switzerland) 19th May 2000, Accepted 28th July 2000
First published as an Advance Article on the web

Selective β-polynitration of Zn–5,10,15,20-tetrakis(2,6-dichlorophenyl)porphyrin, Zn(TDCPP), is achieved by controlled titration with the HNO_3–CF_3SO_3H–$(CF_3SO_2)_2O$ system, and affords a full series of Zn porphyrins bearing one through to eight β-nitro groups in high yield and exhibiting a wide range of reduction potentials (from −920 to +155 mV *vs.* SCE); an X-ray structure of the first reported β-pernitrated Zn porphyrin Zn(TDCPN$_8$P)(EtOH)$_2$·2EtOH confirms the synthetic methodology.

Iron and manganese meso-tetraaryl porphyrins bearing electron-withdrawing β-substituents have been shown to be efficient catalysts for cytochrome P450-mimetic oxygenations of hydrocarbons.[1] In an effort to obtain metalloporphyrins with significantly altered redox potentials and unusual reactivities, we have attempted to synthesize metalloporphyrins bearing as many electron-withdrawing β-nitro substituents as possible.[2] Nitration of TDCPPH$_2$[3] with red fuming HNO_3 led us to mixtures of β-pentanitro- and β-hexanitro-TDCPPH$_2$.[2a] More recently, we reported that a more powerful nitrating agent, consisting of a mixture of HNO_3 and $(CH_3CO)_2O$ in the presence of K10 montmorillonite, reacted with Zn(TDCPP) to afford the corresponding β-heptanitroporphyrin, Zn(TDCPN$_7$P), in 50% yield.[2b] However all the nitrating systems that we have used so far suffered from two main drawbacks, (i) they did not pernitrate the porphyrin to the β-octanitro level, and (ii) they did not act as general nitrating agents to produce all the desired β-polynitroporphyrins, Zn(TDCPN$_x$P) (x = 1–8), as the number of nitrating equivalents was increased. Indeed, selective formation of any one TDCPN$_x$P porphyrin required a different nitrating system[2] for each value of x.

We have now developed a nitrating system based on HNO_3 and the superacid CF_3SO_3H in the presence of $(CF_3SO_2)_2O$ that acts as a general nitrating agent for the selective synthesis of the full TDCPN$_x$P series. We describe here the successful use of this nitrating procedure to prepare all eight members of the Zn(TDCPN$_x$P) series in high yield, present the first X-ray structure of a β-pernitroporphyrin, Zn(TDCPN$_8$P), prepared by this method, and report the strikingly wide range of redox potentials now accessible *via* the eight members of the Zn(TDCPN$_x$P) series.

Titration of Zn(TDCPP) with 1, 2, 3, 4 or 6 equiv. of red fuming HNO_3 and CF_3SO_3H (1:1)[4] selectively led to Zn(TDCPN$_x$P) with x = 1, 2, 3, 4 or 6, respectively with yields between 50 and 70% (Table 1). However, the use of 5 equiv. of HNO_3–CF_3SO_3H led to a complex mixture of Zn(TDCPN$_x$P) with x = 4, 5 and 6. Moreover, low yields of Zn(TDCPN$_8$P) were obtained (*ca.* 25%, Table 1) when using the same system.

A slightly modified system consisting of red fuming HNO_3 in the presence of < 1 equiv. of CF_3SO_3H and $(CF_3SO_2)_2O$, in order to limit side reactions [demetallation and destruction of Zn(TDCPP)], allowed us to prepare each compound of the Zn(TDCPN$_x$P) series in much higher yields. Thus, titration of Zn(TDCPP) with increasing amounts of the HNO_3–CF_3SO_3H–$(CF_3SO_2)_2O$ (1:0.12:0.06) mixture selectively led to each compound of the Zn(TDCPN$_x$P) series (x = 1–7) with yields between 78 and 95%. Formation of the desired porphyrin was followed by thin-layer chromatography and addition of the nitrating agent was stopped after complete formation of the target product. The pernitrated Zn(TDCPN$_8$P) was selectively obtained with a satisfactory 50% yield by the same method under the conditions described in Table 1. The full range of β-nitro products obtained with this system contrasts sharply with

† Electronic supplementary information (ESI) available: ORTEP plots for **1**, bond distances and displacements from the plane of the porphyrin core. See http://www.rsc.org/suppdata/cc/b0/b004160m/

Table 1 Synthesis and reduction potentials of Zn(TDCPN$_x$P)

	x							
	1	2	3	4	5	6	7	8
Synthesis method	Yield (%)							
HNO_3–CF_3SO_3H (1:1)[a]	60	62	67	63	—[b]	60	53	25
HNO_3–CF_3SO_3H–$(CF_3SO_2)_2O$ (1:0.12:0.06)[c]	78	90	86	93	80	95	90	50
$E_{1/2}$ (first reduction)/mV *vs.* SCE[d]	−920	−750	−595	−470	−300	−150	0	+155

[a] Yields of Zn(TDCPN$_x$P) after addition of x equiv. of red fuming HNO_3 and CF_3SO_3H (1:1) to 5.2×10^{-5} M Zn(TDCPP) in CH_2Cl_2 at 20 °C and 0.5, 1, 2, 4, 5, 24, 48 and 72 h reaction time for x = 1 to 8, respectively. For x = 7 and 8, 10 and 40 equiv. of nitrating agent were added, respectively. [b] Only case in which Zn(TDCPN$_x$P) was not largely predominant. [c] Yields of Zn(TDCPN$_x$P) after titration of Zn(TDCPP) with the HNO_3–CF_3SO_3H–$(CF_3SO_2)_2O$ mixture. For $1 \leqslant x \leqslant 5$, reactions at 20 °C in CH_2Cl_2 for 24 h after addition of 1.1, 3.5, 6.5, 9 and 11 equiv. of HNO_3, respectively. For x = 6, 7 and 8, reactions at 30 °C in $MeNO_2$ for 1, 2 and 5 days and after addition of 18, 150 and 380 equiv. of HNO_3, respectively. [d] $E_{1/2}$ for the first one-electron reduction of Zn(TDCPN$_x$P), 10^{-3} M in CH_2Cl_2 containing 0.1 M NBu_4PF_6; $E_{1/2}$ for Zn(TDCPP) = −1285 mV.[2b]

DOI: 10.1039/b004160m

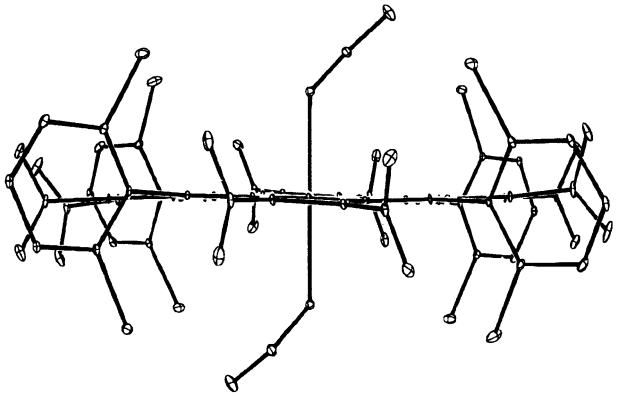

Fig. 1 Edge-on-view of $Zn(TDCPN_8P)(EtOH)_2$ **1**. Thermal ellipsoids have been reduced to 1% to illustrate the planarity of the porphyrin skeleton and the orientations of the substituents.

the classical nitrating HNO_3–H_2SO_4 system which was found to be efficient only for the preparation of the first four members of the $Zn(TDCPN_xP)$ series (yield *ca.* 80%).

All the $Zn(TDCPN_xP)$ compounds (x = 1–8) were completely characterized by elemental analysis and UV–VIS, ^1H NMR spectroscopy and mass spectrometry. Additional details of the syntheses and full characterizations will be presented elsewhere. It is of note that Zn(TDCPNP), $Zn(TDCPN_7P)$ and $Zn(TDCPN_8P)$ are single pure compounds while the other members of the $Zn(TDCPN_xP)$ series are mixtures of regioisomers with different relative positions of the β-nitro substituents.

The molecular structure of the first β-pernitrated porphyrin to be reported, $Zn(TDCPN_8P)(EtOH)_2$ **1**, was confirmed by an X-ray crystallographic study of **1**·2EtOH obtained by crystallization from CH_2Cl_2–EtOH.[5] As shown in Fig. 1, the Zn is axially coordinated by two molecules of EtOH with Zn–O distances of 2.272(10) Å and average Zn–N distances to the pyrrole nitrogens of 2.075(8) Å. The Zn–O and Zn–N distances are, respectively, the shortest and longest bond distances reported to date for hexacoordinated Zn porphyrins with oxygen donor axial ligands.[6] The tight axial bonds and the expanded porphyrin core are readily attributable to the multiple electron-withdrawing groups of **1**. In spite of the 12 peripheral substituents, which generally result in severe skeletal distortions,[7] the macrocycle of **1** is essentially planar with an average deviation from the 24-atom porphyrin plane of only 0.035 Å, and maximum displacements of only 0.08 and 0.07 Å at any one β or meso carbon, respectively. Macrocycle planarity is achieved by orienting all the peripheral substituents nearly orthogonal to the porphyrin plane: the two crystallographically independent phenyl rings align at 80 and 90° to the porphyrin plane whereas the four independent nitro groups subtend angles of 76, 82, 87, 77° to the same plane.

As established by cyclic voltammetry, all eight $Zn(TDCPN_xP)$ undergo a reversible one-electron reduction leading to the formation of π-anion radicals. Formation of such radicals[8] is confirmed by controlled-potential electrolysis of $Zn(TDCPN_8P)$ at 0 V *vs.* SCE in CH_2Cl_2 which yields a species that exhibits new absorption bands centered at 900 nm and a singlet EPR spectrum centered at g = 2.00.[9] Table 1 compares the reduction potentials of each ZnP/ZnP^- couple for all eight nitro derivatives. The potentials increase in a linear manner, the introduction of each additional β nitro group causing a shift of *ca.* +150 mV. Thus, the incorporation of eight β-nitro groups in Zn(TDCPP) leads to a strikingly large positive shift of *ca.* 1.4 V of the reduction potential and thus readily explains why the π-anion radical of $Zn(TDCPN_8P)$ forms under such mild reducing conditions, even in the presence of O_2.

In conclusion, we have developed a new general method for selective β-polynitration of Zn(TDCPP) in high yield based on controlled titration of the starting porphyrin with HNO_3–CF_3SO_3H–$(CF_3SO_2)_2O$. The method leads to a complete series of porphyrins bearing 1–8 β-nitro groups with a wide span of reduction potentials that range from −920 to +155 mV. Similar results were obtained with Ni(TDCPP) and methods for selective demetallation of the Zn and Ni polynitroporphyrins have been recently developed. Use of metallo–β-polynitroporphyrins in catalysis, and application of the nitration method to other polyaromatic molecules are under investigation.

This work was supported by CNRS, Université Paris V and the Division of Chemical Sciences, U.S. Department of Energy under Contract no. DE-ACO_2-98CH10886 at BNL.

Notes and references

1 For general reviews see: B. Meunier, *Chem. Rev.*, 1992, **92**, 1411; D. Mansuy, *Coord. Chem. Rev.*, 1993, **125**, 129; R. A. Sheldon, *Metalloporphyrins in Catalytic Oxidations*, M. Dekker, New York, 1994; J. T. Groves and Y. Z. Han, in *Cytochrome P450: Structure, Mechanism and Biochemistry*, ed. P. Ortiz de Montellano, Plenum Press, New York, 1995, p. 3; D. Dolphin, T. G. Traylor and L. Xie, *Acc. Chem. Res.*, 1998, **31**, 155.

2 (*a*) J. F. Bartoli, P. Battioni, W. R. De Foor and D. Mansuy, *J. Chem. Soc., Chem. Commun.*, 1994, 23; (*b*) K. Ozette, P. Leduc, M. Palacio, J. F. Bartoli, K. M. Barkigia, J. Fajer, P. Battioni and D. Mansuy, *J. Am. Chem. Soc.*, 1997, **119**, 6442; (*c*) K. Ozette, P. Battioni, P. Leduc, J. F. Bartoli and D. Mansuy, *Inorg. Chim. Acta*, 1998, **272**, 4.

3 TDCPP = dianion of 5,10,15,20-tetrakis(2,6-dichlorophenyl)porphyrin, SCE = saturated calomel electrode.

4 The HNO_3–CF_3SO_3H system has been previously used for nitration of aromatic compounds: C. L. Coon, W. G. Blucher and M. E. Hill, *J. Org. Chem.*, 1973, **38**, 4243; G. A. Olah, *Angew. Chem., Int. Ed.*, 1993, **32**, 767.

5 *Crystal data* for **1**·2EtOH (two EtOHs are bound to the Zn and two EtOHs are in the lattice): $C_{52}H_{36}Cl_8N_{12}O_{20}Zn$, M = 1497.90, triclinic, space group $P\bar{1}$ (no. 2), dark blue blocks, a = 11.792(3), b = 11.993(2), c = 12.279(4) Å, α = 106.04(2), β = 90.24(3), γ = 106.87(3)°, V = 1590.4(7) Å^3, μ = 4.343 mm^{-1}, D_c = 1.564 g cm^{-3}, Z = 1, T = 293 K, 4210 reflections measured, 3973 unique, $R1$ = 0.094, $wR2(F^2)$ = 0.317 (3971 data), GOF = 1.031. Data were measured on an Enraf-Nonius CAD4 diffractometer with graphite-monochromated Cu-Kα radiation (λ = 1.54178 Å). The structure was solved by direct methods (SIR92) and refined by full-matrix least squares (SHELXL-93) on F^2. CCDC 182/1732. See http://www.rsc.org/suppdata/cc/b0/b004160m/ for crystallographic files in .cif format.

6 For hexacoordinated Zn porphyrins, see Cambridge Structural Data Base, F. H. Allen and O. Kennard, *Chem. Des. Automat. News*, 1993, **8**(1), 1; F. H. Allen and O. Kennard, *Chem. Des. Automat. News*, 1993, **8**(1), 31.

7 For examples of severely nonplanar dodecasubstituted Zn porphyrins, see: K. M. Barkigia, M. D. Berber, J. Fajer, C. J. Medforth, M. W. Renner and K. M. Smith, *J. Am. Chem. Soc.*, 1990, **112**, 8851; M. O. Senge, *J. Porphyrins Phthalocyanines*, 1998, **2**, 93; K. M. Barkigia, D. J. Nurco, M. W. Renner, D. Melamed, K. M. Smith and J. Fajer, *J. Phys. Chem. B*, 1998, **102**, 322.

8 K. M. Kadish, *Prog. Inorg. Chem.*, 1986, **34**, 435; K. M. Kadish, E. Van Caemelbecke and G. Royal, in *The Porphyrin Handbook*, ed. K. M. Kadish, K. M. Smith and R. Guilard, Academic Press, New York, 1999, vol. 8, pp. 1–97.

9 For properties of metalloporphyrin π-anion radicals, see: R. H. Felton, in *The Porphyrins*, ed. D. Dolphin, Academic Press, New York, 1978, vol. 5, pp. 53–125; P. Bhyrappa and V. Krishnan, *Inorg Chem.*, 1991, **30**, 239; M. W. Renner, L. R. Furenlid, K. M. Barkigia, A. Forman, H. K. Shim, D. J. Simpson, K. M. Smith and J. Fajer, *J. Am. Chem. Soc.*, 1991, **113**, 6891.

Constrained phenylalanyl peptides *via* a [2+2+2]-cycloaddition strategy

Sambasivarao Kotha,* Kumar Mohanraja and Susheel Durani

Department of Chemistry, Indian Institute of Technology, Bombay, Mumbai 400 076 India.
E-mail: srk@chem.iitb.ernet.in

Received (in Cambridge, UK) 11th July 2000, Accepted 21st August 2000
First published as an Advance Article on the web

Peptide modification potentially valuable for peptidomimetic and combinatorial chemistry applications is described involving a [2+2+2]-cycloaddition reaction leading to conformationally constrained phenylalanyl peptides.

Aromatic amino acids like phenylalanine and tyrosine are often important elements of peptide pharmacophores. Novel methods to generate conformationally restrained analogs from suitable precursor peptides evoke interest,[1–3] particularly for combinatorial chemistry applications. A variety of benzenoid molecules are accessible through [2+2+2] or [4+2]-cycloaddition reactions.[4] Applied to suitable peptide precursors, the reaction may provide an approach to conformationally constrained aryl amino acid residues *in situ*. Artificial amino acids with olefin, diene, allene or acetylene groups in the side chain have been described[5] and could be useful synthons for conformationally constrained aryl amino acid residues approachable in a [2+2+2]-type cycloaddition reaction. Conversion of a suitable diacetylenic dipeptide precursor **1** into a constrained phenylalanyl peptide **2** in a [2+2+2]-cycloaddition reaction catalyzed by Wilkinson's catalyst[6] is illustrated in Scheme 1.† The reaction conditions are mild enough to be compatible with the acid and base labile protecting groups that are normally required for peptide synthesis.

The precursor peptide **1** could be easily made in a standard peptide synthesis protocol starting from the dipropargyl glycine **6** as the specific building block amino acid. The Boc-protected form of **6** was easily made from ethyl isocyanoacetate **3** serving as the glycine synthon.[7] Dipropargylation in refluxing acetonitrile–K_2CO_3 in the presence of tetrabutylammonium hydrogen sulfate as the phase transfer catalyst furnished the isonitrile derivative **4** in good yield (69%). Acid catalysed hydrolysis, followed by Boc-protection gave **5**. Saponification of **5** furnished the Boc protected amino acid **6**.

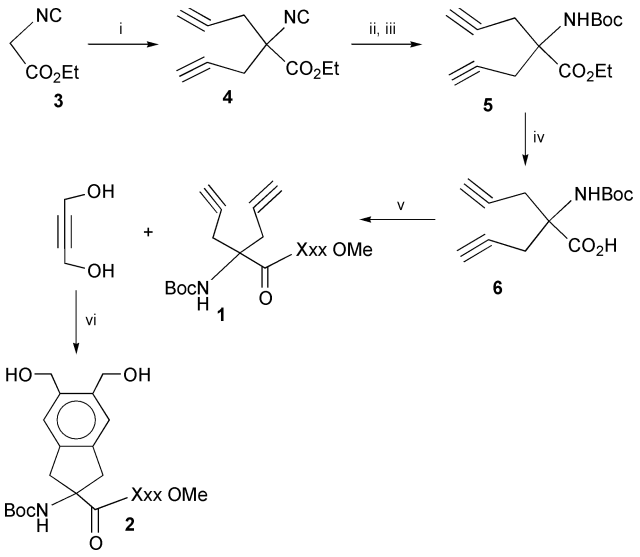

Scheme 1 *Reagents*: (i) K_2CO_3, propargyl bromide, $^nBu_4NHSO_4$; (ii) HCl, EtOH; (iii) $CHCl_3$, $(Boc)_2O$; (iv) aq NaOH, MeOH; (v) HCl H_2N Xxx CO_2Me, HOBt, THF, NMM; (vi) $(Ph_3P)_3RhCl$, EtOH, reflux.

Table 1 Representative constrained phenylalanyl peptides

Starting peptide	[2+2+2]-Cycloaddition product	Yield (%)[a]
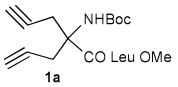 1a	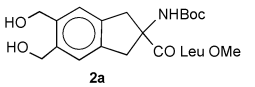 2a	66
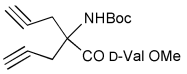 1b	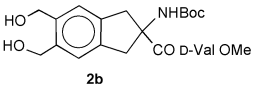 2b	54
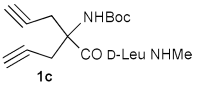 1c	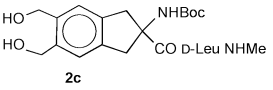 2c	75
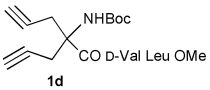 1d	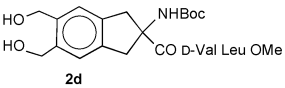 2d	70
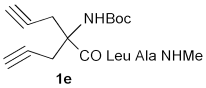 1e	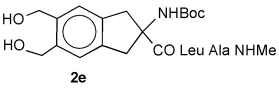 2e	65

[a] Yields refers to [2+2+2]-cycloaddition product

Condensation of the Boc-protected building block amino acid **6** with various amino acid ester derivatives in a standard DCC-mediated peptide procedure[8] furnished the dipeptide (*e.g.*) **1a** or longer peptides Boc-Dprg-Xxx-OMe (with Xxx = L-Leu, D-Val, D-Leu, D-Val-L-Leu, L-Leu-L-Ala, L-Leu-D-Val-L-Leu). Treatment with five-fold excess of but-2-yn-1,4-diol, a model monoyne so chosen as to avoid the formation of diastereomers, furnished representative constrained phenylalanyl peptides shown in Table 1.

The additional methylene bridge connecting the α-carbon with the aromatic ring not only restrains the phenylalanyl moiety but also the backbone, restricting its conformational freedom, and this has potential to influence the pharmacological profile[9] of the parent Phe or Tyr peptide variant. Additional structural variations are feasible and can add to the versatility of the combinatorial chemistry approaches. For instance, the diol functionality in the product peptides here is a useful site for possible further molecular manipulations.

In summary, a peptide modification capable of generating constrained phenylalanyl peptide variants in a [2+2+2]-cycloaddition reaction is reported and could be potentially useful for both peptidomimetic and combinatorial chemistry applications.

We gratefully acknowledge the DST for financial support, RSIC-Mumbai for recording the spectral data and CDRI-Lucknow for mass spectral data. K. M. thanks IIT-Bombay for the fellowship.

Notes and references

† Dprg = dipropargyl glycine. Boc = *tert*-butoxycarbonyl. The peptides were purified by silica gel column chromatography or by HPLC. The purity of the peptides was judged by TLC and high field (300 MHz) NMR spectroscopy.

(**1a**) ^{1}H NMR 300 MHz, $CDCl_3$) δ 7.02 (broad, 1H), 5.38 (broad s, 1H), 4.60–4.67 (td, *J* = 8.6, 5.1 Hz, 1H), 3.72 (s, 3H), 2.86–3.05 (m, 4H), 2.09–2.14 (m, 2H), 1.58–1.67 (m, 3H), 1.46 (s, 9H), 0.93 (t, *J* = 6.9 Hz, 6H). $[\alpha]_D$ −38.89° (*c*. 1). Mass: 378 (M + H).

(**1b**) ^{1}H NMR (300 MHz, $CDCl_3$) δ 7.13 (broad, 1H), 5.35 (broad s, 1H), 4.56 (dd, *J* = 8.6, 4.5 Hz, 1H), 3.73 (s, 3H), 2.87–3.06 (m, 4H), 2.16–2.22 (m, 1H), 2.10–2.13 (m, 2H), 1.46 (s, 9H), 0.96 (d, *J* = 6.7 Hz, 3H), 0.91 (d, *J* = 6.9 Hz, 3H). $[\alpha]_D$ +11.71° (*c*. 1). Mass: 364 (M + H).

(**1c**) ^{1}H NMR (300 MHz, $CDCl_3$) δ 7.00 (broad s, 1H), 6.54 (d, *J* = 8.0 Hz, 1H), 5.34 (s, 1H), 4.45–4.52 (m, 1H), 2.80–3.20 (m, 4H), 2.74 (d, *J* = 4.7 Hz, 3H), 2.17 (t, *J* = 2.7 Hz, 1H), 2.12 (t, *J* = 2.5 Hz, 1H), 1.68–1.95 (m, 3H), 1.47 (s, 9H), 0.93 (d, *J* = 2.7 Hz, 3H), 0.90 (d, *J* = 2.5 Hz, 3H). $[\alpha]_D$ −11.87° (*c*. 1). Mass: 377 (M + H).

(**1d**) ^{1}H NMR (300 MHz, $CDCl_3$) δ 7.24 (broad, 1H), 6.68 (d, *J* = 8.0 Hz, 1H), 5.29 (s, 1H), 4.52–4.56 (m, 1H), 4.30 (dd, *J* = 7.8, 3.6 Hz, 1H), 3.67 (s, 3H), 2.84–3.20 (m, 4H), 2.19 (t, *J* = 2.9 Hz, 1H), 2.13 (t, *J* = 2.5 Hz, 1H), 1.91–1.96 (m, 1H) 1.67–1.73 (m, 3H), 1.47 (s, 9H), 0.90–0.93 (t, 12H). $[\alpha]_D$ + 10.55° (*c*. 1). Mass: 378 (M + H). $[\alpha]_D$ + 0.011° (*c*. 1). Mass: 477 (M + H).

(**1e**) ^{1}H NMR (300 MHz, $CDCl_3$) δ 7.41 (d, *J* = 8.0 Hz, 1H), 6.81 (d, *J* = 4.0 Hz, 1H), 6.71 (d, *J* = 4.7 Hz, 1H), 5.43 (s, 1H), 4.47–4.53 (m, 1H), 4.21–4.27 (m, 1H), 2.81–3.15 (overlapped two ABq, 4H), 2.77 (d, *J* = 4.67 Hz, 3H), 2.22 (t, *J* = 3.0 Hz, 1H), 2.13 (t, *J* = 2.7 Hz, 1H), 1.71–1.85 (m, 2H), 1.46 (s, 9H), 1.42 (d, *J* = 7.2 Hz, 3H), 0.98 (d, *J* = 6.2 Hz, 3H), 0.94 (d, *J* = 6.0 Hz, 3H). $[\alpha]_D$ + 10.55° (*c*. 1). Mass: 448 (M + H).

(**1f**) ^{1}H NMR (300 MHz, $CDCl_3$) δ 7.10 (broad, 1H), 6.78 (d, 1H), 6.69 (d, 1H), 5.26 (s, 1H), 4.48–4.56 (m, 1H), 4.35–4.42 (m, 1H), 4.18–4.25 (m, 1H), 3.69 (s, 3H), 2.77–3.10 (m, 4H), 2.12–2.30 (m, 3H), 1.60–1.85 (m, 3H), 1.46 (s, 9H), 0.91–0.98 (m, 18H). $[\alpha]_D$ − 24.52° (*c*. 1). Mass: 590 (M + H).

(**2a**) ^{1}H NMR (300 MHz, $CDCl_3$) δ 7.20 (s, 1H), 7.17 (s, 1H), 6.91 (broad, 1H), 5.20 (s, 1H), 4.71 (q, *J* = 11.0 Hz, 4H), 4.59–4.65 (m, 1H), 3.70 (s, 3H), 3.72 (1/2 ABq, *J* = 16.8 Hz, 1H), 3.54 (1/2 ABq, *J* = 16.4 Hz, 1H), 3.15–3.25 (m, 2H), 1.51–1.61 (m, 3H), 1.42 (s, 9H), 0.92 (t, *J* = 5.8 Hz, 6H). $[\alpha]_D$ +15.14° (*c*. 1). Mass: 464 (M + H).

(**2b**) ^{1}H NMR (300 MHz, $CHCl_3$) δ 7.17 (s, 1H), 7.15 (s, 1H), 7.11 (d, *J* = 7.6 Hz, 1H), 5.36 (s, 1H), 4.65 (q, *J* = 12.0 Hz, 4H), 4.52–4.56 (m, 1H), 3.72 (s, 3H), 3.69 (1/2 ABq, *J* = 16.4 Hz, 1H), 3.51 (1/2 ABq, *J* = 16.5 Hz, 1H), 3.18 (dd, *J* = 26.8, 17.5 Hz, 2H), 2.17–2.19 (m, 1H), 1.42 (s, 9H), 0.95 (d, *J* = 6.9 Hz, 3H), 0.87 (d, *J* = 6.9 Hz, 3H). $[\alpha]_D$ −4.36° (*c*. 1). Mass: 450 (M + H).

(**2c**) ^{1}H NMR (300 MHz, CD_3OD) δ 8.01 (d, *J* = 8.0 Hz, 1H), 7.84 (broad, 1H), 7.24 (s, 3H), 4.62 (s, 4H), 4.36–4.41 (m, 1H), 3.71 (1/2 ABq, *J* = 16.4 Hz, 1H), 3.43 (1/2 ABq, 16.4 Hz, 1H), 3.10 (dd, *J* = 16.3, 6.9 Hz, 2H), 2.73 (d, *J* = 4.39 Hz, 3H), 1.65 (m, 3H), 1.44 (s, 9H), 0.94 (d, *J* = 5.85 Hz, 3H), 0.89 (d, *J* = 5.49 Hz, 3H). $[\alpha]_D$ + 13.11° (*c*. 1). Mass: 463 (M + H).

(**2d**) ^{1}H NMR (300 MHz, $CDCl_3$) δ 7.27 (broad, 1H), 7.22 (s, 1H), 7.18 (s, 1H), 6.75 (d, *J* = 5.4 Hz, 1H), 5.36 (s, 1H), 4.62–4.80 (m, 4H), 4.48–4.55 (m, 1H), 4.29 (dd, *J* = 7.8, 4.3 Hz, 1H), 3.86 (1/2 ABq, *J* = 17.2 Hz, 1H), 3.68 (s, 3H), 3.52 (1/2 ABq, *J* = 16.4 Hz, 1H), 3.0 (dd, *J* = 40.0, 16.8 Hz, 2H), 2.44 (m, 1H), 1.66 (m, 3H), 1.42 (s, 9H), 0.91–0.97 (t, 12H). $[\alpha]_D$ −13.31° (*c*. 1). Mass: 563 (M + H).

(**2e**) ^{1}H NMR (300 MHz, $CDCl_3$) δ 7.54 (d, *J* = 7.6 Hz, 1H), 7.22 (s, 1H), 7.19 (s, 1H), 6.91 (d, *J* = 3.6 Hz, 1H), 6.77 (d, 5.4 Hz, 1H), 5.81 (s, 1H), 4.61–4.78 (m, 4H), 4.46–4.51 (m, 1H), 4.23–4.29 (m, 1H), 3.95 (1/2 ABq, *J* = 16.8 Hz, 1H), 3.41 (1/2 ABq, *J* = 16.8 Hz, 1H), 3.04 (d, *J* = 16.8 Hz, 2H), 2.71 (d, *J* = 4.3 Hz, 3H), 1.70 (broad, 3H), 1.42 (s, 12H), 0.98 (d, *J* = 6.2 Hz, 3H), 0.94 (d, *J* = 6.3 Hz, 3H). $[\alpha]_D$ −7.89° (*c*. 1). Mass: 534 (M + H).

(**2f**) ^{1}H NMR (300 MHz, $CDCl_3$) δ 7.43 (d, 2H), 6.24 (d, 2H), 5.32–5.38 (m, 2H), 4.58–4.65 (m, 3H), 4.18–4.23 (m, 4H), 3.72 (s, 3H), 2.78–2.81 (m, 2H), 2.32–2.37 (m, 2H), 2.21 (m, 1H), 1.63 (m, 6H), 1.25 (s, 9H), 0.93–0.98 (m, 18H). $[\alpha]_D$ + 4.96° (*c*. 1). Mass: 713 (M + HCl).

1 A. Giannis and T. Kolter, *Angew. Chem., Int. Ed. Engl.*, 1993, **32**, 1244; C. Cativiela and M. D. Diaz-de-Villegas, *Tetrahedron: Asymmetry*, 2000, **11**, 645; S. E. Gibson, N. Guillo and M. J. Tozer, *Tetrahedron*, 1999, **55**, 585.

2 R. M. J. Liskamp, *Recl. Trav. Chim. Pays-Bas*, 1994, **113**, 1.

3 D. Seebach, A. K. Beck and A. Studer, in *Modern Synthetic Methods*, vol. 7, ed. B. Ernst and C. Leumann, VCH, Weinheim, 1995, pp. 1 and references cited therein; G. Apitz, M. Jager, S. Jaroch, M. Kratzel, L. Schaffeler and W. Steglich, *Tetrahedron*, 1993, **49**, 8223; C. J. Easton, I. M. Scharfbillig and E. W. Tan, *Tetrahedron Lett.*, 1988, **29**, 1565; D. Ranganathan, N. K. Vaish and K. Shah, *J. Am. Chem. Soc.*, 1994, **116**, 6545; M. N. Yousaf and M. Mrksich, *J. Am. Chem. Soc.*, 1999, **121**, 4286; Tetrahedron Symposium-in-print, ed. J. A. Bristol, *Tetrahedron*, 1997, **53**, 6573; N. K. Terret, in *Combinatorial Chemistry*, Oxford University Press, Oxford, 1998 and references cited therein.

4 C. P. Dell, *J. Chem. Soc., Perkin. Trans.*, **1**, 1998, 3873 and reference cited therein; S. Kotha and N. Sreenivasachary, *J. Chem. Soc., Chem. Commun.*, 2000, 503; S. Kotha and N. Sreenivasachary, *Bioorg. Med. Chem. Lett.*, 2000, **10**, 1413; S. Kotha, N. Sreenivasachary and E. Brahmachary, *Tetrahedron Lett.*, 1998, **39**, 2805; S. Kotha, E. Brahmachary and N. Sreenivasachary, *Tetrahedron Lett.*, 1998, **39**, 4095; S. Kotha and E. Brahmachary, *Tetrahedron Lett.*, 1997, **38**, 3561.

5 D. C. Roberts and F. Vellaccio, in *The Peptides*, vol. 5, ed. E. Gross and J. Meienhofer, Academic Press, New York, 1983, pp 341.

6 R. Grigg, R. Scott and P. Stevenson, *J. Chem. Soc., Perkin. Trans. 1*, 1988, 1357.

7 S. Kotha and E. Brahmachary, *J. Org. Chem.*, 2000, **65**, 1359.

8 M. Bodanszky and A. Bodanszky, *The Practice of Peptide Synthesis*, Springer-Verlag, New York, 1984.

9 K. H. Hsieh, T. R. LaHann and R. C. Speth, *J. Med. Chem.*, 1989, **32**, 898; I. Torrini, G. P. Zecchini, M. P. Paradisi, G. Lucente, E. Gavuzzo, F. Mazza, G. Pochetti, S. Spisani and A. L. Giuliani, *Int. J. Peptide Protein Res.*, 1991, **38**, 495.

ChemComm

Simple amphiphilic liquid crystalline *N*-alkylimidazolium salts. A new solvent system providing a partially ordered environment†

Ching K. Lee, Hsin W. Huang and Ivan J. B. Lin*

Department of Chemistry, Fu-Jen Catholic University, Hsinchuang, Taipei 242, Taiwan.
E-mail: Chem1001@fujens.fju.edu.tw; Fax: +886-2-29023209

Received (in Cambridge, UK) 5th June 2000, Accepted 25th August 2000
First published as an Advance Article on the web

Easily accessible liquid crystals of 1-alkylimidazolium salts having a bilayer structure, are good solvents providing a partially ordered reaction environment.

Molecular thermotropic liquid crystals, which have been extensively studied and documented, are usually molecules composed of an extended rigid aromatic core and terminal flexible alkyl chains. Ionic liquid crystals (ILCs), which have been less well studied[1–6] in comparison to neutral LCs, are amphiphiles having a hydrophilic cationic or anionic head group and hydrophobic long alkyl chains. A classic example of an ILC is an alkali metal soap, in which the anion possesses a negatively charged head group with a long alkyl chain. However, ILCs with positively charged mesomorphic cations, such as alkylammonium,[1] alkyl phosphonium,[1b,d,2] *N*-alkylpyridinium[3] and *N*,*N*-dialkylimidazolium[3a,b,4] salts have also been reported. These cationic amphiphiles have many interesting properties and are potentially useful as synthetic membranes,[5] antimicrobial agents,[6] gellators[7,1b,d] NLO[8] and surfactants,[9] to name a few.

Recently rt ionic liquids (ILs) have been considered as a new generation of green solvents for organic reactions.[10] ILs not only provide solvent properties different from any other organic solvent, but can also be recycled very easily. Furthermore, ILs possessing liquid crystal properties further provide a partially ordered environment and may give a better selectivity for organic reactions. A few examples of liquid crystalline ionic liquids of imidazolium salts have been reported.[4,3b,c] In this paper we report the mesomorphic behavior of a new series of 1-alkylimidazolium salts prepared simply by the addition of acids to 1-alkylimidazoles (Scheme 1). In order to appraise the usefulness of this system as a solvent, we have begun a study of the Diels–Alder condensation. A stereoselectivity different from that of the known reactions has been found.

1-Alkylimidazoles‡ were synthesized according to the literature methods.[11] 1-Alkylimidazolium salts (n = 10, 12, 14, 16, 18) were prepared by adding a slight excess of concentrated acids dropwise to the 1-alkylimidazoles. Salts with the formula [R-imH][NO_3], [R-imH]Cl·H_2O and [R-imH][BF_4] were obtained after recrystallization from THF or CH_2Cl_2–hexane. Anhydrous chloride salts were obtained by heating the hydrated samples at 140 °C under vacuum for 3 h. Under such conditions, no decomposition has been observed as evidenced by ^{1}H NMR spectroscopy. The completeness of the dehydration has been confirmed by thermal gravimetric analysis. The chemical shift of the NH proton depends on the anion. With an alkyl chain length of n = 14, the chloride salt has the lowest chemical shift at 16.0 ppm, the nitrate salt has 15.5 ppm and the $[BF_4]^-$ salt has the highest chemical shift at 12.3 ppm. A similar trend is observed for the 2-CH protons (Cl^-, 9.4; $[NO_3]^-$, 9.2; $[BF_4]^-$, 8.7 ppm). These trends may reflect the strength of the H-bonding between the respective protons and anions and have been reported.[12]

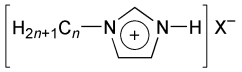

X = NO_3^-, Cl^-, BF_4^-; n = 10, 12, 14, 16, 18

Scheme 1 *N*-alkylimidazolium salts.

In research on the packing of charged surfactant molecules, studies of the crystal structures of imidazolium based salts are rare.[3b,4a] Therefore, the molecular structure of [$C_{14}H_{29}$-imH][NO_3] was determined by single crystal X-ray diffraction and is shown in Fig. 1. 1-Alkyl chains are parallel to the imidazole planes. The nitrate planes are also parallel to the imidazole planes. Interdigitation of alkyl chains forms a bilayer lamellae with a repeating layer distance of 16.9 Å. Each bilayer is further linked with anions through hydrogen bonds.

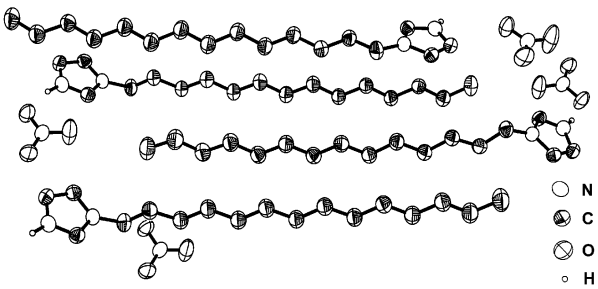

Fig. 1 ORTEP drawing of [$C_{14}H_{29}$-imH][NO_3] (50% thermal ellipsolids), hydrogens being omitted for clarity (except for N–H).

The liquid crystal properties of 1-alkylimidazolium salts were examined by optical polarized microscopy and differential scanning calorimetry. The nitrate salts with n = 14, 16 and 18 exhibit liquid crystal behavior. Characteristic focal conic fan and oily streak textures with spontaneous homeotropic phenomena are observed during the process of heating and cooling, suggesting a lamellar SmA mesophase (Fig. 2). The chloride and tetrafluoroborate salts also show SmA mesophases. The Cl^- salt of n = 10 is a rt ILC and for the salt of n = 12, the process of crystallization needs several days when cooling to rt. The $[BF_4]^-$ salt with n = 12 exhibits monotropic liquid crystal properties. In general, the temperature range of mesophase increases with increasing chain length (Fig. 3). Among the three different anions of [C_nH_{2n+1}-imH]X (X = Cl^-, $[NO_3]^-$,

Fig. 2 The fan texture of the mesophase of [$C_{14}H_{29}$-imH][NO_3] at 70 °C.

DOI: 10.1039/b004462h

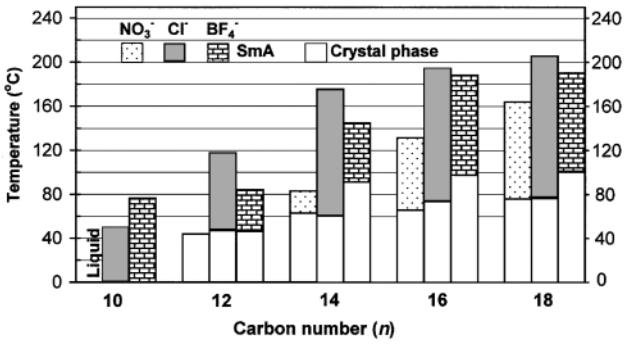

Fig. 3 The phase transition diagram of $[C_nH_{2n+1}$-imH]X from DSC at 10 °C min^{-1}. (X = Cl, BF_4, second heating step; X = NO_3, first heating step; X = BF_4, monotropic; X = Cl, n = 10 and X = NO_3, n = 14 from POM). For clarity the crystal to crystal phase transitions are not shown.

$[BF_4]^-$), the chloride salts have the widest temperature range of mesophase. This result may reflect the strength of H-bonding between the cation and the chloride anion. The nitrate salt of n = 12 and chloride salts of n = 10, 12, 14 exhibit lyotropic behavior in water, acidic water and THF. For example, both the nitrate and chloride salts of n = 12 in H_2O (> 20% by weight concentration) are liquid crystals having a fan texture with a spontaneous homeotropic behavior at rt.

To demonstrate the effect of the lamellar phase on the stereoselectivity of Diels–Alder reactions, a preliminary condensation reaction[13] of cyclopentadiene (0.063 g, 0.3 mmol) with diethyl maleate (0.024 g, 0.3 mmol) in an ionic liquid crystalline solvent system (a mixture of 0.42 g of $C_{12}H_{25}$-im and 0.15 mL of 12 M HCl) at rt was examined. Optical observation indicated that under these reaction conditions the reaction mixture retained the lamellar mesophase structure. The selectivity of *exo/endo* product was 54 : 46. A parallel reaction carried out in EtOH, gave an *exo/endo* ratio of 12 : 88. This preference for *exo* over *endo* product in the ionic liquid crystalline solvent is different from that observed when the reaction is carried out it EtOH and, in those earlier studies, simple ionic liquids,[13c,d] water[13a–c] or organic solvents.[13a–c] This result indicates that the lamellar mesophase has a strong influence on the selectivity of the reaction product.

In summary, we prepared a new series of thermotropic liquid crystalline 1-alkyl-substituted imidazolium salts. The chloride salts of n = 10, 12, 14 and the nitrate salts of n = 12 also exhibit lyotropic properties. The thermotropic and special lyotropic properties possessed by this series of ILCs make them alternative solvents for organic reactions, such as Diels–Alder condensations, and metal-catalyzed reactions.

We thank the National Science Council of Taiwan, R. O. C. (NSC90-2113-M-030-001) for the support of this work.

Notes and references

† *Crystal data* for $[C_{14}H_{29}$-imH][NO_3]: $C_{17}H_{33}N_3O_3$, M = 303.44, triclinic, a = 8.962(3), b = 19.793(18), c = 22.363(7) Å, α = 99.606(17), β = 92.371(18), γ = 98.307(18)°, V = 3862(2) $Å^3$, T = 298 K, space group $P\bar{1}$, Z = 10, μ = 0.090 mm^{-1}, σ_{calcd} = 1.305 mg m^{-3}, 1.52 < θ < 25.00. Of 16247 reflections measured, 13442 were unique. Data were collected on a Siemens P4 diffractometer with graphite monochromatized Mo-Kα radiation (λ = 0.71073 Å) in ω scan mode. The structure was solved by direct methods and refined (based on F^2 using all independent data) by full matrix least squares methods (Siemens SHELXTL V. 5.03). All the non-hydrogen atoms were refined anisotropically. The hydrogen atoms, located by Fourier difference synthesis, were isotropically refined with a common thermal parameter. R values are reported for $R1$ = 0.0505 (based on observed data, $I > 2\sigma$) and $wR2$ = 0.1390 (based on all data). CCDC 182/1768. See http://www.rsc.org/suppdata/cc/b0/b004462h/ for crystallographic files in .cif format. ^{1}H-NMR (ppm, $CDCl_3$, 25 °C): 0.87 (t, ^3J = 7 Hz, $-CH_3$, 3H), 1.25–1.32 (m, $-CH_2$, 22H), 1.87 (m, $-CH_2$, 2H), 4.28 (t, ^3J = 7 Hz, $-NCH_2$, 2H), 7.11 (s, CH, 1H), 7.40 (s, –CH, 1H), 9.36 (s, –CH, 1H), 15.53 (s, –NH, 1H). Anal. Calcd. for $C_{17}H_{33}N_3O_3$: C 62.35; H 10.16; N 12.83. Found: C 62.17; H 10.14; N 12.76%.

‡ 1-Alkylimidazolium nitrates (n = 10, 12, 14, 16, 18) were prepared by adding a slight excess of concentrated nitric acid dropwise to the 1-alkylimidazoles at 0 °C in ether. Immediate white precipitates formed when n = 12, 14, 16 ,18. The nitrate salt with n = 10 is a liquid, which was purified by successive washing with ether followed by vacuum drying. Chloride salts (n = 10, 12, 14, 16, 18) were prepared by using concentrated hydrochloric acid as the acid source. Tetrafluoroborate salts (n = 10, 12, 14, 16, 18) were prepared by adding excess of tetrafluoroboric acid (32% in water) to 1-alkylimidazoles in water–THF.

1 (*a*) M. Dreja, S. Gramberg and B. Tieke, *Chem. Commun.*, 1998, 1371; (*b*) D. J. Abdallah, R. E. Bachman, J. Perlstein and R. G. Weiss, *J. Phys. Chem. B*, 1999, **103**, 9269; (*c*) M. Arkas, D. Tsiourvas, C. M. Paleos and A. Skoulios, *Chem. Eur. J.*, 1999, **5**, 3202; (*d*) D. J. Abdallah, A. Robertson, H.-F. Hsu and R. G. Weiss, *J. Am. Chem. Soc.*, 2000, **122**, 3053; (*e*) S. Ujiie and Y. Yano, *Chem. Commun.*, 2000, 79.

2 (*a*) W. Gao, L. Dickinson, F. G. Morin and L. Reven, *Chem. Mater.*, 1997, **9**, 3113; (*b*) A. Kanazawa, O.Tsutsumi, T. Ikeda and Y. Nagase, *J. Am. Chem. Soc.*, 1997, **119**, 7670.

3 (*a*) C. J. Bowlas, D. W. Bruce and K. R. Seddon, *Chem. Commun.*, 1996, 1625; (*b*) C. M. Gordon, J. D. Holbrey, A. R. Kennedy and K. R. Seddon, *J. Mater. Chem.*, 1998, **8**, 2627; (*c*) F. Neve, A. Crispini and O. Francescangen, *Inorg. Chem.*, 2000, **39**, 1187 and reference therein.

4 (*a*) K. M. Lee, C. K. Lee and I. J. B. Lin, *Chem. Commun.*, 1997, 899; (*b*) J. D. Holbrey and K. R. Seddon, *J. Chem. Soc., Dalton Trans.*, 1999, 2133.

5 T. Kunitake, *Angew. Chem., Int. Ed. Engl.*, 1992, **31**, 709.

6 A. Kanazawa, T. Ikeda and T. Endo, *Antimicrob. Agents Chemother.*, 1994, **38**, 945.

7 D. J. Abdallah and R. G. Weiss, *Chem. Mater.*, 2000, **12**, 406.

8 A. Kanazawa, T. Ikeda and J. Abe, *Angew. Chem., Int. Ed.*, 2000, **39**, 612.

9 D. Demus, J. Goodby, G. W. Gray, H. W. Spiess and V. Vill, *Handbook of Liquid Crystals, Amphiphilic Liquid Crystals*, Wiley-VCH, New York, 1998, Vol. 3, p. 303.

10 T. Welton, *Chem. Rev.*, 1999, **99**, 2071 and references therein.

11 V. McKee, M. Zvagulis, J. V. Dagdigian, Marianne G. Patch and C. A. Reed, *J. Am. Chem. Soc.*, 1984, **106**, 4765.

12 (*a*) A. A. Fannin, Jr., L. A. King, J. A. Levisky and J. S. Wilkes, *J. Phys. Chem.*, 1984, **88**, 2609; (*b*) A. G. Avent, P. A. Chaloner, M. P. Day, K. R. Seddon and T. Welton, *J. Chem. Soc., Dalton Trans.*, 1994, 3405.

13 (*a*) R. Braun, F. Schuster and J. Sauer, *Tetrahedron Lett.*, 1986, **27**, 1285; (*b*) H. J. Schneider and N. K. Sangwan, *Angew. Chem., Int. Ed. Engl.*, 1987, **26**, 896; (*c*) D. A. Jaeger and C. E. Tucker, *Tetrahedron Lett.*, 1989, **30**, 1785; (*d*) T. Fischer, A. Sethi, T. Welton and J. Woolf, *Tetrahedron Lett.*, 1999, **40**, 793.

The selective detection of uranium(VI) on a microchip using a derivatized 4-sulfonic calix[6]arene

Qin Lu,[a] John H. Callahan[b] and Greg E. Collins*[b]

[a] *GeoCenters, Inc., 1801 Rockville Pike, Suite 405, Rockville, MD 20852, USA*
[b] *Naval Research Laboratory, Chemistry Division, Code 6116, Washington DC 20375-5342, USA. E-mail: gcollins@ccf.nrl.navy.mil; Fax: 1(202)404-8119; Tel.: +1(202)404-3337*

Received (in Columbia, MO, USA) 12th April 2000, Accepted 15th August 2000
First published as an Advance Article on the web 18th September 2000

4-Sulfonic calix[6]arene is derivatized with lissamine rhodamine B to give a fluorescent ligand, L, which is applied to a capillary electrophoresis microchip for the selective detection of uranium(VI).

Environmental concerns associated with the remediation of radioactive waste sites have generated considerable interest in the development of a portable, rapid and selective monitor for radioactive contaminants, such as uranium. This need has been prompted by the costly and time-consuming delays which have resulted from submitting samples to external laboratories for analytical characterization before, during and after the application of remediation methodologies to contaminated groundwater or structural materials encountered at these sites. In this communication, we report the application of a derivative of the 'super-uranophile', 4-sulfonic calix[6]arene, which has been tagged with a long wavelength fluorophore, lissamine rhodamine B, for the selective detection of uranyl ion, UO_2^{2+}, on a glass microchip. The experimental design employed here combines the superior selectivity of 4-sulfonic calix[6]arene for the UO_2^{2+} ion,[1] the high sensitivity and diminished overlap of impurity fluorescence inherent with utilizing long wavelength fluorescence detection,[2] and the numerous advantages associated with performing glass microchip separations, including short analysis times, minimal sample consumption and waste generation, and portable instrumentation.[3]

The calixarene derivative, **L**, was synthesized through the coupling reaction of 4-sulfonic calix[6]arene with lissamine rhodamine B sulfonyl chloride in a mixed solvent of methanol and water in the presence of excess 4-sulfonic calix[6]arene (Scheme 1). The mono-derivatized product, **L**, was isolated by column chromatography (methanol/ethyl acetate) and verified by electrospray mass spectrometry.[4] Excitation of **L** at 532 nm gives an intense fluorescence peak at 593 nm in water, differing only slightly from the parent fluorophore, lissamine rhodamine B sulfonyl chloride, at 583 nm.

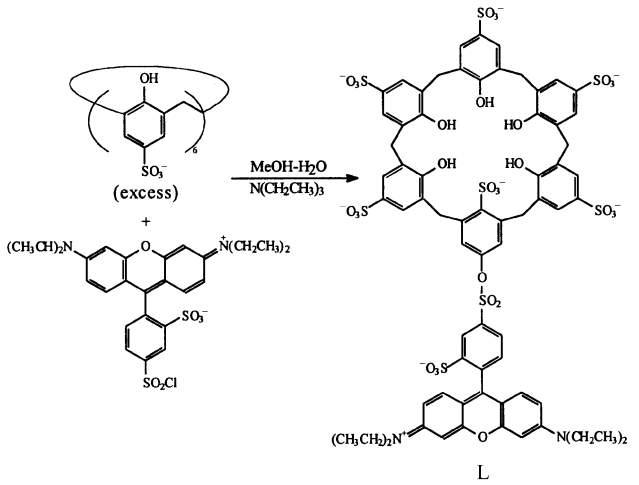

Scheme 1 Synthetic coupling of lissamine rhodamine B to 4-sulfonic calix[6]arene.

The microchips utilized for performing the separation were microfabricated in Borofloat glass to contain a simple cross pattern, lithographically etched into the glass substrate (20 μm deep × 50 μm wide) to define the sample loading and separation microchannels (see Fig. 1).[5] A glass cover plate pre-drilled to contain four access holes was thermally bonded to the microfabricated glass plate. Sample, buffer, and waste reservoirs were constructed by inserting pipette tips into these holes. The lengths of the loading and separation channels were 10 and 85 mm, respectively, with an effective separation length of 80 mm. Through computer control of the potentials applied to the different reservoirs, sample analyte was loaded into the intersection of the two channels and subsequently separated down the length of the separation channel. The separation was monitored by focussing light from a compact, 15 mW Nd/YAG laser (532 nm) onto the end of the separation channel, collecting the fluorescent light with a microscope objective (20×) positioned at 90°, and directing the light onto a miniature, red-shifted photomultiplier tube (Hamamatsu).

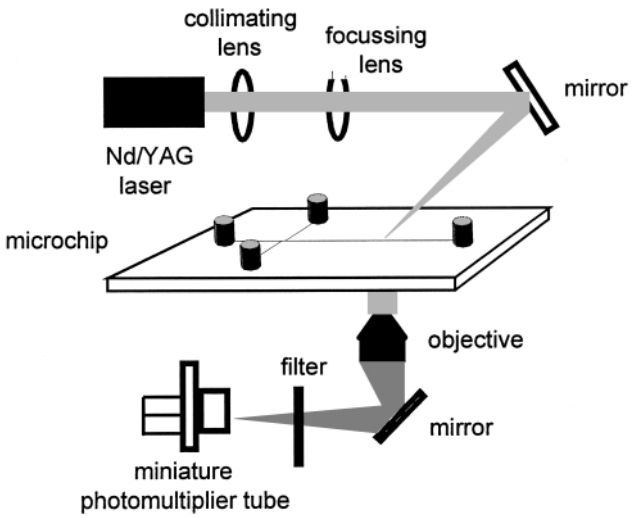

Fig. 1 Instrumental layout for performing microchip separations.

Microchip separations were performed using a buffer solution containing 10 mM sodium borate, 50 mM boric acid, and 2 mM $MgCl_2$ (pH = 8.3). Under this pH condition, in addition to the complete deprotonation of the six sulfonic groups of ligand **L**, previous studies establish that two of the five phenol groups will also likely be deprotonated to give $\mathbf{L}^{8-}$.[6] In experiments run without the addition of $MgCl_2$ in the buffer solution, **L** was detected under positive polarity (+1000 V cm^{-1}) with long migration times (over 100 s) and poor peak shapes. Furthermore, following the addition of UO_2^{2+} to the analyte reservoir, the resolution obtained on the microchip was insufficient to separate the uranyl bound ligand from the free ligand, **L**. The addition of 2 mM $MgCl_2$, however, allowed **L**

and its uranyl ion complex to be completely resolved under negative polarity (−1000 V cm^{-1}) with significantly reduced migration times and improved peak shape (Fig. 2a, b). A similar enhancement in the resolution was reported for the capillary electrophoretic separation of *p*-sulfonated calixarenes following the addition of Mg^{2+} to the background supporting electrolyte.[7] The uranyl complex formed with **L** is believed to further deprotonate the remaining three phenols, giving a planar complex, $[\mathbf{L}\cdot UO_2]^{9-}$, which is more negatively charged than the parent molecule, $\mathbf{L}^{8-}$. This observation helps explain the shorter retention time obtained for the uranyl complex, $[\mathbf{L}\cdot UO_2]^{9-}$, due to its enhanced electrophoretic mobility under the applied electric field. Microchip evaluations of the electroosmotic flow using the neutral marker, rhodamine B, demonstrate that the electroosmotic flow was significantly reduced by the addition of $MgCl_2$, but not reversed. The detection limit for UO_2^{2+} under these conditions was 4.2 μM.

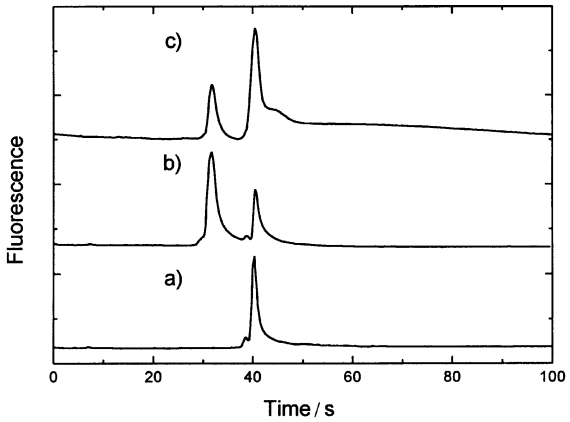

Fig. 2 Microchip separations obtained using 10^{-4} M **L** in a buffer solution containing 10 mM sodium borate, 50 mM boric acid and 2 mM $MgCl_2$ (pH = 8.3), (a) 0 mg L^{-1} UO_2^{2+}; (b) 10 mg L^{-1} UO_2^{2+}; (c) 10 mg L^{-1} UO_2^{2+}, Cu^{2+}, Pb^{2+}, Cd^{2+}, Th^{4+} and Nd^{3+}.

The effective detection of UO_2^{2+} on the microchip requires a pre-complexation step between the ligand, **L**, and uranyl ion. In general, the binding rates of UO_2^{2+} by calixarenes are relatively slow, due to the geometric rearrangement requirements imposed on the calixarene for conforming to the pseudoplanar geometry which permits binding of the uranyl ion in a hexacoordinate structure. The half-life of the binding reaction between the super-uranophile, 4-sulfonic calix[6]arene, and UO_2^{2+} is about an hour.[1b] The high thermodynamic stability constant and slow dissociation kinetics of the uranyl ion complex, $[\mathbf{L}\cdot UO_2]^{9-}$, however, explain why the complex does not dissociate and become undetectable as it travels down the separation column, a problem which plagues the majority of capillary electrophoresis separations of strongly complexed metal ions when the complexing ligand is absent from the separation buffer.[8]

Studies were performed on the detection of UO_2^{2+} in the presence of six competing metal ions, Cu^{2+}, Zn^{2+}, Pb^{2+}, Cd^{2+}, Th^{4+}, and Nd^{3+}, each at a concentration of 10 mg L^{-1}. Introduction of these six impurity metal ions to **L** in the absence of UO_2^{2+} resulted in no change to the electropherogram recorded for **L**. The subsequent addition of UO_2^{2+}, however, gave the electropherogram shown in Fig. 2c, indicating the capability for **L** to selectively complex UO_2^{2+} despite the presence of a matrix of six impurity metal ions. The underivatized form of the ligand utilized here, 4-sulfonic calix[6]arene, has been termed a super-uranophile, due to the extremely large selectivity factors, 10^{12-17}, determined for the binding of uranyl ion in the presence of competing Ni^{2+}, Zn^{2+}, and Cu^{2+} ions.[1] The selective binding of UO_2^{2+} ion by **L** in the presence of other metal ions results from the fact that **L** provides a pseudoplanar, hexacoordinate geometry which suits UO_2^{2+} uniquely. Any weakly bound metal complexes and/or complexes bearing fast dissociation kinetics will be unresolved due to their rapid dissociation from the fluorescent ligand as the complexes travel down the separation column.

In conclusion, by synthetically coupling the super-uranophile, 4-sulfonic calix[6]arene, to the long wavelength, fluorescent dye, lissamine rhodamine B, we have developed a new ligand, **L**, which is ideally suited for selectively detecting uranium on a glass microchip platform. **L** has a coordination site which is highly selective for binding UO_2^{2+} ion in the presence of numerous impurity metal ions, and a fluorescent tag whose red shifted emission wavelength enables a compact, portable laser to be utilized, minimizing any background fluorescence arising from impurities apparent in real samples. The results of this study have exciting implications with respect to methods for preparing molecular and metal recognition molecules for application to the burgeoning field of microchip capillary electrophoresis.

The authors gratefully acknowledge the Environmental Management Science Program of the Department of Energy for funding support of this study.

Notes and references

1 (*a*) S. Shinkai, H. Koreishi, K. Ueda, T. Arimura and O. Manabe, *J. Am. Chem. Soc.*, 1987, **109**, 6371; (*b*) T. Nagasaki, K. Kawana, K. Araki and S. Shinkai, *J. Chem. Soc., Perkin Trans. 2*, 1991, 1325.

2 (*a*) G. Patonay and M. D. Antoine, *Anal. Chem.*, 1991, **63**, 321A; (*b*) L. C. Shriver-Lake, J. P. Golden, G. Patonay, N. Narayanan and F. S. Ligler, *Sens. Actuators B*, 1995, **29**, 25.

3 (*a*) D. J. Harrison, K. Fluri, K. Seiler, Z. Fan, C. S. Effenhauser and A. Manz, *Science*, 1993, **261**, 895; (*b*) H. Salimi-Moosavi, T. Tang and D. J. Harrison, *J. Am. Chem. Soc.*, 1997, **119**, 8716; (*c*) S. C. Jacobson, A. W. Moore and J. M. Ramsey, *Anal. Chem.*, 1995, **67**, 2059.

4 Compound **L** was verified by NMR and electrospary mass spectrometry. The negative ion mode of the mass spectrometer yielded three major clusters of peaks, corresponding to doubly, triply and quadruply charged species. The most abundant cluster of peaks corresponded to the following species: $[M - 2H]^{2-}$, *m/z* 828.1; $[M - 3H + Na]^{2-}$, *m/z* 839.1; $[M - 4H + 2Na]^{2-}$, *m/z* 850.1; $[M - 5H + 3Na]^{2-}$, *m/z* 861.1; $[M - 6H + 4Na]^{2-}$, *m/z* 872.1. A second cluster of peaks, corresponding to triply charged ions, was observed at the following *m/z* ratios: $[M - 3H]^{3-}$, *m/z* 551.7; $[M - 4H + Na]^{3-}$, *m/z* 559.0; $[M - 5H + 2Na]^{3-}$, *m/z* 566.4; $[M - 6H + 3Na]^{3-}$, *m/z* 573.7. The cluster of quadruply charged ions was observed at the following *m/z* ratios: $[M - 4H]^{4-}$, *m/z* 413.5; $[M - 5H + Na]^{4-}$, *m/z* 419.0; $[M - 6H + 2Na]^{4-}$, *m/z* 424.5. Mass assignments were confirmed to 0.1 u using a high resolution scanning mode.

5 Alberta Microelectronic Corporation, Edmonton, Alberta, Canada.

6 (*a*) J.-P. Scharff, M. Mahjoubi and R. Perrin, *New J. Chem.*, 1991, **15**, 883; (*b*) J. L. Atwood, D. L. Clark, R. J. Juneja, G. W. Orr, K. D. Robinson and R. L.Vincent, *J. Am. Chem. Soc.*, 1992, **114**, 7558.

7 (*a*) Y. Zhang and I. M. Warner, *J. Chromatogr. A*, 1994, **688**, 293; (*b*) I. Rodriguez, H. K. Lee and S. F. Y. Li, *Talanta*, 1998, **45**, 683.

8 (*a*) M. Macka and P. R. Haddad, *Electrophoresis*, 1997, **18**, 2482; (*b*) M. Macka, P. Nesterenko, P. Andersson and P. R. Haddad, *J. Chromatogr. A*, 1998, **803**, 279; (*c*) B.-F. Liu, L.-B. Liu and J.-K. Cheng, *Anal. Chim. Acta*, 1998, **358**, 157.

ChemComm

Molecular recognition directed porphyrin chemosensor for selective detection of nicotine and cotinine

Gollapalli R. Deviprasad and Francis D'Souza*

Department of Chemistry, Wichita State University, Wichita, KS 67260-0051, USA.
E-mail: dsouza@wsuhub.uc.twsu.edu

Received (in Corvallis, OR, USA) 25th July 2000, Accepted 14th August 2000
First published as an Advance Article on the web 18th September 2000

The first example of a metalloporphyrin based fluorescent chemosensor for selective detection of dinitrogen alkaloids such as nicotine and cotinine in solution by using a 'two-point' binding strategy and a modified fluorescence analysis procedure is reported.

Nicotine, a dinitrogen alkaloid is a major drug of abuse, acting as a potent agonist of the nicotinic acetylcholine receptor (*n*AChR). Recently, nicotinic agonists and antagonists have been considered as promising therapeutic agents for a variety of conditions including the treatment of pain, cognitive and attention deficits, Parkinson's disease, Tourette's syndrome, and anxiety.[1] Nicotine is also the most abundant and potent pharmacological agent in tobacco and tobacco smoke, hence, it is of considerable interest to medicine and society.[2] Several methods using HPLC, GC-MS or capillary electrophoresis are available for quantification of nicotine in tobacco, tobacco smoke, pharmaceutical agents, atmospheric air (an issue related to passive smoking), and in urine samples (involves cotinine, a metabolic product of nicotine).[3] Though these methods offer good detection sensitivity, they often suffer from low selectivity. Hence, a selective method for sensitive detection of nicotine and cotinine is highly desirable.

The development of sensors/biosensors for selective detection of analytes and improved transduction methods for higher detection sensitivity is considered to be a challenge in modern chemistry.[4] Among the different techniques utilized for developing chemical sensors, molecular fluorescence is an important one because of its high sensitivity of detection down to a single molecule, recognition and/or self-assembly directed selectivity, on–off switchability, sub-nanometer spatial resolution with sub-micron visualization, and sub-millisecond temporal resolution.[5] Among the different fluorophores that could be utilized to develop fluorescent sensors/chemosensors, porphyrins are attractive candidates because of their relatively high fluorescence quantum yields and the many different established synthetic procedures of functionalization.[6] In porphyrin based chemosensors, sensing is often achieved either by having suitable receptors at the ring periphery, by metal axial ligation, or a combination of both.[6] In the present study, we have successfully designed a porphyrin based fluorescence chemosensor for selective detection of nicotine and cotinine in solution. Our approach utilizes: (i) a 'two-point' binding mechanism which involves axial ligation of the nicotine pyridine entity through the zinc ion of the porphyrin cavity, and, hydrogen bonding of the pyrrolidine ring nitrogen to a carboxylic acid or amide group located on one of the phenyl rings of a tetraphenylporphyrinatozinc macrocycle and (ii) a modified porphyrin fluorescence data analysis procedure.

The binding of the dinitrogen alkaloid, **1** or **2**, to the newly synthesized, receptor porphyrin,† **3** or **4** was studied by ^{1}H NMR and UV-visible absorption spectral methods. Fig. 1 depicts ^{1}H NMR spectra of **1**, **3**, and, a mixture of **1** and **3** in $CDCl_3$. Upon binding to **3**, the *o*-pyridyl protons of **1** experience a shielding up to 5 ppm while the *m*- and *p*-pyridyl protons and the pyrrolidine ring protons of **1** experience less shielding (1–2 ppm). The protons of the substituted phenyl ring of **3** experience

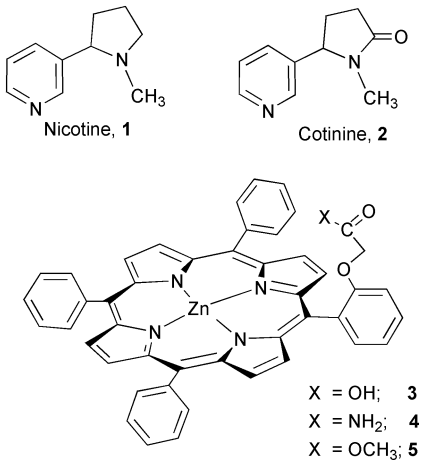

a deshielding effect (up to 0.5 ppm) upon binding to **1**. Control experiments performed using *meso*-tetraphenylporphyrinatozinc, (TPP)Zn, (a compound without the side pendant arm) or compound **5**, bearing a methyl ester group at the substituted phenyl ring, reveal similar large deshielding of pyridyl protons of **1** indicating that the pyridyl group of **1** binds to the central zinc.[9]

The UV-visible absorption spectral studies reveal red shifted Soret and visible bands upon addition of **1** to a solution of the investigated receptor porphyrins confirming that the pyridyl entity of **1** binds to the central zinc.[10] The formation constant *K*

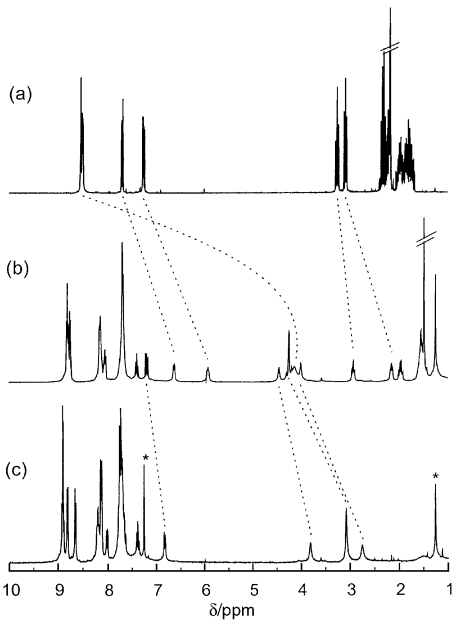

Fig. 1 ^{1}H NMR spectrum of (a) nicotine, **1** (31 mM), (b) **1** (31 mM) + porphyrin, **3** (27 mM), and (c), **3** (12 mM) in $CDCl_3$ at 298 K.

DOI: 10.1039/b006055k

Table 1 Formation constant, *K*, and the thermodynamic parameters for zinc porphyrin–alkaloid complexes in toluene

Porphyrin	Alkaloid	K_a, M^{-1} [a]	ΔG, KJ mol^{-1} [a]	ΔH, KJ mol^{-1}	ΔS, J K^{-1} mol^{-1}
3	**1**	455.6×10^3	−32.28	−65.75	−112.31
	2	42.3×10^3	−26.39	−47.21	−69.87
4	**1**	63.1×10^3	−27.38	−49.12	−72.96
	2	17.5×10^3	−24.21	−40.25	−53.83
5	**1**	6.4×10^3	−21.69	−26.13	−14.89
	2	7.0×10^3	−21.92	−26.44	−15.17
(TPP)Zn	**1**	6.9×10^3	−21.91	−26.34	−14.87
	2	7.0×10^3	−21.93	−26.33	−14.77

[a] At 298 K.

calculated from the Scatchard method[11] of UV-visible absorption titration curves, is listed in Table 1. The binding constants for (TPP)Zn binding to alkaloids under these solution conditions is also given for comparison. The *K* values for **1** binding to **3** is found to be nearly two orders of magnitude higher than that observed for binding of either **1** to **5** or **1** to (TPP)Zn. The binding of alkaloids, **1** or **2** to porphyrins **3** or **4** are stronger as revealed by the *K* values and this effect could be attributed to the 'two-point' mode of binding. As expected, the *K* values for binding of **1** or **2** to **5** are comparable to that observed for alkaloid binding to (TPP)Zn indicating the absence of any hydrogen bonding between the methyl ester group of **5** with the pyrrolidine ring nitrogen of either **1** or **2**. The calculated thermodynamic parameters from the Van't Hoff plots of ln*K vs.* T^{-1} for **5** or (TPP)Zn binding to **1** or **2** also draw similar conclusions. Interestingly, both ΔH and ΔS decrease upon binding to **3** or **4** as compared to that observed for binding to **5** or (TPP)Zn. These results indicate that the enthalpy change is a main factor responsible for the observed higher stability of the 'two-point' bound porphyrin–alkaloid systems.

Fig. 2 shows the fluorescence emission spectra of porphyrin **3** in the presence of various amounts of **1** in toluene. The zinc porphyrin emission bands located at 605 and 650 nm decrease in intensity with the appearance of an isosbestic point at 670 nm indicating the presence of only one equilibrium in solution. It is observed that the decrease in intensity of the 650 nm band is much more than the 605 nm band.‡ Similar spectral features are observed for porphyrin **3** or **4** binding with either compound **1** or **2**.

In order to quantitate these results, we monitored the intensity ratio of these two bands as a function of alkaloid concentration.

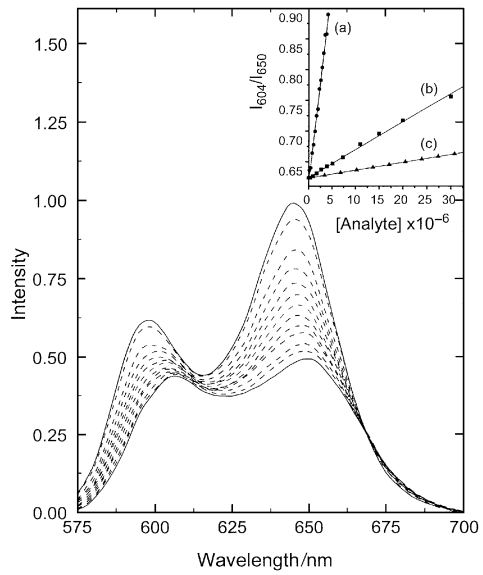

Fig. 2 Fluorescence emission spectrum of **3** (3.8 μM) in the presence of various amounts of **1** in toluene (λ_{ex} = 420 nm). The inset figure shows the relationship between the intensity ratio of the emission bands, I_{604}/I_{650} of **3** in the presence of (a) nicotine, (b) cotinine and, (c) pyridine substrates.

The inset in Fig. 2 shows such plots obtained for nicotine and cotinine binding. A linear relationship is obtained for the emission peak intensity ratio against the alkaloid concentration. This procedure is found to work well in non-coordinating solvents such as toluene, *o*-dichlorobenzene or acetonitrile. These plots offer the much-needed selectivity with respect to the presence of other axially coordinating nitrogenous bases. As shown in the inset of Fig. 2, the intensity ratio of the emission bands for a strongly coordinating ligand such as pyridine does not change significantly in the employed concentration range. These results along with the higher binding constants suggest that the present 'two-point' binding and fluorescence analysis procedure offers the much-needed selectivity for dinitrogen alkaloid detection. Further studies to expand this novel approach of employing a 'two-point' binding and modified fluorescence analysis procedure for developing porphyrin chemosensors for selective detection of compounds of biological and societal importance are in progress.

The authors are thankful to the donors of the Petroleum Research Fund, administered by the American Chemical Society, and Wichita State University for financial help.

Notes and references

† Free-base forms of porphyrins **3**–**5** were synthesized by reacting stoichiometric amounts of pyrrole, benzaldehyde and the appropriate *ortho* substituted benzaldehyde in propionic acid followed by column chromatography purification on either basic alumina or silica gel. The *ortho* substituted benzaldehydes, (2-formylphenoxy)acetic acid and (2-formylphenoxy)acetamide were synthesized according to the literature procedure given in ref. 7*a* and 7*b*, respectively. Zinc insertion was carried out according to the standard procedure (ref. 8). The molecular integrity of all the synthesized free-base and zinc porphyrins was established from FAB mass, elemental analysis and ^{1}H NMR studies (see Fig. 1 and text for ^{1}H NMR results).

‡ The details of the fluorescence quenching mechanism will be published elsewhere.

1 (*a*) A. W. Banon, M. W. Decker, M. W. Holladay, P. Curzon, D. Donnelly-Robers, P. S. Puttfarcken, R. S. Bitner, A. Diaz, A. H. Dickenson, R. D. Porsolt, M. Williams and S. P. Arneric, *Science*, 1998, **279**, 77; (*b*) M. W. Holladay, M. J. Dart and J. K. Lynch, *J. Med. Chem.*, 1997, **40**, 4169; (*c*) R. M. Elgen, J. C. Hunter and A. Dray, *Trends Pharmacol. Sci.*, 1999, **20**, 337; (*d*) M. B. Brennan, *Chem. & Eng. News*, 2000, **78**, 23.

2 (*a*) N. L. Benowitz, *Annu. Rev. Med.*, 1986, **37**, 21; (*b*) P. E. McBride, *Med. Clin. North Am.*, 1992, **76**, 333; (*c*) I. P. Stolerman and M. J. Jarvis, *Psychopharmacology*, 1995, **117**, 2; (*d*) K. A. Perkins, N. Benowitz, J. Henningfield, P. Newhouse, O. Pomerleau and G. Swan, *Addiction*, 1996, **91**, 129.

3 (*a*) H. W. A. Teeuwen, F. J. W. Aalders and J. M. V. Rossum, *Mol. Biol. Rep.*, 1989, **13**, 165 and references cited therein; (*b*) B. Siegmund, E. Leitner and W. Pfannhauser, *J. Agric. Food Chem.*, 1999, **47**, 3117 and references cited therein.

4 See for example, (*a*) *Handbook of Biosensors and Electronic Noses, Medicine, Food, and the Environment*, ed. E. Kress-Rogers, CRC Press, 1997; (*b*) *Biosensor and Chemical Sensor Technology*, eds. K. R. Rogers, A. Mulchandani, W. Zhou, ACS Symposium Series 613, American Chemical Society, Washington, DC, 1995; (*c*) *Biosensor Technology, Fundamentals and Applications*, eds. R. P. Buck, W. E. Hatfield, M. Umana, E. F. Bowden, Marcel Dekker, Inc., 1990; (*d*) B. Eggins, *Biosensors, An Introduction*, Wiley, New York, 1996.

5 (*a*) *Fluorescent Chemosensors for Ion and Molecule Recognition*, ed. A. W. Czarnik, ACS Symposium Series 538, American Chemical Society, Washington, DC, 1993; (*b*) A. P. de Silva, H. Q. N. Gunaratne, T. Gunnlaugsson, A. J. M. Huxley, C. P. McCoy, J. T. Rademacher and T. E. Rice, *Chem. Rev.*, 1997, **97**, 1515; (*c*) J. R. Lakowicz, *Principles of Fluorescence Spectroscopy*, 2nd Edn. Kluwer/Plenum, New York, 1999.

6 *The Porphyrin Handbook*, ed. K. M. Kadish, K. M. Smith and R. Guilard, vol 6, Academic Press, New York, 2000.

7 (*a*) *Org. Synth.*, 1966, **46**, 28; (*b*) *Org. Synth. Coll. Vol. 4*, 1963, 486.

8 G. D. Dorough, J. R. Miller and F. M. Huennekens, *J. Am. Chem. Soc.*, 1951, **73**, 4315.

9 F. D'Souza, Y.-Y. Hsieh and G. R. Deviprasad, *Inorg. Chem.*, 1996, **35**, 5747.

10 M. Nappa and J. S. Valentine, *J. Am. Chem. Soc.*, 1978, **100**, 5075.

11 G. Scatchard, *Ann. N. Y. Acad. Sci.*, 1949, **51**, 661.

The effect of solvent on the α-effect: the MeCN–H_2O solvent system†

Ik-Hwan Um,[a] Young-Min Park[a] and Erwin Buncel*[b]

[a] *Department of Chemistry, Ewha Womans University, Seoul 120-750, Korea*
[b] *Department of Chemistry, Queen's University, Kingston, Ontario K7L 3N6, Canada. E-mail: buncele@chem.queensu.ca; Tel: 613-533-2635; Fax: 613-533-6669*

Received (in Corvallis, OR, USA) 10th July 2000, Accepted 23rd August 2000
First published as an Advance Article on the web 18th September 2000

The increasing α-effect observed in MeCN–H_2O solvent mixtures, which contrasts with the previously found bell-shaped dependence on solvent composition in the DMSO–H_2O system, is attributed to the differential solvent effect on basicities of the α- and normal nucleophiles in the former case.

Among the possible causes of the α-effect, that is the enhanced reactivity of nucleophiles having an unshared pair of electrons adjacent to the nucleophilic centre,[1] the effect of solvent has been particularly controversial.[2–9] As one possible approach to the problem, in 1986 we examined the reactivities of an α-nucleophile, butane-2,3-dione monoximate (Ox^-), and a normal nucleophile, *p*-chlorophenoxide ($ClPhO^-$) with *p*-nitrophenyl acetate (PNPA) in dimethyl sulfoxide (DMSO)–H_2O mixtures,[7a] due to the unique properties of this solvent system.[10] Unexpectedly, we observed a bell-shaped profile for the dependence of the α-effect on solvent composition, with a maximum at *ca*. 50 mol % DMSO.[7a] More recently, we observed a similar bell-shaped α-effect trend for the corresponding reactions of *p*-nitrophenyl diphenyl phosphinate (PNPDPP).[7b] However, a contrary result was reported for the reaction of PNPA with *O*-iodosylbenzoate (IBO^-) and $ClPhO^-$: the α-effect showed no maximum but decreased steadily as the DMSO content in the reaction medium increased.[9] Clearly, more work is called for in order to understand the effect of solvent on the α-effect.

We have now extended our study to a different solvent system, acetonitrile (MeCN)–H_2O mixtures, and have found a new type of solvent effect on the α-effect, namely an increasing α-effect. A plausible cause of this trend for the reaction of PNPA with Ox^- and $ClPhO^-$ (eqn. 1) in MeCN–H_2O mixtures is herein presented.

$$CH_3C(O)OC_6H_4NO_2\text{-}p + Nu^- \rightarrow CH_3C(O)\text{-}Nu + p\text{-}NO_2C_6H_4O^-$$
$$Nu^- = CH_3C(O)C(CH_3)=NO^- (Ox^-), \text{ an } \alpha\text{-nucleophile}$$
$$p\text{-}ClC_6H_4O^- (ClPhO^-), \text{ a normal nucleophile} \quad (1)$$

Kinetic studies were performed spectrophotometrically under pseudo-first-order conditions with the nucleophile in excess. Pseudo-first-order rate constants (k_{obs}) were obtained from linear plots of ln ($A_\infty - A_t$) *vs*. *t*. Second-order rate constants (k^{Ox-} and k^{ClPhO-}) were calculated from the slope of the linear plot of k_{obs} *vs.* nucleophile concentration. As shown in Fig. 1, the magnitude of the α-effect (k^{Ox-}/k^{ClPhO-}) increases as the mol % MeCN in the medium increases, from *ca.* 100 in H_2O to 500 in 90 mol % MeCN. Recently, we found a decreasing α-effect trend for the reaction of PNPA with hydroxamates in MeCN–H_2O mixtures, and a shift in equilibrium from an OH acid to an NH acid upon addition of MeCN to H_2O was attributed as responsible for the observed α-effect trend.[8b]

Transition-state stabilization is one possible cause of the α-effect[11] and recently the bell-shaped α-effect trend observed for the reaction of PNPA in DMSO–H_2O mixtures has been explained through a dissection of ground-state and transition-state contributions.[7c] In that system the basicities of the α-Nu (Ox^-) and normal-Nu ($ClPhO^-$) exhibit a parallel dependence on the DMSO–H_2O composition.[7]

The addition of MeCN to H_2O could influence not only the reaction rate but also the basicity of the anionic nucleophiles. Although the pK_a values for some phenols, carboxylic acids and amines in pure MeCN are available,[12a,b] very few pK_a data have been reported for MeCN–H_2O mixtures.[8b] Therefore, we have measured the relative basicity of Ox^- and $ClPhO^-$ in MeCN–H_2O mixtures using piperazine as a reference base. One can define ΔpK_a as the pK_a difference between the conjugate acids of the nucleophile (Ox^- or $ClPhO^-$) and piperazine, *i.e.* ΔpK_a = pK_a of the conjugate acid of the nucleophile (Ox^- or $ClPhO^-$) − pK_a of the conjugate acid of the reference base (piperazine). Hence, the magnitude of ΔpK_a represents the relative basicities of these nucleophiles. We determined ΔpK_a values spectrophotometrically using the relationship: $\Delta pK_a = \log [HA]_{eq}[B]_{eq}/[A^-]_{eq}^2$, in which $[HA]_{eq}$ represents the equilibrium concentration of the conjugate acid of the nucleophile, and $[B]_{eq}$ and $[A^-]_{eq}$ represent the equilibrium concentration of the reference base (piperazine) and the nucleophile, respectively. The ΔpK_a values thus determined in MeCN–H_2O mixtures are summarized in Table 1. As shown in the table, the ΔpK_a values of Ox^- and $ClPhO^-$ in H_2O are −0.38 and −0.44, respectively. The pK_a values of the conjugate acids of Ox^-, $ClPhO^-$ and piperazine in H_2O at 25 °C, have been reported to be 9.44,[7b] 9.38[12c] and 9.82,[12c] respectively, *i.e.* the ΔpK_a data determined in H_2O in the present study are identical to the literature values. It is also noted that Ox^- and $ClPhO^-$ are less basic than piperazine in H_2O but appear to be more basic upon addition of MeCN. This is consistent with the report that the increase in pK_a values upon changing medium from H_2O to MeCN is more significant for phenols than for amines: the pK_a enhancements were reported to be 12–17 and 7–8 in pK_a units for phenols and for the conjugate acids of alicyclic secondary

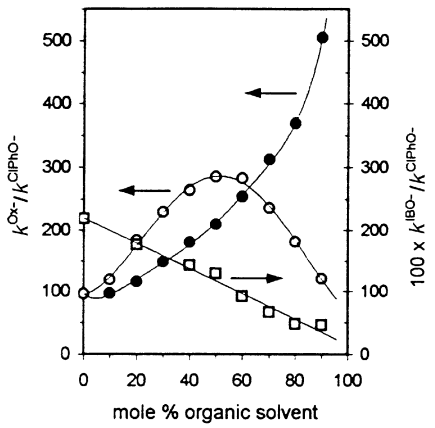

Fig. 1 Plots showing the effect of solvent on the α-effect ($k^{\alpha-Nu}/k^{normal-Nu}$) for the reaction of PNPA at 25.0 °C: k^{Ox-}/k^{ClPhO-} in MeCN–H_2O (●); k^{Ox-}/k^{ClPhO-} in DMSO–H_2O (○);[7b] k^{IBO-}/k^{ClPhO-} in DMSO–H_2O (□).[9]

† Electronic supplementary information (ESI) is available: second-order rate constants for the reaction of *p*-nitrophenyl acetate with butane-2,3-dione monoximate and *p*-chlorophenoxide in MeCN–H_2O mixtures at 25 °C. See http://www.rsc.org/suppdata/cc/b0/b005610n/

Table 1 Summary of the relative basicity of the nucleophile (ΔpK_a = pK_a of the conjugate acid of the nucleophile—pK_a of the conjugate acid of the reference base, piperazine) in MeCN–H_2O mixtures of varying compositions at 25.0 ± 0.1 °C[a]

Mol % MeCN	ΔpK_a (Ox^-)	ΔpK_a ($ClPhO^-$)	$\Delta\Delta pK_a$[b]
0	−0.38	−0.44	0.06
10	0.58	0.43	0.15
20	1.17	0.90	0.27
30	1.80	1.44	0.36
40	2.32	1.89	0.43
50	2.69	2.19	0.50
60	3.43	2.84	0.59
70	3.90	3.20	0.70
80	4.96	4.18	0.78
90	5.85	4.90	0.95

[a] The uncertainty in ΔpK_a values is estimated to be less than ±0.03 pK_a units. [b] $\Delta\Delta pK_a$ = ΔpK_a (Ox^-) − ΔpK_a ($ClPhO^-$).

amines (*e.g.* piperidine and morpholine), respectively, upon solvent change from H_2O to MeCN.[12a,b]

The difference in the relative basicity between Ox^- and $ClPhO^-$ can be expressed as $\Delta\Delta pK_a$, *i.e.* $\Delta\Delta pK_a$ = $\Delta pK_a(Ox^-)$ − ΔpK_a ($ClPhO^-$). As shown in Table 1, $\Delta\Delta pK_a$ increases as the mol % MeCN in the medium increases, *i.e.* Ox^- is more basic than $ClPhO^-$ by 0.06, 0.50 and 0.95 pK_a units in H_2O, 50 and 90 mol % MeCN, respectively, which contrasts with the situation, noted above, for DMSO–H_2O mixtures. We propose therefore, that the differential solvent effect on the basicity of these nucleophiles is the cause of the contrasting α-effect trends observed for the reaction of PNPA with Ox^- and $ClPhO^-$ in DMSO–H_2O and in MeCN–H_2O mixtures.

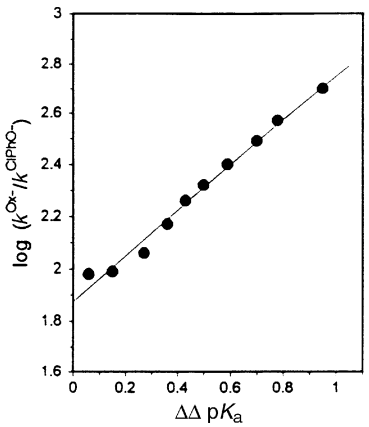

Fig. 2 Plot of log k^{Ox-}/k^{ClPhO-} *vs.* $\Delta\Delta pK_a$ for the reaction of PNPA with Ox^- and $ClPhO^-$ in MeCN–H_2O mixtures at 25.0 ± 0.1 °C.

Furthermore, it is found that a plot of log k^{Ox-}/k^{ClPhO-} against $\Delta\Delta pK_a$ is linear with a slope of 0.85 (Fig. 2). This provides evidence that the increase in the $\Delta\Delta pK_a$ values is almost fully reflected in the increase in the α-effect for the reaction of PNPA with Ox^- and $ClPhO^-$ upon addition of MeCN into the reaction medium.

I. H. U. is grateful for financial support from KOSEF of Korea (1999-2-123-003-5). E. B. thanks NSERC of Canada for a research grant.

Notes and references

1 J. O. Edwards and R. G. Pearson, *J. Am. Chem. Soc.*, 1962, **84**, 16.
2 Reviews: (*a*) E. Buncel and S. Hoz, *Isr. J. Chem.*, 1985, **26**, 313; (*b*) A. P. Grekov and V. Y. Veselov, *Usp. Khim.*, 1978, **47**, 1200; (*c*) N. J. Fina and J. O. Edwards, *Int. Chem. Kinet.*, 1973, **5**, 1.
3 (*a*) C. F. Bernasconi and C. Murray, *J. Am. Chem. Soc.*, 1986, **108**, 5251; (*b*) D. J. Palling and W. P. Jencks, *J. Am. Chem. Soc.*, 1984, **106**, 4869.
4 (*a*) G. Moutiers, E. Guevel, L. Villien and F. Terrier, *J. Chem. Soc., Perkin Trans. 2*, 1997, 710; (*b*) F. Terrier, G. Moutiers, L. Xiao, E. Guevel and F. Guir, *J. Org. Chem.*, 1995, **60**, 1748.
5 (*a*) I. H. Um, J. S. Lee and S. M. Yuk, *J. Org. Chem.*, 1998, **63**, 9152; (*b*) K. R. Fountain, T. W. Dunkin and K. D. Patal, *J. Org. Chem.*, 1997, **62**, 2738; (*c*) E. Buncel, C. Chuaqui and H. Wilson, *J. Am. Chem. Soc.*, 1982, **104**, 4896.
6 W. L. Jorgensen, *J. Am. Chem. Soc.*, 1987, **109**, 2349.
7 (*a*) E. Buncel and I. H. Um, *J. Chem. Soc., Chem. Commun.*, 1986, 595; (*b*) R. M. Tarkka and E. Buncel, *J. Am. Chem. Soc.*, 1995, **117**, 1503; (*c*) I. H. Um and E. Buncel, *J. Org. Chem.*, 2000, **65**, 577.
8 (*a*) I. H. Um, D. S. Kwon and G. J. Lee, *Bull. Korean Chem. Soc.*, 1989, **10**, 620; (*b*) I. H. Um, H. W. Yoon, J. S. Lee and H. J. Moon, *J. Org. Chem.*, 1997, **62**, 5939.
9 R. A. Moss, S. Swarup and S. Ganguli, *J. Chem. Soc., Chem. Commun.*, 1987, 860.
10 E. Buncel and H. Wilson, *Adv. Phys. Org. Chem.*, 1977, **14**, 133.
11 (*a*) E. Buncel and S. Hoz, *Tetrahedron Lett.*, 1983, **24**, 4777; (*b*) S. Hoz and E. Buncel, *Tetrahedron Lett.*, 1984, **25**, 3411; (*c*) K. R. Fountain, D. B. Tad-y, T. W. Paul and M. V. Golynskiy, *J. Org. Chem.*, 1999, **64**, 6547; (*d*) K. R. Fountain and K. D. Patel, *J. Org. Chem.*, 1997, **62**, 4795.
12 (*a*) M. K. Chantooni and I. M. Kolthoff, *J. Phys. Chem.*, 1976, **80**, 1306; (*b*) J. F. Coetzee and G. R. Padmanabhan, *J. Am. Chem. Soc.*, 1965, **87**, 5005; (*c*) W. P. Jencks and J. Regenstein, in *Handbook of Biochemistry. Selected Data for Molecular Biology*, ed. H. A. Sober, The Chemical Rubber Co., Cleveland, OH, 1968.

Sialidase-catalyzed transsialylation using polymer-supported solution-phase techniques†‡

Dirk Schmidt and Joachim Thiem*

Institute of Organic Chemistry, University of Hamburg, Martin-Luther-King-Platz 6, D-20146 Hamburg, Germany. E-mail: thiem@chemie.uni-hamburg.de

Received (in Cambridge, UK) 17th May 2000, Accepted 22nd August 2000
First published as an Advance Article on the web 18th September 2000

By combination of glycosidase-catalyzed transglycosylation with polyethylene glycol ω-monomethyl ether (MPEG; mw 5000) based solution phase synthesis, various terminally sialylated di- and trisaccharides were synthesized.

Sialyl oligosaccharides are involved in many diseases and function as the receptor determinants for viruses, lectins, toxins and certain tumor-specific antibodies.[1,2] To further investigate the biological functions of these components efficient methodologies for their synthesis are needed.

It has been demonstrated that sialidases are effective sialylation tools[3–5] supplying the stereoselective efficiency of a sialyltransferase while avoiding its complex donor-regeneration cycles and the need for intermediate protection and deprotection sequences of classical chemical procedures. Limitations in efficiency of classical chemical and enzymatic glycosylation methods resulting from time-consuming work-up and purification procedures after each glycosylation step can be overcome by application of polymer-supported solution-phase techniques which previously have been shown to be powerful tools in classical chemical synthesis.[6] Whereas solid-phase techniques suffer from various problems due to the heterogenous nature of reactions on the insoluble resin, soluble polymer supports enable standard solution-based reaction conditions to be used while preserving the possibility of exploiting the macromolecular properties of the resin in the purification steps. Combining the glycosidase-catalyzed transglycosylation technique with solid-phase supported work-up procedures, the terminally α(2-3)- and α(2-6)-sialylated oligosaccharides **5**–**12** (Scheme 1) were synthesized from the precursors **1**–**4** employing MPEG as polymeric support using a procedure based on the solubility of the polymer under reaction conditions and its insolubility during work-up in various ethers.[7]† In order to facilitate final cleavage, an α,α′-dioxyxylyl linker (DOX) is introduced.[8] Thus, glycosylation can be performed in the aqueous solution phase whereas work-up is performed in the solid phase.

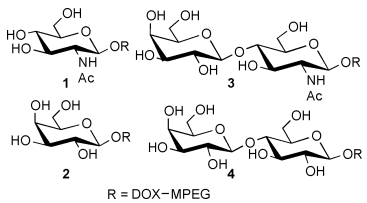

Essentially, all reactions proceed following the same sequence: TRANSSIALYLATION → CODISTILLATION (with toluene) → REDISSOLUTION (in dichloromethane) → PRECIPITATION (with *tert*-butyl methyl ether) → FILTRATION → RECRYSTALLIZATION (from ethanol).

Employing incubation conditions broadly identical to standard procedures for transsialylation the oligosaccharides **5**–**12** were obtained in yields corresponding to non-polymer-supported acceptor molecules.[5]

As sialidases can display a variety of regioselectivities depending on their biological source, extreme care has to be taken in order to achieve product formation of a single regioisomer. Among a variety of sialidases that not only display the necessary regioselectivity but are also commercially available in sufficient quantitity and purity the sialidases from *Vibrio cholerae* and *Salmonella typhimurium* proved to be the most suitable transsialylation catalysts.§ While the sialidase

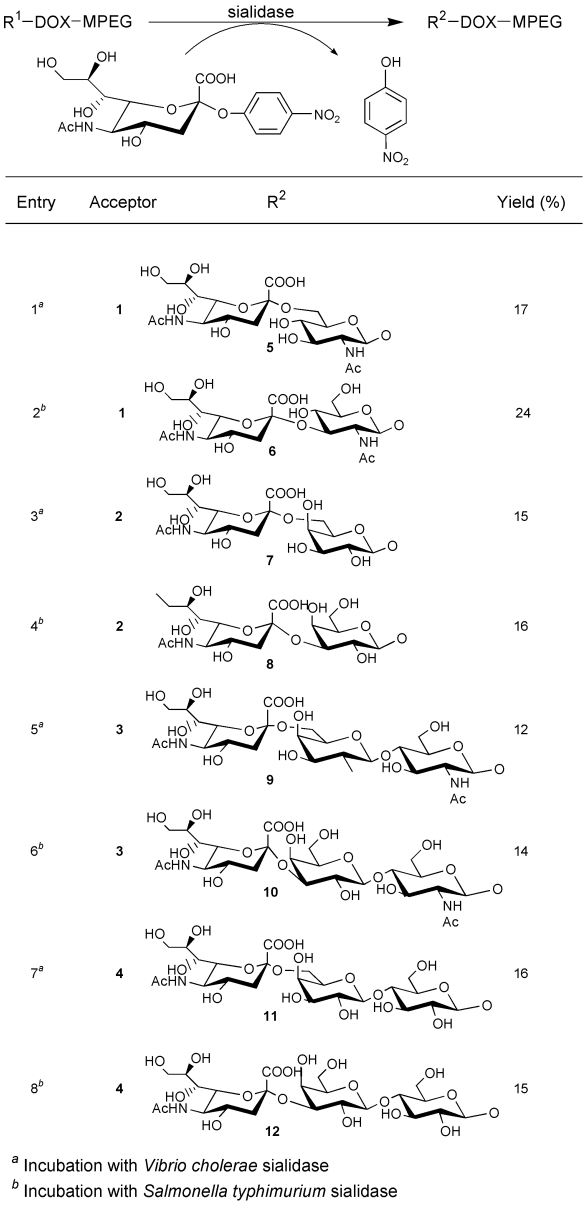

Scheme 1 Chemoenzymatic transsialylation of **1**–**4** using *Vibrio cholerae* and *Salmonella typhimurium* sialidase.

† Electronic supplementary information (ESI) available: Further experimental data. See http://www.rsc.org/suppdata/cc/b0/b003943h/

from *V. cholerae* preferentially catalyzes transsialylation in the α(2-6)-position the sialidase from *S. typhimurium* displays a pronounced regioselectivity for the α(2-3)-directed sialylation.

Sialylation of the monosaccharide acceptors **1** and **2** afforded slightly higher yields than the respective disaccharide conjugates **3** and **4**. The relatively high yield of 24% for **6** was achieved by twofold repetition of the transsialylation after intermediate work-up, giving **6** in 13% after the first and 21% yield after the second cycle. Unfortunately, only in this one case could the yield be raised considerably. Increases in yields of 2–3% after renewed incubation did not justify repeated transsialylation cycles for the other acceptor molecules. Instead it proved to be more profitable to run the same reaction in several small batches. The reactions could be scaled up to 100 μmol of product oligosaccharide without great loss in yields. In all instances described, a completely regiospecific transfer of *N*-acetylneuraminic acid could be achieved by careful monitoring of the reaction course by ^{1}H NMR spectroscopy. Regioisomeric transfer ratios were determined on-resin by integration of the axial and equatorial H-3 protons of neuraminic acid, applying the structural-reporter group concept.[9] The shifts of the *N*-acetylneuraminic acid H-3 protons are not only located outside the bulk signal region but also contain characteristic information about the type and linkage position of the glycosidically coupled saccharide. In some cases incubations had to be interrupted before maximum overall product formation was achieved in order to obtain a single regioisomer.

Even with an acceptor turnover rate of 10–25%, 75–90% of unreacted polymer-bound acceptor is still present. Cleavage from the resin at this stage would require an additional chromatographic step. This can be avoided by exploiting the capability of *exo*-glycosidases to stereoselectively hydrolyze specific terminal glycosyl units while leaving internal ones intact. Treatment of **9** with β-galactosidase from *Bacillus circulans* and β-*N*-acetylhexosaminidase from *Aspergillus oryzae* using standard incubation protocols yields MPEG-bound sialyllactosamine while free galactose and *N*-acetylglucosamine are removed as above by precipitation and filtration (Scheme 2). Owing to similar incubation conditions, the reaction in this case can be carried out as a one-pot reaction.

Prior to the cleavage of the product from the polymer, the carboxy function of the sialyl unit is protected by a methyl ester using standard procedures. Final cleavage of the product is achieved by application of a recently published method using scandium(III) trifluoromethanesulfonate and acetic anhydride,[10] which results in cleavage of the C–O bond between the dioxyxylyl unit and the terminal oxygen of the MPEG. Furthermore, all free hydroxy groups of the oligosaccharide are acetylated, which facilitates chromatographic purification of the product by flash chromatography.

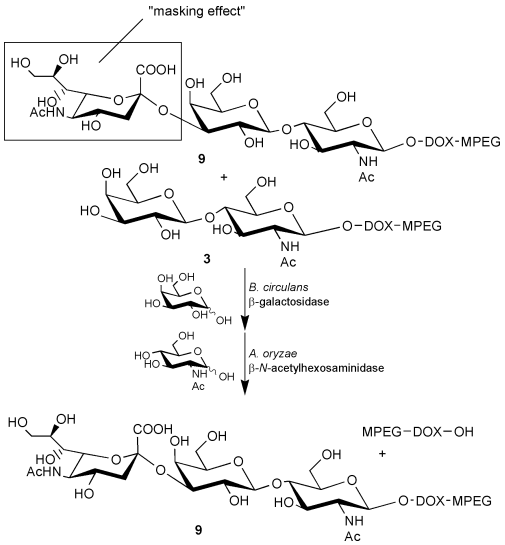

Scheme 2 Down-trimming of the polymer.

In conclusion, we have demonstrated for the first time a combination of glycosidase-catalyzed transglycosylation methodology with polymer-supported solution-phase techniques and have been able to synthesize various terminally α(2-3)- and α(2-6)-sialylated di- and trisaccharides, thus, providing a simple and useful method for the synthesis of heterooligosaccharides.

Notes and references

‡ *Transsialylation assay using V. cholerae sialidase.* Solutions of *p*Np-Neu5Ac (21 mg, 50 μmol) and acceptor (120–160 mg, 25 μmol, donor–acceptor ratio 2 : 1) in degassed incubation buffer (150 μl, 0.1 M NaOAc, 0.5 mM $CaCl_2$, pH5.5) are incubated with *V. cholerae* sialidase (1 U) at 30 °C. Compounds **5** (24 mg, 17%), **7** (21 mg, 15 %), **9** (17 mg, 12 %) and **11** (22 mg, 16%) were obtained as white powders. The amounts refer to the calculated absolute amounts of polymer-bound product, whereas the percentages are relative to polymer-bound acceptor units.

Transsialylation assay using S. typhimurium sialidase. Solutions of *p*Np-Neu5Ac (21 mg, 50 μmol) and acceptor (110–150 mg, 20 μmol, donor–acceptor ratio 2.5 : 1) in degassed incubation buffer (150 μl, 0.1 M NaOAc, pH 5.1) are incubated with *S. typhimurium* sialidase (1 U) at 30 °C. Compounds **6** (34 mg, 24%), **8** (23 mg, 16%), **10** (21 mg, 14%) and **12** (23 mg, 15%) were obtained as amorphous solids.

General procedure. The course of the reaction is followed photometrically at 400 nm and by TLC (EtOH–1 M ammonium acetate (pH 7.4) 5 : 1) using resorcinol spraying reagent for *N*-acetylneuraminic acid detection. The incubation is terminated by addition of 0.1 M Na_2CO_3 (1 ml) followed by ultrasonification for 3 min. The mixture is acidified to pH 6.8 with Dowex 50WX8 H^+ cation exchanger and centrifuged. The supernatant is decanted and codistilled twice with toluene (10 ml). The residue is taken up in dry dichloromethane (10 ml) and precipitated with *tert*-butyl methyl ether (200 ml). The precipitate is filtered, rinsed with *tert*-butyl methyl ether (50 ml) and recrystallized from EtOH.

Cleavage of the product from the resin exemplified for compound **3**. 160 mg of polymer-bound trisaccharide **11** (0.032 mmol) is dissolved in dry dichloromethane (1.5 ml). Acetic anhydride (1.5 ml) and scandium(III) trifluoromethanesulfonate [$Sc(OTf)_3$, 10 mg, 0.02 mmol] are added sequentially. After stirring under argon for 6 h the mixture is cooled to 0 °C in an ice bath and *tert*-butyl methyl ether (150 ml) is added to precipitate the cleaved polymer. The filtrate is concentrated to dryness. The residue is suspended in dry MeOH (10 ml) and 100 mg cation exchange resin (DOWEX 50W-X8 H^+) is added. After stirring for 6 h at rt the resin is filtered off. The filtrate is concentrated and purified by flash chromatography (petrol ether–ethyl acetate 3 : 1 to 1 : 1) to yield *p*-*O*-acetyl-[DOX]yl [methyl(5-acetamido-4,7,8,9-tetra-*O*-acetyl-3,5-dideoxy-D-*glycero*-α-D-*galacto*-2-nonulopyranosyl)onate]-(2-3)-*O*-(2,3,4-tri-*O*-acetyl-β-D-galactopyranosyl)-(1-4)-*O*-2,3,6-tri-*O*-acetyl-*β*-D-glucopyranoside (1.8 mg, 14% relative to polymer bound **4**, 88% relative to **11**).

§ Sialidase (E.C. 3.2.1.18) from *V. cholerae* was a kind gift from Chiron Behring GmbH, Germany. Recombinant sialidase (E.C.3.2.1.18) from *S. typhimurium* was purchased from New England Biolabs GmbH, Germany. 2-*O*-(*p*-Nitrophenyl)-5-acetamido-3,5-dideoxy-D-*glycero*-α-D-*galacto*-nonulopyranusonic acid (*p*Np-Neu5Ac) was prepared by the method of Rothermel *et al.*[11] Acceptor **1** was prepared by a procedure developed by Hodosi *et al.*[12]

For further experimental detail see ESI†.

1 A. Varki, *Glycobiology*, 1993, **3**, 97.
2 R. Schauer and J. P. Kamerling, in *Glycoproteins II*, ed. J. Montreuil, J. F. G. Vliegenthart and H. Schachter, Elsevier Science, 1997, p. 243.
3 J. Thiem and B. Sauerbrei, *Angew. Chem., Int. Ed. Engl.*, 1991, **30**, 1503.
4 K. Ajisaka, H. Fujimoto and M. Isomura, *Carbohydr. Res.*, 1994, **259**, 103.
5 D. Schmidt, B. Sauerbrei and J. Thiem, *J. Org. Chem.*, in the press.
6 D. J. Gravert and K. D. Janda, *Chem. Rev.*, 1997, **97**, 589.
7 S. P. Douglas, D. M. Whitfield and J. J. Krepinsky, *J. Am. Chem. Soc.*, 1991, **113**, 5095.
8 S. P. Douglas, D. M. Whitfield and J. J. Krepinsky, *J. Am. Chem. Soc.*, 1995, **118**, 2116.
9 J. F. G. Vliegenthart, L. Dorland and H. von Halbeek, *Adv. Carbohydr. Chem. Biochem.*, 1983, **41**, 209.
10 S. Mehta and D. M. Whitfield, *Tetrahedron Lett.*, 1998, **39**, 5907.
11 J. Rothermel and H. Faillard, *Carbohydr. Res.*, 1990, **196**, 29.
12 G. Hodosi and J. J. Krepinsky, *Synlett*, 1996, 159.

ChemComm

Remarkable enhancement of photocurrent generation by ITO electrodes modified with a self-assembled monolayer of porphyrin†

Hiroko Yamada,[a] Hiroshi Imahori,*[a] Yoshinobu Nishimura,[b] Iwao Yamazaki*[b] and Shunichi Fukuzumi*[a]

[a] *Department of Material and Life Science, Graduate School of Engineering, Osaka University, CREST, JAPAN Science and Technology Corporation, Suita, Osaka 565-0871, Japan. E-mail: imahori@ap.chem.eng.osaka-u.ac.jp; fukuzumi@ap.chem.eng.osaka-u.ac.jp*

[b] *Department of Molecular Chemistry, Graduate School of Engineering, Hokkaido University, Sapporo 060-8628, Japan. E-mail: yamiw@eng.hokudai.ac.jp*

Received (in Cambridge, UK) 27th July 2000, Accepted 21st August 2000
First published as an Advance Article on the web

Quantum yield of the photocurrent generation by an ITO electrode modified with a self-assembled monolayer of porphyrin was remarkably enhanced by a factor of *ca.* 280, as compared to that of the corresponding porphyrin monolayer on a gold electrode.

In recent years organized assemblies of porphyrins have attracted much attention directed toward the development of photovoltaic devices, catalysis, and sensors.[1] In particular, formation of self-assembled monolayers (SAMs)[2] of porphyrins on the material surface is a potential approach for fabricating highly ordered functional thin films. In this context, we[3–5] and others[6] have reported the photoelectrochemical properties of porphyrin and porphyrin-containing donor–acceptor SAMs on gold electrodes. However, the photocurrent generation, initiated from the porphyrin excited singlet state ($^1P^*$) in the porphyrin SAMs on the gold electrodes, has been hampered by the competing energy transfer (EN) quenching of $^1P^*$ by the gold surface. Such an undesirable EN process may be avoided by employing semiconductor electrodes such as indium tin oxide (ITO) instead of metal electrodes.[7,8] However, there has so far been no report on the photoelectrochemical properties of porphyrin-containing donor–acceptor SAMs on conductive ITO support, although porphyrin SAMs on oxide surfaces or gold nanoparticles have been extensively studied.[9–12] As such, no quantitative comparison of such quenching effect has ever been reported for porphyrin SAMs on semiconductor and metal electrodes.

We report herein the first quantitative comparison of photocurrent generation in porphyrin SAMs on ITO and gold electrodes. A remarkable 280-fold enhancement of photocurrent generation has been observed in the porphyrin SAM on the ITO, as compared to the corresponding porphyrin SAM on the gold surface. The present study thereby provides valuable information for the construction of highly efficient photovoltaic cells.

In order to evaluate the EN quenching effect accurately, we designed porphyrin SAMs where the porphyrin is tethered to ITO (denoted as **1**/ITO) and gold electrodes (denoted as **2**/Au) with a spacer of the same number of atoms, respectively, as shown in Fig. 1. Bulky *tert*-butyl groups were introduced into the *meta*-positions of the *meso*-phenyl groups on the porphyrin to preclude self-quenching of the $^1P^*$ due to the porphyrin aggregation.[4,13] The general strategy employed for synthesizing the SAMs is summarized in Scheme 1. ITO electrodes (1900–2000 Å ITO on transparent glass slides) were treated with aminopropyltrimethoxysilane by refluxing for 3 h in toluene.[11] Activated porphyrin **4**, prepared from porphyrin carboxylic acid **3** and pentafluorophenol,[11] was coupled to the aminopropylsilylated glass by refluxing for 3 h in toluene to give **1**/ITO.[11] **2**/Au was prepared by following the same procedures as described previously.[4]‡ Porphyrin references **5** and **6**[4] were also synthesized.

Fig. 2 displays absorption spectra of **1**/ITO and reference **5** in $CHCl_3$. The Soret band of **1**/ITO becomes broader than that of reference **5** in $CHCl_3$. The λ_{max} value of the Soret band of **1**/ITO is nearly identical to that of **5** in $CHCl_3$, whereas the λ_{max} value of **2**/Au was reported to be red-shifted (4 nm) as compared to that of reference **6** in $CHCl_3$.[4] This indicates that the porphyrin environment of **1**/ITO is less perturbed than that of **2**/Au.

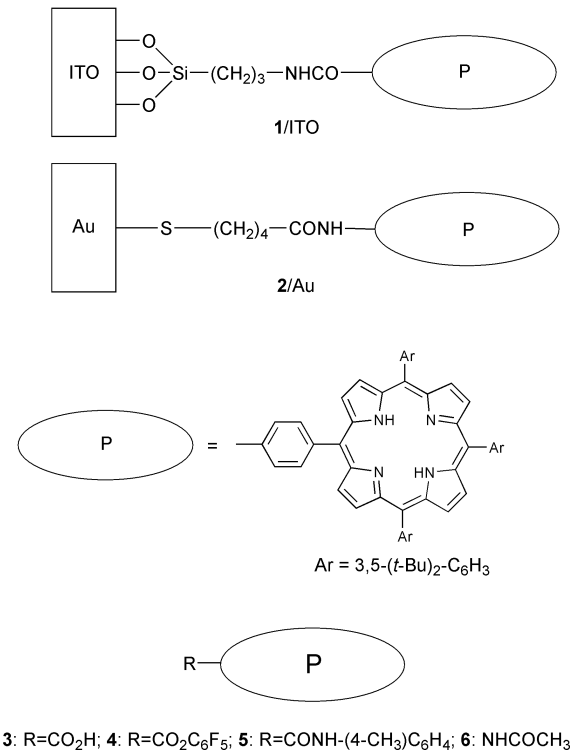

3: R=CO_2H; **4**: R=$CO_2C_6F_5$; **5**: R=CONH-(4-CH_3)C_6H_4; **6**: $NHCOCH_3$

Fig. 1 **1**/ITO and **2**/Au and porphyrin derivatives used in this study.

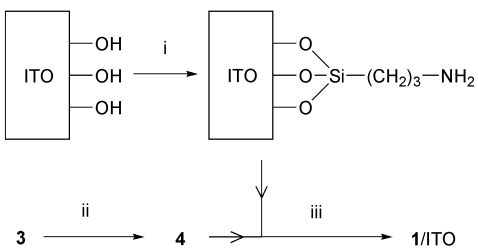

Scheme 1 *Reagents and conditions*: i, $(MeO)_3Si(CH_2)_3NH_2$, isopropylamine, dry toluene, argon, reflux 3 h; ii, DCC, 4-pyrrolidinopyridine, pentafluorophenol, dry CH_2Cl_2, 96%; iii, dry toluene, argon, reflux 3 h.

† Electronic supplementary information (ESI) available: Fig. A cyclic voltammograms of **1**/ITO and **2**/Au. See http://www.rsc.org/suppdata/cc/b0/b006108p/

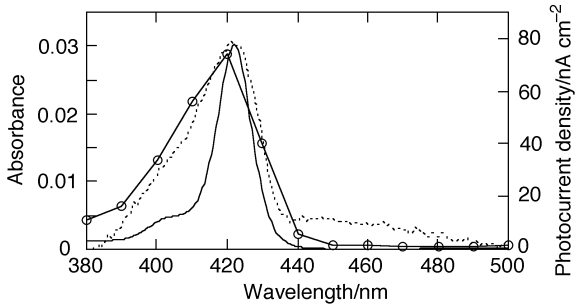

Fig. 2 UV-visible absorption spectra of **1**/ITO (dotted line) and **5** in $CHCl_3$ (solid line) and action spectrum of the ITO/**1**/TEA/Pt cell (solid line with circles); 100 μW cm^{-2}, +400 mV *vs*. Ag/AgCl, an argon-saturated 0.1 M Na_2SO_4 aqueous solution containing 50 mM TEA. The spectra are normalized at the Soret band for comparison.

A cyclic voltammetric experiment using **1**/ITO (electrode area, 0.48 cm^2) in CH_2Cl_2 containing 0.2 M $Bu^n_4NPF_6$ electrolyte with a sweep rate of 0.1 V s^{-1} was performed to estimate the surface coverage.[4,5]‡ The adsorbed amount of the porphyrin on **1**/ITO was calculated from the anodic peak of the porphyrin as 2.4×10^{-10} mol cm^{-2} (69 Å^2). Assuming that packing densities of the porphyrins are similar in **1**/ITO and **2**/Au (1.0×10^{-10} mol cm^{-2}, 170 Å^2),[4] the roughness factor of ITO is estimated as 2.5.

Photoelectrochemical measurements were carried out in an argon-saturated 0.1 M Na_2SO_4 aqueous solution containing 50 mM triethanolamine (TEA) as an electron sacrificer using **1**/ITO or **2**/Au as the working electrode, Pt counter electrode, and Ag/AgCl (sat. KCl) reference electrode (hereafter represented by ITO/**1**/TEA/Pt and Au/**2**/TEA/Pt, respectively, where / denotes an interface).[4,5] A stable anodic photocurrent from the electrolyte to the ITO appeared immediately upon irradiation of the ITO electrode with $\lambda = 419.5 \pm 5.3$ nm light with 100 μW cm^{-2}. The photocurrent fell down instantly when the illumination was cut off. In the absence of TEA, the anodic photocurrent was negligible under otherwise the same experimental conditions. The anodic photocurrent increases monotonically with increasing positive bias to the ITO electrode (−0.2–+0.4 V), whereas the dark current remains constant, as shown in Fig. 3. This demonstrates that photocurrent flows from the electrolyte to the ITO electrode *via* the porphyrin SAM. The agreement of the action spectrum with absorption spectrum of **1**/ITO from 380–500 nm (Fig. 1) demonstrates clearly that the porphyrin is the photoactive species.

The photocurrent generation efficiency becomes much lower when the ITO/**1**/TEA/Pt cell was replaced by the Au/**2**/TEA/Pt cell under the same experimental conditions. The quantum yield (3.4%) of the ITO/**1**/TEA/Pt cell determined under the optimized conditions ($\lambda = 419.5 \pm 5.3$ nm light with 100 μW cm^{-2} and at +0.4 V *vs*. Ag/AgCl)§ is *ca*. 280 times higher than the value (0.012%) for the Au/**2**/TEA/Pt cell.

Time-resolved, single-photon counting fluorescence studies were made for **1**/ITO and **2**/Au as well as **5** and **6** in solutions with the excitation wavelength at 435 nm. In each case the decay of the fluorescence intensity due to the $^1P^*$ was monitored at 655 nm. The decay curve could be fitted as a single exponential except for the case of **1**/ITO. The fluorescence lifetimes of **1**/ITO (1.0 (74%) and 3.7 ns (26%))¶ are significantly longer than that of **2**/Au (15 ps), although the lifetimes are shorter than those of **5** (7.7 ns) and **6** (7.6 ns) in $CHCl_3$.[4] This clearly indicates that the EN quenching efficiency of $^1P^*$ on the ITO is much suppressed as compared to that on the gold surface. Based on the electrochemical data, it is concluded that an electron transfer takes place from TEA (+0.61 V)[15] to the singlet excited state $^1P^*$ (+0.62 V *vs*. Ag/AgCl)[14] rather than the excited triplet state $^3P^*$ (+0.12 V *vs*. Ag/AgCl),[14] yielding the porphyrin radical anion ($P^{\bullet -}$). The formation efficiency of $P^{\bullet -}$ in **1**/ITO should become much larger than that in **2**/Au as observed experimentally because of the suppression of undesirable EN quenching of $^1P^*$ by the electrode as compared to the **2**/Au system. The resulting $P^{\bullet -}$ (−1.28 V *vs*. Ag/AgCl) gives an electron to the ITO electrode, resulting in the anodic photocurrent generation.

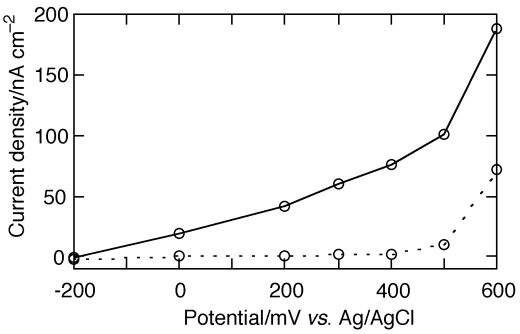

Fig. 3 Photocurrent *vs*. applied potential curves for the ITO/**1**/TEA/Pt cell (solid line with open circles): $\lambda = 419.5$ nm (100 μW cm^{-2}), an argon-saturated 0.1M Na_2SO_4 aqueous solution containing 50 mM TEA. The dark current is shown as a dotted line with open circles.

In conclusion, we have successfully demonstrated that the quantum yield of photocurrent generation for the porphyrin SAM cell on ITO becomes 280 times larger as compared to the quantum yield on the gold electrode due to the suppression of undesirable EN quenching of $^1P^*$ by the electrode.

H. I. thanks the Sumitomo Foundation for financial support.

Notes and references

‡ For electrochemical and photoelectrochemical measurements, gold electrodes (**2**/Au) (roughness factor $R = 1.1$) were prepared by a vacuum deposition technique with titanium (5–10 nm) and gold (20–100 nm) in a sequence onto a Si(100) wafer, whereas for UV-visible absorption measurements, gold (20 nm) was evaporated onto a transparent glass slide to give **1**/Au ($R = 1.5$).[4,5]

§ $\phi = (i/e)/[I(1 - 10^{-A})]$, $I = (W\lambda)/(hc)$ where i is the photocurrent density, e is the elementary charge, I is number of photons per unit area and unit time, λ is the wavelength of light irradiation, A is absorbance of the adsorbed dyes at λ nm, W is light power irradiated at λ nm, c is the light velocity, and h is the Planck constant; ITO/**1**/TEA/Pt: $i = 74$ nA cm^{-2}, $A = 0.029$; Au/**2**/TEA/Pt: $i = 0.28$ nA cm^{-2}, $A = 0.030$ (including the reflection at 419.5 nm).[4,5]

¶ In the case of 5,10,15,20-tetrakis(3,5-di-*tert*-butylphenyl)porphyrin (TBP) and octadecylamine (ODA) Langmuir–Blodgett multilayers on a glass slide, two-component emission decay was observed with lifetimes of 1–2 ns and 2–4 ns at a high ratio of TBP–ODA (> 0.11).[13]

1 S. Fukuzumi and H. Imahori, *Electron Transfer in Chemistry*, ed. V. Balzani, Wiley–VCH, Weinheim, 2000, in press.
2 A. Ulman, *An Introduction to Ultrathin Organic Films*, Academic Press, San Diego, 1991.
3 H. Imahori and Y. Sakata, *Eur. J. Org. Chem.*, 1999, 2445.
4 H. Imahori, H. Norieda, Y. Nishimura, I. Yamazaki, K. Higuchi, N. Kato, T. Motohiro, H. Yamada, K. Tamaki, M. Arimura and Y. Sakata, *J. Phys. Chem. B*, 2000, **104**, 1253.
5 H. Imahori, H. Yamada, Y. Nishimura, I. Yamazaki and Y. Sakata, *J. Phys. Chem. B*, 2000, **104**, 2099.
6 K. Uosaki, T. Kondo, X.-Q. Zhang and M. Yanagida, *J. Am. Chem. Soc.*, 1997, **119**, 8367.
7 S. Suto, W. Uchida, M. Yashima and T. Goto, *Phys. Rev. B*, 1987, **35**, 4393.
8 B. Choudhury, A. C. Weedon and J. R. Bolton, *Langmuir*, 1998, **14**, 6199.
9 M. Lahav, T. Gabriel, A. N. Shipway and I. Willner, *J. Am. Chem. Soc.*, 1999, **121**, 258.
10 D. Li, B. I. Swanson, J. M. Robinson and M. A. Hoffbauer, *J. Am. Chem. Soc.*, 1993, **115**, 6975.
11 D. W. J. McCallien, P. L. Burn and H. L. Anderson, *J. Chem. Soc., Perkin Trans. 1*, 1997, 2581.
12 D. L. Pilloud, X. Chen, P. L. Dutton and C. C. Moser, *J. Phys. Chem. B*, 2000, **104**, 2868.
13 M. Anikin, N. V. Tkachenko and H. Lemmetyinen, *Langmuir*, 1997, **13**, 3002.
14 C. Luo, D. M. Guldi, H. Imahori, K. Tamaki and Y. Sakata, *J. Am. Chem. Soc.*, 2000, **122**, 6535.
15 T. Morita, S. Kimura, S. Kobayashi and Y. Imanishi, *J. Am. Chem. Soc.*, 2000, **122**, 2850.

Novel liquid-crystalline and amorphous materials containing oxadiazole and amine moieties for electroluminescent devices

Hiroyuki Mochizuki,[a] Takahiro Hasui,[a] Masuki Kawamoto,[a] Takeshi Shiono,[a] Tomiki Ikeda,*[a] Chihaya Adachi,[b] Yoshio Taniguchi[b] and Yasuhiko Shirota[c]

[a] *Chemical Resources Laboratory, Tokyo Institute of Technology, 4259 Nagatsuta, Midori-ku, Yokohama 226-8503, Japan. E-mail: tikeda@res.titech.ac.jp*

[b] *Department of Functional Polymer Science, Faculty of Textile Science and Technology, Shinshu University, Ueda, Nagano 386-8567, Japan*

[c] *Department of Applied Chemistry, Faculty of Engineering, Osaka University, Yamadaoka, Suita, Osaka 565-0871, Japan*

Received (in Cambridge, UK) 12th July 2000, Accepted 10th August 2000
First published as an Advance Article on the web 13th September 2000

Three 1,3,4-oxadiazole derivatives with an amine and an alkyl tail were designed and synthesized as novel electroluminescent materials; it was found that the length of alkyl tail and the structure of the amine strongly affect the phase structure of the oxadiazole derivatives.

Functional organic materials have been the subject of recent research work in relation to their optical and electronic properties as well as their industrial applications in many fields such as electroluminescent (EL) devices, transistors, batteries, sensors, photoreceptors and displays.[1] However, practical products made of organic compounds are solely photoreceptors and displays. Thus, the advantages of organic compounds are not sufficiently utilized in practical materials and devices.

Liquid-crystalline (LC) phases and amorphous states of organic materials have been known to show unique morphology. LC materials are quite attractive in terms of possessing both self-organizing capability and fluidity. On the other hand, amorphous materials are promising in terms of their excellent processability, flexibility, transparency, non-existence of grain boundaries and isotropic properties. Recently, much attention has been paid to low-molecular-weight materials which form stable amorphous glasses above rt.[2] It is of interest and of significance to develop photo- and electroactive amorphous molecular materials, which consist of π-electron systems and have glass transition temperature (T_g) higher than rt, for use in electronic devices.

In 1990, it was found that 2-(biphenyl-4-yl)-5-(4-*tert*-butylphenyl)-1,3,4-oxadiazole (PBD) functioned very well as an excellent electron transport material (ETM) in an organic multilayer EL diode.[3] After this report, many researchers began to use various kinds of oxadiazole molecules to obtain high EL performances. Furthermore, in recent studies of polymer light-emitting diodes, the oxadiazole moieties were demonstrated to possess high potential for electron transport.[4]

Introduction of the oxadiazole moieties to polymer main chains and to mesogens of LC compounds is expected to tune EL efficiencies and electron transport properties. EL polymers with *p*–*n* diblock structures were reported, in which thiophene and 1,3,4-oxadiazole moieties connected alternately to form fully conjugated rigid-rod polymers: one has been successfully used to fabricate single layer EL devices showing blue emission.[5] Likewise, LC compounds containing oxadiazole moieties were reported to exhibit a high electron transport capability and blue EL emission.[6]

In this study, we report the synthesis and properties of a novel class of oxadiazole derivatives for photo- and electroactive materials, emphasizing that the length and structure of the introduced moieties strongly affect the phase structure of the oxadiazole derivatives.

The oxadiazole derivatives in this study were prepared starting from 4-(4-*n*-alkylphenyl)benzoic acid by the synthetic route shown in Scheme 1. 4-(4-*n*-Alkylphenyl)benzoic acid was reacted with an excess of thionyl chloride. The resulting 4-(4-*n*-alkylphenyl)benzoyl chloride was reacted with aminophenyltetrazole derivatives in dry pyridine at 135 °C, yielding the products: 2-(4′-propylbiphenyl-4-yl)-5-(4-*N*,*N*-dimethylaminophenyl)-1,3,4-oxadiazole (**3-OXD-Me**), 2-(4′-heptylbiphenyl-4-yl)-5-(4-*N*,*N*-dimethylaminophenyl)-1,3,4-oxadiazole (**7-OXD-Me**) and 2-(4′-heptylbiphenyl-4-yl)-5-(4-*N*,*N*-diphenylaminophenyl)-1,3,4-oxadiazole (**7-OXD-Ph**).[7] These products were purified by column chromatography on silica gel, followed by recrystallization from toluene–ethanol. The overall yields were about 55%. The oxadiazole derivatives were characterized as obtained by FT-IR, ^{1}H NMR and elemental analysis.

Thermotropic and LC behaviors were evaluated by means of DSC (heating and cooling rate: 2 °C min^{-1}) and polarizing microscopy. Fig. 1 shows DSC thermograms of **3-OXD-Me** and **7-OXD-Me** on the third cooling. It was found that **3-OXD-Me** showed only a sharp exothermic peak corresponding to a melting point (T_m) at 174 °C. By contrast, **7-OXD-Me** exhibited two exothermic peaks at 143 and 138 °C. It seems that the peak at 143 °C is due to isotropic (I)-nematic (N) phase transition and another peak at 138 °C is due to N-crystal phase transition. Fig. 2 shows the textures observed with a polarizing microscope at 140 and 100 °C, respectively. Referring to the Schlieren texture, the phase could be assigned to an N phase at 140 °C, and then a typical crystal texture was observed at 100 °C. As **7-OXD-Me** showed no LC phase on heating but an N phase on cooling, it seems to be a monotropic LC material.

DSC thermograms of **7-OXD-Ph** on the first and the second heating are shown in Fig. 3. When the crystalline sample of **7-OXD-Ph** obtained by recrystallization from ethanol–toluene was heated, **7-OXD-Ph** exhibited T_m at 166 °C to give an I phase. **7-OXD-Ph** in the I phase was then cooled by standing in

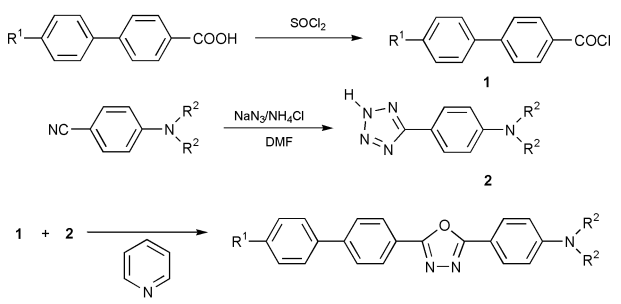

3-OXD-Me: R^1, -(CH$_2$)$_2$CH$_3$; R^2, -CH$_3$
7-OXD-Me: R^1, -(CH$_2$)$_6$CH$_3$; R^2, -CH$_3$
7-OXD-Ph: R^1, -(CH$_2$)$_6$CH$_3$; R^2, -C$_6$H$_5$

Scheme 1 Synthetic route for compounds used in this study with abbreviations.

DOI: 10.1039/b005550f

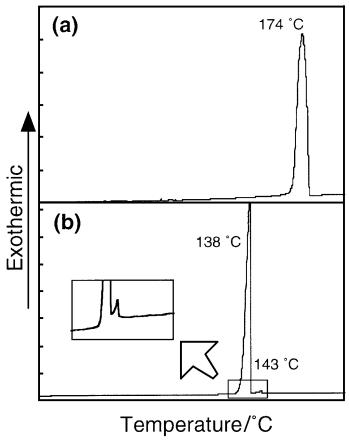

Fig. 1 DSC thermograms on the third cooling. (a), **3-OXD-Me**; (b), **7-OXD-Me**.

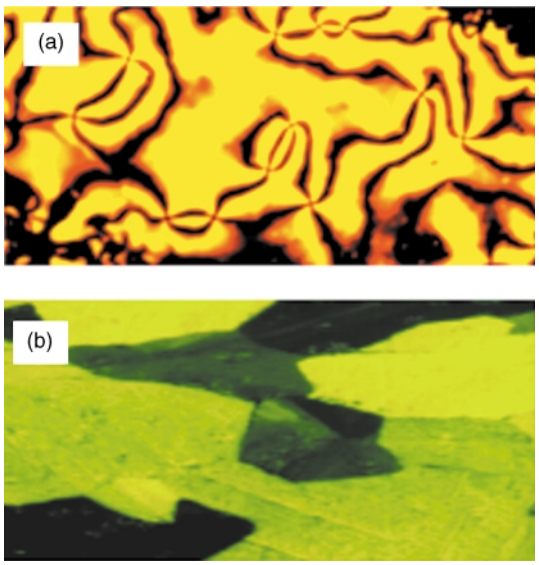

Fig. 2 Polarizing optical micrographs of the texture of **7-OXD-Me**. (a), at 140 °C (N phase); (b), 100 °C (crystalline phase).

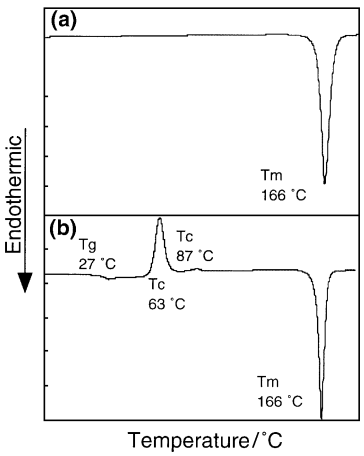

Fig. 3 DSC thermograms of **7-OXD-Ph**. (a), on the first heating; (b), on the second heating.

air, and it formed spontaneously the supercooled liquid state, which changed into the amorphous glassy state. On the second heating, T_g was observed at 27 °C, and then the first exothermic peak owing to crystallization appeared at around 60 °C. Subsequently, another crystallization occurred at 87 °C and the crystal melted at 166 °C. These phenomena of crystallization from the melt were confirmed with a polarizing microscope, however, the structure of each crystal was beyond identification.

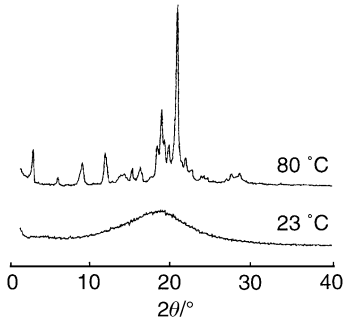

Fig. 4 X-Ray diffraction patterns of **7-OXD-Ph** at 23 and 80 °C.

The formation of an amorphous glass was evidenced in the X-ray diffraction patterns of **7-OXD-Ph** at rt (23 °C) and 80 °C, as exhibited in Fig. 4. **7-OXD-Ph** showed no sharp signals but only broad halos, when cooled from an I state to 23 °C, indicating that **7-OXD-Ph** is in an amorphous state. On the other hand, several sharp signals appeared at 80 °C, suggesting that **7-OXD-Ph** is in a crystalline state. **7-OXD-Ph** did not show an LC phase but an amorphous state; steric hindrance between two clusters of benzene rings of **7-OXD-Ph** may contribute to formation of the amorphous glass.

All materials investigated in this work emitted strong blue fluorescence with high quantum yields (0.81–0.91); emission peaks of **3-OXD-Me** and **7-OXD-Me** were 420 nm, and that of **7-OXD-Ph** was 436 nm. It is assumed that these compounds show an excellent EL performance. The present study will enable us to perform molecular design of various compounds based on oxadiazole for developing photo- and electroactive materials. These materials are expected to find potential application as functional materials, *e.g.* charge transport and luminescent materials for photoreceptors and electroluminescent devices.

In summary, 1,3,4-oxadiazole derivatives with amine and alkyl tails were designed and prepared as novel EL materials: the phase structures and optical properties of the oxadiazole derivatives were investigated in this study. We found that the length of the alkyl tail and the structure of the amine strongly affected the phase structure of the oxadiazole derivatives.

Notes and references

1 C. W. Tang and S. A. VanSlyke, *Appl. Phys. Lett.*, 1987, **51**, 913; J. H. Burroughes, D. D. C. Bradley, A. R. Brown, R. N. Marks, K. Mackay, R. H. Friends, P. L. Burn and A. B. Holmes, *Nature*, 1990, **347**, 539; A. J. Epstei, *MRS Bulletin*, June 1997, 16; G. P. Wiederrecht, A. B. Yoon and M. R. Wasielewski, *Science*, 1995, **270**, 1794; T. Ikeda and O. Tsutsumi, *Science*, 1995, **268**, 1873.
2 Y. Shirota, T. Kabata and N. Noma, *Chem. Lett.*, 1989, 1145; A. Higuchi, H. Inada, T. Kabata and Y. Shirota, *Adv. Mater.*, 1991, **3**, 549; H. Inada and Y. Shirota, *J. Mater. Chem.*, 1993, **3**, 319; W. Ishikawa, K. Noguchi, K. Kuwabara and Y. Shirota, *Adv. Mater.*, 1993, **5**, 559; K. Katsuma and Y. Shirota, *Adv. Mater.*, 1998, **10**, 223.
3 C. Adachi, T. Tsutsui and S. Saito, *Appl. Phys. Lett.*, 1990, **56**, 799; C. Adachi, T. Tsutsui and S. Saito, *Appl. Phys. Lett.*, 1990, **57**, 513.
4 C. Hosokawa, N. Kawasaki, S. Sakamoto and T. Kuzumoto, *Appl. Phys. Lett.*, 1992, **62**, 2503; Q. Pei and Y. Yang, *Chem. Mater.*, 1995, **7**, 1568.
5 W. Huang, H. Meng, W. Yu, J. Gao and A. J. Heeger, *Adv. Mater.*, 1998, **10**, 593.
6 H. Tokuhisa, M. Era and T. Tsutsui, *Appl. Phys. Lett.*, 1998, **72**, 2639.
7 N. Tamoto, C. Adachi and K. Nagai, *Chem. Mater.*, 1997, **9**, 1077.

ChemComm

A one-step, enantioselective reduction of ethyl nicotinate to ethyl nipecotinate using a constrained, chiral, heterogeneous catalyst†

Stuart A. Raynor,[ab] John Meurig Thomas,*[a] Robert Raja,[ab] Brian F. G. Johnson,*[b] Robert G. Bell[b] and Mike D. Mantle[c]

[a] *Davy-Faraday Research Laboratory, The Royal Institution of Great Britain, 21 Albemarle Street, London, UK W1X 4BS. E-mail: jmt@ri.ac.uk*
[b] *University of Cambridge, Department of Chemistry, Lensfield Road, Cambridge, UK CB2 1EW*
[c] *Department of Chemical Engineering, The University of Cambridge, New Museum Site, Cambridge, UK CB2 3QZ*

Received (in Liverpool, UK) 12th July 2000, Accepted 29th August 2000
First published as an Advance Article on the web

A chiral catalyst derived from 1,1′-bis(diphenylphosphino)-ferrocene and anchored within MCM-41 displays remarkable increases in both enantioselectivity and activity, in the hydrogenation of ethyl nicotinate to ethyl nipecotinate, when compared to an analogous homogeneous model compound.

It is acknowledged that, in view of their biological activity, the enantioselective synthesis of chiral saturated ring systems involving piperidine or cyclohexane is of considerable practical interest. Previously, efforts to hydrogenate enantioselectively an aromatic ring such as that in ethyl nicotinate (Scheme 1) have resulted in values of enantiomeric excess (ee) that are less than 6%.[1] However, very recently, a two-step process, involving initial hydrogenation in high yield to the comparatively stable 1,4,5,6-tetrahydronicotinate, followed by subsequent hydrogenation in the presence of a dihydrocinchonidine modified noble metal catalyst, yielded a quite high ee of the nipecotinate. The best activity reported by Blazer *et al.* [using a Pd on carbon (plus cinchonidine) catalyst for step (ii)] was 19% ee at 12% conversion.[2] Using the principle, first conceived five years ago,[3] of chirally constraining a designed active centre attached to a chiral ligand and tethered to the inner walls of mesoporous silica, as schematized in Fig. 1, we have produced an effective enantioselective catalyst for the direct hydrogenation of ethyl nicotinate to ethyl nipecotinate, with an ee of 17% and conversions in excess of 50%.

We have previously demonstrated that in the allylic amination of cinnamyl acetate, the enantiomeric excess achieved by the spatially confined (tethered) catalyst, which is derived from 1,1′-bis(diphenylphosphino)ferrocene (dppf), far exceeds that attained with the same active site when it is unconfined.[4] Mesoporous silica of the M41S type (used earlier as the support for several high performance catalysts[5]) was used to confine the designed catalyst, thereby creating the chiral space. The confinement is a crucial feature of the enantioselectivity of our catalyst. When an alkyl silsesquioxane with the same tethered, designed catalyst is subjected to identical conditions, degrees of conversion are appreciably lower and the catalyst exhibits no enantiodiscrimination.

Our approach in the synthesis of the heterogeneous catalyst was to design a homogeneous, metal-containing ferrocenyl precursor which possessed a functionality capable of reacting directly with a silica surface. This precursor could be characterized in detail using solution spectroscopic techniques, and then anchored to the surface of the mesoporous silica support in a one-step reaction. The synthetic strategy involved the reaction between (*S*)-1-[(*R*)-1,2′-bis(diphenylphosphino)ferrocenyl]-ethyl acetate[6,7] and 3-(methylamino)propyltrimethoxysilane to form a silane functionalised ferrocenyl ligand (**1**), the incorporation of palladium dichloride to which forms the target ferrocenyl precursor (**2**) (Scheme 2). The ferrocenyl precursor **2** was then reacted with the mesoporous silane MCM-41, the outer walls of which were previously deactivated *via* treatment with [Ph_2SiCl_2], a method which we have already shown to be applicable in this situation.[8]

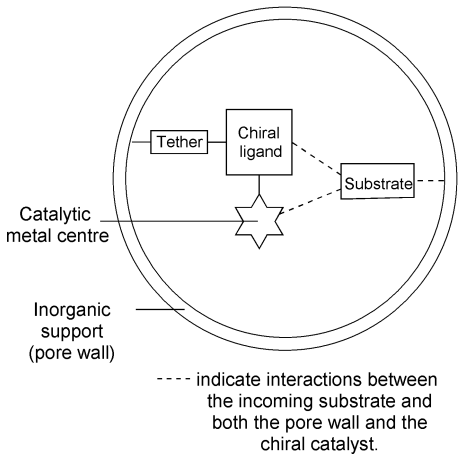

Fig. 1 Schematic diagram of the chiral catalyst constrained within a mesopore.

The anchored catalyst was characterised using ^{13}C and ^{31}P MAS NMR spectroscopy (ESI†). The ^{13}C spectrum was fully assignable when compared to that of (*S*)-1-[(*R*)-1,2′-bis(diphenylphosphino)ferrocenyl]ethylallylamine palladium dichlor-

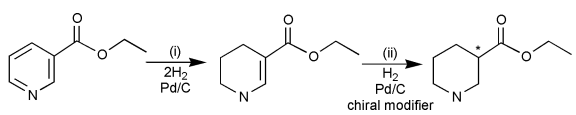

Scheme 1 The two-step hydrogenation of ethyl nicotinate to ethyl nipecotinate *via* 1,4,5,6-tetrahydronicotinate.

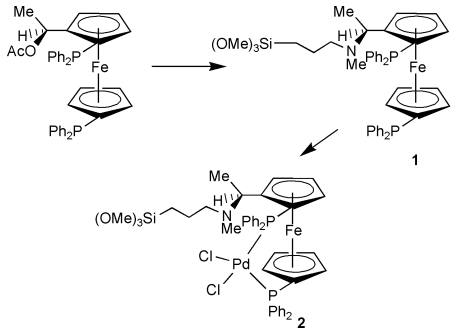

Scheme 2 The synthesis of the ferrocenyl precursor **2** from a chiral ferrocenyl acetate, *via* the silane functionalised ferrocenyl ligand **1**.

† Electronic supplementary information (ESI) available: ^{1}H, ^{13}C and ^{31}P NMR spectroscopic data for the ferrocenyl precursor **2**, the anchored heterogeneous catalyst and the silsesquioxane-bound homogeneous catalyst. See http://www.rsc.org/suppdata/cc/b0/b005689h/

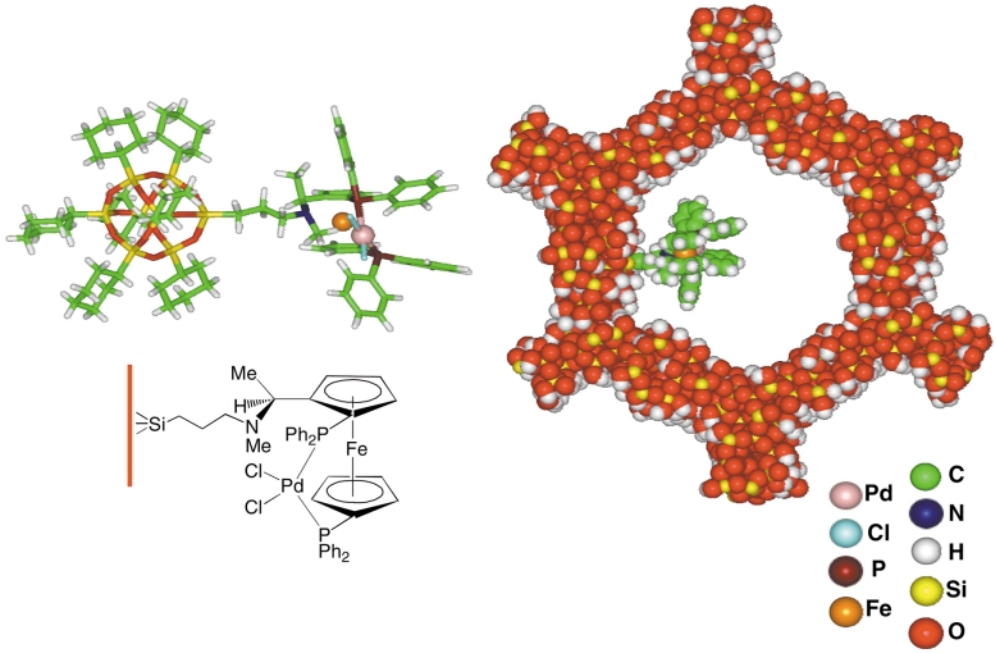

Fig. 2 Depiction of the catalytically active centre attached to a soluble silsesquioxane moiety and bound in a constrained manner inside mesoporous silica.

ide.[9] The spectrum showed two broad peaks centred at δ 135 and 75 which may be attributed to the phenyl and cyclopentadienyl rings, respectively. There is a peak at δ 12 which may be assigned to the methyl group bound to the chiral carbon and the carbon bound to the silicon. The central carbon in the propyl tether may be assigned to the peak at δ 22, whilst the final carbon of the tether, that bound to the nitrogen, can be attributed to the peak at δ 52. The final peaks in the spectrum are at δ 41 and 58 and may be assigned to the methyl group of the amine and the chiral carbon, respectively. The ^{31}P MAS NMR spectrum revealed a broad, split signal centred around δ 30, which is comparable to that observed with the ferrocenyl precursor **2**.

The ferrocenyl precursor **2** was also reacted with an incompletely condensed silsesquioxane cube,[10] to form a homogeneous model of the anchored heterogeneous catalyst. Solution ^{1}H NMR spectroscopy in C_4D_8O was used to characterise the model compound (ESI†), and the absence of the peaks for the hydroxy protons of the box at δ 6.97 and the methoxy protons of **2** at δ 3.47, are diagnostic in this regard. The MCM-41 bound catalyst and the silsesquioxane catalyst are illustrated in Fig 2.

The two catalysts were tested in the one-step hydrogenation of ethyl nicotinate to ethyl nipecotinate.‡ The catalysis was performed under mild conditions (20 bar H_2, 40 °C) and in both cases proceeded with the formation of the desired nipecotinate. However, analysis of the products revealed that the MCM-41 anchored species catalysed the reaction with a 17% ee whilst the use of the homogeneous silsesquioxane complex resulted in a racemic product. This remarkable change in stereoselectivity demonstrates the profound importance of confinement in the catalysis. The free catalyst shows no enantioselectivity whilst chiral confinement results in a catalyst that shows greater selectivity by almost a *threefold* margin than any other reported.[1] The confined catalyst also displayed a higher degree of activity (TON = 291) compared to the homogeneous form (TON = 98), after a reaction time of 72 h, and is remarkably stable. The reaction mixture of the anchored catalyst contained less than 3 ppb of metal (by ICP analysis), thereby ruling out the possibility of any leaching.

These results show the considerable potential that this type of catalyst offers, and how, by careful design of an active centre, a heterogeneous catalyst may be engineered, the performance of which is far superior than its free, homogeneous analogue.

We thank EPSRC for a rolling grant to J. M. T. and an award to B. F. G. J. We also wish to thank ICI for a case studentship to S. A. R. M.S.I. Inc. is gratefully acknowledged for the molecular modelling software. We are also grateful for assistance from Professor L. F. Gladden.

Notes and references

‡ The catalytic testing was performed in a high-pressure stainless steel reactor (Cambridge Reactor Design) lined with PEEK (polyether ether ketone). The catalyst (250 mg MCM-anchored, 100 mg box) was added to 5 g of ethyl nicotinate in 100 ml solvent (90 ml THF, 10 ml methanol). The vessel was pressurised to 20 bar with hydrogen and heated to 40 °C, whilst stirring was maintained at 400 rpm. During the reaction small aliquots were removed, using a mini-robot autosampler, to enable the kinetics to be studied. The products of the reaction were analysed by gas chromatograpy (GC, Varian, Model 3400 CX) employing a BPX5 capillary column (25 m × 0.32 mm) and flame ionisation detector. The ee was determined on the same machine *via* the conversion of the nipecotinate to a diastereomeric amide using (*R*)-(−)-Mosher's acid chloride.[2]

1 (*a*) R. M. Laine, G. Hum, B. J. Wood and M. Dawson, *Stud. Surf. Sci. Catal.*, 1981, **7**, 1478; (*b*) K. Nasar, F. Fache, M. Lemaire, J.-C. Beziat, M. Besson and P. Gallezot, *J. Mol. Catal.*, 1994, **87**, 107; (*c*) C. Exl, E. Ferstl, H. Honig and R. Rogi-Kohlenprath, *Chirality*, 1995, **7**, 211.
2 H.-U. Blazer, H. Honig, M. Studer and C. Wedemeyer-Exl, *J. Mol. Catal. A: Chem.*, 1999, **139**, 253.
3 (*a*) T. Maschmeyer, Unpublished Presentation at the Annual Progress Meeting of the Davy-Faraday Research Laboratories, 17 March 1995; (*b*) J. M. Thomas, *Philos. Trans. R. Soc. London, Ser. A*, 1990, **333**, 173; (*c*) J. M. Thomas, T. Maschmeyer, B. F. G. Johnson and D. S. Shephard, *J. Mol. Catal.*, 1999, **141**, 139.
4 B. F. G. Johnson, S. A. Raynor, D. S. Shephard, T. Mashmeyer, J. M. Thomas, G. Sankar, S. Bromley, R. Oldroyd, L. Gladden and M. D. Mantle, *Chem. Commun.*, 1999, 1167.
5 (*a*) T. Maschmeyer, F. Rey, G. Sankar and J. M. Thomas, *Nature*, 1995, **378**, 159; (*b*) R. D. Oldroyd, J. M. Thomas and G. Sankar, *Chem. Commun.*, 1997, 2025.
6 G. W. Gokel and I. K. Ugi, *J. Chem. Educ.*, 1972, **49**, 294.
7 T. Hayashi, T. Mise, M. Fukushima, M. Kagotani, N. Nagashima, Y. Hamada, A. Matsumoto, S. Kawakami, M. Konishi, K. Yamamoto and M. Kumada, *Bull. Chem. Soc. Jpn.*, 1980, **53**, 1138.
8 D. S. Shephard, W. Z. Zhou, T. Mashmeyer, J. M. Matters, C. L. Roper, S. Parsons, B. F. G. Johnson and M. Duer, *Angew. Chem., Int. Ed.*, 1998, **37**, 2719.
9 S. A. Raynor, R. Raja, J. M. Thomas, B. F. G. Johnson and M. D. Mantle, manuscript in preparation.
10 F. J. Feher, D. A. Newman and J. F. Walzer, *J. Am. Chem. Soc.*, 1989, **111**, 1741.

Triazacyclohexane complexes of chromium as highly active homogeneous model systems for the Phillips catalyst†‡§

Randolf D. Köhn,*[a] Matthias Haufe,[a] Shahram Mihan*[b] and Dieter Lilge[b]

[a] *Department of Chemistry, University of Bath, Bath, UK BA2 7AY. E-mail: r.d.kohn@bath.ac.uk*
[b] *BASF AG, Kunststofflaboratorium, Abteilung Polyolefine ZKP/E-M 505, D-67056 Ludwigshafen, Germany. E-mail: shahram.mihan@basf-ag.de*

Received (in Cambridge, UK) 19th July 2000, Accepted 30th August 2000
First published as an Advance Article on the web

MAO activated 1,3,5-triazacyclohexane complexes of chromium(III) are highly active ethene polymerisation catalysts that resemble the Phillips catalyst in many important properties and may represent the first good homogeneous model system.

The heterogeneous Phillips catalysts[1] based on CrO_3/SiO_2 for the polymerisation of ethene without co-catalysts produce a large fraction of the world production of HDPE (>7 M ton a^{-1}).[2] The molecular weight of the polymer depends on the reaction temperature. When activated with metal alkyls the Phillips catalyst can also trimerise ethene to 1-hexene (as well as some dimers) which is *in-situ* co-polymerised giving a polymer with butyl side chains and other unusual end groups including additional methyl groups, vinylidene and some internal olefinic groups. In contrast to the Ziegler–Natta systems, the nature of the active species and the origin of the end groups is still a matter of debate. Many homogeneous model systems[3] show only limited activity[4] and most of them fail to reproduce the properties of the Phillips catalyst and a true model has yet to be found.

For several years we have been investigating the coordination chemistry of 1,3,5-triazacyclohexanes **1**.[5] The results suggest that it should be possible to generate cationic alkyl chromium complexes with low steric demand due to the small N–Cr–N angle which may be able to catalyse ethene polymerisation. Indeed, complex **2a** reacts with methylaluminoxane (MAO) to give a highly active catalyst. However, good solubility of the complexes is crucial to achieve high productivities. This solubility problem is solved by introducing longer alkyl chains as substituents in **2b**–**d** according to Scheme 1. The solubility increases dramatically and **2c** and especially **2d** become highly soluble in toluene. Complexes **2c** and **2d** can be prepared from $CrCl_3$ (stored under air), **1**, toluene and zinc powder by simple heating under a stream of argon.[6]

Since the ligands **1c**,**d** can also be prepared by heating the corresponding primary amine and paraformaldehyde in toluene a simple one-pot synthesis of **2** is possible.

The systems **2**/MAO have much higher activity than the best co-catalyst free complex **3**[7] and the best non-Cp system **4**/MAO[8] (Scheme 2). The activity is comparable to

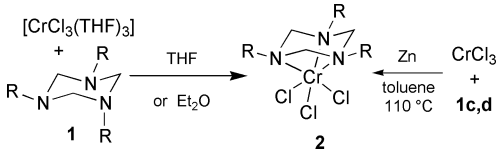

Scheme 1 Syntheses of the complexes **2**.

† Electronic supplementary information (ESI) available: synthetic, spectroscopic and analytical details of new compounds and the ethene polymerisation experiments. See http://www.rsc.org/suppdata/cc/b0/b005842o/
‡ Dedicated to Prof. H. Schumann on the occasion of his 65th birthday.
§ Chemistry of 1,3,5-triazacyclohexane complexes, Part 8. [Part 7, is ref. 5(*a*)].

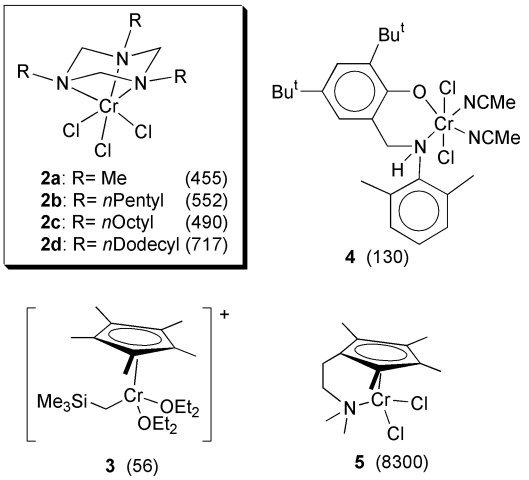

Scheme 2 Chromium complexes in ethene polymerisation (comparison of activity in [kg (mol Cr)$^{-1}$ h^{-1}]) (**2** at 40 °C and 1 bar ethene in toluene over 1 h).

$[(nBuCp)_2ZrCl_2]$/MAO under the same condition (650 kg (mol Cr)$^{-1}$ h^{-1}) and the only more active chromium system is **5**/MAO from Jolly *et al*.[4]

Maximum activity is reached at MAO : Cr $\approx$ 300. Activation of **2** can also be achieved with 1.6 eq. DMAB (dimethylanilinium tetrakis(pentafluorophenyl)borate) and 20–50 eq. $Al(iBu)_3$, giving similar activity (590 for **2a** and 390 for **2d**).

The molecular weights of the polymers under these conditions are around 40 000 (M_w) with M_w/M_n = 2–4 which is typical for a single-site catalyst.

End group analysis of the polymers (IR, ^{13}C NMR) shows more methyl groups than expected and additional vinylidene and some internal olefin as well as the expected vinyl end groups in a distribution that is typical for end groups produced by the Phillips catalyst. Since the molecular weights of the polymers differ, the end groups are best compared relative to the total number of olefinic groups (set to 100%) (Table 1).

In addition, 1-hexene as the trimer of ethene and some decenes as 'co-trimers' of 1-hexene and ethene can be found in the solution, and butyl side chains in the polyethene are indicative of some 1-hexene built into the polymer. Thus, our system is also able to reproduce the selectivity for trimerisation.[9] Interestingly, analysis of the decene isomers by NMR

Table 1 Relative end group distribution with the sum of olefinic groups set to 100%

End group	CH_2=CHR	CH_2=CR_2	RHC=CHR	Me
PE (Phillips)[a]	84–92%	7–13%	1–4%	150–300%
PE (**2d**)	82%	12%	6%	240%
decenes (**2d**)	87%	8%	5%	200%

[a] IR analyses of commercially available (BASF) Phillips HDPE products. Typical range under various conditions.

DOI: 10.1039/b005842o

shows an end group distribution similar to the polymers (Table 1). Addition of 1-hexene to the solution increases the content of butyl side chains substantially and a co-polymer can be obtained. Similar to the Phillips catalyst, activated **2** gives molecular weights of polyethene that are highly dependent on the reaction temperature.

Thus, activated **2** represents the first true homogeneous model for the Phillips catalyst that can reproduce many important properties and the results indicate that the typical end group distribution may be closely linked to a required trimerisation activity. A comprehensive discussion of substituent effects and the link between trimerisation and polymerisation activity will follow in separate publications.

R. D. K. thanks the Deutschen Forschungsgemeinschaft and the Fonds der Chemischen Industrie as well as Professor H. Schumann (TU Berlin) for support. We thank BASF for support.

Notes and references

1 J. P. Hogan and R. L. Banks, Phillips Petroleum, *US Pat.* 2 825 721, 1958; *Chem. Abstr.*, 1958, 52:8621h; M. P. McDaniel, *Adv. Catal.*, 1985, **33**, 47; C. E. Marsden, *Plast. Rubber Compos. Process. Appl.*, 1994, **21**, 193; T. E. Nowlin, *Prog. Polym. Sci.*, 1985, **11**, 29; S. M. Augustine and J. P. Blitz, *J. Catal.*, 1996, **161**, 641.

2 M. Rätzsch, *Polymerwerkstoffe '98 Merseburg, 23–25 September 1998; Kunststoffe*, 1996, **86**, 6; R. Messere, A. F. Noels, P. Dournel, N. Zandona and J. Breulet, *Proceedings of Metallocenes '96, 6–7 March 1996, Düsseldorf*, p. 309.

3 K. H. Theopold, *Eur. J. Inorg. Chem.*, 1998, 15.

4 G. J. P. Britovsek, V. C. Gibson and D. F. Wass, *Angew. Chem.*, 1999, **111**, 448; *Angew. Chem., Int. Ed. Engl.*, 1999, **38**, 428; A. Döhring, J. Göhre, P. W. Jolly, B. Kryger, J. Rust and G. P. J. Verhovnik, *Organometallics*, 2000, **19**, 388.

5 (*a*) M. Haufe, R. D. Köhn, G. Kociok-Köhn and A. C. Filippou, *Inorg. Chem. Commun.*, 1998, **1**, 263; (*b*) R. D. Köhn and G. Kociok-Köhn, *Angew. Chem.*, 1994, **106**, 1958; *Angew. Chem., Int. Ed. Engl*, 1994, **33**, 1877; (*c*) R. D. Köhn, G. Kociok-Köhn and M. Haufe, *J. Organomet. Chem.*, 1995, **501**, 303; (*d*) M. Haufe, R. D. Köhn, R. Weimann, G. Seifert and D. Zeigan, *J. Organomet. Chem.*, 1996, **520**, 121.

6 All new compounds were completely characterised. Experimental details are available in the electronic supplementary information (ESI).†

7 P. A. White, J. Calabrese and K. H. Theopold, *Organometallics*, 1996, **15**, 5473.

8 V. C. Gibson, C. Newton, C. Redshaw, G. A. Solan, A. J. P. White and D. J. Williams, *J. Chem. Soc., Dalton Trans.*, 1999, 827.

9 α-Olefins react to give trimers exclusively: R. D. Köhn, M. Haufe, G. Kociok-Köhn, S. Grimm, P. Wasserscheid and W. Keim, *Angew. Chem.*, in press.

Comment on the preparation of the ionic liquid 1-ethyl-3-methylimidazolium ethanoate: a unique monomeric, homoleptic pentacoordinate lead ethanoate complex

Jennifer T. Hamill,[a] Chris Hardacre,[a] Mark Nieuwenhuyzen,*[a] Kenneth R. Seddon,[ab] Sarah A. Thompson[b] and Brian Ellis[c]

[a] *School of Chemistry, The Queen's University of Belfast, Stranmillis Road, Belfast, UK BT9 5AG. E-mail: woody.m@qub.ac.uk*
[b] *The QUILL Centre, The Queen's University of Belfast, Stranmillis Road, Belfast, UK BT9 5AG*
[c] *BP Amoco Chemicals, Chertsey Road, Sunbury-on-Thames, Middlesex, UK TW16 7LN*

Received (in Cambridge, UK) 14th June 2000, Accepted 22nd August 2000
First published as an Advance Article on the web

Atomic absorption spectroscopy of the ionic liquid 1-ethyl-3-methylimidazolium ethanoate ($[emim]_2[O_2CMe]$), prepared according to International Patent WO 96/18459, showed it to contain large amounts of lead impurity: (*ca.* 0.5 M): $[emim]_2[Pb(O_2CMe)_4]$ was isolated and shown crystallographically to contain the first known example of a monomeric, homoleptic pentacoordinate lead(II) carboxylate complex, with a stereochemically active lone-pair.

Ionic liquids are well-established media for clean synthesis,[1,2] and consequently an essential requirement is their purity. In particular, heavy metal and halide impurities pose problems with regard to human and environmental health, catalysis and corrosion. Thus it is important to develop routes that yield pure products. A number of methods for the synthesis of ionic liquids have been cited in the literature.[2,3] As part of our general work in this area, we have examined a BP Chemicals patent that describes the use of lead(II) salts in the synthesis of ionic liquids.[4] It is claimed that the ionic liquid 1-ethyl-3-methylimidazolium ethanoate ($[emim][O_2CMe]$) could be synthesised *via* the metathesis of lead(II) ethanoate and [emim]Cl or [emim]Br. Analysis by atomic absorption spectroscopy of the ionic liquid thus obtained showed that large amounts of lead remained in the product (*ca.* 0.5 M). Crystals of the dissolved lead complex were obtained from the $[emim][O_2CMe]$ produced *via* a modification of this method that precludes the addition of water.†

A review of BIDS[5] and the Cambridge Structural Database[6] for lead(II) carboxylate complexes identified a total of 25 structures: 18 were polymeric with the carboxylate moiety acting as a bridging ligand; three others that, although monomeric, contained either the sterically demanding $[edta]^{2-}$ ligand or bulky crown ethers; and one containing hexanuclear units.[7] The remaining three compounds, $Pb(C_8H_{11}N_4S)(O_2CMe)$,[8] $[Pb(C_{16}H_{36}N_4)(O_2CMe)][O_2CMe]\cdot 2H_2O$[9] and $Pb(C_{12}H_{10}N_3SO)(O_2CMe)$,[10] are compared and contrasted with $[emim]_2[Pb(O_2CMe)_4]$ below.

The data for $[emim]_2[Pb(O_2CMe)_4]$ were collected using our usual methodology.‡ The asymmetric unit consists of one $[Pb(O_2CMe)_4]^{2-}$ unit and two $[emim]^+$ cations. The four ethanoate anions are involved in two different bonding modes: three are bonded *via* one oxygen atom, and one is chelating, Fig. 1. The three non-coordinated oxygen atoms are involved in C–H···O hydrogen bonds with the cations, and extend towards the void associated with the lead(II) centre, Fig. 2. Two $[emim]^+$ cations lie either side of this void and act as spacers between the $[Pb(O_2CMe)_4]^{2-}$ units. The large void in the coordination sphere around the lead(II) centre is indicative of a stereochemically active lone-pair, the existence of which is usually attributed to the '*inert-pair effect*'. The $[Pb(O_2CMe)_4]^{2-}$ units in $[emim]_2[Pb(O_2CMe)_4]$ are hydrogen bonded to four cations forming an infinite chain *via* C–H···O interactions in the $<0\,0\,1>$ plane, Fig. 2.

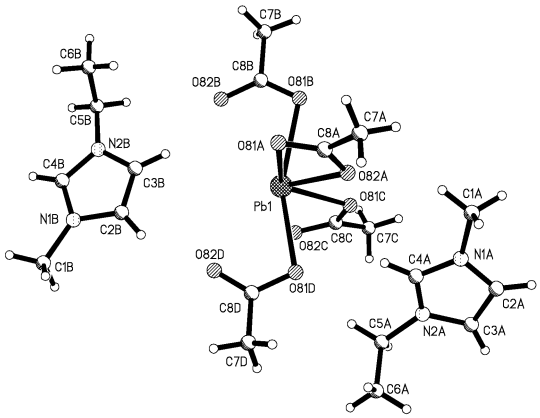

Fig. 1 Atomic numbering scheme for $[emim]_2[Pb(O_2CMe)_4]$ emphasising the void created by the stereochemically active lone-pair on the lead(II) centre.

Although the term '*inert-pair effect*' is the subject of some controversy, the structural consequences of the $6s^2$ lone-pair are well documented. Shimoni-Livny *et al.*[11] identified some conditions in which the lone-pair is likely to be stereochemically active; namely, hard donor atoms, a low coordination number and attractive interactions between ligands. The structure of $[emim]_2[Pb(O_2CMe)_4]$ fits well with these findings and the criteria are satisfied.

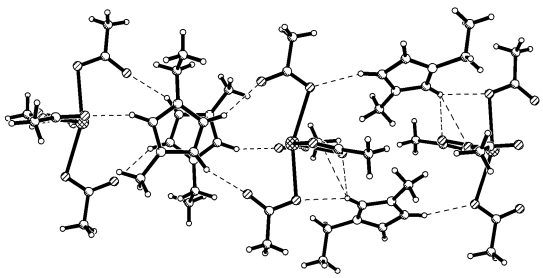

Fig. 2 A view illustrating the alternating C–H···O hydrogen bonded chains in $[emim]_2[Pb(O_2CMe)_4]$ (the dashed lines represent hydrogen bonds). Hydrogen bond lengths (Å) and angles (°), (H···A), (D···A), (D–H···A): C2A–H2A···O81B′ 2.32, 3.15(3), 147; C3A–H3A···O81A″; 2.64, 3.45(3), 144; C4A–H4A···O81C 2.79, 3.22(2), 109; C4A–H4A···O81D 2.37, 3.20(2), 149; C4A–H4A···O82A 2.65, 3.38(2), 135; C2B–H2B···O82D 2.16, 3.01(3), 149; C3B–H3B···O82B 2.28, 3.14(3), 153; C4B–H4B···O82C‴ 2.03, 2.93(3), 160. Symmetry codes: ′ = $1-x, 1-y, 1-z$; ″ = $x, 1+y, z$; ‴ = $-x, -y, -z$.

DOI: 10.1039/b005095o

The dominant feature of the three monomeric lead complexes obtained from the CSD is the presence of a rigid organic ligand, which restricts the possible geometries available to the metal centres. In $Pb(C_8H_{11}N_4S)(O_2CMe)$[8] and $[Pb(C_{16}H_{36}N_4)(O_2CMe)][O_2CMe]\cdot 2H_2O$[9] this leads to the orientation of the inert lone-pairs associated with adjacent lead atoms towards one another with Pb···Pb contacts of 3.905 and 4.165 Å, respectively: they essentially exist as dinuclear complexes. As with $[emim]_2[Pb(O_2CMe)_4]$, the ethanoate ions are monodentate with the free oxygen atoms extending towards the void associated with the lone-pair. In $Pb(C_{12}H_{10}N_3SO)(O_2CMe)$[10] the use of a rigid ligand still influences the coordination geometry of the lead(II) centres. However, the distance between the metal centres is much longer which suggests that they are not associated with each other (Pb···Pb distance 4.822 Å). Again, the ethanoate ions are monodentate with the free oxygen atoms associated with the void. Moreover, these free oxygen atoms are also associated with the lead centre of the adjacent molecule (Pb···O distance 3.001 Å). The only common feature of these compounds and $[emim]_2[Pb(O_2CMe)_4]$ is that the monodentate ethanoate ligands are associated with the lone-pair on the metal centre. Unlike the previous complexes, the lead centres in $[emim]_2[Pb(O_2CMe)_4]$ do not show any lone-pair orientation effects and $[emim]_2[Pb(O_2CMe)_4]$ can be considered mononuclear.

A recent study by Hall *et al.*[12] on lead(II) complexes containing aromatic ligands highlighted the difficulties of determining the presence or absence of a stereochemically active lone-pair. They found that in many of the materials the so-called '*lone-pair*' regions were either (a) associated with longer contacts with the oxygen atoms from anions (*e.g.* $[ClO_4]^-$, $[NO_3]^-$), leading to polynuclear motifs with consequent orientation of the lone-pairs towards each other as above, or (b) associated with inter-ring interactions between the aromatic ligands which occupied the void region. In $[emim]_2[Pb(O_2CMe)_4]$, although the cations are associated with this lone-pair region and are involved in C–H···O hydrogen bonds with the ethanoate anions, the emim cations do not occupy the void associated with the '*inert lone-pair*'.

Furthermore, the presence or absence of a stereochemically active lone-pair has implications for the design of new materials using the Group 14 elements. The use of hydrogen-bond donor cations, in conjunction with hydrogen-bond acceptors on the coordination complex anions, results in '*capping*' of the voids, which may be a useful generic strategy for the rational design of materials containing these elements. The possible application of this approach to crystal engineering is illustrated by the isolation of $[emim]_2[Pb(O_2CMe)_4]$.

In conclusion, we have isolated and structurally characterised a new and novel lead(II) homoleptic complex. Preliminary XAFS data§ show that this unusual (for lead) metal coordination environment is stable even at moderate temperature (*ca.* 373 K), which will be the subject of a further communication. This, and the previously reported $[SbCl_3][AlCl_4]$,[13] also indicates that ionic liquids may be useful media for the stabilisation and study of unusual metal coordination environments; more specifically those metals that contain stereochemically active lone-pairs.

Furthermore, the presence of this lead(II) complex, which was produced in an attempted preparation of an ionic liquid, highlights the problems inherent in the use of metathetic reactions of metal salts as a preparative methodology for ionic liquids in general. We are currently critically examining the extant methods and developing more general procedures for ionic liquid production.

We would like to thank Unilever (J. T. H and S. A. T) for financial support and the EPSRC and Royal Academy of Engineering for the Award of a Clean Technology Fellowship (K. R. S).

Notes and references

† *Preparation*: [emim]Cl and $Pb(O_2CMe)_2\cdot 3H_2O$ (Aldrich) were separately dissolved in solutions of methanol–water (4:1 v/v). Upon mixing the two solutions a precipitate of $PbCl_2$ was produced which was removed by filtration after cooling at −20 °C overnight. The solvent was removed from the filtrate by rotary evaporation. Analysis by ^{1}H NMR spectroscopy showed that this was insufficient to remove the water, and this was accomplished after heating at *ca.* 130 °C under vacuum for 24 h. The product was a viscous liquid, pale yellow in colour before drying and pale brown in colour after drying. In order to eliminate the need for drying, the above method was modified slightly to eliminate the use of water. This was achieved by placing the lead ethanoate in a Soxhlet extractor. The product obtained was a mixture of crystalline solid and viscous liquid. Single crystal X-ray analysis showed the crystalline material to be the salt $[emim]_2[Pb(O_2CMe)_4]$.

‡ *Crystallographic data* were collected on a Siemens P4 diffractometer using omega scans. A crystal was sealed into a Lindemann tube under an inert atmosphere and then mounted on to the diffractometer at room temperature. The structure was solved using direct methods using the SHELX program packages.[14] *Crystal data* for $[emim]_2[Pb(O_2CMe)_4]$: M = 665.70, triclinic, space group $P\bar{1}$, a = 7.9761(9), b = 10.4439(9), c = 16.8872(15) Å, α = 100.222(7), β = 99.228(9), γ = 94.712(9), U = 1357.6(2) Å^{-3}, Z = 2, μ = 0.117 mm^{-1}, R_{int} = 0.0607. A total of 3743 reflections were measured for the angle range $4 < 2\theta < 50$ and 3455 independent reflections were used in the refinement. Final parameters were wR_2 = 0.1815 and R_1 = 0.0556 [$I > 2\sigma(I)$].

CCDC 182/1758. See http://www.rsc.org/suppdata/cc/b0/b005095o/ for crystallographic files in .cif format.

§ *XAFS spectra* were recorded at the Synchrotron Radiation Source at Daresbury using station 9.3 on the Pb L_{II} edge using our usual method.[15]

1 J. D. Holbrey and K. R. Seddon, *Clean Processes Products*, 1999, **1**, 233.
2 T. Welton, *Chem. Rev.*, 1999, **99**, 2071.
3 J. S. Wilkes and M. J. Zaworotko, *J. Chem. Soc., Chem. Commun.*, 1992, **13**, 965.
4 B. Ellis, *Int. Pat.*, WO 96/18459, 1996.
5 BIDS copyright © (1998) Institute for Scientific Information Inc.®
6 Cambridge Structural Database Version 5.17 (January 2000), O. Kennard and F. H. Allen, *Chem. Des. Automat. News*, 1993, **8**, 3137.
7 G. D. Fallon, L. Spicca, B. O. West and Q. Zhang, *Polyhedron*, 1997, **16**, 19.
8 A. Castineiras, R. Domingues, L. Bresolin, A. J. Bortoluzzi, R. A. Burrow and M. Horner, *Z. Naturforsch., Teil B*, 1998, **53**, 81.
9 J. M. Harrowfield, H. Miyamae, T. M. Shand, B. W. Skelton, A. A. Soudi and A. H. White, *Aust. J. Chem.*, 1996, **49**, 1051.
10 P. C. Christidis, I. A. Tossidis and C. A. Hondroudis, *Z. Kristallogr.*, 1994, **209**, 607.
11 L. Shimoni-Livny, J. P. Glusker and C. W. Brock, *Inorg. Chem.*, 1988, **37**, 1853.
12 A. K. Hall, J. M. Harrowfield, A. Morsali, A. A. Soudi and A. Yanovsky, *CrystEngComm*, 2000, 13.
13 P. Coleman, M. Nieuwenhuyzen, H. N. Rutt and K. R. Seddon, *J. Chem. Soc., Chem. Commun.*, 1995, 2369.
14 G. M. Sheldrick, SHELXTL PC, An Integrated System for Data Collection, Processing, Structure Solution and Refinement, Siemens Analytical X-Ray Instruments, Madison, WI, 1990; G. M. Sheldrick, SHELXL 97, Siemens Analytical X-Ray Instruments, Madison, WI, 1997.
15 A. Carmichael, J. D. Holbrey, C. Hardacre, M. Nieuwenhuyzen and K. R. Seddon, *Anal. Chem.*, 1999, **71**, 4572.

Remarkable activity, selectivity and stability of polymer-supported Pt catalysts in room temperature, solvent-less, alkene hydrosilylations

Robert Drake,[a] Russell Dunn,[b] David C. Sherrington*[b] and Steven J. Thomson[b]

[a] *Dow Corning, Barry, S. Glamorgan, UK CF63 2YL*
[b] *Department of Pure and Applied Chemistry, University of Strathclyde, Glasgow, UK G1 1XL. E-mail: m.p.a.smith@strath.ac.uk*

Received (in Liverpool, UK) 19th July 2000, Accepted 25th August 2000
First published as an Advance Article on the web

A polystyrene-resin supported Pt catalyst displays higher conversion, remarkably improved selectivity and excellent recyclability relative to Speier's catalyst in the room temperature solvent-less hydrosilylation of oct-1-ene using trichlorosilane.

Alkene hydrosilylation is an important reaction both on a laboratory and an industrial scale. Though many metal complexes have been reported as useful catalysts,[1] since the discovery by Speier *et al.* in 1957 that hexachloroplatinic acid is a potent catalyst even under ambient conditions,[2] Pt complexes have become the catalysts of choice. The remarkable turnover frequencies displayed by Pt-based species, and the fact that they can be used not only with alkyl and alkoxysilanes but also with chlorosilanes, explain their dominance in industrial processes. Paradoxically, however, these high activities coupled with the exothermicity of alk-l-ene hydrosilylation can lead to a rapid temperature rise in reactions, and the occurrence of a significant level of alkene isomerisation. The so-formed internal alkenes react much more slowly, and in any event limit the conversion of alk-l-enes to useful terminally silylated products.

There has been significant earlier work on the immobilisation of Pt-based catalysts using both inorganic and polymer supports, aimed at producing experimentally and technologically convenient analogues of soluble catalysts.[3,4] Likewise Rh-based species,[5] and recently Mn-based catalysts,[6] have been examined in this context. While these reports have demonstrated active heterogeneous catalysts, data on the activity and selectivity with prolonged use are rare, particularly with the more difficult chlorosilane reactants, and equally importantly meticulous evaluation of the contribution from leached soluble catalyst has generally been absent. We now make a preliminary report on our studies of in-house prepared polystyrene and polymethacrylate resin-supported Pt catalysts in the hydrosilylation of oct-l-ene using trichlorosilane in the absence of any solvent, and at ambient temperature.

Precursor resins (PR1–PR5) were prepared by suspension polymerisation[7] using the comonomer mixtures shown in Table 1. The functional group content [–CH_2Cl from vinylbenzyl chloride (VBC) or epoxide from glycidyl methacrylate (GMA)] and surface area of the resultant resins are also shown in Table 1. PR1–PR5 were aminated by treatment with excess trimethylethylene diamine/NaH in THF at 60 °C for 48 h to yield AFRI–AFR5 (Table 2), and finally each of these was loaded with Pt by treatment with an excess of K_2PtCl_4 in water to yield polymer catalysts C1–C5 (Scheme 1, Table 2). The activity and selectivity of C1–C5 were assessed in the reaction of oct-l-ene (20 mmol) and trichlorosilane (10 mmol) in 8 cm^3 sealed Pyrex vials in the absence of any solvent at room temperature. Polymer catalysts containing 10^{-3} mmol of Pt were employed

Table 2 Analytical data for catalyst resins

	Amine functionalised resin		Pt catalyst resin	
Precursor resin	Code	Diamine content[a]/ mmol g^{-1}	Code	Pt content[b]/ mmol g^{-1}
PR1	AFR1	2.85	C1	1.4
PR2	AFR2	1.5	C2	0.9
PR3	AFR3	1.5	C3	0.9
PR4	AFR4	0.9	C4	0.4
PR5	AFR5	1.7	C5	0.5

[a] Calculated from N% content. [b] ICPES analysis of acid digested resins.

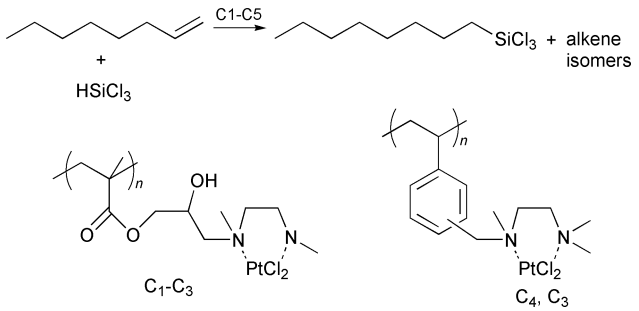

Scheme 1 Oct-1-ene hydrosilylation using trichlorosilane catalysed by polymer catalysts C1–C5.

Table 1 Composition of precursor resins

	Comonomer mixture (vol %)[b]							Resin properties	
Precursor resin[a]	EGDMA	GMA	DVB	Est	St	VBC	Porogen (Porogen/ monomer vol ratio)	Epoxide/ CH_2Cl content/ mmol g^{-1}	Surface area[c]/m^2 g^{-1}
PR1-Me-G	2	98	—	—	—	—	None	6.9/—	~0
PR2-Me-M	50	50	—	—	—	—	Toluene (2:1)	3.5/—	113
PR3-Me-M	50	50	—	—	—	—	Octan-2-one (2:1)	3.5/—	119
PR4-St-M	—	—	53	13	0	34	Isooctane (1:1)	—/2.3	100
PR5-St-CM	—	—	10	2	53	34	2-Ethylhexanoic acid (1:1)	—/2.3	33

[a] Me = methacrylate-type; St = styrene-type; G = gel-type; M = macroporous type; CM = collapsed macroporous.[8] [b] EGDMA = ethyleneglycol dimethacrylate; GMA = glycidyl methacrylate; DVB = divinylbenzene. [c] N_2 sorption, BET analysis.

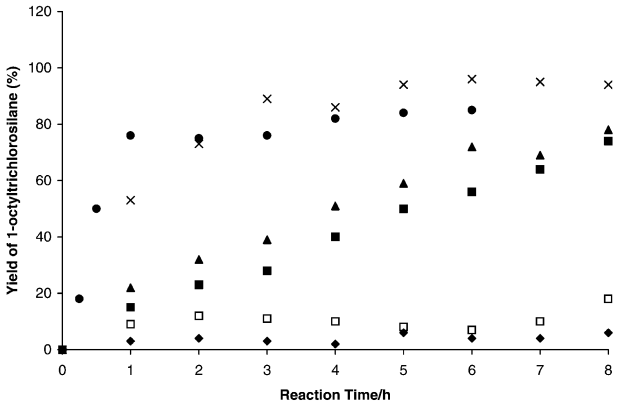

Fig. 1 Yield of 1-octyltrichlorosilane as a function of time in oct-1-ene hydrosilylations using trichlorosilane catalysed by: (●) Speier's catalyst; (◆), C1; (■), C2; (▲), C3; (×) C4; (□), C5.

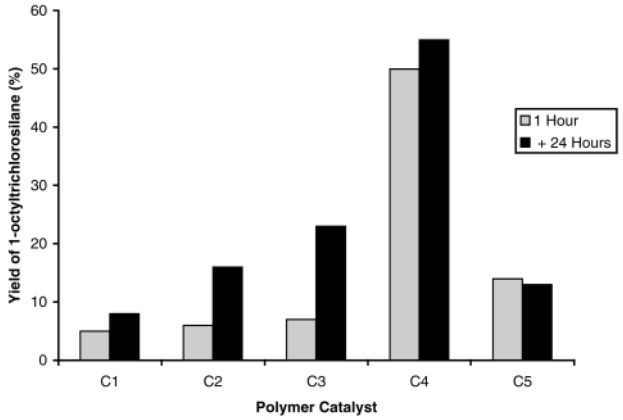

Fig. 2 Yield of 1-octyltrichlorosilane from oct-l-ene and trichlorosilane catalysed by C1–C5 with the heterogeneous catalyst removed after 1 h.

and compared to the performance of soluble Speier's catalyst (5 wt% H_2 $PtCl_6 \cdot 6H_2O$ in isopropyl alcohol using 10^{-3} mmol Pt). The appearance of l-octyltrichlorosilane and octene isomers (oct-2-, -3- and -4-enes as a non-resolved group) was monitored by GC analysis using nonane as an internal standard. The mole ratio of oct-l-ene: trichlorosilane of 2 : 1 was chosen to highlight any isomerisation induced by the catalyst while minimising competition from the hydrosilylation reaction, *i.e.* isomerisation was deliberately given a competitive advantage. In addition, to demonstrate the high activity and stability of the polymer catalysts (identified in preliminary ligand screening experiments) each sample reported here was utilised in four previous reactions, *i.e.* the data here refer to the fifth cycle of use in each case. Data for Speier's catalyst refer to its first use. No attempt was made to recover and re-use this homogeneous species.

The results of the catalytic studies are summarised in Fig. 1. The behaviour of the homogeneous catalyst is as expected from the literature. The conversion of trichlorosilane to l-octyltrichlorosilane reached *ca.* 75% in *ca.* 1 h. However, simultaneously the isomerisation of oct-l-ene to internal alkenes was *ca.* 60%. (Note initial mole ratio oct-l-ene : trichlorosilane is 2 : 1.) The performance of the polymer catalysts varies considerably. Catalyst C1 shows very low activity. Since this is a polar gel-type methacrylate-based resin, it would not be expected to swell in the non-polar reaction mixture and presumably therefore catalytic Pt sites are accessed only very inefficiently as a result of poor mass transport. Likewise though catalyst C5 is a non-polar styrene-based resin, and is nominally macroporous, in fact the surface area of this species is very low (*ca.* 30 $m^2\ g^{-1}$), and we believe the morphology is substantially collapsed.[8] Catalysts C2 and C3 perform well yielding *ca.* 70% l-octyltrichlorosilane after *ca.* 6 h. Though these are polar methacrylate-based resins, they have permanent macroporous morphologies with good surface area (*ca.* 110–120 $m^2\ g^{-1}$). Catalyst C4 is significantly the most active yielding *ca.* 70% l-octyltrichlorosilane after 2 h, and ultimately delivering *ca.* 90%. In this respect it performs better than Speier's catalyst. C4 is a non-polar styrene-based resin and is macroporous with a good surface area (*ca.* 100 $m^2\ g^{-1}$). It clearly offers no significant mass transfer limitations. Furthermore with C4 the level of oct-l-ene isomerisation is only *ca.* 9%, and indeed less than *ca.* 4% with the other polymer catalysts. C4 therefore is also significantly more selective in favour of hydrosilylation than Speier's catalyst. These results are even more remarkable when it is borne in mind that these data refer to the fifth cycle of use of this sample of C4.

Overall it is tempting to conclude that the heterogenised Pt complexes are highly selective in favour of the hydrosilylation reaction, and the low level of alkene isomerisation observed may be due to very low levels of leached Pt species acting as a less selective homogeneous catalyst.

Some assessment of the level of Pt leaching with C1–C5 was obtained from a sixth cycle of use of these samples in which hydrosilylations were run as before for 1 h, and then the reaction mixtures decanted from the resin beads, and the mixtures monitored for a further 24 h. The results are shown in Fig. 2. The left-hand bar in each case shows the percentage of 1-octyltrichlorosilane formed after 1 h in the presence of polymer catalysts, and the right-hand bar the conversion after a further 24 h in the absence of polymer catalysts. Though some increase in l-octyltrichlorosilane is seen, particularly with C2 and C3 (presumably reflecting the presence of some soluble catalytic species), the effect is not large. With C4 the small additional conversion seen after 24 h is within the analytical experimental error. In addition no measurable increase in the amount of isomerised alkene is observed, which remains very low. Thus it seems that the level of Pt leached is itself very low, or any species in solution is inactive as a catalyst either in hydrosilylation or in isomerisation.

Thus we have succeeded in producing a polymer-supported Pt alkene hydrosilylation catalyst (C4) with activity comparable to that of Speier's catalyst, with greatly enhanced selectivity in terms of minimising concurrent alkene isomerisation, and with considerable long term recycling stability along with minimal Pt leaching characteristics. The catalyst performs well with trichlorosilane as the silylating agent and displays considerable potential for both small- and large-scale application. We are currently undertaking a more detailed investigation to improve our understanding of this catalyst system.

R. D. and S. J. T. acknowledge the receipt of studentships from Dow Corning. The gift of vinylbenzyl chloride from the Dow Chemical Company is appreciated. The useful discussions with Z. M. Michalska are warmly acknowledged.

Notes and references

1 B. Marciniec, J. Gulinski, W. Urbaniak and Z. W. Kornetka in *Comprehensive Handbook on Hydrosilylation*, ed. B. Marciniec, Pergamon Press, Oxford, UK, 1992, ch. 2, p. 8.
2 J. L. Speier, J. A. Webster and C. H. Barnes, *J. Am. Chem. Soc.*, 1957, **79**, 974.
3 For a summary of work prior to 1985, see F. R. Hartley, *Supported Metal Complexes—A New Generation of Catalysts*, D. Reidel Pub. Co., Dordrecht, Germany, 1985, ch. 7, p. 204.
4 For a further summary of work to 1992 see ref 1. p. 84.
5 Z. M. Michalska, K. Strzelec and J. W. Sobczak, *J. Mol. Catal. A*, 2000, **156**, 91; Z. M. Michalska, B. Ostaszewski and K. Strzelec, *J. Organomet. Chem.*, 1995, **496**, 19; Z. M. Michalska, B. Ostaszewski, K. Strzelec, R. Kwiatkowski and A. Wlochowicz, *React. Polym.*, 1994, **23**, 85.
6 H. S. Hilal, M. A. Suleiman, W. J. Jondi, S. Khalaf and M. M. Masoud, *J. Mol. Catal. A*, 1999, **144**, 47.
7 P. M. van Berkel and D. C. Sherrington, *Polymer*, 1996, **37**, 1431.
8 S. M. Howdle, K. Jerabeck, V. Leocorbo, P. C. Marr and D. C. Sherrington, *Polym. Commun.*, 2000, **41**, 7273.

ChemComm

Novel bis-*N*-[2-(diphenylphosphino)ferrocenylcarbonyl]diaminocyclohexane ligands: application in asymmetric allylic alkylation of imino esters with simple allyl carbonate

Shu-Li You, Xue-Long Hou,* Li-Xin Dai,* Bo-Xun Cao and Jie Sun

Laboratory of Organometallic Chemistry, Shanghai Institute of Organic Chemistry, Chinese Academy of Sciences, 354 Fenglin Lu, Shanghai 200032, China. E-mail: xlhou@pub.sioc.ac.cn or dailx@pub.sioc.ac.cn

Received (in Cambridge, UK) 12th May 2000, Accepted 18th August 2000
First published as an Advance Article on the web

Several derivatives of ferrocene ligands with planar chirality were investigated in palladium-catalysed asymmetric allylic alkylation of iminoesters, in which bis-ferrocene ligand 7 containing a chiral pocket showed good enantiocontrol in this reaction; the products having a quaternary chiral center were obtained with up to 75.3% ee.

Chiral α,α-dialkyl-α-amino acids are an important class of non-coded amino acids and have attracted an ever growing interest in biological and pharmacological problems.[1] The quaternary chiral center leads to many of the desirable properties associated with this class of amino acid, but offers a significant challenge with respect to asymmetric synthesis.[2] Many methods reported to date involve either the use of chiral auxiliaries or strategies that utilize self-regeneration of stereocenters.[3] The catalytic asymmetric hydrogenation of dehydroamino acids is not applicable to synthesis of quaternary amino acids.[4] Thus, the procedure of their catalytic asymmetric synthesis remains to be established. Imino esters as nucleophiles in Pd-catalyzed asymmetric allylic alkylation reactions give chiral α-mono-alkylated amino acids,[5,6] however, the ee was not high when simple allyl acetate was used. Though a significant improvement of the asymmetric alkylation of a glycine Schiff's base under PTC conditions has been reported, an amino acid with a quaternary chiral centre could not be easily constructed in general.[7] Recently, Trost and Ariza reported the asymmetric synthesis of α-alkylated amino acids by using their chiral pocket strategy in catalytic asymmetric allylic alkylation and good to excellent results were obtained when substituted allyl acetates were used—for the simplest member of this family, the allyl acetate, only 40% ee value was provided.[8]

In the course of studying the synthesis and applications of ferrocenyl derivatives with planar chirality in metal-catalysed asymmetric reactions,[9] we investigated the role of planar chirality and found that the enantioselectivity could be affected by planar chirality, and that high enantioselectivity would be reached when the ligand contained a pair of matched chiralities. Combining these results and Trost's chiral pocket concept[10] we designed new planar chiral ligands **7** and **8** and used them in a synthesis of α-alkylated amino ester derivatives with a quaternary chiral carbon center through catalytic asymmetric allylic alkylation. Herein we would like to report our preliminary results.

The reaction of imino esters **1** with allyl ethyl carbonate in the presence of $[Pd(\eta^3\text{-}C_3H_5)Cl]_2$ and ligands **3**–**8** was carried out [eqn. (1)]† and results were summarized in Table 1.

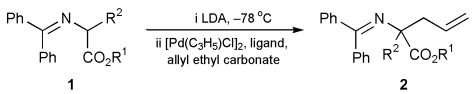

1 **2** (1)

a, R^1 = Me, R^2 = Bn; **b**, R^1 = Me, R^2 = Me; **c**, R^1 = Bu^t, R^2 = Me; **d**, R^1 = Bu^t, R^2 = H; **e**, R^1 = Et, R^2 = H; **f**, R^1 = Me, R^2 = H.

From Table 1, we found that planar chirality showed great influence on the enantioselectivity of the product. By using (*S*, *R*$_p$)-ligand **5** the product with 34.5% ee was given but only 2% ee for (*S*, *S*$_p$)-ligand **4** (entries 3 and 4), apparently central and planar chirality in ligand **5** is matched in this reaction. With BINAP as the ligand, the product was isolated in high yield but low ee. Ligand **6**, developed by Trost's group, showed high enantioselectivity in many kinds of asymmetric alkylation reactions due to its 'chiral pocket effect'.[10] Only 40% ee was given when it was used in this reaction. This value is the same as in the reaction of allyl acetate and azalactone reported by Trost.[8] Above all, we deduced that both planar chirality and the chiral pocket could improve the enantioselectivity of the product. Therefore, ligands **7** or **8**, the ferrocene modification of the chiral pocket, were synthesized in high yields from **4** [eqn.

Table 1 Palladium-catalysed asymmetric allylation of **1a** with different ligands†

Entry	Ligand	Base	Yield (%)[a]	Ee (%)[b]	Optical rotation[c]
1	**(S)-BINAP**	LDA	95	18.2	–
2	**3**	LDA	—	—	–
3	**4**	LDA	91	2.0	–
4	**5**	LDA	89	34.5	–
5	**5**	KHMDS	77	9.3	–
6	**6**	LDA	93	40.0	+
7	**7**	LDA	87	57.4	+
8	**8**	LDA	93	3.8	+
9[d]	**7**	LDA	91	22.2	+
10[e]	**7**	LDA	81	50.0	+

[a] Isolated yield based on imino esters. [b] Determined by HPLC (chiralcel OJ column). [c] Detected in trichloromethane. [d] 2 mmol% $[Pd(\eta^3\text{-}C_3H_5)Cl]_2$ and 4 mmol% ligand were used as catalyst. [e] After completion of addition, the reaction mixture was allowed to stir at 0 °C.

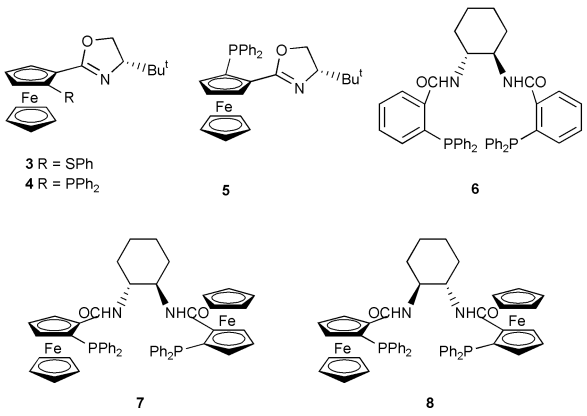

(2)].[12] As expected, when ligand **7** was injected into the above

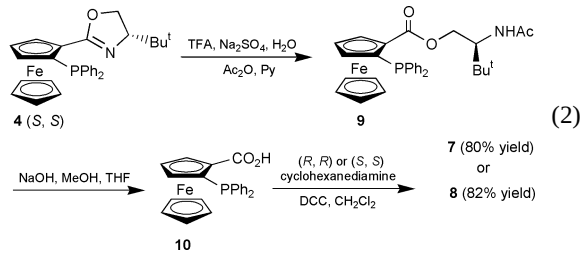

reaction, the enantioselectivity of the product was raised to 57.4% ee. On the other hand, the product with 3.8% ee was produced when ligand **8**, derived from (*S*,*S*)-cyclohexanediamine, was used. Obviously, ligand **7** possesses the matched chiralities. In addition, changing reaction temperature or the ratio between ligand and palladium did not improve the enantioselectivity (entries 9 and 10). The enantioselectivity of the product decreased greatly when the base was changed to KHMDS with ligand **5** (entry 5).

Several imino esters were examined with ligand **7** under the optimized conditions. The results are summarized in Table 2. It can be seen that different R^1 of the esters has a great influence on the enantioselectivities of the products. It was improved by increased steric demand of R^1 substitution. The ee values of the products were 56.9% (entry 5, R^1 = Bu^t), 52.6% (entry 6, R^1 = Et), 24.6% (entry 7, R^1 = Me), respectively, This effect was also operated in the α-methyl substituted imino esters which are important in the synthesis of quaternary carbon centers. When **1b** and **1c** were injected into this reaction, ee values of products were 53.6% (entry 2, R^1 = Me) and 75.3% (entry 4, R^1 = Bu^t), respectively. It was very strange that the product from **1b** achieved 71.6% ee when equimolar amounts of palladium and ligand were used as catalyst. The changing of the ratio of palladium to ligand has no effect in the case of **1c**.

Ligand **7** was viewed more clearly by its crystal structure (Fig. 1).‡ It was easy to deduce that the two Cp rings could become a part of a better pocket if the two phosphorus atoms were coordinated with palladium, which might be responsible for the better enantiocontrol.

Table 2 Palladium-catalysed asymmetric allylation of different amino esters with ligand **7**†

Entry	Substrate	Yield (%)[a]	Ee (%)[b]
1	**1a**	87	57.4
2	**1b**	93	53.6
3[c]	**1b**	92	71.6
4	**1c**	95	75.3
5[d]	**1d**	94	56.9
6[d]	**1e**	93	52.6
7[d]	**1f**	92	24.6

[a] Isolated yield based on imino esters. [b] Determined by HPLC. [c] 2 mmol% $[Pd(\eta^3\text{-}C_3H_5)Cl]_2$ and 4 mmol% ligand were used as catalyst. [d] 110 mmol% LDA and 110 mmol% allyl ethyl carbonate were used.

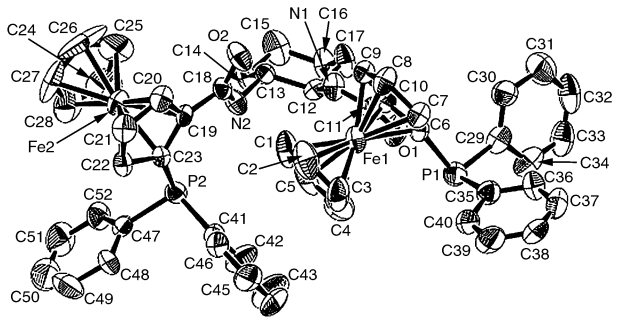

Fig. 1 ORTEP view of **7**·$2H_2O$ (hydrogen atom and water molecule omitted for clarity).

In conclusion, the catalytic asymmetric allylic alkylation between imino esters and chiral palladium allylic intermediates can be used to construct a chiral quaternary carbon center. Combination of planar chirality and a chiral pocket effect in the same ligand may provide product with a higher enantioselectivity. Up to 75% ee was realized by using ligand **7**. To the best of our knowledge, this is the highest ee value for a simple allyl system in this type of reaction. This concept for designing new ligands is worth further study. We are now exploring the application of ligand **7** and its analogues in other asymmetric reactions.

This research was financially supported by the National Natural Science Foundation of China, the Major Basic Research Development Program (grant No. G2000077506), National Outstanding Youth Fund, Chinese Academy of Sciences, and Shanghai Committee of Science and Technology.

Notes and references

† To a solution of 1 mL of THF and 103 mg (0.3 mmol) of ester **1a** was added 0.23 mL (0.45 mmol, 2 M heptane–THF–ethylbenzene) of LDA at −78 °C. The solution was stirred for 1 h, then charged with a solution containing 2.2 mg (0.006 mmol) of $[Pd(\eta^3\text{-}C_3H_5)Cl]_2$, 16.3 mg (0.018 mmol) of chiral ligand **7** in 0.5 mL of THF, and a solution of 59 mg (0.45 mmol) allyl ethyl carbonate in 0.25 mL THF. The reaction was allowed to proceed at rt to completion. Work up as usual and purification by column chromatography [EtOAc–petroleum ether (1/20), the silica gel was eluted with Et_3N in advance] afforded 100 mg of **2a** in 87% yield, 57.4% ee, determined by HPLC [Chiralcel OJ Column, hexane–isopropyl alcohol (96/4)].

‡ *Crystal data* for **7**·$2H_2O$: $C_{52}H_{52}N_2O_4Fe_2P_2$, M = 942.64, monoclinic, space group $P2_1$(no. 4), a = 11.195(2), b = 14.972(2), c = 14.316(3) Å, β = 96.43(2)°, V = 2384.6(7) Å^3, Z = 2, D_c = 1.313 g cm^{-3}, T = 293 K, Mo-Kα radiation (λ = 0.7107 Å, μ = 7.21 cm^{-1}, 4610 measured reflections, 4377 observed reflections, R_{int} = 0.052, S = 0.02, Δ_{max}, Δ_{min} = 0.94, −0.35 Å^{-3}.

CCDC 182/1751. See http://www.rsc.org/suppdata/cc/b0/b008304k/ for crystallographic files in .cif format.

1 G. Jung and A. G. Beck-Sickinger, *Angew. Chem., Int. Ed. Engl.*, 1992, **31**, 367; A. Giannis and T. Kolter, *Angew. Chem., Int. Ed. Engl.*, 1993, **32**, 1244.

2 For some reviews, see: R. M. Williams, *Synthesis of Optically Active Amino Acids*, Pregamon Press, Oxford, 1989, vol. 7; H. Heimgartner, *Angew. Chem., Int. Ed. Engl.*, 1991, **30**, 238; I. Ojima, *Acc. Chem. Res.*, 1995, **28**, 383; T. Wirth, *Angew. Chem., Int. Ed. Engl.*, 1997, **36**, 225.

3 J. Seyden-Penne, *Chiral Auxiliaries and Ligands in Asymmetric Synthesis*, Wiley, New York, 1995; D. Seebach, A. R. Sting and M. Hoffmann, *Angew. Chem., Int. Ed. Engl.*, 1996, **35**, 2708; U. Kazmaier and C. Schneider, *Synlett*, 1996, 975.

4 R. Noyori, *Asymmetric Catalysis in Organic Synthesis*, Wiley, New York, 1994, ch. 2.

5 J.-P. Genet, S. Juge, S. Achi, S. Mallart, J. Ruiz-Montes and G. Levif, *Tetrahedron*, 1988, **44**, 5263.

6 I. C. Buldwin, J. M. J. Williams and R. P. Beckett, *Tetrahedron: Asymmetry*, 1995, **6**, 1515.

7 E. J. Corey, F. Xu and M. C. Noe, *J. Am. Chem. Soc.*, 1997, **119**, 12 414; M. J. O'Donnell, F. Delgado, C. Hostettler and R. Schwesinger, *Tetrahedron Lett.*, 1998, **39**, 8775.

8 B. M. Trost and X. Ariza, *Angew. Chem., Int. Ed. Engl.*, 1997, **36**, 2635; B. M. Trost and X. Ariza, *J. Am. Chem. Soc.*, 1999, **121**, 10 727.

9 S.-L. You, Y.-G. Zhou, X.-L. Hou and L.-X. Dai, *Chem. Commun.*, 1998, 2765; W.-P. Deng, X.-L. Hou, L.-X. Dai, Y.-H. Yu and W. Xia, *Chem. Commun.*, 2000, 285; L.-X. Dai, X.-L. Hou, W.-P. Deng, S.-L. You and Y.-G. Zhou, *Pure Appl. Chem.*, 1999, **71**, 1401.

10 Reviews: B. M. Trost and D. L. Van Vranken, *Chem. Rev.*, 1996, **96**, 395; B. M. Trost, *Acc. Chem. Res.*, 1996, **29**, 355.

11 M. J. O'Donnell and R. L. Polt, *J. Org. Chem.*, 1982, **47**, 2663.

12 A. M. Warshawsky and A. I. Meyers, *J. Am. Chem. Soc.*, 1990, **112**, 8090; T. D. Nelson and A. I. Meyers, *J. Org. Chem.*, 1994, **59**, 2655.

A photochromic system based on photochemical or thermal chelate exchange on $Ru(phen)_2L^{2+}$ (L = diimine or dinitrile ligand)

Etienne Baranoff, Jean-Paul Collin,* Yoshio Furusho, Anne-Chantal Laemmel and Jean-Pierre Sauvage*

Laboratoire de Chimie Organo-Minérale, UMR 7513 du CNRS, Université Louis Pasteur, Faculté de Chimie, 4, rue Blaise Pascal, 67070 Strasbourg Cedex, France. E-mail: sauvage@chimie.u-strasbg.fr

Received (in Cambridge, UK) 21st June 2000, Accepted 25th August 2000
First published as an Advance Article on the web

In the presence of a bidentate chelate containing two convergent nitrile groups, $Ru(phen)_2L^{2+}$ (L = sterically hindering aromatic diimine ligand; phen = 1,10-phenanthroline) undergoes a photochemical reaction leading to quantitative replacement of the diimine by the bis-nitrile ligand; the reverse reaction takes place upon heating, also quantitatively.

Multicomponent molecular systems for which certain parts can be set into motion while others can be considered as motionless are promising models of biological molecular machines and motors as well as potential switches.[1,2] The signals sent to the molecules in order to trigger the movement can be of an electrochemical[3] or chemical[4] nature, photoinduced redox processes being also used in a few cases.[5] In the search for non-sacrificial photochemical reactions usable for moving molecular fragments,[6] it occurred to us that ligand-field (LF) excited states of d^6 transition metal complexes are strongly antibonding and can lead, in some cases, to effective ligand exclusion and substitution by solvent molecules.[7] In the present work, we would like to describe a system in which two different chelates, an aromatic diimine and a dinitrile, can be efficiently and cleanly interchanged under the action of light or heat. In addition, significant photochromism is observed. The ligands used are represented in Fig. 1.

The aromatic diimines 6,6′-dmbp and biq are sterically hindering so that their removal from a ruthenium(II) trischelate complex will be favoured over that of phen, also considering that rotation about the C–C bond between both halves of the chelate facilitates stepwise decoordination. The bis-nitrile dCN has been previously described and used by Angelici *et al*. to make a few complexes (Mn(I), Fe(II) and Pt(II)).[8] Although no structural data are available, dCN is expected to behave as a bidentate chelate.

The following photochemical reactions have been shown to take places quantitatively under light irradiation (300 nm $\leqslant \lambda \leqslant$ 800 nm):[9]

$$Ru(phen)_2L^{2+} + dCN \xrightarrow[L = 6,6'\text{-dmbp or biq}]{h\nu} Ru(phen)_2(dCN)^{2+} + L \quad (1)$$

The efficiency of reaction (1) is solvent dependent, the best solvents being acetone or 1,2-dichloroethane (1,2-DCE). The photoproduct, $Ru(phen)_2(dCN)^{2+}$, was isolated quantitatively and authenticated by comparison with a separately prepared sample.[10] To our knowledge, it is the first example of a photochemical chelate-to-chelate exchange reaction. Crystals were grown from MeOH–*p*-xylene and an X-ray structure of the compound was obtained.[11] The ORTEP diagram is shown in Fig. 2. The ruthenium–nitrogen bond lengths range from 2.04(1) to 2.085(8) Å and are similar to those observed in the $Ru(phen)_3^{2+}$ and $Ru(phen)_2(dpq)^{2+}$ complexes[12] (dpq = dipyrido[3,2-*d*:2′,3′-*f*]quinoxaline). As also indicated by the N–Ru–N angles the geometry about ruthenium atom is distorted from octahedral. The most noticeable feature is the constraint imposed on the dCN ligand as reflected by the Ru–N(6)–C(40) and Ru–N(5)–C(2) angles (167 and 168° respectively) as well as the large dihedral angle between the two phenyl groups.

In order to demonstrate that dCN and 6,6′-dmbp or biq can be interchanged, it was essential to show that the starting complex can be regenerated. This is indeed the case: reaction (2) takes place quantitatively.

$$Ru(phen)_2(dCN)^{2+} + L \xrightarrow[L = 6,6'\text{-dmbp or biq}]{\Delta} Ru(phen)_2L^{2+} + dCN \quad (2)$$

For example, a yellow solution of $Ru(phen)_2(dCN)^{2+}$ and biq in ethyleneglycol was heated at 190 °C for 4 h in the dark. The colour of the solution changed to deep red. After removal of the solvent followed by chromatography, $Ru(phen)_2(biq)^{2+}$ was obtained in 91% yield. Moreover, the photochemical reaction (6,6′-dmbp or biq release) and the thermal back reaction (dCN

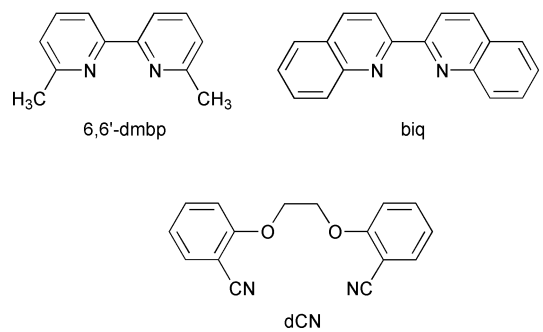

Fig. 1 The various chelates used in photochemically active ruthenium complexes.

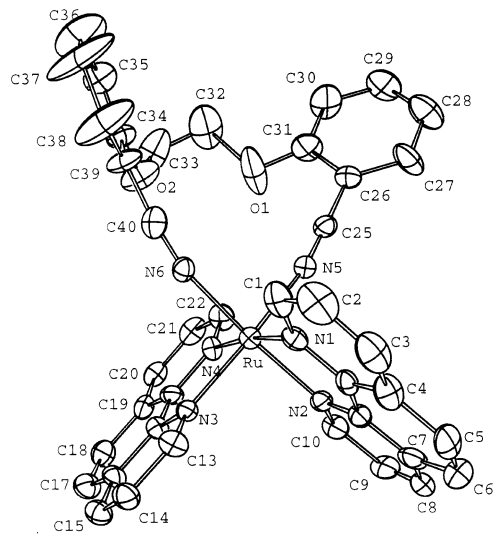

Fig. 2 ORTEP view of the cationic part of $[Ru(phen)_2(dCN)](PF_6)_2(p\text{-xylene})_2(MeOH)$ with partial labelling scheme. Ellipsoids are scaled to enclose 30% of the electronic density. Hydrogen atoms are omitted for clarity. Selected distances (Å) and angles (°): Ru–N(1) 2.059(9), Ru–N(2) 2.054(9), Ru–N(3) 2.061(9), Ru–N(4) 2.085(8), Ru–N(5) 2.05(1), Ru–N(6) 2.04(1), N(5)–Ru–N(6) 85.1(3), Ru–N(5)–C(25) 168(1), Ru–N(6)–C(40) 167(1), C(26)–C(25)–N(5) 177(1), C(39)–C(40)–N(6) 172(1).

DOI: 10.1039/b004982o

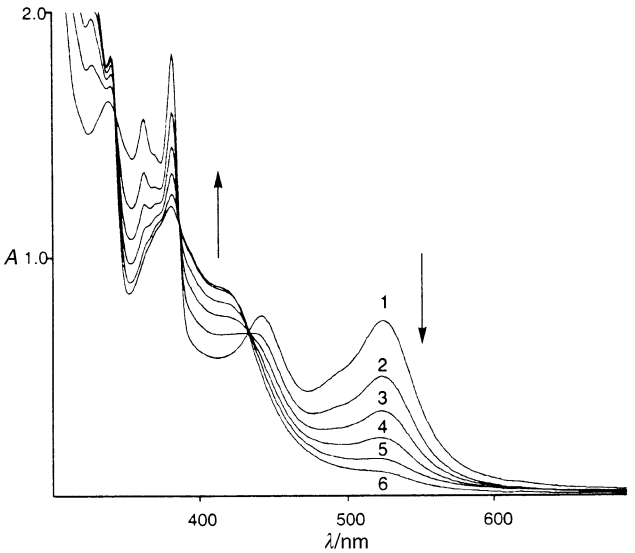

Fig. 3 Electronic spectra of a 1,2-DCE solution of $Ru(phen)_2(biq)^{2+}$ in the presence of dCN (10 eq) after visible light irradiation: **1** (0 s); **2** (20 s); **3** (40 s); **4** (60 s); **5** (90 s); **6** (120 s).

release with recoordination of 6,6′-dmbp or biq) could be carried out on the same reaction mixture containing an excess of both ligands, dCN and the aromatic diimine, in addition to the starting ruthenium(II) complex. The solvent, $EtOCH_2CH_2OCH_2CH_2OH$, in which all the components (ligands and complexes) are soluble, turned out to be compatible with both photochemical and thermal processes.

Interestingly, the absorption spectra of $Ru(phen)_2(dCN)^{2+}$ and $Ru(phen)_2(biq)^{2+}$, for instance, are significantly different. dCN is a poor σ-donor and good π-acceptor, stabilizing the d_π orbitals of $Ru(t_{2g})$ and thus leading to a relatively high MLCT (Ru → phen) excited state. In $Ru(phen)_2(biq)^{2+}$, the nature of the MLCT bond is different: biq is a better π-acceptor than phen so that the charge transfer is directed from the metal centre to biq and no more to the phen ligands. The photochromism of the system is illustrated in Fig. 3.

Without displaying colour changes as large as those obtained with organic photochromic compounds,[13,14] $Ru(phen)_2(biq)^{2+}$ (deep red; λ_{max} = 525 nm in 1,2-DCE) changes colour under irradiation to afford an orange solution of $Ru(phen)_2(dCN)^{2+}$ (λ_{max} = 382 nm in 1,2-DCE) within a few tens of seconds.

In conclusion, the present system is particularly promising for the construction of molecular photomechanical devices, combining motion and photochromism.

This work was performed with financial support from CNRS and the European Community. We thank André De Cian and Jean Fischer for the X-ray structure. A. C. L. acknowledges support from the French Ministry of Education and Y. F. thanks Osaka Prefecture (Japan) for a fellowship.

Notes and references

1 (*a*) J. E. Walker, *Angew. Chem., Int. Ed.*, 1998, **37**, 2308; (*b*) T. Elston, H. Wang and G. Oster, *Nature*, 1998, **391**, 510; (*c*) H. Noji, R. Yasuda, M. Yoshida and K. Kinosita, Jr., *Nature*, 1997, **386**, 299; (*d*) K. Kitamura, M. Tokunaga, A. H. Iwane and T. Yanagida, *Nature*, 1999, **397**, 129.

2 (*a*) V. Balzani, M. Gómez-López and J. F. Stoddart, *Acc. Chem. Res.*, 1998, **31**, 405; (*b*) J.-P. Sauvage, *Acc. Chem. Res.*, 1998, **31**, 611.

3 (*a*) R. A. Bissel, E. Còrdova, A. E. Kaifer and J. F. Stoddart, *Nature*, 1994, **369**, 133; (*b*) A. Livoreil, C. O. Dietrich-Bucheker and J.-P. Sauvage, *J. Am. Chem. Soc.*, 1994, **116**, 9399; (*c*) L. Zelikovich, J. Libman and A. Shanzer, *Nature*, 1995, **374**, 790.

4 (*a*) P. R. Ashton, R. Ballardini, V. Balzani, M. Gomez-Lopez, S. E. Lawrence, M.-V. Martinez-Diaz, M. Montaldi, A. Piersanti, L. Prodi, M. Venturi, D. Philp, H. G. Ricketts and J. F. Stoddart, *J. Am. Chem. Soc.*, 1997, **119**, 10 641; (*b*) T. R. Kelly, H. De Silva and R. A. Silva, *Nature*, 1999, **401**, 150; (*c*) R. Ballardini, V. Balzani, A. Credi, M. T. Gandolfi, S. J. Langford, S. Menzer, L. Prodi, J. F. Stoddart, M. Venturi and D. J. Williams, *Angew. Chem., Int. Ed. Engl.*, 1996, **35**, 978; (*d*) D. B. Amabilino, C. O. Dietrich-Buchecker, A. Livoreil, L. Perez-Garcia, J.-P. Sauvage and J. F. Stoddart, *J. Am. Chem. Soc.*, 1996, **118**, 3905.

5 (*a*) R. Ballardini, V. Balzani, M. T. Gandolfi, L. Prodi, M. Venturi, D. Philp, H. G. Ricketts and J. F. Stoddart, *Angew. Chem., Int. Ed. Engl.*, 1993, **32**, 1301; (*b*) A. Livoreil, J.-P. Sauvage, N. Armaroli, V. Balzani, L. Flamigni and B. Ventura, *J. Am. Chem. Soc.*, 1997, **119**, 12 114; (*c*) N. Armaroli, V. Balzani, J.-P. Collin, P. Gaviña, J.-P. Sauvage and B. Ventura, *J. Am. Chem. Soc.*, 1999, **121**, 4397.

6 N. Koumura, R. W. J. Zijistra, R. A. van Delden, N. Harada and B. L. Ferringa, *Nature*, 1999, **401**, 152.

7 (*a*) A. von Zelewsky and G. Gremaud, *Helv. Chim. Acta*, 1988, **71**, 1108; (*b*) B. Durham, J. L. Walsh, C. L. Carter and T. J. Meyer, *Inorg. Chem.*, 1980, **19**, 860; (*c*) P. J. Steel, F. Lahousse, D. Lerner and C. Marzin, *Inorg. Chem.*, 1983, **22**, 1488; (*d*) H. Hichida, S. Tachiyashiki and Y. Sasaki, *Chem. Lett.*, 1989, 1579; (*e*) B. E. Buchanan, P. Degn, J. M. Pavon Velasco, H. Hughes, B. S. Creaven, C. Long, J. G. Vos, R. A. Howie, R. Hage, J. H. van Diemen, J. G. Haasnoot and J. Reedijk, *J. Chem. Soc., Dalton Trans.*, 1992, 1177; (*f*) B. E. Buchanan, H. Hughes, J. H. van Diemen, R. Hage, J. G. Haasnoot, J. Reedijk and J. G. Vos, *J. Chem. Soc., Chem. Commun.*, 1991, 300; (*g*) A.-C. Laemmel, J.-P. Collin and J.-P. Sauvage, *Eur. J. Inorg. Chem.*, 1999, 383.

8 (*a*) R. J. Angelici, M. H. Quick and G. A. Kraus, *Inorg. Chim. Acta*, 1980, **44**, 137; (*b*) R. J. Angelici, M. H. Quick, G. A. Kraus and D. T. Plummer, *Inorg. Chem.*, 1982, **21**, 2178.

9 Photoirradiation was performed in a quartz UV cell (l = 1.0 cm) or in a NMR tube (ϕ = 5.0 mm) by the use of a Hanimex side projector (150 W halogen lamp).

10 A mixture of dCN (79 mg) and *cis*-$Ru(phen)_2Cl_2$ (0.272 mmol), EtOH (10 mL) and H_2O (10 mL) was refluxed for 2 h under an argon atmosphere. To the mixture was added a KPF_6 aqueous solution to form a yellow-orange solid, which was filtered off and washed with water. Chromatography (SiO_2, acetone/H_2O/KNO_3(aq.) = 100/10/1) followed by anion exchange gave $[Ru(phen)_2(dCN)](PF_6)_2$ as a yellow solid in 53% yield. ^{1}H NMR (400 MHz, CD_2Cl_2) δ 9.93 (dd, J = 5.21 Hz, 1.26 Hz, 2H, phen-2H), 8.82 (dd, J = 8.12 Hz, 1.22 Hz, 2H, phen-4H), 8.46 (dd, J = 8.26 Hz, 1.22 Hz, 2H, phen-7H), 8.33 (dd, J = 8.29 Hz, 5.22 Hz, 2H, phen-3H), 8.30 (d, J = 8.88 Hz, 2H, phen-5H), 8.17 (d, J = 8.88 Hz, 2H, phen-6H), 7.89 (dd, J = 5.30 Hz, 1.24 Hz, 2H, phen-9H), 7.65 (ddd, J = 8.92 Hz, 7.60 Hz, 1.72 Hz, 2H, dCN-5H), 7.59 (dd, J = 8.24 Hz, 5.30 Hz, 2H, phen-8H), 7.46 (dd, J = 7.79 Hz, 1.69 Hz, 2H, dCN-3H), 7.18 (d, J = 8.61 Hz, 2H, dCN-6H), 7.06 (dt, J = 7.64 Hz, 0.52 Hz, 2H, dCN-4H), 4.61 (s, 4H, dCN-CH_2); UV/Vis (1,2-DCE): λ_{max} (ε) = 382 nm (14 100 L mol^{-1} cm^{-1}).

11 Crystal data for $C_{57}H_{52}F_{12}N_6O_3P_2Ru$:$[Ru(phen)_2(dCN)(PF_6)_2](p$-xylene$)_2$(MeOH), yellow crystal: M = 1257.06, orthorhombic, a = 17.9740(6), b = 21.1890(9), c = 29.793(1) Å, U = 11 346(1) Å^3, T = 294 K, space group *Pbca*, Z = 8, D_c = 1.47 g cm^{-3}, μ = 0.422 mm^{-1}. Crystal dimensions: 0.20 × 0.18 × 0.14 mm, F_{000}: 5112, wavelength: 0.71073 Å, radiation: Mo-Kα graphite monochromated, diffractometer: KappaCCD, ϕ and ω scans, *hkl* limits: 0.22/ − 27,27/ − 38,38, θ limits: 2.5/27.49°, number of data measured: 22153, number of data with $I > 3\sigma(I)$: 4186, weighting scheme: $4F_o^2/(\sigma^2(F_o^2) + 0.0064\,F_o^4)$, number of variables: 727, $R(F)$: 0.066, $R(F)w$: 0.095, GOF: 1.553, largest peak in final difference: 0.940 e Å^{-3}. Package used: OpenMolen, Interactive Structure Solution, Nonius B.V., Delft, The Netherlands, 1997. CCDC 182/1761. See http://www.rsc.org/suppdata/cc/b0/b004982o/ for crystallograhic files in .cif format.

12 (*a*) J. Breu and A. J. Stoll, *Acta Crystallogr., Sect. C*, 1996, **52**, 1174; (*b*) J. G. Collins, A. D. Sleeman, J. R. Aldrich-Wright, I. Greguric and T. W. Hambley, *Inorg. Chem.*, 1998, **37**, 3133.

13 M. Inouye, K. Akamatsu and H. Nakazumi, *J. Am. Chem. Soc.*, 1997, **119**, 9160.

14 M. Irie, K. Sakemura, M. Okinaka and K. Uchida, *J. Org. Chem.*, 1995, **60**, 8305.

Amorphous calcium carbonate stabilised by poly(propylene imine) dendrimers

Jack J. J. M. Donners,[a] Brigid R. Heywood,[b] E. W. Meijer,[a] Roeland J. M. Nolte,[ac] Cristina Roman,[a] Albertus P. H. J. Schenning[a] and Nico A. J. M. Sommerdijk*[a]

[a] *Laboratory for Macromolecular and Organic Chemistry, Eindhoven University of Technology, Post Office Box 513, 5600 MB Eindhoven, The Netherlands. E-mail: N.Sommerdijk@tue.nl; Fax: +31-40-2451036*

[b] *Birchall Centre for Inorganic Chemistry and Materials Science, Chemistry Department, Keele University, Keele, Staffordshire, UK*

[c] *Department of Organic Chemistry, NSR Centre, University of Nijmegen, Nijmegen, The Netherlands*

Received (in Cambridge, UK) 19th June 2000, Accepted 24th August 2000
First published as an Advance Article on the web

In the presence of octadecylamine, poly(propylene imine) dendrimers modified with long alkyl chains self-assemble to form well-defined aggregates that stabilise for periods exceeding 14 days the normally unstable amorphous calcium carbonate (ACC) which persists in competition with the thermodynamic product, calcite.

Templates that consist of organised biomacromolecules are known to direct the formation of most biominerals, in many cases leading to materials with unique shapes and properties.[1] In synthetic assays, the use of ordered supramolecular assemblies, such as micelles,[2] monolayers,[3] vesicles,[4] inverted micelles[5] and lyotropic liquid crystalline systems,[6] allows for the controlled nucleation of inorganic materials on molecular templates with well-defined structure and surface chemistry. One of the most abundant biological minerals is calcium carbonate, the main constituent of mollusc shells, for example.[7] In nature, all three crystalline calcium carbonate polymorphs, calcite, aragonite and the metastable vaterite, are observed. In addition, amorphous calcium carbonate, which is normally unstable at room temperature and pressure, has been reported.[8] In synthetic milieu this amorphous phase is unstable and transforms readily into one of the crystalline polymorphs. Here we report on a synthetic system in which aggregates consisting of assemblies of poly(propylene imine) dendrimers modified with long hydrocarbon chains and single chain surfactants stabilise spheroids of amorphous calcium carbonate (ACC) for extended periods of time.

Poly(propylene imine) dendrimers modified with long aliphatic chains are a new class of amphiphiles which display a variety of aggregation states due to their conformational flexibility.[9] Globular aggregates are formed when C_{16}-modified 5th generation dendrimer **1** is dispersed in aqueous media.[10] In the present work we have modified the outer surface of this dendrimer assembly by addition of **1** to aqueous solutions containing single chain surfactants (octadecylamine, OA, and cetyltrimethylammonium bromide, CTAB) at concentrations below their CMC (Scheme 1). In this way we were able to generate solid self-reinforced aggregates with different shape, size and surface chemistry depending on the choice of surfactant.† It was found that aggregates arising from the interaction of **1** and octadecylamine (OA) expressed a persistent polyhedral shape,[11] as well as a narrow size distribution (Fig. 1a,b). The extremely high fluorescence depolarization anisotropy values found for the aggregates at room temperature (r = 0.32) indicate that they have a very rigid structure.‡ When the dendrimer was mixed with CTAB, spherical aggregates with a narrow distribution and an average size of 20 nm (determined by DLS) were formed (not shown). Fluorescence depolarisation measurements showed that these aggregates are less rigid (r = 0.24) with respect to the dendrimer/octadecylamine aggregates.

The remarkable rigidity and the well-defined size and shape of the aggregates consisting of **1** and OA prompted us to exploit them as 3D templates in calcium carbonate crystallisation

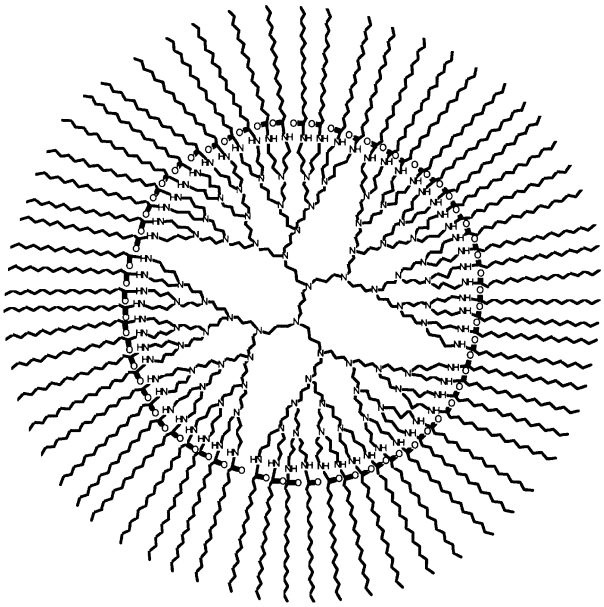

1

assays.§ The addition of these novel templates to such an assay catalysed the formation of amorphous calcium carbonate. Indeed, calcified aggregates, which had retained their polyhedral shape, were recovered after only 15 min (Fig. 1c). FTIR showed strong peaks characteristic for hydrated ACC at 3433 and 1070 cm^{-1},[12] whereas only minor peaks characteristic of calcite were observed (1420, 875 and 712 cm^{-1}). Selected area electron diffraction analyses confirmed that the vast majority of these particles consisted of amorphous material.

Over the course of 4 days a discrete population of {10.4} rhombohedral calcite crystals was also identified in the bulk solution of **1**/OA doped assays, alongside large isolated ACC particles (diameter $\geqslant$ 10 μm; Fig. 1d) a small portion of which still possessed a polyhedral shape (Fig. 1c, inset). It is notable that 80% of the rhombohedra enveloped an ACC sphere (Fig. 1e). The spatial juxtaposition of the two $CaCO_3$ phases argues

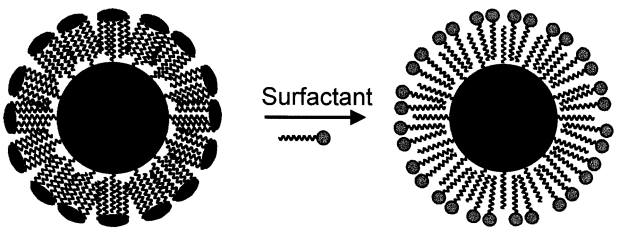

Scheme 1 Schematic representation of the modification of the outer layer of dendrimer-based aggregates using single chain surfactants.

DOI: 10.1039/b004867o

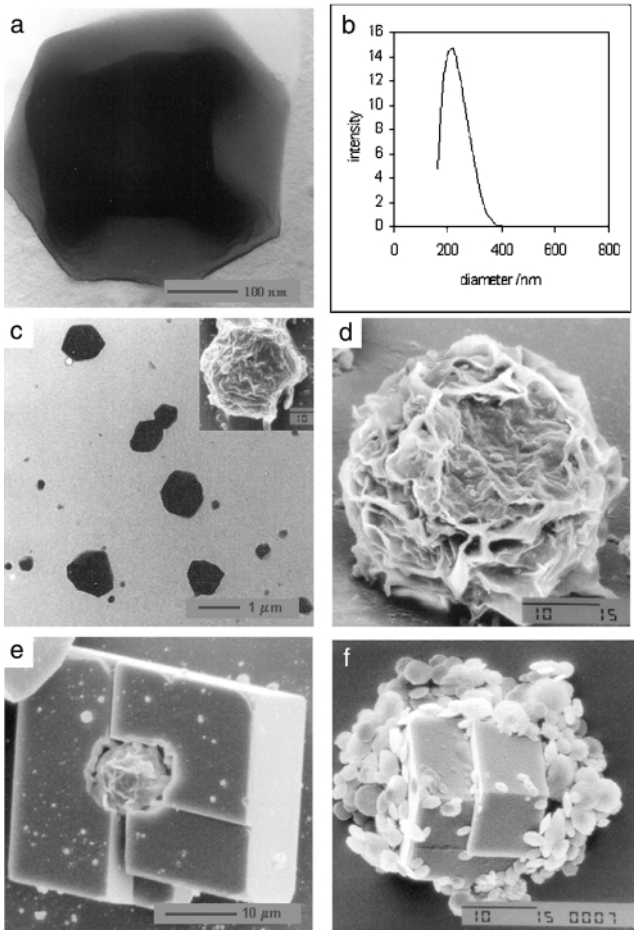

Fig. 1 (a) Transmission electron microscopy (TEM) image (platinum shadowing) of an aqueous dispersion of **1**/OA. (b) Size distribution of aggregates of **1**/OA as determined by dynamic light scattering. (c) TEM image of the crystallisation assay doped with **1**/OA after 15 min, inset: scanning electron microscopy (SEM) image of the assay after 1 h. (d–f) SEM images of the assay doped with (d,e) **1**/OA and (f) **1**/CTAB. Images were recorded (d,f) after 4 days and (e) after 14 days.

strongly for a critical role of the spheres in fostering the nucleation and growth of the crystalline form.

Another notable feature of the **1**/OA doped crystallisation assays was the persistent formation of ACC spheres at the air/solution interface. It is our contention that the continuous formation of spheres at this location is linked to the active adsorption of the **1**/OA aggregates at the air/solution interface. It is significant that particle size analysis of spheres harvested from this location over a fourteen day period revealed a population of ACC spheres with diameters consistently in the range of 1–10 μm. In contrast, the particle size profile of ACC spheres recovered from bulk solution over the same time period showed a gradual shift in size to larger dimensions (> 10 μm). This was accompanied by a diminution in the total number of isolated spheres and an increase in the proportion of spheres which were associated with calcite. The ACC spheres allied with calcite were very uniform in size having diameters of 8 μm, but comprised only 10% of the population. From the integration of FTIR spectra it was concluded that at this stage 20% of the calcium carbonate was still present in the form of spherical ACC.

Aggregates prepared of **1** alone also templated the formation of ACC spheres. However, in this case the amount of ACC was reduced and the transformation to calcite was more rapid than observed previously with the OA modified aggregates: after 24 h 80% of the sample had been converted to calcite compared to 16% in the case of the **1**/OA aggregates. The use of aggregates prepared from **1** and CTAB did not lead to the generation of ACC. Instead, the formation of calcite crystals covered with disc-shaped vaterite crystals was observed (Fig. 1f). Over a period of 5 days these vaterite discs disappeared and only calcite crystals remained.

The gradual dissolution of the small ACC particles and maturation of larger ones can be attributed to the process of Ostwald ripening wherein particles with a high surface to volume ratio provide a continuous source of materials for those with lower surface activity.[13] In the present case this process also effects the gradual release of the **1**/OA aggregates originally occluded within the calcium carbonate spheres. Thus, the depletion of polymeric complex, which accompanies ACC formation at the air/solution interface, will be offset by the dynamic adsorption of surfactant/dendrimer aggregates released into bulk solution from the proportion of small ACC spheres which dissolves. One outcome of this activity will be the iterative formation of an active organic template, capable of inducing the kinetic precipitation of calcium carbonate at the air/solution interface leading to a high local nucleation density of ACC.

Although ACC has been observed as a short-lived intermediate in the presence of various scale prevention agents, to our knowledge only biological systems allow the coexistence of amorphous and crystalline calcium carbonate for extended periods of time.[12] The nucleation of the kinetic product at the expense of the thermodynamically stable form, calcite, and the stabilisation of the amorphous phase against transformation results in the formation of a unique inorganic–organic hybrid material.

Notes and references

† A solution of 18.5 mg of **1** and 15.5 mg surfactant in 100 μl THF/EtOH (2 : 1 v:v) was injected into 6 ml Ultrapure water at 60 °C and sonicated for 1 hour. Subsequently, 1.0 ml aggregate suspension was injected into 25 ml Ultrapure water at room temperature. A detailed investigation of the structures of these aggregates will be published elsewhere.

‡ Fluorescence depolarization was carried out using DPH which in a frozen system has an intrinsic anisotropy value of $r_0 = 0.362$.[14]

§ The aggregate dispersion (1.0 ml) was injected into 25 ml of a supersaturated solution of calcium carbonate ([Ca^{2+}] = 9 mM; [**1**] = 5.3 μM; [surfactant] = 0.37 mM).[15]

1 S. Mann, *Nature*, 1993, **365**, 499; A. Berman, *Science*, 1993, **259**, 776.
2 S. Förster and M. Antonietti, *Adv. Mater.*, 1998, **10**, 195.
3 S. Mann, D. D. Archibald, J. M. Didymus, T. Douglas, B. R. Heywood, F. C. Meldrum and N. J. Reeves, *Science*, 1993, **261**, 1286; J. Aizenberg, A. J. Black and G. M. Whitesides, *Nature*, 1999, **398**, 495.
4 S. Mann, J. P. Hannington and R. J. P. Williams, *Nature*, 1998, **324**, 565.
5 M. Meyer, C. Wallberg, K. Kurihara and J. H. Fendler, *J. Chem. Soc., Chem. Commun.*, 1984, 90.
6 H. Yang, N. Coombs and G. A. Ozin, *Nature*, 1997, **386**, 692; H. Yang, G. A. Ozin and C. T. Kresge, *Adv. Mater.*, 1998, **10**, 883; S. I. Stupp and P. V. Braun, *Science*, 1997, **227**, 1242.
7 L. Addadi and S. Weiner, *Angew. Chem., Int. Ed. Engl.*, 1992, **31**, 153.
8 A. Berman, L. Addadi and S. Weiner, *Nature*, 1988, **331**, 546.
9 S. Stevelmans, J. C. M. van Hest, J. F. G. A. Jansen, D. A. F. J. van Boxtel, E. M. M. de Brabander-van den Berg and E. W. Meijer, *J. Am. Chem. Soc.*, 1996, **118**, 7398.
10 A. P. H. J. Schenning, C. Elissen-Roman, J.-W. Weener, M. W. P. L. Baars, S. J. van der Gaast and E. W. Meijer, *J. Am. Chem. Soc.*, 1998, **20**, 8199.
11 See also: A. E. Blaurock and R. C. Gamble, *J. Membr. Biol.*, 1979, **50**, 187.
12 J. Aizenberg, G. Lambert, L. Addadi and S. Weiner, *Adv. Mater.*, 1996, **8**, 222.
13 A. Burger and R. Ramberger, *Microchim. Acta II*, 1979, 259.
14 M. Shinitzky and Y. Barenholz, *J. Biol. Chem.*, 1974, **249**, 2652.
15 S. Rajam, B. R. Heywood, J. B. A. Walker, S. Mann, R. J. Davey and J. D. Birchall, *J. Chem. Soc., Faraday Trans.*, 1991, **87**, 727.

ChemComm

[2]Rotaxane molecular shuttles employing 1,2-bis(pyridinium)ethane binding sites and dibenzo-24-crown-8 ethers†

Stephen J. Loeb* and James A. Wisner

School of Physical Sciences, Chemistry & Biochemistry, University of Windsor, Windsor, Ontario, Canada N9B 3P4. E-mail: loeb@uwindsor.ca

Received (in Columbia, MO, USA) 5th June 2000, Accepted 15th August 2000
First published as an Advance Article on the web

Symmetrical and unsymmetrical axles containing two binding sites of the 1,2-bis(pyridinium)ethane type are threaded with a single molecule of dibenzo-24-crown-8 ether (DB24C8) resulting in [2]rotaxane *molecular shuttles* that display translational isomerism.

One of the most intriguing developments in supramolecular chemistry is the ability to construct mechanically linked molecular systems that display switching properties resulting from the relative positioning of the internal components of the supermolecule.[1] An elegant example of this is the [2]rotaxane *molecular shuttle* pioneered by Stoddart *et al.* in which a single 'wheel' component can occupy either of two binding sites on a dumbbell shaped 'axle'.[2]

We have recently reported the synthesis of symmetrical and unsymmetrical [3]rotaxanes, **1** and **2**, employing extended axles

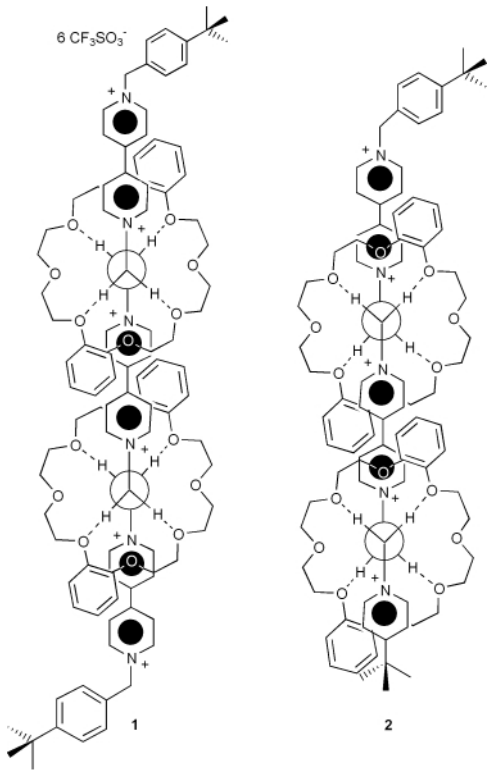

containing two binding sites of the 1,2-bis(pyridinium)ethane type each occupied by a dibenzo-24-crown-8 ether (DB24C8) molecule.[3] Although these [3]rotaxanes are saturated and therefore display no translational isomerism, it is possible to prepare [2]rotaxane molecular shuttles with this template and this work is reported herein.

The [2]rotaxanes **5** and **8**‡ were prepared by mixing **3** and **6** respectively with two equivalents of DB24C8 in MeCN solution followed by a 2-fold excess of the required equivalents of *tert*-butylbenzyl bromide (Scheme 1).[4] The mixtures were stirred at room temperature for 2 days, the salts precipitated by the addition of Et_2O and the products isolated as the chloride salts by column chromatography on silica gel ($MeOH/MeNO_2$/2.0 M NH_4Cl(aq), 3:1:1). Anion exchange with $NaCF_3SO_3$ and $NaBF_4$ respectively in aqueous solution produced **5** and **8** in overall yields of 13 and 19% as orange crystalline solids, which were soluble in organic solvents such as MeCN, $MeNO_2$ and CH_2Cl_2.

Noncovalent interactions between axle and wheel can be inferred by significant chemical shift differences ($\Delta\delta$) in the solution (MeCN-d_3) ^{1}H NMR spectra of **5** and **8** when compared to the respective axles **4** and **7** and free DB24C8.[5] C–H···O hydrogen bonds from axle protons to crown ether O-atoms are evident from the significant *downfield* shifts for all α^+-pyridinium and $^+NCH_2$ protons, while π-stacking between the electron-rich catechol and electron-poor pyridinium rings is indicated by *upfield* shifts observed for the β-pyridinium protons and crown aromatic protons. There exists the possibility of two translational isomers; *i.e.* the crown ether can *shuttle* from one binding site to the other. That this dynamic phenomenon occurs is supported by the fact that only one set of resonances is observed at room temperature and there is a slight exchange broadening of the axle protons interacting with the crown oxygen atoms. It was concluded that the crown ether is undergoing fast exchange between the two binding sites and the observed room temperature chemical shifts for **5** and **8** are

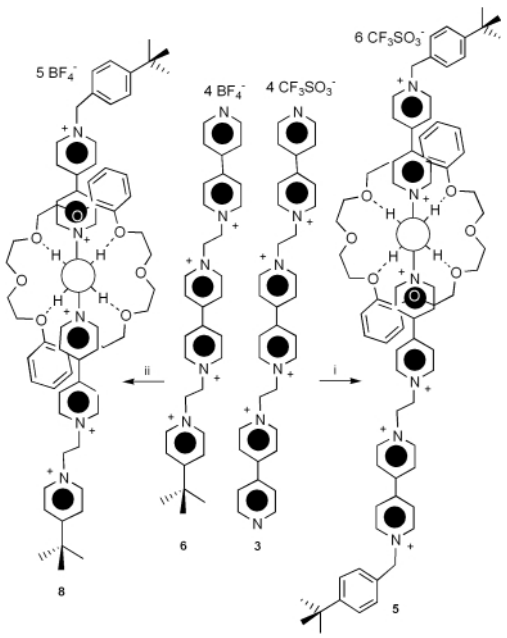

Scheme 1 *Reagents and conditions:* i, 4 equiv. of 4-*tert*-butylbenzyl bromide, 2 equiv. of DB24C8, MeCN, RT, 2 days, SiO_2 ($MeOH/MeNO_2$/2.0 M NH_4Cl(aq), 3:1:1), R_f = 0.35, $NaCF_3SO_3$(aq), 13%; ii, 2 equiv. of 4-*tert*-butylbenzyl bromide, 2 equiv. of DB24C8, MeCN, RT, 2 days, SiO_2 ($MeOH/MeNO_2$/2.0 M NH_4Cl(aq), 3:1:1), R_f = 0.31, $NaBF_4$(aq), 19%.

† Electronic supplementary information (ESI) available: ^{1}H NMR chemical shifts. See http://www.rsc.org/suppdata/cc/b0/b004784h/

DOI: 10.1039/b004784h

weighted averages of the resonances attributable to the individual occupied and vacant sites.

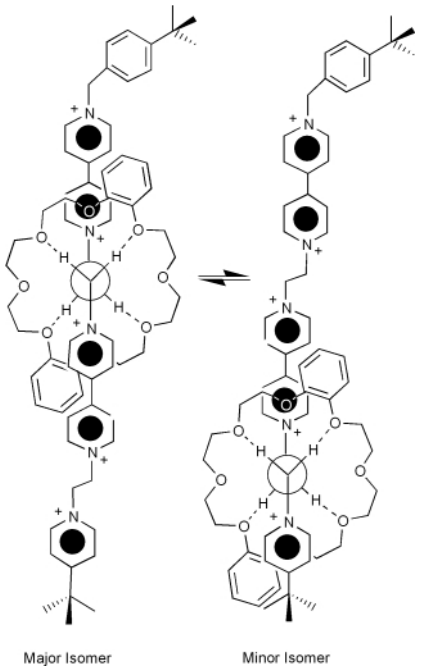

The ^{1}H NMR spectrum of **5** coalesced at 293 K yielding a rate of exchange between the equally populated binding sites of 320 Hz with $\Delta G^{\ddagger}$ = 57.5 kJ mol^{-1}. Similarly, **8** reached coalescence at 273 K with an exchange rate of 222 Hz and $\Delta G^{\ddagger}$ = 54.3 kJ mol^{-1}. For this unsymmetrical [2]rotaxane, the aryl crown ether resonances were used to determine the occupancy of each site. Integration of these signals at 243 K yielded a 2 : 1 ratio of isomers with the bis(4,4′-bipyridinium)ethane site being favoured. This preference is likely due to two factors: (i) the 4,4′-bipyridinium rings are the most electron-poor resulting in more favourable π-stacking and (ii) there are steric problems caused by the *t*Bu-pyridinium group which disfavour π-stacking.

An X-ray crystal structure determination§ of **8** verified the nature of the interactions observed in solution; a ball-and-stick representation is shown in Fig. 1. The DB24C8 ring is threaded on the unsymmetrical axle such that the S-shaped crown ether ring occupies the more favoured bis(4,4′-pyridinium) moiety. The unoccupied bis(pyridinium)ethane group adopts a *gauche* conformation in the solid state.

It has been demonstrated that the 1,2-bis(pyridinium)ethane/24-crown-8 ether templating motif can be used for the synthesis of symmetrical and unsymmetrical molecular shuttles. Future work will focus on controlling this switching process by external perturbations.

We thank the Natural Sciences and Engineering Council of Canada for financial support of this research and J. A. W. thanks the Ontario Graduate Scholarship program for funding.

Notes and references

‡ All new compounds were successfully characterized by ^{1}H NMR spectroscopy (500 MHz, 298 K) and LSI-MS or ESI-MS. NOESY experiments were used make individual ^{1}H NMR assignments. Synthetic note: > 3 equivalents of DB24C8 produces exclusively [3]rotaxane;[4] < 3 equivalents of DB24C8 produces a mixture of [3]rotaxane, [2]rotaxane and thread with the optimum yield of [2]rotaxane produced with 2 equivalents.

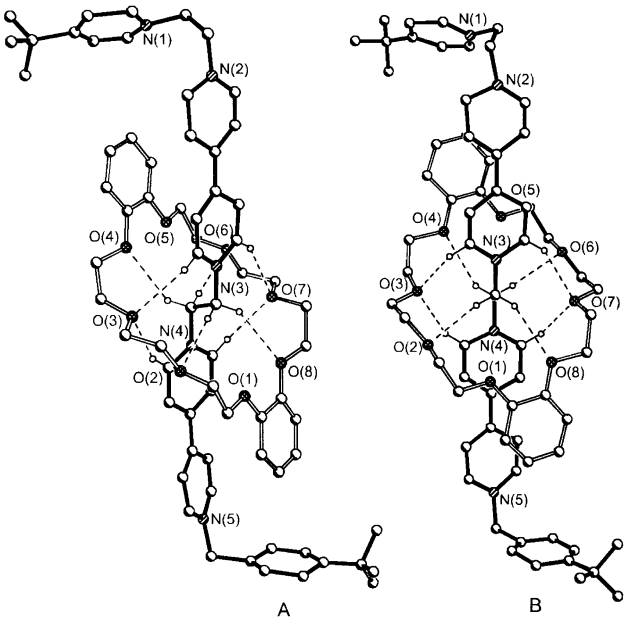

Fig. 1 Ball and stick representations of the X-ray crystal structure of the [2]rotaxane molecular shuttle **8**. (A) showing the basic numbering scheme and (B) a view down the ethane C(22)–C(23) bond. Significant N$^+$···O distances (Å): N(3)···O(4) 3.54, N(3)···O(5) 3.48, N(4)···O(1) 3.56, N(4)···O(8) 3.55. C–H···O distances (Å) and angles (°): H(19A)···O(3) 2.63, C(19)–H(19A)···O(3) 135.0; H(20A)···O(7) 2.47, C(20)–H(20A)···O(7) 151.2; H(22A)···O(2) 2.52, C(22)–H(22A)···O(5) 163.5; H(22B)···O(8) 2.70, C(22)–H(22B)···O(8) 148.7; H(23A)···O(4) 2.65, C(23)–H(23A)···O(4) 147.3; H(23B)···O(6) 2.59, C(23)–H(23B)···O(6) 166.1; H(24A)···O(3) 2.33, C(24)–H(24A)···O(3) 155.3; H(28A)···O(7) 2.57, C(28)–H(28A)···O(2) 138.3.

Selected data for **5**: ^{1}H NMR (CD_3CN): δ 9.22 (m, 8H), 9.00 (d, 4H, J = 7.63 Hz), 8.35 (br, 8H), 8.28 (d, 4H), 7.57 (d, 4H, J = 8.72 Hz), 7.47 (d, 4H), 6.68 (m, 4H), 6.49 (m, 4H), 5.81 (s, 4H), 5.48 (br, 8H), 4.03 (m, 24H), 1.33 (s, 18H). ESI-MS: m/z 2012.7 ([M − OTf]$^+$). **8**: ^{1}H NMR (CD_3CN): δ 9.28 (br, 4H), 9.12 (br, 2H), 9.01 (d, 2H), 8.83 (br, 2H), 8.28 (br, 8H), 8.06 (br, 2H), 7.59 (d, 2H, J = 8.29 Hz), 7.50 (d, 2H), 6.69 (m, 4H), 6.54 (m, 4H), 5.83 (s, 2H), 5.55 (br, 4H), 5.35 (br, 2H), 5.28 (br, 2H), 4.06 (m, 24H), 1.38 (s, 9H), 1.34 (s, 9H). ESI-MS: m/z 1446.6 ([M − BF_4]$^+$).

§ *Crystal data* for **8**: $C_{68}H_{84}B_5F_{20}N_5O_8$, M = 1533.45, monoclinic, a = 40.78(2), b = 15.808(5), c = 12.336(4) Å, β = 98.48(2)°, U = 7866(5) Å^3, T = 293(2) K, Cc, Z = 4, μ = 0.115 mm^{-1}, 10068 independent reflections [R(int) = 0.0631], $R1$ = 0.0997, $wR2$ = 0.2451 [$I > 2\sigma I$], $R1$ = 0.1982, $wR2$ = 0.2999 [all data], Goodness-of-fit (F^2) = 0.929. Data were collected on a Siemens SMART CCD instrument and solutions performed using the SHELXTL 5.03 Program Library for Structure and Solution and Molecular Graphics, Siemens Analytical Instrument Division, Madison, WI, USA, 1997. CCDC 182/1753. See http://www.rsc.org/suppdata/cc/b0/b004784h/ for crystallographic files in .cif format.

1 (*a*) A. C. Benniston, *Chem. Soc. Rev.*, 1996, 428; (*b*) V. Balzani, M. Gómez-López and J. F. Stoddart, *Acc. Chem. Res.*, 1998, **31**, 405; (*c*) P. R. Ashton, R. Ballardini, V. Balzani, I. Baxter, A. Credi, M. C. T. Fyfe, M. T. Gandolfi, M. Gómez-López, M.-V. Martínez-Díaz, A. Piersanti, N. Spencer, J. F. Stoddart, M. Venturi, A. J. P. White and D. J. Williams, *J. Am. Chem. Soc.*, 1998, **120**, 11 932; (*d*) L. Raehm, J.-M. Kern and J.-P. Sauvage, *Chem. Eur. J.*, 1999, **5**, 3310; (*e*) C. P. Collier, E. W. Wong, M. Belohradsky, F. M. Raymo, J. F. Stoddart, P. J. Kuekes, R. S. Williams and J. R. Heath, *Science*, 1999, **285**, 391.

2 A. P. Lucio, N. Spencer and J. F. Stoddart, *J. Am. Chem. Soc.*, 1991, **113**, 5131.

3 S. J. Loeb and J. A. Wisner, *Chem. Commun.*, 2000, 845.

4 J. McGeachie and L. A. Summers, *Z. Naturforsch., Teil B*, 1986, **41**, 1255.

5 (*a*) S. J. Loeb and J. A. Wisner, *Angew. Chem.*, 1998, **110**, 3010; *Angew. Chem., Int. Ed.*, 1998, **37**, 2838; (*b*) S. J. Loeb and J. A. Wisner, *Chem. Commun.*, 1998, 2757.

Replacement of selenium by antimony in $MoSe_2$: interconnection of the MoSbSe layers by Sb–Sb bonding

Holger Kleinke*

Department of Chemistry, University of Waterloo, Waterloo, Ontario, Canada N2L 3G1. E-mail: kleinke@uwaterloo.ca

Received (in Oxford, UK) 21st June 2000, Accepted 22nd August 2000
First published as an Advance Article on the web

The replacement of every other Se atom in layered $MoSe_2$ by two Sb atoms led to the formation of $MoSb_2Se$; within its lattice, Sb atoms interconnect the MoSbSe sheets to form a truly three-dimensional structure, thereby enlarging the octahedral cavities.

The layered dichalcogenides of the valence-electron-poor transition metal atoms have attracted the interest of various different interdisciplinary research groups owing to potential applications such as solid lubricants, and intercalation reactions and electronic instabilities leading to energy storage applications[1] and charge density waves.[2] Consequently, extensive theoretical work (based on the Extended Hückel calculations) was performed to investigate the different physical properties[3] as well as the different metal clustering which are both dependent upon the electron count.[4]

For packing considerations, metal atoms, M, fill the octahedral voids of every other layer in the hexagonal close-packing of chalcogen atoms, Q, (realized in the CdI_2 lattice type, as observed for $ZrSe_2$[5]); different electron configurations of the M atoms bring about different distortions in the structures. For example, in going from $ZrSe_2$ through the polymorph $NbSe_2$[6] to $MoSe_2$,[7] the d electron configuration of the M^{4+} atom changes from $4d^0$ to $4d^1$ to $4d^2$: this leads to significant shifts of the atomic positions in the layers of $NbSe_2$ and $MoSe_2$, which produce in part bonding M–M contacts that do not occur in the undistorted CdI_2 type structure. $MoSe_2$ and α-$MoTe_2$[8] crystallize as the MoS_2 type, with Mo atoms surrounded in a trigonal prismatic arrangement. This is—for d^2 ions—one of the two energetically favorable deviations from ideal hexagonal close-packing of the chalcogen atoms. Here, the electronic stabilization results from lowering of the one filled d orbital in the trigonal prismatic ligand field. The other favorable configuration, realized in β-$MoTe_2$ and WTe_2,[9] is the formation of M–M zigzag chains, stabilized by the occurrence of two single bonds per M atom, *i.e.* by lowering the one filled d orbital of the t_{2g} set. Linearly linked rhomboidal clusters would be favorable for a d^3 count as in $ReSe_2$.[10] The latter two distortions can be deduced to arise from a Peierls distortion associated with the partially filled t_{2g} band.

The intercalation chemistry of the layered chalcogenides, MQ_2, known to date is substantive.[11] Usually, intercalation of cations increases the number of M-centered d electrons and thus enhances M–M bonding within the MQ_2 layers. Examples include $M'_{0.5}NbSe_2$ (M′ = Ti, V, Cr)[12] and Cu_xNbTe_2,[13] while $Zr_{1+x}Te_2$ represents a notable exception.[14]

Intercalation of anions is less favorable due to anion–anion repulsions. The problem can be avoided by connecting the anions to the MQ_2 layers *via* covalent bonds. To achieve this, one must either oxidize the Q^{2-} anions or exchange Q for less electronegative atoms, such as the heavier pnictogen atoms like antimony. Since the Sb atoms tend to form Sb–Sb bonds even in metal-rich antimonides of the valence-electron-poor transition metals, *e.g.* in $(Hf,Ti)_7Sb_4$,[15] $(Zr,V)_{11}Sb_8$,[16] $(Zr,V)_{13}Sb_{10}$[17] and (Zr,Ti)Sb,[18] and the only known molybdenum antimonide, Mo_3Sb_7, comprises Sb–Sb bonds as well,[19] it seemed most promising to use the latter method with Sb atoms as replacements for the chalcogen atoms, Q.

Subsequently, reactions aimed at hypothetical $Sb_xMo(Sb,Se)_2$ were carried out by heating the elements in the stoichiometric ratios in sealed silica tubes at 800 °C with addition of traces of iodine to promote crystal growth. Thereby, the new antimonide selenide $MoSb_2Se$ formed and was characterized by EDX and crystal structure analysis.[20] $MoSb_2Se$ crystallizes in its own structure type, which can be described based on MoSbSe layers being interconnected by additional Sb atoms (Sb3 and Sb4), as depicted in Fig. 1.

The MoSbSe layers closely resemble the $MoTe_2$ layers of β-$MoTe_2$, with the Sb atoms capping the longer Mo–Mo distances > 450 pm and the smaller Se atoms capping the Mo–Mo bonds of 281 pm (Mo–Mo in β-$MoTe_2$: 289–290 pm). This suggests a d^2 configuration of the Mo atoms, *i.e.* Mo^{4+}, as in $Mo^{4+}(Se^{2-})_2$. Correspondingly, the Mo–Se distances are very similar in both compounds, ranging from 250–252 pm in $MoSb_2Se$, compared to 253 pm in $MoSe_2$. Also, the Mo–Sb distances in $MoSb_2Se$ (282–284 pm) compare well to the longer one in Mo_3Sb_7 (285 pm), to which the Sb atoms with Sb–Sb bonding contribute.

Every Sb atom of the MoSbSe layers forms one homonuclear bond to one interlayer Sb atom, the length of which (285 pm) suggests a typical single bond, as also found in KSb (283 and 285 pm),[21] *cyclo*-Sb_5^{5-} (between 281–291 pm),[22] and Sb_{11}^{3-} (276–285 pm).[23] Furthermore, each of these intralayer Sb atoms takes part in four longer bonds (325–330 pm, dashed lines in Figs. 1 and 2). These distances are indicative of weak but clearly present interactions.[24] Ignoring them in a first approximation and applying the $(8 - N)$ rule, we assign the oxidation state of 2− to the intralayer Sb atoms, which leads to neutral interlayer Sb atoms, *i.e.* $Sb^0Mo^{4+}Sb^{2-}Se^{2-}$. The latter readily explains the presence of three Sb–Sb single bonds per interlayer Sb atom

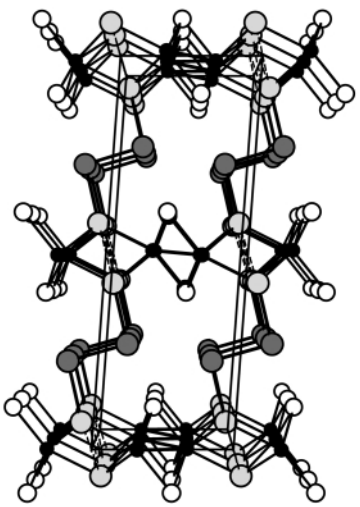

Fig. 1 Projection of the structure of $MoSb_2Se$ along [010]. Horizontal, *a* axis; Mo (●), Se (○), Sb1, Sb2 (◍), Sb3, Sb4 (◍); dashed lines, $325 < d_{Sb-Sb} < 330$ pm.

DOI: 10.1039/b005062h

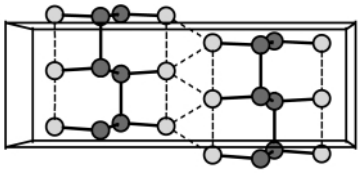

Fig. 2 Projection of the Sb atom substructure along [100]. Horizontal, *c* axis; solid lines, 285 < *d* < 292 pm; dashed lines, 325 < *d* < 330 pm.

(bond lengths 285–292 pm), which requires doubling of the monoclinic axis (Fig. 2). The doubling of the *b* axis led to only weak superstructure reflections because only the Sb3 and Sb4 atoms were shifted to form alternating short and long distances of 292 and 357 pm. These shifts are reflected in the differences in the *y* parameters of Sb3 and Sb4, while all other atoms are pairwise related, *e.g.* Mo1 *x*, *y*, *z*, Mo2 *x*, *y* + ½, *z*.

The situation is somewhat more complicated as discussed above, since the Sb–Sb bonds classified as single bonds are up to 10 pm longer than regular single bonds, and because of the presence of the four weaker bonds per intralayer Sb atom. These details suggest the oxidation states of the different Sb atoms being more similar, leading to a formulation of $Sb^{x-}Mo^{4+}Sb^{(2-x)-}Se^{2-}$ with $0 < x < 1$.

Although interlayer atoms are already present in $MoSb_2Se$, the structure is still susceptible for intercalation of cations. The distances between the layers increase by going from $MoSe_2$ through $MoTe_2$ to $MoSb_2Se$, *i.e.* from 366, to 386, to 561 pm, measured between the Se and Te atoms, respectively. As a consequence, an octahedral void remains, which is even larger in $MoSb_2Se$ than in $MoSe_2$.

Therefore, we are currently investigating possible intercalation reactions for $MoSb_2Se$. Reducing $MoSb_2Se$ might lead to reduced interlayer Sb atoms thus breaking the Sb–Sb bonds parallel to the *b* axis, which would eliminate the superstructure. Also of interest are attempts to place more Sb atoms between the MoSbSe layers by forming (hypothetical) compounds like $MoSb_3Se$ or $MoSb_4Se$.

Financial support from the Natural Science and Engineering Research Council of Canada (NSERC) is gratefully acknowledged.

Notes and references

1 J. Rouxel and R. Brec, *Annu. Rev. Mater. Sci.*, 1986, **16**, 137.
2 J. A. Wilson and F. J. DiSalvo, *Adv. Phys.*, 1975, **24**, 117.
3 E. Canadell and M.-H. Whangbo, *Inorg. Chem.*, 1990, **29**, 1398.
4 E. Canadell, A. LeBeuze, M. Abdelaziz El Khalifa, R. Chevrel and M.-H. Whangbo, *J. Am. Chem. Soc.*, 1989, **111**, 3778.
5 A. Gleizes and Y. Jeannin, *J. Solid State Chem.*, 1970, **1**, 180.
6 B. E. Brown and D. J. Beerntsen, *Acta Crystallogr.*, 1965, **18**, 31; M. Marezio, P. D. Dernier, A. Menth and G. W. Hull, Jr., *J. Solid State Chem.*, 1972, **4**, 425.
7 K. D. Bronsema, J. L. De Boer and F. Jellinek, *Z. Anorg. Allg. Chem.*, 1986, **540**, 15.
8 D. Puotinen and R. E. Newnham, *Acta Crystallogr.*, 1961, **14**, 691.
9 B. E. Brown, *Acta Crystallogr.*, 1966, **20**, 268.
10 M. Kertesz and R. Hoffmann, *J. Am. Chem. Soc.*, 1984, **106**, 3453.
11 F. Lévy, *Structural Chemistry of Layer-Type Phases*, Reidel, Dordrecht, The Netherlands, 1976.
12 A. Meerschaut and J. Rouxel, *C. R. Seances Acad. Sci., Ser. C.*, 1977, **277**, 163; A. Meerschaut, M. Spiesser, J. Rouxel and O. Gorochov, *J. Solid State Chem.*, 1980, **31**, 31.
13 W. Tremel, U. Wortmann, T. Vomhof and W. Jeitschko, *Chem. Ber.*, 1994, **127**, 15.
14 C. Wang, C. Eylem and T. Hughbanks, *Inorg. Chem.*, 1998, **37**, 390.
15 H. Kleinke, *Inorg. Chem.*, 1999, **38**, 2931.
16 H. Kleinke, *J. Mater. Chem.*, 1999, **9**, 2703.
17 H. Kleinke, *Chem. Commun.*, 1998, 2219.
18 H. Kleinke, *J. Am. Chem. Soc.*, 2000, **122**, 853.
19 A. Brown, *Nature*, 1965, **206**, 502.
20 *Crystal data*: $MoSb_2Se$, M = 418.4, space group $P2_1/c$, a = 657.28(4), b = 649.41(3), c = 1829.9(1) pm, β = 94.246(8)°, Z = 8; μ = 26.0 mm^{-1}, 2214 independent reflections, $R(F)$ = 0.021, $R_w(F^2)$ = 0.044 for 1403 observed reflections [$I > 2\sigma(I)$]. Atomic positions [atom *x*, *y*, *z*, U_{eq} (pm^2)]: Mo1 0.32480(4), 0.1251(3), 0.99414(2), 32.4(8); Mo2 0.32494(4), 0.6247(3), 0.99426(2), 31.7(8); Sb1 0.07475(3), 0.3744(3), 0.07598(1), 47.1(7); Sb2 0.07472(3), 0.8747(3), 0.07582(1), 48.4(7); Sb3 0.20296(7), **0.3499(2)**, 0.22816(3), 119(2); Sb4 0.20267(7), **0.8999(2)**, 0.22806(3), 122(2); Se1 0.41395(5), 0.6249(4), 0.39800(2), 53.0(8); Se2 0.41440(5), 0.1247(4), 0.39798(2), 53.2(8). CCDC 182/1764. See http://www.rsc.org/suppdata/cc/b0/b005062h/ for crystallographic files in .cif format.
21 W. Hönle and H.-G. von Schnering, *Z. Kristallogr.*, 1981, **155**, 307.
22 N. Korber and F. Richter, *Angew. Chem., Int. Ed. Engl.*, 1997, **36**, 1512.
23 U. Bolle and W. Tremel, *J. Chem. Soc., Chem. Commun.*, 1992, 91.
24 For an overview see: H. Kleinke, *Chem. Soc. Rev.*, 2000, **29**, in press.

ChemComm

Formation and pH-controlled assembly of amphiphilic gold nanoparticles

Joseph Simard, Cheryl Briggs, Andrew K. Boal and Vincent M. Rotello*

Department of Chemistry, University of Massachusetts, Amherst, MA 01003, USA. E-mail: rotello@chem.umass.edu

Received (in Columbia, MO, USA) 23rd May 2000, Accepted 16th August 2000
First published as an Advance Article on the web

Alkanethiolate-protected gold nanoclusters are solublized through place exchange reaction with ω-thiocarboxylic acids.

Thiolate monolayer-protected gold clusters (MPCs) provide versatile precursors for the fabrication of nanoscale systems.[1] These colloidal MPCs can be readily modified through place exchange reactions,[2] providing a direct route to mixed monolayer-protected clusters (MMPCs) featuring a broad array of functionality. This functional diversity, coupled with the combinatorial nature of the place exchange process, has made MMPCs central in the creation of numerous nanoparticle-based materials and devices.

One potentially powerful application of MMPCs is biomolecular recognition.[3] In recent investigations, we have demonstrated that the mobility of thiolate ligands on nanoparticles can be exploited to create templated multivalent receptors.[4] The extension of this methodology to the recognition of protein surfaces[5] has been limited by the inaccessibility of water-soluble amphiphilic MMPCs. Recently, Murray and co-workers have demonstrated the formation of water-soluble MPCs and place exchange reactions to produce the corresponding MMPCs.[6] In both the colloid formation and place exchange steps, however, purification of the resulting colloids required lengthy dialysis to remove unreacted thiols. More significantly, attempts to exchange hydrophobic groups into water-soluble MPCs resulted in the formation of insoluble aggregates.[6c] To provide an alternative route to the formation of amphiphilic colloids we have explored the exchange of polar functionality with gold nanoparticles featuring non-polar monolayer coverage. We report here the direct formation of water-soluble amphiphilic colloids through place exchange of alkanethiolate MPCs with an ω-thiol carboxylic acid.

To obtain a system that would provide water solubility with non-polar groups present, we prepared the carboxylic acid-functionalized colloid AuCOOH through place exchange of 2 nm octanethiol colloids[7] with 11-thioundecanoic acid **1** (Scheme 1).[8] After washing with dichloromethane, the AuCOOH nanoparticles were dissolved in D_2O/NaOD, and characterized by NMR. The end-group analysis of the ^{1}H NMR spectrum of the resulting $AuCOO^-$ colloids indicated that the ratio of ω-thiol carboxylic acid to octanethiol was *ca.* 1 : 1.

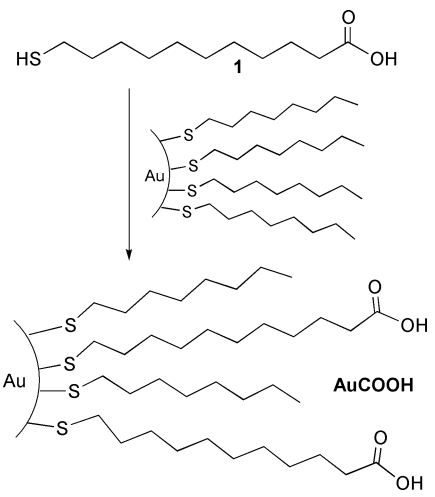

Scheme 1

The functionalized colloids were also characterized by pH titration. Acid/base titrations of nanoparticles with ionizable monolayer moieties have been carried out previously.[6c,9] Fig. 1A shows the titration of $AuCOO^-$, which exhibited a pK_a of about 4.0. This corresponds closely to previous work done on carboxylate-terminated MPCs featuring a C_{12} monolayer, where a pK_a of 4.5 was reported,[8] and is considerably lower than the pK_a of 5.56 observed with tipronin (C_4)-functionalized MPCs. This disparity in pH provides further evidence of the distance dependence of sidechain–sidechain interactions arising from the radial nature of MPC systems.[10]

During titrations, aggregation of particles was observed at pH < 5. This is attributed to interparticle interactions: at low pH the carboxylic acid groups facilitate interparticle interactions through both hydrogen bonding and an increase in hydrophobicity, resulting in the formation of particle aggregates. At high pH, however, particle aggregation is disfavored due to repulsive interactions between negatively charged carboxylate particles.[11] Transmission electron microscopy (TEM) was used to better understand the aggregation process.[8,9] Samples were prepared by initially dissolving AuCOOH nanoparticles in pH 10 buffer. A portion of this solution was neutralized to pH ~ 7 with 0.1 M HCl which was then diluted with pH 7 or pH 4 buffer, producing three solutions with pH 10, 7, and 4. All the solutions were diluted with sufficient buffer to yield a final colloid concentration of 1 mg mL^{-1}. A single drop of the desired solution was deposited on a TEM grid.[12] At pH 10, there was very little aggregation, as would be expected for a highly charged colloid (Fig. 2a). When this system was deposited from a neutral pH 7 solution (Fig. 2b) both small loosely packed aggregates and individual particles were observed. At pH 4, (Fig. 2c), aggregation was increased, with very few free particles observed. Additionally, these aggregates are much larger and denser than those observed at pH 7.

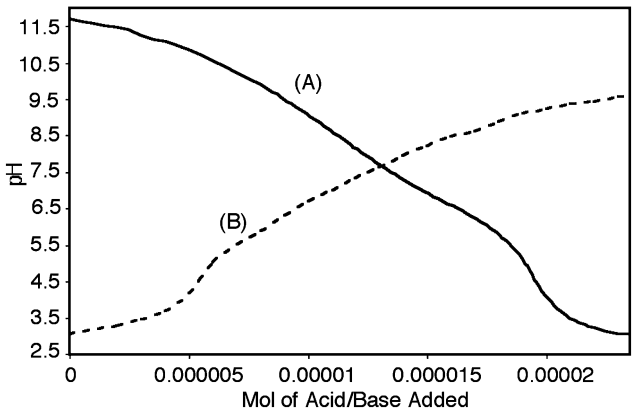

Fig. 1 Titration curves of AuCOOH. The colloid was first dissolved in a small amount of 0.1 M NaOH and brought up to a volume of 3.3 ml with distilled water. (A) Original solution titrated with aliquots of 10–50 μL 0.01 M HCl. (B) Back titration of solution. Titrated with aliquots of 10 μL 0.1 M NaOH. The pH was recorded initially and after each addition of either the acid or base.

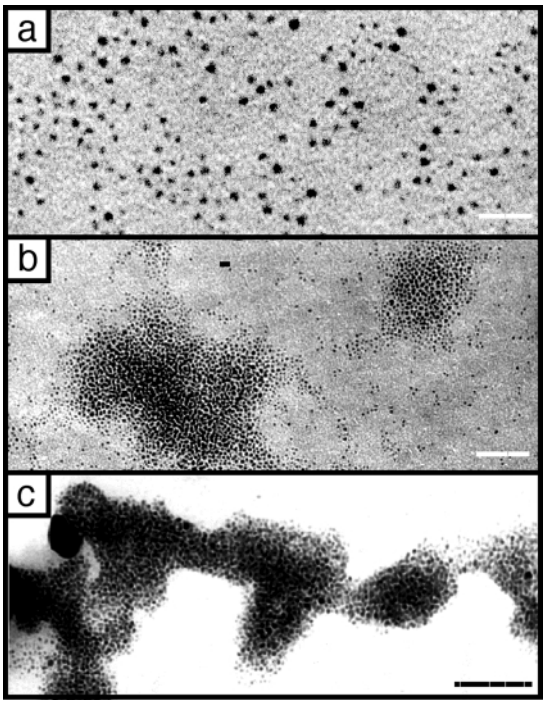

Fig. 2 TEM micrographs of ω-thiol carboxylic acid functionalized colloid at (a) pH 10, (b) pH 7, and (c) pH 4. Scale bars represent 10 nm, 25 nm, and 50 nm, respectively.

In summary, we have demonstrated the effective fabrication of a water-soluble amphiphilic MMPC through place-exchange processes. We have also shown that aggregation of these particles can be directly controlled through modulation of pH. The application of these water-soluble MMPCs to molecular and biomolecular recognition is currently underway, and will be reported in due course.

This research was supported by the National Science Foundation (CHE 9905492 to V. M. R.; DMR-9809365 for MRSEC instrumentation), and the National Institutes of Health (GM-59249). V. M. R. acknowledges the Petroleum Research Fund of the ACS, the Alfred P. Sloan Foundation, the Camille and Henry Dreyfus Foundation, and is a Cottrell scholar of Research Corporation.

Notes and references

1 J. Liu, R. L. Xu and A. E. Kaifer, *Langmuir*, 1998, **14**, 7337.
2 M. J. Hostetler, A. C. Templeton and R. W. Murray, *Langmuir*, 1999, **15**, 3782.
3 A. P. Alivisatos, K. P. Johnsson, X. G. Peng, T. E. Wilson, C. J. Loweth, M. P. Bruchez and P. G. Schultz, *Nature*, 1996, **382**, 609; B. Johne, K. Hansen, E. Mork and J. Holtlund, *J. Immunol. Methods*, 1995, **183**, 167; C. A. Mirkin, R. L. Letsinger, R. C. Mucic and J. J. Storhoff, *Nature*, 1996, **382**, 607; G. P. Mitchell, C. A. Mirkin and R. L. Letsinger, *J. Am. Chem. Soc.*, 1999, **121**, 8122; O. D. Velev and E. W. Kaler, *Langmuir*, 1999, **15**, 3693.
4 A. K. Boal and V. M. Rotello, *J. Am. Chem. Soc.*, 2000, **122**, 734.
5 For recent examples of protein surface recognition using other synthetic scaffolds, see: H. S. Park, Q. Lin and A. D. Hamilton, *J. Am. Chem. Soc.*, 1999, **121**, 8; L. E. Strong and L. L. Kiessling, *J. Am. Chem. Soc.*, 1999, **121**, 6193.
6 (*a*) A. C. Templeton, M. J. Hostetler, E. K. Warmoth, S. W. Chen, C. M. Hartshorn, V. M. Krishnamurthy, M. D. E. Forbes and R. W. Murray, *J. Am. Chem. Soc.*, 1998, **120**, 4845; (*b*) A. C. Templeton, D. E. Cliffel and R. W. Murray, *J. Am. Chem. Soc.*, 1999, **121**, 7081; (*c*) A. C. Templeton, S. W. Chen, S. M. Gross and R. W. Murray, *Langmuir*, 1999, **15**, 66.
7 D. G. Duff, A. Baiker and P. P. Edwards, *J. Chem. Soc., Chem. Commun.*, 1993, 96.
8 In a typical procedure, 11-thioundecanoic acid (740 mg, 3.4 mmol) in 4 mL of THF was added to 140 mg of C_8-functionalized nanoparticles.[4] The resulting solution was stirred under argon for two days at room temperature, forming a black precipitate of AuCOOH. Solvent was removed *in vacuo*, and the resulting solid purified by repeated suspension, centrifugation, and decanting with dichloromethane. The resulting AuCOOH colloid was soluble in polar organic solvents such as methanol, and ethanol, and slightly soluble in THF. Solublization of AuCOOH colloid aqueous solution was achieved using aqueous solution at pH 10. This solution of AuCOOH could be acidified to pH ~5 before precipitation occurred.
9 C. S. Weisbecker, M. V. Merritt and G. M. Whitesides, *Langmuir*, 1996, **12**, 3763.
10 A. C. Templeton, M. P. Wuelfing and R. W. Murray, *Acc. Chem. Res.*, 2000, **33**, 27.
11 S. H. Chen and K. Kimura, *Langmuir*, 1999, **15**, 1075.
12 The samples were analyzed using a JEOL 100CX electron microscope, on 300 mesh Cu grid with carbon film.

ChemComm

Gold nanoparticles from self-assembled gold(I) amine precursors†

Silvia Gomez,[a] Karine Philippot,[a] Vincent Collière,[a] Bruno Chaudret,*[a] François Senocq[b] and Pierre Lecante[c]

[a] *Laboratoire de Chimie de Coordination du CNRS, 205, route de Narbonne, 31077 Toulouse Cédex 04, France*
[b] *CIRIMAT, UMR CNRS 5085, E.N.S.C.T., 118, route de Narbonne, 31077 Toulouse Cédex 04, France*
[c] *Centre d'Elaboration des Matériaux et d'Etudes Structurales du CNRS, 29, rue Jeanne Marvig BP 4347, 31055 Toulouse Cédex 04, France*

Received (in Cambridge, UK) 3rd July 2000, Accepted 21st July 2000
First published as an Advance Article on the web

The reaction of AuCl(THT) (1) with long chain primary amines ($C_nH_{2n+1}NH_2$; n = 8, 12, 16) leads to the formation of the complexes $AuCl(NH_2R)$ (R = C_8H_{17}, 2; $C_{12}H_{25}$, 3; $C_{16}H_{33}$, 4) which are characterized by classical methods and shown to self-organize in the solid state into a fibrous material; decomposition of the complexes inside the supramolecular framework yields a monolayer of ordered gold nanoparticles.

There is presently a considerable interest for the physical properties of nanomaterials (electronics, magnetism, catalysis, mechanical properties, …). If one excepts near field experiments, the study of these properties implies an ordering of the materials in 1, 2 or 3 dimensions.[1–4] It has been proposed recently that the formation of self-assembled gold nanowires could be an alternative to photolithography.[4] In many cases, gold appears as a metal of choice for applications regarding, *e.g.* microelectronics but, while the synthesis of gold nanoparticles has been known for 150 years,[5] a study of the recent literature reveals the need for new preparative methods leading to monodisperse particles of adjustable size and shape.[6–12]

Gold particles are commonly prepared by chemical reduction of a chloride precursor. For example, the well-known Turkevich method involves reduction of $HAuCl_4$ by sodium citrate in water[13] while Schmid has demonstrated that the reduction of $AuCl(PR_3)$ by B_2H_6 leads to Au_{55} nanoclusters.[14] Several new methods have been developed in the last few years which involve the reduction of gold chlorides by sodium borohydride or super-hydride.[11,12] The stabilization of the particles is generally performed by thiolate ligands or by a polymer (PVA, PVP) but, recently, amines have also been used as stabilizers.[15] It has for example been possible, using a two phase method in the presence of a long chain quaternary ammonium salt as phase transfer agent, to produce particles of regular size which could be assembled into a mono- or a bi-layer.[16–20] Alternative syntheses involve vacuum deposition onto graphite[6] or silica[7] or UV irradiation of aqueous $HAuCl_4$ solution in the presence of a polymer.[8]

In our group, we have been interested for some time in the synthesis of metal nanoparticles from organometallic precursors.[21–23] The reasons for this interest were (i) the possibility to control the kinetic of the decomposition of the precursor and therefore the size of the particles, (ii) the possibility to prepare novel structures because of the mild conditions involved and (iii) the control of the surface contamination.[22,23] Concerning gold, no readily available and purely organometallic precursor was known but some gold(I) complexes have been reported to be unstable.[24,25] We have previously shown that the chloride gold(I) complex AuCl(THT)[26] (**1**; THT = tetrahydrothiophene) could be decomposed by CO or H_2 in the presence of a polymer (PVP or nitrocellulose).[24] This prompted us to investigate the decomposition of AuCl(THT) in the presence of amine which could act as HCl acceptor. We use in this study primary amines containing long alkyl chains since these compounds are known to self-assemble and have been used as templating agents for the synthesis of mesoporous materials.[27]

We describe here the synthesis of three new gold(I) amine complexes, their supramolecular arrangement and their decomposition into gold nanoparticles.

The reaction of AuCl(THT) (**1**) in toluene at room temperature leads within a few minutes to the precipitation of gold as a polycrystalline powder. GLC-MS analysis of the solution demonstrates the formation of chlorotoluene as a mixture of its three isomers and the decoordination of THT. This indicates that, unexpectedly and probably through a mechanism analogous to that of the Friedel–Crafts reaction, toluene is a good reductant of Au(I). However, the same reaction, when carried out in the presence of one equivalent of a primary long chain amine ($C_nH_{2n+1}NH_2$; n = 8, 12, 16), leads to the formation of a white powder, insoluble in toluene, soluble in THF and acetone for n = 8, and only slightly soluble in THF and DMSO for n = 12 and 16. The solutions are however not very stable and change colour to purple after a few minutes in DMSO and a few hours in THF and acetone. These powders correspond to the complexes $AuCl(NH_2R)$ (R = C_8H_{17}, **2**; $C_{12}H_{25}$, **3**; $C_{16}H_{33}$, **4**); they were characterized by microanalysis, infrared and ^1H and ^{13}C NMR spectroscopy, and TGA.† Mass spectra obtained using the DCI or the FAB techniques only evidenced the presence of the free amine ligand because of the decomposition of the compounds. It was however possible to follow the decomposition of **2**–**4** in the solid state by TGA experiments which demonstrate the successive elimination of the chloride and amine ligands. GLC-MS analysis of the solution shows the presence of free THT but chlorotoluene is not detected. All these data are in agreement with a simple substitution of THT by amine.

A powder of complex **2** was investigated by TEM (Transmission Electron Microscopy; see Fig. S1, ESI†). At the microscopic level, the powder is formed from nanocrystals the size of which is found near 2 nm see Fig. S1(*b*), ESI.† It is possible to determine by WAXS analysis (WAXS: Wide Angle X-ray Scattering) that these nanocrystals are ordered and that the first Au–Au distance is *ca.* 3.25 Å. This result rules out the presence of metal–metal bonds (Au–Au distance in bulk gold: 2.88427 Å) but is in agreement with the presence of aurophilic contacts such as the ones recently found in the crystal structure of AuCl(piperidine) (Au···Au: 3.301(5) Å).[25]

In the solid state, complexes **2**–**4** are stable under argon but, when slightly heated or left in air, their decomposition into metallic gold is visible through the colour change of the materials from white to purple and eventually to gold. The reaction can be monitored by infrared spectroscopy. For example, in the case of **2**, a change in the N–H stretching bands, from sharp peaks at 3251 and 3211 cm^{-1} to a broad signal in the same region, indicates the decoordination of the amine ligand. The powder XRD spectra (XRD: X-ray Diffraction) of complex **2** illustrates this transformation: at room temperature several features are visible which were not attributed but, when heated at 70 °C, new peaks are visible which correspond to metallic

† Electronic supplementary information (ESI) available: experimental details and full characterization of complexes **2**–**4**, powder XRD spectra of **2** and TEM micrographs of **2** and gold nanoparticles. See http://www.rsc.org/suppdata/cc/b0/b005327i/

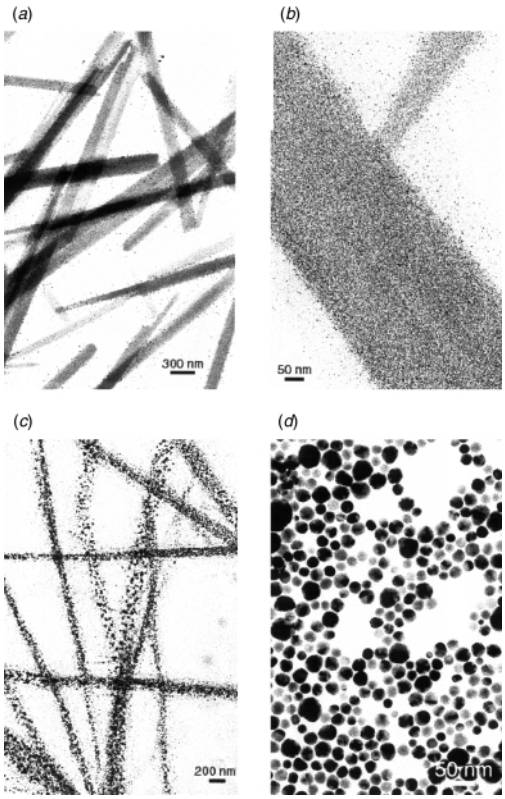

Fig. 1 TEM micrographs of $AuCl(NH_2C_8H_{17})$ (**2**) after deposition using a microinjector for ordering (*a*, *b*) and decomposition in the solid state into gold nanoparticles (*c*, *d*).

gold. At 80 °C, the transformation is complete and sharp peaks corresponding to well-crystallised fcc gold are observed (see Fig. S2, ESI).†

At the mesoscopic level, the nanoparticles of these complexes display a supramolecular organization into a fibrous material as shown in Figs. S1(*a*), 1(*a*) and 1(*b*).† These fibers are composed of interconnected self-assembled cylinders which organize spontaneously at the surface of the microscopy grid and are presumably present in solution. This probably accounts for the unexpected low solubility of these materials. Attempts at orienting the fibers were made by depositing a drop of a solution of **2** onto a microscopy grid using a microinjector; it is visible on Figs. 1(*a*), 1(*b*) that fibers can adopt privileged directions but further developments are necessary in order to achieve regular arrays.† In agreement with the XRD experiments, the transformation of the gold(I) complexes into gold nanoparticles can also be observed on a microscopy grid prepared by deposition and evaporation of a droplet of a solution (suspension) of **2**–**4** in THF. When a grid supporting complex **2** is left in air for a few days, the initial complex nanocrystals transform into regular gold nanocrystals within the frame of the supramolecular arrangements described here-above (see Figs. 1(*c*), 1(*d*)). The size distribution of the nanoparticles is at the end of the growth process relatively broad and centred at 23 nm [±6 nm; Fig. 1(*d*)]. This order of magnitude of size is frequently obtained for gold nanoparticles and suggests a poor, if any, control of the particle growth by the amine ligands. This is not unexpected since the poor stabilization of the soft gold centres by the hard amine ligands has already been discussed in the literature.

The decomposition of **2** can also be carried out in a THF solution under 3 bars H_2 at room temperature, in the presence or not of an excess of amine. After 15 hours, the resulting purple solution does not contain any precursor any more but well-crystallised gold nanoparticles of *ca.* 10 nm (±3 nm) which self-assemble on the microscopy grid used for TEM characterizations as shown in Fig. S3.† After several days, no gold is present in solution any more and a gold mirror is observed on the walls of the Fisher-Porter bottle.

In conclusion, we have described a new method for the preparation of gold nanoparticles using a gold(I) amine precursor. If this method does not appear to allow a good control of the particles size, it leads surprisingly to a good control of the size dispersity and, which is unexpected and more important, it allows a self-organization of the particles. There is presently a growing need for the controlled deposition of nanoparticles on physical or microelectronic devices. Several routes are possible and employed: sputtering, OMCVD, sol–gel, deposition of organized solutions of nanoparticles, … The growth of nanoparticles, in the solid state, as monolayers within the frame of a supramolecular arrangement is an alternative process of interest, for example for gold deposition onto microstructures. These studies are presently in progress.

We thank the CNRS, EC through the TMR network ‘CLUPOS’ for support of this research and TEMSCAN service of the ‘Université Paul Sabatier’ for electron microscopy facilities.

Notes and references

1 P. C. Ohara, J. R. Heath and W. M. Gelbart, *Angew. Chem., Int. Ed. Engl.*, 1997, **36**, 1078.
2 M. P. Pileni, *New J. Chem.*, 1998, **22**, 693.
3 G. Schmid, M. Bäumle and N. Beyer, *Angew. Chem., Int. Ed.*, 2000, **39**, 181.
4 T. Oku and K. Suganuma, *Chem. Commun.*, 1999, 2355.
5 M. Faraday, *Philos. Trans. R. Soc. London*, 1857, **147**, 145.
6 K. Honda, N. Yamada, M. Sano and S. Yoshimura, *J. Mater. Res.*, 1999, **14**, 968.
7 S. Rubin, G. Bar, T. N. Taylor, R. W. Cutts and T. A. Zawodzinski Jr., *J. Vac. Sci. Technol. A*, 1996, **14**, 1870.
8 Y. Zhou, C. Y. Wang, Y. R. Zhu and Z. Y. Chen, *Chem. Mater.*, 1999, **11**, 2310.
9 M. Y. Han, C. H. Quek, W. Huang, C. H. Chew and L. M. Gan, *Chem. Mater.*, 1999, **11**, 1144.
10 A. Mayer and M. Antonietti, *Colloid Polym. Sci.*, 1998, **276**, 769.
11 M. Brust, M. Walker, D. Bethell, D. J. Schiffrin and R. Whyman, *J. Chem. Soc., Chem. Commun.*, 1994, 801.
12 C. K. Yee, R. Jordan, A. Ulman, H. White, A. King, M. Rafailovich and J. Sokolov, *Langmuir*, 1999, **15**, 3486.
13 J. Turkevich, P. C. Stevenson and J. Hillier, *Discuss. Faraday Soc.*, 1951, **11**, 55.
14 (*a*) G. Schmid, R. Pfeil, R. Boese, F. Bandermann, S. Meyer, G. H. M. Calis and J. W. A. Van der Velden, *Chem. Ber.*, 1981, **114**, 3634; (*b*) G. Schmid, *Chem. Rev.*, 1992, **92**, 1709.
15 F. Tian and K. J. Klabunde, *New J. Chem.*, 1998, **22**, 1275.
16 (*a*) M. Brust, J. Fink, D. Bethell, D. J. Schiffrin and C. Kiely, *J. Chem. Soc., Chem. Commun.*, 1995, 1655; (*b*) M. Brust, D. Bethell, D. J. Schiffrin and C. J. Kiely, *Adv. Mater.*, 1995, **7**, 795.
17 (*a*) M. J. Hostetler and R. W. Murray, *Curr. Opin. Colloid Interface Sci.*, 1997, **2**, 42; (*b*) M. J. Hostetler, C. J. Zhong, B. K. H. Yen, J. Andereeg, S. M. Gross, N. D. Evans, M. Porter and R. W. Murray, *J. Am. Chem. Soc.*, 1998, **120**, 9396.
18 J. Fink, C. J. Kiely, D. Bethell and D. J. Schiffrin, *Chem. Mater.*, 1998, **10**, 922.
19 X. M. Lin, C. M. Sorensen and K. J. Klabunde, *Chem. Mater.*, 1999, **11**, 198.
20 C. J. Zhong, W. X. Zhang, F. L. Leibowitz and H. H. Eichelberger, *Chem. Commun.*, 1999, 1211.
21 C. Pan, K. Philippot, C. Amiens, B. Chaudret, F. Dassenoy, M.-J. Casanove, P. Lecante and A. Mosset, *J. Phys. Chem. B*, 1999, **103**, 10 098.
22 M. Verelst, T. Ould Ely, C. Amiens, E. Snoeck, P. Lecante, A. Mosset, M. Respaud, J. M. Broto and B. Chaudret, *Chem. Mater.*, 1999, **11**, 2702.
23 O. Vidoni, K. Philippot, C. Amiens, B. Chaudret, O. Balmes, J.-O. Malm, J.-O. Bovin, F. Senocq and M.-J. Casanove, *Angew. Chem., Int. Ed.*, 1999, **38**, 3736.
24 D. de Caro, V. Agelou, A. Duteil, B. Chaudret, R. Mazel, C. Roucau and J. S. Bradley, *New. J. Chem.*, 1995, **19**, 1265.
25 B. Ahrens, P. G. Jones and A. K. Fischer, *Eur. J. Inorg. Chem.*, 1999, 1103.
26 R. Uson, A. Laguna and M. Laguna, *Inorg. Synthesis*, 1989, **26**, 85.
27 S. Biz and M. L. Occelli, *Catal. Rev.-Sci. Eng.*, 1998, **40**, 329 and references cited therein.

An intramolecular π–π interaction has no effect on the lifetime of an aryl radical cation

Xiaoming Liu,[ab] Li Mei Lindy Chia,[c] Colin A. Kilner,[a] Lesley J. Yellowlees,[b] Mark Thornton-Pett,[a] Swiatoslaw Trofimenko[d] and Malcolm A. Halcrow*[a]

[a] *School of Chemistry, University of Leeds, Woodhouse Lane, Leeds, UK LS2 9JT. E-mail: M.A.Halcrow@chem.leeds.ac.uk*
[b] *Department of Chemistry, The University of Edinburgh, West Mains Road, Edinburgh, UK EH9 3JJ*
[c] *Department of Chemistry, University of Cambridge, Lensfield Road, Cambridge, UK CB2 1EW*
[d] *Department of Chemistry and Biochemistry, University of Delaware, Newark, DE 19716-2522, USA*

Received (in Cambridge, UK) 25th July 2000, Accepted 23rd August 2000
First published as an Advance Article on the web

The lifetimes of electrochemically generated $[Cu(L^{1\cdot+})(Tp^{Ph})]^{2+}$ and $[Cu(L^{1\cdot+})(Tp^{Cy})]^{2+}$ are identical to within experimental error.

We have recently reported that the complexes $[Cu(L^1)(Tp^R)]BF_4$ (L^1 = 1-{pyrid-2-yl}-3-{2′,5′-dimethoxyphenyl}pyrazole; $[Tp^R]^-$ = tris-[3-arylpyrazolyl]borate: **1**·BF_4–**3**·BF_4, Scheme 1) exhibit an unusual, fully reversible L^1-based 1-electron oxidation by cyclic voltammetry in CH_2Cl_2/0.5 M $NBu^n_4PF_6$ at 298 K.[1] This led us to suggest that an intramolecular π–π stacking interaction observed in **1**·BF_4–**3**·BF_4 might be kinetically stabilising the $[L^{1\cdot}]^+$-containing oxidation products. This would not be without precedent, in that others have detected unusual reversible voltammetric oxidations of intramolecularly π–π-stacked monocyclic aryl moieties in sesterbenzobicyclo[2.2.2]octane[2] and *ortho*-cyclophane[3] derivatives. In addition, a related $n \rightarrow \pi^*$ charge-transfer interaction leads to a 1000-fold increase in the lifetime of sulfanyl radical cations in aromatic, compound to chlorinated, solvents.[4] If true, such a result would be of relevance to the properties of proteins such as galactose oxidase (GOase), which contains a tyrosyl radical that is involved in a π–π interaction with a tryptophan indole ring.[5] This π–π interaction is vital to the function of the enzyme,[6] although its detailed role in catalysis is unknown. We now report the synthesis of a complex closely related to **1**·BF_4–**3**·BF_4 but lacking the π–π interaction, which has allowed us to quantify the effects of π–π stacking on the properties of $[L^{1\cdot}]^+$. We also describe the spectroelectrochemical characterisation of the aryl radical complex products $\mathbf{1}^{2+}$ and $\mathbf{2}^{2+}$.

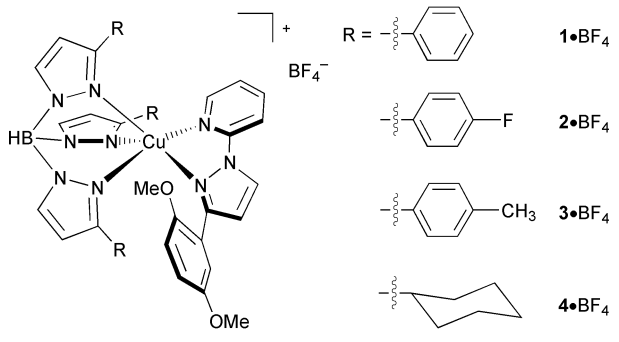

Scheme 1

Treatment of hydrated $Cu(BF_4)_2$ with one molar equivalent of L^1 and $K[Tp^{Cy}]$[7] in CH_2Cl_2 affords, following concentration and layering with hexanes, a dark green compound analysing as $[Cu(L^1)(Tp^{Cy})]BF_4$ (**4**·BF_4) in 55% yield.† This complex exhibits a d–d absorption in CH_2Cl_2 at $\nu_{max} = 15.6 \times 10^3$ cm^{-1} (ε_{max} = 104 M^{-1} cm^{-1}), which bears a low-energy shoulder. X-band EPR spectroscopy of **4**·BF_4 in 10:1 CH_2Cl_2:toluene shows $\langle g \rangle$ = 2.13, $\langle A\{^{63,65}Cu\} \rangle$ = 65 G, $\langle A\{^{14}N\} \rangle$ = 14 G at 298 K and $g_\parallel$ = 2.25, $g_\perp$ = 2.04, $A_\parallel\{^{63,65}Cu\}$ = 167 G at 77 K. The close correspondence of these parameters to those shown by **1**·BF_4–**3**·BF_4, which exhibit square pyramidal geometries in the solid state and in solution,[1] strongly suggests that the molecular structure of **4**·BF_4 is essentially identical to those of our earlier compounds. A single crystal X-ray analysis‡ confirmed the proposed molecular connectivity (Fig. 1). Apart from the short apical distance Cu(1)–N(2) (Fig. 1), which we have found to be a very plastic parameter in square-pyramidal Cu(II)/trispyrazolylborate complexes,[8] the co-ordination geometry at Cu differs insignificantly from that of **1**·BF_4.[1]

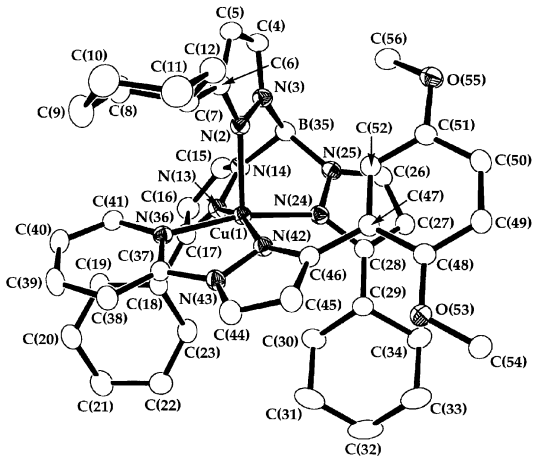

Fig. 1 View of the complex cation in the crystal of **4**·BF_4·$2CHCl_3$ with 35% probability ellipsoids, showing the atom numbering scheme employed. For clarity, all H atoms have been omitted. Selected distances (Å) and angles (°): Cu(1)–N(2) 2.153(2), Cu(1)–N(13) 2.024(2), Cu(1)–N(24) 1.984(2), Cu(1)–N(36) 2.029(2), Cu(1)–N(42) 2.0596(19), N(2)–Cu(1)–N(13) 92.41(8), N(2)–Cu(1)–N(24) 93.80(8), N(2)–Cu(1)–N(36) 98.86(8), N(2)–Cu(1)–N(42) 102.66(8), N(13)–Cu(1)–N(24) 85.70(8), N(13)–Cu(1)–N(36) 94.34(8), N(13)–Cu(1)–N(42) 164.25(8), N(24)–Cu(1)–N(36) 167.32(8), N(24)–Cu(1)–N(42) 97.69(8), N(36)–Cu(1)–N(42) 78.99(8).

The cyclic voltammogram of **4**·BF_4 in CH_2Cl_2/0.5 M $NBu^n_4BF_4$ at 298 K exhibits all the processes shown by **1**·BF_4–**3**·BF_4 in this solvent.[1] Hence, a chemically reversible L^1-based 1-electron oxidation is obseved at $E_{\frac{1}{2}}$ = +1.06 V *vs.* ferrocene/ferrocenium (ΔE_p = 96 mV),§ which is 60–90 mV more positive than the values we have recorded for **1**·BF_4–**3**·BF_4. In order to quantify any kinetic stabilisation of $\mathbf{1}^{2+}$–$\mathbf{3}^{2+}$ afforded by intramolecular π–π stacking, we have measured the half-lives of $\mathbf{1}^{2+}$, $\mathbf{2}^{2+}$ and $\mathbf{4}^{2+}$ at 298 K in the electrochemical cell using convolution methods.[9] The values obtained are almost identical within experimental error: $\mathbf{1}^{2+}$, $t_{\frac{1}{2}}$ = 1.7(2) s; $\mathbf{2}^{2+}$, $t_{\frac{1}{2}}$ = 1.39(17) s; and $\mathbf{4}^{2+}$, $t_{\frac{1}{2}}$ = 0.98(11) s. Although it is unclear whether the assumption of first-order decomposition kinetics employed by the convolution procedure is valid in our system, it is clear that

DOI: 10.1039/b006005o

the kinetic stabilities of $\mathbf{1}^{2+}$, $\mathbf{2}^{2+}$ and $\mathbf{4}^{2+}$ are essentially identical.

Attempts to electrogenerate bulk samples of $\mathbf{1}^{2+}$ and $\mathbf{2}^{2+}$ for EPR measurements were unsuccessful, resulting in appreciable decomposition of the sample over the timescale of the experiment. *In situ* spectroelectrochemical characterisation of the oxidised species $\mathbf{1}^{2+}$ and $\mathbf{2}^{2+}$ was therefore undertaken. Electrooxidation of $\mathbf{1}\cdot BF_4$ in CH_2Cl_2/0.5 M $NBu^n_4BF_4$ at 243 K at a potential corresponding to the $\mathbf{1}^{+}/\mathbf{1}^{2+}$ couple using an optically transparent electrode proceeds isosbestically and results in substantial changes in the UV, vis and NIR regions of the spectrum (Fig. 2). The oxidised solution for $\mathbf{1}^{2+}$ shows ν_{max} = 12.4 (ε_{max} = 1000), 19 (sh), 22.2 (3 400), 26 (sh) and 32.5 $\times$ 10^3 cm^{-1} (15 500 M^{-1} cm^{-1}) at 243 K (Fig. 2). The absorption spectrum of $\mathbf{2}^{2+}$ generated under identical conditions is barely distinguishable from those of $\mathbf{1}^{2+}$. Re-reduction of both samples at 0 V also proceeds isosbestically and quantitatively regenerates $\mathbf{1}^{+}$ or $\mathbf{2}^{+}$, demonstrating the chemical reversibility of this process under these conditions.

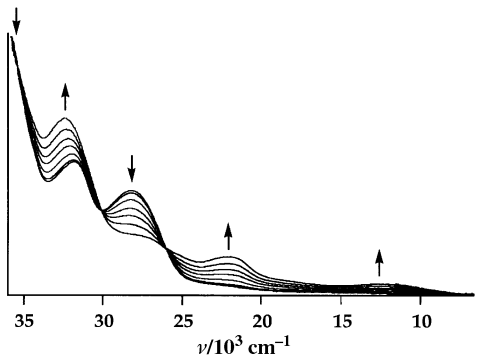

Fig. 2 Oxidation of $\mathbf{1}^{+}$ to $\mathbf{1}^{2+}$ by controlled potential electrolysis in CH_2Cl_2/0.5 M $NBu^n_4PF_6$ at 243 K.

The $[C_6H_4(OMe)_2$-1,4·$]^+$ radical cation exhibits ν_{max} = 21.7 (ε_{max} = 9 540 M^{-1} cm^{-1}), 23.3 (9 040) and 33.3 $\times$ 10^3 cm^{-1} (13 000) in aqueous solution,[10] but is optically transparent in the range 11–21 $\times$ 10^3 cm^{-1}.[11] The 22.2, 26 and 32.5 $\times$ 10^3 cm^{-1} bands from $\mathbf{1}^{2+}$ and $\mathbf{2}^{2+}$ quite closely match those shown by $[C_6H_4(OMe)_2$-1,4·$]^+$; we therefore assign these bands to local excitation transitions within the $[L^{1\cdot}]^+$ moiety. The 12.4 $\times$ 10^3 cm^{-1} absorption can be attributed to a $[Tp^{Ph}]\rightarrow[L^{1\cdot}]^+$ LLCT transition. By comparison, the $[(C_6H_6)(C_{10}H_8)]^{\cdot+}$ complex exhibits a gas-phase intra-dimer CT band at 10.9 $\times$ 10^3 cm^{-1},[12] while $[(C_6H_6)(C_7H_8)]^{\cdot+}$ exhibits three such bands, at 8.5, 10.8 and 14.9 $\times$ 10^3 cm^{-1}.[13] The observation of such a transition for $\mathbf{1}^{2+}$ and $\mathbf{2}^{2+}$ is clear evidence that the intramolecular π–π-stacking interaction in these complexes is retained following oxidation. The assignment of the shoulder near 19 $\times$ 10^3 cm^{-1} is uncertain; we tentatively suggest that this may correspond to a second LLCT transition, or to a $Cu\rightarrow[L^{1\cdot}]^+$ MLCT band.

To conclude, we have demonstrated that the intramolecular π–π interaction exhibited by $\mathbf{1}^{+}$ and $\mathbf{2}^{+}$ is retained following their 1-electron oxidation, but that this interaction has no measurable effect on the kinetic stability of the resultant aryl radical. The unusual longevity of the dimethoxyphenyl radical cation species $\mathbf{1}^{+}$ and $\mathbf{2}^{+}$, and those formed from sesterbenzobicyclo[2.2.2]octane[2] and *ortho*-cyclophane[3] derivatives, presumably originates rather in steric protection of the radical center afforded by the overlying aryl ring. These results demonstrate that the tyrosyl/tryptophan π–π interaction in GOase probably has little or no effect on the chemical reactivity of the tyrosyl radical in this enzyme, except to shield it from external solvent. We are continuing to investigate the effects of π–π stacking on the spectroscopic and luminescent properties of aryl radicals and their complexes, and will report these results in due course.

The authors would like to thank Sanja Radojevic and Professor Mary McPartlin (University of North London) for a preliminary X-ray study of $\mathbf{4}\cdot BF_4$. Funding by The Royal Society (M. A. H.), the government of Singapore (L. M. L. C.), the Committee of Vice-Chancellors and Principles and EPSRC (X. L.) is gratefully acknowledged.

Notes and references

† *Analytical data* for $\mathbf{4}\cdot BF_4$: Found: C 58.1, H 6.2, N 13.8%: calcd. for $C_{43}H_{55}B_2CuF_4N_9O_2$: C 58.0, H 6.2, N 14.1%.

‡ *Crystal data* for $\mathbf{4}\cdot BF_4\cdot 2CHCl_3$: $C_{45}H_{57}B_2Cl_6CuF_4N_9O_2$, M_r = 1129.86, monoclinic, $P2_1/n$, green prism, 0.56 $\times$ 0.49 $\times$ 0.30 mm, a = 11.8709(2), b = 20.8196(3), c = 21.6065(4) Å, β = 98.7150(11)°, U = 5278.34(15) Å^3, Z = 4, T = 150(2) K, μ(Mo-Kα) = 0.778 mm^{-1}; Enraf-Nonius KappaCCD diffractometer, 34102 measured reflections, 11965 independent, R_{int} = 0.058; $R(F)$ = 0.053, w$R(F^2)$ = 0.151, S = 1.019. Both solvent molecules were disordered, one over two equally occupied orientations and one over three orientations with occupancies of 0.5, 0.25 and 0.25. All C–Cl bonds were restrained to 1.75(2) Å, and Cl···Cl distances to 2.86(2) Å. All non-H atoms with occupancy ≥0.5 were refined anisotropically. CCDC 182/1760. See http://www.rsc.org/suppdata/cc/b0/b006005o/ for crystallographic files in .cif format.

§ In addition to these oxidative voltammetric processes, $\mathbf{4}\cdot BF_4$ exhibits an irreversible Cu(II/I) reduction at E_{pc} = −0.58 V, with an associated daughter wave at E_{pa} = +0.25 V. A weak daughter wave at E_{pa} = +0.03 V becomes apparent following multiple scanning of the $\mathbf{4}^{+}/\mathbf{4}^{2+}$ oxidation.

1 M. A. Halcrow, E. J. L. McInnes, F. E. Mabbs, I. J. Scowen, M. McPartlin, H. R. Powell and J. E. Davies, *J. Chem. Soc., Dalton Trans.*, 1997, 4025.
2 W. Grimme, H. T. Kämmerling, J. Lex, R. Gleiter, J. Heinze and M. Dietrich, *Angew. Chem., Int. Ed. Engl.*, 1991, **30**, 205.
3 S. Mataka, K. Shigaki, T. Sawada, Y. Mitoma, M. Taginuchi, T. Thiemann, K. Ohga and N. Egashira, *Angew. Chem., Int. Ed. Engl.*, 1998, **37**, 2532.
4 D. Werst, *J. Phys. Chem.*, 1992, **96**, 3640.
5 J. P. Klinman, *Chem. Rev.*, 1996, **96**, 2541.
6 A. J. Baron, C. Stevens, C. Wilmot, K. D. Seneviratne, V. Blakeley, D. M. Dooley, S. E. V. Phillips, P. F. Knowles and M. J. McPherson, *J. Biol. Chem.*, 1994, **269**, 25 095.
7 A. L. Rheingold, B. S. Haggerty and S. Trofimenko, *Angew. Chem., Int. Ed. Engl.*, 1994, **33**, 1983.
8 M. A. Halcrow, L. M. L. Chia, X. Liu, E. J. L. McInnes, L. J. Yellowlees, F. E. Mabbs, I. J. Scowen, M. McPartlin and J. E. Davies, *J. Chem. Soc., Dalton Trans.*, 1999, 1753; L. M. L. Chia, S. Radojevic, I. J. Scowen, M. McPartlin and M. A. Halcrow, *J. Chem. Soc., Dalton Trans.*, 2000, 133.
9 F. E. Woodward, R. D. Goodin and P. J. Kinlen, *Anal. Chem.*, 1984, **56**, 1920.
10 P. O'Neill, S. Steenken and D. Schulte-Frohlinde, *J. Phys. Chem.*, 1975, **79**, 2773.
11 C. T. Johnston, T. Tipton, D. A. Stone, C. Erickson and S. L. Trabue, *Langmuir*, 1991, **7**, 289.
12 M. Matsumoto, Y. Inokuchi, K. Ohashi and N. Nishi, *J. Phys. Chem. A*, 1997, **101**, 4574.
13 K. Ohashi, Y. Nakane, Y. Inokuchi, Y. Nakai and N. Nishi, *Chem. Phys.*, 1998, **239**, 429.

Synthesis of ene-1,1-diamines and pyrrolo[1,2-*a*]imidazolediones by 4,5-dihydroimidazole *N*-oxide cycloaddition and isoxazoline ring opening

Raymond C. F. Jones,*[a] Jason N. Martin,[b] Paul Smith,[c] Tomas Gelbrich,[d] Mark E. Light[d] and Michael B. Hursthouse[d]

[a] *Department of Chemistry, Loughborough University, Leics., UK LE11 3TU*
[b] *Department of Chemistry, The Open University, Walton Hall, Milton Keynes, UK MK7 6AA*
[c] *SmithKline Beecham Pharmaceuticals, New Frontiers Science Park North, Harlow, Essex, UK CM19 5AW*
[d] *EPSRC National Crystallography Service, Department of Chemistry, University of Southampton, Highfield, Southampton, UK SO17 1BJ*

Received (in Cambridge, UK) 10th July 2000, Accepted 18th August 2000
First published as an Advance Article on the web

Dihydroimidazole *N*-oxides 1 undergo 1,3-dipolar cycloaddition with alkyne dipolarophiles and the cycloadducts suffer isoxazoline N–O bond cleavage to afford ene-1,1-diamines, with subsequent cyclisation to pyrrolo[1,2-*a*]imidazole-5,6-diones if possible.

We have recently described the synthesis of 4,5-dihydroimidazolium 3-oxide **1**, and its diastereoselective 1,3-dipolar cycloaddition reactions with alkenes to produce the rarely reported imidazo[1,2-*b*]isoxazoles (Scheme 1).[1] These latter, on N–O reduction and recyclisation, are potential sources for chiral pyrroloimidazoles and thence for pyrrolidines. Whilst exploring the reactions of this dipole with alkynes we isolated unexpected ene-1,1-diamine products which correspond to a C–C bond formation at C-2 of the dihydroimidazole ring with transfer of the nitrone oxygen atom to the new side-chain. Where possible, a second cyclisation to give pyrroloimidazole-5,6-diones is observed. We report these results herein and account for them in terms of the predicted 1,3-dipolar cycloadditions followed by isoxazoline ring opening. Ene-1,1-diamines are useful reagents in heterocyclic synthesis and in some cases possess biological activities.[2] Our results represent a new approach to such systems, that is very different from 'traditional' enediamine synthesis, *e.g.* from diamines with ketene acetals, or cyclic ureas with active methylene compounds,[2] or from acylation of 2-methyl cyclic amidines.[3] Biological activity has also been recorded for some pyrrolo[1,2-*a*]imidazoles.[4]

The nitrone **1** as its hydrochloride salt was prepared *in situ* from the aminohydroxylamine **2** dihydrochloride as previously described,[1] by treatment with triethyl orthoformate (toluene, 60 °C), and used directly. Reaction of the nitrone hydrochloride solution with methyl propynoate (1.25 eq., Et_3N, 2.1 eq., 60 °C, 18 h) led to isolation of the formyl alkoxycarbonyl enediamine **3a** (Scheme 2, Table 1). Similar reactions were observed with ethyl, 2-propyl and *tert*-butyl propynoates to afford further enediamines **3b**–**d** (Scheme 2, Table 1). With other 2-alkynoates (namely ethyl but-2-ynoate, methyl oct-2-ynoate, methyl and ethyl non-2-ynoate, and ethyl 3-phenylpropynoate) as reaction partner for the nitrone **1**, the corresponding alkanoyl alkoxycarbonyl enediamines **3e**–**i** were observed as the products.[5,6]

The products **3** are represented as the enaminoketone tautomer A (Fig. 1), although they may in principle also exist as the imino–enol tautomer B. Solution spectroscopy suggests the enaminoketone representation. All of **3a**–**i** display a peak in the

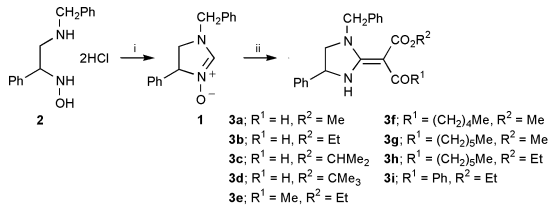

Scheme 2 *Reagents*: i, $(EtO)_3CH$, toluene, 60 °C; $R^1C{\equiv}CCO_2R^2$, Et_3N, 60 °C.

Table 1 1,1-Enendiamines **3** from reaction of imidazoline 1-oxide **1** and 2-alkynoates (Scheme 2)

R^1	R^2	1,1-Enendiamines **3** (yield %)
H	Me	**3a** (37)
H	Et	**3b** (18)
H	$CHMe_2$	**3c** (55)
H	CMe_3	**3d** (45)
Me	Et	**3e** (58)
$(CH_2)_4Me$	Me	**3f** (80)
$(CH_2)_5Me$	Me	**3g** (56)
$(CH_2)_5Me$	Et	**3h** (48)
Ph	Et	**3i** (51)

^{13}C NMR spectrum for a conjugated aldehyde (δ 186–187 for **3a**–**d**) or ketone (δ 193–197 for **3e**–**i**), respectively. The resonances for the enamine double bond are observed in the ranges δ 85–90 (NC=*C*CO) and δ 165–170 (N*C*=CCO). In the ^1H NMR spectra of **3a**–**d**, the signal observed at δ 9.7–9.75 (1H, s) is consistent with the aldehydic proton, whilst a broad singlet, δ 9.5–10.4 represents the NH. The geometry of the enediamine is shown with the formyl/alkanoyl substituent *syn* (and potentially hydrogen-bonding) to the NH of the heterocyclic ring (N-3), as supported by the ^{13}C NMR chemical shifts of the C=O carbons, see above, and our experience with related structures.[7]

We have further probed the questions of tautomerism and geometry in the solid state by X-ray crystal structure analysis of enediamines **3f** and **3g**. We have previously shown that related enediamine **4** exists in the solid state as the *syn*-enaminoketone form.[7] In the current work, it was found that compound **3f** displays an NH proton and a dihedral angle N-1/C-2/C(α)/

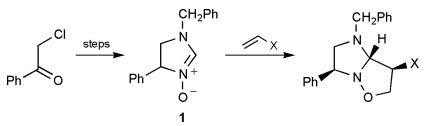

Scheme 1

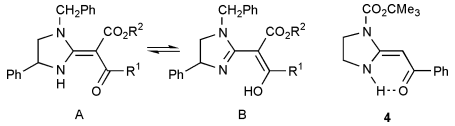

Fig. 1 Tautomerism of enediamines **3**.

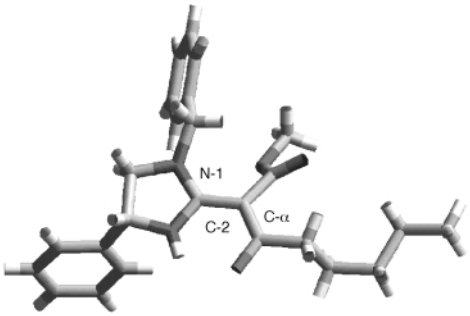

Fig. 2 X-Ray crystal structure of enediamine **3f**.

CO_2Me of 21° (Fig. 2).† This near-planarity suggests that hydrogen bonding is operating from N-3(H) to the keto-carbonyl group, consistent with the enaminoketone tautomer in the solid state. On the other hand, compound **3g** reveals two independent molecules in the unit cell, dihedral angles N-1/C-2/C(α)/CO_2Me of 100° (Fig. 3) and 113°, with some alkyl chain conformational differences.† These large deviations from planarity, precluding a C-2,C(α) double bond, and the location of a proton on oxygen rather than N-3 (Fig. 3), imply that the hydrogen bonding is absent and that the imino–enol tautomer B is present in this instance.

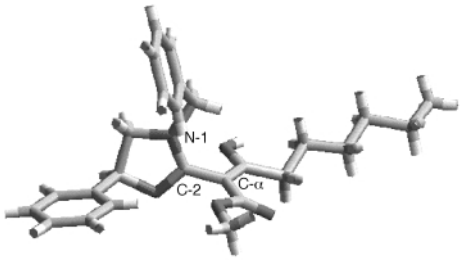

Fig. 3 X-Ray crystal structure of enediamine **3g**; two independent molecules per unit cell.

The formation of the enediamine **3** can be best rationalised through N–O cleavage of the expected imidazoisoxazole products **5** of an initial 1,3-dipolar cycloaddition of nitrone **1** (Scheme 3). Two possibilities can then be envisaged, pathways A and B of Scheme 3. Pathway A postulates a sigmatropic 1,5-H shift of the bridgehead hydrogen atom and bond reorganisation that would not be possible for the cycloadducts of alkene dipolarophiles (Scheme 1). Alternatively, pathway B suggests loss of the bridgehead proton and N–O bond cleavage, followed by reprotonation.[5] This elimination has a triply stabilised enolate as a leaving group, which would not be the case in the cycloadducts formed from alkenes.

A further unexpected reaction was observed when alkyne-1,2-dicarboxylates were reacted with nitrone **1**. Using dimethyl

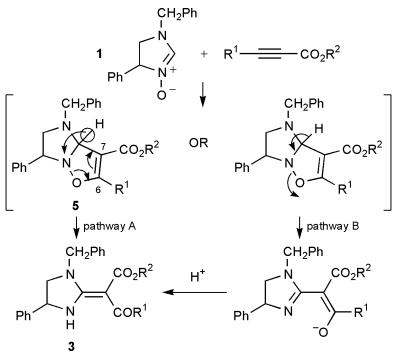

Scheme 3

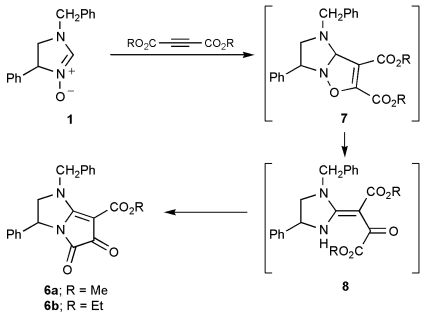

Scheme 4

or diethyl butyn-1,4-dioates, the 2,3,5,6-tetrahydro-1*H*-pyrrolo[1,2-*a*]imidazole-5,6-diones **6a** and **6b**, respectively, were isolated (58 and 20%), Scheme 4. Again, formation of these bicyclic products can be rationalised by initial dipolar cycloaddition to afford imidazoisoxazoles **7**. N–O cleavage *via* either of the pathways proposed in Scheme 3 would lead to an enediamine intermediate that now carries an electrophilic ester group suitably disposed to permit the secondary recyclisation.[8]

We have thus shown that dihydroimidazolium nitrones **1** undergo 1,3-dipolar cycloaddition with alkyne dipolarophiles, and that the cycloadducts suffer N–O bond cleavage to afford enediamines, and subsequent cyclisation where possible.

We thank EPSRC & SB Pharmaceuticals for a CASE studentship and the Open University for financial support (J. N. M.), Dr J. N. Iley for useful discussion, the EPSRC for its support of the National X-Ray Crystallography Service Centre, and the EPSRC National Mass Spectrometry Service Centre (Swansea) for some MS data.

Notes and references

† *Crystal data for* **3f**: $C_{25}H_{30}N_2O_3$, M = 406.51, monoclinic, a = 26.9087(10), b = 6.8778(4), c = 24.9780(10) Å, α = 90, β = 106.211(3), γ = 90°, U = 4438.9(4) Å^3, T = 150(2) K, space group $C2/c$, monochromated Mo-Kα radiation, λ = 0.71073 Å, Z = 8, D_c = 1.217 Mg m^{-3}, $F(000)$ = 1744, colourless needles, dimensions 0.12 × 0.02 × 0.02 mm, μ(Mo-Kα) = 0.080 mm^{-1}, 3.06 < 2θ < 24.00°, 8729 reflections measured, 3468 unique reflections. The structure was solved by direct methods and refined by full-matrix least-squares on F^2. The final cycle (for 301 parameters) converged with wR_2 = 0.1059 (for all data) and R_1 = 0.0662 [$I > 2\sigma(I)$].

Crystal data for **3g**: $C_{26}H_{32}N_2O_3$, M = 420.54, triclinic, a = 9.4057(2), b = 11.341(2), c = 33.051(7) Å, α = 92.243(4), β = 99.513(4), γ = 103.536(4)°, U = 2360.5(3) Å^3, T = 150(2) K, space group $P\bar{1}$, monochromated Mo-Kα radiation, λ = 0.71073 Å, Z = 4, D_c = 1.181 Mg m^{-3}, $F(000)$ = 900, colourless plates, dimensions 0.10 × 0.10 × 0.05 mm, μ(Mo-Kα) = 0.077 mm^{-1}, 3.02 < 2θ < 21.97°, 12951 reflections measured, 5590 unique reflections. The structure was solved by direct methods and refined by full-matrix least-squares on F^2. The final cycle (for 564 parameters) converged with wR_2 = 0.1129 (for all data) and R_1 = 0.0621 [$I > 2\sigma(I)$]. CCDC 182/1759. See http://www.rsc.org/suppdata/cc/b0/b005530l/ for crystallographic files in .cif format.

1 R. C. F. Jones, J. N. Martin and P. Smith, *Synlett*, 2000, 967.
2 Z.-T. Huang and M.-X. Wang, in *The Chemistry of Enamines*, ed. Z. Rappoport, Wiley, New York, 1994, p. 1303.
3 See, for example: M. W. Anderson, M. J. Begley, R. C. F. Jones and J. Saunders, *J. Chem. Soc., Perkin Trans. 1*, 1984, 2599.
4 See, for example: T. F. Gallagher and J. L. Adams, *Tetrahedron Lett.*, 1989, **30**, 6599.
5 *Cf.* S. Takahashi and H. Kano, *Tetrahedron Lett.*, 1963, 1687; S. Takahashi and H. Kano, *Chem. Pharm. Bull. Jpn.*, 1964, 1290.
6 S. Takahashi and H. Kano, *J. Org. Chem.*, 1965, **30**, 1118.
7 R. C. F. Jones and P. Dimopoulos, *Tetrahedron*, 2000, **56**, 2061.
8 See: H. Seidl, R. Huisgen and R. Knorr, *Chem. Ber.*, 1969, **102**, 904, for a related observation with 3,4-dihydroisoquinoline *N*-oxide.

$LiSb_3O_8$: the first tetrarutile structure†

M. Elmina Lopes,[a] Caroline A. Kirk,[a] Susan M. Blake,[b] James Marr[b] and Anthony R. West[a]

[a] *University of Sheffield, Department of Engineering Materials, Mappin Street, Sheffield, UK S1 3JD. E-mail: a.r.west@sheffield.ac.uk*

[b] *University of Aberdeen, Department of Chemistry, Meston Walk, Aberdeen, UK AB24 3UE*

Received (in Cambridge, UK) 21st July 2000, Accepted 1st September 2000
First published as an Advance Article on the web

The new phase, $LiSb_3O_8$, synthesised by solid state reaction at 900 °C, has an ordered rutile structure with 1:3 cation order and monoclinic symmetry: a = 10.2578(9), b = 4.7063(3), c = 5.6017(5) Å, β = 96.467(7)°, space group $P2_1/a$.

The rutile structure is found in a variety of oxides (*e.g.* TiO_2, SnO_2) and halides (*e.g.* MgF_2). More complex, ordered rutile structures with 1:1 cation order occur in dirutiles (*e.g.* $CoReO_4$), although with different cation arrangements, and with 1:2 order in trirutiles (*e.g.* $ZnSb_2O_6$).[1] We present here, the first example of 1:3 cation order in the new phase $LiSb_3O_8$, the structure of which can therefore be described as a tetrarutile.

$LiSb_3O_8$ is a thermodynamically stable phase, synthesised by solid state reaction of Li_2CO_3 and Sb_2O_3 powder mixtures in Pt foil boats in air, initially at 700 °C for 2 h to expel CO_2 and finally at 900 °C for 2–3 days, with intermittent regrinding. The powder X-ray diffraction (XRD) pattern (Stoe Stadi diffractometer, Cu-Kα_1 radiation) was indexed by trial-and-error, using the TREOR program in the Stoe software package, on a monoclinic unit cell, a = 10.2578(9), b = 4.7063(3), c = 5.6017(5) Å, β = 96.467(7)°. The first 20 indexed lines are given in Table 1. A search through both the International Centre for Diffraction Data file and the Inorganic Crystal Structure Database did not reveal any similar powder pattern or unit cell and therefore, $LiSb_3O_8$ probably had a previously unreported structure type.

† Electronic supplementary information (ESI) available: Fig. 2: experimental, calculated and difference XRD profiles. Table 3: bond lengths and selected bond angles for $LiSb_3O_8$. Table 4: oxygen–oxygen distances in $LiSb_3O_8$. See http://www.rsc.org/suppdata/cc/b0/b005915n/

The structure was determined *ab initio* using the EXPO software package. First, the Sb positions were located by direct methods. Refinement of the partial structure (Sb only) was then carried out using the program GSAS followed by difference Fourier analysis to locate the oxygen atoms. At this stage, a drawing of the crystal structure was made which showed the existence of octahedral sites for Sb within an oxygen array that approximated to hexagonal close packed. Additional octahedrally coordinated sites, which corresponded to positions with some residual electron density in a difference map, were located and assigned to Li. The structure converged fully upon Rietveld refinement of the XRD data with the final coordinates given in Table 2. The refinement was entirely satisfactory apart from the U_{iso} value for Li, which refined to a slightly negative value and was therefore fixed at 0.025 in the final stages of refinement. This could indicate difficulties in the refinement of the light atom Li in the presence of Sb or a small amount of cross-substitution ($\leqslant$ 1%) between Li and Sb sites so as to increase the effective electron concentration on the Li sites. Neutron diffraction studies are planned to resolve this question.

Bond lengths and a selection of bond angles are given in Table 3 (ESI†); projections of the structure are given in Fig. 1 and a profile fit is shown in Fig. 2 (ESI†). The structure has a rutile-like subcell, with a supercell caused by 1:3 ordering of Li:Sb on octahedral sites in the columns of edge-sharing octahedra parallel to c in the rutile subcell; $V_{supercell} = 4V_{subcell}$; Z = 2; $a_{supercell}//[102]_{subcell}$; $c_{supercell}//[10\bar{1}]_{subcell}$. *ac* Projections of the subcell and supercell are shown in Fig. 1(a) as dotted and continuous lines, respectively. The columns of edge-sharing octahedra run vertically in the plane in Fig. 1(a) and therefore, run obliquely through the supercell. These columns are seen edge-on in Fig. 1(b), as a $[10\bar{1}]$ projection of the

Table 1 Indexed X-ray powder diffraction data for $LiSb_3O_8$

$2\theta_{obs}$/Å	h	k	l	$2\theta_{calc}$/Å	$\Delta(2\theta)$	d_{obs}/Å	d_{calc}/Å	I_{obs}	I_{calc}
15.892	0	0	1	15.910	−0.018	5.5722	5.5660	13	12
17.370	2	0	0	17.387	−0.017	5.1012	5.0963	15	14
20.759	1	1	0	20.772	−0.013	4.2754	4.2728	18	18
22.256	−2	0	1	22.267	−0.011	3.9911	3.9892	13	11
24.743	0	1	1	24.754	−0.011	3.5954	3.5938	4	1
24.941	2	0	1	24.963	−0.022	3.5672	3.5641	8	7
25.644	−1	1	1	25.657	−0.012	3.4710	3.4693	12	11
26.867	1	1	1	26.877	−0.010	3.3157	3.3145	100	100
29.320	−2	1	1	29.326	−0.006	3.0436	3.0431	2	< 1
31.454	2	1	1	31.461	−0.007	2.8419	2.8413	2	< 1
32.133	0	0	2	32.137	−0.004	2.7833	2.7830	4	3
32.473	3	1	0	32.476	−0.004	2.7550	2.7547	7	7
34.956	−2	0	2	34.922	0.034	2.5647	2.5672	50	17
	−3	1	1	34.971	−0.015		2.5637		35
35.186	4	0	0	35.192	−0.006	2.5485	2.5481	20	17
37.091	−4	0	1	37.082	0.009	2.4219	2.4225	2	1
37.698	−1	1	2	37.702	−0.004	2.3843	2.3840	9	6
	3	1	1	37.705	−0.007		2.3839		3
38.213	0	2	0	38.216	−0.003	2.3533	2.3531	9	9
38.521	2	0	2	38.534	−0.013	2.3352	2.3344	9	9
39.289	1	2	0	39.262	0.027	2.2913	2.2928	2	< 1
39.422	1	1	2	39.434	−0.013	2.2839	2.2832	2	1

DOI: 10.1039/b005915n

Table 2 Atomic positions and isotropic thermal parameters for $LiSb_3O_8$

Atom	Site	*x*	*y*	*z*	Site occupancy	U_{iso}
Sb(1)	4e	0.25108(7)	−0.47980(2)	0.2375(1)	1	1.33(2)
Sb(2)	2b	0.5	0	0.5	1	1.34(3)
O(1)	4e	0.3266(7)	−0.774(2)	0.477(2)	1	1.6(2)
O(2)	4e	0.4210(7)	−0.291(2)	0.276(2)	1	0.8(2)
O(3)	4e	0.8264(7)	0.192(2)	−0.013(2)	1	1.0(2)
O(4)	4e	0.5799(7)	0.174(1)	0.230(2)	1	1.3(2)
Li	2a	0	0	0	1	0.025[a]

[a] Not refined; default value used. $\chi^2 = 3.168$, $R_{wp} = 10.05\%$, $R_p = 7.76\%$.

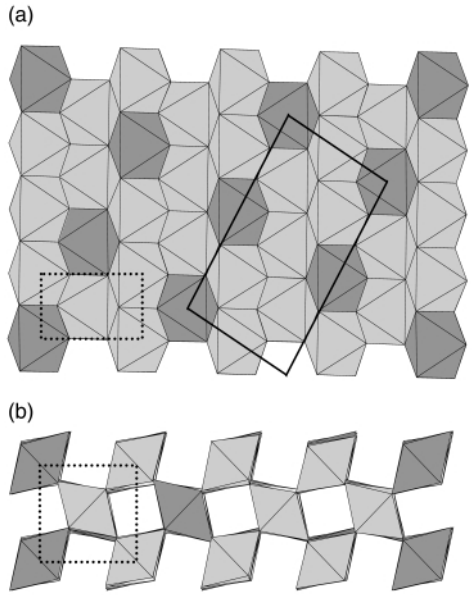

Fig. 1 Projections of the $LiSb_3O_8$ structure. Dark octahedra: LiO_6; light octahedra: SbO_6. (a) Projection in the *ac* plane showing subcell (dotted) and supercell (continuous); (b) projection down [10$\bar{1}$] showing columns of edge-sharing octahedra with corrugated *tp* oxide layers running horizontally and vertically.

supercell. As with rutile, edge-sharing of octahedra leads to structural distortion associated with cation repulsion effects and this reduces the O–Sb–O and O–Li–O angles facing the shared edges to *ca*. 80° (Table 3). Li–O and Sb–O distances are in the ranges 1.99–2.11 and 1.95–2.10 Å, respectively, giving very similar sized LiO_6 and SbO_6 octahedra.

The structure may be described in two rather different ways: either as filling of half the octahedral sites in a distorted hexagonal close packed (*hcp*) oxide array; or, as filling of all the (undistorted) octahedral sites in a tetragonal packed (*tp*) array.[2,3] The latter viewpoint is a more accurate description; although the structure does not possess fourfold symmetry (unlike the parent rutile structure), the corrugated *tp* layers are seen running horizontally and vertically in Fig. 1(b), together with the diamond-shaped (in projection) columns of edge-sharing octahedra and the square-shaped columns containing empty distorted tetrahedral and distorted octahedral interstitial sites. The *tp* nature of the oxide ion array is further demonstrated by consideration of the oxygen–oxygen closest distances. In *hcp*, 12 equidistant oxygens are expected; in *tp*, ideally there are 11 equidistant oxygens, plus 2 somewhat further away. The distribution of distances in $LiSb_3O_8$ clearly falls into the second category (Table 4, ESI†): for the four crystallographically distinct oxygens, there are 11 O–O distances in the range 2.60–3.13 Å and 2 O–O distances at 3.34–3.49 Å; the next shortest O–O distances are at 3.92 Å.

Antimonates are often isostructural with compositionally similar niobates and tantalates. The rutile-related structure of $LiSb_3O_8$ is, however, distinct from that of both $LiNb_3O_8$ and $LiTa_3O_8$. $LiNb_3O_8$ has a cation-ordered α-PbO_2 structure in which cations occupy half the octahedral sites in an *hcp* oxide array.[4,5] The distribution of occupied octahedral sites gives rise to zigzag chains of edge-sharing octahedra, rather than the linear chains in $LiSb_3O_8$ and other rutile derivatives; also the oxide array is *hcp* instead of *tp*. $LiTa_3O_8$ exists in three polymorphic forms. The L polymorph is isostructural with $LiNb_3O_8$.[5] The M polymorph also has an α-PbO_2 superstructure but with a different cation arrangement to that of the L polymorph[6,7] and is isostructural with the mineral wodginite. The structure of the H polymorph is quite different and contains a mixture of TaO_7 pentagonal bipyramids and TaO_6 octahedra.[8–12]

$LiSb_3O_8$ is the first rutile derivative structure with 1:3 cation order and may therefore be described as a tetrarutile. It is possible that other $M(I)M(V)_3O_8$ phases may have the same structure (although not with $LiNb_3O_8$ and $LiTa_3O_8$, apparently). It is also possible that other tetrarutile structures may form with different cation arrangements, in the same way that different dirutile cation arrangements exist.[1]

Notes and references

1 W. H. Baur, *Z. Kristallogr*, 1994, **209**, 143.
2 W. H. Baur, *Mater. Res. Bull.*, 1981, **16**, 339.
3 A. R. West and P. G. Bruce, *Acta Crystallogr., Sect. B*, 1982, **38**, 1891.
4 M. Lundberg, *Acta Chem. Scand.*, 1971, **25**, 3337.
5 B. M. Gatehouse and P. Leverett, *Cryst. Struct. Commun.*, 1972, **1**, 83.
6 B. M. Gatehouse, T. Negas and A. S. Roth, *J. Solid State Chem.*, 1976, **18**, 1.
7 A. Santoro, A. S. Roth and D. Minor, *Acta Crystallogr., Sect. B*, 1977, **33**, 3945.
8 A. G. Nord and J. O. Thomas, *Acta Chem. Scand. Ser. A*, 1978, **32**, 539.
9 P. E. Werner, B. O. Marinder and A. Magneli, *Mater. Res. Bull.*, 1978, **13**, 1371.
10 G. D. Fallon, B. M. Gatehouse, R. S. Roth and A. S. Roth, *J. Solid State Chem.*, 1979, **27**, 255.
11 M. Pouchard and J. P. Chaminade, *Compt. Rend. Acad. Seances – Ser. C*, 1972, **274**, 1739.
12 J. L. Houdeau, M. Marezio, A. Santoro and A. S. Roth, *J. Solid State Chem.*, 1984, **51**, 275.

A novel polymeric Ag^I complex consisting of two three-dimensional networks which are enantiometric and interpenetrating†

Xian-He Bu,*[ab] Kumar Biradha,[cd] Tadashi Yamaguchi,[e] Mayumi Nishimura,[e] Tasuku Ito,*[e] Kentaro Tanaka[a] and Mitsuhiko Shionoya*[a]

[a] *Department of Chemistry, Graduate School of Science, The University of Tokyo, Hongo, Bunkyo-ku, Tokyo 113-0033, Japan. E-mail: shionoya@chem.s.u-tokyo.ac.jp*
[b] *Department of Chemistry, Nankai University, Tianjin 300071, P.R. China*
[c] *Institute for Molecular Science, Myodaiji, Okazaki 444-8585, Japan*
[d] *Department of Applied Chemistry, School of Engineering, Nagoya University, Chikusa, Nagoya 464-8603, Japan*
[e] *Department of Chemistry, Graduate School of Science, Tohoku University, Sendai 980-8578, Japan*

Received (in Columbia, MO, USA) 13th April 2000, Accepted 28th August 2000
First published as an Advance Article on the web

One-pot reaction of $AgNO_3$ and a large aromatic bridging ligand, diquinoxalino[2,3-a:2′,3′-c]phenazine, which has three bidentate coordination sites, afforded a Ag^I complex consisting of two independent three-dimensional (3D) networks which are enantiometric and interpenetrating.

A major goal of the polymer-based approach to crystal engineering is to develop new robust materials with useful electronic, magnetic, electrochemical, optical or catalytic properties. Among various types of molecular-based frameworks, interpenetrating networks are of particular interest with regard to the topological types of 3D nets postulated by Wells.[1] Since the groups of Robson[2] and Ciani[3] reported their first pioneering works on '3D racemates' using suitable metal ions and polydentate ligands, in which two enantiomeric interpenetrating networks are included, compounds bearing two or more metal chelating sites have often been used as connecting units for the generation of interpenetrating 3D networks.[4–6]

In our effort to construct novel 3D coordination polymer networks, diquinoxalino[2,3-a:2′,3′-c]phenazine (L) has attracted our attention. This ligand is a nitrogeneous aromatic compound with three bidentate sites, which was expected to provide a coordination network characterized by a delocalized π-electron system. We report here, the synthesis and X-ray crystal structure of a novel Ag^I complex[7] **1** with L, consisting of an interpenetrating enantiomorphic pair of nets.

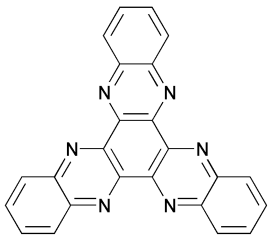

L

Complex **1** was prepared in the dark by carefully layering a solution of $AgNO_3$ in MeCN on top of a solution of L in CH_2Cl_2. After *ca.* two weeks, yellow–orange crystals of **1** $\{(Ag_3L_2)(NO_3)_3\cdot solvent\}$ were isolated in *ca.* 90% yield. The structure of **1** was established by single-crystal X-ray diffraction.‡

Each Ag^I center in **1** acts as a two-connecting node by connecting two ligands of L. Interestingly, **1** exhibits twofold interpenetrating networks with the two-connected (Ag^I) and three-connected (L) nodes. A single cationic network of the doubly interpenetrating networks is shown Fig. 1(a). The basic building block of the network contains distorted tetrahedral Ag^I atoms and two types of ligand L with B ligands parallel to the *xy*-plane [Fig. 1(a)]. The coordination geometry around each Ag^I center is not perfectly tetrahedral. A ligands in the building block make an interplanar angle of 100° with B ligands and arranged in a propeller fashion around them. These basic building blocks are linked by Ag^I atoms to form a 3D network. A ligands along the *z*-axis are connected by Ag^I atoms to form a one-dimensional threefold helical network [see the bold lines in Fig. 1(b)]. A crystallographic C_3 axis exists perpendicular to ligand B. Interestingly, these helices are interlinked with ligands

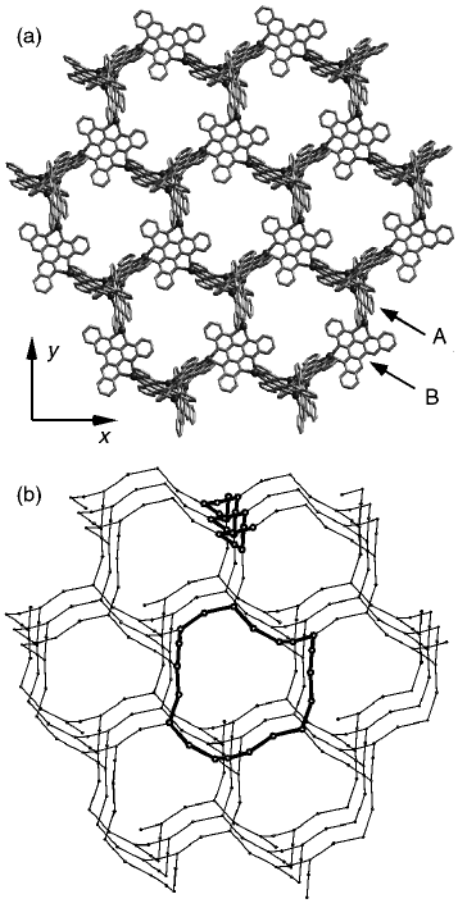

Fig. 1 Representations of (a) a single 3D network in complex **1**, where metal atoms are shown as spheres and (b) a schematic view of a single network with the ligands replaced by trigonal nodes; one of the 20-gons and a helix are highlighted by bold lines.

† Electronic supplementary information (ESI) available: experimental procedure for complex **1**. See http://www.rsc.org/suppdata/cc/b0/b003183f/

DOI: 10.1039/b003183f

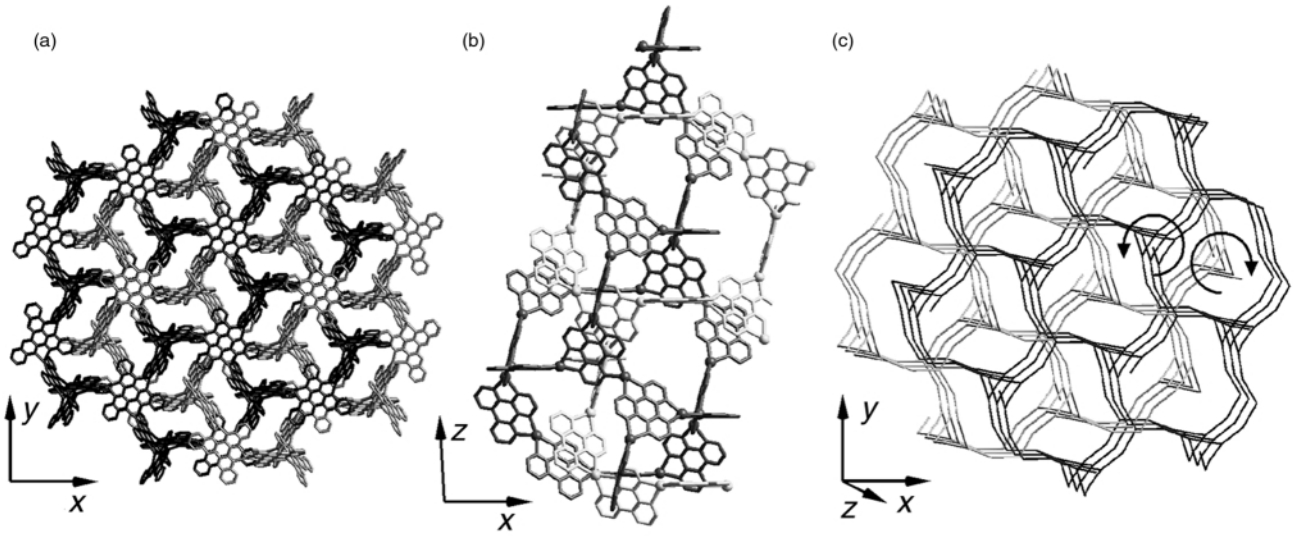

Fig. 2 Representations of (a) a top view of the doubly interpenetrating networks of **1**, where the two networks are colored black and gray, (b) a side view of the two interpenetrating networks of **1**, where the outer phenyl rings of the ligands are omitted for clarity and (c) a schematic view of the 3D nets in which the ligands are replaced by trigonal nodes. Note the difference in the handedness of the helical networks in each 3D net.

B *via* Ag^{I} atoms to form a 3D network with large channels. The shortest loop in the network is a 20-gon that is constituted of 10 Ag^{I}-atoms and 10 ligands [see the bold lines in Fig. 1(b)]. The structure can be regarded as a 3D network in which half of the nodes are replaced by three-fold helices, and is quite different from that of the Ag^{I} complex with Hat (1,4,5,8,9,12-hexaazatriphenylene) which similarly has three bidentate sites but differs in the size of the π-plane. In the Hat complex, all the Ag^{I} centers are chelated by three Hat ligands to form an octahedral coordination environment.[5a]

The extended structure of **1** reveals interesting twofold interpenetrating networks as shown in Fig. 2(a) and (b). These two interpenetrating networks are topologically equivalent but differ in the handedness of the threefold helices [see Fig. 2(c)], where the two arrows show the handedness of helices. Thus complex **1** contains an interpenetrating enantiomorphic pair of nets with a (10,3)-a type topology[1a] consisting of Ag^{I} ions coordinated by nitrogeneous aromatic ligands in a tetrahedral fashion. This type of interpenetration of 3D nets was referred to by Wells as 'a 3D racemate'.[1a] The interactions observed between the two interpenetrating networks are aromatic edge-to-face interactions between A ligands in one network and adjacent B′ ligands in the other, with no face-to-face interactions between B and B′ ligands observed in the structure. Although the channels in one network are occupied by another network, there are still large vacant spaces between the two, corresponding to the 53% of crystal volume, which is filled by solvent molecules and the counter anions. However, some of the solvent molecules and counter ions were found to be disordered owing to the high symmetry of the network.

This study has revealed a one-pot, high-yield synthesis of a Ag^{I} complex consisting of doubly interpenetrating 3D networks with nitrogeneous heterocyclic bridging ligands L. Furthermore, L has a large delocalized π-electron system which may allow facile d–π interactions between ligands and remote metal centers throughout extended 3D networks.

Support from Ministry of Education, Science, Sports and Culture, Japan (Grant-in-Aid for Scientific Research on Priority Areas (No. 11136255 and 10149102, 'Metal-assembled Complexes') to M. S. and T. I. respectively, and partial support from the Natural Science Foundation of China (No. 29771022) to X. H. B. are gratefully acknowledged. M. S. is also grateful to Novartis Foundation for the Promotion of Science, Nagase Science and Technology Foundation and Uehara Memorial Foundation for support.

Notes and references

‡ Reflection data were collected on a Bruker CCD SMART system with Mo-Kα radiation (λ = 0.71073 Å) at 193 ± 2 K. The structure was solved by direct methods using the SHELXTL program.[8] Non-hydrogen atoms of the complex were refined with anisoptropic thermal parameters. Refinement was done by full-matrix least squares on F^2.

Crystal data for **1**: M = 1580.04, crystal size 0.20 × 0.15 × 0.15 mm, trigonal, space group $R\bar{3}$, $a = b$ = 32.223(2), c = 20.827(2) Å, V = 18728(2) Å^3, Z = 12, μ = 1.258 mm^{-1}, D_c = 1.681 g cm^{-3}, min./max. transmission = 0.8031/0.8468, 1.22 < θ < 27.93°, $R(R_w)$ = 0.0790(0.2077) for 9985 (R_{int} = 0.1083) independent reflections out of a total of 47197 reflections with $I > 2\sigma(I)$ and 506 parameters, and $R(R_w)$ = 0.1711(0.2417) for all the data. The goodness-of-fit on F^2 is 1.241, and the residual electron density (min./max.) is −1.041/1.646e Å^{-3}.

Yellow–orange crystals of $Ag_3L_2(PF_6)_3{\cdot}0.75CHCl_3{\cdot}2.25CH_3CN$ were obtained using $AgPF_6$ in place of $AgNO_3$. This compound has the same 3D interpenetrating networks as compound **1**. Crystal data (at 223 K): trigonal, space group $R\bar{3}$, $a = b$ = 33.936(2), c = 20.462(2) Å, V = 20407(1) Å^3, Z = 12.

CCDC 182/1773. See http://www.rsc.org/suppdata/cc/b0/b003183f/ for crystallographic files in .cif format.

1 (*a*) A. F. Wells, *3D Nets and Polyhedra*, Wiley-Interscience, New York, 1977; (*b*) *Further Studies of Three-dimensional Nets*, ACA Monograph No. 8, American Crystallographic Association, 1979.
2 B. F. Abrahams, S. R. Batten, H. Hamit, B. F. Hoskins and R. Robson, *Chem. Commun.*, 1996, 1313.
3 L. Carlucci, G. Ciani, D. M. Proserpio and A. Sironi, *Chem. Commun.*, 1996, 1393.
4 S. R. Batten and R. Robson, *Angew. Chem., Int. Ed.*, 1998, **37**, 1460 and references therein.
5 (*a*) B. F. Abrahams, P. A. Jackson and R. Robson, *Angew. Chem., Int. Ed.*, 1998, **37**, 2656; (*b*) B. F. Abrahams, S. R. Batten, M. J. Grannas, H. Hamit, B. F. Hoskins and R. Robson, *Angew. Chem., Int. Ed.*, 1999, **38**, 1475.
6 L. Carlucci, G. Ciani and D. M. Proserpio, *Angew. Chem., Int. Ed.*, 1999, **38**, 3488; L. Carlucci, G. Ciani, P. Macchi, D. M. Proserpio and S. Rizzato, *Chem. Eur. J.*, 1999, **5**, 237.
7 Y. Suenaga, T. Kuroda-Sowa, M. Kaekawa and M. Munakata, *J. Chem. Soc., Dalton Trans.*, 1999, 2737 and references therein; G. B. Gardner, D. Venkataraman, J. S. Moore and S. Lee, *Nature*, 1995, **374**, 792.
8 SHELXTL version 5.03, Siemens Analytical X-Ray Instruments, Inc., Madison, WI, 1994.

High yield synthesis and crystal structures of the Ru_6–Sn cluster compounds $[Ru_6C(CO)_{16}SnCl_2]$ and $[Ru_6C(CO)_{16}SnCl_3]^-$

Sophie Hermans and Brian F. G. Johnson*

Department of Chemistry, University of Cambridge, Lensfield Road, Cambridge, UK CB2 1EW. E-mail: bfgj1@cam.ac.uk

Received (in Cambridge, UK) 8th June 2000, Accepted 18th August 2000
First published as an Advance Article on the web

Addition of two molar equivalents of $SnCl_4$ to $[Ru_6C(CO)_{16}]^{2-}$ yields first the new $[Ru_6C(CO)_{16}SnCl_3]^-$ cluster anion and then $[Ru_6C(CO)_{16}SnCl_2]$, the latter being also the single product of the direct addition of $SnCl_2$ to $[Ru_6C(CO)_{17}]$.

We are currently investigating the preparation and catalytic activity of bimetallic nanoparticles derived from fully characterised bimetallic cluster compounds.[1–3] Recent results have indicated that, once formed within the cavities of the mesoporous solid MCM-41, such nanoparticles exhibit a surprising stability and resist sintering even under moderately vigorous conditions. To this end, we have established a need for nanoparticles containing Ru–Sn cores. This association of metals is known to be highly versatile, and is used in both selective oxidation and hydrogenation catalysis.[4] However, few Ru–Sn mixed-metal clusters have been reported.[5–9] In this paper we report the synthesis of the new bimetallic clusters $[Ru_6C(CO)_{16}SnCl_2]$ **2** and $[Ru_6C(CO)_{16}SnCl_3]^-$ **4**. We regard these new cluster species as derivatives of Sn(IV) containing *formally* the bidentate ligand $[Ru_6C(CO)_{16}]^{2-}$.

The reaction sequence for the preparation of the compound $[Ru_6C(CO)_{16}SnCl_2]$ **2** and the anion $[Ru_6C(CO)_{16}SnCl_3]^-$ **4** is outlined in Scheme 1. Direct reaction of $[Ru_6C(CO)_{17}]$ **1** with stannous chloride in dichloromethane is slow but over a period of several days under reflux, product **2** may be obtained in good yield (91%). The mechanism by which this reaction occurs is uncertain but would appear to take place first by simple carbon monoxide extrusion followed then by the addition of $SnCl_2$. However, the *formal* oxidation state of the Sn in **2** is (IV)† indicating that a redox process of the type $[Ru_6C(CO)_{16}]$ to $[Ru_6C(CO)_{16}]^{2-}$ occurs at some stage during the reaction sequence. In this sense, the reaction might be described as a oxidative-addition to Sn(II), leading to reduction of the cluster fragment.

In agreement, reactions of the dianionic cluster $[Ru_6C(CO)_{16}]^{2-}$ with stannic chloride in dichloromethane produce the same Sn(IV) cluster **2** and in addition the anion $[Ru_6C(CO)_{16}SnCl_3]^-$ **4** (as its PPN^+ salt). Anion **4** is obtained in 67% yield when equimolar amounts of $[Ru_6C(CO)_{16}]^{2-}$ **3** and $SnCl_4$ are reacted. Treatment of **4** with further stannic chloride (1 mole) results in Cl^- ion abstraction and the formation of **2**. The other product of this reaction is the Sn(IV) anion $[SnCl_5]^-$. This reaction is easily reversed, and addition of Cl^- {as [PPN]Cl} to **2** results in the formation of **4**. The ease with which cluster **2** accepts the additional Cl^- to generate a coordinated $SnCl_3^-$ group is of interest and in line with the established chemistry of $SnCl_4$. This emphasises the view of compound **2** as an adduct of the type $XSnCl_2$, where X = the bidentate dianionic ligand $[Ru_6C(CO)_{16}]^{2-}$.

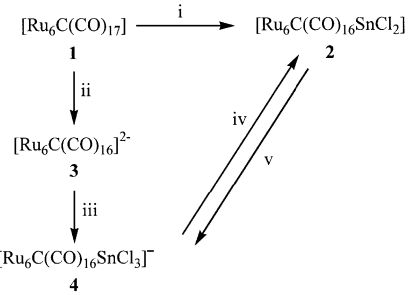

Scheme 1 Synthesis of the cluster species $[Ru_6C(CO)_{16}SnCl_2]$ and $[Ru_6C(CO)_{16}SnCl_3]^-$ **3**. *Reagents and conditions*: i, reaction with $SnCl_2$ in dichloromethane, reflux, 4 days; ii, reaction with KOH–MeOH; iii, reaction with $SnCl_4$ in dichloromethane at room temperature; iv, reaction with $SnCl_4$ in dichloromethane under reflux; v, reaction with [PPN]Cl in dichloromethane at room temperature.

Clusters **2** and **4** have been fully characterised by the usual spectroscopic and analytical techniques, and their molecular structure established by single crystal X-ray diffraction.[10]

The mass spectrum of **4**, obtained by ESI-MS run in negative mode, consists of a peak at *m/z* 1289, corresponding to the formulation $[Ru_6C(CO)_{16}SnCl_3]$. The IR spectra of **4** in the ν_{CO} stretching region consists of peaks at 2086, 2056, 2035, 2026, 1987 and 1973 cm^{-1} corresponding to terminal carbonyls, and a broad peak at 1825 cm^{-1} corresponding to bridging CO.

The molecular structure of the anion $[Ru_6C(CO)_{16}SnCl_3]^-$ **4** is shown in Fig. 1, together with selected bond lengths and angles. It consists of the intact core of the $Ru_6C(CO)_{16}$ cluster, with one Ru–Ru edge bridged by a $SnCl_3$ fragment. It is

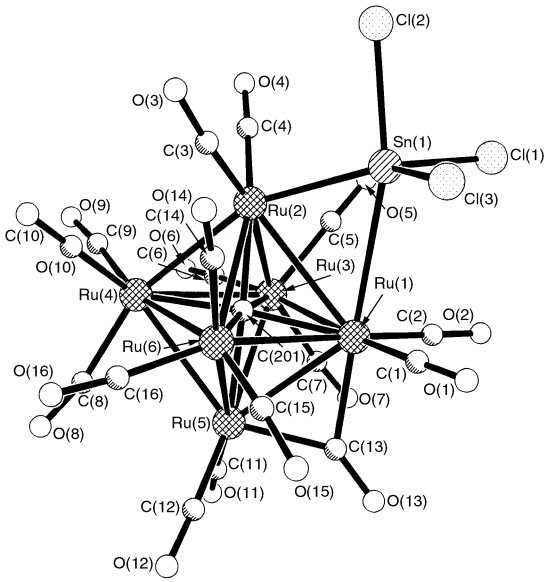

Fig. 1 Molecular structure of $[Ru_6C(CO)_{16}SnCl_3]^-$ **4** with atom numbering scheme. Selected bond lengths (Å) and angles (°): Molecule 1: Ru(1)–Sn(1) 3.140(2), Ru(2)–Sn(1) 2.581(3), Sn(1)–Cl(1) 2.391(6), Sn(1)–Cl(2) 2.459(5), Sn(1)–Cl(3) 2.406(5), Ru(1)–Ru(2) 3.039(3), Ru–Ru (mean) 2.89(2), C–O (mean) 1.177(8), Ru(1)–Sn(1)–Ru(2) 63.28(6), Cl(1)–Sn(1)–Cl(2) 164.13(13), Cl(2)–Sn(1)–Cl(3) 93.70(19), Cl(1)–Sn(1)–Cl(3) 101.1(2). Molecule 2: Ru(7)–Sn(2) 2.583(3), Ru(8)–Sn(2) 3.102(2), Sn(2)–Cl(5) 2.478(6), Sn(2)–Cl(6) 2.371(6), Sn(2)–Cl(4) 2.386(5), Ru(7)–Ru(8) 3.043(3), Ru–Ru (mean) 2.90(3), C–O (mean) 1.17(1), Ru(7)–Sn(2)–Ru(8) 63.97(6), Cl(4)–Sn(2)–Cl(6) 101.6(2), Cl(6)–Sn(2)–Cl(5) 93.1(3), Cl(5)–Sn(2)–Cl(4) 93.8(2).

DOI: 10.1039/b004585n

monoanionic and the asymmetric unit of the structure contains two independent anions and two PPN^+ cations. Fifteen carbonyl ligands are terminally bound to the ruthenium atoms, and one is bridging a Ru–Ru bond.

The geometry of the Ru_6C octahedron has remained almost unchanged, with the mean Ru–Ru bond distance of 2.89(2) Å in molecule 1 and 2.90(3) Å in molecule 2 identical to that of 2.90(2) Å found in $[Ru_6C(CO)_{17}]$.[11] The Ru–Ru bond spanned by the tin atom is the longest (Ru(1)–Ru(2) 3.039(3) Å in molecule 1 and Ru(7)–Ru(8) 3.043(3) Å in molecule 2), as has been previously observed in other Ru–Sn mixed-metal clusters.[5–9] The Ru(2)–Sn(1) (2.581(3) Å) in molecule 1 and the Ru(7)–Sn(2) (2.583(3) Å) in molecule 2 bond lengths are within the range observed previously, as in $[(\mu\text{-}H)_2(\mu_3\text{-}S)(\mu\text{-}Cl)Ru_3(CO)_8(SnCl_3)]$ (Ru–Sn 2.571(1) Å),[5] $[Ru_3(\mu\text{-}H)(\mu_3,\eta^2\text{-amphy})\{\mu,\eta^1:\eta^2\text{-}PhC{=}C(H)Ph\}(SnPh_3)(CO)_7]$ (Ru–Sn 2.662(1) Å),[6] $[Ru_3(\mu\text{-}H)(\mu_3,\eta^2\text{-amphy})\{\mu,\eta^1{:}\eta^2PhC{=}C(H)Ph\}(SnPh_3)(CO)_7]$ (different isomer, Ru–Sn 2.623(1) Å),[6] in which a SnR_3 fragment is terminally bound to a ruthenium atom; and $[Me_3Sn(CO)_3Ru(SnMe_2)]_2$ (Ru–Sn 2.638(2)–2.694(2) Å),[7] $[Ru_3(CO)_{10}(SnR_2)_2]$ (Ru–Sn 2.733(2)–2.739(2) Å),[8] $[Ru_3(CO)_9(\mu\text{-}SnR'_2)_3]$ (Ru–Sn 2.715(2)–2.734(2) Å),[9] $[Ru_3(CO)_9(\mu\text{-}SnR_2)(\mu\text{-}SnR'_2)_2]$ (Ru–Sn 2.705(2)–2.750(2) Å),[9] $[Ru_3(CO)_9(\mu\text{-}SnR_2)_2(\mu\text{-}SnR'_2)]$ (Ru–Sn 2.641(2)–2.729(2) Å),[9] and $[Ru_2(CO)_6(\mu\text{-}SnR_2)(dppm)]$ (Ru–Sn 2.699(1)–2.715(1) Å),[9] in which SnR_2 fragments are bridging Ru–Ru edges. The Ru(1)–Sn(1) and the Ru(8)–Sn(2) bonds (3.140(2) and 3.102(2) Å, respectively) in **4** are much longer but still within bonding distance, implying that the $SnCl_3$ fragment forms an asymmetrical bridge, intermediate between the symmetrically bridging and terminal bonding modes observed in other Ru–Sn clusters.[5–9] This confers to the tin atom a nearly perfect trigonal bipyramidal coordination geometry, with Ru(1) or Ru(8) equatorial, and Ru(2) or Ru(7) in axial position.

The IR spectrum of compound $[Ru_6C(CO)_{16}SnCl_2]$ **2** contains CO stretching bands attributable to terminal carbonyl ligands only. Compound **2** has been characterised by positive electron impact mass spectrometry, and its spectrum consists of the parent ion at *m/z* 1256 followed by peaks corresponding to loss of CO ligands.

The molecular structure of $[Ru_6C(CO)_{16}SnCl_2]$ **2** is shown in Fig. 2, together with selected bond lengths and angles. As with anion **4**, it consists of a $Ru_6C(CO)_{16}$ octahedron edge-bridged by a $SnCl_2$ fragment. Each ruthenium atom bears three terminally bound carbonyl ligands, except for the two ruthenium atoms supporting the Sn(IV) bridge, which bear two carbonyl ligands only. The Ru_6C core remains unchanged. Again the Ru–Ru edge bearing the $SnCl_2$ fragment is the longest (Ru(1)–Ru(2) 3.0559(11) Å [3.039(3) Å in **4**]), with the other Ru–Ru bonds ranging from 2.8280(10) to 2.9429(10) Å [2.89(2) Å (mean) in **4**]. The Ru–Sn bonds (2.5907(11) and 2.5733(12) Å) are very similar to the shortest Ru–Sn bond in **4** (2.581(3) Å), and within the range observed in previously reported Ru–Sn clusters (2.571(1)–2.750(2) Å).[5–9]

In this work we have demonstrated that simple derivatives of Sn(IV) containing the 'ligand' $[Ru_6C(CO)_{16}]^{2-}$ may be readily obtained. The coordination chemistry about the central Sn(IV) ion would appear to be normal (tetrahedral or tbp). This fundamental idea has been extended to other metal systems and, for example, related derivatives of square planar Pt(II) have been obtained similarly. These new Ru–Sn clusters have been shown to be ideal precursors to catalytically active Ru–Sn nanoparticles.

We gratefully acknowledge Dr Neil Feeder and Dr John E. Davies for data collection and structure refinement and the European Commission for a TMR grant to B. F. G. J. and for a Marie Curie Fellowship to S. H.

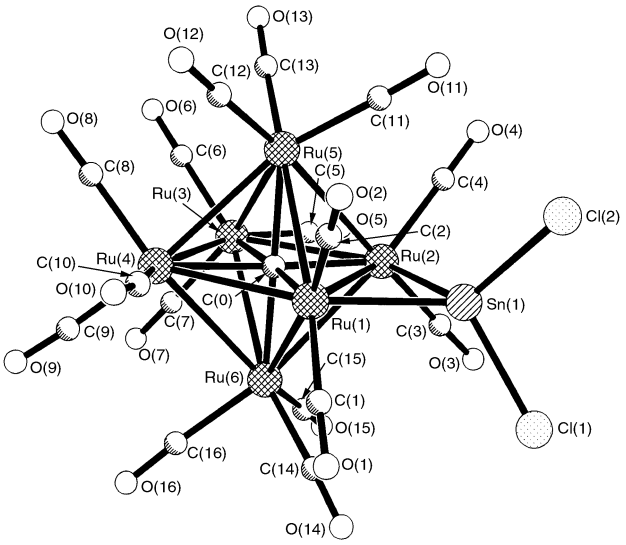

Fig. 2 Molecular structure of $[Ru_6C(CO)_{16}SnCl_2]$ **2** with atom numbering scheme. Selected bond lengths (Å) and angles (°): Ru(1)–Sn(1) 2.5907(11), Ru(2)–Sn(1) 2.5733(12), Sn(1)–Cl(1) 2.2454(15), Sn(1)–Cl(2) 2.343(2), Ru(1)–Ru(2) 3.0559(11), Ru–Ru (mean) 2.91(2), C–O (mean) 1.131(2), Ru(1)–Sn(1)–Ru(2) 72.56(2), Cl(1)–Sn(1)–Cl(2) 100.24(6), Cl(1)–Sn(1)–Ru(1) 118.07(4), Cl(1)–Sn(1)–Ru(2) 121.54(5).

Notes and references

† We derive this oxidation state (+4) by removing the 'ligand' $[Ru_6C(CO)_{16}]$ in its closed shell configuration, *i.e.* as $[Ru_6C(CO)_{16}]^{2-}$.

1 D. S. Shephard, T. Maschemeyer, B. F. G. Johnson, J. M. Thomas, G. Sankar, D. Ozkaya, W. Zhou, R. D. Oldroyd and R. G. Bell, *Angew. Chem., Int. Ed. Engl.*, 1997, **36**, 2242.

2 D. S. Shephard, T. Maschmeyer, G. Sankar, J. M. Thomas, D. Ozkaya, B. F. G. Johnson, R. Raja, R. D. Oldroyd and R. G. Bell, *Chem.-Eur. J.*, 1998, **4**, 1214.

3 R. Raja, G. Sankar, S. Hermans, D. S. Shephard, S. Bromley, J. M. Thomas, B. F. G. Johnson and T. Maschemeyer, *Chem. Commun.*, 1999, 1571.

4 See for example: Y. Pouilloux, F. Austin, C. Guimon and J. Barrault, *J. Catal.*, 1998, **176**, 215; Y. Moritomo and E. B. Yeager, *J. Electroanal. Chem.*, 1998, **444**, 95.

5 R. D. Adams and D. A. Katahira, *Organometallics*, 1982, **1**, 53.

6 J. A. Cabeza, S. Garcia-Granda, A. Llamazares, V. Riera and J. F. Van der Maelen, *Organometallics*, 1993, **12**, 157.

7 S. F. Watkins, *J. Chem. Soc. A*, 1969, 1552.

8 C. J. Cardin, D. J. Cardin, G. A. Lawless, J. M. Power and M. B. Power, *J. Organomet. Chem.*, 1987, **325**, 203.

9 C. J. Cardin, D. J. Cardin, M. A. Convery, Z. Dauter, D. Fenske, M. M. Devereux and M. B. Power, *J. Chem. Soc., Dalton Trans.*, 1996, 1133.

10 *Crystallographic data*: $[Ru_6C(CO)_{16}SnCl_2]$ **2**: $C_{17}Cl_2O_{16}Ru_6Sn$, M = 1256.18, monoclinic, a = 16.740(6), b = 16.500(7), c = 20.941(9) Å, β = 90.96(2)°, U = 5783.3(41) Å^3, T = 180(2) K, space group $C2/c$, Z = 8, μ = 4.153 mm^{-1}, 9762 measured reflections, 5103 independent reflections (R_{int} = 0.0565), refinement method: full-matrix least squares on F^2, final R_1 = 0.0330, wR_2 = 0.0601 [$I > 2\sigma(I)$], R_1 = 0.0413, wR_2 = 0.0624 (all data). A final Fourier-difference electron-density synthesis revealed maximum and minimum residual electron density peaks of 1.192 and −1.164 e Å^{-3}. $[PPN][Ru_6C(CO)_{16}SnCl_3]$ **4**: $C_{53}H_{30}Cl_3NO_{16}P_2Ru_6Sn$, M = 1830.18, monoclinic, a = 10.540(8), b = 34.655(7), c = 32.571(5) Å, β = 90.19(4)°, U = 11897(10) Å^3, T = 200(2) K, space group $P2_1/c$, Z = 8, μ = 2.150 mm^{-1}, 18999 measured reflections, absorption correction using ψ scans (T_{max} = 0.994, T_{min} = 0.820), 18617 independent reflections (R_{int} = 0.0876), refinement method: full-matrix least squares on F^2, final R_1 = 0.0904, wR_2 = 0.1837 [$I > 2\sigma(I)$], R_1 = 0.1923, wR_2 = 0.2341 (all data). A final Fourier-difference electron-density synthesis revealed maximum and minimum residual electron density peaks of 1.360 and −1.397 e Å^{-3}. One of the PPh_3 groups of one of the PPN^+ cations is disordered over two sites, and some disorder is also associated with two carbonyl ligands. Common, isotropic temperature factors were used for these disordered atoms, hence the relatively high R-values. CCDC 182/1750. See http://www.rsc.org/suppdata/cc/b0/b004585n/ for crystallographic files in .cif format.

11 A. Sirigu, M. Bianchi and E. Benedetti, *Chem. Commun.*, 1969, 596.

High-field (high-frequency) EPR spectroscopy and structural characterization of a novel manganese(III) corrole

Jesper Bendix,[a] Harry B. Gray,*[a] Galina Golubkov[b] and Zeev Gross*[b]

[a] *Beckman Institute, California Institute of Technology, Pasadena, California 91125, USA*
[b] *Department of Chemistry and Institute of Catalysis Science and Technology, Technion - Israel Institute of Technology, Haifa 32000, Israel. E-mail: chr10zg@tx.technion.ac.il*

Received (in Cambridge, UK) 2nd August 2000, Accepted 30th August 2000
First published as an Advance Article on the web

The X-ray structure, magnetic susceptibility, and high-field (high-frequency) EPR spectrum of manganese 5,10,15-tris-(pentafluorophenyl) corrole unambiguously establish that the complex contains an isolated, slightly rhombic, manganese(III) center.

Manganese(III) porphyrins are very efficient catalysts for functionalization of hydrocarbons in processes that involve high valent intermediates.[1,2] Spectroscopic identification of odd-spin manganese(IV) and spin-coupled manganese(V) porphyrins by magnetic resonance measurements is relatively straightforward, *via* utilization of EPR and NMR, respectively.[3–6] However, even-spin manganese(III) porphyrins are EPR-silent (X-band) and their NMR spectra are not easily interpretable. For example, an early assignment of the origin of the paramagnetic shifts in manganese(III) porphyrins was recently revised,[7] and there is some evidence indicating that the complexes might better be described as manganese(II) porphyrin radical cations.[8] A recent development relevant to this question is the utilization of high-field (high-frequency) EPR (HF-EPR) spectroscopy for elucidation of the electronic structures of high-spin manganese(III) complexes.[9]

The close relationship of porphyrins and corroles suggests that metallocorroles could also be very interesting catalysts. This proposal was only recently explored, taking advantage of the novel electron-poor 5,10,15-tris(pentafluorophenyl)corrole, H_3tpfc,[10] whose substitution pattern matches that of the most active porphyrin-based catalysts. First, it was demonstrated that the iron and rhodium complexes of H_3tpfc are potent catalysts for oxygen and carbene transfer to olefins and alkanes,[11] followed by full characterization of H_3tpfc[12] and its $Cr^{V}O$, $Fe^{IV}Cl$ and $Rh^{III}(PPh_3)$ complexes.[13,14] The manganese corrole [(tpfc)Mn] was also found to be an epoxidation catalyst, as well as an excellent precursor to a relatively stable oxomanganese(V) corrole.[1b,15] The apparent importance of this result together with the rather limited information on the electronic structures of manganese corroles[16,17] were the driving forces for the current investigations. A combination of HF-EPR spectroscopy, X-ray crystallography, and magnetic susceptibility measurements, led to the conclusion that [(tpfc)Mn($OPPh_3$)] is an authentic manganese(III) complex that does not experience significant intermolecular interactions.

Obtaining X-ray quality crystals of [(tpfc)Mn] was a difficult task; NMR examination of material from different crystallization batches revealed significant variations in chemical shifts. Since we suspected that these differences were due to solvent coordination, we added external ligands to the recrystallization mixtures. These attempts finally met with success: with triphenylphosphine oxide as additive, X-ray quality crystals of [(tpfc)Mn($OPPh_3$)] were isolated.[18] The structure of [(tpfc)Mn($OPPh_3$)] (Fig. 1) is quite different from that of the previously reported square planar manganese(III) corrole, [(e-7,13-mc)Mn].[1b,16] In the latter complex the metal is located almost perfectly within the N_4 plane and the macrocycle is planar, whereas in [(tpfc)Mn($OPPh_3$)] the manganese is 0.29 Å out of both the N_4 and the corrole core planes. This causes some

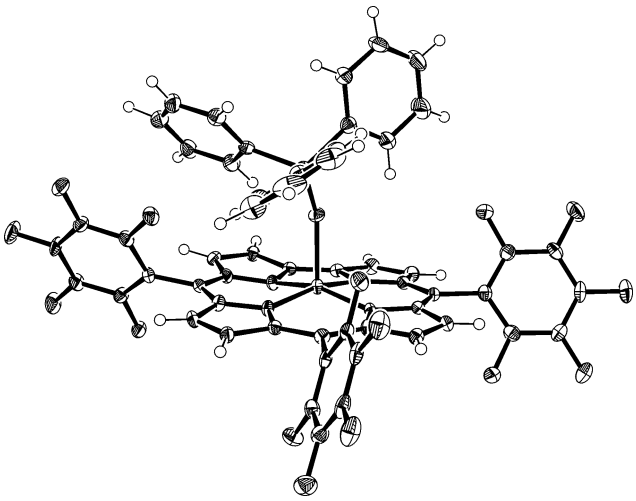

Fig. 1 ORTEP view of [(tpfc)Mn($OPPh_3$)].

elongation of the average Mn–$N_{pyrrole}$ bonds {from 1.894 in [(e-7,13-mc)Mn] to 1.916 Å in [(tpfc)Mn($OPPh_3$)]} with slight deviations of the tpfc atoms from the mean plane. Another significant difference is the absence of interactions between the corroles in [(tpfc)Mn($OPPh_3$)], which is a dominant factor in the structure of [(e-7,13-mc)Mn]. Rather, the potential empty space is occupied by the triphenylphosphine oxide ligand (Fig. 2).

The absence of intermolecular interactions is also reflected in the magnetic susceptibility measurements on [(tpfc)Mn($OPPh_3$)], performed in the temperature range 2–300 K.[19] The magnetic moment of 4.88 μ_B confirms that the complex possesses a simple high-spin (S = 2) ground state; and the very flat plateau in the μ_{eff} *vs*. temperature plot down to 10 K (Fig. 3) is perfectly in line with the molecular packing deduced from the X-ray structure (Fig. 2).

Since the consequences of lowered symmetry on the electronic structures of corrole *vs*. porphyrin complexes have

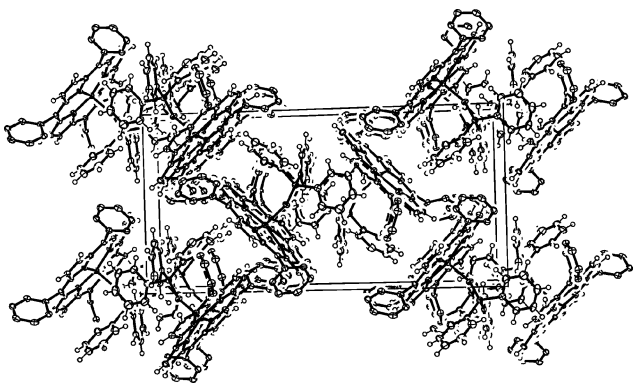

Fig. 2 Unit cell of [(tpfc)Mn($OPPh_3$)], approximately along the *a*-axis. Fluorine atoms have been omitted for clarity.

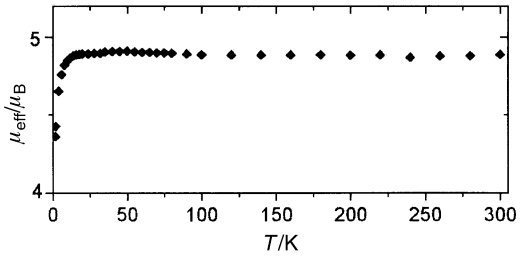

Fig. 3 Variation of the magnetic moment of [(tpfc)Mn(OPPh$_3$)] with temperature.

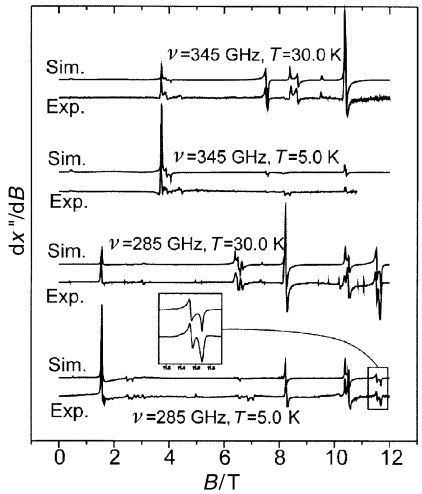

Fig. 4 Experimental and simulated HF-EPR spectra of [(tpfc)Mn(OPPh$_3$)].

not yet been quantified experimentally, we measured HF-EPR spectra of [(tpfc)Mn(OPPh$_3$)] at two different frequencies (285 and 345 GHz) and at two different temperatures (5 and 30 K). The spectra shown in Fig. 4 are very well reproduced by simulations of randomly oriented powder samples employing the following parameters: $g_{||}$ = 1.980(4), $g_{\perp}$ = 1.994(4), D = 2.69(2) cm^{-1}, E = 0.030(3) cm^{-1}, $W_{1/2}$ = 150 G (T = 5 K), $W_{1/2}$ = 180 G (T = 30 K).[20] One of the most sensitive lines to g-value rhombicity is that centered at 8 T (285 GHz), which consists of the transitions ($|-1> \rightarrow |0>$) and ($|0> \rightarrow |+1>$). The fact that this line is not split puts an upper limit of 0.005 on the difference between g_x and g_y. An expansion of one of the easily observed line splittings attributable to the rhombic zero-field splitting is shown in the insert of Fig. 4. The rhombic zero-field splitting is small compared to that found in tris(β-diketonate) complexes of manganese(III) (E = 0.26 cm^{-1}, E/D = −0.06),[9b] but we emphasize that the corresponding line is not split in the spectra of manganese(III) porphyrins and phthalocyanines. Although the lower molecular symmetry of metallocorroles compared to metalloporphyrins is also pronounced for systems with no preferred coordination geometry,[21] the *electronic* deviation from axiality is quite small. We thus conclude that treating a corrolate as a trianionic porphyrinate is not unreasonable.

We have fully characterized a manganese complex of H$_3$tpfc. Employing three different methods, we have shown that [(tpfc)Mn(OPPh$_3$)] contains an authentic, isolated S = 2 manganese(III) center.

We thank Dr M. W. Day (Beckman Institute) for assistance with the crystal structure determination and Ms S. Mossin (University of Copenhagen) and Dr A.-L. Barra (CNRS, Grenoble) for recording the HF-EPR spectra. This research was supported by the Fund for the Promotion of Research at the Technion (Z. G.), the National Science Foundation (H. B. G.), and grant # 9800549 from the Danish Natural Science Research Council (J. B.).

Notes and references

1 (*a*) A major part of this work was first presented as Poster 23 in *Contemp. Inorg. Chem.- II*, March 12–15, 2000, College Station, Texas, and as Paper 293 in the 219th national ACS meeting in San Francisco, March 26–30, 2000; (*b*) abbreviations: tpfc and e-7,13-mc; the trianions of 5,10,15-tris(pentafluorophenyl)corrole and 2,3,8,12,17,18-hexaethyl-7,13-dimethylcorrole, respectively.
2 (*a*) B. Meunier, in *Metalloporphyrin Catalyzed Oxidations*, ed. F. Montanari and L. Casella, Kluwer Academic Publishers, Dordrecht, 1994, pp. 1–48; (*b*) J. T. Groves, in *Cytochrome P450: Structure, Mechanism, and Biochemistry*, ed. P. R. Ortiz de Montellano, Plenum Press, New York, 2nd edn., 1995, pp. 1–48.
3 L. Kaustov, M. E. Tal, A. I. Shames and Z. Gross, *Inorg. Chem.*, 1997, **36**, 3503.
4 H. Volz and W. Muller, *Chem. Ber.*, 1997, **130**, 1099, and references therein.
5 N. Jin and J. T. Groves, *J. Am. Chem. Soc.*, 1999, **121**, 2923.
6 J. T. Groves and T. Takahashi, *J. Am. Chem. Soc.*, 1983, **105**, 2073.
7 Z. Gross, A. Mahammed and C. M. Barzilay, *Chem. Commun.*, 1998, 1505.
8 P. Turner and M. J. Gunter, *Inorg. Chem.*, 1994, **33**, 1406.
9 (*a*) D. P. Goldberg, J. Telser, J. Krzystek, A. G. Montalban, L.-C. Brunel, A. G. M. Barrett and B. M. Hoffman, *J. Am. Chem. Soc.*, 1997, **119**, 8722; (*b*) A.-L. Barra, D. Gatteschi, R. Sessoli, G. L. Abbati, A. Cornia and A. C. Fabretti, *Angew. Chem., Int. Ed. Engl.*, 1997, **36**, 2329; (*c*) J. Krzystek, J. Telser, L. A. Pardi, D. P. Goldberg, B. M. Hoffman and L.-C. Brunel, *Inorg. Chem.*, 1999, **38**, 6121.
10 (*a*) Z. Gross, N. Galili and I. Saltsman, *Angew. Chem., Int. Ed.*, 1999, **38**, 1427; (*b*) H$_3$(tpfc) is commercially available (Strem Chemicals Inc.).
11 Z. Gross, L. Simkhovich and N. Galili, *Chem. Commun.*, 1999, 599.
12 Z. Gross, N. Galili, L. Simkhovich, I. Saltsman, M. Botoshansky, D. Bläser, R. Boese and I. Goldberg, *Org. Lett.*, 1999, **1**, 599.
13 A. E. Meier-Callahan, H. B. Gray and Z. Gross, *Inorg. Chem.*, 2000, **39**, 3605.
14 L. Simkhovich, N. Galili, I. Saltsman, I. Goldberg and Z. Gross, *Inorg. Chem.*, 2000, **39**, 2704.
15 Z. Gross, G. Golubkov and L. Simkhovich, *Angew. Chem., Int. Ed.*, 2000, **39**, in press.
16 S. Licoccia, E. Morgante, R. Paolesse, F. Polizio, M. O. Senge, E. Tondello and T. Boschi, *Inorg. Chem.*, 1997, **36**, 1564.
17 C. Erben, S. Will and K. M. Kadish, in *The Porphyrin Handbook*, ed. K. M. Kadish, K. M. Smith and R. Guilard, Academic Press, 2000, vol. 2, p. 233.
18 *Crystal data*: (tpfc)Mn(OPPh$_3$), $C_{55}H_{23}F_{15}MnN_4OP$: M = 1126.68, monoclinic, space group $P2_1/n$, a = 13.883(2), b = 12.802(1), c = 25.952(3) Å, β = 100.31(1)°, V = 4537.9(9) Å^3, Z = 4, T = 98 K, D_c = 1.649 g cm^{-3}, μ(Mo-Kα) = 0.44 mm^{-1}, 10384 unique reflections, $R1$ = 0.044 for 5262 observations with $F_o > 4\sigma(F_o)$, $R1$ = 0.117 (wR = 0.075) for all unique data, $|\Delta\rho| \leqslant 0.44$ e Å^{-3}. CCDC 182/177l. See http://www.rsc.org/suppdata/cc/b0/b006299p/ for crystallographic files in .cif format.
19 The measurement was done on a pressed powder sample in a static field of 100 G on a Quantum Design MPMS SQUID magnetometer.
20 Simulations were done by use of the full-matrix-diagonalization program SIM vers. 13.12.99, by H. Weihe, Univ. of Copenhagen. See also: J. Glerup and H. Weihe, *Acta Chem. Scand.*, 1991, **45**, 444.
21 L. Simkhovich, I. Goldberg and Z. Gross, *J. Inorg. Biochem.*, 2000, **80**, 235; J. Bendix, I. J. Dmochowski, H. B. Gray, A. Mahammed, L. Simkhovich and Z. Gross, *Angew. Chem. Int. Ed.*, 2000, **39**, in press.

ChemComm

$RbCuPO_4$ – a maximum copper tetrahedral framework adopting the zeotype ABW structure

Paul F. Henry, Robert W. Hughes, Suzanna C. Ward and Mark T. Weller*

Department of Chemistry, University of Southampton, Highfield, Southampton, UK SO17 1BJ. E-mail: mtw@soton.ac.uk

Received (in Cambridge, UK) 7th August 2000, Accepted 5th September 2000
First published as an Advance Article on the web

The sky blue $RbCuPO_4$-ABW is the first reported maximum copper (framework ratio 1 : 1) zeotype framework, consisting of alternating PO_4 and flattened CuO_4 (Cu–O 1.89–1.95 Å) tetrahedra; a second metastable very pale green–blue phase can also be produced by quenching, with conversion to the purely four-coordinate copper material accomplished by application of slight mechanical pressure.

The incorporation of transition metals into frameworks, including zeolites, is of great interest due to the properties potentially imparted by the presence of d-metal centres including catalytic activity, colour and magnetic ordering phenomena. Zeolite structures containing first row transition metals have received most attention, although in general the levels of substitution have been low, presumably due to the reduced stability of tetrahedral coordination over higher coordination environments (5- and 6-fold) in the aqueous media used to synthesise the majority of framework materials. Work to date has centred on the first row transition metals that do show appreciable tetrahedral coordination chemistry to oxygen, namely Co^{2+} and Zn^{2+}. Frameworks containing high levels of Co^{2+} were first described by Chippindale *et al.*[1] and were extended by Stucky and coworkers, using hydrothermal methods, to include the ABW and related semi-condensed frameworks such as $NaCoPO_4$, $KCoPO_4$, NH_4CoPO_4 and $RbCoPO_4$.[2] We completed this series by synthesising $CsCoPO_4$ ABW using a solid state route.[3] Until recently, the levels of other transition metals that could be doped into most zeolite structure types remained low, at around 5% of the tetrahedral sites. However, synthesis of other maximum transition-metal ABW related frameworks has now been achieved by our group to include $CsFeSiO_4$[4] and $RbNiPO_4$.[5]

We have found that the zeotype structures that permit high levels of transition metal substitution are generally denser, in terms of tetrahedral units per unit volume, and exist with low levels of hydration, for example the ABW, CAS, ANA and BIK zeolite families.[6] In terms of transition metal substitutions, the ANA structure type is the most versatile with transition metal substituted leucite[7] and pollucite[8,9] phases described in the literature. However the levels of substitution in this system are limited through compound stoichiometry at 16.6% of the framework sites, *i.e.* to the one trivalent tetrahedral site.

Here we describe the synthesis and structural characterisation of the ABW-type structure material $RbCuPO_4$, where half of the tetrahedral framework sites are occupied by copper.

A polycrystalline sample of $RbCuPO_4$-ABW was produced as follows. Stoichiometric amounts of $Cu(MeCO_2)_2$ (Aldrich, 99.9%), $(NH_4)_2HPO_4$ (Aldrich, 99%) and RbOH (Aldrich, 50% solution by weight in water) were dissolved in dilute nitric acid. 100 ml ethanol was then added to the solution and the pH slowly raised by the addition of ammonia solution until precipitation occurred. The resulting mixture was slowly evaporated to give a thick gel paste, which was decomposed over 12 h in a furnace at 250 °C. The powder was thoroughly ground in an agate pestle and mortar before being fired at 650 °C and then 750 °C, each for 12 h. Soluble impurities were removed by washing with deionised water followed by firing for 12 h at 750 °C. Powder X-ray diffraction patterns were collected for preliminary phase identification and subsequent Rietveld analysis using a Siemens D5000 diffractometer (Cu-Kα_1 radiation; λ = 1.54056 Å). GSAS was used for Rietveld refinement of the powder X-ray data.[10]

Differential thermal analysis (DTA) and thermogravimetric analysis (TGA) were performed using a Polymer Laboratories STA1500 DTA/TGA balance. The sample was heated in air at a rate of 5 °C min^{-1} from room temperature to 600 °C, held for 30 min at this temperature and then cooled back to room temperature at 10 °C min^{-1}. Diffuse reflectance UV–VIS spectra were obtained from a Lambda19 spectrophotometer with solid state attachment. The Kubelka–Munk function was applied to the data to compensate for the effects of particle size. Elemental analysis was carried out using a JEOL JSM-6400 SEM equipped with a TRACOR series II energy dispersive X-ray analysis system.

Inspection of the powder X-ray diffraction (PXD) pattern of the as-synthesised material showed that the majority phase present could be indexed on an orthorhombic unit cell with a = 8.5262(4) Å, b = 5.3562(3) Å and c = 8.9064(4) Å. There were also several weaker peaks that were indexed on a monoclinic unit cell with a = 5.0424(8) Å, b = 8.5880(2) Å, c = 9.6434(2) Å and α = 91.51(1)°. Both unit cells were consistent with structure types that have been previously reported for the ABW-type framework.[11]

Grinding the product followed by further PXD pattern collection showed that the proportion of the two phases present was altered, with the orthorhombic phase growing in intensity. Quenching the reaction from above 600 °C to RT without any grinding gave the monoclinic phase as the major phase (*ca.* 9 : 1 ratio). Pelletisation of the product under 6 tonnes cm^{-2} for 10 min followed by regrinding gave essentially *only* the orthorhombic product and increased the intensity of the blue colouration of the product. We have also recently found that nickel doping into $RbCuPO_4$ stabilises the monoclinic ABW subtype and details of the new sub-structure will be published elsewhere.[12]

Data for Rietveld profile analysis on the orthorhombic phase were collected over a period of 16 h between 10 and 110° using a step size of 0.02°. The initial model used for the refinement was that of Henry and Weller for $CsFeSiO_4$.[4] Weak constraints (standard deviation 0.01 Å) were placed upon bond lengths in the refinement due to the poor definition of the oxygen positions from powder X-ray diffraction data. A few weak impurity peaks (< 5% of the maximum peak intensity) were also excluded from the refinement. The final refinement profile is illustrated in Fig. 1 and the structural model is given in Table 1. Derived bond lengths and relevant framework bond angles are given in Table 2. It can be seen from Table 2 that the phosphate tetrahedra are much more regular than the cuprate polyhedra, which are flattened in accordance with the expected Jahn–Teller distortion found in other four-coordinate Cu^{II} compounds.[13]

TGA showed the orthorhombic phase to be a non-hydrated framework, as no weight losses were observed between RT and 800 °C. Fig. 2 illustrates the DTA trace obtained for the orthorhombic phase between RT and 600 °C. It can be seen that

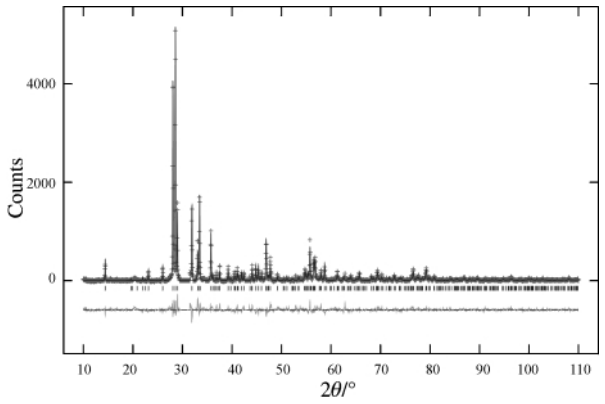

Fig. 1 Final profile fit obtained from the powder X-ray diffraction data for $RbCuPO_4$. The observed data are crosses, the calculated profile pattern the solid line and the lower continuous line the difference plot. Tick marks show the allowed reflection positions.

Table 1 Atomic coordinates for $RbCuPO_4$[a]

Atom	Multiplicity	*x*	*y*	*z*	$10^2U_{iso}/Å^2$
Rb	4*e*	0.1768(4)	0.4719(20)	0.5199(4)	2.80(14)
Cu	4*e*	0.4140(9)	−0.0303(20)	0.3268(7)	4.48(25)
P	4*e*	0.0791(18)	−0.0146(27)	0.1837(14)	4.0(3)
O1	4*e*	0.1419(25)	0.028(5)	0.0294(14)	4.4(7)
O2	4*e*	−0.0621(23)	−0.1769(27)	0.1682(33)	4.4(7)
O3	4*e*	0.0534(31)	0.2262(30)	0.2667(24)	4.4(7)
O4	4*e*	0.2302(23)	−0.1355(34)	0.2249(31)	4.4(7)

[a] Space group $Pc2_1n$: a = 8.5261(4) Å, b = 5.3562(2) Å, c = 8.9064(4) Å, R_p = 12.57%, R_{wp} = 16.72%, R_{F^2} = 17.06% for 315 observations.

Table 2 Derived bond distances (Å) and angles (°) for $RbCuPO_4$ (e.s.d.s are given in parentheses)

P–O1	1.490(6)	O1–P–O2	107.0(17)
P–O2	1.492(6)	O1–P–O3	112.1(19)
P–O3	1.504(7)	O1–P–O4	90.1(16)
P–O4	1.486(6)	O2–P–O3	115.3(17)
Cu–O1	1.892(11)	O2–P–O4	117.9(17)
Cu–O2	1.905(12)	O3–P–O4	112.2(15)
Cu–O3	1.951(12)	O1–Cu–O2	80.9(12)
Cu–O4	1.896(12)	O1–Cu–O3	132.1(11)
		O1–Cu–O4	107.3(12)
		O2–Cu–O3	127.5(12)
		O2–Cu–O4	113.3(12)
		O3–Cu–O4	95.8(12)

there are two phase transitions on heating, at 410 and 550 °C, only one of which is reversible on cooling. It is thought that the first transition is the orthorhombic–monoclinic phase transition but the second transition is yet to be characterised. The first transition can be assigned as the orthorhombic–monoclinic phase interconversion because it is absent on cycling and rapid cooling is known to give the monoclinic phase. Further investigation is planned using variable temperature powder neutron diffraction in order to study the copper coordination sphere, the orthorhombic–monoclinic phase transition and the high temperature polymorph.

Elemental analysis using EDAX confirmed the ratio of Rb:Cu:P to be 1:1:1 within experimental error and the UV–VIS spectrum showed an absorption centred at approximately 610 nm in the visible region, which is consistent with that expected for copper coordinated to four oxygen atoms, *e.g.* $CaCu(MeCO_2)_4.6H_2O$,[13] and the observed sky blue colour.

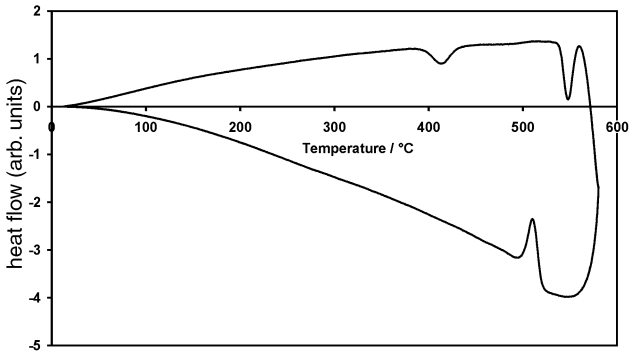

Fig. 2 DTA trace of $RbCuPO_4$ between RT and 600 °C showing two transitions, the first at 410 °C is irreversible under the experimental conditions and the second at 550 °C in the heating cycle and 510 °C in the cooling cycle is reversible.

In this case, the small pore size, illustrated by the fact that the extra-framework counter cation cannot be ion exchanged, either in solution or by melt methods, means that the material is very unlikely to be a selective catalyst, with any activity being restricted to the surfaces of the particles. However, we have shown that high levels of transition metals can be doped into zeotype frameworks using this experimental route, which may lead to new catalytic materials in the future.

We have successfully synthesised the first maximum copper framework (1:1 framework species ratio) with a zeolite topology, $RbCuPO_4$-ABW. Two structurally similar phases exist at room temperature with the proportions being determined by the final heating regime, cooling conditions and subsequent grinding. Slow cooling followed by grinding gives a framework containing purely four-coordinate copper whereas quenching without grinding gives a metastable monoclinic phase as the major phase (*ca.* 9:1 ratio). This second phase, which is very pale green-blue, can be converted back to the purely four-coordinate Cu containing framework by the application of moderate pressure (*e.g.* mechanical grinding or pelletisation). This transition is readily observed by the marked colour change.

We would like to thank the EPSRC for financial support for R. W. H. and the Southampton oceanographic centre for access to SEM facilities.

Notes and references

1 A. M. Chippindale, A. R. Cowley, J. S. Chen, Q. M. Gao and R. R. Xu, *Acta Crystallogr., Sect. C*, 1999, **55**, 845.
2 P. Y. Feng, X. H. Bu, S. H. Tolbert and G. D. Stucky, *J. Am. Chem. Soc.*, 1997, **119**, 2497.
3 P. F. Henry, E. M. Hughes and M. T. Weller, *J. Chem. Soc., Dalton Trans.*, 2000, 555.
4 P. F. Henry and M. T. Weller, *Chem. Commun.*, 1998, 2723.
5 P. F. Henry, R. W. Hughes and M. T. Weller, *Inorg. Chem.*, submitted.
6 W. M. Meier, D. H. Olsen and Ch. Baerlocher, *Zeolites*, 1996, **17**, 1.
7 A. M. T. Bell and C. M. B. Henderson, *Acta Crystallogr., Sect. C*, 1994, **50**, 1531.
8 L. M. Torres-Martinez and A. R. West, *Z. Kristallogr.*, 1986, **175**, 1.
9 A. R. Heinrich and C. Baerlocher, *Acta Crystallogr., Sect. C*, 1991, **47**, 237.
10 A. C. Larson and R. B. Von Dreele, *Generalised Structure Analysis System*, Los Alamos National Laboratory, 1994.
11 X. H. Bu, P. Y. Feng, T. E. Gier and G. D. Stucky, *Zeolites*, 1997, **19**, 200.
12 P. F. Henry, R. W. Hughes, S. C. Ward and M. T. Weller, to be submitted.
13 B. J. Hathaway and D. E. Billing, *Coord. Chem. Rev.*, 1970, **5**, 143.

Stabilised $(H_2)Al–E(H)R$ species, E = P or As, $R^- = C(SiMe_3)_2$-(6-Me-2-pyridyl)$^-$

Philip C. Andrews, Colin L. Raston* and Brett A. Roberts

Department of Chemistry, Monash University, Clayton, Melbourne, Victoria 3800 Australia.
E-mail: c.raston@sci.monash.edu.au

Received (in Columbia, MO, USA) 12th May 2000, Accepted 15th August 2000
First published as an Advance Article on the web

Reaction of $RECl_2$ ($R^- = C(SiMe_3)_2$(6-Me-2-pyridyl)$^-$, E = P or As) with $LiAlH_4$ in THF affords directly bonded aluminium hydride–pnictide hydride complexes as weakly associated hydride bridged dimers, $[RE(H)–Al(H)_2]_2$; a strong solvent dependency of these reactions, which had previously been observed with the formation of the disecondary diphosphane in Et_2O (E = P), is further confirmed by the formation of $RAsH_2$ from $RAsCl_2$ and $LiAlH_4$ in Et_2O.

Compounds containing group 13–15 bonds are of interest as potential precursors to group 13–15 ceramic and semiconductor materials.[1,2] Access to the class of compounds possessing aluminium(III) to phosphorus(III) or arsenic(III) bonds has mainly involved dehydrosilylation reactions of $E(SiMe_3)_3$ with lithium aluminium hydride, $LiAlH_4$,[3] or the trimethylamine adduct of alane, H_3AlNMe_3,[1] affording $(Et_2O)_2Li\{\mu\text{-}E(SiMe_3)_2\}_2AlH_2$, $[H_2Al\{\mu\text{-}P(SiMe_3)_2\}_3]$ and $[H_2AlAs(SiMe_3)_2(NMe_3)]$. Analogous compounds with gallium to phosphorus or arsenic bonds have similarly been prepared.[4,5] Another approach to making compounds with group 13–15 bonds where the metal has exclusively hydrido anionic ligands, other than the simple Lewis base adducts MH_3,[6–9] is transmetallation involving $H_2(X)MPCy_3$ and $LiPCy_2(THF)_n$, Cy = cyclohexyl, M = Ga, X = Cl,[10] M = In, X = H.[9] All the aforementioned phosphide and arsenide compounds are based on secondary phosphines or arsines, the pnictide bearing two substituents, either a trimethylsilyl group or a C-centred ligand. The prospect of forming dihydrido metal complexes based on primary phosphines and arsines is a synthetic challenge because of the likely propensity of spontaneous elimination of hydrogen and formation of polymeric material, although we have noted in earlier studies that secondary amine adducts of alane can be stabilised by the bulk of the amine ligand itself; 2,2,6,6-tetramethylpiperidine forms a stable Lewis base adduct with alane,[6] as does $H\{N(SiMe_3)_2\}$ for which the adduct is a distillable liquid.[7]

Our approach in gaining access to dihydridoaluminium(III) compounds based on primary phosphide and arsenide species, $(H_2)Al–P/As(H)R$, is to incorporate a bulky alkyl group bearing an N-donor centre on the pnictide, notably (6-Me-2-pyridyl)$(SiMe_3)_2C^-$ (= R^-), which has been shown to stabilise unusual bonding configurations, as has the related ligand, C(2-$(SiMe_3)_2$(2-pyridyl)$^-$, allowing access to a range of new compounds.[11–17] The combined steric hindrance of R^- coupled with the N-donor group has the tendency to reduce the degree of aggregation of the target species. In this context its noteworthy that $[H_2Al\{\mu\text{-}P(SiMe_3)_2\}_3]$ is trimeric whereas the NMe_3 adduct of the arsenic analogue is monomeric, $[H_2Al-As(SiMe_3)_2(NMe_3)]$.[1] Herein we report the synthesis of the first alane compounds based on primary phosphine and arsenine moieties, and also the synthesis of a primary arsine, $RAsH_2$, and its structure determination, a first for this class of compound.

The new phosphide and arsenide compounds, $(H_2)Al–P/As(H)R$, **1** (P) and **2** (As), were prepared by the reaction of $RECl_2$ with $LiAlH_4$ in THF, Scheme 1.† The choice of solvent in their synthesis is crucial. We have previously reported that

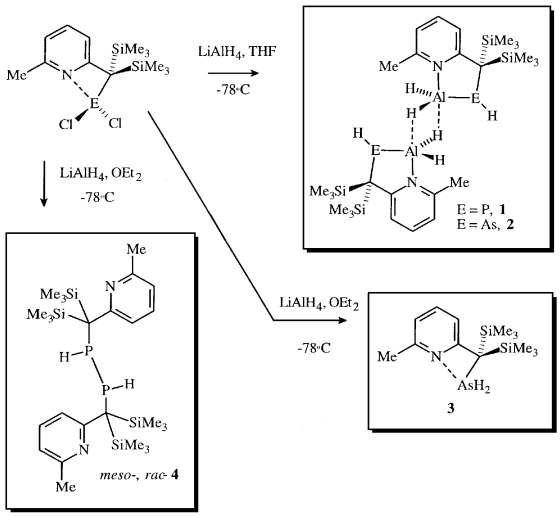

Scheme 1

the reaction of $RPCl_2$ with $LiAlH_4$ in Et_2O affords reproducibly the disecondary diphosphane, **4**, as a mixture of the *rac* and *meso* isomers, and not the expected dihydride species,[12] Scheme 1. In contrast we have now established that the analogous reaction of $RAsCl_2$ with $LiAlH_4$ in Et_2O does in fact result in the target dihydride species, $RAsH_2$, **3**.†

Single crystals of **1**, **2** (Fig. 1) and **3** suitable for single crystal X-ray diffraction were obtained from hexane solutions at −30 °C.‡ Compound **1** decomposes at temperatures above

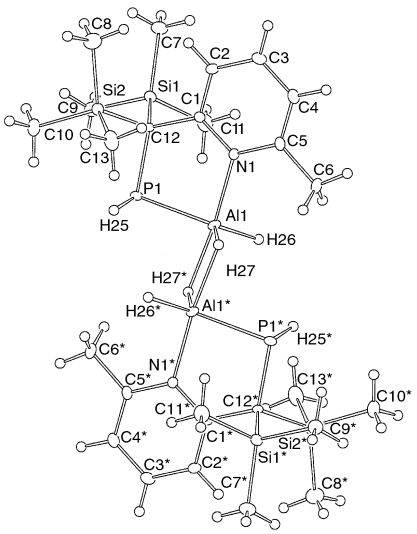

Fig. 1 Projection of $[H_2Al\{P(H)R\}]_2$, **1**. Important bond distances (Å) and angles (°) (values for the arsenic analogue, **2**, in square brackets: Al–N 2.040(2) [2.043(1)], Al–E 2.330(1) [2.4184(5)], Al–H, 1.668, 1.633 [1.60, 1.52(20)], E–H 1.303 [1.54], E–C, 1.913(2) [2.041(2)]; N–Al–P 88.85(6) [89.96(4)], Al–E–C 96.29(8) [92.76(5)], Al–N–C 119.2(2), 120.9(2) [119.5(1), 120.5(1)], Al–E–H 94.6 [93.8].

DOI: 10.1039/b003990j

116 °C to a dark red oil, whereas **2** melts at 206–208 °C. **3** decomposes above 50 °C, darkening in colour from yellow to orange at around 120 °C and at 160 °C it becomes dark red and gradually melts.

Complexes **1** and **2** are isostructural in the solid state (monoclinic, $P2_1/n$) and are dimeric, being weakly associated *via* metal–hydride bridging. The central feature of the two structures is the novel five membered heteroatomic rings containing Al–E bonds, with bond distances of 2.330(1) and 2.418(5) for Al–P and Al–As respectively. The P–Al bond distance is short in comparison to other alkylaluminium–phosphorus complexes, in particular 2.681(4) Å in $[(Me_3C\text{-}CH_2)_3Al{\cdot}P(SiMe_3)_3]$, 2.498(7) Å in $[(Me_3SiCH_2)_2(Br)\text{-}Al{\cdot}P(SiMe_3)_3]$, 2.436(2) Å in $[(Me_3SiCH_2)_3AlP(SiMe_3)_2]_2$,[2] 2.3916(16) Å and 2.4041(14) Å in $[H_2AlP(SiMe_3)_2]_3$[1] and 2.4001(13) Å in $[(Et_2O)_2Li[\mu\text{-}P(SiMe_3)_2]_2AlH_2$,[3] a factor most likely attributable to the steric crowding around the metal centre. The Al–As bond distance is comparable to that found in $[H_2AlAs(SiMe_3)_2]{\cdot}NMe_3$,[1] 2.438(2) Å, and in $[(Et_2O)_2Li[\mu\text{-}P(SiMe_3)_2]_2AlH_2$,[3] 2.4934(7) Å, while it is shorter than in $[(Me_3SiCH_2)(Br)AlAs(SiMe_3)_2]_2$, $[(Me_3CCH_2)_3AlAs\text{-}(SiMe_3)_3]$ and $[(Me_3SiCH_2)_2AlAs(SiMe_3)_2]_2$[2] which have Al–As bond distances of 2.505(3) Å, 2.72(2) Å and 2.567(2) Å respectively. For **1** and **2**, the H atom on E and the bridging H on Al are coplanar; however, in geometrical terms they point away from each other, and at 3.185 Å, **1**, and 3.263 Å, **2**, there is no significant interaction. The non-bridging H on Al and the H on E point away from each other in **1** and **2**.

Despite many attempts we have been unable to obtain a satisfactory refinement for the crystals of $RAsH_2$, **3**, as we have for **1** and **2**. This is due to an inherent twinning disorder and as such the *R*-factor converged at 18%. Although this prejudices discussion on bond distances and angles within the crystal lattice, it is evident that the As centre is involved in a planar four membered chelate with the pyridine ring, through a N···As interaction, similar to that observed in $RECl_2$. Complex **3** is the only arsenic dihydride complex to exhibit N–As connectivity. Given the thermal instability of arsenic hydride it is not surprising that only four other AsH_2 complexes have been structurally characterised[18–20] in the solid state, and these have been stabilised through attachment either to a transition metal, *e.g.* $[Ir(CO)ClH(Pet_3)_2(AsH_2)]$,[18] or to silicon in $[(2,4,6\text{-}i\text{Pr}_3C_6H_2)(^t\text{Bu})Si(AsH_2)_2]$.[20]

In order to assess the potential of complexes **1** and **2** as possible single source precursors for CVD the solids were slowly heated *in vacuo* to 200 °C which resulted in decomposition to an orange solid for **1** and a black solid for **2**. Microprobe analysis on the decomposed solids showed an approximate 1 : 1 ratio for Al : P for **1**, but not so for the As : Al ratio for **2**, which was 1 : 26. There was also evidence of a high percentage of Si present in the samples, indicating that decomposition *via* β-hydrogen transfer to form an intermediate HAl=ER, followed by β-hydrogen elimination of HR, is not evident. While it appears that compounds **1** and **2** are not a direct route to aluminium phosphide and arsenide, a new class of compounds has been established, and the ability of N-functionalised donor alkyl ligands to stabilise an unusual bonding configuration is noteworthy; extending the work to other donor alkyl ligand systems (group 15 and 16), and to the heavier group 13 elements is a synthetic challenge.

We are grateful to the Australian Research Council for support of this work.

Notes and references

† All ^1H and ^{13}C NMR spectra were referenced internally to d_6-benzene. ^{31}P NMR was referenced to a 5% solution of H_3PO_3.

Synthesis of $[H_2Al\{P(H)R\}]_2$, **1**: $LiAlH_4$ 0.44 g, 11.57 mmol, thf 30 ml, $R'PCl_2$ 1.85 g, 5.26 mmol (yield 42%). Mp > 116 °C (decomp). ^1H NMR (400 MHz, C_6D_6, 298 K): δ 0.15 (18H, s, $SiMe_3$), 1.63, 2.18 (1H, d, $^1J_{PH}$ 164 Hz), 2.49 (3H, s, Me), 4.96 (2H, br, AlH_2), 5.97 (1H, m, H_3), 6.64 (1H, m, H_5), 7.11 (1H, m, H_4). ^{13}C NMR (75.0 MHz, C_6D_6, 298 K): δ 1.27 ($SiMe_3$), 24.00 (C_7), 25.76 (C_1), 120.75 (C_5), 123.97 (C_3), 138.44 (C_4), 157.48 (C_6), 170.45 (C_2). $^{31}P\{^1H\}$ (162 MHz, C_6D_6, 298 K): δ −192.20. ^{31}P (162 MHz, C_6D_6, 298 K): δ −194.91, −192.17 ($^1J_{PH}$ 164 Hz). Microanalysis: Calc. (found) C 50.13 (49.85), H 8.74 (8.74), N 4.50 (4.37%). IR (Nujol mull): Al–H 1821.6 cm^{-1}.

Synthesis of $[H_2Al\{As(H)R\}]_2$ **2**: $LiAlH_4$ 0.28 g, 7.38 mmol, thf 30 ml, $R'AsCl_2$ 1.34 g, 3.39 mmol (yield 35%). Mp 206–208 °C. NMR: (^1H, 400 MHz, C_6D_6, 298 K): δ 0.22 (18H, s, $SiMe_3$), 1.84 (1H, s, As–H), 2.26 (3H, s, Me), 4.91 (2H, br, AlH_2), 6.07 (1H, m, H_3), 6.74 (1H, m, H_5), 6.96 (1H, m, H_4); (^{13}C, 75.0 MHz, C_6D_6, 298 K): δ 1.17 ($SiMe_3$), 24.26 (C_7), 26.45 (C_1), 120.25 (C_5), 123.75 (C_3), 138.62 (C_4), 157.46 (C_6), 169.35 (C_2). Microanalysis: Calc. (found) C 43.98 (44.10), H 7.66 (7.92), N 3.94 (4.00%). IR (Nujol mull): Al–H 1819.8 cm^{-1}, As–H 2096 cm^{-1}.

Synthesis of **3** ($R'AsH_2$): $LiAlH_4$ 0.17 g, 4.54 mmol, Et_2O 30 ml, $R'AsCl_2$ 0.90 g, 2.27 mmol (yield 0.45 g, 60.3%). Mp > 50 °C decomp. (orange)–120 °C (red) > 160 °C (melt). NMR: (^1H, 400 MHz, C_6D_6, 298 K): δ 0.057 (18H, σ, $SiMe_3$), 2.43 (3H, s, Me), 3.91 (2H, br, As–H_2), 6.78 (1H, m, H_3), 6.88 (1H, m, H_5), 7.51 (1H, s, H_4); (^{13}C, 75.0 MHz, C_6D_6, 298 K): δ 1.2 ($SiMe_3$), 21.2 (C_7), 50.9 (C_1), 119.1 (C_5), 120.3 (C_3), 137.9 (C_4), 155.7 (C_6), 163.6 (C_2). Microanalysis: Calc. (found) C 47.68 (47.69), H 8.00 (8.26), N 4.28 (4.21%).

‡ *Crystal data*: $[H_2Al\{P(H)R\}]_2$, **1**: $C_{26}H_{54}N_2Al_2P_2Si_4$, monoclinic, $P2_1/n$ (no. 14), a = 9.3949(2), b = 13.7790(3), c = 14.2939(3) Å, β = 99.330(2)°, V = 1825.90(6) Å^3, F(000) = 648, D_{calc} = 1.089 g cm^{-3}, μ(Mo-Kα) = 3.14 cm^{-1}, 0.16 × 0.13 × 0.39 mm^3, Z = 2; Enraf-Nonius CCD diffractometer, Mo-Kα radiation, T = 123 K, 4510 unique reflections (3554 observed, $I > 2.0\sigma(I)$), 2θ = 70.8°, R = 0.051, R' = 0.057 (sigma weights, n = 4 × 10^{-4}).

$[H_2Al\{As(H)R\}]_2$, **2**: $C_{26}H_{54}N_2Al_2As_2Si_4$, monoclinic, $P2_1/n$ (no. 14), a = 9.4334(2), b = 13.7645(3), c = 14.4634(2) Å, β = 99.734(1)°, V = 1850.97(6) Å^3, F(000) = 744, D_{calc} = 1.27 g cm^{-3}, μ(Mo-Kα) = 20.00 cm^{-1}, 0.15 × 0.15 × 0.40 mm^3, Z = 4; Enraf-Nonius CCD diffractometer, Mo-Kα radiation, T = 123 K, 5445 unique reflections (4150 observed, $I > 3.0\sigma(I)$), 2θ = 60.1°, R = 0.030, R' = 0.030 (sigma weights, n = 4 × 10^{-4}).

$[RAsH_2]$ **3**: $C_{13}H_{26}NAsSi_2$, triclinic, $P\bar{1}$ (no. 2), a = 8.7896(7), b = 9.1611(7), c = 11.7955(6) Å, α = 100.069(5), β = 96.977(5)°, V = 854.6(1) Å^3, F(000) = 344, D_{calc} = 1.272 g cm^{-3}, μ(Mo-Kα) = 21.13 cm^{-1}, 0.12 × 0.13 × 0.35 mm^3, Z = 2; Enraf-Nonius CCD diffractometer, Mo-Kα radiation, T = 123 K, 4208 unique reflections (3087 observed, $I > 3.0\sigma(I)$), 2θ = 60.1°, R = 0.183, R' = 0.233 (sigma weights, n = 4 × 10^{-4}).

CCDC 182/1752. See http://www.rsc.org/suppdata/cc/b0/b003990j/ for crystallographic files in .cif format.

1 J. F. Janik and R. L. Wells, *Inorg. Chem.*, 1998, **37**, 3561 and references therein.
2 R. L. Wells and E. E. Foos, *Organometallics*, 1998, **17**, 2869.
3 J. F. Janik and R. L. Wells, *Oragnometallics*, 1998, **17**, 2361 and references therein.
4 J. F. Janik, R. L. Wells, V. G. Young Jr., A. L. Rheingold and I. A. Guezi, *J. Am. Chem. Soc.*, 1998, **120**, 532.
5 J. F. Janik, R. L. Wells, V. G. Young Jr. and J. A. Halfen, *Organometallics*, 1997, **16**, 3022.
6 J. L. Atwood, G. A. Koutsantonis, F.-C. Lee and C. L. Raston, *J. Chem. Soc., Chem. Commun.*, 1994, 91.
7 M. G. Gardiner, G. A. Koutsantonis, S. M. Lawrence, F.-C. Lee and C. L. Raston, *Chem. Ber.*, 1996, **129**, 545.
8 M. G. Gardiner and C. L. Raston, *Coord. Chem. Rev.*, 1997, **166**, 1.
9 M. L. Cole, D. E. Hibbs, C. Jones and N. A. Smithies, *J. Chem. Soc., Dalton Trans.*, 2000, 545.
10 F. M. Elms, G. A. Koutsantonis and C. L. Raston, *J. Chem. Soc., Chem. Commun.*, 1995, 1669.
11 T. R. van den Ancker and C. L. Raston, *J. Organomet. Chem.*, 1995, **500**, 289 and references therein.
12 P. C. Andrews, S. J. King, C. L. Raston and B. A. Roberts, *Chem. Commun.*, 1998, 547.
13 P. C. Andrews, C. L. Raston, B. W. Skelton, V.-A. Tolhurst and A. H. White, *Chem. Commun.*, 1998, 575.
14 P. C. Andrews, C. L. Raston, B. W. Skelton and A. H. White, *Chem. Commun.*, 1997, 1183.
15 P. C. Andrews, C. L. Raston, B. W. Skelton and A. H. White, *Organometallics*, 1998, **17**, 779.
16 P. C. Andrews, C. L. Raston, P. C. Nichols and B. A. Roberts, *Organometallics*, 1999, **21**, 4247.
17 P. C. Andrews, S. J. King, C. L. Raston, B. A. Roberts, B. W. Skelton and A. H. White, unpublished results.
18 E. A. V. Ebsworth, R. O. Gould, R. A. Mayo and M. Walkinshaw, *J. Chem. Soc., Dalton Trans.*, 1987, 2831.
19 J. von Seyerl, A. Frank and G. Hunter, *Cryst. Struct. Commun.*, 1981, **10**, 97.
20 M. Driess and H. Pritzkow, *Chem. Ber.*, 1994, **127**, 477.

Development of a family of β-amino alcohol ligands with two stereocenters for highly efficient enantioselective trimethylsilylcyanation of aldehydes

Jing-Song You,† Han-Mou Gau*[a] and Michael C. K. Choi*[b]

[a] *Department of Chemistry, National Chung-Hsing University, Taichung, Taiwan 402. E-mail: hmgau@dragon.nchu.edu.tw*

[b] *Union Laboratory of Asymmetric Synthesis and Department of Applied Biology and Chemical Technology, The Hong Kong Polytechnic University, Hong Kong*

Received (in Cambridge, UK) 28th July 2000, Accepted 30th August 2000
First published as an Advance Article on the web

The asymmetric addition of Me_3SiCN to aldehydes catalyzed by titanium(IV) complexes of *N*-sulfonylated derivatives of β-amino alcohols gave excellent ee's up to 96% ee.

Optically pure cyanohydrins are important chiral building blocks for a wide variety of chiral products such as α-hydroxy acids, α-hydroxy aldehydes, α-hydroxy ketones, β-hydroxy amines, β-amino alcohols and α-amino acid derivatives.[1] Therefore, in recent years, a number of synthetic methods have been reported employing enzymes, synthetic peptides, and chiral metal complexes.[1,2] Of chiral metal complexes reported so far, titanium-based Lewis acids have attracted the most interest, and the chiral ligands used include TADDOLs,[3] BINOLs,[4] sulfoximines,[5] peptides,[6] Schiff bases[7] and others.[8–10] For examples, the TADDOL–Ti(O-*i*-Pr)$_2$Cl$_2$ catalytic system reported by Narasaka *et al*. gave a 96% ee for benzaldehyde as a substrate at −65 °C.[3] However, for aliphatic aldehydes, the catalytic system gave low ee values of 68–77% ee. With the use of 20 mol% of the sulfoximine–Ti(O-*i*-Pr)$_4$ catalyst reported by Bolm and Müller, the ee values could be up to 91% ee.[5] Recently, Belokon *et al.* reported a very efficient [(salen)Ti(μ-O)]$_2$ catalyst to give the best ee value of 92% ee with the use of only 0.1 mol% of the catalyst.[7] In these studies, the best enantioselectivities were reported by Uang *et al*. with the use of the diamide–Ti(O-*i*-Pr)$_4$ catalytic system giving ee values higher than 96% ee.[9] Despite extensive studies, limitations such as poor enantioselectivities, the lack of wide-range substrate generality, high catalyst loading, or even a stoichiometric use of chiral ligand, were usually encountered. This makes the development of practical and highly effective catalytic systems for the preparation of chiral cyanohydrins much more challenging. Herein we report the synthesis of a new family of *N*-sulfonylated β-amino alcohols with one or two stereocenters as chiral ligands, and the asymmetric addition of Me_3SiCN to aldehydes was conducted‡ (eqn. 1).

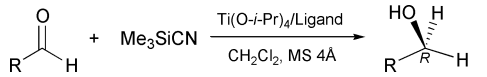

(1)

In this study, we first synthesized the *N*-sulfonylated β-amino alcohols (*S*)-**3** and (*S*)-**4** with only one stereocenter. Unfortunately, the catalytic reaction using (*S*)-**3** or (*S*)-**4** with an equimolar amount of Ti(O-*i*-Pr)$_4$ as a catalyst gave no conversion or low enantioselectivity of 7% ee at 0 °C (entries 1 and 2, Table 1). These results prompted us to develop a novel family of β-amino alcohols with two stereocenters, and based on the route described by Reetz *et al.*,[11] the β-amino alcohols **5** and their *N*-sulfonylated derivatives **6** and **7** with two stereocenters were prepared. The synthetic strategy provides a tremendous pool of various β-amino alcohols *via* variation of both R and R′ groups. While creating the second stereogenic carbon center, it was found that the second stereocenter is controlled by the original amino chiral carbon center, and the major (*R*,*S*)-stereomer and the minor (*S*,*S*)-stereomer can be easily separated by chromatography.

In using the (*R*,*S*)-**6**–Ti(O-*i*-Pr)$_4$ system, the asymmetric addition of Me_3SiCN to benzaldehyde afforded the cyanohydrin in only 14% yield at 0 °C (entry 3). In contrast, employing (*R*,*S*)-**7a** resulted in significant improvement of ee values to 68% ee

Table 1 Enantioselective addition of trimethylsilyl cyanide (Me_3SiCN) to aldehydes catalyzed by *in situ*-formed **3**–**7**–Ti(O-*i*-Pr)$_4$ systems for 48 h

Entry	Ligand/mol%	Aldehyde	Temp./°C	Yield[b] (%)	% ee[c] (Config.)
1	(*S*)-**3** (10)	Benzaldehyde (**1a**)	0	0	—
2	(*S*)-**4** (10)	Benzaldehyde (**1a**)	0	67 (58)	7 (*R*)
3	(*R*,*S*)-**6** (10)	Benzaldehyde (**1a**)	0	14	8 (*R*)
4	(*R*,*S*)-**7a** (10)	Benzaldehyde (**1a**)	0	100	68 (*R*)
5	(*R*,*S*)-**7a** (10)	Benzaldehyde (**1a**)	−40	100	79 (*R*)
6	(*R*,*S*)-**7a** (10)	Benzaldehyde (**1a**)	−65	100 (93)	96 (*R*)
7[a]	(*R*,*S*)-**7a** (10)	Benzaldehyde (**1a**)	−65	52	77 (*R*)
8	(*R*,*S*)-**7a** (5)	Benzaldehyde (**1a**)	−65	90 (81)	94 (*R*)
9	(*R*,*S*)-**7b** (10)	Benzaldehyde (**1a**)	−65	82	62 (*R*)
10	(*R*,*S*)-**7c** (10)	Benzaldehyde (**1a**)	−65	85 (73)	38 (*R*)
11	(*S*,*S*)-**7a** (10)	Benzaldehyde (**1a**)	−65	51 (41)	8 (*S*)
12	(*R*,*S*)-**7a** (10)	4-Chlorobenzaldehyde (**1b**)	−65	93 (85)	90 (*R*)
13	(*R*,*S*)-**7a** (10)	4-Methoxybenzaldehyde (**1c**)	−65	100 (92)	94 (*R*)
14	(*R*,*S*)-**7a** (10)	2-Methoxybenzaldehyde (**1d**)	−65	100 (92)	86 (*R*)
15	(*R*,*S*)-**7a** (10)	2-Naphthaldehyde (**1e**)	−65	95 (88)	96 (*R*)
16	(*R*,*S*)-**7a** (10)	1-Naphthaldehyde (**1f**)	−65	100 (91)	77 (*R*)
17	(*R*,*S*)-**7a** (10)	(*E*)-Cinnamaldehyde (**1g**)	−65	100 (89)	93 (*R*)
18	(*R*,*S*)-**7a** (10)	Isobutyraldehyde (**1h**)	−65	100 (91)	95 (*R*)

[a] Without addition of powdered molecular sieves. [b] Yields were based on ^{1}H NMR analyses of the mixture of cyanohydrin and unreacted aldehyde. In parentheses, isolated yield. [c] Determined by HPLC with Chiralcel OD column for **1a**–**1f**, Chiralcel AS for **1g** and Chiralpak OJ for **1h** after protected as acetyl esters except **1h** as a benzoyl ester. Absolute configurations were determined by comparison of optical rotations with literature values.

DOI: 10.1039/b006128j

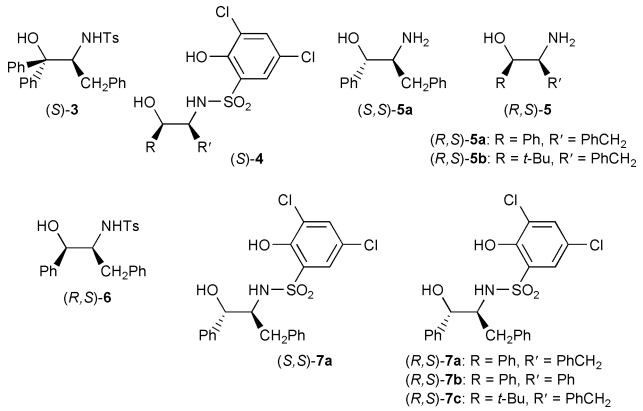

(entry 4). From entries 5 and 6, a significant temperature effect was observed with enantioselectivities of 79% ee at −40 °C (entry 5) and 96% ee at −65 °C (entry 6). Another key factor for the successful practice of highly efficient enantioselective trimethylsilylcyanation of aldehydes is the use of powdered 4 Å molecular sieves. In the absence of molecular sieves, the ee value significantly decreased from 96 to 77% ee with the yield decreased to 52% (entry 7). When as little as 5 mol% of (*R*,*S*)-**7a** was used, an excellent enantioselectivity was still obtained with 94% ee (entry 8). Replacing (*R*,*S*)-**7a** with (*R*,*S*)-**7b** gave a lower enantioselectivity of 62% ee (entry 9). When (*R*,*S*)-**7c** with a benzyl substituent at the amino carbon and a *tert*-butyl substituent at the hydroxy carbon was used, a much lower ee value of 38% ee was obtained (entry 10). For (*S*,*S*)-**7a**, which is a diastereomer of (*R*,*S*)-**7a**, the reaction gave only 8% ee of *S* configuration (entry 11). In addition, other metallic reagents such as $AlMe_3$, $AlEt_3$, Et_2AlCl, $Ti(O\text{-}i\text{-}Pr)_2Cl_2$, $Ti(O\text{-}i\text{-}Pr)Cl_3$ and $TiCl_4$ were also examined. However, the reactions gave low enantioselectivities with the best ee value of only 37% ee. Solvent effect was also studied, and CH_2Cl_2 was the best choice.

The enhanced unique reactivity of the *N*-sulfonylated amino alcohol (*R*,*S*)-**7a** has been suggested to arise from the following factors: (a) phenoxides are known to form strong bonds to group 4 transition metals, and with electron withdrawing halogen groups, the phenoxide moiety may lead to enhanced Lewis acidity at the metal center to improve the reactivity; (b) the phenolic ring further enhances conformational rigidity of these tridendate ligands, which may be an important factor in the transfer of asymmetry.

From entries 12–18, the generality of the asymmetric catalytic reactions employing the (*R*,*S*)-**7a**–$Ti(O\text{-}i\text{-}Pr)_4$ catalytic system was conducted. For aromatic aldehydes (entries 12–16), the asymmetric cyanosilylations gave (*R*)-cyanohydrins with excellent ee values except in the cases of 2-methoxybenzaldehyde (86% ee) and 1-naphthaldehyde (77% ee). The best ee value of 96% ee was obtained for benzaldehyde (entry 6) or 2-naphthaldehyde (entry 15). It is worth noting that, in this study, ee values of 95 and 93% ee were obtained for aliphatic isobutyraldehyde and α,β-unsaturated (*E*)-cinnamaldehyde (entries 17 and 18), respectively.

In conclusion, the first example of highly effective asymmetric addition of a cyano group to aldehydes using *N*-sulfonylated β-amino alcohols as ligands has been reported with excellent enenatioselectivities and with broad substrate generality. Besides, the similar sulfoxamide ligands were also applied to asymmetric diethylzinc addition to aldehydes.[12] This study clearly demonstrates that differences in ligand structures strongly influence the enantioselectivity, and several trends were noted. First, the generation of the second stereocenter greatly improved enantioselectivities. Second, substitution of a flexible benzyl group at the amino carbon ((*R*,*S*)-**7a**) for a rigid phenyl group ((*R*,*S*)-**7b**) resulted in a significant drop in the ee value. Third, aryl substituents on the stereogenic center at the alcoholic carbon proved to be superior to alkyl substituents. The mechanistic study of the catalytic systems and their further applications are currently underway.

Notes and references

† Postdoctoral research fellow from Department of Chemistry, Sichuan University, Peoples Republic of China.

‡ *General procedures for asymmetric cyanosilylation of aldehydes*: Under dry dinitrogen atmosphere, 0.05 mmol of the chiral ligand, 0.05 mmol of $Ti(O\text{-}i\text{-}Pr)_4$, and 100 mg of powdered 4 Å molecular sieves were mixed in 2.0 mL of dry DCM at rt. The mixture was stirred for 1 h and cooled to −65 °C. To the resulting yellow solution were added 1.5 mmol of Me_3SiCN and 0.5 mmol of aldehyde. After the solution was stirred at this temperature for 48 h, the reaction was quenched with 1 M HCl, and the mixture was then vigorously stirred for 4 h. The aqueous phase was extracted with ethyl acetate (3 × 10 mL), and the combined organic layers were dried over $MgSO_4$, and concentrated *in vacuo*. Flash chromatography of the residue on silica gel (elution with 5:1 hexane–ethyl acetate) gave a cyanohydrin. ee was determined by HPLC after protection as acetyl esters (except **1h**, which was protected as a benzoyl ester).

1 R. J. H. Gregory, *Chem. Rev.*, 1999, **99**, 3649; F. Effenberger, *Angew. Chem., Int. Ed. Engl.*, 1994, **33**, 1555; C. G. Kruse in *Chirality in Industry*, ed. A. N. Collins, G. N. Schedrake and J. Crosby, Wiley, Chichester, 1992, chapter 14.
2 M. North, *Synlett*, 1993, 807.
3 D. E. Ward, M. J. Hrapchak and M. Sales, *Org. Lett.*, 2000, **2**, 57; K. Narasaka, T. Yamada and H. Minamikawa, *Chem. Lett.*, 1987, 2073.
4 M. Mori, H. Imma and T. Nakai, *Tetrahedron Lett.*, 1997, **38**, 6229.
5 C. Bolm and P. Müller, *Tetrahedron Lett.*, 1995, **36**, 1625.
6 H. Nitta, D. Yu, M. Kudo, A. Mori and S. Inoue, *J. Am. Soc.*, 1992, **114**, 7969.
7 L. Z. Flores-Lopéz, M. Parra-Hake, R. Somanathan and P. J. Walsh, *Organometallics*, 2000, **19**, 2153; Y. N. Belokon, S. Caveda-Cepas, B. Green, N. S. Ikonnikov, V. N. Khrustalev, V. S. Larichev, M. A. Moscalenko, M. North, C. Orizu, V. I. Tararov, M. Tasinazzo, G. I. Timofeeva and L. V. Yashkina, *J. Am. Chem. Soc.*, 1999, **121**, 3968; X. Zhou, J. Huang, P. Ko, K. Cheung and C. Che, *J. Chem. Soc., Dalton Trans.*, 1999, 3303; V. I. Tararov, D. E. Hibbs, M. B. Hursthouse, N. S. Ikonnikov, K. M. A. Malik, M. North, C. Orizu and Y. N. Belokon, *Chem. Commun.*, 1998, 387; Y. Jiang, L. Gong, X. Feng, W. Hu, W. Pan, Z. Li and A. Mi, *Tetrahedron*, 1997, **53**, 14 327; M. Hayashi, T. Inoue, Y. Miyamoto and N. Oguni, *Tetrahedron*, 1994, **50**, 4385; M. Hayashi, Y. Miyamoto, T. Inoue and N. Oguni, *J. Org. Chem.*, 1993, **58**, 1515.
8 J. M. Brunel, O. Legrand and G. Buono, *Tetrahedron: Asymmetry*, 1999, **10**, 1979.
9 C. Hwang, D. Hwang and B. Uang, *J. Org. Chem.*, 1998, **63**, 6762.
10 D. Callant, D. Stanssens and J. G. de Vries, *Tetrahedron: Asymmetry*, 1993, **4**, 185.
11 M. T. Reetz, M. W. Drewes and A. Schmitz, *Angew. Chem., Int. Ed. Engl.*, 1987, **26**, 1141.
12 J. Qiu, C. Guo and X. Zhang, *J. Org. Chem.*, 1997, **62**, 2665; J. Balsells and P. J. Walsh, *J. Am. Chem. Soc.*, 2000, **122**, 3250.

Chemo- and regioselective crossed alkyne cyclotrimerisation of 1,6-diynes with terminal monoalkynes mediated by Grubbs' catalyst or Wilkinson's catalyst†

Bernhard Witulski,* Thomas Stengel and Jesús M. Fernández-Hernández

Fachbereich Chemie, Universität Kaiserslautern, Erwin Schrödinger Straße, D-67663 Kaiserslautern, Germany. E-mail: witulski@rhrk.uni-kl.de

Received (in Liverpool, UK) 7th July 2000, Accepted 30th August 2000
First published as an Advance Article on the web

A novel protocol for crossed alkyne cyclotrimerisations mediated by Grubbs' catalyst [$RuCl_2$(=CHPh)(PCy_3)$_2$] allows the efficient synthesis of 4,6-substituted indolines with high regioselectivity, and it is complementary to alkyne cyclotrimerisations mediated by Wilkinson's catalyst [RhCl(PPh_3)$_3$] allowing the regioselective synthesis of the corresponding 4,5-substituted isomers in many cases.

The transition metal catalysed cyclotrimerisation of alkynes has been recognised as a versatile synthetic approach for highly substituted benzenes.[1] While the intramolecular version has been established as an efficient synthetic method, the efficiency of the conceptually more flexible crossed cyclotrimerisation of tethered diynes with monoalkynes has to be evaluated by the ability to gain control over the chemo- and regioselectivity of this process.[2] Only a few reports appear using differently substituted diynes and monoalkynes in crossed cyclotrimerisation reactions,[2d,h,m,3] and in most cases the observed regioselectivity was either dependent on a reactivity preference of a given substrate or limited by the use of sterically encumbered substituents.

Recently, we reported a novel synthesis of indolines based on a rhodium-catalysed crossed cyclotrimerisation with *N*-functionalised alk-1-ynylamides, a process which provides flexible access to 4-, or 7-, as well as to 4- and 7-substituted indolines.[3] While servicing a number of objectives in indole synthesis, this method has not yet been applicable for the regioselective synthesis of indolines bearing substituents in the 4,6-, or 4,5-position—a feature of numerous compounds of synthetic and medicinal interest.[4] We propose below a solution to this challenging issue by using either Grubbs' catalyst [$RuCl_2$(=CHPh)(PCy_3)$_2$] **A** or Wilkinson's catalyst [RhCl(PPh_3)$_3$] **B** in crossed alkyne cyclotrimerisations.

At the outset of our studies we anticipated that a crossed alkyne cyclotrimerisation based on a cascade of metathesis steps could contribute to the above problem set, because metathesis catalytic cycles usually begin with a regioselective addition of the ylidene-transition metal complex to the less hindered site of an olefinic or acetylenic substrate.[5] Based on the findings of Blechert and Roy, that the complex **A** caused a fully intra- or intermolecular alkyne cyclotrimerisation,[6] we projected a catalytic cycle as outlined in Scheme 1. The preferred addition of complex **A** to the least substituted alkyne moiety of the 1,6-diyne should be supported by a coordination of the remaining triple bond to the ruthenium complex, thus causing the chemo- and regioselectivity of this process. A cascade of intra- and intermolecular, as well as ring closing metathesis steps, which are related to the well established enyne and olefin metathesis,[7] would finally result in the liberation of the ruthenium benzylidene catalyst and in the preferred formation of the corresponding *meta*-isomer.

A first set of examples was obtained by the reaction of the 1,6-diyne **1** (0.02 M in CH_2Cl_2) with the monoalkynes **2a–d** (5 eq.) in the presence of 5 mol% **A** at 40 °C (Scheme 2, Table 1). During a period of 10–20 h the starting material was consumed giving the isoindolines **3a–d** in 81–89% yield after chromatography on silica gel (entries 1–4). Although in some cases the amount of **2** could be reduced to 2 eq., best results were obtained using 5 eq., which effectively suppressed a competitive cotrimerisation of **1**. In agreement with our mechanistic hypoth-

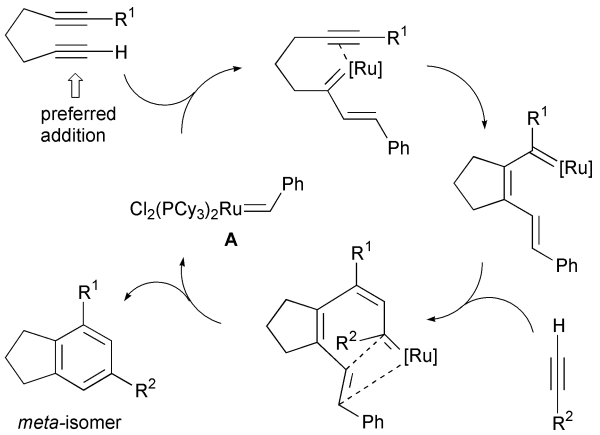

Scheme 1

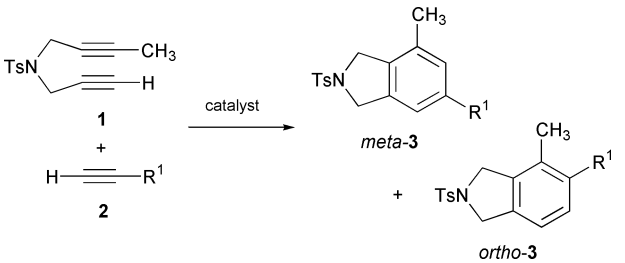

Scheme 2

Table 1 Cycloaddition of **1** with **2a–d** mediated by Grubbs'catalyst **A** or Wilkinson's catalyst **B**‡[a]

Entry	**2**	R^1	Catalyst (mol%)	Yield (%)[b]		*meta*:*ortho*[c]
1	**2a**	Ph	**A** (5)	**3a**	82	5:1
2	**2b**	C_3H_7	**A** (5)	**3b**	92	6:1
3	**2c**	CH_2OH	**A** (5)	**3c**	81	6:1
4	**2d**	$(CH_2)_2OH$	**A** (5)	**3d**	89	6:1
5	**2a**	Ph	**B** (5)	**3a**	52	1:8
6	**2b**	C_3H_7	**B** (5)	**3b**	61	1:4
7	**2c**	CH_2OH	**B** (5)	**3c**	90	1:10
8	**2d**	$(CH_2)_2OH$	**B** (5)	**3d**	79	1:1.5

[a] *Reaction conditions:* monoalkyne (5 eq.), reactions with catalyst **A** [$RuCl_2$(=CHPh)(PCy_3)$_2$] were run in CH_2Cl_2 at 40 °C in a sealed tube for various reaction times (10–20 h), reactions with catalyst **B** [RhCl(PPh_3)$_3$] were run in toluene at rt for various reaction times (10–15 h). [b] Yield after purification by silica gel chromatography. [c] Determined by ^{1}H-NMR.

† Electronic supplementary information (ESI) available: experimental procedures and analytical data for **3**, **4** and **5**. See http://www.rsc.org/suppdata/cc/b0/b005636g/

DOI: 10.1039/b005636g

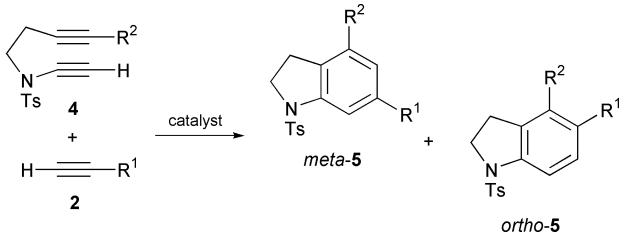

Scheme 3

Table 2 Cycloaddition of **4a**–**b** with **2b**–**e** mediated by Grubbs' catalyst **A** or Wilkinson's catalyst **B**‡[a]

Entry	4	R^2	2	R^1	Catalyst (mol%)	Yield (%)[b]	*meta*:*ortho*[c]
1	**4a**	CH_3	**2c**	CH_2OH	**A** (5)	**5a** 70	9:1
2	**4a**	CH_3	**2d**	$(CH_2)_2OH$	**A** (10)	**5b** 51	9:1
3	**4a**	CH_3	**2e**	$(CH_2)_3OH$	**A** (10)	**5c** 57	9:1
4	**4b**	Ph	**2c**	CH_2OH	**A** (10)	**5d** 60	9.5:1
5	**4a**	CH_3	**2b**	C_3H_7	**B** (5)	**5e** 54	1:10
6	**4a**	CH_3	**2c**	CH_2OH	**B** (5)	**5a** 67	1:20
7	**4a**	CH_3	**2d**	$(CH_2)_2OH$	**B** (5)	**5b** 66	1:3
8[d]	**4b**	Ph	**2c**	CH_2OH	**B** (5)	**5f** 70	1:1

[a] *Reaction conditions:* monoalkyne (5 eq.), reactions with catalyst **A** [$RuCl_2$(=CHPh)(PCy_3)$_2$] were run in CH_2Cl_2 at 40 °C in a sealed tube for various times (10–20 h), reactions with catalyst **B** [$RhCl(PPh_3)_3$] were run in toluene at rt for various reaction times (10–15 h). [b] Yield after purification by silica gel chromatography. [c] Determined by ^{1}H-NMR. [d] Reaction run at 100 °C.

esis, well pronounced selectivities were observed with ratios of *meta*:*ortho* = 5:1 and 6:1 for **3a** and **3b**–**d**, respectively.‡

Most strikingly, when the same set of compounds was treated with 5 mol% Wilkinson's catalyst **B** in toluene at 20 °C, the regioselectivities of the above reactions could be reversed giving the *ortho*-isomers of **3a**–**d** as major products with ratios of *meta*:*ortho* = 1:8, 1:4, 1:10, and 1:1.5, respectively (Table 1, entries 5–8).§ However, in the case of complex **B**—a catalyst that is assumed to operate through rhodacyclooligoolefins as intermediates in alkyne cyclotrimerisations—the outcome of regioselectivity was markedly dependent on the substituent of the monoalkyne **2**.

Finally, we applied our findings to the regioselective synthesis of 4,6- and 4,5-substituted indolines using either complex **A** or **B** as catalyst and the 1,6-diynes **4a** (R^2 = Me) or **4b** (R^2 = Ph) together with the monoalkynes **2b**–**e** (Scheme 3, Table 2).[8] When complex **A** was applied in CH_2Cl_2 at 40 °C the indolines **5a**–**d** were obtained in 51–70% yield, and once again with excellent *meta*-selectivities of *meta*:*ortho* = 9:1 and 9.5:1 for **5a**–**c** and **5d**, respectively (entries 1–4). However, a higher catalyst load of 10 mol% **A** was in some cases necessary for the completion of the reaction. Notably, nearly uniform isomer ratios were observed being independent of the substitution pattern of the alkynes used. These uniform ratios and comparably higher selectivities for the formation of the 4,6-substituted indolines *meta*-**5a**–**d** should be attributed to the electron richness of the alk-1-ynylamide moiety in **4a** and **4b** causing a clear and distinct preference for the addition of the electrophilic ruthenium benzylidene complex **A** to this electron rich triple bond and thus underlying our mechanistic hypothesis.

Gratifyingly, when the 1,6-diyne **4a** and the monoalkynes **2b**,**c** were treated with 5 mol% Wilkinson's catalyst **B** in toluene at 20 °C, again a switch in regioselectivity was observed, allowing the regioselective synthesis of 4,5-substituted indolines.§ Under these conditions the products **5e** and **5b** were obtained in 54 and 67% yield with excellent selectivities of *meta*:*ortho* = 1:10, and 1:20, respectively (entries 5 and 6). However, only a moderate preference for the *ortho*-isomer of **5b** (*meta*:*ortho* = 1:3) was found in the reaction of **4a** (R^2 = CH_3) with but-3-yn-1-ol **2d**, and the reaction of **4b** (R^2 = Ph) with **2c** occurred without a significant selectivity. Obviously crossed alkyne cyclotrimerisation catalysed by complex **B** are more sensitive to steric hindrance and the substitution pattern of the alkynes, than those catalysed by **A**.

In conclusion, we have achieved a new protocol for chemo- and regioselective crossed alkyne cyclotrimerisations mediated by Grubbs' complex **A**, which is most likely based on a cascade of metathesis steps. This novel catalytic protocol offers an efficient, flexible and highly regioselective access to 4,6-substituted indolines. Moreover, in many cases the regioselectivity of the alkyne cyclotrimerisation could be switched affording the corresponding 4,5-substituted indolines, when Wilkinson's catalyst **B** was used. Notably, both catalysts are commercially available and tolerate a wide range of functionalities.

Financial support of this work by the Deutsche Forschungsgemeinschaft (Wi-1696) is gratefully acknowledged.

Notes and references

‡ All new compounds exhibited satisfactory spectra and elemental analyses. The regioisomers could be separated by simple flash chromatography on silica gel.

§ Regioselectivities of crossed alkyne cyclotrimerisations using catalyst **B** were solvent dependent. Best selectivities were obtained with non-polar solvents like toluene. A detailed discussion on the solvent-dependency of this process will be presented in the full account of this study.

1 D. B. Grotjahn in *Comprehensive Organometallic Chemistry II*, ed. L. S. Hegedus, E. W. Abel, F. G. A. Stone and G. Wilkinson, Pergamon, Oxford, 1995, vol. 12, p. 741; N. E. Shore, in *Comprehensive Organic Synthesis: Selectivity, Strategy, and Efficiency in Modern Organic Chemistry*, ed. B. M. Trost and I. Fleming, Pergamon, Oxford, 1991, vol. 5, p. 1129.

2 (*a*) E. Müller, *Synthesis*, 1974, 761; (*b*) R. Grigg, R. Scott and P. Stevenson, *Tetrahedron Lett.*, 1982, **23**, 2691; (*c*) R. L. Hillard III, C. A. Parnell and K. P. C. Vollhardt, *Tetrahedron*, 1983, **39**, 905; (*d*) K. P. C. Vollhardt, *Angew. Chem., Int. Ed. Engl.*, 1984, **23**, 539; (*e*) R. Grigg, R. Scott and P. Stevenson, *J. Chem. Soc., Perkin Trans. 1*, 1988, 1357; (*f*) P. Bahataran and E. H. Smith, *J. Chem. Soc., Perkin Trans 1*, 1992, 2163; (*g*) D. F. Taber and M. Rahimizadeh, *Tetrahedron Lett.*, 1994, **35**, 9139; (*h*) F. E. McDonald, H. Y. H. Zhu and C. R. Holmquist, *J. Am. Chem. Soc.*, 1995, **117**, 6605; (*i*) D. M. Duckworth, S. Lee-Wong, A. M. Z. Slawin, E. H. Smith and D. J. Williams, *J. Chem. Soc., Perkin Trans. 1*, 1996, 815; (*j*) Y. Sato, K. Ohashi and M. Mori, *Tetrahedron Lett.*, 1999, **40**, 5231; (*k*) R. Grigg, V. Sridharan and J. Zhang, *Tetrahedron Lett.*, 1999, **40**, 8277; (*l*) A. Bradley, W. B. Motherwell and F. Ujjainwalla, *Chem. Commun.*, 1999, 917; (*m*) Y. Yamamoto, R. Ogawa and K. Itoh, *Chem. Commun.*, 2000, 549.

3 B. Witulski and T. Stengel, *Angew. Chem., Int. Ed.*, 1999, **38**, 2426.

4 R. J. Sundberg in *Indoles*, Academic Press, London, 1996; G. W. Gribble, *J. Chem. Soc., Perkin Trans. 1*, 2000, 1045.

5 W. J. Zuercher, M. Scholl and R. H. Grubbs, *J. Org. Chem.*, 1998, **63**, 4291; S.-H. Kim, N. Bowden and R. H. Grubbs, *J. Am. Chem. Soc.*, 1994, **116**, 10 801.

6 J.-U. Peters and S. Blechert, *Chem. Commun.*, 1997, 1983; S. K. Das and R. Roy, *Tetrahedron Lett.*, 1999, **40**, 4015.

7 R. H. Grubbs and S. Chang, *Tetrahedron*, 1998, **54**, 4413; M. Mori, *Top. Organomet. Chem.*, 1998, **1**, 133; S. K. Armstong, *J. Chem. Soc., Perkin Trans. 1*, 1998, 371; M. Schuster and S. Blechert, *Angew. Chem., Int. Ed. Engl.*, 1997, **36**, 2036.

8 For the synthesis of alky-1-ynylamides see: B. Witulski and M. Gößmann, *Chem. Commun.*, 1999, 1879; B. Witulski and T. Stengel, *Angew. Chem., Int. Ed.*, 1998, **37**, 489; and ref. 3.

ChemComm

A novel hyperbranched polyether by melt transetherification

M. Jayakannan and S. Ramakrishnan*

Department of Inorganic and Physical Chemistry, Indian Institute of Science, Bangalore 560012, India. E-mail: raman@ipc.iisc.ernet.in; Fax: 91-80-360-1552

Received (in Cambridge, UK) 10th July 2000, Accepted 24th August 2000
First published as an Advance Article on the web

Melt self-condensation of 1-(2-hydroxyethoxy)-3,5-bis-(methoxymethyl)-2,4,6-trimethylbenzene in the presence of an acid catalyst *via* a transetherification process yielded a soluble high molecular weight hyperbranched polyether, whose structure was established by NMR spectroscopy.

Highly branched macromolecules, such as dendrimers and hyperbranched polymers, adopt compact conformations and possess a large number of terminal functional groups. This drastically alters both their solution and bulk properties. Several reviews have appeared in the recent literature, that describe the synthesis, structural properties and applications of dendrimers and hyperbranched polymers.[1–4] Despite the presence of significant levels of structural imperfections, hyperbranched polymers present one major advantage over their structurally perfect cousins and that is the ease of synthesis, which is most often a one-pot self-condensation of an AB_2-type monomer. More importantly, several of the interesting *dendrimeric* properties, such as low melt-viscosity and high functionality, are also exhibited by hyperbranched polymers, thereby making them excellent alternatives to the synthetically cumbersome dendrimers for certain kinds of applications. A large variety of hyperbranched polymers, namely polyesters, polyurethanes, polyamides, polyphenylenes, polysiloxanes, polycarbonates and polyethers have been reported.[3,4] One important feature of the polyether class is their high solubility in common organic solvents, which make them more readily amenable for the study and exploitation of their properties in solution. Hyperbranched polyethers of several types have also been reported in the literature.[5–8] Most of these procedures yielded moderate to high molecular weight polymers, however, they lack adaptability toward structural variation, in that they always require a phenolic group and an aryl/benzyl halide.

Recently, we reported a melt transetherification methodology for the synthesis of linear polyethers.[9] Fully substituted bisbenzyl methyl ethers readily underwent *melt-condensation* with diols in the presence of an acid catalyst to give polyethers of moderate molecular weights. In this report the transetherification methodology is extended for the preparation of a hyperbranched polyether under *melt* condition. For this purpose an AB_2 monomer having a hydroxy group (A) and two benzyl methyl ether groups (B) was targeted. An additional requirement for the transetherification approach to function effectively without crosslinking is the preclusion electrophilic aromatic substitution, which is fulfilled by complete substitution of all the aromatic sites in the monomer.[9] The simplest monomer that meets all these criteria is 1-(2-hydroxyethoxy)-3,5-bis(methoxymethyl)-2,4,6-trimethylbenzene (**3**), which is readily prepared from commercially available mesitol, as shown in Scheme 1. Mesitol was bis-chloromethylated and reacted with $NaOCH_3$–methanol to give the intermediate **2** in good yield. It was then treated with 2-chloroethanol to give the monomer **3**. This monomer was readily polymerized at 145–150 °C in the presence of toulene-*p*-sulfonic acid (PTSA) as catalyst. Typically, the polymerization is carried out under N_2 purge for 30 min and then under reduced pressure (0.01 mm of Hg) for an additional 15 min to attain high molecular weight. To start with, the contents of the reaction vessel formed a clear melt but as the condensation proceeded it transformed into a solid mass. The solid polymer was dissolved in THF, filtered to remove any unwanted insoluble material, and then precipitated into methanol. The precipitate was isolated and dried to give the polymer in 82% yield. The expected structure of the resulting hyperbranched polyether is shown in Scheme 1.

The ^{1}H-NMR spectra of the monomer **3** and the polymer are shown in Fig. 1, along with the assignments of the various peaks. Comparison of the spectrum of the monomer with that of the polymer reveals several interesting features. Firstly, as expected for high conversions, there is a 50% decrease in the relative intensity of the peak **d**, corresponding to Ar-CH_2OCH_3 protons, and a complete disappearance of the peak **b**, corresponding to the –CH_2OH protons, in the spectrum of the polymer (Fig. 1-B). Furthermore, two types of benzylic protons (**a**$_1$ and **a**$_2$) of equal intensity—one corresponding to the unreacted benzyl methyl ether (Ar-CH_2OCH_3) and the other to the reacted one (Ar-CH_2OR–), are seen in the polymer spectrum. These observations confirm that the transetherification process has indeed occurred to very high conversions to yield a polymer with the expected structure. One other interesting feature is the transformation of the peaks corresponding to the aromatic methyl groups from two singlets (**e** and **f**) in the monomer to a cluster of at least five well-resolved peaks (six inclusive of a shoulder), suggesting the presence of several distinct chemical environments in which they are present.

In general, hyperbranched polymers are expected to have different types of subunits, such as dendritic (D), linear (L) and terminal (T) units. Most often, the presence of these various units is established and quantified based on the ^{1}H-NMR signals corresponding to the aromatic protons belonging to them. Interestingly, in the present polyether a significantly more intense Ar-CH_3 signal appears to reveal the presence of these subunits. A total of six aromatic methyl signals (in the region between 2.3–2.5 ppm) are seen, as opposed to a total of seven that might be expected if no coincidental overlaps are present—two each corresponding to dendritic and terminal units and three to the linear unit. As expected, the sum total of the intensities of these Ar-CH_3 peaks is in the expected ratio with respect to the other peaks, **c** and **d**. In order to calculate the degree of branching (DB), it is essential to identify and quantify the mole fraction of the various subunits D, L and T, in such hyperbranched structures. Based on topological considerations

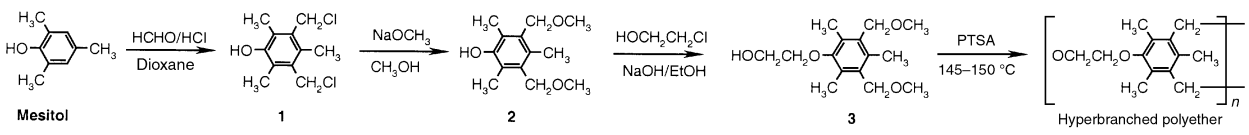

Scheme 1

DOI: 10.1039/b005552m

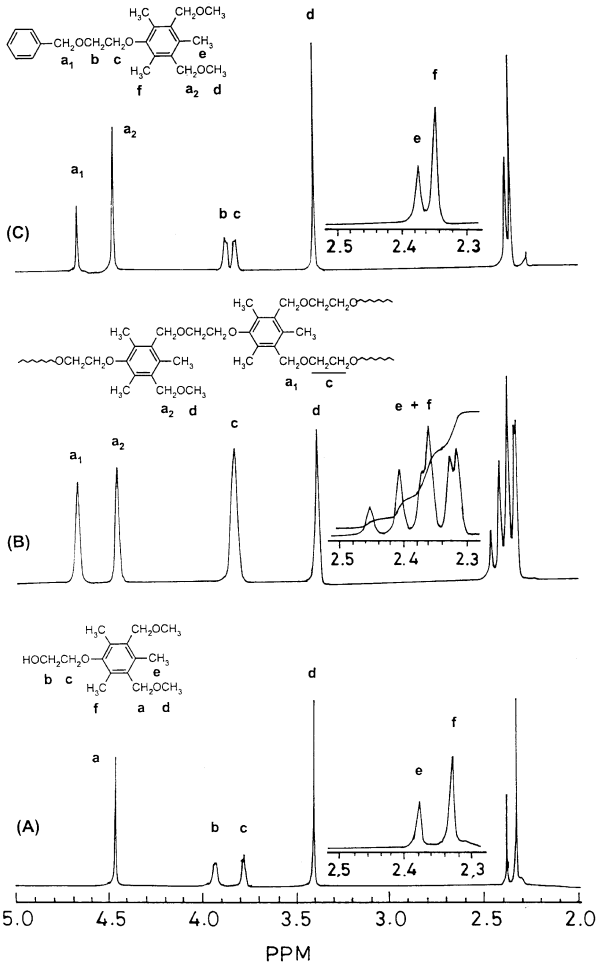

Fig. 1 500 MHz ^{1}H-NMR spectra of the monomer (A), polymer (b) and model compound (C), in $CDCl_3$.

it has been shown that hyperbranched structures will always possess equal number of D and T units (at high conversions), and the DB has been calculated for several polymers using a simplified expression (eqn. 1), from the mole fraction of the terminal units alone.[8,10–13]

$$\mathrm{DB} = \frac{[\mathrm{D}]+[\mathrm{T}]}{[\mathrm{D}]+[\mathrm{L}]+[\mathrm{T}]} = \frac{2[\mathrm{T}]}{[\mathrm{D}]+[\mathrm{L}]+[\mathrm{T}]} \quad (1)$$

In order to identify the methyl peaks belonging to the terminal units, a model compound **4** (see Fig. 1-C) was prepared by reacting **2** with 2-benzyloxy-1-chloroethane in presence of a base, and its ^{1}H-NMR spectrum is shown in Fig. 1. Upon comparison of the spectrum of the model compound with that of the polymer, it is clear that the peaks between 2.34–2.39 ppm in the polymer corresponds to the Ar-CH_3 protons of the terminal unit. The sensitivity of the chemical shifts of these methyl protons to its chemical environment is apparent when one compares the spectrum of model compound **4** with that of the monomer; the transformation of a remote hydroxy group to a benzyl ether causes a significant downfield shift of the two *ortho*-methyl protons peak, **f**. Thus, a non-exact match between the chemical shifts of model compound **4** and the polymer is not surprising; the *ortho*-methyl signal **f** appears slightly further downfield in the polymer. Thus, the DB was calculated from the relative intensities of the two peaks assigned to the terminal unit (between 2.34–2.39 ppm) with respect to the total intensity of all the methyl signals (between 2.3–2.49 ppm), as per the above formula. This number works out to be 0.78 suggesting that a fairly high degree of branching has been achieved. In the absence of the dendritic model compound,[13] we rely on the *ca.* 1 : 2 intensity ratio of the shoulder to peak (**e** : **f**) in the polymer spectrum to confirm the absence of peaks due to other subunits within this one. Typical values for DB quoted in the literature range from 0.4–0.8.[14] Special efforts using a gradual addition of the AB_2 monomer to a polyfunctional B-type core monomer (B_f), are often needed to further increase the degree of branching.[15]

The molecular weight of the polymer was determined by GPC using polystyrene standards and it showed a broad distribution with M_W of 103 000 and a polydispersity of 5.8. The high polydispersity is typical of such hyperbranched structures. The DSC thermogram of the polymer was recorded under a dry N_2 purge, and the sample was first heated to 150 °C and then quenched to −100 °C at 30 °C min^{-1}. It was then reheated from −100 to 150 °C at 10 °C min^{-1} and cooled at the same rate to record the thermograms. No crystallization and melting transitions were observed either during the heating or cooling runs, which suggests that the samples were completely amorphous. A glass transition temperature (T_g) was, however, clearly visible at 28 °C.

In conclusion, we have shown that the *melt transetherification* approach can be readily adapted for the preparation of hyperbranched polyethers. More importantly, the intermediate **2** is readily amenable to a variety of structural variation by incorporation of various types of alkyl and oligoethyleneoxy spacers, to generate a wide range of AB_2 monomers. Such an inclusion of spacer segments into hyperbranched polyethers is not readily possible using most other previous methods, which makes this approach especially useful for preparing a range of hyperbranched structures starting from a single intermediate. A particularly interesting series of hyperbranched polyethers would be the one that incorporates oligoethyleneoxy segments. This would lead essentially to branched polyethylene oxides, which could serve as potential candidates for solid polymer electrolyte applications.[16,17] Work along these lines is currently in progress and will be reported shortly.

We would like to thank Department of Science and Technology, New Delhi, for financial support, and Dr Shiv Venkataramani, 3M-Center, St. Paul, for GPC analysis.

Notes and references

1 A. W. Bosman, H. M. Janssen and E. W. Meijer, *Chem. Rev.*, 1999, **99**, 1665.
2 C. J. Hawker, *Adv. Polym. Sci.*, 1999, **147**, 144.
3 Y. H. Kim, *J. Polym. Sci., Polym. Chem. Ed.*, 1998, **36**, 1685.
4 A. Hult, M. Johansson and E. Malmstrom, *Adv. Polym. Sci.*, 1999, **143**, 1.
5 V. Percec and M. Kawasumi, *Macromolecules*, 1992, **25**, 3843.
6 K. E. Uhrich, C. J. Hawker and J. M. J. Frechet, *Macromolecules*, 1992, **25**, 4583.
7 T. M. Miller, T. X. Neenan, E. W. Kwock and S. M. Stein, *J. Am. Chem. Soc.*, 1993, **115**, 356.
8 C. J. Hawker and F. Chu, *Macromolecules*, 1996, **29**, 4370.
9 M. Jayakannan and S. Ramakrishnan, *Macromol. Chem. Phys.*, 2000, **201**, 759.
10 K. L. Wooley, C. J. Hawker, R. Lee and J. M. J. Frechet, *Polym. J.*, 1994, **26**, 187.
11 D. Yan, A. H. E. Muller and K. Matyjaszewski, *Macromolecules*, 1997, **30**, 7024.
12 H. R. Kricheldorf, O. Stober and D. Lubbers, *Macomolecules*, 1995, **28**, 2118.
13 Attempts to prepare the dendritic model compound using standard approaches did not yield the desired product, and hence the unequivocal confirmation of the absence of coincidental overlap is yet to be established.
14 D. Holter, A. Burgath and H. Frey, *Acta Polym.*, 1997, **48**, 30.
15 D. Holter and H. Frey, *Acta Polym.*, 1997, **48**, 298.
16 C. J. Hawker, F. Chu, P. J. Pomery and D. J. T. Hill, *Macromolecules*, 1996, **29**, 3831.
17 A. Kumar and S. Ramakrishnan, *Macromolecules*, 1996, **29**, 2524.

ChemComm

Quadruple hydrogen bonded oligo(*p*-phenylene vinylene) dimers

Abdelkrim El-ghayoury, Emiel Peeters, Albertus P. H. J. Schenning and E. W. Meijer*

Laboratory of Macromolecular and Organic Chemistry, Eindhoven University of Technology, PO Box 513, 5600 MB Eindhoven, The Netherlands

Received (in Cambridge, UK) 21st July 2000, Accepted 23rd August 2000
First published as an Advance Article on the web

Direct self-assembly of π-conjugated oligomers *via* self-complementary quadruple hydrogen bonding is achieved and the first steps towards supramolecular polymers with functional side chains are described.

Conjugated polymers are investigated for a manifold of electronic semiconductor applications.[1] It is also widely accepted that well-defined oligomers will play a crucial role in the future advancement of π-conjugated materials, since their precise chemical structure and conjugation length stand for defined functional properties and facilitate enhanced control over their supramolecular architecture.[2,3] Synthetic efforts have been mainly directed towards the synthesis of extended linear conjugated oligomers of length of 5–10 nm, but cyclic,[4] bicyclic,[5] spiro[6] and dendritic[7] structures have also been reported. Further, different π-conjugated functionalities have been combined in a large number of well-defined donor–acceptor molecules. The major challenge is now to obtain control of the supramolecular ordering over length scales extending into the macroscopic regime.[8] Only a few examples have been reported on spatial organization of functional π-conjugated entities by making use of hydrogen bonding motifs. Self-assembled fibers of mono and bisthiophene bisurea compounds have been reported and showed efficient charge transport within these fibers.[9] Superstructure formation of π-conjugated materials has also been obtained by hydrogen bonding complexation of perylene bisimide derivatives with a ditopic melamine compound[10] and with chlorine singlet excited-state electron donor and a naphthalene bisimide acceptor.[11]

Recently, we have reported supramolecular polymers which exhibit real macroscopic polymeric properties.[12] These polymeric systems are based on the strong dimerization of quadruple hydrogen-bonding self-complementary 2-ureido-4[1*H*]-ureido-pyrimidinone units. These recent developments pave the way to combine the specific electronic and optical properties of conjugated oligomers with the material properties of polymers, by incorporating well-defined π-conjugated moieties in these supramolecular polymeric assemblies. Here we report on the synthesis of the ureidopyrimidinone derivatives **OPV3UP**, **OPV4UP1** and **OPV4UP2** (depicted in Schemes 1 and 2) and on their supramolecular ordering.

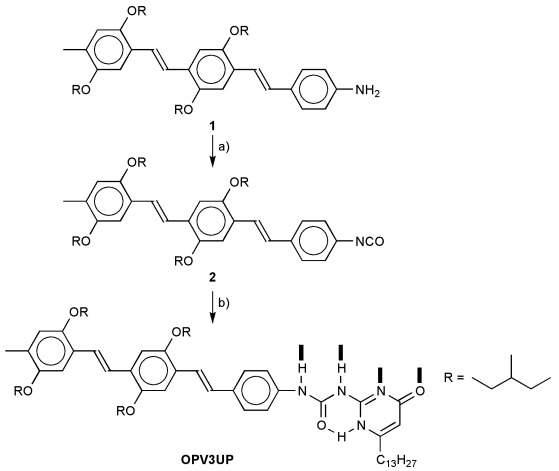

Scheme 1 Synthesis of **OPV3UP**. (a) di-*tert*-butyl tricarbonate, CH_2Cl_2, 100%; (b) 6-tridecylisocytosine, pyridine, 90 °C, 26%.

Compound **OPV3UP** was prepared starting from the amino functionalized oligomer. Using di-*tert*-butyl tricarbonate the amine functionality was quantitatively converted to the isocyanate **2**.[13] Reaction of **2** with 1.5 eq. of 6-tridecylisocytosine

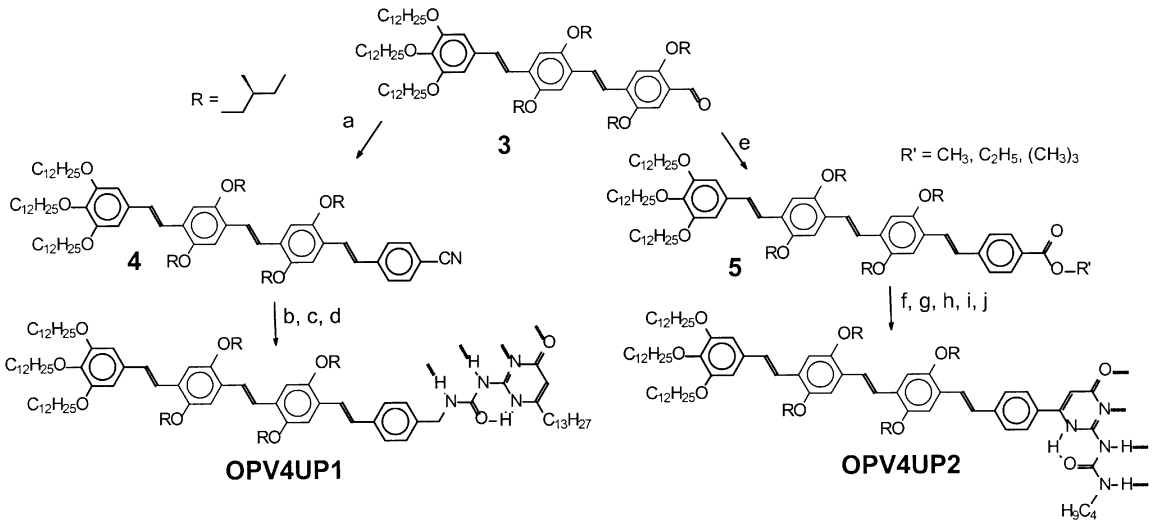

Scheme 2 Synthesis of **OPV4UP1** and **OPV4UP2**. (a) diethyl 4-cyanobenzylphosphonate, *t*-BuOK, DMF, 91%; (b) $LiAlH_4$, Et_2O, 93%; (c) $COCl_2$, toluene, 100 °C, 100%; (d) 6-tridecylisocytosine, pyridine, 90 °C, 52%; (e) diethyl 4-(methylbenzoate)phosphonate, *t*-BuOK, DMF, THF; (f) KOH, EtOH, 80 °C, 100%; (g) $(COCl)_2$, CH_2Cl_2, DMF, 100%; (h) $MgCl_2$, Et_3N, EtOAc, HCl aq., 30%; (i) $(NH_2)_2C{=}NH{\cdot}HCO_3$, EtOH, 90%; (j) n-$C_4H_9NCO$, pyridine, 90 °C.

DOI: 10.1039/b005903j

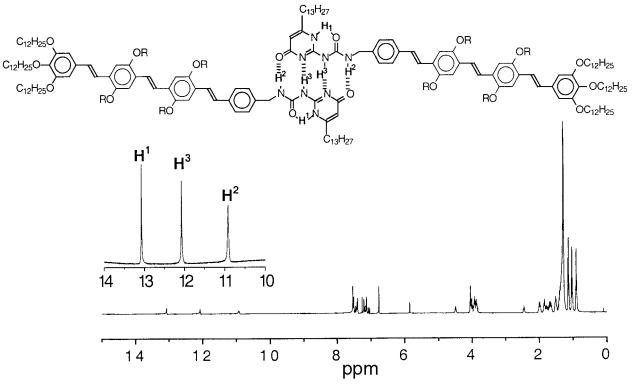

Fig. 1 ^{1}H-NMR spectra of **OPV4UP1** recorded in $CDCl_3$.

in anhydrous pyridine at 90 °C afforded **OPV3UP** in 26% yield after column chromatography. The low yield of **OPV3UP** is probably due to the relatively low reactivity of aromatic isocyanates. Therefore, benzylic isocyanates were used for the preparation of **OPV4UP1**. To obtain the benzylic isocyanate, aldehyde **3** was allowed to react with diethyl 4-cyanobenzylphosphonate in a Wittig–Horner reaction to give the nitrile compound in 91% yield. The nitrile functionality was subsequently reduced using LAH to afford the benzylic amine. The pure compound was isolated after work-up and precipitation in 93% yield. The amine derivative was reacted with phosgene in refluxing toluene to give the isocyanate. Reaction of the latter with 6-tridecylisocytosine in anhydrous pyridine at 90 °C gave **OPV4UP1** in 52% yield. In order to obtain full conjugation between the OPV and hydrogen bonding unit, **OPV4UP2** was synthesized. Reaction of aldehyde **3** with diethyl 4-(methylbenzoate)phosphonate in a Wittig–Horner reaction afforded a mixture of esters **5**. Saponification of these esters gave quantitatively the acid, which was quantitatively converted to the acid chloride using oxalylchloride in DCM and DMF. The β-ketoester was obtained in 30% yield by reaction of the acid chloride with potassium ethylmalonate in presence of triethylamine and magnesium chloride. Reaction of the β-ketoester with guanidinium carbonate yielded quantitatively the isocytosine. The desired compound **OPV4UP2** was finally obtained in 90% yield by reaction of the isocytosine and *n*-butylisocyanate in anhydrous pyridine at 90 °C.

All the compounds **OPV3UP**, **OPV4UP1** and **OPV4UP2** were fully characterized.† These π-conjugated oligomers form quadruple hydrogen bonded **DDAA**-dimers in solution as is evident from the ^{1}H-NMR spectra (Fig. 1). The large downfield shift for the N–H protons gives direct evidence for the involvement of these protons in strong hydrogen bonding.[14] The electronic absorption spectra recorded in $CHCl_3$ solution display a weak band in the visible spectral region (λ_{max} = 409 nm) for the less extended π-conjugated **OPV3UP**. In the case of tetrameric oligophenylene vinylene, **OPV4UP1** and **OPV4UP2**, the absorption maxima are located at λ_{max} = 431 and 446 nm, respectively. The red shift of the absorption maxima of **OPV4UP2** indicates conjugation between the OPV segment and the hydrogen bonding unit. In addition, in dilute $CHCl_3$ solution (*ca.* 10^{-5} M) these hydrogen bonded species are present in dimeric form since the association constant of the ureidopyrimidinone units is extremely high ($K_{dim} = 6 \times 10^7$ M^{-1} in $CHCl_3$ solutions).[15] In dodecane solution, both the dimers of **OPV4UP1** and **OPV4UP2** aggregate into larger architectures and circular dichroism (CD) spectroscopy shows an exciton coupling of the π–π* transition in this solvent. In other words, the side-chain chirality is expressed at the supramolecular level.[16] In the bulk, the two trialkoxybenzene capped dimers are liquid crystalline, but investigation concerning their detailed structure is in progress.

In conclusion, directed self-assembly of π-conjugated oligomers *via* self-complementary quadruple hydrogen bonding has been achieved. It opens new possibilities for the design of electronically active supramolecular materials in which the specific properties of well-defined oligomers can be combined with the material properties of polymers.

We thank Michel Fransen for the synthesis of the starting materials, Joost van Dongen for MALDI-TOF MS measurements, and Dr Rint Sijbesma for fruitful and helpful discussions. This work has been supported by Netherlands Organization for Scientific Research (NWO) and the Royal Netherlands Academy of Arts and Sciences.

Notes and references

† Full synthetic details will be given elsewhere. All new compounds were authenticated by ^{1}H and ^{13}C NMR, FT-IR, MALDI-TOF MS and elemental analyses. *Selected data*: for **OPV3UP**: δ_{N-H} ($CDCl_3$) 12.91, 12.35, 12.11, MALDI-TOF MS (MW = 974.68) *m/z* = 974.77 $[M]^+$, elemental analyses C, 74.46 (75.11), H, 9.28 (9.30), N, 5.96 (5.74%); **OPV4UP1**: δ_{N-H} ($CDCl_3$) 13.06, 12.07, 10.89, MALDI-TOF MS (MW = 1629.28) *m/z* = 1629.89 $[M]^+$, elemental analyses C, 77.68 (77.35), H, 10.77 (10.39), N, 3.26 (3.44%); **OPV4UP2**: δ_{N-H} ($CDCl_3$) 13.91, 12.03, 10.29, MALDI-TOF MS (MW = 1490.24) *m/z* = 1490.09 $[M]^+$, elemental analyses C, 75.99 (76.60), H, 9.58 (10.00), N, 3.45 (3.80%); calculated values in parenthesis.

1 R. H. Friend, R. W. Gymer, A. B. Holmes, J. H. Burroughes, R. N. Marks, C. Taliani, D. C. C. Bradley, D. A. Dos Santos, J. L. Brédas, M. Logdlund and W. R. Salaneck, *Nature*, 1999, **397**, 121.
2 R. E. Martin and F. Diederich, *Angew. Chem., Int. Ed.*, 1999, **38**, 1350.
3 J. M. Tour, *Chem. Rev.*, 1996, **84**, 303.
4 Z. Hu, J. L. Atwood and M. P. Cava, *J. Org. Chem.*, 1994, **59**, 8071; K. P. Baldwin, R. S. Simons, J. Rose, P. Zimmerman, D. M. Hercules, C. A. Tessier and W. J. Youngs, *J. Chem. Soc., Chem. Commun.*, 1994, 1257; C. J. Walter and J. K. M. Sanders, *Angew. Chem., Int. Ed. Engl.*, 1995, **34**, 217; J. Zhang, D. J. Pesak, J. L. Ludwick and J. S. Moore, *J. Am. Chem. Soc.*, 1994, **116**, 4227.
5 Z. Wu, S. Lee and J. S. Moore, *J. Am. Chem. Soc.*, 1992, **114**, 8730.
6 J. M. Tour, R. Wu and J. S. Schumm, *J. Am. Chem. Soc.*, 1991, **113**, 7065; R. Wu, J. S Schumm, D. L. Pearson and J. M. Tour, *J. Org. Chem.*, 1996, **61**, 6906; J. Salbeck, F. Weissörtel and J. Bauer, *Macromol. Symp.*, 1997, **125**, 121.
7 Z. Xu and J. S. Moore, *Angew. Chem., Int. Ed.*, 1993, **32**, 1354.
8 D. Goldhaber-Gordon, M. S. Montemerlo, J. C. Love, G. J. Opiteck and J. C. Ellenbogen, *Proceedings of the IEEE*, 1997, **85**, 521; D. L. Pearson, L. Jones III, J. S. Schumm and J. M. Tour, *Synth. Met.*, 1997, **84**, 303.
9 F. S. Schoonbeek, J. H. van Esch, B. Wegewijs, D. B. A. Rep, M. P. de Haas, T. M. Klapwijk, R. M. Kellog and B. L. Feringa, *Angew. Chem., Int. Ed.*, 1999, **38**, 1393.
10 F. Würthner, C. Thalacker and A. Sautter, *Adv. Mater.*, 1999, **11**, 754.
11 J. L. Sessler, C. T. Brown, D. O'Conner, S. L. Springs, R. Wang, M. Sathiosatham and T. Hirose, *J. Org. Chem.*, 1998, **63**, 7370.
12 R. P. Sijbesma, F. H. Beijer, L. Brunsveld, B. J. B. Folmer, J. H. K. K. Hirschberg, R. F. M. Lange, J. K. L. Lowe and E. W. Meijer, *Science*, 1997, **278**, 1601; B. J. B. Folmer, R. P. Sijbesma, R. M. Versteegen, J. A. J. van der Rijt and E. W. Meijer, *Adv. Mater.*, 2000, **12**, 874; L. Brunsveld, B. J. B. Folmer and E. W. Meijer, *MRS Bull.*, 2000, **25**, 49; J. H. K. K. Hirschberg, F. H. Beijer, H. A. van Aert, P. C. M. M. Magusin, R. P. Sijbesma and E. W. Meijer, *Macromolecules*, 1999, **32**, 2696.
13 H. W. I. Peerlings and E. W. Meijer, *Tetrahedron Lett.*, 1999, **40**, 1021.
14 F. H. Beijer, R. P. Sijbesma, H. Kooijman, A. L. Spek and E. W. Meijer, *J. Am. Chem. Soc.*, 1998, **120**, 6761.
15 S. H. M. Söntjens, R. P. Sijbesma, M. H. P. van Genderen and E. W. Meijer, *J. Am. Chem. Soc.*, in press.
16 See *e.g.* E. Peeters, M. P. T. Christiaans, H. F. M. Schoo, H. P. J. M. Dekkers and E. W. Meijer, *J. Am. Chem. Soc.*, 1997, **119**, 9909; B. M. W. Langeweld-Voss, D. Beljone, Z. Shuai, R. A. J. Janssen, S. C. J. Meskers, E. W. Meijer and J.-L. Brédas, *Adv. Mater.*, 1998, **10**, 1343.

Typeset and printed by Black Bear Press Limited, Cambridge, England

The bioinorganic chemistry of zinc: synthetic analogues of zinc enzymes that feature tripodal ligands

Gerard Parkin

Department of Chemistry, Columbia University, New York, New York 10027, USA.
E-mail: parkin@chem.columbia.edu

Received (in Cambridge, UK) 15th June 2000, Accepted 18th August 2000
First published as an Advance Article on the web 29th September 2000

Zinc, as a constituent of more than 300 enzymes, plays essential roles in biological systems. The active sites of these enzymes feature a zinc center attached to the protein backbone by three or four amino acid residues, the nature of which influences the specific function of the enzyme. In order to understand why different zinc enzymes utilize different amino acid residues at the active site, it is necessary to understand how, and why, the chemistry of zinc is modulated by its coordination environment. Answers to these questions are being provided by a study of synthetic analogues of zinc enzymes, *i.e.* small molecules that resemble the enzyme active sites. This article provides an account of those studies that have specifically used tripodal ligands to mimic the active site protein residues in an effort to ascertain the bioinorganic chemistry of zinc.

1. Introduction

Once dubbed a 'boring element',[1] zinc is now experiencing a dramatic renaissance in its chemistry due to the important roles that it plays in biological systems.[2] For example, an average adult human contains *ca*. 3 grams of zinc,[3] and its bioavailability has been shown to have an effect on the occurrence of malaria, pneumonia, and also the common cold.[2,3] To a large degree, the primary influence of zinc in biological systems resides with its presence in *ca*. 300 enzymes. The active sites of many of these enzymes feature a tetrahedrally coordinated zinc center that is attached to the protein backbone by three amino acid residues, with the fourth site being occupied by a water molecule (Fig. 1).[2,4] The specific function performed by each of these enzymes is dictated by both *(i)* the nature of the residues which bind zinc to the protein, typically His (N), Glu (O), Asp (O), and Cys (S), and *(ii)* the amino acid spacer lengths between the active site residues. For example, a selection of zinc enzymes and their functions, which differ according to the composition of the active site, are illustrated in Table 1 and Fig. 2. While it is recognized that the prevalent use of zinc in biological systems is a manifestation of the unique characteristics associated with the Zn^{2+} ion (Table 2),[5] the factors that are responsible for modifying the detailed properties of the active sites of zinc enzymes are not known with certainty. For this

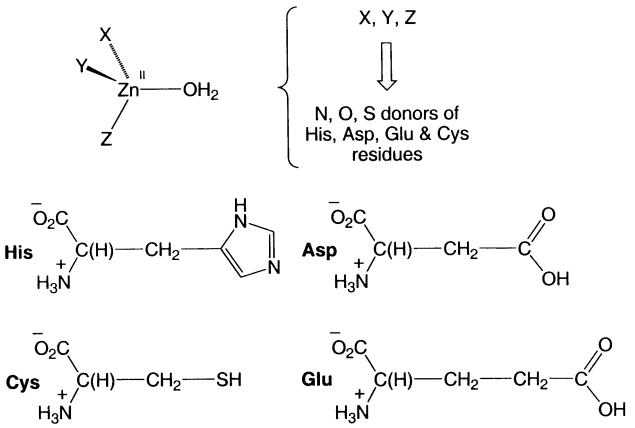

Fig. 1 A common structural feature of zinc enzymes.

Table 1 Coordination motifs in representative mononuclear [{XYZ}Zn^{II}-(OH_2)] zinc enzymes and their functions

X, Y, Z	Enzyme	Function
His, His, His	Carbonic anhydrase	Hydration of CO_2
His, His, Glu	Carboxypeptidase Thermolysin Neutral protease	Exo peptidase Endo peptidase Endo peptidase
His, His, Asp	Protease from streptomyces caespitosus	Endo peptidase
His, His, Cys	Bacteriophage T7 lysozyme	Cleavage of the amide bond between L-alanine and *N*-acetylmuramate moieties in polysaccharides
His, Asp, Cys	Farnesyl protein transferase	Transfer of a farnesyl isoprenoid to a cysteine residue
His, Cys, Cys	Alcohol dehydrogenase Cytidine deaminase	Oxidation of alcohols to aldehydes and ketones Hydrolytic deamination of cytidine to uridine
Cys, Cys, Cys	5-Aminolevulinate dehydratase	Synthesis of porphobilinogen from 5-aminolevulinic acid

Gerard Parkin received his B. A., M. A., and D. Phil degrees from the Queen's College, Oxford University. Both his graduate and undergraduate research was carried out under the guidance of Professor Malcolm L. H. Green. In 1985, he moved to the California Institute of Technology as a NATO post-doctoral fellow to work with Professor John E. Bercaw. He joined the faculty of Columbia University as Assistant Professor in 1988 and was promoted to Associate Professor in 1991 and to Professor in 1994. He is currently Chairman of the Department. Among other awards, he is a recipient of the Presidential Faculty Fellowship Award, the American Chemical Society Award in Pure Chemistry, and the Royal Society of Chemistry Corday Morgan Medal. His principal research interests are in the areas of synthetic, structural, and mechanistic inorganic chemistry.

DOI: 10.1039/b004816j

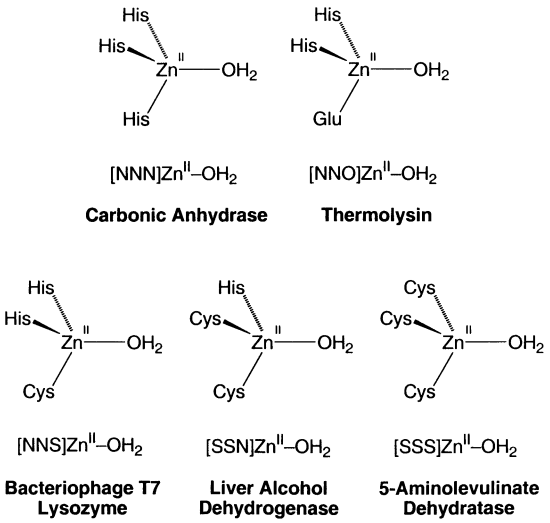

Fig. 2 Active site coordination motifs in representative zinc enzymes.

Table 2 Properties of Zn^{II} that are pertinent to its role in enzymes (information taken from refs. 2 and 3)

Redox properties	The divalent zinc ion is exceptionally stable with respect to oxidation and reduction and so it does not participate in redox reactions, in contrast to Mn, Fe, and Cu.
Coordination geometries	The d^{10} configuration of Zn^{2+} indicates that zinc complexes are not subject to ligand field stabilization effects and so coordination number and geometry is only dictated by ligand size and charge. In enzymes, zinc shows a strong preference for tetrahedral coordination which enhances both the Lewis acidity of a zinc center and the Brønsted acidity of a coordinated water molecule. Only Cu^{II} is a better Lewis acid.
Ligand binding properties	Zinc is an element of borderline hardness, so that nitrogen, oxygen and sulfur ligands can all be accommodated, in contrast to magnesium and calcium which favor binding to oxygen. Therefore, zinc binds strongly to many proteins.
Ligand exchange	The flexibility in coordination geometry makes ligand exchange more facile than for Ni or Mg and enhances the ability of zinc to effect a catalytic cycle.
Ligand nucleophilicity	Anions such as OH^-, OR^- and SR^- retain nucleophilic character when coordinated to zinc. Only Mn^{II}, Fe^{III}, and Cu^{II} are better in this regard.

reason, a number of research groups are actively studying the chemistry of synthetic analogues of zinc enzymes (*i.e.* small molecules that resemble the enzyme active sites) as part of a concerted effort to establish how, and why, the chemistry of zinc is modulated by its coordination environment.[6] The purpose of this article is to provide an account of those studies that have specifically used tripodal ligands to mimic the active site protein residues in an effort to ascertain the bioinorganic chemistry of zinc.

2. Tripodal ligands as mimics for protein binding

The importance of studying synthetic analogues of zinc enzymes resides with the fact that such species are more amenable to structural, spectroscopic, and mechanistic studies than the enzymes themselves. As such, these studies enable the bioinorganic chemistry of zinc to be established for well defined systems. Accurate synthetic analogues of zinc enzymes are not, however, trivial to obtain. A simple illustration of this statement is provided by the fact that whereas *pseudo*-tetrahedral coordination geometry is prevalent in zinc enzymes, higher coordination numbers are common for simple zinc complexes in both the solid state and solution.[4e,7,8] Furthermore, binuclear degradatory pathways are inhibited for the enzyme by virtue of the fact that the active sites are located in its interior. To circumvent such problems involving departures from tetrahedral coordination and oligomerization, considerable attention must be given to ligand design in order to procure synthetic analogues that mimic well the enzyme active sites. Since the active sites of most zinc enzymes are of the composition [{XYZ}Zn^{II}–OH_2], where X, Y, and Z are three protein residues (Table 1 and Fig. 2), a rational approach towards obtaining synthetic analogues is to use tridentate ligands which incorporate the requisite X, Y and Z donor groups to mimic the protein ligation. A further refinement of this approach is to use a *tripodal* ligand in which the X, Y, and Z groups are attached to a common tetrahedral (or trigonal pyramidal) center.

There are at least three advantages of using tripodal ligands, rather than acyclic or cyclic ligands, to support tetrahedral zinc centers. Specifically:

(i) As a result of its trigonal nature, a tripodal ligand enforces the 'facial' (as opposed to 'T-shaped') binding that is required to create a tetrahedral metal center (Fig. 3). In contrast, acyclic

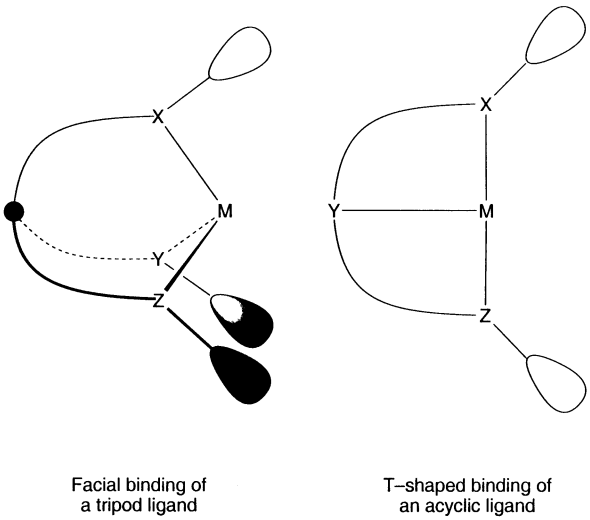

Fig. 3 Comparison of the facial coordination of a tripodal ligand with the T-shaped binding of an acyclic ligand.

tridentate ligands often bind in a 'T-shaped' manner that has no significant biological relevance.

(ii) Tripodal ligands typically possess only a single relevant binding conformation, whereas macrocyclic ligands are more conformationally flexible.

(iii) The directional nature of tripodal ligands is such that it is possible to incorporate substituents that directly influence the steric environment about the metal center. In contrast, substituents in macrocyclic ligands are not, in general, suitably placed to have a profound impact on the sterics of the coordination pocket.

Trofimenko's tris(pyrazolyl)borate ligand system, [$Tp^{RR'}$] (Fig. 4),[9] which features prominently in this article, provides an

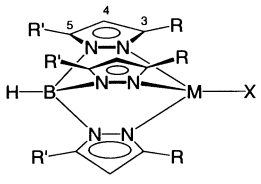

Fig. 4 The tris(pyrazolyl)hydroborato ligand system, [$Tp^{RR'}$]MX.

exemplary illustration of the above virtues of a tripodal ligand. Indeed, with bulky *tert*-butyl substituents on the 3-position of

the pyrazolyl groups, the ligand has been referred to as a 'tetrahedral enforcer' due to its tendency to favor tetrahedral coordination.[10] Not only can the substituents at the 3-position be used to modify the size of the coordination pocket, they may also be used to influence the electronic properties of the metal center. For example, in addition to simple alkyl and aryl substituents, electron withdrawing perfluoroalkyl groups, *e.g.* CF_3, may be incorporated.[9] Finally, it should be noted that substituents such as Bu^t provide a valuable ^{1}H NMR spectroscopic probe that facilitates reactivity and mechanistic studies.

3. Synthetic analogues of zinc enzymes incorporating tripodal ligands

In view of the very large number of zinc enzymes known, a systematic and comprehensive investigation of synthetic analogues for all of these enzymes is yet to be conducted. For this reason, the selection of enzymes discussed in this article is eclectic, with the specific intention being to illustrate aspects of the chemistry of those enzymes which feature mononuclear tetrahedral active sites of the type [{XYZ}Zn^{II}–OH$_2$]. The chemistry will be discussed according to the nature of the {XYZ} ligand complement at the active site, ranging from nitrogen rich carbonic anhydrase, [(His)$_3$Zn^{II}–OH$_2$], to sulfur rich 5-aminolevulinate dehydratase [(Cys)$_3$Zn^{II}–OH$_2$].

(a) The [(His)$_3$Zn^{II}–OH$_2$] motif: carbonic anhydrase

Carbonic anhydrase, the first enzyme recognized to contain zinc, has played a pivotal role in the development of zinc enzymology.[11] It is recognized to be an 'ancient' enzyme since it has widespread occurrence in prokaryotes, it is ubiquitous in nature, and is one of the most efficient enzymes known. As implied by its name, its physiological function is to catalyse the reversible hydration of carbon dioxide (Scheme 1), and thus

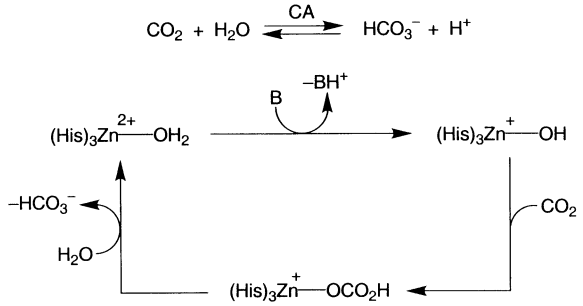

Scheme 1

carbonic anhydrase plays an important role in respiration and intracellular CO_2/HCO_3^- equilibration. X-Ray diffraction studies demonstrate that the zinc center of the active site is coordinated to the protein by the imidazole groups of three histidine residues and a water molecule (or hydroxide ion, depending upon pH) (Fig. 5), and the overall features of the mechanism of action are illustrated in Scheme 1.[11]

Numerous studies have been performed using tridentate nitrogen donor ligands to model the structure and function of the active site carbonic anhydrase.[6] However, very few of these studies have successfully enabled the isolation of structurally-characterized mononuclear four-coordinate zinc–hydroxide or zinc–aqua complexes that mimic the active site of carbonic anhydrase. It is, therefore, significant that the first such complexes were obtained using sterically demanding tris(pyrazolyl)borato ligands, namely [Tp$^{RR'}$]ZnOH.[12] For example, [Tp$^{Bu^t,Me}$]ZnOH, the first monomeric terminal zinc hydroxide complex to be isolated, has been synthesized by (*i*) the direct reaction between equimolar amounts of $Zn(ClO_4)_2 \cdot 6H_2O$, K[Tp$^{Bu^t,Me}$] and KOH in methanol, and (*ii*) by metathesis of [Tp$^{Bu^t,Me}$]ZnI with Bu$^n_4$NOH (Scheme 2).

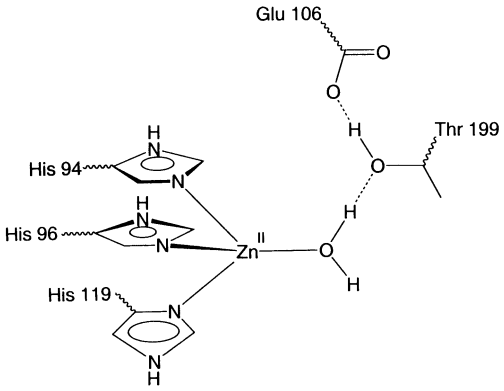

Fig. 5 Active site of carbonic anhydrase.

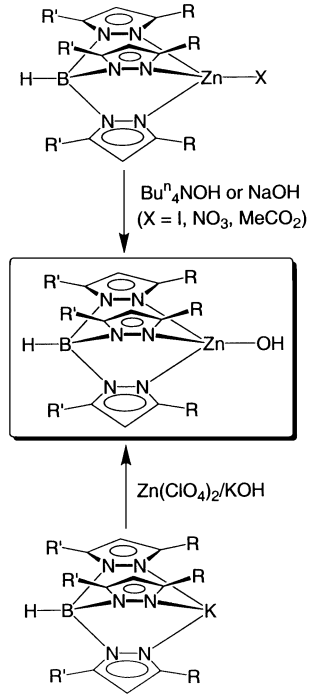

Scheme 2

The molecular structures of [Tp$^{Bu^t,Me}$]ZnOH and [Tp^{Cum,Me}]-ZnOH have been determined by X-ray diffraction, thereby confirming the monomeric and tetrahedral nature of the complexes, as illustrated for [Tp$^{Bu^t,Me}$]ZnOH in Fig. 6. It is important to emphasize that the presence of bulky substituents (*e.g.* Bu^t and $C_6H_4Pr^i$) is essential for the successful isolation of the four-coordinate [Tp$^{RR'}$]ZnOH terminal hydroxide complexes. For example, a simple phenyl substituent in the 3-position of [Tp^{Ph}]ZnOH does not afford a stable derivative.[13] Furthermore, the absence of bulky susbtituents on simple macrocyclic ligands results in oligomerization *via* either hydroxy-bridges, *e.g.* $\{[\{Me_3[9]aneN_3\}Zn(\mu\text{-}OH)]\}_2^{2+}$,[14] or hydrogen bonding interactions, *e.g.* $[\{[12]aneN_3\}Zn(OH)]_3(ClO_4)_3 \cdot (HClO_4)$.[15] More recently, a monomeric five-coordinate anionic zinc hydroxide with a trigonal-bipyramidal geometry, $\{[\eta^4\text{-}N\{CH_2CH_2NC(O)NHBu^t\}_3]ZnOH\}^{2-}$,[16] has been synthesized; notably, this complex also features bulky amide substituents that provide a hydrogen bonding cavity in which the hydroxide ligand resides.[17]

In addition to being structurally determined by X-ray diffraction, the hydroxide ligand in [Tp$^{RR'}$]ZnOH is well characterized spectroscopically, as illustrated by the IR and NMR spectroscopic data listed in Table 3. For example, the ^{1}H NMR spectrum of [Tp$^{Bu^t,Me}$]ZnOH in C_6D_6 illustrates that the hydroxide proton is observed as a sharp signal at δ −0.07 ppm.

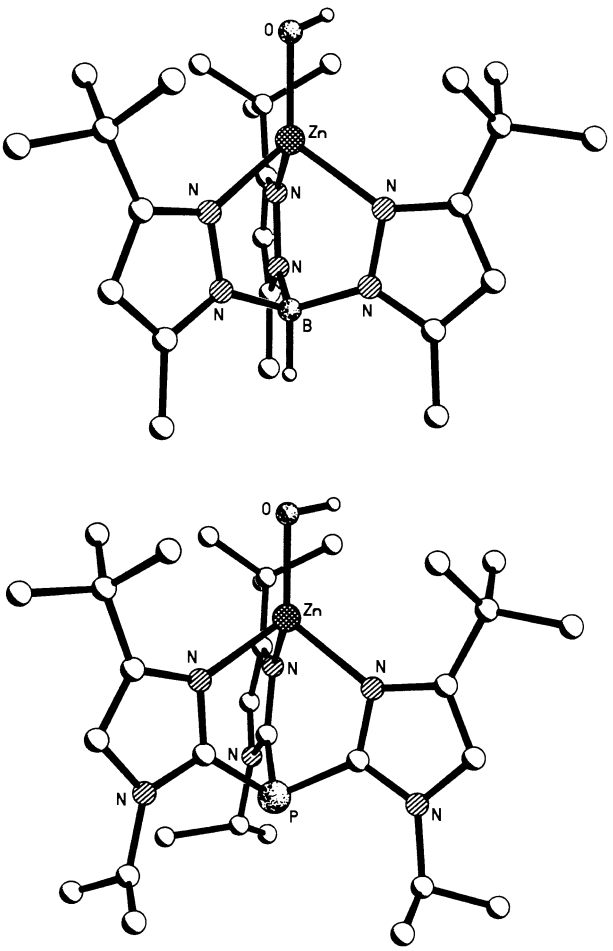

Fig. 6 Molecular structures of $[Tp^{Bu^t,Me}]ZnOH$ and $\{[Pim^{Pr^i,Bu^t}]ZnOH\}^+$.

Table 3 Spectroscopic data for $[Tp^{RR'}]ZnOH$ complexes (data taken from ref. 9*b*)

$[Tp^{RR'}]ZnOH$	ν(O–H)/cm^{-1}	δ(^{1}H)	δ(^{17}O)
$[Tp^{Bu^t,Me}]ZnOH$	3676	−0.07	−8
$[Tp^{Pr^i_2}]ZnOH$	3668	−0.29	−36
$[Tp^{Ar_2}]ZnOH$[a]	3558		
$[Tp^{Cum,Me}]ZnOH$	3647		

[a] Ar = *p*-$C_6H_4Bu^t$

While the $[Tp^{RR'}]ZnOH$ complexes represent a major advance in bioinorganic zinc chemistry by providing the first well characterized tetrahedral zinc hydroxide complexes, their structural similarity to the enzyme is limited by the fact that the nitrogen donors are not of the imidazolyl type, but are rather pyrazolyl-based. Nevertheless, a tetrahedral terminal zinc hydroxide complex has been obtained by the use of the sterically demanding neutral tris[2-(1-isopropyl-4-*tert*-butylimidazolyl)]phosphine ligand, $[Pim^{Pr^i,Bu^t}]$. Specifically, the hydroxide complex $\{[Pim^{Pr^i,Bu^t}]ZnOH\}^+$ was isolated as the perchlorate derivative upon reaction of $[Pim^{Pr^i,Bu^t}]$ with $Zn(ClO_4)_2{\cdot}6H_2O$ (Scheme 3).[18] The molecular structure of $\{[Pim^{Pr^i,Bu^t}]ZnOH\}^+$ has been determined by X-ray diffraction, as illustrated in Fig. 6, which emphasizes the strong relationship with that of $[Tp^{Bu^t,Me}]ZnOH$. The Zn–O and Zn–N bond length data listed in Table 4 reinforce this similarity, and also the relationship with carbonic anhydrase. Since $\{[Pim^{Pr^i,Bu^t}]ZnOH\}^+$ is the only structurally characterized monomeric tetrahedral zinc hydroxide derivative with three imidazole moieties attached to zinc, the complex represents the best structural model for carbonic anhydrase to date.

As with the tris(pyrazolyl)borate derivatives, $[Tp^{RR'}]ZnOH$, the importance of bulky substituents in enabling the isolation of

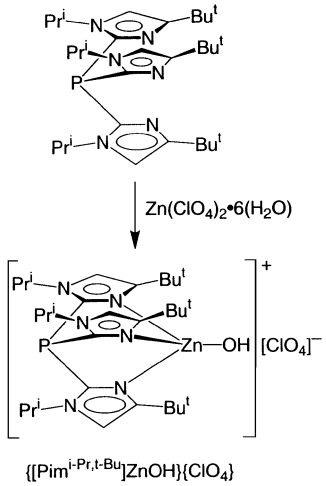

Scheme 3

Table 4 Comparison of Zn–O and Zn–N bond lengths in carbonic anhydrase with those of synthetic analogues

	d(Zn–O)/Å	*d*(Zn–N)/Å
$\{[Pim^{Bu^t,Pr^i}]ZnOH\}^+$	1.86	2.08
$[Tp^{Bu^t,Me}]ZnOH$	1.85	2.05
$[Tp^{Cum,Me}]ZnOH$	1.85	2.05
$\{[Tp^{Bu^t,Me}]Zn(OH_2)\}^+$	1.94	2.02
CAI	1.9	1.9
CAII	2.05	2.11

$\{[Pim^{Pr^i,Bu^t}]ZnOH\}^+$ is underscored by the fact that analogous zinc hydroxide complex species have not been isolated using other tris(imidazolyl)phosphine ligands with less sterically demanding substituents.[6*f*] Furthermore, tris(imidazolyl)carbinol and tris(imidazolyl)alkane ligands have likewise failed to yield structurally characterized terminal zinc hydroxide complexes.[6*f*]

The first essential step in the proposed mechanism of action of carbonic anhydrase (Scheme 1) involves reversible proton transfer which interconverts the aqua and hydroxide forms of the active site, $[(His)_3Zn–OH_2]^{2+}$ and $[(His)_3Zn–OH]^+$. However, while several studies have addressed the factors that influence the pK_a of zinc-bound water molecules in a general sense,[8,15,19] there is to date only a single report demonstrating reversible deprotonation/protonation of a four-coordinate $[Zn–OH_2]^{2+}/[Zn–OH]^+$ pair of complexes. The paucity of such examples is due to the fact that protonation of a zinc hydroxide moiety is typically accompanied by displacement of the aqua ligand by the counter anion (Scheme 4),[20] as illustrated by the

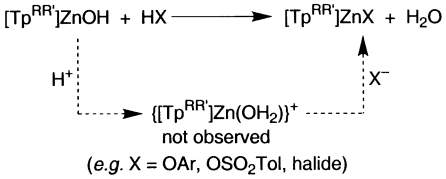

Scheme 4

reaction of $[Tp^{Bu^t,Me}]ZnOH$ with *p*-$TolS(O)_2OH$ to give $[Tp^{Bu^t,Me}]ZnOS(O)_2Tol$.[20*d*] It is, therefore, significant that $[Tp^{Bu^t,Me}]ZnOH$ may be protonated by $(C_6F_5)_3B(OH_2)$ to give a zinc aqua derivative $\{[Tp^{Bu^t,Me}]Zn(OH_2)\}[HOB(C_6F_5)_3]$ in which the water molecule is *not* displaced by the counter ion (Scheme 5).[21] Furthermore, the reaction is reversible and subsequent treatment of $\{[Tp^{Bu^t,Me}]Zn(OH_2)\}^+$ with Et_3N regenerates $[Tp^{Bu^t,Me}]ZnOH$.

The molecular structure of $\{[Tp^{Bu^t,Me}]Zn(OH_2)\}$-$[HOB(C_6F_5)_3]$ has been determined by X-ray diffraction, as

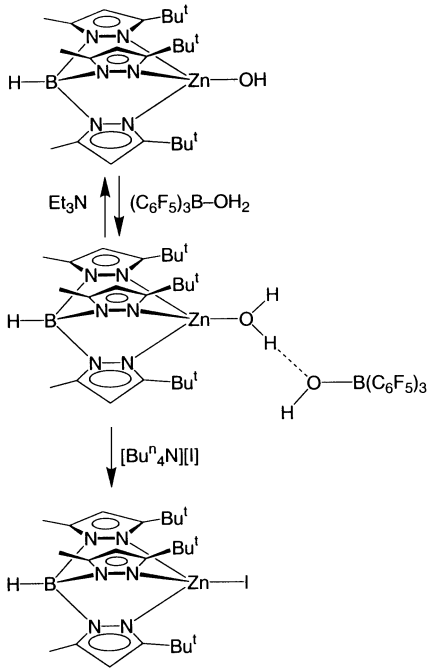

Scheme 5

illustrated in Fig. 7. A notable feature of the structure of {[Tp$^{Bu^t,Me}$]Zn(OH$_2$)}[HOB(C$_6$F$_5$)$_3$] is that the Zn–O bond [1.937(2) Å] is significantly longer than that in [Tp$^{Bu^t,Me}$]ZnOH

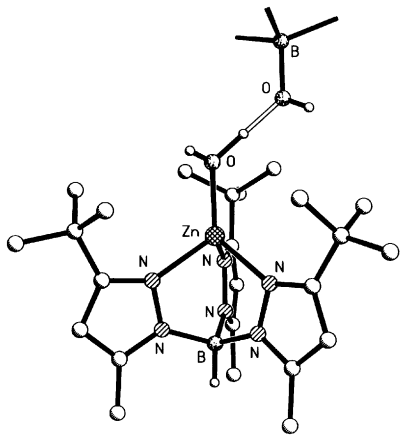

Fig. 7 Molecular structure of {[Tp$^{Bu^t,Me}$]Zn(OH$_2$)}[HOB(C$_6$F$_5$)$_3$].

[1.850(8) Å]. Such lengthening is in accord with the fact that the hydroxide ligand has been protonated. Another interesting aspect of the structure of {[Tp$^{Bu^t,Me}$]Zn(OH$_2$)}[HOB(C$_6$F$_5$)$_3$] is the existence of a hydrogen bond interaction between the coordinated water molecule and the [(C$_6$F$_5$)$_3$BOH]$^-$ counter anion, which bears an analogy to that between the zinc-bound water molecule in carbonic anhydrase and the Thr-199 residue (Fig. 5). The existence of these hydrogen bonding interactions is consistent with the water molecule attached to a tetrahedral Zn^{II} center being acidic. Although the pK_a of {[Tp$^{Bu^t,Me}$]Zn(OH$_2$)}$^+$ has not been accurately determined due to the complications mentioned above, an estimate of *ca*. 6.5 has been cited,[6b] which is comparable to the value of *ca*. 7 for carbonic anhydrase.

Following deprotonation of the zinc-bound water molecule, the second key step of the mechanism of action of carbonic anhydrase involves the reaction of the nucleophilic zinc–hydroxide group with carbon dioxide to give a bicarbonate intermediate. An excellent precedent for this transformation is provided by the reaction of [Tp$^{Bu^t,Me}$]ZnOH with CO_2 to generate the bicarbonate complex [Tp$^{Bu^t,Me}$]Zn(OCO$_2$H), as illustrated in Scheme 6.[12c] IR spectroscopic studies demonstrate that the bicarbonate ligand is characterized by absorptions at

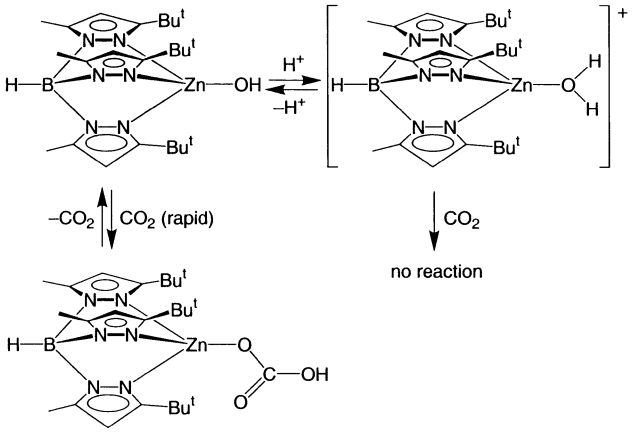

Scheme 6

1302 and 1675 cm^{-1}, which are indicative of unidentate coordination.

Also of relevance to a catalytic cycle, the formation of the bicarbonate complex [Tp$^{Bu^t,Me}$]Zn(OCO$_2$H) is reversible, and removal of the CO_2 atmosphere results in regeneration of the hydroxide derivative [Tp$^{Bu^t,Me}$]ZnOH (Scheme 6).[12c] Furthermore, ^{1}H NMR spectroscopic studies demonstrate that the equilibration is rapid on the NMR time-scale. Thus, upon addition of CO_2 to [Tp$^{Bu^t,Me}$]ZnOH, the sharp signal attributed to the hydroxide ligand broadens substantially and merges into the base line. The spectroscopic transformation is reversible, and the signal of the hydroxide complex gradually reappears upon progressive removal of the CO_2 atmosphere. The tris(pyrazolyl)hydroborato system has, therefore, allowed direct observation of all three zinc species that correspond to the proposed zinc intermediates of the mechanism of action of carbonic anhydrase, namely aqua, hydroxide, and bicarbonate complexes (Scheme 7). Moreover, their interconversion has

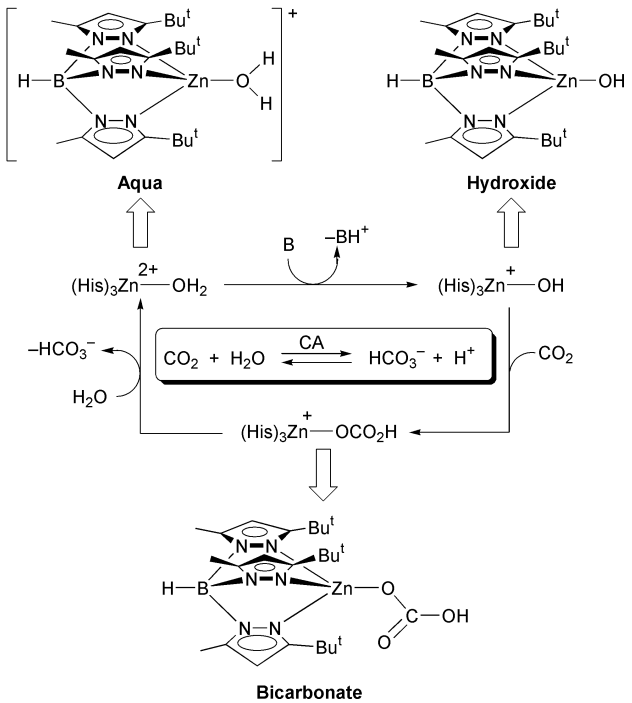

Scheme 7

been shown to be facile. As such, {[Tp$^{Bu^t,Me}$]ZnOH$_2$}$^+$, [Tp$^{Bu^t,Me}$]ZnOH and [Tp$^{Bu^t,Me}$]Zn(OCO$_2$H) represent to date the most thoroughly characterized synthetic analogue system corresponding to carbonic anhydrase.

The functional equivalence of [Tp$^{Bu^t,Me}$]ZnOH as a synthetic analogue of carbonic anhydrase has been established by using

^{17}O NMR spectroscopy which demonstrates that [Tp$^{Bu^t,Me}$]Zn-OH is capable of catalyzing the exchange of oxygen atoms between CO_2 and $H_2{}^{17}O$ [eqn. (1)],[12c] a reaction that is also catalyzed by carbonic anhydrase.

$$CO_2 + H_2{}^{17}O \rightleftharpoons CO^{17}O + H_2O \quad (1)$$

Specifically, ^{17}O NMR spectroscopy indicates that, in the presence of a [Tp$^{Bu^t,Me}$]ZnOH catalyst and CO_2, the ^{17}O NMR spectroscopic signal for $H_2{}^{17}O$ in benzene solution is rapidly replaced by the signal for $CO^{17}O$. Under comparable conditions, but in the absence of a [Tp$^{Bu^t,Me}$]ZnOH catalyst, a mixture of $H_2{}^{17}O$ and CO_2 takes several days to reach isotopic equilibrium in benzene solution, thereby clearly demonstrating the efficiency of [Tp$^{Bu^t,Me}$]ZnOH as a functional carbonic anhydrase mimic. Related to the exchange of oxygen atoms between [Tp$^{Bu^t,Me}$]ZnOH and CO_2, the hydroxide complex [Tp^{Ph,Me}]ZnOH reacts with CS_2 to give [Tp^{Ph,Me}]ZnSH and COS.[22]

Another aspect of the reaction between [Tp$^{Bu^t,Me}$]ZnOH and CO_2 which deserves mention is that of the condensation reaction between [Tp$^{Bu^t,Me}$]Zn(OCO_2H) and [Tp$^{Bu^t,Me}$]Zn-OH.[12c] Thus, as a result of the facile interconversion between [Tp$^{Bu^t,Me}$]Zn(OCO_2H) and [Tp$^{Bu^t,Me}$]ZnOH, condensation of the latter two molecules may occur to generate a bridging carbonate complex {[Tp$^{Bu^t,Me}$]Zn}$_2$(μ-η^1,η^1-CO_3) which may be isolated over a period of days by virtue of its lower solubility (Scheme 8). The bridging carbonate complex {[Tp$^{Bu^t,Me}$]-

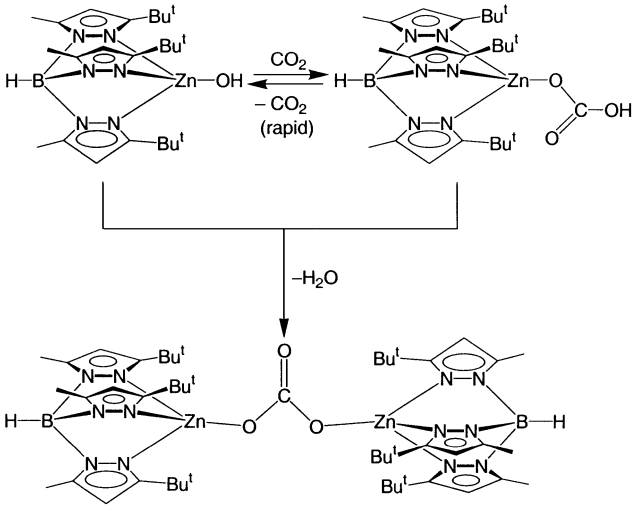

Scheme 8

Zn}$_2$(μ-η^1,η^1-CO_3) is, however, extremely sensitive towards water, thereby regenerating the hydroxide derivative [Tp$^{Bu^t,Me}$]ZnOH.[12c]

The course of the reaction between [Tp$^{RR'}$]ZnOH and CO_2 is strongly influenced by the nature of the pyrazolyl substituents, as illustrated by the reactivity of [Tp$^{Pr^i_2}$]ZnOH towards CO_2 (Scheme 9). Thus, in contrast to the {[Tp$^{Bu^t,Me}$]Zn} system, the bicarbonate complex [Tp$^{Pr^i_2}$]Zn(OCO_2H) is insufficiently stable to be spectroscopically detected and [Tp$^{Pr^i_2}$]ZnOH reacts rapidly with CO_2 to yield the bridging carbonate complex {[Tp$^{Pr^i_2}$]Zn}$_2$(μ-η^1,η^2-CO_3) (Scheme 9), which also differs from that of the {[Tp$^{Bu^t,Me}$]Zn}$_2$(μ-η^1,η^1-CO_3) counterpart by virtue of the nature of the carbonate bridge. In particular, whereas the carbonate ligand in {[Tp$^{Bu^t,Me}$]Zn}$_2$(μ-η^1,η^1-CO_3) binds in a symmetric manner, with unidentate coordination to each zinc center, that in {[Tp$^{Pr^i_2}$]Zn}$_2$(μ-η^1,η^2-CO_3) binds asymmetrically, with unidentate coordination to one zinc center and bidentate coordination to the other zinc center (Scheme 9); the bidentate coordination mode is presumably a consequence of the lower steric demands of the [Tp$^{Pr^i_2}$] ligand. It is also noteworthy that the reactivity of the carbonate ligand towards water is strongly influenced by the nature of the bridge. Thus,

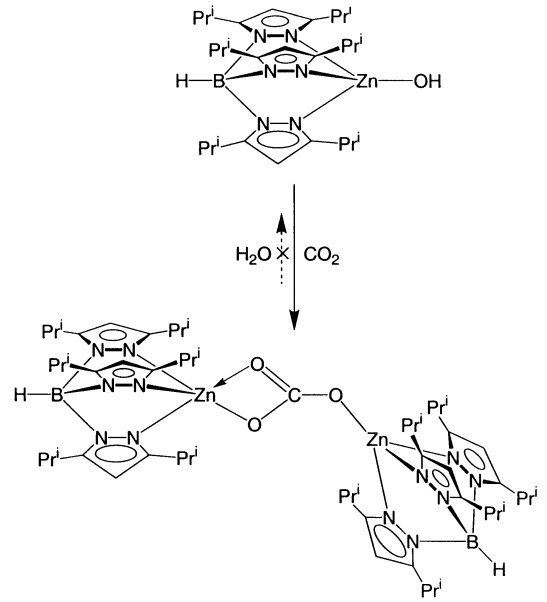

Scheme 9

{[Tp$^{Pr^i_2}$]Zn}$_2$(μ-η^1,η^2-CO_3) is stable towards water (Scheme 9), whereas {[Tp$^{Bu^t,Me}$]Zn}$_2$(μ-η^1,η^1-CO_3) reacts instantaneously to give [Tp$^{Bu^t,Me}$]ZnOH. The significant difference in reactivity emphasizes the extent to which the coordination mode of a carbonate ligand and, by inference, that of a bicarbonate ligand, dictates its stability towards water. Since the final step of the proposed mechanism of action of carbonic anhydrase involves displacement of bicarbonate by water, the above difference in reactivity of {[Tp$^{Pr^i_2}$]Zn}$_2$(μ-η^1,η^2-CO_3) and {[Tp$^{Bu^t,Me}$]-Zn}$_2$(μ-η^1,η^1-CO_3) towards H_2O suggests that factors which promote bidentate coordination of a bicarbonate ligand could inhibit the catalytic cycle. In support of this notion, the increased catalytic activity of [{[12]aneN_4}ZnOH]$^+$ over that of [{[12]aneN_3}ZnOH]$^+$ towards hydration of CO_2 has also been attributed to the greater tendency of the former to form a unidentate, rather than bidentate, bicarbonate intermediate.[23,24]

A final issue concerned with the formation of the bicarbonate intermediate of the catalytic cycle (Scheme 1) is that it requires that the coordinated water be deprotonated prior to reaction with CO_2. Comparative studies on both the hydroxide [Tp$^{Bu^t,Me}$]Zn-OH and aqua {[Tp$^{Bu^t,Me}$]Zn(OH_2)}[HOB(C_6F_5)$_3$] complexes allows this proposal to be confirmed. Thus, whereas [Tp$^{Bu^t,Me}$]-ZnOH reacts rapidly with CO_2 to yield the bicarbonate derivative [Tp$^{Bu^t,Me}$]Zn(OCO_2H), the aqua complex {[Tp$^{Bu^t,Me}$]Zn(OH_2)}$^+$ is inert under comparable conditions (Scheme 6).

(b) The [(His)$_2$(Glu)Zn^{II}–OH_2] motif: thermolysin, carboxypeptidase and neutral protease

Thermolysin (TLN), carboxypeptidase (CP) and neutral protease are a class of related zinc proteases that are responsible for catalyzing the hydrolysis of peptide bonds [eqn. (2)].

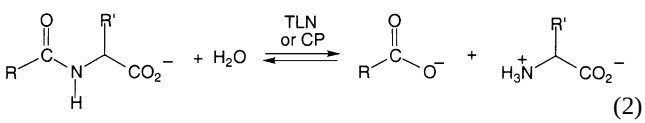

(2)

The active sites of carboxypeptidase, thermolysin, and neutral protease bear a close resemblance, with the zinc centers of each being bound to the protein by a combination of one glutamate and two histidine residues. The similarity between thermolysin

and carboxypeptidase is further emphasized by the fact that the glutamate residue of each enzyme is capable of binding in both a unidentate and bidentate manner. Efforts to obtain synthetic analogues of these enzymes have focused on the use of a variety of tridentate ligands with $[N_2O]$ donor arrays,[25–29] but many of these ligands do not enforce tetrahedral coordination geometries akin to those in the enzymes. For example, ligands such as bis[(3,5-diisopropylpyrazolyl)ethyl] ether, $O(CH_2CH_2pz^{Pr^i_2})_2$, bind with a 'T-shaped' configuration, rather than with the facial configuration required to mimic the tetrahedral coordination in enzymes.[26] The use of a $[N_2O]$ tripod ligand, however, ensures facial binding. Interestingly, such ligands may be constructed directly on the zinc center by insertion of R_2CO (R = H, Ph) or CO_2 into the B–H bond of a bis(pyrazolyl)hydroborato derivative (Scheme 10).[30] The formate derivative $[\eta^3$-$(HCO_2)Bp^{Bu^t,Pr^i}]ZnCl$ that is obtained by reaction of CO_2 with $[Bp^{Bu^t,Pr^i}]ZnCl$ is particularly significant because it is the first structurally characterized tetrahedral zinc complex of a tridentate $[N_2O]$ ligand in which the O-donor is a carboxylate group. Since only one oxygen coordinates to zinc, the complex is better regarded as a synthetic analogue of thermolysin or carboxypeptidase B rather than of carboxypeptidase A. In addition to using boron as a tripod linker, carbon has also been used as a linker atom to prepare the $[N_2O]$ donor ligand $[HC(pz^{Me_2})(C_6H_2MeBu^tO)]^-$, from which the zinc complexes $[HC(pz^{Me_2})(C_6H_2MeBu^tO)]ZnX$ (X = Cl, Me) have been synthesized (Fig. 8).[28]

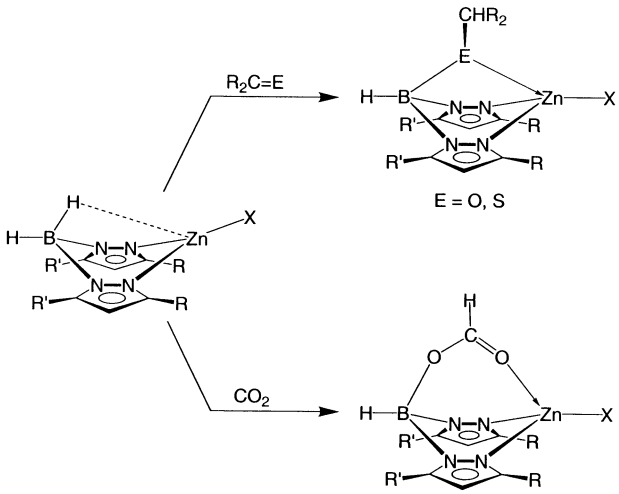

Scheme 10

(c) The $[(His)_2(Cys)Zn^{II}–OH_2]$ motif: bacteriophage T7 lysozyme and peptide deformylase

The active site of bacteriophage T7 lysozyme, a zinc enzyme which destroys bacteria by cleaving the amide bond between L-alanine and *N*-acetylmuramate moieties of polysaccharide components within their cell walls, consists of a tetrahedral zinc center which is bound to the protein backbone *via* one sulfur and two nitrogen donors of cysteine and histidine residues, with the fourth site being occupied by a water molecule (Fig. 2).[31] The active site of peptide deformylase is similar to that of T7 lysozyme, but recent studies suggest that the zinc form has low activity and that the active form of the enzyme which is responsible for the hydrolytic cleavage of a formyl group [eqn. (3)] is actually an *iron* enzyme.[32]

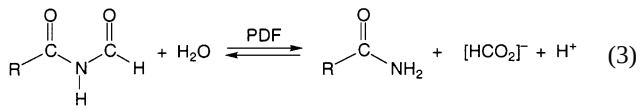

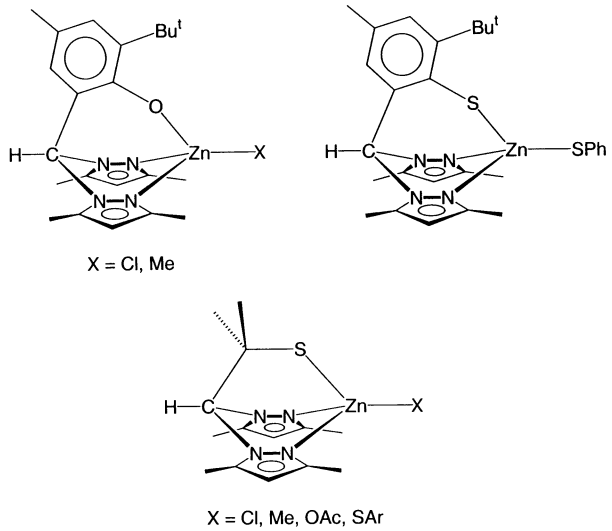

Fig. 8 [NNO] and [NNS] ligands based on the bis(pyrazolyl)methane fragment.

In part due to the propensity of sulfur to act as a bridge between metal centers, tridentate $[N_2S]$ ligands that support monomeric tetrahedral zinc centers analogous to the active sites of peptide deformylase and T7 lysozyme are not common. A second problem is that a variety of studies indicate that the ability of sulfur to coordinate to zinc is very sensitive to the nature of the ligand. For example, the sulfur atom of the thioether derivative $[S(CH_2CH_2pz^{Me_2})_2]ZnCl_2$ does *not* coordinate to zinc.[33] Nevertheless, the use of a tripod construction enforces 'facial' binding of a $[N_2S]$ donor ligand and, by analogy with the $[N_2O]$ ligands $[\{R_2C(H)O\}Bp^{Bu^t,Pr^i}]$ described above, the tetrahedral zinc complex, $[\eta^3$-$\{Ph_2C(H)S\}Bp^{Bu^t,Pr^i}]ZnI$ may be obtained by insertion of Ph_2CS into a B–H bond of $[Bp^{Bu^t,Pr^i}]ZnI$ (Scheme 10).[34] Related complexes, $[HC(pz^{Me_2})_2(C_6H_2MeBu^tS)]ZnSPh$ and $[HC(pz^{Me_2})_2(CMe_2S)]ZnX$ (Fig. 8), derived from $[N_2S]$ ligands that use a carbon, rather than boron, atom linker have also been synthesized.[28,35] Although mononuclear zinc hydroxide complexes of the type $\{[N_2S]ZnOH\}$ have yet to be structurally characterized, it is worth noting that a related dinuclear species has recently been isolated. Thus, only one of the two thioether linkages of the $[N_2S_2]$ bmnpa ligands in the bridging hydroxide complex $\{[(bmnpa)Zn(\mu\text{-}OH)]_2\}^{2+}$ coordinates to each zinc center, such that each zinc adopts a $\{[N_2S]Zn(\mu\text{-}OH)_2\}$ coordination environment [bmnpa = *N*-bis-2-(methylthio)ethyl-*N*-(6-neopentylamino-2-pyridylmethyl)amine].[36a] A dinuclear hydroxide complex with a similar motif, but in which thiosulfate $[S_2O_3]^{2-}$ provides the sulfur ligand, has also been reported.[36b]

(d) The $[(His)(Cys)_2Zn^{II}–OH_2]$ motif: liver alcohol dehydrogenase

Alcohol dehydrogenases (ADH) belong to an important class of enzymes that catalyze the biological oxidation of primary and secondary alcohols. The oxidations proceed *via* the formal transfer of a hydride anion to the oxidized form of nicotinamide adenine dinucleotide (NAD^+), coupled with the release of a proton [eqn. (4)].

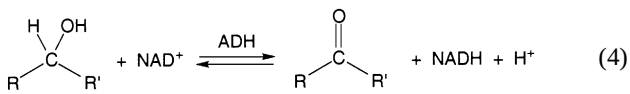

Liver alcohol dehydrogenase (LADH) is the most widely studied of this class of enzymes. X-Ray diffraction studies demonstrate that the active site consists of a zinc center which is coordinated in a distorted tetrahedral manner to a histidine and two cysteine residues of a single polypeptide chain, with a

water molecule occupying the fourth coordination site (Fig. 2). In addition to the catalytic site, there is also a zinc center that is coordinated tetrahedrally to four cysteine residues, which plays a structural role. Although the sulfur-rich composition of the active site of LADH is relatively uncommon for zinc enzymes, two other examples that have similar active sites are spinach carbonic anhydrase[37] and cytidine deaminase.[38] The coordination environment of the catalytic site in LADH is also not well precedented in zinc chemistry. For example, even though a variety of tridentate [NS_2] donor ligands have been synthesized with a view to modeling LADH,[39–41] none of these previous studies has yielded structurally characterized mononuclear tetrahedral complexes that mimic the active site of LADH. The principal problems of these ligands are associated with (*i*) the proclivity of thiolate groups to act as bridging ligands and thus form oligonuclear structures, and (*ii*) the preference of certain tridentate [NS_2] ligands to bind with a meridional (*i.e.* 'T'-shaped) geometry, rather than the facial binding required to mimic the active site of LADH.

A suitable tridentate [NS_2] donor ligand has, nevertheless, been obtained by reaction of pyrazole with a bis(mercaptomethylimidazolyl)borate derivative.[42] Specifically, the reaction of $LiBH_4$ with methimazole (2 equivalents) yields [Bm^{Me}]Li, from which the [NS_2] donor [$pzBm^{Me}$]Li may be obtained by reaction with pyrazole (Scheme 11). Subsequent transfer of the [NS_2] ligand to zinc is readily achieved by treatment of [$pzBm^{Me}$]Li with ZnI_2, thereby resulting in the formation of [$pzBm^{Me}$]ZnI. Alternatively, [$pzBm^{Me}$]ZnI may be obtained *via* reaction of the [Bm^{Me}]ZnI with pyrazole (Scheme 11).

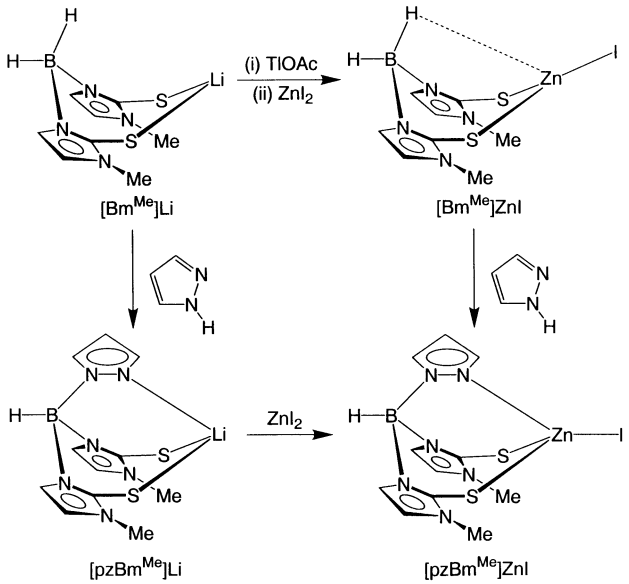

Scheme 11

The molecular structure of the zinc iodide complex, [$pzBm^{Me}$]ZnI, has been determined by X-ray diffraction which demonstrates that it is indeed mononuclear with a distorted tetrahedral coordination geometry about zinc, and Zn–N and Zn–S bond lengths that are comparable to those within the enzyme. As noted above, the ability of [$pzBm^{Me}$] to provide a facial set of donors is associated with the use of a tetrahedral center as a point of attachment for the donor groups. In this regard, Riordan and coworkers have also recently used tripodal phenylborato ligands to provide [NS_2] donation that is capable of stabilizing monomeric structures, as illustrated by [$Ph(pz)(CH_2SBu^t)_2$]ZnBr and [$Ph(pz^{Bu^t})(CH_2SBu^t)_2$]ZnSPh.[43]

A simplified version of the postulated mechanism of action of LADH is illustrated in Scheme 12, with the essential features involving (*i*) binding NAD^+ (nicotinamide adenine dinucleotide), (*ii*) displacement of the water molecule by alcohol, (*iii*) deprotonation of the coordinated alcohol affording a zinc alkoxide intermediate,[44] *(iv)* hydride transfer from the alkoxide to NAD^+ giving a zinc-bound aldehyde, (*v*) displacement of the aldehyde by water, and (*vi*) release of NADH. The role of the zinc center is, therefore, to facilitate the formation of an alkoxide and thereby enhance hydride transfer to NAD^+. Conversely, in the reverse direction, coordination of the ketone or aldehyde to the zinc center serves to enhance the electrophilicity of the carbonyl carbon atom and thereby promote reduction.

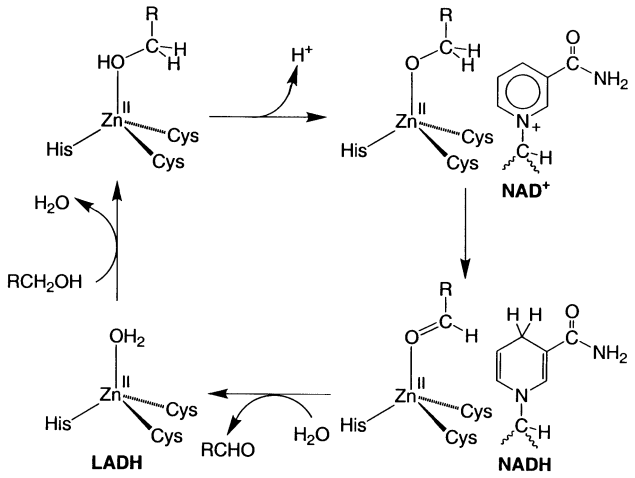

Scheme 12

Interestingly, although the generation of a four-coordinate zinc alkoxide intermediate is an essential step in the catalytic cycle of LADH (Scheme 12), until recently, there was little precedent for the formation of simple aliphatic alkoxide complexes from either zinc aqua or hydroxide derivatives. In view of the non-existence of well defined mononuclear zinc hydroxide complexes with a pseudo-tetrahedral {[NS_2]$Zn^{II}X$} structure, such studies have necessarily focused on complexes with a different structural motif, and specifically those supported by tris(pyrazolyl)hydroborato ligation for which a series of [$Tp^{RR'}$]ZnOH complexes are known. Significantly, ^{1}H NMR spectroscopy demonstrates that the zinc hydroxide [$Tp^{Bu^t,Me}$]-ZnOH complex reacts with ROH (R = Me, Et, Pr^i) to generate the alkoxides [$Tp^{Bu^t,Me}$]ZnOR (Scheme 13);[45] however, in contrast to the reactions of [$Tp^{RR'}$]ZnOH with acidic alcohols (*e.g.* phenols and trifluoroethanol),[46] the simple alkoxides [$Tp^{Bu^t,Me}$]ZnOR (R = Me, Et, Pr^i, Bu^t) are only formed as minor components in an equilibrium mixture (Fig. 9).[45] As such, the alkoxides [$Tp^{Bu^t,Me}$]ZnOR are not readily isolated from the reaction of [$Tp^{Bu^t,Me}$]ZnOH with ROH. It is, therefore, significant that the alkoxides [$Tp^{Bu^t,Me}$]ZnOR may be isolated from the reaction of the hydride complex [$Tp^{Bu^t,Me}$]ZnH with the respective alcohol (Scheme 13). The molecular structure of [$Tp^{Bu^t,Me}$]ZnOEt has been determined by X-ray diffraction, thereby demonstrating its mononuclear tetrahedral nature and confirming its relationship to the proposed intermediate in the mechanism of action of LADH.

An understanding of the factors which influence the stability of tetrahedral zinc alkoxide complexes with respect to hydrolysis is critical to understanding the mechanism of action of LADH. The data presented in Fig. 9 indicate that the equilibrium constant for formation of [$Tp^{Bu^t,Me}$]ZnOR from [$Tp^{Bu^t,Me}$]ZnOH and ROH (R = Me, Et, Pr^i, Bu^t) is highly dependent upon the nature of R, decreasing markedly in the sequence: Me > Et > Pr^i > Bu^t, a trend that is a result of steric and electronic influences (Table 5). Therefore, in an effort to identify the relative importance of these components, the equilibria involving the reactions of [$Tp^{Bu^t,Me}$]ZnOH with a series of *para*-substituted phenols, *p*-XC_6H_4OH, for which electronic substituent parameters (*e.g.* Hammett σ constants) are available, have been studied.[47] Significantly, the data

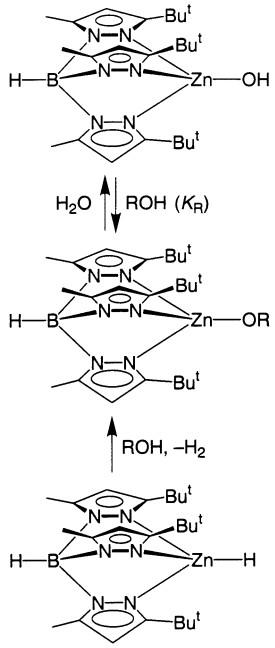

Scheme 13

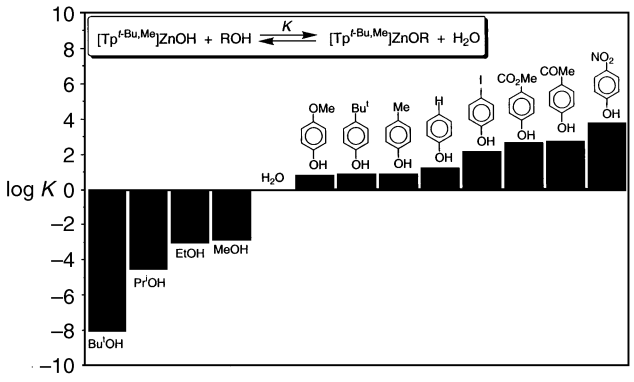

Fig. 9 Variation in alcoholysis equilibrium constant as a function of R.

Table 5 Equilibrium constant and thermodynamic data for alcoholysis reactions of [Tp$^{Bu^t,Me}$]ZnOH with ROH (data taken from ref. 45)

R	K_R(300 K)
Me	$1.4(2) \times 10^{-3}$
Et	$9(2) \times 10^{-4}$
Pr^i	$3(1) \times 10^{-5}$
Bu^t	$\approx 10^{-8}$

presented in Fig. 9 demonstrate that the alcoholysis reactions are very sensitive to electronic influences, being strongly favored for electron withdrawing substituents. Thus, a Hammett plot of log *K vs.* σ gives a good linear correlation with a ρ value of 2.8. The alcoholysis reactions have also been studied computationally using DFT calculations (B3LYP) and the results are in excellent agreement with the experimental results.[47]

The computational study demonstrates that the trend illustrated by the Hammett plot is a consequence of electron withdrawing substituents increasing Zn–OAr BDEs to a greater extent than the corresponding H–OAr BDEs.[47] Thus, rather than exhibit the 1:1 correlation between M–X and H–X bond energies that has been reported for certain other systems,[48] the Zn–OAr BDE is substantially more sensitive to the *para* substituent than is the H–OAr BDE (Fig. 10), *i.e.* D(Zn–OAr) = 1.48 D(H–OAr) − 61 kcal mol^{-1}.[47]

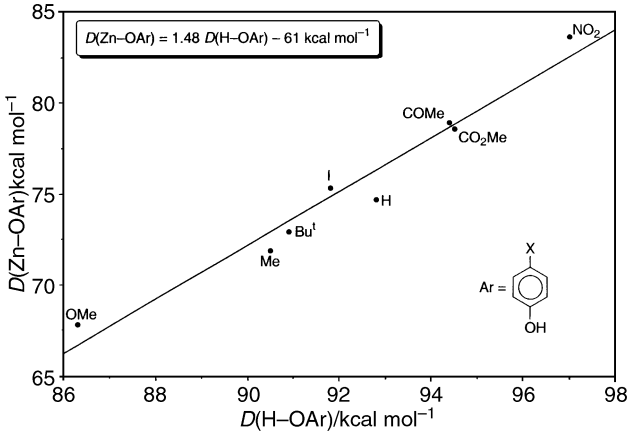

Fig. 10 Correlation of calculated [Zn]–OAr and H–OAr BDEs.

Theoretical studies on phenols have rationalized that the ability of an electron withdrawing *para* substituent to increase the H–OAr BDE is a result of preferential stabilization of the ground state by increasing the delocalization of the electron density from the oxygen atom.[49] On the other hand, electron-donating *para* substituents decrease the H–OAr BDE, but the effect is principally due to stabilization of the ArO• radical, with destabilization of ArOH contributing only to a small degree. The greater influence of an electron withdrawing substituent on the Zn–OAr *vs.* H–OAr BDE is proposed to be a consequence of the $Zn^{\delta+}$–$OAr^{\delta-}$ bond being more polar than the $H^{\delta+}$–$OAr^{\delta-}$ bond, *i.e.* an electron withdrawing substituent would exert a greater influence in stabilizing the partial negative charge on the oxygen atom in [Tp$^{Bu^t,Me}$]ZnOAr than in ArOH.

Calculations on the alkoxides [Tp$^{Bu^t,Me}$]ZnOR (R = Me, Et, Pr^i, Bu^t) indicate that the observed trend is a result of the homolytic Zn–OR BDE decreasing rapidly upon increasing the bulk of R as compared to that for the corresponding H–OR BDE. The greater sensitivity of the Zn–OR BDEs to the bulk of R has been attributed to steric interactions between R and the *tert*-butyl substituents of the [Tp$^{Bu^t,Me}$] ligand in [Tp$^{Bu^t,Me}$]Zn-OR playing a more important role that the interactions between R and H in ROH.[47]

In view of the unfavorable thermodynamics for the formation of the alkoxide derivatives [Tp$^{Bu^t,Me}$]ZnOR from [Tp$^{Bu^t,Me}$]-ZnOH, it is noteworthy that the use of the related tris(mercapto-mesitylimidazolyl)borate ligand [Tm^{Mes}], which features [S_3] rather than [N_3] coordination, favors the formation of an *alcohol* adduct. Thus, the alcohol complex {[Tm^{Mes}]Zn(HOMe)}$^+$ is obtained by reaction of Li[Tm^{Mes}] with $Zn(ClO_4)_2$ in methanol (Scheme 14).[50] This observation indicates that the sulfur rich coordination environment provided by [Tm^{Mes}] stabilizes alcohol binding to zinc and thereby suggests that one of the reasons why LADH utilizes a sulfur rich coordination environment is to increase the stability of the required alcohol intermediate with respect to that of an aqua species.

The alcohol coordination mode in {[Tm^{Mes}]Zn(HOMe)}$^+$ resembles aspects of that in LADH. For example, the Zn–O bond length in {[Tm^{Mes}]Zn(HOMe)}$^+$ (1.99 Å) is effectively identical to that in the $C_6F_5CH_2OH$ adduct of LADH (2.0 Å) and the hydroxy group of the coordinated methanol participates in a hydrogen bonding interaction with an additional molecule of methanol, which resembles the hydrogen bond network at the active site of LADH. For example, the hydrogen bonded O···O separation of 2.58 Å in {[Tm^{Mes}]Zn(HOMe)(HOMe)}$^+$ is effectively identical to that between the zinc-bound alcohol at the active site of LADH and Ser-48 (2.6 Å).

A final issue concerned with the proposed role of zinc alkoxide intermediates is their potential for 'hydride' transfer to NAD$^+$. Studies employing *p*-nitrobenzaldehyde as a NAD$^+$ hydride acceptor mimic[51] provide evidence that the alkoxide complexes [Tp$^{Bu^t,Me}$]ZnOR (R = Et, Pr^i) are indeed capable of

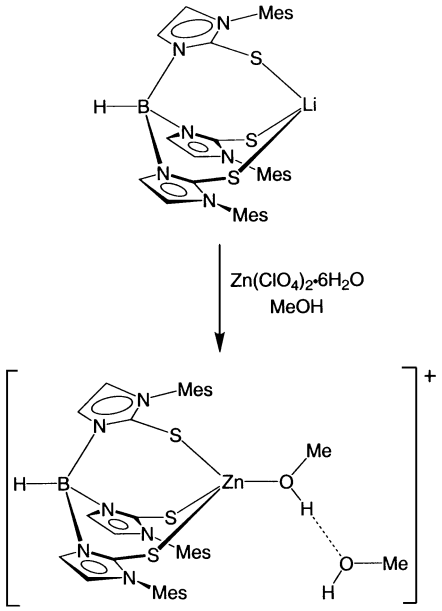

Scheme 14

such a transformation. For example, [Tp$^{Bu^t,Me}$]ZnOEt reacts with ArCHO (Ar = *p*-$C_6H_4NO_2$) in benzene to yield [Tp$^{Bu^t,Me}$]ZnOCH_2Ar and MeCHO (Scheme 15). Furthermore, solutions of ArCHO in ROH (R = Me, Et, Pr^i) yield ArCH_2OH at *ca*. 90 °C in the presence of [Tp$^{Bu^t,Me}$]ZnOH.

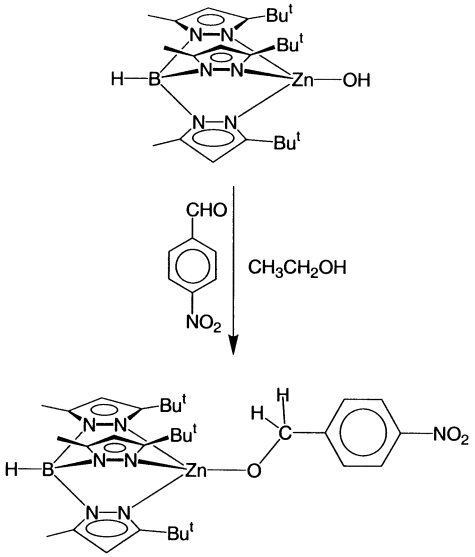

Scheme 15

(e) The [(Cys)$_3$Zn^{II}–OH$_2$] motif: 5-aminolevulinate dehydratase

5-Aminolevulinate dehydratase (ALAD), also known as porphobilinogen synthase (PBGS), catalyzes the dimerization of 5-aminolevulinic acid (ALA) to porphobilinogen, a monopyrrole (Scheme 16).[52] This transformation is of considerable importance since it is the first step in the biological synthesis of tetrapyrroles (including heme, chlorophyll and cobalamins). ALAD is a zinc dependent enzyme, containing both catalytic and structural zinc sites, of which the catalytic site possesses the unusual composition of [(Cys)$_3$Zn^{II}(OH$_2$)] (Fig. 2).[53] As discussed above for liver alcohol dehydrogenase, due to the proclivity of sulfur containing ligands to bridge more than one zinc center, mononuclear tetrahedral zinc complexes with sulfur rich coordination environments that mimic the active site of ALAD are not common. Nevertheless, the sterically demanding

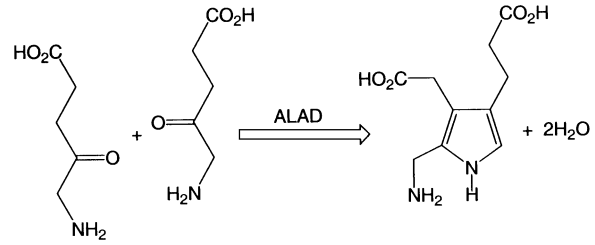

Scheme 16

tris(mercaptoarylimidazolyl)borate ligands, [Tm^{Ar}] (Ar = Ph, Mes), described above may be considered to provide the requisite motif which mimics the three cysteine residues at the active site of ALAD. Thus, a series of [Tm^{Ar}]ZnX complexes have been prepared, *e.g.* [Tm^{Ph}]ZnX (X = I, NO_3) and [Tm^{Mes}]ZnX (X = Cl, I),[50] as illustrated in Scheme 17.

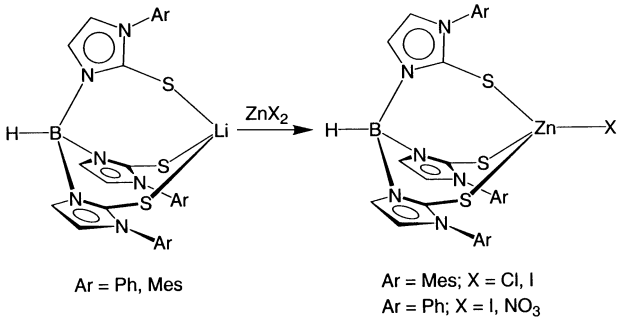

Scheme 17

An important aspect of the chemistry of ALAD is concerned with lead poisoning. Specifically, lead is the most commonly encountered toxic metal pollutant in the environment,[54] and its toxicological properties are associated with its interactions with proteins and, in particular, ALAD.[55] The existence of a series of [Tm^{Ar}]ZnX derivatives has enabled the replacement of zinc by lead in complexes which mimic aspects of the coordination environment in the active site of ALAD to be studied. Significantly, both [Tm^{Ph}]ZnI and {[Tm^{Ph}]Zn(NCMe)}(ClO_4) react rapidly with Pb(ClO_4)$_2$•*x*H_2O to give the lead complex {[Tm^{Ph}]Pb}(ClO_4) (Scheme 18).[56]

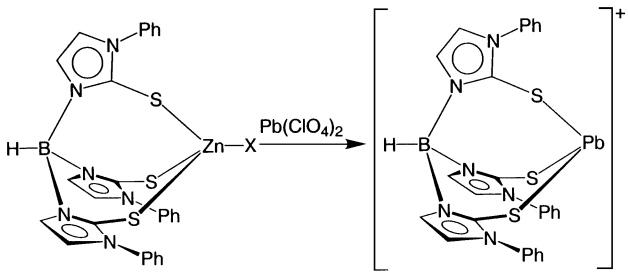

Scheme 18

The molecular structure of {[Tm^{Ph}]Pb}$^+$ has been determined by X-ray diffraction (Fig. 11), thereby demonstrating that the trigonal-pyramidal geometry bears a close correspondence to the active site of Pb^{II}–ALAD.[57] For example, {[Tm^{Ph}]Pb}$^+$ and Pb^{II}–ALAD have very similar average Pb–S bond lengths of 2.7 and 2.8 Å, respectively. It is also important to emphasize that the lead coordination environment in {[Tm^{Ph}]Pb}$^+$ is in marked contrast to that of zinc in {[Tm^{Ph}]Zn(NCMe)}$^+$, an observation which clearly indicates that trigonal-pyramidal lead centers have a reduced tendency to bind an additional ligand compared to that of zinc. The reduced Lewis acidity of a three coordinate Pb^{II} center is of significance to the inactivity of Pb^{II}–ALAD since the mechanism of action has been proposed to involve activation of ALA by interaction of the ketone group with the

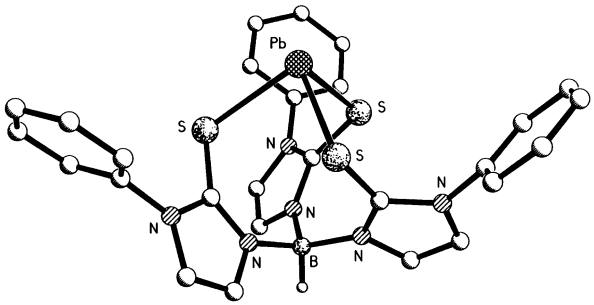

Fig. 11 Molecular structure of {[Tm^{Ph}]Pb}$^{+}$.

Zn^{II} center.[52] The reduced Lewis acidity of a three coordinate Pb^{II} center indicates that the formation of the required tetrahedral intermediate [(Cys)$_3$Pb^{II}–ALA] would be inhibited.

The binding preferences of lead and zinc to ligands which mimic the coordination motif in ALAD is of relevance to obtaining a thorough understanding of the factors responsible for the debilitating effects of lead poisoning. It is, therefore, significant that a study of the equilibrium involving ligand exchange between {[Tm^{Ph}]Pb}(ClO$_4$) and Zn(ClO$_4$)$_2$ in MeCN [eqn. (5)] indicates that the preference of [Tm^{Ph}] to coordinate Pb^{II} over Zn^{II} in this system is *ca.* 500 : 1. This value is substantially greater than the *ca.* 25 : 1 relative affinity of these metals to reside at the active site of human erythrocyte ALAD.[58]

$$\{[Tm^{Ph}]Pb\}^{+} + Zn^{2+} + MeCN \overset{K}{\rightleftharpoons} \{[Tm^{Ph}]Zn(NCMe)\}^{+} + Pb^{2+} \qquad (5)$$

More interestingly, despite the fact that [Tm^{Ph}] prefers to bind to Pb^{II} rather than Zn^{II}, the lead in {[Tm^{Ph}]Pb}$^{+}$ may be replaced by zinc in the presence of NaI. Thus, addition of NaI to a mixture of {[Tm^{Ph}]Pb}(ClO$_4$) and Zn(ClO$_4$)$_2$ in acetonitrile results in the formation of {[Tm^{Ph}]Zn(NCMe)}$^{+}$ due to the equilibrium being shifted to the right by precipitation of Pb^{II} as PbI$_2$. This observation is of relevance since a completely effective means to reverse the toxic effects of lead in the human body are not yet known, despite efforts to develop lead complexing agents.[59]

(f) The [(Cys)$_4$Zn^{II}] motif: The Ada DNA repair protein

In addition to the ubiquitous [{XYZ}Zn^{II}–OH$_2$] motif in which the coordinated water molecule plays a critical role, recent studies indicate that zinc may also play an important role by activating thiols towards nucleophilic attack. For example, alkylation of zinc thiolates has been proposed to be a step in the mechanism of action of the Ada DNA repair protein which is responsible for demethylating DNA in a stoichiometric manner (Scheme 19);[60] related zinc thiolate reactivity has also been proposed for other enzymes.[61] The active site of the Ada repair protein possesses a [(Cys)$_4$Zn] motif and has been modeled by the anion [Zn(SPh)$_4$]$^{2-}$.[62] Thus, Wilker and Lippard have reported that [Me$_4$N]$_2$[Zn(SPh)$_4$] reacts with (MeO)$_3$PO to form PhSMe, (MeO)$_2$PO$_2^-$, and [Zn(SPh)$_3$]$^-$ *via* initial heterolytic dissociation generating an incipient thiolate anion. More recently, the thiolate complex [Tm^{Ph}]ZnSPh (Scheme 20) has been introduced as a model for the Ada repair protein, in which the [Tm^{Ph}] ligand mimics the three cysteine residues that remain bound to zinc during the course of the alkylation reaction.[63] The phenylthiolate ligand in [Tm^{Ph}]ZnSPh also possesses nucleophilic character and is alkylated by MeI to give PhSMe and [Tm^{Ph}]ZnI, a transformation that is analogous to the reactivity exhibited by tris(pyrazolyl)borate complexes [Tp$^{RR'}$]ZnSR[64] and other scorpionate thiolates.[65]

Methionine synthases are a class of enzymes related to the Ada protein in that thiolate alkylation is a common feature.[61*a*] The active sites of the various methionine synthases also feature cysteine coordination, and Riordan and coworkers have recently

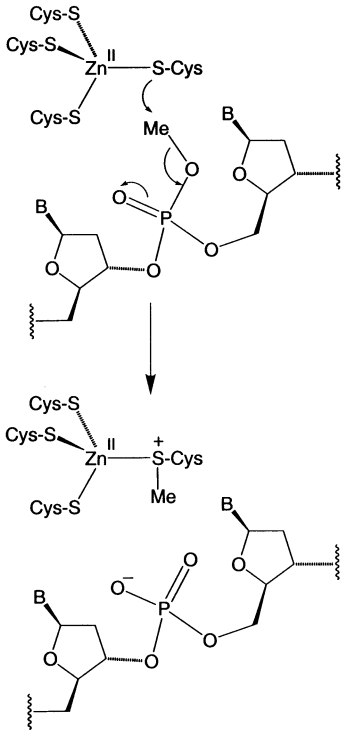

Scheme 19

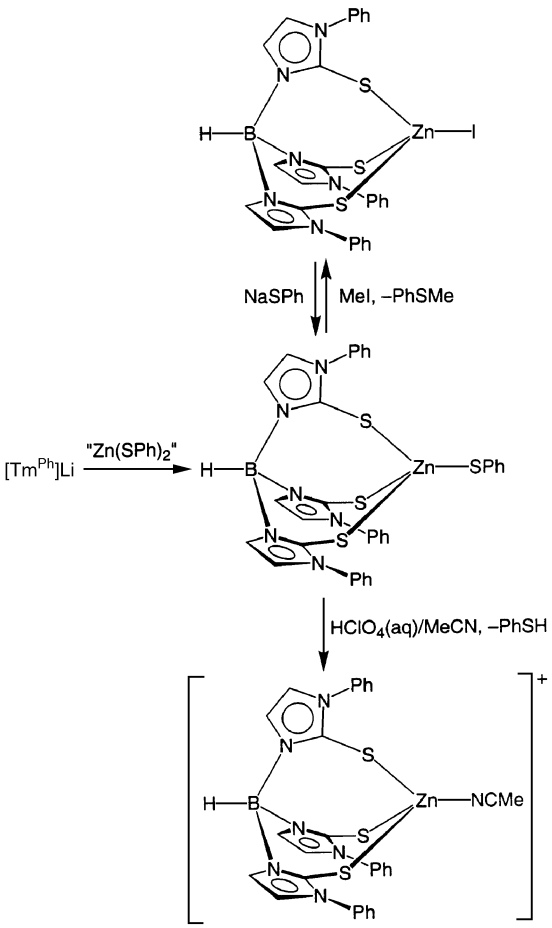

Scheme 20

introduced the use of the phenylborato ligands [PhB(CH$_2$SBu^t)$_3$] and [Ph(pz$^{Bu^t}$)(CH$_2$SBu^t)$_2$] as [S$_3$] and [NS$_2$] donors to mimic the active sites in these enzymes (Fig. 12).[43]

In addition to alkylation of zinc–cysteine thiolates, proteolytic cleavage of such groups is of relevance to the mechanism

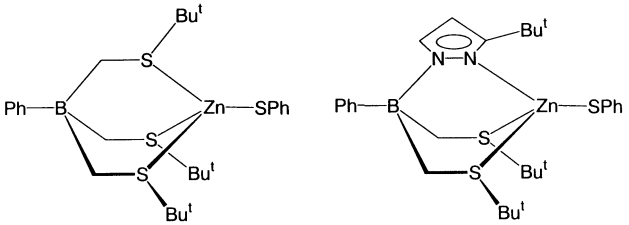

Fig. 12 Methionine synthase mimics.

of action of matrix metalloproteinases (matrixins) which are an important group of zinc enzymes responsible for degradation of the extracellular matrix components.[66] One of the mechanisms for activating the proenzyme involves proteolytic cleavage of the cysteine thiolate residue and a chemical model for this process is provided by the reactivity of $[Tm^{Ph}]ZnSPh$ towards H^+. Specifically, treatment of $[Tm^{Ph}]ZnSPh$ with $HClO_4$ in acetonitrile results in elimination of PhSH and formation of $\{[Tm^{Ph}]Zn(NCMe)\}(ClO_4)$, as illustrated in Scheme 20.

4. Metal ion substitution for probing zinc enzymes

As a result of the poor spectroscopic properties of Zn^{II}, it is difficult to obtain information concerning the structure of the active site of the enzyme and the nature of the intermediates involved in the catalytic cycle. For this reason, considerable effort has been directed towards investigating enzymes in which the zinc has been replaced by various other metals in an effort to incorporate a spectroscopic probe, *e.g.* Co^{II} (UV–vis) and Cd^{II} (NMR).[67] However, the various metal substituted enzymes often exhibit markedly different activities, and so the use of metal ion substitution to provide insight into the mechanism of action depends critically on a knowledge of the chemistry of various metal ions in coordination environments that are closely related to the enzyme active site. Therefore, in an effort to provide such information, the chemistry of other metals in coordination environments related to those of zinc enzymes has also been investigated.

(a) Influence of the metal on active site coordination geometry

Cobalt is the metal that is most commonly substituted into zinc enzymes because it has distinct electronic spectroscopic properties and also has a strong tendency to form tetrahedral complexes. However, structural studies on a series of closely related metal complexes indicate that substitution of zinc in enzymes by other metals is actually likely to have a significant impact on the structure of the active site,[68] as illustrated by the carbonic anhydrase synthetic analogues $\{[Tp^{Pr^i_2}]M(\mu\text{-}OH)\}_n$. Thus, of these derivatives, only the zinc complex $[Tp^{Pr^i_2}]ZnOH$ exists as a tetrahedral terminal hydroxide derivative, whereas the manganese, iron, cobalt, nickel and copper derivatives exist as five-coordinate dinuclear complexes with bridging hydroxide ligands, $\{[Tp^{Pr^i_2}]M(\mu\text{-}OH)\}_2$ (M = Mn, Fe, Co, Ni, Cu)[12d] (Fig. 13).

Interesting differences as a function of metal are also observed for complexes obtained using tris(imidazolyl)phosphine ligands. For example, the reactions of $[Pim^{Pr^i,Bu^t}]$ with $M(ClO_4)_2{\cdot}6H_2O$ (M = Zn, Cd) yield $\{[Pim^{Pr^i,Bu^t}]ZnOH\}^+$ and $\{[Pim^{Pr^i,Bu^t}]Cd(OH_2)(OClO_3)\}^+$ which, as illustrated in Fig. 14, possess significantly different structures.[69] Thus, the zinc complex $\{[Pim^{Pr^i,Bu^t}]ZnOH\}^+$ exists as a simple tetrahedral hydroxide derivative, whereas the cadmium counterpart is a *five*-coordinate *aqua* complex, $\{[Pim^{Pr^i,Bu^t}]Cd(OH_2)(OClO_3)\}^+$. In addition to the different structures, the fact that

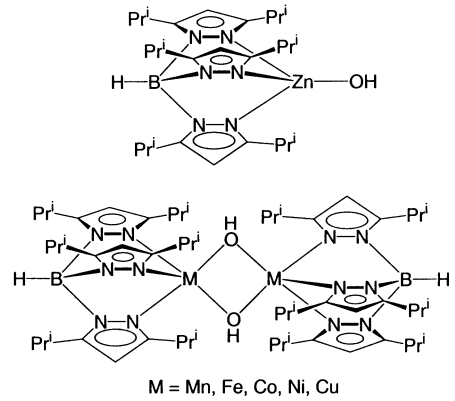

Fig. 13 Mononuclear and dinuclear metal hydroxides.

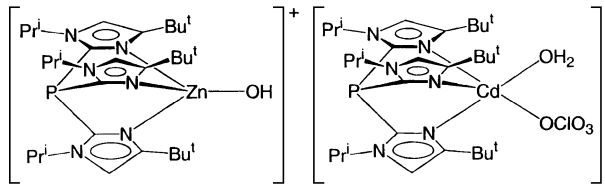

Fig. 14 Comparison of the structures of $\{[Pim^{Pr^i,Bu^t}]ZnOH\}^+$ and $\{[Pim^{Pr^i,Bu^t}]Cd(OH_2)(OClO_3)\}^+$.

the cadmium center binds a ligand as weakly coordinating as perchlorate is particularly interesting because it indicates that biologically more pertinent anions should also coordinate to a tetrahedral $[\{N_3\}Cd^{II}(OH_2)]$ center and thereby suggests that Cd^{II}–carbonic anhydrase may not be tetrahedral.

The observation that the cadmium complex $\{[Pim^{Pr^i,Bu^t}]Cd(OH_2)(OClO_3)\}^+$ also exists as an aqua species provides a rationalization for the reduced activity of Cd^{II}–carbonic anhydrase since access to a hydroxide species is required for efficient carbonic anhydrase activity. The reluctance of the aqua complex $\{[Pim^{Pr^i,Bu^t}]Cd(OH_2)(OClO_3)\}^+$ to convert to a hydroxide species is a consequence of the coordinated perchlorate ligand since the acidity of a coordinated water molecule is reduced considerably upon the binding of an anionic ligand, *i.e.* the pK_a of the monocation $\{[Pim^{Pr^i,Bu^t}]Cd(OH_2)(OClO_3)\}^+$ would be expected to be greater than that of dicationic $\{[Pim^{Pr^i,Bu^t}]Zn(OH_2)\}^{2+}$. The fact that Cd^{II}–carbonic anhydrase only exhibits significant activity at higher pH (corresponding to the ionization of a cadmium-bound water molecule with a pK_a of *ca.* 9) is in accord with the isolation of the aqua species $\{[Pim^{Pr^i,Bu^t}]Cd(OH_2)(OClO_3)\}^+$, with a higher pH being necessary to generate the requisite hydroxide species.

An investigation of the reaction of $Co(ClO_4)_2{\cdot}6H_2O$ with $[Pim^{Pr^i_2}]$ in methanol also indicates the reluctance of cobalt to form simple tetrahedral cobalt hydroxide complexes by forming the six-coordinate aqua–methanol–perchlorate complex $\{[Pim^{Pr^i_2}]Co(OH_2)(HOMe)(OClO_3)\}^+$ (Scheme 21).[70]

Structural studies on a series of complexes of the bis(2-mercapto-1-methylimidazolyl)(pyrazolyl)hydroborato $[NS_2]$ donor ligand also indicate interesting differences in coordination mode as a function of the metal. Thus, of the $[pzBm^{Me}]_2Zn$, $[pzBm^{Me}]_2Co$ and $[pzBm^{Me}]_2Cd$ derivatives (Fig. 15), only the zinc complex has a tetrahedral $M[S_4]$ structure which resembles the $[(Cys)_4Zn]$ structural sites in enzymes such as LADH. In contrast, the cobalt and cadmium derivatives, $[pzBm^{Me}]_2Co$ and $[pzBm^{Me}]_2Cd$, exhibit structures in which the B–H groups also interact with the metal center. The non-tetrahedral nature of the latter complexes indicates that zinc has a greater preference for tetrahedral $M[S_4]$ coordination, which is in accord with its prevalent role in the structural sites of enzymes.

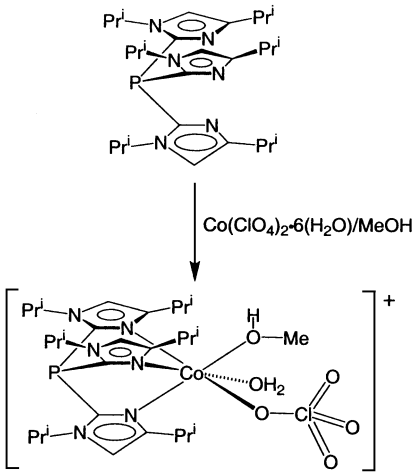

Scheme 21

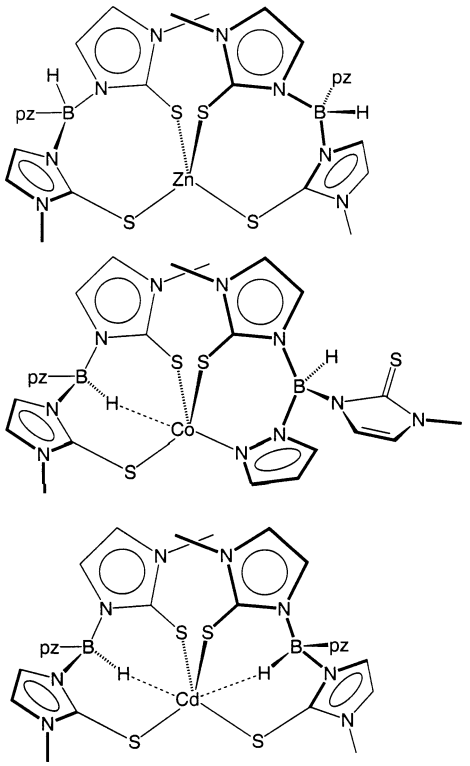

Fig. 15 Structures of $[pzBm^{Me}]_2M$ (M = Zn, Co, Cd) indicating the greater preference of zinc to adopt tetrahedral $M[S_4]$ coordination.

(b) Nitrate ligands as a probe for trends in bicarbonate coordination modes in metal-substituted carbonic anhydrases

The final step of the carbonic anhydrase catalytic cycle, *i.e.* displacement of a bicarbonate ligand by water, is undoubtedly dependent on the coordination mode of the bicarbonate ligand. For example, Co^{II}–carbonic anhydrase is less active than the zinc enzyme and X-ray diffraction studies indicate that the bicarbonate ligand binds in a bidentate manner. An appreciation of the factors that influence the coordination mode of a bicarbonate ligand is, therefore, critical to understanding the relative activities of metal-substituted carbonic anhydrases. However, such a study is presently not possible due to the general instability of bicarbonate complexes, with no zinc bicarbonate complex having been structurally characterized. For this reason, the nitrate ligand has been employed as a probe to provide an indication of the structural variations that would be expected for a series of bicarbonate complexes.[12c,68] Specifically, since bicarbonate and nitrate ligands are isoelectronic and sterically similar, the *variation* in nitrate coordination mode (Fig. 16) for a series of analogous metal complexes is anticipated to correlate with the *trend* observed for analogous bicarbonate complexes.

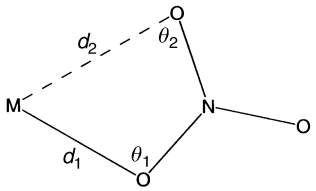

Fig. 16 Parameters used in classifying nitrate coordination mode.

The variation in nitrate ligand coordination mode has been examined for the tris(pyrazolyl)hydroborato and tris(imidazolyl)phosphine complexes, $[Tp^{Bu^t,R}]M(NO_3)$ and $\{[Pim^{Pr^i,Bu^t}]M(NO_3)\}^+$,[68] as summarized in Table 6. Nitrate ligand coordination modes may be classified as either bidentate ($\Delta d < 0.3$ Å; $\Delta\theta < 14°$), anisobidentate ($0.3 < \Delta d < 0.6$ Å; $28 < \Delta\theta < 14°$), or unidentate ($\Delta d > 0.6$ Å; $\Delta\theta > 28°$), depending upon the degree of asymmetry. The data listed in Table 6 indicate that the bidenticity increases in the sequence Zn < Hg < Co < Cu ≈ Ni ≈ Cd, reflecting the different electronic properties of the metals. Steric effects are also important in influencing the coordination mode, as illustrated by the observation that the asymmetry of the nitrate coordination mode decreases across the series $[Tp^{Bu^t}]Zn(NO_3)$,[68a] $[Tp^{Ph}]Zn(NO_3)$,[71] and $[Tp]Zn(NO_3)$[72]

Table 6 Comparison of nitrate coordination mode of $LM(NO_3)^{Q+a}$ with activity of M^{II}–CA (data taken from ref. 68*d*)

M	M^{II}–CA activity (%)	Δd/Å		$\Delta\theta$/°	
		$[Pim^{Pr^i,Bu^t}]$	$[Tp^{Bu^t,R}]^b$	$[Pim^{Pr^i,Bu^t}]$	$[Tp^{Bu^t,R}]^b$
Zn	100	0.53	0.60	24.4	29.6
Co	50	0.27	0.34	10.8	15.8
Ni	2	—	0	—	0
Cu	0	0.13	0	5.9	0
Cd	2	0.13	0.23	7.4	1.8
Hg	0	0.39	—	19.3	—

[a] $Q = 1$ for L = $[Pim^{Pr^i,Bu^t}]$; $Q = 0$ for L = $[Tp^{Bu^t,R}]$. [b] R = H for M = Zn, Co, Cu, Ni; R = Me for M = Cd.

Interestingly, with the exception of mercury, the nitrate coordination mode in these complexes correlates with the activity of metal substituted carbonic anhydrases: Zn > Co >> Cu ≈ Ni ≈ Cd ≈ Hg (Table 6). Specifically, those metals with almost symmetric bidentate coordination are inactive, whereas those with significant asymmetry (Zn and Co) are active. In this regard, it is also noteworthy that the carbonate ligand in the complexes $\{[Tp^{Pr^i_2}]M\}_2(\mu\text{-}CO_3)$ (M = Mn, Fe, Co, Ni, Cu)[12d] exhibits varying degrees of asymmetry that closely parallel the series of nitrate complexes described above, and thereby provides further support for the notion that nitrate is a good model for bicarbonate.

(c) Spectroscopic models

Finally, another use for synthetic analogues is to provide spectroscopic signatures that enable the assignment of the coordination environments of the active sites of metalloenzymes. For example, (*i*) the similarity of the electronic spectrum of blue $[Tp^{Bu^t}]CoCl$[68b] with that of the high pH form of Co^{II}–carbonic anhydrase is consistent with the notion that the active site exhibits a pseudo-tetrahedral coordination geometry,[67] (*ii*) comparison of the electronic spectra of purple $[Tp^{Bu^t}]NiCl$, yellow $[Tp^{Bu^t}]Ni(\eta^2\text{-}O_2NO)$ and green $[Tp^{Me_2}]Ni(\eta^2\text{-}O_2NO)(THF)$,[68b] with the electronic spectrum of Ni^{II}–carbonic anhydrase supports the notion that nickel is six-coordinate in the enzyme at neutral pH, and (*iii*) comparison of the electronic spectrum of Cu^{II}–carbonic anhydrase with those

of [Tp$^{Bu^t}$]CuCl and [Tp$^{Bu^t}$]Cu(η^2-O_2NO) indicates a greater similarity to the five-coordinate structure.[68b]

Acknowledgements

I sincerely wish to thank the students and postdoctoral researchers who carried out portions of the research described in this article, which was supported by the National Institutes of Health (Grant GM46502).

Notes and references

1 H. Vahrenkamp, *Chem. Unserer Zeit*, 1988, **22**, 73.
2 (*a*) B. L. Vallee and D. S. Auld, *Acc. Chem. Res.*, 1993, **26**, 543; (*b*) W. N. Lipscomb and N. Sträter, *Chem. Rev.*, 1996, **96**, 2375; (*c*) D. S. Auld, *Struct. Bonding (Berlin)*, 1997, **89**, 29; (*d*) J. E. Coleman, *Curr. Opin. Chem. Biol.*, 1998, **2**, 222; (*e*) S. Rahuel-Clermont and M. F. Dunn, *Copper Zinc Inflammatory Degener. Dis.*, 1998, 47.
3 C. F. Mills, *Zinc in Human Biology*, Springer-Verlag, New York, 1989.
4 See, for example: I. L. Alberts, K. Nadassy and S. J. Wodak, *Protein Sci.*, 1998, **7**, 1700.
5 R. J. P. Williams, in *Zinc in Human Biology*, ed. I. Macdonald, Springer-Verlag, New York, 1989, ch 2.
6 For lead references, see: (*a*) E. Kimura and E. Kikuta, *J. Biol. Inorg. Chem.*, 2000, **5**, 139; (*b*) H. Vahrenkamp, *Acc. Chem. Res.*, 1999, **32**, 589; (*c*) H. Vahrenkamp, *Bioinorganic Chemistry—Transition Metals in Biology and their Coordination Chemistry*, Wiley-VCH, Weinheim, 1997, pp. 540–551; (*d*) R. S. Brown, *NATO ASI Ser., Ser. C*, 1990, **314**, 145; (*e*) L. Banci, I. Bertini, C. Luchinat and J. M. Moratal, *NATO ASI Ser., Ser. C*, 1990, **314**, 181; (*f*) G. Parkin, in *Probing of Proteins by Metal Ions and Their Low-Molecular-Weight Complexes, Met. Ions Biol. Syst.*, ed. A. Sigel and H. Sigel, M. Dekker, New York, vol. 38, in press.
7 C. W. Bock, A. K. Katz and J. P. Glusker, *J. Am. Chem. Soc.*, 1995, **117**, 3754.
8 H. Sigel and R. B. Martin, *Chem. Soc. Rev.*, 1994, **23**, 83.
9 For recent reviews, see: (*a*) S. Trofimenko, *Scorpionates – The Coordination Chemistry of Polypyrazolylborate Ligands*, Imperial College Press, London, 1999; (*b*) G. Parkin, *Adv. Inorg. Chem.*, 1995, **42**, 291; (*c*) N. Kitajima and W. B. Tolman, *Prog. Inorg. Chem.*, 1995, **43**, 419.
10 S. Trofimenko, J. C. Calabrese and J. S. Thompson, *Inorg. Chem.*, 1987, **26**, 1507.
11 See, for example: (*a*) S. Lindskog, *Pharmacol. Ther.*, 1997, **74**, 1; (*b*) D. N. Silverman, *Can. J. Bot.*, 1991, **69**, 1070.
12 (*a*) R. Alsfasser, S. Trofimenko, A. Looney, G. Parkin and H. Vahrenkamp, *Inorg. Chem.*, 1991, **30**, 4098; (*b*) R. Alsfasser, M. Ruf, S. Trofimenko and H. Vahrenkamp, *Chem. Ber.–Recl.*, 1993, **126**, 703; (*c*) A. Looney, R. Han, K. McNeill and G. Parkin, *J. Am. Chem. Soc.*, 1993, **115**, 4690; (*d*) N. Kitajima, S. Hikichi, M. Tanaka and Y. Morooka, *J. Am. Chem. Soc.*, 1993, **115**, 5496; (*e*) M. Ruf and H. Vahrenkamp, *Inorg. Chem.*, 1996, **35**, 6571; (*f*) A. Looney, G. Parkin, R. Alsfasser, M. Ruf and H. Vahrenkamp, *Angew. Chem., Int. Ed. Engl.*, 1992, **31**, 92.
13 F. Hartmann, W. Kläui, A. Kremer-Aach, D. Mootz, A. Strerath and H. Wunderlich, *Z. Anorg. Allg. Chem.*, 1993, **619**, 2071.
14 P. Chaudhuri, C. Stockheim, K. Wieghardt, W. Deck, R. Gregorzik, H. Vahrenkamp, B. Nuber and J. Weiss, *Inorg. Chem.*, 1992, **31**, 1451.
15 E. Kimura, T. Shiota, T. Koike, M. Shiro and M. Kodama, *J. Am. Chem. Soc.*, 1990, **112**, 5805.
16 A. S. Borovik, personal communication.
17 For the cobalt analogue, see: B. S. Hammes, V. G. Young, Jr. and A. S. Borovik, *Angew. Chem., Int. Ed.*, 1999, **38**, 666.
18 C. Kimblin, W. E. Allen and G. Parkin, *J. Chem. Soc., Chem. Commun.*, 1995, 1813.
19 (*a*) I. Bertini, C. Luchinat, M. Rosi, A. Sgamellotti and F. Tarantelli, *Inorg. Chem.*, 1990, **29**, 1460; (*b*) M. Sola, A. Lledos, M. Duran and J. Bertran, *Inorg. Chem.*, 1991, **30**, 2523.
20 (*a*) M. Ruf, K. Weis and H. Vahrenkamp, *J. Chem. Soc., Chem. Commun.*, 1994, 135; (*b*) M. Ruf, K. Weis, I. Brasack and H. Vahrenkamp, *Inorg. Chim. Acta*, 1996, **250**, 271; (*c*) M. Ruf, K. Weis and H. Vahrenkamp, *Inorg. Chem.*, 1997, **36**, 2130; (*d*) T. Brandsch, F. A. Schell, K. Weis, M. Ruf, B. Muller and H. Vahrenkamp, *Chem. Ber.–Recl.*, 1997, **130**, 283; (*e*) S. Hikichi, M. Tanaka, Y. Morooka and N. Kitajima, *J. Chem. Soc., Chem. Commun.*, 1992, 814; (*f*) U. Hartmann and H. Vahrenkamp, *Inorg. Chem.*, 1991, **30**, 4676; (*g*) U. Hartmann and H. Vahrenkamp, *Chem. Ber.*, 1994, **127**, 2381.
21 C. Bergquist and G. Parkin, *J. Am. Chem. Soc.*, 1999, **121**, 6322.
22 M. Bräuer, E. Anders, S. Sinnecker, W. Koch, M. Rombach, H. Brombacher and H. Vahrenkamp, *Chem. Commun.*, 2000, 647.
23 (*a*) X. Zhang and R. Van Eldik, *Inorg. Chem.*, 1995, **34**, 5606; (*b*) X. Zhang, R. van Eldik, T. Koike and E. Kimura, *Inorg. Chem.*, 1993, **32**, 5749.
24 (*a*) X. Zhang, C. D. Hubbard and R. van Eldik, *J. Phys. Chem.*, 1996, **100**, 9161; (*b*) S. Schindler, C. D. Hubbard and R. van Eldik, *Chem. Soc. Rev.*, 1998, **27**, 387.
25 C. Dowling and G. Parkin, *Polyhedron*, 1996, **15**, 2463 and references therein.
26 C. Dowling, V. J. Murphy and G. Parkin, *Inorg. Chem.*, 1996, **35**, 2415.
27 P. Ghosh and G. Parkin, *J. Chem. Soc., Dalton Trans.*, 1998, 2281.
28 S. S. Tandon, S. Chander, L. K. Thompson, J. N. Bridson and V. McKee, *Inorg. Chim. Acta*, 1994, **219**, 55.
29 B. S. Hammes and C. J. Carrano, *Inorg. Chem.*, 1999, **38**, 4593.
30 (*a*) C. Dowling and G. Parkin, *Polyhedron*, 1996, **15**, 2463; (*b*) P. Ghosh and G. Parkin, *J. Chem. Soc., Dalton Trans.*, 1998, 2281.
31 X. Cheng, X. Zhang, J. W. Pflugrath and F. W. Studier, *Proc. Natl. Acad. Sci. USA*, 1994, **91**, 4034.
32 (*a*) P. T. R. Rajagopalan, X. C. Yu and D. Pei, *J. Am. Chem. Soc.*, 1997, **119**, 12418; (*b*) A. Becker, I. Schlichting, W. Kabsch, D. Groche, S. Schultz and A. F. V. Wagner, *Nat. Struct. Biol.*, 1998, **5**, 1053; (*c*) S. Ragusa, S. Blanquet and T. Meinnel, *J. Mol. Biol.*, 1998, **280**, 515.
33 P. Ghosh, M. Wood, J. B. Bonanno, T. Hascall and G. Parkin, *Polyhedron*, 1999, **18**, 1107.
34 P. Ghosh and G. Parkin, *Chem. Commun.*, 1998, 413.
35 (*a*) B. S. Hammes and C. J. Carrano, *Inorg. Chim. Acta*, 2000, **300**, 427; (*b*) B. S. Hammes and C. J. Carrano, *J. Chem. Soc., Dalton Trans.*, 2000, 3304.
36 (*a*) L. M. Berreau, R. A Allred, M. M. Makowska-Grzyska and A. M. Arif, *Chem. Commun.*, 2000, 1423; (*b*) S. Baggio, M. I. Pardo, R. Baggio and M. T. Garland, *Acta Crystallogr., Sect. C*, 1997, **53**, 551.
37 M. H. Bracey, J. Christiansen, P. Tovar, S. P. Cramer and S. G. Bartlett, *Biochemistry*, 1994, **33**, 13126.
38 S. B. Xiang, S. A. Short, R. Wolfenden and C. W. Carter, *Biochemistry*, 1996, **35**, 1335.
39 (*a*) R. M. Kellogg and R. P. Hof, *J. Chem. Soc., Perkin Trans. 1*, 1996, 1651; (*b*) B. Kaptein, G. Barf, R. M. Kellogg and F. Vanbolhuis, *J. Org. Chem.*, 1990, **55**, 1890; (*c*) B. Kaptein, L. Wang-Griffin, G. Barf and R. M. Kellogg, *Chem. Commun.*, 1987, 1457; (*d*) B. Koning, R. Hulst, A. Bouter, J. Buter, A. Meetsma and R. M. Kellogg, *Chem. Commun.*, 1997, 1065.
40 N. J. Curtis and R. S. Brown, *Can. J. Chem.*, 1981, **59**, 65.
41 U. Brand and H. Vahrenkamp, *Z. Anorg. Allg. Chem.*, 1996, **622**, 213.
42 C. Kimblin, T. Hascall and G. Parkin, *Inorg. Chem.*, 1997, **36**, 5680.
43 S.-J. Chiou, J. Innocent, C. G. Riordan, K.-C. Lam, L. Liable-Sands and A. L. Rheingold, *Inorg. Chem.*, 2000, **39**, 4337.
44 The observation of a hydrogen-bond interaction between methanol and a thiolate ligand in five-coordinate zinc complexes with [N_3S_2]Zn coordination, has led to the suggestion that the alcohol substrate may interact with the cysteine groups in a similar manner and that this interaction may possibly promote deprotonation before interaction with the zinc center. See: S. C. Shoner, K. J. Humphreys, D. Barnhart and J. A. Kovacs, *Inorg. Chem.*, 1995, **34**, 5933.
45 C. Bergquist and G. Parkin, *Inorg. Chem.*, 1999, **38**, 422.
46 (*a*) R. Walz, K. Weis, M. Ruf and H. Vahrenkamp, *Chem. Ber.–Recl.*, 1997, **130**, 975; (*b*) M. Ruf, F. A. Schell, R. Walz and H. Vahrenkamp, *Chem. Ber.–Recl.*, 1997, **130**, 101.
47 C. Bergquist, H. Storrie, L. Koutcher, B. M. Bridgewater, R. A. Friesner and G. Parkin, submitted.
48 See, for example: H. E. Bryndza, P. J. Domaille, W. Tam, L. K. Fong, R. A. Paciello and J. E. Bercaw, *Polyhedron*, 1988, **7**, 1441.
49 R. M. Borges dos Santos and J. A. Martinho Simões, *J. Phys. Chem. Ref. Data*, 1998, **27**, 707.
50 C. Kimblin, B. M. Bridgewater, D. G. Churchill and G. Parkin, *Chem. Commun.*, 1999, 2301.
51 Kimura *et al.* have also used *p*-nitrobenzaldehyde as a NAD^+ mimic in model studies. See: E. Kimura, M. Shionoya, A. Hoshino, T. Ikeda and Y. Yamada, *J. Am. Chem. Soc.*, 1992, **114**, 10134.
52 E. K. Jaffe, *Acta Crystallogr. Sect. D: Biol. Crystallogr.*, 2000, **56**, 115.
53 (*a*) P. T. Erskine, N. Senior, S. Awan, R. Lambert, G. Lewis, I. J. Tickle, M. Sarwar, P. Spencer, P. Thomas, M. J. Warren, P. M. Shoolingin-Jordan, S. P. Wood and J. B. Cooper, *Nat. Struct. Biol.*, 1997, **4**, 1025;

(*b*) P. T. Erskine, E. Norton, J. B. Cooper, R. Lambert, A. Coker, G. Lewis, P. Spencer, M. Sarwar, S. P. Wood, M. J. Warren and P. M. Schoolingin-Jordan, *Biochemistry*, 1999, **38**, 4266.

54 (*a*) M. J. Hynes and B. Jonson, *Chem. Soc. Rev.*, 1997, **26**, 133; (*b*) N. Castellino, P. Castellino and N. Sannolo, *Inorganic Lead Exposure: Metabolism and Intoxication*, Lewis Publishers, Boca Raton, FL, 1995.

55 See, for example: (*a*) I. A. Bergdahl, *Analusis*, 1998, **26**, M81; (*b*) A. C. Todd, J. G. Wetmur, J. M. Moline, J. H. Godbold, S. M. Levin and P. J. Landrigan, *Environ. Health Perspect.*, 1996, **104**, 141.

56 B. M. Bridgewater and G. Parkin, *J. Am. Chem. Soc.*, 2000, **122**, 7140.

57 M. J. Warren, J. B. Cooper, S. P. Wood and P. M. Shoolingin-Jordan, *Trends Biochem. Sci.*, 1998, **23**, 217.

58 T. J. B. Simons, *Eur. J. Biochem.*, 1995, **234**, 178.

59 See, for example: K. Abudari, T. B. Karpishin and K. N. Raymond, *Inorg. Chem.*, 1993, **32**, 3052.

60 (*a*) L. C. Myers, M. P. Terranova, A. E. Ferentz, G. Wagner and G. L. Verdine, *Science*, 1993, **261**, 1164; (*b*) L. C. Myers, F. Jackow and G. L. Verdine, *J. Biol. Chem.*, 1995, **270**, 6664

61 (*a*) R. G. Matthews and C. W. Goulding, *Curr. Opin. Chem. Biol.*, 1997, **1**, 332; (*b*) K. E. Hightower and C. A. Fierke, *Curr. Opin. Chem. Biol.*, 1999, **3**, 176; (*c*) C. L. Strickland and P. C. Weber, *Curr. Opin. Drug Discovery Dev.*, 1999, **2**, 475.

62 (*a*) J. J. Wilker and S. J. Lippard, *Inorg. Chem.*, 1997, **36**, 969; (*b*) J. J. Wilker and S. J. Lippard, *J. Am. Chem. Soc.*, 1995, **117**, 8682.

63 B. M. Bridgewater and G. Parkin, *J. Chem. Soc., Dalton Trans.*, submitted.

64 (*a*) U. Brand, M. Rombach and H. Vahrenkamp, *Chem. Commun.*, 1998, 2717; (*b*) R. Burth and H. Vahrenkamp, *Z. Anorg. Allg. Chem.*, 1998, **624**, 381.

65 C. R. Warthen, B. S. Hammes and C. J. Carrano, *J. Biol. Inorg. Chem.*, in press.

66 (*a*) W. Bode, C. Fernandez-Catalan, H. Tschesche, F. Grams, H. Nagase and K. Maskos, *Cell. Mol. Life Sci.*, 1999, **55**, 639; (*b*) H. Nagase and J. F. Woessner, Jr., *J. Biol. Chem.*, 1999, **274**, 21491.

67 See, for example: L. Banci, I. Bertini, C. Luchinat, A. Donaire, M. J. Martinez and J. M. Moratal Mascarell, *Comments Inorg. Chem.*, 1990, **9**, 245 and references therein.

68 (*a*) R. Han and G. Parkin, *J. Am. Chem. Soc.*, 1991, **113**, 9707; (*b*) R. Han, A. Looney, K. McNeill, G. Parkin, A. L. Rheingold and B. S. Haggerty, *J. Inorg. Biochem.*, 1993, **49**, 105; (*c*) A. Looney, A. Saleh, Y. Zhang and G. Parkin, *Inorg. Chem.*, 1994, **33**, 1158; (*d*) C. Kimblin, V. J. Murphy, T. Hascall, B. M. Bridgewater, J. B. Bonanno and G. Parkin, *Inorg. Chem.*, 2000, **39**, 967.

69 C. Kimblin and G. Parkin, *Inorg. Chem.*, 1996, **35**, 6912.

70 C. Kimblin, B. M. Bridgewater, D. G. Churchill and G. Parkin, *J. Chem. Soc., Dalton Trans.*, 2000, 2191.

71 (*a*) R. Alsfasser, A. K. Powell, S. Trofimenko and H. Vahrenkamp, *Chem. Ber.–Recl.*, 1993, **126**, 685; (*b*) R. Alsfasser, A. K. Powell and H. Vahrenkamp, *Angew. Chem., Int. Ed. Engl.*, 1990, **29**, 898.

72 A. Looney and G. Parkin, *Inorg. Chem.*, 1994, **33**, 1234.

Palladium-catalysed annulation reaction of allenyltins with β-iodo vinylic acids: selective synthesis of α-pyrones

Séverine Rousset,[a] Mohamed Abarbri,[a] Jérôme Thibonnet,[a] Alain Duchêne*[a] and Jean-Luc Parrain*[b]

[a] *Laboratoire de Physicochimie des Interfaces et des Milieux Réactionnels, Faculté des Sciences de Tours, Parc de Grandmont, 37200 Tours, France. E-mail: duchene@delphi.phys.univ-tours.fr*

[b] *Laboratoire de Synthèse Organique associé au CNRS (ESA 6009), Faculté des Sciences de Saint Jérôme, Avenue Escadrille Normandie-Niemen, 13397 Marseille Cedex 20, France. E-mail: jl.parrain@lso.u-3mrs.fr*

Received (in Liverpool, UK) 18th July 2000, Accepted 1st September 2000
First published as an Advance Article on the web 21st September 2000

Palladium-catalysed regio- and stereoselective annulation of allenyl stannanes by β-iodo vinylic acids gives the corresponding α-pyrones in high yields. This annulation most probably proceeds through a Stille reaction/cyclisation sequence.

Five- and six-membered ring unsaturated lactones (butenolides or pyrones) constitute an important class of biologically active compounds and their synthesis has been the focus of considerable attention in synthetic organic chemistry[1] as well as in medicinal chemistry.[2] Numerous methods reported in the last decade for the synthesis of these structures involve transition metal (Ag, Hg, Rh, Pd) promoted intramolecular additions of carboxylic acids to alkynes.[3] In general, the lactonisation reaction of alk-4-ynoic acids proceeds through a stereoselective *trans* addition reaction *via* a *5-exo* process. In addition to the formation of γ-alkylidenebutenolides, in some cases six-membered lactones resulting from the *6-endo* mode have been obtained as minor products. This problem of regioselectivity was recently solved by Larock *et al.* who demonstrated that substituted isocoumarins or α-pyrones could be prepared by treating β-halogeno α,β-unsaturated esters with internal alkynes in the presence of a palladium catalyst.[4] Nevertheless, two α-pyrone regioisomers were obtained in the case of non-symmetric alkynes. On the other hand, we have previously described the synthesis of dienoic acids or enynes bearing a carboxylic acid function from β-iodovinylic acids and vinyltin or alkynylzinc reagents.[5] This methodology was then applied to the synthesis of γ-tributyltin methylidenebutenolides.[6] To broaden our synthesis strategy and to design a system suitable for *6-endo* lactonization, we planned the preparation of allenyl substituted alkenoic acids which we thought would exclusively undergo *6-endo* mode cyclisation mediated by a palladium complex (Scheme 1).[7]

We report here the selective one pot synthesis of α-pyrones under palladium complex catalysis. Our investigation began with the coupling of tributylstannylallene[8] with (*Z*)-3-iodoprop-2-enoic acid[5] under conditions previously defined by our group.[6] Unfortunately, neither allenyl substituted propenoic acid nor cyclised products (5- or 6-membered ring lactones) were detected. Only a large amount of tin by-products were recovered, among them the tributylstannyl ester of the starting iodovinylic acid. In order to avoid the proteolysis of allenylstannane and to promote the cross coupling reaction, we examined the reaction under various conditions (solvent, catalyst, presence of additives,...). First the influence of the nature of the carboxylic acid derivative on conversion rates was examined. In DMF and in the presence of 1% of tetrakis(triphenylphosphine)palladium,† the ethyl ester of **1a** yielded exclusively ethyl hex-2-en-4-ynoate. The use of tributyltin carboxylate (Table 1 entry 4) under identical conditions to those used for the synthesis of tributyltin methylidenebutenolides, led to 52% yield of 6-methylpyran-2-one **3a**, without any trace of hexa-2,4,5-trienoic acid. Finally, we found that an 83% yield of **3a** could also be obtained from **1a** at rt in DMF using 5% palladium acetate, triphenylphosphine, sodium carbonate and tetrabutylammonium bromide.

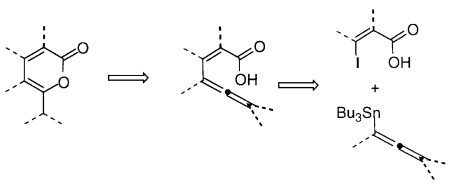

Scheme 1

Next the nature of the solvent and of the palladium complexes were examined. THF was found to be ineffective whereas acetonitrile afforded a very poor yield (< 25%) of cyclised product. We also observed that phosphine-liganded palladium appeared to be more efficient than other palladium salts such as

Table 1 Synthesis of αpyrones

Entry	R (**1**)	Allenylstannane	α-Pyranone	Yield (%)
1	H (**1a**)	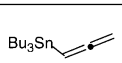	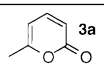 **3a**	83
2	Me (**1b**)	"	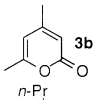 **3b**	85
3	*n*-Pr (**1c**)	"	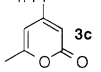 **3c**	81
4	Ph (**1d**)	"	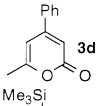 **3d**	87
5	Me_3Si (**1e**)	"	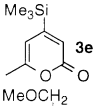 **3e**	79
6	CH_2OMe (**1f**)	"	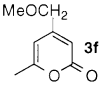 **3f**	84
7	Me (**1b**)	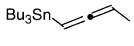	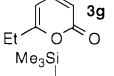 **3g**	85
8	Me_3Si (**1e**)	"	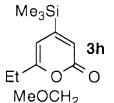 **3h**	86
9	CH_2OMe (**1f**)	"	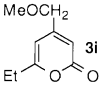 **3i**	84
10	Me (**1b**)	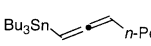	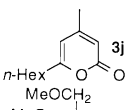 **3j**	84
11	CH_2OMe (**1f**)	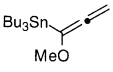	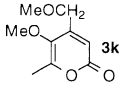 **3k**	82

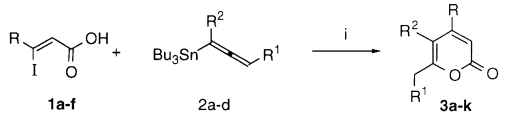

Scheme 2 $Pd(OAc)_2$ (5%), PPh_3 (10%), Na_2CO_3 (4 eq.), *n*-Bu_4NBr (1 eq.), DMF, rt.

palladium acetate (without additional triphenylphosphine) or bis(acetonitrile)palladium chloride. Tetrakis(triphenylphosphine)palladium gave approximately identical yields to the $Pd(OAc)_2/PPh_3$ couple.

The reaction of tributylstannylallene with a range of (*Z*)-3-substituted 3-iodoprop-2-enoic acids under regio- and stereocontrol gave good yields of 4-substituted-6-methylpyranones **3a**–**f** as the sole products (Table 1 entries 1–6) (Scheme 2). Other allenylstannanes were used under similar conditions in order to determine the scope of the reaction. High regioselectivity was observed in each case. The use of 3-alkylallenylstannanes (entries 7–10) showed that the regioselective heteroannulation reaction occurred only on carbons 1 and 2 of the allenyltin. On the other hand, γ-alkylidenepyranones previously obtained by Larock *et al*. from a reaction of allenes with (*Z*)-3-iodopropenoic acids were not observed. This almost certainly indicates a different mechanism to those proposed by Larock and Yamamoto respectively.[9,10]

A plausible mechanism for the heteroannulation reaction is shown in Scheme 3. First, a Stille mechanism[11] would yield 3-allenylpropenoic acid **6** by oxidative addition, transmetallation (formation of **5**) and reductive elimination. Cyclisation would then occur *via* an attack on the carboxylate function at the β-position of the allenyl moiety, which would give the π-allylpalladium intermediate. The latter would subsequently provide α-pyrone and regenerate the palladium(0) catalyst.[12]

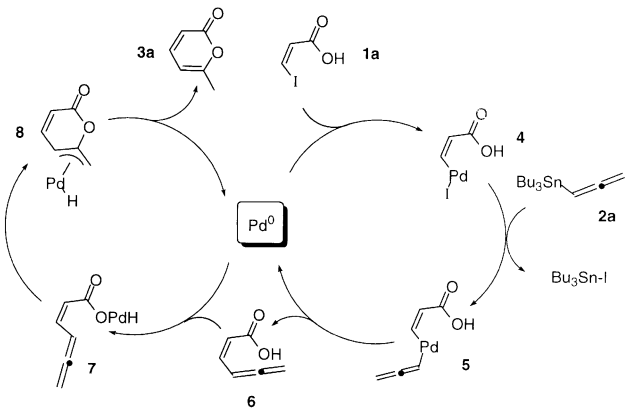

Scheme 3 Postulated mechanism for heteroannulation.

An alternative pathway involving the attack of **4** on the central carbon atom of the stannylallene **2a** could be excluded on the basis of the experiments conducted with 1 or 3-substituted allenylstannanes since other regioisomers should have been obtained rather than **3h**–**g**‡.[9]

In conclusion, under palladium complex catalysis, β-iodovinylic α,β-unsaturated acids react with allenyl stannanes *via* heteroannulation selectively to provide diverse α-pyrones. Studies to extend this reaction to other γ-halogeno pronucleophiles are currently under way and will be reported in due course.

Notes and references

† General procedure for the heteroannulation summarised in Table 1: palladium acetate (112 mg, 0.5 mmol), triphenylphosphine (131 mg, 0.5 mmol), tetrabutylammonium bromide (3.2 g, 10 mmol) and sodium carbonate (5.3 g, 50 mmol) were progressively added to a degassed solution of 3-substituted-3-iodopropenoic acid **1** (10 mmol) in anhydrous DMF (40 mL). The mixture was stirred at rt for 10 min and allenylstannane **2** (10 mmol) was then added. The reaction mixture was stirred for 4 h. After conversion was complete (checked by TLC; reaction time < 10 h), the reaction was quenched with aqueous NH_4Cl solution. After ether extraction (3 × 20 mL) and usual treatments, the crude products were chromatographed on silica gel to obtain compounds **3a**–**k**. All new compounds were fully characterised spectroscopically.

‡ Selected data for **3k**: δ_H(200 MHz, $CDCl_3$) 2.18 (3H, s), 3.40 (3H, s), 3.59 (3H, s), 4.27 (2H, s), 6.15 (1H, s); δ_C(50.3 MHz, $CDCl_3$) 15.3, 59.7, 62.5, 68.9, 109.7, 138.5, 154.2, 154.6, 162.4. MS (70 ev): *m/z* = 184 (*M*, 23%), 169 (22), 141 (22), 45 (14), 43 (100), 39 (14).

1 For reviews on butenolides see: (*a*) Y. S. Rao, *Chem. Rev.*, 1976, **76**, 625; (*b*) Y. S. Rao, *Chem. Rev*., 1964, **64**, 353; (*c*) D. W. Knight, *Contemp. Org. Synth.*, 1994, **1**, 287. For a discussion of the chemistry of α-pyrones see: (*d*) J. Staunton, in *Comprehensive Organic Chemistry*, ed. P. G. Sammes, Pergamon Press, Oxford, England, 1979, **4**, 629–646. 2*H*-Pyran-2-one and its derivatives are commonly referred to as 2-pyrones or α-pyrones; (*e*) G. H. Posner, *Acc. Chem. Res.*, 1987, **20**, 72.

2 M. T. Davies-Coleman and D. E. A. Rivett, *Progress in the Chemistry of Organic Natural Products*, 1989, **55**, 1; V. Kvita and W. Fischer, *Chimia*, 1992, **46**, 457; V. Kvita and W. Fischer, *Chimia*, 1993, **47**, 3; G. H. Posner, T. Nelson, C. Kinter and N. Johnson, *J. Org. Chem.*, 1992, **57**, 4083.

3 For recent synthesis of butenolides using Pd or Ag catalysts see C. Xu and E. Negishi, *Tetrahedron Lett.*, 1999, **40**, 431; S. Ma and Z. Shi, *J. Org. Chem.*, 1998, **63**, 6387; R. Rossi, F. Bellina, M. Biagetti and L. Mannina, *Tetrahedron Lett.*, 1998, **39**, 7799; R. Rossi, F. Bellina, M. Biagetti and L. Mannina, *Tetrahedron Lett.*, 1998, **39**, 7599; R. Rossi, F. Bellina and L. Mannina, *Tetrahedron Lett.*, 1998, **39**, 3017; R. Rossi, F. Bellina, C. Bechini, L. Mannina and P. Vergamini, *Tetrahedron*, 1998, **54**, 135; J. A. Marshall, M. A. Wolf and E. M. Wallace, *J. Org. Chem.*, 1997, **62**, 367; J. A. Marshall, M. A. Wolf and E. M. Wallace, *J. Org. Chem.*, 1995, **60**, 796; J. A. Marshall, M. A. Wolf and E. M. Wallace, *J. Org. Chem.*, 1996, **61**, 3238; Y. Ogawa, M. Maruno and T. Wakamatsu, *Heterocycles*, 1995, **41**, 2587; Y. Ogawa, M. Maruno and T. Wakamatsu, *Synlett*, 1995, 871.

4 R. C. Larock, M. J. Doty and X. Han, *J. Org. Chem.*, 1999, **64**, 8770.

5 A. Duchêne, M. Abarbri, J.-L. Parrain, M. Kitamura and R. Noyori, *Synlett*, 1994, 524; M. Abarbri, J.-L. Parrain and A. Duchêne, *Tetrahedron Lett.*, 1995, **36**, 2469; M. Abarbri, J.-L. Parrain, J.-C. Cintrat and A. Duchêne, *Synthesis*, 1996, 82.

6 S. Rousset, M. Abarbri, J. Thibonnet, A. Duchêne and J.-L. Parrain, *Org. Lett.*, 1999, **1**, 701.

7 B. Cazes, *Pure Appl. Chem.*, 1990, **62**, 1867 and references cited therein.

8 Allenyltin reagents were prepared from 3-bromoprop-1-yne, magnesium and tributyltin chloride under lead(II) bromide catalysis. H. Tanaka, A. K. M. A. Hai, H. Ogawa and S. Torii, *Synlett*, 1993, 835.

9 R. C. Larock, Y. He, W. W. Leon, X. Han, M. D. Refvik and M. J. Zenner, *J. Org. Chem.*, 1998, **63**, 2154.

10 Y. Yamamoto, M. Al-Masum and N. Fujiwara, *Chem. Commun.*, 1996, 381.

11 J. K. Stille, *Angew. Chem., Int. Ed. Engl.*, 1986, **25**, 508; T. N. Mitchell, *Synthesis*, 1992, 803.

12 M. Al-Masum and Y. Yamamoto, *J. Am. Chem. Soc.*, 1998, **120**, 3809.

Formation of pure intermediate spin complexes in highly nonplanar iron(III) porphyrins

Takahisa Ikeue,[a] Takashi Saitoh,[b] Tatsuya Yamaguchi,[a] Yoshiki Ohgo,[a] Mikio Nakamura,*[ab] Masashi Takahashi*[c] and Masuo Takeda[c]

[a] *Department of Chemistry, Toho University School of Medicine, Ota-ku, Tokyo 143-8540, Japan. E-mail: mnakamu@med.toho-u.ac.jp*
[b] *Division of Biomolecular Science, Graduate School of Science, Toho University, Funabashi 274-8510, Japan*
[c] *Department of Chemistry, Faculty of Science, Toho University, Funabashi 274-8510, Japan. E-mail: takahasi@chem.sci.toho-u.ac.jp*

Received (in Cambridge, UK) 25th July 2000, Accepted 29th August 2000
First published as an Advance Article on the web 27th September 2000

Bis(thf)(porphyrinato)iron(III) complexes with highly S_4-ruffled and S_4-saddled porphyrin cores are determined to be very pure intermediate spin complexes on the basis of NMR, EPR, Mössbauer, and magnetic data.

Iron(III) porphyrins with an intermediate spin state (S = 3/2) have attracted much attention since Maltempo pointed out the important contribution of this spin state in certain bacterial heme proteins known as cytochromes c′.[1] Among various attempts to prepare complexes with the intermediate spin state, the use of anionic ligands with a very weak ligand field, such as ClO_4^-, has brought about successful results.[2–5] In general, iron(III) ions of these complexes are in the admixed intermediate spin state represented as S = 5/2,3/2.[6] Thus, Reed and Guiset ranked the relative field strengths of weak axial ligands on the basis of the characteristics of the admixed spin state and called the hierarchy a magnetochemical series.[7] Cheng and coworkers reported that highly saddle shaped [Fe(OETPP)Cl] is in the admixed S = 5/2,3/2 spin state in spite of the presence of the much stronger chloride ligand at the axial position.[8,9] Weiss and coworkers quite recently reported, however, that the S = 3/2 character in these complexes is much smaller than originally reported.[10] We have been interested in the effects of nonplanar porphyrin rings on the physicochemical properties of iron(III) porphyrin complexes.[11–13] We have anticipated that the iron(III) complexes of highly nonplanar porphyrins such as [Fe(T^{i}PrP)(THF)$_2$]ClO_4 (**1**) and [Fe(OETPP)(THF)$_2$]ClO_4 (**2**)

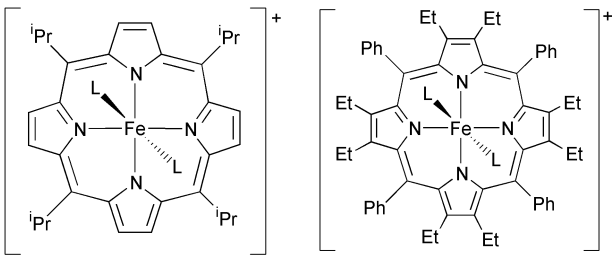

[Fe(T^{i}PrP)(L)$_2$]ClO_4
1: L = THF

[Fe(OETPP)(L)$_2$]ClO_4
2: L = THF

could show a very pure intermediate spin state as compared with well characterized [Fe(TPP)(THF)$_2$]ClO_4, since the $d_{x^2-y^2}$ orbitals in the deformed porphyrin complexes are destabilized by the short Fe–N bond lengths.[8,13] In this paper, we report that strongly S_4-ruffled **1** and S_4-saddled **2** actually show very pure intermediate spin states.

1 was prepared from $AgClO_4$ and [Fe(T^{i}PrP)Cl] in THF solution. The purple crystals were recrystallized from THF/heptane. The ^{1}H NMR spectrum taken at 233 K showed the pyrrole signal at −52.1 ppm and the CH and CH_3 signals at 9.8 and 4.8 ppm, respectively. Two signals at 14.4 and 20.5 ppm,

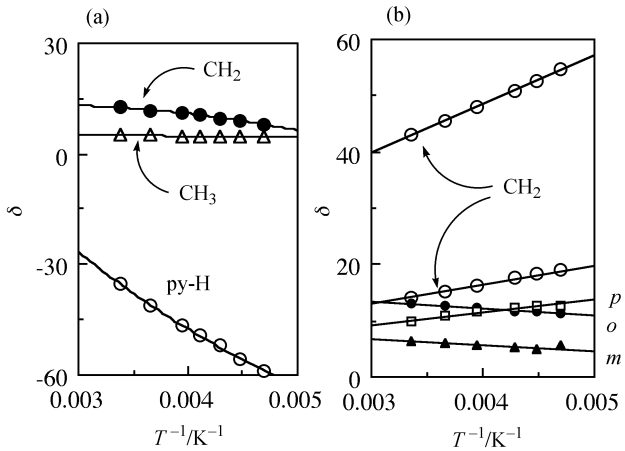

Fig. 1 Temperature dependence of the ^{1}H NMR chemical shifts of some protons in (a) **1** and (b) **2** taken in CD_2Cl_2 solution.

each corresponding to 8H, were assigned to the methylene protons of the coordinated THF ligands; these signals disappeared when the sample recrystallized from THF-d_8/heptane was used. Fig. 1a shows the temperature dependence of the chemical shifts of some protons. The existence of the extremely upfield shifted pyrrole signal indicates that **1** is in the admixed intermediate (S = 3/2,5/2) spin state where the S = 3/2 state is the main contributor.[7] The downfield shift of the THF signals can be explained in terms of the occupancy of an unpaired electron in the d_{z^2} orbital; the unpaired electron in this orbital is transferred to the axial ligand *via* σ bonding to induce downfield shifts of the ligand signals. Fig. 2a shows the EPR spectrum taken in frozen CH_2Cl_2 solution at 4.2 K. The g values were

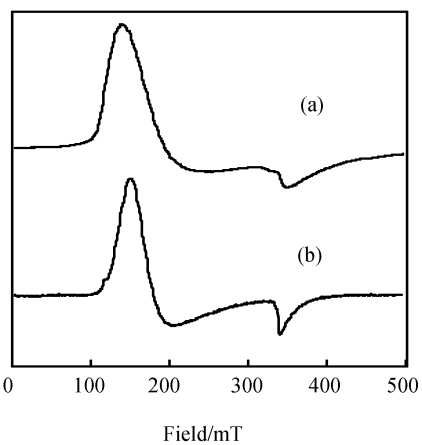

Fig. 2 EPR spectra of (a) **1** and (b) **2** taken in frozen CH_2Cl_2 solution at 4.2 K.

DOI: 10.1039/b006006m

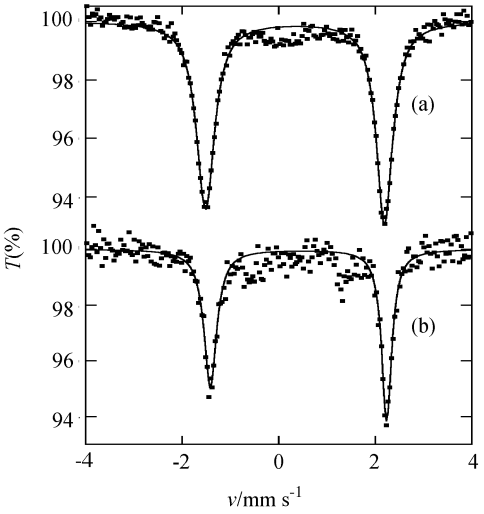

Fig. 3 Mössbauer spectra of (a) **1** taken at 76 K and (b) **2** taken at 290 K.

estimated to be 3.99 and 1.97, suggesting that the spin state of **1** should be regarded as $S = 3/2$ at 4.2 K. Magnetic moments taken for the solid sample by SQUID showed almost constant values, 3.90 ± 0.10 μ_B at 50–300 K, which are quite close to the spin only value $\mu = 3.87$ μ_B expected for $S = 3/2$ complexes. Fig. 3a shows the Mössbauer spectrum measured on a microcrystalline sample at 76 K. The isomer shift (δ; relative to α-iron foil) and quadrupole splitting (ΔE_q) were determined to be 0.34 and 3.71 mm s^{-1}, respectively. Large ΔE_q values are usually observed for complexes with $S = 3/2$ or $S = 3/2,5/2$.[14] Taken together, it is concluded that **1** is a highly pure intermediate spin complex.

2 was similarly prepared from [Fe(OETPP)Cl] and $AgClO_4$ in THF solution. The coordination of the THF ligands was confirmed by ^{1}H NMR analysis. Fig. 1b shows the temperature dependence of the chemical shifts of some protons. Fairly large downfield shifts of the methylene signals, 51.0 and 17.5 ppm at 233 K, clearly indicate that the β-pyrrole carbons have a considerable amount of π-spin density. Fig. 2b shows the EPR spectrum taken in frozen CH_2Cl_2 solution at 4.2 K. The *g* values were 4.01 and 2.00, suggesting that the spin state of **2** should also be represented as $S = 3/2$ at 4.2 K. The spin state was further confirmed by the magnetic moments determined by the Evans method in CH_2Cl_2 solution as well as by SQUID magnetometry in the solid; the former showed the magnetic moment to be 4.0 ± 0.1 μ_B at 193–303 K, and the latter gave values 3.85 ± 0.05 μ_B at 20–300 K. Fig. 3b shows the Mössbauer spectrum measured on a microcrystalline sample at 290 K. The δ and ΔE_q values were determined to be 0.50 and 3.50 mm s^{-1}, respectively. Taken together, it is concluded that **2** is also a very pure intermediate spin complex.

Formation of the very pure intermediate spin complexes, **1** and **2**, indicates that the $S = 3/2$ state is stabilized in both ruffled and saddled porphyrin complexes. The major reason must be the short Fe–N(porphyrin) bond lengths commonly observed in highly deformed porphyrin complexes.[8,15] We have recently determined the crystal structure of **1**.[16] As expected, **1** has a strongly S_4-ruffled porphyrin core with the *meso*-carbons deviating above and below the average porphyrin plane by *ca*. 0.68 Å. The Fe–N(porphyrin) bond distances of **1**, av. 1.967(12) Å, are significantly shorter than those of other bis(THF) complexes such as $[Fe(OEP)(THF)_2]ClO_4$ (av. 1.994 Å),[4] $[Fe(TEtP)(THF)_2]ClO_4$ (av. 2.006 Å)[17] and $[Fe(TPP)(THF)_2]ClO_4$ (av. 2.016 Å).[18]

In conclusion, we have shown that highly S_4-ruffled **1** and S_4-saddled **2** are highly pure intermediate spin complexes on the basis of the NMR, EPR, Mössbauer, and magnetic data.

This work was supported by a Grant-in-Aid for Scientific Research (No. 10640551) from the Ministry of Education, Science, Culture and Sports of Japan. Thanks are due to the Research Center for Molecular Materials, the Institute for Molecular Science, for assistance in obtaining the low-temperature spectra. The authors are grateful to Dr Hiroshi Fujii, Dr Yasuhiro Funahashi, and Mr Masahiro Sakai of the Institute for Molecular Science for assistance with the SQUID measurements.

Notes and references

1 M. M. Maltempo, *J. Chem. Phys.*, 1974, **61**, 2540.
2 D. H. Dolphin, J. R. Sams and T. B. Tsin, *Inorg. Chem.*, 1977, **16**, 711.
3 C. A. Reed, T. Mashiko, S. P. Bentley, M. E. Kastner, W. R. Scheidt, K. Spartalian and G. Lang, *J. Am. Chem. Soc.*, 1979, **101**, 2948.
4 H. Masuda, T. Taga, K. Osaki, H. Sugimoto, Z. I. Yoshida and H. Ogoshi, *Inorg. Chem.*, 1980, **19**, 950.
5 G. E. Toney, L. W. terHaar, J. E. Savrin, A. Gold, W. E. Hatfield and R. Sangaiah, *Inorg. Chem.*, 1984, **23**, 2561.
6 A. D. Boersma and H. M. Goff, *Inorg. Chem.*, 1982, **21**, 581.
7 C. A. Reed and F. Guiset, *J. Am. Chem. Soc.*, 1996, **118**, 3281.
8 R.-J. Cheng, P.-Y. Chen, P.-R. Gau, C.-C. Chen and S.-M. Peng, *J. Am. Chem. Soc.*, 1997, **119**, 2563.
9 Abbreviations: OETPP, T^{i}PrP, TEtP, and OEP are the dianions of 2,3,7,8,12,13,17,18-octaethyl-5,10,15,20-tetraphenylporphyrin, 5,10,15,20-tetraisopropylporphyrin, 5,10,15,20-tetraethylporphyrin, and 2,3,7,8,12,13,17,18-octaethylporphyrin, respectively.
10 V. Schünemann, M. Gerdan, A. X. Trautwein, N. Haoudi, D. Mandon, J. Fischer, R. Weiss, A. Tabard and R. Guilard, *Angew. Chem., Int. Ed.*, 1999, **38**, 3181.
11 M. Nakamura, T. Ikeue, H. Fujii and T. Yoshimura, *J. Am. Chem. Soc.*, 1997, **119**, 6284.
12 T. Ikeue, Y. Ohgo, T. Saitoh, M. Nakamura, H. Fujii and M. Yokoyama, *J. Am. Chem. Soc.*, 2000, **122**, 4068.
13 T. Ikeue, Y. Ohgo, A. Uchida, M. Nakamura, H. Fujii and M. Yokoyama, *Inorg. Chem.*, 1999, **38**, 1276.
14 K. Keutel, L. Käpplinger, E.-G. Jäger, M. Grodzicki, V. Schünemann and A. X. Trautwein, *Inorg. Chem.*, 1999, **38**, 2320.
15 L. D. Sparks, C. J. Medforth, M.-S. Park, J. R. Chamberlain, M. R. Ondrias, M. O. Senge, K. M. Smith and J. A. Shelnutt, *J. Am. Chem. Soc.*, 1993, **115**, 581.
16 Y. Ohgo, T. Saitoh and M. Nakamura, *Acta Crystallogr., Sect. C*, submitted.
17 Y. Ohgo, T. Saitoh and M. Nakamura, *Acta Crystallogr., Sect. C*, 1999, **55**, 1284.
18 L. Chen, G.-B. Yi, L.-S. Wang, U. R. Dharmwardana, A. C. Dart, M. A. Khan and G. B. Richter-Addo, *Inorg. Chem.*, 1998, **37**, 4677.

ChemComm

Synthesis and characterization of the monomer Ga{(NDippCMe)$_2$CH} (Dipp = C$_6$H$_3$Pr$^i_2$-2,6): a low valent gallium(I) carbene analogue

Ned J. Hardman, Barrett E. Eichler and Philip P. Power*

Department of Chemistry, University of California, Davis, One Shields Avenue, Davis California, 95616, USA. E-mail: pppower@ucdavis.edu

Received (in Irvine, CA, USA) 12th July 2000, Accepted 6th September 2000
First published as an Advance Article on the web 27th September 2000

The reaction between solvent free Li{(NDippCMe)$_2$CH} (Dipp = C$_6$H$_3$Pr$^i_2$-2,6), 'GaI' and potassium in toluene afforded Ga{(NDippCMe)$_2$CH} 1 which features a V-shaped, two-coordinate, six-electron gallium(I) center electronically analogous to a singlet carbene carbon.

Neutral, molecular derivatives of low-valent gallium usually exist as Ga–Ga bonded tetramers[1] or hexamers[2] of formula $(GaR)_4$ or $(GaR)_6$ which may dissociate to monomers in either the vapor or the solution phase.[3] Lower degrees of aggregation than four are extremely rare in the solid state, and the monomeric compound Ga(Tp$^{Bu^t_2}$) [Tp$^{Bu^t_2}$ = tris(3,5-di-*tert*-butylpyrazolyl)hydroborato] is the only such example to have been well characterized. In this species, the bulky tridentate Tp$^{Bu^t_2}$ ligand prevents association by coordinatively saturating the gallium center to afford a complex with four electron pairs in the metal valence shell.[4] In related work it has been demonstrated that the anion of the salt [K(18-crown-6)(thf)$_2$][Ga{N(Bu^t)CH}$_2$] contains a two-coordinate gallium center that has just three valence electron pairs and is electronically analogous to a carbene carbon.[5] In addition, the use of extremely bulky terphenyl ligands in the compounds MC$_6$H$_3$Trip$_2$-2,6 (M = In or Tl; Trip = C$_6$H$_2$Pr$^i_3$-2,4,6) has shown that unassociated, low valent, one-coordinate, monomers with only two electron pairs in the metal valence shell can be stabilized.[6]† In attempting to extend this work to lower valent gallium we were struck by the close steric resemblance (Fig. 1) between the terphenyl ligand C$_6$H$_3$Trip$_2$-2,6[7] and the Dipp substituted β-diketiminate ligand (NDippCMe)$_2$CH (Dipp = C$_6$H$_3$Pr$^i_2$-2,6).[8] This led to the hypothesis that the use of a crowded β-diketiminate ligand should stabilize a Ga(I) derivative with a low degree of aggregation. The synthesis and characterization of such a compound are now described.

Yellow crystals of Ga{(NDippCMe)$_2$CH} **1** were obtained‡ by the reaction of Li{(NDippCMe)$_2$CH} with "GaI"[9] and subsequent treatment with potassium to reduce any I$_2$Ga{(NDippCMe)$_2$CH} formed in the reaction. Compound **1** was characterized by ^{1}H and ^{13}C NMR spectroscopy, UV-VIS and IR spectroscopy and C, H elemental analyses. These data were consistent with the structure (Fig. 2) obtained by X-ray crystallography§ which showed that the molecule is monomeric and has a V-shaped two-coordinate geometry at gallium. The central GaN$_2$C$_3$ ring atoms, the C(4) and C(5) methyl carbons, and the *ipso*-carbons C(6) and C(18) are essentially coplanar. The substituent aryl (Dipp) ring planes are oriented at angles of 88.2 and 89.2° with respect to the plane of the GaN$_2$C$_3$ ring. The C–C and N–C distances within this ring are similar to those previously reported for this ligand.[10]

The most interesting structural features in **1** concern; (a), the two-coordinate environment at gallium, (b), the Ga–N distances which average 2.054(2) Å, and (c) the NGaN angle of 87.56(6)°. The Ga–N distances in **1** are relatively long in view of the low coordination number of the gallium atom, and do not support the presence of significant multiple Ga–N bond character which might have arisen from delocalization of the π-electrons of the C$_3$N$_2$ ring moiety. Instead, the bonding in **1** is probably best viewed as involving a Ga$^+$ ion complexed by the bidentate, monoanionic ligand [(NDippCMe)$_2$CH]$^-$. The increased ionic and less directional character of the Ga–N bonds are also consistent with the narrow N–Ga–N angle. The Ga–N distances in **1** are shorter than the 2.230(5) Å observed in Ga(Tp$^{Bu^t_2}$)[4] as a result of the lower metal coordination number. On the other hand, the Ga–N distances in [Ga{N(Bu^t)CH}$_2$]$^-$ [Ga–N 1.985(6) Å][5] are shorter than those observed in **1**, probably as a result of the lower steric effects of the {N(Bu^t)CH}$_2$ ligand.¶ The relatively long Ga–N distances in these monovalent complexes are underlined by the fact that the trivalent digallium species {HC(Bu^t)N}$_2$Ga–Ga{N(Bu^t)CH}$_2$[11] {which has the same ligand as that in [Ga{N(Bu^t)CH}$_2$]$^-$} has Ga–N distances of 1.836(4) and 1.839(6) Å. These values are typical of those found for three-coordinate Ga–N bond lengths in trivalent complexes with similarly sized ligands.[12]

A significant feature of interest in **1** is the presence of a lone pair of electrons at gallium which suggests that this ligand will display significant Lewis base chemistry. Experiments on this aspect of **1** are in progress.

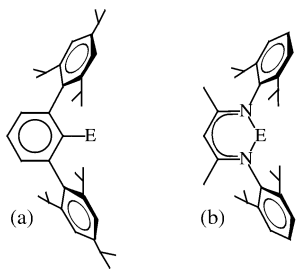

Fig. 1 Schematic drawing of the C$_6$H$_3$Trip$_2$-2,6 (Trip = C$_6$H$_2$Pr$^i_3$-2,4,6) and (NDippCMe)$_2$CH (Dipp = C$_6$H$_3$Pr$^i_2$-2,6) ligands illustrating their steric resemblance and the protection they afford the bound site E.

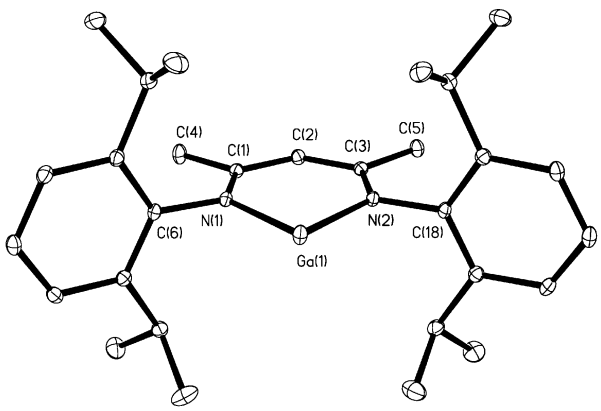

Fig. 2 Thermal ellipsoid (30%) plot of **1**. H atoms are not shown. Selected bond distances (Å) and angles (°): Ga(1)–N(1) 2.0528(14), Ga(1)–N(2) 2.0560(13), N(1)–C(1) 1.337(2), N(1)–C(6) 1.446(2), N(2)–C(3) 1.338(2), N(2)–C(18) 1.442(2), C(1)–C(2) 1.399(2), C(2)–C(3) 1.401(3); N(1)–Ga(1)–N(2) 87.53(5), Ga(1)–N(1)–C(1) 129.04(1), Ga(1)–N(2)–C(3) 129.31(11), N(1)–C(1)–C(2) 123.44(15), C(1)–C(2)–C(3) 127.74(16), C(2)–C(3)–N(2) 122.91(14).

DOI: 10.1039/b005686n

We thank the National Science Foundation for financial support.

Notes and references

† $GaC_6H_3Trip_2$-2,6 has been stabilized as an iron carbonyl complex in which the gallium is two coordinate.[6c]

‡ All manipulations were carried out under anaerobic and anhydrous conditions. Crystals of Li{$(NDippCMe)_2CH$} were synthesized by the reaction of H{$(NDippCMe)_2CH$}[8] with Bu^nLi and grown from toluene. The structure of this lithium salt consists of weakly associated monomers in the crystal phase. Crystals of Li{$(NDippCMe)_2CH$} (2.2 g, 5.2 mmol) in toluene (30 mL) were added dropwise to a well stirred slurry of 'GaI'[9] (1.5 g, 7.6 mmol) in toluene with cooling in a dry ice/acetone bath. The mixture was allowed to come to room temperature overnight and cooled again with a dry ice/acetone bath, whereupon excess potassium (0.5 g, 12.8 mmol) was added by a solids-addition tube. After stirring for 1 h the solution was allowed to warm to room temperature overnight. The resultant red solution was filtered and the volume was reduced to incipient crystallization (10 mL). Storage at *ca*. −20 °C for 48 h afforded yellow crystals of **1** (0.97 g, yield 39%); Anal. Calc. (found) for $C_{29}H_{41}GaN_2$: C, 71.46 (71.90), H, 8.48 (8.86)%. Mp 202–204 °C; UV–VIS λ_{max} = 340 nm; ^{1}H NMR (300 MHz C_6D_6) δ 7.17 (m, 6H, aromatic H of Dipp group, partially obscured by resonances due to impurities in the solvent C_6D_6) 5.19 (s, 1H, methine CH), 3.14, (sept, $^3J_{HH}$ 6.9 Hz, 4H, C*H*Me_2), 1.67 (s, 6H, C*Me*), 1.25 (d, $^3J_{HH}$ 6.9 Hz, 12H, CH*Me*$_2$), 1.11 (d, $^3J_{HH}$ = 6.9 Hz, 12H, CH*Me*$_2$): ^{13}C{^{1}H} NMR (75 MHz, C_6D_6) δ 163.49 (*p*-C), 143.65 (*C*Me) 142.92 [*o*-C(Dipp)], 126.49 [*p*-C(Dipp], 123.96 [*m*-C(Dipp], 99.55 (γ-C), 28.76 (*C*HMe_2), 25.72 (CH*Me*$_2$), 24.02 (C*Me*), 23.85 (CH*Me*$_2$).

§ *Crystal data* at 90 K for **1** with Mo-Kα radiation (λ = 0.71073 Å): $C_{29}H_{41}GaN_2$, M = 487.36, yellow parallelpipeds, monoclinic, space group $P2_1/n$, a = 12.6570(4), b = 15.9025(6), c = 13.9390(5) Å, β = 105.099(1)°, V = 2689.49(16) Å, Z = 4, D_c = 1.204 g cm^{-3}, μ = 1.041 mm^{-1}, $R1$ = 0.0375 for 6190 [$I > 2\sigma(I)$] data. CCDC 182/1774. See http://www.rsc.org/suppda/cc/b0/b005686n/ for crystallographic files in .cif format.

¶ In this compound the formal valence of the gallium is two (one unit higher than that in **1**) although its formal oxidation state is +1.

1 W. Uhl, W. Hiller, M. Layh and W. Schwartz, *Angew. Chem., Int. Ed. Engl.*, 1992, **31**, 1364; G. Linti and W. Köster, *J. Organomet. Chem.*, 1996, **520**, 107; G. Linti and W. Köster, *Angew. Chem., Int. Ed. Engl.*, 1997, **36**, 2644; W. Uhl and A. Jantschak, *J. Organomet. Chem.*, 1998, **555**, 263; G. Linti and A. Rodig, *Chem. Commun.*, 2000, 127.

2 D. Loos, E. Baum, A. Ecker, H. Schnöckel and A. J. Downs, *Angew. Chem., Int. Ed. Engl.*, 1997, **36**, 860.

3 A. Haaland, K.-G. Martinsen, H. V. Volden, D. Loos and H. Schnöckel, *Acta Chem. Scand.*, 1994, **48**, 172; A. Haaland, K.-G. Martinsen, H. V. Volden, W. Kaim, E. Waldhör, W. Uhl and U. Schutz, *Organometallics*, 1996, **15**, 1146.

4 M. C. Kuchta, J. B. Bonanno and G. Parkin, *J. Am. Chem. Soc.*, 1996, **118**, 10 914.

5 E. S. Schmidt, A. Jockisch and H. Schmidbaur, *J. Am. Chem. Soc.*, 1999, **121**, 9758.

6 (*a*) S. T. Haubrich and P. P. Power, *J. Am. Chem. Soc.*, 1998, **120**, 2202; (*b*) M. Niemeyer and P. P. Power, *Angew. Chem., Int. Ed.*, 1998, **37**, 1277; (*c*) J. Su, X.-W. Li, R. C. Crittendon, C. F. Campagna and G. H. Robinson, *Organometallics*, 1997, **16**, 4511.

7 B. Schiemenz and P. P. Power, *Organometallics*, 1996, **15**, 958.

8 J. Feldman, S. J. McLain, A. Parthasarathy, W. J. Marshall, J. C. Calabrese and S. D. Arthur, *Organometallics*, 1997, **16**, 1514.

9 M. H. L. Green, P. Mountford, G. J. Smout and S. R. Speel, *Polyhedron*, 1990, **9**, 2763.

10 B. Qian, D. L. Ward and M. R. Smith, III, *Organometallics*, 1998, **17**, 3070.

11 D. S. Brown, A. Decken and A. H. Cowley, *J. Am. Chem. Soc.*, 1995, **117**, 5421.

12 P. J. Brothers and P. P. Power, *Adv. Organomet. Chem.*, 1996, **39**, 1; P. P. Power, *Chem. Rev.*, 1999, **99**, 3463.

ChemComm

Remarkable cumulative stereoselectivity in cyclopropanation with supramolecular Cu(I) catalytic complexes

Tomislav Portada, Marin Roje, Zlata Raza, Vesna Čaplar, Mladen Žinić* and Vitomir Šunjić*

Department of Organic Chemistry and Biochemistry, Rudjer Bošković Institute, 10001 Zagreb, Croatia. E-mail: zinic@rudjer.irb.hr

Received (in Liverpool, UK) 24th July 2000, Accepted 30th August 2000
First published as an Advance Article on the web 27th September 2000

Supramolecular Cu(I) catalyst 1 exhibited 77% cumulative (dia- and enantio-) stereoselectivity and one of the highest diastereoselectivities (86% de) obtained to date in the cyclopropanation of styrene with ethyl diazoacetate.

Enantioselective transformations based on the use of chiral organometallic catalysts present one of the most important strategies for production of enantiomerically pure compounds.[1,2] On the other hand, extensive development of supramolecular chemistry enabled syntheses of the cavity-containing receptor molecules capable of binding and recognition of selected substrate molecules.[3,4] Design of cavity-containing supramolecular catalysts with a built in organometallic catalytic center presents an attractive but until now lesser explored possibility.[5]

Here we describe the first approach to a chiral supramolecular catalyst for enantioselective cyclopropanation. In the classical cyclopropanation of styrene with ethyl diazoacetate (Scheme 1), chiral bidentate bisoxazoline–Cu(I) catalytic complexes possessing C_2-symmetry are most frequently used.[2a–d] The cumulative stereochemical outcome of the reaction is evaluated by ee and de of the formed cyclopropanes. While with some catalysts very high enantioselectivity (more than 90% ee) is achieved, diastereoselectivity is usually low to medium, in the range 40–50% de. Our new strategy toward supramolecular catalysts for cyclopropanation is based on the design of cavity-containing ligands with a built-in bisoxazoline unit (Fig. 1). Since the bridge connects two centers of C_2-symmetric bisoxazoline unit, a certain degree of helicity is induced to the bridge. According to the proposed reaction mechanism of bisoxazoline–Cu(I) catalyzed cyclopropanations, a cyclopropane ring forms by the electrophilic attack of Cu(I) bound carbene to prochiral alkene.[6] Consequently, with a macrocyclic supramolecular catalyst of sufficient size, the reaction should occur inside the helical cavity. In this way, the local C_2 chirality at the metallic center is to a certain degree extended to the reaction space defined by the size of the cavity. Compared to classical acyclic bisoxazoline–Cu(I) catalysts, this strategy offers the advantage of stereochemically more defined catalyst topology beyond the catalytic site that could result in the improved diastereo- and enantioselectivity of the cyclopropanation reaction.

To test this hypothesis, the macrocyclic ligands **1**–**4** (Scheme 2, **1**–**4** obtained in 29, 27, 49 and 25% yields, respectively),

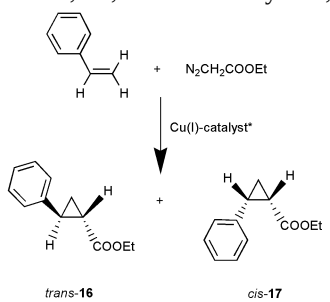

trans-**16** *cis*-**17**

Scheme 1 Cyclopropanation of styrene with ethyl diazoacetate catalysed by chiral bisoxazoline–Cu(I) complexes.

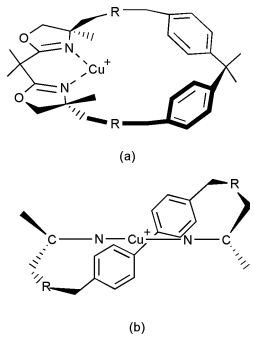

Fig. 1 General structure of C_2-symmetric supramolecular Cu(I) catalyst (*a*); helicity of the macrocycle connecting stereogenic centers of the bisoxazoline unit (*b*).

possessing different sizes of the macrocyclic ring, have been prepared and their Cu(I) complexes used in cyclopropanation of styrene with diazoacetate.[7]

The enantio- and diastereoselectivities obtained in the cyclopropanations with Cu(I) complexes of the macrocyclic ligands **1**–**4** at two standard ligand/Cu(I) ratios,[2b] are collected in Table 1 and compared to those obtained with the Cu(I) complexes of the acyclic bisoxazoline ligands **14** and **15**.[2b] It turns out that the complexes of the two smallest macrocyclic ligands, **1** and **2**, exibit the highest diastereoselectivity (86% de for **1**) and enantioselectivity (81% ee for **2**) affording nearly the same cumulative stereoselectivity (75–77%). For the two larger macrocycles **3** and **4** both de and ee dropped; for the former de is somewhat higher (50–54% de) than for the latter (42% de), whereas ee in both cases remains quite similar (66–68%). As compared to acyclic precursor **14**, however, the cumulative stereoselectivity for the *trans*-**16** isomer obtained with **1** and **2** is 20% higher than that for **14** (57–58%) and also higher than that obtained with the best bisoxazoline in the acyclic series, ligand **15**[2b] (69–70%). The cumulative stereoselectivity increase for **1**–**4** shows clear dependence on the size of the macrocycle cavity being the lowest for the most flexible, **4**, and the highest for the most rigid, **1**. In the series acyclic **14**–macrocyclic **4** to **1** the remarkable increase of de from 38 to 86% is observed. Interestingly the ee's in the series are rather similar (65–68%) except for the peak value for **2** (81%). These results reveal the importance of the catalyst topology for the diastereoselectivity outcome of the reaction and show the advantage of macrocyclic over acyclic catalysts. The exceptional diastereoselectivity observed for the **1**–Cu(I) catalyst can be explained by high degree of stereoselection induced by the helicity of the bridge which strongly favors formation of *trans*-**16** over *cis*-**17** (Fig. 2).

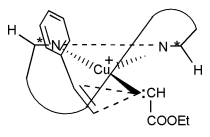

Fig. 2 Schematic presentation of helical topology and *trans*-position of the larger groups of reactants in the **1**–Cu(I) carbene catalytic complex reaction with styrene.

DOI: 10.1039/b006057g

Table 1 Cyclopropanation reaction of styrene with ethyl diazoacetate in 1,2-dichloroethane solution catalysed by macrocyclic **1**–**4**- and **14**, **15**-Cu(I) complexes

Ligand	Ligand/Cu(I)	Yield[a]	*cis*-**17**–*trans*-**16** ratio[b]; (de %)	*cis*-**17**[b] ee %	*trans*-**16**[b] ee %	Cumulative stereoselectivity[c] (%)
1, *n* = 2	1.2	58	7:93; (86)	60.0 (1*S*,2*R*)	65.1 (1*S*,2*S*)	77
	2.0	55	7:93; (86)	59.4 (1*S*,2*R*)	65.0 (1*S*,2*S*)	77
2, *n* = 3	1.2	55	17:83; (66)	70.1 (1*S*,2*R*)	80.5 (1*S*,2*S*)	75
	2.0	58	16:84; (68)	72.9 (1*S*,2*R*)	81.3 (1*S*,2*S*)	76
3, *n* = 4	1.2	54	25:75; (50)	51.0 (1*S*,2*R*)	66.1 (1*S*,2*S*)	62
	2.0	57	23:77; (54)	53.5 (1*S*,2*R*)	68.7 (1*S*,2*S*)	65
4, *n* = 5	1.2	67	29:71; (42)	60.5 (1*S*,2*R*)	66.5 (1*S*,2*S*)	59
	2.0	62	29:71; (42)	62.3 (1*S*,2*R*)	67.7 (1*S*,2*S*)	59
14	1.2	77	30:70; (40)	54.0 (1*S*,2*R*)	64.8 (1*S*,2*S*)	58
	2.0	79	31:69, (38)	54.2 (1*S*,2*R*)	65.3 (1*S*,2*S*)	57
15	1.2	75	28:72; (44)	95 (1*R*,2*S*)	96 (1*R*,2*R*)	70
	2.0	80	29:71; (42)	95 (1*R*,2*S*)	96 (1*R*,2*R*)	69

[a] Isolated, not optimised yields. [b] Determined by chiral GC analysis, using Chirasil Dex-CB column. [c] Cumulative (diastereo- and enantio-) selectivity calculated in % of (1*S*,2*S*)-*trans*-**16** and (1*R*,2*R*)-*trans*-**16** formed in catalytic reactions by using ligands **1**–**4**, **14** and the ligand **15**, respectively.

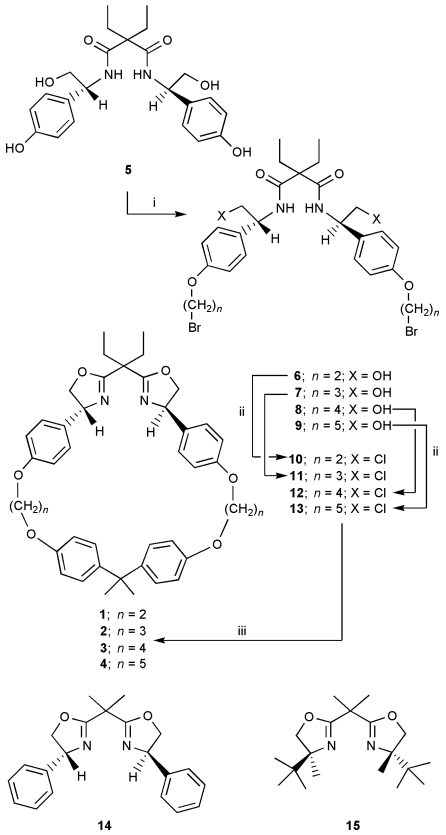

Scheme 2 (i) $Br(CH_2)_nBr$ (*n* = 2-5); K_2CO_3,MeCN; (ii) $(Cl_3CO)_2CO$; PPh_3, CH_2Cl_2 or $SOCl_2$; (iii) Cs_2CO_3, MeCN. Structures of the reference ligands **14** and **15**. All prepared compounds have correct spectroscopic and elemental analysis data.

In conclusion, we report on the synthesis of the first supramolecular Cu(I) catalysts comprising macrocyclic ligands **1**–**4** and their application in stereoselective cyclopropanations of styrene with ethyl diazoacetate. The macrocyclisation principle used with such catalysts which produced the highest cumulative stereoselectivity in cyclopropanations reported to date could be of general value considering variety of catalytic transformations based on C_2-symmetric organometallic ligands.[1,2] Our work on the cavity-tuning of the supramolecular Cu(I) catalysts, and their applications in other catalytic enantioselective reactions is in progress.

The financial support from the Croatian Ministry of Science and Technology (Program 009807) is gratefully acknowledged.

Notes and references

1 (*a*) *Comprehensive Asymmetric Catalysis*, eds. E. N. Jacobsen, A. Pfalz and H. Yamamoto, Springer, Berlin, Heidelberg, 1999; (*b*) R. Noyori, *Asymmetric Catalysis in Organic Synthesis*, J. Wiley & Sons, New York, 1994.

2 (*a*) R. E. Loewenthal, A. Abiko and S. Masamune, *Tetrahedron Lett.*, 1990, **31**, 6005; (*b*) D. A. Evans, K. A. Woerpel, M. M. Hinman and M. M. Paul, *J. Am. Chem. Soc.*, 1991, **113**, 726; (*c*) D. A. Evans, K. A. Woerpel and M. J. Scott, *Angew. Chem., Int., Ed. Engl.*, 1992, **31**, 430; (*d*) C. Bolm, *Angew. Chem., Int. Ed. Engl.*, 1991, **30**, 542.

3 (*a*) J.-M. Lehn, *Supramolecular Chemistry. Concepts and Perspectives*, VHC, Weinheim, 1995; (*b*) J.-M. Lehn, *Angew. Chem., Int. Ed. Engl.*, 1988, **27**, 1726.

4 (*a*) D. J. Cram and J. M. Cram, *Container Molecules and Their Guests*, RSC, Cambridge, 1994; (*b*) *Frontiers in Supramolecular Organic Chemistry and Photochemistry*, eds. H.-J. Schneider and H. Dürr, VCH, Weinheim, 1991; (*c*) F. Diederich, *Cyclophanes*, RSC, Cambridge, 1991; (*d*) F. Vögtle, *Supramolecular Chemistry*, Wiley, New York, 1991.

5 (*a*) H. K. A. C. Coolen, J. A. M. Meeuwis, P. W. N. M. van Leeuwen and R. J. M. Nolte, *J. Am. Chem. Soc.*, 1995, **117**, 11906; (*b*) M. Komiyama and Y. Matsumoto, *J. Am. Chem. Soc.*, 1989, 719; (*c*) D. R. Benson, R. Valentekovich and F. Diederich, *Angew, Chem., Int. Ed. Engl.*, 1990, **29**, 191; (*d*) H.-J. Schneider and F. Xiao, *J. Chem. Soc., Perkin Trans. 2*, 1992, 387; (*e*) T. Akiike, Y. Nagauo, Y. Yamamoto, A. Nakamura, H. Ikeda, A. Ueno and F. Toda, *Chem. Lett.*, 1994, 1089.

6 H. Fritschi, U. Leutenegger and A. Pfaltz, *Helv. Chim. Acta*, 1988, **71**, 1553.

7 Manuscript in preparation.

ChemComm

G-quartets as a self-assembled scaffold for circular porphyrin arrays†

Stefano Masiero,* Giovanni Gottarelli and Silvia Pieraccini

Dipartimento di Chimica Organica 'A. Mangini', Università di Bologna, Via S. Donato, 15, I-40127, Bologna, Italy. E-mail: masiero@alma.unibo.it

Received (in Cambridge, UK) 31st July 2000, Accepted 4th September 2000
First published as an Advance Article on the web 27th September 2000

A new lipophilic guanosine carrying a porphyrin chromophore on the ribose moiety has been prepared: evidence is reported for the formation of a supramolecular complex based on G-quartets and containing an array of eight porphyrins.

Understanding and mimicking natural photosynthesis with the goal of producing molecular electronic devices and eventually clean energy is currently one of the areas of major investigation in chemistry.[1]

A particular impetus to the field has been the solution of crystal structures for the reaction centres of photosynthetic bacteria *Rhodopseudomonas viridis* and *Rhodobacter sphaeroides* R-26,[2] as well as the structure elucidation of the antenna complex of *Rhodopseudomonas acidophila*.[3] In particular, the so-called light harvesting system LH2 is an elegant supramolecular assembly in which two distinct sets of 18 and 9 bacteriochlorophylls-a, respectively, are arranged in a circular disposition.

Several synthetic models for such a system have been proposed in the literature, wherein porphyrin arrays were obtained by covalent synthesis.[4] An alternative, and more attractive approach, has been based on the supramolecular strategy of having porphyrin-carrying subunits spontaneously self-assemble to give organised chromophore arrays.[5]

For several years, we have been studying the self-assembly of lipophilic guanosine derivatives in chlorinated organic solvents.[6] These compounds, in the presence of alkali metal ions, form octameric[6b] [Fig. 1(a)] or polymeric[6c] [Fig. 1(b)] species based on the hydrogen-bonded G-quartet.[7] In particular, while 3′,5′-diacyl-2′-deoxyguanosines form octamers or polymers depending on the amount of alkali metal ion added, 5′-acyl-2′,3′-isopropylidene guanosine derivatives form only discrete octamers.[8] The basic structure of the G8 octamer appeared to us to be an ideal non-covalent scaffold for the formation of porphyrin arrays.

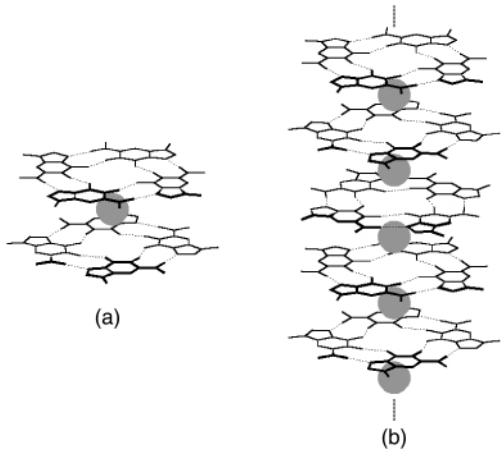

Fig. 1

We report here the preparation of a self-assembled porphyrin array consisting of eight chromophores arranged in a circular disposition.

Porphyrin-carrying lipophilic guanosine **1** was synthesized starting from 5-(4′-hydroxyphenyl)-10,15,20-tritolylporphyrin **2**[9] and commercially available 2′,3′-isopropylidene guanosine **3** according to Scheme 1.

Hydroxyporphyrin **2** was alkylated with 4-bromobutyric acid methyl ester, and the resulting ester **4** (93%) was then hydrolysed to give carboxylic acid **5** (95%), which was converted into the corresponding acyl chloride **6**.

Isopropylidene guanosine **3** was converted into the *N*(2)-Fmoc derivative **7**[10] (56%) and condensed with porphyrin acid chloride **5** to give ester **8** (31%). Deprotection of ester **8** gave the porphyrin-functionalised guanosine **1** (76%). All of the compounds were characterized by NMR, ESI mass spectrometry and elemental analysis (ESI†).

Derivative **1** self-assembles in chloroform in the presence of potassium picrate giving rise to octamers consisting of two G-quartets, as inferred from UV–VIS, CD, 1D and 2D ^{1}H NMR studies.

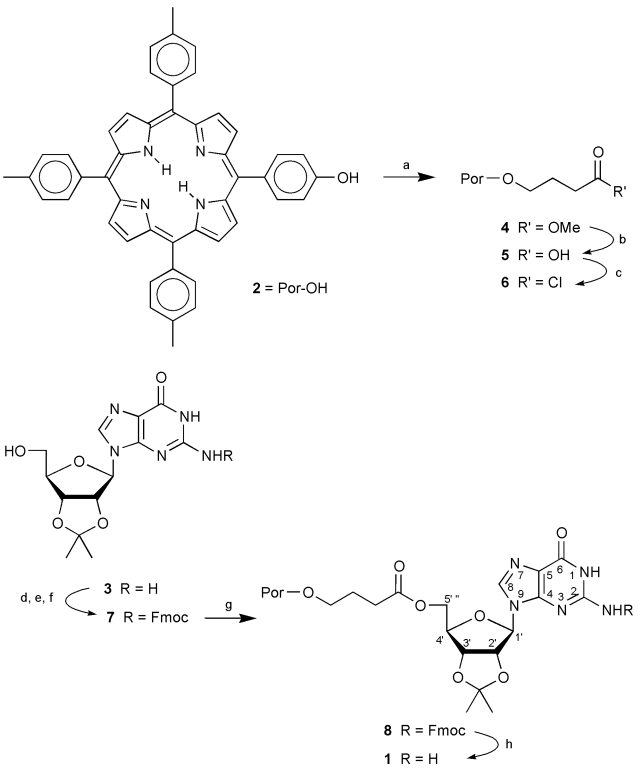

Scheme 1 *Reagents and conditions*: (a) $BrCH_2CH_2CH_2CO_2Me$, K_2CO_3, DMF; (b) KOH, dioxane, MeOH, H_2O, 80 °C then dil. AcOH; (c) $SOCl_2$, THF, reflux; (*d*) Me_3SiCl, pyridine; then (e) FmocCl then (f) H_2O; (g) **6**, CH_2Cl_2, pyridine; (h) piperidine, CH_2Cl_2.

† Electronic supplementary information (ESI) available: 1. ESI-MS spectrum of **1** in methanol–dichloromethane and elemental analysis results. 2. ^{1}H NMR and NOESY spectra (400 MHZ) of 2 mM $[\mathbf{1}]_8$–Kpic in $CDCl_3$ at −10 °C. 3. Tentative structure of the octameric complex, as evinced from preliminary data. See http://www.rsc.org/suppdata/cc/b0/b006160n/

DOI: 10.1039/b006160n

Proton NMR spectra (ESI†) show the characteristic features of G-quartet formation upon K^+ complexation. Thus, the broad singlet at 6.37 ppm for the N(2)H2 splits into two signals centred at 9.69 ppm [H-bonded N(2)H] and 6.43 ppm [free N(2)H], respectively, at −10°C. These separate signals for the exocyclic amine, already visible although broader at room temperature, are diagnostic of G-quartet formation.[13] The NOESY spectrum shows cross peaks among both these N(2)H2 protons and the N(1)H imino proton at 12.52 ppm.[6b,13] Conversely, there is no significant shift of any other signal in the ^{1}H NMR spectrum upon complexation.[14]

In the present case, the nucleoside protons for porphyrin-functionalised guanosine **1** are not split upon K^+ coordination, as was previously observed for the 3′,5′-diacyl deoxyG-derivatives,[6a,b] and NMR data indicate an exclusive *syn* conformation of the nucleobases around the glycosidic bond (*e.g.* a strong NOE cross peak between H8 at 7.31 ppm and H1′ at 6.04 ppm). So far, all the 5′-alkanoyl-2′,3′-isopropylidene G derivatives that we have investigated have behaved in this way.[8]

The visible spectra of ester **4** and derivative **1** in $CHCl_3$ before K^+ extraction are nearly superimposable, as would be expected if no electronic interaction between the guanine and porphyrin chromophores takes place.[5a] In addition, the spectrum of **1** after K^+ extraction does not change, ruling out a self-assembling process in which porphyrin stacking is involved. This stacking in fact would lead to strong electronic interactions with consequent modification of the absorption. The stoichiometric ratio of 8 molecules of derivative **1** per picrate ion can be deduced from quantitative absorption measurements.

The CD spectra of **1** before and after complexation with K^+ picrate are shown in Fig. 2. Before K^+ extraction, the signal is very weak and no exciton couplets can be observed. Complexation of the cation produces a dramatic effect in the CD spectrum, as exciton couplets appear both in the guanine absorption region (*ca.* 270 nm) and in the Soret region (*ca.* 417 nm). While the couplet centered at 270 nm is diagnostic of the assembly of guanine bases into an octamer,[11] that corresponding to the Soret band indicates a weak, intermolecular, electronic interaction between porphyrin chromophores:[12] this demonstrates that porphyrins are disymmetrically arrayed around the $[G]_8K^+$ complex. The relatively low intensity of this signal is likely to be due to the conformational freedom of the porphyrin chromophores, which are attached by flexible linkers to the G-quartet platforms.

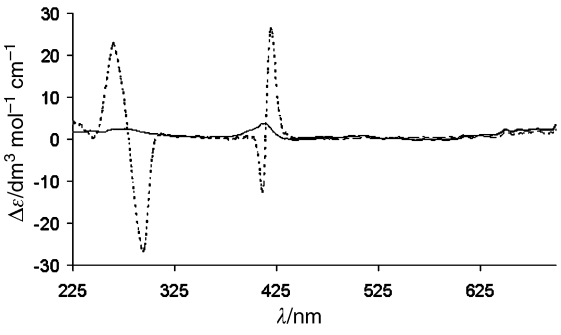

Fig. 2 CD spectra of **1** (0.3 mM in $CHCl_3$) before (——) and after (·····) K^+ extraction.

In conclusion, we have synthesized a new porphyrin derivative which responds to K^+ ions by forming a supramolecular array of eight porphyrins with a circular disposition (see ESI for a tentative structure†). The detailed stereochemistry of the aggregate is now under investigation, as well as the photochemical energy transfer processes possible in this octameric system. Preparation of new derivatives capable of forming aggregates with a larger number of porphyrins arranged circularly around the G-quartets is also being pursued.

We are indebted to Professor J. T. Davis (Maryland) for helpful discussions and suggestions, and to Dr E. Cortini for technical assistance. Financial support by MURST (cofin. 99, ex 40%), CNR (Rome) and University of Bologna (ex 60%) is gratefully acknowledged.

Notes and references

1 For recent reviews see: M. R. Wasielewski, *Chem. Rev.*, 1992, **92**, 453; S. Fukuzumi, in *The Porphyrin Handbook*, ed. K. M. Kadish, K. M. Smith and R. Guilard, Academic Press, New York, 1999, vol. 8, p. 115; D. Gust and T. A. Moore, *The Porphyrin Handbook*, ed. K. M. Kadish, K. M. Smith and R. Guilard, Academic Press, New York, 1999, vol. 8, 153.

2 J. P. Allen, G. Feher, T. O. Yeates, H. Komiya and D. C. Rees, *Proc. Natl. Acad. Sci. USA*, 1987, **84**, 5730; H. Komiya, T. O. Yeates, D. C. Rees, J. P. Allen and G. Feher, *Proc. Natl. Acad. Sci. USA*, 1988, **85**, 9012; T. O. Yeates, H. Komiya, A. Chirino, D. C. Rees, J. P. Allen and G. Feher, *Proc. Natl. Acad. Sci. USA*, 1988, **85**, 7993; J. P. Allen, G. Feher, T. O. Yeates, D. C. Rees, J. Deisenhofer, H. Michel and R. Huber, *Proc. Natl. Acad. Sci. USA*, 1986, **83**, 8589.

3 G. McDermott, S. M. Prince, A. A. Freer, A. Hawthornthwaite-Lawless, M. Z. Papiz, R. J. Cogdel and N. W. Isaacs, *Nature*, 1995, **374**, 517.

4 For recent reviews see: M. G. H. Vicente, L. Jaquinod and K. M. Smith, *Chem. Commun.*, 1999, 1771; A. K. Burrel and M. R. Wasielewski, *J. Porphyrins Phthalocyanines*, 2000, **4**, 401.

5 (*a*) J. L. Sessler, B. Wang and A. Harriman, *J. Am. Chem. Soc.*, 1995, **117**, 704; (*b*) C. M. Drain, K. C. Russel and J.-M. Lehn, *Chem. Commun.*, 1996, 337; (*c*) J.-P. Collin, A. Harriman, V. Heitz, F. Odobel and J.-P. Sauvage, *J. Am. Chem. Soc.*, 1994, **116**, 5679; (*d*) C. M. Drain, F. Nafiatis, A. Vasenko and J. D. Batteas, *Angew. Chem., Int. Ed.*, 1998, **37**, 2344.

6 (*a*) G. Gottarelli, S. Masiero and G. P. Spada, *J. Chem. Soc., Chem. Commun.*, 1995, 2555; (*b*) A. L. Marlow, E. Mezzina, G. P. Spada, S. Masiero, J. T. Davis and G. Gottarelli, *J. Org. Chem.*, 1999, **64**, 5116; (*c*) E. Mezzina, P. Mariani, R. Itri, S. Masiero, S. Pieraccini, G. P. Spada, F. Spinozzi, J. T. Davis and G. Gottarelli, *Chem.-Eur. J.*, in press.

7 S. L. Forman, J. C. Fettinger, S. Pieraccini, G. Gottarelli and J. T. Davis, *J. Am. Chem. Soc.*, 2000, **122**, 4060; J. L. Sessler, M. Sathiosatham, K. Doerr, V. Lynch and K. A. Abboud, *Angew. Chem., Int. Ed.*, 2000, **39**, 1300.

8 J. Davis, G. Gottarelli, S. Masiero and E. Mezzina, in preparation.

9 R. G. Little, J. A. Anton, P. A. Loach and J. A. Ibers, *J. Heterocycl. Chem.*, 1975, **12**, 343.

10 L. H. Koole, H. M. Moody, N. L. H. L. Broeders, P. J. L. M. Quaedflieg, W. H. A. Kuijpers, M. H. P. van Genderen, A. J. J. M. Coenen, S. van der Wal and H. M. Buck, *J. Org. Chem.*, 1989, **54**, 1657.

11 G. Gottarelli, S. Masiero and G. P. Spada, *Enantiomer*, 1998, **3**, 429.

12 *Circular Dichroism—Principles and Applications*, ed. N. Berova, K. Nakanishi and R. W. Woody, Wiley-VCH, 2nd edn., 2000, p. 360.

13 K. J. Address and J. Feigon, in *Bioorganic Chemistry—Nucleic Acids*, ed. S. M. Hecht, Oxford University Press, 1996, p. 163.

14 H. A. M. Biemans, A. E. Rowan, A. Verhoeven, P. Vanoppen, L. Latterini, J. Foekema, A. P. H. J. Schenning, E. W. Meijer, F. C. de Schryver and R. J. M. Nolte, *J. Am. Chem. Soc.*, 1998, **120**, 11 054.

ChemComm

Influence of ion exchange conditions on the defect chemistry and performance of cobalt doped layered lithium manganese oxide based intercalation compounds†

Alastair D. Robertson, A. Robert Armstrong and Peter G. Bruce*

School of Chemistry, University of St. Andrews, North Haugh, St. Andrews, Fife, UK KY16 9ST. E-mail: p.g.bruce@st-andrews.sc.uk

Received (in Oxford, UK) 3rd May 2000, Accepted 8th August 2000
First published as an Advance Article on the web 28th September 2000

It is shown that by varying the conditions used to exchange Na by Li in layered sodium manganese oxide based compounds, not only are the guest ions exchanged but the defect chemistry of the host is modified and this has an important effect on the reversibility of lithium intercalation; in particular, defect 2.5% Co doped layered lithium manganese oxide exhibits a capacity to store lithium equivalent to 200 mA h g^{-1} which fades by only 0.08% per cycle on cycling at 25 mA g^{-1}.

One of the greatest challenges in the field of rechargeable lithium batteries is to replace the $LiCoO_2$ positive electrode with an alternative lithium intercalation compound that is safer, cheaper and less toxic, such as a lithium manganese oxide. The spinel, $LiMn_2O_4$, has been widely studied in this regard.[1–4] Recently, we reported the first synthesis of the layered intercalation compound, $LiMnO_2$, which involved the low temperature ion exchange of Na by Li in $NaMnO_2$.[5,6] The present interest in layered $LiMnO_2$ based materials is significant.[5–12] When doped with Co, high capacities to store Li are obtained but reversibility on cycling is insufficient. Here, we report that varying the ion exchange conditions has an important effect on the defect chemistry in these layered materials, and this has a critical influence on the all-important reversibility of the lithium intercalation reaction.

The layered sodium manganese cobalt oxide phases, $Na_xMn_{1-y}Co_yO_2$, were prepared as described previously.[11] The initial reaction mixture contained 1 mol of Na per transition metal ion, *i.e.* $x = 1$. Ion exchange was carried out using an 8-fold excess of LiBr in either ethanol at 80 °C for 48 h or hexanol at 160 °C for 8 h. Following ion exchange the materials were washed with ethanol and water. Powder X-ray diffraction was carried out on a Stoe STADI/P diffractometer in transmission mode and using an Fe-Kα_1 source ($\lambda = 1.936$ Å). Neutron diffraction data were collected on the GEM diffractometer at RAL. Chemical analysis was carried out using well established methods; for Li and Na this was conducted by flame emission whereas atomic absorption spectroscopy was employed for Mn and Co. Oxidation states were obtained by $KMnO_4$/iron(II) ammonium sulfate titration.[13] BET measurements indicated that the surface areas were between 5 and 10 m^2 g^{-1}.

Powder X-ray diffraction patterns of the as-prepared Na materials revealed that they contain two phases, one may be indexed based on the layered phase whereas the other exhibits the characteristic peaks of Na_2CO_3. Evidently the Na_2CO_3 has not reacted completely and by implication the layered sodium phase is Na deficient, *i.e.* $x < 1$. The Na_2CO_3 is removed during the ion exchange and subsequent washing in ethanol–water. Focussing on the layered lithium phases, powder neutron diffraction patterns for these phases prepared in either hexanol or ethanol exhibit a single phase that may be indexed based on the layered O3 structure of $LiCoO_2$ (space group $R\bar{3}m$, structure type α-$NaFeO_2$). For the Co doped materials prepared in hexanol, full structure refinements have been reported previously.[11] Before discussing further Rietveld refinement of the ethanol samples it is instructive to consider the results of chemical analysis (Table 1). Several conclusions may be drawn from these results. First the sodium phase is alkali metal deficient ($x < 1$), consistent with the XRD data, and this is carried through to the Li phases after ion exchange. There is evidence of a somewhat greater alkali metal content after ion exchange than before indicating that some lithium intercalation accompanies the ion exchange process. Table 1 also reveals that the Na phase contains vacancies on the transition metal sites, these vacancies are retained in ethanol samples prepared at 80 °C whereas ion exchange in hexanol at 160 °C eliminates almost all the vacancies. The transition metal vacancies in the Na phase will be associated with negative effective charges which are likely to trap some of the Na^+ ions; this can explain the retention of a small amount of Na during the ethanol exchange. The ion exchange conditions used here are somewhat reducing, and this is sufficient to result in some lithium intercalation in ethanol and hexanol. The more aggressive conditions of reflux in hexanol at 160 °C cause, in addition, reduction of the host with the associated elimination of the transition metal vacancies, without the transition metal vacancies to trap Na^+, the ion exchange process is more complete. Overall it is evident that the ion exchange process is not

† Electronic supplementary information (ESI) available: powder neutron diffraction profile for $Li_x(Mn_{0.975}Co_{0.025})O_2$ prepared in ethanol. See http://www.rsc.org/suppdata/cc/b0/b002552f/

Table 1 Compositional analysis of as-prepared 2.5% Co Na phase[a] and ion exchanged Li phases for layered $A_xMn_{1-y}Co_yO_2$ materials

Nominal Co content	A = Na or Li; Ion exchange conditions	Composition	Average TM oxidation state	No. of TM vacancies	Mn^{3+} occupancy of TM sites
0.025	Na	$Na_{0.53}Mn_{0.92}Co_{0.025}O_2$[a]	3.672+	5.5%	28.5%
0.025	Li; Ethanol, 80 °C	$Na_{0.048}Li_{0.58}Mn_{0.91}Co_{0.025}O_2$	3.610+	6.5%	33.8%
0.025	Li; Hexanol, 160 °C	$Na_{0.009}Li_{0.62}Mn_{0.96}Co_{0.028}O_2$	3.412+	1.2%	55.3%
0.1	Li; Ethanol, 80 °C	$Na_{0.035}Li_{0.54}Mn_{0.87}Co_{0.087}O_2$	3.579+	4.3%	31.5%
0.1	Li; Hexanol, 160 °C	$Na_{0.012}Li_{0.64}Mn_{0.90}Co_{0.094}O_2$	3.368+	0.6%	53.4%

[a] Content of Na determined by CHN analysis, thereby allowing the amount of Na_2CO_3 and Na in the main phase to be calculated.

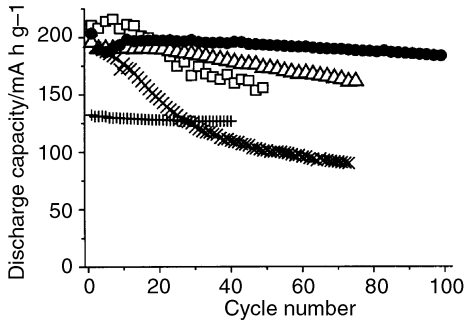

Fig. 1 Discharge capacities as a function of the number of charge–discharge cycles carried out at 25 mA g^{-1} (C/7) and 30 °C between potential limits of 2.4 and 4.6 V for; (●) 2.5% Co prepared in ethanol: (△) 2.5% Co prepared in hexanol: (□) 10% Co prepared in hexanol: (X) $Li_{1.07}(Mn_{1.78}Co_{0.05})O_4$ spinel and (+) $LiCoO_2$ cycled between 3.3 and 4.2 V.

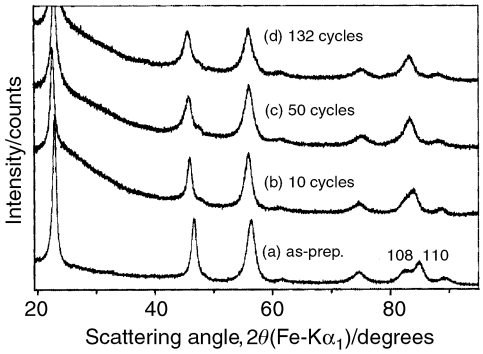

Fig. 2 Powder X-ray diffraction patterns collected on $Li_x(Mn_{0.975}Co_{0.025})O_2$, prepared in ethanol at 80 °C, (a) before cycling, (b) after 10 cycles, (c) after 50 cycles and (d) after 132 cycles. Cycling was carried out at 25 mA g^{-1} and over the range 2.4–4.6 V.

restricted to the anticipated simple exchange of Na by Li, instead it plays a critical role in controlling the defect chemistry/non-stoichiometry of the transition metal host.

Returning to the neutron data for the 2.5% Co doped ethanol sample (ESI†), Rietveld refinement was carried out based on the O3-$LiCoO_2$ structure, which possesses cubic close packed oxide ions. Li and Na were placed in the octahedral sites (3b) of the alkali metal layers and Mn and Co in the octahedral sites (3a) of the transition metal layers. The Na and Co occupancies were fixed at values obtained from the chemical analysis ($Na_{0.048}Li_{0.58}Mn_{0.91}Co_{0.025}O_2$). The Li and Mn occupancies were allowed to vary freely. The refined occupancies are in good agreement with the chemical analysis. A good fit to the observed data was obtained and the crystallographic data are presented in ref. 14. $LiMnO_2$ is monoclinic owing to a cooperative Jahn–Teller distortion promoted by the high spin Mn^{3+} ions. For the Co doped materials it has been shown that cobalt is in the trivalent state.[11] The presence of Co^{3+} along with the alkali metal deficiency and, in the case of the ethanol samples, vacancies on the transition metal sites conspire to reduce the occupancy of the octahedral sites by Mn^{3+} to a level where they can no longer promote a cooperative distortion which typically occurs at *ca.* 50% occupancy of the transition metal octahedral sites by Mn^{3+}. As a result none of the samples exhibit a monoclinic distortion.

What effect does the presence of transition metal vacancies have on the behaviour of these materials as intercalation electrodes? The variation of discharge capacity with cycle number is shown in Fig. 1. Considering first the hexanol samples, reducing the Co content from 10 to 2.5% improves the capacity retention on cycling. However the highest degree of reversibility is obtained from the 2.5% Co doped sample prepared in ethanol; this corresponds to a capacity fade of only 0.08% per cycle. High capacities to store Li are of no value for application in rechargeable lithium batteries unless accompanied by a high degree of reversibility of the intercalation reaction. This is now becoming recognised as a key feature that must be built into the chemistry of intercalation compounds for rechargeable lithium battery electrodes. The capacity of $LiCoO_2$, used as the positive electrode in the current generation of rechargeable lithium batteries, is also shown for comparison. The layered manganese based materials may be particularly relevant to the market in sub 3 V electronics for which high capacity cathodes delivering their charge above 2.4 V could be combined with graphite anodes to yield high capacity low voltage cells for such electronic applications. This is one of the most rapidly growing markets for rechargeable lithium batteries.

We have shown previously that Co doped materials prepared in hexanol convert to spinel on cycling.[11] This is also the case for the samples prepared in ethanol. The merging of the 108 and 110 peaks is indicative of the transformation (Fig. 2). It is interesting to compare the capacity fade of the layered compounds prepared in hexanol and ethanol which convert to spinel *in situ*, with a directly prepared cobalt doped lithium manganese spinel cycled over the same voltage range. The chosen spinel, which was prepared by conventional solid state reaction, has a very similar composition to the 2.5% Co doped material prepared in ethanol containing, as it does, a similar concentration of vacancies on the transition metal sites. Whereas spinels are known to cycle well when confined to a potential range around 4 V, the irreversibility of the intercalation process on cycling over the wider voltage range is clearly severe even for Co doped samples (Fig. 1), yet this is not the case for the *in situ* spinels.

The results presented here show that by changing the mild ion exchange conditions, it is possible to modify the defect chemistry/stoichiometry of the host. In particular, by forming a layered lithium manganese oxide based spinel with Co and vacancies on the transition metal sites it is possible to improve significantly the reversibility of the intercalation process which is a critical property for applications as an electrode material.

P. G. B. is indebted to the EPSRC for financial support and RAL for the provision of neutron facilities.

Notes and references

1 M. M. Thackeray, W. I. F. David, P. G. Bruce and J. B. Goodenough, *Mater. Res. Bull.*, 1983, **18**, 461.
2 R. J. Gummow, A. De Kock and M. M. Thackeray, *Solid State Ionics*, 1994, **69**, 59.
3 J. M. Tarascon, W. R. McKinnon, F. Coowar, T. N. Bowmer, G. Amatucci and D. Guyomard, *J. Electrochem. Soc.*, 1994, **141**, 1421.
4 Y. Gao and J. R. Dahn, *J. Electrochem. Soc.*, 1996, **143**, 100.
5 A. R. Armstrong and P. G. Bruce, *Nature*, 1996, **381**, 499.
6 F. Capitaine, P. Gravereau and C. Delmas, *Solid State Ionics*, 1996, **89**, 197.
7 S. K. Mishra and G. Ceder, *Phys. Rev. B*, 1999, **59**, 6120.
8 Y.-I. Jang, B. Huang, Y.-M. Chiang and D. R. Sadoway, *Electrochem. Solid State Lett.*, 1998, **1**, 13.
9 P. G. Bruce, A. R. Armstrong and R. L. Gitzendanner, *J. Mater. Chem.*, 1999, **9**, 193.
10 A. R. Armstrong, R. Gitzendanner, A. D. Robertson and P. G. Bruce, *Chem. Commum.*, 1998, 1833.
11 A. R. Armstrong, A. D. Robertson, R. Gitzendanner and P. G. Bruce, *J. Solid State Chem.*, 1999, **145**, 549.
12 J. M. Paulsen and J. R. Dahn, *Solid State Ionics*, 1999, **126**, 3.
13 M. J. Katz, R. C. Clarke and W. F. Nye, *Anal. Chem.*, 1956, **28**, 507.
14 *Crystallographic data* for $Li_xMn_{0.975}Co_{0.025}O_2$ prepared by ion exchange under reflux in ethanol: space group $R\bar{3}m$, a = 2.86605(2), c = 14.5752(5) Å, Li/Na (3b) (0.0, 0.0, 0.5), B_{iso} = 0.23(13), occupancies: Li = 0.595(14), Na = 0.048 (fixed from analysis). Mn/Co (3a) (0.0, 0.0, 0.0), B_{11} = B_{22} = 0.95(8), B_{33} = 1.7(2), B_{12} = 0.48(4), occupancies: Mn = 0.897(10), Co = 0.025 (fixed from analysis). O1 (6c) (0.0, 0.0, 0.2624(1)), B_{11} = B_{22} = 0.70(2), B_{33} = 1.01(3), B_{12} = 0.351(8). *R*-factors: R_{exp} = 1.2%, R_{wp} = 3.4%, R_p = 2.9%, R_I = 3.4%.

Differential electronic effects and the selective protonation of mutually *trans* ligands

Valerie Autissier,[a] Richard A. Henderson*[a] and Christopher J. Pickett[b]

[a] *Department of Chemistry, Bedson Building, University of Newcastle, Newcastle-upon-Tyne, UK NE1 7RU. E-mail: r.a.henderson@ncl.ac.uk*

[b] *Department of Biological Chemistry, John Innes Centre, Norwich Research Park, Norwich, UK NR4 7UH*

Received (in Cambridge, UK) 2nd August 2000, Accepted 5th September 2000
First published as an Advance Article on the web 27th September 2000

The rate of protonation of the nitrile carbon in *trans*-[Mo(N$_2$)(NCC$_6$H$_4$R-4)(Ph$_2$PCH$_2$CH$_2$PPh$_2$)$_2$] (R = MeO, Me, H, Cl, MeCO or NO$_2$) shows an unusual non-linear dependence on the identity of R, revealing how both kinetic and thermodynamic factors control the site of protonation in complexes containing a variety of protonatable ligands.

Understanding the factors which define where protons bind to metal complexes is important in gaining insight into the reactivity of certain metalloenzymes,[1] and in controlling the regio-, stereo- and product-specificities of metal-mediated reactions.[2,3] However, we are still some way from being able to predict where protons will bind to complexes containing a variety of potential sites, as is evident when we consider the reactions shown in Fig. 1.

Some years ago,[4] protonation of *trans*-[Mo(N$_2$)(NCPr^n)(Ph$_2$PCH$_2$CH$_2$PPh$_2$)$_2$] was found to occur at dinitrogen, forming the corresponding hydrazide (top line). However recently, the analogous *trans*-[Mo(N$_2$)(NCPh)(Ph$_2$PCH$_2$CH$_2$PPh$_2$)$_2$] was shown to protonate at the nitrile carbon[5] (bottom line). This observation is rather unexpected since earlier investigations[6,7] showed that protonation of end-on coordinated dinitrogen is rapid (probably diffusion-controlled), whereas protonation at carbon sites is usually several orders of magnitude slower, even when bound to electron-rich metal centres[2,3,8] indicating that hydrazides would always be formed in such reactions. Given that in *trans*-[Mo(N$_2$)(NCPh)(Ph$_2$PCH$_2$CH$_2$PPh$_2$)$_2$] both dinitrogen and nitrile are bound to the same centre it is difficult to reconcile why carbon should be the preferred protonation site. Herein, we report kinetic studies on the family of reactions represented in eqn. (1) (R = MeO, Me, H, Cl, MeCO or NO$_2$),[9] and show that R affects the protonation chemistry of the dinitrogen and nitrile ligands in quite different ways.

trans-[Mo(N$_2$)(NCC$_6$H$_4$R-4)(Ph$_2$PCH$_2$CH$_2$PPh$_2$)$_2$] + HCl ⟶
trans-[MoCl(NCH$_2$C$_6$H$_4$R-4)(Ph$_2$PCH$_2$CH$_2$PPh$_2$)$_2$]$^+$ + Cl$^-$ (1)

When the reaction between *trans*-[Mo(N$_2$)(NCPh)(Ph$_2$PCH$_2$CH$_2$PPh$_2$)$_2$] and an excess of anhydrous HCl is studied in thf, using stopped-flow spectrophotometry, a single exponential absorbance–time curve is observed. Under all conditions, the initial absorbance corresponds to the reactant and final absorbance† to *trans*-[MoCl(NCH$_2$Ph)(Ph$_2$PCH$_2$CH$_2$PPh$_2$)$_2$]$^+$. The kinetics of this reaction exhibit a first order dependence on the concentration of *trans*-[Mo(N$_2$)(NCPh)(Ph$_2$PCH$_2$CH$_2$PPh$_2$)$_2$] but the dependence on the concentration of HCl is markedly non-linear, such that at high concentrations of HCl the rate is independent of the concentration of acid (Fig. 2).

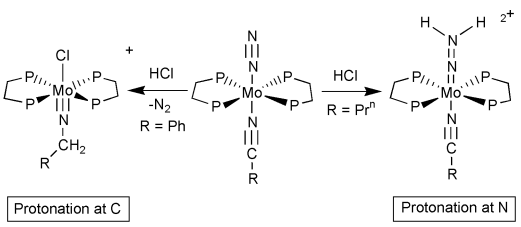

Fig. 1 Protonation of dinitrogen *vs.* nitrile in *trans*-[Mo(N$_2$)(NCR)(Ph$_2$PCH$_2$CH$_2$PPh$_2$)$_2$].

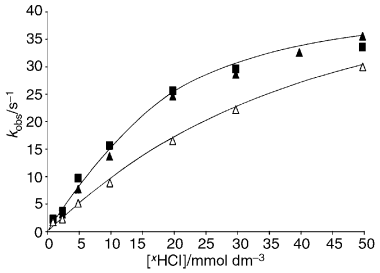

Fig. 2 Dependence on the concentration of ^{x}HCl for the reaction with *trans*-[Mo(N$_2$)(NCPh)(Ph$_2$PCH$_2$CH$_2$PPh$_2$)$_2$] in thf at 25.0 °C. The data points correspond to: [Mo] = 0.2 mmol dm^{-3} (■) and [Mo] = 0.4 mmol dm^{-3} (▲). Data collected in the reaction with ^{2}HCl (△) are also shown. The data were analysed by plotting $1/k_{obs}$ *vs.* 1/[HCl], from the straight line the intercept = $1/k_2$ and gradient = $1/k_1$.

These observations are consistent with the mechanism shown in Fig. 3. Initial protonation of the nitrile carbon (k_1) generates [Mo(N$_2$)(NCHPh)(Ph$_2$PCH$_2$CH$_2$PPh$_2$)$_2$]$^+$. Protonation of the nitrile diminishes the electron density at the metal, and because dinitrogen is a strong π-acceptor ligand, this has two effects on its reactivity: (i) decreasing the basicity of dinitrogen thus suppressing protonation and (ii) increasing the lability of dinitrogen. Dissociation of dinitrogen (k_2) and subsequent rapid binding of chloride facilitates further protonation of carbon to form *trans*-[MoCl(NCH$_2$Ph)(Ph$_2$PCH$_2$CH$_2$PPh$_2$)$_2$]$^+$. An analogous mechanism has been proposed for the reactions of acid with *trans*-[Mo(N$_2$)$_2$(R$_2$PCH$_2$CH$_2$PR$_2$)$_2$][6,7] (R = Ph or Et), involving rapid protonation of one dinitrogen followed by rate-limiting dissociation of the other. The important difference in the two systems is that for *trans*-[Mo(N$_2$)(NCPh)(Ph$_2$PCH$_2$-

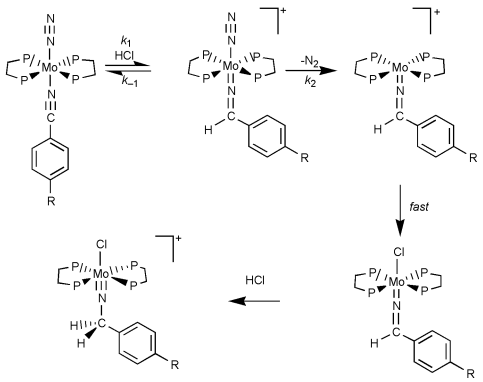

Fig. 3 Mechanism for the formation of *trans*-[MoCl(NCH$_2$C$_6$H$_4$R-4)(Ph$_2$PCH$_2$CH$_2$PPh$_2$)$_2$] in the reactions of anhydrous HCl with *trans*-[Mo(N$_2$)(NCC$_6$H$_4$R-4)(Ph$_2$PCH$_2$CH$_2$PPh$_2$)$_2$].

DOI: 10.1039/b006302i

$CH_2PPh_2)_2$] the protonation at carbon is rate-limiting at low concentrations of HCl, and consequently the reaction with DCl is associated with a primary isotope effect (k_1^H/k_1^D = 1.8; Fig. 2). Only at high concentrations of acid does the unimolecular dissociation of dinitrogen become rate-limiting, and under these conditions there is no isotope effect (k_2^H/k_2^D = 1.0).

Studies on *trans*-[Mo(N_2)(NCC_6H_4R-4)($Ph_2PCH_2CH_2PPh_2)_2$] (R = MeO, Me, Cl, MeCO or NO_2) show analogous behaviour to that of *trans*-[Mo(N_2)(NCPh)($Ph_2PCH_2CH_2PPh_2)_2$] and allow investigation into how k_1 and k_2 are affected by the electronic influences of R (Fig. 4).

The effect of R on the lability of dinitrogen (k_2) is not unexpected. As R is varied and becomes more electron-releasing, the dinitrogen becomes less labile. This is in line with the labilities of dinitrogen previously observed in the reactions of *trans*-[Mo(N_2)$_2${(4-RC_6H_4)$_2PCH_2CH_2P(C_6H_4$R-4)$_2$}$_2$] (R = CF_3, Cl, H, Me or MeO).[10] The effect of R on the rate of protonation at the nitrile carbon is less straightforward. It is anticipated that k_1 would be affected by both the electron density at the carbon and the barrier to structural rearrangement (rehybridisation).[11] Certainly, there is a general increase in the rate of protonation as R becomes more electron-releasing but the trend is markedly non-linear, and with the most strongly electron-releasing substituents the rate of protonation is essentially independent of the nature of R. The reason R affects protonation of the nitrile and dinitrogen ligands so differently becomes clearer after considering the effect R has on the IR stretching frequencies, $\upsilon(N_2)$ and υ(CN) (Fig. 4, insert).[9] It is evident that R affects $\upsilon(N_2)$ and υ(CN) in a manner which parallels the rates of dinitrogen dissociation and protonation of carbon, respectively. The values of $\upsilon(N_2)$ and υ(CN) reflect the bond orders in these groups, which are affected by the backbonding from {Mo($Ph_2PCH_2CH_2PPh_2)_2$} to each of the π-acceptor ligands. The substituent R will modulate this effect, but because it is sited on the nitrile, R affects the backbonding to dinitrogen and nitrile differently.

For the *trans*-dinitrogen, as R is varied and made more electron-releasing the backbonding from Mo to dinitrogen is reinforced resulting in a decrease in $\upsilon(N_2)$ and dinitrogen lability (k_2) (and, as noted above, an increase in basicity). In contrast, the effect of an electron-releasing R will oppose the backbonding from Mo to nitrile. This counterbalance of the electron-releasing effect of R and the backbonding from Mo results in the increasing insensitivity of υ(CN) and the rate of protonation of the nitrile carbon as R becomes more electron-releasing ($k_1^{max} \approx 1 \times 10^4$ dm^3 mol^{-1} s^{-1}). Understanding the electronic origins of these effects allows us to appreciate that it is a combination of kinetic and thermodynamic factors which control product-selectivity in the reactions of acid with *trans*-[Mo(N_2)(NCR)($Ph_2PCH_2CH_2PPh_2)_2$] (Fig. 1).

As noted above, the π-backbonding from the {Mo($Ph_2PCH_2CH_2PPh_2)_2$} site affects both the lability and the basicity of dinitrogen.[12] In *trans*-[Mo(N_2)(NCC_6H_4R-4)($Ph_2PCH_2CH_2PPh_2)_2$], the aryl group is poorly electron-releasing and consequently the *trans*-dinitrogen is only weakly basic. Indeed, we can estimate an upper limit for the proton-affinity of the dinitrogen in these systems [eqn. (2)]. Even at the highest concentration of HCl (50 mmol dm^{-3}), there is no spectroscopic or kinetic evidence for dinitrogen being protonated, and hence $K_3^{Ph} \leqslant 4 \times 10^{-5}$. Since $K_3^{Ph} = k_3^{Ph}/k_{-3}^{Ph}$ and assuming the thermodynamically favourable k_{-3}^{Ph} step is diffusion controlled, we can estimate $k_3^{Ph} \leqslant 4 \times 10^5$ dm^3 mol^{-1} s^{-1}. Hence in these systems, the rates of protonation of dinitrogen and the nitrile carbon are not necessarily appreciably different. Since the exclusive product is always *trans*-[MoCl(NCC_6H_4R-4)($Ph_2PCH_2CH_2PPh_2)_2$] thermodynamic factors must be controlling the outcome of the reaction.

$$Mo{-}N{\equiv}N + HCl \underset{}{\overset{K_3}{\rightleftharpoons}} Mo{=}N{=}\overset{+}{N}\overset{H}{\diagdown} + Cl^- \qquad (2)$$

As indicated above, a natural consequence of the mutually *trans* dinitrogen and nitrile both being π-acceptor ligands is that protonation at one suppresses protonation at the other. However, the unfavourable value of K_3^{Ph} means that the parent dinitrogen complex is the major component of the protolytic equilibrium mixture and is able to react by the irreversible, protonation of the nitrile carbon, resulting in the ultimate formation of *trans*-[MoCl($NCH_2C_6H_4$R-4)($Ph_2PCH_2CH_2PPh_2)_2$]$^+$.

Consider now the situation where the nitrile is *very* electron-releasing, as is the case in *trans*-[Mo(N_2)(NCPr^n)($Ph_2PCH_2CH_2PPh_2)_2$]. The Pr^{n}CN ligand is sufficiently electron-releasing[4] that dinitrogen binds two protons even with [HCl] = 10 mmol dm^{-3}, giving $K_3^{Pr} \geqslant 0.36$ and hence $k_3^{Pr} \geqslant 3.6 \times 10^9$ dm^3 mol^{-1} s^{-1} (*i.e.* close to the diffusion-controlled limit). However, the data in Fig. 4 indicate that protonation of carbon will not exceed $k_1 \approx 1 \times 10^4$ dm^3 mol^{-1} s^{-1}. Consequently both the kinetics and thermodynamics favour protonation at dinitrogen, and *trans*-[Mo(NNH_2)(NCPr^n)($Ph_2PCH_2CH_2PPh_2)_2$]$^{2+}$ is formed (Fig. 1).

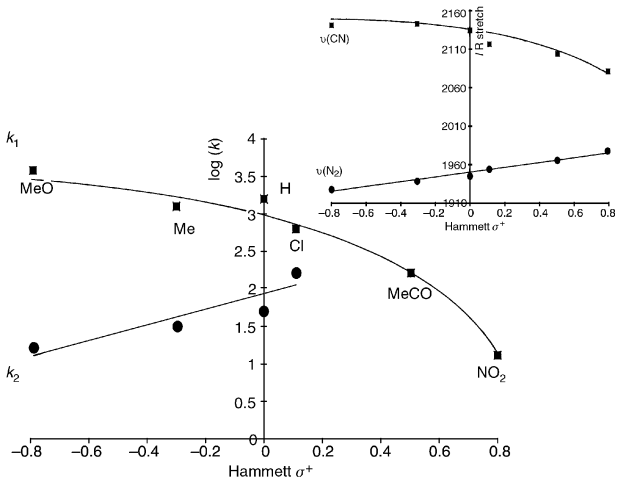

Fig. 4 Correlation of log(k) with Hammett σ^+ for the protonation of the nitrile carbon, k_1 (■) and dissociation of dinitrogen, k_2 (●) in the reactions of HCl with *trans*-[Mo(N_2)(NCC_6H_4R-4)($Ph_2PCH_2CH_2PPh_2)_2$] (R = NO_2, MeCO, Cl, H, Me or MeO) in thf at 25.0 °C. Insert: correlation of Hammett σ^+ with υ(CN) (■) and $\upsilon(N_2)$ (●).

Notes and references

† The identity of the product was confirmed by $^{31}P\{^1H\}$ NMR spectroscopy and comparison of the spectra with those reported in the literature.[5]

1 D. J. Evans, R. A. Henderson and B. E. Smith, *Bioinorganic Catalysis*, ed. J. Reedijk and E. Bouwman, Marcel Dekker Inc., New York, 2nd edn., 1999, ch 7, and references therein.
2 R. A. Henderson, *Angew. Chem.*, 1996, **35**, 946 and references therein.
3 K. W. Kramarz and J. R. Norton, *Prog. Inorg. Chem.*, 1994, **42**, 1 and references therein.
4 J. Chatt, G. J. Leigh, H. Neukomm, C. J. Pickett and D. R. Stanley, *J. Chem. Soc., Dalton Trans.*, 1980, 121.
5 H. Seino, Y. Tanabe, Y. Ishii and M. Hidai, *Inorg. Chim. Acta*, 1998, **280**, 163.
6 R. A. Henderson, *J. Chem. Soc., Dalton Trans.*, 1982, 917.
7 R. A. Henderson, *J. Chem. Soc., Dalton Trans.*, 1984, 2259.
8 R. A. Henderson and K. E. Oglieve, *J. Chem. Soc., Dalton Trans.*, 1996, 3397 and references therein.
9 T. Tatsumi, M. Hidai and Y. Uchida, *Inorg. Chem.*, 1975, **14**, 2530.
10 W. Hussain, G. J. Leigh, H. Mohd Ali, C. J. Pickett and D. A. Rankin, *J. Chem. Soc., Dalton Trans.*, 1984, 1703.
11 R. P. Bell, *The Proton in Chemistry*, Chapman & Hall, London, 2nd edn., 1973, ch 7.
12 J. Chatt, *J. Organomet. Chem.*, 1975, **100**, 17.

ChemComm

Measurement of nanotube content in pyrolytically generated carbon soot

Jonathan N. Coleman,*[a] Diarmuid F. O'Brien,[a] Alan B. Dalton,[b] Brendan McCarthy,[a] Bernd Lahr,[a] Anna Drury,[a] Robert C. Barklie[a] and Werner J. Blau[a]

[a] *Materials Ireland Polymer Research Center, Department of Physics, University of Dublin, Trinity College, Dublin 2, Republic of Ireland. E-mail: colemaj@tcd.ie*

[b] *School of Physics, Dublin Institute of Technology, Kevin St, Dublin 8, Republic of Ireland*

Received (in Cambridge, UK) 31st July 2000, Accepted 5th September 2000
First published as an Advance Article on the web 27th September 2000

Carbon nanotubes can be efficiently separated from impurity material in carbon soot using a conjugated polymer filtration system as monitored by EPR, allowing the calculation of purity of the crude carbon soot.

Carbon nanotubes have generated interest in all areas of science owing to their novel structural, mechanical and electronic properties. In the physical sciences nanodevices have already been demonstrated including transistors[1] and rectifying heterojunctions.[2] In microbiology they have been used as probes to study the structure of biomolecules[3,4] and as templates for the self assembly of proteins.[5] However, at present, as-produced carbon soot remains low in nanotube content.[6] Furthermore, neither quantitative techniques to analyse soot content nor methods to measure nanotube content exist. This work presents the first measurement of nanotube content in impure carbon soot. Using a conjugated polymer as a nanotube 'filter', carbon nanotubes are separated from all other soot components. An absolute value for the nanotube content can then be calculated for the first time using electron paramagnetic resonance and thermogravimetric measurements. This is a vital step towards making nanotubes a practical material for novel scientific developments.

The necessity for a technique to measure nanotube content in carbon soot is apparent when the present fabrication and purification methods are examined. During nanotube production unwanted carbon species such as turbostratic graphite (TSG) and carbon onions are invariably formed. Purification by oxidation[7] destroys many nanotubes and alters the electronic properties of the remaining tubes. Chromatographic techniques[8] have succeeded in purifying carbon soot but no quantitative measure of purity has been obtained. Furthermore, scale-up of these processes is problematic. The process outlined in this work approaches these issues in a novel manner *via* the production of a polymer nanotube composite. Thus a quantifiable purification method for carbon soot is presented which leads logically to a measurement of the purity of that soot.

In order to produce the polymer nanotube composites used in this work 80 mg of poly(*m*-phenylene-*co*-2,5-dioctyloxy-*p*-phenylenevinylene) (PmPV) were mixed with 25.5 mg of multiwall nanotube (MWNT) containing arc-generated carbon soot in 4 ml of toluene. The PmPV was synthesised using a standard polycondensation reaction,[9] while the carbon soot was generated in a Krätschmer generator.[10] The mixture was sonicated for 2 min using a high power sonic tip and then for 2 h in a low power sonic bath to ensure complete dispersion of the Krätschmer generated carbon soot. This was carried out for seven composite solutions with identical constituents. These solutions were then allowed to stand undisturbed for various amounts of time, from 30 min to 90 h. At the end of its settling time each solution was carefully decanted into a new sample bottle, leaving a black sediment at the bottom of the old bottle. These sediments were then dried and weighed.

To determine the natures of the sediment and remaining solute, EPR spectroscopy was used. This technique measures microwave-induced transitions between electron spin energy levels in the presence of a magnetic field. Unpaired electrons in different environments may be distinguished using this technique by differences in their resonance spectra. To prepare samples for EPR, *ca.* 0.3 ml of each of the separated solutions was drop cast onto spin free quartz plates, giving *ca.* 7 mg of solute after the solvent had evaporated. In addition all the recovered sediments were carefully weighed and *ca.* 7 mg of each placed in spin free quartz tubes. EPR spectra were recorded for all samples and carbon soot. The carbon soot was dispersed in toluene in a spin free glass tube to reduce the interaction of the spins within neighbouring particles, and to match more closely the environment of the spins in a polymer host.

Fig. 1 shows EPR derivative spectra for the dispersed carbon soot, the sediment and solute samples for both the shortest and longest settling times. In all cases these spectra could well be fitted to the superposition of two symmetric absorption lines of Lorentzian shape. In the case of the dispersed carbon soot and the various sediments, *g* values determined from the line positions, of *ca.* 2.011 and 2.020 and peak-to-peak line widths, ΔB_{pp}, of close to 11 and 12 G, respectively, were observed. Similar results were obtained for the solute spectra which could be fitted to two lines with *g* values of *ca.* 2.011 and 2.020 and widths of 7 and 18 G, respectively. This demonstrates that the carbon soot consists of the same two components as are in the solutes and sediments. The variation in linewidth between sediment and solute is probably due to small environmental variations between the two phases. Two such components have been observed by other authors who attribute them to paramagnetic centers in nanotubes[6,11] and TSG.

In addition to *g* values and linewidths, signal intensities can be measured for both the MWNT and TSG. In each case the signal intensity of the MWNT or TSG line is proportional to the mass of the MWNT or TSG present in the measured sample. Assuming that the measured fraction is representative of the whole mass of sediment or solute, the signal intensities can be normalized to represent all the unpaired spins in the total mass of sediment or solute. This normalized signal intensity (*NSI*) is achieved by multiplying the measured signal intensity by a

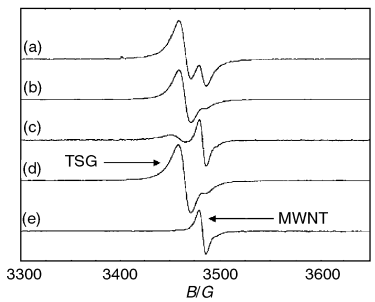

Fig. 1 EPR derivative spectra for some of the samples studied in this work. EPR spectra of (a) carbon soot dispersed in toluene, (b) the sediment formed after 30 min settling time, (c) the solute remaining after 30 min settling time, (d) the sediment formed after 90 h settling time and (e) the solute remaining after 90 h settling time. Note that in all spectra except E two components, TSG and MWNT (denoted by arrows), are clearly present. For spectrum E the sole component present is that of the MWNT.

DOI: 10.1039/b006164f

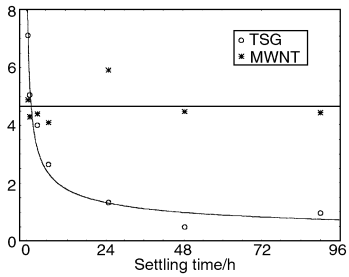

Fig. 2 Normalised signal intensities (*NSI*) for the nanotube and TSG components of the solute formed for various settling times. The *NSI* values are proportional to the entire mass of each component for each solute. Note that while the nanotube component remains approximately constant the turbostratic graphite component decreases as the TSG falls out of solution.

factor of M_T/M_{EPR} where M_T is the total sediment or solute mass and M_{EPR} is the mass of the sample measured.

These normalized signal intensities, for both nanotube and TSG components of the solute are shown in Fig. 2 as a function of sample settling time. It is clear from this diagram that the nanotube component of the various solutes is approximately constant for all the settling times. The TSG component however shows a sharp decrease. After 48 h settling time there is virtually no TSG present in the solute. Therefore the PmPV holds carbon nanotubes in solution while the TSG gradually settles out to give solutions rich in nanotubes. Thus nanotubes can be effectively separated from other unwanted forms of carbon present in carbon soot.

For the 48 h settling time we can calculate the percentages of both MWNT and TSG that have remained in solution. This can be calculated for a given species from

$$\% = 100 \times \frac{NSI_{solution}}{NSI_{solution} + NSI_{sediment}} \quad (1)$$

where % is the percentage of the given species (MWNT or TSG) in solution, $NSI_{solution}$ and $NSI_{sediment}$ are the normalized signal intensities for the same species in solution and sediment, respectively. For the 48 h settling sample $NSI_{solution}$(MWNT) = 4.5 while $NSI_{sediment}$(MWNT) = 2.6 (in arbitrary units). By comparison for the same sample $NSI_{solution}$(TSG) = 0.5 while $NSI_{sediment}$(TSG) = 26.5. Using this we can calculate that 63% of the added nanotubes go into solution while only 1.9% of the added TSG remains in solution.

While this allows us to make relative comparisons of amounts of nanotubes present in a given sample using the *NSI* values, EPR alone does not give us enough information to make absolute measurements of nanotube content. In order to do this we need to be able to calculate a nanotube signal intensity per unit mass, *k*, such that we can write an equation of the form

$$S_i = k_i m_i \quad (2)$$

where S_i is a signal intensity for a given mass m_i of a given species (MWNT or TSG) *i*. This will allow us to calculate the mass of nanotubes in a given sample from the EPR spectrum provided we know *k*.

In order to calculate the mass of nanotubes present in a purified composite sample with only trace amounts of TSG we use thermogravimetric analysis (TGA). In this technique the sample is heated in air and the sample mass monitored as it is oxidised. This was carried out for the carbon soot, PmPV and a highly separated solute sample (settling time 48 h). The TGA traces for these samples are shown in Fig. 3. By 650 °C the PmPV sample is almost completely oxidised (except for some impurities), while the carbon soot only begins to burn at *ca.* 700 °C. For the composite sample, between these two temperatures, no oxidisation occurs as demonstrated from the horizontal part of the trace in this region. Thus the stable mass in this temperature region represents nanotubes and some polymer impurities. It is possible to account for the polymer impurities and hence calculate the mass of nanotubes present in the composite using these data. For the composite solute

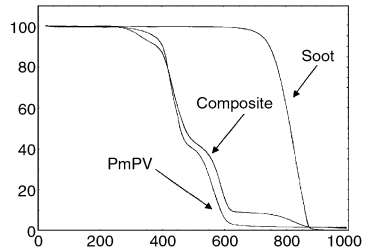

Fig. 3 Thermogravitational analysis trace for PmPV, a highly separated composite film and carbon soot. Note that PmPV stops burning at *ca.* 600 °C while the carbon soot only begins to burn at 750 °C. For the composite sample there is no oxidation between these temperatures. This allows us to calculate the mass of nanotubes in this sample.

measured here the nanotube mass was calculated at 5.1% of the total composite mass. This allows us to calculate the actual mass of nanotubes present in the (same) sample measured by EPR. As we know the nanotube EPR signal intensity (S_n) for this sample we can calculate a signal intensity per mass of nanotubes, k_n. This works out to be 1.04 per mg in our system of units.

From this it is possible to calculate the nanotube content in the carbon soot. As described above we can obtain a *NSI* for the nanotube component in the carbon soot. This was measured as 0.53 for the 1.5 mg of carbon soot dispersed in toluene, giving a nanotube component in this sample of carbon soot a mass of $m_n = S_n/k_n = 0.53/1.04\ mg^{-1} = 0.51$ mg. This allows us to calculate the nanotube content of the carbon soot as 34%. This value is consistent with estimates of nanotube content in various carbon soots from scanning electron microscopy and transmission electron microscopy.

In conclusion we have demonstrated a preparation method which allows us to isolate nanotubes from unwanted carbon components with a high nanotube yield. This allows us to use EPR and TGA to calculate the nanotube content (purity) of the soot. For the carbon soot used in this study, the nanotube content was 34% by mass.

While calculation of carbon soot purity is the most obvious benefit of this technique many other potential advantages exist. To date no technique exists which can give quantitative measurements of nanotube content in any environment. In the past nanotube researchers in all fields have relied on purely qualitative methods such as measuring ratios of ill-defined Raman peaks or counting nanotubes in SEM or TEM micrographs. This present technique will eradicate these issues and finally solve the fundamental problem of high yield nanotube extraction. Furthermore we believe that this work is the first step toward the ability to design specific polymer architectures to select tubes of given chirality or diameter. This is considered to be one of the most important potential developments needed to make nanoelectronics using nanotubes a reality.

The authors wish to thank the Irish Higher Educational Authority for partly funding this work.

Notes and references

1 S. J. Tans, A. R. M. Verschueren and C. Dekker, *Nature*, 1998, **393**, 49.
2 J. Hu, M. Ouyang, P. Yang and C. M. Lieber, *Nature*, 1999, **399**, 48.
3 J. Li, A. M. Cassell and H. Dai, *Surf. Interface Anal.*, 1999, **28**, 8.
4 P. Wagner, S. Nock, J. A. Spudich, W. D. Volkmuth, S. Chu, R. L. Cicero, C. P. Wade, M. R. Linford and C. E. D. Chidsey, *J. Struct. Biol.*, 1997, **119**, 18.
5 F. Balavoine, C. Richard, T. W. Ebbesen, C. Mioskowski and P. Schulz, *Biol. Cell*, 1998, **90**, 283.
6 S. Bandow, *J. Appl. Phys.*, 1996, **80**, 1020.
7 T. W. Ebbesen, P. M. Ajayan, H. Hiura and K. Tanigaki, *Nature*, 1994, **367**, 519.
8 G. S. Duesberg, M. Burghard, J. Muster, G. Philipp and S. Roth, *Chem. Commun.*, 1998, **3**, 435.
9 W. Holzer, A. Penzkofe, S. H. Gong, A. Bleyer and D. D. C. Bradley, *Adv. Mater.*, 1996, **8**, 974.
10 W. Krätschmer, L. D. Lamb, K. Fostiropoulos and D. R. Huffman, *Nature*, 1990, **347**, 354.
11 O. Chauvet, L. Forro, W. Bacsa, D. Ugarte, B. Doudin and W. A. de Heer, *Phys. Rev. B.*, 1995, **52**, R6963.

ChemComm

Intramolecular benzylic C–H activation: palladium-catalyzed synthesis of hexahydromethanofluorenes†

Marta Catellani,*[a] Elena Motti[a] and Stefano Ghelli[b]

[a] *Dipartimento di Chimica Organica e Industriale dell'Università, Parco Area delle Scienze, 17/A, I-43100 Parma, Italy. E-mail: catell@unipr.it*
[b] *Spin Co., Via Tamagno, 3, I-42048 Rubiera, Italy*

Received (in Cambridge, UK) 28th June 2000, Accepted 5th September 2000
First published as an Advance Article on the web 27th September 2000

C–H activation of benzylic methyl groups has been realized catalytically under mild conditions through intramolecular reaction on a palladium complex.

Aromatic and aliphatic C–H activation catalyzed by transition metal complexes is an area of increasing interest in view of the elaboration of selective methodologies for the functionalisation of arenes and alkanes.[1] Cyclometallation and, in particular, cyclopalladation reactions are valuable tools to achieve intramolecular C–H bond cleavage.[1f–h]

We previously reported[2] a new methodology for selective aromatic substitution which implies C–H activation and *o*,*o*′-dialkylation of the hexahydropalladafluorene **1**. As shown in the simplified Scheme 1, the reaction proceeds through oxidative addition of alkyl halides, alkyl group migration on the aryl site of the palladacycle **1** and spontaneous expulsion of norbornene **4** to give the *o*,*o*′-dialkylated arylpalladium species **3**.

The reaction could be made catalytic by causing the final complex **3** to undergo further reaction so that palladium(0) could be formed.[3] An example is shown by the reaction of iodobenzene, *n*-propyl bromide, norbornene and phenylboronic acid to form 2,6-di-*n*-propyl-1,1′-biphenyl in 90% isolated yield.[3c]

We have now found that in the presence of a methyl group the reaction can take a completely different course, norbornene no longer being expelled as in Scheme 1, but instead undergoing ring closure on the methyl group.

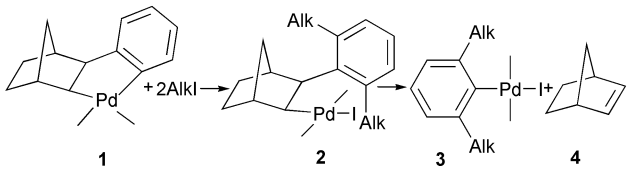

Scheme 1

Compounds **6** and **7** (Scheme 2) are formed by heating an *N*,*N*-dimethylformamide (DMF, 5 mL) solution of norbornene (49 mg, 0.52 mmol) and *o*,*o*′-dimethyliodobenzene (103 mg, 0.44 mmol) at 105 °C for 18 h under nitrogen in the presence of $Pd(OAc)_2$ (10 mg, 0.044 mmol) as the catalyst and K_2CO_3 (61 mg, 0.44 mmol) as the base. *cis*,*exo*-Hexahydromethanofluorenes **6** (30%) and **7** (two diastereoisomers, 11%) correspond to palladium-catalyzed C–H activation of a benzylic methyl group. Yields of **6** and **7** could be raised to 60 and 28%, respectively, by using KOAc instead of K_2CO_3 as a base.

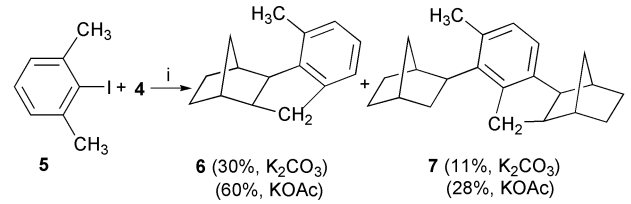

Scheme 2 *Reagents and conditions*: i, 10% mol $Pd(OAc)_2$, KOAc, DMF, N_2, 18 h, 105 °C, 91% conversion.

† Electronic supplementary information (ESI) available: selected spectroscopic data for compounds **6**, **7**, **15** and **16**. See http://www.rsc.org/suppdata/cc/b0/b005182i/

The positive influence of KOAc on the conversion of the disubstituted aryl iodide **5** could be ascribed to the favourable action exerted by the acetate anion on norbornene insertion,[4] this step being adversely affected by the steric hindrance of the two *ortho* methyl groups. The proposed course of the reaction leading to compounds **6** and **7** is shown in Scheme 3.

Complex **2** (Alk = CH_3) instead of undergoing norbornene deinsertion as previously observed (see Scheme 1), prefers to activate the methyl group to give the palladacyclohexene complex **8**. This means that the tendency of palladium to react with a suitably positioned methyl group, possibly through agostic interaction,[1h,5] is strong enough relative to C–C bond cleavage so preventing norbornene deinsertion. Complex **8** can either undergo $C(sp^3)$–$C(sp^3)$ coupling to give compound **6** or ring opening catalyzed by protonic species HX in the manner previously described[6] and thoroughly investigated by Carmona's group in a recent study.[7] Norbornene then inserts into the new alkylpalladium complex **9** to form **10**; the latter gives the new disubstituted *cis*,*exo*-hexahydromethanofluorene **7** through the intermediacy of a six-membered palladacycle of type **11**.

Since compound **7** must originate from a benzylpalladium complex of type **9**, which in turn requires the palladacyclohex-

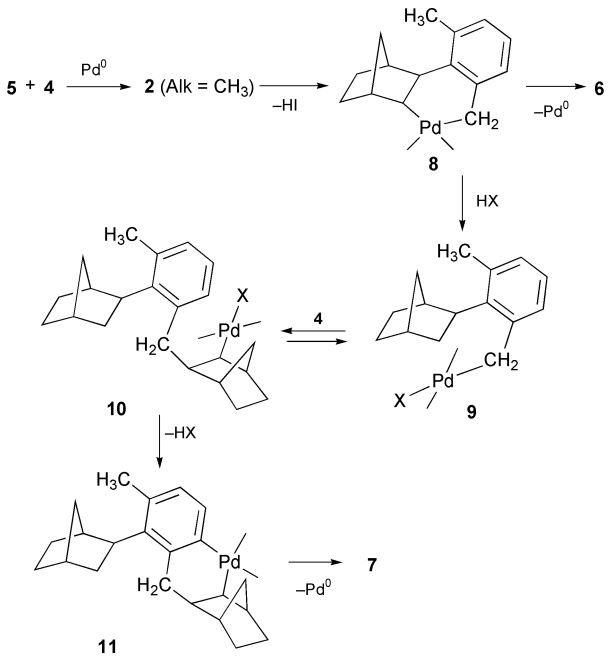

Scheme 3 Proposed mechanism for the palladium-catalyzed synthesis of **6** and **7**. Solvent or reagent molecules as ligands are omitted for simplicity.

DOI: 10.1039/b005182i

ene **8** as precursor, its presence unequivocally confirms the proposed mechanism.

The reaction shows some analogy with those of *o*-*tert*-butyliodobenzene and *o*-iodoanisole described by Dyker[8] which, however, imply palladium-catalyzed C–H activation at a *tert*-butyl group and at a methoxy group, respectively, and end up with a $C(sp^3)$–$C(sp^2)$ ring closure.

To further support these results we carried out the stoichiometric reaction of the dimeric *o*-tolylnorbornylpalladium chloride complex **2** (one Alk = CH_3, the other being H)[9] (52 mg, 0.08 mmol) with methyl iodide (23 mg, 0.16 mmol) in the presence of K_2CO_3 (33 mg, 0.24 mmol) in DMF (5 mL) at room temperature for 5 h under nitrogen. The cyclopentene derivative **6** was obtained in 73% yield.

At this point we wondered whether a catalytic reaction involving benzylic activation could be possible also using *o*-iodotoluene in place of *o*,*o*′-dimethyliodobenzene. Poor results were obtained with KOAc while using K_2CO_3 led to the formation of four products. Thus compounds **15**–**18** (Scheme 4) were obtained by heating a DMF (25 mL) solution of norbornene (57 mg, 0.6 mmol) and *o*-iodotoluene (109 mg, 0.5 mmol) in the presence of $Pd(OAc)_2$ (11 mg, 0.05 mmol) as catalyst and K_2CO_3 (70 mg, 0.5 mmol) as the base under the conditions previously reported. The formation of products **15** (63%) and **16** (two diastereoisomers, 5%) implies the same type of C–H activation of a benzylic methyl group as observed for **6** and **7**.

The reaction pathway involves the intermediacy of palladacycle **13** and its further reaction with a second molecule of *o*-iodotoluene to form eventually **14**.[9c] Once the *o*,*o*′-disubstituted aromatic is formed the reaction proceeds as shown in Scheme 3 for *o*,*o*′-dimethyliodobenzene.

Although the cyclisation reaction leading to **15** could be expected to occur between one molecule of iodotoluene and one of norbornene, it surprisingly takes place only after a second tolyl unit has been introduced into the free *ortho* position. This fact can be explained considering that, as long as one *ortho* methyl group only is present, coordination with the aromatic ring is preferred. This point has been recently highlighted by Crabtree and coworkers.[1g,10]

The formation of **17** (10%)[11] and **18** (two diastereoisomers, 4%) does not involve benzylic C–H activation. However, since it can readily be explained according to a pathway previously described,[11] it will not be examined further. Yields are strongly influenced by reaction conditions (such as temperature, concentration, solvent) as well as by the base used and the addition of ligands and salts. For example by adding tetrabutylammonium bromide to the reaction mixture, compound **16** becomes the main product, being obtained in 37% yield together with compounds **15**, **17** and **18** in 23, 6 and 14% yield, respectively.

Compounds **6**, **7**, **15** and **16** were fully characterised by spectroscopic methods and by elemental analysis (ESI).†

In conclusion we have shown that C–H bonds of benzylic methyl groups can be activated catalytically with formation of cyclopentene rings. The use of the appropriate organometallic precursors allows the reaction to occur stoichiometrically even at room temperature. The generality of the reaction is being investigated.

This work was supported by Italian MURST and CNR (Rome).

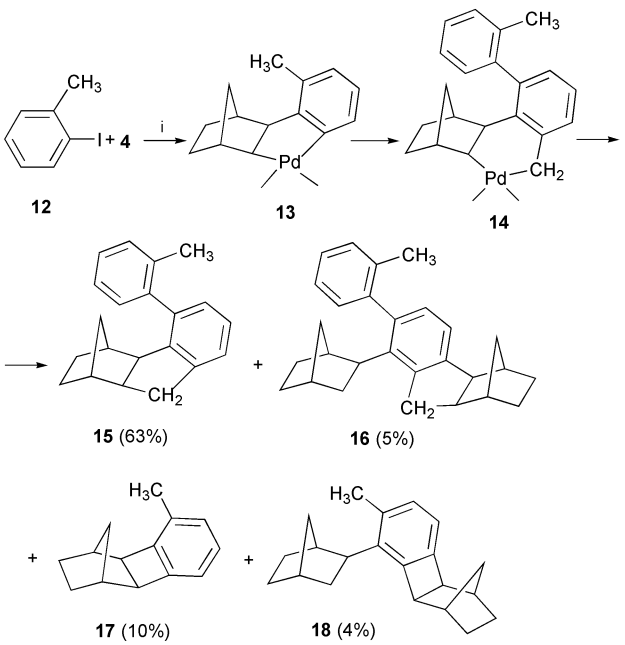

Scheme 4 *Reagents and conditions*: i, 10% mol $Pd(OAc)_2$, K_2CO_3, DMF, N_2, 18 h, 105 °C, 93% conversion.

Notes and references

1 (*a*) G. Dyker, *Angew. Chem., Int. Ed.*, 1999, **38**, 1698; (*b*) A. E. Shilov and G. B. Shul'pin, *Chem. Rev.*, 1997, **97**, 2879; (*c*) R. G. Bergman, *Acc. Chem. Res.*, 1995, **28**, 154; (*d*) A. Sen, *Acc. Chem. Res.*, 1988, **21**, 421; (*e*) R. H. Crabtree, *Chem. Rev.*, 1985, **85**, 245; (*f*) J. Dehand and M. Pfeffer, *Pure Appl. Chem.*, 1992, **3**, 335; (*g*) A. D. Ryabov, *Chem. Rev.*, 1990, **90**, 403; (*h*) M. Brookhart and M. L. H. Green, *J. Organomet. Chem.*, 1983, **250**, 395.

2 M. Catellani and M. C. Fagnola, *Angew. Chem., Int. Ed. Engl.*, 1994, **33**, 2421.

3 (*a*) M. Catellani, F. Frignani and A. Rangoni, *Angew. Chem., Int. Ed. Engl.*, 1997, **36**, 119; (*b*) M. Catellani and F. Cugini, *Tetrahedron*, 1999, **55**, 6595; (*c*) M. Catellani, E. Motti and M. Minari, *Chem. Commun.*, 2000, 157; (*d*) M. Lautens and S. Piguel, *Angew. Chem., Int. Ed.*, 2000, **39**, 1045.

4 M. C. Gallazzi, L. Porri and G. Vitulli, *J. Organomet. Chem.*, 1975, **97**, 131.

5 W. Baratta, E. Herdtweck and P. Rigo, *Angew. Chem., Int. Ed.*, 1999, **38**, 1629; M. A. Cinellu, G. Minghetti, M. V. Pinna, S. Stoccoro, A. Zucca and M. Manassero, *J. Chem. Soc., Dalton Trans.*, 1999, 2823; H. D. Empsall, P. N. Neys and B. L. Shaw, *J. Chem. Soc., Dalton Trans.*, 1978, 257; A. Immirzi and A. Musco, *J. Chem. Soc., Chem. Commun.*, 1974, 400.

6 G. Bocelli, M. Catellani and G. P. Chiusoli, *J. Organomet. Chem.*, 1985, **279**, 225; B. A. Markies, P. Wijkens, H. Kooijman, A. L. Spek, J. Boersma and G. van Koten, *J. Chem. Soc., Chem. Commun.*, 1992, 1420; A. J. Canty and G. van Koten, *Acc. Chem. Res.*, 1995, **28**, 406.

7 J. Cámpora, J. A. López, P. Palma, P. Valerga, E. Spillner and E. Carmona, *Angew. Chem., Int. Ed.*, 1999, **38**, 147.

8 G. Dyker, *Angew. Chem., Int. Ed. Engl.*, 1994, **33**, 103; G. Dyker, *Angew. Chem., Int. Ed. Engl.*, 1992, **31**, 1023.

9 (*a*) C.-S. Li, C.-H. Cheng, F.-L. Liao and S.-L. Wang, *J. Chem. Soc., Chem. Commun.*, 1991, 710; (*b*) M. Portnoy, Y. Ben-David, I. Rousso and D. Milstein, *Organometallics*, 1994, **13**, 3465; (*c*) M. Catellani and E. Motti, *New J. Chem.*, 1998, 759.

10 M. Lavin, E. M. Holt and R. H. Crabtree, *Organometallics*, 1989, **8**, 99.

11 M. Catellani, G. P. Chiusoli and L. Ferioli, *Synthesis*, 1996, **286**, 769.

A novel C–C bond formation by Baylis–Hillman type reaction mediated by SmI_2: an effective approach to α-hydroxyalkylacrylamide synthesis

So Won Youn, Heui Sul Park and Yong Hae Kim*

Center for Molecular Design & Synthesis and Department of Chemistry, Korea Advanced Institute of Science and Technology, 373-1, Kusong Dong, Yusong Gu, Taejon, 305-701, Korea. E-mail: kimyh@sorak.kaist.ac.kr

Received (in Cambridge, UK) 15th August 2000, Accepted 5th September 2000
First published as an Advance Article on the web 28th September 2000

α-Bromoacrylamides (1) reacted with aldehydes or ketones, in the presence of SmI_2 at −78 °C in THF, within 5 min to produce Baylis–Hillman type reaction products (2) through an anionic process using vinylsamarium Grignard species in good yields (52–89%).

The construction of C–C bonds has been one of the most fundamental reactions in organic synthesis. The Baylis–Hillman reaction[1] produces multifunctional molecules that can be used for the synthesis of natural and unnatural products[2] through C–C bond formation between the α-position of activated alkene and carbon electrophiles having an electron-deficient sp^2 carbon atom under a basic catalyst, in particular a tertiary amine. But the reaction suffers from being inconveniently slow.[1] Furthermore, under normal circumstances acrylamides, crotonic derivatives, and ketones are inert substrates for the Baylis–Hillman reaction.[1,3] Therefore a number of attempts[2g,4,5] have been made to provide the corresponding adduct including the use of microwave irradiation and high pressure.[6]

Samarium diiodide has become a useful reagent for various organic reactions.[7] Especially, SmI_2 can be used to generate radicals and to reduce alkyl radicals to alkylsamarium reagents that can be trapped by a variety of electrophiles to form a new C–C bond.[7–9] However, there have been arguments that in general, vinyl- and aryl radicals do not usually undergo further reduction to vinyl- or arylsamarium reagents.[9] We report here the first example of reactions *via* vinylsamarium species.

It has been found that α-bromoacrylamides (**1**) reacted with a variety of aldehydes or ketones in the presence of SmI_2 to give α-hydroxyalkylacrylamides (Baylis–Hillman adducts, **2**) within 5 min at −78 °C in THF in good yields (Scheme 1).

The reaction works best when 1 eq. of aldehyde and 3 eq. of SmI_2 are used in THF (run 2–5, Table 1). The crotonic derivative gave only the (*Z*)-isomer which was readily confirmed by ^1H NMR spectroscopy[5a,b,d,f] and a variety of aldehydes and enolizable ketones also proceeded successfully in good yields. The results obtained are summarized in Table 1. Benzaldehyde and α,β-unsaturated carbonyl compounds are reduced to the corresponding alcohols without undergoing Baylis–Hillman type reaction: reduction of carbonyl groups must be faster than Baylis–Hillman type reaction.

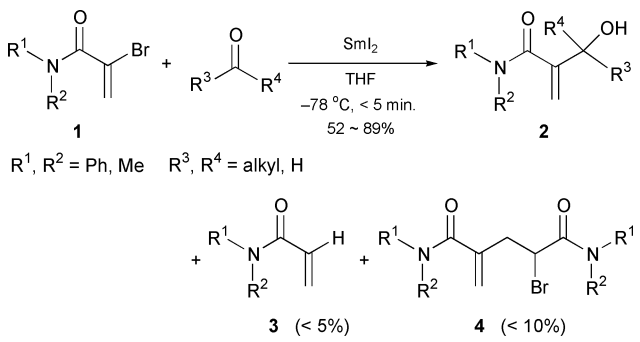

Scheme 1

Table 1 The reactions of acrylamides with various aldehydes and ketones[a]

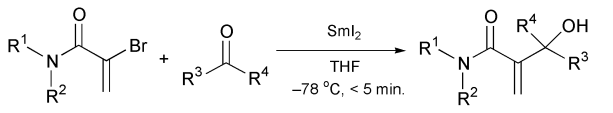

Run	Acrylamide	R^3	R^4	Product	Yield[b] (%)
1		Me	H	**2a**	81
2		Et	H	**2b**	19[c]
3		Et	H	**2b**	43[d]
4		Et	H	**2b**	51[c]
5	**1a**	Et	H	**2b**	62
6		$PhCH_2CH_2$	H	**2c**	70
7		c-Hex	H	**2d**	88
8		t-Bu	H	**2e**	63
9		Me	Et	**2f**	89
10		Me	CH_2CO_2Me	**2g**	52
11		Me	CH_2Ph	**2b**	62
12		$-(CH_2)_4-$		**2i**	63
13		Et	H	**2j**	76
14		c-Hex	H	**2k**	77
15		t-Bu	H	**2l**	77
16	**1b**	Me	Et	**2m**	73
17		Et	H	**2n**	81
18	**1c**	c-Hex	H	**2o**	53

[a] All reactions were performed with SmI_2 (3 eq.) and aldehyde or ketone (1 eq.) in THF at −78 °C, unless otherwise noted. [b] Isolated Yields. [c] Performed with SmI_2 (1 eq.). [d] Performed with SmI_2 (2 eq.). [e] Performed with SmI_2 (2.5 eq.).

Here a question is raised as to whether the reaction proceeds *via* anionic or radical species. Treatment of **1a** with SmI_2 (3 eq.)–CD_3OD (1 eq.) in THF afforded **3a** (67%, 80% deuterated product) as the main product as shown in eqn. 1. The amount of

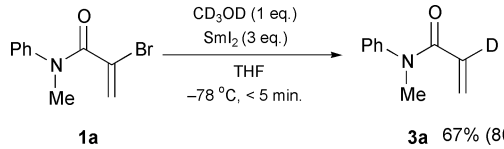

(1)

deuterium incorporation was determined by ^1H NMR and mass spectroscopy. On the other hand, when **1a** was treated with SmI_2 (1 eq.) and THF-d_8 as a solvent, no deuterated acrylamide was detected, whereas α-bromoacrylamides acted as an electrophile to form **4a** (eqn. 2).[7a,10] If the vinyl radical species (**A**) exists for long time it should abstract one D from THF-d_8. If the reaction undergoes samarium Grignard type reaction, it should require more than 2 eq. of SmI_2 to consume the starting acrylamide.

DOI: 10.1039/b006495p

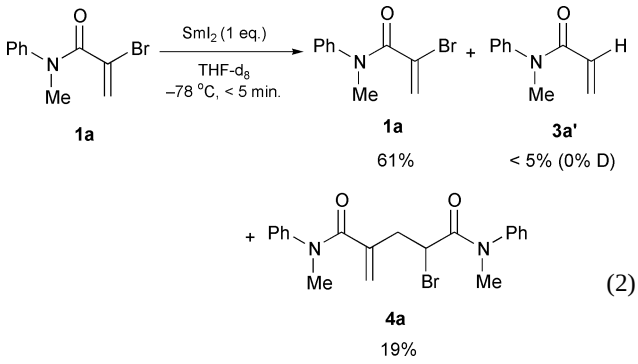

Judging from the three observations, an anion species (**B**) appears to be involved in the reaction (Fig. 1). The reaction might proceed *via* an allenoate intermediate (**C**).[5,11] Ethyl α-bromoacrylate or 2-bromocyclohex-2-en-1-one did not give the desired products. A phenyl group in the amide seems to enable the formation of the vinylsamarium intermediate (**B**). The α-carbon of the acrylamide bearing phenyl group is more electron-deficient than other moieties bearing alkyl or hydrogen. Therefore, the vinyl radical can undergo further reduction to vinylsamarium reagent **B** by a further mole of SmI_2. These results imply that the reduction of the vinyl radical should be faster than hydrogen abstraction from THF. To our knowledge, *this is the first example of the generation of the vinyl samarium intermediate by means of the reduction of bromovinyl compounds!* It is noteworthy that the reaction with enolizable ketones also affords the Baylis–Hillman products.

In summary, it has been demonstrated that the reaction of α-bromoacrylamides with aldehydes or ketones in the presence of SmI_2 can provide Baylis–Hillman adducts through an anionic process, solving several problems of Baylis–Hillman reaction. Baylis–Hillman reactions require long reaction times and a tertiary amine as a catalyst and its scope is limited to aldehydes as acrylamides, crotonic derivatives and ketones are not reactive. However, a Baylis–Hillman type reaction mediated by SmI_2 is available for both aldehydes and ketones under mild reaction conditions and with short reaction times.

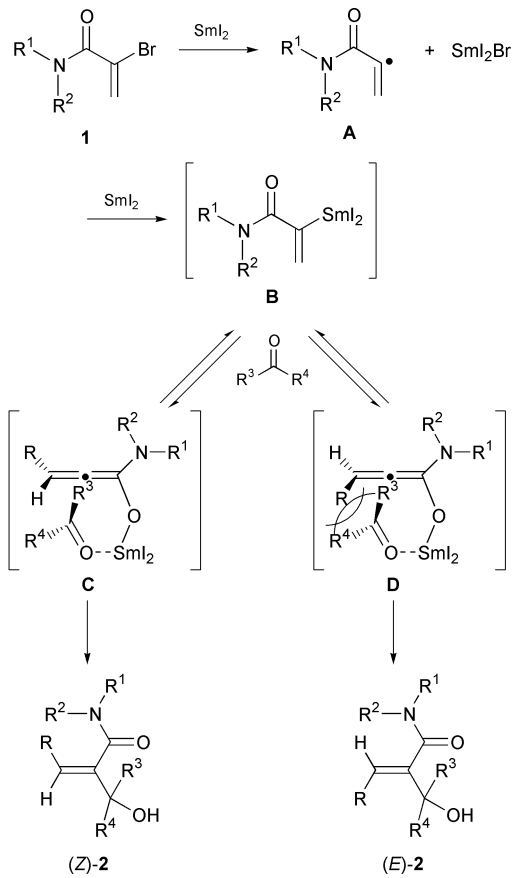

Fig. 1 Possible mechanism.

This work was partially supported by graduate School of Molecular Science of MOE.

Notes and references

1 Reviews: (*a*) D. Basavaiah, P. D. Rao and R. S. Hyma, *Tetrahedron*, 1996, **52**, 8001; (*b*) S. E. Drewes and G. H. P. Roos, *Tetrahedron*, 1988, **44**, 4653; (*c*) E. Ciganek, in *Organic Reactions*, ed. L. A. Paquette, John Wiley & Sons, New York, 1997, vol. 51, pp. 201 and references cited therein.

2 (*a*) J. M. Brown, *Angew. Chem., Int. Ed. Engl.*, 1987, **26**, 190; (*b*) A. H. Hoveyda, D. A. Evans and G. C. Fu, *Chem. Rev.*, 1993, **93**, 1307; (*c*) T. Jenn and D. Heissler, *Synlett*, 1995, 607; (*d*) R. Annunziata, M. Benaglia, M. Cinquini, F. Cozzi and L. Raimond, *J. Org. Chem.*, 1995, **60**, 4697; (*e*) P. Perlmutter and M. Tabone, *J. Org. Chem.*, 1995, **60**, 6515; (*f*) C. M. Marson, J. H. Pink and C. Smith, *Tetrahedron Lett.*, 1995, **36**, 8107; (*g*) Y. Génisson, C. Massardier, I. Gantier-Luneau and A. E. Greene, *J. Chem. Soc., Perkin Trans. 1*, 1996, 2869; (*h*) D. Basavaiah, M. Bakthadoss and S. Pandiaraju, *Chem. Commun.*, 1998, 1639.

3 M. L. Bode and P. T. Kaye, *J. Chem. Soc., Perkin Trans. 1*, 1993, 1809.

4 (*a*) M. Brand, S. E. Drewes, N. D. Emslie and A. A. Khan, *Synth. Commun.*, 1991, **21**, 727; (*b*) J. Auge, N. Lubin and A. Lubineau, *Tetrahedron Lett.*, 1994, **35**, 7947; (*c*) V. K. Aggarwal, G. J. Tarver and R. McCague, *Chem. Commun.*, 1996, 2713; (*d*) S. Rafel and J. W. Leahy, *J. Org. Chem.*, 1997, **62**, 1521; (*e*) T. Kataoka, T. Iwama and S. Tsujiyama, *Chem. Commun.*, 1998, 197; (*f*) V. K. Aggarwal, A. Mereu, G. J. Tarver and R. McCague, *J. Org. Chem.*, 1998, **63**, 7183.

5 For methods using Al, Cu, and others: (*a*) Y. Sato and S. Takeuchi, *Synthesis*, 1983, 734; (*b*) J. P. Marino and R. J. Linderman, *J. Org. Chem.*, 1983, **48**, 4621; (*c*) T. Tsuda, T. Yoshida and T. Saegusa, *J. Org. Chem.*, 1988, **53**, 1037; (*d*) G. Li, H.-X. Wei and S. Willis, *Tetrahedron Lett.*, 1998, **39**, 4607; (*e*) H.-X. Wei, S. Willis and G. Li, *Tetrahedron Lett.*, 1998, **39**, 8203; (*f*) P. V. Ramachandran, M. V. R. Reddy, M. T. Rudd and J. R. De Alaniz, *Tetrahedron Lett.*, 1998, **39**, 8791; (*g*) G. Li, H.-X. Wei, B. R. Whittlesey and N. N. Batrice, *J. Org. Chem.*, 1999, **64**, 1061; (*h*) H.-X. Wei, J. D. Hook and K. A. Fitzgerald, *Tetrahedron: Asymmetry*, 1999, **10**, 661.

6 (*a*) J. S. Hill and N. S. Isaacs, *Tetrahedron Lett.*, 1986, **27**, 5007; (*b*) J. S. Hill and N. S. Isaacs, *J. Chem. Res. (S)*, 1988, 330; (*c*) G. H. P. Roos and P. Rampersadh, *Synth. Commun.*, 1993, **23**, 1261; (*d*) M. K. Kunda, S. B. Mukherjee, N. Balu, R. Padmakumar and S. V. Bhat, *Synlett*, 1994, 444.

7 Recent reviews: (*a*) G. A. Molander, *Chem. Rev.*, 1992, **92**, 29; (*b*) D. P. Curran, T. L. Fevig, C. P. Jasperse and M. J. Totleben, *Synlett*, 1992, 943; (*c*) G. A. Molander, in *Organic Reactions*, ed. L. A. Paquette, John Wiley & Sons, New York, 1994, vol. 46, pp. 211; (*d*) G. A. Molander and C. R. Harris, *Chem. Rev.*, 1996, **96**, 307; (*e*) T. Skrydstrup, *Angew. Chem., Int. Ed. Engl.*, 1997, **36**, 345; (*f*) G. A. Molander and C. R. Harris, *Tetrahedron*, **1998**, **54**, 3321; (*g*) A. Krief and A.-M. Laval, *Chem. Rev.*, 1999, **99**, 745 and references cited therein.

8 (*a*) G. A. Molander and C. Kenny, *J. Am. Chem. Soc.*, 1989, **111**, 8236; (*b*) G. A. Hasegawa and D. P. Curran, *Tetrahedron Lett.*, 1993, **34**, 1717.

9 (*a*) M. Matsukawa, J. Inagana and M. Yamaguchi, *Tetrahedron Lett.*, 1987, **28**, 5877; (*b*) J. Inagana, M. Ishikawa and M. Yamaguchi, *Chem. Lett.*, 1987, 1485; (*c*) T. L. Fevig, R. L. Elliott and D. P. Curran, *J. Am. Chem. Soc.*, 1988, **110**, 5064; (*d*) D. P. Curran and B. Yoo, *Tetrahedron Lett.*, 1992, **33**, 6931; (*e*) D. P. Curran and M. J. Totleben, *J. Am. Chem. Soc.*, 1992, **114**, 6050; (*f*) M. Kunishima, K. Hioki, S. Tani and A. Kato, *Tetrahedron Lett.*, 1994, **35**, 7253; (*g*) L. Capella and P. C. Montevecchi, *Tetrahedron Lett.*, 1994, **35**, 8445; (*h*) L. Capella, P. C. Montevecchi and M. L. Navacchia, *J. Org. Chem.*, 1995, **60**, 7424; (*i*) X. H. Du and R. W. Armstrong, *Tetrahedron Lett.*, 1998, **39**, 2281.

10 Organosamarium intermediates appear to be initiated but unstable in solution.[7] In the absence of electrophiles such as aldehydes or ketones, the organosamarium species reacted with the substrate itself to form **4a** together with the dehalogenated byproduct **3a′**.

11 (*a*) J. P. Marino and R. J. Linderman, *J. Org. Chem.*, 1981, **46**, 3696; (*b*) T. Tsuda, T. Yoshida, T. Kawamoto and T. Saegusa, *J. Org. Chem.*, 1987, **52**, 1624.

ChemComm

Enantiomerically-enriched organic reagents *via* polymer synthesis: enantioselective copolymerization of cycloalkene oxides and CO_2 using homogeneous, zinc-based catalysts†

Ming Cheng, Nicholas A. Darling, Emil B. Lobkovsky and Geoffrey W. Coates*

Department of Chemistry and Chemical Biology, Baker Laboratory, Cornell University, Ithaca, NY 14853, USA. E-mail: gc39@cornell.edu

Received (in Irvine, CA, USA) 3rd July 2000, Accepted 18th August 2000
First published as an Advance Article on the web

Enantiomerically pure zinc complexes have been designed and synthesized for the enantioselective copolymerization of cycloalkene oxides and CO_2.

The desymmetrization of *meso* molecules with chiral catalysts or reagents is rapidly emerging as valuable strategy for the synthesis of enantiomerically-enriched products.[1,2] *Meso* epoxides are particularly attractive substrates for desymmetrization reactions: ring-opening with a variety of nucleophiles yields a range of valuable synthetic intermediates.[3] Remarkable advances in the development of chiral catalysts have yielded highly enantioselective systems for the delivery of halide, azide, alcohol, thiol, cyano and carboxylic acid nucleophiles to epoxides. Despite the recent intense interest in developing enantioselective catalysts for the synthesis of optically-active polymers,[4,5] there are few examples of *meso*-desymmetrization in polymerization reactions.[6,7] We have recently developed a new class of single-site catalysts (**1**, Scheme 1)[8] for the

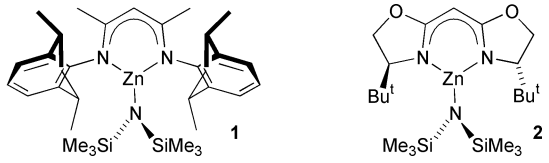

Scheme 1

copolymerization of CO_2 and cyclohexene oxide (CHO); (Scheme 2).[9,10] Following reaction of the amido ligand with CO_2, extrusion of trimethylsilyl isocyanate and reinsertion of CO_2,[11–13] the ring-opening of the epoxide monomer in this system occurs with inversion of stereochemistry thus producing stereogenic centers in the polymer backbone. We reasoned that a chiral ligand set would have the potential to control the

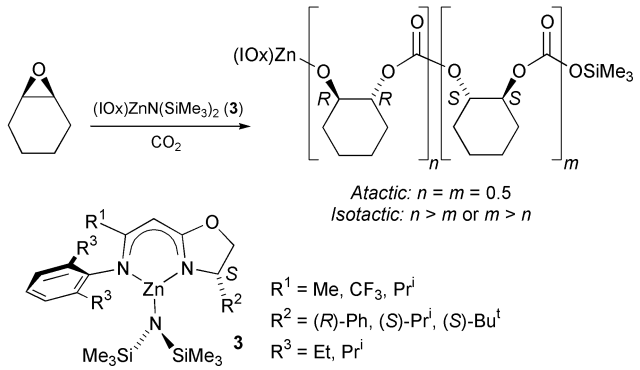

Scheme 2

† Electronic supplementary information (ESI) available: experimental procedures, X-ray data for and molecular structure of **3e**, and characterization data of CHO/CO_2 polymers. See http://www.rsc.org/suppdata/cc/b0/b005537i/

absolute stereochemistry of the ring-opening process, and that hydrolysis of the resultant polycarbonate[14] would yield valuable enantiomerically-enriched diols.[8] During the course of our research Nozaki and coworkers reported a chiral catalyst system for the enantioselective copolymerization of CO_2 and CHO,[15] prompting us to communicate our preliminary results. Herein we report a chiral, homogeneous catalyst system which exhibits unprecedented activity, stereoselectivity and molecular weight control for the polymerization of CO_2 with both cyclopentene and cyclohexene oxide, even under mild reaction conditions.

Owing to the well-defined nature of β-diiminate zinc complexes (**1**) for the synthesis of aliphatic polycarbonates, we first decided to investigate structurally-related bisoxazoline-derived zinc complexes (**2**) to attempt stereochemical control. Complex **2** was readily formed in quantitative yield from the reaction of the bisoxazoline ligand with $Zn[N(SiMe_3)_2]_2$. Despite the structural similarity of the diimine and bisoxazoline ligands, complex **2** is inactive for the copolymerization of CO_2 and CHO at 20 °C. Although the cause of inactivity is currently unknown, we believe that either decomposition to a bis-ligated zinc species or irreversible aggregation of the catalytic species occurs early in the polymerization reaction. To impede such deleterious processes we designed a hybrid imine–oxazoline ligand (IOx) that is sterically incapable of forming strongly aggregated or bis-ligated complexes (**3**, Scheme 2). Despite lacking the high symmetry which is often the hallmark of highly selective catalysts, these ligands have the advantage that efficient synthetic strategies allow the systematic variation of the ligand structure to optimize catalyst behavior. The ligands are formed by the nucleophilic attack of imidoyl chlorides with chiral, deprotonated 2-methyloxazolines.[16–18] Reaction of the ligand with $Zn[N(SiMe_3)_2]_2$ gives **3** in quantitative yield.

Complexes of type **3** are active catalysts for the copolymerization of cycloalkene oxides and CO_2 (Table 1). In general, the reaction of a 2.5 M solution of CHO in toluene under 100 psi of CO_2 at 20 °C using 1 mol% **3** yields an alternated polycarbonate (ether linkages cannot be detected by ^{1}H NMR) with narrow molecular weight distribution (M_w/M_n is significantly less than 2). To optimize this class of catalysts with respect to stereoselectivity, we employed a condensed version of an improvement strategy earlier described by Snapper and Hoveyda.[19,20] By investigating the variation of substituent R^1 (**3a** Me; **3b** CF_3; **3c** Pr^i) while keeping the structures of R^2 (*R*-Ph) and R^3 (Pr^i) constant, we found that the methyl and isopropyl substituents had the best enantioselectivities. Owing to the higher activity of **3c**, we selected the isopropyl group as the substituent to fix at R^1. To probe the effect of R^2 on stereoselectivity, we examined ligands whose chirality was derived from phenylglycine (**3c**), valine (**3d**), and *tert*-leucine (**3e**). Interestingly, complex **3e** exhibits both the highest activity and stereoselectivity, producing a quantitative yield of polymer with an *RR*:*SS* ratio of 86:14. With R^1 fixed as isopropyl and R^2 set as *tert*-butyl, we investigated the effect of varying R^3. Unfortunately, modification of the *ortho*-aryl with the less bulky ethyl group significantly diminishes the activity and slightly decreases the stereoselectivity of the catalyst. Owing to

Table 1 Enantioselective copolymerization of cycloalkene oxides and CO_2 using **3**[a]

Catalyst	R^1	R^2	R^3	Monomer[b]	*t*/h	Conversion (%)	M_n ($\times 10^{-3}$)[c] (g mole^{-1})	M_w/M_n[c]	*RR*:*SS* (*n*:*m*)[d]
3a	Me	(*R*)-Ph	Pr^i	CHO	24	17	1.37	1.24	29:71
3b	CF_3	(*R*)-Ph	Pr^i	CHO	10	100	11.8	1.13	39:61
3c	Pr^i	(*R*)-Ph	Pr^i	CHO	24	45	7.69	1.12	31:69
3d	Pr^i	(*S*)-Pr^i	Pr^i	CHO	24	26	4.81	1.20	82:18
3e	Pr^i	(*S*)-Bu^t	Pr^i	CHO	24	100	14.7	1.35	86:14
3f	Pr^i	(*S*)-Bu^t	Et	CHO	24	23	3.56	1.13	84:16
3g	CF_3	(*S*)-Bu^t	Pr^i	CHO	10	100	27.1	1.78	82:18
3e	Pr^i	(*S*)-Bu^t	Pr^i	CPO	24	48	12.4	1.21	88:12

[a] All reactions performed in 2.5 M epoxide solution (toluene) at 20 °C and 100 psi CO_2 using 1 mol % catalyst. [b] CHO = cyclohexene oxide; CPO = cyclopentene oxide. [c] Measured using gel-permeation chromatography *versus* polystyrene standards. [d] Measured by hydrolyzing the polymer and analyzing the resultant diol by chiral GC.

the high activity of the CF_3-substituted complex **3b**, we decided to investigate the related complex **3g** with the substituents at R^2/R^3 presumably optimized as *tert*-butyl/isopropyl. Although the high activity of the complex was retained, the stereoselectivity of the complex was inferior to that of **3e** (*RR*:*SS* ratio 82:18). Complex **3e** was also investigated for the copolymerization of cyclopentene oxide and CO_2: the polymer formed contained 88% *RR*-units in the main chain. This result represents not only the first successful asymmetric polymerization of this monomer, but also the highest degree of asymmetric induction achieved to date in a CO_2/epoxide copolymerization.

With complex **3e** identified as the most selective catalyst for the copolymerization we obtained a molecular structure of this catalyst precursor using X-ray diffraction.†,‡ Complex **3e** is a rare example of a three-coordinate zinc complex; the steric bulk of the IOx and the amido ligands precludes dimerization or coordination of Lewis-basic solvents. In agreement with other zinc diimine and bisoxazoline complexes, the aryl group is perpendicular to the nearly planar IOx–Zn chelate,[8] and the *tert*-butyl group adopts a staggered conformation. The origins of asymmetric induction are not understood at the current time, although we anticipate that mechanistic studies currently underway on complexes of type **1** will facilitate the more rational design of improved variants of **3**.

We have studied the chemical structure and physical properties of the CHO/CO_2 polymer derived from **3e** in detail. The carbonyl region (δ_C 152–154) of the ^{13}C NMR spectrum of the polymer appears to exhibit partial tetrad resolution based on comparison of experimental and predicted intensities assuming an enantiomorphic-site control mechanism.§ The large peak at δ_C 153.8 is assigned to the chemical shift equivalent m-centered tetrads ([mmm], [mmr] and [rmr]),[15] while the small shifts at δ_C 153.3 and 153.2 are assigned to the [mrm]/[rrr] tetrads (they cannot be unambiguously determined due to their statistical equivalence in the polymer). Finally, the peak at δ_C 153.1 is assigned to the [mrr] tetrad. The T_g and T_m of the polycarbonate are 120 and 220 °C, respectively. The application of these complexes for other asymmetric transformations, as well as the development of improved catalysts for CHO/CO_2 polymerization, is currently underway in our laboratory.

We thank the NSF (Career Award CHE-9875261) and the Cornell University Center for Biotechnology, A New York State Center for Advanced Technology supported by the New York State Science and Technology Foundation and industrial partners for support of this research. This work made use of the Cornell Center for Materials Research facilities (supported by the NSF; DMR-9632275) and the Cornell Department of Chemistry and Chemical Biology X-Ray Facility (supported by the NSF; CHE-9700441). Dr W. Paul Mar (SynChem) generously provided us with a sample of *tert*-leucinol. G. W. C. gratefully acknowledges a Camille and Henry Dreyfus New Faculty Award, a Research Corporation Research Innovation Award, an Alfred P. Sloan Research Fellowship, an Arnold and Mabel Beckman Foundation Young Investigator Award, a Camille Dreyfus Teacher–Scholar Award, a 3M Untenured Faculty Grant, an IBM Partnership Award and a Union Carbide Innovation Recognition Award.

Notes and references

‡ *Crystal data* for **3e**: $C_{30}H_{55}N_3OSi_2Zn$, M = 595.32, monoclinic, space group $P2_1$, a = 11.4881(1), b = 13.9886(1), c = 22.0242(3) Å, U = 3426.23(6) Å^3, T = 173(2) K, Z = 4, μ(Mo-Kα) = 0.811 mm^{-1}, 20704 reflections measured, 14040 unique (R_{int} = 0.0867) which were used in all calculations. Final $wR(F^2)$ was 0.1158 (all data).

CCDC 182/1767. See http://www.rsc.org/suppdata/cc/b0/b005537i/ for crystallographic files in .cif format.

§ The expressions for the tetrad concentrations in terms of the enantioselectivity parameter (α) are: [mmm] = $\alpha^4 + (1-\alpha)^4$; [mmr] = [mrr] = $2[\alpha^3(1-\alpha) + \alpha(1-\alpha)^3]$; [rmr] = [mrm] = [rrr] = $2\alpha^2(1-\alpha)^2$. For the CHO/CO_2 polymer formed using **3e** (α = 0.86), the observed (predicted) tetrad concentrations are: [mmm] + [mmr] + [rmr] = 0.76 (0.76); [rrr]/[mrm] = 0.04 (0.03); [mrm]/[rrr] = 0.02 (0.03); [mrr] = 0.18 (0.18).

1 M. C. Willis, *J. Chem. Soc., Perkin Trans. 1*, 1999, 1765.
2 R. S. Ward, *Chem. Soc. Rev.*, 1990, **19**, 1.
3 D. M. Hodgson, A. R. Gibbs and G. P. Lee, *Tetrahedron*, 1996, **52**, 14361.
4 G. W. Coates, 'Polymerization Reactions' in *Comprehensive Asymmetric Catalysis*, ed. E. N. Jacobsen, A. Pfaltz and H. Yamamoto, Springer, Berlin, 1999, vol. 3, pp. 1329.
5 Y. Okamoto and T. Nakano, *Chem. Rev.*, 1994, **94**, 349.
6 T. M. Ovitt and G. W. Coates, *J. Am. Chem. Soc.*, 1999, **121**, 4072.
7 N. Spassky, P. Dumas, A. Le Borgne, A. Momtaz and M. Sepulchre, *Bull. Soc. Chim. Fr.*, 1994, **131**, 504.
8 M. Cheng, E. B. Lobkovsky and G. W. Coates, *J. Am. Chem. Soc.*, 1998, **120**, 11018.
9 M. S. Super and E. J. Beckman, *Macromol. Symp.*, 1998, **127**, 89.
10 D. J. Darensbourg and M. W. Holtcamp, *Coord. Chem. Rev.*, 1996, **153**, 155.
11 M. Cheng, E. B. Lobkovsky and G. W. Coates, manuscript in preparation.
12 R. A. Andersen, *Inorg. Chem.*, 1979, **18**, 2928.
13 L. R. Sita, J. R. Babcock and R. Xi, *J. Am. Chem. Soc.*, 1996, **118**, 10912.
14 S. Inoue, H. Koinuma, Y. Yokoo and T. Tsuruta, *Makromol. Chem.*, 1971, **143**, 97.
15 K. Nozaki, K. Nakano and T. Hiyama, *J. Am. Chem. Soc.*, 1999, **121**, 11008.
16 S. Fustero, A. Navarro, D. Diaz, M. G. de la Torre, A. Asensio, F. Sanz and M. L. Gonzalez, *J. Org. Chem.*, 1996, **61**, 8849.
17 S. Fustero, M. G. de la Torre, B. Pina and A. S. Fuentes, *J. Org. Chem.*, 1999, **64**, 5551.
18 S. K. Bertilsson, L. Tedenborg, D. A. Alonso and P. G. Andersson, *Organometallics*, 1999, **18**, 1281.
19 B. M. Cole, K. D. Shimizu, C. A. Krueger, J. P. A. Harrity, M. L. Snapper and A. H. Hoveyda, *Angew. Chem., Int. Ed. Engl.*, 1996, **35**, 1668.
20 K. D. Shimizu, B. M. Cole, C. A. Krueger, K. W. Kuntz, M. L. Snapper and A. H. Hoveyda, *Angew. Chem., Int. Ed. Engl.*, 1997, **36**, 1704.

ChemComm

Carbonyl propargylation by 1-substituted prop-2-ynyl mesylates and carbonyl allenylation by 3-substituted prop-2-ynyl mesylates with tin(II) iodide and tetrabutylammonium iodide

Yoshiro Masuyama,*† Akiko Watabe, Akihiro Ito and Yasuhiko Kurusu

Department of Chemistry, Sophia University, 7-1 Kioicho, Chiyoda-ku, Tokyo 102-8554, Japan

Received (in Cambridge, UK) 14th August 2000, Accepted 5th September 2000
First published as an Advance Article on the web 28th September 2000

1-Substituted prop-2-ynyl mesylates cause propargylation of aldehydes with tin(II) iodide, tetrabutylammonium iodide and sodium iodide in 1,3-dimethylimidazolidin-2-one to produce 2-substituted but-3-yn-1-ols, while 3-substituted prop-2-ynyl mesylates cause allenylation of aldehydes under the same conditions as those of the propargylation by 1-substituted prop-2-ynyl mesylates to produce 2-substituted buta-2,3-dien-1-ols.

Table 1 Allenylation by prop-2-ynyl mesylate with SnI_2 and TBAI[a]

R^3	Time/h	Yield (%)[b] **2** + **3**	**2**:**3**[c]
C_6H_5	45	85	78:22
ClC_6H_4	48	80	75:25
$CH_3OC_6H_4$	70	74	78:22
$CH_3(CH_2)_5$	71	66	66:34
c-C_6H_{11}	72	68	81:19

[a] The reaction of prop-2-ynyl mesylate (1.5 mmol) with aldehydes (1.0 mmol) was carried out using SnI_2 (1.5 mmol), TBAI (0.10 mmol) and NaI (1.5 mmol) in DMI (3 ml) at 10 °C. [b] Yields of a mixture of **2** and **3**. [c] The ratio was determined by ^{1}H NMR analysis (JEOL Λ-500).

Alkynes and allenes have formed an attractive chemistry for high reactivities with metal complexes or reagents.[1] Thus, the preparation of alkynes and allenes becomes an important theme. Barbier-type carbonyl propargylation or allenylation with propargylic halides is one of the most convenient methods for the introduction of propargyl or allenyl functions.[2–7] However, it is not easy to control selectivity between Barbier-type propargylation and allenylation with propargylic halides. We have established both selective propargylation and allenylation by 1-haloprop-2-yne with tin(II) halide and tetrabutylammonium halide (TBAX) through choice of reaction conditions: carbonyl propargylation occurs with 1-bromoprop-2-yne, $SnCl_2$ and TBABr at 50 °C in water, while carbonyl allenylation occurs with 1-chloroprop-2-yne, SnI_2 and TBAI at 25 °C in 1,3-dimethylimidazolidin-2-one (DMI).[8] ^{1}H NMR observations (JEOL Λ-500) have confirmed that prop-2-ynyltriiodotin (propargyltin), derived from 1-chloroprop-2-yne with SnI_2 and NaI at 25 °C in DMF-d_7, does not isomerize to propa-1,2-dienyltriiodotin (allenyltin) at 25 °C but does so at 50 °C.[8,9] We thus hoped that this kind of isomerization of propargyltin to allenyltin would be prohibited by the steric effect of a 3-substituent in 1-haloprop-2-ynes and be promoted by the steric effect of a 1-substituent in 1-haloprop-2-ynes.[10] We here

Table 2 Selective carbonyl propargylation or allenylation mediated by steric effects[a]

R^1	R^2	R^3	Time/h	Yield (%)[b] **2** + **3**	**2**:**3**[c]	**3** *syn*:*anti*[c]
H	CH_3	C_6H_5	48	58	~100:0	
H	CH_3	ClC_6H_4	47	65	~100:0	
H	CH_3	$CH_3C_6H_4$	55	52	~100:0	
H	CH_3	$C_6H_5CH{=}CH$	71	21[d]	94:6	
H	CH_3	$C_6H_5CH_2CH_2$	51	62	90:10	
H	CH_3	$CH_2{=}CH(CH_2)_8$	50	57	89:11	
H	CH_3	$CH_3(CH_2)_5$	67	65	90:10	
H	CH_3	c-C_6H_{11}	79	41	84:16	
H	C_6H_5	C_6H_5	71	81	~100:0	
H	C_6H_5	ClC_6H_4	63	84	~100:0	
H	C_6H_5	$CH_3C_6H_4$	90	76	~100:0	
H	C_6H_5	$C_6H_5CH_2CH_2$	79	56	90:10	
H	C_6H_5	$CH_2{=}CH(CH_2)_8$	75	32	98:2	
H	C_6H_5	$CH_3(CH_2)_5$	70	35	98:2	
H	C_6H_5	c-C_6H_{11}	71	48	93:7	
CH_3	H	C_6H_5	71	71	12:88	49:51
CH_3	H	ClC_6H_4	79	83	6:94	48:52
CH_3	H	$CH_3C_6H_4$	75	65	6:94	47:53
CH_3	H	2-Furyl	70	41	0:~100	50:50
CH_3	H	$C_6H_5CH{=}CH$	72	75	0:~100	47:53
CH_3	H	$C_6H_5CH_2CH_2$	70	66	1:99	19:81
CH_3	H	$CH_2{=}CH(CH_2)_8$	47	55	1:99	26:74
CH_3	H	$CH_3(CH_2)_5$	71	48	10:90	35:65
CH_3	H	c-C_6H_{11}	70	44	14:86	—[e]
Pr	H	C_6H_5	75	66	2:98	48:52
Pr	H	ClC_6H_4	72	85	1:99	50:50
Pr	H	$CH_3(CH_2)_5$	75	41	8:92	22:78

[a] The reaction of 1- or 3-substituted prop-2-ynyl mesylates (1.5 mmol) with aldehydes (1.0 mmol) was carried out using SnI_2 (2.0 mmol), TBAI (0.20 mmol) and NaI (2.0 mmol) in DMI (3 ml) at rt. [b] Yields of a mixture of **2** and **3**. [c] The ratios were determined by ^{1}H NMR analysis (JEOL Λ-500). For the ratio of *syn* to *anti*, see ref. 8. [d] The reaction was carried out in the presence of MS 4Å in THF. [e] The ratio was not confirmed.

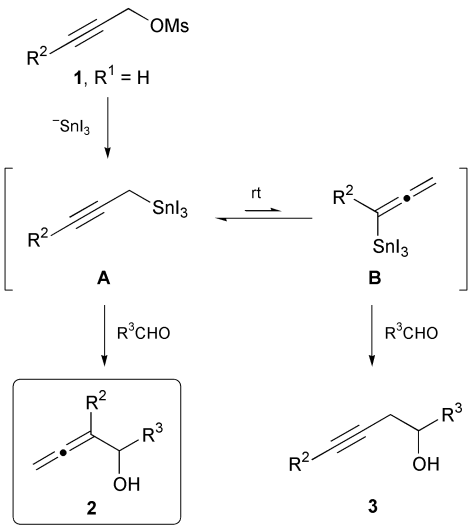

Scheme 1 Allenylation.

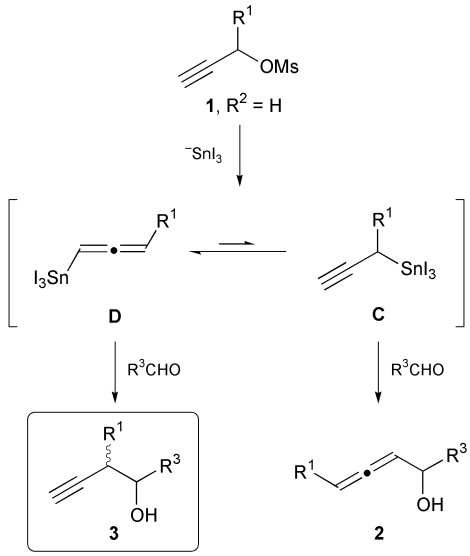

Scheme 2 Propargylation.

report on selective Barbier-type carbonyl propargylation and allenylation mediated by steric effects, using the 1- or 3-substituted prop-2-ynyl mesylates‡ as Barbier-type propargylating or allenylating reagents, rather than the more usual corresponding halides (1-haloprop-2-ynes), because the mesylates are superior to the halides for ease of preparation and the stability of propargylic substrates.[11]

The reaction of prop-2-ynyl mesylate (**1**; R^1, R^2 = H) with some aldehydes was carried out using SnI_2, TBAI and NaI under the same conditions as those reported for the carbonyl allenylation by 1-chloroprop-2-yne [eqn. (1)].[8] The results are

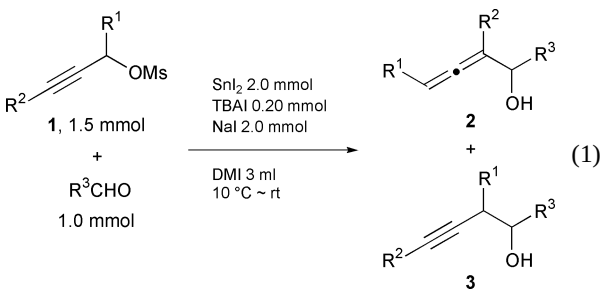

(1)

summarized in Table 1. Prop-2-ynyl mesylate (**1**; R^1, R^2 = H) proved to be as available as 1-chloroprop-2-yne for the selective carbonyl allenylation with SnI_2 and TBAI. Thus, we investigated whether the 1- or 3-substituents of prop-2-ynyl mesylates affect the selectivity between propargylation and allenylation under the same conditions as those of prop-2-ynyl mesylate (**1**; R^1, R^2 = H) [eqn. (1)]. The results are summarized in Table 2. 3-Substituted prop-2-ynyl mesylates (**1**; R^1 = H, R^2 = CH_3 and R^1 = H, R^2 = C_6H_5) caused the same allenylation of various aldehydes as that of **1** (R^1, R^2 = H). In particular, with aromatic aldehydes, only allenyl carbinols **2** were obtained. The reaction of cinnamaldehyde in DMI afforded 1-phenylhexa-1,3-dien-5-one derivatives that were probably formed by the hydration of the corresponding allenyl carbinols **2** (R^2 = CH_3, C_6H_5) followed by dehydration.[4,8] 1-Substituted prop-2-ynyl mesylate (**1**; R^1 = CH_3, R^2 = H and R^1 = Pr, R^2 = H) caused the preferential propargylation of various aldehydes. The selectivity for this propargylation was enhanced by the use of THF–H_2O (1 : 1) as a solvent instead of DMI: R^1 = CH_3, R^2 = H, R^3 = C_6H_5; rt, 72 h; 92%, **2** : **3** = 0 : ~100, *syn*:*anti* = 46:54.

A plausible mechanism for the allenylation is illustrated in Scheme 1. 3-Substituent R^2 (CH_3 or C_6H_5), being bulkier than H, probably prohibits propargyltin intermediate **A** from isomerizing to allenyltin intermediate **B**. Thus allenyl carbinols **2** are produced more selectively than in the allenylation by prop-2-ynyl mesylate (**1**; R^1, R^2 = H), *via* nucleophilic addition of the propargyltin **A** at the γ-position.[8] A plausible mechanism for the propargylation is illustrated in Scheme 2. 1-Substituent R^1 (CH_3 or Pr) probably promotes the isomerization of the initially prepared propargyltin **C** to allenyltin **D**, even at room temperature, or mediates a direct preparation of allenyltin **D**.§ The allenyltin **D** then undergoes nucleophilic addition to aldehydes at the γ-position to afford homopropargyl alcohols **3**.

Notes and references

† E-mail: y-masuya@hoffman.cc.sophia.ac.jp

‡ The 1- or 3-substituted prop-2-ynyl mesylates were prepared from 1- or 3-substituted prop-2-yn-1-ols and methanesulfonyl chloride with triethylamine in ether on an ice-bath. 1-Phenylprop-2-ynyl mesylate was not prepared under the conditions described above: see I. S. Aidhen and R. Braslau, *Synth. Commun.*, 1994, **24**, 789.

§ It was shown by ^{1}H NMR analysis (JEOL Λ-500) that the reaction of 1-methylprop-2-ynyl mesylate with SnI_2 and NaI in DMF-d_7 produced 3-methylprop-1,2-dienyltriiodotin **D** (R^1 = CH_3) at 25 °C; δ 1.73 (dd, J = 7.2, 2.6 Hz, 3H), 5.21 (quintet, J = 6.7 Hz, 1H), 6.09 (dq, J = 5.6, 2.6 Hz, 1H).

1 *Modern Acetylene Chemistry*, ed. P. J. Stang and F. Diederich, VCH, Weinheim, 1995; H. Yamamoto, in *Comprehensive Organic Synthesis*, ed. I. Fleming and B. M. Trost, Pergamon Press, Oxford, 1991, vol. 2, p. 81; H. F. Schuster and G. M. Coppola, *Allenes in Organic Synthesis*, Wiley, New York, 1984.
2 T. Mukaiyama and T. Harada, *Chem. Lett.*, 1981, 621.
3 G. P. Boldrini, E. Tagliavini, C. Trombini and A. Umani-Ronchi, *J. Chem. Soc., Chem. Commun.*, 1986, 685.
4 M. Iyoda, Y. Kanao, M. Nishizaki and M. Oda, *Bull. Chem. Soc. Jpn.*, 1989, **62**, 3380.
5 A. Kundu, S. Prabhakar, M. Vairamani and S. Roy, *Organometallics*, 1999, **18**, 2782.
6 H. Tanaka, T. Hamatani, S. Yamashita and S. Torii, *Chem. Lett.*, 1986, 1461.
7 K. Belyk, M. J. Rozema and P. Knochel, *J. Org. Chem.*, 1992, **57**, 4074.
8 Y. Masuyama, A. Ito, M. Fukuzawa, K. Terada and Y. Kurusu, *Chem. Commun.*, 1998, 2025.
9 J. A. Marshall, R. H. Yu and J. F. Perkins, *J. Org. Chem.*, 1995, **60**, 5550.
10 For selective formation of propargylmetals and allenylmetals utilizing steric effects, see: J. Nokami, T. Tamaoka, T. Koguchi and R. Okawara, *Chem. Lett.*, 1984, 1939; L.-J. Zhang, Y.-Z. Huang and Z.-H. Huang, *Tetrahedron Lett.*, 1991, **32**, 6579; S. Kobayashi and K. Nishio, *J. Am. Chem. Soc.*, 1995, **117**, 6392.
11 For selective propargylation by propargylic mesylates with Et_2Zn or InI in the presence of Pd^{II} catalysts, see: J. A. Marshall and N. D. Adams, *J. Org. Chem.*, 1999, **64**, 5201; J. A. Marshall and C. M. Grant, *J. Org. Chem.*, 1999, **64**, 8214.

ChemComm

Unusual *tri*substitutions on (η⁶-arene)tricarbonylchromium(0) complexes and evidence for the formation of a *tri*anion

Susan E. Gibson (née Thomas), Sandra A. Saladin and Surojit Sur*

Department of Chemistry, King's College London, Strand, London, UK WC2R 2LS

Received (in Liverpool, UK) 25th July 2000, Accepted 4th September 2000
First published as an Advance Article on the web 28th September 2000

A one-pot *tri*substitution on a representative range of (η⁶-arene)tricarbonylchromium(0) complexes is described and evidence for the formation of a *tri*anion is presented.

(η⁶-Arene)tricarbonylchromium(0) complexes have been studied extensively[1] and have a wide range of applications from their use in total synthesis[2] through their growing importance as chiral building blocks[3] to their current involvement in ligand design for asymmetric catalysis.[4] The characteristic enhanced kinetic acidity of the ring protons has been utilised regularly in the introduction of a single substituent *via* a deprotonation/electrophilic quench sequence and has been the subject of numerous synthetic and mechanistic studies.[1b] In contrast, reports regarding the introduction of two new substituents employing a similar sequence are relatively few.[5] Although such double functionalisation has been mentioned in the literature, this reactivity has never been the target of a systematic study. Furthermore, to the best of our knowledge, there exist only two examples of *tri*substitution.† In the first, chlorination of (η⁶-chlorobenzene)tricarbonylchromium(0) afforded a tetrasubstituted complex as a side product in poor yield.[5g] In the second report, we observed a *tri*substitution reaction as part of a wide ranging study on the reactivity of an electron-deficient sulfone complex.[5e] We wish to report here the results of a recent study which indicate (a) this reaction involves the formation of a rare *tri*anionic species, and (b) this extraordinary reactivity is not limited to a single, electron deficient substrate and may be viewed as an inherent feature of (η⁶-arene)tricarbonylchromium(0) complexes.

Initially, the sulfone complex **1a**,[5e] was examined. Treatment of **1a** with 3.0 eq. of 2,2,6,6-tetramethylpiperidine (LiTMP) in THF (−78 °C for 2 h) was followed by a Me_3SiCl quench. The reaction mixture was allowed to warm up to rt and worked up. Column chromatography yielded the *tri*silylated complex **2a** in 50% yield (Table 1, entry 1). In order to gain insight into the species involved in this *tri*substitution, we subsequently performed a reaction under identical conditions using deuteroacetic acid as the electrophilic quench. The mass spectrum of the product mixture showed four molecular ion peaks corresponding to unreacted **1a** and its mono-, di- and trideuterated analogues in the ratio 14 : 38 : 35 : 13.‡ It can thus be concluded that a *tri*anionic species is a significant component (13%) of the reaction mixture prior to quenching.

We next decided to study the electron rich complex (η⁶-anisole)tricarbonylchromium(0), **1b**, in order to start to define the scope of the trisubstitution reaction. Treatment of **1b** with 3.0 eq. of LiTMP in THF (−78 °C for 2 h) was followed by a Me_3SiCl quench. Column chromatography yielded the novel *tri*silylated complex **2b**[6] in 42% yield along with a 9% yield of **3b** (Table 1, entry 2).[5f] A deuteration experiment under identical conditions was once again performed. Analysis of the mass spectrum revealed the presence of unreacted **1b**, and its mono-, di- and trideuterated analogues in a 24 : 45 : 25 : 6 ratio.‡

Encouraged by the *tri*substitution of electron rich **1b**, we then progressed to the electronically neutral complex **1c**. In this case, reaction with LiTMP followed by an electrophilic quench with Me_3SiCl afforded almost equal amounts of the *tri*-substituted complexes **2c** and 2,5-disubstituted complex **3c**, both previously unknown compounds (Table 1, entry 3).

The prospect of C_{3v}-symmetric arenes being accessible through this route encouraged us to attempt the reaction on unsubstituted (η⁶-benzene)tricarbonylchromium(0) which led to novel **5a** and **6a**.[7] Optimisation experiments demonstrated that use of LDA at −40 °C afforded the desired C_{3v}-symmetric product **5a** in the highest yield (Table 2, entry 1). A control experiment was then performed on uncomplexed benzene under identical conditions. This resulted in recovery of unreacted starting material (≥ 95%), confirming beyond doubt that the *tri*substitution reaction requires the presence of the tricarbonylchromium(0) moiety.

Having established that the one-pot *tri*substitution is not limited to electron deficient arene complexes, we decided to further test the scope of this reaction by using other electrophiles. Considering the utility of tin containing compounds in coupling reactions we chose Me_3SnCl as the electrophile: pleasingly, *tri*substitution afforded the novel complex **5b** in good yield with **6b**[8] as the minor product (Table 2, entry 2). The possibility of gaining access to C_{3v}-symmetric phosphine ligands led us to use PPh_2Cl as the next electrophile. The novel

Table 1 Reaction of complexes **1a–c**

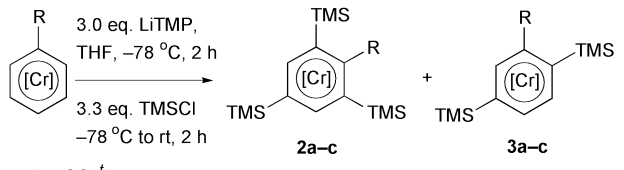

1a, R = $SO_2{}^tBu$
1b, R = OMe
1c, R = CH_2NMe_2

[Cr] = $Cr(CO)_3$

Entry	R	Yield of **2** (%)	Yield of **3** (%)
1	$SO_2{}^tBu$	50	[a]
2	OMe	42	9
3	CH_2NMe_2	40	48

[a] **3a** was not observed.

Table 2 Reaction of complex **4** with various electrophiles

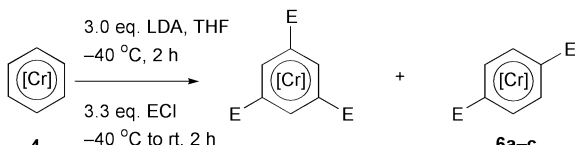

4

[Cr] = $Cr(CO)_3$

5a, E = TMS
5b, E = $SnMe_3$
5c, E = PPh_2

Entry	E	Yield of **5** (%)	Yield of **6** (%)
1	TMS	42	48
2	$SnMe_3$	58	7
3	PPh_2	29	[a]

[a] **6c** was observed, but was not isolated.

DOI: 10.1039/b006105k

*tri*substituted complex **5c** was isolated by fractional crystallisation, fully characterised and its structure confirmed by X-ray crystallography.[9]

In summary, we have presented evidence for the formation of a *tri*anionic species in an unusual one-pot *tri*substitution reaction. Furthermore, we have broadened the scope of this reaction sufficiently to demonstrate for the first time that it is an inherent feature of the reactivity of (η^6-arene)tricarbonylchromium complexes.

Notes and references

† An example of trisubstitution in two discrete steps has also been reported: see ref. 5*d*.

‡ The product mixture was also analyzed using ^{1}H and ^{2}H NMR spectroscopy; these gave results consistent with the mass spectral data.

1 For reviews in this area, see: (*a*) M. F. Semmelhack, in *Comprehensive Organometallic Chemistry II*, ed. E. W. Abel, F. G. A. Stone and G. Wilkinson, Pergamon, Oxford, 1995, vol. 12, p979; (*b*) M. F. Semmelhack, in *Comprehensive Organometallic Chemistry II*, ed. E. W. Abel, F. G. A. Stone and G. Wilkinson, Pergamon, Oxford, 1995, vol. 12, p1017; (*c*) S. G. Davies and T. D. McCarthy, in *Comprehensive Organometallic Chemistry II*, ed. E. W. Abel, F. G. A. Stone and G. Wilkinson, Pergamon, Oxford, 1995, vol. 12, p1039.

2 For recent examples, see: L. G. Monovich, Y. LeHuérou, M. Ronn and G. A. Molander, *J. Am. Chem. Soc.*, 2000, **122**, 52; D. Hörstermann, H.-G. Schmalz and G. Kociok-Köhn, *Tetrahedron*, 1999, **55**, 6905; T. Tanaka, H. Mikamiyama, K. Maeda, C. Iwata, Y. In and T. Isada, *J. Org. Chem.*, 1998, **63**, 9782; K. Schellhaas, H.-G. Schmalz and J. W. Bats, *Chem. Eur. J.*, 1998, **4**, 57.

3 S. E. Gibson (née Thomas) and E. G. A.. Reddington, *Chem. Commun.*, 2000, 989; A. Solladié-Cavallo, in *Advances in Metal–Organic Chemistry*, ed. L. S. Liebeskind, JAI Press, 1991, vol. 1, p. 99; M. Uemura, in *Advances in Metal–Organic Chemistry*, ed. L. S. Liebeskind, JAI Press, 1991, vol. 2, p. 231.

4 C. Bolm and K. Muñiz, *Chem. Soc. Rev.*, 1999, **28**, 51; C. Bolm, K. Muñiz and C. Ganter, *New J. Chem.*, 1998, 1371; G. B. Jones and M. Guzel, *Tetrahedron:Asymmetry*, 1998, **9**, 2023; G. B. Jones, M. Guzel and B. J. Chapman, *Tetrahedron:Asymmetry*, 1998, **9**, 901.

5 (*a*) T. Volk, D. Bernicke, J. W. Bats and H.-G. Schmalz, *Eur. J. Inorg. Chem.*, 1998, 1863; (*b*) A. Ariffin, A. J. Blake, W.-S Li and N. S. Simpkins, *Synlett*, 1997, 1453; (*c*) R. A. Ewin, A. M. MacLeod, D. A. Price, N. S. Simpkins and A. P. Watt, *J. Chem. Soc., Perkin Trans. 1*, 1997, 401 and references cited therein; (*d*) H.-G. Schmalz, T. Volk, D. Bernicke and S. Huneck, *Tetrahedron*, 1997, **53**, 9219; (*e*) S. E. Gibson (née Thomas), N. Guillo, A. J. P. White and D. J. Williams, *J. Chem. Soc., Perkin Trans. 1*, 1996, 2575; (*f*) H.-G. Schmalz and K. Schellhaas, *Tetrahedron Lett.*, 1995, **36**, 5515; (*g*) P. G. Gassman and P. A. Deck, *Organometallics*, 1994, **13**, 1934; (*h*) H.-G. Schmalz, A. Schwarz and G. Dürner, *Tetrahedron Lett.*, 1994, **35**, 6861; (*i*) R. J. Card and W. Trahanovsky, *J. Org. Chem.*, 1980, **45**, 2560; (*j*) M. F. Semmelhack, J. Bisaha and M. Czarny, *J. Am. Chem. Soc.*, 1979, **101**, 768.

6 All novel complexes were characterized by their IR, ^{1}H NMR, ^{13}C NMR spectroscopic, mass spectrometric and microanalytical data.

7 M. E. Wright, *Organometallics*, 1989, **8**, 407.

8 T. P. Poeth, P. G. Harrison, T. J. Long, B. R. Willeford and J. J. Zuckermann, *Inorg. Chem.*, 1971, **10**, 522.

9 S. E. Gibson, J. W. Steed and S. Sur, unpublished results.

1,2-Hopobactin: a hydroxamate analog of enterobactin

Haim Weizman,† and Abraham Shanzer*

Department of Organic Chemistry, The Weizmann Institute of Science, Rehovot, 76100, Israel

Received (in Cambridge, UK) 20th June 2000, Accepted 1st September 2000
First published as an Advance Article on the web 28th September 2000

Hopobactin is a 1-hydroxy-2-oxopyridine-6-carboximide analog of enterobactin that forms isostructural complexes.

Enterobactin is a catechol-based siderophore that is one of the strongest ferric iron binders.[1] The remarkable binding properties of enterobactin are attributed to a unique binding cavity that stabilizes the metal complex.[2] This hexacoordinate cavity is composed of a trislactone ring where three 2,3-dihydroxybenzamide units are attached to the L-serine α-amino groups (Fig 1). Upon Fe^{3+} binding, the lactone ring allows for coplanarity of the amide bond and the coordinated catecholate moiety. The conjugation with the amide increases the acidity of the phenol groups and results in an inter-chain hydrogen bond between the amide NH and the 2-catecholate oxygen. As a consequence of the trislactone chirality and the hydrogen bonds, the natural enterobactin iron complex preferentially adopts a Δ configuration. Synthetic analogs of enterobactin have demonstrated that deviations from the enterobactin structure result in less profound properties.[3] Here we present the synthesis of a hydroxamic acid analog of enterobactin, 1,2-hopobactin (HOPO = 1-hydroxy-2-oxopyridine-6-carboximide, Fig. 1). The HOPO ligand and its anion have resonance forms that are isoelectronic with pyrocatechol and have a similar structure. Attaching the HOPO moiety through an amide linkage to the trislactone results in a perfect structural analog of enterobactin that forms neutral complexes.

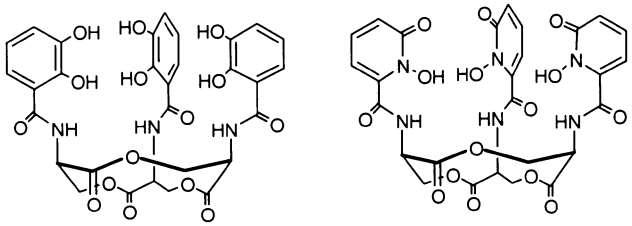

Fig. 1 Enterobactin (left) and its hydroxamic acid analog (right).

Two enantiomeric trilactones were prepared from L and D-serine (Scheme 1).[4a] 1,2-dihydro-1-hydroxy-2-oxopyridine-6-carboxylic acid [4b] was protected with benzyl groups, activated and coupled with the trislactone. Hydrogenolysis of the protected product gave a mixture of products and the desired compound could not be isolated.[5] Yet, by addition of ferric or gallium acetylacetonates to the mixture, the corresponding complexes could be purified by preparative TLC in very low yields. The complexes were characterized by NMR (for Ga), IR and MS.[6] Removal of the benzyl protecting groups was accomplished quantitatively using Lewis acids like $FeCl_3$ or $GaCl_3$. After the reaction was complete, the pH was adjusted to 8 and the complexes were purified by chromatography. The spectroscopic data for the ferric and gallium complexes were identical to those of the complexes isolated by addition of ferric and gallium acetylacetonate as described above.

Both gallium complexes I-D-Ga and I-L-Ga were characterized by NMR (Table 1). Since Ga^{3+} has the same charge as Fe^{3+} and a similar radius, it is a good diamagnetic equivalent of iron.[7] I-L-Ga displays one set of signals in the NMR time scale. Due to the homochirality of the trislactone, the formation of the diasteromeric complexes (L,L,L-Δ and L,L,L-Λ) would be expected to form two sets of NMR signals. The observance of only one set indicates the formation of only one diastereoisomer (within the limits of detection of NMR). The possibility of fast exchange between the two isomers can be disregarded, as isomerization reactions of hydroxamates are slow enough to allow detection of two geometrical isomers.

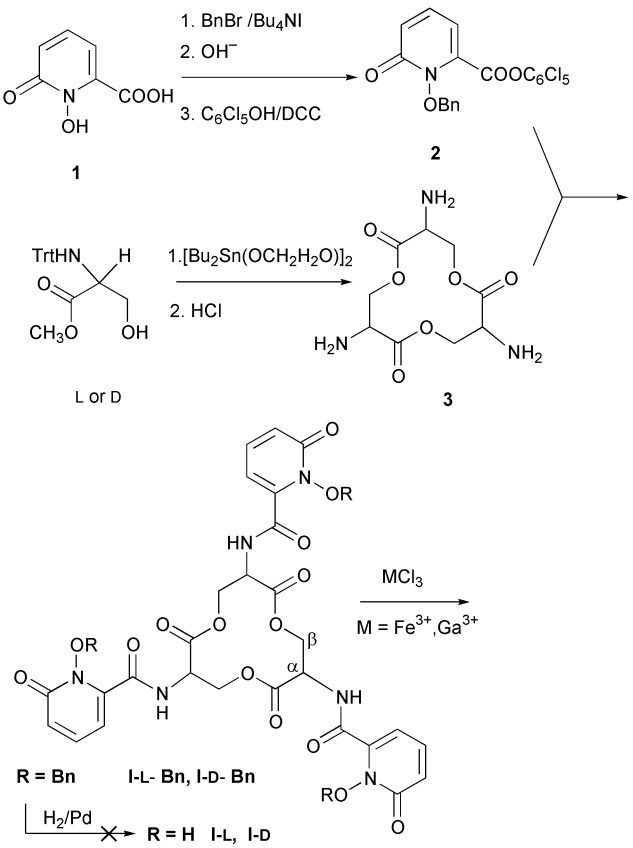

Scheme 1 Synthetic scheme for the preparation of 1,2-hopobactin (I-L) and enantioenterobactin (I-D).

I-D-Ga gave an NMR spectrum identical to that of I-L-Ga. Because the two compounds are based on enantiomeric trislactones, the identical spectra reveal that the complexes are

Table 1 ^1H NMR Spectra of enterobactin and analogs

Compound	H^{α}	$H^{\beta}{}_1$	$H^{\beta}{}_2$	H^{N}
Enterobactin[a]	4.94 (m)	4.66 (dd)	4.41 (dd)	9.06
	J = 8.06, 4.19	*J* = 8.06, 10.8	*J* = 4.19, 10.8	*J* = 6.52
Enterobactin-Ga[a]	5.12	5.22	3.80	11.72
		J = 10.68	*J* = 10.68	*J* = 9.83
I-protected[b]	4.80 (d)	4.76 (d)	3.68 (d)	8.12
	J = 10.9	*J* = 10.9	*J* = 10.3	
I-D-Ga[b]	5.37 (t of d)	5.56 (dd)	3.96 (dd)	10.70 (d)
I-L-Ga[b]	*J* = 1.3, 6.4	*J* = 1.1, 7.2	*J* = 1.7, 7.2	*J* = 6.3
TBA[c]	5.05 (m)	4.91 (dd)	4.65 (dd)	7.25
	J = 7.8	*J* = 3.1, 11.5	*J* = 3.3, 11.5	

[a] Data for enterobactin in DMSO-d_6.[8] [b] $CDCl_3$. [c] Trisbenzylamide enterobactin $CDCl_3$.[2a]

DOI: 10.1039/b004880l

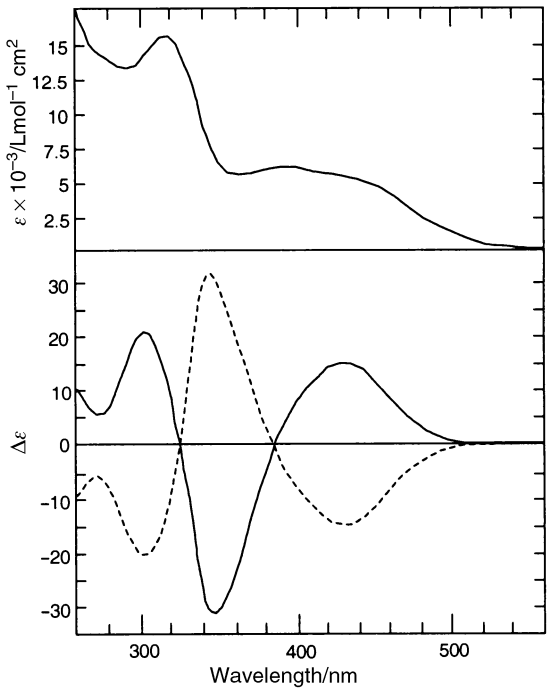

Fig. 2 UV/CD spectra of I-L-Fe (…..) and I-D-Fe (__) in $CHCl_3$.

enantiomers and that the D,D,D trislactone is directing the formation of a complex with opposite helicity. Therefore, the NMR indicates that the enterobactin skeleton serves as a stereospecific template for the formation of exclusively one stereoisomer depending on the chirality of the serine units.

For I-Ga, the vicinal proton–proton coupling constants for the $C_\alpha H$-$C_{\beta 1}H$ and $C_\alpha H$-$C_{\beta 2}H$ were both small (J = 1.1 and 1.7 Hz). These values indicate equatorial–equatorial and axial–equatorial relationships between the vicinal protons and, therefore, an axial arrangement of the HOPO ring. The pronounced shift of the amide proton to a lower field upon Ga^{3+} complexation compared to the protected I-D is compatible with hydrogen-bonding. A similar shift was previously observed in enterobactin and several triscatecholamides as well. In enterobactin the shift was attributed to a hydrogen bond between the amide NH and the 2-catecholate oxygen in the complex. This suggestion was supported by theoretical calculations, and it was shown experimentally that replacement of the NH with *N*-Me results in a lower binding affinity. It is suggested that a similar stabilization occurs in I-Ga between the amide proton and the HOPO N-oxygen.

The isolated iron complexes exhibit two absorption maxima at 321 nm (ε = 16430 M^{-1} cm^{-1}) and 398 nm (ε = 6375 M^{-1} cm^{-1}) in chloroform (Fig. 2). The LMCT band has an additional shoulder at 450 nm (ε = 5575 M^{-1} cm^{-1}). The CD spectra of I-L-Fe and I-D-Fe showed opposite Cotton effects. The fact that the spectra are mirror images confirms that the enantiomeric trislactone skeleton induced opposite helicity around the iron center.

The determination of metal center chirality of the metal complex in solution is possible through comparison of the solution CD spectra. However, the correlation of the rotary power with left or right-handed helical stereochemistry requires an absolute assignment based on crystal structure data. As this data is not available, the ferric enterobactin CD spectrum was used as a reference.[9a] This comparison is based on the high structural and electronic similarity between the HOPO and enterobactin complexes together with the resemblance in their CD spectral shape.[9b] This correlation suggests that I-L induces the formation of the Δ iron complex while the I-D ligand induces the formation of the Λ isomer. This chiral induction is compatible with the one observed for enterobactin.

These results indicate that the unique structure of the enterobactin complex is preserved in the HOPO analog. This work demonstrates that careful design of ligands allows for the mimicking of the unique features of enterobactin while changing only desired properties. While the enterobactin complex is negatively charged and, therefore, water-soluble, hopobactin forms neutral M^{3+} complexes that are soluble in non polar organic solvents. Therefore, hopobactin is a potential ligand for liquid-membrane separations. The evaluation of these complexes as siderophore mimics is underway.

Notes and references

† Current address: Department of Chemistry and Biochemistry, University of California San Diego, La Jolla, CA, 92093.

1 K. N. Raymond and C. J. Carrano, *Acc. Chem. Res.*, 1979, **12**, 183; L. D. Loomis and K. N. Raymond, *Inorg. Chem.*, 1991, **30**, 906.
2 (*a*) A. Shanzer, J. Libman, S. Lifson and C. E. Felder, *J. Am. Chem. Soc.*, 1986, **108**, 7609; (*b*) T. B. Karpishin, T. M. Dewey and K. N. Raymond, *J. Am. Chem. Soc.*, 1993, **115**, 1842.
3 W. R. Harris and K. N. Raymond, *J. Am. Chem. Soc.*, 1979, **101**, 6534; Y. Tor, J. Libman, A. Shanzer, C. E. Felder and S. Lifson, *J. Am. Chem. Soc.*, 1992, **114**, 6661.
4 (*a*) R. J. A. Ramirez, L. Karamanukyan, S. Ortiz and C. G. Gutierrez, *Tetrahedron Lett.*, 1997, **38**, 749; (*b*) R. C. Scarrow, P. E. Riley, K. Abu-Dari, D. L. White and K. N. Raymond, *Inorg. Chem.*, 1985, **24**, 954.
5 The hydrogenolysis of HOPO resulted in hydrogenation of the ring or reduction to the lactam.
6 **I-Fe**: IR ($CDCl_3$)ν cm^{-1}: 3258 (NH), 1768 (COOC), 1676 (CONO, CONH) 1610 (CONO-Fe). FAB-MS *m/z* 725.20 [L-Fe]$^+$. **I-Ga**: IR ($CDCl_3$)ν cm^{-1}: 3286 (NH), 1766 (COOC), 1676 (CONO, CONH) 1610 (CONO-Ga). FAB-MS *m/z* 738.04 [L-^{69}Ga]$^+$.
7 B. A. Borgias, S. J. Barclay and K. N. Raymond, *J. Coord. Chem.*, 1986, **15**, 109.
8 M. Llinas, D. M. Wilson and J. B. Neilands, *Biochemistry*, 1973, **12**, 3836.
9 (*a*) H. J. Rogers, C. Synger, B. Kimber and P. M. Bayley, *Biochim. Biophys. Acta*, 1977, **497**, 548; (*b*) M. Meyer, J. R. Telford, S. M. Cohen, D. J. White, J. Xu and K. N. Raymond, *J. Am. Chem. Soc.*, 1997, **119**, 10 093.

Unusual addition reactions of lithium alkoxides to 2,4,6-tri-*tert*-butyl-1,3,5-triphosphabenzene†

M. Krein, U. Bergsträßer, C. Peters, S. G. Ruf and M. Regitz*

Fachbereich Chemie der Universität Kaiserslautern, Erwin-Schrödinger-Straße, D-67663 Kaiserslautern, Germany. E-mail: regitz@rhrk.uni-kl.de

Received (in Cambridge, UK) 21st January 2000, revised manuscript received 18th August 2000, Accepted 21st August 2000
First published as an Advance Article on the web

2,4,6-Tri-*tert*-butyl-1,3,5-triphosphabenzene (1) reacts selectively with a mixture of the primary lithium alkoxides 2a,b and the corresponding alcohols 3a,b to afford the novel 2,4,6-tri-*tert*-butyl-1,3,5-alkoxy-1,3,5-triphosphacyclohexane derivatives 4a,b; treatment of 4a with sulfur results in oxidation of all phosphorus atoms to furnish the triphosphane sulfide 5.

The polarity of the P/C double bond resulting from the electronegativity difference between phosphorus and carbon generally favours the addition of H-acidic compounds.[1] In this process, the proton is added to the carbon atom of the phosphaalkene unit while the nucleophilic part is attached to the positively polarised phosphorus atom.[2,3] It has recently been shown that the addition of alcohols to isolated P/C double bonds is particularly successful when a mixture of a lithium alkoxide with at least an equimolar amount of the corresponding alcohol in THF as solvent is used.[4] In the course of these studies we posed the question of whether this reagent system would be able to undergo addition to phosphaalkene units incorporated in a delocalised, heteroaromatic[5] bonding system. For this purpose, we have chosen 2,4,6-tri-*tert*-butyl-1,3,5-triphosphabenzene[6] (**1**) as a reaction partner. To date, only the unusual addition of water to a η^1-bonded 2,4,6-tri-*tert*-butyl-1,3,5-triphosphabenzene platinum(II) complex has been reported.[7]

When the triphosphabenzene **1** was allowed to react with three equivalents of the lithium alkoxides **3a**,**b** and an excess of the respective alcohol **2a**,**b**, a highly regio- and stereoselective, three-fold addition of alcohol to all three P/C double bonds of **1** was indeed observed. The products are the 1,3,5-trialkoxy-1,3,5-triphosphabenzenes **4a**‡ (84%, mp 51 °C) and **4b** (72%, 74 °C) obtained as microcrystalline solids (Scheme 1). For the reaction of **1** + **2a**/**3a** we found that the use of merely 10% of the stoichiometric amount of lithium ethoxide can also result in the same product yield when a longer reaction time is allowed. The rate-determining step is most certainly the 1,2- or 1,4-addition of the first equivalent of the alcohol which destroys the aromaticity of **1**.[5] The thus-formed 1,3,5-triphosphacyclohexa-1,3(or 1,4)-diene then reacts much more rapidly so that intermediates cannot be detected by ^{31}P NMR spectroscopic monitoring of the reaction.

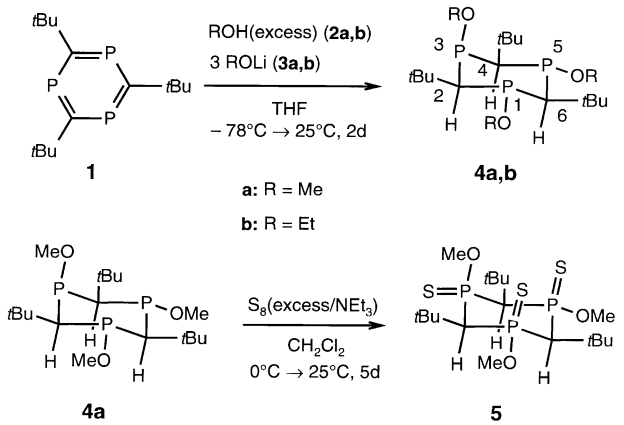

Scheme 1

The ^{31}P and ^{13}C NMR spectra of **4a** and **4b** are in accord with the assumed saturation of the double bonds of the heteroarene **1** (^{31}P: δ = 232.6 , ^{13}C: δ = 211.8). The ^{31}P NMR signals of **4a** are shifted to higher field in comparison to those of **1** and appear at δ = 162.8 (d, P-1/P-5) and δ = 162.4 (t, P-3) with $^2J_{P,P}$ coupling constants of 3.1 Hz. The corresponding signals for **4b** show the same splitting pattern but are slightly diagmagnetically shifted (δ = 156.3 and δ = 155.5, respectively). Also noteworthy are the high-field shifts of the signals of the ring carbon atoms of **4a** and **4b** appearing at δ = 57.2 and 56.9 (C-2/C-4) and δ = 60.7 and 59.9 (C-6), respectively.

For the structural elucidation of the 1,3,5-triphosphacyclohexanes **4a**,**b** it is justifiable to assume that the framework prefers the chair form in analogy to the cyclohexane system. The sterically demanding *tert*-butyl substituents should adopt an equatorial arrangement for energetic reasons. However, a conclusive assignment of the configurations of the three phosphorus atoms is not possible at this stage.

The final structure elucidation was established by an X-ray crystallographic analysis of **4a** (Fig. 1).§ The highly distorted, chair conformation of the ring skeleton with equatorial linked *tert*-butyl substituents is clearly apparent.

In the crystal the two methoxy substituents at P-1 and P-5 occupy approximately equatorial positions while that at P-3 is in an axial position. The P/C bond lengths measured in the ring range from 1.824(3) Å to 1.874(3) Å and thus exhibit only minor deviations from the average literature value.[8] Other characteristic features in the crystal structure of compound **4a**

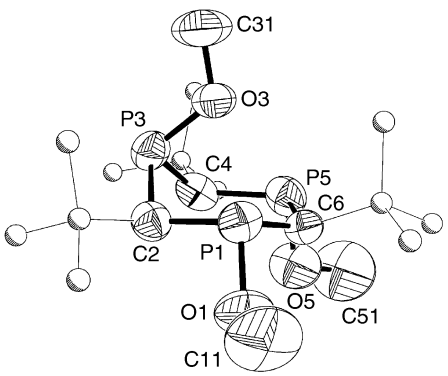

Fig. 1 Crystal structure of **4a**. Selected bond lengths (Å) and angles (°): P(1)–C(2) 1.843(3), P(1)–C(6) 1.870(3), P(3)–C(2) 1.840(3), P(3)–C(4) 1.824(3), P(5)–C(4) 1.834(3), P(5)–C(6) 1.874(3), P(1)–O(1) 1.660(2), P(3)–O(3) 1.653(2), P(5)–O(5) 1.656(2); C(2)–P(1)–C(6) 104.34(11), C(4)–P(3)–C(2) 99.10(12), C(4)–P(5)–C(6) 107.51(12), P(1)–C(2)–P(3) 109.93(14), P(3)–C(4)–P(5) 112.33(14), P(1)–C(6)–P(5) 126.15(14).

† Part 152 of the series of papers in Organophosphorus Compounds. For part 151, see: S. G. Ruf, J. Dietz and M. Regitz, *Tetrahedron*, 2000, **56**, 6259.

DOI: 10.1039/b006795o

are the widely differing folding angles between the planes defined by the atoms P-1/C-6/P-5 and C-2/P-3/C-4 to that defined by the atoms C-2/P-1/P-5/C-4 (23.9 and 112.8°, respectively). The widely opened endocyclic bonding angle at C-6 [126.15(14)°] is comparable to that of a 1,3-diphosphorinane described in the literature.[9]

Since the novel products **4a**,**b** represent the first members of a new class of compounds we have also investigated their functionalisation reactions with chalcogens. The reaction of **4a** with an excess of sulfur in the presence of triethylamine proceeded with coordination increases at all phosphorus atoms to furnish the triphosphane trisulfide **5** (74%, colourless solid, mp 84 °C).¶ The ^{13}C NMR data for compound **5** confirm the retention of the cyclic structure while the absorption at ν = 1261 cm^{-1} in the IR spectrum is characteristic for the newly introduced P/S double bonds. We also assume that the configurations at the phosphorus atoms remain unchanged by this reaction. The oxidation of **4a** with bis(trimethylsilyl) peroxide proceeded analogously to furnish **5** (O in place of S) but this product still contains traces of impurities (^{31}P NMR).

We thank the Fonds der Chemischen Industrie for graduate grants (to C. P. and S. R.) and the Deutsche Forschungsgemeinschaft (Graduate College Phosphorus as Connecting Link between Various Chemical Disciplines) for generous financial support.

Notes and references

‡ *Selected data* for **4a**: δ_P (81 MHz, C_6D_6) 162.8 (d, $^2J_{P,P}$ 3.1, P-1, P-5), 162.4 (d, $^2J_{P,P}$ 3.1, P-3); δ_H (400 MHz, C_6D_6) 1.34 [s, 18 H, $C(CH_3)_3$], 1.49 [s, 9 H, $C(CH_3)_3$], 2.12 (d, 2H, $^2J_{H,P}$ 1.7, H-2, H-4), 2.20 (t, 1H, $^2J_{H,P}$ 3.8, H-6), 3.19 (d, 3H, $^3J_{H,P}$ 12.1, OCH_3), 3.40 (m, 6H, OCH_3); δ_C (100.6 MHz, C_6D_6) 30.4 [m, $C(CH_3)_3$], 30.9 [t, $^3J_{C,P}$ 11.8, $C(CH_3)_3$], 34.3 [m, $C(CH_3)_3$], 35.6 [t, $^2J_{C,P}$ 24.3, $C(CH_3)_3$], 55.3 (m, OCH_3), 57.2 (m, C-2, C-4), 60.7 (t, $^1J_{C,P}$ 49.3, C-6); IR (CCl_4) ν = 2958 (vs), 2827 (m), 1464 (m), 1398 (m), 1362 (w), 1219 (s), 1047 (m), 796 (s), 772 (s), 748 (m), 727 (s); *m/z* (EI, 70 eV): 396 (93) $[M]^+$, 381 (100) $[M - CH_3]^+$, 365 (13) $[M - OMe]^+$, 339 (18) $[M - {}^tBu]^+$, 57 (14) $[{}^tBu]^+$. (Calc. for $C_{18}H_{39}O_3P_3$: C, 54.40; H, 9.90. Found C, 54.35; H, 10.09%).

§ *Crystal data for* **4a**: $C_{18}H_{39}O_3P_3$, M = 396.43 g mol^{-1}, monoclinic, space group $P2_1/n$, a = 9.384(2), b = 24.807(5), c = 10.901(2) Å, β = 111.90(3)°, V = 2354.8 $Å^3$, Z = 4, D_c = 1.118 Mg m^{-3}, μ = 0.265 mm^{-1}, $F(000)$ = 864. Crystal dimensions 0.80 × 0.50 × 0.30 mm^3, 15039 reflections collected, 3641 independent reflections (R_{int} = 0.0579), 2731 reflections with $I > 2\sigma(I)$, goodness-of-fit on F^2: 1.279, $R[I > 2\sigma(I)]$ = 0.0478, wR_2 = 0.1223; R (all data) = 0.0618, wR_2 = 0.1315; maximum and minimum residual density 0.543 and 0.223 e $Å^{-3}$. Data were collected on a STOE Imaging Plate Diffraction System at room temperature with Mo-Kα radiation (λ = 0.71073 Å). The structure was solved with SHELXS-86 [ref. 10(*a*)] and refined with SHELXL-93 [ref. 10(*b*)]. CCDC 182/1755. See http://www.rsc.org/suppdata/cc/b0/b006795o/ for crystallographic files in .cif format.

¶ *Selected data* for **5**: δ_P (81 MHz, C_6D_6) 99.5 (s, P-1, P-5), 123.5 (s, P-3); δ_H (400 MHz, C_6D_6) 1.29 [s, 18 H, $C(CH_3)_3$], 1.75 [s, 9 H, $C(CH_3)_3$], 2.74 (pseudo t, 2 H, $^2J_{H,P}$ 19.2, H-2, H-4), 3.11 (m, 1 H, H-6), 3.47 (d, 6 H, $^2J_{H,P}$ 14.1, OCH_3), 3.52 (d, 3 H, $^2J_{H,P}$ 12.1, OCH_3); δ_C (100.6 MHz, C_6D_6) 30.2 [m, $C(CH_3)_3$], 31.7 [t, $^3J_{C,P}$ 6.0, $C(CH_3)_3$], 36.2 [dd, $^2J_{P,C}$ 19.9, 1.8, $C(CH_3)_3$], 39.2 [m, $C(CH_3)_3$], 49.5 (m, OCH_3), 57.2 (d, $^2J_{C,P}$ 22.6, OCH_3), 60.4 (dd, $^1J_{C,P}$ 49.9, 27.3, C-2, C-4), 66.0 (t, $^1J_{C,P}$ 51.8 Hz, C-6); IR (CCl_4) ν = 2956 (vs), 1466 (m), 1393 (m), 1261 (m), 1364 (m), 1047 (vs), 825 (s), 790 (s), 783 (vs), 763 (s), 745 (s); *m/z* (EI, 70 eV): 492 (6) $[M]^+$, 461 (16) $[M - OMe]^+$, 460 (62) $[M - S]^+$, 403 (26) $[M - {}^tBuS]^+$, 57 (70) $[{}^tBu]^+$. $C_{18}H_{39}O_3P_3S_3$.

1 R. Appel, in *Multiple Bonds and Low Coordination in Phosphorus Chemistry*, ed. M. Regitz and O. J. Scherer, Thieme, Stuttgart, 1990, p. 157.
2 Th. C. Klebach, R. Lourens and F. Bickelhaupt, *J. Am. Chem. Soc.*, 1978, **100**, 4886.
3 R. Appel and U. Kündgen, *Angew. Chem.*, 1982, **94**, 227; R. Appel and U. Kündgen, *Angew. Chem., Int. Ed. Engl.*, 1982, **21**, 219.
3 S. G. Ruf, U. Bergsträßer and M. Regitz, *Eur. J. Org. Chem.*, 2000, 2219.
5 R. Gleiter, H. Lange, P. Binger, J. Stannek, C. Krüger, J. Bruckmann, U. Zenneck and S. Kummer, *Eur. J. Inorg. Chem.*, 1998, 1619.
6 More simple access: F. Tabellion, A. Nachbauer, S. Leininger, C. Peters and M. Regitz, *Angew. Chem.*, 1998, **110**, 1318; F. Tabellion, A. Nachbauer, S. Leininger, C. Peters and M. Regitz, *Angew. Chem., Int. Ed.*, 1998, **37**, 1233. First synthesis: P. Binger, S. Leininger, J. Stannek, B. Gabor, R. Mynott, J. Bruckmann and C. Krüger, *Angew. Chem.*, 1995, **107**, 2411; P. Binger, S. Leininger, J. Stannek, B. Gabor, R. Mynott, J. Bruckmann and C. Krüger, *Angew. Chem., Int. Ed. Engl.*, 1995, **34**, 2227.
7 S. B. Clendenning, P. B. Hitchcock and J. F. Nixon, *Chem. Commun.*, 1999, 1377.
8 *CRC Handbook of Chemistry and Physics*, ed. D. R. Lide, CRC Press, Boca Raton, FL, 1992, p. 9.
9 P. J. Jones and A. Wienkauf, *Acta Crystallogr., Sect. C*, 1998, **54**, 1449.
10 (*a*) G. M. Sheldrick, SHELXS-86, a program for the solution of crystal structures, Göttingen, Germany, 1986; (*b*) G. M. Sheldrick, SHELXL-93, a program for structure refinement, Göttingen, Germany, 1993.

ChemComm

Outstanding stability of immobilized recombinant α(1→3/4)-fucosyltransferases exploited in the synthesis of Lewis a and Lewis x trisaccharides

Claudine Augé,*[a] Annie Malleron,[a] Halima Tahrat,[b] Annie Marc,[b] Jean-Louis Goergen,[b] Martine Cerutti,[c] Wim F. A. Steelant,†[d] Philippe Delannoy[d] and André Lubineau[a]

[a] *Laboratoire de Chimie Organique Multifonctionnelle, UMR 8614, Université Paris-Sud, 91405 Orsay Cedex, France. E-mail: clauauge@icmo.u-psud.fr*
[b] *Laboratoire des Sciences du Génie Chimique, CNRS-INPL, BP 172, 54505 Vandoeuvre lès Nancy, France*
[c] *Laboratoire de Pathologie Comparée, Unité de Biologie Cellulaire et Moléculaire, URA 2209 and UPR INRA 27, 30380 Saint Christol lez Alès, France*
[d] *Laboratoire de Chimie Biologique, Unité de Glycobiologie Structurale et Fonctionnelle, UMR 8576 Université des Sciences et Technologies de Lille, 59655 Villeneuve d'Ascq, France*

Received (in Cambridge, UK) 28th July 2000, Accepted 24th August 2000
First published as an Advance Article on the web 28th September 2000

Recombinant human α(1→3/4)-fucosyltransferases (FucT-III) expressed in CHO cells or baculovirus-infected insect cells, immobilized on Ni^{2+}-agarose through a 6His tag, exhibit a marked stability, which was exploited in the synthesis of Lewis a and Lewis x trisaccharides.

Glycosyltransferases have become widely used over the past decade as efficient tools for glycosylation because they catalyze sugar unit transfer with complete regio- and stereoselectivity. Early work in this area suffered from the low availability of these membrane-bound enzymes isolated from natural sources, but nowadays, thanks to genetic engineering, the expression of secreted forms of recombinant glycosyltransferases offers the opportunity of producing active enzymes in large quantities. Fucosyltransferases comprise a family of enzymes that catalyze the transfer of a fucose residue from GDP-fucose, the sugar-nucleotide donor, to a disaccharide acceptor. Among this family, α(1→3/4)-fucosyltransferase (FucT-III), is responsible for both the synthesis of the Lewis a trisaccharide Gal*p*-(1→3)-[α-L-Fuc*p*-(1→4)]-β-D-GlcNAc*p* from β-D-Gal*p*-(1→3)-β-D-GlcNAc*p* (type 1 disaccharide), and to a smaller extent the synthesis of the Lewis x trisaccharide Gal*p*-(1→4)-[α-L-Fuc*p*-(1→3)]-β-D-GlcNAc*p* from β-D-Gal*p*-(1→4)-β-D-GlcNAc*p* (type 2 disaccharide). FucT-III, consist of a short NH_2-terminal cytoplasmic tail, a transmembrane domain and a stem region followed by a large globular COOH-terminal catalytic domain. Previous works have reported cloning of the human FucT-III, expression of a soluble form in COS cells and in BHK-21 cell lines.[1] Besides, another construct of recombinant FucT-III turned out to be very efficient to produce sialyl Lewis a libraries.[2]

Within a French network devoted to the production and studies of recombinant glycosyltransferases, the cDNA coding for the human FucT-III gene[1] deleted of the part corresponding to the transmembrane domain was again expressed in three different expression systems: *Pichia pastoris* yeast,[3] Chinese Hamster Ovary (CHO) cells and baculovirus-infected insect cells. In CHO and baculovirus-infected insect cells, a 6His tag was added to the sequence, at the *C*-terminal end in the first case, at the *N*-terminal end in the latter case.[4]

We wish to report here an efficient procedure for concentration, immobilization and stabilization of FucT-III, relying on the His tag of the recombinant enzymes.

In each expression system, CHO and baculovirus-infected insect cells, a functional soluble form of FucT-III was produced. The specificities of both recombinant enzymes were compared (see Table 1). The highest activity was noticed when type 1 disaccharide was substituted by a galactose residue. Activity with the type 2 acceptor increased when concentration changed from 10 to 20 mM, which clearly showed evidence of the low affinity for β-D-Gal*p*-(1→4)-β-D-GlcNAc*p* and β-D-Gal*p*-(1→4)-β-D-Glc*p* disaccharides. No significant difference in substrate specificity has been observed between both FucT-III. Furthermore, a novel fluorescent assay was developed as an alternative to radioactive assays routinely used for glycosyltransferases. For this purpose, new disaccharide derivatives **3**

Table 1 α1,4 and α1,3 activities of recombinant FucT-III expressed in CHO or baculovirus-infected insect cells on various acceptors

	CHO Vrel[a]	Baculovirus Vrel[a]
β-D-Gal*p*-(1→3)-β-D-GlcNAc*p*-O$(CH_2)_7CH_3$[c]	100	100
α-D-Gal*p*-(1→3)-β-D-Gal*p*-(1→3)-β-GlcNAc*p*-O$(CH_2)_7CH_3$[c]	125	112
α-D-NeuAc*p*-(2→3)-β-D-Gal*p*-(1→3)-β-D-GlcNAc*p*-OBn[c]	42	53
β-D-Gal*p*-(1→4)-β-D-GlcNAc*p*-OBn[b]	9.5	4.5
β-D-Gal*p*-(1→4)-β-D-GlcNAc*p*[c]	25	15
β-D-Gal*p*-(1→4)-β-D-GlcNAc*p*[d]	38	38
β-D-Gal*p*-(1→4)-β-D-Glc*p*[c]	37	26
β-D-Gal*p*-(1→4)-β-D-Glc*p*[d]	50	46

[a] Relative velocities with 0.14 mM GDP-[^{14}C]Fuc. [b] Tested at 6 mM because of low solubility in water. [c] Tested at 10 mM. [d] Tested at 20 mM.

Table 2 Kinetic constants of recombinant FucT-III expressed in CHO and baculovirus-infected insect cells, towards dansyl disaccharides **3** and **4**. Enzyme assay conditions with fluorescent acceptors: 50 mM sodium cacodylate buffer pH 7.4, 5 mM ATP, 20 mM $MnCl_2$, 0.2 mM GDP-Fuc, 0.05 to 1 mM disaccharide **3** or **4**. The mixture was incubated at 37 °C for 15 to 60 min with 10-fold concentrated culture supernatant. Samples were analyzed by HPLC on a Waters 600 equipped with a reversed phase column (Nucleosil). Detection was done with a Luminescence Spectrometer LS50B from Perkin–Elmer. Fluorescence of substrate and product was read at 385 nm excitation/540 nm emission.

	Baculovirus	CHO
Vmax for **3**, mU mL^{-1}	22.5	15.5
KM for **3**, mM	0.9	0.4
Vmax for **4**, mU mL^{-1}	2[b]	Nd[a]
KM for **4**, mM	9.9[b]	Nd[a]

[a] Nd: not determined. [b] Because of low solubility of disaccharide **4** in water, 5% DMSO was added.

† Recipient of a fellowship of the European Carbohydrate Research Network Carenet 2.

Table 3 Immobilization of recombinant FucT-IIIs on Ni^{2+}-NTA-agarose. Culture supernatant (23 mL) was immobilized on 1 mL of gel

	Initial soluble enzyme activity mU mL^{-1}[a]	Gel-bound enzyme activity mU mL^{-1}[a]	Immob. yield %[b]
CHO	1.3	28	92
Baculovirus	2.1	41	87

[a] U represents the enzyme unit number defined as the quantity of enzyme that catalyzes transformation of 1 μmole of substrate per min. [b] Immobilization yield is expressed as the ratio of immobilized activity to that initially present in the solution.

and **4** bearing, an aminohexyl chain substituted by a dansyl group at the anomeric center were prepared. Kinetic parameters for these substrates are reported for both enzymes in Table 2.

Recombinant FucT-III were tagged with a polyhistidine tail: indeed a stretch of six His is now commonly appended to the primary sequence of recombinant proteins, in order to facilitate their purification by Ni^{2+} affinity chromatography, according to strong interactions between Ni^{2+} immobilized on agarose through ligands such as nitriloacetic (NTA) and the polyhistidine tag.[5] Thus the 6His-tagged FucT-IIIs were immobilized on Ni^{2+}-NTA-agarose at 4 °C according to a batch procedure. Prior to the binding step, the culture media must be dialyzed, in order to adjust the pH and remove any interfering components. Irrespective of the position of the His tag, the *N*-terminal and *C*-terminal tagged FucT-IIIs were immobilized in quantitative yield (see Table 3). However it is worth noting that attempts to elute enzymes from the gel were troublesome and unsuccessful; imidazole turned out to be a strong inhibitor of FucT-III, and less than 5% of enzyme activity was recovered in the dialyzed eluate. On the contrary, the immobilisation of FucT-III on Ni^{2+}-agarose presented two major advantages. First it turned out to be a very efficient procedure for concentrating enzyme activity (by a 15–20 factor), much better than ultrafiltration bringing about some protein denaturation. Secondly immobilized FucT-III exhibited an outstanding stability under enzymatic incubation conditions at 37 °C with an half-life of three weeks (Fig. 1). On the other hand, CHO culture supernatant incubated in the same conditions proved to be very unstable (Fig. 1).

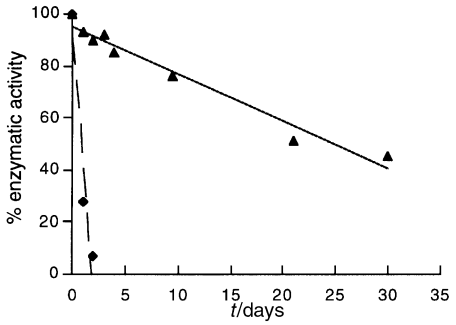

Fig. 1 Percentage of remaining enzymatic activity as a function of incubation time, expressed in days, for FucT-III immobilized on Ni^{2+}-NTA-agarose (▲) and crude CHO culture supernatant (◆) both incubated at 37 °C in 0.1 M sodium cacodylate buffer pH 7.4.

Disaccharide **2** was incubated with GDP-fucose and Mn^{2+} in the presence of the recombinant CHO FucT-III adsorbed on Ni^{2+}-agarose to afford the Lewis x trisaccharide **7** (Scheme 1). Fucosylation of this disaccharide required a long incubation time (10 d) because of its low affinity, but could finally be achieved in 80% yield. At the end of the incubation almost 50% of enzyme activity still remained. Then the same immobilized enzyme could be used two more times for the synthesis of Lewis a trisaccharides **8** and **9** in quantitative yields from the best disaccharide substrates **1** and **3** (Scheme 1).‡

To our knowledge there was one previous report on the use of a recombinant mannosyltransferase immobilized on Ni^{2+}-agarose for synthesis on a microscale, but the increased stability of the immobilized biocatalyst was not highlighted.[6]

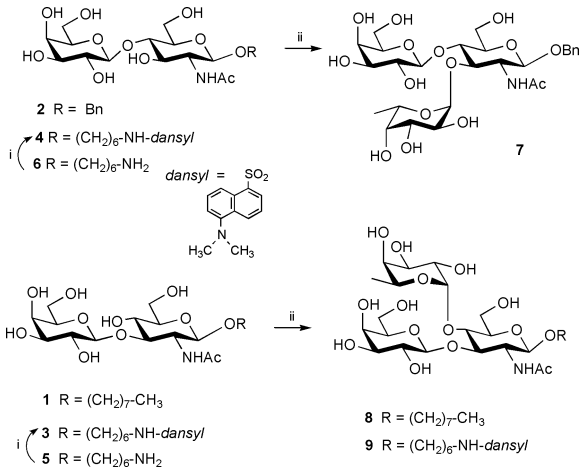

Scheme 1 *Reagents*: i, dansyl chloride, Na_2CO_3, acetone; ii, FucT-III adsorbed on Ni^{2+}–agarose, GDP-Fuc, 5 mM $MnCl_2$.

Work is now in progress to extend immobilisation on Ni^{2+} to other His-tagged recombinant glycosyltransferases and to apply such immobilized enzymes to the supported enzymatic synthesis of oligosaccharides.

This work has been achieved in the frame of the French GTrec Network, supported by MENRT (ACC SV n° 951411) and CNRS (Programmes Interdisciplinaires PCV Génie des et Procédés).

Notes and references

‡ Benzyl-β-D-*N*-acetyllactosamine **2** (0.015 g, 0.032 mmol) was incubated at 37 °C with FucT-III immobilized on Ni^{2+}-NTA-agarose (0.070 U) and GDP-Fuc (0.047 in sodium cacodylate buffer pH 7.4 (3 mL) containing 0.01% NaN_3, $MnCl_2$ (0.015 mmol) and intestine phosphatase (4 U). At the end of incubation, the gel was filtered off and the filtrate was applied onto Sep-Pak C_{18} cartridges; the products were eluted from Sep-Pak with MeOH. The gel could be recycled twice, first with disaccharide **1** (0.032 mmol), secondly with disaccharide **3** (0.016 mmol).

Trisaccharide **7**: 80% yield; δ_H (CD_3OH) 1.10 (d, 3 H, $J_{5,6}$ 6.5 Hz, CH_3), 1.85 (s, 3 H, NAc), 4.41 (d, 1 H, $J_{1,2}$ 7.5 Hz, H-1), 4.52 (d, 1 H, $J_{1',2'}$ 8 Hz, H-1′), 4.62 (d, 1 H, *J* 12 Hz, C-H), 5.00 (d, 1H, $J_{1'',2''}$ 4 Hz, H-1″), 7.35 (5 H, Ph). LRMS: calc. for $C_{27}H_{41}O_{15}N$: *m/z* 619.6; found 642.3 ($M + Na^+$).

Trisaccharide **8:** quant. yield; δ_H (CD_3OH) 0.8 (t, 3 H, CH_3), 1.11 (d, 3 H, $J_{5,6}$ 6.5 Hz, CH_3), 1.22 (m, 12 H, 6 CH_2), 1.48 (m, 2 H, CH_2), 1.98 (d, 3 H, NAc), 4.43 (d, 1 H, $J_{1,2}$ 7.5 Hz, H-1), 4.45 (d, 1 H, $J_{1',2'}$ 8 Hz, H-1′), 4.96 (d, 1H, $J_{1'',2''}$ 3.Hz, H-1″). LRMS: calc. for $C_{28}H_{51}O_{15}N$: *m/z* 641.7; found 664.3 ($M + Na^+$).

Trisaccharide **9**: quant. yield; δ_H (CD_3OH) 1.18 (d, 3 H, $J_{5,6}$ 6.5 Hz, CH_3), 1.92 (s, 3 H, NAc), 2.87 (s, 6 H, $N(CH_3)_2$), 4.36 (d, 2 H, $J_{1',2'} = J_{1,2}$ 7 Hz, H-1′, H-1), 5.3 (d, 1 H, $J_{1'',2''}$ 3.7 Hz, H-1″), 7.25, 7.58, 8.19, 8.3, 8.55 (6 H, dansyl). LRMS: calc. for $C_{38}H_{59}O_{17}N_3S$: *m/z* 861.9; found 884.4 ($M + Na^+$).

1 J. F. Kukowska-Latallo, R. P. Nair, R. D. Larsen and J. B. Lowe, *Genes & Dev.*, 1990, **4**, 1288; T. de Vries, C. A. Srnka, M. M. Palcic, S. J. Swiedler, D. H. van den Eijnden and B. A. Macher, *J. Biol. Chem.*, 1995, **270**, 8712; J. Costa, E. Grabenhorst, M. Nimtz and H. S. Conradt, *J. Biol. Chem.*, 1997, **272**, 11 613.

2 G. Baisch, R. Öhrlein, M. Streiff and F. Kolbinger, *Bioorg. Med. Chem. Lett.*, 1998, **8**, 755.

3 P. F. Gallet, H. Vaujour, J.-M. Petit, A. Maftah, A. Oulmouden, R. Oriol, C. Le Narvor, M. Guilloton and R. Julien, *Glycobiology*, 1998, **8**, 919.

4 C. Benslimane, S. Chenu, H. Tahrat, V. Deparis, C. Augé, M. Cerutti, J. L. Goergen and A. Marc, in *Animal Cell Technology: Products from Cells, Cells as Products*, ed. A. Bernard *et al.*, KAP, Dordrecht, 1999, pp. 251–253.

5 E. Hochuli, H. Döbeli and A. Schacher, *J. Chromatogr.*, 1987, **411**, 177.

6 G. M. Watt, L. Revers, M. C. Webberley, I. B. H. Wilson and S. L. Flitsch, *Carbohydr. Res.*, 1997, **305**, 533.

ChemComm

Non-covalent ternary systems (DNA-acridine hybrid/DNA/lanthanide(III)) for efficient and site-selective RNA scission†

Akinori Kuzuya and Makoto Komiyama*

Research Center for Advanced Science and Technology, The University of Tokyo, 4-6-1 Komaba, Meguro, Tokyo, 153-8904 Japan. E-mail: komiyama@mkomi.rcast.u-tokyo.ac.jp

Received (in Cambridge, UK) 17th August 2000, Accepted 30th August 2000
First published as an Advance Article on the web 2nd October 2000

The target phosphodiester linkage in RNA is activated by the combination of acridine-attached DNA and unmodified DNA, so that the RNA is site-selectively hydrolysed at this linkage by free Lu^{III} ion.

Interests in sequence-selective RNA hydrolysis have been rapidly growing.[1] The most common strategy is to tether chemical scissors (either organic or inorganic) to DNA oligomers.[2] However, non-covalent systems, which involve no tethering and are obtainable without complicated organic synthesis, are also valuable for practical applications.[3] Here we show that non-covalent systems, composed of (i) DNA oligomer bearing an acridine residue, (ii) unmodified DNA, and (iii) free lanthanide(III) ion, selectively and efficiently hydrolyse RNA at the target site. The corresponding phosphodiester linkage is notably activated by non-covalent interactions with the DNAs ((i) and (ii)), and thus the site-selective scission by the metal ion promptly proceeds under physiological conditions. The predominant role of the acridine residue is evidenced.

The substrate RNA (36-mer: ^{32}P-labeled at its 5′-end) and the DNA oligomers are presented in Fig. 1a. When the DNA bears an acridine at the 5′-end (DNA_1-Acr), another DNA (DNA_2), and $LuCl_3$ are combined, the RNA is efficiently and site-selectively hydrolysed (lane 3 in Fig. 2).[4] Here, all the ribonucleotides in the RNA, except for U-19, are forming Watson–Crick base-pairs with either DNA_1-Acr or DNA_2. The selective scission occurs at the 3′-sides of C-18 and U-19 (Fig. 1b). The C-18/U-19 ratio is around 3. When the position of unpaired ribonucleotide in the RNA is moved from U-19 to C-18 by using appropriate DNAs, the site of selective scission accordingly shifts to the 3′-sides of U-17 and C-18 (Electronic Supplementary Information (ESI) Fig. 1a). In the absence of these DNA oligomers, however, RNA scission by Lu^{III} (and by other lanthanide(III) ions also) takes place almost randomly (lane 1 in Fig. 2).

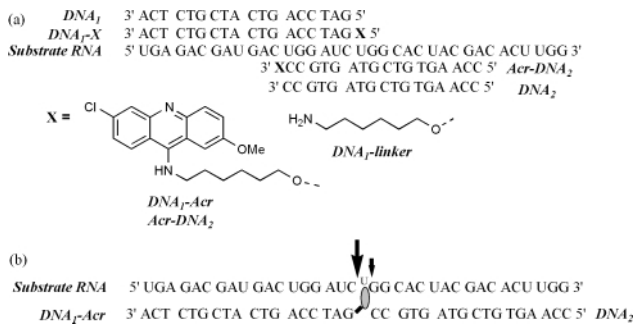

Fig. 1 Structures of the substrate RNA and the DNA oligomers used in the present study (a), and the scission pattern by the DNA_1-Acr/DNA_2/Lu^{III} system (b). The hatched ellipse shows the acridine residue, and the length of arrow corresponds to the scission efficiency.

† Electronic supplementary information (ESI) is available: supplementary Figs. 1–3 and Scheme 1. See http://www.rsc.org/suppdata/cc/b0/b006772p/

Quite significantly, the site-selective RNA scission is far more (> 30 fold)[5] efficient than that by the DNA_1/DNA_2/Lu^{III} system (compare lane 3 in Fig. 2 with lane 2). Furthermore, this selective scission is faster than the scission (at the corresponding site) in the absence of the DNAs (lane 3 *vs.* lane 1). Apparently, the target phosphodiester linkage is significantly activated by the acridine moiety of DNA_1-Acr. A similar site-selective scission is achieved, when Acr-DNA_2 bearing an acridine at the 3′-end is combined with DNA_1 (lane 4). The scission by the DNA_1-Acr/Acr-DNA_2/Lu^{III} system is also selective, but less efficient (lane 5).

Both DNA_1-Acr and DNA_2 (as well as the relevant combinations) are essential for prompt and site-selective scission. When only one of them is used, the whole single-stranded portion in RNA is hydrolysed without any specific selectivity (lanes 2 and 3 in Fig. 3). The DNA bearing only the linker moiety (DNA_1-linker) is also poor in the activity (lane 5), further substantiating the necessary role of the acridine. In the absence of the lanthanide ions, no scission occurs. Site-selective scission is also successful, when two ribonucleotides in the RNA are unpaired (lane 3 in ESI Fig. 1b). Without any unpaired ribonucleotide, however, no scission takes place (lane 1).[6]

One of the most important characteristics of the present non-covalent ternary systems is that the RNA hydrolysis comes up near to completion under physiological conditions. At pH 8.0 and 37 °C ($[LuCl_3]_0$ = 100 μmol dm^{-3}), more than half of the

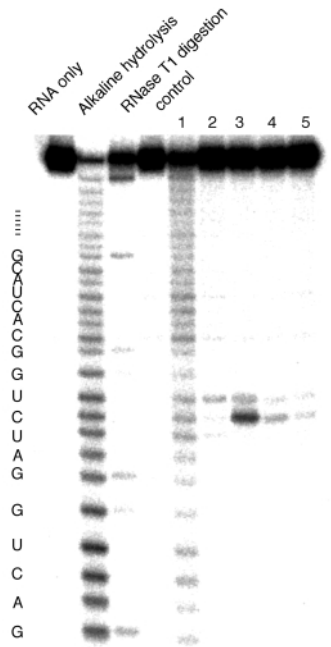

Fig. 2 RNA scission by the ternary systems composed of two DNAs and Lu^{III}. Lane 1, Lu^{III} only; lane 2, DNA_1/DNA_2/Lu^{III}; lane 3, DNA_1-Acr/DNA_2/Lu^{III}; lane 4, DNA_1-Acr/DNA_2/Lu^{III}; lane 5, DNA_1-Acr/Acr-DNA_2/Lu^{III}. At pH 8.0 and 37 °C for 2 h; $[RNA]_0$ = 1, [each of modified or unmodified DNAs]$_0$ = 10, and $[LuCl_3]_0$ = 100 μmol dm^{-3}; $[NaCl]_0$ = 200 mmol dm^{-3}.

DOI: 10.1039/b006772p

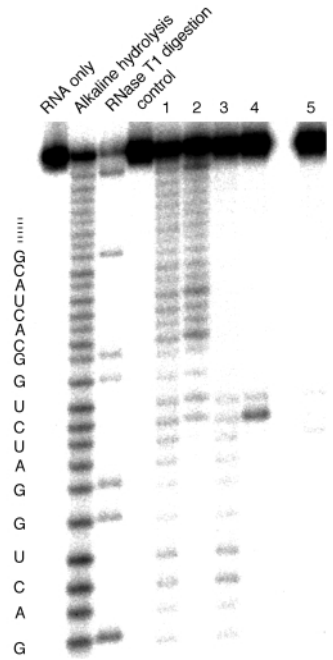

Fig. 3 RNA scission by various non-covalent systems. Lane 1, Lu^{III} only; lane 2, DNA_1-Acr/Lu^{III}; lane 3, DNA_2/Lu^{III}; lane 4, DNA_1-Acr/DNA_2/Lu^{III}; lane 5, DNA_1-linker/DNA_2/Lu^{III}. The reaction conditions are presented in the legend for Fig. 2.

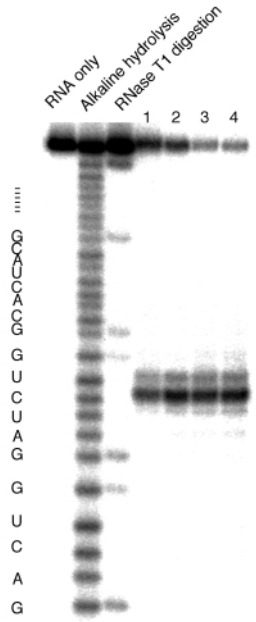

Fig. 4 Time-course of the sequence-selective RNA scission by the DNA_1-Acr/DNA_2/Lu^{III} system: lane 1, 13 h; lane 2, 23 h; lane 3, 40 h; lane 4, 48 h.

RNA is hydrolysed in 13 h by the DNA_1-Acr/DNA_2/Lu^{III} system (lane 1 in Fig. 4). The conversion is nearly 90 mol% at 48 h (lane 4).[7]

In the DNA_1-Acr/DNA_2/RNA system, the UV-visible absorption band of acridine (380–480 nm) shows a clear-cut hypochromicity. In the DNA_1-Acr/RNA system, however, hypochromicity is marginal. These results indicate that the acridine (bound to the 5′-end of DNA_1) is sandwiched by the DNA–RNA base-pair (G–C) at the 5′-terminus of DNA_1 and the C–G base-pair at the 3′-terminus of DNA_2 (see Fig. 1b). Consistently, the fluorescence from the acridine is significantly quenched (ESI Fig. 3).[8] Assumedly, the conformation of the RNA near the sandwiching site is perturbed, and the attacking 2′-OH is brought closer to the P-atom for facile nucleophilic attack. These arguments fairly agree with the fact that neither DNA_1-Acr nor DNA_2 alone activates the RNA (note that the scission efficiencies at C-18 and U-19 in lanes 2 and 3 in Fig. 3 are almost the same as those in lane 1). Only by combining both of them is the target phosphodiester linkage efficiently activated (lane 4). Applications of the present findings are currently under way.

This study was partially supported by a grant from the ‘Research for the Future’ Program of the Japan Society for the Promotion of Science (JSPS-RFTF97I00301) and Grants-in-Aid for Scientific Research from the Ministry of Education, Science, and Culture, Japan.

Notes and references

1 B. N. Trawick, A. T. Daniher and J. K. Bashkin, *Chem. Rev.*, 1998, **98**, 939; M. Oivanen, S. Kuusela and H. Lönnberg, *Chem. Rev.*, 1998, **98**, 961; M. Komiyama, N. Takeda and H. Shigekawa, *Chem. Commun.*, 1999, 1443.

2 K. Matsumura, M. Endo and M. Komiyama, *J. Chem. Soc., Chem. Commun.*, 1994, 2019; J. Hall, D. Hüsken and R. Häner, *Nucleosides Nucleotides*, 1997, **16**, 1357; D. Magda, M. Wright, S. Crofts, A. Lin and J. L. Sessler, *J. Am. Chem. Soc.*, 1997, **119**, 6947; M. Komiyama, T. Inokawa and K. Yoshinari, *J. Chem. Soc., Chem. Commun.*, 1995, 77. J. Hovinen, A. Guzaev, E. Azhayeva, A. Azhayev and H. Lönnberg, *J. Org. Chem.*, 1995, **60**, 2205; M. A. Reynolds, T. A. Beck, P. B. Say, D. A. Schwartz, B. P. Dwyer, W. J. Daily, M. M. Vaghefi, M. D. Metzler, R. E. Klem and L. J. Arnold, Jr., *Nucleic Acids Res.*, 1996, **24**, 760; S. Matsuda, A. Ishikubo, A. Kuzuya, M. Yashiro and M. Komiyama, *Angew. Chem., Int. Ed.*, 1998, **37**, 3284; W. C. Putnam and J. K. Bashkin, *Chem. Commun.*, 2000, 767.

3 Non-covalent systems for site-selective RNA scission were previously reported: D. Hüsken, G. Goodall, M. J. J. Blommers, W. Jahnke, J. Hall, R. Häner and H. E. Moser, *Biochemistry*, 1996, **35**, 16 591; A. Kuzuya, M. Akai and M. Komiyama, *Chem. Lett.*, 1999, 1035.

4 The RNA cleavage was achieved at pH 8.0 (10 mmol dm^{-3} Tris buffer: [NaCl] = 200 mmol dm^{-3}) and 37 °C, and analysed by denaturing polyacrylamide gel electrophoresis. The melting temperatures of the RNA–DNA hetero-duplexes are significantly higher than the reaction temperature, so that they are almost completely formed in the reaction mixtures. The phosphoramidite monomer bearing an acridine was synthesized according to ESI Scheme 1.

5 This value is evaluated from the ratio of band intensities at C-18 and U-19 in lane 3 to those in lane 2. The weak scission in lane 2 is mainly at U-19.

6 When bulge structures were formed in the RNA by using appropriate DNAs (without an acridine residue), the RNA was cleaved at several positions around near the bulge (see ESI Fig. 2).

7 The RNA is hydrolysed mostly at C-18 and U-19, although a minor scission occurs at U-17.

8 The G-20 and G-21 of RNA and the 5′-terminal G of DNA_1-Acr are fixed near the acridine residue, and their guanine residues quench the fluorescence.

ChemComm

Chiral molecular patterns of self-assembled ion pairs composed of (*R*,*S*), (*S*)-16-methyloctadecanoic acid and 4,4′-bipyridine†

Pu Qian,*[a] Hiroshi Nanjo,[a] Toshiro Yokoyama,[a] Toshishige M. Suzuki,*[a] Kazuaki Akasaka[b] and Hiroshi Orhui[b]

[a] *Tohoku National Industrial Research Institute, 4-2-1 Nigatake, Miyagino-ku, Sendai, 983-8551 Japan. E-mail: suzuki@tniri.go.jp; B.Sen@tniri.go.jp (P. Qian); nanjo@tniri.go.jp*

[b] *Graduate School of Agricultural Science, Tohoku University, 1-1 Tsutsumidori-Amamiyamachi Aoba-ku, Sendai, 981-8555 Japan. E-mail: bunseki@agri.tohoku.ac.jp*

Received (in Cambridge, UK) 26th June 2000, Accepted 7th September 2000
First published as an Advance Article on the web 29th September 2000

Self-assembled monolayers of stearic acid, (*R*,*S*) and (*S*)-16-methyloctadecanoic acid ion-paired with 4,4′-bipyridine have been observed on a solution–graphite interface by a scanning tunneling microscope (STM) and the observed macro-scale molecular patterns have been interpreted in terms of absolute chirality of the constituent molecule.

Scanning tunneling microscopy (STM) has provided molecular images of self-assembled molecules at atomic resolution.[1] Monolayers of self-assembled amphiphiles including fatty acids, alkylated amines, amides and alcohols have been directly imaged at solution–solid interfaces.[2] Recently, determination of absolute configuration of chiral molecules from the STM and AFM images has attracted considerable attention.[3] Determination of the absolute stereochemistry is very important for accessing the biological and toxicological properties of enantiomers. Walba and his group have obtained the STM images of several chiral mesogens aligned on a graphite surface.[4] In this case, the macro-scale chiral structure of the domain has been controlled by the molecular chirality of individual molecules. Flynn's group has observed STM images of (*R*,*S*)-2-bromodecanoic acid aligned on graphite.[5] Although they used a racemic mixture, it was possible to assign the absolute configuration of right handed and left handed molecules from the relative location of the bromine atom, long alkyl chain and hydrogen bonded carboxylic acid. These functional groups provided relative contrast in the image and therefore acted as 'chemical markers'.

In the present paper we have attempted to observe directly the molecular patterns of a chiral and racemic 16-methyloctadecanoic acid (16MeC18) which was synthesized from 2-methylbutanol of known absolute configuration.[6] Such branched fatty acids are found in mammalian tissues and play biologically important roles.[7] In order to confirm the relative position of fatty acid in the observed images, we have attempted to insert 4,4′-bipyridine (bpy) between the carboxy groups as a marker. The observed molecular pattern in the macro-scale order has been correlated with the chirality of the constituent molecule.

For the measurement of STM, sample crystals were dissolved in phenyloctane to near saturation and a drop of solution was applied on the surface of freshly cleaved highly oriented pyrolytic graphite (HOPG). The STM images were obtained in both constant current mode and constant height mode using NanoScope IIIa STM (Digital Instruments). The tunneling tip was a Pt–Ir purchased from Digital Instruments or a tungsten wire which was sharpened by electrochemical etching prior to use. Edges of multilayers were not observed in any STM images, indicating that the observed images are those of monolayers.

Fig. 1 shows the STM image of (*S*)-16MeC18 over a scan area of 12 × 12 nm. Unlike stearic acid, these molecules appear to orient parallel to each other forming a centro-symmetric molecular pattern. An interdigitated geometry, in which the head groups alternately point in opposite directions, has been observed for the molecular alignment of stearic acid and other *n*-alkanoic acids.[8] Steric repulsion between the carboxy group and the branched end group may prevent the molecules from aligning interdigitally. Although a small change in the carbon number of *n*-alkanes and straight chain fatty acids has little effect on the molecular pattern, introduction of a single methyl group on the chain dramatically influences the self-assembled molecular pattern. In Fig. 1, the dark area corresponds to hydrogen bonded carboxy groups associated head-to-head,[8] whereas bright bands can be attributed to the branched alkyl ends. Since most unsubstituted fatty acids do not show such marked contrast in the methylene chain, the alkyl end group in this molecule may locate away from the graphite basal plane.

Stearic acid as well as (*S*)-16MeC18 readily formed 2 : 1 ion pairs with 4,4′-bipyridine (bpy) in octylbenzene solution and generated a stable monolayer on HOPG. Their STM images are given in Figs. 2 and 3, along with their possible molecular alignments. The remarkably bright areas in the image correspond to bpy moieties since areas of higher electronic conductance tend to give brighter images.[9] Therefore a conjugate system like bpy can act as a marker, which provides unusual contrast in the obtained image. Obviously, the bpy moiety is sandwiched by two molecules of fatty acid, as depicted in Figs. 2(b) and 3(b). The molecular axis of the stearic acid appears to incline at an angle of 70° with respect to the bpy array, and that of (*S*)-16MeC18 is inclined as well. It is of note that the bpy salt of stearic acid generates two enantiomeric domains in the macro-scale molecular pattern (Fig. 2(a)). Some achiral molecules are known to form mirror image domains in long-range order when assembled on substrate.[3,4] Thus, sponta-

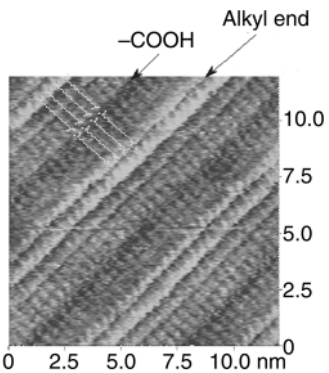

Fig. 1 The STM image of (*S*)-16MeC18 at an interface of phenyloctane and graphite over a scan area of 12 × 12 nm (bias voltage and tunneling current were 1.85 V (tip positive) and 247 pA, respectively).

† Electronic supplementary information (ESI) is available: colour versions of Figs. 1–4. See http://www.rsc.org/suppdata/cc/b0/b005112h/

DOI: 10.1039/b005112h

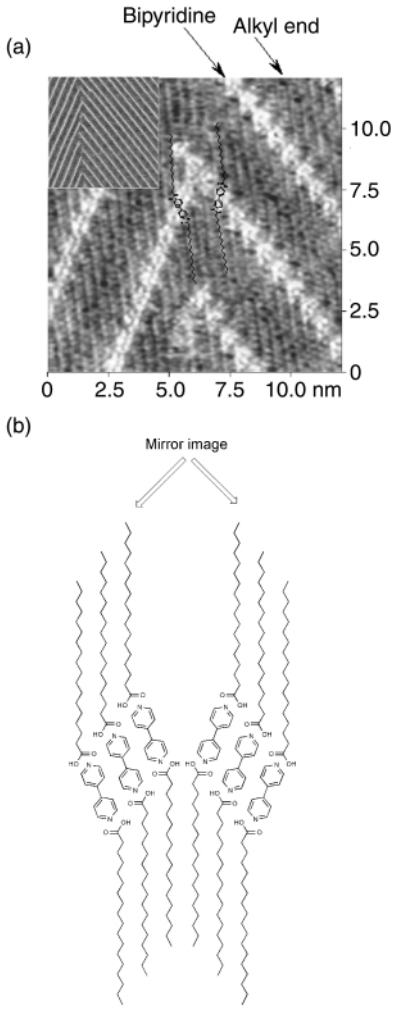

Fig. 2 (a) The STM image of an ion pair composed of stearic acid and 4,4′-bipyridine (2 : 1) over a scan area of 12 × 12 nm (bias voltage and tunneling current were 1.32 V (tip positive) and 234 pA, respectively). A 50 × 50 nm image is inserted in the corner. (b) The schematic drawing of the possible geometry.

neous segregation of achiral bpy salt has taken place upon self-assembly. However, under repeated experiments only a single domain was observed for (*S*)-16MeC18/bpy, as given in Fig.

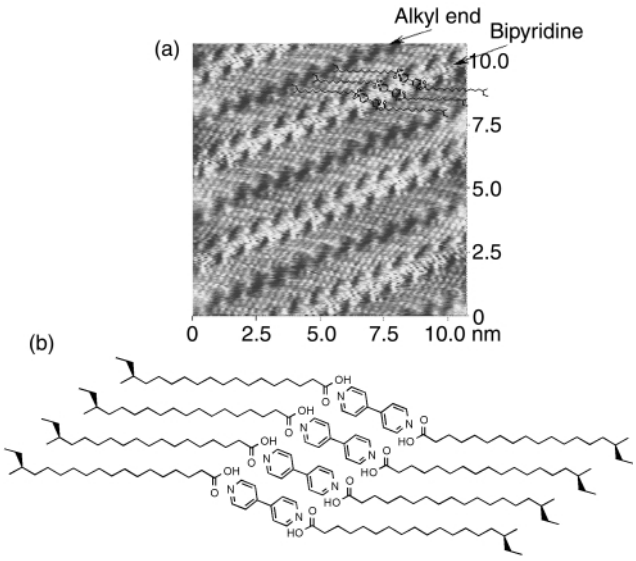

Fig. 3 (a) High resolution STM image of an ion pair composed of (*S*)-16MeC18 and 4,4′-bipyridine (2 : 1) over a scan area of 10.5 × 10.5 nm (bias voltage and tunneling current were 1.85 V (tip positive) and 243 pA, respectively). (b) Proposed molecular alignment of the (*S*)-16MeC18/bpy.

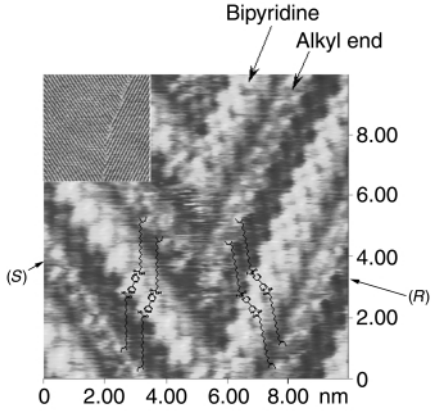

Fig. 4 The STM image of an ion pair composed of (*R*,*S*)-16MeC18 and 4,4′-bipyridine (2 : 1) over a scan area of 10 × 10 nm (bias voltage and tunneling current were 1.80 V (tip positive) and 318 pA, respectively).

3(a). We can clearly see the alkyl chains of the fatty acid as brighter spots. Under careful observation, the alkyl terminal appears to locate out of the straightly stretched alkyl chain. The obtained image is consistent with an (*S*) configuration provided that the bright spot at the alkyl terminal is assigned to the ethyl group, as depicted in Fig. 3(b). Fig. 4 shows the STM image of (*R*,*S*)-16MeC18–bpy over a scan area of 10 × 10 nm, where the racemate mixture appears to segregate into two domains. Thus two different domains of pure enantiomers have grown on the graphite surface from the racemate solution. Since macro-scale morphology of the aligned molecule has been defined by the handedness of the constituent molecule, we can assign the configuration of molecules in each domain by comparison with the macro molecular pattern of (*S*)-16MeC18.

Notes and references

1 J. P. Rabe and S. Buchholz, *Science*, 1991, **253**, 442; A. A. Grewirth and B. K. Niece, *Chem. Rev.*, 1997, **97**, 1129.

2 D. M. Cyr, B. Venkataraman, G. W. Flynn, A. Black and G. M. Whitesides, *J. Phys. Chem.*, 1996, **100**, 13 747; C. L. Claypool, F. Francesco, W. A. Goddard III, H. B. Gray, N. S. Lewis and R. A. Marcus, *J. Phys. Chem. B*, 1997, **101**, 5978; Pu Qian, H. Nanjo, T. Yokoyama and T. M. Suzuki, *J. Chem. Soc., Chem. Commun.*, 1999, 1197.

3 G. P. Lopinski, D. J. Moffatt, D. D. M. Wayner and R. A. Wolkow, *Nature*, 1998, **392**, 909; R. Viswanathan, J. A. Zasadzinski and D. K. Schwartz, *Nature*, 1994, **368**, 440; C. J. Eckhardt, N. M. Peachey, D. R. Swanson, J. M. Takacs, M. A. Khan, X. Gong, J.-H. Kim, J. Wang and R. A. Uphaus, *Nature*, 1993, **362**, 614.

4 D. M. Walba and F. Stevens, *Acc. Chem. Res.*, 1996, **29**, 591; F. Stevens, D. J. Dyer and D. M. Walba, *Angew. Chem., Int. Ed. Engl.*, 1996, **35**, 900.

5 H. Fang, L. C. Giancarlo and G. W. Flynn, *J. Phys. Chem. B*, 1998, **102**, 7311.

6 Racemic and (*S*)-16-methyloctadecanoic acids ((*R*,*S*) and (*S*)-16MeC18) were prepared from racemic and (*S*)-2-methyl-1-butyl tosylate as follows. 1-Benzyloxy-14-methylhexadecane was prepared from 2-methyl-1-butyltosylate by Grignard coupling reaction with 12-benzyloxy-1-dodecylmagnesium bromide. After debenzylation of 1-Benzyloxy-14-methylhexadecane and tosylation, the tosylate was reacted with allylmagnesium bromide to produce 17-methyl-1-nonadecene. Then, it was oxidized to 16-methyloctadecanoic acid by $KMnO_4$ in water–CH_2Cl_2 in the presence of tetrabutylammonium bromide as a phase-transfer reagent. The structures of (*R*,*S*)- and (*S*)-16MeC18 were confirmed by their ^{1}H-NMR and high resolution MS spectra.

7 K. Akasaka and H. Ohrui, *Biosci. Biotechnol. Biochem.*, 1999, **63**, 1209.

8 M. Hibino, A. Sumi and I. Hatta, *Jpn. J. Appl. Phys.*, 1995, **34**, 610; *Jpn. J. Appl. Phys.*, 1995, **34**, 3354.

9 P. Sautet, *Chem. Rev.*, 1997, **97**, 1097.

Rapid enantiomeric determination of α-hydroxy acids by electrospray ionization tandem mass spectrometry

W. Andy Tao, Lianming Wu and R. Graham Cooks*

Department of Chemistry, Brown Laboratories, Purdue University, West Lafayette, IN 47907 USA. E-mail: cooks@purdue.edu; Fax: (765) 494-9421

Received (in Corvallis, OR, USA) 31st July 2000, Accepted 29th August 2000
First published as an Advance Article on the web 28th September 2000

Direct chirality measurement of tartaric and other α-hydroxy acids at very low enantiomeric excess (ee) using a fast new mass spectrometric method.

Tartaric acid is a special molecule in the history of chirality. As the first compound resolved[1] it triggered the concept of molecular chirality and for more than 150 years it has been used to explore new chiral technologies. For instance, tartaric acid has recently been absorbed on a copper surface to study heterogeneous enantioselectivity.[2] Herein, tartaric acid, along with other α-hydroxy acids, is employed as a model compound to study chiral analysis by mass spectrometry. Previously, ester derivatives of tartaric acid, although not the acid itself, were extensively studied for gas-phase chiral recognition.[3–5] These studies, along with most other mass spectrometric experiments attempting to achieve gas-phase chiral recognition,[6,7] were qualitative. We report the first enantiomeric quantification of tartaric acid and other α-hydroxy acids in the gas phase, on the basis of a newly developed method[8,9] that employs cluster ions comprised of the analyte, a chiral reference and a transition metal. Chiral discrimination is achieved in the dissociation of these cluster ions and evaluated by the kinetic method[10,11] that is sensitive to small energy differences between diastereomers. Two independent parallel reactions are used to monitor the chiral distinction and measurements of the ratio of product ion abundances allow the quantification of enantiomeric mixtures, even at low enantiomeric excess (ee). This simple chiral analysis method employs a standard commercial instrument.[12]

Electrospray ionization (ESI) was performed on an aqueous methanol solution containing a mixture of an analyte (α-hydroxy acid, A, as an enantiomeric mixture A_R and A_S, 100 μM), a chiral reference compound (chiral amino acid, ref*,100 μM), and a transition metal ion (Co(II), 25 μM). The electrosprayed solution formed abundant singly-charged cluster ions $[Co^{II}(ref^*)_2(A) - H]^+$ which were mass-selected and dissociated in a quadrupole ion trap to competitively form the dimeric complexes $[Co^{II}(A)(ref^*) - H]^+$ and $[Co^{II}(ref^*)_2 - H]^+$ by the loss of neutral reference compound, ref*, and analyte, A, respectively. The difference in stability of the diastereomeric ions $[Co^{II}(A)(ref^*) - H]^+$ due to the two configurations of the analyte A, results in different abundances, relative to the abundance of the $[Co^{II}(ref^*)_2 - H]^+$ ion. The relative abundance ratio R (eqn. 1) depends on the enantiomeric composition of the analyte, A:

$$R = [Co^{II}(A)(ref^*) - H]^+ / [Co^{II}(ref^*)_2 - H]^+ \quad (1)$$

When the analyte is enantiomerically pure, R equals R_R or R_S. Therefore, the ratio of R_R to R_S, defined as R_{chiral}, measures the degree of chiral distinction:[13]

$$R_{chiral} = R_R / R_S = \frac{[Co^{II}(A_R)(ref^*) - H]^+ / [Co^{II}(ref^*)_2 - H]^+}{[Co^{II}(A_S)(ref^*) - H]^+ / [Co^{II}(ref^*)_2 - H]^+} \quad (2)$$

Tartaric and four other α-hydroxy acids (malic acid, mandelic acid, 3-phenyllactic acid, citramalic acid) were selected for chiral analysis. Chiral references were chosen for their capability to produce large steric interactions and for structural similarity to the analyte. Such similarity allows the complexes to form easily and it also allows accurate relative abundance ratios to be measured, otherwise dissociation proceeds overwhelmingly to form the more stable product. Amino acids (α-aminocarboxylic acids) having similar structures to the analyte (α-hydroxy acid) and the nineteen natural chiral α-amino acids, plus numerous other amino acids, provide an array of choices. Aromatic amino acids were observed to provide the greatest chiral distinction.[8,9] The use of Co(II) ion as the central ion rather than Cu(II) or Ni(II) previously used for chiral recognition of amino acids[8,9] is because of its ready binding to hydroxy groups. By contrast, Cu(II) and Ni(II) bind to amino groups so strongly that loss of the hydroxy acid is the only observed dissociation channel.

Typical spectra showing the distinction of D- and L-malic acid, using L-tyrosine as the chiral reference, are shown in Fig. 1. The chiral recognition of five α-hydroxy acids is summarized in Table 1. Abundance ratios showed standard deviations of 2%. Chiral selectivity (R_{chiral})[13] values for the five α-hydroxy acids ranged from 0.67 to 1.43. Among them, tartaric acid shows moderate chiral selectivity (R_{chiral} = 1.29). Mandelic acid shows a low affinity for Co(II) and there is no chiral distinction between *R* and *S*-mandelic acids with L-alanine as reference. However, when a chiral aromatic compound, L-3-phenyllactic acid, is used as reference, chiral distinction is observed with an

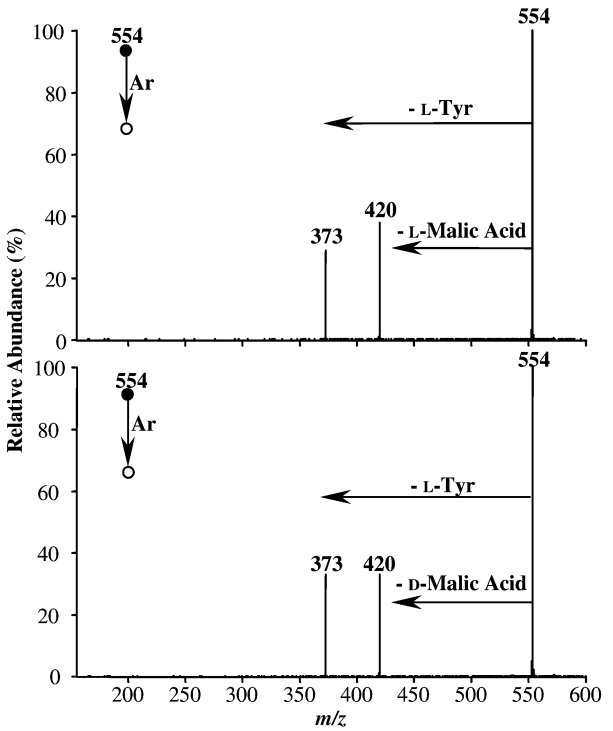

Fig. 1 MS/MS product ion spectra of (a) $[Co^{II}$(L-malic acid)$(L\text{-Tyr})_2 - H]^+$ (*m/z* 554); (b) $[Co^{II}$(D-malic acid)$(L\text{-Trp})_2 - H]^+$ (*m/z* 554). The CID activation level is chosen as 11%, corresponding to approximately 275 mV AC.

DOI: 10.1039/b006277o

Table 1 Chiral recognition of α-hydroxy acids.[a,b]

A	Ref*	$[Co^{II}(ref^*)(A) - H]^{+\cdot}/[Co^{II}(ref^*)_2 - H]^{+\cdot}$	R_{chiral}
D-Tartaric acid	L-Tyr	0.823	1.29
L-Tartaric acid		0.640	
D-Malic acid	L-Tyr	1.11	1.43
L-Malic acid		0.775	
R-Mandelic acid	L-Ala	1.00	1.00
S-Mandelic acid		1.02	
R-Mandelic acid	L-3-Phenyllactic acid	0.175	0.81
S-Mandelic acid		0.216	
D-3-Phenyllactic acid	L-Pro	0.168	1.29
L-3-Phenyllactic acid		0.130	
D-3-Phenyllactic acid	L-Phe-d_5	0.0226	0.67
L-3-Phenyllactic acid		0.0337	
R-Citramalic acid	L-Tyr	5.81	1.35
S-Citramalic acid		4.30	

[a] R_{chiral} is defined in eqn. 2. [b] CID activation level is optimized in each experiment and then kept constant for the measurement of enantiomers.

R_{chiral} value of 0.81. Chiral recognition of D- and L-3-phenyllactic acids shows the largest chiral effect using L-phenylalanine-d_5 as the reference (an isotopically labelled compound was used for convenience, since there is only one-dalton mass difference between phenylalanine and 3-phenyllactic acid). As expected,[8,9] when a non-aromatic compound, for example L-proline, is used as reference the chiral selectivity is smaller.

Quantification of tartaric acid was performed using an enantiomerically pure chiral reference (L-tyrosine) and tartaric acid in various ee. The experiments focused on mixtures with extreme ee values, since these are particularly difficult to analyze accurately and yet combinatorial syntheses frequently yield such samples. The ratio (*R*) of the two fragment ions was measured in a single tandem (MS/MS) spectrum as a function of the ee of the tartaric acid. A linear relationship of ln (*R*) *versus* ee was obtained (Fig. 2) with a correlation coefficient (r^2) of 0.9945. Such a linear correlation between the logarithm of the fragment ion abundance ratio and the ee is intrinsic to the kinetic method[10,11] and is the result of the logarithmic relationship between relative ion abundance and energy that characterizes this method.[14] On the basis of such an experimentally established semi-log plot, two-point calibrations can be performed using a racemic sample and a sample of known ee and quantitative chiral analysis carried out by measuring the ratio of two fragment ions in a single spectrum, within a time of about 1 min.

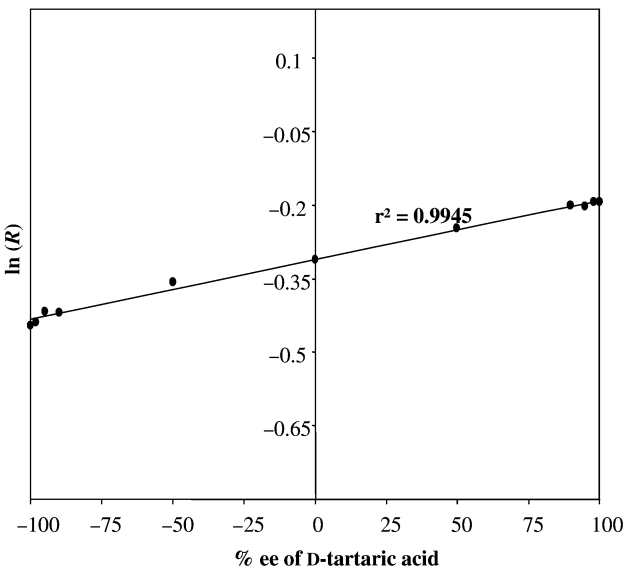

Fig. 2 Calibration curve for chiral analysis of tartaric acid using L-tyrosine as the reference.

The present study has described a novel method for rapid enantiomeric determination. At low %ee values, where the error is greatest, tartaric acid samples whose ee values differ by 2% (3 and 5%) can be distinguished at the σ confidence level in the current experiments.[15] When applying the method to real mixtures, matrix effects may influence its accuracy. Note that the chiral resolution (R_{chiral}) achieved for tartaric acid is only 1.29, and further improvement in chiral selectivity will further improve the method. The experiment, along with the previous observation of chiral analysis of other types of chiral compounds, represents a general mass spectrometric method for gas-phase chiral analysis. The measurements are simple, rapid, and only require very small amounts of sample for analysis. Further extension of this work to the study of other chiral compounds, such as chiral drugs is in progress.

This work was supported financially by the United States Department of Energy, Office of Energy Research. A Fellowship from Triangle Pharmaceuticals (to W.A.T.) is gratefully acknowledged.

Notes and references

1 L. C. R. Pasteur, *Hebd. Seance Acad. Sci. Paris*, 1848, **2**, 535.
2 M. O. Lorenzo, C. J. Baddeley, C. Muryn and R. Raval, *Nature*, 2000, **404**, 376.
3 E. V. Denisov, V. Shustryakov, E. N. Nikolaev, F. J. Winkler and R. Medina, *Int. J. Mass Spectrom.*, 1997, **167**, 259.
4 T. T. Dang, S. F. Pedersen and J. A. Leary, *J. Am. Soc. Mass Spectrom.*, 1994, **5**, 452.
5 E. N. Nikolaev, E. V. Denisov, V. S. Rakov and J. H. Futrell, *Int. J. Mass Spectrom.*, 1999, **183**, 357.
6 M. Sawada, *Mass Spectrom. Rev.*, 1997, **16**, 73.
7 A. Filippi, A. Giardini, S. Piccirillo and M. Speranza, *Int. J. Mass Spectrom.*, 2000, **198**, 137.
8 W. A. Tao, D. Zhang, F. Wang, P. Thomas and R. G. Cooks, *Anal. Chem.*, 1999, **71**, 4427.
9 W. A. Tao, D. Zhang, E. N. Nikolaev and R. G. Cooks, *J. Am. Chem. Soc.*, in the press.
10 R. G. Cooks and P. S. H. Wong, *Acc. Chem. Res.*, 1998, **31**, 379.
11 R. G. Cooks, J. S. Patrick, T. Kotiaho and S. A. McLuckey, *Mass Spectrom. Rev.*, 1994, **13**, 287.
12 All experiments were performed using a commercial LCQ ion trap mass spectrometer (Finnigan, San Jose, CA), equipped with an ESI source and operated in the positive ion mode. Spectra shown represent the average of about 50 scans, each requiring 0.2 s. The sample was infused *via* a syringe pump at a flow rate of 1–2 μL min^{-1}. The collision-induced dissociation (CID) conditions were optimized for each analyte.
13 R_{chiral} is equivalently defined as the ratio of R_D to R_L (nomenclature commonly used for chiral acids). The further the R_{chiral} value is from unity, the higher the degree of chiral recognition. $R_{chiral} = 1$ indicates no chiral discrimination, which means that the particular combination of Co(II) ion and reference ligand fails to create stereochemically-distinctive interactions with the enantiomers under the observation conditions employed.
14 From the kinetic method, ln (*R*) is linearly proportional to the energy change $\Delta Co^{II}BDE\{(A)(ref^*)\}$, where $\Delta Co^{II}BDE\{(A)(ref^*)\}$ is defined as energy of the reaction $[Co^{II}(ref^*)_2 - H]^+ + A \rightarrow [Co^{II}(ref^*)(A) - H]^+ + ref^*$, and the designation $\Delta Co^{II}BDE\{(A)(ref^*)\}$ is used to recognize that the energy term involves both deprotonation and binding to Co. The quantity $\Delta Co^{II}BDE\{(A)(ref^*)\}$ is linearly proportional to the ee of the analyte A, therefore ln (*R*) changes linearly with ee. Detailed derivation is available in ref. 9.
15 Multiple injections were used to determine these values which refer to standard deviation σ.

Natural bond orbital dissection of fluorine–fluorine through-space NMR coupling ($J_{F,F}$) in polycyclic organic molecules

J. E. Peralta,[a] R. H. Contreras*[b] and J. P. Snyder*[a]

[a] *Departamento de Física, Facultad de Ciencias Exactas y Naturales, Universidad de Buenos Aires, Argentina*
[b] *Department of Chemistry, Emory University, Atlanta, GA 30322, USA. E-mail: snyder@euch4e.chem.emory.edu*

Received (in Corvallis, OR, USA) 1st August 2000, Accepted 1st September 2000
First published as an Advance Article on the web 29th September 2000

A new approach to deconvolute DFT and *ab initio* Fermi contact-derived NMR coupling constants into conceptually familiar localized orbital contributions (NJC analysis) is exemplified by analysis of through-space *J*(F,F) couplings in a few illustrative cases.

Large NMR spin–spin coupling between two proximate atoms that are otherwise separated by a considerable number of formal bonds, through-space coupling, has been observed for many years. Very early, the idea that spin polarization associated with the Fermi contact coupling mechanism can be transmitted between such atoms was advanced.[1] Since that time, both experimental and theoretical evaluations of through-space coupling has stimulated useful insights on how such a mechanism operates.[2–6] Most known theoretical approaches are semiempirical in nature. They partition the total coupling according to the electronic mechanisms involved in spin polarization transmission.[7–9] One attempt to extend the IPPP[9] method to the *ab initio* level proved to be intractable for systematic study of practical problems.[10]

Recently, very efficient and reliable implementations of Finite Perturbation Theory[11] within the Gaussian suite of programs[12] permit calculation of the Fermi contact contribution to spin–spin couplings, J^{FC}(A,B). Both single (FPT-1) and double perturbation (FPT-2) approaches have been reported and reviewed.[13,14] For calculating J^{FC}(A,B) within the FPT-1 method, the Fermi contact operator is introduced as a perturbation placed at only one of the two coupled nuclei, *e.g.* A. The resulting interaction spin-polarizes the electronic environment to define a spin density at nucleus B proportional to J^{FC}(A,B).

Ordinarily, the spin density is written in terms of canonical molecular orbitals. However, if localized molecular orbitals are employed instead, then each localized orbital contribution to J^{FC}(A,B) can be rationalized in terms of familiar chemical concepts. In this way, a practical and intuitive theoretical approach to dissecting J^{FC}(A,B) couplings into different transmission mechanisms is achieved.

In the present work, natural localized molecular orbitals (NLMO) provided by natural bond orbital analysis, NBO,[15] are utilized to express the spin density. The latter and, consequently, J^{FC}(A,B) can then be rewritten as a sum of contributions in terms of core orbitals, CR, non-bonding electron pairs, LP, and bonding orbitals, BD, as in eqn. (1). We refer to the method as natural *J*-coupling (NJC) analysis and consider it a complement to natural chemical shielding analysis (NCS).[16] All calculations of Fermi contact terms reported here were carried out with the Gaussian 98 suite of programs[12] at the DFT B3LYP/6-311G** level.

$$J^{FC}(A,B) = J_{CR}(A,B) + J_{LP}(A,B) + J_{BD}(A,B) \qquad (1)$$

Eqn. (1) is particularly suited to the study of through-space *J*-coupling originating from lone-pair overlap between atoms which are proximate in space, a problem of considerable current interest.[6,17] Three examples illustrate mechanistic insights obtained from the approach. The first case concerns the hydrogen fluoride dimer as a model for pure intermolecular F–F coupling. In this very simple system evaluated for different planar configurations (**1**), the coupling mechanisms can be

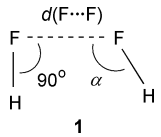

1

understood on intuitive grounds. Fig. 1 displays the total J^{FC}(F,F) coupling and the J_{LP}(F,F), J_{CR}(F,F) and J_{BD}(F,F) contributions as a function of F···F distance for α = 90°. Several features of the plots are noteworthy. The total J^{FC}(F,F) coupling decreases rapidly with increasing *d*(F···F) following the same trend as the absolute values for the different components. The J_{LP}(F,F) and J_{CR}(F,F) contributions correspond to positive decrements, while J_{BD}(F,F) is negative. In agreement, several experimental reports on *J*(H,H) and *J*(F,H) couplings offer evidence that through-space transmission as a result of direct overlap between two bonds elicits a negative contribution.[3,18] With respect to different lone pairs within the HF dimer, the J_{LP}(F,F) breakdown suggests that (a) the lone pairs of both fluorine atoms whose NLMOs are of π-symmetry do not participate in through-space transmission; (b) the NLMOs of lowest energy yield the largest and positive contribution to J^{FC}(F,F); and (c) the *J*-contribution of the lone pairs of highest energy are negative but of notably smaller absolute value than that described in (b). However, actual values of each component depend strongly on α for a given *d*(F···F) distance. Thus, for *d*(F···F) = 2.3 Å and α = 90°, J^{FC}(F,F), J_{LP}(F,F), J_{CR}(F,F) and J_{BD}(F,F) are calculated to be 245, 210, 53 and −18 Hz, respectively. On the other hand, for α = 120° at the same distance, the values are 351, 330, 90 and −70 Hz, respectively. These NJC variations call for caution when *J*(F,F) couplings dominated by a through-space mechanism are correlated with only the *d*(F···F) parameter.

Our second example is taken from compound **2**, in which $^4J(F_a,F_b)$ and $^4J(F_a,F_c)$ were reported to be 37 and 24 Hz, respectively.[19] In order to study the behavior of the through-

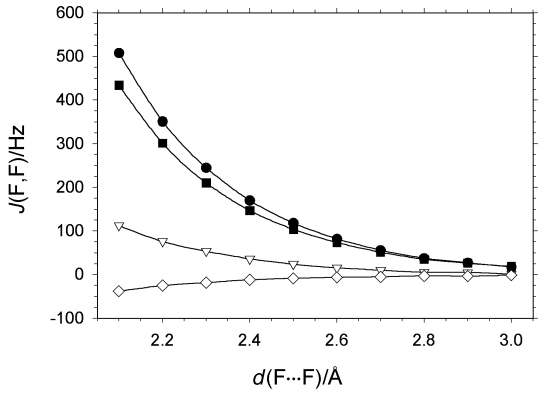

Fig. 1 Plots of J^{FC}(F,F), ●, in the hydrogen fluoride dimer **1** and its J_{LP}(F,F), ■, J_{CR}(F,F), ▽, and J_{BD}(F,F), ◇, contributions as a function of *d*(F···F); α = 90°.

DOI: 10.1039/b006283i

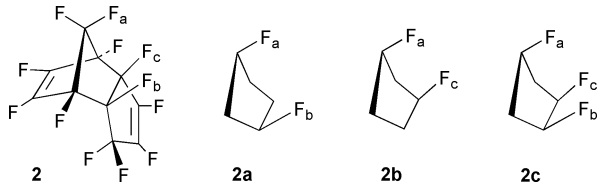

space components of the two couplings for fluorine atoms with the same configuration, the structure of **2** was first optimized with the MM3*/MacroModel.[20] The five-membered ring structures **2a**–**c** were then constructed from optimized **2** by preserving local heavy atom geometries; that is, both distance and angular relationships between the fluorine atoms are unchanged. The lone pair contributions to $^4J^{FC}(F_a,F_b)$ and $^4J^{FC}(F_a,F_c)$ in **2a**–**c** are compared with their respective total $^4J^{FC}(F,F)$ couplings in Table 1. While the latter calculated values do not accurately reproduce the corresponding experimental values in **2**, a number of qualitative trends are evident. $^4J_{LP}(F,F)$ and $^4J_{CR}(F,F)$ are positive and correspond to contributions transmitted through-space. On the other hand, the negative term $\Delta^4J(F,F)$ is composed of both through-space and through-bond contributions, the former originating in the direct superposition of two C–F bonds. Not surprisingly, the absolute value of $\Delta^4J(F_a,F_b)$ (16–20 Hz) is considerably larger than that for $\Delta^4J(F_a,F_c)$ (3–5 Hz) (Table 1). To interpret the difference, we note that the fluorine pairs F_a/F_b and F_a/F_c are linked by four bonds, while the fluorine atoms in each pair are separated by 2.56 and 2.92 Å, respectively. A reasonable assumption is that the −3 to −5 Hz exhibited by $\Delta^4J(F_a,F_c)$ is an upper limit for through-bond coupling. Thus, the −16 to −20 Hz calculated for $\Delta^4J(F_a,F_b)$ can be viewed primarily as a C–F bond through-space effect, a result in harmony with the HF dimer model calculations.

In the final example, we perform an NJC analysis for the *peri*-$^4J^{FC}(F,F)$ coupling in compounds **3a** and **3b**. The total $J^{FC}(F,F)$

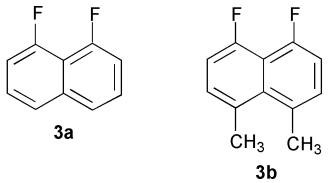

coupling and the $J_{LP}(F,F)$, $J_{CR}(F,F)$ and $J_{BD}(F,F)$ contributions to these *peri*-$^4J^{FC}(F,F)$ couplings are compared in Table 2. While the total $J^{FC}(F,F)$ couplings are underestimated by 12–15%, they follow experiment nicely. All contributions are in agreement with expections based on molecular geometry. For instance, the larger absolute values of $^4J_{LP}(F,F)$, $^4J_{CR}(F,F)$ and $\Delta^4J(F,F)$ in **3b** with the smaller $d(F\cdots F)$ (Table 2), parallel the trends described above for the FH dimer (Fig. 1). Similar to **2a**–**c**, the combined and negative through-bond and through-space term, $\Delta^4J(F,F)$, is larger for the shorter distance. As before, we assume a similar ^4J through-bond coupling (both σ and π) for **3a** and **3b**. The calculated difference of −11.8 Hz can thus be attributed to the C–F bonds contribution to coupling in the latter compound.

Table 1 Becke3LYP/6-311G**/NBO values for $^4J^{FC}(F,F)$ (Hz) and component couplings in **2a**–**c**

Coupling	**2a**		**2b**	**2c**
	$^4J(F_a,F_b)$	$^4J(F_a,F_c)$	$^4J(F_a,F_b)$	$^4J(F_a,F_c)$
$^4J^{FC}(F,F)$	68.0	7.6	67.7	9.0
$^4J_{LP}(F,F)$	72.9	11.8	71.1	12.6
$^4J_{CR}(F,F)$	14.5	0.4	13.0	0.2
Δ^4J $(F,F)^a$	−19.4	−4.6	−16.4	−3.8
$d(F\cdots F)^b$	2.56	2.92	2.56	2.92

[a] $\Delta^4J(F,F) = {}^4J^{FC}(F,F) - [{}^4J_{LP}(F,F) + {}^4J_{CR}(F,F)]$. [b] From MM3*/MacroModel[19] optimized **2**(Å).

Table 2 Becke3LYP/6-311G**/NBO and experimental values for $^4J^{FC}(F,F)$ (Hz) and component couplings in **3a** and **3b**

Coupling	**3a**	**3b**
$^4J^{FC}(F,F)$	52.1	73.2
$^4J_{LP}(F,F)$	58.2	86.4
$^4J_{CR}(F,F)$	10.8	15.5
Δ^4J $(F,F)^a$	−16.9	−28.7
Jexp[b]	59.0	85.2
$d(F\cdots F)^c$	2.580	2.508

[a] $\Delta^4J(F,F) = {}^4J^{FC}(F,F) - [{}^4J_{LP}(F,F) + {}^4J_{CR}(F,F)]$. [b] Taken from F. B. Mallory, *et al*.[17] [c] MM3*/MacroModel optimized **3a** and **3b** (Å). X-ray of 1,8-difluoronaphthalene, $d(F\cdots F)$ = 2.584 Å; P. A. Meresse, C. Courseille, F. Leroy and N. B. Chanh, *Acta Crytallogr. B*, 1975, **31**, 1236.

In summary, the main features of dissection of $J(F,F)$ couplings transmitted through-space in compounds such as **2**–**3** are in good agreement with currently accepted mechanisms, especially the lone-pair overlap proposal of Mallory and co-workers.[17] However, in addition to presenting a novel tool for *J*-analysis, we also highlight the previously unrecognized importance of angular effects and X–F bond–bond coupling contributions. Future NJC analyses will explore these phenomena in detail.

R. H. C. and J. E. P. gratefully acknowledge financial support from CONICET, UBATEC and ANPCyT. R. H. C. also acknowledges the kind hospitality of the Emerson Center (Department of Chemistry, Emory University) during his visit as an Emerson Fellow.

Notes and references

1 L. Petrakis and C. H. Sederholm, *J. Chem. Phys.*, 1961, **35**, 1243; D. R. Davis, R. P. Lutz and J. D. Roberts, *J. Am. Chem. Soc.*, 1961, **83**, 246.
2 J. Hilton and L. H. Sutcliffe, *Prog. NMR Spectrosc.*, 1975, **10**, 27.
3 R. H.Contreras, M. A. Natiello and G. E. Scuseria, *Magn. Reson. Rev.*, 1985, **9**, 239.
4 F. B. Mallory and C. W. Mallory, in *Encyclopedia of Nuclear Magnetic Resonance*, ed. D. M. Grant and R. K. Harris, J. Wiley & Sons, Chichester, 1996, vol. 3, p. 1491.
5 R. H. Contreras and J. C. Facelli, *Ann. Rep. NMR Spectrosc.*, 1993, **27**, 255.
6 R. H. Contreras and J. E. Peralta, *Prog. NMR Spectrosc.*, in the press.
7 M. Barfield, *J. Am. Chem. Soc.*, 1980, **102**, 1.
8 A. R. Engelmann, R. H. Contreras and J. C. Facelli, *Theoret. Chim. Acta*, 1981, **59**, 17.
9 A. R. Engelmann and R. H. Contreras, *Int. J. Quantum Chem.*, 1983, **23**, 1033.
10 P. Lazzeretti, M. Malagoli, R. Zanasi, E. W. Della, I. J. Lochert, C. G. Giribet, M. C. Ruiz de Azúa and R. H. Contreras, *J. Chem. Soc., Faraday Trans.*, 1995, **91**, 4031.
11 J. A. Pople and D. L. Beveridge, *Approximate Molecular Orbital Theory*, McGraw–Hill, New York (1970).
12 Gaussian 98, Revision A.7, Gaussian Inc., Pittsburgh, PA, 1998.
13 R. H. Contreras, J. E. Peralta, M. C. Ruiz de Azúa, C. G. Giribet and J. C. Facelli, *Ann. Reps. NMR Spectrosc.*, 2000, **41**, 55.
14 J. E. Peralta, M. C. Ruiz de Azúa and R. H. Contreras, *Theoret. Chem. Acc.*, in the press.
15 J. P. Foster and F. Weinhold, *J. Am. Chem. Soc.*, 1980, **102**, 7211; A. E. Reed, L. A. Curtis and F. Weinhold, *Chem. Rev.*, 1988, **88**, 899; NBO version 3.1, E. D. Glendening, A. E. Reed, J. E. Carpenter and F. Weinhold (in ref. 12).
16 J. A. Bohmann, F. Weinhold and T. C. Farrar, *J. Chem. Phys.*, 1997, **107**, 1173.
17 F. B. Mallory, C. W. Mallory, K. E. Butler, M. B. Lewis, A. Q. Xia, E. D. Luzik Jr., L. E. Fredenburgh, M. M. Ramanjulu, Q. N. Van, M. M. Francl, D. A. Freed, C. C. Wray, C. Hann, M. Nerz-Stormes, P. J. Carroll and L. E. Chirlian, *J. Am. Chem. Soc.*, 2000, **122**, 4108.
18 T. Schaefer, S. Kroeker and D. M. McKinnon, *Can. J. Chem.*, 1995, **73**, 2208.
19 R. Fields, M. Green and A. Jones, *J. Chem. Soc. B*, 1967, 270.
20 MacroModel web site: http://www.schrodinger.com/macromodel.html

Synthesis and structural characterisation of the first hexaphosphastrontocene $[Sr(\eta^5\text{-}P_3C_2Bu^t_2)_2]$ and its pyrazine adduct

Matthew D. Francis, Peter B. Hitchcock and John F. Nixon*

School of Chemistry, Physics and Environmental Sciences, University of Sussex, Falmer, Brighton, UK BN1 9QJ. E-mail: j.nixon@sussex.ac.uk

Received (in Cambridge, UK) 20th July 2000, Accepted 1st September 2000
First published as an Advance Article on the web 28th September 2000

Treatment of SrI_2 with 2 equivalents of $K[P_3C_2Bu^t_2]$ affords the hexaphosphastrontocene $[\{Sr(\eta^5\text{-}P_3C_2Bu^t_2)_2\}_\infty]$ which is polymeric in the solid state; treatment of this complex with an excess of pyrazine leads to the corresponding Lewis base adduct $[\{Sr(\eta^5\text{-}P_3C_2Bu^t_2)_2(\mu\text{-}C_4H_4N_2)\}_\infty]$ which is also polymeric in the solid state.

There has been increasing interest in the structure and bonding in metallocene complexes of the heavier alkaline earth elements (Ca, Sr, Ba) in recent years and several reviews have appeared.[1–3] With the exception of $[Ca(\eta^5\text{-}C_5H_5)_2]$ which is a three-dimensional polymer, these compounds are generally monomeric in the solid state or weakly associated, the degree of association depending on both the steric bulk of the cyclopentadienyl ligand and size of the central metal. Moreover, where the cyclopentadienyl ligands are not excessively bulky (typified by encapsulated metallocenes), additional coordination of Lewis bases may occur.

In contrast, however, sandwich compounds of the alkaline earth metals with heteroatom substituted cyclopentadienyl ligands are extremely rare. To the best of our knowledge only two structurally characterised examples, incorporating the 2,5-di-*tert*-butylpyrrolyl ligand and coordinated THF have been reported[4] namely $[M(\eta^5\text{-}NC_4H_2Bu^t_2)_2(THF)]$ **1** (M = Ca, Sr). Westerhausen and co-workers[5,6] showed that the 2,5-diphenyl-3,4-bis(trimethylsilyl)phospholyl ligand coordinates in an η^1-fashion to the metal dications $[M(THF)_4]^{2+}$ (M = Ca, Sr), however unpublished calculations by the same authors on the solvent free systems favour an η^5-ligating mode. Motivated by our recent observation[7] that the complex $[In(\eta^5\text{-}P_3C_2Bu^t_2)]$, containing the aromatic 3,5-di-*tert*-butyl-1,2,4-triphospholyl anion **2**, is a source of pure InP by chemical vapour deposition, we decided to react **2** with alkaline earth metal halides. We now report the first synthesis and structural characterisation of the hexaphosphastrontocene, $[\{Sr(\eta^5\text{-}P_3C_2Bu^t_2)_2\}_\infty]$ **3** and its pyrazine adduct $[\{Sr(\eta^5\text{-}P_3C_2Bu^t_2)_2(N_2C_4H_4)\}_\infty]$ **4**.

Thus, treatment of a THF solution of SrI_2 with two equivalents of **2** (Scheme 1) leads to the formation of air and moisture sensitive, but thermally stable, $[\{Sr(\eta^5\text{-}P_3C_2Bu^t_2)_2\}_\infty]$ **3** (*ca.* 50% yield). Complex **3**, which is a pale yellow solid, can be extracted from the initial reaction residue with toluene but sublimation or prolonged evacuation of the extracted residue renders it insoluble in all but donor solvents. We believe the initially formed complex is a THF solvated monomeric species $[Sr(\eta^5\text{-}P_3C_2Bu^t_2)_2(THF)_n]$ which readily loses THF to afford polymeric strands of **3** (*vide infra*). This behaviour also occurs in the case of strontocenes such as $[Sr(\eta^5\text{-}C_5H_4Bu^t)(THF)_2]$ and $[Sr\{\eta^5\text{-}C_5H_3(SiMe_3)_2\}_2(THF)]$ which both readily desolvate on sublimation, although they remain monomeric.[8,9]

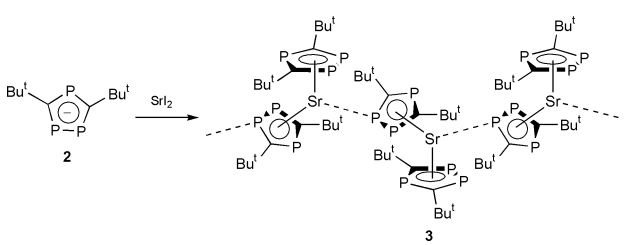

Scheme 1

The $^{31}P\{^1H\}$ NMR spectrum of **3**† is consistent with η^5 ligated triphospholyl rings and the chemical shifts are similar to those of $[K(\eta^5\text{-}P_3C_2Bu^t_2)]$ (δ 252.8 and 244.8). This is in contrast to the generally observed *upfield* shift in the ^{31}P resonances of **2** upon coordination to transition metals {*e.g.* AB_2 pattern at δ 65 in $[Ru(\eta^5\text{-}P_3C_2Bu^t_2)_2]$}[10] and this may indicate a significant degree of ionic character in the metal–ligand bonding in **3** in solution. The EI mass spectrum of **3** exhibits a strong molecular ion (*m/z* 550, 58%) but no higher peaks, suggesting that in the gas phase **3** exists primarily as a monomeric species.

A single crystal X-ray diffraction study‡ reveals that in the solid state, **3** consists of bent sandwich units linked in chains along the crystallographic *c*-glide plane (Fig. 1). Each unit bears one solely η^5 bound triphospholyl ligand and a second η^5 ligand which also acts as a bridge linking the molecules into extended chains *via* a further η^1 interaction involving one of the two adjacent phosphorus ring atoms. This strontium–phosphorus bond distance [3.2200(7) Å] is only marginally longer than the average strontium–phosphorus distances within the sandwich unit (3.1837 Å) and all lie within the sum of the van der Waals radii for the two elements. The centroid–metal–centroid angle of 141.50(7)° in **3** is larger than that observed in analogous strontocenes bearing substituted cyclopentadienyl ligands of comparable steric bulk {*e.g.* 122 and 124° in **1**[4] and 134° in $[Sr\{\eta^5\text{-}C_5H_3(SiMe_3)_2\text{-}1,3\}_2]$ **5**).[8] Similarly, the metal–centroid distances of 2.692(3) and 2.788(3) Å in **3** are somewhat larger than those in **1** (2.525 Å) and **5** (2.551 Å), which probably results from replacement of three ring carbon atoms with the

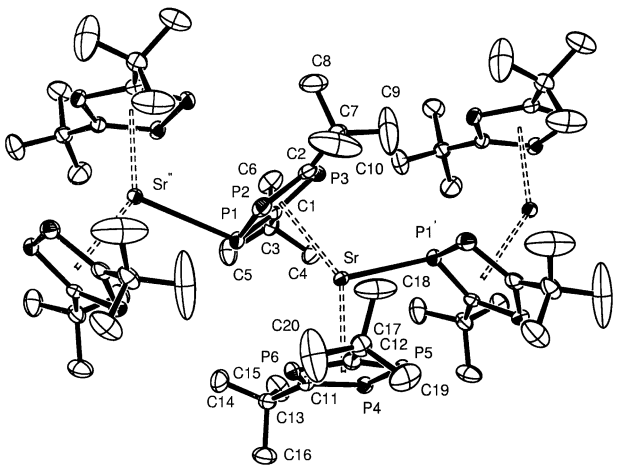

Fig. 1 Solid state structure of **3**. Selected bond distances (Å) and angles (°): M(1)–Sr–M(2) 141.50(7); Sr–M(1) 2.788(3), Sr–M(2) 2.692(3), P(1)–P(2) 2.1150(11), P(2)–C(2) 1.749(3), C(2)–P(3) 1.745(3), P(3)–C(1) 1.749(3), C(1)–P(1) 1.753(3), P(4)–P(5) 2.1069(11), P(5)–C(12) 1.756(3), C(12)–P(6) 1.755(3), P(6)–C(11) 1.751(3), C(11)–P(4) 1.759(3). M(1) and M(2) are the centroids of the rings defined by C(1), C(2), P(1), P(2), P(3) and C(11), C(12), P(4), P(5), P(6), respectively.

DOI: 10.1039/b005855f

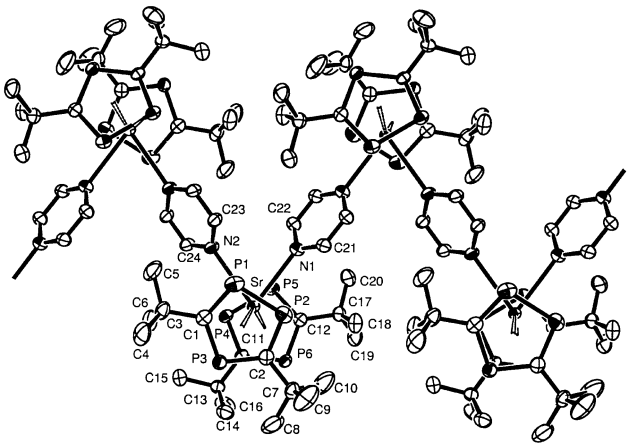

Fig. 2 Solid state structure of **4**. Selected bond distances (Å) and angles (°): M(1)–Sr–M(2) 146.73(6); Sr–M(1) 2.794(2), Sr–M(2) 2.791(2), P(1)–P(2) 2.1073(10), P(2)–C(2) 1.751(3), C(2)–P(3) 1.748(2), P(3)–C(1) 1.754(2), C(1)–P(1) 1.746(3), P(4)–P(5) 2.1101(9), P(5)–C(12) 1.748(2), C(12)–P(6) 1.755(2), P(6)–C(11) 1.750(2), C(11)–P(4) 1.749(2). M(1) and M(2) are the centroids of the rings defined by C(1), C(2), P(1), P(2), P(3) and C(11), C(12), P(4), P(5), respectively.

larger phosphorus atoms. The bridging strontium–phosphorus interaction in **3**, not possible in the related strontocenes, obviates the need for any additional ligation to THF or other donor solvent molecules.

However, treatment of **3** with an excess of pyrazine in refluxing toluene leads *quantitatively* to $[\{Sr(\eta^5\text{-}P_3C_2Bu^t_2)_2(\mu\text{-}C_4H_4N_2)\}_\infty]$ **4** in which the strontium–phosphorus bridges of **3** have been broken and replaced with pyrazine units. Complex **4**, which is an orange solid, is insoluble in all but donor solvents but could be recrystallised from a hot saturated toluene solution. The room temperature mass spectrum of **4**† indicates a ready loss of pyrazine and at higher temperature the spectrum is essentially that of the parent complex **3**. Furthermore, the NMR spectroscopic data for **3** and **4** are essentially identical, suggesting that **4** undergoes complete dissociation into **3** and free pyrazine in solution.†

The solid state, polymeric structure of **4** determined by a single crystal X-ray diffraction study‡ is shown in Fig. 2. The pyrazine units act as bridges linking the hexaphosphastrontocene molecules into zigzag chains, each sandwich unit being related to the next by a crystallographic inversion centre lying at the middle of the pyrazine ring. The *intra*ring parameters of **4** do not differ significantly from those in **3**: the average phosphorus–carbon (1.750 Å) and phosphorus–phosphorus (2.1087 Å) distances within the strontium hexaphosphametallocene unit in **4** are very similar to those observed in **3** (1.752 and 2.1109 Å, respectively). Moreover, the centroid–metal–centroid angle in **4** is 146.73(6)° compared with 141.50(7)° in **3** and the two individual metal–centroid distances of 2.791(2) and 2.794(2) Å are similar to those in **3** [2.692(3) and 2.788(3) Å].

The Engineering and Physical Sciences Research Council (EPSRC) is gratefully acknowledged for financial support of this work.

Notes and references

† *Spectroscopic data*: for **3**: NMR (C_5D_5N, 298 K): δ_H(300 MHz) 1.95 (s, 36H, Bu^t). δ_P(121.68 MHz) 256.4 (t, $^2J_{PP}$ 48.3 Hz), 235.3 (d, $^2J_{PP}$ 48.3 Hz) δ_C(125.16 MHz) AMXX′ spin system 38.0 (m, $^3J_{P(M)C}$ 10.86, $\Sigma^3J_{P(X')C}$ + $^4J_{P(X)C}$ 10.78 Hz, C*C*H$_3$), 40.8 (m, $^2J_{P(M)C}$ 22.85, $\Sigma^2J_{P(X')C}$ + $^3J_{P(X)C}$ 14.27 Hz, *C*CH$_3$), 208.4 (m, $^1J_{P(M)C}$ 58.8, $\Sigma^1J_{P(X')C}$ + $^2J_{P(X)C}$ 82.8 Hz, PCP), EI mass spectrum: *m/z* (%) 550 (58) M$^+$, 319 (100) [M − $P_3C_2Bu^t_2$]$^+$. Microanalysis: found: C, 42.0; H, 6.3. Calc.: C, 43.6; H, 6.6%.

For **4**: NMR (C_5D_5N, 298 K): δ_H(300 MHz) 1.95 (s, 36H, Bu^t), 8.59 (s, 4H, pyrazine). δ_P(121.68 MHz) 257.0 (t, $^2J_{PP}$ 48.3 Hz), 235.1 (d, $^2J_{PP}$ 48.3 Hz) δ_C(125.16 MHz) AMXX′ spin system 38.3 (m, $^3J_{P(M)C}$ 10.9, $\Sigma^3J_{P(X')C}$ + $^4J_{P(X)C}$ 10.8 Hz, C*C*H$_3$), 41.7 (m, $^2J_{P(M)C}$ 22.9, $\Sigma^2J_{P(X')C}$ + $^3J_{P(X)C}$ 14.5 Hz, *C*CH$_3$), 208.8 (m, $^1J_{P(M)C}$ 58.0, $\Sigma^1J_{P(X')C}$ + $^2J_{P(X)C}$ 82.9 Hz, PCP), EI mass spectrum: *m/z* (%) (low temp.) 80 (90) $[C_4H_4N_2]^+$, 464 (100) $[P_3C_2Bu^t_2H]^+$; (high temp.) 319 (100) $[SrP_3C_2Bu^t_2]^+$, 550 (43) $[Sr(P_3C_2Bu^t_2)_2]^+$. Microanalysis: found: C, 45.7; H, 6.3; N, 4.9. Calc.: C, 45.8; H, 6.4; N, 4.5%.

‡ *Crystal data*: for **3**: $C_{20}H_{36}P_6Sr$, M = 549.93, monoclinic, space group $P2_1/c$ (no. 14), a = 11.2175(3), b = 22.0485(5), c = 11.6287(2) Å, β = 112.272(2)°, V = 2661.5(1) Å^3, T = 173(2) K, Z = 4, μ = 2.39 mm^{-1}, λ = 0.71073 Å, 25843 reflections collected, 6302 independent (R_{int} = 0.057), R_1 = 0.040, wR_2 = 0.083 for $I > 2\sigma(I)$, R_1 = 0.059, wR_2 = 0.091 for all data.

For **4**: $C_{24}H_{40}N_2P_6Sr$, M = 630.02, triclinic, space group $P\bar{1}$, a = 9.8797(3), b = 11.5540(3), c = 15.8655(4) Å, α = 71.134(2), β = 74.932(2), γ = 68.190(2)°, V = 1570.80(7) Å^3, T = 173(2) K, Z = 2, μ = 2.04 mm^{-1}, λ = 0.71073 Å, 25418 reflections collected, 9025 independent (R_{int} = 0.051), R_1 = 0.041, wR_2 = 0.076 for $I > 2\sigma(I)$, R_1 = 0.059, wR_2 = 0.082 for all data.

The SHELX-97 suite of programs for crystal structure analysis were used for solution and refinement of both structures.[11]

CCDC 182/1772. See http://www.rsc.org/suppdata/cc/b0/b005855f/ for crystallographic files in .cif format.

1 P. Jutzi and N. Burford, *J. Chem. Soc., Dalton Trans.*, 2000, 2237; P. Jutzi and N. Burford, *Chem. Rev.*, 1999, **99**, 969.
2 T. P. Hanusa, *Chem. Rev.*, 1993, **93**, 1023.
3 T. P. Hanusa, *Polyhedron*, 1990, **9**, 1345.
4 H. Schumann, J. Gottfriedsen and J. Demtschuk, *Chem. Commun.*, 1999, 2091.
5 M. Westerhausen, M. H. Digeser, H. Noth, W. Ponikwar, T. Seifert and K. Polborn, *Inorg. Chem.*, 1999, **38**, 3207.
6 M. Westerhausen, M. H. Digeser, C. Guckel, H. Noth, J. Knizek and W. Ponikwar, *Organometallics*, 1999, **18**, 2491.
7 M. D. Francis J. F. Nixon and W. S. Rees Jr., manuscript in preparation.
8 M. G. Gardiner, C. L. Raston and C. H. L. Kennard, *Organometallics*, 1991, **10**, 3680.
9 L. M. Engelhardt, P. C. Junk, C. L. Raston and A. L. White, *J. Chem. Soc., Chem. Commun.*, 1988, 1500.
10 P. B. Hitchcock, R. M. Matos and J. F. Nixon, *J. Organomet. Chem.*, 1995, **490**, 155.
11 G. M. Sheldrick, SHELX-97, University of Göttingen, Göttingen, Germany, 1997.

Olefination reactions through phosphazenes

Emma Peralta Pérez and Fernando López Ortiz*

Universidad de Almería, Área de Química Orgánica,Carretera de Sacramento, 04120 Almería, Spain. E-mail: flortiz@ualm.es

Received (in Liverpool, UK) 4th August 2000, Accepted 22nd August 2000
First published as an Advance Article on the web 28th September 2000

The first synthesis of di-, tri- and tetrasubstituted alkenes through reaction of lithium *P*-diphenyl(alkyl)(*N*-carboxymethyl)phosphazenes with aldehydes and ketones is reported.

Phosphorus-stabilized carbanions are very important reactive intermediates in the stereoselective synthesis of olefins. Since the breakthrough of the Wittig reaction between phosphorus ylides and carbonyl compounds[1] in carbon–carbon double bond forming reactions, the usefulness of other phosphorus derivatives in this type of process has been demonstrated. The most relevant members of this class of compounds are phosphonates,[2] phosphonamides[3] and phosphine oxides.[4]

Phosphazenes are isoelectronic with phosphorus ylides and phosphine oxides. They are well known for the large number of synthetic applications of the P–N bond,[5] particularly in the preparation of heterocycles[6] based on the aza-Wittig reaction. However, the chemistry of their α-carbanions has received much less attention.[7] We have shown that lithiated *P*-diphenyl(alkyl)(*N*-phenyl)phosphazenes **1** add to aldehydes with a high diastereoselectivity yielding the corresponding β-hydroxy derivatives (Scheme 1).[8] These compounds are easily isolated and no trace of olefins were observed in the reaction even when forcing conditions were used.

Recently, in a synthesis of cyclopentenones **3** obtained by reaction of lithium *P*-diphenyl(alkyl)(*N*-phenyl)phosphazenes with dimethylacetylene dicarboxylate (DMAD) (Scheme 1) we proposed a reaction mechanism in which one intermediate phosphazene participated in an olefination step similar to the Horner carbon–carbon double bond synthesis using phosphine oxides.[9] No experimental evidence could be obtained regarding the structure of any reactive intermediate involved in the synthesis.

Here we report the first application of phosphazenes to the synthesis of di-, tri- and tetrasubstituted alkenes. The phosphazenes **4** used in this study are readily obtained, either by alkylation of the anion Ph_2P^- (generated by reaction of Ph_3P with lithium) followed by *in situ* addition of N_3CO_2Me, or through alkylation of simpler lithiated phosphazenes (Scheme 2). *P*-diphenyl(alkyl)(*N*-carboxymethyl)phosphazenes **4** were metallated with *n*-BuLi in THF at −35 °C over a 30 min period. The appropriate aldehyde or ketone was then added and the mixture was stirred for 4–20 h at rt. Aqueous work-up followed by distillation or filtration through a short path silica-gel chromatography column afforded the olefins **8**(*Z*)/**9**(*E*)

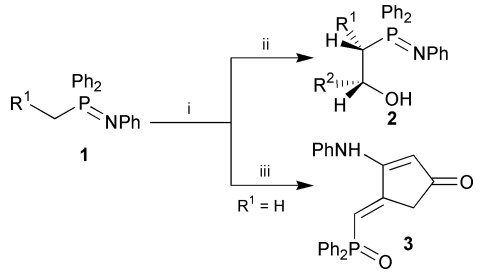

Scheme 1 *Reagents and conditions*: i, *n*-BuLi, −30 °C, THF; ii, R^2CHO, −70 °C; iii, DMAD, −70 °C.

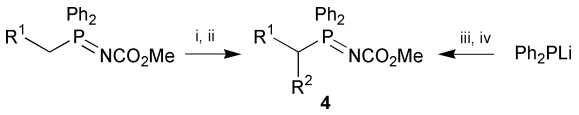

Scheme 2 *Reagents and conditions*: i, *n*-BuLi, −35 °C, THF; ii, R^2Br, −70 °C; iii, R^1R^2CHBr, −35 °C, THF; iv, N_3CO_2Me.

(Scheme 3).† The diphenylphosphinamide **11** by-product was completely eliminated in the aqueous layer.

A list of the compounds obtained, as well as the isolated yields and the diastereomeric ratios observed are given in Table 1.[10] The stereochemistry of the tri-substituted alkenes was easily assigned through 2D NOESY spectra measured from the mixture of isomers. For the di-substituted derivatives the geometry of the double bond was deduced from the magnitude of the vicinal coupling constants or chemical shifts of the olefinic protons.

Reaction yields were higher than 90% in all cases except for the phosphazene having R^1 = Me and R^2 = ^{n}Bu. In this case only a 16% yield of the *E*/*Z* alkenes was obtained under the standard conditions. However, this yield increased to 70% without changes in the isomeric ratio when a large excess of aldehyde (10 equiv.) was used. Worthy of note is the high yield obtained when benzophenone is used as electrophile giving rise to the tetrasubstituted alkene **8j**. The olefin *E* predominates in all cases except for phosphazenes bearing a benzyl group where the *Z* alkene is favoured (Table 1, entries 7, and 8). Good to excellent stereoselectivies are obtained for phosphazenes with R^1 = Ph, CO_2Me and R^2 = H (Table 1, entries 1–5). Using the synthesis of alkenes **8/9d** as reference, under the same reaction conditions the appropriate phosphazene, phosphine oxide, phosphonate, and phosphonium salt afforded essentially the *E* isomer (*Z*:*E* 1:99) in similar yields. Curiously, the stereoselectivity of the Wittig reaction showed a slight decrease (*Z*:*E* 4:96) when the olefination was carried out with the isolated phosphorus ylide. However, the reported reactions of Ph_3P=CHPh with benzaldehyde using BuLi or PhLi as a base

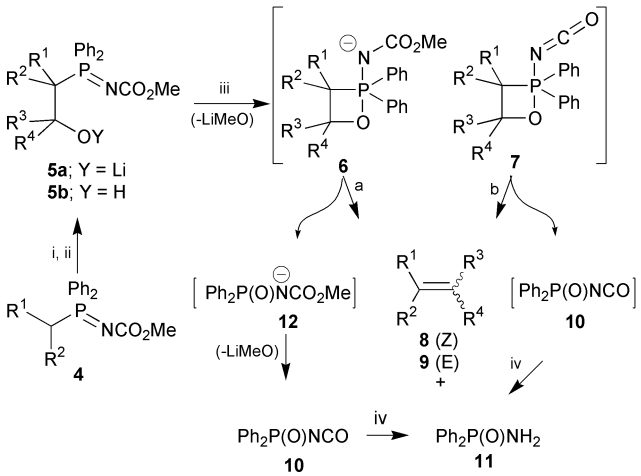

Scheme 3 *Reagents and conditions*: i, *n*-BuLi, −35 °C, THF; ii, R^3R^4CO, rt; iii, 4–20 h; iv, H_2O.

Table 1 Alkenes **8**, **9** obtained, including isomeric ratio of the mixture and isolated yield

	Alkene	R^1	R^2	R^3	R^4	$Z:E$ (%)[a]	Yield (%)
1	**8**, **9a**	Ph	H	H	Ph	17:83	92
2	**8**, **9b**	Ph	H	H	$(CH_3)_3C$	4:96	95
3	**8**, **9c**	CO_2Me	H	H	Ph	1:99	85
4	**8**, **9d**	CO_2Me	H	H	*p*-Cl-C_6H_4	1:99	88
5	**8**, **9e**	CO_2Me	H	H	C_6H_{11}	4:96	90
6	**8**, **9f**	Me	$CH_3(CH_2)_2CH_2$	H	Ph	34:66	16 (70)[b]
7	**8**, **9g**	$PhCH_2$	$CH_3(CH_2)_2CH_2$	H	*p*-Cl-C_6H_4	72:28	86
8	**8**, **9h**	Me	$PhCH_2$	H	$(CH_3)_3C$	74:26	85
9	**8**, **9i**	Me	CH_2=$CHCH_2$	H	*p*-MeO-C_6H_4	32:68	90
10	**8j**	Me	CH_2=$CHCH_2$	Ph	Ph		85

[a] Determined from the integrals of the olefinic protons and/or the methyl signals in the ^{1}H NMR spectrum of the mixture. [b] When a large excess of aldehyde is used.

are clearly less stereoselective (*Z*:*E* 34:66 and 30:70, respectively)[1b,11] than the analogous synthesis of stilbene through phosphazenes (Table 1, entry 1). The olefination reported here is sensitive to the degree of substitution in the carbanion and modest *Z*/*E* ratios are obtained when α,α-disubstituted phosphazenes are used (*cf*. entries 6–9 in Table 1). This is a known characteristic of Horner olefination.[5]

A reaction mechanism explaining the formation of **8**, **9**, and **11** is shown in Scheme 3. First, one carbon–carbon bond is formed by addition of the C_α-metallated phosphazene to the carbonylic carbon of the electrophile affording the alkoxy intermediate **5a**. The nucleophilic oxygen of this adduct attacks the electrophilic phosphorus intramolecularly to yield an oxaphosphetane heterocycle **6** as proposed for the Wittig[1] and Horner[12] reactions. In this particular case, the oxaphosphetane **6** may break down to the alkenes **8**/**9** (route a) or may eliminate lithium methoxide affording the isocyanate derivative **7**. Ring opening of **7** would yield the alkenes **8**/**9** and diphenylphosphinoyl isocyanate **10** (route b), which by reaction with water would produce the diphenylphosphinamide **11**. Alternatively the isocyanate **10** may be formed by elimination of lithium methoxide from the lithium phosphinamide **12** (route a).

The intermediate adducts **5b** can be isolated as the corresponding (β-hydroxy)phosphazenes when the carbonyl compound is added at −70 °C and the reaction is stirred for 2 h at this temperature. Aqueous work-up yields a mixture of diastereomeric compounds **5b** in the same ratio as observed for the respective olefins. Therefore, the diastereoselectivity of the synthesis is determined by the addition step and no interconversion occurs between the two isomers. The (β-hydroxy)-phosphazenes **5b** are converted quantitatively into the corresponding olefins by lithiation under the same reactions conditions used in the one-pot process.

Support for the participation of phosphinoyl isocyanates as intermediates in the formation of phosphinamides in the olefination reaction described above has been obtained from phosphinamide **13** synthesized by reaction of methoxycarbonyl azide with diphenylphosphine oxide. Compound **13** was treated with one equiv. of *n*-BuLi in THF at −30 °C (Scheme 4) and the reaction was stirred for 4 h at rt.[13] After aqueous work-up the phosphinamide **11** was isolated quantitatively.[14]

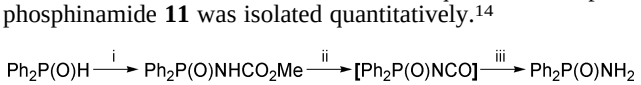

Scheme 4 *Reagents and conditions*: i, N_3CO_2Me, THF, rt; ii, *n*-BuLi, THF, −35 °C to rt; iii, H_2O.

In conclusion, the application of phosphazenes to the synthesis of alkenes through reaction with carbonyl compounds is described for the first time. The phosphazenes are readily available through conventional reactions, analogous to the preparation of phosphine oxides. High yields of di-, tri and tetrasubstituted olefins are obtained. The stereoselectivity depends on the substituents on the alkyl group bonded to phosphorus and for α-substituted phosphazenes the stereocontrol achieved is comparable to that obtained in the Wittig, Horner, and Wadsworth–Emmons reactions. A reaction mechanism is proposed which involves the sequential formation of an isolable (β-hydroxy)phosphazene and an oxaphosphetane intermediate.

Financial support from the Ministerio de Educación y Cultura (PB96-1503) is gratefully acknowledged.

Notes and references

† Synthesis of methyl cinnamate **8**, **9c**: to a Schlenk with $MeO_2CCH_2(Ph)_2P$=NCO_2Me (0.2 g, 6×10^{-4} mol) dissolved in 25 mL of dry THF was added a solution of *n*-BuLi (0.45 mL of a 1.6 M solution in hexane, 7.2×10^{-4} mol) at −35 °C. After 30 min of metallation the temperature was lowered to −70 °C and benzaldehyde (61 μL, 6×10^{-4} mol) was added. The reaction mixture was stirred for 6 h and allowed to reach rt. Work-up (A): addition of diethyl ether (15 mL) to the reaction crude produced a white precipitate of $Ph_2P(O)NH_2$ (0.102 g, 78%), which was filtered off. The filtrate was evaporated to dryness and distilled under vacuum. Methyl cinnamate **8**, **9c** (*Z*:*E* 1:99) was isolated as a colourless liquid bp $122^{0.1}$ °C (lit. $120–125^{0.1}$ °C)[15], (79×10^{-3} g, 81%). Work-up (B): Addition of water (25 mL) followed by extraction with CH_2Cl_2 (3×15 mL) and solvent evaporation under vacuum afforded one (almost pure) oil, which was further purified by distillation under vacuum bp $122^{0.1}$ °C (83×10^{-3} g, 85%). The same yields were obtained by filtration through a short path column of silica gel 60 (40–63 μm) using ethyl acetate:hexane (1:4) as eluent.

1 G. Wittig and G. Geissler, *Liebigs Ann. Chem.*, 1953, **580**, 44. For recent references see: O. I. Kolodiazhnyi, *Phosphorus Ylides. Chemistry and Application in Organic Synthesis*, Wiley-VCH, Weinheim, 1999; P. J. Murphy and S. E. Lee, *J. Chem. Soc., Perkin Trans. 1*, 1999, 3049.

2 L. Horner, H. Hoffmann, H. G. Wippel and G. Klahre, *Chem. Ber.*, 1959, **92**, 2499; W. S. Wadsworth and W. D. Emmons, *J. Am. Chem. Soc.*, 1961, **83**, 1733.

3 E. J. Corey and G. T. Kwaitkowsky, *J. Am. Chem. Soc.*, 1966, **88**, 5652.

4 L. Horner, H. Hoffmann and H. G. Wippel, *Chem. Ber.*, 1958, **91**, 61; J. Clayden and S. Warren, *Angew. Chem., Int. Ed. Engl.*, 1996, **35**, 241.

5 A. W. Johnson, *Ylides and Imines of Phosphorus*, John Wiley, New York, 1993.

6 H. Wamhoff, G. Richard and S. Stölben, *Adv. Heterocycl. Chem.*, 1995, **64**, 159 and references therein.

7 J. M. Álvarez-Gutiérrez and F. López-Ortiz, *Tetrahedron Lett.*, 1996, **37**, 2841 and references therein

8 J. Barluenga, F. López-Ortiz and F. Palacios, *Synthesis*, 1988, 562

9 J. M. Álvarez-Gutiérrez and F. López-Ortiz, *Chem. Commun.*, 1996, 1583.

10 Compounds **8**, **9g**–**j** are new. They gave satisfactory elemental analysis. Full structural characterisation will be given elsewhere.

11 L. D. Bergelson, L. I. Barsukov and M. M. Shemyakin, *Tetrahedron*, 1967, **23**, 2709.

12 P. O. Norrby, P. Brandt and T. Rein, *J. Org. Chem.*, 1999, **64**, 5854; K. Ando, *J. Org. Chem.*, 1999, **64**, 6815.

13 Diphenylphosphinoyl isocyanate is a stable compound previously prepared by reaction of diphenylphosphinic chloride and silver cyanate. K. Utvary and R. Hagenauer, *Monatsh. Chem.*, 1963, **94**, 797.

14 The addition of amines and alcohols to diphenylphosphinoyl isocyanate has been described. K. Utvary, E. Freundlinger and V. Gutmann, *Monatsh. Chem.*, 1966, **97**, 348.

15 C. Cardellicchio, A. R. Cicciomessere, F. Naso and P. Tortorella, *Gazz. Chim. Ital.*, 1996, **126**, 555.

ChemComm

The first vanadium-catalyzed oxidation of aryl allylic selenides with *in situ* [2,3] sigmatropic rearrangement†

Rich G. Carter* and T. Campbell Bourland

Department of Chemistry and Biochemistry, University of Mississippi, Oxford, MS 38677 USA. E-mail: rgcarter@olemiss.edu

Received (in Corvallis, OR, USA) 28th July 2000, Accepted 1st September 2000
First published as an Advance Article on the web 28th September 2000

The efficient synthesis of a series of 2° allylic alcohols from a vanadium-catalyzed oxidation of suitably disposed allylic selenides with tandem [2,3] sigmatropic rearrangement is outlined.

The rapid growth of metal-catalyzed transformations in recent decades has contributed to the construction of evermore complex synthetic targets. For example, the catalytic oxidation of sulfides is well documented using several transition metal catalysts.[1] This methodology has proven useful in both racemic and enantioselective pathways. Recently, Bolm and co-workers showcased the use of vanadium for the enantioselective oxidation of prochiral sulfides.[2] In addition, the Ellman laboratory has reported an elegant use of a similar catalytic system for the enantioselective oxidation of alkyl disulfides.[3] Despite these encouraging results, relatively little attention has been paid to the corresponding oxidation of selenium. In particular, the tandem oxidation of suitably disposed allylic selenides with *in situ* [2,3] sigmatropic rearrangement has been limited to stoichiometric oxidants such as oxaziridines, peracids or peroxides.[4] Scattered asymmetric methods have also been developed for these transformations utilizing primarily stoichiometric titanium–tartrate complexes[5] or chiral oxaziridines.[6] In addition, several groups have studied the effect of a chiral auxiliary on selenium.[7] None of these systems, however, have been exploited in a sub-stoichiometric sense for this transformation.[8] We herein report the first catalytic method for oxidation of allylic selenides with tandem *in situ* [2,3] sigmatropic rearrangement.

Our initial exploits in this area were directed toward the use of titanium-mediated oxidation based on previously described conditions;[9] however, this proved to be ineffective in our hands due to lack of generality, slow reaction times, and the need for stoichiometric amounts of the metal catalyst. Our interest then turned to the use of vanadyl(IV) acetylacetonate as a potential candidate for the desired transformation. Synthesis of the selenide precursors was readily accomplished from the corresponding alcohol using tributylphosphine and *o*-nitrophenyl selenocyanate in high yield.[10]

The standard reaction conditions involved a 0.3 M solution of the selenide **1** in methylene chloride with vanadyl(IV) acetylacetonate (10 mol%) in the presence of powdered 4 Å molecular sieves (Scheme 1). This green solution was then cooled to −10 °C in an ice–acetone bath and cumene hydroperoxide (1.8 equiv.) was added to the stirred solution. After the reaction was judged to be complete, tributylphosphine (1.2 equiv.) was added to convert the intermediate selenenate **3** to the desired allylic alcohol **4**. This efficient and rapid method for cleavage of the selenenate species **3** is noteworthy because of its tolerance for sterically demanding systems such as the adamantyl selenide **1c**. Previous described methods for selenenate cleavage (such as pyridine and water) proved to be slow and capricious in our hands. The vanadium metal catalyst is

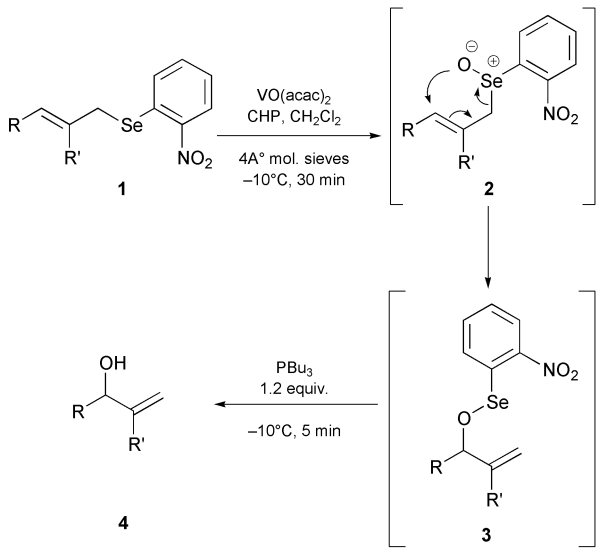

Scheme 1 Selenide oxidation, sigmatropic rearrangement and selenenate cleavage sequence.

critical for the dual reaction sequence to proceed; the blank experiment without $VO(acac)_2$ resulted in no conversion of the selenide under the prescribed reaction conditions.[11] It has been previously reported that phenyl selenides can be oxidized using *tert*-butyl hydroperoxide in the absence of a metal catalyst;[12] however, the decreased reactivity of the selenium to oxidation that is observed may be due to the electron withdrawing nature of the *o*-nitro substituent.

A variety of substituents on the alkene were studied in order to investigate the utility of this methodology as shown in Table 1. These results suggest that the oxidation and rearrangement occur rapidly, regardless of the steric environment located at the allylic position. In addition, the vanadium-mediated conditions occur equally effectively with conjugated and non-conjugated olefins. These results are in contrast to preliminary studies in our laboratory with titanium-mediated reactions in which substitution on the alkene function had a dramatic impact on the efficiency of the reaction. Furthermore, the rearrangement does not seem to be influenced by a stereogenic center located in the allylic position. For example, treatment of selenides **1f** and **5c** yielded the resultant allylic alcohol in nearly 1:1 selectivity. This result is in good agreement with Davis and co-workers who have shown that the stereochemical outcome of the resultant alcohol in acyclic substrates appears to be determined by the oxidation of the selenide.[6] Finally, the results in Table 2 demonstrate that this methodology is equally effective for the *cis* olefin geometry.

In conclusion, the first vanadium-catalyzed method for oxidation of selenides is reported with tandem [2,3] sigmatropic rearrangement. This methodology is effective on a broad range of substrates, regardless of steric environment, thereby expanding the scope and utility of selenoxide rearrangements. Furthermore, tributylphosphine is shown to be a rapid and

† Electronic supplementary information (ESI) available: typical experimental procedure for synthesis of **1**–**6**. See http://www.rsc.org/suppdata/cc/b0/b006278m/

Table 1 Selected data for *trans* disposed allylic selenides[a]

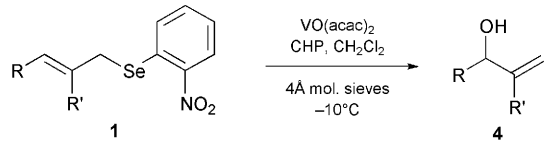

1 4

Entry	R	R′	Yield[b] (d.s.)
a[c]		H	70%
b		H	75%
c		H	84%
d	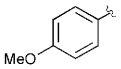	H	66%[d]
e		CH_3	70%
f		H	60% (1.1:1)

[a] All reactions unless otherwise noted were performed at 0.3 M substrate concentration using 1.2 equiv. tributylphosphine to quench the selenenate intermediate. [b] All yields are isolated yields after chromatography over silica gel. [c] This reaction was quenched with triphenylphosphine. [d] *tert*-Butyl hydroperoxide was substituted for cumene hydroperoxide to simplify purification.

Table 2 Selected data for *cis* disposed allyl selenides[a]

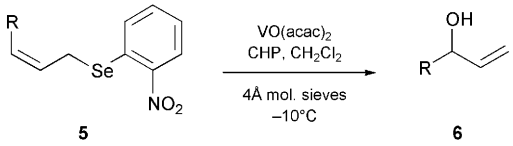

5 6

Entry	R′	Yield[b] (d.s.)
a[c]		89%
b		71%[d]
c		71% (1.2:1)

[a] All reactions unless otherwise noted were performed at 0.3 M substrate concentration using 1.2 equiv. tributylphosphine to quench the selenenate intermediate. [b] All yields are isolated yields after chromatography over silica gel. [c] This reaction was quenched with triphenylphosphine. [d] *tert*-Butyl hydroperoxide was substituted for cumene hydroperoxide to simplify purification.

general method for selenenate cleavage and a viable alternative to traditional methods. In addition, it should be possible to effect catalytic asymmetric oxidation of selenium with tandem sigmatropic rearrangement using the appropriate multidentate ligand–vanadium system. We are actively pursuing this area and will report our results in due course.

The authors wish to thank the University of Mississippi for their generous support of this work.

Notes and references

1 K. K. Andersen, *The Chemistry of Sulfones and Sulfoxides*, ed. S. Patai, Z. Rappaport and C. J. M. Stirling, Wiley & Sons, New York, 1988, pp. 56–94.
2 C. Bolm and F. Bienewald, *Angew. Chem., Int. Ed. Engl.*, 1995, **34**, 2640. See also: K. Nakajima, K. Kojima, M. Kojima and J. Fujita, *Bull. Chem. Soc. Jpn.*, 1990, **63**, 2630.
3 D. A. Cogen, G. Liu, K. Kim, B. J. Backes and J. A. Ellman, *J. Am. Chem. Soc.*, 1998, **120**, 8011.
4 Y. Nishibayashi and S. Uemura, *Organoselenium Chemistry-A Practical Approach*, ed. T. G. Back, Oxford University Press, Oxford, 1999, pp. 207–21.
5 N. Komatsu, Y. Nishibayashi and S. Uemura, *Tetrahedron Lett.*, 1993, **34**, 2339.
6 F. A. Davis and R. T. Reddy, *J. Am. Chem. Soc.*, 1992, **57**, 2599.
7 K. Fujita, M. Kanakubo, H. Ushijima, A. Oishi, Y. Ikeda and Y. Taguchi, *Synlett*, 1998, 987; N. Kurose, T. Takahashi and T. Koizumi, *Tetrahedron*, 1997, **53**, 12 115; Y. Nishibayashi, J. D. Singh, S. Fukuzawa and S. Uemura, *J. Org. Chem.*, 1995, **60**, 4114; H. J. Reich and K. E. Yelm, *J. Org. Chem.*, 1991, **56**, 5673; T. Wirth, *Tetrahedron*, 1999, **55**, 1.
8 Nitrogen oxide catalysis: E. Bosch and J. K. Kochi, *J. Chem. Soc., Perkin Trans. 1*, 1996, 2731; Enzymatic catalysis: G.-P. Chen and D. M. Zielger, *Arch. Biochem. Biophys.*, 1994, **312**, 566; T. P. M. Akerboom, H. Sies and D. M. Ziegler, *Arch. Biochem. Biophys.*, 1995, **316**, 220.
9 T. Shimizu, M. Kobayashi and N. Kamigata, *Bull. Chem. Soc. Jpn.*,1989, **62**, 2099; M. Tiecco, M. Tingoli, L. Testaferri and D. Bartoli, *Tetrahedron Lett.*, 1987, **28**, 3849.
10 D. L. Comins and A. Dehgagani, *J. Org. Chem.*, 1995, **60**, 794.
11 For example, treatment of selenide **1f** with excess cumene hydroperoxide in the absence of $VO(acac)_2$ at rt led to < 5% conversion after 24 h.
12 T. F. Woiwode and T. J. Wandless, *J. Org. Chem.*, 1999, **64**, 7670.

ChemComm

Tandem 1,3-azaprotio cyclotransfer–cycloaddition reactions between aldoximes and divinyl ketone. The effect of oxime *E*/*Z*-isomerism on cycloaddition stereoselectivity

Peter J. Dunn,[b] Alison B. Graham,[a] Ronald Grigg,*[a] Paul Higginson[b] and Imaad S. Saba[a]

[a] *Molecular Innovation, Diversity and Automated Synthesis (MIDAS) Centre, School of Chemistry, The University of Leeds, Leeds, UK LS2 9JT. E-mail: R.Grigg@chem.leeds.ac.uk*

[b] *Pfizer Global Research & Development (UK), Sandwich, Kent, UK CT13 9NJ*

Received (in Cambridge, UK) 5th July 2000, Accepted 11th September 2000
First published as an Advance Article on the web 2nd October 2000

The tandem 1,3-azaprotiocyclotransfer–cycloaddition reaction between aldoximes and divinyl ketone affords mixtures of *exo*- and *endo*-isomers of substituted 1-aza-8-oxabicyclo[3.2.1]octan-4-ones, the ratio of which is dependent on the *E*/*Z* geometry of the starting oxime and its ability to isomerise under the thermal reaction conditions.

We recently reported that the tandem 1,3-azaprotio cyclotransfer–cycloaddition reaction between symmetrical ketoximes (R′ = R) and divinyl ketone **2** (or its equivalents) is selective for cycloadducts **3** or **4**, depending on solvent or additive.[1] Reductive cleavage of **3** and **4** can afford *piperidones* **5** and *perhydroazepinones* **6**, potentially making these Class 2 cascades viable routes to various alkaloids and other related natural products (Scheme 1).[2] We have been exploring the

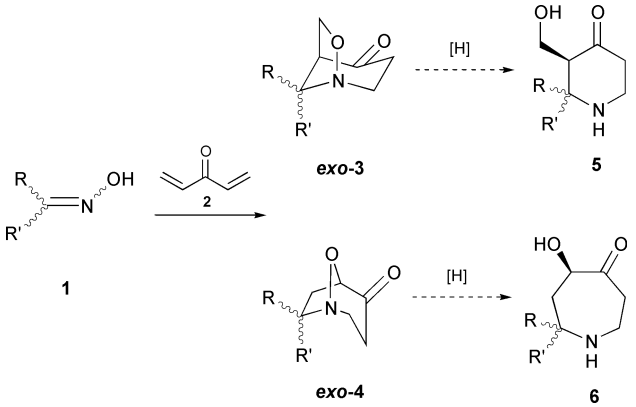

Scheme 1

scope of this reaction with aldoximes **1** (R or R′ = H). Under thermal reaction conditions (81 °C, acetonitrile) symmetrical ketoximes (R = R′) afford mixtures of **3** and **4**, whereas aldoximes (R or R′ = H) afford **4** only (as a mixture of *exo*- and *endo*-isomers) (Scheme 2).

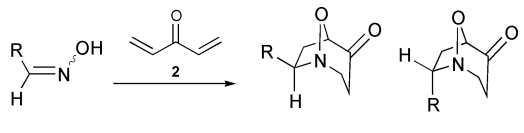

Scheme 2

Under thermal reaction conditions aldoximes isomerise to a mixture of *E*- and *Z*-isomers. The rate of *E*/*Z* equilibration is dependent on temperature and the nature of the aldoxime R group. The desired 1,3-azaprotiocyclotransfer process (herein referred to as 1,3-APT) (Scheme 3) can occur between either *E*- or *Z*-oxime isomer and **2** to form respective *E*- and *Z*-nitrones. Nitrones are not expected to isomerise under the reaction conditions.[3] Intramolecular 1,3-dipolar cycloaddition then proceeds completely regioselectively from the *Z*-nitrone affording *exo*-**4** (*path a*) or the *E*-nitrone affording *endo*-**4** (*path b*).[4] A survey of aldoximes **1a**–**f** showed that the diastereoselectivity of the reaction is dependent on the size of the aldoxime R group (Table 1). Increasing the size of the R group (aldoximes **1b**–**d**) resulted in a decrease in *exo*-selectivity. However, the case of **1e** perturbed this trend, affording *exo*-**4e** as the sole product.

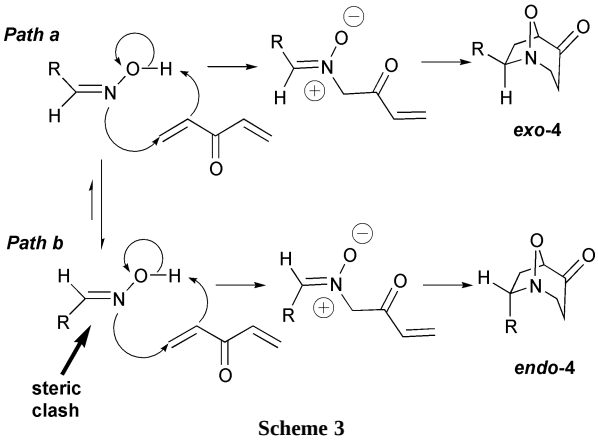

Scheme 3

It is proposed that *path a* and *path b* can have different rate determining steps. In *path a*, oxime isomerism can become the rate determining step when the steric clash resulting from the *cis*-relationship of the R and hydroxy moieties in the *Z*-oxime is severe or due to the electronic properties of R (*vide infra*). In contrast, 1,3-APT is rate determining in *path b* because the R group impedes the reactivity of the lone pair. The ratio of *exo*- and *endo*-products is determined by the relative rates of these steps and this is determined by the nature of R. Predominant formation of *exo*-**4** (*e.g.* for aldoximes **1a**,**b**) indicates that oxime *E*/*Z*-isomerism is faster than *E*-oxime 1,3-APT.

Though an increase in the size of the R group will decrease both the rate of oxime isomerism and *E*-oxime 1,3-APT, we propose that the effect is more pronounced on the oxime isomerism step due to the increased steric clash between the R and hydroxy moieties. The *E*-oxime 1,3-APT step can occur

Table 1[a]

Oxime **1**	R	Conv. (%)[b]	*exo*-**4**:*endo*-**4**[b]	Yield (%)[c]
a	Bn	> 95	3:1	65
b	Me	> 95	3.4:1	59
c	Et	> 95	2:1	41
d	Pr^{i}	90	1.5:1	34
e	Bu^{t}	25	*exo*-**4e** only	11
f	Ph	10	*endo*-**4f** only	—

[a] Reaction conditions: divinyl ketone (1.2 eq.), acetonitrile, 48 h, carried out in a STEM block at 80 °C. [b] Determined by ^{1}H NMR. [c] Combined yield isolated by column chromatography.

DOI: 10.1039/b005393g

Table 2

X	Isomer	Conv. (%)[a]	*exo*-**4**[b]	*endo*-**4**[b]	Yield (%)[c]
H	*E*-	10	1	> 20	—
H	*Z*-	> 95	> 20	1	79
CF_3	*E*-	< 5	—	—	—
CF_3	*Z*-	> 95	> 20	1	76
CN	*E*-	< 5	—	—	—
CN	*Z*-	90	> 20	1	44
NO_2	*E*-	< 5	—	—	—
NO_2	*Z*-	55	> 20	1	19
MeO	*E*-	80	4	1	55
MeO	*Z*-	> 95	7	1	78
Cl	*E*-	> 95	10	1	61
Cl	*Z*-	> 95	8	1	76
F	*E*-	> 95	8	1	72
F	*Z*-	> 95	12	1	70

[a] Reaction conditions: Divinyl ketone (1.2 eq.), acetonitrile, 80 °C, 48 h. [b] Determined by ^{1}H NMR. Where the ratio of isomers is > 20 : 1 no trace of the minor isomer was detected. [c] Yield isolated by column chromatography.

provided the oxime R substituent contains an α-hydrogen (as in **1a**–**d**). This allows conformations where a C–H bond, as opposed to a C–R′ bond, impedes the reactivity of the lone pair. As the size of R increases, the increasingly sluggish nature of the *E*-oxime 1,3-APT step is reflected in the lower yields and conversions (Table 1). Where the oxime contains no α-hydrogens (**1e**) severe impediment of the lone pair's reactivity is unavoidable and 1,3-APT can only proceed *via* the *Z*-oxime (*path a*). The sluggish nature of the oxime isomerism step for **1e** is reflected in the low conversion (25% after 48 h) and yield (11%).

Unlike aliphatic oximes (*E*)-benzaldoxime **1f** does not isomerise at 81 °C. Both *E*- and *Z*-isomers can be prepared and stored separately.[5,6] The observation that (*E*)-**1f** forms *endo*-**4f** exclusively while (*Z*)-**1f** affords *exo*-**4f** exclusively (Table 2) supports our hypothesis. In order to determine the effect of the electronic nature of the aryl ring on oxime isomerism we carried out the cascade with both *E*- and *Z*-isomers of *para*-substituted benzaldoximes (Table 2). We observed that the presence of electron donating groups promotes oxime isomerism, affording mixtures of *exo*- and *endo*-isomers. The presence of electron withdrawing groups in the aromatic ring does not promote oxime isomerism and instead 'switches off' the 1,3-APT step for *E*-oxime isomers. Switching to the *Z*-isomers in the case of these electron deficient benzaldoximes allows the reactions to proceed, leading to *exo*-**4** exclusively.

Increasing the reaction temperature from 80 to 95 °C (closed system) resulted in an increase in the propensity of aliphatic aldoximes to form the *exo*-isomer (Table 3). We were able to utilise this effect in the case of phenyl acetaldehyde oxime (**1a**), attaining *exo*-selectivity of 8 : 1 (81%) when the reaction temperature was 120 °C (closed system) (Table 3). Similarly, **1b** afforded an 8 : 1 ratio of *exo*-**4b** and *endo*-**4b** (65%). Increasing the temperature of the system further (150 °C) resulted in identical *exo*-selectivity, however. It is proposed that high temperatures facilitate higher rates of *E*/*Z*-oxime equilibration, leading to enhanced *exo*-selectivity.[7]

In conclusion we have demonstrated that this tandem 1,3-APT-cycloaddition cascade between aldoximes and divinyl ketone can afford single diastereomers with predictable *exo*- or *endo*-stereochemistry by a correct choice of conditions: high temperatures for aliphatic aldoximes and correct choice of starting oxime for aromatic aldoximes.

Table 3[a]

Oxime **1**	R	Temp/°C	Conv. (%)[d]	*exo*-**4** : *endo*-**4**[d]	Yield (%)[e]
a	Bn	95[b]	> 95	4.3 : 1	57
a	Bn	120[c]	> 95	8 : 1	81
b	Me	95[b]	> 95	5.6 : 1	59
b	Me	120[c]	> 95	8 : 1	65
c	Et	95[b]	> 95	2.7 : 1	53
d	Pr^i	95[b]	90	2 : 1	54
e	Bu^t	95[b]	45	*exo*-**4e** only	37
f	Ph	95[b]	30	*endo*-**4f** only	14

[a] Reaction conditions: Divinyl ketone (1.2 eq.), acetonitrile, STEM block at 95 °C, 48 h. [b] Temperature of STEM block. [c] Temperature of closed system. [d] Determined by ^{1}H NMR. [e] Combined yield of *exo*-**4** and *endo*-**4** isolated by column chromatography.

Notes and References

1 I. S. Saba, M. Frederickson, R. Grigg P. Dunn and P. Levett, *Tetrahedron Lett.*, 1997, **38**, 6099.
2 I. S. Saba, PhD Thesis, 1997, University of Leeds.
3 R. Grigg, F. Heaney, S. Surendrakumer and W. Warnock, *Tetrahedron*, 1991, **47**, 4477.
4 The reasons for this regioselective formation of **4** are discussed in the proceeding communication.
5 R. Grigg, F. Heaney, S. Surendrakumar and W. Warnock, *Tetrahedron*, 1991, **47**, 4477.
6 R. Grigg, M. Dorrity, F. Heaney, J. Malone, S. Rajviroongit, V. Sridharan and S. Surendrakumar, *Tetrahedron*, 1991, **47**, 8297.
7 A mixture of *exo*-**3b** and *endo*-**3b** was recovered unchanged, in good recovery after heating in a closed system at 120 °C. Thus proving that a cycloreversion–cycloaddition is not responsible for the increased *exo*-selectivity.

Tandem 1,3-azaprotiocyclotransfer–cycloaddition reactions between aldoximes and divinyl ketone. Remarkable rate enhancement and control of cycloaddition regiochemistry by hafnium(IV) chloride

Peter J. Dunn,[b] Alison B. Graham,[a] Ronald Grigg*[a] and Paul Higginson[b]

[a] *Molecular Innovation, Diversity and Automated Synthesis (MIDAS) Centre, School of Chemistry, The University of Leeds, Leeds, UK LS2 9JT. E-mail: R.Grigg@chem.leeds.ac.uk*
[b] *Pfizer Global Research & Development (UK), Sandwich, Kent, UK CT13 9NJ*

Received (in Cambridge, UK) 5th July 2000, Accepted 11th September 2000
First published as an Advance Article on the web 2nd October 2000

The tandem 1,3-azaprotiocyclotransfer–cycloaddition reaction between aldoximes and divinyl ketone affords the *exo*-isomers of substituted 1-aza-8-oxabicyclo[3.2.1]octan-4-ones when a substoichiometric amount of hafnium(IV) chloride is added.

As part of our continuing interest in cascade cycloaddition reactions of oximes we recently outlined our efforts to incorporate divinyl ketone **2** as a bifunctional azaprotiophile/dipolarophile component[1] in Class 2 processes.[2] The reaction between **2** and symmetrical ketoximes **1** (R′ = R) proceeds smoothly to afford a regioisomeric mixture of isoxazolidinones **3** and **4**, where **4** is the major product (Scheme 1). We were able to obtain **3** (R = R′) as the major product by the addition of a stoichiometric amount of zinc bromide and to bias the cascade in favour of **4** (R = R′) by a judicious choice of solvent. Preliminary investigations of aldoxime **1** (R′ or R = H)-**2** cascades gave **4** as the major product and **3** was rarely detected.[3] The *exo*-:*endo*-ratio was shown to be dependent on the geometry of the starting oxime and its propensity to isomerise under thermal conditions. The addition of zinc bromide was found to be much less effective for aldoxime cascades than for symmetrical ketoxime cascades, prompting us to seek an alternative Lewis acid. We now report a regio- and stereoselective hafnium(IV) chloride catalysed aldoxime-**2** cascade.

The reaction between an achiral aldoxime **1** (R or R′ = H) and **2** can in principle occur *via* a number of pathways, including the synthetically less useful *O*-Michael addition. Polymerization of **2** is also a potential problem. Generally both *E*- and *Z*-aldoxime isomers can undergo 1,3-azaprotiocyclotransfer (herein referred to as 1,3-APT) to afford *E*- and *Z*-nitrones respectively.[3] Subsequent cycloaddition of each nitrone can afford four possible diastereomeric products *exo*-**3**, *exo*-**4**, *endo*-**3** and *endo*-**4** (Scheme 2). Under thermal conditions (81 °C, acetonitrile) *exo*-**4** and *endo*-**4** are the exclusive products.

Amongst the Lewis acids tested were salts of lanthanides, titanium, indium and magnesium. These have been reported to catalyze 1,3-dipolar cycloaddtions.[4] The majority of these salts directed the regioselectivity of the cascade towards *exo*-**3** but the results were capricious in terms of yield. Hafnium(IV) chloride appeared to be the least detrimental and was selected for further optimisation. The mode 2 conditions outlined in Table 1 afford reproducible results.[5]

Thus treatment of aryl and aliphatic aldoximes **1a**–**j** with hafnium(IV) chloride resulted in complete reversal of the

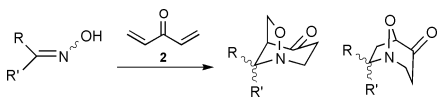

Scheme 1

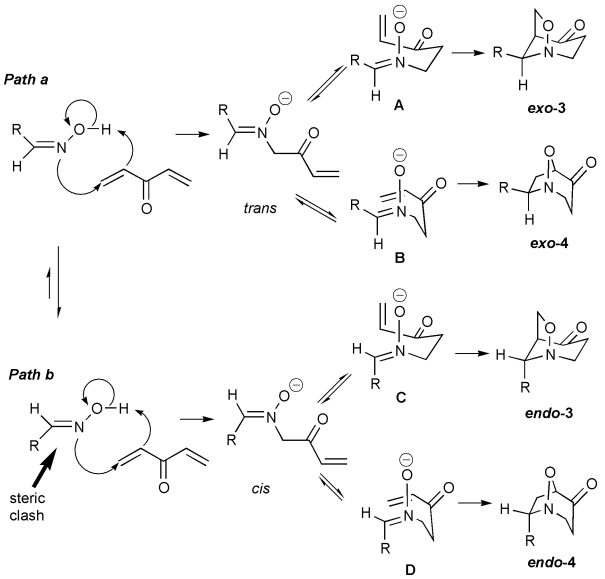

Scheme 2

selectivity of the thermally controlled cascade, giving exclusive formation of *exo*-**3a**–**j** (Table 1). The scope of the reaction includes aliphatic aldoximes (entries **a**–**c**), electron deficient aryl aldoximes (entries **f, g, h**) and electron rich aryl aldoximes (entry **i**). In many cases the addition of hafnium(IV) chloride was necessary for a reaction to occur (entries **f**, **g**, **h**).

Both *E*- and *Z*-isomers of benzaldoxime (**1d**,**e**) afford the same product under the hafnium(IV) chloride catalysed conditions. In the absence of hafnium(IV) chloride **1d** and **e** each afford different *exo*- and *endo*-diastereomers of **4**, due to the inability of these oxime isomers to equilibrate at 81 °C.[2,3] Thus hafnium(IV) chloride promotes oxime isomerism. This may be by co-ordination of hafnium to the oxime *via* the hydroxy moiety and the subsequent lowering of its pK_a or the release of a catalytic amount of HCl from hafnium(IV) chloride and traces of water.[6,7] Only a small equilibrium concentration of the *Z*-oxime is required for exclusive formation of the *Z*-nitrone.[8] Though we have evidence to suggest that hafnium(IV) chloride enhances the rate of the 1,3-APT step, it's precise role is a matter of conjecture at this time.[9]

The regiochemistry, which is dictated by the relative magnitudes of the interacting orbital coefficients, is completely reversed by the addition of hafnium(IV) chloride. This particular cycloaddition is expected to be $HOMO_{nitrone}$–$LUMO_{alkene}$ controlled and is predicted to result in bond formation between the oxygen and the terminal alkene carbon as in **A**, ultimately leading to **3**.[10] However, Gandolfi and co-workers have shown experimentally that only strongly electron withdrawing alkenes (*e.g.* nitroethylene) and electron rich nitrones (*e.g.* triphenyl nitrones) react in this way.[11] Otherwise, mixtures of regio-

Table 1

		MODE 1: **2** (1.2 eq.), MeCN, 81 °C, 48 h			MODE 2: **2** (1.5 eq.), $HfCl_4$ (0.5 eq), THF, 66 °C, 30 min		
Oxime **1**[a]		Conv.[b] (%)	*exo*-**3**:**4**[b,c]	Yield (%)[d]	Conv.[b] (%)	*exo*-**3**:**4**[b,c]	Yield[d] (%)
a		>95[e]	1:>20	65	>95	>20:1	45
b		25[e]	1:>20	11	>95	>20:1	78
c		>95[e]	1:>20	41	>95	>20:1	37
d	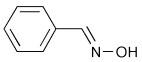	10[e]	1:>20	—	90	>20:1	64 (71)
e	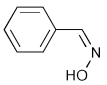	>95	1:>20	79	90	>20:1	55 (61)
f	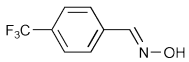	<5	—	—	85	>20:1	70 (82)
g	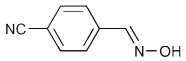	<5	—	—	85	>20:1	62 (73)
h	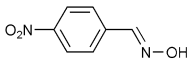	<5	—	—	70	>20:1	63 (90)
i	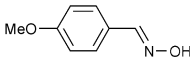	80	1:2.5	55	>95	>20:1	49
j	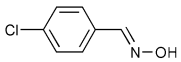	>95	1:11	61	85	>20:1	57 (63)

[a] The *E*/*Z* stereochemistry of the oxime is as illustrated. [b] Mixtures of *exo*-**4** and *endo*-**4** were formed. [c] Ratios determined by ^{1}H NMR, in cases where the ratio is >20:1 no traces of the minor isomer were detected. [d] Yield isolated by column chromatography, values in parentheses indicate yields based on 100% conversion of oxime. [e] Reaction carried out in a STEM block at 80 °C.

isomers are formed. Co-ordination of the hafnium to the ketone as depicted in Fig. 1 will alter the relative magnitudes of the atomic coefficients favouring **A** (leading to *exo*-**3**) over **B** (leading to *exo*-**4**).

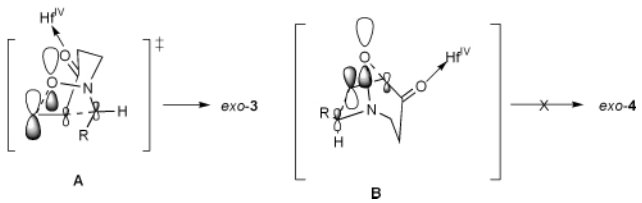

Fig. 1

Hafnium(IV) chloride is a highly effective catalyst for aldoxime–divinyl ketone cascades. There are only a few reports[12] of the use of hafnium salts in organic synthesis. To the best of our knowledge this is the first example of a hafnium promoted 1,3-dipolar cycloaddition.

Notes and references

1 I. S. Saba, M. Frederickson, R. Grigg, P. Dunn and P. Levett, *Tetrahedron Lett.*, 1997, **38**, 6099.
2 R. Grigg, F. Heaney, S. Surendrakumer and W. Warnock, *Tetrahedron*, 1991, **47**, 4477.
3 P. Dunn, A. B. Graham, R. Grigg, P. Higginson and I. S. Saba, *Chem. Commun.*, preceding communication (DOI: 10.1039/b005389i).
4 K. V. Gothelf and K. A. Jorgensen, *Chem. Rev.*, 1998, **98**, 863, and references cited therein.
5 Hafnium(IV) bromide, hafnocene(IV) dichloride, hafnium(IV) ethoxide and hafnium(IV) fluoride were found to be less effective than $HfCl_4$.
6 (*E*)-Benzaldoxime was heated in the absence of divinyl ketone under otherwise identical reaction conditions and the reaction was quenched after 30 min without being allowed to cool. The formation of (*Z*)-benzaldoxime (7%) was visible by ^{1}H NMR.
7 Reaction between (*E*)-benzaldoxime and **2** did not proceed on treatment of the reaction mixture with a small amount of HCl gas. ^{1}H NMR of the reaction mixture indicated oxime isomerism had not occurred.
8 The rate of 1,3-APT from (*Z*)-benzaldoxime is expected to be significantly faster than that from the corresponding (*E*)-benzaldoxime due to steric factors. For a full account see ref. 3.
9 The rate enhancement is not simply due to oxime isomerism. The *Z*-isomer of **1f** reacts after 48 h in >95% conversion to afford *exo*-**4f** but after 30 min in THF at 66 °C only starting material is recovered.
10 K. N. Houk, J. Sims, R. E. Duke, R. W. Strozier and J. K. George, *J. Am. Chem. Soc.*, 1973, **95**, 7287; K. N. Houk, J. Sims, C. R. Watts and C. J. Luskus, *J. Am. Chem. Soc.*, 1973, **95**, 7301.
11 M. Burdisso, R. Gandolfi and P. Grunanger, *Tetrahedron*, 1989, **45**, 5579.
12 I. Hachiya, M. Moriwaki and S. Kobayashi, *Tetrahedron Lett.*, 1995, **35**, 409; I. Hachiya, M. Moriwaki and S. Kobayashi, *Bull. Chem. Soc. Jpn.*, 1995, **68**, 2053; S. Kobayashi, M. Moriwaki and I. Hachiya, *Tetrahedron Lett.*, 1996, **37**, 2053; E. Yoshikawa, V. Gevorgyan, N. Asao and Y. Yamamoto, *J. Am. Chem. Soc.*, 1997, **119**, 6781.

ChemComm

An ultimate species in the substrate oxidation process by cytochrome P-450

Masayuki Hata,* Tyuji Hoshino and Minoru Tsuda

Laboratory of Physical Chemistry, Faculty of Pharmaceutical Sciences, Chiba University, Chiba 263-8522, Japan. E-mail: hata@pn120.p.chiba-u.ac.jp

Received (in Cambridge, UK) 3rd August 2000, Accepted 31st August 2000
First published as an Advance Article on the web 2nd October 2000

We propose a structure for the ultimate species which gives a straightforward explanation of the major results in the oxidation of hydrocarbons by cytochrome P-450 where the stereochemistry is retained and the isotope effect is small.

In the substrate oxidation process by cytochrome P-450 it was believed that the ultimate species is compound **I** [(heme)Fe=O] (Fig. 1).[1] Recently, Harris and Loew[2] showed that the spin-density of compound **I** in the spin doublet state (the ground state of this compound) is localized at the oxygen atom that is bound to the Fe atom of the heme, *i.e.* the spin-density is 0.92, indicating that the oxygen atom has the character of a free radical. The summation of the spin-densities shared by the heme and the fifth ligand gives a value of 0.08. We re-confirmed this spin-density distribution of compound **I** by performing similar calculations using density functional theory (DFT).[3]

It is well known that a free radical abstracts a hydrogen atom from hydrocarbons.[7] We found that compound **I** abstracts a hydrogen atom from hydrocarbons and produces Fe–OH with an activation energy of 15.5 kcal mol^{-1}. The hydrogen abstraction from hydrocarbons has been considered to be one of the plausible mechanisms caused by the ultimate species, compound **I**, and the substrate oxidation process by cytochrome P-450 should be as in the two-step mechanism shown in Fig. 1(a).[1,8] This two-step mechanism has the characteristics that (*i*) the stereochemistry is lost, and (*ii*) an isotope effect is clearly observed.[1,8]

The hydroxylation of a hydrocarbon by cytochrome P-450, however, generally occurs with retention of stereochemistry and a small isotope effect.[1,8] The concerted insertion of an oxygen atom into a hydrocarbon C–H bond [Fig. 1(b)] is therefore, favorable from this viewpoint. In order to examine the possibility of the one-step mechanism [Fig. 1(b)], a theoretical study has been preformed.

Firstly, we carried out the molecular dynamics (MD) simulations for 300 ps at 310 K on oxy-ferrous P-450cam in water, and showed that the substrate–oxygen molecule interaction is maintained in the heme pocket of cytochrome P-450cam, *i.e.* the distance between the C5 atom of d-camphor and the oxygen atom which is not directly bound to the Fe atom of the heme (the distal oxygen atom, O2) is *ca.* 3.0–3.5 Å (3.22 Å in Fig. 2). It is considered that the interaction between the substrate and the oxygen molecule bound to the Fe atom of the heme is always effective throughout the substrate oxidation process by cytochrome P-450. Experiments by Tuckey and Kamin[14] support the existence of the substrate–oxygen molecule interaction in the heme pocket, *i.e.* the 1-electron-reduced–oxygenated complex of cytochrome P-450 is kinetically stabilized by the binding of the substrate.

From Fig. 2 it is natural to consider that the distal oxygen atom is inserted into the C5–H bond of d-camphor. From this the revised ultimate species shown in Fig. 3 is proposed. Because it exists at a minimum in the potential energy hypersurface, the structure of this compound is stable. The potential energy of the structure is 59.8 kcal mol^{-1} higher than the sum of the potential energies of compound **I** and H_2O. However, it is considered that formation of the revised ultimate species could occur, because reduced oxy-ferrous heme is stabilized by > 700 kcal mol^{-1} upon binding of two protons to form each ultimate species. For the revised ultimate species

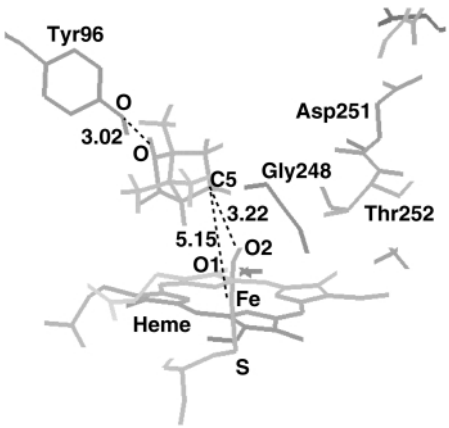

Fig. 2 Schematic of oxy-ferrous P-450cam obtained by 300-ps MD simulation at 310 K. Numerals are inter-atomic distances in Å. Computational program is AMBER 4.1.[9] A united-atom force field[10] was applied except for d-camphor, for which an all-atom force field[11] was used. Calculations of the non-bonded term were accelerated by the use of a hardware accelerator (MD Engine).[12] A cutoff distance (8 Å) was applied for computation of van der Waals forces (r^{-6} and r^{-12}). The electrostatic term (r^{-1}) was calculated with no cutoff, taking full advantage of the MD Engine. The SHAKE constraint,[13] where all of the bonds are kept at equilibrium distances, was used.

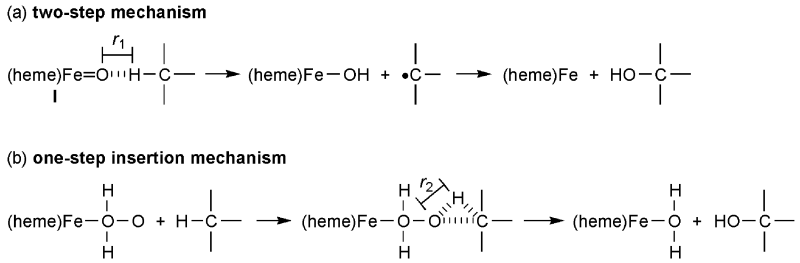

Fig. 1 Two processes in the substrate oxidation by cytochrome P-450: (a) two-step mechanism by the currently believed ultimate species, compound **I**, which has an active oxygen atom in the spin doublet state; (b) one-step insertion mechanism by the newly proposed ultimate species which has an active oxygen atom in the spin singlet state. The existence of these two processes gives complicated results in the oxidation products by cytochrome P-450.

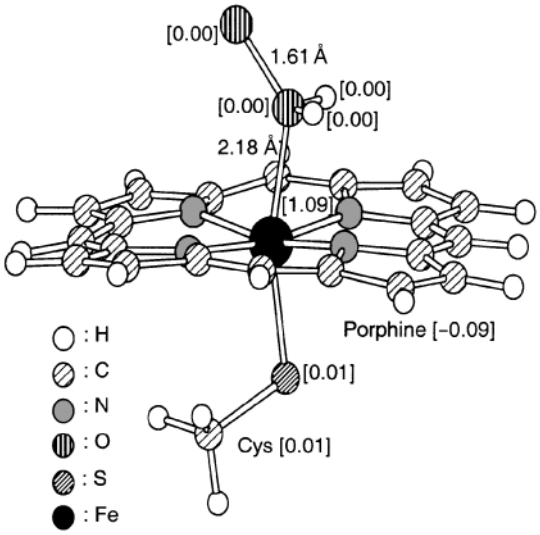

Fig. 3 Spin-density distribution of the stable structure of the newly proposed ultimate species for the mono-oxygenation reaction by cytochrome P-450. Numerals in parentheses are the spin-densities. The total electronic charge of the model compound is neutral and the total spin multiplicity is that of a doublet.

(Fig. 3) it should be noted in the spin-density distribution that the distal oxygen atom is in the spin singlet state, and it has already been suggested that a spin singlet state oxygen atom ^{1}D operates a one-step insertion mechanism.[15] The activation energy of the insertion reaction of this singlet oxygen atom to the C5–H bond of d-camphor was calculated to be 4.2 kcal mol^{-1}. This value is very small, compared with the activation energy (13 kcal mol^{-1}) of singlet oxygen atom ^{1}D insertions into hydrocarbons,[15] suggesting the important role of the heme-protein in the substrate oxidation. It is clear that this revised ultimate species gives a straightforward explanation of the major results in the oxidation of hydrocarbons by cytochrome P-450, where the stereochemistry is retained and the isotope effect is small. The formation process of the ultimate species may be followed by the same experiment which support the formation of compound **I** except in the final process, where the conventional mechanism postulates the formation of the compound **I** and a free water molecule, but the new mechanism considers the oxygenated hydrocarbon and a water molecule which binds to the Fe atom of the heme. Provided that the interaction between a substrate and the distal oxygen in the heme pocket is weak enough that the interaction is not maintained throughout the substrate oxidation process, the conventional ultimate species (compound **I**) may be produced. It is well known that compound **I** is produced in the substrate oxidation process by peroxidase where the isotope effect is clearly observed.[16]

The mechanism shown in Fig. 1 is clearly explained by the existence of these two ultimate species. The two kinds of the ultimate species generated in the substrate oxidation process by cytochrome P-450 explains in a straightforward manner the reasons why a variety of products have been reported in the literature.[1,8]

The authors thank the Computer Center of the Institute for Molecular Science, Okazaki, for the use of the IBM SP2 computer. The computations were also carried out by DRIA System at the Faculty of Pharmaceutical Sciences, Chiba University.

Notes and references

1 Y. Ishimura, in *Cytochrome P-450*, ed. T. Omura, Y. Ishimura and Y. Fujii-Kuriyama, Kodansha, Tokyo, 1993, p. 80.
2 D. L. Harris and G. H. Loew, *J. Am. Chem. Soc.*, 1998, **120**, 8941.
3 Exchange and correlation functionals used for the DFT calculations in this study are Becke's three parameter function[4] and the Lee–Yang–Parr function,[5] respectively. Basis set is 3-21G**. Computational program is Gaussian 98.[6]
4 A. D. Becke, *J. Chem. Phys.*, 1993, **98**, 5648.
5 C. Lee, W. Yang and R. G. Parr, *Phys. Rev. Sect. B*, 1988, **37**, 785.
6 M. J. Frisch, G. W. Trucks, H. B. Schlegel, G. E. Scuseria, M. A. Robb, J. R. Cheeseman, V. G. Zakrzewski, J. A. Montgomery Jr., R. E. Stratmann, J. C. Burant, S. Dapprich, J. M. Millam, A. D. Daniels, K. N. Kudin, M. C. Strain, O. Farkas, J. Tomasi, V. Barone, M. Cossi, R. Cammi, B. Mennucci, C. Pomelli, C. Adamo, S. Clifford, J. Ochterski, G. A. Petersson, P. Y. Ayala, Q. Cui, K. Morokuma, D. K. Malick, A. D. Rabuck, K. Raghavachari, J. B. Foresman, J. Cioslowski, J. V. Ortiz, A. G. Baboul, B. B. Stefanov, G. Liu, A. Liashenko, P. Piskorz, I. Komaromi, R. Gomperts, R. L. Martin, D. J. Fox, T. Keith, M. A. Al-Laham, C. Y. Peng, A. Nanayakkara, C. Gonzalez, M. Challacombe, P. M. W. Gill, B. Johnson, W. Chen, M. W. Wong, J. L. Andres, C. Gonzalez, M. Head-Gordon, E. S. Replogle and J. A. Pople, *Gaussian 98, Revision A.7*, Gaussian, Inc., Pittsburgh PA, 1998.
7 For example, see Y. Tomoda and M. Tsuda, *Nature*, 1961, **190**, 905; Y. Tomoda and M. Tsuda, *J. Polym. Sci*., 1961, **54**, 321; R. T. Morrison and R. N. Boyd, in *Organic Chemistry*, Allyn and Bacon, Inc., Newton, MA, 5th edn., 1987, ch. 15.
8 P. R. Ortiz de Montellano, in *Cytochrome P-450, Structure, Mechanism, and Biochemistry*, ed. P. R. Ortiz de Montellano, Plenum Press, New York, 1986, p. 217.
9 D. A. Pearlman, D. A. Case, J. W. Caldwell, W. S. Ross, T. E. Cheatham, III, D. M. Ferguson, G. L. Seibel, U. C. Singh, P. K. Weiner and P. A. Kollman, *AMBER 4.1*, University of California, San Francisco, 1995.
10 S. J. Weiner, P. A. Kollman, D. A. Case, U. C. Singh, C. Ghio, G. Alagona, S. Profeta, Jr. and P. Weiner, *J. Am. Chem. Soc.*, 1984, **106**, 765.
11 S. J. Weiner, P. A. Kollman, D. T. Nguyen and D. A. Case, *J. Comput. Chem.*, 1986, **7**, 230.
12 S. Toyoda, H. Miyagawa, K. Kitamura, T. Amisaki, E. Hashimoto, H. Ikeda, A. Kusumi and N. Miyakawa, *J. Comput. Chem.*, 1999, **20**, 185.
13 J. Richaert, G. Ciccotti and H. J. C. Berenedsen, *J. Comput. Phys.*, 1977, **23**, 327.
14 R. C. Tuckey and H. Kamin, *J. Biol. Chem.*, 1982, **257**, 9309.
15 M. Nakajima, M. Tsuda and S. Oikawa, *Chem. Pharm. Bull.*, 1987, **35**, 941.
16 G. T. Miwa, J. S. Walsh, G. L. Kedderis and P. F. Hollenberg, *J. Biol. Chem.*, 1983, **258**, 14 445; O. Okazaki and F. P. Guengerich, *J. Biol. Chem.*, 1993, **268**, 1546; F. P. Guengerich, C.-H. Yun and T. L. Macdonald, *J. Biol. Chem.*, 1996, **271**, 27 321.

An important application of the 1,8-diketone ring formation reaction: a concise synthesis of 5,6-diphenyl[1,3]dithiolo[4,5-*b*][1,4]dithiine-2-thione and its coupling product

Erdal Ertas and Turan Ozturk*

TUBITAK, Marmara Research Centre, Chemistry Department, Organic Chemistry, Gebze Kocaeli, Turkey. E-mail: turan@mam.gov.tr

Received (in Corvallis, OR, USA) 8th May 2000, Accepted 28th August 2000
First published as an Advance Article on the web 2nd October 2000

Syntheses of fully unsaturated 5,6-diphenyl[1,3]dithiolo[4,5-*b*][1,4]dithiine-2-thione and its coupling product, a fully unsaturated analogue of BEDT-TTF, have been achieved by a 1,8-diketone ring formation reaction.

There has been wide interest in the synthesis of derivatives of bis(ethylenedithio)tetrathiafulvalene, BEDT-TTF (or ET) **1**.

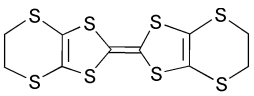

1

This is due to its electron donating ability, which makes it exhibit conducting and superconducting properties as charge transfer salts with electron acceptors such as TCNQ and mono anions.[1] The highest superconducting critical temperature, T_c, observed to date for an organic superconductor is 12.8 K with K-(BEDT-TTF)Cu[$N(CN)_2Br$].[2]

One of the important features, which has been the subject of efforts by various research groups, is the introduction of an increased conjugation, which would allow the system to have an extended π-electron delocalisation. So far, such an extension has been achieved in the middle of the molecule.[1b] However, there are limited examples of introduction of conjugation at the peripheral ethylene groups.[3]

Recently, we have reported a convenient method of synthesising fused 1,4-dithiin systems with various functional groups (**2**, **3**).[4] This method has allowed us to introduce four phenyl

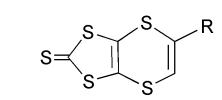

R = Ph, 4-CH_3OPh, 4-NO_2Ph, CH_3, [7] 4-BrPh[7]

2

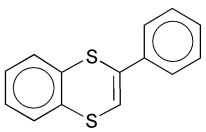

3

groups on to the peripheral ethylene bridges of BEDT-TTF, that is the synthesis of a tetra-phenyl substituted and fully unsaturated analogue, 5,5′,6,6′-tetraphenyl-2,2′bi([1,3]dithiolo[4,5-*b*][1,4]dithiinylidene) **11**, which has been the subject of research by other groups.[5] Unfortunately, their attempts have been unsuccessful so far, although trace amount of 5,6-diphenyl[1,3]dithiolo[4,5-*b*][1,4]dithiine-2-thione **10** was claimed to have been obtained.[5c] We report here that our 1,8-diketone ring-closure reaction smoothly gives the precursor **10** in a relatively high yield, 65%, which proves that this reaction may be an important tool in the formation of fused and fully substituted 1,4-dithiin rings.

In our previous report,[4] we disclosed that refluxing the 1,8-diketones in toluene with Lawesson's Reagent (LR) **4**

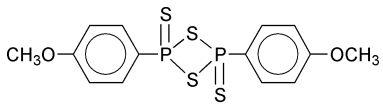

4

yielded fused thiophenes and 1,4-dithiins. The precursor **7**, which is the subject of the cyclisation reaction in this study, was easily obtained from the reaction of readily available dianion **5**[6] and desyl chloride† **6** in dry ethanol at rt in 90% yield (Scheme 1). Following the previous reaction conditions, the 1,8-diketone **7** was allowed to react with LR in boiling toluene overnight (Scheme 2). In agreement with the result reported by Noh *et al.*,[5b] fused thiophene rather than dithiin was isolated. Considering our preliminary results that such a ring formation reaction could be carried out with P_4S_{10} and tended to give 1,4-dithiin in a shorter reaction time, in another experiment, we treated **7** with P_4S_{10} in refluxing toluene.[7] Interestingly, this reaction, after 3 h reflux, gave **9** as one of the products, possessing a benzylphenyldithiole ring, along with the thiophene **8**, in 25 and 30% yields, respectively. This result suggested that, since there was no loss of sulfur, the initially *in situ* formed 1,4-dithiin derivative **10** rearranged radically to give benzylphenyldithiole **9**. Obviously, in the presence of sulfur as a source of radicals such a mechanism is likely. In view of all these experiences, cyclisation was performed with P_4S_{10} in refluxing toluene in the dark. After the consumption of starting material **7**, which took *ca*. 3 h, column chromatography of the crude reaction product (3 : 1, hexane–CH_2Cl_2) gave three compounds, thiophene **8** (20%), benzylphenyldithiole **9** (trace) and 1,4-dithiin **10**[8] (65%). The structures of **8**, **9** and **10** were confirmed by X-ray single-crystal diffraction analysis and the results will be published elsewhere.

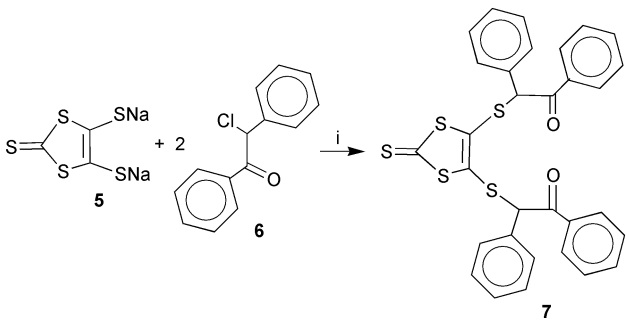

5 **6** **7**

Scheme 1 *Reagents and conditions*: i, EtOH (dry), N_2, rt, overnight.

With this fully unsaturated compound **10** in hand, which does not require storage under nitrogen, coupling product **11** was prepared following the well-established reaction scheme (Scheme 3). The thione sulfur atom in **10** was converted to oxygen with mercury acetate in a quantitative yield. Subsequent heating of the reaction product in neat triethylphosphite

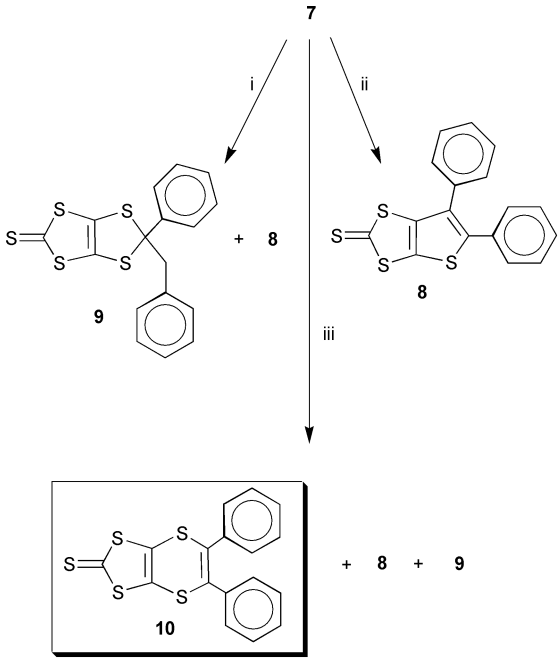

Scheme 2 *Reagents and conditions*: i, P_4S_{10}, toluene, reflux, 3 h; ii, LR, toluene, reflux, overnight; iii, P_4S_{10}, toluene, reflux, dark, 3 h.

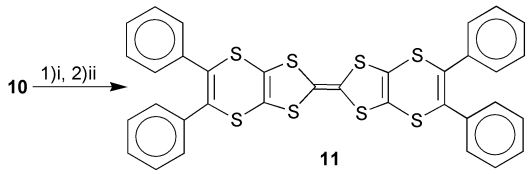

Scheme 3 *Reagents and conditions*: i, $Hg(OAc)_2$–AcOH, $CHCl_3$, 3 h, rt; ii, $(EtO)_3P$, 110 °C, N_2, 2 h.

(110 °C) for 2 h resulted a yellow precipitate of **11**,[9] which was collected in 90% yield. Contrary to the result reported for the coupling of the saturated analogue **12**, which gave tetrakis(ethylthio)tetrathiafulvalene **13** rather than its self-coupled product **14**,[5a,c] the fully unsaturated **10** yielded **11** smoothly in a high yield. This result further suggests that unsaturated dithiin ring contributes to the stability of the molecule through conjugation.

In conclusion, we have demonstrated that a fully substituted and fused 1,4-dithiin derivative can easily be prepared by a 1,8-diketone ring-formation reaction, using P_4S_{10}, and also a fully unsaturated analogue of BEDT-TTF has been prepared in an efficient procedure and in a good yield. The precursor **10** and the analogue **11** themselves could prove useful as electronic materials.

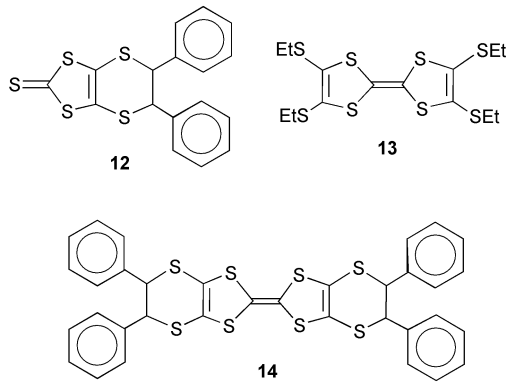

Notes and references

† The IUPAC name for desyl chloride is 2-chloro-2-phenylacetophenone.

1 (*a*) J. M. Williams, J. R. Ferraro, R. J. Thorn, K. D. Carlson, U. Geiser, H. H. Wang, A. M. Kini and M.-H. Whangbo, *Organic Superconductors (Including Fullerenes)*, Prentice Hall, Englewood Cliffs, 1992; (*b*) M. R. Bryce, *J. Mater. Chem.*, 1995, **5**, 1481; (*c*) M. R. Bryce, *J. Mater. Chem.*, 2000, **10**, 589.

2 A. M. Kini, U. Geiser, H. H. Wang, K. D. Carlson, J. M. Williams, W. K. Kwok, K. G. Vandervoort, J. E. Thompson, D. L. Stupka, D. Jung and M.-H. Whangbo, *Inorg. Chem.*, 1990, **29**, 2555.

3 (*a*) J.-I. Yamada, S. Satoki, H. Anzai, K. Hagiya, M. Tamura, Y. Nishio, K. Kajita, E. Watanabe, M. Konno, T. Sato, H. Nishikawa and K. Kikuchi, *Chem. Commun.*, 1996, 1955; (*b*) T. Nakamura, S.-I. Iwasaka, H. Nakano, K. Inoue, T. Nogami and H. Mikawa, *Bull. Chem. Soc. Jpn.*, 1987, **60**, 365; (*c*) T. Nogami, K. Inoue, T. Nakamura, S.-I. Iwasaka, H. Nakano and H. Mikawa, *Synth. Met.*, 1987, **19**, 539; (*d*) P. J. Skabara, I. M. Serebryakov, D. M. Roberts, I. F. Perepichka, S. J. Coles and M. B. Hursthouse, *J. Org. Chem.*, 1999, **64**, 6418; (*e*) M. R. Bryce, A. K. Lay, A. S. Batsanov and J. A. K. Howard, *Tetrahedron Lett.*, 1999, **40**, 801; (*f*) W. Xu, D. Zhang, H. Li and D. Zhu, *J. Mater. Chem.*, 1999, **9**, 1245.

4 (*a*) T. Ozturk, *Tetrahedron Lett.*, 1996, **37**, 2821.

5 (*a*) D.-Y. Noh, H.-J. Lee, J. Hong and A. E. Underhill, *Tetrahedron Lett.*, 1996, **37**, 7603; (*b*) H.-J. Lee, Y.-Y. Kim and D.-Y. Noh, *Bull. Korean Chem. Soc.*, 1998, **19**, 1011 (*c*) H.-J. Lee and D.-Y. Noh, *Bull. Korean Chem. Soc.*, 1998, **19**, 340.

6 N. Svenstrup and J. Becher, *Synthesis*, 1995, 215.

7 T. Ozturk and F. Turksoy, unpublished results.

8 5,6-Diphenyl[1,3]dithiolo[4,5-*b*][1,4]dithiine-2-thione **10**: mp 113–114 °C. HRMS *m/z* calculated 373.9386; measured 373.9397 for $C_{17}H_{10}S_5$. Calc. C 54.5, H 2.69; found C 54.44, H 2.66%. IR ν 1080 cm^{-1} (C=S). UV λ_{max} (CH_3CN) 391 nm. δ_H(250 MHz, $CDCl_3$) 7.09–7.34 (m, 10H). δ_H(67.8 MHz, $CDCl_3$) 213.9 (C=S), 136.2 (C-*q*), 134.7 (C-*q*), 129.9 (C-*q*), 129.5 (C-*t*), 128.7 (C-*t*), 128.6 (C-*t*).

9 5,5′,6,6′-Tetraphenyl-2,2′bi([1,3]dithiolo[4,5-*b*][1,4]dithiinylidene) **11**: mp 249 (decomp.). HRMS *m/z* calculated 683.9330; measured 683.9329 for $C_{34}H_{20}S_8$. Calculated C 59.6, H 2.9; found C 59.71, H 2.79%. δ_H(250 MHz, $CDCl_3$) 7.14–7.30 (m, 20H). δ_c(67.8 MHz, $CDCl_3$) 136.8 (C-*q*), 135.3 (C-*q*), 134.2 (C-*q*), 129.6 (C-*t*), 128.8 (C-*t*), 128.4 (C-*t*).

Synthesis of microporous surfactant-templated aluminosilicates

David P. Serrano,*[a] José Aguado,[a] José M. Escola[a] and Eduardo Garagorri[b]

[a] *Department of Experimental Sciences and Engineering, ESCET, Rey Juan Carlos University, c/Tulipán s/n 28933, Móstoles, Madrid, Spain. E-mail: dserrano@escet.urjc.es*

[b] *Department of Chemical Engineering, Complutense University, Av. Complutense s/n, 28040 Madrid, Spain.*

Received (in Cambridge, UK) 31st July 2000, Accepted 7th September 2000
First published as an Advance Article on the web 2nd October 2000

Microporous aluminosilicates have been synthesized in the presence of organic surfactants according to a procedure based on a two-step sol–gel process at room temperature; varying the surfactant chain length and/or the Si/Al ratio, materials with pore diameters adjustable in the range 1.0–2.5 nm have been obtained; the Al atoms in the as-synthesized samples present tetrahedral coordination, even for materials with high Al content (Si/Al = 6).

The M41S family of surfactant-templated mesoporous silicates and aluminosilicates was discovered and characterized in 1992 by Mobil Oil researchers.[1] The presence of Al atoms incorporated into the walls and large pores provide these materials with interesting properties for the catalytic conversion of bulky molecules.[2–4] In past years, a number of studies have been published aimed to the synthesis of mesoporous materials with increasing pore size by incorporation of swelling agents to the synthesis medium or by using block copolymer surfactants.[5–8] Accordingly, micelle-templated silicates and aluminosilicates have been prepared with uniform pore sizes in the range 2–10 nm.[9–13] However, less attention has been devoted to the synthesis of surfactant-templated materials with pore diameters below 2.0 nm. This is an interesting goal as it would contribute to fill the pore size gap existing between microporous zeolitic materials (D_p < 1 nm) and surfactant-templated mesoporous solids (D_p > 2 nm). Moreover, materials with uniform pore size in the range 1.0–2.0 nm are expected to exhibit interesting shape-selectivity properties in the conversion of large substrates.

Several papers have recently appeared with the aim of obtaining surfactant templated materials with small pore diameters. Thus, a novel method for tailoring the pore opening size of MCM-41 materials has been reported,[14] although based on a complex post-synthesis treatment with three steps. A completely different approach has been developed by Bagshaw and Haymann,[15] which has led to silicates with pore sizes in the range 1.4–2.0 nm through the use of a new family of ω-hydroxy-bolaform surfactants. However, at present it is not clear whether this last alternative would also allow microporous aluminosilicates to be synthesized.

In a recent work,[16] we have reported a new method for the preparation of Al-containing micelle-templated silica (Al-MTS) based on a sol–gel process at room temperature. We have found that when increasing the aluminium content, materials with pore sizes in the range 1.5–2.0 nm are obtained. In the present work we show that this method is also useful for the synthesis of Al-MTS solids with pore sizes that can be tailored in the range 1.0–2.0 nm through the variation of both surfactant alkyl chain length and Al content.

The materials were synthesized at room temperature according to the following procedure. The silica and aluminium sources (tetraethyl orthosilicate, TEOS, and aluminium isopropoxide, IPA) were first hydrolyzed under acidic conditions (aqueous HCl), the starting Si/Al ratio being varied within the range 5–30. The surfactant was added and the mixture obtained was stirred and kept under acidic conditions for 1 h (TEOS/Surf. molar ratio = 0.3). Both cetyltrimethylammonium chloride (CTMACl) and dodecyltrimethylammonium bromide (DTMABr) were employed as surfactants. In a second step, condensation reactions were promoted by dropwise addition of 2 wt% aqueous NH_3 until the gel point is reached. The solid material so obtained was filtered off, washed with deionized water and dried at 110 °C overnight. Finally, it was calcined in N_2 flow at a heating rate of 1 °C min^{-1} up to 550 °C and then kept in air flow at this temperature for 5 h.

Table 1 summarizes the physicochemical properties of different Al-MTS materials prepared. Although in general the samples obtained show Al contents lower than those of the synthesis mixture, a close correspondence is observed among them, even for the synthesis with the lowest Si/Al ratios. TG analysis of the as-synthesized samples show the presence of the surfactant molecules occluded in the pores with weight losses in the range 40–55 wt%, confirming that they can be regarded as micelle-templated materials. Fig. 1 illustrates the XRD spectra of samples prepared with surfactants of different chain length, a sharp diffraction peak at low angle being observed, which is

Table 1 Synthesis conditions and physicochemical properties of the synthesized materials

			N_2 adsorption isotherm (77 K)		
Surfactant	Si/Al (medium)	Si/Al (product)	Pore volume[a]/ $cm^3\ g^{-1}$	BET surface area[b]/ $m^2\ g^{-1}$	Surfactant content[c] (wt%)
CTMACl	30	45.2	0.93	1180	55
CTMACl	20	31.5	0.66	1020	52
CTMACl	10	18.9	0.56	910	50
CTMACl	5	8.3	0.45	790	43
DTMABr	20	42.4	0.47	960	46
DTMABr	15	18.9	0.40	840	42
DTMABr	8	10.4	0.39	820	35
DTMABr	5	6.3	0.32	770	40

[a] Measured at p/p_o = 0.9. [b] Measured within the range p/p_o = 0.01–0.125. [c] Determined from the TGA weight loss in the range 150–450 °C.

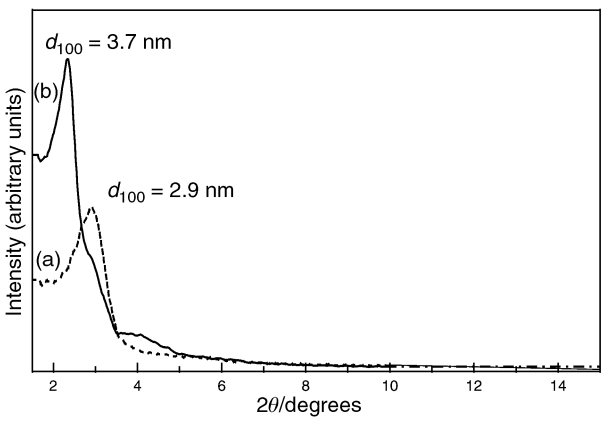

Fig. 1 XRD spectra of calcined samples: (a) DTMABr, Si/Al = 6.3 and (b) CTMACl, Si/Al = 45.2.

DOI: 10.1039/b006186g

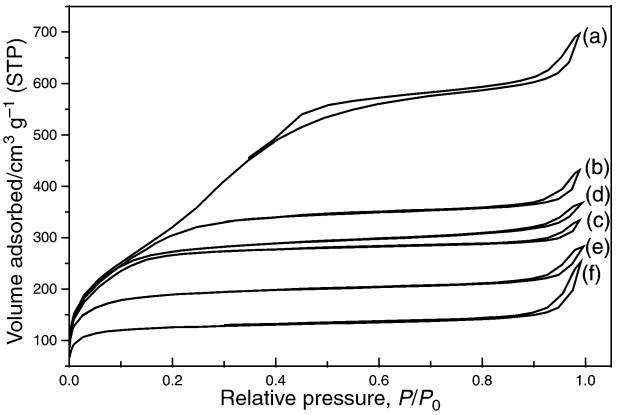

Fig. 2 N_2 adsorption–desorption isotherms: (a) CTMACl, Si/Al = 45.2; (b) CTMACl, Si/Al = 31.5; (c) CTMACl, Si/Al = 8.3; (d) DTMABr, Si/Al = 42.4; (e) DTMABr, Si/Al = 18.9; (f) DTMABr, Si/Al = 6.3.

characteristic of M41S amorphous structured materials. The *d*-spacings of the calcined samples prepared with DTMABr are higher than those obtained with CTMACl, which shows that a lower chain length of the surfactant leads to a reduction in the unit cell size.

Fig. 2 compares the N_2 adsorption–desorption isotherms at 77 K of a number of samples synthesized varying both the surfactant and the starting Si/Al ratio. A type IV isotherm is obtained for the sample prepared using CTMACl and Si/Al = 45.2, which is typical of a mesoporous material. This sample shows a pore diameter of 2.5 nm, calculated by the BJH method. However, increasing the Al content and/or reducing the alkyl chain length of the surfactant leads to type I isotherms, typical of microporous solids, which is accompanied by a decrease in both surface area and pore volume. Fig. 3 shows the variation in the pore size of these samples *vs.* the Al content. For both surfactants, the pore diameter is progressively reduced as the Al content is increased, showing that the presence of aluminium species during the synthesis process strongly affects the ionic surfactant-templated mechanism. For the samples prepared using CTMACl, the lowest pore diameter obtained is 1.5 nm, clearly within the micropore region. Interestingly, this limit can be reduced using DTMABr as surfactant, which leads to the synthesis of materials with pore sizes in the range 1.0–1.7 nm.

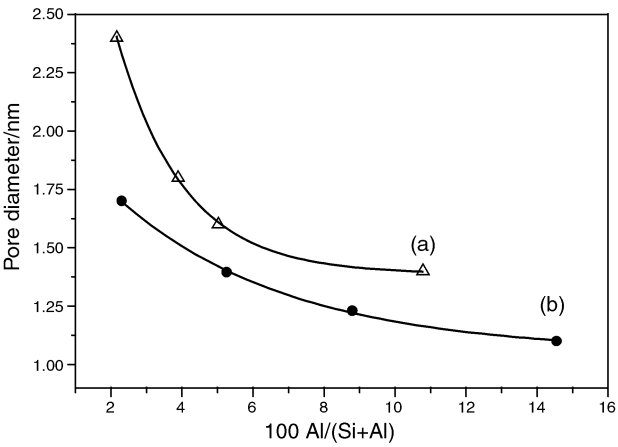

Fig. 3 Relationship between the pore diameter and the aluminium content of the samples: (a) CTMACl (pore diameters calculated according to the BJH method) and (b) DTMABr (pore diameters calculated according to the Saito–Foley method).

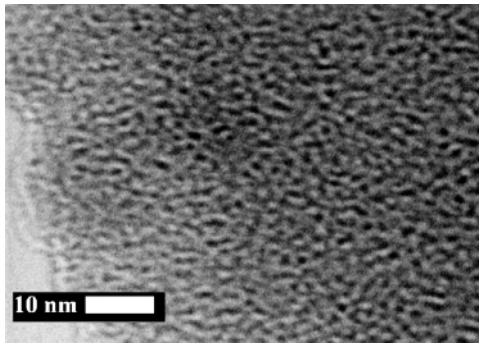

Fig. 4 TEM micrograph of the sample with Si/Al = 6.3 synthesized using DTMABr as surfactant.

These results are further confirmed by TEM micrographs of the samples (see Fig. 4). The pore diameters measured in these micrographs agree well with those derived from the N_2 adsorption measurements. Moreover, from XRD spacings and pore diameters, a large wall thickness (1.5–2.0 nm) is obtained. This result may be also important in terms of the stability of these materials.

In order to study the Al environment in the samples, ^{27}Al MAS NMR spectra were measured, which show that in the as-synthesized materials all the Al atoms present tetrahedral coordination. This result indicates that even for samples with high aluminium content (Si/Al = 6), most of the Al species are effectively incorporated into the pore walls.

In summary, it can be concluded that using this new synthesis method, and through a suitable combination of surfactant chain length and Al content, Al-MTS materials with pore size adjustable in the range 1.0 - 2.5 nm can be prepared.

This work was funded by the Spanish Comisión Interministerial de Ciencia y Tecnología (CICYT), project number AMB-97/0530, and by Comunidad de Madrid, Strategic Group Project.

Notes and references

1 C. T. Kresge, M. E. Leonowicz, W. J. Roth, J. C. Vartuli and J. S. Beck, *Nature*, 1992, **359**, 710.
2 A. Corma, A. Martínez, V. Martínez.Soria and J. B. Montón, *J. Catal.*, 1995, **153**, 25.
3 J. Aguado, J. L. Sotelo, D. P. Serrano, J. A. Calles and J. M. Escola, *Energy Fuels*, 1997, **11**, 1225.
4 D. P. Serrano, J. Aguado, J. L. Sotelo, R. Van Grieken, J. M. Escola and J. M. Menéndez, *Stud. Surf. Sci. Catal.*, 1998, **117**, 437.
5 I. Díaz, J. Pérez Pariente and E. Sastre, *Stud. Surf. Sci. Catal.*, 1999, **125**, 53.
6 M. Janicke, D. Kumar, G. D. Stucky and B. F. Chmelka, *Stud. Surf. Sci. Catal.*, 1994, **84**, 243.
7 S. A. Bagshaw, E. Prouzet and T. J. Pinnavaia, *Science*, 1995, **269**, 1242.
8 Y. Yue, A. Gedeón, J. Bonardet, N. Melosh, J. D'Espinose and J. Fraissard, *Chem. Commun.*, 1999, 1967.
9 C. Y. Chen, H. X. Li and M. E. Davis, *Microporous Mater.*, 1993, **2**, 17.
10 Z. Luan, C. Cheng, W. Zhou and J. Klinowski, *J. Phys. Chem.*, 1993, **99**, 1018.
11 K. R. Kloetstra, H. W. Zandbergen and H. Van Bekkum, *Catal. Lett.*, 1995, **33**, 157.
12 R. Mokaya and W. Jones, *Chem. Commun.*, 1996, 981.
13 P. T. Tareu and T. J. Pinnavaia, *Science*, 1996, **271**, 1267.
14 X. S. Zhao, G. Q. Lu and X. Hu, *Chem. Commun.*, 1999, 1391.
15 S. A. Bagshaw and A. R. Hayman, *Chem. Commun.*, 2000, 533.
16 J. Aguado, D. P. Serrano and J. M. Escola, *Microporous Mesoporous Mater.*, 2000, **34**, 43.

Blue photoluminescent zinc coordination polymers with supertetranuclear cores†

Jun Tao,[a] Ming-Liang Tong,[a] Jian-Xin Shi,[a] Xiao-Ming Chen*[a] and Seik Weng Ng[b]

[a] *State Key Laboratory of Ultrafast Laser Spectroscopy and School of Chemistry & Chemical Engineering, Zhongshan University, Guangzhou, 510275, P.R. China. E-mail: cescxm@zsu.edu.cn*

[b] *Institute of Postgraduate Studies and Research, University of Malaya, 50603 Kuala Lumpur, Malaysia*

Received (in Cambridge, UK) 17th July 2000, Accepted 11th September 2000
First published as an Advance Article on the web

Two photoluminescent two- and three-dimensional coordination polymers consisting of Zn_4O [or $Zn_4(OH)_2$] cores, dicarboxylate (isophthalate or fumarate) and 4,4′-bipyridine ligands as building blocks have been hydrothermally synthesized and structurally characterized.

The construction of supramolecular architectures are currently of great interest owing to their intriguing network topologies and potential functions as new classes of materials.[1] Polynuclear d^{10} metal (Cu^I, Ag^I, Au^I, Zn^{II} or Cd^{II}) complexes have been found to exhibit intriguing structural and photoluminescent properties.[2–5] We have been pursuing synthetic strategies for non-interpenetrating open frameworks with variable cavities or channels using simple units as building blocks.[6] We now extend to work towards extended networks based on metal clusters as building blocks, and report here the preparation and crystal structures of two novel coordination polymers constructed by zinc cluster cores, 4,4′-bipyridine (4,4′-bpy) and dicarboxylate ligands, namely $[Zn_4O(ip)_3(4,4'\text{-bpy})]$ (ip = isophthalate) **1** and $[Zn_4(OH)_2(fa)_3(4,4'\text{-bpy})_2]$ (fa = fumarate) **2**.

The hydrothermal reactions of zinc salts with the dicarboxylates and 4,4′-bpy in molar ratio 1 : 1 : 1 at 180 °C (7 days) and 140 °C (60 h) led to the formation of colourless **1** and **2**, respectively. Elemental analysis confirmed the formulae of **1** and **2**.‡ Thermogravimetric analysis (TGA) performed on the polycrystalline samples indicate that they are thermally stable up to 380 °C, in accord with the fact that hydrothermal products are usually stable.

X-Ray single-crystal analysis§ has revealed that **1** contains two-dimensional polymeric grids with supertetranuclear Zn_4O cores as building units, in which each zinc atom is coordinated by the central μ_4-oxo atom, two oxygen atoms from two μ-carboxylate, and a monodentate carboxylate or 4,4′-bpy groups to furnish tetrahedral coordination, as shown in Fig. 1. The average Zn–O length (1.971 Å) is somewhat longer than that (av. 1.939 Å) found in $[Zn_4O(O_2CPh)_6]$.[5] The ip ligands in **1** act in both bisbidentate and bismonodentate modes, though the Zn(2)–O(4) distance of 2.547(2) Å suggests a non-negligible interaction, or semi-chelate coordination mode for the bismonodentate tp ligand.[7] The different coordination environments around two crystallographically independent zinc atoms may be attributed to the different Zn–O(oxo) distances, the Zn(2)–O(5) bond (1.993 Å) is much longer than that (1.931 Å) of Zn(1)–O(5).

The most striking feature of **1** is the connection of Zn_4O cores *via* organic ligands to form infinite two-dimensional networks with two different types of cavities (8.7 × 8.7 and 8.7 × 10.4 Å), as shown in Fig. 2. The Zn_4O cores are bridged by bismonodentate and bisbidentate ip ligands into infinite one-dimensional ladder-like $[Zn_4O(ip)_3]$ chains, and adjacent ladders are interlinked through μ-4,4′-bpy spacers, resulting in a novel two-dimensional grid. It is noteworthy that the topology of **1** can be simplified to (4,4) if we connect only the core (O5) of the supertetrahedra.

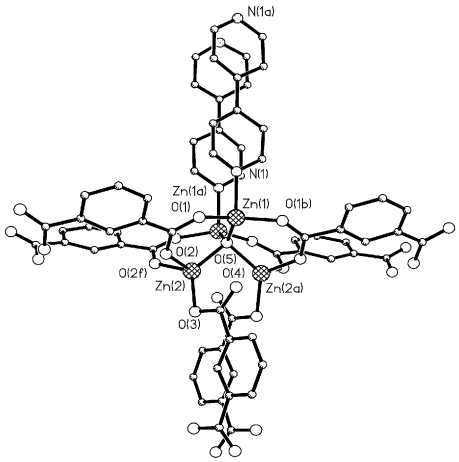

Fig. 1 The coordination environments of zinc atoms in **1**. Selected bond distances (Å) and angles (°): Zn(1)–O(1) 1.970(2), Zn(1)–O(5) 1.931(1), Zn(2)–O(2) 1.989(2), Zn(2)–O(3) 1.969(3), Zn(2)–O(5) 1.993(2), Zn(1)–N(1) 2.076(3); O(1)–Zn(1)–N(1) 96.4(1), O(1)–Zn(1)–O(5) 113.1(1), O(5)–Zn(1)–N(1) 117.0(1), O(2)–Zn(2)–O(3) 94.0(1), O(2)–Zn(2)–O(5) 108.3(1), O(3)–Zn(2)–O(5) 128.8(1).

Complex **2** is made up of an infinite interpenetrating three-dimensional framework with $Zn_4(\mu_3\text{-}OH)_2$ cores and organic bridges. Unlike **1**, the tetranuclear core in **2** is unprecedented in zinc coordination chemistry, and similar to the butterfly-like tetranuclear manganese complexes.[8] Atom Zn(1) is in a distorted octahedral geometry, coordinated by two μ_3-OH groups, one 4,4′-bpy group, and three oxygen atoms from one chelate and one monodentate carboxylate groups (Fig. 3). The Zn–O(hydroxo) distances are compatible to those documented

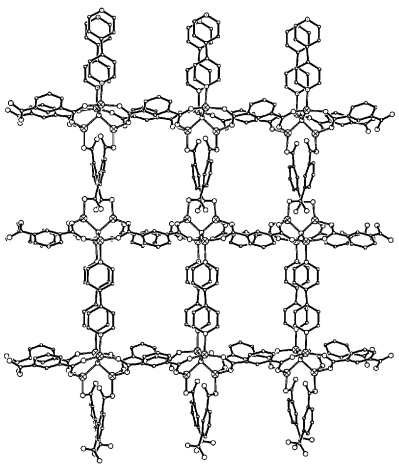

Fig. 2 Perspective view of the two-dimensional framework of **1**.

† Electronic supplementary information (ESI) available: X-ray powder diffraction data for complexes **1** and **2**. See http://www.rsc.org/suppdata/cc/b0/b005753n/

DOI: 10.1039/b005753n

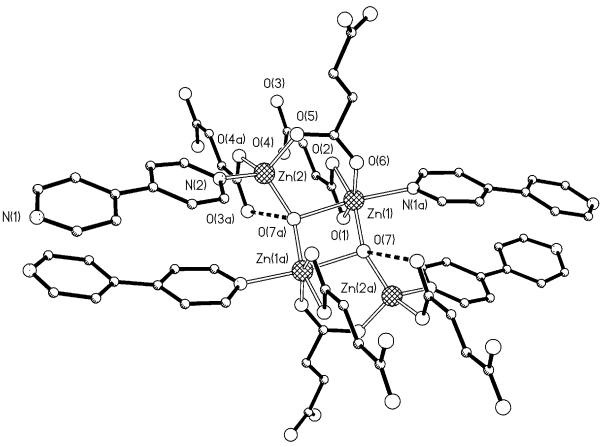

Fig. 3 The coordination environments of zinc atoms in **2**. Selected bond distances (Å) and angles (°): Zn(1)–O(1) 2.367(4), Zn(1)–O(2) 2.089(4), Zn(1)–O(6) 2.054(4), Zn(1)–O(7) 2.015(3), Zn(1)–N(1a) 2.192(4), Zn(2)–O(4a) 1.973(4), Zn(2)–O(5) 1.955(3), Zn(2)–O(7a) 1.950(3), Zn(2)–N(2) 2.054(4), O(7a)···O(3a) 2.755(5); O(1)–Zn(1)-O(2) 58.8(1), O(6)–Zn(1)–O(7) 95.0(1), O(7)–Zn(1)–N(1a) 95.5(1), O(4a)–Zn(2)-O(7a) 109.4(1), O(5)–Zn(2)–O(7a) 110.9(1), O(7a)–Zn(2)–N(2) 116.8(2), O(4a)–Zn(2)–N(2) 105.0(1), O(5)–Zn(2)–N(2) 100.0(2).

in the literature.[9] The μ_3-OH group is also hydrogen-bonded to the monodentate carboxylate [O(7a)···O(3a) 2.755(5)Å]. Zn(2) atom is tetrahedrally coordinated by μ_3-OH, one 4,4′-bpy group and two oxygen atoms from two fa ligands. The $Zn_4(OH)_2$ cores are interlinked by the carboxylate groups of six fa ligands in both bisbidentate and chelate-monodentate fashions, resulting in infinite two-dimensional $[Zn_4(OH)_2(fa)_3]$ sheets [Fig. 4(a)], which are pillared by the 4,4′-bpy ligands to generate an infinite three-dimensional prismatic-like framework [Fig. 4(b)]. The actual crystal structure has two such 3D frameworks that interpenetrate each other. The topology of **2** can be related to the simple cubic α-Po two-fold interpenetrated lattice.

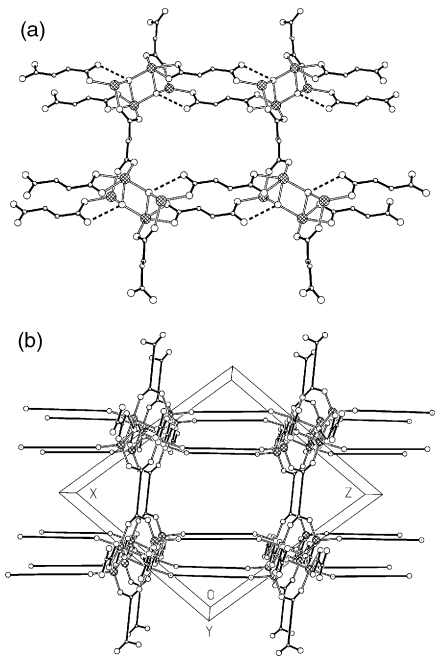

Fig. 4 Perspective views of the two-dimensional framework of $[Zn_4(OH)_2(fa)_3]$ (a) and the building unit of three-dimensional framework (b) of **2**. For clarity, both the 4,4′-bpy ligands and the ethylene groups of fa ligands in (b) are shown as solid lines.

It is noteworthy that **1** and **2** are the first examples of coordination polymers constructed by oxo or hydroxo metal clusters with mixed bridging organic ligands, though the first three-dimensional framework constructed by Zn_4O cores and dicarboxylates has recently been documented in $[Zn_4O(BDC)_3](DMF)_8(C_6H_5Cl)$ (BDC = 1,4-benzenedicarboxylate).[10]

In the solid state **1** and **2** exhibit intense photoluminescence upon photoexcitation at 320 and 398 nm, respectively. The emissions of **1** (λ_{max} = 432 nm) and **2** (λ_{max} = 453 nm) may be assigned as ligand-to-metal charge transfer (LMCT).[11] They may be good candidates for blue-light emitting diode devices, since these condensed materials are highly thermally stable and insoluble in common polar and non-polar solvents.

In conclusion, we have synthesised two stable polynuclear zinc polymers under hydrothermal conditions, providing a new synthetic route for metal coordination polymers with promising photoelectronic properties.

This work was supported by the NSFC (No. 29625102, 29971033).

Notes and references

‡ Anal. Calc. for $C_{34}H_{20}N_2O_{13}Zn_4$ **1**: C, 44.10; H, 2.18; N, 3.02. Found: C, 43.85; H, 2.07; N, 2.90%. Calc. for $C_{32}H_{24}N_4O_{14}Zn_4$ **2**: C, 40.45; H, 2.55; N, 5.90. Found: C, 40.30; H, 2.45; N, 5.72%.

§ *Crystal data* for **1**: $C_{34}H_{20}N_2O_{13}Zn_4$, M_r = 926.00, tetragonal, space group $P4_2/mnm$ (no. 136), a = 17.346(2), c = 10.428(2) Å, V = 3137.6(8) Å^3, Z = 4, D_c = 1.960 g cm^{-3}, μ (Mo-Kα) = 3.099 cm^{-1}. **2**: $C_{32}H_{24}N_4O_{14}Zn_4$, M_r = 950.03, monoclinic, space group $P2/n$ (no. 13), a = 17.096(7), b = 11.183(6), c = 18.607(12) Å, β = 103.52(1)°, V = 3459(3) Å^3, Z = 4, D_c = 1.824 g cm^{-1}, μ(Mo-Kα) = 2.817 cm^{-1}. Data collections ($2 \leqslant \theta \leqslant 30°$ for **1**, $2 \leqslant \theta \leqslant 27°$ for **2**) were performed at 293 K on Bruker CCD and Siemens R3m diffractometers (Mo-Kα, λ = 0.71073 Å) for **1** and **2**, respectively. The structures were solved with direct methods (SHELXS-97)[12] and refined by full-matrix least squares (SHELXL-97),[13] giving for **1** a final R_1 value of 0.0294 for 164 parameters and 1845 unique reflections with $I \geqslant 2\sigma(I)$ and wR_2 of 0.0859 for all 2295 reflections, and for **2** a final R_1 value of 0.0431 for 487 parameters and 5414 unique reflections with $I \geqslant 2\sigma(I)$ and wR_2 of 0.1119 for all 6801 reflections.

CCDC 182/1775. See http://www.rsc.org/suppdata/cc/b0/b005753n/ for crystallographic files in .cif format.

1 S. R. Batten and R. Robson, *Angew. Chem., Int. Ed.*, 1998, **37**, 1460; O. M. Yaghi, H. Li, C. Davis, D. Richardson and T. L. Groy, *Acc. Chem. Res.*, 1998, **31**, 474; P. J. Hagrman, D. Hagrman and J. Zubieta, *Angew. Chem., Int. Ed.*, 1999, **38**, 2639.

2 P. D. Harvey and H. B. Gray, *J. Am. Chem. Soc.*, 1988, **110**, 2145; Y. Ma, H.-Y. Chao, Y. Wu, S. T. Lee, W.-Y. Yu and C.-M. Che, *Chem. Commun.*, 1998, 2491.

3 K. R. Kyle, C. K. Ryu, J. A. DiBenedetto and P. C. Ford, *J. Am. Chem. Soc.*, 1991, **113**, 2954; M. Henary and J. I. Zink, *J. Am. Chem. Soc.*, 1989, **111**, 7407.

4 P. C. Ford, E. Cariati and J. Bourassa, *Chem. Rev.*, 1999, **99**, 3625.

5 W. Clegg, D. R. Harbron, C. D. Homan, P. A. Hunt, J. R. Little and B. P. Straughan, *Inorg. Chim. Acta*, 1991, **186**, 51.

6 M.-L. Tong, S.-L. Zheng and X.-M. Chen, *Chem. Commun.*, 1999, 561; M.-L. Tong, X.-M. Chen, B.-H. Ye and L.-N. Ji, *Angew. Chem., Int. Ed.*, 1999, **38**, 2237; M.-L. Tong, S.-L. Zheng and X.-M. Chen, *Chem.-Eur. J.*, 2000, **6**, in press.

7 C. C. Addison, N. Logan, S. C. Wallwork and N.-L. Chang, *Q. Rev. Chem. Soc.*, 1971, **25**, 289; G. Guilera and J. W. Steed, *Chem. Commun.*, 1999, 1563.

8 G. Christou, *Acc. Chem. Res.*, 1989, **22**, 328.

9 T. Konno, K. Okamoto and J. Hidaka, *Bull. Chem. Soc. Jpn.*, 1994, **67**, 101.

10 H. Li, M. Eddaoudi, M. O'Keeffe and O. M. Yaghi, *Nature*, 1999, **402**, 276.

11 A. Meijerink, G. Blasse and M. Glasbeek, *J. Phys.: Condens. Matter*, 1990, **2**, 6303; R. Bertoncello, M. Bettinelli, M. Cassrin, A.Gulino, E. Tondello and A. Vittadini, *Inorg. Chem.*, 1992, **31**, 1558.

12 G. M. Sheldrick, SHELXS-97, Program for Crystal Structure Solution, University of Göttingen, Germany, 1997.

13 G. M. Sheldrick, SHELXS-97, Program for Crystal Refinement, Solution, University of Göttingen, Germany, 1997.

Persistent phosphinyl radicals from a bulky diphosphine: an example of a molecular jack-in-the-box†

Sarah L. Hinchley,[a] Carole A. Morrison,[a] David W. H. Rankin,*[a] Charles L. B. Macdonald,[b] Robert J. Wiacek,[b] Alan H. Cowley,[b] Michael F. Lappert,[c] Grete Gundersen,[d] Jason A. C. Clyburne[e] and Philip P. Power[f]

[a] *Department of Chemistry, University of Edinburgh, West Mains Road, Edinburgh, UK EH9 3JJ. E-mail: dwhr01@holyrood.ed.ac.uk*
[b] *Department of Chemistry and Biochemistry, The University of Texas at Austin, Austin, Texas 78712, USA.*
[c] *School of Chemistry, Physics and Environmental Sciences, University of Sussex, Falmer, Brighton, UK BN1 9RH*
[d] *Department of Chemistry, University of Oslo, Box 1033, Blindern, N-0315 Oslo, Norway*
[e] *Department of Chemistry, Acadia University, Wolfville, NS, B0P 1X0, Canada*
[f] *Department of Chemistry, The University of California, Davis, Davis, California 95616, USA*

Received (in Columbia, MO, USA) 8th June 2000, Accepted 22nd August 2000
First published as an Advance Article on the web 2nd October 2000

The structure of the phosphinyl radical, $\dot{P}R_2$ [R = $CH(SiMe_3)_2$], has been determined by gas-phase electron diffraction (GED) together with *ab initio* molecular orbital calculations, and that of the corresponding diphosphine, $(PR_2)_2$, has been established by X-ray crystallography; the diphosphine behaves as an energy storage reservoir.

In considering the homolytic cleavage of the E–E single bond of molecules of the general type $R'_nEER'_n$, the formation of the corresponding $R'_nE\cdot$ radicals is expected to be favoured by increased steric bulk of the substituents, R′. The conventional view is that such increases of steric strain would be manifested primarily in elongation of the E–E bond and that beyond a critical point of steric loading this bond would rupture. Herein we describe the X-ray crystal structure of the sterically encumbered diphosphine, $(PR_2)_2$ (**1**) (R = $CH(SiMe_3)_2$), and the gas-phase electron diffraction (GED) structure of the corresponding homolysis product, PR_2 (**2**), the exclusive species found in both solution and in the gas phase.[1] In conjunction with *ab initio* calculations on **2**, comparisons of the structural features of the radical with those of the cognate dimer **1** provide new insights into the origins of the stabilisation of **2** and related species.

Diphosphine **1** was prepared by the reduction of a hexane solution of $ClPR_2$ (**3**) as described previously[1] or by variations thereof.[2] Slow cooling of the filtered reaction mixture afforded both yellow crystals of **1** and colourless crystals of **3**, which were separated manually. Phosphinyl radical **2** was produced by melting or vaporising **1**.

One of the most interesting features of the crystal structure of **1**‡ (Fig. 1) is the P–P bond length [2.3103(7) Å]. While this is the longest such bond yet reported for a diphosphine, it is only ~0.1 Å longer than those reported for other diphosphines. Moreover, this modest lengthening amounts to a diminution of only ~4 kJ mol^{-1} in terms of the P–P bond dissociation energy. Previously reported distances for uncoordinated diphosphines $(PR'_2)_2$ include 2.260(1) Å (R′ = Mes),[3a] 2.246(2) Å (R′ = CF_3),[3b] 2.215(3) Å (R′ = Cy),[3c] 2.211(2) and 2.206(2) Å (R′ = Ph,C(O)Bu^t),[3d] 2.212(1) Å (R′ = Me)[3e] and 2.2051(11) Å (R′ = C_4Ph_4).[3f] Another noteworthy feature of the structure of **1** is the *syn,anti* orientation of the R ligands on each PR_2 fragment, which allows for a more efficient packing of the ligands around the P–P core than does the corresponding *syn,syn* orientation.

GED data†§ in conjunction with *ab initio* theoretical results revealed that **2** exists as a single *syn,syn* conformer of symmetry

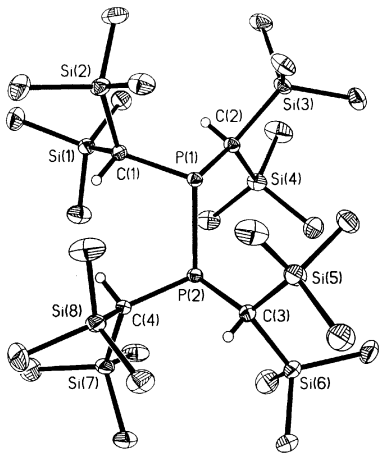

Fig. 1 Thermal ellipsoid plot (30% probability level) of $(PR_2)_2$ (**1**; R = $CH(SiMe_3)_2$). Selected bond lengths (Å), bond angles (°) and dihedral angles (°): P(1)–P(2) 2.3103(7), P(1)–C(1) 1.892(2), P(1)–C(2) 1.896(2), P(2)–C(4) 1.892(2), P(2)–C(3) 1.893(2), Si(1)–C(1) 1.905(2), Si(2)–C(1) 1.915(2), Si(3)–C(2) 1.918(2), Si(4)–C(2) 1.894(2), Si(5)–C(3) 1.892(2), Si(6)–C(3) 1.926(2), Si(7)–C(4) 1.921(2), Si(8)–C(4) 1.896(2), C(1)–P(1)–C(2) 103.57(9), C(1)–P(1)–P(2) 107.92(7), C(2)–P(1)–P(2) 104.83(6), C(4)–P(2)–C(3) 103.00(9), C(4)–P(2)–P(1) 106.98(6), C(3)–P(2)–P(1) 105.27(7), C(1)–P(1)–P(2)–C(4) 32.0(1), C(2)–P(1)–P(2)–C(3) 109.0(1), H(111)–C(11)–P(1)–C(12) 124.6, H(112)–C(12)–P(1)–C(11) 7.8, H(113)–C(13)–P(2)–C(14) −4.6, H(114)–C(14)–P(2)–C(13) 122.9.

C_2 in the gas phase [*cf.* the *syn,anti* found for $(PR_2)_2$]. The electron diffraction data for **2** in the C_2 geometry were fitted by use of the SARACEN method.[4] The final experimental structure (Fig. 2) is in reasonable agreement with that calculated by the Density Functional Theory (DFT) method at the UB3LYP/DZP level. The computed bond lengths generally exceed the experimental values by ~0.01–0.02 Å and the calculated angles within 1–2° of the GED values.

The change from the *syn,syn* to the *syn,anti* conformation represents the most obvious difference between the local geometries of the PR_2 fragments in **1** and **2**, and is a consequence of the packing requirements of the ligands about the P–P core of **1**. However, the price of this packing is that there is substantial steric strain, (a) within each R group, *i.e.* between the two $SiMe_3$ groups, (b) between the two R groups attached to each P atom, and (c) between the R groups on the two halves of the molecule. The steric strain is considerably greater in the diphosphine than in the radical, as evidenced by the distortions of the metrical parameters of **1** compared with those of **2**. For example, in **2** the root-mean-square variances from the means of the angles at carbon and silicon are 3.9 and

† Electronic supplementary information (ESI) available: summary of GED details and theoretical results. See http://www.rsc.org/suppdata/cc/b0/b004889p/

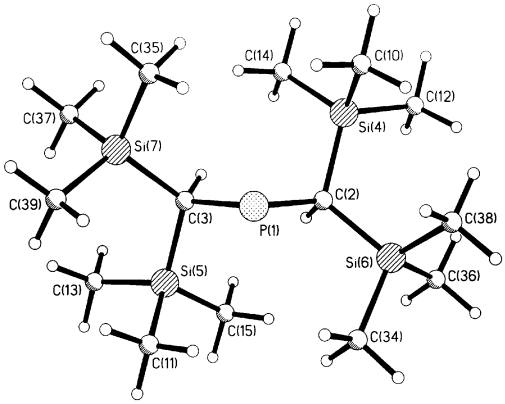

Fig. 2 Gas-phase electron diffraction structure of $\dot{P}R_2$ (**2**; R = $CH(SiMe_3)_2$). Selected bond lengths (Å), bond angles (°) and dihedral angles (°): P(1)–C(2) 1.856(9), C(2)–Si(6) 1.902(2), C(2)–Si(4) 1.905(2), Si(4)–C(10) 1.878(2), Si(4)–C(12) 1.878(2), Si(4)–C(14) 1.876(2), Si(6)–C(34) 1.880(2), Si(6)–C(36) 1.879(2), Si(6)–C(38) 1.875(2), C(2)–P(1)–C(2a) 103.9(10), P(1)–C(2)–H(8) 108.1(13), avg. P(1)–C(2)–Si 109.4(4), avg. Si(4)–C–Si(6) 117.5(5), H(8)–C(2)–P(1)–C(3) −26.4(8).

2.4° respectively, whereas in **1** they are significantly larger (15.3 and 4.1°). There are also increases in many of the bond lengths of the R ligands in **1**, the largest of which are close to the P–P core. In general, there is an attenuation of such bond length increases towards the molecular periphery.

In essence, the whole structure of **1** represents an energy storage reservoir, somewhat like a compressed spring, which, upon dissolution, melting or evaporation, is used to effect cleavage of the P–P bond. In sharp contrast, other diphosphines $P_2R'_4$ with sterically demanding substituents retain their P–P bonding in both solution and the gas phase. To gain further insights, we estimated the magnitude of steric relaxation in the dissociation process using DFT calculations, summarised in Fig. 3 (see ESI† for details). Single-point calculations on **1** (C–H bond lengths fixed at 1.08 Å) and the two fragments formed by breaking the P–P bond, $\mathbf{1A_1}$ and $\mathbf{1A_2}$, predict a P–P homolysis energy of 95 kJ mol^{-1}. The hydrogen atom positions in $\mathbf{1B_2}$ were then optimised. This energy change, which reflects the correction for unrefined placement of hydrogen atoms in the crystal, was 239 kJ mol^{-1}. The remaining atom positions in $\mathbf{1B_2}$ were then relaxed, to give structure $\mathbf{1C_2}$ releasing 52 kJ mol^{-1}. Finally, rotation of one of the R ligands around the P–C bond to form the optimised *syn,syn* conformation (**2**), analogous to that observed experimentally, releases a further 33 kJ mol^{-1} per radical. Thus, while the initial step in the homolysis reaction is endothermic, the relaxation and rotation of the R ligands releases at least 135 kJ mol^{-1}, more than sufficient to render the overall process exothermic.

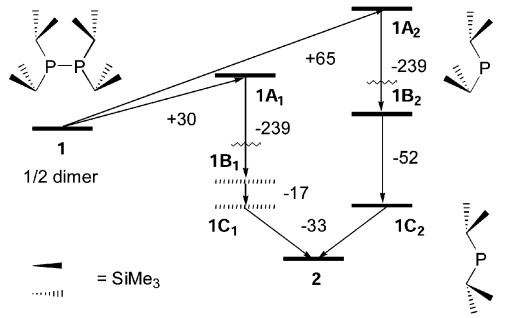

Fig. 3 Summary of DFT calculation results for diphosphine **1** in the solid-state geometry, the *syn,anti* phosphinyl radicals with solid-state geometries $\mathbf{1A_1}$ and $\mathbf{1A_2}$, with hydrogen atom positions relaxed ($\mathbf{1B_1}$ and $\mathbf{1B_2}$), the *syn,anti* phosphinyl radical in the optimised geometry **1C** (the same for both radical fragments), and the *syn,syn* phosphinyl radical in the optimised geometry **2**. Energies in kJ mol^{-1}.

An informative comparison can be made with some closely-related group 14 species. Analogous *syn,anti* to *syn,syn* conformational changes and similar dissociation energies are observed in the cleavage of $(MR_2)_2$ (M = Ge, Sn) into the MR_2 carbenoid fragments.[5] Again, the M–M distances in the solid are very similar to those in sterically less encumbered $M_2R'_4$ molecules. In contrast, the related $\{M[N(SiMe_3)_2]_2\}$ (M = Ge, Sn, Pb) species, while remaining monomeric in both the gas and the solid, change their conformations.[6]

In conclusion, the homolytic behaviour of **1** permits a new understanding concerning the functioning of bulky substituents. The shape and flexibility of the $CH(SiMe_3)_2$ ligands allows for the formation of the P–P bond in **1**. However, in the process of bond formation (and crystallisation) the molecule accumulates a large store of potential energy and is primed to spring apart upon release from the solid state. The potential energy of steric repulsion is not manifested in an elongated P–P bond, but is evidenced primarily by the deformation of the ligands. In this sense, the malleable R substituents act as the springs in a molecular jack-in-the-box.

We thank the EPSRC (UK), the National Science Foundation (USA) and the Robert A. Welch Foundation (UT) for financial support. We also thank R. Seip (Oslo) for collection of electron diffraction data, Dr. V. Typke of the University of Ulm for the variable-array version of ASYM40, and the UK Computational Chemistry Facility (admin: Department of Chemistry, King's College London, Strand, London, UK WC2R 2LS) for the computing time on Columbus.

Notes and references

‡ *Crystal data* for **1**: $C_{28}H_{76}P_2Si_8$, M = 699.55, yellow blocks, monoclinic, $P2_1/c$, a = 18.341(2), b = 13.4240(10), c = 19.033(2) Å, β = 110.650(10)°, V = 4385.0(7) $Å^3$, Z = 8, D_{calcd} = 1.060 g cm^{-3}, μ(Mo-Kα) = 0.335 mm^{-1}. A suitable single crystal of **1** was covered with mineral oil and mounted on a Siemens P4 diffractometer at 183 K. A total of 9263 reflections was collected in the range 2.38° < 2θ < 50.13° using Mo-Kα radiation (λ = 0.71073 Å). Of these, 7709 were considered observed (I > 2.0$\sigma(I)$) and were used to solve (direct methods) and refine (full matrix, least squares on F^2) the structure of **1**; R_w = 0.1159, R = 0.0375. CCDC 182/1770. See http://www.rsc.org/suppdata/cc/b0/b004889p/ for crystallographic files in .cif format.

§ *GED data* for **2**: Electron scattering intensities for **2** were recorded on the Balzers' gas electron diffraction apparatus in Oslo. See ESI for details.†

1 (*a*) M. J. S. Gynane, A. Hudson, M. F. Lappert, P. P. Power and H. Goldwhite, *J. Chem. Soc., Chem. Commun.*, 1976, 623; (*b*) M. J. S. Gynane, A. Hudson, M. F. Lappert, P. P. Power and H. Goldwhite, *J. Chem. Soc., Dalton Trans.*, 1980, 2428.

2 R. A. Kemp, Ph.D. Dissertation, The University of Texas at Austin, 1982.

3 (*a*) S. G. Baxter, A. H. Cowley, R. E. Davis and P.E. Riley, *J. Am. Chem. Soc.*, 1981, **103**, 1699; (*b*) G. Becker, W. Golla, J. Grobe, K. W. Klinkhammer, D. L. Van, A. H. Maulitz, H. Oberhammer and M. Sachs, *Inorg. Chem.*, 1999, **38**, 1099; (*c*) V. R. Richter, J. Kaiser, J. Sieler, U. H. Hartung and C. Peter, *Acta Crystallogr., Sect. B*, 1977, **33**, 1887; (*d*) V. G. Becker, O. Mundt and M. Rössler, *Z. Anorg. Allg. Chem.*, 1980, **468**, 55; (*e*) O. Mundt, H. Riffel, G. Becker and A. Simon, *Z. Naturforsch., Teil B*, 1988, **43**, 952; (*f*) P. Wei, J. Su, B. C. Beck, S. D. Goodwin and G. H. Robinson, *Chem. Commun.*, 2000, 1037.

4 (*a*) A. J. Blake, P. T. Brain, H. McNab, J. Miller, C. A. Morrison, S. Parsons, D. W. H. Rankin, H. E. Robertson and B. A. Smart, *J. Phys. Chem.*, 1996, **100**, 12 280; (*b*) P. T. Brain, C. A. Morrison, S. Parsons and D. W. H. Rankin, *J. Chem. Soc., Dalton Trans.*, 1996, 4589.

5 (*a*) T. Fjeldberg, A. Haaland, B. E. R. Schilling, M. F. Lappert and A. J. Thorne, *J. Chem. Soc., Dalton Trans.*, 1986, 1551; (*b*) D. E. Goldberg, P. B. Hitchcock, M. F. Lappert, K. M. Thomas, T. Fjeldberg, A. Haaland and B. E. R. Schilling, *J. Chem. Soc., Dalton Trans.*, 1986, 2387.

6 (*a*) T. Fjeldberg, H. Hope, M. F. Lappert, P. P. Power and A. J. Thorne, *J. Chem. Soc., Chem. Commun.*, 1983, 639; (*b*) R. W. Chorley, P. B. Hitchcock, M. F. Lappert, W.-P. Leung, P. P. Power and M. M. Olmstead, *Inorg. Chim. Acta*, 1992, **201**, 121.

ChemComm

Combining ionic liquids and supercritical fluids: *in situ* ATR-IR study of CO_2 dissolved in two ionic liquids at high pressures†

Sergei G. Kazarian,*[a] Brian J. Briscoe[a] and Thomas Welton[b]

[a] *Department of Chemical Engineering and Chemical Technology, Imperial College of Science, Technology and Medicine, London, UK SW7 2BY. E-mail: s.kazarian@ic.ac.uk*

[b] *Department of Chemistry, Imperial College of Science, Technology and Medicine, London, UK SW7 2BY*

Received (in Cambridge, UK) 10th July 2000, Accepted 5th September 2000
First published as an Advance Article on the web 2nd October 2000

An *in situ* ATR (attenuated total reflectance)-IR study of CO_2 dissolved in two ionic liquids at high pressures has demonstrated the effects of the anionic species of the ionic liquids on the molecular state of the dissolved CO_2.

In the search for alternatives to conventional solvents partly driven by the need for 'green' chemistry and sustainable technology, but primarily because of the potential for novel synthetic routes, a number of media have been explored recently. These include supercritical fluids (SCF) and room-temperature ionic liquids (IL).[1] One of the challenges that exist in the use of ionic liquids is that it is often difficult to separate products from reactants, catalyst or solvent. Distillation of the solvent cannot be applied for separation because of the low vapour pressure of ionic liquids. The possibility of combining chemical reactions in IL with separations using SCF is of potential value.

Very recent work has demonstrated that supercritical (sc) CO_2 is highly soluble in certain ionic liquids while these ionic liquids are not measurably soluble in the $scCO_2$ phase.[2] This observation indicates that there is a potentially useful opportunity to separate $scCO_2$-soluble products from ionic liquids using SCF/liquid extraction. The 'tunable' solvent power of the supercritical fluid, owing to its variable (with pressure or temperature) solvent density may be utilised for extraction and separation of the products of chemical processing in ionic liquids (without, for example, removing catalyst from IL). Synthetic procedures and catalytic processes using IL media have been recently summarised[3] and the applications of SCF solvents for extraction, and in particular the role of spectroscopy in monitoring these processes, have also been reviewed.[4] The preliminary data showed that naphthalene could be extracted from an ionic liquid into $scCO_2$ phase.[2] However, the same authors later indicated that the presence of water in the IL had a significant effect on CO_2 solubility.[5] In this work the authors also speculated about the origins of the high solubility of CO_2 in ionic liquids, and the role of different anions.

A molecular-level insight into the state of CO_2 dissolved in IL is needed to elucidate the fundamental origin of this phenomenon. Here, we report an *in situ* ATR-IR study of CO_2 dissolved in two ionic liquids at high pressures. The advantage of a very shallow penetration (few microns) of the IR light in ATR-IR spectroscopy has been utilised to measure the spectrum of CO_2 dissolved in two ionic liquids. Ionic liquids based on the 1-alkyl-3-methylimidazolium cation in conjunction with either $[PF_6]^-$ or $[BF_4]^-$ {[bmim][PF_6] **I** and [bmim][BF_4] **II**}, were synthesised by established procedures.[3] ATR-IR spectroscopy overcomes some of the limitations inherent to other techniques when the objective is to gain spectra of molecules dissolved in highly absorbing media. It would be very difficult, if not impossible, to measure the IR spectrum of the bending mode of CO_2 dissolved in ionic liquids using transmission spectroscopy because of the strong absorbance of these ionic liquids in the important region of the bending mode of CO_2. The current ATR-IR method uses a modified commercial diamond ATR accessory (Specac, Ltd., UK) and a miniature high-pressure flow cell.[6] Diamond's ability to withstand high pressure was used to measure the spectra of CO_2 dissolved in IL at various pressures and temperatures. IR spectra were measured using an Equinox-55 FTIR spectrometer (Bruker) with DTGS and MCT detectors; resolution was 2 cm^{-1}. The cell was pressurised with CO_2 up to 200 bar at room temperature, equilibrated for periods from several hours to a few days, and the spectra were measured. The temperature of the cell could readily be varied from room temperature to 200 °C (for a schematic view of the cell see ESI†).

The IR spectrum of CO_2 dissolved in two ILs shows the bands corresponding to antisymmetric (not illustrated) and bending modes of CO_2. There was no difference in position of the bands corresponding to the ν_3 antisymmetric stretching modes of CO_2 dissolved in **I** and **II**. Both bands appear with the peak maximum at *ca*. 2338 cm^{-1} with the shoulder on the low-wavenumber side of the band. The position of this band of CO_2 dissolved in IL is very close to that of CO_2 dissolved in glassy polymers, such as PMMA[7] rather than the CO_2 incorporated in halogen salts of alkali metals[8] where the bands are observed in the region of 2150–2200 cm^{-1}. The absorbance of the ν_3 band is 0.35 for CO_2 dissolved in **I** at 68 bar and 40 °C. *In situ* ATR-IR spectroscopy provides a direct but approximate measurement of the solubility of CO_2 in IL; the effective pathlength for this band is *ca*. 1.5 μm, and using the same molar absorptivity for CO_2 as for CO_2 dissolved in water at high pressures[9] the solubility of CO_2 in **I** at these conditions is *ca*. 0.6 mol fraction (2 M). The absorbance of the ν_3 band of CO_2 dissolved in **II** is approximately 40% lower indicating the lower solubility of CO_2 in **II**.

Fig. 1 shows the normalised spectra of CO_2 in the ν_2 region in **I** and **II** at 68 bar and 40 °C. There are two important

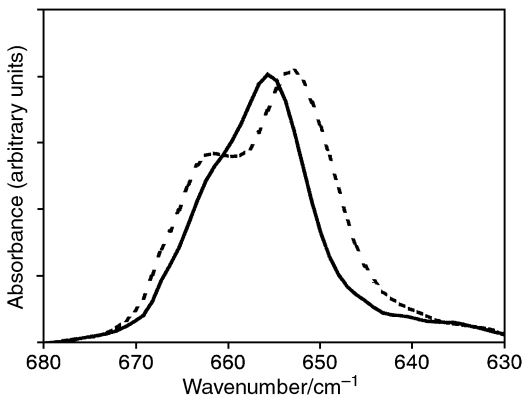

Fig. 1 ATR-IR spectra of CO_2 in the ν_2 mode region: spectrum of CO_2 dissolved in **II** (- - - -) and **I** (———). The absorbance scales of these spectra have been normalized to the absorbance of the stronger band (the maximum absorbance for **I** was *ca*. 0.2).

† Electronic supplementary information (ESI) available: schematic view of the miniature high-pressure flow cell. See http://www.rsc.org/suppdata/cc/b0/b005514j/

DOI: 10.1039/b005514j

observations: (i) the band is split into a doublet comprising of two bands; (ii) the magnitude of the splitting is different for CO_2 dissolved in **I** compared with **II**; the bands are strongly overlapped in **I** while the bands are distinct in **II**. The splitting of the bending mode of CO_2 indicates that the double degeneracy has been removed. This occurs due to a small bending of the CO_2 molecule. The angle of the bending is, probably, just a few degrees since we did not detect the appearance of the band corresponding to the symmetric stretching mode of CO_2. By analogy with the reported specific interaction between CO_2 and Lewis bases, which also results in the splitting of the bending mode,[7] it is reasonable to speculate that the splitting of the bending mode of CO_2 dissolved in ionic liquids indicates an interaction of CO_2 with a negatively charged fluorinated anion in **I** and **II**. These anions could act as weak Lewis bases, and CO_2 appears to be a useful probe to sense the extent of their basicity. The width of the ν_2 mode, measured as an effective average width of the split band (the average width represents the width of the doublet at the half-maximum of the absorbance) is an estimate of the strength of the interaction of CO_2 with the Lewis bases: the width increases with the increase of the strength of the interaction.[7] The observation of the striking differences in the band widths for CO_2 dissolved in **I** and **II** suggests that $[BF_4]^-$ is a stronger Lewis base in its interaction with CO_2 than $[PF_6]^-$. The average width of ν_2 for CO_2 dissolved in **II** reaches 19 cm^{-1}, the ν_2 width of CO_2 in **I** is just 15 cm^{-1}. The degree of the splitting also indicates that CO_2 molecules are more strongly bent and interactive with **II** than with **I** as was observed previously for CO_2 dissolved in organic solvents and supported by *ab initio* calculations.[10] Thus $[BF_4]^-$ acts as a stronger Lewis base towards CO_2 than $[PF_6]^-$. This conclusion contradicts the proposal by Brennecke and coworkers[5] that the strength of the interaction between CO_2 with $[PF_6]^-$, in ionic liquids, should be stronger than with $[BF_4]^-$. The current spectroscopic data provide strong evidence that the trend is the opposite, the $[BF_4]^-$ anion interacting more strongly with CO_2 than $[PF_6]^-$. This could also be a result of the strength of interaction decreasing with the increase of anion size. Thus, the strength of these interactions cannot be solely responsible for the solubility of CO_2 in these ionic liquids, and, presumably, a free volume contribution in the IL plays a significant role.[5] The strength of anion–cation interaction in the IL affects the available free volume, and one would anticipate that a weaker interacting anion leads to more free volume being available.

The spectroscopic ATR-IR method also facilitates the estimation of the swelling of ionic liquids subjected to high-pressure CO_2. The bands corresponding to the vibrations of the ionic liquids decrease in intensity as the pressure of CO_2 increases which would indicate that the evanescent wave in ATR spectroscopy probes a smaller number of ions in the vicinity of the ATR crystal due to the swelling of the liquid. This indicates that the interaction of CO_2 molecules with anions in ionic liquids facilitates swelling by decreasing anion–cation interactions for ions that are already largely mobile at room temperature in ionic liquids compared to other salts. The swelling of **I** is greater than of **II** presumably due to the weaker anion–cation interactions in **I**; it was noted earlier that the estimated solubility of CO_2 in **II** was *ca*. 40% less than for **I**, consistent with the differences in swelling. We have also observed a small (a few cm^{-1}) shift to the high-frequency region of the some of the bands corresponding to the stretching ν_3 modes of anions in **I** and **II** (relative to the bands of these ionic liquids in absence of dissolved CO_2) which also indicates that CO_2 interacts with the anions in these ILs. This shift also indicates a weakening of the interactions of the anions with their environment as CO_2 molecules weakly interact with the anions and act as a 'shield' reducing stronger interactions. The interactions between the CO_2 molecule and anion are probably of Lewis acid–base type, with the axis of the O=C=O molecule orienting towards the anion in perpendicular arrangement to P–F or B–F bonds. If the interaction of the CO_2 molecule with the cation in IL was *via* the CO_2 oxygen atom one would expect the ν_3 band to appear in a higher frequency range (2345–2360 cm^{-1}), the appearance of the ν_1 band and no splitting of the bending mode ν_2. This was observed in a number of studies on CO_2 adsorption in zeolites.[11] The influence of the negative charge density of the oxygen atoms in some zeolite networks reduces the ν_3 frequency,[11] which is consistent with the current proposal for the origin of the CO_2/anion interactions. The variation of the temperature of the **I**/CO_2 system in the range 40–60 °C shows that the absorbance bands of CO_2 dissolved in IL decrease in intensity as temperature increases; the interaction between CO_2 and **I** is exothermic which is typical for Lewis acid–base type interactions.

These data for the CO_2 interactions with IL is remarkably similar to those observed for CO_2 interactions with polymers.[7] There it was shown that the bending mode ν_2 of dissolved CO_2 is a very informative probe in elucidating its interactions with electron-donating functional groups in polymers. It is significant that the splitting of the bending mode of CO_2 in **II** exceeded any of the corresponding splittings observed for CO_2 in the polymers,[7] and the splitting for both **I** and **II** is significantly larger than that observed in fluorine-containing polymers indicative of the role of the negative charge in IL. There is a report implying that $[BF_4]^-$ is a stronger Lewis base than $[PF_6]^-$ based on the measurements of the coordinating ability of these anions.[12] Our spectroscopic assignment of the strength of interaction between CO_2 and anions in the two ionic liquids is also consistent with recent work[13] on the interactions between methanol and various anions where it was shown that $[BF_4]^-$ is a stronger proton acceptor relative to $[PF_6]^-$. Preliminary results for ionic liquids containing anions that are stronger bases, compared to [bmim][PF_6] and [bmim][BF_4], *e.g.* $[CF_3CO_2]^-$, has shown that the bending mode of CO_2 dissolved in this ionic liquid is split even further reflecting the greater basicity of this anion.

In summary, these spectroscopic data provide a first direct indication of the effect of an anion in the weak Lewis acid–base interactions with CO_2 molecules, and also provides a way to study phase partition behaviour of supercritical CO_2/IL systems, and hence to facilitate the design and optimisation of IL/SCF synthetic and separation routes.

We are particularly grateful to the RSC for a Journals Grant for International Authors in 1997. We thank EPSRC for support, Dr P. Turner (Bruker), Dr D. Coombs (Specac, Ltd.), Dr L. Lancaster, Dr C. J. Lawrence and Mr N. M. B. Flichy (Imperial College) for their support.

Notes and references

1 K. R. Seddon, *J. Chem. Tech. Biotechnol.*, 1997, **68**, 351; J. G. Huddleston, H. D. Willauer, R. P. Swatloski, A. E. Visser and R. D. Rogers, *Chem. Commun.*, 1998, 1765; C. M. Gordon and A. McCluskey, *Chem. Commun.*, 1999, 1431.
2 L. A. Blanchard, D. Hancu, E. J. Beckman and J. F. Brennecke, *Nature*, 1999, **399**, 28.
3 T. Welton, *Chem. Rev.*, 1999, **99**, 2071.
4 S. G. Kazarian, *Appl. Spectrosc. Rev.*, 1997, **32**, 301.
5 Z. Gu, L. A. Blanchard, D. Hancu, E. J. Beckman and J. F. Brennecke, in *Proceedings of 5th International Symposium on Supercritical Fluids*, Atlanta, USA, 2000.
6 S. G. Kazarian, B. J. Briscoe, D. Coombs and G. Poulter, *Spectrosc. Eur.*, 1999, **11**, 10.
7 S. G. Kazarian, M. F. Vincent, F. V. Bright, C. L. Liotta and C. A. Eckert, *J. Am. Chem. Soc.*, 1996, **118**, 1729.
8 M. H. Jamroz, J. C. Dobrowolski and M. Glice, *J. Mol. Struct.*, 1992, **267**, 365.
9 P. G. Maiella, J. W. Schoppelrei and T. B. Brill, *Appl. Spectrosc.*, 1999, **53**, 351.
10 M. H. Jamroz, J. C. Dobrowolski, K. Bajdor and M. A. Borowiak, *J. Mol. Struct.*, 1995, **349**, 9.
11 H. Knozinger and S. Huber, *J. Chem. Soc., Faraday Trans.*, 1998, **94**, 2047; B. Bonelli, B. Onida, B. Fubini, C. Otero Arean and E. Garrone, *Langmuir*, 2000, **16**, 4976; V. B. Kazansky, V. Y. Borovkov, A. I. Serykh and M. Bulow, *Phys. Chem. Chem. Phys.*, 1999, **1**, 3701.
12 H. G. Mayfield and W. E. Bull, *J. Chem. Soc. A.*, 1971, 2279.
13 O. Kristiansson and M. Schuisky, *Acta Chem. Scand.*, 1997, **51**, 270.

A convenient, one-step, synthesis of β-*C*-glycosidic ketones in aqueous media

Filipe Rodrigues, Yves Canac* and André Lubineau*

Laboratoire de Chimie Organique Multifonctionnelle, Associé au CNRS, Institut de Chimie Moléculaire d'Orsay, Université Paris Sud, 91405 Orsay, France. E-mail: yvescanac@icmo.u-psud.fr; lubin@icmo.u-psud.fr

Received (in Liverpool, UK) 9th August 2000, Accepted 13th September 2000
First published as an Advance Article on the web 2nd October 2000

Condensation of pentane-2,4-dione with different unprotected sugars in alkaline aqueous media gave quantitatively in one step β-*C*-glycosidic ketones.

C-Glycosides are becoming useful as building blocks for the synthesis of various types of natural products and as potential enzyme inhibitors.[1] In addition, they are used as a model in enzymatic and metabolic studies, indeed it has been shown that the conformational differences between the *O*- (or *N*-) glycosides and the *C*-linked analogue are minimal.[2] Moreover, *C*-glycosides are essentially inert to degradation because the natural anomeric centre has been transformed from a hydrolytically labile O or N acetal link to an ether. As a result, significant attention has been focused in the last decade on the development of new routes for their syntheses.

The most common method for C–C bond formation at the anomeric centre involves nucleophilic attack on this naturally electrophilic carbon atom.[3] A wide variety of electrophilic sugars have been employed such as reducing sugars, alkyl glycosides, anomeric esters, anomeric trichloroacetimidates, or glycosyl halides. The carbon nucleophiles that have been used include cyanides, allyl- and propargylsilanes, silyl enol ethers, silyl ketenes, enamines and organometallics such as Grignard reagents, organolithiums, cuprates, or aluminates.[4] In most cases, these procedures require specific, awkward reaction conditions and generally suffer from low yields.

Recently, there have been several advances in C–C bond formation in aqueous media. These milder methods include the coupling of unprotected sugars with malonate-derived nucleophiles such as barbituric derivatives[5] or Meldrum acid,[6] with Wittig-type reagents,[7] or with allyl bromides promoted by tin or indium in Barbier-type reactions.[8] In fact, water is now recognised as an attractive medium for many organic reactions[9] but curiously, for the most part, sugar chemistry stays away from this development of organic synthesis in water. Yet, the use of water-soluble unprotected reducing carbohydrates would allow syntheses without the tedious protection–deprotection protocol.

The Knoevenagel condensation,[10] a century-old reaction, consists of the condensation of aldehydes with active methylene-containing derivatives such as malonic acid or its ester. Despite the Knoevenagel reaction being a net dehydration, this reaction was surprisingly in some cases favoured in aqueous media.[11]

In this communication, we describe the very efficient one-step synthesis of β-*C*-glycosidic ketones in alkaline aqueous media from unprotected carbohydrates *via* the Knoevenagel condensation.

C-Glycosidic ketones are normally prepared in anhydrous conditions from an activated protected sugar by addition of a suitable nucleophile such as silyl enol ether[12] or enamines[13] to give generally the α-*C*-glycoside anomers as the major stereoisomer. Alternatively they can be obtained through multistep chemical transformations of allyl *C*-glycosides or using Wittig-type reaction on reducing sugars.[14]

We describe here the reaction in water of pentane-2,4-dione with D-glucose (**1**), D-mannose **(2)** or D-cellobiose (**3**) in the presence of sodium bicarbonate, which gave quantitatively in one step the β-*C*-glycosidic ketones (**4**–**6**).† The results and conditions are summarised in Table 1.

It is worth pointing out that compound **4** derived from D-glucose and **6** derived from D-cellobiose have been prepared only recently, respectively in six and seven steps in overall low yields from commercial 2,3,4,6-tetrabenzylglucopyranose.[15] In the case of the still unknown compound **5**, the structure and particularly the configuration at the anomeric centre was determined through ^{1}H, ^{13}C and NOESY NMR spectra.‡ Indeed a strong correlation between H-1 with both H-3 and H-5 in the NOESY spectrum along with a small coupling constant $J_{1,2}$ of 1 Hz indicates a β-configuration.

In fact, the reaction of pentane-2,4-dione with reducing sugars had already been studied in acidic medium ($ZnCl_2$, MeOH) and was shown[16] to give in the case of glucose the furan derivative (**7**) which further cyclises to **8** (32% overall yield), or, in aqueous acetone in the presence of sodium carbonate with reducing amino sugars such as glucosamine, the pyrrole derivative (**9**).[17]

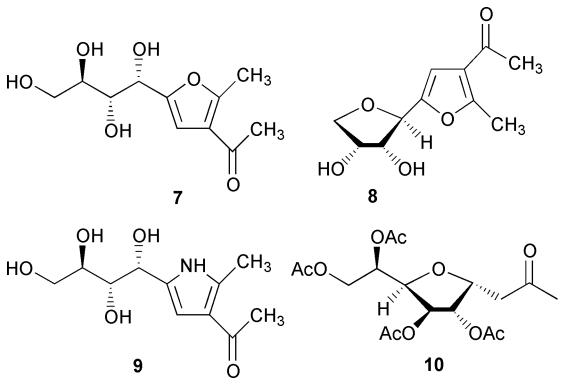

In our case, the formation of compounds (**4**–**6**) results from the initial condensation of the carbanion of the β-diketone with the starting sugar (**1**–**3**), β-elimination of water and then cyclisation to the intermediate *C*-glycoside which undergoes a retro-Claisen aldolisation under the basic conditions with concomitant sodium acetate elimination, as shown in Scheme 1.

The exclusive formation of the β-pyranoside stereoisomer in the reaction at 90 °C came from thermodynamic control in the

Table 1 Addition of pentane-2,4-dione onto unprotected carbohydrates in water

Substrates	Conditions	Products and stereoselectivity[b]	Total yields (%)[a]
D-Glucose (**1**)	$NaHCO_3$ (1.5 eq.), 6 h, 90 °C	**4** (100% β)	96
	$Yb(OTf)_3$ (0.1 eq.) 20 h, 60 °C	**7** (58%)[a] + **8** (39%)[a]	97
D-Mannose (**2**)	12 h, 90 °C	**5** (100% β)	95
D-Cellobiose (**3**)	12 h, 90 °C	**6** (100% β)	93

[a] Isolated yields. [b] Determined by ^{1}H and ^{13}C NMR spectroscopy.

DOI: 10.1039/b006642g

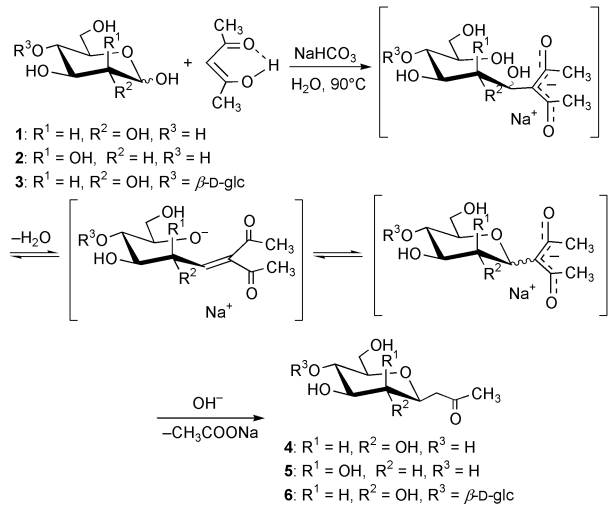

1: R^1 = H, R^2 = OH, R^3 = H
2: R^1 = OH, R^2 = H, R^3 = H
3: R^1 = H, R^2 = OH, R^3 = β-D-glc

4: R^1 = H, R^2 = OH, R^3 = H
5: R^1 = OH, R^2 = H, R^3 = H
6: R^1 = H, R^2 = OH, R^3 = β-D-glc

Scheme 1

presence of sodium bicarbonate. Effectively, at rt after 24 h we get a mixture of the four possible α,β-furanosides and α,β-pyranosides stereoisomers in which the α-furanoside predominates.§ Indeed, it has been shown that equilibration under basic conditions of protected α,β-*C*-glucofuranoside analogues having an activated methylene group adjacent to the anomeric carbon favored the α-anomer through an α,β-unsaturated keto-intermediate.[18] By contrast, in the case of a mixture of α,β-glucopyranosides, equilibration led to the practically exclusive formation of the β-glucopyranoside.[19] In our case, the reaction with D-glucose, including the equilibration towards the pure β-*C*-glucopyranoside, is complete after 6 h at 90 °C whereas for the reaction with D-mannose a longer reaction time is required (12 h at 90 °C) as a result of a slower equilibration process. In the case of cellobiose, pure β-*C*-glycoside was obtained along with a trace of starting cellobiose (< 4%) which still existed after 12 h at 90 °C and which was removed after crystallisation of the β-*C*-glycosidic ketone.

Recently, ytterbium trifluoromethanesulfonate was shown to promote acid-catalysed reactions in water under rather smooth conditions. This encouraged us to try the reaction of pentane-2,4-dione with D-glucose in water in the presence of $Yb(OTf)_3$ at neutral pH. Indeed, after 20 h at 60 °C, we obtained a 1.5 : 1 mixture of compounds **7** and **8**, formerly prepared under rather drastic conditions,[16] in near quantitative yield which could be further separated by flash chromatography into pure **7** (58%) and **8** (39%).

In summary, the Knoevenagel condensation under aqueous conditions presented in this paper represents a very convenient method for the preparation of pure β-*C*-glycosidic ketones in one step directly from the unprotected sugar. Application of this method to other bi-functional compounds as well as the use of these compounds in the preparation of more elaborate *C*-glycosides are at present under investigation in our laboratory.

Notes and references

† *General procedure for the condensation of pentane-2,4-dione with unprotected sugars*: to a solution of D-glucose, D-mannose or D-cellobiose (1 mmol) in water (4 ml) were added sodium bicarbonate (1.5 mmol) and pentane-2,4-dione (1.2 mmol). After stirring at 90 °C for the given time, the reaction mixture was washed with CH_2Cl_2 (5 ml) and treated with Dowex resin (50X8-200, H^+ form). After concentrating the aq. mixture, the residues looked pure by NMR spectroscopy except for **6** which still contained 4% of unreacted cellobiose. Analytical samples were obtained after flash chromatography (AcOEt–iPrOH–H_2O 8 : 1 : 1) or crystallization (MeOH–Et_2O) for **5** and **6**. Compounds **4** and **6** were found identical with those described in literature,[15] except that in our hands **6** crystallized from MeOH–ether mp, 88–89 °C.

‡ (**5**): white powder; mp 125–127 °C (CH_3OH–Et_2O); $[\alpha]_D^{27}$: −10° (*c* 1.2, MeOH); δ_H(200 MHz, D_2O): 2.26 (s, 3H, CH_3), 2.78 (dd, $J_{3a',1}$ 4.4, 1H, H-3a′), 2.98 (dd, $J_{3a',3b'}$ 17.1, $J_{3b',1}$ 8.3, 1H, H-3b′), 3.32–3.41 (ddd, $J_{5,4}$ 9.3, 1H, H-5), 3.55 (t, $J_{4,3}$ 9.3, 1H, H-4), 3.67 (dd, $J_{6a,6b}$ 12.2, $J_{6a,5}$ 6.4, 1H, H-6a), 3.68 (dd, $J_{3,2}$ 3.4, 1H, H-3), 3.85 (dd, $J_{1,2}$ 1.0, 1H, H-2), 3.88 (dd, $J_{6b,5}$ 2.4, 1H, H-6b), 4.05 (ddd, 1H, H-1); δ_C(62.9 MHz, D_2O): 29.8 (C-1′), 44.5 (C-3′), 61.1 (C-6), 66.9, 70.7, 73.7, 74.0, 79.9 (C-1), 212.7 (C-2′); υ_{max}(KBr)/cm^{-1}: 1712 (C=O). Calc. for $C_9H_{16}O_6$: C, 49.09; H, 7.32; O, 43.59. Found: C, 48.88; H, 7.27; O, 43.39%.

§ After 24 h at rt the mixture contained four stereoisomers in a 2 : 1 : 1 : 1 ratio in *ca*. 35% total yield from which the major stereoisomer could be separated by flash chromatography (AcOEt–iPrOH 8 : 2). It was fully characterized after peracetylation (Ac_2O, pyridine, 16 h at rt) and shown to be the α-*C*-glucofuranoside (**10**) by ^{1}H NMR. Indeed, we found H-4 at 4.29 ppm while H-5 moves downfield to 5.17 ppm showing clearly the presence of an acetate at OH-5. Moreover, NOESY experiment shows strong correlations between H-1 and H-5 and between H-1 and H-2 but not between H-1 and H-3, indicating an α configuration.

(**10**): colorless oil; $[\alpha]_D^{25}$: +18° (*c* 1.1, CH_2Cl_2); δ_H(200 MHz, $CDCl_3$): 1.99, 2.08, 2.13, 2.19 (s, 4 CH_3), 2.58 (dd, $J_{3a',1}$ 5.9, 1H, H-3a′), 2.80 (dd, $J_{3a',3b'}$ 17.1, $J_{3b',1}$ 7.3, 1H, H-3b′), 4.10 (dd, $J_{6a,6b}$ 12.2, $J_{6a,5}$ 5.4, 1H, H-6a), 4.29 (dd, $J_{4,5}$ 9.5, $J_{4,3}$ 3.7, 1H, H-4), 4.55 (dd, $J_{6b,5}$ 2.5, 1H, H-6b), 4.69 (ddd, $J_{1,2}$ 3.4, 1H, H-1), 5.17 (ddd, 1H, H-5), 5.21 (dd, $J_{2,3}$ 1.0, 1H, H-2), 5.43 (dd, 1H, H-3); δ_C(62.9 MHz, $CDCl_3$): 20.7 (CH_3CO), 30.4 (C-1′), 42.8 (C-3′), 63.4 (C-6), 67.8, 74.6, 76.2, 76.7, 76.9, 169.1, 169.7, 170.6 (CO), 205.1 (C-2′). Calc. for $C_{17}H_{24}O_{10}$: C, 52.57; H, 6.23; O, 41.20. Found : C, 52.43; H, 6.12; O, 40.93%.

1 S. Hanessian, *Total Synthesis of Natural Products: the Chiron Approach*, Pergamon, Oxford, 1983; J. N. BeMiller, M. P. Yadav, V. N. Kalabokis and R. W. Myers, *Carbohydr. Res.*, 1990, **200**, 111; R. R. Schmidt and H. Dietrich, *Angew. Chem., Int. Ed.*, 1991, **30**, 1328; F. Nicotra, *Top. Curr. Chem.*, 1997, **187**, 55.

2 T. C. Wu, P. G. Goekjian and Y. Kishi, *J. Org. Chem.*, 1987, **52**, 4819; A. Wei, A. Haudrechy, C. Audin, H. S. Jun, N. Haudrechy-Bretel and Y. Kishi, *J. Org. Chem.*, 1995, **60**, 2160 and references therein.

3 Nucleophilic reactivity at C-1 is also feasible. J. M. Beau and T. Gallagher, *Top. Curr. Chem.*, 1997, **187**, 1.

4 M. H. D. Postema, *Tetrahedron*, 1992, **48**, 8545; D. E. Levy and C. Tang, *The Chemistry of C-Glycosides*, Pergamon, Oxford, 1995; M. H. D. Postema, *C-Glycoside Synthesis*, CRC Press, Boca Raton, FL, 1995.

5 G. Wulff and G. Clarkson, *Carbohydr. Res.*, 1994, **257**, 81; M. B. Martinez, F. Z. Mata, A. M. Ruiz, J. A. G. Perez and C. J. Cardiel, *Carbohydr. Res.*, 1990, **199**, 235.

6 F. Z. Mata, M. B. Martinez and J. A. G. Perez, *Carbohydr. Res.*, 1990, **201**, 223.

7 A. H. Davidson, L. R. Hughes, S. S. Qureshi and B. Wright, *Tetrahedron Lett.*, 1988, **29**, 693; S. K. Chung and S. H. Moon, *J. Chem. Soc., Chem. Commun.*, 1992, 77.

8 W. Schmid and G. M. Whitesides, *J. Am. Chem. Soc.*, 1991, **113**, 6674; T. H. Chan and C. J. Li, *J. Chem. Soc., Chem. Commun.*, 1992, 747; J. Gao, R. Härter, D. M. Gordon and G. M. Whitesides, *J. Org. Chem.*, 1994, **59**, 3714.

9 C. J. Li, *Chem. Rev.*, 1993, **93**, 2023; A. Lubineau, J. Augé and Y. Queneau, *Synthesis*, 1994, 741; F. Fringuelli, G. Pani, O. Piermatti and F. Pizzo, *Tetrahedron*, 1994, **50**, 11 499; A. Lubineau, *Chem. Ind.*, 1996, **4**, 123; *Organic Synthesis in Water*, ed. P. Knochel, Thomson Sciences, London, 1998.

10 E. Knoevenagel, *Chem. Ber.*, 1896, **29**, 172; E. Knoevenagel, *Chem. Ber.*, 1898, **31**, 730; L. F. Tietze and U. Beifuss, in *Comprehensive Organic Synthesis*, ed. B. M. Trost, I. Fleming, C. H. Heathcock, Pergamon, Oxford, 1991, Vol. 2, Chapter 1.11, p. 341.

11 F. Bigi, L. Chesini, R. Maggi and G. Sartori, *J. Org. Chem.*, 1999, **64**, 1033.

12 P. Allevi, M. Anastasia, P. Ciuffreda, A. Fiecchi and A. Scala, *J. Chem. Soc., Chem. Commun.*, 1987, 1245.

13 P. Allevi, M. Anastasia, P. Ciuffreda, A. Fiecchi and A. Scala, *J. Chem. Soc., Chem. Commun.*, 1988, 57.

14 V. Aucagne, D. Gueyrard, A. Tatibouët, A. Quinsac and P. Rollin, *Tetrahedron*, 2000, **56**, 2647 and references therein; Y. A. Zhdanov and V. A. Polenov, *J. Gen. Chem. USSR*, 1969, **39**, 1091.

15 S. Howard and S. G. Withers, *J. Am. Chem. Soc.*, 1998, **120**, 10 326.

16 A. P. Kozikowski, G. Q. Lin and J. P. Springer, *Tetrahedron Lett.*, 1987, **28**, 2211; F. Garcia Gonzalez, *Adv. Carbohydr. Chem.*, 1956, **11**, 97.

17 F. Garcia Gonzalez and A. Gomez Sanchez, *Adv. Carbohydr. Chem.*, 1965, **20**, 303.

18 H. Ohrui, G. H. Jones, J. G. Moffatt, M. L. Maddox, A. T. Christensen and S. K. Bryam, *J. Am. Chem. Soc.*, 1975, **97**, 4602; M. C. Clingerman and J. A. SecristIII, *J. Org. Chem.*, 1983, **48**, 3141.

19 P. Allevi, M. Anastasia, P. Ciuffreda, A. Fiecchi and A. Scala, *J. Chem. Soc., Perkin Trans. 1*, 1989, 1275.

ChemComm

New fluorous ionic liquids function as surfactants in conventional room-temperature ionic liquids

Travis L. Merrigan, Eleanor D. Bates, Scott C. Dorman and James H. Davis, Jr.*

Department of Chemistry, University of South Alabama, Mobile, Alabama 36688 USA. E-mail: jdavis@jaguar1.usouthal.edu

Received (in Columbia, MO, USA) 23rd June 2000, Accepted 13th September 2000
First published as an Advance Article on the web 2nd October 2000

Ionic liquids formulated from imidazole cations with appended fluorous tails function as surfactants when added to conventional ionic liquids, facilitating the emulsification of fluoroalkanes with IL phases.

The development of less-polluting, 'neoteric' solvents is a key element in an emerging agenda for sustainable industrial development.[1] The alternatives receiving the most attention as neoteric solvents are ionic liquids (ILs), supercritical CO_2 (sc-CO_2), supercritical/near-critical H_2O, and perfluorocarbons.[2] Despite the intense interest in them, much of the basic chemistry of ionic liquids remains to be explored. Indeed, an understanding of this basic chemistry is of vital importance to the development of ionic liquids for 'green' applications.[1,3]

The thrust of our work with ionic liquids is the design and synthesis of salts composed of ions that incorporate structural or functional features that imbue them with particular properties.[1d,4] In a recent paper, we reported the synthesis of the first imidazolium ion with a long fluorous 'ponytail', with which we formulated a low-melting salt, *cf.*, a fluorous ionic liquid.[5,6] Our observation of the formation of a liquid crystalline phase by this structurally complex, fluorinated IL led us to speculate that the fluorocarbon tails of such ionic-liquid component cations associate. We subsequently reasoned that this property might be exploited to address a question of fundamental importance with regard to ionic liquid chemistry—the capacity of a designed, IL-based surfactant to alter the properties of a more conventional IL phase. Further, we deemed it feasible to capitalize upon such compounds to achieve a result of potential utility in biphasic systems—the use of the surfactant to promote and stabilize dispersions of a fluorous phase into an ionic liquid, two ordinarily immiscible neoteric solvent types. Note that Brennecke, Johnson and Rogers have all recently demonstrated the potential importance of biphasic systems in which both solvent components were neoteric materials.[7]

Here, we report the synthesis of four new fluorinated ionic liquids. The new compounds, **1**–**4**, differ substantially from the handful of known fluorine-containing ionic liquids in that the cation head-group structure is conventional and the fluorous appendage long (Fig. 1).[8,9] All of the new compounds are surfactants that promote the formation and stabilization of dispersions of perfluorocarbons in a conventional ionic liquid, 1-hexyl-3-methylimidazolium hexafluorophosphate, [6-mim]PF_6. Ours is the first report of the action of a fluorous surfactant on an ionic liquid, and only the second report of any surfactant action on or in an ionic liquid solvent.[10,11]

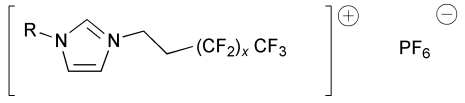

1 R = Me, *x* = 5
2 R = n-Bu, *x* = 5
3 R = Me, *x* = 7
4 R = n-Bu, *x* = 7

Fig. 1 General structure of the new fluorous ionic liquids.

The new fluorous ionic liquids are readily prepared from commercially available starting materials. Using an approach similar to that used to prepare our earlier fluorous IL, the imidazole cores 1-methyl- and 1-butylimidazole are dissolved in toluene, treated with a slight molar deficiency of 1,1,1,2,2,3,3,4,4,5,5,6,6-tridecafluoro-8-iodooctane or 1,1,1,2,2,3,3,4,4,5,5,6,6,7,7,8,8-heptadecafluoro-10-iododecane and heated under reflux overnight. Cooling to rt followed by removal of the solvent *in vacuo* leaves soft, off-white waxes. These iodide salts are readily metathesized in acetone using $AgPF_6$, giving ILs **1**–**4** in good yields.[12]

Compounds **1**–**4** manifest several behaviors common to surfactants. Simple capillary-rise measurements reveal that the surface tensions of saturated solutions (0.3 mass percent, ~ 1–4 mmolar) of **1**–**4** in [6-mim]PF_6 range from 10 to 15% less than the surface tensions of the conventional ionic liquid alone. Further, Ostwald viscosimetry establishes that increases in the viscosity of [6-mim]PF_6 occur upon addition of compounds **1**–**4**, a behavior common to known surfactants.[13] Still, the most dramatic surfactant behavior manifested by the new ILs is their capacity to act as agents to promote and stabilize dispersions of perfluorohexane in the 'conventional' IL [6-mim]PF_6. In the absence of the new fluorous ILs, the IL and perfluorohexane phases remain well defined. Controlled, timed mechanical agitation of the two-phase system results in the dispersal of droplets of the fluorous phase into the IL, but the droplets are quite large and individually distinguishable. They visibly begin to coalesce back into a bulk phase upon cessation of agitation. When this experiment is repeated using saturated solutions of **1**–**4** dissolved in [6-mim]PF_6, the dispersions that are formed persist for weeks without visible change.

Transmittance spectroscopy of the dispersions of perfluorohexane in the fluorous/conventional ionic liquid solution *versus* time graphically demonstrates the enhanced stability of those systems (Fig. 2).[14] Without fluorous IL, the initial turbidity of the system as determined by transmittance is slightly more than 40%. When any of the compounds **1**–**4** is dissolved in the bulk IL phase, the initial transmittance values are all near 10%. The rapid coalescence of the dispersed perfluorohexane droplets is apparent in the system without any

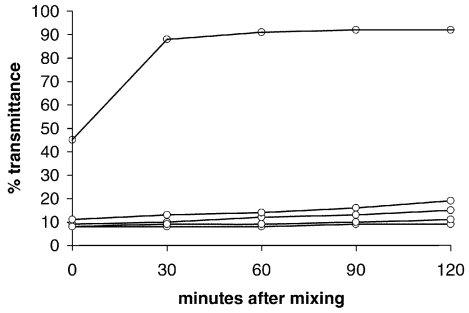

Fig. 2 Transmittance of perfluorohexane dispersions in [6-mim]PF_6 as a function of time with *(top to bottom)* no added fluorous IL; added **2**; added **1**; added **4**; added **3**. The enhanced stability of the dispersions in the presence of the fluorous ILs is apparent.

DOI: 10.1039/b005418f

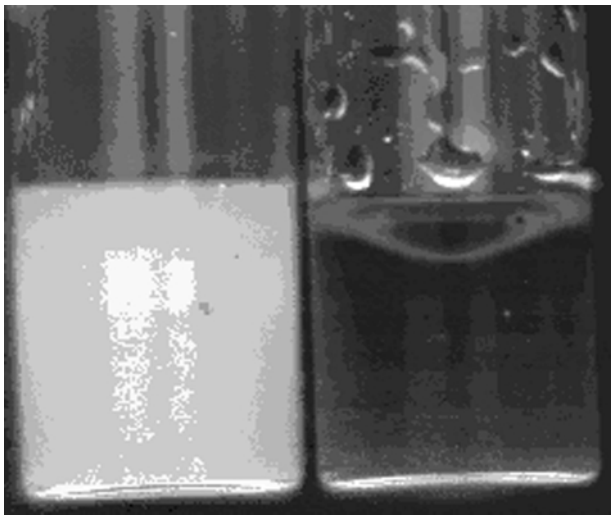

Fig. 3 Solution of **3**/[6-mim]PF_6 with emulsified perfluorohexane *(left)* and a mixture of [6-mim]PF_6–perfluorohexane *(right)*, both with added thymol blue. Note the turbidity of the stabilized emulsion, which has been aged one week, in contrast to the phase separation apparent in the system without FIL, aged five minutes. Also note the more efficient wetting of the container surface by the system containing fluorous IL.

fluorous IL, the transmittance of the system rising to 85% after 30 minutes. After similar time intervals, all four dispersions with added fluorous IL remain below 15% transmittance. This marked disparity persists with time. Over a four-hour interval, the transmittance of the IL–perfluorohexane mixture rises to 92%, while the transmittance values of the dispersions containing fluorous ILs range between 12 and 28%. This stability persists for extended time periods, dispersions of perfluorohexane and [6-mim]PF_6 with added **3** enduring for several weeks. Over periods of time greater than a month, the dispersions gradually decay with the formation of flocs.

In an effort to explore putative changes in the solvent environment arising from the presence of dissolved fluorous salt, we exploited a recent discovery by Rogers that, dissolved in conventional IL phases, thymol blue functions as an effective visual probe of such differences.[15] Systems containing [6-mim]PF_6–perfluorohexane and **3**–[6-mim]PF_6–perfluorohexane were prepared in identical fashion, solid thymol blue being added to each after the initial IL phases had been pre-equilibrated with pH 7.2 buffer. The mixtures were mechanically agitated for 15 min during which time the thymol blue dissolved. Upon dissolution of the thymol blue, the [6-mim]PF_6–perfluorohexane suspension became red, the color remaining in the IL phase as the two component liquids coalesced back into bulk phases. In the case of the **3**–[6-mim]PF_6–perfluorohexane mixture, a persistent suspension was formed which was brilliant yellow (Fig. 3). The yellow coloration was also observed in a mixture of **3** and [6-mim]PF_6 in the absence of perfluorohexane, indicating that the presence of the fluorous IL solute in the conventional IL phase is responsible for the observed difference in color. The effect does not appear to be linked to an electron-withdrawing effect of the fluorous appendage upon the imidazolium ion. Proton NMR spectra of **1**–**4** reveal that the chemical shifts of the imidazole ring C-2 protons—the most acidic within the cation structure—are similar to those of non-fluorinated ILs, suggesting that they are not rendered more acidic by the fluorous appendage.[16]† However, the presence of the fluorous appendage is likely to alter the capacity of the conventional IL to hold trace quantities of water, and the effect of such variations in water content within the IL phase on the behavior of the dye is unknown. Consequently, the basis of the difference in the color, whether pH based, solvatochromic, *etc*. is unclear. Studies to address this issue and other facets of the chemistry of fluorous ionic liquids are in progress, and will be reported in due course.

J. H. D. wishes to thank the Research Corporation for support of this work. We also wish to thank Dr Joseph Serafin for helpful advice and consultation with the turbidimetric and surface tension measurements, and Mr Michael Laurila for acquiring NMR spectra for us. Finally, we wish to thank Dr Ray Hoobler for providing the photograph appearing in this paper.

Notes and references

† ^{1}H-NMR (CD_3CN), δ. **1**: 2.81 (m, 2H, -C$H_2$$CF_2$-), 3.83 (s, 3H, N-$CH_3$), 4.50 (t, 2H, N-$CH_2$$CH_2$-), 7.37 (m, 1H, CH), 7.45 (m, 1H, CH), 8.50 (s, 1H, N-CH-N). **2**: 0.89 (t, 3H, CH_2CH_3), 1.34 (m, 2H, CH_2C$H_2$$CH_3$), 2.00 (m, 2H, C$H_2$$CH_2$$CH_3$), 2.80 (m, 2H, -$CH_2$$CF_2$-) 4.11 (m, N-$CH_2$-), 4.48 (m, N-$CH_2$-), 7.40 (m, 1H, CH), 7.44 (m, 1H, CH), 8.51 (s, 1H, N-CH-N). **3**: 2.81 (m, 2H, -C$H_2$$CF_2$-), 3.83 (s, 3H, N-$CH_3$), 4.50 (t, 2H, N-C$H_2$$CH_2$-), 7.36 (m, 1H, CH), 7.45 (m, 1H, CH), 8.48 (s, 1H, N-CH-N). **4**: 0.91 (t, 3H, CH_2CH_3), 1.34 (m, 2H, CH_2C$H_2$$CH_3$), 2.02 (m, 2H, C$H_2$$CH_2$$CH_3$), 2.80 (m, 2H, -C$H_2$$CF_2$-) 4.10 (m, N-$CH_2$-), 4.50 (m, N-$CH_2$-), 7.39 (m, 1H, CH), 7.44 (m, 1H, CH), 8.46 (s, 1H, N-CH-N).

1 (*a*) K. R. Seddon, *Kinet. Catal.*, 1996, **37**, 693; (*b*) K. R. Seddon, *J. Chem. Tech. Biotech.*, 1997, **68**, 351; (*c*) Y. Chauvin and H. Olivier-Bourbigou, *CHEMTECH*, 1995, **25**, 26; (*d*) T. Welton, *Chem. Rev.*, 1999, **99**, 2071; (*e*) M. Freemantle, *Chem. Eng. News*, 2000, **78** [May 15], 37.

2 P. E. Savage, *Chem Rev.*, 1999, **99**, 603; P. Zurrer, *Chem. Eng. News*, 2000, **78** [Jan. 3], 26.

3 K. R. Seddon, *Novel Chemistries in Ionic Liquids*, Green Industrial Applications of Ionic Liquids, Proceeding of the NATO Advanced Research Workshop, Heraklion, Greece, April 12–16, 2000, ed. R. D. Rogers, Kluwer, Dordrecht.

4 J. H. Davis, Jr., *Ionic Liquids Derived from Natural Products and Other Novel Chemistries*, Green Industrial Applications of Ionic Liquids, Proceeding of the NATO Advanced Research Workshop, Heraklion, Greece, April 12–16, 2000, ed. R. D. Rogers, Kluwer, Dordrecht.

5 J. H. Davis, Jr., K. J. Forrester and T. Merrigan, *Tetrahedron Lett.*, 1998, **39**, 8955.

6 A useful guideline for the upper limit of melting points for salts described as ionic liquids is *ca*. 150 °C, the temperature around which the lowest-melting purely 'inorganic' or 'classical' salt eutectics melt. For a recent example of the use as solvents of ionic liquids with melting points above rt, see: N. Karodia, S. Guise, C. Newlands and J.-A. Andersen, *Chem. Commun.*, 1998, 2341.

7 L. A. Blanchard, D. Hancu, E. J. Beckman and J. F. Brennecke, *Nature*, 1999, **399**, 28; J. G. Huddleston, H. D. Willauer, R. P. Swatlowski, A. E. Visser and R. D. Rogers, *Chem. Commun.*, 1998, 1765; K. P. Johnston, K. L. Harrison, M. J. Clarke, S. M. Howdle, M. P. Heitz, F. V. Bright and C. Carlier, *Science*, 1996, **271**, 624.

8 V. R. Koch,. C. Nanjundiah and R. T. Carlin, U.S. Patent 5,827,602 1998; P. Bonhôte and A.-P. Dias, U.S. Patent 5,683,832 1997; P. Bonhôte, A.-P. Dias, N. Papageorgiou, K. Kalyanasundaram and M. Grätzel, *Inorg. Chem.*, 1996, **35**, 1168.

9 During the preparation of this manuscript, the synthesis of the iodide salt of the cation of **3** was reported, as was its use as the precursor for the formation of a fluorous imidazolidene carbene ligand. See: L. Xu, W. Chen, J. F. Bickley, A. Steiner and J. Xiao, *J. Organomet. Chem.*, 2000, **598**, 409.

10 T. A. Hoefling, R. M. Enick and E. J. Beckman, *J. Phys. Chem.*, 1991, **95**, 7127.

11 S. E. Friberg, Q. Yin, F. Pavel, R. A. Mackay, J. D. Holbrey, K. R. Seddon and P. A. Aikens, *J. Dispersion Science & Technology*, 2000, **21**, 185.

12 The respective melting and clearing points for **1**–**4** are: **1**, 61°/109°; **2**, 88°/134°; **3**, 87°/130°; **4**, 97°/145°.

13 B. Vincent, in *Emulsions and Foams Surfactants*, ed. T. F. Tadros, Academic Press, London, 1984, p. 175.

14 R. S. Farinato and R. L. Powell, *Optical Properties of Emulsions*, Encyclopedia of Emulsion Technology, vol. 1, ed. P. Becker, Dekker, New York, 1983, p. 439.

15 A. E. Visser, R. P. Swatlowski and R. D. Rogers, *Green Chem.*, 2000, **2**, 1.

16 M. R. Grimmett, *Imidazole and Benzimidazole Synthesis*, 1997, Academic Press, London.

Pyrazole and benzothiazole palladacycles: stable and efficient catalysts for carbon–carbon bond formation

Xinjie Gai,[a] Ronald Grigg,*[a] M. Imran Ramzan,[a] Visuvanathar Sridharan,[a] Simon Collard[b] and Jayne E. Muir[b]

[a] *Molecular Innovation, Diversity and Automated Synthesis (MIDAS) Centre, School of Chemistry, Leeds University, Leeds, UK LS2 9JT. E-mail: R.Grigg@chem.leeds.ac.uk*
[b] *Johnson Matthey, Orchard Road, Royston, Herts, UK SG8 5HE*

Received (in Cambridge, UK) 1st August 2000, Accepted 11th September 2000
First published as an Advance Article on the web 2nd October 2000

Cyclopalladated phosphine free pyrazole complexes 1 and benzothiazole complexes 2 are excellent catalysts for the Heck vinylation of aryl iodides and termolecular queuing cascades, leading to turnover numbers of $>10^6$ in some cases, at moderate temperatures; these catalysts show high thermal stability and are not sensitive to moisture and air.

Palladium salts/complexes are exceptionally versatile and robust catalysts for the construction of carbon–carbon and carbon–heteroatom bonds. Recently a number of novel phosphapalladacycles[1–7] as well as cyclometallated imine complexes[8] have been used in the Heck coupling of aryl halides and acrylates with TONs (turnover numbers) of 10^5–10^6. Suzuki[1,5,8,9] and Stille cross couplings[1,5] have also been performed using some of these palladacycle catalysts with varying TONs of 10^2–10^6. These catalysts exhibit higher air and thermal stability compared with conventional Pd(0) catalysts *e.g.* $Pd(PPh_3)_4$.

The use of phosphine free, nitrogen based ligands in the Heck reaction is a neglected area. We report here that palladacycles **1** and **2**[10] are outstanding catalysts for the Heck reaction and

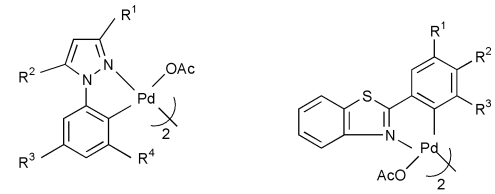

a R^1 = Me, R^2 = Me, R^3 = F, R^4 = H
b R^1 = CF_3, R^2 = Me, R^3 = F, R^4 = H
c R^1 = Me, R^2 = CF_3, R^3 = F, R^4 = H
d R^1 = Me, R^2 = Me, R^3 = F, R^4 = F
e R^1 = CF_3, R^2 = Me, R^3 = F, R^4 = F
f R^1 = Me, R^2 = CF_3, R^3 = F, R^4 = F

a R^1 = F, R^2 = H, R^3 = H
b R^1 = H, R^2 = OMe, R^3 = H
c R^1 = F, R^2 = H, R^3 = F
d R^1 = CF_3, R^2 = H, R^3 = H
e R^1 = CF_3, R^2 = H, R^3 = F
f R^1 = OMe, R^2 = H, R^3 = H

TONs of $>10^6$ can be achieved at 70–110 °C. Palladium complexes **1** and **2** are easily prepared, show high thermal stability and are not sensitive to moisture or air. Recently Milstein and coworkers reported non-phosphine cyclopalladated imine complexes for Heck reactions.[8]

Initially we explored the Heck reaction between iodobenzene and *n*-butyl acrylate (Scheme 1) in the presence of 1 mol% catalyst in DMF at 100 °C (Table 1).

Introducing fluorine (−I and π donor) substituents in the heterocyclic ligand *para* and/or *ortho* to the C–Pd bond increases the rate of the reaction (Table 1, entries 1, 4 and 9). Dual *o*- and *p*-fluoro substituents enhance this trend (Table 1,

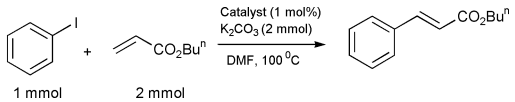

Scheme 1

Table 1 Heck coupling of iodobenzene with *n*-butyl acrylate using pyrazole and benzothiazole palladacycles at 100 °C in DMF

Entry	Catalyst (1 mol %)	*T*/°C	*t*/min	Conversion[a] (%)
1	**1a**	100	60	100
2	**1b**	100	15	100
3	**1c**	100	90	100
4	**1d**	100	45	100
5	**1e**	100	15	100
6	**1f**	100	60	100
7	**2a**	110	180	95
8	**2b**	110	180	93
9	**2c**	100	30	100
10	**2f**	110	180	100

[a] Conversion estimated by NMR spectroscopy.

entries 4 and 9). Exchanging the R^1 and R^2 methyl groups for an electron withdrawing trifluoromethyl group in **1** also perturbs the rate. Thus replacing the C(3) methyl group in **1a** by CF_3 results in a more active catalyst (Table 1, entries 1 and 2; entries 4 and 5) whilst replacing the C(5) methyl group does not produce rate acceleration (Table 1, entries 1 and 3; entries 4 and 6). The role of the fluoro and trifluoromethyl substituents is to perturb the C–Pd covalent bond, and N–Pd dative bond. When these substituents are optimally located they facilitate a controlled breakdown of the Pd(II) complexes **1** and **2** furnishing the active catalytic species. These palladacycles could operate *via* a Pd(II)/Pd(IV)[12] or Pd(0)/Pd(II) catalytic cycle. It appears probable, on our current evidence that the active species are Pd(0) nanoparticles.[13,14]

Next we briefly studied the effects of base in the Heck reaction employing milder conditions. These results are summarised in Table 2.

Although in some cases competitive reduction of the aryl iodide bond was observed, the use of sodium and potassium formate was found to accelerate the rate of the reaction. When potassium carbonate was employed as the base, the product was furnished in 80% isolated yield (entry 5) after 2 h. However lower isolated yields of product (65–70%) were obtained after

Table 2 Effect of base on the Heck coupling of iodobenzene with *n*-butyl acrylate using pyrazole and benzothiazole palladacycles at 70 °C in DMF

Entry	Catalyst (1 mol%)	Base (2 eq.)	*t*/h	Conversion[a] (%)
1	**1b**	HCO_2Na	1	100
2	**1b**	K_2CO_3	2	61
3	**1b**	HCO_2K	1	100
4	**1b**	$MeCO_2Na$	1	29
5	**1e**	K_2CO_3	2	93
6	**1e**	HCO_2Na	1	100
7	**1e**	HCO_2K	1	100

[a] Conversion estimated by NMR spectroscopy.

DOI: 10.1039/b005452f

Table 3 Heck coupling of iodobenzene (1 mmol) with *n*-butyl acrylate (2 mmol) using pyrazole and benzothiazole palladacycles for 48 h at 90–110 °C in DMF

Entry	Catalyst/mmol	Base (2 mmol)	*T*/°C	Conversion[a] (%)	TON[b]	Yield[c] (%)
1	**1b** (5×10^{-7})	HCO_2Na	100	75	1.5×10^6	—
2	**1b** (5×10^{-7})	$MeCO_2Na$ or $MeCO_2Cs$	100	< 10	—	—
3	**1e** (5×10^{-7})	HCO_2Na	100	74	1.48×10^6	—
4	**1e** (5×10^{-7})	$MeCO_2Na$	100	0	—	—
5	**1f** (5×10^{-7})	HCO_2Na	100	93	1.8×10^6	—
6	**1a** (5×10^{-7})	HCO_2Na	100	100	2×10^6	50
7	**1a** (5×10^{-7})	K_2CO_3	110	100	2×10^6	78
8	**2c** (1×10^{-6})	K_2CO_3	90	78	7.8×10^5	—
9	**2b** (1×10^{-5})	K_2CO_3	90	98	9.8×10^4	—
10	**2e** (1×10^{-5})	K_2CO_3	90	98	9.8×10^4	—
11	**2f** (1×10^{-5})	K_2CO_3	90	100	1×10^5	—

[a] Conversion estimated by NMR spectroscopy. [b] TON based on consumption of iodobenzene. [c] Isolated yields.

1 h when either sodium or potassium formate were used (entries 1, 3, 6 and 7). Sodium acetate was the least effective of the bases evaluated (entry 4), with only 29% conversion after 1 h.

Turnover numbers are summarised in Table 3 for the Heck reaction of iodobenzene (1 mmol) and *n*-butyl acrylate (2 mmol) using either HCO_2Na (2 mmol) or K_2CO_3 (2 mmol) as base in DMF at 90–110 °C for 48 h.

Although TONs of up to 2×10^6 can be achieved when employing sodium formate as base (entry 6) competitive reduction of the aryl iodide bond results in lower isolated yield of Heck product (50%). Employing potassium carbonate as base resulted in a TON of 2×10^6 (entry 7) and 78% isolated yield.

Finally we have briefly explored the scope of these catalysts in a three-component cascade process.[15] Typical examples are shown in Scheme 2.

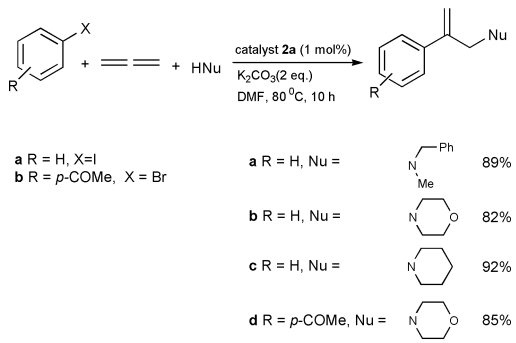

Scheme 2

In conclusion, we have developed a range of non-phosphine palladacycles which are efficient catalysts with high TONs for Heck reactions under mild conditions and with relatively short reaction times. Studies on other Heck substrates and the mechanism are in progress.

We thank Leeds University, the ORS (X. G.) and Johnson Matthey for support.

Notes and references

1 For a recent review, see: W. A. Herrmann, V. P. W. Bohm and C.-P. Reisinger, *J. Organomet. Chem.*, 1999, **576**, 23.
2 W. A. Herrmann, C. Brossmer, K. Ofele, C.-P. Riesinger, T. Priermeier, M. Beller and H. Fischer, *Angew. Chem., Int. Ed. Engl.*, 1995, **34**, 1844; M. Beller, H. Fischer, W. A. Herrmann, K. Ofele and C. Brossmer, *Angew. Chem., Int. Ed. Engl.*, 1995, **34**, 1848.
3 M. Ohff, A. Ohff, M. E. Van der Boom and D. Milstein, *J. Am. Chem. Soc.*, 1997, **119**, 11 687; K. Kiewel, Y. Liu, D. E. Bergbreiter and G. A. Sulikowski, *Tetrahedron Lett.*, 1999, **40**, 8945.
4 B. L. Shaw, S. D. Perera and E. E. Staley, *Chem. Commum.*, 1998, 2095.
5 D. A. Albisson, R. B. Bedford, S. E. Lawrence and P. N. Scully, *Chem. Commun.*, 1998, 2095.
6 F. Miyazaki, K. Yamaguchi and M. Shibasaki, *Tetrahedron Lett.*, 1999, **40**, 7379.
7 I. P. Beletskaya, A. V. Churchurjukin, H. P. Dijkstra, G. P. M. Van Klink and G. VanKoten, *Tetrahedron Lett.*, 2000, **41**, 1075.
8 M. Ohff, A. Ohff and D. Milstein, *Chem. Commun.*, 1999, 357; H. Weissman and D. Milstein, *Chem. Commun.*, 1999, 1901; D. A. Alonso, C. Najera and M. C. Pacheco, *Org. Lett.*, 2000, **13**, 1823.
9 W. A. Herrmann, M. Elison, J. Fischer, C. Kocher and G. R. J. Artus, *Angew. Chem., Int. Ed. Engl.*, 1995, **34**, 2371; W. A. Herrmann, C.-P. Reisinger and M. J. Splieger, *J. Organomet. Chem.*, 1998, **557**, 93.
10 **1a–f** and **2a–f** are new compounds prepared from the ligand (1 eq.) and $Pd(OAc)_2$ (1 eq.) in acetic acid and 100–120 °C over 2–5 h. The ligands were prepared by conventional ring synthetic methods for pyrazoles and benzothiazoles.[11]
11 Pyrazoles: J. Elguero, in *Comprehensive Heterocyclic Chemistry*, ed. A. R. Katritsky and C. W. Rees, Pergamon, 1st edn., 1984, vol. 5, p. 167 *et seq*; benzothiazoles: J. Metzger, *Comprehensive Heterocyclic Chemistry*, ed. A. R. Katritsky and C. W. Rees, Pergamon, 1st edn., 1984, vol. 6, p. 235 *et seq*.
12 B. L. Shaw, *New J. Chem.*, 1998, 77.
13 D. G. Blackmond, J. S. Bradly, J. Lebers and U. Specht, *Langmuir*, 1999, **15**, 7621.
14 M. Reetz and A. Westermann, *Angew. Chem., Int. Ed.*, 2000, **39**, 165.
15 R. Grigg and V. Sridharan, *J. Organomet. Chem.*, 1999, **576**, 65.

First evidence for the coexistence of four-, five- and six-coordinated silicon in glasses prepared at ambient pressure

M. Golam Mortuza,*[ab] M. Rafiqul Ahsan,[b] John A. Chudek[a] and Geoffrey Hunter[a]

[a] *Department of Chemistry, University of Dundee, Dundee, UK DD1 4HN. E-mail: m.g.mortuza@dundee.ac.uk*
[b] *Department of Physics, University of Rajshahi, Rajshahi 6205 Bangladesh*

Received (in Cambridge, UK) 1st August 2000, Accepted 11th September 2000
First published as an Advance Article on the web 2nd October 2000

At ambient pressure, a series of cadmium phosphosilicate glasses has been prepared in which, at certain phosphorus concentrations, the coexistence of four-, five- and six-coordinated silicon has been observed by ^{29}Si MAS solid state NMR spectroscopy.

In 1932 Zachariasen postulated that four coordinated silicon (Si^{iv}) is the building block of silicate glasses.[1] Indeed, several unsuccessful attempts were made subsequently to show that higher silicon coordination numbers would impose periodic long range order and consequent crystallinity.[2,3] However, in 1987 a peak −213 ppm (characteristic of Si^{vi}) was first observed in the ^{29}Si NMR spectrum of a 1 : 2 alkali metal silicate glass containing > 30 mol% P_2O_5 and prepared at ambient pressure.[4] Other reports of higher coordination numbers (Si^{v} and Si^{vi}) occurring in alkali and alkaline-earth silicate glasses have appeared subsequently.[5–8] Such knowledge of the local order of network forming silicon is needed to understand the physicochemical behaviour of silicate melts, magmas and plasmas at both ambient and high pressures.[8–10] Generally, the transition of Si^{iv} to Si^{v} and to Si^{vi} is favoured at high pressures. We now report the first evidence of the coexistence of Si^{iv}, Si^{v}, and Si^{vi} in a series of cadmium phosphosilicate single phase glasses prepared at *ambient* pressure and which were wholly vitreous within the detection limit of X-ray diffraction.

The cadmium phosphosilicate single phase glasses were made using appropriate amounts of analytical grade $CdCO_3$, SiO_2 and P_2O_5. A 20 g batch of nominal composition for xCdO·$(1-x-z)$$SiO_2$·$zP_2O_5$ was mixed together in a glass bottle and shaken for 8 h to achieve a homogeneous mixture. Powder batches in an alumina crucible were heated to 1250 °C by an electric furnace for 2.5 h. In order to maintain ambient pressure the crucibles in the furnace were open to the atmosphere. The glass melt was splat cooled using two steel plates at room temperature to give xCdO·$(1-x-z)$$SiO_2$·$zP_2O_5$ as a transparent homogeneous glass which was wholly vitreous within the detection limit of X-ray diffraction and, on optical inspection, did not show any evidence of phase separation. The ratio x:$(1-x-z)$ was kept constant at 1.5 while the value of z was varied between 0.50 and 0.70. The detailed composition of the samples and their nomenclature are given in Table 1.

All magic angle spinning (MAS) NMR spectra were obtained using a Chemagnetics AMX 300 Lite spectrometer operating at 59.61 MHz for ^{29}Si and 121.46 MHz for ^{31}P. Pulses of 5 μs (π/4) followed by a delay of 120 s were employed for the investigation of the ^{29}Si nuclei; 1 μs (π/4) with a 20 s delay for ^{31}P. The delays between pulses were chosen to ensure unsaturated signals. The samples were spun in 7.5 mm o.d. zirconia rotors at 6.5 kHz for ^{29}Si to put the spinning sidebands outside the −110 ppm to −215 ppm range. A higher rotational rate of *ca*. 14 kHz in 4.0 mm o.d. zirconia rotors was used for ^{31}P nuclei. The chemical shifts and peak positions were measured with respect to TMS for ^{29}Si and 85% H_3PO_4 for ^{31}P. The powdered samples were kept in a desiccator prior to spectral acquisition.

Fig. 1 shows the ^{29}Si spectra of CdSP1–CdSP4 and the NMR spectral parameters are presented in Table 1. Incorporation of phosphorus at > 30 mol% is known to rupture Si–O–Si bonds in some alkali metal silicate glasses, leading to Si^{iv}–O–P and Si^{vi}–O–P bonds characterised by ^{29}Si resonances at −120 ppm and −213 ppm, respectively.[3–7] The spectrum of CdSP1 (z = 0.50) glass showed an asymmetry on the high field side of the peak at −120 ppm suggesting the presence of a very small amount of a different species resonating at *ca*. −127.0 ± 1.0 ppm. This shift corresponds to an environment in which two adjacent silicon atoms are replaced by two phosphorus atoms while preserving the tetrahedral network.[11]

The ^{29}Si NMR spectra obtained for the glasses of composition $0.55 \leqslant z \leqslant 0.70$ differed significantly from those glasses with both lower and higher values of z. For z = 0.55 a new resonance of low intensity at −165.0 ± 0.5 ppm, characteristic of Si^{v}, along with a Si^{vi} resonance at −213.0 ± 0.5 ppm were observed. Both of these resonances increased in relative intensity with further addition of P_2O_5 up to z = 0.60. The coexistence of four-, five- and six-coordinated silicon in glasses at atmospheric pressure is unprecedented. Moreover, in contrast

Table 1 Composition and spectral properties of the cadmium phosphosilicate base glasses

				NMR spectral parameters (ppm) ± 0.5						
	Nominal composition (mol%)			^{29}Si		^{31}P [a]		Relative intensities (%)		
Sample	CdO	SiO_2	P_2O_5	chemical shift	FWHM	chemical shift	FWHM	Si^{iv}	Si^{v}	Si^{vi}
CdSP1	30.0	20.0	50.0	−118.4	17.5	−18.4	22.0	100.0	0.0	0.0
CdSP2	27.0	18.0	55.0	−119.0	16.4	−16.8	17.1	91.6 ± 3.5	2.8 ± 0.2	5.6 ± 0.3
				−164.5	13.4	−34.6	26.6			
				−213.2	10.7					
CdSP3	24.0	16.0	60.0	−119.4	17.4	−16.9	16.6	75.0 ± 3.0	7.1 ± 0.3	17.9 ± 0.8
				−165.0	13.1	−36.0	30.0			
				−212.8	10.4					
CdSP4	18.0	12.0	70.0	−119.6	17.2	−16.2	17.7	86.5 ± 3.5	3.9 ± 0.2	9.6 ± 0.5
				−165.1	12.8	−34.5	29.2			
				−213.6	11.3					

[a] ^{31}P chemical shifts and linewidths were obtained by deconvoluting the spectra.

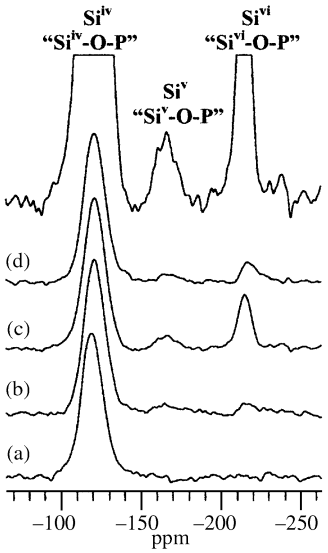

Fig. 1 ^{29}Si spectra of xCdO·(1 − x − z)SiO$_2$·zP$_2$O$_5$ for z = (a) 0.50, (b) 0.55, (c) 0.60 and (d) 0.70. The top spectrum is spectrum c ×8 multiplication.

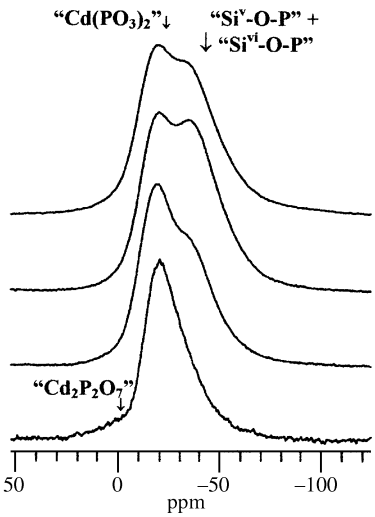

Fig. 2 ^{31}P spectra of xCdO·(1−x−z)SiO$_2$·zP$_2$O$_5$ for z = (a) 0.50, (b) 0.55, (c) 0.60 and (d) 0.70. Only the isotropic band is shown for clarity.

to alkali-metal phosphosilicate glasses, in the CdO–SiO$_2$–P$_2$O$_5$ system increasing z beyond 0.70 led to a *decrease* in the concentrations of the higher coordination number silicon environments. Integration of the unsaturated ^{29}Si NMR signals gave accurate measures of the Si^{iv}:Si^{v}:Si^{vi} ratios in the splat cooled base samples (Table 1). The Si^{v}:Si^{vi} ratio remained constant at 0.42 ± 0.03 for those samples in which higher coordinated silicon could be detected.

The reported shift of −150 ppm for Si^{v} in a K$_2$Si$_4$O$_9$ glass[8] is lower than that assigned to this environment in the cadmium phosphosilicate single phase glasses. We attribute this upfield shift to the silicon being surrounded by five oxygen atoms that are in turn bonded to phosphate species, phosphorus being of higher electronegativity.[4] The Si^{vi} chemical shift, −213 ppm, observed for the cadmium phosphosilicate glasses corresponds almost exactly to that reported for SiP$_2$O$_7$ species.[4–7]

Although the glass melt had been maintained at ambient pressure, quenching *via* splat cooling might have led to the metastable retention of a coordination multiplicity which was appropriate only to high temperatures. As CdSP3 had the highest concentrations of Si^{v} and Si^{vi}, this sample was chosen to observe the effects of slow cooling of the melt. There was a successive diminution of the higher coordination number species with slower cooling rates, corresponding to the removal of structural defects in the glass on annealing. The decrease in Si^{v} abundance is consistent with similar observations for K$_2$Si$_4$O$_9$ glass.[8] However, the decrease in the abundance of Si^{vi} contrasts with the situation for both phosphosilicate[3] and alkali metal phosphosilicate systems where annealing leads to the transformation of Si^{iv} into Si^{vi}. This suggests that the cadmium phosphosilicate system has different thermodynamic properties to those of the alkali metal-based glasses. This could lead to different optical properties for the CdO–SiO$_2$–P$_2$O$_5$ glasses.

Fig. 2 illustrates the ^{31}P NMR spectra of the glasses and the corresponding spectral parameters are given in Table 1. The sample CdSP1 (z = 0.50) showed only one resonance at −18.0 ppm, characteristic of cadmium metaphosphate species, accompanied by asymmetry on both the low and high field sides of the peak. That at lower field is due to the presence of cadmium pyrophosphate, whereas that at higher field may be due to a small amount of phosphosilicate species in which the silicon is four-coordinated. This could be the same species causing the asymmetry in the Si^{iv} peak of the ^{29}Si spectrum. With increasing P$_2$O$_5$ concentration another distinct resonance at −35.0 ppm, characteristic of phosphosilicate species with higher Si coordination numbers,[4] and a metaphosphate peak at *ca*. −16.0 ppm were observed. Relative to the metaphosphate peak, the former increased in intensity for CdSP2 and CdSP3 but then decreased for CdSP4. This change in intensity is consistent with that observed for the ^{29}Si resonances of the phosphosilicate species.

In general, we would expect two ^{31}P resonances corresponding to Si^{v}–O–P and Si^{vi}–O–P environments, but such was not observed. However, the linewidth of the resonance at −35.0 ppm (FWHM *ca*. 30.0 ppm) was far greater than that reported for Si^{vi}–O–P species (17.0 ppm) in alkali metal phosphosilicate systems.[4] This substantiated the presence of peaks attributable to Si^{v}–O–P species within the envelope of the resonance at −35.0 ppm. The unresolved spectral data suggest that the chemical shift difference between the two ^{31}P local orders is smaller than the difference in the linewidth of the resonances.

Further experiments are being performed to determine the variation of Si^{v} and Si^{vi} concentrations with CdO content. The thermodynamical and optical properties of the glasses are also being investigated and will be presented elsewhere.

We thank the Association of Commonwealth Universities in the United Kingdom for the award of a Commonwealth Fellowship (M. G. M).

Notes and references

1 W. H. Zachariasen, *J. Am. Chem. Soc.*, 1932, **54**, 3841.
2 I. N. Chakraborty and R. A. Condrate, *Phys. Chem. Glasses*, 1985, **26**, 68.
3 T. L.Weeding, B. H. W. S. de Jong, W. S.Veeman and B. G. Aitken, *Nature*, 1985, **318**, 352.
4 R. Dupree, D. Holland and M. G. Mortuza, *Nature*, 1987, **328**, 416.
5 R. Dupree, D. Holland, M. G. Mortuza, J. A. Collins and M. W. G. Lockyer, *J. Non-Cryst. Solids*, 1988, **106**, 403.
6 R. Dupree, D. Holland, M. G. Mortuza, J. A. Collins and M. W. G. Lockyer, *J. Non-Cryst. Solids*, 1989, **112**, 111.
7 M. Nogami, K. Miyamura, Y. Kawasaki and Y. Abe, *J. Non-Cryst. Solids*, 1997, **211**, 208.
8 J. F. Stebbins, *Nature*, 1991, **351**, 638.
9 X. Xue, J. F. Stebbins, M. Kanzaki and R. G. Tronnes, *Science*, 1989, **245**, 962.
10 J. F. Stebbins and M. Kanzaki, *Science*, 1991, **251**, 294.
11 M. G. Mortuza, J. A. Chudek and G. Hunter, *J. Mater. Sci. Lett.*, submitted.

ChemComm

Synthesis of amorphous, microporous silica with adamantanamine as a templating agent

Tao Sun,† Michael S. Wong and Jackie Y. Ying*

Department of Chemical Engineering, Massachusetts Institute of Technology, Cambridge, MA 02139, USA. E-mail: jyying@mit.edu

Received (in Irvine, CA, USA) 7th February 2000, Accepted 31st August 2000
First published as an Advance Article on the web 2nd October 2000

Amorphous, microporous silica with a spherical particle morphology has been prepared with adamantanamine, and its unusual structural properties suggest a non-zeolitic templating synthesis pathway.

Templating agents have been widely used in directing the formation of porous inorganic structures.[1,2] Traditionally, small organic molecules have been used as individual *molecular* templates in constructing the pore openings and cage-like cavities in microporous zeolites (pores < 20 Å).[2] In contrast, long-chained surfactant molecules are used as *supramolecular* templating agents in the preparation of amorphous mesoporous M41S-type silicates (pores > 20 Å).[3–6] The amphiphilic molecules interact with inorganic precursors and organize into micellar domains to form mesostructured metal oxide/surfactant composites. Mesoporous materials are produced after removal of the organic templating agents. Microporous transition metal oxide analogues prepared with short-chain surfactant-like molecules[7] and bifunctional surfactants[8] have recently been reported.

Here, we describe the formation of amorphous microporous silica using adamantanamine. Adamantanamine is a small, bulky molecule (axial length of *ca.* 5.9 Å) used as a molecular template in the preparation of zeolites, *e.g.* deca-dodecasil 3R (DD3R).[9]

In the synthesis of silicate/adamantanamine composites, 120 mol equivalents of water were added to an ethanolic solution consisting of 4 g of tetraethylorthosilicate and adamantanamine with an adamantanamine/Si molar ratio of 0.4. After stirring the reaction mixture at room temperature for 48 h, the white precipitate obtained was collected by filtration and washed with water. The resulting solid powder, designated as Si-TMS7, gave the X-ray diffraction (XRD) pattern shown in Fig. 1(a). Upon calcination at 540 °C for 3 h in air to remove the adamantanamine from the inorganic/organic composite, Si-TMS7 retained its XRD pattern [Fig. 1(b)]. The resulting silicate has an effective BET surface area of 737 $m^2\ g^{-1}$ and a pore volume of 0.35 $cm^3\ g^{-1}$. The type I nitrogen adsorption isotherm in Fig. 2 clearly illustrates the microporous nature of Si-TMS7.

The XRD patterns of Si-TMS7 (Fig. 1) have an intense low-angle diffraction peak, with *d*-spacings of 21.5 and 20.4 Å before and after calcination at 540 °C, respectively. The patterns resemble more closely those of surfactant-templated mesoporous materials than those of any zeolites. The lack of higher-order diffraction peaks indicates the absence of long-range pore ordering. The lone diffraction peak represents a common distance between the pore walls, as is usually observed in supramolecular-templated mesoporous materials with local pore ordering, *e.g.* KIT-1,[10] MSU-1[6] and L_3-phase silica gels.[11]

The particle morphology of calcined Si-TMS7 is predominated by *ca.* 1 μm spheres, as shown by transmission electron microscopy (TEM) [Fig. 3(a)]. These spheres are very monodisperse in size, as also confirmed by scanning electron microscopy. The morphology of Si-TMS7 is similar to the 200–500 μm spherical particles of MCM-41 prepared through surfactant–templating within butanol-in-water emulsions.[12] An emulsion-like system of adamantanamine, ethanol and water could be responsible for the spherical shapes of Si-TMS7 particles.

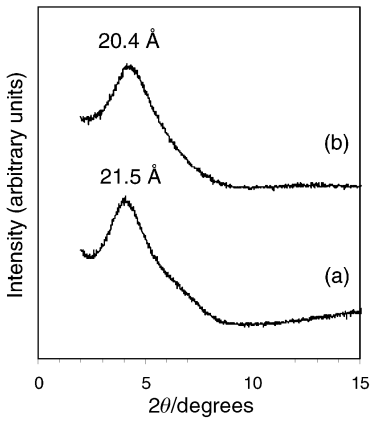

Fig. 1 XRD patterns of Si-TMS7 synthesized with adamantanamine templates at room temperature: (a) as-synthesized and (b) after calcination at 540 °C. The XRD patterns were obtained with a Siemens D5000 θ–θ diffractometer with Cu-Kα radiation (λ = 1.5406 Å).

The Si-TMS7 spheres were microtomed to reveal their amorphous, microporous structure [Fig. 3(b)]. Highly packed, randomly ordered pores appear throughout the particle. The pore size is estimated to be in the 13–17 Å range, more than twice the size of a single adamantanamine molecule (*ca.* 5.9 Å). We speculate that aggregates of adamantanamine may be directing the formation of the pores, distinct from the surfactant micellar domains prominent in mesoporous materials synthesis.

The temperature was found to be a very important parameter in the synthesis of Si-TMS7. Mesostructured Si-TMS7 could only be derived under ambient conditions; hydrothermal treatment at elevated temperatures resulted in amorphous, non-

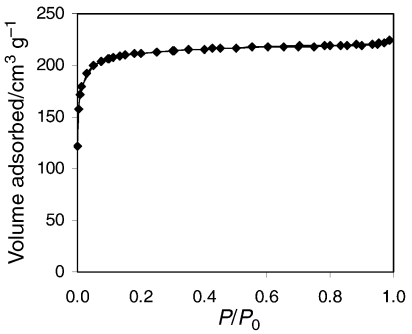

Fig. 2 N_2 adsorption isotherm of Si-TMS7 after adamantanamine removal by calcination at 540 °C in air. The isotherm was collected on a Micromeritics 2010 Gas Adsorption Analyzer after degassing the sample at 150 °C and 10^{-3} mmHg for 6 h.

† Current Address: Corporate R&D-Chemical Sciences Laboratory, The Dow Chemical Company, Midland, MI 48674 USA.

DOI: 10.1039/b001079k

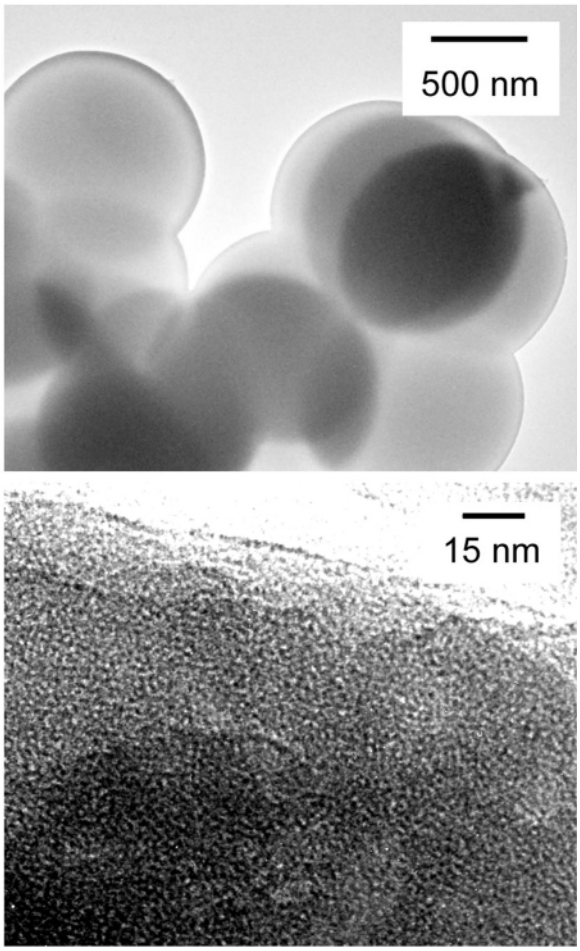

Fig. 3 TEM images of calcined Si–TMS7 (a) before and (b) after microtoming. The thinned sections were prepared by setting the calcined powder in acrylic resin. The microscopy was performed on a JEOL 2010 operating at 200 kV with a LaB_6 gun.

mesostructured materials. The interaction between the adamantanamine and the silicon alkoxide is most likely characterized by hydrogen bonding, which would be too weak to be sustained at high temperatures.[5,13] Other important factors that determine the templated inorganic structure are solubility and hydrophobicity of the templates, as shown by the fact that linear amines with only hydrocarbon chain length of > 6 are capable of leading to porous silicas with self-assembled templating structures.[13]

In conclusion, adamantanamine was used to prepare silicate/organic composites and was successfully removed without structural collapse of the resulting microporous silica. The unique structure and large 13–17 Å micropores provide evidence for collective templating of the small rigid adamantanamine molecules. Through such a synthesis pathway, other non-zeolitic microporous metal oxides can be attained.

This work was supported by the David and Lucile Packard Foundation and the Camille and Henry Dreyfus Foundation. We thank the MIT-NSF CMSE for use of the microscopy facilities, and Dr A. J. Reed and M. Frongillo for their assistance with the TEM studies.

Notes and references

1 E. M. Flanigen, *Adv. Chem. Ser.*, 1973, **121**, 114.
2 M. E. Davis and R. F. Lobo, *Chem. Mater.*, 1992, **4**, 756.
3 C. T. Kresge, M. E. Leonowicz, W. J. Roth, J. C. Vartuli and J. S. Beck, *Nature*, 1992, **359**, 710.
4 D. Zhao, J. Feng, Q. Huo, N. Melosh, G. H. Fredrickson, B. F. Chmelka and G. D. Stucky, *Science*, 1998, **279**, 548.
5 P. T. Tanev and T. J. Pinnavaia, *Science*, 1995, **267**, 865.
6 S. A. Bagshaw, E. Prouzet and T. J. Pinnavaia, *Science*, 1995, **269**, 1242.
7 T. Sun and J. Y. Ying, *Nature*, 1997, **389**, 704.
8 T. Sun and J. Y. Ying, *Angew. Chem., Int. Ed.*, 1998, **37**, 664.
9 H. Gies, B. Marler and U. Werthmann, in *Molecular Sieves: Science and Technology*, ed. H. G. Karge, J. Weitkamp, Springer-Verlag, Berlin, 1998, vol. 1, pp. 65–96.
10 R. Ryoo, J. M. Kim, C. H. Ko and C. H. Shin, *J. Phys. Chem.*, 1996, **100**, 17718.
11 K. M. McGrath, D. M. Dabbs, N. Yao, I. A. Aksay and S. M. Gruner, *Science*, 1997, **277**, 552.
12 Q. Huo, J. Feng, F. Schüth and G. D. Stucky, *Chem. Mater.*, 1997, **9**, 14.
13 T. Sun, L. Zhang, M. S. Wong and J. Y. Ying, *Chem. Mater.*, to be submitted.

N-Sulfonylimines as an excellent acceptor for intermolecular radical reactions

Hideto Miyabe, Masafumi Ueda and Takeaki Naito*

Kobe Pharmaceutical University, Motoyamakita, Higashinada, Kobe 658-8558, Japan.
E-mail: taknaito@kobepharma-u.ac.jp

Received (in Cambridge, UK) 10th August 2000, Accepted 13th September 2000
First published as an Advance Article on the web

The intermolecular carbon radical addition to *N*-sulfonylimines proceeded effectively under either iodine atom-transfer reaction conditions or zinc-mediated aqueous-medium reaction conditions.

The carbon–nitrogen double bond of imine derivatives has emerged as a radical acceptor and, thus, numerous synthetically useful intramolecular carbon–carbon bond-forming reactions are available.[1] However, the intermolecular radical reaction of imine derivatives has not been widely investigated except for a few examples.[2] We reported recently that the intermolecular carbon radical addition to unactivated oxime ethers proceeded smoothly in the presence of $BF_3{\cdot}OEt_2$;[3] subsequently, the screening of more reactive imino radical acceptors has been the focus of our efforts. We now report an intermolecular radical reaction of electron deficient *N*-sulfonylimines which exhibit excellent reactivity toward nucleophilic alkyl radicals even in the absence of strong Lewis acids.

As a preliminary experiment, we investigated a simple intermolecular addition of an ethyl radical to *N*-sulfonylimine **1A** [eqn. (1)]. The reaction was run in dichloromethane at 25 °C

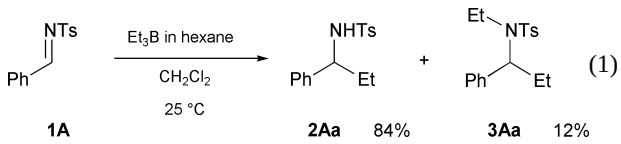

(1)

by using Et_3B as an ethyl radical source to give the desired ethylated product **2Aa** in 84% yield accompanied with a small amount of the diethylated product **3Aa**. It is important to note that the radical addition to benzaldehyde *O*-benzyloxime did not proceed under similar reaction conditions.[3] Good chemical yields were also observed in the radical addition using different radical precursors such as isopropyl, cyclohexyl, and cyclopentyl iodides under the iodine atom-transfer reaction conditions in the absence of tin hydride (Scheme 1). We also examined the stannyl radical-mediated radical reaction of **1A**;

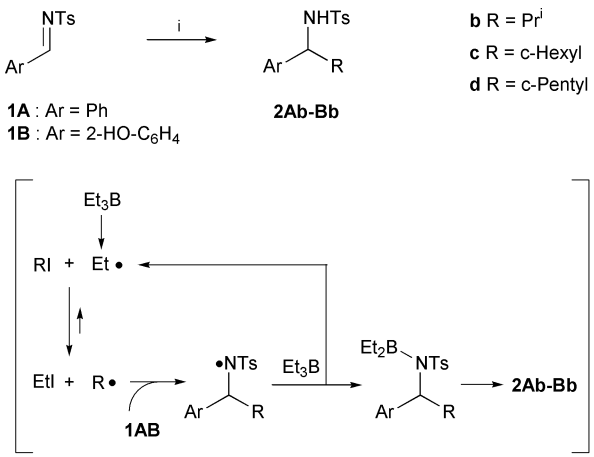

Scheme 1 *Reagents and conditions*: i, RI (30 equiv.), Et_3B 5 equiv. 3 times), CH_2Cl_2, 25 °C; **2Ab**: R = Pr^i (80%), **2Ac**: R = c-Hexyl (55%), **2Ad**: R = c-Pentyl (54%), **2Bb**: R = Pr^i (89%).

however, the use of Bu_3SnH effected tin hydride-mediated reduction of the carbon–nitrogen double bond to give a significant amount of the corresponding *N*-sulfonylbenzylamine. Thus, the iodine atom-transfer reaction using RI and Et_3B in the absence of toxic tin hydride is an effective method for using *N*-sulfonylimine as a radical acceptor. Moreover, the reaction with more nucleophilic secondary alkyl radicals proceeded selectively and did not give the diethylated products, in contrast with the reaction with a primary ethyl radical. In this reaction, Et_3B would act as a reagent for trapping the intermediate aminyl radicals to regenerate an ethyl radical, and therefore more than a stoichiometric amount of Et_3B is required. As expected, *N*-sulfonylimine **1B**, which is activated by the intramolecular hydrogen bond by a 2-hydroxy group, was more reactive than *N*-sulfonylimine **1A** and therefore the isopropyl radical addition to **1B** proceeded effectively to give the desired product **2Bb** in 89% yield.

The use of water as a solvent has generated considerable interest from both economic and environmental points of view.[4] We recently have demonstrated that radical reactions of imine derivatives such as oxime ethers, hydrazones, and nitrones proceed in aqueous media using Et_3B.[5] In the case of *N*-sulfonylimine **1A**, a similar reaction procedure did not give good results in the radical addition reaction because of the competitive hydrolysis to $TsNH_2$. On the other hand, we have now found that the formation of the desired alkylated products **2Ab**–**Af** was observed in the zinc-mediated radical reaction of **1A** in aqueous media [eqn. (2)].[6] To a micro tube containing

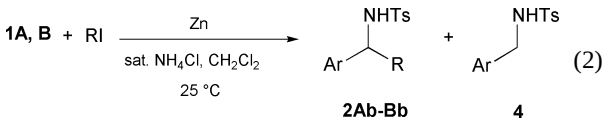

(2)

N-sulfonylimine **1A**, Pr^{i}I, zinc, and dichloromethane as a co-solvent was added dropwise saturated aq. NH_4Cl over 15 min at 25 °C (Table 1, entry 1). The isopropylated product **2Ab** was obtained in 73% yield along with the reductive product **4** as a by-product. Not only a secondary alkyl but also the bulky *tert*-

Table 1 Zinc-mediated radical addition to **1A**, **B** in aq. media[a]

			Yield (%)[b]		
Entry	Sulfonylimine	RI	**2**		**4**
1	**1A**	Pr^{i}I	**2Ab**	73	8
2	**1A**	c-Hexyl I	**2Ac**	71	12
3	**1A**	c-Pentyl I	**2Ad**	64	18
4	**1A**	Bu^{s}I	**2Ae**	56	10
5	**1A**	Bu^{t}I	**2Af**	66	20
6[c]	**1A**	MeI	**2Ag**	—	16
7	**1B**	Pr^{i}I	**2Bb**	64	8
8[d]	**1A**	Pr^{i}I	No reaction		

[a] Reactions of **1A** or **1B** (50 mg) were carried out with Zn (7 equiv.), RI (5 equiv.), and sat. NH_4Cl (1 cm^3) in CH_2Cl_2 (0.1 cm^3) at 25 °C. [b] Isolated yields. [c] $TolSO_2NH_2$ was obtained in 65% yield. [d] Reactions of **1A** (50 mg) were carried out with Zn (7 equiv.) and Pr^{i}I (5 equiv.) in CH_2Cl_2 (1 cm^3) at 25 °C.

DOI: 10.1039/b006574i

butyl radical worked well under similar reaction conditions (entries 1–5). The methylated product **2Ag** was not obtained in the reaction using a less reactive methyl radical because of the competitive hydrolysis and reduction (entry 6). The isopropyl radical addition to another *N*-sulfonylimine **1B** also proceeded smoothly (entry 7). However, the reaction of **1A** using zinc in dichloromethane in the absence of aq. NH_4Cl did not proceed (entry 8). The known examples of metal-mediated carbon–carbon bond-forming reactions in aqueous media are mainly limited to allylation of carbonyl compounds;[7] thus, it is noteworthy that this reaction involves the alkylation of imine derivatives. The alkylation and reduction reactions would proceed as indicated in Scheme 2.

In conclusion, we have demonstrated the utility of *N*-sulfonylimines as radical acceptors under two different reaction conditions. These are the first examples of the reaction of *N*-sulfonylimines with carbon radicals and are a convenient method for preparing a wide range of amine derivatives.

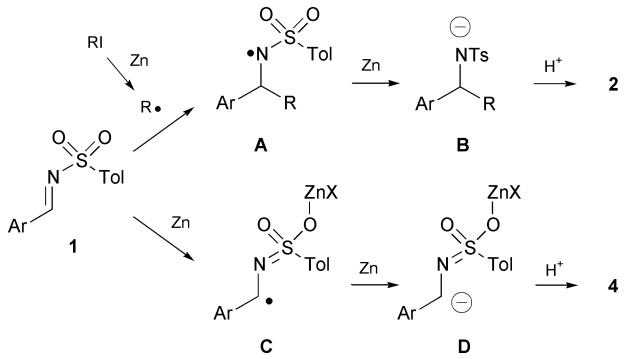

Scheme 2

This work was supported by research grants from the Ministry of Education, Science, Sports and Culture of Japan and the Science Research Promotion Fund of the Japan Private School Promotion Foundation. Partial support for this work was also provided (to H. M.) by the Nissan Chemical Industries Award in Synthetic Organic Chemistry, Japan. H. M. gratefully acknowledges financial support from Takeda Science Foundation and Fujisawa Foundation, Japan.

Notes and references

1 For reviews, see: T. Naito, *Heterocycles*, 1999, **50**, 505; A. G. Fallis and I. M. Brinza, *Tetrahedron*, 1997, **53**, 17543.
2 D. J. Hart and F. L. Seely, *J. Am. Chem. Soc.*, 1988, **110**, 1631; H. Miyabe, C. Ushiro, M. Ueda, K. Yamakawa and T. Naito, *J. Org. Chem.*, 2000, **65**, 176 and references cited therein; M. P. Bertrand, L. Feray, R. Nouguier and P. Perfetti, *J. Org. Chem.*, 1999, **64**, 9189 and references cited therein.
3 H. Miyabe, R. Shibata, M. Sangawa, C. Ushiro and T. Naito, *Tetrahedron*, 1998, **54**, 11 431.
4 P. P. Garner, D. T. Parker, J. J. Gajewski, A. Lubineau, J. Angé, Y. Queneau, I. P. Beletskaya, A. V. Cheprakov, F. Fringuelli, O. Piermatti, F. Pizzo and S. Kobayashi, *Organic Synthesis in Water*, ed. P. A. Grieco, Blackie Academic & Professional, London, 1998.
5 H. Miyabe, M. Ueda and T. Naito, *J. Org. Chem.*, 2000, **65**, 5043.
6 Alkyl radical can be generated *via* sonication of alkyl iodide in the presence of Zn–CuI in water. See: C. Petrier, C. Dupuy and J. L. Luche, *Tetrahedron Lett.*, 1986, **27**, 3149; B. Giese, W. Damm, M. Roth and M. Zehnder, *Synlett*, 1992, 441; P. Erdmann, J. Schäfer, R. Springer, H.-G. Zeitz and B. Giese, *Helv. Chim. Acta*, 1992, **75**, 638.
7 For reviews, see: C. J. Li, *Chem. Rev.*, 1993, **93**, 2023; A. Lubineau, J. Angé and Y. Queneau, *Synthesis*, 1994, 741; C. J. Li, *Tetrahedron*, 1996, **52**, 5643.

Opto-electronic multifunctional chiral diamondoid-network coordination polymer: bis{4-[2-(4-pyridyl)ethenyl]benzoato}zinc with high thermal stability†

Ren-Gen Xiong,[a] Jing-Lin Zuo,[a] Xiao-Zeng You,*[a] Brendan F. Abrahams,[b] Zhi-Ping Bai,[a] Chi-Ming Che[c] and Hoong-Kun Fun[d]

[a] *Coordination Chemistry Institute, State Key Laboratory of Coordination Chemistry, Nanjing University, Nanjing, 210093, P.R. China. E-mail: xyz@netra.nju.edu.cn*
[b] *School of Chemistry, University of Melbourne, Parkville, Victoria 3052, Australia*
[c] *Department of Chemistry, The University of Hong Kong, Pokfulam Road, Hong Kong*
[d] *X-Ray Crystallography Unit, School of Physics, Universiti Sains Malaysia, 11800 Penang*

Received (in Cambridge, UK) 21st June 2000, Accepted 8th September 2000
First published as an Advance Article on the web

A novel 8-fold interpenetration diamondoid-like chiral condensed neutral coordination polymer, bis{4-[2-(4-pyridyl)ethenyl]benzoato}zinc [Zn(PEBA)$_2$] 1, synthesized by the hydrothermal reaction between $Zn(ClO_4)_2{\cdot}6H_2O$ and 4-[2-(4-pyridylethenyl)]benzenecarbonitrile (PEBC), displays very strong blue fluorescent emission and SHG response (*ca.* 1.5 × that of urea) as well as high thermal stability (up to *ca.* 430 °C).

Within the family of blue-luminescent compounds previously used in EL devices or light-emitting diodes (LED), most of them are aromatic organic molecules,[1] conjugated organic polymers,[2] organometallic compounds[3] or metal–chelate compounds such as metal complexes based on 8-hydroxyquinoline, 2-methylquinolin-8-ol, azomethine, azaindole, oxadiazole and bipyridyl derivatives.[4] More recently, boron complexes with 8-hydroxyquinoline derivatives have been shown to display very highly efficient blue-light emission.[5] However, blue-luminescent emission coordination polymers with high thermal stability (up to 400 °C) are, as far as we are aware, relatively rare. Condensed coordination polymers could play a key role in the development of LED materials because one can tune the emission color and stability of the complex readily by manipulating the ligand and the coordination environment around the central atom. Recently, the crystal engineering strategy has been utilized in the construction of acentric diamondoid metal–organic coordination polymers by using asymmetric bridging ligands as building blocks since the utilization of asymmetric ligands can introduce electronic asymmetry (push–pull effect) which is essential for a second harmonic generation (SHG) response.[6,7] However, coordination polymers which display both very strong blue fluorescent emission and SHG response in the solid state still remain, to the best of our knowledge, unexplored. The condensed neutral diamondoid-like coordination polymer, bis{4-[2-(4-pyridyl)-ethenyl]benzoato}zinc (**1**)‡ represents the first example of such materials with strong blue-lumienscent emission and an SGH response (1.5× as that of urea), as well as high stability up to 430 °C.

The three-dimensional polymeric structure of **1** was revealed by an X-ray single crystal diffraction investigation.§ The local coordination environment around Zn1 and Zn2 ions in **1** can best be described as distorted octahedral and tetrahedral, respectively, as shown in Fig. 1. Each asymmetric unit of **1** contains two Zn atom centers in which the Zn1 center coordinates to four oxygen atoms from two different PEBA groups in bidentate chelating mode and to two pyridine nitrogen atoms of two other PEBA groups, resulting in the formation of a distorted octahedral geometry. In contrast to the octahedral coordination of Zn1 centers, the Zn2 center coordinates to two pyridine nitrogen atoms of two PEBA groups and to two carboxylate oxygen atoms of two other PEBA groups in a monodentate fashion. If the chelating carboxylates are treated as one connecting point, Zn1 centers also have a pseudotetrahedral environment. Thus, both Zn1 and Zn2 centers are connected to four Zn centers through PEBA bridges to form a diamondoid-like net (Fig. 1). The crystal contains eight independent interpenetrating diamondoid networks with Zn···Zn separations in each network in the range 15.36–15.49 Å while[6,7] Zn···Zn···Zn angles are in the range 91.7–128.8° which represents a significant distortion from the ideal tetrahedral angle of 109.5° found in diamond. Thus, although the connectivity of the network is the same as diamond, the symmetry is lower. Two schematic representations of the 3D diamond-like network and the eight interpenetrating nets are shown in Fig. 2(a) and (b), respectively. As a result of the unsymmetrical nature of PEBA, **1** crystallizes in a chiral space group *C*2, which belongs to the crystal class 2 where optical activity can occur as specific physical effects.[8] Preliminary experimental results show that **1** displays strong powder SHG efficiencies, *ca.* 1.5× that of urea (see ESI†), probably due to its diamondoid structural type which is similar to that of potassium dideuterophosphate (KDP), the only known nonlinear optical (NLO)-active diamondoid network.[9] On the other hand, the protonated free ligand HPEBA also finds wide applications in second-order NLO films using organic molecular beam deposition techniques. However, because of the absence of strong donor/acceptor substituents in HPEBA, it is unlikely to display a high nonlinearity or substantial SHG response.[10] Thus, **1** combines the advantages of both pure organic and inorganic

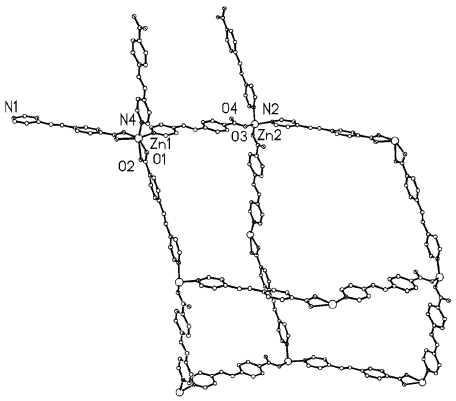

Fig. 1 A chiral diamondoid-like net representation of the coordination polymer [Zn(PEBA)$_2$] **1**. Hydrogen atoms are omitted for clarity. Selected bond lengths (Å) Zn(1)–O(1) 2.088(5), Zn(1)–O(2) 2.297(6), Zn(1)–N(4) 2.085(6), Zn(2)–O(3) 1.953(5), Zn(2)–N(2) 2.077(5).

† Electronic supplementary information (ESI) available: schematic representation of the 8-fold interpenetrating diamondoid-like network and second harmonic generation (SHG) measurements for **1**. See http://www.rsc.org/suppdata/cc/b0/b004980h/

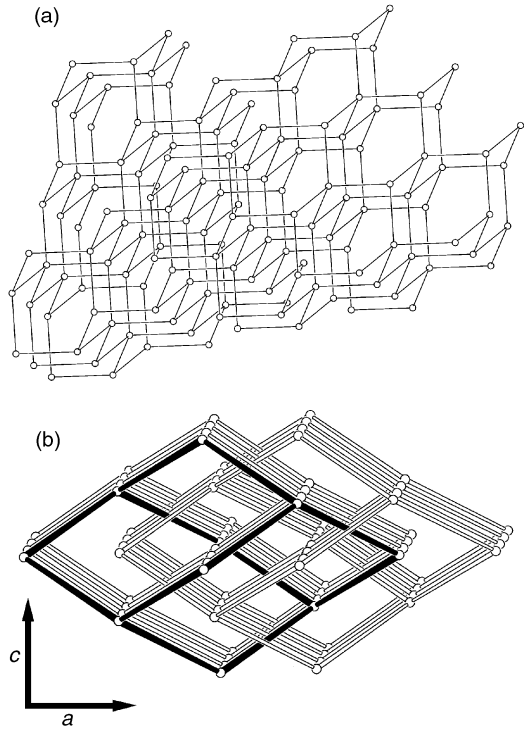

Fig. 2 (a) 3D diamond-like network representation (circles and straight lines denote Zn atoms and PEBA ligands, respectively). The other seven interpenetrating diamandoid nets are omitted for clarity. (b) A schematic representation of the eight interpenetrating diamond nets, with one net highlighted. Three other nets are related by unit cell translations in the *b*-direction. A second set of four nets is related by a translation of 1/2 + *x*, 1/2 + *y*, *z* (see also ESI).

NLO materials and such hybrid inorganic–organic NLO materials have recently been widely investigated as NLO materials.[11]

To study the thermal stability of the compound **1** thermogravimetric analysis (TGA) was performed on a polycrystalline sample, indicating that no strikingly clean weight loss step occurred below 430 °C, indicating that **1** is stable up to this temperature while HPEBA only remains intact up to 350 °C. The most important feature of the structure of **1** is that its three-dimensionally condensed polymeric structure leads to significant enhancement of fluorescent intensity, which is larger than that of free ligand (HPEBA) by a factor of *ca.* 10 (Fig. 3), probably due to the enhanced rigidity of **1**, compared to the free ligand. This phenomenon is similar to that found in Cd(TPT)(PY) (TPT = terephthalato, PY = pyridine).[4] The emission of **1** with λ_{max} = 460 nm is neither MLCT (metal-to-ligand charge transfer) nor LMCT (ligand-to-metal charge transfer) in nature, and can be probably assigned to intraligand fluorescent emission since a weakly similar emission with λ_{max} at 466 nm

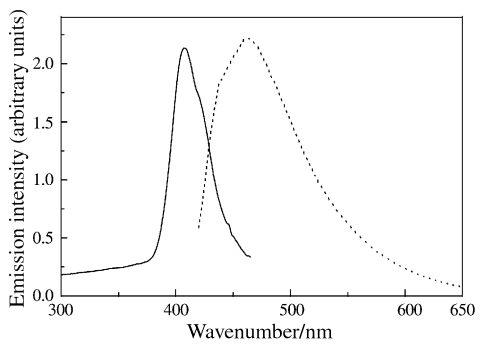

Fig. 3 Fluorescent emission spectrum of **1** in the solid state at room temperature.

is also observed for HPEBA. On the other hand, the diffuse reflectance spectrum of **1** is dominated by an intraligand π–π* transition at 423 nm. The blue fluorescent emission of **1** suggests that it may be used as an advanced material for blue LED devices. Condensed coordination polymer **1** appears to be an excellent candidate since, in addition to its high thermal stability and SHG response, it is virtually insoluble in most solvents such as ethanol, chloroform, ethyl acetate, acetone, acetonitrile, benzene and water.

This work was funded by The Major State Basic Research Development Program (Grant No. G2000077500) and the National Natural Science Foundation of China as well as the Distinguished Young Scholar Fund to C. M. C. from the National Natural Science Foundation of China (NSF29929001). F. H. K. thanks the Malaysian Government R&D Grant 305/pfizik/610942.

Notes and references

‡ *Preparation* of $Zn(PEBA)_2$ **1**: hydrothermal treatment of $Zn(ClO_4)_2{\cdot}6H_2O$ (1.2 mmol), PEBC (1 mmol), pyridine (1 ml) and water (10 ml) for 2 days at 140 °C gave a yellowish platy crystalline product (single pure phase).[12] The yield of **1** *ca.* 35% based on PEBC. Anal. Calc. for $C_{18}H_{20}N_2O_4Zn$: C, 65.50; H, 3.90; N, 5.46 . Found: C, 65.35; H, 4.02; N, 5.62%. IR(KBr, cm^{-1}): 3448br, 3014w, 1737m, 1718m, 1613s, 1549m, 1498w, 1416m (sh), 1373s, 1226m, 1216m, 1177w, 1071w, 1024m, 983w, 854m, 814m, 774m, 684m, 542m.

§ *Crystal data* for **1**: $C_{28}H_{20}N_2O_4Zn$, monoclinic, space group *C*2, a = 21.4550(2), b = 8.8584(2), c = 13.2661(1) Å, β = 93.8150(10)°, V = 2515.73(7) $Å^3$, Z = 4, M = 513.83, D_c = 1.357 Mg m^{-3}, R_1 = 0.0565, wR_2 = 0.1638 (4927 reflections). T = 293 K, μ = 1.012 mm^{-1}. Flack parameter value χ = 0.08(2). CCDC 182/1776. See http://www.rsc.org/suppdata/cc/b0/b004980h/ for crystallographic files in .cif format.

1 C. W. Tang and S. A. VanSlyke, *Appl. Phys. Lett.*, 1987, **51**, 913; C. W. Tang, S. A. VanSlyke and C. H. Chen, *J. Appl. Phys.*, 1989, **65**, 3611; C. H. Chen, J. Shi and C. W. Tang, *Macromol. Symp.*, 1997, **125**, 1.
2 R. H. Friend, R. W. Gymer, A. B. Holms, J. H. Burroughes, R. N. Marks, C. Taliani, D. C. Bradley, D. A. Dos Santos, J. L. Brédas, M. Lögdlund and W. R. Salaneck, *Nature*, 1999, **397**, 121.
3 W.-Y. Wong, K.-H. Choi and K.-W. Cheah, *J. Chem. Soc., Dalton Trans.*, 2000, 113.
4 N.-X. Hu, M. Esteghamatian, S. Xie, Z. Popovic, A.-M. Hor, B. Ong and S. Wang, *Adv. Mater.*, 1999, **11**, 1460; Q. Wu, M. Esteghamatian, N.-X. Hu, Z. Popovic, G. Enright, S. R. Breeze and S. Wang, *Angew. Chem., Int. Ed.*, 1999, **38**, 985; K.-Y. Ho, W.-Y. Yu, K.-K. Cheung and C.-M. Che, *Chem. Commun.*, 1998, 2101.
5 T. Noda, Y. Shirota and Y. Chujo, *J. Am. Chem. Soc.*, 1998, **120**, 9714; N. Matsumi, K. Naka and Y. Chujo, *J. Am. Chem. Soc.*, 1998, **120**, 5112; X. T. Tao, H. Suzuki, T. Wada, S. Miyata and H. Sasabe, *J. Am. Chem. Soc.*, 1999, **121**, 9447.
6 O. R. Evans, R.-G. Xiong, Z. Wang, G. K. Wong and W. Lin, *Angew. Chem., Int. Ed.*, 1999, **38**, 536; K. A. Hirsch, S. R. Wilson and J. S. Moore, *Chem.-Eur. J.*, 1997, **3**, 765.
7 S. R. Batten and R. Robson, *Angew. Chem., Int. Ed.*, 1998, **37**, 1461; M. J. Zaworotko, *Chem. Soc. Rev.*, 1994, 283; K. A. Hirsch, R. S.Wilson and J. S. Moore, *Chem.-Eur. J.*, 1997, **3**, 765; O. Ermer, *J. Am. Chem. Soc.*, 1988, **110**, 3747.
8 T. Hahn and H. Klapper, *International Tables for Crystallography*, Reidel, Dordrecht, The Netherlands, 1993, Vol. A, ch. 10.5, p. 780; S. K. Kurtz and T. T. Perry, *J. Appl. Phys.*, 1968, **39**, 3798.
9 S. Endo, T. Chino, S. Tsuboi and K. Koto, *Nature*, 1989, **340**, 452; B. C. Frazer and R. Pepnsky, *Acta Crystallgr.*, 1953, **6**, 273.
10 C. Cai, M. M. Bösch, B. Müller, Y. Tao, A.Kündig, C. Bosshard, Z. Gan, I. Biaggio, I. Liakatas, M. Jäger, H. Schwer and P. Günter, *Adv. Mater.*, 1999, **11**, 745; C. Cai, B. Müller, J. Weckesser, J. V. Barth, Y. Tao, M. M. Bösch, A. Kündig, C. Bosshard, I. Biaggio and P. Günter, *Adv. Mater.*, 1999, **11**, 750.
11 C. Janiak, T. G. Scharmann, P. Albrecht, F. Marlow and R. Macdonald, *J. Am. Chem. Soc.*, 1996, **118**, 6307; H. Zhang, X. Wang and B. K. Teo, *J. Am. Chem. Soc.*, 1996, **118**, 11 813; W. Lin, O. R. Evans, R.-G. Xiong and Z. Wang, *J. Am. Chem. Soc.*, 1998, **120**, 13 272.
12 R.-G. Xiong, S. R. Wilson and W. Lin, *J. Chem. Soc., Dalton Trans.*, 1998, 4089; R.-G. Xiong, J.-L. Zuo, X.-Z. You, H.-K. Fun and S. S. S. Raj, *New J. Chem.*, 1999, **23**, 1108; O. R. Evans, Z. Wang, R.-G. Xiong, B. M. Foxman and W. Lin, *Inorg. Chem.*, 1999, **38**, 2969.

Highly efficient sensitization of nanocrystalline TiO_2 films with styryl benzothiazolium propylsulfonate

Zhong-Sheng Wang, Fu-You Li and Chun-Hui Huang*

State Key Laboratory of Rare Earth Materials Chemistry and Applications, Peking University–The University of Hong Kong Joint Laboratory in Rare Earth Materials and Bioinorganic Chemistry, Peking University, Beijing 100871, P. R. China. E-mail: hch@chemms.chem.pku.edu.cn

Received (in Cambridge, UK) 7th August 2000, Accepted 18th September 2000
First published as an Advance Article on the web

Near 100% of maximum incident photon-to-electron conversion efficiency (IPCE) and > 15 mA cm^{-2} of short-circuit photocurrent under 94.6 mW cm^{-2} simulated solar light from a xenon lamp were obtained from a thin layer sandwich-type solar cell based on a 2-[4-bis(methyl)aminostyryl]benzothiazolium propylsulfonate (BTS) sensitized nanocrystalline TiO_2 film.

Dye-sensitized nanocrystalline TiO_2 is a promising material for solar cell applications since it is expected to be fabricated at a relatively low cost and can generate efficiencies of up to 10%.[1–3] The most efficient charge transfer sensitizers employed so far are polypyridyl-type complexes of ruthenium[2–4] that have been widely studied in the past ten years.[5,6] Pure organic dyes, owing to their small size, large extinction coefficients and much lower cost, are also promising sensitizers. However, with poor solar energy conversion efficiency (η) below 1%, they are insufficient for solar cell applications.[7,8] Recently Arakawa and coworkers reported that some efficient merocyanine dyes generated 4.2% overall yield on a porous TiO_2 electrode,[9] which suggests good application prospects of these organic dyes on Grätzel cells. Our previous work centered on the photoelectric conversion of hemicyanine derivatives with a π-conjugation bridge between the donor and acceptor groups (D-π-A), and some promising dyes have been selected by molecular design and use of the Langmuir-Blodgett technique.[10–12] In order to advance the development of the Grätzel cell, it is worthwhile to investigate the sensitization of nanocrystalline TiO_2 with pure organic dyes, such as hemicyanine derivatives. Here, we report an outstanding organic sensitizer for nanocrystalline TiO_2 films. A thin layer sandwich-type solar cell fabricated with this dye-modified nanocrystalline TiO_2 film generated an exceptional, high IPCE near unity between 480 and 500 nm and 15.1 mA cm^{-2} of short-circuit photocurrent, amongst the highest values reported so far.[1–3,7–9]

2-[4-Bis(methyl)aminostyryl]benzothiazolium propylsulfonate (BTS) (Fig. 1) was synthesized[12,13] by condensing its methyl azolium propylsulfonate precursor with 4-[bis(methyl)-amino]benzaldehyde. [Elemental analysis: found (calc. for $C_{20}H_{22}N_2S_2O_3{\cdot}H_2O$): C, 56.73 (57.12); H, 5.86 (5.75); N, 6.54 (6.66)%]. The absorption and fluorescence emission spectra of BTS were measured in chloroform solution. While the absorption peak in the visible region is at 557 nm, the maximum of the fluorescence is located at 590 nm. Interestingly, the emission is entirely quenched when BTS is adsorbed onto a nanocrystalline TiO_2 film, indicating efficient electron injection from the excited singlet state of the dye into the conduction band (CB) of TiO_2. Cyclic voltammetry of BTS in MeCN was measured using $LiClO_4$ as supporting electrolyte. The oxidation and reduction potentials are 0.87 and 0.80 V (*vs.* SCE), respectively, from which $E_{1/2}$ is derived to be 0.84 V (*vs.* SCE). When BTS is adsorbed onto a TiO_2 film, the absorption threshold is extended to *ca.* 700 nm. Combining the redox potential with the absorption threshold of BTS, the first excited state level of BTS is estimated to be −0.93 V (*vs.* SCE), above the flat band potential (−0.90 V *vs.* SCE) of nanocrystalline TiO_2 film in aprotic solvent containing no less than 0.1 M Li^+ ion.[14] Therefore, one can conclude that electron injection from the excited dye molecules to the CB of TiO_2 is thermodynamically possible. A 7 μm-thick nanocrystalline TiO_2 film,[2] coated onto conducting glass (fluorine doped SnO_2 sheet, resistance 20 Ω per square), was protonated by soaking for 2 h in a HCl solution at pH 2 and dried in a hot air flow before dipping it in a 1×10^{-4} M solution in chloroform for 4 h. The visible band in the absorption spectrum of BTS on TiO_2 film is red shifted by 12 nm with the half width increased from 55 to 90 nm upon previous treatment of the TiO_2 film with HCl solution, as seen in Fig. 2(a) and (b). These changes are favorable to photoelectric conversion. It is of note that HCl treatment does not significantly affect the adsorbed quantity of BTS on the TiO_2 [Fig. 2(a) and (b)]; the height of the absorption peak remains almost the same while the shape of spectrum changes drastically upon treating the TiO_2 film with HCl solution.

The photocurrent action spectra are shown in Fig. 2(c) and (d) where IPCE is plotted as a function of wavelength. After HCl treatment, IPCE values are increased by more than 50% between 400 and 700 nm with respect to the untreated TiO_2 film, but remain almost unchanged above 700 nm. Obviously, IPCE is improved remarkably upon HCl pretreatment of the TiO_2 film. The surface of nanocrystalline TiO_2 is hydroxylated

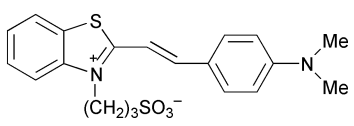

Fig. 1 Schematic structure of BTS.

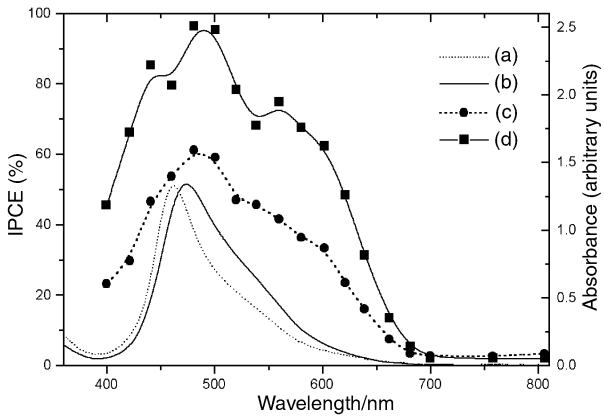

Fig. 2 Absorption spectra of BTS on nanocrystalline TiO_2 film (2 μm), corrected for the absorption of TiO_2 film and the conducting glass support: (a) untreated TiO_2 film and (b) HCl pretreated TiO_2 film. Photocurrent action spectra for BTS-coated nanocrystalline TiO_2 film (7 μm): (c) untreated TiO_2 film and (d) HCl pretreated TiO_2 film. A sandwich-type cell configuration was used to measure the action spectra. The redox electrolyte was 0.5 M LiI–0.05 M I_2 in propylene carbonate solvent. IPCE data were corrected for the absorption of the conducting glass.

DOI: 10.1039/b006427k

under preparation conditions.[15] BTS, which is adsorbed onto TiO_2 *via* coordination bonds between RSO_3^- and Ti^{4+},[2] may show a weakened interaction due to the repulsive force between RSO_3^- and deprotonated hydroxyl groups on neutral TiO_2. However, after pretreatment of the nanocrystalline TiO_2 film with HCl solution, the surface of nanocrystalline TiO_2 is protonated which enables BTS to adsorb onto the TiO_2 surface more strongly, which is consequently favorable for electron injection.[15] Another reason for the improvement in performance is that the decrease of flat band potential of nanocrystalline TiO_2 film due to the adsorption of H^+ ion can increase the driving force for electron injection.[14] Under illumination of simulated solar light from a 500 W Xe lamp (Ushio Electric, Japan), while a sandwich-type solar cell fabricated with this dye-sensitized nanocrystalline TiO_2 film in conjunction with a 0.5 M LiI–0.05 M I_2 redox electrolyte in propylene carbonate (PC) generated 9.0 mA cm^{-2} of short-circuit photocurrent (I_{sc}), 413 mV open-circuit photovoltage (V_{oc}) and 0.410 for the fill factor (FF) with an overall yield (η) of 1.6%, a value of 2.1% for η (15.1 mA cm^{-2} I_{sc}, 410 mV V_{oc} and 0.315 FF) was obtained from a HCl treated film under the same conditions. It is interesting that while V_{oc} remains almost unchanged, I_{sc} is increased by 68% upon HCl pretreatment of the nanocrystalline TiO_2 film. It is believed that the overall yield will be greatly improved after optimization of FF and V_{oc}.[2] The maximum IPCE and short-circuit photocurrent are the highest values among pure organic sensitizers so far studied.[9] For stability examination, this solar cell was illuminated with 94.6 mW cm^{-2} white light from a xenon lamp for 10 h, and the short-circuit photocurrent was almost unchanged after this period. Longer-term tests will be studied in detail.

Our results indicate that hemicyanine derivatives are promising sensitizers for solar cell applications. The notable improvement of photoelectric properties upon treating nanocrystalline TiO_2 film with HCl solution indicates that surface treatment is very important in photoelectric conversion. Preliminary experimental results show that this method for surface treatment of TiO_2 can also improve performance parameters for other hemicyanine dyes containing SO_3^- groups. Therefore, these findings open up a new pathway for designing new efficient sensitizers and aid the development of the Grätzel cell. As the cost of hemicyanine-group dye is much lower than that of ruthenium polypyridine complexes, the overall cost of dye-sensitized solar cells could be further reduced. Detailed study of BTS is now in progress.

The State Key Program of Fundamental Research (G 1998061310), the NNSFC (20023005 and 59872001), and Doctoral Program Foundation of High Education (99000132) are gratefully acknowledged for financial support of this work.

Notes and references

1 B. O'Regen and M. Grätzel, *Nature*, 1991, **353**, 737.
2 M. K. Nazeeruddin, A. Kay, I. Rodicio, R. Humphry-Baker, E. Müller, P. Liska, N. Vlachopoulos and M. Grätzel, *J. Am. Chem. Soc.*, 1993, **115**, 6382.
3 P. Péchy, F. P. Rotzinger, M. K. Nazeeruddin, O. Kohle, S. M. Zakeeruddin, R. Humphry-Baker and M. Grätzel, *J. Chem. Soc., Chem. Commun.*, 1995, 65.
4 Z.-S. Wang, C.-H. Huang, B.-W. Zhang, Y.-J. Hou, P.-H. Xie, H.-J. Qian and K. Ibrahim, *New J. Chem.*, 2000, **24**, 567.
5 D. Cahen, G. Hodes, M. Grätzel, J. F. Guillemoles and I. Riess, *J. Phys. Chem. B*, 2000, **104**, 2053.
6 S. Södergren, A. Hagfelt, J. Olsson and S.-E. Lindquist, *J. Phys. Chem.*, 1994, **98**, 5552.
7 H. Tsubomura, M. Mastumura, Y. Nomura and T. Amamiya, *Nature*, 1976, **261**, 402.
8 K. Sayama, M. Sugino, H. Sugihara, Y. Abe and H. Arakawa, *Chem. Lett.*, 1998, 753.
9 K. Sayama, K. Hara, N. Mori, M. Satsuki, S. Suga, S. Tsukagoshi, Y. Abe, H. Sugihara and H. Arakawa, *Chem. Commun.*, 2000, 1173.
10 A.-D. Lang, J. Zhai, C.-H. Huang, L.-B. Gan, Y.-L. Zhao, D.-J. Zhou and Z.-D. Chen, *J. Phys. Chem. B*, 1998, **63**, 4240.
11 F.-Y. Li, J. Zheng, C.-H. Huang, L.-P. Jin, J.-Y. Zhuang, J.-Q. Guo, X.-S. Zhao and T.-T. Liu, *J. Phys. Chem. B*, 2000, **104**, 5090.
12 J. Zheng, D.-G. Wu, J. Zhai, C.-H. Huang, W.-W. Pei and X.-C. Gao, *Phys. Chem. Chem. Phys.*, 1999, **1**, 2345.
13 A. Hassner, D. Birnbaum and L. M. Loew, *J. Org. Chem.*, 1984, **49**, 2546.
14 G. Redmond and D. Fitzmaurice, *J. Phys. Chem.*, 1993, **97**, 1426.
15 A. Hagfeldt and M. Grätzel, *Chem. Rev.*, 1995, **95**, 49.

ChemComm

P–N bond formation as a route to highly electron rich phosphine ligands

Matthew L. Clarke, David J. Cole-Hamilton, Alexandra M. Z. Slawin and J. Derek Woollins*

School of Chemistry, University of St. Andrews, St. Andrews, Fife, UK KY16 9ST. E-mail: jdw3@st-andrews.ac.uk

Received (in Cambridge, UK) 7th June 2000, Accepted 18th September 2000
First published as an Advance Article on the web

Phosphines containing two N-bound pyrrolidine groups and one alkyl or aryl group are unusually electron rich σ-donor ligands when compared to either tris(*N*-pyrrolidinyl)phosphine or trialkyl- and triaryl-phosphines.

One of the many attractive features of phosphine ligands is their wide range of electronic properties.[1,2] Metal complexes of strongly electron donating alkyl phosphines undergo many reactions which are not possible with aryl phosphines,[3] and these types of metal complexes have recently found important applications in homogenous catalysis.[4–6] Tris(alkylamino)-phosphines are strongly electron donating phosphine ligands. The high basicity (σ-donor strength) of the P atom is thought to arise from donation towards the P from the N lone pair. X-Ray crystal structures of tris(alkylamino)phosphines and their metal complexes[2,7] show these ligands to contain two short P–N bonds with planar N, and one long P–N bond with a non-planar N atom (**1** and **2**). This suggested to us that only two of the N lone pairs could donate electron density towards P, while the third N substituent acts merely as an electronegative atom bound to the P, and therefore reduces the overall basicity of the phosphine.

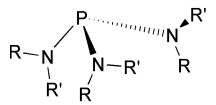

1

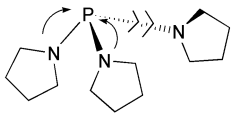

2

If this were the case, a 'hybrid' ligand that contains one electron donating alkyl group and two electron donating amino groups might be an extremely electron rich phosphine ligand, and have numerous applications in catalysis. Here, we describe the preparation of these new di(*N*-pyrrolidinyl)alkylphosphines and preliminary experiments which suggest that the new phosphine ligands are amongst the most electron rich phosphines known.

The aminophosphines described in this study were prepared by the addition of an excess of pyrrolidine to the appropriate phosphine dichloride (pyrrolidine was chosen as it is a very basic secondary amine) (Scheme 1).

^{31}P and ^{1}H NMR spectra of the air and moisture sensitive phosphine products showed them to be 90–98% pure, and they were therefore purified no further. They were further characterised by their conversion to the metal complexes described below. Molloy and Petersen have previously prepared tris(*N*-pyrrolidinyl)phosphine and shown it to be a highly electron rich ligand, in contrast to tris(*N*-pyrrolyl)phosphine which has exceptional π-acceptor character. The method they used to gauge the electronic characteristics of their ligands was measurement of ν_{CO} in the IR spectrum of the *trans*-$(R_3P)_2Rh(CO)Cl$ complexes. These are readily formed in high purity from $[Rh(CO)_2Cl]_2$ and an excess of ligand.[8] As the position of ν_{CO} in these complexes is known for a huge variety

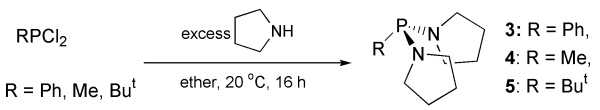

Scheme 1

of phosphines (and is always in agreement with the expected σ-donor strength of the phosphine) this does seem to be an excellent spot test to gauge the donor characteristics of a particular phosphine.

As can be seen from Table 1, the position of ν_{CO} for $PhMe_2P$ is, as expected, in between electron rich Me_3P and the less basic Ph_3P. PhP(*N*-pyrr)$_2$, however, has ν_{CO} at lower wavenumber than P(*N*-pyrr)$_3$, and therefore can be assumed to be a more electron rich ligand. This is evidence [along with the properties of MeP(*N*-pyrr)$_2$ and Bu^{t}P(*N*-pyrr)$_2$] that only two pyrrolidinyl groups can contribute towards the strong donor strength of *N*-pyrrolidinyl phosphines. The values of ν_{CO} for MeP(*N*-pyrr)$_2$ and Bu^{t}P(*N*-pyrr)$_2$ are significantly lower than those of most other highly electron rich alkylphosphines (compare entries 11 and 12 to 5 and 6) which are often applied in catalysis. Tri-*tert*-butylphosphine, which is generally thought of as the most electron donating phosphine, actually forms a tetrahedral $(R_3P)_2Rh(CO)Cl$ complex and cannot be directly compared.[13] The new ligands may be of particular use as they deliver a donor strength that is normally reserved for very bulky ligands, as defined by their large cone angle. It is expected that the ligands **3**–**5** (especially **4**) will have relatively small cone angles. We also note here that iron(II) complexes of type $CpFe(CO)I(PR_3)$ can also be prepared from the four *N*-pyrrolidinyl phosphines by the method of Colville *et al.*[14] The position of ν_{CO} in the IR spectrum of these four compounds is less informative than the Rh compounds, but is at significantly lower wavenumber than the iron complexes of Ph_3P, $PhMe_2P$ or Bz_3P.

Finally, we have also characterised the dichloroplatinum complexes, $(R_3P)_2PtCl_2$, of the four *N*-pyrrolidinyl phosphines $[(pyrr)_3P]_2PtCl_2$ **6**, $[(pyrr)_2PhP]_2PtCl_2$ **7**, $[(pyrr)_2MeP]_2PtCl_2$ **8** and $[(pyrr)_2Bu^tP]_2PtCl_2$ **9**. These are formed quantitatively from $Pt(cod)Cl_2$ and 2 equivalents of phosphine. The sizes of $^1J_{PPt}$ reflect the reduction in coupling constant observed when a phenyl group is replaced by an alkyl group, and the increased size of $^1J_{PPt}$ observed for compounds containing P–N or P–O bonds.[8] The molecular structures[15] (determined by X-ray crystallography) of $[P(N\text{-pyrr})_3]_2PtCl_2$ and $[MeP(N\text{-pyrr})_2]_2PtCl_2$ are shown in Fig. 1 and 2, respectively.

Table 1 Comparison of ν_{CO} of *trans*-$L_2Rh(CO)Cl$ complexes for pyrrolidine based ligands with other phosphines

Entry	L	υ_{CO}[a] [$L_2Rh(CO)Cl$]	Ref.
1	$(PhO)_3P$	(2016)	9
2	$(p\text{-}CF_3C_6H_4)_3P$	(1990)	2
3	Ph_3P	1965 (1966)	2[b]
4	$PhMe_2P$	(1965)	10
5	Me_3P	(1960)	2
6	Et_3P	(1956)	11
7	Cy_3P	1943 (1942)	12[b]
8	$P(NMe_2)_3$	(1959)	2
9	P(*N*-pyrr)$_3$[c]	1951 (1952)	[b,d]2
10	PhP(*N*-pyrr)$_2$	1949	[b,d]
11	MeP(*N*-pyrr)$_2$	1947	[b,d]
12	Bu^{t}P(*N*-pyrr)$_2$	1942	[b,d]

[a] To ensure the accuracy and validity of our values, we have reprepared *trans*-$(R_3P)_2Rh(CO)Cl$ complexes of (*N*-pyrr)$_3$P, Ph_3P and Cy_3P. The values quoted above are those found on our spectrometer (lit. values in parentheses). [b] IR spectra recorded as KBr discs. [c] pyrr = pyrrolidinyl. [d] This work.

DOI: 10.1039/b004893n

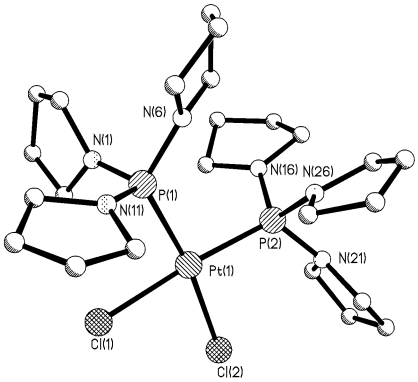

Fig. 1 Ball and stick representation of $[P(N\text{-pyrr})_3]_2PtCl_2$ **6**. Selected bond lengths (Å) and angles (°): Pt–P(1) 2.246(3), Pt–P(2) 2.270(3), Pt–Cl(1) 2.398(3), Pt–Cl(2) 2.371(3); P(2)–Pt–P(1) 98.24(10), Cl(2)–Pt–Cl(1) 85.08(11).

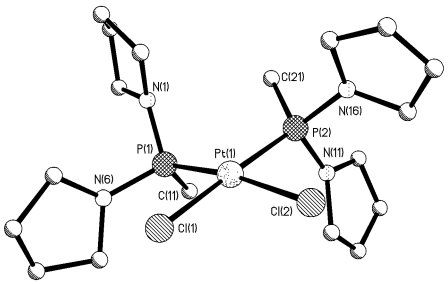

Fig. 2 Ball and stick representation of $[MeP(N\text{-pyrr})_2]_2PtCl_2$ **8**. Selected bond lengths (Å) and angles (°): Pt–P(1) 2.226(2), Pt–P(2) 2.255(2), Pt–Cl(1) 2.372(2), Pt–Cl(2) 2.391(2); P(2)–Pt–P(1) 93.37(7), Cl(1)–Pt–Cl(2) 86.14(8).

The X-ray structure of *trans*-$[P(N\text{-pyrr})_3]_2Rh(CO)Cl$ [2] shows two of the pyrrolidine rings in a given $P(N\text{-pyrr})_3$ fragment to have planar N atoms (sum of angles around N = 354–360°) and one tetrahedral N atom (sum of angles around N = 347, 350°) with a 0.02 Å longer P–N bond length [av. 1.667(3) *vs*. 1.688(3) Å]. We therefore expected the crystal structure of $[P(N\text{-pyrr})_3]_2PtCl_2$ to show this phenomenon. The crystal structure of $[P(N\text{-pyrr})_3]_2PtCl_2$ shows the expected *cis* square planar Pt complex, but to our surprise, the sum of angles around each N was similar (356–360°) and planar. The P–N bond lengths [1.628(10), 1.721(11), 1.642(11), 1.659(10), 1.678(12) and 1.678(9) Å] do not show any particular pattern.

The crystal structure of $[MeP(N\text{-pyrr})_2]_2PtCl_2$ **8** has two independent molecules in each unit cell, but there are no drastic differences between the two molecules. Complex **8** shows a similar coordination environment to complex **6**, with fairly similar Pt–Cl and Pt–P bond lengths. The angle P(1)–Pt(1)–P(2) between the phosphines is considerably smaller than in complex **6** [93.90(8), 93.37(7) *vs*. 98.24(10)°], and indicates that $MeP(N\text{-pyrr})_2$ is less sterically demanding than $P(N\text{-pyrr})_3$. As a result of this, the angle between the Cl ligands is slightly larger in complex **8** [87.01(9), 86.14(8) *vs*. 85.08(11)°]. The bond lengths and angles about the N atoms are again somewhat surprising. Each phosphine has one planar N (sum of angles from the four phosphine ligands in the two independent molecules: 356.6, 359.5, 359.5, 356.4°), and in each of the four phosphine molecules present, the other N atom shows a slight tetragonal distortion (sum of angles: 353.3, 353.5, 354.0, 351.8°), and slightly longer P–N bond length [average bond lengths: 1.683(6) *vs*. 1.643(7) Å].

The crystallographically determined cone angles of $P(pyrr)_3$ and $MeP(pyrr)_2$ are 122 and 110°, respectively. These values refer to 2/3 of the sum of the largest possible angle observed between the Pt centre and the centre H atoms on the phosphine substituents. This value differs from the Tolman cone angle (determined by molecular modelling) by using the centre of the H atom and the real Pt–P bond length. It is also likely to differ due to the volume of space occupied by the phosphine being partly determined by the coordination environment provided by the Pt. The values obtained clearly confirm the smaller size of ligand **4** with respect to ligand **2**. It has been estimated that the Tolman cone angle of **2** is 145°.[2]

The crystal structure of **6** reveals different structural features to the other crystal structure studies of tris(dialkylamino)phosphines. This may suggest that the bonding observed in these compounds is slightly more subtle than we originally supposed, and could also be related to the exact coordination environment of the ligand. The coordination environment provided by the Pt complex is also likely to have an effect on the ligand structure observed within that of complex **8**. In conclusion, we have prepared three new phosphine ligands and shown them to be especially strong donor ligands. Studies to evaluate the potential uses of these ligands in catalysis are now underway.

We are grateful to the EPRSC for financial support, and the Joint Research Equipment Initiative for an equipment grant.

Notes and references

1 C. A. Tolman, *Chem Rev.*, 1977, **77**, 313; Md. M. Rahman, H.-Y. Lie, K. Eriks, A. Prock and W. P. Giering, *Organometallics*, 1989, **8**, 1 and references therein; M. F. Ernst and D. M. Roddick, *Inorg. Chem.*, 1989, **28**, 1624.
2 K. G. Molloy and J. L. Petersen, *J. Am. Chem. Soc.*, 1995, **117**, 7696.
3 M. C. Simpson and D. J. Cole-Hamilton, *Coord. Chem. Rev.*, 1996, **155**, 163 and references therein.
4 Catalytic C–H bond activation: T. Sakakura, T. Sodeyama, K. Sasaki, K. Wada and M. Tanaka, *J. Am. Chem. Soc.*, 1990, **112**, 7221 and references therein.
5 Hydroformylation: J. K. MacDougall, M. C. Simpson, M. J. Green and D. J. Cole-Hamilton, *J. Chem. Soc., Dalton Trans.*, 1996, 1161 and references therein.
6 Pd catalysed substitutions of aryl chlorides: A. F. Littke and G. C. Fu, *J. Org. Chem.*, 1999, **64**, 10; *Angew. Chem., Int. Ed.*, 1999, **38**, 2411; J. P. Wolfe, R. A. Singer, B. H. Yang and S. L. Buchwald, *J. Am. Chem. Soc.*, 1999, **121**, 9550; B. C. Hamann and J. F. Hartwig, *J. Am. Chem. Soc.*, 1998, **120**, 7370.
7 A. H. Cowley, M. Lattman, P. M. Stricklen and J. G. Verkade, *Inorg. Chem.*, 1982, **21**, 453; C. Romming and J. Songstad, *Acta Chem. Scand., Ser. A.*, 1978, **32**, 689; C. Romming and J. Songstad, *Acta Chem. Scand., Ser. A.*, 1979, **33**, 187; C. Romming and J. Songstad, *Acta Chem. Scand., Ser. A.*, 1982, **36**, 665.
8 NMR parameters for Rh and Pt complexes: $[(pyrr)_3P]_2Rh(CO)Cl$: δ 98.5, 146 Hz; $[(pyrr)_2PhP]_2Rh(CO)Cl$: δ 88.2, 136 Hz; $[(pyrr)_2MeP]_2Rh(CO)Cl$: δ 95.2, 130 Hz; $[(pyrr)_2Bu^tP]_2Rh(CO)Cl$: δ 114.6, 133 Hz. Pt complexes: **6**: δ 40.7, 4950 Hz; **7**: δ 46.1, 4358 Hz; **8**: δ 46.4, 4232 Hz; ligand **5** does not give *cis*-L_2PtCl_2 on reaction with $Pt(cod)Cl_2$. A *trans*-L_2PtCl_2 complex can most conveniently be prepared from Zeise's Salt, $K[PtCl_3(C_2H_4)]$ δ 83.5, 2716 Hz.
9 S. Vastag, B. Heil and L. Marko, *J. Mol. Catal.*, 1979, **5**, 189.
10 D. de Montauzon and R. Poilblanc, *J. Organomet. Chem.*, 1975, **93**, 397.
11 S. Franks and F. R. Hartley, *Inorg. Chim. Acta*, 1981, **47**, 235.
12 W. Strohmeier, W. Rehder-Strirnweiss and G. Reischig, *J. Organomet. Chem.*, 1971, **17**, 393.
13 R. L. Harlow, S. A. Westcott, D. L. Thorn and R. T. Baker, *Inorg. Chem.*, 1992, **31**, 323.
14 N. J. Colville, E. A. Darling, A. W. Hearn and P. Johnston, *J. Organomet. Chem.*, 1987, **328**, 375.
15 *Crystal data* for **6**: $C_{24.50}H_{49}Cl_3N_6P_2Pt$, M = 791.08, orthorhombic, a = 18.3979(9), b = 10.7098(6), c = 17.2722(6) Å, U = 3403.3(3) Å^3, T = 293 K, space group $Pna2_1$, Z = 8, μ = 4.476 mm^{-1}, 14076 reflections measured, 4808 independent reflections (R_{int} = 0.0983), Final R_1 = 0.0428, Final $wR(F^2)$ was 0.0929. For **8**: $C_{18}H_{38}Cl_2N_4P_2Pt$, M = 638.45, monoclinic, a = 8.5068(3), b = 26.2926(10), c = 21.6988(8) Å, β = 90.27(1)°, U = 4853.2(3) Å^3, T = 293 K, space group $P2_1/n$, Z = 8, μ = 6.146 mm^{-1}, 21101 reflections measured, 6979 independent reflections (R_{int} = 0.0520), Final R_1 = 0.0366, Final $wR(F^2)$ was 0.0774 (all data). CCDC 182/1778. See http://www.rsc.org/suppdata/cc/b0/b004893n/ for crystallographic files in .cif format.

Electrochemiluminescence of 2′,6′-difluorophenyl 10-methyl-9,10-dihydroacridine-9-carboxylate

Robert Wilson,*[a] Hashem Akhavan-Tafti,[b] Renuka DeSilva[b] and A. Paul Schaap[b]

[a] *Robert Wilson, Department of Chemistry, Liverpool University, Liverpool, UK L69 7ZD. E-mail: R.Wilson@liv.ac.uk*

[b] *Lumigen, Inc., 24485 W. Ten Mile Rd., Southfield, MI 48034, USA. E-mail: aps@lumigen.com*

Received (in Cambridge, UK) 20th April 2000, Accepted 8th September 2000
First published as an Advance Article on the web

Electrochemical oxidation of the acridine ester 2′,6′-difluorophenyl 10-methyl-9,10-dihydroacridine-9-carboxylate yields the corresponding acridinium ester which reacts with H_2O_2 to generate intense chemiluminescence.

Electrochemiluminescence (ECL) has received widespread attention during the previous decade, especially in the field of chemical analysis.[1] It combines the well known sensitivity of chemiluminescence (CL) with the precise control over the time and position of light emitting reactions afforded by electrochemistry. As an alternative approach for conducting immunoassays and nucleotide assays it offers advantages such as increased sensitivity and precision, reduction in time and labor, and the elimination of radioisotopes.[2] In order to exploit the full potential of this technology there is a requirement for new CL compounds which can be initiated electrochemically. In this communication we show for the first time how acridinium ester CL can be triggered by electrochemical oxidation of 2′,6′-difluorophenyl 10-methyl-9,10-dihydroacridine-9-carboxylate (DMC).

Prior to the present communication ruthenium chelates[3] and luminol† derivatives[4] are the only compounds that have been used in a significant number of analytical applications involving ECL. Ruthenium chelates have been used for enzyme assays,[5] but their most significant impact has been as labels for immunoassays[6] and nucleotide assays.[7] Luminol has also been used for enzyme assays[8] and immunoassays.[9] Light is emitted when electrochemically oxidized luminol reacts with H_2O_2, which allows the reaction to be coupled to oxidase enzymes such as glucose oxidase.[10] The latter enzyme has been used as an antibody label in ECL enzyme immunoassays which constitute a further consolidation of existing technology.[9] The chemiluminescence reaction of luminol is also catalyzed by electrochemically oxidized ferrocenes[11] suggesting that these compounds could be used as labels in an ECL system resembling the one based on ruthenium chelates.

Acridinium esters have been used as labels in chemiluminescence immunoassays for many years.[12] The CL reaction of these compounds does not require a catalyst and is usually triggered by addition of an acidic solution of H_2O_2 followed by a NaOH solution. The acidic solution ensures that inactive pseudo-base is converted to the active acridinium ester and the alkali triggers the CL oxidation of the ester by a H_2O_2.[13] Two advantages of these compounds which do not appear to have been fully exploited are freedom from interference in matrices such as whole blood[14] and their ability to intercalate into the double helix of polynucleotides.[12] Intercalation of an acridinium ester into an oligonucleotide duplex shields it from attack by hydroxide and forms the basis of homogenous hybridization protection assays for RNA.[15]

Recently a large number of esters derived from 9,10-dihydroacridines (reduced acridinium esters and thioesters) based on the *N*-alkyldihydroacridinecarboxylate nucleus, including DMC, have been made at Lumigen.[16] These dihydroacridine compounds are stable in the presence of H_2O_2 and do not form an inactive pseudo-base. Light emission can be triggered by oxidising the acridan with horseradish peroxidase (HRP) in the presence of H_2O_2 and an enhancer such as *p*-iodophenol. HRP oxidizes the 9,10-dihydroacridine to the corresponding acridinium ester, which is immediately subject to nucleophillic attack by the peroxide anion (OOH^-) at the 9 position of the acridinium nucleus; the possibility of pseudo-base formation does not arise because peroxide is several orders of magnitude more nucleophillic than hydroxide.[13] Nucleophillic attack results in the formation of a dioxetanone which decomposes to form the singlet excited state of *N*-methylacridone. This relaxes to the ground state accompanied by the emission of intense blue light with a maximum wavelength of 430 nm. By using these compounds as a substrate for HRP it has been possible to detect as little as 0.1 amol of this enzyme in a 15 min assay.[16]

Although there have been several reports of ECL in aqueous solutions involving acridinium esters[17] and the related compound lucigenin[18] they are all based on the reduction of dissolved oxygen to H_2O_2; this has two disadvantages: reliance on dissolved oxygen concentration and the susceptibility of the acridinium ester to pseudo-base formation.[13] These drawbacks are avoided when DMC is used because the acridinium ester is produced *in situ* from a passive precursor.

Cyclic voltammetry and linear sweep voltammetry with luminometric detection were carried out using an experimental arrangement described previously;[11] all potentials *vs.* Ag/AgCl. The concentrations of DMC and the corresponding acridinium ester were 50 and 5 μM respectively. The second cyclic voltammogram (CV) of DMC shown in Fig. 1 has three peaks located at 0.76 V (peak A), −0.25 (peak B) and −0.11 V (peak C). A plot of light intensity at 430 nm against applied potential for DMC in the presence of H_2O_2 (Fig. 2) has a single peak at 0.75 V corresponding closely to the position of peak A in Fig. 1. This suggests that peak A represents the two electron oxidation of DMC to the corresponding acridinium ester as shown in Scheme 1a, which then reacts with H_2O_2 to generate chemiluminescence as shown in Scheme 1b. Peaks B and C in

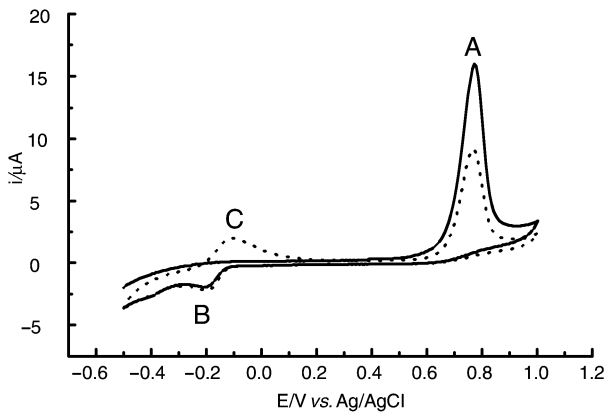

Fig. 1 Two successive cyclic voltammograms of 50 μM DMC in 10 mM Tris buffer with 0.1 M NaCl, 10 mM H_2O_2, and 0.025% Tween-20. Scan rate 100 mV s^{-1}, 1st scan (solid line); 2nd scan (dashed line).

DOI: 10.1039/b003158p

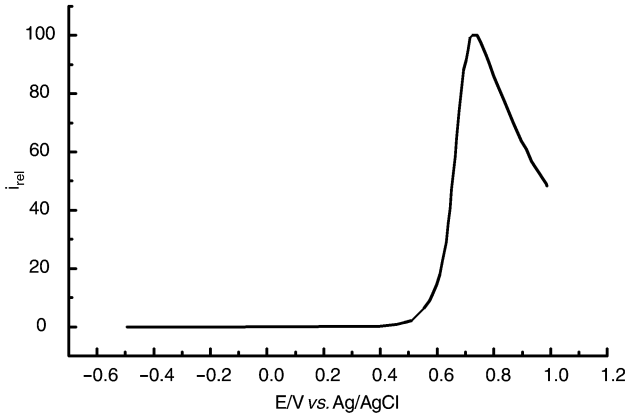

Fig. 2 Dependence of electrochemiluminescence on potential for 50 μM DMC at pH 8.0, in 10 mM Tris buffer with 0.1 M NaCl, 10 mM H_2O_2, 1 mM EDTA and 0.025% Tween-20. Scan rate 10 mV s^{-1}.

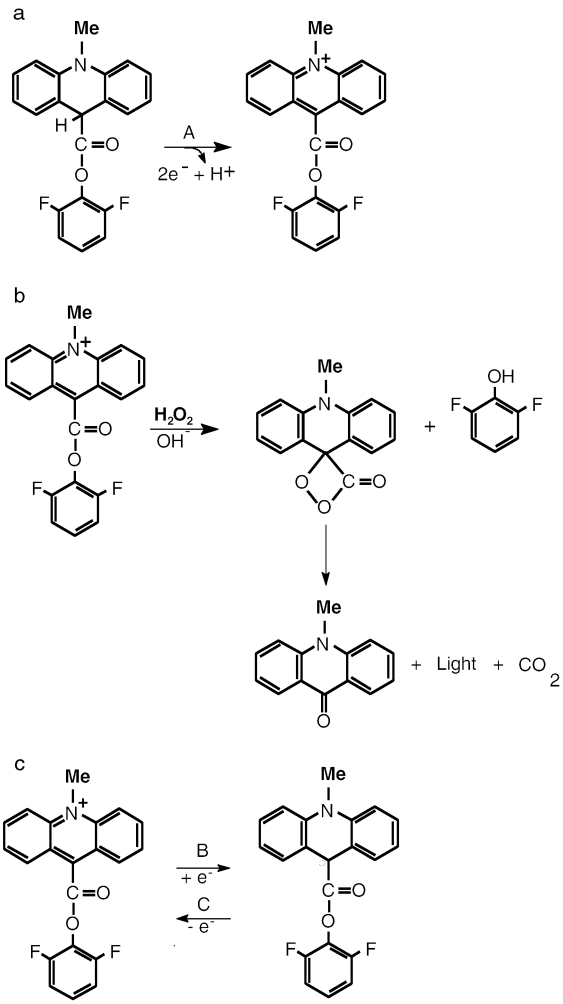

Scheme 1 Large capital letters refer to peaks in CV. (a) Two-electron oxidation of DMC to acridinium ester; (b) CL reaction of acridinium ester with H_2O_2; (c) one-electron redox reactions of acridinium ester/radical couple.

Fig. 1 only appear in the CV after oxidation of DMC and therefore peak B must represent the reduction of an oxidation product. Light emission in the presence of H_2O_2 indicates that an acridinium ester is produced when DMC is oxidized and the simplest explanation for peak B is that it represents reduction of this product as shown in Scheme 1c. This is supported by the observation that peak B is almost absent when a CV is obtained in the presence of H_2O_2, as would be expected if the compound responsible reacts with peroxide. Further investigation of this hypothesis with an authentic sample of the acridinium ester corresponding to DMC[16] gave a CV with two peaks identical to B and C in Fig. 1.

Enzymatic oxidation of DMC by HRP has been reported to occur in two one-electron oxidation steps separated by a non-enzymatic deprotonation.[16] The corresponding electrochemical pathway would be a classic ECE mechanism[19] in which the two enzymatic steps are replaced by electrochemical oxidations. Previous work on acridans, however, has suggested an alternative mechanism in which the second oxidation step occurs in solution as a result of disproportionation between protonated and unprotonated radical intermediates.[20] Further work is required to reveal which mechanism applies to DMC.

We have shown for the first time that CL of the dihydroacridine ester DMC can be triggered by electrochemical oxidation in the presence of H_2O_2. Presently work is in progress to extend this investigation to other 9,10-dihydroacridine esters in order to build up a detailed picture of the mechanism, and the relationship between electrochemiluminescence and molecular structure. ECL of 9,10-dihydroacridines in matrices where light emission from compounds such as luminol is quenched[14] will also be investigated as will the effect of nucleotide duplexes on ECL. The latter investigation is based on the assumption that if intercalation of an acridinium ester into a nucleotide double helix can shield it from hydrolysis it may also shield a 9,10-dihydroacridine ester from oxidation by an electrode.

Notes and references

† The IUPAC name for luminol is 5-amino-2,3-dihydrophthalazine-1,4-dione.

1 A. W. Knight and G. M Greenway, *Analyst*, 1994, **119**, 879; W. Y. Lee, *Mikrochim. Acta*, 1997, **127**, 19; A. W. Knight, *TRAC. Trends Anal. Chem.*, 1999, **18**, 47.
2 D. R. Deaver, *Nature*, 1995, **377**, 758.
3 J. K. Leland and M. J. Powell, *J. Electrochem. Soc.*, 1990, **137**, 3127.
4 S. Sakura, *Anal. Chim. Acta*, 1992, **262**, 49.
5 F. Jameison, R. I. Sanchez, L. Dong, J. K. Leland, D. Yost and M. T. Martin, *Anal. Chem.*, 1996, **68**, 1298.
6 D. L. Gatto-Menking, H. Yu, J. G. Bruno, M. T. Goode, M. Miller and A. W. Zulich, *Biosensors*, 1995, **10**, 501; H. Yu, *J. Immunol. Methods*, 1996, **192**, 163.
7 S. Zhao, U. Consoli, R. Arceci, J. Pfeifer, W. S. Dalton and M. Andreeff, *BioTechniques*, 1996, **21**, 726; C. D. O'Connel, A. Juhasz, C. Kuo, D. J. Reeder and D. S. B. Hoon, *Clin. Chem.*, 1998, **44**, 1161.
8 J. Kremeskötter, R. Wilson, D. J. Schiffrin, B. J. Luff and J. S. Wilkinson, *Meas. Sci. Technol.*, 1995, **6**, 1325; R. Wilson, J. Kremeskötter, D. J. Schiffrin and J. S. Wilkinson, *Biosens. Bioelectron.*, 1996, **11**, 805.
9 R. Wilson, M. H. Barker, D. J. Schiffrin and R. Abuknesha, *Biosens. Bioelectron.*, 1997, **12**, 277.
10 R. Wilson and A. P. F. Turner, *Biosens. Bioelectron.*, 1992, **7**, 165.
11 R. Wilson and D. J. Schiffrin, *Anal. Chem.*, 1996, **68**, 1254; R. Wilson and D. J. Schiffrin, *J. Electroanal. Chem.*, 1998, **448**, 125.
12 I. Weeks, M. Sturges, R. C. Brown and J. S. Woodhead, in *Methods In Enzymology*, ed. M. DeLuca and W. D. McElroy, Academic Press, London, 1986, vol. 133, p. 366; M. J. Pringle, in *Advances In Clinical Chemistry*, ed. H. E. Spiegel, Academic Press, London, 1993, vol. 30, p. 89.
13 I. Weeks, I. Beheshti, F. McCapra, A. K. Campbell and J. S. Woodhead, *Clin. Chem.*, 1983, **29**, 1474; I. Weeks, *Chemiluminescence Immunoassay*, Elsevier, London, 1992, pp. 35–39.
14 F. McCapra, D. Watmore, F. Sumum, A. Patel, I. Beheshti, K. Ramakrishnan and J.Branson, *J. Biolumin. Chemilumin.*, 1989, **4**, 51.
15 N. C. Nelson, P. W. Hammond, W. A. Weise and L. J. Arnold in *Luminescence Immunoassay and Molecular Applications*, ed. K. Van Dyke and R. Van Dyke, CRC Press, Boca Raton, Fl, 1990, p. 293.
16 H. Akhavan-Tafti, K. Sugioka, Z. Arghavani, R. DeSilva, R. S. Handley, Y. Sugioka, R. A. Eickholt, M. P. Perkins and A. P. Schaap, *Clin. Chem.*, 1995, **41**, 1368; H. Akhavan-Tafti, R. DeSilva, Z. Arghavani, R. A. Eickholt, R. S. Handley, B. A. Schoenfelner, K. Sugioka and A. P. Schaap, *J. Org. Chem.*, 1998, **63**, 930.
17 J. S. Littig and T. A. Neeman, *Anal. Chem.*, 1992, **64**, 1140.
18 K. D. Legg and D. M. Hercules, *J. Am. Chem. Soc.*, 1969, **91**, 1902.
19 C. Amatore, M. Gareil and J. M. Savéant, *J. Electroanal. Chem.*, 1983, **147**, 1.
20 P. Hapiot, J. Moiroux and J. M. Savéant, *J. Am. Chem. Soc.*, 1990, **112**, 1337.

Typeset and printed by Black Bear Press Limited, Cambridge, England

ChemComm
FEATURE ARTICLE

Theoretical and experimental aspects of enantiomeric differentiation using natural abundance multinuclear nmr spectroscopy in chiral polypeptide liquid crystals

Muriel Sarfati, Philippe Lesot,* Denis Merlet and Jacques Courtieu*

Laboratoire de Chimie Structurale Organique, Université de Paris-Sud, Bât. 410, ICMO CNRS ESA n°8074, 91405 Orsay cedex, France. E-mail: philesot@icmo.u-psud.fr; courtieu@icmo.u-psud.fr

Received (in Liverpool, UK) 1st August 2000, Accepted 16th August 2000
First published as an Advance Article on the web 18th September 2000

Liquid crystalline organic solutions of poly-γ-benzyl-L-glutamate generate a sufficient differential ordering effect to visualize enantiomers using multinuclear high-resolution NMR spectroscopy at natural isotopic abundance levels. Chiral discrimination can be observed through a difference in the order-sensitive NMR observables, namely: proton–proton, carbon–proton and carbon–carbon residual internuclear dipolar couplings, carbon chemical shift anisotropies, and deuterium quadrupolar splittings. In most cases, the enantiodifferentiation is large enough to allow determation of the enantiomeric excesses satisfactorily. All theoretical considerations and significant experimental parameters that affect the efficiency of this methodology are presented and discussed. The various possible anisotropic NMR techniques provide a very reliable and powerful alternative to the current analytical techniques which operate in the isotropic phase.

Muriel Sarfati was born in Saint Denis, France, in 1974. She received her degree in chemistry in 1998 and is now doing a Ph.D at the University of Paris XI with Dr. P. Lesot and Professor J. Courtieu on natural abundance deuterium NMR spectroscopy in oriented solvents.

Philippe Lesot has been a scientific researcher at the CNRS since 1998. He was born in Paris, France, in 1967. He did his Ph.D at the University of Paris XI under the supervision of Professor J. Courtieu (1992–95). He then received a postdoctoral grant from the Royal Society of Chemistry and joined the Professor J. W. Emsley's NMR group at the Chemistry Department of the University of Southampton (1995–96). In 1997–98 he was appointed as lecturer in Chemistry at the University of Paris XI.

Denis Merlet was born in Etampes, France, in 1970. He received his Ph.D from the University of Paris VII in 1998 (Professor J. Courtieu). He was a postdoctoral fellow of the French Foreign Office and spent one year with the NMR group of Professor J.W. Emsley at Southampton (1998–99). In 1999 he returned to the University of Paris XI to take up his present position as a lecturer in Chemistry.

Jacques Courtieu is Professor of Chemistry at the University of Paris XI since 1983. He was born in Saint-Marcellin, France, in 1944. He sustained a Ph.D thesis at the University of Paris XI (Professor J. Jullien), and subsequently was a postdoctoral fellow of the University of Utah, Salt Lake City, for two years with Professor D. M. Grant's NMR team (1976–78). He is currently Chairman of the Orsay Institute for Molecular Chemistry (I.C.M.O.). In 1999, he has received the Grammaticakis-Neuman award from the French Academy of Sciences.

The research interests of the authors focus mainly on the design and the development of new NMR methodologies using oriented solvents with applications in structural chemistry. Their current work includes the enantiodifferentiation of chiral molecules using 1 D and 2 D NMR spectroscopy in chiral liquid-crystalline media.

Introduction

The sustained interest in enantioselective synthesis and the necessity of providing reliable quality control tests for marketed or new candidate synthetic chiral drugs in the pharmaceutical industry, have strongly stimulated the development of novel, convenient and efficient techniques for enantiomeric purity analysis. Among them NMR spectroscopy is widely used. Various NMR methods using isotropic solvents, nicely reviewed by Parker,[1,2] are available for determining enantiomeric excesses (ee's), but all suffer of a lack of generality. For instance, derivatization of chiral molecules using chiral derivatizing agents requires the presence of a reactive function and great care is required to ensure that neither kinetic resolution nor racemization occur during the derivatization. The preparation of specific complexing agents is needed when using chiral solvating agents dependent on the functional groups in the chiral molecule under study. Also the use of chiral lanthanide shift reagents works only when the enantiomers may complex the paramagnetic center in equilibrium at the NMR timescale. Last, but not least, the final result is not always satisfactory as in almost all cases, only the variation of a chemical shift is utilised for discrimining between isomers.

To provide an alternative when usual isotropic NMR methods fail and to avoid some of their main disadvantages, we have developed an analytical approach based on the use of chiral liquid crystals (CLC). The best results, to date, have been obtained with a chiral anisotropic solvent comprised of a synthetic polypeptide, poly-γ-benzyl-L-glutamate (PBLG), dissolved in various organic solvents such as chloroform, dichloromethane, dimethyl formamide, *etc.*[3–6]

NMR spectra of chiral solutes in this liquid crystalline medium are extremely rich in their information because they are affected not only by the usual scalar couplings and chemical shifts, but also by anisotropic interactions such as dipolar couplings, chemical shift anisotropy (CSA) and if the nuclei have a spin $I > 1/2$, by quadrupolar interactions. It is differences in these anisotropic interactions which provide the chiral discrimination. We have shown that this effect originates from the fact that enantiomers are not oriented in the same manner in this chiral anisotropic medium. The great advantage that this new NMR analytical method has over the more established techniques, which use isotropic solvents, is that

chiral discrimination can be achieved for a very wide range of compounds, including those in which there are no functional groups, such as saturated hydrocarbons. A second important advantage is that there are a number of NMR nuclei which can be exploited, and for a specific molecule there are usually many NMR parameters which can be measured, with varying sensitivities to chirality. In this review, we will illustrate this point through the investigation of a single chiral compound, (±)-1-chloropropan-2-ol [(±)-CP] for which we will show that it is possible to discriminate its *S* and *R* isomers using proton, carbon-13 and deuterium NMR spectroscopy, the enantiodifferentiation being based on a difference in their ^{1}H–^{1}H, ^{1}H–^{13}C residual dipolar couplings, carbon-13 CSA or ^{2}H residual quadrupolar splittings. In addition we will report the first successful enantiomeric discrimination based on differences of ^{13}C–^{13}C residual dipolar couplings.

To introduce chemists to this non-conventional area of NMR spectroscopy, all essential theoretical and practical aspects of NMR in chiral anisotropic solvents, particularly when using the PBLG system, are reviewed. Consequently, this article is not a comprehensive survey of successful results already obtained using this methodology, but is rather intended to describe and assess the respective pratical interests of various 1D and 2D multinuclear NMR tools in natural isotopic abundance systems that have been used or specifically developed to visualize enantiomers dissolved in the PBLG phase. Thus, all experimental parameters or useful details that can affect the efficiency of each of the NMR tools proposed will be examined and discussed. It is important to emphasise that all NMR spectra of (±)-CP reported in this work were obtained in natural isotopic abundance.

NMR in chiral oriented solvents: background

Since the pioneering work of Snyder and coworkers, it is known that enantiomers may give different NMR spectra when dissolved in a chiral anisotropic material.[7,8] This situation arises because the difference in the enantioselective interactions between the *S* and *R* isomers and the CLC generally generates a sufficient differential ordering effect (DOE) to discriminate between them using order-sensitive NMR observables.[9,10] These various observables, which are averaged to zero due to the isotropic motion of solutes in the liquid state, are the chemical shift anisotropy, ($\Delta\sigma_i$), the spin–spin coupling anisotropy (ΔT_{ij}) and the quadrupolar splitting for spin $I > 1/2$ nuclei ($\Delta\nu_{Q_i}$).[11] It should be noted that (ΔT_{ij}) is due to the purely anisotropic dipolar couplings (D_{ij}) and to the anisotropy of the scalar coupling, (ΔJ_{ij}), the latter being generally considered small in comparison to D_{ij}. In the following, we will assume that ΔJ_{ij} is negligible, thus reducing ΔT_{ij} to D_{ij}. A rough classification of the sensitivity of these anisotropic interactions towards the DOE of enantiomers indicates that $|\Delta\nu_{Q_i}| > |\Delta T_{ij}| > |\Delta\sigma_i|$.[11]

The analysis of NMR spectra obtained in CLC differs from their isotropic analogues, but the numerous anisotropic interactions provide interesting tools as far as enantiodiscrimination is concerned. Regarding the various active NMR nuclei intrinsically included in any chiral organic compounds and their natural magnetic properties, namely, ^{1}H ($I = 1/2$, 99.985%), ^{13}C ($I = 1/2$, 1.108%) and ^{2}H ($I = 1$, 0.015%), it appears that, theoretically, there are ten possible NMR observables for detecting the DOE, namely $\Delta\sigma_H$, $\Delta\sigma_C$, $\Delta\sigma_D$, ΔT_{HH}, ΔT_{HD}, ΔT_{DD}, ΔT_{CC}, ΔT_{CH}, ΔT_{CD} and $\Delta\nu_{QD}$. However, some of these will not provide an efficient tool for our purpose because the weakness of the natural isotopic abundance of the involved nuclei. For instance, the present sensitivities of routine spectrometers do not permit the observation of ΔT_{CD} or ΔT_{DD}, in natural abundance NMR. In contrast, when enantiomers under investigation exhibit other X-active nuclei of spin $I = 1/2$ (fluorine-19, phosphorus-31,…) or $I > 1/2$ (boron-10, boron-11,…), additional NMR observables such as $\Delta\sigma_X$, ΔT_{HX}, ΔT_{CX} or $\Delta\nu_{QX}$ are available and therefore increase the probability to reveal an enantiomeric discrimination.[12,13] Finally, as all these anisotropic NMR interactions are order-sensitive and therefore temperature-, concentration- and solvent-dependent, we have three further variables at our disposal to control the DOE, thus enhancing the probability to detect a chiral differentiation. Consequently, this analytical strategy offers undoubtfully better possibilities for discriminating between enantiomers compared with current isotropic NMR techniques in which only the variation of a chemical shift is used.[1,2] As we will show throughout this work, the two main features of this non-conventional approach generally involving a single NMR sample preparation are, therefore, both its analytical potentialities and high adaptability from the NMR point of view.

Description of the chiral liquid crystalline solvent

The chiral recognition principle in the liquid crystalline state is based on the ability for the chiral phase to orientate differently the two enantiomers as schematically depicted in Fig. 1, and so the choice of the solvent is crucial.[8,9,14,15] As a consequence, we need to have a system able to interact enantioselectively with almost all enantiomers (functionalized or not) and give sufficiently large orientational differences which can be revealed using NMR spectroscopy. This condition supposes therefore that the enantioselective electrostatic interactions as well as geometric shape recognition play an important role in the discrimination mechanisms. Actually, this situation is very similar to that involved for enzymatic enantioselectivity in biological systems.

From the NMR point of view, the liquid crystal should ideally solubilize almost all organic compounds, provide a very homogeneous anisotropic mesophase with low viscosity at about room temperature, and its NMR spectrum should not interfere with that of the dissolved molecules. In addition, the DOE is not directly related with the magnitude of orientational order parameters and in fact it is advantageous to use an anisotropic solvent exhibiting low molecular ordering for solutes. This is firstly because in the majority of cases the proton and proton-coupled X spectra can be easily analysed in a similar way as for isotropic spectra. Second, the contribution to NMR linewidths of order inhomogeneities in the sample is rather small, hence a higher signal-to-noise (*S/N*) ratio may be achieved. This is a key point to observe chiral discriminations for very low-sensitive quadrupolar nuclei such as deuterons at natural abundance level.[16–18]

Among the CLC examined up to now, the most valuable mesophase satisfying all criteria mentioned above is the lyotropic system poly-γ-benzyl-L-glutamate (PBLG) or its enantiomer poly-γ-benzyl-D-glutamate (PBDG), in solution with various organic helicogenic co-solvents.[19–22] In such co-solvents, the main chain of the synthetic homo-polypeptide adopts a rigid α-helical conformation similar to that observed for some naturally occuring polypeptides[23] while the glutamate side chains, which branch from the main helix, also form a secondary molecular helix.[22,24–26]

Within a certain concentration range, organic solutions of PBLG are liquid crystals. Spontaneously, the PBLG chiral fibers orientate to form a macroscopic, supramolecular helical structure of directors in the mesophase, typical of that exhibited by cholesteric liquid crystals. However, when submitted to a routine NMR magnetic field, the supramolecular helix unwinds, and the system behaves like a chiral nematic phase with positive anisotropy of the molecular diamagnetic susceptibility ($\Delta\chi_m > 0$), with the director, $\boldsymbol{n}$, homogeneously aligned parallel to the static magnetic field $\boldsymbol{B}_o$ (Fig. 1).[27,28] Various possible co-organic solvents may be used. Chloroform, dichloromethane, dioxane, DMF and THF are among the most convenient to dissolve a wide variety of organic materials.[24,29,30] However,

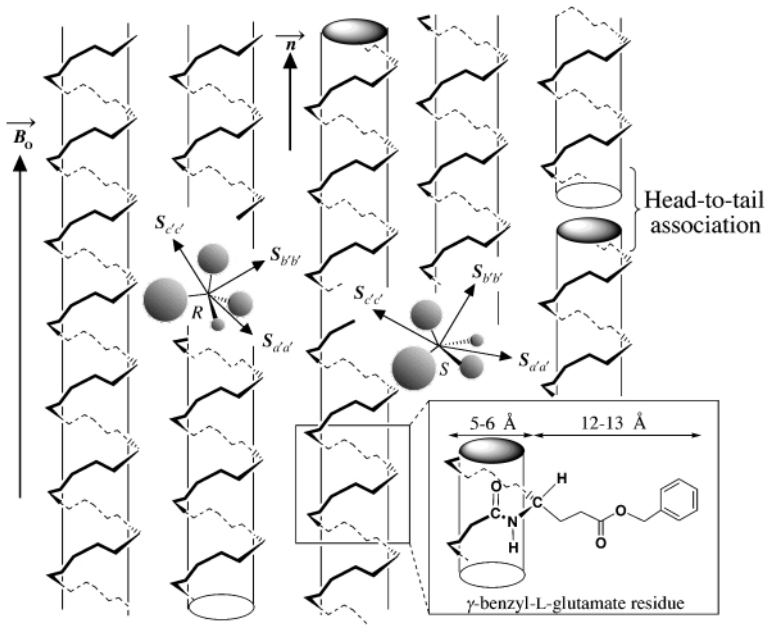

Fig. 1 Schematic illustration of the differential ordering effect for two enantiomers dissolved in the PBLG phase. To clarify the drawing, the glutamate side chains of the polypeptide and the co-solvent molecules were not displayed. The assignments *S* and *R* and the space representation of the orientational principal axis system (a',b',c') of enantiomers should be regarded as arbitrary. The PBLG and chiral solutes are not plotted to scale. Note the head-to-tail associations between two PBLG fibers.

for DMF or dioxane, it is necessary to heat the mixture in order to dissolve the polymer during the sample preparation. In all cases the organic co-solvent employed has to homogeneously dissolve the polypeptide and preserve the α-helical structure of the polymer. For instance, trifluoroacetic acid and DMSO are not suitable co-solvents since they form strong intermolecular hydrogen bonds with the polypeptide chain, giving rise to a random coil conformation for the PBLG, and consequently, the liquid crystalline properties of the solvent disappear.[24] Studies for the optimisation of the ternary mixture, 'PBLG/co-solvent/chiral material', have established that the best NMR results are generally obtained for samples prepared with a concentration in PBLG which varies between 12 and 25% by weight. Except for molecules that are able to precipitate the PBLG fibers, the addition of a reasonable amount of solute (1–20%) in PBLG/co-solvent mixtures does not disrupt the liquid crystalline properties of the solvent. The average molecular weight of PBLG is another important factor for the quality of the enantiodiscrimination. Indeed, this parameter as well as the concentration of the polymer and the nature of the organic co-solvent determine the sample viscosity. Using the same co-solvent and keeping the PBLG concentration constant, the viscosity of the phase significantly decreases when the molecular weight of the polymer is reduced. Generally, a greater fluidity of the liquid crystalline phase provides longer apparent transversal relaxation times for solutes (T_2*), and hence a better spectral resolution and *S/N* ratio. Therefore, we suggest using a PBLG whose degree of polymerisation (DP) is in the range 350–600.[4,5] Under these conditions, the sample temperature can be optimized between 285 and 340 K depending on both the organic co-solvent used and the solute under investigation. Finally we note that a DP below 200 is not convenient for our purpose because the liquid crystal range of the sample is either too small or non-existent.

Theoretical considerations

Analysis of the order-dependent NMR observables involved in chiral differentiation

When embedded in a liquid crystal, solute molecules are partially ordered.[11] This situation arises also using chiral liquid crystals, but in this case, the difference of interactions between the enantiomers and the PBLG molecules generally produces a measurable difference in their orientational ordering.[8,9,31] Consequently, the molecular order of *S* and *R* isomers must be described by two distinct second-rank order tensors, $\boldsymbol{S}^S$ and $\boldsymbol{S}^R$, denoted Saupe matrices, whose elements can be expressed as:[11]

$$S_{\alpha\beta}^{S\text{ or }R} = \frac{1}{2}\left\langle 3\cos\theta_{\alpha_z}^{S\text{ or }R}\cos\theta_{\beta_z}^{S\text{ or }R} - \delta_{\alpha\beta}^{S\text{ or }R}\right\rangle \qquad (1)$$

In this equation, $\alpha,\beta = a,b,c$ are the axes of the molecular fixed reference frame, $\theta_{\alpha_z}^{S\text{ or }R}$ is the angle between the magnetic field and the molecule fixed α axis in the *S* or *R* isomers (the *z* laboratory axis is assumed parallel to the $\boldsymbol{B}_o$ axis). $\delta_{\alpha\beta}$ is the Kronecker symbol (unity if $\alpha = \beta$ and zero otherwise). The angular brackets denote a statistical average over all orientations of the molecule as well as over all intramolecular motions. From the components of $\boldsymbol{S}^{S\text{ or }R}$, we can derive the order parameter, $S_{ij}^{S\text{ or }R}$, of any direction along a vector $\boldsymbol{v}_{ij}$ in the molecular axis system (a,b,c):

$$\begin{aligned} S_{ij}^{S\text{ or }R} &= \sum_{\alpha,\beta=a,b,c}\cos\theta_{ij\alpha}^{S\text{ or }R}\cos\theta_{ij\beta}^{S\text{ or }R}S_{\alpha\beta}^{S\text{ or }R} \\ &= \frac{1}{2}\left(3\cos^2\theta_{ija}^{S\text{ or }R}-1\right)S_{aa}^{S\text{ or }R} \\ &+ \frac{1}{2}\left(\cos^2\theta_{ijb}^{S\text{ or }R}-\cos^2\theta_{ijc}^{S\text{ or }R}\right)\left(S_{bb}^{S\text{ or }R}-S_{cc}^{S\text{ or }R}\right) \\ &+ 2\left(\cos\theta_{ija}^{S\text{ or }R}\cos\theta_{ijb}^{S\text{ or }R}\right)S_{ab}^{S\text{ or }R} \\ &+ 2\left(\cos\theta_{ija}^{S\text{ or }R}\cos\theta_{ijc}^{S\text{ or }R}\right)S_{ac}^{S\text{ or }R} \\ &+ 2\left(\cos\theta_{ijb}^{S\text{ or }R}\cos\theta_{ijc}^{S\text{ or }R}\right)S_{bc}^{S\text{ or }R} \end{aligned} \qquad (2)$$

where the $\cos\theta_{ij\alpha}^{S\text{ or }R}$ are the director cosines of the vector $\boldsymbol{v}_{ij}$ in the molecular fixed frame. All the order-dependent NMR interactions are related to these order parameters as we will see in the next sections.

As a consequence of the DOE and of the non-zero averaging of order-dependent NMR interactions, the total static spin-Hamiltonian which describes the NMR spectra of each diamagnetic enantiomer in CLC must be written as the sum of four distinct terms:

$$\mathcal{H}_{\text{tot}}^{S\text{ or }R} = \mathcal{H}_{\text{cs}}^{S\text{ or }R} + \mathcal{H}_{\text{J}}^{S\text{ or }R} + \mathcal{H}_{\text{D}}^{S\text{ or }R} + \mathcal{H}_{\text{Q}}^{S\text{ or }R} \quad (3)$$

where $\mathcal{H}_{\text{cs}}^{S\text{ or }R}$ is the Zeeman term including the electronic shielding contribution, $\mathcal{H}_{\text{J}}^{S\text{ or }R}$ and $\mathcal{H}_{\text{D}}^{S\text{ or }R}$ are the indirect electron-coupled and direct through-space spin–spin interactions and $\mathcal{H}_{\text{Q}}^{S\text{ or }R}$ is the quadrupolar interaction caused by electric field gradients acting on quadrupolar nuclei ($I > 1/2$). In this respect, magnetic interactions for liquid crystalline solutions are not different from those of solid state NMR, except that molecules are free to diffuse and tumble, leading to line narrowing, and hence high resolution spectra.

Let us now treat in detail the various order-dependent NMR observables involved in the analysis of NMR spectra of enantiomers in chiral anisotropic media.

Chiral discrimination arising from chemical shift anisotropy

In a chiral anisotropic solvent, the resonance frequency ν_i of a nucleus i contains both an isotropic, σ_i^{iso}, and an anisotropic, $\Delta\sigma_i$, contribution to the electronic shielding and may be written for two enantiomers such as:[11]

$$\nu_i^{R\text{ or }S} = \frac{\gamma}{2\pi}\left[1 - \sigma_i^{\text{iso}} - \Delta\sigma_i^{S\text{ or }R}\right] B_{\text{o}} \quad (4)$$

Expressed in a molecular frame (a,b,c), the terms σ_i^{iso} and $\Delta\sigma_i$ at the ith site are defined as:

$$\sigma_i^{\text{iso}} = \frac{1}{3}\left(\sigma_{iaa} + \sigma_{ibb} + \sigma_{icc}\right) \text{ and}$$

$$\Delta\sigma_i^{S\text{ or }R} = \frac{2}{3}\sum_{\alpha,\beta=a,b,c}\sigma_{i\alpha\beta}S_{\alpha\beta}^{S\text{ or }R} \quad (5)$$

Eqn. (4) indicates clearly that chiral discrimination is detected in NMR spectra when $\nu_i^S - \nu_i^R \neq 0$ as depicted in Fig. 2(a), *i.e.* when Δs_i^S significantly differs from $\Delta\sigma_i^R$. However, the quantity

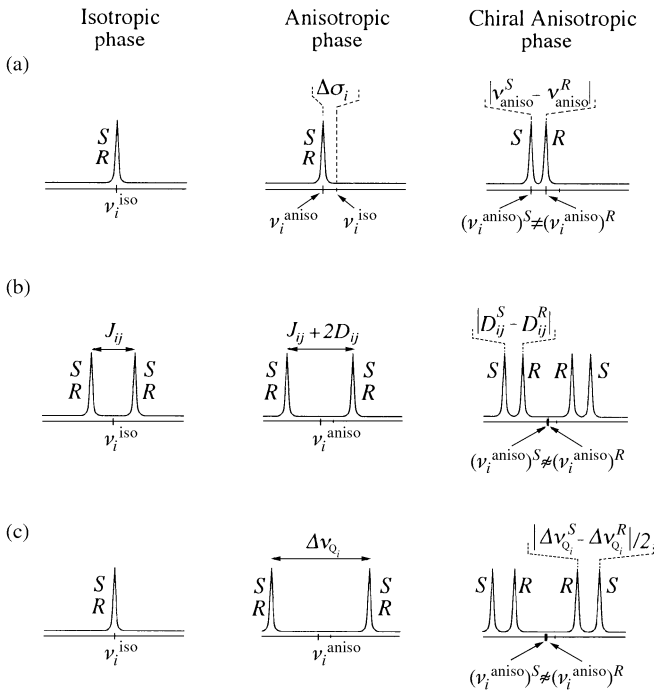

Fig. 2 Principle of the enantiomeric discrimination in CLC based on (a) a difference of chemical shift anisotropies, $\Delta\sigma_i$, (b), residual dipolar couplings, D_{ij}, and (c) residual quadrupolar splittings, $\Delta\nu_{\text{Q}_i}$, for $I = 1$ nuclei (deuterium). For all examples, we have assumed that $\Delta\sigma_i$, was negative. In addition (b) and (c) are depicted assuming the CSA difference ($\Delta\sigma_i^S - \Delta_i^R$) between the enantiomers in the chiral anisotropic phase was negligible. D_{ij}^S and D_{ij}^R were chosen to be smaller than J_{ij}, and having a positive and negative sign, respectively. $\Delta\nu_{\text{Q}_i}$ can be positive or negative. The various spectra are not plotted to scale. The assignments S and R given in all spectra are arbitrary.

$\Delta\sigma_i^{S\text{ or }R}$ is not trivial to analyse as from eqn. (5) it depends both on the elements of the shielding tensor and on the orientational order parameters, $S_{\alpha\beta}^{S\text{ or }R}$, in the same reference frame. In order to consider the various factors governing this quantity, it is more convenient to recast the previous equation into:

$$\begin{aligned}\Delta\sigma_i^{S\text{ or }R} = {} & \frac{2}{3}\left[\sigma_{iaa} - \frac{1}{2}\left(\sigma_{ibb} + \sigma_{icc}\right)\right]S_{aa}^{S\text{ or }R} \\ & + \frac{1}{3}\left(\sigma_{ibb} - \sigma_{icc}\right)\left(S_{bb}^{S\text{ or }R} - S_{cc}^{S\text{ or }R}\right) \\ & + \frac{4}{3}\left(\sigma_{iab}S_{ab}^{S\text{ or }R} + \sigma_{iac}S_{ac}^{S\text{ or }R} + \sigma_{ibc}S_{bc}^{S\text{ or }R}\right)\end{aligned} \quad (6)$$

For each nucleus i of both enantiomers, there exists a principal frame (a'_i, b'_i, c'_i), where the chemical shift tensor is diagonal. Consequently the relationship (6) can be rewritten as:

$$\begin{aligned}\Delta\sigma_i^{S\text{ or }R} = {} & \frac{2}{3}\left[\sigma_{ia'a'} - \frac{1}{2}\left(\sigma_{ib'b'} + \sigma_{ic'c'}\right)\right]S_{ia'a'}^{S\text{ or }R} \\ & + \frac{1}{3}\left(\sigma_{ib'b'} - \sigma_{ic'c'}\right)\left(S_{ib'b'}^{S\text{ or }R} - S_{ic'c'}^{S\text{ or }R}\right)\end{aligned} \quad (7)$$

with

$$S_{ia'a'}^{S\text{ or }R} = \sum_{\alpha,\beta=a,b,c}\cos\theta_{ia'\alpha}^{S\text{ or }R}\cos\theta_{ia'\beta}^{S\text{ or }R}S_{\alpha\beta}^{S\text{ or }R}$$

where $\theta_{ia'\alpha}$ are the angles between the principal axis system of the chemical shift tensor of a nucleus i and the molecular frame.

In eqn. (7), the quantity $\sigma_{ia'a'} - (\sigma_{ib'b'} + \sigma_{ic'c'})/2$ corresponds to the anisotropy of the electronic shielding of atom i, σ_i^{aniso}, while ($\sigma_{ib'b'} - \sigma_{ic'c'}$) may be seen as the asymmetry of the electronic shielding, σ_i^{asym}. An examination of the relationship (7) shows clearly that σ_i^{aniso} and σ_i^{asym} as well as the order parameter differences ($S_{ia'a'}^S - S_{ia'a'}^R$) and [($S_{ib'b'}^S - S_{ic'c'}^S$) − ($S_{ib'b'}^R - S_{ic'c'}^R$)], should both be large in order to detect any frequency difference, $|\nu_i^S - \nu_i^R|$, between the NMR signals of nucleus i for each enantiomer. Consequently, all factors which would increase either the difference in order parameters between enantiomers or the electronic shielding anisotropy of nucleus i (such as the nature of the substituents bonded to nucleus i or its hybridization state) will increase the magnitude of $\Delta\sigma_i$. As the magnitude of the shielding anisotropy, however, is rather small for almost all nuclei involved in classical organic molecules compared with other NMR interactions, only nuclei having the largest CSAs such as sp or sp^2 carbon atoms or fluorine atoms may provide appropriate spy nuclei allowing enantiomers to be differentiated on the basis of a CSA difference.[11,32,33] In contrast, deuterium, proton or sp^3 carbon atoms are rather poor in regard to CSA.

Chiral discrimination using the internuclear dipolar coupling interactions

In the spectra of enantiomers dissolved in chiral liquid crystalline solutions, dipolar interactions between atoms are not averaged to zero. In this case each pair of interacting nuclei i and j for both isomers may produce a direct dipolar coupling defined in Hz as:[11]

$$D_{ij}^{S\text{ or }R} = -k_{ij}\left\langle\frac{S_{ij}^{S\text{ or }R}}{r_{ij}^3}\right\rangle \text{ with } k_{ij} = \frac{\mu_{\text{o}}}{4\pi}\frac{h\gamma_i\gamma_j}{4\pi^2} \quad (8)$$

In this equation, γ_i and γ_j are the magnetogyric ratios of nuclei i and j, and μ_{o} is the permeability constant of a vacuum. The angular brackets denote an (ensemble or time) average over molecular tumbling and internal motions (vibrational motions,

conformational changes…), r_{ij} is the internuclear distance between nuclei i and j and $S_{ij}^{S\text{ or }R}$ is the order parameter for the internuclear vector $\boldsymbol{r}_{ij}$. Note that the magnitude of k_{ij} depends on the nuclear isotopes involved. For intance, the k_{ij} values are 7.59, 28.4, 30.19, 112.96, 120.07 kHz Å^{-3} for ^{13}C–^{13}C, ^{19}F–^{13}C, ^{1}H–^{13}C, ^{19}F–^{1}H, ^{1}H–^{1}H, interacting pairs, respectively.

Disregarding any discrepancies in the molecular geometry between two enantiomers, eqn. (8) shows that the chiral discrimination between enantiomers occurs when the internuclear order parameters, $S_{ij}^{S\text{ or }R}$, are different for the S and R isomers [Fig. 2(b)]. Although $S_{ij}^{S\text{ or }R}$ can be related to the molecular order matrix elements, $S_{\alpha\beta}^{S\text{ or }R}$, using eqn. (2), it is also convenient and often easier to express this parameter relative to the $\boldsymbol{B}_o$ axis as:

$$S_{ij}^{S\text{ or }R} = \frac{1}{2}\left\langle 3\cos^2\theta_{ij}^{S\text{ or }R} - 1\right\rangle \qquad (9)$$

where $\theta_{ij}^{S\text{ or }R}$ is now the angle between the internuclear vector $\boldsymbol{r}_{ij}$ and $\boldsymbol{B}_o$. It must be emphasised that the dipolar coupling difference, $D_{ij}^S - D_{ij}^R$, measured from spectra varies with the relative position of the internuclear vectors $\boldsymbol{r}_{ij}^S$ and $\boldsymbol{r}_{ij}^R$ with respect to $\boldsymbol{B}_o$. This point will be discussed in detail for the quadrupolar interaction.

Finally as underlined in the Introduction, the presence of internuclear dipolar interactions has a profound impact on the spectrum of a molecule dissolved in liquid crystals (chiral or not). As a consequence, the analysis of dipolar spectra may appear rather puzzling compared to those recorded in an isotropic medium. For instance, a first order splitting, denoted T_{ij}, observed between two coupled anisochronous nuclei i and j, is now equal to $J_{ij} + 2\Delta T_{ij}$, where J_{ij} is the isotropic part of the scalar coupling and ΔT_{ij} is the anisotropic part of the total coupling that we limit to the dipolar contribution, D_{ij} [see Fig. 2(b)]. Consequently, as the sign of D_{ij} can be negative or positive, the first order splitting between two non-equivalent nuclei may be zero when $J_{ij} = -2D_{ij}$, producing a fortuitous decoupling. This situation is often encountered for weakly ordered liquid crystals such as organic solutions of PBLG because in this case dipolar and scalar couplings are of the same order of magnitude. Furthermore, dipolar couplings are observable between magnetically equivalent nuclei, contrary to scalar couplings. Thus, in proton liquid crystal NMR, the nuclei of an isolated methyl group produce a 1:2:1 triplet, while a methylene group produces a 1:1 doublet. In both cases the splittings are equal to $3D_{HH}$. Actually, in an anisotropic medium, the spectrum of any n-fully equivalent $I = 1/2$ nuclei consists of an n-multiplet with line spacing $3D$ and a binomial distribution of intensities.

Chiral discrimination using the quadrupolar coupling interaction

NMR spectra of quadrupolar nuclei (spin $I > 1/2$) in oriented solvents are dominated by the nuclear quadrupole–electric field gradient interaction. Disregarding spin–spin couplings, the spectrum, to first order, consists of equally spaced $2I$ peaks corresponding to the various $m \leftrightarrow m + 1$ transitions. The separation between the lines, denoted, $\Delta\nu_{Q_i}$, is referred to as the quadrupolar splitting as shown in Fig. 2(c). For two enantiomers oriented differently in a chiral ordered environment and assuming that the quadrupole term is much smaller than the Zeeman term, the quadrupolar Hamiltonian can be written in frequency units as:[11]

$$\mathcal{H}_Q^{S\text{ or }R} = \frac{1}{h}\sum_i \frac{e^2 Q_i q_{izz}^{S\text{ or }R}}{4I_i(2I_i-1)}\left[3I_{zi}I_{zi} - I_i(I_i+1)\right] \qquad (10)$$

where eQ_i is the nuclear electric quadrupole moment of nucleus i, $eq_{izz}^{S\text{ or }R}$ is the component of the electric field gradient (EFG) tensor along the magnetic field (z axis) at the nucleus i for each enantiomer. In this equation, eq_{izz}, is related to the elements of the EFG tensor in the molecular frame, $eq_{i\alpha\beta}$, using:

$$eq_{izz}^{S\text{ or }R} = \frac{2}{3}\sum_{\alpha,\beta=a,b,c} eq_{i\alpha\beta} S_{\alpha\beta}^{S\text{ or }R} \qquad (11)$$

For most quadrupolar nuclei, the relaxation induced by the purely anisotropic quadrupolar interaction broadens the signals so strongly that the analytical potential produced by the DOE in a chiral mesophase is lost. However, the relaxation behaviour for some nuclei, such as boron-10 ($I = 3$), boron-11 ($I = 3/2$) or deuterium atoms ($I = 1$), resembles that of spin-1/2 nuclei in small molecules owing to their small quadrupole moment, and produces high-resolution quadrupolar NMR spectra.[13] In the case of deuterons, which are monovalent atoms, the EFG is usually assumed to lie along the C–D bond direction and to be axially symmetric. Choosing one of the principal axes along the C–D bond, and safely neglecting any asymmetry parameter the quadrupolar splitting between the two lines [Fig. 2(c)] can be written as:

$$\Delta\nu_{Q_i}^{S\text{ or }R} = \frac{3}{2}K_{C-D_i}\, S_{C-D_i}^{S\text{ or }R} \text{ with } K_{C-D_i} = \frac{e^2 Q_{D_i} q_{C-D_i}}{h} \qquad (12)$$

where $S_{C-D_i}^{S\text{ or }R}$ is the order parameter of the C–D$_i$ axis for the R or S enantiomers and K_{C-D_i} is the deuterium quadrupolar coupling constant. Note that K_{C-D_i} varies depending on the hybridization state of the carbon bonded to a given deuteron. Thus K_{C-D_i} is approximately equal to 170 ± 5 kHz, 185 ± 5 kHz and 210 ± 5 kHz, for sp^3, sp^2 and sp carbons, respectively.[11,34]

Similarly to eqn. (9), the order parameter associated with the EFG for a C–D bond can be related to the molecular order parameters through eqn. (2) and is expressed relative to $\boldsymbol{B}_o$ as:

$$S_{C-D_i}^{S\text{ or }R} = \frac{1}{2}\left\langle 3\cos^2\theta_{C-D_i}^{S\text{ or }R} - 1\right\rangle \qquad (13)$$

As already described for the dipolar interaction, eqn. (12) shows that chiral differentiation $|\Delta\nu_{Q_i}^S - \Delta\nu_{Q_i}^R| \neq 0$ occurs when $|S_{C-D_i}^S - S_{C-D_i}^R| \neq 0$. Eqn. (13) indicates, however, that order parameters, $S_{C-D_i}^{S\text{ or }R}$, are composite quantities as they depend both on the angle $\theta_{C-D_i}^{S\text{ or }R}$ and on the motional averaging ($\langle \ldots \rangle$). Consequently whenever two-order parameters are different between enantiomers, we generally do not know if this happens from a purely geometrical reason, $\theta_{C-D_i}^S \neq \theta_{C-D_i}^R$, or from a difference involving motional averaging, or both. However assuming that the motional averaging for enantiomers is more or less the same, it appears that the magnitude of the differentiation should depend strongly on the relative position of the EFG direction for both isomers with respect to $\boldsymbol{B}_o$ (Fig. 3). These variations occur because the trigonometric function, $(3\cos^2\theta - 1)/2$, is very steep for angles around the magic angle, $\theta_m = 54.7°$ (for which the function is null, and hence $S_{C-D_i}^{S\text{ or }R} = 0$), and rather flat in the angular ranges of [−5, +5°] and [+85, +95°]. Analyzing the evolution of the calculated quadrupolar splitting difference, assuming $\theta_{C-D_i}^S = \theta_{C-D_i}^R + 10°$, and the corresponding spectra plotted in Fig. 3, we can easily see that larger chiral discriminations are obtained when θ_{ij}^S and θ_{ij}^R vary in the interval $\theta_m \pm 20°$. This range of angles corresponds also to the smallest values for $S_{C-D_i}^{S\text{ or }R}$ and subsequently to the smallest magnitudes of quadrupolar splittings. As shown in Fig. 3, there exist several particular spectral situations corresponding to either the cancellation of quadrupolar splitting for one of the enantiomers ($\theta_{ij}^S = \theta_m$ or $\theta_{ij}^R = \theta_m$) or the disappearance of the chiral discrimination ($S_{ij}^S = S_{ij}^R$). Note that the various spectral situations simulated here in the case of spins-1 could be also observed for two dipolar coupled magnetically equivalent spins-1/2. The great efficiency of deuterium NMR in the discrimination of enantiomers in PBLG mainly originates from the relatively large magnitude of the deuterium quadrupolar coupling constants, K_{C-D}, compared with almost all k_{ij},

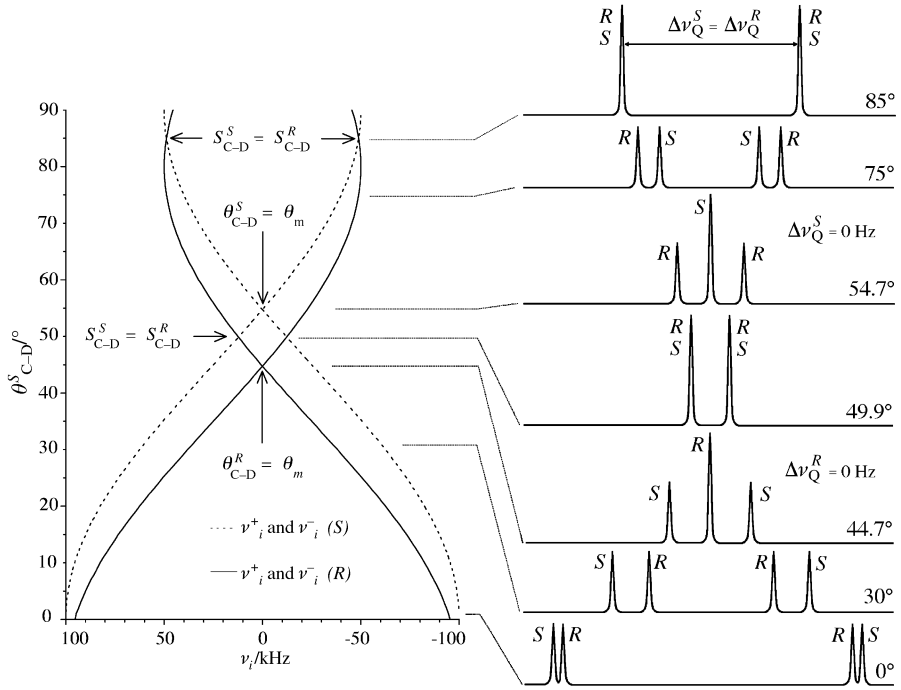

Fig. 3 Theoretical evolution of the two components (ν_i^- and ν_i^+) of a quadrupolar doublet associated with two enantiomers, versus the angle θ_{C-D}^S. We have assumed that K_{C-D} = 133 kHz and the difference $\theta_{C-D}^S - \theta_{C-D}^R$ = +10° for all values. On the right of the figure, the expected spectra for various angles θ_{ij} are shown. Note the four particular situations corresponding to $\theta_{C-D}^R = \theta_m$, $S_{C-D}^S = S_{C-D}^R$ when $\theta_{C-D}^S < \theta_m$, $\theta_{C-D}^S = \theta_m$ and $S_{C-D}^S = S_{C-D}^R$ when $\theta_{C-D}^S > \theta_m$, respectively. The *S* and *R* assignment given for the initial spectrum is arbitrary.

involved in the dipolar interaction. Indeed, even when the DOE between two enantiomers is rather small, the magnitude of the deuterium quadrupolar coupling constant for a C–D bond can make the difference in their residual quadrupolar splittings, $|\Delta\nu_{Q_i}^S - \Delta\nu_{Q_i}^R|$, measurable.

Experimental and NMR technical considerations

In this technique, PBLG sample preparation is very important because it may affect strongly the quality of NMR spectra, in particular the linewidths. The typical procedure to prepare a PBLG sample consists of directly weighing 2–100 mg of racemic material, 80–100 mg of PBLG and adding about 350–500 mg of co-solvent into a 5 mm NMR tube. Note that the viscosity of the mixture and the evaporation of the co-solvent preclude the possibility of preparing and handling the sample outside the NMR tube. Under these conditions, the total volume of the sample is optimal compared to the length of the coil of a 5 mm diameter dual probe-head. In this study we have added 100 mg of PBLG (DP = 562, MW ≈ 120 000), 100 mg of 1-chloropropan-2-ol (CP) in racemic mixture and 350 mg of dry chloroform. The polymer was purchased from Sigma and used with no further purification, however numerous preparative methods of PBLG are possible and have been described in the literature.[24,35–37] It is recommended to wait for slow dissolution of the compounds in the NMR tube (which was sealed to prevent any co-solvent evaporation) and then to centrifuge the sample in both directions until an optically homogeneous birefringent phase is obtained. Finally, before measuring the NMR spectra, the sample was kept for about 15 min in the magnetic field in order to achieve a good thermal equilibration and the complete unwinding of the cholesteric pitch prior to starting the shimming procedure.

NMR experiments in PBLG can be performed on any routine spectrometer and no special hardware equipment is required. Nevertheless, using a high magnetic field is a strong advantage to increase the chemical shift dispersion and to record low sensitivity nuclei at natural abundance level such as deuterium. In this work, all NMR spectra were obtained on a Bruker DRX-400 high-resolution NMR spectrometer equipped with an inverse 5 mm multinuclear probe, the operating frequencies being 400.1, 100.6 and 61.4 MHz for ^{1}H, ^{13}C and ^{2}H, respectively. The NMR probehead was tuned and matched very carefully to minimize losses in probe efficiency. This is of importance for detecting nuclei of very low natural isotopic abundance such as deuterons. The NMR tube was not spun in the magnet and the temperature of the sample was regulated carefully at 298.0 ± 0.1 K by the Bruker BVT 3000 temperature unit in order to prevent substantial temperature fluctuations. Note here that the sample rotation does not produce a significant improvement in the spectral resolution when the magnetic field homogeneity is good whereas a good long term thermal stability ensures an optimal spectral resolution. The field-frequency lock was not used, but the field drift of our magnet is small enough to allow for a long time accumulation without significant line broadening. When long term field stability is poor, field-frequency lock on a deuterium signal is possible, one component of the quadrupolar doublet of the deuterated solvent providing the lock signal for instance. The recording of natural abundance deuterium spectra of solutes is, however, not possible in this case. One solution consists of using a fluorine-19 signal as lock signal. Thus a few drops of $CFCl_3$ can be added to the co-solvent without perturbing the PBLG phase, but this technical solution requires a fluorine-19 lock device and a suitable probe. In order to avoid possible sample heating which can produce some line broadening, proton-decoupled carbon or deuterium spectra are recorded applying broadband proton decoupling using the WALTZ-16 composite pulse sequence (≈ 0.5 W of rf power).[38] Note here that the proton decoupling in PBLG does not necessitate more power than for isotropic samples because of the rather small amplitude of the residual heteronuclear dipolar interactions. Other specific experimental details for each technique will be given in the figure captions.

Description and analysis of various anisotropic NMR tools in PBLG

Proton NMR spectroscopy

Proton spectra of oriented molecules in classical thermotropic LCs are dominated by the residual dipolar couplings and yield

usually non-trivial second order spectra. The reason for this is that the magnitude of partially averaged ^{1}H–^{1}H dipolar couplings are often much larger than the chemical shift differences.[11] Actually, this analytical circumstance is less often encountered using organic solutions of PBLG because of the weak degree of molecular orientation in PBLG. The value of order parameters are in the range 10^{-3} to 10^{-5}, and consequently the dipolar couplings are often small (negative or positive) values compared to Larmor frequency differences.[9,10] Consequently, the analysis of proton spectra in PBLG may often be carried out at first order and allows detection of a possible chiral discrimination.

To illustrate our purpose, Fig. 4 shows the proton signals of the methyl group in (±)-CP where two different spectral

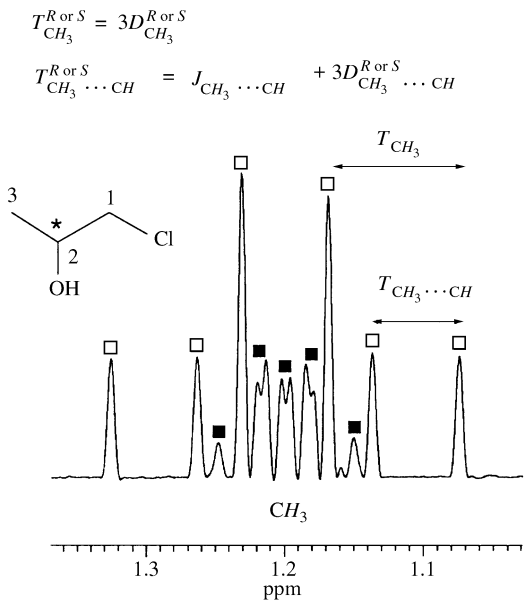

Fig. 4 Proton signal of the methyl group of (±)-CP. The spectrum was Fourier transformed after adding 256 scans. The peaks due to each enantiomer are labelled by (□) and (■). Zero filling, digital gaussian filtering (GB = 40% and LB = −9 Hz) and a baseline correction were applied to increase the digital resolution and enhance the spectral aspect.

patterns, centred on the same chemical shift, may be observed, one for each enantiomer. As already suggested in the theoretical section, this situation illustrates perfectly that the very weak sensitivity of proton CSA toward the DOE does not generally allow a chemical shift difference between enantiomers to be measured on the ^{1}H spectra (even at 400 MHz). In contrast, the superposition of two spectral patterns for the methyl shows the chiral separation of enantiomers through a difference in the residual ^{1}H–^{1}H dipolar couplings. Thus, for one of the enantiomers (labelled using white squares) we obtain a doublet of triplets due to the dipolar couplings between the three equivalent protons of the methyl group and to the coupling with the proton directly attached to the asymmetric carbon. From the values T_{CH_3} and $T_{CH_3\cdots CH}$, measured directly from the spectrum, we can determine the ^{1}H–^{1}H residual dipolar constants. We find here $|D_{CH_3}| = 12.4$ Hz and $|D_{CH_3\cdots CH}| = 9.1$ Hz. The spectral pattern associated to methyl group of the other enantiomer (labelled using black squares) is more complicated than the first because the dipolar couplings between the protons of CH_3 and the diastereotopic protons of the CH_2 group are not averaged to zero as previously. This perfectly emphasises the variation of dipolar couplings between the *S* and the *R* isomers and shows the influence of the DOE on the spectral analysis in chiral liquid crystals. However as the order parameters and subsequently the D_{ij} values are temperature-sensitive, we can modify the spectral patterns by changing the sample temperature and, hopefully, simplify the analysis. The determination of all dipolar couplings is not trivial and requires the use of spectral simulation programs such as PANIC.[39] For the *R* enantiomer of CP, we have measured $|D_{CH_3}| = 4.2$ Hz, $|D_{CH_3\cdots CH}| = 3.2$ Hz and $|D_{CH_3\cdots CH_2}| = 3.3$ Hz. Finally, it is noteworthy that the chiral discrimination may also be seen on the NMR signal of the methylene and methine groups through ^{1}H–^{1}H dipolar coupling differences, but they are not shown here.

Although chiral differentiation was visualized in this example using ^{1}H NMR, it is clear that when the number of interacting protons in the molecules becomes larger, the analysis of the ^{1}H spectra becomes very difficult. In this case, the chiral discrimination between enantiomers cannot always be unambiguously established because doubling of peaks may arise, for instance, from the long distance dipolar couplings. Two solutions can be suggested to check if a chiral discrimination occurs or not. First, it is always convenient to apply a selective decoupling of protons which are susceptible to interact with the signal suspected to give a chiral discrimination. When doubt still arises, the spectra in a racemic mixture of PBLG and its enantiomer, PBDG, dissolved in $CHCl_3$ may then be recorded.[22,31] Indeed in such a mixture, the fast exchange between chiral solutes and the vicinity of PBLG and PBDG eliminates the chiral discrimination, and hence results in a significant simplification of spectra, which can give valuable information with regard to chiral discrimination.[31] This latter solution can be also successfully applied using the other NMR spectroscopies described below such as carbon-13 or deuterium NMR. However in proton NMR, these alternatives will remain limited for large, chiral molecules because the numerous long distance dipolar couplings together with the superposition of the ^{1}H spectra for each enantiomer can yield either significant line broadening of the resonances or an excessive peak overlap which totally prevents their analysis. We reach, then, the limits of the applicability of the proton NMR spectroscopy in PBLG solvent. In such cases, carbon-13 NMR spectroscopy can offer a first and reliable alternative.

Carbon-13 NMR spectroscopy in natural abundance

In spite of the lower natural isotopic abundance of carbon-13 atoms, the advantages of using carbon-13 NMR in PBLG are obvious compared with proton NMR.[5,32] In the first place, the spectral analysis of rare spins in anisotropic medium is considerably simplified due to the absence of coupling between two dilute spins. Second, the magnetic fields used in routine NMR are sufficiently strong to reach a satisfying *S/N* ratio with a relatively small amount of material and short experimental times. Moreover because of its high molecular weight and liquid crystalline nature, the broad carbon-13 NMR resonances arising from PBLG do not interfere with the analysis of the solute signals. Consequently in a second approach, we have demonstrated that natural abundance carbon-13 NMR may be successfully applied to visualize enantiomeric discrimination, through a difference of ^{13}C–^{1}H dipolar interactions and/or C-13 chemical shift anisotropies when proton NMR gives rather poor or unconvincing results.[5]

1D proton-coupled carbon-13 experiments. Fig. 5(a), shows the proton-coupled carbon-13 signal of the methyl group of (±)-CP. Here again, we distinguish two spectral patterns, namely a doublet of quartets for each enantiomer, clearly indicating chiral differentiation. To check this analysis, we have recorded the carbon-13 signal of the methyl carbon applying a selective decoupling of the proton attached on the asymmetric carbon. In this case, we eliminate the dipolar splitting, $T_{CH_3\cdots H}$, and we observe only two distinct quartets, corroborating unambiguously the discrimination of enantiomers. Note that recording the proton-coupled carbon-13 signal of the methyl in a racemic mixture of PBLG and PBDG would give a single dedoubled quartet, showing that chiral discrimination occurred in the PBLG phase. From the values of $^nT_{CH}$ (*n* is the number of

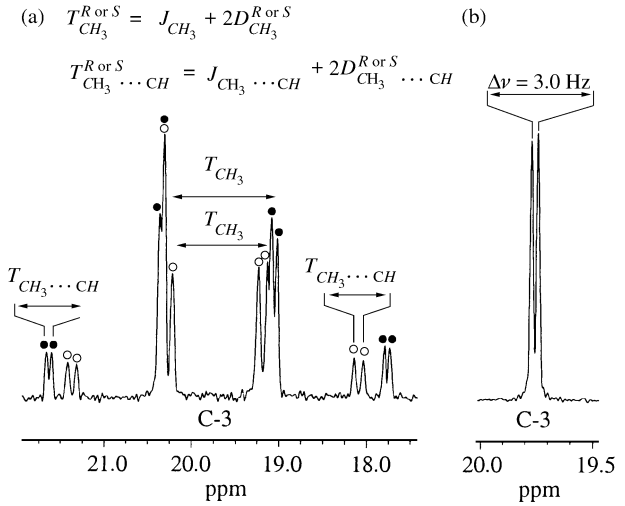

Fig. 5 (a) Carbon-13 and (b) ^{13}C-{^{1}H} signal of the methyl group of (±)-CP. The spectra were obtained after adding 2000 and 1000 scans of 16 K data points, respectively. The recycling delay was 2 s. For spectrum (a), proton decoupling was applied during the relaxation delay period in order to gain a nuclear Overhauser effect. The peaks arising from each enantiomer are labelled (○) and (●).

bonds separating the two coupled nuclei in the molecular skeleton), measured directly from the spectrum, we can calculate the residual dipolar coupling constants, $^nD_{CH}$. As the sign of $^1J_{CH}$ and $^3J_{CH}$ are known to be positive[33] and considering that $^1J_{CH}$ and $^3J_{CH}$ are larger than $^1D_{CH}$ and $^3D_{CH}$, in the PBLG phase,[9,10] we are able to determine the absolute sign of those dipolar couplings. In contrast, the sign of $^2J_{CH}$ can be positive or negative, consequently the sign of $^2D_{CH}$ cannot be ascertained directly. In this example, the four corresponding residual dipolar couplings derived from the spectrum analysis are D_{CH_3} = −8.5 Hz and $D_{CH_3\cdots CH}$ = +3.8 Hz (○) and D_{CH_3} = +1.5 Hz and $D_{CH_3\cdots CH}$ = +1.7 Hz (●) assuming that $J_{CH_3\cdots CH}$ and $T_{CH_3\cdots CH}$ are positive. Note here that at 298 K, we are not able to measure the dipolar couplings between the methyl group and the diastereotopic protons on the methylene group. Disregarding the fortuitous elimination of dipolar splittings (J + 2D = 0 Hz) and lack of spectral resolution, we may assume that the large internuclear distance ($r_{CH_3\cdots CH_2}$ > 2.8 Å) and the small magnitude of order parameters in PBLG give a negligible dipolar interaction between those protons and the methyl carbon. Consequently no further splittings are visible in the spectral pattern. We can also remark that the spectral patterns are not perfectly centered on the same chemical shift owing to a small but measurable difference of carbon-13 CSA. As we will see in the next section, this small difference is more clearly visible on the proton-decoupled carbon-13 spectrum. Finally it can be stated that a chiral discrimination has also been detected on the other two carbons on the basis of a difference in dipolar couplings, but they are not presented here.

In this example, we were able to clearly visualize a chiral discrimination based on a difference of ^{13}C–^{1}H residual dipolar couplings. It is clear, however, that such well-resolved spectra will not always be obtained when the molecule under study possesses a large number of interacting nuclei. Actually for medium to large sized molecules, we may reach again the limits of the applicability of the proton-coupled carbon-13 NMR similar to the situation which is encountered in overcrowded proton NMR spectra. For chiral compounds exhibiting an isolated group (such as a methyl group) far removed from other protons in the molecule, it may be convenient to record the proton-coupled carbon-13 spectrum in order to detect the separation of enantiomers through a difference in the ^{13}C–^{1}H dipolar couplings. When proton-coupled carbon-13 spectra cannot be conveniently resolved it becomes necessary to cancel out all dipolar interactions. By recording the proton-decoupled carbon-13 spectrum, we can, therefore, expect to distinguish between enantiomers through a difference in their carbon-13 CSA.

1D proton-decoupled carbon-13 experiments. The major advantage of proton-decoupled carbon-13 NMR (^{13}C-{^{1}H}) in PBLG is the simplicity of the spectral analysis. First, with broadband proton decoupling, carbon-13 spectra of solutes usually show resolved peaks which can be assigned to all non-equivalent individual carbon atoms in the molecule, similar to that for an isotropic sample. When the difference in C-13 chemical shift anisotropy between the *S* and *R* isomers for a given carbon *i* is large enough, then we observe two distinct resonance lines located at ν_i^S and ν_i^R as depicted in Fig. 2(a). Second, as the carbon-13 CSAs are rather small in PBLG, the chemical shifts of each carbon are very close to those observed in the isotropic solvent. Consequently the assignment of the C-13 resonances in PBLG is often trivial and comparison with the isotropic spectrum readily reveals the carbons of the chiral molecule which are discriminated.

Although the carbon-13 chemical shift anisotropies are much greater than for the proton, the chemical shift differences measured in almost all spectra are typically just a few Hz (typically 3–15 Hz), except for some sp carbon atoms for which chiral discriminations of up to 40 Hz have already been measured.[5] Nevertheless these small differences allow the visualization and the measurement of enantiomeric excess using classical numerical integration or iterative curve-fitting. As for overcrowded ^{1}H and ^{13}C spectra, it is clear that a good homogeneity of both sample and magnetic field is required to reach an optimal enantiomeric discrimination. Under the experimental conditions described above, the linewidths at half-height commonly observed in ^{13}C-{^{1}H} spectra are *ca.* 2–4 Hz. Note that when this spectral resolution is not reached, it can be useful to slightly increase the sample temperature. Indeed a greater fluidity of the phase may give an important improvement in the spectral resolution. When no significant effect is obtained, it is recommended to heat the sample for a few hours prior to centrifuging the sample in both directions again. In fact this latter procedure can produce a more homogenous distribution of each component in the mixture, thus avoiding possible concentration gradients in the sample.

Finally, compared with proton-coupled carbon-13 NMR, ^{13}C-{^{1}H} NMR offers an important advantage in terms of sensitivity and *S/N* ratio, since all signals are concentrated in only one resonance for each carbon. This situation enhances considerably the quantitative aspects of this approach through the greater precision that can be reached in measuring the ee values. Usually a sufficient *S/N* ratio is obtained after an experimental time varying between 1 and 5 h depending on the available amount of solute and its molecular weight. The experimental enantiomeric excess determined on such spectra by integration can be within 2% of the true value.[6] Generally, we estimate that the accuracy on the enantiomeric excess measurements is about 5% of the true value when the spectrum is recorded and processed using standard conditions.[40,41]

Fig. 5(b), shows a small but visible chiral discrimination ($|\nu_i^S - \nu_i^R|$ = 3 Hz) on the signal of the methyl group for (±)-CP. Although the probability for detecting a chiral discrimination is generally greater for carbons having an sp and sp^2 hybridization state, the discrimination on sp^3 carbons is also possible as seen in this example. However, we must note that none of the carbons bonded to the heteroatoms in the molecule displays a line separation. The result is rather surprising if we consider that the strength of the carbon-13 CSA increases with the electronegativity of the substituents.[33] However, as already emphasised in the theoretical section, the electronic shielding anisotropy and the asymmetry term are not the only parameters involved in the chiral discrimination, and the order parameter differences ($S^S_{ia'a'} - S^R_{ia'a'}$) and [($S^S_{ib'b'} - S^S_{ic'c'}$) − ($S^R_{ib'b'} - S^R_{ic'c'}$)],

may have a large effect on the frequency difference of both isomers for a given carbon. In this particular example, we may suppose that the angle, θ, between the magnetic field and one of the principal axes of the CSA tensor for the methylene and methine carbon are located in the region where the function $(3\cos^2\theta - 1)/2$ is rather flat and produces a negligible DOE, thus leading to absence of chiral discrimination.

In contrast with the homo- and hetero-nuclear spin–spin coupling interactions that are independant of magnetic field magnitude, eqn. (4) shows that the sensitivity of CSA to the DOE increases with $\boldsymbol{B}_o$. Consequently, the use of NMR spectrometers operating at higher magnetic fields enhances considerably the possibility to detect enantiomeric discriminations on all non-equivalent carbons of the chiral molecule. Thus, when recording the ^{13}C-{^1H} spectra of (±)-CP at 201.2 MHz (18.4 T), the chemical shift difference of 3.0 Hz measured for the methyl carbon would become around 6 Hz under the same experimental conditions. Such a difference would offer a very comfortable separation between these signals which are associated with an sp^3 carbon. In addition, we may expect to observe a chemical shift difference for the two other carbon signals of the molecule, thus increasing the probability to detect a chiral discrimination.

2D ^{13}C–^{13}C INADEQUATE experiments. The detection of coupled dilute spin systems such as two carbon-13 nuclei in a CLC solvent is not trivial to achieve for three reasons. First, the probability for observing chiral isotopomers possessing two carbon-13 nuclei is only 1/10000 and the intensity of the corresponding resonances will be a factor 200 lower than the intensity of signals from the isolated carbon-13 nuclei. Second, the k_{CC} parameter for two interacting carbon-13 nuclei is small ($\gamma_C\gamma_C/\gamma_C\gamma_H \approx 0.25$) and the larger internuclear distances between adjacent carbon-13 atoms (1.20–1.54 Å *cf.* 1.09 Å for a ^{13}C–^1H bond) significantly reduces the sensitivity of ^{13}C–^{13}C dipolar interaction to the DOE compared with that of the ^{13}C–^1H dipolar interaction. Finally the detection of two coupled carbon-13 spins is not simple, and hence requires usually the creation of double quantum coherences using the well-known 2D INADEQUATE experiment, the basic pulse sequence of which is shown in Fig. 6(a).[42–44] The condition for optimum transfer of one quantum into double-quantum coherence is satisfied with the delay $\tau = (2n + 1)/(4T_{CC})$ where n is an integer, and consequently the choice of the τ value is important. In the PBLG phase, the very small magnitude of one-bond ^{13}C–^{13}C dipolar couplings (a few Hz) compared with the range of one-bond ^{13}C–^{13}C scalar couplings (20–200 Hz, depending on hybridization state of coupled carbons)[33] allows the assumption that $^1T_{CC} \approx {}^1J_{CC}$. Consequently, despite the fact that the exact values of $^1D_{CC}$ are unknown, the loss of signal during the single-to-double quantum transfer, due to a non-ideal value of τ is weak and the detection of double quantum remains possible. Note here that the magnitude of long-distance ^{13}C–^{13}C dipolar couplings is generally too small to be experimentally detected. Finally the α read pulse (α = 90, 120 or 135°) depends on the phase cycling employed and allows either optimization of the double quantum coherence or suppression of the quadrature images in the F_1 dimension.[43,45]

Related to such 2D experiments, Levitt and coworkers were the first to report the measurements of ^{13}C–^{13}C dipolar couplings of liquid crystalline molecules using the 2D INADEQUATE sequence.[46] In our case, the low concentration of chiral solutes in the PBLG phase reduces further the sensitivity of this experiment, thus raising another difficulty. In other words, the visualization of enantiomeric discrimination based on a difference of ^{13}C–^{13}C dipolar couplings is a difficult but challenging task.

Fig. 6(b) displays part of the 2D INADEQUATE experiment of (±)-CP recorded in PBLG after 15 h of experimental time

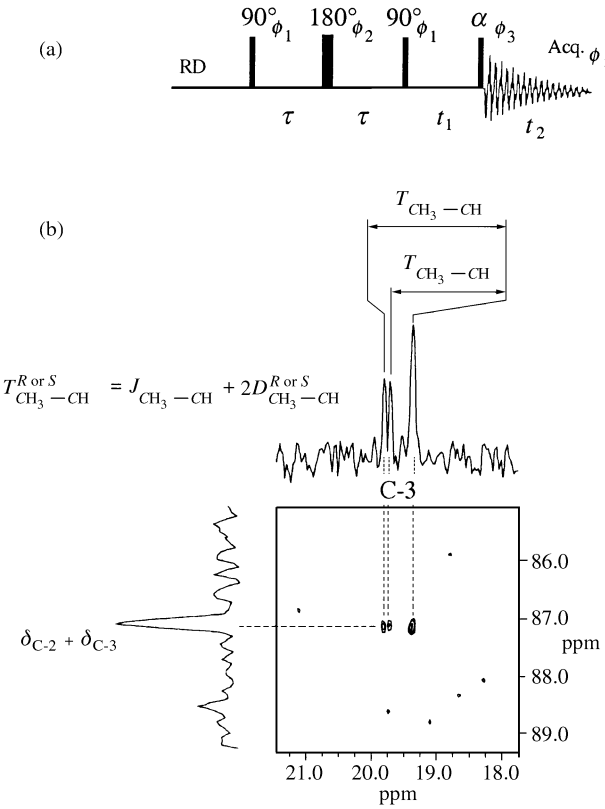

Fig. 6 (a) Basic INADEQUATE pulse scheme for carbon-13 2D NMR spectroscopy. (b) 100.6 MHz INADEQUATE 2D spectrum of (±)-CP in PBLG. The spectrum was recorded with data matrix of 384 (t_1) × 2048 (t_2) data points. The recycle delay and the preparation time τ were set to 2 s and 6.3 ms, respectively. The number of free induction decays added for each t_1 increment was 256. No apodization was applied. The 2D contour plot is presented in magnitude mode.

(overnight). As in an isotropic solvent, all dipolar coupled two-spin systems straddle the skew diagonal of slope 2, each being located at the sum of their Larmor frequency, $\nu_i + \nu_j$, in the F_1 double-quantum dimension. Two slices parallel to the ω_2 axis were observed in the 2D contour plot and permit the unambiguous identification of each ^{13}C–^{13}C doublet, and assignment of each of them on the basis of chemical shifts. On the 2D contour plot, we can observe two partially overlapping dipolar doublets associated with the carbon-13 atom of the methyl group, thus showing two different ^{13}C–^{13}C dipolar couplings between the C-2 and C-3 carbons, one for each enantiomer. This situation occurs when the two dipolar doublets are not centered on the same chemical shift due to a CSA difference between enantiomers (here *ca.* 3 Hz). This part of the 2D spectrum unambiguously evidences chiral discrimination. This result was also confirmed by recording the 2D INADEQUATE spectrum of (±)-CP in the isotropic state at 298 K because in this instance, only a single doublet was detected between this pair of adjacent carbons. The residual dipolar constant D_{CH_3-CH} measured on the 2D spectrum is +2.6 and −1.1 Hz for one enantiomer and the other, the scalar coupling measured in isotropic solution, J_{CH_3-CH}, between the two components being equal to +38.9 Hz ($^1J_{CC}$ is always positive).

It is of note that this is the first enantiomeric discrimination of a chiral molecule using ^{13}C–^{13}C dipolar interaction since no successful results using this NMR technique have, up to now, been recorded. Even though the natural sensitivity of the 2D INADEQUATE experiment is rather poor, this result establishes that enantiomeric discrimination based on a difference of ^{13}C–^{13}C dipolar coupling is possible and should not be neglected. However, it is clear that the analytical potential of this tool is rather limited because the condition for optimum transfer into double-quantum coherence subtantially restricts its

use for accurate quantitative measurements of enantiomeric excess.

Deuterium NMR spectroscopy in natural abundance

As already mentioned in the theoretical section, the deuterium quadrupolar interaction is the most sensitive interaction to the DOE of enantiomers. Consequently, in the earliest studies, we have focused on chiral discrimination using labelled materials.[14,47] Among successful results already reported, the great sensitivity of this approach allowed us to visualize the chirality of almost all investigated chiral molecules.[4,5,48,49] Among the compounds known to be very difficult to analyse, but showing a chiral discrimination in PBLG, are ethers, monohalogenated hydrocarbons and non-functionalised cycloalkenes.[4] Also we have reported the discrimination of molecules that are chiral by virtue of isotopic substitution.[3] Although synthetic methods for selectively introducing deuterium in chiral molecules are numerous and well documented, it is clear that this is not always possible or easy to do, and may be time-consuming.[4,5] Consequently, isotopic labelling may be a serious limitation to this investigation technique.

To eliminate the synthetic step, we have recently demonstrated that isotopic enrichment of chiral solutes was not necessary to yield observable deuterium resonances in PBLG, despite its very low sensitivity (1.45×10^{-6} with respect to proton).[16] Actually, calculations indicate that NAD-NMR experiments have sensitivities comparable with those of the above 2D INADEQUATE experiments. However for the same experimental time, NAD-NMR experiments are more advantageous in terms of *S/N* ratio because the deuterium T_1 relaxation values of solutes dissolved in PBLG ($\approx$ 0.8–1 s) are generally much shorter than the T_1 values of carbon-13, allowing a faster repetition rate of the pulsing. Consequently, enantiomeric differentiation of chiral compounds using natural abundance deuterium (NAD) NMR is perfectly possible using standard NMR equipments, and provides, therefore, a second and interesting alternative to other previous techniques.[6,16,50]

Assuming that the detection of a rare spin such as deuterium in natural abundance is not an insurmountable obstacle in terms of signal sensitivity, site-specific labelling of the molecules would, therefore, not be required. Furthermore, it would permit the simultaneous probing of all possible deuterated sites of the molecule, thus increasing the probability to visualize a chiral differentiation between enantiomers. At natural abundance level, ^{2}H–^{2}H spin–spin couplings are not detected (owing to the very low probability of observing two interacting deuterons in the same isotopomer). Consequently, as all the couplings with protons are eliminated through decoupling, the natural abundance ^{2}H-{^{1}H} spectra in organic solutions of PBLG consist of the superposition of independent quadrupolar doublets corresponding to all non-equivalent deuterons in each of the enantiomers.[6,16,50] Thus, disregarding the doublets originating from organic co-solvent, we can expect 2*n* doublets (4*n* peaks) to be observed in the NAD spectrum for a racemic mixture of enantiomers possessing *n* non-equivalent deuterons, assuming that all deuterated chiral isotopomers are discriminated and neither line overlaps nor null quadrupolar splittings occur. This evaluation can be, however, reduced to $2n - 1$ doublets for molecules possessing an –OD or –ND group, since no chiral discrimination has (until now) been detected for such groups, owing to the fast exchange of their deuteron. In the case of (±)-CP and disregarding solvent quadrupolar doublets (one doublet for $CDCl_3$), eight different chiral isotopomers exist in the mixture and a maximum of eight quadrupolar doublets are expected to be detected if all deuterated sites show chiral differentiation. This is because (±)-CP contains two diastereotopic nuclei associated with deuterons of the methylene group. For this group, four quadrupolar doublets corresponding to the (*S*, pro-*S*), (*S*, pro-*R*), (*R*, pro-*S*), (*R*, pro-*R*) deuterons of the *S* and *R* isomers can be expected to be seen in the NAD-NMR spectrum (when all isomers are discriminated and without peak overlapping). Traditionally we use the term '*semi-isotopic*' diastereoisomers for all deuterated isotopomers bearing a classical asymmetric carbon and an asymmetric carbon by virtue of isotopic substitution.

It must be clear that for larger molecules, the correlation between the two components for each quadrupolar doublet will not always be simple to achieve, mainly due to overlapping of peaks, and will require the use of proton-decoupled deuterium 2D-NMR experiments.[6,50,51] Consequently, we have developed several two-dimensional autocorrelation deuterium NMR experiments referred to as QUOSY (for QUadrupole Ordered SpectroscopY), which facilitate the analysis of overcrowded NAD spectra. Among them, the Q-COSY and Q-resolved experiments and their composite pulse variants were found to be the most useful 2D sequences for applications in NAD-NMR or when the problem of sensitivity is crucial (very low degree of deuteration). The optimised sequences using pulse composites and the corresponding full phase cycling are described in refs. 6 and 51.

Fig. 7 shows the 2D NAD Q-COSY spectrum of (±)-CP recorded over 14 h (overnight) with digital filtering and oversampling in order to enhance the dynamic range of the analogue-to-digital converter (ADC).[52,53] The 2D contour plot is symmetrized prior to the tilt procedure and is displayed in

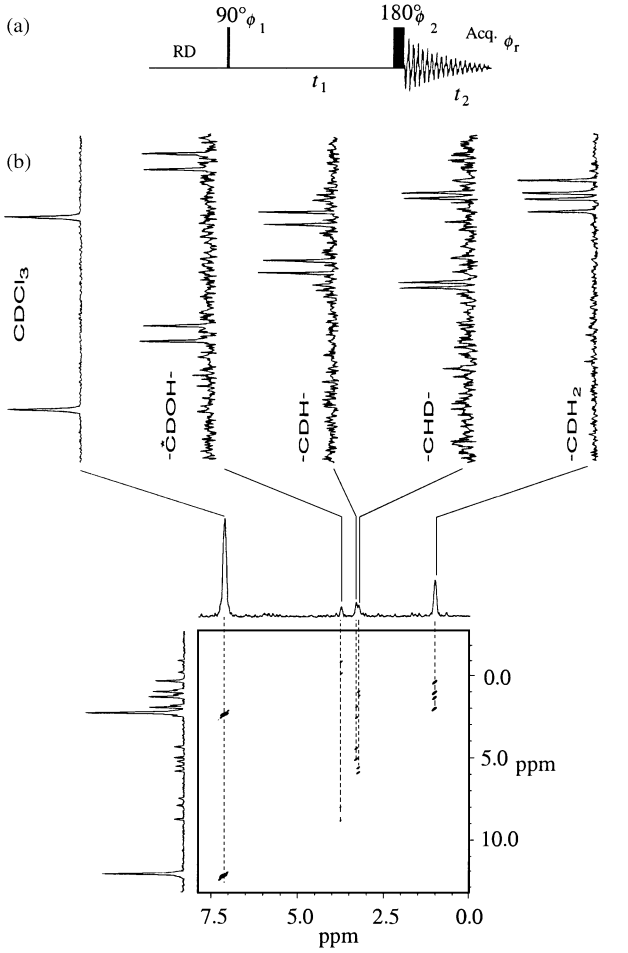

Fig. 7 (a) Basic Q-COSY pulse scheme for deuterium 2D NMR spectroscopy in partially ordered solvents. (b) 61.4 MHz tilted NAD Q-COSY 2D spectrum of the (±)-CP in PBLG and slices parallel to the ω_1 axis corresponding to the deuterium spectrum of each monodeuterated isotopomer in the mixture. The number of free induction decays added for each t_1 increment is 384. The recycling delay was 0.5 s and the spectral width in both dimensions was 2500 Hz. The data matrix of 300 (t_1) $\times$ 1400 (t_2) was weighted with a gaussian window (GB_1 = 50%, LB_1 = −2.0 Hz and GB_2 = 45%, LB_2 = −1.5 Hz) in t_1 and t_2 dimensions, respectively, and zero-filled to 512 (t_1) $\times$ 2048 (t_2) prior to 2D FT.

magnitude mode in order to cancel out the phase-twist lineshapes.[6] In this 2D spectrum, the chemical shift of each non-equivalent deuteron appears in the F_2 dimension. From each of them, we can observe the deuterium signals of the corresponding isotopomers in the mixture, the most unshielded trace (7.3 ppm) being the chloroform quadrupolar doublet. The analysis of each slice indicates that all deuterons in the molecule exhibit two quadrupolar doublets, one for each enantiomer. In particular the two diastereotopic deuterons of the methylene group distinctly show two pairs of quadrupolar doublets which are not centered on the same chemical shift. Strong differences of *S/N* ratio for each extracted slice are observed. This situation reflects that the number of equivalent deuterons (magnetic equivalence) for the various possible isotopomers is different. Thus, the signals associated with the deuteron attached to the asymmetric carbon are three times smaller than the signal of the methyl group, and hence the strong reduction of *S/N* ratio observed on the corresponding trace. The precision of the enantiomeric measurement for (±)-CP was not investigated here, but previous results have shown that such determination is possible within an accuracy of *ca.* 10% for reasonable *S/N* ratio, thus already giving a valuable estimation of the enantiomeric excess.[6]

Finally it should be noted that chloroform is the most efficient solvent for NAD NMR in PBLG. Apart from the fact that it dissolves a wide range of organic compounds, the linewidths at half-height of solutes measured on the ^{2}H-{^{1}H} spectra are usually low (2–8 Hz). Second, this solvent contains a single deuterated isotopomer giving rise only to a single additional quadrupolar doublet in the NAD spectrum. Third, the number of deuterons per unit volume is not excessively large relative to those of the chiral solutes, thus minimizing the digitization problems associated with the dynamic range of the ADC. Fourth, the deuterium signal of chlorofom can be used as an internal reference for the NAD spectra.

With this last analytical approach, we show that the enantiomeric discrimination of (±)-CP in 2D NAD-NMR using a 9.4 T field and standard NMR equipment is possible. These present results confirm the feasibility, potential and usefulness of NAD NMR spectroscopy, thus providing a further practical solution to DOE measurements in PBLG without site-specific isotopic labelling. In spite of the natural low sensitivity of deuterium, there is no doubt that, by taking advantage of higher magnetic field NMR spectrometers, it should be possible to acquire NAD spectra with shorter experimental times or determine enantiomeric excesses to a higher precision.[6] Indeed the *S/N* ratio is proportional to $(B_o)^{3/2}$ for a given experimental time t_{exptl} while t_{exptl} is proportional to $(B_o)^3$ for a given *S/N* ratio. To illustrate this, Fig. 8 shows the relationship between the total experimental time t_{exptl} and the *S/N* ratio with respect to values calculated with our 9.4 T spectrometer. Thus, when recording the NAD spectra of (±)-CP at 122.8 MHz (18.8 T), the *S/N* ratios would be increased by a factor of 2.8 for the same t_{exptl}. Conversely, the t_{exptl} would be reduced by a factor of 8 to obtain the same *S/N* ratio that is obtained at 400 MHz. This, incidently, means that the *S/N* ratio of 20 measured here for the methyl group on the NAD spectra of (±)-CP would become *ca.* 60 at 18.4 T under the same experimental conditions. Such a *S/N* ratio would then result in an acceptable error in the determination of enantiomeric excesses. Another and probably cheaper solution to improve the *S/N* ratio of NAD spectra would consist in using selective, deuterium cryogenic probes. Indeed the present developments and studies of such cryoprobes have shown a very significant gain of the signal sensitivity (a factor 3 to 4) compared with standard high resolution probes.[54] Consequently the use of both higher field and deuterium cryoprobes should quickly establish that NAD 2D NMR spectroscopy is the most general and powerful technique for analysing chiral molecules in PBLG.

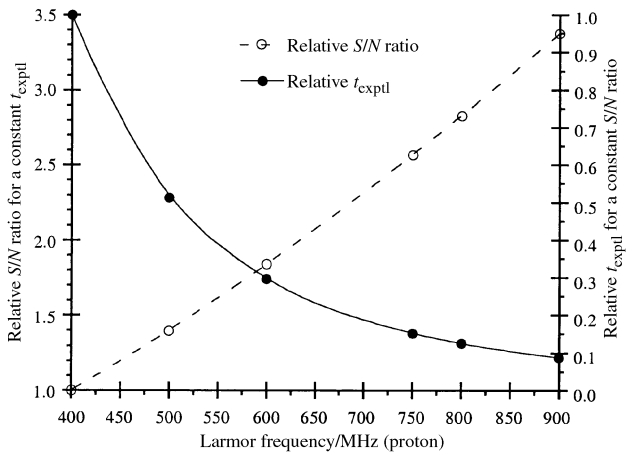

Fig. 8 Evolution of the relative *S/N* ratio and the relative t_{exptl} as a function of the Larmor frequency with respect to a 9.4 T (400 MHz for proton) spectrometer. The reference value at 400 MHz is 1.

Comparison of the various analytical potentialities of each technique

To compare and discuss the analytical potentialities of these various natural abundance NMR approaches, we have reported their respective features in terms of NMR and enantiomeric analysis in Table 1. Each of these NMR tools possesses advantages and drawbacks in terms of resolution, signal sensitivity, data presentation, complexity of spectral analysis, quality of chiral discrimination and accuracy in enantiomeric measurements. The choice of the technique to be used depends therefore on both chemical as well as NMR features of the chiral molecule (size of the molecule, functional groups, isolated group of nuclei, hybridization state of carbons, equivalent nuclei in deuterated isotopomers,…) and the available amount of material under investigation in comparison with its molecular weight.

Although too large a number of interacting protons in the molecule yields generally unresolved, overcrowded ^{1}H spectra in PBLG and prevents their analysis, it is always worthwhile to record such spectra to detect any separation of enantiomers through a difference in the residual ^{1}H–^{1}H dipolar couplings for small, chiral, functionalized molecules (which are usually precursors of larger target molecules) or compounds having isolated groups far removed from other protons in the molecule. Indeed for such compounds, we may expect well resolved spectral patterns for both enantiomers, allowing the ee to be measured to a high accuracy.

For larger molecules, proton-decoupled carbon-13 NMR spectroscopy is an excellent alternative to ^{1}H NMR since it prevents overcrowded carbon-13 NMR spectra. The spectra are relatively easy to analyse and the measurement of ee values is possible and reliable[40,41] with a reasonable amount of compound. However when ^{13}C-{^{1}H} NMR fails by a lack of spectral resolution or negligible DOEs, the proton-coupled carbon-13 NMR can provide a useful alternative, in particular, for chiral derivatives exhibiting an isolated group (such as a methyl group) in the molecule. Finally, whilst noting the problem of deuterium sensitivity, NAD 2D NMR spectroscopy seems particularly well adapted for medium to large, functionalised or non-functionalised, chiral molecules because of the strong sensitivity of the quadrupolar interaction toward the DOE and the relatively simple analysis of 2D Q-COSY spectra.

Pragmatically, it is clear that chiral molecules possessing sp^2 or sp carbons have a strong probability to be differentiated using ^{13}C-{^{1}H} NMR with a satisfactory accuracy (*ca.* 5%) on the measurement of enantiomeric excess while no significant chiral discrimination would be expected to occur for chiral, non-functionalised molecules such as alkanes or cycloalkanes; conversely, NAD 1D and 2D NMR spectroscopy seems to be

Table 1 Comparative table of various natural abundance NMR experiments for the chiral analysis in PBLG phases using a high resolution 400 MHz spectrometer

Nuclei observed	Natural isotopic abundance (%)	NMR sequence used	Useful anisotropic observables	Spectral analysis	Sensitivity to chiral differentiation	Signal sensitivity	Required amount for a racemic mixture[c]/mg	Average experimental time[c]/h	Estimated error on ee (%)
^{1}H	99.9	1D S.P.A.[a]	^{1}H–^{1}H dipolar couplings	Difficult or impossible[b]	Low	Very high	2–10	< 0.5	< 5
^{13}C	1.1	1D S.P.A.[a]	^{13}C–^{1}H dipolar couplings	Simple to difficult	Low to good	Low	20–60	2–8	5–10
^{13}C-{^{1}H}	1.1	1D S.P.A.[a]	^{13}C CSA	Simple	Low to good	Low to high	20–50	1–4	3–5
^{13}C–^{13}C	0.012	2D (INADEQUATE)	^{13}C–^{13}C dipolar couplings	Simple to difficult	Very low	Very low	80–100	12–15	15–20
^{2}H-{^{1}H}	0.015	1D S.P.A. 2D (Q-COSY)	^{2}H quadrupolar splittings	Simple	Strong	Very low	50–100	12–15	10–15

[a] S.P.A = single pulse-acquisition sequence. [b] Impossible when the line broadenings give unresolved spectra. [c] Values assuming that the MW of enantiomers to be studied is in the range 100–200.

more adapted for such compounds for which ^{13}C-{^{1}H} NMR is of less value. Indeed we may assume that the difference in the interactions between *S* and *R* isomers and the polypeptide will generate a rather small DOE and consequently only a very sensitive order-dependent NMR interaction such as the quadrupolar interaction may reveal an enantiomeric discrimination.[55] In addition, if the chiral molecule possesses magnetically equivalent deuterons (a methyl group), we may reach an adequate *S/N* ratio using a reasonable quantity of chiral material after an overnight acquisition. Although to date the accuracy on the measurements of enantiomeric excesses for reasonable signal-to-noise ratios are not better than 10%, the obtained experimental results already provide a very valuable estimation of ee values. In addition this technique allows a rapid and simple determination of the best site of chiral discrimination in the molecule and subsequently, may aid in selection of the most suitable synthetic strategy for introducing a deuteron in the molecule.

For all possible anisotropic natural abundance NMR techniques in PBLG the advantages of using higher magnetic field and/or a cryoprobe are obvious both in terms of chemical shift dispersion and *S/N*, the main benefit resulting in the higher precision in the calculation of ee values. We may expect that the approaches described here provide a very reliable alternative to current analytical techniques in the isotropic phase.

Conclusion

The differentiation and the study of enantiomers is a challenging task. In this field, multinuclear NMR spectroscopy in the PBLG phase provides an efficient and convenient analytical tool to differentiate almost all possible enantiomers. The major interest of this methodology is that the polypeptide helices are able to interact enantioselectively with almost all enantiomers and give sufficiently large orientational differences to be revealed by almost all the routine NMR tools. In addition, the advent of routine high magnetic fields has made possible the observation of nuclei with very low sensitivity with acceptable *S/N* ratios such as deuterium at the natural abundance level. Here, we have shown, as illustrative examples, that it is possible to discriminate the *S* and *R* isomers of (±)-1-chloropropan-2-ol using proton, carbon-13 and deuterium spectroscopy on a single NMR sample. For almost all of the NMR methods reviewed, quantitative determination of enantiomeric purity is possible with a sufficient accuracy from simple peak integration. Nevertheless, each technique described here possesses both advantages and drawbacks in terms of signal sensitivity, complexity of spectral analysis, quality of chiral discrimination and accuracy in measurements of ee values. The choice of the best NMR technique for a given compound will depend on both the chemical and NMR features of the chiral molecule and obviously the available amount of material. This choice, however, does not exclude the examination of other possible NMR techniques in PBLG when the results obtained are not convincing. In comparison to other NMR methods for chiral discrimination, the use of this emerging methodology offers therefore important advantages in terms of flexibility and versatility and provides a useful new NMR analytical tool. Besides, it has the valuable advantage that no labelling or any chemical modification of the chiral material is needed and the NMR requirements are not different compared to those for other isotropic methods.

This analytical method, characterized by its simplicity and adequate sensitivity, should certainly be considered as a powerful alternative to classical chiroptical, chromatographic or other NMR techniques. In this review, we have attempted to point out that this non-familiar tool for organic chemists is probably the most general method for the purpose of enantiomeric analysis. Finally, there is no doubt that by routinely taking advantage of higher magnetic field NMR spectrometers and/or using double tuned (carbon-13 and deuterium) cryogenic probe systems, the present potentialities of all these techniques should become evident and definitely establish the significant advantages of this strategy in the very near future.

In order to further evaluate the applicability, advantages and limitations of this methodological approach, additional work is still required and is currently being undertaken.

Acknowledgements

We gratefully thank Professor J. W. Emsley and Professor A. Loewenstein for stimulating discussions.

Notes and references

1 D. Parker, *Chem. Rev.*, 1991, **91**, 1441.
2 D. Parker and R. J. Taylor, *Asymmetric Synthesis*, Chapman and Hall, University Press, Cambridge, 1992.
3 A. Meddour, I. Canet, A. Loewenstein, J. M. Péchiné and J. Courtieu, *J. Am. Chem. Soc.*, 1994, **116**, 9652.
4 I. Canet, J. Courtieu, A. Loewenstein, A. Meddour and J. M. Péchiné, *J. Am. Chem. Soc.*, 1995, **117**, 6520.
5 A. Meddour, P. Berdagué, A. Hedli, J. Courtieu and P. Lesot, *J. Am. Chem. Soc.*, 1997, **119**, 4502.
6 D. Merlet, B. Ancian, J. Courtieu and P. Lesot, *J. Am. Chem. Soc.*, 1999, **121**, 5249.
7 E. E. Sackmann, S. Meiboom and L. C. Snyder, *J. Am. Chem. Soc.*, 1968, **90**, 2183.
8 E. E. Sackmann, S. Meiboom, L. C. Snyder, A. E. Meixner and R. E. Dietz, *J. Am. Chem. Soc.*, 1968, **90**, 3567.
9 P. Lesot, Y. Gounelle, D. Merlet, A. Loewenstein and J. Courtieu, *J. Phys. Chem.*, 1995, **99**, 14871; (correction), 1995, **100**, 14569.
10 P. Lesot, D. Merlet, T. P. Rantala, J. Jokisaari, J. W. Emsley and J. Courtieu, *J. Phys. Chem. A*, 1997, **101**, 5719.
11 J. W. Emsley and J. C. Lindon, *NMR Spectroscopy Using Liquid Crystal Solvents*, Pergamon Press, Oxford, 1975.

12 M. Jakubcova, A. Meddour, J. M. Péchiné, A. Baklouti and J. Courtieu, *J. Fluorine Chem.*, 1997, **86**, 149.
13 E. Graf, R. Graf, M. W. Hosseini, C. Huguenard and F. Taulelle, *Chem. Commun.*, 1997, 1459.
14 E. Lafontaine, J. P. Bayle and J. Courtieu, *J. Am. Chem. Soc.*, 1989, **111**, 8294.
15 J. Courtieu, E. Lafontaine, J. M. Péchiné and C. L. Mayne, *Liq. Cryst.*, 1990, **7**, 293.
16 P. Lesot, D. Merlet, A. Loewenstein and J. Courtieu, *Tetrahedron Asymmetry*, 1998, **9**, 1871.
17 K. Tabayashi and K. Akasaka, *Liq. Cryst.*, 1998, **1**, 127.
18 C. L. Khetrapal, K. V. Ramanathan, N. Suryaprakash and S. Vivekanandan, *J. Magn. Reson.*, 1998, **135**, 265.
19 A. Elliot and E. J. Ambrose, *Discuss. Faraday Soc.*, 1950, **9**, 246.
20 C. Robinson, *Trans. Faraday Soc.*, 1956, **52**, 571.
21 C. Robinson, *Mol. Cryst.*, 1966, **1**, 467.
22 K. Czarniecka and E. T. Samulki, *Mol. Cryst. Liq. Cryst.*, 1981, **63**, 205.
23 A. L. Lehninger, *Biochemistry*, Worth Publishers, Inc, New York, 1978.
24 P. Doty, J. H. Bradbury and A. M. Holtzer, *J. Am. Chem. Soc.*, 1956, **78**, 947.
25 L. Pauling, R. B. Corey and H. R. R. Brandson, *Proc. Natl. Acad. Sci.*, 1951, **37**, 205.
26 T. J. McMaster, H. J. Carr, M. J. Miles, P. Cairns and V. J. Morris, *Macromolecules*, 1991, **24**, 1428.
27 M. Panar and W. D. Phillips, *J. Am. Chem. Soc.*, 1968, **90**, 3880.
28 E. T. Samulski and A. V. Tobolsky, *Macromolecules*, 1968, **1**, 155.
29 P. Doty, J. H. Bradbury and A. M. Holtzer, *J. Am. Chem. Soc.*, 1956, **78**, 947.
30 J. C. Mitchell, A. E. Woodward and P. Doty, *J. Am. Chem. Soc.*, 1957, **79**, 3955.
31 C. Canlet, D. Merlet, P. Lesot, A. Meddour, A. Loewenstein and J. Courtieu, *Tetrahedron: Asymmetry*, 2000, **11**, 1911.
32 P. Lesot, D. Merlet, A. Meddour, A. Loewenstein and J. Courtieu, *J. Chem. Soc., Faraday Trans.*, 1995, **91**, 1371.
33 H. O. Kalinowski, S. Berger and S. Braun, *Carbon-13 NMR Spectroscopy*, Wiley and Sons, Chichester, 1984.
34 E. H. Hardy, R. Witt and M. D. Zeidler, *J. Magn. Reson.*, 1998, **134**, 300.
35 E. R. Blout, R. H. Karlson, P. Doty and B. Hargitay, *J. Am. Chem. Soc.*, 1954, **76**, 4492.
36 E. R. Blout and R. H. Karlson, *J. Am. Chem. Soc.*, 1954, **76**, 941.
37 R. Albert, J. Danklmaier, H. Honig and H. Kandolf, *Synthesis*, 1987, 635.
38 A. J. Shaka, J. Keeler and R. Freeman, *J. Magn. Reson.*, 1983, **53**, 335.
39 The simulation program 'PANIC' is marketed by Bruker SA.
40 V. Madiot, P. Lesot, D. Gree, J. Courtieu and R. Gree, *Chem. Commun.*, 2000, 169.
41 O. Dirat, C. Kouklovsky, Y. Langlois, P. Lesot and J. Courtieu, *Tetrahedron: Asymmetry*, 1999, **10**, 3197.
42 R. R. Ernst, G. Bodenhausen and A. Wokaun, *Principles of Nuclear Magnetic Resonance in One and Two Dimensions*, Clarendon Press, Oxford, 1987.
43 G. Wagner and E. R. P. Zuiderweg, *Biochem. Biophys. Res. Commun.*, 1983, **113**, 854.
44 G. Otting and K. Wüttrich, *J. Magn. Reson.*, 1986, **66**, 359.
45 A. Bax, *Two-dimensional Nuclear Magnetic Resonance in Liquids*, Delft University Press, Dordrecht, Holland, 1984.
46 D. Sandstrom, K. T. Summamen and M. H. Levitt, *J. Am. Chem. Soc.*, 1994, **116**, 9357.
47 J. P. Bayle, J. Courtieu, E. Gabetty, A. Loewenstein and J. M. Péchiné, *New J. Chem.*, 1992, **16**, 837.
48 I. Canet, A. Meddour, J. Courtieu, J. L. Canet and J. Salaün, *J. Am. Chem. Soc.*, 1994, **116**, 2155.
49 W. Smadja, S. Auffret, P. Berdagué, D. Merlet, C. Canlet, J. Courtieu, J. Y. Legros, A. Boutros and J. C. Fiaud, *Chem. Commun.*, 1997, 2031.
50 D. Merlet, B. Ancian, W. Smadja, J. Courtieu and P. Lesot, *Chem. Commun.*, 1998, 2301.
51 D. Merlet, M. Sarfati, B. Ancian, J. Courtieu and P. Lesot, *Phys. Chem. Chem. Phys.*, 2000, **2**, 2283.
52 R. Freeman, *A Handbook of Nuclear Magnetic Resonance*, A. W. Longman Limited, Essex, 2nd edn., 1997, p. 258.
53 A. Belguise, *Analusis*, 1995, **23**, M57.
54 Y. W. Kim, W. L. Earl and R. E. Norberg, *J. Magn. Reson.*, 1995, **116**, 139.
55 M. Sarfati, J. Courtieu and P. Lesot, *Chem. Commun.*, 2000, 1113.

Copper(I) mediated radical polymerisation of uridine and adenosine monomers on a silica support†

Andrew Marsh,* Afzal Khan, Margarita Garcia and David M. Haddleton

Department of Chemistry, University of Warwick, Coventry, UK CV4 7AL. E-mail: a.marsh@warwick.ac.uk

Received (in Cambridge, UK) 19th July 2000, Accepted 14th September 2000
First published as an Advance Article on the web 3rd October 2000

Copper(I) mediated radical polymerisation is used to polymerise uridine and adenosine substituted methacrylates onto a silica surface giving supported polymers with potential as re-usable templates and for interaction with nucleic acids.

The immobilisation of polymers on solid supports and surfaces is of considerable interest for a number of applications. For example, derivatisation of surfaces for biocompatibility[1] and the production of sensors[2] is of interest to the biotechnology industry and new resins are being sought for application to solid supported organic synthesis.[3] Automated synthesis of oligonucleotides on solid supports is performed routinely for the production of short strands of DNA and RNA or their synthetic analogues.[4] Solid supported oligonucleotides are finding applications in medical diagnostics[5] and hence numerous methods have appeared in the literature for derivatising solid supports for oligonucleotide synthesis and attaching oligonucleotides to support media.[6] Having placed an oligonucleotide onto a solid support it has been shown to be possible to employ this as a re-usable template to synthesise complementary strands of DNA. Ashley and MacDonald[7] attached a naturally occurring segment of DNA directly to diazobenzyloxymethyl-cellulose and then used this to synthesise complementary strands of DNA which could be washed away and the template re-used repeatedly. This work involved using enzymes and primers however, and the solid supported template was only made on a very small scale. We have recently shown that it is possible to carry out the templated polymerisation of an unnatural backbone polyacryloylnucleoside by using non-polar solvents to maximise interactions between complementary base pairs.[8] This communication describes the synthesis of a re-usable template prepared on a silica support for use in such a polymerisation reaction.

Transition metal mediated living radical polymerisation[9] is an efficacious method for the preparation of narrow polydispersity (PDI) methacrylic and styrenic polymers, as it allows controlled synthesis of structurally diverse polymers due to its living or pseudo-living nature.[10] Such polymerisations can be performed in the presence of many functional groups and solvents which other living polymerisation methods, such as ionic or group transfer polymerisations cannot tolerate.[11] Metal mediated radical polymerisation on solid supports has been the subject of a number of recent reports. Tsujii and co-workers modified the surface properties of silica by immobilising a chlorosulfonyl phenyl moiety on silica wafers and using this for living polymerisation of MMA.[12] Matyjaszewski and co-workers carried out atom transfer radical polymerisation of styrene and acrylates on silica wafers to give homopolymers and block co-polymers.[13] Nitroxide mediated polymerisation has been utilized on Merrifield resin to produce 'designer resins' with functional properties.[14] This present work describes the application of copper(I) mediated radical polymerisation to the biologically significant nucleoside derivatives 5′-methacryloyluridine **1** and 5′-methacryloyladenosine **2** on silica gel functionalised with a bromoisobutyrate initiator (**3** or **4**) to give surfaces of considerable potential (Fig. 1).

† Electronic supplementary information (ESI) available. Experimental procedures and details. See http://www.rsc.org/suppdata/cc/b0/b005832g/

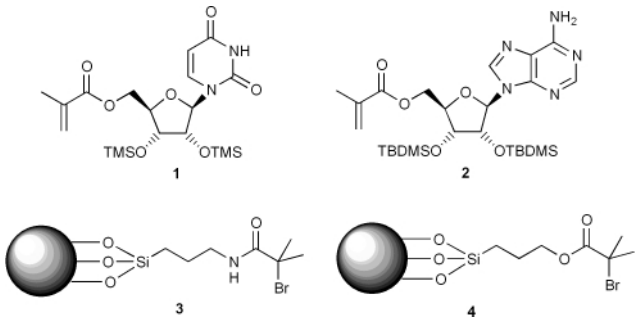

Fig. 1 Monomers and silica supported initiators used in this study.

The 5′-methacryloyluridine **1** and 5′-methacryloyladenosine **2** were synthesised using a modified procedure of Moris and Gotor,[15] using the enzyme *Candida antarctica lipase* 435 (CAL 435) with an activated acetoneoxime ester.[16] In order to make these monomers soluble in suitable polymerisation solvents and to aid polymer characterisation the 2′- and 3′-hydroxy groups were protected as silyl ethers. The adenosine monomer, being more polar, required the larger *tert*-butyldimethylsilyl (TBDMS) protecting groups. The amidic initiator **3** was synthesised using commercially available 3-aminopropylsilica and bromoisobutyroyl bromide in the presence of triethylamine base and THF solvent. The ester initiator **4** was synthesised as follows (Scheme 1). Firstly bromoisobutyroyl bromide was reacted with allyl alcohol in the presence of triethylamine to give **5** in 98% yield.[17] This was then treated with trimethoxysilane in the presence of a catalytic amount of hexachloroplatinic acid[18] to give the trimethoxysilyl bromoisobutyrate initiator **6** in 62% yield. The derivatised silica was then prepared by refluxing trimethoxysilyl bromoisobutyrate **6** with TLC grade silica gel in toluene for 22 h (Scheme 1). TLC grade silica gel was used because of its larger surface area and it has been shown previously that attachment of a trimethoxysilyl group to silica gel gives better loading than powdered silica due to the former having porous particles.[19] This was found to have a loading of 0.61 mmol g^{-1} as determined by Thermal Gravimetric Analysis (TGA).

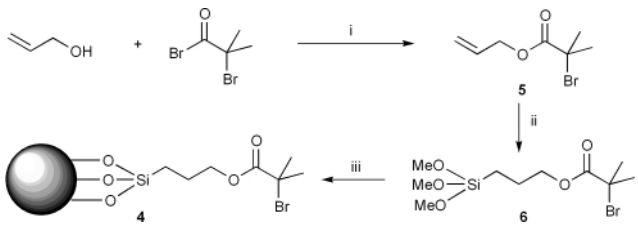

Scheme 1 *Reagents and conditions*: i, Et_3N, THF (98%); ii, $(MeO)_3SiH$, H_2PtCl_6 (98%); iii, silica gel, PhMe, reflux.

Copper(I) mediated radical polymerisation of uridine monomer **1** with the amidic solid supported initiator **3** was attempted using *N*-(*n*-pentyl)-2-pyridylmethanimine (NPMI) as a ligand in conjunction with copper(I) bromide (Scheme 2). However, this initiator was found to give a loading of only 0.87 mmol g^{-1} (Table 1). Changing the ligand to Me_6Tren[20] gave a slightly

DOI: 10.1039/b005832g

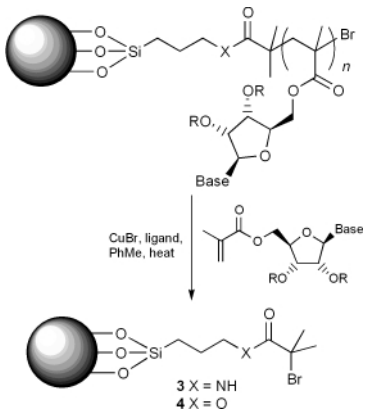

Scheme 2 Copper(I) mediated radical polymerisation of 5'-methacryloylnucleosides.

Table 1 Monomer loading for initiators **3** and **4**

Initiator	Monomer	Ligand	Loading (mmol g^{-1})	Increase in initiator weight(%)
3	**1**	NPMI	0.87	53
3	**1**	Me_6Tren	0.80	48
4	**1**	NPMI	1.51	188
4	**2**	NPMI	1.11	117
4	**1**/**2**	NPMI	1.04	105

lower loading of 0.80 mmol g^{-1}. It has been suggested by Matyjaszewski that amidic initiators are prone to intramolecular reactions in the early stages of living radical polymerisation caused by the nitrogen lone pair.[21] The non-amidic solid supported initiator **4** was therefore synthesised. Use of this initiator for polymerisation of **1** almost doubled the loading to 1.51 mmol g^{-1} using NPMI as the ligand. Fig. 2 shows the FT-IR of the immobilised polymer clearly demonstrating the broad N–H signal from 3700–2900 cm^{-1} and the carbonyl stretch at 1683 cm^{-1}. Polymerisation of 5′-methacryloyladenosine **2** using initiator **4** gave a lower loading of 0.96 mmol g^{-1}. This reflects the lower yields obtained with this functionally more complex monomer during solution phase copper(I) mediated radical polymerisations (see ref. 16). Statistical co-polymerisation of **1** and **2** was also successful giving a loading of 1.04 mmol g^{-1}. This was calculated by taking into account the ^{1}H NMR of the unreacted monomers in the filtrate which showed a 15:85 ratio of **1**:**2**, indicating that the co-polymer is rich in uridine.

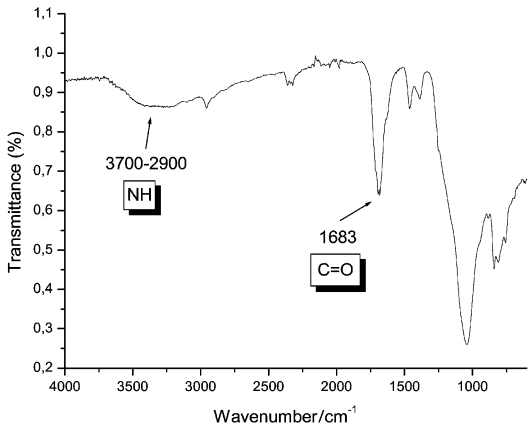

Fig. 2 IR of poly(5′-methacryloyluridine) on silica.

In summary it has been shown that copper(I) mediated radical polymerisation of the multifunctional nucleosides uridine and adenosine methacrylates is possible using a bromoisobutyrate initiator bound to silica giving surface attached homopolymers and statistical co-polymers with good loading. Although we cannot unequivocably describe this polymerisation as *living* from these experiments, we know that similar conditions bring about a controlled polymerisation. Other work has shown[22] that these conditions favour narrow polydispersity products, indicative of a living radical polymerisation.[23] To our knowledge this is the first time controlled radical polymerisation has been used to immobilise biologically important nucleosides to a solid support. Investigations into the use of these immobilised biopolymers as re-usable templates for polymerisations and their interaction with nucleic acids are under way.

We are grateful to the University of Warwick for a postdoctoral fellowship (A. K.), the EPSRC for a Fast Stream Studentship (M.G.; GR/L71933) and Novo Nordisk for a generous donation of CAL 435. We also thank Dr Stefan Bon for supplying the amidic solid supported initiator **3**.

Notes and references

1 M. Mrksich and G. M. Whitesides, *Ann. Rev. Biophys. Biomol. Struct.*, 1996, **25**, 55.
2 *Sensors: a Comprehensive Survey*, ed. W. Göpel, J. Hesse and J. N. Zemel, VCH, Weinheim, 1991, vols. 2 and 3.
3 B. Yan, *Acc. Chem. Res.*, 1998, **31**, 621; A. G. M. Barrett, S. M. Cramp and R. S. Roberts, *Org. Lett.*, 1999, **1**, 1083.
4 M. H. Caruthers, *Science*, 1985, **230**, 281; S. Iwai, T. Sasaki and E. Ohtsuka, *Tetrahedron*, 1990, **46**, 6673.
5 P. O. Brown and D. Botstein, *Nat. Genet.*, 1999, **21**, 33 (supplement).
6 M. J. O'Donnell-Maloney, C. L. Smith and C. R. Cantor, *Trends Biotechnol.*, 1996, **14**, 401.
7 P. L. Ashley and R. J. Macdonald, *Anal. Biochem.*, 1984, **140**, 95.
8 A. Khan, D. M. Haddleton, M. J. Hannon, D. Kukulj and A. Marsh, *Macromolecules*, 1999, **32**, 6560.
9 M. Kato, M. Kamigaito, M. Sawamoto and T. Higashimura, *Macromolecules*, 1995, **28**, 1721; J. S. Wang and K. Matyjaszewski, *J. Am. Chem. Soc.*, 1995, **117**, 5614.
10 M. Sawamoto and M. Kamigaito, *Trends Polym. Sci.*, 1996, **4**, 371; T. E. Patten and K. Matyjaszewski, *Acc. Chem. Res.*, 1999, **32**, 89.
11 O. W. Webster, *Science*, 1991, **251**, 887.
12 M. Ejaz, S. Yamamoto, K. Ohno, Y. Tsujii and T. Fukuda, *Macromolecules*, 1998, **31**, 5934.
13 K. Matyjaszewski, P. J. Miller, N. Shukla, B. Immaraporn, A. Gelman, B. B. Luokala, T. M. Siclovan, G. Kickelbick, T. Vallant, H. Hoffmann and T. Pakula, *Macromolecules*, 1999, **32**, 8716.
14 J. C. Hodges, L. S. Harikrishnan and S. Ault-Justus, *J. Comb. Chem.*, 2000, **2**, 80.
15 F. Moris and V. Gotor, *J. Org. Chem.*, 1993, **58**, 653.
16 A. Marsh, A. Khan, D. M. Haddleton and M. J. Hannon, *Macromolecules*, 1999, **32**, 8725.
17 R. T. Arnold and S. T. Kulenovic, *J. Org. Chem.*, 1978, **43**, 3687.
18 F. Effenberger and S. Heid, *Synthesis*, 1995, 1126.
19 G. Kickelbick, H. J. Paik and K. Matyjaszewski, *Macromolecules*, 1999, **32**, 2941.
20 *N*, *N*′, *N*″-Hexamethyl tris(2-aminoethyl)amine: M. Ciampolini and N. Nardi, *Inorg. Chem.*, 1966, **5**, 41.
21 M. Teodorescu and K. Matyjaszewski, *Macromolecules*, 1999, **32**, 4826.
22 S. Angot, S. A. F. Bon, N. Ayres and D. M. Haddleton, *Macromolecules*, submitted.
23 T. R. Darling, T. P. Davis, M. Fryd, A. A. Gridnev, D. M. Haddleton, S. D. Ittell, R. R. Matheson, G. Moad and E. Rizzardo, *J. Polym. Sci. Part A - Polym. Chem.*, 2000, **38**, 1706.

ChemComm

Metallacyclophanes formed by a tetrapyrazolyl ligand and copper(II) cation

Abdelaziz Jouaiti, Marielle Loï, Mir Wais Hosseini* and André De Cian

Laboratoire de Chimie de Coordinaiton Organique, Université Louis Pasteur, F-67000 Strasbourg, France, UMR CNRS 7513. E-mail: hasseini@chimie.u-strasbg.fr

Received (in Cambridge, UK) 15th August 2000, Accepted 18th September 2000
First published as an Advance Article on the web 19th October 2000

Using a tetrakis(pyrazolyl)benzene ligand and $CuCl_2$ or $Cu(CF_3SO_3)_2$ salts, binuclear metallamacrocycles of cyclophane type have been exclusively obtained; structural characterisation by X-ray on single-crystal reveals that in both cases, chloride or triflate anions are coordinated to Cu metal centres adopting a square pyramial coordination geometry.

Metallamarocycles, macrocyclic frameworks based on interconnection of organic ligands by metal cations, have been attracting much attention over the past decade. Although the first examples were reported by Saalfrank *et al.*[1] and Fujita,[2] many other groups are now active in the design and synthesis of metallamacrocyles.[3] However, as connecting metallic centres the majority of examples reported so far are based on the use of diamagnetic transition metals such as Pd(II) and Pt(II) requiring square coordination geometry. Thus, using these metals, a variety of metallamacrocycles has been reported using ligands such as 4,4′-bipyridine, pyrimidine, bipyrazine, 4,7-phenanthroline or bis-pyridines interconnected by rigid or flexible spacers.[4] Using pyrazolyl based ligands, we have previously reported the formation of metallamacrocycles and metallatubulanes.[5]

Here, we report the design of new ligands based on pyrazolyl units as coordination sites and its self-assembly into binuclear metallamacrocycles using pentacoordinated paramagnetic Cu(II) cation.

Ligands **1** and **2** (Scheme 1), both based on aromatic cores (benzene or biphenyl) and bearing four pyrazolyl units, are designed to act as tetradentate ligands. For ligand **1**, two different arrangements of the coordination sites may be envisaged leading to either a seven (**1A**) or an eight membered ring cyclic system (**1B**) upon chelating to metal cations (Scheme 1). In both cases, owing to the disposition of the coordination sites ligand **1** may form metallamacrocyles in the presence of metals requiring square, octahedral or square pyramidal coordination geometry. For the latter case, the two possibilities (**4A** and **4B**) are shown (Scheme 1). Ligand **2** was designed as an extended analogue of ligand **1** thus allowing an increase in the size of the metallamacrocycle.

Ligand **1** was first prepared in 8% yield by reacting 1,2,4,5-tetrachlorobenzene with sodium pyrazolate in DMF at 95 ° C for 3 d. The yield could be increased to 68% by using 1,2,4,5-tetrabromobenzene and under reflux for 72 h. Pure compound **1** was obtained as a colourless solid after chromatography (SiO_2, CH_2Cl_2–MeOH) and was characterised by X-ray crystallography† (Fig. 1) which revealed the following relevant bond distances and angles (d_{NN} = 1.37 Å, $d_{C(Ph)N}$ = 1.42 Å; NNCC dihedral angles of −25.8 and −77.2°). Ligand **2** was prepared by a nickel coupling reaction using $NiBr_2(PPh_3)_2$[6] in the presence of Zn and NEt_4I in THF using compound **3** as the starting material. The latter was obtained upon treatment of 1,3,5-benzene by sodium pyrazolate in DMF at 95 °C for 4 d in 22% yield after chromatography [Al_2O_3, CH_2Cl_2–hexane (8/2)].

Cu(II) was selected as the metal ion because of its paramagnetic nature and the fact that it forms pentacoordinated complexes. Both the chloride and triflate Cu(II) complexes have been obtained as single-crystals upon slow diffusion of a MeOH solution of $CuCl_2$ or $Cu(OTf)_2$ (5 mg) into a $CHCl_3$ solution of ligand **1** (2 mg). For both complexes, their structure was investigated in the cystalline state by X-ray crystallography.

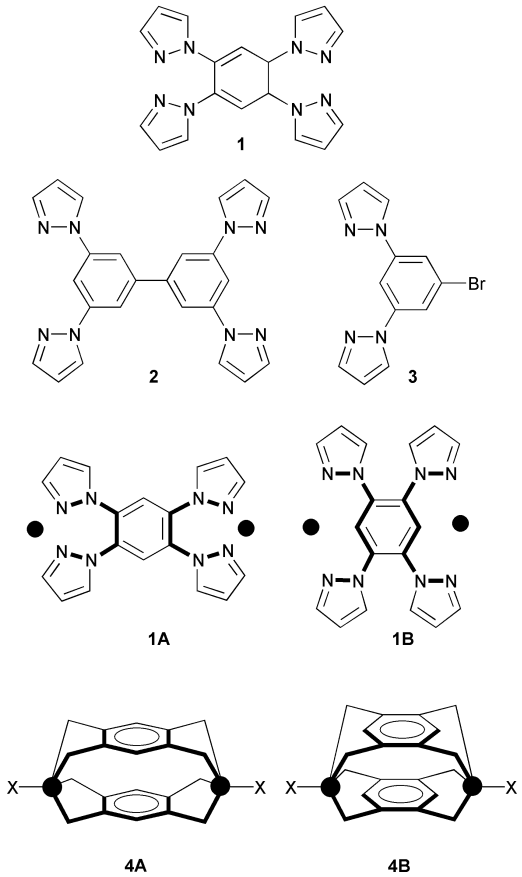

Scheme 1

The reaction of **1** and $CuCl_2$ in $CHCl_3$–MeOH afforded a green crystalline material which was structurally characterised by X-ray diffraction (Fig. 2).† The solid contains the complex unit [$\mathbf{1}_2Cu_2(Cl_2(CuCl_4)_2)$] and two MeOH and $CHCl_3$ solvent molecules with no specific interactions with the complex. The cationic part of the complex is indeed a metallamacrocycle composed of two ligands **1**, two Cu(II) cations and two Cl^-

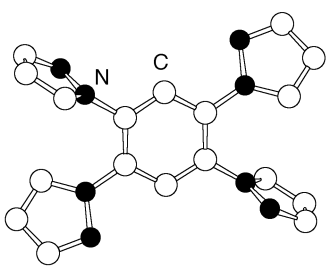

Fig. 1 The X-ray structure of free ligand **1**. H atoms are omitted for clarity, for bond length and distances see text.

DOI: 10.1039/b006665f

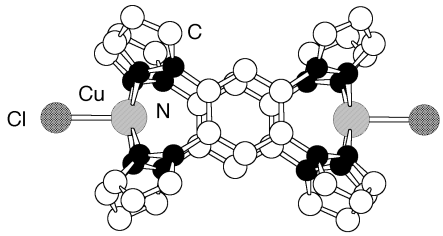

Fig. 2 The X-ray structure of the metalloamacrocycle $[\mathbf{1}_2Cu_2Cl_2]^{2+}$ obtained between **1** and $CuCl_2$. H atoms, anions and solvent molecules are omitted for clarity.

anions. Owing to the parallel orientation of the two phenyl rings, the binuclear metallamacrocycle is of the cyclophane type with an internal cavity of 4.29 × 7.42 Å (Scheme 1). The coordination sphere around the pentacoordinated Cu(II) cations is composed of four nitrogen atoms belonging to two ligands **1** and one chloride anion with a slightly distorted square pyramidal geometry. The two poles of the ligand **1**, composed each of two pyrazolyl moieties (d_{NN} = 1.37 Å, $d_{C(Ph)N}$ = 1.42 Å; NNCC dihedral angle of 57.8°) and occupying the square base in the coordination sphere around the metal, act as bidentate units and form two seven membered metallarings of type **4A** (Scheme 1) with Cu–N distances of *ca*. 2.01 Å and NCuN angles of 86.9–91.4° (Scheme 1). The axial position is occupied by a Cl anion with Cu–Cl distance of 2.44 Å. The two positive charges on the $[\mathbf{1}_2Cu_2Cl_2]^{2+}$ complex are neutralised by a $[CuCl_4]^{2-}$ anion with d_{CuCl} = 2.283 Å and ClCuCl angle of 90° (Fig. 3).

The $[\mathbf{1}_2Cu_2(CF_3SO_3)_2(CF_3SO_3)_2]$ complex was obtained as a blue-violet crystalline solid upon reaction of **1** and $Cu(CF_3SO_3)_2$ in $CHCl_3$–MeOH. The latter complex was also structurally characterised by X-ray diffraction (Fig. 4).† The solid contains the complex unit $[\mathbf{1}_2Cu_2(CF_3SO_3)_2(CF_3SO_3)_2]$ and two CH_2Cl_2 solvent molecules with no specific interactions with the complex. The triflate anions are disordered. The cationic part of the complex of type **4A** (Scheme 1) shows almost identical structural features as the above chloride complex (Scheme 1). Again a metallamacrocycle (internal cavity of 4.16 Å × 7.29 Å) composed of two ligands **1**, two Cu(II) cations and two triflate anions is observed. The coordination sphere around the pentacoordinated Cu(II) cations is, as in the chloride case, comprised of four nitrogen atoms belonging to two ligands **1** and one triflate anion (d_{NN} = 1.38 Å $d_{C(Ph)N}$ = 1.42 Å; NNCC dihedral angles of −59.6 and 58.9°, Cu–N distances of *ca*. 1.99 Å and NCuN angles of 87.4–92.6°. Interestingly, the axial position is occupied by a triflate anion with Cu–O distance of 2.20 Å. The two positive charges on the $[\mathbf{1}_2Cu_2(CF_3SO_3)_2]^{2+}$ complex are neutralised by two external triflate anions (Fig. 4).

We have previously reported examples of metallatubulanes based on interconnection of metallamacrocyles into infinite 1-D

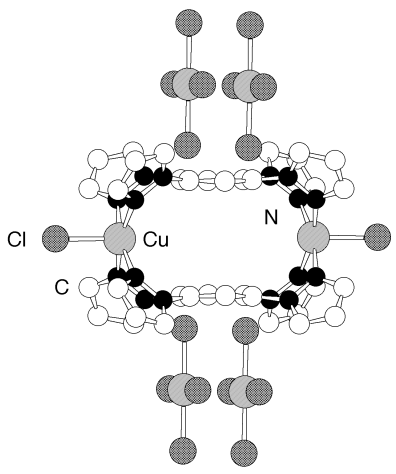

Fig. 3 The packing of the dicationic metallamacrocycle $[\mathbf{1}_2Cu_2Cl_2]$ and $CuCl_4^{2-}$ anions. H atoms and solvent molecules are not presented for clarity.

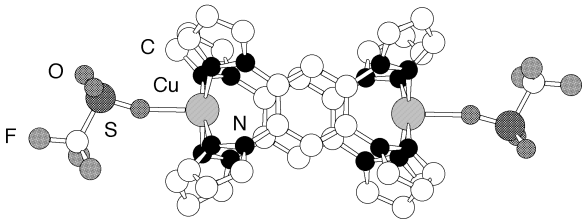

Fig. 4 The X-ray structure of the metallamacrocycle $[\mathbf{1}_2Cu_2(CF_3SO_3)_2]^{2+}$ obtained between **1** and $Cu(CF_3SO_3)_2$. Then triflate anions are disordered. H atoms, anions and solvent molecules are omitted for clarity.

coordination networks with tubular topology.[5,7,8] In relation to this, it may be of interest that, since the two anions occupying the summit of the square pyramid on each Cu centre are oriented in a divergent fashion, by interconnecting the metalloacyclophanes new types of coordination polymers may be obtained using bridging bidentate anionic ligands such as azido or isocyanato anions.

In conclusion, the synthesis of paramagnetic binuclear copper metallacyclophanes has been achieved and their solid state structural elucidation revealed that the Cu(II) cation adopts a slightly distorted square pyramidal geometry with the axial position occupied either by chloride or triflate anion. The formation of extended metallacyclophanes using ligand **2** is being currently pursued. Furthermore, the interconnection of the obtained metallamacrocyles leading to paramagnetic coordination networks through the substitution of monodentate coordinated anions by bidentate anions is currently under investigation.

Notes and references

† *Crystal data*: (colourless, 294 K), $C_{18}H_{14}N_8$, M = 342.37, triclinic, a = 6.384(1), b = 7.007(1), c = 9.941(1) Å, α = β = 76.00, γ = 80.00, U = 416.5(2) Å^3, Z = 1, space group $P\bar{1}$, D_c = 1.36 g cm^{-3}, μ = 0.089 mm^{-1}, 1508 data with $I > 3\sigma(I)$, R = 0.040, R_w = 0.0649. [($\mathbf{1}_2Cu_2Cl_2(CuCl_4)$)], (green, 294 K), $2(CuClC_{18}H_{14}N_8)\cdot CuCl_4\cdot 2CHCl_3\cdot 2MeOH$, M = 1390.91, orthorhombic, a = 10.0302(5), b = 11.3568(6), c = 23.5388(7) Å, U = 2681.3(4) Å^3, Z = 2, *Immm*, D_c = 1.72 g cm^{-3}, μ = 1.830 mm^{-1}, 1486 data with $I > 3\sigma(I)$, R = 0.042, R_w = 0.052. [$\mathbf{1}_2Cu_2(CF_3SO_3)_2(CF_3SO_3)_2$], (blue-violet, 173 K), $C_{38}H_{28}Cu_2F_6N_{16}O_6S_2\cdot 2CF_3SO_3\cdot 2CH_2Cl_2$ M = 1577.95, orthorhombic, a = 19.7081(7), b = 17.9293(6), c = 17.1966(6) Å, U = 6076.5(6) Å^3, Z = 4, space group *Cmca* D_c = 1.72 g cm^{-3}, μ = 1.121 mm^{-1}, 2127 data with $I > 3\sigma(I)$, R = 0.077, R_w = 0.096. Data for all 3 structures have been obtained on a Nonius Kappa CCD (Mo-Kα) diffractometer Structural determinations were performed using the Nonius OpenMolenN package.[9] CCDC 182/1781. See http://www.rsc.org/suppdata/cc/b0/b006665f/ for crystallographic data in .cif format.

1 R. W. Saalfrank, A. Stark, K. Peters and H.-G. von Schnering, *Angew. Chem., Int. Ed.*, 1988, **27**, 851.

2 M. Fujita, in *Comprehensive Supramolecular Chemistry*, ed. J. L. Atwood, J. E. D. Davies, D. D. MacNicol and F. Vögtle, Vol. 9 (ed. J. P. Sauvage and M. W. Hosseini, Elsevier, 1996, p. 253).

3 J. K. M. Sanders, *in Comprehensive Supramolecular Chemistry*, ed. J. L. Atwood, J. E. D. Davies, D. D. MacNicol and F. Vögtle, Vol. 9 (ed. J. P. Sauvage and M. W. Hosseini), Elsevier, 1996, p. 131; P. J. Stang and B. Olenyuk, *Acc. Chem. Res.*, 1997, **30**, 502; C. M. Drain and J.-M. Lehn, *J. Chem. Soc., Chem. Commun.*, 1994, 2313; T. Beissel, R. E. Powers and K. N. Raymond, *Angew. Chem., Int. Ed. Engl.*, 1996, **35**, 1084.

4 C. V. Krishnamohan Sarma, S. T. Griffin and R. D. Rogers, *Chem. Commun.*, 1998, 215; R.-D. Schnebeck, L. Radaccio, E. Zangrando and B. Lippet, *Angew. Chem., Int. Ed.*, 1988, **37**, 119; J. R. Hall, S. J. Loeb, G. K. H. Shimizu and G. P. A. Yap, *Angew. Chem., Int. Ed.*, 1998, **37**, 121; R. Schneider, M. W. Hosseini, J.-M. Planeix, A. De Cian and J. Fischer, *J. Chem. Soc., Chem. Commun.*, 1988, 1625.

5 M. Loï, M. W. Hosseini, A. Jouaiti, A. De Cian and J. Fischer, *Eur. J. Inorg. Chem.*, 1999, 1981.

6 M. Iyoda, H. Otsuka, K. Sato, N. Nisato and M. Oda, *Bull. Chem. Soc. Jpn.*, 1990, **63**, 80; V. K. Yamamoto, *Bull. Chem. Soc. Jpn.*, 1954, **27**, 501.

7 G. Mislin, E. Graf, M. W. Hosseini, A. De Cian, N. Kyritsakas and J. Fischer, *Chem. Commun.*, 1998, 2545.

8 C. Klein, E. Graf, M. W. Hosseini, A. De Cian and J. Fischer, *Chem. Commun.*, 2000, 239.

9 OpenMolenN, Interactive Structure Solution, Nonius B. V., Delft, The Netherlands, 1997.

Nitrogen ligands on a phosphinic Lewis acceptor including a 2,2′-dipyridyl chelate complex

Neil Burford,*[a] T. Stanley Cameron,[a] Katherine N. Robertson,[a] Andrew D. Phillips[a] and Hilary A. Jenkins[b]

[a] *Department of Chemistry, Dalhousie University, Halifax, Nova Scotia, B3H 4J3, Canada. E-mail: burford@is.dal.ca*

[b] *Department of Chemistry, Saint Mary's University, Halifax, Nova Scotia, B3H 3C3, Canada*

Received (in Irvine, CA, USA) 28th June 2000, Accepted 12th September 2000
First published as an Advance Article on the web 9th October 2000

In the context of the developing coordination chemistry of lone pair bearing phosphinic centers as acceptors, synthesis and characterisation for new complexes of the phosphadiazonium cation with nitrogen donors are described, including the first dipyridyl chelate.

The coordination chemistry of phosphorus(V) as an acceptor is well established[1,2] and is highlighted by hexacoordinated centers such as PF_6^- and the pyridine complex of PF_5.[3] The Lewis acidity of phosphines represents a more recent and developing area and demonstrates interesting bonding properties by virtue of the non-bonding electron pair at the acceptor site. Systems **1**, **2** and **3**, containing coordinatively unsaturated

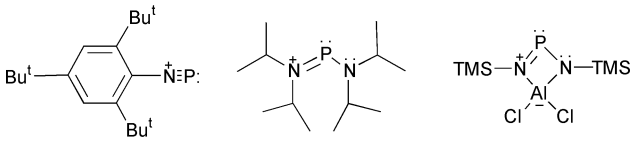

1 **2** **3**

phosphinic centers form complexes with amines,[4–7] phosphines,[8] carbenes[9] and arenes,[10] and an example of a bis-ligand complex has been mentioned.[11] We have now developed the coordination chemistry of the phosphadiazonium cation **1** with nitrogen donors, and have isolated the first chelate complex.

Reactions of [**1**][OSO_2CF_3][12] with equimolar amounts of quinuclidine (1-azabicyclo[2.2.2]octane, quin) or 2,2′-dipyridyl (dipyr) proceed almost instantaneously and quantitatively at RT as shown by ^{31}P NMR spectra of reaction mixtures, which are consistent with those for solutions of isolated crystalline products.†‡ Comprehensive characterisation, including X-ray crystallographic analysis, confirm 1:1 association of the reagents and the compounds are best represented as coordination complexes [**1**·quin][OSO_2CF_3] and [**1**·dipyr][OSO_2CF_3] involving phosphorus as an acceptor. Selected structural features for **1**·quin and **1**·dipyr are presented in Table 1 in comparison with analogous parameters for related complexes.

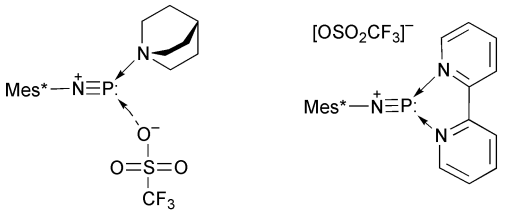

[**1**•quin][OSO_2CF_3] [**1**•dipyr][OSO_2CF_3]

Mes* = 2,4,6-tri-*tert*-butylphenyl

The N→P interactions are weak and variable in distance (*cf.* N–P single bond distance 1.800(4) Å),[13] but effect extension of the P–O(triflate) cation–anion interaction, which is most pronounced for the ionic material [**1**·dipyr][OSO_2CF_3]. The chelate complexation of **1** by dipyr, illustrated in Fig. 1, is

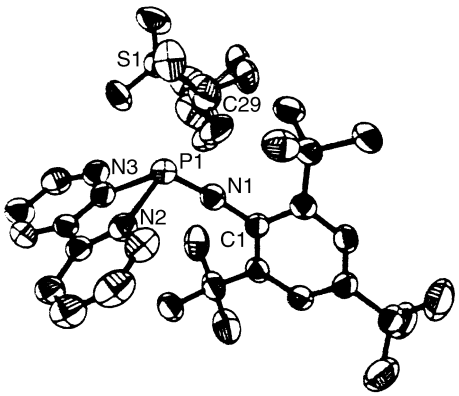

Fig. 1 Crystallographic view of [**1**·dipyr][OSO_2CF_3] with 50% probability displacement ellipsoids. The hydrogen atoms and dichloromethane solvate have been omitted. The CF_3 group of the triflate anion is disordered.

Table 1 Selected structural parameters for complexes of **1**, **2** and **3** with nitrogen donors (pyr = pyridine, DBN = 1,5-diazabicyclo[4.3.0]non-5-ene, tmeda = tetramethylethylenediamine)

Compound	N–P (Å)	N→P/Å	P–O/Å	Mes*N–P–N/°	(Mes*)C–N–P/°	Ref.
1	1.467(4)	—	1.923(3)	—	176.4(3)	12
[**1**·quin][OSO_2CF_3]	1.519(2)	1.933(2)	2.697(3)	103.7(1)	143.9(2)	This work
[**1**·pyr][OSO_2CF_3]	1.472(8)	1.958(8)	2.712(7)	107.8(4)	161.7(7)	9
[**1**·dipyr][OSO_2CF_3]	1.497(4)	2.065(4), 2.066(4)	3.490(6)	106.3(2), 113.0(2)	169.4(4)	This work
[**2**·DBN][Cl]	1.661(4), 1.666(4)	1.796(3)	—	101.6(2), 99.1(2)	—	5,6
3·quin	1.686(9), 1.660(9)	2.038(9)	—		—	7
(**3**)$_2$·tmeda	1.658(5), 1.661(5)	2.110(6)	—		—	7

DOI: 10.1039/b005265p

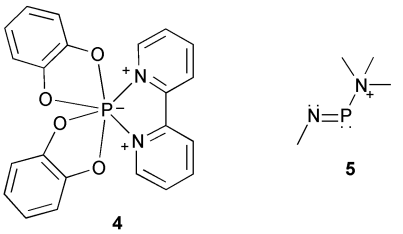

4

5

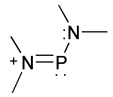

6

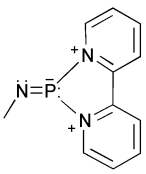

7

defined by two indistinguishable N→P interactions, contrasting the asymmetric chelate-like cation–anion contact reported for the diselenophosphinate salt of **1**,[14] and complementing the established series of 2,2′-dipyridyl complexes of $AsCl_3$,[15] $SbCl_3$,[16] and $BiCl_3$[17] that could not be extended to PCl_3.[18]

A pyramidal geometry for phosphorus in **1**·dipyr accommodates the non-bonding electron pair and offers interesting comparisons with the hexafluorophosphate salt of phosphonium **4**,[2] which involves a distorted octahedral site. The 'bite' (N–P–N) angle in **1**·dipyr (75.1(2)°) is substantially less than in **4** (81.7(2)°), due to significantly longer N→P bond distances (*cf.* **4**, 1.896(4) and 1.898(4) Å). Coordinate interactions are demonstrated in both complexes by the small N–C–C(bridge) angles (**1**·dipyr, 111.9(4), 113.6(4)°; **4**, 112.0(4), 112.2(4)°).

Complexes of nitrogen ligands on phosphinic centers provide access to new bonding environments for phosphorus in that [**1**·quin]$^+$ represents a novel structural isomer **5** of a diaminophosphenium cation **6** and **1**·dipyr represents a cationic iminophosphide[9] bonding environment **7**, both of which are synthetically accessible only *via* the coordination chemistry of phosphorus as an acceptor.

We thank the Natural Sciences and Engineering Research Council of Canada (N. B, T. S. C.) and the Killam Foundation (N. B.) for funding, the Walter Sumner Foundation for a scholarship (A. D. P.), the Atlantic Regional Magnetic Resonance Centre for the use of instrumentation and Dr D.J. LeBlanc for helpful discussion.

Notes and references

† Procedures described in ref. 19, equimolar combinations in benzene, crystals obtained by liquid/liquid (CH_2Cl_2 and n-hexane) diffusion; [**1**·quin][OSO_2CF_3]: yield 0.07 g, 21%; mp 176–178 °C; Anal. Calcd.: C, 56.71; H, 7.69; N, 5.09. Found: C, 57.10; H, 8.38; N, 5.12%. IR (cm^{-1}, ranked intensities): 516(16), 637(2), 752(10), 763(13), 877(17), 891(20), 923(19), 966(15), 1005(14), 1026(1), 1147(9), 1163(8), 1226(7), 1241(3), 1257(5), 1278(6), 1339(11), 1365(4), 1417(12), 1600(18). NMR (ppm, in CD_2Cl_2): ^{1}H 1.31 (s, 9H, *p*-(CH_3)$_3$C), 1.47 (s, 18H, *o*-(CH_3)$_3$C), 1.98, (m, 6H, HC(CH_2)$_3$), 2.16 (sept, $^3J(^1H,^1H)$ = 3.35 Hz, 1H, *H*C(CH_2)$_3$), 3.43 (m, 6H, (CH_2)$_3$N), 7.40 (d, $^5J(^{31}P,^1H)$ = 1.53 Hz, 2H, *m*-C*H*); ^{13}C{^{1}H} 20.8 (s, H*C*(CH_2)$_3$), 24.6 (s, HC(CH_2)$_3$), 31.4 (s, *o*-(CH_3)$_3$C), 31.5 (s, *p*-(CH_3)$_3$C), 35.5 (s, *p*-(CH_3)$_3$*C*), 36.5 (s, *o*-(CH_3)$_3$*C*), 48.1 (s, N(*C*H_2)$_3$), 121.3 (q, $^1J(^{19}F,^{13}C)$ = 319 Hz, *C*F_3), 123.2 (s, *m*-CH), 136.9 (d, $^2J(^{31}P,^{13}C)$ = 26.2 Hz, *i*-*C*NP), 140.4 (d, $^3J(^{31}P,^{13}C)$ = 8.11 Hz, *o*-(CH_3)$_3$C*C*), 150.0 (s, *p*-(CH_3)$_3$C*C*); ^{19}F{^{1}H} −78.8 (s, $^1J(^{19}F,^{13}C)$ = 319 Hz); ^{31}P{^{1}H} 144 (s). [**1**·dipyr][OSO_2CF_3]: yield 0.29 g, 84%; mp 201 °C. CH_2Cl_2 of crystallisation has precluded determination of elemental analysis. IR (cm^{-1}, ranked intensity): 1602(14), 1491(8), 1446(5), 1392(18), 1364(15), 1314(16), 1280(2), 1275(3), 1256(4), 1226(11), 1160(7), 1151(9), 1032(1), 1014(10), 778(12), 768(17), 755(20), 651(13), 639(6), 518(19); NMR (ppm, in CD_2Cl_2): ^{1}H 1.27 (s, 9H, *p*-(CH_3)$_3$C), 1.31 (s, 18H, *o*-(CH_3)$_3$C), 7.31 (d, $^5J(^{31}P,^1H)$ = 1.83 Hz, 2H, *m*-C*H*) 7.99 (m, $^3J(^1H,^1H)$ = 6.95 Hz, $^3J(^1H,^1H)$ = 7.55 Hz, 2H, 5,5′-C*H*), 8.54 (m, $^3J(^1H,^1H)$ = 6.95 Hz, $^3J(^1H,^1H)$ = 5.43, 2H, 4,4′-C*H*), 8.88 (mm, $^3J(^1H,^1H)$ = 7.55 Hz, 2H, 3,3′-C*H*), 8.99 (m, $^3J(^1H,^1H)$ = 5.43 Hz, 2H, 6,6′-C*H*); ^{13}C{^{1}H} 30.1 (s, *o*-(CH_3)$_3$C), 31.4 (s, *p*-(CH_3)$_3$*C*), 35.3 (s, *p*-(CH_3)$_3$*C*), 35.8 (s, *o*-(CH_3)$_3$*C*), 121.2 (q, $^1J(^{19}F,^{13}C)$ = 320 Hz, *C*F_3), 122.3 (s, 3,3′-CH), 122.6 (s, *m*-*C*H), 123.9 (s, 5,5′-*C*H), 128.5 (s, 4,4′-*C*H), 133.9 (d, $^3J(^{31}P,^{13}C)$ = 46.7 Hz, *i*-*C*NP), 144.6 (s, 6,6′-*C*H), 145.2, (s, 2,2′-N*CC*N), 145.5 (d, $^3J(^{31}P,^{13}C)$ = 14.3 Hz, *o*-(CH_3)$_3$C*C*), 148.6 (d, $^5J(^{31}P,^{13}C)$ = 4.29 Hz, *p*-(CH_3)$_3$C*C*); ^{19}F{^{1}H} −78.8 (s, $^1J(^{19}F,^{13}C)$ = 320 Hz); ^{31}P{^{1}H} 54 (s).

‡ *Crystal data*: for $C_{26}H_{42}F_3N_2O_3PS$. M = 550.65 g mol^{-1}, orthorhombic, $P2_12_12_1$, a = 29.469(2), b = 10.0650(6), c = 9.7745(6), Å, V = 2899.2(3) Å^3, T = 193 K, Z = 4, μ(Mo-Kα) = 0.215 mm^{-1}, 18488 measured reflections, 6851 unique, 326 refined parameters, $R[I^2 > 2\sigma(I^2)]$ = 0.0530, $wR2(F^2)$ = 0.1294, S = 1.037. For $C_{30}H_{39}Cl_2F_3N_3O_3PS$. M = 680.57 g mol^{-1}, monoclinic, $P2_1/a$, a = 18.4174(9), b = 10.9488(6), c = 19.213(1) Å, β = 116.924(1)°, V = 3454.3(3) Å^3, T = 193 K, Z = 4, μ(Mo-Kα) = 0.345 mm^{-1}, 20945 measured reflections, 8094 unique, 404 refined parameters with 29 restraints, $R[I^2 > 2\sigma(I^2)]$ = 0.1000, $wR2(F^2)$ = 0.2381, S = 1.173. CCDC 182/1780.

1 R. R. Holmes, *Chem. Rev.*, 1996, **96**, 927; R. R. Holmes, *Acc. Chem. Res.*, 1998, **31**, 535; F. Carre, C. Chuit, R. J. P. Corriu, P. Monforte, N. K. Nayyar and C. Reye, *J. Organomet. Chem.*, 1995, **499**, 147; K. Kamijo, A. Otoguro, K. Toyota and M. Yoshifuji, *Bull. Chem. Soc. Jpn.*, 1999, **72**, 1335; M. Meisel, P. Lonnecke, A. R. Grimmer and D. Wulff. Molder, *Angew. Chem., Int. Ed. Engl.*, 1997, **36**, 1869.

2 W.S. Sheldrick, A. Schmidpeter and T. von Criegern, *Z. Naturforsch., Teil B*, 1978, **33**, 583.

3 W. S. Sheldrick, *J. Chem. Soc., Dalton Trans.*, 1974, 1402.

4 R. W. Kopp, A. C. Bond and R. W. Parry, *Inorg. Chem.*, 1976, **15**, 3042; C. Payrastre, Y. Madaule, J. G. Wolf, T. C. Kim, M. R. Mazières, R. Wolf and M. Sanchez, *Heteroat. Chem.*, 1992, **3**, 157; T. Kaukorat, I. Neda and R. Schmutzler, *Coord. Chem. Rev.*, 1994, **137**, 53; Y. V. Balitzky, S. E. Pipko, A. D. Sinitsa, A. N. Chernega and Y. G. Gololobov, *Phosphorus Sulfur, Silicon*, 1993, **75**, 167; F. Carre, C. Chuit, R. J. P. Corriu, A. Mehdi and C. Reye, *J. Organomet. Chem.*, 1997, **529**, 59.

5 R. Reed, R. Réau, F. Dahan and G. Bertrand, *Angew. Chem., Int. Ed. Engl.*, 1993, **32**, 399.

6 G. Bouhadir, R. W. Reed, R. Reau and G. Bertrand, *Heteroat. Chem.*, 1995, **6**, 371.

7 N. Burford, P. Losier, P. K. Bakshi and T. S. Cameron, *Chem. Commun.*, 1996, 307.

8 N. Burford, T. S. Cameron, J. A. C. Clyburne, K. Eichele, K. N. Robertson, S. Sereda, R. E. Wasylishen and W. A. Whitla, *Inorg. Chem.*, 1996, **35**, 5460; R. W. Alder, D. D. Ellis, J. K. Hogg, A. Martin, A. G. Orpen and P. N. Taylor, *Chem. Commun.*, 1996, 537; R. W. Alder, D. D. Ellis, A. G. Orpen and P. N. Taylor, *Chem. Commun.*, 1996, 539; G. David, E. Niecke, M. Nieger, J. Radseck and W. W. Schoeller, *J. Am. Chem. Soc.*, 1994, **116**, 2191; N. Burford, T. S. Cameron, D. J. LeBlanc, P. Losier, S. Sereda and G. Wu, *Organometallics*, 1997, **16**, 4712.

9 N. Burford, T. S. Cameron, D. J. LeBlanc, A. D. Phillips, T. E. Concolino, K. C. Lam and A. L. Rheingold, *J. Am. Chem. Soc.*, 2000, **122**, 5413.

10 N. Burford, J. A. C. Clyburne, P. K. Bakshi and T. S. Cameron, *Organometallics*, 1995, **14**, 1578.

11 M. Blättner, A. Ruban, D. Gudat, M. Nieger and E. Niecke, *Phosphorus Sulfur, Silicon*, 1999, **147**, 31.

12 E. Niecke, R. Detsch, M. Nieger, F. Reichert and W.W. Schoeller, *Bull. Soc. Chim. Fr.*, 1993, **130**, 25.

13 T. S. Cameron, C. Chan and W. J. Chute, *Acta Crystallogr., Sect. B*, 1980, **36**, 2391.

14 E. Niecke, M. Nieger, F. Reichert and W. W. Schoeller, *Angew. Chem., Int. Ed. Engl.*, 1988, **27**, 1713.

15 J. U. Cameron and R. C. G. Killean, *Cryst. Struct. Commun.*, 1972, **1**, 31.

16 A. Lipka and H. Wunderlich, *Z. Naturforsch., Teil B*, 1980, **35**, 1548.

17 G. A. Bowmaker, F. M. M. Hannaway, P. C. Junk, A. M. Lee, B. W. Skelton and A. H. White, *Aust. J. Chem.*, 1988, **51**, 331.

18 W. R. Roper and C. J. Wilkins, *Inorg. Chem.*, 1964, **3**, 500.

19 N. Burford, J. Müller and T. M. Parks, *J. Chem. Educ.*, 1994, **71**, 807.

ChemComm

Chemical fixation of carbon dioxide to styrene carbonate under supercritical conditions with DMF in the absence of any additional catalysts

Hajime Kawanami*[ab] and Yutaka Ikushima[ab]

[a] *National Industrial Research Institute of Tohoku, 4-2-1 Nigatake, Miyagino-ku, Sendai 983-8551, Japan. E-mail: h-kawa@tniri.go.jp*
[b] *CREST, (JST), Tokyo 102-8666, Japan Science and Technology Corporation, Japan*

Received (in Cambridge, UK) 15th August 2000, Accepted 19th September 2000
First published as an Advance Article on the web 9th October 2000

Chemical fixation of carbon dioxide to styrene carbonate proceeds effectively under supercritical conditions with DMF even in the absence of any additional catalysts, giving a maximum yield of 85% in the near-critical region.

From the standpoint of the protection of environment, the development of an environmentally benign process utilizing carbon dioxide, which is one of the greenhouse-effect gases, has drawn current interest in industrial chemistry and biotechnology. Chemical fixation of carbon dioxide is one of the most attractive methods for the development of a truly environmentally benign process since there are many possibilities for carbon dioxide to be used as a safe and cheap C_1 component to produce useful organic compounds. The conversion of carbon dioxide into carbonates has been carried out in conventional organic solvents using catalysts such as dialkyltin methoxide,[1] organoantimony halide,[2] alkali metal salts[3] and Mg–Al mixed metal oxide.[4] In particular, the conversion of epoxides into five-membered cyclic carbonates is industrially of great importance. However, these reactions using metallic catalysts have disadvantages, such as poor solubility of the catalyst[3] and difficulties in catalyst recycling,[2] whereas $scCO_2$ has advantageous features such as the disappearance of a gas–liquid phase boundary and easily tunable properties with pressure and temperature which make $scCO_2$ an alternative to conventional solvents.[5] The reactions of epoxides with CO_2 under supercritical CO_2 conditions have been studied in the presence of zinc catalysts; however, they give a biphasic mode of operation leading to poor reaction rates.[6] It has recently been found that the reaction with epoxide and CO_2 proceeds in DMF alone without any catalysts at temperatures around 135 °C and atmospheric CO_2 pressure, but the yield of styrene carbonate still remains low.[4,7] This low reactivity may be due to a much lower mass transfer of epoxide in DMF solution, although DMF is considered to catalyze the reaction in a manner similar to the Mg–Al mixed catalysts.[4] Thus, our conception of using a co-solvent such as DMF both as a catalyst as well as a solvent in $scCO_2$ has emerged to improve the poor reaction rates, which are due to limitations in liquid–liquid mass transfer and/or low solubility of reactants.[5] DMF itself catalyzes the reactions of CO_2 with epoxides dissolved in DMF–$scCO_2$ which allows to advantage a reduction in viscosity and an increase in diffusion rate as compared with the DMF liquid phase.[8] Here we demonstrate integration of $scCO_2$ and DMF to accelerate the reaction of styrene oxide with CO_2 and to be a very powerful tool in the chemical fixation of CO_2 (Scheme 1).†

Carboxylation of styrene oxide with CO_2 has been conducted without additional catalysts under various conditions (see Table 1). Under these conditions, carbonate was the main product with trace amounts of a few by-products.‡ In acetone and acetonitrile, styrene oxide did not react with CO_2 and styrene carbonate was not obtained (runs 2 and 3). It is noteworthy that the conversion proceeds successfully even in the absence of the metallic catalysts used so far when DMF is used in the place of acetone and acetonitrile (run 1). This is believed to be due to catalysis by DMF itself because the substrates, styrene oxide and CO_2, have similarly finite solubilities in acetone and acetonitrile as well as DMF. When $scCO_2$ alone was used as medium instead of DMF, a very poor reaction was obtained (run 7), and the catalytic action of $scCO_2$ for this reaction was found to be negligibly small. In the case of the CO_2–DMF system at lower pressures such as 2.0 MPa (run 1), the yield of styrene

Scheme 1

Table 1 Carboxylation of epoxides with carbon dioxide in different reaction systems

Run	Reaction type	Substrate	Catalyst	Solvent system	Pressure/ MPa	Temperature/°C	Yield of carbonate (%)[a]
1	Biphasic		None	DMF–CO_2	2.0	135	29
2[b]	Biphasic		None	Acetone–CO_2	2.0	135	0
3[b]	Biphasic		None	Acetonitrile–CO_2	2.0	135	0
4	Biphasic		None	DMF–CO_2	2.0	107	0
5	Homogeneous		None	DMF–$scCO_2$	7.9	100	20
6	Homogeneous		None	DMF–$scCO_2$	7.9	150	85
7	Homogeneous		None	$scCO_2$	7.9	120	3.2
8[c]	Biphasic		MgO	DMF–CO_2	2.0	135	60
9	Homogeneous		None	DMF–$scCO_2$	7.9	120	83
10[d]	Biphasic	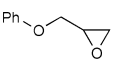	Mg–Al mixed oxide	DMF–CO_2	0.5	100	90(86)[e]

[a] The yields are determined by GC analysis based on the area ratio of tridecane or tetradecane as the internal references. [b] Reaction conditions: acetonitrile 5 mmol or acetone 5 mmol; styrene oxide 5 mmol; reaction time 15 h. [c] Ref. 7. [d] Ref. 4. [e] K. Yamaguchi *et al*. reported similar yields of the carbonate.

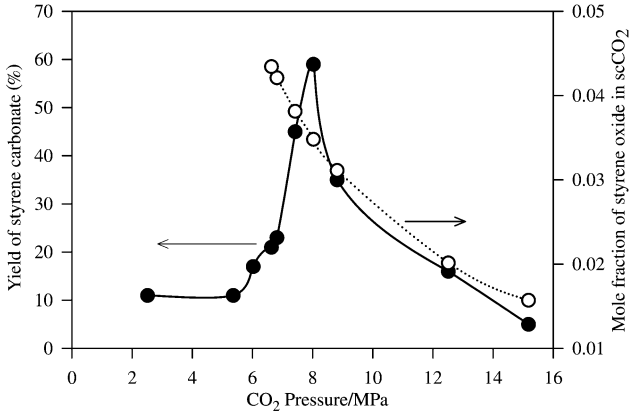

Fig. 1 Pressure dependence of the yield of styrene carbonate in CO_2 in the presence of DMF at 120 °C, and mole fraction of styrene oxide in $scCO_2$. Reaction time is 15 h. Mole fraction of styrene oxide was calculated using PROPATH Ver.10.2.

carbonate remains as low as 29%, whereas $scCO_2$–DMF (run 6) provides a much better yield compared with the CO_2–DMF system (29 to 85%) and the DMF–MgO system (60 to 85%). Furthermore, it was found that in the $scCO_2$–DMF system (run 5) styrene carbonate can be successfully synthesized even at lower temperatures around 100 °C, giving a better yield than that in the CO_2–DMF system (run 4) at 107 °C (0 to 20%). Gas–liquid–liquid mass transfer together with liquid–liquid mass transfer (solubility of substrate in catalyst or solvent phase) are important parameters for controlling the reaction yield. Visual observation through a sapphire window confirms that this $scCO_2$–DMF system forms a homogeneous reaction system, resulting in complete elimination of gas–liquid mass transfer, so that transport to and from the DMF phase is no longer a limiting factor. This is considered to be one of the most effective factors that cause the significant increase in yield as observed in Table 1.§ We have further attempted the conversion into another epoxide, 1,2-epoxy-3-phenoxypropane, using the $scCO_2$–DMF system at 7.9 MPa and 120 °C (run 9). This $scCO_2$–DMF system gives a good conversion to 3-phenoxy-1,2-propylcarbonate, the yield being comparable to that of the DMF–Mg/Al mixed oxide system (run 10). So this system can be available for acceleration of conversion from epoxides to carbonates.

Fig. 1 shows the pressure dependence of the yield of styrene carbonate in CO_2 in the presence of DMF at 120 °C. One can see an interesting pressure dependence in which the yield significantly increases, reaching a maximum yield at 7.9 MPa near the critical pressure of CO_2, and then sharply decreases with increasing pressure. In the lower pressure range below about 7 MPa, the yields are very small; DMF remains insoluble (by visual observation), leading to a much lower transfer of the epoxide. However, approach to the critical pressure with increasing pressure, which can dissolve DMF, significantly increases the rate of reaction and a higher yield is observed. On the other hand, the remarkable decrease in yield observed at higher pressures beyond 7.9 MPa near the critical pressure cannot be fully explained by the thermodynamic pressure effect, in which an increase in pressure is predicted to cause an enhancement in the reaction rate.[9] All experiments in the higher pressure range were confirmed by visual observation to take place in a single phase. To explain the decrease in yield with increasing pressure, we have attempted to introduce the mole fraction of styrene oxide in $scCO_2$ as shown in Fig. 1. It is evident that the extent of the decrease in yield of styrene carbonate is in agreement with that in mole fraction of styrene oxide except at 7.9 MPa near the critical pressure. If the reaction of styrene oxide with CO_2 is to take place by the catalysis of DMF, the molecules of styrene oxide and DMF must come into contact or very nearly so. Consequently, the decrease in mole fraction of styrene oxide in the higher pressure region prevents contact with DMF and reduces the yield of styrene carbonate. However, in the near-critical region the yield at 7.9 MPa is significantly higher than that expected from the relationship in Fig. 1, which cannot be accounted for only by the change in mole fraction of styrene oxide. It is likely that the increased local concentration[10,11] of the styrene oxide and/or CO_2 around the DMF is influencing the reaction, which becomes more pronounced at lower pressures in the near-critical region.[12,13] Thus, in the present conversion to styrene carbonate, the local concentration of reactants would be very large at 7.9 MPa near the critical pressure, resulting in the significant increase of the yield as seen in Fig. 1.

In conclusion, $scCO_2$–DMF was shown to be a good alternative catalytic system for conventional biphasic catalytic systems. It was further demonstrated that the yield of carbonates can be enhanced just by pressure manipulation of the $scCO_2$–DMF system.

Notes and references

† Typical experimental procedure is as follows: styrene oxide (5 mmol) was dissolved in DMF (5 mmol) in a 50 cm^3 reactor at rt, and then the mixture was heated up to the desired temperature and CO_2 (7.9 MPa) was introduced into the reactor. In the case of the $scCO_2$–DMF system, liquid CO_2 was subsequently charged into the reactor using a high-pressure liquid pump and compressed to the desired pressure. Pressure control was achieved by a back-pressure regulator. The reactions in both the CO_2–DMF and $scCO_2$–DMF systems were started by stirring the mixture and continued for 15 h. After the reaction, the pressure was released and the crude product was analyzed by NMR and GC-MS spectroscopy. The yields of carbonates were determined by GC-MS using tridecane or tetradecane as an internal standard.

‡ The total amount of these minor products is less than 1% from the GC analyses.

§ Another factor is thought to be solvation effect of CO_2, and studies on the solvation effect by IR and NMR are now in progress.

1 There are too many reports to list here. One of the latest reports dealing with carbonate is: J.-C. Choi, T. Sakakura and T. Sako, *J. Am. Chem. Soc.*, 1999, **121**, 3793.
2 H. Matsuda, A. Ninagawa, R. Nomura and T. Tuschida, *Chem. Lett.*, 1979, 573.
3 N. Kihara, N. Hara and T. Endo, *J. Org. Chem.*, 1993, **58**, 6198.
4 K. Yamaguchi, K. Ebitani, T. Yoshida, H. Yoshida and K. Kaneda, *J. Am. Chem. Soc.*, 1999, **121**, 4526.
5 P. G. Jessop, T. Ikariya and R. Noyori, *Nature*, 1994, **368**, 687; Y. Ikushima and M. Arai, *Chemical Synthesis using Supercritical Fluids*, P. G. Jessop and W. Leitner, eds., Wiley-VCH, Weinheim, 1999, ch. 4.3.
6 D. J. Darensbourg, N. W. Stafford and T. Katsurao, *J. Mol. Catal. A: Chem.*, 1995, **104**, L1.
7 T. Yano, H. Matsui, T. Koike, H. Ishiguro, H. Fujihara, M. Yoshihara and T. Maeshima, *Chem. Commun.*, 1997, 1129.
8 B. M. Bhanage, Y. Ikushima, M. Shirai and M. Arai, *Tetrahedron Lett.*, 1999, **40**, 6427; B. M. Bhanage, Y. Ikushima, M. Shirai and M. Arai, *Chem. Commun.*, 1999, 1277.
9 J. B. Ellington and J. F. Brennecke, *J. Chem. Soc., Chem. Commun.*, 1993, 1094.
10 Y. Ikushima, N. Saito, M. Arai and H. W. Blanch, *J. Phys. Chem.*, 1995, **99**, 8941.
11 T. W. Randolph, D. S. Clark, H. W. Blanch and J. M. Prausnitz, *Science*, 1988, **239**, 387.
12 S. Kim and K. P. Johnston, *AIChE J.*, 1987, **33**, 1603.
13 R. Wu, L. L. Lee and H. D. Cochran, *Ind. Eng. Chem. Res.*, 1990, **29**, 977.

ChemComm

Self-assembled organogels formed by monoalkyl derivatives of oxamide

Xuzhong Luo, Chun Li and Yingqiu Liang*

Institute of Mesoscopic Solid State Chemistry and State Key Laboratory of Coordination Chemistry, Nanjing University, Nanjing 210093, Peoples Republic of China

Received (in Cambridge, UK) 26th July 2000, Accepted 21st September 2000
First published as an Advance Article on the web 9th October 2000

The monoalkyloxamide amphiphiles self-assemble to form ordered bilayer aggregates in a number of organic liquids and gelatinize the liquids.

In recent years the study on the gelation of organic solvents by low molecular weight organic compounds has been growing into a challenging research field.[1–4] Some attempts have been made to correlate the properties of the gels and the structures of the gelators.[5–7] Nevertheless, to date, only a limited number of small molecular gelators have been found and it is impossible to select a molecule that will definitively gel a selected liquid.[1–7] It has been known that some amphiphiles containing amide groups and chiral centers can gel a number of organic liquids even at a very low concentration, while those lacking chiral centers or racemic compounds usually exhibit no gelling ability.[2] Herein, we report simple diamide amphiphiles, monoalkyloxamide containing no chiral centers, which can form ordered bilayer aggregates in a number of organic liquids and gelatinize the liquids.

The oxamide derivatives, **1**–**7**,† used here were prepared in our laboratory. A typical procedure for studying gel formation

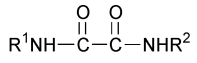

1 $R^1 = C_{14}H_{29}$, $R^2 = H$ **5** $R^1 = C_{14}H_{29}$, $R^2 = C_4H_9$
2 $R^1 = C_{18}H_{37}$, $R^2 = H$ **6** $R^1 = R^2 = C_{12}H_{25}$
3 $R^1 = C_{12}H_{25}$, $R^2 = H$ **7** $R^1 = R^2 = C_4H_9$
4 $R^1 = C_4H_9$, $R^2 = H$

ability is as follows: a weighed sample was mixed with an organic liquid (1 mL) in a sealed test tube and the mixture was heated until the solid dissolved. The resulting solution was cooled at 25 °C for 2 h and then the gelation was studied. Upon formation the organogel is stable and the tube can be inverted without any change of shape of the organogel.

The minimum gel concentrations of **1** necessary for gelation are summarized in Table 1. From Table 1, it is clear that **1** can form stable physical organogels and gelatinize a number of organic fluids even at a very low concentration. For example, the amounts of **1** necessary to gel one litre of carbon tetrachloride, benzene, toluene, *o*-xylene and dichloromethane are 3, 3, 3, 4 and 6 g, respectively.

The FT-IR spectrum of the KBr pellet of **1** is similar to that of the toluene gel, suggesting that the pattern of hydrogen bonding in the gel is close to that in the crystal. The FT-IR spectrum of the toluene gel of **1** is characterized by bands near 3386 (ν_{asNH2}), 3214 (ν_{sNH2}) and 1692 cm^{-1} ($\nu_{C=O}$ of primary amide) which are close to those of solid oxamide.[8,9] It has been known that the oxamide crystal has triclinic layer structure and the molecules within the layers are linked together by hydrogen bonds.[10] Therefore, it suggests that in the gel the primary amide groups (-$CONH_2$) of the amphiphiles are connected with each other by hydrogen bonds in the same way as in solid oxamide. FT-IR measurement also reveals a shift of NH stretching and secondary amide I ($\nu_{C=O}$) bands from 3440, 1680 cm^{-1} for a free secondary amide group (-NHCO-) to 3315, 1648 cm^{-1}, respectively.[11] These changes demonstrate that hydrogen bonds have formed between neighboring secondary amides. The above FT-IR results indicate that in the gel three self-complement intermolecular hydrogen bonds have been formed between an oxamido-group and its neighboring ones, and thus they form a hydrogen bond network.

The TEM image of a toluene gel of **1** is shown in Fig. 1. It reveals a number of fibers, juxtaposed and intertwined by several long slender aggregations with widths of *ca.* 30–100 nm. The X-ray diffraction patterns (Fig. 2) of the gel cast film show periodical diffraction peaks, indicating that **1** indeed assembles into an ordered structure. The long spacing (D) of the aggregate obtained by the XRD method is about 3.27 nm, which is smaller than twice the evaluated molecular length of **1** (2.35 nm, by the CPK model) but larger than the length of one molecule of **1**. According to the XRD and FT-IR results, it can be deduced that the gel aggregates consist of a repeating bilayer unit, which bears the head-to-head packing model and highly tilted alkyl chains relative to the bilayer

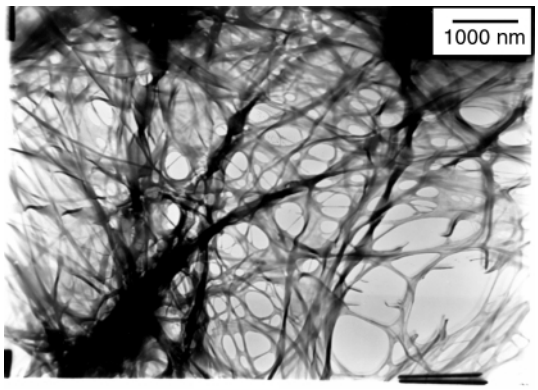

Fig. 1 TEM image of a toluene gel of **1** (4 g L^{-1}). The sample was prepared by picking up the gel on a carbon grid.

Table 1 Minimum gel concentration, *c*, of **1** (g L^{-1} solvent) necessary for gelation at 25 °C

Solvent	*c*	Stable period[a]	Solvent	*c*	Stable period[a]
Carbon tetrachloride	3	> 3 Months	Benzene	3	> 3 Months
Toluene	3	> 3 Months	*o*-Xylene	4	> 3 Months
Dichloromethane	6	> 3 Months	Acetonitrile	5	> 3 Months
1,2-Dichloroethane	6	> 3 Months	Aniline	6	> 3 Months
Tetrachloroethylene	6	> 3 Months	1,1,2-Trichloroethane	6	> 3 Months
Epichlorohydrin	5	> 3 Months	1,1,2,2-Tetrachloroethane	6	> 3 Months

[a] Stable period: the time which a gel persists in a sealed tube at 25 °C.

DOI: 10.1039/b005904h

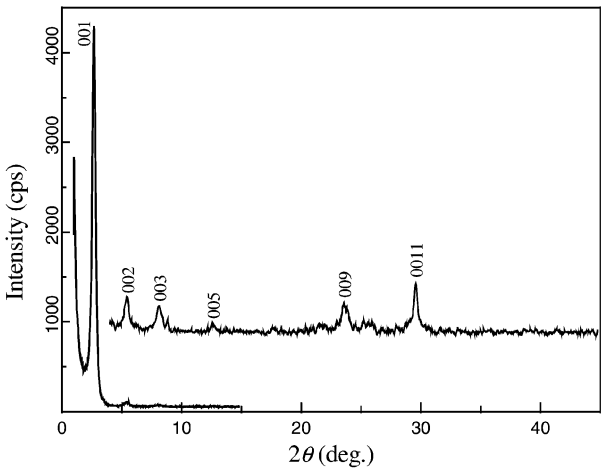

Fig. 2 XRD pattern of a cast film from toluene gel of **1**. (The XRD pattern has been adjusted by subtracting the diffraction of glass substrate in the range of (2θ) 16–32°).

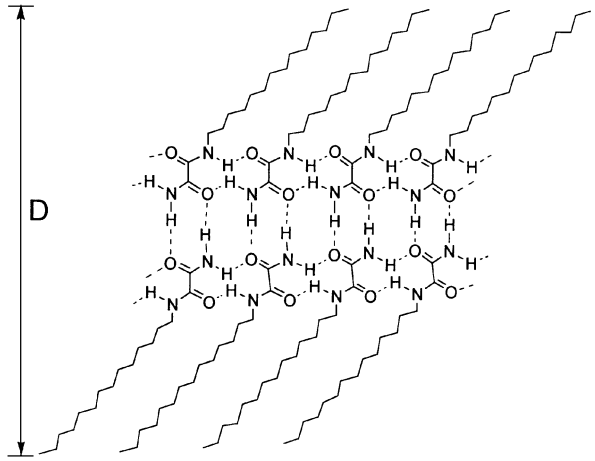

Fig. 3 Local microstructure of the bilayer aggregates of **1** in organogel.

normal (Fig. 3). Within the bilayer unit, the amphiphiles are connected with intra- and inter-layer hydrogen bonds.

The gelling abilities of some structurally related compounds, **2**, **3** (gel-forming) and **4**–**7** (non-gel-forming), have been inspected. None of the related compounds involving *N*,*N*′-disubstituted oxamide exhibit gelling ability. It may be due to the fact that after substituting one of the two hydrogen atoms of the primary amide by an alkyl group, no interlayer hydrogen bonds between the head-to-head arrangements can be formed and the amphiphiles fail to self-assemble to form ordered bilayer aggregates. Therefore the intermolecular hydrogen bonding is unable to meet the need for gelation. Furthermore, the introduction of a long lypophilic chain is essential for gelation, since organogels fail to form when the tail chain is shortened to four carbon atoms. From these observations and analyses, it can be concluded that: (i) gelling ability strongly depends on the oxamido-group; (ii) the hydrophile–lypophile balance is a significant factor for gelation; (iii) the formation of the ordered bilayer aggregates plays an important role in gel-forming.

In conclusion, this paper has shown that simple diamide amphiphiles, monoalkyloxamide, can form ordered bilayer aggregates, through intermolecular hydrogen bonding in a number of organic liquids, which are juxtaposed and interlocked by van der Waals interaction, and finally gelatinize the organic liquids.

We acknowledge the State Science and Technology Commission of China and National Nature Science Foundation of China for financial support of this work.

Notes and references

† Alkylamine reacts with diethyl oxalate in a molar ratio of 1 : 8 in EtOH at 70 °C for 4 h to give *N*-alkyloxamethane‡. The compounds, **1**–**7,** were prepared by reacting *N*-alkyloxamethane with excess concentrated ammonia (for **1**–**4**) or corresponding alkylamine (for **5**–**7**) in EtOH at 30 °C for 3 h. Satisfactory ^{1}H NMR data were obtained for all oxamide derivatives after recrystallization.

‡ The IUPAC name for oxamethane is oxamic acid, ethyl ester.

1 L. Lu, T. Mattew Cocker, R. E. Bachman and R. G. Weiss, *Langmuir*, 2000, **16**, 20; T. Pierre and R. G. Weiss, *Chem. Rev.*, 1997, **97**, 3133; E. Otsumi, P. Kamaras and R. G. Weiss, *Angew. Chem., Int. Ed. Engl.*, 1996, **35**, 1324.
2 T. Kato, G. Kondo and K. Hanabusa, *Chem. Lett.*, 1998, 193; K. Hanabusa, R. Tanaka, M. Suzuki, M. Kimura and H. Shirai, *Adv. Mater.*, 1997, **9**, 1095; K. Hanabusa, M. Yamada, M. Kimura and H. Shirai, *Angew. Chem., Int. Ed. Engl.*, 1996, **35**, 1949; K. Hanabusa, J. Tange, Y. Taguchi, T. Koyama and H. Shirai, *J. Chem. Soc. Chem. Commun.*, 1993, 390; K. Hanabusa, J. Tange, Y. Taguchi, T. Koyama and H. Shirai, *J. Chem. Soc., Chem. Commun.*, 1992, 1371.
3 R. Oda, I. Huc and S. J. Candau, *Angew. Chem., Int. Ed.*, 1998, **37**, 2689.
4 K. Oishi, T. Ishi-i, M. Sano and S. Shinkai, *Chem. Lett.*, 1999, 1089.
5 Y. Lin, B. Kachar and R. G. Weiss, *J. Am. Chem. Soc.*, 1989, **111**, 5542.
6 K. Murata, M. Aoti, T. Suzuki, T. Harada, H. Kawabata, T. Komori, F. Ohseto, K. Ueda and S. Shinkai, *DIC Tech. Rev.*, 1996, (2), 39, and references cited therein.
7 C. M. Garner, P. Terech, J.-J. Allegraud, B. Mistrot, P. Nguyen, A. de Geyer and D. Rivera, *J. Chem. Soc., Faraday Trans.*, 1998, **94**, 2173.
8 T. A. Scott Jr and E. L. Wagner, *J. Chem. Phys.*, 1959, **30**, 465.
9 J. Chouteau, *Bull. Soc. Chim. Fr.*, 1953, 1148.
10 E. M. Ayerst and J. R. C. Duke, *Acta Cryst.*, 1954, **7**, 588.
11 R. S. Clegg and J. E. Hutchison, *Langmuir*, 1996, **12**, 5239.

ChemComm

New, efficient and chemoselective method of thioacylation, starting from carboxylic acids†

Leszek Doszczak and Janusz Rachon*

Department of Organic Chemistry, Chemical Faculty, Technical University of Gdansk, ul. Narutowicza 11/12, 80-952 Gdansk, Poland

Received (in Liverpool, UK) 19th July 2000, Accepted 19th September 2000
First published as an Advance Article on the web 9th October 2000

_S_-Acylation of dithiophosphoric acids yields mixed anhydrides 3; they readily isomerize to _O_-thioacyl 4 and _S_-thioacyl monothiophosphates 5, which treated with the excess of dithiophosphoric acid 2 can be easily converted into thioacyl dithiophosphates 6, excellent thioacylating reagents.

Thioacyl derivatives are mainly obtained by treating acyl derivatives with a thionating agent such as phosphorus pentasulfide or Lawesson's reagent.[1,2] Numerous other examples of sulfurating reagents have been reported (*e.g.* R_3OBF_4–NaHS,[3] R_2PSX,[4] $POCl_3$–$(Me_3Si)_2S$,[5] $(Et_2Al)_2S$,[1] B_2S_3[1] or SiS_2[1]) but are less well-known. Another strategy is to thioacylate nucleophiles with active derivatives of thiocarboxylic acids. Unfortunately, the known thioacylating agents (*e.g.* thioacyl halides,[1] thioacyl benzimidazolones,[6] thioacyl imidazoles, triazoles or tetrazoles,[1] thioacyloxybenzotriazoles,[7] thioacyl trifluorosulfonyl sulfides,[8] phenylmercury dithiocarboxylates[9] or bis(thioacyl) sulfides[10] *etc*.) show many disadvantages. They are generally unstable, expensive or their synthesis is complicated. In the case of less reactive reagents (like thioesters) reaction times are very long or the product cannot be obtained at all.[1] Most of the described reagents can only be prepared from dithiocarboxylic acids, which are scarcely obtainable commercially and are not easy to synthesise in high yield or to handle in pure form.

Here we report a new procedure for thioacylation with *S*-thioacyldithiophosphates, starting from carboxylic acids and dithiophosphoric acid. The usefulness of those kinds of reagents (namely thioacyl diphenylthiophosphinic sulfides) have been described by Kato *et al*.[11] but only derivatives of aromatic dithioacids were prepared by his group and the method of synthesis required cesium (or piperidinium) salts of dithiocarboxylic acids (general drawback). Moreover thioacyl diphenyldithiophosphinates are less reactive than dithiophosphates. We would like to describe a new and efficient method of synthesis of corresponding species and expand the scope of their applications (Scheme 1).‡

Acylation of dithiophosphoric acids (at the moment our best choice is 5,5-dimethyl-2-thiolo-2-thiono-1,3,2-dioxaphosphorinane[12] (**2**)) yields mixed anhydrides of type **3** almost quantitatively (see Table 1). These compounds in solution isomerize to *O*-thioacylmonothiophosphates **4** and *S*-thioacylmonothiophosphates **5** (as we have proved, potential thioacylating reagents) but in an equilibrium mixture compounds **3** generally predominate.§ However, we have found that treatment of that mixture with excess of dithiophosphoric acid leads to the formation of mixed anhydrides of type **6** in high yields (see Table 2). Compounds of type **6** are relatively inert towards water and oxygen and are very good thioacylating agents. They react immediately with nitrogen and sulfur nucleophiles at rt. Thioacyl derivative **7** can be easily separated from water-soluble salts of thiophosphoric acids. Anhydrides **6** chemoselectively thioacylate nitrogen or sulfur nucleophiles in the presence of hydroxy groups. This property allows us to obtain *e.g.* hydroxythioamides (Table 3, **7g**, **7l**) or hydroxydithioesters (**7m**) or thiohydroxamic acids (**7e**, **7f**, **7k**) as well, from substrates with an unprotected oxygen atom. It is worth mentioning that these kinds of compound are not available *via* thionation of unprotected hydroxyamides, hydroxythiolesters or hydroxamic acids with Lawesson's reagent.[13]

In summary we have developed a new strategy of thioacylation, starting from carboxylic acids. In one pot the exchange of C=O into C=S occurs and at the same time activation of the thiocarboxyl function is performed. The method is simple and efficient and cheap reagents are used. The thioacylating agents formed are stable and can be stored for months without noticeable changes. Even thioanhydrides derived from aliphatic acids can be handled without special precautions. The reaction with *N*- or *S*-nucleophiles is very fast under ambient conditions and isolation of the product is very simple.

Our efforts to apply the isomerization of anhydrides of type **3** for the synthesis of thioacylating reagents are focused on a search for dithiophosphoric acids better suited for the described procedure. Our results will be published in a full paper soon.

We gratefully acknowledge the Polish State Committee for Scientific Research for financial support (Grant No. 3 T09A 061 16).

Table 1 Acylation of dithiophosphoric acid **2**

Entry	R	Chemical shift (ppm) ^{31}P NMR	Yield (%)
3a	1-Naphthyl	69.6	100
3b	Ph	69.1	98
3c	4-PhOMe[a]	70.1	85
3d	4-PhNO_2	65.9	85
3e	CH=CH_2Ph[a]	69.7	93
3f	Me	69.1	89
3g	Pr	70.1	92
3h	iPr	70.6	98
3i	tBu	70.8	96
3j	CH_2NPht	65.8	82
3k	CH_2CH_2NPht	67.7	93
3l	CH_2OPh	67.9	90
3m	$(CH_2)_4$COOMe	69.2	100

[a] Due to fast isomerization obtained in mixtures with anhydride **4** (chemical shift ^{31}P NMR of **4c**: 50.1 ppm; **4e**: 50.3 ppm).

Table 2 Thioacyl dithiophosphates **6**

Entry	R	Chemical shift (ppm) ^{31}P NMR	Time/h	Yield (%)
6a	1-Naphthyl	67.8	1.5	90
6b	Ph	68.6	2	94
6f	Me	68.4	3	88
6g	Pr	68.5	3	92
6i	tBu	70.7	4	91
6m	$(CH_2)_4$COOMe	67.2	4	88

† Presented in part at 13th ICOS, Warsaw 2000, Poland, pp. 139.

DOI: 10.1039/b005911k

Table 3 Thioacylations with dithiophosphates **6**

Entry	R	Nucleophile	Product	Yield (%)
7a	Ph	Aq. NH_3	$PhCSNH_2$	95
7b	Ph	$PhNH_2$–NEt_3	PhCSNHPh	99
7c	Ph	$(CH_2)_5NH$–NEt_3	$PhCSN(CH_2)_5$	98
7d	Ph	MeOH–NEt_3	PhCSOMe	0
7e	Ph	MeNHOH·HCl–NEt_3	PhCSN(OH)Me	68
7f	Ph	iPrNHOH·HCl–NEt_3	PhCSN(OH)iPr	73
7g	Ph	$HOCH_2CH_2NH_2$–NEt_3	$PhCSNHCH_2CH_2OH$	94
7h	Me	$PhNH_2$–NEt_3	MeCSNHPh	88[a]
7i	Pr	$PhNH_2$–NEt_3	PrCSNHPh	96[a]
7j	tBu	$PhNH_2$–NEt_3	tBuCSNHPh	92
7k	tBu	MeNHOH·HCl–NEt_3	tBuCSN(OH)Me	71
7l	tBu	2-$HOPhNH_2$–NEt_3	2-tBuCSNHPhOH	99
7m	tBu	$HOCH_2CH_2SH$–NEt_3	$tBuCSSCH_2CH_2OH$	97
7n	$(CH_2)_4COOMe$	$(CH_2)_5N$–NEt_3	$MeOCO(CH_2)_4CSN(CH_2)_5$	88[a]

[a] Procedure B.

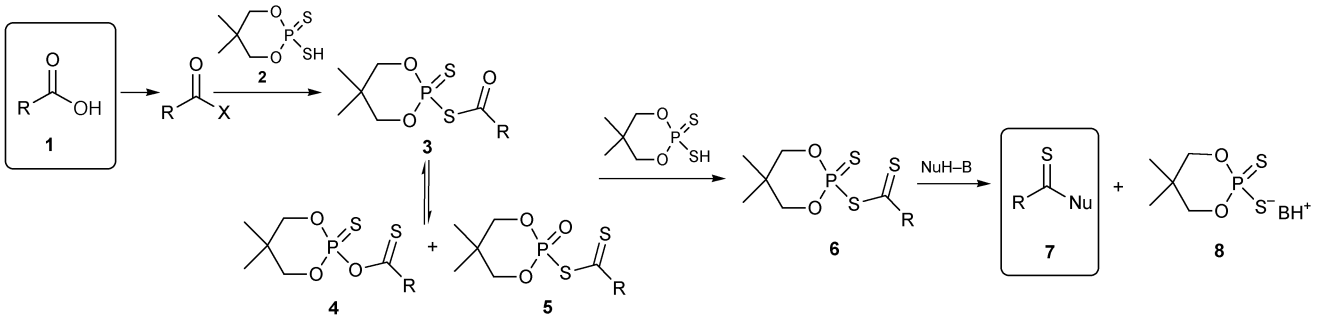

Scheme 1 Conversion of carboxylic acids into thioacylating reagents and their reaction with nucleophiles.

Notes and references

‡ *Acyl dithiophosphates* **3**, *typical procedure*: acyl chloride (5 mmol) is added to a solution of 5,5-dimethyl-2-thiolo-2-thiono-1,3,2-dioxaphosphorinane (**2**) (5 mmol) in 15 ml of benzene. The solution is cooled with iced water and subsequently pyridine or triethylamine (5 mmol) is added dropwise. Immediately, ammonium chloride precipitates. After 15 minutes the reaction mixture is filtered through a short layer of silica gel. Following solvent evaporation a pure enough product is obtained.

Thioacyl dithiophosphates **6**, *typical procedure*: A solution of 5 mmol of acyl 2-(5,5-dimethyl-2-thiono-1,3,2-dioxaphosphorinanyl) sulfide (**3**) and 5,5-dimethyl-2-thiolo-2-thiono-1,3,2-dioxaphosphorinane (**2**) (10 mmol) in 35 ml of benzene is heated under reflux for 2–6 h. Subsequently phosphoric thioacids **2** and **8** are removed by washing with an aq. solution of sodium carbonate and then water. The organic layer is then dried with magnesium sulfate and the benzene is evaporated. The crude product is used for thioacylation without further purification, or if necessary is purified by means of silica gel chromatography or crystallization.

Thioacylation with thioacyl dithiophosphates **6**, *typical procedure A:* A solution of amine or thiol (5 mmol) and pyridine or triethylamine (5.5 mmol) in benzene is added dropwise to a solution of thioacyl 2-(5,5-dimethyl-2-thiono-1,3,2-dioxaphosphorinanyl) sulfide (**6**). Triethylammonium (or pyridinium) dithiophosphate precipitates and can be removed by means of filtration or washing with water and aq. sodium carbonate. Drying and evaporation of the solvent generally yields pure enough product. If necessary, the thioacyl derivative can be purified by means of chromatography or crystallisation.

Typical procedure B: A solution of acyl 2-(5,5-dimethyl-2-thiono-1,3,2-dioxaphosphorinanyl) sulfide (**3**) (5 mmol) and 5,5-dimethyl-2-thiolo-2-thiono-1,3,2-dioxaphosphorinane (**2**) (10 mmol) in 35 ml of benzene is heated under reflux for 2–6 h. A solution of amine or thiol (5 mmol) and pyridine or triethyl amine (16.5 mmol) in benzene is then added. The resulting mixture is worked up as above.

§ On the basis of our ^{31}P NMR experiments we were able to estimate the composition of the equilibrium mixtures and additionally we managed to isolate a few examples of *S*- and *O*-thioacylmonothiophosphates (*e.g.* **4b**, **5a**,**b**,**i**) and to fully characterize them. Reactivity and the mechanism of formation of the species are under investigation. We would like to emphasize that apart from not well proven reports[14] of isomerization of anhydrides of type **3** to **4**, formation of compounds type **5** from **3** (or a mixture of **3** and **4**) have not been previously reported in the literature (excluding the speculations of Cherkasov,[15] which however do not agree with our results).

1 S. Scheithauer and R. Mayer, in *Thio- and Dithiocarboxylic Acids and their Derivatives*, A. Senning, ed., Thieme, Stuttgart, 1979, vol. 4.
2 R. Cherkasov, G. Kutyriev and A. Pudovik, *Tetrahedron*, 1985, **41**, 2567; M. Cava and M. Levinson, *Tetrahedron*, 1985, **41**, 5061.
3 J. Bodine and M. Kaloustian, *Synth. Commun.*, 1982, **12**, 787.
4 B. Pedersen and S. Lawesson, *Bull. Soc. Chem. Belg.*, 1977, **86**, 693.
5 D. Smith, S. Lee and P. Fuchs, *J. Org. Chem.*, 1994, **59**, 348.
6 B. Zacharie, G. Sauve and C. Penney, *Tetrahedron*, 1993, **49**, 10 489.
7 T. Hoeg-Jensen, C. Olsen and A. Holm, *J. Org. Chem.*, 1994, **59**, 1257.
8 A. Katritzky, J. Moutou and Z. Yang, *Synthesis*, 1995, 1497.
9 S. Kato, E. Hattori, H. Sato, M. Mizuta and M. Ishida, *Z. Naturforsch.*, 1981, **86b**, 783.
10 S. Kato, H. Shibahashi, T. Katada, T. Tagaki, I. Noda, M. Mizuta and M. Goto, *Lieb. Ann. Chem.*, 1982, 1229.
11 S. Kato, M. Goto, R. Hattori, K. Nishivaki, M. Mizuta and M. Ishida, *Chem. Ber.*, 1985, **118**, 1668.
12 Acid **2** can be obtained from P_2S_5 and 2,2-dimethylpropane-1,3-diol according to R. Edmundson, *Tetrahedron*, 1965, **21**, 2379.
13 W. Przychodzeń and A. Chimiak, *Phosphorus, Sulfur Silicon Relat. Elem.*, 1998, **143**, 77.
14 N. Yousif, U. Pedersen, B. Yde and S. Lawesson, *Tetrahedron*, 1984, **40** (14), 2663; A. V. Alfonsof, D. Pudovik, E. Batyeva and A. Pudovik, *Zh. Obshch. Khim.*, 1985, **55**, 2303; N. Yuosif and M. Salama, *Phosphorus, Sulfur Silicon Relat. Elem.*, 1987, **32**, 51; N. Yuosif, *Phosphorus, Sulfur Silicon Relat. Elem.*, 1989, **46**, 79.
15 N. Zabirov, F. Schamsevaliev and R. Cherkasov, *Zh. Obshch. Khim.*, 1991, **61**(3.1), 558.

Preparation of mesoporous SnO_2–SiO_2 composite as electrodes for lithium batteries

Fanglin Chen, Zhong Shi and Meilin Liu*

School of Materials Science and Engineering, Georgia Institute of Technology, Atlanta, GA 30332-0245, USA. E-mail: meilin.liu@mse.gatech.edu

Received (in Irvine, CA, USA) 29th March 2000, Accepted 12th September 2000
First published as an Advance Article on the web 9th October 2000

Mesoporous SnO_2–SiO_2 composite stable up to 600 °C with a BET surface area of 350 m^2 g^{-1} and an average pore size of 3.4 nm is successfully prepared, which exhibits promising cycling properties as anodes for lithium batteries.

Following the discovery of the M41S family of mesoporous silicates using supramolecular templating approach,[1,2] mesoporous materials have attracted considerable attention because of their tunable pore size, narrow pore size distribution, and remarkably large surface areas, which make them ideal candidates for catalysts, molecular sieves, and electrodes for solid-state ionic devices. The ordering in these materials is a consequence of a self-assembly process in an aqueous solution containing organic surfactants (anionic, cathodic, or neutral) and inorganic cations or anions. To date, a wide range of mesoporous materials have been prepared using the structure-directing functions of electrostatic, hydrogen-bonding, covalent bonding and van der Waals interactions associated with amphiphilic surfactant molecules.[3–10]

Tin-based composite oxides are promising candidates for anodes in lithium batteries because of their much larger reversible capacity compared to carbonaceous materials. In this study, mesoporous SiO_2 stable up to 600 °C has been prepared using Brij 56 as a structure-directing agent and TEOS as precursor in an aqueous solution.† Further, a tin compound is introduced into porous SiO_2 using a sol-gel technique to form SnO_2–SiO_2 composite. The objective of our study is to create a nano-structured SnO_2–SiO_2 electrodes for lithium batteries. The structural stability of the tin-based materials during cycling is a major barrier to the successful application of this material as anodes in Li-batteries.[11] Our approach to improving the structural stability is to incorporate a tin compound into a mesoporous SiO_2 matrix, which is structurally stable and hence offers structural stability to the nanocomposite electrode. The mesoporous SnO_2–SiO_2 structure will facilitate the penetration of the liquid electrolyte into the electrodes and hence increase the rate of charge and discharge.

Shown in Fig. 1 are XRD patterns of mesoporous SiO_2 powder samples before and after calcination at 600 °C for 2 h prepared using Brij 56 as surfactant. The XRD pattern of the as-synthesized powders indicates that the surfactant molecules were organized into a hexagonal structure when aged at room temperature for 2 d. The peak at about 1.2° corresponds to the (100) reflection, which has a *d*-spacing of 6.8 nm. Thermogravimetric analysis shows that Brij 56 surfactant is completely removed upon calcination in air at 400 °C for 1 h. The appearance of a low-angle diffraction peak of the SiO_2 powder calcined at 600 °C for 2 h indicates that mesoscopic order is preserved upon removal of the surfactant by calcination, although the structure contracted slightly as evidenced from a slight shift of the XRD peak to a higher angle. The corresponding *d*-spacing is reduced to about 6.3 nm. The increased intensity of the XRD peak of the calcined SiO_2 indicates that the ordering of the mesostructure is improved during calcination. Shown in Fig. 1(*c*) is the XRD pattern of a SnO_2–SiO_2 composite. The peak is broader than that of pure SiO_2, suggesting that either the degree of ordering was reduced or the size distribution of the mesopores was broadened. However, the position of the peak did not change, implying that the *d*-spacing remained the same upon incorporating tin species into the pores of the mesoporous SiO_2. Further, the wide-angle XRD pattern shown in the inset in Fig. 1 indicates that the SnO_2 incorporated into the mesoporous SiO_2 is crystalline, rather than amorphous.

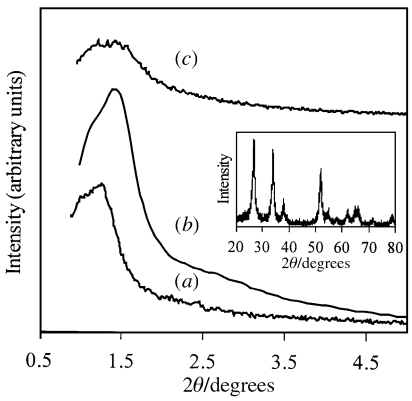

Fig. 1 Representative small-angle X-ray powder diffraction patterns of (*a*) as-synthesized SiO_2, (*b*) SiO_2 calcined at 600 °C for 2 h, and (*c*) SnO_2–SiO_2 composite calcined at 600 °C for 2 h. The wide-angle X-ray diffraction pattern of SnO_2–SiO_2 composite is shown in the inset.

Shown in Fig. 2 are representative TEM images of SiO_2 and SnO_2–SiO_2 samples after calcination at 600 °C for 2 h. Mesostructures with short-range hexagonal order can be seen and the corresponding *d*-spacings are 6.3 nm for both SiO_2 and SnO_2–SiO_2 composite, which are close to those determined from the XRD patterns. The nitrogen adsorption isotherms of the SiO_2 and SnO_2–SiO_2 samples after calcination at 600 °C for 2 h are shown in Fig. 3 and the calculated Brunauer–Emmett–Teller (BET) surface areas are 1100 m^2 g^{-1} for SiO_2 and 350 m^2 g^{-1} for SnO_2–SiO_2 composite, respectively. The gas-accessible surface area of the mesoporous SnO_2–SiO_2 composite was greatly reduced due to partial occupation of the pores by

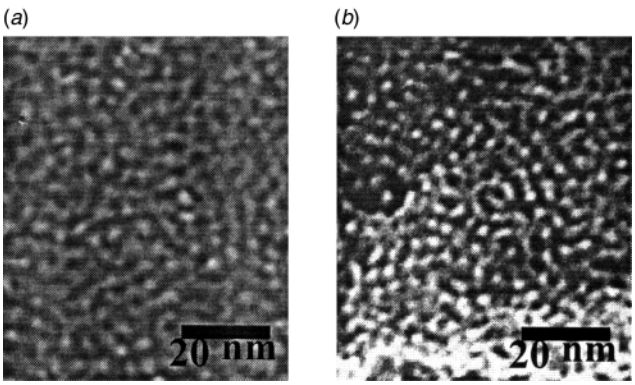

Fig. 2 TEM micrographs of (*a*) 600 °C calcined mesoporous SiO_2 and (*b*) mesoporous SnO_2–SiO_2 composite.

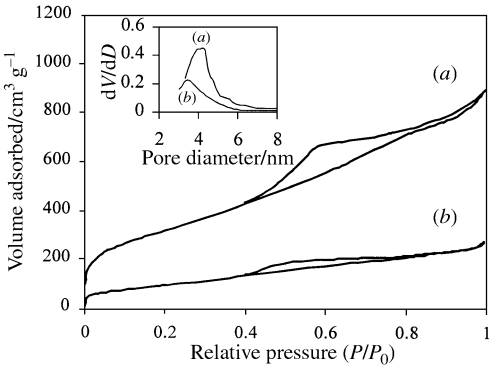

Fig. 3 Representative nitrogen adsorption and desorption isotherms for (*a*) SiO_2 and (*b*) SnO_2–SiO_2 composite after calcination at 600 °C for 2 h. Corresponding BJH pore size distributions are shown in the inset.

the tin species incorporated into the mesoporous SiO_2. Both nitogren isotherm curves have a well-defined step for the relative pressure P/P_0 ranging from 0.4 to 0.8, a characteristic of the filling of the framework-confined mesopores,[12] suggesting that both SiO_2 and SnO_2–SiO_2 samples are mesoporous after calcination at 600 °C for 2 h. As shown in the inset in Fig. 3, the average pore size in the SiO_2 structure is 4.0 nm while that in the SnO_2–SiO_2 composite is 3.4 nm, implying that a thin SnO_2 layer has been incorporated into the channel surface of the mesoporous SiO_2.

The electrochemical behavior of the obtained SnO_2–SiO_2 composite oxide is further studied using cyclic voltammetry. Shown in Fig. 4 are the cyclic voltammograms (CVs) of a mesoporous SnO_2–SiO_2 composite, as studied using a powder microelectrode in the potential range between 2.0 and 0 V (*vs.* Li^+/Li) with a scan rate of 0.2 mV s^{-1}. The potential was swept from 2.0 V in the cathodic direction down to the set limit (0 V) and then in the anodic direction. Two very small irreversible reduction peaks appeared near 0.6 and 0.9 V, respectively, in the CV of the first cycle. This is quite different from the CVs observed for tin-based composite electrodes in the literature,[13,14] in which there is only one large irreversible reduction peak around 0.9 V in the first sweep. It is well known that this large irreversible reduction peak is due to the *in situ* electrochemical reduction of SnO or SnO_2 by lithium to metallic tin and Li_2O,[15] representing a large irreversible capacity loss for tin-based composite materials in the first cycle, which is still a major barrier to the successful application of these materials as anodes in Li-batteries.[14] In this work, even though it is still not

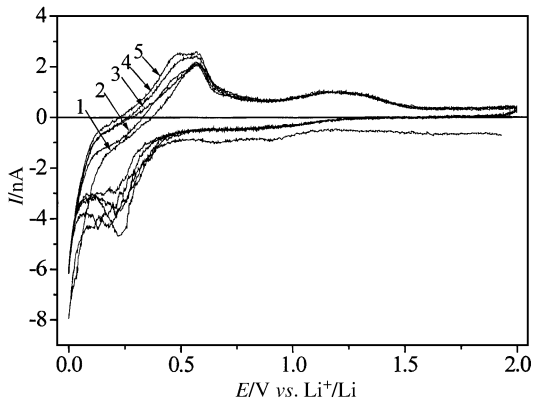

Fig. 4 Cyclic voltammograms (CVs) of a mesoporous SnO_2–SiO_2 composite as studied electrode using a powder microelectrode technique. The number adjacent to each CV represents the order of the cycles.

clear what the two tiny irreversible reduction peaks (observed for the mesoporous SnO_2–SiO_2 composite) correspond to, it is anticipated that the mesoporous SnO_2–SiO_2 composite as an anode for a lithium battery would display much less irreversible capacity loss during the first cycle. Further, the reversible redox peaks in the range of 0.1–0.7 V in the first five cycles of the CVs show very little change, an indication of good cyclability of such a mesoporous SnO_2–SiO_2 composite electrode. The electrochemical behavior of SnO_2 in mesoporous SnO_2–SiO_2 composites as well as the long-term charge–discharge cycling behavior of the composite electrodes in a lithium cell are still under investigation and will be reported in subsequent communications.

We gratefully acknowledge partial support of this research by the National Science Foundation under Award No. CTS-9819850 and by the Georgia Institute of Technology Molecular Design Institute, under prime contract N00014-95-1-1116 from the Office of Naval Research.

Notes and references

† In a typical preparation using Brij 56 as the structure-directing agent, 1.093 g Brij 56 was dissolved in 80 ml H_2O by stirring at room temperature. 2.667 g tetraethyl orthosilicate (TEOS) was added to the Brij 56 solution and the solution was stirred at room temperature for 2 h. Subsequently, 1.333 ml 0.2 M NaF was added to the above solution and the solution was stirred at room temperature for 2 h while a milky sol was obtained. The milky sol was placed at room temperature for 2 d and a white precipitate formed progressively. The precipitate was finally filtered off, washed 5 times using distilled H_2O, dried at 60 °C in a vacuum oven and finally calcined in air at 600 °C for 2 h to remove the surfactant. Incorporation of tin compound into the pores of SiO_2 was achieved by immersing mesoporous SiO_2 powder into tin nitrate solution and then drying at 40 °C under vacuum. Mesoporous SnO_2–SiO_2 composite was obtained by calcining the dried tin nitrate–SiO_2 powder at 600 °C for 2 h in air. A powder microelectrode was used to study the electrochemical performance of mesoporous SnO_2–SiO_2 composite in 1 M $LiN(SO_2CF_3)_2$/EC+DMC electrolyte solution.

1 C. T. Kresge, M. E. Leonowicz, W. J. Roth, J. C. Vartuli and J. S. Beck, *Nature*, 1992, **359**, 710.
2 J. S. Beck, J. C. Vartuli, W. J. Roth, M. E. Leonowicz, C. T. Kresge, K. D. Schmitt, C. T.-W. Chu, D. H. Olson, E. W. Sheppard, S. B. Mccullen, J. B. Higgins and J. L. Schlenker, *J. Am. Chem. Soc.*, 1992, **114**, 10 834.
3 A. Sayari, *Chem. Mater.*, 1996, **8**, 1840.
4 Z. R. Tian, W. Tong, J. Y. Wang, N. G. Duan, V. V. Krishnan and S. L. Suib, *Science*, 1997, **276**, 926.
5 Q. Huo, D. I. Margolese, U. Ciesla, D. G. Demuth, P. Feng, T. E. Gier, P. Sieger, A. Firouzi, B. F. Chmelka, F. Schuth and G. D. Stucky, *Chem. Mater.*, 1994, **6**, 1176.
6 D. M. Antonelli and J. Y. Ying, *Angew. Chem., Int. Ed. Engl.*, 1995, **34**, 2014; *Chem. Mater.*, 1996, **8**, 874; D. M. Antonelli, A. Nakahira and J. Y. Ying, *Inorg. Chem.*, 1996, **35**, 426.
7 F. Chen and M. Liu, *Chem. Commun.*, 1999, 1829.
8 D. Zhao, J. Feng, Q. Huo, N. Melosh, G. Fredrickson, B. Chmelka and G. D. Stucky, *Science*, 1998, **279**, 548.
9 E. Prouzet and T. J. Pinnavaia, *Angew. Chem., Int. Ed. Engl.*, 1997, **36**, 516.
10 P. Yang, D. Zhao, D. I. Margolese, B. F. Chemelka and G. D. Stucky, *Nature*, 1998, **396**, 152.
11 S. Machill, T. Shodai, Y. Sakuraai and J. Yamaki, *J. Power Sources*, 1998, **73**, 216.
12 S. Cabrera, J. E. Haskouri, J. Alamo, A. Beltran, D. Beltran, S. Mendioroz, M. D. Marcos and P. Amoros, *Adv. Mater.*, 1999, **11**, 379.
13 J. Li, H. Lim, Z. Wang, X. Huang and L. Chen, *J. Power Sources*, 1999, **81–82**, 346.
14 S. Machill, T. Shodai, Y. Sakurai and J. Yamaki, *J. Power Sources*, 1998, **73**, 216.
15 I. A. Courtney and J. R. Dahn, *J. Electrochem. Soc.*, 1997, **144**, 2045.

ChemComm

Synthesis and characterization of poly(*p*-phenylenephosphine)s

Brett L. Lucht* and Nicole O. St. Onge

Department of Chemistry, University of Rhode Island, Kingston, Rhode Island 02881, USA. E-mail: blucht@chm.uri.edu

Received (in Columbia, MO, USA) 12th April 2000, Accepted 28th August 2000
First published as an Advance Article on the web 9th October 2000

***P*-Substituted poly(*p*-phenylenephosphine)s were prepared *via* palladium catalyzed carbon–phosphorus bond formation.**

There has been substantial recent interest in the synthesis and properties of π-conjugated polymers. These polymers have found important uses for a variety of optoelectric applications such as rechargeable battery electrodes, light-emitting diodes, and chemical sensors.[1] While many conjugated polymers contain only sp and sp^2 hybridized carbon atoms along the polymer backbone, two of the most important and widely investigated conjugated polymers, polyaniline[2] and polythiophene,[3] contain heteroatoms as a vital component of the conjugation path (Scheme 1). Other interesting conjugated polymers have been prepared which contain heteroatoms in the backbone including poly(*p*-phenyleneborane)s,[4] poly(*p*-phenyleneselenide)s,[5] and poly(*p*-phenylenesulfide).[6] The presence and properties of the heteroatom have a profound impact on the optoelectronic properties of the polymer. A substantial increase in the doped conductivity is observed upon moving from poly(*p*-phenyl-eneoxide) to poly(*p*-phenylenesulfide).[6] While phosphorous containing polymers have found a variety of important uses including flame retardants, ionic conduting materials, and easily separable supports for metal catalysts,[7] the incorporation of phosphorus into the backbone of a conjugated polymer has been limited. The few cases include poly(ferrocenylphosphine),[8] oligophospholes,[9] and the trace incorporation of phosphorus into soluble poly(*p*-phenylene)s *via* catalyst ligand decomposition.[10]

Palladium catalysis has been used extensively in organic chemistry for the formation of new sp^2–sp^2 and sp^2–sp hybridized carbon–carbon bonds with high yields and is useful for the preparation of π-conjugated polymers.[11] Recent investigations by Buchwald[12] and Hartwig[13] have expanded the utility of palladium mediated cross coupling to include carbon–nitrogen bond formation. The new synthetic method couples arylhalides or aryltosylates with amines and has generated considerable interest for the preparation of arylamine containing materials such as polyanilines, oligoanilines, and arylamine dendrimers.[14] Analogous nickel[15] and palladium[16] mediated carbon–phosphorus bond forming reactions have been reported and recently utilized for the synthesis of phosphorus containing polymers.[7e] We report the synthesis and optoelectric investigation of the phosphorus analog to *N*-substituted polyanilines, *P*-substituted poly(*p*-phenylenephosphine)s, *via* palladium catalyzed carbon–carbon phosphorus bond formation.

In this paper, we describe the palladium catalyzed condensation polymerization of monoalkyl and monoaryl phosphines with 1,4-diiodobenzene (Scheme 2). A typical experiment is conducted as follows. Palladium tetrakis(triphenylphosphine) (0.310, 0.27 mmol) and diiodobenzene (1.77 g, 5.37 mmol) were dissolved in 1 : 1 dry oxygen free THF–toluene (10 ml). To this solution was added isobutylphosphine (0.63 ml, 5.37 mmol) followed by triethylamine (2.0 ml). Upon the addition of the triethylamine a white precipitate was observed indicating the formation of $Et_3N{\cdot}HI$. The reaction mixture was heated at 70 °C for 72 h and turned burnt orange. The reaction mixture was poured into rapidly stirring 5 : 1 MeOH–aq. NH_3 (500 ml) to precipitate the polymer, which was collected by filtration. The polymer was redissolved in THF, reprecipitated in MeOH, filtered, washed with MeOH, and dried under high vacuum for 8 h to yield polymer **1a** as a light pink solid (0.73 g, 83% yield).

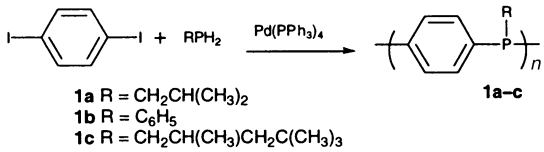

Scheme 2 Synthesis of poly(*p*-phenylenephosphine)s.

The structures of polymers **1a**–**c** are supported by ^1H, ^{13}C, and ^{31}P NMR and IR spectroscopy and the molecular weights are estimated by gel permeation chromatography (Table 1).† The ^1H NMR spectra of **1a** contain four broad resonances with appropriate chemical shifts and integrated intensities. The ^{31}P NMR spectra contain a single broad resonance at −19.81 ppm suggesting that the environment is similar for most of the P nuclei. The ^{13}C NMR spectra contain five resonances each with scalar coupling to ^{31}P. The resonance at 132.66 ppm is coupled to two different ^{31}P nuclei characteristic of ^2J (^{31}P–^{13}C, 19.1 Hz) and ^3J(^{31}P–^{13}C, 6.1 Hz) as expected for the C nuclei not directly bound to P.[17] The IR spectra include absorptions characteristic of aromatic ring stretches but contain no observable P=O absorptions. Polymers **1a** and **c** are entirely soluble in THF, toluene, and $CHCl_3$ while **1b** is only partially soluble.

The UV-visible spectra of polymers **1a**–**c** in $CHCl_3$ suggest significant π-conjugation along the polymer backbone *via* the lone pair on P. A red shift of the optical absorption upon increasing the number of phenyl phosphine units is observed, as evidenced by the shift of the absorbance maximum for the π–π* transition for the following series of phosphines: triphenylphosphine (λ_{max} = 263 nm), 1,4-bis(diphenylphosphino)benzene (**2**) (λ_{max} = 275 nm), and polymer **1b** (λ_{max} = 291 nm). In addition, polymer **1b** has a second small absorption maximum at 434 nm (Fig. 1). We suspect that this lower energy absorption results from an n–π* transition. The absorption is observed due to an increase in intensity resulting from electron delocalization in the polymer.

Table 1 Optical and molecular weight data for polymers **1a**–**c**

Polymer	R	M_n[a]	n[b]	PDI	λ_{max} Abs
1a	Isobutyl	1,700	10	1.3	278, 415
1b	Phenyl	1,300	7	1.4	291, 434
1c	2,4,4-Trimethylpentyl	3,100	14	1.5	276, 422

[a] Molecular weights were determined by GPC *vs*. polystyrene standards in THF. [b] The value *n* corresponds to the average number of repeat unit in the polymer.

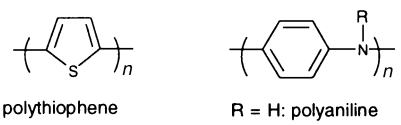

Scheme 1 Heteroatom containing conjugated polymers.

DOI: 10.1039/b003989f

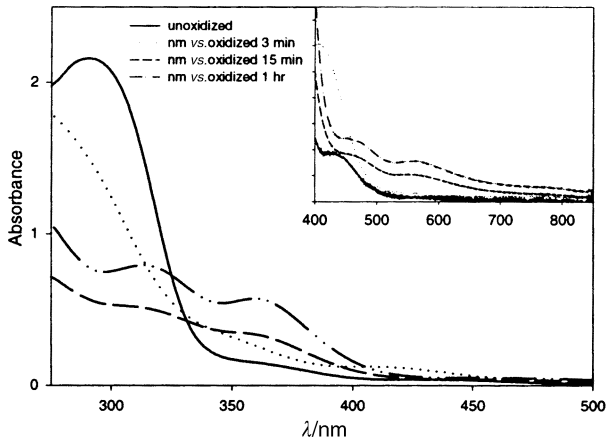

Fig. 1 UV-visible spectra of the oxidation of polymer **1b** with $FeCl_3$ in $CHCl_3$.

Chemical oxidation provides additional support for the electronic delocalization of poly(*p*-phenylenephosphine)s. Oxidation of polymer **1b** with $FeCl_3$ in the absence of O_2 and H_2O results in the formation of several new absorption bands and a shift of the band edge past 800 nm (Fig. 1). The spectral properties of these polymers are related to poly(*N*-arylaniline)s.[14a] The NMR spectra of polymers **1a**–**c** are also altered upon oxidation with $FeCl_3$. We are unable to observe ^{31}P or ^{1}H NMR spectra for oxidized polymers **1a**–**c**. The lack or severe broadening of NMR resonances is consistent with paramagnetism resulting from declocalized electrons along the polymer chain. The oxidized polymer is stable in solution for several hours in the absence of O_2 and H_2O. While we do not fully understand the spectroscopic properties of these polymers, the data support an extension of the conjugation path through P and electronic delocalization along the polymer chain.

Since phosphines are well known to undergo rapid oxidation to phosphine oxides, we investigated the oxidation of the polymers by hydrogen peroxide (Scheme 3). Addition of (30%) H_2O_2 to $CHCl_3$ solutions of **1b** resulted in a color change to deep red along with a dramatic change of the UV-visible spectroscopic properties, the primary absorption (291 nm) is blue shifted while the low energy band (434 nm) is red shifted to 550 nm and severely broadened. A change in the structure of the polymer is supported by NMR and IR spectroscopy. The ^{31}P NMR absorption for polymer **1b** cleanly shifts from −5.2 ppm to 28.6 ppm suggesting near quantitative conversion of **3b**.‡ IR spectra of polymer **3b** contain two strong absorptions at 1120 and 1188 cm^{-1} characteristic of phosphine oxides.[18] Polymers **1a**–**c** are mildly sensitive to atmospheric oxygen and are converted to **3a**–**c** over 4–6 days in solution ($CHCl_3$) and 4–6 months in the solid state.

We have described the synthesis and spectroscopic investigation of a series of poly(*p*-phenylenephosphine)s. Polymers **1a**–**c** were synthesized *via* palladium catalyzed cross coupling of diiodobenzene with primary phosphines. The investigations suggest significant electronic delocalization through P along the backbone of the polymer. We are currently further evaluating the properties of these interesting polymers and investigating additional routes to incorporate P into conjugated polymers.

The authors of this paper would like to thank the University of Rhode Island for financial support of this research, Professor William Euler for valuable help obtaining UV-visible spectra data and for thoughtful discussions, and Cytec Canada Inc. for a generous donation of primary phosphines.

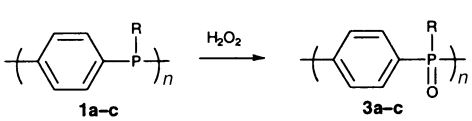

Scheme 3 Oxidation of poly(*p*-phenylenephosphine).

Notes and references

† Characterization data for polymer **1a**. δ_H(400 MHz, $CDCl_3$) 1.01 (d, *J* 6.2, 6H, CH_3), 1.63 (non, *J* 6.6, 1H, CH), 1.94 (d, *J* 7.0, 2H, CH_2), 7.33 (s, 4H, C_6H_4); δ_C(100 MHz, $CDCl_3$) 24.27 (d, J_{CP} 9.0, CH_3), 26.22 (d, J_{CP} −14.5, CH_2), 38.43 (d, J_{CP} 13.3, CH), 139.53 (d, J_{CP} −17.2, C_6H_4), 132.66 (dd, J^2_{CP} 19.1 J^3_{CP} 6.1, C_6H_4); δ_P(162. MHz, $CDCl_3$) −19.81 (s); ν(film, KBr)/cm^{-1} 2953, 2924, 2867, 2360, 1474, 1461, 1455, 1381, 1364, 1110, 1046, 1014, 1004, 814, 795, 758, 547; (Calc. for $C_{10}H_{13}P$: C, 73.13; H, 7.98. Found: C, 64.08; H, 7.20%). While the absolute values of the elemental analysis are a few percent low the calculated and found C : H ratios are 9.17 and 8.90 respectively; we suspect the difference in absolute values is the result of polymer end-groups. Assuming the polymers are quantitatively capped with *p*-iodophenyl substituents provides better correlation to experimental elemental analysis. (Calc. for $C_{106}H_{134}P_{10}I_2$; C, 64.56; H, 6.86%).

‡ The chemical shift for the ^{31}P NMR resonances of Ph_3P and $Ph_3P{=}O$ are −4.6 ppm and 29.7 ppm respectively.

1 *Conjugated Polymers: The Novel Science of Technology of Highly Conducting and Nonlinear Optically Active Materials*, ed. J. L. Bredas and R. Silbey, Kluwer Academic Publishers, Dordrecht, 1991; J. M. Tour, *Chem. Rev.*, 1996, **96**, 537; T. M. Swager, *Acc. Chem. Res.*, 1998, **31**, 201.
2 A. G. MacDiarmid and A. J. Epstein, *Faraday Discuss. Chem. Soc.*, 1989, **31**, 317.
3 A. O. Patil, A. J. Heeger and F. Wudl, *Chem. Rev.*, 1988, **88**, 183.
4 N. Matsumi, K. Naka and Y. Chujo, *J. Am. Chem. Soc.*, 1998, **88**, 10 776.
5 E. Tsuchida, M. Jikei, K. Miyatake, K. Yamamoto and H. Nishide, *Macromolecules*, 1993, **26**, 4732.
6 R. H. Baughman, J. L. Bredas, R. R. Chance, R. L. Elsenbaumer and L. W. Shacklette, *Chem. Rev.*, 1982, **82**, 209.
7 (*a*) W. C. Kuryla and A. J. Papa, *Flame Retardancy of Polymeric Materials Vol. 1–5*, Marcel Dekker, New York, 1973; (*b*) H. Ghassemi and J. E. McGrath, *Polymer*, 1997, **38**, 3139; (*c*) D. B. Bergbreiter and Y. Liu, *Tetrahedron Lett.*, 1997, **38**, 7843; (*d*) H. R. Allcock, D. L. Olmeiger and J. M. O'Connor, *Macromolecules*, 1998, **31**, 753; (*e*) T. Kanbara, S. Takase, K. Izumi, S. Kagaya and K. Hasegawa, *Macromolecules*, 2000, **33**, 657.
8 T. J. Peckham, J. A. Massey, C. H. Honeyman and I. Manners, *Macromolecules*, 1999, **32**, 2830.
9 E. Deschamps, L. Ricard and F. Mathey, *Angew. Chem., Int. Ed. Engl.*, 1994, **96**, 537.
10 F. E. Goodson, T. I. Walow and B. M. Novak, *Macromolecules*, 1998, **31**, 2047.
11 M. Rehahn, A.-D. Schluter, G. Wegner and W. J. Feast, *Polymer*, 1989, **30**, 1060; D. L. Trumbo and C. S. Marvel, *J. Polym. Sci. Part A: Polym. Chem.*, 1987, **25**, 839.
12 J. P. Wolfe, S. Wagaw and S. L. Buchwald, *J. Am. Chem. Soc.*, 1996, **118**, 7215; J. P. Wolfe, S. Wagaw, J.-F. Marcoux and S. L. Buchwald, *Acc. Chem. Res.*, 1998, **31**, 805.
13 M. S. Driver and J. F. Hartwig, *J. Am. Chem. Soc.*, 1996, **118**, 7217; J. F. Hartwig, *Acc. Chem. Res.*, 1998, **31**, 852.
14 (*a*) F. E. Goodson, S. I. Hauck and J. F. Hartwig, *J. Am. Chem. Soc.*, 1999, **121**, 7527; (*b*) J. Louie, J. F. Hartwig and A. J. Fry, *J. Am. Chem. Soc.*, 1997, **119**, 11 695; (*c*) R. A. Singer, J. P. Sadighi and S. L. Buchwald, *J. Am. Chem. Soc.*, 1988, **120**, 213; (*d*) J. P. Sadighi, R. A. Singer and S. L. Buchwald, *J. Am. Chem. Soc.*, 1998, **120**, 4960.
15 D. Cai, J. F. Payack, D. R. Bender, D. L. Huges, D. L. Hughes, T. R. Verhoeven and P. J. Reider, *J. Org. Chem.*, 1994, **59**, 1780.
16 T. Hirao, T. Masaunaga, N. Yamada, Y. Oshiro and T. Agawa, *Bull. Chem. Soc. Jpn.*, 1982, **55**, 909; S. E. Tunney and J. K. Stille, *J. Org. Chem.*, 1987, **52**, 748; O. Herd, A. Hessler, M. Hingst, M. Tepper and O. Stelzer, *J. Organomet. Chem.*, 1996, **522**, 69; J. H. Hillhouse, U.S. Patent No. 5550295 (to Cytec), 1996; M. A. Zhuravel, PhD Thesis, Darmouth College, Hannover, NH, 2000.
17 F. W. Wehrli, A. P. Marchand and S. Wehrli, *Interpretation of Carbon-13 NMR Spectra*, 2nd ed., John Wiley Sons, New York, 1988, Chapter 2.
18 L. C. Thomas and R. A. Chittenden, *Spectrochim. Acta*, 1964, **20**, 467.

Control of metal/ligand stoichiometry and structure in aminopyridinato complexes of zirconium: *N*-alkyl is better than trimethylsilyl†

Colin Morton, Paul O'Shaughnessy and Peter Scott*

Department of Chemistry, University of Warwick, Coventry, UK CV4 7AL. E-mail: peter.scott@warwick.ac.uk

Received (in Cambridge, UK) 11th August 2000, Accepted 21st September 2000
First published as an Advance Article on the web 12th October 2000

_N_-Adamantyl-2-aminopyridines (HL) readily form C_2-symmetric aminopyridinato complexes with zirconium [ZrL_2X_2] (X = Cl, NMe_2, CH_2Ph, CH_2Bu^t) which are stable with respect to ligand redistribution and lead to catalysts for ethylene polymerisation with similar productivity to the related [Zr(benzamidinate)$_2X_2$] system.

Of the many ligand sets that may provide an alternative to cyclopentadienyl,[1] the amidinates have been among the most productive in terms of both new stoichiometric chemistry and catalytic activity.[2] Of particular note recently are reports that complexes such as **I** support an impressive range of ancillary

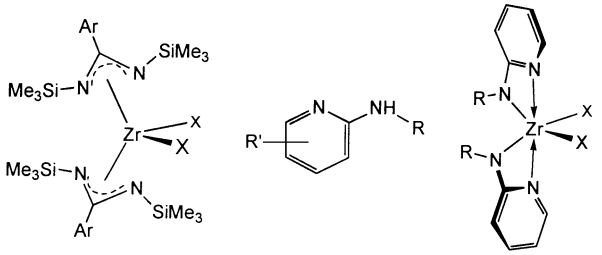

I **II** **III**

ligand- and metal-centred reactivity,[3] and are catalysts for alkene oligomerisation[4] and the synthesis of isotactic poly(propylene).[5] For the closely related aminopyridinato complexes of zirconium,[6] most commonly based on **II** (R = $SiMe_3$),[7] control of the number of such ligands about each metal centre is challenging. For example, treatment of [$Zr(NEt_2)_2Cl_2$] with aminopyridines **II** (R = $SiMe_3$) gave complexes with one or three (but not two) aminopyridinato ligands, depending on substitution at pyridine R′. Complexes of the type **III** analogous to **I** have thus never been isolated, although for the lighter congener titanium unsymmetric complexes [Ti(2-PyNR)$_2$(N-Me_2)Cl] (Py = 2-C_5H_3N; R = Me, Ph) have been crystallographically characterised.[8]

Inspired by the success of alkylanilide ligands in early transition and actinide chemistry,[9] we began to investigate the coordination chemistry of aminopyridines with sterically demanding alkyl (as opposed to trialkylsilyl) substituents R. We report here our initial findings, and in particular that control of metal/ligand stoichiometry and synthesis of catalytically competent species can be achieved.

The Buchwald arylation of amines[10] is particularly successful in the case where arene = pyridine, and we were able to synthesise the 1-adamantyl-2-pyridyl amines HL^1 and HL^2 in good yield from commercially available bromopyridines and 1-adamantylamine using this methodology (Scheme 1).‡

The lithium amide LiL^1 generated *in situ* from HL^1 and lithium butyl§ gave the complex [$L^1{}_2ZrCl_2$] **1a** on reaction with $ZrCl_4$ in diethyl ether. The free amine HL^1 reacted smoothly with [$Zr(NMe_2)_4$], [$Zr(CH_2Ph)_4$] and [$Zr(CH_2Bu^t)_4$] in toluene to give the target complexes [$L^1{}_2Zr(NMe_2)_2$] **2a**,

† Electronic supplementary information (ESI) available: characterisation data. See http://www.rsc.org/suppdata/cc/b0/b006603f/

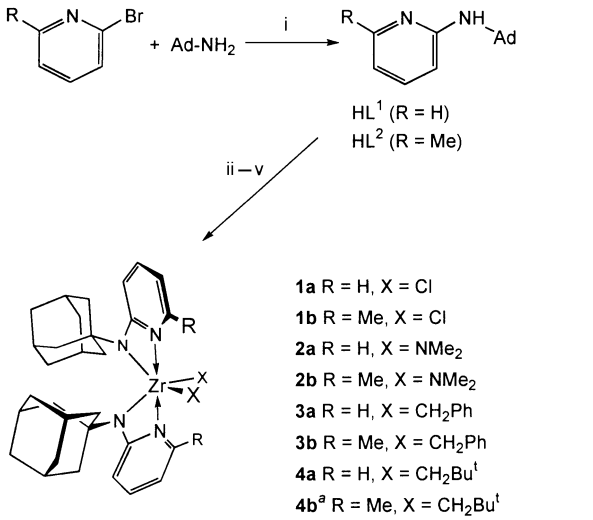

Scheme 1 Synthesis of proligands and complexes **1**–**4**. *Reagents and isolated yields*: i, [$Pd_2(dba)_3$], dppp, $NaOBu^t$, toluene, 60% (L^1), 52% (L^2); ii, Bu^nLi, $ZrCl_4$, diethyl ether, 56% (**1a**), 49% (**1b**); iii, [$Zr(NMe_2)_4$], toluene, 70% (**2a**), pentane, 78% (**2b**); iv, [$Zr(CH_2Ph)_4$], toluene, 86% (**3a**), pentane, 59% (**3b**); v, [$Zr(CH_2Bu^t)_4$], toluene, 63% (**4a**). [a] **4b** not isolated (see text).

[$L^1{}_2Zr(CH_2Ph)_2$] **3a** and [$L^1{}_2Zr(CH_2Bu^t)_2$] **4a**, respectively. NMR tube scale experiments showed that these reactions are essentially quantitative. The analogous complexes **1b**–**3b** of L^2 were prepared similarly. In no instance was a complex of the type [L_3ZrX][6a] detected, although an intermediate [$\{L^1Zr(CH_2Bu^t)_3\}_n$] was observed by NMR spectroscopy when the synthesis of **4a** was conducted in d^8-toluene. The reaction of HL^2 with [$Zr(CH_2Bu^t)_4$] gives a similar monosubstituted intermediate which is converted slowly to **4b**. 2-Methyl substitution on the pyridine ring in L^2 thus appears to have a profound steric effect in the complex, as further evidenced by the broadness of the ^1H NMR spectrum of **4b** in the aliphatic (adamantyl) region. Steric compression in the auxiliary ligand sphere is probably also responsible for the slow thermal decomposition of this compound with elimination of neopentane. In contrast, **4a** and the other alkyls did not decompose in solution over a period of several days at room temperature.

The molecular structure of the six-coordinate neopentyl complex **4a** is shown in Fig. 1.¶ The neopentyl methylene groups and amido N atoms occupy mutually *cis* positions with C(31)–Zr(1)–C(36) and N(2)–Zr(1)–N(4) angles of 98.18(15) and 99.82(11)°, respectively. The two pyridine N atoms are mutually *trans* [N(3)–Zr–N(1) 174.85(11)°]. The overall structure is thus closely related to the bis(benzamidinate)dichlorozirconium complex[3b,5c] but is very different from the *ansa*-bis(aminopyridonato) complexes of titanium in which the quadridentate ligand adopts a planar disposition.[11]

The C_2-symmetry of **4a** is apparent from Fig. 2. The angle between the planes formed by C(36), Zr(1), C(31) and N(2), Zr(1), N(4) is *ca.* 61.85°. It is clear from space-filling models that the conformation of the neopentyl ligands serves to minimise steric interactions between their *tert*-butyl groups and

DOI: 10.1039/b006603f

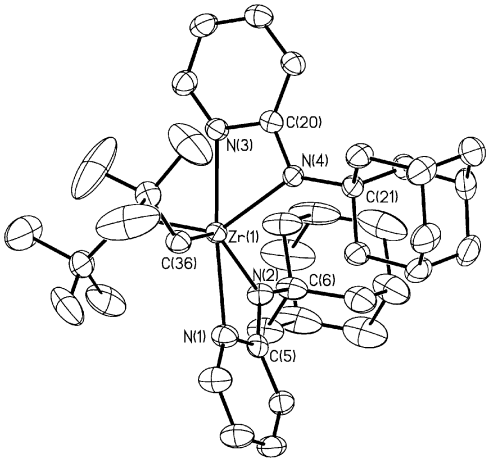

Fig. 1 Thermal ellipsoid plot of the molecular structure of **4a**; hydrogen atoms omitted. Selected bond lengths (Å) and angles(°) Zr(1)–N(4) 2.201(3), Zr(1)–N(2) 2.208(3), Zr(1)–C(36) 2.279(4), Zr(1)–C(31) 2.279(4), Zr(1)–N(3) 2.346(3), Zr(1)–N(1) 2.356(3); N(4)–Zr(1)–N(2) 99.82(11), C(36)–Zr(1)–C(31) 98.18(15).

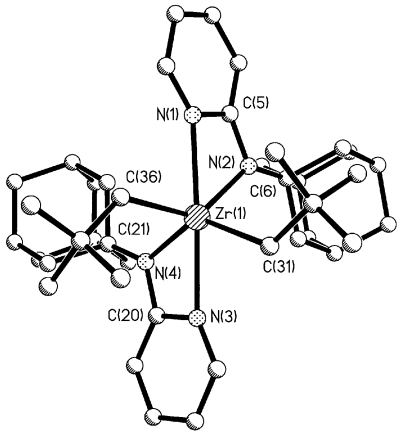

Fig. 2 Molecular structure of **4a** viewed along the approximate C_2 axis.

the pyridine rings. As we suggested above, a methyl group in the 1-position of the ring (as in L[2]) would lead to excessive steric compression in these positions, at least for a ligand as large as neopentyl.

The structures of the complexes in solution are similar to that observed in the solid state for **4a** as judged from NMR spectra. In all instances only one set of resonances for the aminopyridinato ligands is observed at accessible temperatures, and the metal-bound methylene groups in both sets of complexes **3** and **4** appear as pairs of AB doublets in the ^{1}H spectra at room temperature. At elevated temperatures these latter signals coalesce indicating that the complexes racemise, presumably through rotation of the aminopyridinato ligands. From lineshape analysis of the spectra of **3a** a value $\Delta G^{\ddagger}_{298}$ = 60(1) kJ mol^{-1} was extracted. The related amidinate complexes have much lower barriers to inversion, and for example [Zr{CyNC(Me)NCy}$_2$Cl$_2$] has spectroscopically equivalent cyclohexyl groups.[12]

The new complexes are moderately active[1] procatalysts for the polymerisation of ethene. For example, **1a**/MAO in toluene at 25 °C exposed to *ca.* 1 atm. of ethylene gave a reproducible productivity of 20 kg mol^{-1} h^{-1} bar^{-1} for a 1 h run. This exceeds significantly that obtained with previously reported aminopyridinates,[11] and compares favourably with that for the comprehensively studied benzamidinates.[5c] Although the nature of the catalytic system for ethene polymerisation produced from **1a** is as yet unknown it is likely to be of similar nature to the 'alkyl cation' [ZrCp$_2$R]$^+$ implicated in metallocene based catalysis.[13] The reactions of **3a** and **3b** with B(C$_6$F$_5$)$_3$ give species which ^{1}H NMR spectra indicate are the cations [ZrL$_2$(CH$_2$Ph)][B(C$_6$F$_5$)$_3$(CH$_2$Ph)] or ionisation isomers thereof.

We have thus shown that control of ligand stoichiometry and structure can be achieved in aminopyridinato chemistry of zirconium by careful choice of amido *N*-substituent; in this respect alkyl is better than trialkylsilyl. Given that the adamantyl group is close in steric demand to the commonly used SiMe$_3$ the dramatic disparity in the properties of the two systems is likely to arise from the electronic influence of the Si atom on the amido N–Zr bonds in the latter.[14] We note Jordan's comments to the effect that control of ligand stoichiometry in pyridine(alkoxide) complexes of zirconium depends on the proton acidity of the ligand as much as its steric demand.[15] The bis(alkylaminopyridinato) unit is thus established as a robust ligand set for the stabilisation of zirconium complexes with halide, amide and alkyl ligands. We will report further chemistry of these versatile ligands and more detailed catalysis studies in due course.

P.S. wishes to thank EPSRC for postdoctoral fellowships (to C.M. and P.O.'S.).

Notes and references

‡ We have synthesised several related ligands from sterically demanding alkyl and aryl amines and we will report their chemistry in due course.

§ The aminopyridines are also rapidly deprotonated with sodium and potassium hydrides.

¶ *Crystal data* for **4a**: M = 760.29, triclinic, a = 11.456(2), b = 13.352(3), c = 14.019(3) Å, α = 89.456(4), β = 79.991(5), γ = 87.587(4)°, U = 2109.9(7) A^3, T = 180(2) K, space group $P\bar{1}$, Z = 2, μ(Mo-Kα) = 0.295 mm^{-1}, 20512 reflections measued, 10117 unique (R_{int} = 0.0711), R_1 [for 10117 reflections with $I > 2\sigma(I)$] = 0.0674, $wR2$ = 0.1495. Data were collected on a Siemens SMART CCD. The structure was solved by direct methods with additional light atoms found by Fourier methods.

CCDC 182/1787. See http://www.rsc.org/suppdata/cc/b0/b006603f/ for crystallographic files in .cif format.

1 G. J. P. Britovsek, V. C. Gibson and D. F. Wass, *Angew. Chem., Int. Ed.*, 1999, **38**, 428.
2 F. T. Edelmann, *Coord. Chem. Rev.*, 1994, **137**, 403.
3 (*a*) J. R. Hagdahorn and J. Arnold, *Organometallics*, 1998, **17**, 1355; (*b*) J. R. Hagdahorn and J. Arnold, *J. Chem. Soc., Dalton Trans.*, 1997, 3087.
4 E. A. C. Brussee, A. Meetsma, B. Hessen and J. H. Teuben, *Chem. Commun.*, 2000, 497.
5 (*a*) V. Volkis, M. Schmulinson, C. Averbuj, A. Livovskii, F. T. Edelmann and M. S. Eisen, *Organometallics*, 1998, **17**, 3155; (*b*) C. Averbuj, E. Tish and M. S. Eisen, *J. Am. Chem. Soc.*, 1998, **120**, 8640; (*c*) D. Herskovics-Korine and M.S. Eisen, *J. Organomet. Chem.*, 1998, **503**, 307.
6 (*a*) R. Kempe, S. Brenner and P. Arndt, *Organometallics*, 1996, **15**, 1071; (*b*) M. Oberthür, G. Hillebrand, P. Arndt and R. Kempe, *Chem. Ber.*, 1997, **130**, 789; (*c*) H. Fuhrmann, S. Brenner, P. Arndt and R. Kempe, *Inorg. Chem.*, 1996, **35**, 6742.
7 C. L. Raston, B. W. Skelton, V. A. Tolhurst and A. H. White, *J. Chem. Soc., Dalton Trans.*, 2000, 1279; H. K. Lee, Y.-L. Wong, Z.-Y. Zhou, Z.-Y. Zhang, D. K. P. Ng and T. C. W. Mak, *J. Chem. Soc., Dalton Trans.*, 2000 539 and references 10–15 therein.
8 R. Kempe and P. Arndt, *Inorg. Chem.*, 1996, **35**, 2644.
9 C. C. Cummins, *Chem. Commun.*, 1998, 1777.
10 J. P. Wolfe, H. Tomori, J. P. Sadighi, J. Yin and S. L. Buchwald, *J. Org. Chem.*, 2000, **65**, 1158.
11 M. Oberthür, P. Arndt and R. Kempe, *Chem. Ber.*, 1996, **129**, 1087.
12 A. Littke, N. Sleiman, C. Bensimon, D. S. Richeson, G. P. A. Yap and S. J. Brown, *Organometallics*, 1998, **14**, 446.
13 H. H. Brintzinger, D. Fischer, R. Mulhaupt, B. Rieger and R. M. Waymouth, *Angew. Chem., Int. Ed. Engl.*, 1995, **34**, 1143.
14 M. F. Lappert, P. P. Power, A. R. Sanger and R. C. Srivastava, *Metal and Metalloid Amides*, Ellis Horwood, Chichester, 1980, p. 244.
15 T. Tsukahara, D. C. Swenson and R. F. Jordan, *Organometallics*, 1997, **16**, 3303.

Calculated amide/enol of amide energy differences for several interesting amide systems†

Zvi Rappoport*[a] and Hiroshi Yamataka*[b]

[a] *Department of Organic Chemistry and the Minerva Center for Computational Quantum Chemistry, The Hebrew University, Jerusalem 91904, Israel. E-mail: zr@vms.huji.ac.il*

[b] *Institute of Scientific and Industrial Research, Osaka University, Ibaraki, Osaka 567-0047, Japan. E-mail: yamataka@sanken.osaka-u.ac.jp*

Received (in Cambridge, UK) 1st August 2000, Accepted 21st September 2000
First published as an Advance Article on the web 9th October 2000

The calculated pK_{Enol} values for the enols of amides $Me_2CHCON(Me)Ph$ and $XCH_2CH(NH_2)CONHMe$ (X = H,OH) are lower by only 1.1–2.7 units than that of acetamide, and therefore these enols should not display unusual stability.

Although 'simple' enols (*i.e.* those lacking a β-electron-withdrawing substituent)[1] of aldehydes and ketones are much less stable than their aldehyde or ketone tautomers unless the enols are specially stabilised, they play an important role in several reactions.[2] Simple enols of carboxylic acid derivatives such as esters and amides are even much more unstable compared with the acid derivatives than the corresponding carbonyl/enol pair, owing to the stabilisation of the acid derivative by the alkoxy or amino substituent.[3] Recent calculations had shown that the equilibrium constant for the parent pair $MeCONH_2/CH_2{=}C(OH)NH_2$ expressed as pK_{Enol} (= $-\log K_{Enol}$; K_{Enol} = [Enol]/[Amide] at equilibrium) is 21.3 in the gas phase.[4] It is therefore not surprising that, from what we presently know, the role of enols of amides as reaction intermediates is limited.

A process in which enols of amides may play a role is peptide racemisation, since ketonisation of an intermediate planar enol of amide will give both *R* and *S* species of the amide. D-Serine and D-aspartate are observed in significant amount in mammalian tissues[5] and the enzyme responsible for serine isomerisation was recently isolated[5a] so that *in vivo* racemisation is possible.

Hegarty *et al.* reported recently experimental results which suggest that the enol 1-*N*-methylanilino-2-methylpropen-1-ol **2** of the amide *N*-methylanilino-2-methylpropionamide **1** exists in observable concentration in water-containing media and underwent tautomerisation to **1** at measurable rates.[6] Enols of amides as simple as **2** were not hitherto observed and, based on the shorter life times for related enols of acids,[7] they are not expected to have such a long lifetime. Since **2** resembles the intermediate enols expected in peptide racemisation we performed theoretical calculations for **1** and **2** as well as for two simple pairs of amides/enols of serine and alanine amides in order to find out if the enols are unusually thermodynamically stable, so that this may be reflected in their kinetic stability.

The relative stabilities of the amide **1** and the enol **2** as well as that of the other compounds in Table 1 were computationally determined by means of density functional theory at the B3LYP/6-31G** level.[8,9] This method has been extensively used in recent calculations of enols of carboxylic acid derivatives, and the calculated pK_{Enol} values were shown to be within *ca.* 2 pK_{Enol} units of the values measured in water.[4,10]

Several conformational isomers were examined for **1** and **2** and the most stable ones are shown in Fig. 1. with others given as ESI.† The phenyl ring of amide **1** is *anti* to the C=O bond and is perpendicular to the amide moiety, facing the isopropyl group. Another conformation with the phenyl ring coplanar to the amide moiety is not on a local minimum and converges to the structure shown in Fig. 1. The conformer with the carbonyl group and the phenyl ring *syn* to each other is 12.7 kJ mol^{-1} higher in energy than **1**. In enol **2**, the ethenol and the anilino moieties are twisted (O–C–N–Ph dihedral angle of 64°) and the enolic hydrogen is directed toward the Ph ring. Attempted optimisation of a planar conformation gave the twisted structure. Another conformer with the OH pointing away from the Ph ring is 4.0 kJ mol^{-1} less stable.

Table 1 Amide–enol isomerisation free energies ΔG (kJ mol^{-1}), electronic energies (ΔE) (kJ mol^{-1}) (in parentheses) and pK_{Enol} of amides calculated at the B3LYP/6-31G** level at 25 °C

Amide/enol	$\Delta G(\Delta E)$	pK_{Enol}
$Me_2CHCON(Me)Ph$ **(1)**/$Me_2C{=}C(OH)$-N(Me)Ph (**2**)	105.3 (103.2)	18.5
$MeCONH_2$ **(3)**/$CH_2{=}C(OH)NH_2$ **(6)**	121.2 (114.5)	21.3[4]
$HOCH_2CH(NH_2)CONHMe$ **(4)**/$HOCH_2C(NH_2){=}$C(OH)NHMe (**7**)	119.1 (123.7)	20.1
$MeCH(NH_2)CONHMe$ (**5**)/$MeC(NH_2){=}C(OH)NHMe$ (**8**)	112.7 (113.3)	19.8

The calculated energy difference between **1** and **2** is 103.2 kJ mol^{-1} in electronic energy and 105.3 kJ mol^{-1} in free energy, which corresponds to a pK_{Enol} value of 18.5 at 25 °C. This value is 2.8 pK_{Enol} units lower than that calculated for the parent acetamide system.[4] The pK_{Enol} value is much higher than those of enols of acids which were observed by flash photolysis, but had shorter lifetimes owing to a faster decomposition to the corresponding acids.[7] Clearly the unexpectedly long lifetime of enol **2**[6] does not reflect an unusual thermodynamic stability of the enol. The calculated gas phase K_{Enol} value for **1**, taking into account that the calculated solvent effects on pK_{Enol} values are small[4,11] suggests that **2** will not be observable in aqueous organic media at room temperature, based on data of pK_{Enol} values and the lifetimes of simple enols.[12] Indeed, the other observable simple enols of amides having two bulky β-Tip (Tip = 2,4,6-$Pr^i_3C_6H_2$) groups, *i.e.* $Tip_2C{=}C(OH)NR_2$[13] should have pK_{Enol} values of *ca.* 8, based on the calculated K_{Enol} of 9.3

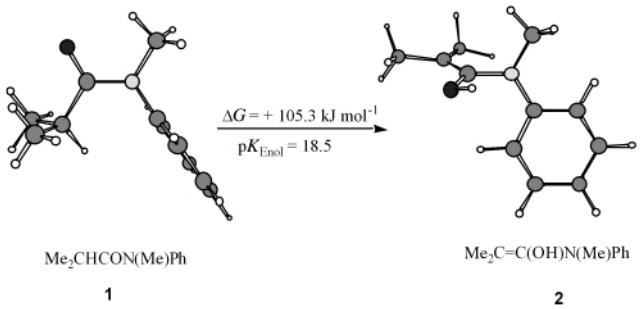

Fig. 1 Most stable conformational isomers for **1** and **2**.

† Electronic supplementary information (ESI) available: optimised structures of various conformers. See http://www.rsc.org/suppdata/cc/b0/b006216m/

for ditipylacetic acid[10] and the lower pK_{Enol} for acetamide than for AcOH.[4] The $t_{1/2}$ for the tautomerisation of diTip *N*,*N*-dimethylacetamide is *ca.* 20 min in 5:1 CD_3CN–THF-d_8 at 273 K.[13a]

Table 1 summarises the keto–enol isomerisation energies for the amide/enol pairs of the *N*-methyl amides of serine and alanine. Again, several conformations were found for each species (these are given in the ESI†) and the energy differences and the derived pK_{Enol} values in Table 1 are based on the most stable conformation of both species. For the two *N*-methylamides the pK_{Enol} values are *ca.* 1 unit lower than for the parent acetamide system but the 1,2-diaminoenols are still so unstable compared with the corresponding amide forms, that if a correlation between thermodynamic and kinetic stability exists in these cases, the isomerisation of peptides including serine and aspartic acid *via* the enol route is inferred to be very slow.[14]

Dissection of the overall effect of the C_β and nitrogen substituents to their individual effects on the amide and the enol is obtained by using the isodesmic reactions (1) and (2). All

$$XX'CHCONYY' + MeMe \rightleftharpoons XX'CHCH_2NYY' + MeCH{=}O \quad (1)$$

reaction free energies at 25 °C in kJ mol^{-1}

1: X=X′=Me, Y=Me, Y′=Ph	108.5
3: X=X′=Y = Y′=H	115.4
4: X=$HOCH_2$, X′=NH_2, Y=H, Y′=Me	129.5
5: X=Me, X′=NH_2, Y=H, Y′=Me	124.4

$$XX'C{=}C(OH)NYY' + MeMe \rightleftharpoons XX'CHCH_2NYY' + H_2C{=}CHOH \quad (2)$$

2: X=X′=Me, Y=Me, Y′=Ph	59.3
6: X=X′=Y=Y′=H	50.2
7: X=$HOCH_2$, X′ = NH_2, Y=H, Y′=Me	66.5
8: X=Me, X′=NH_2, Y=H, Y′=Me	67.7

reactions were found to be endothermic indicating that the interaction of the amino groups with either the carbonyl or the enol function stabilises the system and more so for the amide form. For the amino acid amides the amide forms (**4** and **5**) are more stabilised than acetamide by 9–14 kJ mol^{-1}, whereas the higher stabilisation of the enol forms (**7** and **8**) by *ca.* 17 kJ mol^{-1} result in lower pK_{Enol} values for the amino acid amides. The stabilisation of enol **2** is small, being only 9.1 kJ mol^{-1}, but the amide form **1** is less stabilised by 6.9 kJ mol^{-1} compared with acetamide and this destabilising interaction is responsible for the lower pK_{Enol} for **1**.

Numerical calculations were in part carried out at the Research Center for Computational Science, Okazaki, Japan. Z. R. is indebted to the Israel Science Foundation for support, to Professors A. J. Kresge, M. Goodman and R. Mechoulam for discussions and to Professor A. F. Hegarty for correspondence.

Notes and references

1 H. Hart, *Chem. Rev.*, 1979, **79**, 515.
2 *The Chemistry of Enols*, ed. Z. Rappoport, Wiley, Chichester, 1990.
3 A. F. Hegarty and P. O'Neill in ref. 2, ch. 10, p. 639.
4 S. Sklenak, Y. Apeloig and Z. Rappoport, *J. Am. Chem. Soc.*, 1998, **120**, 10 359.
5 H. Wolosker, K. N. Sheth, M. Takahashi, J.-P. Mothet, R. O. Brady, Jr., C. D. Ferris and S. H. Snyder, *Proc. Natl. Acad. Sci. USA*, 1999, **96**, 721; H. Wolosker, S. Blackshaw and S. H. Snyder, *Proc. Natl. Acad. Sci. USA*, 1999, **96**, 13 409.
6 A. F. Hegarty, S. J. Eustance and C. Relihan, *7th European Symposium on Organic Reactivity (ESOR 7)*, Ulm, Germany, August 22–27, 1999, *Book of Abstracts*, A8, p. 68.
7 For a summary, see: A. J. Kresge, *Chem. Soc. Rev.*, 1996, **25**, 275.
8 A. D. Becke, *Phys. Rev. A*, 1988, **38**, 3098; C. Lee, W. Yang and R. G. Parr, *Phys. Rev. B*, 1988, **37**, 785.
9 All calculations were performed using the Gaussian 98 program: Gaussian 98, Revision A.6, M. J. Frisch, G. W. Trucks, H. B. Schlegel, G. E. Scuseria, M. A. Robb, J. R. Cheeseman, V. G. Zakrzewski, J. A. Montgomery, Jr., R. E. Stratmann, J. C. Burant, S. Dapprich, J. M. Millam, A. D. Daniels, K. N. Kudin, M. C. Strain, O. Farkas, J. Tomasi, V. Barone, M. Cossi, R. Cammi, B. Mennucci, C. Pomelli, C. Adamo, S. Clifford, J. Ochterski, G. A. Petersson, P. Y. Ayala, Q. Cui, K. Morokuma, D. K. Malick, A. D. Rabuck, K. Raghavachari, J. B. Foresman, J. Cioslowski, J. V. Ortiz, B. B. Stefanov, G. Liu, A. Liashenko, P. Piskorz, I. Komaromi, R. Gomperts, R. L. Martin, D. J. Fox, T. Keith, M. A. Al-Laham, C. Y. Peng, A. Nanayakkara, C. Gonzalez, M. Challacombe, P. M. W. Gill, B. Johnson, W. Chen, M. W. Wong, J. L. Andres, C. Gonzalez, M. Head-Gordon, E. S. Replogle and J. A. Pople, Gaussian, Inc., Pittsburgh PA, 1998.
10 H. Yamataka and Z. Rappoport, *J. Am. Chem. Soc.*, 2000, **122**, in press.
11 J. Gao, *J. Mol. Struct. (THEOCHEM)*, 1996, **370**, 203.
12 J. Toullec, ch. 6 in ref. 2; J. R. Keeffe and A. J. Kresge, ch. 7 in ref. 2.
13 (*a*) J. Frey and Z. Rappoport, *J. Am. Chem. Soc.*, 1996, **118**, 3994; (*b*) Z. Rappoport, J. Frey, M. Sigalov and E. Rochlin, *Pure Appl. Chem.*, 1997, **69**, 1933.
14 Since the α-hydrogen to the amide function is acidic, ionization to a planar enolate ion is still a possible mechanistic route for racemisation of peptides.

Cation-triggered 'switching on' of the red/near infra-red (NIR) fluorescence of rigid fluorophore–spacer–receptor ionophores

Knut Rurack,*[a] Ute Resch-Genger,[a] Julia L. Bricks[b] and Monika Spieles[a]

[a] *Dept. I.3902, Federal Institute for Materials Research and Testing (BAM), Richard-Willstaetter Str. 11, D-12489 Berlin, Germany. E-mail: knut.rurack@bam.de*

[b] *Institute of Organic Chemistry, National Academy of Sciences of the Ukraine, Murmanskaya 5, 253660, Kiev-94, Ukraine*

Received (in Liverpool, UK) 3rd August 2000, Accepted 22nd September 2000
First published as an Advance Article on the web 9th October 2000

Fluorophore–spacer–receptor ionophores 1 and 2 show a strong cation-induced enhancement of the fluorescence at λ > 650 nm in the presence of Hg^{II} and Ag^{I} (1) or Pb^{II}, alkaline-earth and alkali metal ions (2).

Molecular signaling systems relying on drastic changes in fluorescence intensity and/or band position upon binding to an inorganic/organic substance have lately received much attention as photonic molecular devices.[1] As functionalized hosts for inorganic guests such as main group, heavy, and transition metal ions or anions, ionophores that consist of an ion-responsive receptor and a (potentially, *i.e.* in the 'switched on' state) highly emissive chromophore, separated by a short alkyl spacer thus preventing pronounced electronic interaction in the ground state, are of particular interest.[2] This molecular constitution allows to combine an electron-donating receptor with a reducable chromophore to invoke fast signaling processes such as intramolecular electron transfer (ET).[3] Among composite ET fluoroionophores, dyes containing a small and rigid spacer are especially advantageous in terms of minimally separated molecular subunits with efficient transduction capability. Recently, such probe molecules based on the Δ^2-pyrazoline chromophore were introduced, showing a cation-induced 'switching on' of the fluorescence upon binding to main group[4] and/or heavy metal ions.[4b] In these substituted 1,3,5-triaryl-Δ^2-pyrazolines, not only does the spacer-separated receptor at the 5-position acts as an electron donor but the main chromophore itself (including the ring fragment C(3)=N(2)–N(1)) consists of a donor (D: N(1) and 1-substituent) and an acceptor (A: C(3) = N(2) and 3-substituent) subunit, and thus the intramolecular ET reaction from the 5-donor does not quench a chromophore-localized state (as, for instance in donor–alkyl-substituted anthracenes or pyrenes)[5] but rather a highly emissive charge transfer (CT) excited state.[4b] This constitution harbors two important advantages for rational probe design: (i) rigidized D–A-fluorophores with allowed CT transtitions (*e.g.* the basic 1,3-diaryl-Δ^2-pyrazoline chromophore)[4b] usually show broad and largely Stokes-shifted absorption and emission bands often accompanied by high fluorescence quantum yields and (ii) the tuning of composite D–A-chromophores by combining specific D and A units is synthetically well feasible. Here, we extended this design concept to the red/near infra-red (NIR) region by the introduction of the strong *N*-phenyl-1,8-naphthalimide (PhNI) acceptor to the 3-position of the Δ^2-pyrazoline ring yielding **1**–**4**. **1** and **2** are equipped with cation-sensitive anilino crown units showing strongly different ion binding preferences and **3** and **4** act as model compounds.

The efficient separation of the electron donating 5-*p*-receptor unit and the main 1,3-diaryl-Δ^2-pyrazoline chromophore by the rigid spacer is suggested from the nearly identical positions of

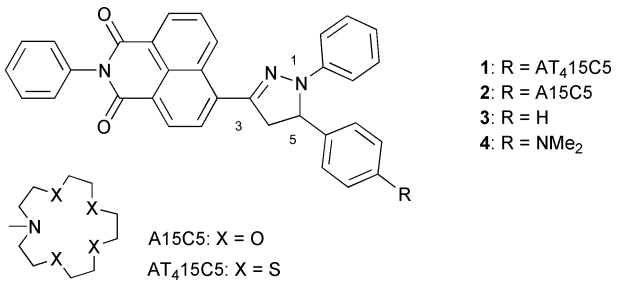

the absorption and emission bands of **1**–**4** in acetonitrile, the solvent we used for the complexation studies (Table 1). The broad, structureless and largely Stokes-shifted absorption and emission bands underline the CT character of the optical transitions in the 1,3-chromophore. In accordance with results obtained for their 3-benzothiazol-2-yl-substituted analogues,[4b] both, the intensive low energy absorption band ($\varepsilon \approx 2 \times 10^4$ M^{-1} cm^{-1} for all the dyes) and the considerably high fluorescence quantum yield of the reference compound **3** reveal that allowed CT transitions determine the spectroscopic properties of the 3-PhNI-Δ^2-pyrazolines. When comparing the fluorescence quantum yield and lifetime data of **3** with those of **1**, **2** and **4**, the quenching electron transfer interaction (virtually no changes in spectral band position, see above) of a 5-*p*-anilino donor is evident. Since the radiative rate constants $k_f = \phi_f/\tau_f$ of **1**–**4** are very similar ($k_f \approx 0.9 \times 10^8$ s^{-1}), the rate constant of the ET quenching process in **1**, **2** and **4** can be calculated from

Table 1 Spectroscopic data of **1** and its Hg^{II} and Ag^{I} complexes, **2** and its Li^{I}, Na^{I}, K^{I}, Mg^{II}, Ca^{II}, Sr^{II}, Ba^{II} and Pb^{II} complexes, **3** and **4** in acetonitrile at room temperature[a]

	λ_{abs}/nm	λ_{em}/nm	ϕ_f	τ_f/ns	log K_S
1	488	680	0.007[b]	0.076	—
1⊂Hg^{II}	483	667	20[c]	1.57	> 5.2[d]
1⊂Ag^{I}	484	673	15[c]	1.22	4.95
2	493	679	0.003[b]	0.029	—
2⊂Li^{I}	489	675	11[c]	0.35	2.92
2⊂Na^{I}	487	673	17[c]	0.65	2.47
2⊂Mg^{II}	484	669	40[c]	1.14	2.99
2⊂Ca^{II}	484	668	43[c]	1.08	4.40
2⊂Sr^{II}	484	668	39[c]	1.23	3.74
2⊂Ba^{II}	485	670	37[c]	0.99	3.68
2⊂Pb^{II}	483	667	47[c]	1.53	> 5.2[d]
3	490	682	0.18[b]	1.32	—
4	484	670	0.002[b]	0.017	—

[a] *Experimental conditions*: *c* (dye) = 5×10^{-6} M, $\lambda_{exc} \approx 480$ nm (at the respective isosbestic points) for steady-state, 480 nm for time-resolved fluorescence measurements. The cation selectivity is identical to that of related pairs of aza-oxa and aza-thia crowns.[4b,9] [b] Fluorescence quantum yield determined relative to fluorescein 27 in 0.1 M NaOH ($\phi_f = 0.90 \pm 0.03$).[12] [c] Relative fluorescence enhancement with respect to ϕ_f of the corresponding free dye. [d] Too high to be determined with acceptable accuracy with the method employed.

† Electronic supplementary information (ESI) available: experimental details including synthesis of **1**–**4** and optical spectroscopy. See http://www.rsc.org/suppdata/cc/b0/b006430k/

DOI: 10.1039/b006430k

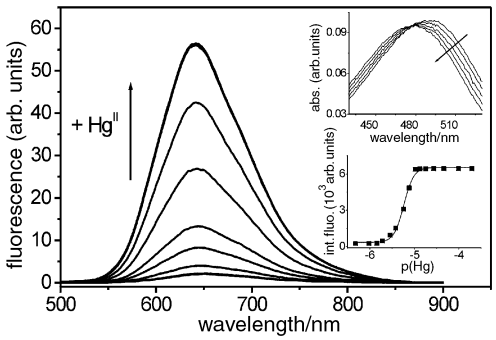

Fig. 1 Fluorescence titration spectra (λ_{exc} = 478 nm) of **1** (5×10^{-6} M) with $Hg(ClO_4)_2$ (concentration range: 5×10^{-7} to 2×10^{-3} M) in acetonitrile. Upper inset: selected absorption titration spectra (isosbestic point: 478 nm; arrow indicates the direction of change upon Hg^{II} addition). Lower inset: fit (——) of the integrated intensity (■) of the fluoroescence titration.

the measured fluorescence lifetime according to $k_{ET} = \tau_f^{(X)-1} - \tau_f^{(3)-1}$ with X = **1**, **2**, **4** by using that of **3** as a reference (Table 1). This yields k_{ET} of 12, 34 and 58 ns^{-1} for **1**, **2** and **4**, respectively. These rate constants are rather small and are thus not related to the solvent relaxation time (the longitudinal solvent relaxation time in acetonitrile was determined to 0.2 ps)[6] suggesting a nonadiabatic electron transfer process.

Upon cation addition to **1** and **2**, the changes in spectral band position are comparatively small (Table 1 and, as an example, the titration of **1** with $Hg(ClO_4)_2$ shown in Fig. 1) as is expected for an ET signaling mechanism. Accordingly, binding of a cation to the electron donating 5-*p*-receptor strongly alters its redox potential and weakens its donor strength thus decelerting the ET quenching process. As is evident from Table 1, the cation-induced changes in fluorescence quantum yield and lifetime are drastic and are directly related to the charge density of the metal ion, *i.e.* the inhibition of the ET reaction being stronger for Hg^{II} than for Ag^{I} (for **1**) and for alkaline-earth metal ions relative to alkali metal ions (for **2**). For the complexes with divalent Hg^{II}, Ca^{II} and Pb^{II}, all of them tightly binding to the fluorescent sensor molecules, even a complete 'switching off' of the ET process is manifested by rate constants of radiative and non-radiative deactivation which are nearly identical to those of the reference compound **3**, lacking a 5-*p*-anilino donor. In all the cases, the fit of the spectrofluorometric titration data[4b,7] yielded a 1 : 1 complex stoichiometry.

Besides the favorable fluorescence enhancement characteristics, the cation selectivity can easily be directed by tuning of the 5-*p*-receptor. Whereas **1**, containing four 'soft'[8] sulfur donor atoms in the 15-crown-5 receptor, only binds to the thiophilic heavy and transition metal ions Hg^{II} and Ag^{I} (for a detailed discussion of ion selectivities and preferences, see refs 4(*b*) and 9), **2** with a monoaza-tetraoxa-15-crown-5 unit shows changes in its spectroscopic properties in the presence of the 'hard'[8] group I and II metal ions as well as Pb^{II}. The power of the present design concept, especially for Hg^{II} (**1**) and Pb^{II} (**2**) commonly known as fluorescence quenchers[10] and for sensing applications in the red/NIR, is apparent.[11]

In summary, we have shown that upon combining intramolecular charge and electron transfer processes in a simple fluorophore–spacer–receptor ionophore with a small but rigid spacer, an efficient cation-triggered 'switching on' of the intramolecular charge transfer fluorescence can selectively be achieved even with advantageous emission features such as broad and largely Stokes shifted bands and considerably high fluorescence quantum yields in the red/NIR spectral region.

We gratefully acknowledge the financial support by the Deutsche Forschungsgemeinschaft and the Bundesministerium für Bildung und Forschung.

Notes and references

1 (*a*) T. D. James, P. Linnane and S. Shinkai, *Chem. Commun.*, 1996, 281; (*b*) P. D. Beer, *Chem. Commun.*, 1996, 689; (*c*) A. P. de Silva, H. Q. N. Gunaratne, C. McVeigh, G. E. M. Maguire, P. R. S. Maxwell and E. O'Hanlon, *Chem. Commun.*, 1996, 2191; (*d*) M.-P. Teulade-Fichou, J. P. Vigneron and J.-M. Lehn, *J. Chem. Soc., Perkin Trans. 2*, 1996, 2169; (*e*) D. Parker, K. Senanayake and J. A. G. Williams, *Chem. Commun.*, 1997, 1777; (*f*) M. A. Mortellaro and D. G. Nocera, *J. Am. Chem. Soc.*, 1996, **118**, 7414; (*g*) S. Weidner and Z. Pikramenou, *Chem. Commun.*, 1998, 1473; (*h*) A. P. de Silva and T. E. Rice, *Chem. Commun.*, 1999, 163; (*i*) J. J. La Clair, *Angew. Chem., Int. Ed.*, 1999, **38**, 3045; (*j*) G. McSkimming, J. H. R. Tucker, H. Bouas-Laurent and J.-P. Desvergne, *Angew. Chem., Int. Ed.*, 2000, **39**, 2167; (*k*) A. P. de Silva, H. Q. N. Gunaratne, T. Gunnlaugsson, A. J. M. Huxley, C. P. McCoy, J. T. Rademacher and T. E. Rice, *Chem. Rev.*, 1997, **97**, 1515.

2 For examples on anions: D. H. Vance and A. W. Czarnik, *J. Am. Chem. Soc.*, 1994, **116**, 9397; H. Miyaji, P. Anzenbacher, Jr., J. L. Sessler, E. R. Bleasdale and P. A. Gale, *Chem. Commun.*, 1999, 1723; for examples on heavy and transition metal cations: P. Ghosh, P. K. Bharadwaj, S. Mandal and S. Ghosh, *J. Am. Chem. Soc.*, 1996, **118**, 1553; B. Ramachandram and A. Samanta, *Chem. Phys. Lett.*, 1998, **290**, 9; for examples on alkali and alkaline-earth cations: A. P. de Silva, H. Q. N. Gunaratne and G. E. M. Maguire, *J. Chem. Soc., Chem. Commun.*, 1994, 1213; K. Yoshida, T. Mori, S. Watanabe, H. Kawai and T. Nagamura, *J. Chem. Soc., Perkin Trans. 2*, 1999, 393; for reviews: see refs. 1*b*, *k*.

3 R. A. Bissell, A. P. de Silva, H. Q. N. Gunaratne, P. L. M. Lynch, G. E. M. Maguire, C. P. McCoy and K. R. A. S. Sandanayake, *Top. Curr. Chem.*, 1993, **168**, 223.

4 (*a*) A. P. de Silva, H. Q. N. Gunaratne, T. Gunnlaugsson and M. Nieuwenhuizen, *Chem. Commun.*, 1996, 1967; (*b*) K. Rurack, J. L. Bricks, B. Schulz, M. Maus, G. Reck and U. Resch-Genger, *J. Phys. Chem. A*, 2000, **104**, 6171.

5 A. P. de Silva and S. A. de Silva, *J. Chem. Soc., Chem. Commun.*, 1986, 1709; E. U. Akkaya, M. E. Huston and A. W. Czarnik, *J. Am. Chem. Soc.*, 1990, **112**, 3590; S. Draxler and M. E. Lippitsch, *Appl. Opt.*, 1996, **35**, 4117; H.-F. Ji, R. Dabestani, G. M. Brown and R. L. Hettich, *Photochem. Photobiol.*, 1999, **69**, 513.

6 M. A. Kahlow, T. J. Kang and P. F. Barbara, *J. Phys. Chem.*, 1987, **91**, 6452; P. J. Rossky and J. D. Simon, *Nature*, 1994, **370**, 263.

7 S. Fery-Forgues, M.-T. Le Bris, J.-P. Guetté and B. Valeur, *J. Phys. Chem.*, 1988, **92**, 6233; J. Bourson, J. Pouget and B. Valeur, *J. Phys. Chem.*, 1993, **97**, 4552.

8 R. G. Pearson, *J. Am. Chem. Soc.*, 1963, **85**, 3533.

9 K. Rurack, J. L. Bricks, G. Reck, R. Radeglia and U. Resch-Genger, *J. Phys. Chem. A*, 2000, **104**, 3087.

10 A. W. Varnes, R. B. Dodson and E. L. Wehry, *J. Am. Chem. Soc.*, 1972, **94**, 946; H. Masuhara, H. Shioyama, T. Saito, K. Hamada, S. Yasoshima and N. Mataga, *J. Phys. Chem.*, 1984, **88**, 5868.

11 It is interesting that the corresponding substituted chalcone-type dyes (PhNI–CO–CH=CH–C_6H_4R with R = H, NMe_2 or crowns), which were obtained as intermediates within the Δ^2-pyrazoline synthesis (see ESI†), do not fluoresce ($\phi_f < 1 \times 10^{-5}$) and thus cannot be exploited for sensing purposes as, for instance their benzothiazole derivatives.[9] This is most probably due to the close neighborhood of the carbonyl and the PhNI group, since electron acceptors at the 4-position of the naphthalimide chromophore are known to quench its fluorescence.[13]

12 J. Olmsted, III, *J. Phys. Chem.*, 1979, **83**, 2581.

13 A. Pardo, J. M. L. Poyato and E. Martin, *J. Photochem.*, 1987, **36**, 323.

Controlling the energy-transfer direction: an oligophenylenevinylene–phenanthroline dyad acting as a proton triggered molecular switch

Nicola Armaroli,*[a] Jean-François Eckert[b] and Jean-François Nierengarten*[b]

[a] *Istituto di Fotochimica e Radiazioni d'Alta Energia (FRAE) del CNR, via Gobetti 101, 40129 Bologna, Italy. E-mail: armaroli@frae.bo.cnr.it*

[b] *Groupe des Matériaux Organiques, Institut de Physique et Chimie des Matériaux de Strasbourg, Université Louis Pasteur et CNRS, 23 rue du Loess, 67037 Strasbourg, France. E-mail: niereng@ipcms.u-strasbg.fr*

Received (in Cambridge, UK) 31st July 2000, Accepted 20th September 2000
First published as an Advance Article on the web 11th October 2000

In a two-component system combining an oligophenylenevinylene (OPV) group with a protonable phenanthroline unit, the direction of intercomponent photoinduced energy transfer can be tuned by proton input, thus allowing on/off switching of the luminescence of the OPV moiety.

A molecular switching device exists in two (or more) different states that can be reversibly interconverted and present different characteristic properties.[1–4] Typically, the switching work is carried out by photons, electrons, or external chemical species.[3] Of course it is crucial to be able to distinguish between the different states, and one of the most powerful tools is fluorescence spectroscopy.[2] For instance, a large variety of molecular recognition events taking place on molecular receptors has been revealed by switching or tuning the luminescence of nearby signaling moieties.[2,3,5]

Oligophenylenevinylenes (OPVs) are strongly fluorescent molecules widely used in materials science for the preparation of light emitting devices (LEDs), field-effect transistors (FETs) or photovoltaic cells.[6,7] Such compounds appear also to be attractive functional building blocks for the construction of new molecular and supramolecular photoactive devices. Here, we describe the preparation and the electronic properties in CH_2Cl_2 solution of the two-component array 3PV-Phen, combining an OPV unit with a protonable phenanthroline group. The related compounds 3PV[8] and Phen have been used as reference compounds for the photophysical studies.

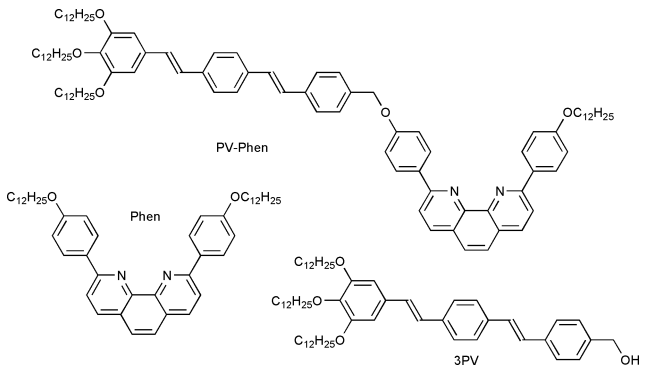

Interestingly, 3PV-Phen can act as a proton triggered molecular switch. Effectively, the intense fluorescence of the 3PV-type moiety can be quenched (*off* state) by protonation of the phenanthroline unit upon addition of acid, whereas the starting emission can be restored (*on* state) by adding a base. The functioning of the 3PV-Phen switch is schematically represented in Fig. 1.

The synthesis of 3PV-Phen is depicted in Scheme 1. Treatment of *p*-bromododecyloxyphenyl with Bu^{t}Li in THF at −78 °C followed by quenching with 1,10-phenanthroline, hydrolysis and oxidation with MnO_2 gave **1** (85% yield). Reaction of **1** with *p*-lithio[(*tert*-butyldimethylsilyl)oxy]-phenyl[9] followed by hydrolysis and oxidation (MnO_2) yielded **2**

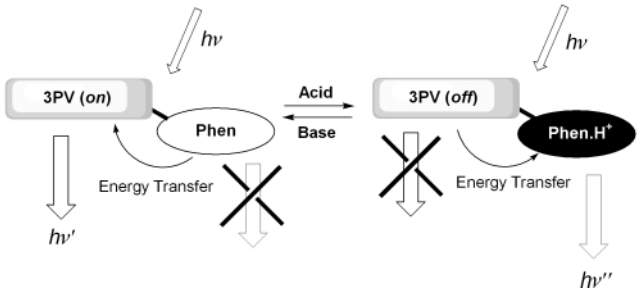

Fig. 1 Schematic representation showing the functioning of the 3PV-Phen molecular switch.

which after deprotection (TBAF) gave **3** in an overall yield of 33%. The reaction of **3** with 3PV under Mitsunobu conditions afforded 3PV-Phen in 71% yield. All of the spectroscopic studies and elemental analysis results were consistent with the proposed molecular structures.

The electronic absorption and emission properties of the model compounds 3PV and Phen [Fig. 2(a)] are very similar to those of previously investigated OPVs[7] and substituted phenanthrolines.[10] Both molecules are strongly fluorescent in the VIS spectral region; 3PV exhibits a band with λ_{max} = 460 nm, τ = 1.3 ns and Φ_{fl} = 0.77, whereas Phen displays λ_{max} = 398 nm, τ = 2.1 ns and Φ_{fl} = 0.35.†

Addition of increasing amounts of trifluoroacetic acid (TFA) to a 1.5×10^{-5} M solution of Phen causes dramatic changes in the absorption spectrum, that are leveled off at *ca.* 10 equivalents of acid added. Isosbestic points are maintained at 296, 314 and 356 nm indicating that a single chemical process occurs, *i.e.* protonation of the phenanthroline;[10] interestingly, the initially transparent solution becomes yellow at the end of the titration. In parallel with the changes in the absorption spectra, remarkable variation in the fluorescence properties are recorded. The intense luminescence band of Phen progressively disappears while a new band characteristic of $PhenH^+$ grows at

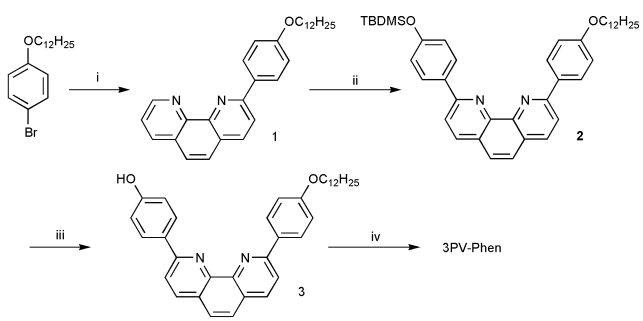

Scheme 1 *Reagents and conditions*: i, Bu^{t}Li, THF, −78 °C, 1 h, then 1,10-phenanthroline, −78 to 0 °C, 3 h, then H_2O, then MnO_2, room temp., 1 h; ii, *p*-lithio[(*tert*-butyldimethylsilyl)oxy]phenyl, THF, 0 °C, 4 h, then H_2O, then MnO_2, room temp., 1 h; iii, TBAF, THF, 0 °C, 2 h; iv, 3PV, DEAD, PPh_3, THF, reflux, 72 h.

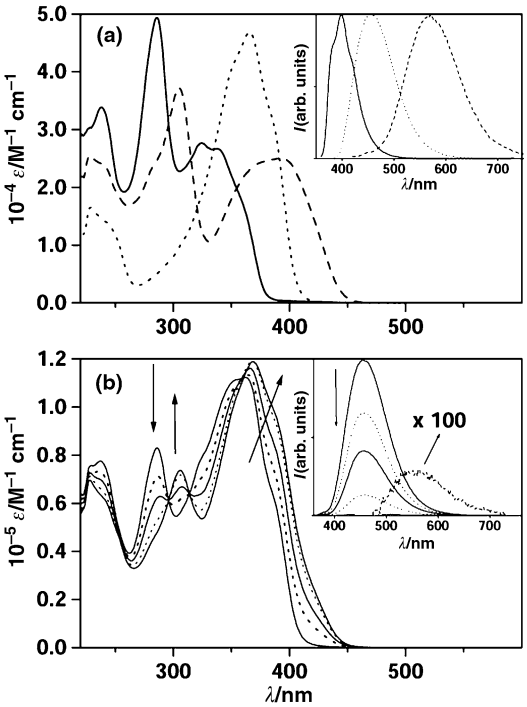

Fig. 2 (a) Absorption and (inset) fluorescence spectra of 3PV (·····), Phen (——), and $PhenH^+$ (– – –). (b) Absorption and (inset) fluorescence (λ_{exc} = 314 nm, isosbestic point) spectra of a 1.5×10^{-5} M CH_2Cl_2 solution of 3PV-Phen containing 0, 1, 2, 4 or 20 equivalents of trifluoroacetic acid. The weak red-shifted band is obtained for the solution containing 20 equiv., after subtraction of the residual 3PV luminescence (see text).

570 nm, with τ = 12.2 ns and Φ_{fl} = 0.048; the luminescence color switches from purple (Phen) to yellow ($PhenH^+$). Addition of an organic base [diazabicyclo[4.3.0]non-5-ene (DBN)] restores the initial absorption and luminescence properties. Importantly, no changes of such properties are observed upon addition of a large excess of TFA or DBN to 3PV solutions.

The absorption spectrum of 3PV-Phen matches the sum of the spectra of the reference compounds within ±10% error, showing one diagnostic band for each component unit with maxima at 286 (Phen) and 360 nm (3PV). Only the typical fluorescence band of the 3PV fragment is observed (λ_{max} = 460 nm, τ = 1.3 ns, Φ_{fl} = 0.70); the excitation spectrum (λ_{em} = 460 nm) matches the absorption profile, indicating that excitation of the Phen moiety is followed by quantitative energy transfer to the 3PV unit. One can thus conclude that, in 3PV-Phen, only the OPV luminescence is *on* since a photoinduced quenching process featuring a Phen → 3PV direction is active (Fig. 1).

Addition of increasing amounts of (TFA) to a 1.5×10^{-5} M solution of 3PV-Phen causes dramatic changes in the absorption spectrum [Fig. 2(b)]. A clear analogy with the protonation reaction of Phen is found: the same amount of acid is required to complete the reaction, isosbestic points are located at 296, 314 and 359 nm. Importantly, the final spectrum matches the sum of the spectra of 3PV and Phen.H^+ within ±10% error, and the reaction is reversible upon addition of DBN. These findings suggest that the 3PV-$PhenH^+$ species is formed.

The addition of acid also leads to dramatic changes in the emission properties (λ_{exc} = 359 nm, isosbestic point): the characteristic blue 3PV luminescence is progressively suppressed and a much weaker green-yellow emission (λ_{max} = 556 nm, τ = 12.7 ns‡) is detected, attributable to the $PhenH^+$ moiety (see above). The luminescence quenching of 3PV, observed also in a rigid matrix at 77 K, is attributable to energy transfer to the $PhenH^+$ moiety. The energy transfer efficiency is difficult to estimate, since some residual 3PV fluorescence (< 0.5%, relative to the initial value) is present, even when a large excess of acid is added. Such residual emission, likely arising from unprotonated 3PV-Phen in the acid–base equilibrium, overlaps the much weaker $PhenH^+$ emission, thus making difficult clean excitation spectroscopy. In any case one can conclude that, in an acid environment, the OPV luminescence of 3PV-Phen is *off* due to an intercomponent quenching process displaying a 3PV → Phen direction [Fig. 1].

In terms of electronic energy levels our bipartite system has been designed in order to achieve the following: in one component (3PV) the energy of the fluorescent level (E_1) is insensitive to protons; by contrast, in the other component (Phen), a proton input tunes the fluorescent levels between two energy values (E_2 and E_3). The key feature is that the energy of E_1 is intermediate between that of E_2 and E_3, thus enabling an energy transfer in the desired direction *via* the chemical (proton) input. The energy scaling ($E_2 > E_1 > E_3$) is reflected in the spectral position of the corresponding fluorescence bands [Fig. 2(a), inset].

In conclusion, we have shown a simple way to reversibly switch *on* and *off* the widely exploited fluorescence of OPVs. Also, it is worth pointing out that this is one of the rare cases of multicomponent systems where the direction of the photo-induced energy transfer can be controlled.[11–12] To the best of our knowledge, this is the first example where such control can be reversibly accomplished by chemical inputs.

This work was supported by the Italian CNR and the French CNRS. We thank L. Oswald for technical help and Professor J.-F. Nicoud for his interest and support.

Notes and references

† Fluorescence spectra, lifetimes (time resolution 0.5 ns), and quantum yields were obtained as described in detail in ref. 7; experimental uncertainties are ±2 nm, ±8% and ±20%, respectively. For emission quantum yields anthracene in cyclohexane (Φ = 0.34) and quinine sulfate in 0.05 M H_2SO_4 (Φ = 0.546) were used as standards.

‡ In this case the decay is biexponential and 12.6 ns refers to the longest component. A shorter component (1.3 ns) accounts for the residual 3PV fluorescence (see text).

1 M. Irie, *Chem. Rev.*, 2000, **100**, 1685; J.-M. Lehn, *Supramolecular Chemistry–Concepts and Perspectives*, VCH, Weinheim, 1995.
2 A. P. de Silva, H. Q. N. Gunaratne, T. Gunnlaugsson, A. J. M. Huxley, C. P. McCoy, J. T. Rademacher and T. E. Rice, *Chem. Rev.*, 1997, **97**, 1515.
3 L. Fabbrizzi, M. Licchelli and P. Pallavicini, *Acc. Chem. Res.*, 1999, **32**, 846.
4 L. Gobbi, P. Seiler and F. Diederich, *Angew. Chem., Int. Ed.*, 1999, **38**, 674.
5 T. D. James, P. Linnane and S. Shinkai, *Chem. Commun.*, 1996, 281.
6 K. Müllen and G. Wegner, *Electronic Materials: The Oligomer Approach*, Wiley-VCH, Weinheim, 1998.
7 J.-F. Eckert, J.-F. Nicoud, J.-F. Nierengarten, S.-G. Liu, L. Echegoyen, F. Barigelletti, N. Armaroli, L. Ouali, V. Krasnikov and G. Hadziioannou, *J. Am. Chem. Soc.*, 2000, **122**, 7467.
8 J.-F. Eckert, J.-F. Nicoud, D. Guillon and J.-F. Nierengarten, *Tetrahedron Lett.*, 2000, **41**, 6411.
9 E. Fernández-Megía, J. M. Iglesias-Pintos and F. J. Sardina, *J. Org. Chem.*, 1997, **62**, 4770.
10 N. Armaroli, L. De Cola, V. Balzani, J.-P. Sauvage, C. O. Dietrich-Buchecker and J.-M. Kern, *J. Chem. Soc., Faraday Trans.*, 1992, **88**, 553; N. Armaroli, P. Ceroni, V. Balzani, J.-M. Kern, J.-P. Sauvage and J.-L. Weidmann, *J. Chem. Soc., Faraday Trans.*, 1997, **93**, 4145; C. O. Dietrich-Buchecker, J.-P. Sauvage, N. Armaroli, P. Ceroni and V. Balzani, *New J. Chem.*, 1996, **20**, 801.
11 D. J. Cárdenas, J.-P. Collin, P. Gaviña, J.-P. Sauvage, A. De Cian, J. Fischer, N. Armaroli, L. Flamigni, V. Vicinelli and V. Balzani, *J. Am. Chem. Soc.*, 1999, **121**, 5481.
12 S. Serroni, S. Campagna, R. Pistone Nascone, G. S. Hanan, G. J. E. Davidson and J.-M. Lehn, *Chem. Eur. J.*, 1999, **5**, 3523.

ChemComm

Hydrothermal crystal engineering using hard and soft acids and bases: synthesis and X-ray crystal structures of the metal hydroxide-based phases $M_3M'_2(OH)_2[NC_5H_3(CO_2)_2$-2,4$]_4(H_2O)_4$ (M = Co, Ni, Zn; M′ = Pd, Pt)†

Lee A. Gerrard and Paul T. Wood*

School of Chemical Sciences, University of East Anglia, Norwich, UK NR4 7TJ. E-mail: p.wood@uea.ac.uk

Received (in Cambridge, UK) 27th July 2000, Accepted 20th September 2000
First published as an Advance Article on the web 12th October 2000

Solvothermal reaction of $K_2M'Cl_4$ (M′ = Pd, Pt) with pyridine dicarboxylate and excess base produces isostructural coordination solids in which 'complex ligands' containing palladium or platinum coordinate to metal hydroxide chains.

The use of solvothermal techniques to prepare hybrid organic–inorganic materials inaccessible by other means is a rapidly expanding area.[1,2] One current challenge is to prepare materials of increasing compositional complexity in which the individual components confer different physical properties or have different structural influences. This goal is exemplified by hydrolytic phases containing oxide or hydroxide moieties in addition to metal ions and ligands.[2] We are particularly interested in this area as judicious choice of ligands can lead to important target materials such as porous solids and low-dimensional magnets. The size of the organic ligand plays an important role in our approach to both of these classes of material as it controls both the size of the pores and the separation between low-dimensional magnetic structures. A logical choice of ligand type to fulfil the role of large 'spacer' would be polycyclic aromatic carboxylates such as 4,4′-biphenyl dicarboxylic acid or 3,4,9,10-perylene tetracarboxylic acid, however, these have proved unsuccessful in our hands,[3] possibly owing to their solubility characteristics. Subsequently we have investigated a strategy based on 'metal complex ligands' which we report here.

A multi-component ligand equivalent in size to those suggested above can be constructed by relying on the principle that hard and soft bases will coordinate to like acids.[4] By coordinating ligands with both hard and soft donor sites to a soft metal we can generate a large but soluble anionic ligand which is terminated by hard (carboxylate) donor groups and as such is analogous to the ligands we have already found to be successful in simpler reactions. Pyridine-2,*x*-dicarboxylates are known to be stable to solvothermal conditions[2] and also to form stable complexes with soft metals *via* N-coordination.[5] The existence of three isomers also presents the opportunity to study the effect of substitution pattern on product structure. This is actually a very important variable with the 2,4 isomer yielding much more straightforward chemistry hence it is this ligand on which we concentrate here.

The method we have previously developed for preparing hydrolytic phases of the 3d transition metals involves the reaction of a carboxylate salt with $M(OH)_2$ prepared *in situ*, a variation of this technique is used here. Three aqueous solutions are first prepared containing (i) K_2PtCl_4 (0.1 mmol) in H_2O (2.5 ml); (ii) pyridine-2,4-dicarboxylic acid (0.2 mmol) and 1 M KOH (0.7 mmol) in H_2O (5 ml); (iii) MCl_2 hydrate (0.2 mmol) in H_2O (2.5 ml). Solutions (i) and (ii) are first mixed, followed by (iii) which results in formation of $M(OH)_2$. Hydroxide formation is evident for cobalt-containing solutions from the slight blue colour produced which we have previously observed to be indicative of the onset of Co(II) hydrolysis.[3] This gives a Pt:metal:ligand:base ratio of 1:2:2:7. The mixture was placed in a 23 cm^3 Teflon-lined autoclave and heated at 200 °C for 15 h, followed by slow cooling to room temperature over a period of 8 h. The solid was filtered off and purified by brief ultrasonic treatment of an aqueous slurry followed by decanting. The material was then filtered off, washed with water and air dried. The palladium-containing materials are made in analogous fashion from K_2PdCl_4 on a 0.12 mmol scale with a Pd:metal:ligand:base ratio of 1:2:2:6.

These methods produce $M_3M'_2(OH)_2[NC_5H_3(CO_2)_2$-2,4$]_4(H_2O)_4$ as crystalline solids in good yields; **1a**, Co/Pd, pale pink (62 mg, 89%); **1b**, Co/Pt, orange–pink (52 mg, 78%); **2a**, Ni/Pd, pale green (52 mg, 75%); **2b**, Ni/Pt, green (44 mg, 66%); **3a**, Zn/Pd, yellow (57 mg, 82%); **3b**, Zn/Pt, yellow (49 mg, 72%). Satisfactory microanalytical data were obtained for all compounds (ESI†).

IR spectra for the six compounds are essentially superimposable showing only the slight shifts in frequency expected on isomorphous substitution (ESI†). The band which is indicative of the formation of these materials is the sharp, medium intensity O–H stretch due to the bridging hydroxide ligand: ν_{max}(KBr) = 3598, 3604, 3606, cm^{-1} for Co, Ni and Zn, respectively. The position of the band is insensitive to the presence of Pd or Pt.

The X-ray crystal structures‡ of a representative sample of the compounds (**1a** and **3a**) along with the unit cell dimensions for **1b**, **2a**, **2b** and **3b**, were determined showing that the materials are indeed isostructural (ESI†). The secondary building unit (SBU) is the $M'M_2L_2$ fragment (Fig. 1) which has two environments for the hard (octahedral) metal. The SBUs are held together by two different types of linkage, the overall effect of which is to produce layers lying parallel to [0 1 −1]. The first type of linkage consists of infinite chains with a –MLM′LMLM′– repeat unit running parallel to the *bc* bisector. The second type is a series of metal hydroxide strips containing chains of edge- and vertex-sharing $M_3(\mu_3$-OH) triangles which run parallel to the *a* axis (Fig. 2). Each individual layer has metal hydroxide 'ribs' which are linked to their nearest neighbours by a row of LM′L moieties. The ligands form the upper and lower faces of the layer (Fig. 3) with an average intra-

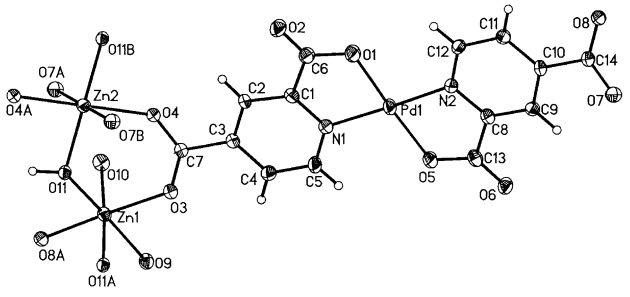

Fig. 1 The basic building block of the title complexes (illustrated here for **3a**) showing the atom numbering scheme. Ellipsoids are drawn at the 30% probability level.

† Electronic supplementary information (ESI) available: elemental analysis, IR data, unit cell parameters and selected bond lengths and angles. See http://www.rsc.org/suppdata/cc/b0/b006094l/ for crystallographic files in .cif format.

DOI: 10.1039/b006094l

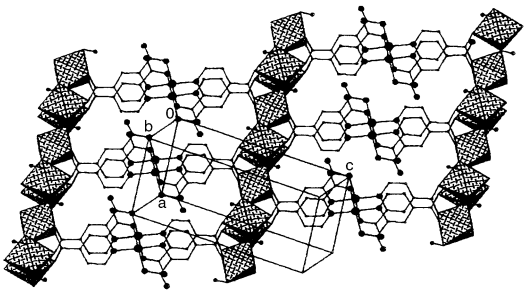

Fig. 2 View showing the chains of vertex sharing metal octahedra (running down the crystallographic *a* axis) and their linkage *via* the LML moiety.

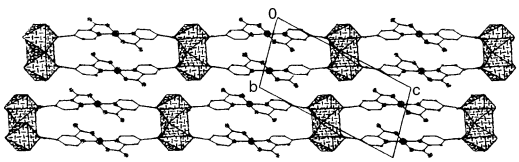

Fig. 3 View down the crystallographic *a* axis showing the packing of layers.

layer distance of 3.42(1) Å. There is a second π-stacking interaction between the sheets with an average separation of 3.56(1) Å. The π stacks and metal hydroxide strips run along orthogonal axes, this leads to the formation of a tightly packed three-dimensional structure. We believe that the stacking interaction hampers the formation of pores within these materials. It is also noteworthy that when porous materials have been prepared[3] the ligands bridge in the plane of the metal triangles, rather than above and below as seen here. All bond lengths and angles are normal with the metal–ligand distances showing small deviations from ideal square and octahedral geometry (ESI†). For example the palladium square planar angles range from 82.5(2) to 100.1(2)°. The two octahedral zinc geometries show a greater distortion for the metal that is not on an inversion centre, Zn(1). The angles range from 82.2(2) to 96.9(2)° and 172.1(2) to 176.8(2)° for Zn(1) in comparison with 86.6(1) to 93.2(1)° and exactly 180° for Zn(2). The formation of the particularly stable five-membered chelate ring for the soft metal helps to stabilise it against decomposition to intractable material, which we believe to be oxide, at the relatively high pH required for hydrolysis of the divalent 3d metal ions.

This material can be synthesised using a range of metal : metal′ : ligand : base ratios provided that the pH is kept relatively high. The optimum reaction conditions found for the platinum compounds require a ratio of 1 : 2 : 2 : 7 resulting in a pH in the range 7.7–8.8 depending on the metal. The palladium compounds can be obtained in pure form from a ratio of 1:2:2:6 which gives pH values in the range 6.7–7.8. In general the production of the platinum compounds requires more base than is needed for the palladium-containing materials. Hydrolysis of the metal salts occurs prior to heating and therefore the pH values measured for the reaction mixtures are lower than expected considering the excess base used. Accurate control of hydroxide content is essential as there is a very narrow range in which these materials may be formed. There is little overlap between the conditions required for the formation of M(OH)-containing materials and those required for stabilisation of the soft metal complex.

The reactions are also sensitive to temperature and duration. To obtain an optimum yield of pure product the reactions should be performed at temperatures in the range 180–220 °C for 15 h. Lower temperatures result in contamination by other products whilst higher temperatures result in decomposition. We have also investigated the chemistry of isomeric ligands under similar conditions. Reactions with pyridine-2,3-dicarboxylate yield only decomposition products whilst pyridine-2,5-dicarboxylate gives a range of highly complex products with structures sensitive to both the hard and soft metal.

We have shown that hard and soft donor sites on a metal can preferentially bind hard and soft metal ions from a binary mixture. This provides another tool in our armoury for engineering materials with specific properties such as magnetism and porosity.

We wish to thank Johnson-Matthey for the generous loan of precious metal salts and the University of East Anglia for funding.

Notes and references

‡ *Crystal data*: for **1a**: $C_{28}H_{22}N_4O_{22}Pd_2Co_3$, M = 1156.09, triclinic, space group $P\bar{1}$, a = 6.531(1), b = 8.027(2), c = 16.595(3) Å, α = 76.46(3), β = 89.39(3), γ = 85.14(3)° , V = 842.7(3) Å^3, Z = 1, D_c = 2.278 g cm^{-3}, $F(000)$ = 567, μ = 2.596 mm^{-1}, T = 293(2) K, crystal dimensions 0.16 × 0.14 × 0.04 mm. Data were collected on a Rigaku R-axis II image plate diffractometer equipped with a rotating anode X-ray source using graphite-monochromated Mo-Kα radiation (λ = 0.71073 Å). Total no. of reflections was 4959 of which 2698 were unique (R_{int} = 0.0439). The structure was solved by direct methods and refined using full-matrix least squares on F^2 to give $R1$ = 0.0363 for $F > 4\sigma(F)$ and $wR2$ = 0.1585, S = 1.006 for all data.

For **3a**: $C_{28}H_{22}N_4O_{22}Pd_2Zn_3$, M = 1175.41, triclinic, space group $P\bar{1}$, a = 6.529(1), b = 8.124(2), c = 16.719(3) Å, α = 75.94(3), β = 88.73(3), γ = 84.78(3)°, V = 856.7(3) Å^3, Z = 1, D_c = 2.278 g cm^{-3}, $F(000)$ = 567, μ = 3.202 mm^{-1}, T = 293(2) K, crystal dimensions 0.14 × 0.10 × 0.08 mm. Data collected as above. Total no. of reflections was 5386 of which 2862 were unique (R_{int} = 0.0630). The structure was solved by direct methods and refined using full-matrix least squares on F^2 to give $R1$ = 0.0412 for $F > 4\sigma(F)$ and $wR2$ = 0.1348, S = 0.976 for all data.

CCDC 182/1785. See http://www.rsc.org/suppdata/cc/b0/b006094l/ for crystallographic files in .cif format.

1 P. T. Wood, W. T. Pennington, J. W. Kolis, B. Wu and C. J. O'Connor, *Inorg. Chem.*, 1993, **32**, 129; M. I. Khan, Y. S. Lee, C. J. O'Connor, R. C. Haushalter and J. Zubieta, *J. Am. Chem. Soc.*, 1994, **116**, 4525; B. K. Das and M. G. Kanatzidis, *Inorg. Chem.*, 1995, **34**, 5721; S. O. H. Gutschke, A. M. Z. Slawin and P. T. Wood, *J. Chem. Soc., Chem. Commun.*, 1995, 2197; O. M. Yaghi and G. M. Li, *J. Am. Chem. Soc.*, 1995, **117**, 10 401; W. Bensch, C. Nather and M. Schur, *Chem Commun.*, 1997, 1773.

2 D. Hagrman, P. J. Hagrman and J. Zubieta, *Angew. Chem., Int. Ed.*, 1999, **38**, 3165; A. Distler, D. L. Lohse and S. C. Sevov, *J. Chem. Soc., Dalton Trans.*, 1999, 1805; R. Kuhlman, G. L. Schimek and J. W. Kolis, *Inorg. Chem.*, 1999, **38**, 194; C. Serre and G. Férey, *Inorg. Chem.*, 1999, **38**, 5370; S. O. H. Gutschke, M. Molinier, A. K. Powell and P. T. Wood, *Angew. Chem., Int. Ed. Engl.*, 1997, **36**, 991; D.Yufit, D. J. Price, J. A. K. Howard, S. O. H. Gutschke, A. K. Powell and P. T. Wood, *Chem. Commun.*, 1999, 1561.

3 S. O. H. Gutschke, L. A. Gerrard, E. Stothers and P. T. Wood, unpublished work.

4 R. G. Pearson, *J. Am. Chem. Soc.*, 1963, **85**, 3533.

5 R. Song, K. M. Kim and Y. S. Sohn, *Inorg. Chim. Acta*, 1999, **292**, 238; S. Jayasree, A. Seayad and R. V. Chaudhari, *Chem. Commun.*, 2000, 1239.

Planar chirality: a fascinating symmetry breaking which leads to ferroelectricity in ferrocenyl liquid crystals

Thierry Chuard,[a] Stephen J. Cowling,[b] Maria Fernandez-Ciurleo,[a] Isabelle Jauslin,[a] John W. Goodby*[b] and Robert Deschenaux*[a]

[a] *Institut de Chimie, Université de Neuchâtel, Avenue de Bellevaux 51, Case postale 2, CH-2007 Neuchâtel, Switzerland. E-mail: robert.deschenaux@unine.ch*

[b] *Department of Chemistry, University of Hull, Hull, UK HU6 7RX. E-mail: j.w.goodby@chem.hull.ac.uk*

Received (in Cambridge, UK) 12th July 2000, Accepted 9th August 2000
First published as an Advance Article on the web 11th October 2000

We describe the synthesis, characterization and properties of the first optically-active 1,3-unsymmetrically disubstituted ferrocene derivative which is to exhibit smectic C* and smectic A* phases.

Symmetry breaking operations and chirality have held centre stage in the fundamental investigations and applications of liquid crystals.[1,2] Furthermore, recent studies on mesogens with banana-shaped molecular structures have shown that chiral induction in self-organizing systems is possible even though the materials are themselves achiral.[3,4] The search for new chiral effects in mesomorphic systems prompted us to synthesize unsymmetrically 1,3-disubstituted ferrocene-containing liquid crystals,[5] where the different substituents at the 1- and 3-positions generate structures with planar chirality (Fig. 1). A representative example is illustrated by compound **1** (see Scheme 1); the two substituents are differentiated by the length of the alkyl chains and the orientation of the outer ester groups. Homologues of this material were prepared in racemic form from (±)-**2**[5] (see Scheme 1). Over the entire range of the compounds studied, smectic C (SmC) and smectic A (SmA) phases were observed, and in some cases an additional nematic phase was detected.

The presence of the SmC phase in this family of compounds provided a unique challenge to make the materials optically active (SmC*) and thereby ferroelectric. Of course symmetrically 1,3-disubstituted ferrocene derivatives have the potential to exhibit ferro- or antiferro-electricity if the packing constraints of the molecules within the layers induce a restricted rotation of the molecules about their long axes. Within this packing constraint, the V-shaped molecules will pack together to give a non-symmetric arrangement thereby leading to the induction of non-linear properties.

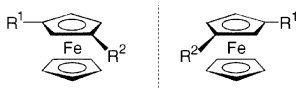

Fig. 1 Planar chirality in unsymmetrically 1,3-disubstituted Fc derivatives. Planar chirality: chirality resulting from the arrangement of out-of-plane groups with respect to a reference plane, called the 'chiral plane'.[6]

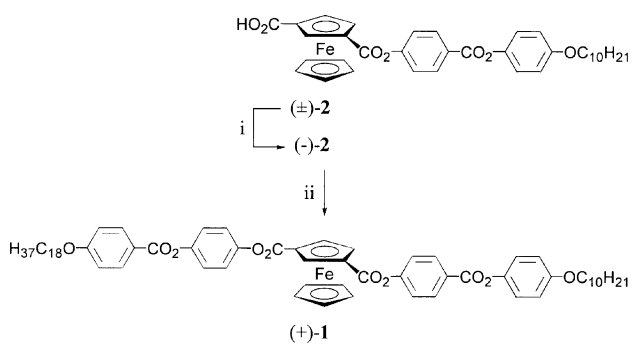

Scheme 1 *Reagents and conditions*: i, (+)-phenylethylamine [(+)-PEA], CH_2Cl_2; ii, (a) oxalyl chloride, pyridine, CH_2Cl_2, reflux, 3 h; (b) 4-hydroxyphenyl 4-(octadecyloxy)benzoate,[10] triethylamine, CH_2Cl_2, reflux, 3 h.

Ferroelectric liquid crystals are of considerable interest in switchable, half-wave plate, bistable light-valves. For ferrocenyl liquid crystals, SmC* phases have been reported only for two mono-substituted derivatives.[7,8] Chirality was introduced into the peripheral side-chain by means of asymmetric carbon atoms, but for the two materials no ferroelectric behavior was described.

In addition to the investigation of the dependency of ferroelectricity on planar chirality, this study allowed us to probe the influence of the chiral unit, which is embedded in the central region of the molecular structure, on the self-organization process and mesophase formation. In metallomesogens, planar chirality was elegantly exploited by Malthête and coworkers who reported optically-active butadiene–tricarbonyliron liquid crystal complexes.[9] The spontaneous polarization of one of the complexes was determined, and a value of 32 nC cm^{-2} was obtained (response time: 9 ms).[9b]

We report, herein, the synthesis, mesomorphic behavior and ferroelectric properties of the liquid-crystalline Fc derivative (+)-**1** (Scheme 1). The latter structure was selected because the corresponding racemic analogue gave the broadest SmC range among the family of homologues studied.[5]

The preparation of (+)-**1** is shown in Scheme 1. Optical resolution of acid (±)-**2** with (+)-phenylethylamine [(+)-PEA] gave (−)-**2**.† Treatment of (−)-**2** with oxalyl chloride gave the corresponding acid chloride derivative, which was condensed with 4-hydroxyphenyl 4-(octadecyloxy)benzoate[10] to furnish (+)-**1**.‡

Derivatization of the acid (−)-**2** with (+)-PEA gave the amide **3a**,§ which served for the determination of the enantiomeric excess (ee) of (−)-**2** by ^{1}H NMR and HPLC techniques. We assumed that the reactions used to prepare **3a** and (+)-**1** did not alter the optical purity of (−)-**2**. Therefore, the determination of the diastereomeric excess (de) of **3a** is a measure of the ee of (−)-**2** and, consequently, of (+)-**1**. The 1:1 diastereomeric mixture of **3a**:**3b** synthesized from (±)-**2** and (+)-PEA was used to fix the analytical conditions. The ^{1}H NMR and HPLC characteristics of diastereoisomer **3b** [from (+)-**2** and (+)-PEA] were deduced by comparing the data of the 1:1 diastereomeric mixture with that of **3a**.

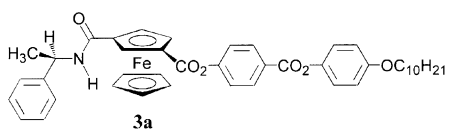

3a

In the ^{1}H NMR spectrum of the 1:1 diastereomeric mixture, each diastereoisomer gave well separated signals for the five protons of the unsubstituted cyclopentadienyl (Cp) ring (**3a**:

4.28 ppm; **3b**: 4.33 ppm) and the two Cp protons *ortho* to the amide function (**3a**: 5.70 and 5.19 ppm; **3b**: 5.65 and 5.24 ppm). For these signals, the five Cp protons gave two sharp singlets with baseline resolution, and appeared to be suitable for the determination of the de of **3a**. HPLC analysis (column Nucleosil 120 RP-C_{18} (250 × 4 mm) equipped with a precolumn Nucleosil 120 RP—C_{18} (30 × 4 mm); solvent, acetonitrile–water (80:20); elution rate, 1.5 ml min^{-1}) of the 1:1 diastereomeric mixture furnished two peaks (**3a**: 40.2 min; **3b**: 38.0 min) with almost baseline resolution. Both techniques led to reliable and reproducible results.

Optical resolution of (±)-**2** by (+)-PEA proved to be efficient: ^{1}H NMR and HPLC methods gave a de of 98% for **3a**, leading to an ee value of 98% for (+)-**1**.

The absolute configuration of the Fc in (+)-**1**, (−)-**2** and **3a** is shown arbitrarily. So far, crystallization of the salt (+)-PEA/(−)-**2** and amide **3a** failed to give crystals suitable for X-ray analysis.

The liquid-crystalline properties were investigated by differential scanning calorimetry (DSC, 10 °C min^{-1}, under N_2) and polarized optical microscopy.¶ Ferrocene (+)-**1** gave enantiotropic SmC* and SmA* phases (Cr → SmC*: 170 °C; SmC* → SmA*: 198 °C; SmA* → I: 202 °C; onset point, first heating run). The SmC* to SmA* phase transition was not detected by DSC (second order transition). No decomposition or racemization was observed for (+)-**1**. Similar transition temperatures were obtained for racemic (±)-**1** (Cr → SmC: 166 °C; SmC → SmA: 198 °C; SmA → I: 200 °C).[5] No mesomorphic behavior was observed for the acid (−)-**2** and amide **3a**.

Fig. 2 shows the value of the spontaneous polarization as a function of temperature.‖ At the Curie point, the spontaneous polarization increased rapidly to a value of *ca*. 1.36 nC cm^{-2}, at which point it increased almost linearly as the temperature was lowered. At a temperature of 30 °C below the Curie point, a value of only 2.8 nC cm^{-2} was reached (response time: *ca*. 200 ms).

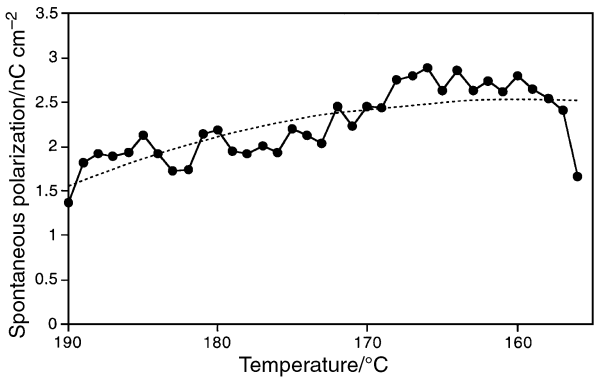

Fig. 2 The spontaneous polarization measured as a function of temperature from the Curie point for (+)-**1**.

An appreciable scatter in the data was observed because of the weak ferroelectric properties. The results obtained indicate firstly that planar chirality can induce ferroelectric properties, and secondly the induced effects are weak, revealing a poor coupling between the chirality associated with the Fc moiety at the centre of the molecular structure, the strongly polar functional groups in the material, and the liquid-crystalline environment. The weak ferroelectric properties are probably linked to the fact that the two arms attached to the Fc unit are not greatly different in length or polarity.

R. D. acknowledges the Swiss National Science Foundation for financial support.

Notes and references

† *Optical resolution* of (±)-**2**[5] (1.45 g, 2.31 mmol) in dry CH_2Cl_2 (130 ml), was added a solution of (+)-PEA (140 mg, 1.16 mmol) in dry CH_2Cl_2 (15 ml). The solution was allowed to stand overnight at room temperature. The salt was recovered by filtration, dried (743 mg), and crystallized in a 1:1 mixture of dry CH_2Cl_2–acetone (75 ml); yield: 554 mg. A mixture of the salt (554 mg), CH_2Cl_2 (40 ml) and 5 M HCl (40 ml) was vigorously shaken and the layers were separated. The organic layer was washed (water), dried ($MgSO_4$), and evaporated to dryness. Crystallization (CH_2Cl_2–hexane) of the solid residue gave (−)-**2** (327 mg, 45% with respect to the desired enantiomer) of ee = 98%. Mp 170 °C. $[\alpha]_D$ −18 (*c* 0.45, CH_2Cl_2). δ_H(200 MHz, acetone-d_6) 8.27 (d, 2 H, arom.), 7.52 (d, 2 H, arom.), 7.22 (d, 2 H, arom.), 7.01 (d, 2 H, arom.), 5.52 (t, 1 H, Cp), 5.19 (dd, 1 H, Cp), 5.14 (dd, 1 H, Cp), 4.44 (s, 5 H, Cp), 4.03 (t, 2 H, OCH_2), 1.80 (m, 2 H, OCH_2CH_2), 1.60–1.20 [m, 14 H, $O(CH_2)_2(CH_2)_7$], 0.89 (t, 3 H, CH_3). Anal. Calc. for $C_{35}H_{38}O_7Fe$ (626.53): C, 67.10; H, 6.11. Found: C, 67.08; H, 6.27%.

‡ *Synthesis* of (+)-**1**: *first step*: a mixture of (−)-**2** (250 mg, 0.441 mmol), oxalyl chloride (670 mg, 5.29 mmol), pyridine (5 drops) and dry CH_2Cl_2 (15 ml) was heated under reflux for 3 h, and evaporated to dryness. The solid residue was extracted with hot light petroleum (bp 60–90 °C) until the extracts remained colorless. Evaporation of the solvent gave the acid chloride derivative (273 mg, 96%), which was used in the next step without further purification. δ_H(400 MHz, $CDCl_3$) 8.29 (d, 2 H, arom.), 7.33 (d, 2 H, arom.), 7.13 (d, 2 H, arom.), 6.94 (d, 2 H, arom.), 5.74 (t, 1 H, Cp), 5.34 (dd, 1 H, Cp), 5.21 (dd, 1 H, Cp), 4.50 (s, 5 H, Cp), 3.97 (t, 2 H, OCH_2), 1.79 (m, 2 H, OCH_2CH_2), 1.60–1.20 [m, 14 H, $O(CH_2)_2(CH_2)_7$], 0.89 (t, 3 H, CH_3). *Second step*: a solution of the above acid chloride derivative (250 mg, 0.39 mmol), 4-hydroxyphenyl 4-(octadecyloxy)benzoate[10] (188 mg, 0.39 mmol), triethylamine (40 mg, 0.39 mmol) in dry CH_2Cl_2 (15 ml) was heated under reflux for 3 h, cooled to room temperature, and evaporated to dryness. Purification of the solid residue twice by column chromatography (CC) [first CC: silica gel, CH_2Cl_2–AcOEt (50:1); second CC: silica gel, CH_2Cl_2–AcOEt (100:1)], and crystallization (CH_2Cl_2–EtOH) gave (+)-**1** (232 mg, 54%) of ee = 98%. $[\alpha]_D$ +3 (*c* 0.42, CH_2Cl_2). δ_H(200 MHz, $CDCl_3$) 8.29 (d, 2 H, arom.), 8.15 (d, 2 H, arom.), 7.35 (d, 2 H, arom.), 7.27 (d, 4 H, arom.), 7.12 (d, 2 H, arom.), 6.98 (d, 2 H, arom.), 6.94 (d, 2 H, arom.), 5.79 (t, 1 H, Cp), 5.27 (br s, 2 H, Cp), 4.47 (s, 5 H, Cp), 4.06 (t, 2 H, OCH_2), 3.97 (t, 2 H, OCH_2), 1.80 (m, 4 H, OCH_2CH_2), 1.60–1.20 (m, 44 H, aliph.), 0.89 (2 × t, 6 H, CH_3). Anal. Calc. for $C_{66}H_{82}O_{10}Fe$ (1091.21): C, 72.65; H, 7.57. Found: C, 72.79; H, 7.77%.

§ **3a**: prepared analogously to the synthesis of (+)-**1**, from (−)-**2** (3.00 mg) and (+)-PEA. Purification by column chromatography [silica gel, CH_2Cl_2–AcOEt (98:2)] gave the desired product of de = 98%. δ_H(200 MHz, acetone-d_6) 8.26 (d, 2 H, arom.), 7.74 (d, 1 H, NH), 7.56–7.27 (m, 5 H, arom.), 7.48 (d, 2 H, arom.), 7.21 (d, 2 H, arom.), 7.01 (d, 2 H, arom.), 5.70 (t, 1 H, Cp), 5.28 (qut., 1 H, $CHCH_3$), 5.19 (dd, 1 H, Cp), 5.10 (dd, 1 H, Cp), 4.28 (s, 5 H, Cp), 4.03 (t, 2 H, OCH_2), 1.84-1.73 (m, 2 H, OCH_2CH_2), 1.57 (d, 3 H, $CHCH_3$), 1.55–1.25 [m, 14 H, $O(CH_2)_3(CH_2)_7$], 0.89 (t, 3 H, CH_3). Anal. Calc. for $C_{43}H_{47}NO_6Fe$ (729.69): C, 70.78; H, 6.49, N, 1.92. Found: C, 70.60; H, 6.61, N, 1.90%.

¶ For instrumentation, see: B. Dardel, R. Deschenaux, M. Even and E. Serrano, *Macromolecules*, 1999, **32**, 5193.

‖ Electro-optic studies on the ferroelectric properties were carried out using homogeneously aligned cells (Linkam) which were constructed from ITO coated glass, treated with antiparallel-buffed polyimide (PI) coated layers so as to give sites for planar, homogeneous growth of the liquid-crystalline state. The cell gap (*ca*. 5 μm) maintained by glass spacers was verified by UV–VIS interferometry. The effective electrode areas of the cells used were 0.9 cm^2. The cells were filled by capillary action at atmospheric pressure with (+)-**1** in the isotropic phase. Good alignment was achieved by cooling slowly (< 0.1 °C min^{-1}) from the isotropic liquid into the liquid-crystalline state. The spontaneous polarization was determined using the triangular wave method.

1 J. W. Goodby, *J. Mater. Chem.*, 1991, **1**, 307.
2 J. W. Goodby, R. Blinc, N. A. Clark, S. T. Lagerwall, M. A. Osipov, S. A. Pikin, T. Sakurai, K. Yoshino and B. Zeks, in *Ferroelectric Liquid Crystals—Principles, Properties and Applications*, Gordon and Breach, Philadelphia and Reading, 1991.
3 R. H. Tredgold, *J. Phys. D: Appl. Phys.*, 1990, **2**, 119.
4 T. Niori, T. Sekine, J. Watanabe, T. Furukawa and H. Takezoe, *J. Mater. Chem.*, 1996, **6**, 1231.
5 R. Deschenaux and J. Santiago, *Tetrahedron Lett.*, 1994, **35**, 2169.
6 E. L. Elliel and S. H. Wilen, in *Stereochemistry of Organic Compounds*, Wiley, New York, 1994.
7 C. Imrie and C. Loubser, *J. Chem. Soc., Chem. Commun.*, 1994, 2159.
8 T. Seshadri and H.-J. Haupt, *Chem. Commun.*, 1998, 735.
9 (*a*) L. Ziminsky and J. Malthête, *J. Chem. Soc., Chem. Commun.*, 1990, 1495; (*b*) P. Jacq and J. Malthête, *Liq. Cryst.*, 1996, **21**, 291.
10 R. Deschenaux, J.-L. Marendaz and J. Santiago, *Helv. Chim. Acta*, 1993, **76**, 865.

$[Ni(edt\text{-}CN)_2]^{-\cdot}$, a novel paramagnetic nickel dithiolene complex analog of $Ni(mnt)_2^{-\cdot}$ with two cyano groups only

Marc Fourmigué* and Josep N. Bertran

Sciences Moléculaires aux Interfaces, CNRS FRE 2068, Institut des Matériaux Jean Rouxel, 2, rue de la Houssinière, BP32229, 44322 Nantes cedex 3, France. E-mail: fourmigue@cnrs-imn.fr

Received (in Cambridge, UK) 7th August 2000, Accepted 18th September 2000
First published as an Advance Article on the web 12th October 2000

The preparation, X-ray crystal structures and electrochemical properties of bis(2-cyano-1,2-ethanedithiolate)-nickelate $[Ni(edt\text{-}CN)_2]^{2-/-\cdot}$ are described for both oxidation states together with the singlet–triplet behaviour of the PPh_4^+ salt of the paramagnetic $[Ni(edt\text{–}CN)_2]^{-\cdot}$ complex.

The construction of conducting or magnetic solids from the assembling of transition metal centers and organonitrile anion radical molecules[1] such as $TCNE^{-\cdot}$, $DCNQI^{-\cdot}$ or $TCNQ^{-\cdot}$ has

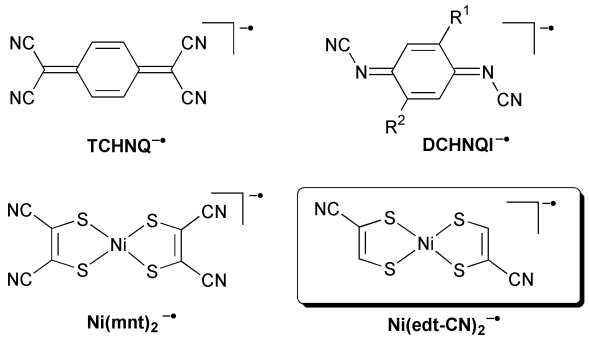

revealed extraordinary materials such as the metallic $Cu(DCNQI)_2$,[2] the electrically bistable[3] Cu(TCNQ) or a bulk ferromagnet from V with TCNE (TCNE = tetracyanoethylene).[4] By comparison and most surprisingly, the parallel coordination chemistry of the corresponding nickel dithiolene complexes with the maleonitriledithiolate ligand (mnt^{2-}) is virtually untouched and only a few salts of the diamagnetic $Ni(mnt)_2^{2-}$ have been reported with $Ag(PPh_3)_2^+$ and CuI.[5,6] The crystalline salts derived from DCNQI anions incorporating only two nitrile groups as well as the rich chemistry of the mnt^{2-} complexes[7] prompted us to investigate the numerous possibilities that would be offered by the unknown corresponding nickel dithiolene complex bearing only two cyano groups, *viz.* bis(2-cyano-1,2-ethanedithiolate)nickelate $[Ni(edt\text{-}CN)_2]^{n-}$ (n = 1 or 2). We describe here the synthesis of this novel complex system together with its electrochemical properties and report and analyse the X-ray crystal structures of the PPh_4^+ salts of both the diamagnetic $[Ni(edt\text{-}CN)_2]^{2-}$ dianion and the paramagnetic radical anion $[Ni(edt\text{-}CN)_2]^{-\cdot}$. This complex offers extensive possibilities for the elaboration of promising materials with conducting or magnetic properties by varying the nature of the counter cation, closed-shell inorganic (Na^+, Cu^+, Ag^+ or NH_4^+) or organic (R_4N^+, PyH^+, ...) cations as well as open shell organic ($TTF^{+\cdot}$, $BEDT\text{-}TTF^{+\cdot}$) or organometallic ($Cp^*{}_2Fe^{+\cdot}$) cations.

The dithiocarbonate **4**† precursor of the dithiolene ligand was prepared by a novel route (Scheme 1) which avoids the use of cyanoacetylene[8] in the reported preparation of **3** or that of activated Zn complexes in the reported preparation of **4**.[9] The easily available ester **1**[10] was successively converted into the corresponding amide **2** with NH_3 in MeOH in 72% yield, into the nitrile **3** by $POCl_3$ dehydration[11] in 75% yield before oxymercuration to the dithiocarbonate **4** in 84% yield. Treatment of **4** with 2 equiv. of MeONa followed by addition of 0.5 equiv. $NiCl_2{\cdot}6H_2O$ and PPh_4Cl afforded the air-stable dianionic

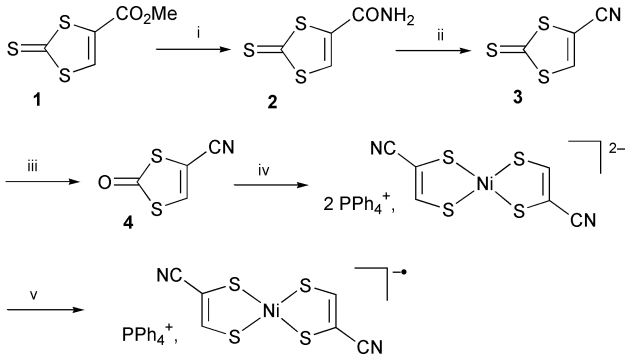

Scheme 1 *Reagents and conditions*: i, NH_3/MeOH; ii, 1 equiv. $POCl_3$, tetramethylene sulfone, 100 °C, 7 h; iii, $Hg(OAc)_2$, $CHCl_3$–AcOH, 2 h; iv, 2 equiv. MeONa, MeOH, 0.5 $NiCl_2{\cdot}6H_2O$, PPh_4Cl/H_2O; v, 0.5 I_2.

diamagnetic $[PPh_4^+]_2[Ni(edt\text{-}CN)_2{}^{2-}]$ salt. The corresponding one-electron oxidation product, $[PPh_4^+][Ni(edt\text{-}CN)_2{}^{-\cdot}]$, was obtained by iodine oxidation and recrystallisation from methanol. Cyclic voltammetry of the dianionic $Ni(edt\text{-}CN)_2{}^{2-}$ salt (Fig. 1) shows that it oxidises reversibly to the monoanionic $Ni(edt\text{-}CN)_2{}^{-\cdot}$ at −0.31 V *vs.* SCE while an irreversible process is observed at +0.65 V, a behaviour also observed for $Ni(mnt)_2{}^{n-}$ (0.226 V for $Ni(mnt)_2{}^{2-/-}$ with an ill-defined oxidation wave around 1 V)[12] but with a cathodic shift attributable to the presence of only two cyano groups. Single crystal X-ray structures‡ of both salts show that the nickel complexes adopt the same square-planar structure in the two different oxidation states (Fig. 2) with a *trans* orientation of the two cyano groups. It is likely that both *cis* and *trans* orientations are in equilibrium in solution while the most symmetrical *trans* isomer exhibits a lower solubility. The observed shortening of the Ni–S and C–S bonds upon oxidation of the dianion to the monoanion is in accordance with the antibonding character of

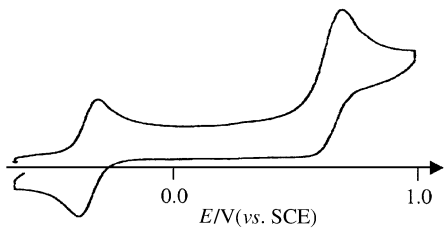

Fig. 1 Cyclic voltammetry of $[PPh_4]_2[Ni(edt\text{-}CN)_2]$, in MeCN with 0.5 M $NBu^n_4PF_6$ as electrolyte at a scan rate of 100 mV s^{-1}.

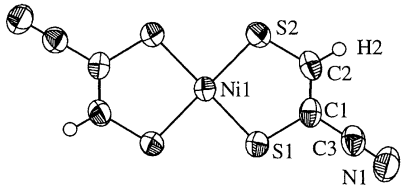

Fig. 2 ORTEP view (with 50% probability displacement ellipsoids) of the radical anion $[Ni(edt\text{-}CN)_2]^{-\cdot}$ in the 1:1 $[PPh_4][Ni(edt\text{-}CN)_2]$ salt.

DOI: 10.1039/b006440h

Table 1 Important bond distances (Å) in $[Ni(edt\text{-}CN)_2]^{2-/-\cdot}$ together with a representation of the π-type HOMO of $[Ni(edt\text{-}CN)_2]^{2-}$

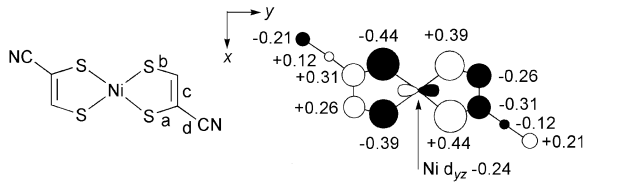

	$[Ni(edt\text{-}CN)_2]^{2-}$	$[Ni(edt\text{-}CN)_2]^{-\cdot}$
Ni–S	2.188(2)	2.148(3)
S–C (bond a)	1.756(5)	1.736(3)
S–C (bond b)	1.720(5)	1.706(4)
C=C (bond c)	1.342(7)	1.341(4)
C–C (bond d)	1.426(8)	1.427(4)
C≡N	1.148(7)	1.141(3)

those bonds in the dianion HOMO shown in Table 1. Similarly the antibonding character of the C≡N bonds is reflected by an increase in ν(C≡N), from 2180 cm^{-1} in the dianion to 2205 cm^{-1} in the monoanion. In the 2:1 $[PPh_4^+]_2[Ni(edt\text{-}CN)_2^{2-}]$ salt, two crystallographically independent dianions, each of them on an inversion centre, are fully isolated from each other by the bulky PPh_4^+ cations. On the other hand, in the 1:1 $[PPh_4^+][Ni(edt\text{-}CN)_2^{-\cdot}]$ salt, the open-shell anions, in general positions in the unit cell, associate into inversion-centered diads with a unusual overlap (Fig. 3) and a short plane-to-plane distance of 3.519(3) Å. The temperature dependence of the SQUID magnetic susceptibility for this salt (Fig. 4) exhibits a maximum at 23 K and is satisfactorily fitted with the Bleaney–Bowers[13] expression of the susceptibility[14] of singlet–triplet behaviour with $|J/k| = 37.5(2)$ K, in accordance with the diad structure. Preliminary metathesis experiments show that a highly insoluble precipitate is obtained upon addition of $AgBF_4$ to $[PPh_4^+][Ni(edt\text{-}CN)_2^{-\cdot}]$ solutions while the Cu^+ salt obtained from $Cu(MeCN)_4BF_4$ is much more soluble. Charge-transfer salts are also being investigated with organic ($TTF^{+\cdot}$) and organometallic ($Cp^*_2Fe^{+\cdot}$) radical cations as well as with functionalized TTF molecules bearing hydrogen bonding groups or halogen atoms able to interact in the solid state with the cyano group.

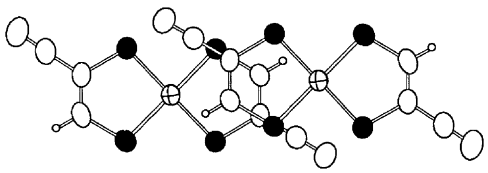

Fig. 3 The peculiar overlap between two $[Ni(edt\text{-}CN)_2]^{-\cdot}$ radical anions in the 1:1 $[PPh_4][Ni(edt\text{-}CN)_2]$ salt.

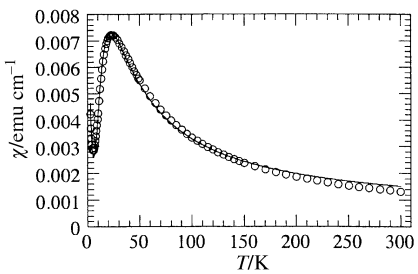

Fig. 4 Temperature dependence of the magnetic susceptibility of the 1:1 $[PPh_4][Ni(edt\text{-}CN)_2]$ salt. The solid line is a fit to the Bleaney–Bowers equation (see text) together with a low-temperature Curie tail encompassing 2.7% magnetic defects.

Notes and references

† *Selected data* for **2**: yellow crystals; mp 225–226 °C (MeOH), δ_H(400 MHz, d_6-DMSO), 3.36 (s, 2H, NH_2), 8.18 (s, 1H, CH); δ_C(100 MHz, d_6-DMSO), 134.2 (CH), 143.7 ($CCONH_2$), 160.0 (C=O), 213.9 (C=S). ν_{max}(KBr)/cm^{-1}; 1651 (C=O), 1084 (C=S). MS (EI) *m/z* (%) 177 (100, $M^{+\cdot}$) (Anal. Calc. for $C_4H_3NOS_3$ (177.35): C, 27.19; H, 1.71; N, 7.90; S, 54.27. Found: C, 27.19; H, 1.67; N, 7.71; S, 53.32%). For **3**: yellow crystals; mp 96 °C (lit.:[8] 100–101 °C, δ_H(400 MHz, $CDCl_3$), 7.73 (s, 1H, CH); δ_C(100 MHz, $CDCl_3$), 109.7 (*C*CN), 112.2 (C≡N), 142.3 (CH), 207.7 (C=S). ν_{max}(KBr)/cm^{-1}; 1058 (C=S), 2218 (C≡N). MS (EI) *m/z* (%) 159 (100, $M^{+\cdot}$) (Anal. Calc. for C_4HNS_3 (159.257): C, 30.17; H, 0.63; N, 8.80; S, 60.40. Found: C, 30.14; H, 0.70; N, 8.28; S, 60.1%). For **4**: white crystals; mp 60–63 °C, δ_H(400 MHz, $CDCl_3$), 7.61 (s, 1H, CH); δ_C(100 MHz, $CDCl_3$), 103.7 (*C*CN), 111.3 (C≡N), 134.0 (CH), 188.0 (C=O). ν_{max}(KBr)/cm^{-1}; 1636 (C=O), 2229 (C≡N). (lit.:[9] 1638, 2235), MS (EI) *m/z* (%) 143 (100, $M^{+\cdot}$) (Anal. Calc. for C_4HNOS_2 (143.190): C, 33.57; H, 0.70; N, 9.79; S, 44.76. Found: C, 33.78; H, 0.83; N, 9.43; S, 43.68%). For $[PPh_4]_2[Ni(edt\text{-}CN)_2]$: ν_{max}(KBr)/cm^{-1}; 2180 (C≡N). (Anal. Calc. for $C_{54}H_{42}N_2NiPS_4$ (967.85): C, 67.01; H, 4.37; N, 2.89; S, 13.25. Found: C, 66.61; H, 4.21; N, 2.84; S, 13.41%). For $[PPh_4][Ni(edt\text{-}CN)_2]$: ν_{max}(KBr)/cm^{-1}; 2204 (C≡N). (Anal. Calc. for $C_{30}H_{22}N_2NiPS_4$ (628.45): C, 57.34; H, 3.53; N, 4.46. Found: C, 57.09; H, 3.47; N, 4.32%).

‡ *X-Ray data* for $[PPh_4]_2[Ni(edt\text{-}CN)_2]$ and $[PPh_4][Ni(edt\text{-}CN)_2]$ were collected on a Stoe Imaging Plate diffractometer (IPDS) with Mo-Kα radiation, $\lambda = 0.71073$ Å at $T = 293(2)$ K. The structures were solved by direct methods and refined against F^2 using the SHELXTL5.04 set of programs. Hydrogen atoms were introduced at calculated positions and not refined (riding model).

Crystal data for $[PPh_4]_2[Ni(edt\text{-}CN)_2]$: $C_{54}H_{42}N_2NiP_2S_4$, $M = 967.79$, monoclinic, space group $P2_1/n$, $a = 20.523(4)$, $b = 11.220(2)$, $c = 21.304(4)$ Å, $\beta = 107.33(3)°$, $V = 4683(1)$ Å^3, $Z = 4$, $D_c = 1.373$ g cm^{-3}, $\mu = 0.701$ mm^{-1}, data collected = 35954, unique data = 9096 ($R_{int} = 0.061$) of which 5396 with $I > 2\sigma(I)$, $R(F) = 0.058$, $wR(F^2) = 0.163$ for 571 parameters.

For $[PPh_4][Ni(edt\text{-}CN)_2]$: $C_{30}H_{22}N_2NiPS_4$, M = 628.42, triclinic, space group $P\bar{1}$, $a = 11.394(1)$, $b = 11.510(1)$, $c = 12.826(1)$ Å, $\alpha = 64.264(10)$, $\beta = 72.777(12)$, $\gamma = 83.074(12)°$, $V = 1447.2(3)$ Å^3, $Z = 2$, $D_c = 1.442$ g cm^{-3}, $\mu = 1.037$ mm^{-1}, data collected = 14189, unique data = 5232 ($R_{int} = 0.042$) of which 3582 with $I > 2\sigma(I)$, $R(F) = 0.0343$, $wR(F^2) = 0.0713$ for 343 parameters.

CCDC 182/1779. See http://www.rsc.org/suppdata/cc/b0/b006440h/ for crystallographic files in .cif format.

1 W. Kaim and M. Morderosch, *Coord. Chem. Rev.*, 1994, **129**, 157.
2 A. Aumüller, P. Erk, G. Klebe, S. Hünig, J. von Schütz and H. Werner, *Angew. Chem., Int. Ed. Engl.*, 1986, **25**, 740; P. Erk, H.-J. Gross, S. Hünig, H. Meixner, H.-P. Werner, J. U. von Schütz and H. C. Wolf, *Angew. Chem., Int. Ed. Engl.*, 1989, **28**, 1245; R. Kato, H. Kobayashi and A. Kobayashi, *J. Am. Chem. Soc.*, 1989, **111**, 5224; S. Hünig, *J. Mater. Chem.*, 1995, **5**, 1469.
3 S. K. Hoffmann, P. J. Corvan, P. Singh, C. N. Sethulekshmi, R. M. Metzger and W. E. Hatfield, *J. Am. Chem. Soc.*, 1983, **105**, 4608; M. Schwartz and W. E. Hatfield, *Inorg. Chem.*, 1987, **26**, 2823; R. A. Heintz, H. Zhao, X. Ouyang, G. Grandinetti, J. Cowen and K. R. Dunbar, *Inorg. Chem.*, 1999, **38**, 144 and references therein.
4 J. M. Manriquez, G. T. Yee, R. S. McLean, A. J. Epstein and J. S. Miller, *Science*, 1991, **252**, 1415.
5 D. Coucouvanis, N. C. Baenziger and S. M. Johnson, *Inorg. Chem.*, 1974, **13**, 1191; F. J. Hollander, Y. L. Yp and D. Coucouvanis, *Inorg. Chem.*, 1976, **15**, 2230.
6 K. Sugimoto, T. Kuroda-Sowa, M. Maekawa and M. Munakata, *Chem. Commun.*, 1999, 455.
7 F. J. Weiher, L. R. Melby and R. E Benson, *J. Am. Chem. Soc.*, 1964, **86**, 4329; P. I. Clemenson, *Coord. Chem. Rev.*, 1990, **106**, 171; A. T. Comber, D. Beljonne, R. H. Friend, J. L. Bredas, A. Charlton, N. Robertson, A. E. Underhill, M. Kurmoo and P. Day, *Nature*, 1996, **380**, 144; N. Robertson, C. Bergemann, H. Becker, P. Agarwal, S. R. Julian, R. H. Friend, N. J. Hatton, A. E. Underhill and A. Kobayashi, *J. Mater. Chem.*, 1999, **9**, 1713.
8 B. R. O'Connor and F. N. Jones, *J. Org. Chem.*, 1970, **35**, 2002.
9 R. J. Pafford, J.-H.Chou and T. B. Rauchfuss, *Inorg. Chem.*, 1999, **38**, 3779.
10 C. U. Pittman, Jr., M. Narita and Y. F. Liang, *J. Org. Chem.*, 1976, **41**, 2855; G. C. Papavassiliou, D. J. Lagouvardos and W. C. Kakounis, *Z. Naturforsch. Teil B*, 1991, **46**, 1730.
11 G. V. Tormos, M. G. Bakker, P. Wang, M. V. Lakshmikantham, M. P. Cava and R. M. Metzger, *J. Am. Chem. Soc.*, 1995, **117**, 8528.
12 A. Davison, N. Edelstein, R. H. Holm and A. H. Maki, *Inorg. Chem.*, 1963, **2**, 1227.
13 B. Bleaney and K. D. Bowers, *Proc. R. Soc. (London) Ser. A*, 1952, **214**, 451.
14 O. Kahn, in *Molecular Magnetism*, VCH, Weinheim, 1993, ch. 6.

A cyclic tetranuclear Cu_2Gd_2 complex with an $S = 8$ ground state derived from ferromagnetic spin-coupling between copper(II) and gadolinium(III) ions arrayed alternately

Takafumi Kido, Shigeyuki Nagasato, Yukinari Sunatsuki and Naohide Matsumoto*

Department of Chemistry, Faculty of Science, Kumamoto University, Kurokami 2-39-1, Kumamoto 860-8555, Japan. E-mail: naohide@aster.sci.kumamoto-u.ac.jp

Received (in Cambridge, UK) 7th August 2000, Accepted 27th September 2000
First published as an Advance Article on the web 12th October 2000

A cyclic tetranuclear $Cu^{II}_2Gd^{III}_2$ complex, in which Cu^{II} and Gd^{III} ions are arrayed alternately, has an $S = 8$ spin ground state, due to the ferromagnetic spin coupling between $S_{Gd} = 7/2$ and $S_{Cu} = 1/2$.

The field of molecular-based magnetic compounds has shown spectacular advances in the last two decades, especially in the metal-complex based magnetic materials.[1] Hetero-metal assembly complexes with multi-dimensional extended structures and versatile magnetic behavior[1] as well as single molecule magnets derived from large ground spin state and large magnetic anisotropy[2] have attracted special attention. These interesting magnetic materials consist of a d-transition metal ion, and the magnetic chemistry of d–f and f–f transition metal complexes is the forthcoming target in this field. Since ferromagnetic coupling between Cu^{II} and Gd^{III} ions was first observed in 1985 in a trinuclear complex,[3] several polynuclear Cu_2Gd_2, Cu_2Gd and other d–f complexes have been reported.[4] However, the coexisting antiferromagnetic coupling such as within a Cu_2 pair often concealed the weak ferromagnetic coupling and resulted in net antiferromagnetic behavior. Thus, recent efforts have been focused on strictly binuclear d–f complexes,[5] in order to obtain accurate information on the magnetic properties. If a d–f cluster compound without the d–d and the f–f magnetic interactions was synthesized, it could be a single molecule with a large spin state.[6] If a d–f extended multi-dimensional compound without d–d and the f–f magnetic interactions was synthesized, it would be a magnetic material exhibiting spontaneous magnetization.[7] Here we report a cyclic tetranuclear Cu_2Gd_2 complex $[CuLGd(hfac)_2]_2$, where H_3L = 1-(2-hydroxybenzamido)-2-(2-hydroxy-3-methoxybenzylideneamino)ethane[8] and Hhfac = hexafluoroacetylacetone. The tetranuclear Cu_2Gd_2 complex assumes an $S = 8$ ground state derived from ferromagnetic spin-coupling between Cu^{II} and Gd^{III} ions arrayed alternately, in which the Cu^{II}–Cu^{II} and Gd^{III}–Gd^{III} magnetic interactions are weak.

The copper(II) complex K[CuL] was used as a '*ligand complex*' in order to construct an alternate array of Cu^{II} and Gd^{III} ions, because it is well-known that phenoxo-, methoxy- and amido-oxygen atoms can coordinate to a lanthanide ion,[9] and further it is expected that the amido oxygen atom at the opposite side serves as a bridge to provide an alternate array of the d–f metal ions.[10] As a counterpart, the gadolinium(III) complex $[Gd(hfac)_3(H_2O)_2]$ was used, because the hexafluoroacetylacetonato (hfac) ion can be easily substituted with external donor atoms and can also function as a capping or terminal ligand. The reaction of K[CuL] with an equimolar amount of $[Gd(hfac)_3(H_2O)_2]$ in methanol at ambient temperature produced dark reddish purple crystals of $[CuLGd(hfac)_2]$.[11]

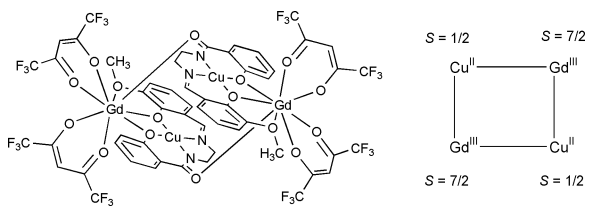

Scheme 1

The structure was determined by a single-crystal X-ray diffraction analysis.[12] Fig. 1 shows an ORTEP drawing of the cyclic Cu_2Gd_2 tetranuclear structure, in which the Cu^{II} and Gd^{III} ions are arrayed alternately and the molecule has an inversion center. The Cu^{II} ion has square planar coordination geometry with the N_2O_2 donor atoms of the unequivalent tetradentate ligand (see chemical structure). The Cu–N and Cu–O distances of the 2-oxybenzamido moiety (Cu–N1 = 1.913(4), Cu–O2 = 1.903(4) Å) are considerably shorter than the corresponding values of the 2-oxy-3-methoxybenzaldehyde moiety (Cu–N2 = 1.931(4), Cu–O3 = 1.952(3) Å). In the cyclic structure, the Cu(II) complex functions as a '*ligand complex*' with the two Gd^{III} ions. The two phenoxo (O2 and O3) and the methoxy (O4) atoms at the one side of the planar Cu(II) complex coordinate to a Gd^{III} ion as a tridentate ligand with the distances of Gd–O2 = 2.468(3), Gd–O3 = 2.350(3), Gd–O4 = 2.550(3) Å, and Cu–Gd = 3.433(1) Å. The amido oxygen atom (O1) at the opposite side of the Cu(II) complex coordinates to another Gd ion as a monodenate ligand with the distance of Gd–O1 = 2.274(3) and Cu–Gd = 5.618(2) Å. Including the coordination of the two hfac ions as a bidentate chelate ligand (Gd–O = 2.347(4)–2.405(4) Å), the Gd^{III} ion has an octacoordinate geometry with the O_8 oxygen atoms. It should be noted that the Gd–O bond distance with the amido oxygen is the shortest among the eight Gd–O bonds. In a cyclic structure, there is no bridging ligand between the two Cu^{II} ions or between the two Gd^{III} ions. The Cu–Cu and Gd–Gd distances in the cyclic structure are 4.952(2) and 7.885(3) Å, respectively, indicating that each metal ion pair is well separated.

The magnetic susceptibilities were measured under a 1 T applied magnetic field in the 2–300 K temperature range.[13] The

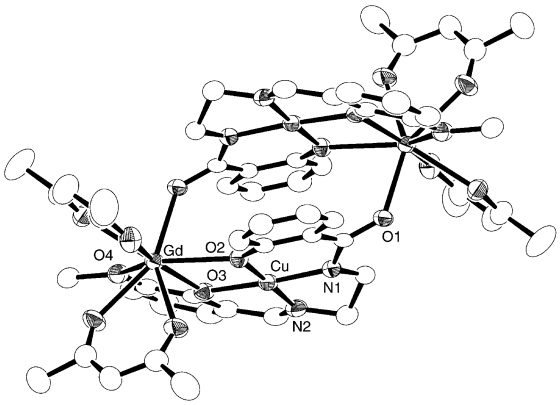

Fig. 1 ORTEP view of the cyclic Cu_2Gd_2 tetranuclear complex with 30% thermal probability ellipsoids and selected atom labeling scheme. The hydrogen and fluorine atoms are omitted for clarity.

DOI: 10.1039/b006445i

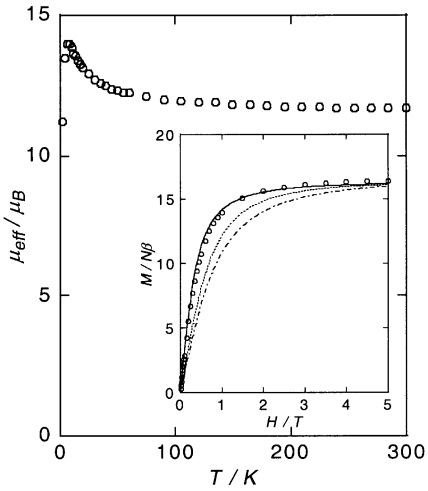

Fig. 2 Plot of the effective magnetic moment (μ_{eff}) per Cu_2Gd_2 *vs.* temperature. The inserted figure shows the field dependence of the magnetization at 2 K. The solid line represents the theoretical curve for g = 2.02 and S = 8 spin state produced by ferromagnetic coupling of the spin system (1/2, 7/2, 1/2, 7/2). The dotted and broken lines represent the theoretical curves for two isolated S = 4 spin states and for an isolated spin state of (1/2, 7/2, 1/2, 7/2).

magnetic behavior is shown in Fig. 2, as the μ_{eff} *vs.* T plot, where μ_{eff} is the effective magnetic moment per Cu_2Gd_2. The μ_{eff} at 300 K is 11.61 μ_B, which is slightly larger than the spin-only value of 11.49 μ_B expected for independently existing two Cu^{II} (S = 1/2) and two Gd^{III} (S = 7/2) ions and g = 2.00. On lowering the temperature, the μ_{eff} increases gradually to reach a maximum value, 13.98 μ_B, at 8.0 K and then decreases abruptly. The increase at the higher temperature region indicates the operation of ferromagnetic interaction between the Cu^{II} and Gd^{III} ions. The maximum value of the μ_{eff} is larger than the spin-only value, 12.65 μ_B, expected for two isolated S = 4 spins resulting from ferromagnetic coupling between the Cu^{II} and Gd^{III} ions of the binuclear complex, although the value is smaller than the spin-only value, 16.97 μ_B, expected for an S = 8 spin. The abrupt decrease in the μ_{eff} at the lower temperature region can be ascribed to weak intermolecular antiferromagnetic interaction.

To confirm the spin ground state of the cyclic tetranuclear complex, the field dependence of the magnetization was measured up to 5 T at several temperatures. The inserted plots in Fig. 2 show the experimental values of $M/N\beta$ *vs.* H at 2 K, together with the theoretical curves for the sum of the Brillouin functions of isolated two Cu^{II} (S = 1/2) and two Gd^{III} (S = 7/2) ions, for sum of two S = 4 spins, and for an S = 8 spin derived from the ferromagnetic coupling of the spin-system (1/2, 7/2, 1/2, 7/2), respectively. The magnetization data are larger than those for two independent S = 4 spins and for a magnetically isolated (1/2, 7/2, 1/2, 7/2) system. The magnetization data are well reproduced by the Brillouin function with S = 8 and g = 2.02. The slight difference is due to an incomplete population of the S = 8 state.

This study revealed that a discrete molecule with a large spin could be easily synthesized even in a d–f transition metal complex. The analogous synthetic approach should produce single molecules with larger spin states and with magnetic anisotropy. Magnets with an extended multidimensional structure can be obtained by substitution of the terminal ligand.

We are grateful to Dr J.-P. Costes for fruitful discussion and to Dr M. Nakamura for help in synthesis.

Notes and references

1 O. Kahn, *Molecular Magnetism*, VCH, Weinheim, 1993.
2 R. Sessoli, D. Gatteschi, A. Caneschi and M. A. Novak, *Nature*, 1993, **365**, 141.
3 A. Bencini, C. Benelli, A. Caneschi, R. L. Carlin, A. Dei and D. Gatteschi, *J. Am. Chem. Soc.*, 1985, **107**, 8128.
4 C. Benelli, A. Caneschi, D. Gatteschi, O. Guillou and L. Pardi, *Inorg. Chem.*, 1990, **29**, 1750; C. Benelli, A. C. Fabretti and A. Giusti, *J. Chem. Soc., Dalton Trans.*, 1993, 409; A. Bencini, C. Benelli, A. Caneschi, A. Dei and D. Gatteschi, *Inorg. Chem.*, 1986, **25**, 572; M. L. Kahn, C. Mathoniere and O. Kahn, *Inorg. Chem.*, 1999, **38**, 3692; C. Benelli, M. Murrier, S. Parsons and R. E. P. Winpenny, *J. Chem. Soc., Dalton Trans.*, 1999, 4125; R. E. P. Winpenny, *Chem. Soc. Rev.*, 1998, **27**, 447.
5 J.-P. Costes, F. Dahan and A. Dupuis, *Inorg. Chem.*, 2000, **39**, 165; J.-P. Costes, F. Dahan, A. Dupuis and J.-P. Laurent, *Inorg. Chem.*, 2000, **39**, 169; J.-P. Costes, F. Dahan, A. Dupuis and J.-P. Laurent, *Inorg. Chem.*, 1997, **36**, 3429; J.-P. Costes, F. Dahan, A. Dupuis and J.-P. Laurent, *Inorg. Chem.*, 1997, **39**, 4284; M. Sasaki, K. Manseki, H. Horiuchi, M. Kumagai, M. Sakamoto, H. Sakiyama, Y. Nishida, M. Sakai, Y. Sadaoka, M. Ohba and H. Okawa, *J. Chem. Soc., Dalton Trans.*, 2000, 259.
6 Recently, the same synthetic approach has been developed: J.-P. Costes and F. Dahan, *C. R. Seances Acad. Sci.*, accepted in special issue number dedicated to the late Olivier Kahn, 'Assembling ferromagnetically coupled (Cu, Gd) pairs: toward higher spin entities'.
7 O. Guillou, P. Bergerat, O. Kahn, E. Bakalbassis, K. Boubekeur, P. Batail and M. Guillot, *Inorg. Chem.*, 1992, **31**, 110.
8 H_3L was synthesized by the 1:1:1 condensation of methyl salicylate, ethylenediamine and 3-methoxysalicylaldehyde. The crude product was washed well with dichloromethane. K[CuL] was obtained as reddish purple crystals by the reaction of H_3L, copper(II) acetate monohydrate and potassium *tert*-butoxide in the molar ratio of 1:1:3 in methanol.
9 J.-P. Costes, F. Dahan, A. Dupuis and J.-P. Laurent, *Chem. Eur. J.*, 1998, **4**, 1616.
10 Y. Sunatsuki, T. Matsuo, M. Nakamura, F. Kai, N. Matsumoto and J.-P. Tuchagues, *Bull. Chem. Soc. Jpn.*, 1998, **71**, 2611; Y. Sunatsuki, M. Mimura, H. Shimada, F. Kai and N. Matsumoto, *Bull. Chem. Soc. Jpn.*, 1998, **71**, 167.
11 Synthesis of [CuLGd(hfac)$_2$]: a methanolic solution (20 mL) of K[CuL] (104 mg, 0.25 mmol) was added to a methanolic solution (20 mL) of [Gd(hfac)$_3$(H$_2$O)$_2$] (204 mg, 0.25 mmol) at ambient temperature. The mixture was allowed to stand for several days. Meanwhile, dark reddish purple crystals which formed were collected (205 mg). Anal.: calcd. for $C_{27}H_{17}N_2O_8F_{12}CuGd$: C 34.27, H 1.81, N, 2.96; found: C 34.37, H 1.85, N, 2.95%.
12 *Crystal data*: $C_{27}H_{17}N_2O_8F_{12}CuGd$, M = 946.22, triclinic, space group = $P\bar{1}$ (no. 2), a = 11.054(4), b = 16.173(4), c = 10.284(3) Å, α = 105.96(2), β = 114.61(2), γ = 80.47(3)°, V = 1604(1) Å^3, Z = 2, F(000) = 916, D_c = 1.958 g cm^{-3}, D_m = 1.91 g cm^{-3}, λ = 0.71069 Å, T = 20 ± 1 °C, μ(Mo-Kα) = 28.37 cm^{-1}, R = 0.033, R_w = 0.034, (R = $\Sigma||F_o|-|F_c||/\Sigma|F_o|$ and R_w = $[\Sigma w(|F_o|-|F_c|)^2/\Sigma w|F_o|^2]^{1/2}$). Data were collected over the 2θ range 2.5–50° on a Rigaku AFC-7R X-ray diffractometer with Mo-Kα radiation. A total of 5981 reflections were collected, of which 5661 were independent. Convergence to the final R values was achieved using 5060 unique reflections (R_{int} = 0.012) with $I > 2.00\ \sigma(I)$ and a maximum/residual peak of −0.61/0.91 e Å^{-3}. CCDC 182/1792. See http://www.rsc.org/suppdata/cc/b0/b006445i/ for crystallographic files in .cif format,
13 Magnetic susceptibilities were measured with a MPMS5 SQUID susceptometer (Quantum Design, Inc.) in the 2–300 K temperature range under an external magnetic field of 1 T. The calibrations were done with palladium. Corrections for diamagnetism were applied using Pascal's constants. Effective magnetic moments were calculated with the equation μ_{eff} = $2.828(\chi_M T)^{1/2}$, where χ_M is the magnetic susceptibility per tetrameric molecule.

Synthesis of a novel triphosphate analogue: nucleoside α-*P*-borano, α-*P*-thiotriphosphate

Jinlai Lin and Barbara Ramsay Shaw*

Paul M. Gross Chemical Laboratory, Department of Chemistry, Duke University, Durham, North Carolina 27708-0346, USA. E-mail: brs@chem.duke.edu

Received (in Covallis, OR, USA) 22nd June 2000, Accepted 10th August 2000
First published as an Advance Article on the web 11th October 2000

The first boranothiotriphosphate compound, thymidine 5′-[α-*P*-borano, α-*P*-thio]triphosphate, in which borane and sulfur replace the two non-bridging oxygens of the α-phosphate in natural nucleoside triphosphates (NTPs), has been synthesized; some chemical properties of this borane–sulfur disubstituted nucleoside triphosphate analogue have been investigated. The synthetic approach reported here should be applicable for preparation of any α-borano, α-thio modified NTP or deoxy NTP; potential applications are discussed.

Modifications of nucleoside triphosphates (NTPs) [Fig. 1a] have received much attention in searches for potential diagnostic and therapeutic agents and as probes in a multitude of biological processes.[1,2] Of these modified NTPs, only the nucleoside 5′-[α-thio]triphosphates[1] [Fig. 1b] and nucleoside 5′-[α-borano]triphosphates[2] [Fig. 1c] can substitute for normal NTP and be readily incorporated into DNA and RNA by DNA or RNA polymerases.[1,2] Yet once in DNA or RNA, the phosphorothioate[3] and boranophosphate[4] linkages are more resistant to *exo*- and *endo*-nucleases than normal phosphate diesters. By structurally combining the phosphorothioate [S–P=O]$^-$ and boranophosphate [O=P–BH_3]$^-$, we recently reported the first example of a boranothiophosphate moiety [S=P–BH_3]$^-$, dithymidine boranphosphorothioate,[5] which is stable from pH 3 to 11 and is a more nuclease resistant and highly lipophilic phosphodiester analogue of DNA. We expected that the corresponding NTP analogue, nucleoside [α-borano, α-thio]triphosphate (Fig. 1d), wherein one of the two non-bridging oxygen atoms of the α-phosphate group is replaced by a sulfur atom and the other is replaced by a borane group, should be more lipophilic than the parent NTP and have other useful properties. The borano-, thio-disubstitution of nucleoside triphosphate could greatly increase the stability of the molecule against enzymatic cleavage, thus facilitating studies of enzymes which utilize NTPs and enabling studies of the nature of phosphate ester bond formation and cleavage.

Here, we report the first example of a novel boranothiotriphosphate compound, specifically the thymidine 5′-[α-*P*-borano, α-*P*-thio]triphosphate **5**, its synthesis and properties.

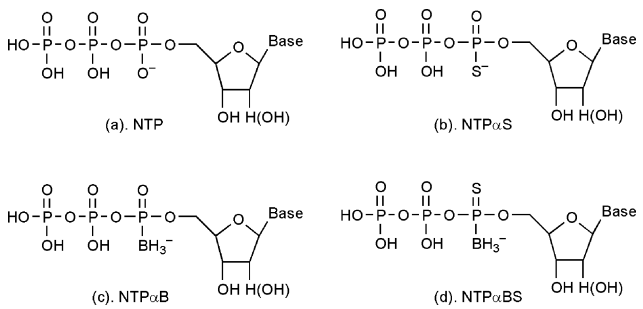

Fig. 1 Nucleoside triphosphate analogue structures and abbreviations. (a) Nucleoside triphosphates (NTP). (b) Nucleoside [α-thio]triphosphates (NTPαS). (c) Nucleoside [α-borano]triphosphates (NTPαB). (d) Nucleoside [α-borano, α-thio]triphosphates (NTPαBS).

The general procedure[6] for the one-pot synthesis of nucleoside 5′-[α-borano, α-thio]triphosphates shown in Scheme 1 is an extension of a method reported by us[2c,d] for the synthesis of boranotriphosphates and by Ludwig and Eckstein[1c] for the synthesis of thiotriphosphates. The overall yield of thymidine 5′-[α-*P*-borano, α-*P*-thio]triphosphate **5** (TTPαBS) was about 26%. The chemical structure of **5** (^{31}P NMR, δ: 153.1 ppm(br) for disubstituted α-*P*) was established *via* spectroscopic methods.[7] Successful separation of the two diastereomers (*R*p and *S*p) of **5** was achieved by reverse-phase HPLC.[7b] The first eluted isomer TTPαBS I (**5a**) and second eluted isomer TTPαBS II (**5b**) were characterized by ^{31}P NMR and ^{1}H NMR.[7c] The method here should be applicable for the synthesis of any deoxy- or ribonucleoside [α-borano, α-thio]triphosphate.

The [S=P–BH_3]$^-$ α-triphosphate is the only known non-bridging-disubstituted chiral α-triphosphate with a negative charge.[8] The borano-, thio-disubstitution in a nucleotidic linkage will result in changes in polarity of the phosphate, as well as its interactions with metal ions.[2f,g] These properties coupled with ready synthesis of isotopic [NTPα^{35}S=P–BH_3] compounds from Li_2S^* (S^* = ^{35}S) could make this modification useful as a probe for nucleotide binding sites in enzymes, for elucidating the stereochemical course and role of metal ions of phosphoryl and nucleotidyl transfer reactions, and for probing whether a non-bridging oxygen is absolutely necessary in these reactions.

To summarize, the synthesis of a new type of doubly modified nucleoside triphosphate analogue, the first [S=P–BH_3]$^-$ triphosphate, opens the possibility of preparing an entirely new and intriguing class of borane–sulfur modified phosphate analogues. Their potential utility as substrates, cofactors, or inhibitors of polymerases and nucleotide binding and metabolizing enzymes, as molecular probes, and as carriers of ^{35}S for radiolabeling and radiation therapy,[9] make the

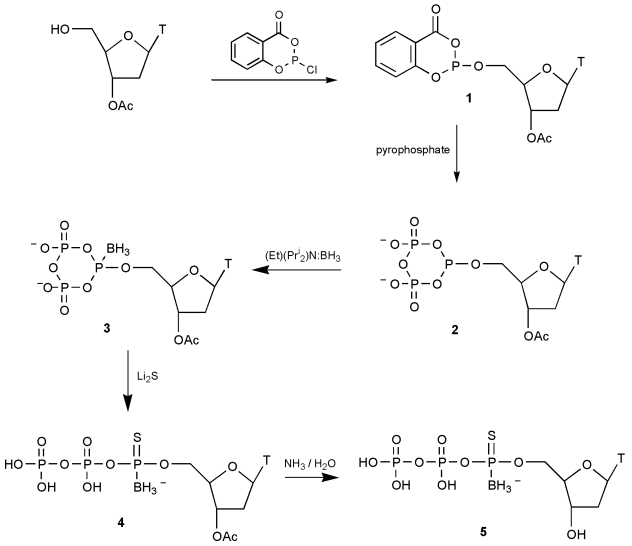

Scheme 1 Synthesis of thymidine [α-*P*-borano, α-*P*-thio]triphosphate.

DOI: 10.1039/b005059h

nucleoside boranothiotriphosphate a promising candidate for further mechanistic, diagnostic and therapeutic applications.

We thank Drs Vladimir Rait, Dmitri S. Sergueev, Zinaida Sergueeva and Kaizhang He for their encouragement and suggestions. This work was supported by grants 1R01-GM57693-01 from NIH and DE-FG05-97ER62376 from DOE to B. R. S.

Notes and references

1 (*a*) F. Eckstein, *Angew. Chem., Int. Ed. Engl.*, 1983, **22**, 423; (*b*) J. Ludwig and F. Eckstein, *J. Org. Chem.*, 1989, **54**, 631; (*c*) J. Ludwig and F. Eckstein, *J. Org. Chem.*, 1991, **56**, 1777; (*d*) G. Gish and F. Eckstein, *Science*, 1988, **240**, 1520; (*e*) P. Sideras, K. Funa, I. Zalcberg-Quintana, K. G. Xanthopoulos, P. Kisielow and R. Palacios, *Proc. Natl. Acad. Sci. U.S.A.*, 1988, **85**, 218; (*f*) S. Verma and F. Eckstein, *Ann. Rev. Biochem.*, 1998, **67**, 99.

2 (*a*) J. Tomasz, B. R. Shaw, K. Porter, B. F. Spielvogel and A. Sood, *Angew. Chem., Int. Ed. Engl.*, 1992, **31**, 1373; (*b*) K. W. Porter, J. D. Briley and B. R. Shaw, *Nucleic Acids Res.*, 1997, **25**, 1611; (*c*) K. He, A. Hasan, B. Krzyzanowska and B. R. Shaw, *J. Org. Chem.*, 1998, **63**, 5769; (*d*) B. Krzyzanowska, K. He, A. Hasan and B. R. Shaw, *Tetrahedron*, 1998, **54**, 5119; (*e*) K. He, K. W. Porter, A. Hasan, J. D. Briley and B. R. Shaw, *Nucleic Acids Res.*, 1999, **27**, 1788; (*f*) B. R. Shaw, D. Sergueev, K. He, K. Porter, J. Summers, Z. Sergueeva and V. Rait, *Methods Enzymol.*, 1999, **313**, 226; (*g*) J. S. Summers, D. Roe, P. D. Boyle, M. Colvin and B. R. Shaw, *Inorg. Chem.*, 1998, **37**, 4158; (*h*) J.-L Lin, K. He and B. R. Shaw, *Helv. Chim. Acta*, 2000, **83**, 1392.

3 (*a*) P. M. J. Burgers and F. Eckstein, *Biochemistry*, 1979, **18**, 592; (*b*) P. M. J. Burgers and F. Eckstein, *Proc. Natl. Acad. Sci. U.S.A.*, 1978, **75**, 4798.

4 (*a*) A. Sood, B. R. Shaw and B. F. Spielvogel, *J. Am. Chem. Soc.*, 1990, **112**, 9000; (*b*) Y.-Q. Chen, F.-C. Qu and Y.-B. Zhang, *Tetrahedron Lett.*, 1995, **36**, 745; (*c*) D. S. Sergueev and B. R. Shaw, *J. Am. Chem. Soc.*, 1998, **120**, 9417.

5 J.-L. Lin and B. R. Shaw, *Chem. Commun.*, 1999, 1517.

6 The following procedure for the preparation of nucleoside [α-borano, α-thio]triphosphates is representative: 3′-*O*-acetylthymidine (0.5 mmol, 142 mg) was phosphitylated with 2-chloro-4*H*-1,3,2-benzodioxaphosphorin-4-one (0.55 mmol, 112 mg in 0.8 ml anhydrous DMF) at 0 °C for 10 min to yield two diastereomers of **1**. They were identified by the appearance of a doublet around 127 ppm in the ^{31}P NMR spectra. Instead of introducing the borane group at this stage, **1** was treated with tributylammonium pyrophosphate (240 mg in 1.0 ml anhydrous DMF) and 0.15 ml triethylamine at rt for 1 h to form a cyclic intermediate **2**. The upfield shift from around 127 to 107 ppm for trivalent phosphorus P^{III} together with a doublet around −18 ppm for pentavalent phosphorus P^{V} in ^{31}P NMR confirmed the formation of **2**. The borane group was introduced by the reaction of **2** with excess borane–diisopropylethylamine complex (1 ml) at rt for 2 h to afford **3**. The critical step in the synthesis is ring-opening of the cyclic boronated triphosphate **3** by the treatment with 2 eq. lithium sulfide at 55 °C for 1 h to yield **4**, which was converted to compound **5** with NH_3–H_2O–CH_3OH (aq. NH_3–CH_3OH = 1 : 1, v/v) at rt for 4 h. The low boiling point solvents were removed under reduced pressure and the residue was extracted with ethyl acetate (16 ml) and water (10 ml). The organic layer was washed twice with 2 ml water. The water portions were combined and concentrated to 2 ml. The resulting crude mixture was applied to ion-exchange chromatography on a QA-Cellulose (HCO_3^-) column eluted with a linear gradient of 0.005–0.20 M NH_4HCO_3 (pH = 9.56, 700 ml each) and appropriate portions were collected to give **5** as the ammonium salt. Further purification of **5** (one-sixth of total amount) by HPLC using a linear gradient of 50 mM triethylammonium acetate (TEAA, pH 7.0) and CH_3CN (from 0 to 18% in 40 min) gave pure **5**, R_t = 21.4 min (HPLC conditions: Sphereclone 5 μ ODS(2), 10 × 250 mm column; flow rate, 3.0 ml min^{-1}). The desired fraction was dried by lyophilization, and excess salt was removed by repeated lyophilization with deionized water to yield the triethylammonium salt of **5** (13 mg).

7 Characterization and separation of **5** and its two diastereomers (**5a** and **5b**): (*a*) TTP$^{\alpha}$BS (**5**): UV λ_{max} = 267 nm; δ_P (D_2O, 161.9 MHz) 153.1 (br) for α-*P*, −22.4 and −22.7 for β-*P* and −10.0 and −10.1 for γ-*P*; δ_H (D_2O, 400 MHz) 7.62, 7.57 (2s, 2 isomers, 1 H, H6), 6.16 (unresolved, 1 H, H1′), 4.54–4.46 (m, 1 H, H3′), 4.29–4.15 (m, 1 H, H4′), 4.02–3.99 (m, 2 H, H5′), 2.15 (2 H, H2′), 1.78, 1.74 (2s, 3 H, 5-CH_3), 0.92–0.54 (br, 3 H, BH_3); MS (FAB$^-$): *m*/*z* for M^- 495; HRMS (FAB$^-$) calc. for $C_{10}H_{19}O_{12}N_2P_3SB$ M^- 494.9963, found 494.9942; (*b*) *HPLC conditions:* Sphereclone 5 μ ODS(2), 10 × 250 mm column; eluants were 10% MeOH and 90% 50 mM triethylammonium acetate (pH 7.0); flow rate, 3.0 ml min^{-1}. R_t (**5a**) = 24.9 min. R_t (**5b**) = 30.4 min. (*c*) *Two diastereomers: TTP$^{\alpha}$BS I* (**5a**): δ_P (D_2O, 161.9 MHz) 152.3 (br) for α-*P*, −21.20, −21.33, −21.44 and −21.57 for β-*P* and −5.72 and −5.85 for γ-*P*; δ_H (D_2O, 400 MHz) 7.62 (s, 1 H, H6), 6.18 (t, 1 H, *J* = 7.0 Hz, H1′), 4.51–4.48 (m, 1 H, H3′), 4.32–4.28 (m, 1 H, H4′), 4.05–4.01 (m, 2 H, H5′), 2.19–2.15 (m, 2 H, H2′), 1.79 (s, 3 H, 5-CH_3), 0.90–0.30 (br, 3 H, BH_3). *TTP$^{\alpha}$BS II* (**5b**): δ_P (D_2O, 161.9 MHz) 151.3 (br) for α-*P*, −21.28, −21.41, −21.50 and −21.63 for β-*P* and −7.03 and −7.15 for γ-*P*; δ_H (D_2O, 400 MHz) 7.57 (s, 1 H, H6), 6.16 (t, 1 H, *J* = 7.0 Hz, H1′), 4.51 (m, 1 H, H3′), 4.20–4.16 (m, 1 H, H4′), 4.12–4.06 (m, 2 H, H5′), 2.19–2.16 (m, 2 H, H2′), 1.78 (s, 3 H, 5-CH_3), 0.90–0.30 (br, 3 H, BH_3).

8 S/CH_3 phosphate analogues, in which the two non-bridging oxygens in a phosphate are replaced by S and CH_3 moieties, carry no charge; S_2 (dithio) phosphate analogues,[1c] in which the two non-bridging oxygens in a phosphate are replaced by S atoms, are achiral.

9 M. F. Hawthorne, *Angew. Chem., Int. Ed. Engl.*, 1993, **32**, 950.

Deactivation of a [PPN][Rh(CO)$_4$]-based catalytic system [PPN$^+$ = (PPh$_3$)$_2$N$^+$]. The first decomposition reaction of PPN$^+$ and the formation of [Rh$_{10}$P(CO)$_{22}$]$^{3-}$†

Fabio Ragaini,*[a] Angelo Sironi[b] and Alessandro Fumagalli[c]

[a] *Dipartimento di Chimica Inorganica, Metallorganica e Analitica and CNR Center, via G. Venezian 21, 20133 Milano, Italy. E-mail: ragaini@csmtbo.mi.cnr.it*
[b] *Dipartimento di Chimica Strutturale e Stereochimica Inorganica, via G. Venezian 21, 20133 Milano, Italy*
[c] *Dipartimento di Biologia Strutturale e Funzionale, Università dell'Insubria, via J. H. Dunant 3, 21100 Varese, Italy*

Received (in Cambridge, UK) 28th July 2000, Accepted 20th September 2000
First published as an Advance Article on the web 12th October 2000

Decomposition of [PPN][Rh(CO)$_4$] [PPN$^+$ = (PPh$_3$)$_2$N$^+$] at 200 °C under CO pressure affords [Rh$_{10}$P(CO)$_{22}$]$^{3-}$, featuring the first decomposition reaction of PPN$^+$ and explaining the reason for the deactivation of [PPN][Rh(CO)$_4$]-based catalytic systems.

Tetraalkyl and aryl ammonium and phosphonium cations are widely used to improve isolability and solubility of anionic organometallic complexes in organic solvents. However, they usually suffer from limited chemical stability, especially in basic media. In contrast, the PPN$^+$ cation [PPN$^+$ = (PPh$_3$)$_2$N$^+$], first isolated by Appel,[1] is generally considered as a chemically very stable and little interacting counter cation. For these reasons, it has found an increasingly important use in organometallic chemistry and homogeneous catalysis. Although the 'non-interacting' character of PPN$^+$ has later been questioned,[2] to the best of our knowledge its chemical stability is still undisputed.

In recent years, some of us have been involved in the use of [PPN][Rh(CO)$_4$] as a catalyst for the reduction reactions of nitroarenes by CO/MeOH[3] or CO/H$_2$O[4] to afford respectively methyl arylcarbamates (ArNHCO$_2$Me) or anilines (Scheme 1).

Despite the high catalytic activity of [PPN][Rh(CO)$_4$] in these reactions, deactivation of the catalytic system was observed upon prolonged use. We thus decided to investigate the fate of rhodium in these reactions. Since the products of reduction and carbonylation of nitroarenes are difficult to separate from the small amounts of catalyst-derived complexes, we examined the behaviour of [PPN][Rh(CO)$_4$] under similar experimental conditions, but in the absence of any nitroarene.

Heating [PPN][Rh(CO)$_4$] in acetone–water (instead of nitrobenzene–water) at 200 °C and under 60 bar CO for 4 h afforded a brown precipitate. Only very weak carbonyl bands were observed in the IR spectrum of the solution. The IR spectrum of the residue dissolved in CH$_2$Cl$_2$ showed a strong band at 1990 cm^{-1} (in CH$_2$Cl$_2$), with several shoulders, and a series of overlapping bands between 1840 and 1775 cm^{-1}. No [Rh(CO)$_4$]$^-$ was detected either in solution or in the solid residue.

When this last residue was used in place of [PPN][Rh(CO)$_4$] as catalyst for the reduction of nitrobenzene to aniline,[4] only trace amounts of the amine were obtained, indicating that the formed compound(s) is catalytically inactive.

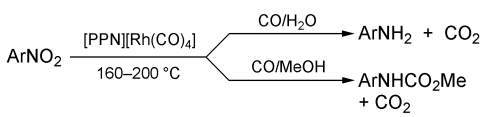

Scheme 1

Recrystallisation of the residue from acetonitrile + acetone (1 : 1)–diisopropyl ether afforded crystals of a cluster that was identified by single-crystal X-ray diffraction as [PPN]$_3$[Rh$_{10}$P(CO)$_{22}$],‡ having an interstitial phosphorus atom. [PPN]$_3$[Rh$_{10}$P(CO)$_{22}$] crystallises in the centrosymmetric triclinic space group $P\bar{1}$ with two independent (half) [Rh$_{10}$P(CO)$_{22}$]$^{3-}$ anions disordered about two distinct centres of symmetry. Two independent PPN cations are in general position while the third one consists of two (ordered, independent) halves lying about two distinct centres of symmetry. The [Rh$_{10}$P(CO)$_{22}$]$^{3-}$ anion which has a bicapped square antiprismatic metal core (see Fig. 1) has been previously structurally characterised as a triethylbenzylammonium salt[5] but, owing to the intrinsic centrosymmetric nature of its ligand envelope (all the external oxygen atoms were actually ordered), suffered of a similar disorder. The present, more accurate, structure determination confirms most of the previous stereochemical observations but also shows the marked effect of different packing environments by comparing the actual values of the distances, and their averages, in the three independent anions (Table 1, ESI†).

The identification of a cluster species having an interstitial phosphorus atom is very informative, since this atom can only derive from decomposition of the PPN$^+$ counter cation. The

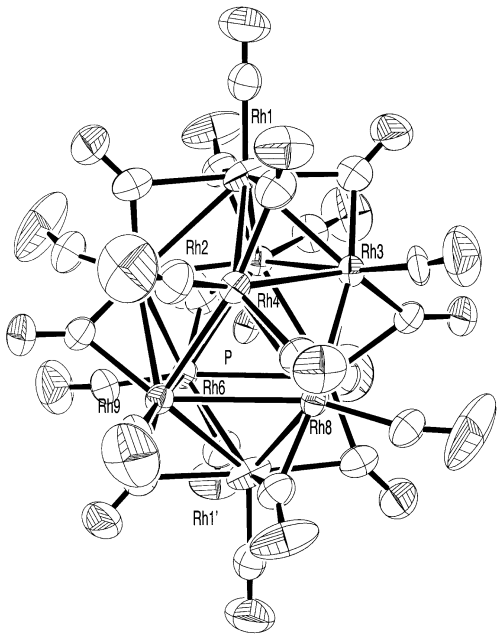

Fig. 1 ORTEP drawing of the [Rh$_{10}$P(CO)$_{22}$]$^{3-}$ anion (B). Thermal ellipsoids are drawn at the 50% probability level.

† Electronic supplementary information (ESI) available: Table 1: selected bond lengths (Å) for [PPN][Rh$_{10}$P(CO)$_{22}$]. See http://www.rsc.org/suppdata/cc/b0/b006135m/

decomposition must be initiated by a rhodium complex, since no acids or bases are present in the reaction mixture. To the best of our knowledge, this is the first time a decomposition product of PPN^+ is identified. The formation of $[Rh_{10}P(CO)_{22}]^{3-}$ also explains the loss of activity of the catalytic system. Indeed, whereas many rhodium clusters are known to convert to mononuclear species under high CO or CO/H_2 pressures,[6] this phosphido cluster has been shown to be remarkably stable even under CO/H_2 pressures much higher than that used both in our studies and in most of those from other laboratories.[5] The formation of $[Rh_{10}P(CO)_{22}]^{3-}$ must thus be considered as irreversible in most if not all catalytic systems and represents a warning against the use of PPN^+ as a counter cation when very long catalyst lives are required, as in industrial applications.

We thank MURST (ex 40%) for financial support.

Notes and references

‡ *X-Ray crystallography*: the diffraction experiment was performed using a suitable crystal (of dimensions 0.23 × 0.17 × 0.15 mm), on a Siemens SMART CCD area-detector diffractometer, by measuring 2100 frames (20 s per frame; ω scan method, $\Delta\omega$ = 0.3°; sample-detector distance fixed at 5 cm) which, upon data reduction, afforded almost all reflections belonging to the sphere with $2\theta < 55°$. The first 100 frames were recollected at the end to monitor crystal decay, which was not observed; an absorption correction was applied (SADABS).[7] The structure was solved by direct methods (SIR97)[8] and refined with full-matrix least squares (SHELX97);[9] anisotropic temperature factors were assigned to all atoms except phenyl hydrogens which were allowed to ride on their carbon atoms with individual isotropic displacement parameters 1.2 times that of the pertinent carbon atom. Data/restraints/parameters 24974/55/1702, GOF (on F^2) = 0.983; R = 0.0372, $wR2$ = 0.0767, for $I > 2\sigma(I)$, R = 0.0705, $wR2$ = 0.0886, for all data; largest difference peak and hole 0.95 and −1.06 e Å^3.

Crystal data: $C_{130}H_{90}N_3O_{22}P_7Rh_{10}$, M = 3291.94, triclinic, space group $P\bar{1}$, a = 16.2084(7), b = 16.3039(7), c = 23.9367(11) Å, α = 91.241(1), β = 94.880(1), γ = 90.067(1)°, U = 6301.1(5) Å^3, Z = 2, D_c = 1.735 Mg m^{-3}, T = 298(2) K, μ(Mo-Kα) = 1.431 mm^{-1}, F(000) = 3244. 66631 Reflections collected 24974 unique (R_{int} = 0.0432).

CCDC 182/1784. See http://www.rsc.org/suppdata/cc/b0/b006135m/ for crystallographic files in .cif format.

1 R. Appel and A. Hauss, *Z. Anorg. Allg. Chem.*, 1961, **311**, 290.
2 M. Darensbourg, H. Barros and C. Bornan, *J. Am. Chem. Soc.*, 1977, **99**, 1647; M. Tilset, A. A. Zlota, K. Folting and K. G. Caulton, *J. Am. Chem. Soc.*, 1993, **115**, 4113.
3 F. Ragaini, S. Cenini, A. Fumagalli and C. Crotti, *J. Organomet. Chem.*, 1992, **428**, 401; F. Ragaini, S. Cenini and F. Demartin, *Organometallics*, 1994, **13**, 1178; F. Ragaini, E. Gallo and S. Cenini, *J. Organomet. Chem.*, 2000, **593**–**594**, 109.
4 F. Ragaini and S. Cenini, *J. Mol. Catal. A.*, 1996, **105**, 145.
5 J. L. Vidal, W. E. Walker and R. C. Schoening, *Inorg. Chem.*, 1981, **20**, 238.
6 J. L. Vidal and W. E. Walker, *Inorg. Chem.*, 1980, **19**, 896; C. Fyhr and M. Gardland, *Organometallics*, 1993, **12**, 1753.
7 G. M. Sheldrick, SADABS, University of Göttingen, Germany, 1996.
8 A. Altomare, M. C. Burla, M. Camalli, G. L. Cascarano, C. Giacovazzo, A. Guagliardi, A. G. G. Moliterni, G. Polidori and R. Spagna, *J. Appl. Crystallogr.*, 1999, **32**, 115.
9 G. M. Sheldrick, SHELX97-Program for the refinement of crystal structure, University of Göttingen, Germany, 1997.

ChemComm

Rapid synthesis of high quality MCM-41 silica with ultrasound radiation†

Xianghai Tang,‡ Suwen Liu, Yanqin Wang, Weiping Huang, Elena Sominski, Oleg Palchik, Yuri Koltypin and Aharon Gedanken*

Department of Chemistry, Bar-Ilan University, Ramat-Gan 52900, Israel. E-mail; gedanken@mail.biu.ac.il

Received (in Oxford, UK) 27th July 2000, Revised manuscript received 10th September 2000, Accepted 14th September 2000
First published as an Advance Article on the web 11th October 2000

High quality MCM-41 silica with thick walls and a very narrow distribution of mesopore size has been synthesized in a relatively short time *via* ultrasound radiation.

Recently, great efforts have been dedicated to improving the synthesis of mesoporous MCM-41 silica[1] by lowering the temperature, shortening the crystallization time as well as controlling the particle size.[2] However, due to the amorphous nature within the pore wall,[3,4] the products synthesized in alkaline media at low temperature have been much less stable than those obtained at higher temperatures,[5] which imposes a strict limitation on their applications. To achieve highly stable MCM-41 silica, a number of papers have focused on thickening the pore wall in order to obtain a more condensed and longer range ordered framework, either by modifying the assembly pathways[6] or by post-synthesis treatments.[7] The drawbacks of these procedures obviously lie within the time-consuming and complicated processing strategies. Therefore it is more desirable to synthesize stable MCM-41 silica by a quick and direct way.

Ultrasound has been introduced to a variety of material syntheses[8,9] owing to its sonochemical effects based on acoustic cavitation, a property which results from the continuous formation, growth and implosive collapse of bubbles within a liquid.[10] We have found it possible, for the first time, to quickly synthesize MCM-41 silica with small particle size and enhanced pore wall thickness by a sonochemical process.

To synthesize all-silica MCM-41 in the present work, a mixture with initial molar ratio of 1.0 Na_2SiO_3:0.33 CTAB:1.86 EtAc:450 H_2O was first prepared in the following manner; CTAB and EtAc are cetyltrimethylammonium bromide and ethyl acetate, respectively. Typically, to an aqueous solution containing 4.90 g CTAB, 11.65 g $Na_2SiO_3{\cdot}9H_2O$ and 325 mL distilled water, 6.70 g EtAc was quickly injected under either vigorous stirring or sonication. A white precipitate appeared after *ca*. 1 min. The slurry was then divided into six parts for further treatment, the synthesis conditions of which are summarized in Table 1.

Powder X-ray diffraction (PXRD) shows differences among the as-synthesized as well as the calcined products. Except for the calcined sample A, all samples exhibit at least three well resolved reflections in the 2θ range between 2 and 10°. The patterns can be indexed to an ordered hexagonal lattice typical of MCM-41.[1] Interestingly, the full width at half maximum height (FWHM) of the (100) reflections of the samples synthesized with ultrasound is slightly narrower than those obtained without ultrasound (Table 2). It is well known that both structural disorder and a decrease in particle size may result in diffraction line broadening. In fact, under TEM the particles of samples A and F are much smaller and poorly

† Electronic supplementary information (ESI) available: PXRD patterns (Fig. S1) TEM and SAED pattern (Fig. S2). See http://www.rsc.org/suppdata/cc/b0/b007442j/

‡ Permanent address: Department of Chemistry, Nankai University, Tianjin 300071, P.R. China. E-mail: xhtang@public.tpt.tj.cn

Table 1 Synthesis conditions used to prepare samples A–F and their crystalline phases[a]

Sample	Synthesis conditions	Sample	a_0[b]/Å
A	Aged for 4.5 h without stirring under ambient conditions	MCM-41	44.1
B	Sonicated for 3.5 h under ambient conditions	MCM-41	46.4
C	Heated at 358 K for 28 h then sonicated for 3.5 h under ambient conditions	MCM-41	47.6
D	Aged for 28 h then sonicated for 3.5 h under ambient conditions	MCM-41	47.5
E	Heated at 358 K for 56 h without stirring	MCM-41	47.4
F	Aged for 56 h under ambient conditions without stirring	MCM-41	47.5

[a] Sonication is carried out in a 50 mL sonication cell with a high-intensity ultrasonic horn (Sonic and Materials, model VC-600, 0.5 in Ti horn, 20 kHz, 100 W cm^{-2}). [b] Unit cell constant of the as-synthesized sample, $a_0 = 2d_{100}/\sqrt{3}$, where d_{100} is the *d*-spacing of (100) reflection.

Table 2 Textural properties of samples A–F after calcination in air at 823 K for 4 h and further at 923 K for 1 h

Sample	Solid	FWHM[a]/°	a_0[b]/Å	S_{BET}[c]/ $m^2\ g^{-1}$	V_T[d]/ mL g^{-1}	V_F[e]/ mL g^{-1}	V_{Tx}[f]/ mL g^{-1}	D[g]/Å	W[h]/Å	V_F/V_T	W/a_0
A	Amorphous	—	—	833	0.386	—	—	—	—	—	—
B	MCM-41	0.16	44.9	853	0.794	0.656	0.138	24.8	20.1	0.827	0.448
C	MCM-41	0.16	43.4	835	0.783	0.611	0.172	23.3	20.1	0.780	0.463
D	MCM-41	0.18	42.5	931	0.920	0.660	0.260	22.6	19.9	0.717	0.468
E	MCM-41	0.20	42.5	1041	1.264	0.771	0.493	23.5	19.0	0.610	0.447
F	MCM-41	0.28	40.9	1042	1.109	0.776	0.433	23.5	17.4	0.700	0.425

[a] Full width at half maximum height of (100) reflection. [b] Unit cell constant, $a_0 = 2d_{100}/\sqrt{3}$, where d_{100} is the *d*-spacing of (100) reflection. [c] BET surface area, calculated from the linear part of the BET plot (p/p_0 = 0.1–0.2). [d] Total pore volume, taken from the volume of N_2 adsorbed at p/p_0 = 0.995. [e] Framework pore volume, derived from the volume of N_2 adsorbed at p/p_0 = 0.54. [f] Textural pore volume, obtained from the difference ($V_T - V_F$). [g] Average pore diameter, estimated using the adsorption branch of the isotherm and the Barrett–Joyner–Halenda (BJH) formula. [h] Pore wall thickness, estimated from the difference ($a_0 - D$).

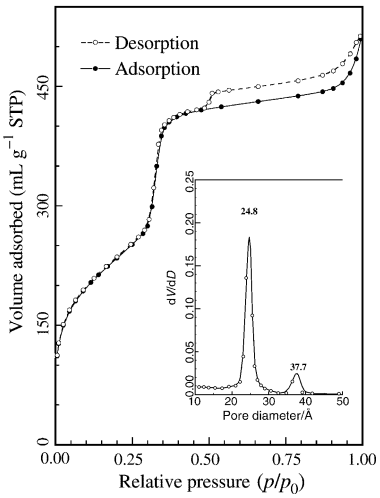

Fig. 1 N_2 adsorption–desorption isotherms of calcined sample B. *Inset*: the pore size distribution calculated by the use of the adsorption data.

aggregated than those of samples B–E, though samples A and F are more uniform in size. Moreover, all samples suffer a framework contraction upon calcination as indicated by the d_{100}-spacings' diminution, except for sample A whose framework collapses. This implies that the samples synthesized without ultrasound are less ordered and of lower stability than those synthesized with ultrasound.

The results from liquid N_2 adsorption–desorption measurements shed more light on the sonochemical effect upon the synthesis. Fig. 1 shows the N_2 adsorption–desorption isotherm as well as the pore size distribution of calcined sample B, and the structural features of the products are detailed in Table 2. The results indicate that samples B–F retain their hexagonal mesophase and exhibit narrow pore size distributions after removal of the organic templates. Though the BJH method may systematically underestimate the pore size by up to 1.0 nm,[11] and although many recent papers have developed more accurate methods for pore size calculation,[12] we think that the data obtained by applying the same method are comparable, and therefore the quantitative results based on these data are credible. It is quite obvious that the ultrasonic processing favors a thicker wall formation. Though acoustic cavitation etched the particles, resulting in a coarse outer surface whereas the inside channels retained the hexagonal arrangement, the electron diffraction pattern shows higher order spots, which provide evidence that both the pore array and pore walls are highly ordered. The processing time of sample B is relatively short; however, a highly ordered, stable mesostructure was fabricated. It was previously reported that MCM-41 can be prepared in a few hours under ambient conditions but, unfortunately, no data regarding the stability have been presented.[13] In our case, the pore wall thicknesses of samples B–D are larger than those of samples E and F. This is quite promising since high quality MCM-41 can be synthesized by a simpler procedure as well as in a shorter time than by the conventional methods. The unit cell constants of the samples decrease in the order B > C > D ≈ E > F after calcination *vs*. C ≈ D ≈ E ≈ F > B before calcination, which means that the frameworks of samples B–D suffer less shrinkage than those of samples E and F. This implies that the pore walls of the sonochemically prepared samples are more condensed or ordered than those of the conventionally prepared ones. The ^{29}Si MAS NMR of calcined sample D is measured and reveals that the framework consists primarily of a fully cross-linked Q^4 unit and a smaller fraction of Q^3 sites. The calculated Q^4:Q^3 ratio is 6.7:1; normally, calcined silica mesostructures prepared by conventional methods have Q^4:Q^3 values near 3.[1] The Q^4:Q^3 ratio of calcined sample D is much higher than those prepared with special treatment,[7c] and is comparable to those of MSG silicas with ratios in the range 6.2–7.4.[6d] In fact, when sample D was refluxed for 6 h in boiling water its crystallinity changed very little. It decreased by *ca*. 35% after refluxing for 12 h, while in the literature[14] the MCM-41 prepared using conventional hydrothermal methods became amorphous after refluxing for 12 h. This can be an advantage of the sonochemical effects. During the formation of the framework, despite the agitation of the ultrasound which helps to disperse the small silica oligomers more homogeneously in the mixture, the formation of hot spots within the surfactant–silicate interface may accelerate the silica polymerization which is slow and rate-limited under normal conditions. Thus the fabrication of the mesostructure can be achieved more efficiently. On the one hand, acoustic cavitation etches the surface of surfactant–silicate micelles which results in a coarse outer surface. On the other hand, hot spots accelerate the condensation of surface silanol groups among micelles, and by this way ultrasound radiation accelerates the formation of the MCM-41 framework and the growth of particles. This two-fold function of ultrasound radiation results in the particles of samples B–E being bigger and more aggregated than those of samples A and F, though samples A and F are more uniform in size.

In conclusion, a novel synthesis route has been developed to prepare high quality MCM-41 within a relatively short time by involving ultrasound. The as-prepared material, whose mesopore size shows a very narrow distribution, possesses thick and condensed wall and is therefore thermally stable.

X. H. T., S. W. L. and W. P. H. thank the Fred and Barbara Kort Sino–Israel Postdoctoral Fellowships Foundation for financial support and the China Scholarship Council for its support. The authors would like to thank Professor K. Kay for editorial assistance. The authors also thank Dr S. Kabaya and Professor S. Vega from the Weizmann Institute of Science for performing the NMR experiments.

Notes and references

1 C. T. Kresge, M. E. Leonowicz, W. J. Roth, J. C. Vartuli and J. S. Beck, *Nature*, 1992, **359**, 710; J. S. Beck, J. C. Vartuli, W. J. Roth, M. E. Leonowicz, C. T. Kresge, K. D Schmitt, C. T.-W. Chu, D. H. Olson, E. W. Sheppard, S. B. McCullen, J. B. Higgins and J. L. Schlenker, *J. Am. Chem. Soc.*, 1992, **114**, 10 0834.
2 A. Corma, *Chem. Rev.*, 1997, **97**, 2373.
3 C. Y. Chen, H. X. Li and M. E. Davis, *Microporous Mater.*, 1993, **2**, 17.
4 J. M. Kim, J. H. Kwak, S. Jun and R. Ryoo, *J. Phys. Chem.*, 1995, **99**, 16 742.
5 (*a*) P. T. Tanev, M. Chibwe and T. J. Pinnavaia, *Nature*, 1994, **368**, 321; (*b*) K. J. Edler and J. W. White, *J. Chem. Soc., Chem. Commun.*, 1995, 155; (*c*) G. D. Stucky, A. Monnier, F. Schuth, Q. Huo, D. I. Margolese, D. Kumar, M. Krishnamurty, P. Petroff, A. Firouzi, M. Janicke and B. F. Chmelka, *Mol. Cryst. Liq. Cryst.*, 1994, **240**, 187.
6 (*a*) R. Ryoo and J. M. Kim, *J. Chem. Soc., Chem. Commun.*, 1995, 711; (*b*) C.-F. Cheng, W. Zhou and J. Klinowski, *Chem. Phys. Lett.*, 1996, **263**, 247; (*c*) D. Zhao, J. Feng, Q. Huo, N. Melosh, G. H. Fredrickson, B. F. Chmelka and G. D. Stucky, *Science*, 1998, **279**, 548; (*d*) S. S. Kim, W. Zhang and T. J. Pinnavaia, *Science*, 1998, **282**, 1302; (*e*) W. Zhang, B. Glomski, T. R. Pauly and T. J. Pinnavaia, *Chem. Commun.*, 1999, 1803.
7 (*a*) D. Khushalani, A. Kuperman, G. A. Ozin, K. Tanaka, J. Garces, M. M. Olken and N. Coombs, *Adv. Mater.*, 1995, **7**, 842; (*b*) A. Sayari, P. Liu, M. Kruk and M. Jaroniec, *Chem. Mater.*, 1997, **9**, 2499; (*c*) L. Chen, T. Horiuchi, T. Mori and K. Maeda, *J. Phys. Chem. B*, 1999, **103**, 1216; (*d*) R. Mokaya, *J. Phys. Chem. B*, 1999, **103**, 10 204.
8 K. S. Suslick, S. B. Choe, A. A. Cichowlas and M. W. Grinstaff, *Nature*, 1991, **353**, 414; T. Hyeon, M. Fang and K. S. Suslick, *J. Am. Chem. Soc.*, 1996, **118**, 5492.
9 J. Zhu, Y. Koltypin and A. Gedanken, *Chem. Mater.*, 2000, **12**, 73.
10 K. S. Suslick, *Science*, 1990, **247**, 1439; K. S. Suslick and G. J. Price, *Ann. Rev. Mater. Sci.*, 1999, **29**, 295.
11 J. C. P. Broekhoff and J. H. de Boer, *J. Catal.*, 1967, **9**, 8.
12 M. Kruk, M. Jaroniec, Y. Sakamoto, O. Terasaki, R. Ryoo and C. H. Ko, *J. Phys. Chem. B*, 2000, **104**, 292; M. Kruk and M. Jaroniec, *Chem. Mater.*, 2000, **12**, 222.
13 W. Lin, Q. Cai, W. Pang and Y. Yue, *Chem. Commun.*, 1998, 2473.
14 R. Ryoo, J. M. Kim, C. H. Ko and C. H. Shin, *J. Phys. Chem. B*, 1996, **100**, 17 718; R. Ryoo and S. Jun, *J. Phys. Chem. B*, 1997, **101**, 317.

ChemComm

Control of the microporosity within the pore walls of ordered mesoporous silica SBA-15

Kohji Miyazawa and Shinji Inagaki*

Toyota Central R&D Labs., Inc., Nagakute, Aichi 480-1192, Japan. E-mail: inagaki@mosk.tytlabs.co.jp

Received (in Oxford, UK) 21st June 2000, Accepted 21st September 2000
First published as an Advance Article on the web 11th October 2000

Microporosity within the pore walls of ordered mesoporous silica SBA-15 was confirmed by physisorption; the micropore volume could be systematically controlled by varying the synthesis temperature and the TEOS/surfactant ratio.

Mesoporous molecular sieves, such as MCM-41[1] and FSM-16,[2] have attracted much attention as catalysts and adsorbents owing to their large pore dimensions compared to microporous zeolites. It is, however, difficult to obtain mesoporous materials exhibiting specific catalysis and adsorption properties such as the uniform acidity and the strong adsorption properties characteistic of zeolites, owing to the amorphous pore walls and large pore dimensions. Although some efforts have been made to crystallize the pore walls of mesoporous materials in order to endow them with a specific functionality,[3–5] it is well known that crystallization of thin pore walls (1–6 nm) is not easy. The generation of microporosity within the amorphous pore walls of mesoporous materials is a promising strategy for endowing them with a specific functionality. Such a material possessing a bimodal pore system, *i.e*. one in which micropores exist within the walls of mesopores, is an ideal porous material for catalysts and adsorbents, because molecules are first transported through mesopore channels and then strongly adsorbed in the micropores. The synthesis of a material with micro- and meso-porous properties would be of great interest. Although there have been some reports suggesting microporosity within the pore walls of MCM-41[6,7] and SBA-15,[8,9] a systematic study for confirmation and control of the microporosity within the pore walls of an ordered mesoporous material has not been reported. Here, we report that the micropore volume of SBA-15 can be controlled systematically by the synthesis temperature and the Si/surfactant ratio in the starting mixture, and micropores are certainly established within the pore wall of SBA-15 material.

A triblock copolymer, Pluronic P104 (BASF), EO_{17}-$PO_{58}EO_{17}$ (EO = $–CH_2CH_2O–$, PO = $–CH_2CH(CH_3)O–$), was used as a structure-directing agent for the synthesis of mesoporous materials. In a typical preparation, 0.8 g of P104 was dissolved in 53 cm^3 of deionized water at 45 °C, and then 10 cm^3 of an aqueous 36% HCl solution was added to the solution. After 2.1–5.6 g of TEOS had been added to the solution, the mixtures was maintained at 45 °C for 8 h with vigorous stirring, followed by heating at 80–100 °C for 8 h under static conditions. The solid products were filtered off and then washed with deionized water repeatedly. After drying at 45 °C overnight, the powders were calcined at 550 °C for 6 h in air. The chemical composition of the reaction mixtures was 0.18 mmol P104: 0.010–0.027 mol TEOS: 0.12 mol HCl: 3.3 mol H_2O. The SBA-15 materials reported previously[10,11] were synthesized with a higher concentration of a surfactant (33.7 g L^{-1}) than the concentration (15.2 g L^{-1}) used in this study. Triblock copolymer P104 has not been previously used for the synthesis of an SBA-15 material. The X-ray diffraction patterns of the products had 2–4 peaks in the low angle region (2θ(Cu-Kα) = 0.7–3.5°) indicating the formation of ordered mesoporous materials with hexagonal (*p*6*mm*) symmetry. Table 1 lists the lattice constants, BJH pore diameters, BET surface areas and pore wall thicknesses of the mesoporous products prepared with different TEOS/P104 ratios and synthesis temperatures.

The adsorption isotherms of the mesoporous materials synthesized under various conditions using the triblock copolymer surfactant exhibited sharp increases in adsorption at $P/P_0 <$ 0.1 and P/P_0 = 0.4–0.7 as shown in Fig. 1(a) and (b). The MS-1 material (Fig. 1(a)) showed a type IV isotherm according to the IUPAC classification,[12] which is typically observed for conventional mesoporous materials such as MCM-41[1] and SBA-15.[10] The first increase in adsorption at $P/P_o < 0.1$ is due to multilayer adsorption on the surface while the second increase at P/P_0 = 0.5–0.7 arises from capillary condensation in the mesopores with nitrogen multilayers adsorbed on the inner surface.[12] The ratio of the first to second feature is higher for MS-6 (Fig. 1(b)) than for MS-1. This suggests that the MS-6 material not only has mesopores but also micropores, since a microporous material shows a type I isotherm,[12] which exhibits a sharp increase in adsorption at $P/P_0 < 0.1$ and a plateau at $P/P_0 > 0.1$.

A comparative plot of the nitrogen adsorption isotherm[7,12] was used to confirm the microporosity and to estimate the micropore volume in the mesoporous materials, similarly to previous reports.[8,9] The t-plots were obtained by using a

Table 1 Physical properties of ordered mesoporous silicas prepared using different TEOS/P104 ratios and temperatures

Sample	TEOS/P104 molar ratio	Synthesis temperature/°C	Lattice constant[a]/nm	Pore diameter[b]/nm	Surface area[c]/m^2 g^{-1}	Pore-wall thickness[d]/nm	Micropore volume[e]/cm^3 g^{-1}
MS-1	60	100	10.4	6.4	646	4.0	~0
MS-2	60	80	9.9	5.8	565	4.1	0.07
MS-3	90	80	10.7	5.4	506	5.3	0.10
MS-4	120	100	10.4	5.8	619	4.6	0.08
MS-5	120	90	10.0	5.0	734	5.0	0.13
MS-6	120	80	10.8	4.7	401	6.2	0.15
MS-7	150	80	11.3	4.9	436	6.5	0.19
MS-6[f]	120	80	10.7	5.0	249	5.7	~0
MS-6[g]	120	80	10.3	5.1	410	5.2	0.11

[a] $2d_{100}/1.732$. [b] Calculated from the adsorption branch of the N_2 isotherm. [c] Calculated by the BET method. [d] Lattice constant−pore diameter. [e] Calculated by the t-plot method. [f] As-synthesized form of MS-6. [g] Surfactant-depleted MS-6 material after solvent extraction.

DOI: 10.1039/b005128o

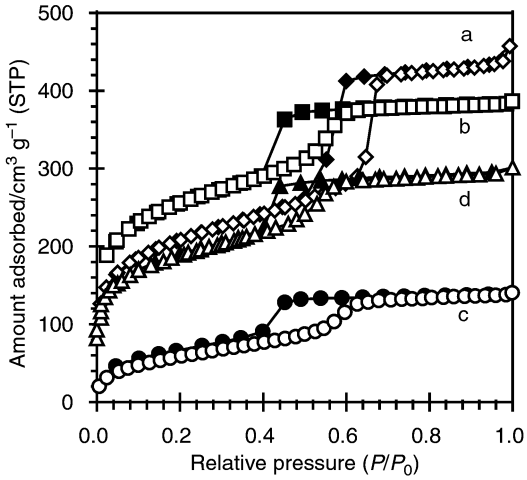

Fig. 1 Nitrogen adsorption–desorption isotherms for mesoporous materials prepared under different conditions: (a) MS-1, (b) MS-6, (c) as-synthesized form of MS-6 and (d) surfactant-depleted MS-6 material after solvent extraction.

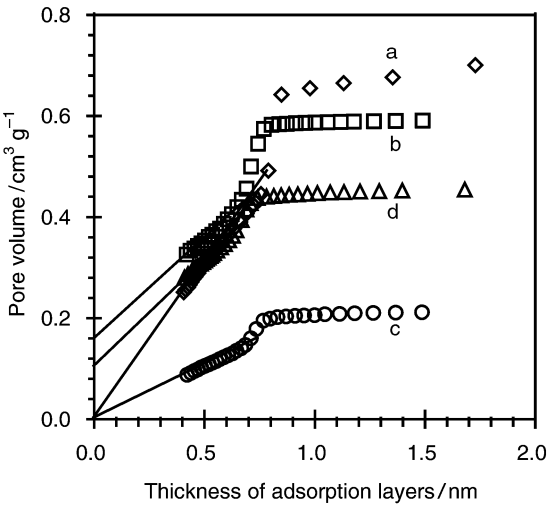

Fig. 2 t-Plots of nitrogen adsorption isotherms for mesoporous materials: (a) MS-1, (b) MS-6, (c) as-synthesized form of MS-6 and (d) surfactant-depleted MS-6 material after solvent extraction.

reference isotherm obtained for a non-porous silica described in a previous report.[13] The t-plots for MS-1 and MS-6 are shown in Fig. 2(a) and (b).

The t-plot for MS-1 gave a straight line at t = 0.40–0.75 nm (t = thickness of adsorbed layer) and the extrapolation line went through the origin, indicating that the MS-1 material has no micropores. Although the MS-6 material also showed a straight line in the same t-value region in the t-plot, the extrapolation line cut the y-axis at 0.15 cm^3 g^{-1}. This indicates that the MS-6 material has a micropore volume of 0.15 cm^3 g^{-1} with a pore radius of < 0.4 nm. A t-plot calculation with the same reference isotherm as for the nitrogen adsorption isotherm of the SBA-15 described in the previous report[10] revealed the absence of microporosity.

The microporosity in the mesoporous materials changed systematically with variation of the synthesis temperature and the TEOS/P104 ratio, as shown in Table 1. Microporosity was not observed for the mesoporous material (MS-1) prepared with a TEOS/P104 molar ratio of 60 and a temperature of 100 °C. A decrease in the temperature from 100 to 80 °C with a constant TEOS/P104 molar ratio of 120 increased the micropore volume from 0.08 to 0.15 cm^3 g^{-1}. An increase in the TEOS/P104 molar ratio from 60 to 150 with a constant temperature of 80 °C also increased the micropore volume from 0.10 to 0.19 cm^3 g^{-1}. These are the first results on the systematic control of microporosity for SBA-15. The increase in microporosity was accompanied by enlargement of the pore-wall thickness (Table 1). The density of micropores in the walls, obtained by dividing the micropore volume by the pore-wall volume, increased with enlargement of the pore walls. The generation of microporosity can be explained by penetration of hydrophilic poly(ethylene oxide) chains of triblock coplymer in the silica wall, as reported by Kruk *et al*.[9] who also suggested that the micropore volume should decrease at elevated temperatures, owing to dehydration of ethylene oxide blocks.[9] The result obtained in this study clearly shows this relationship between the micropore volume and the synthesis temperature. An increase in TEOS/surfactant ratio in the starting mixture is also found to be an effective method to increase the micropore volume of SBA-15. The TEOS/surfactant ratio affects the siloxane network structure in the pore walls, and thereby results in changes of microporosity. There are many variations in the siloxane network structure in a silica gel, which give different pore sizes and porosity.[14] The systematic change of the micropore volume and pore-wall thickness of the mesoporous materials also indicates the existence of micropores within the mesopore walls.

The nitrogen adsorption isotherm and t-plot for the as-synthesized MS-6 material are shown in Fig. 1(c) and Fig. 2(c), respectively. They indicate that the as-synthesized MS-6 material contains surfactant in the mesopore spaces (73% occupation of the mesopore space) with no microporosity. The as-synthesized MS-6 material (1 g) was treated with an ethanol solution (30 cm^3) at room temperature three times to remove the surfactant. The treated MS-6 material showed a micropore volume of 0.11 cm^3 g^{-1}, which was confirmed by the t-plot (Fig. 2(d)) of the nitrogen adsorption isotherm (Fig. 1(d)). The removal of the surfactant from the mesopore spaces made it possible for nitrogen molecules to gain access to the micropores within the mesopore walls. This strongly suggests that micropores exist within the mesopore walls, and that MS-6 is not a physical mixture of mesoporous and microporous materials.

In conclusion, t-plot analysis of nitrogen adsorption isotherms strongly suggests the formation of micropores within the mesopore walls of mesoporous materials. The microporosity can be controlled *via* the synthesis conditions. A novel porous material possessing an ideal bimodal pore system should exhibit high performance catalysis and adsorption properties.

Notes and references

1 C. T. Kresge, M. E. Leonowicz, W. J. Roth, J. C. Vartuli and J. S. Beck, *Nature*, 1992, **359**, 710.
2 S. Inagaki, Y. Fukushima and K. Kuroda, *J. Chem. Soc., Chem. Commun.*, 1993, 680.
3 K. R. Kloetstra, H. van Bekkum and J. C. Jansen, *Chem. Commun.*, 1997, 2281.
4 P. Yang, D. Zhao, D. Margolese, B. F. Chmelka and G. D. Stucky, *Nature*, 1998, **396**, 152.
5 P. Yang, D. Zhao, D. I. Margolese, B. F. Chmelka and G. D. Stucky, *Chem. Mater.*, 1999, **11**, 2813.
6 Y. Long, T. Xu, Y. Sun and W. Dong, *Langmuir*, 1998, **14**, 6173.
7 S. Storck, H. Bretinger and W. F. Mair, *Appl. Catal. A*, 1998, **174**, 137.
8 W. W. Lukens, Jr., P. S-Winkel, D. Zhao, J. Feng and G. D. Stucky, *Langmuir*, 1999, **15**, 5403.
9 M. Kruk, M. Jaroniec, C. H. Ko and R. Ryoo, *Chem. Mater.*, 2000, **12**, 1961.
10 D. Zhao, J. Feng, Q. Huo, N. Melosh, G. H. Fredrickson, B. F. Chmelka and G. D. Stucky, *Science*, 1998, **279**, 548.
11 D. Zhao, Q. Huo, J. Feng, B. F. Chmelka and G. D. Stucky, *J. Am. Chem. Soc.*, 1998, **120**, 6024.
12 S. J. Gregg and K. S. W. Sing, *Adsorption, Surface Area and Porosity*, Academic Press, New York, 1982.
13 M. R. Bhambhani, P. A. Cutting, K. S. W. Sing and D. H. Turk, *J. Colloid Interface Sci.*, 1972, **38**, 109.
14 R. K. Iler, *The Chemistry of Silica*, Wiley-Interscience, New York, 1979.

ChemComm

Amperometric biosensor for inert organic solvents based on a sol–gel hybrid material

Bingquan Wang, Jingzhong Zhang, Guangjin Cheng and Shaojun Dong*

Laboratory of Electroanalytical Chemistry, Changchun Institute of Applied Chemistry, Chinese Academy of Sciences, Changchun, 130022, P. R. China. E-mail; dongsj@ns.ciac.jl.cn

Received (in Cambridge, UK) 21st June 2000, Accepted 25th September 2000
First published as an Advance Article on the web 11th October 2000

A unique sol–gel enzyme electrode for inert organic solvents is developed that is based on the partition equilibrium of the substrate between water–organic solvent media and the enzyme membrane.

Since the introduction of the first enzyme electrode over 30 years ago, growing interest in biosensors has resulted in increasingly widespread development. The development direction of biosensors can be divided into two aspects: First, the scope of the detection medium was expanded. In order to meet specific requirements, biosensors were developed from the aqueous phase, then to organic solvents saturated with water,[1] then to pure organic solvents,[2] and finally to a universal organic solvent.[3] Second, the scope of the determinable substance was expanded. Enzyme electrodes were first used to detect various substrates,[4,5] later inhibitors could be quantified due to their inhibition of enzyme activity.[6] Recently, Wang[7] applied biosensors to water determination based on the effect of water content on enzyme activity in organic solvents. In this study, we further expand the application of biosensors to inert organic solvent determination.

Recently the use of sol–gel glass as a biosensor encapsulation matrix has recieved much interest because of its high stability.[8] We have fabricated a sol–gel/hydrogel hybrid material, which retained the high activity of enzymes and exhibited negligible swelling.[9] In order to eliminate the influence of matrix swelling on the response, a tyrosinase enzyme electrode based on this hybrid material was chosen to demonstrate the feasibility of the biosensor for the determination of polar organic solvents. The preparations of fresh sol-gel solution and the enzyme electrode have been described elsewhere.[9]†

Steady-state amperometry was used to characterize the enzyme electrode, and Fig. 1(A) shows the typical steady-state current–time responses for successive addition of 50 μl acetonitrile in the presence of catechol. The first 'jump' in the current resulted from the response of catechol to the enzyme electrode, after the steady-state current reached a plateau, injection of acetonitrile caused a current drop. The current decrease is proportional to the content of the organic solvents added [Fig. 1(B)], therefore, electrochemically inert organic solvents can be amperometrically quantified by the enzyme electrode. Fig. 1(B) also shows the effect of enzyme loading upon the response for acetonitrile. Obviously, the response for acetonitrile increases upon increasing the enzyme loading between 266 and 400 units. Therefore, the increase in the enzyme loading can improve detection sensitivity, consequently decreasing the detection limit.

The dilution effect on the substrate in the solution can be ruled out by the control experiments because the injection of the same volume of buffer into the solution did not produce obvious current changes.[11] Thus the mechanism can be ascribed to the change of the sol–gel enzyme membrane due to the addition of organic solvent. Sol–gel encapsulation provides a sufficiently hydrophilic microenvironment that would both retain the essential hydration layer and exclude potentially denatured solvent components,[2,4,8] so it has a stabilization function on the enzyme system. Moreover, the content of organic solvent in this system is considerably lower than that in non-aqueous media,[1–3] so the addition of small amounts of organic solvent will not greatly influence the activity of the sol–gel encapsulated enzyme.[10] If the addition of organic solvent will inhibit the enzyme activity to a large degree, then after the 12th injection of polar organic solvents, the biosensor should exhibit a small current response to the same concentration of catechol. This was not the case. Hupp also found the sol–gel-encapsulated enzyme could retain its catalytic activity when alcohol and aldehyde were successively added into the enzyme monolith.[4]

To accurately demonstrate the response mechanism, we did steady-state QCM experiments at sol–gel modified gold electrodes. Fig. 2 shows the frequency changes following the injection of catechol and acetonitrile when the solution was under rapid stirring. When no enzyme was added into the sol–gel film, the injection of organic solvent did not produce noticeable changes in the frequency (curve *a*). Therefore, the nature of the sol–gel/electrode interface does not change on addition of solvent, which further proves the high stability of the sol–gel hybrid material.[8,9] The responses of the enzyme electrode are shown in curve *b*. With a constant frequency established at time T1, injection of catechol caused a frequency decrease. This can be explained by the fact that catechol diffuses

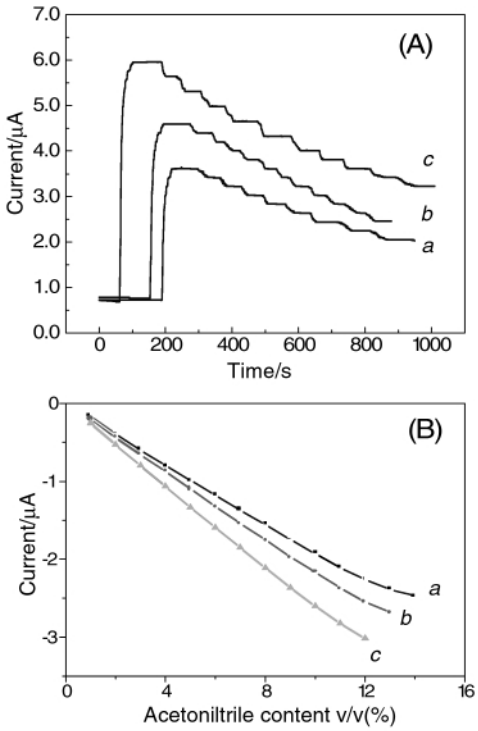

Fig. 1 (A) Amperometric responses of biosensors with different enzyme loadings to addition of 60 μM catechol, followed by successive additions of 50 μl acetonitrile to 5 ml PBS. (B) Corresponding calibration curve for acetonitrile. Enzyme loading, (a) 266 units, (b) 320 units, (c) 400 units; potential, −100 mV *vs* Ag/AgCl (sat. KCl).

DOI: 10.1039/b004967k

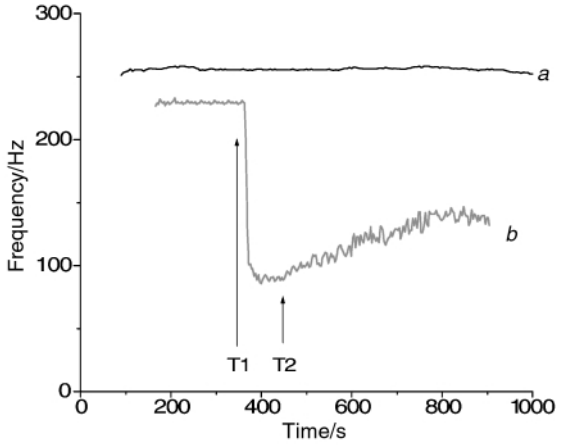

Fig. 2 Frequency–time response curves at the sol-gel-modified gold electrodes with 0 (a) and 320 units tyrosinase (b). At time T1, injections of 60 μM catechol; at time T2, injection of 1% (*v*/*v*) acetonitrile.

into the enzyme membrane and causes an increase in mass, accordingly the frequency decreases. When the response reached a steady state at time T2, injection of acetonitrile caused a frequency increase, which illustrates that the mass of the enzyme membrane does not increase but decreases. If the addition of organic solvent mainly inhibits the enzyme activity, then the mass of the enzyme membrane would not decrease. Therefore, this phenomenon further proves that organic solvent will not greatly inhibit the enzyme activity. In the enzyme membrane, only the amount of catechol may change; therefore, we attribute the current decrease to the extraction effect of organic solvent on the catechol in the enzyme membrane.[11] The solubility of catechol in organic solvents is much greater than in water, and the injected polar organic solvent quickly hydrates and concentrates catechol in the solution, which causes a decrease of the substrate concentration in the solution. Because of the dynamic distribution balance of the substrate between membrane and solution, the catechol in the membrane diffuses toward the solution; this brings about the substrate decrease in the enzyme membrane, accordingly, the response of the biosensor decreases. This mechanism is consistent with our previous report.[11] Both the working electrode and the configuration of the electrochemical cell in QCM experiments are different from those used in Fig. 1, so the response is relatively slower in Fig. 2. Moreover, because of the high sensitivity of QCM (~ng), the noise in Fig. 2 is larger than that in Fig. 1(A).

The sensitivity of the enzyme electrode to organic solvent is solvent dependent. The dielectric constant (ε) and the viscosity (λ) of organic solvents influence the response of the biosensor. The higher the $1/\varepsilon\lambda$, the lower the frictional resistance forces of the solvents on the substrate. This will bring about a higher diffusion of the substrate through the sol–gel film, therefore resulting in a greater sensitivity.[12] In addition, the hydrophobicity of the organic solvent plays an important role in the sensitivity of the biosensor. Methanol, *n*-propanol and *n*-butanol were selected to study the relationship between the sensitivity and the hydrophobicity of organic solvents, because they have similar molecular structures. The biosensor showed a sensitivity sequence as *n*-butanol > *n*-propanol > methanol. log *P* values for *n*-butanol, *n*-propanol and methanol are 0.88, −0.16 and −0.76, respectively. log *P* is a measure of the hydrophobicity of an organic solvent (*P* is the partition coefficient of a solvent in a standard octanol–water two-phase system[13]). The higher the log *P* value is, the more hydrophobic the organic solvent.[14] Obviously, the sensitivity sequence for the three organic solvents conforms to the hydrophobicity sequence. This is because the solubilities of catechol in the three solvents are in the sequence: *n*-butanol > *n*-propanol > methanol.

The biosensor proposed here determines organic solvents well. The response time for acetonitrile is about 40 s, and the detection limit of 1,4-dioxane, an explosive compound, is 0.023% *v*/*v* (*S*/*N* = 3). Moreover, the biosensor can be used to determine some organic solvents such as acetone, dimethylformamide, tetrahydrofuran *etc*., for which no specific enzyme has been found to fabricate a specific biosensor.

We acknowledge the National Natural Science Foundation (China) for financial support.

Notes and references

† The enzyme electrodes were prepared as follows: a suitable amount of tyrosinase (E.C.1.14.18.1) was dissolved in 30 μl of phosphate buffer solution (PBS, pH 7.0), and then 20 μl of hydrogel and 10 μl of silica sol were added. After complete mixing, 10 μl of the mixture was dropped on a glassy carbon electrode (diameter 4 mm). The film was allowed to dry at 4 °C for 16 h and then washed thoroughly with PBS.

1 N. Pena, M. Romero, F. J. M.Villena, A. J. Reviejo and J. M. Pingarron, *Electroanaysis*, 1999, **11**, 85.
2 S. Dong and Y. Guo, *J. Chem. Soc., Chem. Commun.*, 1995, **67**, 1357.
3 Y. Guo and S. Dong, *Anal. Chem.*, 1997, **69**, 1904.
4 A. K. Williams and J. T. Hupp, *J. Am. Chem. Soc.*, 1998, **120**, 4366.
5 A. Bardea, E. Katz, A. F. Buckmann and I. Willner, *J. Am. Chem. Soc.*, 1997, **119**, 9114.
6 J. Wang, E. Dempsey, A. Eremenko and M. R. Smyth, *Anal. Chim. Acta.*, 1993, **279**, 203.
7 J. Wang and A. J. Reviejo, *Anal. Chem.*, 1993, **65**, 845.
8 For example, see: I. Gill and A. Ballesteros, *J. Am. Chem. Soc.*, 1998, **120**, 8587; B. C. Dave, B. Dunn, J. S. Valentine and J. I. Zink, *Anal. Chem.*, 1994, **66**, 1120A.
9 B. Wang, B. Li, Z. Wang, G. Xu, Q. Wang and S. Dong, *Anal. Chem.*, 1999, **71**, 1935.
10 J. S. Dordick, *Enzyme Microb. Technol.*, 1989, **11**, 194.
11 J. Zhang, B. Wang, B. Xu, G. Cheng and S. Dong, *Anal. Chem.*, 2000, **72**, 3455.
12 O. Adeyoju, E. I. Iwuoha and M. R. Smyth, *Electroanalysis*, 1995, **7**, 924.
13 E. I. Iwuoha, M. R. Smyth and M. E. G. Lyons, *J. Electroanal. Chem.*, 1995, **390**, 35.
14 S. Saini, G. F. Hall, M. E. A. Downs and A. P. F. Turner, *Anal. Chim. Acta.*, 1991, **249**, 1.

Mesoporous Sn–TiO_2 composite electrodes for lithium batteries

Zuoyan Peng, Zhong Shi and Meilin Liu*

School of Materials Science and Engineering, Georgia Institute of Technology, Atlanta, GA, 30332-0245SA. E-mail: meilin.liu@mse.gatech.edu

Received (in Irvine, CA, USA) 9th May 2000, Accepted 12th September 2000
First published as an Advance Article on the web 11th October 2000

Mesoporous TiO_2 is prepared stable up to 500 °C with BET surface area of 603 m^2 g^{-1} and pore size 6.9 nm, and Sn–TiO_2 composites based on the mesoporous TiO_2 show good potential as an electrode for lithium batteries with large capacity and structural integrity.

Since mesoporous materials (*e.g.* MCM-41) were first prepared in 1992,[1,2] surfactant-templated synthesis procedures have been widely used for the preparation of highly-ordered mesoporous or nanostructured materials which would be difficult to prepare otherwise. The ordering in these materials is a consequence of a self-assembly process in an aqueous solution containing organic surfactants (anionic, cationic or neutral) and inorganic (oligo-) cations or anions. A wide range of mesoporous materials have been prepared using the structure-directing functions of electrostatic, hydrogen-bonding, and van der Waals interactions associated with amphiphilic molecules.[3–14] Mesoporous TiO_2 was first prepared using a phosphate surfactant through a modified sol–gel process.[13] Since a significant amount of phosphorus still remained in these materials, they are not pure titanium oxides. Recently, mesoporous TiO_2 has been prepared using amphiphilic poly(alkylene oxide) block copolymers as structure-directing agents and titanium inorganic salts as precursors in a non-aqueous solution.[15] The mesoporous structure was stable up to 400 °C with BET (Brunauer–Emmett–Teller) surface area of about 200 m^2 g^{-1}. The use of amine surfactants resulted in mesoporous TiO_2 with BET surface area about 700 m^2 g^{-1} (for as-synthesized powders) while heat treatment of the obtained materials in dry air at 300 °C led to loss of surface area and disappearance of the low angle diffraction peak in X-ray diffraction (XRD) patterns.[16] In this study, mesoporous TiO_2 stable up to 500 °C has been successfully prepared using tri-block copolymers, $(EO)_n$–$(PO)_m$–$(EO)_n$, as directing agents and titanium butoxide as precursor in an aqueous solution. Further, tin oxide was introduced into the mesoporous TiO_2 using a sol–gel process and then reduced in an atmosphere containing hydrogen to form a Sn–TiO_2 composite electrode for lithium ion batteries. The objective of our study is to create a nano-structured Sn–TiO_2 electrode for lithium ion batteries because tin-based compounds may offer much larger capacity than a lithiated carbon electrode. The structural stability of the tin-based materials during cycling is a major concern.[17] Our approach to improve the structural stability was to incorporate tin compound into a mesoporous TiO_2 matrix, which is structurally stable and hence offers structural stability to the nanocomposite electrode.

Shown in Fig. 1 are small-angle XRD patterns of TiO_2 powder samples prepared using a tri-block polymer surfactant (Pluronic 103). The XRD pattern of the as-synthesized sample, Fig. 1(*a*), implies that the surfactant molecules were organized into a hexagonal superstructure after being aged at 50 °C for one week. In addition to the major peak at about 1° due to the (100) reflection, which corresponds to a *d*-spacing of 8.4 nm, small peaks due to the (110) and (200) reflections are also observable. The XRD pattern of the as-calcined sample, Fig. 1(*b*), indicates that the mesoporous structure was retained during the removal of the surfactant by calcination at 500 °C in air for 1 h, although the superstructure had contracted slightly as evidenced by a slight shift of the XRD peaks toward larger angle. The

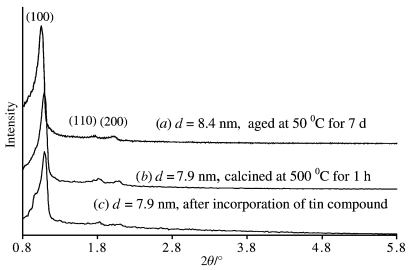

Fig. 1 XRD patterns of (*a*) as-synthesized (aged at 50 °C for 1 week) and (*b*) as-calcined (at 500 °C in air for 1 h) TiO_2 samples prepared using Pluronic 103 as surfactant and (*c*) XRD pattern of a Sn–TiO_2 sample.

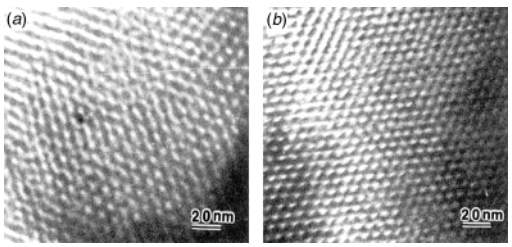

Fig. 2 TEM images of (*a*) as-synthesized (aged at 50 °C for 1 week) and (*b*) as-calcined (at 500 °C in air for 1 h) TiO_2 samples prepared using Pluronic 103 as surfactant.

corresponding *d*-spacing was reduced from 8.4 nm for the as-synthesized sample to about 7.9 nm for the as-calcined sample. Shown in Fig. 1(*c*) is a small-angle XRD pattern of a Sn–TiO_2 sample, which is nearly identical to the XRD pattern of the as-synthesized TiO_2 shown in Fig. 1(*b*), implying that the periodicity of the mesoporous TiO_2 remain unchanged during the incorporation of tin compounds into the mesoporous TiO_2 and the reduction of tin oxide to tin metal.

Shown in Fig. 2 are TEM images of the as-synthesized and as-calcined samples. The periodicities of the mesoporous superstructure as determined from the TEM images are consistent with those determined from XRD analysis. The corresponding pore sizes are about 7.6 and 6.9 nm, respectively. The N_2 adsorption isotherms of the as-synthesized and as-calcined TiO_2 powder are shown in Fig. 3(*a*). Both adsorption isotherm curves have a well-defined step for the relative pressure P_s/P_0 ranging from 0.6 to 0.8, a characteristic of the filling of the framework-confined mesoporous, suggesting that both as-synthesized and as-calcined samples are mesoporous. However, the calculated BET surface area was increased from 203 m^2 g^{-1} for the as-synthesized sample to 603 m^2 g^{-1} for the as-calcined sample, indicating that the gas-accessible surface area was dramatically increased after the surfactant was removed. Further, the average pore size in the as-calcined mesoporous superstructure is about 6.9 nm with a narrow size distribution, as shown in the insert in Fig. 3(*a*).

After the incorporation of tin compound into the pores of the mesoporous TiO_2, the surface area and pore size were reduced to 441 m^2 g^{-1} and 6 nm, respectively, as determined from the absorption isotherm and pore size distribution data shown in Fig. 3(*b*). This implies that the tin compound was formed inside the pores of the mesoporous TiO_2, an ideal configuration of a

DOI: 10.1039/b007687m

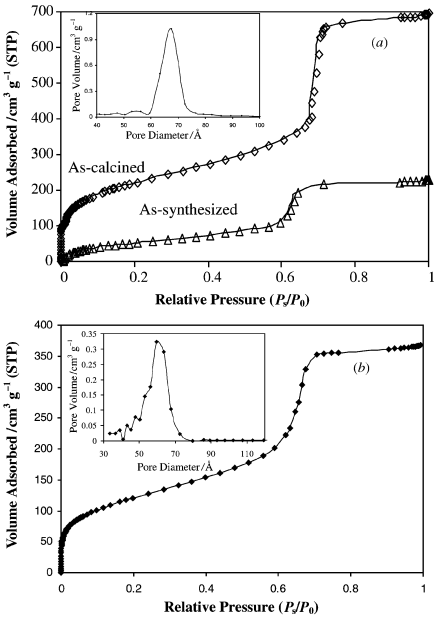

Fig. 3 (*a*) Nitrogen isotherm plots of as-synthesized (aged at 50 °C for 1 week) and as-calcined (at 500 °C in air for 1 h) TiO_2 samples prepared using Pluronic 103 as surfactant (the insert curve is the pore size distribution for the as-calcined TiO_2 sample calculated from the BET curve); (*b*) nitrogen isotherm plots of a Sn–TiO_2 composite sample (the insert curve is the pore size distribution for the composite calculated from the BET curve).

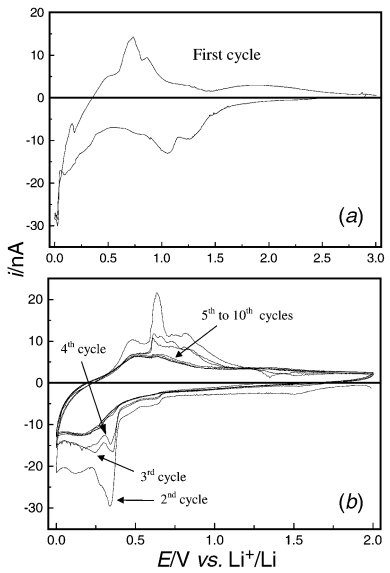

Fig. 4 Cyclic voltammograms of a mesoporous Sn–TiO_2 composite as studied using a powder microelectrode: (*a*) the cycle 1; (*b*) the 2 to 10 cycles. The potential sweep rate was 0.5 mV s^{-1}.

composite electrode for lithium batteries with desired structural stability.

Shown in Fig. 4 are the first several cyclic voltammograms of a mesoporous Sn–TiO_2 composite electrode as studied using a powder microelectrode. Clearly, the CV curve for the first cycle is very different from those commonly observed for most tin-based composite electrodes.[18] It is noted that there is no cathodic peak at 0.85 V (or 2.6 V), corresponding to electrochemical reduction of SnO or SnO_2,[18] indicating that most tin oxides had been chemically reduced to tin metal in the mesocomposite during the exposure to hydrogen. However, there are two small reduction peaks between 1 and 1.5 V in the first cycle, which disappeared after the first cycle. Several pairs of redox peaks appear in the voltammograms after the second cycle. The peak currents decreased during the first few cycles but remained relatively constant later on, as shown in Fig. 4(*b*). There was little change from 5th to 10th cycle, implying that the composite electrode may have good cycleability. Long-term cycling behavior of the composite electrode is still under investigation using constant current charge–discharge cycling test and will be reported in the near future.

In a typical preparation, 10 g titanium butoxide was dissolved in 20 ml absolute ethanol and 2.92 ml acetylacetone at room temperature before 10 ml distilled water was added, followed by stirring for another 2–3 h. In a separate beaker, 5 g Pluronic 103 was dissolved in 20 ml ethanol and 100 ml 2 M HCl solution. This surfactant solution was then slowly added to the titanium butoxide solution. The resulting solution was subsequently kept at 50 °C with continuous stirring for one week. The obtained solid product was washed and centrifuged three times using distilled water and then dried at 60 °C for 24 h and 120 °C for 5 d. The dried powder was fired at 500 °C for 1 h in air using an alumina boat to remove the surfactant.

To incorporate Sn into the pores of the mesoporous TiO_2, $SnCl_4$ was dissolved in water, to which NH_3(aq) was added to ensure all Sn^{4+} was hydrolyzed and precipitated. The solid product was washed and centrifuged three times using distilled water and was then dissolved in nitric acid to obtain a solution containing Sn^{4+}. The mesoporous TiO_2 powder was then immersed in the solution containing Sn^{4+} for a few days. The resulting powder was obtained after drying at 80 °C for one day and at 120 °C for another day, followed by reduction at 300 °C for 24 h in a hydrogen atmosphere.

The electrochemical properties of the mesoporous Sn–SiO_2 electrode were studied in 1 M $LiN(SO_2CF_3)_2$/EC+DMC electrolyte solution using a powder microelectrode[19] technique.

We gratefully acknowledge the support of this research by the National Science Foundation (under Grant No. CTS-9819850) and the Caleb Corporation.

Notes and references

1 C. T. Kresge, M. E. Leonowicz, W. J. Roth, J. C. Vartuli and J. S. Beck, *Nature*, 1992, **359**, 710.
2 J. S. Beck, J. C. Vartuli, W. J. Roth, M. E. Leonowicz, C. T. Kresge, K. D. Schmitt, C. T-W. Chu, D. H. Olson, E. W. Sheppard, S. B. Mccullen, J. B. Higgins and J. L. Schlenker, *J. Am. Chem. Soc*., 1992, **114**, 10 834.
3 A. Sayari, *Chem. Mater.*, 1996, **8**, 1840.
4 Q. Huo, R. Leon, P. M. Petroff and G. D. Stucky, *Science*, 1995, **268**, 1324.
5 Q. Huo, D. I. Margolese, U. Ciesla, D. G. Demuth, P. Feng, T. E. Gier, P. Sieger, A. Firouzi, B. F. Chmelka, F. Schuth and G. D. Stucky, *Chem. Mater.*, 1994, **6**, 1176.
6 A. Monnier, F. Schüth, Q. Huo, D. Kumar, D. Margoless, R. S. Maxwell, G. D. Stucky, M. Krishnamurty, P. Petroff, A. Firouzi, M. Janicke and B. F. Chmelka, *Science*, 1993, **261**, 1299.
7 U. Ciesla, S. Schacht, G. Stucky, K. Unger and F. Schüth, *Angew. Chem., Int. Ed. Engl.*, 1996, **35**, 541.
8 U. Ciesla, M. Fröba, G. Stucky and F. Schüth, *Chem. Mater.*, 1999, **11**, 227.
9 M. Fröba and O. Muth, *Adv. Mater.*, 1999, **11**, 564.
10 Z. R. Tian, W. Tong, J. Y. Wang, N. G. Duan, V. V. Krishnan and S. L. Suib, *Science*, 1997, **276**, 926.
11 M. Thieme and F. Schüth, *Microporous Mesoporous Mater.*, 1999, **27**, 193.
12 V. Luca, D. J. Maclachlam, J. M. Hook and R. Whiters, *Chem. Mater.*, 1995, **7**, 2220.
13 D. M. Antonelli and J. Y. Ying, *Angew. Chem., Int. Ed. Engl.*, 1995, **34**, 2014; *Chem. Mater.*, 1996, **8**, 874; D. M. Antonelli, A. Nakahira and J. Y. Ying, *Inorg. Chem.*, 1996, **35**, 426.
14 D. Zhao, J. Feng, Q. Huo, N. Melosh, G. Fredrickson, B. Chmelka and G. D. Stucky, *Science*, 1998, **279**, 548.
15 P. Yang, D. Zhao, D. I. Margolese, B. F. Chemelka and G. D. Stucky, *Nature*, 1998, **396**, 152.
16 D. M. Antonelli, *Microporous Mesoporous Mater.*, 1999, **30**, 315.
17 R. A. Huggins, *Solid State Ionics*, 1998, **113–115**, 57.
18 S. Machill, T. Shodai, Y. Sakuraai and J. Yamaki, *J. Power Sources*, 1998, **73**, 216.
19 C. S. Cha, C. M. Li, H. X. Yang and P. F. Liu, *J. Electroanal. Chem.*, 1994, **368**, 47.

ChemComm

Synthesis of aza-*C*-disaccharides using cycloaddition reactions of a functionalized cyclic nitrone

Fraser J. Duff, Vincent Vivien and Richard H. Wightman*

Department of Chemistry, Heriot-Watt University, Riccarton, Edinburgh, UK EH14 4AS. E-mail: cherhw@hw.ac.uk

Received (in Liverpool, UK) 18th July 2000, Accepted 14th September 2000
First published as an Advance Article on the web

Cycloaddition reactions of a functionalized nitrone with sugar alkenes gives stereoselective access to aza-*C*-disaccharide analogues of α-D-Lyx(1→6)-α-D-Man and α-D-Lyx(1→6)-D-Gal.

Iminosugars have attracted much attention in recent years[1] due to their ability to act as inhibitors of glycosidases, and hence to have potential application in the treatment of a number of disparate disease states such as viral infections,[2] diabetes[3] and tumour metastasis.[4] It has been theorised that glycosidase inhibitors which permit interaction with the aglycon binding site should be more potent than those which lack this ability,[5] and the validity of this concept has been demonstrated.[6] The attachment of a second aglycone-mimicking sugar unit to an iminosugar has been done in a number of ways, as for example in the α,β-trehalose analogue **1**[6a] or by attachment *via*

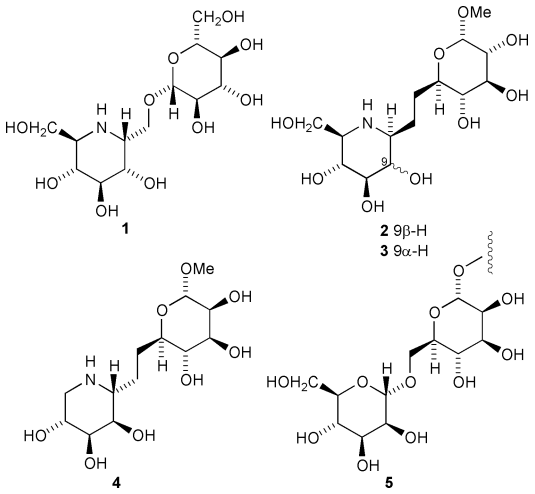

nitrogen,[6c,7] but the aza-analogues of disaccharides which can be regarded as being closest in structure to the natural sequences are those with an all-carbon link, namely the aza-*C*-disaccharides prepared in the laboratories of Johnson[8] and of Vogel and van Boom,[9] such as **2**[8a,9] and **3**.[8c,9]

In this communication we describe our preliminary results on the synthesis of aza-*C*-disaccharides by a different synthetic approach to those previously employed,[8,9] and in which stereoselective cycloaddition reactions between functionalized cyclic nitrones and sugar alkenes are employed to establish the disaccharide analogue; our approach is illustrated by the synthesis of **4**, related to the sequence α-D-Man(1→6)-α-D-Man **5**, which is hydrolysed by Golgi α-mannosidase II during the processing of *N*-linked glycans of glycoproteins,[10] and of a related aza-*C*-disaccharide **20**.[11]

Treatment of 2,3-*O*-isopropylidene-D-lyxose **6**[12] with TsCl-pyridine (Scheme 1) gave in high yield the solid but somewhat unstable tosylate **7**, which was directly treated with excess hydroxylamine to give predominantly (44–47%) the nitrone **8**,† together with smaller amounts (3–8%) of the nitrone **9** with a five-membered ring. We consider that **9** is formed *via* intermediates **A** and **B** (Scheme 1), whilst **8** is derived predominantly by direct cyclisation of **A**,[13] but also to a lesser extent by 6-*endo*- ring closure of **B**.‡ In support of this, we have shown that epoxide **10**, on treatment with hydroxylamine, gives (54%) a mixture of the enantiomers of **8** and **9** in a 1 : 1 ratio.

Methyl α-D-mannopyranoside was converted routinely (66% overall) into **11** (see Scheme 2), which was oxidised and converted to alkene **12**. Reaction of **12** and nitrone **8** in toluene at reflux led to the isolation of a crystalline cycloadduct **13** in 84% yield. The stereostructure of **13**, which corresponds to reaction on the face of **8** *anti*- to the isopropylidenedioxy group, and *via* an *exo*-transition state,§ was indicated by NOESY data, which were obtained at high temperature (120 °C) since at lower temperatures signal-broadening was found, presumably due to slow inversion at nitrogen. Strong interactions were observed between 6-H and 7β-H, and between 7α-H and both 5-H and 8-H. The structure of **13** was subsequently confirmed by X-ray crystallography.¶ The stereoselectivity of this cycloaddition is enhanced (double stereodifferentiation) by the known facial preference of chiral allylic ethers in cycloadditions, such that an *erythro*-relationship between the stereocentres at C-5′ and C-8 will be preferred.[14]

The cycloadduct **13** was acetylated, whereupon reductive cleavage of the N–O bond was carried out using $Mo(CO)_6$ in aqueous acetonitrile,[15] to give after protection of the amine the benzyloxycarbonyl derivative **14**. Deoxygenation to give **15** was carried out through the intermediacy of the imidazolyl-thiocarbonyl derivative, but we observed that it was necessary to carry out the reaction of **14** with thiocarbonyldiimidazole at high concentrations and with excess of reagent in order to obtain a high yield, an observation recently reported by others during the synthesis of *C*-disaccharides.[16] Routine deprotection of **15** then led to the aza-*C*-disaccharide **4**, isolated as its hydrochloride (44% overall from **13**).†

As a further example of this approach to aza-*C*-disaccharides, reaction of nitrone **8** with the D-galactopyranosyl alkene **16**[17] gave in 88% yield the *anti*-, *exo*-cycloadduct **17**† (Scheme 3), together with 1% of the *syn*-, *exo*-isomer. The stereochemistry of **17** again followed from NOESY spectra run at elevated temperatures, with strong interactions being observed between

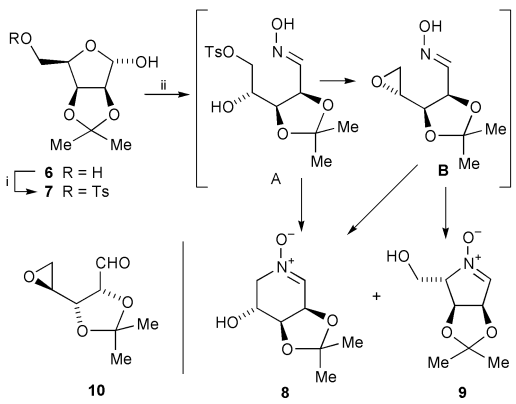

Scheme 1 *Reagents and conditions*: i, TsCl, pyridine–$CHCl_3$, 5 h (76%); ii, $NH_2OH{\cdot}HCl$, $NaHCO_3$, MeOH–H_2O, rt, 20h (44–47% **8**, 3–8% **9**).

DOI: 10.1039/b005984f

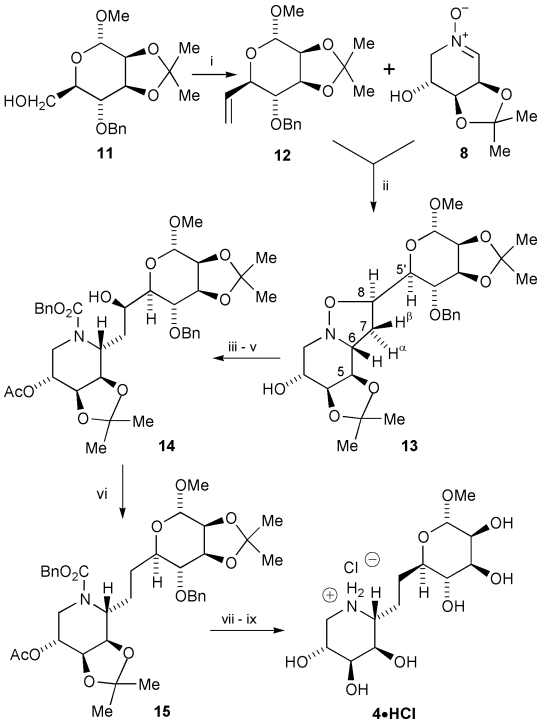

Scheme 2 *Reagents and conditions*: i, PCC, DCM, then $Ph_3PMe{\cdot}Br$, KHMDS, −78 °C to rt; ii, toluene, reflux (84%); iii, Ac_2O, DMAP, pyridine; iv, $Mo(CO)_6$, MeCN–H_2O, reflux; v, BnOCOCl, Na_2CO_3, acetone (67% from **13**); vi, excess $(Im)_2C{=}S$, $(CH_2Cl)_2$, reflux, 2 h, then Bu_3SnH, AIBN, toluene, reflux (81% from **14**); vii, NaOMe, MeOH; viii, H_2, Degussa Pd/C, MeOH; ix, HCl, MeOH (80% from **15**).

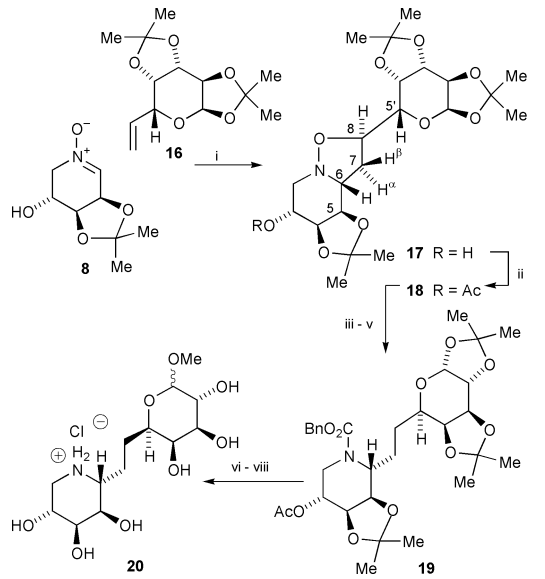

Scheme 3 *Reagents and conditions*: i, toluene, reflux (88%); ii, Ac_2O, DMAP, pyridine (82%); iii, $Mo(CO)_6$, MeCN–H_2O, reflux; iv, BnOCOCl, Na_2CO_3, acetone; v, excess $(Im)_2C{=}S$, $(CH_2Cl)_2$, reflux, then Bu_3SnH, AIBN, toluene, reflux; vi, NaOMe, MeOH, rt, 1.5 h; vii, H_2, Pd/C, MeOH; viii, HCl, MeOH, rt, 24h (48% overall from **18**).

6-H and 7β-H, between 7α-H and both 5-H and 8-H, and between 5′-H and both 6-H and 7β-H; these last interactions, and the observed value of 7.4 Hz for $J_{5',8}$ imply a preferred rotamer about the C-8–C-5′ bond as indicated in **17** (for **13**, $J_{5',8}$ = 2.4 Hz). This, and the configuration of **17**, was confirmed by X-ray crystallography of the crystalline *O*-acetyl derivative **18**. Reduction of **18**, followed by *N*-protection and deoxygenation under conditions of high concentration, gave **19**, deprotected as indicated in Scheme 3 to give the aza-*C*-disaccharide **20**, as an anomeric mixture (α:β, 5:2), in 48% overall yield from **18**.

We thank EPSRC for financial support (GR/K97301) and for access to facilities at the National Mass Spectrometry Service Centre, and Dr Georgina Rosair for X-ray crystallography.

Notes and references

† Selected data (*J* values in Hz): **8**: mp 162–164 °C; $[\alpha]_D$ +235.2 (*c* 1.05, $CHCl_3$); δ_H (400 MHz, $CDCl_3$) 1.39 (6H, s, C*Me*$_2$), 3.90 (1H, dd, J_{gem} 15.2, *J* 0.9, 6_a-H), 4.07 (1H, dd, J_{gem} 15.2, *J* 1.1, 6_b-H), 4.34 (1H, m, 4-H), 4.39 (1H, m, 5-H), 4.87 (1H, dd, *J* 5.1, 3.8, 3-H), 7.12 (1H, t, *J* 2.9, 2-H); **4·HCl**: $[\alpha]_D$ +52.2 (*c* 0.67, MeOH); δ_H (400 MHz, CD_3OD) 1.74–1.82 (1H, m, 6_a-H), 1.89–2.13 (3H, m, 6_b-H and 7-H_2), 3.06 (1H, dd, J_{gem} 12.8, $J_{12a,11}$ 2.4, 12_a-H), 3.26 (1H, br ddd, *J* ~ 10, ~ 8, 2.9, 8-H), 3.31 (1H, dd, J_{gem} 12.8, $J_{12b,11}$ 1.8, 12_b-H), 3.36 (3H, s, OMe), 3.44–3.54 (2H, m, 4-H, 5-H), 3.64 (1H, dd, $J_{3,4}$ 9.1, $J_{3,2}$ 3.2, 3-H), 3.80 (1H, dd, $J_{2,3}$ 3.2, *J* 1.8, 2-H), 3.86–3.93 (2H, m, 9-H, 10-H), 4.00 (1H, m, 11-H), 4.62 (1H, d, $J_{1,2}$ 1.8, 1-H). **17**: $[\alpha]_D$ −53.5 (*c* 0.99, $CHCl_3$); δ_H [400 MHz, $(CDCl_2)_2$, 120 °C] 2.10 (1H, dt, J_{gem} 12.6, $J_{7\alpha,6}$ ~ $J_{7\alpha,8}$ ~ 9.0, 7α-H), 2.20 (1H, br s, OH), 2.45 (1H, ddd, J_{gem} 12.6, $J_{7\beta,6}$ 7.0, $J_{7\beta,8}$ 3.8, 7β-H), 2.93–3.00 (1H, m, H-6), 2.96 (1H, dd, J_{gem} 11.0, $J_{2\beta,3}$ 3.5, 2β-H), 3.03 (1H, dd, J_{gem} 11.0, $J_{2\alpha,3}$ 6.0, 2α-H), 3.57 (1H, dd, $J_{5',8}$ 7.4, $J_{5',4'}$ 1.75, 5′-H), 3.92 (1H, br q, *J* ~ 4.4, 3-H), 4.00 (1H, t, *J* ~ 5.0, 4-H), 4.15 (1H, t, *J* ~ 5.7, 5-H), 4.17 (1H, dd, $J_{2',1'}$ 4.95, $J_{2',3'}$ 2.3, 2′-H), 4.20 (1H, dd, $J_{4',3'}$ 7.9, $J_{4',5'}$ 1.8, 4′-H), 4.22 (1H, ddd, $J_{8,7\alpha}$ 8.65, $J_{8,5'}$ 7.5, $J_{8,7\beta}$ 3.8, 8-H), 4.48 (1H, dd, $J_{3',4'}$ 7.9, $J_{3',2'}$ 2.3, 3′-H), 5.38 (1H, d, $J_{1',2'}$ 4.95, 1′-H).

‡ It is possible that the cyclisations of **A** and/or **B** occur through the intermediacy of geminal bis(hydroxylamine)s (see ref. 13). In a similar cyclisation to form a stereoisomer of **8**, we have also isolated and fully characterised an *N*-hydroxy-2-hydroxylaminopiperidine as a byproduct (V. Vivien, unpublished results).

§ *endo*-Transition states are disfavoured for cyclic nitrones on steric grounds; see, *e.g.* J. J. Tufariello in *1,3-Dipolar Cycloaddition Reactions*, Vol 2, ed. A. Padwa, Academic Press, New York, 1983, p. 83.

¶ CCDC 182/1789. See http://www.rsc.org/suppdata/cc/b0/b005984f/ for crystallographic files in .cif format.

1 *Iminosugars as Glycosidase Inhibitors: Nojirimycin and Beyond*, ed. A. E. Stütz, Wiley–VCH, Weinheim, 1999.
2 *e.g.* A. Karpas, G. W. J. Fleet, R. A. Dwek, S. Petursson, S. K. Namgoong, N. G. Ramsden, G. S. Jacob and T. W. Rademacher, *Proc. Natl. Acad. Sci. USA*, 1988, **85**, 9229.
3 G. D. Dimitriadis, P. Tessari, V. L. W. Go and J. E. Gerich, *Metabolism*, 1985, **34**, 261.
4 M. J. Humphries, K. Matsumoto, S. L. White and K. Olden, *Cancer Res.*, 1986, **46**, 5215; P. E. Goss, M. A. Baker, J. P. Carver and J. W. Dennis, *Clin. Cancer Res.*, 1995, **1**, 935.
5 *e.g.* G. Legler, in *Carbohydrate Mimics*, ed. Y. Chapleur, Wiley–VCH, Weinheim, 1998, p. 463.
6 *e.g.* (*a*) P. B. Anzeveno, L. J. Creemer, J. K. Daniel, C.-H. R. King and P. S. Liu, *J. Org. Chem.*, 1989, **54**, 2539; (*b*) M. Horsch, L. Hoesch, A. Vasella and D. M. Rast, *Eur. J. Biochem.*, 1991, **197**, 815; (*c*) W. Dong, T. Jespersen, M. Bols, T. Skrydstrup and M. R. Sierks, *Biochemistry*, 1996, **35**, 2788.
7 L. Sun, P. Li, N. Amankulor, W. Tang, D. W. Landry and K. Zhao, *J. Org. Chem.*, 1998, **63**, 6472.
8 (*a*) B. A. Johns, Y. T. Pan, A. D. Elbein and C. R. Johnson, *J. Am. Chem. Soc.*, 1997, **119**, 4856; (*b*) C. R. Johnson and B. A. Johns, *Tetrahedron Lett.*, 1997, **38**, 7977; (*c*) J. L. Asensio, F. J. Cañada, A. García-Herrero, M. T. Murillo, A. Fernández-Mayoralas, B. A. Johns, J. Kozak, Z. Zhu, C. R. Johnson and J. Jiménez-Barbero, *J. Am. Chem. Soc.*, 1999, **121**, 11 318.
9 M. A. Leewenburgh, S. Picasso, H. S. Overkleeft, G. A. van der Marel, P. Vogel and J. H. van Boom, *Eur. J. Org. Chem.*, 1999, 1185.
10 For a review, see: K. W. Moremen, R. B. Trimble and A. Herscovics, *Glycobiology*, 1994, **4**, 113.
11 For the synthesis by a different approach of another aza-*C*-disaccharide involving the same iminoalditol see: C. Marquis, S. Picasso and P. Vogel, *Synthesis*, 1999, 1441.
12 M. Morita, E. Sawa, K. Yamaji, T. Sakai, T. Natori, Y. Kuezuka, H. Fukushima and K. Akimoto, *Biosci. Biotech. Biochem.*, 1996, **60**, 288.
13 For a similar cyclisation to give a nitrone related to L-fucose, see A. Peer and A. Vasella, *Helv. Chim. Acta*, 1999, **82**, 1044.
14 M. Ito, M. Maeda and C. Kibayashi, *Tetrahedron Lett.*, 1992, **33**, 3765, and references therein.
15 S. Cicchi, A. Goti, A. Brandi, A. Guarna and F. De Sarlo, *Tetrahedron Lett.*, 1990, **31**, 3351.
16 O. Jarreton, T. Skrydstrup, J.-F. Espinosa, J. Jiménez-Barbero and J.-M. Beau, *Chem. Eur. J.*, 1999, **5**, 430.
17 A. J. Blake, R. O. Gould, R. M. Paton and A. A. Young, *J. Chem. Res.*, 1993, (*S*) 482, (*M*) 3173, and refs. therein.

The synthesis and structure of a new oxide fluoride, $LaSrMnO_4F$, with staged fluorine insertion

L. D. Aikens, R. K. Li and C. Greaves*

School of Chemistry, University of Birmingham, Birmingham, UK B15 2TT. E-mail: c.greaves@bham.ac.uk

Received (in Cambridge, UK) 30th August 2000, Accepted 21st September 2000
First published as an Advance Article on the web 13th October 2000

$LaSrMnO_4F$ has been synthesised and shown to have a staged structure in which the insertion of F atoms into the parent $LaSrMnO_4$ structure has occurred only in alternate (La,Sr)O rocksalt blocks.

In recent years the synthesis of materials which are superconducting or exhibit high magnetoresistance behaviour has been the focus of much attention from solid state chemists. Interestingly, although the detailed mechanistic principles for both classes of materials remain incomplete, the structural and electronic requirements are sufficiently clear to allow the design and synthesis of new materials. The two-dimensional structural features and mixed valence (generally Cu^{2+}/Cu^{3+}) observed in high temperature superconductors are now well known, and similar criteria appear to be important for some oxides which show high magnetoresistance at fairly low magnetic fields. The importance of such materials was illustrated in the $n = 2$ Ruddlesden–Popper phase $La_{1.2}Sr_{1.8}Mn_2O_7$,[1] which contains Mn^{3+}/Mn^{4+} and double layers of MnO_6 octahedra linked through corners. We have previously shown that for both superconductors and layered manganese oxides, low temperature fluorine insertion reactions provide not only the means for achieving controlled increases in cation oxidation states (associated with reduction of F atoms to F^- ions), but also new low dimensional oxide–fluoride structures. This is exemplified by the reactions of F_2 gas with Sr_2CuO_3 or $La_{1.2}Sr_{1.8}Mn_2O_7$ to form, respectively, superconducting $Sr_2CuO_2F_{2.3}$ and ferromagnetic $La_{1.2}Sr_{1.8}Mn_2O_7F_2$.[2,3] In both reactions, fluorine inserts between two adjacent AO rocksalt layers (these rocksalt 'bilayers' exist in both precursor oxides, with A = Sr for the former compound and A = Sr/La for the latter). The insertions cause increases in transition metal oxidation states, from Cu^{2+} to $Cu^{2.3+}$ and $Mn^{3.4+}$ to $Mn^{4.4+}$.

Here, we report the structure and basic magnetic properties of a new phase, $LaSrMnO_4F$, in which fluorine is inserted between *alternate* rocksalt bilayers. This is an example of a staged insertion reaction for which the product contains layers with fully occupied interstitial sites, regularly spaced between completely empty layers, rather than a random distribution of inserted species in all layers. Although staging occurs for the intercalation of alkali metal and halogen atoms into graphite,[4] and has also been reported for other layered materials, *e.g.* Ag_xTiS_2,[5] we believe $LaSrMnO_4F$ provides the first example relating to fluorine insertion in oxides. Synthetically the observation could be significant, especially for magnetic systems such as manganese oxides. For example, the successful synthesis of a series of staged manganese oxide–fluorides with different fluorine contents would produce materials with not only a gradual change in Mn oxidation state, but also a gradation of magnetic exchange interactions perpendicular to the 'MnO_2' layers.

The precursor oxide $LaSrMnO_4$ was prepared as described in previous reports,[6,7] and fluorination was achieved by exposing the sample to a $10\%F_2/90\%N_2$ gas mixture for 2 h at 200 °C. Chemical analysis of the fluorinated phase (mass change on fluorination, Mn oxidation state *via* titrimetry and F content *via* thermogravimetric decomposition in $10\%H_2/90\%N_2$) suggested the approximate composition $LaSrMnO_4F_{1.7}$, which is indicative of incomplete filling of the interstitial sites between the rocksalt layers, since full occupancy would correspond to $LaSrMnO_4F_2$. In order to prepare $LaSrMnO_4F$, the original fluorinated sample was mixed with an appropriate amount of the precursor oxide (mole ratio 1.2 : 0.8) followed by heating the mixture in air at 300 °C for 12 h. Iodometric titration indicated a manganese oxidation state of 3.93(3)+, in satisfactory agreement with the value of 4.0 expected for stoichiometric $LaSrMnO_4F$. Thermogravimetric analysis (to 600 °C, $10\%H_2/90\%N_2$) revealed a 3.5% weight loss during decomposition to give a multi-phase product consisting of SrF_2, $La_{2-x}Sr_xMnO_4$ and MnO according to X-ray powder diffraction (XRPD) analysis. The weight loss is sensitive to the F content and agrees well with that expected (3.3%) for 1 mol of $LaSrMnO_4F$ producing $\frac{1}{2}SrF_2 + \frac{3}{4}La_{1.333}Sr_{0.667}MnO_4 + \frac{1}{4}MnO$. In addition, phase analysis of the product using Rietveld refinement procedures[8] indicated a $SrF_2 : La_{1-x}Sr_xMnO_4$ ratio of 0.72, slightly higher than the 0.67 ratio expected for $LaSrMnO_4F$. The analytical data support a composition close to stoichiometric $LaSrMnO_4F$, although a small amount of F substitution at O sites may have occurred ($LaSrMnO_{3.93}F_{1.07}$ would correspond to $Mn^{3.93+}$ and produce a $SrF_2 : La_{1-x}Sr_xMnO_4$ ratio of 0.73).

In order to obtain an insight into the structural characteristics of $LaSrMnO_4F$, XRPD data were collected (Siemens D5000, primary Ge monochromator, PSD). It was clear that a fairly close structural relationship existed between $LaSrMnO_4F$ and its parent oxide $LaSrMnO_4$, and the pattern was satisfactorily indexed on a tetragonal unit cell (*P*4/*nmm*, $a = 3.7749(1)$ Å, $c = 14.1049(3)$ Å). Fluorination results in a symmetry reduction and a significant expansion of *ca.* 7.3% along *c* compared to the precursor oxide $LaSrMnO_4$ (*I*4/*mmm*, $a = 3.7952(1)$ Å, $c = 13.1410(9)$ Å). Structure refinement, using the program FULLPROF[8] was performed. Several structural models were examined including those with F atoms statistically occupying interstitial sites between all the (La/Sr)O rocksalt layers and those where occupancy is confined to alternate layers only. Only the latter model provided a basis to achieve satisfactory agreement between the calculated and experimental XRPD patterns. The F^- ions are located in the ideal interstitial positions between one of the two (La/Sr)O bilayers in the unit cell, and are tetrahedrally coordinated to 4 La/Sr sites. The fitted profile is shown in Fig. 1 and Table 1 gives the refined atomic coordinates and selected interatomic bond distances. In the refinement, all sites occupied by a given ion were constrained to have equal thermal parameters. The refined structure (Fig. 2) clearly displays the staged arrangement of guest F^- ions within the $LaSrMnO_4$ host structural framework. Although O and F atoms cannot be differentiated by XRPD, the anion assignments in Table 1, which restrict F to only one of the two interstitial positions, are supported by Madelung energy calculations.[9] This analysis, based purely on electrostatic arguments, indicates that the Madelung energy for the proposed anion distribution (24 110 kJ mol^{-1}) is the highest of all possible arrangements; the next highest (22 880 kJ mol^{-1}) corresponds to F occupying the neighbouring O2 apical site. Bond valence sum calculations[10] for the Mn–O bonds using r_o for Mn(IV) yields a value of 4.2 at the Mn site indicating that the Mn coordination is consistent with Mn^{4+}. The structure refinement clearly indicates that fluorine insertion has occurred between alternate rocksalt layers only. As a result, two quite different Mn–O apical bonds

DOI: 10.1039/b007045i

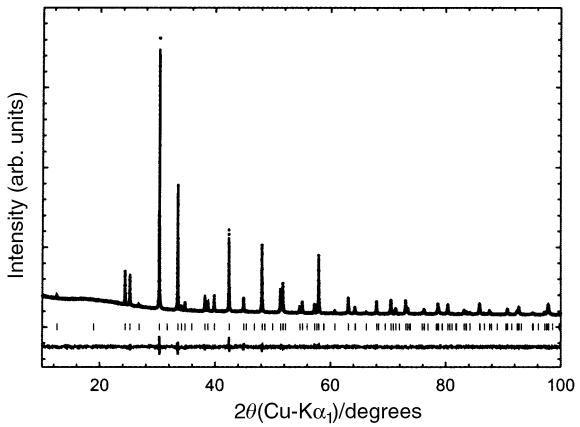

Fig. 1 Rietveld structure refinement based on XRPD data: solid curves calculated and difference profiles; dots, observed profile; vertical bars, reflection positions.

Table 1 Refined atomic coordinates and selected bond lengths for $LaSrMnO_4F$

Atom	*x/a*	*y/b*	*z/c*	*B*/Å²	Unit cell occupancy
La1/Sr1	0.75	0.75	0.1167(1)	0.431(3)	1.00/1.00
La2/Sr2	0.75	0.75	0.4020(1)	0.431(3)	1.00/1.00
Mn	0.25	0.25	0.2720(2)	0.30(8)	2.00
O1	0.25	0.75	0.2781(6)	0.8(1)	4.00
O2	0.25	0.25	0.1483(8)	0.8(1)	2.00
O3	0.25	0.25	0.4197(8)	0.8(1)	2.00
F	0.25	0.75	0.0	0.3(2)	2.00
	Bond lengths (Å):				
	Mn–O1 (×4)		1.889(1)	O2–F 2.817(8)	
	Mn–O2		1.745(12)		
	Mn–O3		2.083(12)		

*P*4/*mmm*; $a = 3.77486(8)$, $c = 14.1049(3)$; $R_{wp} = 2.53\%$. $R_{exp} = 1.4\%$, $\chi^2 = 2.97$.

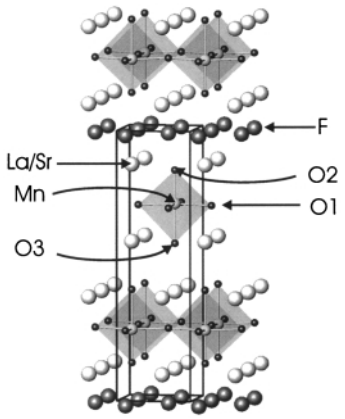

Fig. 2 Structure of $LaSrMnO_4F$ showing the unit cell.

are present (Table 1 and Fig. 2): Mn–O2 bonds, which point towards the F-containing layers, are significantly shorter than the *trans*-Mn–O3 bonds owing to the influence of F–O2 repulsions.

Studies of the magnetic properties of this material (Cryogenics S100 SQUID, Fig. 3) revealed paramagnetic behaviour

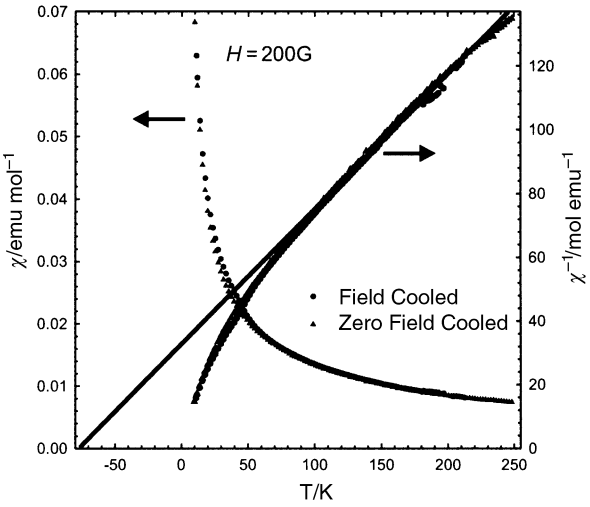

Fig. 3 Variation of magnetic susceptibility (χ) and χ^{-1} with temperature (T).

above 10 K. Above 95 K, application of the Curie–Weiss law [$\chi = C/(T - \theta)$], provides a negative value of the Curie–Weiss constant ($\theta = -80$ K), suggesting antiferromagnetic interactions are taking place. The effective moment, $\mu_{eff} = 4.3\ \mu_B$, estimated from the linear part of the $1/\chi$ *vs.* T plot (Fig. 3), is slightly higher than that expected for Mn^{4+} (spin-only moment $3.9\ \mu_B$), and is consistent with the presence of some Mn^{3+}. At temperatures below 95 K we see the appearance of a ferromagnetic component to the magnetic interactions. Further studies are required to establish whether these are intrinsic or extrinsic to the bulk $LaSrMnO_4F$ phase.

$LaSrMnO_4F$ has been synthesised and the most important structural characteristics determined by XRPD. For the first time, staged insertion of fluorine has been demonstrated such that only alternate rocksalt regions of the parent structure have been subject to intercalation. This is the first example of this type of fluorinated oxide and suggests that other staged products may be possible, not only for $n = 1$ Ruddlesden–Popper phases such as $LaSrMnO_4$ studied here, but for family members with higher n. Such possibilities are currently under investigation.

We thank EPSRC for financial support including the provision of a studentship to L. D. A.

Notes and references

1 Y. Moritomo, A. Asamitsu, H. Kuwahara and Y. Tokura, *Nature (London)*, 1996, **360**, 141.
2 M. Al-Mamouri, C. Greaves, P. P. Edwards and M. Slaski, *Nature (London)*, 1994, **369**, 382.
3 C. Greaves, J. L. Kissick, M. G. Francesconi, L. D. Aikens and L. J. Gillie, *J. Mater. Chem.*, 1999, **9**, 111.
4 A. F. Wells, *Structural Inorganic Chemistry*, 5th edn., Oxford University Press, 1987.
5 K. K. Bardham, G. Kirczenow, G. Jackle and J. C. Irwin, *Phys. Rev. B*, 1986, **33**, 4149.
6 A. Benabad, A. Daoudi, R. Salmon and G. Le Flem, *J. Solid State Chem.*, 1977, **22**, 121.
7 R. K. Li and C. Greaves, *J. Solid State Chem.*, 2000, **153**, 34.
8 J. Rodriguez-Carvajal, FULLPROF, version 3.2, based on the original code by D. B. Wiles and R. A. Young, *J. Appl. Crystallogr.*, 1981, **14**, 149.
9 J. W. Weenk and H. A. Harwig, *J. Phys. Chem. Solids*, 1977, **38**, 1047.
10 I. D. Brown and D. Altermatt, *Acta Crystallogr., Sect. B*, 1985, **41**, 244.

Synthesis by conjugate radical addition of new heterocyclic amino acids with nucleic acid bases in their side chains

Raymond C. F. Jones,*† Didier J. C. Berthelot and James N. Iley*

Department of Chemistry, The Open University, Walton Hall, Milton Keynes, UK MK7 6AA

Received (in Cambridge, UK) 21st August 2000, Accepted 20th September 2000
First published as an Advance Article on the web 13th October 2000

_N_-(2-Iodoethyl) and _N_-(3-iodopropyl)pyrimidines and purines undergo stereoselective conjugate radical addition with an optically active oxazolidinone acceptor to give _syn_-adducts that can be converted into pyrimidine and purine amino acids.

Peptide-based nucleic acid analogues (PNAs) have attracted much attention as molecules with the potential to interact with nucleic acid chains.[1] Suggested applications include antisense properties.[2] Nielsen's PNA has been shown to form duplexes with the complementary DNAs.[1] DNA recognition using analogues with a 'real' peptide backbone has, however, proved more elusive. Substituted alanine oligomers **1** (B = pyrimidine or purine base) and homologues **2** (termed α-PNA[3]) do not demonstrate hybridisation with DNA and insufficient flexibility of the polypeptide chain has been suggested as the cause,[4] whereas triplex formation between tetrapeptides of type **2** and poly(dT) or poly(dU) has been reported.[5] Our interest in unusual amino acids led us to propose the homologous amino acids **4** carrying the nucleic acid bases with a 3- or 4-methylene tether to the peptide backbone, as components for PNA variant **3**. Residues **4** are also analogues of natural pyrimidine and purine amino acids.[6] We report here our flexible methodology based on stereospecific radical chemistry.[7]

In contrast to published routes to residues with C_2 tethers,[3,5,8] we determined to link preformed heterocycles with the peptide backbone by forming a *carbon–carbon* bond in the tether, and proposed to generate the C(β)–C(γ) bond by conjugate radical addition to chiral acceptor **7** (Scheme 1).[9] The (*S*)-acceptor **8** was prepared from *S*-methyl-(*R*)-cysteine (Scheme 2) by adaptation of a published sequence to the *N*-benzoyl analogue.[10] *syn*-Sulfone **7** was formed as a 10:1 mixture with its *anti*-diastereoisomer **6** [57% overall from *S*-methyl-(*R*)-cysteine] and easily separated by column chromatography.[10] The *syn*-configuration was supported *inter alia* by mutual NOE enhancements between C-2(H) and C-4(H). Base treatment afforded (*S*)-oxazolidinone **8** as a crystalline solid.

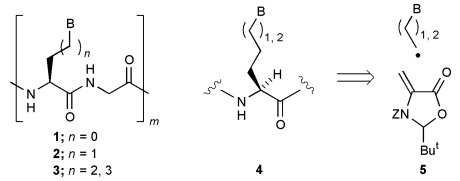

Scheme 1

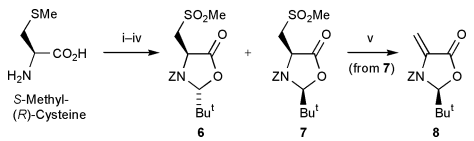

Scheme 2 *Reagents*: i, NaOH aq.; Bu^{t}CHO, Dean-Stark; iii, $PhCH_2OCOCl$ (ZCl); iv, oxone®, MeCN–H_2O; v, DBU.

† Current address: Department of Chemistry, Loughborough University, Leicestershire, UK LE11 3TU; e-mail r.c.f.jones@lboro.ac.uk

The radical precursors were haloalkyl pyrimidines and purines, prepared from the appropriately protected heterocyclic base and an ω-haloalcohol.[11] Thus 3-benzoylthymine **9**[12] was coupled with 2-bromoethanol or 3-bromopropanol (DIAD, Ph_3P) to afford the 1-(ω-bromoalkyl) derivatives **10a,b**, respectively (Scheme 3). Attempts to generate radicals from these bromides proved fruitless, so they were converted directly to the iodoalkyl compounds **10c,d**, respectively (NaI, propanone reflux; 85, 87% from **9**).

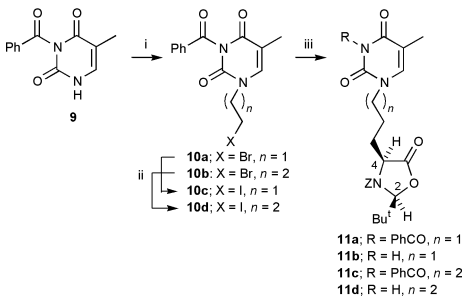

Scheme 3 *Reagents*: i, $HO(CH_2)_{n+1}Br$, $Pr^iO_2CN{=}NCO_2Pr^i$, Ph_3P; ii, NaI, Me_2CO reflux; iii, Method A: **10** (1 mol equiv.), Bu_3SnH (1 mol equiv.), AIBN (0.1 mol equiv.), toluene reflux; Method b: **8** (2 mol equiv.), Bu_3SnCl (0.3 mol equiv.), $NaBH_3CN$ (2 mol equiv.), AIBN (0.1 mol equiv.).

Iodide **10c** was treated under two protocols differing in the method for radical generation;[9] method A: with oxazolidinone **8** (1 mol equiv.) in toluene at reflux containing AIBN (0.1 mol equiv.) and dropwise addition of Bu_3SnH (1 mol equiv.); or method B: with oxazolidinone **8** (2 mol equiv.), Bu_3SnCl (0.3 mol equiv.), $NaBH_3CN$ (2 mol equiv.) and AIBN (0.1 mol equiv.) in *tert*-BuOH at reflux. Method A afforded the conjugate addition product **11a** (26%) and reduction product **12a** (24%), whereas method B after 16 h afforded 54% of conjugate addition products consisting of the adduct **11a** (24%) and the 3-debenzoylated derivative **11b** (30%), with no reduced material. The extent of debenzoylation was time dependent; a reaction time of 40 h led to **11b** as the sole addition product (47%). This suggests the deacylation may be *via* hydride-mediated reduction of the out-of-plane benzoyl carbonyl group, a possibility supported by an observed decrease in debenzoylation when less $NaBH_3CN$ is used in method B, and that debenzoylation of **10** occurs in the presence of $NaBH_3CN$ alone.[13] When 1-iodopropylthymine derivative **10d** was treated under method B, adduct **11c** was not found and deacylated adduct **11d** was isolated (25%) along with reduction product **12b** (75%).

We elected to extend these standard protocols (method B preferred) to other pyrimidines and purines rather than optimise each conjugate addition. Thus 3-benzoyluracil **13**[12] was

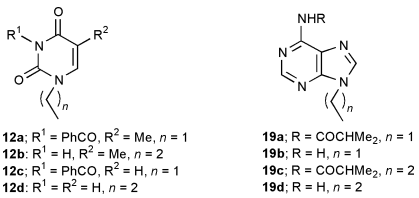

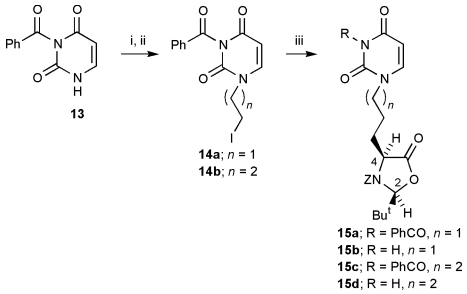

Scheme 4 *Reagents*: i, ii as Scheme 3; iii, Method B.

converted into the 1-(iodoalkyl) derivatives **14a,b** (Scheme 4). Method B applied to **14a** afforded addition product **15a** (41%) and reduction product **12c** (46%); when the reaction was left for 2 days, deacylated addition product **15b** (51%) was isolated. Homologue **14b** gave debenzoylated adduct **15d** (44%) with reduced material **12d** (51%).‡ In the purine series, the 9-(iodoalkyl)adenines **17a,b** were prepared from (2-methylpropionyl)adenine **16**[14] (Scheme 5). Using method B, iodoethyl compound **17a** led to the expected mixture of conjugate addition [40%; acylated **18a** (26%) and deacylated **18b** (14%)] and reduction [36%; acylated **19a** (17%) and deacylated **19b** (19%)]. Iodopropyl derivative **17b** likewise gave adducts [22%; acylated **18c** (12%) and deacylated **18d (**10%)] and reduced compounds [34%; acylated **19c** (11%) and deacylated **19d** (23%)]. Finally, a protected guanine **20a**[15] was converted into the 9-iodoethyl derivative **20b** (Scheme 6) and method A led to adduct **21** (21%) and reduction to **20c** (20%).

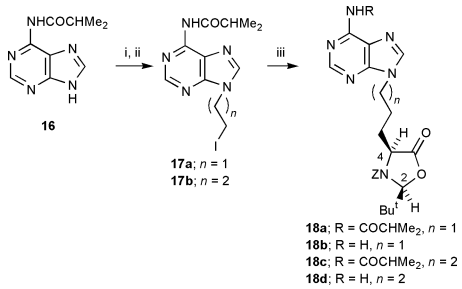

Scheme 5 *Reagents*: i, ii as Scheme 3; iii, Method B.

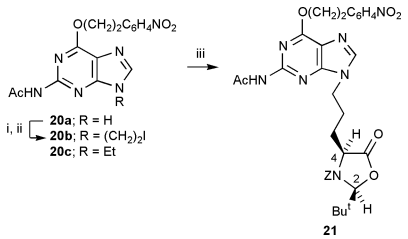

Scheme 6 *Reagents*: i, ii as Scheme 3; iii, Method A.

The illustrated conjugate radical addition products were all *syn*-adducts, as determined by NOE studies [enhancements between C-2(H) and C-4(H)]. Only one diastereoisomer was visible in the ^{1}H NMR spectra at 300 MHz. All of these *syn*-oxazolidinones could be easily and efficiently converted into *N*-benzyloxycarbonyl-(*S*)-amino acids (suitable for peptide coupling) by base hydrolysis (LiOH, aq. THF, 0 °C, 30–60 min; 70–98%). Thus the three thymine-substituted Z-amino acids **22a–c** (having 3- or 4-carbon tethers for the pyrimidine) were prepared from the adducts **11a**,**b**,**d**, respectively. The uracil Z-amino acids **22d–g** were likewise prepared from adducts **15a–d**, respectively, as were adenine derivatives **23a–d** (from **18a–d**, respectively) and guanine Z-amino acid **24a** (from **21**). To monitor optical purity, the Z group was removed by hydrogenolysis (Pd–C, EtOH–H_2O; 60–80%) to afford the amino

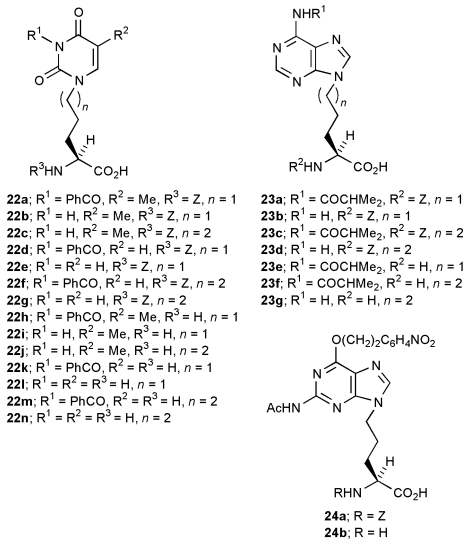

acids **22h–n**, **23e–g** and **24b**, analysed by esterification (AcCl, EtOH, reflux) and subsequent conversion to the Mosher amides (*R*-3,3,3-trifluoro-2-methoxy-2-phenylpropanoyl chloride, pyridine);[16] ^{19}F NMR spectroscopy revealed, *e.g.* 86–91% e.e. for the amino acids **22i**,**j**,**l**,**m**, and **23f**.

We have thus made available a range of novel pyrimidinyl and purinyl amino acids for application, for example, in PNA variants.

We thank the Open University for financial support (competitive studentship to D. J. C. B.) and the EPSRC National Mass Spectrometry Service Centre (Swansea) for some MS data.

Notes and references

‡ The yield of **15d** could be increased to 62% by using 5 mol equiv. of acceptor **8** in method B, but we more usually used 2 mol equiv. of this valuable optically active intermediate. When less than 2 mol equiv. $NaBH_3CN$ was used, some of the benzoylated adduct **15c** was isolated.

1 For recent reviews, see: B. Hyrup and P. E. Nielsen, *Bioorg. Med. Chem.*, 1996, **4**, 5; P. E. Nielsen and G. Haaima, *Chem. Soc. Rev.*, 1997, **26**, 73.
2 H. K. Larsen, T. Bentin and P. E. Nielsen, *Biochim. Biophys. Acta*, 1999, **1489**, 159.
3 N. M. Howarth and L. P. G. Wakelin, *J. Org. Chem.*, 1997, **62**, 5441.
4 See: M. Kuwahara, M. Arimitsu and M. Sisido, *Tetrahedron*, 1999, **55**, 10 067, and refs. therein.
5 T. Yamakazi, K. Komatsu, H. Umemiya, Y. Hashimoto, K. Shudo and H. Kagechika, *Tetrahedron Lett.*, 1997, **38**, 8363.
6 See, for example: R. M. Adlington, J. E. Baldwin, D. Catterick and G. J. Pritchard, *J. Chem. Soc., Perkin Trans. 1*, 1999, 855.
7 See: C. J. Easton, *Chem. Rev.*, 1997, **97**, 53, for a review of radical reactions in amino acid synthesis.
8 A. Lenzi, G. Reginato and M. Taddei, *Tetrahedron Lett.*, 1995, **36**, 1713.
9 J. R. Axon and A. L. J. Beckwith, *J. Chem. Soc., Chem. Commun.*, 1995, 549, and refs. therein.
10 S. G. Pyne, B. Dikic, P. A. Gordon, B. W. Skelton and A. H. White, *Aust. J. Chem.*, 1993, **46**, 73.
11 *Cf.* G. Cadet, C.-S. Chan, R. Y. Daniel, C. P. Davis, D. Guiadeen, G. Rodriguez, T. Thomas, S. Walcott and P. Scheiner, *J. Org. Chem.*, 1998, **63**, 4574.
12 K. A. Cruickshank, J. Jiricny and C. B. Reese, *Tetrahedron Lett.*, 1984, **25**, 681.
13 *Cf.* S. Kim, T. A. Lee and Y. Song, *Synlett*, 1998, 471, for radical addition to imides.
14 J. Zhou, K. Bouhadir, T. R. Webb and P. B. Shevlin, *Tetrahedron Lett.*, 1997, **38**, 4037.
15 J. Zhou, J.-Y. Tsai, K. Bouhadir and P. B. Shevlin, *Synth. Commun.*, 1999, **29**, 3003.
16 J. A. Dale, D. L. Dull and H. S. Mosher, *J. Org. Chem.*, 1969, **34**, 2543.

ChemComm

Conformationally stressed phthalocyanines: the non-planarity of the 1,4,8,11,15,18,22,25-octaisopentyl derivative

Isabelle Chambrier, Michael J. Cook* and Paul T. Wood

School of Chemical Sciences, University of East Anglia, Norwich, UK NR4 7TJ

Received (in Cambridge, UK) 25th August 2000, Accepted 21st September 2000
First published as an Advance Article on the web

An X-ray crystal structure determination reveals that 1,4,8,11,15,18,22,25-octaisopentylphthalocyanine adopts a saddle conformation, a geometry which shows modified spectroscopic properties and reduced photostability relative to planar ring structures.

Phthalocyanines (Pcs) are important commercial dyes and pigments[1] but their interesting photophysical and conducting properties[2] also render them suitable for a number of 'high-tech' applications. Examples are used as charge carriers in photocopiers, as dyes in laser/LED printing[3] and as laser light absorbers for optical data storage systems.[4] Others are promising candidates for exploitation in devices such as solar cells,[5] gas sensors[6] and optical limiters[7] and, in medicine, as singlet oxygen photosensitizers for photodynamic therapy (PDT)[8] and as a therapy for transmissible spongiform encephalopathies.[9] Such developments have benefited from the ease of tuning or modifying the properties of the ring system. Principal strategies involve ring substitution and incorporation of a metal ion or metalloid element at the centre of the ring. However, the effect of ring conformation on properties has not been adequately addressed, a situation in marked contrast with studies of ring distortion of the related porphyrin[10] and tetrabenzoporphyrin[11] systems. X-Ray structure determinations[12] show that **1** is essentially planar, allowing maximum delocalisation of the π electron system. Analogues of **1** metallated with first row transition metal ions are similar but larger metal ions, *e.g.* Pb and Sn, distort the geometry.[12] The present paper is concerned with the use of substituents alone to distort ring geometry through conformational stress. Previous X-ray studies on substituted Pcs, though few,[12] include those for two non-peripherally substituted metal-free derivatives, **2**[13] and **3**.[14] The macrocyclic cores show some limited distortion from planarity, *vide infra*, but potential conformational stress involving substituents is largely relieved through the location of some of them orthogonal to the ring. Here we report results for **4**,[15] an octaalkyl derivative in which the point of branching of the chain is one bond closer to the core than in **3**. The greater steric congestion leads to a saddle shaped conformation of the ring without precedent in the published literature on non-metallated Pc derivatives.[16] Solution phase spectroscopic properties and photostability of **4** are compared with those of **2** and the straight chain isomer of **4**, *viz.*, **5**.

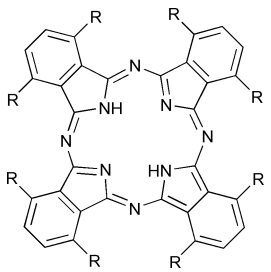

1 R = H
2 R = $(CH_2)_5CH_3$
3 R = $O(CH_2)_2CH(CH_3)_2$
4 R = $(CH_2)_2CH(CH_3)_2$
5 R = $(CH_2)_4CH_3$

DSC analysis of **4**, recrystallised from THF–MeOH, indicated there is a crystal to crystal transition at 263 K. The X-ray crystal structure of **4**† at rt shows that the compound crystallises in the centrosymmetric space group *C*2/*c*. The asymmetric unit consists of half a molecule with the other half being generated by a 2-fold rotation axis. However, there is disorder in the positions of some of the atoms in the alkyl chains and evidence of considerable thermal motion. An attempt to model the disorder better by determining the crystal structure at low temperature was thwarted by the structural phase transition at 263 K. On approaching this temperature the crystal began to lose integrity as shown by smearing out of the diffraction spots into arcs.

The rt data reveal unambiguously that the central core of the molecule deviates markedly from planarity forming a saddle shape, Fig. 1a and 1b. The dihedral angles between the pair of planes formed by the isoindole units on either side of the core are both 32.0°. The two crystallographically distinct five membered rings make angles at 18.0 and 11.3° with the mean plane generated by the four pyrrole type nitrogens. The calculated positions of the hydrogen atoms attached to nitrogen are therefore out of this plane. The molecules pack together to form stacks, Fig. 1b, which run along the crystallographic *c* axis. This involves a number of π-stacking interactions, the shortest of which is 3.686 Å. The ring conformation of **4** differs significantly from that adopted by **2**,[13] shown in Fig. 1c for comparison. Here isoindole units on opposite sides of the ring are located in parallel planes. The distances between one pair of planes is 0.3 Å, for the other it is 0.15 Å.

Table 1 includes spectroscopic data for **2**, **4** and **5**. Comparison of those for **2** and **4**, the two compounds for which crystal structure data are now available, shows there are clear differences. In particular, the visible region absorption bands, Q_x and Q_y, of **4** show a bathochromic shift and lowering of the extinction coefficient relative to those of **2.** This is consistent with the trend detected upon distortion from planarity of the 18 π electron system of porphyrins[10] and indicates that the non-planar structure of **4** persists in the solution phase.

^{1}H-NMR spectral data obtained from dilute solutions at 50 °C, conditions devised to limit aggregation, show that the N-*H* signal of **4** is to lower field than for **2**. This may point to differences in the degree of aggregation for the two compounds and/or indicate a weaker ring current in **4** attributable to the greater departure of the cyclic π electron system from planarity. ^{1}H-NMR spectra of **4** recorded down to −70 °C in THF-d_8 solution showed broadening and separation of two sets of signals for the benzylic protons. However, there is no coupling between them and we therefore assign the phenomenon to slowing of N–H tautomerism rather than slowing of conformational inversion of a saddle structure for the ring itself. The latter would render the CH_2 protons diastereotopic.

Spectral data for **5** are more similar to those of **2** than **4**. The Q-band extinction coefficient and shielding of the N–H protons is highest for **5** and offers an indication that the core of **5** may be the least distorted of all three compounds. The data highlight the potential for using spectroscopic parameters for assessing Pc ring conformation in the solution phase.

Phthalocyanines are known to undergo photooxidative cleavage, particularly in the solution phase, leading to phthalimide derivatives.[17] Though a potential problem for the use of these compounds in devices, photobleaching of Pc photosensitizers in PDT treatment may provide a means of facilitating their removal from patients. Photobleaching of **2**, **4** and **5** as solutions

DOI: 10.1039/b006935n

Table 1 Comparative spectroscopic and photodecomposition data for compounds **2**, **4** and **5**.

Solvent or medium	Parameter	Compound **2**	Compound **4**	Compound **5**
THF	λ_{max} Q$_x$ ($\varepsilon \times 10^{-5}$)[a]	728 nm (1.68)	731 nm (1.55)	728 nm (1.77)
THF	λ_{max} Q$_y$[a]	696 nm (1.47)	701 nm (1.34)	696 nm (1.54)
KBr disc	ν_{N-H}	3297 cm^{-1}	3302 cm^{-1}	3297 cm^{-1}
$CHCl_3$	ν_{N-H}	3308 cm^{-1}	3310 cm^{-1}	3308 cm^{-1}
10^{-3}M, C_6D_6	δ_{N-H} (50 °C)	−0.148 ppm	−0.052 ppm	−0.165 ppm
THF	rel. k $_{(photodecomp.)}$[b]	1.13	1.43	1.00

[a] ε values were obtained from the Beer–Lambert plots over the concentration range 5×10^{-7} to 5×10^{-5}M. The plots remained linear up to 1×10^{-4} M. [b] Relative pseudo first order rates of photodecomposition in aerated solutions of compounds upon irradiation using UV lamps, starting molarity 10^{-5} M.

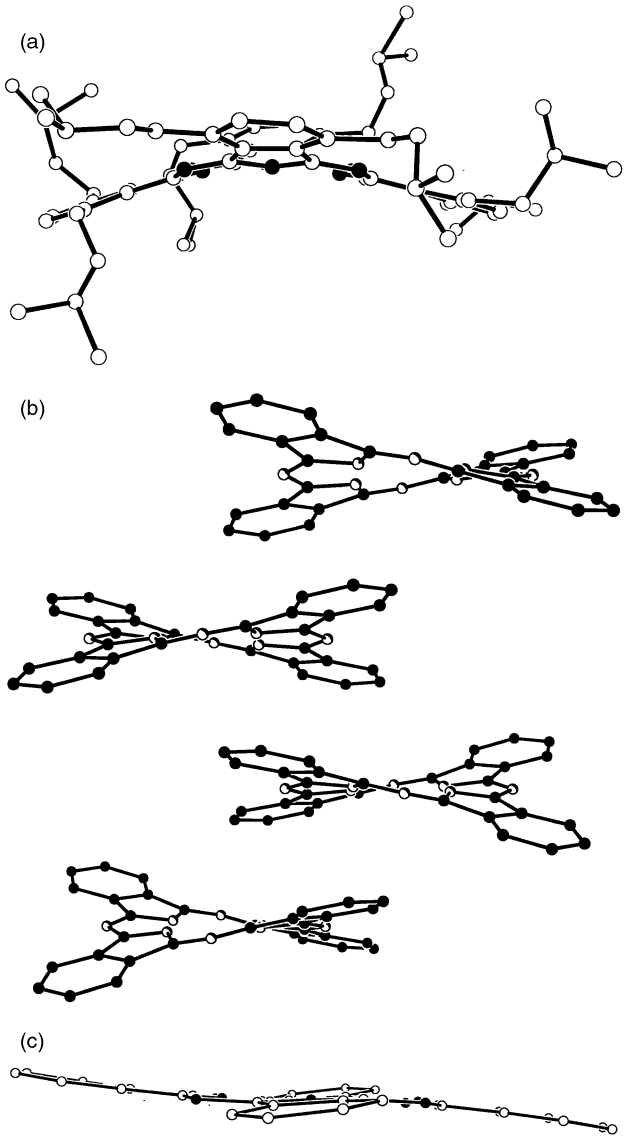

Fig. 1 (a) Representation of the molecular structure of 1,4,8,11,15,18,22,25-octaisopentylphthalocyanine, **4**. (b) The structure with the alkyl chains removed for clarity and illustrating the stacking of the molecules within a column. (c) A view of the ring conformation of compound **2**[13] with the hexyl groups removed.

in THF was monitored by the disappearance of the Q-band on UV irradiation (S.Y.L.V.A.N.I.A. Blacklight-blue, 8 W), (Table 1). The consumption of compound followed first order kinetics with the rate of photobleaching slowest for **5** and fastest for **4**. This is likely to be a further manifestation of the significant ring distortion of **4**.

In conclusion, the work demonstrates that the conformation of the Pc ring can be adjusted by judicious choice and location of substituents leading to a concomitant fine tuning of spectroscopic properties and photochemical stability.

This work was undertaken as a contribution to projects run under the auspices of CEC COST programme 514 and CEC RTN contract HPRN-CT-2000-00020.

Notes and references

† Crystal data for $C_{72}H_{98}N_8$: M = 1075.58, monoclinic, $C2/c$, a = 20.433(5), b = 33.873(4), c = 10.025(4) Å, β = 110.12(2)°, Z = 4, ρ_{calcd} = 1.097 Mg m^{-3}, 10287 reflections were collected of which 5349 were unique (R_{int} = 0.584), $2\theta_{max}$ = 51.02°, graphite-monochromated Mo-kα radiation (λ = 0.71073 Å). Data were collected using a Rigaku R-AXIS IIc area detector and corrected for Lorentz and polarisation factors but no absorption correction was applied (μ = 0.064 mm^{-1}). The structure was solved by direct methods (SHELXTL-PLUS) and refined using full-matrix least-squares on F^2 using SHELX-93 software. The hydrogen atoms associated with the ordered part of the molecule were placed on idealised positions and allowed to ride on their parent atoms, no hydrogens were placed on the disordered portion of the side chain. 384 parameters refined, $R1$ = 0.1073 for $F > 4\sigma(F)$, $wR2$ = 0.3911 for all data S = 0.939, maximum residual electron density (largest electron hole) 0.449 (−0.260) e Å^{-3}. CCDC 182/1786. See http://www.rsc.org/suppdata/cc/b0/b006935n/ for crystallographic files in .cif format.

1 F. H. Moser and A. L. Thomas, *The Phthalocyanines, Vol. 2 Manufacture and Applications*, CRC Press, Boca Raton, FL 1983.
2 *Phthalocyanines: Properties and Applications, Vols. 1-4*, ed. C. C. Leznoff and A. B. P. Lever, VCH Publishers, New York, 1989, 1993, 1996; N. B. McKeown, *Phthalocyanine Materials: Synthesis, Structure and Function*, Cambridge University Press, Cambridge, 1998.
3 P. Gregory, *J. Porphyrins Phthalocyanines*, 2000, **4**, 432.
4 D. Birkett, *Chem. Ind.*, 2000, 178.
5 H. Eichhorn, *J. Porphyrins Phthalocyanines*, 2000, **4**, 88.
6 J. D. Wright, *Prog. Surf. Sci.*, 1989, **31**, 1; A. W. Snow and W. R. Barger in *Phthalocyanines—Properties and Applications*, ed. C. C. Leznoff and A. B. P. Lever, VCH Publishers, New York, 1989, 341.
7 J. S. Shirk, R. G. S. Pong, S. R. Flom, H. Heckmann and M. Hanack, *J. Phys. Chem.*, 2000, **104**, 1438; G. de la Torre, P. Vázquez, F. Agulló-López and T. Torres, *J. Mater. Chem.*, 1998, **8**, 1671.
8 H. Hasrat and J. E. van Lier, *Chem. Rev.*, 1999, **99**, 2379.
9 S. A. Priola, A. Raines and W. S. Caughey, *Science*, 2000, **287**, 1503.
10 M. O. Senge, C. J. Medforth, T. P. Forsyth, D. A. Lee, M. M. Olmstead, W. Jentzen, R. K. Pandey, J. A. Shelnutt and K. M. Smith, *Inorg. Chem.*, 1997, **36**, 1149.
11 R.-J. Cheng, Y.-R. Chen, S. L. Wang and C. Y. Cheng, *Polyhedron*, 1993, **12**, 1353.
12 M. K. Engel, *Kawamura Rikagaku Kenkyusho Hokoku, (English)*, 1996, 11–54; *Chem. Abs.*, 1997, **127**, 313213.
13 I. Chambrier, M. J. Cook, M. Helliwell and A. K. Powell, *J. Chem. Soc., Chem. Commun.*, 1992, 444.
14 M. J. Cook, J. McMurdo and A. K. Powell, *J. Chem. Soc., Chem. Commun.*, 1993, 903.
15 N. B. McKeown, M. J. Cook and I. Chambrier, *J. Chem. Soc., Perkin Trans. 1*, 1990, 1169.
16 During the preparation of this paper, Dr N. B. McKeown, University of Manchester, UK, informed us of unpublished work on a hexadeca substituted Pc derivative which also adopts a saddle conformation.
17 A. K. Sobbi, D. Wöhrle and D. Schlettwein, *J. Chem. Soc., Perkin Trans. 2*, 1993, 481; M. J. Cook, I. Chambrier, S. J. Cracknell, D. A. Mayes and D. A. Russell, *Photochem. Photobiol.*, 1995, **62**, 542.

Zirconium complexes of a tacn-derived amido ligand and ring-opening to form a new diamido-amino pincer

Garth R. Giesbrecht, Alex Shafir and John Arnold*

Department of Chemistry, University of California, Berkeley, and the Chemical Sciences Division, Lawrence Berkeley National Laboratory, Berkeley, CA, 94720-1460. E-mail: arnold@socrates.berkeley.edu

Received (in Cambridge, UK) 13th July 2000, Accepted 19th September 2000
First published as an Advance Article on the web

The tribenzyl complex (Pr^i_2tacn)Zr(CH_2Ph)$_3$ eliminates toluene upon heating with concomitant ring-opening of the anionic ancillary macrocycle to yield [CH_2=CHNCH_2-CH_2N(Pr^i)CH_2CH_2NPr^i]Zr(CH_2Ph)$_2$; the latter features a new class of dianionic pincer ligand.

Non-metallocene complexes of Group IV metals have recently been the subject of renewed interest due to the realization that new ligand environments might result in novel patterns of reactivity.[1–3] For example, Group IV metal complexes bearing bi-[4–8] or tridentate[9–15] diamide ligands have attracted attention as potential alternatives to the classical homogeneous Ziegler–Natta polymerization catalysts that are mostly based on bis- or monocyclopentadienyl ligands. In contrast, tridentate mono-amide ligands have received scant attention, an exception being the tridentate, acyclic monoanion, [($Me_2NCH_2SiMe_2$)$_2$N]$^-$, for which Ti, Zr and Hf derivatives have been described.[16]

We[17] and others[18] recently described the use of the lithium salt of diisopropyltriazacyclonone as a synthon in the development of new constrained-geometry ligand systems.[17,18] By utilizing a ligand system in which the nitrogen donors are part of a macrocycle, we reasoned that metal complexes would necessarily bind the azamacrocycle facially, in closer analogy to cyclopentadienyl complexes. Here we report the use of this fragment as an anionic, tridentate diamino-amido ancillary ligand for the stabilization of zirconium complexes and the conversion of this ligand into a dianionic acyclic variant.

As shown in Scheme 1, {(Pr^i_2tacn)Li}$_2$ reacts with $ZrCl_4(THF)_2$ in THF to yield the mono-ligand complex, (Pr^i_2tacn)$ZrCl_3$ **1** as an analytically-pure pale yellow solid in low yield. Alternately, **1** can be synthesized *via* a two-step process in nearly 90% overall yield: reaction of (Pr^i_2tacn)H with Zr(NEt_2)$_4$ quantitatively generates (Pr^i_2tacn)Zr(NEt_2)$_3$ **2** as a yellow oil which is sufficiently clean to be used without further purification. The latter reacts smoothly with excess Me_3SiCl in hot toluene to give **1**, which precipitates in pure form. Compound **1** is soluble in methylene chloride and only sparingly soluble in solvents such as THF, diethyl ether or toluene.

(Pr^i_2tacn)H reacts with Zr(CH_2Ph)$_4$ in diethyl ether to form the tribenzyl species (Pr^i_2tacn)Zr(CH_2Ph)$_3$ **3** in good yield. Compound **3** may also be synthesized from the trichloride **1** and 3 equiv. of benzyl Grignard, although the former reaction is substantially cleaner. The ^{1}H NMR spectrum of **3** shows a doublet for the diastereotopic isopropyl resonances and the methylene protons of the triazacyclononane ring appear as broad singlets. Also, the two isopropyl methyl groups give rise to a single peak in the {^{1}H}^{13}C NMR spectrum (18.9 ppm) in contrast to the two distinct singlets observed for **1** (19.5 and 18.1 ppm). The six benzylic protons are equivalent on the NMR time scale, resulting in a singlet in the ^{1}H NMR spectrum (2.71 ppm) and a broad resonance in the {^{1}H}^{13}C NMR spectrum (76.1 ppm).

Compound **3** is monomeric in the solid-state (see Fig. 1)† with the triazacyclononane ring attached facially to the metal through all three nitrogen atoms. The zirconium center is best described as distorted octahedral, with the N–Zr–C_{trans} angles ranging from 152.06(8) to 159.46(7)°; additionally, the three C–Zr–C angles vary from 91.10(8) to 96.33(9)°. Two of the benzyl

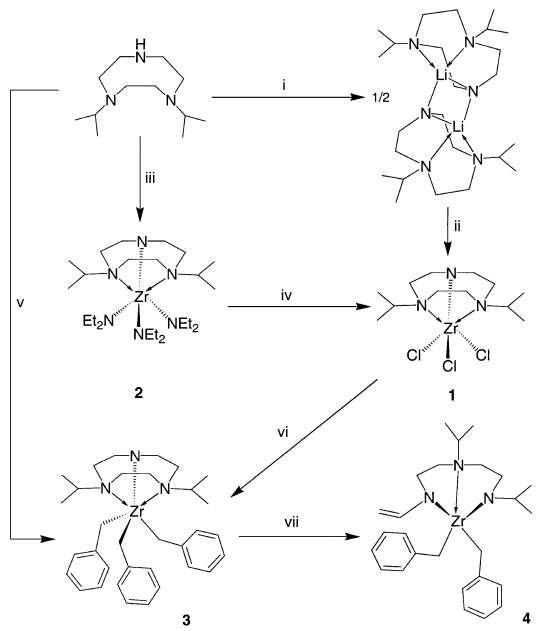

Scheme 1 i, BuLi, Et_2O, −78 °C; ii, $ZrCl_4(THF)_2$, THF, rt; iii, Zr(NEt_2)$_4$, Et_2O, −78 °C; iv, xs Me_3SiCl, toluene, 90 °C; v, Zr(CH_2Ph)$_4$, Et_2O, −78 °C; vi, 3 BzMgCl, Et_2O, −78 °C; vii, 90 °C, benzene, 24 h.

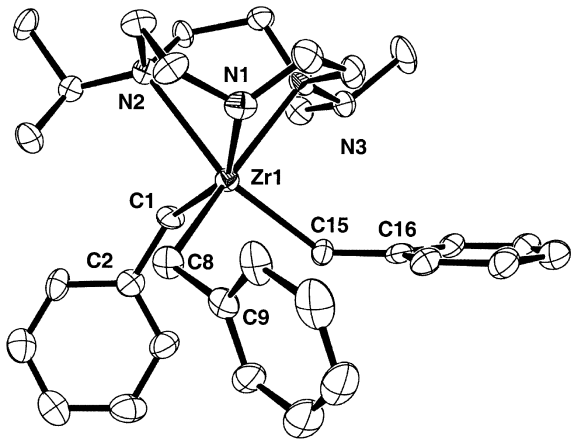

Fig. 1 ORTEP view of (Pr^i_2tacn)Zr(CH_2Ph)$_3$ **3** drawn with 50% probability ellipsoids. Selected bond distances (Å) and angles (°): Zr1–N1 2.073(2), Zr1–N2 2.604(2), Zr1–N3 2.479(2), Zr1–C1 2.347(2), Zr1–C8 2.326(2), Zr1–C15 2.303(2); N1–Zr1–N2 70.00(7), N1–Zr1–N3 73.04(7), N1–Zr1–C1 152.06(8), N1–Zr1–C8 88.12(8), N1–Zr1–C15 115.99(8), N2–Zr1–N3 73.01(6), N2–Zr1–C1 82.50(7), N2–Zr1–C8 108.67(8), N2–Zr1–C15 155.46(7), N3–Zr1–C1 104.15(8), N3–Zr1–C8 159.46(7), N3–Zr1–C15 85.79(7), C1–Zr1–C8 96.33(9), C1–Zr1–C15 91.10(8), C8–Zr1–C15 95.54(8), Zr1–C1–C2 116.3(2), Zr1–C8–C9 113.7(2), Zr1–C15–C16 133.5(2).

DOI: 10.1039/b005675h

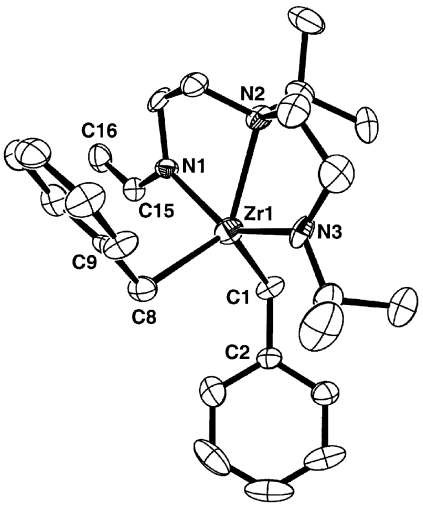

Fig. 2 ORTEP view of $[CH_2{=}CHNCH_2CH_2N(Pr^i)CH_2CH_2N\text{-}Pr^i]Zr(CH_2Ph)_2$ **4** drawn with 50% probability ellipsoids. Selected bond distances (Å) and angles (°): Zr1–N1 2.131(5), Zr1–N2 2.410(5), Zr1–N3 2.043(5), Zr1–C1 2.289(6), Zr1–C8 2.295(6), C15–C16 1.317(9); N1–Zr1–N2 71.3(2), N1–Zr1–N3 142.3(2), N1–Zr1–C1 100.5(2), N1–Zr1–C8 94.3(2), N2–Zr1–N3 71.5(4), N2–Zr1–C1 124.3(2), N2–Zr1–C8 125.1(2), N3–Zr1–C1 105.3(2), N3–Zr1–C8 101.9(2), C1–Zr1–C8 110.2(2), Zr1–C1–C8 114.7(2), Zr1–C8–C9 109.2(4).

ligands are positioned with their phenyl rings pointing downwards with respect to the tacn ring, while the third has its phenyl ring pointing upwards, being disposed almost parallel to the azamacrocycle. Two of the benzyl groups possess normal Zr–C–C bond angles (113.7(2) and 116.3(2)°) while the third displays an angle that is larger than expected (Zr1–C15–C16 = 133.5(2)°). The disposition of the benzyl groups is similar to that found for $Cp^*Ti(CH_2Ph)_3$, in which a single anomalous Ti–C–C angle is a consequence of a double agostic CH_2–Ti interaction.[19] Owing to the broadness of the peak arising from the benzylic methylene groups in the $\{^1H\}^{13}C$ NMR spectrum, we were unable to extract the C–H coupling constant to determine if any additional interaction was present in our case; it is likely that this unusually large angle is a result of packing forces in the crystal.

Heating $(Pr^i_2tacn)Zr(CH_2Ph)_3$ **3** for 24 h at 80 °C results in elimination of one equiv. of toluene and complete conversion to a new metal complex. The ^1H NMR spectrum reveals a total lack of symmetry in solution as evidenced by the presence of four isopropyl methyl doublets and separate multiplets for each of the methylene protons of the ligand backbone. Particularly diagnostic of this new species are resonances consistent with a vinyl group; a doublet of doublets corresponding to one olefinic proton is present at 7.92 ppm ($^3J_{H\text{-}H'}$ = 8.4, $^3J_{H\text{-}H''}$ = 14.8 Hz) with the other two protons of the vinyl unit giving rise to two doublets farther upfield (4.12 ppm, $^3J_{H\text{-}H'}$ = 8.4 Hz; 3.93 ppm, $^3J_{H\text{-}H''}$ = 14.8 Hz). These conclusions are supported by $\{^1H\}^{13}C$ NMR spectroscopy which shows four separate isopropyl methyl peaks, two isopropyl methine resonances and distinct peaks for four methylene groups of the ancillary ligand. ^{13}C DEPT experiments allowed the vinyl resonances to be assigned (143.1 and 79.0 ppm); the presence of a vinyl group is visible in the IR spectrum which shows a strong absorption in the olefinic region (*ca.* 1600 cm^{-1}).

To further investigate the structure of the thermolysis product, we turned to X-ray diffraction (Fig. 2).† The ORTEP of **4** shows that the zirconium center is coordinated by two benzyl groups and a new tacn-derived pincer ligand in which the original anionic, macrocyclic, diamino-amido ligand has been transformed into a dianionic, acyclic, diamido-amino moiety. Additionally, one of the ethylene units of the triazacyclononane ring has been converted into a vinyl group (C15–C16). The zirconium center is best described as distorted trigonal bipyramidal, with N1 and N3 occupying the axial sites (N1–Zr1–N3 = 142.3(2)°). Both amido nitrogens in **4** display trigonal planar geometries, with the sum of the three angles subtended by nitrogen approaching 360°. The metal center displays two short zirconium–nitrogen bonds (Zr1–N1 = 2.131(5), Zr1–N3 = 2.043(5) Å) and one longer bond (Zr1–N2 = 2.410(5) Å) consistent with a diamido-amino ligand. The benzyl groups are unremarkable (Zr–C–C_{benzyl} = 109.2(4), 114.7(4)°), although they are inequivalent by ^1H and ^{13}C NMR spectroscopy. This implies that the structure observed in the solid state is maintained in solution, and the benzyl groups are not averaged by some fluxional process as is observed for tribenzyl **3**.

In order to test the generality of this reaction, $(Pr^i_2tacn)ZrCl_3$ **1** was reacted with three equiv. of RLi (R = Me, CH_2SiMe_3, Ph). The NMR spectra of these products also indicate the formation of $[CH_2{=}CHNCH_2CH_2N(Pr^i)CH_2CH_2NPr^i]ZrR_2$ with the elimination of the corresponding alkane. A related ligand decomposition has been observed for the tantalum species $[N_3N]TaMe_2$ ($[N_3N] = [N(CH_2CH_2NSiR_3)_3]^{3-}$, R = Me[20], Et[21]). Thermolysis of the deuterated complex $(Pr^i_2\text{-}tacn)Zr(CD_2C_6D_5)_3$ affords C_7D_7H, ruling out α-hydrogen abstraction and a benzylidene intermediate. A more detailed study of the kinetics and mechanism of this ring-opening reaction will be reported shortly, along with other examples of the synthetic utility of $(Pr^i_2tacn^-)$.

This work was supported by the Department of Energy contract no. DE-AC03-76SF00098.

Notes and references

† *Crystal data*: for **3**: $C_{33}H_{47}N_3Zr$, M = 576.97, trigonal, a = 39.6517(3), b = 39.6517(3), c = 9.7469(1) Å, V = 13 271.5(2) Å^3, T = 173 K, space group R-3(h) (no. 148), Z = 18, μ(Mo-Kα) = 0.4 mm^{-1}, 20082 reflections measured, 5097 unique (R_{int} = 0.035), D_{calc} = 1.30 g cm^{-3}, R = 0.024, R_w = 0.028. For **4**: $C_{26}H_{39}N_3Zr$, M = 484.83, monoclinic, a = 8.881(5), b = 25.936(2), c = 11.7707(7) Å, β = 112.017(1)°, V = 2513.5(6) Å^3, T = 164 K, space group $P2_1/c$ (no. 14), Z = 4, μ(Mo-Kα) = 0.45 mm^{-1}, 11 204 reflections measured, 4314 unique (R_{int} = 0.082), D_{calc} = 1.28 g cm^{-3}, R = 0.043, R_w = 0.054. CCDC 182/1783. See http://www.rsc.org/suppdata/cc/b0/b005675h/ for crystallographic files in .cif format.

1 G. J. P. Britovsek, V. C. Gibson and D. F. Wass, *Angew. Chem., Int. Ed.*, 1999, **38**, 428.
2 R. Kempe, *Angew. Chem., Int. Ed.*, 2000, **39**, 468.
3 L. H. Gade, *Chem. Commun.*, 2000, 173.
4 J. D. Scollard, D. H. McConville and J. J. Vittal, *Organometallics*, 1995, **14**, 5478.
5 J. D. Scollard, D. H. McConville, N. C. Payne and J. J. Vittal, *Macromolecules*, 1996, **29**, 5241.
6 J. D. Scollard and D. H. McConville, *J. Am. Chem. Soc.*, 1996, **118**, 10 008.
7 F. G. N. Cloke, T. J. Geldbach, P. B. Hitchcock and J. B. Love, *J. Organomet. Chem.*, 1996, **506**, 343.
8 C. H. Lee, Y. H. La and J. W. Park, *Organometallics*, 2000, **19**, 344.
9 M. Aizenberg, L. Turculet, W. M. Davis, F. Schattenmann and R. R. Schrock, *Organometallics*, 1998, **17**, 4795.
10 R. Baumann, W. M. Davis and R. R. Schrock, *J. Am. Chem. Soc.*, 1997, **119**, 3830.
11 F. G. N. Cloke, P. B. Hitchcock and J. B. Love, *J. Chem. Soc., Dalton Trans.*, 1995, 25.
12 F. Guerin, D. H. McConville and J. J. Vittal, *Organometallics*, 1996, **15**, 5586.
13 F. Guerin, D. H. McConville and N. C. Payne, *Organometallics*, 1996, **15**, 5085.
14 F. Guerin, D. H. McConville, J. J. Vittal and G. A. P. Yap, *Organometallics*, 1998, **17**, 5172.
15 R. R. Schrock, F. Schattenmann, M. Aizenberg and W. M. Davis, *Chem. Commun.*, 1998, 199.
16 M. D. Fryzuk, V. Hoffmann, J. E. Kickham, S. J. Rettig and S. Gambarotta, *Inorg. Chem.*, 1997, **16**, 3480.
17 G. R. Giesbrecht, A. Gebauer, A. Shafir and J. Arnold, *J. Chem. Soc., Dalton Trans.*, 2000, in press.
18 B Qian, L. M. Henling and J. Peters, *Organometallics*, 2000, **19**, 2805.
19 M. Mena, M. A. Pellinghelli, P. Royo, R. Serrano and A. Tiripicchio, *J. Chem. Soc., Chem. Commun.*, 1986, 1118.
20 J. S. Freundlich, R. R. Schrock and W. M. Davis, *J. Am. Chem. Soc.*, 1996, **118**, 3643.
21 J. S. Freundlich, R. R. Schrock and W. M. Davis, *Organometallics*, 1996, **15**, 2777.

Hydride transfer reactions in dimolybdenum compounds: a simple route to the novel μ-η¹:η¹-tetrahydroboride complex $[Mo_2Cp_2(\mu\text{-}SMe)_3(\mu\text{-}BH_4)]$

Philippe Schollhammer,[a] Nolwenn Cabon,[a] François Y. Pétillon,*[a] Jean Talarmin[a] and Kenneth W. Muir*[b]

[a] *UMR CNRS 6521, Chimie, Electrochimie Moléculaires et Chimie Analytique, Faculté des Sciences, Université de Bretagne Occidentale, BP 809, 29285 Brest-Cedex, France. E-mail: francois.petillon@univ-brest.fr*
[b] *Chemistry Department, University of Glasgow, Glasgow, Scotland, UK G12 8QQ*

Received (in Cambridge, UK) 7th August 2000, Accepted 27th September 2000
First published as an Advance Article on the web

The reaction of $NaBH_4$ with the bis-nitrile compound $[Mo_2Cp_2(\mu\text{-}SMe)_3(MeCN)_2](BF_4)$ 1 unexpectedly gives rise to the rare, stable μ-(η¹-H):(η¹-H) tetrahydroborato complex $[Mo_2Cp_2(\mu\text{-}SMe)_3(\mu\text{-}BH_4)]$ 2, in addition to the expected azavinylidene product $[Mo_2Cp_2(\mu\text{-}SMe)_3(\mu\text{-}\eta^1\text{-}NCHMe)]$ 3.

The versatility shown by the tetrahydroborate anion in binding to transition metal ions is well known: it can bind *end-on* to a single metal atom through one, two or three hydrogen atoms [η¹-H, η²-H,H or η³-H,H,H modes] or *side-on via* an η²-B,H interaction.[1,2] The same variable hapticity is observed in metal clusters: BH_4^- can link two metal atoms through μ-(η³-H,H,H):(η³-H,H,H), μ-(η²-H,H):(η²-H,H), μ-(η¹-H):(η¹-H) or μ-(η²-H,H):(η¹-H) bridges.[2] Of these four bridge types only the $\{M_2(\mu\text{-}\eta^2\text{:}\eta^2\text{-}BH_4)\}$ core, which is a straightforward modification of the *end-on* η²-H,H mode of coordination, is relatively common. The $\{M_2(\mu\text{-}\eta^1\text{:}\eta^1\text{-}BH_4)\}$ bridge is particularly rare: we know only of single structurally characterized examples for three metals: Ir, Ru and Mn.[3–5] The three complexes involved each contain H^- as well as BH_4^- ligands and were obtained during studies of the synthesis and reactivity of polyhydride complexes in whose formation they are thought to be intermediate.[3,4]

We now report that $NaBH_4$ in acetonitrile reacts readily at room temperature with the bis-nitrile compound $[Mo_2Cp_2(\mu\text{-}SMe)_3(MeCN)_2](BF_4)$**1**[6] to afford a true μ-η¹-η¹-tetrahydroborate bridge in the novel, diamagnetic complex $[Mo_2Cp_2(\mu\text{-}SMe)_3(\mu\text{-}BH_4)]$ **2**, together with the azavinylidene product $[Mo_2Cp_2(\mu\text{-}SMe)_3(\mu\text{-}\eta^1\text{-}NCH(Me)]$ **3**. Formation of **2** involves substitution of the two acetonitrile ligands by BH_4^-, while the azavinylidene species **3** arises from the transfer of hydride to a coordinated acetonitrile (Scheme 1). Complexes **2** and **3** were obtained in different ratios which depend upon the solvent: **2**:**3** = 80:20 in MeCN but 20:80 in THF. They were separated by chromatography on a silica gel column using hexane–dichloromethane as eluent. Recrystallisation of **2** and **3** from diethyl ether afforded orange crystals.† **2** and **3** have been fully characterized by NMR and IR spectroscopy, microanalysis, and single crystal X-ray analysis.‡§

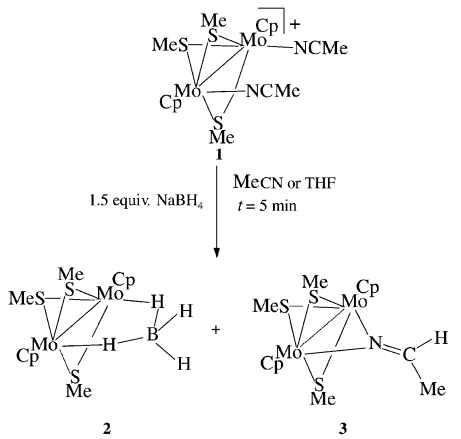

Scheme 1

The IR and $^{11}B\{^1H\}$ NMR spectra both revealed the presence of coordinated borohydride in **2**. In the $^{11}B\{^1H\}$ NMR spectrum a single broad resonance at δ −27.0 confirmed these assignments. The ^1H NMR spectrum displayed a broad high-field resonance at δ −15.79 (in $CDCl_3$) assignable to two equivalent Mo–H–B bridges. The detection of the two terminal hydrogens bound to the boron atom, at δ 2.32 and 1.28, required the recording of a ^1H spectrum with selective ^{11}B decoupling. The results of 2D ^1H–^1H and ^1H–^{11}B correlation NMR experiments are in accord with these assignments. A ^{11}B-decoupled ^1H–^1H 2D-experiment showed the two resonances at δ 2.32 and 1.28, to be coupled to each other and also to the peak at δ −15.79 (in toluene-d_8), and a ^1H–^{11}B inverse-correlation experiment confirmed that these protons are bound to the boron atom. The well resolved $^2J_{HH}$ couplings (*ca.* 18, 3 and 3 Hz) suggested significant deviations from regular tetrahedral coordination at the boron atom. Moreover, the observation of these couplings at room temperature and further variable temperature NMR experiments between 293 and 363 K implies that the commonly observed interchange of bridging and terminal hydrogens in BH_4 does not occur in **2** in this temperature range. The structure of **2** (Fig. 1)§ involves covalent interaction of the $\{Mo_2Cp_2(\mu\text{-}SMe)_3\}^+$ moiety with a BH_4^- anion through two bent 3c–2e Mo–H–B bonds [Mo–H_b 1.87(5), 1.84(5); B–H_b 1.19(5), 1.20(5) Å; Mo–H–B 121(3), 125(3)°]. The molecule contains a distorted tetrahedral μ-η¹:η¹-BH_4 ligand in which the bridging B–H_b bonds are somewhat longer than the terminal B–H_t bonds

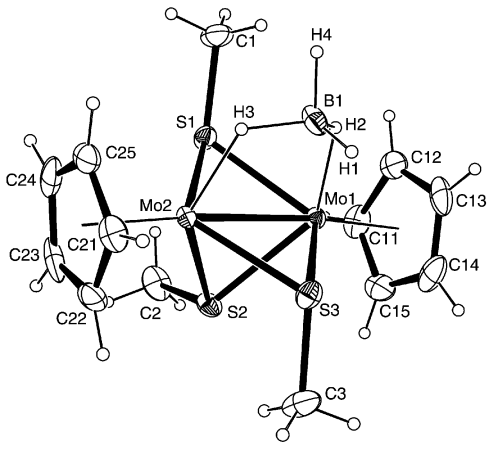

Fig. 1 An ORTEP drawing (20% thermal ellipsoids) of the complex $[Mo_2Cp_2(\mu\text{-}SMe)_3(\mu\text{-}BH_4)]$ **2**. Selected bond lengths (Å) and angles (°): Mo1–Mo2 2.653(1), Mo1–S1 2.4544(12), Mo1–S2 2.4313(12), Mo1–S3 2.4499(12), Mo2–S1 2.4513(11), Mo2–S2 2.4280(12), Mo2–S3 2.4531(12); Mo2–S1–Mo1 65.48(3); Mo2–S2–Mo1 66.18(3), Mo2–S3–Mo1 65.52(3); Mo1–H2 1.87(5), Mo2–H3 1.84(5), B1–H2 1.19(5), B1–H3 1.20(5), B1–H1 1.08(5), B1–H4 1.11(5); H2–B1–H4 96(3), H3–B1–H4 98(3), H1–B1–H2 118(4), H1–B1–H3 115(4), H2–B1–H3 110(3), H1–B1–H4 116(4), Mo1–H2–B1 125(3), Mo2–H3–B1 121(3). Minor disorder sites of the bridging ligands [occupancy 5.6(2)%] are not shown.

DOI: 10.1039/b006457m

[B–H_t 1.08(5), 1.11(5) Å]. The Mo–B distances [2.681(6), 2.711(6) Å] are nearly equal and their length suggests that there is little or no direct Mo–B bonding. Indeed, they are longer than the single Mo–Mo bond [2.653(1) Å]. In all other {$M_2(\mu\text{-}\eta^1:\eta^1\text{-}BH_4)$} bridge systems the M–B distances are shorter than the M–M bond length. Thus, in the diiridium complex [$Ir_2(C_5Me_5)_2H_3(\mu\text{-}BH_4)$] the Ir–B distances are 2.214(4) Å, compared with an Ir–Ir bond length of 2.823(1) Å. In this case it has been suggested that the two bridging hydrogen atoms of the BH_4^- ligand are almost completely transfered to the iridium atoms and that the BH_4^- coordination should be described as $\mu\text{-}(\eta^2\text{-}B,H):(\eta^2\text{-}B,H)$ rather than $\mu\text{-}(\eta^1:\eta^1\text{-}BH_4)$.[3] In the dimanganese species [$Mn_2(\mu\text{-}H)(\mu\text{-}BH_4)(CO)_6(\mu\text{-}Ph_2PCH_2PPh_2)$][5,7] the Mn–B distances [2.557(3), 2.607(4) Å] are again shorter than the Mn–Mn bond length [2.989(1) Å] and may indicate some direct Mn–B bonding. The Mn–H bond lengths [1.65(4), 1.68(4) Å] are slightly shorter than the Mo–H distances in **2**. The B–H_b [1.24(4), 1.18(4) Å] and B–H_t [1.08(4), 1.09(4) Å] distances are comparable with those in **2** indicate that hydrogen transfer from boron to the metal atoms is small compared with the Ir_2 complex. The third example of a $\mu\text{-}(\eta^1:\eta^1\text{-}BH_4)$ ligand is found in [$Ru_2(C_5Me_5)_2H_3(\mu\text{-}BH_4)$].[4] The Ru–B distances [2.406(4) Å] are consistent with closed 3c–2e Ru–H–B interactions though they are again shorter than the Ru–Ru bond [2.895(1) Å].[8] Two features of complex **2** appear therefore to be unprecedented: (i) the presence of a $\mu\text{-}\eta^1:\eta^1$-tetrahydroborate bridge which involves very weak or no direct interaction between boron and the metal atoms and (ii) the stability of this bridge which does not depend on the presence of H^-, as is the case with the Ir, Mn and Ru species.

The hydride transfer from BH_4^- to the dimolybdenum site is stopped at a very early stage in **2**. The reaction can also continue to completion, with hydride adding to one acetonitrile ligand, as is shown by the isolation and characterization of **3**.‡ In the IR spectrum of **3** a C≡N bond was revealed by a typical band at 1624 cm^{-1}. In the ^1H NMR spectrum a quadruplet at δ 7.69 and a doublet at δ 1.82 (J_{HH} 4.6 Hz) indicate that a hydride has been transferred to one of the acetonitrile ligands. The structure of **3** was confirmed by X-ray analysis (Fig. 2).§ It was found to consist of a typical [$Mo^{III}_2Cp_2(\mu\text{-}SMe)_3$] unit[6] bridged by the nitrogen atom of the azavinylidene N=C(H)Me ligand.

The reaction of BH_4^- with transition metal halides is a standard route to the borohydride complexes which are thought to be intermediates in the conversion of metal halides to metal hydrides.[2a] The simultaneous formation of **2** and **3** reveals a competition between the incomplete transfer of hydride to the bimetallic site and the reduction of one acetonitrile ligand (MeC≡N) into an azavinylidene group (MeCH=N), this latter transformation being favored in THF rather than in acetonitrile. Finally, the four known structural examples of $M_2(\mu\text{-}BH_4)$ system may represent different stages in the double σ-activation of an XH_4 entity at a bimetallic site: in **2** and in the Mn complex the H atoms bridge M and B atoms which do not interact directly; in the Ir complex H transfer is nearly complete and the Ir–B distance is close to the value expected for a single bond; an intermediate stage between these extremes is illustrated by the Ru complex. Further experiments to convert **2** into dimolybdenum hydride and dimolybdenum borane complexes of higher nuclearity are now under investigation.

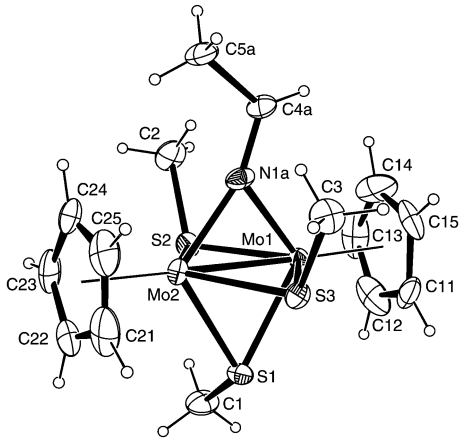

Fig. 2 An ORTEP drawing (20% thermal ellipsoids) of the complex [$Mo_2Cp_2(\mu\text{-}SMe)_3(\mu\text{-}\eta^1\text{-}N{=}CHCH_3$] **3**. Selected bond lengths (Å) and angles (°): Mo1–Mo2 2.564(1), Mo1–S1 2.446(2), Mo1–S2 2.450(2), Mo1–S3 2.467(2), Mo2–S1 2.448(2), Mo2–S2 2.456(2), Mo2–S3 2.472(2), Mo1–N1A 2.089(8), Mo2–N1A 2.067(8), N1A–C4A 1.38(2), C4A–C5A 1.58(3); Mo1–S1–Mo2 63.18(5), Mo1–S2–Mo2 63.01(5), Mo1–S3–Mo2 62.54(5), Mo1–N1A–Mo2 76.2(2). Random disorder of the azavinylidene C atoms over two sites is not shown.

Notes and references

† *Experimental procedure:* A solution of **1** (0.2 g, 0.32 mmol) in acetonitrile (10 mL) [or a suspension of **1** in thf (10mL)] was treated with $NaBH_4$ (20 mg, 0.53 mmol) at room temperature. The red solution turned readily to orange. After stirring for 5 min the solvent was removed under vacuum and the residue was extracted with diethyl ether. This extract was chromatographed on a silica gel column and elution with hexane–dichloromethane gave two orange bands of **2** and **3**. Recrystallisation from diethyl ether of the two fractions afforded orange crystals of **2** (92 mg, 60%, in MeCN) and **3** (8 mg, 5%, in MeCN). Anal. for $C_{13}H_{23}BMo_2S_3$ **2**. Calc.: C, 32.6; H, 4.8; B, 2.3. Found: C, 32.4; H, 4.8; B, 2.0%. Anal. for $C_{15}H_{23}NMo_2S_3$ **3**. Calc.: C, 35.6; H, 4.6; N, 2.8. Found: C, 35.9; H, 4.7; N, 2.8%.

‡ *Selected spectroscopic data*: for **2**: IR (KBr pellet, cm^{-1}): ν(BH)$_t$: 2449s, 2375s, 2245w; ν(BH)$_b$:1871. $^1H\{^{11}B\}$ NMR (toluene-d_8), δ 4.94 (s, 10H, C_5H_5), 2.32 [td, J_{HH} 18.3, J_{HH} 3.0 Hz, 1H, $Mo_2(\mu\text{-}H)_2BH_2$], 1.89 (s, 3H, SCH_3), 1.65 (s, 3H, SCH_3), 1.42 (s, 3H, SCH_3), 1.28 [br m, 1H, $Mo_2(\mu\text{-}H)_2BH_2$], −15.53 [dd, J_{HH} 18.3, J_{HH} 3.0 Hz, 2H, $Mo_2(\mu\text{-}H)_2BH_2$]. ^{11}B NMR ($CDCl_3$), δ −27.0 (br s, $Mo_2(\mu\text{-}H)_2BH_2$]. For **3**: IR (KBr pellet, cm^{-1}): ν(C=N), 1624. ^1H NMR ($CDCl_3$), δ 7.69 (q, J_{HH} 4.6 Hz, 1H, $Mo_2\text{-}\mu\text{-}N{=}CHCH_3$), 5.41 (s, 5H, C_5H_5), 5.23 (s, 5H, C_5H_5), 1.82 (d, J_{HH} 4.6 Hz, 3H, CH_3), 1.72 (s, 3H, SCH_3), 1.26 (s, 3H, SCH_3), 1.22 (s, 3H, SCH_3). $^{13}C\{^1H\}$ NMR ($CDCl_3$), δ 167.7 (br s, $Mo_2\text{-}\mu\text{-}N{=}CHCH_3$), 93.0 ($C_5H_5$), 91.1 ($C_5H_5$), 29.7, 23.4 15.4 ($N{=}CHCH_3$ + SCH_3).

§ *Crystal data*: for **2**: $C_{13}H_{23}BMo_2S_3$, M = 478.18, monoclinic, space group $P2_1/n$, a = 11.7445(13), b = 10.4279(7), c = 14.196(2) Å, β = 100.77(1)°, U = 1707.9(3) Å^3, Z = 4, D_c = 1.860 Mg m^{-3}, μ = 1.819 mm^{-1}, F(000) = 952. 8632 reflections measured, 3366 unique (R_{int} = 0.011) used in refinement. R1[2373 with $I > 2\sigma(I)$] = 0.027, wR2(all data) = 0.070. For **3**: $C_{15}H_{23}Mo_2NS_3$, M = 505.40, orthorhombic, space group $P2_12_12_1$, a = 10.1071(12), b = 13.1712(17), c = 14.0181(18) Å, U = 1866.1(4) Å^3, Z = 4, D_c = 1.779 Mg m^{-3}, μ = 1.672 mm^{-1}, F(000) = 1008. 4219 reflections measured, 3961 unique (R_{int} = 0.051) used in refinement. R1[3296 with $I > 2\sigma(I)$] = 0.057, wR2(all data) = 0.16. Flack absolute structure parameter x = 0.21(12).[9]

CCDC 182/1791. See http://www.rsc.org/suppdata/cc/b0/b006457m/ for crystallographic files in .cif format.

1 R. H. Crabtree, *Angew. Chem., Int. Ed. Engl.*, 1993, **32**, 789; M. Brookhart, M. L. H. Green and L. L. Wong, *Prog. Inorg. Chem.*, 1988, **36**, 1.

2 (*a*) T. J. Marks and J. R. Kolb, *Chem. Rev.*, 1977, **77**, 263; (*b*) Z. Xu and Z. Lin, *Coord. Chem. Rev.*, 1996, **156**, 139.

3 T. M. Gilbert, F. J. Hollander and R. G. Bergman, *J. Am. Chem. Soc.*, 1985, **107**, 3508.

4 M. Jahncke, G. Mester, G. Rheiwald, H. Stoekli-Evans and G. Suss-Fink, *Organometallics*, 1997, **16**, 1137.

5 R. Carreno, V. Riera, M. A. Ruiz, Y. Jeannin and M. Philoche-Levisalles, *J. Chem. Soc., Chem. Commun.*, 1990, 15.

6 F. Barrière, Y. Le Mest, F. Y. Pétillon, S. Poder-Guillou, P. Schollhammer and J. Talarmin, *J. Chem. Soc., Dalton Trans.*, 1996, 3967.

7 R. Carreno, V. Riera, M. A. Ruiz, C. Bois and Y. Jeannin, *Organometallics*, 1993, **12**, 1946.

8 R. W. Parry and G. Kodama, *Coord. Chem. Rev.*, 1993, **128**, 245; R. Bau, R. G. Teller, S. W. Kirtley and T. F. Koetzle, *Acc. Chem. Res.*, 1979, **12**, 176; J. E. McMurry and T. Lectka, *J. Am. Chem. Soc.*, 1993, **115**, 10 167.

9 Programs used: SHELX97—Programs for Crystal Structure Analysis (Release 97-2). G. M. Sheldrick, Institüt für Anorganische Chemie der Universität, Tammanstrasse 4, D-3400 Göttingen, Germany, 1998; WinGX—A Windows Program for Crystal Structure Analysis, L. J. Farrugia, *J. Appl. Crystallogr.*, 1999, **32**, 837.

ChemComm

The synthesis of the largest perfluoro macrocycles; perfluoro [60]-crown-20 and perfluoro [30]-crown-10†

Han-Chao Wei and Richard J. Lagow*

Department of Chemistry and Biochemistry, University of Texas at Austin, Austin, TX 78712-1167, USA. E-mail: rjlagow@mail.utexas.edu

Received (in Columbia, MO, USA) 23rd May 2000, Accepted 22nd August 2000
First published as an Advance Article on the web 16th October 2000

The largest perfluoro macrocycles, perfluoro [60]-crown-20 and perfluoro [30]-crown-10, have been synthesized using the new continuous addition solution phase direct fluorination technique and characterized using ^{19}F NMR and mass spectrometry.

The syntheses of perfluoro crown ethers were first reported in 1985.[1] Perfluoro macrocycles have important medical applications such as ^{19}F NMR imaging and oxygen carrier applications.[2,3] Perfluoro crown ethers generally do not form stable complexes with cations because the basicities of perfluoro crown ethers dramatically decrease as the amount of fluorine substitution increases.[4,5] However, perfluoro crown ethers form complexes with anions, such as O_2^- and F^-, in gas phase reactions.[6] Prior to 1997, only thirteen perfluoro macrocycles were reported and all were synthesized by members of our fluorine research group using low temperature, below room temperature, direct fluorination synthetic techniques.[1,3,7–9] In this paper, we have explored the possible synthesis of perfluorinated organic compounds at higher temperature, above room temperature, during the initial stage of fluorination. The largest perfluoro macrocycles, perfluoro [60]-crown-20 **1** and perfluoro [30]-crown-10 **2**, have been successfully synthesized by using a new continuous addition solution phase direct fluorination technique. In the future, the synthesis of higher molecular weight perfluoro macrocycles will enable us to further explore the chemistry of the perfluoro macrocycles, such as ion complex chemistry and oxygen carrier applications.

In general, the rate of fluorination must be slow enough to allow vibrational energy relaxation processes to occur by collisions in an inert solvent. Many direct fluorination reactions are performed below room temperature during the initial stage of fluorination because reaction rates are so fast that excessive fragmentation occurs and a much lower temperature is required. We initially lowered the fluorination temperature to minimize possible ring opening reactions during fluorination of [60]-crown-20. Several first attempts to perfluorinate [60]-crown-20 at lower temperatures, 0, −10, −20 and −30 °C, during the initial stage of fluorination were unsuccessful. Interestingly, as the temperature of the initial stage of fluorination decreased, the degree of fluorination decreased and only partial fluorination occurred. These observations were confirmed by ^{1}H, ^{19}F NMR spectroscopy and mass spectrometry. Therefore, we increased the initial stage reaction temperature to 26 °C and succeeded in the synthesis of perfluoro [60]-crown-20 **1**.

At room temperature, [60]-crown-20 molecules are conformationally flexible[8] and hydrogen atoms can be replaced by fluorine even at sites which are sterically protected by the configuration of the carbon skeleton of [60]-crown-20 during fluorination. In contrast, the [60]-crown-20 molecules are less flexible at lower temperatures. Once the 'surface' hydrogen atoms of [60]-crown-20 are replaced by fluorine, the non-bonding electron cloud of the fluorine atoms tends to repel the oncoming fluorine molecules as they approach the [60]-crown-20 molecules and only partially fluorinated products are obtained. Under such vigorous fluorination conditions, higher temperature solution phase fluorination, fragmentation products were also obtained and the yield of perfluoro [60]-crown-20 was 14%. However, perfluoro [30]-crown-10 **2** was synthesized in 50% yield using the direct fluorination method with reaction temperatures escalating from −20 to 26 °C, as described in the literature.[9,10] The spectral data were in agreement with the structural assignments of perfluoro [60]-crown-20 **1** and perfluoro [30]-crown-10 **2**.[11]

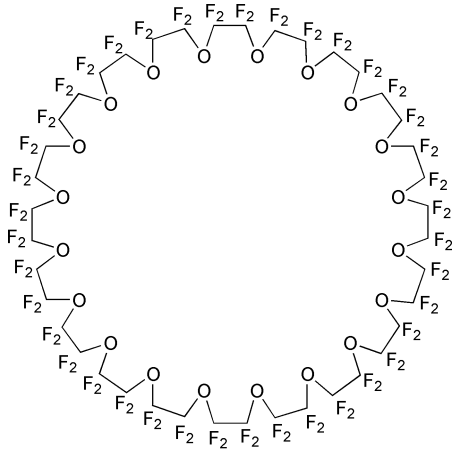

1

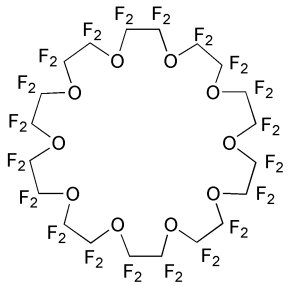

2

In conclusion, the largest perfluoro macrocycle, perfluoro [60]-crown-20 **1** and perfluoro [30]-crown-10 **2**, were synthesized by direct fluorination and characterized using ^{19}F NMR spectroscopy and mass spectrometry. Perfluoro [60]-crown-20 **1** and perfluoro [30]-crown-10 **2** are expected to be biologically inert, in contrast to their hydrocarbon analogues, and may be useful in biological or medical applications where physiologically inert or oxygen carrying fluids are required. Perfluoro [60]-crown-20 **1** has also shown potential as a very clean, high mass compound for use as a mass spectral marker material in the chemical ionization negative mode.

The authors are grateful for the financial support from the National Science Foundation (CHE 9972888).

† Electronic supplementary information (ESI) available: experimental details. See http://www.rsc.org/suppdata/cc/b0/b004168h/

Notes and references

1 W. H. Lin, W. I. Bailey and R. J. Lagow, *J. Chem. Soc., Chem. Commun.*, 1985, 1350.
2 F. K. Schweighardt and J. A. Rubertone, *US Pat.*, 4 838 274, 1989.
3 T.-Y. Lin and R. J. Lagow, *J. Chem. Soc., Chem. Commun.*, 1991, 12.
4 M. Shionoya, E. Kimura and Y. Iitaka, *J. Am. Chem. Soc.*, 1990, **112**, 9237.
5 E. Kimura, M. Shionoya, M. Okamoto and H. Nada, *J. Am. Chem. Soc.*, 1989, **110**, 3679.
6 (*a*) J. S. Brodbelt, C.-C. Liou, S. Maleknia, T.-Y. Lin and R. J. Lagow, *J. Am. Chem. Soc.*, 1993, **115**, 11 069; (*b*) J. S. Brodbelt, S. Maleknia, R. J. Lagow and T.-Y. Lin, *J. Chem. Soc., Chem. Commun.*, 1991, 1075; (*c*) J. S. Brodbelt, S. Maleknia, C.-C. Liou and R. J. Lagow, *J. Am. Chem. Soc.*, 1991, **113**, 5913; (*d*) S. Maleknia and J. S. Brodbelt, *J. Am. Chem. Soc.*, 1992, **114**, 4295; (*e*) C.-C Liou and J. S. Brodbelt, *J. Am. Chem. Soc.*, 1992, **114**, 6761; (*f*) C.-C Liou and J. S. Brodbelt, *J. Am. Soc. Mass Spectrom.*, 1992, **3**, 543; (*g*) H. Zhang, I. Chu, S. Leming and D. A. Dearden, *J. Am. Chem. Soc.*, 1991, **113**, 7415.
7 (*a*) W. D. Clark, T.-Y. Lin, S. D. Maleknia and R. J. Lagow, *J. Org. Chem.*, 1990, **55**, 5933; (*b*) T.-Y. Lin, H. W. Roesky and R. J. Lagow, *Synth. Commun.*, 1993, **23**, 2451; (*c*) T.-Y. Lin, W.-H. Lin, W. D. Clark, R. J. Lagow, S. B. Larson, S. H. Simonsen, V. M. Lynch, J. S. Brodbelt, S. D. Maleknia and C.-C. Liou, *J. Am. Chem. Soc.*, 1994, **116**, 5172.
8 R. Chenevert and L. D'Astous, *J. Heterocycl. Chem.*, 1986, **23**, 1785.
9 H. C. Wei, V. M. Lynch and R. J. Lagow, *J. Org. Chem.*, 1997, **62**, 1527.
10 H. C. Wei, S. Corbelin and R. J. Lagow, *J. Org. Chem.*, 1996, **61**, 1643.
11 The starting materials, [60]-crown-20 and [30]-crown-10, were synthesized by the following procedures from the literature (ref. 8). *Synthesis of perfluoro [60]-crown-20*. In a typical reaction, the direct fluorination reaction was performed in a similar manner to the reactions that have been described in the literature (ref. 9 and 10). [60]-Crown-20 (1 g) was dissolved in 1,1,2-trichloro-1,1,2-trifluoroethane (300 mL) and chloroform (3 mL), then the solution was slowly introduced into a stainless steel reactor which contained 1,1,2-trichloro-1,1,2-trifluoroethane (600 mL), sodium fluoride (100 g) and a fluorine–helium mixture. During the next 72 h the relative fluorine concentration was slowly increased. Filtration of the solution and removal of 1,1,2-trichloro-1,1,2-trifluoroethane by simple distillation produced a white waxy solid and a viscous oil. The product was purified by preparative gas chromatography on an OV-210 column at 200 °C. Pure perfluoro [60] crown-20 was collected by preparative GC as white waxy solid in 14% yield. Negative chemical ionization mass spectrometry: *m/z* (formula, identification, intensity) 2320 ($C_{40}F_{80}O_{20}$, M^-, 100). The elemental compositions were studied by high resolution mass spectrometry in chemical ionization negative mode. The results were consistent with $C_{40}F_{80}O_{20}$ (Calc.: 2319.7706; Found: 2319.7688). ^{19}F NMR ($CFCl_3$) δ −89.45 (s, 80F). *Synthesis of perfluoro[30]-crown-10*. Perfluoro [30]-crown-10 was synthesized in a similar manner to perfluoro [60]-crown-20. The product was purified by preparative gas chromatography on a OV-210 column at 150 °C. Pure perfluoro [30]-crown-10 was collected by preparative GC as a colorless liquid in 50% yield. Fast atom bombardment (FAB) mass spectral analysis (negative mode): *m/z* (formula, identification, intensity) 1159 ($C_{20}F_{40}O_{10}$, M^-, 100). The elemental compositions were studied by high resolution mass spectrometry in FAB negative mode. The results were consistent with $C_{20}F_{40}O_{10}$ (Calc.: 1159.8853; Found: 1159.8844). ^{19}F NMR ($CFCl_3$) δ −89.48 (s, 40F). More experimental details are described in ESI.†

ChemComm

Structure and magnetic properties of a nickel(II) complex of a tridentate verdazyl radical: strong ferromagnetic metal-radical exchange coupling†

Tosha M. Barclay,[a] Robin G. Hicks,*[b] Martin T. Lemaire[b] and Laurence K. Thompson[c]

[a] *Department of Chemistry, Box 9573, Mississippi State University, Mississippi State MS 39762-9573, USA*
[b] *Department of Chemistry, University of Victoria, PO Box 3065, Victoria, B.C. V8W 3V6, Canada. E-mail: rhicks@uvic.ca*
[c] *Department of Chemistry, Memorial University of Newfoundland, St. Johns, Nfld. A1B 3X7, Canada*

Received (in Irvine, CA, USA) 1st August 2000, Accepted 25th September 2000
First published as an Advance Article on the web

Magnetic susceptibility measurements on a structurally characterized nickel(II) complex of a tridentate verdazyl radical indicate very strong ferromagnetic Ni–verdazyl intramolecular exchange interactions (J > +200 cm^{-1}).

Metal complexes of coordinated radicals have been actively pursued as components of new molecular magnetic materials. A principal advantage of paramagnetic ligands is that direct magnetic exchange coupling between metal and ligand spins is possible. Although a large number of metal–radical systems have been studied, the *variety* of radical-based ligands is somewhat limited. Most work has been carried out with ligands based on the nitroxide family[1–3] and TCNE[4] and TCNQ[5] radical anions, although there has been a growing interest in exploring alternative radicals as ligands.[6] Derivatives of the verdazyl radical family[7] offer an attractive alternative to the conventional radical ligands because of their abundance of donor atoms. Verdazyls such as pyvd and bvd possess chelating environments that are excellent structural mimics of 2,2′-bipyridine and 2,2′-bipyrimidine, respectively, and transition metal complexes of both radicals have been reported.[8–11] Given the huge interest and success in employing oligopyridines as ligands in metallo-supramolecular chemistry,[12–14] it is appealing to consider creating oligopyridine analogues in which one or more of the heterocyclic rings is replaced by a verdazyl radical. The preservation of the chelating environment makes such systems attractive both for self-assembly processes and for the desirable metal–radical exchange coupling. As an initial foray in this direction, we present the synthesis, coordination chemistry, and magnetic properties of a nickel complex of the tridentate verdazyl 1,5-dimethyl-3-(2,2′-bipyridin-6-yl)-6-oxoverdazyl, bipyvd, a radical that possesses a coordination pocket analogous to that of 2,2′:6′,2″-terpyridine.

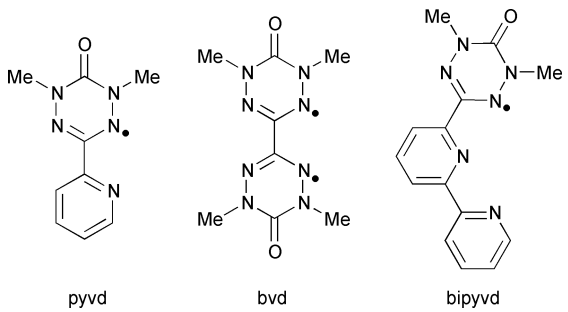

The bipyvd ligand was prepared[15] from 2,2′-bipyridine-6-carbaldehyde[16] using established procedures.[17,18] Reactions of bipyvd with $NiCl_2$ in the presence of $NaPF_6$ produced Ni(bipyvd)$_2^{2+}$·2PF_6^- (**1**) which crystallized as an acetone solvate.‡ Fig. 1 shows the molecular structure of the cation of **1**, which consists of two tridentate bipyvd ligands surrounding the nickel ion in a pseudo-octahedral coordination sphere.§ The local geometry at the nickel is D_{2d} distorted from ideal octahedral geometry, as is also the case for structurally characterized Ni(terpy)$_2^{2+}$ complexes.[19,20] The six Ni–N bonds occur in three pairs with a distinct progression of bond lengths: two short bonds to each of the central pyridine nitrogens (N5 and N11, mean bond length 1.996 Å), two slightly longer bonds to the terminal pyridine nitrogens (N6 and N12, 2.098 Å) and two yet longer bonds to the verdazyl ring nitrogens (N1 and N7, 2.211 Å). The structural features of the verdazyl rings of the ligands are quite similar to other 1,5-dimethyl-6-oxoverdazyls, although there is a slight asymmetry in the bond lengths and angles induced by coordination to nickel (see supporting information). Each of the two bipyvd ligands are essentially planar and are oriented perpendicular to one another, with an interligand dihedral angle of 92.4°. Overall, the general structural features of this complex, particularly with respect to the local coordination environment at Ni, are strongly reminiscent of Ni(terpy)$_2^{2+}$-based systems,[19,20] further validating the *structural* analogy between oligopyridine-substituted verdazyls and the 'parent' oligopyridines.

The UV–visible spectrum of **1** exhibits an absorption maximum at 438 nm (ε = 5700 L mol^{-1} cm^{-1}), which is slightly red shifted with respect to the spectrum of free bipyvd (λ_{max} = 400 nm, ε = 1900). The complex is therefore appropriately described as consisting of a nickel(II) center and two radicals. The temperature dependence of the effective

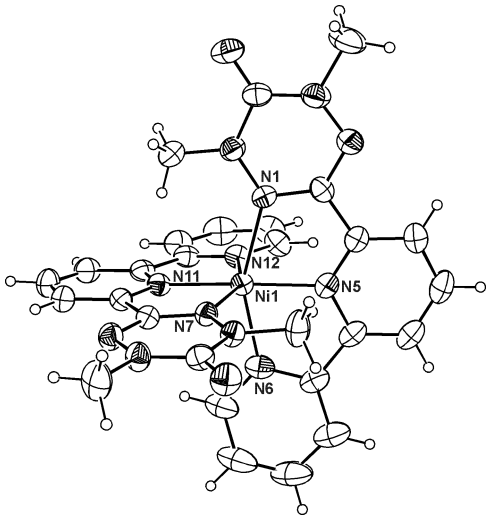

Fig. 1 Molecular structure of the Ni(bipyvd)$_2^{2+}$ dication of **1** (30% probability thermal ellipsoids). Selected bond lengths (Å) and angles (°) Ni(1)–N(1) 2.209(3), Ni(1)–N(5) 2.000(3), Ni(1)–N(6) 2.101(3), Ni(1)–N(7) 2.212(3), Ni(1)–N(11) 1.991(3), Ni(1)–N(12) 2.094(3); N(1)–Ni(1)–N(6) 154.59(12), N(7)–Ni(1)–N(12) 155.58(11), N(5)–Ni(1)–N(11) 175.08(11).

† Electronic supplementary information (ESI) available: partial packing diagram for **1**. See http://www.rsc.org/suppdata/cc/b0/b006520j/

DOI: 10.1039/b006520j

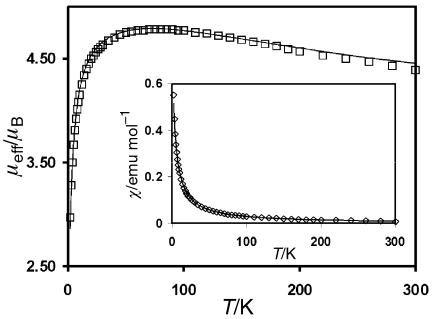

Fig. 2 Plot of μ_{eff} *vs.* T for **1**. The solid line corresponds the model fit according to parameters described in the text. The inset displays the corresponding χ *vs.* T profile.

magnetic moment of **1** is presented in Fig. 2.¶ The room temperature value (4.4 μ_B) is significantly higher than that expected for a non-interacting $S = 1$ Ni^{II} ion and two $S = \frac{1}{2}$ radicals (3.9 μ_B for $g = 2.1$). As the temperature decreases, μ_{eff} increases to a maximum value of 4.8 μ_B at 85 K and then rapidly decreases on further cooling. The high temperature behaviour provides evidence for strong ferromagnetic interactions between the Ni^{II} spins and each of the two radical centers. The magnetic data were fitted to a three-spin model in which the two radicals ($S_{A1} = S_{A2} = \frac{1}{2}$) are both ferromagnetically coupled to a nickel ion ($S_B = 1$) by exchange constant J_1 and coupled to each other with value J_2. Attempts to model the magnetic behaviour of **1** yielded several different solutions with essentially the same quality fits to the experimental data. In these various solutions, the radical–radical coupling J_2 varied from +40 to −70 cm^{-1}, precluding any firm conclusions regarding the nature of the magnetic interactions between coordinated radicals. The metal–radical exchange J_1 was also variable, although the *smallest* acceptable fitted value was +200 cm^{-1} (and values of up to +330 cm^{-1} were obtained in some solutions). This implies that the observed magnetic properties are largely determined by the very strong ferromagnetic metal–radical coupling. The uncertainty in the coupling parameters may be a reflection of the difficulties associated with quantifying exchange integrals in strongly ferromagnetically coupled systems.[21] We are currently preparing analogous bipyvd complexes of diamagnetic metal ions in order to explicitly determine the radical–radical coupling. In the absence of any knowledge regarding the true value of J_2 we arbitrarily set it equal to zero, producing the following parameters: $J_1 = +320$ cm^{-1}, $J_2 = 0$ cm^{-1}, $g = 2.11$, $\theta = -5$ K, TIP (temperature-independent paramagnetism) = 0.00022 cm^3 mol^{-1}, ρ (fraction of paramagnetic impurity) = 0.014 ($R = 0.0321$; $R = [\Sigma(\chi_{obs} - \chi_{calc})^2/\Sigma(\chi_{obs})^2]^{1/2}$). The Weiss-like constant θ was employed as a pseudo-intermolecular exchange parameter necessary to model the low temperature magnetic behaviour; analysis of the molecular packing in **1** reveals neighbouring verdazyl rings in somewhat close proximity (ESI†). The overlap of adjacent verdazyl moieties offers a probable intermolecular exchange pathway, although zerofield splitting of the high-spin Ni^{II} ground state may also contribute to the low temperature behaviour.

We recently reported similarly strong coupling in a nickel complex of pyvd which contains two hfac ligands.[11] In this system the ferromagnetic verdazyl–nickel coupling was explained by invoking well-established orbital orthogonality arguments.[21] The intramolecular exchange coupling in compound **1** is similar in nature and establishes that verdazyl–nickel ferromagnetic coupling is a general phenomenon and is not dependent on the nature of the ancillary ligands. This stands out in sharp contrast to the behaviour of virtually all other metal-radical complexes described to date, in which strong *anti*-ferromagnetic or weak ferromagnetic coupling is the rule. The only other complexes which we are aware of with comparable ferromagnetic exchange properties are semiquinone complexes of Ni^{II} and Cu^{II}.[22] Moreover, the structural similarities of verdazyl–metal binding to that seen in complexes of oligopyridines brings a significant component of structural design into the construction of metal–radical assemblies because of the well-established binding modes of oligopyridines. We are enthusiastic about the prospects of making new high-spin clusters and solids based on nickel(II) and oligopyridine-based verdazyls.

Notes and references

‡ A solution of $NiCl_2 \cdot 6H_2O$ (103 mg, 0.433 mmol) in 5 mL of water was added to a slurry of bipyvd (240 mg, 0.853 mmol) in 5 mL of methanol, causing immediate dissolution of the ligand and formation of a deep cherry red solution. The mixture was stirred for 20 minutes and a solution of $NaPF_6$ (143 mg, 0.851 mmol) in 2 mL of water was added, giving a red precipitate. The reaction mixture was concentrated to about 3 mL and placed in an ice bath. The product **1** was vacuum filtered as a deep red powder and washed with cold distilled water. Yield: 290 mg (74%). The product was recrystallized by slow evaporation of a 1 : 1 acetone–ethanol solution, giving deep red plates. ν/cm^{-1} (KBr) 1709(s), 1602(m), 1574(m), 1496(m), 1460(s), 1437(m), 1359(w), 1306(m), 1275(s), 1216(w), 1177(w), 1158(w), 1090(w), 1057(w), 1037(m), 1012(m), 844(s), 777(s), 748(m), 713(m), 685(s), 643(w), 559(s), 503(w). UV–Vis (CH_3CN) λ_{max}(nm) (ε/M^{-1}cm^{-1}) 438 (5691). FAB-MS 764.9(22) [M − PF_6]$^+$. Anal. Calcd for $C_{28}N_{12}O_2$-$H_{26}NiP_2F_{12} \cdot C_3H_6O$: C, 38.41; H, 3.33; N, 17.34. Found: C, 38.25; H, 3.18; N, 17.27.

§ *Crystal data* for **1**: $C_{31}H_{32}F_{12}N_{12}NiO_3P_2$, $M = 969.34$, monoclinic, $a = 11.2095(16)$, $b = 17.362(2)$, $c = 20.494(3)$ Å, $V = 3986.8(10)$ Å^3, $T = 293$ K, space group $P2_1/c$, $Z = 4$, λ(Mo-Kα) = 0.71073 Å, 20965 reflections measured, 7033 unique ($R_{int} = 0.026$). The final $wR(F^2)$ was 0.155 (all data). CCDC 182/1796. See http://www.rsc.org/suppdata/cc/b0/b006520j/ for crystallographic files in .cif format.

¶ Variable temperature magnetic data (2−300 K) were obtained with a Quantum Design MPMS5S Squid magnetometer operating at 0.1–0.5 T. Calibrations were carried out with a palladium standard cylinder, and temperature errors were determined with $[H_2TMEN][CuCl_4]$ (D. S. Brown, V. H. Crawford, J. W. Hall and W. E. Hatfield, *J. Phys. Chem.*, 1977, **81**, 1303). The spin Hamiltonian for **1** has the form $H = J_1(S_{A1}S_B + S_{A2}S_B) - J_2S_{A1}S_{A2}$.

1 A. Caneshi, D. Gatteschi and P. Rey, *Prog. Inorg. Chem.*, 1991, **39**, 331.
2 K. Inoue, T. Hayamizu, H. Iwamura, D. Hashizume and Y. Ohashi, *J. Am. Chem. Soc.*, 1996, **118**, 1803.
3 H. Oshio and T. Ito, *Coord. Chem. Rev.*, 2000, **198**, 329.
4 J. M. Manriquez, G. T. Yee, S. MacLean, A. J. Epstein and J. S. Miller, *Science*, 1991, **252**, 1415.
5 H. Zhao, R. A. Heintz, X. Ouyang, K. R. Dunbar, C. F. Campana and R. D. Rogers, *Chem. Mater.*, 1999, **11**, 736.
6 D. A. Shultz and S. H. Bodnar, *Inorg. Chem.*, 1999, **38**, 591.
7 F. A. Neugebauer, *Angew. Chem., Int. Ed. Engl.*, 1973, **12**, 455.
8 D. J. R. Brook, V. Lynch, B. Conklin and M. A. Fox, *J. Am. Chem. Soc.*, 1997, **119**, 5155.
9 D. J. R. Brook, S. Fornell, J. E. Stevens, B. Noll, T. H. Koch and W. Eisfeld, *Inorg. Chem.*, 2000, **39**, 562.
10 D. J. R. Brook, S. Fornell, B. Noll, G. T. Yee and T. H. Koch, *J. Chem. Soc., Dalton Trans.*, 2000, 2019.
11 R. G. Hicks, M. T. Lemaire, L. K. Thompson and T. M. Barclay, *J. Am. Chem. Soc.*, 2000, **122**, 8077.
12 E. C. Constable, *Prog. Inorg. Chem.*, 1994, **42**, 67.
13 J. M. Lehn, *Chem. Eur. J.*, 2000, **6**, 2097.
14 S. Leininger, B. Olenyuk and P. J. Stang, *Chem. Rev.*, 2000, **100**, 853.
15 R. G. Hicks and M. T. Lemaire, manuscript in preparation.
16 F. R. Heirtzler, M. Neuberger, M. Zehnder and E. C. Constable, *Liebigs Ann./Recueil*, 1997, 297.
17 F. A. Neugebauer, H. Fischer and R. Siegel, *Chem. Ber.*, 1988, **121**, 815.
18 C. L. Barr, P. A. Chase, R. G. Hicks, M. T. Lemaire and C. L. Stevens, *J. Org. Chem.*, 1999, **64**, 8893.
19 M. I. Arriotua, T. Rojo, J. M. Amigo, G. Germain and J. P. Declerq, *Bull. Soc. Chim. Belg.*, 1982, **91**, 337.
20 E. C. Constable, J. Lewis, M. C. Liptrot and P. R. Raithby, *Inorg. Chim. Acta*, 1990, **178**, 47.
21 O. Kahn, R. Prins, J. Reedijk and J. S. Thompson, *Inorg. Chem.*, 1987, **26**, 3557.
22 C. Benelli, A. Dei, D. Gatteschi and L. Pardi, *Inorg. Chem.*, 1988, **27**, 2831.

ChemComm

The first Janus [2]rotaxane

Tatsuhiko Fujimoto, Yoshiteru Sakata and Takahiro Kaneda*

The Institute of Scientific and Industrial Research, Osaka University, Ibaraki, Osaka 567-0047, Japan. E-mail: kaneda@sanken.osaka-u.ac.jp

Received (in Cambridge, UK) 17th August 2000, Accepted 25th September 2000
First published as an Advance Article on the web 16th October 2000

The first Janus [2]rotaxane 3 has been synthesized by bis-azo coupling of 2-naphthol-3,6-disulfonic acid with a Janus [2]pseudorotaxane 2 prepared by dimerization of 6-*O*-[(4-aminophenylazo)phenyl]-permethylated α-cyclodextrin 1 and characterized by MALDI-TOF-MS and ^{1}H NMR methods.

Mechanically interlocked compounds such as rotaxanes and catenanes have become of interest since the first creative development of molecular machines associated with a so-called mechanical bond characteristic of such compounds.[1] Recently, we have reported the rare lipophilic [2]supercyclodextrins with a 'doubly pseudorotaxaned' superstructure, corresponding to the cyclic homo-dimers of azophenol-branched permethylated α-cyclodextrins (CDs).[2] Although such double-[2]pseudorotaxanes[3] have a tendency to exist only under limited conditions of the temperature, concentration, and medium, they must be regarded as fascinating precursors for so far unknown double-rotaxanes. To fix the dissociable structures of the precursors by capping with bulky stoppers on the terminal groups, azo coupling reactions provide a promising approach because of their practical feasibility in aqueous solutions at low temperatures, with low activation energies. In fact, Anderson *et al*. have succeeded in preparing azo dye [2]- and [3]-rotaxanes in this manner.[4] Here, we describe the synthesis of the first 'Janus [2]rotaxane'[5] **3**[6] from a lipophilic α-CD monomer **1** bearing a diazotizable 4-aminoazobenzene *via* dimerization to a [2]pseudodoublerotaxane **2**.

Competitive substitution reaction of 6-*O*-monotosyl permethylated α-CD[2] with an excess of 4-amino-4′-hydroxyazobenzene as a bifunctional nucleophile gave a mixture of 6-*O*-[(4-aminophenylazo)phenyl]- and 6-deoxy-6-[(4-hydroxyphyenylazo)phenylamino]-permethylated α-CDs (Scheme 1). The former desired compound **1** could be separated from the latter by extraction with toluene from the alkaline aqueous phase, and obtained in 38% yield after purification by preparative GPC column chromatography.[7]

The self-association of monomer **1** has been examined by solvent-, temperature- and concentration-dependent ^{1}H NMR methods. A spectrum observed at ambient temperature from a solution of **1** in CD_3OD–D_2O (6 : 1) is understood in terms of an equilibrium mixture of two species, **1** and its complex **2** [Fig. 1(b)]. The complexed species disappeared completely at 55 °C to result in the uncomplexed species alone, the spectrum of which [Fig. 1(a)] is similar to that of **1** obtained in $CDCl_3$. By contrast, the association complex **2** was found to exist exclusively in CD_3OD–D_2O (1 : 1) at 23 °C [Fig. 1(c)]. The superstructure of the Janus [2]pseudorotaxane **2** is confirmed by both the determination of the value $n = 2.0$[8] of the degree of association according to the method[2b] reported previously and the appearance of the four sets of doublets due to the aromatic protons. The spectral features mentioned above indicate that the dimerization equilibrium in Scheme 1, for which the association constant K_a was evaluated to be 430 M^{-1},[8] occurred in hydrophilic media at room temp. and that its exchange rate was slow but the free rotations of the guest azobenzene-rods were fast on the NMR timescale. Similar phenomena have been described in other lipophilic α-CD–azobenzene dyads.[2]

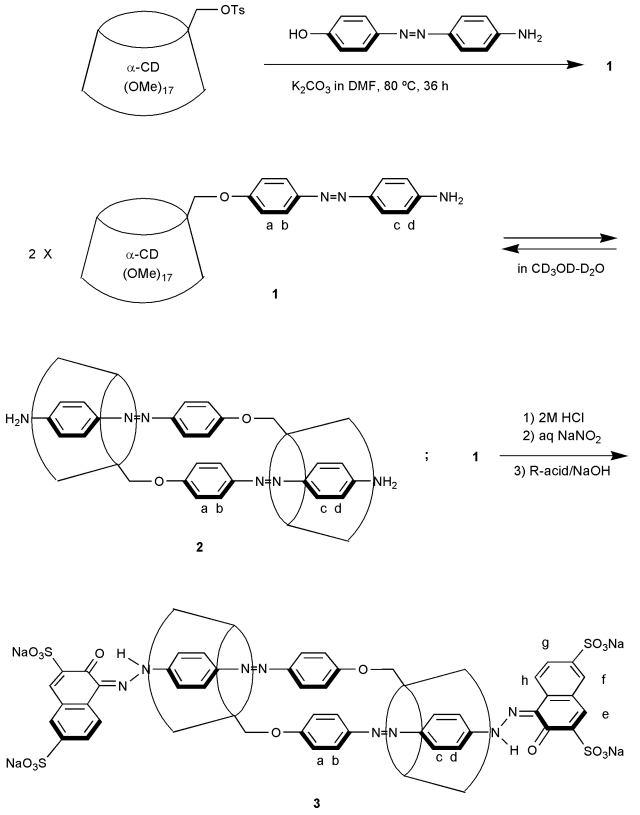

Scheme 1

The aromatic protons of **2**[9] were assigned by difference NOE and decoupling experiments in CD_3OD–D_2O (6 : 1) and (1 : 1), respectively. The observations of two correlations due to H_a–H_b and H_c–H_d and of the chemical exchange involving H_c and H_d are compatible with the assignment shown in Fig. 1(c). The up-

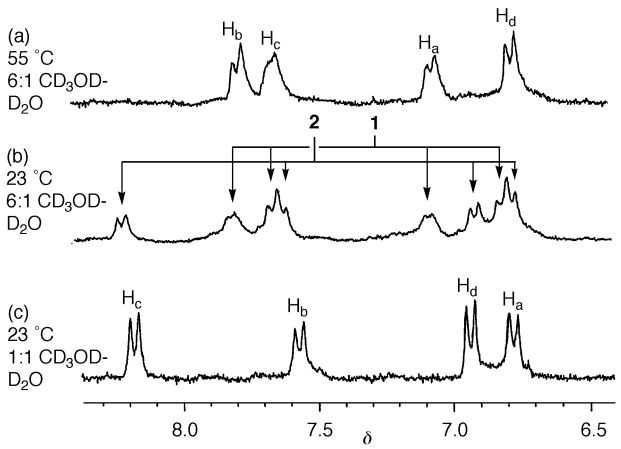

Fig. 1 270 MHz ^{1}H NMR spectra of solutions of **1**.

and down-field shifts of H_a (−0.27), H_b (−0.19), H_c (+0.56) and H_d (+0.12 ppm) after the dimerization resemble those observed previously with the other [2]supercyclodextrins[2] and therefore, these shifts also support the Janus [2]pseudorotaxane **2** for which a cyclophane-like π–π stacking between the two phenol residues and the binding of the terminal aniline residues with the CD cavities are characteristic.

Bis-azo coupling experiments to introduce two bulky naphthols as stoppers were carried out as follows. To prepare the bis-diazonium salt of **2**, a cold aqueous solution of sodium nitrite was added in portions to a cold solution of the aniline derivative **1** in 2 M HCl. The reaction mixture was treated with an alkaline solution of 2-naphthol-3,6-disulfonic acid (R-acid) at room temperature for 3 h. After neutralization followed by purification by reverse phase column chromatography, the desired Janus [2]rotaxane **3**[10] was isolated in 84% yield as red–purple solid. The symmetrical and dimeric structure of **3** has been confirmed by the observations of a 1 : 1 ratio of the naphthol to the azobenzene moiety in its ^{1}H NMR spectrum and of a peak at *m/z* 3549 corresponding to $[M+Na]^+$ in its MALDI-TOF-MS spectrum. It is interesting that the possible coupling product of **1** with the R-acid could not be detected. Thus, it is unlikely that the bis-aniline **2**, its dihydrochloride and the corresponding bis-diazonium salt dissociate into the monomeric species during the coupling processes.

The ^{1}H NMR spectral features of **3** reflect its Janus [2]rotaxane skeleton. It was anticipated that the stoppers introduced at the terminal ends have substantial substituent effects on the aromatic protons H_d situated at the *ortho* positions while this is not so for H_a and H_b which lie further away. Indeed, the following reasonable differences in their chemical shifts were found: $\Delta\delta = \delta(\mathbf{3}) - \delta(\mathbf{2})$, −0.04 for H_a, −0.04 (H_b), +0.17 (H_c), and +1.21 ppm (H_d). Further, no difference between the spectra of **3** recorded at 24 and 90 °C in D_2O was observed, supporting the fixed superstructure. At present, there is no evidence for a potential oscillation, like the stretching vibration of the covalent bond for a diatomic molecule, with respect to the mechanical bond between the two components of **3**.

In conclusion, we have demonstrated that a [2]supercyclodextrin prepared by self-assembly of an α-cyclodextrin–azobenzene dyad serves as a precursor for a very rare Janus [2]rotaxane. Synthesis of other Janus [2]rotaxanes are currently in progress in our laboratory.

We are grateful to Dr. Ken-ichi Sugiura in our laboratory for his helpful discussions.

Notes and references

1 P.-L. Anelli, P. R. Ashton, R. Ballardini, V. Balzani, M. Delgado, M. T. Gandolfi, T. T. Goodnow, A. E. Kaifer, D. Philp, M. Pietraszkiewicz, L. Prodi, M. V. Reddington, A. M. Z. Slawin, N. Spencer, J. F. Stoddart, C. Vicent and D. J. Williams, *J. Am. Chem. Soc.*, 1992, **114**, 193; for excellent reviews: V. Balzani, M. Gomez-Lopez and J. F. Stoddart, *Acc. Chem. Res.*, 1998, **31**, 405; F. M. Raymo and J. F. Stoddart, *Chem. Rev.*, 1999, **99**, 1643.

2 (*a*) T. Fujimoto, Y. Uejima, H. Imaki, N. Kawarabayashi, J. H. Jung, Y. Sakata and T. Kaneda, *Chem. Lett.*, 2000, 564; (*b*) T. Fujimoto, Y. Sakata and T. Kaneda, *Chem. Lett.*, 2000, 764.

3 Double-[2]pseudorotaxanes as cyclic hetero-dimers or cyclic pseudorotaxane dimers have been reported recently: N. Yamaguchi and H. W. Gibson, *Angew. Chem., Int. Ed.*, 1999, **38**, 143; N. Yamaguchi and H. W. Gibson, *Chem. Commun.*, 1999, 789.

4 (*a*) S. Anderson, T. D. W. Claridge and H. L. Anderson, *Angew. Chem., Int. Ed. Engl.*, 1997, **36**, 1310; (*b*) S. Anderson, W. Clegg and H. L. Anderson, *Chem. Commun.*, 1998, 2379; (*c*) M. R. Craig, T. D. W. Claridge, M. G. Hutchings and H. L. Anderson, *Chem. Commun.*, 1999, 1537.

5 This term is used for a unique face-to-face dimeric structure of **3** according to a referee's suggestion.

6 Although there is no information about the isomeric structure for the naphthol-azo units at present, they are represented here as the hydrazo tautomer rather than as the azo tautomer according to its solid state geometry [see ref. 4(*b*)].

7 **1**: yellow solid. Anal. Found: C, 55.46; H, 7.47; N, 2.80%. Calc. for $C_{65}H_{103}O_{30}N_3$: C, 55.51; H, 7.38; N, 2.99%. MALDI-TOF-MS: *m/z* 1434 $[M+Na]^+$. δ_H(270 MHz, $CDCl_3$, 23 °C): 7.83 (d, *J* 8.9 Hz, 2H, H_b), 7.74 (d, *J* 8.6 Hz, 2H, H_c), 7.03 (d, *J* 8.9 Hz, 2H, H_a), 6.73 (d, *J* 8.6 Hz, H_d), 5.2–4.9 (m, 6H, CD-H_1), 4.5–3.0 (m, CD-H).

8 The following three sets of the parameters (C_0/mM, I_x, I_y) in Scheme 1 of ref. 2(*b*) were used for the determination of the association number *n* and constant K_a: (1.97, 41, 38), (0.99, 56, 30) and (0.66, 54, 22) in CD_3OD–D_2O (5 : 1) at 23 °C.

9 **2**: Selected ^{1}H NMR data: δ_H(270 MHz, CD_3OD–D_2O (6 : 1), 23 °C): 6.79 (d, *J* 8.9 Hz, H_a), 7.64 (d, *J* 8.9 Hz, H_b), 8.23 (d, *J* 8.9 Hz, H_c), 6.93 (d, *J* 8.9 Hz, H_d).

10 **3**: MALDI-TOF-MS: *m/z* 3555 $(M+Na)^+$ for $C_{150}H_{212}O_{74}N_8S_4Na_5$. Selected ^{1}H NMR data: δ_H (270 MHz, D_2O, 23 °C): 8.40 (d, *J* 8.9 Hz, 4H, H_c), 8.39 (s, 2H, H_e), 8.18 (d, *J* 8.9 Hz, 2H, H_h), 8.14 (d, *J* 8.9 Hz, 4H, H_d), 8.08 (s, 2H, H_f), 7.82 (d, *J* 8.9 Hz, 2H, H_g), 7.60 (d, *J* 8.4 Hz, 4H, H_b), 6.75 (d, *J* 8.4 Hz, 4H, H_a).

ChemComm

$Ge_8O_{16}[(OH)^-(MeNH_3)^+(MeNH_2)]$: one OH-templated germanium zeotype

Concepción Cascales, Enrique Gutierrez-Puebla,* Marta Iglesias, M. Angeles Monge,* Caridad Ruiz-Valero and Natalia Snejko

Instituto de Ciencia de Materiales de Madrid, CSIC Cantoblanco, E-28049 Madrid, Spain.
E-mail: amonge@icmm.csic.es or egutierrez@icmm.csic.es

Received (in Oxford, UK) 30th August 2000, Accepted 20th September 2000
First published as an Advance Article on the web

A new type of zeolite is found for the title microporous germanate whose peculiar connectivity between the 3- and 9-ring layers creates cages in which an extra-framework hydroxy group is confined.

Zeolites have found a number of applications in fields of commercial importance, notably as catalyst, adsorbents and ion exchangers.[1–4] Relating to the germanium zeotypes, the possibility of designing new open frameworks increases greatly due to the possible co-existence of different coordination polyhedra around Ge (tetrahedra, octahedra and trigonal bipyramid), which implies different charged frameworks without doping with trivalent cations. Nevertheless, novel microporous germanium frameworks had not been synthesized until recently.[5–11]

In terms of our interest in the structure–properties relationship for this kind of compound, we were concerned in the design and study of precise atomic architectures of zeotypes. In previous work the existence of $Ge_7O_{15}^{2-}$ (ICMM1)[12,13] and $Ge_9O_{19}^{2-}$ (ICMM2)[14] were reported. Here, we report the structure ICMM3, the first zeotype in which it is clear that one confined hydroxy group acts as a template.

ICMM3 was synthesized hydrothermally from a reaction mixture containing GeO_2, $MeNH_2$, H_2O and ethylene glycol in molar ratios 1 : 8 : 25 : 15. The mixture was introduced and sealed in a Teflon-lined stainless steel autoclave and heated at 170 °C for 4 days. After optimizing the reaction conditions, the yield was 100%. The purity of the resulting solid product was checked by X-ray powder diffraction.†

A suitable crystal of the compound with hexagonal platelike features was selected and mounted in a diffractometer equipped with a CCD detector. Crystals were pseudo-hexagonally twinned so that the space group appeared to have a pseudo-6_3 axis along *b*, however, the structure was solved and refined in the monoclinic space group $P2_1$ with *a* and *c* equal and β = 120°. Upon determining the crystal structure, the composition was found to be $Ge_8O_{16}(OH)^-(MeNH_3)^+MeNH_2$ in which the eight Ge atoms are at the center of more or less distorted tetrahedra [range of Ge–O bond lengths 1.72(2)–1.79(2) Å; O–Ge–O bond angles 95.5(7)–120.1(8)°, Ge–O–Ge 110.2(7)–143.5(7)°]. The tetrahedra are linked together in the *ac* plane giving rise to infinite GeO_2 layers which are constructed from a secondary structural building unit (SBU) denoted 4 = 1, joined by 3-tetrahedra rings into an infinite 9-tetrahedra ring containing sheet. This arrangement was also present in ICMM1 and in ICMM2. In the former zeotype, GeO_6 octahedra were involved in both 3- and 9-rings.

Every two GeO_2 adjacent sheets are joined through the three free oxygen atoms of the 3-ring tetrahedra creating thick blocks. These connections give rise to cages which are formed by six germanium atoms (three of each layer) and the three bringing oxygen atoms (Figs. 1 and 2). Inside these cages one atom of oxygen is found which corresponds to a confined OH^- anion the hydrogen atom of which was located and isotropically refined [O–H 0.8(1) Å]. This oxygen interacts with the six germanium atoms of the cage at distances in the range 2.12(2)–2.44(2) Å. Depending on these distances the surrounding germanium polyhedra are distorted to a greater or lesser degree, distortion ranging from the nearly regular tetrahedron of Ge(1) to what can be considered as trigonal bypiramids of Ge(4) and Ge(6) when including the fifth Ge–O interaction.

Cohesion between blocks is established, as also found in ICMM2, through the only oxygen atom [O(8)] not involved in connectivities within double layers. Also, as in ICMM2, the blocks are mutually shifted.

This 3D structure contains intersecting tunnels along the three directions: one set of tunnels runs in a zigzag fashion along the *b* direction as a consequence of the shifted pillaring of the $9R_b$ 9-rings. Perpendicular to the *b* direction 8-ring 8R intersecting tunnels can be seen along the (101), (100) and (001) directions accordingly with the pseudo-hexagonal symmetry present in the crystals.

There are two crystallographically independent molecules of methylamine in the asymmetric unit, situated in the 8R channels

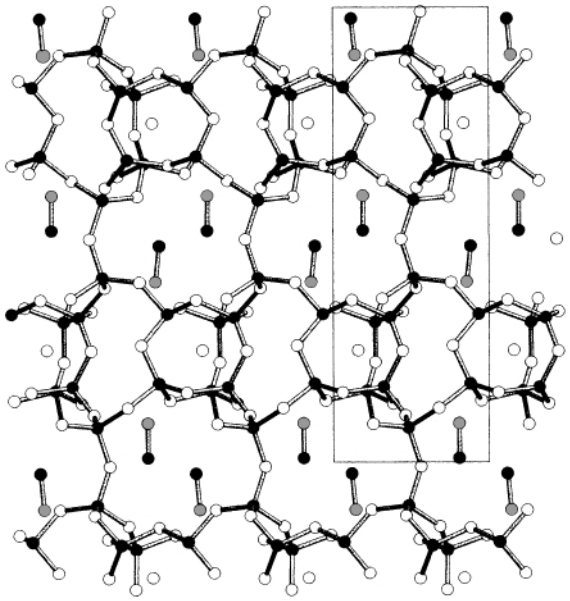

Fig. 1 View of the structure of ICMM3, showing the blocks and connectivity between them. Black, white and gray spheres are Ge, O and atoms of the amines, respectively.

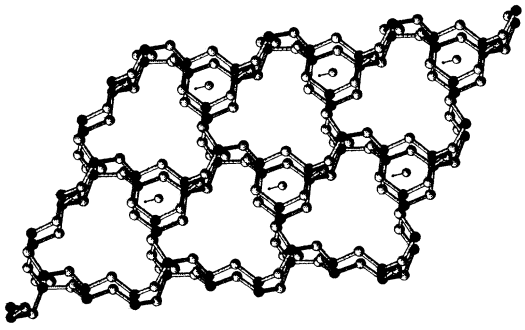

Fig. 2 View along the *b* direction of the double layer showing the confined OH group.

DOI: 10.1039/b007054h

formed between blocks. They are bonded to different oxygen atoms of the framework through hydrogen bonds. Although hydrogen atoms involving amines could not be reliably located, the range of the N···O distances [2.86(1)–3.08(1) Å], as well as their number, seem to indicate that many of these hydrogen bonds are bifurcated. Owing to the existence of one OH^- anion, it is clear that to maintain electrical neutrality, a protonated amine is required. Protonation is established through the different C–N bond lengths [1.56(4) and 1.41(4) Å] as well as by spectroscopy. The IR spectrum shows a band at 3400 cm^{-1} due to the stretching vibrations of the OH groups while bands at 2792 and 2876 cm^{-1} arise from N–H vibrations, which are characteristic of a primary amine in its protonated form. Stretching vibrations of non-protonated amine sites occur at 3100 and 3164 cm^{-1}.

TGA–DTA in N_2 atmosphere (50 ml min^{-1}) shows one progressive weight loss between 375 and 550 °C accompanied by an endothermic effect corresponding to the loss of both methylamine molecules and the OH^- group. Powder X-ray diffraction and IR spectra show that the structure is maintained upon heating to 375 °C during 4 h in air but collapses to give amorphous GeO_2 after prolonged heating.

In conclusion, a zeolite type microporous germanate has been synthesized. Its framework exhibits a peculiar connectivity between the 3- and 9-ring layers. Every two of these layers are joined through the three free oxygen atoms of the 3-ring tetrahedra. This joining creates cages in which an extra-framework hydroxy group is trapped. The negative charge of this OH^- group is compensated by one intratunnel protonated methylamine molecule.

This work was supported by the Spanish CICYT MAT98-1735-E and DGESIC PB97-1200.

Notes and references

† *Crystal data* for ICMM3: $(OH)^-[MeNH_3]^+[MeNH_2]Ge_8O^{16}$ monoclinic, space group $P2_1$, (pseudo-$P6_3$ hexagonal) a = 7.4933(8), b = 19.145(2), c = 7.4944(8) Å, β = 120.01(2)°, V = 931.0(2) Å^3, Z = 2, M_w = 916.9, D_c = 3.271 Mg cm^{-3}, μ(Mo-Kα) = 12.81 mm^{-1}. Dimensions: 0.10 × 0.10 × 0.01 mm. SADABS absorption correction, max., min. transmission coefficients: 0.51, 1.00. Data were collected on a CCD Siemens diffractometer, using ω scans in the range $3 < \theta < 32°$. The total number of reflections measured was 8132, of which 5751 were independent. The structure was solved by direct methods (G. M. Sheldrick, SHELX-86, Program for Crystal Structure Determination, University of Cambridge, 1992).[15] The hydrogen atom of the OH group was located in a difference Fourier map and isotropically refined, those of the amine molecules were geometrically situated. Refinement was carried out by full-matrix least-squares analysis with anisotropic thermal parameters for the germanium atoms and isotropic for the remaining atoms. $R(F)$ = 0.05 for $I > 2\sigma(I)$ and 0.06 for all reflections.

CCDC 182/1790. See http://www.rsc.org/suppdata/cc/b0/b007054h/ for crystallographic files in .cif format.

1 A. Corma, *Chem. Rev.*, 1997, **97**, 2373.
2 A. K. Cheetham, G. Férey and T. Loiseau, *Angew. Chem., Int. Ed.*, 1999, **38**, 3268.
3 J. M. Thomas, *Angew. Chem., Int. Ed.*, 1999, **38**, 3588.
4 T. E. Gier, X. Bu, P. Feng and G. D. Stucky, *Nature*, 1998, **395**, 154.
5 H. Li, M. Eddaoudi, D. A. Richardson and O. M. Yaghi, *J. Am. Chem. Soc.*, 1998, **120**, 8567.
6 H. Li and O. M. Yaghi, *J. Am. Chem. Soc.*, 1998, **120**, 10 569.
7 X. Bu, P. Feng and G. D. Stucky, *J. Am. Chem. Soc.*, 1998, **120**, 11204.
8 X. Bu, P. Feng, T. E. Gier, D. Zhao and G. D. Stucky, *J. Am. Chem. Soc.*, 1998, **120**, 13 389.
9 H. Li, M. Eddaoudi and O. M. Yaghi, *Angew. Chem., Int. Ed.*, 1999, **38**, 653.
10 M. O'Keeffe and O. M. Yaghi, *Chem. Eur. J.*, 1999, **5**, 2796.
11 X. Bu, P. Feng and G. D. Stucky, *Science*, 1997, **278**, 2080.
12 C. Cascales, E. Gutiérrez-Puebla, M. A. Monge and C. Ruiz-Valero, *Angew. Chem.*, 1998, **110**, 135; C. Cascales, E. Gutiérrez-Puebla, M. A. Monge and C. Ruiz-Valero, *Angew. Chem., Int. Ed.*, 1998, **37**, 129.
13 C. Cascales, E. Gutiérrez-Puebla, M. A. Monge and C. Ruiz-Valero, *Int. J. Inorg. Mater.*, 1999, **1**, 181.
14 C. Cascales, E. Gutiérrez-Puebla, M. Iglesias, M. A. Monge and C. Ruiz-Valero, *Angew. Chem.*, 1999, **111**, 2592; C. Cascales, E. Gutiérrez-Puebla, M. Iglesias, M. A. Monge and C. Ruiz-Valero, *Angew. Chem., Int. Ed.*, 1999, **38**, 2436.
15 SHELXTL, Siemens Energy & Automation Inc., Analytical Instrumentation, 1996.

Efficient photodecarboxylation of aroyl-substituted phenylacetic acids in aqueous solution: a general photochemical reaction

Musheng Xu and Peter Wan*

Department of Chemistry, Box 3065, University of Victoria, Victoria, British Columbia, Canada V8W 3V6. E-mail: pwan@uvic.ca

Received (in Corvallis, OR, USA) 15th August 2000, Accepted 18th September 2000
First published as an Advance Article on the web

Photolysis (254–350 nm) of a variety of aroyl-substituted phenylacetic acids and *p*-acetylphenylacetic acid in aqueous solution at pH > pK_a resulted in efficient photodecarboxylation (Φ = 0.2–0.7), to give in most cases a single product arising *via* the corresponding arylmethyl carbanion, indicating that photodecarboxylation is an efficient and general reaction for these types of compounds.

The photodecarboxylation of organic carboxylates and carboxylic acids continues to be an area of active research interest.[1–3] This is an example of a simple photochemical extrusion reaction that is comparable to the well-known photodecarbonylation of ketones. However, mechanistically, photodecarboxylation of carboxylic acids is more complex. The mechanism in which carbon dioxide is eliminated from photoexcited (organic) carboxylic acids has been classified into several types with the simple heterolytic and homolytic mechanisms being the most readily visualized.[1] Some recent papers dealing with photodecarboxylation of some non-steroidal anti-inflammatory drugs (NSAIDs) suggest that new insights and potentially new reactive systems await discovery.[2,3*a–e*] A particular example that attracted our attention is the highly efficiently (Φ = 0.75) photodecarboxylation of ketoprofen [**1**, eqn. (1)] in aqueous solution orginally reported by

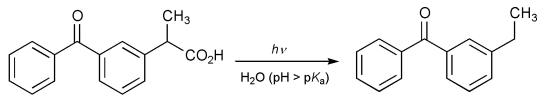

1 (1)

Costanzo *et al.*[2] At least two groups[3*a–e*] have studied the mechanism of the photodecarboxylation. The latest report we are aware of is from Scaiano and co-workers[3*a*] who showed that the reaction proceeds from the singlet excited state of the carboxylate form and that water is not essential (but probably helpful). Singlet state reactivity is unusual for benzophenone photochemistry. The nature of the primary photochemical step remains an issue. It could be either (a) a simple heterolytic cleavage mechanism to generate the carbanion directly or (b) a mesolytic mechanism in which there is an electron transfer from the carboxylate oxygen to the ketone to generate a biradical anion, followed by bond cleavage to give the carbanion.

Ketoprofen (**1**) is an aroyl-substituted phenylacetic acid. Compounds of this general structural type are readily available by routine synthesis. The high (and clean) reactivity of **1** suggested to us that other aroyl-substituted phenylacetic acids might react in a similar manner and that a general type of efficient photodecarboxylation awaits discovery. The availability of compounds of similar structural type that also react will certainly help in the elucidation of the reaction mechanism. We have now made five analogs of **1**, *viz.*, **2**–**6**. Acids **2** and **3** are simple analogs of ketoprofen (**1**). If the photodecarboxylation of **1** is respresentative of a general process, compounds **2** and **3** should react, neglecting of course any dramatic substituent effects on excited state reactivity that we have not taken into account. Compounds **4** and **5** have a different carbonyl chromophore (anthraquinone and acetophenone, respectively). If the reaction is general for other types of carbonyl chromophores, these compounds might be expected to show reactivity as well. Finally, we have changed the nature of the 'leaving group' in **6**. Here, the leaving group is formally formaldehyde, which is much less labile than CO_2. If **6** reacts in an analogous manner (*i.e.* deformylation to give the corresponding carbanion), then the reaction is indeed much more general than ever suspected. In this report, we show that all of **2**–**6** react in the manner anticipated (with varying degrees of efficiency, all generally high) demonstrating that the photodecarboxylation of aroyl and acetoyl-substituted phenylacetic acids is a general reaction. Moreover, less labile leaving groups such as formaldehyde may also be used.

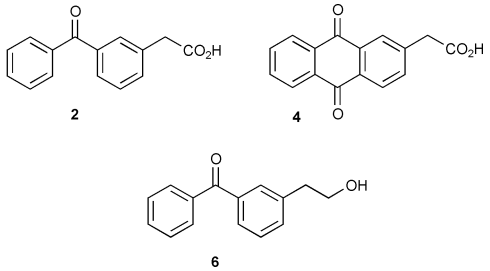

Carboxylic acids **2**–**5** were readily made by conversion of the corresponding commercially available methyl-substituted derivative to the α-bromo compound (NBS–CCl_4), followed by reaction with NaCN–EtOH and then hydrolysis using either conc. HCl or aqueous H_2SO_4. All of the acids were purified by repeated crystallization from aqueous EtOH to achieve > 98% purity.† Keto-alcohol **6** was readily prepared by BH_3–THF reduction of **2**.

Photolysis of **2**–**4** in 1 : 1 H_2O–CH_3CN (50 mL total volume; water portion set to pH 7 with dilute NaOH after adding compound to ensure complete dissociation of the acid; ≈ 10^{-3} M substrate; Rayonet photochemical reactor; 254, 300 or 350 nm lamps; quartz vessel; solution cooled with a cold-finger to ≈ 15 °C; purged continuously with argon; 5–20 min) gave cleanly the corresponding photodecarboxylation product [*e.g.*, eqn. (2)] in high yield (up to 100% on sufficiently long

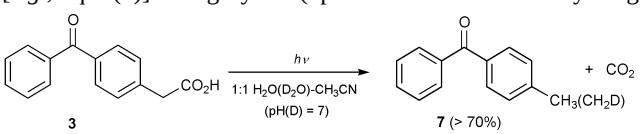

3 **7** (> 70%) (2)

photolysis time). No reaction was observed when the solution was kept in the dark. Quantum yields for photodecarboxylation were estimated using the reaction of ketoprofen (**1**) as a secondary standard (Φ = 0.75, in neat water, pH 7)[2] and ^{1}H NMR to monitor conversions. These experiments gave high quantum yields for the photodecarboxylations for **2**–**4** (in 1 : 1 H_2O-CH_3CN, pH 7): **2** (Φ = 0.66); **3** (Φ = 0.62); **4** (Φ = 0.22). Photolysis of **2**–**5** in neat CH_3CN under photolysis times used above gave no more than 5% reaction and the compounds could be essentially recovered unchanged.

It's clear from these results that (efficient) photodecarboxylation is a general photoreaction for aroyl-substituted phenyl-

DOI: 10.1039/b006724p

acetic acids. Quantum yields decreased on lowering the pH‡ which is consistent with the carboxylate form being reactive, consistent with the latest findings for ketoprofen (**1**) reported by Scaiano and co-workers.[3a] Furthermore, photolysis of **2** and **3** in D_2O–CH_3CN (as above) gave exclusively the corresponding α-deutero-methyl product, consistent with a carbanion intermediate [eqn. (2)]. Interestingly, photolysis of acetophenone derivative **5** gave two products in a 7 : 3 mole ratio (Φ for loss of substrate ≈ 0.2), respectively [eqn. (3)]: the expected simple decarboxylation product (*p*-methylacetophenone) *via* a simple phenylmethyl carbanion and a 'dimeric' product formally derivable from the phenylmethyl radical *via* coupling. Independent photolysis of *p*-methylacetophenone under identical conditions gave no reaction. Although radical coupling products have not been observed for ketoprofen (**1**) or from any of **2**–**4**, the fact that it is observed for **5** indicates that a radical-type mechanism (*e.g.* initial electron transfer from the carboxylate to the ketone)[3a–c] cannot be excluded for the photodecarboxylation. The reactivity of acetophenone derivative **5** allows for detailed investigations on this reaction pathway.

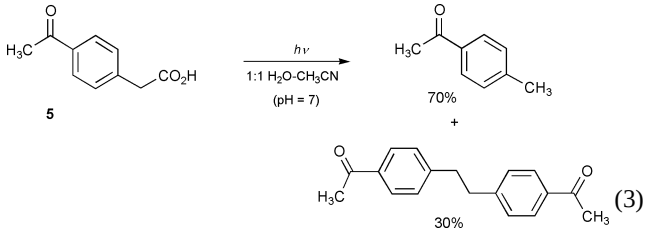

(3)

The generally high reactivity towards photodecarboxylation of the above aroyl (and acetoyl) substituted phenylacetic acids prompted us to think about the possible driving force for these reactions. A simple rationalization (assuming S_1 reactivity) is that the excited singlet states of these compounds have highly polarized π electron densities, shifted towards the keto oxygen. This would favour loss of CO_2 *via* benzylic C–C bond heterolysis, and subsequent generation of the carbanion. This mechanism bypasses the need for an initial electron transfer from the carboxylate oxygen to the carbonyl group, which appears to be warranted only for **5**. In any event, we wanted to test the former proposal and have made derivative **6** to test whether a similar reaction could operate using a much poorer 'leaving group', *viz.*, formaldehyde, and a moiety incapable of efficient electron transfer to the carbonyl group. To our surprise, photolysis of **6** in 1 : 1 H_2O–CH_3CN gave the anticipated deformylated product [*p*-methylbenzophenone (**7**)] although with yields that are several fold (5–10%) less than observed for the corresponding acid **2**, along with what appears to be major product(s) derived from photoreduction of the ketone. However, photolysis at pH 12 resulted in clean deformylation (> 70% yield) consistent with a hydroxide ion catalyzed process which would be required for deformylation *via* a carbanion intermediate. These initial results suggest that the aroylphenylmethyl group may be thought of as 'photolabile' carbanion leaving group which is able to induce a variety of benzylic C–C bond heterolysis in appropriately designed molecular systems. This is akin to the nitrobenzyl group[4] and selected diarylmethyl systems[5] that are known to have this ability.

In summary, we have shown that the photodecarboxylation of aroyl and acetoyl-substituted phenylacetic acids is a general reaction, all proceeding with high quantum yields. Less labile 'leaving groups' such as formaldehyde may also be used. In this way, one may visualize the aroyl-substituted phenylmethyl group to be a photolabile carbanion leaving group. This type of general reactivity may have application in the design of photolabile protecting groups and other photochemical applications in addition to providing new structural types for the elucidation of detailed reaction mechanism.

We acknowledge the continued support of the Natural Sciences and Engineering Research Council (NSERC) of Canada and the University of Victoria.

Notes and references

† All compounds had satisfactory ^{1}H NMR (300 MHz) and mass spectral data.

‡ We have preliminary results indicating that the *meta* isomer **2** becomes increasingly more reactive at acidities greater than pH 2 (and into the Hammett acidity region) suggesting that a new mechanism for photodecarboxylation is available for this compound in acid involving the acid form.

1 (*a*) D. Budac and P. Wan, *J. Photochem. Photobiol., A*, 1992, **67**, 135; (*b*) S. A Fleming and J. A. Pincock, *Molecular and Supramolecular Photochemistry*, Vol. 3, V. Ramamurthy and K. Schanze, eds., M. Dekker Inc., New York, 1999, p. 211.

2 L. L. Costanzo, D. DeGuidi, G. Conderelli, A. Cambria and M. Fama, *Photochem. Photobiol.*, 1989, **50**, 359.

3 (*a*) G. Cosa, L. J. Martínez and J. C. Scaiano, *Phys. Chem. Chem. Phys.*, 1999, **1**, 3533; (*b*) J. L. Martínez and J. C. Scaiano, *J. Am. Chem. Soc.*, 1997, **119**, 11 066; (*c*) S. Monti, S. Sortino, G. De Guidi and G. Marconi, *J. Chem. Soc., Faraday Trans.*, 1997, **93**, 2269; (*d*) S. Sortino and J. C. Scaiano, *Photochem. Photobiol.*, 1999, **69**, 167; (*e*) F. Boscá and M. A. Miranda, *Photochem. Photobiol.*, 1999, **70**, 853; (*f*) F. L. Cozens, W. Ortiz and N. P. Schepp, *J. Am. Chem. Soc.*, 1998, **120**, 13543; (*g*) T. M. Bockman, S. M. Hubig and J. K. Kochi, *J. Org. Chem.*, 1997, **62**, 2210; (*h*) H. Koshima, E. Hayashi, K. Shirafuji, M. Hamada, D. Matsushige, M. Miyauchi and T. Matsuura, *J. Photochem. Photobiol., A*, 1999, **129**, 121; (*i*) H. Yokoi, T. Nakano, W. Fujita, K. Ishiguro and Y. Sawaki, *J. Am. Chem. Soc.*, 1998, **120**, 12 453; (*j*) H. Görner and H. J. Kuhn, *J. Chem. Soc., Perkin Trans. 2*, 1999, 2671; (*k*) C. K. Lee and P. Wan, *J. Photochem. Photobiol., A*, 1993, **76**, 39.

4 P. Wan and S. Muralidharan, *J. Am. Chem. Soc.*, 1988, **110**, 4336.

5 E. Krogh and P. Wan, *J. Am. Chem. Soc.*, 1992, **114**, 705.

Highly regioselective addition of an ester enolate equivalent to α,β-unsaturated ketones: selective formation of both isomers derived from 1,2- and 1,4-additions using α-stannyl ester with additives

Makoto Yasuda, Yozo Matsukawa, Keishi Okamoto, Toshifumi Sako, Noriko Kitahara and Akio Baba*

Department of Applied Chemistry, Faculty of Engineering, Osaka University, 2-1 Yamadaoka, Suita, Osaka 565-0871, Japan. E-mail: baba@ap.chem.eng.osaka-u.ac.jp

Received (in Cambridge, UK) 15th June 2000, Accepted 26th September 2000
First published as an Advance Article on the web

The reaction of α-stannyl ester with α,β-unsaturated ketones in the presence of stannous chloride ($SnCl_2$) and chlorosilanes (Me_3SiCl or Me_2SiCl_2) gave 1,2- and 1,4-addition products, respectively.

The regioselective addition of a nucleophile to α,β-unsaturated carbonyl compounds (1,2- or 1,4-addition) has been focused on in modern organic syntheses. An enolate or its equivalent is often used for the functionalised nucleophile to unsaturated carbonyls. Heathcock reported excellent results using lithium enolate in which either kinetic or thermodynamic conditions effectively control the regioselectivity.[1] The correlation between the character of the metal in the enolate and the regioselectivity was also investigated.[2] We have recently reported the 1,4-addition of organotin ketone enolate using a high coordination method.[3] An organotin ester enolate, however, has significantly different reactivity and character as compared with an organotin ketone enolate and is not suitable for the reaction conditions developed for ketone enolates. For the organotin ester enolates, the equilibrium between *O*-stannylated and *C*-stannylated forms largely lies towards the *C*-stannylated species above 0 °C.[4] The stannylation of lithium ester enolate is reported to give only a *C*-stannylated ester compound (the α-stannyl ester) after distillation,[5] although stannyl ketone enolate generally exists as an equilibrium mixture of both forms.[6] Since enol forms generally show higher reactivity than keto forms, the α-stannyl ester has a lower reactivity than ketone enolates.[7,8] During our study of the activation methodology of α-stannyl ester, we found a novel approach to regiocontrol in the reaction of α,β-unsaturated ketones with α-stannyl ester as an ester enolate equivalent.

First, we examined additives for the reaction of α-stannyl ester **1** with chalcone **2a** and the results are summarized in Table 1. An attempt without additives resulted in no reaction (entry 1). The use of $BF_3{\cdot}OEt_2$ as an additive was not effective at all (entry 2). $TiCl_4$ afforded a low yield of 1,4-addition product **4a** (entry 3). Recently, we have reported a carbonyl allylation system using tributylallyltin(IV) and $SnCl_2$ in which transmetallation occurs to generate an active species.[9,10] This activation methodology was applied to the reaction of **1** in the presence of $SnCl_2$ to give β-hydroxy ester **3a** in 63% yield with excellent selectivity in 1,2-addition manner (entry 4). On the other hand, the addition of chlorotrimethylsilane gave selectively **4a** in practical yields, which were influenced by the solvents used. Nitromethane was the solvent of choice and gave the sole product **4a** in 95% yield (entry 6). These results encouraged us to develop these reaction systems using α-stannyl ester for regioselective addition to α,β-unsaturated ketones.

Next, we explored the generality of this regiocontrolled system using either $SnCl_2$–MeCN or Me_3SiCl–$MeNO_2$ with various types of enones **2a**–**e**, and showed the results in Table 2.† Excellent regiocontrol was observed in the reaction with phenyl ketone **2b**, which has an alkyl substituent on the terminal olefinic carbon (entries 3 and 4). In the reaction with alkyl ketone **2c** using $SnCl_2$, the low yield of **3c** in entry 5 was ascribed to the polymerization of the starting enone, although regioselectivity was high (entry 5). Chlorotrimethylsilane gave 83% yield of products with high selectivity (entry 6). The cyclic substrate **2d** was also applied to these systems. When

Table 1 Effect of additives on regioselective addition of **1** to enone **2a**[a]

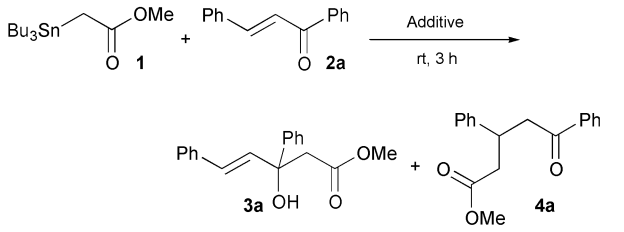

Entry	Additive	Solvent	Yield (%)	Ratio of **3a**/**4a**
1	None	MeCN	0	—
2[b]	$BF_3{\cdot}OEt_2$	CH_2Cl_2	0	—
3[b]	$TiCl_4$	CH_2Cl_2	19	< 1/99
4	$SnCl_2$	MeCN	63	> 99/1
5[c]	Me_3SiCl	MeCN	47	< 1/99
6[c]	Me_3SiCl	$MeNO_2$	95	< 1/99

[a] All reactions were carried out in solvent (1 mL) using **1** (1.2 mmol), unsaturated ketone **2a** (1.0 mmol), and additive (1.2 mmol). [b] Reaction temperature −78 °C to rt. [c] Additive (2.0 mmol) was used.

Table 2 Control of regioselectivity in addition of **1** to various enones **2**[a]

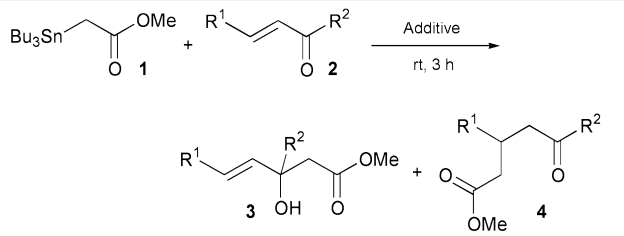

Entry	Enone	Additive	Solvent	Yield (%)	Ratio of **3**/**4**
1	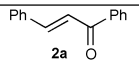	$SnCl_2$	MeCN	63	> 99/1 (**3a**/**4a**)
2		Me_3SiCl	$MeNO_2$	95	< 1/99
3	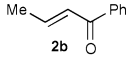	$SnCl_2$	MeCN	91	> 99/1 (**3b**/**4b**)
4		Me_3SiCl	$MeNO_2$	92	< 1/99
5	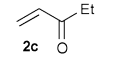	$SnCl_2$	MeCN	23	> 99/1 (**3c**/**4c**)
6		Me_3SiCl	$MeNO_2$	83	5/95
7	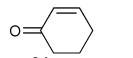	$SnCl_2$	MeCN	50	> 99/1 (**3d**/**4d**)
8		Me_3SiCl	$MeNO_2$	90	< 1/99
9	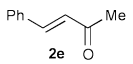	$SnCl_2$	MeCN	80	> 99/1 (**3e**/**4e**)
10		Me_3SiCl	$MeNO_2$	59	46/54
11		Me_2SiCl_2	$MeNO_2$	63	5/95

[a] All reactions were carried out in solvent (1 mL) using **1** (1.2 mmol), unsaturated ketone **2** (1.0 mmol). Either $SnCl_2$ (1.2 mmol) or chlorosilanes (2.0 mmol) were used as additives.

DOI: 10.1039/b004817h

acetonitrile was used as a solvent in the reactions with **2a**–**d** in the presence of chlorotrimethylsilane, the same or lower yields were observed but selectivity was not significantly affected. In the reaction with 4-phenylbut-3-en-2-one **2e**, the 1,2-adduct **3e** was obtained in good yield with perfect selectivity (entry 9). However, the reaction using chlorotrimethylsilane did not give selective 1,4-addition (**3e**/**4e** = 46/54, entry 10). The low selectivity is ascribed to the conjugation of the phenyl group with the olefinic moiety which could be kept by 1,2-addition and broken by 1,4-addition.[11] Unexpectedly, Michael adduct **4e** was favored (**3e**/**4e** = 5/95) when dichlorodimethylsilane was used as an additive instead of chlorotrimethylsilane (entry 11).

Although the exact reaction mechanism for either course using stannous chloride or chlorosilanes is not clear, the regiocontrol can be explained by the following assumption at the present stage. In the $SnCl_2$ system, the active tin(II) species generated by transmetallation has high Lewis acidity.[9,10] The strong interaction between carbonyl oxygen and the tin center in the nucleophile effectively accelerates the carbostannylation. The resulting Sn–O bond is strong enough for irreversible reaction. In order to examine the chlorosilane system, an NMR study was performed. The mixture of **1** and chlorotrimethylsilane in acetonitrile underwent transmetallation to give tributylchlorostannane and silylketene acetal, as determined by NMR.[12,13] After standing for 48 h at rt, the silylketene acetal completely disappeared and α-silyl ester was observed by NMR.[14,15] This resulting solution including silyl ester and tributylchlorostannane was inert to chalcone **2a**. These results suggest that tributylchlorostannane would act as a Lewis acid for Mukaiyama-type Michael addition of silylketene acetal.[16] Another possibility, namely, that further transmetallation to give stannylketene acetal from chlorostannane and silylketene acetal, which would have high reactivity and a short life time under the conditions employed in this procedure, is not completely ruled out at this stage.[4] The difference in active species generated in each system causes the highly regiocontrolled reactions.

The solvent effect of acetonitrile or nitromethane on yields probably relates to their coordination ability to the concerned active species. The additive effect of chlorosilanes on selectivity of **3e**/**4e** is still not clear.

In conclusion, regioselective addition of α-stannyl ester to α,β-unsaturated ketones was achieved in 1,2- and 1,4-addition manner by using stannous chloride and chlorosilanes as additives, respectively. The transmetallation of stannyl ester with these additives generates the key reactive intermediates with proper selectivities. α-Stannyl esters will be attractive functionalized nucleophiles with these activation methodologies because they are easy to prepare and handle and can be stored for months owing to their moderate stability. The detailed reaction mechanism is now under investigation and will be reported in a full account.

This work was supported by a Grant-in-Aid for Scientific Research from the Ministry of Education, Science, Sports, and Culture, of the Japanese Government. Thanks are due to Mr H. Moriguchi, Faculty of Engineering, Osaka University, for assistance in obtaining MS spectra.

Notes and references

† *Experimental procedure* for the synthesis of **3**: see the representative experimental procedure in our previous paper[9] (use an α-stannyl ester instead of allylstannane). *General procedure* for the synthesis of **4**: to a mixture of chlorosilane (Me_3SiCl or Me_2SiCl_2, 2.0 mmol) and an α-stannyl ester **1** (1.2 mmol) in nitromethane (1 mL) was added α,β-unsaturated ketones **2** (1.0 mmol) under nitrogen. The mixture was stirred for 3 h at ambient temperature. The reaction mixture was poured into the mixed solvent of Et_2O (30 mL) and aqueous NH_4F (15%; 15 mL) with vigorous stirring for 10 min. The resulting Bu_3SnF was filtered off. The filtrate was extracted with Et_2O (30 mL × 2) and washed by aq.HCl (1 M, 20 mL × 2) and $NaHCO_3$ (20 mL × 1) and dried ($MgSO_4$) and evaporated. The crude reaction mixture was purified by column chromatography and recrystallisation or distillation gave pure products **4**.

1 D. A. Oare and C. H. Heathcock, *J. Org. Chem.*, 1990, **55**, 157.
2 J. Bertrand, L. Gorrichon, P. Maroni and R. Meyer, *Tetrahedron Lett.*, 1982, **23**, 3267.
3 M. Yasuda, N. Ohigashi, I. Shibata and A. Baba, *J. Org. Chem.*, 1999, **64**, 2180; M. Yasuda, K. Hayashi, Y. Katoh, I. Shibata and A. Baba, *J. Am. Chem. Soc.*, 1998, **120**, 715.
4 *O*-Stannylated ketene acetal can be obtained as a kinetic product from ketene and trialkyltin alkoxide and used at low temperature. E. Shimada, K. Inomata and T. Mukaiyama, *Chem. Lett.*, 1974, 689.
5 A. Zapata and C. Acunâ, *Syn. Commun.*, 1984, **14**, 27.
6 M. Pereyre, B. Bellegarde, J. Mendelsohm and J. Valade, *J. Organomet. Chem.*, 1968, **11**, 97; M. Yasuda, Y. Katoh, I. Shibata, A. Baba, H. Matsuda and N. Sonoda, *J. Org. Chem.*, 1994, **59**, 4386.
7 J. G. Noltes, F. Verbeek and H. M. J. C. Creemers, *Organomet. Chem. Synth.*, 1970/1971, **1**, 57.
8 Enol forms generally show higher reactivity than keto forms. K. Kobayashi, M. Kawanisi, T. Hitomi and S. Kozima, *Chem. Lett.*, 1983, 851.
9 M. Yasuda, Y. Sugawa, A. Yamamoto, I. Shibata and A. Baba, *Tetrahedron Lett.*, 1996, **37**, 5951.
10 M. Yasuda, M. Tsuchida and A. Baba, *Chem. Commun.*, 1998, 563.
11 In the case of 1,4-addition to **2a**, a new conjugation with another phenyl group could appear in the resultant enolate which is first generated in this reaction course before quenching.
12 A mixed solution of **1** (1.0 mmol) and chlorotrimethylsilane (2.0 mmol) in CD_3CN (0.5 mL) in a sealed tube at rt for 10 min showed a signal corresponding to tributylchlorostannane at 122 ppm in ^{119}Sn NMR. The silylketene acetal was also observed in ^{29}Si NMR (21 ppm) and in ^1H NMR (3.16 and 3.12 ppm, each signal has a doublet with J = 2.7 Hz).
13 (*a*) G. S. Burlachenko, B. N. Khasapov, L. I. Petrovskaya, Yu. I. Baukov and I. F. Lutsenko, *Zh. Obshch. Khim.*, 1966, **36**, 512; (*b*) S. E. Denmark, R. A. Stavenger, S. B. D. Winter, K.-T. Wong and P. A. Barsanti, *J. Org. Chem.*, 1998, **63**, 9517.
14 ^{29}Si NMR (3.5 ppm), ^1H NMR (1.9 ppm).
15 The transformation from silylketene acetal to silylester is accelerated in the presence of mercury salt (ref. 13*a*).
16 K. Narasaka, K. Soai and T. Mukaiyama, *Chem. Lett.*, 1974, 1223; K. Narasaka, K. Soai, Y. Aikawa and T. Mukaiyama, *Bull. Chem. Soc., Jpn.*, 1976, **49**, 779.

ChemComm

Enantiopure arene dioxides: chemoenzymatic synthesis and application in the production of *trans*-3,4-dihydrodiols

Derek R. Boyd,* Narain D. Sharma, Colin R. O'Dowd and Francis Hempenstall

School of Chemistry, The Queen's University of Belfast, Belfast, UK BT9 5AG

Received (in Cambridge, UK) 21st August 2000, Accepted 27th September 2000
First published as an Advance Article on the web

Enantiopure *syn*- and *anti*-arene dioxides are synthesised from *cis*-dihydrodiol metabolites; *anti*-benzene dioxides are reduced to enantiopure *trans*-3,4-dihydrodiols while *syn*-benzene dioxides racemise thermally *via* 1,4-dioxocins.

The metabolism of monocyclic arenes by bacteria (procaryotes) occurs *via* dioxygenase-catalysed dihydroxylation to yield *cis*-dihydrodiols (*e.g.* metabolite **3** from benzene **1**, R = H).[1] In fungi or animals (eucaryotes) however, benzene ring metabolism proceeds *via* monooxygenase-catalysed epoxidation to yield a rapidly equilibrating arene oxide–oxepine tautomeric mixture (*e.g.* metabolites **2** ⇌ **4** from benzene **1,** R = H, Scheme 1).[2]

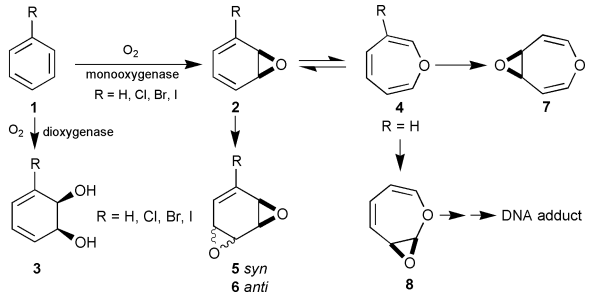

Scheme 1

When further oxidation of benzene oxide–oxepine, **2** ⇌ **4** (R = H), was carried out using dimethyl dioxirane (DMD) as oxidant epoxidation occurred exclusively on the oxepine valence tautomer **4**. The minor symmetrical oxepine epoxide **7** was isolated but the major oxepine epoxide **8** rearranged spontaneously to *Z*,*Z*-muconaldehyde.[3] Oxepine epoxide **8** and *Z*,*Z*-muconaldehyde have been implicated in DNA adduct formation and possibly the carcinogenicity of benzene (Scheme 1).[4] Evidence that arene dioxides can be formed in eucaryotic systems is provided by the isolation of the *anti*-naphthalene dioxide **9** as a liver metabolite of naphthalene,[5] and the *syn*-benzene dioxide **10** as a fungal metabolite.[6]

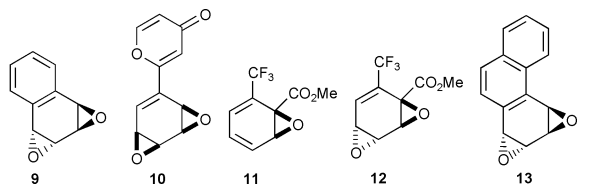

Following earlier studies of remote site epoxidation of arene oxide derivatives of polycyclic arenes using DMD,[7] we have extended this method to the synthesis of *anti*-arene dioxides in mono- and polycyclic arenes. Thus the stable benzene oxide metabolite **11**[8] was found to yield only *anti*-benzene dioxide **12** upon treatment with DMD. The formation of **12** from a benzene oxide tautomer, and of oxirane **7** from an oxepine tautomer,[3] indicates that epoxidation can occur on either form. The DMD epoxidation of configurationally stable (+)-1*R*,2*S*-naphthalene oxide ([α]$_D$ +145, $CHCl_3$) gave only (+)-1*R*,2*R*,3*R*,4*R*-*anti*-naphthalene dioxide **9** ([α]$_D$ +1, $CHCl_3$).† Conversely phenanthrene 3,4-oxide was found to spontaneously racemise *via* an undetected oxepine intermediate and only the racemic form of *anti*-dioxides **13** could be obtained by DMD oxidation. The spontaneous racemization of benzene oxides[9] similarly precludes the synthesis of enantiopure *anti*-benzene dioxides by the chemical oxidation route.

Racemic samples of *syn*-**5**[10] (R = Br, CO_2H, CHO) and *anti*-benzene dioxides **6**[11–13] (R = H) were synthesised earlier by multistep routes; only compound **6** (R = H) was obtained in enantiopure form.[12,13] The availability of *cis*-dihydrodiol enantiomers **3** (R = Cl, Br, I) from bacterial metabolism,[1,2] prompted the following new approach to the synthesis of enantiopure *syn*-**5** and *anti*-benzene dioxides **6**, (Scheme 2). A mixture of *syn*- (**14**, 85%) and *anti*-tetraol (**17,** 15%) derivatives of *cis*-dihydrodiols **3** (R = Cl, Br, I), obtained (80% yield) using the osmylation procedure reported by Donohoe *et al.*,[14] was separated (charcoal–Celite chromatography, EtOH–H_2O as eluent). Reaction of *syn*-tetraols **14** (R = Cl, Br, I) with 2-acetoxyisobutyryl bromide afforded *bis*-bromoacetates **15** (R = Cl, Br, I) in *ca*. 86% yield. Cyclization using NaOMe yielded the 3*S*,4*S*,5*S*,6*S*-*syn*-benzene dioxides **5** (R = Cl, Br, I, in *ca*. 75% yield) with [α]$_D$ values of −59, −56, and −56 in $CHCl_3$ respectively. Reaction of the *bis*-acetonide derivative of *syn*-tetraol **14** (R = I) with PhMgBr, and deprotection of the acetonide groups, yielded *syn*-tetraol **14** (R = Ph), which was similarly converted to 3*S*,4*S*,5*R*,6*R*-*syn*-benzene dioxide **5** (R = Ph, [α]$_D$ −42, $CHCl_3$). Application of this method to *anti*-tetraols **17** (R = Cl, Br, I) gave 3*R*,4*R*,5*S*,6*S*-*anti*-benzene dioxides **6** (R = Cl, Br, I, 78 % yield) with [α]$_D$ values of −115, −54, and −6 in $CHCl_3$ respectively (Scheme 2). Hydrogenolysis (H_2, Pd/C, NaOAc, MeOH) of the 3,4-acetonide derivative of *anti*-tetraol **17** (R = I), and deprotection, yielded the parent compound conduritol E, **17** (R = H), [α]$_D$ − 320, H_2O; it was converted to 1*R*,2*R*,3*R*,4*R*-*anti*-benzene dioxide **6** (R = H, [α]$_D$ −319, $CHCl_3$) using the method shown in Scheme 2.

The method of conversion of *cis*-dihydrodiols to *anti*-arene dioxides (Scheme 2) was also applied to polycyclic arenes. Thus, 1*R*,2*R*,3*R*,4*R*-*anti*-naphthalene dioxide **9** ([α]$_D$ + 1, $CHCl_3$; +14, MeOH)† was synthesised from the available *cis*-1*R*,2*S*-dihydrodiol metabolite of naphthalene ([α]$_D$ + 247, $CHCl_3$). Similarly the *cis*-3*S*, 4*R*-dihydrodiol metabolite of

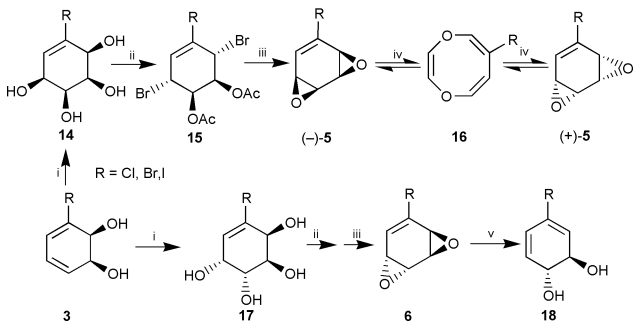

Scheme 2 *Reagents*: i, OsO_4, CH_2Cl_2, TMNO; ii, $AcOCMe_2COBr$, MeCN; iii, NaOMe, Et_2O; iv, toluene, 85 °C; v, CO, $Pd(OAc)_2$, K_2CO_3, THF–H_2O.

DOI: 10.1039/b006837n

phenanthrene ($[\alpha]_D$ + 35, MeOH) was converted to an enantiopure sample of 1*R*,2*R*,3*R*,4*R*-*anti*-phenanthrene dioxide **13** ($[\alpha]_D$ + 47, MeOH).

Attempts to form the carbomethoxy-substituted *anti*-benzene dioxide **6** (R = CO_2Me) from the corresponding vinyl iodide **6** (R = I), using a reported[15] palladium-catalysed carbonylation procedure for aryl iodides (CO, $Pd(OAc)_2$, K_2CO_3, THF–H_2O, rt) formed *trans*-3,4-dihydrodiol **18** (R = I, $[\alpha]_D$ −145, MeOH) in excellent yield (>85%) after 0.75 h. The *anti*-benzene dioxides **6** (R = Cl, Br) also yielded 1*R*,2*R*-*trans*-3,4-dihydrodiols **18** (R = Cl, $[\alpha]_D$ −176, MeOH) and **18** (R = Br, $[\alpha]_D$ −253, MeOH) in high yields; a complex mixture of products was obtained from the corresponding *syn*-benzene dioxides **5** (R = Cl, Br, I). The mechanism of conversion of *anti*-benzene dioxides **6** to the corresponding *trans*-3,4-dihydrodiols **18** may involve opening of one epoxide ring followed by formation of a π-allyl palladium complex and rearrangement, *via* an oxetane intermediate, with CO acting as a reducing agent.

The *trans*-dihydrodiols **18** (R = H, Cl, Br) have been detected as minor metabolites of the parent benzene substrates in animal liver systems and have been converted to diol epoxides which are implicated in DNA adduct formation and mutagenicity.[16,17] Palladium-catalysed reaction of *trans*-dihydrodiol **18** (R = I) under similar conditions (CO, $Pd(OAc)_2$, NaOAc, MeOH, rt), but for an extended period (18 h) resulted in the substitution of the iodine atom with a carbomethoxy group to give the 3*R*,4*R*-*trans*-dihydrodiol **18** (R = CO_2Me, $[\alpha]_D$ −94, MeOH) in 80% yield. The *trans*-3,4-dihydroxy-3,4-dihydrobenzoic acid **18** (R = CO_2H), a hydrolysis product of chorismic acid, appears to be a growth promoter.[17] The four step approach to the synthesis of single enantiomer *trans*-3,4-dihydrodiols **18** (R = Cl, Br, I) from *cis*-2,3-dihydrodiols (Scheme 2) represents a significant improvement over earlier routes requiring eight[9] or more[16] steps. The *syn*-benzene dioxides **5** (R = Cl, Br, I, Ph), in common with other *syn*-benzene dioxides **5** (R = H, CO_2H, CHO),[8] were found to undergo a retro-Diels–Alder cycloaddition reaction to yield the corresponding 1,4-dioxocins **16** at relatively low (~85 °C) temperature. Since an enantiopure sample of a *syn*-benzene dioxide was available, a thermal racemization study on the (−)-*syn*-dioxide of iodobenzene **5** (R = I) was carried out (toluene, 85 °C). Total racemization occurred over 2 h (HPLC by Chiralcel OB, α 1.32, iPrOH:hexane, 1:5). NMR analysis showed that the equilibrium mixture contained both the residual *syn*-benzene dioxide **5** (R = I), as a minor component (12%), and the corresponding 1,4-dioxocin isomer **16** (R = I) as a major component (88%). Chromatographic separation of compounds **16** and **5** (R = I) followed by heating either component as before yielded the same equilibrium mixture. This unusual example of a concerted racemisation of four chiral centres in one enantiomer was not observed for the *anti*-benzene dioxide **6** (R = I).

In conclusion we have shown that: (i) arene oxides yield isolable *anti*-arene dioxides by DMD oxidation, (ii) enantiopure samples of *syn*-**5** and *anti*-arene dioxides **6**, **9**, **13** are obtained in high yields from the corresponding *cis*-dihydrodiol metabolites, (iii) *anti*-benzene dioxides **6** are precursors for a new route to *trans*-3,4-dihydrodiols **18**, (iv) racemisation of a *syn*-benzene dioxide enantiomer containing four chiral centres occurs thermally.

We thank Dr R. Agarwal for assistance with preliminary work on the synthesis of polycyclic arene dioxides, Professor D. B. Harper and Dr J. Hamilton for a sample of arene oxide metabolite **11**, Dr R. Schobert for helpful discussion and the Queen's University of Belfast for financial support (CRO'D, FH).

Notes and references

† The $[\alpha]_D$ values observed for the enantiopure *anti*-arene dioxides **6** (R = H) and **9** are significantly different from those reported,[12] furthermore, the stereochemistry of (+) *anti*-dioxide **9** was incorrectly assigned.[12]

1 D. R. Boyd and G. N. Sheldrake, *Nat. Prod. Rep.*, 1998, 309; T. Hudlicky, D. Gonzalez and D. T. Gibson, *Aldrichimica Acta*, 1999, **32**, 34.
2 D. R. Boyd and N. D. Sharma, *Chem. Soc. Rev.*, 1996, 289.
3 C. Bleasdale, R. Cameron, C. Edwards and B. T. Golding, *Chem. Res. Toxicol.*, 1997, **10**, 1314.
4 C. Bleasdale, B. T. Golding, G. Kennedy, J. O. MacGregor and W. P. Watson, *Chem. Res. Toxicol.*, 1993, **6**, 407.
5 W. G. Stillwell, O. J. Bouwsma, J. P. Thenot, M. G. Horning, G. W. Griffin, K. Isikawa and M. Takaku, *Res. Commun. Chem. Pathol. Pharmacol.*, 1978, **20**, 509.
6 D. B. Borders, P. Shu and J. E. Lancaster, *J. Am. Chem. Soc.*, 1972, **94**, 2540.
7 S. K. Agarwal, D. R. Boyd, W. B. Jennings, R. M. McGuckin and G. A. O'Kane, *Tetrahedron Lett.*, 1989, **30**, 123.
8 D. R. Boyd, J. T. G. Hamilton, N. D. Sharma, J. S. Harrison, W. C. McRoberts and D. B. Harper, *Chem. Commun.*, 2000, 1481.
9 D. R. Boyd, N. D. Sharma, H. Dalton and D. Clarke, *Chem. Commun.*, 1996, 45.
10 H. J. Altenbach and E. Vogel, *Angew. Chem., Int. Ed. Engl.*, 1972, **11**, 937; E. Vogel, H. J. Altenbach and D. Gremer, *Angew. Chem. Int. Ed. Engl.*, 1972, **11**, 935; H. J. Altenbach, B. Voss and E. Vogel, *Angew. Chem., Int. Ed. Engl.*, 1983, **22**, 410.
11 E. Vogel, H. J. Altenbach and E. Schmidbauer, *Angew. Chem., Int. Ed. Engl.*, 1973, **12**, 838; H. J. Altenbach, H. Stegelmeier and E. Vogel, *Tetrahedron Lett.*, 1978, 3333.
12 M. Koreeda and M. Yoshihara, *J. Chem. Soc., Chem. Commun.*, 1981, 974.
13 S. Adelt, O. Plettenburg, R. Stricker, G. Reiser, H. J. Altenbach and G. Vogel, *J. Med. Chem.*, 1999, **42**, 1262.
14 T. J. Donohoe, R. Garg and P. R. Moore, *Tetrahedron Lett*, 1996, **37**, 3407.
15 N. A. Bumagin, K. V. Nikitin and I. P. Beletskaya, *J. Organomet. Chem.*, 1988, **358**, 563.
16 M. V. Ganey, R. E. Padykula, G. A. Berchtold and A. G. Braun, *J. Org. Chem.*, 1989, **54**, 2787.
17 G. A. Berchtold and B. A. Chiasson, *J. Am. Chem. Soc.*, 1974, **96**, 2898.

A novel route to advanced model systems for silica-immobilized olefin polymerization catalysts

Frank T. Edelmann,* Stephan Gießmann and Axel Fischer

Chemisches Institut der Otto-von-Guericke-Universität Magdeburg, Universitätsplatz 2, D-39106 Magdeburg, Germany. E-mail: Frank.Edelmann@vst.uni-magdeburg.de

Received (in Basel, Switzerland) 26th April 2000, Revised manuscript received 22nd September 2000, Accepted 28th September 2000
First published as an Advance Article on the web

Constituting a novel synthetic route to model compounds for titanium catalysts immobilized on silica, the disilylated silsesquioxane derivative $Cy_7Si_7O_9(OH)(OSiMe_3)_2$ 2a, has been reacted with the 'tucked-in' fulvene complex Cp*Ti-($C_5Me_4CH_2$) to give the titanium(III) silsesquioxane Cp^*_2Ti-$[Cy_7Si_7O_{10}(OSiMe_3)_2]$ 3, while treatment of Cp*Ti-($C_5Me_4CH_2$) with $Cy_7Si_7O_9(OH)_2(OSiMe_3)$ 2b affords the mono(pentamethylcyclopentadienyl) complex Cp*Ti[Cy_7-$Si_7O_{11}(OSiMe_3)$][$Cy_7Si_7O_{10}(OH)(OSiMe_3)$] 4 which is an advanced model compound for a catalytically active titanium center on a silica surface.

Silsesquioxanes of the general formula $(RSiO_{1.5})_n$ are an unusual class of organosilicon compounds offering numerous exciting applications in catalysis[1] and materials science[2,3] alike. According to Feher *et al*., incompletely condensed silsesquioxanes such as $Cy_7Si_7O_9(OH)_3$ **1** (Cy = cyclohexyl) share structural similarities with β-cristobalite and β-tridymite and are thus quite realistic models for the silanol sites on silica surfaces.[4–10] These include the first trivalent titanasilsesquioxane, blue dimeric $[Cy_7Si_7O_{12}Ti]_2$, which was prepared by treatment of **1** with $Ti[N(SiMe_3)_2]_3$.[7] It is now generally accepted that metallasilsesquioxanes derived from **1** are suitable model systems for heterogeneous silica-supported transition metal catalysts. Moreover, it has turned out that certain metallasilsesquioxanes, especially those of Ti and V, are veritable catalysts themselves *e.g.* in the metathesis, polymerization and epoxidation of olefins.[1] We report here a novel preparative route leading to model compounds for titanium olefin polymerization catalysts immobilized on silica surfaces which involves addition of functionalized silsesquioxane precursors across the Ti–C bond of the 'tucked in' fulvene titanium complex (η^5-C_5Me_5)(η^5,η^1-$C_5Me_4CH_2$)Ti (= Cp*FvTi).[11–13]

Treatment of Cp*FvTi with 1 equivalent of the disilylated silsesquioxane precursor **2a** resulted in clean formation of the titanium(III) silsesquioxane complex **3** which was isolated in the form of air-sensitive, dark green crystals (Scheme 1). The low isolated yield (16%) can be traced back to the very high solubility of **3** even in non-polar organic solvents.

The X-ray structure of **3**‡ (Fig. 1) shows that upon protonation of the coordinated tetramethylfulvene ligand a Cp^*_2Ti unit has been generated which is now coordinated to a 'model silanized silica surface'. The Ti–O bond length in **3** is 1.927(2) Å. In accordance with the presence of a decamethyltitanocene(III) derivative a very broad ^{1}H NMR signal ($\nu_{1/2} \cong$ 1000 Hz) at δ 14.6 could be unambiguously assigned to the C_5Me_5 protons which is in good agreement with values reported by Pattiasina *et al.* for a series of Cp^*_2TiX complexes (X = Cl, Br, I, BH_4, NMe_2, OBu^t, O_2CH; δ 14.1–18.4, $\nu_{1/2}$ = 620–5000 Hz).[12,13]

The new synthetic route using the fulvene precursor Cp*FvTi was also successfully employed in the preparation of a compound which can be regarded as one of the most advanced molecular models for a catalytically active titanium center on a silica surface. Reaction of Cp*FvTi with the monosilylated silsesquioxane precursor **2b** in refluxing toluene afforded a

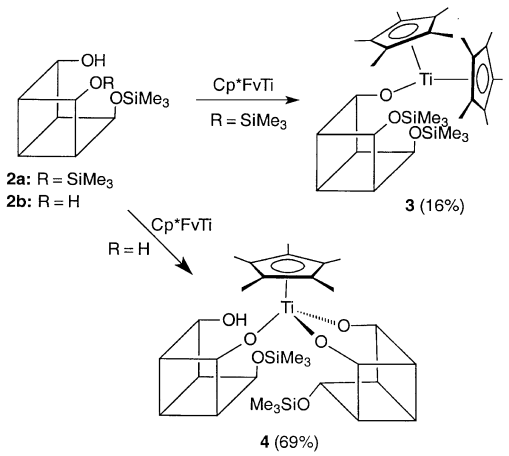

Scheme 1 Synthesis of complexes **3** and **4**.† *Reaction conditions*: toluene, 2 h reflux, crystallization from hexane.

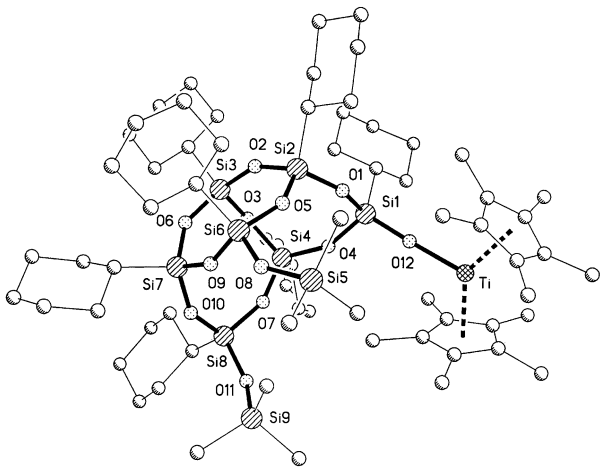

Fig. 1 Structure of **3** in the crystal. Selected interatomic distances (Å) and bond angles (°): Ti–O(12) 1.927(2), Si(1)–O(12) 1.595(2), Ti–C 2.411(3) (av.), Ti–O(12)–Si(1) 177.8(1), Si(6)–O(8)–Si(5) 146.1(1), Si(8)–O(11)–Si(9) 147.7(1).

yellow crystalline material which was shown to be the novel mono-Cp* titanium(IV) silsesquioxane complex Cp*Ti[Cy_7-$Si_7O_{11}(OSiMe_3)$][$Cy_7Si_7O_{10}(OH)(OSiMe_3)$] **4** (69% yield). The surprising outcome of this reaction is the exclusive formation of a Cp^*Ti^{IV} complex in which two silsesquioxanes are bonded in different ways to a single titanium center. In the course of the reaction 1 equivalent of pentamethylcyclopentadiene is eliminated (GC control).

An X-ray diffraction analysis‡ (Fig. 2) clearly shows that **4** is an advanced and highly 'realistic' molecular model for a Ti olefin polymerization catalyst immobilized on a silica surface. A mono(pentamethylcyclopentadienyl) titanium unit resides on

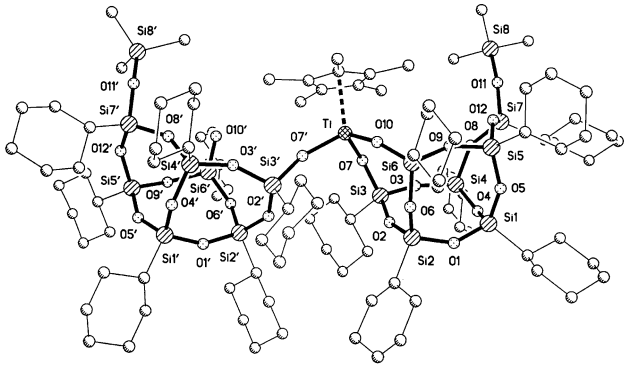

Fig. 2 Structure of **4** in the crystal. Selected interatomic distances (Å) and bond angles (°): Ti–O7 1.789(3), Ti–O7′ 1.794(3), Ti–O10 1.805(3), Ti–C 2.317(5), Si3–O7 1.575(3), Si3′–O7′ 1.571(3), Si6–O10 1.580(3); O7–Ti–O7′ 104.3(2), O7–Ti–O10 103.9(2), O7′–Ti–O10 105.3(2), Ti–O7–Si3 148.9(2), Ti–O7′–Si3′ 162.9(2), Ti–O10–Si6 154.8(2).

a 'model silica surface' formed by one chelating and one monodentate silsesquioxane ligand. With an average of 1.796(3) Å the three Ti–O bond lengths are virtually identical. A highly unusual feature of **4** making this compound a particular 'realistic' model system is a silanol function in close proximity to the Ti center. Very weak hydrogen bonding interaction of this silanol group with a cage oxygen atom (C8′) apparently prevents the molecule from intermolecular protonation of the remaining Cp* ligand, thereby 'taming' the reactivity of the Si–OH function.

We conclude that reactions of the fulvene precursor Cp*FvTi with functionalized silsesquioxanes represent a novel salt-free route to advanced molecular model systems for Ti olefin polymerization catalysts immobilized on a silica surface. The new method should have the potential of being more generally applicable to other silsesquioxane reagents as well as the zirconium analogues.

We thank the Deutsche Forschungsgemeinschaft (Schwerpunktprogramm Siliciumchemie) and the Fonds der Chemischen Industrie for financial support.

Notes and references

† *Selected spectroscopic and analytical data*: **3**: green crystals, mp 294 °C. δ_H($CDCl_3$, 25 °C): 14.6 (br, $\nu_{1/2} \cong$ 1000 Hz, C_5Me_5), 2.2–0.4 (m br, 95H, Cy-CH_2, Cy-CH, $OSiMe_3$). Anal. Calc. for $C_{68}H_{125}O_{12}Si_9Ti$ (1435.38): C, 56.9; H, 8.8. Found: C, 56.0; H, 8.7%. **4**: Yellow crystals, mp 248–252 °C. IR (KBr): 3430w br, 2922vs, 2852vs, 1461vs, 1448vs, 1269s, 1196vs, 1129vs, br, 1016vs br, 939s, 891vs (Si–OH), 849s (Si–OH), 825m, 742m, 508vs br, 471vs cm^{-1}. δ_H($CDCl_3$, 25 °C): 2.97 (s, 1H, Si–OH), 2.43 (s, 15H, C_5Me_5), 2.17 (m, br, 32H, Cy-CH_2), 1.77 (m, br, 69H, Cy-CH_2), 1.36 (m, br, 39H, Cy-CH_2), 1.07 (m, br, 14H, Cy-CH), 0.36 (s, 9H, $OSiMe_3$), 0.33 (s, 9H, $OSiMe_3$). δ_C(C_6D_6, 25 °C): 127.4 (C_5Me_5), 28.8–27.3 (m, Cy-CH_2), 26.5–23.9 (m, Cy-CH), 12.9 (C_5Me_5), 2.5 ($OSiMe_3$), 2.3 ($OSiMe_3$). ^{29}Si NMR (C_6D_6, 25 °C): δ 9.6, 7.9 ($OSiMe_3$); −66.3 to −69.1 (m). Anal. Calc. for $C_{100}H_{187}O_{24}Si_{16}Ti$ (2270.82): C, 52.9; H, 8.3. Found: C, 53.4; H, 8.3%.

‡ *Crystal data*: the measurements on **3** and **4** were performed at −100 °C using a Siemens SMART CCD system with Mo-Kα X-radiation (λ = 0.71073 Å) and graphite monochromator. Selected crystals of **3** and **4** were coated with mineral oil, mounted on a glass fibre and transferred to the cold nitrogen stream (Siemens LT-2 attachment). Full hemispheres of the reciprocal space were scanned by ω in three sets of frames of 0.3°. As an absorption correction the SADABS routine was applied.

3: $C_{68}H_{125}O_{12}Si_9Ti\cdot 0.5\ C_7H_8$, M = 1481.46, monoclinic, space group $P2_1/n$, a = 13.087(1), b = 26.163(1), c = 24.449(2) Å, β = 97.616(3)°, U = 8297.5 Å^3, Z = 4, D_c = 1.186 Mg m^{-3}, F(000) = 3208, μ(Mo-Kα) = 0.29 mm^{-1}, max./min. transmission 1.00/0.57, green prism 0.88 × 0.41 × 0.36 mm. A total of 54689 reflections were collected, over a range $1.7 < \theta < 28.3°$, of which 20363 were independent (R_{int} = 0.053). The structure was solved by direct methods. Refinement was by full-matrix least squares on F^2 and converged to $R1$ = 0.054 (conventional) and $wR2$ = 0.136 (all data), with goodness of fit = 1.02, 844 refined parameters, weighting scheme $[\sigma^2(F_o^2) + 0.0822P)^2 + 1.1511P]$, where $P = (F_o^2 + 2F_c^2)/3$.

4: $C_{100}H_{188}O_{24}Si_{16}Ti\cdot 1.5C_7H_8$, M = 2410.04, triclinic, space group $P\bar{1}$, a = 12.0428(3), b = 22.461(2), c = 25.540(2) Å, α = 106.667(3), β = 99.602(3), γ = 100.045 (3)°, U = 6342 Å^3, Z = 2, D_c = 1.262 Mg m^{-3}, F(000) = 2602, μ(Mo-Kα) = 0.28 mm^{-1}, max./min. transmission 1.00/0.79, pale yellow prism 0.45 × 0.35 × 0.30 mm. A total of 31546 reflections were collected, over a range of $0.9 < \theta < 26.7°$, of which 24118 were independent (R_{int} = 0.034). The structure was solved by direct methods.[14] Refinement was by full-matrix least squares on F^2 and converged to $R1$ = 0.080 (conventional) and $wR2$ = 0.194 (all data), with goodness of fit = 1.040, 1382 refined parameters, weighting scheme $[\sigma(F_o^2) + 0.0487P)^2 + 17.2592P]$, where $P = (F_o^2 + 2F_o^2)/3$.[15]

CCDC 182/1793. See http://www.rsc.org/suppdata/cc/b0/b007854i/ for crystallographic files in .cif format.

1 H. C. L. Abbenhuis, *Chem. Eur. J.*, 2000, **6**, 25.
2 P. G. Harrison, *J. Organomet. Chem.*, 1997, **542**, 141.
3 J. D. Lichtenhan, *Comments Inorg. Chem.*, 1995, **117**, 15.
4 M. G. Voronkov and V. L. Lavrentyev, *Top. Curr. Chem.*, 1982, **102**, 199.
5 F. J. Feher, D. A. Newman and J. F. Walzer, *J. Am. Chem. Soc.*, 1989, **111**, 1741.
6 (*a*) F. J. Feher, T. A. Budzichowski, R. L. Blanski, K. J. Keller and J. W. Ziller, *Organometallics*, 1991, **10**, 2526; (*b*) F. J. Feher and T. A. Budzichowski, *Polyhedron*, 1995, **14**, 3239.
7 (*a*) F. J. Feher, S. L. Gonzales and J. W. Ziller, *Inorg. Chem.*, 1988, **27**, 3440; (*b*) F. J. Feher and J. F. Walzer, *Inorg. Chem.*, 1990, **29**, 1604.
8 P. G. Harrison, *J. Organomet. Chem.*, 1997, **542**, 141.
9 R. Murugavel, A. Voigt, M. G. Walawalkar and H. W. Roesky, *Chem. Rev.*, 1996, **96**, 2205.
10 T. W. Hambley, T. Maschmeyer and A. F. Masters, *Appl. Organomet. Chem.*, 1992, **6**, 253.
11 J. E. Bercaw, *J. Am. Chem. Soc.*, 1974, **96**, 5087.
12 J. W. Pattiasina, C. E. Hissink, J. L. de Boer, A. Meetsma and J. H. Teuben, *J. Am. Chem. Soc.*, 1985, **107**, 7785.
13 J. W. Pattiasina, Ph.D. Thesis, Rijksuniversiteit Groningen, 1988.
14 G. M. Sheldrick, SHELXTL, Structure Determination Software Programs, Version 5.03 (PC), Siemens Analytical X-Ray Instruments, Madison, WI, 1995.
15 G. M. Sheldrick, SHELXL-97, A program for crystal structure refinement, Universität Göttingen, 1997.

ChemComm

Synthesis and structural characterisation of Fe(II) and Cu(I) complexes of a new tetrafunctional N-donor ligand with dodecahedral or tetrahedral binding domains†

Sardar Ameerunisha,[a] Jörg Schneider,[a] Thomas Meyer,[a] Panthapally S. Zacharias,[b] Eckhard Bill[c] and Gerald Henkel*[a]

[a] *Institut für Synthesechemie der Gerhard-Mercator-Universität, Lotharstr. 1, D-47048, Duisburg, Germany. E-mail: biohenkel@uni-duisburg.de*
[b] *School of Chemistry, University of Hyderabad, Hyderabad - 500 046, India. E-mail: pszsc@uohyd.ernet.in*
[c] *Max-Planck-Institut für Strahlenchemie, D-45413, Mülheim an der Ruhr, Germany*

Received (in Cambridge, UK) 13th July 2000, Accepted 21st September 2000
First published as an Advance Article on the web

The tetrafunctional N-donor ligand 1 is able to form homoleptic complex cations with dodecahedral ($[Fe\{C_{12}H_6N_2(CHNC_6H_4SMe)_2\}_2]^{2+}$ 2) or tetrahedral ($[Cu_2\{C_{12}H_6N_2(CHNC_6H_4SMe)_2\}_2]^{2+}$ 3) binding domains.

Polyfunctional ligands which are able to either act as fully chelating systems towards one metal ion or to divide their donor functions into separate domains to bind different metal ions offer fascinating perspectives in the synthesis of complexes with complementary topological properites.[1–3]

Though principally ambivalent in this sense, 1,10-phenanthroline systems normally act in a chelating fashion due to steric hindrances caused by the polycyclic aromatic system.[4,5] We report herein the first instance where a Schiff-base derivative of 1,10-phenanthroline containing four nitrogen donor functions—namely $C_{12}H_6N_2(CHNC_6H_4SMe)_2$ **1**—behaves in an ambivalent fashion towards different metal ions in homoleptic bis-ligand complex cations and describe the structural properties of $[Fe\{C_{12}H_6N_2(CHNC_6H_4SMe)_2\}_2]^{2+}$ **2** and of $[Cu_2\{C_{12}H_6N_2(CHNC_6H_4SMe)_2\}_2]^{2+}$ **3**.

Ligand **1** (ESI†) was synthesised from 2,9-diformylphenanthroline[6] and 2-methylmercaptoaniline. The mononuclear iron(II) complex cation **2** was obtained by reaction of **1** with $FeCl_2{\cdot}4H_2O$ and isolated as $[Fe\{C_{12}H_6N_2(CHNC_6H_4SMe)_2\}_2]_2[Cl_3FeOFeCl_3][ClO_4]_2{\cdot}4DMF$.‡ The dinuclear copper(I) cation **3** was obtained by reaction of **1** with $Cu(MeCN)_4BF_4$[7] or with $Cu(ClO_4)_2{\cdot}6H_2O$ and isolated as $[Cu_2\{C_{12}H_6N_2(CHNC_6H_4SMe)_2\}_2][BF_4]_2$ or as $[Cu_2\{C_{12}H_6N_2(CHNC_6H_4SMe)_2\}_2][ClO_4]_2{\cdot}3DMF$ respectively.

The crystal structure of **2**§ (Fig. 1) shows that the eight nitrogen donor atoms of the two ligands define a distorted triangulated dodecahedron around Fe(II) which is composed of two sets of trapezoidal arrangements in perpendicular orientations. These sets belong to different ligands and form two interpenetrating tetrahedra, a flattened one consisting of N(1), N(2), N(5) and N(6) and an elongated one defined by N(3), N(4), N(7) and N(8). The shortest Fe–N bonds [N(2), N(6): 2.180 Å; N(1), N(5): 2.242 Å] are formed by the aromatic donor functions which define the flattened tetrahedron. The elongated tetrahedron is composed of the imine donor functions and makes two slightly longer Fe–N_{imino} bonds [N(3), N(7): 2.389 Å] and two substantially longer ones [N(4), N(8): 2.769 Å]. According to this distance distribution, the overall coordination around iron(II) should be described as a distorted 4 + 2 + 2 dodecahedral geometry. The two phen moieties are planar within experimental error (mean deviation 0.026 and 0.037 Å, respectively) and nearly perpendicular (interplanar angle 100.7°) to each other. The complex anion $[Cl_3FeOFeCl_3]^{2-}$ has crystallographically imposed inversion symmetry resulting in an apparently linear Fe–O–Fe bridge [Fe–O 1.759(1) Å]. From an inspection of the atomic displacement parameters, however, it cannot be ruled out that the linear bridge represents only the mean geometry of slightly bent molecules which are distributed throughout the crystal in a disordered fashion. This dinuclear iron(III) species has been described frequently in the literature in compounds with a variety of different counter cations.[8]

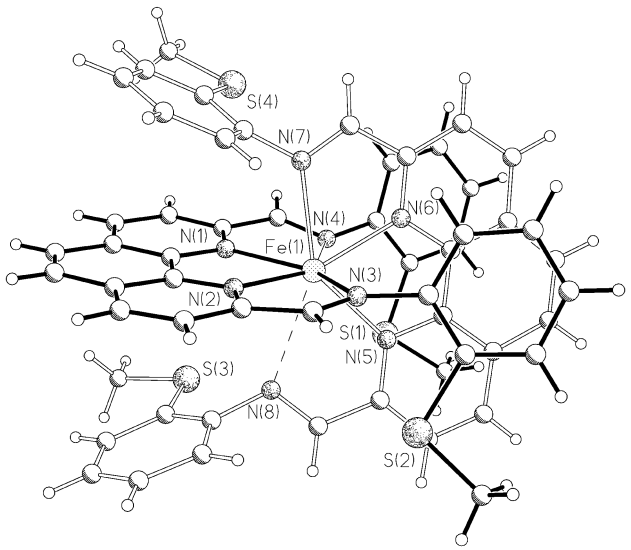

Fig. 1 Structure of $[Fe\{C_{12}H_6N_2(CHNC_6H_4SMe)_2\}_2]^{2+}$ **2** in crystals of $[Fe\{C_{12}H_6N_2(CHNC_6H_4SMe)_2\}_2][Cl_3FeOFeCl_3][ClO_4]_2{\cdot}4DMF$. Selected bond distances (Å): Fe(1)–N(1) 2.246(3), Fe(1)–N(2) 2.178(3), Fe(1)–N(3) 2.397(3), Fe(1)–N(4) 2.809(3), Fe(1)–N(5) 2.238(3), Fe(1)–N(6) 2.183(3), Fe(1)–N(7) 2.399(3), Fe(1)–N(8) 2.729(3).

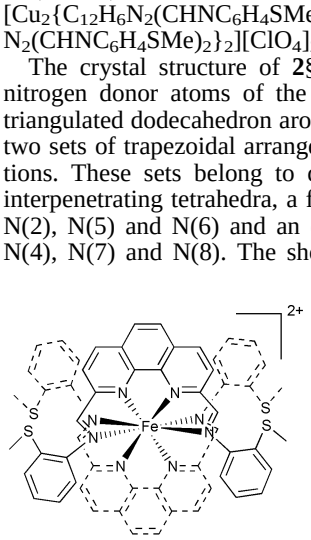

2

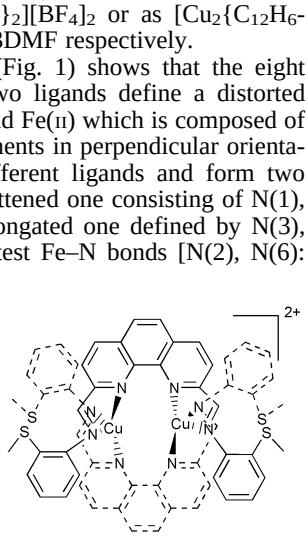

3

The structure of **3** is shown in Fig. 2. Though the spatial distribution of the nitrogen donor functions within the complex cation is closely related to that observed in **2**, the overall symmetry is remarkably higher in this case. Cation **3** belongs to the point group D_2 with the principal twofold axis passing through the Cu atoms. The second rotation axis passes through

† Electronic supplementary information (ESI) available: synthesis, characterisation, Mössbauer and NMR data, structure of **1**. See http://www.rsc.org/suppdata/cc/b0/b005671p/

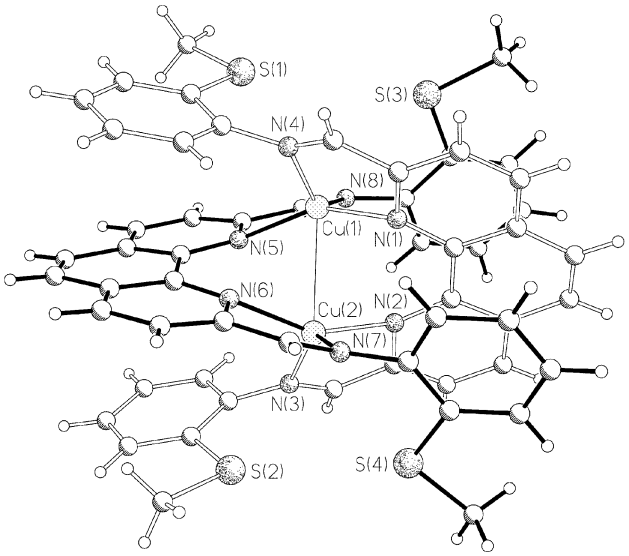

Fig. 2 Structure of $[Cu_2\{C_{12}H_6N_2(CHNC_6H_4SMe)_2\}_2]^{2+}$ **3** in crystals of $[Cu_2\{C_{12}H_6N_2(CHNC_6H_4SMe)_2\}_2][ClO_4]_2\cdot 3DMF$. Selected bond distances (Å): Cu(1)–N(1) 2.052(2), Cu(1)–N(4) 2.044(2), Cu(1)–N(5) 2.057(2), Cu(1)–N(8) 2.048(2), Cu(2)–N(2) 2.060(2), Cu(2)–N(3) 2.041(2), Cu(2)–N(6) 2.061(2), Cu(2)–N(7) 2.046(2).

the midpoints of the homonuclear six-membered carbon rings of the phenanthroline systems, and the third axis is normal to the others. None of these axes is crystallographically imposed. The dodecahedral (bitetrahedral) nitrogen framework around iron in **2** is now split into two distinct sub-sites hosting the copper ions in a fashion completely different from the mononuclear iron complex. Each copper ion is in a highly distorted tetrahedral environment formed by two phenanthroline-type and two imine-type nitrogen atoms from different ligands each. The angles defined by those CuN_2 triangles which are bisected by the principal twofold axis are 74.8° for Cu(1) and 74.3° for Cu(2), and the corresponding N–Cu–N angles within these triangles are 152.1(1) and 138.0(1)° for Cu(1) and 154.1(1) and 137.0(1)° for Cu(2). The N-donor functions of both phen systems are bonded to two different metal atoms each which are located at opposite sides of the aromatic plane. This type of bonding introduces steric strain to the ligand and leads to a significant twisting of the individual rings of the polycyclic aromatic system. Consequently, the N–C–C–N fragments are no longer planar, and the corresponding torsion angles are 9.4° [N(1), N(2)] and 10.4° [N(5), N(6)] respectively. The copper atoms are 2.695(1) Å apart from each other. Cation **3** is an extremely rare example of a complex containing 1,2-bifunctional nitrogen donor ligands with phenanthroline-like rigid geometries which do not act as chelating groups towards metal ions. To our knowledge, the only other example is the binuclear complex cation $[Cu_2\{C_{12}H_6N_2(CHNC_6H_4F)_2\}_2]^{2+}$.[4]

The structures of the complex cations **2** and **3** show some striking similarities. The close relationship between them can best be explained by removing the binuclear copper system and placing a divalent iron atom into the centroid of the molecule. This system has a highly symmetrical nitrogen environment around the central metal which can be described in terms of a triangulated dodecahedron with center-to-vertex distances of 2.182 Å (mean of 4) for the compressed tetrahedron and of 2.828 Å (mean of 4) for the elongated one. The hypothetical complex cation thus derived can easily be transformed to the complex cation **2** by a formal relaxation process which shortens two of the four long nitrogen–iron contacts within the elongated nitrogen tetrahedron to *ca.* 2.398 Å. This process is accompanied by a rotation of the methylthio-substituted phenyl rings which are attached to the conserved nitrogen donor functions of the elongated nitrogen tetrahedron around the N–C bond by 180°.

The Mössbauer spectra of a crystalline sample of $[Fe\{C_{12}H_6N_2(CHNC_6H_4SMe)_2\}_2]_2[Cl_3FeOFeCl_3]$-$[ClO_4]_2\cdot 4DMF$ in the range 80–300 K show a superposition of two quadrupole doublets (I) and (II) with an intensity ratio of close to unity (48 : 52) at 80 K. We assign subspectrum (I) to cation **2** and subspectrum (II) to $[Cl_3FeOFeCl_3]^{2-}$. The parameters of the subspectrum (I) (δ 1.18 mm s^{-1}; ΔE_Q = 2.45 mm s^{-1}) are surprisingly close to those typical for ferrous iron in octahedral environments.[9] They do not reflect any particularity in the electronic structure that could be related to the eight-coordination of iron in **2**.

The results presented here indicate that the highly conjugated ligand **1** acts either as a normal chelating tetradentate ligand or as a binucleating bis-didentate ligand depending on the nature of the central metal ion.

We thank the Deutsche Forschungsgemeinschaft (DFG), the Bundesminister für Bildung, Wissenschaft, Forschung und Technologie (BMBF) and the Fonds der Chemischen Industrie for financial support. S. A. thanks the Alexander von Humboldt Stiftung (AvH) for a post doctoral fellowship. J. S. thanks the Stiftung Stipendienfonds des Verbandes der Chemischen Industrie for granting a Kekulé fellowship.

Notes and references

‡ **CAUTION**: perchlorate salts of metal complexes are potentially explosive. Only small amounts of the materials should be handled and this has to be done with great caution.

§ *X-Ray structure analysis*: Siemens P4RA four-circle diffractometer, Mo-Kα radiation (λ = 0.71073 Å), graphite monochromator, rotating anode generator, scintillation counter, 150 K, empirical absorption corrections, SHELXTL-Plus and SHELXL97 programs,[10] direct methods, full-matrix least-squares refinement on F^2, one scaling factor, one isotropic extinction parameter.

Crystal data: for $[Fe\{C_{12}H_6N_2(CHNC_6H_4SMe)_2\}_2]_2[Cl_3FeOFeCl_3]$-$[ClO_4]_2\cdot 4DMF$: M = 2857.85, monoclinic, a = 11.760(4), b = 21.356(5), c = 25.690(8) Å, β = 100.66(2)°, V = 6340.6 Å^3, space group $P2_1/c$, Z = 2, D_c = 1.497 g cm^{-3}, μ(Mo-Kα) = 0.819 mm^{-1}, transmission range 0.801–0.688, crystal dimensions *ca.* 0.45 × 0.23 × 0.18 mm, ω scan, $2\theta_{max}$ = 54°, 13 833 unique reflections, $R1(wR2)$ = 0.0589 (0.1297) for 9226 observed reflections [$I > 2\sigma(I)$], 802 variables, non-hydrogen atoms anisotropic, H atoms at idealized positions.

For $[Cu_2\{C_{12}H_6N_2(CHNC_6H_4SMe_3)_2\}_2][ClO_4]_2\cdot 3DMF$: M = 1502.50, triclinic, a = 11.188(3), b = 16.587(4), c = 17.538(4) Å, α = 89.54(2), β = 84.40(2), γ = 87.11(2)°, V = 3234.9 Å^3, space group $P\bar{1}$, Z = 2, D_c = 1.543 g cm^{-3}, μ(Mo-Kα) = 0.94 mm^{-1}, transmission range 0.843–0.707, crystal dimensions *ca.* 0.75 × 0.23 × 0.15 mm, ω scan, $2\theta_{max}$ = 54°, 14 130 unique reflections, $R1(wR2)$ = 0.0435 (0.0929) for 10 639 observed reflections [$I > 2\sigma(I)$], 862 variables, non-hydrogen atoms anisotropic, H atoms at idealized positions.

CCDC 182/1788. See http://www.rsc.org/suppdata/cc/b0/b005671p/ for crystallographic files in .cif format.

1 J.-M. Lehn, *Supramolecular Chemistry*, VCH, Weinheim, 1995; D. P. Funeriu, J.-M. Lehn, K. M. Fromm and D. Fenske, *Chem. Eur. J.*, 2000, **6**, 2103.
2 E. C. Constable, *Nature*, 1990, **346**, 314; G. Baum, E. C. Constable, D. Fenske, C. E. Housecraft and T. Kulke, *Chem. Eur. J.*, 1999, **5**, 1862; E. C. Constable, S. M. Elder, M. J. Hannon, A. Martin, P. R. Raithby and D. A. Tocher, *J. Chem. Soc., Dalton Trans.*, 1996, 2423; E. C. Constable, *Prog. Inorg. Chem.*, 1994, **42**, 67.
3 E. C. Constable, T. Kulke, M. Neuburger and M. Zehnder, *Chem. Commun.*, 1997, 489; P. C. Rüttimann, G. Bernardinelli, B. Bocquet and A. Williams, *J. Am. Chem. Soc.*, 1992, **114**, 4230.
4 R. Ziessel and J. Suffert, *J. Chem. Soc., Chem. Commun.*, 1990, 1105; R. Ziessel, A. Harriman, J. Suffert, M.-T. Youinuo, A. de Cian and J. Fischer, *Angew. Chem.*, 1997, **109**, 2621; *Angew. Chem., Int. Ed. Engl.*, 1997, **36**, 2509.
5 S. Ameerunisha and P. S. Zacharias, *Polyhedron*, 1994, **13**, 2327.
6 C. J. Chandler, L. W. Deady and J. A. Reiss, *J. Heterocycl. Chem.*, 1981, **18**, 599.
7 H. Meerwein, V. Hederick and K. Wunderlich, *Arch. Pharm.*, 1958, **63**, 541.
8 G. Haselhorst, K. Wieghardt, S. Keller and B. Schrader, *Inorg. Chem.*, 1993, **32**, 520 and references therein.
9 N. N. Greenwood and T. C. Gibb, *Mössbauer Spectroscopy*, Chapman and Hall Ltd, London, 1971.
10 G. M. Sheldrick, SHELXTL-Plus, Structure Determination Software Programs, Siemens Analytical X-ray Instruments Inc., Madison, WI, USA, 1990; G. M. Sheldrick, SHELXL97, Program for the refinement of crystal structures, University of Göttingen, Germany, 1997.

ChemComm

Catalytic epoxidation of alkenes with hydrogen peroxide over first mesoporous titanium-containing zeolite

Iver Schmidt,[a,b] Anne Krogh,[a,c] Katrine Wienberg,[a,c] Anna Carlsson,[a] Michael Brorson[a] and Claus J. H. Jacobsen*[a]

[a] *Haldor Topsøe Research Laboratories, Nymøllevej 55, DK-2800 Lyngby, Denmark. E-mail: chj@topsoe.dk*
[b] *Leverhulme Centre for Innovative Catalysis, University of Liverpool, Liverpool, UK L69 3BX*
[c] *Inter-Disciplinary Research Center for Catalysis (ICAT), Technical University of Denmark, DK-2800 Lyngby, Denmark*

Received (in Cambridge, UK) 7th August 2000, Accepted 2nd October 2000
First published as an Advance Article on the web

Novel mesoporous TS-1 catalyst is shown to be active in epoxidation of oct-1-ene and significantly more active in epoxidation of cyclohexene than conventional TS-1.

Since the first report by Taramasso *et al.*[1] there have been numerous demonstrations of the outstanding catalytic properties of titanium silicalite 1 (TS-1) for selective oxidation and epoxidation of various organic compounds with aqueous hydrogen peroxide. However, TS-1 suffers from intracrystalline diffusion limitations owing to the small size of the zeolite micropores; this limitation is most pronounced for low-temperature liquid phase reactions with bulky reactants and products. This has stimulated research into zeolites with larger pores (*e.g.* BEA, UTD-1) and amorphous mesoporous titanium-containing materials. Mesoporous materials only exhibit high selectivities towards epoxides if organic peroxides are used as oxidants.[2] This reduces the environmental and economic advantages, since management of by-products due to reduced selectivities and decomposition of the organic oxidant becomes an important issue. Comparative studies of TS-1 and Ti-BEA have shown that different catalytic behaviour and lifetime are to be expected,[3] *i.e.* the excellent catalytic properties of TS-1 might not be observed for Ti-BEA. The diffusional properties of TS-1 catalysts can be altered by preparation of nanosized TS-1 (*e.g.* by the recently developed Confined Space Synthesis method[4,5]), but separation of the finely crystalline catalyst from the product mixture might involve costly high-speed centrifugation or flash distillation.

Recently we reported the preparation of mesoporous zeolite single crystals that compared with conventional zeolite crystals, exhibiting significantly improved diffusional properties.[6] Typical mesoporous zeolite single crystals of $1.0 \times 0.5 \times 0.5$ mm^3 incorporate an interconnected network built from more than 1500 primary carbon particles during growth. Contrary to nanosized TS-1, separation of mesoporous TS-1 from the product mixture can be performed by simple filtration. Here, the catalytic performance of mesoporous TS-1 in the epoxidation of linear and cyclic alkenes is compared with that of conventional TS-1.

Carbon Black Pearls 700® (supplied by Carbot Corp.) with an average particle diameter of 18 nm (ASTM D-3249) were impregnated to incipient wetness with a clear solution of tetrapropylammonium hydroxide, water and ethanol. After evaporation of the ethanol, the carbon particles were impregnated with 20% excess (relative to incipient wetness) of a mixture of tetraethylorthotitanate and tetraethylorthosilicate. The composition of the resulting synthesis gel was 20 TPA_2O:TiO_2:100 SiO_2:200 H_2O, and the resulting zeolite concentration *ca.* 20 wt%. After ageing for a minimum of 3 h at room temperature, the impregnated carbon black was introduced into a stainless steel autoclave containing sufficient water to produce saturated steam. The autoclave was heated slowly (0.5 °C min^{-1}) to 170 °C and maintained at this temperature for 72 h. After cooling the autoclave to room temperature, the product was suspended in water and isolated by suction filtration. The product was washed four times as a suspension with water and then dried at 110 °C for 10 h. The carbon black was removed in a muffle furnace by controlled combustion in air at 550 °C for 8 h. In this manner a white material was obtained which according to chemical analysis was shown to contain < 0.5 wt% C.

Micron-sized TS-1 with a similar titanium content, prepared according to ref. 7, was used as a reference.

XRPD showed that both samples consisted of highly crystalline MFI-structured material. Characterisation by diffuse UV–VIS reflectance spectroscopy and Raman spectroscopy verified the presence of titanium in the zeolite framework while no extra-framework anatase was detected. Chemical analysis of the two TS-1 samples gave Si/Ti ratios of 110 in both cases. Electron microscopy of the conventional TS-1 revealed a highly crystalline material consisting of twinned coffin-shaped crystals with a narrow size distribution of *ca.* 1.5 μm as shown in Fig. 1.

Transmission electron micrographs were recorded with a Philips CM200 FEG, operating at 200 kV. The sample was suspended in ethanol and dispersed on a copper grid coated with lacey carbon film.

Relatively large (*ca.* 0.3–1.2 μm) and well shaped crystals are obtained by hydrothermal crystallisation in carbon black, and a representative crystal is shown in Fig. 2. Inspection of high-resolution transmission electron micrographs revealed lattice fringes extending through the entire crystal. The significant mesoporosity was observed as bright spots, *ca.* 20 nm in diameter, dispersed throughout the entire crystal. This diameter matches that of the carbon primary particles (18 nm) which occupy these positions prior to combustion. It was shown by N_2 adsorption/desorption that the mesoporous TS-1 exhibited a

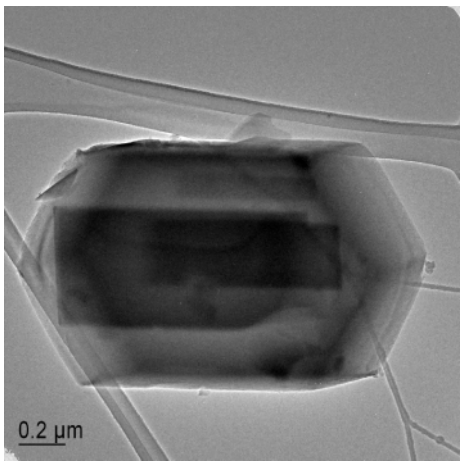

Fig. 1 Transmission electron microscopy image of a conventional TS-1 crystal.

DOI: 10.1039/b006460m

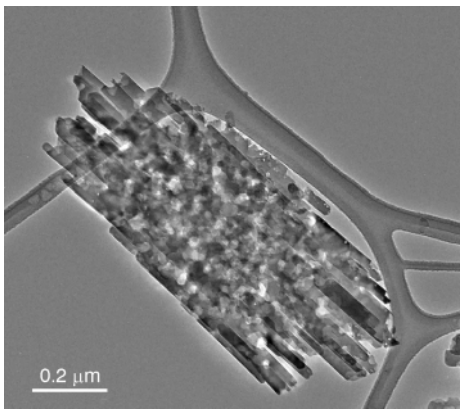

Fig. 2 Transmission electron microscopy image of mesoporous TS-1 single crystal.

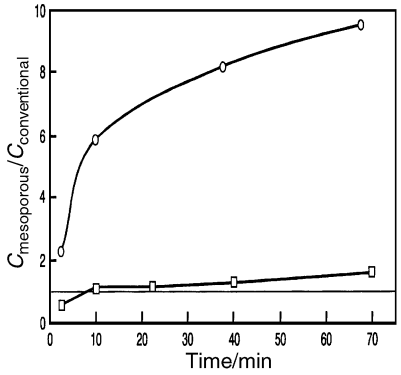

Fig. 3 Ratio of product concentrations [sum of epoxide and secondary products; (■) from oct-1-ene and (●) from cyclohexene] obtained with mesoporous and conventional TS-1 as a function of the contact time. It is seen that mesoporous TS-1 has a similar activity for oct-1-ene epoxidation as conventional TS-1. However, the mesoporous TS-1 is significantly more active for cyclohexene epoxidation.

porosity similar to that reported previously for ZSM-5 prepared by a similar route.[6]

The two TS-1 samples were tested as catalysts for epoxidation of oct-1-ene and cyclohexene with aqueous hydrogen peroxide using methanol as solvent and *n*-heptane as internal standard. The reaction was performed at ambient pressure in a magnetically stirred round-bottomed flask fitted with a condenser and placed in a thermostated oil bath. Alkene (4.2 ml of oct-1-ene or 2.7 ml of cyclohexene), 20.0 ml methanol, 0.75 ml *n*-heptane (internal standard) and 0.18 g of TS-1 catalyst were added to the flask and preheated to the reaction temperature (40 °C). The kinetic experiment was started when 0.50 ml 35 wt% H_2O_2 was added; samples of the reaction mixture were taken at regular intervals. The samples were cooled, the zeolite catalyst removed by filtration and analysed by GC. The initial hydrogen peroxide/olefin molar ratio was 0.25, and the H_2O_2/titanium molar ratio was *ca.* 230. The selectivities towards the corresponding epoxides were > 90% in all cases. The catalytic performance of the two types of TS-1 is compared by plotting the ratio of product concentrations as a function of time. This is illustrated in Fig. 3 for the epoxidation of oct-1-ene and cyclohexene.

Similar product concentrations ($C_{mesoporous}/C_{conventional} = 1$) are obtained when the epoxidation of oct-1-ene is catalysed by mesoporous and by conventional TS-1. This suggests that the epoxidation of oct-1-ene is not limited by intra-crystalline diffusion and therefore not dependent on whether or not the crystals are mesoporous. The results also suggest that the intrinsic activity of mesoporous TS-1 is similar to conventional TS-1. In contrast, the epoxidation of cyclohexene exhibits a product concentration ratio, which exceeds a value of 10 within the contact times studied. Since the experiments with oct-1-ene suggest similar intrinsic activity of the two types of TS-1, the enhanced catalytic performance of the mesoporous sample must be due to a better accessibility of the active sites. Experiments using cyclooctene have also been performed, showing a similar pattern as observed for cyclohexene. Thus, the improved catalytic activity of the mesoporous TS-1 is attributed to its improved diffusional properties compared with conventional micron-sized TS-1.

Compared with conventional TS-1, mesoporous TS-1 improves the catalytic performance without changing the product distribution, which might be an advantage compared with the alternative of using titanium-containing zeolites with larger pores. Generally, it seems possible to prepare mesoporous crystals of most zeolites with the present technique. This may lead to improved new catalysts for many different zeolite catalysed reactions. Particularly, in bifunctional catalysis it appears attractive to disperse another catalytic functionality 'inside' every individual zeolite crystal.

Notes and references

1 M. Taramasso, G. Perego and B. Notari, *US Pat.*, 4 410 501, 1983.
2 M. C. Capel-Sanchez, J. M. Campos-Martin, J. L. G. Fierro, M. P. de Frutos and A. Padilla Polo, *Chem. Commun.*, 2000, 855.
3 A. Carati, C. Flego, E. Previde Massara, R. Millini, L. Carluccio, W. O. Parker, Jr. and G. Bellussi, *Microporous Mesporous Mater.*, 1999, **30**, 137.
4 C. Madsen and C. J. H. Jacobsen, *Chem. Commun.*, 1999, 673.
5 I. Schmidt, C. Madsen and C. J. H. Jacobsen, *Inorg. Chem.*, 2000, **39**, 2279.
6 C. J. H. Jacobsen, J. Houzvicka, I. Schmidt, C. Madsen and A. Carlsson, *J. Am. Chem. Soc.*, 2000, **122**, 7116.
7 A. J. H. P van der Pol and J. H. C. van Hooff, *Appl. Catal. A.*, 1992, **92**, 93.

Aqueous solutions of hypovalent gallium; reductions using gallium(I)†

Shawn Swavey* and Edwin S. Gould*

Department of Chemistry, Kent State University, Kent, Ohio 44242, USA

Received (in Cambridge, UK) 19th June 2000, Accepted 25th September 2000
First published as an Advance Article on the web

Solutions 0.2 mol dm^{-3} in Ga^{I}, prepared by dissolving Ga_2Cl_4 in dry acetonitrile, are stable for more than seven days and may be diluted 300- to 1000-fold with O_2-free water to give Ga^{I} preparations that may be handled by conventional techniques; these Ga^{I}(aq) solutions readily reduce I_3^-, Br_2(aq), $IrCl_6^{2-}$, $Fe(bipy)_3^{3+}$ and aquacob(III)alamin (B_{12a}) but are inert to $Co(NH_3)_5Cl^{2+}$ and $Co(NH_3)_5Br^{2+}$; reduction of $HCrO_4^-$ in 2-ethyl-2-hydroxybutanoate buffers yields the Cr^{IV} chelate of the buffering anion.

Accounts of the generation of gallium(I) species in aqueous solution are exceedingly scarce,[2,3] and no redox studies of this unusual state appear to have been described. A standard potential for Ga(III,I), −0.755 V (25 °C) has been documented.[2]

The crystalline compound 'gallium dichloride' (Ga_2Cl_4) is known to feature equal numbers of Ga(I) and Ga(III) centers ($Ga^{I}Ga^{III}Cl_4^-$).[4] Employing this as a source of hypovalent gallium, we have prepared aqueous Ga(I) solutions which have allowed us, utilizing conventional methods, to compare rates at which this s^2-center reacts with a variety of oxidants.

Manipulations of Ga_2Cl_4 (Aldrich) were carried out under high purity N_2 or Ar. Solutions were prepared by dissolving 1.25 g of this halide in 8.0 ml of anhydrous MeCN under a constant flow of protective gas. After 5 min of stirring, a silver-colored precipitate separates. The clear yellow supernatant solution, which was obtained by centrifuging, was found to be 0.20 mol dm^{-3} in Ga^{I} (spectrophotometric redox titration *vs.* KI_3 at 353 nm) and remained unchanged on standing for seven days. Aqueous solutions for kinetic experiments, prepared by 300- to 1000-fold dilutions of the MeCN solutions with O_2-free water, were stable for 10–15 min in the absence of electrolyte. For slow reactions (*e.g.* reduction of vitamin B_{12a}) fresh aqueous solutions were prepared for each individual run. The rate of the Ga(I)–I_3^- reaction was not appreciably changed by increasing [MeCN] from 0.02 to 0.50 mol dm^{-3}, or by adding $GaCl_3$ in concentration three times that of Ga^{I}.

Solutions of Ga(I) rapidly reduce I_3^-, Br_2(aq), $IrCl_6^{2-}$, $HCrO_4^-$, $Fe(CN)_6^{3-}$ and $Fe(bipy)_3^{3+}$. Reduction of B_{12a} [aquacob(III)alamin] is slow, and there is no perceptible reaction with $Co(NH_3)_5Cl^{2+}$ or $Co(NH_3)_5Br^{2+}$. Each mol of Ga(I) consumes very nearly 1.0 mol of I_3^- or Br_2 but 2.0 mol of the le$^-$ oxidants $IrCl_6^{2-}$ and $Fe(bipy)_3^{3+}$, reflecting the expected conversion to Ga^{III} with oxidants of either type [eqn. (1) and (2)]:

$$Ga^{I} + Br_2 \rightarrow Ga^{III} + 2Br^- \quad (1)$$

$$Ga^{I} + 2\ Fe(bipy)_3^{3+} \rightarrow Ga^{III} + 2\ Fe(bipy)_3^{2+} \quad (2)$$

Oxidation by $HCrO_4^-$ utilizes 0.64 ± 0.01 mol of Cr^{VI} in 0.01 M $HClO_4$ but 1.1 mol of oxidant when carried out in 2-ethyl-2-hydroxybutanoic acid buffer (EHBA/EHB$^-$, pH 3.3), indicating predominant conversion to Cr^{III} in the absence of this chelating ligand [eqn. (3)] but formation of Cr^{IV} in its presence [eqn. (4)]:

$$3Ga^{I} + 2\ Cr^{VI} \rightarrow 3\ Ga^{III} + 2\ Cr^{III}\ (\text{pH 1–2}) \quad (3)$$

$$Ga^{I} + Cr^{VI} \xrightarrow[\text{buffer}]{\text{EHBA}} Ga^{III} + Cr^{VI}\ (\text{EHB}^-\ \text{complex}) \quad (4)$$

The pink product of eqn. (4) showed a strong peak at 510 nm, typical of EHB-chelated Cr^{IV}.[5]

The reactions listed in Table 1 are first order in each of the redox partners. Although oxidations by $IrCl_6^{2-}$ and $Fe(bipy)_3^{3+}$ almost certainly pass through the intermediate state Ga^{II}, kinetic profiles for these oxidants exhibit no discontinuity attributable to the accumulation or decay of this odd-electron species, implying a two-step sequence (5), in which

$$Ga^{I} \xrightarrow[\text{slow}]{Ir^{IV}} Ga^{II} \xrightarrow[\text{rapid}]{Ir^{IV}} Ga^{III} \quad (5)$$

the initial step is rate-determining and the more rapid follow-up step is kinetically silent. The relative rates of the two steps suggest that Ga^{II}, the s^1 intermediate, is much more strongly reducing than the parent s^2 cation, a difference applying also to the related p-block triads, Tl(III,II,I),[7] In(III,II,I)[8] and Ge(IV,III,II).[9]

As has been recently noted[1] for Ge^{II} (an isoelectronic state), Ga^{I} resists oxidation by both $Co(NH_3)_5Cl^{2+}$ and by its Co(III)Br counterpart. These Co(III) oxidants offer remarkably facile inner-sphere le$^-$ paths to aqua complexes of d- and f-block reductants,[10] but such routes are denied to this pair of $4s^2$ species which react primarily as 2e$^-$ donors. This marked mechanistic shift probably results in part from less effective halo-ligation to this main group center and, in part, from its modestly reducing $E°$(I,II) value (in contrast to the more negative potential for its II–III conversion).

In contrast, we find the cobalt(III) corrin derivative, aquacob(III)alamin (B_{12a}) to be reduced smoothly to its Co(II) analog. We suspect that this reaction is initiated by the two-unit reduction (very likely by oxo-transfer) to the known Co^{I} complex, B_{12s} [cob(I)alamin], a hypovalent species which has been shown[11] to undergo very rapid comproportionation with B_{12a} [eqn. (6)]:

$$Co^{III} \xrightarrow{Ga^{I}} Co^{I} \xrightarrow{Co^{III}} 2\ Co^{II} \quad (6)$$

Table 1 Reductions with aqueous gallium(I)[a]

Oxidant	Product	k/dm^3 mol^{-1} s^{-1}
I_3^-	I^-	(1.47 ± 0.09) × 10^4
Br_2 (aq)	Br^-	(2.05 ± 0.05) × 10^4
$IrCl_6^{2-}$	$IrCl_6^{3-}$	(7.3 ± 0.05) × 10^2
$Fe(bipy)_3^{3+}$	$Fe(bipy)_3^{2+}$	(8.9 ± 0.2) × 10^4
$HCrO_4^-$ (pH 2.0)	Cr^{III}	(2.7 ± 0.1) × 10^3
B_{12a} (Co^{III})	B_{12r} (Co^{II})[b]	7.1 ± 0.3
$[Co(NH_3)_5Br]^{2+}$		< 0.02
$[Co(NH_3)_5Cl]^{2+}$		< 0.01

[a] Reactions at 25 °C; μ = 0.5 M ($NaClO_4$, LiCl or KI); [H$^+$] = 0.01–0.05 M; [Ga^{I}] = (1.0–12.0) × 10^{-4} M; [oxidant] = (4.0–12.0) × 10^{-5} M. [b] Spectrum of product corresponded to that reported by Pratt.[6]

We are grateful to the National Science Foundation for support of this work and to Ms Arla McPherson and Ms Carol Haven for technical assistance.

Notes and references

† Electron Transfer, part 145. For part 144, see ref. 1.

1 O. A. Babich and E. S. Gould, *Inorg. Chem.*, 2000, **39**, 4119.
2 L. Ph. Kozin, N. M. Openko and T. A. Tishura, *Ukr. Khim. Zh. (Eng. Ed.)*, 1993, **59**, 227.

3 L. Ph. Kozin, V. N. Statsyuk and A. K. Bogdanova, *Ukr. Khim. Zh. (Russ. Ed.)*, 1985, **51**, 496; *Chem. Abstr.*, 1985, **103**, 94986.
4 G. Garton and H. M. Powell, *J. Inorg. Nucl. Chem.*, 1957, **4**, 84.
5 M. C. Ghosh and E. S. Gould, *Inorg. Chem.*, 1990, **29**, 4238.
6 J. M. Pratt, *Inorganic Chemistry of Vitamin B_{12}*, Academic Press, New York, 1972, p. 104.
7 H. A. Schwarz, D. Comstock, J. K. Yandell and R. W. Dodson, *J. Phys. Chem.*, 1974, **78**, 488.
8 A. M. Al-Ajlouni and E. S. Gould, *Res. Chem. Intermed.*, 1998, **24**, 653.
9 O. A. Babich, M. C. Ghosh and E. S. Gould, *Chem. Commun.*, 2000, 907.
10 See, for example: A. G. Lappin, *Redox Mechanisms in Inorganic Chemistry*, Ellis Horwood, New York, 1994, ch. 3.
11 D. A. Ryan, J. H. Espenson, D. Meyerstein and W. A. Mulac, *Inorg. Chem.*, 1978, **17**, 3725.

Fabrication of hollow zeolite spheres

X. D. Wang,[a] W. L. Yang,[b] Y. Tang,*[a] Y. J. Wang,[a] S. K. Fu[b] and Z. Gao[a]

[a] *Department of Chemistry, Fudan University, Shanghai 200433, P. R. China. E-mail: yitang@fudan.edu.cn*
[b] *Department of Macromolecular Science and Key Laboratory of Molecular Engineering of Polymers, Fudan University, Shanghai 200433, P. R. China*

Received (in Cambridge, UK) 9th August 2000, Accepted 21st September 2000
First published as an Advance Article on the web

Hollow spheres of zeolite have been fabricated through a layer-by-layer technique using polystyrene spheres as templates and nanozeolites as 'building blocks', followed by calcination.

Hollow spheres have found many applications in chemistry, biotechnology and materials science owing to their characteristic macroscopic structure.[1,2] Fabrication of hollow spheres with well defined nanoscaled pores on the shell may open up possibilities for various new application fields, such as controlled release capsules, artificial cells, chemical sensors, shape-selective adsorbents and catalysts. Up to now, only hollow spheres of mesoporous silica have been obtained by spray drying and emulsion/phase separation techniques.[3–5] Zeolites are ideal construction materials for the shell of hollow spheres owing to their high thermal stability, large microporosity, high shape-selectivity and intrinsic chemical activity. However, the present methods of preparing hollow mesoporous silica spheres cannot be used to fabricate hollow zeolite spheres, because the synthetic conditions and formation mechanisms of mesoporous silica and zeolites are totally different. Recently, a layer-by-layer (LbL) technique based on electrostatic interaction or hydrogen bonding has been widely adopted to fabricate films on the surfaces of flat and spherical substrates.[6,7] It has been noticed that colloidal zeolites are negatively charged in basic solution and can aggregate readily to form hierarchical structures such as membranes, fibers and micro/macroporous zeolite monoliths.[8,9] The electrostatic attraction between a negatively charged nanozeolite and an oppositely charged polymer is an effective driving force for the self-assembly of zeolite–polymer multilayers on colloidal templates. A new procedure for fabricating hollow zeolite spheres involving polystyrene (PS) latex templated electrostatic LbL self-assembly of nanozeolite/polymer multilayers followed by removal of the template and the polymer is reported in this work.

Nanocrystals of zeolite β (40 ± 5 nm), silicalite-1 (50±10 and 80 ± 10 nm) were prepared according to the literature methods,[10,11] and characterized by XRD, IR and SEM. The nanozeolites were centrifuged, washed and dispersed in 0.1 mol L^{-1} NaCl solution at pH 9.5. The fabrication procedure for hollow zeolite spheres is depicted in Scheme 1. First, the positively charged PS latex templates were prepared by depositing five layers of polyelectrolytes of cationic poly(diallyldimethylammonium chloride) (PDDA) and anionic poly(styrenesulfonate, sodium salt) (PSS) in the order of PDDA/PSS/PDDA/PSS/PDDA.[2,7] Then, the nanozeolite and PDDA were alternately deposited on the positively charged PS substrates to form homogeneous nanozeolite/PDDA multilayers. All the above adsorption steps were performed in 0.1 mol L^{-1} NaCl solution with a liquid/solid volume ratio of 50 at pH 9.5 and ambient temperature for 20 min, and after each adsorption step the sample was centrifuged, washed and redispersed. To remove the PS latex template and the polymers, the samples were heated to 873 K at a heating rate of 5 K min^{-1} in nitrogen, and kept at 873 K in nitrogen for 4 h and subsequently in air for 8 h.

Homogeneous deposition of nanozeolite particles on PS latex templates is a crucial step in the preparation of hollow zeolite spheres using the LbL technique. The success of this process largely depends on the electrostatic interaction between the nanozeolite and PDDA. Hence, pH and ionic strength of the colloidal solution are important. In neutral solution, most of the coated spheres are coalesced and have very rough surfaces [Fig. 1(a)]. In addition, the nanozeolite particles form aggregates in solution. This is probably because the charge density on the nanosilicalite-1 surface is rather low near its isoelectric point (pH = 7).[12] At pH 11, discontinuous defects [see arrows in Fig. 1(c)] on the sphere surface are observed even after four nanozeolite/PDDA layer pairs are deposited. Under such conditions, most of the silanol groups on the surface of the nanozeolite particles exist in the form of Si–O^-, which increases the repulsive force between the particles and inhibits the formation of a compact coat. The best result is obtained at pH 9.5 [Fig. 1(b)], when the amount of negative charge on the zeolite particles is just adequate for them to deposit onto the positively charged PS spheres densely and compactly. NaCl was added into the solution to adjust the ionic strength. Without adding salt, defects were observed on the sphere surface even after four layers of zeolites were deposited. As the salt concentration was increased to 0.1 mol L^{-1}, the coat on the sphere surface became uniform and dense. This shows that a proper ionic strength of the solution is necessary to screen the nanozeolite particles from mutual repulsion and to facilitate the formation of a uniform and compact zeolite coat on the templates.[13]

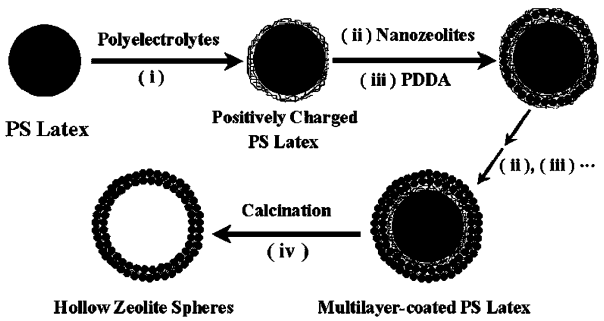

Scheme 1 The procedure for preparing hollow zeolite spheres.

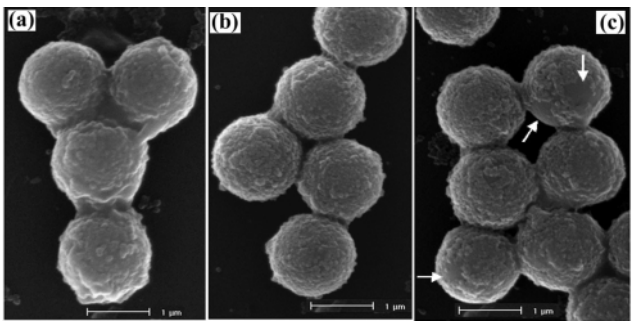

Fig. 1 SEM micrographs of polyelectrolyte-modified PS latices deposited with two nanosilicalite-1/PDDA layer pairs, (a) in neutral solution, (b) at pH = 9.5 and (c) four nanosilicalite-1/PDDA layer pairs at pH = 11.0.

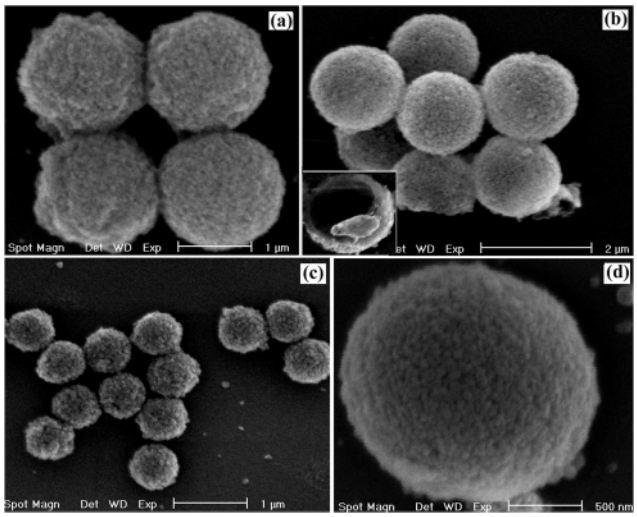

Fig. 2 SEM micrographs of samples deposited with four nanozeolite/PDDA layer pairs, (a) PS latices (ϕ = 1.47 μm) coated with zeolite β, (b) hollow zeolite β sphere templated by PS latices (ϕ = 1.47 μm), (c) hollow zeolite β sphere templated by PS latices (ϕ = 0.53 μm), (d) hollow silicalite-1 sphere templated by PS latices (ϕ = 1.47 μm).

SEM micrographs of hollow spheres of zeolite β and silicalite-1 templated by PS latices with diameters ϕ of 1.47 and 0.53 μm are shown in Fig. 2. The PS latices are homogeneously covered with zeolite nanoparticles. The inset in Fig. 2(b) shows that the spheres are hollow after calcination and the thickness of the shell is rather uniform. The surface of the hollow spheres is smoother than the coated PS latices, implying that the zeolite nanoparticles are more closely packed after calcination. Also, it was observed that the smaller the PS latices and the nanozeolite particles employed, the easier it was to keep the hollow spheres intact. Almost all the hollow spheres were intact, when the samples were prepared by depositing four layers of 40 nm zeolite β onto PS latices of 0.53 μm [Fig. 2(c)]. The percentage of intact spheres in the final product was also influenced by the number of deposited nanozeolite layers. Hollow spheres were not formed if only one layer of zeolite was deposited, but the formation of such spheres did occur, under the appropriate conditions, when two layers were deposited. The shell thickness of the hollow spheres could be tailored through varying the number of deposited nanozeolite layers. The thickness of shells composed of two, four and six layers of zeolite β nanocrystals was *ca.* 70, 140 and 200 nm, respectively.

XRD patterns of calcined hollow spheres of zeolite β and silicalite-1 are shown in Fig. 3. The patterns are almost the same as those of the original nanozeolites of zeolite β and silicalite-1, indicating that the crystalline structure and crystal size of the zeolites are unaltered after fabrication. Energy dispersive X-ray analysis established that the elemental composition of the shell is in accord with the nanozeolites used. Only characteristic bands of the zeolites appear in the IR spectra of the calcined samples,[10,11] indicating the PS latex core and other organic species are totally removed. Such novel materials are expected to have potential applications as controlled release capsules, artificial cells and catalysts owing to their unique 'cage structure' with microporous shells.

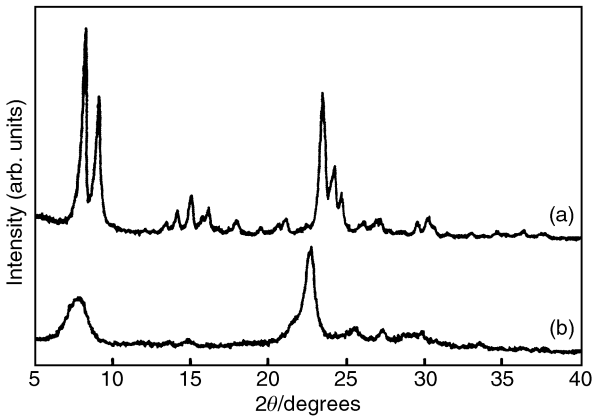

Fig. 3 XRD patterns of hollow spheres of silicalite-1 (a) and zeolite β (b).

In conclusion, hollow spheres of zeolite β and silicalite-1 with different sizes were fabricated efficiently and conveniently through LbL self-assembly of nanozeolite–polymer multilayers on a PS latex, coupled with removal of the core by calcination. The pH and ionic strength of the colloidal solution, crystal size of nanozeolites and size of PS latex templates are factors affecting the fabrication of hollow zeolite spheres. Hollow spheres of other zeolites such as ZSM-5 and TS-1 have also been successfully fabricated in the same manner (to be published). Currently, the application of these novel materials in catalysis, separation and delivery systems is in progress in our laboratory.

This work is supported by the Major State Basic Research Development Program (Grant No. 2000077500), the NNSFC (Grant No. 29873011) and the Foundation for University Key Teacher by the Ministry of Education.

Notes and references

1 D. L. Wilcox, M. Berg, T. Bernat, D. Kellerman and J. K. Cochran, *Hollow and Solid Spheres and Microspheres: Science and Technology Associated with Their Fabrication and Application*, Materials Research Society Proceedings, Pittsburgh, 1995, vol. 372.
2 F. Caruso, *Chem. Eur. J.*, 2000, **6**, 413.
3 S. Schacht, Q. Huo, I. G. Voigt-Martin, G. D. Stucky and F. Schuth, *Science*, 1996, **273**, 768.
4 P. J. Bruinsma, A. Y. Kim, J. Liu and S. Baskaran, *Chem. Mater.*, 1997, **9**, 2507.
5 H. Lin, Y. Cheng and C. Mou, *Chem. Mater.*, 1998, **10**, 3772.
6 G. Decher, *Science*, 1997, **277**, 1232.
7 F. Caruso, R. A. Caruso and H. Mohwald, *Science*, 1998, **282**, 1111.
8 L. M. Huang, Z. B. Wang, J. Y. Sun, L. Miao, Q. Z. Li, Y. S. Yan and D. Y. Zhao, *J. Am. Chem. Soc.*, 2000, **122**, 3530.
9 Y. J. Wang, Y. Tang, Z. Ni, W. M. Hua, W. L. Yang, X. D. Wang, W. C. Tao and Z. Gao, *Chem. Lett.*, 2000, 510.
10 M. A. Camblor, A. Corma, A. Mifsud, J. Perez-Pariente and S. Valencia, *Stud. Surf. Sci. Catal.*, 1997, **105**, 341.
11 R. Ravishankar, C. Kirschhock, B. J. Schoeman, P. Vanoppen, P. J. Grobet, S. Storck, W. F. Maier, J. A. Martens, F. C. De Schryver and P. A. Jacobs, *J. Phys. Chem. B*, 1998, **102**, 2633.
12 J. Sterte, S. Mintova, G. Zhang and B. J. Schoeman, *Zeolites*, 1997, **18**, 387.
13 C. J. Brinker and G. W. Scherer, *Sol–Gel Science: The Physics and Chemistry of Sol–Gel Processing*, Academic Press, Inc., New York, 1990, ch. 3, p. 97.

Multilayer ultrathin films of molecular titania nanosheets showing highly efficient UV-light absorption

Takayoshi Sasaki,*[a] Yasuo Ebina,[a] Mamoru Watanabe[a] and Gero Decher[b]

[a] *National Institute for Research in Inorganic Materials, 1-1 Namiki, Tsukuba, Ibaraki 305-0044, Japan. E-mail: sasaki@nirim.go.jp*

[b] *Université Louis Pasteur and CNRS, Institut Charles Sadron, 6, rue Boussingault, F-67083 Strasbourg Cedex, France*

Received (in Cambridge, UK) 16th August 2000, Accepted 27th September 2000
First published as an Advance Article on the web

Titania nanosheet crystallites have been self-assembled layer-by-layer with poly(dimethyldiallyl ammonium chloride) onto substrates to produce ultrathin nanostructured films which exhibit highly efficient optical absorption with a sharp peak at 266 nm.

In the past decade, titania thin films have attracted tremendous attention for their optical and photochemical applications, *e.g.* UV-light shielding, solar energy conversion and detoxification of pollutants.[1] For these applications, it is of great importance to fabricate titania thin films with a well controlled nanostructure. Among a range of film growth strategies, the Langmuir–Blodgett technique and self-assembly procedure *via* sequential adsorption[2] are the most feasible and widely applicable to tailor stable and high-quality films on a nanometer-scale range. Recently these approaches have been applied for the synthesis of multilayer titania films by several groups.[3–6] These preparations incorporated titania particles of several nm in size as a film component. Hence, the resulting multilayer films were composed of alternating layers of two-dimensionally packed nanoparticles and organic substances as a binder. The titania nanoparticles were synthesized by hydrolyzing an appropriate Ti salt. It is sometimes difficult to prepare extremely small sized particles in high quality, particularly in terms of crystallinity, uniform shape and size, which is essential for fabrication of well organized films.

Recently we have demonstrated that colloidal titania nanosheets of composition $Ti_{1-\delta}O_2$ ($\delta \approx 0.09$) can be derived by completely delaminating a layered titanate.[7] The obtained semiconductor crystallite, as the elementary fragment of the layered crystals prepared at a high temperature, is characterized by its very high two-dimensionality, with a thickness of molecular dimension as well as high crystallinity, which leads to novel physicochemical properties which are distinct from those of titania nanoparticles.[8] These features of the nanosheet crystallites may have some advantages to better control nanostructures in the layering process and some enhanced physical properties may be expected for resulting multilayer assemblies in comparison with films composed of nanoparticles. Here, we report the layer-by-layer construction of a well organized multilayer system of titania semiconductor nanosheets and organic polymers, which efficiently absorb UV light with a wavelength below 300 nm.

The titania nanosheet crystallites, $Ti_{1-\delta}O_2$ ($\delta \approx 0.09$), were obtained by chemically delaminating a protonic titanate of γ-FeOOH type layered structure, $H_{0.7}Ti_{1.825}\square_{0.175}O_4{\cdot}H_2O$ (□ = vacancy),[9] into its colloidal single layers upon action of an aqueous solution of tetrabutylammonium hydroxide (TBAOH).[7] The multilayer films were prepared by repeating the following adsorption procedures for the desired number of cycles.

Each cycle involves the immersion of a substrate such as Si wafer or quartz glass into the colloidal suspension of the titania nanosheets for 20 min, rinsing with Milli-Q filtered water (> 17 MΩ cm^{-1}), and then dipping in an aqueous solution of poly(dimethyldiallyl ammonium chloride) (PDDA) for 20 min, and finally washing with water. A polycation such as PDDA was employed as a counterpart for the self-assembly process because the titania nanosheets are negatively charged. The substrates were cleaned prior to the film deposition by a method described in the literature[10] and then primed with poly(ethylenimine), PEI, to introduce positive charge onto their surface. The concentration of the titania suspension and the PDDA solution were 0.08 and 20 g dm^{-3}, respectively. The pH values of both were adjusted to *ca*. 9 by adding an appropriate amount of HCl or TBAOH. The PDDA was added as a 0.5 mol dm^{-3} NaCl solution.

Consecutive adsorption procedures as described above yielded visibly transparent thin films, the growth process of which was followed by several characterization techniques. UV–VIS absorption spectra show progressive enhancement as a function of the layer pair number (Fig. 1). The spectral profile with a pronounced peak at 266 nm is characteristic of titania nanosheets in aqueous suspension.[8] The polycations, PDDA and PEI, do not show substantial absorption in the energy region shown. Consequently, the nearly linear growth of the absorption peak indicates that an approximately equal amount of $Ti_{1-\delta}O_2$ was deposited for each adsorption procedure. The modest increase in background at a wavelength of > 300 nm may arise from light scattering by the nanosheet crystallites oriented parallel to the substrate surface with lateral sizes in the submicro- to micro-meter range.

X-Ray diffraction patterns (Fig. 2) illustrate the evolution of a Bragg peak suggesting a periodicity of 1.4 nm. This diffraction peak is attributable to a so-called superlattice reflection of the inorganic/organic repeating nanostructure. The nanosheet crystallite $Ti_{1-\delta}O_2$ has an atomic architecture of γ-FeOOH type in which TiO_6 octahedra at two different levels along the sheet normal are connected with each other *via* edge-sharing to produce the two-dimensional sheet.[8] Its thickness is

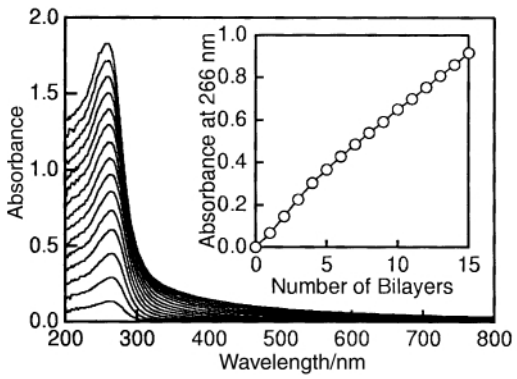

Fig. 1. UV–VIS absorption spectra of $Ti_{1-\delta}O_2$/PDDA multilayer films grown on SiO_2 glass; 0.5 × the observed absorbance at 266 nm is plotted in the inset taking into account the presence of the film on both sides of the substrate.

DOI: 10.1039/b006720m

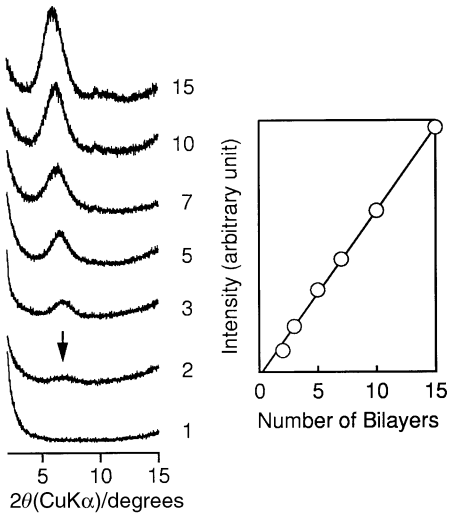

Fig. 2. X-Ray diffraction patterns of $Ti_{1-\delta}O_2$/PDDA films on SiO_2 glass with the number of layer pairs indicated.

estimated to be 0.75 nm taking into account the outermost edges of surface oxygen atoms. Accordingly, the thickness for the PDDA layer should be 0.65 nm. This dimension is reasonable for the PDDA molecular structure at the salt concentration under which the film was grown.

The intensity of the basal diffraction series for a system of N parallel nanosheets can be calculated using eqn. (1):[11]

$$I(0k0) = \frac{1}{N}\frac{1+\cos^2 2\theta}{\sin^2\theta\cos\theta}F^2(0k0)\frac{\sin^2(\pi Nk)}{\sin^2(\pi k)} \qquad (1)$$

where the second, third and fourth terms are the Lorentz-polarization factor, structure factor and interference function, respectively. Since the latter term is proportional to N^2 at $k = \pm 1, 2, 3$, the $0k0$ peak intensity is linearly dependent on N. This was experimentally observed as shown in inset, suggesting successful construction of the multilayer film.

The diffraction peak was detectable even for the two-unit system, *i.e.* PEI/$Ti_{1-\delta}O_2$/PDDA/$Ti_{1-\delta}O_2$. The well ordered nature of this multilayer system is principally explained by the fact that the interpenetration of inorganic and organic components is strongly reduced owing to the two-dimensional architecture of the rigid inorganic nanosheets. This is in sharp contrast to other multilayer films composed of organic polymers where neighboring layers intermingle considerably.[2]

The ultrathin titania films obtained in this study have a molecularly ordered array of the components. The film architecture is based on platelets rather than particles as found for titania films reported previously.[3–6] The multilayer repeat dimension of 1.4 nm is finer than for such previously reported films (> 3 nm).

The optical properties are also noteworthy, particularly in terms of sharp and highly efficient absorption in the UV region (< 300 nm). The sharp absorption edge, which is significantly blue-shifted relative to bulk TiO_2, may be associated with exciton confinement in the two-dimensional semiconductor crystallites which are of sub-nm thickness.[8] Theoretical calculations predict very small values, 0.3–1.9 nm, for the Bohr radius of the first exciton in TiO_2, or the threshold at which quantum size effects manifest themselves.[12,13] On the basis of the experimental data, Serpone *et al.*[14] have claimed that the exciton radius is < 1 nm. Titania nanoparticles reported so far are mostly larger in size than this size-quantization threshold. On the other hand, the nanosheet thickness is small enough to expect carrier confinement. To our knowledge, a dimension as small as 0.75 nm (the nanosheet thickness) has not previously been reported for titania systems.

The absorption efficiency was several times higher than for films incorporated with titania nanoparticles.[3–6] The optical density at a wavelength of 266 nm was 0.065 for one titania-nanosheet layer (inset in Fig. 1). Comparable data for multilayer films with titania nanoparticles and amino acid capped particles are reported to be 0.016 ± 0.008 (at 190 nm) and 0.017 (232 nm), respectively.[4,6] Note that the optical density for the nanosheet system was higher despite its smaller thickness of the titania layer (0.75 nm) in comparison with those of nanoparticles (2.3–3 nm). Although there are several factors to be considered for the origin of this intense absorption, we speculate that the size effect on oscillator strength is a likely explanation. Its significant enhancement with decreasing the size of semiconductor nanocrystallites has been theoretically predicted and has been experimentally observed for CdS nanoclusters.[15] The findings here strongly suggest promising potential of the present system for its use as photovoltaic, photochromic and catalytic devices and sensors.

Notes and references

1 A. Hangfeldt and M. Grätzel, *Chem. Rev.*, 1995, **95**, 49.
2 G. Decher, *Science*, 1997, **277**, 1232.
3 S. Doherty and D. Fitzmaurice, *J. Phys. Chem.*, 1996, **100**, 10732.
4 Y. Liu, A. Wang and R. Claus, *J. Phys. Chem. B*, 1997, **101**, 1385.
5 N. Kovtyukhova, P. J. Ollivier, S. Chizhik, A. Dubravin, E. Buzaneva, A. Gorchinskiy, A. Marchenko and N. Smirnova, *Thin Solid Films*, 1999, **337**, 166.
6 T. Cassagneau, J. H. Fendler and T. E. Mallouk, *Langmuir*, 2000, **16**, 241.
7 T. Sasaki and M. Watanabe, *J. Am. Chem. Soc.*, 1998, **120**, 4682.
8 T. Sasaki and M. Watanabe, *J. Phys. Chem. B*, 1997, **101**, 10159.
9 T. Sasaki, M. Watanabe, Y. Michiue, Y. Komatsu, F. Izumi and S. Takenovchi, *Chem. Mater.*, 1995, **7**, 1001.
10 Y. Lvov, G. Decher and H. Möhwald, *Langmuir*, 1993, **9**, 481.
11 R. C. Reynolds, Jr., in *Modern Powder Diffraction*, ed. D. L. Bish and J. E. Post, Mineralogical Society of America, Washington, DC, 1989.
12 C. Kormann, D. W. Bahnemann and M. R. Hoffmann, *J. Phys. Chem.*, 1988, **92**, 5196.
13 M. Grätzel, *Heterogeneous Photochemical Electron Transfer*, CRC Press, Boca Raton, FL, 1989.
14 N. Serpone, D. Lawless and R. Khairutdinov, *J. Phys. Chem.*, 1995, **99**, 16646.
15 T. Vossmeyer, L. Katsikas, M. Giersig, I. G. Popovic, K. Diesner, A. Chemseddine, A. Eychmüller and H. Weller, *J. Phys. Chem.*, 1994, **98**, 7665.

ChemComm

First definitive spectroscopic evidence for a stable intermediate in a sulfinyl-transfer reaction: reaction of dibenzo[1,2]oxathiin-6-oxide with sodium ethoxide in anhydrous ethanol†

Ik-Hwan Um,* Myung-Jin Kim and Hye-Won Lee

Department of Chemistry, Ewha Womans University, Seoul 120-750, Korea. Tel: 822 3277-2349, Fax: 822 3277-2844, E-mail: ihum@mm.ewha.ac.kr

Received (in Cambridge) 7th August 2000, Accepted 25th August 2000
First published as an Advance Article on the web

The UV spectral changes along with the kinetic results for the title reaction suggest that the reaction proceeds through a rapidly formed stable intermediate which decomposes slowly to the product.

Acyl-transfer and related reactions such as phosphoryl- and sulfonyl-transfer reactions are central to our understanding of biochemical pathways. Consequently, there has been considerable interest in examining this large class of reactions.[1–11] Acyl-transfer reactions may proceed either through a stepwise mechanism with an addition intermediate or through a concerted mechanism, depending upon the nature of the nucleophile and structure of the substrate.[1–11] For example, it has generally been understood that reactions of esters with amines proceed through a stepwise mechanism, in which the rate-determining step (RDS) changes from breakdown to formation of the intermediate as the attacking amine becomes more basic than the leaving group by 4–5 pK_a units.[2–4] However, the corresponding reactions with anionic nucleophiles are still controversial.[5–11]

Buncel *et al.* have suggested that acyl-transfer reactions proceed through a stepwise mechanism, based on Hammett plots obtained from reactions of a series of substituted phenyl acetates, phosphinates and sulfonates with anionic nucleophiles.[5,6] Recently, Okuyama *et al.* arrived at a similar conclusion for buffer catalyzed hydrolysis of sulfinate esters.[7] By contrast, Williams *et al.* have concluded that acyl-transfer reactions with anionic nucleophiles proceed through a concerted mechanism, based on linear Brønsted-type plots obtained from reactions of *p*-nitrophenyl acetate and related phosphinate and sulfonate esters with a series of substituted phenoxides.[8] The cross interaction correlations of Jencks,[9] isotope effect studies by Hengge[10] and Marcus analysis by Guthrie[11] have all supported the concerted process.

However, there has been no definitive evidence such as spectroscopic data for any intermediate. We now report, along with kinetic evidence for a stepwise mechanism, the first spectroscopic observation of an intermediate in the reaction of a sulfinate ester (**1**, dibenzo[1,2]oxathiin-6-oxide) with EtONa in anhydrous EtOH, as shown in Scheme 1.

Fig. 1 shows UV spectral changes for the reaction of **1** with EtONa in EtOH. The first spectrum from the top has been taken from the substrate alone in EtOH, and the next ones have been recorded immediately after addition of EtONa at intervals of 180 s. The time between the first and the next spectrum is less than 3 s, but even with this short period the spectral change between the two is significant. Furthermore, there is no isosbestic point discernable in the UV spectra. In subsequent experiments with different concentrations of EtONa, a similar result is found, *i.e.* rapid spectral change upon addition of nucleophile followed by slow modification of the spectrum, but the initial spectral change becomes more significant with increasing concentration of EtONa. Such spectral changes, as well as the absence of isosbestic points, definitely suggest that the present reaction proceeds through rapid formation of a stable intermediate which decomposes slowly to the product.

The initial spectral change has been followed using a stopped-flow spectrophotometer and is illustrated in Fig. 2. These spectral changes were monitored for 16 ms at an interval of 2 ms. Two isosbestic points are observed in Fig. 2, indicating that there is no stable intermediate during this fast process. Therefore, based on the spectroscopic data, it is proposed that the present reaction proceeds in two steps with rapid formation of an intermediate shown as **2**, that decomposes slowly to the product **3**,[12] as shown in Scheme 1.

Further support for the stepwise mechanism can be provided by determination of the microscopic rate constants, k_1, k_{-1}, and k_2 in Scheme 1. Therefore, a kinetic study was performed to determine the k_1 value in Scheme 1 using a stopped-flow technique under pseudo-first-order conditions. The plot of pseudo-first-order rate constants (k_{obs}) *vs.* the concentration of EtONa exhibits good linearity with a large positive intercept (Table 1, ESI†). In a separate control experiment, **1** was shown to be inert in EtOH in the absence of EtONa, indicating that the positive intercept in the plot of k_{obs} *vs.* [EtONa] cannot be ascribed to ethanolysis of **1**, but represents the reverse reaction, k_{-1}. Therefore, the microscopic rate constants (k_1 and k_{-1}) of

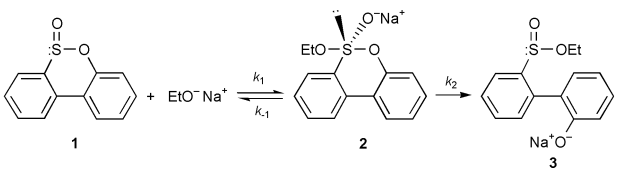

Scheme 1

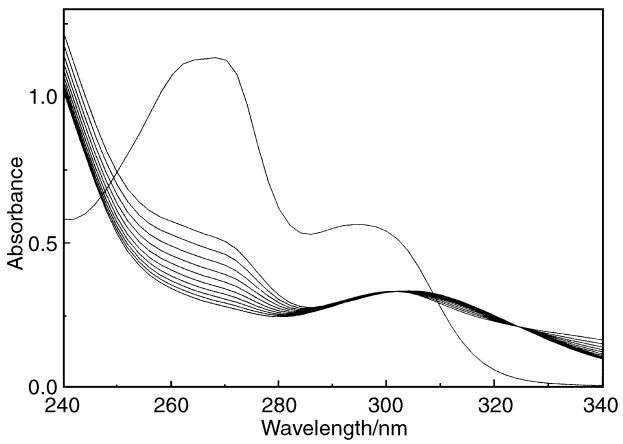

Fig. 1 Repetitive scanning of the UV spectra for the reaction of **1** with EtONa (**1** ⇌ **2** → **3**) in anhydrous EtOH at 25.0 ± 0.1 °C. [**1**] = 7.50×10^{-5} M, [EtONa] = 12.1×10^{-3} M. Time interval less than 3 s for the first and second spectrum from the top, and 180 s for the remainder. See text.

† Electronic supplementary information (ESI) available: summary of kinetic results for reaction of **1** with EtONa. See http://www.rsc.org/suppdata/cc/b0/b006439o/

DOI: 10.1039/b006439o

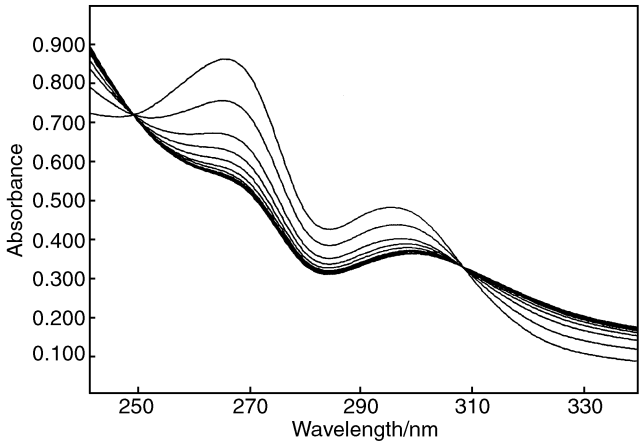

Fig. 2 Repetitive scanning of the stopped-flow spectra for the reaction of **1** with EtONa (**1** ⇌ **2**) in anhydrous EtOH at 25.0 ± 0.1 °C. [**1**] = 8.12×10^{-5} M, [EtONa] = 13.0×10^{-3} M. Time interval = 2 ms.

the fast equilibrium process (**1** ⇌ **2**) can be calculated according to eqn. (1), *i.e*. from the slope and intercept of the plot of k_{obs} *vs*. [EtONa]. The k_1 and k_{-1} values determined in this way are 14,500 $M^{-1}s^{-1}$ and 30.5 s^{-1}, respectively.

$$k_{obs} = k_1[\text{EtONa}] + k_{-1} \quad (1)$$

In order to determine the k_2 value in Scheme 1, the slow reaction process (**1** ⇌ **2** → **3**) has been monitored. The plot of k_{obs} *vs*. [EtONa] yields a curvilinear trace that levels off as the concentration of EtONa increases (Table 2, ESI†). Eqn. (2) may be derived for a reaction which proceeds through a rapid pre-equilibrium as in the present system.[13]

$$k_{obs} = k_1k_2\,[\text{EtONa}]/\{k_1[\text{EtONa}] + k_{-1} + k_2\} \quad (2)$$

Eqn. (2) resembles the Michaelis–Menten equation[14] which accounts for enzyme catalyzed reactions. In this case, the plot of k_{obs} *vs*. [EtONa] should reach a maximum and then flatten out as the concentration of EtONa increases, as found in the present system. Rearrangement of eqn. (2) gives eqn. (3).

$$1/k_{obs} = 1/k_2 + \{k_{-1} + k_2\}/\{k_1k_2\,[\text{EtONa}]\} \quad (3)$$

Consequently, if the present reaction proceeds as in Scheme 1, the plot of $1/k_{obs}$ *vs*. 1/[EtONa] should be linear. In fact, a linear plot has been obtained (Fig. S1, ESI†). From the intercept of the linear plot, the $1/k_2$ value has been calculated. The k_2 value determined in this way is 1.36×10^{-3} s^{-1}, which is much smaller than the k_{-1} value. The relative magnitude of these microscopic rate constants is clearly consistent with the preceeding proposal based on the spectral data shown in Figs. 1 and 2. The small k_2 (1.36×10^{-3} s^{-1}) as compared to k_{-1} (30.5 s^{-1}) would permit observation of the putative intermediate **2**.

Since ethoxide is more basic than aryloxide by 4–5 pK_a units in EtOH,[6b] one might expect EtO^- would be a poorer leaving group than aryloxide. However, in fact, the k_{-1} value has been determined to be over 10^4 times larger than the k_2 value in the present system. Therefore, the present result is quite surprising, and suggests that basicity alone does not determine nucleofugality in this system. Since cyclic sulfinate esters have been suggested to be thermodynamically stable,[15–17] one might suggest that thermodynamic stability of **1** would accelerate the k_{-1} step and retard the k_2 step in Scheme 1. This argument gains support from the fact that the product (**3**) reverts quantitatively to the reactant (**1**) upon acidification of the reaction mixture. However, solvent effect may also be important in the present system. Note that reaction of **1** with OH^- in H_2O is much faster than the corresponding reaction with EtONa in EtOH,[7a] and there is no accumulation of intermediate in H_2O (Fig. S2, ESI†, *e.g*. good isosbestic points at 242 and 306 nm). Furthermore, we have noticed that the reaction of **1** with EtONa is accelerated significantly by addition of H_2O into the reaction medium, even in very small amounts.

However, more systematic studies are required in order to elucidate how the solvent stabilizes or destabilizes reactants, TS and intermediate. Reactions of **1** with various nucleophiles and in different solvents are currently under way to investigate further the reaction mechanism.

The authors are grateful for the financial support from KOSEF (1999-2-123-003-5 and 2000-123-02-2).

Notes and references

1 N. J. Baxter, L. J. M. Rigoreau, A. P. Laws and M. I. Page, *J. Am. Chem. Soc.*, 2000, **122**, 3375; M. Zhong and J. I. Brauman, *J. Am. Chem. Soc.*, 1999, **121**, 2508; H. Adalsteinsson and T. C. Bruice, *J. Am. Chem. Soc.*, 1998, **120**, 3440.
2 W. P. Jencks and M. Gilchrist, *J. Am. Chem. Soc.*, 1968, **90**, 2622.
3 E. A. Castro, M. Cubillos, J. G. Santos and J. Tellez, *J. Org. Chem.*, 1997, **62**, 2512; E. A. Castro, M. Cubillos and J. G. Santos, *J. Org. Chem.*, 1996, **61**, 3501.
4 I. H. Um, J. S. Min and H. W. Lee, *Can. J. Chem.*, 1999, **77**, 659; H. K. Oh, S. Y. Woo, C. H. Shin, Y. S. Park and I. Lee, *J. Org. Chem.*, 1997, **62**, 5780.
5 E. Buncel, I. H. Um and S. Hoz, *J. Am. Chem. Soc.*, 1989, **111**, 971; R. M. Tarkka and E. Buncel, *J. Am. Chem. Soc.*, 1995, **117**, 1503.
6 (*a*) I. H. Um, E. K. Chung and D. S. Kwon, *Tetrahedron Lett.*, 1997, **38**, 4787. (*b*) I. H. Um, Y. J. Hong and D. S. Kwon, *Tetrahedron*, 1997, **53**, 5973.
7 (*a*) T. Okuyama, H. Takano and K. Senda, *Bull. Chem. Soc. Jpn.*, 1996, **69**, 2639; (*b*) T. Okuyama, J. P. Lee and K. Ohnish, *J. Am. Chem. Soc.*, 1994, **116**, 6480; (*c*) T. Okuyama, H. Takano, K. Ohnishi and S. Nagase, *J. Org. Chem.*, 1994, **59**, 472; (*d*) T. Okuyama, *Heteroat. Chem.*, 1993, **4**, 459.
8 (*a*) A. Williams, *Acc. Chem. Res.*, 1989, **22**, 387; (*b*) S. Ba-Saif, A. K. Luthra and A. Williams, *J. Am. Chem. Soc.*, 1987, **109**, 6362; (*c*) N. Bourne, E. Chrystiuk, A. M. Davis and A. Williams, *J. Am. Chem. Soc.*, 1988, **110**, 1890; (*d*) T. Deacon, C. R. Farra, B. J. Sikkel and A. Williams, *J. Am. Chem. Soc.*, 1978, **100**, 2625.
9 D. Stefanidis, S. Cho, S. Dhe-Paganon and W. P. Jencks, *J. Am. Chem. Soc.*, 1993, **115**, 1650.
10 R. A. Hess, A. C. Hengge and W. W. Cleland, *J. Am. Chem. Soc.*, 1997, **119**, 6980; A. C. Hengge and R. A. Hess, *J. Am. Chem. Soc.*, 1994, **116**, 11 256; A. C. Hengge, W. A. Edens and H. Elsing, *J. Am. Chem. Soc.*, 1994, **116**, 5045.
11 J. P. Guthrie, *J. Am. Chem. Soc.*, 1996, **118**, 12878; J. P. Guthrie, *J. Am. Chem. Soc.*, 1991, **113**, 3941.
12 Due to high solubility in basic solution and the reverse reaction to yield the reactant **1** in neutral or in acidic medium, the ethyl sulfinate **3** was hydrolyzed by adding a small amount of NaOH solution into the reaction mixture. The hydrolyzed product was identified as disodium 2′-oxidobiphenyl-2-sulfinate by mass and ^{1}H NMR spectroscopy (Supplementary ^{1}H NMR spectrum). ^{1}H NMR (DMSO-d_6) δ 7.77(d, J = 7.5Hz, 1H), 7.18(m, 2H), 6.87(d, J = 7.5Hz, 1H), 6.71(m, 2H), 6.18(d, J = 7.5Hz, 1H), 5.97(t, J = 7.5Hz, 1H); HRMS (FAB) calcd. for $C_{12}H_8Na_2O_3S$ [(M − Na)$^-$] 255.0092, found 255.0087.
13 J. H. Espenson, in *Chemical Kinetics and Reaction Mechanisms*, 2nd Ed., McGraw-Hill, Inc., New York, 1995, p. 90.
14 L. Michaelis and M. L. Menten, *Biochem. Z.*, 1913, **2**, 333.
15 C. W. Perkins and J. C. Martin, *J. Am. Chem. Soc.*, 1983, **105**, 1377.
16 R. A. McClelland and L. J. Santry, *Acc. Chem. Res.*, 1983, **16**, 394; B. Capon, A. K. Ghosh and D. M. A. Grieve, *Acc. Chem. Res.*, 1981, **14**, 306.
17 T. Okuyama, *Bull. Chem. Soc. Jpn.*, 1996, **69**, 3281; R. A. Hayes and J. C. Martin, in *Organic Sulfur Chemistry*, F. Bernardi, I. G. Csizmadia and A. Mangini, eds., Elsevier, Amsterdam, 1985, Ch. 8.

Stabilisation of nanostructured $Ce_{0.2}Zr_{0.8}O_2$ solid solution by impregnation on Al_2O_3: a suitable method for the production of thermally stable oxygen storage/release promoters for three-way catalysts

R. Di Monte,[a] P. Fornasiero,[a] J. Kašpar,*[a] M. Graziani,[a] J. M. Gatica,[b] S. Bernal[b] and A. Gómez-Herrero[c]

[a] *Dipartimento di Scienze Chimiche, Università di Trieste, 34127 Trieste, Italy. E-mail: kaspar@univ.trieste.it*
[b] *Departamento de Ciencia de los Materials e Ingeniería Metalúrgica y Química Inorgánica, Universidad de Cádiz, Apartado 40, 11510 Puerto Real, Spain*
[c] *Centro de Microscopía Electrónica, Universidad Complutense de Madrid, E28040 Madrid, Spain*

Received (in Cambridge, UK) 15th August 2000, Accepted 25th September 2000
First published as an Advance Article on the web

By impregnating γ-Al_2O_3 with cerium/zirconium citrate solutions and subsequent calcination, nanostructured $Ce_mZr_{1-m}O_2$ mixed oxides supported on Al_2O_3 are obtained, which feature remarkably high oxygen storage even after calcination at 1100 °C for 24 h.

The oxygen storage/release capacity (OSC) of a three-way catalyst (TWC) is a measure of the ability to attenuate the negative effects of rich/lean oscillations of exhaust gas composition through the Ce^{3+}/Ce^{4+} redox process.[1] By maintaining a stoichiometric composition at the catalyst, the highest conversion efficiency of the exhaust is attained. Accordingly, the efficiency of the OSC is monitored by the vehicle emission on-board diagnostics; decline of OSC being an indication of TWC failure, which makes its substitution mandatory by environmental regulations. In modern TWCs, the OSC is achieved by adding a CeO_2–ZrO_2 mixed oxide component.[2,3] Advent of the 'light-off catalyst', *i.e.* a secondary converter close coupled to the engine, exposes the TWCs to very high temperatures, which requires their thermal stability up to 1100 °C.[4]

$Ce_mZr_{1-m}O_2$ (13 wt%)/γ-Al_2O_3 (m = 1, 0.6, 0.2, denoted as CZXX/Al_2O_3, XX = 100, 60, 20) were prepared by using a modified citrate complexation method;[5] by a single-step wet impregnation of the resulting citrate-containing solution on γ-Al_2O_3 (BET surface area 186 $m^2\ g^{-1}$, pore volume 1.03 ml g^{-1}). $Ce(NO_3)_3{\cdot}6H_2O$ (99.99%, Aldrich) was dissolved in water and mixed with an aqueous solution of $ZrO(NO_3)_2$ (20% ZrO_2, MEL Chemicals), then a water solution of citric acid (99.7%, Prolabo) was added. The metal cation to ligand ratio was 1 to 2.1. The resulting solution was stirred at 75 °C for 5 h, then at room temperature (r.t.) for 12 h, and finally concentrated to perform the 'incipient wetness' impregnation of the support. The resulting material was dried at 120 °C for 12 h, heated to 500 °C at a rate of 3 °C min^{-1} and then calcined at this temperature for 5 h to obtain a yellow powder. These samples are indicated as being 'fresh'. Catalysts were aged by calcination in air. Temperature programmed reduction (TPR) was carried out in a conventional instrument.[3] Dynamic-OSC was measured by alternately pulsing CO (100 μl) and O_2 (100 μl) over the sample (30–100 mg, maintained in a flow of Ar of 25 ml min^{-1}).[3] Powder XRD spectra were collected on a

Table 1 Oxygen storage and textural/structural characterisation of the CeO_2–ZrO_2 and CeO_2–ZrO_2/Al_2O_3 catalysts

Sample	Calcination		BET surface area/ $m^2\ g^{-1}$	Phase composition (%)				CZ Crystallite size/nm	OSC[b]/ml O_2 $g_{solid\ solution}^{-1}$		
				Al_2O_3							
	T/ °C	t/h		γ	θ[c]	α	CZ[a]		400 °C	500 °C	600 °C
Al_2O_3	700	5	186	100			—	—	0	0	0
	1100	5	58		56	44	—	—	—	—	—
	1100	24	12			100	—	—	—	—	—
$Ce_{0.2}Zr_{0.8}O_2/Al_2O_3$	500	5	180	100			—	—	0.2	2.2	5.8
	1000	5	115		100		t (100)	7	0.6	2.5	4.6
	1000	48	104		100		t (100)	9	0.4	1.8	4.9
	1100	5	68		100		t (100)	11	0.1	1.1	3.5
	1100	24	63		98	2	t (100)	11	0.3	1.3	3.6
$Ce_{0.6}Zr_{0.4}O_2/Al_2O_3$	500	5	168	100			—	—	1.7	8.6	16.9
	1000	5	105		100		c (90) t (10)	12 (c) 7 (t)	1.4	5.8	9.2
	1000	48	103		100		c (90) t (10)	12 (c) 7 (t)	1.7	5.2	9.1
	1100	5	71		100		c (74) t (26)	14 (c) 7 (t)	0.5	3.1	8.7
	1100	24	55		80	20	c (75) t (25)	18 (c) 10 (t)	0.2	1.6	6.0
CeO_2/Al_2O_3	500	5	180	100			—	—	3.2	9.3	13.8
	1100	5	60		100		c (100)	20	0.3	0.9	1.6
	1100	24	32		34	66	c (100)	28	0.4	1.0	1.9
$Ce_{0.2}Zr_{0.8}O_2$	500	5	24	—	—	—	t (100)	6	0.3	1.6	3.4
	1100	5	1	—	—	—	t (100)	35	0	0	0.1
$Ce_{0.6}Zr_{0.4}O_2$	500	5	42	—	—	—	t″(100)	5	0.9	3.1	5.8
	1100	5	1	—	—	—	c (85) t (15)	20 (c) 15 (t)	0	0.1	0.6

[a] t″, t′ and t are tetragonal phases (space group $P4_2/nmc$) with pseudo-cubic cell parameter ratio (c/a), respectively, of 1.000, 1.002–1.010 and 1.02; c phase: cubic fluorite type of lattice (space group $Fm3m$).[2] When a mixture of phases was detected the approximate composition was evaluated: c phase: $Ce_{0.8}Zr_{0.2}O_2$; t phase $Ce_{0.2}Zr_{0.8}O_2$. [b] For consistency OSC (O_2 uptake) is given per g of CZ mixed oxide. Dynamic-OSC measured at the indicated temperatures. Total-OSC was measured as O_2 uptake at 427 °C after a TPR up to 1000 °C and assuming a full re-oxidation.[2] 5–7, 15–18 and 18–20 ml O_2 $g_{solid\ solution}^{-1}$ were obtained, respectively, for CZ20/Al_2O_3, CZ60/Al_2O_3 and CZ100/Al_2O_3. [c] Some δ-Al_2O_3 was also detected in a few samples and the sum of θ- and δ-Al_2O_3 is given.

DOI: 10.1039/b006674p

Siemens Kristalloflex Mod.F Instrument (Ni-filtered Cu-Kα radiation). The profile fitting of the XRD patterns was performed by a Rietveld analysis program (RIETAN94). High resolution electron microscopy (HREM) measurements were performed using a JEOL 4000-EX microscope equipped with a top-entry specimen holder with 0.18 nm point resolution with an accelerating voltage of 400 kV. Digital processing was carried out by using a CCD camera and the SEMPER 6+ software package.

Table 1 reports the effects of calcination of the fresh samples on textural, structural and OSC properties. Calcination at 700–1100 °C progressively transforms γ-Al_2O_3 into θ-Al_2O_3 and α-Al_2O_3, the latter being the only phase detected after 24 h at 1100 °C. Consistent with the literature, these transformations are hindered by the presence of either CeO_2[6] or ZrO_2.[7] This effect is noticeable after calcination at 1100 °C for 24 h; the highest surface area (63 m^2 g^{-1}) being observed for CZ20/Al_2O_3. XRD analysis by Rietveld refinement of CZ20/Al_2O_3 calcined at 1100 °C for 5 h revealed the presence of a single phase CZ solid solution. Lattice parameters a = 3.6296(5) and c = 5.2317(5) Å were calculated for the tetragonal cell, which compare well with a = 3.6396(1) and c = 5.2382(1) Å obtained for CZ20 after calcination at 1000 °C. This indirectly confirmed that no appreciable phase segregation occurred. Some CeO_2 non-incorporated into the mixed oxide was detected for CZ60/Al_2O_3, in accord with a previous observation that compositional inhomogeneities are favoured at intermediate compositions.[7] There is a synergic stabilisation between the CZ and Al_2O_3 component, since the sintering of CZ is retarded by the presence of Al_2O_3, particularly at high ZrO_2 content. For CZ20/Al_2O_3 calcined at 1100 °C a crystallite size of 11 nm was evaluated from the XRD analysis. These findings were confirmed by HREM analysis which revealed the presence of tetragonal $Ce_{0.2}Zr_{0.8}O_2$ particles in the range 9–20 nm [Fig. 1(a)]. The nanosized nature of the CZ component seems attributable to the presence of zirconia rather then ceria, since significantly higher particle sizes were detected by XRD for CZ100/Al_2O_3.

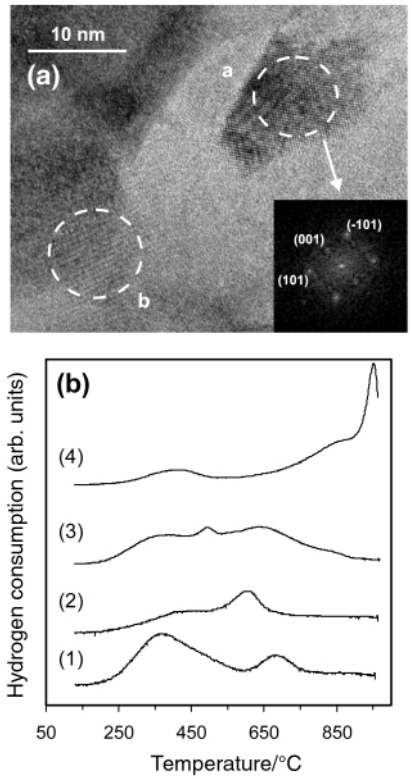

Fig. 1 (a) HREM image of $Ce_{0.2}Zr_{0.8}O_2/Al_2O_3$ calcined at 1100 °C for 5 h. The digital diffraction pattern of area 'a' was indexed as tetragonal $Ce_{0.2}Zr_{0.8}O_2$ viewed along the [0,1,0] axis. In the zone marked 'b', interplanar distances typical of θ-Al_2O_3 were found; (b) Comparison of TPR profiles of $Ce_{0.2}Zr_{0.8}O_2/Al_2O_3$ (1) fresh, (2) calcined at 1100 °C for 5 h, and CeO_2/Al_2O_3 (3) fresh and (4) calcined at 1100 °C for 5 h.

Fig. 1(b) compares the TPR profiles of fresh and calcined (1100 °C) samples of CZ20/Al_2O_3 and CZ100/Al_2O_3. High temperature ageing leads to most reduction occurring at high temperatures in CZ100/Al_2O_3, consistent with the relatively high CeO_2 particle size.[6] In contrast, reduction at relatively low temperature persists in CZ20/Al_2O_3 even after high temperature calcination. Either $CeAlO_3$ or crystalline CeO_2 were detected by XRD after the TPR/oxidation at 427 °C experiment carried out on CZ100/Al_2O_3. Dispersing CeO_2 over Al_2O_3 led to deactivation of OSC in CeO_2/Al_2O_3 owing to formation of $CeAlO_3$.[8] Within the sensitivity of the XRD method (estimating an upper limit of *ca*. 5% $CeAlO_3$ with respect to the CZ phase in the CZ/Al_2O_3 material for non-detection) no formation of $CeAlO_3$ was detected in any of the CZ20/Al_2O_3 samples. This indicates that incorporation of ZrO_2 into CeO_2 prevents this undesirable deactivation pathway. The more ZrO_2 is added to CeO_2, the more effective stabilisation is achieved, highlighting the crucial role of ZrO_2 in improving the stability of these systems. Phase separation into CeO_2-rich and ZrO_2-rich phases was indeed detected at 1100 °C in CZ60/Al_2O_3, leading to partial formation of $CeAlO_3$ after TPR/oxidation at 427 °C.

The effects of addition of Al_2O_3 to CZ on the dynamic-OSC are remarkable (Table 1): (i) there is a strong improvement of the dynamic-OSC in the fresh CZ/Al_2O_3 samples compared to the unsupported ones; (ii) thermal ageing at 1000–1100 °C leads to an almost complete deactivation of the dynamic-OSC in unsupported CZ; (iii) such ageing decreases dynamic-OSC of CZ/Al_2O_3 compared to fresh samples, however, appreciably high OSC persists, which is comparable or higher than that of fresh CZ; (iv) thermally stable dynamic-OSC was detected in CZ20/Al_2O_3, which remarkably did not decline by increasing the calcination time at 1100 °C up to 24 h. We tentatively attribute these improved properties to an intimate contact between the CZ20 and Al_2O_3 phases generated by the synthesis method, which stabilises high dispersion of the CZ component (by contrast physical mixtures of CZ and Al_2O_3 calcined at 1100 °C for 5 h showed negligible dynamic-OSC). In summary, materials, which are highly suitable for thermally demanding redox reactions, such as those mediated by TWCs, can be obtained by supporting zirconia rich CeO_2–ZrO_2 mixed oxides over Al_2O_3.

Helpful discussions with Drs José J. Calvino and José A. Pérez-Omil (University of Cadiz) are gratefully acknowledged. The CNR (Roma) Programmi Finalizzati 'Materiali Speciali per Tecnologie Avanzate II', Contract n. 97.00896.34, Regione Friuli Venezia-Giulia, Fondo regionale per la ricerca L.R. 3/1998, Fondo Trieste – 1999, and Project CiCYT (MAT-99-0570) are gratefully acknowledged for financial support.

Notes and references

1 H. C. Yao and Y. F. Yu Yao, *J. Catal.*, 1984, **86**, 254.
2 J. Kašpar, P. Fornasiero and M. Graziani, *Catal. Today*, 1999, **50**, 285 and references therein.
3 N. Hickey, P. Fornasiero, J. Kašpar, M. Graziani, G. Blanco and S. Bernal, *Chem. Commun.*, 2000, 357.
4 A. J. Zarur and J. Y. Ying, *Nature*, 2000, **403**, 65.
5 C. Marcilly, P. Courty and B. Delmon, *J. Am. Ceram. Soc.*, 1970, **53**, 56.
6 A. Trovarelli, *Catal. Rev.-Sci. Eng.*, 1996, **38**, 439.
7 M. H. Yao, R. J. Baird, F. W. Kunz and T. E. Hoost, *J. Catal.*, 1997, **166**, 67.
8 J. Z. Shyu, W. H. Weber and H. S. Gandhi, *J. Phys. Chem.*, 1988, **92**, 4964.

ChemComm

Hydrothermal synthesis and crystal structures of two novel hybrid open-frameworks and a two-dimensional network based on tungsten(VI) oxides

Bangbo Yan,*† Yan Xu, Ngoh K. Goh and Lian S. Chia

Division of Chemistry, School of Science, Nanyang Technological University, Singapore 259756, Republic of Singapore

Received (in Cambridge, UK) 3rd July 2000, Accepted 13th September 2000
First published as an Advance Article on the web

Three new tungsten(VI) oxide hybrid materials, $[WO_3(pyz)_{0.5}]$ (pyz = pyrazine) 1, $[WO_3(bpy)_{0.5}]$ (bpy = 4,4′-bipyridyl) 2 and $[W_3O_{10}(enH_2)]$ 3, have been hydrothermally synthesized: 1 and 2 exhibit covalent/coordination hybrid framework connectivities while the structure of 3 consists of novel layers comprised of distorted $\{WO_6\}$ octahedra linked through edge- and corner-sharing interactions.

Crystal engineering of low-dimensional and porous materials is the main concern of many current research projects, owing to their potential applications in catalysis, sorption, separation and photochemistry.[1–6] Hydrothermal crystallization, in the presence of organic templating species, has been demonstrated to be a versatile technique for the synthesis of these kinds of materials.[4–6] Of significant importance is the ability of the organic molecules to influence profoundly the structure of synthesized products, and to direct their formation with particular structural and physical properties. The exquisite control over the detailed topology of the anionic framework that can be achieved by altering the steric and electronic properties of the template has been exploited to synthesize materials with an astonishingly diverse range of structural characteristics. In addition to silicon, aluminium and phosphorus,[6,7] a wide variety of other main group and transition metals such as Ga,[8] Mo,[9] V[10] and Fe[11] have been incorporated into the three-dimensional framework and two-dimensional network structures through hydrothermal synthesis in the presence of organic templating agents.

The chemistry of tungsten oxide clusters and their derivatives has been extensively studied owing to their unusual magnetic properties, potential medical uses derived from their antiviral and antibacterial activities, relevance in the design and development of new materials, proven roles in catalysis, and promise as catalysts for chemical transformations.[12] Although organic amines have been extensively used as templating or structure-directing agents in hydrothermal reactions, little work has been reported on their use in the hydrothermal synthesis of new tungsten oxides with the exception of $[H_3N(CH_2)_6NH_3]_4[W_{18}P_2O_{62}]\cdot H_2O$[13] and a few Keggin species.[14] Here, we report the hydrothermal synthesis and structural characterization of three novel tungsten(VI) oxide hybrid materials: $[WO_3(pyz)_{0.5}]$ **1**, $[WO_3(bpy)_{0.5}]$ **2** and $[W_3O_{10}(enH_2)]$ **3**.

Compounds **1**–**3** were prepared from hydrothermal mixtures of $Na_2WO_4\cdot 2H_2O$, $MCl_2\cdot nH_2O$ (M = Cu, Zn), organoamines and H_2O, heated to 140–160 °C for 120–264 h.‡ Crystal structures were solved from the data collected using a Siemens P4 X-ray diffractometer.§ The IR spectra of **1**–**3** exhibited strong bands in the range 910–960 cm^{-1} attributed to ν(W=O). Thermogravimetric analysis indicated weight losses corresponding to the loss of ligands.¶

The structure of $[WO_3(pyz)_{0.5}]$ **1** consists of layers of corner-sharing $\{WO_5N\}$ octahedra parallel to the *ab*-plane linked through pyz molecules into a 3-D tungsten oxide/pyz framework [Fig. 1(a)]. The 3-D architecture of **1** can be described as an interwoven net of inorganic metal oxide layers and organic tethers. The tungsten oxide layers are stacked along the *c* axis in an ABAB… sequence. The connectivity between the tungsten oxide layers and pyz molecules results in one-dimensional rectangular channels along the *b* axis circumscribed by six $\{WO_5N\}$ octahedra and two pyz molecules. The dimensions of the channels are *ca.* 7.7 × 5.2 Å. The coordination geometry at the W site is defined by one terminal oxo group, four bridging oxo groups and one pyz nitrogen donor with W–O bond lengths of 1.680(2), 4 × 1.8741(3) Å and W–N bond length of 2.440(3) Å. The significant lengthening in the W–N distance reflects the strong *trans* effects of the terminal oxo group.

Compound $[WO_3(bpy)_{0.5}]$ **2** has a similar topology to compound **1**. As shown in Fig. 1(b), the structure of **2** consists of W/O/N layers, parallel to the *ab*-plane, of corner sharing $\{WO_5N\}$ octahedra bridged through bpy ligands into a 3-D covalent/coordination hybrid framework. The connectivity between the tungsten oxide layers and bpy molecules results in one-dimensional rectangular channels along the [1 1 0] direction circumscribed by six $\{WO_5N\}$ octahedra and two pyz molecules. The dimensions of the one-dimensional rectangular channels are *ca.* 11.9 × 5.2 Å. Each W site receives

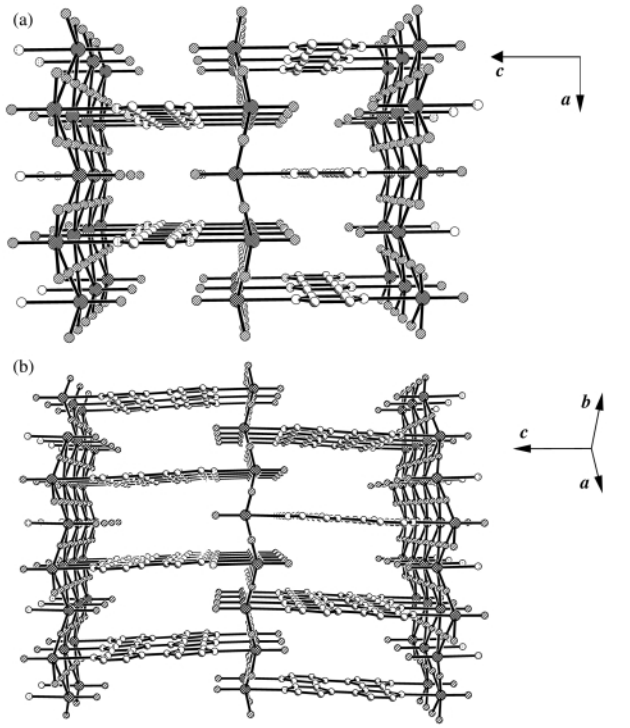

Fig. 1 (a) Crystal structure of $[WO_3(pyz)_{0.5}]$ **1** viewed along the *b* axis. (b) Crystal structure of $[WO_3(bpy)_{0.5}]$ **2** viewed along the [1 1 0] direction. Coordination of ligands (pyrazine or 4,4′-bipyridyl) to tungsten oxide layers results in a 3-D inorganic–organic framework with 1-D rectangular channels.

† Current address: School of Science, Nanyang Technological University, 469 Bukit Timah Road, Singapore 259756, Republic of Singapore. E-mail: yanbangbo@hotmail.com

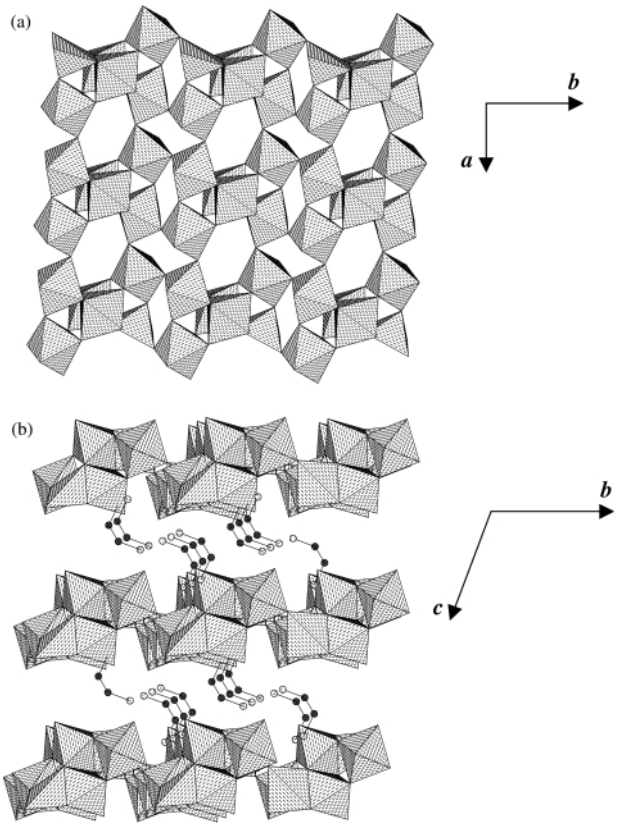

Fig. 2 (a) A polyhedral packing view of the $[W_3O_{10}]^{2-}$ layers of $[W_3O_{10}(enH_2)]$ **3** showing the puckered six-membered rings. (b) A polyhedral and ball-and-stick view of $[W_3O_{10}(enH_2)]$ **3.**

contributions from four bridging oxo groups, one terminal oxo group and one nitrogen donor with W–O bond lengths of 1.678(11), 2 × 1.8936(4), 1.851(13) and 1.897(12) Å, and W–N bond length of 2.409(14) Å.

The inorganic layers of compounds **1** and **2** are analogous to that of three-dimensional ReO_3-type WO_3 (r-WO_3).[15] However, the inorganic layers in r-WO_3 are connected through shared corners forming a three-dimensional structure whereas the tungsten oxide layers in compounds **1** and **2** are cross-linked by organodiamines through coordination bonds giving rise to their three-dimensional organic/inorganic hybrid structures. It is noteworthy that the synthesis conditions of compounds **1** and **2** differ from their molybdenum isostructures, $MoO_3(pyz)_{0.5}$ and $MoO_3(bpy)_{0.5}$.[16,17] It should also be noted that some carbon atoms in compounds **1** and **2** are disordered over two sites.

In contrast to the three-dimensional covalent/coordination hybrid frameworks of **1** and **2**, the structure of $[W_3O_{10}(enH_2)]$ **3** consists of $[W_3O_{10}]^{2-}$ layers [Fig. 2(a)], separated by interlamellar enH_2^{2+} cations [Fig. 2(b)]. The tungsten oxide layers contain infinite ribbons, two polyhedra thick, of edge- and corner-sharing {WO_6} octehedra running parallel to the *b* axis. These infinite ribbons are connected by shared corners resulting in the layer structure of **3**. The {WO_6} octohedra are distorted with W–O distances in the range 1.722(9)–2.307(7) Å. The layer structure of compound **3** exhibits a puckered six-membered ring circumscribed by six tungsten octahedra as shown in Fig. 2(a). Ethylenediamine cations are located between adjacent layers and are linked to the oxygen atoms of the tungstate units *via* hydrogen bonds.

It should be noted that the structure of anionic layer of compound **3** is quite different from that of $K_2W_3O_{10}$[18] although the tungstate anions in these two compounds have the same stoichiometry. The three-dimensional framework of $K_2W_3O_{10}$ consists of corner- and edge-sharing {WO_6} octahedra. Moreover, the structures of known trimolybdates $[Mo_3O_{10}]^{2-}$ are composed of infinite chains of polymolybdate anions,[19,20] and the existence of a layered trimolybdate $[Mo_3O_{10}]^{2-}$ has not yet been reported. More interestingly, a one-dimensional example of compound **3** has also been isolated from hydrothermal media.[21]

The success in synthesizing compounds **1**–**3** provides innovative examples of the utility of the template-mediated hydrothermal method for the construction of versatile tungsten oxide hybrid solids. It further demonstrates the multifunctional roles of organoamines functioning as ligands bound to the tungsten oxide skeleton, as in compounds **1** and **2**, and as a simple counter ion in compound **3** in the cooperative assembly of organic/tungsten oxide hybrid materials. The current success opens up an exciting area of research in which the structural versatility of tungsten oxide materials can be evolved from the introduction of appropriate templates and optimization of reaction conditions.

Notes and references

‡ Hydrothermal reactions were carried out in sealed Teflon-lined stainless steel autoclave reactors. *Reaction conditions*: **1**: mol ratio $Na_2WO_4{\cdot}2H_2O$: $CuCl_2{\cdot}2H_2O$: pyz : H_2O = 1.0 : 0.70 : 1.9 : 1096, at 160 °C for 120 h; **2**: mol ratio $Na_2WO_4{\cdot}2H_2O$: $ZnCl_2$: bpy : H_2O = 1.0 : 0.2 : 0.6 : 539, at 140 °C for 255 h; **3**: mol ratio $Na_2WO_4{\cdot}2H_2O$: $CuCl_2{\cdot}2H_2O$: en : H_2O = 2.0 : 1.0 : 1.2 : 1110, at 160 °C for 264 h.

§ *Crystal data*: $[WO_3(pyz)_{0.5}]$ **1**: $C_{0.25}H_{0.25}W_{0.125}N_{0.125}O_{0.375}$, M_w = 33.959, tetragonal, space group *I*4/*mmm*, a = 5.2288(7), c = 14.175(3) Å, V = 387.55(10) Å^3, Z = 32, D_c = 4.660 g cm^{-3}, μ = 29.664 mm^{-1}, T = 296 K, yellow plate, crystal size *ca.* 0.12 × 0.08 × 0.04 mm, R_1/wR_2 = 0.0302/0.0802 (R_1/wR_2 = 0.0314/0.0805 for all data). $[WO_3(bpy)_{0.5}]$ **2**: $C_5H_4W_1N_1O_3$, M_w = 309.94, orthorhombic, space group *Cmca*, a = 7.4733(15), b = 7.3927(15), c = 22.570(4) Å, V = 1246.9(4) Å^3, Z = 16, D_c = 3.302 g cm^{-3}, μ = 18.462 mm^{-1}, T = 296 K, yellow plate, crystal size *ca.* 0.10 × 0.09 × 0.04 mm, R_1/wR_2 = 0.0336/0.0776 (R_1/wR_2 = 0.0441/0.0809 for all data). $[W_3O_{10}(enH_2)]$ **3**: $C_2H_{10}W_3N_2O_{10}$, M_w = 773.67, triclinic, space group $P\bar{1}$, a = 7.343(2), b = 7.373(3), c = 9.889(3) Å, α = 93.99(2), β = 109.714(16), γ = 91.23(2)°, V = 502.2(3) Å^3, Z = 2, D_c = 5.116 g cm^{-3}, μ = 34.326 mm^{-1}, T = 296 K, colorless plate, crystal size *ca.* 0.25 × 0.20 × 0.08 mm, R_1/wR_2 = 0.0403/0.0970 (R_1/wR_2 = 0.0502/0.1021 for all data).

CCDC 182/1777. See http://www.rsc.org/suppdata/cc/b0/b005303l/ for crystallographic files in .cif format.

¶ *TGA data*: weight loss for **1**: 14.35% (calc. 14.76%, 507–576 °C); **2**: 25.20% (calc. 25.24%, 498–572 °C); **3**: 8.08% (calc. 8.03%, 342–392 °C).

1 T. Chirayil, P. Y. Zavalij and M. S. Whittingham, *Chem. Mater.*, 1998, **10**, 2629.
2 S. L. Brock, N. Duan, Z. R. Tian, O. Giraldo, H. Zhou and S. L. Suib, *Chem. Mater.*, 1998, **10**, 2619.
3 P. J. Hagrman, D. Hagrman and J. Zubieta, *Angew. Chem., Int. Ed.*, 1999, **38**, 2638.
4 R. M. Barrer, *Hydrothermal Chemistry of Zeolites*, Academic Press, London, 1982.
5 B. M. Lok, T. R. Cannon and C. A. Messina, *Zeolites*, 1983, **3**, 282.
6 M. E. Davis and R. F. Lobo, *Chem. Mater.*, 1992, **4**, 756.
7 S. T. Wilson, B. M. Lok, C. A. Messina, T. R. Cannon and E. M. Flanigen, *ACS Symp. Ser.*, 1983, **218**, 79.
8 T. Loiseau and G. Férey, *J. Mater. Chem.*, 1996, **6**, 1073.
9 R. C. Haushalter and L. A. Mundi, *Chem. Mater.*, 1992, **4**, 31.
10 V. Soghomanian, Q. Chen, R. C. Haushalter, J. Zubieta and J. O'Connor, *Science*, 1993, **259**, 1596.
11 K. H. Lii, Y. F. Huang, V. Zima, C. Y. Huang, H. M. Lin, Y. C. Jiang, F. L. Liao and S. L. Wang, *Chem. Mater.*, 1998, **25**, 2599, and references therein.
12 A. Muller, M. T. Pope and D. Gatteschi, *Chem. Rev.*, 1998, **98**, 239; D. E. Katsoulis, *Chem. Rev.*, 2998, **98**, 359.
13 M. Hölscher, U. Englert, B. Zibrowius and W. F. Hölderich, *Angew. Chem., Int. Ed.*, 1999, **33**, 2491.
14 P. Zavalij, J. Guo, M. S. Whittingham, R. A. Jacobson, V. Pecharsky, C. K. Bucher and S. Hwu, *J. Solid State Chem.*, 1996, **123**, 83.
15 A. F. Wells, *Structural Inorganic Chemistry*, Oxford University Press, Oxford, 1984.
16 Y. Xu, J. Lu and N. K. Goh, *J. Mater. Chem.*, 1999, **9**, 1599.
17 J. W. Johnson, A. J. Jacobson, S. M. Rich and J. F. Brody, *J. Am. Chem. Soc.*, 1981, **103**, 5246.
18 K. Okada, H. Morikawa, F. Marumo and S. Iwai, *Acta Crystallogr., Sect. B*, 1976, **32**, 1522.
19 M. I. Khan, Q. Chen and J. Zubieta, *Inorg. Chim. Acta*, 1993, **213**, 325.
20 N. Guilou and G. Férey, *J. Solid State Chem.*, 1997, **132**, 224.
21 B. Yan, Y. Xu, N. K. Goh and L. S. Chia, *Inorg. Chem. Commun.*, 2000, **3**, 379.

Second-generation fluorous chiral (salen) manganese complexes

Marco Cavazzini, Amedea Manfredi, Fernando Montanari, Silvio Quici and Gianluca Pozzi*

Centro CNR and Dipartimento di Chimica Organica e Industriale dell'Università, Via Golgi 19, I-20133 Milano, Italy. E-mail: gianluca.pozzi@unimi.it

Received (in Cambridge, UK) 29th August 2000, Accepted 14th September 2000
First published as an Advance Article on the web

Sterically hindered chiral (salen)manganese complexes bearing long perfluoroalkyl substituents are synthesized and successfully employed as catalysts in the enantioselective (ee = 50–87%) epoxidation of alkenes under fluorous biphasic conditions.

Following the pioneering work of Horváth and Rábai,[1] a number of reagents and catalysts bearing appropriate perfluoroalkyl substituents ('fluorous compounds') have been prepared and used in 'fluorous biphase chemistry'.[2] Catalytic reactions in fluorous biphasic systems present several advantages over their classical homogeneous counterparts.[3] Fluorous chemistry has also a great potential for enantioselective transformations, offering both an easy way to recover precious chiral reagents or catalysts and unusual solvation effects. Nevertheless, only a few chiral fluorous compounds have been prepared to date and the actual influence of perfluoroalkyl substituents (R_F) and perfluorocarbon solvents on the outcome of asymmetric reactions is virtually unknown.[4] We have reported the first example of a fluorous biphasic enantioselective reaction, namely the epoxidation of alkenes in the presence of the optically active fluorous (salen)Mn^{III} complexes Mn-**1** and Mn-**2** (Jacobsen–Katsuki catalysts, Fig. 1).[4a] Good chemoselectivity and efficiency were observed in the epoxidation of several substrates, and recycling of the catalysts was also demonstrated. However, high levels of enantioselectivity were not attained, except in the epoxidation of indene (ee = 90%). This behaviour was tentatively ascribed to the low steric hindrance of the R_F groups in the 3,3'- and 5,5'-positions of the ligands and to the inadequate electronic shielding of the metal site from the strong electron-withdrawing effect of these substituents.[4c]

Second-generation (salen)Mn^{III} complexes Mn-**3** and Mn-**4** (Fig. 1) were designed with these assumptions in mind. In order to better shield the metal site, the R_F substituents in 5,5'-positions were replaced by perfluoroalkyl-substituted aryl moieties. Moreover, sterically demanding *tert*-butyl substituents were introduced in the key-positions 3,3' of ligands **3** and **4**.

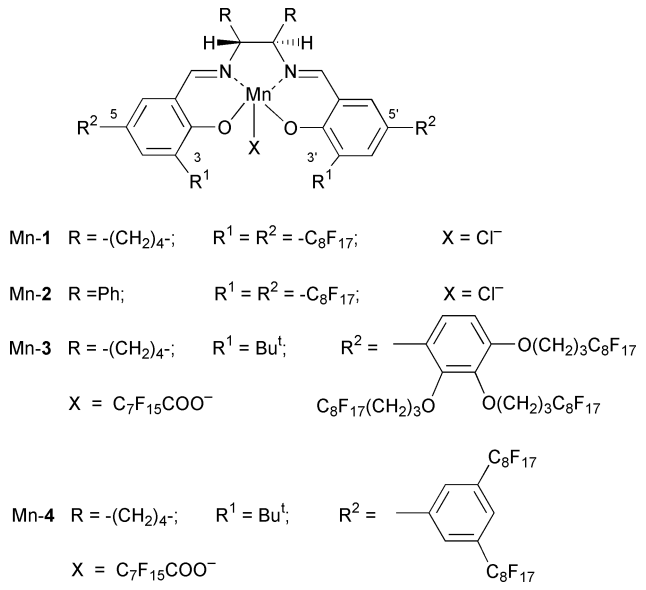

Fig. 1 First- (Mn-**1**, Mn-**2**) and second-generation (Mn-**3**, Mn-**4**) fluorous chiral (salen)Mn complexes.

Both salicylaldehydes **7** and **10**, the key intermediates for the synthesis of ligands **3** and **4**, were prepared starting from aldehyde **5**,[5] as shown in Scheme 1. Pd^0-catalyzed cross-coupling reaction of **5** with boronic acid **6** (yield = 86%),[6] followed by *O*-deprotection (89%) and *O*-alkylation with $C_8F_{17}(CH_2)_3I$ (37%), afforded the fluorous salicylaldehyde **7**. Mono- and bis-*O*-alkylated biaryl compounds were isolated from the reaction mixture by column chromatography and reused in following runs.

In the case of salicylaldehyde **10,** aldehyde **5** was used as a precursor of aryl boronic acid **8**, whereas perfluoroalkyl-substituted aryl bromide **9** was prepared by copper-mediated cross-coupling reaction of 1,3,5-tribromobenzene with 2 equiv. of $C_8F_{17}I$. The bis(perfluoroalkyl) derivative was obtained as the main product and isolated in reasonable yields (60%) after crystallization from CH_2Cl_2 and then from Et_2O. Pd^0-catalyzed cross-coupling reaction of crude aryl boronic acid **8** with **9**, followed by deprotection with BBr_3 gave the desired salicylaldehyde **10** in 62% yield.

Condensation of two equivalents of salicylaldehyde **7** or **10** with (1*R*,2*R*)-(−)-1,2-diaminocyclohexane in boiling ethanol afforded the fluorous salen ligands **3** (72%) and **4** (95%), respectively.[7] Mn^{III} complexes Mn-**3** and Mn-**4** were prepared by reaction of the corresponding ligand with an excess of $Mn(OAc)_2{\cdot}4H_2O$ in refluxing ethanol under aerobic conditions, followed by anion exchange with LiCl and then $C_7F_{15}COONH_4$. The exchange of Cl^- for the fluorophilic

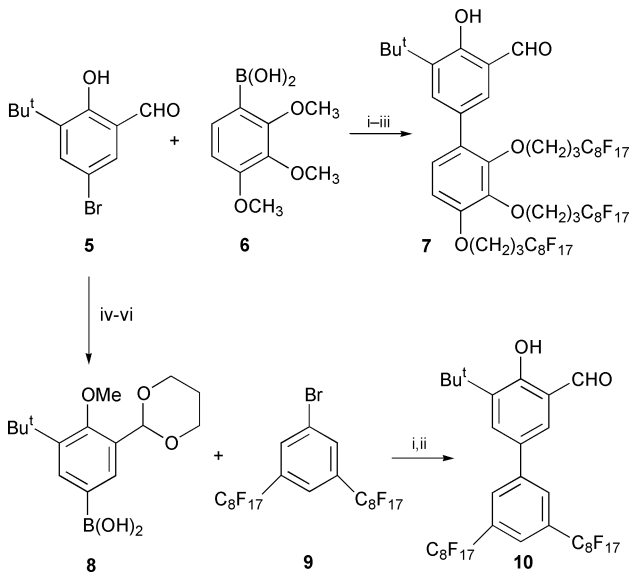

Scheme 1 *Reagents and conditions*: i, $Pd(OAc)_2/PPh_3$, Pr^iOH, aqueous Na_2CO_3, 110 °C; ii, BBr_3, CH_2Cl_2, 0 °C; iii, $C_8F_{17}(CH_2)_3I$, K_2CO_3, CH_3CN, 70 °C; iv, $(CH_3)_2SO_4$, K_2CO_3, acetone, r.t.; v, $HO(CH_2)_3OH$, *p*-TsOH, toluene, reflux; vi, BuLi, −78 °C, THF, 45 min, then $B(OCH_3)_3$, −78 to 0 °C, aqueous HCl.

DOI: 10.1039/b007053j

$C_7F_{15}COO^-$ anion resulted in the sought preferential solubility of Mn-**3** and Mn-**4** in perfluorocarbons, as verified by partition experiments in biphasic mixtures *n*-perfluorooctane/organic solvents. Partition coefficients, determined by UV–Vis spectroscopy at 25 °C,[8] were found to be quite similar for the two complexes, ranging from 1.21 for Mn-**3** in *n*-perfluorooctane/hexane, to >1000 for Mn-**3** and Mn-**4** in *n*-perfluorooctane/CH_3CN and *n*-perfluorooctane/toluene.

First- and second-generation (salen)Mn^{III} complexes were initially compared in the homogeneous epoxidation of 1,2-dihydronaphthalene in CH_2Cl_2/benzotrifluoride, using *meta*-chloroperbenzoic acid/ *N*-methylmorpholine *N*-oxide (*m*-CPBA/NMO) as the oxidant at −50 °C.[9] Second-generation catalysts afforded ee values much higher than those obtained with Mn-**1** and Mn-**2** (63% *vs*. 16 and 12%, respectively) and slightly improved epoxide yields (70% with Mn-**3** and Mn-**4** *vs*. 60% with Mn-**1** and Mn-**2**). Other oxidising agents commonly used in association with (salen)Mn^{III} complexes were also tested and the superiority of the new complexes was confirmed.

PhIO together with small amounts of pyridine *N*-oxide (PNO) was used as the oxidising system in the next fluorous biphasic reactions that were run in *n*-perfluorooctane/CH_3CN (Table 1).† This set of conditions was chosen taking into account the favourable partition coefficients of the catalysts and considering that homogeneous epoxidation reactions with PhIO/PNO are conveniently carried out in CH_3CN at 0–25 °C.[10] Both reaction yield and enantioselectivity rose with temperature under fluorous biphasic conditions: the best results were obtained at 100 °C, corresponding to the boiling point of *n*-perfluorooctane (Table 1, entries 1–5). Blank experiments evidenced that only traces of epoxide are formed at this temperature in the absence of the fluorous catalysts. The results obtained in the fluorous biphasic epoxidation of 1,2-dihydronaphthalene with PhIO/PNO at 100 °C (entry 5) compare favourably to those reported for the same reaction in CH_3CN in the presence of Jacobsen's catalyst, a commercially available, standard (salen)Mn^{III} complex (yield = 70%, ee = 46%).[11]

The fluorous layer, easily separated upon cooling, could be reused up to three times after the first run as exemplified in the case of triphenylethylene (entries 8–10). Catalytic activity generally dropped in the fourth run due to the oxidative decomposition of the catalyst, as evidenced by the progressive disappearence of the characteristic UV–Vis absorption bands of the (salen)Mn^{III} in the fluorous phase and by the absence of such bands in the organic phase. Such behaviour is in agreement with previous literature reports dealing with (salen)Mn^{III} complexes immobilised by other techniques.[11]

The use of the second-generation (salen)Mn^{III} complexes considerably widen the scope of the fluorous biphasic epoxidation reaction, since these catalysts not only afford good epoxide yields, but also ee ranging from 50 to 87% with several substrates. This finding strongly supports our aforementioned hypotheses about the role of R_F substituents on the catalytic activity of (salen)Mn^{III} complexes. The relative importance of electronic and steric effects in determining the enantioselectivity of fluorous (salen)Mn^{III} complexes and the design of new chiral fluorous catalysts are currently investigated in this laboratory.

We thank the COST Action D12 'Fluorous medium: a tool for environmentally compatible oxidation processes'.

Table 1 Asymmetric epoxidation of alkenes with PhIO/PNO in CH_3CN/perfluorooctane.[a]

Entry	Catalyst	Substrate	*T*/°C	*t*/h	Yield[b](%)	Ee[c](%)
1	Mn-**4**	1,2-dihydronaphthalene	0	3	4.5	8
2	Mn-**4**	1,2-dihydronaphthalene	20	3	46	26
3	Mn-**4**	1,2-dihydronaphthalene	40	3	76	32
4	Mn-**4**	1,2-dihydronaphthalene	70	2	74	42
5	Mn-**4**	1,2-dihydronaphthalene	100	1	77	50
6	Mn-**3**	1,2-dihydronaphthalene	100	1	68	50
7	Mn-**4**	triphenylethylene	100	0.5	98	87[g]
8	Mn-**4**[d]	triphenylethylene	100	0.5	96	85[g]
9	Mn-**4**[e]	triphenylethylene	100	0.5	92	83[g]
10	Mn-**4**[f]	triphenylethylene	100	1	80	71[g]
11	Mn-**3**	triphenylethylene	100	0.5	98	80[g]
12	Mn-**4**	benzosuberene	100	0.5	92	68
13	Mn-**3**	benzosuberene	100	0.5	84	69
14	Mn-**4**	1-methylindene	100	0.5	98	77
15	Mn-**3**	1-methylindene	100	0.5	96	70
16	Mn-**4**	1-methylcyclohexene	100	0.5	91	58
17	Mn-**3**	1-methylcyclohexene	100	0.5	95	52

[a] See footnote †. [b] Determined by GC analysis (HP-5 5% phenyl methyl siloxane column), internal standard method. [c] Determined by GC analysis (Cyclodex-B chiral column). [d] First, [e] second and [f] third reuse of the fluorous layer. [g] Determined by ^1H NMR spectroscopy in the presence of the chiral shift reagent Eu(hfc)$_3$.

Notes and references

† General procedure for the asymmetric epoxidation of alkenes under fluorous biphasic conditions: in a 10 ml Schlenk vessel placed in a thermoregulated bath at 100 °C, 1 ml of a 0.2 M solution of alkene in CH_3CN containing *o*-dichlorobenzene (0.1 M, internal standard for GC) and 0.2 ml of a 0.25 M solution of pyridine *N*-oxide (PNO) in CH_3CN were added under nitrogen to 1 ml of a solution of the catalyst in *n*-perfluorooctane. PhIO (67 mg, 0.3 mmol) was quickly added under a nitrogen stream. The two-phase mixture was magnetically stirred at 1300 ± 50 rpm and cooled to room temperature at the end of the reaction. The brown fluorous layer was separated, washed with CH_3CN (2 × 0.5 ml) and reused in further runs (see Table 1). The combined organic layers were washed with saturated aqueous Na_2SO_3 (1 ml), brine (1 ml) and dried ($MgSO_4$). Epoxide yield and enantiomeric excess were determined by gas-chromatographic analysis of the organic solution.

1 I. T. Horváth and J. Rábai, *Science*, 1994, **266**, 72.
2 I. T. Horváth, *Acc. Chem. Res.*, 1998, **31**, 641.
3 Recent reviews: (*a*) L. P. Barthel-Rosa and J. A. Gladysz, *Coord. Chem. Rev.*, 1999, **192**, 587; (*b*) R. H. Fish, *Chem. Eur. J.*, 1999, **5**, 1677; (*c*) E. De Wolf, G. van Koten and B.-J. Deelman, *Chem. Soc. Rev.*, 1999, **28**, 37; (*d*) M. Cavazzini, F. Montanari, G. Pozzi and S. Quici, *J. Fluorine Chem.*, 1999, **94**, 183; (*e*) E. G. Hope and A. M. Stuart, *J. Fluorine Chem.*, 1999, **100**, 75.
4 (*a*) G. Pozzi, F. Cinato, F. Montanari and S. Quici, *Chem. Commun.*, 1998, 877; (*b*) Y. Takeuchi, Y. Nakamura, Y. Ohgo and D. P. Curran, *Tetrahedron Lett.*, 1998, **39**, 8691; (*c*) G. Pozzi, M. Cavazzini, F. Cinato, F. Montanari and S. Quici, *Eur. J. Org. Chem.*, 1999, 1947; (*d*) H. Kleijn, E. Rijnberg, J. T. B. H Jastrzebski and G. van Koten, *Org. Lett.*, 1999, **1**, 853; (*e*) Y. Takeuchi, Y. Nakamura, Y. Ohgo and D. P. Curran, *Tetrahedron Lett.*, 2000, **41**, 57; (*f*) Y. Takeuchi, Y. Nakamura, Y. Ohgo and D. P. Curran, *Tetrahedron*, 2000, **56**, 351.
5 J. F. Larrow, E. N. Jacobsen, Y. Gao, Y. Hong, X. Nie and C. M. Zepp, *J. Org. Chem.*, 1994, **59**, 1939.
6 M. G. Banwell, J. M. Cameron, M. P. Collins, G. T. Crisp, R. W. Gable, E. Hamel, J. N. Lambert, M. F: Mackay, M. E. Reum and J. S. Scoble, *Aust. J. Chem.*, 1991, **44**, 705.
7 (*a*) W. Zhang, J. L. Loebach, S. R. Wilson and E. N. Jacobsen, *J. Am. Chem. Soc.*, 1990, **112**, 2801; (*b*) R. Irie, K. Noda, Y. Ito, N. Matsumoto and T. Katsuki, *Tetrahedron Lett.*, 1990, **31**, 7345.
8 S. Colonna, N. Gaggero, F. Montanari, G. Pozzi and S. Quici, *Eur. J. Org. Chem.*, 2000, in the press.
9 M. Palucki, P. J. Pospisil, W. Zhang and E. N. Jacobsen, *J. Am. Chem. Soc.*, 1994, **116**, 9333.
10 H. Sasaki, R. Irie and T. Katsuki, *Synlett*, 1993, 300.
11 J. M. Fraile, J. I. Garcia, J. Massam and J. A. Mayoral, *J. Mol. Catal. A: Chem.*, 1998, **136**, 47 and references cited therein.

Typeset and printed by Black Bear Press Limited, Cambridge, England

ChemComm
FEATURE ARTICLE

On the organometallic chemistry of gallium and the dynamics of Ga–Ga bond formation

Gregory H. Robinson

Department of Chemistry, The University of Georgia, Athens, GA 30602-2556, USA.
E-mail: robinson@chem.uga.edu

Received (in Cambridge, UK) 23rd August 2000, Accepted 26th September 2000
First published as an Advance Article on the web 31st October 2000

Recent advances in the organometallic chemistry of gallium are presented with an historical perspective and a particular emphasis toward the dynamics of the Ga–Ga bond.

Introduction

Due to the fortuitously combined efforts of Dmitri Mendeleev and Paul-Émile Lecoq de Boisbaudran, the main group metal gallium holds a paradoxically unique distinction of having many of its physical and chemical properties foretold *prior* to its actual discovery. While developing the theory of chemical periodicity in 1870, Mendeleev not only predicted the existence of a yet to be discovered element thought to reside between aluminium and indium, *eka-aluminium*, in his periodic arrangement of the elements, but he also boldly and accurately predicted a number of properties of this mystery element. Indeed, Mendeleev proposed a value of 5.9 g cm^{-3} for the density of eka-aluminium and predicted that this element would be discovered using spectroscopic analysis.[1] The fact that the actual events regarding the discovery of gallium and the subsequent development of organogallium chemistry would rival a compelling work of fiction only adds to the lore.

In the summer of 1875, following more than a decade of fundamental research upon which the science of spectroscopy would ultimately rest, Lecoq de Boisbaudran observed the first spectroscopic evidence of what he believed to be a new chemical element. While working in Paris in September 1875 Lecoq de Boisbaudran proudly obtained more than a gram of this mysterious element after having begun with several hundred kilograms of the appropriate zinc blende ore. Lecoq de Boisbaudran aptly named this new element *Gallia*, in honor of his beloved France (Latin, *Gallia*: France). Upon the determination of several chemical and physical properties of gallium, it became increasingly apparent that this low-melting metal was indeed the element which had been so confidently predicted by Mendeleev in 1870. The genius, if not the persistence, of Mendeleev emerged once more when Lecoq de Boisbaudran initially reported the density of gallium as 4.7 g cm^{-3}. Mendeleev wrote to Lecoq de Boisbaudran suggesting that he re-examine the value of 4.7 g cm^{-3} as it was at odds with his predicted value of 5.9 g cm^{-3}.[2] The correct value for the density of gallium is 5.904 g cm^{-3}.

The historical development of the organometallic chemistry of gallium is no less dramatic than that just offered concerning its discovery. Triethylgallium, Et_3Ga, as described by Dennis and Patnode in 1932, was the first reported organometallic compound of gallium.[3] The saga of the synthesis of triethylgallium is of an unusually intriguing, if not tragic, nature. Clearly noted in the 1932 article, another graduate student, Mr. H. A. Lovenberg, had been pursuing the synthesis of the first organogallium compounds and had actually begun the preparation of triethylgallium several years prior to the Dennis and Patnode 1932 article. Shortly after the flask had been charged with the ethylmagnesium bromide/gallium bromide reaction mixture and the flask had been sealed and secured, Mr. Lovenberg met an untimely death. This same flask containing the $EtMgBr/GaBr_3$ reaction mixture remained untouched, perhaps even lost, until Mr. Pathode happened upon it in January 1931 and continued the synthesis.[3] Triethylgallium monoetherate was isolated by Dennis and Pathnode as a colorless, moderately viscous, pyrophoric liquid [eqn. (1)]:

$$3EtMgBr + GaBr_3 \xrightarrow[Et_2O]{} 3MgBr_2 + Et_3Ga(Et_2O) \quad (1)$$

Dennis and Patnode also reported that ether-free triethylgallium could be isolated by reaction of gallium metal with diethylmercury. In an ironic postscript, the contribution of Mr. Lovenberg did not result in his being granted posthumous co-authorship on the 1932 article.

Although the simple gallium alkyls share some similarities to aluminium alkyls (*i.e.*, colorless, air-sensitive liquids), there are notable differences. For example, simple aluminium alkyls, such as trimethylaluminium,[4] are dimeric, bridging through electron deficient three center–two electron, 3c–2e, bonds, while the corresponding organogallium compounds are exclusively monomeric. In addition, the pyrophoric nature of aluminium alkyls is generally more substantial than that observed for gallium alkyls.

For decades following their discovery, organogallium compounds garnered limited attention and were largely considered little more than laboratory curiosities. Indeed, Pauling once opined that the chemistry of gallium [along with indium and thallium] was limited and of 'little practical importance'.[5] Insofar as this may have been a perfectly accurate description of the chemistry of gallium of the day, the organometallic chemistry of gallium (and indium and thallium) has since been shown to be as rich as it is varied. This Feature Article will examine some of the more significant recent discoveries in organogallium chemistry with a particular emphasis on ster-

Gregory H. Robinson (b. 1958) gained a B.S. degree in chemistry from Jacksonville State University (1980) and a Ph.D. degree at The University of Alabama (1984), working under the direction of Professor Jerry L. Atwood. Beginning his academic career at Clemson University (1985), he was promoted to full professor in 1995. Robinson was awarded an Alexander von Humboldt Research Fellowship in 1994 conducting research at the Technische Universität Berlin in the laboratory of Prof. Dr Herbert Schumann. In 1995 he joined the faculty at The University of Georgia where he now holds the title of Distinguished Research Professor of Chemistry. His research interests are in the organometallic chemistry of the main group elements.

DOI: 10.1039/b006905l

ically demanding organogallium compounds and the nature of the gallium–gallium bond.

Sterically demanding organogallium compounds

Generally, the phenyl substituent is not considered to be very bulky or sterically demanding. Nonetheless, the phenyl ligand is quite significant as it serves as the base unit from which very important sterically demanding ligands are derived. Much like trimethylaluminium, triphenylaluminium was shown to be dimeric,[6] bridging through a carbon atom of the phenyl ring. In contrast, triphenylgallium was demonstrated to be monomeric.[7] Interestingly, the phenyl rings of Ph_3Ga were observed to only be slightly out of the plane of the GaC_3 core. The nearly coplanar nature of the phenyl rings with the gallium core in Ph_3Ga allowed for secondary interactions of each gallium center with the *meta*-carbon atoms of other Ph_3Ga moieties in the unit cell.

The fact that sixteen years passed between the structural characterization of triphenylgallium and its next logical aryl derivative of trimesitylgallium, $(Me_3C_6H_2)_3Ga$, belies the latent development of this chemistry. Ironically, the preparation of $(Me_3C_6H_2)_3Ga$ in 1986 was analogous to that employed more than five decades earlier in the 1932 synthesis of triethylgallium, namely the reaction of the appropriate Grignard reagent with a gallium halide [eqn. (2)].[8]

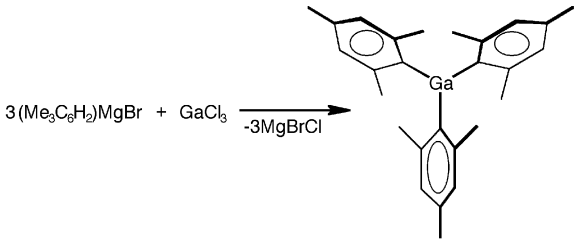

(2)

Trimesitylgallium was isolated as colorless, air-sensitive crystals. It is an interesting coincidence that the synthesis and molecular structure of trimesitylaluminium[9] and trimesitylgallium[8] were published as consecutive articles in the same issue of the journal *Organometallics*. Although the molecular structure of $(Me_3C_6H_2)_3Ga$ revealed the gallium center to be in a virtually idealized trigonal planar environment, the aromatic rings of the mesityl ligands assumed a propellor-like arrangement about the gallium center at an angle of 55.9° between each ring and the metal coordination plane. This is most unlike the case for triphenylgallium wherein the aromatic rings were only slightly out of the metal center plane. As a consequence of the steric crowding about the metal center, trimesitylgallium was shown to be a very weak Lewis acid incapable of forming stable adducts with either Et_2O or THF.

Significant developments in the organometallic chemistry of sterically demanding organogallium compounds were few for the next ten years at which point an even more sterically demanding ligand system was examined relative to gallium. The ligand system which was chosen by this laboratory was the substituted *m*-terphenyl ligands initially reported by Hart and coworkers.[10] In notable contrast to the syntheses of triethylgallium and trimesitylgallium, wherein Grignard reagents were utilized in the syntheses, we employed lithium derivatives of *m*-terphenyl ligands. Reaction of 2,6-dimesitylphenyllithium with gallium chloride affords bis(2,6-dimesitylphenyl)gallium chloride, $[(Me_3C_6H_2)_2C_6H_3]_2GaCl$ (Fig. 1).[11] This organometallic compound was the first example of an *m*-terphenyl ligand being attached to a main group metal. Secondly, it is noteworthy that two such bulky ligands were accommodated by the gallium atom. This point is particularly manifested in the geometry about the metal center. Unlike triethylgallium and trimesitylgallium, in which the metal center is trigonal planar, the steric interaction between the two *m*-terphenyl ligands in

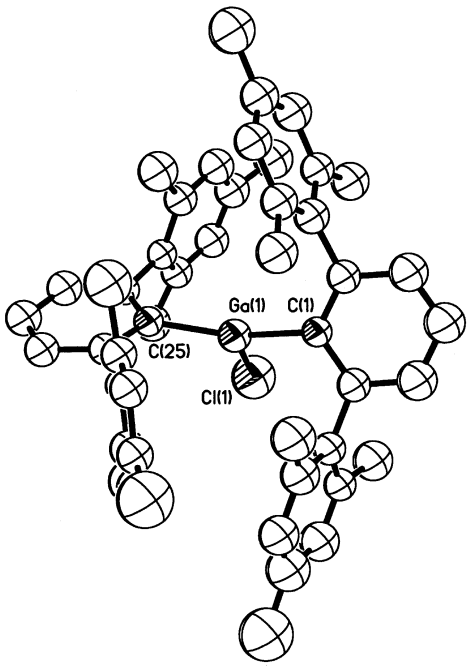

Fig. 1 Crystal structure of $[(Me_3C_6H_2)_2C_6H_3]_2GaCl$.

$[(Me_3C_6H_2)_2C_6H_3]_2GaCl$ was such that the C–Ga–C bond angle was widened substantially beyond the 120° expected for trigonal planar to 154°. This is sufficient to warrant the description of this compound as T-shaped. Normally, the T-shaped orientation is reserved for the well known interhalogen compounds such as ClF_3 and BrF_3 wherein the central atom has two lone pairs of electrons to assist in stabilizing this rather obscure geometry. Thus, $[(Me_3C_6H_2)_2C_6H_3]_2GaCl$ is the first unambiguous example of a Group 13 metal organometallic complex assuming a T-shaped geometry. The synthesis and molecular structure of the corresponding T-shaped bis(2,6-dimesitylphenyl)gallium bromide has also been recently reported.[12]

Perhaps the only tri(aryl)-based molecule possibly more sterically crowded than the T-shaped bis(2,6-dimesitylphenyl)gallium halides is (2,6-dimesitylphenyl)(dimesityl)gallium, $(Me_3C_6H_2)_2C_6H_3Ga(C_6H_2Me_3)_2$.[12] This compound, isolated from reaction of $(Me_3C_6H_2)_2C_6H_3GaCl_2$ with two equivalents of mesityllithium, arguably, represents the most sterically crowded gallium center ever observed. The aromatic rings about the GaC_3 core approach orthogonality at angles of 82.4, 82.4 and 86.3°.

Gallium(II) halides: useful synthetic reagents

As recently as 1979 the notion of discrete 'gallium(II) dihalides' was a novel concept. A study by Beamish, Small, and Worrall offered an unambiguous perspective on the existence of gallium(II) halides with the synthesis and molecular structure of $Ga_2Cl_4(dioxane)_2$,[13] isolated from recrystallization of Ga_2Cl_4 from 1,4-dioxane at 0 °C. The gallium atoms are clearly four-coordinate, each bonding to two chlorine atoms, one dioxane adduct, and the other gallium atom with a Ga–Ga distance of 2.406(1) Å.

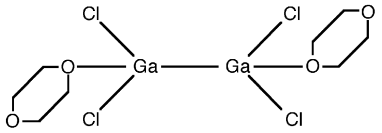

The bromide derivative, $Ga_2Br_4(dioxane)_2$, has a similar structure along with a Ga–Ga bond distance of 2.395(6) Å.[14] Gallium(II) chloride bis(dioxane) will prove pivotal in the

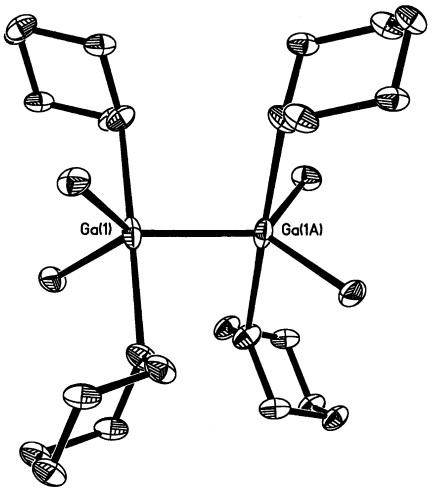

Fig. 2 Crystal structure of $Ga_2Cl_4(dioxane)_4$.

development of the stabilization of the Ga–Ga bond in some organometallic gallanes (*vide infra*).

Recently we made a surprising discovery concerning 1,4-dioxane adducts of gallium(II) chloride. Upon slow room temperature (as opposed to 0 °C) recrystallization of Ga_2Cl_4 from 1,4-dioxane we isolated a tetrameric dioxane adduct, $Ga_2Cl_4(dioxane)_4$.[15] Both gallium atoms in $Ga_2Cl_4(dioxane)_4$ reside in almost idealized trigonal bipyramidal environments [O–Ga–O 179.10(10)°] about the two gallium atoms (Fig. 2).

The five-coordinate trigonal bipyramidal gallium atoms of $Ga_2Cl_4(dioxane)_4$ are easily compared with the four-coordinate tetrahedral gallium atoms of $Ga_2Cl_4(dioxane)_2$ which was prepared more than twenty years earlier. Surprisingly, the Ga–Ga bond distance of 2.3825(9) Å in $Ga_2Cl_4(dioxane)_4$ is shorter than the values reported for $Ga_2Cl_4(dioxane)_2$ [2.406(1) Å] and $Ga_2Br_4(dioxane)_2$ [2.395(6) Å]. The Ga–O bond distance in $Ga_2Cl_4(dioxane)_4$ (2.4087 Å), however, is notably longer than that reported for $Ga_2Cl_4(dioxane)_2$ [2.027(2) Å]. The Ga–Cl bonds are generally unremarkable. While very weak secondary $Cl_{(Ga)}\cdots H_{(dioxane)}$ interactions were suggested in the original paper, this compound is perhaps best described as a monomeric unit. It is important to note that the tetra-dioxane adduct bears a striking resemblance to an indium compound containing an In–In bond and stabilized by four THF units, $In_2Cl_4(THF)_4$, recently reported by Schmidbaur and coworkers.[16] Ga_2Cl_4-$(dioxane)_4$ is a rare example of five-coordinate gallium atoms engaging in Ga–Ga bond formation.

Gallium(II) dichloride bis(dioxane), $Ga_2Cl_4(dioxane)_2$,[13] proved critical in the preparation of the first organometallic compound unambiguously shown to contain a Ga–Ga bond. Uhl *et al*. prepared $[(Me_3Si)_2HC]_2Ga–Ga[CH(SiMe_3)_2]_2$ (below) by reaction of $Ga_2Cl_4(dioxane)_2$ with $LiCH(SiMe_3)_2$.[17]

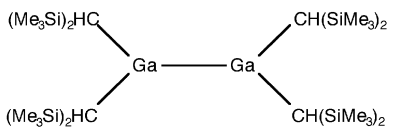

The Ga–Ga bond distance in $[(Me_3Si)_2HC]_2Ga–Ga[CH(SiMe_3)_2]_2$ was shown to be 2.541(1) Å.

In an effort to approach a measure of multiple bond character in the Ga–Ga bond, the same workers reduced $[(Me_3Si)_2HC]_2Ga–Ga[CH(SiMe_3)_2]_2$ with ethyllithium to afford red–black crystals of the corresponding radical anion, $[(Me_3Si)_2HC]_2Ga–Ga[CH(SiMe_3)_2]_2^{\bullet-}$,[18] to yield a 'one electron π-bond'. Both EPR and single crystal X-ray diffraction were in support of this description. The Ga–Ga bond distance of 2.301(1) Å in $[(Me_3Si)_2HC]_2Ga–Ga[CH(SiMe_3)_2]_2^{\bullet-}$ represents a decrease of 0.240 Å from the neutral gallane.

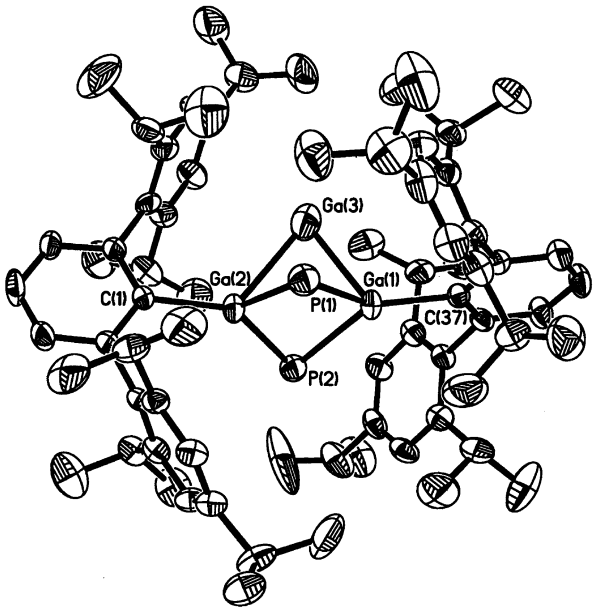

Fig. 3 Crystal structure of $[(Pr^i_3C_6H_2)_2C_6H_3]Ga\{H_2PGa(H)PH_2\}$-$Ga[C_6H_3(C_6H_2Pr^i_3)_2]$.

Although *m*-terphenyl ligands have been shown by this laboratory to be effective in the stabilization of compounds containing Ga–Ga bonds, their general reactivity had not been examined relative to Lewis bases. Recently we explored the reaction of $[(Pr^i_3C_6H_2)_2C_6H_3]GaCl_2$ with the sterically demanding Lewis base tris(trimethylsilyl)phosphine, $P(SiMe_3)_3$. This reaction affords the unusual organometallic compound $[(Pr^i_3C_6H_2)_2C_6H_3]Ga\{H_2PGa(H)PH_2\}Ga[C_6H_3(C_6H_2Pr^i_3)_2]$ (Fig. 3).[19]

The isolation of this compound was as unexpected as it was interesting. Noteworthy is the fact that the compound contains a –Ga–Ga–Ga– linkage. Just as striking is the *m*-terphenyl ligand stripping from the central gallium atom (being replaced by a hydrogen atom) and the stripping of the tris(trimethylsilyl) groups from the two phosphorus atoms (being replaced by two hydrogen atoms each). While it may be reasonable to dismiss the five hydrogen atoms, two on each of the two phosphorus atoms and one on the central gallium atom, as having originated from the stripped *m*-terphenyl ligand, there are other possibilities. For example, it is also reasonable that the ligand stripping may have initiated hydride abstraction from the solvent (or *vice versa*). The phosphine hydrogen atoms and the gallium hydride were prominently manifested in IR and NMR spectroscopy. Moreover, theoretical calculations of IR bands on the model molecule $MeGa\{H_2PGa(H)PH_2\}GaMe$ are in good agreement with the experimental IR spectrum.[19] The asymmetric nature of the Ga(1)–Ga(3)–Ga(2) linkage, at distances of 2.5145(13) and 2.7778(14) Å for Ga(1)–Ga(3) and Ga(2)–Ga(3), respectively, is interesting. It should be noted, however, that this compound is not strictly governed by a symmetry element (*i.e.*, mirror plane or two-fold axis) which would impose a symmetrical –Ga–Ga–Ga– linkage. Even as the Ga–Ga bond distances in $[(Pr^i_3C_6H_2)_2C_6H_3]Ga\{H_2PGa(H)PH_2\}Ga[C_6H_3(C_6H_2Pr^i_3)_2]$ are somewhat elongated, they compare well with other Ga–Ga bond distances observed in tetrahedra or heteronuclear trigonal bipyramids (*vide infra*).

The literature reveals another compound containing a Ga–Ga–Ga linkage in $Ga_3I_5{\cdot}3PEt_3$ (below), isolated from ultrasonic irradiation of gallium and diiodine in the presence of triethylphosphine.[20]

In this mixed-valent compound, a Ga(I) centre is the bridging moiety for two Ga(II) units with Ga–Ga distances of 2.451(1) and 2.4560(1) Å. The Ga–I bond distances in the two terminal GaI_2 units [2.610(1) Å] are slightly shorter than the central Ga–I [2.627(1) Å]. The Ga–Ga–Ga bond angle is 121.9(1)°. This

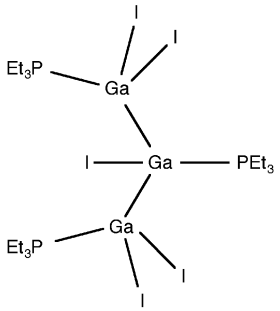

value is compared with 69.68° for the corresponding Ga–Ga–Ga bond angle observed in $[(Pr^i_3C_6H_2)_2C_6H_3]Ga\{H_2P\text{-}Ga(H)PH_2\}Ga[C_6H_3(C_6H_2Pr^i_3)_2]$, a striking difference of almost 50°.

Cyclogallenes: metalloaromatic compounds

Even though gallium has demonstrated limited catenation abilities, as evidenced by the synthesis of (previously discussed) compounds containing –Ga–Ga–Ga– linkages, reports of an entirely new class of organogallium compounds are perhaps more substantial. Sodium metal reduction of the *m*-terphenylgallium dichloride $[(Me_3C_6H_2)_2C_6H_3]GaCl_2$ in diethyl ether has been shown by this laboratory (below) to afford dark red crystals of $Na_2[(Me_3C_6H_2)_2C_6H_3Ga]_3$ [eqn. (3)].[21]

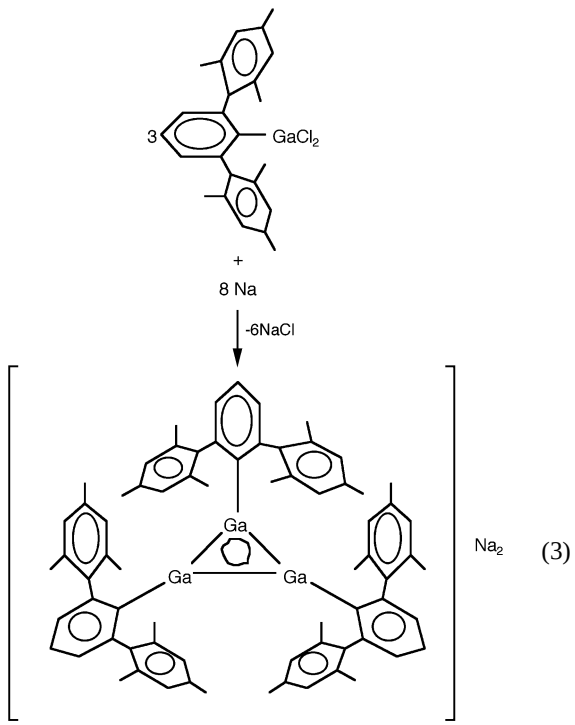

(3)

The X-ray crystal structure of $Na_2[(Me_3C_6H_2)_2C_6H_3Ga]_3$ (Fig. 4) reveals a perfectly planar gallium three-membered ring, Ga–Ga bond distances of 2.441(1) Å, and Ga–Ga–Ga bond angles within the ring of 60.01°.

Upon closer examination a more intriguing aspect of the $Na_2[(Me_3C_6H_2)_2C_6H_3Ga]_3$ compound began to emerge. The gallium atoms are taken to be sp^2 hybridized along with one unhybridized p orbital on each gallium atom. Moreover, the three p orbitals are populated by two electrons, one from each of the two sodium atoms. Thus, this first example of a gallium ring compound, a cyclogallene, is also a 2π aromatic system. The synthesis and molecular structure of a potassium based cyclogallene, $K_2[(Me_3C_6H_2)_2C_6H_3Ga]_3$, was subsequently reported (similar bond distances and angles were observed).[22] The Ga–Ga bonds within these rings are shorter than most of the

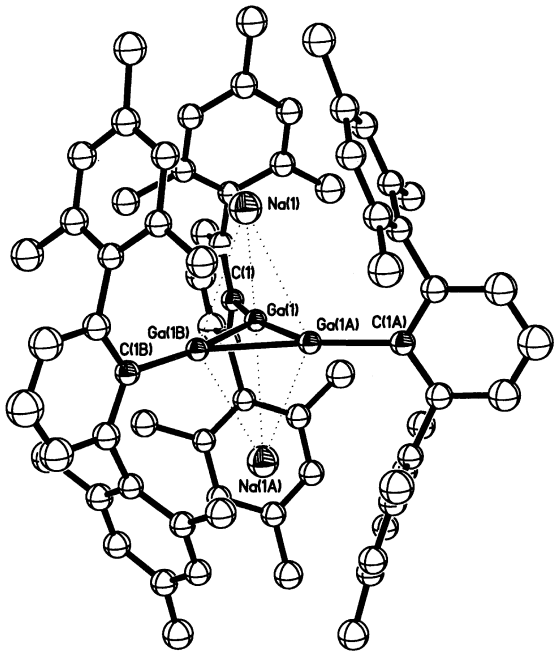

Fig. 4 Crystal structure of $Na_2[(Me_3C_6H_2)_2C_6H_3Ga]_3$.

reported gallanes. In addition, these ring compounds bear a striking resemblance to the smallest aromatic moiety—the triphenylcyclopropenium cation reported by Breslow more than four decades ago.[23]

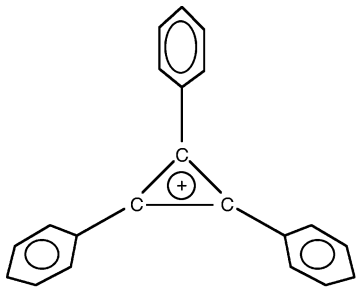

The nucleus independent chemical shifts (NICS) values[24] calculated for cyclogallenes[25] were supportive of aromatic behavior. Thus, the term *metalloaromaticity*,[22] intended to denote traditional aromatic behavior derived from a metallic ring system, was deemed warranted for these novel compounds. Metallic ring systems demonstrating traditional aromatic behavior present a serious challenge to borazine's long held position as the most important inorganic aromatic system.[26]

The gallium–gallium triple bond: a provocative compound, a vigorous debate

Even as it is the simplest of all alkynes, it is generally accepted that acetylene is also the most important compound possessing the iconic carbon–carbon triple bond. Moreover, the chemical bonding in acetylene is elegantly simplistic as interpreted by valence bond theory: a perfectly linear H–C–C–H molecular structure, as a consequence of sp hybridized carbon atoms, coupled with a tubular-shaped electron density. To be sure, the concept of a main group metal compound being analogous to acetylene would prove formidable.

In an effort to ascertain the extent to which slight modifications in the *m*-terphenyl ligand would affect the nature of the resulting organometallic compound we sought to modify the ligand. We slightly modified the peripheral substituents on the *m*-terphenyl ligand from methyl groups (in the case of cyclogallenes) to isopropyl groups. Thus, we prepared the $[(Pr^i_3C_6H_2)_2C_6H_3]Li$ lithium salt and allowed it to react with gallium chloride. Sodium metal reduction of the resulting

sterically demanding gallium based *m*-terphenyl, $[(Pr^i_3C_6H_2)_2C_6H_3]GaCl_2$, which is dimeric in the solid state, bridging through two chlorine atoms,[27] affords Na_2-$[\{(Pr^i_3C_6H_2)_2C_6H_3\}Ga{\equiv}Ga\{C_6H_3(C_6H_2Pr^i_3)_2\}]$ [eqn. (4)].

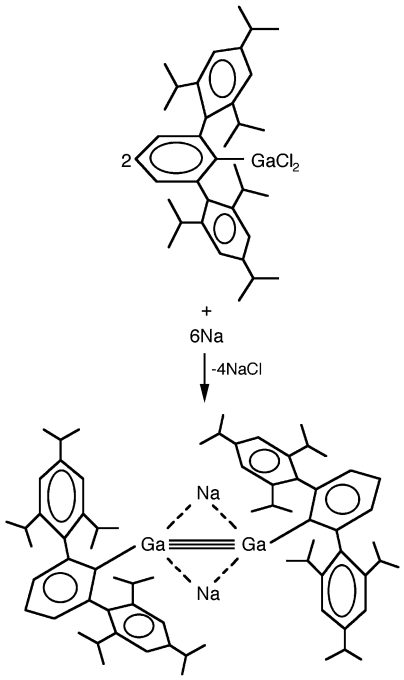

(4)

The article which reported the synthesis and molecular structure of this reaction product, entitled *How Short is a –Ga≡Ga– Triple Bond?*[28] made a most provocative claim: that the $[\{(Pr^i_3C_6H_2)_2C_6H_3\}Ga{\equiv}Ga\{C_6H_3(C_6H_2Pr^i_3)_2\}]^{2-}$ dianion represented a digallium analog of acetylene, or a *gallyne*, the first moiety claiming to contain a Ga≡Ga triple bond. The molecular structure of $Na_2[\{(Pr^i_3C_6H_2)_2C_6H_3\}Ga{\equiv}Ga\{C_6H_3$-$(C_6H_2Pr^i_3)_2\}]$ is shown in Fig. 5.

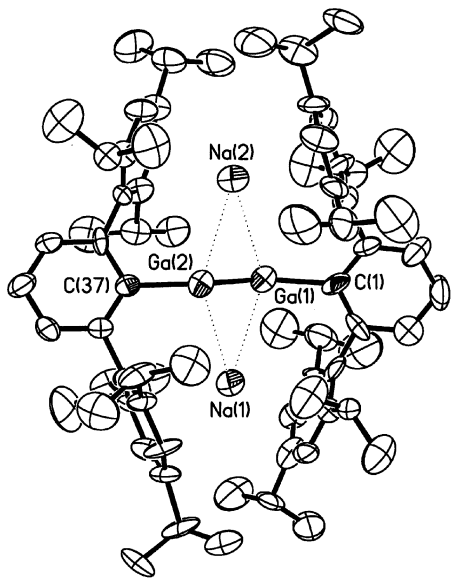

Fig. 5 Crystal structure of $Na_2[\{(Pr^i_3C_6H_2)_2C_6H_3\}Ga{\equiv}Ga\{C_6H_3$-$(C_6H_2Pr^i_3)_2\}]$.

The inherent significance of such a claim is evidenced by the fact that it resulted in two highly publicized reports in *Chemical & Engineering News*.[29,30] The Ga–Ga bond distance in the dianion of 2.341 Å is among the shortest distances reported for a compound containing a gallium–gallium bond. However, the decidedly nonlinear C–Ga–Ga–C core linkage of 127 and 134° was most *unacetylenic*. Our justification in describing the metal–metal bonding as a gallium–gallium triple bond goes far beyond the short Ga–Ga bond distance. Indeed, *where heavier main group element compounds (beyond carbon) are concerned, short bond distances are neither necessary nor sufficient to constitute multiple bonding*. Essentially, the nature of a chemical bond is first and foremost determined by the electronic structure, not by the molecular geometry. Theoreticians and computational quantum chemists have been predicting for years (prior to the gallyne report) that if such a main group metal compound could be synthesized possessing a homonuclear diatomic triple bond, its structure would *not* be linear (as in the case of acetylene), but rather it would possess a non-linear *trans*-bent structure,[31] as in the gallyne. Perhaps most informative, workers such as Kobayashi and Nagase[32] (and references cited therein) have long predicted that, at the expense of the linear disilyne model H–Si≡Si–H ($D_{\infty h}$), the *trans*-bent disilyne model H–Si≡Si–H (C_{2h}) would be favored.

Opposition to the gallium–gallium triple bond was swift and vigorous.[30] Utilizing density functional theory (DFT) Cotton, Cowley, and Feng (CCF)[33] examined a number of main group element moieties containing multiple bonds including P_2, P≡C–R, R–P=P–R, R_2–Ge=Ge–R_2. These results were compared with calculations on the closely related (2,6-diphenyl)-phenyl gallyne model, $Na_2[(Ph_2C_6H_3)Ga{\equiv}Ga(C_6H_3Ph_2)]$. The principal conclusion put forth by CCF (beyond a discussion on the presence and/or absence of a gallium hydride in the gallyne): 'With or without hydrogen atoms, there can only be a Ga=Ga double bond [one σ bond and one π bond which may be described by two canonical molecular orbitals], namely, Na_2[R–Ga=Ga–R], rather than Na_2[R–Ga≡Ga–R] for the case of no hydrogen atoms.' Importantly, the CCF effort, in posing an argument against a Ga≡Ga triple bond, failed to address the concept of bond orders, an obvious and puzzling omission. Allen, Fink and Power[34] also argued against the gallium–gallium triple bond in the gallyne. These workers simply, if pejoratively, stated (among other things) that 'there is no GaGa σ bond [in the gallyne].' Furthermore, these workers proceeded to address bond orders *without providing or calculating a bond order for the Ga–Ga interaction in question*. Allen, Fink and Power summarily stated, 'The results of these studies provide strong evidence that the Ga–Ga or Ge–Ge bond orders in such molecules are significantly less than three and, in the case of the gallium species, *very probably between one and two*.' Our calculated bond orders of 2.36 and 3.02 {for $[HGa{\equiv}GaH]^{2-}$ (C_{2h})} and 2.79 for $Na_2[(Ph_2C_6H_3)Ga{\equiv}Ga(C_6H_3Ph_2)]$ would appear to refute this work (*vide infra*).

Offering a rebuttal to the more credible CCF position, we also published a detailed DFT study firmly in support of the gallyne model and the Ga≡Ga triple bond, entitled '*The Nature of the Gallium–Gallium Triple Bond*'.[35] Our position is unambiguous: the $Na_2[\{(Pr^i_3C_6H_2)_2C_6H_3\}Ga{\equiv}Ga\{C_6H_3(C_6H_2Pr^i_3)_2\}]$ gallyne consists of two donor–acceptor bonds and one π bond, thus resulting in a gallium–gallium triple bond, albeit a *weak triple bond*. Klinkhammer,[36] utilizing the Natural Bond Orbitals technique (NBO), states that the bonding (of the gallyne) bears a striking similarity to that put forth by Lappert[37] in 1976 for the distannene $[(Me_3Si)_2CH]_2Sn{=}Sn[CH(SiMe_3)_2]_2$: namely, the Sn=Sn double bond is constituted by two donor–acceptor bonds resulting in 'a "bent" and weak Sn–Sn double bond.' Specifically, one may interpret the bonding in the gallyne, writes Klinkhammer, as two donor–acceptor bonds (as in the distannene) which are 'augmented by an additional π bond to yield a Ga≡Ga triple bond (below).'

Indeed, Power and Brothers,[38] describing $[(Me_3$-$Si)_2CH]_2Sn{=}Sn[CH(SiMe_3)_2]_2$ as 'a tin analogue of a substituted ethene,' prophetically opined: 'The discovery of such compounds [as $[(Me_3Si)_2CH]_2Sn{=}Sn[CH(SiMe_3)_2]_2$] has shown that the classical σ/π-model of the double bond in carbon, nitrogen, or oxygen compounds does not necessarily apply to the heavier elements.'

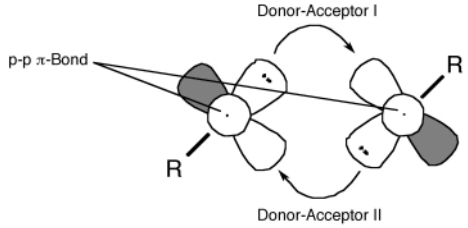

Thus, an interesting dichotomy emerges most unlike the case for multiple bonds involving carbon: even as the bonding in the gallyne is described as a triple bond, this interaction is admittedly *weak*. Indeed, a recent study examining force constants given by DFT frequency calculations shows that the gallium–gallium bond in $Ga_2H_2^{2-}$ is only slightly strengthened with respect to the Ga–Ga single bond in $Ga_2H_6^{2-}$.[39] Another recently published work entitled '*How Strong is the Gallium ≡Gallium Triple Bond?*', found that the gallium–gallium bond strength in the Na_2[H–GaGa–H] gallyne model is weaker than the gallium=gallium double bond in the $Na_2[H_2Ga{=}GaH_2]$ model gallene.[40] The fact that these workers conclude that the gallium–gallium bond is weak is perfectly consistent with our original position. Other workers have also referred to the gallyne as having a weak Ga≡Ga triple bond.[41]

Relative to bond orders, there are a number of ways in which they may defined and calculated. Nonetheless, if the same method is applied to a series of moieties, logical trends should emerge. Thus, in this work we calculated the bond orders by the Wiberg Bond Index (WBI)[42] and the Natural Localized Molecular Orbital Natural Population Analysis (NLMO/NPA)[43] obtaining values of 2.36 and 3.02, respectively, for the *trans*-bent $[H–Ga{\equiv}Ga–H]^{2-}$ (C_{2h}) gallyne model. These bond orders are, at minimum, supportive of a multiple bond considerably beyond that of a double bond. The bond order of 3.02 is clearly deserving of the triple bond label.

Earlier this year we published a second detailed theoretical examination of the gallyne in a more realistic model: we used the same gallyne model that Cotton had used, namely $Na_2[(Ph_2C_6H_3)Ga{\equiv}Ga(C_6H_3Ph_2)]$.[44] A cursory examination of the optimized $Na_2[(Ph_2C_6H_3)Ga{\equiv}Ga(C_6H_3Ph_2)]$ gallyne model (Fig. 6) reveals that this molecule is very similar to the experimentally prepared gallyne, differing only in the absence of the six isopropyl substituents.

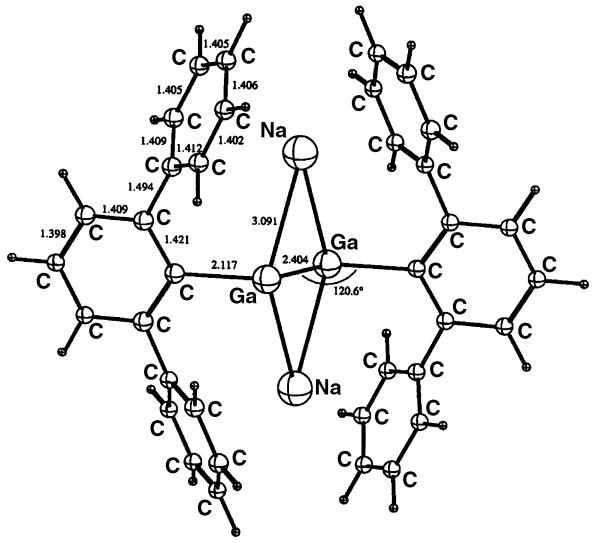

Fig. 6 Geometry (C_{2h}) of the $Na_2[(Ph_2C_6H_3)Ga{\equiv}Ga(C_6H_3Ph_2)]$ molecule optimized at the B3LYP level of theory with a basis set of 836 contracted Gaussian functions.

The $Na_2[(Ph_2C_6H_3)Ga{\equiv}Ga(C_6H_3Ph_2)]$ structure was fully optimized with the B3LYP method utilizing a substantial basis set of 836 contracted Gaussian functions. In this work we obtained a NLMO/NPA bond order of 2.79 for $Na_2[(Ph_2C_6H_3)Ga{\equiv}Ga(C_6H_3Ph_2)]$, thus offering support for a weak Ga≡Ga triple bond in the model compound and in the experimental gallyne.

The associated bond distances and angles are similar to the experimental values. The calculated Ga–Ga bond distance of 2.404 Å, although similar to, is somewhat shorter than that reported for the simplest gallyne model, Na_2[H–Ga≡Ga–H] (2.441 Å), and considerably shorter than the methyl gallyne derivative, Na_2[Me–Ga≡Ga–Me] (2.508 Å). There should be little cause for concern with this trend, however. A similar trend is observed in the disilyne model series H–Si≡Si–H (2.111 Å), Me–Si≡Si–Me (2.123 Å) and R–Si≡Si–R (2.095 Å) (R = large substituent).[32] As suggested by CCF, we also observed that the optimized structure allows for twisting of the four substituent phenyl rings toward the sodium atoms at a distance of 2.8 Å. This has the effect of shortening the Ga–Ga distance (as compared to those simpler gallyne models which do not have aryl substituents). It is important to point out, however, that our optimized Ga–Ga distance is longer than that reported in the CCF study. We believe that this is due to the relatively small basis sets used by these workers (6-31G and 6-311G, without polarization and diffuse functions).

Relative to the Ga–Ga bond distances, our calculated bond distance of 2.404 Å is 0.085 Å longer than the experimental value of 2.319(3) Å. We view this as an indication that the gallium–gallium bond in the experimental compound may be a bit more substantial than for the gallyne model. The experimental Ga–C bond distance of 2.044 Å compares to a calculated value of 2.117 Å. In contrast, the experimental Ga–Na (3.081 Å) distances compare well to the calculated value (3.091 Å). Finally, a NLMO/NPA bond order of 2.79 was obtained for $Na_2[(Ph_2C_6H_3)Ga{\equiv}Ga(C_6H_3Ph_2)]$.

An elegantly detailed examination of homonuclear multiple bonding between main group elements was recently put forth by Grützmacher and Fässler.[45] While presenting an informative historical perspective on chemical bonding and the development of the symbols used to denote bonding, these workers utilized electron localization function (ELF) to examine and interpret the bonding in the gallyne and other heavier main group moieties involving multiple bonds. Grützmacher and Fässler reached an unambiguous conclusion regarding the heavier main group elements:

> "The classical multiple bond indicators—bond lengths and bond strengths—have no meaning for multiple bonds in which elements from the higher periods are involved. However, they are valid for an exceptional element: carbon."

This striking position, also put forth by Klinkhammer,[36] underscores the awkward reality that most of our theories of structure and bonding are based upon the element carbon. The resulting implication: What holds for carbon need not necessarily hold for the heavier main group elements. The conclusion of Grützmacher and Fässler relative to the gallyne: these workers refer to the Ga–Ga interaction as a 'slipped triple bond' as compared to an 'unslipped triple bond' in the case of acetylene. Grützmacher and Fässler[45] further add, 'Clearly this compound [the gallyne] has a [Ga≡Ga] triple bond.'

Concluding remarks

The synthesis and molecular structure of organogallium compounds are an interesting area of study. A number of novel compounds have been prepared in recent years. Few topics in organogallium chemistry have generated more interest than the report of a compound containing a Ga≡Ga triple bond.[46] The fact that this compound has served as a substrate upon which fundamental questions of structure and bonding may be pondered and debated is most significant. It would appear that

some of our long-standing theories of structure and bonding may be inadequate to describe sufficiently novel organometallic compounds.

Acknowledgements

This research was support by the National Science Foundation and the Petroleum Research Fund, administered by the American Chemical Society. The author is woefully indebted to a number of gifted coworkers without whom the discoveries from this laboratory would not have been possible. Their names are cited in the references.

Notes and references

1 M. E. Weeks and H. M. Leicester, in *Discovery of the Elements*, Journal of Chemical Education, Easton, 7th edn., 1968, p. 642.
2 N. N. Greenwood and A. Earnshaw, in *Chemistry of the Elements*, Pergamon Press, New York, 1984, pp. 243–246.
3 L. M. Dennis and W. Patnode, *J. Am. Chem. Soc.*, 1932, **54**, 182.
4 R. G. Vranka and E. L. Amma, *J. Am. Chem. Soc.*, 1967, **89**, 3121.
5 L. Pauling, in *General Chemistry*, Dover Publications (Republication of the 3rd edn., published by W. H. Freeman and Company, San Francisco, CA, 1970), Mineola, NY, 1988, p. 719.
6 J. F. Malone and W. S. McDonald, *Chem. Commun.*, 1967, 444.
7 J. F. Malone and W. S. McDonald, *J. Chem. Soc. A*, 1970, 3362.
8 O. T. Beachley, M. R. Churchill, J. C. Pazik and J. W. Ziller, *Organometallics*, 1986, **6**, 1814.
9 J. J. Jerius, J. M. Hahn, A. F. M. M. Rahman, O. Mols, W. H. Ilsley and J. P. Oliver, *Organometallics*, 1986, **5**, 1812.
10 C.-J. F. Du, H. Hart and K.-K. Ng, *J. Org. Chem.*, 1986, **51**, 3162.
11 X.-W. Li, W. T. Pennington and G. H. Robinson, *Organometallics*, 1995, **14**, 2109.
12 R. C. Crittendon, X.-W. Li, J. Su and G. H. Robinson, *Organometallics*, 1997, **16**, 2443.
13 J. C. Beamish, R. W. H. Small and I. J. Worrall, *Inorg. Chem.*, 1979, **18**, 220.
14 R. W. H. Small and I. J. Worrall, *Acta Crystallogr., Sect. B*, 1982, **38**, 250.
15 P. Wei, X.-W. Li and G. H. Robinson, *Chem. Commun.*, 1999, 1287.
16 F. P. Gabbaï, A. Schier, J. Riede and H. Schmidbaur, *Inorg. Chem.*, 1995, **34**, 3855.
17 W. Uhl, M. Layh and T. Hildenbrand, *J. Organomet. Chem.*, 1989, **364**, 289.
18 W. Uhl, W. Schütz, W. Kaim and E. Waldhör, *J. Organomet. Chem.*, 1995, **501**, 79.
19 X.-W. Li, P. Wei, B. C. Beck, Y. Xie, H. F. Schaefer, J. Su and G. H. Robinson, *Chem. Commun.*, 2000, 453.
20 A. Schnepf, C. Doriat, E. Möllhausen and H. Schnöckel, *Chem. Commun.*, 1997, 2111.
21 X.-W. Li, W. T. Pennington and G. H. Robinson, *J. Am. Chem. Soc.*, 1995, **117**, 7578.
22 X.-W. Li, Y. Xie, P. R. Schreiner, K. D. Gripper, R. C. Crittendon, C. F. Campana, H. F. Schaefer and G. H. Robinson, *Organometallics*, 1996, **15**, 3798.
23 R. Breslow, *J. Am. Chem. Soc.*, 1957, **79**, 5318.
24 P. v. R. Schleyer, C. Maerker, A. Dransfeld, H. Jiao and N. J. R. v. E. Hommes, *J. Am. Chem. Soc.*, 1996, **118**, 6317.
25 Y. Xie, P. R. Schreiner, H. F. Schaefer, X.-W. Li and G. H. Robinson, *J. Am. Chem. Soc.*, 1996, **118**, 10 635.
26 Y. Xie, P. R. Schreiner, H. F. Schaefer, X.-W. Li and G. H. Robinson, *Organometallics*, 1998, **17**, 114.
27 J. Su, X.-W. Li and G. H. Robinson, *Chem. Commun.*, 1998, 2015.
28 J. Su, X.-W. Li, R. C. Crittendon and G. H. Robinson, *J. Am. Chem. Soc.*, 1997, **119**, 5471.
29 R. Dagani, *Chem. Eng. News*, 1997, **75** (June 16), 9.
30 R. Dagani, *Chem. Eng. News*, 1998, **76** (March 16), 31.
31 R. S. Grev, *Adv. Organomet. Chem.*, 1991, **33**, 125.
32 K. Kobayashi and S. Nagase, *Organometallics*, 1997, **16**, 2489.
33 F. A. Cotton, A. H. Cowley and X. Feng, *J. Am. Chem. Soc.*, 1998, **120**, 1795.
34 T. L. Allen, W. H. Fink and P. P. Power, *J. Chem. Soc., Dalton Trans.*, 2000, 407.
35 Y. Xie, R. S. Grev, J. Gu, H. F. Schaefer, P. v. R. Schleyer, J. Su, X.-W. Li and G. H. Robinson, *J. Am. Chem. Soc.*, 1998, **120**, 3773.
36 K. W. Klinkhammer, *Angew. Chem., Int. Ed. Engl.*, 1997, **36**, 2320.
37 D. E. Goldberg, D. H. Harris, M. F. Lappert and K. M. Thomas, *J. Chem. Soc., Chem. Commun.*, 1976, 261.
38 P. P. Power and P. J. Brothers, in *Advances in Organometallic Chemistry. Multiply Bonded Main Group Metals and Metalloids*, ed. F. G. Stone and R. West, Academic Press, New York, 1994, pp. 1–70.
39 R. Köppe and H. Schnöckel, *Z. Anorg. Allg. Chem.*, 2000, **626**, 1095.
40 J. Grunenberg and N. Goldberg, *J. Am. Chem. Soc.*, 2000, **122**, 6045.
41 I. Bytheway and Z. Lin, *J. Am. Chem. Soc.*, 1998, **120**, 12133.
42 K. B. Wiberg, *Tetrahedron*, 1968, **24**, 1083.
43 A. E. Reed and P. v. R. Schleyer, *Inorg. Chem.*, 1988, **27**, 3969.
44 Y. Xie, H. F. Schaefer and G. H. Robinson, *Chem. Phys. Lett.*, 2000, **317**, 174.
45 H. Grützmacher and T. F. Fässler, *Chem. Eur. J.*, 2000, **6**, 2317.
46 G. H. Robinson, *Acc. Chem. Res.*, 1999, **32**, 773.

Rare earth alkoxides as inorganic precursors for olefin polymerization: an alternative to traditional lanthanocene chemistry

Jérome Gromada,[a] Thomas Chenal,[a] André Mortreux,*[a] Joseph W. Ziller,[b] Frédéric Leising[c] and Jean-François Carpentier*[a]

[a] *Laboratoire de Catalyse de Lille, UPRESA CNRS 8010, ENSCL, B.P. 108-59652, Villeneuve d'Ascq Cedex, France. E-mail: carpentier@ensc-lille.fr*
[b] *University of California, Department of Chemistry, Irvine, 92697 CA, USA*
[c] *Rhodia Recherches, 52 rue de la Haie Coq 93308 Aubervilliers Cedex, France*

Received (in Cambridge, UK) 24th August 2000, Accepted 2nd October 2000
First published as an Advance Article on the web 23rd October 2000

The combination of the neodymium *tert*-butoxide [$Nd_3(\mu_3\text{-}OBu^t)_2(\mu\text{-}OBu^t)_3(OBu^t)_4(THF)_2$] 1 with 1 equivalent of a dialkylmagnesium reagent affords an efficient catalyst for the pseudo-living polymerization of ethylene.

Trivalent rare earth metal hydrides and alkyl complexes stabilized by two cyclopentadienyl-type ligands, Cp_2LnR have attracted much attention because of their high efficiency in polymerizing ethylene.[1] Currently, there is considerable interest in developing related organolanthanide complexes involving ancillary ligands other than the commonly used Cp-type ligands. In this respect, hard, electronegative ligands such as alkoxides are particularly attractive because they offer strong metal–oxygen bonds that are expected to stabilize complexes.[2] Although the mixed Cp*–aryloxide system $[Y(C_5Me_5)(OC_6H_3\text{-}Bu^t_2\text{-}2,6)(\eta\text{-}H)]_2$ has been shown to be active for the polymerization of α-olefins,[3] no equivalent Cp-free alkoxy catalyst system had been developed to date.[4] We report here that some lanthanide *tert*-alkoxides are efficient inorganic precatalysts, when combined with dialkylmagnesium compounds, for the pseudo-living polymerization of ethylene and ethylene–MMA block copolymerization.

The reaction of $NdCl_3$ with 3 equiv. of $NaOBu^t$ in THF at 25 °C for 3 days gives a single primary product **1**, that can be isolated in 80–90% yield as a very air-sensitive compound. An X-ray crystallographic study revealed that **1** is a trimetallic compound with the formula $[Nd_3(\mu_3\text{-}OBu^t)_2(\mu\text{-}OBu^t)_3(OBu^t)_4(THF)_2]$ (Fig. 1).[5] Some lanthanum analogues isostructural to **1** have been reported: $La_3(OBu^t)_9(THF)_2$ **2**, prepared by ionic metathesis,[6] and $[La_3(\mu_3\text{-}OBu^t)_2(\mu\text{-}OBu^t)_3(OBu^t)_4(HOBu^t)_2]$ **3**, obtained by alcoholysis of $La\{N(SiMe_3)_2\}_3$.[7] Complexes **2** and **3** are, however, respectively, much less efficient than **1** and totally inefficient for the polymerization catalysis described hereafter.

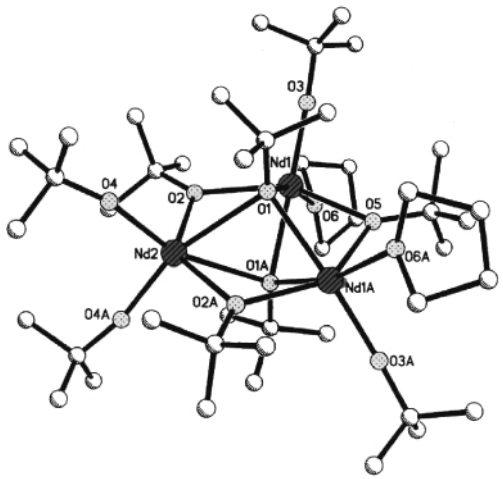

Fig. 1 Molecular structure of **1** in the crystal. Selected bond lengths (Å): Nd1–O3 2.147(4), Nd1–O2 2.333(3), Nd1–O5 2.399(3), Nd1–O1 2.409(3), Nd1–O1A 2.520(3), Nd1–O6 2.661(4), Nd1–Nd1A 3.6318(6), Nd1–Nd2 3.7161(4), Nd2–O4 2.163(3), Nd2–O2 2.458(3), Nd2–O1 2.624(3).

The addition of 1 equivalent of di(*n*-hexyl)magnesium to **1** in toluene solution at 0 °C offers an active catalyst for ethylene polymerization. The typical ethylene flow rate for a batch experiment conducted under 1.1 atm is shown in Fig. 2. The maximum consumption of ethylene, reached after a few minutes, corresponds to the appearance of insoluble polymer. The typical average catalytic activity calculated over 1 h on the basis of the amount of Nd initially introduced is *ca.* 10 g $mmol^{-1}$ h^{-1} atm^{-1} at 0 °C. This places this new catalyst system on a moderate rate of effectiveness on Gibson's scale,[1d] and compares well to traditional alkyl–lanthanocenes under similar conditions. The Mg(*n*-hex)$_2$–**1** system gives linear high density and highly crystalline (>80%) polyethylene (T_m = 139–141 °C) with M_n = (3–4) × 10^5 and M_w/M_n = 2.3–2.5. GPC analysis of aliquots revealed that the molecular weight and the polydispersity do not increase significantly during the reaction course. These results are tentatively ascribed to slow *in situ* catalyst generation, rapid propagation relative to the rate of initiation and/or concomitant heterogenezation due to precipitation of long-chain metal–alkyl species from solution. The monomodality of the GPC curves is, however, consistent with the generation of one type of active species. Progressive deactivation of the catalyst system was observed above 20 °C, resulting in lower productivities and formation of low molecular weight PE (*e.g.* at 80 °C: $[a]_{1h}$ = 0.6 g $mmol^{-1}$ h^{-1} atm^{-1}, M_n = 1720, M_w/M_n = 1.55, 29% vinyl terminations).

When the polymerization was carried out at 0 °C in the presence of $PhSiH_3$ as a transfer agent[8] (10 equiv. *vs.* Nd), the activity profile and the productivity over 1 h were the same as those observed in the absence of this reagent. The polymer recovered after MeOH quenching and work-up was shown by ^1H and ^{13}C NMR to be end-capped $PhSiH_2$–polyethylene, with M_n = 14 300 and broad polydispersity (M_w/M_n = 25). Using 2% of H_2 in ethylene as an alternative transfer agent[9] resulted in

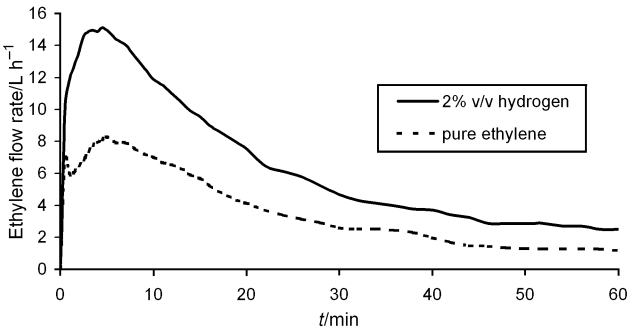

Fig. 2 Typical ethylene consumption plots observed with the **1**–Mg(*n*-hex)$_2$ system with pure C_2H_4 and a 98 : 2 v/v C_2H_4–H_2 mixture (0.33 mmol **1**, 1.0 mmol Mg, 100 mL toluene, 0 °C, 1.1 atm ethylene kept constant).

DOI: 10.1039/b006941h

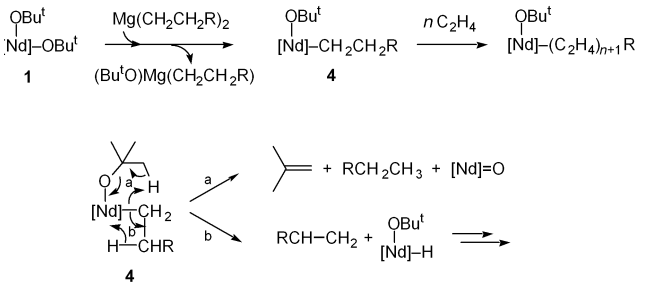

Scheme 1 Schematic presentation of proposed activation (up) and deactivation (down) pathways.

a *ca*. 25% increase in the catalyst productivity (Fig. 2) and formation of polyethylene with M_n = 17 000 (constant value ± 500 for five samples collected every 10 min) and broad polydispersity (M_w/M_n = 5.8). In both cases, no end-group associable with conventional (*e.g.* β-H elimination) chain transfer processes was detected by NMR in the polymers. Further evidence for the pseudo-living character of the Mg(*n*-hex)$_2$–**1** catalyst system at 0 °C is provided by the possibility of achieving ethylene–MMA block copolymerization through initial homopolymerization of ethylene and sequential addition of MMA.[10]

All of these results support a polymerization mechanism for the present system similar to that established for traditional lanthanocenes. We assume that alkylation of **1** by the dialkylmagnesium[11] *in situ* generates an active alkyl–Nd species **4** (Scheme 1). Preliminary NMR investigations of Mg(CH$_2$CH$_2$R)$_2$–**1** systems (R = H, Et, Bu) show the formation, at as low as −60 °C, of the corresponding alk-1-ene, RCH=CH$_2$, in 15–40% yield *vs*. Nd. This is consistent with the formation of an alkyl–Nd species **4** which further evolves, *e.g. via* β-H elimination (a). Also, the slow formation of isobutene in 2–40% yield *vs*. Nd with concomitant release of the alkane [clearly evidenced with SiMe$_4$ upon using Mg(CH$_2$SiMe$_3$)$_2$] supports the generation of **4** and indicates that *tert*-butoxy ligands are likely involved in the degradation of the active species (b).[12]

Among the large variety of alkylating reagents so far investigated in combination with **1**, only dialkylmagnesium derivatives, in particular those bearing long alkyl chains, led to appreciable ethylene polymerization activity. Best activities are obtained with 1.0 equiv. of MgR$_2$ *vs*. Nd, as deviation from this stoichiometry resulted in a rapid drop in catalytic activity. Other tris(alkoxy)lanthanide complexes have been investigated as precatalysts, among which some show similar properties but contrasting performances; *e.g.* the Sm^{III} *tert*-butoxide–Mg(*n*-hex)$_2$ system gives low molecular weight PE ([*a*]$_{1h}$ = *ca*. 2 g mmol^{-1} h^{-1} atm^{-1}, M_n = 2500, M_w/M_n = 6.1). On the other hand, alkoxylanthanide precursors such as **3** or its Nd equivalent, both prepared by alcoholysis of amide precursors, are totally inactive. In fact, alkoxy ligands having no hydrogen in the β-position, the absence of coordinated protic solvent and of chloro ligands, as well as structural constraints in the nuclearity of the complex appear to be prerequisites for the successful development of these new-generation lanthanide catalysts.

This work was supported by Rhodia, the Ministère de l'Industrie and the CNRS. We thank Dr J. Vaissermann, Paris, for initial efforts in elucidating the crystal structure and Professor R. F. Jordan, Chicago, for GPC facilities.

Notes and references

1 (*a*) D. G. H. Ballard, A. Courtis, J. Holton, J. McMeeking and R. Pearce, *Chem. Commun.*, 1978, 994; (*b*) P. L. Watson and G. W. Parshall, *Acc. Chem. Res.*, 1985, **18**, 51; (*c*) G. Jeske, H. Lauke, H. Mauermann, P. N. Swepston, H. Schumann and T. J. Marks, *J. Am. Chem. Soc.*, 1985, **107**, 8091; (*d*) G. J. P. Britovsek, V. C. Gibson and D. F. Wass, *Angew. Chem., Int. Ed.*, 1999, **38**, 428.

2 J. W. Bruno, T. J. Marks and L. R. Morss, *J. Am. Chem. Soc.*, 1983, **105**, 6824.

3 C. J. Schaverien, *Organometallics*, 1994, **13**, 69.

4 To our knowledge, only the dialkyl(aryloxy)yttrium complex (Me$_3$SiCH$_2$)$_2$Y(OC$_6$H$_3$Bu$^t_2$-2,6)(THF)$_2$ shows (very low) ethylene polymerization activity [9 × 10^{-3} g mmol^{-1} h^{-1} atm^{-1} at room temp. (RT)]: W. J. Evans, R. N. R. Broomhall-Dillard and J. W. Ziller, *J. Organomet. Chem.*, 1998, **569**, 89; Sc complexes containing amide-diphosphane and triaza ligands, as well as benzamidinate yttrium complexes have been recently shown to polymerize ethylene with very low activity; see ref. 1(*d*).

5 *Crystal data*: C$_{44}$H$_{97}$O$_{11}$Nd$_3$, *M* = 1234.92, orthorhombic, space group *Pbcn*, *a* = 17.0538(10), *b* = 20.0343(12), *c* = 17.7400(11) Å, *V* = 6061.1(6) Å^3, *T* = 158 K, *Z* = 4, μ(Mo-Kα) = 2.581 mm^{-1}. 38059 reflections collected, 7315 unique. Hydrogen atoms were included using a riding model. The *tert*-butoxide ligand located on the two-fold axis and the THF ligand were disordered. The carbon atoms associated with these ligands were included using multiple components with partial site occupancy factors. There was also one disordered THF solvent molecule present per formula unit. Hydrogen atoms associated with the disordered *tert*-butoxide ligand and with the solvent molecule not included in the refinement. Final *R* values [$F > 2\sigma(F)$]: *R*1 = 0.0410, *wR*2 = 0.1044. CCDC 182/1798. See http://www.rsc.org/suppdata/cc/b0/b006941h/ for crystalographic files in .cif format.

6 W. J. Evans, M. S. Sollberger and T. P. Hanusa, *J. Am. Chem. Soc.*, 1988, **110**, 1841.

7 D. C. Bradley, H. Chudzynska, M. B. Hursthouse and M. Motevalli, *Polyhedron*, 1991, **10**, 1049.

8 P.-F. Fu and T. J. Marks, *J. Am. Chem. Soc.*, 1995, **117**, 10 747.

9 W. J. Evans, D. M. Decoster and J. Greaves, *Macromolecules*, 1995, **28**, 7929.

10 The MgR$_2$–**1** (1 : 5) system initiates the living polymerization of MMA at 0 °C to give syndiotactic PMMA [75–80% *rr*; M_n = (60–130) × 10^3, M_w/M_n = 1.07–1.12]: J. Gromada, T. Chenal, A. Mortreux, F. Leising and J.-F. Carpentier, *Fr. Pat.*, 99 08648, 1999; H. Yasuda, M. Furo, H. Yamamoto, A. Nakamura, S. Miyake and N. Kibino, *Macromolecules*, 1992, **25**, 5115.

11 V. A. Schreider, E. P. Turevskaya, N. L. Koslova and N. Y. Turova, *Inorg. Chim. Acta*, 1981, **53**, L73; H. Schumann, W. Genthe and N. Brunks, *Organometallics*, 1982, **1**, 1194; A. Gulino, N. Casarin, V. P. Conticello, J. G. Gaudiello and T. J. Marks, *Organometallics*, 1988, **7**, 2360.

12 R. Duchateau, T. Tuinstra, E. A. C. Brussee, A. Meetsma, P. T. van Duijnen and J. H. Teuben, *Organometallics*, 1997, **16**, 3511 and references therein.

ChemComm

An approach to open-chain 1,5-stereocontrol using a silyl group

Ian Fleming* and Chandrashekar Ramarao

Department of Chemistry, Lensfield Road, Cambridge, UK CB2 1EW. E-mail: if10000@cam.ac.uk

Received (in Liverpool, UK) 7th August 2000, Accepted 26th September 2000
First published as an Advance Article on the web 23rd October 2000

Nucleophilic attack by an ethylcuprate on the α,β-unsaturated ketone 3 takes place *anti* to the silyl group to give largely (96:4) a single product 4, fragmentation of which removes the silyl group, and reveals a pair of stereogenic centres having an open-chain 1,5 relationship 9.

We have developed a substantial body of chemistry in which a stereogenic centre carrying a silyl group controls the stereochemistry of electrophilic attack on a C=C double bond in the sense **1**,[1] and we have also adapted these reactions to control

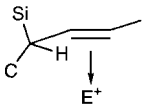

1

more distant open-chain relationships, including 1,4 in the course of syntheses of tetrahydrolipstatin[2] and of nonactin,[3] and 1,6 in an S_E2'' reaction.[4] The use of a silyl group to control 1,4-relationships has also been exploited by Procter[5] and by Panek.[6] We have now developed a method for the control of a 1,5-relationship, which we describe here. The essence of our approach is successively to set up two 1,3-relationships, moving the stereochemistry three atoms along the chain each time. By using a silyl group in the middle, we can remove the intervening functionality and stereochemistry to reveal the open-chain 1,5-relationship.

We began with the well established 1,3-control seen in conjugate additions to 5-substituted cyclohexenones,[7] which we already knew was well behaved when the nucleophile was a silyl group.[8] On this occasion we used the phenyldimethylsilylzincate reagent[9] with 5-methylcyclohex-2-enone **2** (Scheme 1), and the intermediate zinc enolate readily underwent an aldol reaction with acetaldehyde to give a β-hydroxy ketone as a mixture of diastereoisomers. Dehydration gave, as far as we could tell, a single α,β-unsaturated ketone **3** with the C-5 methyl and C-3 silyl groups *trans* to each other and the exocyclic double bond with a *Z* configuration (COSY and NOESY). This set up the first 1,3-relationship, and we set up the second by conjugate addition of an ethylcuprate reagent in the presence of *tert*-butyldimethylsilyl chloride. This gave a silyl enol ether **4** as a single diastereoisomer (^{1}H-NMR, >95:5), which proved (see below) to have the relative configuration illustrated.

We carried out the complementary sequence, trapping the zinc enolate with propionaldehyde instead of acetaldehyde, and adding a methylcuprate to the α,β-unsaturated ketone **5**, which gave largely (86:14) the alternative stereoisomer **6** (Scheme 2).

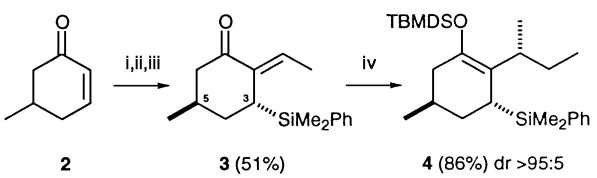

2 **3** (51%) **4** (86%) dr >95:5

Scheme 1 *Reagents and conditions*: i, $PhMe_2SiZnMe_2$ Li, THF, −78 °C, 1 h; ii, MeCHO, −78 °C, 2 h; iii, MsCl, Py, $CHCl_3$, reflux, 16 h; iv, TBDMSCl, Et_2CuLi LiCN, THF, −78 °C, 1 h.

This time we could clearly see the signals (^{1}H-NMR) of the minor isomer, which were identical to those we had already seen for the isomer **4**. Clearly, the reaction had been stereochemically highly controlled, and either stereoisomer, **4** or **6**, could be obtained with nearly equal ease.

We hydrolysed the silyl enol ether **4**, and obtained a single diastereoisomer of the ketone **7**, which was unaffected by treatment with sodium methoxide, suggesting that it was the thermodynamically favourable isomer (Scheme 3). We then applied a fragmentation reaction developed by Nishiyama and Itoh,[10] using the oxime acetate **8**, and obtained the alkene **9** with the 1,5-relationship between C-3 and C-7 revealed in an open chain. That the alkene had a *trans* double bond showed that the relative stereochemistry assigned (COSY and NOESY) to C-2 in the ketone **7** was correct, since Itoh has shown that this type of fragmentation is stereospecifically *anti*.

We proved the relative stereochemistry between the 1,5-related centres, by carrying out the same sequence using enantiomerically pure (5*R*)-methylcyclohex-2-enone **1**,[11] and obtained the nitrile **9** enantiomerically pure at C-3. Ozonolysis and borohydride reduction gave 2-methylbutanol, derivatisation of which with Mosher's acid gave us the known esters (Scheme 4).[12] The major component **10** was the *R*,*R*-diastereoisomer (^{1}H-NMR), and a minor component (4%) was now detectable and identifiable as the *R*,*S*-diastereoisomer, allowing us to measure, more accurately than it had been possible to from the earlier NMR spectra, the degree to which we had been successful in the conjugate addition step **3** → **4**.

We suggest that, if the silyl group in the α,β-unsaturated ketone **3** were equatorial **11**, it would suffer from steric compression with the methyl group on the exocyclic double

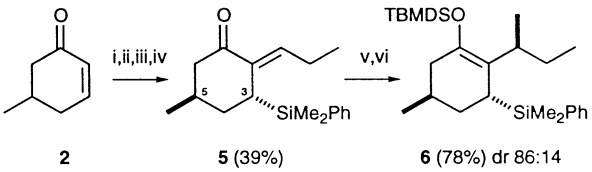

2 **5** (39%) **6** (78%) dr 86:14

Scheme 2 *Reagents and conditions*: i, $PhMe_2SiZnMe_2$ Li, THF, −78 °C, 1 h; ii, EtCHO, −78 °C, 2 h; iii, MsCl, Et_3N, CH_2Cl_2, 0 °C, 2 h; iv, DBU, toluene, reflux, 4 h, or NaH, THF, 0 °C → rt, 12 h; v, Me_2CuLi LiCN, THF, −78 °C, 40 min; vi, TBDMSCl, HMPA, Et_3N, −78 °C, 1 h.

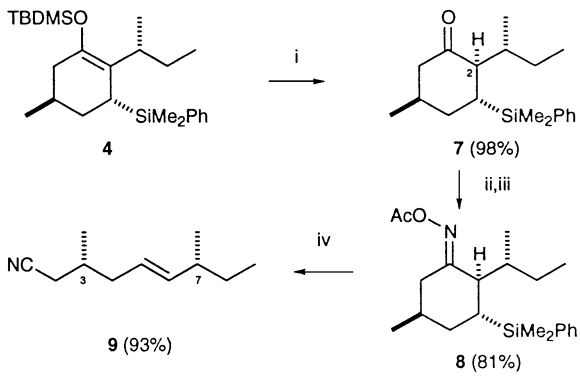

4 **7** (98%) **8** (81%) **9** (93%)

Scheme 3 *Reagents and conditions*: i, HCl, H_2O, THF, rt, 14 h; ii, NH_2OH HCl, Py, EtOH, reflux, 12 h; iii, Ac_2O, Py, CH_2Cl_2, 0 °C → rt, 4 h; iv, Me_3SiOTf, CH_2Cl_2, 0 °C, 4 h.

DOI: 10.1039/b006515n

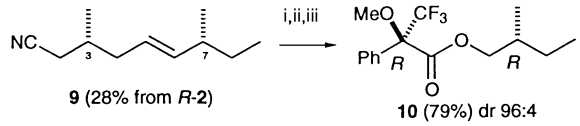

9 (28% from *R*-**2**) **10** (79%) dr 96:4

Scheme 4 *Reagents and conditions*: i, O_3, Et_2O, −78 °C, 10 min; ii, $NaBH_4$, H_2O, 0 °C, 1 h; iii, Mosher's *R*-acid, DCC, DMAP, CH_2Cl_2, rt, 16 h.

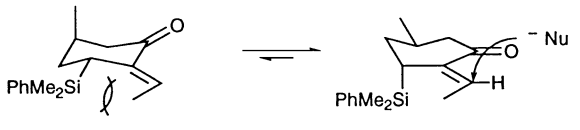

11 **12**

bond. In consequence, even though a trimethylsilyl group has a larger A-value than a methyl group (2.5[13] and 1.74, respectively), the lower-energy conformation of the enone **3** probably has the methyl group equatorial and the silyl group axial **12**, where, in any case, it only has one 1,3-diaxial interaction. With the silyl group held on the lower surface, nucleophilic attack can be expected to take place on the top surface *anti* to the bulky group **12** (arrow), and hence give the silyl enol ether with the relative configuration **4**.

To support this argument, we carried out molecular modelling calculations (Macromodel), which confirmed that the conformation with the silyl group axial **12** had the lowest energy,[14] with the stereo drawings **13** giving a more accurate

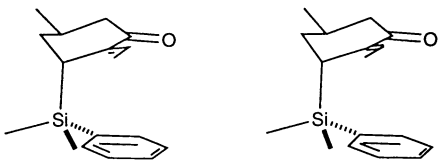

13

picture of the minimised structure. Looking at the space-filling versions **14** (from above) and **15** (from below) illustrates the difference between the two surfaces of the enone **3**—the β-carbon (darker grey) in the top view is exposed, but in the bottom view it is hindered by the substituents on the silyl group.[15]

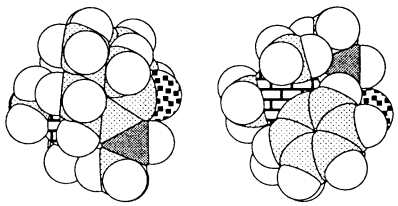

14 top view **15** bottom view

Furthermore, the calculation for the second α,β-unsaturated ketone **5** revealed why it suffered a lower degree of stereocontrol in the conjugate addition step—the methyl group of the ethyl group was oriented upwards, hindering the top surface more than the top surface of the α,β-unsaturated ketone **3** = **12** = **13**.

The stereocontrol in this system is interesting from two points of view. In the first place, it shows that the silyl group is not so hindering that it cannot adopt the axial position, and yet simultaneously it does hinder the approach of the incoming nucleophile. The long Si–C bond takes the silyl group far enough away from the cyclohexane ring to make 1,3-diaxial interactions less severe than they would be for a carbon-based group, and yet the length of the Si–C bonds to the three other substituents on the silicon atom causes them to occupy much of the space below the double bond. In the second place, this is the first reaction that we have studied in which the double bond

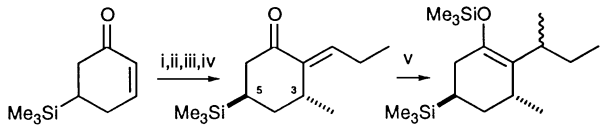

16 **17** (41%) **18** (74%) dr 50:50

Scheme 5 *Reagents and conditions*: i, Me_2CuLi, THF, −78 °C, 1 h; ii, TBDMSCl, HMPA, Et_3N, −78 °C → rt, 1 h; iii, EtCHO, $TiCl_4$, CH_2Cl_2 −78 °C, 2 h; iv, TsOH, toluene, reflux, 1 h; v, Me_2CuLi, THF, −78 °C, 1 h; vi, TMSCl, HMPA, Et_3N, −78 °C → rt, 1 h.

adjacent to the stereogenic centre carrying a silyl group has undergone *nucleophilic* attack. All our work in the past has involved electrophilic attack. Since the sense of attack, *anti* to the silyl group **1**, is the same, it may be that we have here some indication that the stereocontrol is largely steric in origin. This conclusion stems from the prejudice that nucleophilic attack and electrophilic attack would take place in opposite senses if purely electronic effects were operative.

Although this may be a little too simplistic, we can be sure that the silyl group is an important component in ensuring the high levels of diastereocontrol that we have seen, for we have carried out a similar set of reactions with the C-5 methyl group and the C-3 silyl group in **5** interchanged (Scheme 5). Starting with the silicon-containing cyclohexenone **16**,[16] and using a methylcuprate to set up the 1,3-related centres in the enone **17**. This time, the conjugate addition of the methylcuprate gave both possible diastereoisomers **18** in equal amounts. Presumably a methyl group on C-3, although surely held axial, shields the bottom surface from attack to the same extent as the upturned methyl group on the side chain shields the top surface.

We thank Avra Laboratories, Hyderabad, for a maintenance grant (C. R.), and Setu P. Roday for help with the molecular modelling.

Notes and references

1 Summarised in: I. Fleming, *J.. Chem. Soc., Perkin Trans. 1*, 1992, 3363.
2 I. Fleming and N. J. Lawrence, *J. Chem. Soc., Perkin Trans. 1*, 1998, 2679.
3 M. Ahmar, C. Duyck and I. Fleming, *J. Chem. Soc., Perkin Trans. 1*, 1998, 2721; I. Fleming and S. K. Ghosh, *J. Chem. Soc., Perkin Trans. 1*, 1998, 2733.
4 I. Fleming and C. P. Leslie, *J. Chem. Soc., Perkin Trans. 1*, 1996, 1197.
5 G. Procter, A. T. Russell, P. J. Murphy, T. S. Tan and A. N. Mather, *Tetrahedron*, 1988, **44**, 3953.
6 C. E. Masse and J. S. Panek, *Chem. Rev.*, 1995, **95**, 1293.
7 N. L. Allinger and C. K. Riew, *Tetrahedron Lett.*, 1966, 1269. For the most recent discussion, see S. Mori and E. Nakamura, *Chem. Eur. J.*, 1999, **5**, 1534. For the first application in synthesis, see G. Stork, R. A. Kretchmer and R. H. Schlessinger, *J. Am. Chem. Soc.*, 1968, **90**, 1647; G. Stork, *Pure Appl. Chem.*, 1968, **17**, 383.
8 I. Fleming, R. Henning, D. C. Parker, H. E. Plaut and P. E. J. Sanderson, *J. Chem. Soc., Perkin Trans. 1*, 1995, 317.
9 R. A. N. C. Crump, I. Fleming and C. J. Urch, *J. Chem. Soc., Perkin Trans. 1*, 1994, 701.
10 H. Nishiyama, K. Sakuta, N. Osaka, H. Arai, M. Matsumoto and K. Itoh, *Tetrahedron*, 1988, **44**, 2413.
11 D. Caine, K. Procter and R. A. Cassell, *J. Org. Chem.*, 1984, **49**, 2647.
12 H. Oikawa, I. Matsuda, T. Kagawa, A. Ichihara and K. Kohmoto, *Tetrahedron*, 1994, **50**, 13 347.
13 W. Kitching, H. A. Olszowy, G. M. Drew and W. Adcock, *J. Org. Chem.*, 1982, **47**, 5153.
14 The chair conformation with the silyl group equatorial is 46.5 kJ mol^{-1} higher in energy, and there are two families of boat conformations in between, at 13 and 40 kJ mol^{-1} above the minimum.
15 Although the calculation places the phenyl group under the carbonyl group, a methyl group would be nearly as much hindrance at the β-carbon; we do not think that the high degree of selectivity is dependent upon the presence of the phenyl group on silicon.
16 M. Laguerre, J. Dunoguès R. Calas and N. J. Duffaut, *J. Organomet. Chem.*, 1975, **93**, C17; M. Asaoka, K. Shima and H. Takei, *Tetrahedron Lett.*, 1987, **28**, 5669.

ChemComm

Synthesis and crystal structure of [IBa(OBu^t)$_4${Li(thf)}$_4$(OH)]: a mixed ligand heterometallic cluster with an unusual low coordination number for barium

Katharina M. Fromm,*[a] Estelle D. Gueneau[a] and H. Goesmann[b]

[a] *University of Geneva, Sciences II, 30, Quai Ernest-Ansermet, CH-1211 Geneva 4, Switzerland. E-mail: Katharina.Fromm@chiam.unige.ch*

[b] *Institut für Anorganische Chemie, Universität Karlsruhe, Engesserstr., Geb. 30.45, D-76128 Karlsruhe, Germany*

Received (in Cambridge, UK) 12th July 2000, Accepted 5th October 2000
First published as an Advance Article on the web 25th October 2000

The reaction of [BaI$_2$(thf)$_5$] with LiOBu^t in THF in the presence of hydroxide yields a volatile mixed alkali and alkaine earth metal cluster with an unusually low coordination number for the alkaline earth cation; due to the presence of the alkoxide groups, the cluster is volatile at temperatures below 200 °C.

Recently, many organolithium compounds have been structurally investigated, their structure being of interest for the elucidation of possible reaction mecanisms in organic metallation reactions. Thus, it has been shown that metallated organic compounds tend to form aggregated species in the solid state as well as in solution. For example, LiMe, NaMe and MOBu^t, M = Rb, K, form tetrahedral tetramers,[1,2] LiEt forms hexameric units[3] and NaOBu^t has been shown to have one hexameric and one nonameric molecule in its structure.[4] LiOBu^t forms a hexameric aggregate in the gas phase as well as in solution and the solid state.[5] We here describe the reaction of this compound with [BaI$_2$(thf)$_5$] in THF which yields the mixed metal cluster [IBa(OBu^t)$_4${Li(thf)}$_4$(OH)] **1**.†

In our attempts to make alkaline earth metal cluster compounds in analogy to transition metal clusters, we use an alkaline earth metal halide and an alkali metallated organic compound in order to eliminate alkali halide and to enforce aggregation of the alkaline earth compound.[6] Herein, we report on the reaction of BaI$_2$ with LiOBu^t in THF preceded by the synthesis and isolation of LiOBu^t.[5]

The reaction of 4 equiv. of LiOBu^t dissolved in THF under partial hydrolysis or directly in the presence of LiOH with a THF-solution of 1 equiv. of BaI$_2$ containing [BaI$_2$(thf)$_5$][7] at −20 °C yields colorless blocks of **1** [eqn. (1)], suitable for single crystal X-ray analysis.[8]

$$[BaI_2(thf)_5] + 4\,[Li(OBu^t)] + OH^- \rightarrow [IBa(OBu^t)_4\{Li(thf)\}_4(OH)]\ \mathbf{1} + I^- \quad (1)$$

The compound crystallises in the tetragonal space group *P*4/*nmm* (No. 129) with two molecules per unit cell. The structure can be described as a square antiprism formed by four Li atoms in one plane and four O atoms of the OBu^t ligands in the other square plane, the Li-face being capped by an OH-group and the O-face by a Ba–I unit leading to an overall almost spherical entity. Its formation can be explained by the successful substitution of one iodide and five thf molecules of [BaI$_2$(thf)$_5$] by a [LiOBu^t]$_4$-unit and a μ_4-capping OH-group (Fig. 1), the latter being introduced by partial hydrolysis of the THF solution of LiOBu^t or LiOH. In fact, compound **1** can be obtained in a yield of up to 65% when the reaction is carried out in the presence of 1 equiv. of LiOH relative to BaI$_2$. The coordination sphere of barium is built up by the one remaining iodide and four OBu^t-groups to give a tetragonal pyramidal geometry. Barium has thus a coordination number of five which is unusually low for such a big cation (ionic radius of 1.36 Å for a coordination number of 6)[9] and only possible by the steric protection by the OBu^t-ligands. The four thf molecules, each one coordinating a lithium ion to yield a tetrahedral coordination sphere for the alkali metal, form a calix[4]arene-like cavity of an average diameter of 7.5 Å, this diameter taking into account the disorder positions of the thf molecules. The μ_4-capping OH-group presents an oxygen with five bonding partners.

The alkaline earth cation Ba lies on a crystallographic 4*mm* site (0, $\frac{1}{2}$, *z* (*c*)) as do the halide I and the O3-hydroxy group. The Li-atom is found on a crystallographic mirror plane *m* (*y*, 0, −*z* (*i*)), the oxygen atom O1 of the OBu^t-groups are on a crystallographic mirror plane *m* (-*x*+$\frac{1}{2}$, *x*, −*z* (*j*)) together with the attached C1 atom and one of the three methyl groups C2. The main symmetric features of the molecule are thus the four-fold axes through I, Ba and O3 as well as the two mirror planes through Li and O1. In the crystal, the neutral clusters are arranged along the C_4-axis with rather long I–O3(H3) hydrogen bonds of 3.935 Å.[6]

The terminal Ba–I distance at 3.344(2) Å is extremely short due to the low coordination number of barium and even shorter than the smallest Ba–I distance in solid BaI$_2$ of 3.38 Å.[10] In [BaI$_2$(thf)$_5$],[7] the terminal Ba–I distances are 3.374(2) and 3.3822(2) Å for a coordination number of seven for the barium. The Ba–O distances in **1** are 2.597(6) Å and thus shorter than in the six-coordinate [Ba(OBu^t)$_2$(HOBu^t)$_2$]$_4$ (2.673(8) Å).[11] The four OBu^t-groups form, together with the four Li(thf) units a square antiprism, the two square faces being twisted by 41.85° to each other. The Li–Li contacts at 2.716(18) Å are shorter than in elemental lithium (3.0390 Å), but longer than in similar

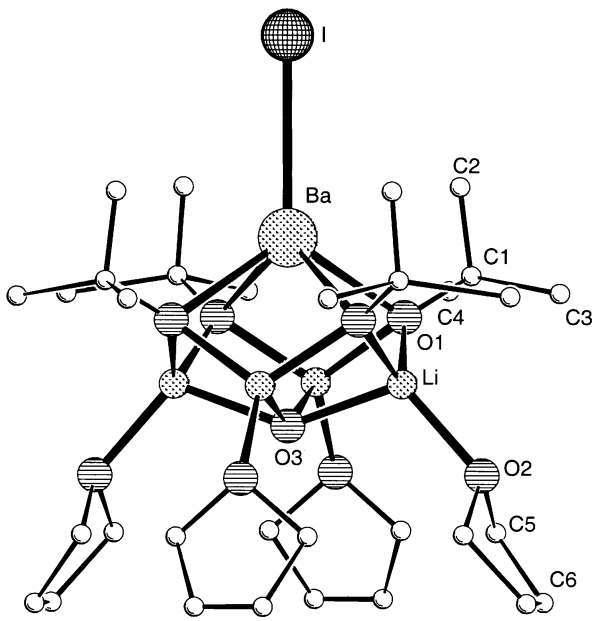

Fig. 1 Crystal structure of **1**. Selected bond lengths [Å] and angles [°]: Ba–I 3.344(2), Ba–O1 2.597(6), Ba–O3 3.115(10), Li–O1 1.962(8), Li–O2 1.997(14), Li–O3 2.035(14), Ba–Li 3.108(13), Li–Li 2.716(18), O1–Ba–I 120.77(12), O1–Ba–O1(*trans*) 118.5(2), O1–Li–O2 122.3(4), O1–Li–O3 91.3(5), O2–Li–O3 113.7(8), Li–O3–Li(*trans*) 141.4(9), cavity diameter (thf) 7.5 Å in average.

compounds like $[Ph_2P(NSiMe_3)]_2CLi_2$[12] with 2.393–2.410 Å. The enlargement relative to the literature data is probably due to the short Ba–O3 contact of 3.115(10) Å in which the alkaline earth cation strongly attracts the OH^- anion which caps the Li_4-square. This also leads to the formation of the very flat square antiprism in which the plane containing the four Li atoms is only 1.115 Å apart from the plane containing the oxygen atoms of the OBu^t groups. Thus, the O3 atom is 0.672 Å above the Li_4 plane, and the Ba atom is 1.328 Å below the O_4 plane. For the Li–O3 and the Li–O2 bonds, bond lengths of 2.035(14) Å and 1.997(14) Å, respectively are observed.

Similar structures containing a square arrangement of four alkali metals are the above mentioned $[Ph_2P(NSiMe_3)]_2CLi_2$,[12] $[Na_4][P\{Si(F)R_2\}(SiPr^i_3)]_2$, (R = 2,4,6-$Pr^i_3C_6H_2$),[13] $[(LiOBu^t)_{10}(LiOH)_6]$,[14] $[Me_2C(CH_2)_3CMe_2NLi]_4$,[15] $[\{Li(NBu^t)_3S\}_2]$[16] or $[Li_4L{\cdot}LiOH{\cdot}4hmpa]$, ($H_4L$ = *tert*-butylcalix[4]arene)[17] as well as $[(Bu^tO)_8Li_4K_4]$.[18] In the $[(LiOBu^t)_{10}(LiOH)_6]$ structure, one can also find the square Li_4O_4-antiprism which is capped on one side by an HO ligand. This fragment shows similar Li–OBu^t and Li–OH bond lengths to **1** at 1.877(10)–2.063(9) and 1.905(11)–2.066(10) Å, respectively.

Similar low coordination spheres for barium are known for instance in the sterically hindered molecule $[(thf)Ba_3(\mu_4\text{-}PSiBu^t_3)_2\{\mu_2\text{-}P(H)SiBu^t_3\}_2]_2$[19] where coordination numbers 5 and 4 for Ba are stabilised by THF or agostic interactions with Bu^t-groups respectively. In the case of **1**, one can also discuss agostic interactions with neighbouring Bu^t-groups since the Ba–(C2)CH_3 distances are in the range of 3.41(3) Å. Other examples for the stabilized low coordination number of 5 for barium are the compounds $[\{BaNP(NMe_3)_2NP(NMe_2)_2NSiMe_3\}_4]$,[20] $[Ba_2\{(C_6H_{11})NC(Me)CHC(Me)N(C_6H_{11})\}_3\{(SiMe_3)_2N\}]$,[21] $[(Et_3PO)_2Ba_2Cu_4(OBu^t)_8]$[22] and $[H_3Ba_6(O)(OBu^t)_{11}(OCEt_2CH_2O)(thf)_3]$[23] for which the Ba–O($\mu_3$-$OBu^t$) distances at 2.76(1) Å are much longer than in **1**. An even lower coordination sphere of 4 in $[BaY_2\{\mu\text{-}OCH(CF_3)_2\}_4(thd)_4]$ (thd = 2,2,6,6-tetramethylheptane-3,5-dionato),[24] $[Ba\{N(SiMe_3)_2\}_2(thf)_2]$ and $[Ba\{N(SiMe_3)_2\}_2(thf)]_2$[25] or 3 in $[Ba\{N(SiMe_3)_2\}_2]$[25] for the alkaline earth metal cation is observed. Another molecular cluster compound combining lithium and barium is the $\{[Ba_6Li_3O_2][OC(CH_3)_3]_{11}(OC_4H_8)_3\}$ in which an oxygen-centered Ba_6-octahedron is fused *via* one triangular face to an oxygen-centered Li_3Ba_3-prism.[26]

As compound **1** is volatile in vacuum at temperatures lower than 200 °C due to the presence of alkoxide groups, its potential application as a barium source in *chemical vapour deposition* processes in order to synthesise high temperature superconductors will be tested. The syntheses of further mixed metal clusters are also under current investigation.

This work was financed by the Swiss National Foundation and the University of Geneva. The authors are grateful to Professor A. F. Williams and Professor C. Piguet for their support, Dr E. Rivara-Minten for ^{7}Li NMR measurements.

Notes and references

† *Experimental* : BaI_2 was dried under vacuum at 200 °C and the reaction carried out under nitrogen atmosphere. 20 ml of a 0.2 M (4 mmol) solution of Bu^tOLi in THF was added to 0.391 g (1 mmol) of BaI_2 and 0.024 g (1 mmol) of LiOH dissolved in 20 ml freshly dried and distilled THF in order to yield a milky white solution after 30 min of stirring. The solution was cooled to −20 °C to give colorless crystals of **1**. Yield: 65% (for BaI_2). ^{1}H NMR (d_8-THF, 20 °C) δ 1.147 (s, CH_3), 1.78 (m, thf), 3.62 (m, thf), 4.5 (s, OH); ^{13}C NMR (d_8-THF, 20 °C) δ 31.78 (CH_3); ^{7}Li NMR (d_8-THF, 20 °C, LiCl 1M/D_2O) δ 0.84, T1 = 1.8 s. ν/cm^{-1} (CsI, Nujol) 3584(s, sharp), 3050(vs, Nujol), 1596(s, Nujol), 1440(s, Nujol), 1374(s, Nujol), 1260(m), 1100(w), 1020(w), 802(m), 497(s, broad), 275(s), 238(w). MS: EI (low resolution): (M^+) = 889 (6%), (M^+−Bu^tOH) = 815 (8%), (M^+− 2Bu^tOH) = 741 (7%), plus degradation compounds at 355 (10%), 281 (56%), 207 (100%), 133 (16%), 73 (38%) and 59 (3%).

1 E. Weiss and E. A. C. Lucken, *J. Organomet. Chem.*, 1964, **2**, 197; E. Weiss and G. Hencken, *J. Organomet. Chem.*, 1978, **21**, 265.
2 J. E. Davies, J. Kopf and E. Weiss, *Acta Crystallogr., Sect B*, 1982, **38**, 2251.
3 D. Seebach, Proceedings of the Robert A. Welch Foundation. Conferences on Chemical Research XXVII. Stereospecificity in Chemistry and Biochemistry, Houston, TX, 1984.
4 E. Weiss, H. Alsdorf, H. Kühr and H. F. Grützmacher, *Chem. Ber.*, 1968, **101**, 3777.
5 M. Braun, D. Waldmüller and B. Mayer, *Angew. Chem., Int. Ed.*, 1989, **28**, 895, (see ref. 4 within); G. E. Hartwell and T. L. Brown, *Inorg. Chem.*, 1966, **5**, 1257; J. D. Kahn, A. Haag and P. v. R. Schleyer, *J. Phys. Chem.*, 1988, **92**, 212; V. Halaska, L. Lochmann and D. Lim, *Collect. Czech. Chem. Commun.*, 1968, **33**, 3245; R. D. Thomas, S. G. Bott, P. W. Gravelle and H. D. Nguyen, *Abstracts of Papers of the American Chemical Society*, 1998, **215**, 291.
6 K. M. Fromm, *Chem. Commun.*, 1999, 1659.
7 K. M. Fromm, *Angew. Chem.*, 1997, **24**, 2876; K. M. Fromm, *Angew. Chem., Int. Ed. Engl.*, 1997, **24**, 2799.
8 *Single crystal data* for **2**: $C_{32}H_{69}O_9BaILi_4$, M = 889.87 g mol^{-1}, tetragonal, space group $P4/nmm$ (No. 129), a = 15.574(2), c = 10.395(2) Å, V = 2521.5(7) Å^3, Z = 4, T = 200 K, $\mu(Mo_{Ka})$ = 1.435 mm^{-1}, 4721 reflections of which 1313 unique and 1313 observed, 86 parameters refined, R(int) = 0.1139, $R1$ = $\Sigma|F_o-F_c|/\Sigma F_o$ = 0.0807, $wR2$ = 0.2014 for $I > 2\sigma$ and $R1$ = 0.1138, $wR2$ = 0.2343 for all data. Crystals of **2** were measured on an ENRAF-NONIUS four-circle diffractometer on a crystal of 0.3 × 0.3 × 0.65 mm and with an absorption correction by analytical integration. The structure was solved with direct methods and refined by full matrix least squares on F^2 with the SHELX-97 package.[27] Disorder was observed for the thf molecules bound to Li as well as for the methyl groups of the *tert*-butanolate ligands. All heavy atoms of the cluster could be refined anisotropically. CCDC 182/1803. See http://www.rsc.org/suppdata/cc/b0/b005638n/ for crystallographic files in .cif format.
9 R. D. Shannon, *Acta Crystallogr., Sect. A.*, 1976, **32**, 751.
10 E. B. Brackett, T. E. Brackett and R. L. Sass, *J. Phys. Chem.*, 1963, **67**, 2132.
11 B. Borup, J. A. Samuels, W. E. Streib and K. G. Caulton, *Inorg. Chem.*, 1994, **33**, 994.
12 A. Kasani, R. P. Kamalesh Babu, R. McDonald and R. G. Cavell, *Chem. Commun.*, 1999, **38**, 1483.
13 M. Driess, H. Pritzkow, M. Skipinski and U. Winkler, *J. Am. Chem. Soc.*, 1998, **120**, 10774.
14 C. Lambert, F. Hampel, P. v. R. Schleyer, M. G. Davidson and R. Snaith, *J. Organomet. Chem.*, 1995, **487**, 139.
15 R. E. Mulvey, *Chem. Soc. Rev.*, 1998, **27**, 339 (see ref. 30 within).
16 R. Fleischer and D. Stalke, *Coord. Chem. Rev.*, 1998, **176**, 431 (see ref. 31 and 32 within).
17 M. G. Davidson, J. A. K. Howard, S. Lamb and C. W. Lehmann, *Chem. Commun.*, 1997, 1607.
18 W. Clegg, A. M. Drummond, S. T. Liddle, R. E. Mulvey and A. Robertson, *Chem. Comm.*, 1999, 1569.
19 M. Westerhausen, M. H. Digeser, M. Krofta, N. Wiberg, H. Nöth, J. Knizek, W. Ponikwar and T. Seifert, *Eur. J. Inorg. Chem.*, 1999, 743.
20 S. K. Pandey, A. Steiner, H. W. Roesky and D. Stalke, *Angew. Chem., Int. Ed. Engl.*, 1993, **34**, 596.
21 W. Clegg, S. J. Coles, E. K. Cope and F. S. Mair, *Angew. Chem., Int. Ed.*, 1998, **37**, 796.
22 B. Borup, J. C. Huffman and K. G. Caulton, *J. Organomet. Chem.*, 1997, **536**, 109.
23 K. G. Caulton, M. H. Chisholm, S. R. Drake and K. Folting, *J. Chem. Soc., Chem. Commun.*, 1990, 1349.
24 F. Labrize, L. G. Hubert-Pfalzgraf, J.-C. Daran and S. Halut, *J. Chem. Soc., Chem. Commun.*, 1993, 1556.
25 M. Westerhausen, *Inorg. Chem.*, 1991, **30**, 96; B. A. Vaartstra, J. C. Huffman, W. E. Streib and K. G. Caulton, *Inorg. Chem.*, 1991, **30**, 121.
26 H. Bock, A. John, C. Näther and Z. Havlas, *J. Am. Chem. Soc.*, 1995, **117**, 9367.
27 G. M. Sheldrick, SHELX-97, University of Göttingen, Göttingen 1997.

ChemComm

Copolymers of vinyl epoxides with carbon monoxide†

Jong Tae Lee and Howard Alper*

Centre for Catalysis Research and Innovation, Department of Chemistry, University of Ottawa, 10 Marie Curie, Ottawa, Ontario, Canada K1N 6N5

Received (in Corvallis, OR, USA) 11th August 2000, Accepted 7th September 2000
First published as an Advance Article on the web 23rd October 2000

Highly functionalized alternating polyketones which possess epoxide groups in the side chains are synthesized by cationic palladium(II) complex catalyzed copolymerization of vinyl epoxides (non-conjugated diene monoepoxides) with carbon monoxide. Catalytic amounts of formic acid and 1,4-naphthoquinone promote the copolymerization significantly without effecting the epoxide group, with $[Pd(L)(MeCN)_2](BF_4)_2$ (L = (*R*,*R*)-Me-DUPHOS) as the catalyst.

Alternating aliphatic polyketones, a new class of engineering thermoplastics made from alk-1-enes and CO, have attracted great interest in polymer science in recent years.[1] The monomers are readily available in high purity and at a relatively low cost, and the polyketones have interesting and unique properties, and may replace conventional engineering thermoplastics in several areas of application (*e.g.* polyketone derived from ethylene and CO).[2]

Another important aspect of polyketones is the presence of carbonyl groups in the polymer backbone that makes them suitable for functional group modifications,[3] and hence polyketones which possess other functional groups in the side chains can serve as excellent starting materials or pre-polymers for other classes of valuable polymers. One of the major goals in this area is the synthesis of highly functionalized polyketones from functionalized alkenes and CO. There are very few examples of the copolymerization of functionalized alkenes with CO.[4–9]

A number of cationic palladium(II) complexes with weakly or non-coordinating counteranions, and phosphine or nitrogen ligands, have been used for the copolymerization of olefins with CO. In the case of higher α-olefins, using a chiral bidentate ligand can afford optically active copolymers with nearly complete head-to-tail regioselectivity and isotacticity, higher molecular weights and higher polymer yields compared to other achiral bidentate ligands.[5,7–9]

The epoxide group is one of the most versatile and important functional groups in organic synthesis. We now wish to report the synthesis of alternating highly functionalized polyketones, which possess epoxide groups in the side chains, *via* cationic palladium(II) catalyzed copolymerization of vinyl epoxides with CO. Given the facility with which epoxides undergo palladium catalyzed rearrangment[10] and other reactions of epoxides, the selectivity for the olefinic unit in the reactions described herein, is indeed impressive.

We first examined the copolymerization of 1,2-epoxyhex-5-ene with CO as a model reaction using, as catalyst, various kinds of cationic palladium(II) complexes with bidentate or monodentate chiral and achiral phosphine ligands [reaction (1)].

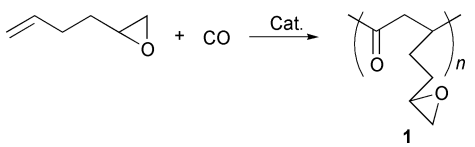

(1)

1

† Electronic supplementary information (ESI) available: general procedure for the copolymerization of vinyl epoxides with CO and spectral data of copolymers. See http://www.rsc.org/suppdata/cc/b0/b006641i/

Among the reported catalyst systems, only $[Pd(L)(MeCN)_2](BF_4)_2$ (L = (*R*,*R*)-Me-DUPHOS, Me-DUPHOS = 1,2-bis(2,5-dimethylphospholano)benzene) previously used for the copolymerization of functionalized (–CO_2H or −OH) alkenes with CO by Sen and co-workers,[5] gave traces of co-oligomer when 1,2-epoxyhex-5-ene was reacted with CO (1000 psi) at 40 °C, in nitromethane and $CHCl_3$ (run 1, Table 1). Quinones are known to promote the copolymerization,[11] so we examined the effect of quinones as a promoter. 1,4-Naphthoquinone gave better results than other quinones such as 1,4-benzoquinone or 2-*tert*-butyl-1,4-benzoquinone. Repetition of the same reaction in the presence of a catalytic amount (3.1 mol%) of 1,4-naphthoquinone afforded the corresponding copolymer (**1**) in moderate molecular weight but in only 10% yield (run 2, Table 1). We then searched for another promoter or coinitiator which could enable this copolymerization to occur without effecting the epoxide group. It was found that a catalytic amount of HCO_2H can significantly improve the yield of the epoxypolyketone. When the copolymerization was performed in the presence of a catalytic amount of 1,4-naphthoquinone and HCO_2H as promoters, as well as the palladium complex, up to 63% yield of copolymer **1** was obtained in moderate molecular weight (run 4, Table 1). Even HCO_2H alone can be used as a promoter with copolymer **1** formed in 26% yield but the molecular weight was lower than using only 1,4-naphthoquinone (compare runs 2 and 7, Table 1). The exact role of HCO_2H is not clear but it can possibly generate palladium hydride, which is known as an active catalyst [reaction (2)].[1c,12] The effect of monomer concentration

$$(\text{Me-DUPHOS})(\text{MeCN})_2\text{Pd}^{2+} + \text{HCO}_2\text{H} \xrightarrow[-\text{MeCN}]{} (\text{Me-DUPHOS})(\text{MeCN})\text{Pd}^{+}\text{H} + \text{CO}_2 + \text{H}^{+} \quad (2)$$

Table 1 Copolymerization of 1,2-epoxyhex-5-ene with CO[a]

		Promotor			Result	
Run	[Epoxide]/M	1,4-NQ/mmol	HCO_2H/mmol	Time/h	Yield (%)	M_w[b] M_w/M_n
1	2	—	—	24	trace	—
2	2	0.25	—	24	10	19 700 1.99
3	2	0.25	0.3	18	40	12 900 1.58
4	2	0.25	0.6	18	63	15 500 1.72
5	1.33	0.25	0.6	18	47	12 300 1.61
6	1.33	0.25	0.6	30	67	10 900 1.97
7	2	—	0.6	24	26	12 200 1.62
8[c]	2	0.25	0.6	24	46	11 600 2.03
9[d]	2	0.25	0.6	24	Trace	—

[a] Condition: 1,2-epoxyhex-5-ene 8 mmol, solvent; CH_3NO_2 + $CHCl_3$ (ratio 1:1) 4 ml ([Sub]/M = 2); $[Pd(MeCN)_4](BF_4)_2$, 0.02 mmol (0.25 mol%); (*R*,*R*)-Me-DUPHOS, 0.02 mmol (0.25 mol%), CO, 1000 psi, temp. 40 °C. [b] Molecular weights were measured by GPC relative to polystyrene standards. [c] CH_3NO_2 only as solvent. [d] $CHCl_3$ only as solvent.

DOI: 10.1039/b006641i

Table 2 The copolymerization of vinyl epoxides with CO[a]

Run	Epoxide	Time/h	Result	
			Copolymer, yield (%)	M_w (M_w/M_n)[b]
1	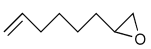	40	**3**, 58	30 500 (1.97)
2	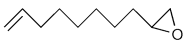	40	**4**, 52	33 600 (1.41)
3	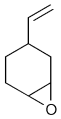	18	**5**, 41	28 500 (3.40)
4	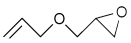	48	**6**, 77	3 350 (1.28)
5		24	—	—

[a] Reaction conditions were the same as for run 4 in Table 1. [b] Molecular weights were measured by GPC relative to polystyrene standards.

was not critical but higher concentrations afforded higher molecular weights for the epoxypolyketones (run 4–6, Table 1). A 1:1 (v/v) mixture of nitromethane and $CHCl_3$ was the best solvent system. Use of only chloroform as the solvent gave trace amounts of copolymer **1** (run 9, Table 1) while use of only nitromethane gave lower yields than the mixed solvent system (run 8, Table 1).

The above results indicate that the optimum conditions for the copolymerization of 1,2-epoxyhex-5-ene with CO are 0.25 mol% of $[Pd(MeCN)_4](BF_4)_2$, 0.25 mol% of (*R*,*R*)-Me-DUPHOS, 3.1 mol% of 1,4-naphthoquinone and 7.5 mol% of HCO_2H in nitromethane and solvent at 40 °C under 1000 psi of CO (run 4, Table 1).

Under the optimum reaction conditions, principally the poly(1,4-ketone) structure (**1**) of the corresponding copolymer was obtained and soluble in organic solvents like CH_2Cl_2, THF or DMSO. However if the copolymerization was performed for an extended reaction time (more than 24 h) or isolated as a pure solid, the structure of the copolymer was that of a poly(spiroketal-1,4-ketone) which is insoluble in common organic solvents and even in fluorinated alcohols. The solid state ^{13}C NMR spectrum of the poly(spiroketal-1,4-ketone) indicated a 1:1 ratio of the poly(1,4-ketone) and poly(spiroketal), with resonances of 1,4-keto groups and spiroketal groups appearing at 211.5 and 110.5 ppm respectively. The values of 1,4-keto and spiroketal groups of other polyketones (higher α-olefins or other functionalized alkenes and CO) occur at 211–214 and 112–114 ppm respectively.[5,8] The structure of the copolymer **1** (*i.e*. poly(1,4-ketone)) was determined by ^{13}C NMR and IR, and was supported by elemental analysis.† The IR spectrum displays a carbonyl stretching band at 1706 cm^{-1}, and the epoxy group bands appeared at 1260, 914 and 835 cm^{-1}. The ^{13}C NMR spectrum (DMSO-d_6) showed a resonance at 211.8 ppm due to the carbonyl group, and resonances at 44.5 and 43.5 ppm which are due to the CH_2CH units in the polymer backbone. Resonances at 51.5 and 46.5 ppm are due to the epoxide carbons in the side chains and the $(CH_2)_2$ units in the side chains appeared at 29.4 and 27.3 ppm. The chemical shift values for the carbonyl and main chain carbons of the ^{13}C NMR spectrum, and the simplicity of the spectrum, support the copolymerization as a highly regio (head-to-tail) and diastereoselective (isotactic) process.[5,7,8]

Several other vinyl epoxides were copolymerized with CO under the optimum reaction conditions found for the copolymerization of CO and 1,2-epoxyhex-5-ene (run 4, Table 1), and the results are summarized in Table 2.†

In the case of 1,2-epoxyoct-7-ene, where the epoxy group is far from the olefinic unit compared with 1,2-epoxyhex-5-ene, the copolymerization was slower but the molecular weight of the copolymer **3** was higher than that of **1** (run 1, Table 2). 1,2-Epoxydec-9-ene gave similar results to that of 1,2-epoxyoct-7-ene, affording **4** but with narrower polydispersity when compared with 1,2-epoxyhex-5-ene and 1,2-epoxyoct-7-ene (compare run 6, Table 1, run 1 and 2, Table 2). The copolymerization of 4-vinyl-1,2-epoxycyclohexane (*cis* and *trans* mixture) with CO afforded the corresponding copolymer **5** in reasonable yield and molecular weight, but with broad polydispersity (M_w/M_n = 3.40, run 3, Table 2). Allyl glycidyl ether, which has not been successfully copolymerized with CO in the past,[4] can also undergo smooth copolymerization under the reaction conditions described above, affording the copolymer **6** in 77% yield. Interestingly, the molecular weight was very low (M_w = 3350, run 4, Table 2) compared to vinyl epoxides not having an ether group. The copolymer **6** was slightly soluble in DMSO, and the molar optical rotation was + 3.4° (*c* = 6.1 mg ml^{-1}, DMSO). Finally in the case of conjugated diene monoxide, 1,2-epoxybut-3-ene, the copolymerization with CO did not proceed under the usual conditions, and the starting epoxide was recovered unchanged (run 5, Table 2).

In conclusion, the copolymerization of vinyl epoxides and CO proceeds in good yields and moderate molecular weights, in the presence of $[Pd((R,R)\text{-Me-DUPHOS})(MeCN)_2](BF_4)_2$ as the catalyst, with HCO_2H and 1,4-naphthoquinone as promoters. Complete chemoselectivity was observed, even in the presence of a reactive epoxide group. These polyketones, with epoxides in the pendant chain, will be of considerable value as precursors to novel polymeric materials by ring opening reactions of the epoxide groups.

We are grateful to Dow Chemical Co. for support of this research. We are indebted to Drs Marv Dettloff and Jerry White of Dow Chemicals for their excellent suggestions regarding this project.

Notes and references

1 Reviews: A. S. Abu-Surrah and B. Rieger, *Top. Catal.*, 1999, **7**, 165; E. Drent and W. W. Jager, *Polym. Mater. Sci. Eng.*, 1997, **76**, 100; E. Drent and P. H. M. Budzelaar, *Chem. Rev.*, 1996, **96**, 663; A. Sen, *Acc. Chem. Res.*, 1993, **26**, 303.
2 C. E. Ash and J. E. Flood, *ACS Proceedings*, 1997, **76**, 110; J. G. Bonner and A. K. Powell, *ACS Proceedings*, 1997, **76**, 108; B. J. Lommerts, *Eur. Pat.*, 1991, 456 306.
3 M. M. Brubaker, D. D. Coffman and H. H. Hoehn, *J. Am. Chem. Soc.*, 1952, **74**, 1509; M. J. Green, A. R. Lucy, S. Lu and R. M. Paton, *J. Chem. Soc., Chem. Commun.*, 1994, 2063; A. Sen, *Chemtech.*, 1986, 48; A. Sen, *Adv. Polym. Sci.*, 1986, **73/74**, 1.
4 E. Drent, *Eur. Pat.*, 1988, 272 727 (*Chem. Abstr.*, 1988, **109**, 191 089); E. Drent, *Eur. Pat. Appl.*, 1992, 463 689 (*Chem. Abstr.*, 1992, **116**, 129 879).
5 S. Kacker, Z. Jiang and A. Sen, *Macromolecules*, 1996, **29**, 5852.
6 H. A. Klok, M. Schmid, A. S. Abu-Surrah, M. Moller and B. Rieger, *Makromol. Chem. Phys.*, 1997, **198**, 2759.
7 With propene: Z. Jiang, S. E. Adams and A. Sen, *Macromolecules*, 1994, **27**, 2694; S. Bronco, G. Consiglio, R. Hutter, A. Batistini and U. W. Suter, *Macromolecules*, 1994, **27**, 4436; K. Nozaki, N. Sato and H. Takaya, *J. Am. Chem. Soc.*, 1995, **117**, 9911; K. Nozaki, N. Sato, Y. Tonomura, M. Yasutomi, H. Takaya, T. Hiyama, T. Matsubara and N. Koga, *J. Am. Chem. Soc.*, 1997, **119**, 12 779.
8 With aliphatic α-olefins: Z. Jiang and A. Sen, *J. Am. Chem. Soc.*, 1995, **117**, 4455.
9 With styrene derivatives: M. Brookhart, M. I. Wagner, G. G. A. Balavoine and H. A. Haddou, *J. Am. Chem. Soc.*, 1994, **116**, 364; M. Sperrle, A. Aeby, G. Consiglio and A. Pfaltz, *Helv. Chim. Acta.*, 1996, **79**, 1387.
10 Recent publication: S. Kulasegaram and R. J. Kulawiec, *Tetrahedron*, 1998, **54**, 1361.
11 E. Drent, J. A. M. Van Broekhoven and J. M. Doyle, *J. Organomet. Chem.*, 1991, **417**, 235.
12 D. Zargarian and H. Alper, *Organometallics*, 1993, **12**, 712.

Reduction of aldehydes using trialkylboranes in ionic liquids

George W. Kabalka* and Rama R. Malladi

Departments of Chemistry and Radiology, The University of Tennessee, Knoxville, TN 37996-1600 USA. E-mail: kabalka@utk.edu

Received (in Corvallis OR, USA) 1st September 2000, Accepted 25th September 2000
First published as an Advance Article on the web 31st October 2000

Non-aqueous ionic liquids, molten salts, have been found to enhance organoboron mediated reductions of aldehydes.

In recent years, chemists have developed new synthetic methodologies which are environmentally benign.[1] For example, ionic liquids have been found to be useful in many environmentally sensitive industrial applications.[2] More recently, ionic liquids have attracted interest as reaction media in organic and organometallic synthetic manipulations such as hydrogenation,[3] allylation,[4] Heck-vinylation,[5] epoxidation,[6] Diels–Alder reactions,[7] and Suzuki cross-coupling reactions.[8] These solvents possess a number of interesting properties, which include a lack of vapor pressure, ease of reuse, absence of flammability and a tolerance for large temperature variations.

The reduction of aldehydes by organoborane reagents is an important organic transformation. Generally, boron hydrides are utilized as reducing agents due to their facile reactivity.[9] Trialkylboranes, most notably the pinanyl derivatives, have also been found to be especially useful reducing reagents.[10,11] However, reductions involving simple trialkylboranes generally require reaction temperatures in excess of approximately 150 °C.[12] We have discovered that ionic liquids, such as 1-butyl-3-methylimidazolium tetrafluoroborate ([Bmim][BF_4]),[13] 1-ethyl-3-methylimidazolium tetrafluoroborate ([Emim][BF_4]), and 1-ethyl-3-methylimidazolium hexafluorophosphate ([Emim][PF_6]) enhance the rate of trialkylborane reductions. For example, tributylborane reduces benzaldehyde at rt in [Emim][PF_6] although the reaction can be carried out more rapidly at 100 °C (Table 1).

Both aromatic and aliphatic aldehydes are reduced by tributylborane in ionic liquids (Table 2). The presence of a *para*-substituted electron-donating group appears to hinder the reaction. Only one alkyl group is utilized, and thus an equimolar ratio of aldehyde and tributylborane is required. Presumably this is a consequence of the weaker Lewis acidity of the dialkylborinic ester generated after the first reduction, reaction 1.

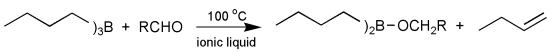

(1)

The fact that the organic products are readily removed from the ionic liquids *via* extraction is especially appealing. We routinely recycled the ionic solvents and found no decrease in reduction yields.

The reduction of benzaldehyde is representative: benzaldehyde (106 mg, 1.00 mmol) and [Emim][PF_6] (250 mg) were placed in a 10 mL round-bottomed flask. Tributylborane (182 mg, 1.00 mmol) was added and the mixture stirred at rt for 48 h. The product was extracted into ether (2 × 5 mL) the extracts were combined and dried over anhydrous $MgSO_4$. The solvent was removed under reduced pressure and then purified by silica gel chromatography to yield 102 mg (94%) of benzyl alcohol.[14]

Table 1 Reduction of benzaldehyde with tributylborane in different ionic liquids

Ionic liquid	Time/h	Yield (%)[c]
[Bmim BF_4]	16[a]	93
[Emim BF_4]	16[a]	90
[Emim PF_6]	16[a]	96
[Emim PF_6]	48[b]	94

[a] Reactions were carried out at 100 °C. [b] Reaction was carried out at rt. [c] Isolated yield.

Table 2 Reduction of aldehydes with tributylborane in [Emim][PF_6]

Aldehydes	Time/h	Yield (%)[c]
C_6H_5CHO	16[a]	100
p-BrC_6H_4CHO	16[a]	100
m-BrC_6H_4CHO	16[a]	100
o-FC_6H_4CHO	16[a]	100
p-FC_6H_4CHO	16[a]	100
p-CH_3OC_4CHO	24[a]	40
o-$CH_3C_6H_4CHO$	16[a]	98
p-$CH_3C_6H_4CHO$	16[a]	96
$C_{10}H_{20}O$	48[b]	100
$C_{10}H_{20}O$	24[a]	100
$(CH_3)_3CCHO$	48[b]	100

[a] Reactions were carried out at 100 °C. [b] Reactions were carried out at rt. [c] NMR yield.

Ionic liquids are excellent solvents in which to carry out reductions using trialkylboranes. The reaction proceeds readily with aromatic and aliphatic aldehydes. Separation of the products from the ionic liquid is straightforward as is recycling of the solvent.

We wish to thank the U.S. Department of Energy and the Robert H. Cole Foundation for support of this research.

Notes and references

1 G. W. Kabalka and R. M. Pagni, *Tetrahedron*, 1997, **53**, 7999.
2 Michael Freemantle, *Chem. Eng. News*, May 15, 2000, 37.
3 P. J. Dyson, D. J. Ellis, D. G. Parker and T. Welton, *Chem. Commun.*, 1999, 25.
4 C. M. Gordon and A. McCluskey, *Chem. Commun.*, 1999, 1431.
5 V. P. W. Bohm and W. A. Hermann, *Chem. Eur. J.*, 2000, **6**, 1017.
6 C. E. Song and E. J. Roh, *Chem. Commun.*, 2000, 837.
7 (*a*) M. J. Earle, P. B. McCormac and K. R. Seddon, *Green Chem.*, 1999, **1**, 23; (*b*) T. Fisher, A. Sethi, T. Welton and J. Woolf, *Tetrahedron Lett.*, 1999, **40**, 793.
8 C. J. Mathews, P. J. Smith and T. Welton, *Chem. Commun.*, 2000, 1249.
9 N. M. Yoon, *Pure Appl. Chem.*, 1996, **68**, 843.
10 M. M. Midland, A. Tramontan and S. A. Zderic, *J. Am. Chem. Soc.*, 1977, **99**, 5211.
11 M. M. Midland, *Chem. Rev.*, 1989, **89**, 1553.
12 B. M. Milkhailov, Yu. N. Bubnov and V. G. Kiselev, *J. Gen. Chem. USSR*, 1966, **36**, 65.
13 J. S. Wilks and M. J. Zaworotko, *J. Chem. Soc., Chem. Commun.*, 1992, 965.
14 In the absence of the molten salt, essentially no reduction occurs.

ChemComm

A possible antimalarial action mode of qinghaosu (artemisinin) series compounds. Alkylation of reduced glutathione by *C*-centered primary radicals produced from antimalarial compound qinghaosu and 12-(2,4-dimethoxyphenyl)-12-deoxoqinghaosu

Dong-Ye Wang and Yu-Lin Wu

State Key Laboratory of Bio-organic & Natural Products Chemistry, Shanghai Institute of Organic Chemistry, Chinese Academy of Sciences, 354 Fenglin Road, Shanghai 200032, China. E-mail: ylwu@pub.sioc.ac.cn

Received (in Cambridge, UK) 23rd August 2000, Accepted 3rd October 2000
First published as an Advance Article on the web 31st October 2000

Antimalarial compound qinghaosu (1) and its phenyl derivative 2 were reacted with reduced glutathione (GSH) and Fe(II/III) to give, besides other known degradation products, an interesting adduct from a primary *C*-centered free radical and GSH. Because GSH plays a very important role in the cell cycle, this finding may eventually lead to a new understanding of its mode of action.

Qinghaosu (artemisinin, **1**) originally isolated from a traditional Chinese herb,[1] and its derivatives are the most promising antimalarial medicines. Their unique 1,2,4-trioxane peroxy

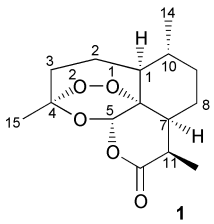

1

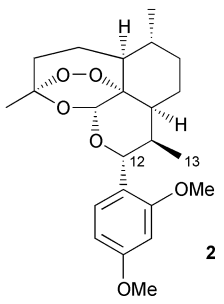

2

structure has been proved to be essential for antimalarial activity[2] and is entirely different from that of previous generations of antimalarial drugs such as quinine and chloroquine. Cell-biological studies showed that qinghaosu's toxicity appeared to be the consequence of the membrane damage that might result from protein alkylation.[3] On the other hand, alkylation of a simplified heme *in vitro* has also been reported,[4] but this does not provide a full description of the antimalarial mechanism of qinghaosu and its derivatives. We have reported the reaction mechanism of the Fe(II)-induced cleavage of the peroxide bond in qinghaosu and its derivatives and certified the presence of *C*-centered radicals derived from this cleavage and the following radical rearrangement.[5,6] At the same time the DNA damage associated with this process has also been observed in our laboratory.[5] A parallel correlation[7] between the chemical reactivity of Fe(II)-induced cleavage of the peroxide in qinghaosu's derivatives and their antimalarial activity *in vivo* and also the intermolecular interaction[8]—abstraction of a hydrogen atom from cysteine and attachment to the cysteine sulfur atom—of the primary *C*-centered radicals involved in the degradation of qinghaosu have been found in our previous work. Continuing these explorations we have synthesized a pair of C-11 epimers of 12-(2,4-dimethoxyphenyl)-12-deoxoqinghaosu (**2**) and found once again the parallel relationship of reactivity of their Fe(II)-induced cleavage and antimalarial activity. In the presence of cysteine and catalytical ferrous or ferric ion a stable product from cysteine and the primary free radical from phenyl qinghaosu **2** could be isolated and identified. These experimental results[9] provided further evidence for the participation of a primary carbon centered free radical in the antimalarial action of qinghaosu compounds.

With the adduct of cysteine and the primary free radical derived from qinghaosu and its derivatives in hand, it would be interesting to observe if an adduct could form from glutathione and this free radical. Malaria parasite infected red cells have a high concentration of the reduced glutathione (GSH, the main reducing agent in physiological systems).[10] It was also reported that an excess GSH in the parasite may be responsible for protecting the parasite from the toxicity of heme.[11] In general, GSH takes part in many biological functions, including the detoxification of cytosolic hydrogen peroxide and organic peroxides and then protects cells from oxidative stress. Therefore, depletion of GSH or inhibiting glutathione reductase in tumor or parasite cell will induce oxidative stress and then kill these cells,[12] which may explain the mechanism of some antitumor or antiparasite agents. In addition, an alternative promising approach to finding new antitumor or antiparasite agents is provided.

Here we report that the *C*-centered radicals of compound **2** and qinghaosu (**1**) can abstract a hydrogen atom from GSH, and, the novel adducts between **2**, **1** and GSH are characterized.

The 12-(2,4-dimethoxyphenyl)-12-deoxoqinghaosu (**2**) prepared from dihydroqinghaosu is a UV detectable, stable, lipophilic and hence easily handled qinghaosu derivative. It is also a more active antimalarial agent than qinghaosu and artermether. Therefore compound **2** was firstly used as the substrate to react with GSH in the presence of catalytic amounts of ferrous sulfate. Thus, a mixture of GSH, AcONa, a catalytic amount of $FeSO_4 \cdot 7H_2O$ and 0.5 equivalents of compound **2** in aq. MeCN was stirred at rt for 3 days. From the organic extract, starting material **2** (20%) and known compounds[9] **3**, **4**, **5**, and **6** (43%, 26%, 2%, and 4%, respectively) were obtained. On the other hand adduct **7**[13] (1%) was isolated from the aqueous layer by column chromatography (RP-C-18) (Scheme 1).

It is reasonable to propose that adduct **7** is formed by coupling the primary *C*-centered free radical and GSH. Adduct **7** gives a typical ESI mass spectrum peak at $m/z = 735$ ($M + Na - 1$) and all the corresponding proton resonances in the NMR spectra. Adduct **7** tends to rearrange to give compound **8** in acidic medium, partial rearrangement could be observed even in deuteriated water in the NMR tube.

The successful isolation of adduct **7** encouraged us to explore the reaction of GSH with qinghaosu–Fe(II/III) and search for the products from both the organic and water phases. The reaction of qinghaosu (**1**) with 2 equivalents of GHS and 0.04 equivalent Fe(II) was performed at 37 °C under argon. After 12 hours all qinghaosu was consumed to yield known compounds **9**[8] (5%), **10**[6] (41%), **11**[6] (26.4%), and **12** (1%, a C-3 epimer of known compound), all collected from the organic phase, and **13**[14] (4%) collected from the aqueous phase of the reaction mixture after work-up (Scheme 2). The reaction also proceeds wider acid conditions in the range pH 1–7, giving slight variations in the yields of **9** and **13**.

The most interesting adduct **13** is a highly polar, water soluble compound, which was recovered from the reaction

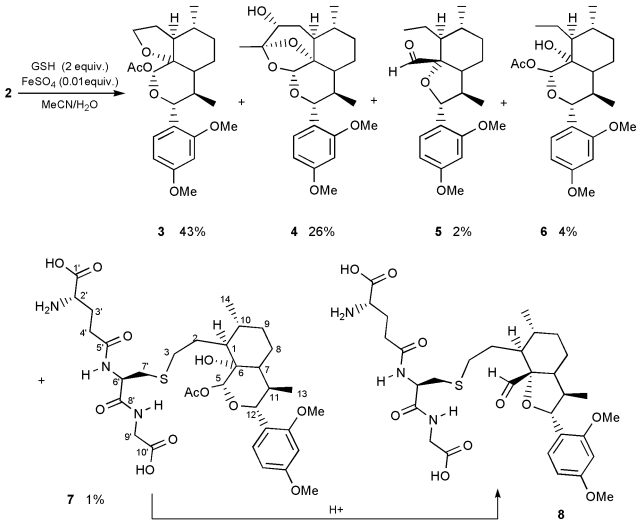

Scheme 1

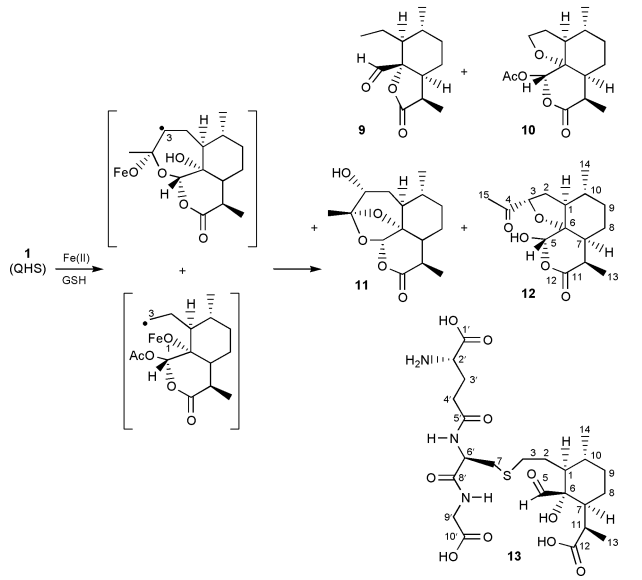

Scheme 2

mixture by chromatography on reverse phase silica gel (RP-C18, H_2O). On thin-layer chromatography (TLC, with 3 : 1 : 1 n-BuOH–AcOH–H_2O) **13** could be visualized by 0.5% ninhydrin in EtOH as a pink spot. The mass spectrum (ESI) exhibited typical peaks at *m/z* 548 $(M + H)^+$, 570 $(M + Na)^+$, and 586 $(M + K)^+$. Its high resolution mass spectrum (SI) exhibited the peaks at *m/z* 570.2090 $(M + Na)^+$, and 592.1916 $(M - H + 2Na)^+$. NMR analyses were performed in D_2O, including ^1H and ^{13}C NMR, DEPT, DQ-COSY, NOESY, HMQC (^1J) and long-range (^3J) proton-carbon correlation (HMBC). Compound **13** showed several cross-peaks (H-7′/H-3, H-6′/H-3) in NOESY and (H-7′/C-3, H-3/C-7′) in HMBC spectrum. The data undoubtedly showed that a σ-bond was present between the sulfur of the glutathione residue and C-3 in the qinghaosu part. Compound **13** was therefore the result of an adduct between primary carbon-radical derived from qinghaosu and GS$^{\cdot}$.

In conclusion, qinghaosu (**1**) and its phenyl derivative **2** could be degraded in the presence of reduced glutathione (GSH) and a catalytical amount of Fe(II/III). Besides known products previously isolated from the reaction of qinghaosu and its derivative with ferrous ion, an interesting adduct from the primary *C*-centered free radical derived from qinghaosu and *S*-centered free radical from GSH was isolated and structurally elucidated by NMR and other spectroscopy. In *Plasmodium* parasite the GSH concentration is maintained by means of the glutathione reductase catalyzed reduction of glutathione disulfide (GSSG) at the expense of NADPH. GSH plays an important role in protecting the parasite from oxidative stress. The formation of a GSH–qinghaosu adduct reduces the amount of GSH and the adduct itself might also cause inhibition of the glutathione reductase in the parasite. Therefore the present finding may lead to a new understanding of the mode of action of these antimalarial drugs.

This work was supported by the Chinese Academy of Sciences (no. KJ951-A1-504-04), the National Natural Science Foundation (no. 29572075, 09561423, 29832020, 39870899), and the Ministry of Science and Technology of China (no. 970211006-6). We also thank Dr Yikang Wu for the helpful discussion.

Notes and references

1 (*a*) J.-M. Liu, M.-Y. Ni, Y.-F. Fan, Y.-Y.Tu, Z.-H. Wu, Y.-L. Wu and W.-S. Chou, *Huaxue Xuebao*, 1979, **37**, 129; (*b*) D. L. Klayman, *Science*, 1985, **228**, 1049; (*c*) A. R. Butler and Y.-L. Wu, *Chem. Soc. Rev.*, 1992, 85.

2 (*a*) Y. Li, P.-L. Yu, Y.-X. Chen, L.-Q. Li, Y.-Z. Gai, D.-S. Wang and Y.-P. Zheng, *Yaoxue Xuebao*, 1981, **16**, 429; (*b*) Y.-L. Wu and Y. Li, *Med. Chem. Res.*, 1995, **5**, 569.

3 S. R. Meshnick, T. E. Taylor and S. Kamchonwongpaisan, *Microbiol. Rev.*, 1996, **60**, 301, and references cited therein.

4 (*a*) A. Robert and B. Meunier, *Chem. Soc. Rev.*, 1998, **27**, 273; (*b*) A. Robert and B. Meunier, *J. Am. Chem. Soc.*, 1997, **119**, 5968.

5 W.-M. Wu, Z.-J. Yao, Y.-L. Wu, K. Jiang, Y.-F. Wang, H.-B. Chen, F. Shan and Y. Li, *J. Chem. Soc., Chem. Commun.*, 1996, 2213.

6 W.-M. Wu, Y.-K. Wu, Y.-L. Wu, Z.-J. Yao, C.-M. Zhou, Y. Li and F. Shan, *J. Am. Chem. Soc.*, 1998, **120**, 3316, and references cited therein.

7 D.-Y. Wang, Y.-K. Wu, Y.-L. Wu, Y. Li and F. Shan, *J. Chem. Soc., Perkin Trans. 1*, 1999, 1827.

8 Y. Wu, Z.-Y. Yue and Y.-L. Wu, *Angew. Chem., Int. Ed.*, 1999, **38**, 2580.

9 D.-Y. Wang, Y.-L. Wu, Y. Wu, J. Liang and Y. Li, *J. Chem. Soc., Perkin Trans. 1*, submitted for publication.

10 H. Atamna and H. Ginsburg, *Eur. J. Biochem.*, 1997, **250**, 670.

11 (*a*) H. Ginsburg, O. Famin, J. Zhang and M. Krugliak, *Biochem. Pharmacol.*, 1998, **56**, 1305; (*b*) O. Famin, M. Krugliak and H. Ginsburg, *Biochem. Pharmacol.*, 1999, **58**, 59.

12 R. H. Schirmer, J. G. Muller and R. L. Krauth-Siegel, *Angew. Chem., Int. Ed. Engl.*, 1995, **34**, 141.

13 Compound **7**: mp: > 210 °C. ^1H NMR (600 MHz, D_2O) δ: 7.37 (d, 1H, J = 7.8 Hz, Ar-H), 6.60 (d, 1H, J = 8.4 Hz, Ar-H), 6.56 (d, 1H, J = 2.4 Hz, Ar-H), 6.15 (s, 1H, H-5), 4.70 (m, 1H, H-12), 4.50 (m, 1H, H-6′), 3.76 (6H, $2OCH_3$), 3.74 (2H, 2H-9′), 3.08 (m, 1H, H-2′), 3.02 (m, 1H, H-7′), 2.80 (m, 1H, H-7′), 2.64 (m, 1H, H-3), 2.57 (m, 1H, H-11), 2.47 (m, 1H, H-3), 2.40 (m, 2H, 2H-4′), 2.22 (m, 1H, H-2), 2.04 (s, 3H, Ac), 1.98 (m, 2H, 2H-3′), 1.78–1.61 (m, 4H, H-9β, H-8α, H-7, H-8β), 1.39 (m, 1H, H-10), 1.26 (m, 1H, H-2), 1.12 (m, 1H, H-1), 1.05 (m, 1H, H-9α), 0.85 (d, 3H, J = 6.6 Hz, CH_3 at C-10), 0.50 (d, 3H, J = 6.6 Hz, CH_3 at C-11); MS (ESI) *m/z*: 779 ($M - 1 + 3Na$), 757 ($M + 2Na$), 735 ($M + 1 + Na$).

14 Compound **13** ^1H NMR (600 MHz, D_2O) δ: 9.98 (s, 1H, CHO), 4.63 (m, 1H, H-6′), 3.85 (m, 3H, 2H-9′ and H-2′), 3.14 (dd, 1H, J = 14.1, 5.1 Hz, H-7′), 2.93 (dd, 1H, J = 14.1, 8.7 Hz, H-7′), 2.62 (m, 4H, 2H-4′, 2H-3), 2.47 (m, 1H, H-11), 2.24 (m, 2H, 2H-3′), 1.98 (m, 1H, H-9ß), 1.82-1.91 (m, 3H, H-10, H-7, H-8α), 1.79 (m, 1H, H-8β), 1.63 (m, 1H, H-2), 1.56 (m, 1H, H-2), 1.39 (m, 1H, H-1), 1.31 (m, 1H, H-9α), 1.16 (d, 3H, J = 7.2 Hz, CH_3 at C-11), 1.04 (d, 3H, J = 6.6 Hz, CH_3 at C-10); ^{13}C NMR (75 MHz, $CDCl_3$) δ: 209.99 (HC=O), 187.32 (C-12), 178.97 (C-10′), 177.59 (C-5′), 176.72 (C-1′), 174.67 (C-8′), 86.01(q, C-6), 56.95 (C-1 or C-2′), 56.86 (C-2′ or C-1), 55.75 (C-6′), 53.45 (C-7), 46.50 (C-11), 46.13 (C-9′), 37.89 (C-10), 37.52 (C-9), 35.44 (C-7′), 34.67 (C-4′ or C-3), 34.11 (C-4′ or C-3), 30.43 (C-2), 28.94 (C-3’ or C-8), 28.88 (C-3′ or C-8), 23.00 (CH_3 at C-1), 20.26(CH_3 at C-11); MS (ESI) *m/z*: 548 ($M^+ + 1$), 570 (M + Na); HRMS (SI) *m/z:* Calcd for $C_{23}H_{37}O_{10}N_3S$ + Na: 570.2092; Found: 570.2090; Calcd for $C_{23}H_{37}O_{10}N_3S - H + 2Na$: 592.1911; Found: 592.1916.

Wittig reactions in the ionic solvent [bmim][BF_4]

Virginie Le Boulaire and René Grée

Laboratoire de Synthèses et Activations de Biomolecules, CNRS UMR 6052, Ecole Nationale Supérieure de Chimie de Rennes, Avenue du Général Leclerc, 35700 Rennes Beaulieu, France. E-mail: rene.gree@ensc-rennes.fr; Tel: (33)(0)2 99 87 13 83; Fax: (33)(0)2 99 87 13 84

Received (in Liverpool, UK) 14th August 2000, Accepted 26th September 2000
First published as an Advance Article on the web 31st October 2000

The ionic salt [bmim][BF_4] is an attractive solvent for Wittig reactions, allowing both easier separation of alkenes from Ph_3PO together with efficient reuse of the solvent.

Ionic liquids are a new class of solvents which have attracted growing interest over the past few years due to their unique physical and chemical properties.[1] They usually consist of poorly coordinating ion pairs, and a classical example is the readily accessible 1-butyl-3-methylimidazolium tetrafluoroborate [bmim][BF_4], which is a colourless mobile but non-volatile liquid with no smell (Fig. 1).[2] Since such solvents easily dissolve metal salts and transition metal catalysts interesting developments have recently appeared in synthesis using organometallic reagents.[3] Some applications of these solvents in organic chemistry have also been reported, for instance in alkylations,[4] benzoin condensation,[5] and Diels–Alder[6] and Friedel–Crafts[7] type reactions. Furthermore, their possible use for selective extraction of organic compounds has been noted recently.[8]

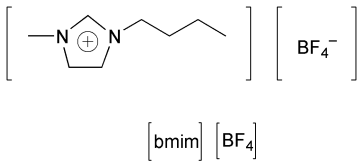

Fig. 1

The Wittig reaction is amongst the most popular methods for C=C bond formation, giving in most cases good to excellent stereocontrol.[9] The separation of the alkene from the by-product (Ph_3PO) is a classical problem: it is usually done by crystallisation and/or chromatography. In this communication we demonstrate the usefulness of the ionic solvent [bmim] [BF_4] as a medium to perform Wittig reactions using stabilized ylides allowing both easier separation of alkenes from Ph_3PO and also the recycling of the solvent. Phosphorane **1a** and benzaldehyde were selected as first models (Scheme 1) to develop this method and study the selectivity in the extraction by appropriate solvents.

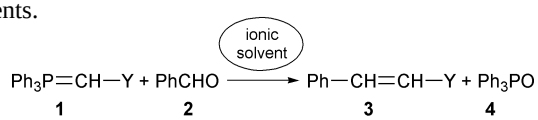

a: Y = COMe; **b**: Y = CO_2Me; **c**: Y = CN

Scheme 1

The reaction was complete in 2.5 h at 60 °C and the results obtained with different solvents are reported in Table 1.†

Table 1 Recovery of **3a** in three different combinations of solvents

	Exp. 1		Exp. 2		Exp. 3	
	Ether[a]	Tol[b]	tBuOME[a]	Tol[b]	Hexane[a]	Tol[b]
3a yield (%)	79	—	87	—	49	41
Ph_3PO yield (%)	21	72	11	78	1	54

[a] First solvent of extraction. [b] Second solvent of extraction.

Extraction of the reaction mixture with Et_2O gave **3a**‡ (79% isolated yield after filtration on a short SiO_2 pad) and Ph_3PO (21%). Further extraction with toluene removed almost completely the residual Ph_3PO and phosphorane.

Careful ^1H and ^{13}C NMR analysis of the ionic solvent after these successive extractions gave no evidence for residual PhCHO and **3a** (less than 2% for both compounds). Only residual **1a** and a small amount ($\approx$5%) of Ph_3PO could be detected. Slightly better results were obtained with tBuOMe as the first solvent (87% of **3a** with only 11% of Ph_3PO). Extraction with hexane was not convenient, even though very little Ph_3PO was obtained in that case.

One of the advantages of ionic solvents is ease of recycling. As indicated in Table 2, such is indeed the case for this Wittig reaction since excellent yields of **3a** were obtained, even after 6 consecutive runs.

Table 2 Reuse of [bmim]BF_4] in the reaction of **1a** + **2**

Run	1	2	3	4	5	6
3a Yield (%)[a]	82	83	86	82	90	91
3a Yield (%)[b]	86	88	93	92	88	92

[a] Extraction with Et_2O. [b] Extraction with tBuOMe.

A more difficult challenge was to reuse the solvent, *but for two different Wittig reactions*. This was established in the following way (Scheme 2): the reaction of **1a** with *o*-tolualdehyde gave **6** in excellent yield (95%). Then, the *same* ionic solvent was used for the reaction of **1a** with benzaldehyde: careful ^1H and ^{13}C NMR analysis of the product isolated in the latter reaction indicated that **3a** was obtained, with no trace ($\leqslant$2%) of **6**.

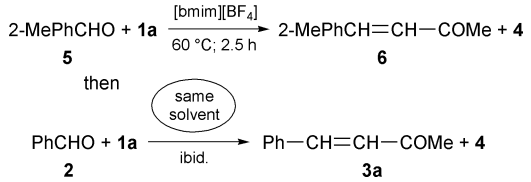

Scheme 2

Other stabilized ylides can also be used the obtain alkenes **3** in good yields (Table 3).

Finally, this method could also be extended to other aldehydes (Table 4). Various aromatic and aliphatic aldehydes,

Table 3 Reaction of phosphorus ylides **1** with **2** in [bmim][BF_4]

Y	**3** Yield (%)	*E*/*Z*[a]
COMe	82	97/3
CO_2Me	90	96/4
CN	79	50/50
CN[b]	66	77/23

[a] Established using ^1H NMR. [b] For comparison, reaction in toluene (60 °C, 2.5 h) was also performed.

DOI: 10.1039/b006666o

Table 4 Reaction of ylide **1a** with different aldehydes in [bmin][BF_4] at 60 °C

RCHO + **1a**		RCH=CHCOMe + Ph_3PO	
R	Time/h	Yield olefin (%)	*E*/*Z*[a]
4-Cl-Ph-	2.5	86	97/3
4-NO_2-Ph	2.5	44[b]	98/2
4-MeO-Ph-	72	82	96/4
2-Me-Ph-	4	95	96/4
Cyclohexyl-	4	80	85/15
C_5H_{11}	12	82	98/2
i-Butyl-	4	84	98/2
(*E*) Ph-CH=CH-	12	86	90/10
(*E*) Me-CH=CH-	12	88	95/5

[a] Established using ^{1}H NMR. [b] Low solubility of this olefin in either.

as well as enals react with **1a** to give corresponding alkenes in good yield and selectivity. In the case of the *para*-nitro derivative however athough the Wittig reaction was complete, the corresponding alkene was isolated in lower yield due to the low solubility of the product in ether. For these stabilized ylides, the *E*-stereoselectivity in the ionic solvent appears at least equivalent, if not better, than the reactions performed in the usual organic solvents.[9] The only exception was **1c** which is a little less selective (see Table 3).

In conclusion, Wittig reactions of stabilized ylides with aldehydes are easily performed in the ionic solvent [bmim][BF_4]. This method offers attractive possibilities for selective extraction of alkenes and Ph_3PO. Furthermore it is possible to efficiently reuse the ionic solvent.

Notes and references

† Representative procedure, preparation of **3a**: a solution of benzaldehyde **2** (0.2 mL, 2 mmol) and phosphorane **1a** (0.689 g, 2.16 mmol) in the [bmim][BF_4] salt (2 mL) was heated at 60 °C, under magnetic stirring, for 2.5 h. The reaction mixture was extracted first with tBuOMe (3 × 3mL) and then with toluene (3 × 3 mL). The extracts were evaporated *in vacuo*. Filtration of the tBuOMe extract on a short SiO_2 pad gave **3a** (0.254 g, 87% yield) and then Ph_3PO (0.061 g, 11% yield). Similarly, the toluene extract yielded Ph_3PO (0.434 g, 78% yield).

‡ All isolated compounds gave spectra (^{1}H and ^{13}C NMR) consistent with indicated structures and in agreement with literature data. For the alkenes, isolated yields refer to the (*E* + *Z*) mixtures.

1 T. Welton, *Chem. Rev*., 1999, **99**, 2071, and references cited therein.
2 P. A. Z. Suarez, J. E. L. Dullius, S. Einloft, R. De Souza and J. Dupont, *Polyhedron*, 1996, **15**, 1217.
3 For recent examples see: P. J. Dyson, D. J. Ellis, D. G. Parker and T. Welton, *Chem. Commun.*, 1999, 25; C. De Bellefon, E. Pollet and P. Grenouillet, *J. Mol. Catal. A*:*Chem.*, 1999, **145**, 121; A. J. Carmichael, M. J. Earle, J. D. Holbrey, P. B. Mc Cormac and K. R. Seddon, *Org. Lett.*, 1999, **1**, 997; V. P. W. Böhm and W. A. Herrmann, *Chem. Eur. J.*, 2000, **6**, 1017; C. E. Song and E. J. Roh, *Chem. Commun.*, 2000, 837.
4 M. J. Earle, P. B. McCormack and K. R. Seddon, *Chem. Commun.*, 1998, 2245.
5 J. H. Davis Jr. and K. J. Forrester, *Tetrahedron Lett.*, 1999, **40**, 1621.
6 M. J. Earle, P. B. McCormac and K. R. Seddon, *Green Chemistry*, 1999, 23, and references cited therein.
7 C. J. Adams, M. J. Earle, G. Roberts and K. R. Seddon, *Chem. Commun.*, 1998, 2087, and references cited therein.
8 J. G. Huddleston, H. D. Willauer, R. P. Swatloski, A. E. Visser and R. D. Rogers, *Chem. Commun.*, 1998, 1765; L. A. Blanchard, D. Hancu, E. J. Beckman and J. F. Brennecke, *Nature*, 1999, **399**, 28.
9 J. March, *Advanced Organic Chemistry, Reactions, Mechanisms and Structure*, Wiley, New York, 4th Edition, 1992, p. 956; J. I. G. Cadogan, *Organophosphorus Reagents in Organic Synthesis*, Acedemic Press, New York, 1979, 17; B. E. Maryanoff and A. B. Reitz, *Chem. Rev.*, 1989, **89**, 863; O. I. Kolodiazhnyi, *Phosphorus Ylides, Chemistry and Application in Organic Synthesis*, Wiley CH, Weinheim, 1999 and references cited therein.

ChemComm

Highly selective formation of 2:2 macrocycles from a novel hydroxybenzaldehyde derivative and diamines†

Hirohiko Houjou, Sung-Kil Lee, Yukio Hishikawa, Yoshinobu Nagawa and Kazuhisa Hiratani*

National Institute for Advanced Interdisciplinary Research, 1-1-4 Higashi, Tsukuba, Ibaraki 305-8562, Japan

Received (in Cambridge, UK) 10th July 2000, Accepted 27th September 2000
First published as an Advance Article on the web 31st October 2000

A hydroxybenzaldehyde derivative which has isobutenyl linkage reacts with a variety of diamines to efficiently result in a 2:2 macrocyclic compound.

Macrocyclic compounds are extensively studied from the viewpoints of molecular recognition, artificial catalyst, supramolecular structures, and so on.[1] In general, their preparation is not very efficient because competitive reactions may occur, resulting in several kinds of oligomeric compounds. In order to selectively obtain a desired macrocycle, researchers have developed several techniques such as template-assisted or preorganization-assisted syntheses combined with the high dilution method. Since the high dilution method is effective only when an individual reaction is fast enough, each reactant needs to have high activity, which must be maintained during a long period of dropwise addition in a carefully assembled apparatus. In spite of such efforts, the yield usually reaches only 30–60% at most.[2] Even if intramolecular hydrogen bonding works well for the preorganization,[3] stepwise syntheses are necessary to achieve a sufficient yield.

In contrast to kinetic control by, for example, the high dilution method, the concept of self-organization or self-assembly could be useful as another way for an efficient preparation of macrocycles if a desired compound is thermodynamically favoured. In this communication, we report on a hydroxybenzaldehyde derivative that reacts with a variety of diamines to give a 2:2 macrocyclic compound in a good yield under relatively mild and simple conditions. Herein we discuss the role of intramolecular hydrogen bonding that controls the direction of functional groups during the cyclisation step.

A procedure to prepare **1** and **2** is shown in Scheme 1. The second step is a tandem Claisen rearrangement,[4] in which an isobutenyl aryl ether is transformed into the corresponding bisphenol compound. By heating **1** at 220 °C for 10 h under reduced pressure, **2** was obtained in 79% isolated yield. Compounds **1** and **2** were recrystallized from ethyl acetate and MeOH, respectively.‡

Fig. 1(a) and (b) show the X-ray crystal structures of **1** and **2**, respectively,§ which provide information about hydrogen bonding in each compound. In **1**, the aldehyde hydrogen is positioned towards the phenolic ether oxygen, indicating a hydrogen bonded pseudo five-membered ring. In **2**, each carbonyl oxygen is positioned towards the neighbouring hydroxy group to form a hydrogen bonded pseudo six-membered ring. These hydrogen bonding structures are reflected in the ^{1}H NMR spectra: the signal of the aldehyde proton of **1** appears at 10.49 ppm, whereas that of **2** appears at 9.88 ppm. The downfield shift of 0.61 ppm in **1** was caused by the hydrogen bond between ether oxygen and aldehyde hydrogen atoms. For **2**, the relatively lowfield signal of phenolic OH proton (11.27 ppm) implies the hydrogen bonding between the hydroxy group and carbonyl oxygen.

THF solutions of **2** (0.1 M) and *p*-phenylenediamine (0.1 M) were mixed and stirred over 30 h at rt. Then, MeOH was slowly

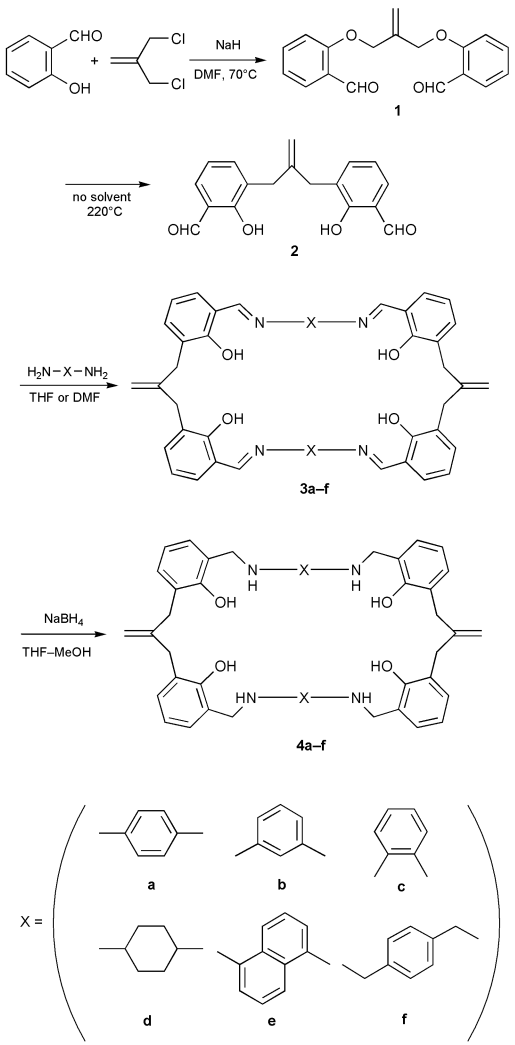

Scheme 1

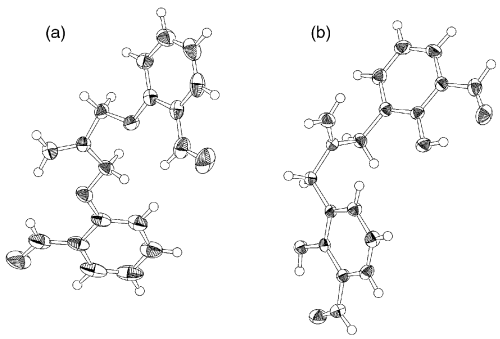

Fig. 1 X-ray crystal structures of (a) **1** and (b) **2**.

† Electronic supplementary information (ESI) available: characterisation data for new compounds. See http://www.rsc.org/suppdata/cc/b0/b005536k/ for crystallographic files in .cif format.

Table 1 The yields (%) of tetraimine (**3a**–**f**) and tetramine (**4a**–**f**) from a variety of diamines (**a**–**f**)

	3a–**f**[a]	**4a**–**f**[b]
a *p*-phenylenediamine	76–89	47–69
b *m*-phenylenediamine	58–64	61–81
c *o*-phenylenediamine	90–97	53–59
d *trans*-1,4-cyclohexanediamine	57–79	87
e naphthalene-1,5-diamine	80–90	70–79
f *p*-xylylenediamine	33	75

[a] Yields of crude solid. [b] Yields of **4a**–**f** from **3a**–**f**.

added to the solution until a yellowish orange solid precipitated (crude yield >80 %). FAB MS and ^{1}H NMR measurements revealed that the solid was 2:2 adduct **3a**, and that the amount of higher oligomeric compounds was too small to accurately determine their structures and yields. Since it was difficult to purify **3a** by recrystallisation or column chromatography due to its low solubility, it was used for the next step after washing with $CHCl_3$. To a THF–MeOH suspension (v/v = 7/3) of **3a** (0.736 g/50 ml), four equiv. of sodium borohydride were added at rt, resulting in cyclic polyamine **4a** as a colorless solid (69 %).‡ Similarly, by using *o*-phenylenediamine, *m*-phenylenediamine, *trans*-1,4-cyclohexanediamine, naphthalene-1,5-diamine, and *p*-xylylenediamine instead of *p*-phenylenediamine, **4b**–**f** were prepared respectively (Scheme 1).‡ In the case of naphthalene-1,5-diamine, DMF was used as solvent in the cyclisation step. In some cases, a catalytic amount of hydrochloric acid was used for the Schiff base formation. The yields are summarized in Table 1.

It is noteworthy that the reaction selectively affords the 2:2 compounds in a relatively concentrated solution. For *p*-phenylenediamine, it is confirmed that a major product in an early stage of this reaction is the linear imine **5** (see Fig. 2) resulting from 1:1 condensation of **2** and the diamine, suggesting that the reaction proceeds as illustrated in Scheme 2. This scheme can be applied to the cases of the other diamines. For aromatic amines (X = **a**, **b**, **c**, and **e**), the Schiff base formation is slow enough so that the reaction can proceed stepwise, resulting in high yields of the 2:2 macrocycles. Similarly, *trans*-1,4-cyclohexanediamine (X = **d**), which has aliphatic amine groups, afforded the 2:2 compound in a good yield. On the other hand, the yield for *p*-xylylenediamine (X = **f**), which also has aliphatic amine groups, was relatively low.

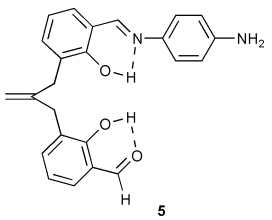

5

Fig. 2 Presumptive hydrogen bonding for *p*-phenylenediamine Schiff base of **2**.

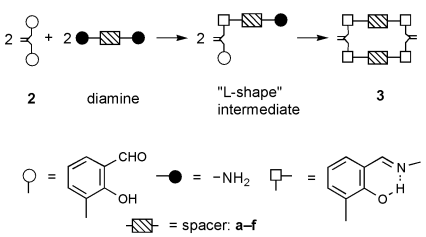

Scheme 2

These results imply that the yield is much affected by the flexibility of the amine rather than its reactivity.

In contrast to **2**, attempts to prepare macrocycles from **1** were not successful. Although the products have not been characterised in detail, the reaction might give a mixture of several oligomeric compounds. Although there is a difference in substitution position between **1** and **2**, these results suggest that the hydroxy groups of **2** play an important role in selectively forming the 2:2 macrocycles.

A typical ^{1}H chemical shift of such an hydroxy group for **3a**–**f** was 13–14 ppm, indicating a strong interaction between the hydroxy and imine groups by making a pseudo six-membered ring even in solution. For **5**, the corresponding ^{1}H NMR peak was observed at 13.88 ppm, indicating similar hydrogen bonding. Such a hydrogen bond can fix this molecule into an 'L-shape' (Fig. 2), and thereby prevents it from making an intramolecular Schiff base linkage to give a 1:1 macrocycle. As shown in Scheme 2, if two L-shaped molecules are present in high concentration, the probability of the formation of 2:2 macrocycles will increase. For the Schiff base of **1**, however, one can not expect so strong a hydrogen bond that the conformational freedom of the molecule is reduced. This would be a reason why a selective macrocyclisation of **1** and diamine is not successful.

In summary, a novel bishydroxybenzaldehyde that we synthesized *via* tandem Claisen rearrangement is a useful building block for preparation of a new series of macrocyclic polyamine compounds. These compounds can be regarded as derivatives of salophane,[5] and therefore are expected to act as good metal ligands. Furthermore, taking advantage of hydrogen bonding interactions, these cyclic salophanes might act as molecular hosts, artificial catalysts, and so on. In fact, recently **4a** has been found to react selectively with *p*-quinones to reduce them into hydroquinones. We will describe an electrochemical study on this system elsewhere.[6]

Notes and references

‡ Compound **1**: ^{1}H NMR (500 MHz, $CDCl_3$): δ 4.80 (s, Ar-O-CH_2-), 5.53 (s, -C(=CH_2)-), 7.02 (d, -O-*Ar*-), 7.07 (t, −O-*Ar*-), 7.55 (m, -O-*Ar*-), 7.84 (m, -O-*Ar*-), 10.49 (s, Ar-C*H*O). Precise MS calcd. for $C_{18}H_{16}O_4$ 296.1048, found 296.1069.

Compound **2**: ^{1}H NMR (500 MHz, $CDCl_3$): δ 3.42 (s, Ar-CH_2-C(=CH_2)), 4.81 (s, -C(=CH_2)-), 6.97 (t, -*Ar*(OH)-), 7.44 (d, -*Ar*(OH)-), 7.44 (d, -*Ar*(OH)-), 9.88 (s, Ar-C*H*O), 11.27 (s, -Ar(O*H*)-). Precise MS calcd. for $C_{18}H_{16}O_4$ 296.1048, found 296.1098.

§ Crystal data for **1**: $C_{18}H_{16}O_4$, *M*w = 296.32, crystal system = monoclinic, space group $P2_1/n$(#14), Z = 4 in a cell of dimensions: a = 7.7307(3), b = 13.7793(6), c = 14.5413(4) Å, β = 101.431(1)°, V = 1519.50(10) Å^3, D_{calcd} = 1.29 g cm^{-3}. The data were collected at −80 °C on a Rigaku RAXIS-RAPID Imaging Plate diffractometer, λ(Mo-Kα) = 0.7107 Å, μ = 0.91 cm^{-1}, 3572 measured and 3427 unique reflections ($2\theta_{max}$ = 55.00, R_{int} = 0.023). R = 0.103, R_w = 0.073.

Crystal data for **2**: $C_{18}H_{16}O_4$, *M*w = 296.32, crystal system = monoclinic, space group $P2_1/a$(#14), Z = 4 in a cell of dimensions: a = 7.9346(4), b = 14.3035(8), c = 13.3949(7) Å, β = 102.18(2)°, V = 1486.0(1) Å^3, D_{calcd} = 1.32 g cm^{-3}. The data were collected at −80 °C on a Rigaku RAXIS-RAPID Imaging Plate diffractometer, λ(Mo-Kα) = 0.7107 Å, μ = 0.93 cm^{-1}, 3555 measured and 3410 unique reflections ($2\theta_{max}$ = 55.00, R_{int} = 0.021). R = 0.085, R_w = 0.078. CCDC 182/1801.

1 J.-M. Lehn, *Supramolecular Chemistry: Concepts and Perspectives*, VHC, Weinheim, 1995.
2 *Macrocycle Synthesis*, ed. D. Parker, Oxford University Press, New York, 1996.
3 F. J. Carver, C. A. Hunter and R. J. Shannon, *J. Chem. Soc., Chem. Commun.*, 1994, 1277.
4 K. Hiratani, K. Kasuga, M. Goto and H. Uzawa, *J. Am. Chem. Soc.*, 1997, **119**, 12 677.
5 D. A. Atwood, *Coordination Chem. Rev.*, 1997, **165**, 267.
6 H. Houjou, S.-K. Lee, Y. Nagawa and K. Hiratani, in preparation.

ChemComm

Toward benign syntheses of pyridines involving sequential solvent free aldol and Michael addition reactions

Gareth W. V. Cave and Colin L. Raston*

Centre for Green Chemistry, School of Chemistry, Monash University, Clayton, Melbourne, Victoria, 3800, Australia. E-mail: c.raston@sci.monash.edu.au

Received (in Cambridge, UK) 13th September 2000, Accepted 27th September 2000
First published as an Advance Article on the web 31st October 2000

Kröhnke type pyridines are readily accessible *via* a sequential solventless aldol condensation and Michael addition involving solid NaOH, followed by treatment with ammonium acetate in acetic acid, as a one pot reaction, which enables both symmetrical and unsymmetrical 2,6-bisaryl substituted pyridines to be isolated in high yield, typically > 75%.

Kröhnke type pyridines[1] and other substituted pyridines including the related terpyridines[2-4] are prominent building blocks in supramolecular chemistry with their π-stacking ability, and directional H-bonding and coordination. In general, conventional methods used in the synthesis of substituted pyridines use volatile organic solvents and display only moderate to low yields.[2,5,6] In developing a more versatile route to such compounds, where possible adopting the principles of 'Green Chemistry',[7] we have established that using solventless conditions involving sequential aldol and Michael addition reactions results in a dramatic improvement in yield, and indeed allows access to a range of compounds not accessible using conventional methods involving organic solvents. Overall, this versatile new approach can be applied to the synthesis of a range of symmetrical and unsymmetrical terpyridines, and pyridines in general bearing aryl groups in the 2, 4 and 6 positions.

The significance of our findings also relates to reducing the use of organic solvents as potentially toxic and hazardous materials,[7] as well as its simplicity and mild conditions, and inherent lower costs, with more likely industrial applications. Moreover, the findings are further credence to challenge the conventional view of using organic solvents in synthesis even in the absence of reasons to do so.[8] The use of solventless reactions is gaining prominence with recent advances in solventless reactions under mild conditions including the aldol condensation,[8–12] and others recently reviewed by Tanaka and Toda.[8]

Synthetic details are summarised in Scheme 1.† In a typical experiment, the benzaldehyde **1** and acetylpyridine **2** analogues were mixed together as liquids with a pestle and mortar in the presence of NaOH. Over a period of *ca*. 10 min constant aggregating, the reaction solidified as the aldol condensation product **3**. For the same reaction using two equiv. of the acetylpyridine **2**, the initial product **3** underwent a Michael addition to form the diketone **4**. The addition of a second acetylpyridine **1** to the condensation product **3** provided a direct route to unsymmetrical diketones. The facile formation of **3** and **4** is essentially quantitative and subsequently does not require isolation from the reaction mixture before the tertiary step whereby the diketone **4** was consequently treated with ammonium acetate in acetic acid to generate the terpyridyl product **5** in high yield, > 75%. The structure of the 4,4″ isomer of **5**, R = OC_8H_{17}, *viz*. 4′-(4-octyloxyphenyl)-4,2′:6′,4″-terpyridine, Fig. 1, has been determined from X-ray diffraction data‡ as a representative of compounds prepared thus far using this new synthetic strategy.

The new method herein has also been applied to a number of analogues including the formation of a series of 2,6-bis(4-iodophenyl)-4-phenylpyridines (**6**), 2,4,6-triphenylpyridines (**7**) and bipyridines (**8**).

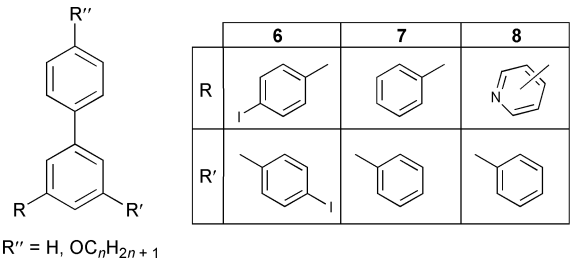

A synthetic route to a diketone similar (pyridine nitrogens in the 2′ position, R = ^{t}Bu) to the intermediate **4** was reported to yield the Michael addition product, *ca*. 40% yield, by reacting two equiv. of 2-acetylpyridine with the *para*-substituted benzaldehye in the presence of NaOH, in EtOH.[13] All of our corresponding reactions, conducted using the solventless conditions described above, were determined to be essentially quantitative by ^{1}H and ^{13}C NMR techniques. This therefore allows the intermediate **4** to be reacted on to form the product **5** and thus dispense with extensive recrystallisation and/or chromatographic purification steps. It is noteworthy that when these solvent based methods are adopted in an attempt to prepare 4′-(4-alkoxyphenyl)-4,2′:6′,4″-terpyridines, only the cyclohexyl product **9** is isolated from the complex reaction mixture which is devoid of target molecules. Compound **9**, which was characterised using NMR data, R = OC_4H_9, and X-ray diffraction data, R = H, does however incorporate the expected intermediate **4**.[14]

Typically unsymmetrical Kröhnke type pyridines have been synthesised by reacting the aldol product **3** with a *N*-[1-oxo-

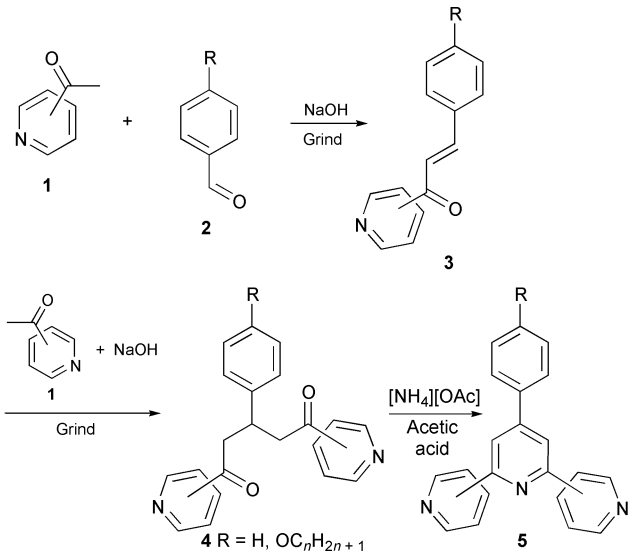

Scheme 1

DOI: 10.1039/b007431o

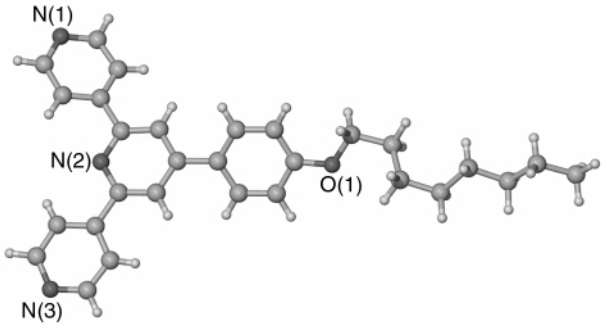

Fig. 1 Molecular structure of 4′-(4-octyloxyphenyl)-4,2′: 6′,4″-terpyridine.

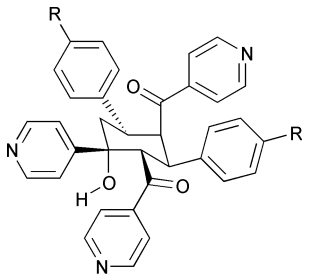

9 R = H, OC_nH_{2n+1}

(2-aryl)ethyl]pyridinium iodide or bromide and ammonium acetate.[2,3] These reactions seldom afford the products in more than a 45% yield, and this coupled with the fact that the pyridinium halide often has to be synthesised can lead to an expensive, time consuming protocol. The versatility of the solventless reactions is demonstrated by the facile inexpensive formation of such unsymmetrical Kröhnke type pyridines as **5** and **8** in high yield.

The above solventless reactions involve the reaction of liquids formed by mixing two organic compounds, at most only one of them being a solid, with the solid intermediate (**3**) reacted with a liquid. At no time was there a reaction of a solid with a solid, athough this is possible given our previous endeavours with solventless aldol condensation involving two organic solids which show that the primary process is the formation of a eutectic mixture with a melting point below rt. This mixture then reacts with the solid NaOH *en route* to the product, rather than two solids reacting through crystal deformation mechanisms.[8,15]

We thank the Australian Research Council for the support of this work, and Michaele Hardie for assistance in the crystallography.

Notes and references

† *Synthesis*: *e.g.* 4′-(4-butyloxyphenyl)-4,2′:6′,4″-terpyridine, **5**: 4-acetylpyridine (3.02 g, 24.9 mmol) and freshly distilled 4-butyloxybenzaldehyde (2.22 g, 12.5 mmol) and NaOH pellets (1.00 g, 25.0 mmol) were crushed together with a pestle and mortar until a pale yellow powder was formed (*ca*. 15 min). [Diketone **5**: MS (ESI+) for $C_{25}H_{26}N_2O_3$ ([*M* + Na]$^+$): calcd: 425.48; found: 425.3. FT-IR: $\nu_{(C=O)}$ 1695 cm^{-1} KBr]. The powder was added to a stirred solution of ammonium acetate (5.00 g, excess) in glacial acetic acid (300 cm^3). The reaction was heated at reflux (2 h), affording a dark green solution. The reaction mixture was neutralised with saturated potassium carbonate, extracted with $CHCl_3$ (3 × 100 cm^3) and dried (magnesium sulfate). All volatiles were removed under *vacuo* yielding a viscous dark green oil. The white product was recrystallised from MeOH. Yield: 3.63 g (76%, 9.53 mmol). Mp 185.2 °C. Anal. found (expected): C 78.58 (78.71), H 5.96 (6.08), N 10.86 (11.02)%. MS (EI+, 70 eV, 200 °C) for $C_{25}H_{23}N_3O$ ([M]$^+$): calcd: 381.47; found: 381.^{1}H NMR (300 MHz, $CDCl_3$, 300.0 K): δ = 8.76 (AA'XX', 4H, pyridine *ortho* to N), 8.04 (AA'XX', 4H, pyridine *meta* to N, *ortho* to trisubstituted pyridine), 7.96 (s, 2H, pyridine *ortho* to phenyl), 7.58 (AA'XX', 2H, phenyl *meta* to OC_4H_9 chain), 7.04 (AA'XX', 2H, phenyl *ortho* to OC_4H_9 chain), 4.04 (t, J = 6.5 Hz, 2H, OCH_2), 1.81 (m, 2H, OCH_2CH_2), 1.52 (m, 2H, CH_2CH_3), 0.99 (t, J = 7.4 Hz, 3H, CH_3). ^{13}C NMR (75 MHz, $CDCl_3$, 300.0 K): δ = 159.62, 154.12, 149.64, 149.42, 145.23, 128.77, 127.29, 120.22, 117.32, 114.32, 66.97, 30.24, 18.23, 12.82. 2,6-bis(4-iodophenyl)-4-phenylpyridines, **6**: the reaction proceeded as above *via* the addition of 4′-iodoacetophenone (3.00 g, 12.2 mmol) and 4-octyloxybenzaldehyde (1.43 g, 6.09 mmol) in the absence of light. The product (**7**) separated as a colourless oil from the acetic acid solution, the analytically pure product solidified on further cooling. Yield: 3.45 g (85%, 5.20 mmol). Mp 120 °C. Anal. found (expected): C 54.08 (54.17), H 4.67 (4.55), N 1.96 (2.04)%. MS (EI+, 50 eV, 200 °C) for $C_{31}H_{31}I_2NO$ ([M]$^+$): calcd: 687.39; found: 688.0. ^{1}H NMR (300 MHz, $CDCl_3$, 300.0 K): δ = 7.89 (AA'XX', 4H, *meta* to I), 7.82 (AA'XX', 4H, *ortho* to I), 7.79 (s, 2H, pyridine), 7.64 (AA'XX', 2H, phenyl *meta* to OC_8H_{17} chain), 7.02 (AA'XX', 2H, phenyl *ortho* to OC_8H_{17} chain), 4.02 (t, J = 7.0 Hz, 2H, OCH_2), 1.85 (m, 2H, OCH_2CH_2), 1.43 (m, 12H, alkyl chain), 0.90 (t, J = 7.4 Hz, 3H, CH_3). ^{13}C NMR (75 MHz, $CDCl_3$, 300.0 K): δ = 198.67, 157.65, 137.90, 137.83, 136.19, 132.82, 129.44, 129.26, 128.82, 114.63, 100.87, 68.08, 40.61, 31.80, 29.35, 29.22, 26.05, 22.64, 14.07.

‡ *Crystallographic data* for 4′-(4-octyloxyphenyl)-4,2′:6′,4″-terpyridine: $C_{29}H_{31}N_3O$ crystals suitable for structural analysis were grown from EtOH. A yellow prism (dimensions 0.18, 0.14, 0.12 mm) was mounted with oil on a thin quartz fiber. The molecular structure is largely unexceptional with an absence of both directional H-bonding and π-stacking of the aromatics. Monoclinic, space group, *C*2/*c*, a = 19.7473(3), b = 10.8189(3), c = 23.8391(7) Å, β = 114.033(1)°, V = 4651.57 Å^3, D_c = 1.2496 g cm^{-3}, Mo-Kα radiation (λ = 0.71073 Å) for Z = 2. Least-squares refinement based on 59925 reflections with $I_{net} > 3\sigma(I_{net})$ (out of 293 unique reflections) led to final value of R = 0.0625.

The intensity data was collected at 123 K using a Enraf-Nonius KappaCCD diffractometer. The structure was solved by direct methods using SHELXS and refined using SHELXL software. Crystallographic data have been deposited with the CCDC (12 Union Road, Cambridge, CB2 1EZ, UK) and are available on request quoting the deposition number CCDC 182/1797). See http://www.rsc.org/suppdata/cc/b0/b007431o/ for crystallographic files in .cif format.

1 F. Kröhnke, *Synthesis*, 1976, 1.
2 F. Neve, A. Crispini and S. Campagna, *Inorg. Chem.*, 1997, **36**, 6150.
3 L. R. MacGillivray, P. R. Diamente, J. L. Reid and J. A. Ripmeester, *Chem. Commun.*, 2000, 359.
4 B. Olenyuk, J. A. Whiteford, A. Frechtenkötter and P. J. Stang, *Nature*, 1999, **398**, 796.
5 M. L. Turonek, P. Moor and W. Errington, *J. Chem. Soc., Dalton Trans.*, 2000, 441.
6 E. C. Constable, P. Harverson, D. R. Smith and L. A. Whall, *Tetrahedron*, 1994, **50**, 7799.
7 *Green Chemistry, Theory and Practice*, P. T. Anastas and J. C. Warner, Oxford University Press, 1998.
8 K. Tanaka and F. Toda, *Chem. Rev.*, 2000, **100**, 1025.
9 F. Toda, K. Tanaka and K. Hamai, *J. Chem. Soc., Chem. Commun.*, 1990, 3207.
10 J. L. Scott and C. L. Raston, *Green Chem.*, 2000, **2**, 49.
11 J. L. Scott, D. R. MacFarlane, C. L. Raston and C. M. Teoh, *Green Chem.*, 2000, **2**, 123.
12 J. L. Scott and C. L. Raston, *Green Chem.*, in press.
13 M. G. B. Drew, P. B. Iveson, M. J. Hudson, J. O. Liljenzin, L. Spjuth, P.-Y. Cordier, A. Enarsson, C. Hill and C. Madic, *J. Chem. Soc., Dalton Trans.*, 2000, 821.
14 G. W. V. Cave and C. L. Raston, unpublished results.
15 G. Rothenberg, A. Downie, C. L. Raston and J. L. Scott, *J. Am. Chem. Soc.*, submitted.

(1*R*,2*S*)-(+)-*cis*-1-Methoxycarbonyl-2-methylcyclobutane

Jacob S. Alexander, John E. Baldwin,* Richard C. Burrell and Karin Ruhlandt-Senge

Department of Chemistry, Syracuse University, Syracuse, New York 13244-4100, USA. E-mail: jbaldwin@syr.edu

Received (in Corvallis, OR, USA) 7th August 2000, Accepted 19th September 2000
First published as an Advance Article on the web 31st October 2000

An X-ray crystallographic structure determination for the related (*R*)-(−)-2-phenylglycinol derived amide demonstrates that (+)-*cis*-1-methoxycarbonyl-2-methylcyclobutane is the (1*R*,2*S*) isomer.

In the course of work requiring synthetically useful amounts of chiral 2-methylcyclobutanecarboxylic acid derivatives of securely known absolute stereochemistry we prepared a sample of (+)-*cis*-1-methoxycarbonyl-2-methylcyclobutane, 99% ee by GC on an Astec 10-m octakis(2,6-di-*O*-pentyl-3-trifluoroacetyl) γ-cyclodextrin capillary column. The observed rotation of our sample, $[\alpha]_D$ +58 ($CHCl_3$), seemed hardly consistent with a report[1] that the (+)-enantiomer of this ester of better than 97% ee had a rotation of $[\alpha]_D$ +22.4 ($CHCl_3$). An X-ray crystallographic structure determination[2] for the corresponding amide (**2**) derived from (*R*)-(−)-2-phenylglycinol quickly settled the stereochemical point (Scheme 1, Fig. 1).

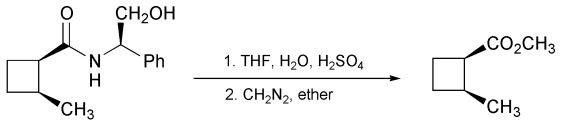

2 (1*R*,2*S*)-(+)-**1**

Scheme 1

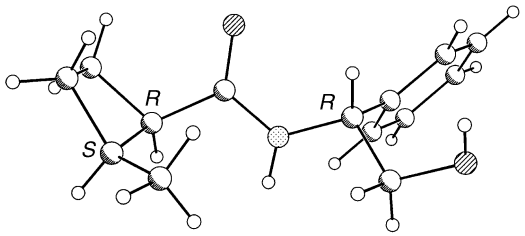

Fig. 1 X-ray crystallographic structure based drawing of *N*-[(*R*)-α-(hydroxymethyl)benzyl]-(1*R*,2*S*)-*cis*-2-methylcyclobutanecarboxamide (**2**).

The relative stereochemistry provided by the X-ray structure and the known absolute stereochemistry of the (*R*)-phenylglycinol unit[3] provide unambiguous evidence for a sure assignment of absolute stereochemistry: (+)-*cis*-1-methoxycarbonyl-2-methylcyclobutane, $[\alpha]_D$ +58 ($CHCl_3$), is (1*R*,2*S*)-(+)-**1**.

The earlier assignment of (1*S*,2*R*) absolute stereochemistry for (+)-**1**[1] must be reversed, and some assignments of absolute stereochemistry for related structures need to be reconsidered. The concerns are of more than academic interest, for structural correlations leading to configurational assignments based on links to (1*R*,2*S*)-(+)-**1** extend to numerous natural products as well as patented analogs of leukotriene, oxetanocin A, prostaglandins, and spermine.[4]

The original stereochemical assignment depended on a structural correlation from the bicyclic lactone (1*S*,5*R*)-(+)-**3** to (+)-**1** (Scheme 2). A sample of (+)-**3**, $[\alpha]_D$ +116.7 ($CHCl_3$), was combined with HBr in CH_3OH to give *cis*-1-methoxycarbonyl-2-(bromomethyl)cyclobutane; reduction of the CH_2Br group to CH_3 with Bu_3SnH gave (+)-**1**, $[\alpha]_D$ +22.4 ($CHCl_3$), in 97% yield.[1] Since the stereochemical correlation of Scheme 2 leads

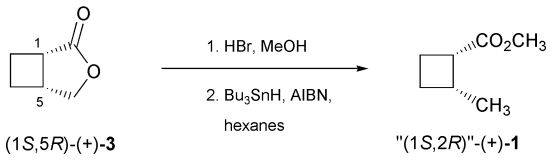

(1*S*,5*R*)-(+)-**3** "(1*S*,2*R*)"-(+)-**1**

Scheme 2 Reported[1] structural correlation.

to the wrong assignment of absolute sterechemistry for (+)-**1**, either the stereochemical assignment for (+)-**3** must be reversed, or the synthetic chemistry involved must, somehow, be misformulated.

The reference compound (+)-**3** had been assigned (1*S*,5*R*) stereochemistry based on a correlation with a chiral sample of *trans*-1,2-di(hydroxymethyl)cyclobutane (Scheme 3).[5] Lactone (+)-**3** ($[\alpha]_D$ +118.7 ($CHCl_3$), 100% ee) was hydrolyzed and epimerized to afford a *trans*-2-(hydroxymethyl)cyclobutanecarboxylic acid as a viscous oil, $[\alpha]_D$ −32.4 ($CHCl_3$), in 52% yield.[5] Reduction gave "(1*R*,2*R*)"-(−)-**5**, $[\alpha]_D$ −4.8 (EtOH), in 97% yield. The literature cited for the "(1*R*,2*R*)" *trans*-diol reported $[\alpha]_D$ −4.3 (EtOH),[6] a seemingly fair match. The reference diol (−)-**5** was thought to be essentially 100% ee, based on criteria related to circular polarization of luminescence;[7] it was derived from (−)-*trans*-cyclobutane-1,2-dicarboxylic acid,[7] a compound of securely known (1*R*,2*R*) absolute stereochemistry.[8]

In the published account of the conversion of (−)-*trans*-cyclobutane-1,2-dicarboxylic acid to the "(1*R*,2*R*)" *trans*-diol,[7] no sign of rotation for the diol was cited[9,10] Reduction of (1*S*,2*S*)-(+)-*trans*-cyclobutane-1,2-dicarboxylic acid ($[\alpha]_D$ +156.4 (H_2O)) with $LiAlH_4$ gives (1*S*,2*S*)-(−)-**5**, $[\alpha]_D$ −67.1 (benzene).[11] In an independent study, the (1*R*,2*R*)-(−)-diacid was reduced to (1*R*,2*R*)-(+)-**5**, $[\alpha]_D$ +64 (benzene).[12]

The chemical correlation steps in Scheme 3 apparently involve a great loss of optical purity. For *trans*-diol "(1*R*,2*R*)"-(−)-**5** $[\alpha]_D$ −4.8 (EtOH) was reported,[5] far from the value more recently determined for the (1*S*,2*S*) isomer, $[\alpha]_D$ −67.1 (benzene).[11] The base-catalyzed reaction in Scheme 3, conducted with conc. aq. NaOH in a stainless steel tube at 130 °C over 8 days,[5] may well have involved more than a simple epimerization at C1 adjacent to the carboxylic acid (carboxylate anion) function.[13]

Given the poor preservation of stereochemical integrity and the faulty reference sample employed, the synthetic steps in Scheme 3 cannot provide a sure designation of configuration for lactone (+)-**3**. Nevertheless we believe that lactone (+)-**3** is indeed the (1*S*,5*R*) isomer, even though the original grounds for the assignment now appear to be indecisive, since it has been converted through a rational synthetic sequence to a sample of enantiomerically pure (+)-grandisol.[14]

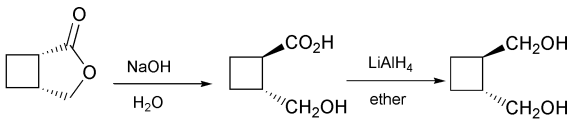

(+)-**3** "(1*R*,2*R*)"-(−)-**4** "(1*R*,2*R*)"-(−)-**5**

Scheme 3 Reported[5] correlation of (+)-**3** with *trans*-diol (−)-**5**.

DOI: 10.1039/b006639g

A related stereochemical puzzle is posed by various reports of pig liver esterase (ple) catalyzed hydrolyses of *cis*-1,2-di(methoxycarbonyl)cyclobutane (Scheme 4): the reported $[\alpha]_D$ values of the ester-acid products are −3.6 ($CHCl_3$),[15] −3.0 ($CHCl_3$),[16] +1.6 ($CHCl_3$),[17] +2.7 (EtOH)[18] and +4.4 (EtOH).[19]

Correlations establishing the absolute stereochemistry of ester-acid **6** are outlined in Scheme 4. A levorotatory sample of **6** ($[\alpha]_D$ −3.0 ($CHCl_3$)) was converted as shown to (+)-**3**, $[\alpha]_D$ +106.7 ($CHCl_3$), estimated to be of 97% ee.[16] Thus the assignment is (1*R*,2*S*)-**6**. A dextrorotatory sample of **6** ($[\alpha]_D$ +4.4 (EtOH)) was correlated with (1*S*,2*S*)-(+)-1,2-di(methoxycarbonyl)cyclobutane,[8] (1*S*,2*S*)-(+)-**7** (86% ee by chiral GC; $[\alpha]_D$ +120 (acetone), +119 ($CHCl_3$)), confirming the assignment (1*R*,2*S*)-**6**.[19]

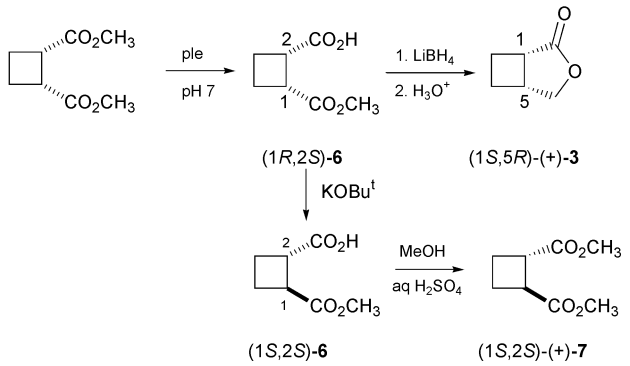

Scheme 4 Correlations[16,19] of (1*R*,2*S*)-**6** with lactone (+)-**3** and diester (+)-**7**

We believe that all enantioselective ple-catalysed hydrolyses of *cis*-1,2-di(methoxycarbonyl)cyclobutane favor formation of (1*R*,2*S*)-(−)-**6**, and that its specific rotation is small. During hydrolyses and isolation procedures a base-catalysed epimerization might occur to a small extent, converting *cis* product (1*R*,2*S*)-(−)-**6** to *trans* ester-acid (1*S*,2*S*)-(+)-**6** having a much larger specific rotation.[8] A minor amount of (1*S*,2*S*)-(+)-**6** in a product mixture might well escape detection and yet have a major impact on the observed specific rotation.

Accordingly, samples of **6** having $[\alpha]_D$ −3.0 ($CHCl_3$)[16] and $[\alpha]_D$ +4.4 (EtOH)[19] are not enantiomeric:[19] both samples are more likely to be largely (1*R*,2*S*)-(−)-**6**, containing different, small, easily overlooked amounts of (1*S*,2*S*)-(+)-**6**. Similarly, samples of **6** with reported $[\alpha]_D$ values of +1.6 ($CHCl_3$)[17] and −1.8 ($CHCl_3$)[20] are not enantiomeric, and the stereochemical assignment "(1*S*,2*R*)"-(−)-**6** suggested by Lukas[20] must be reversed. The "(1*S*,2*R*)"-(−)-**6** sample was obtained from (1*R*,2*S*)-(+)-1-(methoxycarbonyl)cyclobut-3-ene-2-carboxylic acid[21] through a catalytic hydrogenation and correlated with an enantiomer of **3** that could only be formed from (1*R*,2*S*)-**6**.[20]

The present work establishes that (+)-**1** is the (1*R*,2*S*) isomer. We believe that (+)-**3** is (1*S*,5*R*), and that all ple hydrolyses of *cis*-1,2-di(methoxycarbonyl)cyclobutane give predominantly (1*R*,2*S*)-(−)-**6**, in spite of reports of variable and sometimes positive $[\alpha]_D$ values, for under the reaction conditions small amounts of (1*S*,2*S*)-(+)-**6** may be formed.

We thank the National Science Foundation for support through CHE-9532016, CHE-9902184 and CHE-9527898; Syracuse University, and the W. M. Keck Foundation; and C. L. Habraken (University of Leiden) for helpful correspondence.

Notes and references

1 E. J. Toone and J. B. Jones, *Tetrahedron: Asymmetry*, 1991, **2**, 207.

2 *Crystal data* for **2**: $C_{14}H_{19}NO_2$, M_r = 233.30 g mol^{-1}, crystals (mp 138–139 °C) from hexanes–ethyl acetate, colorless plates of dimensions 0.80 × 0.50 × 0.28 mm^3. Mo-Kα (0.71073 Å), 95 K. Tetragonal, space group $P4_12_12$, a = 9.4318(2), c = 27.989(1) Å, V = 2489.87(10) Å^3, Z = 8. ρ calc. 1.245 g cm^{-3}, μ Mo = 0.083 mm^{-1}, 3070 independent reflections ($2.28 < \theta > 28.29$), R_1 (all data) = 0.0347, wR_2 (all data) = 0.0770. CCDC 182/1807. See http://www.rsc.org/suppdata/cc/b0/b006639g/ for crystallographic files in .cif format.

3 *Dictionary of Organic Compounds*, 6th Ed.; exec. ed. J. Buckingham and F. Macdonald, Chapman & Hall, Cambridge University Press, New York, 1996, Vol. 1, p. 371, A-0-03421. (*R*)-(−)-2-Phenylglycinol as obtained from Aldrich had $[\alpha]_D$ −29 (1 M HCl), a value close to the specific rotation given on the label, $[\alpha]_D$ −31.7 (1 M HCl).

4 *Inter alia*: W. Skuballa, B. Buchmann, J. Heindl, W. Froehlich, R. Ekerdt and C. Giesen, *Ger. Offen.*, DE 4,108,351, 17 Sept 1992 (*Chem. Abstr.*, 1993, **118**, P59492v); *Ger. Offen.*, DE 4,127,193, 18 Feb 1993 (*Chem. Abstr.*, 1993, **119**, P8671r); M. E. Jung and A. W. Sledeski, *J. Chem. Soc., Chem. Commun.*, 1993, 589; W. D. Woessner, C. J. Sih, H. C. Kluender, H. C. Arndt and W. G. Biddlecom, *Ger. Offen.*, 2,705,613, 18 Aug 1977 (*Chem. Abstr.*, 1978, **88**, P6406a); V. K. Reddy, A. Valasinas, A. Sarkar, H. S. Basu, L. J. Marton and B. Frydman, *J. Med. Chem.*, 1998, **41**, 4723; B. J. Frydman, L. J. Marton, V. K. Reddy, A. L. Valasinas and D. T. Witiak, *US Pat.*, 5,889,061, 30 Mar 1999 (*Chem. Abstr.*, 1999, **130**, P252086s).

5 I. J. Jakovac, H. B. Goodbrand, K. P. Lok and J. B. Jones, *J. Am. Chem. Soc.*, 1982, **104**, 4659.

6 J. C. A. Windhorst, *PhD Thesis*, 1975, Rijksuniversiteit Te Leiden, The Netherlands, p. 28; cited in ref 5.

7 J. C. A. Windhorst, *J. Chem. Soc., Chem. Commun.*, 1976, 331.

8 Y. Inouye, S. Sawada, M. Ohno and H. M. Walborsky, *Tetrahedron*, 1967, **23**, 3237; J. A. Berson and P. B. Dervan, *J. Am. Chem. Soc.*, 1973, **95**, 267, and refs. therein; W. von E. Doering and A. R. Mastrocola, *Tetrahedron*, 1981, **37**, Suppl. 1, 329.

9 *Atlas of Stereochemistry*, 2nd Ed., ed. W. Klyne and J. Buckingham, Oxford University Press, New York, 1978, Vol. 2, p. A31'.

10 *Dictionary of Organic Compounds*, 6th Edn., exec. ed. J. Buckingham and F. Macdonald, Chapman & Hall, Cambridge University Press, New York, 1996, Vol. 2, p. 1604, C-0-04032.

11 J.-J. Brunet, A. Herbowski and D. Neibecker, *Synth. Commun.*, 1996, **26**, 483.

12 P. Aviron-Violet, Y. Colleuille and J. Varagnat, *J. Mol. Catal.*, 1979, **5**, 41.

13 'Based on the new configurational assignment of (+)-**1**, Professors Jones and Toone speculate that in the vigorous conditions required in their correlation, the C-1 center epimerized to some degree, either during the acid-catalyzed ring opening of cyclobutane lactone (+)-**3**, or from hydrogen atom migration to give a tertiary radical in the subsequent tin hydride mediated reduction step (reactions ii and iii of Scheme 1 of ref. 1), giving compound **1** with an invalid sign of rotation. They also note that the active site model interpretation of the ple-catalyzed hydrolysis of (±)-**1** must be revised, with the cyclobutyl ring occupying the H_L site. They suggest that this interesting, and unexpected, situation is dictated by the fact that the previously anticipated preferred binding of **1** depicted in Fig. 2 of ref. 1 is less favorable than having BOTH the hydrophobic groups binding in hydrophobic sites. This extra benefit is achievable with the cyclobutyl group of the (1*R*,2*S*)-**1** substrate located in the H_L site and the methyl group in the H_S site, which is then in accord with a (1*S*,2*R*) configuration for the recovered ester **1**, as required by the present study. They feel that this preferred binding mode is a special case elicited by the particular substitution pattern of **1**, and do not expect this intriguing facet of ple specificity to apply to substrates with larger hydrophobic group differences.' (J. B. Jones, private communication).

14 J. B. Jones, M. A. W. Finch and I. J. Jakovac, *Can. J. Chem.*, 1982, **60**, 2007.

15 M. Martin-Vila, C. Minguillon and R. M. Ortuno, *Tetrahedron: Asymmetry*, 1998, **9**, 4291.

16 G. Sabbioni, M. L. Shea and J. B. Jones, *J. Chem. Soc., Chem. Commun.*, 1984, 236; G. Sabbioni and J. B. Jones, *J. Org. Chem.*, 1987, **52**, 4565; L. K. P. Lam, C. M. Brown, B. De Jeso, L. Lym, E. J. Toone and J. B. Jones, *J. Am. Chem. Soc.*, 1988, **110**, 4409.

17 M. Schneider, N. Engel, P. Hönicke, G. Heinemann and H. Görisch, *Angew. Chem., Int. Ed. Engl.*, 1984, **23**, 67.

18 P. Mohr, N. Waespe-Sarcevic, C. Tamm, K. Gawronska and J. K. Gawronski, *Helv. Chim. Acta*, 1983, **66**, 2501.

19 Y. N. Ito, X. Ariza, A. K. Beck, A. Bohác, C. Ganter, R. E. Gawley, F. N. M. Kühnle, J. Tuleja, Y. M. Wang and D. Seebach, *Helv. Chim. Acta*, 1994, **77**, 2071.

20 K. L. Lukas, *Ger. Offen.*, DE 86-3,613,312, 1987 (*Chem. Abstr.*, 1988, **109**, P6399c. Available through http://dips-2.dips.org/

21 I. Harvey and D. H. G. Crout, *Tetrahedron: Asymmetry*, 1993, **4**, 807.

ChemComm

Energy transfer cassettes based on BODIPY® dyes†

Armin Burghart,[a] Lars H. Thoresen,[a] Jiong Chen,[a] and Kevin Burgess,*[a] Fredrik Bergström[b] and Lennart B.-Å. Johansson[b]

[a] *Department of Chemistry, Texas A & M University, PO Box 30012, College Station, TX 77842-3012*
[b] *Department of Chemistry: Biophysical Chemistry, Umeå University, S-901 87 Umeå, Sweden*

Received (in Corvallis, OR) 16th August 2000, Accepted 8th September 2000
First published as an Advance Article on the web 31st October 2000

The donor–acceptor dye cassettes 1–4 were designed to capture energy at a single wavelength and to convert it to well-resolved, intense fluorescence emissions; in practice, Stokes' shifts of 40–148 nm, quantum yields of 0.12–0.60, and efficient energy transfer was demonstrated.

Many biological experiments involve irradiating sets of different fluorescent labels with a single excitation source.[1,2] To be effective in such multiplexing experiments, dyes must give fluorescence emission peaks that are both well resolved and intense. These requirements place conflicting demands on the labels. Having sets of dyes that emit close to the excitation wavelength causes resolution problems, while including dyes that emit far from the excitation wavelength gives loss of intensity. In response to this problem, radiationless electronic energy transfer has been used to improve resolution and/or intensities in multiplexing.[3] Systems which exploit this characteristic relay energy from a donor-dye (that absorbs at relatively short wavelengths) to an acceptor-dye that fluoresces at longer wavelengths. Experimentally, it is most convenient if the donor and acceptor components of such systems are introduced simultaneously as a single unit, *i.e.* in an "energy transfer cassette". A challenge in this emerging field[3] is to form cassettes that circumvent the limitations of the classical fluorescein–rhodamine systems (*e.g.* resolution, pH dependence, gel mobility shifts). To address this issue, our group is preparing cassettes wherein the donors and acceptors are linked *via* rigid conjugated linkers that allow radiationless electronic energy transfer through bonds (Dexter and superexchange mechanisms) and/or through-space (Förster mechanism).[4] This communication describes synthesis and spectroscopic studies of new cassettes based on the 4,4-difluoro-4-bora-3a,4a-diaza-*s*-indacene (BODIPY®) dyes shown below.

To access the cassettes, iodoaryl-substituted BODIPY®s were prepared[5,6] then transformed into the corresponding alkynes by Sonogashira couplings (trimethylsilylethyne, cat. $Pd(PPh_3)_4$, CuI, NEt_3, THF; then removal of the silane, Bu_4NF, THF, −78 °C, 10 min). Invariably, the yields for these two reactions were very high (up to 99%). Sonogashira reactions were also used to assemble the cassettes from the BODIPY® starting materials. Scheme 1 outlines a synthesis of a linear cassette **1**. The branched derivatives **2**–**4** were obtained *via* similar sequences featuring Sonogashira couplings.

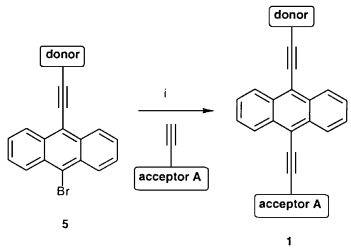

Scheme 1 *Reagents and conditions*: i, cat. $Pd(PPh_3)_4$, CuI, DABCO, toluene, 80 °C, 26 h (51%).

Cassette **1** was prepared mainly to assess its spectroscopic properties; it does not have a functional group that could be conveniently used to link to a biomolecule. A succinimide ester was incorporated into cassette **2** so that, in subsequent work, this dye could be used as a label. Activated esters of aromatic acids, however, are less active than their aliphatic analogs, hence cassettes **3** and **4** were functionalized with glycine attachment points. These variations have no effect on the spectroscopic properties of the dyes reported in this communication; this discussion is only included here to explain how these differences between the structures are consistent with the overall direction of this project.

Table 1 summarizes some light spectroscopic properties of the cassettes dissolved in $CHCl_3$. Using EtOH as the solvent had little effect (a few nm blue-shift relative to $CHCl_3$) on the position and band shape of the fluorescence and absorption spectra (data not shown). The UV absorption spectra of the cassettes resemble those that would be obtained by superimposing the donor and acceptor spectra, indicative of two independent dye fragments. However, when irradiated at the absorption maxima of the donor, the donor fluorescence is almost completely quenched. Thus energy is absorbed at wavelengths corresponding to the donor fragment and emitted at wavelengths governed by the acceptor part, hence large *pseudo*-Stokes' shifts result. Förster radii of the cassettes were determined and found to be significantly greater than the calculated donor–acceptor distances, hence the calculated energy transfer efficiencies were high.[7,8] Experimentally, it was shown that the energy transfer efficiencies (E_{expt}) were very high, meaning the cassettes are very effective. These are slightly

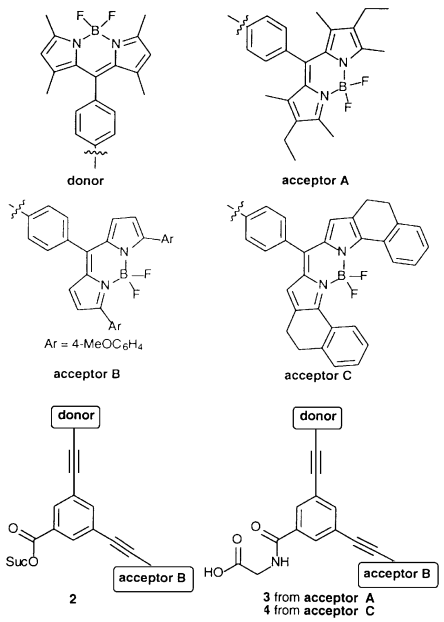

† Electronic supplementary information (ESI) available: absorption and emission spectra of donor and acceptor A and of **1** and experimental details for the spectroscopic measurements. See http:www.rsc.org/suppdata/cc/b0/b006769p/

DOI: 10.1039/b006769p

Table 1 Selected light spectroscopic data for compounds **1**–**4**

Parameter[a]	Compound (in $CHCl_3$) **1**	**2**	**3**	**4**
$\lambda_{max\ abs}$ of donor in cassette/nm	504	504	504	504
$\varepsilon_{max} \times 10^{-3}$ ($mol^{-1}\ dm^3\ cm^{-1}$)	75.8 (donor) 46.3 (acc.)	75.8 (donor) 54.1 (acc.)	75.8 (donor) 46.3 (acc.)	75.8 (donor) 115 (acc.)
$\lambda_{max\ em}$ of acceptor in cassette/nm	544	632	545	652
Pseudo-Stokes' shift/nm	40	128	41	148
Förster radii/Å[b]	50.0 ± 1.0	47.2 ± 1.0	50.0 ± 1.0	39.4 ± 1.0
Calc. donor–acceptor distance/Å[c]	24.5	19.9	19.9	19.9
Calc. energy transfer efficiency[d]	0.982	0.994	0.996	0.983
Expt. energy transfer efficiency[e]	0.968	0.936	0.941	0.946
Fluorescence quantum yield[f]	0.54	0.15	0.58	0.42
Fluorescence quantum yield[g]	0.60 ± 0.03	0.12 ± 0.02	0.56 ± 0.03	0.41 ± 0.03

[a] Additional data (not shown here) was obtained on the donor and acceptor fragments A–C as the corresponding aryl iodides to calculate some of the parameters listed. [b] Calculated from molar absorptivity of the acceptor and corrected fluorescence spectrum of the donor *via* a literature procedure;[8] the κ^2-values (average angular dependence of dipole–dipole coupling in the dynamic limit) used were 0.5 for **1** and 0.665 for **2**–**4**.[10] [c] Estimated using standard bond lengths. [d] From Förster theory as described; uncertainties of the values are within 0.010.[11] [e] From steady-state fluorescence and absorption measurements; uncertainties of the values are within 0.010.[11] [f] From $\phi^{DA} = \phi^{A}E_{expt}(\tau^{A,DA})(\tau^{A})^{-1}$ where $\tau^{A,DA}$ and τ^{A} denote the fluorescence lifetime of the acceptor in the presence and absence of the donor, respectively. [g] Determined using fluorescence and absorption spectra.[9] As references of fluorescence quantum yields were used; *N*,*N*′-bis(1-hexylheptyl)-3,4:9,10-perylene-bis(dicarboximide) in CH_2Cl_2 (Φ = 0.99[12]), 3,3′,4,4′-difluoro-1,3,5,7-tetramethyl-4-borata-3a-azonia-4a-aza-*s*-indacene in MeOH (Φ = 0.94[13]) and Cresyl violet in MeOH (Φ = 0.54[14]).

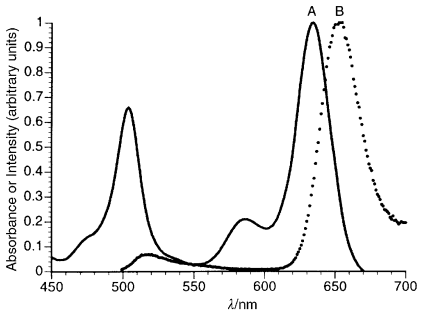

Fig. 1 Absorption ——— (A) and emission •••••• (B) spectra for cassette **4**.

lower than the calculated values, perhaps because the calculations assume energy transfer *via* the dipole–dipole coupling mechanism, which is not a good approximation when distances of interaction are compatible with the molecular size.[7] For all systems studied, the fluorescence decays were not perfectly well described by a single exponential function. Instead bi-exponential fits were found to be acceptable (data not shown). Weighted residuals, reduced χ^2 parameter and the Durbin-Wattson parameter judged upon the goodness of fit. Values considered acceptable were, of the reduced χ^2 parameter < 1.2 and of the Durbin-Wattson parameter > 1.7. The origin to the non-exponential relaxation is not known, but a possible explanation could be connected to a non-homogeneous distribution of the mutual donor and acceptor orientations. Average fluorescence lifetimes varied from 0.9 to 4.2 ns. The fluorescence quantum yields upon exciting the donor (Φ^{DA}) were calculated in two ways for the cassettes, namely; from fluorescence lifetime data (see table text) and by using fluorescence and absorption spectra.[9] The corresponding fluorescence quantum yields (Table 1) are lower than those of the acceptor fragments (data not shown). The fact that there is also a discrepancy in fluorescence lifetimes may partly be assigned to non-radiative processes, other than the Förster mechanism. Despite this, the energy transfer efficiencies are high.

Data from cyclic voltammetry studies demonstrated that the donor and acceptor parts of the cassettes do not communicate electronically in the ground state. For example, cassette **4** displays four distinct redox waves (in CH_3CN at 100 mVs^{-1}, glassy carbon electrode). These are two oxidative ($E_{1/2}$ = +0.62 and +0.78 V *vs.* ferrocene), and two reductive ($E_{1/2}$ = −1.19 and −1.52 V) waves; all four of which can be assigned to redox processes of the single dye portions. This confirms the conclusion from the spectroscopic studies that the donor and acceptors behave as distinct entities, rather than a unified, conjugated system.

In conclusion, this work shows that the BODIPY® fluorophores conjugated in cassettes **1**–**4** exhibit extremely high energy transfer from the donor to the acceptor giving enhanced resolution and intensities for the system when irradiated at the donor absorption maxima. The *pseudo*-Stokes' shifts for the dyes vary between 40 and 148 nm, and their quantum yields are from 0.12 to 0.60. It appears that in these systems *para* or *meta*-orientations (*cf.* **1** and **3**) make no significant difference. Even though these dyes have donor and acceptor fragments that are connected *via* a conjugated linker, steady-state and time-resolved fluorescence measurements are consistent with highly efficient energy transfer according to the Förster mechanism alone.

We thank Ben Lane for running the ^{11}B NMR spectra for this study. Financial support for this work was provided by the NIH (HG01745), The Swedish Natural Science Research Council (NFR K6501981724/2000), The Kempe Foundation, and The Robert A. Welch Foundation.

Notes and references

1 S.-C. Hung, R. M. Mathies and A. N. Glazer, *Anal. Biochem.*, 1997, **252**, 78.
2 S.-I. Kawahara, T. Uchimaru and S. Murata, *Chem. Commun.*, 1999, 563.
3 L. G. Lee, S. L. Spurgeon, C. R. Heiner, S. C. Benson, B. B. Rosenblum, S. M. Menchen, R. J. Graham, A. Constantinescu, K. G. Upadhya and J. M. Cassel, *Nucleic Acids Res.*, 1997, **25**, 2816.
4 S. Speiser, *Chem. Rev.*, 1996, **96**, 1953.
5 A. Burghart, H. Kim, M. B. Welch, L. H. Thoresen, J. Reibenspies, K. Burgess, F. Bergström and L. B.-A. Johansson, *J. Org. Chem.*, 1999, **64**, 7813.
6 J. Chen, A. Burghart, A. Derecskei-Kovacs and K. Burgess, *J. Org. Chem.*, 2000, **65**, 2900.
7 N. L. Vekshin, *Energy Transfer in Macromolecules*, Spie Press, 1997.
8 T. Förster, *Ann. Phys.*, 1948, **2**, 55.
9 F. R. Lipsett, *Prog. Dielectr.*, 1967, **7**, 217.
10 L. B.-Å. Johansson, F. Bergström, P. Edman, I. V. Grechishnikova and J. G. Molotkovsky, *J. Chem. Soc., Faraday Trans.*, 1996, **92**, 1563.
11 J. R. Lakowicz, *Principles of Fluorescence Spectroscopy*, Kluwer Academic/Plenum Publishers, 1999.
12 H. Langhals, J. Karolin and L. B.-Å. Johansson, *J. Chem. Soc., Faraday Trans.*, 1998, **94**, 2919.
13 I. A. Johnson, H. C. Kang and R. P. Haugland, *Anal. Biochem.*, 1991, **198**, 228.
14 D. Magde, J. H. Brannon, T. L. Cremers and J. Olmsted III, *J. Phys. Chem.*, 1979, **83**, 696.
15 H. Langhals, J. Karolin and L. B.-A. Johansson, *J. Chem. Soc., Faraday Trans.*, 1998, **94**, 2919.
16 D. Magde and J. H. Brannon, *J. Phys. Chem.*, 1979, **83**, 696.

Azidohydroperoxidation of pinenes: stereoselectivity pattern and the first X-ray structure of a 2-azidohydroperoxide

Axel G. Griesbeck,* Johann Lex, Kurt M. Saygin and Jörg Steinwascher

Institute of Organic Chemistry, University of Cologne, Greinstr. 4, D-50939 Köln, Germany. E-mail: griesbeck@uni-koeln.de

Received (in Liverpool, UK) 17th July 2000, Accepted 2nd October 2000
First published as an Advance Article on the web

The photoinduced electron transfer of azide anions in the presence of an excited organic dyestuff, oxygen, and α- or β-pinene, respectively, gave 2-azidohydroperoxides in excellent regio- and good diastereoselectivity.

Photooxygenation in the presence of azide anions leads to difunctionalized products which can derive either from an azide trapping reaction of cyclic peroxidic intermediates or from an oxygen trapping reaction of intermediary α-azido carbon radicals.[1–3] The resulting 2-azidohydroperoxides have seldom been isolated and are usually reduced to the corresponding azido- or aminoalcohols.[4] Recent investigation by Workentin *et al.* showed that azidyl radicals are produced under photoinduced electron transfer (PET) conditions and these highly reactive azidyl radicals readily add to nucleophilic alkenes.[5]

In order to evaluate the facial selectivity of the azidyl radical addition in combination with simple diastereoselectivity originating from the secondary attack of molecular oxygen, we investigated the enantiomerically pure α- and β-pinene as substrates. The trisubstituted α-pinene (**1**) was among the most reactive alkenes when irradiated with visible light in the presence of azide anions, oxygen and an organic dye (Scheme 1). The crude reaction mixture consisted of a mixture of diastereoisomeric azidohydroperoxides **2a**–**c** (d.r. 90:8:2) and the corresponding azidoalcohols **3** which could be separated chromatographically (total yield 58%). The hydroperoxide–alcohol ratio could be altered by use of different PET-sensitizers and variation of the water content and was optimal (79:21) for rhodamine B in a 95:5 MeOH–H_2O mixture. Stern–Volmer analysis of the fluorescence quenching gave a rate constant for PET from N_3^- to rhodamine B of $k_{ET} = 1.6 \times 10^9$ M^{-1} s^{-1} (Fig. 1) comparable with the rate constants determined for 9,10-dicyanoanthracene[6] and thioxanthone.[7]

The configuration of the major diastereoisomer **2a** was determined by NOE-spectroscopy and by comparison of the aminoalcohol **4a** which resulted from the LAH-reduction of **2a**

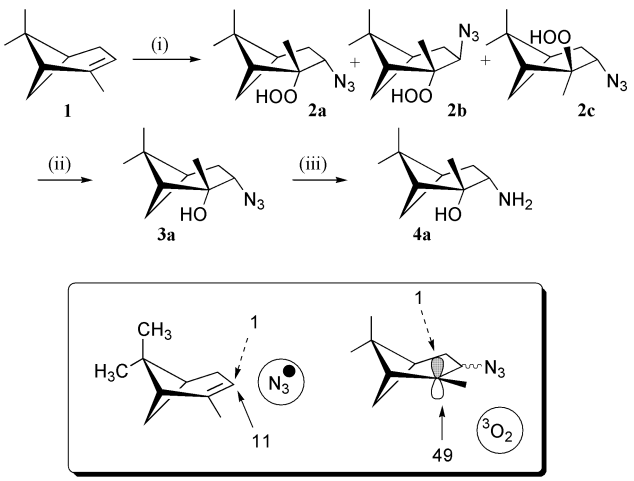

Scheme 1 *Reagents and conditions*: (i) NaN_3, O_2, Rh-B, *hν*, MeOH–H_2O, (ii) $NaBH_4$, MeOH, (iii) $LiAlH_4$, Et_2O.

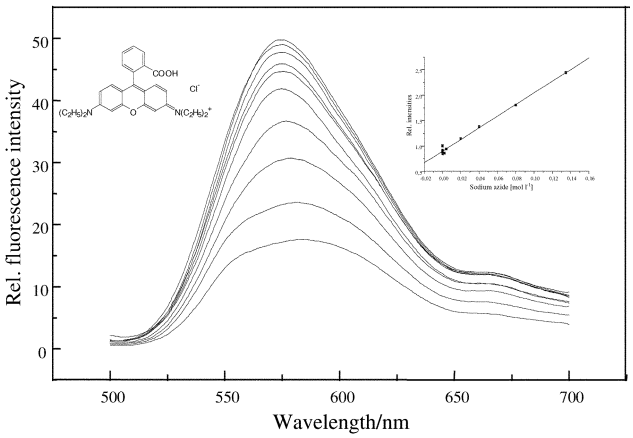

Fig. 1 Fluorescence quenching of rhodamine B by azide anions.

with the literature-known compound.[8] The relative configuration of the two minor components were determined from the $^3J_{HH}$ coupling constants of the hydrogen proximal to the azido group. Thus, the primary attack of the azidyl radical proceeds with a 11:1 *endo*-selectivity and the subsequent oxygen attack with a 49:1 *endo*-selectivity.

Unexpectedly, β-pinene (**5**) also showed noticeable reactivity under standard reaction conditions (Scheme 2): the azidohydroperoxides **6a**,**b**† (Fig. 2) were formed with a dr of 76:24 (72% based on converted **5b**). The addition of molecular oxygen was again directed by the shielding effect of the dimethylmethylene bridge in **5**. From both the azidohydroperoxides **6a,b** as well as the azidoalcohol **7a** the aminoalcohol **8a**, was generated by LAH-reduction. Crystallization from hexane–ethyl acetate gave single crystals of the azidohydroperoxide **6a**. X-Ray structure analysis of **6a** revealed that the molecules are connected by intermolecular hydrogen bonds between the OOH group and the internal nitrogen of the azido function.

Thus, this procedure serves as a simple synthetic approach to aminoalcohols from unsaturated substrates from the 'chiral pool'. Additionally, the pinene skeleton offered the opportunity to study the rate of oxygen addition due to the highly reactive cyclobutylcarbenium radicals (radical clocks) formed after azidyl radical addition. The corresponding ring-opening processes have been studied in free radical additions to α- and β-

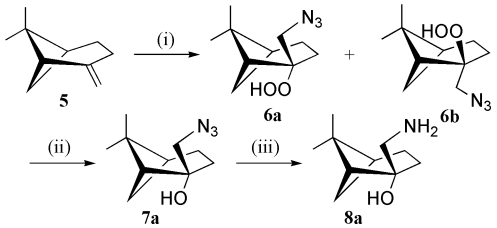

Scheme 2 *Reagents and conditions*: (i) NaN_3, O_2, Rh-B, *hν*, MeOH–H_2O, (ii) $NaBH_4$, MeOH, (iii) $LiAlH_4$, Et_2O.

DOI: 10.1039/b005834n

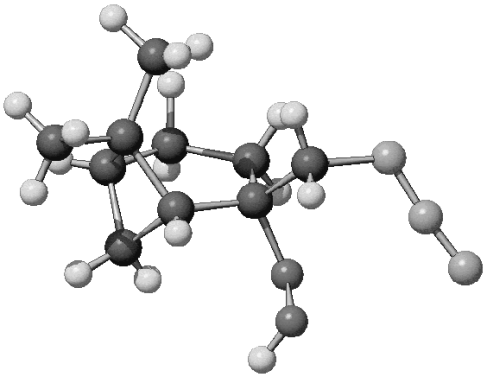

Fig. 2 Structure of the azidohydroperoxide **6a** in the crystal (SCHAKAL).

pinene and rate constants of 8×10^5 s^{-1} were determined.[9] In our hands, less than 5% of ring-opening products (from **2** and **5**) were detected in the crude NMR-spectra. From this data, a bimolecular rate constant for the oxygen addition step of $> 5 \times 10^9$ l M^{-1} s^{-1} resulted. This value is in good agreement with the rate constants determined for the reaction of triplet oxygen with benzylic radicals ($1.6–4.9 \times 10^9$ l M^{-1} s^{-1}).[10] Decreasing the oxygen concentration, *e.g.* by use of air instead of a pure oxygen gas flow gave a number of products. These could not be identified.

The azidohydroperoxidation reaction was also applied for the allylic hydroperoxide **9** (available *via* photooxyenation of α-pinene **1**) and proceeded smoothly to give the corresponding azido *bis*-hydroperoxide which was reduced *in situ* to the azidodiol **10** (Scheme 3).

This work was supported by the Deutsche Forschungsgemeinschaft (project GR 881/9-2) the Fonds der Chemischen Industrie and the Universität zu Köln.

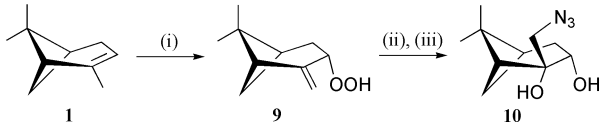

1 **9** **10**

Scheme 3 *Reagents and conditions*: (i) $^1O_2$, MeOH, (ii) NaN_3, O_2, Rh-B, *hν*, MeOH–H_2O, (iii) $NaBH_4$, MeOH.

Notes and references

† *Crystal data*: $C_{10}H_{17}N_3O_2$ (from hexane–ethyl acetate 3:1) **6a**: M = 211.27, monoclinic, a = 10.070(1), b = 11.071(1), c = 10.418(1) Å, β = 91.180(1)°, space group $P2_1$, Mo-K_α, 9958 reflections measured, 4376 reflections with $I > 2\sigma(I)$ R_1 = 0.0367, wR_2 = 0.0870. CCDC 182/1810. See http://www.rsc.org/suppdata/cc/b0/b005834n/ for crystal data in tabular format.

1 W. Fenical, D. R. Kearns and P. Radlick, *J. Am. Chem. Soc.*, 1969, **91**, 7771; C. S. Foote, T. T. Fujimoto and Y. C. Chang, *Tetrahedron Lett.*, 1972, 45; K. Gollnick, D. Haisch and G. Schade, *J. Am. Chem. Soc.*, 1972, **94**, 1747; N. Hasty, P. B. Merkel, P. Radlick and D. R. Kearns, *Tetrahedron Lett.*, 1972, 49.
2 A. Guarini and P. Tundo, *J. Org. Chem.*, 1987, **52**, 3501.
3 A. G. Griesbeck, T. Hundertmark and J. Steinwascher, *Tetrahedron Lett.*, 1996, **37**, 8367.
4 R. Hernández, E. I. León, P. Moreno and E. Suárez, *J. Org. Chem.*, 1997, **62**, 8974.
5 M. S. Workentin, B. D. Wagner, J. Lusztyk and D. D. M. Wayner, *J. Am. Chem. Soc.*, 1995, **117**, 119; M. S. Workentin, B. D. Wagner, F. N. Negri, M. Zgierski, J. Lusztyk, W. Siebrand and D. D. M. Wayner, *J. Phys. Chem.*, 1995, **99**, 94.
6 K. A. Abdullah and T. J. Kemp, *J. Photochem.*, 1985, **28**, 61.
7 K. A. Abdullah and T. J. Kemp, *J. Chem. Soc., Perkin Trans. 2*, 1985, 1279.
8 M. Masui and T. Shioiri, *Tetrahedron*, 1995, **51**, 8363.
9 B. Maillard and J. C. Walton, *J. Chem. Soc., Perkin Trans.2*, 1985, 443.
10 B. Maillard, K. U. Ingold and J. C. Scaiano, *J. Am. Chem. Soc.*, 1983, **105**, 5095.

ChemComm

Stereo- and regiospecific polymerization of cyclic conjugated dienes using highly active nickel catalysts†

Mitsuru Nakano,* Qing Yao, Arimitsu Usuki, Shinobu Tanimura and Takaaki Matsuoka

Functional Polymer Synthesis Laboratory and Computational Materials Engineering Laboratory, Toyota Central R&D Labs., Inc., Yokomichi 41-1, Nagakute, Aichi 480-1192, Japan. E-mail: mnakano@mosk.tytlabs.co.jp; Fax: +81-561-63-6137; Phone: +81-561-63-5251

Received (in Cambridge, UK) 15th August 2000, Accepted 2nd October 2000
First published as an Advance Article on the web 31st October 2000

A markedly active and selective nickel catalyst, bis(allylnickel bromide)–methylaluminoxane, has been developed for cyclohexa-1,3-diene polymerization; the obtained crystalline polymer is a 1,4-linked *cis*-syndiotactic structure as determined by NMR and molecular dynamics using the COMPASS force field.

Interest in cyclic olefin polymers has been growing dramatically over the past decade due to their thermal and chemical stabilities and high mechanical strength and modulus that originates from the restricted molecular motion of a cyclic group. In addition, cyclic olefin polymers are recognized as promising optical materials because of their low birefringence. Among the various cyclic unsaturated compounds, we have focused on cyclohexa-1,3-diene (CHD) because it can be converted from cyclohexene, a known inexpensive by-product from ε-caprolactam synthesis. However, the monomer is so bulky that most catalysts are not effective for CHD polymerization.[1] Grubbs and coworkers reported that bis[(η^3-allyl)(trifluoroacetato)nickel(II)] catalyzed the polymerization of CHD derivatives, though the catalytic activity was not high enough for rapid CHD homopolymer production.[2] Recently, *n*-BuLi–TMEDA was developed for living anionic polymerization of CHD by Natori *et al*.[3] In this anionic polymerization system, however, the regio- and stereostructure of poly(CHD) were poorly controlled. To our knowledge, there are very few reports of initiators having high regio- and stereoselectivity *and* high catalytic activity. We herein report a markedly active bis(allylnickel bromide) (ANiBr)–methylaluminoxane (MAO) catalyst for CHD polymerization. Furthermore, the polymer obtained from the catalyst system exhibited a very high regio- and stereoregular structure, which was fully characterized by NMR and molecular dynamics using the COMPASS force field.

CHD polymerization catalyzed by ANiBr–MAO was rapidly completed at rt.[4] As shown in Table 1, the polymer yields are quite high, especially in halogenated aromatics or in cyclohexane. On the other hand, both the zirconium- and titanium-based catalysts had low activities for CHD polymerization, resulting in low yields of polymer. Late transition metal catalysts such as neutral allylnickel and cationic allylpalladium complexes were also ineffective for CHD polymerization. The ANiBr–MAO catalyst exhibited extremely high activity for the following reasons: (1) allylnickel should have an identical structure with the propagating species, allowing immediate initiation. (2) MAO activates ANiBr to form a highly electron-deficient species. (3) ANiBr has very high solubility in various organic solvents. (4) Allylnickel species should have enough space for the sterically demanding monomer.

In order to explore the polymerization mechanism, we synthesized the well-structured single component Ni complex[5] [(η^3-allyl)Ni(cycloocta-1,5-diene)]$^+$B(C_6F_5)$_4^-$ for CHD polymerization. Although the complex exhibited slightly lower catalytic activity than ANiBr–MAO, the obtained polymer showed the same regio- and stereostructure as the one produced using ANiBr–MAO (*vide infra*), which means that the cationic allylnickel is presumably the true propagating species in the CHD polymerization.

Since the CHD homopolymer[6] is insoluble in any organic solvents, buta-1,3-diene (BD) was copolymerized with CHD to determine the regiostructure of the polymer obtained.[7] Since no signals of the 1,2-poly(BD) units were observed around 114 and 143 ppm in the ^{13}C NMR spectrum of the copolymer, only the 1,4-poly(BD) units were taken into account to assign the ^{1}H NMR signals of poly(BD). Based on ^{1}H COSY spectra,† all signals were assigned as follows (Fig. 1). For the poly(CHD) unit, protons of H_o, H_a and H_b are identified with peak A at 5.73 ppm, peak D at 2.01 ppm and peak E at 1.56 ppm, respectively. On the other hand, peaks B and C are due to protons of H_o' and H_a' in the 1,4-poly(BD) unit, respectively. Assuming that the integral value of peak B is 2.0, peak A can be estimated to be 5.27. Concerning the number of protons in poly(CHD), H_o is equal to H_a in the 1,4-unit while H_o is 3/2 of H_a in the 1,2-unit. Therefore, the calculated value of the integral area of peaks C

† Electronic supplementary information (ESI) available: ^{1}H COSY spectra of the CHD–BD copolymer. See http://www.org/suppdata/cc/b0/b006676l/

Table 1 Polymerization of cyclohexa-1,3-diene using various transition metal catalysts[a]

Entry	Catalyst	Cocatalyst	[Al]/[Cat]	Solvent	Time	Polymer yield (%)
1	ANiBr	MAO	100	Toluene	5 min	78
2	ANiBr	MAO	100	Chlorobenzene	< 1 min	88
3	ANiBr	MAO	100	*o*-Dichlorobenzene	< 1 min	96
4	ANiBr	MAO	100	Cyclohexane	< 1 min	92
5	(EBTHI)$ZrCl_2$[b]	MAO	1000	Toluene	5 days	10
6	$CpTiCl_3$	MAO	1000	Toluene	4 days	30
7	[(η^3-C_3H_5)Ni($OC(O)CF_3$)]$_2$	None		Toluene	34 hours[c]	40
8	[(η^3-C_3H_5)Pd]$^+$ SbF^-	None		Dichloromethane	7 days	10
9	[(η^3-C_3H_5)Ni(cod)]$^+$ [B(C_6F_5)$_4$]$^-$	None		*o*-Dichlorobenzene	20 min	72

[a] Polymerization conditions: $[CHD]_o$ = 1.5 mol l^{-1}, $[CHD]_o/[Cat]$ = 500, at rt. [b] (EBTHI)$ZrCl_2$: *rac*-Ethylenebis(4,5,6,7-tetrahydro-1-indenyl)zirconium dichloride. [c] Polymerization was carried out at rt for 24 h followed by 50 °C for 10 h.

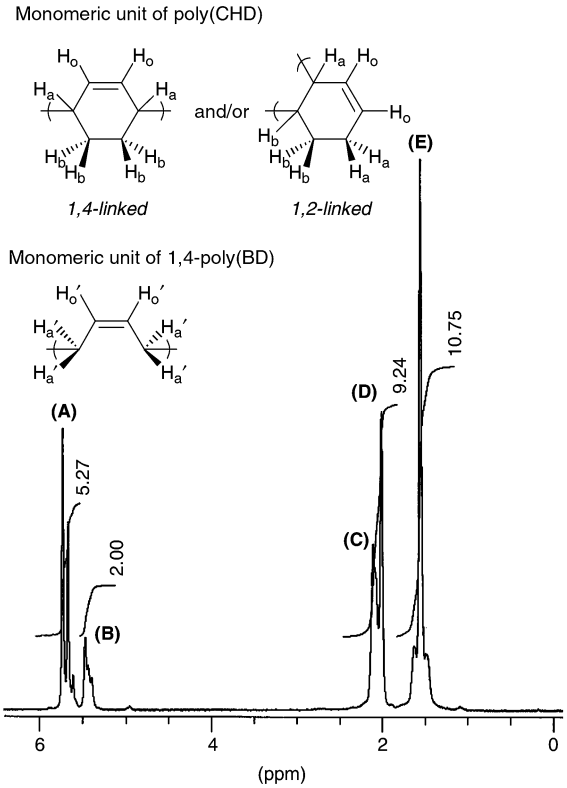

Fig. 1 ^{1}H NMR spectrum of CHD–BD copolymer catalyzed by ANiBr–MAO (polymer composition of [CHD]/[BD] = 72/28).

and D should be in the region from 9.27 (= 2.00 × 2 + 5.27) to 11.91 (= 2.00 × 2 + 5.27 × 3/2). The observed value of 9.24 is practically the same as 9.27, which means the CHD segment is perfectly 1,4-linked as well as the poly(BD) segment. In addition, the observed integral value of peak E is also very close to the calculated one, leading us to postulate that 1,4-linkage is dominant in the poly(CHD) main chain. Another experiment confirming the regiostructure was the synthesis of CHD oligomer anchored by a soluble poly(norbornene) with high molecular weight. The propagating species of norbornene polymerization initiated with ANiBr–MAO was long-lived enough to produce a soluble norbornene–CHD diblock copolymer. The ^{1}H NMR spectrum showed a sharp single peak of olefinic protons at 5.75 ppm, which is totally different from the doublet signal of anionically polymerized CHD.[3]

As shown in Fig. 2(a), the poly(CHD) catalyzed by *n*-BuLi-based initiator revealed the typical amorphous XRD pattern even when the polymer main chain consisted of >90% 1,4-units.[3] On the other hand, the poly(CHD) obtained with the ANiBr–MAO catalyst was found to be highly crystalline with

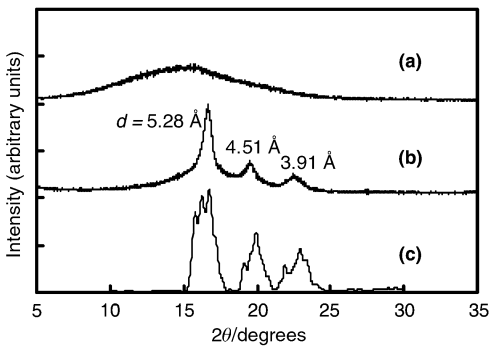

Fig. 2 X-ray diffraction patterns of (a) poly(CHD) obtained from *n*-BuLi–TMEDA, (b) poly(CHD) obtained from ANiBr–MAO, (c) *cis*-syndiotactic 1,4-poly(CHD) simulated using the COMPASS force field.

three major peaks based on a X-ray powder diffraction (XRD) spectrum (Fig. 2(b)). Additionally, the crystalline XRD pattern did not change when the poly(BD) unit was introduced into the main chain though the peak intensity decreased. The crystallinity of poly(CHD) initiated with ANiBr–MAO catalyst should originate from the stereoregular structure. In general, there are four stereoisomers, *i.e. cis*-isotactic, *cis*-syndiotactic, *trans*-isotactic and *trans*-syndiotactic in 1,4-linked poly(CHD).[8] We performed constant-temperature and constant-pressure molecular dynamics simulations of the crystalline poly(CHD) at 300 K and under zero pressure using the COMPASS force field. By use of the simulated atomic coordinates of the crystalline poly(CHD), time-averaged X-ray powder diffraction spectra were calculated. Interestingly, it was confirmed that only the simulated crystalline structure of the *cis*-syndiotactic 1,4-linked poly(CHD) could reproduce the experimental XRD pattern shown in Fig. 2(c). Although Ni-catalyzed poly(CHD) is believed to be a *cis*-rich structure from a *syn*-coordinative mechanism,[9] this simulation is the first evidence of the stereoregular structure of poly(CHD).

In summary, it was found that the ANiBr–MAO catalyst showed remarkably high activity for the CHD polymerization. The obtained polymer was a *cis*-syndiotactic 1,4-linked structure, which induced crystallization. In order to precisely control the poly(CHD) structure, further intensive studies using other nickel catalysts with dimine or phenanthroline ligands are in progress.

The authors are grateful to Ms K. Fukumoto for the NMR analyses.

Notes and references

1 G. Lefebvre and F. Dawans, *J. Polym. Sci., Part A*, 1964, **2**, 3277; P. E. Cassidy, C. S. Marvel and S. Ray, *J. Polym. Sci., Part A*, 1965, **3**, 1553; Y. Imanishi, T. Yamane, S. Kohjiya and S. Okamura, *J. Macromol. Sci.-Chem.*, 1969, **A3**, (**2**), 243; Y. Imanishi, K. Matsuzaki, T. Yamane, S. Kohjiya and S. Okamura, *J. Macromol. Sci.-Chem.*, 1969, **A3**, (**2**), 249; B. A. Dolgoplosk, S. I. Beilin, Yu. V. Korshak, G. M. Chernenko, L. M. Vardanyan and M. P. Teterina, *Eur. Polym. J.*, 1973, **9**, 895; A. Sen and T. Lai, *Organometallics*, 1982, **1**, 415; H. R. Allcock, G. K. Dudley and E. N. Silverberg, *Macromolecules*, 1994, **27**, 1039.

2 D. L. Gin, V. P. Conticello and R. H. Grubbs, *J. Am. Chem. Soc.*, 1994, **116**, 10507.

3 I. Natori, *Macromolecules*, 1997, **30**, 3696; I. Natori and S. Inoue, *Macromolecules*, 1998, **31**, 4687.

4 A typical polymerization was performed with stirring at rt in a 20 ml glass bottle which was successively charged with 4.5 ml of toluene, 1 g (12.5 mmol) of CHD, 4.4 mg (24 μmol) of ANiBr, and 0.95 g of MAO (toluene solution, 2.6 mmol of Al). The polymerization solution immediately became heterogeneous at rt as a white precipitate formed. The reaction was quenched in a solution containing 500 ml MeOH and 10 ml 1 M HCl with a small amount of 2,6-di-*tert*-butyl-4-methylphenol as the antioxidant reagent. After drying under vacuum, an off-white powdery polymer was obtained.

5 J. Ascenso, A. R. Dias, P. T. Gomes, C. C. Romao, D. Neibecker, I. Tkatchenko and A. Revillon, *Makromol. Chem.*, 1989, **190**, 2773.

6 CP–MAS ^{13}C NMR (300 MHz): δ 130 (–*C*H$_2$=), 40 (–H*C*<), 25(–*C*H$_2$–). Elemental analysis. Calcd for $(C_6H_8)_n$: C, 90.0; H,10.0. Found : C, 87.4; H, 9.8. The obtained polymer was stable up to 320–330 °C under N_2 and the melting point was not observed below 320 °C by DSC or a polarized microscopy.

7 The copolymerization of CHD with BD was accomplished by ANiBr–MAO catalyst to produce a copolymer almost quantitatively (yield 95%). While the monomer feed ratio was [CHD]/[BD] = 70/30, the polymer composition was determined to be [CHD]/[BD] = 72/28 by ^{1}H NMR. Based on GPC in *o*-dichlorobenzene at 135 °C, M_n, M_w and PDI were estimated to be 29.3 × 10^3, 63.0 × 10^3 and 2.15 (*vs.* polystyrene standards), respectively. Although the relative reactivity of CHD was somewhat higher than that of BD in the copolymerization, the regiostructure of the CHD segment did not change throughout the polymerization.

8 In this context, *cis–trans* means that bridging C–C bonds between monomer units are in a *cis–trans* relationships on the face of the cyclohexenyl ring.

9 L. Porri and M. Aglietto, *Makromol. Chem.*, 1976, **177**, 1465.

Oxidation of alkanes with H_2O on $Ir(acac)_3$ supported on a carbon fiber-anode

Ichiro Yamanaka,* Taishi Furukawa and Kiyoshi Otsuka

Department of Applied Chemistry, Graduate School of Science and Engineering, Tokyo Institute of Technology, Ookayama, Meguro-ku, Tokyo 152-8552, Japan. E-mail: yamanaka@o.cc.titech.ac.jp

Received (in Cambridge, UK) 27th July 2000, Accepted 6th October 2000
First published as an Advance Article on the web 31st October 2000

$Ir(acac)_3$ supported on a carbon fiber-anode catalyzed the oxidations of alkanes (cyclohexane, *n*-hexane, adamantane) by generating strong electrophilic oxygen species from H_2O at 1.3 V (Ag|AgCl) with high current efficiency, for example, 45% for cyclohexanone formation.

Direct oxidation of alkanes is one of the key oxidation processes expected in the 21st century. On the other hand, the electroorganic synthesis of chemicals is also expected to be a key technology in green chemistry because the electrolysis can be operated under mild conditions. However, it is not so easy to realize direct oxidation of alkanes by electrolysis because their redox potentials [1.85 V (*vs.* NHE) for cyclohexane to 2.25 V for methane in aqueous solutions at pH = 0[1]] are higher than those of solvents and electrolytes. Some work on the anodic oxidation of alkanes in aqueous media >358 K has been reported but current densities were <0.1 mA cm^{-2} and the product was CO_2.[2] In non-aqueous media, oxidation of adamantane to adamantane derivatives was performed at >2.0 V and 303 K but the current density was <4 mA cm^{-2}.[3] Most of all successful electrochemical systems for the oxidation of alkanes applied an electrochemical reductive activation of O_2 at the cathode, indirect electrochemical oxidation, though the current efficiency of the produced oxygenates were low at <10%.[4]

We have recently reported an indirect anodic epoxidation of propene to propene oxide on PtO_2/Pt-anode and oxidation of benzene to benzoquinone on a carbon fiber-anode at 293 K.[5,6] A membrane electrolysis cell was assembled as [reactant|porous anode|silica wool membrane impregnated with H_3PO_4 aq.|porous Pt-graphite-cathode|H_2O(g), He]. An advantage of this system compared with conventional ones is that the separation procedure of the products from electrolyte is quite easy. We proposed that a nascent oxygen species generated on the anode from H_2O would oxidize propene and benzene, *i.e.* indirect electrochemical oxidation at the anode.[5,6] However, the two anodes mentioned above were not active at all for the oxidation of alkanes. Therefore, the purpose of this work was to design a new active anode for the oxidation of alkanes with H_2O by using the membrane electrolysis cell.

Fig. 1 shows the catalytic activities of various anodes for the oxidation of cyclohexane during electrolysis of H_2O in H_3PO_4 (aq) (0.7 mol l^{-1}) at 298 K. The anodes were prepared by the hot-press method from various electrocatalyst powders [metal blacks and metal compounds (0.5 mol%) supported on carbon fibers (CF)] and poly(tetrafluoroethylene) (PTFE) powder[4] with a geometric surface of *ca.* 2 cm^2. The membrane electrolysis cell attached to various anodes was assembled and the anode compartment was filled with pure cyclohexane (40 ml). The electrocatalytic oxidation of cyclohexane with H_2O was carried out by applying the anode potential; 1.5 V (Ag|AgCl) at Pd-black, Pt-black, Ir-powder, Ir-black anodes and 1.8 V at FeCl(TPP)/CF, Co_2O_3/CF, MnO_2/CF, Ir/CF, IrO_2, $IrCl_3$/CF, $IrCl_4$/CF anodes. Products were cyclohexanone (CyO), cyclohexanol (CyOH), adipic acid (AA), CO_2 and O_2. The results in Fig. 1 indicate that Ir compounds, especially $Ir(acac)_3$ supported on carbon fiber (CF), are active for the CyO formation, though current efficiencies (CE) estimated from eqn. (1) were not good.

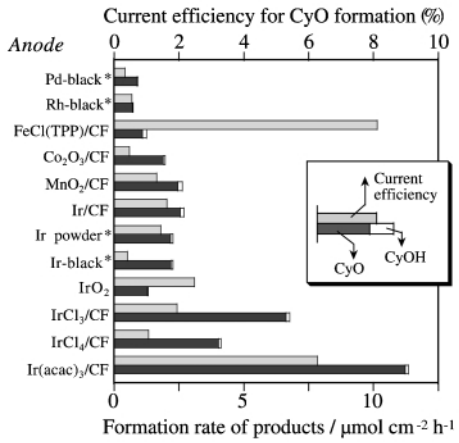

Fig. 1 Electrocatalytic oxidation of cyclohexane with H_2O over various anodes at 1.8 V (Ag|AgCl) or 1.5 V(*) at 298 K.

Therefore, attention was paid to the electrocatalytic function of the most active $Ir(acac)_3$/CF anode.

$$\text{cy-}C_6H_{12} + H_2O \rightarrow \text{cy-}C_6H_{10}O + 4\ H^+ + 4\ e^- \qquad (1)$$

To increase electrocatalytic activity for the oxidation of cyclohexane, (i) preparation conditions of the Ir-anode [types of carbon material, amounts of $Ir(acac)_3$ loading (0–2 mol%), amounts of PTFE (1–50 mg) and impregnation methods] were tested. The best components of the Ir-anode were [$Ir(acac)_3$ (0.025 mol%)/CF] (50 mg) and PTFE (5 mg). (ii) The study on the effects of various electrolytes (H_3PO_4, HCl, $HClO_4$, H_2SO_4, HNO_3, Na_2SO_4, NaOH and KOH) in the membrane and their concentrations on the oxidation of cyclohexane indicated that the best electrolyte was H_2SO_4 (aq) (1 mol l^{-1}).

Fig. 2(a) shows the formation rates of the products as a function of the anode potential by using the best anode and electrolyte described above. In the upper part (b), the current density and the current efficiency (CE) were plotted. When the anode potential was increased above 1.3 V (Ag|AgCl), the current density and the formation rates of CyO and CO_2 rapidly increased. The potential of 1.3 V for the onset of oxidation is far lower than the theoretical oxidation potential of 1.65 V (1.85 V *vs.* NHE) at pH = 0.[1] This result suggest that an indirect electrochemical oxidation of cyclohexane proceeds on the Ir-anode. The maximum formation rate of CyO was obtained at *ca.* 1.5 V. Here, the turnover number of Ir for CyO formation exceeded 110 in 1 h. In contrast, the formation rates of CO_2 and O_2 continuously increased when increasing the anode potential further. The decrease in the formation rate of CyO above 1.5 V may be due to the desorption of active oxygen species on the Ir-anode to the gas phase or to the consumption of the active oxygen in the successive oxidation of CyO to adipic acid or CO_2. Thus, the CE for the CyO formation decreased from 20 to 8% upon increasing the anode potential.

Effects of solvents (CH_2Cl_2, CCl_4, Et_2O, DMF and THF) on the oxidation were studied to optimize the oxidation. When a mixture of CH_2Cl_2 and cyclohexane (50:50 vol%) was used for the oxidation at 1.5 V, the CE for CyO formation dramatically

DOI: 10.1039/b006107g

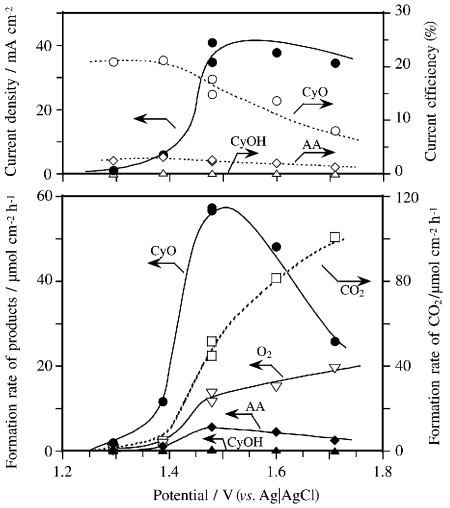

Fig. 2 Effects of anode potentials on (a) the formation rates of products and (b) current and current efficiency for the oxidation of cyclohexane on the $Ir(acac)_3$/CF anode with H_2O at 289 K.

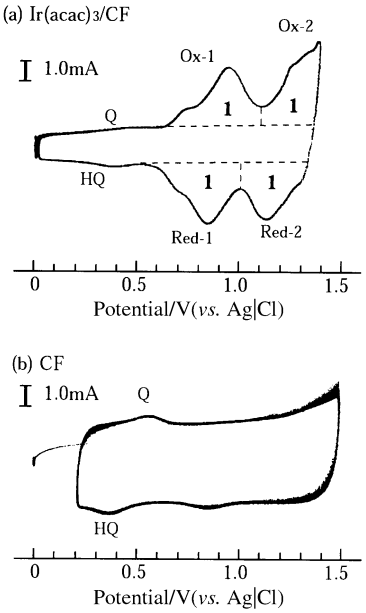

Fig. 3 Cyclic voltammograms of $Ir(acac)_3$/CF and CF electrodes in H_2SO_4 (aq) (1 mol l^{-1}) at atmospheric pressure of Ar. Scan speed 0.5 V s^{-1}.

increased from 15 to 45% while retaining a high formation rate of CyO. The increase in the CE was due to the decrease in both current and formation rates of CO_2 and O_2. If these by-products are formed through eqns. (2)–(4), their CE are estimated to be 18, 0.1, 10 and 15% for adipic acid, CyOH, CO_2 and O_2 respectively, giving a sum of CE of 88% at 1.5 V.

$$\text{cy-}C_6H_{12} + 4\ H_2O \rightarrow C_4H_8(CO_2H)_2 + 10\ H^+ + 10\ e^- \quad (2)$$

$$\text{cy-}C_6H_{12} + 12\ H_2O \rightarrow 6\ CO_2 + 36\ H^+ + 36\ e^- \quad (3)$$

$$\text{cy-}C_6H_{12} + H_2O \rightarrow \text{cy-}C_6H_{11}OH + 2\ H^+ + 2\ e^- \quad (4)$$

On the other hand, the CE for the formation of H_2 at the cathode was almost 100% within experimental error of ±2%. These results suggest the formation of undetectable products or oxidation of the anode itself.

A conventional H-type cell with the same [$Ir(acac)_2$ (0.025 mol%)/CF] anode was applied for the oxidation of cyclohexane dissolved in MeCN or dispersed as micelles in aqueous H_2SO_4. However, the oxidation of cyclohexane did not proceed at all. Our membrane electrolysis method is unique for the oxidation. After the oxidation, no Ir compounds were present in the reaction mixture or H_2SO_4 (aq) in the membrane according to ICP analysis. This result strongly suggests that Ir species are fixed on the CF.

Fig. 3 shows cyclic voltammograms (CV) of (a) the [0.025 mol% $Ir(acac)_2$/CF] electrode and (b) the CF electrode in aqueous H_2SO_4 under atmospheric pressure of Ar (geometric areas of both electrodes was 0.02 cm^2). Several redox couples were observed in the CV (a) of $Ir(acac)_3$/CF not observed in the CV (b) of CF, except for the redox couple due to quinone/hydroquinone groups present on carbon surfaces. A redox couple at 0.8–0.9 V (Ag|AgCl) (Ox-1/Red-1) can be assigned to Ir^{3+}/Ir^0.[7] The ratio of peak areas of Ox-1, Red-1, Ox-2 and Red-2 in Fig. 3(a) were roughly estimated to be 1 : 1 : 1 : 1. These facts suggested that the couple at higher potential (Ox-2/Red-2) can be ascribed to the transfer of three electrons, probably the redox couple Ir^{6+}/Ir^{3+} according to eqn. (5) or (6).

$$Ir^{3+} \rightarrow Ir^{6+} + 3\ e^- \quad (5)$$

$$Ir^{3+} + H_2O \rightarrow [IrO]^{4+} + 2\ H^+ + 3\ e^- \quad (6)$$

We believe that the formation of such high oxidation state Ir species[8] on CF would catalyse the oxidation of cyclohexane at > 1.3 V(Ag|AgCl).

To gain information about the reactivity of active species, oxidations of CyOH (4.8 mol l^{-1}), CyO (4.8), hexane (3.8) and adamantane (0.25) dissolved in CH_2Cl_2 were studied at an anode potential of 1.5 V (Ag|AgCl). CyOH was efficiently oxidized to CyO with a high CE of 73% (assuming $2e^-$ oxidation). On the other hand, CyO was oxidized to adipic acid with a low CE of 17% ($6e^-$ oxidation). These results suggest that active species generated on the Ir-anode oxidizes cyclohexane to CyO through CyOH. Deep oxidations of CyO to adipic acid and CO_2 were not fast. In oxidation of hexane, hexan-2-one (CE 14.0%, assuming $4e^-$ oxidation), hexan-3-one (13.9%, $4e^-$ oxidation) and hexanoic acid (0.4%, $6e^-$ oxidation) were produced. The relative reactivities of secondary and primary C–H bonds (2° : 1°) in hexane were estimated from the quantities of the oxygenated products and found to 250 : 1 when normalized per C–H bond. Thus the secondary C–H bond was selectively oxygenated on the Ir-anode. In oxidation of adamantane, 1-adamantanol (CE 4.9%, assuming $2e^-$ oxidation) and 2-adamantanone (0.7%, $4e^-$ oxidation) were produced. The low CE observed here was due to the low solubility of adamantane in CH_2Cl_2 solvent. The relative reactivities of tertiary and secondary C–H bonds (3° : 2°) was 42 : 1. These results suggest that the active species has very strong electrophilicity for the oxidation of alkanes. This strong electrophilicity must be caused by the high oxidation state of Ir species suggested by CV experiments (Fig. 3).

Notes and references

1 A. E. Shilov, *Activation of Saturated Hydrocarbons by Transition Metal Complexes*, D. Reidel, Dordrecht, 1984.
2 J. O'M. Bockris, E. Gileadi and G. E. Stoner, *J. Electrochem. Soc.*, 1969, **73**, 427.
3 G. J. Edwards, S. R. Jones and J. M. Mellor, *J. Chem. Soc., Chem. Commun.*, 1975, 816; G. J. Edwards, S. R. Jones and J. M. Mellor, *Tetrahedron Lett.*, 1976, **8**, 631.
4 K. Otsuka and I. Yamanaka, *Catal. Today*, 2000, **57**, 71; E. R. Savinova, A. O. Kuzmin, F. Frusteri, A. Parmaliana and V. N. Parmon, *Stud. Surf. Sci. Catal.*, 1998, **119**, 429; R. L. Cook and A. F. Sammels, *J. Electrochem. Soc.*, 1990, **137**, 2007.
5 I. Yamanaka, K. Satio and K. Otsuka, *Electrochem. Solid State Lett.*, 1999, **2**, 131; K. Otsuka, T. Ushiyama, I. Yamanaka and K. Ebitani, *J. Catal.*, 1995, **157**, 450.
6 I. Yamanaka, T. Furukawa and K. Otsuka, *Chem. Lett.*, 1998, 1059.
7 Ir^{3+}/Ir^0 = 1.15 V (NHE), *Lange's Handbook of Chemistry*, ed. J. A. Dean, McGraw-Hill, New York, 1985.
8 L. A. Arasmaskova, A. V. Romanemko and Y. I. Yemakov, *React. Kinet. Catal. Lett.*, 1980, **13**, 391.

Catalytic asymmetric homo-aldol reaction of pyruvate—a chiral Lewis acid catalyst that mimics aldolase enzymes

Karsten Juhl, Nicholas Gathergood and Karl Anker Jørgensen*

Center for Metal Catalysed Reactions, Department of Chemistry, Aarhus University, DK-8000 Aarhus C, Denmark

Received (in Cambridge, UK) 4th September 2000, Accepted 27th September 2000
First published as an Advance Article on the web 31st October 2000

The first catalytic asymmetric homo-aldol reaction of ethyl pyruvate leading to diethyl-2-hydroxy-2-methyl-4-oxoglutarate in up to 96% enantiomeric excess is reported; this reaction has been investigated for various catalysts, amines and solvents, and it is demonstrated that this new reaction leads to a simple synthetic procedure for the formation of optically active isotetronic acid derivatives.

The aldol reaction is one of the most powerful methods for the formation of C–C bonds. The ability to control the absolute configuration of the newly formed stereogenic centre is of fundamental importance. Nature has solved this problem using enzymes and a variety of different aldolase enzymes can catalyse the aldol reaction.[1] For the chemist, the search for methods that predictably transfer chirality catalytically and efficiently by reagent control is a challenging goal. In recent years a number of methods have been developed for the catalytic asymmetric aldol reaction with both high efficiency and enantioselectivity.[2]

In nature aldolase enzymes typically catalyse the stereoselective addition of a ketone donor to a carbonyl acceptor, while the chemical methods normally require more reactive species such as silyl enol ethers,[3] enol-methyl ethers,[4] or ketene silyl acetals,[3a–c,5] except for the multifunctional catalyst systems, containing a Lewis acid and a Brønsted base.[6] This communication presents the first chiral Lewis acid complex acting as a 'pyruvate-dependent aldolase', *i.e.* a type II aldolase, that catalyses a highly enantioselective homo-aldol reaction of ethyl pyruvate.[7] Furthermore, it will be shown that the reaction can be used for the synthesis of an optically active isotetronic acid derivative in two steps, a significant improvement compared with recent multi-step and complex synthetic approaches.[8]

Chiral bisoxazoline–metal(II) complexes are known to act as effective catalysts for enantioselective addition reactions to carbonyl groups.[9] Ethyl pyruvate **1** reacts in the presence of chiral bisoxazoline–metal(II) complexes[3c,d,10] in a homo-aldol reaction to give diethyl-2-hydroxy-2-methyl-4-oxoglutarate **2** [eqn. (1)] and some representative results are shown in Table 1.

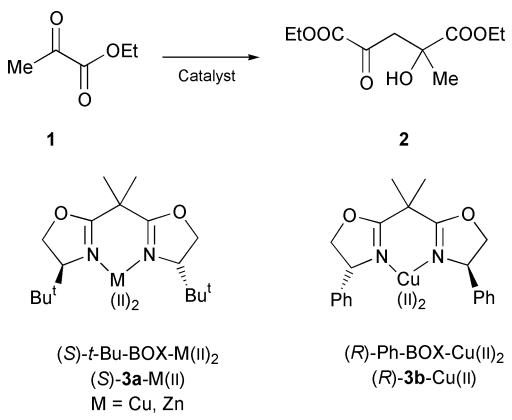

(1)

The homo-aldol reaction of ethyl pyruvate **1** proceeds with > 80% conversion. The reaction of **1** catalysed by (*S*)-**3a**-Cu(OTf)$_2$ (10 mol%) gives diethyl-2-hydroxy-2-methyl-4-oxoglutarate **2** with 65% ee (entry 1). The (*S*)-**3a**-Zn(OTf)$_2$ complex can also catalyse the homo-aldol reaction of **1**, but the other enantiomer of **2** is formed with low ee (entry 2). The addition of *N*,*N*-dimethylaniline (DMA) to the reaction increases the ee of **2** and for the reaction catalysed by (*S*)-**3a**-Cu(OTf)$_2$ (10 mol%) and DMA (5 mol%) 96% ee is achieved (entries 3, 4). The enantioselectivity of the homo-aldol reaction is dependent on the amine added. For the other amines tested the highest ee is 93% using PhNBn$_2$ (entry 7), while *e.g.* 60% ee is obtained for Et$_3$N (entry 9).

The enantioselectivity of the homo-aldol reaction of ethyl pyruvate **1** catalysed by (*S*)-**3a**-Cu(II) is dependent on the copper(II) counterion, the solvent and amine as shown in Table 2. For the reaction catalysed by (*S*)-**3a**-Cu(OTf)$_2$ in the presence of 10 mol% DMA in Et$_2$O and THF, 79% ee and 69% ee of the same enantiomer of **2** are obtained, respectively (entries 1, 2). Changing the solvent to CH$_2$Cl$_2$ leads to a change of enantioselection to 12% of the other enantiomer of **2** in the presence of 10 mol% DMA (entry 3). The homo-aldol reaction is also dependent on the counterion. Changing the counterion from OTf to SbF$_6$ in CH$_2$Cl$_2$, in the absence of an amine, leads to a drop in enantioselectivity of **2** from 11% ee to 0% ee (entries 4, 5). This counterion effect in CH$_2$Cl$_2$ is more dramatic in the presence of 10 mol% DMA, as a change in ee from 12% to 63% was observed (entries 3, 7). When using the (*S*)-**3a**-Cu(SbF$_6$)$_2$ catalyst an increase in ee of homo-aldol product **2** by adding 10 mol% DMA occurs in CH$_2$Cl$_2$ (entries 5, 7). To study the effect of different amines on the enantioselectivity of the (*S*)-**3a**-Cu(SbF$_6$)$_2$ catalysed reaction in CH$_2$Cl$_2$, Et(i Pr)$_2$N, PhNBn$_2$ and CyNMe$_2$ were screened. A drop in ee from 63% in the presence of DMA (entry 8) to 30% was found for Et(i Pr)$_2$N (entry 11), but we were pleased to observe an increase in ee to 75% and 77% for PhNBn$_2$ and CyNMe$_2$, respectively (entries 9, 10).

It is important to note that the enantioinduction of the (*S*)-**3a**-Cu(II) catalytic system can be switched by changing only one

Table 1 Homo-aldol reaction of ethyl pyruvate **1** in the presence of (*S*)-**3a**-M(OTf)$_2$ (M = Cu, Zn) and (*R*)-**3b**-Cu(OTf)$_2$ and various amines in Et$_2$O at room temperature[a]

Entry	Catalyst/ (mol%)[b]	Amine (mol%)[b]	Ee[c,d] (%)
1	(*S*)-**3a**-Cu(OTf)$_2$ (10)	—	(−)-65
2	(*S*)-**3a**-Zn(OTf)$_2$ (10)	—	(+)-7
3	(*S*)-**3a**-Cu(OTf)$_2$ (10)	DMA[e] (10)	(−)-79
4	(*S*)-**3a**-Cu(OTf)$_2$ (10)	DMA[e] (5)	(−)-96
5	(*S*)-**3a**-Zn(OTf)$_2$ (10)	DMA[e] (10)	(+)-16
6	(*R*)-**3b**-Cu(OTf)$_2$ (10)	DMA[e] (10)	(+)-28
7	(*S*)-**3a**-Cu(OTf)$_2$ (10)	PhNBn$_2$ (10)	(−)-93
8	(*S*)-**3a**-Cu(OTf)$_2$ (10)	CyNMe$_2$[f] (10)	(−)-50
9	(*S*)-**3a**-Cu(OTf)$_2$ (10)	Et$_3$N (10)	(−)-60
10	(*S*)-**3a**-Cu(OTf)$_2$ (10)	Et(i Pr)$_2$N (10)	(−)-67

[a] All reactions give > 80% conversion, except for entry 2 which gives 40% conversion. [b] Relative to ethyl pyruvate. [c] Ee measured by GC using a Chrompack CP-Chirasil Dex CB (β-PM) column. [d] (+)/(−), sign of the optical rotation of isotetronic acid derivative (**4**). [e] DMA = *N*,*N*-dimethylaniline. [f] Cy = cyclohexyl.

DOI: 10.1039/b007125k

Table 2 Homo-aldol reaction of ethyl pyruvate **1** catalysed by (*S*)-**3a**-Cu(II) in the presence of OTf and SbF_6 as counterions and various amines in different solvents[a]

Entry	Catalyst (mol%)[b]	Amine (mol%)[b]	Solvent	Ee[c,d] (%)
1	(*S*)-**3a**-Cu(OTf)$_2$ (10)	DMA[e] (10)	Et_2O	(−)-79
2	(*S*)-**3a**-Cu(OTf)$_2$ (10)	DMA[e] (10)	THF	(−)-69
3	(*S*)-**3a**-Cu(OTf)$_2$ (10)	DMA[e] (10)	CH_2Cl_2	(+)-12
4	(*S*)-**3a**-Cu(OTf)$_2$ (10)	—	CH_2Cl_2	(−)-11
5	(*S*)-**3a**-Cu(SbF_6)$_2$ (10)	—	CH_2Cl_2	0
6	(*S*)-**3a**-Cu(SbF_6)$_2$ (10)	—	Et_2O	(−)-50
7	(*S*)-**3a**-Cu(SbF_6)$_2$ (10)	DMA[e] (10)	CH_2Cl_2	(+)-63
8	(*S*)-**3a**-Cu(SbF_6)$_2$ (10)	DMA[e] (10)	Et_2O	(+)-24
9	(*S*)-**3a**-Cu(SbF_6)$_2$ (10)	$PhNBn_2$ (10)	CH_2Cl_2	(+)-75
10	(*S*)-**3a**-Cu(SbF_6)$_2$ (10)	$CyNMe_2$[f] (10)	CH_2Cl_2	(+)-77
11	(*S*)-**3a**-Cu(SbF_6)$_2$ (10)	Et(^{i}Pr)$_2$N (10)	CH_2Cl_2	(+)-30

[a] All reactions give 70–80% conversion, except entry 11 (25% conversion). [b] Relative to ethyl pyruvate. [c] Ee measured by GC using Chrompack CP-Chirasil Dex CB (β-PM) column. [d] (+)/(−), sign of the optical rotation of isotetronic acid derivative (**4**). [e] DMA = *N*,*N*-dimethylaniline. [f] Cy = cyclohexyl.

parameter: the solvent (entry 1 *vs*. 3; Et_2O *vs*. CH_2Cl_2), the counterion (entry 1 *vs*. 8; OTf *vs*. SbF_6) or the presence of an amine (entry 6 *vs*. 8; no amine *vs*. 10 mol% DMA). At the present stage of investigations we are not able to fully account for the change in reaction course, but work is ongoing to elucidate the reaction mechanism.

The chiral bisoxazoline–metal(II) complex, (*S*)-**3a**-Cu(II) (M = OTf, SbF_6), is thus a simple chiral Lewis acid complex which mimics the pyruvate-dependent type II aldolase. This new catalytic enantioselective reaction can be used for the synthesis of the optically active isotetronic acid derivative **4** [eqn. (2)].

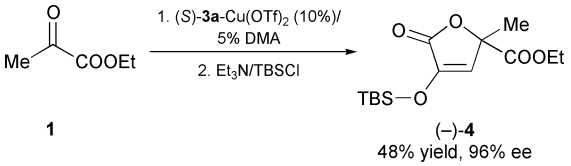

1 (−)-**4** 48% yield, 96% ee (2)

Isotetronic acids have been found to exhibit important biological effects such as aldose reductase inhibitory activity[11] and antitumor activity.[12] Reaction of the homo-aldol product **2** with Et_3N and TBSCl gives **4** in 48% isolated yield (from **1**)† under non-optimised reaction conditions.[13] The formation of **4** where the catalytic enantioselective approach is the first step, is a significant improvement compared to the multi-step and complex synthetic approaches previously reported.[8]

In summary, a catalytic highly enantioselective homo-aldol reaction of ethyl pyruvate giving diethyl-2-hydroxy-2-methyl-4-oxoglutarate in up to 96% ee has been developed. This reaction which mimics the pyruvate-dependent aldolase can be used for the preparation of optically active isotetronic acid derivatives in two steps.

We are indebted to The Danish National Research Foundation for financial support.

Notes and references

† Representative procedure for the catalytic asymmetric homo-aldol reaction: To an oven or flame dried Schlenk flask Cu(OTf)$_2$ (36.2 mg, 0.10 mmol) and 2,2′-isopropylidenebis[(4*S*)-4-*tert*-butyl-2-oxazoline] (32.4 mg, 0.11 mmol) were added. The mixture was stirred under vacuum for 2 h and filled with Ar. Dry solvent (2 mL) was added and the solution was stirred for 2 h. The amine was added followed by the addition of ethyl pyruvate (110 μL, 1.0 mmol). The reaction mixture was stirred for 40 h and was then flushed through a plug of silica with Et_2O as the eluent. Solvent was removed *in vacuo* and the residue was redissolved in CH_2Cl_2 followed by the addition of dry Et_3N (200 μL, 1.5 mmol) and TBSCl (196 mg, 1.3 mmol). The solution was stirred overnight and was purified by FC (SiO_2, 12% Et_2O–pentane) to yield 3-*tert*-butyldimethylsilyloxy-5-methyl-2-oxo-2,5-dihydrofuran-5-carboxylic acid ethyl ester (**4**) as a clear colourless oil (72 mg, 0.24 mmol, 48%).^{1}H-NMR (400 MHz, $CDCl_3$) δ 6.23 (s, 1H), 4.21 (q, J = 7.2, 2H), 1.69 (s, 3H), 1.27 (t, J = 7.2, 3H), 0.96 (s, 9H), 0.24 (s, 6H); ^{13}C-NMR (100 MHz, $CDCl_3$) δ 169.0, 168.1, 143.2, 124.4, 81.7, 62.4, 25.4, 22.9, 18.3, 14.0, 1.0; IR : ν/cm^{-1}: 2958 (m), 2934 (m), 2861 (m), 1890 (s), 1745 (s), 1656 (s), 1473 (w), 1330 (w), 1257 (s), 1208 (s), 1097 (s); HRMS: calcd. for $C_{14}H_{24}O_5Si$ [M + Na]$^+$ 323.1291, found 323.1290; $[\alpha]_D^{23}$ = −84 (c = 0.01, CH_2Cl_2) 96% ee by chiral GC using a Chrompack CP-Chirasil Dex CB (β-PM) column, τ(major) = 20.3 min, τ(minor) = 20.6 min.

1 See *e.g.* (*a*) C.-H. Wong and G. M. Whitesides, *Enzymes in Synthetic Organic Chemistry*, Pergamon, Oxford, 1994; (*b*) K. Drauz and H. Waldmann, *Enzyme Catalysis in Organic Synthesis*, VCH, Weinheim, 1995; (*c*) B. L. Horecker, O. Tsolas and C.-Y. Lai, *The Enzymes*, vol. VII, ed. P. D. Boyer, Academic Press, New York, 1975, p. 213; (*d*) W. D. Fessner and C. Walter, *Bioorg. Chem.*, 1997, **184**, 97.

2 See *e.g.* T. D. Machajewski and C.-H. Wong, *Angew. Chem., Int. Ed.*, 2000, **39**, 1353.

3 See *e.g.* (*a*) G. E. Keck and D. Krishnamurthy, *J. Am. Chem. Soc.*, 1995, **117**, 2363; (*b*) K. Mikami and S. Matsukawa, *J. Am. Chem. Soc.*, 1994, **116**, 4077; (*c*) D. A. Evans, M. C. Kozlowski, J. A. Murry, C. S. Burgey, K. R. Campos, B. T. Connell and R. J. Staples, *J. Am. Chem. Soc.*, 1999, **121**, 669; (*d*) D. A. Evans, C. S. Burgey, M. C. Kozlowski and S. W. Tregay, *J. Am. Chem. Soc.*, 1999, **121**, 686; (*e*) K. Mikima, S. Matsukawa, M. Nagashima, H. Funabashi and H. Morshima, *Tetrahedron Lett.*, 1997, **38**, 579; (*f*) R. A. Singer and E. M. Carreria, *Tetrahedron Lett.*, 1997, **38**, 927; (*g*) E. M. Carreria, R. A. Singer and W. S. Lee, *J. Am. Chem. Soc.*, 1994, **116**, 8837; (*h*) K. Ishimaru, K. Monda, Y. Yamamoto and K.-y. Akiba, *Tetrahedron*, 1998, **54**, 727; (*i*) T. K. Hollis and B. Bosnich, *J. Am. Chem. Soc.*, 1995, **117**, 4570; (*j*) S. Kobayashi, Y. Fujishita and T. Mukaiyama, *Chem. Lett.*, 1990, 1455; (*k*) T. Mukaiyama, *Aldrichimica Acta.*, 1996, **29**, 59.

4 See *e.g.* E. A. Carreira, W. Lee and R. A. Singer, *J. Am. Chem. Soc.*, 1995, **117**, 3649.

5 See *e.g.* (*a*) R. A. Singer and E. M. Carreria, *J. Am. Chem. Soc.*, 1995, **117**, 12 360; (*b*) Y. Kim, R. A. Singer and E. M. Carreria, *Angew. Chem., Int. Ed.*, 1998, **37**, 1261; (*c*) S. D. Rychnovsky, U. R. Khire and G. Yang, *J. Am. Chem. Soc.*, 1997, **119**, 2058.

6 (*a*) Y. M. A. Yamada, N. Yoshikawa, H. Sasai and M. Shibasaki, *Angew. Chem., Int. Ed.*, 1997, **36**, 1871; (*b*) R. Kuwano, H. Miyazaki and Y. Ito, *Chem. Commun.*, 1998, 71.

7 The 'pyruvate-dependent aldolase' enzyme catalysing this reaction in nature is 4-hydroxy-2-oxo-4-methyl glutarate aldolase (EC4.1.3.17), see ref. 2.

8 See *e.g.* (*a*) D. Enders, H. Dyker and F. R. Leusink, *Chem. Eur. J.*, 1998, **4**, *2*, 311; (*b*) E. Guichard, P. Etievant, R. Henry and A. Mosandl, *Z. Lebensm.-Unters.-Forsch.*, 1992, **195**, 540; (*c*) I. Blank, J. Lin, R. Fumeaux, D. H. Welti and L. B. Fay, *J. Agric. Chem.*, 1996, **44**, 1851; (*d*) J. Bigorra, J. Font, C. Ochoa de Echagueun and R. M. Ortuno, *Tetrahedron*, 1993, **49**, 6717; (*e*) A. G. M. Barrett and H. G. Sheth, *J. Org. Chem.*, 1983, **48**, 5017; (*f*) S. V. Attword and A. G. M. Barrett, *J. Chem. Soc., Perkin Trans. 1*, 1984, 1315.

9 For recent reviews see (*a*) J. S. Johnson and D. A. Evans, *Acc. Chem. Res.*, 2000, **33**, 325; (*b*) K. A. Jørgensen, M. Johannsen, S. Yao, H. Audrain and J. Thorhauge, *Acc. Chem. Res.*, 1999, **32**, 605; (*c*) A. K. Ghosh, P. Mathivanan and J. Cappiello, *Tetrahedron: Asymmetry*, 1998, **9**, 1.

10 S. Yao, M. Johannsen, H. Audrain, R. G. Hazell and K. A. Jørgensen, *J. Am. Chem. Soc.*, 1998, **120**, 8599.

11 J. R. Anderson, R. L. Edwards and A. J. S. Whalley, *J. Chem. Soc., Perkin Trans. 1*, 1982, 215.

12 (*a*) I. Ushida, Y. Itoh, T. Namiki, M. Nishikawa and M. Hashimoto, *Tetrahedron Lett.*, 1986, **27**, 2015; (*b*) T. Namiki, Y. Suzuki, K. Sawada, Y. Itoh, T. Oku, Y. Kitaura and M. Hashimoto, *Chem. Pharm. Bull.*, 1987, **35**, 2594; (*c*) T. Namiki, M. Nishikawa, Y. Itoh and I. Uchida, *J. Antibiot.*, 1987, **40**, 1400; (*d*) T. Namiki, Y. Baba, Y. Suzuki, M. Nishikawa, K. Sawada, Y. Itoh, T. Oku, Y. Kitaura and M. Hashimoto, *Chem. Pharm. Bull.*, 1988, **36**, 1404; (*e*) M. Nishikawa, K. Yoshiko, M. Okamoto and M. Kohsaka, *J. Antibiot.*, 1990, **43**, 1186; (*f*) M. Nishikawa, K. Yoshida, M. Okamoto, Y. Itoh and M. Kohsaka, *J. Antibiot.*, 1991, **44**, 441; (*g*) A. Zask, *J. Org. Chem.*, 1992, **57**, 4558.

13 Problems isolating the unprotected isotetronic acid have been encountered before see ref. 8*a*.

ChemComm

New insights into the *endo–exo* stereoselectivity of the intramolecular Diels-Alder reaction of 1,3,8-nonatrienes†

Michael J. Lilly,[a] Michael N. Paddon-Row,*[b] Michael S. Sherburn*[c] and Craig I. Turner[c]

[a] *Institute of Fundamental Sciences, Massey University, Private Bag 11222, Palmerston North, New Zealand*
[b] *School of Chemistry, University of New South Wales, Sydney, NSW 2052, Australia. E-mail: m.paddonrow@unsw.edu.au*
[c] *School of Chemistry, University of Sydney, Sydney, NSW 2006, Australia. E-mail: m.sherburn@chem.usyd.edu.au*

Received (in Cambridge, UK) 8th August 2000, Accepted 27th September 2000
First published as an Advance Article on the web

B3LYP/6-31G(d) theory predicts the experimental *endo–exo* selectivity of intramolecular Diels-Alder reactions of C9-substituted 1,3,8-nonatrienes: the reactions are concerted but the transition structures are remarkably asynchronous.

The intramolecular Diels-Alder (IMDA) cycloaddition is a strategy-level reaction in synthesis[1] that is being viewed increasingly as a biosynthetic event.[2] If this process is to reach its optimum synthetic potential and be fully understood in its biological setting, the stereochemical outcome of IMDA reactions must be more readily predicted and understood. *Exo* and *endo* transition structures (TSs) have been located for the prototype 1,3,8-nonatriene and 1,3,9-decatriene IMDA reactions at the HF/3-21G level of theory.[3,4] These structures were used to construct empirical force field models for a wide range of IMDA reactions.[5] While this hybrid quantum mechanics–molecular mechanics model reproduces many experimentally determined diastereoselectivities with remarkable accuracy, terminally activated 1,3,8-nonatrienes in which the dienophile activating group is disposed in a *Z*-orientation are predicted to form *cis*-fused bicyclic cycloadducts when, in fact, the *trans*-fused stereoisomer is the major observed product.[5]

In studies directed towards unearthing the reasons for the *exo* preference‡ of IMDA reactions of terminally activated 1,3,8-nonatrienes, we have examined the intramolecular cycloadditions of **1**, **2** and several related compounds using B3LYP/6-31G(d) theory. Thus, *exo* and *endo* TSs for nine related systems have been located at a higher level of theory than in any previous investigation into IMDA reactions. Our results confirm the asymmetric stretch–twist asynchronous transition state model proposed for 1,3,8-nonatriene IMDA reactions,[6] reveal hidden TS features and shed new light on their *endo–exo* preferences.

To confirm the experimental *exo* preference of terminally activated trienes, two IMDA precursors differing only in dienophile geometry were prepared and cyclised.[7] Triene precursors **1** and **2** (Fig. 1)§ were prepared by esterification of 2,4-hexadien-1-ol with maleic anhydride–diazomethane[8] and methyl fumaroyl chloride[9] respectively. Thermolysis of the *Z*-dienophile precursor **1** in dilute toluene solution at 110 °C was complete within 2 h to afford a 79 : 21 mixture of *exo* and *endo* stereoisomers. Intramolecular cycloaddition of *E*-dienophile precursor **2** proceeded more slowly to afford a 65 : 35 mixture of *exo* and *endo* stereoisomers, again in good yield. The *exo* preference of the IMDA reaction of both **1** and **2**, and the increased *exo* selectivity of the *Z*-dienophile precursor are mirrored in the trimethylene tether series.[10] That these thermal intramolecular cycloadditions are under kinetic control was demonstrated by subjecting pure samples of each of the

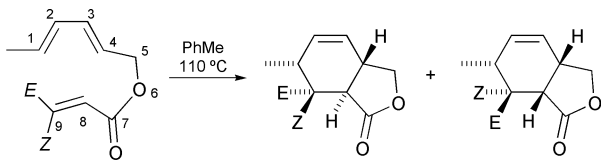

1 (*E* = H, *Z* = CO_2Me; 2h, 79%) **3** *exo* 79:21 **4** *endo*
2 (*E* = CO_2Me, *Z* = H; 23h, 85%) **5** *exo* 65:35 **6** *endo*

Fig. 1 *Exo*-selective IMDA reactions of **1** and **2**.

† Electronic supplementary information (ESI) available: final optimised coordinates for stationary points in all transition structures. See http://www.rsc/org/suppdata/cc/b0/b006483l/

Table 1 B3LYP/6-31G(d) *exo–endo* IMDA TS energy differences and predicted ratios, TS partial bond lengths and dihedrals

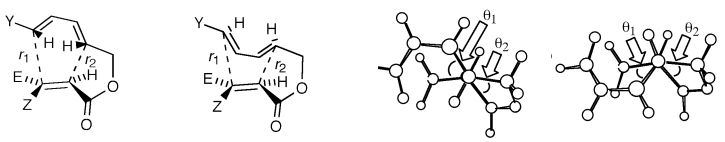

	Substituents					*exo*		*endo*		*exo*		*endo*	
Entry	Y	Z	E	ΔE^a	*exo–endo*[b]	r_1	r_2	r_1	r_2	θ_1	θ_2	θ_1	θ_2
1	H	H	H	1.3	40:60	2.357	2.165	2.314	2.230	61.7	44.6	42.6	42.4
2	H	NH_2	H	−7.0	90:10	2.654	1.875	2.551	1.956	70.8	37.5	40.4	38.8
3	H	H	NH_2	1.25	40:60	2.629	1.944	2.460	2.051	58.4	44.6	47.2	43.9
4	H	CN	H	−7.9	92:8	2.634	1.985	2.477	2.084	70.8	35.5	41.6	36.8
5	H	H	CN	1.3	40:60	2.549	2.035	2.477	2.092	63.6	43.2	45.3	42.6
6	H	CO_2Me	H	−9.7	95:5	2.676	1.994	2.558	2.055	73.8	33.0	34.7	30.0
7	H	H	CO_2Me	−0.79	56:44	2.543	2.036	2.472	2.098	62.8	42.5	45.3	41.5
8	Me	CO_2Me	H	−10.7	97:3	2.741	1.972	2.631	2.004	73.6	32.9	34.7	29.6
9	Me	H	CO_2Me	−0.57	55:45	2.678	1.957	2.581	2.016	64.3	41.2	46.4	40.8

[a] $E(exo) - E(endo)$, kJ mol^{-1}. [b] Boltzmann populations from ΔE values (plus zpe correction) at 110 °C.

DOI: 10.1039/b006483l

stereoisomers **3**–**6** to the cycloaddition reaction conditions. In each case, no isomerisation was observed.

Table 1 presents data for fully optimised B3LYP/6-31G(d) *endo* and *exo* IMDA TSs¶ of related ester-linked 1,3,8-nonatrienes.‖ An *endo* selective IMDA reaction is predicted for the parent acrylate derivative (Table 1, entry 1).** The calculations correctly predict the qualitative trends in *exo*–*endo* selectivity for **1** and **2**, *i.e.* strong *exo* selectivity for **1** (entry 8) and less so for **2** (entry 9). Three important conclusions may be drawn from the data of Table 1: (1) For C9-substituted trienes, the *exo*–*endo* selectivity is strongly dependent on the *E*–*Z* stereochemistry of the dienophile. Thus, *Z*-dienophiles (entries 2, 4, 6 and 8) are predicted to be significantly *exo* selective, while the *E*-dienophiles exhibit either a less pronounced shift towards the *exo* product (entries 7 and 9) or no change (entries 3 and 5). The presence of a terminal diene substituent (Y) has a negligible effect upon this preference (compare entries 6 *vs.* 8; 7 *vs.* 9). (2) In stark contrast to IMDA reactions of C1-substituted trienes,[11] the *exo*–*endo* selectivity is scarcely affected by the electronic demands of the C9-substituent (compare data for NH_2 *vs.* CN or CO_2Me). (3) All TSs display substantial bond forming asynchronicity which is particularly pronounced for the C9-substituted systems. In all cases the developing *internal* bond is more advanced than the developing *peripheral* bond, as indicated by the difference between their lengths, Δr ($= r_2 - r_1$): upon introduction of a C9 substituent (either *E* or *Z*), Δr increases from 0.19 Å (entry 1) to 0.51–0.77 Å, for the *exo* TSs, and from 0.08 Å to 0.37–0.63 Å, for the *endo* TSs. The large Δr values for the substituted systems is mainly due to much longer developing peripheral bonds in these TSs, with r_2 becoming as long as 2.74 Å (entry 8, *exo* TS).††

Our calculations support the Houk twist-asynchronous model[1,4,5,6] for explaining the influence of C9-substituents on the stereochemistry of IMDA reactions. In this model, applied to a trimethylene tether,[6] attention is focussed on strain in the developing cyclopentane ring in the IMDA TS. This strain is alleviated by reducing the magnitude of the C5–C4–C8–C7 dihedral angle θ_2 which may be achieved by twisting the TS about the C4–C8 bond such that C9 rotates in the *exo* (*outside*)[6] direction for the *exo* TS, and in the *endo* (*inside*)[6] direction for the *endo* TS. For a C9-substituted triene, this twisting is more facile for the *exo* TS than for the *endo* TS, since *endo* twisting in the *endo* TS probably leads to increased Pauli overlap repulsion‡‡ between the C9-substituent and the diene. The θ_1 (C3–C4–C8–C9 dihedral angle) values for the *Z*-substituted systems are consistent with this conjecture, with θ_1 displaying a large *exo* twist of 9–12° for the *exo* TSs, but a smaller *endo* twist of 1–8° for the *endo* TSs, relative to the unsubstituted system.

In contrast, the enhanced twist-asynchronicity seen in the *Z*-substituent TSs is absent in the corresponding *E*-substituent TSs since the θ_1 values for these TSs are similar to that for the unsubstituted TS (entry 1). This lack of enhanced twist asynchronicity is consistent with the reduced *exo* selectivity calculated for the *E*-substituted systems, compared to the corresponding *Z*-substituent series. What is the origin of this reduced *exo* preference for *E*-substituted nonatrienes?

Fig. 2 shows the *exo* and *endo* TSs for the parent acrylate compound (Table 1, entry 1), as viewed from the developing *peripheral* (C1–C9) bond. The preferred direction of asynchronous twist of the dienophile about the shorter *internal* (C4–C8) bond is depicted by a curved arrow. The approximate direction of the π electron density surface vector of the diene is depicted by solid arrows. The position of C9 substituents are indicated by *E* and *Z*.

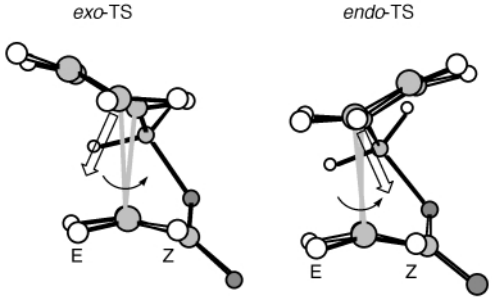

Fig. 2 Fully optimised B3LYP/6-31G(d) *exo* and *endo* TSs for the parent acrylate (Table 1, entry 1). See main text for key to arrows.

In the *exo* TS, preferred *exo* twisting of the dienophile about the C4–C8 axis moves the *Z*-substituent further from the diene, thereby reducing diene–substituent overlap repulsion. In contrast, preferred *endo* twisting in the *endo* TS moves the *Z*-group further into the diene region and overlap repulsion should increase, but slightly (because of the canting of the diene plane with respect to the dienophile). These effects combine to give strong *exo* selectivity for *Z*-substituted systems. For the *E*-substituted systems, *exo* twisting in the *exo* TS brings the substituent closer to the π electron density (once again, due to the canting of the diene), resulting in increased overlap repulsion. This outcome occurs also for preferred *endo* twisting in the *endo* TS. Consequently, on the basis of our refined Houk twist-asynchronicity model, reduced *exo*–*endo* selectivity is *expected* for *E*-substituted nonatrienes.

The authors thank The Australian Research Council for the award of a Senior Research Fellowship (to MNP-R) and a project grant (to MSS) and the New South Wales Centre for Parallel Computing for allocation of CPU time (to MNP-R).

Notes and references

‡ In intramolecular Diels-Alder reactions, we use the terms *endo* and *exo* to describe the orientation of the dienophile tether connection with respect to the diene. An *endo* orientation of the dienophile tether 'substituent' affords the *cis*-fused bicycle; an *exo* orientation of the dienophile tether furnishes the *trans*-fused cycloadduct.

§ For ease of comparison between the all-carbon prototype and other derivatives (such as the substituted esters described here), 1,3,8-nonatriene numbering is retained throughout.

¶ For entries 6–9, two discrete orientations of the terminal ester group with respect to the dienophile C=C bond are possible, namely s-*cis*- and s-*trans*. Both s-*cis* and s-*trans* TSs gave similar *exo*:*endo* product ratios and only data for the slightly lower energy s-*cis* TSs are given in Table 1.

‖ All TSs were fully optimised and characterised by B3LYP/6-31G(d) harmonic frequency calculations.

** Our B3LYP6-31G(d) calculations correctly predict predominant *endo* selectivity for the IMDA reaction of the trimethylene tether analogue of entry 1 (Table 1): the calculated *endo*:*exo* ratio is 83:17, compared to the experimentally observed value of 69:31.[3]

†† IRC calculations carried out on several substituted systems depicted in Table 1 show that these IMDA reactions are concerted, notwithstanding their marked asynchronicity.

‡‡ Electrostatic repulsion and secondary orbital overlap effects may also play a role.

1 Reviews: D. Craig, *Chem. Soc. Rev.*, 1987, **16**, 187; W. R. Roush, in *Comprehensive Organic Synthesis*, ed. B. M. Trost, I. Fleming and L. A. Paquette, Pergamon, Oxford, 1991, vol. 5, p. 513.
2 Recent reports of natural products possibly biosynthesised by IMDA reactions: *VM55599*, E. M. Stocking, J. F. Sanz-Cervera and R. M. Williams, *J. Am. Chem. Soc.*, 2000, **122**, 1675; *Solanapyrone*, H. Oikawa, T. Kobayashi, K. Katayama, Y. Suzuki and A. Ichihara, *J. Org. Chem.*, 1998, **63**, 8748; *Ligulaverin*, Y. Zhao, S. Parsons, B. A. Smart, R. X. Tan, Z. J. Jia, H. D. Sun and D. W. H. Rankin, *Tetrahedron*, 1997, **53**, 6195.
3 M. K. Diederich, F.-G. Klarner, B. R. Beno, K. N. Houk, H. Senderowitz and W. C. Still, *J. Am. Chem. Soc.*, 1997, **119**, 10 255.
4 F. K. Brown, U. C. Singh, P. A. Kollman, L. Raimondi, K. N. Houk and C. W. Bock, *J. Org. Chem.*, 1992, **57**, 4862.
5 L. Raimondi, F. K. Brown, J. Gonzalez and K. N. Houk, *J. Am. Chem. Soc.*, 1992, **114**, 4796.
6 F. K. Brown and K. N. Houk, *Tetrahedron Lett.*, 1985, **26**, 2297.
7 For related reactions on citraconate esters, see J. D. White and B. G. Sheldon, *J. Org. Chem.*, 1981, **46**, 2273.
8 M. J. Lilly and M. S. Sherburn, *Chem. Commun.*, 1997, 687.
9 M. J. Batchelor and J. M. Mellor, *J. Chem. Soc., Perkin Trans. 1*, 1989, 985.
10 W. R. Roush, A. I. Ko and H. R. Gillis, *J. Org. Chem.*, 1980, **45**, 4264.
11 T.-C. Wu and K. N. Houk, *Tetrahedron Lett.*, 1985, **26**, 2293.

A density functional theory study of π-facial stereoselectivity in intramolecular Diels–Alder reactions†

Michael N. Paddon-Row*[a] and Michael S. Sherburn[b]

[a] *School of Chemistry, University of New South Wales, Sydney, NSW 2052, Australia. E-mail: m.paddonrow@unsw.edu.au*
[b] *School of Chemistry, University of Sydney, Sydney, NSW 2006, Australia*

Received (in Cambridge, UK) 8th August 2000, Accepted 27th September 2000
First published as an Advance Article on the web 31st October 2000

B3LYP/6-31G(d) theory has been used to construct a transition structure model which correctly accounts for the observed π-diastereofacial selectivity in intramolecular Diels-Alder reactions induced by allylic substituents attached to the diene.

In addition to the extraordinary number of synthetic studies reported on the intramolecular Diels-Alder (IMDA) reaction,[1] there is growing interest in its stereochemical interpretation by computational methods.[2] The stereochemical outcome of IMDA reactions is complicated by *endo–exo*- and π-facial attributes, factors which allow up to four stereoisomeric products for each concerted process. We recently reported some of the first examples of IMDA reactions in which the stereocontrolling group is at the terminus of the diene (Fig. 1).[3] Whilst *exo* cycloadducts were formed exclusively in all cases, the level of π-diastereofacial selectivity was tuned by altering the substituents at the allylic stereocentre (C*) of **1**. The source of the *exo* preference of this general class of IMDA reactions was discussed in the previous communication.[4] Herein we explain our observed *π-facial* selectivities using transition structure (TS) models based on B3LYP/6-31G(d) theory, which has been shown to give good descriptions of TSs for the intermolecular Diels-Alder reaction.[5]

The origin of the observed π-facial selectivity in the IMDA reaction of **1** (Fig. 1), in terms of identifying the preferred disposition of the allylic substituents R, X and H among the *inside* (*in*), *anti* (*an*), or *outside* (*ou*) positions in TS **7** (Fig. 2), was investigated by carrying out B3LYP/6-31G(d) density functional theory calculations on the TSs for the IMDA reaction of **4**, which serves as a good simulacrum of **1**. In addition to the three conformations about the C1–C* bond, three conformations about the allylic C*–O bond and s-*cis*–s-*trans* orientations of the C9–CO_2CH_3 bond are possible (see **8**, Fig. 2). Thus, in principle, there are 18 diastereomeric TSs for *each* diastereomeric *exo* cycloadduct, **5** and **6**.‡ Two sets of six fully optimised lowest energy TSs associated with the different C1–C* conformations **7** were located, one set with the *Z*-ester adopting the s-*cis* conformation and the other with the *Z*-ester group in the s-*trans* conformation.

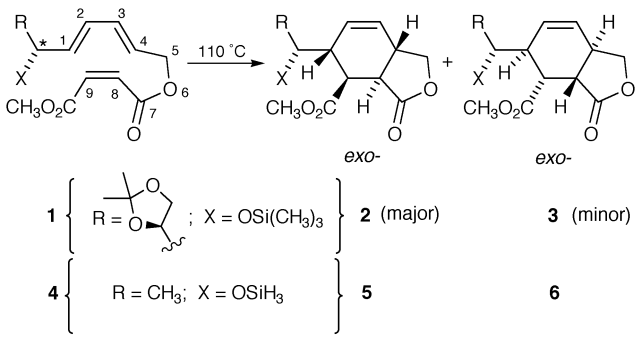

Fig. 1 The reported IMDA reaction (**1** → **2** + **3**) and the reaction under scrutinity by DFT (**4** → **5** + **6**).

† Electronic supplementary information (ESI) available: final optimised coordinates for stationary points in all transition structures. See http://www.rsc/org/suppdata/cc/b0/b006486f/

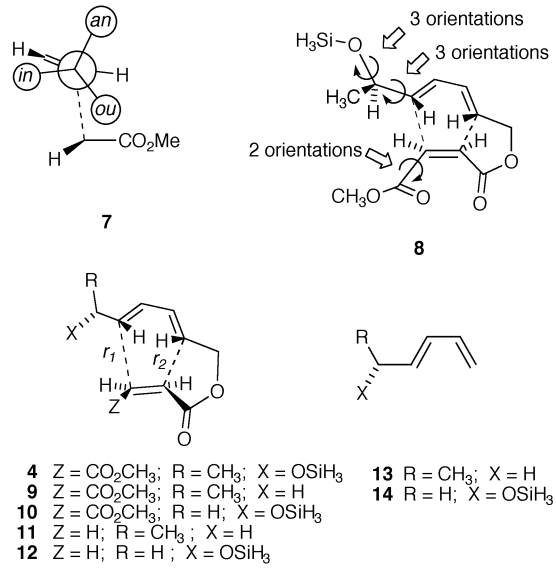

Fig. 2 Positioning of substituents in the IMDA TSs of **4** (**7** and **8**) and structures under investigation (**4**, **9**–**14**).

The relative energies, together with B3LYP/6-31G(d) zpe corrections, of the six diastereomeric TSs **4a**–**4f** for the IMDA reaction of **4**, in which the *Z*-ester adopts the s-*cis* conformation, are given in Table 1 and the profiles of the structures are shown

Table 1 B3LYP/6-31G(d) relative energies (kJ mol^{-1})[a]

Structure	*in*	*an*	*ou*	E_{rel}
4a[b]	$OSiH_3$	CH_3	H	0.0 (0.0)
4b[b]	H	$OSiH_3$	CH_3	4.0 (4.2)
4c[b]	CH_3	H	$OSiH_3$	14.5 (14.6)
4d[b]	$OSiH_3$	H	CH_3	4.8 (4.6)
4e[b]	CH_3	$OSiH_3$	H	10.5 (11.3)
4f[b]	H	CH_3	$OSiH_3$	5.55 (5.4)
9a[c]	H	CH_3	H	0.0 (0.0)
9b[c]	H	H	CH_3	5.4 (5.5)
9c[c]	CH_3	H	H	2.3 (2.0)
10a[c]	$OSiH_3$	H	H	0.0 (0.0)
10b[c]	H	$OSiH_3$	H	5.9 (6.8)
10c[c]	H	H	$OSiH_3$	12.6 (12.7)
11a	H	CH_3	H	0.0 (0.0)
11b	H	H	CH_3	4.5 (3.9)
11c	CH_3	H	H	4.3 (4.1)
12a	$OSiH_3$	H	H	0.0 (0.0)
12b	H	$OSiH_3$	H	2.2 (3.15)
12c	H	H	$OSiH_3$	2.1 (1.75)

[a] Relative energies corrected for zero point energy in parentheses. [b] s-*cis* ester conformation. [c] s-*trans* ester conformation.

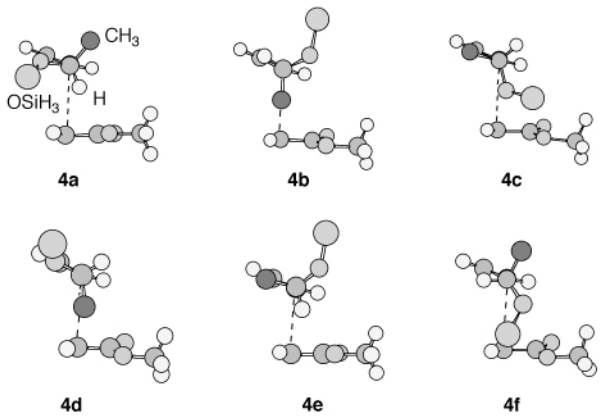

Fig. 3 The six TSs located for the IMDA reaction of **4**, as viewed down the C1–C4 axis (*cf.* **7**, Fig. 2). The developing *peripheral* C1–C9 bond is shown as a dashed line. Tether atoms are omitted for clarity.

in Fig. 3. The other set of six TSs associated with the s-*trans* conformation of the *Z*-ester are slightly higher in energy, by 2.5–6.0 kJ mol^{-1}, with respect to their corresponding s-*cis* congeners. In all other respects, the two sets of TSs show similar trends and so, unless stated otherwise, the following discussion refers to the *s-cis* set of TSs. The following five important points emerge from this study: (1) The lowest energy TS is **4a**, in which the silyloxy group adopts the *inside* position and the methyl group the *anti* position. This TS leads to formation of **5**, possessing the same configuration as **2**, the observed major product. The same major product is predicted from analysis of the TSs associated with the *Z*-ester adopting the s-*trans* conformation. (2) The three TSs **4a**–**4c** give **5**, whereas the three TSs **4d**–**4f** give the minor product **6** having the same configuration as the observed minor adduct **3**. A Boltzmann analysis of the two sets of conformations at 110 °C, including zpe corrections, gives a predicted product distribution of **5**:**6** = 74:26. A similar analysis carried out on the two sets of three TSs associated with the s-*trans Z*-ester conformations predicts a product distribution of **5**:**6** = 81:19. These analyses are in very good qualitative agreement with the experimental product distribution of **2**:**3** = 82:18 for the IMDA reaction of **1** (refluxing toluene) and provide compelling evidence in support of the reliability of our theoretical model. (3) The preferences of the methyl and silyloxy groups for the *anti* and the *inside* positions, respectively, in the lowest energy TS **4a** are a consequence of their respective innate tendencies to adopt these positions, irrespective of the presence of the other substituent. This conclusion is borne out by the calculations on **9** and **10**, each of which contains only one of these substituents. Thus, the most favourable TS for **9** is **9a**, with methyl in the *anti* position, and that for **10** is **10a**, with silyloxy in the *inside* position. The same trend is found for **11** and **12** in which the C9-ester substituent is absent, thereby demonstrating that the presence of this group is not required for inducing the conformational preferences of the methyl and silyloxy groups in these systems.§ (4) Inspection of the profiles of the TSs **4a**–**4f** (Fig. 3) reveals that the allylic substituents show little staggering about the forming *peripheral* bond (r_2) that is normally characteristic of additions to allylic systems.[6] Indeed, the C1–C* conformations in these TSs are essentially the same as those for isolated allylic ethers, with one substituent eclipsing the double bond.[7] This is hardly a surprising finding, given the extended length of the developing *peripheral* bond[4] (the *peripheral* bond length reaches a peak at 2.93 Å for **4d**). Model B3LYP/6-31G(d) calculations on the planar 1-ethyl-s-*cis*-butadiene **13**¶ show that the staggered conformer is favoured over the eclipsed conformer by 2.7 kJ mol^{-1}, which is similar to the energetic preference of the *anti* conformation over the *inside* conformation in the TSs for both **9** and **11**. In contrast, the calculations for **14** demonstrate that the eclipsed conformation is favoured over the staggered conformation by 2.7 kJ mol^{-1}, in reasonable agreement with the results for the TSs for **10** and **12**. (5) Our model for the favoured TS for IMDA reactions, in which the silyloxy group adopts the *inside* position and the alkyl group the *anti* position, is reminiscent of that proposed for *intermolecular* 1,3-dipolar cycloadditions of nitrile oxides to chiral allylic ethers.[6,8]

In conclusion, our model may be used to predict the degree of π-facial selectivity of IMDA reactions with substituents at the allylic position of the diene. The preferred TS, with the C* alkyl substituent *anti* and RO group *inside*, will be further favoured energetically by increasing the size of the alkyl group, for steric reasons, and by increasing the electron density at the oxygen atom of the RO group, for electrostatic reasons. The *inside* preference for the RO group may arise from an attractive electrostatic interaction between the oxygen atom and the hydrogen atom at C2. This would explain why greater π-facial selectivity is observed in IMDA reactions of silyl ethers (*e.g.* **1**) than the corresponding alcohol (Fig. 1; X = OH).[3] Our calculations predict even stronger selectivity for a metal alkoxide (Fig. 1; X = OM).

The authors thank the Australian Research Council for the award of a Senior Research Fellowship (to MNP-R) and a project grant (to MSS) and the New South Wales Centre for Parallel Computing for allocation of CPU time (to MNP-R).

Notes and references

‡ Cycloadducts **5** and **6** result from dienophile approach from below and above the plane of the diene respectively to enantiomerically pure **4**. For simplicity, the π-facial selectivity of this IMDA reaction was evaluated computationally by locating IMDA TSs for dienophile approach to the lower face of the diene for each enantiomer of **4**: *cf.* S. S. Wong and M. N. Paddon-Row, *J. Chem. Soc., Chem. Commun.*, 1991, 327.

§ With the exception of **4c**, the energetic ordering of the TSs calculated for **4a**–**4f** may be correctly deduced from the monosubstituted allylic systems **9** and **10** by simply adding the relative energies of the various pairs of TSs.

¶ The butadiene moiety in **4a**–**4f** is only *ca.* 5° off planarity.

1 Reviews: D. Craig, *Chem. Soc. Rev.*, 1987, **16**, 187; W. R. Roush, in *Comprehensive Organic Synthesis*, ed. B. M. Trost, I. Fleming and L. A. Paquette, Pergamon, Oxford, 1991, vol. 5, p. 513.

2 M. K. Diederich and F.-G. Klarner, *J. Am. Chem. Soc.*, 1998, **120**, 6212; M. K. Diederich, F.-G. Klarner, B. R. Beno, K. N. Houk, H. Senderowitz and W. C. Still, *J. Am. Chem. Soc.*, 1997, **119**, 10 255; L. Raimondi, F. K. Brown, J. Gonzalez and K. N. Houk, *J. Am. Chem. Soc.*, 1992, **114**, 4796; F. K. Brown, U. C. Singh, P. A. Kollman, L. Raimondi, K. N. Houk and C. W. Bock, *J. Org. Chem.*, 1992, **57**, 4862; F. K. Brown and K. N. Houk, *Tetrahedron Lett.*, 1985, **26**, 2297.

3 M. J. Lilly and M. S. Sherburn, *Chem. Commun.*, 1997, 687.

4 M. J. Lilly, M. N. Paddon-Row, M. S. Sherburn and C. I. Turner, *Chem. Commun.*, 2000, 2213.

5 O. Wiest and K. N. Houk, *Top. Curr. Chem.*, 1996, **183**, 1.

6 K. N. Houk, M. N. Paddon-Row, N. G. Rondan, Y.-D. Wu, F. K. Brown, D. C. Spellmeyer, J. T. Metz, Y. Li and R. J. Loncharich, *Science*, 1986, **231**, 1108.

7 B. W. Gung, M. A. Wolf and Z. Zhu, *J. Org. Chem.*, 1993, **58**, 3350.

8 K. N. Houk, S. R. Moses, Y.-D. Wu, N. G. Rondan, V. Jäger, R. Schohe and F. R. Fronczek, *J. Am. Chem. Soc.*, 1984, **106**, 3880.

Why are B_2O_2 rings rare?

Jacquelyn M. Burke, Mark A. Fox, Andrés E. Goeta, Andrew K. Hughes and Todd B. Marder*

Department of Chemistry, University of Durham, Durham, UK DH1 3LE. E-mail: Todd.Marder@durham.ac.uk

Received (in Cambridge, UK) 15th August 2000, Accepted 6th October 2000
First published as an Advance Article on the web

The single-crystal X-ray structure of $\{[HPPh_3]^+\}_2[B_4F_{10}O_2]^{2-}$ 2 reveals trigonal planar oxygen atoms in a rare example of a B_2O_2 ring; extended Hückel and *ab initio* molecular orbital calculations provide insight into the bonding and the geometry about oxygen.

As part of a study of the solid-state structures and NMR spectra of $R_3P{\cdot}BX_3$ adducts, we found that addition of $BF_3{\cdot}OEt_2$ to a hexane solution of PPh_3 yielded $Ph_3P{\cdot}BF_3$ **1**† as a white precipitate. Adduct **1** was previously synthesised from BF_3 and PPh_3 in CH_2Cl_2.[1,2] Attempts to grow single crystals of **1** from CH_2Cl_2–toluene led to the formation of several cube-shaped crystals. X-Ray diffraction studies showed these to be $\{[Ph_3PH]^+\}_2[B_4O_2F_{10}]^{2-}$ **2**,‡ which contains an unusual B_2O_2 ring. This salt apparently resulted from hydrolysis of **1** due to traces of adventitious water.

The novel dianion in the crystal of **2** (Fig. 1) lies on a centre of inversion and thus the B_2O_2 ring is rigorously planar. The B–O bond distances in the ring are 1.498(2) and 1.505(2) Å. The ring is nearly square, with O–B–O and B–O–B internal angles of 88.8(1) and 91.2(1)°, respectively. A BF_3 group is co-ordinated to each oxygen atom, with the B–O bond distance of 1.512(2) Å, and two fluorine atoms are bonded to each ring boron atom. The B–F bond distances in the BF_2 and BF_3 groups are very similar, averaging 1.362(3) and 1.374(5) Å, respectively. Interestingly, the coordination about oxygen is trigonal planar with the sum of the angles being 359.9(2)°.

Although fluoroborates with rings containing five or more atoms are known,[3,4] the dianion in **2** represents the only structurally well characterised discrete ring consisting solely of boron, fluorine and oxygen atoms. Unlike the common six-membered rings containing alternating boron and oxygen,[5] and four-membered rings containing alternating aluminium and oxygen,[6] only four crystal structures containing four-membered B_2O_2 rings have been reported.[7–10] Three of the structurally characterised compounds contain trigonal planar oxygens at the B_2O_2 ring: the porphyrin complex,[7] $[B_2O_2(BCl_3)_2(TpClpp)]$ (TpClpp = dianion of 5,10,15,20-tetra-*p*-chlorophenyl-porphyrin), neutral $[Me_2B–O–BMe_2]_2$,[8] and the 4-oxa-3-borahomoadamantane dimer.[10] A further example of trigonal planar oxygen was recently described by Schröder's group[11] in a complex with alkoxide bridging between BF_3 and a copper atom. In $\{C_6F_4\text{-}1,2\text{-}[B(C_6F_5)_2]_2(\mu\text{-}OR)\}^-$ (R = Me, C_6F_5), it was suggested[12] that the planar geometry about the oxygen could be due either to the bulky groups about O, or to the bite angle of the bidentate moiety coordinated to it. Our dianion $B_4O_2F_{10}^{2-}$ in **2** is simple and elegant with only 16 atoms, making it ideal for theoretical studies.

We have carried out extended Hückel and *ab initio* MO calculations to gain insight into the bonding within the ring and the geometrical preference at oxygen in **2**. EHMO calculations[13,14] were performed on both the dianion $B_4O_2F_{10}^{2-}$ and the $B_2O_2F_4^{2-}$ fragment, and the resulting energy level diagram is shown in Fig. 2, along with plots of the frontier orbitals of the $B_2O_2F_4^{2-}$ fragment; lower lying orbitals include the B–F bonds, fluorine p electrons and the oxygen and boron s orbitals. The bonding in the $B_2O_2F_4^{2-}$ square can be seen to arise from the B–O σ bonds in HOMO-3 and HOMO-4. The in- and out-of-plane combinations of the other oxygen p orbitals produce the four remaining orbitals drawn at the left side of Fig. 2; from the HOMO downwards these are O–O σ*, π*, π, σ. The Lewis basicity of the $B_2O_2F_4^{2-}$ square arises from the in-plane HOMO and HOMO-5 which overlap with the out-of-phase and in-phase combinations of BF_3 acceptor orbitals in the $B_4O_2F_{10}^{2-}$ dianion. The O–O π* and π orbitals are not involved in bonding to the BF_3 groups. The fact that O–O σ* is the $B_2O_2F_4^{2-}$ HOMO is thus likely responsible for the observed trigonal planar coordination at oxygen.

Ab initio MO calculations (GAUSSIAN94)[15] on the $B_2O_2F_4^{2-}$ fragment at the MP2/6-31G* level of theory revealed the energies of the frontier orbitals to be in the same order as in Fig. 2 with the O–O σ* and σ orbitals (HOMO and HOMO-5) significantly lower in relative energies. On coordinating two BF_3 groups to $B_2O_2F_4^{2-}$ to generate **2**, the O–O σ and σ* orbitals provide the electrons used in O–BF_3 bonding and are significantly lowered in energy; as a result the unperturbed O–O π* and π orbitals become HOMO and HOMO-1 respectively.

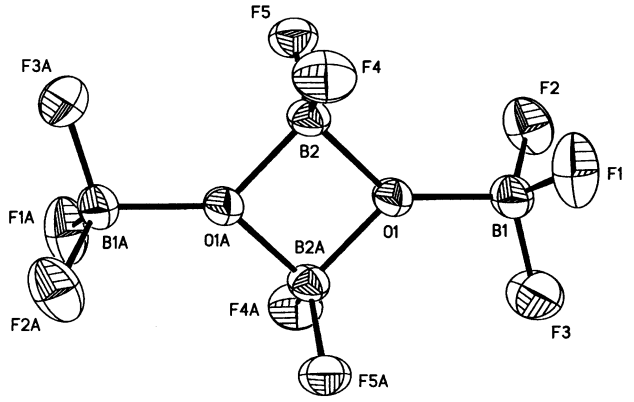

Fig. 1 Structure of the $B_4O_2F_{10}^{2-}$ dianion in **2** drawn with 50% probability ellipsoids showing the atom numbering. Selected bond distances (Å) and angles (°) for **3**: B(1)–O(1) 1.512(2), B(2)–O(1) 1.498(2), B(2)–O(1A) 1.505(2), B(1)–F(1) 1.380(3), B(1)–F(2) 1.372(2), B(1)–F(3) 1.369(3), B(2)–F(4) 1.362(2), B(2)–F(5) 1.362(2); O(1)–B(2)–O(1A) 88.83(12), B(2)–O(1)–B(2A) 91.17(12), B(1)–O(1)–B(2) 136.21(14), B(1)–O(1)–B(2A) 132.48(14).

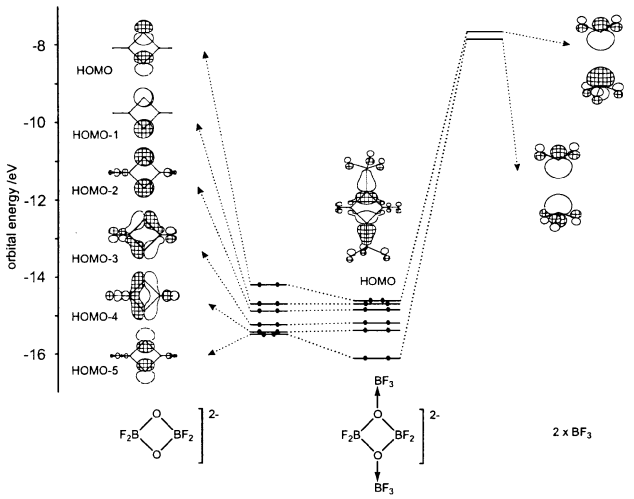

Fig. 2 Extended Hückel molecular orbital interaction diagram for the $B_4O_2F_{10}^{2-}$ anion in **2**.

DOI: 10.1039/b006685k

Geometry optimization of the dianion $B_4O_2F_{10}^{2-}$ in **2** at MP2/6-31G* revealed a minimum virtually identical to that found experimentally with O–B–O and B–O–B internal angles of 89.1 and 90.9° respectively. However, geometry optimization of the discrete fragment $B_2O_2F_4^{2-}$, resulted in a minimum with O–B–O and B–O–B internal angles of 97.5 and 82.5° respectively, and the O–O π* orbital as the HOMO. Thus, coordination of the two BF_3 Lewis acids to the in-plane oxygen orbitals stabilises the antibonding O–O σ* level without the need for significant lengthening of the O–O separation *via* distortion of the B_2O_2 square.

Alternative structures involving pyramidalisation at each oxygen atom can be accounted for by a mixing of the oxygen in- and out-of-plane orbitals (HOMO/HOMO-1 and HOMO-2/HOMO-5) to generate donor orbitals in either *cisoid* or *transoid* arrangements. These have been examined through qualitative Walsh diagrams (Fig. 3) with the observed structure at the energy minimum.

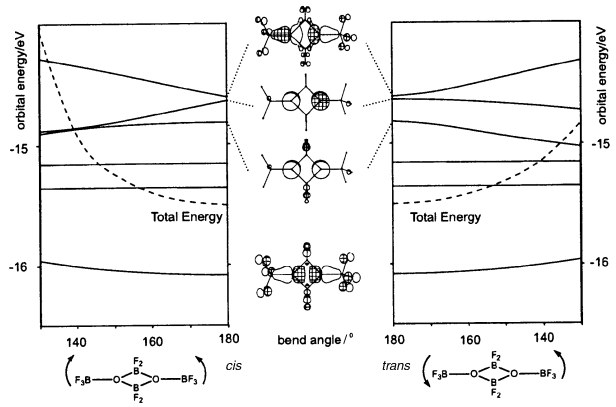

Fig. 3 Walsh diagrams for pyramidalisation at oxygen in the $B_4O_2F_{10}^{2-}$ dianion, calculated at the extended Hückel level. Total energies (in eV): planar, −2229.245; 130° *trans*, −2228.578; 130° *cis*, −2227.807.

Clearly, B_2O_2 rings are inherently destabilised by four-electron interactions of both σ- and π-symmetry between the oxygen atoms. Stable systems can be formed by complexation of Lewis acids such as BX_3, or, in the case of Al_2O_2 systems, by increasing the separation between the oxygen centres.

We thank EPSRC for a studentship (J. M. B.), for a research grant GR/M2308 (T. B. M.) and an Advanced Research Fellowship (M. A. F.). We also thank Dr D. Apperley for obtaining the solid-state ^{31}P NMR spectrum of **1**.

Notes and references

† Yield 84%. $C_{18}H_{15}BF_3P$ requires: C, 65.50; H, 4.58; Found: C, 65.03; H, 4.52%. Solid-state $^{31}P\{^1H\}$ NMR: δ −8.8. Partial characterisation of **1** has been reported.[2]

‡ *Crystal data* for **2**: $C_{18}H_{16}B_2F_5OP$, M = 395.90, monoclinic, a = 11.638(3), b = 12.174(3), c = 13.542(3) Å, β = 93.688(3)°, U = 1914.6(8) Å^3, T = 150 K, space group $P2_1/n$ (no. 14), Z = 4, μ(Mo-Kα) = 0.194 mm^{-1}, 22662 reflections measured on a Bruker SMART-CCD diffractometer, 5437 unique (R_{int} = 0.039) which were used in all calculations. Final $wR(F^2)$ = 0.1287 (all data) and $R(F)$ = 0.0482 [for 3923 data with $I > 2\sigma(I)$]. CCDC 182/1806. See http://www.rsc.org/suppdata/cc/b0/b006685k/ for crystallographic files in .cif format.

1 E. Muylle, G. P. van der Kelen and Z. Eeckhaut, *Spectrochim. Acta, Part A*, 1975, **31**, 1039.
2 E. Muylle, G. P. van der Kelen and E. G. Claeys, *Spectrochim. Acta, Part A*, 1976, **32**, 1149.
3 H. Binder, W. Matheis, G. Heckmann, H.-J. Deiseroth and H. Fu-Son, *Z. Naturforsch., Teil B*, 1985, **40**, 934 and references therein.
4 H. Schmidbaur, B. Brachthäuser, O. Steigelmann and H. Beruda, *Chem. Ber.*, 1992, **125**, 2705.
5 N. N. Greenwood and A. Earnshaw, *Chemistry of the Elements*, Pergamon Press, Oxford, 2nd edn., 1997, ch. 6, p. 205; F. A. Cotton, G. Wilkinson, C. A. Murillo and M. Bochmann, *Advanced Inorganic Chemistry*, Wiley-Interscience, New York, 6th edn., 1999, ch. 5, p. 171; however, see also: B. Pachaly and R. West, *J. Am. Chem. Soc.*, 1985, **107**, 2987 and M. Ito, N. Tokitoh and R. Okazaki, *Tetrahedron Lett.*, 1997, **38**, 4451.
6 J. P. Oliver and R. Kumar, *Polyhedron*, 1990, **9**, 409 and references therein; for an exception to this, see: O. Saied, M. Simard and J. D. Wuest, *Organometallics*, 1996, **15**, 2345.
7 W. J. Belcher, M. Breede, P. J. Brothers and C. E. F. Rickard, *Angew. Chem., Int. Ed.*, 1998, **37**, 1112.
8 H. Borrmann, A. Simon and H. Vahrenkamp, *Angew. Chem., Int. Ed. Engl.*, 1989, **28**, 180.
9 E. Hanecker, H. Nöth and U. Wietelmann, *Chem. Ber.*, 1986, **119**, 1904.
10 L. G. Vorontsova, O. S. Chizhov, L. S. Vasilév, V. V. Veselovskii and B. M. Mikhailov, *Isv. Akad. Nauk. SSSR, Ser. Khim.*, 1981, 353; L. G. Vorontsova, O. S. Chizhov, L. S. Vasilév, V. V. Veselovskii and B. M. Mikhailov, *Bull. Acad. Sci. USSR, Div. Chem. Sci. (Engl. Transl.)*, 1981, 273.
11 L. R. Sutton, A. J. Blake, P. A. Cooke and M. Schröder, *Chem. Commun.*, 2000, 563.
12 V. C. Williams, G. J. Irvine, W. E. Piers, Z. Li, S. Collins, W. Clegg, M. R. J. Elsegood and T. B. Marder, *Organometallics*, 2000, **19**, 1619.
13 EHMO calculations were performed with EH and CACAO; C. Mealli and D. M. Proserpio, *J. Chem. Educ.*, 1990, **67**, 399.
14 R. Hoffmann and W. N. Lipscomb, *J. Chem. Phys.*, 1962, **36**, 2179; R. Hoffmann, *J. Chem. Phys.*, 1963, **39**, 1397.
15 *Ab initio* calculations were performed with the GAUSSIAN94 package; GAUSSIAN94, Revision E.2, M. J. Frisch, G. W. Trucks, H. B. Schlegel, P. M. W. Gill, B. G. Johnson, M. A. Robb, J. R. Cheeseman, T. Keith, G. A. Petersson, J. A. Montgomery, K. Raghavachari, M. A. Al-Laham, V. G. Zakrzewski, J. V. Ortiz, J. B. Foresman, J. Cioslowski, B. B. Stefanov, A. Nanayakkara, M. Challacombe, C. Y. Peng, P. Y. Ayala, W. Chen, M. W. Wong, J. L. Andres, E. S. Replogle, R. Gomperts, R. L. Martin, D. J. Fox, J. S. Binkley, D. J. Defrees, J. Baker, J. P. Stewart, M. Head-Gordon, C. Gonzalez and J. A. Pople, Gaussian, Inc., Pittsburgh, PA, 1995.

ChemComm

Design, synthesis and structural investigation of a 2-D coordination network based on the self-assembly of the tetracarboxylate derivative of tetrathiacalix[4]arene and silver cation

Huriye Akdas,[a] Ernest Graf,[a] Mir Wais Hosseini*[a] André De Cian[a] and Jack McB. Harrowfield[b]

[a] *Laboratoire de Chimie de Coordination Organique, Université Louis Pasteur, F-67000 Strasbourg, France, UMR CNRS 7513. E-mail: hosseini@chimie.u-strasbg.fr*

[b] *University of Western Australia, Nedlands, Western Australia 6009, Australia*

Received (in Cambridge, UK) 25th September 2000, Accepted 5th October 2000
First published as an Advance Article on the web

The fully deprotonated tetrathiacalix[4]arene 1^{4-} in 1,3-alternate conformation and bearing four carboxylate units was shown to act as a tecton leading, in the presence of Ag^+ cation, to a 2-D coordination network in the crystalline phase which can be described as discrete binuclear [1^{4-}, $(Ag^+)_2]^{2-}$ complexes interconnected by Ag^+ cations.

Molecular networks are defined as infinite architectures possessing translational symmetry of assembling nodes (interaction patterns) and are obtained under self-assembly conditions from molecular components capable of reversible and mutual interactions. Coordination networks, based on exo-ligands and metal cations, form a subclass of molecular networks and are currently under active investigation.[1] The majority of coordination networks reported to date are based on two component systems composed of an organic exo-ligand bearing coordination sites oriented in a divergent manner and a metal cation. Furthermore, the ligands employed so far are mainly of the bis-monodentate,[2] bis-bidentate,[3] tetrakis monodentate[4] or bis-tridentate[5] types bearing almost exclusively nitrogen atoms as coordination sites.

For the design of coordination networks, instead of considering a two component system for which both the metal centre and the free exo-ligand act as tectons, a further conceptually new design principle may be based on the use of a metal complex acting as a metallatecton and a metal cation. The design of such a system may be based on a ligand bearing multiple coordination sites allowing, on one hand, the formation of a endomolecular complex with a metal cation M, and on the other, the interconnection of the latter complex into a coordination network using either the same metal cation M or another metallic centre M′. A similar strategy, based on the simultaneous use of coordination and hydrogen bonds has already been investigated with success.[6]

In the present contribution we report, to the best of our knowledge, the first example of a 2-D coordination network based on the use of the above mentioned strategy.

Compound **1**,[7] a tetrathiacalix[4]arene derivative in 1,3-alternate conformation and bearing four carboxylic acid groups, presents several interesting features (Scheme 1). In its fully deprotonated form, $\mathbf{1}^{4-}$ possesses a total of 16 heteroatoms (12 O and 4 S atoms) which may participate in the coordination of metal cations. Its 1,3-alternate conformation[7] allows the positioning of two coordination poles (one may define a coordination pole as a set of coordination sites located in close proximity and capable of coordinating to metal centres) below and above the main plane of the backbone with a 90° angle between them. Each coordination pole is composed of two carboxyl units and two ether junctions. Importantly, owing to the connection of the carboxyl groups to O atoms of the calix by a CH_2 unit, the ether O atom and one of the two oxygen atoms of the carboxyl group may adopt a *syn* conformation leading to a chelate of the glycol type capable of binding metal cations. Thus, within each coordination pole, two such units may bind a metal cation leading to a discrete binuclear metal complex (Fig. 1). This type of coordination mode has been previously observed and structurally proven for the dipotassium salt of a calix[4]arene derivative in 1,3-alternate conformation and bearing amide groups[8] and for the sodium salt of a calix[4]diquinone derivative which was also found to form a 1-D network.[9] It is worth noting that upon formation of the binuclear complex, the remaining O atoms on carboxylate groups would be blocked and oriented in a divergent fashion. Thus, for the formation of coordination networks, the discrete binuclear complex mentioned above which may act as a tetrakis monodentate metallatecton, may be interconnected using metal cations through the remaining O atoms (Fig. 2). The dimensionality of the coordination networks which may be formed using ligand **1** depends on the coordination requirements (coordination number and geometry) of the metal cation used. In principle, either 2- or 3-D networks may be expected.

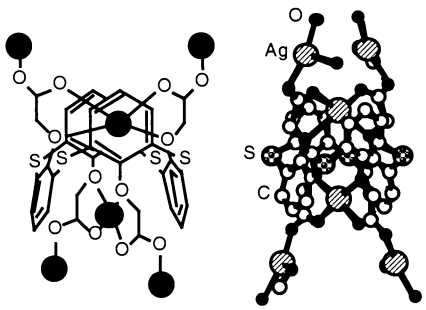

Fig. 1 Schematic representation of the binding mode of Ag^+ cations by ligand $\mathbf{1}^{4-}$ (left) and a portion of the X-ray structure showing the two modes of coordination for the cations with H atoms omited for clarity. For distances and angles see text.

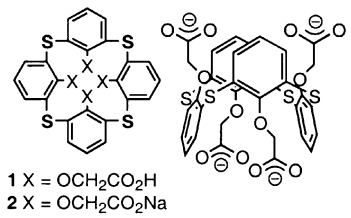

Scheme 1

Dealing with the metal cation, as mentioned above, owing to the fact that the formation of coordination networks using the ligand $\mathbf{1}^{4-}$ requires two different binding modes, silver appeared to be the most suitable cation. Indeed, Ag^+ forms kinetically labile complexes and shows rather loose coordination requirements since it may tolerate bi-, tri- or tetra-dentate ligands with linear, trigonal or tetrahedral coordination geometries. The Ag^+ cation has been extensively used for the formation of coordination networks.[10] In our own studies, Ag^+

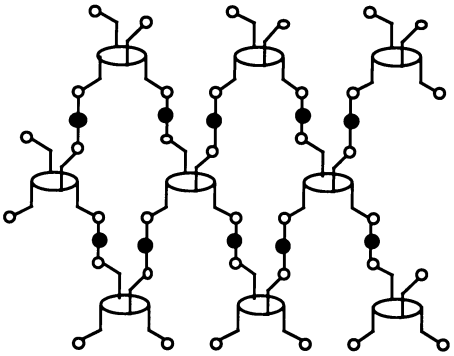

Fig. 2 Schematic representation of the 2-D network formed through interconnection of [$\mathbf{1}^{4-}$, $(Ag^+)_2]^{2-}$ units by Ag^+ cations. For clarity, the Ag^+ cations forming the binuclear complex are not shown.

has been used to form metallamacrocycle,[11] linear,[4] helical[12] and tubular[4b,11b] coordination polymers.

Compound **1** was prepared[7] in four steps stating with *p-tert*-butyltetrathiacalix[4]arene[13] and its 1,3-alternate conformation was established by X-ray diffraction on a single crystal.[7] [$\mathbf{1}^{4-}$, $(Na^+)_4$] was generated upon treatment of **1** in MeOH by addition of 4 eq. of NaOH in H_2O. The removal of volatiles afforded a white solid which was dried in vacuum overnight. Upon slow diffusion at r.t. of a MeOH solution (1 ml) containing [$\mathbf{1}^{4-}$, $(Na^+)_4$] (10 mg) into an aqueous solution (1 ml) of $AgNO_3$ (2 mg), colourless crystals were obtained after three days. An X-ray study† on a single crystal showed the following relevant features (Figs. 1–3): the crystal is composed of $\mathbf{1}^{4-}$, $4Ag^+$, MeOH and H_2O solvent molecules. $\mathbf{1}^{4-}$ adopts the 1,3-alternate conformation thus presenting two carboxylate moieties on each face. The $OCH_2CO_2^-$ fragments adopt a *syn* conformation (OCCO dihedral angles of 14.0 and 11.9° on one side and −9.2 and −11.6° on the other). For the carboxylate units the C–O distance varies between *ca*. 1.23 and 1.27 Å. Dealing with silver, among the four present, two types of Ag^+ cation are observed. For the first variety composed of two Ag^+ cations, both are coordinated, one on each face, to the ligand thus affording the binuclear [$\mathbf{1}^{4-}$, $(Ag^+)_2]^{2-}$ complex. Both Ag^+ cations are tetracoordinated to four O atoms with two short (2.2–2.3 Å) and two long (2.6–2.9 Å) O–Ag distances and adopt a strongly distorted square planar coordination geometry (OAgO angles varying from *ca*. 63 to 171°). However, owing to the fact that on each side of the complex the Ag^+ cations are located in close proximity to two carbon atoms belonging to two opposite aromatic rings (d_{C-Ag} = 3.2–3.3 Å, with CAgC angle of 8.8°), one may describe the coordination geometry around the silver cation as distorted octahedral.

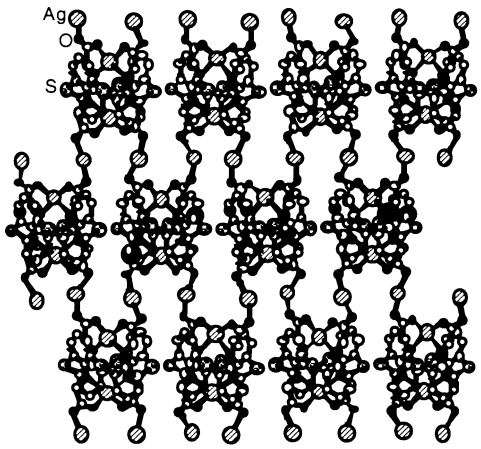

Fig. 3 A portion of the X-ray structure of the 2-D network formed between $\mathbf{1}^{4-}$ and Ag^+. H atoms and solvent molecules are not shown for clarity. For distances and angles see text.

The other type of Ag^+ cations serve to interconnect the dianionic binuclear [$\mathbf{1}^{4-}$, $(Ag^+)_2]^{2-}$ complexes which act as tectons, thus leading to the formation of a 2-D coordination network (Fig. 2). The interconnection is achieved through Ag–O bonds (d_{Ag-O} varying between *ca*. 2.2 and 2.4 Å) engaging the remaining O atoms on the carboxylate units (d_{C-O} = 2.24–2.26 Å) (Fig. 3). The coordination sphere around the metal centres is composed of three O atoms among which one MeOH (d_{Ag-O} of *ca*. 2.40 Å) or one H_2O (d_{Ag-O} of *ca*. 2.39–2.69 Å) solvent molecules with distorted trigonal coordination geometry (OAgO angles of 89.4, 117.4 and 151.2° for Ag^+ coordinated to MeOH and 95.8, 124.0 and 140.0° for Ag^+ coordinated to H_2O).

In conclusion, using the tetraanionic form of the thiacalix-[4]arene bearing four carboxylate units and Ag^+ cation, a 2-D coordination network has been obtained and structurally characterised in the crystalline phase. The network was composed of discrete binuclear [$\mathbf{1}^{4-}$, $(Ag^+)_2]^{2-}$ complexes acting as metallatectons interconnected by Ag^+ cations. The effect of the number of negative charge on the calix unit on the formation of coordination network, as well as the nature of the connecting cation are currently under investigations.

Notes and references

† *Crystal data* for **1**: colourless, 173 K, $C_{65}H_{45}Ag_8O_{26}S_8 \cdot 4CH_3OH \cdot 4H_2O$, M = 2561.77, monoclinic, a = 16.6647(6), b = 24.7585(5), c = 19.9024(7) Å, β = 91.224(5), U = 8209.7(8) Å^3, Z = 4, space group $P2/n$, D_C = 2.07 g cm^{-3}, Nonius Kappa CCD, Mo-Kα radiation (λ = 0.71073 Å), μ = 2.157 mm^{-1}, 6997 data with $I > 3\sigma(I)$, R = 0.059, R_w = 0.062. Structural determination was achieved using the Nonius OpenMolenN package.[14] CCDC 182/1802. See http://www.rsc.org/suppdata/cc/b0/b007761p/ for crystallographic files in .cif format.

1 S. R. Batten and R. Robson, *Angew. Chem., Int. Ed.*, 1998, **37**, 1460.
2 O. M. Yaghi, H. L. Li, C. Davis, D. Richardson and T. L. Groy, *Acc. Chem. Res.*, 1998, **31**, 474; T. L. Hennigar, D. C. MacQuarrie, P. Losier, R. D. Rogers and M. J. Zaworotko, *Angew. Chem., Int. Ed. Engl.*, 1997, **36**, 972; A. J. Blake, N. R. Champness, S. S. M. Chung, W.-S. Li and M. Schröder, *Chem. Commun.*, 1997, 1675.
3 U. Velten and M. Rehahn, *Chem. Commun.*, 1996, 2639.
4 (*a*) G. Mislin, E. Graf, M. W. Hosseini, A. De Cian, N. Kyritsakas and J. Fischer, *Chem. Commun.*, 1998, 2545; (*b*) C. Klein, E. Graf, M. W. Hosseini, A. De Cian and J. Fischer, *Chem. Commun.*, 2000, 239.
5 E. C. Constable and A. M. W. Cargill Thompson, *J. Chem. Soc., Dalton Trans.*, 1992, 3467; S. J. Loeb and G. K. H. Shimizu, *Chem. Commun.*, 1993, 1395; M. Ferigo, P. Bonhôte, W. Marty and H. Stoeckli-Evans, *J. Chem. Soc. Dalton Trans.*, 1994, 1549; M. Loï, E. Graf, M. W. Hosseini, A. De Cian and J. Fischer, *Chem. Commun.*, 1999, 603.
6 A. D. Burrows, D. M. P. Mingos, A. J. P. White and D. Williams, *Chem Commun.*, 1996, 97; C. B. Aakeröy, A. M. Beatty and D. S. Leinen, *Angew. Chem., Int. Ed.*, 1999, **38**, 1815; A. S. Batsanov, P. Hubberstey, C. E. Russell and P. H. Walton, *J. Chem. Soc., Dalton, Trans.*, 1997, 2667; J. C. M. Rivas and L. Brammer, *New J. Chem.*, 1998, **22**, 1315.
7 H. Akdas, W. Jaunky, E. Graf, M. W. Hosseini, A. De Cian and J. Fischer, *Tetrahedron Lett.*, 2000, **41**, 3601.
8 P. D. Beer, M. G. B. Drew, P. A. Gale, P. B. Leeson and M. I. Ogden, *J. Chem. Soc., Dalton Trans.*, 1994, 3479.
9 P. D. Beer, P. A. Gale, Z. Chen, M. G. B. Drew, J. A. Heath, M. I. Ogden and H. R. Powell, *Inorg. Chem.*, 1997, **36**, 5880.
10 D. Perreault, M. Drouin, A. Michel and P. D. Harvey, *Inorg. Chem.*, 1992, **31**, 3688, K. A. Hirsch, S. R. Wilson and J. S. Moore, *Inorg. Chem.*, 1997, **36**, 2960; B. F. Abrahams, S. J. Egan, B. F. Hoskins and R. Robson, *Chem. Commun.*, 1996, 1099; F.-Q. Liu and T. Don Tilley, *Inorg. Chem.*, 1997, **36**, 5090.
11 (*a*) R. Schneider, M. W. Hosseini, J.-M. Planeix, A. De Cian and J. Fischer, *Chem. Commun.*, 1998, 1625; (*b*) M. Loï, M. W. Hosseini, A. Jouaiti, A. De Cian and J. Fischer, *Eur. J. Inorg. Chem.*, 1999, 1981.
12 C. Kaes, M. W. Hosseini, C. E. F. Rickard, B. W. Skelton and A. White, *Angew. Chem., Int. Ed.*, 1998, **37**, 920.
13 H. Kumagai, M. Hasegawa, S. Miyanari, Y. Sugawa, Y. Sato, T. Hori, S. Ueda, H. Kamiyama and S. Miyano, *Tetrahedron Lett.*, 1997, **38**, 3971.
14 OpenMolenN, Interactive Structure Solution, Nonius B. V., Delft, The Netherlands, 1997.

Understanding negative thermal expansion and 'trap door' cation relocations in zeolite rho

Barbara A. Reisner,†[a] Yongjae Lee,[b] Jonathan C. Hanson,[c] Glover A. Jones,[d] John B. Parise,*[be] David R. Corbin,[d] Brian H. Toby,[a] Andrea Freitag,[c] John Z. Larese[c] and Volker Kahlenberg[bf]

[a] *NIST Center for Neutron Research, National Institute of Standards and Technology, Gaithersburg, MD 20899-8562, USA. E-mail: John.Parise@sunysb.edu*
[b] *Geosciences and [e] Chemistry Departments, State University of New York, Stony Brook, NY 11794-2100, USA*
[c] *Chemistry Department, Brookhaven National Laboratory, Upton, NY 11973-5000, USA*
[d] *Central Research and Development, Du Pont Company, Experimental Station, P.O.Box 80262, Wilmington DE 19880-0262, USA*
[f] *Fachbereich Geowissenschaften (Kristallographie), Universität Bremen, Klagenfurter Strasse, D-28359 Bremen, Germany*

Received (in Irvine, CA, USA) 18th August 2000, Accepted 3rd October 2000
First published as an Advance Article on the web 31st October 2000

***In situ* time-resolved synchrotron X-ray and neutron powder diffraction studies indicate that the negative thermal expansion and 'trap door' cation relocations observed in zeolite rho result from water-mediated chemical changes that occur during dehydration.**

Zeolite rho exhibits exceptional flexibility, and its structure is particularly sensitive to cation identity, temperature, and hydration.[1] For example, Sr^{2+}-exchanged zeolite rho (Sr-rho) shows a large negative thermal expansion.[2] A more dramatic effect has been observed in Cd-rho, where Cd^{2+} cations relocate upon heating in a 'trap door' mechanism opening the access to the pores of RHO.[3,4] Both transformations have been previously attributed to temperature-driven phase transitions. To better understand the origin of these structural changes, time-resolved *in situ* synchrotron X-ray powder diffraction and neutron powder diffraction were performed using Pb-rho and Cd-rho. We found that both phenomena result from chemical changes that occur during dehydration rather than being a result of composition-independent, purely temperature-driven effects.

The RHO topology is composed of a body-centered cubic arrangement of truncated cuboctahedra or α-cages linked *via* double 8-rings of corner-connected tetrahedra. Three sites with unique coordination environments can accommodate charge-balancing, extra-framework cations: the single 8-ring (S8R), double 8-ring (D8R) and single 6-ring (S6R) sites. Each site has a distinct coordination environment, and cations preferentially occupy one of these sites depending upon their ionic radii. The framework can adopt a centric (C-form, $Im\bar{3}m$) or acentric (A-form, $I\bar{4}3m$) structure depending upon the unit cell composition and the temperature.[5,6]

Na,Cs-rho, the parent material used for cation-exchange, was prepared using a modification of the method described by Robson.[7] Pb-rho and Cd-rho were then prepared using standard ion-exchange techniques.‡ Time-resolved X-ray powder diffraction data were collected on the X7B beamline at the National Synchrotron Light Source (NSLS) using an *in situ* dehydration cell with an imaging plate detector.§[8] Neutron powder diffraction data were collected on the BT-1 powder diffractometer at the National Institute of Standards and Technology (NIST) Center for Neutron Research. Rietveld structure refinements[9] were performed with the GSAS package.[10]

Upon heating Pb-rho in the *in situ* synchrotron X-ray diffraction experiment, two distinct regions of cell contraction are observed (Fig. 1): a rapid decrease in cell length between 25 and 75 °C, and a second, more gradual decrease up to a temperature of approximately 500 °C. Rietveld refinements using these data indicate that the abrupt cell contraction is related to a conversion from the centric to the acentric form and that the gradual decrease in the unit cell length is coupled with a migration of Pb^{2+} from the S8R to the D8R site. Neutron powder diffraction studies were performed on partially deuterated Pb-rho.¶ Data were collected at room temperature on the sample dehydrated under vacuum at 250 °C. This sample was then heated to 550 °C under active vacuum ($< 10^{-4}$ Pa), and additional data were collected at this temperature and, after cooling *in vacuo*, at room temperature. Difference Fourier analysis of the neutron powder diffraction data collected on the sample dehydrated at 250 °C reveals the presence of D_2O at the D8R site and Pb^{2+} at the S8R site. In contrast, no D_2O is found when the sample is heated to 550 °C, nor when this sample is cooled to room temperature; in these models, Pb^{2+} ions are located at the D8R site, consistent with the changes in the Pb^{2+} occupancy observed from the *in situ* synchrotron X-ray powder diffraction data. The small difference between cell constants in these two samples is consistent with normal thermal expansion ($\approx 0.2\%$).

These results indicate that Pb-rho is not completely dehydrated under the gentle heating conditions that are typically used for dehydration, 200 °C $\leqslant T \leqslant$ 300 °C. Both regions of unit cell contraction are attributable to the loss of water. The first region corresponds to the loss of unbound water, while contraction in the second region can be attributed to the loss of water coordinated to Pb^{2+}. Up to a temperature of approx-

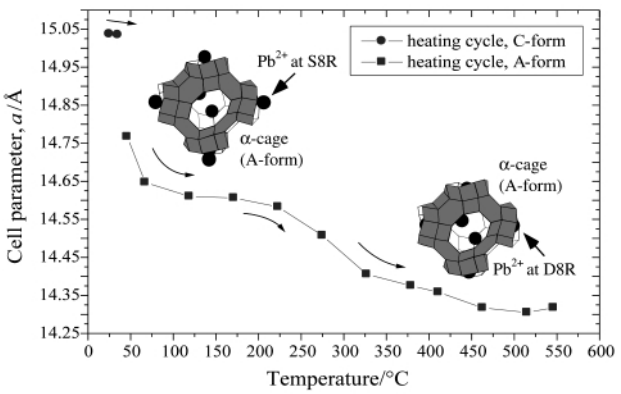

Fig. 1 The cell parameter of Pb-rho heated under air. Schematic diagrams illustrate the α-cages of the C- and A-forms and the siting of Pb^{2+}. (Vertices represent tetrahedrally coordinated Al or Si. Oxygen atoms are omitted for clarity).

† *Current address*: Department of Chemistry, James Madison University, Harrisonburg, VA 22807.

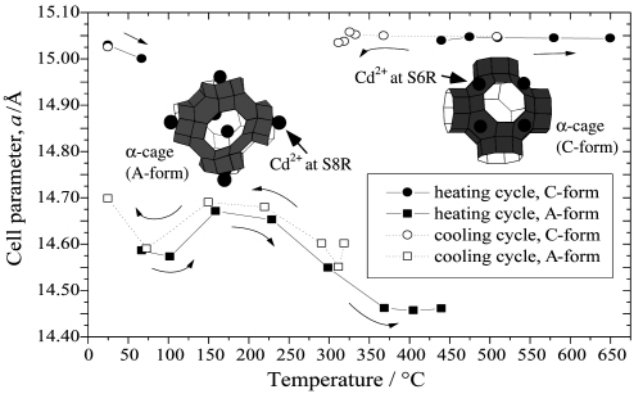

Fig. 2 The cell parameter of Cd-rho heated under air. Schematic diagrams illustrate the siting of Cd^{2+} in the α-cages.

imately 450 °C, both the cell parameter and the composition of the sample are still changing. It is likely that the presence of water strongly correlates with the siting of Pb^{2+} since they change in a concerted manner as a function of temperature. As water leaves the framework, Pb^{2+} must shift towards the D8R site, which provides a better coordination environment for Pb^{2+} in the absence of water. These observations may clarify the observation of the large negative thermal expansion observed for Sr-rho.[2] Since the large-volume, low-temperature phase was collected *in vacuo* at 100 °C and the small-volume, high-temperature phase was collected after heating at 200 °C, it is likely that dehydration was incomplete in the low-temperature phase and the observed negative thermal expansion can be attributed to dehydration.

In situ synchrotron X-ray powder diffraction data indicate that water plays an important role in the greater than 5 Å 'trap door' motion of Cd^{2+} in Cd-rho.[3] Upon heating in either air (Fig. 2) or vacuum (Fig. 3), there is an initial decrease in cell parameter from 25 to 75 °C due to the loss of unbound water, a more gradual change in cell parameter between 75 and 450 °C, then a large increase in the cell parameter which is accompanied by a change from the acentric to centric structure and a relocation of Cd^{2+} from the S8R site to the S6R site. There is a marked difference in the behavior of Cd-rho when cooling under ambient atmosphere (Fig. 2) and vacuum (Fig. 3). With the exception of a small temperature hysteresis, the reaction pathway is directly reversed upon cooling under ambient atmosphere. In contrast, these changes *do not occur* upon cooling under vacuum. These observations indicate that water plays a role in the relocation from the S6R back to the S8R. It is also likely that water acts as a transport agent in the original cation relocation from the S8R to the S6R site; the cell parameter of Cd-rho at 450 °C (14.45 Å) is larger than that of Pb-rho (14.35 Å) although the cationic radius of Cd^{2+} (1.09 Å) is smaller than that of Pb^{2+} (1.33 Å). *In situ* neutron diffraction

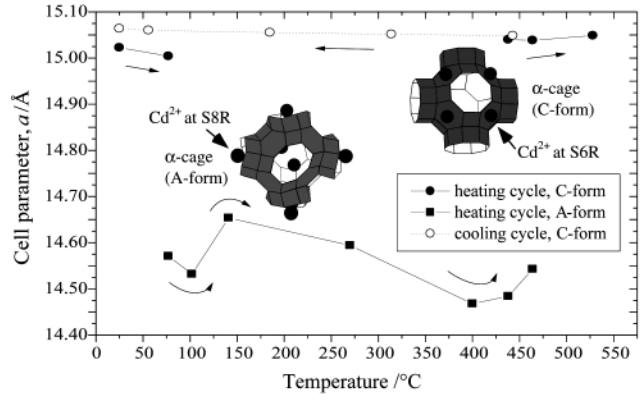

Fig. 3 The cell parameter of Cd-rho heated under vacuum. In the absence of water, there is no phase transformation upon cooling. Schematic diagrams illustrate siting of Cd^{2+} in the α-cages.

studies are planned to determine the siting of D_2O at intermediate temperatures.

There are two modes of cation relocation in zeolite rho: the transition from the S8R site to the D8R site and the 'trap door' relocation from the S8R site to the S6R site. The present work indicates that these relocations are mediated by water. As coordinating water is removed from the structure, extra-framework cations must change their coordination environments by migrating to new sites in order to satisfy their coordination requirements. While dehydration is the driving force for cation relocations, cationic size appears to determine which relocation mechanism occurs. In hydrated samples, all divalent cations studied reside at the S8R site. Even though this site is large, all cations can have their coordination requirements met by binding with water in the sample. Dehydration, and the resulting loss of coordinated water, has a large effect on the cation coordination sphere. Larger cations such as Ca^{2+}, Sr^{2+}, Pb^{2+}, Ba^{2+}, can have their bonding requirements met by relocating to the D8R site. To satisfy the bonding requirements of a smaller cation such as Cd^{2+}, a larger framework distortion must occur. Because of its smaller size, the S6R site presents an attractive binding site in the absence of water. Through water mediation, Cd^{2+} can relocate to this site. Rather than being purely temperature-driven transformations, all cation relocations and the dramatic negative thermal expansion effects observed in zeolite rho appear to be a result of chemical changes that arise from dehydration.

This work was supported by a grant from the National Science Foundation (DMR 97-13375). This work made use of the X7B beamline at the NSLS, supported by the U.S. Department of Energy, Division of Materials Sciences and Division of Chemical Sciences (DEAC02-98CH10886).

Notes and references

‡ Chemical analysis by ICP and microprobe gave unit cell compositions of $Pb_{6.7}Cs_{0.7}Al_{11.7}Si_{36.3}O_{96}{\cdot}wH_2O$ and $Cd_{5.5}Cs_{0.3}Al_{11.7}Si_{36.3}O_{96}{\cdot}wH_2O$ for Pb-rho and Cd-rho, respectively.

§ The sample to detector distance, zero point, and imaging plate tilt were determined from LaB_6 (NIST SRM 660a) prior to the experiment[11] (Cd-rho: λ = 0.9372 Å; Pb-rho: λ = 0.9042 Å). Approximately 3 mg of powdered sample loaded in a 0.5 mm quartz capillary was exposed either to vacuum (< 1 Pa) or ambient atmosphere. A continuous heating or cooling rate between 3 °C min^{-1} and 6 °C min^{-1} was used. Temperatures were calibrated against the thermal expansion of an Ag standard. Data were integrated using FIT2D.[11] Anomalous scattering terms for Cd (f' = −0.53 electrons and f'' = 1.97 electrons) and Pb (f' = −8.76 electrons and f'' = 9.30 electrons) were taken from FPRIME.[10,12]

¶ Samples were deuterated by several cycles of vacuum dehydration at 200 °C (< 10^{-2} Pa) followed by contact with D_2O vapor at room temperature.

1 D. R. Corbin, L. Abrams, G. A. Jones, M. M. Eddy, W. T. A. Harrison, G. D. Stucky and D. E. Cox, *J. Am. Chem. Soc.*, 1990, **112**, 4821.
2 A. Bieniok and W. H. Baur, *J. Solid State Chem.*, 1991, **90**, 173.
3 J. B. Parise, X. Liu, D. R. Corbin and G. A. Jones, in *Synthesis/Characterization and Novel Applications of Molecular Sieve Materials*, ed. R. L. Bedard, T. Bein, M. E. Davis, J. Garces, V. A. Maroni and G. D. Stucky, Materials Research Society, Pittsburgh, PA, 1991, pp. 267–272.
4 J. B. Parise, D. R. Corbin and L. Abrams, *Microporous Mater.*, 1995, **4**, 99.
5 J. B. Parise, T. E. Gier, D. R. Corbin and D. E. Cox, *J. Phys. Chem.*, 1984, **88**, 1635.
6 R. X. Fischer, W. H. Baur, R. D. Shannon, R. H. Staley, L. Abrams, A. J. Vega and J. D. Jorgensen, *Acta Crystallogr., Sect. B*, 1988, **44**, 321.
7 H. E. Robson, D. P. Shoemaker, R. A. Ogilvie and P. C. Manor, in *Molecular Sieves*, ed. W. M. Meier and J. B. Uytterhoven, American Chemical Society, Washington, D.C., 1973, pp. 106–114.
8 P. Norby, *J. Appl. Crystallogr.*, 1997, **30**, 21.
9 H. M. Rietveld, *J. Appl. Crystallogr.*, 1969, **2**, 65.
10 A. C. Larson and R. B. VonDreele, 'GSAS; General Structure Analysis System', Report LAUR 86-748, Los Alamos National Laboratory, New Mexico, 1986.
11 A. P. Hammersley, *FIT2D: V9.129 Reference Manual V3.1*, ESRF Internal Report ESRF98HA01T, Grenoble, France, 1998.
12 D. T. Cromer, *J. Appl. Crystallogr.*, 1983, **16**, 437.

First binuclear complex of an *N*,*N*′,*N*″,*N*‴-tetraalkyl 2,5-diamino-1,4-benzoquinonediimine†

Olivier Siri and Pierre Braunstein*

Laboratoire de Chimie de Coordination, UMR 7513 CNRS, Université Louis Pasteur, 4, rue Blaise Pascal, F-67070 Strasbourg Cedex, France. E-mail: braunst@chimie.u-strasbg.fr

Received (in Cambridge, UK) 24th September 2000, Accepted 10th October 2000
First published as an Advance Article on the web

A new method for the synthesis of *N*,*N*′,*N*″,*N*‴-tetraalkyl 2,5-diamino-1,4-benzoquinonediimines is described together with the structure of a binuclear Pt(II) complex with such a bridging ligand which provides an extended π-system.

The coordination complexes derived from 2,5-dihydroxy-1,4-benzoquinone **1** display many interesting features and possess a rich redox chemistry. Indeed, the deprotonated, enolate form of **1** can react with metal ions to form dinuclear complexes of particular interest owing to the specific electronic properties induced by the quinone system.[1–3] The related 2,5-diamino-1,4-benzoquinonediimines **2a**,**b** could give access to a wider range of metal complexes because of the suitable overlap between the nitrogen and metal orbitals.

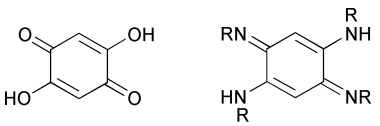

1 **2a**: R = alkyl **2b**: R = H

Such compounds are expected to increase the scope of bonding patterns and electronic delocalization compared to other bridging nitrogen ligands such as terpyridine systems,[4] Creutz–Taube species[5] and *p*-benzoquinonediimine-bridged ligands.[6,7] The direct use of **2b** has been shown to be unsuitable since coordination of metal fragments renders the benzoquinonediimine bridge more susceptible to nucleophilic attack.[8] In contrast, *N*-substitution by electron-donating groups should lead to more stable complexes toward dioxygen and/or water. Since ligands of type **2a** are only accessible by self-condensation of aniline and/or 1,4-diaminobenzene,[9–12] one faces considerable limitations in the nature of the substituents on both types of nitrogen atoms. Here we describe a new strategy to access such ligands and demonstrate their ability to function as bridging chelates in dinuclear chemistry.

Compound **3**·4 HCl was first reacted smoothly in MeCN and excess NEt_3 at room temperature with trimethylacetyl chloride (4 equiv.) to afford **4** which is almost insoluble in most solvents so that only characterization in the solid state is reported (Scheme 1).‡ Reduction of **4** with $LiAlH_4$ in CCl_4 did not lead to the corresponding tetraamino derivative **5** but to yellow **6** which is formed in 18% yield during aerobic work-up. A single crystal X-ray analysis (Fig. 1) established its *p*-benzoquinonediimine form.§ The C(2)–C(3′) bond length of 1.508(3) Å is indicative of the lack of conjugation between the two halves of this 12π electron system[13] and is even slightly longer than the corresponding distance in Bandrowski's base [1.485(6) Å].[14] The π-electron conjugation is thus confined to the upper and lower halves of the ligand. A fast intramolecular double proton transfer involving two tautomers generates in solution a structure of higher symmetry, which accounts for the NMR data.[15]‡

† Dedicated to Professor B. T. Heaton on the occasion of his 60th birthday, with our warmest congratulations and best wishes.

The metallation reaction of **6** with $[PtCl_2(cod)]$ (2 equiv.) at room temperature in CH_2Cl_2 required basic conditions and afforded **7** (*ca*. 15% yield) the ^1H NMR spectrum of which revealed no NH resonances. The molecular structure of **7** was elucidated by X-ray crystallography (Fig. 2).§

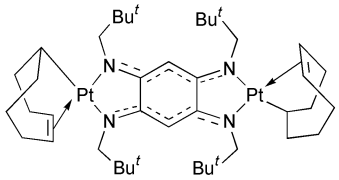

7

The molecule is centrosymmetric and the dianion-derived from **6** chelates each of the two Pt centres, thus acting as a tetradentate bridging ligand. The coordination geometry around the platinum centre is square planar, with the metal being only slightly out the molecular plane. The Pt atom completes its coordination with a Pt–C(19) σ-bond [2.12(1) Å] and a Pt–olefinic π-bond [with Pt–C distances of 2.17(2) and 2.140(9) Å]. Accordingly, the Pt···C(18) separation of 2.677(1) is non-bonding. The most striking feature of **7** is that electronic delocalization of the π-system occurs, in contrast to **6**, and is confined to the upper and lower halves of the ligand, as shown by the C(1)–C(2) bond length of 1.53(1) Å. The delocalization pathway also differs from that in complexes where the metal centres are linked by substituted *p*-benzoquinonediimines.[6,7] This important feature may be of wider occurrence in such systems than previously believed.[16,17] The molecular structure of **7** indicates that π-backbonding from the Pt orbitals into a π* orbital of the quinonediimine is occurring: the N(1)=C(1), C(1)–

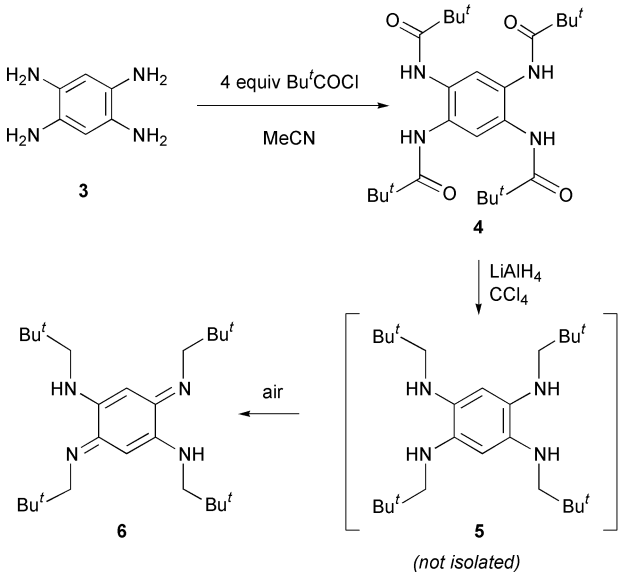

3 **4** **6** **5** *(not isolated)*

Scheme 1 Synthesis of **6** from **3**.

DOI: 10.1039/b005952h

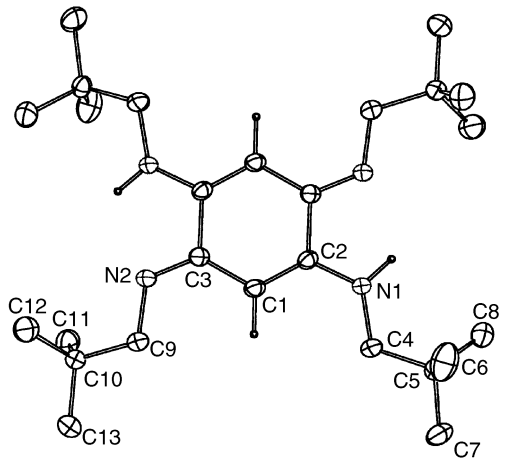

Fig. 1 View of the structure of **6** in the crystal. Selected bond lengths (Å) and bond angles (°): C(1)–C(2) 1.358(4), C(1)–C(3) 1.437(3), C(2)–C(3′) 1.508(3), C(2)–N(1) 1.346(3), C(3)–N(2) 1.286(3); C(2)–N(1)–C(4) 124.7(2), C(3)–N(2)–C(9) 120.1(2), C(2)–C(1)–C(3) 121.9(2), C(1)–C(2)–C(3′) 120.8(2), C(1)–C(2)–N(1) 125.7(2), C(1)–C(3)–N(2) 127.7(2), C(3′)–C(2)–N(1) 113.5(2).

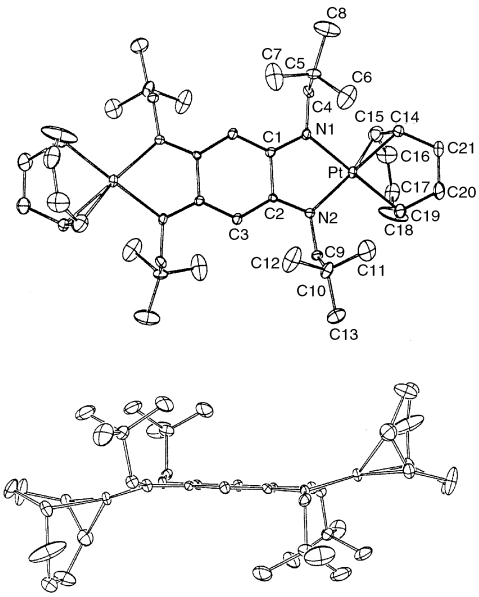

Fig. 2 Top- and side-views of the structure of **7** in the crystal. Selected bond lengths (Å) and bond angles (°): Pt–N(1) 2.082(7), Pt–C(14) 2.140(9), Pt–C(15) 2.17(2), Pt–C(19) 2.12(1), N(1)–C(1) 1.33(1), C(1)–C(2) 1.53(1), C(1)–C(3′) 1.40(1), C(2)–C(3) 1.37(1), C(2)–N(2) 1.33(1); N(1)–Pt–N(2) 78.2(3), N(1)–Pt–C(19) 174.2(4), N(2)–Pt–C(19) 99.6(3), C(14)–Pt–C(15) 36.4(4), Pt–N(1)–C(1) 114.5(6), N(1)–C(1)–C(2) 113.5(7), N(1)–C(1)–C(3′) 127.6(7), N(2)–C(2)–C(3) 127.1(7), C(1)–C(2)–C(3) 117.5(7).

C(3′), C(3′)=C(2′) and C(2′)–N(2′) bonds of the bridge show alternating lengthening and shortening relative to those of the free ligand (Table 1). Such differences are also observed in *p*-benzoquinonediimine systems.[7] Complex **7** is the first example of a binuclear complex bridged with ligands of type **2a** and extends previous results on related mononuclear complexes.[18,19] The electronic spectrum of **7** reveals a metal-to-ligand charge transfer (MLCT) absorption at λ_{max} = 504 nm.

Table 1 Comparison of interatomic distances (Å)

	C=N	C–C	C=C	C–N
6	1.286(3)	1.437(3)	1.358(4)	1.346(3)
7	1.33(1)	1.37(1)	1.40(1)	1.33(1)

Further studies on the electronic properties of **7** and analogous molecules are in progress as well as the synthesis of potential new mixed-valence dimers based on **6**.

We thank the Ministère de l'Education Nationale, de la Recherche et de la Technologie and the CNRS for financial support and Dr A. DeCian and N. Kyritsakis for the X-ray structure determinations.

Notes and references

‡ *Selected data*: for **4**: MS(EI) *m/z* 474 (M^+); Anal. Calc. for $C_{26}H_{42}N_4O_4$: C, 65.78; H, 8.92; N, 11.81. Found: C, 66.31; H, 8.85; N, 11.86%. For **6**: NMR ($CDCl_3$): δ_H 1.00 (36H, s, CH_3), 2.95 (8H, s, CH_2), 5.16 (2H, s, Ph-H), 6.75 (2H, s, NH); δ_C 27.8 (CMe_3), 31.9 (CMe_3), 57.7 (CH_2N), 83.9 (C=C), 150.1 (C=N). UV–VIS (CH_2Cl_2): λ_{max} = 340 nm (intraquinone transition).

§ *Crystal data*: for **6**: $C_{26}H_{48}N_4$, M = 416.70, triclinic, space group $P\bar{1}$; a = 5.8950(7), b = 9.4081(9), c = 12.695(2) Å, α = 85.059(5), β = 77.180(5), γ = 88.044(5)°, V = 683.9(2) Å^3, Z = 1, μ(Mo-Kα) = 0.060 mm^{-1}, T = 173 K, 1384 data with $I > 3\sigma(I)$, final R = 0.051, R_w = 0.071, GOF = 1.126.

For **7**: $C_{42}H_{70}N_4Pt_2$, M = 1021.23, monoclinic, space group $P2_1/c$; a = 9.829(1), b = 22.615(1), c = 10.618(1) Å, β = 117.474(5)°, V = 2094.0(6) Å^3, Z = 2, μ(Mo-Kα) = 6.705 mm^{-1}, T = 173 K, 3184 data with $I > 3\sigma(I)$, final R = 0.047, R_w = 0.068, GOF = 1.289. Although the cod-derived ligands are disordered in the solid state structure, their $\sigma + \pi$-type bonding with the metals was unambiguously established.

CCDC 182/1814. See http://www.rsc.org/suppdata/cc/b0/b005952h/ for crystallographic files in .cif format.

1 M. D. Ward, *Inorg. Chem.*, 1996, **35**, 1712.
2 M. A. Calvo, A. M. Manotti-Lanfredi, L. A. Oro, M. T. Pinillos, C. Tejel, A. Tiripicchio and F. Ugozzoli, *Inorg. Chem.*, 1993, **32**, 1147.
3 F. Tinti, F. M. Verdaguer, O. Kahn and J. M. Savariault, *Inorg. Chem.*, 1987, **26**, 2380.
4 J. V. Folgado, R. Ibanez, E. Coronado, D. Beltran, J. M. Savariault and J. Galy, *Inorg. Chem.*, 1988, **27**, 19.
5 M. D. Ward, *Chem. Soc. Rev.*, 1995, **24**, 121.
6 S. Joss, H. Reust and A. Ludi, *J. Am. Chem. Soc.*, 1981, **103**, 981.
7 S. Joss, H. B. Bürgi and A. Ludi, *Inorg. Chem.*, 1985, **24**, 949.
8 H. Masui, A. L. Freda, M. C. Zerner and A. B. P. Lever, *Inorg. Chem.*, 2000, **39**, 141.
9 E. Bandrowski, *Monatsh. Chem.*, 1889, **10**, 123.
10 E. Bandrowski, *Chem. Ber.*, 1894, **27**, 480.
11 O. Fischer and E. Hepp, *Ber. Dtsch. Chem. Ges.*, 1888, **21**, 676.
12 C. Kimish, *Ber. Dtsch. Chem. Ges.*, 1875, **8**, 1026.
13 S. Dähne and D. Leupold, *Angew. Chem.*, 1966, **78**, 1029.
14 A. J. Blake, P. Hubberstey and D. J. Quinlan, *Acta Crystallogr., Sect. C*, 1996, **52**, 1774.
15 H. Rumpel and H. H. Limbach, *J. Am. Chem. Soc.*, 1989, **111**, 5429.
16 K. Heinze, G. Huttner and L. Zsolnai, *Z. Naturforsch., Teil B*, 1999, **54**, 1147.
17 H. Y. Cheng, G. H. Lee and S. M. Peng, *Inorg. Chem. Acta*, 1992, **191**, 25.
18 J. Rall, A. F. Stange, K. Hübler and W. Kaim, *Angew. Chem., Int. Ed.*, 1998, **37**, 2681.
19 M. L. Hsieh, M. C. Cheng and S. M. Peng, *Inorg. Chim. Acta*, 1988, **145**, 1.

ChemComm

Solid-state polymerization of bis(but-3-enoato)zinc: the generation of a stereoregular oligomer

Michael J. Vela,[a] Vera Buchholz,[b] Volker Enkelmann,[b] Barry B. Snider[a] and Bruce M. Foxman*[a]

[a] *Department of Chemistry, Mail Stop 015, Brandeis University, Waltham, MA 02454-9110, USA. E-mail: foxman1@brandeis.edu*

[b] *Max-Planck-Institut für Polymerforschung, Ackermannweg 10, Mainz, Germany 55128*

Received (in Columbia, MO, USA) 17th July 2000, Accepted 5th October 2000
First published as an Advance Article on the web

Irradiation (^{60}Co γ-rays) of crystalline bis(but-3-enoato)-zinc, a two-dimensional coordination polymer with a bilayer packing motif, affords isotactic zinc poly(but-3-enoate).

Nearly four decades ago, Morawetz and Rubin demonstrated that ^{60}Co γ-irradiation of alkali metal acrylates and methacrylates produced high molecular weight, atactic polymer.[1] Irradiation of crystalline potassium acrylate **1** (2–8 kGy) led to high molecular weight polyacrylate (M_w = 100 000–400 000) with yields in the range 3–34%. Fankuchen reported that crystals of **1** were orthorhombic, space group $P2_12_12_1$, with a = 20.5, b = 4.15 and c = 5.73 Å.[2] Although structure–reactivity relationships have never been established for this interesting system, the short repeat distance of 4.15 Å requires that the crystal structure of **1** contains short contacts of *ca.* 4.15 Å, and the observed reactivity implies that the intermolecular orientation is appropriate for polymerization. In a recent study, we observed that upon ^{60}Co γ-irradiation, aquabis(but-3-enoato)-calcium **2** undergoes solid-state polymerization to high molecular weight polymer (M_w = 400 000) in high yield (97%).[3] The polybutenoates thus formed are again atactic, as also observed in a recent reinvestigation of polystyrenes formed by heating or irradiation of solid styryl monomers.[4] The crystal structure of **2** contains short –C=C–···–C=C– contacts (3.73–3.90 Å), usually considered as an important criterion for the onset of solid-state reactivity.[5] By contrast to the behavior of salts of vinylic monomers, irradiation or heating of *trans*-but-2-enoates affords a single dimer or trimer in cases where two, four or eight diastereomers are possible.[6–8] The relatively few examples of solid-state polymerization of metal salts of vinylic acids suggested to us that the 'structure–reactivity database' was too small to conclude that stereocontrol during polymerization was either unlikely or impossible for such materials. As part of our program in the discovery of new solid-state reactions, we undertook a study of the structure and reactivity of bis(but-3-enoato)zinc. Preliminary screening of several M^+ and M^{2+} systems with small radii, low coordination number and a high potential for bilayer formation[9] indicated that the zinc salt was both highly crystalline and sensitive to ^{60}Co γ-irradiation.

Anhydrous bis(but-3-enoato)zinc **3** was prepared readily by the slow addition of but-3-enoic acid to a stirred aqueous suspension of $ZnCO_3$. After stirring overnight, excess $ZnCO_3$ was removed by filtration; evaporation of the filtrate gave crystalline **3** in high yield (70–80%). Single crystals of **3** decomposed quickly at room temperature in an X-ray beam, suggesting that this was a highly reactive material. Exposure of **3** to large γ-ray doses resulted in a maximum conversion to polymer **4** of *ca.* 50%. NMR spectra of the crude material indicated the presence of monomer, polymer and a small amount of side product(s). Examples of dose/conversion data to polymer, based on extraction of monomer and side products: 61 kGy/2.9%; 102 kGy/9.8%; 316 kGy/21.9%; 592 kGy/47.8%. Further irradiation did not lead to significantly higher degrees of conversion (1570 kGy/48.9%). The NMR spectrum of the purified product, as the free acid in D_2O–DC1, showed the probable formation of a poly(but-3-enoate): δ_H 1.9–2.2 (2H, br d, CH_2CO_2H), 1.6–1.7 (1H, br), 1.3–1.5 (1H, br), 0.9–1.2 (1H, br); δ_C 180 (C), 29.0–40.5 (CH_2, CH). The stereochemistry of **4** was assigned as isotactic by analogy to the ^{1}H NMR spectrum of polypropylene and the expected shift due to a carboxy group. The backbone methylene protons are non-equivalent in isotactic polypropylene; thus three absorptions are seen for the backbone methylene and methine protons with an integration of 1 : 1 : 1 as in **4**.[10] The backbone methylene protons are equivalent in syndiotactic polypropylene, so that there are only two absorptions for the backbone protons with an integration of 1 : 2. A more complex pattern is observed in atactic polypropylene. The molecular weight of **4**, $\bar{M}_w$ = 2128, $\bar{M}_n$ = 1801, D = 1.2, determined by GPC, is consistent with the formation of a low molecular weight oligomer, containing 8–10 monomer units.

Solid-state polymerization of alkali and alkaline earth acrylates and methacrylates (^{60}Co γ-rays),[1] as well as crystalline styryl monomers (^{60}Co γ-rays or heating)[4] leads to *atactic* polymer. Despite the observed lack of stereocontrol, it now seems apparent that topochemical effects are responsible for at least the *onset* of reactivity in a number of cases;[4,8] later, other factors (*e.g.* crystal degradation) intervene such that the product obtained is atactic. However, elegant studies of methacrylate solid-state polymerization have demonstrated that stereocontrol is indeed operative in the *early* stages of solid-state polymerization.[11,12] The dearth of structural information available for reactive, solid materials containing terminal vinyl groups limits our understanding of the structural factors responsible for solid-state reactivity. With this in mind, but also perhaps in order to provide insight into the isotactic nature of the product as well as the maximum *ca.* 50% conversion, we carried out an X-ray structure determination of **3**. The structure determination was carried out at 173 K on a Nonius Kappa-CCD diffractometer in order to prevent the X-ray induced decomposition observed at room temperature on a conventional diffractometer; no decomposition was observed at 173 K on the CCD instrument.

The crystal structure of **3** consists of tetrahedral zinc ions, bridged infinitely by two symmetry-independent but-3-enoate moieties.† The result, shown in Fig. 1, is a two-dimensional coordination polymer, roughly parallel to crystal *bc* planes. As

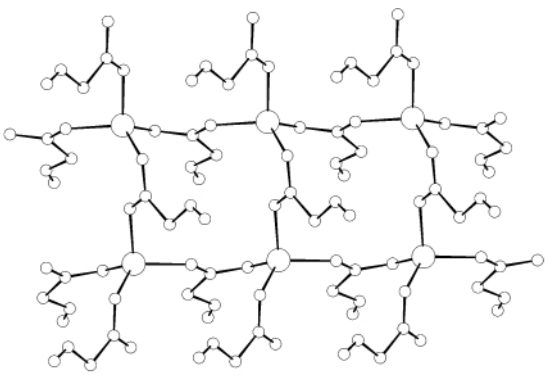

Fig. 1 View of the two-dimensional coordination polymer in **3** showing zinc ions bridged in a *syn, anti*-fashion by the but-3-enoate ligands.

DOI: 10.1039/b007334m

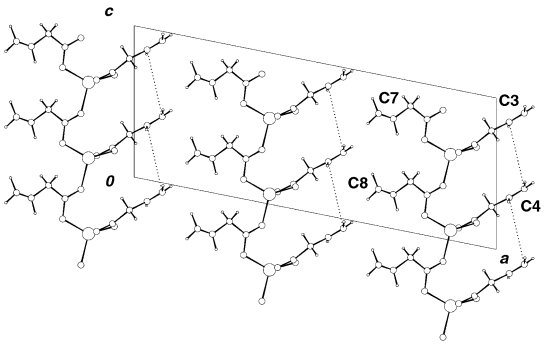

Fig. 2 View of the unit cell of **3**, showing C(3)···C(4) contacts of 4.21 Å (dotted lines), and identification of the 'unreactive' vinyl group [C(7), C(8)], separated by 4.42 Å (no connection shown).

shown in Fig. 2, the two-dimensional coordination polymers pack in a bilayer motif. Bilayer packing arrangements occur with >90% frequency for metal carboxylate coordination polymers where the acids have ⩾4 carbon atoms.[9] As we have described previously, the two-dimensional coordination polymer, generated by metal carboxylate interactions, including carboxylate bridging, serves as a bifunctional template.[13] The first function of such a template is to generate a bilayer structure: the organic tails of the carboxylate groups will be oriented in a roughly perpendicular direction to the bilayer. Secondly, depending on the nature of the bridging, the tails may be forced into very short contact. In the crystal structure of compound **3** (Fig. 2), one set of but-3-enoates is nearly parallel (interplanar angle 9.1°), with a C(3)–C(4) ($x, -2-y, z-\frac{1}{2}$) distance of 4.21 Å. The other set of but-3-enoates are separated, within the bilayer, by a minimum distance C(7)–C(8) ($x, -2-y, z-\frac{1}{2}$) of 4.42 Å and an interplanar angle of 119.0°. There are pairs of 'dimeric' contacts *across* the bilayer [C(3)–C(8) ($\frac{1}{2}+x, \frac{1}{2}+y, z$), 4.01 Å, not shown in Fig. 2]. While such contacts might lead to a dimeric product and may account for observed traces of side product, the resultant reaction pathway cannot account for polymer formation. Thus the 'head-to-head', nearly parallel arrangement shown in Fig. 2 leads to isotactic polymer, in a genuine topochemical fashion.[5] Further, since the C(7)=C(8) double bonds are separated by an amount significantly greater than 4.2 Å,[5] no reactivity is observed (or expected) for this set of but-3-enoates, and the maximum yield possible will be 50%. Topochemical factors thus control both the product stereochemistry and the extent of reaction.

In summary, we have discovered a new solid-state reaction that leads to isotactic oligomer. Such an event is unprecedented for reactive solid materials containing terminal vinyl groups. The present case, as well as the trimerization of sodium *trans*-but-2-enoate[7] to yield sodium (2*R**,3*R**,4*S**,5*R**)-2,4-dimethylhept-6-ene-1,3,5-tricarboxylate **5** represent the only two examples of high-yield, solid-state oligomerization reactions of compounds containing RCH=CH– groups that lead to stereoregular products. The formation of both **4** and **5** lend strong support to the ideas advanced some time ago by the groups of Morawetz and Lando, that the early stages of solid-state polymerization often show strong evidence of stereoregularity, and thus likely occur under topochemical control.[11,12] Further, the stereoregularity observed for **4** and **5** may represent a 'snapshot' of the early stages of a broader class of solid-state polymerization reactions. The synthesis, structure determination and solid-state polymerization of related new materials will help to uncover additional examples that clarify this issue. Such experiments, as well as conventional and 'tail' UV-irradiation[14] of **3**, are underway in our laboratories.

We thank the National Science Foundation (DMR-9629994) for the partial support of this research.

Notes and references

† *Crystal data* for **3**: $C_8H_{10}O_4Zn$, M = 235.54, monoclinic, space group *Cc* (no. 9), colorless plates, a = 22.6251(18), b = 4.8003(4), c = 9.2901(11) Å; β = 101.2915(50)°; Z = 2; U = 989.44 Å^3; D_m = 1.58(3), D_c = 1.581 g cm^{-3}; T = 173 K. Data were collected on a Nonius Kappa-CCD diffractometer [λ(Mo-Kα) = 0.710 73 Å]; no absorption corrections were made. Full matrix least squares refinement (based on $|F|$) of positional and anisotropic displacement parameters for all nonhydrogen atoms, and isotropic displacement parameters for H atoms (fixed at geometric positions; total parameters = 119) led to R = 0.0371 and R_w = 0.0400, using 997 data for which $I > 1.96\sigma(I)$; maximum residual ρ 0.47 e Å^{-3}]. Programs used: SIR92,[15] CRYSTALS,[16] CAMERON.[16] Bond lengths and angles lie in normal ranges (C(3)–C(4) and C(7)–C(8) bond lengths are affected by disorder of atoms C(4) and C(8)).

CCDC 182/1805. See http://www.rsc.org/suppdata/cc/b0/b007334m/ for crystallographic files in .cif format.

1 H. Morawetz and I. D. Rubin, *J. Polym. Sci.*, 1962, **57**, 669.
2 I. Fankuchen, unpublished observations, quoted in ref. 1.
3 M. J. Vela, B. B. Snider and B. M. Foxman, *Chem. Mater.*, 1998, **10**, 3167.
4 L. Di and B. M. Foxman, *Supramol. Chem.*, 2000, in press.
5 (*a*) M. D. Cohen and G. M. J. Schmidt, *J. Chem. Soc.*, 1964, 1996; (*b*) F. L. Hirshfeld and G. M. J. Schmidt, *J. Polym. Sci., Sect. A*, 1964, **2**, 2181.
6 K. Naruchi, S. Tanaka, M. Yamamoto and K. Yamada, *Nippon Kagaku Kaishi*, 1983, 1291; *Chem. Abstr.*, 1983, **99**, 195488q; K. Naruchi and M. Miura, *J. Chem. Soc., Perkin Trans. 2*, 1987, 113.
7 G. C. D. de Delgado, K. A. Wheeler, B. B. Snider and B. M. Foxman, *Angew. Chem., Int. Ed. Engl.*, 1991, **30**, 420.
8 T. H. Cho, B. Chaudhuri, B. B. Snider and B. M. Foxman, *Chem. Commun.*, 1996, 1337.
9 M. J. Vela and B. M. Foxman, *Cryst. Eng.*, 2000, **3**, 11.
10 (*a*) R. C. Ferguson, *Polym. Prepr. (Am. Chem. Soc. Div. Poly. Chem.)*, 1967, **8**, 1026; (*b*) R. C. Ferguson, *Trans. N.Y. Acad. Sci.*, 1967, **29**, 495; (*c*) F. Heatley and A. Zambelli, *Macromolecules*, 1969, **2**, 618; (*d*) A. Zambelli, D. E. Dorman, A. I. R. Brewster and F. A. Bovey, *Macromolecules*, 1973, **6**, 925; (*e*) F. A. Bovey, *Chain Structure and Conformation of Macromolecules*, Academic Press, New York, 1982, pp. 75–84.
11 (*a*) H. Morawetz and T. A. Fadner, *Makromol. Chem.*, 1959, **34**, 162; (*b*) J. B. Lando and H. Morawetz, *J. Polym. Sci., Part C*, 1964, **4**, 789.
12 J. B. Lando and J. Semen, *J. Polym. Sci., Polym. Chem. Ed.*, 1972, **10**, 3003.
13 B. M. Foxman and M. J. Vela, *Trans. Am. Cryst. Assn.*, 1998, **33**, 75.
14 K. Novak, V. Enkelmann, G. Wegner and K. B. Wagener, *Angew. Chem., Int. Ed. Engl.*, 1993, **32**, 1614; V. Enkelmann, G. Wegner, K. Novak and K. B. Wagener, *J. Am. Chem. Soc.*, 1993, **115**, 10 390.
15 A. Altomare, G. Cascarano, C. Giacovazzo, A. Guagliardi, M. C. Burla, G. Polidori and M. J. Camalli, *J. Appl. Crystallogr.*, 1994, **27**, 435.
16 D. J. Watkin, C. K. Prout, J. R. Carruthers, P. W. Betteridge and R. I. Cooper, *CRYSTALS Issue 11*, Chemical Crystallography Laboratory, University of Oxford, Oxford, 1999; D. J. Watkin, C. K. Prout and L. J. Pearce, CAMERON, Chemical Crystallography Laboratory, University of Oxford, Oxford, 1996.

ChemComm

First totally diastereoselective opening of chiral triquinphosphoranes. A new access to enantiopure oxazaphospholidines†

Caroline Marchi, Guillaume Delapierre, Frédéric Fotiadu and Gérard Buono*

Laboratoire de Synthèse Asymétrique, UMR 6516, ENSSPICAM, Avenue Escardrille Normandie-Niemen, 13397 Marseille cedex 20, France. E-mail: buono@spi-chim.u-3mrs.fr; Fax: +33 4 91 28 82 47

Received (in Liverpool, UK) 18th July 2000, Accepted 3rd October 2000
First published as an Advance Article on the web

Asymmetric addition of isocyanate compounds on chiral triquinphosphoranes, tricyclic hydridophosphoranes, led by a total diastereoselective opening of the diazaphospholidine ring. This provides chiral bicyclic oxazaphospholidines in which an eight-membered ring is fused to the oxazaphospholidine ring by the P–N bond.

Chiral tricoordinated organophosphorus compounds containing an oxazaphospholidine ring have been applied with success in enantioselective catalysis[1] and in asymmetric synthesis.[2] We wish to report herein an original synthesis of new enantiopure bicyclic oxazaphospholidines based on the reaction between isocyanate compounds and chiral triquinphosphoranes.‡ This new class of chiral tricyclic phosphoranes was synthesized from enantiopure diaminodiols having a C_2 symmetry axis.[3] Those phosphoranes exist as two trigonal bipyramid structures (TBP) with opposite absolute configuration at the phosphorus atom, R_P and S_P, in fast equilibrium by a Berry pseudorotation process *via* a SP transition state (Scheme 1).[3,4] We have described the first asymmetric addition of chiral triquinphosphorane **1c** to ketopantolactone and to $BH_3{\cdot}SMe_2$ complex leading to chiral alkoxyphosphorane[3c] **2** and chiral triquinphosphorane–borane[3b] adduct **3**, respectively. The X-ray diffraction structure of **3** revealed that the borane group coordinated to the axial nitrogen atom of the TBP structure is in the *syn* position with respect to the P–H bond and in the *anti* position with respect to the adjacent pseudoaxial isopropyl substituent.[3b,5] Phenyl isocyanate **4** and (*R*)-phenylethyl isocyanate **5** reacted readily with the triquinphosphoranes **1a**–**e**[6] to afford chiral bicyclic oxazaphospholidines **6a**–**e** and **7a**–**e**, respectively, in which an eight-membered ring is fused to the oxazaphospholidine ring by the P–N bond (Scheme 1).

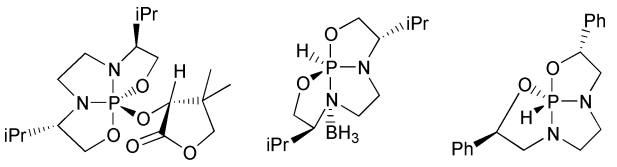

2 **3** **9**

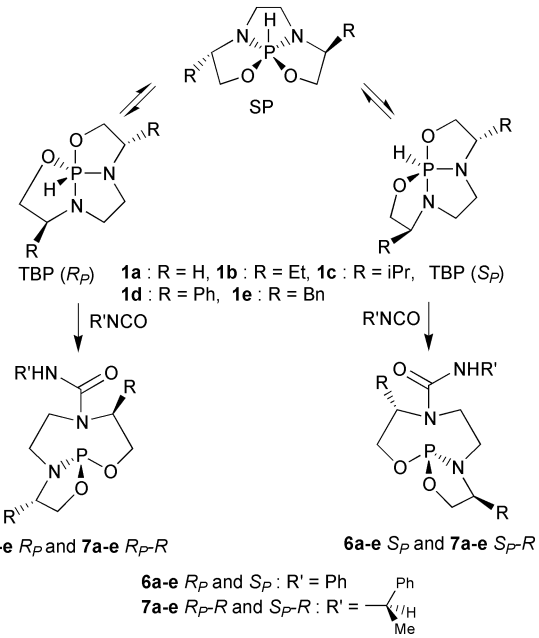

Scheme 1 Pseudorotation process and addition of isocyanates **4** and **5** on triquinphosphoranes.

Oxazaphospholidines **6a** and **7a** were formed in quantitative yield by direct reaction of the parent triquinphosphorane **1a** with isocyanates **4** and **5**, respectively, in toluene solution at −30 °C. The exclusive formation of these new compounds could be monitored by ^{31}P NMR spectroscopy showing only one downfield singlet at 130.1 ppm for racemic **6a** and two signals at 130.70 and 130.77 ppm for **7a** in a 1:1 ratio corresponding to the diastereomers **7a**-R_P and **7a**-S_P. Due to the high energy barrier for the epimerization of the tricoordinated phosphorus atom (30–35 kcal mol^{-1}),[7] this result shows that no dynamic chiral discrimination occurred during the attack of chiral isocyanate **5** on the two enantiomeric structures **1a**-R_P and **1a**-S_P in fast equilibrium.

In the case of chiral triquinphosphoranes **1b**–**e**, ^{31}P NMR monitoring showed that condensation of isocyanates **4** and **5** occurred with a total diastereoselective opening of the diazaphospholidine ring, to afford a single diastereomer as shown by the ^{13}C and ^{31}P NMR spectra. Compound **7e** reacted with $BH_3{\cdot}SMe_2$ complex in toluene solution to give the borane adduct **8** in which the borane is coordinated to the phosphorus atom (δ ^{31}P: 120.3 ppm). The structure of adduct **8** and the absolute configuration of the phosphorus atom were determined by single X-ray diffraction (Fig. 1).[8] The nitrogen, oxygen, and boron atoms around the phosphorus center adopt a slightly distorted tetrahedral arrangement with bond angles between 95.0 and 119.8°. Because the complexation of borane occurs with retention of configuration at the phosphorus atom, the borane adduct shows that the diastereoselective opening of the diazaphospholidine ring led to a tricoordinated compound with the S_P absolute configuration. The shortness of the P1–N6 bond [1.637(5) Å instead of 1.67–1.70 Å usually][9] can in part be assigned to negative hyperconjugation, due to electron donation from π_N to σ^*_{P-B} orbitals.[10] In fact the N6 nitrogen exhibits a planar configuration [sum of bond angles 359.8(4)°].

The newly formed eight-membered ring adopts a twist–boat–chair conformation and the five-membered ring a slightly flattened envelope conformation with the C19 atom as the tip. The benzyl group bound to the C11 carbon of the oxazaphospholidine ring is in the *syn* position with respect to the boron atom whereas the benzyl group bound to the C9 carbon of the eight-membered ring is in the *anti* position.

Taken together, these results suggest that just like borane,[3b] isocyanates attack preferentially the least hindered axial nitrogen atom of the S_P phosphorane diastereomer (Scheme 2).

† Electronic supplementary information (ESI) available: experimental procedures and characterization of compounds **6a**–**e**, **7a**–**e**, **8**. See http://www.rsc.org/suppdata/cc/b0/b005884j/

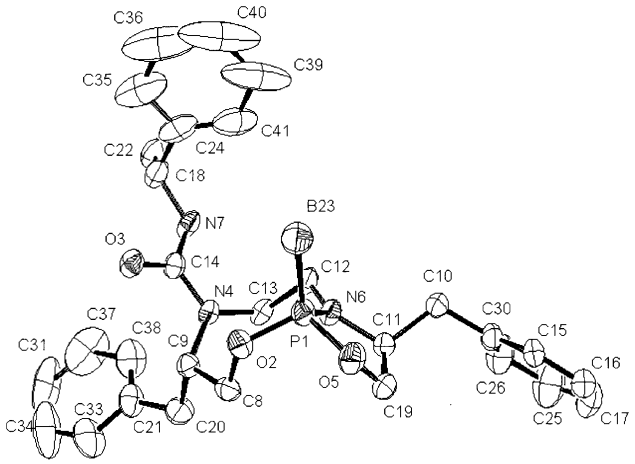

Fig. 1 ORTEP drawing of **8**. For more clarity, we omitted hydrogen atoms and used 30% probability ellipsoids. Selected bond lengths [Å]: O2–P1, 1.581(4); O5–P1, 1.592(4); N6–P1, 1.637(5); N4···P, 3.472(4); B23–P1, 1.888(7). Bond angles [°]: B23–P1–O2, 109.3(3); B23–P1–O5, 113.9(3); B23–P1–N6, 119.8(4); N6–P1–O5, 95.0(2); N6–P1–O2, 108.9(2); O2–P1–O5, 109.0(2); P1–N6–C11, 113.6(3); P1–N6–C12, 125.0(3); C8–O2–P1, 122.4(3); C19–O5–P1, 112.3(3); C11–N6–C12, 121.2(3); C9–N4–C13, 119.1(4); C9–N4–C14, 118.2(4); C13–N4–C14, 122.8(5).

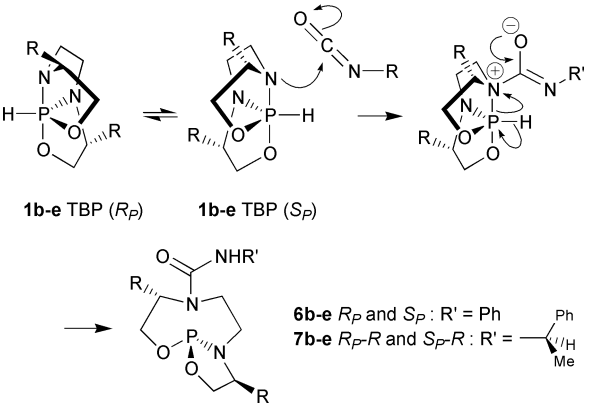

Scheme 2 Addition mechanism of isocyanates **4** and **5** on triquinphosphoranes **1b**–**e**.

In fact, the TBP-S_P, the pseudoaxial substituent is in an *anti* position with respect to the lone pair of the axial nitrogen atom whereas it is in a *syn* position in TBP-R_P. The diastereoselectivity observed can thus be rationalized in terms of a kinetically controlled process in which the minor triquinphosphorane diastereomer (29%) reacts faster than the major one (71%) to afford only one diastereomeric oxazaphospholidine.[4]

The importance of steric factors was further confirmed by the fact that the diastereoselectivity of the isocyanate addition depends on the position of the substituents. Indeed, in the case of triquinphosphorane **9**,[11] in which the phenyl substituents are β to the nitrogen atom, the diastereoselectivity of the addition of isocyanates **4** and **5** decrease to 77 and 93%, respectively.

In summary, we disclose for the first time the formation of enantiomerically pure P^{III} oxazaphospholidines from chiral pentacoordinated phosphoranes. These new compounds feature an eight-membered ring, difficult to synthesize with classical methods.[12] Research to evaluate the efficiency of these new compounds in asymmetric catalysis either as ligands or as catalysts is in progress.

We gratefully acknowledge financial support from the CNRS and fellowships from the MNRT (C. M. and G. D.). We thank Dr M. Giorgi and Professor M. Pierrot from the 'Université d'Aix-Marseille' for the X-ray structure determinations.

Notes and references

‡ The IUPAC name for triquinphosphorane is hexahydro-11 λ⁵-[1,3,2]oxazaphospholo[2′,3′:2,3][1,3,2]diazaphospholo[2,1-*b*][1,3,2]oxazaphosphole.

1 G. Buono, O. Chiodi, M. Gamble and M. Wills, *Synlett*, 1999, **4**, 377.
2 O. I. Kolodiazhnyi, *Tetrahedron: Asymmetry*, 1998, **9**, 1279.
3 (*a*) Y. Vannoorenberghe and G. Buono, *J. Am. Chem. Soc.*, 1990, **112**, 6142; (*b*) C. Marchi, F. Fotiadu and G. Buono, *Organometallics*, 1999, **18**, 915; (*c*) C. Marchi and G. Buono, *Tetrahedron Lett.*, 1999, **40**, 9251.
4 Semi empirical AM1 MO calculations predict that the TBP (R_P) and TBP (S_P) ground-state species are in equilibrium through a SP transition state, the activation barrier being about 5 kcal mol^{-1}. Calculations predict a marked predominance of the (R_P) form [71:29 for **1e**], see ref. 3*b*.
5 Compounds **2** and **3** have been studied by X-ray diffraction. They exhibit a percentage of deformation from the ideal TBP structure along the Berry pseudorotation pathway of 66 and 6.9%, respectively.
6 Triquinphosphoranes **1b**–**e** were prepared from *N*,*N*′-bis[(1*S*)-1-alkyl-2-hydroxyethyl]ethylenediamine. See ref. 3(*b*).
7 (*a*) K. Mislow, *Pyramidal Inversion Barriers of Phosphines and Arsines* in *Organophosphorus Stereochemistry part I: Origin and P(III and IV) Compounds*, eds. W. E. McEwen and K. D. Berlin, Dowden, Hutchinson and Ross, Inc., Stroudsburg, Pennsylvania, 1975, p. 195–210; (*b*) D. G. Gilheany, *Structure and Bonding in Organophosphorous (III) Compounds* in *The Chemistry of Organophosphorous Compounds vol. 1*, eds. F. R. Hartley and S. Patai, J. Wiley & Sons Publication, New York, 1990, p. 9–49.
8 Crystal data for **8**: $C_{29}H_{37}BN_3O_8P$, M_r = 517.42, hexagonal, space group *P*61, *a* = 13.0505(5), *c* = 29.9705(7) Å, *Z* = 6, *V* = 4420.3(3) Å, ρ_{calcd} = 1.166 g cm^{-3}, $\mu(Mo_{K\alpha})$ = 0.126 cm^{-1}, final *R*1 and *wR*2 are 0.0734 and 0.1745 for 368 parameters and 3328 unique observed reflections with $I > 2.0\sigma(I)$. CCDC 182/1811. See http://www.rsc.org/suppdata/cc/b0/b005884j/ for crystallographic files in .cif format.
9 J. M. Dupart, A. Grand, S. Pace and J. G. Riess, *Inorg. Chem.*, 1984, **23**, 3776.
10 (*a*) D. G. Gilheany, *Chem. Rev.*, 1994, **94**(5), 1339; (*b*) P. von R. Schleyer and A. J. Kos, *Tetrahedron*, 1983, **39**, 1141.
11 Triquinphosphorane **9** was prepared from *N*,*N*′-bis[2(*S*)-2-phenyl-2-hydroxyethyl]ethylenediamine.
12 L. D. Quin, in *Conformational Analysis of Medium-Sized Heterocycles*, ed. R. S. Glass, VCH, 1988, chap. 5, p. 181–216.

ChemComm

Synthesis of SO_4^{2-}/ZrO_2/MCM-41 as a new superacid catalyst†

Q.-H. Xia, K. Hidajat and S. Kawi*

Department of Chemical & Environmental Engineering, National University of Singapore, Singapore 119260, Republic of Singapore. Email: chekawis@nus.edu.sg

Received (in Cambridge, UK) 26th July 2000, Accepted 3rd October 2000
First published as an Advance Article on the web 31st October 2000

A new SO_4^{2-}/ZrO_2/MCM-41 superacid catalyst has been successfully synthesized and is *ca*. 2.5–3 times more active than the conventional SO_4^{2-}/ZrO_2 superacid catalyst for MTBE synthesis and *n*-pentane isomerization.

It is well known that zirconia, when modified with anions such as sulfate, forms a highly acidic or superacidic catalyst. In recent years, sulfated zirconia superacids have attracted increasing attention because these catalysts are found to be well suited for catalyzing reactions of industrial importance, such as hydrocarbon isomerization, etherification reactions, *etc*.[1–8] However the non-uniform pore size and relatively small surface area of SO_4^{2-}/ZrO_2 may limit its potential application for catalyzing bulky molecules. The use of M41s and other mesoporous materials,[9–12] which have very uniform mesopores and very high surface area, as catalyst supports for SO_4^{2-}/ZrO_2 should greatly expand the catalytic properties and capabilities of SO_4^{2-}/ZrO_2 for some applications. This is because such mesoporous materials, which have relatively small diffusion hindrance, can aid the diffusion of bulky organic molecules in and out of their mesopores quite easily.[9] Although many superacid catalysts have been developed using silica, alumina and microporous zeolites as supports,[2–8] there are still many limitations in their applications because of diffusion problems. Although a direct preparation of mesoporous sulfated zirconia has been recently reported,[13] the resulting materials had relatively small surface areas compared to that of conventional SO_4^{2-}/ZrO_2 and they were not tested for a particular reaction. Up to now, no silica-based M41s superacid materials nor gas-phase synthesis of MTBE from methanol and *tert*-butyl alcohol on acidic mesoporous catalysts have been reported. In this work, the active superacid SO_4^{2-}/ZrO_2 component has been successfully supported on the surface of MCM-41 to form a new SO_4^{2-}/ZrO_2/MCM-41 superacid catalyst, which is found to be 2.5–3 times more active than the conventional SO_4^{2-}/ZrO_2 superacid catalyst for MTBE synthesis and *n*-pentane isomerization.

$Zr(OH)_4$ was supported onto the surface of MCM-41 through chemical liquid deposition and hydrolysis of $Zr(OPr^n)_4$. Pre-dried siliceous MCM-41 powder having a BET surface area of 1311 $m^2\ g^{-1}$ and a pore diameter of 31.1 Å was dispersed into a mixed solution of $Zr(OPr^n)_4$ and *n*-hexane under vigorous stirring. After evaporating off the solvent, the solid was transferred into a glass container containing an NaCl-saturated aqueous solution at the bottom of the container in order to achieve complete hydrolysis at room temp. overnight. Pure $Zr(OH)_4$ was also prepared through hydrolysis of anhydrous $ZrCl_4$ in ammonia solution with a pH of 9–10.[3] After drying both samples at 100 °C overnight, the two resulting solids were immersed into 0.5 M H_2SO_4 solution at room temp. for 30 min. The sulfated $Zr(OH)_4$/MCM-41 and $Zr(OH)_4$ were then filtered off, dried at 100 °C overnight and calcined at 600 °C in air for 3 h to form SO_4^{2-}/ZrO_2/MCM-41 and SO_4^{2-}/ZrO_2. The content of ZrO_2 in the SO_4^{2-}/ZrO_2/MCM-41 catalyst was analyzed by ICP to be *ca*. 41 wt%. It should be noted that, when $ZrCl_4$ was used as a precursor in the preparation of $Zr(OH)_4$/MCM-41, the mesoporous structure of MCM-41 collapsed in the basic medium required for the hydrolysis of $ZrCl_4$.

XRD was used to characterize the regular mesoporous structure of MCM-41 and the resulting crystalline phase of bulk and supported ZrO_2. Fig. 1 shows that, for SO_4^{2-}/ZrO_2 calcined at 600 °C, three intense diffraction peaks at *ca*. 30, 50 and 60° and several small peaks at *ca*. 35 and 62° can be observed. These diffraction peaks show the presence of the tetragonal ZrO_2 crystalline phase, rather than the monoclinic ZrO_2 phase, and the absence of other impurities. This result shows that the introduction of SO_4^{2-} anions can remarkably stabilize the metastable tetragonal ZrO_2 phase, which is known to be an ideal crystalline phase for high catalytic activity.[2,4,6] The XRD pattern of SO_4^{2-}/ZrO_2/MCM-41 shows three clear and intense peaks below 10°, showing that the regular hexagonal mesostructure of the MCM-41 support is still maintained even after it has gone through the processes of chemical liquid deposition of ZrO_2, impregnation of sulfuric acid and high-temperature calcination. Furthermore, only a very small XRD peak at *ca*. 30° is observed on SO_4^{2-}/ZrO_2/MCM-41, showing that most of the ZrO_2 has been highly dispersed on the MCM-41. However, when this XRD picture is enlarged 5 ×, three diffraction peaks at *ca*. 30, 50 and 60° can be observed. This shows that, under very high loading of zirconia, a very small amount of ZrO_2 clusters (present as tetragonal ZrO_2 phase) might be formed within or outside the MCM-41 structure. BET analyses show that SO_4^{2-}/ZrO_2/MCM-41 (686 $m^2\ g^{-1}$) has a much larger surface area than SO_4^{2-}/ZrO_2 (101 $m^2\ g^{-1}$). The pore size of SO_4^{2-}/ZrO_2/MCM-41 (29.1 Å) is less than that of MCM-41 (31.1 Å), showing that the supported ZrO_2 has been dispersed onto the surface of mesopores of MCM-41.

The *in situ* FTIR spectrum of SO_4^{2-}/ZrO_2 measured after evacuation at 400 °C for 2 h shows an absorption band at 1378 cm^{-1}, corresponding to the asymmetric stretching frequency of covalent S=O; this band is often regarded as the characteristic

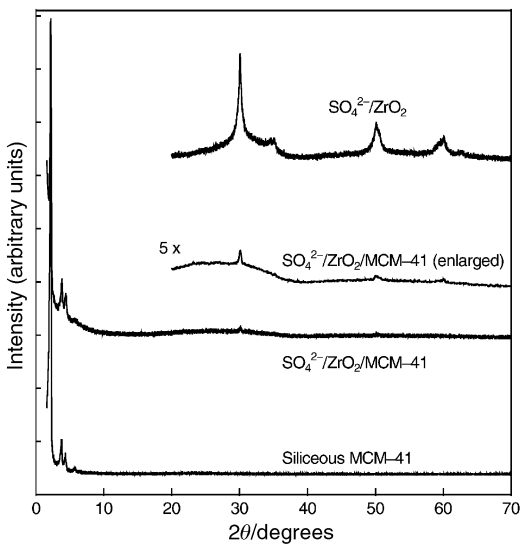

Fig. 1 XRD patterns of SO_4^{2-}/ZrO_2 and SO_4^{2-}/ZrO_2/MCM-41 superacid catalysts calcined in air at 873 K for 3 h and of siliceous MCM-41.

† Electronic supplementary information (ESI) available: characterization data for catalysts. See http://www.rsc.org/suppdata/cc/b0/b006051h/

DOI: 10.1039/b006051h

band of SO_4^{2-} on promoted superacids.[2–4,6] This band shifts to 1363 cm^{-1} for SO_4^{2-}/ZrO_2/MCM-41; the shifting is attributed to the influence of the interaction between ZrO_2 and framework SiO_2. TGA spectra show that both samples display common double-stage weight-loss features: the first below 200 °C (due to the evaporation of physically adsorbed water and other molecules), and the second between 580 and 900 °C (attributed to the removal of SO_4^{2-} species interacting with ZrO_2). The similarities of the decomposition temperature between these two samples indicate that the distribution of SO_4^{2-} species on both SO_4^{2-}/ZrO_2 and SO_4^{2-}/ZrO_2/MCM-41 is quite similar. Based on the amount of weight loss, SO_4^{2-}/ZrO_2 and SO_4^{2-}/ZrO_2/MCM-41 calcined at 600 °C contain 5.8 and 7.6 wt% of sulfate ions, respectively. Since the ZrO_2 content in SO_4^{2-}/ZrO_2/MCM-41 is nearly half of that in SO_4^{2-}/ZrO_2, this result shows that the highly dispersed ZrO_2 on MCM-41 can expose more ZrO_2 and adsorb more SO_4^{2-} anions than bulk crystalline ZrO_2.

The acid strengths of SO_4^{2-}/ZrO_2 and SO_4^{2-}/ZrO_2/MCM-41 samples calcined at 600 °C for 3 h were measured by the change of the color of a Hammet indicator added to the dried powder sample dissolved in the solvent. Both samples are found to have an H_0 value around −13.8 (measured in 2,4-dinitrotoluene), a typical value for superacids,[2–6] showing that they are *ca.* $10^4\times$ more acidic than 100% H_2SO_4. After calcination at 650 °C for 3 h, the acid strengths for both samples were increased to H_0 *ca.* −16.0 (measured in 1,3,5-trinitrobenzene).

Pyridine adsorption *in-situ* IR spectra were measured for both samples to measure the presence of Bronsted and Lewis acid sites. This was done by first pretreating a self-supporting wafer (15 mg) of the sample at 400 °C for 3 h under a vacuum of 10^{-6} mbar before adsorbing an excess of pure pyridine at room temperature, followed by evacuation at 200 °C for 30 min.[8] FTIR spectra on these two superacid catalysts show that they contain strong Bronsted acidity (at 1540 cm^{-1}) and Lewis acidity (at 1450 cm^{-1}). The intensities of Bronsted acid (having an integrated area of 1.20) and Lewis acid (having an integrated area of 1.43) sites of SO_4^{2-}/ZrO_2/MCM-41 are much stronger than the Bronsted acid (0.70) and Lewis acid (1.00) sites of SO_4^{2-}/ZrO_2. Both TGA and FTIR results show that SO_4^{2-}/ZrO_2/MCM-41 has more exposed Bronsted and Lewis acid sites than SO_4^{2-}/ZrO_2.

For the isomerization of *n*-pentane, which is a model reaction for characterizing the catalytic properties of these superacid catalysts, 0.5 g of powder catalyst was placed in a glass batch reactor and activated in vacuum at 250 °C for 3 h before 1 ml of pure *n*-pentane was introduced into the reactor and the reaction carried out at 60 °C under vigorous stirring. For the gas-phase synthesis of MTBE from MeOH and Bu^tOH in a fixed-bed reactor, the catalyst (0.20 g) was dehydrated in a flow of helium before a mixture of MeOH and Bu^tOH (with a molar ratio of 10:1 and a WHSV of 10 h^{-1}) was pumped into the reactor heated at 140 °C. Table 1 shows that both superacid catalysts have rather high activities for both reactions, with SO_4^{2-}/ZrO_2/MCM-41 always showing higher catalytic activity than SO_4^{2-}/ZrO_2. For the isomerization of *n*-pentane, the TON of SO_4^{2-}/ZrO_2/MCM-41 is almost 3 × that of SO_4^{2-}/ZrO_2, while the selectivity of product to isopentane is 98–99% for both catalysts. Increasing the batch reaction time gradually increases the TON of both catalysts to approach the equilibrium value. For the synthesis of MTBE, the TON of SO_4^{2-}/ZrO_2/MCM-41 is nearly 2.5 × that of SO_4^{2-}/ZrO_2, while a complete selectivity to MTBE is obtained on both catalysts. With an increase of reaction time, the TON of both catalysts remain almost unchanged. The reaction results show that the higher catalytic activity of SO_4^{2-}/ZrO_2/MCM-41, as compared to SO_4^{2-}/ZrO_2, is attributed to the increase of the number of active acid sites due to the highly exposed and easily accessible active sites of SO_4^{2-}/ZrO_2 on the surface of MCM-41. All of these results further elucidate the advantages of using a high BET surface area and uniform mesoporous material as a support for superacid catalysts for MTBE synthesis and other acid-catalyzed organic reactions in the future.

Table 1 Catalytic activities of SO_4^{2-}/ZrO_2 and SO_4^{2-}/ZrO_2/MCM-41 superacid catalysts

		SO_4^{2-}/ZrO_2		SO_4^{2-}/ZrO_2/MCM-41	
Reactant	*t*/min	TON[a]	Selec.(%)	TON[a]	Selec.(%)
n-Pentane	60	0.27	98[b]	0.81	100[b]
	200	0.41	98	1.19	99
	360	0.50	98	1.36	99
	600	0.54	98	1.42	99
MeOH + Bu^tOH	60	4.11	100[c]	10.10	100[c]
	180	4.13	100	10.13	100
	360	4.11	100	10.12	100
	600	4.12	100	10.10	100

[a] TON: mol of products/mol of Zr in the catalyst. [b] Selectivity of isopentane. [c] Selectivity to MTBE.

Notes and references

1 K. Arata, *Adv. Catal.*, 1990, **37**, 165.
2 G. D. Yadav and J. J. Nair, *Microporous Mesoporous Mater.*, 1999, **33**, 1.
3 Y. D. Xia, W. M. Hua, Y. Tang and Z. Gao, *Chem. Commun.*, 1999, 1899.
4 T. Jin, T. Yamaguchi and K. Tanabe, *J. Phys. Chem.*, 1986, **90**, 4797.
5 G. D. Yadav and N. Kirthivasan, *J. Chem. Soc., Chem. Commun.*, 1995, 203.
6 M. Hino and K. Arata, *J. Chem. Soc., Chem. Commun.*, 1979, 1148; M. Hino and K. Arata, *J. Chem. Soc., Chem. Commun.*, 1980, 851.
7 F. R. Chen, G. Coudurier, J. F. Joly and J. C. Vederine, *J. Catal.*, 1993, **143**, 616.
8 T. Lei, J. S. Xu, Y. Tang, W. M. Hua and Z. Gao, *Appl. Catal. A: General*, 2000, **192**, 181.
9 S. Biz and M. L. Occeli, *Catal. Rev.-Sci. Eng.*, 1998, **40**, 329.
10 S. Kawi and M. W. Lai, *Chem. Commun.*, 1998, 1407.
11 A. M. Liu, K. Hidajat, S. Kawi and D. Y. Zhao, *Chem. Commun.*, 2000, 1145.
12 R. Anwander, C. Palm, G. Gerstberger, O. Groeger and G. Engelhard, *Chem. Commun.*, 1998, 1811.
13 D. J. McIntosh and R. A. Kydd, *Microporous Mesoporous Mater.*, 2000, 281.

Bilayer nanoporous electrodes for dye sensitized solar cells

A. Zaban,*[a] S. G. Chen,[a] S. Chappel[a] and B. A. Gregg[b]

[a] *Chemistry Department, Bar-Ilan University, Ramat-Gan, 52900, Israel. E-mail: zabana@mail.biu.ac.il*
[b] *National Renewable Energy Laboratory, Golden, CO, 80401, USA*

Received (in Cambridge, UK) 21st July 2000, Accepted 3rd October 2000
First published as an Advance Article on the web 31st October 2000

The fabrication of a new bilayer TiO_2/Nb_2O_5 nanoporous electrode that improves the performance of dye sensitized solar cells by more than 35% is reported.

The high light-to-energy conversion efficiencies achieved with dye sensitized solar cells (DSSCs) may be attributed to the nanoporous TiO_2 electrodes.[1] These electrodes consist of nanosize semiconductor colloids that are sintered on a transparent conducting substrate resulting in a porous geometry and a very large surface area. Both the low absorbance of dye monolayers and the low efficiency of dye multilayers necessitate the large surface area. However, the resulting electrode geometry introduces special characteristics, some of which reduce the performance of the DSSCs.[2–4] One of these characteristics relates to the small size of the individual colloidal particles that cannot support a high space charge.[2,4,5] In other words an energy barrier is not formed at the electrode–electrolyte interface.

Upon illumination of a DSSC, an electron is injected from the dye into the TiO_2 film followed by a hole transfer to the electrolyte[1,6] The injected electrons must cross the TiO_2 film and reach the conducting substrate, while the oxidized ions diffuse towards the back electrode where they are re-reduced.[1,6] The porous geometry that permits the presence of the electrolyte through the entire electrode provides a high surface area for recombination between the injected electrons and the holes in solution[2,7] In the absence of an energy barrier at the electrode–electrolyte interface, the rate of this recombination process may be very high depending on the properties of the hole carrier.[2,5,8,9] For this reason, DSSCs utilizing the I^-/I_3^- redox couple perform better than similar cells consisting of faster couples.[10] Furthermore, part of the low efficiencies observed with solid electrolytes is attributed to this recombination process.[3] The formation of an energy barrier at the surface of the TiO_2 electrode that will enable the use of various mediators has the prospect of improving the performance of DSSCs significantly.

We report here on the fabrication of a nanoporous wide band gap semiconductor electrode that has an inherent energy barrier at its surface. To the best of our knowledge, this is the first time such an electrode has been reported. The new electrode consists of an inner nanoporous TiO_2 matrix covered with a thin layer of Nb_2O_5. The conduction band potential of Nb_2O_5 (0 V *vs.* NHE at pH 0) is *ca.* 100 mV more negative than that of the TiO_2.[11] As illustrated in Fig. 1, this potential difference forms an energy barrier at the electrode–electrolyte interface, which can reduce the rate of recombination processes of the photoinjected electrons. A comparison of two similar DSSCs that differ only in their nanoporous electrodes, shows that the new bilayer electrode is superior to the standard one with respect to all cell parameters. This superiority measured with many cells results in a 35% increase of the overall conversion efficiency.

The TiO_2 nanoporous matrix of 6 μm thickness was prepared from colloids with particles of 23 nm diameter. The colloid and the matrix preparation methods are reported elsewhere.[12] The Nb_2O_5 coating was prepared by dipping the sintered TiO_2 matrix in a dry solution of 0.005 M niobium isopropoxide in isopropyl alcohol for 30 s, followed by washing with dry isopropyl alcohol and sintering at 500 °C in air for 30 min. The dipping was performed under dry nitrogen atmosphere. The thickness of the electrode measured with a Mitutoyo, Surftest SV 500 profilometer did not change upon coating. XPS measurements of the coated electrodes show that the average metal mol fraction of Nb was 36% with the remainder Ti. Given this molar ratio, a 2.7 nm thick Nb_2O_5 layer is calculated when assuming that the TiO_2 colloids are spherical and single sized, and that the Nb_2O_5 coating is uniform.

A sandwich-type configuration was employed to measure the DSSCs. A Pt coated F-doped SnO_2 film was used as a counter electrode, and 0.5 M Li/0.05 M I_2 in 1 : 1 acetonitrile–NMO was used as electrolyte. The dye [*cis*-di(isothiocyanato)-*N*-bis(4,4′-dicarboxy-2,2′-bipyridine)ruthenium(II), (N3)] was adsorbed by immersing the electrodes overnight in a 0.5 mM ethanol solution of the dye. The oxidation potential of the dye (*ca.* 1.09 V *vs*. NHE in acetonitrile) is sufficient to allow injection into both TiO_2 and Nb_2O_5.[11] The amount of dye adsorbed on the electrode was measured by visible absorption of the electrode using a HP 8453 spectrophotometer. Illumination of the cell was conducted using a calibrated Xe lamp. IPCE measurements were performed using a ScinceTech 9010 monochromator scaled to 6 nm bandwidth.

We describe here a comparison of two typical DSSCs that differ in their type of electrode. One cell contained the new bilayer electrode and the other served as a reference, consisting of a standard nanoporous TiO_2 electrode. Both cells were studied under similar conditions. The reference electrode and the TiO_2 matrix were made from the same batch and separated only after the first sintering process. After the Nb_2O_5 coating of the TiO_2 matrix was performed, both electrodes were sintered again to ensure similarity. The thickness of both electrodes was 6 μm, and the same amount of dye was adsorbed on both films as confirmed by absorption spectra. Finally, the undyed electrodes had the same transparent appearance showing transmission spectra that differed slightly only in the band gap region. Under illumination equivalent to sunlight, Nb_2O_5 coating of the TiO_2 resulted in an increase of all cell parameters. The photocurrent increased from 10.2 to 11.4 mA cm^{-2}, the photovoltage from 659 to 732 mV, and the fill factor from 51.1 to 56.4%. As a result, the maximum power of the cell was increased from 3.45 to 4.70 mW cm^{-2}.

The improved cell performance achieved by the new bilayer electrode may be attributed to the energy barrier formed by the

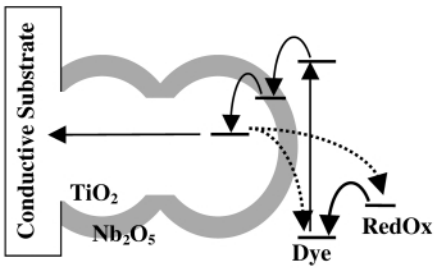

Fig. 1 A schematic view of the new bilayer nanoporous electrode which consists of a nanoporous TiO_2 matrix covered with a thin layer of Nb_2O_5. The Nb_2O_5 coating forms an inherent energy barrier at the electrode–electrolyte interface, which reduces the recombination rate of the photoinjected electrons.

DOI: 10.1039/b005921h

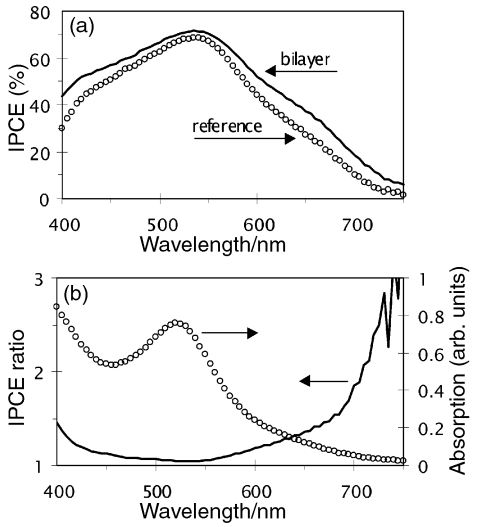

Fig. 2 (a) IPCE curves of the reference dye sensitized solar cell and the cell containing the bilayer electrode. The IPCE curves resemble the absorption spectrum of the electrodes shown in (b) which shows the ratio between the IPCE values of the two solar cells as a function of the illumination wavelength revealing its wavelength dependence.

deposition of the thin Nb_2O_5 layer. The Nb_2O_5 layer apparently decreases the rate of recombination of the photoinjected electrons with the dye and the electrolyte. This phenomenon is revealed best from incident photon to current efficiency (IPCE) measurements for the two cells. As shown in Fig. 2(a) the curves of both cells resemble the absorption spectrum of the N3 dye. The measured IPCE values of the cell containing the bilayer electrode are higher than those of the reference cell throughout the visible spectrum. However, the improvement in the conversion efficiency is wavelength dependent as indicated by the ratio between the IPCE values of the two cells (the improvement factor). Fig. 2(b) shows that this factor increases at illumination wavelengths in which the absorption coefficient of the dye becomes low.

The improved performance evident from Fig. 2(a) is not necessarily the result of a change in the collection efficiency. This improvement can be related to other factors, such as the injection yield.[1] However, the wavelength dependence of the improvement factor can be directly related to the electron collection.[13] The mean distance a photoinjected electron must diffuse in order to reach the current collector increases as the absorption coefficient of the dye decreases thus changing the light absorption profile. This phenomenon means that recombination events are expected to increase as the absorption coefficient of the dye decreases.[13] In other words, a change in the rate of recombination is expected to have a more significant effect at the low dye absorption coefficient regions. Fig. 2(b) indicates that this is the case of the new bilayer electrode.

The results presented above clearly demonstrate that the bilayer electrodes are superior to the standard single material nanoporous electrodes in terms of the performance of DSSCs. These results suggest that the improvement is achieved by the formation of an energy barrier at the electrode–electrolyte interface, which slows the recombination process. However at this stage of research we lack information on the quality of the coating with respect to its homogeneity throughout the film which affects the ability to determine the exact thickness of the coating. In addition, it is still unclear to what extent the new electrode can improve the performance of DSSCs in which mediators other than the I^-/I_3^--based electrolyte are used. Research towards better understanding of this system and further performance improvement are currently being undertaken.

We thank the National Center for Photovoltaics at NREL and The Israel Science Foundation founded by The Israel Academy of Science and Humanities for supporting this research.

References

1 K. Kalyanasundaram and M. Gratzel, *Coord. Chem. Rev.*, 1998, **77**, 347.
2 A. Hagfeldt, S. E. Lindquist and M. Gratzel, *Sol. Energy Mater. Sol. Cells*, 1994, **32**, 245.
3 A. Zaban, A. Meier and B. A. Gregg, *J. Phys. Chem. B*, 1997, **101**, 7985.
4 J. Bisquert, G. Garcia-Belmonte and F. Fabregat-Santiago, *J. Solid State Electrochem.*, 1999, **3**, 337.
5 L. Kavan, M. Gratzel, S. E. Gilbert, C. Klemenz and H. J. Scheel, *J. Am. Chem. Soc.*, 1996, **118**, 6716.
6 B. O'Regan and M. Gratzel, *Nature*, 1991, **353**, 737.
7 Y. Tachibana, J. E. Moser, M. Gratzel, D. Klug and J. R. Durrant, *J. Phys. Chem.*, 1996, **100**, 20 056.
8 I. Bedja, S. Hotchandani and P. V. Kamat, *Ber. Bunsen-Ges. Phys. Chem. Chem. Phys.*, 1997, **101**, 1651.
9 C. Nasr, P. V. Kamat and S. Hotchandani, *J. Electroanal. Chem.*, 1997, **420**, 201.
10 F. Pichot and B. A. Gregg, *J. Phys. Chem. B*, 2000, **104**, 6.
11 K. Sayama, H. Sugihara and H. Arakawa, *Chem. Mater.*, 1998, **10**, 3825.
12 A. Zaban, S. T. Aruna, S. Tirosh, B. A. Gregg and Y. Mastai, *J. Phys. Chem. B*, 2000, **104**, 4130.
13 G. Hodes, I. D. J. Howell and L. M. Peter, *J. Electrochem. Soc.*, 1992, **139**, 3136.

First synthesis of alkynyltriphenylbismuthonium salts and their dual reaction modes in sulfonylation

Yoshihiro Matano*

Department of Chemistry, Graduate School of Science, Kyoto University, Sakyo-ku, Kyoto 606-8502, Japan. E-mail: matano@kuchem.kyoto-u.ac.jp

Received (in Cambridge, UK) 23rd August 2000, Accepted 2nd October 2000
First published as an Advance Article on the web

Treatment of triphenylbismuth difluoride with alkynyldiisopropoxyboranes in the presence of BF_3·OEt_2 in CH_2Cl_2 gives alkynyltriphenylbismuthonium tetrafluoroborates, which react with sodium *p*-toluenesulfinate in dual reaction modes depending on the solvents employed.

The chemistry of onium salts with an acetylenic group on the cationic heteroatom constitutes an attractive area of study in terms of both heteroatom and acetylene chemistry.[1] In general, three reaction sites are conceivable for this class of compounds: the heteroatom center, the acetylenic α-carbon and the acetylenic β-carbon. Owing to this diversity, such compounds have recently been utilized as versatile reagents in organic synthesis.[1] However, no information is yet available for alkynylbismuthonium salts owing to the lack of a general method for constructing a Bi–C_{sp} bond. Recently, the Lewis acid-promoted reactions of triarylbismuth difluorides with organometallic reagents have proven to be efficient methods for the preparation of various types of bismuthonium salts bearing a Bi–C_{sp^3} or Bi–C_{sp^2} bond ($[Ar_3BiR^+][X^-]$; R = alkyl, alkenyl, aryl).[2] Owing to the high leaving ability of the triarylbismuthonio group, this class of compounds has been shown to have unique reactivities that differ significantly from those of lighter element counterparts. These results have led me to disclose the nature of the Bi–C_{sp} bond in bismuthonium salts. Reported here are the first synthesis, crystal structure and reactions of alkynyltriphenylbismuthonium salts.

As shown in Scheme 1, alkynyltriphenylbismuthonium tetrafluoroborates **3a–d** were prepared by the reaction of triphenylbismuth difluoride **1** with the corresponding alkynyldiisopropoxyboranes **2a–d**[3,4] in the presence of BF_3·OEt_2 (Table 1).† No Bi–C_{sp} coupling took place in the absence of the Lewis acid, as was observed in the reaction of **1** with other types of organoboronic acids.[2f,g] Compounds **3** were isolated as colorless solids in 88–93% yields by recrystallization from CH_2Cl_2–Et_2O and characterized by NMR, IR and mass spectrometry.

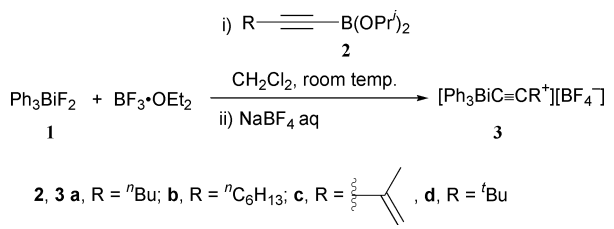

Scheme 1

Table 1 Alkynyltriphenylbismuthonium tetrafluoroborates **3**

Entry	**3**	Yield (%)	Mp/°C
1	**3a** ($[Ph_3Bi^+C{\equiv}C^nBu][BF_4^-]$)	88	137–138
2	**3b** ($[Ph_3Bi^+C{\equiv}C^nC_6H_{13}][BF_4^-]$)	93	83–85
3	**3c** ($[Ph_3Bi^+C{\equiv}CC(Me){=}CH_2][BF_4^-]$)	89	139–141
4	**3d** ($[Ph_3Bi^+C{\equiv}C^tBu][BF_4^-]$)	90	160–161

The structure of **3d** was further determined by X-ray crystallography (Fig. 1).‡ The bismuth center of **3d** adopts a pseudotrigonal bipyramidal (TBPY) geometry with three phenyl *ipso* carbons at the equatorial sites and an acetylenic α carbon and a fluorine atom at the apical sites. The Bi···F(1) distance of 2.749(4) Å is longer than the sum of their covalent radii (2.10 Å) but much shorter than the sum of their van der Waals radii (3.75 Å),[5] indicating that the tetrafluoroborate anion interacts strongly with the cationic bismuth center. Owing to this interaction, the B–F(1) bond is slightly longer than other B–F bonds. The TBPY geometry observed for **3d** may be attributable to the steric as well as electronic character of the acetylenic group: known alkyl-, alkenyl- and aryl-triphenylbismuthonium tetrafluoroborates all adopt a distorted tetrahedral geometry with the spatially separated BF_4^- anion.[2a,b,d,f,g] The Bi–C(1) bond length [2.151(8) Å] is slightly shorter than the Bi–C_{Ph} bond lengths [2.179(9)–2.235(9) Å], reflecting the difference in electronic properties between the C_{sp} and C_{sp^2} atoms. The C(1)–C(2) bond length [1.19(1) Å] is almost identical to that of a typical C≡C triple bond (1.20 Å), and the acetylenic moiety is bent slightly at the C(1) atom. Although the reason for this bent conformation is not clear at present, it might be due to the steric effect caused by the neighboring molecules. In $CDCl_3$, the *ortho* protons of the phenyl groups of **3** were observed at relatively lower field (δ 8.25) than those of tetrahedral bismuthonium salts (δ 7.7–7.8), suggesting that the TBPY geometry of **3** is also maintained in solution.

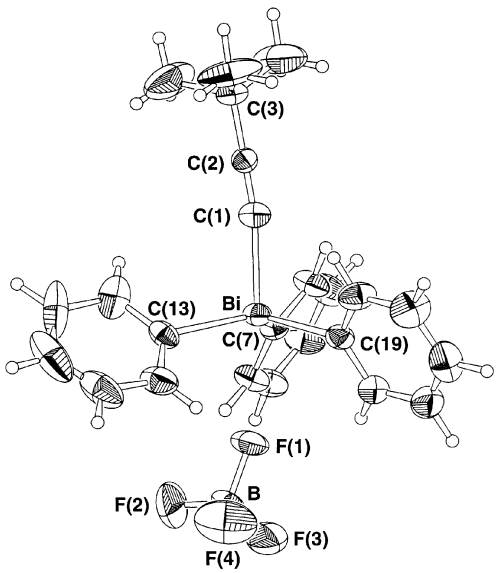

Fig. 1 ORTEP diagram (30% probability ellipsoids) of **3d**. Selected bond lengths (Å) and angles (°): Bi–C(1) 2.151(8), Bi–C(7) 2.210(8), Bi–C(13) 2.235(9), Bi–C(19) 2.179(9), B–F(1) 1.38(1), B–F(2–4) 1.29(1)–1.33(1), C(1)–C(2) 1.19(1), C(2)–C(3) 1.47(1), Bi···F(1) 2.749(4); C(1)–Bi–C(7) 100.1(3), C(1)–Bi–C(13) 98.6(3), C(1)–Bi–C(19) 102.6(3), C(7)–Bi–C(13) 122.1(3), C(7)–Bi–C(19) 111.9(3), C(13)–Bi–C(19) 116.4(3), Bi–C(1)–C(2) 170.9(8), C(1)–C(2)–C(3) 178.6(10).

DOI: 10.1039/b006881k

Alkynylbismuthonium salts **3** were slowly hydrolyzed in open air or in wet solution to give μ-oxobis(triphenylbismuth) bis(tetrafluoroborate)[2a] and parent acetylenes (Scheme 2). Thus, it is reasonable to assume that the hydroxy group of water is bound to the bismuth atom. This mode of hydrolysis is in marked contrast to that observed for methyltriphenylbismuthonium tetrafluoroborate, which produces methanol, triphenylbismuthine and fluoroboric acid.[2g] In this case, the hydroxy group is bound to the methyl group. These two results reflect the difference in reactivity between the Bi–C_{sp} and Bi–C_{sp^3} bonds in bismuthonium salts.

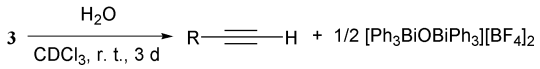

Scheme 2

The reaction of alkynyltriphenylbismuthonium salts **3** with a sulfinate anion was examined (Scheme 3). The treatment of **3a** with 2 equiv. of sodium *p*-toluenesulfinate **4** in MeOH afforded (*Z*)-1,2-bis(*p*-toluenesulfonyl)hex-1-ene **5a** (R = ^{n}Bu) in 48% yield together with triphenylbismuthine **6**.§ The (*Z*)-configuration of **5a** was determined by comparison with the spectral properties of analogous compounds[6] as well as by NOE experiment. Compounds **3b** and **3c** also reacted with **4** in MeOH to give the corresponding disulfones **5b** (R = ^{n}C_6H_{13}, 43%) and **5c** [R = C(Me)=CH_2, 42%], respectively, with good recovery of **6**. By contrast, when a similar reaction of **3a** was carried out in DMF, 1-sulfonyl-3-methylcyclopentene **7** was obtained as a major product (33%) and **5a** was not formed at all.§

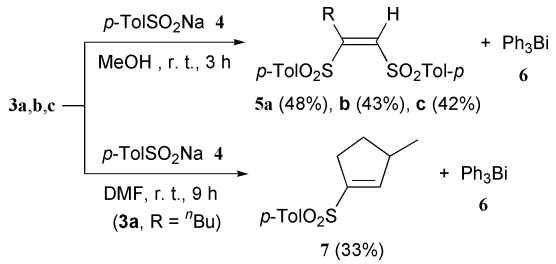

Scheme 3

Plausible mechanisms for the sulfonylations of **3a** are depicted in Scheme 4. The initial stage in both reactions would be a Michael addition of the sulfinate anion to the β-alkynyl carbon. In MeOH, the resulting ylide **8** would be protonated to produce an alkenylbismuthonium intermediate **9**, which subsequently reacts with the sulfinate anion to give **5** with retention of the configuration.[2d] In DMF, ylide **8** would eliminate bismuthine **6** to generate an alkylidene carbene intermediate **10**, which undergoes 1,5-C–H insertion to give cyclopentene **7**. Similar types of tandem bis-sulfonylation and sulfonylation/C–H insertion reactions were reported for alkynylselenonium[7] and alkynyliodonium salts,[8] respectively. Interestingly, alkynylbismuthonium salts **3** react with the same nucleophile *via* two different pathways depending on the solvents employed.

This work was partially supported by a Grant-in-Aid (No. 12640516) from the Ministry of Education, Science, Sports and Culture of Japan. The author thanks Professor Hiroyuki Furuta and Mr Hazumi Nomura for their assistance with the X-ray crystallography.

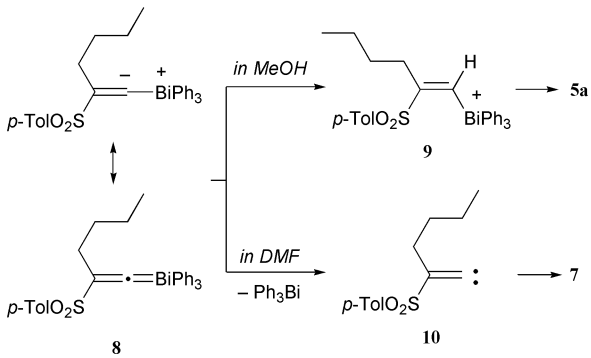

Scheme 4

Notes and references

† *A typical example:* to a mixture of **1** (1.17 g, 2.44 mmol), BF_3·OEt_2 (0.35 cm^3, 2.7 mmol) and CH_2Cl_2 (10 cm^3) was added **2a** (858 mg, 3.00 mmol) at 0 °C. The resulting solution was stirred at room temp. After 15 h, an aqueous solution (10 cm^3) of $NaBF_4$ (2.2 g, 20 mmol) was added, and the resulting two-phase solution was vigorously stirred for 1 min. The organic phase was separated, dried over $MgSO_4$ and concentrated under reduced pressure to leave an oily residue, which was recrystallized from Et_2O–CH_2Cl_2 (10 : 1) to afford **3a** as a colorless crystalline solid (1.31 g, 88%): δ_H 0.96 (t, 3H, *J* 7.2), 1.36–1.74 (m, 4H), 2.48 (t, 2H, *J* 7.0), 7.52–7.75 (m, 9H), 8.25 (d, 6H, *J* 7.8); IR ν_{max} 2147 (C≡C), 1200–1000 (BF_4^-) cm^{-1}; FABMS *m/z* 521 $[M - BF_4]^+$. Found: C, 47.46; H, 4.09. $C_{24}H_{24}BBiF_4$ requires C, 47.39; H, 3.98%. **3b**: δ_H 0.90 (t, 3H, *J* 6.5), 1.20–1.75 (m, 8H), 2.48 (t, 2H, *J* 6.9), 7.53–7.80 (m, 9H), 8.25 (d, 6H, *J* 7.6); IR ν_{max} 2151 (C≡C), 1200–1000 (BF_4^-) cm^{-1}; FABMS *m/z* 549 $[M - BF_4]^+$. Found: C, 48.19; H, 4.37. $C_{26}H_{28}BBiF_4$ requires C, 49.08; H, 4.44%. **3c**: δ_H 2.00 (s, 3H), 5.51 (s, 1H), 5.60 (s, 1H), 7.50–7.80 (m, 9H), 8.25 (d, 6H, *J* 7.2); IR ν_{max} 2130 (C≡C), 1200–900 (BF_4^-) cm^{-1}; FABMS *m/z* 505 $[M - BF_4]^+$. Found: C, 46.53; H, 3.32. $C_{23}H_{20}BBiF_4$ requires C, 46.65; H, 3.40%. **3d**: δ_H 1.37 (s, 9H), 7.59 (t, 3H, *J* 7.2), 7.68 (t, 6H, *J* 7.6), 8.24 (d, 6H, *J* 7.6); IR ν_{max} 2130 (C≡C), 1200–1000 (BF_4^-) cm^{-1}; FABMS *m/z* 521 $[M - BF_4]^+$. Found: C, 47.25; H, 4.01. $C_{24}H_{24}BBiF_4$ requires C, 47.39; H, 3.98%.

‡ The crystal structure of **3d** consists of two isolated molecules which differ little from each other as to the configuration of the central bismuth atom. The ORTEP diagram and selected bond parameters in Fig. 1 are those of the selected molecule. *Crystal data*: $C_{48}H_{48}B_2Bi_2F_8$, *M* = 1216.48, monoclinic, *a* = 17.863(1), *b* = 13.7651(8), *c* = 19.835(1) Å, β = 98.235(2)°, *V* = 4826.8(5) Å^3, *T* = 296 K, space group $P2_1/a$ (no. 14), *Z* = 4, D_c = 1.674 g cm^{-3}, μ(Mo-Kα) = 73.30 cm^{-1}, 40421 reflections measured, 10596 unique (R_{int} = 0.057) refined to R_w = 0.108, R_1 = 0.039 [$I > 2.0\sigma(I)$]. CCDC 182/1812. See http://www.rsc.org/suppdata/cc/b0/b006881k/ for crystallographic files in .cif format.

§ **5a**: Mp 61–62 °C; δ_H 0.83 (t, 3H, *J* 6.9), 1.10–1.22 (m, 4H), 2.39 (t, 2H, *J* 7.6), 2.46 (s, 6H), 6.72 (s, 1H), 7.36 (d, 4H, *J* 8.1), 7.92 (d, 2H, *J* 8.1), 7.97 (d, 2H, *J* 8.1); FABMS *m/z* 393 $[M + 1]^+$. Found: C, 61.26; H, 6.26. $C_{20}H_{24}O_4S_2$ requires C, 61.20; H, 6.16%. Satisfactory spectroscopic and analytical data are available for **5b**,**c**. **7**: δ_H 1.08 (d, 3H, *J* 7.1), 1.55 (m, 1H), 2.23 (m, 1H), 2.44 (s, 3H), 2.45–2.63 (m, 2H), 2.92 (m, 1H), 6.58 (dd, 1H, *J* 1.7, 3.8), 7.33 (d, 2H, *J* 8.0), 7.77 (d, 2H, *J* 8.0); FABMS *m/z* 237 $[M + 1]^+$.

1 M. Ochiai, M. Kunishima, Y. Nagao, K. Fuji, M. Shiro and E. Fujita, *J. Am. Chem. Soc.*, 1986, **108**, 8281; A. C. Dema, X. Li, C. M. Lukehart and M. D. Owen, *Organometallics*, 1991, **10**, 1197; V. V. Zhdankin, P. J. Stang and N. S. Zefirov, *J. Chem. Soc., Chem. Commun.*, 1992, 578; P. J. Stang, *Angew. Chem., Int. Ed. Engl.*, 1992, **31**, 274; T. Kitamura, L. Zheng, T. Fukuoka, Y. Fujiwara, H. Taniguchi, M. Sakurai and R. Tanaka, *J. Chem. Soc., Perkin Trans. 2*, 1997, 1511; A. Varvoglis, *Tetrahedron*, 1997, **53**, 1179; T. Kataoka, S. Watanabe and K. Yamamoto, *Tetrahedron Lett.*, 1999, **40**, 931; V. V. Zhdankin and P. J. Stang, *Tetrahedron*, 1998, **54**, 10 927

2 (*a*) Y. Matano, N. Azuma and H. Suzuki, *J. Chem. Soc., Perkin Trans. 1*, 1994, 1739; (*b*) Y. Matano, N. Azuma and H. Suzuki, *J. Chem. Soc., Perkin Trans. 1*, 1995, 2543; (*c*) Y. Matano, M. Yoshimune and H. Suzuki, *Tetrahedron Lett.*, 1995, **36**, 7475; (*d*) Y. Matano, M. Yoshimune, N. Azuma and H. Suzuki, *J. Chem. Soc., Perkin Trans. 1*, 1996, 1971; (*e*) Y. Matano, M. M. Rahman, M. Yoshimune and H. Suzuki, *J. Org. Chem.*, 1999, **64**, 6924; (*f*) Y. Matano, S. A. Begum, T. Miyamatsu and H. Suzuki, *Organometallics*, 1999, **18**, 5668; (*g*) Y. Matano, *Organometallics*, 2000, **19**, 2258.

3 H. C. Brown, N. G. Bhat and M. Srebnik, *Tetrahedron Lett.*, 1988, **29**, 2631.

4 Quite recently, Zhdankin *et al.* reported a convenient method for the preparation of alkynyliodonium salts from alkynylboronates and hypervalent iodine reagents: V. V. Zhdankin, P. J. Persichini III, R. Cui and Y. Jin, *Synlett*, 2000, 719.

5 J. Emsley, *The Elements*, Oxford University Press, Oxford, 3rd edn., 1998.

6 M. Ochiai, Y. Kitagawa, M. Toyonari, K. Uemura, K. Oshima and M. Shiro, *J. Org. Chem.*, 1997, **62**, 8001.

7 T. Kataoka, Y. Banno, S. Watanabe, T. Iwamura and H. Shimizu, *Tetrahedron Lett.*, 1997, **38**, 1809.

8 M. Ochiai, M. Kunishima, S. Tani and Y. Nagao, *J. Am. Chem. Soc.*, 1991, **113**, 3135.

ChemComm

Phase-boundary catalysis: a new approach in alkene epoxidation with hydrogen peroxide by zeolite loaded with alkylsilane-covered titanium oxide

Hadi Nur, Shigeru Ikeda and Bunsho Ohtani*

Catalysis Research Center, Hokkaido University, Sapporo 060-0811, Japan. E-mail: ohtani@cat.hokudai.ac.jp

Received (in Cambridge, UK) 1st August 2000, Accepted 4th September 2000
First published as an Advance Article on the web 31st October 2000

An NaY zeolite, modified with partly alkylsilane-covered titanium oxide and located at the boundary between aqueous and organic phases (a phase-boundary catalyst), acts as a catalyst for alkene epoxidation without stirring or the addition of a co-solvent to drive liquid–liquid phase transfer.

Utilization of hydrogen peroxide (H_2O_2) as an oxidant for organic substrates has received much attention in recent years because of its environmental implications; it gives only water as a product in a wide range of oxidation reactions. Moreover, it is less expensive and more accessible than other oxidizing agents, such as organic peracids or hydroperoxides. However, H_2O_2 is generally supplied as an aqueous solution, and when the substrate to be oxidized is insoluble in water, it is necessary to add a co-solvent to obtain a homogeneous reaction mixture.[1,2] Here, we propose a novel integrated chemical system, which we have termed 'phase-boundary catalysis', using aqueous H_2O_2 for the oxidation of organic compounds without any co-solvent. For this system, a particulate zeolite catalyst has been designed and prepared in order to be placed at the phase boundary between aqueous H_2O_2 and an organic substrate. Several authors have reported a 'triphase system' in which the homogeneous modification of a particulate catalyst loaded with metal ions or their complexes as active sites induced or accelerated the oxidation of organic substrates with H_2O_2 in aqueous solution.[3–7] In such triphase systems, however, vigorous stirring, leading to sufficient mass transfer, is required to drive the reaction. However, our strategy is different from those previously reported because we aim at placing the bifunctional particles, containing both hydrophilic and hydrophobic regions, at the phase boundary in order to catalyze the epoxidation reaction without requiring an emulsion containing the catalyst by stirring.

Modified zeolite on which the external surface was partly covered with alkylsilane was prepared in two steps. First, titanium(IV) tetraisopropoxide [$Ti(OPr^i)_4$, Wako Pure Chemical] was impregnated from benzene solution into NaY zeolite powder (JRC-Z-Y5.5, supplied by the Catalysis Society of Japan) and heated at 383 K overnight to give sample W-Ti-NaY. 500 μmol of Ti was used per gram of NaY unless otherwise stated. In the second step, *n*-octadecyltrichlorosilane (OTS, Tokyo Kasei) in toluene was impregnated into the W-Ti-NaY powder containing water (0.5 cm^3 g per g of NaY) and heated at 383 K overnight. Due to the hydrophilicity of the W-Ti-NaY surface, addition of a small amount of water (0.5 g per g of W-Ti-NaY) led to aggregation owing to the capillary force of water between particles. Under these conditions, it is expected that only the outer surface of aggregates, in contact with the organic phase can be modified with OTS, and indeed almost all of the particles were located at the phase boundary when added to an immiscible water–organic solvent (W/O) mixture. The partly modified sample is denoted W/O-Ti-NaY. Fully modified Ti-NaY (O-Ti-NaY), prepared without the addition of water in the above second step, is readily suspended in an organic solvent as expected. At present, it is not clear whether the position of alkylsilane attachment is on the zeolite, on the Ti oxide (hydroxide), or on both.

In the water adsorption experiment at room temperature, it was observed that the adsorption capacity of modified zeolites (8 mmol g^{-1} for both W/O-Ti-NaY and O-Ti-NaY) was not greatly different from that of the parent NaY zeolite (11 mmol g^{-1}), suggesting that alkylsilane modification did not block the pores of zeolites. This observation is in agreement with the finding reported by Singh and Dutta.[8]

Oct-1-ene (Kanto Chemical, 97%) was purified by passing it through a column of basic alumina and was used as a substrate for epoxidation reaction. Typically, oct-1-ene (4 ml), 30% aqueous H_2O_2 (1 ml) and catalyst powder (50 mg) were placed in a glass tube, and the reaction was performed with or without stirring for 20 h at ambient temperature. As can be seen in Table 1, all of the modified zeolites showed activity for epoxidation of oct-1-ene to give 1,2-epoxyoctane. GC analyses (Shimadzu GC-14B) indicated that 1,2-epoxyoctane was the sole product, and other probable by-products, such as octanone, octan-1-ol, octan-2-ol or octane-1,2-diol, were not produced. NaY modified by Ti-species only (W-Ti-NaY) was hydrophilic in nature, and was suspended in water when added to a W/O mixture. W-Ti-NaY showed appreciable epoxidation ability only under vigorous stirring, *i.e.* in the W/O emulsion, but was negligibly active without stirring, as shown in Fig. 1. Modification of Ti-NaY by alkylsilane led to a significant rate enhancement. In particular, partial modification by alkylsilane (W/O-Ti-NaY, entry 3) led to better activity than full modification (O-Ti-NaY, entry 4). A reference experiment using non-porous silica (Wako Pure Chemical, < 200 mesh) was also carried out. Silica was modified in a similar manner to that of W/O-Ti-NaY. The epoxidation result showed that the yield of 1,2-epoxyoctane was lowered ten-fold compared to W/O-Ti-NaY (entry 8), suggesting that the pores might be playing a role in the catalytic reaction.

Table 1 Catalytic room-temperature epoxidation of oct-1-ene[a]

Entry	Catalyst	Epoxide yield/μmol	TON for Ti
1	None	0.1	—
2	W-Ti-NaY	2.5	0.1
3	W/O-Ti-NaY	27.4	1.1
4	O-Ti-NaY	5.9	0.2
5	(Solution)[b]	0.1	—
6	W/O-Ti-NaY (reused)[c]	16.4	0.7
7	W/O-Ti-NaY[d]	22.7	45.4
8	W/O-Ti-silica[e]	2.9	0.1

[a] All reactions were carried out at room temperature for 20 h with oct-1-ene (4 ml), 30% H_2O_2 (1 ml) and catalyst (50 mg) with vigorous stirring; the concentration of Ti and alkylsilane = 500 μmol g^{-1}. [b] The aqueous phase of entry 3 after the reaction. The reaction was conducted for 9 h. [c] The reaction was performed after washing and drying of the catalyst. [d] Concentration of Ti = 10 μmol g^{-1}. [e] Nonporous silica (Wako Pure Chemical, < 200 mesh) was modified in a similar way to that of W/O-Ti-NaY.

The recovered and dried W/O-Ti-NaY catalyst was reused in a fresh W/O mixture and showed *ca.* 60% activity. To the remaining reaction mixture, without the catalyst, was added 30% H_2O_2 aqueous solution, and the mixture was vigorously

DOI: 10.1039/b006207n

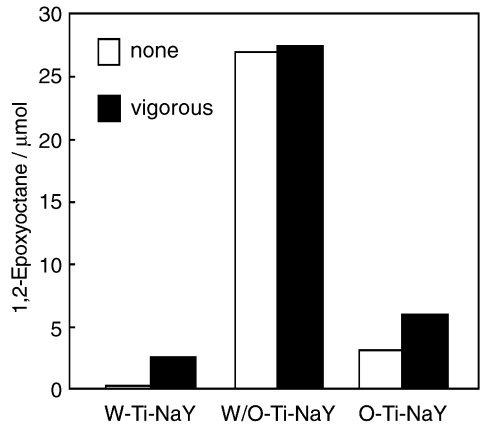

Fig. 1 Effect of stirring on the yield of 1,2-epoxyoctane.

stirred at ambient temperature. A negligible increase in the amount of epoxide could be seen. These facts suggest that epoxide formation occurs at the phase boundary, and not from any leached Ti species. Although the turnover number (TON), the molar ratio of the epoxide to the loaded Ti, was almost unity for the reaction with W/O-Ti-NaY (entry 3) for relatively larger Ti loading, W/O-Ti-NaY with a lower Ti concentration (10 μmol g^{-1}) (entry 7) gave a TON of *ca.* 45, indicating catalytic action of the Ti species. Higher loading might induce aggregation leading to inner inactive sites. One of the most striking features of W/O-Ti-NaY is shown in Fig. 1; the partial alkylsilane modification not only enhanced the epoxidation but also changed the mode of reaction. As described above, W-Ti-NaY showed activity only under vigorous stirring, and a similar behavior was seen for the O-Ti-NaY system in which the epoxide yield under static conditions was almost half of that of the stirred reaction mixture. On the other hand, the activity of W/O-Ti-NaY was not dependent on the stirring rate, *i.e.* this catalyst does not require the formation of W/O emulsion, completely at variance with previously reported results for the 'triphase system'.[7] The amphiphilic nature of W/O-Ti-NaY, enabling it to sit just at the W/O phase boundary, may account for the constant activity. Therefore, the rate of this phase-boundary catalysis depends only on the apparent area of the W/O interphase. In fact, when a narrow-bore reaction tube was used to decrease the apparent interphase area, the activity was reduced, as expected (data not shown).

All of the results mentioned above seem consistent with the mechanism of phase-boundary catalysis; amphiphilic particles having active sites (Ti-species) lie at the W/O interphase to catalyze the chemical reaction. However, the apparent rate of epoxidation was much lower than those previously reported.[4] One of the reasons for the low activity in our catalysts is the presence of few four-coordinate Ti species which are considered to be the most active species in olefin epoxidation.[9] It should be noted that we used the Ti-loaded NaY zeolite as an easily available material and the catalyst and the reaction conditions have not been optimized. Further study for improvement of catalytic activity by generating four-coordinated Ti species in the catalytic system is now underway. Thus, we have shown a new concept of phase-boundary catalysis, that is applicable when amphiphilic particles, molecular assemblies, or films with adequate active sites are used, to a wide range of catalytic reactions.

H. N. thanks the Japan Society for the Promotion of Science (JSPS) for granting a Postdoctoral Fellowship. We are grateful to the Catalysis Society of Japan for the supply of zeolite samples. This research was partly supported by a Grant-in-Aid for Encouragement of Young Scientists (No. 99302) from Ministry of Education, Science, Sports and Culture, Japan. Dr Hisashi Semba (Nippon Shokubai) is acknowledged for his stimulating suggestions and discussion.

Notes and references

1 M. Hudlický, *Oxidations in Organic Chemistry*, ACS Monograph 186, Washington, DC, 1990, p. 7.
2 A. A. Rao and H. R. Mohan, in *Encyclopedia of Reagents for Organic Synthesis*, ed. L. A. Paquette (Editor-in-Chief), John Wiley and Sons, 1995, p. 2731–2735.
3 R. Kumar and A. Bhaumik, *Microporous Mesoporous Mater.*, 1998, **21**, 497.
4 T. Tatsumi, K. A. Koyano and N. Igarashi, *Chem. Commun.*, 1998, 325.
5 R. Neumann and T.-J. Wang, *Chem. Commun.*, 1997, 1915.
6 M. Dusi, T. Mallat and A. Baiker, *Catal. Rev-Sci. Eng.*, 2000, **42**, 213.
7 D. R. C. Huybrechts, Ph. L. Buskens and P. A. Jacobs, *Stud. Surf. Sci. Catal.*, 1992, **72**, 21.
8 R. Singh and P. K. Dutta, *Microporous Mesoporous Mater.*, 1999, **32**, 29.
9 B. Notari, *Adv. Catal.*, 1996, **41**, 253.

Chiral synthesis of the CD ring unit of paclitaxel from D-glucal

Takayuki Momose, Masaki Setoguchi, Toshiki Fujita, Hitoshi Tamura and Noritaka Chida*

Department of Applied Chemistry, Faculty of Science and Technology, Keio University, Hiyoshi, Kohoku-ku, Yokohama 223-8522, Japan. E-mail: chida@applc.keio.ac.jp

Received (in Cambridge, UK) 31st July 2000, Accepted 5th October 2000
First published as an Advance Article on the web 31st October 2000

The chiral synthesis of the fully functionalized CD ring unit of paclitaxel 3 is described; the three component coupling reaction of a cyclohexenone derived from D-glucal by way of Ferrier's carbocyclization with vinyl cuprate and formaldehyde effectively constructed the carbon framework of 3.

Paclitaxel (Taxol®) **1** is a well-documented natural diterpenoid and is known to show highly promising antitumor activity.[1] The challenging structure as well as important biological activities of **1** has attracted much attention of the synthetic community, and six successful total syntheses of **1** have been reported to date.[2] Our own synthetic endeavor to paclitaxel required the fully functionalized CD ring unit **3** as the key intermediate; the formyl function at C-3 (paclitaxel numbering) would be utilized for the coupling reaction with a paclitaxel A-ring **2**, and the vinyl group at C-8 would serve as the key functionality for the construction of a taxane skeleton. Successful precedents for preparation of taxane tricarbocyclic structures by way of final B-ring closure of connected AC ring systems revealed the possibility of this approach.[3] The highly oxygenated structure of **3**, which contains five contiguous chiral centers including a quaternary carbon and a strained oxetane ring is synthetically fascinating, and it is a significant aim to establish an effective synthetic route to **3** from readily available material for the development of a novel approach to the clinically important compounds.[4] In this communication, we report a synthesis of **3**, which utilized commercially available tri-*O*-acetyl-D-glucal **4** as a chiral starting material.

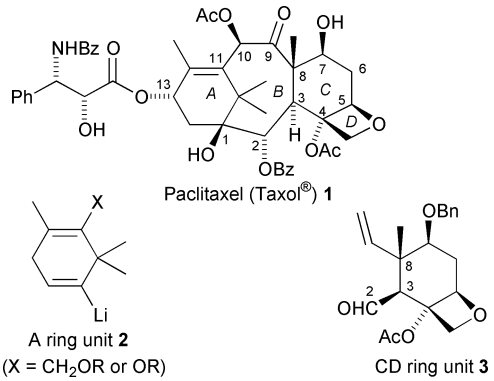

The known methyl glycoside **5**,[5]† derived from **4** in a two step reaction (90% overall yield) (Scheme 1) was converted into primary iodide **6**† in 87% yield, which was then treated with NaH and benzyl bromide to afford enopyranoside **7**† in 80% yield. Ferrier's carbocyclization[6] of **7** using a catalytic amount of $Hg(OCOCF_3)_2$,[7] followed by β-elimination cleanly generated cyclohexenone **8** (80% yield). Reaction of **8** with MeLi gave 1,2-adduct **9**, whose oxidation with PCC afforded **10** in 83% yield from **8**.

With a chiral cyclohexenone **10** in hand, generation of the quaternary carbon at C-8 and the C–C bond at C-3 by a three component coupling reaction[8]‡ of **10**, a vinyl metal species, and formaldehyde in a one-pot reaction was investigated. Treatment of **10** with higher order vinylcuprate [$(vinyl)_2$-$CuCNLi_2$] in Et_2O at −78 °C caused the stereoselective conjugated addition of the vinyl group to give an enolate intermediate,§ which was then reacted with a THF solution of formaldehyde at −60 °C to provide **11** {mp 50–52 °C; $[\alpha]_D^{23}$ + 12 (*c* 1.0, $CHCl_3$)} and its C-3 isomer **12** {$[\alpha]_D^{23}$ + 93 (*c* 1.0, $CHCl_3$)} in 62 and 33% isolated yields, respectively. The observed coupling constants and NOE unambiguously supported the structure of **11** (Scheme 2). Base-induced epimerization of **12** gave an additional amount of **11** (44% yield, **12** was recovered in 51% yield); thus **11** was obtained in 76% overall yield from **10** after one-cycle epimerization of **12**. Protection of the hydroxy group in **11** as a THP ether afforded **14** in 90% yield. To introduce an hydroxy function at C-5, ketone **14** was treated with LiHMDS at −78 °C, and the resulting kinetic enolate was trapped with TMSCl to provide silylenol ether, which was then reacted with MCPBA at −20 °C followed by treatment with TMSCl and triethylamine to give **15** and **16** in 53 and 26% isolated yields, respectively. Reaction of **15** with Tebbe's reagent[9] and subsequent removal of the silyl protecting group under basic conditions afforded *exo*-alkene **17** in 64% yield.¶ Vanadium catalyzed epoxidation[10] of **17** gave **18** as a single isomer in 81% yield. Reaction of **18** with potassium acetate in DMF, followed by treatment with acetic anhydride and pyridine at rt gave **19** in 95% yield. The secondary hydroxy group in **19** was mesylated to afford **20** (96% yield). Removal of the *O*-acetyl group, followed by reaction with DBU[4c] in toluene at 100 °C cleanly generated oxetane **21** in 65% yield. Acetylation of tertiary alcohol in **21** afforded **22** (100%). Deprotection of the *O*-THP group in **22** with CAN[11]‖ gave **23**, which was oxidized with TPAP[12] to furnish the desired aldehyde **3** {$[\alpha]_D^{23}$ −137 (*c* 0.07, $CHCl_3$)} in 80% yield from **22**. The observed NOE between the methyl at C-8 and the formyl hydrogen, H-20, and H-6_β, and between H-7 and H-3 clearly supported the assigned structure.

We thank Professor Takashi Takahashi and Dr Takayuki Doi (Tokyo Institute of Technology, Japan) for valuable discussions and information. Financial support of the Grant-in Aid for Scientific Research on Priority Area from the Ministry of

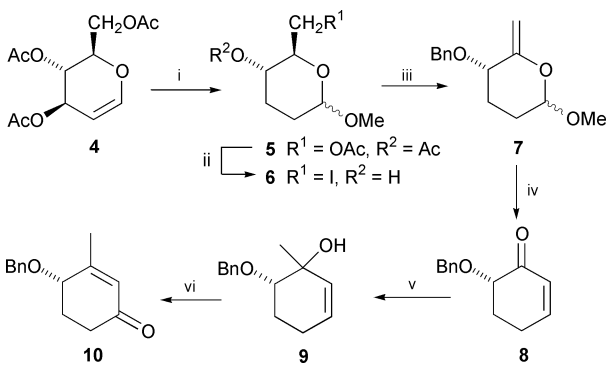

Scheme 1 Bn = $-CH_2Ph$. *Reagents and conditions*: i, MeOH, $BF_3{\cdot}OEt_2$, PhH, 0 °C, then H_2, 10% Pd-C, EtOAc, rt; ii, MeONa, MeOH, 0 °C, then I_2, Ph_3P, imidazole, THF, rt; iii, NaH, DMF, 0 °C, then BnBr, *n*-Bu_4NI, DMF, 0 °C; iv, $Hg(OCOCF_3)_2$ (5 mol%), acetone–H_2O (2:1), 0 °C, then MsCl, Et_3N, CH_2Cl_2, 0 °C; v, MeLi, Et_2O, −78 °C; vi, PCC, molecular sieves 4 Å (powder), CH_2Cl_2, rt.

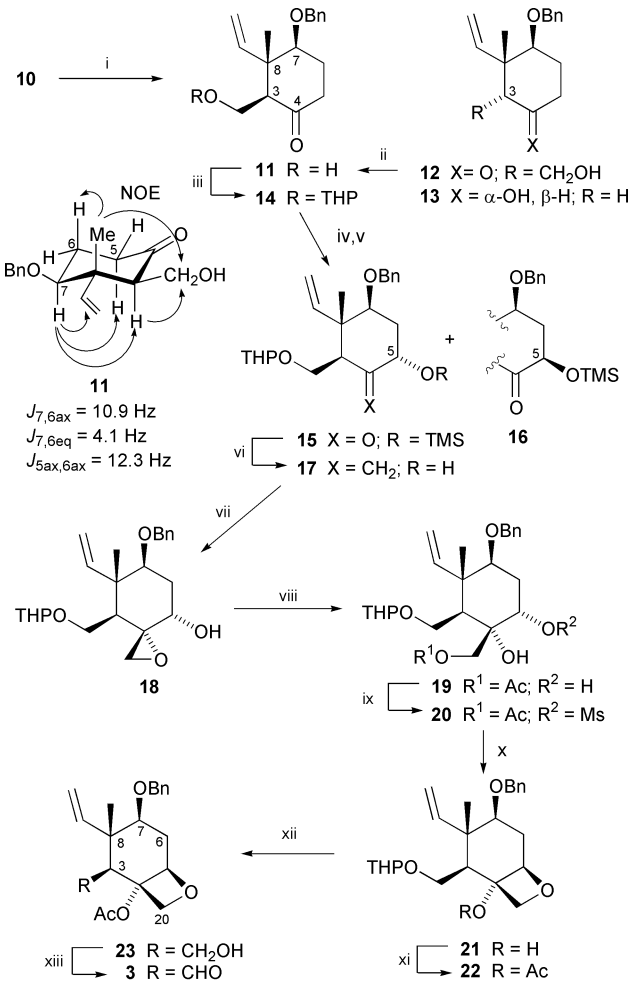

Scheme 2 THP = tetrahydropyran-2-yl, TBS = $-SiMe_2(t\text{-Bu})$, Ms = $-SO_2Me$. *Reagents and conditions*: i, CuCN (2 eq.), vinyllithium (4 eq.), Et_2O, −78 °C, 10 min, then formaldyhyde in THF (1 mol l^{-1}, excess amount), −60 °C, 15 min; ii, K_2CO_3, MeOH, rt; iii, 3,4-dihydro-2*H*-pyran, PPTS, CH_2Cl_2, rt; iv, LiHDMS, THF, −78 °C, then TMSCl–Et_3N (1 : 1, v/v), −78 °C; v, MCPBA , −20 °C, CH_2Cl_2, then TMSCl, Et_3N, CH_2Cl_2; vi, Tebbe reagent, THF, rt, then K_2CO_3, MeOH, rt.; vii, *t*-BuOOH, $VO(acac)_2$, rt; viii, AcOK, 18-crown-6, DMF, 100 °C, then acetic anhydride, pyridine, rt; ix, MsCl, DMAP, CH_2Cl_2, rt; x, K_2CO_3, MeOH, rt; then DBU, toluene, 100 °C; xi, acetic anhydride, DMAP, pyridine, 40 °C; xii, CAN (3 mol%), CH_3CN–borate buffer (pH 8, 1 : 1), 50 °C; xiii, TPAP, NMO, rt.

Education, Science, Sports and Culture, Japanese Government is gratefully acknowledged.

Notes and references

† This compound was an anomeric mixture (α : β = *ca.* 4 : 1), and used in the next reaction without separation.

‡ A similar approach (starting from D-glucose) has been reported by Ermolenko, see ref 4*d*.

§ Conjugated addition of the vinyl group to enone **10** was found to proceed highly stereoselectively. When the intermediate enolate was treated with aqueous NH_4Cl, a 1,4-adduct was obtained as a single isomer in 95% yield. Reduction of the 1,4-adduct with $NaBH_4$ afforded a cyclohexanol derivative **13**, which was acylated with (*R*)- and (*S*)-acetylmandelic acid (DCC, DMAP) to give (*R*)- and (*S*)-acetylmandelate derivatives, respectively. ^1H NMR analyses of the acetylmandelates revealed that they showed quite different spectra, and no signal due to the (*R*)-isomer was observed in the spectrum of the (*S*)-isomer, indicating the cyclohexanol **13** possessed high optical purity (~100% ee), and no racemization had occurred during the preparation of **8** and **10** and the 1,4-addition process.

¶ When compound **16** was subjected to the same reaction conditions, no reaction took place resulting in the recovery of **16**.

‖ Under the conditions of deprotection of the *O*-THP group with PPTS in EtOH, the primary hydroxy group in the resulting **23** further attacked the oxetane ring to generate a significant amount of a THF derivative.

1 Isolation of paclitaxel, see (*a*) M. C. Wani, H. L. Taylor, M. E. Wall, P. Coggon and A. T. McPhail, *J. Am. Chem. Soc.*, 1971, **93**, 2325. Biological activity, see (*b*) *Taxane Anticancer Agents: Basic Science and Current Status'* ed. I. Georg, T. T. Chen, I. Ojima and D. M. Vyas, ACS Symposium Series 583, American Chemical Society, Washington DC, 1995.

2 (*a*) R. A. Holton, H.-B. Kim, C. Somoza, F. Liang, R. J. Biediger, P. D. Boatman, M. Shindo, C. C. Smith, S. Kim, H. Nadizadeh, Y. Suzuki, C. Tao, P. Vu, S. Tang, P. Zhang, K. K. Murthi, L. N. Gentile and J. H. Liu, *J. Am. Chem. Soc.*, 1994, **116**, 1599 and references therein; (*b*) K. C. Nicolaou, Z. Yang, J.-J. Liu, H. Ueno, P. G. Nantermet, R. K. Guy, C. F. Claiborne, J. Renaud, E. A. Couladouros, K. Paulvannan and E. J. Sorensen, *Nature*, 1994, **367**, 630; K. C. Nicolaou, H. Ueno, J.-J. Liu, P. G. Nantermet, Z. Yang, J. Renaud, K. Paulvannan and R. Chadha, *J. Am. Chem. Soc.*, 1995, **117**, 653 and references therein; (*c*) J. J. Masters, J. T. Link, L. B. Snyder, W. B. Young and S. J. Danishefsky, *Angew. Chem., Int. Ed. Engl.*, 1995, **34**, 1723; S. J. Danishefsky, J. J. Masters, W. B. Young, J. T. Link, L. B. Snyder, T. V. Magee, D. K. Jung, R. C. A. Isaacs, W. G. Bornmann, C. A. Alaimo, C. A. Coburn and M. J. Di Grandi, *J. Am. Chem. Soc.*, 1996, **118**, 2843; (*d*) P. A. Wender, N. F. Badham, S. P. Comway, P. E. Floreancig, T. E. Glass, J. B. Houze, N. E. Krauss, D. Lee, D. G. Marquess, P. L. McGrane, W. Meng, M. G. Natchus, A. J. Shuker, J. C. Sutton and R. E. Taylor, *J. Am. Chem. Soc.*, 1997, **119**, 2757 and references therein; (*e*) I. Shiina, H. Iwadare, H. Sakoh, M. Hasegawa, Y. Tani and T. Mukaiyama, *Chem. Lett.*, 1998, 1; I. Shiina, K. Saitoh, I. Fréchard-Ortuno and T. Mukaiyama, *Chem. Lett.*, 1998, 3; T. Mukaiyama, I. Shiina, H. Iwadare, M. Saitoh, T. Nishimura, N. Ohkawa, H. Sakoh, K. Nishimura, Y. Tani, M. Hasegawa, K. Yamada and K. Saitoh, *Chem. Eur. J.*, 1999, **5**, 121; (*f*) K. Morihira, R. Hara, S. Kawahara, T. Nishimori, N. Nakamura, H. Kusama and I. Kuwajima, *J. Am. Chem. Soc.*, 1998, **120**, 12980; H. Kusama, R. Hara, S. Kawahara, T. Nishimori, H. Kashima, N. Nakamura, K. Morihara and I. Kuwajima, *J. Am. Chem. Soc.*, 2000, **122**, 3811.

3 Examples of construction of taxane skeleton involving B-ring closure of AC ring systems by McMurry reaction, see ref. 2*b*. Heck reaction, see ref. 2*c*. Aldol reaction, see ref. 2*f*; R. Hara, T. Furukawa, Y. Horiguchi and I. Kuwajima, *J. Am. Chem. Soc.*, 1996, **118**, 9186; M. R. R. Ferreira, J. I. M. Hernando, J. I. C. Lena, N. Birlirakis and S. Areniyadis, *Synlett*, 2000, 113. Alkylation of cyanohydrin derivatives, see T. Takahashi, H. Iwamoto, K. Nagashima, T. Okabe and T. Doi, *Angew. Chem., Int. Ed. Engl.*, 1997, **36**, 1319. Pinacol coupling with SmI_2, see C. S. Swindell and W. Fan, *Tetrahedron Lett.*, 1996, **37**, 2321; *J. Org. Chem.*, 1996, **61**, 1109.

4 Reports on the synthesis of the fully functionalized paclitaxel CD ring unit, see (*a*) T. V. Magee, W. G. Bornmann, R. C. A. Isaacs and S. J. Danishefsky, *J. Org. Chem.*, 1992, **57**, 3274; (*b*) K. C. Nicolaou, C.-K. Hwang, E. J. Sorensen and C. F. Clairborne, *J. Chem. Soc., Chem. Commun.*, 1992, 1117; (*c*) T. Takahashi, Y. Hirose, H. Iwamoto and T. Doi, *J. Org. Chem.*, 1998, **63**, 5742; representative synthetic approaches, see (*d*) M. S. Ermolenko, T. Shekharam, G. Lukacs and P. Potier, *Tetrahedron Lett.*, 1995, **36**, 2461; M. S. Ermolenko, G. Lukacs and P. Potier, *Tetrahedron Lett.*, 1995, **36**, 2465; (*e*) A. N. Boa, J. Clark, P. R. Jenkins and N. J. Lawrence, *J. Chem. Soc., Chem. Commun.*, 1993, 151; (*f*) M. Nakada, E. Kojima and Y. Iwata, *Tetrahedron Lett.*, 1998, **39**, 313; (*g*) C.-K. Sha, S-J. Lee and W.-H. Tseng, *Tetrahedron Lett.*, 1997, **38**, 2725, and references therein.

5 R. J. Ferrier and N. Presad, *J. Chem. Soc. (C)*, 1969, 570.

6 R. J. Ferrier, *J. Chem. Soc., Perkin Trans., 1*, 1979, 1455; R. J. Ferrier and S. Middleton, *Chem. Rev.*, 1993, **93**, 2779.

7 N. Chida, M. Ohtsuka, K. Ogura and S. Ogawa, *Bull. Chem. Soc. Jpn.*, 1991, **64**, 2118; S. Amano, N. Takemura, M. Ohtsuka, S. Ogawa and N. Chida, *Tetrahedron*, 1999, **55**, 3855.

8 For a review, see R. J. K. Taylor, *Synthesis*, 1985, 364.

9 F. N. Tebbe, G. W. Parshall and G. S. Reddy, *J. Am. Chem. Soc.*, 1978, **100**, 3611; S. H. Pine, R. J. Pettit, G. D. Geib, S. G. Cruz, C. H. Gallego, T. Tijerina and R. D. Pine, *J. Org. Chem.*, 1985, **50**, 1212.

10 K. B. Sharpless and R. C. Michaelson, *J. Am. Chem. Soc.*, 1973, **95**, 6136.

11 I. E. Markó, A. Ates, B. Augustyns, A. Gautier, Y. Quesnel, L. Turet and M. Wiaux, *Tetrahedron Lett.*, 1999, **40**, 5613.

12 S. V. Ley, J. Norman, W. P. Griffith and S. P. Marsden, *Synthesis*, 1994, 639.

Novel synthesis of oxindoles from carbamoyl chlorides *via* palladium catalysed cyclisation–anion capture

Mark R. Fielding,[a] Ronald Grigg*[a] and Christopher J. Urch[b]

[a] *Department of Chemistry, University of Leeds, Woodhouse Lane, Leeds, UK LS2 9JT. E-mail: R.Grigg@chem.leeds.ac.uk*

[b] *Zeneca Agrochemicals, Jealott's Hill Research Station, Bracknell, UK RG42 6ET*

Received (in Cambridge, UK) 17th August 2000, Accepted 5th October 2000
First published as an Advance Article on the web 31st October 2000

The synthesis of 3,3-disubstituted and 3-methyleneoxindoles by palladium(0) catalysed cyclisation of carbamoyl chlorides onto proximate alkene or alkyne groups has been achieved in good yields.

3,3-Disubstituted oxindoles are common structural motifs in a wide range of natural products. Gelsemine,[1] paraherquamides[2] and spirotryprostatins[3] represent classes that possess oxindole cores and have interesting biological profiles. 3-Methyleneoxindoles, on the other hand, are versatile intermediates in synthesis. Recently, Williams *et al.*[4] used a diasterospecific cycloaddition onto a methyleneoxindole in their total synthesis of spirotryprostatin B. Classically, spirooxindoles can be synthesised *via* an oxidative rearrangement of indoles[5] and methyleneoxindoles can be accessed by Wittig–Horner[6] type reactions of isatin. Oxindoles can conceptually be constructed by palladium catalysed processes in a number of ways. There are examples of intramolecular Heck and intramolecular cyclisation–anion capture reactions on acrylamide derivatives of 2-iodoanilines.[7] We have applied our palladium catalysed cyclisation–anion capture methodology to 3,3-disubstituted oxindoles (including spirooxindoles)[8] *via* formation of bond **a** (Fig. 1). We have also developed a 3-component process[9] which constructs bonds **a**, **b**, and **c**. We now describe palladium catalysed cyclisation–anion capture processes involving formation of bond **b** (Fig. 1).

The use of carbamoyl chlorides in palladium catalysed cross-coupling reactions with stannanes was reported by Jousseaume and Dubac.[10] Its use in Heck-type cyclisations[11] is rare, perhaps because the initial reports employed forcing conditions and toxic cosolvents for the synthesis of lactams. Our plan was to use 2-ethynyl- or 2-isopropenyl-phenylcarbamoyl chlorides as oxindole precursors (Fig. 1) in cyclisations which do not terminate *via* β-hydride elimination (as in Heck processes) but involve a group or atom transfer. This process (known as cyclisation–anion capture)[12] allows a large variety of groups to be introduced onto the oxindole. By this route, (*Z*)-3-methyleneoxindoles are stereospecifically formed and 3,3-disubstituted oxindoles can be potentially synthesised by a catalytic, enantioselective process.

The synthesis of the required carbamoyl chlorides was achieved from the appropriate 2-haloaniline in high overall yield (Scheme 1). 2-Iodoaniline **1** is converted to its *N*-benzyl derivative **2** using a reductive amination protocol. Treatment of

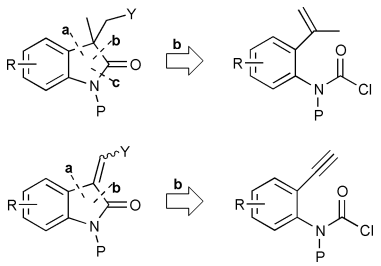

Fig. 1

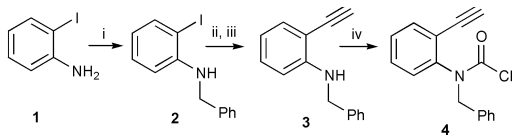

Scheme 1 *Reagents and conditions*: i, PhCHO, MeOH, reflux then $NaBH_4$, reflux (45%, 86% based on 52% conv.); ii, TMSA, $Pd(PPh_3)_4$, CuI, NEt_3, DMF, rt (90%); iii, TBAF, THF–H_2O, rt (91%); iv, $COCl_2$, $NaHCO_3$, DCM–H_2O, 0 °C (93%).

2 with a two step Sonagashira[13]-deprotection procedure then affords the 2-ethynyl derivative **3**. Finally, addition of phosgene[14] to aniline **3** at 0 °C for 10 min affords carbamoyl chloride **4**.

A range of carbamoyl chlorides **4**–**7** were synthesised in a similar way to provide a selection of 5- and 6-membered heterocycle precursors. These carbamoyl chlorides are air and moisture insensitive and can be purified on flash silica. Substrates **4** and **5** are 3-methyleneoxindole precursors, whilst **6**

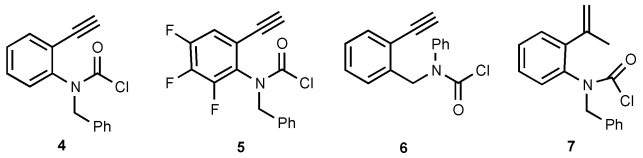

is an example of a 6-ring isoquinolinone precursor. Carbamoyl chloride **7** was synthesised from commercially available 2-isopropenylaniline.

Initially, we focused on the use of tributylstannanes as anion capture agents for these substrates.[15] It was found that treatment of **4** with tributyl(2-thienyl)tin and $Pd(OAc)_2$–tris(2-furyl)phosphine in toluene at 50 °C for 5 min affords the desired 3-methyleneoxindole **8** in 88% yield (Scheme 2). Repetition of this latter reaction using 1 mol% $Pd(OAc)_2$–2 mol% tris(2-furyl)phosphine and a reaction time of 30 min afforded **8** in 91% yield emphasising the scope for considerable reduction in catalyst loading. The use of tributyl(phenylethynyl)tin also resulted in a high yield of product (81%), whilst vinyl transfer affords a 4 : 3 mixture of geometrical isomers **10** and **11** in 76% overall yield. Cyclisation–anion capture employing tributyl(2-furyl)tin was also complete within 5 min at 50 °C, and afforded (*Z*) **12** in 78% yield.

This methodology can also be extended to 6-ring cyclisation–anion capture and to the synthesis of 3,3-disubstituted oxindoles (Scheme 3).

Cyclisation of **6** affords **13** (87%), a 4-methyleneisoquinolin-3-one in 5 min at 50 °C. However, cyclisation onto the isopropenyl group of **7** to form **14** is much slower (4 h), but proceeds in excellent yield (84%). The use of boronic acids as anion capture reagents[8] is currently being studied. A preliminary study involving **7** and phenylboronic acid afforded **15** (50%) (Scheme 3). This reaction was considerably slower (50 h, 90 °C) than those involving organostannane anion capture reagents and since a small amount of water was present

DOI: 10.1039/b006765m

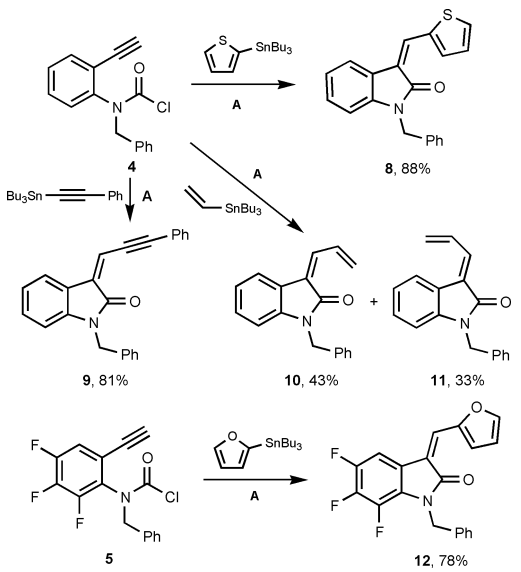

Scheme 2 *Reagents and conditions*: **A** = $Pd(OAc)_2$ (10 mol%), tris(2-furyl)phosphine (20 mol%), 1.1 equiv. Bu_3SnY, toluene, 50 °C. All reactions were complete within 5 min at 50 °C.

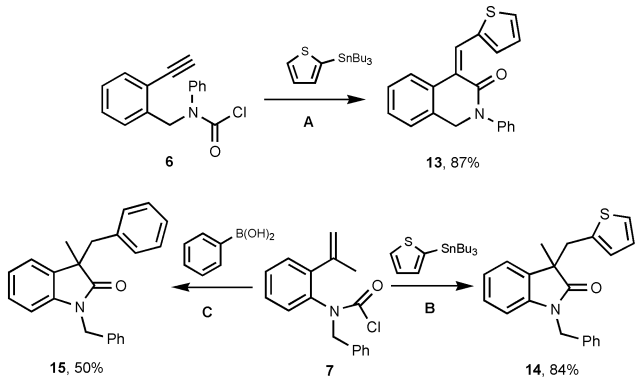

Scheme 3 *Reagents and conditions*: **A** = $Pd(OAc)_2$ (10 mol%), tris(2-furyl)phosphine (20 mol%), 1.1 equiv. Bu_3SnY, toluene, 50 °C, 5 min; **B** = $Pd(OAc)_2$ (10 mol%), tris(2-furyl)phosphine (20 mol%), 1.1 equiv. Bu_3SnY, toluene, 85 °C, 4 h; **C** = $Pd(OAc)_2$ (10 mol%), triphenylphosphine (20 mol%), 2 equiv. $PhB(OH)_2$, toluene, water (2 drops), 90 °C, 50 h.

(Scheme 3, **C**) there was some destruction of the carbamoyl chloride **7**.

The presence of the benzene ring in the above examples is one factor promoting the rapid cyclisation of these carbamoyl chlorides. To extend the scope of this cyclisation–anion capture methodology, we synthesised an example of a non-aryl based carbamoyl chloride. Substrate **16** was derived from but-3-yn-1-ol *via* its tosylate and reacted with benzylamine and then phosgene[14] in the normal fashion. At the typical reaction temperature of 50 °C, only 35% of product **17** was isolated. However, replacing tris(2-furyl)phosphine by the electron rich

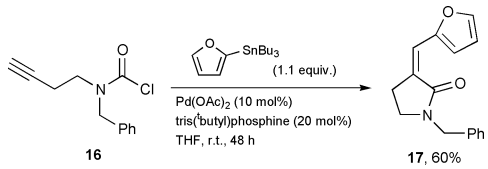

tris(*tert*-butyl)phosphine gave, over 48 h at rt, a 60% yield of lactam **17**.

The two strategic bond formation modes (Fig. 1, **a** and **b**) allow both (*E*)- and (*Z*)-3-methyleneoxindoles to be accessed stereoselectively. Thus formation of bond **a** by palladium catalysed cyclisation onto a proximate alkyne with anion capture affords *E*-isomers[16] whilst formation of bond **b** by palladium catalysed cyclisation affords *Z*-isomers.

In summary, these preliminary results on the palladium catalysed cyclisation–anion capture of carbamoyl chlorides demonstrate that (*Z*)-3-methylene- and 3,3-disubstituted oxindoles can be accessed under mild conditions in high yields. Further studies of these and related processes are in hand.

We thank the EPSRC, University of Leeds and Zeneca Agrochemicals for support.

Notes and references

1 A. Madin, C. J. O'Donnell, T. Oh, D. W. Old, L. E. Overman and M. J. Sharp, *Angew. Chem., Int. Ed.*, 1999, **38**, 2934.
2 T. D. Cushing, J. F. Sanz-Cervera and R. M. Williams, *J. Am. Chem. Soc.*, 1993, **115**, 9323; T. D. Cushing, J. F. Sanz-Cervera and R. M. Williams, *J. Am. Chem. Soc.*, 1996, **118**, 557.
3 S. Edmonson, S. J. Danishefsky, L. Sepp-Lorenzino and N. Rosen, *J. Am. Chem. Soc.*, 1999, **121**, 2147.
4 P. R. Sebahar and R. M. Williams, *J. Am. Chem. Soc.*, 2000, **122**, 5666.
5 E. E. van Tamelen, J. P. Yardley, M. Miyano and W. B. Hinshaw, *J. Am. Chem. Soc.*, 1969, **91**, 7333.
6 H. B. Rasmussen and J. K. MacLeod, *J. Nat. Prod.*, 1997, **60**, 1152.
7 A. Ashimori, T. Matsuura, L. E. Overman and D. J. Poon, *J. Org. Chem.*, 1993, **58**, 6949; M. Ishikura, *J. Chem. Soc., Chem. Commun.*, 1995, 409; M. O. Terpko and R. F. Heck, *J. Am. Chem. Soc.*, 1979, **101**, 5281.
8 R. Grigg, J. M. Sansano, V. Santhakumar, V. Sridharan, R. Thangavelanthum, M. Thorton-Pett and D. Wilson, *Tetrahedron*, 1997, **53**, 11 803; B. Burns, R. Grigg, V. Sridharan, P. Stevenson, S. Sukirthalingam and T. Worakun, *Tetrahedron Lett.*, 1989, **30**, 1135.
9 R. Grigg, B. Putnikovic and C. J. Urch, *Tetrahedron Lett.*, 1996, **37**, 695.
10 B. Jousseaume, H. Kwon, J.-B. Verlhac, F. Denat and J. Dubac, *Synlett*, 1993, **2**, 117; L. Balas, B. Jousseaume, H. Shin, J.-B. Verlhac and F. Wallian, *Organometallics*, 1991, **10**, 366.
11 F. Henin, J. Muzart and J. P. Pete, *Tetrahedron Lett.*, 1996, **52**, 6339.
12 R. Grigg and V. Sridharan, *J. Organomet. Chem.*, 1999, **576**, 65.
13 E-i. Negishi and T. Takahashi, *J. Am. Chem. Soc.*, 1986, **108**, 3402.
14 J. S. Norwick and S. Insaf, *J. Am. Chem. Soc.*, 1997, **119**, 10 903; R. Milcent and G. Barbier, *J. Heterocyclic Chem.*, 1994, **31**, 319 and references therein.
15 P. Fretwell, R. Grigg, J. M. Sansano, V. Sridharan, S. Sukirthalingam, D. Wilson and J. Redpath, *Tetrahedron*, 2000, **56**, 7525.
16 R. Grigg, V. Loganathan, V. Sridharan, P. Stevenson, S. Sukirthalingam and T. Worakun, *Tetrahedron*, 1996, **52**, 11 479; R. Grigg and V. Savic, *Tetrahedron Lett.*, 1996, **37**, 6565.

Palladium catalysed tetramolecular queuing cascades of aryl iodides, carbon monoxide, amines and a polymer supported allene

Ronald Grigg,*[a] William MacLachlan[b] and Marcello Rasparini[a]

[a] *MIDAS Centre, School of Chemistry, University of Leeds, Leeds, UK LS2 9JT. E-mail: R.Grigg@chem.leeds.ac.uk*
[b] *SmithKline Beecham Pharmaceuticals, Third Avenue, Harlow, UK CM19 5AW*

Received (in Cambridge, UK) 6th September 2000, Accepted 5th October 2000
First published as an Advance Article on the web 31st October 2000

Chemo- and regio-specific palladium catalysed four component processes, involving formation of 3 new bonds, initiated by oxidative addition of Pd(0) with aryl iodides followed by sequential incorporation of CO (1 atm), a polymer supported allene and an amine provides complex heterocycles with 3 points of diversity in good yield and excellent purity after cleavage.

A well designed cascade can deliver highly complex molecules whilst avoiding lengthy multistep procedures and the need for protection–deprotection of many functional groups.[1] This approach can be further enhanced by locating one of the reagents on a polymer support thus allowing the pure final product to be isolated by washing the resin and cleavage.

The objective of the present study was to explore the reactivity of a polymer bound allenic alcohol in a palladium catalysed four-component queuing cascade[2] (Scheme 1).

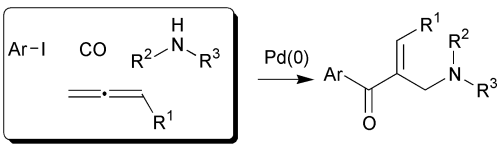

Scheme 1

This cascade is initiated by addition of Pd(0) into the Ar–I bond, followed by CO insertion, allene insertion and capture of the resultant π-allylpalladium(II) complex by a secondary amine (Scheme 2).

In this preliminary study we attached hexa-4,5-dien-1-ol **2** (prepared from the alkyne 1 by a Crabbé[3] reaction) to a gel-type polystyrene resin by means of a traceless silicon linker. The reason for this choice is three-fold: alkyl substituted allenes are particularly stable, the alcohol group is convenient for the introduction of further diversity and the cleavage conditions were anticipated to be particularly mild (Scheme 3).

The silane resin **3** (Argonaut Technologies, loading 1.59 mmol g^{-1} SiH) was chlorinated and immediately loaded[4] with the allenic alcohol **2** to give the resin **5** (loading 1.45 mmol g^{-1}).[5] The colourless resin **5** was characterised by gel-phase ^{1}H NMR (250 MHz, CDCl3) δ = 3.7 (C*H*$_2$CH=C=CH$_2$), 4.7

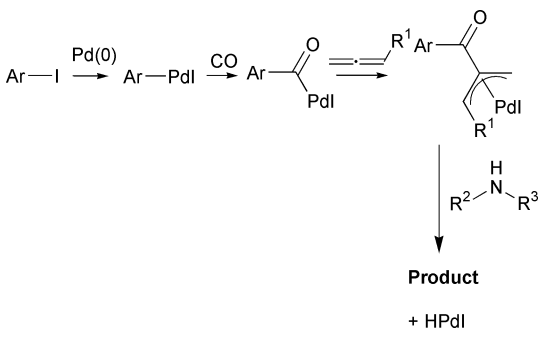

Scheme 2

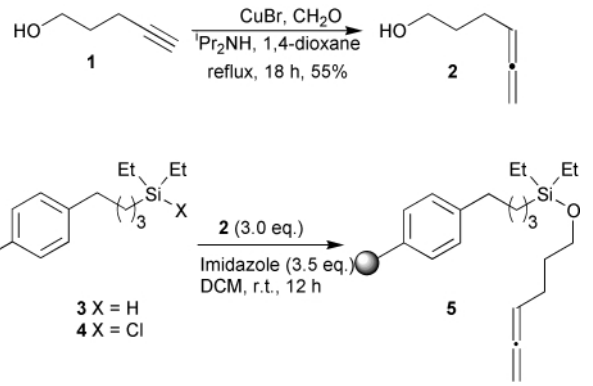

Scheme 3

(C*H*=C=C*H*$_2$), 5.1 (C*H*=C=CH$_2$) and FT-IR (KBr disc) 1953 cm^{-1} (CH=C=CH$_2$ stretch).

The experimental conditions for the palladium-catalysed cascade (Scheme 4) were as follows: resin **5** (1.0 mol eq.), iodobenzene or 2-iodothiophene (4.0 mol eq.), ^{i}Pr$_2$NEt (5.0 mol eq.), piperidine (4.0 mol eq.), Pd(OAc)$_2$ (0.1 mol eq.), tris(2-furyl)phosphine (0.2 mol eq.), toluene (10 ml $mmol^{-1}$) and a balloon containing carbon monoxide attached to the reaction vessel. After all the components were added to the flask containing the resin swollen in toluene, a sequence of evacuation (water pump–CO addition) was performed three times. Subsequently the flask was immersed in an oil bath at 50 °C and magnetically stirred for 24 h.

The reaction was monitored by FT-IR following the disappearance of the allene stretching band at 1953 cm^{-1}. After 24 h a small allenic peak was still present. The resin was washed with DMF, 1:1 DMF–H$_2$O, DCM, MeOH, dried and recycled in a second run to complete the conversion. The reaction was not optimised at this stage. The rate determining step appears to be the oxidative addition of Pd(0) into the Ar–I bond. Thus the iodoacrylamide **8** undergoes complete conversion to product in 18 h. In the case of **8** initial coordination of Pd(0) to the olefinic bond would facilitate the oxidative addition step, which is followed by a facile 5-*exo-trig* cyclisation, carbonylation, allene insertion and amine capture (Scheme 5).

Cleavage of indolinone **9** was achieved using HF/Py (0.4 M HF/Py, THF). Reaction times longer than 25 min led to the formation of a diastereomeric mixture of tetrahydrofurans (1:1

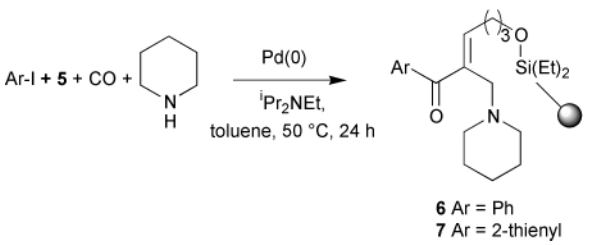

Scheme 4

DOI: 10.1039/b007170f

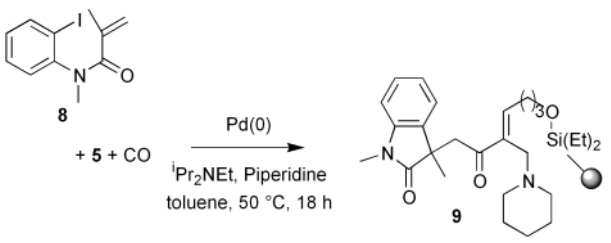

Scheme 5

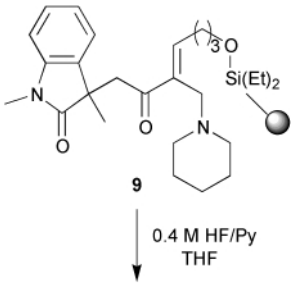

Scheme 6

ratio by HPLC, 70% yield); **10** deriving from acid-catalysed intramolecular Michael addition (Scheme 6).

After exposing the resin for 20 min to the cleavage mixture the filtrate was quenched with a saturated solution of $NaHCO_3$, extracted with AcOEt, the solvent removed *in vacuo* to afford the alcohol (60%) whose purity was 98% by HPLC-MS. The residue was acetylated (Ac_2O, pyridine, DMAP, DCM, 2 h, rt) and the acetate **11** was purified by silica gel chromatography (AcOEt–PE–triethylamine 50 : 50 : 2) and obtained in 90% yield from the alcohol (Scheme 7).

The loading of resin **9** was found to be 1.1 mmol g^{-1} (calculated on the yield of the crude product after cleavage).

Similarly the resins **12**–**14** were prepared. After cleavage and work-up the alcohols **15**–**17** were found to be 98% pure by HPLC-MS and no further purification was carried out.[6]

It is worth noting that all the products **11**–**17** were obtained as single stereoisomers.[7]

In conclusion, the resin supported allene **5** is an excellent scaffold for the construction of complex heterocycles. Further investigations using a broader range of anion capture agents and starter molecules are in progress.

We thank Leeds University, the EU and SmithKline Beecham for support.

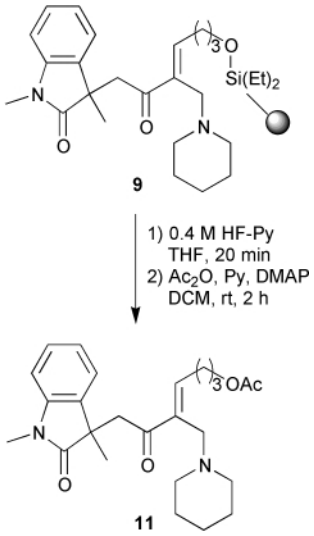

Scheme 7

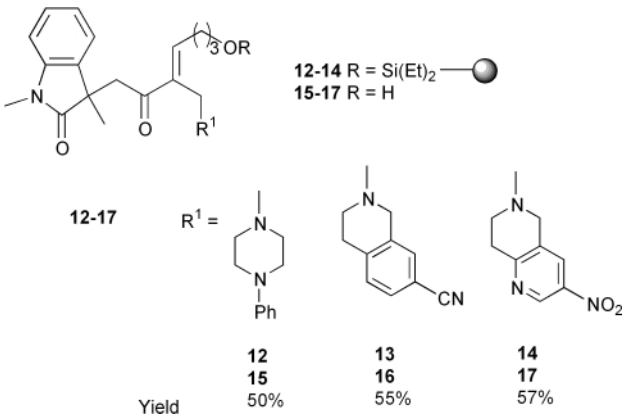

Notes and references

1 R. Grigg and V. Sridharan, *J. Organomet. Chem.*, 1999, **576**, 65.
2 R. Grigg, S. Brown, V. Sridharan and M. Uttley, *Tetrahedron Lett.*, 1997, **38**, 5031.
3 S. Searles, Y. Li, B. Nassim, M. T. Robert Lopes, P. T. Tran and P. Crabbè, *J. Chem. Soc., Perkin Trans. 1*, 1984, 747.
4 Y. Hu, J. A. Porco, J. W. Labadie, O. W. Gooding and B. M. Trost, *J. Org. Chem.*, 1998, **63**, 4518.
5 The loading was the average of two determinations: 1) weight increase after washing and overnight drying *in vacuo*, 2) yield of **2** after cleavage (TBAF, 1.0 M in THF) and chromatographic purification (Et_2O–PE 1 : 1).
6 Overall from **5** to **15**–**17**.
7 In similar experiments we found that the C=C geometry is *Z* (NOE data): this stereochemical outcome is rationalised by attack of the amine on the more stable *anti* π-allylpalladium(II) complex (R. Grigg and M. Rasparini, unpublished data).

A simple, rational synthesis of *meso*-substituted A_2B-corroles†

Daniel T. Gryko*

Institute of Organic Chemistry of Polish Academy of Sciences, Kasprzaka 44/52, 01-224 Warsaw, Poland. E-mail: sfinks@icho.edu.pl

Received (in Liverpool, UK) 14th August 2000, Accepted 3rd October 2000
First published as an Advance Article on the web 31st October 2000

Five unsymmetrically *meso*-substituted corroles have been synthesized from dipyrromethanes and aldehydes in yields of up to 19% *via* a new two-step one-flask procedure.

Although the existence of corroles was reported a long time ago,[1] their chemistry has been overshadowed by the easy accessibility of porphyrin chemistry.[2] Corroles are aromatic tetrapyrrole macrocycles bearing a direct pyrrole–pyrrole link, thereby constituting a bridge between porphyrins (*e.g.* heme) and corrins (*e.g.* vitamin B_{12}). Recently, corrole chemistry has received new impetus due to the discovery of novel ligand properties of this contracted macrocycle[3–5] as well as the advent of efficient synthetic methodologies affording corroles in gram quantities.[6–8] Most of the corrole syntheses known till 1999 (biladiene cyclization,[9] *meso*-carbon or sulfur extrusion of *meso*-thiaporphyrin,[10] or direct synthesis from monopyrrole precursors[11,12]) are lengthy. The very recently reported syntheses of core-modified corroles also require preparation of several precursors.[13,14]

Pioneering studies by Paolesse *et al*.[6] and Gross *et al*.[7,8] have demonstrated that the non-catalyzed reaction of pyrrole with aldehydes results in the formation of *meso*-substituted A_3-corroles. These simple and efficient synthetic methods have already opened a new avenue for in-depth studies of the coordination chemistry of corroles.[5] Nevertheless a potential use of corroles as surrogates for vitamin B_{12} and related compounds in biomimetic models of enzymic catalysis would benefit significantly from the ability to incorporate different groups at distinct sites at the perimeter of the macrocycle. On the other hand it is known that the acid catalyzed reaction of pyrrole with an aldehyde gives an A_4-porphyrin whereas the acid-catalyzed condensation of a dipyrromethane (DPM) with an aldehyde gives the corresponding *trans*-A_2B_2-porphyrin.[15] Hence I assumed that the non-catalyzed reaction of a DPM with a reactive aldehyde would lead to the formation of the corresponding A_2B-type *meso*-substituted corrole. The preliminary results of this study are presented in this paper.

The conditions for the non-catalyzed reaction of pyrrole with aldehydes[6–8] and the stoichiometry of the envisioned reaction prompted me to initiate studies using the following conditions: aldehyde–dipyrromethane ratio, 1:2; reaction time, 2 h; rt; a small amount of solvent; and 1 eq. of DDQ as an oxidant. The reaction of mesityldipyrromethane **1**[16] (a potential precursor of facially-encumbered and hence more soluble corroles) and 2,6-difluorobenzaldehyde **2** (bearing electron-withdrawing substituents) was chosen as a model system for the optimization study (Scheme 1). Indeed, condensation of both substrates in methylene chloride for 2 h followed by subsequent reaction with DDQ smoothly afforded the desired corrole **3** in 11% yield (Table 1, entry 1). This initial success quickly led to the systematic study of reaction conditions. In an effort to improve the yield of corrole **3**, the concentration and ratio of reagents, solvent, time, and amount of DDQ were altered. In addition, the influence of some simple additives (TBABr and TBAF) was examined. The results of this study are presented in Table 1.

† Electronic supplementary information (ESI) available: experimental procedures and spectral data for compounds **3** and **10**–**13**. See http://www.rsc.org/suppdata/cc/b0/b006734m/

When the ratio of aldehyde to DPM was changed to 1:1 (corresponding to the stoichiometry of porphyrin forming reaction) (entry 2), an appreciable increase in the yield of corrole **3** to 17% was obtained. An increased amount of DDQ gave no further increase in the yield of corrole (entry 3). It is well known that the porphyrin-forming reaction as well as many other macrocyclisation reactions require a low concentration of reactants to achieve reasonable yields. Thus, the corrole-forming reaction was carried out under more dilute conditions (entries 4 and 5). The decrease in concentration of both substrates to 0.27 mol dm^{-3} resulted in a slight increase while further dilution caused a sudden drop in the yield of corrole **3**. Use of a large excess of aldehyde **2** did not give any improvement (entry 6). Hence, for further reactions the ratio of reactants was kept constant at 1:1. Because both substrates were still present in the reaction mixture after 2 h, the condensation time was extended (entries 7 and 8). However,

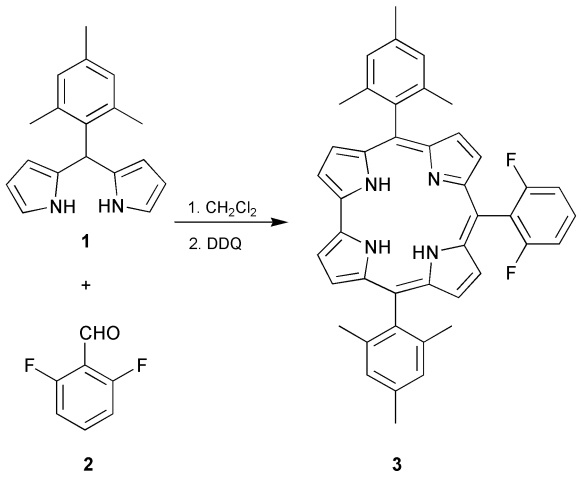

Scheme 1

Table 1 Effects of various conditions on the reaction of mesityldipyrromethane **1** and aldehyde **2**

Entry	DPM **1** (mol dm^{-3})	Ratio **1**:**2**	Time/h[a]	Ratio DDQ: **1**	Yield of corrole **3**[b] (%)
1	0.53	2:1	2	1:1	11
2	0.53	1:1	2	1:1	17
3	0.53	1:1	2	1.5:1	18
4	0.27	1:1	2	1:1	19
5	0.13	1:1	2	1:1	10
6	0.27	1:2	2	1:1	13
7	0.27	1:1	5.5	1:1	19
8	0.53	1:1	16	1:1	0
9[c]	0.27	1:1	2	1:1	12
10[d]	0.27	1:1	2	1:1	0
11	0.53	1:1	2	0.5:1	10
12[e]	0.27	1:1	2	1:1	9

[a] Time of condensation prior to addition of DDQ. [b] Isolated yield. [c] 0.2 eq. of TBABr was added. [d] 0.2 eq. of TBAF was added. [e] $CHCl_3$ was used instead of CH_2Cl_2.

DOI: 10.1039/b006734m

prolonging the reaction time from 2 to 5.5 h did not improve the yield of the product **3** (entry 7). The complete consumption of the substrates was observed after 16 h, then DDQ was added. Surprisingly even traces of corrole **3** were not found in the reaction mixture (entry 8). The idea of adding of soluble inorganic salts was inspired by the beneficial effects of salts observed in the porphyrin-forming reaction.[17] The addition of TBABr resulted in a modest decline in yield whereas no corrole was formed upon reaction in the presence of TBAF (entries 9 and 10). A control experiment with 0.5 eq. of DDQ resulted in a decreased yield of corrole (entry 11). Furthermore, upon changing the solvent from CH_2Cl_2 to $CHCl_3$ the yield of corrole decreased to 9% (entry 12). It is noteworthy to add that no porphyrin was observed under any of these conditions.

The optimized procedure (entry 4) (CH_2Cl_2, conc. of both substrates = 0.27 mol dm^{-3}, 2 h, rt, 1 eq. of DDQ) was applied to a variety of substrates (Scheme 2, Table 2). Reactive aldehydes with various electron-withdrawing groups (F, Cl, NO_2) (**2**, **5**, **6**, **7**, **8**, **9**) were used in conjunction with mesityldipyrromethane **1** and phenyldipyrromethane **4**.[16] In each case with aldehydes possessing at least two fluorine substituents, the corresponding corroles[18] (**10**, **11**, **12** and **13**) were readily isolated in modest yield after straightforward column chromatography. No porphyrin product was observed in these reactions.[19] It was surprising to find that the yields of corroles in the reactions employing 2,4-difluorobenzaldehyde **6** (entry 4) and 2,3,6-trifluorobenzaldehyde **8** (entry 6) were significantly lower than the yield achieved starting from 2,6-difluorobenzaldehyde. On the other hand, 2,6-dichlorobenzaldehyde **5** (entry 3) and 2,4-dinitrobenzaldehyde **7** (entry 5) did not afford any corrole. At present there is no satisfactory explanation for such a significant difference in behavior of these aldehydes. Generally, it is reasonable to assume that a mechanism analogous to that suggested by Gross *et al.*[8] accounts for the formation of corroles from dipyrromethanes. If so, the course of this reaction is not only dependent on the reactivity of the aldehyde (Ar-CHO) but is also influenced by the steric effects of substituents and by the nature of the arylmethylene unit (Ar-CH_2-) as an anionic leaving group.

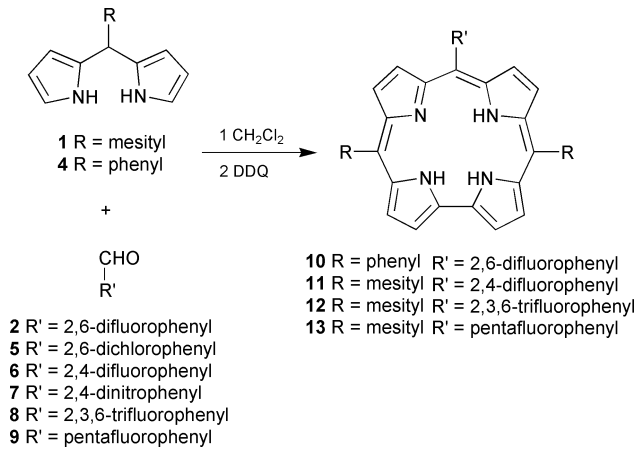

Scheme 2

Table 2 Yield of corroles formed from various dipyrromethanes (DPM's) and aldehydes

Entry	Aldehyde	DPM	Yield (%)[a]
1	**2**	**1**	19
2	**2**	**4**	9
3	**5**	**1**	0
4	**6**	**1**	4[b]
5	**7**	**1**	0
6	**8**	**1**	10
7	**9**	**1**	8

[a] Isolated yield. [b] Condensation of aldehyde and DPM was performed for 5 h prior to addition of DDQ.

In summary, conditions have been identified for a rational two-step synthesis of A_2B-type *meso*-substituted corroles bearing one fluorinated substituent. The main advantages of this method are as follows: (1) a two-step procedure from commercially available materials, (2) short reaction time, (3) straightforward purification, and (4) reaction at high concentration (thereby easy to scale-up). This approach should prove useful for the preparation of a variety of corroles and may open the door to new practical applications of these macrocycles. Further studies aimed at extending the scope of this method and gaining insight into the influence of various factors on the corrole-forming reaction are in progress.

Notes and references

1 A. W. Johnson and I. T. Kay, *J. Chem. Soc.*, 1965, 1620.
2 R. Paolesse, in *Porphyrin Handbook*, ed. K. M. Kadish, K. M. Smith and R. Guilard, San Diego, 2000.
3 S. Licoccia and R. Paolesse, *Struct. Bonding*, 1995, **84**, 71.
4 J. L. Sessler and S. J. Weghorn, *Expanded, Contracted & Isomeric Porphyrins*, Tetrahedron Org. Chem. Series, vol.15, Pergamon, Oxford, 1997, p. 11.
5 L. Simkhovich, N. Galili, I. Saltsman, I. Goldberg and Z. Gross, *Inorg. Chem.*, 2000, **39**, 2704.
6 R. Paolesse, L. Jaquinod, D. J. Nurco, S. Mini, F. Sagone, T. Boschi and K. M. Smith, *Chem. Commun.*, 1999, 1307.
7 Z. Gross, N. Galili and I. Saltsman, *Angew. Chem., Int. Ed.*, 1999, **38**, 1427.
8 Z. Gross, N. Galili, L. Simkhovich, I. Saltsman, M. Botoshansky, D. Blaser, R. Boese and I. Goldberg, *Org. Lett.*, 1999, **1**, 599.
9 S. Licoccia, M. L. DiVona and R. Paolesse, *J. Org. Chem.*, 1998, **63**, 3190.
10 R. B. Woodward and R. Hoffmann, *Angew. Chem., Int. Ed.*, 1969, **8**, 781.
11 R. Paolesse, S. Licoccia, G. Bandoli, A. Dolmella and T. Boschi, *Inorg. Chem.*, 1994, **33**, 1171.
12 R. Paolesse, S. Licoccia, M. Fanciullo, E. Morgante and T. Boschi, *Inorg. Chim. Acta*, 1993, **203**, 107.
13 W.-S. Cho and C.-H. Lee, *Tetrahedron Lett.*, 2000, **41**, 697.
14 C.-H. Lee, W.-S. Cho, J.-W. Ka, H.-J. Kim and P.-H. Lee, *Bull. Korean Chem. Soc.*, 2000, **21**, 429.
15 B. J. Littler, Y. Ciringh and J. L. Lindsey, *J. Org. Chem.*, 1999, **64**, 2864.
16 B. J. Littler, M. A. Miller, C. H. Hung, R. W. Wagner, D. F. O'Shea, P. D. Boyle and J. L. Lindsey, *J. Org. Chem.*, 1999, **64**, 1391.
17 F. Li, K. Yang, J. S. Tyhonas, K. A. MacCrum and J. S. Lindsey, *Tetrahedron*, 1997, **53**, 12339.
18 The purity of each corrole is >99% based on TLC, ^{1}H NMR spectroscopy, and electrospray mass spectrometry. It is noteworthy to add that the ^{1}H NMR spectra of corroles derived from mesityldipyrromethane (**3**, **11**, **12** and **13**) exhibit very sharp signals, in contrast to corrole **10** or 5,10,15-triphenylcorrole[6] which exhibit broad AB patterns.
19 One exception occurred with pentafluorobenzaldehyde **9**, which gave traces (*e.g.* 1%) of 5,15-dimesityl-10,20-bis(pentafluorophenyl)porphyrin.

Enhanced product selectivity in the Mizoroki–Heck reaction using a supercritical carbon dioxide–liquid biphasic system

Yoshihito Kayaki, Yushi Noguchi and Takao Ikariya*

Graduate School of Science and Engineering, Tokyo Institute of Technology and CREST, Japan Science and Technology Corporation, O-okayama, Meguro-ku, Tokyo 152-8552, Japan. E-mail: tikariya@o.cc.titech.ac.jp

Received (in Cambridge, UK) 23rd August 2000, Accepted 2nd October 2000
First published as an Advance Article on the web 31st October 2000

Arylation of ethylene catalysed by Pd complexes bearing triphenyl phosphite ligands proceeds efficiently in a $scCO_2$–liquid biphasic system to give a mixture of arylated products; the selectivity of monoarylated products, styrene derivatives, can be improved by increasing the CO_2 pressure, where the monoarylated products are effectively extracted from the liquid reaction phase into the $scCO_2$ phase to prevent over-reactions to diarylated products.

There has been extensive interest in supercritical fluids (SCFs) as reaction media for molecular catalysis.[1] Their unique physical properties tuned by a small change in the pressure and temperature allows improved performance of molecular catalysts in terms of the reaction rates and selectivities.[2] Besides these benefits for catalysis, the use of SCFs can also offer great opportunities to solve the frequently encountered problem of efficient separation of the molecular catalysts by controlling the pressure of the media.[3] Recently, a biphasic reaction system consisting of a supercritical fluid phase and a solvent phase including H_2O was examined for the purpose of separating and recycling metal catalysts.[4] In the case where CO_2-insoluble substrates form the liquid phase under supercritical or subcritical CO_2 conditions, the high volatility of CO_2 allows it to help selectively remove the CO_2-soluble product from the reaction phase, resulting in a solvent-free reaction. However, the catalyst performance in such a multiphase system has not been systematically investigated except for a recent report on solvent-free synthesis under subcritical CO_2 conditions.[5,6] We now report Mizoroki–Heck arylation of ethylene in a CO_2–liquid biphasic system in which monoarylated products can be preferentially obtained in condensed CO_2 where the selectivity is controllable by a change in the pressure of CO_2.

The arylation of ethylene with aryl halides has been well investigated in liquid solvents.[7] In a single reaction phase, the initial products, styrene derivatives are subject to further reaction with aryl halides to afford stilbenes and 1,1-diphenylethylenes, resulting in a significant decrease in the selectivity for the monoarylation. If one of the desired products, styrene in this case, has high solubility in $scCO_2$ compared to that of the byproducts, the use of $scCO_2$ will enable the separation of the initial product from the liquid phase[8] to suppress the subsequent reactions of styrene (Fig. 1).

We first examined the phase behaviour of iodobenzene, ethylene, $N(C_2H_5)_3$ and styrene under subcritical and supercritical CO_2 conditions.† A visual inspection of these compounds in a window-equipped 50 mL reactor vessel confirmed that 1.0 mmol of styrene was completely dissolved in $scCO_2$ under 100 atm at 130 °C whereas some droplets of iodobenzene were observed under the same conditions. In the presence of subcritical CO_2 gas, these materials, except ethylene, precipitate to form the liquid phase where a neat reaction can be performed. Thus, the significant difference in the solubility of these compounds in $scCO_2$ should allow one to extract styrene preferentially from the liquid phase, leading to the efficient control of the styrene formation.[9]

The screening experiments with Pd catalyst bearing tertiary phosphine or phosphite ligands revealed that

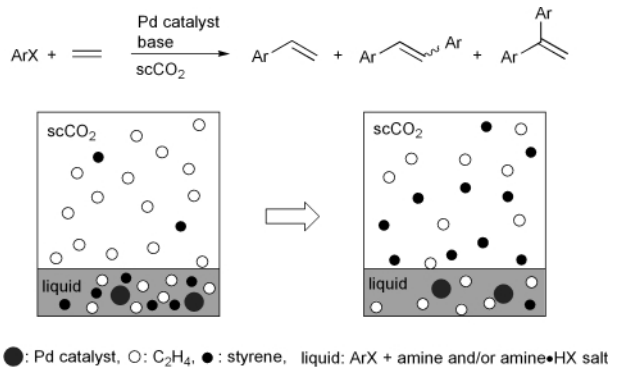

Fig. 1 Schematic illustration of phases during a $scCO_2$–liquid biphasic Mizoroki–Heck reaction. At the initial stage of the reaction, aryl halide, amine and some amine·HX salt are precipitated as a liquid containing the Pd catalyst. At the final stage of the reaction, an excess amount of amine and amine·HX salt form a liquid phase and monoarylated product is extracted into the $scCO_2$ phase. Ar = aryl group, X = I, Br in this case.

$PdCl_2\{P(OC_6H_5)_3\}_2$ (**1**) is the best choice of catalyst for the arylation because of its excellent activity[10] and suitable solubility (discussed later) under the reaction conditions at 130 °C and 100 atm.‡ Although complex **1** has been found to partially dissolve in $scCO_2$ under the same conditions,[11] it should stay in the liquid phase rather than the $scCO_2$ phase because of its higher solubility in the liquid substrates phase.

The reaction of iodobenzene with ethylene (10 atm) catalysed by the $P(OC_6H_5)_3$–Pd complex **1** (substrate/catalyst = 1000 : 1) at 130 °C in the presence of $N(C_2H_5)_3$ as a base proceeded rapidly to an almost quantitative conversion under solvent-free conditions (without CO_2). As listed in Table 1, styrene was obtained in 57% selectivity along with (*E*)-stilbene and 1,1-diphenylethylene in 31 and 11% yields, respectively. Notably, as illustrated in Fig. 2, the selectivity for the styrene formation was remarkably improved with an increase in the pressure of CO_2 above the critical pressure of 73 atm to attain over 80% at 100 atm and the same temperature. Further increase in the pressure above 100 atm resulted in the selectivity approaching 100% albeit with a significant drop in the yield. The decrease in the total efficiency at higher CO_2 pressures was

Table 1 Mizoroki–Heck reaction of iodobenzene with C_2H_4 in $scCO_2$[a]

Run	Medium	Conv. (%)	Styrene Yield (Sel.) (%)	1,1-Diphenylethylene : (*E*)-stilbene
1	—	95	54 (57)	2.8 : 1
2	CO_2, 25 (atm)	> 99	64 (65)	4 : 1
3	CO_2, 50	> 99	68 (69)	3.4 : 1
4	CO_2, 75	95	68 (71)	1.8 : 1
5	CO_2, 100	> 99	82 (83)	3.3 : 1
6	CO_2, 125	32	29 (92)	N.d.
7	CO_2, 150	19	18 (99)	N.d.

[a] Reaction was conducted at 130 °C for 18 h, in a 50 mL reaction vessel containing 10 μmol of Pd catalyst **1**, iodobenzene and triethylamine. Iodobenzene : **1** : $N(C_2H_5)_3$ = 1,000 : 1 : 1,400.

DOI: 10.1039/b006846m

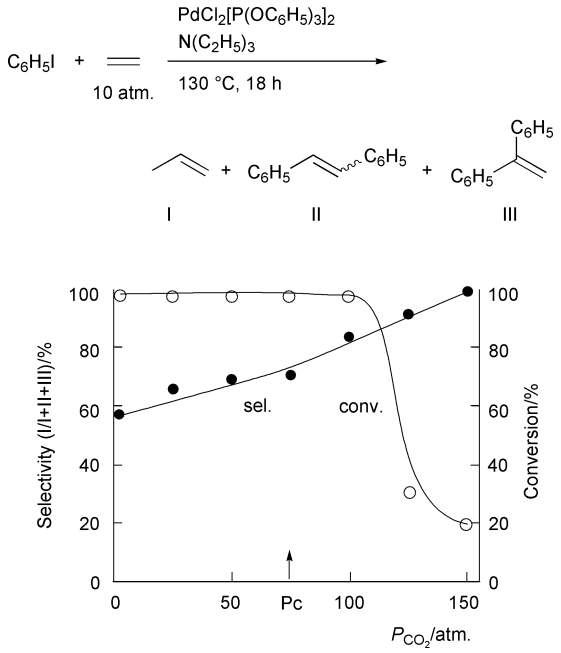

Fig. 2 Selectivity and conversion profile as a function of the CO_2 pressure for the reaction of iodobenzene **2a** and ethylene catalysed by Pd complex **1** in condensed CO_2. Condition: $C_6H_5I:N(C_2H_5)_3$:Pd catalyst = 1000:1400:1, C_2H_4 10 atm.

mainly due to the disappearance of the liquid phase since everything dissolved in the $scCO_2$, where the homogeneous reaction in $scCO_2$ possibly occurred. In fact, separate experiments showed that the arylation using CO_2-soluble trialkyl phosphite–Pd catalysts[12] in the homogeneous $scCO_2$ phase did not provide turnover numbers higher than those obtained in the liquid phase. These results, in addition to the phase behaviour discussed above, clearly indicate that below 100 atm of CO_2 pressure the reaction occurs rapidly mainly in the liquid phase to give the initial product styrene, which is effectively extracted in the $scCO_2$ phase because of its reasonably high vapor pressure (430 mmHg at 125 °C) and high solubility in $scCO_2$ under the reaction conditions. The use of supercritical or even subcritical gaseous CO_2 might help to separate the desired product from the liquid reaction phase into the $scCO_2$ or vapor phase to avoid further reactions which may produce undesired multiarylated products.

A remarkable advantage of this biphasic system can be demonstrated by the reaction of *p*-bromotoluene substrate/catalyst = 100) and ethylene (10 atm) catalysed by complex **1** in the presence of (DBU) and 1-ethylpiperidine (Table 2). A mixture of these bases serves as an efficient promoter for the less reactive bromoarenes possibly because of their strong basicity. Although the reaction of the bromoarene proceeded much more slowly than that of iodoarene, it reacted with ethylene under neat conditions without CO_2 to give products in moderate selectivity as shown in Table 2 (Run 1). Using CH_3CN as a liquid solvent, the reaction proceeded to 74% conversion after 96 h to give the monoarylated product in 82% selectivity (Runs 2 and 3). In contrast to these liquid phase reactions, the outcome of the reaction in the $scCO_2$–liquid biphasic system was significantly improved, the styrene selectivity increasing from 68 to 88% at near complete conversion after 18 h (Run 4).[13]

Table 2 Pd-catalysed reaction of *p*-bromotoluene and ethylene in $scCO_2$ and other media[a]

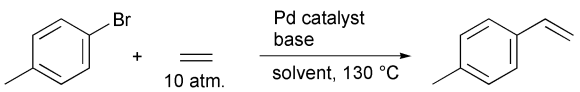

Run	Medium	Time/h	Conversion (%)	Selectivity (%)
1		18	100	68
2	CH_3CN, 10 mL	18	14	100
3	CH_3CN, 10 mL	96	74	82
4	CO_2, 100 atm	18	97	88

[a] Reaction was conducted at 130 °C for 18 h, in a 50 mL reaction vessel containing 100 μmol of Pd catalyst **1**. Base = DBU + 1-ethylpiperidine, *p*-bromotoluene:**1**:DBU:1-ethylpiperidine = 100:1:140:150.

In conclusion, the arylation of ethylene catalysed by Pd complex with phosphite ligands selectively afforded monoarylated products in the $scCO_2$–liquid biphasic system. A combination of the rapid reaction in the liquid phase and the extraction of the product with $scCO_2$ provided a significant improvement in the product selectivity.

Notes and references

† Safety warning: Operators of high-pressure equipment should take proper precautions to minimize the risk of personal injury.

‡ Standard procedure for the arylation: The reactor was charged with argon gas and was placed in the oven at 130 °C before introduction of reagents. A mixture of the substrate (1.0 mmol), base (1.4 mmol) and DMF (0.01 mL) solution of Pd catalyst (0.01 mmol) was added into the reactor with a syringe through an opening against the flow of CO_2. Subsequently, C_2H_4 (10 atm) was introduced, and then CO_2 (0–150 atm) was added with an HPLC pump. After stirring for 18 h, the reactor was cooled in a bath of methanol with dry ice. The mixture of C_2H_4 and CO_2 was vented, and the reactor was slowly warmed to rt. The yields of products were determined by GC analyses.

1 (*a*) P. G. Jessop, T. Ikariya and R. Noyori, *Chem. Rev.*, 1999, **99**, 475; (*b*) *Chemical Synthesis using Supercritical Fluids*, ed. P. G. Jessop and W. Leitner, VCH/Wiley, Weinheim, 1999.

2 (*a*) P. G. Jessop, T. Ikariya and R. Noyori, *Science*, 1995, **269**, 1065.

3 (*a*) A. Fürstner, D. Koch, K. Langemann, W. Leitner and C. Six, *Angew. Chem., Int. Ed. Engl.*, 1997, **36**, 2466; (*b*) D. Koch and W. Leitner, *J. Am. Chem. Soc.*, 1998, **120**, 13 398; (*c*) S. Kaintz, A. Brinkmann, W. Leitner and A. Pfaltz, *J. Am. Chem. Soc.*, 1999, **121**, 6421; (*d*) M. F. Sellin and D. J. Cole-Hamilton, *J. Chem. Soc., Dalton Trans.*, 2000, 1681.

4 (*a*) G. B. Jacobson, C. T. Lee, Jr., K. P. Johnston and W. Tumas, *J. Am. Chem. Soc.*, 1999, **121**, 11 902; (*b*) B. M. Bhanage, Y. Ikushima, M. Shirai and M. Arai, *Chem. Commun.*, 1999, 1277; (*c*) B. M. Bhanage, Y. Ikushima, M. Shirai and M. Arai, *Tetrahedron Lett.*, 1999, **40**, 6427.

5 G. Franciò and W. Leitner, *Chem. Commun.*, 1999, 1663.

6 P. Jessop, D. C. Wynne, S. DeHaai and D. Nakawatase, *Chem. Commun.*, 2000, 693.

7 (*a*) J. E. Plevyak and R. F. Heck, *J. Org. Chem.*, 1978, **43**, 2454; (*b*) W. Heitz, W. Brügging, L. Freund, M. Gailberger, A. Greiner, H. Jung, U. Kampschulte, N. Neißer, F. Osan, H.-W. Schmidt and M. Wicker, *Makromol. Chem.*, 1988, **189**, 119; (*c*) J. Kiji, T. Okano and A. Ooue, *J. Mol. Catal. A*, 1999, **147**, 3.

8 C. A. Eckert, C. L. Liotta, C. W. Culp and D. R. Lamb, *Chemical Synthesis using Supercritical Fluids*, ed. P. G. Jessop and W. Leitner, VCH/Wiley, Weinheim, 1999, p. 446.

9 A similar reaction–extraction system consisting of water and supercritical butene phases is now being used at Idemitsu Petrochemical Co. in Japan. The hydration of butene proceeds in an aqueous phase to give butan-2-ol, which can be extracted by supercritical butene. T. Yamada and T. Muto, *Sekiyu Gakkaishi*, 1991, **34**, 201.

10 Some examples of the catalytic activity of $PdCl_2L_2$ complexes under the same conditions (conversion after 18 h), L = CH_3CN 13%, $P(OC_2H_5)_3$ 44%, $P(n\text{-}C_4H_9)_3$ 52%, $P(OC_6H_5)_3$ 94%, T. Ikariya, to be published.

11 Some examples of the solubility of $PdCl_2L_2$ complexes (mol L^{-1} at 200 atm and 80 °C): L = $P(n\text{-}C_4H_9)_3$ 5.6×10^{-3}; $P(OC_2H_5)_3$ 8.8×10^{-4}; CH_3CN 2.5×10^{-5}; $P(OC_6H_5)_3$ 7.5×10^{-5}. T. Ikariya, to be published.

12 Y. Kayaki, Y. Noguchi, S. Iwasa, T. Ikariya and R. Noyori, *Chem. Commun.*, 1999, 1235.

13 The homogeneous Mizoroki–Heck reaction of aryl iodides and activated olefins such as methyl acrylate in $scCO_2$ has been studied by several groups. However, there are no examples of simple bromoarene as the substrate; (*a*) M. A. Carroll and A. B. Holmes, *Chem. Commun.*, 1998, 1395; (*b*) D. K. Morita, D. R. Pesiri, S. A. David, W. H. Glaze and W. Tumas, *Chem. Commun.*, 1998, 1397; (*c*) N. Shezad, R. S. Oakes, A. A. Clifford and C. M. Rayner, *Tetrahedron Lett.*, 1999, **40**, 2221.

Partial oxidation of alcohols in supercritical carbon dioxide

Gregor Jenzer, David Sueur, Tamas Mallat and Alfons Baiker*

Laboratory of Technical Chemistry, Swiss Federal Institute of Technology, ETH-Zentrum, CH-8092 Zürich, Switzerland. E-mail: baiker@tech.chem.ethz.ch; Phone: +41 1 6323153; Fax: +41 1 6321163

Received (in Cambridge, UK) 1st September 2000, Accepted 3rd October 2000
First published as an Advance Article on the web 31st October 2000

Oxidation of water-insoluble alcohols in supercritical CO_2 over a Pd–Pt–Bi/C catalyst in a continuous fixed bed reactor affords high reaction rates and yields up to 98% of the corresponding ketones, aromatic and α,β-unsaturated aliphatic aldehydes, without the risk of using a flammable organic solvent.

Partial oxidation of alcohols over supported platinum metal catalysts is an attractive, environmentally friendly process: air or oxygen can be used as oxidant in aqueous medium under mild conditions. Primary and secondary alcohols are readily oxidized to carboxylic acids and ketones, respectively, but partial oxidation of primary alcohols to aldehydes is limited to aromatic and α,β-unsaturated aliphatic alcohols where hydration and further dehydrogenation of the intermediate aldehyde is minor.[1–4] Drawbacks of the method are the frequently observed catalyst deactivation necessitating high catalyst–substrate ratio (20–50 mass%),[3,5] and the explosion risk in the case of readily dehydrogenating substrates.[6] Oxidation of water-insoluble alcohols is rather slow in organic solvents[7] and because of safety reasons the process is unattractive even on a laboratory scale.[5]

To overcome these restrictions, the organic solvent can be replaced by supercritical carbon dioxide ($scCO_2$),[8,9] *i.e.* CO_2 under conditions above its critical temperature (T_c = 31.1 °C) and pressure (p_c = 73.8 bar). Supercritical CO_2 has a number of distinct advantages over conventional organic liquid solvents, among which adjustable solvent strength and favorable transport properties are probably the most important. This medium is especially attractive for the oxidation of weakly polar, water-insoluble alcohols, due to the low polarity of $scCO_2$. Besides, CO_2 is relatively inert and non-flammable under oxidizing conditions. Products and solvent can easily be separated by releasing the pressure of the reaction mixture.

There are only two examples of the partial oxidation of alcohols with a solid catalyst in $scCO_2$ reported in the literature. Oxidation of methanol on iron oxide containing aerogels,[10] and ethanol on Pt/TiO_2,[11] affords the corresponding aldehydes in moderate yields (15–30%) compared to the conventional gas phase oxidation of small chain aliphatic alcohols.[12] Here we show that oxidation in $scCO_2$ is an excellent alternative to liquid phase reactions in organic solvents, affording the conversion of water-insoluble alcohols to (deactivated) carbonyl compounds at high rate and selectivity.

The experiments have been performed in a high-pressure continuous fixed bed reactor over a promoted noble metal catalyst (4% Pd–1% Pt–5% Bi/C).† It has been shown before that Bi or Pb promotion can remarkably enhance the performance of Pt and Pd.[4,5] For the study of the influence of reaction parameters, the conditions were chosen to achieve conversions in the range 2–10% in order to minimize the temperature gradients in the catalyst bed. In some cases the contact time and temperature were increased to achieve high conversions, though optimization of the reaction conditions was not attempted. These results, illustrating the potential of the method in the synthesis of activated and non-activated aldehydes and ketones, are collected in Table 1.

Octan-2-ol has been converted to octan-2-one with higher than 99.5% selectivity even at around 70% conversion. Only traces of oct-2-ene (by dehydration) and oct-4-ene (by dehydration and subsequent double bond migration) have been formed. The yield (68%) could be further increased by applying a higher amount of catalyst or lower mass flow rate. The octan-2-one yield increased exponentially with increasing temperature and approximately linearly with contact time. A bell-shaped curve was found for the effect of oxygen concentration in the feed (Fig. 1). The drop after the maximum in yield is attributed to the so-called over-oxidation of the catalyst, a phenomenon commonly observed with platinum metal catalysts.[3,5,6] The rate of oxidative dehydrogenation of alcohols is considerably higher on the reduced metal surface than on the oxygen-covered metal. Though oxygen is necessary to shift the alcohol–carbonyl compound equilibrium by oxidizing the hydrogen abstracted from the substrate, too high surface oxygen coverage reduces the overall reaction rate. An additional effect is the decreasing density of $scCO_2$ with increasing oxygen concentration, which may reduce the solubility of reactant and product. Changes in density of $scCO_2$ can also explain the influence of total pressure in the reactor. At constant temperature the yield reached a maximum at 110–120 bar.

Oxidation of octan-2-ol was relatively slow compared to the conversion of other secondary alcohols, such as 1-phenylethanol (Table 1). The transformation of 1-phenylethanol to acetophenone was nearly quantitative. Only traces of bis(1-

Table 1 Selected examples of the partial oxidation of primary and secondary alcohols to carbonyl compounds in $scCO_2$. Catalyst: 4% Pd–1% Pt–5% Bi/C (3 g), feed flow rate 1.84 to 4.92 mol h^{-1}

Alcohol	Oxygen/ mol%	Alcohol/ mol%	Butanone co-solvent/ mol%	*p*/bar	*T*/°C	Residence time/s	Yield (%)	Sel. (%)
Octan-2-ol	4	2	—	110	140	17	68	> 99.5
1-Phenylethanol	2.7	2.7	5.3	110	140	13	95	> 99.5
1-Phenylethanol	5.3	2.7	5.3	110	140	13	98	99
Octan-1-ol	6	3	—	120	110	9.5	18	34
Octan-1-ol	2.5	5	—	95	80	25	11	82
Benzyl alcohol	2.5	5	—	95	80	13	26	99
Benzyl alcohol	2	2	—	120	100	9.5	65	78
p-Anisyl alcohol	2	2	4	120	110	9.5	70	87
Cinnamyl alcohol	4	2	4	120	110	9.5	78	98
Cinnamyl alcohol	4	2	8	120	110	9.5	61	96

DOI: 10.1039/b007114p

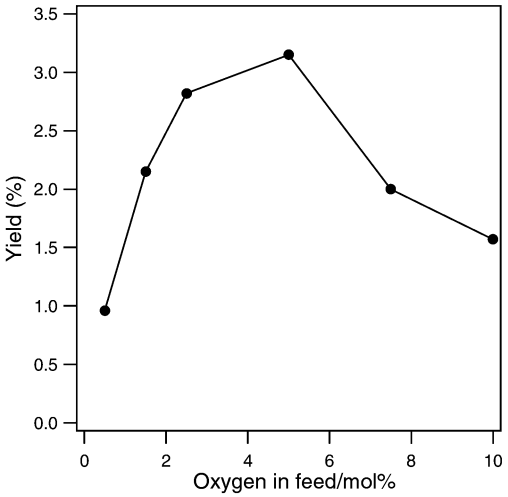

Fig. 1 Effect of oxygen concentration in the feed on the yield of octan-2-one. Conditions: 100 °C, 95 bar, 2 g catalyst, 2.46 mol h^{-1}, 5 mol% octan-2-ol, rest O_2 and CO_2.

phenylethyl) ether were detected. In these reactions the solid substrate was dissolved in butanone for feeding, because the reactor tubes and valves were not heatable. Comparative experiments with octan-2-one indicated that the yield decreased with increasing amount of this co-solvent suggesting that its amount should be kept at a low level (Fig. 2). The change in reaction rate may be connected to H-bonding between the substrate and co-solvent. Formation of H-bonded species (clusters) can change the phase behavior in $scCO_2$.

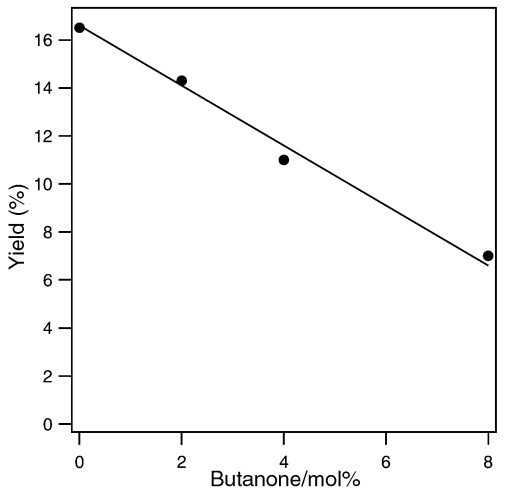

Fig. 2 Dependence of octan-2-one yield on butanone concentration in the feed. Conditions: 120 °C, 120 bar, 2 g catalyst, 3.28 mol h^{-1}, 2 mol% octan-2-ol, 4 mol% O_2, rest CO_2.

Transformation of primary alcohols to aldehydes under similar conditions was fast but non-selective (Table 1). For example, octan-1-ol was oxidized to a mixture of octanal, octanoic acid and octyl octanoate. Oct-2-enal and dioctyl ether were produced in traces. Transient experiments indicated that the acid-catalyzed side reactions (ester and ether formation) were accelerated by the product octanoic acid. In general, the selectivity to octanal decreased rapidly with increasing conversion, especially at high temperature. Relatively good selectivity could be achieved by working at 60–80 °C and high contact time (Table 1). Still, the aldehyde yield was always less than 20%. For comparison, partial oxidation of primary aliphatic alcohols is non-selective also in aqueous medium,[4] due to the high reactivity of aliphatic aldehydes for hydration and subsequent rapid dehydrogenation.

Remarkably better selectivities can be achieved when the product aldehyde is stabilized by an aromatic ring or a C=C double bond. Benzyl alcohol was oxidized to benzaldehyde, benzoic acid and benzyl benzoate. Higher than 99% selectivity for benzaldehyde was obtained at 60–80 °C (Table 1). At 100 °C or higher the selectivity dropped below 80%. Clearly, good yields can be achieved only at moderate temperature and longer contact time (higher amount of catalyst and/or lower mass flow rate). Oxidation of *p*-anisyl alcohol to *p*-anisaldehyde afforded even better yields, presumably due to the electron-releasing methoxy group in the para position (Table 1).

The highest aldehyde yield with high selectivity was obtained in the oxidation of the α,β-unsaturated alkylaromatic alcohol, cinnamyl alcohol. The negative impact of the co-solvent, used for dosing the solid substrate, is confirmed by the last two entries in Table 1. The aldehyde yield dropped from 78 to 61% when the alcohol was diluted with double the amount of butanone. Again, dosing of melted substrate can eliminate this complication.

From the results presented we can conclude that the aerobic oxidation of alcohols to carbonyl compounds in $scCO_2$ is a good alternative to the well-known aqueous phase oxidation on supported platinum metal catalysts. The present method has obvious advantages for the transformation of water-insoluble alcohols, avoiding the application of flammable organic solvents. Aqueous phase oxidations are typically performed at 40–90 °C for 3–10 h reaction time.[2–6] In the present study only 10–25 s residence time was necessary to achieve 65–98% yields of ketones, aromatic and α,β-unsaturated aldehydes. The yields and selectivities may be further improved by applying longer residence times at relatively low temperature, and by direct dosing of melted substrates (without co-solvent). No catalyst deactivation or metal leaching was observed with time-on-stream. Generally, steady-state conditions were reached within 2–3 h. The limitation of the method is similar to that of the aqueous phase oxidation on platinum metal catalysts, namely that primary aliphatic aldehydes cannot be synthesized with good selectivity.

Notes and references

† *Experimental procedure*: The reactions have been performed in a tubular flow reactor with an inner diameter of 13 mm and 38 ml volume. The alcohols were dosed by a Gilson 305 piston pump. Oxygen was supplied to the reactor using a six-port valve dosing 0.05 ml pulses at constant frequency. The constant pressure in the system was maintained by a backpressure regulator with CO_2. The total gas flow was controlled at the vent. The 4% Pd–1% Pt–5% Bi/C catalyst (CEF 196 RA/W, Degussa, BET surface area 930 m^2 g^{-1}) was reduced *in-situ* in hydrogen at 100 °C for 2 h prior to the kinetic measurements. For the parameter study the feed flow consisted of 5 mol% alcohol, 2.5 mol% oxygen and 92.5 mol% CO_2. 2 g catalyst was used, and a feed flow rate of 2.46 mol h^{-1}. The liquid products were separated from CO_2 and identified by GC and GC-MS. Yield and selectivities were determined by GC analysis using the internal standard method.

1 H. van Bekkum, in *Carbohydrates as Organic Raw Materials*, ed. F. W. Lichtenthaler, VCH, Weinheim, 1990, p. 289.
2 P. Vinke, D. de Wit, A. T. J. W. de Goede and H. van Bekkum, *Stud. Surf. Sci. Catal.*, 1992, **72**, 1.
3 T. Mallat and A. Baiker, *Catal. Today*, 1994, **19**, 247.
4 T. Mallat, Z. Bodnar, P. Hug and A. Baiker, *J. Catal.*, 1995, **153**, 131.
5 M. Besson and P. Gallezot, *Catal. Today*, 2000, **57**, 127.
6 J. H. J. Kluytmans, A. P. Markusse, B. F. M. Kuster, G. B. Marin and J. C. Schouten, *Catal. Today*, 2000, **57**, 143.
7 T. Mallat, L. Seyler, M. Mir Alai and A. Baiker, in *Supported Reagents and Catalysts in Chemistry*, ed. B. K. Hodnett, A. P. Kybett, J. H. Clark and K. Smith, Royal Society of Chemistry, Cambridge, 1998, p. 66.
8 P. G. Jessop and W. Leitner, *Chemical Synthesis Using Supercritical Fluids*, Wiley-VCH, Weinheim, 1999, and references therein.
9 A. Baiker, *Chem. Rev.*, 1999, **99**, 453, and references therein.
10 C. T. Wang and R. J. Willey, *Catal. Today*, 1999, **52**, 7.
11 L. B. Zhou and A. Akgerman, *Ind. Eng. Chem. Res.*, 1995, **34**, 1588.
12 M. Kraus, in *Handbook of Heterogeneous Catalysis*, ed. G. Ertl, H. Knözinger and J. Weitkamp, VCH, Weinheim, 1997, p. 2159.

Synthesis of Co-rich CoAPO-CHA molecular sieves in the presence of ethanol and caesium

Weibin Fan,†[a] Robert A. Schoonheydt[a] and Bert M. Weckhuysen*[ab]

[a] *Centrum voor Oppervlaktechemie en Katalyse, Departement Interfasechemie, K.U. Leuven, Kardinaal Mercierlaan 92, B-3001 Heverlee, Belgium. E-mail: Bert.Weckhuysen@agr.kuleuven.ac.be*

[b] *Departement Anorganische Chemie en Katalyse, Debye Instituut, Universiteit Utrecht, Sorbonnelaan 16, PO Box 80083, 3508 TB Utrecht, The Netherlands*

Received (in Oxford, UK) 31st August 2000, Accepted 18th September 2000
First published as an Advance Article on the web

CoAPO-CHA molecular sieves with Co(II) occupying 75% of the framework Al sites can be synthesized in the presence of ethanol and caesium.

Microporous crystalline aluminophosphate ($AlPO_4$-*n*) molecular sieves have a strict alternation of aluminium– and phosphorus–oxygen tetrahedra and their frameworks are neutral and, as a consequence, do not possess ion-exchange or acidic properties.[1] Acidic and redox sites can be generated in these materials by incorporating transition metal ions in the framework positions of these molecular sieves. This incorporation process gives rise to materials with interesting catalytic properties.[1–3] In this respect, the isomorphous substitution of Co(II) in $AlPO_4$-*n* materials has been studied in great detail, although the amounts of framework Co(II) remain still relatively low.[4–8] To the best of our knowledge, the framework Co : Al ratio reported is always < 1 with the exception of some $AlPO_4$-*n* molecular sieves with extremely small pores.[5,6,8] In fact, up to now not more than 38% of the Al(III) sites have been replaced by Co(II) in $AlPO_4$-*n* molecular sieves with pore openings > 3.5 Å. An example is CoAPO-50 with a framework substitution of 37.5%,[9] while for CoAPO-46 *ca*. 26% of the Al(III) sites can be replaced by Co(II).[10] It has also been reported that CoAPO materials with a chabazite structure can be prepared containing *ca.* 30% framework Co(II) by using $[NEt_4]_2CoCl_4$ and tetraethylamine hydroxide as the Co(II) source and template, respectively.[4] In this work, we report on the synthesis of crystalline CoAPO molecular sieves with the CHA structure having a Co : Al ratio substantially > 1. This high substitution degree has been made possible by using ethanol as solvent and by adding appropriate amounts of caesium to the synthesis gel.

CoAPO-CHA materials were prepared with H_3PO_4 (85 wt.%, Acros), $Co(MeCO_2)_2{\cdot}4H_2O$ (97 wt.%, Acros), pseudoboehmite (70 wt.% Al_2O_3, Catapal), caesium chloride (p.a., Acros), triethylamine (TEA, 99%, Acros) and ethanol (99.7–100%, BDH Laboratory) starting from the following gel composition: $(1.0–2.3)TEA{\cdot}(0\text{-}0.8)Cs_2O{\cdot}(0.6–1.6)CoO{\cdot}(0.2–0.7)Al_2O_3{\cdot}P_2O_5{\cdot}(30–60)EtOH$. A typical synthesis procedure is as follows: 2.93 g H_3PO_4 was dissolved into a mixture of 30 ml ethanol and 3.00 g CsCl. Then, 5.22 g $Co(MeCO_2)_2{\cdot}4H_2O$ was added to the solution, followed by the addition of 0.37 g pseudoboehmite and 2.73 g TEA under constant stirring. This mixture was then further stirred for *ca*. 1 h in an ice bath. Finally, the resultant mixture was transferred into a Teflon-lined autoclave and crystallization was carried out at 190 °C for 14 days. The obtained solid was filtered off, washed and dried at 60 °C. ICP was used to analyze the chemical composition of the initial gels and the as-synthesized samples, while XRD was used to identify the crystalline phase of the materials synthesized.

Table 1 gives an overview of the prepared CoAPO-CHA materials, the sample notations and the chemical compositions of the gel materials and final solids. Fig. 1 shows, as examples, the powder X-ray diffraction patterns of CsCoAPO-1.50 and CoAPO-1.50 and indicates that the as-synthesized solids are well crystalline and possess a CHA structure.[4,11] It is also clear that the addition of Cs(I) to the synthesis gel results in a decrease of the intensity of the peaks at lower 2θ values, particularly those at *ca*. 9.4 and 20.5°. It was observed that these peaks further decrease in intensity with increasing Cs(I) content in the synthesis gel, while at the same time the peaks at 2θ *ca.* 24.6,

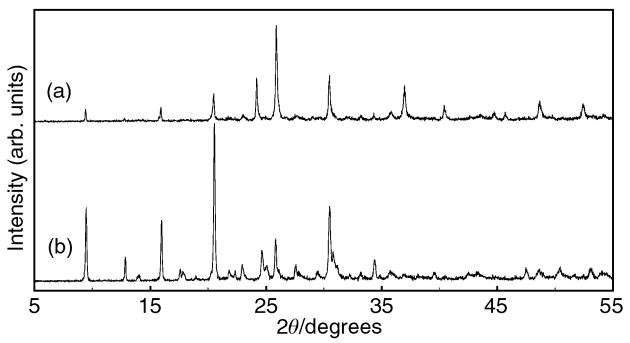

Fig. 1 XRD patterns of the as-synthesized CsCoAPO-1.5 (a) and CoAPO-1.5 (b) molecular sieves.

† On leave from Institute of Special Chemicals, Taiyuan University of Technology, Taiyuan 030024, P.R. China.

Table 1 The chemical compositions of the gels and the as-synthesized CoAPO-CHA materials

	Gels					Products					
Sample	(Co	Al	P)O_2	Co : Al	Cs : Co	(Co	Al	P)O_2	(Co+Al) : P	Co : Al	(P−Al) : Al
CoAPO-0.43	0.15	0.35	0.50	0.43	0.00	0.178	0.366	0.500	1.090	0.487	0.364
CoAPO-0.67	0.20	0.30	0.50	0.67	0.00	0.277	0.318	0.500	1.189	0.869	0.572
CoAPO-1.00	0.25	0.25	0.50	1.00	0.00	0.244	0.333	0.500	1.154	0.734	0.503
CoAPO-1.50	0.30	0.20	0.50	1.50	0.00	0.201	0.348	0.500	1.097	0.579	0.439
CsCoAPO-1.00	0.25	0.25	0.50	1.00	0.80	0.256	0.263	0.500	1.038	0.974	0.910
CsCoAPO-1.50	0.30	0.20	0.50	1.50	0.83	0.348	0.220	0.500	1.136	1.582	1.276
CsCoAPO-2.33	0.35	0.15	0.50	2.33	0.86	0.439	0.176	0.500	1.230	2.494	1.846
CsCoAPO-4.00	0.40	0.10	0.50	4.00	0.88	0.483	0.121	0.500	1.208	3.992	3.123

DOI: 10.1039/b007073o

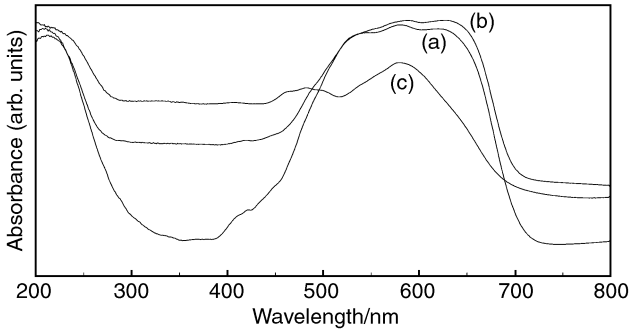

Fig. 2 DRS spectra of as-synthesized (a) and calcined (b) CsCoAPO-4.0, and calcined CoAPO-1.5 (c).

25.8, 30.5 and 37.0° increase in intensity. Such intensity changes are typical for isomorphous substitution processes.

Besides the key factors of the charge and geometry of the structure-directing amine molecules,[5] the solvent also plays a very important role in increasing the concentration of transition metals in the framework. It was reported that the Co : Al ratio of the reaction mixture can be maximized to 0.5 if TEA was used as a template in the hydrothermal synthesis of CoAPO-CHA.[5] We found that attempts to synthesize the samples with reaction mixtures containing higher cobalt contents led to the formation of a pale blue crystalline mixture of CoAPO-5 and an unknown phase. In contrast, when ethanol is used as solvent, pure CoAPO-CHA molecular sieves with an intense blue colour can be synthesized with the synthesis gel having a Co : Al ratio up to 0.67. The framework Co : Al ratio of the as-synthesized material is *ca.* 0.57, as estimated from the (P − Al) : Al ratio (Table 1). The blue colour and the absence of pink materials is indicative of tetrahedral Co(II) in the framework. The amount of framework Co(II) is much higher than that reported previously in the literature. However, further increase of the Co(II) content in the reaction mixture not only results in the formation of pink materials, but also decreases the relative amount of framework Co(II) of the as-synthesized samples. Thus, the more Co(II) in the synthesis gel, the less Co(II) in the framework. In particular, when the Co : Al ratio of the reaction mixture is > 1.5, the pink colour of the material cannot be removed by washing.

It is known that alkali metal cations have a strong influence on the crystallization of molecular sieves. We found that by introduction of Cs(I) cations in the synthesis gel, the Co : Al ratio of the reaction mixture can be dramatically increased to 4.0 for the synthesis of CHA-type Co-containing aluminophosphate molecular sieves. These materials are not contaminated with pink crystalline impurities. These as-synthesized CsCoAPO-*x* (*x* represents the Co : Al ratio of the reaction mixture) samples all have a deep blue colour. This is evident from the diffuse reflectance (DRS) spectrum of CsCoAPO-4.0 shown in Fig. 2(a). The strong triplet bands between 500 and 650 nm confirm that most of the Co(II) ions have been incorporated into the framework lattice, while a broad and weak band around 480 nm indicates the presence of only a small amount of extraframework Co(II).

Table 1 clearly shows that the Co : Al ratio of the CsCoAPO-*x* samples is basically the same as that of the reaction mixture, which is expected if Co(II) isomorphously substitutes for Al(III) in the framework. This behavior is different from that observed for the synthesis conducted in the absence of Cs(I). When the Co : Al ratio of the reaction mixture < 1, the (Co+Al) : P ratio of the as-synthesized solid, *e.g.* CsCoAPO-1.0, is very close to 1. This fact strongly supports the incorporation of most Co(II) in the framework lattice sites. With the addition of more cobalt into the reaction mixture, the (Co+Al) : P ratio is gradually > 1, indicating that a small amount of extraframework Co(II) ions is present in the products. This is in accord with the chemical analysis results. Nevertheless, it can be seen that the (P − Al) : Al ratio of the CsCoAPO-*x* samples maximally reaches about 3.12 (CsCoAPO-4.0), which means that *ca.* 75% framework Al sites have been replaced with Co(II). Table 1 also indicates that the amount of caesium needed in the synthesis increases with increasing cobalt content. The amazing ability of Cs(I) to increase the Co(II) concentration in the framework can be related to its role as a counter cation, possibly resulting in a decrease of framework distortion owing to a stronger Cs–O bond than the TEA–O bond, and consequently an increase of the stability of the as-synthesized CsCoAPO-CHA. Thus, Cs(I) promotes the incorporation of Co(II) into the framework of the CoAPO-CHA material.

As expected, the hydrothermal stability of the as-synthesized products decreases upon increasing the Co : Al ratio. It was found that CsCoAPO-*x* synthesized with reaction mixtures having a Co : Al ratio > 2.33 gradually becomes pale blue upon washing with water. This is further evidenced by the corresponding DRS spectra in which the triplet bands characteristic of tetrahedral Co(II) obviously decrease in intensity at the expense of the appearance of an absorption at 480 nm typical for extraframework octahedral Co(II). This may be due to the hydrolysis of framework Co(II) since this ion shows a strong interaction with water, and competes with Cs(I) for H_2O coordination.[5] Therefore, the products synthesized with high amounts of cobalt should be better washed with ethanol.

On the other hand, Cs(I) as a counter cation can effectively prevent oxidation of Co(II) to Co(III) during calcination. Upon calcination at 550 °C for 6 h, the sample CoAPO-*x* becomes yellow-greenish, and even pink materials are evident when the Co : Al ratio of the synthesis gel is > 0.43. This is evidenced by DRS for the CoAPO-1.5 sample [Fig. 2(c)]. This spectrum is characterized by a band at *ca.* 450–500 nm and a band at *ca.* 320 nm, indicating the presence of octahedral Co(II) and Co(III), respectively. This shows that many framework Co(II) ions have been expelled from the framework, indicating the instability of CoAPO-*x* molecular sieves. In contrast, the calcined CsCoAPO-*x* is still deep-blue, as confirmed by the strong triplet bands at *ca.* 530, 580 and 630 nm in the DRS spectrum of the calcined CsCoAPO-4.0 sample [Fig. 2(b). This proves that the presence of Cs(I) can stabilize tetrahedral Co(II) in the framework of CoAPO-CHA materials.

In conclusion, Co-rich CoAPO molecular sieves with CHA structure have been prepared using ethanol and Cs(I) as solvent and counter cation, respectively. Co(II) can be maximized to occupy about 75% of the framework metal sites. The presence of Cs(I) significantly inhibits the oxidation of Co(II) to Co(III).

This work is supported by the Fonds voor Wetenschappelijk Onderzoek (FWO) and the Geconcerteerde Onderzoeksacties (GOA) of the Flemish Community. W. F. thanks the Research Council of K. U. Leuven for a junior postdoctoral fellowship and B. M. W. acknowledges the FWO for a fellowship.

Notes and references

1 I. W. C. E. Arends, R. A. Sheldon, M. Wallau and U. Schuchardt, *Angew. Chem., Int. Ed. Engl.*, 1997, **36**, 1144.
2 J. Chen and J. M. Thomas, *J. Chem. Soc., Chem. Commun.*, 1994, 603.
3 R. Raja, G. Sankar and J.M. Thomas, *Angew. Chem., Int. Ed.*, 2000, **39**, 2313.
4 S. J. Hill, C. D. Williams and C. V. A. Duke, *Zeolites*, 1996, **17**, 291.
5 P. Feng, X. Bu and G. D. Stucky, *Nature*, 1997, **388**, 735.
6 P. Feng, X. Bu, S. H. Tolbert and G. D. Stucky, *J. Am. Chem. Soc.*, 1997, **119**, 2497.
7 B. M. Weckhuysen, R. R. Rao, J. A. Martens and R. A. Schoonheydt, *Eur. J. Inorg. Chem.*, 1999, 565.
8 H. Yuan, J. Chen, G. Zhu, J. Li, J. Yu, G. Yang and R. Xu, *Inorg. Chem.*, 2000, **39**, 1476.
9 J. M. Bennett and B. K. Marcus, *Stud. Surf. Sci. Catal.*, 1988, **37**, 269.
10 S. T. Wilson and E. M. Flanigen, *Zeolite Synthesis*, ed. M. L. Occelli and H. E. Robson, *ACS Symp. Ser. 398*, 1999, p. 269.
11 M. M. J. Treacy, J. B. Higgins and R. von Ballmoos, *Zeolites*, 1996, **16**, 409.

Unusual RNA and DNA binding properties of a novel pyrrolidine–amide oligonucleotide mimic (POM)†

David T. Hickman,[a] Paul M. King,[b] Matthew A. Cooper,[c] Jonathan M. Slater[b] and Jason Micklefield*[a]

[a] *Department of Chemistry, UMIST, Faraday Building, PO Box 88, Manchester, UK M60 1QD. E-mail: jason.mickelfield@umist.ac.uk*
[b] *Department of Chemistry, Birkbeck College, University of London, 29 Gordon Square, London, UK WC1H 0PP*
[c] *University Chemical Laboratory, Lensfield Road, Cambridge, UK CB2 1EW*

Received (in Cambridge, UK) 23rd August 2000, Accepted 16th October 2000
First published as an Advance Article on the web

A pentameric thymidyl pyrrolidine–amide oligonucleotide mimic (POM) was synthesised and shown to bind with very high affinity to complementary single stranded RNA and DNA, whilst exhibiting kinetic binding selectivity for RNA over DNA.

The sugar–phosphodiester backbone of nucleic acids has been replaced by many alternative neutral and anionic backbones.[1] There have also been reports of zwitterionic and cationic oligonucleotides with pendant aminoalkyl side chains attached to the sugar ring, pyrimidine base, or to various phosphorus internucleoside linkages.[2] Despite this, only a few *de novo* modified oligonucleotides have been reported with positively charged backbones.[3] Here we introduce a novel pyrrolidine–amide oligonucleotide mimic (POM) **1** (Scheme 1), which is derived by replacing the furanose sugar of native nucleic acids with a pyrrolidine ring which will be protonated and positively charged at physiological pH.[3d] An X-ray crystal structure[4] of a protonated pyrrolidine ring, which is stereochemically identical and both electronically and sterically similar to the pyrrolidine ring in **1**, closely resembles the northern (N) conformation of uridine in the crystalline state.[5] Semi-empirical quantum mechanical calculations (MOPAC 6.0) also revealed that the lowest energy conformation of a model pyrrolidine **2** closely resembles the preferred N-conformation of the ribose ring in native RNA. In addition, the rigid amide linkage is a viable replacement for the phosphodiester group in DNA resulting in modified oligonucleotides that form stable duplexes with RNA and DNA.[6]

To begin investigating the nucleic acid binding properties of POM a pentamer, T_5-POM **3**, was synthesised, in solution, from *trans*-4-hydroxy-L-proline *via* the ester **4**[7] (Scheme 2). Lithium borohydride reduction of the ester and benzoyl groups of **4** gave the alcohol **5**, which was subjected to a Mitsunobu reaction to afford the phthalimide derivative **6**. Removal of the phthalimide and Boc groups gave the amines **7** and **8** respectively, which were used as the building blocks for the construction of oligomers by an *N*-alkylation or *N*-acylation strategy. In the former approach primary amine **7** was treated with bromoacetic anhydride to give the bromoacetamide **9** which was coupled

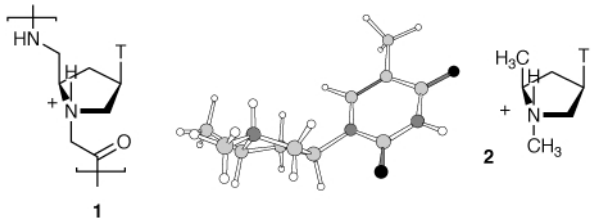

Scheme 1

† Electronic supplementary information (ESI) available: UV thermal denaturation curves, Job plots and SPR sensograms for TS-POM **3** binding to DNA and RNA. See http://www.rsc.org/suppdata/cc/b0/b006903p/

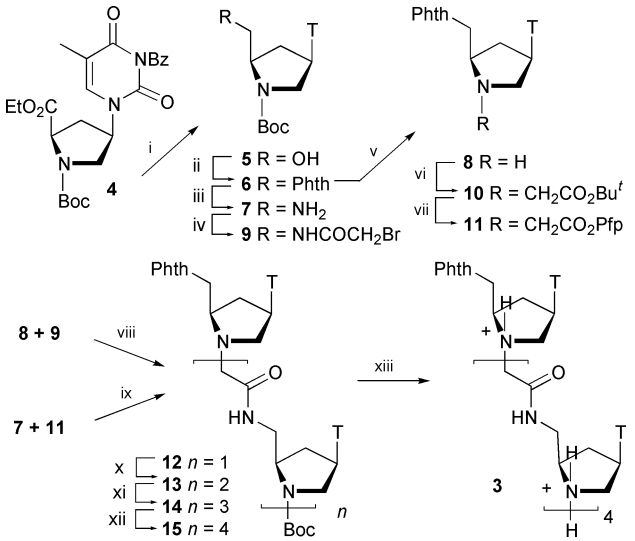

Scheme 2. *Reagents and conditions*: i, $LiBH_4$ (2 eq.), THF, 0 °C → rt, 15 h, 69%; ii, phthalimide, PPh_3, DEAD (all 1.3 eq.) in THF, −15 °C → rt, 15 h, 63%; iii, 25–30% aq. $MeNH_2$, 1 h, 40 °C, 89%; iv, bromoacetic anhydride (1 eq.), AcCN–CH_2Cl_2, −8 °C → rt, 5 min, 97%; v, CH_2Cl_2–CF_3CO_2H (2:1), 4 h, 86%; vi, *tert*-butyl bromoacetate (1.5 eq.), DIPEA (3 eq.), DMF, 0 °C → rt, 18 h, 92%; vii, CH_2Cl_2–CF_3CO_2H (4:1), 3 h, then pyridine (2 eq.), CF_3CO_2Pfp (1.2 eq.), DMF, 2 h, 78%; viii, **8** + **9** (1:1), DIPEA (3 eq.), DMF, rt, 18 h, 98%; ix, **7** + **11** (1:1) CH_2Cl_2, rt, 3 h, 100%; x, CH_2Cl_2–CF_3CO_2H (4:1), rt, 4 h, then DIPEA (5 eq.), DMF, **9**, rt, 97%; xi and xii, repeat conditions for **12** → **13**, 96 and 91%; xiii, MeOH–H_2O (1:1) saturated with $HCl_{(g)}$, rt, 2 h, 95%. DIPEA = diisopropylethylamine, Pfp = pentafluorophenyl, Phth = phthalimide, T = thymidyl. New compounds were characterised by ^1H and ^{13}C NMR, IR, UV, MS, mp, $[\alpha]_D$.

with the secondary amine **8** resulting in the dimer **12**. Boc deprotection of **12** and a second coupling with **9** results in the trimer **13.** These steps were repeated to give the tetramer **14** and pentamer **15**, which on treatment with HCl resulted in T_5-POM **3** as an highly water soluble HCl salt. Alternatively, treatment of the secondary amine **8** with *tert*-butyl bromoacetate followed by acidolysis and esterification with pentafluorophenyl trifluoroacetate gave the Pfp-ester **11** which was used to acylate primary amine **7** to give dimer **12**.

UV thermal denaturation experiments were then carried out with an equimolar mixture of T_5-POM **3** and poly(rA) (Table 1). At pH 7, 0.12 M K^+ a single hyperchromic shift was observed with a melting temperature (T_m) of 49 °C (*ca.* 10 °C per base). In comparison, native $d(T)_5$ showed no hyperchromic shift with poly(rA), above 8 °C under identical conditions, whilst $d(T)_{20}$ formed a duplex with poly(rA) with a T_m of 42 °C (2.1 °C per base). Peptide nucleic acid (PNA) lys-T_5-lysNH_2 exhibited only slightly higher affinity for poly(rA) (T_m = 56 °C). Furthermore, no hyperchromic shifts were observed for T_5-POM **3** with non-complementary poly(rC), (rG) and (rU), whilst Job plots of **3** with poly(rA) revealed a 1:1 binding stoichiometry consistent with the formation of a Watson–Crick base paired duplex.

Table 1 Transition melting temperatures (T_m) of T_5-POM **3** with poly(rA) and poly(dA).

		T_m/°C	
$[K^+]$/M	pH	Poly(rA)[a]	Poly(dA)[b]
0.12	7.0	49 (56)[c]	57 (48)[c]
0.22	7.0	52	n.d.[d]
0.62	7.0	54	42, 66[e]
1.20	7.0	55	61
0.12	8.0	45	n.d.[d]
0.12	7.5	46	n.d.
0.12	6.5	54	n.d.
0.12	6.0	57	35, 64[e]

[a] T_5-POM **3** and poly(rA) (42 μM each in bases) in 10 mM K_2HPO_4(total volume 1 cm³) adjusted to the appropriate ionic strength and pH. UV absorbance (A_{260}) was recorded with heating at 5 °C min^{-1} from 25 to 93 °C, cooling at 0.2 °C min^{-1} to 15 °C and heating at 0.2 °C min^{-1} to 93 °C. The T_m was determined from the first derivative of the final slow heating curve. [b] **3** and poly(dA) (210 μM each in bases) in 10 mM K_2HPO_4 (total volume 0.2 cm³) were incubated for 48–96 h at 25 °C, diluted to 1 cm³ adjusting to the appropriate ionic strength and pH, cooled to 15 °C at 1 °C min^{-1}, heated at 0.2 °C min^{-1} to 93 °C from which the T_m was measured as above. [c] T_m values for lys-T_5-lysNH_2 PNA (PE Biosystems). [d] T_m not determined. [e] Two transitions observed.

Surprisingly however, increasing the salt concentration resulted in slightly higher T_m values. This is in contrast to other cationic modified oligonucleotides that show a marked decrease in duplex and triplex stability with RNA and DNA at higher salt concentration, which is attributed to a reduction in the electrostatic attraction between the oppositely charged backbones.[3] The T_m of **3** with poly(rA) was also highly dependent on pH with more stable duplexes formed at lower pH. This suggests that the extent of protonation of the nitrogen atom of the pyrrolidine ring, is important for binding to RNA. However, factors other than electrostatic attraction, perhaps conformational changes brought about by protonation, are more likely to be the cause of increased duplex stability.

Remarkably no melting was observed between T_5-POM **3** and equimolar poly(dA) under identical conditions. Only after a five-fold increase in concentration of both **3** and poly(dA) followed by an extended period of incubation (48–96 h) was it possible to observe melting, suggesting T_5-POM binds much more slowly to poly(dA) than poly(rA). On the other hand the affinity of **3** for poly(dA) was considerably higher than for poly(rA) (T_m = 57 °C, pH 7, 0.12 M K^+), whilst lys-T_5-lysNH_2 PNA exhibited a lower affinity for poly(dA). Noticeably upon increasing the salt concentration (0.62 M K^+) or lowering the pH to 6, two melting temperatures were observed consistent with triple helix to duplex and duplex to single strand transitions. Job plots of **3** with poly(dA) indicated a 2:1 (T:A) binding stoichiometry consistent of triplex formation.

To investigate the difference in the association kinetics of T_5-POM **3** with DNA and RNA, the change in A_{260} with time was recorded immediately following mixing of equimolar amounts of the polyadenylates with **3** (Fig. 1). With poly(rA) at pH 7, 0.12 M K^+ and a base concentration of 42 μM for each oligomer, a 29% hypochromic shift was observed with a $t_{1/2}$ for association of *ca*. 7 min. Under identical conditions no hypochromic shift was observed with poly(dA) even after 15 h. However, increasing the concentration of both T_5-POM **3** and poly(dA) fivefold resulted in a moderate 6% hypochromic shift with a $t_{1/2}$ of at least 30 min. This clearly shows that T_5-POM **3** binds much more slowly to poly(dA) than (rA). It was also apparent from these experiments that T_5-POM binds faster to poly(rA) at lower pH and salt concentration, suggesting that electrostatic attraction increases the rate of association.

The high affinity, sequence specific binding and relative rates of association of T_5-POM **3** with DNA and RNA were confirmed using surface plasmon resonance (SPR). In these experiments 5′-biotinylated $d(A)_{20}$, $r(A)_{20}$ and a mixed sequence DNA 30–mer were immobilised *via* streptavidin into a dextran matrix upon a gold surface. A solution of T_5-POM **3** was then injected across each surface and the SPR response was measured against time (see ESI†). This revealed that **3** does bind strongly to both $d(A)_{20}$ and $r(A)_{20}$ but associates faster with $r(A)_{20}$ than $d(A)_{20}$. Significantly, the response sensogram of the mixed sequence DNA was identical to the control non–derivatised surface.

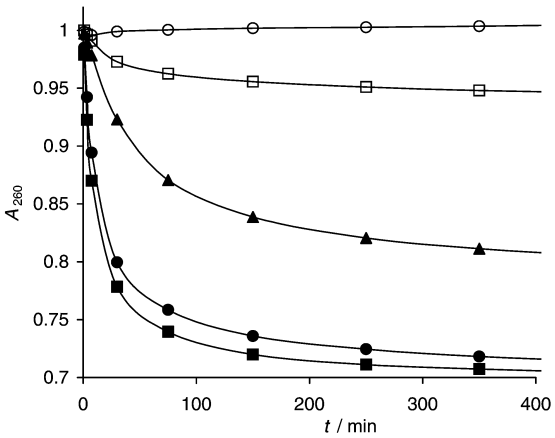

Fig. 1 Normalised UV absorbance (A_{260}) of T_5-POM **3** with poly(rA) and (dA) *vs.* time at 25 °C. **3** and poly(dA) (42 μM each in bases), 0.12 M K^+, pH 7 (○); **3** and poly(dA) (210 μM), 0.12 M K^+, pH 7 (□); **3** and poly(rA) (42 μM), 0.22 M K^+, pH 7 (▲) ; **3** and poly(rA) (42 μM), 0.12 M K^+, pH 7 (●); **3** and poly(rA) (42 μM), 0.12 M K^+, pH 6 (■).

In conclusion we have introduced a novel class of modified nucleic acids with a pyrrolidine–amide backbone and shown that the pentamer T_5-POM **3** binds sequence specifically to both ssDNA and ssRNA with an affinity that is much higher than native nucleic acids. Furthermore, T_5-POM binds much faster to ssRNA than ssDNA. Other oligonucleotides such as 2′,5′-linked RNA and DNA exhibit a thermodynamic binding selectivity for native ssRNA over ssDNA,[8] but as far as we are aware T_5-POM is the first modified oligonucleotide that can kinetically discriminate between the two. This kinetic preference may be due to folding of the polyadenylates induced by base pairing with T_5-POM, given that RNA would be expected to fold more readily than DNA. In addition the formation of tertiary interactions could also explain the high stability of T_5-POM complexes with complementary nucleic acids. The synthesis of longer mixed sequence POMs, using solid phase methods, is underway in order to explore the generality of these findings.

We thank the EPSRC for a studentship to D. T. H.

Notes and references

1 J. F. Milligan, M. D. Matteucci and J. C. Martin, *J. Med. Chem.*, 1993, **36**, 1923; A. De Mesmaeker, R. Häner, P. Martin and H. E. Moser, *Acc. Chem. Res.*, 1995, **28**, 366.

2 B. Cuenoud, F. Casset, D. Hüsken, F. Natt, R. M. Wolf, K.-H. Altmann, P. Martin and H. E. Moser, *Angew. Chem., Int. Ed.*, 1998, **37**, 1288; L. E. Heystek, H.-Q. Zhou, P. Dande and B. Gold, *J. Am. Chem. Soc.*, 1998, **120**, 12 165; T. Horn, S. Chaturvedi, T. N. Balasubramaniam and R. L. Letsinger, *Tetrahedron Lett.*, 1996, **37**, 743.

3 (*a*) R. O. Dempcy, K. A. Browne and T. C. Bruice, *J. Am. Chem. Soc.*, 1995, **117**, 6140; (*b*) B. A. Linkletter, I. E. Szabo and T. C. Bruice, *J. Am. Chem. Soc.*, 1999, **121**, 3888; (*c*) D. P. Arya and T. C. Bruice, *J. Am. Chem. Soc.*, 1998, **120**, 12 419; (*d*) M. D'Costa, V. A. Kumar and K. N. Ganesh, *Org. Lett.*, 1999, **1**, 1513.

4 T. Furuya, S. Fujita, S. Iwanami, A. Takenka and Y. Sasada, *Acta Crystallogr., Sect. C*, 1986, **42**, 1345.

5 E. A. Green, R. D. Rosenstein, R. Shiono, D. J. Abraham, B. L. Trus and R. E. Marsh, *Acta Crystallogr., Sect. B*, 1975, **31**, 102.

6 A. De Mesmaeker, A. Waldner, J. Leberton, P. Hoffmann, V. Fritsch, R. M. Wolf and S. M. Freier, *Angew. Chem., Int. Ed. Engl.*, 1994, **33**, 226.

7 G. L. Baker, S. J. Fritschel, J. R. Stille and J. K. Stille, *J. Org. Chem.*, 1981, **46**, 2954; G. Lowe, T. Vilaivan, *J. Chem. Soc., Perkin Trans. 1*, 1997, 539.

8 P. A. Giannaris and M. J. Damha, *Nucleic Acids Res.*, 1993, **21**, 4742; T. L. Sheppard and R. C. Breslow, *J. Am. Chem. Soc.*, 1996, **118**, 9810.

N-Methylimidazole-functionalized gold nanoparticles as catalysts for cleavage of a carboxylic acid ester

Lucia Pasquato,*[a] Fiorenza Rancan,[a] Paolo Scrimin,*[a] Fabrizio Mancin[a] and Cesare Frigeri[b]

[a] *Centro CNR Meccanismi di Reazioni Organiche (CMRO) and Dipartimento di Chimica Organica, Università di Padova, via Marzolo 1, I-35131 Padova, Italy. E-mail: pasquato@chor.unipd.it*
[b] *CNR-MASPEC, Parco Area della Scienza, 37a, I-43010 Fontanini, Parma, Italy*

Received (in Liverpool, UK) 27th June 2000, Accepted 2nd September 2000
First published as an Advance Article on the web

New *N*-methylimidazole-functionalized gold clusters 2 catalyze, in 6:4 methanol–water solution, the cleavage of 2,4-dinitrophenyl acetate with more than an order of magnitude rate acceleration with respect to acetyl-*N*-methylhistamine 3; comparison with dodecanoyl-*N*-methylhistamine 4 comicellized with Brij 35 reveals that 2 is still a better catalyst than the comicellar system and highlights analogies and differences between the two systems.

The last few years have witnessed a growing interest in nanomaterials for their potential applications ranging from catalysis to technology. Among them monolayer-protected gold clusters (Au-MPCs) appear particularly promising. Since the seminal work by Brust, Schiffrin *et al.*[1] these materials can be easily obtained as systems which are stable,[2] soluble in organic solvents (according to the properties of the protecting monolayer) and rather monodisperse in size. However, in spite of these interesting properties, reports concerning applications of Au-MPCs in catalysis are rather limited. In particular, the potential for cooperativity between several functional groups assembled on gold nanoclusters has not been specifically exploited so far. This communication addresses these aspects of Au-MPCs.

The conventional preparation procedure of the nanoparticles calls for the synthesis *in situ* by reduction of an Au(III) salt in the presence of the functional thiol derivative, followed, when required, by further derivatization[3] or by solution exchange of hydrocarbon-protected Au-MPC with a suitable functional thiol.[4] Following this latter approach we have first prepared gold nanoparticles protected with a monolayer of dodecanthiolates (C12) according to the detailed protocol reported by Murray and coworkers.[5] The resulting Au-MPC-C12 proved to be rather monodisperse by transmission electron microscopy (TEM) with an average core diameter of 2.2 ± 1.0 nm. This result, combined with the elemental analysis, indicates that the clusters are composed mainly of $Au_{225}(C12)_{90}$. Subsequently, we accomplished the place-exchange reaction[4,6] by codissolving MPC-C12 and thiol **1**† in dichloromethane–methanol (1:1) under an entering:exiting ligand ratio of 1:1.5. The resulting material was purified by exclusion chromatography [Sephadex LH-60, CH_2Cl_2–MeOH (1:1)]. Proton NMR spectra‡ reveal that the obtained Au-MPC comprises a 1:1 mixture of dodecane- and *N*-methylimidazole-functionalized thiolates. TEM measurements show that during the place-exchange process the average dimension of the gold core remains unchanged while the size distribution becomes slightly larger. The presence of a 1:1 mixture does not necessarily mean a random distribution. As recently reported,[7] in solution there may be rearrangement of thiols on the Au surface.

In the design of **2** our specific goal was the realization of a catalytically active Au-MPC for the cleavage of a carboxylate ester. Furthermore we wanted to verify the possibility of cooperativity of the active functional groups because of their confinement on the surface of Au-MPC **2**. For this purpose imidazole (or *N*-methylimidazole) appeared to be a suitable

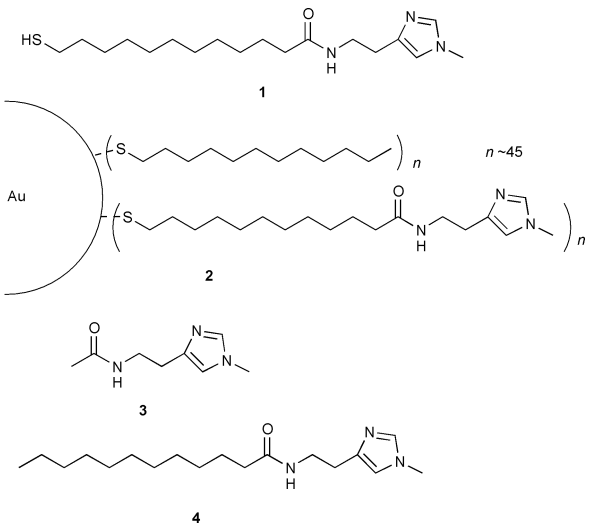

candidate because of its key role as a catalyst in many hydrolytic systems where cooperativity between two such units has been reported.[8,9]

Cleavage of 2,4-dinitrophenyl acetate (DNPA), as a model ester, was studied in a methanol–water (6:4) solution, in which the new MPCs **2** are fully soluble, in the pH range 4.5–7.2. The reactions were monitored by UV–VIS following the formation of the 2,4-dinitrophenolate at 400 nm and 25 °C. For comparison purposes acetyl-*N*-methylhistamine **3** was also used as a reference monomeric catalyst.

The dependence of the second order rate constant, k_2,§ with pH for Au-MPC **2** and monomeric catalyst **3** is shown in Fig. 1 where the remarkable rate acceleration exerted by the nano-

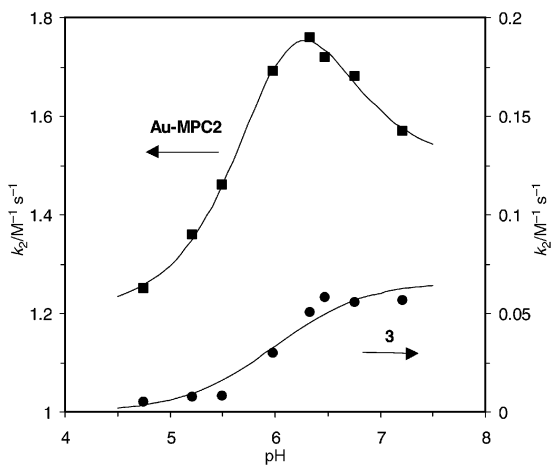

Fig. 1 pH dependence of the second order rate constants for the hydrolysis of 2,4-dinitrophenyl acetate in MeOH–H_2O (6:4) in the presence of Au-MPC **2** (■) or of the model system **3** (●). The solid curves are the best fitting of the experimental points.

DOI: 10.1039/b005244m

particles relative to **3** can be readily appreciated. Although the pK_a of *N*-methylimidazole of **2** could not be determined because of its insolubility at the high concentration required for the potentiometric titration, it is likely to be similar to the value (6.2) determined for **3** in the solvent mixture employed for the kinetic experiments. The low dependence of k_2 from pH in the pH range 5–7, with a small maximum in the proximity of the pK_a, supports cooperativity between two methylimidazoles in the DNPA cleavage by the nanocluster (general acid/general base or nucleophilic catalysis). The solid curves of Fig. 1 represent the computer-generated best fitting of the experimental points assuming a cooperative process (Au-MPC) and nucleophilic catalysis (**3**). A fair comparison between the two systems can be made at the pH values of the maxima of the two curves (pH 7.2 for **3** and 6.1 for **2**). Under these conditions the nanoclusters-catalyzed process is *ca.* 30 times faster than that using monomeric **3**. The kinetic behavior is very similar to that reported by the group of Baltzer[8] who studied four helix bundle-forming hydrolytic peptides bearing multiple imidazole side arms where cooperativity had been clearly demonstrated.

We note here that the system is really catalytic as all kinetic reactions were performed using an excess substrate (up to 7 : 1) over catalyst and the kinetic profile followed, in all cases, a well behaved pseudo-first-order process accounting for all added substrate.

Because gold nanoclusters **2** present structural analogies with a micellar aggregate we also tested the lipophilic *N*-methylhistamine derivative **4** in Brij 35 comicelles. As expected, micellar aggregates exist only in aqueous solution and not in the methanol–water mixture used for the study of **2**, as the hydrophobic effect that is at the basis of monomer aggregation vanishes in this solvent. Consequently, the catalytic efficiency in the mixed solvent is rather poor and similar to that of **3**. Comicellar **4**/Brij 35, however, binds DNPA in water (pH 6.3) with $K_b = 40\ M^{-1}$ and, in this solvent, accelerates the rate of its cleavage with k_{lim}, the pseudo-first-order rate constant for the fully bound substrate, of $2.5 \times 10^{-2}\ s^{-1}$. The comparison between the two systems is complicated by the fact that, because of the mixed solvent and the very low concentration of **2** used, the Au-MPCs are not expected to significantly bind the substrate. For this reason we have determined the second-order rate constant for the micellar system at very low surfactant concentration in the linear part of the rate *vs.* concentration profile above the critical aggregate concentration. At pH 6.2 the rate acceleration over that of the monomeric catalyst **3** is 35 for **2** and 22 for the comicelles indicating a slightly better efficiency of the Au-MPCs.

In conclusion we have reported the very first example of functional gold nanoclusters which are catalytically active in the hydrolysis of an activated ester. These systems present analogies with micellar aggregates although they exist under solvent conditions where micelles do not survive. Furthermore, the cooperative effects of the functional moieties may be exploited at very low concentration of the catalyst because the nanocluster does not require the critical aggregate concentration necessary for the formation of micelles. As for these properties, Au-MPCs resemble dendrimers, although the synthetic effort required for their formation is much less demanding. We believe that these systems present great potentialities as catalysts, and work aimed at the realization of new Au-MPCs bearing different functional groups, as well as small peptides, is in progress in our laboratory.

We are indebted to Professor P. Tecilla for helpful discussion.

Notes and references

† **1** was obtained by hydrolysis of the thioacetylated precursor: δ_H(250 MHz, $CDCl_3$) 1.20–1.40 (m, 14H), 1.43–1.65 (m, 4H), 2.15 (t, 2H, *J* 7.67), 2.52 (q, 2H, *J* 7.43), 2.72 (t, 2H, *J* 6.02), 3.52 (q, 2H, *J* 6.02), 3.64 (s, 3H), 6.5 (br, 1H, NH), 6.66 (s, 1H), 7.34 (s, 1H). δ_C(62.9 MHz, $CDCl_3$) 24.65, 25.71, 28.35, 29.04, 29.27, 29.37, 29.47, 34.03, 35.76, 36.52, 38.2, 118.19, 133.55, 134.75, 174.29. IR (film on KBr) ν/cm^{-1}: 3333, 2917, 2850, 2613, 1738, 1640, 1543, 1471, 1423, 1170, 717, 625.

‡ δ_H(250 MHz, CD_3OD) 0.96 (br s, 3H), 1.08–2.10 (br, 44H), 2.23 (br, 2H), 2.90 (br, 2H), 3.49 (br, 2H), 3.90 (br, 3H), 7.32 (br, 1H), 8.57 (br, 1H). δ_C[600 MHz HMQC (^{13}C–^1H), 400 MHz HMBC (^{13}C–^1H), CD_3OD] 15.01, 24.27, 26.91, 27.47, 29.79, 30.56, 31.27 (br), 33.59, 35.84, 37.56, 39.63, 121.27, (C5-Im, 7.32), 135.14 (C4-Im), 137.26 (C2-Im), 176.42 (C=O). IR (film on KBr), ν/cm^{-1}: 3467, 2919, 2849, 1644, 1465, 1415, 1261, 1167, 1021, 722, 624. Anal Calc. for $Au_{225}(C_{30}H_{57}N_3OS_2)_{45}$: C, 23.66; H, 3.77; N, 2.76; S, 4.21. Found: C, 23.57; H, 3.44; N, 2.50; S, 4.24.

§ Standard reaction conditions are: [DNPA] = $3.35–10.8 \times 10^{-5}$ M, [MI] = 1.54×10^{-5} M ([MI] is the molar concentration of methylimidazole or the methylimidazole head group in Au-MPC. The nanoparticle concentration is *ca.* [MI]/45), 25 °C in MeOH : H_2O (6 : 4). [Buffer] = 2×10^{-2} M. Buffers used were: AcO^-/AcOH pH 4.75, 5.21, 5.5; MES pH 5.98, 6.33, 6.47, 6.76 and HEPES pH 7.21; $k_2 = (k_{obs} - k_0)$/[MI]. For reference k_{obs}/k_0 (pH 6.5 at the above concentration) were *ca.* 1.3 and 10 for **3** and **2**, respectively, with $k_0 = 2 \times 10^{-5}\ s^{-1}$.

1 M. Brust, M. Walker, D. Bethell, D. J. Schiffrin and R. Whyman, *J. Chem. Soc., Chem. Commun.*, 1994, 801.
2 A. C. Templeton, W. P. Wuelfing and R. W. Murray, *Acc. Chem. Res.*, 2000, **33**, 27.
3 For example: A. C. Templeton, M. J. Hostetler, E. K. Warmoth, S. Chen, C. M. Hartshorn, V. M. Krishnamurthy, M. D. E. Forbes and R. W. Murray, *J. Am. Chem. Soc.*, 1998, **120**, 4845.
4 R. S. Ingram, M. J. Hostetler and R. W. Murray, *J. Am. Chem. Soc.*, 1997, **119**, 9175; M. J. Hostetler, A. C. Templeton and R. W. Murray, *Langmuir*, 1999, **15**, 3782.
5 M. J. Hostetler, J. E. Wingate, C.-J. Zhong, J. E. Harris, R. W. Vachet, M. R. Clark, J. D. Londono, S. J. Green, J. J. Stokes, G. D. Wignall, G. L. Glish, M. D. Porter, N. D. Evans and R. W. Murray, *Langmuir*, 1998, **14**, 17.
6 M. J. Hostetler, S. J. Green, J. J. Stokes and R. W. Murray, *J. Am. Chem. Soc.*, 1996, **118**, 4212.
7 A. K. Boal and V. M. Rotello, *J. Am. Chem. Soc.*, 2000, **122**, 734.
8 K. S. Broo, H. Nilsson, J. Nilsson, A. Flodberg and L. Baltzer, *J. Am. Chem. Soc.*, 1998, **120**, 4063.
9 R. Breslow, J. B. Doherty, G. Guillot and C. Lipsey, *J. Am. Chem. Soc.*, 1978, **100**, 3227; E. Anslyn and R. Breslow, *J. Am. Chem. Soc.*, 1989, **111**, 5972.

ChemComm

Supramolecular similarities between a diastereomer pair and their truncated derivative: common tetrameric synthon and isostructurality

Alajos Kálmán,* László Fábián and Gyula Argay

Institute of Chemistry, Chemical Research Center, Hungarian Academy of Sciences, Budapest 114, P.O. Box 17, H-1525, Hungary

Received (in Columbia, MO, USA) 20th June 2000, Accepted 13th September 2000
First published as an Advance Article on the web

A common tetrameric supramolecular synthon and an unexpected isostructurality reveal similarities between the crystal structures of three related cyclopentane derivatives fused together by OH···O and NH···O hydrogen bonds.

Since the fundamental statements of Lehn[1] the concept that crystals are solid state supermolecules built by connecting molecules with intermolecular interactions has been widely accepted by both organic and structural chemists. In particular, Desiraju[2,3] has made relevant contributions to this concept by classifying the governing principles of supramolecular chemistry. He distinguishes anisotropic long range forces (hydrogen bonds) from the similarly important isotropic van der Waals forces. The magnitude of the latter is proportional to the size of the molecule.[4] From this it follows that packing similarities between crystals of small molecules can primarily be attributed to directional interactions. A basic description of these similarities can be given by means of supramolecular synthons.[2,3] When similarities, expressed by synthons and/or the corresponding graph set notations,[5] extend to the three dimensional arrangement of the molecules, crystals may be homo- or even isostructural.[6,7] Present work demonstrates an inherent relationship between graph set notations, synthons and isostructurality.

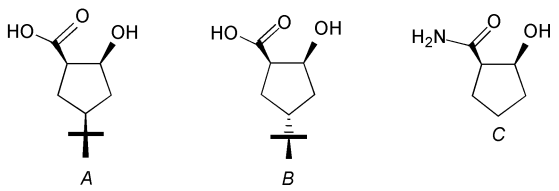

Crystal structures of three chemically-related small molecules *A*, *B* and *C* exemplify:

(1) a common tetrameric supramolecular synthon which establishes a genetical connection between the structures of diastereomers *A* and *B*. They crystallize with the two most frequently occurring space groups in CSD,[8] *i.e.* $P2_1/c$ (20%) and $P\bar{1}$ (35.5%).
(2) an unprecedented form of isostructurality discovered between the monoclinic ($P2_1/c$) structures of *B* and its *tert*-butyl-free derivative *C*. The isostructurality[6] of two small molecules differing substantially both in volume (by 33.5%) and shape forced us to reconsider the early view of Kitaigorodskii[9] on the conditions and limits of isomorphism.

The three crystal structures† **A**, **B** and **C** have a common OH···O=C (No. 1), and an alternative (O=C)–XH···OH (X = O for *A* and *B*, or NH for *C*) hydrogen bond (No. 2), respectively. In structure **C** there is an additional –NH···O=C(–$\underline{\text{N}}\text{H}_2$) hydrogen bond (No. 3). Structure **A**, with space group $P\bar{1}$, is composed from pairs of parallel and infinite rows of the 'all-*cis*' diastereomers *A* bound by the hydrogen bonds No. 1 [Fig. 1(A)]. Each row is homochiral and an enantiomer of the other. Each enantiomer pair is fused together by the No. 2 hydrogen bonds around an inversion center located at 0, ½, ½, closing a 12-membered ring described by graph set notation $R_2^2(12)$. This very closed pattern of the No. 1 and 2 hydrogen bonds topologically hinders the formation of the most common synthon **1**[2] between the well separated carboxyl groups. Instead of synthon **1** (Fig. 2), there is a second ring described by the $R_4^4(12)$ graph set notation which is enlarged by two additional –OH moieties from a third and fourth molecule,[10] respectively. This tetrameric synthon (Fig. 2) is located around the inversion center at ½, ½, ½ and repeated by unit translation.

The triclinic $P\bar{1}$ structure of diastereomer *A* is a *par excellence* case of the simplest molecular self-complementarity. Similarly, diastereomer *B* builds up a canonical structure with the most common space group $P2_1/c$. In structure **B** [Fig. 1(B)] hydrogen bonds No. 1 link the glide plane-related molecules parallel with the *c* axis. Pairs of parallel but folded and heterochiral rows are held together by the same tetrameric synthons recognized in the triclinic structure **A**. The $R_4^4(12)$ rings are closed around inversion centers at 0,0,0, 0,0, ½, *etc.* The 'homochiral parts' of this network are constructed by the No. 2 hydrogen bonds around the screw axes at 0,0,¼, 0,0,¾, *etc.*, forming infinite helices around the *b* axis. Thus, the infinite ribbons in structure **A** maintained by centres of inversion and

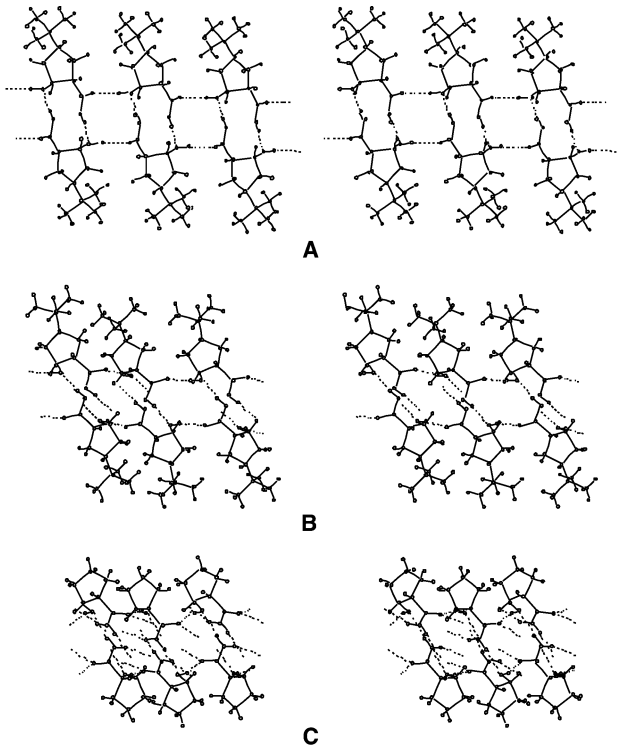

Fig. 1 Stereoview of the structures **A**, **B** and **C**. In **A**, projected in the (−1, −1,0) plane for clarity, hydrogen bonds form C(6) chains and $R_2^2(12)$ dimers. The generated $R_4^4(12)$ rings – identified as a tetrameric synthon – can also be recognized in structures **B** and **C** related by visible degree of isostructurality.

DOI: 10.1039/b005422o

translation are self-organized into 2D-stacks in structure **B** by the homochiral screw axes and heterochiral glide planes. They jointly generate centres of inversion surrounded by the supramolecular synthons **1***. From structure **A** it follows that the formation of this synthon is sterically preferred. *Mutatis mutandis* [*i.e.* $R_2^2(12)$ dimers of **A** are replaced by C(6) helices] this conclusion is also valid for structure **B**. This underscores the genetic relationship between these structures which can be regarded as *configurational* polymorphs.[11] The close relationship between their space groups $P\bar{1}$ and $P2_1/c$ is also shown[12] by migration and multiplication of pseudo-symmetries 2_1* and *c** in oblique unit cells with space group $P\bar{1}$ and $Z = 8$.

Interestingly, the higher ($P2_1/c$) and the lower ($P\bar{1}$) degree of self-complementarity exhibited by the *B* and *A* molecules equally result in the same packing coefficient[13] (0.68) for structures **B** and **A**. Nevertheless, the predominance of the monoclinic molecular array over a triclinic close packing is shown by the structure of molecule *C* [Fig. 1(C)]. It is a truncated (*i.e. tert*-butyl moiety-free) form of both diastereomers *A* and *B* and instead of a CO_2H group it possesses a $CONH_2$ moiety. However, **B** and **C** are homostructural[6,7] (Fig. 1) which implies that the tetrameric synthon is also retained. Naturally, owing to the OH $\rightarrow$ NH_2 replacement, now it is the enlarged form of the dimeric supramolecular synthon **3** (Fig. 2). From these it follows that the directional[4] hydrogen bond network in structure **B** is so stable that it survives the elimination of the bulky *tert*-butyl moiety. In other words, in special circumstances a small molecule such as *B* can maintain nearly isostructural close packing with an even smaller molecule *C*. Even the presence of an additional supramolecular synthon **4** (Fig. 2) built by hydrogen bond No. 3 cannot alter this pattern either.

The supramolecular synthon **1*** or **3*** is a common hallmark of the structural similarity shown by these related structures. It can be attributed to their special feature, *i.e.* two pairs of donor/acceptor functions maintaining the most common supramolecular cements, the OH···O and NH···O hydrogen bonds, which are located in the vicinal position on a small but flexible (pseudo-rotation) spacer. The *synclinal* position of the 1,2-*cis*-substituents on the flexible cyclopentane ring provides genuine steric conditions to the observed supramolecular arrangement.

This raises the question, how does the *cis*$\rightarrow$*trans* isomerization of the vicinal functions modify the close packing found in these structures? Moreover, how does the migration of the bulky *tert*-butyl moiety influence the pattern so stable in structure **B**? Modeling of structure **B** with molecules *A* revealed that such a packing is hindered by very short H···H contacts (*ca.* 1.15 Å). These and further questions will be answered in a full paper[14] to be published elsewhere.

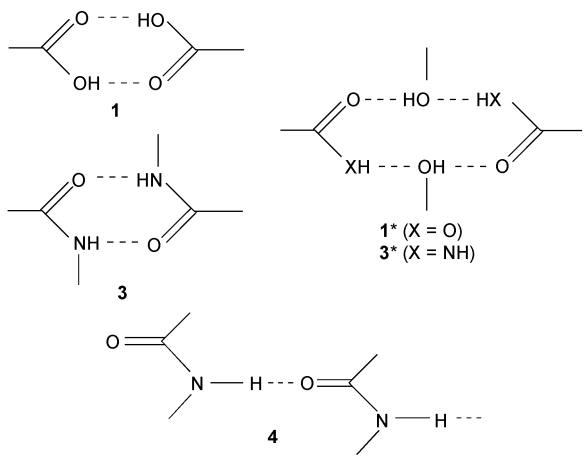

Fig. 2 The tetrameric synthon found in structures **A** and **B**. In **C**, $-CO_2H$ groups are replaced by –CONH moieties. **1**, **3** and **4** are the most common supramolecular synthons as labelled by Desiraju.[2]

Authors thank Professor G. Bernáth (University of Szeged, Hungary) for the crystals and acknowledge support of the Hungarian Research Fund (Grant No. OTKA T023212).

Notes and references

† *Crystal data*: Enraf-Nonius CAD-4, Mo-Kα radiation for **A**, Cu-Kα radiation for **B** and **C**.

For **A**: $C_{10}H_{18}O_3$, M = 186.24, colorless block, triclinic, space group $P\bar{1}$, a = 5.931(1), b = 6.200(1), c = 15.591(3) Å, α = 84.30(4), β = 89.97(4), γ = 62.28(4)°, V = 516.0(2) Å^3, Z = 2, D_c = 1.199 Mg m^{-3}, μ = 0.087 mm^{-1}, T = 293 K, $R(F^2)$ = 0.0477, $R(wF^2)$ = 0.1249, R_{tot} = 0.091, N_o = 2998, N_o/N_v = 24.2.

For **B**: $C_{10}H_{18}O_3$, M = 186.24, colorless block, monoclinic, space group $P2_1/c$, a = 16.862(2), b = 6.104(1), c = 10.519(3) Å, β = 107.03(4)°, V = 1035.2(4) Å^3, Z = 4, D_c = 1.195 Mg m^{-3}, μ = 0.704 mm^{-1}, T = 293 K, $R(F^2)$ = 0.0541, $R(wF^2)$ = 0.1415, R_{tot} = 0.0732, N_o = 2084, N_o/N_v = 16.6.

For **C**: $C_6H_{11}NO_2$, M = 129.16, colorless block, monoclinic, space group $P2_1/c$, a = 11.693(2), b = 7.225(1), c = 7.902(2) Å, β = 103.70(3)°, V = 648.6(2) Å^3, Z = 4, D_c = 1.323 Mg m^{-3}, μ = 0.819 mm^{-1}, T = 293 K, $R(F^2)$ = 0.0406, $R(wF^2)$ = 0.1238, R_{tot} = 0.0437, N_o = 1274, N_o/N_v = 15.2.

CCDC 182/1800. See http://www.rsc.org/suppdata/cc/b0/b005422o/ for crystallographic files in .cif format.

1 J.-M. Lehn, *Angew. Chem., Int. Ed. Engl.*, 1988, **27**, 89; J.-M. Lehn, *Angew. Chem., Int. Ed. Engl.*, 1990, **29**, 1304.
2 G. R. Desiraju, *Angew. Chem., Int. Ed. Engl.*, 1995, **34**, 2311.
3 G. R. Desiraju, *Chem. Commun.*, 1997, 1475.
4 A. Nangia and G. R. Desiraju, *Acta Crystallogr., Sect. A*, 1998, **54**, 934.
5 M. C. Etter,. *Acc. Chem. Res.*, 1990, **23**, 120.
6 A. Kálmán, L. Párkányi and Gy. Argay, *Acta Crystallogr., Sect. B*, 1993, **49**, 1039.
7 A. Kálmán and L. Párkányi, *Advances in Molecular Structure Research*, JAI Press, Greenwich, CT, 1997, vol.3, p.189.
8 F. H. Allen and O. Kennard, *Chem. Des. Autom. News*, 1993, **8**, 31.
9 A. I. Kitaigorodskii, *Organic Chemical Crystallography*, Consultants Bureau, New York, 1961, p. 222.
10 A search in CSD revealed *ca*. 70 entries incorporating $R_4^4(12)$ rings, *e.g.* in B. Ibragimov, K. Beketov, K. Makhkamov and E. Weber, *J. Chem. Soc., Perkin Trans. 2*, 1997, 1349; M. Sugahara, K. Sada and M. Miyata, *Chem. Commun.*, 1999, 293.
11 J. D. Dunitz and J. Bernstein, *Acc. Chem. Res.*, 1995, **28**, 193.
12 A. Kálmán and Gy. Argay, *Acta Crystallogr., Sect. B*, 1998, **54**, 877.
13 A. Gavezzotti, *J. Am. Chem. Soc.*, 1983, **105**, 5220.
14 A. Kálmán, L. Fábián, Gy. Argay, G. Bernáth and F. Fülöp, *Acta Crystallogr., Sect. B*, in press.

ChemComm

Can 4,4′-bipyridine *N*,*N*'-dioxide play the same important role as 4,4′-bipyridine in the construction of metal coordination networks and crystal engineering?†

De-Liang Long, Alexander J. Blake, Neil R. Champness* and Martin Schröder*

School of Chemistry, The University of Nottingham, University Park, Nottingham, UK NG7 2RD. E-mail: neil.champness@nottingham.ac.uk; M.Schroder@nottingham.ac.uk

Received (in Cambridge, UK) 15th August 2000, Accepted 2nd October 2000
First published as an Advance Article on the web

Various binding modes of 4,4′-bipyridine *N*,*N*′-dioxide (L) for crystal engineering are demonstrated in the complexes $[Zn(MeOH)_2L_3](SiF_6)\cdot 3MeOH$ and $[ZnL_6](NO_3)_2$, which include examples of M–L coordination bonds, hydrogen-bonding and π–π stacking interactions.

4,4′-Bipyridine and its analogues containing two 4-pyridyl donor units have been found to be useful bridging ligands in the construction of inorganic networks and crystal engineering, and this has resulted in a plethora of extended assemblies including helical networks and diamondoid, honeycomb, square-grid, ribbon, grid, T-shaped, ladder, brick wall and octahedral frameworks.[1,2] We demonstrated recently the use of 4,4′-bipyridine *N*,*N*′-dioxide (L) in the construction of lanthanide coordination polymers with unusual 2- or 3-D networks.[3] We now extend this work to d-block elements and confirm that L and related *N*-oxide ligands have enormous potential for the construction of unusual networks incorporating these metal ions. We report herein two Zn(II) complexes, $[Zn(MeOH)_2L_3](SiF_6)\cdot 3MeOH$ **1** and $[ZnL_6](NO_3)_2$ **2**, which contain *four* different connection modes of L *via* M–L coordination, hydrogen-bonding and π–π interactions. While **1** has a 3-D open-framework structure whose large pores accommodate methanol solvent molecules, **2** is a mononuclear complex which forms 2-D layers *via* extensive π–π stacking interactions.

Compounds **1** and **2** were prepared by mixing methanolic solutions of $Zn(SiF_6)$ or $Zn(NO_3)_2$, respectively, and 4,4′-bipyridine *N*,*N*′-dioxide.‡ Crystals of **1** were found to be unstable in air and decayed quickly *via* solvent loss. X-Ray analysis of **1** confirms a polymeric structure based on networks of six-coordinate Zn(II) centres linked by 4,4′-pyridine *N*,*N*'-dioxide ligands.§ The Zn(II) ions have an octahedral environment provided by four oxygen atoms from four different *N*-oxide ligands and two others from coordinated molecules of MeOH. The 4,4′-bipyridine *N*,*N*′-dioxide ligands bridge metal centres directly or through combinations of M–L coordination and hydrogen bonds in three distinct fashions A (A′), B and C as shown in Scheme 1 and Fig. 1. The 4,4′-bipyridine *N*,*N*′-dioxide ligands therefore sustain a 3D framework structure through *four* different linkages. If coordination bonds (A or A′) are taken into account alone the structure can be considered as having a two-dimensional brick-wall (6,3) topology. Linkages of type A and A′ propagate along the *a* and *b* axes, respectively, and are chemically equivalent but crystallographically different, the latter having an inversion centre at its midpoint. Ligand A is slightly bent, with the two pyridyl rings twisted by 17.9° and bridging two Zn(II) centres separated by 12.7 Å. Ligand A′ is planar by symmetry and bridges two Zn(II) centres lying 12.3 Å apart. Ligands adopting connection mode C modify the two-dimensional framework by joining the nodes at the centres of the long sides of the rectangle (*i.e.* across the centre of the "brick" in the brick-wall structure) to form a square grid network of (4,4) topology. Strong hydrogen-bonding is confirmed by the short O···O separation [2.571(7) Å] within the O–H···O unit in mode C. Ligands involved in connection mode B [O···O separation 2.652(6) Å] join sheets to build up a 3-D open network with channels of dimensions 10.2 × 14.2 Å extending along the *c* axis (Fig. 2).

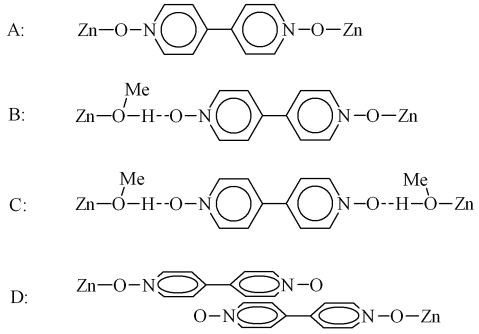

Scheme 1 Modes of connection observed in compounds **1** and **2**.

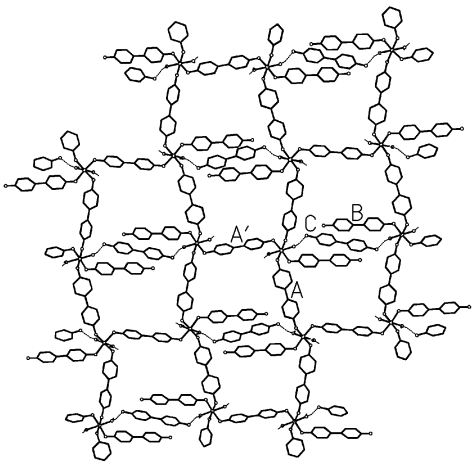

Fig. 1 View of the sheet observed in compound **1**. The $[SiF_6]^{2-}$ anion, methanol solvent molecules and hydrogen atoms are omitted for clarity.

4,4′-Bipyridine and its analogues containing two 4-pyridyl donor units can also adopt these coordination modes when forming complexes with either lanthanide[4,5] or d-block metals[6] but no examples of all three modes occurring in the same compound have been reported previously. The coexistence of three coordination modes for such a bidentate ligand is unique and indicates a real versatility in coordinative behaviour for *N*-oxide ligands.

Compound **2** is composed of discrete $[ZnL_6]^{2+}$ cations and uncoordinated nitrate anions. The Zn(II) centres are octahedral with a ZnO_6 environment, the six oxygen donors being derived from six different terminal 4,4′-bipyridine *N*,*N*′-dioxide ligands. The Zn(II) centre occupies a crystallographic inversion centre which results in three crystallographically independent ligands

† Electronic supplementary information (ESI) available: molecualr structures and labelling schemes for complexes **1** and **2**. See http://www.rsc.org/suppdata/cc/b0/b006679f/

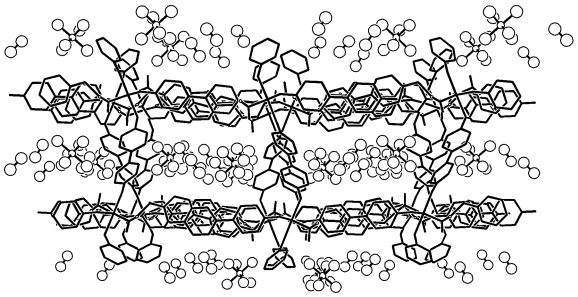

Fig. 2 View of the channels in compound **1**. Methanol solvent molecules and anions are highlighted by large open cycles. Hydrogen atoms are omitted for clarity.

with Zn–O bond lengths falling in the range 2.063(3)–2.109(3) Å, typical for Zn(II) complexes of pyridine *N*-oxide.[7] The pyridyl rings within each of these ligands are twisted with respect to each other, the twist angles ranging from 13.0 to 28.5°. To our knowledge this is the first example of a mononuclear complex of the 4,4′-bipyridine *N*,*N*′-dioxide ligand, which normally acts as a bridge between metal ions, either though M–L coordination or hydrogen bonds.[3]

Although all six 4,4′-bipyridine *N*,*N*′-dioxide ligands act as terminal ligands and the complex is mononuclear, an overall layered polymeric structure is observed for **2** *via* intermolecular π–π interactions. π–π Interactions have been used previously for the construction of coordination networks from discrete molecules,[8] but the mode found here is unique (Fig. 3). The six ligands are distributed alternatively in two planes around the Zn(II) centre so that the molecule has approximate D_{3h} symmetry. Each complex cation is involved in six ligand-to-ligand π–π interactions (mode D, Scheme 1) with six adjacent coplanar molecules to give an unprecedented (3,6) two-dimensional sheet. The plane/centroid distances for these π–π interactions are in the range 3.27–3.39 Å. It is important to note that the use of 4,4′-bipyridine *N*,*N*′-dioxide is crucial here; not only do the reduced steric requirements of the *N*,*N*′-dioxide ligand, compared with 4,4′-bipyridine, allow coordination of six ligands around the metal centre, but the angle subtended at the O-donor (the Zn–O–N bond angles for **2** range from 124.4 to 129.2°) is necessary to allow the construction of the two-dimensional sheet. These differences between donors based on bipyridine and those derived from bipyridine *N*,*N*′-dioxide are crucial to the differing roles they can play in coordination polymer chemistry.

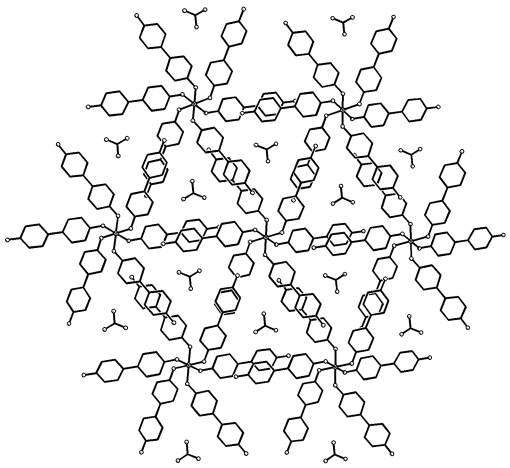

Fig. 3 View of the layer structure of (3,6) topology formed *via* π–π interactions in compound **2**. Hydrogen atoms are omitted for clarity.

Furthermore, comparison of the structures of **1** and **2** gives insight into the templating role of the anion in the construction of coordination polymer networks.[9] Thus for example in **2**, the nitrate anion appears to template the formation of a network of trigonal symmetry (Fig. 3) of specific stoichiometry. Efficient space-filling enables dense-packing to leave small trigonal holes that accommodate nitrate anions. Significantly, the formation of compound **2** is independent of M:L ratio, and is obtained even when a ratio of M:L ratio of 1:2 is used. The influence of the anion, therefore, appears significant enough to influence the oberved coordination of the bridging ligand and stoichiometry of the product isolated. Current works seeks to investigate further the binding of *N*-oxide ligands to d-, f-block and other elements.

This work is supported by the Royal Society K.C. Wong Fellowship and EPSRC. We acknowledge the use of the EPSRC National Service for crystallography at the University of Southampton.

Notes and references

‡ Preparation of $[Zn(MeOH)_2L_3](SiF_6)\cdot 3MeOH$ **1**: 4,4′-bipyridine *N*,*N*′-dioxide (22 mg, 0.10 mmol) in MeOH (6 cm^3) was carefully mixed with a solution of $ZnSiF_6\cdot 6H_2O$ (21 mg, 0.05 mmol) in MeOH (6 cm^3). The reaction gave a colourless crystalline product after several days. $[ZnL_6](NO_3)_2$ **2** was prepared similarly replacing $ZnSiF_6\cdot 6H_2O$ with $Zn(NO_3)_2\cdot 6H_2O$, colourless crystals growing over several days.

§ *Crystal data*: for **1**: $C_{35}H_{44}F_6N_6O_{11}SiZn$, M = 932.22, monoclinic, space group $P2_1/c$ (no. 14), a = 10.174(3), b = 28.313(5), c = 13.865(4) Å, β = 92.06 (3)°, U = 3991(2) $Å^3$, T = 150(2) K, Z = 4, μ(Mo-Kα) = 0.74 mm^{-1}. 7821 unique reflections of which 5277 with $F_o > 4\sigma(F_o)$. Final $R1$ [$I > 2\sigma(I)$] = 0.083, $wR2$ (all data) = 0.166.

For **2**: $C_{60}H_{48}N_{14}O_{18}Zn$, M = 1318.49, triclinic, space group $P\bar{1}$ (no. 2), a = 8.8202(9), b = 11.6805(10), c = 14.006(2) Å, α = 104.589(6), β = 96.265(6), γ = 99.082(6)°, U = 1326.1(3) $Å^3$, T = 150(2) K, Z = 1, μ(Mo-Kα) = 0.55 mm^{-1}. 6140 unique reflections (R_{int} = 0.099) of which 3378 with $F_o > 4\sigma(F_o)$. Final $R1$ [$I > 2\sigma(I)$] = 0.069, $wR2$ (all data) = 0.146.

CCDC 182/1795. See http://www.rsc.org/suppdata/cc/b0/b006679f/ for crystallographic files in .cif format.

1 M. A. Withersby, A. J. Blake, N. R. Champness, P. Hubberstey and M. Schröder, *Coord. Chem. Rev.*, 1999, **183**, 117.
2 O. M. Yaghi, H. Li, C. Davis, D. Richardson and T. L. Groy, *Acc. Chem. Res.*, 1998, **31**, 474.
3 D-L. Long, A. J. Blake, N. R. Champness and M. Schröder, *Chem. Commun.*, 2000, 1369 and references therein.
4 M. Bukowska-Strzyzewska and A. Tosik, *Inorg. Chim. Acta*, 1978, **30**, 189.
5 K. Al-Rasoul and T. J. R. Weakley, *Inorg. Chim. Acta*, 1982, **60**, 191.
6 G. D. Munno, D. Armentano, T. Poerio, M. Julve and J. A. Real, *J. Chem. Soc., Dalton Trans.*, 1999, 1813; A. J. Blake, S. J. Hill, P. Hubberstey and W-S. Li, *J. Chem. Soc., Dalton Trans.*, 1997, 913.
7 S. Jin, M. Nieuwenhuyzen and C. J. Wilkins, *J. Chem. Soc., Dalton Trans.*, 1992, 2071.
8 M. Munakata, L. P. Wu, M. Yamamoto, T. Kuroda-Sowa and M. Maekawa, *J. Am. Chem. Soc.*, 1996, **118**, 3117; O.M. Yaghi, H. Li and T. L. Groy, *Inorg. Chem.*, 1997, **36**, 4292; M. L. Tong, H. K. Lee, X-M. Chen, R-B. Huang and T. C. W. Mak, *J. Chem. Soc., Dalton Trans.*, 1999, 3657.
9 M. A. Withersby, A. J. Blake, N. R. Champness, P. Hubberstey, W. S. Li and M. Schröder, *Angew. Chem., Int. Ed. Engl.*, 1997, **36**, 2327.

Fluoroacetaldehyde: a precursor of both fluoroacetate and 4-fluorothreonine in *Streptomyces cattleya*

Steven J. Moss,[a] Cormac D. Murphy,[abc] John T. G. Hamilton,[b] W. Colin McRoberts,[b] David O'Hagan,*[ac] Christoph Schaffrath[ac] and David B. Harper*[b]

[a] *University of Durham, Department of Chemistry, Science Laboratories, South Road, Durham, UK DH1 3LE*
[b] *Microbial Biochemistry Section, School of Agriculture and Food Science, The Queen's University of Belfast, Newforge Lane, Belfast, UK BT9 5PX*
[c] *University of St. Andrews, School of Chemistry, Purdie Building, North Haugh, St. Andrews, Fife, UK KY16 9ST. E-mail: david.o'hagan@st-andrews.ac.uk*

Received (in Cambridge, UK) 7th September 2000, Accepted 2nd October 2000
First published as an Advance Article on the web

Fluoroacetaldehyde is converted to fluoroacetate and 4-fluorothreonine in *Streptomyces cattleya* indicating that it is the biosynthetic precursor of both of these secondary metabolites.

Organic compounds containing a C–F bond are extremely rare in living organisms; only about a dozen have been identified, the majority in plants.[1] Fluoroacetate (FAc) **1** is the most widespread fluorinated natural product and its biosynthesis in plants has been the subject of investigation and some speculation for the past 50 years. Despite this interest little progress has been achieved in elucidating the mechanism of fluorination or the metabolic route involved.[2] However the discovery that FAc **1** and L-4-fluorothreonine (4-FT) **2** are secondary metabolites of *Streptomyces cattleya* has provided a convenient microbial system in which to study the biosynthesis of the C–F bond.[3]

Our investigations into the origin of these metabolites in *S. cattleya*[4–7] have consistently shown that, in terms of magnitude and regiochemistry, isotope incorporations into C-1 and C-2 of FAc **1** always mirror those into C-3 and C-4 of 4-FT **2** from a given isotopically labelled precursor. This finding suggests a single fluorination enzyme in *S. cattleya*. As the possibility of direct conversion of one fluorometabolite to the other has been eliminated,[4,5] each fluorometabolite must therefore arise by further metabolism of a common fluorinated intermediate. We now report results which indicate that this metabolic precursor is fluoroacetaldehyde **3**.

An aqueous sample of fluoroacetaldehyde **3** was prepared by PDC oxidation of fluoroethanol in dichloromethane, followed by distillation of the volatiles into water. The preparation contained both fluoroacetaldehyde **3** and fluoroethanol (ratio ~1:3). The fluoroacetaldehyde was characterized as the DNP derivative.[8] Incubation of resting cells suspensions[7] of *S. cattleya* with the fluoroacetaldehyde preparation (2 mM with respect to fluoroacetaldehyde in 50 mM MES buffer, pH 6.5, containing 176 mg wet wt cells ml^{-1}) resulted in the efficient and almost stoichiometric conversion of fluoroacetaldehyde **3** to FAc **1** over a 3 h period (Scheme 1). Analysis of the culture supernatant by ^{19}F-NMR indicated that only the fluoroacetaldehyde **3** was converted to FAc **1**, the fluoroethanol remaining unmetabolised. Previous studies have demonstrated[5] that fluoroethanol is metabolically inert in *S. cattleya* and this was confirmed by control experiments with resting cells which did not reveal any oxidation of fluoroethanol to fluoroacetate. To further investigate the conversion of fluoroacetaldehyde **3** to FAc **1** cell-free extracts of *S. cattleya* were prepared with a French press. The extract oxidised fluoroacetaldehyde to fluoroacetate only in the presence of NAD^+ ($NADP^+$ was ineffective), demonstrating that an aldehyde dehydrogenase mediated the conversion. The purified enzyme[9] also oxidised acetaldehyde, chloroacetaldehyde, glycolaldehyde and propionaldehyde (34, 79, 116 and 30% of the enzyme activity with fluoroacetaldehyde respectively) indicating that *S. cattleya* possesses a relatively non-specific NAD^+-dependent aldehyde dehydrogenase which efficiently converts fluoroacetaldehyde **3** to FAc **1**.

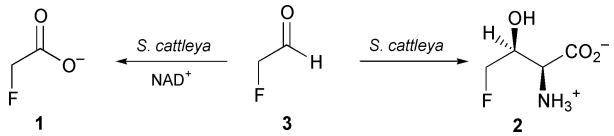

1 **3** **2**

Scheme 1

Sanada *et al.*[3] proposed that 4-FT **2** might arise by an aldol condensation between fluoroacetaldehyde and glycine, such that the latter contributes C-3 and C-4 of the amino acid. However, in experiments using [1-^{13}C]-, [2-^{13}C]- and [1,2-$^{13}C_2$]-glycine we have demonstrated[7] that glycine is not the condensing nucleophile as it is not incorporated directly into C-1 and C-2 of 4-FT **2**, so at present the origin of C-1 and C-2 of 4-FT **2** is unknown. Nevertheless fluoroacetaldehyde is an attractive precursor for C-3 and C-4 of 4-FT **2**. To establish a role for this compound in 4-FT **2** biosynthesis, its effect on 4-FT **2** production by resting cell suspensions of *S. cattleya* was measured by monitoring concentrations in culture supernatants using an HPLC assay.[10] The data from this experiment are presented in Fig. 1. When resting cell suspensions were incubated over a period of 6 h with the fluoroacetaldehyde–fluoroethanol preparation (176 mg wet wt cells ml^{-1} in 50 mM MES buffer pH 6.5, 2 mM fluoroacetaldehyde, 6 mM fluoroethanol), 4-FT **2** concentrations increased linearly with time ultimately attaining 49 μM. In suspensions with no supplementation or those incubated with 6 mM fluoroethanol alone, concentrations of 4-FT **2** did not exceed 7 μM after 6 h. Suspensions supplemented with 2 mM NaF (the optimal F^- concentration for fluorometabolite biosynthesis[4]) yielded 26 μM 4-FT **2** over the same time period. When 2 mM FAc **1** was

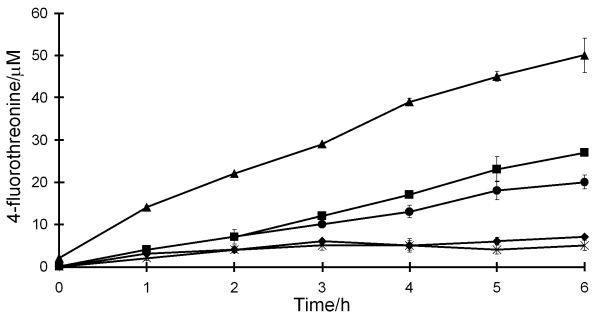

Fig. 1 L-4-Fluorothreonine **2** concentration in supernatant of resting cell suspensions of *S. cattleya* after addition of (a) fluoroacetaldehyde (2 mM)–fluoroethanol (6 mM) (▲); (b) NaF (2 mM) (■); (c) fluoroacetate (2 mM) (●); (d) fluoroethanol (6 mM) (**x**); (e) no supplementation (⧫). Data determined by HPLC analysis.[10] Error bars indicate the SD of triplicate samples.

DOI: 10.1039/b007261n

incubated with cell suspensions a slight enhancement of 4-FT **2** biosynthesis was observed (19 μM after 6 h). As previous investigations involving incubation of [$^2H_2$]-fluoroacetate with cell suspensions of *S. cattleya* had demonstrated no direct conversion of FAc **1** to 4-FT **2**, this increase can probably be attributed to defluorination of FAc **1** and subsequent *de novo* synthesis of 4-FT **2** from F^-. Such cell suspensions are known to have a limited defluorinating activity with FAc **1**.[5] Thus fluoroacetaldehyde clearly stimulates 4-FT **2** biosynthesis in *S. cattleya* almost doubling the rate recorded in suspensions incubated under optimal F^- concentrations, an enhancement which is not explicable in terms of metabolism *via* fluoroethanol or fluoroacetate.

The biosynthetic relationship between fluoroacetaldehyde **3** and 4-FT **2** was further investigated using [1-$^2H_1$]-fluoroacetaldehyde **3a**, a synthesis of which was developed, by an adaptation of a previously reported synthetic route for isotopically labelled ethanol[11] (Scheme 2). The [1-$^2H_1$]-fluoroacetaldehyde preparation contained 5% [1,2-$^2H_2$]-fluoroacetaldehyde as an impurity. [1-$^2H_1$]-Fluoroacetaldehyde **3a** was administered as above to cell suspensions of *S. cattleya* and the incorporation of deuterium into C-3 of 4-FT **2** was monitored by GC-MS[12] over time.

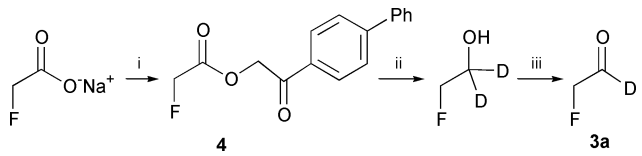

Scheme 2 i. *p*-Phenylphenacyl bromide, 18-crown-6, acetonitrile–toluene (1:1); ii. LiAl^2H_4, diethyl ether, 2-phenoxyethanol quench, distillation; iii. PDC, diethyl ether–dichloromethane (1:9).

The GC-MS data presented in Table 1 show substantial incorporation of a single ^2H atom into (C-2+C-3+C-4) of 4-FT **2** after 7 h. This label can only reside on the C-3–C-4 fragment of 4-FT **1** as there is no significant labelling at C-2. During the same time period there was also a small but significant incorporation (1.7%) of two ^2H atoms into these positions of the amino acid. It is revealing that the ratio of *M*+1:*M*+2 for (C-3+C-4) directly reflects the ratio (~20:1) of $^2H_1$:$^2H_2$ label in the fluoroacetaldehyde administered to the cells. Similar results were obtained for the samples incubated for 20 h. These findings provide compelling evidence that fluoroacetaldehyde **3** is incorporated as an intact unit into C-3 and C-4 of 4-FT **2**. Interestingly the incubation of resting cell suspensions with 0.25 mM chloroacetaldehyde resulted in the detection in the supernatant of small quantities of an amino acid with a mass spectrum similar to that predicted for 4-chlorothreonine.[13] This observation provides further support for the participation of fluoroacetaldehyde in an aldol condensation leading to 4-FT **2** biosynthesis.

Table 1 ^2H Incorporation into 4-FT **2** after labelled fluoroacetaldehyde ([1-^2H]-, 95%; [1,2-$^2H_2$]-, 5%) was incubated with resting cell suspensions of *S. cattleya*. The data are corrected for natural abundances. Means and standard deviations were obtained from 10 replicate analyses

	^2H-Incorporation (%)			
	(C-1+C-2)		(C-2+C-3+C-4)	
Incubation time (h)	M+1	M+2	M+1	M+2
7	< 0.5	< 0.5	33.5 ± 0.09	1.7 ± 0.05
20	< 0.5	< 0.5	22.4 ± 0.10	1.2 ± 0.04

In conclusion we have demonstrated that cell free extracts of *S. cattleya* contain a fluoroacetaldehyde dehydrogenase which efficiently converts fluoroacetaldehyde to FAc **1**. Fluoroacetaldehyde also markedly enhances the biosynthesis of 4-FT **2** by resting cells of *S. cattleya*. Furthermore incubation of resting cells with ^2H-labelled fluoroacetaldehyde indicates incorporation of the compound as an intact unit into C-3 and C-4 of 4-FT **2**. These observations are consistent with a role for fluoroacetaldehyde as the common intermediate in the biosynthesis of both fluorometabolites and it may emerge that fluoroacetaldehyde is the immediate post fluorination product.

We thank the BBSRC and BNFL for financial support and Dr Harold Eccles of BNFL and Dr Roy Bowden of F2-Chemicals for useful discussions.

Notes and references

1 D. O'Hagan and D. B. Harper, *J. Fluorine Chem.*, 1999, **100**, 127.
2 D. B. Harper and D. O'Hagan, *Nat. Prod. Rep.*, 1994, **11**, 4.
3 M. Sanada, T. Miyano, S. Iwadare, J. M. Williamson, B. H. Arison, J. L. Smith, A. W. Douglas, J. M. Liesch and E. Inamine, *J. Antibiotic.*, 1986, **39**, 259.
4 K. A. Reid, R. D. Bowden and D. B. Harper, in *Naturally Produced Organohalogens*, eds. A. Grimvall and E. W. B. de Leer, Kluwer Academic Publishers, Dordrecht, 1995, pp. 269-279.
5 K. A. Reid, J. T. G. Hamilton, R. D. Bowden, D. O'Hagan, L. Dasaradhi, M. R. Amin and D. B. Harper, *Microbiology*, 1995, **141**, 1385.
6 J. Nieschalk, J. T. G. Hamilton, C. D. Murphy, D. B. Harper and D. O'Hagan, *J. Chem. Soc., Chem. Commun.*, 1997, 799.
7 J. T. G. Hamilton, C. D. Murphy, M. R. Amin, D. O'Hagan and D. B. Harper, *J. Chem. Soc., Perkin Trans. 1*, 1998, 759.
8 A dinitrophenylhydrazine (DNP) derivative of fluoroacetaldehyde **3** was prepared by adding the aqueous solution of fluoroacetaldehyde to the DNP solution and the resultant precipitate filtered and recrystallised from ethanol. Melting point: 143–144 °C; ^1H NMR δ_H (400 MHz, $CDCl_3$): 11.17 (1H, s, N*H*), 9.14 (1H, s, (C-3)-*H*), 8.36 (1H, m, (C-5)-*H*), 7.98 (1H, m, (C-6)-*H*), 7.64 (1H, dd, $^3J_{HH}$ = 5.2 Hz, $^3J_{HF}$ = 10.4 Hz, (C-7)-*H*), 5.17 (2H, dd, $^2J_{HF}$ = 46.4 Hz, $^3J_{HH}$ = 5.2 Hz, (C-8)-*H*); δ_C (100 MHz, $CDCl_3$): 80.9 (C-8, d, $^1J_{CF}$ = 166.4 Hz), 114.6 (C-6), 123.2 (C-3), 130.1 (C-5), 138.9 (C-7), 143.5 (C–NO_2), 143.7 (C–NO_2), 144.7 (C-1); δ_F (376 MHz, $CDCl_3$): −222.61 (dt, $^2J_{FH}$ = 46.4 Hz, $^3J_{FH}$ = 6.4 Hz); HRMS (EI) $C_8H_7FN_4O_4$: Calculated (M^+) 242.04513, found 242.0451.
9 Details of the purification of this enzyme will be reported elsewhere.
10 4-FT **2** in culture supernatants was determined using a fluorimetric HPLC procedure similar to that described by L. A. Sternson, J. F. Stobaugh and A. J. Repta *Anal. Biochem.*, 1985, **144**, 233. Precolumn derivatisation with *o*-phthalaldehyde–mercaptopropionic acid reagent was followed by elution from a reversed phase HPLC column. The detection limit of the method was 2 μM in the culture supernatant.
11 D. E. Cane, T.-C. Laing and H. Hasler, *J. Am. Chem. Soc.*, 1982, **104**, 7274.
12 For studies of incorporation of ^2H into 4-FT the per-trimethylsilylated derivative was prepared and analysed by GC-MS.[7] The MS was employed in the selected ion monitoring mode measuring ion currents at *m/z* 218 (M), 219 (M+1) and 220 (M+2) for incorporation onto (C-1+C-2) and at *m/z* 236 (M), 237 (M+1) and 238 (M+2) for incorporation onto (C-2+C-3+C-4).
13 GC-EIMS data for per-trimethylsilyl derivative of 4-chlorothreonine: *m/z* = 218 (100), 252 (45), 254 (15), 73 (38), 116 (14), 147 (10), 354 (3), 356 (1). 4-Chlorothreonine has been reported as a metabolite of *Streptomyces* sp. OH–5093 by H. Yoshida, N. Arai, M. Sugoh, J. Iwabuchi, K. Shioiomi, M. Shinose, Y. Tanaka and S. Omura, *J. Antibiot.*, 1994, **47**, 1165.

Typeset and printed by Black Bear Press Limited, Cambridge, England

ChemComm
FEATURE ARTICLE

Watching solids crystallise using *in situ* powder diffraction

Richard I. Walton† and Dermot O'Hare*

Inorganic Chemistry Laboratory, South Parks Road, Oxford, UK OX1 3QR. E-mail: dermot.ohare@chem.ox.ac.uk

Received (in Cambridge, UK) 26th September 2000, Accepted 17th October 2000
First published as an Advance Article on the web 9th November 2000

The study of the chemical processes that occur during the synthesis of inorganic solids has attracted much recent attention. The ultimate aim of these experiments is the atomic level understanding of reaction mechanisms which lead to the formation of extended inorganic solids, so that rational design of new materials can be achieved. Solid-state syntheses are typically performed under non-ambient temperature and pressures in sealed containers so specialised apparatus must be constructed to allow us to directly probe these reaction mixtures. We review the use of *in situ* powder diffraction to investigate the formation of crystalline solids in real time, and discuss the latest developments in the technology required for these challenging experiments.

1 Introduction

The study of inorganic solid-state chemistry has seen a renaissance in the last 20 years, which has in the most part been brought about by the introduction of new techniques for structural elucidation (CCD cameras for crystallography data collection, and new solid-state NMR techniques, for example), and the investigation of new preparative methods (in particular *chimie douce* methods, such as hydrothermal chemistry and sol–gel techniques).[1,2] An astonishing diversity of novel materials is presently being prepared and characterised, as evidenced by the large numbers of published reports of new inorganic solids. These materials can have technologically valuable properties such microporosity, photophysical properties, electrochemical activity, superconductivity and magnetic behaviour, and thus research in solid-state inorganic chemistry can have significant application focus. A pressing aim of the fundamental research in this area is a quantitative knowledge of the mechanism of nucleation and growth of inorganic solids; this understanding would allow the rational design of new materials for application in the same way that the organic chemist is able to synthesise a complex molecule by use of specific starting materials and reaction conditions. The difficulty in the rational design of new solids is largely due to the lack of mechanistic data currently available, *i.e.* a quantitative understanding at an atomic level of the chemical processes leading to the formation of solids. This is perhaps not too surprising since many materials crystallise from complex heterogeneous mixtures held at elevated pressures or temperatures in sealed, thick-walled reaction vessels.

This article is concerned with recent developments in the use of powder diffraction techniques to follow the course of the synthesis of inorganic solids *in situ* under real reaction conditions. Diffraction clearly is an appropriate technique when following the formation of a crystalline solid and as we will demonstrate, in addition to obtaining qualitative information about the course of a reaction and phase identification at each step, time-resolved diffraction techniques allow quantitative kinetic information to be extracted, since the intensity of a Bragg reflection is directly proportional to the amount of diffracting solid. This information is the first step in being able to postulate reaction mechanisms.

In order to measure powder diffraction data from a reacting mixture of chemicals at non-ambient temperatures (and often pressures) the design and construction of specialised apparatus is required. Powder diffraction patterns of solids under non-ambient temperatures have been recorded since the earliest days of X-ray diffraction,[3] and the construction of furnaces for use in diffraction experiments has been well reviewed.[4] Such high temperature diffraction techniques are now routinely used to investigate the phase transitions and thermal stability of solids, but when the requirement to reproduce real reaction conditions is introduced, for example the use of a solvent or a reactive gas atmosphere, greater constraints are placed upon the experiment. The three most important points to consider when constructing a reaction cell for *in situ* powder diffraction studies are that: (i) the intensity of the radiation used must be high enough to achieve good signal:noise in the diffraction data above diffuse scatter of the amorphous components (solvent for example), (ii) the radiation must be able to penetrate the cell walls and not be obstructed by bulky heating devices or pressure containment, and (iii) the experiment must be optimised to enable rapid data acquisition for kinetic studies. We will limit our discussion to such apparatus, and select examples of experiments that best

† Present address: School of Chemistry, Stocker Road, University of Exeter, Exeter, UK EX4 4QD.

Richard Walton completed his BA degree in Chemistry at the University of Oxford in 1994 after research with Dr A. M. Chippindale into open-framework gallium phosphates which was awarded a university undergraduate thesis prize. In 1997 he received his PhD from the University of Reading following research with Dr S. J. Hibble into the structure of amorphous transition-metal chalcogenides. The same year he returned to Oxford to undertake postdoctoral research with Professor O'Hare on the use and development of in situ *powder diffraction techniques. He has recently been appointed to a university lecturership in Inorganic Chemistry at the University of Exeter.*

Dermot O'Hare obtained his first degree in Chemistry from the University of Oxford in 1982 and then remained at Oxford for his D.Phil under the supervision of Malcolm Green, where he worked on carbon–hydrogen bond activation using metal atom chemistry. In 1990 he was appointed to a University Lectureship in Inorganic Chemistry and Septcentenary Tutorial Fellowship at Balliol College in 1990. His current interests span a wide range of inorganic chemistry from synthetic molecular organometallic chemistry through to solid state chemistry. He received the RSC's Sir Edward Frankland Fellowship in 1996–97. In 1998, he received the RSC Corday–Morgan Medal and Prize and the Exxon Chemicals European Science and Engineering award.

DOI: 10.1039/b007795j

illustrate the various *in situ* diffraction techniques currently in use. We begin our article by briefly discussing recent experiments performed using laboratory X-ray diffractometers, before considering experiments performed at synchrotron X-ray sources and at neutron sources.

2 *In situ* diffraction using laboratory X-ray sources

Many modern laboratory diffractometers can be readily modified to enable data to be collected at elevated temperatures, and some of the commercially available environmental chambers can be adapted for the study of the formation of crystalline inorganic solids. Environmental cells for studying the reactions between mixtures of gases and solids or simply solid-solid reactions have been most commonly described. For example Gavra and McMurray constructed a furnace to study gas/solid reactions at temperatures of up to 300 °C and pressures of 50 atm,[5] and used the cell to study the reaction between $EuNi_5$ and H_2 *in situ* at pressure of up to 50 atm, directly observing the formation of crystalline $EuNi_5H_{5.5}$, a material of potential use for hydrogen storage.[6] Samples were contained in 0.3 mm quartz capillaries. A more robust cell has been described by Puxley *et al.*; their apparatus could operate at temperatures of up 1000 °C using a larger amount of solid placed on a flat plate.[7] Data were collected from catalysts under reactive active gas atmospheres, and during the solid-state reaction between SnO_2 and Bi_2O_3. Another good example of the monitoring of a solid-state reaction in the laboratory with powder diffraction is the work of Bondioli *et al.* who studied the formation of the ferroelectric material $BaTiO_3$ from TiO_2 and $BaCO_3$ as a function of temperature up to 1200 °C. They were able to show that $BaTi_2O_4$ is present as a metastable phase at lower temperatures, and proposed a stepwise course of reaction.[8] A recent example of the use of a laboratory diffractometer to follow the formation of an inorganic material form a liquid medium was described by Rathousky *et al.* who followed the precipitation of the mesoporous silica MCM-41.[9] This study was performed at room temperature from a liquid/solid mixture in a *ca.* 0.5 mm^3 container. A small *d*-spacing region of diffraction data was monitored at 130 s intervals, allowing the appearance of the characteristic low-angle diffraction peak of MCM-41 to be monitored in real time.

Lindén *et al.* also studied the formation of mesoporous MCM-41 in the laboratory, using an ingenious tubular reactor in which reagents were mixed and allowed to flow along the apparatus through an X-ray diffraction cell.[10] By varying the length of the tube, or flow rate, samples of material could be studied *in situ* after different periods of reaction. Although meaningful kinetic data would be difficult to determine using this method, the measurement of diffractograms of material under real conditions allows the time-scale of reaction to be judged efficiently, even for reactions taking place on in sort times (less than 3 minutes for MCM-41). Mechanistic insight was possible for the case of the MCM-41 preparation, since under reaction conditions the material was observed to be less condensed than on isolation since on removal of hydration water de-swelling takes place.

These selected examples of the use of laboratory X-ray diffraction to follow chemical reactions illustrate that simple reaction cells can be constructed and mechanistic inferred during the formation of inorganic solids using readily available apparatus. In general, however, even with the best available rotating anode X-ray sources the time resolution is low (data must be collected on time-scales of minutes) and so it is difficult to extract accurate quantitative kinetic information. In addition, the limited range of X-ray energies available from laboratory diffractometers places severe limits of the amount of sample that can be studied and the size of reaction chamber used, because high levels of X-ray absorption greatly affects the quality of data that may be obtained from the sample within the cell. A point to bear in mind is that when scaling reactions down to very small quantities, genuine laboratory reactions conditions may no longer be reproduced. Problems in sampling a representative small portion of a mixture of reagents could arise, especially when mixtures of solids and liquids are studied, giving rise to results that are difficult to reproduce and/or interpret. Nevertheless laboratory diffractometer-based studies play a valuable rôle; they are readily available and provide a straightforward means to begin mechanistic of reactions producing solid materials.

3 *In situ* diffraction using synchrotron X-ray sources

3.1 Monochromatic radiation (angular dispersive diffraction)

Synchrotron-generated X-rays typically have intensity up to 10 orders of magnitude greater than the most brilliant laboratory-generated X-rays, Fig. 1. The high flux of X-rays from a synchrotron allows diffraction experiments to be performed using bulky sample containers since significant attenuation of the incident beam can be tolerated. Another advantage of synchrotron-generated radiation is that X-rays with short wavelengths (and hence high energies) can be utilised; these are less absorbed than higher wavelength X-rays, and so are useful when sample containers are must be penetrated. The experimental geometry of the experiments which use monochromatic synchrotron-generated X-rays are virtually identical to any laboratory diffractometer, but the time taken to record a diffraction pattern, especially when a static position-sensitive detector is used so that all data are accumulated simultaneously, is dramatically shortened; reactions can be followed in milliseconds rather than minutes.

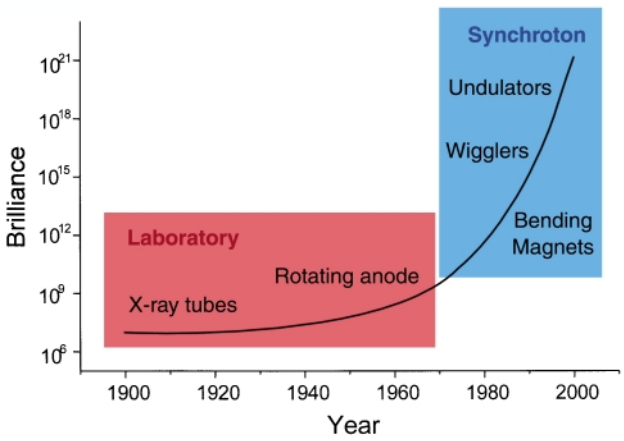

Fig. 1 A schematic of the historical development of available brilliance of X-rays from different sources. Brilliance is defined as number of photons per second per square millimetre per square milliradain per 0.1% bandwidth).

As with the experiments already discussed, much work using synchrotron X-rays has concentrated on the reactions between solids and gases, or solid-solid reactions. Good examples of such experiments are those by Larsen and co-workers who designed a cell to enable self-propagating high-temperature syntheses to be followed in time intervals as short as 10 ms.[11,12] Blocks of solid reagents (*ca.* 0.01 cm^3) are electrically ignited by a tungsten coil and the solid combustion reactions generate temperatures of up to 4000 K; diffraction data are measured by two fixed-angle detectors, each positioned to monitor an area of interest in the diffractogram. The technique has been used to

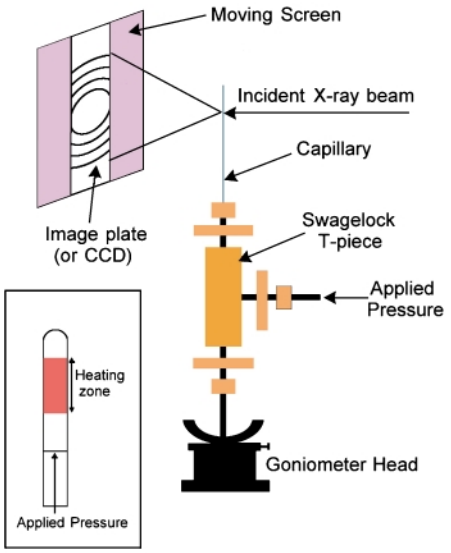

Fig. 2 A schematic of the apparatus developed by Norby and coworkers for time-resolved diffraction studies of hydrothermal crystallisations. The inset shows an enlargement of the capillary.

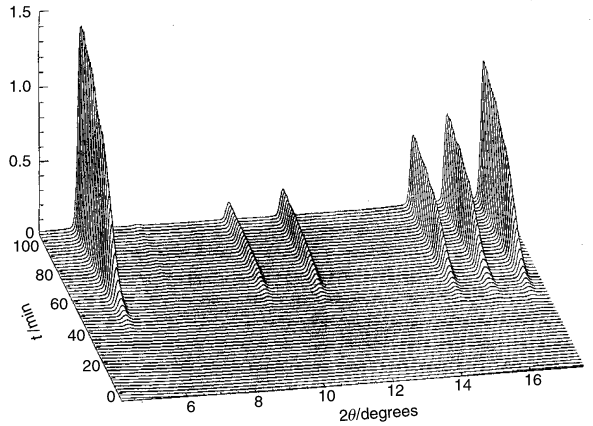

Fig. 3 Time-resolved diffraction patterns measured during the crystallisation of CoAPO-5, a microporous cobalt aluminophosphate from an amorphous gel by Norby and Hanson. Data were recorded at 200 °C in 1 min intervals. Figure reproduced with permission from ref. 19.

study syntheses of the carbide TaC.[13] and the ferroelectric $BaTiO_3$.[14] In the former case, the course of reaction was followed at 50 ms intervals and the material was observed to form *via* Ta_2C from Ta and C, with a total reaction time of only 50 s. This is a dramatic illustration of the power of synchrotron techniques for *in situ* studies of chemical reactions.

Norby *et al.* have developed in the last five years a synchrotron X-ray diffraction cell for study the hydrothermal crystallisation of inorganic materials.[15] This apparatus, Fig. 2, uses a quartz capillary as a sample container, pressure is applied externally to balance the pressure generated during a reaction and a 5 mm part of the tube heated by a hot air flow (up to 250 °C when pressures of 45 atm may be produced). Rapid data collection is made possible by use of a novel translating image plate detector. High resolution angular dispersive data are extracted by scanning the image plate after each experiment. Integration of the image plate data typically gives time resolution of 1–2 minutes.[16] Norby and his collaborators have used the apparatus to great effect in the study of the crystallisation of metal-substituted aluminium phosphates,[17–20] materials with useful catalytic properties. Fig. 3 shows typical diffraction data measured using the technique; in this case the crystallisation of CoAPO-5, a microporous cobalt aluminium phosphate from an amorphous gel.[19] As well as direct observation of the time-scale of reaction, these measurements allowed the determination of quantitative kinetic data by monitoring the area of a Bragg reflections with time and such data analysis has enabled rate constants to be determined, and kinetic models for these crystallisations to be proposed.[18,20] The same hydrothermal apparatus has also been used to follow the crystallisation of aluminosilicate zeolites[21,22] and a microporous manganese germanium sulfide.[23] Gross *et al.* used a similar cell to investigate the stability of silica/surfactant nanocomposites, precursors to mesoporous silicas when heated under hydrothermal conditions at 180 °C.[24]

The hydrothermal capillary apparatus has very recently been developed further to allow reactions under more extreme conditions to be studied. By using high energy X-rays ($\approx$35 keV, $\lambda \approx 0.32$ Å) generated at the European Synchrotron Radiation Facility, France and at Brookhaven National Laboratory, USA, Norby *et al.* showed that it is possible to penetrate a steel capillary.[25] Time-resolved diffraction data were measured at 350 °C, 200 atm during the transformation of a zeolite into a dense aluminosilicate. The *in situ* diffraction patterns obtained were of sufficient quality to allow structural information to be extracted by using the Reitveld method; such detailed structural characterisation of materials under reaction conditions is vital for understanding their properties.

3.2 Polychromatic radiation (energy-dispersive diffraction)

Synchrotron-generated X-rays are produced with high intensity over a wide energy range (typically 10 to 120 keV). This unique feature obviously offers the possibility of selection of a specific X-ray wavelength for any given diffraction experiment, but also the opportunity to perform powder diffraction experiments in the energy dispersive mode, utilising all the incident X-ray flux in a single experiment. In the energy-dispersive X-ray diffraction (EDXRD) experiment the intensity spectrum of scattered X-rays from the sample is measured by a fixed-angle solid-state photon counting and energy discriminating detector, and each Bragg reflection is characterised by an energy which is dependent on the angle of the detector.[26] Since no monochromation is employed and only minimal collimation of the incident X-ray beam is used, the flux incident on the sample is high (*ca.* 10^{10} photons s^{-1}) and of sufficient intensity and energy to probe large volume samples in thick-walled reaction vessels. The geometry is particularly suitable for the use of environmental cells, since the fixed-angle detector means that only small windows are necessary for the passage of X-rays through the apparatus so devices with heaters or bulky pressure containment can easily be constructed.[27] The EDXRD method is widely used for the study of the pressure induced phase-transitions of inorganic solids where very confined cells are used,[28] but because data acquisition can be performed in times of the order of seconds the technique is also very useful for kinetic studies. One particular merit of the EDXRD technique is that reactions cells can be 'laboratory-sized', identical in design to apparatus used in preparative chemistry, so that more realistic, bulk reaction conditions are mimicked; this is in contrast to the techniques discussed in section 2.1, which use scaled-down reaction cells to minimise absorption.

Barnes and coworkers have pioneered the use of EDXRD for the study of chemical reactions, and have followed the reactions involved in the hydration of calcium silicate cements on time-scales down to 0.3 s per diffraction pattern.[29–31] These workers also first described the use of EDXRD methods to follow hydrothermal crystallisations. They designed a reaction cell made from the high performance polymer PEEK, that allowed use at temperatures up to 100 °C. They were able to monitor the crystallisation of sodalite, a dense aluminosilicate zeolite, from the layered material kaolinite and determined crystallisation curves describing extent of reaction as a function of time.[32] The hydrothermal formation of the large pore aluminophosphate VPI-5 was also studied by these workers using the EDXRD

method.[33] The operating temperature of this early cell was limited by its design and the performance characteristics of the PEEK cell material. We have subsequently described the construction of a large-volume hydrothermal reaction cell from which EDXRD data may be collected at up to 250 °C, more typical of the temperatures used in hydrothermal synthesis.[34] This reaction cell is virtually identical in design and construction to the 23 mL Parr hydrothermal autoclaves widely used in many research laboratories, but the steel walls of the cell are thinned to 0.3 mm to minimise absorption of X-rays, Fig. 4 The

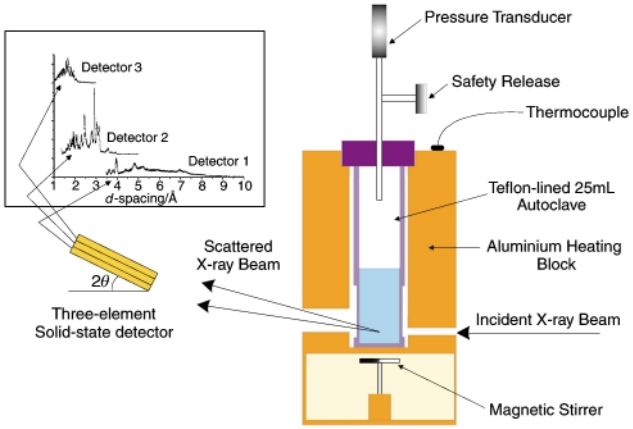

Fig. 4 A schematic of the Oxford/Daresbury hydrothermal autoclave used for energy-dispersive X-ray diffraction studies, developed by us for use on Station 16.4 of the UK synchrotron source at Daresbury Laboratory.

Oxford/Daresbury hydrothermal cell has been used on Station 16.4 of the Daresbury SRS, the UK synchrotron radiation source, to study the crystallisation of a wide range of inorganic materials by several groups. The cell has been much used for studying the formation of microporous solids; our group has studied the formation of porous layered tin sulfides,[35] open-framework gallium fluorophosphates,[36–38] and zeolites,[39,40] and Thomas and coworkers have used the cell to study the formation of transition-metal substituted aluminophosphates.[41–43] One important observation we have made during the study of the crystallisation of gallium fluorophosphates is that under certain reaction conditions previously unknown intermediate crystalline phases are observed to form before the onset of the crystallisation of the expected microporous phase, Fig. 5. For

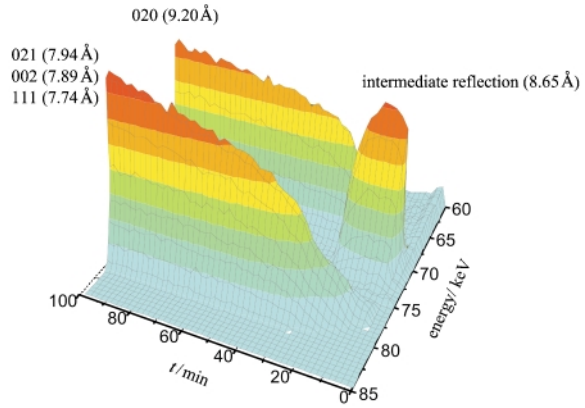

Fig. 5 A small part of energy-dispersive X-ray diffraction data (30 s intervals) measured *in situ* during the crystallisation of the open-framework gallium fluorophosphate ULM-3 from an amorphous phosphate gel at 180 °C. The use of P_2O_5 as a reagent results in the formation of a previously unknown crystalline intermediate phase before the onset of crystallisation of the product.

the case of the microporous phase ULM-3, a transient crystalline intermediate is only stable under hydrothermal conditions; if the reaction cell is allowed to cool when the intermediate is present, transformation into another, as yet unidentified, phase takes place.[38] This is a dramatic illustration of the need to study reactions under real conditions, and of how quenching experiments are not always a reliable method of determining the species present at reaction conditions. In this particular case it has subsequently lead us to discover some new related metastable gallium fluorophosphates.[44,45]

In addition to the direct observation of crystallisation on a short time-scale, the *in situ* EDXRD method has allowed much new information about the kinetics of the crystallisation of microporous solids to be determined. By determination of changing Bragg peak areas, it is possible to extract quantitative kinetic information, since the intensity of a Bragg reflection is directly proportional to the amount of diffracting solid.[46] Fig. 6,

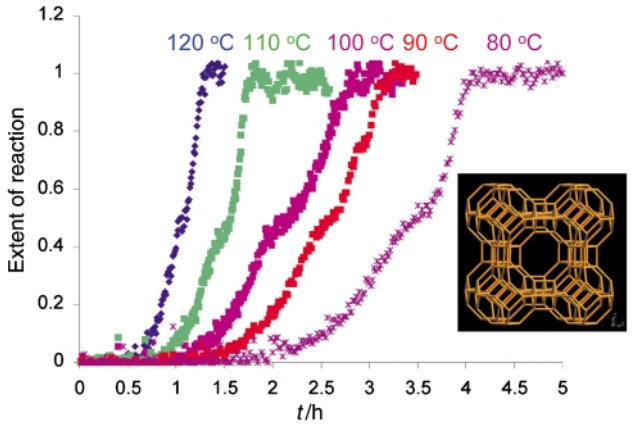

Fig. 6 Crystallisation curves for sodium aluminosilicate zeolite A (inset) determined using the *in situ* EDXRD technique. Diffraction patterns were collected every 30 s while an amorphous aluminosilcate gel was heated in the autoclave.

for example, shows crystallisation curves we have recently obtained from a study of the hydrothermal formation of sodium zeolite A, one of the most widely used microporous materials in many industries.[40] The unusual two-step crystallisation curve has never been reported previously, and was only revealed by continuous monitoring of the reaction with high time resolution (30 s per diffraction pattern). The effect is highly dependent on reaction conditions and is believed to arise from dissolution of an amorphous precursor gel controlling the rate of reaction. Such an observation sheds new light on zeolite crystallisation, and these measurements using EDXRD on short time scales will provide new data for computer modelling studies, and ultimately mechanistic information. A recent development in the use of *in situ* EDXRD is the installation of a three element solid-state photon counting, energy discriminating detector on Station 16.4 of the SRS;[47,48] this allows three *d*-spacing regions of the powder diffraction pattern to be measured simultaneously and permits unambiguous phase identification, which has been particularly useful in the study of microporous materials.[49]

As well as the studying the formation of microporous materials, the Oxford/Daresbury hydrothermal autoclave has been used by other groups to monitor the formation of inorganic solids. Cahill *et al.* studied the formation of iron sulfides using the cell, and were able to establish a pathway of progressive sulfidation of FeS to FeS_2.[50] Shaw *et al.* recently studied the hydrothermal formation of calcium silicate minerals; this study was performed at the Advanced Photon Source, USA, which offers *ca.* 10 times greater X-ray flux than the SRS, enabling reactions to be performed in cells with thicker walls, and consequently at temperatures of up to 330 °C.[51]

EDXRD has been used by our group in Oxford to study the formation and behaviour of a wide range of other inorganic solids. Time-resolved EDXRD studies of intercalation reactions of layered solids have been very important in understanding their mechanism, and this area has recently been reviewed.[52,53] We have also investigated the kinetics and mechanism of formation mesoporous silicas and the different growth mechanism for MCM-41 *versus* the mesoporous silicate FSM-16,

which is derived from kanemite,[54] and of the crystallisation of gibbsite,[55] an important material in aluminium manufacture. The *in situ* EDXRD method is clearly easily extended to following reactions under conditions more extreme conditions than the hydrothermal reactions discussed above, with simple modification of furnace design. We have very recently described the construction of a furnace that operates at 1000 °C and from which EDXRD data can be measured.[56] We have studied the formation of some dense metal oxides at *ca.* 800 °C, both by a traditional ceramic methods using the carbonates of the constituent metals, and by a molten-salt method in liquid alkali-metal halide fluxes. We were able to follow the decay of starting materials, and subsequent growth of the layered perovskite $RbCa_2Nb_3O_{10}$ and show the enhancement of crystallisation rate in the alkali-metal flux.[56] Parkin *et al*. have recently begun a study of self-propagating high-temperature reactions (SHS) using EDXRD on Station 16.4 at the SRS. To study these reactions they have pushed the data collection intervals down to just 100 ms.[57] They also studied the effects of a magnetic field on these reactions using EDXRD.

In summary we anticipate that further advances in apparatus design are likely to follow shortly, and allow reactions over a wide spectrum of temperatures and pressures to be followed by EDXRD.

4 *In situ* diffraction using neutron sources

The complementarity of neutron diffraction and X-ray diffraction for the structural characterisation of materials is well known, in particular the use of neutron diffraction to locate light atoms in the presence of heavy atoms, especially hydrogen atoms, and in the determination of the spin arrangement of magnetically ordered materials.[58] In the context of performing *in situ* diffraction studies, neutron diffraction offers distinct advantages over many of the X-ray diffraction experiments. For example, many materials have very low neutron absorption cross-sections which means that reaction vessels can be constructed which give rise to low backgrounds in diffraction data. Processes involving light atoms, such as reactions involving water can be followed. In additon, use of time-of-flight neutron diffraction with fixed-angle detectors would simplify apparatus construction. One disadvantage of neutron diffraction is the much lower flux available from currently available neutron sources at present compared to synchrotron X-ray sources; this means that at present the time resolution of time-resolved neutron diffraction experiments is relatively poor (of the order of minutes rather than sub-second), but recent development in the area shows the great promise of the method.

Pannetier is well known for his many time-resolved neutron diffraction studies of chemical reactions;[59] he and his coworkers have concentrated on fairly simple systems, such as hydration reactions,[60] and the reactions of solids with gases.[61] Christensen and coworkers performed an extensive study of the reactions between silicates and water under moderate temperatures (up to *ca.* 120 °C) using *in situ* neutron diffraction and were able to measure diffraction data in periods as short as 5 minutes.[62–66] The same workers also performed the first *in situ* neutron diffraction study of a hydrothermal crystallisation, in this case the formation of iron(III) oxides from amorphous iron hydroxides at 120 °C.[67] They were able to measure crystallisation curves and efficiently monitor the effect of experimental parameters on reaction rate. When performing neutron diffraction studies, it is usual to use deuterated reagents to minimise the large incoherent scattering of protons, however the use of protonated reagents can reveal additional information. For example Tuttillas *et al.* studied the calcination of zirconium hydroxide, used to prepare zirconia, with *in situ* powder neutron diffraction at the Institut Laue Langevin (ILL). They were able to detect a massive decrease in background when dehydration was complete (and all protons were lost from the reagents) allowing one step of the reaction to be pinpointed.[68]

Polak *et al.* described the design of an autoclave to allow the acquisition of neutron diffraction data during the hydrothermal crystallisation of tobermorite, a calcium silicate used in cements, and of some zeolites.[69] The cell could operate at temperatures of up to 250 °C, and external pressure was applied. One draw-back of this cell design was the dominance of the Bragg reflections due to the sample containment (aluminium with a Teflon liner) in the measured diffraction data; this could severely limit the amount of structural information available. Our recent work, in collaboration with colleagues at ISIS, the UK neutron spallation source, on the use of neutron diffraction to follow hydrothermal crystallisations has resulted in the design and construction of a novel null-scattering environmental cell from which time-resolved diffraction data can be measured at temperatures of up to 250 °C and pressures of 20 atm.[70] The cell (Fig. 7) is constructed from a Ti-Zr alloy whose

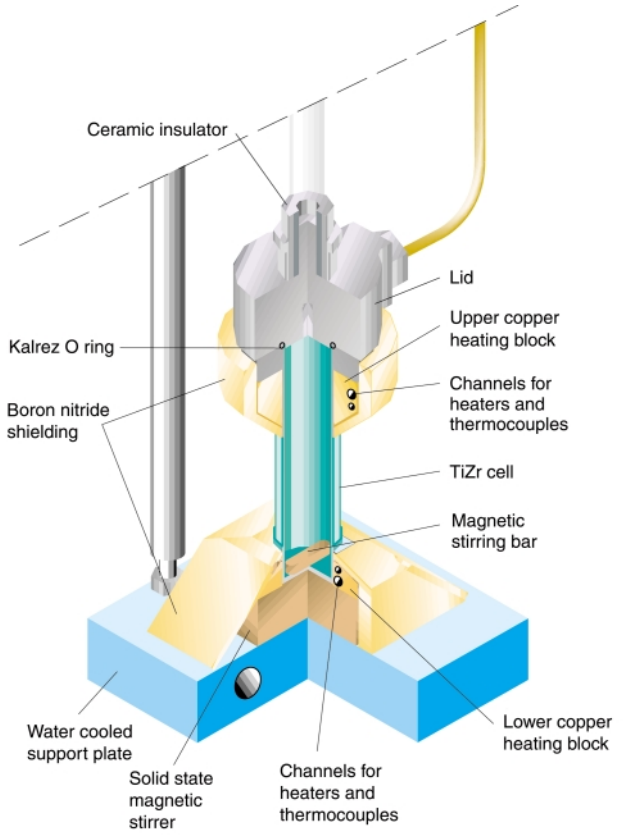

Fig. 7 Schematic of the Oxford/ISIS hydrothermal reaction cell for *in situ* neutron powder diffraction measurements.

component metals are mixed in such a ratio as to cancel their negative (Ti 67.7 atom %, $b = -3.44$ fm) and positive (Zr 32.3 atom%, $b = 7.16$ fm) neutron scattering lengths. The cell is protected from corrosive reagents by a thin internal layer of gold metal, thus the cell is invisible to neutrons and can contain reactive mixtures of solids and liquids. We have commissioned the Oxford/Isis hydrothermal cell on the medium-resolution high-flux diffractometer POLARIS initially and most recently have tested it on GEM, a new neutron diffractometer with a large array of detectors which allows rapid data collection.[71] Our first experiments have addressed the hydrothermal formation of barium titanate, an important ferroelectric material used in the electroceramics industry.[72] The industry requires the crystallisation of the phase pure tetragonal polymorph. The presence of the highly X-ray absorbing barium ions in the sample mixture meant that it was impossible to study this system even using synchrotron X-ray diffraction. However, using *in situ* neutron diffraction we were able to observe directly the dissolution of both the crystalline starting materials, TiO_2

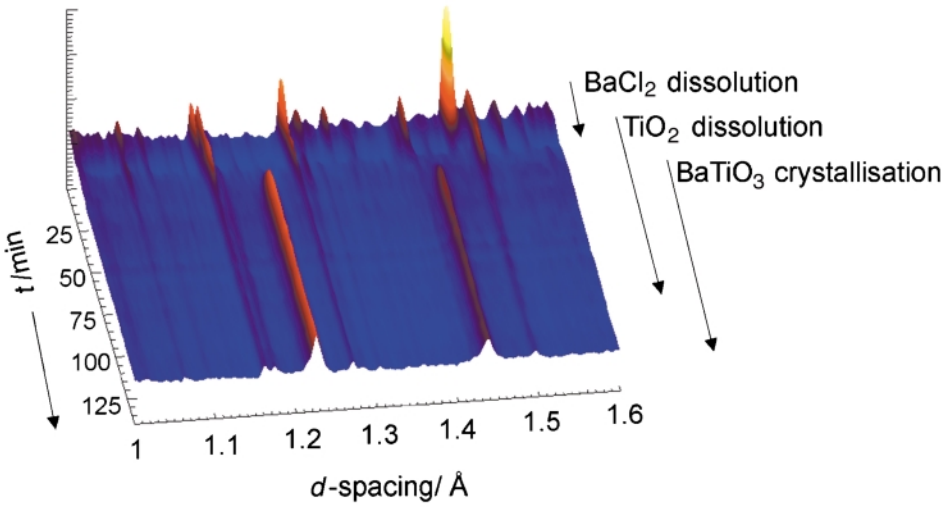

Fig. 8 *In situ* neutron diffraction data measured during the formation of the ferroelectric barium titanate from $BaCl_2$ and TiO_2 in NaOD solution at 200 °C. Data were collected at 5 min intervals using the GEM diffractometer at ISIS.

and $Ba(OD)_2{\cdot}8D_2O$, before the onset of crystallisation of $BaTiO_3$. This allowed us to conclude that a dissolution–precipitation mechanism predominates, rather than a heterogeneous transformation mechanism. Fig. 8 shows *in situ* neutron diffraction data measured using GEM where data were collected in 5 min intervals. As well as the new mechanistic insights, we were able to measure high resolution diffraction data that are suitable for Reitveld profile analysis, Fig. 9. This is a step

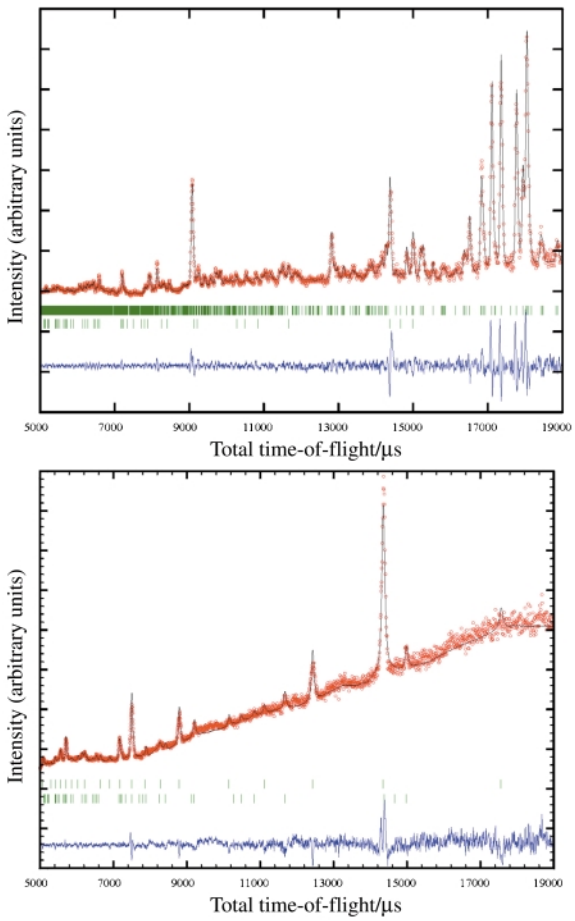

Fig. 9 Neutron diffraction data measured *in situ* during the hydrothermal formation of $BaTiO_3$ from $Ba(OD)_2.8D_2O$ and TiO_2 (a) after 15 min, and (B) after 12 h.

forward in *the in situ* study of hydrothermal reactions, and shows the potential use of neutron diffraction in real time structural determination of crystalline solids under laboratory reaction conditions. We have most recently used the Oxford/ISIS hydrothermal cell to study the formation of some aluminosilicate zeolites, the archetypal materials synthesised hydrothermally. We have followed the crystallisation of sodium zeolite A and monitored its collapse into the dense phase hydroxosodalite.[73]

Other recent highlights in the use of powder neutron diffraction to monitor the formation of inorganic solids include following the crystallisation of superconductors from melt-cast precursors,[74] and a study of the reaction between Nd/Fe/V alloys and nitrogen at 800 °C.[75] In the latter study data were collected in around 5 min intervals, and were of sufficient quality to perform Reitveld refinement, and allowed structural determination *in situ*. This study was performed using the recently constructed D20 diffractometer at the ILL, which offers a combination of high neutron flux and high count rate by a novel large surface area position-sensitive detector.[76] Undoubtedly this instrument will lead to many more kinetic studies of solid-state reactions in the coming years.

5 *In situ* powder diffraction combined with spectroscopic probes

The *in situ* diffraction techniques described above yield information about the growth and decay of crystalline ordered materials during the course of a chemical reaction. As the above discussion demonstrates, these methods allow the course of reactions to be observed in real time, including the detection of crystalline intermediate phases, and kinetic information can be determined. Bragg diffraction, however, does not probe any amorphous phases present. For instance no information about the changing local atomic structure of the gel-precursor to zeolites in a hydrothermal crystallisation is obtained. In order to achieve the monitoring of both long-range crystallographic order and short-range atomic order, several ingenious experiments have been designed, combining *in situ* diffraction with spectroscopic methods. The most powerful of these methods is the use of combined X-ray absorption fine structure spectroscopy and X-ray diffraction (XAFS/XRD). This was first described by Couves *et al.* in 1991,[77] and has since been used to monitor various reactions involving solids such as solid-state transformations,[78–80] polymerisations,[81] thermal decompositions,[82,83] and widely used for monitoring catalytic processes under operating conditions.[84,85] High-intensity synchrotron generated X-rays are required for such studies.

Fig. 10 shows the arrangement of a typical XAFS/XRD experiment. This set-up was used by Sankar *et al.* to follow the formation of a microporous cobalt aluminophosphate from an amorphous gel.[86] XRD data were measured for 220 s, followed

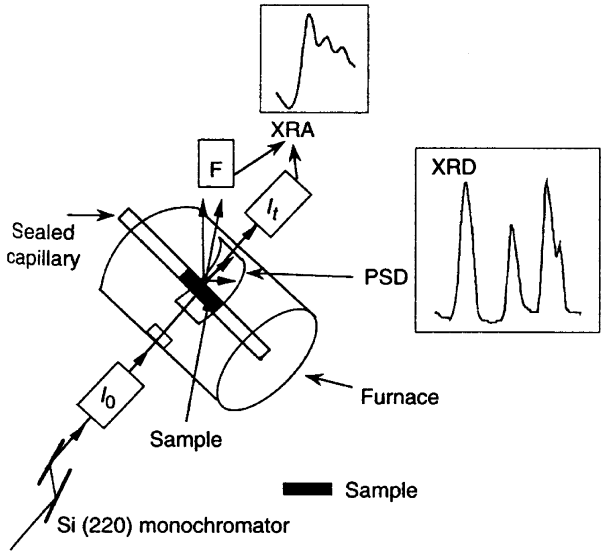

Fig. 10 A schematic of the XAFS/XRD experiment used to follow the crystallisation of a cobalt aluminophosphate. Figure reproduced with permission from ref. 86.

by XAFS data at the cobalt K-edge for the same time (alternation between the two measurements is necessary as the XRD data are acquired with a constant wavelength whilst the XAFS data require a scan over a wavelength range). Changes in the local environment of cobalt were monitored, and related to the changes in long range order apparent in the diffraction pattern, Fig. 11. It was thus shown that the coordination of

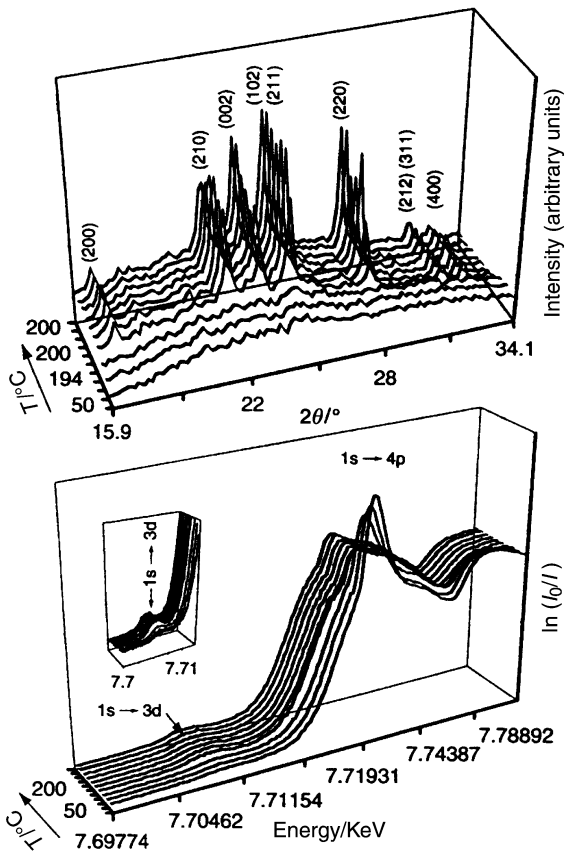

Fig. 11 XRD (top) and Co K-edge EXAFS (bottom) recorded during the crystallisation of CoALPO-5 at 180 °C from an amorphous gel. Figure reproduced with permission from ref. 86.

cobalt changes from octahedral to tetrahedral in the gel immediately prior to crystallisation. The same apparatus was also used to follow the formation of a bismuth molybdate catalyst from a precursor gel,[87] and of small particles of cadmium oxide from a hydroxy gel.[88] In both cases monitoring changes in local atomic environment and relating them to crystallographic order allowed new insights into the reaction mechanism.

6 Conclusions and outlook

The measurement of powder diffraction data during the synthesis of many inorganic materials requires the design and construction of specialised apparatus, but in the last five years much progress has been made. The experiments we have surveyed here represent in most cases the first attempts to determine kinetic and mechanistic information about reactions involving the formation of solids from heterogeneous media. The reactivity and structures of solids under non-ambient conditions have been probed directly for the first time. As is apparent from our review, the most impressive advances have been made in the area of hydrothermal chemistry, with several groups developing apparatus that are now widely used on a routine basis to follow directly the crystallisation of a range of porous materials with useful properties. This undoubtedly reflects the fact that hydrothermal chemistry has found to be an incredibly fertile method for the synthesis of new inorganic solids, and is currently used to prepare a diversity of materials from new zeolitic solids[89] to metastable metal oxides.[90] Given the success in using powder diffraction to follow hydrothermal crystallisations, extension of the methodology to other preparative methods is likely to follow shortly; systems such as alkali-metal–chalcogenide fluxes[91] and solvothermal synthesis in alcohols or amines[92] which are currently the focus of attention in synthetic solid-state chemistry.

With the now almost routine measurements of the course of solid-state reactions, a large amount of kinetic data has been accumulated, as well as much qualitative information about the course of reaction and identification of intermediates. Analysis of these data is one of the first steps in proposing reaction mechanisms, but clearly much more work is required in this new field before the rational design of new materials is possible. Computer modelling will undoubtedly have an important rôle in understanding the data obtained by the techniques we have reviewed, and is an area which is developing rapidly; for example the early stages of the formation of zeolite has been modelled in some detail recently and the energetics of these solution-mediated reactions calculated,[93] and the prediction of the structures of new solids using computer-modelling techniques is currently the focus of much attention.[94,95]

In this article we have emphasised how recent progress in the use of *in situ* powder diffraction methods has been intimately linked to developments at synchrotron and neutron sources. The availability of high intensity synchrotron-generated X-rays over a wide energy range and the design of new neutron diffractometers to enable rapid data collection has instigated many of the experiments we have described. As well as the continued use of the experiments already in use, new developments are likely to enable other new experiments to be designed and realised. In many parts of the world new synchrotron and neutron sources are being constructed, including a third-generation synchrotron source in the UK to replace the SRS, and a new spallation neutron source at Oak Ridge USA. These will offer increasingly higher fluxes of radiation and the possibility of rapid data collection; features vital for the future development of *in situ* powder diffraction methods.

7 Acknowledgements

We thank our many colleagues and collaborators who have been involved in the work we have performed in the field of time-resolved diffraction; in particular the instrument scientists at the Daresbury and Rutherford Laboratories who have made much of our work possible. We thank the Leverhulme Trust and

EPSRC for the award of research grants for this work and which has allowed us access to the CLRC laboratories.

8 References

1 C. N. Rao and J. Gopalakrishnan, *New Directions in Solid State Chemistry*, Cambridge University Press, Cambridge, 1997.
2 A. K. Cheetham and P. Day, *Solid State Chemistry: Compounds*, Clarendon Press, 1992.
3 A. Westgren, *J. Iron Steel Inst.*, 1921, **103**, 303.
4 P. Aldebert, *Rev. Phys. Appl.*, 1984, **19**, 649.
5 Z. Gavra and J. J. Murray, *Rev. Sci. Instrum.*, 1986, **57**, 1590.
6 Z. Gavra, J. J. Murray, L. D. Calvert and J. B. Taylor, *J. Less Common Met.*, 1985, **105**, 291.
7 D. C. Puxley, G. D. Squire and D. R. Bates, *J. Appl. Crystallogr.*, 1994, **27**, 585.
8 K. Bondioli, A. Bonamartini-Corradi, A. M. Ferrari, T. Manfredini and G. C. Pellacani, *Mater. Sci. Forum*, 1998, **278**–**281**, 379.
9 J. Rathousky, G. Schulz-Ekloff, J. Had and A. Zukal, *Phys. Chem., Chem. Phys.*, 1999, **1**, 3053.
10 M. Lindén, S. A. Schunk and F. Schüth, *Angew. Chem., Int. Ed.*, 1998, **37**, 821.
11 J. Wong, E. M. Larson, J. B. Holt, P. A. Waide, B. Rupp and R. Frahm, *Science*, 1990, **249**, 1407.
12 E. M. Larson, P. A. Waide and J. Wong, *Rev. Sci. Instrum.*, 1991, **62**, 53.
13 E. M. Larson, J. Wong, J. B. Holt, P. A. Waide, G. Nutt, B. Rupp and L. J. Terminello, *J. Mater. Res.*, 1993, **8**, 1533.
14 E. M. Larson, J. Wong, J. B. Holt, P. A. Waide and B. Rupp, *Powder Diffraction*, 1999, 111.
15 P. Norby, A. N. Christensen and J. C. Hanson, *Stud. Surf. Sci. Catal.*, 1994, **84**, 179.
16 P. Norby, *J. Appl. Crystallogr.*, 1997, **30**, 21.
17 A. N. Christensen, P. Norby and J. C. Hanson, *Acta Chem. Scand.*, 1997, **51**, 249.
18 A. N. Christensen, T. R. Jensen, P. Norby and J. C. Hanson, *Chem. Mater.*, 1998, **10**, 1688.
19 P. Norby and J. C. Hanson, *Catal. Today*, 1998, **39**, 301.
20 P. Norby, A. N. Christensen and J. C. Hanson, *Inorg. Chem.*, 1999, **38**, 1216.
21 A. Gualtieri, P. Norby, G. Artioli and J. Hanson, *Microporous Mater.*, 1997, **9**, 189.
22 A. Gualtieri, P. Norby, G. Artioli and J. Hansen, *Phys. Chem. Miner.*, 1997, **24**, 191.
23 C. L. Cahill, Y. Ko, J. C. Hansen, K. Tan and J. B. Parise, *Chem. Mater.*, 1998, **10**, 1453.
24 A. F. Gross, E. J. Ruiz and S. H. Tolbert, *J. Phys. Chem. B*, 2000, **104**, 5448.
25 P. Norby, J. C. Hanson, A. N. Fitch, G. Vaughan, L. Flaks and A. Gualtieri, *Chem. Mater.*, 2000, **12**, 1473.
26 B. C. Giessen and G. E. Gordon, *Science*, 1968, **159**, 973.
27 S. M. Clark, A. Nield, T. Rathbone, J. Flaherty, C. C. Tang, J. S. O. Evans, R. J. Francis and D. O'Hare, *Nucl. Instrum Methods B*, 1995, **97**, 98.
28 J. B. Parise, D. J. Weidner, J. Chen and R. C. Liebermann, *Ann. Rev. Mater. Sci.*, 1998, **28**, 349.
29 P. Barnes, S. M. Clark, D. Hausermann, E. Henderson, C. H. Fentiman, M. N. Muhamad and S. Rashid, *Phase Transitions*, 1992, **39**, 117.
30 A. C. Jupe, X. Turrillas, P. Barnes, S. L. Colston, C. Hall, D. Hausermann and M. Hanfland, *Phys. Rev. B*, 1996, **53**, 14 697.
31 P. Barnes, S. L. Colston, B. Craster, C. Hall, A. Jupe, S. Jacques, J. Cockcroft, S. Morgan, M. Johnson, D. O'Connor and M. Bellotto, *J. Synchrotron Radiat.*, 2000, **7**, 167.
32 J. Munn, P. Barnes, D. Hausermann, S. A. Axon and J. Klinowski, *Phase Transitions*, 1992, **39**, 129.
33 H. Y. He, P. Barnes, J. Munn, X. Turrillas and J. Klinowski, *Chem. Phys. Lett.*, 1992, **196**, 267.
34 J. S. O. Evans, R. J. Francis, D. O'Hare, S. J. Price, S. M. Clarke, J. Flaherty, J. Gordon, A. Nield and C. C. Tang, *Rev. Sci. Instrum.*, 1995, **66**, 2442.
35 R. J. Francis, S. J. Price, J. S. O. Evans, S. O'Brien, D. O'Hare and S. M. Clark, *Chem. Mater.*, 1996, **8**, 2102.
36 R. J. Francis, S. J. Price, S. O'Brien, A. M. Fogg, D. O'Hare, T. Loiseau and G. Férey, *Chem. Commun.*, 1997, 521.
37 R. J. Francis, S. O'Brien, A. M. Fogg, P. S. Halasyamani, D. O'Hare, T. Loiseau and G. Férey, *J. Am. Chem. Soc.*, 1999, **121**, 1002.
38 R. I. Walton, T. Loiseau, D. O'Hare and G. Férey, *Chem. Mater.*, 1999, 3201.
39 R. I. Walton and D. O'Hare, *J. Phys. Chem. B*, in press.
40 R. I. Walton, F. Millange, D. O'Hare, A. T. Davies, G. Sankar and C. R. A. Catlow, *J. Phys. Chem. B*, in press.
41 F. Rey, G. Sankar, J. M. Thomas, P. A. Barrett, D. W. Lewis, C. R. A. Catlow, S. M. Clark and G. N. Greaves, *Chem. Mater.*, 1995, **7**, 1435.
42 F. Rey, G. Sankar, J. M. Thomas, P. A. Barrett, D. W. Lewis, C. R. A. Catlow, S. M. Clark and G. N. Greaves, *Chem. Mater.*, 1996, **8**, 590.
43 A. T. Davies, G. Sankar, C. R. A. Catlow and S. M. Clark, *J. Phys. Chem. B*, 1997, **101**, 10 115.
44 R. I. Walton, F. Millange, A. L. Bail, T. Loiseau, C. Serre, D. O'Hare and G. Férey, *Chem. Commun.*, 2000, 203.
45 R. I. Walton, F. Millange, D. O'Hare, C. Paulet, T. Loiseau and G. Férey, *Chem. Mater.*, 2000, **12**, 1977.
46 H. P. Klug and L. E. Alexander, *Diffraction Procedures for Polycrystalline and Amorphous Materials*, John Wiley, 1974.
47 P. Barnes, A. C. Jupe, S. L. Colston, S. D. Jacques, A. G. T. Rathbone, M. Miller, S. M. Clark and R. J. Cernik, *Nucl. Instrum. Methods Phys. Res. Sect. B*, 1998, **134**, 310.
48 S. L. Colston, S. D. M. Jacques, P. Barnes, A. C. Jupe and C. Hall, *J. Synchrotron Radiat.*, 1998, **5**, 112.
49 G. Muncaster, A. T. Davies, G. Sankar, C. R. A. Catlow, J. M. Thomas, S. L. Colston, P. Barnes, R. I. Walton and D. O'Hare, *Phys. Chem. Chem. Phys.*, 2000, **2**, 3523.
50 C. L. Cahill, L. G. Benning, H. L. Barnes and J. B. Parise, *Chem. Geol.*, 2000, **167**, 53.
51 S. Shaw, S. M. Clark and C. M. B. Henderson, *Chem. Geol.*, 2000, **167**, 129.
52 J. S. O. Evans, S. J. Price, H. V. Wong and D. O'Hare, *J. Am. Chem. Soc.*, 1998, **120**, 10 837.
53 D. O'Hare, J. S. O. Evans, A. M. Fogg and S. O'Brien, *Polyhedron*, 2000, **19**, 297.
54 S. O'Brien, R. J. Francis, S. J. Price, D. O'Hare, S. M. Clark, N. Okazaki and K. Kuroda, *J. Chem Soc., Chem. Commun.*, 1995, 2423.
55 J. S. C. Loh, A. M. Fogg, H. R. Watling, G. M. Parkinson and D. O'Hare, *Phys. Chem., Chem. Phys.*, 2000, **2**, 3597.
56 M. J. Geselbracht, R. I. Walton, E. S. Cowell, F. Millange and D. O'Hare, *Rev. Sci. Instrum.*, 2000, in press.
57 I. P. Parkin, Q. A. Pankhurst, L. Affleck, M. D. Aguas and M. V. Kuznetsov, *J. Mater Chem.*, 2000, in press.
58 A. K. Cheetham and A. P. Wilkinson, *Angew. Chem., Int. Ed. Engl.*, 1992, **31**, 1557.
59 J. Pannetier, *Chem. Scr.*, 1985, **26A**, 131.
60 W. Abriel, K. Reisdorf and J. Pannetier, *J. Solid State Chem.*, 1990, **85**, 23.
61 V. Paul-Boncour, C. Lartigue, A. Percheron-Guegan, J. C. Achard and J. Pannetier, *J. Less-Common Met.*, 1988, 143.
62 A. N. Christensen, M. S. Lehman and J. Pannetier, *J. Appl. Crystallogr.*, 1985, **18**, 170.
63 A. N. Christensen, H. Fjellvag and M. S. Lehmann, *Acta Chem. Scand. Ser. A*, 1985, **39**, 593.
64 A. N. Christensen, H. Fjellvag and M. S. Lehmann, *Acta. Chem. Scand. Ser. A*, 1986, **40**, 127.
65 A. N. Christensen, H. Fjellvag and M. S. Lehmann, *Cement Concrete Res.*, 1986, **16**, 871.
66 A. N. Christensen, H. Fjellvag and M. S. Lehmann, *Acta Chem. Scand. Ser. A*, 1988, **42**, 117.
67 A. N. Christensen, P. Convery and M. S. Lehamnn, *Acta Chem. Scand. Ser. A*, 1980, **34**, 771.
68 X. Turrillas, P. Barnes, S. E. Tarling, S. L. Jones, C. J. Norman and C. Ritter, *J. Mater. Sci. Lett.*, 1993, **12**, 223.
69 E. Polak, J. Munn, P. Barnes, S. E. Tarling and C. Ritter, *J. Appl. Crystallogr.*, 1990, **23**, 258.
70 R. I. Walton, R. J. Francis, P. S. Halasyamani, D. O'Hare, R. I. Smith, R. Done and R. Humpreys, *Rev. Sci. Instrum.*, 1999, **70**, 3391.
71 W. G. Williams, R. M. Ibberson, P. Day and J. E. Enderby, *Physica B*, 1997, **241**, 234.
72 R. I. Walton, R. I. Smith, F. Millange, I. J. Clark, D. C. Sinclair and D. O'Hare, *Chem. Commun.*, 2000, 1267.
73 R. I. Walton, R. I. Smith and D. O'Hare, 2000, submitted to *Microporous Mesoporous Mater*.
74 P. S. Whitfield, J. R. Bhakta, J. S. Abell, R. I. Smith and R. Cywinski, *Rev. Sci. Instrum.*, 1998, **69**, 2475.
75 P. Oleinek, O. Isnard, P. Convert, K.-H. Muller, M. Loewenhaupt and L. Schultz, *J. Alloys Compd.*, 2000, **298**, 220.
76 P. Convert, T. Hansen, A. Oed and J. Torregrossa, *Physica B*, 1998, **241**–**243**, 195.

77 J. W. Couves, J. M. Thomas, D. Waller, R. H. Jones, A. J. Dent, G. E. Derbyshire and G. N. Greaves, *Nature*, 1991, **354**, 465.
78 G. Sankar, P. A. Wright, S. Natarajan, J. M. Thomas, G. N. Greaves, A. J. Dent, B. R. Dobson, C. A. Ramsdale and R. H. Jones, *J. Phys. Chem.*, 1993, **97**, 9550.
79 S. R. Coyler, G. N. Greaves, S. W. Carr and K. K. Fox, *J. Phys. Chem. B*, 1997, **101**, 10 105.
80 S. R. Davis, A. V. Chadwick and J. D. Wright, *J. Phys. Chem. B*, 1997, **101**, 9901.
81 M. Epple, G. Sankar and J. M. Thomas, *Chem. Mater.*, 1997, **9**, 3127.
82 R. I. Walton, A. J. Dent and S. J. Hibble, *Chem. Mater.*, 1998, **10**, 3737.
83 R. I. Walton and S. J. Hibble, *J. Mater. Chem.*, 1999, **9**, 1347.
84 B. S. Clausen, *Catal. Today*, 1998, **39**, 293.
85 G. Sankar and J. M. Thomas, *Top. Catal.*, 1999, **8**, 1.
86 G. Sankar, J. M. Thomas, F. Rey and G. N. Greaves, *J. Chem. Soc., Chem. Commun.*, 1995, 2549.
87 L. M. Reilly, G. Sankar and C. R. A. Catlow, *J. Solid. State Chem.*, 1999, **148**, 178.
88 C. Aletru, G. N. Greaves and G. Sankar, *J. Phys. Chem. B*, 1999, **103**, 4147.
89 A. K. Cheetham, G. Férey and T. Loiseau, *Angew. Chem., Int. Ed.*, 1999, **38**, 3268.
90 M. S. Whittingham, *Curr. Op. Solid State Mater. Sci.*, 1996, **1**, 227.
91 M. G. Kanatzidis and A. C. Sutorik, *Prog. Inorg. Chem.*, 1995, **43**, 151.
92 W. S. Sheldrick and M. Wachhold, *Angew. Chem., Int. Ed. Engl.*, 1997, **36**, 206.
93 C. R. A. Catlow, D. S. Coombes and J. C. G. Pereira, *Chem. Mater.*, 1998, **11**, 3249.
94 C. M. Draznieks, J. M. Newsam, A. M. Gorman, C. M. Freeman and G. Férey, *Angew Chem., Int Ed.*, 2000, **39**, 2270.
95 S. M. Woodley, P. D. Battle, J. D. Gale and C. R. A. Catlow, *Phys. Chem. Chem. Phys.*, 1999, **1**, 2535.

Palladium-catalysed asymmetric [4 + 2] cycloaddition of vinylallene with 1,3-diene

Masahiro Murakami,* Ryo Minamida, Kenichiro Itami, Masaya Sawamura† and Yoshihiko Ito*

Department of Synthetic Chemistry and Biological Chemistry, Kyoto University, Yoshida, Kyoto 606-8501, Japan

Received (in Cambridge, UK) 6th September 2000, Accepted 5th October 2000
First published as an Advance Article on the web 7th November 2000

A catalytic asymmetric [4 + 2] cycloaddition reaction of a vinylallene with buta-1,3-diene was developed in which a palladium complex modified by a ferrocene-derived chiral monophosphine ligand acted as a template transferring chirality to the product.

Cycloaddition reactions are among the most powerful methods for the rapid construction of carbocycles and heterocycles alike.[1] The [4 + 2] cycloaddition is most widely used to build six-membered ring carbon skeletons. However, strenuous reaction conditions are required for the combination of 1,3-dienes and dienophiles lacking electron-withdrawing or -donating substituents, which limits the range of the synthetic utility. The use of transition metal complexes as the promoter[2] provides considerably wider substrate scope. The transition metal acts as the template bringing the unsaturated substrates together in an array to promote the cycloaddition reaction. We have developed the palladium-catalysed directed intermolecular [4 + 2] cycloaddition between a vinylallene and an ordinary 1,3-diene.[3–5] The initially formed palladacyclopentene intermediate couples with a 1,3-diene before undergoing a ring-flipping isomerization, resulting in a highly stereospecific reaction [eqn. (1)]. We anticipated that a palladium complex modified by a chiral ligand would possibly differentiate the enantiofaces of vinylallene in its s-*cis* form and that this differentiation would be directly transferred to the product. This paper describes the catalytic asymmetric [4 + 2] cycloaddition of a vinylallene[6] with buta-1,3-diene which employs a palladium complex modified by a ferrocene-derived chiral monophosphine ligand as a template.

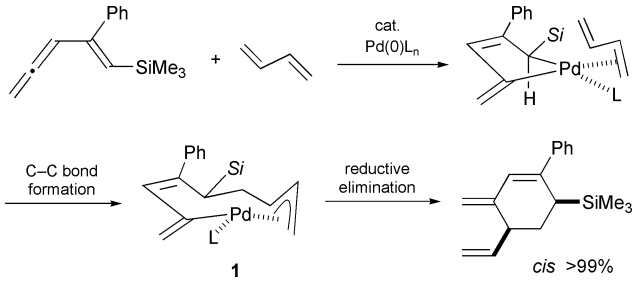

(1)

Initially, a variety of chiral phosphines were screened in the standard test cycloaddition reaction using vinylallene **2a** and buta-1,3-diene (excess). The catalyst complex was prepared by treatment of $[Pd_2(dba)_3{\cdot}CHCl_3]$ with a chiral phosphine ligand *in situ*. Highly reputed bidentate chiral diphosphine ligands like DuPHOS (1,2-bis[2,5-dimethylphospholanyl]benzene) and CHIRAPHOS (2,3-bis(diphenylphosphino)butane gave only low enantioselectivities. No reaction occurred with BINAP. Since our proposed mechanism involves a square planar palladium(II) intermediate **1** in which three of the four coordination sites are occupied by the cycloaddition partners, we supposed that monodentate ligands would be more effective transmitters of chirality. Whereas MOP (2-diphenylphosphino-1,1′-binaphthalene) afforded only 15% ee, a better result was

Table 1 Asymmetric induction in palladium-catalysed directed [4 + 2] cycloaddition of **2a** with buta-1,3-diene

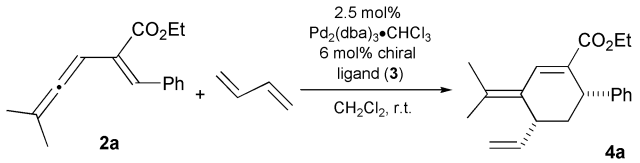

Entry	Chiral ligand	Isolated yield (%) Enantioselectivity	Entry	Chiral ligand	Isolated yield (%) Enantioselectivity
1	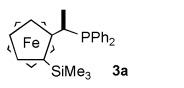 **3a**	90 47 % ee	7	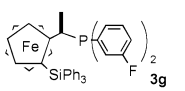 **3g**	85 47 % ee
2	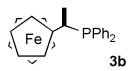 **3b**	62 6 % ee	8	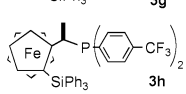 **3h**	77 52 % ee
3	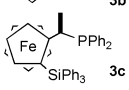 **3c**	82 51 % ee	9	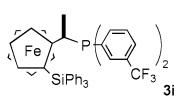 **3i**	87 64 % ee
4	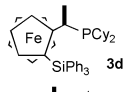 **3d**	80 [a] 18 % ee	10	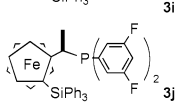 **3j**	74 71 % ee
5	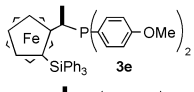 **3e**	30 [a] 40 % ee	11	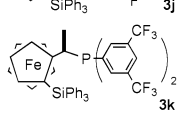 **3k**	85 83 % ee
6	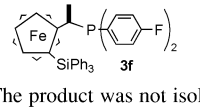 **3f**	90 63 % ee			

[a] Conversion of **2a**. The product was not isolated.

DOI: 10.1039/b007781j

Table 2 Palladium-catalysed asymmetric [4 + 2] cycloaddition of vinylallenes (**2**) with 1,3-dienes[a]

Entry	Vinylallene (**2**)	1,3-Diene	Product (**4**)[b]	Isolated yield (%) Enantioselectivity
1	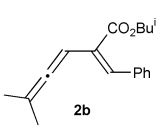 **2b**		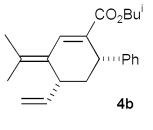 **4b**	63 82 % ee
2	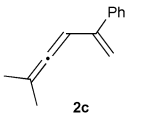 **2c**		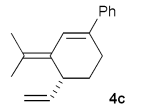 **4c**	89 77 % ee
3	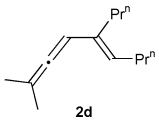 **2d**		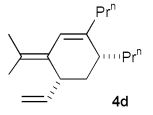 **4d**	76 52 % ee
4	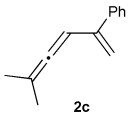 **2c**		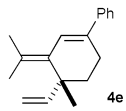 **4e** 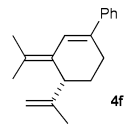 **4f**	89 (**4e**:**4f** = 81:19)[c] **4e** 63 % ee **4f** 65 % ee

[a] The reaction was carried out using 5 mol% of palladium(0) and 6 mol% of **3k** in CH_2Cl_2 at rt. [b] The absolute configuration was not determined. [c] The ratio was determined by HPLC.

obtained with PPFA (2-(1-dimethylaminoethyl)-1-diphenylphosphinoferrocene 27% ee). Among ferrocene-derived ligands, the monodentate phosphine ligand **3a** gave a moderate selectivity (Table 1, entry 1). This result directed our detailed investigation to ligands of analogous structures. The ligands **3b**–**k** listed in Table 1 were prepared‡ and applied to the test reaction. Ligand **3b** lacking a silyl group at the *ortho* position gave a low selectivity (entry 2). The triphenylsilyl-substituted ligand **3c** gave slightly better selectivity than the trimethylsilyl-substituted ligand **3a** (entry 3). Diphenylphosphine-substituted ligands were significantly more effective than dicyclohexylphosphine derivatives (entry 4). The effect of the electronic nature of the diarylphosphinyl group was examined in detail (entries 5–11). Ligands having an electron-withdrawing group gave comparable or better selectivities than **3c**. In particular, the phosphine possessing two 3,5-bis(trifluoromethyl)phenyl groups (**3k**) afforded the highest enantioselectivity of 83% ee.§¶ Although solvents other than DCM were also screened, little effect was observed in terms of the enantioselectivity. The absolute stereochemistry of the major enantiomer was determined to be (4*R*,6*S*) by an X-ray crystallographic study of the amide derived from **4a** and (*S*)-1-phenylethylamine [eqn. (2)].

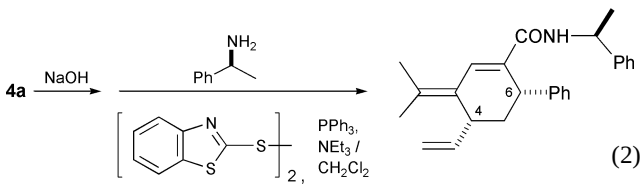

(2)

Thus, **3k** proved to be the ligand of choice, and was applied to the reactions of other vinylallenes with buta-1,3-dienes.‖ The [4 + 2] cycloadducts were produced with moderate to good enantioselectivities in good yields (Table 2). Note that a useful level of asymmetric induction was obtained in the case of **2c** lacking any coordinating heteroatom functionalities (entry 2). For the unsymmetrical 1,3-diene (2-methylbuta-1,3-diene), incorporation of the more substituted C–C double bond was favoured to afford **4e** as the predominant product (entry 4).

A number of highly successful asymmetric [4 + 2] cycloadditions have been reported in which the carbonyl group of an electron-deficient dienophile coordinates to a chiral Lewis acid to induce an excellent enantioselection.[1] On the other hand, it is difficult to gain stereocontrol over a substrate lacking coordinating heteroatom functionalities. The asymmetric [4 + 2] cycloaddition documented herein presents a promising new example which may be applied to such unactivated substrates. The full potential of this new process remains to be elucidated.

Notes and references

† Present address: Department of Chemistry, The University of Tokyo, Hongo, Bunkyo-ku, Tokyo 113-0033, Japan.

‡ The chiral ferrocenyl phosphines **3** were prepared as follows [eqn. (3)]:

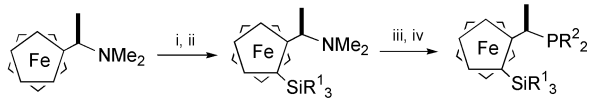

(3)

i, BuLi; ii, Cl-SiR^1_3; iii, Ac_2O; iv, R^2_2P-H /AcOH

ortho-lithiation of (*R*)-*N*,*N*-dimethyl-1-ferrocenylethylamine (**5**) with butyllithium followed by treatment with chlorosilane afforded (*S*)-1-silyl-2-[(*R*)-1-(dimethylamino)ethyl]ferrocene **6**. A diarylphosphinyl group was then introduced by successive treatment of **6** with excess acetic anhydride, and then with diarylphosphine in acetic acid to furnish (*S*)-1-silyl-2-[(*R*)-1-(diarylphosphino)ethyl]ferrocene **3**.

§ The experimental procedure for the formation of **4a** is as follows: to a mixture of $[Pd_2(dba)_3{\cdot}CHCl_3]$ (3.4 mg, 3.3 μmol) and the ligand **3k** (7.4 mg, 7.9 μmol) in CH_2Cl_2 (3 mL) under N_2 at rt were successively added buta-1,3-diene (4.4 M in CH_2Cl_2, 0.3 mL, 1.32 mmol) and the vinylallene **2a** (32.0 mg, 0.132 mmol). The reaction was complete within 10 min. The mixture was evaporated under vacuum, and the residue was subjected to preparative TLC (silica gel, ether–hexane = 1:10) to afford **4a** (33.2 mg, 85%) as a colorless oil. $[\alpha]_D^{20}$ + 12.3 (*c* 1.0, $CHCl_3$). The enantioselectivity was determined to be 83% ee by chiral HPLC analysis [SUMICHIRAL OA-2500-I (4.0 × 250 mm), 1.0 mL min^{-1}, hexane–$ClCH_2CH_2Cl$–EtOH = 2000:20:1, (4*S*,6*R*) t_1 = 17 min, (4*R*,6*S*) t_2 = 19 min].

¶ Platinum was also tested as a metal using $Pt(cod)_2$ and provided 77% ee. However, platinum suffered from low conversion.

‖ Cyclohexa-1,3-diene failed to undergo the cycloaddition, suggesting that 1,3-diene reacts in its s-*cis* form as shown in eqn. (1).

1 For reviews, see: (*a*) W. Carruthers, *Cycloaddition Reactions in Organic Synthesis*, Pergamon, Oxford, 1990; (*b*) *Advances in Cycloaddition*, ed. D. P. Curran, Vol. 1–3, JAI Press, Connecticut, 1994.

2 For a review of transition metal-mediated cycloaddition reactions, see: M. Lautens, W. Klute and W. Tam, *Chem. Rev.*, 1996, **96**, 49.

3 M. Murakami, K. Itami and Y. Ito, *J. Am. Chem. Soc.*, 1997, **119**, 7163.

4 For thermal Diels-Alder reactions of vinylallenes, see: J. Spino, C. Thibault and S. Gingras, *J. Org. Chem.*, 1998, **63**, 5283; U. Koop, G. Handke and N. Krause, *Liebigs Ann.*, 1996, 1487 and refs. therein.

5 For other examples of transition metal-catalysed cycloaddition reactions of vinylallenes, see: (*a*) H. Siegel, H. Hopf, A. Germer and P. Binger, *Chem. Ber.*, 1978, **111**, 3112; (*b*) T. Mandai, S. Suzuki, A. Ikawa, T. Murakami, M. Kawada and J. Tsuji, *Tetrahedron Lett.*, 1991, **32**, 7687; (*c*) M. S. Sigman and B. E. Eaton, *J. Am. Chem. Soc.*, 1996, **118**, 11 783; (*d*) T. Mandai, J. Tsuji and Y. Tsujiguchi, *J. Am. Chem. Soc.*, 1993, **115**, 5865; (*e*) C. Darcel, C. Bruneau and P. H. Dixneuf, *Synlett*, 1996, 218; (*f*) M. Murakami, K. Itami and Y. Ito, *Angew. Chem., Int. Ed. Engl.*, 1995, **34**, 2691; (*g*) M. Murakami, K. Itami and Y. Ito, *J. Am. Chem. Soc.*, 1997, **119**, 2950; (*h*) M. Murakami, M. Ubukata, K. Itami and Y. Ito, *Angew. Chem., Int. Ed.*, 1998, **37**, 2248; (*i*) M. Murakami, K. Itami and Y. Ito, *Organometallics*, 1999, **18**, 1326; (*j*) M. Murakami, K. Itami and Y. Ito, *J. Am. Chem. Soc.*, 1999, **121**, 4340; (*k*) M. Murakami, K. Itami and Y. Ito, *Angew. Chem., Int. Ed.*, 1998, **37**, 3418; (*l*) M. Murakami, K. Itami and Y. Ito, *Synlett*, 1999, 951.

6 For allene-participating [4 + 2] cycloaddition reactions which involve chirality transfer, see: (*a*) I. Ikeda, K. Honda, E. Osawa, M. Shiro, M. Aso and K. Kanematsu, *J. Org. Chem.*, 1996, **61**, 2031; (*b*) P. A. Wender, T. E. Jenkins and S. Suzuki, *J. Am. Chem. Soc.*, 1995, **117**, 1843; (*c*) X. Wang, J. Donovalova, A. Hollis, D. Johnson, A. Rodriguez, G. D. Kennedy, G. Krishnan and H. Banks, *J. Heterocycl. Chem.*, 1994, **31**, 871.

Development of small peptides recognizing a monosaccharide by combinatorial chemistry

Naoki Sugimoto,*[ab] Daisuke Miyoshi[a] and Jin Zou[ac]

[a] *Department of Chemistry, Faculty of Science, Konan University, 8-9-1 Okamoto, Higashinada-ku, Kobe 658-8501, Japan. E-mail: sugimoto@konan-u.ac.jp; Fax: +81-78-435-2539; Phone: +81-78-435-2497*

[b] *High Technology Research Center, Konan University, 8-9-1 Okamoto, Higashinada-ku, Kobe 658-8501, Japan*

[c] *Department of Biological Engineering, School of Chemical Engineering, Heibei University of Technology, Tiaujin 300130, People's Republic of China*

Received (in Cambridge, UK) 18th August 2000, Accepted 9th October 2000
First published as an Advance Article on the web 7th November 2000

Small peptides selected from a library of 62 000 chemically synthesized peptides were able to recognize a monosaccharide specifically and efficiently using both sandwiching and hydrogen bonding interactions, much like sugar-binding proteins (lectins) with the appropriate orientation of amino acid side chains.

Protein–oligosaccharide interactions play a key role in the control of various normal and pathological processes.[1,2] Because of their importance, there has been considerable drive toward the better understanding of the saccharide (carbohydrate) binding specificity of proteins (lectins). Progress has been made using X-ray crystallography, isothermal titration microcalorimetry and site-directed mutagenesis experiments.[3–6] These numerous studies have found diverse mechanisms for saccharide recognition by proteins that have evolved independently but that share some key features. High selectivity for a saccharide is achieved through a combination of hydrogen bonding to the saccharide hydroxy groups and van der Waals packing of the hydrophobic sugar face against aromatic amino acid side chains forming what is called sandwiching interaction.[7,8] Since the binding of saccharides by proteins involves a variety of recognition processes and the proteins themselves exhibit considerable structural diversity, it is difficult to obtain detailed information using thermodynamic and kinetic parameters resulting from the analysis of a large lectin–oligosaccharide complex. Establishing a model system is one of the essential methods to reveal function and mechanism of the specific interactions quantitatively, but there is no good model system that includes the two binding interactions found between proteins and saccharides.

Here, a small oligopeptide–monosaccharide complex was developed as a model system for wild type protein–saccharide complexes which includes the hydrogen bonding and sandwiching recognition mechanisms. Firstly, in order to investigate the relationship between peptide conformation and sandwiching interaction ability, we synthesized alanine-based oligopeptides with one or two tryptophan residues to test the sandwiching interaction between the monosaccharide and the two tryptophan indole side chains, KW (S *i*+0), KWW (S *i*+1), KWAW (S *i*+2), KWAAW (S *i*+3), KWAAAW (S *i*+4), KWAAAAW (S *i*+5) and KWAAAAAW (S *i*+6).† Fig. 1 shows relative fluorescence intensities (ΔF) of these peptides in the presence (F) and absence (F^0) of D-galactose, $\Delta F = (F - F^0) \times 100/F^0$.‡ Because ΔF shows saccharide sandwiching ability of the oligopeptide,[8] these results indicate that the oligopeptide is able to recognize the monosaccharide effectively with W residues at *i* and *i*+4. Aoyama and co-workers showed only two residual peptides, W–W, can recognize maltodextrin *via* sugar–bisindole interaction,[12] as the result of the (S *i*+1) peptide. Our results show that the (S *i*+4) peptide is capable of recognizing a monosaccharide more efficiently than the (S *i*+1) peptide and that the aromatic residues at *i* and *i*+4 have a critical role in this recognition. Previously, tryptophan and porphyrin binding peptides were obtained using combinatorial chemistry and phage display, respectively.[9–11] These peptides also had two aromatic residues and recognized each target molecule using only the sandwiching interaction with these two aromatic residues. Therefore, if both the hydrogen bonding and sandwiching interaction can be introduced suitably in one peptide, more efficient and specific recognition of a monosaccharide could be acquired, even in a small oligopeptide.

We have attempted to put both of the binding modes in the appropriate orientation into a small peptide using combinatorial chemistry. It was shown that the two aromatic residues at *i* and *i*+4 had a critical role for the sandwiching interaction by the fluorescence measurements of (S *i*+0 ~ 6) peptides. Therefore, using a basic split and mix method on a solid phase,[12] a biased combinatorial peptide library with Aro-X-X-X-Aro, where Aro is an L-aromatic amino acid and X is a natural L-amino acid (except C), was synthesized to have sandwiching interaction with *i* and *i*+4 aromatic residues. D-Erythrose ($HOCH_2$-$[CH(OH)]_2CHO$, Sigma–Aldrich Co.) was chosen as a target monosaccharide because D–erythrose is a light yellow syrup and can be followed with visible light.[13] The peptide library and D-erythrose were mixed, gently shaken overnight in a buffer containing 10 mM NaCl, 10 mM Na_2HPO_4, and 1 mM EDTA (pH 7.0) at rt then washed with buffer solution to eliminate any non-specific interactions. It was confirmed that the background signal arising from the non-specific interaction between D-erythrose and the beads in the selection procedure is low enough to select specific colored beads. Using a microscope, 15 beads were then selected from a library theoretically containing

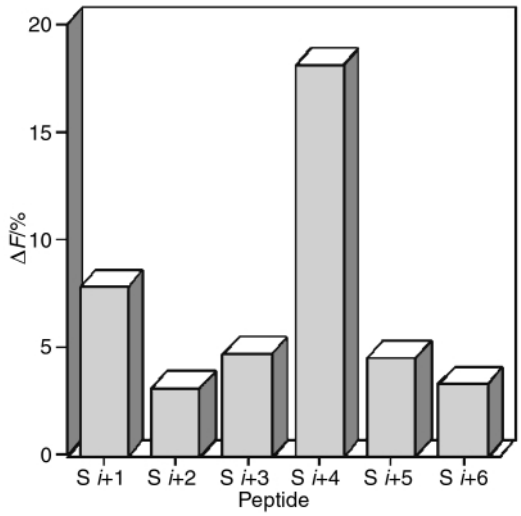

Fig. 1 Ratio of fluorescence intensities (ΔF) of 5 μM peptides at 348 nm and 1.0 °C. All experiments were carried out in a buffer of 10 mM NaCl, 1 mM Na_2HPO_4 and 1 mM EDTA (pH 7.0). The excitation wavelength for Trp is 278 nm and detected at 348 nm.

Table 1 Binding constants and free energies of peptide–saccharide complexes at 1 °C

Peptide sequence	$K_a/10^4$ M[a]		$-\Delta G^0$/kcal mol^{-1} [b]	
	D-Erythrose	D-Galactose	D-Erythrose	D-Galactose
WGDEY	35.0 ± 2.9	5.22 ± 0.42	6.95 ± 0.05	5.91 ± 0.04
WADEF	26.5 ± 2.3	3.81 ± 0.27	6.80 ± 0.05	5.75 ± 0.04
KWAAAW	0.41 ± 0.06	3.89 ± 0.13	4.53 ± 0.06	5.76 ± 0.02

[a] K_a values were estimated by the curve fitting procedure described in the text. [b] $-\Delta G^0$ values were determined with the equation $\Delta G^0 = -RT\ln K_a$

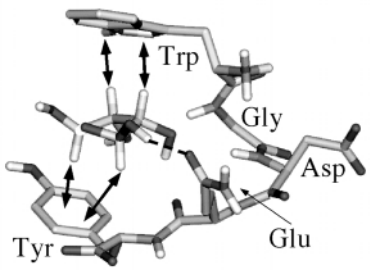

Fig. 2 Minimized energy structure of WGDEY–D-erythrose. Lines and dotted lines indicate CH-π and hydrogen-bonding interaction, respectively.

62 000 kinds of peptides. Ten of the 15 selected peptides had a common motif: WNNNF/T where two of the three N residues were negatively charged amino acids (D or E).

To confirm the highly selective monosaccharide binding by motif peptides and to investigate the motif peptide–D-erythrose interaction, association constants (K_a) of motif peptides for monosaccharides were estimated from fluorescence intensity change by a curve fitting procedure described previously,[14] using the same buffer as the selection experiments. Table 1 shows the K_a of WGDEY and WADEF with D-erythrose and a reference sugar (D-galactose), respectively, and the values of the (S *i*+4) peptide with sugars as references. The difference observed between motif peptides-D-erythrose and motif peptide-D-galactose suggests that motif peptides can recognize a target molecule selectively. Affinity of the lectin for a monosaccharide is usually weak with association constants in the millimolar range, yet it is often highly selective.[2] On the other hand, affinity constants for binding of a simple oligosaccharide to most lectins are estimated to be 10^3–10^6 M^{-1}).[15] Therefore, the K_a value of the motif peptide-D-erythrose is large enough for a monosaccharide recognition protein. The difference between $\Delta G°$ of motif peptides-D-erythrose (−7.0 and −6.8 kcal mol^{-1}) and reference peptide-D-galactose (−4.5 kcal mol^{-1}) is about −2.5 kcal mol^{-1}. The net contributions of an intramolecular hydrogen bond between protein side chains and an intermolecular hydrogen bond between protein and water were estimated to be −2.3 and −1.2 kcal mol^{-1}, respectively.[16] Furthermore, hydrogen bonds in proteins and α-helical peptides were estimated to be −1.3 and −1.0 kcal mol^{-1}, respectively.[17,18] Therefore, one or two appropriate hydrogen bonding interactions were successfully introduced into the selected peptides-D-erythrose interaction using combinatorial chemistry. Fig. 2 shows the minimized energy structure of WGDEY–D-erythrose complex§ which suggests that the peptide sandwiches D-erythrose with W and Y and that a hydrogen bond is formed between the hydroxy group of D-erythrose and a polar side chain of the peptide. Both thermodynamic and molecular modelling results indicate that the motif peptides can bind D-erythrose with the two binding manners as observed in the wild-type saccharide binding proteins. These results also show that all (*i* ~ *i*+4) residues have critical roles for specific monosaccharide recognition. The *i* and *i*+4 aromatic residues are necessary to form a sandwiching interaction, and the acidic residues at *i*+1, *i*+2 and *i*+3 are well suited for hydrogen-bonding interactions. Other selected small residues such as A and G are also important to fit peptide structure for the multi-point saccharide recognition. These delicate residue arrangements were achieved with a combination of rational design studies and a biased combinatorial library.

In summary, the smallest model system of saccharide-binding protein with both hydrogen bonding and the sandwiching interaction was developed using a combination of rational design and combinatorial chemistry. This system is very useful to obtain quantitative parameters of general saccharide–protein interactions.

We thank Dr Angel Maki, Department of Chemistry, Stanford University, for critical reading of the manuscript and helpful comments. This work was supported in part by Grants-in-Aid for Scientific Research from the Ministry of Education, Science, Sports and Culture, Japan, and Grants from 'Research for the Future' Program of the Japan Society for the Promotion of Science.

Notes and references

† All peptides used in this study were synthesized by the Fmoc procedure on a solid support of Fmoc-NH-SAL resin then purified by HPLC. These peptides were named as S *i*+*x* (*x* = 0–6) by means of short oligopeptides which have one or two Trp residues at *i* and *i*+*x*. The peptide sequences were confirmed by peptide sequencing.

‡ All fluorescence spectra were measured from 250 to 350 nm and excited at 278 nm in a 1 cm path length cuvette in the presence and absence of D-Gal at 1.0 °C. All experiments were done in a buffer of 10 mM NaCl, 1 mM Na_2HPO_4 and 1 mM $EDTA_4$ (pH 7.0). Peptide and saccharide concentrations were 5 μM and 50 mM, respectively.

§ The minimized energy structure was obtained after molecular calculation using QUANTA 96/CHARMM 23.2 on a Silicon Graphics Indigo^2 workstation running IRIX 5.3. The energy of the complex was minimized by the parameter of Newton-Raphson and VERLET with an adopted basis set. Dynamics simulation of the minimized energy structure was performed to obtain various conformations as initial coordinates for the calculation. The VERLET algorithm with a time step of 1 fs was used in the dynamics simulation. The system was heated from 0 to 1000 K for the conformational search in the MD simulation.

1 N. Sharon and H. Lis, *Science*, 1989, **246**, 227.
2 L. A. Lasky, *Science*, 1992, **258**, 964.
3 F. A. Quiocho, D. K. Wilson and N. K. Vyas, *Nature*, 1989, **340**, 404.
4 B. W. Sigurskjold and D. R. Bundle, *J. Biol. Chem.*, 1992, **267**, 8371.
5 M. H. Du, U. Spohr and R. U. Lemieux, *Glycoconj. J.*, 1994, **11**, 443.
6 W. I. Weis and K. Drickamer, *Annu. Rev. Biochem.*, 1996, **65**, 441.
7 J. M. Rini, K. D. Hardman, H. Einspahr, F. L. Suddath and J. P. Carver, *J. Biol. Chem.*, 1993, **268**, 10 126.
8 J. Otsuki, K. Kobayashi, H. Toi and Y. Aoyama, *Tetrahedron Lett.*, 1993, **34**, 1945.
9 N. Sugimoto and S. Nakano, *Chem. Lett.*, 1997, 939.
10 N. Sugimoto, H. Kazuta, J. Zou and D. Miyoshi, *Chem. Commun.*, 1999, 677.
11 J. Kawakami, T. Kitano and N. Sugimoto, *Chem., Commun.*, 1999, 1765.
12 K. S. Lam, S. E. Salmon, E. M. Hersh, V. J. Hruby, W. M. Kazmierski and R. J. Knapp, *Nature*, 1991, **354**, 82.
13 K. Sonogashira and M. Nakagawa, *Bull. Chem. Soc. Jpn.*, 1972, **45**, 2616.
14 S. Nakano and N. Sugimoto, *Bull. Chem. Soc. Jpn.*, 1998, **71**, 2205.
15 D. K. Mandal, N. Kishore and C. F. Brewer, *Biochemistry*, 1994, **33**, 1149.
16 K. Tanaka, Y. Yamagata, J. Funahashi, Y. Hioki, S. Kuramitsu and K. Yutani, *Biochemistry*, 1999, **38**, 12 698.
17 J. Fernandez-Recio, A. Romero and J. Sancho, *J. Mol. Biol.*, 1999, **290**, 319.
18 B. J. Stapley and A. J. Doig, *J. Mol. Biol.*, 1997, **272**, 465.

ChemComm

New luminescent and redox-active homometallic dinuclear iridium(III), ruthenium(II) and osmium(II) complexes prepared by metal-catalyzed coupling reactions†

Paul M. Griffiths,* Frédérique Loiseau, Fausto Puntoriero, Scolastica Serroni and Sebastiano Campagna*

Dipartimento di Chimica Inorganica, Chimica Analitica e Chimica Fisica, Università di Messina, Via Sperone 31, I-98166 Messina, Italy. E-mail: photochem@chem.unime.it

Received (in Cambridge, UK) 7th August 2000, Accepted 4th October 2000
First published as an Advance Article on the web 7th November 2000

Four new homometallic dinuclear Ir^{III}, Ru^{II} and Os^{II} complexes are prepared and their luminescence properties and redox behavior are reported; the bis-phenathroline bridging ligand is found to isolate the two components of each dinuclear system because of its unusual nonplanar structure.

Luminescent and redox-active multinuclear metal complexes are extensively investigated because of their interest in the design of novel systems for photochemical energy conversion and for the elaboration of optical information at the molecular level.[1] Beside standardized synthetic methods like the so-called 'complexes as ligands and complexes as metals' approach,[2] metal-catalyzed coupling reactions involving suitable metal precursors are attracting an increasing attention due to the relatively high yields of these reactions and the unambiguity of the products obtained.[3]

In this paper we demonstrate the feasibility of the application of the coupling reaction to suitable Os^{II} polypyridine and Ir^{III} cyclometallated precursors, by the preparation of new luminescent and redox-active homometallic dinuclear Os^{II} and Ir^{III} compounds, and report the absorption spectra, luminescence properties and redox behavior of these new compounds. To the best of our knowledge, it is the first time that this synthetic approach has been applied to luminescent Os^{II} and Ir^{III} complexes. For the sake of completeness, an analogous Ru^{II} polypyridine complex was also prepared and its absorption spectrum, luminescence properties and redox behavior studied. The new compounds synthesized were $[(ppy)_2Ir(phen–phen)Ir(ppy)_2]^{2+}$ (**1**; ppy is the monoanion of 2-phenylpyridine; phen–phen = 5,5′-bis(1,10-phenanthroline)), $[(bpy)_2Ru(phen–phen)Ru(bpy)_2]^{4+}$ (**2**; bpy = 2,2′-bipyridine); $[(bpy)_2Os(phen–phen)Os(bpy)_2]^{4+}$ (**3**) and $[(Me_2bpy)_2Os(phen–phen)Os(Me_2bpy)_2]^{4+}$ (**4**; Me_2bpy = 4,4′-dimethyl-2,2′-bipyridine).‡

The only published procedure for the synthesis of the free bridging ligand phen–phen (5,5-bis(1,10-phenanthroline)) is based on Skraup reactions applied to a benzidine derivative,[4] however this procedure is both toxic and low yielding. The incorporation of coupling methodologies into the synthesis would avoid both, although previous attempts involving copper coupling reactions on 5-bromo-1,10-phenanthroline have failed.[4] We attempted to apply nickel coupling reactions to 5-chloro-1,10-phenanthroline (Cl–phen) to form the free ligand, but this method failed, possibly due to the destabilisation of the nickel tetrakis(triphenylphosphine) catalyst involved in the reaction. However, upon complexation with $Ru(bpy)_2Cl_2$ to yield the new $[Ru(bpy)_2(Cl–phen)]^{2+}$ complex, the phenanthroline moieties couple together in a good yield, 65%, to form the homometallic dimer **2**. Preparation of the new compounds $[Os(bpy)_2(Cl–phen)]^{2+}$, $[Os(Me_2bpy)_2(Cl–phen)]^{2+}$ and $[Ir(ppy)_2(Cl–phen)]^{+}$ by standard literature procedures[5] afforded us suitable precursors to synthesise osmium and iridium homometallic dinuclear compounds by the same coupling reaction. This method yielded the desired compounds **1**, **3**, and **4** (Scheme 1) without particular problems and with comparable yields with respect to the Ru^{II} dimer.

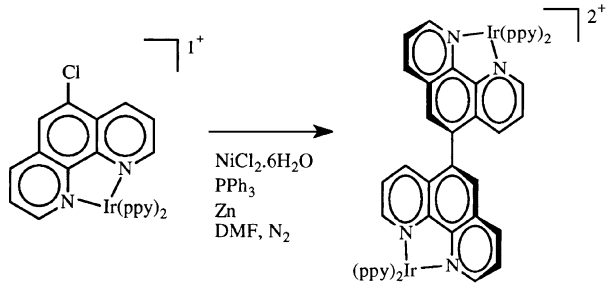

Scheme 1

Each of the four dinuclear compounds exhibits a reversible two-electron oxidation process in acetonitrile solution (Table 1), which can be assigned to simultaneous one-electron oxidation involving the identical metal centres. As expected and in agreement with the above assignment, the osmium species are oxidized at less positive potentials than the ruthenium species. The Ir-centred oxidation process occurs at a typical potential for Ir^{III} cyclometallated species;[5b,6] its reversibility also suggests that an Ir–C^- σ-bond orbital, sometimes playing the role of the donor orbital in the oxidation process,[6] is not involved in such a process in **1**. The coincidence of the two metal-centred oxidation processes in all the complexes indicates that the metal–metal electronic interaction across the phen–phen briding ligand is weak.

The reduction patterns of all the complexes (Table 1) show series of reversible two-electron reductions. The process at less negative potential occurs at similar potentials for all the complexes, and is therefore assigned to the reduction of the two phenanthroline halves of the phen–phen bridging ligand, which is the only polypyridine ligand common to all the species. The two-electron nature of this process suggests that the two phenanthroline halves of the bridge are reduced simultaneously, and indicates that these moieties are isolated from an electrochemical viewpoint. This result is quite surprising on considering the redox behavior of similar systems, such as the $[(bpy)_2Ru(bpy–bpy)Ru(bpy)_2]^{4+}$ complex (bpy–bpy = 4,4′-bis(2,2′-bipyridine)), in which only monoreduction of the

Table 1 Half-wave potentials in argon-purged acetonitrile solution, 298 K. All waves are bielectronic

Compound	$E_{1/2}$ (ox)/V *vs.* SCE	$E_{1/2}$ (red)/V *vs.* SCE
1	+1.28	−1.27; −1.89
2	+1.31	−1.26; −1.47; −1.78
3	+0.86	−1.26; −1.46; −1.77
4	+0.78	−1.23; −1.53

† Electronic supplementary information (ESI) available: spectral data for **1**–**4**, cyclic voltammogram for **3** and absorption and emission spectra for **1**–**3**. See http://www.rsc.org/suppdata/cc/b0/b006456o/

DOI: 10.1039/b006456o

bridge occurs (at −1.10 V *vs*. SCE) before bpy-centred reductions take place;[7] that result suggested that in the bpy–bpy ligand the LUMO orbital in which reduction takes place extends over the two bipyridine halves of the bridging ligand (because the reduction is much easier than in isolated bpy), indicating that the reduced form of the bridging ligand is planar. However, planarity is forbidden in the case of the phen–phen bridging ligand used here, because of strong steric constraints. The absence of planarity is therefore suggested to be responsible for the electrochemical isolation of the two halves of phen–phen.[8] The successive two-electron reduction process of **1** occurs at a potential typical for ppy reduction in cyclometallated complexes[5b] and is attributed to simultaneous one-electron reduction of two ppy ligands coordinated to different metal centres. The second, bielectronic processes of **2** and **3** is attributed to simultaneous one-electron reduction of two bpy ligands coordinated to different metals and the third bielectronic process is assigned to one-electron reduction of the two remaining bpy ligands. The second bielectronic reduction of **4** is analogously assigned to simultaneous one-electron reduction of two Me_2bpy ligands coordinated to different metals, slightly shifted to more negative potentials compared to that of **2** and **3** because the two methyl substituents make the ligand more difficult to reduce. The same reason probably moves the expected reduction of the other Me_2bpy ligands out of the potential window investigated (+2.00 to −2.00 V *vs*. SCE).

The visible region of the absorption spectra of the Ru^{II} and Os^{II} complexes is dominated by moderately intense metal-to-ligand charge-transfer (MLCT) bands, whereas intense ligand-centred (LC) bands dominate the UV region (Table 2).[1a,9] In particular, by comparison among the various compounds and literature data,[9] the bands at about 285 nm can be assigned to spin-allowed bpy-centred transitions, the bands at about 270 nm are assigned to spin-allowed LC transitions involving the phen–phen bridge, the broad absorption features in the 400–500 nm region are attributed to spin-allowed MLCT transitions (with those involving the bridging ligand lower in energy than those involving the peripheral ligands), and the absorption bands at wavelengths longer than 500 nm to spin-forbidden MLCT transitions (such bands are particularly evident in the osmium-containing compounds due to enhanced spin–orbit coupling). For the Ir^{III} dinuclear complex **1** (Table 2), the UV region is also mainly dominated by LC spin-allowed transitions, with spin-allowed MLCT transitions contributing to the absorption spectrum at about 380 nm. The broad, weaker absorption feature in the 400–500 nm region is attributed to spin-forbidden MLCT transitions.[5b,6]

Table 2 Relevant spectroscopic and photophysical data in CH_3CN deaerated solutions at room temperature

Compound	Absorption λ_{max}/nm (ε, M^{-1} cm^{-1})	Luminescence		
		λ_{max}/nm	τ	ϕ
1	265 (108900) 374 (16500)	613	386 ns	0.123
2	284 (126800) 452 (34800)	617	1.3 μs	0.069
3	289 (130200) 432 (29900) 478 (30500)	743	222 ns	0.023
4	288 (118600) 485 (27700)	787	214 ns	0.0044

All the four new dinuclear complexes exhibit relatively intense room temperature luminescence (Table 2). In all the cases, on the basis of the luminescence energies, spectra, lifetimes and quantum yields, emission can be attributed to ^{3}MLCT levels. The redox data also suggest that for all the compounds the emitting ^{3}MLCT state involves the phen–phen bridging ligand. Differences among excited state energies in the various compounds are in line with redox and absorption data. The values calculated for the radiative and radiationless rate constants of the emitting excited state decay in **1**–**4** can be rationalized by considering the energy gap law[10] and the larger singlet character of the emitting level in the osmium and iridium complexes compared to the ruthenium one, which accelerate both the formally forbidden radiative and radiationless decay processes.

We thank MURST (Project: fotosintesi artificiale) and the European Community (TMR Network on nanometer size metal complexes) for financial support.

Notes and references

‡ All the new complexes were isolated as their PF_6 salts, and characterized by elemental analysis, UV-VIS spectra, mass spectra and, where possible, ^{1}H NMR. Relevant characterization data are reported as ESI. Details on the synthesis and on the equipment employed for spectroscopic and electrochemical experiments will be reported elsewhere.

1 (*a*) V. Balzani, A. Juris, M. Venturi, S. Campagna and S. Serroni, *Chem. Rev.*, 1996, **96**, 759; (*b*) C. A. Bignozzi, J. R. Schoonover and F. Scandola, *Prog. Inorg. Chem.*, 1997, **44**, 1; (*c*) J.-P. Collin, P. Gaviña, V. Heitz and J.-P. Sauvage, *Eur. J. Inorg. Chem.*, 1998, 1; (*d*) F. Barigelletti and L. Flamigni, *Chem. Soc. Rev.*, 2000, **29**, 1; (*e*) E. Breuning, M. Ruben, J.-M. Lehn, F. Renz, Y. Garcia, V. Ksenofontov, P. Gütlich, E. Wegelius and K. Rissanen, *Angew. Chem., Int. Ed.*, 2000, **39**, 2504.
2 V. Balzani, S. Campagna, G. Denti, A. Juris, S. Serroni and M. Venturi, *Acc. Chem. Res.*, 1998, **31**, 26, and references therein.
3 See for example: (*a*) M. Beley, J.-P. Collin, R. Louis, B. Metz and J.-P. Sauvage, *J. Am. Chem. Soc.*, 1991, **113**, 8521; (*b*) E. C. Constable, A. M. W. Cargill Thompson and S. Greutlich, *J. Chem. Soc., Chem. Commun.*, 1993, 1444; (*c*) D. Tzalis and Y. Tor, *J. Am. Chem. Soc.*, 1997, **119**, 852; (*d*) S. Fanni, C. Di Pietro, S. Serroni, S. Campagna and J. G. Vos, *Inorg. Chem.*, 2000, **3**, 42; (*e*) K. O. Johansson, J. A. Lotoski, C. C. Tong and G. S. Hanan, *Chem. Commun.*, 2000, 819.
4 F. H. Case, *J. Heterocycl. Chem.*, 1964, **1**, 112.
5 (*a*) E. M. Kober, J. V. Caspar, B. P. Sullivan and T. J. Meyer, *Inorg. Chem.*, 1988, **27**, 4587; (*b*) M. Maestri, V. Balzani, C. Deuschel-Cornioley and A. von Zelewsky, *Adv. Photochem.*, 1992, **17**, 1.
6 F. Neve, A. Crispini, S. Campagna and S. Serroni, *Inorg. Chem.*, 1999, **38**, 2250, and references therein.
7 A. J. Downward, G. E. Honey, L. F. Phillips and P. J. Steel, *Inorg. Chem.*, 1991, **30**, 2259.
8 It should be considered that this does not mean that the phen–phen bridging ligand is not suitable to build up multinuclear systems featuring intercomponent energy or electron transfer. It has been demonstrated that even electronic interactions as small as 10 cm^{-1} (well beyond the limit of the coupling which is possible to evidence by redox experiments) are enough to allow fast energy and electron transfer processes (see: F. Scandola, M. T. Indelli, C. Chiorboli and C. A. Bignozzi, *Top. Curr. Chem.*, 1990, **158**, 73).
9 A. Juris, V. Balzani, F. Barigelletti, S. Campagna, P. Belser and A. von Zelewsky, *Coord. Chem. Rev.*, 1988, **84**, 85 and references therein.
10 J. V. Caspar and T. J. Meyer, *J. Phys. Chem.*, 1983, **87**, 952.

ChemComm

Does *C*-methylcalix[4]resorcinarene always adopt the crown shape conformation? A resorcinarene/bipyridine/decamethylruthenocene supramolecular clathrate with a novel framework structure†

Yuegang Zhang, Christopher D. Kim and Philip Coppens*

Department of Chemistry, State University of New York at Buffalo, Buffalo, New York, 14260-3000, USA. E-mail: coppens@acsu.buffalo.edu

Received (in Columbia, MO, USA) 5th June 2000, Accepted 11th October 2000
First published as an Advance Article on the web 8th November 2000

Decamethylruthenocene acts as the template for the self-assembly of a 2:4:1 *C*-methylcalix[4]resorcinarene/bipyridine/decamethylruthenocene supramolecular structure with large hydrophobic cavities.

As part of a survey of candidates for time-resolved diffraction studies of excited state structures we have previously reported binary phases of 4,4′-dihydroxybenzophenone and *p*-amino-*p*′-nitrobiphenyl and photoinactive 'spacer' molecules.[1,2] Molecular dilution achieved in host–guest crystals has several advantages in time-resolved work, as discussed elsewhere.[3] We report here, on a complex crystalline phase containing decamethylruthenocene (DMR), which has a long-lived triplet state.

MacGillivray *et al*. reported the entrapment of acetylated ferrocene derivatives within the supramolecular deep cavity *C*-methylcalix[4]resorcinarenes (CMCR)/4,4′-bipyridine.[4,5] Though decamethylruthenocene is larger than diacetylferrocene, the cavity formed by *C*-methylcalix[4]resorcinarene, which is extended through hydrogen bonding with the bipyridine molecules, appeared sufficiently flexible to accommodate larger guests.

Needle shape orange crystals of CMCR/4,4′-bipyridine/DMR crystal were grown by slow cooling (one day) of a boiling 96% ethanol (3 mL) solution of *C*-methylcalix[4]resorcinarene (27.2 mg, 0.05 mmol), 4,4′-bipyridine (15.6 mg, 0.10 mmol) and decamethylruthenocene (18.5 mg, 0.05 mmol). Low temperature X-ray structure determination[6] shows an arrangement in which one DMR, two water and two ethanol solvent molecules are located in cavities within a hydrogen-bonded framework formed by the host molecules, with a 2:4:1 CMCR/bipyridine/DMR ratio, as illustrated in Fig. 1. The clathrated DMR molecules occupy one of two center-of-symmetry related positions in a disordered arrangement.

The *C*-methylcalix[4]resorcinarene (CMCR) molecules have a 'flattened cone' conformation (Fig. 2), using the terminology introduced by Gutsche[7] (Fig. 2), different from the crown shape of all the other reported X-ray structures of CMCR. Intramolecular hydrogen bonding is absent in this conformation. While *C*-methylcalix[4]resorcinarene derivatives adopting the 'flattened cone' conformation occur when their hydroxy groups are substituted by ethoxy[8] or trimethylsiloxy groups,[9] or the hydroxy groups are coordinated with metal,[10] which eliminates the possibility of intramolecular hydrogen bonding, this is the first observation of a non-substituted non-metal-atom-containing *C*-methylcalix[4]resorcinarene in this conformation.[11]

Four O–H···O hydrogen bonds link pairs of neighboring resorcinarenes into columns parallel to the crystallographic [011] direction,[12] while O–H···N hydrogen bonds to the nitrogen atoms at each end of the interspersed bipyridine molecules link the columns into 'skewed-brick' sheets parallel to the (1 $\bar{1}$ 1) plane.[13] The DMR molecules serve as templates for the self-assembly of the framework, which is isomeric to MacGillivray's one dimensional polymer.[14] The template-induced architecture of the host framework is of much current interest.[15] Large hydrophobic cavities, in which the guest molecules are located, occur in the space between the bipyridyl molecules (Fig. 3). Successive sheets perpendicular to (1 $\bar{1}$ 1) are linked by weaker interactions, including C-H···O hydrogen bonds. The two independent bipyridine molecules are twisted by 32.04(14) and 17.15(20)°, respectively.

Though crystals of neat DMR are disordered at ambient temperature,[16] low temperature X-ray analysis shows the structure to be fully ordered at 90 K, with a doubling of the unit cell.[6] Comparison of the DMR molecules in the two structures shows only negligible differences, the Ru–Cp distances averag-

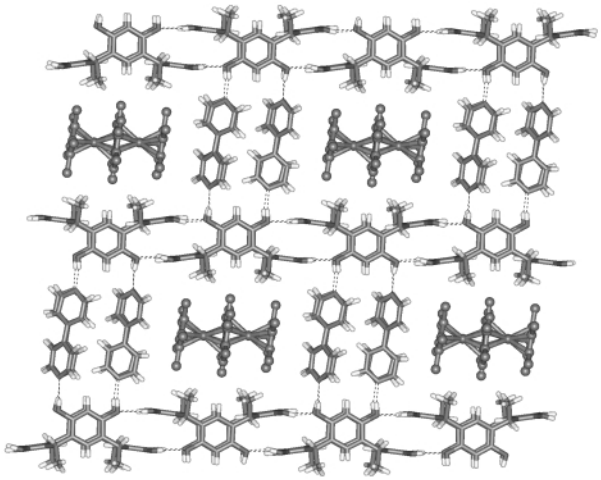

Fig. 1 Hydrogen-bonded layers showing columns of *C*-methylcalix[4]resorcinarene linked by 4,4′-bipyridine molecules. The two half-occupancy decamethylruthenocene molecules are shown. Solvent molecules omitted for clarity.

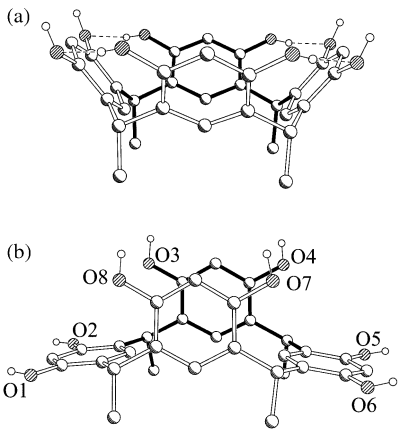

Fig. 2 (a) The bowl-shaped (based on coordinates from ref. 4) and (b) the flattened cone conformation of *C*-methylcalix[4]resorcinarene as determined by X-ray diffraction.

† Electronic supplementary information (ESI): colour version of Fig. 1. See http://www.rsc.org/suppdata/cc/b0/b004783j/

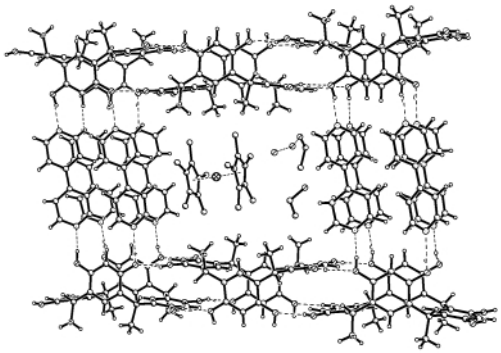

Fig. 3 Detailed view of the cavity including the solvent molecules. Only one of the two center-of-symmetry related positions of the guest molecules is shown.

ing 1.805(16) and 1.792(7) Å respectively in the complex, compared with 1.800(3) and 1.800(3) Å in the neat DMR structure.

The impetus for the current study was the long lifetime of the $^3E_1$ triplet state of DMR, reported as 627 μs (4.2 K), compared with 127 μs for ruthenocene (1.5 K).[17] Spectroscopic experiments[18,19] and calculations[20,21] indicate a significant change in inter-ring distance on excitation of ruthenocene, which is to be investigated by time-resolved synchrotron diffraction methods. Using equipment described elsewhere,[22] we have measured the 16 K lifetimes of the DMR triplet state in both the resorcinarene/DMR complex and neat DMR as 492 and 460 μs, respectively. While the DMR concentration is much lower in the complex crystal (0.602 *vs.* 3.71 M in the neat crystal), the difference could reflect a slightly different temperature.[23] Other measurements on lifetimes in host–guest complexes show no clear relation between excited-state lifetime and molecular concentration.[24]

In summary, decamethylruthenocene acts as the template for the self-assembly of the 2:4:1 *C*-methylcalix[4]resorcinarene/bipyridine/decamethylruthenocene supramolecular crystal. The crystal has a layered structure with two-dimensional planes of hydrogen-bonded molecules, and contains 'flattened cone' shaped calix[4]resorcinarene molecules. The decamethylruthenocene molecules are located in hydrophobic cavities lined by the *C*-methyl groups and the bipyridyl hydrogen atoms. It is likely that other hydrophobic molecules of comparable size can be similarly accommodated in this type of structure, thus suggesting additional applications in crystal engineering and supramolecular chemistry. We have already obtained *C*-methylcalix[4]resorcinarene/bipyridine/benzophenone crystals with similar framework and 'flattened cone' shaped calix[4]resorcinarene molecules.[25]

Support of this work by the National Science Foundation (CHE9981864) and the Petroleum Research Fund of the American Chemical Society (PRF32638AC3) is gratefully acknowledged.

Notes and References

1 Y. Zhang, G. Wu, B. R. Wenner, F. V. Bright and P. Coppens, *Cryst. Eng.*, 1999, **2**, 1.

2 Y. Zhang and P. Coppens, *Chem. Commun.*, 1999, 2425.

3 P. Coppens, *Synchrotron Radiat. News*, 1997, **10**, 26; Y. Zhang, G. Wu, B. R. Wenner, F. V. Bright and P. Coppens, *Cryst. Eng.*, 1999, **2**, 1; P. Coppens, G. Wu, A. Volkov, Y. Abramov, Y. Zhang, W. K. Fullagar and L. Ribaud, *Trans. Am. Crystallogr. Assoc.*, 1999, **34**, 51.

4 L. R. MacGillivray, P. R. Diamente, J. L. Reid and J. A. Ripmeester, *Chem. Commun.*, 2000, 359 and references therein.

5 L. R. MacGillivray, H. A. Spinney, J. L. Reid and J. A. Ripmeester, *Chem. Commun.*, 2000, 517.

6 *Crystal data* for $C_{32}H_{32}O_8{\cdot}2(C_{10}H_8N_2){\cdot}0.5(C_{20}H_{30}Ru){\cdot}C_2H_6O{\cdot}H_2O$: M = 1106.78, triclinic, space group $P\bar{1}$(no. 2), a = 12.5878(4), b = 13.5020(4), c = 17.5000(6) Å, α = 96.0730(10), β = 108.9230(10), γ = 96.7020(10)°, U = 2761.48(15) Å^3, T = 90(1) K, Z = 2, D_c = 1.331 g cm^{-3}, crystal size 0.2 × 0.1 × 0.1 mm, μ(Mo-Kα) = 0.218 mm^{-1}, 25037 reflections, 13375 unique reflections (R_{int} = 0.0346), $2\theta_{max}$ = 58.28°, GOF = 1.058, $R(F)$ = 0.065 for 9166 reflections with $F_o > 4\sigma(F_o)$, $R_w(F^2)$ = 0.203 for all reflections, 1008 parameters. X-Ray data were collected by the oscillation method on a Bruker SMART 1K CCD diffractometer. Reflections were reduced by the SAINT program. The structure was solved by direct methods with XS in SHELXTL, and refined with XL. The decamethylruthenocene, two ethanol and two water molecules were refined with 0.5 occupancy. The two cyclopentadiene rings were constrained to have the same geometry. Hydrogen atoms on the calix[4]resorcinarene molecules were located from difference Fourier peaks and refined isotropically without constraints. For $C_{20}H_{30}Ru$: M = 371.51, monoclinic, space group $P2_1/n$, (no. 14), a = 7.6071(12), b = 14.478(2) c = 16.481(3) Å, β = 99.056(3)°, T = 90(1) K, Z = 4, D_c = 1.377 cm^{-3}, crystal size 0.20 × 0.15 × 0.10 mm, μ(Mo-Kα) = 0.868 mm^{-1}, 12966 reflections, 3745 unique reflections (R_{int} = 0.073), $2\theta_{max}$ = 54.9°, GOF = 0.992, $R(F)$ = 0.029 for 2932 reflections with $Fo > 4\sigma(F_o)$, $R_w(F^2)$ = 0.067 for all reflections, 310 parameters. X-Ray data were collected by the oscillation method on a Bruker SMART 1K CCD diffractometer. Reflections were reduced by the SAINT program. The structure was solved by direct methods with XS in SHELXTL, and refined with XL. CCDC 182/1819. See http://www.rsc.org/suppdata/cc/b0/b004783j/ for crystallographic files in .cif format.

7 C. D. Gutsche, *Calixarenes*, ed. J. F. Stoddart, The Royal Society of Chemistry, Cambridge, 1989.

8 G. Zahn, K. Muller and G. Mann, *Z. Kristallogr.*, 1994, **209**, 470.

9 I. Neda, T. Siedentop, A. Vollbrecht, H. Thonnessen, P. G. Jones and R. Schmutzler, *Z. Naturforsch., Teil B*, 1998, **53**, 841.

10 M. Munakata, L. P. Wu, T. Kuroda-Sowa, M. Maekawa, Y. Suenaga, K. Sugimoto and I. Ino, *J. Chem. Soc., Dalton Trans.*, 1999, 373.

11 After submission of this communication, we learned that the same 'flattened cone' conformation was observed in the ethyl-substituted complex *C*-ethylcalix(4)resorcinarene: M. Nissinen, E. Wegelius, D. Falábu and K. Rissanen, *Cryst. Eng. Commun.*, 2000, 28.

12 O1···O3^{I} 2.785(2) Å, O1–H1D···O3^{I} 171(4)° (I = $-x+1, -y+2, -z+1$); O2···O8^{I} 2.758(3) Å, O2–H2D···O8^{I} 175(4)°; O5···O7^{II} 2.767(3) Å, O5–H5D···O7^{II} 164(4)° (II = $-x+1, -y+1, -z$); O6···O4^{II} 2.722(3) Å, O6–H6D···O4^{II} 162(4)°.

13 O8···N1^{III} 2.723(3) Å, O8–H8D…N1^{III} 165(4)° (III = $x, y+1, z$); O4···N2^{IV} 2.730(3) Å, O4–H4D···N2^{IV} 167(4)° (IV = $-x, -y+1, -z$); O3···N3^{V} 2.729(3) Å, O3–H3D···N3^{V} 168(4)° (V = $x-1, y+1, z$); O7···N4^{II} 2.707(3) Å, O7–H7D···N4^{II} 169(4)°.

14 L.R. MacGillivray, K. T. Hollman and J. L. Atwood, *Cryst. Eng.*, 1998, **1**, 87.

15 C. C. Evans, L. Sukarto and M. D. Ward, *J. Am. Chem. Soc.*, 1999, **121**, 320.

16 M. O. Albers, D. C. Liles, D. J. Robinson, A. Shaver, E. Singleton, M. B. Wiege, J. C. A. Boeyens and D. C. Levendis, *Organometallics*, 1986, **5**, 2321; D. Liles, A. Shaver, E. Singleton and M. B. Wiege, *J. Organomet. Chem.*, 1985, **288**, 33.

17 H. Riesen, E. Krausz, W. Luginbühl, M. Biner, H. U. Güdel and A. Ludi, *J. Chem. Phys.*, 1992, **96**, 4131.

18 G. A. Crosby, G. D. Hager, K. W. Hipps and M. L. Stone, *Chem. Phys. Lett.*, 1974, **28**, 497.

19 G. J. Hollingsworth, K.-S. Kim Shin and J. I. Zink, *Inorg. Chem.*, 1990, **29**, 2501.

20 C. Daul, H. U. Guedel and J. Weber, *J. Chem. Phys.*, 1993, **98**, 4023.

21 F. Gilardoni, J. Weber, A. Hauser and C. Daul, *J. Chem. Phys.*, 1998, **109**, 1425.

22 W. K. Fullagar, G. Wu, C. D. Kim, L. Ribaud, G. Sagerman and P. Coppens, *J. Synchrotron Radiat.*, 2000, **7**, 229.

23 The temperature was measured using the known temperature dependence of the lifetime of a $[Pt_2(H_2P_2O_5)_4]^{4-}$ salt (C. D. Kim, G. Wu, Y. Zhang P. Coppens, to be published).

24 C. D. Kim, G. Wu and P. Coppens, to be published.

25 Y. Zhang, G. Wu, C. D. Kim and P. Coppens, to be published.

The first unambiguous determination of a nitrosyl-to-nitrite conversion in an iron nitrosyl porphyrin

Lin Cheng,[a] Douglas R. Powell,[b] Masood A. Khan[a] and George B. Richter-Addo*[a]

[a] *Department of Chemistry and Biochemistry, University of Oklahoma, 620 Parrington Oval, Norman, OK 73019, USA. E-mail: grichteraddo@ou.edu*

[b] *X-ray Structural Laboratory, Department of Chemistry, University of Wisconsin, 1101 University Avenue, Madison, WI 53706, USA*

Received (in Cambridge, UK) 18th August 2000, Accepted 17th October 2000
First published as an Advance Article on the web 8th November 2000

The picket fence porphyrin complex [Fe(tpivpp)(NO)] undergoes complete conversion to the isolable *N*-bound nitrite derivative [Fe(tpivpp)(NO_2)(py)] in air in the presence of pyridine: reconversion to the starting nitrosyl complex is achieved using triphenylphosphine as reductant.

The study of the reactions of nitric oxide ligands in iron nitrosyl porphyrins is receiving increased attention in bioinorganic chemistry.[1] This is due, in part, to a need to understand the fate of the NO group after it binds to the metal center in heme biomolecules and related model complexes, and to elucidate the chemical processes involved in the conversion of the coordinated NO group to nitrite. There are very interesting results in the literature regarding the formation of coordinated NO_2 groups in iron porphyrins.† For example, Scheidt and coworkers have prepared and structurally characterized a series of [Fe(por)(NO)(NO_2)] complexes by the reaction of $[Fe(por)]_2O$ or [Fe(tpivpp)(NO)] with an excess of NO,[2] and they have proposed the intermediacy of reactive nitrite compounds during the formation of nitrate [Fe(por)(NO_3)] products (por = tpivpp, oep, tpp, ttp) from their nitrosyl precursors.[3,4] Ford and Lorkovic have demonstrated that NO_2 (N_2O_3; derived from reaction of NO gas with trace oxygen) reacts with [Fe(tpp)(NO)] to give [Fe(tpp)(NO)(NO_2)].[5]

Surprisingly, and although it is of fundamental interest in heme–NO chemistry, no direct chemical evidence has been reported on the straightforward conversion of the coordinated NO group in an iron nitrosyl porphyrin to an isolable nitrite complex.‡ We now produce the first unambiguous experimental evidence that the [Fe(tpivpp)(NO)] compound converts to the [Fe(tpivpp)(NO_2)(py)] derivative in air and in the absence of added NO.

The X-ray structure of [Fe(tpivpp)(NO)] is shown in Fig. 1.§¶ Reaction of this compound in $CHCl_3$ with air in the presence of pyridine results in its complete conversion to [Fe(tpivpp)(NO_2)(py)]‖** within 1 h as judged by IR spectroscopy of KBr pellets of dried aliquots.†† When the reaction of [Fe(tpivpp)(NO)] (20–50 mg, 0.018–0.040 mmol) with air and pyridine is performed in a $CHCl_3$–heptane mixture, and the solvent allowed to evaporate over a 3 d period, needle-shaped crystals of the [Fe(tpivpp)(NO_2)(py)]·py product were obtained in 70–80% isolated yields. The observed Fe–NO_2 distances of 1.92–1.97 Å in the [Fe(tpivpp)(NO_2)(py)] products are longer than the axial Fe–NO distance in the precursor [Fe(tpivpp)(NO)] complex (1.65–1.74 Å), and the nitrite O-atoms point towards the HN groups of the picket fence (O···N distances of 3.7–3.8 Å) suggesting possible stabilization of the bound nitrite through weak H-bonding interactions.

The added base is essential for the generation of the stable ferric nitrite derivative, since the reaction of [Fe(tpivpp)(NO)] with air in $CHCl_3$ solution (without added pyridine) results in its quantitative conversion to the known ferric chloro [Fe(tpivpp)(Cl)] complex (λ_{max} = 417 nm).[12,13] We have found that this latter reaction is also enhanced by UV–VIS light (*e.g.* when monitoring the reaction by UV–VIS spectroscopy). We have also confirmed an earlier observation that air oxidation of the non-picket fence [Fe(por)(NO)] compounds (por = tpp, ttp, oep) results in the isolation of the $[Fe(por)]_2O$ oxo dimers,[4] suggesting that the picket fence pocket is indeed crucial for the stabilization of the singly-oxidized nitrite product.

Deoxygenation of the coordinated nitrite to nitrosyl in this picket fence [Fe(tpivpp)(NO_2)(py)] complex in $CHCl_3$ (under a nitrogen atmosphere) is achieved by the addition of triphenylphosphine. The reaction is complete within 15 min, and the five-coordinate nitrosyl [Fe(tpivpp)(NO)] complex is obtained in 80% isolated yield, with triphenylphosphine oxide as the oxidized product. The overall reaction is shown in eqn. (1):

$$[Fe(tpivpp)(NO)] \underset{PPh_3\ (-\ OPPh_3)}{\overset{air,\ py}{\rightleftharpoons}} [Fe(tpivpp)(NO_2)(py)] \quad (1)$$

The conversion of coordinated nitrite to nitrosyl has precedent in iron porphyrin chemistry. For example, (i) the anionic bis-nitro $[Fe(tpivpp)(NO_2)_2]^-$ complex undergoes rearrangement in the presence of boron trifluoride to [Fe(tpivpp)(ONO_2)] and [Fe(tpivpp)(NO)] in some organic solvents,[3] and (ii) oxygen-atom transfer to organic compounds by the [Fe(oep)Cl]/nitrite mixture is believed to occur *via* the intermediacy of '[Fe(oep)(NO_2)]', although this intermediate was not unambiguously identified.[14]

The observation of this base-assisted stabilization of an iron-bound nitrite product derived from its nitrosyl precursor has implications for the reactivity of the bound NO group in nitrosyl heme proteins containing *trans* axial N-bases, and suggests that

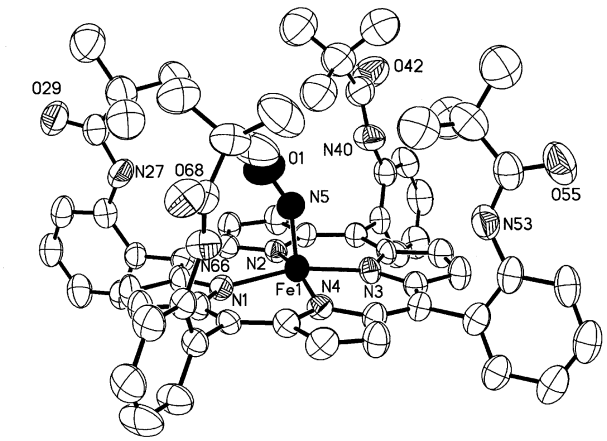

Fig. 1 Molecular structure of [Fe(tpivpp)(NO)]. The nitrosyl group is disordered over two positions, and only one of these positions is shown. Hydrogen atoms have been omitted for clarity. Selected bond distances (Å) and angles (°): Fe(1)–N(por) 1.991(5)–2.007(5), Fe(1)–N(5) 1.65(5), Fe(1)–N(5′) 1.74(6), N(5)–O(1) 1.17(5), N(5′)–O(1′) 1.20(7); Fe(1)–N(5)–O(1) 149(4), Fe(1)–N(5′)–O(1′) 137(4).

DOI: 10.1039/b006775j

iron-bound nitrite could be one of several products or intermediates in some heme–NO ligand oxidations.

We are grateful to the National Science Foundation (CHE-9625065) and the National Institutes of Health (GM-53586), and the Oklahoma Center for the Advancement of Science and Technology (HN97-088) for support for this research. We thank Professor W. Robert Scheidt (U.S.A.) for helpful discussions.

Notes and references

† *Abbreviations*: por = porphyrinato dianion, tpivpp = 'picket fence' tetra(α,α,α,α-*o*-pivalamidophenyl)porphyrinato dianion, oep = octaethylporphyrinato dianion, tpp = tetraphenylporphyrinato dianion, ttp = tetratolylporphyrinato dianion.

‡ Related conversions of cobalt[6] and rhodium[7] nitrosyl porphyrins to nitrite derivatives have been reported.

§ Crystal data for [Fe(tpivpp)(NO)] were collected on a Bruker (Siemens) SMART/CCD diffractometer with Mo-Kα radiation (λ = 0.71073 Å). The structure was solved by direct methods using the SHELXTL system and refined by full-matrix least squares on F^2. *Crystal data*: $C_{64}H_{64}FeN_9O_5$, M = 1095.09, monoclinic, space group $P2_1/n$, a = 17.7905(14), b = 17.6238(13), c = 20.2731(16) Å, β = 99.390(2)°, V = 5913.3(8) Å^3, Z = 4, D_c = 1.230 g cm^{-3}, T = 158(2) K, absorption coefficient = 0.311 mm^{-1}, 7705 independent reflections (R_{int} = 0.0758). Final R (F obs. data) = 0.0709 for 4338 'observed' reflections with [$I > 4\sigma(I)$].

CCDC 182/1820. See http://www.rsc.org/suppdata/cc/b0/b006775j/ for crystallographic files in .cif format.

¶ The X-ray structure of the related [Fe(tpivpp)(NO)][K(NO$_2$)(18-crown-6)] has been reported.[8] The [Fe(por)(NO)] compounds are commonly referred to as ferrous nitrosyls.[1]

‖ This compound was initially prepared from the reaction of the anionic bis-nitro [Fe(tpivpp)(NO$_2$)$_2$]$^-$ complex with pyridine.[9]

** We have obtained three solid-state X-ray structures of this [Fe(tpivpp)(NO$_2$)(py)]·solvate product from these reactions that differ in the nature of the solvate (pyridine, chloroform or dichloromethane). These structures are available in the above .cif file, and are similar to the previously reported structure of [Fe(tpivpp)(NO$_2$)(py)]·PhCl.[9] The structure of the anionic five-coordinate [Fe(tpivpp)(NO$_2$)]$^-$ compound is known.[10] Anionic iron porphyrin nitrites also have rich electrochemistry.[11]

†† KBr pellets were used to observe the ν_{NO} (1675 cm^{-1}) and ν_{NO_2} (1307 cm^{-1}) bands. These bands were confirmed by the use of the ^{15}N-labeled [Fe(tpivpp)(^{15}NO)] (λ_{max} = 409 nm) precursor: $\nu_{^{15}NO}$ of 1641 cm^{-1} for the nitrosyl complex, and $\nu_{^{15}NO_2}$ 1289 cm^{-1} for the nitrite derivative. We have not been able to determine the position of the second ν_{NO_2} band owing to extensive overlap with the porphyrin bands. Also, the UV–VIS spectrum of [Fe(tpivpp)(NO$_2$)(py)] (λ_{max} = 419 nm) is very similar to that of the six-coordinate nitrosyl [Fe(tpivpp)(NO)(py)] complex (λ_{max} = 419 nm), making the monitoring of the reaction by UV-VIS spectroscopy very difficult.

1 L. Cheng and G. B. Richter-Addo, in *The Porphyrin Handbook*, ed. K. M . Kadish, K. M. Smith and R. Guilard, Academic Press, New York, 2000, ch. 33.
2 M. K. Ellison, C. E. Schulz and W. R. Scheidt, *Inorg. Chem.*, 1999, **38**, 100.
3 O. Q. Munro and W. R. Scheidt, *Inorg. Chem.*, 1998, **37**, 2308.
4 M. G. Finnegan, A. G. Lappin and W. R. Scheidt, *Inorg. Chem.*, 1990, **29**, 181.
5 I. M. Lorkovic and P. C. Ford, *Inorg. Chem.*, 2000, **39**, 632.
6 T. S. Kurtikyan, *Russ. J. Inorg. Chem.*, 1999, **25**, 28; P. G. Jene and J. A. Ibers, *Inorg. Chem.*, 2000, **39**, 3823.
7 B. B. Wayland and A. R. Newman, *Inorg. Chem.*, 1981, **20**, 3093.
8 H. Nasri, K. J. Haller, Y. Wang, B. H. Huynh and W. R. Scheidt, *Inorg. Chem.*, 1992, **31**, 3459.
9 H. Nasri, Y. Wang, B. H. Huynh, F. A. Walker and W. R. Scheidt, *Inorg. Chem.*, 1991, **30**, 1483.
10 H. Nasri, Y. Wang, B. H. Huynh and W. R. Scheidt, *J. Am. Chem. Soc.*, 1991, **113**, 717.
11 J. B. Fernandes, D. Feng, A. Chang, A. Keyser and M. D. Ryan, *Inorg. Chem.*, 1986, **25**, 2606.
12 A. Gismelseed, E. L. Bominaar, E. Bill, A. X. Trautwein, H. Winkler, H. Nasri, P. Doppelt, D. Mandon, J. Fischer and R. Weiss, *Inorg. Chem.*, 1990, **29**, 2741.
13 J. P. Collman, R. R. Gagne, C. A. Reed, T. R. Halbert, G. Lang and W. T. Robinson, *J. Am. Chem. Soc.*, 1975, **97**, 1427.
14 S. K. O'Shea, W. Wang, R. S. Wade and C. E. Castro, *J. Org. Chem.*, 1996, **61**, 6388.

Synthesis of bicyclic sugar azido acids and their incorporation in cyclic peptides

Francesco Peri, Laura Cipolla, Barbara La Ferla and F. Nicotra*

Department of Biotechnology and Biosciences, University of Milano-Bicocca, Piazza della Scienza 2, I-20126 Milano, Italy. E-mail: francesco.nicotra@unimib.it; Tel +39.02.64483457; Fax +39.02.64483565

Received (in Cambridge, UK) 31st July 2000, Accepted 13th October 2000
First published as an Advance Article on the web

Bicyclic amino acids derived from the natural sugars D-arabinofuranose and D-fructofuranose have been synthesised; their ability to induce a turn conformation in peptides has been exploited in the preparation of a cyclic RGD loop mimetic.

The conformational rigidity of the pyran and furan rings makes sugar amino acids (SAAs) interesting building blocks in the induction of precise secondary structures in peptides and in the construction of peptidomimetics. In this context, β-D-glucopyranose was used as scaffold in the preparation of the first nonpeptide somatostatin mimetic;[1] in a different biological context the same sugar moiety was employed to present the guanidine group crucial for the biological activity of thrombin inhibitors.[2] By varying the mutual positions of the amino and carboxylic groups in the glucopyranose scaffold, a set of SAAs was designed and found to be capable of inducing linear or β-turn conformations when incorporated into Leu-enkephalin peptide analogues.[3] Oligomers of pyranose sugar amino acids[4] ('carbopeptoids') have been synthesised, and the furanose ring has also been exploited as a building block for carbopeptoid assembling.[5] Homo-oligomers of tetrahydrofuran amino acids derived from the arabinofuranose were shown to adopt a novel repeating β-turn type secondary structure in tetrameric units stabilized by intramolecular hydrogen bond.[6]

We present here the design and the synthesis of novel azido

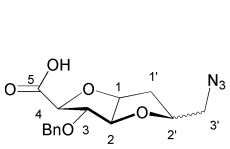

1

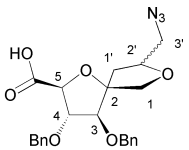

2

acids (**1** and **2**) with bicyclic structures, derived from D-arabinofuranose and D-fructofuranose respectively. Given that the azido group is chemically equivalent to a protected amine, these compounds can be used as building blocks for solid phase assembly of peptoids. Our main goal in the design of this type of SAAs was to lock the furanose ring in a rigid conformation through the formation of fused rings or spiro-bicycles, thus mimicking protein reverse turns (**1**) or constraining a linear peptide conformation (**2**). The transformation of the commercially available starting materials into the corresponding bicyclic azido acids are based on the same synthetic strategy, once the respective allyl-*C*-furanosides have been formed (Schemes 1 and 2).

The 2,3,5-tri-*O*-benzyl-D-arabinofuranose was converted into the anomeric acetate **3**, which was allylated by treatment with allyltrimethylsilane in the presence of catalytic amounts of BF_3–Et_2O. The reaction, effected at rt in dry acetonitrile, afforded **4** as a 1:1 mixture of α and β diastereomers (72% yield). Iodocyclization (Scheme 1) was then carried out with iodine in CH_2Cl_2 at 0 °C. This step is crucial to the formation of the bicyclic structures of the arabino- and fructo-derived compounds and consists of the opening of the intermediate iodonium ion by attack of the γ-benzyloxy groups in the 5-*exo*-

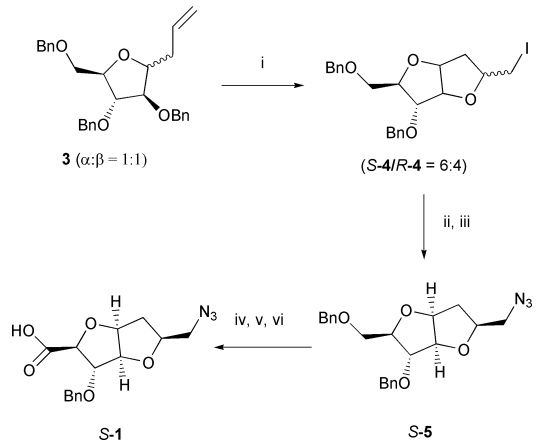

Scheme 1 *Reagents and conditions*: i, I_2, CH_2Cl_2, 0 °C, 12 h; ii, separation of diastereomers by flash chromatography; iii, Bu_4NN_3, toluene, 60 °C; iv, Ac_2O, CF_3COOH, 0 °C; v, MeONa, MeOH; vi, CrO_3–H_2SO_4, acetone–water.

mode with formation of a cyclic iodoether with debenzylation.[7] Obviously, only the β anomer of **4** reacted and this allowed the easy separation from the α-anomer. The bicyclic iodoether **5** was obtained as a mixture of diastereomers (95% yield based on the β anomer), the major isomer having the 2′-(*S*) configuration (20% d.e.). Compounds *R*-**5** and *S*-**5** were separated by flash chromatography and their relative configurations at the C-2′ assigned by NOESY analysis.[8] The reaction of the iododerivative **5** with tetrabutylammonium azide in toluene to give azidoderivative **5** (60 °C, 24 h, 87% yield), as well as the subsequent synthetic steps, were carried out separately on the two diastereoisomers with similar yields. In order to introduce the carboxylic function, **5** was regioselectively debenzylated at the primary hydroxy group by controlled acetolysis (Ac_2O, CF_3COOH, 0 °C), followed by saponification of the acetate and

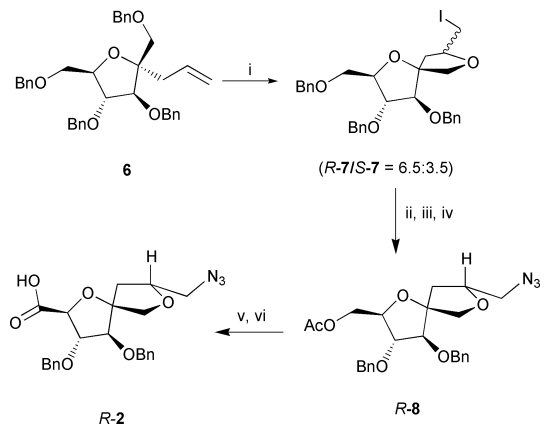

Scheme 2 *Reagents and conditions*: i, I_2, CH_2Cl_2, 0 °C, 12 h; ii, separation of diastereomers by flash chromatography; iii, Bu_4NN_3, toluene, 60 °C; iv, Ac_2O, CF_3COOH, 0 °C; v, MeONa, MeOH; vi, CrO_3–H_2SO_4, acetone–water.

DOI: 10.1039/b006192l

Jones oxidation. Compound **1** was obtained in 48% yield over three steps. The spiro-azido acid **2** was prepared in a similar way, as shown in Scheme 2, the iodocyclization of **6** affording stereoselectively *R*-**7** as the major product[9] (d.e. 33%). The iododerivative was reacted with tetrabutylammonium azide in toluene (60 °C, 24 h) then submitted to acetolysis affording *R*-**10**,[10] and finally converted into azido acid *R*-**2**. The overall yields for the transformation of **3** into **1** and of **6** into **2** were respectively 40% and 35%, *S*-**1**[11] and *R*-**2** being obtained as the major isomers.

NMR and molecular dynamics indicate that both arabino- and fructo-derived bicycles adopt rigid, spatially well-defined conformations. In particular the sugar-amino acids derived from precursors *S*-**1** and *R*-**1** are rigid turn mimetics, both molecules can be incorporated in peptide sequences and used to replace *i* + 1 and *i* + 2 residues of a protein β-turn.

Moreover, these conformationally constrained sugar-amino acids may be incorporated as rigid templates into cyclic peptides in order to lock a bioactive conformation. Several templates have been included in cyclic peptides containing the RGD loop with the aim of obtaining new inhibitors of the adhesive interaction between the $\alpha_v\beta_3$ and the $\alpha_{IIb}\beta_3$-type integrins and their ligands.[12] As example, cyclic peptide **9** was synthesised on solid phase (Scheme 3) by the well-established Fmoc protocol. The dipeptide Arg(Pmc)-Gly was assembled onto Sasrin resin with a loading of 0.47 mmol g^{-1}, then compound *S*-**1** was coupled in the presence of HBTU,[13] HO-Bt and DIPEA. The *N*-terminal azide reduction to the amine and the coupling with Fmoc-Asp(tBu) was effected one-pot in the presence of DIC, Bu_3P, HO-Bt in dry DMF–toluene (2 : 1) at rt for 24 h.[14] This reaction was found to be very efficient and high yielding (as assessed from the loading value calculated after the Fmoc deprotection of the aspartate), in sharp contrast with the inefficiency of other well-established methods we employed to reduce this azide. The tetrapeptide was then cleaved from the resin (1% TFA in CH_2Cl_2 with immediate neutralisation of the effluents with pyridine) maintaining all protecting groups, purified by flash chromatography on silica gel, cyclised in a dilute solution of DMF (peptide conc. 0.5 mM) in the presence of HBTU, HO-Bt and DIPEA and finally totally deprotected with TFA–TIS–water (95 : 2.5 : 2.5), affording **9**[15] in 63% yield over the last two steps.

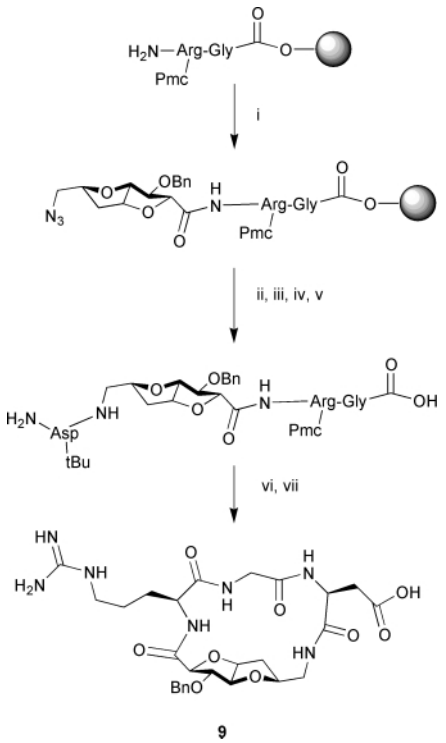

9

Scheme 3 *Reagents and conditions:* i, *S*-**1**, HBTU, HOBt, DIPEA, DMF, rt, 4 h; ii, Bu_3P, DIC, Fmoc-Asp(OtBu), rt, 24 h; iii, piperidine 20% in DMF; iv, 1% TFA in DCM, neutralisation of the effluent with pyridine; v, 0.5 mM peptide in DMF, HBTU, HOBt, DIPEA, 12 h, rt; vi, 95% TFA, 2.5% TIS, 2.5% H_2O, 10 h, rt.

The high efficiency of the synthesis of compounds **1** and **2** is likely to offer opportunities for the preparation of a wide range of carbohydrate-derived bicyclic amino acids with improved conformational rigidity to be used as templates, inducing precise secondary structure conformations in peptides. Detailed conformational analysis of these compounds was carried out by NMR and molecular dynamics and will be reported elsewhere.

We gratefully acknowledge the contribution of Carola Cassani to the experimental work.

Notes and references

1 K. C. Nicolau, J. M. Salvino, K. Raynor, S. Pietranico, T. Reisine, R. M. Freidinger and R. Hirschmann, *Pept. Chem. Struct. Biol. Proc. Am. Chem. Symp. 11th*, 1990; R. Hirschmann, K. C. Nicolau, S. Pietranico, J. Salvino, E. M. Leathy, P. A. Sprengler, G. Furst, A. B. Smith III, C. D. Strader, M. A. Cascieri and M. R. Candelore, *J. Am. Chem. Soc.*, 1992, **114**, 9217; R. Hischmann, W. Yao, M. A. Cascieri, C. D. Strader, L. Maechler, M. A. Cichy-Knight, J. Hines Jr., R. D. van Rijn, P.A. Sprengeler and A. B. Smith III, *J. Med. Chem.*, 1996, **39**, 2441; R. Hischmann, J. Hines Jr., M. A. Cichy-Knight, R. D. van Rijn, P. A. Sprengeler, P. G. Spoors, W. C. Sheakespeare, S. Pietranico-Cole, J. Barbosa, J. Liu, W. Yao, S. Rohrer and A. B. Smith III, *J. Med. Chem.*, 1998, **41**, 1382.

2 H. P. Wessel, D. Banner, K. Gubernator, K. Hilpert, K. Müller and T. Tschopp, *Angew. Chem., Int. Ed. Engl.*, 1997, **36**, 751.

3 E. G. von Roedern, E. Lohof, G. Hessler, M. Hoffmann and H. Kessler, *J. Am. Chem. Soc.*, 1996, **118**, 10 165.

4 E. F. Fuchs and J. Lehmann, *Chem. Ber.*, 1975, **108**, 2254; E. F. Fuchs and J. Lehmann, *J. Carbohydr. Res.*, 1975, **45**, 135; E. F. Fuchs and J. Lehmann, *J. Carbohydr. Res.*, 1976, **49**, 267; K. C. Nicolau, H. M. Florke, G. Egan, T. Barth and V. A. Estevez, *Tetrahedron Lett.*, 1995, **36**, 1775.

5 M. D. Smith, D. D. Long, D. G. Marquess, T. D. W. Claridge and G. W. J. Fleet, *Chem. Commun.*, 1998, 2039.

6 M. D. Smith, T. D. W. Claridge, G. E. Tranter, M. S. P. Sansom and G. W. J. Fleet, *Chem. Commun.*, 1998, 2041.

7 L. Cipolla, L. Lay and F. Nicotra, *J. Org. Chem.*, 1997, **62**, 6678.

8 A consistent NOESY crosspeak (400 MHz, $CDCl_3$) was observed between H-2′ and H-3 protons for the diastereoisomer *R*-**5**, that was absent for *S*-**5**.

9 A sequential NOESY correlation allowed the unambiguous attribution of the configuration at C-2′: for diastereoisomer *R*-**5** H-3/H-1′b and H-2′/H-1′a NOESY crosspeaks were observed thus indicating that H-3 and H-2′ point towards different spatial regions. For diastereoisomer *S*-**8**, H-3/H-1′b and H-2′/H-1′b NOESY crosspeaks were observed.

10 *Selected data for R*-**9**: MALDI-TOF MS*: m/z* 467.9 (M), 491.3 (M + Na), 507.1 (M + K); δ_H (300 MHz, $CDCl_3$) 1.76 (1H, dd, *J* 12.9, 9.8, H-1′a), 2.04 (3H, s, CH_3CO), 2.18 (1H, dd, *J* 12.9, 6.0, H-1′b), 3.19 (1H, dd, *J* 12.9, 4.9, H-3′a) 3.47 (1H, dd, *J* 12.9, 4.0, H-3′b), 3.52–3.64 (1H, m, H-5), 3.82 (1H, d, *J* 9.8, H-1a), 3.87–3.92 (1H, m, H-4), 3.94 (1H, d, *J* 1.4, H-3), 4.08–4.20 (2H, m, H-6), 4.25 (1H, d, *J* 9.8, H-1b), 4.28–4.35 (1H, m, H-2′), 4.42–4.60 (4H, m, CH_2-Ph) 7.20–7.40 (10H, m, H_{arom}).

11 *Selected data for S*-**1**: MALDI-TOF MS: *m/z* 319.9 (M + H); 342.4 (M + Na), 358.4 (M + K); δ_H (300 MHz, $CDCl_3$) 2.09 (1H, m, H-1′b), 2.31 (1H, ddd, *J* 14.2, 6.1, 8.3, H-1′a), 3.30 (1H, dd, *J* 12.8, 3.8, H-3′b), 3.55 (1H, dd, *J* 12.8, 7.3, H-3′a), 4.13 (1H, m, H-2′), 4.35 (1H, bd, *J* 3.3, H-2), 4.42 (1H, bd, *J* 1.7, H-3), 4.61 (1H, bd, *J* 1.8, H-4), 4.66 (2H, AB system, CH_2-Ph), 4.90 (1H, m, H-1), 7.3–7.4 (5H, m, H_{arom}).

12 M. Aumalley, M. Gurrah, G. Müller, J. Calvete, R. Timpl and H. Kessler, *FEBS Lett.*, 1991, **291**, 50; G. Müller, M. Gurrath, H. Kessler and R. Timpl, *Angew. Chem.*, 1992, **31**, 326; R. Haubner, R. Gratias, B. Diefenbach, S. L. Goodman, A. Jonczyk and H. Kessler, *J. Am. Chem. Soc.*, 1996, **118**, 7461; A. Giannis and F. Rübsam, *Angew. Chem.*, 1997, **109**, 606; A. C. Bach II, J. Espina, S. A. Jackson, P. F. W. Stouten, J. L. Duke, S. A. Mousa and W. F. De Grado, *J. Am. Chem. Soc.*, 1996, **118**, 293.

13 *Abbreviations*: DIC, *N*,*N*′-diisopropylcarbodiimide; DIPEA, diisopropylethylamine; HBTU, 2-(1*H*-benzotriazole-1-yl-)-1,1,3,3-tetramethyluronium hexafluorophosphate; HOBt, *N*-hydroxybenzotriazole; Pmc, 2,2,5,7,8-pentamethylchroman-6-sulfonyl; TIS, triisopropylsilane.

14 Z. Tang and J. C. Pelletier, *Tetrahedron Lett.*, 1998, **39**, 4773.

15 *Selected data for* **9**: MALDI-TOF MS*: m/z* 603.3 (M), 626.6 (M + Na), 642.1 (M + K).

Chirality amplification in dynamic helical columns in water

Luc Brunsveld, Bas G. G. Lohmeijer, Jef A. J. M. Vekemans and E. W. Meijer

Laboratory of Macromolecular and Organic Chemistry, Eindhoven University of Technology, P.O. Box 513, 5600 MB Eindhoven, The Netherlands. E-mail: E.W.Meijer@tue.nl

Received (in Cambridge, UK) 15th September 2000, Accepted 13th October 2000
First published as an Advance Article on the web

Extended core discotic molecules self-assemble in water by different secondary interactions to give well-defined, helical columns in which the chirality of one chiral molecule is transferred to on average 12 achiral molecules.

Amplification of chirality, generating homochiral molecules or architectures, is one of the fascinating aspects of life that chemists have repeatedly tackled.[1] Approaches have ranged from crystallization-induced resolution to asymmetric synthesis, while Green pioneered the amplification of chirality at helical macromolecular backbones.[2] We have shown that the addition of small amounts of homochiral seed molecules to dynamic, racemic supramolecular architectures of achiral building blocks in solution generates homochiral supramolecular assemblies.[3,4] For well-defined columns formed by *N*-acylated 3,3′-diamino-2,2′-bipyridine based C_3-extended core discotics, we determined that a single chiral molecule imposes its chirality on 80 achiral molecules at rt.[3] In columnar assemblies of alkyl substituted benzene-1,3,5-tricarboxamides, one chiral seed can even direct the chirality of 200 molecules.[4] For aggregates not formed by directional secondary interactions, such as alkoxy substituted polythiophenes, the amplification of chirality was found to be orders of magnitude lower.[5] The solvents used for the study of these architectures, as well as for other chirality transferring supramolecular systems reported so far,[6] are apolar and organic, favouring specific polar secondary interactions. The creation of well-defined chiral supramolecular architectures in water is a subject of increasing importance and one of the goals in bio-inspired supramolecular chemistry.[7]

In the C_3-extended discotic **1**, oligo(ethylene oxide) side chains have been incorporated. The synthesis and the lyotropic behaviour of chiral **1a** in *n*-butanol, have been described elsewhere.[8] Compound **1a** is molecularly dissolved in $CHCl_3$, but is aggregated in *n*-butanol[9] as evidenced by a red-shift in the UV-Vis spectra with respect to those in $CHCl_3$, broad signals in ^{1}H-NMR spectra and a fluorescent species with a long life time.[8] Furthermore, at low temperatures, the columnar aggregates of **1a** in alcohols are chiral, as evidenced from the appearance of a strong Cotton effect ($g_{abs} = 3 \times 10^{-3}$) in the chromophore corresponding to the aromatic core.[10] We have now synthesized achiral **1b** and studied the self-assembly of **1a**–**1b** mixtures in water. Different interactions are shown to be operative in the self-assembly in water and one chiral molecule is able to induce chirality into 12 achiral molecules at 5 °C.

Compounds **1a**,**b** dissolve in water due to their hydrophilic side chains, but intriguingly, aggregation takes place as evidenced by broad signals in the ^{1}H-NMR spectra and a red shift of the UV-Vis spectra, and a strong intensity of the luminescence compared to solutions in $CHCl_3$. This aggregation in water resembles that of chromonics that are known to aggregate *via* hydrophobic interactions of their aromatic cores.[11] Remarkably and in contrast to chromonics, the architectures are chiral and well-defined as evidenced by the appearance of a Cotton effect for **1a** at the wavelength corresponding to the aromatic core ($g_{abs} = 1.4 \times 10^{-3}$). Apparently, the arene–arene interactions of the aromatic cores create a hydrophobic micro-environment that allows for structuring *via* the specific, solvent-sensitive interactions.[8]

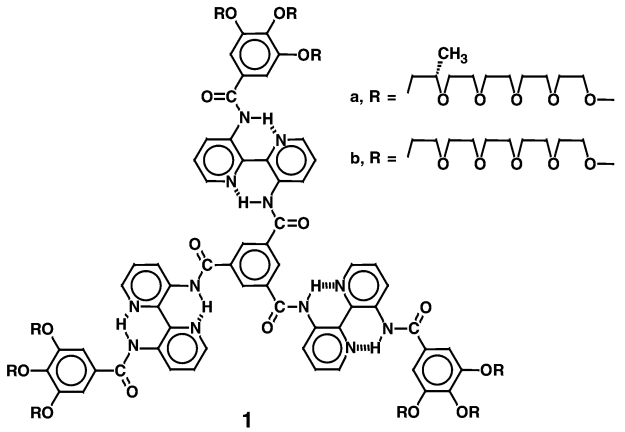

Furthermore, this shows that the peripheral chirality of the individual molecules can be transmitted to the centre of the self-assemblies by cooperative side-chain interactions.

In order to investigate the self-assembly, we studied the solution of **1a** in water as a function of temperature. Raising the temperature from 0 to 90 °C resulted in gradual changes in the UV (Fig. 1, top) and CD spectra (Fig. 1, bottom) as well as the fluorescence characteristics (not shown). In contrast to the *n*-butanol solutions that showed a highly cooperative loss of chirality around 20 °C,[8] the Cotton effect of the aqueous solutions only decreased slowly from 0 to 70 °C. At temperatures as low as 0 °C the Cotton effect is still temperature-sensitive, suggesting that the individual molecules are not yet fully locked in one defined position. The bandshape characteristics of the UV-spectra and the high luminescence suggest that the molecules remain aggregated at all temperatures. The stacking at high temperatures is in contrast with the behaviour of **1** in *n*-butanol[8] and to that of chromonics in general.[11] We attribute this behaviour to the combination of a large aromatic core, allowing for strong arene–arene interactions, and the

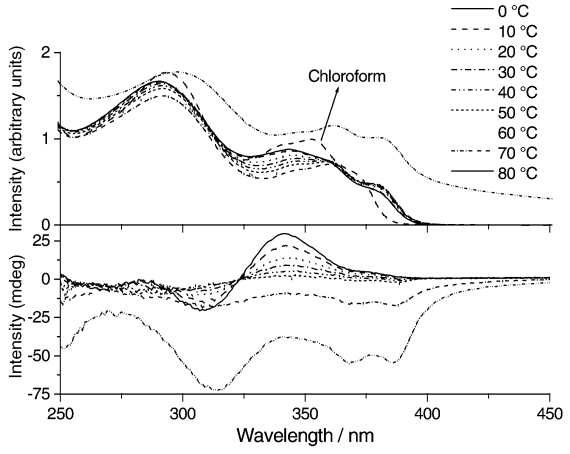

Fig. 1 Temperature dependent UV-Vis (top) and CD (bottom) spectra of **1a** in water (2.6×10^{-5} M). Furthermore, the UV-Vis spectrum of **1a** in chloroform (2.6×10^{-5} M) is shown.

DOI: 10.1039/b007502g

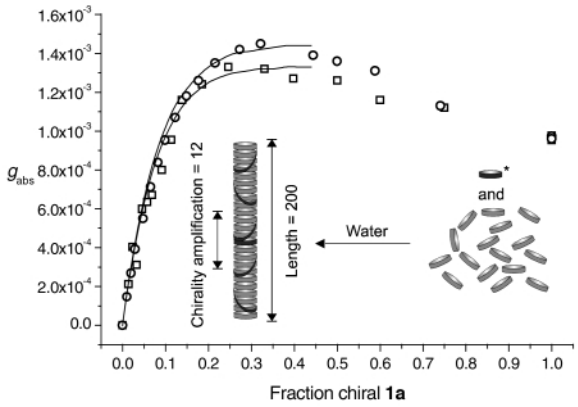

Fig. 2 Dependence of the overall chirality on the mole fraction of chiral **1a** in water at 5 °C, expressed in terms of the *g*-value measured at the maximum of the Cotton effect at 336–341 nm. Measurements were recorded at 10^{-5} M in a 1 cm cell (circles) and at 10^{-4} M in a 1 mm cell (squares). The solid lines represent the best fit to the data using a cooperativity length of 12 molecules and a K_{ass} of 1×10^8 L mol^{-1}.

LCST behaviour of oligo(ethylene oxide)s in water. Dilute solutions of **1a**/**b** in water become turbid around 70 °C (Fig. 1). The turbidity is ascribed to the formation of clusters of columns. At 60 °C a Cotton effect with opposite sign appears (Fig. 1 bottom). Whether this 'inversion' results from the formation of clusters with super-helical structure, or is simply due to scattering of the large particles is not clear yet.

'Sergeant and Soldiers' experiments[12] on **1a**/**1b** mixtures in water were conducted at two different concentrations at 5 °C (Fig. 2) to investigate the possibility of amplification of chirality. Indeed, chirality is amplified in the assembly; the maximal expression of chirality is reached after the addition of 25–30% chiral compound. Adopting the model of Havinga,[3] the association constant (K_{ass}) was calculated to be 1×10^8 L mol^{-1}, with a cooperativity length of 12 molecules. This means that at 10^{-4} M columns with a degree of polymerisation as high as 200 are being formed[13] and that 15–20 chiral molecules are needed to achieve a homochiral column. We are aware of the fact that the model is not exactly suited for the system in water, since it is made for single molecules forming a columnar stack whereas in water non-chiral columns, already present, become chiral. However, to a first approximation the calculated data seem to fit well with the results observed.

The high stability and order of the columns, essential for obtaining chirality amplification, is reflected in a strong time-dependence for the columns to become homochiral; after addition of a small aliquot of chiral **1a** to a solution of achiral **1b** it takes approximately 1.5 h before full amplification of chirality is reached. This phenomenon either results from a diffusion-limited transport of molecules from one stack to the other, or, more likely, is due to an extremely ordered and stable packing of the molecules, both **1a** and **1b**, in the columns.

Fig. 2 clearly shows that in water the intensity of the Cotton effect for particular mixtures is significantly higher than for pure chiral **1a**. In addition, it was established that in water the UV-Vis spectra of **1a** and **1b** differ and as a consequence the CD spectra, for which the maximum has been shifted from 342 nm for pure chiral **1a** to 336 nm for the mixtures with low 'seed' content (Fig. 3). These results demonstrate that the efficiency of packing in columns is different for **1a** and **1b**. The stronger Cotton effect of the mixtures suggests the packing of the achiral molecules to be superior. We attribute the differences in packing to the differing hydrophobicities of **1a** and **1b** and the increased steric hindrance in stacks of **1a** caused by the extra nine branching methyl groups.

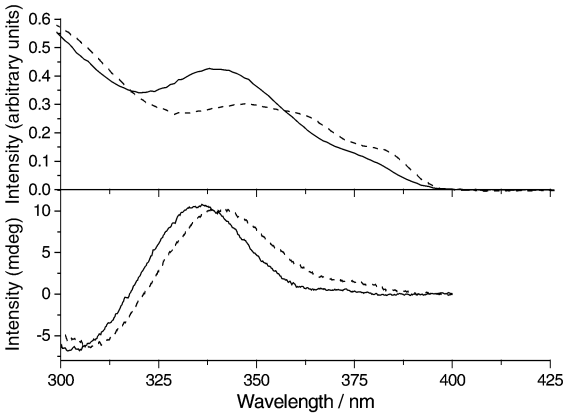

Fig. 3 UV-Vis (top) and CD (bottom) spectra of **1a** (----) and a mixture containing 8% **1a** and 92% **1b** (——) in water at 5 °C at a total constant concentration of 10^{-5} M.

In conclusion, we have demonstrated the creation of well-defined chiral self-assembled structures in aqueous solutions. Although the aggregation process of **1a** in water has similarities with that in organic solvents,[8] the special behaviour in water and the interaction of water with ethylene oxide side-chains results in striking differences. Currently, we are trying to elucidate the specific role of the water in the formation of the (chiral) supramolecular architectures based on **1a** and **1b**.

The National Research School Combination–Catalysis is thanked for funding.

Notes and references

1 B. L. Feringa and R. A. van Delden, *Angew. Chem., Int. Ed.*, 1999, **38**, 3418; M. Avalos, R. Babiano, P. Cintas, J. L. Jiménez and J. C. Palacios, *Chem. Commun.*, 2000, 887.
2 M. M. Green, N. C. Peterson, T. Sato, A. Teramoto and S. Lifson, *Science*, 1995, **268**, 1860.
3 A. R. A. Palmans, J. A. J. M. Vekemans, E. E. Havinga and E. W. Meijer, *Angew. Chem., Int. Ed. Engl.*, 1997, **36**, 2648.
4 L. Brunsveld, A. P. H. J. Schenning, M. A. C. Broeren, H. M. Janssen, J. A. J. M. Vekemans and E. W. Meijer, *Chem. Lett.*, 2000, 292.
5 B. M. W. Langeveld-Voss, R. J. M. Waterval, R. A. J. Janssen and E. W. Meijer, *Macromolecules*, 1999, **32**, 227.
6 R. K. Castellano, C. Nuckolls and J. Rebek Jr.,*J. Am. Chem. Soc.*, 1999, **121**, 11156; L. J. Prins, J. Huskens, F. de Jong, P. Timmerman and D. N. Reinhoudt, *Nature*, 1999, **398**, 498.
7 F. Carsughi, G. Di Nicola, G. Gottarelli, P. Mariani, E. Mezzina, A. Sabatucci, G. P. Spada and S. Bonazzi, *Helv. Chim. Acta*, 1996, **79**, 220; D. H. Appella, J. J. Barchi Jr., S. R. Durell and S. H. Gellman, *J. Am. Chem. Soc.*, 1999, **121**, 2309; W. Blokzijl and J. B. F. N. Engberts, *Angew. Chem., Int. Ed. Engl.*, 1993, **32**, 1545; T. Kunitake, *Angew. Chem., Int. Ed. Engl.*, 1992, **31**, 709; J. H. K. K. Hirschberg, L. Brunsveld, A. Ramzi, J. A. J. M. Vekemans, R. P. Sijbesma and E. W. Meijer, *Nature*, 2000, **407**, 167.
8 L. Brunsveld, H. Zhang, M. Glasbeek, J. A. J. M. Vekemans and E. W. Meijer, *J. Am. Chem. Soc.*, 2000, **122**, 6175.
9 We used *n*-butanol because of its accessible temperature window, but experiments have indicated that the results obtained are general for other low molecular weight alcohols such as methanol and ethanol.
10 In *n*-butanol at 5 °C, chirality is amplified to over 400 molecules. L. Brunsveld, B. G. G. Lohmeijer, J. A. J. M. Vekemans and E. W. Meijer, to be published.
11 J. Lydon, *Curr. Opin. Colloid Interface Sci.*, 1998, **3**, 458.
12 M. M. Green, M. P. Reidy, R. J. Johnson, G. Darling, D. J. O'Leary and G. Wilson, *J. Am. Chem. Soc.*, 1989, **111**, 6454.
13 R. P. Sijbesma, F. H. Beijer, L. Brunsveld, B. J. B. Folmer, J. H. K. K. Hirschberg, R. F. M. Lange, J. K. L. Lowe and E. W. Meijer, *Science*, 1997, **278**, 1601.

ChemComm

Reduction of benzoyl tributylphosphonium chlorides by samarium diiodide as a novel access to 4-benzoylbenzaldehydes

Hatsuo Maeda,* You Huang, Nagomi Hino, Yuji Yamauchi and Hidenobu Ohmori

Graduate School of Pharmaceutical Sciences, Osaka University, 1-6 Yamada-oka, Suita, Osaka 565-0871, Japan

Received (in Cambridge, UK) 6th September 2000, Accepted 17th October 2000
First published as an Advance Article on the web 9th November 2000

Addition of samarium diiodide to a well-stirred THF solution of benzoyl tributylphosphonium chlorides generated *in situ* from benzoyl chlorides and tributylphosphine at −40 °C gave 4-benzoylbenzaldehydes as predominant products from benzoyl chlorides without *para*-substituents, while benzoyl chloride bearing *p*-methyl or chloro groups was exclusively converted into the corresponding α-diketone.

Recently it was found that the reduction potentials of alkanoyl- and benzoyltributylphosphonium ions (**1** and **2**, respectively) (Scheme 1), anodically generated from carboxylic acids and tributylphosphine (Bu_3P) or formed from acid chlorides and Bu_3P, are much more positive than those of the corresponding acid chlorides;[1,2] hence **1** and **2** are converted into aldehydes without over-reduction to alcohols by reduction using a cathode,[1] Zn or Zn–Cu couple[3] more feasibly than the corresponding carboxylic acids or acid chlorides. In addition, electrochemical reduction of **1** was shown to provide a novel tool for the generation of acyl radical or acyl anion equivalents, which are utilized in intramolecular C–C bond formation.[4] However, the synthetically intriguing species generated from **1** or **2** have not been applied to intermolecular reactions. This is probably because **1** and **2** are highly reactive acylating reagents.[4–6] During electrochemical generation of an acyl radical or acyl anion equivalent from **1** or **2**, excess of the acylating reagent remains. Such circumstances may have induced formation of a complex mixture in the cathodic reaction of **1** or **2** with an electrophile or radical acceptor through acylation of all anionic species generated during the electrolysis. Thus, it is speculated that an immediate and total transformation of **1** or **2** into the corresponding acyl radical or acyl anion equivalent prevents such an undesired process. It was reported that benzoyl chlorides **3** were reduced by samarium diiodide (SmI_2)[7] as a one-electron reducing reagent, leading to formation of the corresponding α-diketones (**5**).[8,9] Based on the reduction potentials, it was postulated that **2** will be more feasibly reduced by SmI_2 than the corresponding **3**, namely, that SmI_2-reduction will satisfy the above requirement for the reduced species of **2** to enter intermolecular reaction. Thus, we examined the reduction of **2** itself by SmI_2 as a preliminary study to develop the intermolecular reaction of an acyl radical or acyl anion equivalent generated from **1** or **2**, and obtained interesting results different from those for the case of **3** itself. We report herein that SmI_2–reduction affords benzoylbenzaldehydes **4** as predominant products from **2** without *para*-substituents and **5** exclusively from **2** bearing *para*-substituents (Scheme 1).

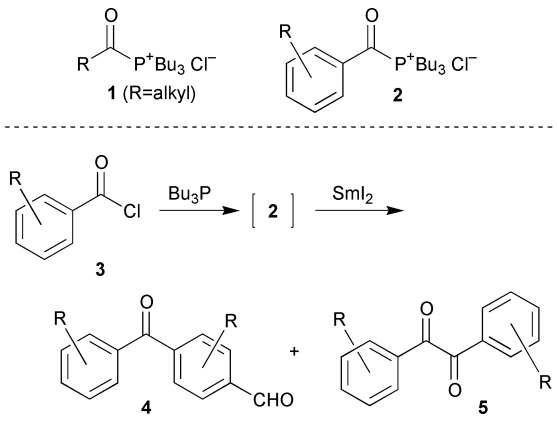

Scheme 1

It was reported that **4** can be prepared by the following methods: (1) SmI_2-induced coupling of benzaldehydes followed by PDC oxidation;[10] (2) benzylic bromination of 4-methylbenzophenone followed by periodate oxidation;[11] (3) oxidative transformation of 4-methylbenzophenone into the corresponding benzaldiacetate followed by acid hydrolysis,[12,13] (4) photolysis of benzaldehyde–cyclodextrin complexes in the solid state.[12] However, the following factors seem to attenuate their synthetic utilities: in the first method, the yields of coupling products from substituted benzaldehydes were rather low; it is unlikely that starting materials with a variety of substituents for the second and the third methods are easily available; the fourth method was applied only to unsubstituted benzaldehyde and its generality is unknown. Thus, it is worthwhile developing a simple and general method for preparing **4**, taking into consideration not only the drawbacks of these methods but also the facts that **4** was used as an important intermediate for synthesis of an HIV-1 integrase inhibitor[11] and antifungal agents.[14]

The typical procedure is as follows: to a THF solution of **3** (1.0 mmol) cooled to −40 °C, Bu_3P (1.1 mmol) was added under an argon atmosphere and the resulting mixture was stirred for 20 min. To the vigorously† stirred mixture, a THF solution (0.1 M, 20 ml) of SmI_2 was added using a syringe. After stirring for 5 min at the same temperature, the reaction was quenched by addition of 1 M HCl (5 ml). The entire mixture was poured into H_2O (20 ml) and extracted with ether (50 ml × 3). The combined organic layer was washed with 5% K_2CO_3 and brine (40 ml each), and dried over $MgSO_4$. After removal of the solvent, the residue was subjected to column chromatography (SiO_2, hexane–AcOEt). Thus obtained products were characterized by ^{1}H-NMR, ^{13}C-NMR, IR, and mass spectra or by comparison with spectroscopic data in the literature.[10,11,15] The regiochemistry in **4b**, **4c**, **6**, and **4f** (*cf.* Table 1) was tentatively assigned to be *para* with respect to the aldehyde groups, based on the results for **2** with *para*-substituents as described below.

The results obtained for benzoyltributylphosphonium chlorides **2** derived from several benzoyl chlorides **3** are shown in Table 1. Reduction of phosphonium chloride **2a** with SmI_2 afforded keto aldehyde **4a** as a sole product in an excellent yield (run 1). Without *in situ* transformation into **2a**, benzoyl chloride was converted only to the corresponding α-diketone in 38% yield under essentially the same conditions, suggesting that reduction of **2** by SmI_2 proceeds in a different manner from that of **3** itself. Similarly, **2b** and **2c** bearing *o*- or *m*-methyl groups were transformed into **4b** and **4c**, respectively, in excellent yields, although formation of the corresponding α-diketone in small amounts was noted (runs 2 and 3). In contrast to the case of **2b** and **2c**, reduction of **2d** with a *p*-methyl group resulted in exclusive formation of α-diketone **5d** (run 4), suggesting that

Table 1 Reduction of benzoyl tributylphosphonium ions (**2**) *in situ* generated from benzoyl chlorides and Bu_3P by SmI_2

Run	2	Product
1	**2a** (R=H)	**4a** (80%)[a,b]
2	**2b** (R=2-CH_3)	**4b** (80%), **5b** (10%)[c]
3	**2c** (R=3-CH_3)	**4c** (71%), **5c** (13%)
4	**2d** (R=4-CH_3)	**5d** (59%)[c]
5	**2e** (R=2-Cl)	**6** (50%)
6	**2f** (R=3-Cl)	**4f** (45%), **5f** (42%)
7	**2g** (R=4-Cl)	**5g** (56%)[c]

[a–c] Physical data are available in ref. 10, 12 and 11 respectively.

SmI_2-reduction of **2** favors formation of **4** *via* coupling at the *para*-position. In reaction with SmI_2, **2f** and **2g** with *m*- or *p*-chloro groups exhibited a tendency similar to **2c** and **2d**; in the former case, **4f** was obtained as a major product and the latter case predominantly afforded α-diketone **5g** (runs 6 and 7). Interestingly, reduction of **2e** bearing an *o*-chloro group led to the formation of a triply coupled product **6** in 50% yield (run 5). These results demonstrated that SmI_2-reduction of **2** provided a novel access to **4** from **3** without *para*-substituents, and the transformation seems to prefer electron-donating substituents to electron-withdrawing substituents on the aromatic ring of **3**. It should be mentioned here that the decanoyl tributylphosphonium ion (**1** with R = n-$C_{10}H_{21}$ in Scheme 1) generated from decanoyl chloride and Bu_3P was reduced under essentially the same conditions, affording only decanal in 39% yield.

For formation of **4** by SmI_2-reduction of **2**, two plausible routes can be considered as depicted in Scheme 2, although the detailed mechanism is not clear at present. By one-electron reduction, characteristic of SmI_2,[7] a neutral radical **7** would be formed from **2**. One of the routes to **4** includes a head-to-tail coupling of the radical (route A). The other comprises radical addition of **7** to **2** (route B). When the procedure with a reverse addition was utilized, namely, when **2** was added to a THF solution of SmI_2 cooled at −40 °C, the yields of **4** were markedly decreased: **4a** (57%) and benzil (9%) from **2a**; **4b** (33%) and **5b** (61%) from **2b**; **4c** (32%) and **5c** (61%) from **2c**. These results suggest that effective formation of **4** needs generation of **7** in the presence of excess **2**, namely, that route B is more likely than route A. In addition, route B seems to provide a reasonable explanation that formation of the triply

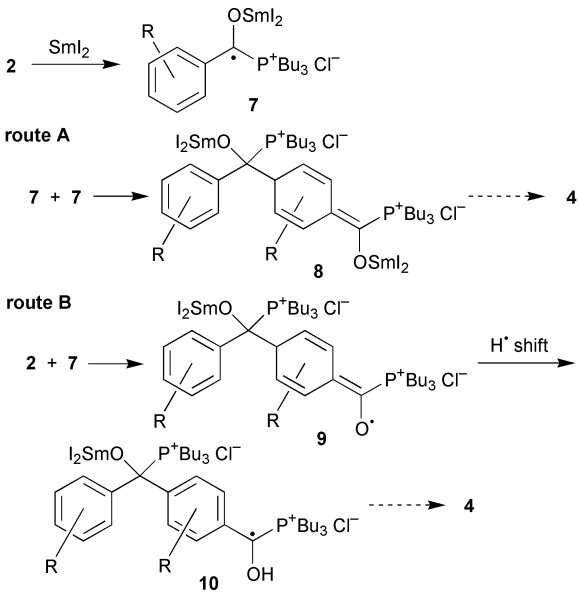

Scheme 2

coupled product **6** is initiated by addition of a radical such as **10** to **2**.

Since benzoyl chlorides **3** with a wide variety of substituents are commercially available and the present transformation is carried out in one-pot, the SmI_2 reduction of benzoylphosphonium ions **2** is thought to be more straightforward and applicable for the preparation of various types of **4**. Further work is under way to examine the generality of the present methodology as a method of preparing **4** and to shed light on the mechanism of its formation.

This work was supported in part by a Grant-in-Aid for Scientific Research on Priority Areas (B) (10208205) from the Ministry of Education, Science, Sports, and Culture, Japan.

Notes and references

† Vigorous stirring was essential for the formation of **4** in high yields, when SmI_2 was added to a THF solution of **2**.

1 H. Maeda, T. Maki and H. Ohmori, *Denki Kagaku oyobi Kogyo Butsuri Kagaku*, 1994, **62**, 1109.
2 H. Maeda, K. Takahashi and H. Ohmori, *Tetrahedron*, 1998, **54**, 12 233.
3 H. Maeda, T. Maki and H. Ohmori, *Tetrahedron Lett.*, 1995, **36**, 2247.
4 H. Maeda and H. Ohmori, *Acc. Chem. Res.*, 1999, **32**, 72.
5 E. Vedejs and S. T. Diver, *J. Am. Chem. Soc.*, 1993, **115**, 3358.
6 E. Vedejs, N. S. Bennett, L. M. Conn, S. T. Diver, M. Gngras, S. Lin, P. A. Oliver and M. J. Peterson, *J. Org. Chem.*, 1993, **58**, 7286.
7 For reviews, H. B. Kagan and J. L. Namy, *Tetrahedron*, 1986, **42**, 6573; J. Inanaga, *Yuki Gosei Kagaku Kyokaishi*, 1989, **47**, 200; J. A. Soderquist, *Aldrichimica Acta*, 1991, **24**, 15; G. A. Molander, *Comprehensive Organic Synthesis*, ed. B. M. Trost and I. Fleming, Pergamon Press, Oxford, 1991, vol. 1, pp. 251–282; G. A. Molander and C. R. Harris, *Chem. Rev.*, 1996, **96**, 307.
8 P. Girard, R. Couffignal and H. B. Kagan, *Tetrahedron Lett.*, 1981, **22**, 3959.
9 J. Collin, J.-L. Namy, F. Dallemer and H. B. Kagan, *J. Org. Chem.*, 1991, **56**, 3118.
10 J.-S. Shiue, M.-H. Lin and J.-M. Fang, *J. Org. Chem.*, 1997, **62**, 4643.
11 H. Zhao, N. Neamati, Y. Pommier and T. R. Burke, Jr., *Heterocycles*, 1997, **45**, 2277.
12 V. P. Rao and N. J. Turro, *Tetrahedron Lett.*, 1989, **30**, 4641.
13 S. B. Liberman and R. Connor, *Organic Syntheses*, 1943, **Coll. Vol. II**, 441.
14 G. Philippe, J. Synese and Z. Rene, EP 401798 A2/1990 (*Chem. Abstr.*, 1990, **114**, 246961).
15 M. Okimoto, T. Itoh and T. Chiba, *J. Org. Chem.*, 1996, **61**, 4835.

ChemComm

Latent chemical behavior revealed in the crystalline state: novel photochemistry of a *cis*-9-decalyl aryl ketone

Eugene Cheung, Ting Kang, John R. Scheffer* and James Trotter

Department of Chemistry, University of British Columbia, Vancouver, B.C., Canada V6T 1Z1. E-mail: scheffer@chem.ubc.ca

Received (in Corvallis, OR, USA) 5th September 2000, Accepted 10th October 2000
First published as an Advance Article on the web 9th November 2000

The case of a ketone whose photochemistry in solution is markedly different from that observed in the crystalline state is reported.

Molecules in crystals may be thought of as residing in reaction cavities whose walls are composed of the neighboring molecules in the lattice.[1,2] When the central molecule in this ensemble is caused to react in some way, for example by UV irradiation, the cavities often restrict certain reaction pathways and allow others, thus generally leading to a reduced number of products compared to reactions carried out in more forgiving fluid media. In some cases, the pathway favored in solution is topochemically forbidden in the solid state (*i.e.* prevented by lattice restraints), and when this is the case, less topochemically demanding reactions leading to new products take over.[3] To put it another way, organic (and inorganic) molecules can be thought of as having *latent reactivity* that is expressed only when they are caused to react in the crystalline state; by restricting chemistry to fluid media, these new reactions would be missed. In the present communication we report an example of this type of behavior in the photochemistry of a *cis*-9-decalyl aryl ketone.

The molecule in question is *cis*-9-decalyl *p*-carbomethoxyphenyl ketone (**1**), mp 85–86 °C (Scheme 1).[4] Irradiation of acetonitrile solutions of this compound (145 mg, 100% conversion) through Pyrex afforded cyclobutanols **6** (47%) and **9** (47%) along with 6% of cyclopentanone **8**. In contrast, when crystals of ketone **1** were irradiated (Pyrex, −20 °C to minimize melting, 76 mg, 100% conversion), the product mixture consisted of cyclobutanol **6** (81%) and the novel cyclopropanol derivative **7** (19%). The structure and stereochemistry of each photoproduct were deduced from FTIR, HRMS, 1D, 2D and NOE difference NMR, and microanalysis. The structures of compounds **6** and **8** were also verified by single crystal X-ray diffraction studies.†

What is responsible for the remarkable difference in product structure and distribution in going from solution to the solid state? To help answer this question, the X-ray crystal structure of ketone **1** was determined (Fig. 1).† This conformation, which is depicted by structure **1a** in Scheme 1, clearly indicates that the ketone oxygen atom is directed toward hydrogen atoms H4 (2.55 Å) and H10 (2.38 Å). This is significant, because these are the very hydrogen atoms abstracted in the first step of the formation of solid state photoproducts **6** and **7**, respectively. Abstraction of H4 takes place through a 6-membered transition state and leads to 1,4-hydroxybiradical **2**, whose closure occurs with retention of configuration at the carbonyl carbon affording cyclobutanol **6**.[5] Abstraction of H10, on the other hand, is a relatively rare 5-membered transition state process that produces 1,3-biradical **3** leading to cyclopropanol **7**.[6] Both biradical closure processes are similar in that they occur without the need for any large molecular motions, *i.e.* they are not topochemically restricted by the confines of the solid state reaction cavity.[7]

Biradicals **2** and **3** are presumably formed in acetonitrile as well, and indeed, photoproduct **6** is a major product in this medium. Cyclopropanol **7** is not formed in solution, however, its place being taken by cyclopentanone **8**. The reason for this difference, we suggest, is that ring closure of biradical **3** to cyclopropanol **7** is slow (ring strain), and in solution, rotation of biradical **3** about the C9 to carbonyl carbon bond to form biradical **4** is faster. This places the aromatic ring in proximity to the radical at C10, and radical coupling of **4** at the *ortho* position followed by tautomerization and oxidation leads to cyclopentanone **8**.[8] Why, then, is no photoproduct **8** formed in the solid state? The simple reason is that the required rotation about the C9 to *carbonyl* carbon bond in biradical **3** is topochemically restricted in the crystal. The aromatic ring would have to sweep through a large volume of space—a motion prohibited by the solid state reaction cavity.

A final point concerns the formation of cyclobutanol **9** in solution but not in the solid state. Formation of this photoproduct necessarily involves abstraction of H2, and this is not possible in the crystal because the C=O···H2 abstraction

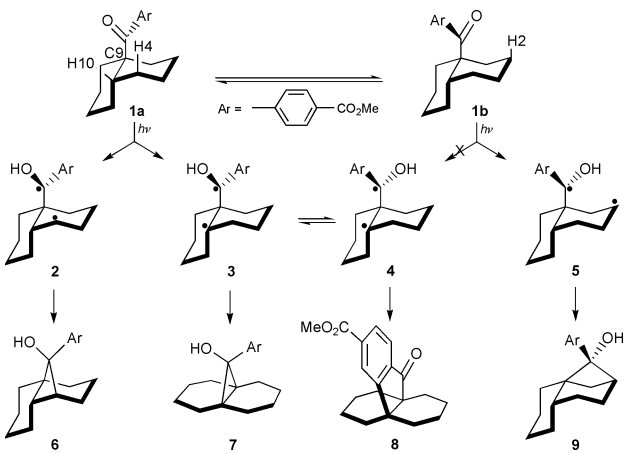

Scheme 1

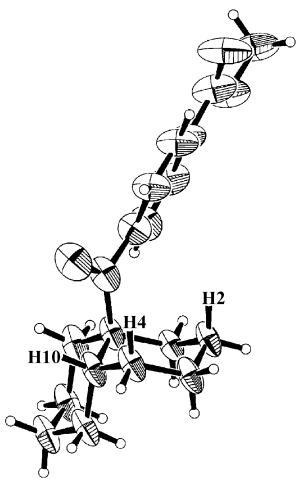

Fig. 1 ORTEP drawing of conformer **1a**

DOI: 10.1039/b007398i

distance in conformer **1a** is too great (3.47 Å).[9] In solution, on the other hand, ketone **1** can adopt alternative low energy conformations that permit abstraction of H2. Molecular mechanics calculations (Hyperchem MM+ and MacroModel MM3*) show that ketone **1** has two lowest energy conformations that differ in energy by only 0.1 kcal mol^{-1}. One of these is **1a**, the conformation adopted in the crystal, and the other is **1b**, in which abstraction of H2 (2.40 Å) is favored geometrically over abstraction of H4 (3.22 Å) or H10 (3.83 Å). We therefore postulate that cyclobutanol **9** is formed in solution from conformer **1b** *via* abstraction of H2 (6-membered transition state) followed by closure of the resulting 1,4-hydroxybiradical **5**.[10]

In summary, the latent solid state photochemical behavior of ketone **1** is manifested by the formation of cyclopropanol **7**, a product not observed in solution. Similarly, irradiation of ketone **1** in solution leads to two new photoproducts (**8** and **9**) not observed in the solid state. These reactivity differences can be explained on the basis of the conformational freedom (or lack thereof) that the reactants and intermediates experience in the two media.

Acknowledgment is made to the donors of the Petroleum Research Fund, administered by the American Chemical Society, for partial support of this research. Financial support by the Natural Sciences and Engineering Research Council of Canada is also gratefully acknowledged.

Notes and references

† *Crystal data*: **1**:$C_{19}H_{24}O_3$, M = 300.40, monoclinic, a = 13.881(5), b = 6.362(2), c = 18.197(8) Å, β = 97.77(4), V = 1591(1) $Å^3$, T = 293 K, space group $P2_1/a$ (no. 14), Z = 4, μ(Mo-Kα) = 0.083 mm^{-1}, 2611 reflections measured, 2503 unique (R_{int} = 0.03), final $R(F^2)$ = 0.062 ($\geqslant 2\sigma$). The achiral space group in this case precludes solid state asymmetric induction studies.

6: $C_{19}H_{24}O_3$, M = 300.40, triclinic, a = 8.8083(3), b = 17.365(7), c = 6.182(2) Å, α = 90.99(3), β = 109.53(3), γ = 79.04(3)°, V = 801.9(5) $Å^3$, T = 293 K, space group $P\bar{1}$ (no. 2), Z = 2, μ(Cu-Kα) = 0.659 mm^{-1}, 3515 reflections measured, 3263 unique (R_{int} = 0.02), final $R(F)$ = 0.060 ($\geqslant 3\sigma$).

8: $C_{19}H_{22}O_3$, M = 298.38, monoclinic, a = 11.209(1), b = 10.149(1), c = 7.5641(8) Å, β = 70.368(9), V = 810.5(2) $Å^3$, T = 293 K, space group $P2_1$ (no. 4), Z = 2, μ(Cu-Kα) = 0.651 mm^{-1}, 1884 reflections measured, 1805 unique (R_{int} = 0.05), final $R(F)$ = 0.041 ($\geqslant 3\sigma$). The absolute structure was not determined.

1 M. D. Cohen, *Angew. Chem., Int. Ed. Engl.*, 1975, **14**, 386; M. D. Cohen, *Mol. Cryst. Liq. Cryst.*, 1979, **50**, 1.
2 R. G. Weiss, V. Ramamurthy and G. S. Hammond, *Acc. Chem. Res.*, 1993, **26**, 530.
3 For examples, see S. Ariel, S. Askari, J. R. Scheffer and J. Trotter, *J. Org. Chem.*, 1989, **54**, 4324; P. R. Pokkuluri, J. R. Scheffer, J. Trotter and M. Yap, *J. Org. Chem.*, 1992, **57**, 1486.
4 E. Cheung, T. Kang, J. R. Raymond, J. R. Scheffer and J. Trotter, *Tetrahedron Lett.*, 1999, **40**, 8729.
5 Cyclobutanol products in Norrish type II photochemistry were first reported by N. C. Yang and D. H. Yang, *J. Am. Chem. Soc.*, 1958, **80**, 2913. For a general review of the Norrish/Yang type II reaction see P. Wagner and B. S. Park, *Organic Photochemistry*, ed. A. Padwa, Marcel Dekker, New York, 1991, Vol. 11, Chapter 4.
6 For a previous example of cyclopropanol formation in a solid state photochemical reaction, see S. Ariel, S. Askari, J.R. Scheffer and J. Trotter, *Tetrahedron Lett.*, 1986, **27**, 783.
7 Competitive β *versus* γ-hydrogen atom abstraction is rare but not unprecedented. See R. A. Cormier, W. L. Schreiber and W. C. Agosta, *J. Chem. Soc., Chem. Commun.*, 1972, 729.
8 For an analogous photoreaction involving cyclization to a 6-membered ring ketone, see M. J. Perkins, N. B. Peynircioglu and B. V. Smith, *J. Chem. Soc., Chem. Commun.*, 1976, 222.
9 For a discussion of the geometric requirements for intramolecular hydrogen atom transfer in the solid state, see H. Ihmels and J. R. Scheffer, *Tetrahedron*, 1999, **55**, 885.
10 Formation of biradical **4** from conformer **1b** is impossible owing to the long C=O···H_{10} distance involved (3.83 Å).[9]

Synthesis of *N*-1-oxypyrimidine 1,3-dioxolane and 1,3-oxathiolane nucleosides

Nghe Nguyen-Ba, Nola Lee, Laval Chan and Boulos Zacharie*

BioChem Pharma Inc. 275 Armand-Frappier Blvd., Laval, Québec, Canada H7V 4A7

Received (in Corvallis, OR, USA) 10th August 2000, Accepted 15th September 2000
First published as an Advance Article on the web 9th November 2000

Two series of 1,3-dioxolanes and 1,3-oxathiolane nucleosides containing *N*-1-oxypyrimidine were synthesized as potential antiviral agents.

The potent activity displayed by 3′-azido-3′-deoxythymidine (AZT)[1] against human immuno-deficiency virus (HIV) prompted further design and evaluation of nucleoside analogues.[2] However, the toxicities associated with these compounds as well as the development of resistant viral strains upon prolonged treatment indicates that there is still a need for novel therapeutic agents.[3] One approach is to replace the carbohydrate moiety of 2′,3′-dideoxynucleoside analogues with other five membered rings.[3b,4] It has been demonstrated that heterosubstitution of these rings has a profound effect on the biological activity of the resulting nucleoside analogue[5] as displayed by (−)-2′-deoxy-3′-thiacytidine (3TC®, Epivir) **1**[5c,6] and (+)-2′-deoxy-3′-oxacytidine (Troxacitabine) **2**.[7]

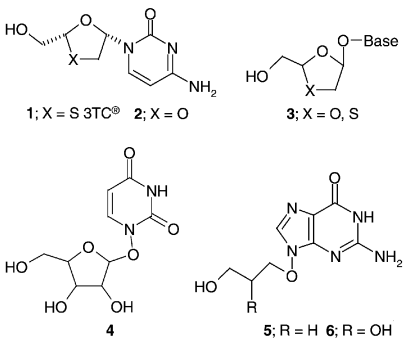

As part of an ongoing search for new antiviral leads, we further explored this class of 3′-heterosubstituted nucleosides. We synthesized a novel class of these compounds where the 1,3-oxathiolane or 1,3-dioxolane ring is linked to the heterocyclic base through a nitrogen–oxygen bond. This is exemplified by the general structure **3**. The structure of these nucleosides are analogous to those of biologically active compounds[8] such as 1-(α-D-ribofuranosyloxy)uracil **4**,[8b] 9-(3-hydroxypropoxy)guanine **5**[8c] and 9-(2,3-dihydroxypropoxy)guanine **6**.[8d] As an example, **6** showed more potent and selective activity than acyclovir against HSV-1, HSV-2 but was less active than acyclovir against VZV.[8c,d]

The synthetic route to (±)-1,3-dioxolane and 1,3-oxathiolane nucleoside analogues **3** is based upon reaction of *N*-1-hydroxyheterocycles **8** with a dioxolane or oxathiolane moiety **7** bearing a suitable leaving group Y (Scheme 1).

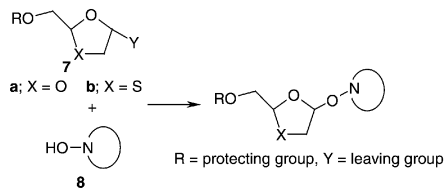

Scheme 1

Our strategy was to build stepwise the *N*-1-hydroxypyrimidine base **8** since its direct synthesis by oxidation of the base has not yet been achieved. *N*-1-Hydroxyuracil **12** was selected as the key base in this series.[9] The preparation of this compound is described in Scheme 2. Treatment of *O*-benzylhydroxylamine with aqueous acidic potassium cyanate afforded urea **9** in 80% yield. This was reacted with sodium hydride followed by ethyl 3,3-dimethoxypropionate to give the protected uracil **10**. This compound was hydrogenated to give *N*-1-hydroxyuracil **12**. Similarly, *N*-1-hydroxythymine **13** was prepared by reacting the urea **9** with ethyl 3,3-diethoxy-2-methylpropionate followed by deprotection of the benzyl group of compound **11**. These pyrimidine bases **12** and **13** were also synthesized by Klötzer using a similar approach.[10] *N*-1-Hydroxycytosine was prepared from its precursor uracil. For example, reaction of *N*-1-benzyloxyuracil **10** with phosphorus oxychloride, triethylamine and triazole gave the triazolo derivative which was treated with ammonia then debenzylated to give *N*-1-hydroxycytosine **15** in 75% yield (Scheme 2).

Unlike 1-(benzyloxy)imidazole which is unstable under alkaline conditions,[8a] the *N*-1-benzyloxypyrimidines **10**, **11**, **14** are stable under a variety of conditions. These include acidic and basic conditions, as well as temperatures (< 90 °C) and catalytic hydrogenation. In addition, the final free *N*-1-hydroxy compounds **12**, **13**, **15** can be stored for months at 0 °C without decomposition.

Two approaches were considered for the preparation of pyrimidine and purine nucleosides. The first route was based upon coupling of a suitably functionalised *N*-1-hydroxy base with 1,3-dioxolane or 1,3-oxathiolane sugars under Mitsunobu conditions. Unfortunately, this reaction appeared to be ineffective and resulted in low yield. In fact, the Mitsunobu reaction between acylated furanose and 1-hydroxybenzotriazole gave similar results.[11] The second approach offers a more general route for the synthesis of these nucleosides. Scheme 3 illustrates a representative example where the sugar moieties of 1,3-dioxolane or 1,3-oxathiolane were reacted with iodo- or bromotrimethylsilane then the solution was treated with a mixture of sodium hydride and *N*-1-hydroxyuracil **12** or

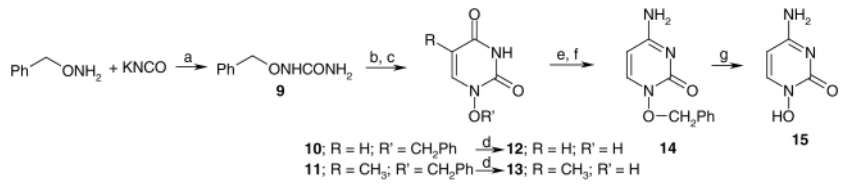

Scheme 2 *Reagents and conditions:* (a) 10% aq. acetic acid; (b) NaH, DMSO, 70 °C, 22 h; (c) Na, EtOH, $(MeO)_2CHCH_2COOEt$; (d)10% Pd/C, cyclohexane, EtOH, 60 °C, 5 h; (e) $POCl_3$, Et_3N, triazole; (f) NH_3; (g) H_2/Pd-C.

DOI: 10.1039/b006600l

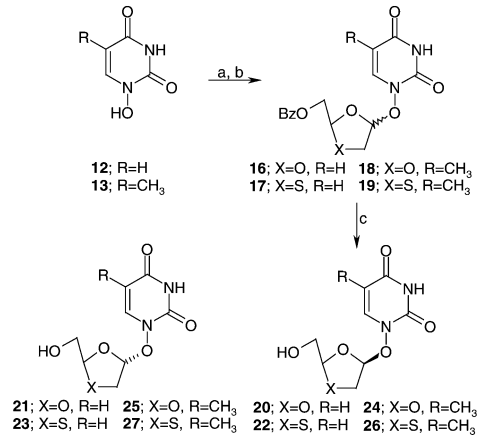

Scheme 3 *Reagents and conditions*: (a) NaH/THF; (b) 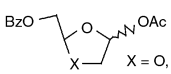 , TMSI or TMSBr, DMF; (c) NH_3/MeOH.

thymidine **13** in DMF. This gave the desired nucleoside **16** and **17** or **18** and **19**, respectively, as a 1 : 1 mixture of *cis* and *trans* isomers in 72 and 66% yields, respectively.[12] Replacement of halotrimethylsilane with trimethylsilyl triflate or the base sodium hydride with triethylamine did not alter the ratio of isomers but reduced the yield. Separation of the isomers **16**–**19** by chromatography followed by deprotection with methanolic ammonia gave the expected nucleosides **20**–**27** in high yields.[13]

Similarly, cytosine derivatives **28**–**31** were produced in a 1 : 1

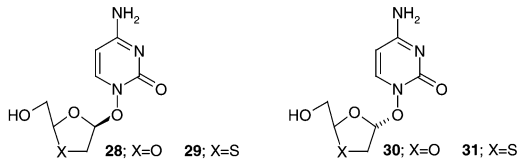

mixture of *cis* and *trans* isomers under the same conditions starting from *N*-1-hydroxycytosine **15**. Direct conversion of uracil nucleoside **16** or **17** to the corresponding cytosine using the triazolo–phosphorus oxychloride–ammonia procedure was not successful and gave low yield of the expected product **28**–**31**.

The anti HIV, HBV, HSV-1 and HSV-2 activities of (±)-1,3-dioxolane and 1,3-oxathiolane nucleoside analogues **20**–**27**, **28**–**31**, were evaluated and compared with 3TC® (Epivir) and AZT. All of them were found to be inactive and non-toxic, except the cytosine derivative **29** which displayed weak inhibition of extracellular HBV.

In summary, described herein is a novel class of (±)-1,3-dioxolane and 1,3-oxathiolane nucleoside analogues. The biological results demonstrate that linking the sugar to the heterocyclic base through an oxygen causes dramatic reduction in antiviral activity in this series of compounds.

We thank Drs R. Storer and T. Bowlin for reading the manuscript, Mrs L. Bernier and J. Dugas for technical assistance with HPLC purification, and Mrs L. Marcil for secretarial and technical assistance.

Notes and references

1 H. Mitsuya, J. K. Weinhold, P. A. Furman, M. H. St-Clair, S. Nusinoff-Lehrman, R. C. Gallo, D. Bolognesi, D. W. Barry and S. Broder, *Proc. Natl. Acad. Sci. U.S.A.*, 1985, **82**, 7096.

2 (*a*) H. Mitsuya and S. Broder, *Proc. Natl. Acad. Sci. U.S.A.*, 1986, **83**, 1911; (*b*) R. Yarchoan, H. Mitsuya, R. V. Thomas, J. M. Pluda, N. R. Hartman, C.-F. Perno, K. S. Marczyk, J.-P. Allain, D. G. Johns and S. Broder, *Science*, 1989, **245**, 412; (*c*) T.-S. Lin, R. F. Schinazi and W. H. Prusoff, *Biochem. Pharmacol.*, 1987, **36**, 2713.

3 (*a*) For a recent review, see: E. De Clerq, *J. Med. Chem.*, 1995, **38**, 2491; (*b*) M. L. Peterson and R. Vince, *J. Med. Chem.*, 1991, **34**, 2787 and references cited therein.

4 (*a*) B. Belleau, L. Brasili, L. Chan, M. DiMarco, B. Zacharie, N. Nguyen-Ba, H. J. Jenkinson, J. A. V. Coates and J. M. Cameron, *Bioorg Med. Chem. Lett.*, 1993, **3**, 1723; (*b*) M. J. Bamford, D. C. Humber and R. Storer, *Tetrahedron Lett.*, 1991, **32**, 271 and references cited therein; (*c*) J. Branalt, I. Kvarnstrom, B. Classon and B. Samuelsson, *J. Org. Chem.*, 1996, **61**, 3604 and references cited therein.

5 (*a*) N. Nguyen-Ba, W. L. Brown, L. Chan, N. Lee, L. Brasili, D. Lafleur and B. Zacharie, *Chem. Commun.*, 1999, 1245; (*b*) N. Nguyen-Ba, W. Brown, N. Lee and B. Zacharie, *Synthesis*, 1998, 759; (*c*) J. A. V. Coates, N. Cammack, H. J. Jenkinson, I. M. Mutton, B. A. Pearson, R. Storer, J. M. Cameron and C. R. Penn, *Antimicrob. Agents Chemother.*, 1992, **36**, 202; (*d*) M. W. Chun, D. H. Shin,.H. R. Moon, J. Lee, H. Park and L. S. Jeong, *Bioorg. Med. Chem. Lett.*, 1997, **7**, 1475.

6 J. M. Camaron, P. Collis, M. Daniel, R. Storer and P. Wilcox, *Drugs of the Future*, 1993, **18**, 319 and references cited therin.

7 K. L. Grove, X. Guo, S.-H. Liu, M. Kukhanova, C. K. Chu and Y.-C. Cheng, *Nucleosides Nucleotides*, 1997, **16**, 1229.

8 (*a*) M. R. Harnden, EP 0319 228 A3; (*b*) E. Grochowski, H. Stepowska, P. Salanski and J. Jurczak, *Carbohydr. Res.*, 1988, **177**, 244; (*c*) S. Bailey, M. R. Harnden, R. L. Jarvest, A. Parkin and M. R. Boyd, *J. Med. Chem.*, 1991, **34**, 57; (*d*) M. R. Harnden, P. G. Wyatt, M. R. Boyd and D. Sutton, *J. Med. Chem.*, 1990, **33**, 187.

9 A similar approach for the synthesis of 1-(hydroxyalkoxy)pyrimidines has been reported by M. R. Harnden, L. J. Jenning and A. Parkin, *Tetrahedron Lett.*, 1988, **29**, 4013.

10 (*a*) W. Klötzer, *Monatsh. Chem.*, 1964, **95**, 1729; (*b*) W. Klötzer and M. Herberz, *Monatsh. Chem.*, 1965, **96**, 1721.

11 E. Grochowski and H. Stepowska, *Synthesis*, 1988, 795.

12 The relative stereochemistry of the *cis* and *trans* products was assigned by difference NOE spectra.

13 Selected data for **22**: mp 190–191 °C; δ_H (DMSO-d_6) 11.58 (br, 1H), 7.92 (d, 1H, *J* 5.4), 6.07 (d, 1H, *J* 4.3), 5.63 (t, 1H, *J* 5), 5.50 (d, 1H, *J* 7.5), 5.23 (t, 1H), 3.67 (m, 1H), 3.63 (m, 1H), 3.54 (m, 2H); δ_C (DMSO-d_6) 163.2, 148.5, 145.1, 109.5, 99.7, 86.8, 64.0, 34.7; HRMS (FAB): M^+ calcd for $C_8H_{11}N_2O_5S$ 247.038868, found 247.038107. For **23**: mp 180-182 °C; δ_H (DMSO-d_6) 11.59 (br, 1H), 7.99 (d, 1H, *J* 3.9), 5.97 (t, 1H, *J* 3.4), 5.52 (d, 1H, *J* 3.6), 5.49 (t, 1H, *J* 6), 5.44 (t, 1H), 3.74 (m, 1H), 3.71 (m, 1H), 3.18 (m, 1H), 3.34 (m, 1H); δ_C (DMSO-d_6) 163.71, 148.61, 145.05, 110.87, 99.62, 88.74, 64.99, 35.56; HRMS (FAB): M^+ calcd for $C_8H_{11}N_2O_5S$ 247.038868, found 247.039700. For **26**: mp 188–189 °C; δ_H (DMSO-d_6) 11.55 (s, 1H), 7.86 (s, 1H), 5.93 (dd, 1H, *J* 1.2, 5.0), 5.38 (m, 2H), 3.73 (m, 1H), 3.63 (m, 1H), 3.44 (dd, 1H, *J* 5.2, 12.6), 3.31 (d, 1H, *J* 12.4), 1.74 (s, 3H); δ_C (DMSO-d_6) 163.35, 148.12, 140.39, 110.53, 107.23, 88.40, 64.90, 35.49, 11.67; LRMS (FAB) *m/z* = 261 (MH^+). For **27**: mp 146–147 °C; δ_H (DMSO-d_6) 11.54 (s, 1H), 7.77 (d, 1H, *J* 1.2), 6.04 (d, 1H, *J* 4.4), 5.62 (t, 1H, *J* 5.0), 5.19 (br s, 1H), 3.64 (m, 1H), 3.52 (m, 1H), 3.35 (dd, 1H, *J* 4.6, 12.3), 3.21 (d, 1H, *J* 12.4), 1.75 (d, 3H, *J* 1.0); δ_C (DMSO-d_6) 163.36, 148.14, 140.22, 108.96, 107.53, 86.46, 63.84, 34.67, 11.73; LRMS (FAB) *m/z* = 261 (MH^+). For **29** mp 210-212 °C; δ_H (DMSO-d_6) 7.83 (d, 1H, *J* 7.5), 7.27 (br d, 2H), 5.92 (dd, 1H), 5.60 (d, 1H, *J* 7.5), 5.43 (t, 1H), 5.37 (t, 1H, *J* 5.0), 3.75 (m, 1H), 3.61 (m, 1H), 3.42 (m, 1H); δ_C (DMSO-d_6) 165.00, 152.07, 144.82, 109.89, 93.07, 88.72, 65.44, 35.81; LRMS (FAB) *m/z* = 246 (MH^+). For **31** mp 183–185 °C; δ_H (DMSO-d_6) 7.78 (d, 1H, *J* 7.4), 7.47 (br d, 2H), 6.08 (dd, 1H), 5.62 (d, 1H, *J* 7.6), 5.59 (t, 1H, *J* 5.0), 5.20 (br s, 1H), 3.67 (m, 1H), 3.55 (m, 1H), 3.48 (m, 2H); LRMS (FAB) *m/z* = 246 (MH^+).

ChemComm

Highly stable cage-like complexes by self-assembly of tetracationic Zn(II) porphyrinates and tetrasulfonatocalix[4]arenes in polar solvents†

Roberto Fiammengo, Peter Timmerman,* Feike de Jong and David N. Reinhoudt

Laboratory of Supramolecular Chemistry and Technology, MESA+ Research Institute, P.O. Box 217, 7500 AE Enschede, The Netherlands. E-mail: d.n.reinhoudt@ct.utwente.nl

Received (in Liverpool, UK) 18th August 2000, Accepted 10th October 2000
First published as an Advance Article on the web 9th November 2000

Tetracationic Zn(II) porphyrinates and tetraanionic calix[4]arenes can be assembled in polar solvents to obtain cage-like complexes in an entropy driven process. These structures are remarkably stable even in the presence of water or competing salts.

Metalloporphyrins are well known for their ability to bind a variety of small molecules[1–6] and for their catalytic properties.[7,8] Moreover, they have been intensively studied with respect to their occurrence in metalloporphyrin-dependent proteins,[9,10] in which they display largely differentiated chemical properties. The chemical behavior of a metalloporphyrin is strongly affected by the surrounding environment.[11] For example, the peptidic backbone in metalloporphyrin-dependent proteins is able to fine-tune the chemical properties of the metal center by means of non-covalent interactions. Most studies with synthetic porphyrins heavily rely on the covalent modification of the macrocyclic structure,[1,12] while studies on porphyrins with a non-covalently organized periphery have hardly been reported so far. In this communication we describe the formation and characterization of cage-like complexes **1·2**, consisting of cationic porphyrins **1** and anionic calix[4]arenes **2** (see Fig. 1), *that are very stable in polar solvents* such as MeOH DMSO and DMPU.‡§

Zinc(II) *meso*-tetrakis(*N*-alkylpyridinium-3-yl)-porphyrins **1a–c** were prepared in three steps starting from pyridine-3-carboxyaldehyde and pyrrole in an overall yield of 14–18% following literature procedures.[5] Tetrasulfonatocalix[4]arene **2** was obtained in 84% yield by sulfonation of the parent 25,26,27,28-tetrakis(2-ethoxyethoxy)calix[4]arene with concentrated sulfuric acid using a slightly modified literature procedure.[13]

The assembly process was first studied by UV spectroscopy. Addition of calix[4]arene **2** to a solution of porphyrins **1** in MeOH ($2–3 \times 10^{-6}$ M) causes a bathochromic shift (3–5 nm) of the porphyrin's Soret band with a concomitant 20–25% decrease in ε (molar absorptivity) at λ_{max}. This behavior is characteristic for cationic pyridiniumyl porphyrins that form ion-pair complexes in water.[14] Non-linear least-squares fitting analysis of the spectral changes using a 1 : 1 binding model gave association constants in the order of 10^7 M^{-1} for the complexes **1·2** (see Table 1). The presence of a well-defined isosbestic point during the titration strongly supports the proposed formation of a 1 : 1 complex. These high values most likely reflect the perfect complementarity in charge distribution of the two interacting molecular ions leading to the formation of strong, cooperative salt bridges. Nevertheless these ion-pair complexes remain highly dynamic structures as we were unable to observe any time dependent phenomenon either by NMR or by UV-vis experiments.

In order to determine the thermodynamic parameters associated with the assembly formation, the stability constant of complex **1a·2** was determined at different temperatures. Van't Hoff analysis of the binding data revealed that the process is strongly entropically driven (129 ± 24 J K^{-1} mol^{-1}) with a very small exothermic contribution (-8.0 ± 6.7 kJ mol^{-1}). Therefore, we conclude that the release of solvent molecules is the

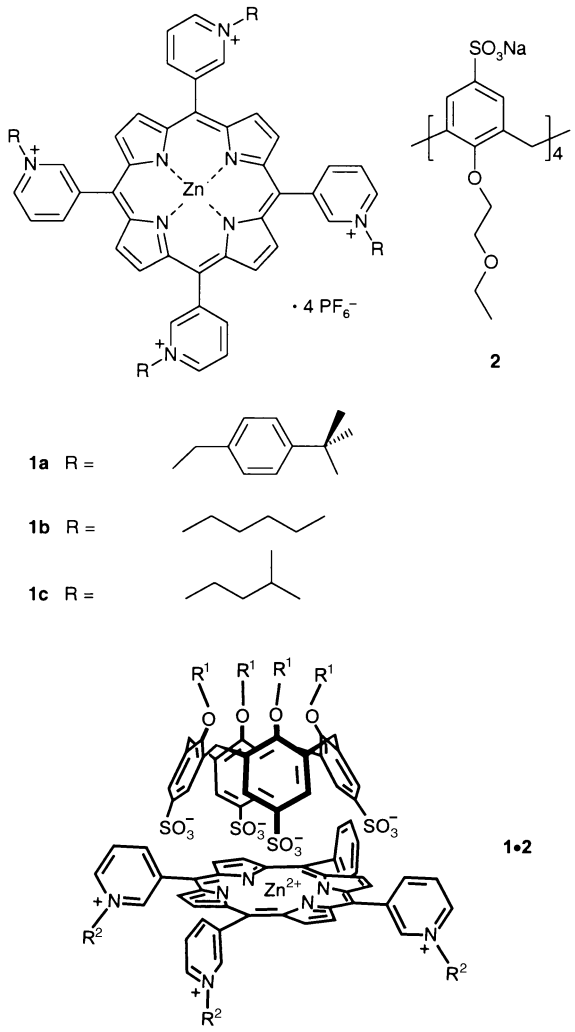

Fig. 1 Molecular structure of components **1**, **2**, and 1 : 1 complex **1·2**.

Table 1 Association constants for the assembly of cationic zinc porphyrinates **1** with the anionic calix[4]arene **2**

Assembly	Solvent	Log $K_{1:1}$
1a·2	CH_3OH	7.11 ± 0.04
1b·2	CH_3OH	7.04 ± 0.20
1c·2	CH_3OH	7.15 ± 0.09
1a·2	DMSO	6.21 ± 0.03
1a·2	DMPU	6.16 ± 0.01
1a·2	H_2O–DMPU x_{water} = 0.26	6.04 ± 0.02

† Electronic supplementary information (ESI) available: Figs. 3–6. See http://www.rsc.org/suppdata/cc/b0/b006960o/

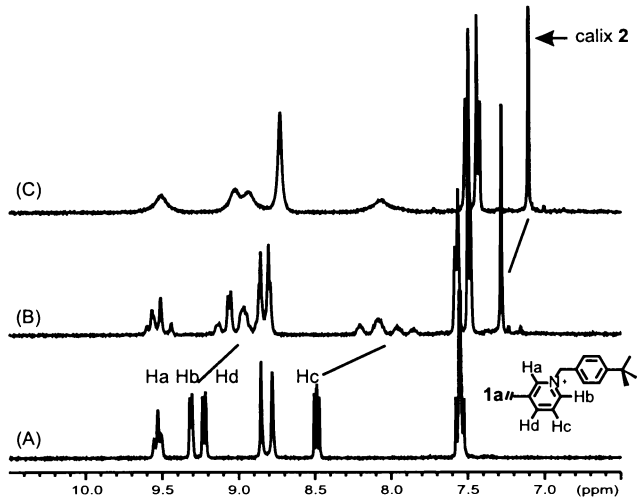

Fig. 2 ^{1}H NMR of (A) porphyrin **1a**, (B) 1:1 mixture of **1a** and **2** at 298 K, (C) 1:1 mixture of **1a** and **2** at 343 K.

main driving force for the formation of the highly stable ion-pair complexes **1·2** in MeOH.[15]

Structural investigation of complex **1a·2** by ^{1}H NMR spectroscopy was performed in CD_3CN–D_2O (6.5:1.5). At ambient temperatures the porphyrin proton signals show a complicated set of signals that indicate the presence of a mixture of isomeric structures with reduced symmetry. The calix[4]arene strongly influences the atropoisomerization equilibrium of the porphyrin,[5] without inducing a particular conformational preference. Coalescence of the various signals occurs at higher temperatures, whereby the position of the averaged signals is significantly shifted upfield in comparison to the corresponding signals in the free porphyrin. The largest shifts are observed for protons H_b, H_c and H_d (0.3–0.7 ppm) (see Fig. 2), which suggests that these protons are located in closest proximity to the calix[4]arene unit. Molecular simulation studies (CHARMm 24.0) support this view and further show that the structure in which the alkyl chains are pointing away from the calix[4]arene minimizes the distance between opposite charges in the two building blocks.¶

The cage-like structure of these ion-pair complexes prompted us to study their formation in other polar solvents such as DMSO and DMPU, from which the individual molecules are more bulky than MeOH. Titration experiments with **1a** and **2** in these solvents also gave well-defined isosbestic spectral variations. However, no shift in the maximum (DMSO) or a 5 nm blue shift (DMPU) was observed. This indicates a different solvation shell around the porphyrin upon formation of the complex in these solvents. Moreover, the $K_{1:1}$ values are one order of magnitude smaller than in MeOH (Table 1), which might indicate that MeOH is probably a very good guest for the cage-like complex‖ and enhances the stability of the system. Further experiments on solvent or guest encapsulation in these cage-like structures are currently ongoing in our laboratories.

Furthermore, we examined the effect of adding salts on the stability of the ion-pair complexes: association constants were determined for assembly **1a·2** in DMSO at different concentrations of $NaClO_4$. A logarithmic plot of $K_{1:1}$ and $[NaClO_4]$ shows a bimodal linear relationship with a slope of 1.91 ± 0.11 for $[NaClO_4] > 2 \times 10^{-3}$ M. This behavior suggests that, at high concentrations of Na^+, calix[4]arene **2** complexes two Na^+ ions in a cooperative fashion, as indicated by the sharp curvature at the breaking point, with $\beta = 2.2\ 10^5\ M^{-2}$. Determination of the $K_{1:1}$ value at 10^{-2} M of Bu_4NClO_4 clearly showed a smaller effect in comparison to $NaClO_4$ at the same concentration ($pK_{1:1}$ = 5.22 ± 0.08 and 4.56 ± 0.03 for Bu_4NClO_4 and $NaClO_4$ respectively). Therefore, it can be concluded that addition of inert salts, as much as 4500 times the concentration of the building blocks, only reduces the stability of the complex by a factor of 10.

Finally, we have found that the influence of the presence of water on the stability of the assemblies is very small. The log $K_{1:1}$ value is 6.04 ± 0.02 in a H_2O–DMPU mixture (x_{water} = 0.26), which is comparable to the value of 6.16 ± 0.01 obtained in pure DMPU (see Table 1).

In conclusion we have shown that stable cage-like complexes are obtained by self-assembly of cationic porphyrins and anionic calix[4]arenes in polar solvents. These assemblies are formed as a result of multiple electrostatic interactions between oppositely charged building blocks and are highly stable in polar solvents, like MeOH DMSO and DMPU. Furthermore, they remain stable even in the presence of water and, to a large extent, upon the addition of electrolytes.

These investigations are supported by the Netherlands Research Council for Chemical Sciences (CW) with financial aid from the Technology Foundation STW.

Notes and references

‡ DMPU = 1,3-dimethyl-3,4,5,6-tetrahydropyrimidin-2(1*H*)-one).

§ Self-assembled molecular capsules formed by means of ionic interactions have been reported using cyclotriveratrylene building blocks[16] or cyclodextrin derivatives.[17] In the first case the authors did not report the formation constant for the 1:1 complex and they observed the presence of oligomers at 7 mM in DMSO-d_6. In the paper dealing with cyclodextrins indirect proof for the existence of the capsules was obtained from the calculation of self-diffusion coefficients *via* ^{1}H NMR techniques.

¶ The symmetrical situation as observed from a gas-phase simulation (see ESI) is likely reflecting the structure of the complex at temperatures higher than rt.

‖ Coordination of MeOH to zinc(II) porphyrin hosts have been observed in several cases.[18]

1 J. P. Collman and L. Fu, *Acc. Chem. Res.*, 1999, **32**, 455.
2 N. Bampos, V. Marvaud and J. K. M. Sanders, *Chem. Eur. J.*, 1998, **4**, 335.
3 H. L. Anderson and K. M. Sanders, *Angew. Chem., Int Ed. Engl.*, 1990, **29**, 1400.
4 T. Mizutani, T. Murakami, T. Kurahashi and H. Ogoshi, *J. Org. Chem.*, 1996, **61**, 539.
5 T. Mizutani, T. Horiguchi, H. Koyama, I. Uratani and H. Ogoshi, *Bull. Chem. Soc. Jpn.*, 1998, **71**, 413.
6 M. Sirish and H.-J. Schneider, *Chem. Commun.*, 1999, 907.
7 J. P. Collman, J. I. Brauman, B. Meunier, T. Hayashi, T. Kodadek and S. A. Raybuck, *J. Am. Chem. Soc.*, 1985, **107**, 2000.
8 J. Bernadou and B. Meunier, *Chem. Commun.*, 1998, 2167.
9 *Cytochrome P-450: Structure, Mechanism and Biochemistry*, ed. P. R. Ortiz de Montellano, Plenum Press, New York, 2nd edn., 1995.
10 *Peroxidases in Chemistry and Biology*, ed. J. Everse, K. E. Everse and M. P. Grisham, CRC Press, Boca Raton, FL, 1991, vol. I and II.
11 D. Liu, D. A. Williamson, M. L. Kennedy, T. D. Williams, M. M. Morton and D. R. Benson, *J. Am. Chem. Soc.*, 1999, **121**, 11 798.
12 D. M. Rudkevich, W. Verboom and D. N. Reinhoudt, *J. Org. Chem.*, 1995, **60**, 6585.
13 A. Casnati, Y. Ting, D. Berti, M. Fabbi, A. Pochini, R. Ungaro, D. Sciotto and G. G. Lombardo, *Tetrahedron*, 1993, **49**, 9815.
14 H.-J. Schneider and M. Wang, *J. Org. Chem.*, 1994, **59**, 7464.
15 B. Linton and A. D. Hamilton, *Tetrahedron*, 1999, **55**, 6027.
16 S. B. Lee and J.-I. Hong, *Tetrahedron Lett.*, 1996, **37**, 8501.
17 B. Hamelin, L. Jullien, C. Derouet, C. Hervé du Penhoat and P. Berthault, *J. Am. Chem. Soc.*, 1998, **120**, 8438.
18 R. P. Bonar-Law and J. K. M. Sanders, *J. Am. Chem. Soc.*, 1995, **117**, 259.

ChemComm

Synthesis of a novel bis-amino-modified thymidine monomer for use in DNA triplex stabilisation

Matthieu Sollogoub,[a] Beatriz Dominguez,[a] Keith R. Fox[b] and Tom Brown*[a]

[a] *Department of Chemistry, University of Southampton, Highfield, Southampton, UK SO17 1BJ. E-mail: tb2@soton.ac.uk*

[b] *Division of Biochemistry and Molecular Biology, School of Biological Sciences, University of Southampton, Bassett Crescent East, Southampton, UK SO16 7PX. E-mail: krf1@soton.ac.uk*

Original manuscript received 2nd August 2000, Revised manuscript received 2nd October 2000, Accepted 16th October 2000
First published as an Advance Article on the web 9th November 2000

A novel thymidine analogue containing both 5-aminopropargyl† and 2′-aminoethoxy modifications has been synthesised and incorporated into a triplex-forming oligonucleotide; the combination of the two amino groups on the same nucleoside greatly enhances triplex stability.

DNA triple-helix formation by sequence-specific triplex-forming oligonucleotides is of considerable interest because of its great potential in a variety of analytical and therapeutic applications, including selective control of gene expression,[1] site-directed mutagenesis,[2] gene repair,[3] *in situ* chromosome labelling and other molecular diagnostics.[4] Although triplex-forming oligonucleotides bind with high specificity, their binding is usually much weaker than that of the underlying DNA duplex. In part this is thought to be due to the charge repulsion resulting from bringing together the three polyanionic DNA strands. Studies by ourselves and others[5] have shown that the introduction of positively charged groups at multiple sites in the backbone, sugar or base can produce stable triplexes, but to date only one such group has been added per nucleoside. Combining two of these modifications in a single nucleoside should produce stable triplexes across a wide range of salt concentrations, particularly under physiological conditions.

To test this hypothesis, we have synthesised a thymidine analogue containing two modifications that individually are known to stabilise triplexes: 5-aminopropargyl[6] and 2′-aminoethoxy.[7] These groups were specifically chosen so that the amines would act at different sites in a cooperative manner. An obvious synthesis for such a compound appears to be alkylation of the 2′-position of the nucleoside as reported for the 2′-aminoethoxy thymidine analogue.[7] However this strategy was not successful for our compound due to side reactions at the 5-position of the pyrimidine. We therefore had to adopt a longer route including a glycosylation step after introduction of the aminoethoxy moiety onto the sugar. The successful synthesis of the doubly modified monomeric thymidine building block **6** is shown in Scheme 1.

Alkylation of the protected β-Me ribofuranoside **1**[8] with methyl bromoacetate in the presence of sodium hydride (74% yield), followed by reduction of the ester by $LiBH_4$ and replacement of the hydroxy group by a phthalimide substituent using Mitsunobu[9] conditions yielded **2** (89% for two steps). Phthalimide is a suitable protecting group for oligonucleotide synthesis because of its stability to the acidic conditions encountered in dimethoxytrityl removal and ease of removal in standard basic conditions at the end of the synthesis. Attempted glycosylations[10] with **2** resulted in ring opening of the sugar. The anomeric position was therefore activated by means of an acetyl group *via* acetolysis with acetic anhydride and a catalytic amount of sulfuric acid in glacial acetic acid. Under these conditions[8] the TIPDS was replaced by acetyls to afford **3** in 95% yield. Triacetate **3** was transformed into the desired nucleoside **4** in 82% yield with silylated 5-iodouracil in the presence of TMSOTf (Vorbrüggen reaction conditions,[11] 82% yield, 2:1 β–α separable mixture). The β-anomer was then deacetylated using NaOMe powder in MeOH and the reaction was quenched by Dowex 50 (pyridinium form) then directly tritylated with freshly recrystallised dry DMTrCl in pyridine to yield **5** (63% for two steps). The aminopropargyl moiety was added protected as the trifluoroacetamide (equally suitable to oligonucleotide synthesis as phthalimide) by a palladium coupling reaction[12] in 89% yield. Conventional phosphitylation of the 3′-hydroxy group in an inert atmosphere using 2-cyanoethoxy(*N*,*N*-diisopropylamino)chlorophosphine afforded the phosphoramidite monomer **6** suitable for oligonucleotide synthesis in 70% yield.

Oligonucleotide syntheses were performed on an ABI 394 automated DNA/RNA synthesiser following standard cycles. The monomer **6** was incorporated in good yield (5 min coupling, > 98.5%) and oligonucleotides were deprotected with concentrated aqueous NH_3 at 55 °C for 5 h. After reversed-phase HPLC purification, the oligonucleotides were desalted (Sephadex G25) and characterised by ESMS.

We synthesised the intramolecular triplex forming oligonucleotide P3 containing a double substitution of the modified monomer **6** and the UV-melting curve was monitored at pH 7 (Table 1). P3 showed an increase in T_m of 22.9 K relative to P2 which contains two aminopropargyl modifications and an increase of 48.7 K relative to unmodified oligonucleotide P1. The general sequence of oligonucleotides P1, P2 and P3 was

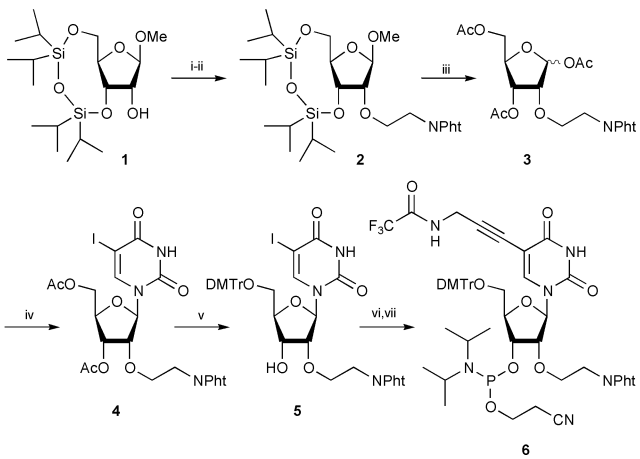

Scheme 1 *Reagents and conditions:* (i) $BrCH_2CO_2Me$ (5 eq.), NaH (2.2 eq.), DMF, RT, 3 h, 74 %; (ii) (a) $LiBH_4$ (2 eq.), THF, MeOH, −20 → 0 °C, 1 h; (b) PhtNH (1.05 eq.), PPh_3 (1.05 eq.), DEAD (1.05 eq.), THF, RT, 30 min, 89 %; (iii) Ac_2O, AcOH, H_2SO_4, RT, 3 h, 95%; (iv) 5-iodouracil-bis-TMS (3 eq.), TMSOTf (3 eq.), $Cl(CH_2)_2Cl$, −20 →0 °C, 3 h, 82% (α:β 1:2); (v) (a) MeONa (3 eq.), MeOH, RT, 5 min; (b) DMTrCl (3 eq.), Py, RT, 3 h, 63%; (vi) $HC{\equiv}CCH_2NHCOCF_3$ (3 eq.), CuI (0.25 eq.), Et_3N (5 eq.), $Pd(PPh_3)_4$ (0.1 eq.), DMF, RT, 16 h, 89%; (vii) $(iPr)_2NP(Cl)OCH_2CH_2CN$ (1.5 eq.), DIPEA (2.2 eq.), CH_2Cl_2, RT, 16 h, 70%.

DOI: 10.1039/b006268p

Table 1 Melting temperatures (T_m) measured at pH 7.0; 50 mM phosphate buffer with 100 mM NaCl : L, octanediol linker; ^{p}U, 5-aminopropargyl modified T; X, bis-amino modified T

	Oligonucleotide	T_m/K
P1	T_6-L_2-T_6-AGTCT-L_2-AGACT-A_6	295
P2	T^{p}UT^{p}UTT-L_2-T_6-AGTCT-L_2-AGACT-A_6	320.8
P3	TXTXTT-L_2-T_6-AGTCT-L_2-AGACT-A_6	343.4

chosen as this motif is known to give clear triplex melting transitions.[6]

Footprinting data from a 9-mer oligonucleotide containing three bis-amino-modified thymidines (XTTXTTCXT) showed a reduction in the intensity of bands within the footprint by 50% at a concentration of 1.0 ± 0.5 μM. This is in contrast to the same sequence with three aminopropargyl T nucleosides which failed to show a footprint at concentrations as high as 50 μM. The footprints were located at a single target site within a 110 base pair fragment indicating that the oligonucleotide retained considerable sequence selectivity.

The above UV-melting data (intramolecular triplexes) and DNase I footprinting experiments (intermolecular triplexes) show that the 5-aminopropargyl/2′-aminoethoxy combination contributes significantly to triplex stabilisation, and is greatly superior to the aminopropargyl substitution alone. Hence the doubly modified nucleotide **6** appears to be a very promising building block for triplex-forming oligonucleotides.

We thank the Cancer Research Campaign for supporting this work.

Notes and references

† The IUPAC name for propargyl is prop-2-ynyl.

1 C. Giovannangeli and C. Helene, *Antisense Nucleic Acid Drug Dev.*, 1997, **7**, 413; C. Giovannangeli, L. Perrouault, C. Escude, N. Thuong and C. Helene, *Biochemistry*, 1996, **35**, 10 539; L. J. Maher, P. B. Dervan and B. Wold, *Biochemistry*, 1992, **31**, 70.
2 G. Wang, D. D. Levy, M. M. Seidman and P. M. Glazer, *Mol. Cell. Biol.*, 1995, **15**, 1759; G. Wang, M. M. Seidman and P. M. Glazer, *Science*, 1996, **271**, 802.
3 S. Broitman, O. Amosova, N. G. Dolinaya and J. R. Fresco, *J. Biol. Chem.*, 1999, **274**, 21 763.
4 M. D. Johnson and J. R. Fresco, *Chromosoma*, 1999, **108**, 181.
5 For a review see: K. R. Fox, *Curr. Med. Chem.*, 2000, **7**, 17.
6 J. Bijapur, M. D. Keppler, S. Bergqvist, T. Brown and K. R. Fox, *Nucleic Acids Res.*, 1999, **27**, 1802.
7 B. Cuenoud, F. Casset, D. Husken, F. Natt, R. M. Wolf, K.-H. Altmann, P. Martin and H. E. Moser, *Angew. Chem., Int. Ed.*, 1998, **37**, 1288.
8 J. P. Schaumberg, G. C. Hokanson and J. C. French, *J. Org. Chem.*, 1985, **50**, 1651.
9 O. Mitsunobu, *Synthesis*, 1981, 1.
10 P. Martin, *Helv. Chem. Acta*, 1996, **79**, 1930.
11 H. Vorbrüggen, K. Krolikiewicz and B. Bennua, *Chem. Ber.*, 1981, **114**, 1234.
12 S. Takahashi, Y. Kuroyama, K. Sonogashira and N. Hagihara, *Synthesis*, 1980, 627; F. W. Hobbs, *J. Org. Chem.*, 1989, **54**, 3420.

Catalytic radical addition of ketones to alkenes by a metal–dioxygen redox system

Takahiro Iwahama, Satoshi Sakaguchi and Yasutaka Ishii*

Department of Applied Chemistry, Faculty of Engineering & High Technology Research Center, Kansai University, Suita, Osaka 564-8680, Japan. E-mail: ishii@ipcku.kansai-u.ac.jp

Received (in Cambridge, UK) 5th September 2000, Accepted 2nd October 2000
First published as an Advance Article on the web 9th November 2000

Radical addition of ketones to alkenes catalyzed by $Mn(OAc)_2$ combined with $Co(OAc)_2$ using dioxygen as oxidant was developed; for instance, the reaction of cyclohexanone with oct-1-ene in the presence of very small amounts of $Mn(OAc)_2$ and $Co(OAc)_2$ under air (1 atm) gave 2-octylcyclohexanone in good selectivity; from styrene, a six-membered cyclic peroxide was isolated in good yield.

Free radical reactions in organic synthesis have been recognized as a powerful tool for the construction of C–C and C–X (X = H or heteroatoms) bonds.[1] However, a limited number of methods have appeared for the generation of α-keto carbon radicals in spite of their synthetic importance.[1,2] Among the methods developed for this purpose, peroxide- and metal-initiated reactions of ketones are often used.[2a–d] Thus, the addition of α-keto radicals to alkenes which leads to α-alkylated ketones is practiced by the use of high oxidation state metal ions such as Mn(III), Ce(IV), Ag(II) and Pb(IV).[2c,d] Unfortunately, most reported procedures call for a large quantity of the metal reagent. To the best of our knowledge, there is only one report on the catalytic addition of α-keto radicals to alkenes *via* a catalytic process using $AgNO_3$ and $Na_2S_2O_3$ as the reoxidant.[3] If the addition of ketones to alkenes can be achieved by using a catalytic amount of metal ions in combination with an appropriate oxidizing agent, the reaction would become an effective tool for the synthesis of α-alkylated ketones. From environmental and economic aspects, molecular oxygen is the best candidate as the oxidant to regenerate the reduced metal ions to a high oxidation state, but such a catalytic system has not yet been developed. Here we wish to report a novel catalytic radical addition of ketones to alkenes by Mn(II) combined with Co(II) under dioxygen [eqn. (1)].

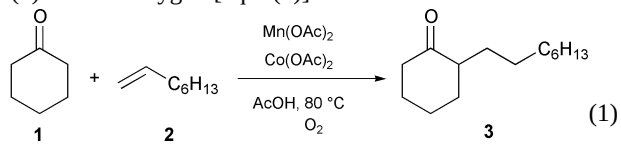

1 2 3 (1)

To highlight the possibility of using dioxygen as reoxidant, the addition of cyclohexanone (**1**) to oct-1-ene (**2**) was carried out in the presence of a catalytic amount of $Mn(OAc)_3$ (0.5 mol%) having one-electron oxidizing ability under either an inert gas (N_2) or air (1 atm) in AcOH at 80 °C for 5 h (Table 1, runs 1 and 2).† The reaction under N_2 led to an adduct, 2-octylcyclohexanone (**3**), in low yield (4%), while the reaction under air afforded **3** in better yield (26%). This fact indicates that the reduced Mn(II) species can be continually reoxidized to Mn(III) by O_2 making use of $Mn(OAc)_2$, which is cheaper than $Mn(OAc)_3$, more viable for reactions under O_2 instead of $Mn(OAc)_3$. In fact, $Mn(OAc)_2$ in the presence of O_2 promoted the reaction to a similar extent as $Mn(OAc)_3$ did (run 3). Needless to say, the reaction did not take place at all by $Mn(OAc)_2$ under N_2 (run 4).

The present reaction was found to be facilitated by adding a small amount of $Co(OAc)_2$ (0.1 mol%) to $Mn(OAc)_2$ (0.5 mol%) to give **3** in 88% selectivity at 41% conversion (run 6), while the reaction was not induced by Co(II) alone (run 7).‡ The addition proceeded smoothly even with a very small amount of $Mn(OAc)_2$ and $Co(OAc)_2$ (run 10). Since Co(II) ions are well-known to react easily with O_2 to form a Co(III)–dioxygen complex such as a superoxocobalt(III) or peroxocobalt(III) complex,[4] it is thought that such a Co(III) species catalyzes the reoxidation of the reduced Mn(II) to Mn(III) under O_2.

Table 1 Reaction of cyclohexanone (**1**) to oct-1-ene (**2**) by $Mn(OAc)_2$ combined with $Co(OAc)_2$ under various conditions[a]

Run	mol% Mn	mol% Co	Oxygen source (N_2–O_2 atm)	Time/h	Conv. (%)[b]	Select. (%)[c]
1[d]	0.5	—	N_2	5	< 10	4[e]
2[d]	0.5	—	Air	5	35	26[e]
3	0.5	—	Air	5	32	69
4	0.5	—	N_2	5	No reaction	
5[d]	0.5	0.1	N_2	5	< 8	5[e]
6	0.5	0.1	Air	5	41	88
7	—	0.5	Air	5	< 2	Trace
8	0.5	0.1	Air	10	57	83
9[f]	0.5	0.1	Air	10	57	85
10[g]	0.01	0.005	Air	10	30	72
11	0.5	0.1	0.9 : 0.1	10	11	80
12	0.5	0.1	0.5 : 0.5	10	72	83
13	0.5	—	0.5 : 0.5	10	49	72
14	0.5	0.1	0.3 : 0.7	10	69	81
15	0.5	0.1	O_2	10	87	62
16	0.1	0.05	0.5 : 0.5	10	70	85

[a] **2** (2 mmol) was allowed to react with **1** (20 mmol) under dioxygen in the presence of $Mn(OAc)_2$ and $Co(OAc)_2$ in AcOH (2 mL) at 80 °C. [b] Conversion of **2**. [c] Based on **2** reacted. [d] $Mn(OAc)_3$ was used instead of $Mn(OAc)_2$. [e] Yield based on **2** used. [f] AcOH (0.5 mL) was used. [g] **1** (5 eq.) was used.

The remarkable effect of oxygen concentration on the reaction of **1** with **2** was observed (runs 11–16). When a mixed gas of 0.5 : 0.5 atm of N_2–O_2 was employed, **3** was obtained in 83% selectivity at 72% conversion (run 12).

On the basis of these results, the addition of various ketones to alkenes was examined under the optimized reaction conditions (Table 2).

Both cyclic and aliphatic ketones were added to **2** to give the corresponding adducts in fair to good yields (runs 1–4). The reaction of an unsymmetrical ketone such as pentan-2-one (**4**) with **2** led to two structural isomers, 3-ethylundecan-2-one (**5**) and tridecan-4-one (**6**), in a ratio of *ca.* 6 : 1. The preferential formation of **5** is believed to be due to the fact that the secondary carbon radical is more easily generated than the primary one.

From isopropenyl acetate, γ-acetoxy ketone was obtained in relatively good selectivity (run 5). The reaction of **1** with styrene (**7**) did not form the expected adduct but gave a cyclic peroxide (**8**) in 41% yield (run 6). Such six-membered cyclic peroxides are known to exhibit significant biological activities.[5] The peroxide **8** may be formed through the reaction path shown in Scheme 1. A benzyl radical (**B**) derived from the addition of an α-keto radical (**A**) to **7** reacts with O_2 rather than **1**, giving an alkylperoxy radical (**C**) which then undergoes intramolecular cyclization leading to **8**.[6] It is believed that the benzyl radical **B** which is stabilized by conjugation with the phenyl group is

Table 2 Reaction of various ketones with alkenes[a]

Run	Ketone	Alkene	Conv. (%)[b]	Products	Select. (%)[c]
1		**2**	78	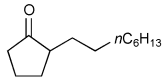	85
2[d]	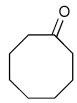	**2**	68	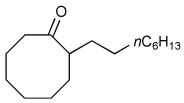	82
3		**2**	73	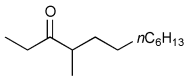	62
4	 **4**	**2**	78	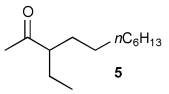 **5** + 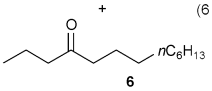 **6**	71 (6 : 1)[e]
5	**1** 		86	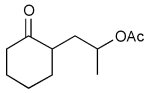	61
6[d,f]	**1**  **7**		92	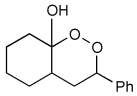 **8**	41[g]
7[d,h]	**1**	**7**	96	**8**	70[i]

[a] Alkenes (2 mmol) were allowed to react with ketones (20 mmol) under 0.5:0.5 atm of N_2–O_2 in the presence of $Mn(OAc)_2$ (0.5 mol%) and $Co(OAc)_2$ (0.1 mol%) in AcOH (2 mL) at 80 °C for 10 h. [b] Conversion of alkenes. [c] Based on alkenes reacted. [d] Ketone (10 mmol) was used. [e] Ratio of **5**:**6**. [f] Reaction was carried out at 70 °C for 3 h. [g] ^{1}H-NMR yield based on **7** used. [h] Reaction was carried out in the absence of $Co(OAc)_2$ under O_2 (1 atm). [i] Isolated yield based on **7** used.

unable to abstract a hydrogen atom from **1**. Since Co ions are known to promote the redox decomposition of the peroxides,[7] the reaction was conducted without Co(II) to give **8** in 70% yield (run 7).

In conclusion, we have developed a novel catalytic method for the addition of ketones to alkenes by the combined use of Mn(II) and Co(II) salts using dioxygen as the reoxidant. This method provides an alternative route to α-alkylated cycloalkanones which are attractive compounds as fine chemicals such as fragrances. Further investigation to extend the present method and to elucidate the role of the Co(II) species is currently in progress.

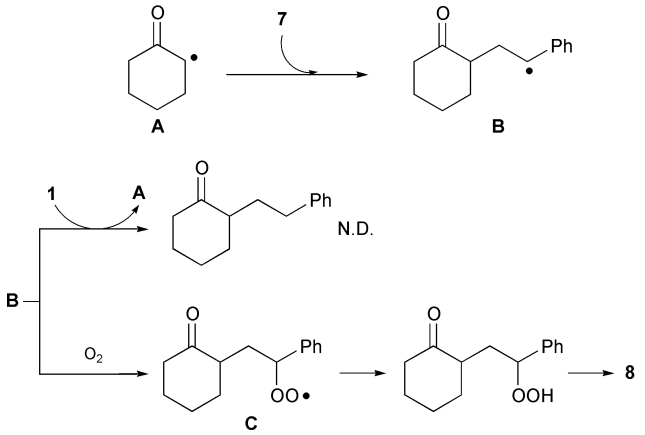

Scheme 1

This work was partly supported by the Japan Society for the Promotion of Science under the Research for the Future program, JSPS.

Notes and references

† *A typical procedure for reaction of cyclohexanone* **1** *with oct-1-ene* **2**: To a solution of **1** (20 mmol), $Mn(OAc)_2$ (0.1–0.5 mol%) and $Co(OAc)_2$ (0.05–0.1 mol%) in AcOH (2 mL) in a two-necked flask equipped with a balloon filled with an appropriate concentration of O_2 was added **2** (2 mmol), and the mixture was stirred at 80 °C for 5 h. After evaporation of AcOH and unreacted **1**, 2-octylcyclohexanone (**3**) was isolated by flash chromatography on silica gel (*n*-hexane–AcOEt = 5:1).

‡ By the reaction using the combined catalytic systems of $Mn(OAc)_2$ with other metals such as $Cu(OAc)_2$, $VO(acac)_2$, $Ni(acac)_2$ and $Fe(acac)_3$, the yield of **3** was not improved.

1 B. Giese, *Radicals in Organic Synthesis: Formation of Carbon–Carbon Bonds*, Pergamon, Oxford, 1986.
2 (*a*) J. C. Allen, J. I. G. Cadogan and D. H. Hey, *J. Chem. Soc.*, 1965, 1918; (*b*) E. I. Heiba and R. M. Dessau, *J. Am. Chem. Soc.*, 1971, **93**, 524; (*c*) M. Hajek and J. Malek, *Synthesis*, 1976, 315; (*d*) M. Hajek, P. Silhavy and J. Malek, *Tetrahedron Lett.*, 1974, **36**, 3193; (*e*) M. S. Kharash, J. Kuderna and W. Nudenberg, *J. Org. Chem.*, 1953, **18**, 1225; (*f*) H. J. Schafer, *Angew. Chem., Int. Ed. Engl.*, 1981, **20**, 911.
3 A. Citterio, F. Ferrario and S. De Bernardinis, *J. Chem. Res. (S)*, 1983, 310.
4 (*a*) R. S. Drago, J. P. Cannady and K. A. Leslie, *J. Am. Chem. Soc.*, 1980, **102**, 6014; (*b*) E. C. Niederhoffer, J. H. Timmons and A. E. Martell, *Chem. Rev.*, 1984, **84**, 137.
5 I. Saito and S. S. Nittala, *The Chemistry of Functional Groups, Peroxides*, ed. S. Patai, Wiley, New York, 1983.
6 C.-Y. Qian, H. Nishino, K. Kurosawa and J. D. Korp, *J. Org. Chem.*, 1993, **58**, 4448.
7 It is well-known that Co ions catalyze the decomposition of alkyl hydroperoxides; R. A. Sheldon and J. K. Kochi, *Metal Catalyzed Oxidations of Organic Compounds*, Academic Press, New York, 1981.

A highly convergent synthesis of a branched *C*-trisaccharide employing a double SmI_2-promoted *C*-glycosylation

Lise Munch Mikkelsen,[a] Sussie Lerche Krintel,[a] Jesús Jiménez-Barbero[b] and Troels Skrydstrup*[a]

[a] *Department of Chemistry, University of Aarhus, Langelandsgade 140, 8000 Aarhus C, Denmark. E-mail: ts@kemi.aau.dk; Fax: +45 8619 6199*

[b] *Instituto de Química Orgánica,CSIC, Juan de la Cierva 3, E-28006 Madrid, Spain*

Received (in Liverpool, UK) 29th August 2000, Accepted 10th October 2000
First published as an Advance Article on the web 9th November 2000

The branched *C*-trisaccharide analogue of α-D-Man-(1→3)-[α-D-Man-(1→6)]-D-Man has been synthesised by the SmI_2-mediated coupling of two mannosyl pyridyl sulfone units to a monosaccharide dialdehyde. This approach represents a highly convergent synthesis of a *C*-oligosaccharide.

C-Disaccharides, in which the interglycosidic linkage has been replaced by a methylene group, have proved to be valuable tools for studying conformational preferences of their parent *O*-glycosides both in solution and protein bound, as well as providing important insight into the mechanism of glycoside cleaving enzymes (glycosidases) owing to the inability of *C*-disaccharides to undergo hydrolysis.[1] Many synthetic approaches to these analogues have therefore been devised, but have mainly been restricted to disaccharides and not higher oligomers thereof owing to the synthetic challenge in preparing such compounds.[2,3] In previous reports, we have shown that reductive samariation of glycosyl pyridyl sulfones in the presence of a *C*-formyl branched sugar is a viable approach for the stereoselective construction of *C*-disaccharides.[4,5] The synthetic approach to these sugar mimics employs intact carbohydrate units as both *C*-glycosyl donors and acceptors, which are complementary to approaches exploited in standard *O*-glycoside synthesis. This suggested the possibility of applying this procedure for the construction of branched *C*-oligosaccharides as well, by a multiple *C*-glycosylation step of a carbohydrate unit containing more than one *C*-formyl chain. In this communication, we report on the success of this goal in the highly convergent construction of the *C*-glycoside analogue of the core region, α-D-Man-(1→3)-[α-D-Man-(1→6)]-D-Man, of the asparagine-linked oligosaccharides.

The synthetic approach to the branched *C*-trisaccharide **1** is illustrated in Fig. 1, comprising of the direct double coupling of dialdehyde **3** with two equivalents of the configurationally stable anomeric samarium species **2**, which in turn may easily be prepared *via* the *in situ* reduction of the anomeric pyridyl sulfone.[4,5] Subsequent radical-based deoxygenation of the two hydroxy groups formed would then complete this short synthesis of the protected *C*-trisaccharide.

We began the synthesis of the branched *C*-trisaccharide with the construction of the dideoxymannosyl unit **9** containing the C3 and C6 formyl groups *via* the stepwise introduction of two alkene groups at the denoted positions, as illustrated in Scheme 1.† Regioselective opening of the easily available epoxide **4** (5 steps from 1,6-anhydroglucose[6]) with excess vinylmagnesium bromide[7] and subsequent dibenzylation afforded the alkene **5** in 42% yield. In order to introduce the second alkene group at C-6, we took advantage of a recent report by Clark *et al.* in their synthetic approach to the marine polycyclic ethers of the brevetoxin and ciguatoxin family.[8] Hence, methanolysis of **5** led to the opening of the anhydro-ring affording only the methyl α-mannoside **6**, which could easily be transformed to the corresponding triflate by treatment with Tf_2O–2,6-lutidine. Alkynylation with the lithium anion of TMSacetylene in THF–HMPA then afforded the C6-alkyne branched sugar **7** (53%, 2

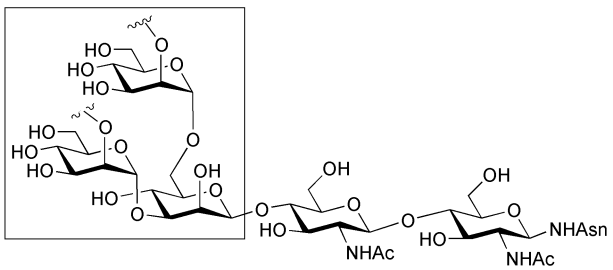

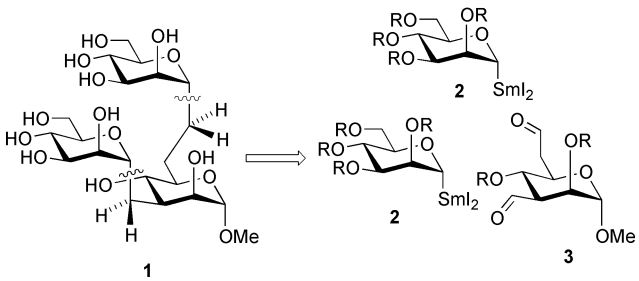

Fig. 1

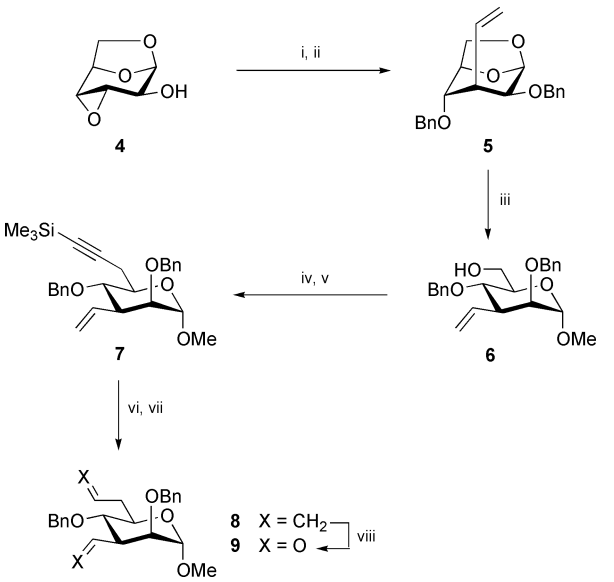

Scheme 1 *Reagents and conditions:* i, 3 equiv. of $CH_2CHMgBr$, THF, 60 °C; ii, NaH, BnBr, DMF, 42% (2 steps); iii, conc. HCl in MeOH, reflux, 56%; iv, Tf_2O, 2,6-lutidine, CH_2Cl_2, −40 °C; v, $Me_3SiCCLi$, THF–HMPA, −78 °C to 20 °C, 53% (2 steps); vi, Bu_4NF, THF, 20 °C; vii, H_2, Lindlar's catalyst, quinoline, EtOAc, 20 °C, 77% (2 steps); viii, O_3, CH_2Cl_2–MeOH, −78 °C, then Ph_3P, 77%.

DOI: 10.1039/b007117j

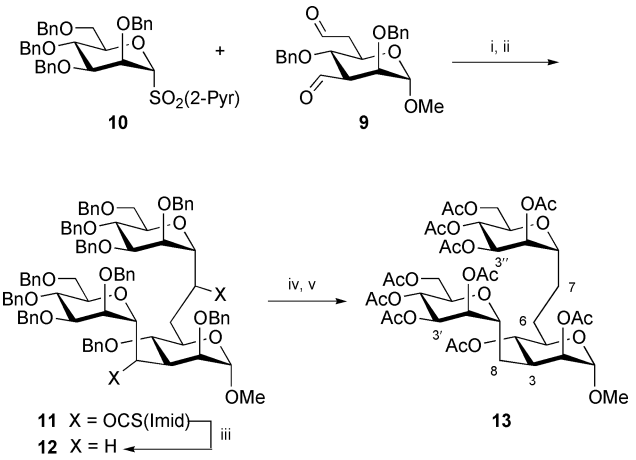

Scheme 2 *Reagents and conditions:* i, 4.7 equiv. of **10**, 10 equiv. of SmI_2, THF, 20 °C; ii, 25 equiv. of $(Imid)_2CS$, CH_3CN, reflux, 67% (2 steps); iii, 4 equiv. of F_5C_6OH, 5.2 equiv. of Ph_3SnH, AIBN (cat.), toluene, 90 °C, 53%; iv, Pd/C, H_2, MeOH–AcOH; v, Ac_2O, DMAP (cat.), pyridine.

steps), which was first desilylated and then hydrogenated with Lindlar's catalyst providing the dialkene **8** in 77% yield (2 steps). Finally, ozonolysis led to the required dialdehyde **9**.

The key coupling step of the dialdehyde with the mannosyl pyridyl sulfone **10** was achieved by quickly adding a 0.1 M solution of SmI_2 (10 equiv.) to a mixture of **9** with excess **10** (4.7 equiv.) at 20 °C leading to the immediate consumption of both reagents (Scheme 2).[4,5] Subsequent work-up led to a complex mixture of diastereomers, which was immediately subjected to a surplus of thiocarbonyldiimidazole (25 equiv.) in refluxing acetonitrile. A quick reaction was observed as monitored by TLC analysis leading to the introduction of a single thiocarbonylimidazole unit, which was most likely to occur at the sterically less encumbered carbon adjacent to C6. However, the slow evaporation of the solvent under heating finally led to the formation of a second more polar product at the expense of the first, which was identified as compound **11** as a mixture of diastereomers containing two functionalised alcohol groups (67% yield, 2 steps). The slow removal of the solvent is necessary for the successful introduction of the second thicarbonylimidazole moiety as previously observed in similar cases for the functionalisation of sterically hindered secondary alcohols.[4]

Finally, radical-based deoxygenation employing our established procedure with the F_5C_6OH–Ph_3SnH–AIBN combination in hot toluene[4] completed this short synthesis of the desired branched *C*-trisaccharide **12**, obtained as a single stereoisomer in 53% yield. Further characterisation of **12** was made by its conversion to the decaacetate **13** easily prepared by a two-step protocol involving catalytic hydrogenation and peracetylation.‡,§

In conclusion, we have successfully applied the SmI_2 promoted *C*-glycosylation procedure to the expedient and convergent synthesis of a branched *C*-trisaccharide related to the core structure of the asparagine-linked oligosaccharides. Work can now commence in studying its conformational behaviour in comparison to its parent *O*-glycoside, the investigation of which will be reported in due course.

We thank the Danish National Science Foundation (THOR programme), The University of Aarhus, and the Carlsberg Foundation for generous financial support.

Notes and references

† We initially attempted several routes to introduce simultaneously the two alkene units into the easily available methyl 2,4-di-*O*-benzyl-α-D-mannopyranoside, although this synthetic pathway was unrewarding.

‡ *Selected data for* **13**: (400 MHz, C_6D_6) δ_H 5.53 (dd, 1H, *J* 6.0, 3.0 Hz, H3′), 5.48 (dd, 1H, *J* 8.8, 3.6 Hz, H3″), 5.45 (dd, 1H, *J* 8.8, 7.6 Hz, H4″), 5.38 (dd, 1H, *J* 3.6, 3.2 Hz, H2″), 5.28 (dd, 1H, *J* 6.4, 3.0 Hz, H2′), 5.25 (dd, 1H, *J* 2.4, 1.6 Hz, H2), 5.23 (dd, 1H, *J* 10.4, 9.2 Hz, H4), 5.17 (dd, 1H, *J* 6.0, 4.8 Hz, H4′), 4.72 (dd, 1H, *J* 11.6, 7.2 Hz, H6a′), 4.64 (d, 1H, *J* 1.6 Hz, H1), 4.48 (dd, 1H, *J* 12.0, 7.2 Hz, H6a″), 4.16 (ddd, 1H, *J* 7.6, 6.4, 4.8 Hz, H1′), 4.04 (dd, 1H, *J* 12.0, 2.8 Hz, H6b″), 4.00 (m, 2H, H5′, H6b′), 3.95 (ddd, 1H, *J* 10.4, 3.6, 3.2 Hz, H1″), 3.89 (ddd, 1H, *J* 7.6, 7.2, 2.8 Hz, H5″), 3.69 (ddd, 1H, *J* 9.2, 9.2, 2.8 Hz, H5), 2.96 (s, 3H, OMe), 2.54 (m, 1H, H3); HR-MS (ES) calcd for $C_{41}H_{58}O_{24}$ (*M* + Na): 957.3215, found 957.3216.

§ The stereochemistry at C1 for both of the non-reducing sugars in **13** was assigned to the α-configuration, based on the similar coupling patterns observed for the H1′ and H1″ protons compared to those observed in the *C*-disaccharides of α-D-Man-(1→3)-D-Man and α-D-Man-(1→6)-D-Man. In addition, all previous reactions performed with the mannosyl pyridyl sulfone **10** have led only to the formation of α-*C*-mannosides.

1 A. Wei, K. M. Boy and Y. Kishi, *J. Am. Chem. Soc.*, 1995, **117**, 9432; J.-F. Espinosa, F. J. Cañada, J. L. Asensio, H. Dietrich, M. Martín-Lomas, R. R. Schmidt and J. Jiménez-Barbero, *Angew. Chem., Int. Ed. Engl.*, 1996, **35**, 303; J.-F. Espinosa, F. J. Cañada, J. L. Asensio, M. Martin-Pastor, H. Dietrich, M. Martín-Lomas, R. R. Schmidt and J. Jiménez-Barbero, *J. Am. Chem. Soc.*, 1996, **118**, 10 862; J.-F. Espinosa, H. Dietrich, M. Martín-Lomas, R. R. Schmidt and J. Jiménez-Barbero, *Tetrahedron. Lett.*, 1996, **37**, 1467; J.-F. Espinosa, E. Montero, A. Vian, J. L. Garcia, H. Dietrich, M. Martín-Lomas, R. R. Schmidt, A. Imberty, F. J. Cañada and J. Jiménez-Barbero, *J. Am. Chem. Soc.*, 1998, **120**, 1309; R. Ravishankar, A. Surolia, M. Vijayan, S. Lim and Y. Kishi, *J. Am. Chem. Soc.*, 1998, **120**, 11 297; J. F. Espinosa, M. Bruix, O. Jarreton, T. Skrydstrup, J.-M. Beau and J. Jiménez-Barbero, *Chem. Eur. J.*, 1999, **5**, 442; J. L. Asensio, J.-F. Espinosa, H. Dietrich, F. J. Cañada, R. R. Schmidt, M. Martín-Lomas, S. André, H.-J. Gabius and J. Jiménez-Barbero, *J. Am. Chem. Soc.*, 1998, **120**, 1309.

2 M. H. D. Postema, *C-Glycoside Synthesis*, CRC Press, Boca Raton, FL, 1995; D. E. Levy and C. Tang, *The Chemistry of C-Glycosides*, Pergamon Press, Exeter, 1995; G. Casiraghi, F. Zanardi, G. Rassu and P. Spanu, *Chem. Rev.*, 1995, **95**, 1677. See also, C. Pasquarello, S. Picasso, R. Demange, M. Malissard, E. G. Berger and P. Vogel, *J. Org. Chem.*, 2000, **65**, 4251, and references therein.

3 For examples of the synthesis of *C*-oligosaccharides, T. Haneda, P. G. Goekjian, S. H. Kim and Y. Kishi, *J. Org. Chem.*, 1992, **57**, 490; A. Wei, A. Haudrechy, C. Audin, H.-S. Jun, N. Haudrechy-Bretel and Y. Kishi, *J. Org. Chem.*, 1995, **60**, 2160; D. P. Sunderlin and R. W. Armstrong, *J. Org. Chem.*, 1997, **62**, 5267; A. Dondoni, M. Kleban, H. Zuurmond and A. Marra, *Tetrahedron Lett.*, 1998, **39**, 7991; Y.-C. Xin, Y.-M. Zhang, J.-M. Mallet, C. P. J. Glaudemans and P. Sinaÿ, *Eur. J. Org. Chem.*, 1999, 471; A. Dondoni, M. Mizuno and A. Marra, *Tetrahedron Lett.*, 2000, **41**, 6657.

4 (*a*) O. Jarreton, T. Skrydstrup and J.-M. Beau, *Chem. Commun.*, 1996, 1661; (*b*) L. Andersen, L. M. Mikkelsen, J.-M. Beau and T. Skrydstrup, *Synlett*, 1998, 1393; (*c*) O. Jarreton, T. Skrydstrup, J.-F. Espinosa, J. Jiménez-Barbero and J.-M. Beau, *Chem. Eur. J.*, 1999, **5**, 430; (*d*) S. L. Krintel, J. Jiménez-Barbero and T. Skrydstrup, *Tetrahedron Lett.*, 1999, **40**, 7565.

5 For a recent review, T. Skrydstrup and J.-M. Beau, in *Advances in Free Radical Chemistry*, ed. S. Z. Zard, Jai Press, Stamford, 1999, vol. 2, p. 89.

6 J. Dolezalová, T. Trnka and M. Cerny, *Collect. Czech. Chem. Commun.*, 1982, **47**, 2415.

7 T. Inghardt and T. Frejd, *Synthesis*, 1990, 285.

8 J. S. Clark and O. Hamelin, *Angew. Chem., Int. Ed.*, 2000, **39**, 372.

ChemComm

Dynamic kinetic asymmetric synthesis of β-aminoalcohols from racemic epoxides in cyclodextrin complexes under solid state conditions†

L. Rajender Reddy, N. Bhanumathi and K. Rama Rao*

Organic Chemistry Division-I, Indian Institute of Chemical Technology, Hyderabad-500 007, India. E-mail: ramaraok@iict.ap.nic.in

Received (in Cambridge, UK) 12th June 2000, Accepted 16th October 2000
First published as an Advance Article on the web 9th November 2000

It has been shown for the first time that enantiopure β-aminoalcohols can be prepared from racemic epoxides by dynamic kinetic resolution involving enantio-differentiating racemisation in cyclodextrin complexes under solid state conditions.

The novel phenomenon of converting racemic substrates into a single enantiomer of the product by dynamic kinetic resolution *via* racemisation of the substrates has been a formidable challenge in asymmetric synthesis.[1] Recently, it has been receiving increasing attention and attempts are being made to achieve every useful asymmetric synthesis by dynamic kinetic resolution since it overcomes the severe limitation of the conventional kinetic resolution where the maximum yield of one stereoisomer of the starting material or product is only 50%. But, so far there is no report on the dynamic kinetic asymmetric synthesis of β-aminoalcohols of great significance from the easily accessible and inexpensive racemic epoxides. The β-aminoalcohol moiety is present in many natural products and drugs and acts as an intermediate in various asymmetric transformations.[2] The approaches hitherto reported from the racemic epoxides involve only kinetic resolution.[3] Further to our studies on cyclodextrins as chiral templates for the enantioselective synthesis of a variety of chiral building blocks,[4] we report herein the first biomimetic approach for the synthesis of a single enantiomer of β-aminoalcohols from the corresponding racemic epoxides by dynamic kinetic resolution involving enantio-differentiating racemisation in cyclodextrin complexes.[5]

The cyclodextrins are cyclic oligosaccharides possessing hydrophobic cavities and they mimic enzymes in their capability to bind substrates selectively and catalyse chemical reactions by supramolecular catalysis involving reversible formation of host–guest complexes with substrates through non-covalent bonding. Apart from this, with the cyclodextrin cavity being chiral it can induce asymmetric reactions.[6] It requires the following criteria to be fulfilled to ensure rigidity for chiral recognition by cyclodextrins: (i) a phenyl ring which can fit into the cyclodextrin cavity to form an inclusion complex, (ii) a functional group at the stereogenic center to form a strong interaction at the cyclodextrin cavity entrance. Since aryloxyepoxides **1** fulfil these criteria, they have been chosen as substrates.

The inclusion complexes of aryloxyepoxides **1** with β-cyclodextrin (β-CD) were prepared as described earlier.[4] The reaction of these cyclodextrin complexes of epoxides **1** with amines **2** or **3** (Scheme 1) when carried out in water as the reaction medium, yielded aminoalcohols that were nearly racemic (ee 2%). This may be due to free movement of the guest molecule in solution. Hence, it was planned to carry out these reactions in the solid state where the movement of the guest molecule would be restricted, resulting in better chiral recognition.

An intimate mixture of the epoxide **1**–β-cyclodextrin complex (1:1) and the amine **2** or **3** was mixed in equimolar amounts in an agate mortar using a pestle and the mixing continued until the starting epoxide disappeared on TLC (3–12 h). The time taken was always dependent on the frequency of mixing. However, in the case of amine **2**, it was added in excess due to its volatility and was added intermittently during the course of mixing. The resulting aminoalcohols **4** and **5** were extracted with ethyl acetate and purified through the formation followed by release of their hydrochlorides. The isolated yield of the product was always in the range 70–79% and the enantioselectivity was excellent in some of the compounds (Table 1). Compounds **4b** and **5b** have shown 100% ee followed by compound **4c** (ee 89%) and **4d** (ee 85%). The enantiomeric excesses (ee) of the products (**4** and **5**) were determined by chiral HPLC analysis. These aminoalcohols **4** and **5** have been shown to have *R* configuration by comparison of the sign of rotation with those of the known compounds.[7] However, these reactions when carried out using α-cyclodextrin inclusion complexes, gave enantioselectivities that were far lower than those obtained with β-cyclodextrin. This may be due to ineffective complexation.

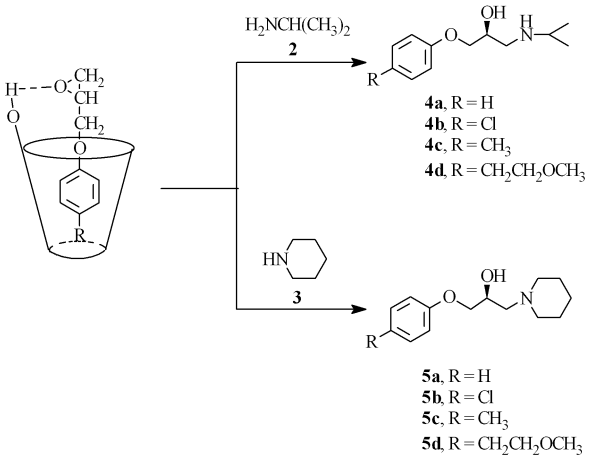

Scheme 1

The formation of enantiopure β-aminoalcohols (**4** and **5**) from the racemic epoxides **1** may be postulated as follows:

Table 1 Solid state asymmetric synthesis of β-aminoalcohols

Entry	Product	ee (%)[a]	Yield (%)[b]
1	4a	73.8	79
2	4b	100	75
3	4c	89	72
4	4d	85	70
5	5a	1.4	74
6	5b	100	70
7	5c	0.8	76
8	5d	3.5	73

[a] Determined by HPLC analysis with the chiral column 'Diacel Chiralcel OD' (0.46 cm ϕ × 25 cm) using hexane: propan-2-ol: diethylamine (80:20:0.1) as eluent at a flow rate of 0.5 ml min^{-1} using UV detection (254 nm). [b] Isolated yields.

DOI: 10.1039/b004643o

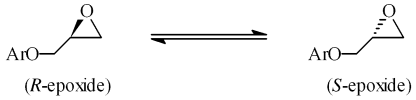

Scheme 2

The fact that the epoxide **1** isolated from the cyclodextrin complex is racemic and the yields of the aminoalcohols **4** and **5** were always more than 50%, suggests that kinetic resolution is not operating under these conditions as then only a maximum of 50% conversion can be expected. Hence, in the present investigation, to get a single enantiomer of the product (**4** or **5**) from the racemic starting epoxide **1**, it requires interconversion of one of the enantiomers of the epoxide **1** (Scheme 2). This is possible through racemisation which is controlled by entropy effects.[8] Racemisation can take place in the present case by the interconversion of the epoxide enantiomer facilitated under solid state conditions. Though racemisation is quite a slow process in the absence of suitable driving mechanism *i.e.* the external amine in the present case, the racemisation of the β-CD complexes of the individual *R* and *S* epoxides of **1a** (R = H) has been attempted by grinding them intimately for 5 h and analysing by chiral HPLC.[9] It is observed that racemisation does indeed take place only with *S*-enantiomer to an extent of ≅2% as seen by the change in %ee. This reaction also further substantiates the process of dynamic kinetic resolution *i.e.* as the *R*-enantiomer of the epoxide (**1**) in the CD complex reacts with the amine, the *S*-epoxide gets converted to the *R*-epoxide to take the reaction forward, leading to only the *R*-enantiomer of the product (**4**).

Thus, when one of the enantiomeric forms of the epoxide **1** in the β-cyclodextrin cavity, due to its favourable geometry, is captured selectively by the external amine (**2** or **3**), the phenomenon of dynamic kinetic resolution sets in under the reaction conditions. Hence, by dynamic kinetic resolution through racemisation of the starting epoxide, it is possible to get enantiomerically pure aminoalcohols (**4** and **5**). This has also been confirmed from the individual experiments utilizing either *R* or *S* epoxides (Scheme 3). Both *R* and *S* epoxides gave the aminoalcohol (**4a**) mainly as the *R* enantiomer (90% ee by HPLC). This gives further evidence to show that racemisation of the starting epoxide and dynamic kinetic resolution are operating under the reaction conditions to give a single enantiomer of the product.

Thus, in conclusion, it has been shown for the first time that enantiopure β-aminoalcohols of high potential can be made from the easily accessible and inexpensive racemic epoxides. This can be achieved by dynamic kinetic resolution involving

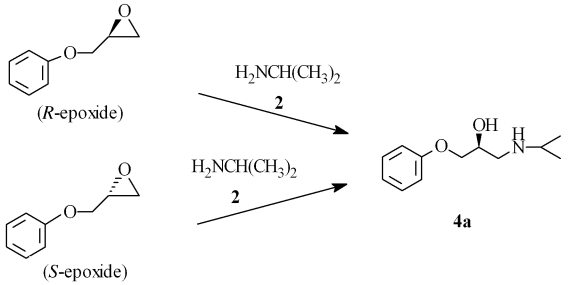

Scheme 3

enantio-differentiating racemisation in cyclodextrin complexes under solid state reaction conditions.

We thank the Director, Dr K. V. Raghavan for constant encouragement and support during the course of this work and CSIR, New Delhi, India for the award of research fellowship to LRR.

Notes and references

† IICT Communication No. 4579.

1 (*a*) R. S. Ward, *Tetrahedron Asymmetry*, 1996, 1475; (*b*) F. Toda and K. Tanaka, *Chem. Lett.*, 1983, 661.

2 (*a*) *Pharmacological Basis of Therapeutics*, ed. L. S. Goodman and A. Gilman, 6th edn., MacMillan, New York, 1980; (*b*) A. S. Rao, S. K. Paknikar and J. G. Kirtane, *Tetrahedron*, 1983, **39**, 2323; (*c*) Bo. Lamn, K. Ankener and M. Frantsi, *Acta Chem. Scand.*, 1987, **B41**, 202; (*d*) C. K. Juslen, M. Kuhn, H. R. Loosli, T. J. Petcher, H. P. Weber and A. V. Wartburg, *Tetrahedron Lett.*, 1976, 4147; (*e*) J. S. Zewig, J. L. Luche, E. Barreiro and P. Crabbe, *Tetrahedron Lett.*, 1975, 2355.

3 (*a*) N. Matsuo and N. Ohno, *Tetrahedron Lett.*, 1985, **26**, 5533; (*b*) H. S. Bevinakatti and A. A. Banerji, *J. Org. Chem.*, 1991, **56**, 5372; (*c*) W. E. Lander and G. M. Whitesides, *J. Am. Chem. Soc.*, 1984, **106**, 7250; (*d*) J. F. Larrow, S. E. Schaus and E. N. Jacobsen, *J. Am. Chem. Soc.*, 1996, **118**, 7420.

4 (*a*) K. Rama Rao and P. B. Sattur, *J. Chem. Soc., Chem. Commun.*, 1989, 342; (*b*) K. Rama Rao and H. M. Sampth Kumar, *Synth. Commun.*, 1993, **23**, 1877.

5 K. Rama Rao, N. Bhanumathi and L. Rajender Reddy, *Indian Pat. Appl. No.* 127/DEL/2000, *US Pat. Appl. No.* 09/535 384, 2000.

6 K. Takahashi, *Organic Reactions Mediated by Cyclodextrins, Chem. Rev.*, 1998, **98**, 2013.

7 H. Takahashi, S. Sakuraba, H. Takeda and K. Achiwa, *J. Am. Chem. Soc.*, 1990, **112**, 5876.

8 (*a*) Y. Izumi and A. Tai, *Stereodifferentiating reactions, the nature of asymmetric reactions*, Academic Press, New York, 1977, p. 169–177; (*b*) E. L. Eliel and S. H. Wilen, *Stereochemistry of Organic Compounds*, John Wiley and Sons, Inc., New York, 1994, 424.

9 We would like to thank one of the referees who has suggested this set of experiments which has given further proof to our results.

ChemComm

A pH sensitive fluorescent cyanine dye for biological applications

Mark S. Briggs, D. Dougal Burns, Michael E. Cooper* and Susan J. Gregory

Drug Discovery, Amersham Pharmacia Biotech, Forest Farm, Whitchurch, Cardiff, UK CF14 7YT. E-mail: michael.cooper@eu.apbiotech.com

Received (in Cambridge, UK) 1st September 2000, Accepted 10th October 2000
First published as an Advance Article on the web 9th November 2000

A pentamethine cyanine dye has been synthesised that is fluorescent when protonated, becoming non-fluorescent upon proton abstraction. The probe has a pK_a of 7.5, with observable changes in the fluorescent emission properties across a pH range of 6.0–8.0, therefore providing a useful probe for studying pH in biological media.

Cyanine dye[1] fluorescent probes are useful markers for flow cytometry,[2] sequencing assays[3] and high throughput screening.[4] These probes have high extinction coefficients (> 200000 l mol^{-1} cm^{-1}), can be designed with long excitation and maximum fluorescent emission wavelengths (> 600 nm) and with lower molecular weights than the majority of commercially available natural fluorophores.[5] These fluorescent cyanine dyes also have the added value of containing reactive functional groups, such as an *N*-hydroxysuccinimidyl ester or an isothiocyanate facilitating a covalent link to a biomolecule. More recently, attention has also focussed on the synthesis of more specialised probes,[6] or "functional dyes", that can act as molecular and optical switches.[7] Indeed, many of these dyes are designed to be environmentally sensitive, acting as ionophores for protons, Ca^{2+}, Na^+ or K^+ or as small molecule sensors for cyclic adenosine monophosphate[8] or inositol phosphate.[9]

One subject of ongoing interest is acidity regulation in mammalian cells.[10] Monitoring small changes in proton concentration is important for the study of numerous signal transduction pathways and ligand interactions with G-protein coupled receptors. The majority of commercially available pH sensitive fluorescent dyes employed in intracellular studies[5] provide a reduced fluorescent signal in acidic media or alternatively the pK_a of the dye is outside the critical intracellular pH window of between 5–8 pH units.

We now report an example of a fluorescent pentamethine cyanine dye (Cy5™) that is sensitive to proton concentration over a pH range of 6–9 (Fig. 1). The intensity of the fluorescent emission (665 nm) for this probe increases with increasing proton concentration. This probe is analogous to a number of previously reported benzothiazolium[11] trimethine cyanine dyes with pH sensitive UV/visible absorption properties, although in addition, the design of our fluorescent probe includes several other important elements. The presence of a sulfonic acid functional group aids solubility in aqueous media and the position of such functional groups is also known to reduce probe aggregation in solution.[12] There is also a pendant carboxylic acid group that can be easily converted to the reactive *N*-hydroxysuccinimidyl ester for biolabelling. Furthermore, unlike previously reported cyanine dyes,[1] the pH sensitivity is introduced *via* a non-*N*-alkylated indolium moiety whereupon protonation and deprotonation occurs depending upon the localised hydrogen ion concentration.

The probe exists in two forms, as either the fluorescent cyanine dye or the complementary non-fluorescent base (Fig. 1). The intense cyanine dye absorption and emission properties are largely due to a resonance effect between the two nitrogen atoms of the two indole rings *via* the conjugated pentamethine bridge. Abstraction of a proton from this system destroys this resonance, and subsequently leads to the non-fluorescent base form. Moreover, this property provides excellent resolution at long wavelengths (> 600 nm) where little else in a biological sample is likely to absorb.

The probe was synthesised by standard cyanine dye methods.[1] 1-Ethyl-2,3,3-trimethyl-3*H*-indol-1-ium-5-sulfonate[1] and 5-carboxymethyl-2,3,3-trimethyl-2,3-dihydroindole[13] were condensed with malonaldehyde bis(phenylimine) in the presence of acetic acid, acetic anhydride and pyridine at 70 °C . The product was purified by reverse phase HPLC[14] and conversion to the NHS (*N*-hydroxysuccinimidyl) ester is facile by standard methods. A typical conversion to the NHS ester involves reacting the dye in DMSO with 1 eq. of PyBOP (benzotriazol-1-yloxytripyrrolidinophosphonium hexafluorophosphate, *N*-hydroxysuccinimide and 1.1 eq. of diisopropylethylamine. Stirring for 1 h gives quantitative conversion. TLC analysis (10% methanol–DCM on SiO_2) observes a fast running blue spot R_f = 0.60. R_f of the free acid = 0.41. Hydrolysis of this material gives the free acid by TLC.

The fluorescent properties of this dye can be seen in Fig. 2. Equimolar solutions of the dye were made up in phosphate buffers[15] over a pH range of between 4.5–9. It can be observed that the fluorescent characteristics of the probe are greatly reduced as the buffers become less acidic in nature. This is due to increased deprotonation of the cyanine dye and leads to a larger population of the non-fluorescent base species. Similar experiments with a commercial bis(*N*-alkylated) sample of

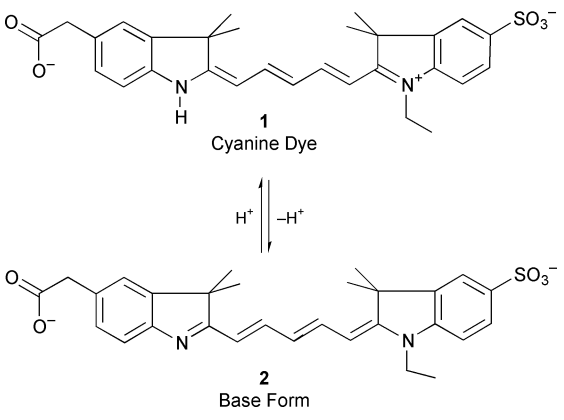

Fig. 1 The cyanine dye-base form of the pH sensitive fluorescent probe.

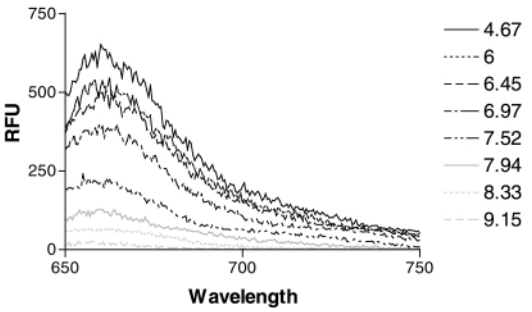

Fig. 2 Fluorescence characteristics of the pH sensitive probe as a function of pH (~ 0.1 μmol of complex, λ_{ex} = 630 nm, 295 K. Readings were made using a Perkin-Elmer LS50B fluorimeter in fluorescence mode, with excitation and emission slits set at 2.5 nm and with 3 ml quartz cuvettes).

Cy5™ showed no change in the emission properties of the probe over the same pH range. Furthermore, the photostability of the fluorescent form of this probe was comparable to the non-pH sensitive cyanine pentamethine dyes (Cy5™) routinely used in biological studies.

Further proof of this acid–base equilibrium can be achieved by observation of the UV/visible spectra of **1** in phosphate buffers of different pH (Fig. 3). It can be seen that as the buffer solutions become less acidic, the characteristic absorption maximum for the pentamethine cyanine dye at 645 nm is greatly reduced as a new peak evolves at 480 nm. This absorption peak is due to the increased presence of the base form (**2**) of the probe by proton abstraction from the pentamethine cyanine dye. A further observation is the presence of an isosbestic point at 545 nm. This gives a good indication that the solutions are all of similar ionic strength.[16] It is therefore likely that the proton concentration alone is responsible for the different observed spectra, and that this phenomenon cannot be attributed to the differing concentrations of any other ions present in the buffer solution.

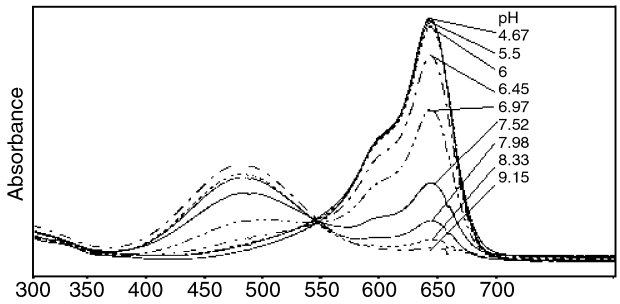

Fig. 3 UV/visible absorption spectra of **1** (and **2**) as a function of pH (from a Hewlett Packard 8453 UV/vislble spectrophotometer with diode array detector, 1 cm pathlength quartz cuvettes).

Fig. 4 illustrates the pH response of probe **1** as a function of I/I_{max} *vs.* pH, where I is the measured fluorescent emission at that pH, and I_{max} is the maximum output of the probe. It can be seen that a regular sigmoidal response is observed for this probe in response to pH. The pK_a of **1** can be estimated where I/I_{max} is 0.5. This provides a pK_a value of 7.5 (296 K) for this probe.

A current limitation in the application of many current pH sensitive fluorescent probes is due to lack of any specific labelling functionality present on the dye such as an NHS ester. The presence of these groups allows specific biomolecules or particular functional groups, *e.g*. primary amines to be targeted, and a subsequent range of bioassays to be performed using the dye-labelled biomolecule. The presence of a pendant carboxylic acid allows rapid conversion to the *N*-hydroxysuccinimidyl ester and therefore facilitates the labelling of biological molecules such as proteins or antibodies.[17] The reactive form of this probe has been employed to label aliphatic amine groups present on the outer membrane of a CHO cell. Upon constitutive endocytosis the probe becomes internalised into acid vesicles with a subsequent increase in fluorescent emission.[18] Furthermore, the pK_a of the probe when bioconjugated did not change implying that the carboxylic acid present in the free form of the probe does not affect the pH sensitive fluorescent properties. Details of these cellular studies will be reported elsewhere.

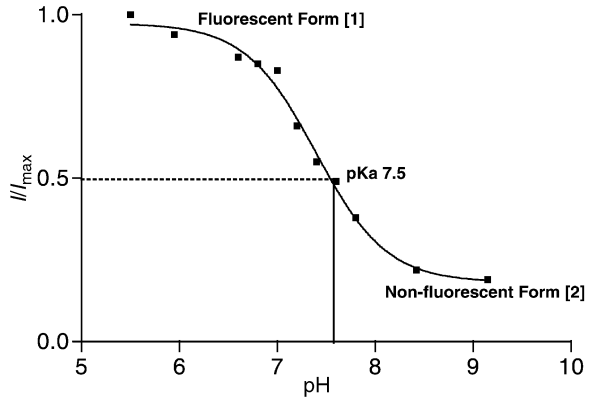

Fig. 4 pH Dependence of **1** (I/I_{max}) at 295 K in phosphate buffers of differing pH (λ_{exc} = 630 nm λ_{em} = 665 nm. Readings were made using a Perkin-Elmer LS50B fluorimeter in fluorescence mode, with excitation and emission slits set at 2.5 nm and with 3 ml quartz cuvettes. Each point is the average of 10 measurements).

Furthermore many other probes offer a reduced fluorescent emission in acidic conditions and the spectral data acquired often requires deconvolution due to both protic and non-protic forms being fluorescent and thus, these probes are of interest for ratiometric pH studies. In contrast, this pH sensitive cyanine probe has only one fluorescent form and is therefore useful for high throughput studies whereby a change in fluorescent emission can be easily and rapidly observed. The long emission wavelength of this pentamethine pH sensitive cyanine dye is also of value for biological studies, due to the increased light penetration into cell tissue of the excitation lasers. A range of homologous pH sensitive fluorescent pentamethine cyanine dyes is now being synthesised and evaluated and will be reported in subsequent communications.

MEC thanks Adam Colebrook and Tony Rees for the accurate mass spectroscopic analysis and J. Tony Smith and Martyn Birch for stimulating discussion.

Notes and references

1 R. B. Mujumdar, L. A. Ernst, S. R. Mujumdar, C. J. Lewis and A. S. Waggoner, *Bioconjugate Chem.*, 1993, Vol. 4, No. 2., 105–111.

2 L. A. Ernst, R. K. Gupta, R. B. Mujumdar and A. S. Waggoner, *Cytometry*, 1989, **10**, 11.

3 Z. Zhu, J. Chao, H. Yu and A. S. Waggoner, *Nucleic Acids Res.*, 1994, **22**, 3418.

4 M. E. Cooper, *Fluorescence Microscopy and Fluorescent Probes 3*, ed. A. Kotyk, Espero Publishing, Prague, 1999, 37–57.

5 R. P. Haugland, *Handbook of Fluorescent Probes Seventh Edn.*, Molecular Probes Inc., Oregon, USA, 1999.

6 W. T. Mason, *Fluorescent and Luminescent Probes for Biological Activity, 2nd edn.*, ed. W. T. Mason, Academic Press, 1999.

7 (*a*) M. P. Lowe and D. P. Parker, *Chem. Commun.*, 2000, 707; (*b*) L. Fabbrizzi, M. Licchelli, L. Parodi, A. Poggi and A. Taglietti, *Eur. J. Inorg. Chem.*, 1999, 35; (*c*) I. García-Ochoa, M.-Á. Díez López, M. H. Viñas, L. Santos, E. Martínez Atáz, F. Amat-Guerri and A. Douhal, *Chem. Eur. J.*, 1999, 5, 3, 897.

8 P. Turkewitsch, B. Wandelt, G. D. Darling and W. S. Powell, *Anal. Chem.*, 1998, **70**, (13), 2771.

9 K. Niikura, A. Metzger and E. V. Anslyn, *J. Am. Chem. Soc.*, 1998, **120** (33), 8533.

10 T. J. Rink, R. Y. Tsien and T. Pozzan, *J. Cell. Biol.*, 1982, **95**, 189.

11 L. G. S. Brooker, R. H. Sprague, C. P. Smyth and G. L. Lewis, *J. Chem. Soc.*, 1940, **62**, 1116.

12 S. R. Mujumdar, R. B. Mujumda, C. M. Grant and A. S. Waggoner, *Bioconjugate Chem.*, 1996, **7**, 356.

13 P. L. Southwick, J. G. Cairns, L. A. Ernst and A. S. Waggoner, *Org. Prep. Proced. Int.*, 1988, **20** (3), 279.

14 NMR data: 200 MHz ^{1}H-NMR, (d_6-DMSO), δ 8.3–8.1 (m, 2H, β,β′-protons in bridge), 7.76 (d, 1H, *J* = 4H-Ar), 7.62 (d, 1H, 7H-Ar, *J* = 8.3), 7.45 (s, 1H, 4H-Ar′), 7.27 (d, 1H, 7H-Ar, J = 7.8) 7.19 (d 6H-Ar, *J* = 8.3) 7.14 (d, 1H, Ar-6H, *J* = 7.8), 6.49 (t, 1H, γ′-proton in bridge), 6.27 (d, 1H, α-proton in bridge) 6.16 (d, 1H, α′-proton in bridge) 4.09 (q, 2H, α-CH_2, 1.63 (s, 6H, (-CH_3)$_2$, 1.56 (s, 6H, −CH_3)$_2$), 1.25 (t, 3H, β-CH_3). MS (electrospray, negative mode) *m*/*z* (%) = 521.2110 (100%).

15 *U.S. Pharmacopeia. The National Formulary*, Mach Printing Co., Easton, PA, USA, 1990, pp. 1784–1785.

16 V. Good, *pH Measurements, Their Theory and Practice*, Methuen Publ., London, 1956.

17 M. Aslam and A. Dent, *Bioconjugation. Protein Coupling Techniques for the Biomedical Sciences*, Macmillan Reference Ltd Publ., London, 1998.

18 E. Adie, *et al.*, *Measurement of Receptor Translocation using pH Sensitive Cyanine Dyes*. Presented at *Society for Biomolecular Screening 6th Annual Conference*, Vancouver, 2000.

ChemComm

Synthesis, cytotoxicity and DNA cross-linking activity of symmetrical dimers based upon the epoxide domain of the azinomycins

John A. Hartley,[a] Ali Hazrati,[a] Timothy J. Hodgkinson,[b] Lloyd R. Kelland,[c] Ruzwana Khanim,[a] Michael Shipman*[b] and Franck Suzenet[b]

[a] *CRC Drug-DNA Interactions Research Group, Department of Oncology, Royal Free & University College Medical School, University College London, 91 Riding House Street, London, UK W1P 8BT*
[b] *School of Chemistry, University of Exeter, Stocker Road, Exeter, UK EX4 4QD. E-mail: m.shipman@exeter.ac.uk; Fax: +44-1392-263434; Phone: +44-1392-263469*
[c] *CRC Centre for Cancer Therapeutics, Institute of Cancer Research, Sutton, Surrey, UK SM2 2NG*

Received (in Liverpool, UK) 15th August 2000, Accepted 13th October 2000
First published as an Advance Article on the web 9th November 2000

A series of dimeric compounds 1a–c designed around the epoxide domain of the azinomycins have been synthesised and demonstrated to be highly efficient DNA interstrand cross-linking agents.

Chemical agents capable of inducing DNA interstrand cross-links (ISC's) comprise an extremely important class of clinical cancer chemotherapeutic agent.[1] Indeed, several important drugs used for the treatment of this disease (*e.g.* cisplatin, chlorambucil and melphalan) are known to induce ISC formation. In 1986, two new cytotoxic agents named azinomycin A and B were isolated from the culture broths of *Streptomyces griseofuscus* S42227 which were shown to possess significant *in vivo* anti-tumour activity (Fig. 1).[2] Using synthetic oligonucleotide duplexes, Armstrong *et al.* demonstrated that azinomycin B causes interstrand cross-links in the major groove of DNA by alkylation at N-7 of guanine (G) and reaction with another purine residue (A or G) two bases along on the complementary DNA strand.[3] More recently, Fujiwara *et al.* provided the first direct evidence for the involvement of the electrophilic epoxide and aziridine moieties in the DNA cross-linking event using self-complementary oligodeoxynucleotide $[d(TAGCTA)_2]$.[4] Whilst reactions with the nucleophilic purine residues of DNA is clearly essential for ISC formation, the poor chemical stability of these agents especially the 1-azabicyclo-[3.1.0]hexane ring system is undesirable from the point of view of possible drug development. Indeed, the high reactivity of this heterocyclic system has severely hampered efforts to complete the total synthesis of these natural products.[5] Since several studies have determined that simplified derivatives based upon the epoxide domain of the azinomycins are highly cytotoxic,[6] we reasoned that dimeric structures based upon this motif joined by a suitable linker might serve as effective DNA cross-linking agents (Fig. 1). Such compounds might be expected to display enhanced chemical stability with respect to the natural products. Furthermore, by fine tuning the nature of the aromatic residues and the linker, agents capable of targeting specific base sequences can be imagined.

To test our hypothesis, we chose to prepare three bisepoxides **1a–c** containing flexible hydrocarbon linker units of varying lengths between the two epoxide subunits. The synthesis of these bisepoxides was accomplished in a straightforward fashion from enantiomerically pure epoxy ester (2*S*,3*S*)-**2**.[7] Selective cleavage of the benzyl ester by hydrogenation and coupling of the resultant acid with 0.5 molar eq. of ethylenediamine furnished bisepoxide **1a** in 69% yield (Scheme 1).† Similarly, (2*S*,3*S*)-**2** was transformed into bisepoxides **1b** and **1c** using 0.5 molar eq. of 1,4-diaminobutane and 1,6-diaminohexane, respectively. All three bisepoxides were produced as crystalline solids which displayed good thermal and hydrolytic stability.‡

With these bisepoxides in hand, we turned our attention to studying their interstrand cross-linking activities using an agarose gel assay.[8] Monoepoxide **3**[7] was used as a control in these experiments. In contrast to epoxide **3** which displays no ISC activity at concentrations up to 50 μM, bisepoxide **1a** induces cross-links at concentrations as low as 0.1 μM and effects 100% cross-linking at 10 μM (Fig. 2). Bisepoxides **1b** and **1c** bearing progressively longer linkers between the two epoxide centres also induce ISC in double stranded DNA. Bisepoxide **1b** induces some ISC's at 0.1 μM with 100% ISC's being observed at just 1 μM; **1c** induces appreciable levels of cross-linking at the somewhat higher concentration of 10 μM. It is interesting to observe that bisepoxides **1a** and **1b** are more effective ISC agents in this assay than the clinically important anti-cancer drugs cisplatin, melphalan and chlorambucil (data not shown). To gain preliminary information concerning the

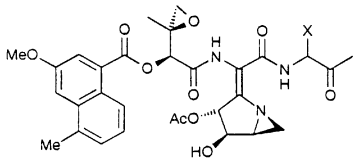

Azinomycin A (X = H); Azinomycin B (X = CHO)

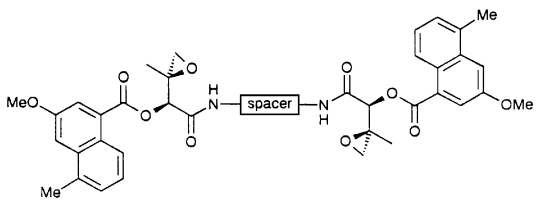

dimeric epoxides: chemically stable DNA interstrand cross-linking agents?

Fig. 1

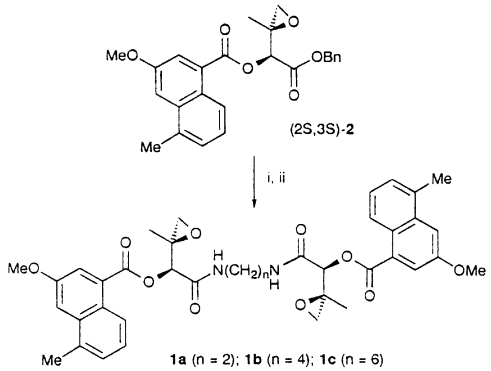

1a (n = 2); **1b** (n = 4); **1c** (n = 6)

Scheme 1 *Reagents and conditions*: (i) 10% Pd/C, H_2, MeOH, 1 h; (ii) diamine (see text), PyBOP®, Et_3N, HOBt, DMF, 69% (**1a**), 46% (**1b**), 80% (**1c**). PyBOP = benzotriazol-1-yloxytripyrrolidinophosphonium hexafluorophosphate.

DOI: 10.1039/b006723g

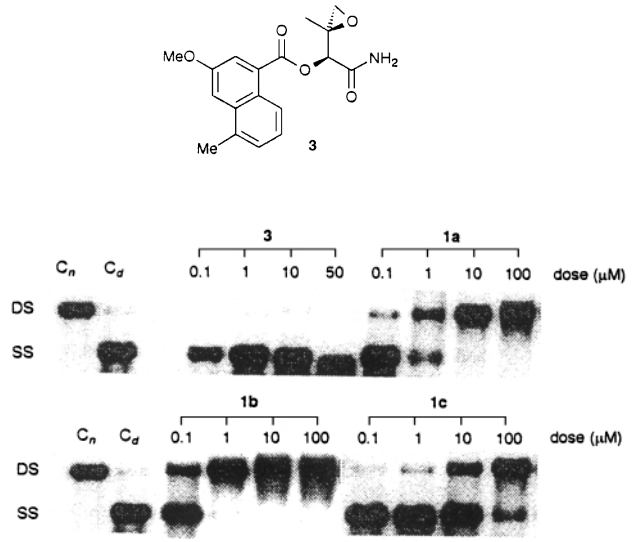

Fig. 2 Agarose cross-linking gel for bisepoxides **1a–c** and epoxide **3**. Plasmid DNA was treated with the agents at the concentrations shown for 2.5 h prior to denaturation and gel electrophoresis. C_n and C_d are control non-denaturated and denatured samples, respectively. DS and SS indicate the positions of double and single stranded DNA, respectively.

Table 1 Cytotoxicity data for **1a–c**

Human tumour cell lines	IC_{50} (μM)[a]		
	1a	**1b**	**1c**
A2780	< 0.05	0.065	0.11
CH1	< 0.05	< 0.05	0.08
CH1cisR[b]	< 0.05	< 0.05	0.08
SKOV-3	1.4	0.82	1.2
HT29	0.42	0.55	0.50
K562	0.067	0.027	0.062

[a] Dose of drug inhibiting growth by 50% following a 96 h exposure (1 h in the case of K562) as determined by the SRB assay[10] (MTT assay[11] in the case of K562). [b] Cell line with acquired resistance to cisplatin.

sequence selectivity of bisepoxides **1a–c**, we have evaluated them in a Taq DNA polymerase stop assay.[9] All three bisepoxides and epoxide **3** induce Taq stops preferentially at G residues indicating alkylation at these bases. Interestingly, the bisepoxides block polymerase at fewer bases than the corresponding monoepoxide **3**, indicating enhanced sequence specificity.

The cytotoxicity of bisepoxides **1a–c** was determined against a small panel of human tumour cell lines [A2780, CH1, SKOV-3 (all ovarian), HT-29 (colon), K-562 (leukemia)] (Table 1). All the compounds display potent cytotoxicity in a range of cell lines including one with acquired resistance to the drug cisplatin (CH1cisR) where no cross resistance was observed. In some cell lines, epoxide **3** shows comparable potency to these bisepoxides (*e.g.* CH1, IC_{50} 0.056 μM), however in other lines it is markedly less potent (*e.g.* K562, IC_{50} 0.493 μM).

In conclusion, we have demonstrated that the chemically stable bisepoxides **1a–c** are easy to prepare and are highly effective ISC agents. Our findings suggest that a spacer consisting of a chain of approximately four carbon atoms is optimal for cross-linking ability. Furthermore, we have determined that these bisepoxides are highly cytotoxic. In future studies, we plan to determine how the nature of the aromatic residue and the conformational flexibility of the linker influence ISC activity and how the sequence specificity of these agents can be enhanced.

The authors gratefully acknowledge the financial support provided by the CRC and the EPSRC. We are indebted to the EPSRC National Mass Spectrometry Centre for performing mass spectral measurements, and the EPSRC Chemical Database Service at Daresbury.[12]

Notes and references

† *Selected physical and spectroscopic data*: **1a**: mp 66–68 °C; $[\alpha]_D^{20}$ = +76.6 (*c* 0.57, $CHCl_3$); ν_{max} (Nujol®)/cm^{-1} 3369 (NH), 1726 (ester C=O), 1685 (amide C=O); δ_H (400 MHz; $CDCl_3$) 8.62 (2H, m, ArH), 7.98 (2H, d, *J* = 2.6 Hz, ArH), 7.37 (2H, d, *J* = 2.6 Hz, ArH), 7.32–7.27 (4H, m, ArH), 6.96 (2H, br s, NH), 5.31 (2H, s, H-2), 3.88 (6H, s, OCH_3), 3.56–3.37 (4H, m, CONHCH_2-), 2.96 (2H, d, *J* = 4.7 Hz, H-4), 2.66 (2H, d, *J* = 4.7 Hz, H-4′), 2.62 (6H, s, $ArCH_3$), 1.49 (6H, s, CH_3); δ_C (100.6 MHz; $CDCl_3$) 167.6 (s, C=O), 165.5 (s, C=O), 155.8 (s, ArC), 134.3 (s, ArC), 133.1 (s, ArC), 127.71 (s, ArC), 127.68 (d, ArCH), 127.0 (s, ArC), 125.1 (d, ArCH), 123.8 (d, ArCH), 122.5 (d, ArCH), 108.2 (d, ArCH), 76.0 (d, C-2), 56.0 (s, C-3), 55.4 (q, OCH_3), 52.6 (t, C-4), 39.0 (t, CONHCH_2), 20.0 (q, Ar-CH_3), 18.0 (q, CH_3); Observed (MH^+): 685.2760; $C_{38}H_{41}N_2O_{10}$ requires 685.2760. **1b**: mp 95 °C; $[\alpha]_D^{20}$ = +32 (*c* 0.31, $CHCl_3$); Observed (M^+): 712.2993; $C_{40}H_{44}N_2O_{10}$ requires 712.2996. **1c**: mp 105 °C; $[\alpha]_D^{20}$ = +50 (*c* 0.43, $CHCl_3$); Observed (M^+): 740.3310; $C_{42}H_{48}N_2O_{10}$ requires 740.3309; found: C, 68.15; H, 6.63; N, 3.49. $C_{42}H_{48}N_2O_{10}$ requires C, 68.09; H, 6.53; N, 3.78%.

‡ No degradation was observed after stirring **1a** in DMSO and pH 7.4 buffer (1 : 1) for 7 days.

1 S. R. Rajski and R. M. Williams, *Chem. Rev.*, 1998, **98**, 2723.
2 (*a*) K. Nagaoka, M. Matsumoto, J. Onoo, K. Yokoi, S. Ishizeki and T. Nakashima, *J. Antibiot.*, 1986, **39**, 1527; (*b*) K. Yokoi, K. Nagaoka and T. Nakashima, *Chem. Pharm. Bull.*, 1986, **34**, 4554; (*c*) S. Ishizeki, M. Ohtsuka, K. Irinoda, K.-I. Kukita, K. Nagaoka and T. Nakashima, *J. Antibiot.*, 1987, **40**, 60.
3 R. W. Armstrong, M. E. Salvati and M. Nguyen, *J. Am. Chem. Soc.*, 1992, **114**, 3144.
4 T. Fujiwara, I. Saito and H. Sugiyama, *Tetrahedron Lett.*, 1999, **40**, 315.
5 For examples, see (*a*) M. Hashimoto and S. Terashima, *Heterocycles*, 1998, 59; (*b*) R. S. Coleman, *Synlett*, 1998, 1031.
6 (*a*) M. Hashimoto, M. Matsumoto, K. Yamada and S. Terashima, *Tetrahedron Lett.*, 1994, **35**, 2207; (*b*) K. Shishido, S. Haruna, H. Iitsuka and M. Shibuya, *Heterocycles*, 1998, **49**, 109; (*c*) T. J. Hodgkinson, L. R. Kelland, M. Shipman and F. Suzenet, *Biorg. Med. Chem. Lett.*, 2000, **10**, 239; (*d*) J. A. Hartley, A. Hazrati, L. R. Kelland, R. Khanim, M. Shipman, F. Suzenet and L. F. Walker, *Angew. Chem., Int. Ed.*, 2000, **39**, 3467; (*e*) K. S. Gates and H. Zang, *Abstr. Pap. Am. Chem. Soc.*, 1999, **218**, 368–ORGN.
7 H. J. Bryant, C. Y. Dardonville, T. J. Hodgkinson, M. B. Hursthouse, K. M. A. Malik and M. Shipman, *J. Chem. Soc., Perkin Trans. 1*, 1998, 1249.
8 J. A. Hartley, M. D. Berardini and R. L. Souhami, *Anal. Biochem.*, 1991, **193**, 131.
9 M. Ponti, S. M. Forrow, R. L. Souhami, M. D'Incalci and J. A. Hartley, *Nucl. Acid Res.*, 1991, **19**, 2929.
10 P. Skehan, R. Storeng, D. Scudiero, A. Monks, J. McMahon, D. Vistica, J. T. Warren, H. Bokesch, S. Kenney and M. R. Boyd, *J. Nat. Cancer Inst.*, 1990, **82**, 1107.
11 J. Carmichael, W. G. DeGraff, P. F. Gazdar, J. D. Minna and J. B. Mitchell, *Cancer Res.*, 1987, **47**, 936.
12 D. A. Fletcher, R. F. McMeeking and D. Parkin, *J. Chem. Inf. Comp. Sci.*, 1996, **36**, 746.

ChemComm

Generation of aminoacyl radicals from 1-carbamoyl-1-methylcyclohexa-2,5-dienes: a new tin-free homolytic route to β- and γ-lactams

Leon V. Jackson and John C. Walton*

University of St. Andrews, School of Chemistry, St. Andrews, Fife, UK KY16 9ST. E-mail: jcw@st-and.ac.uk

Received (in Cambridge, UK) 13th September 2000, Accepted 3rd October 2000
First published as an Advance Article on the web 9th November 2000

Radical induced homolyses of 1-carbamoyl-1-methylcyclohexa-2,5-dienes took place cleanly to yield aminoacyl radicals, with no competition from the alternative dissociation to methyl radicals: β- and γ-lactams were obtained from ring closures of suitably unsaturated model compounds.

The quest for 'cleaner' free-radical precursors, independent of tin and other toxic metal involvement, and hence suitable for pharmaceutical syntheses,[1] was aided by the discovery that esters of 1-methylcyclohexa-2,5-diene-1-carboxylic acid and of 2,5-dihydrofuran-2-carboxylic acid selectively furnished alkyl radicals on induced homolysis.[2] These reagents were employed with moderate success in benign chain alkylations of olefins, and in cyclisations, affording product yields in the range 35–65%.[3] The main limitation to the scope of their deployment was unwanted competition from an alternative dissociation of intermediate 1-methyl-1-carboxylatocyclohexadienyl radicals, that generated methyl radicals and benzoate esters as by-products. These findings triggered the idea that analogous amides **1** might function as sources of aminoacyl radicals **3**. It was anticipated that the greater stability of aminoacyl radicals, in comparison to alkoxyacyls, would favour the desired dissociation of the delocalised radical **2** to aminoacyl **3**, over the alternative dissociation to Me˙ and amide **4** (Scheme 1). Moreover, it was expected that aminoacyls would not decarbonylate at moderate temperatures and hence could be incorporated in free-radical chain cyclisations.

To test this possibility, amide **7** was prepared as illustrated in Scheme 2. Benzylimine **5** was reduced to *N*-but-3-enylbenzylamine **6** with sodium borohydride and hence, by reaction with 1-methylcyclohexa-2,5-diene-1-carbonyl chloride,[3] to amide **7**. Preliminary observations were carried out using EPR spectroscopy to monitor radical intermediates generated on photolysis of a solution of **7** in di-*tert*-butyl peroxide (DTBP) as initiator (In). Below about 30 °C the EPR spectrum showed a single radical with hyperfine splittings (hfs) and *g*-factor entirely as expected for cyclohexadienyl radical **8**; and similar to parameters previously reported for related radicals.[3,4] Above this temperature the spectrum of radical **8** weakened and by about 60 °C was entirely replaced by a new spectrum consisting of a simple nitrogen triplet (g = 2.0018, a(N) = 2.21 mT, DH_{pp} = 0.24 mT). These EPR parameters are very similar to those of archetype aminoacyls *e.g.* EtNHC˙(O) (*trans*-radical: g = 2.0018, a(N) = 2.24 mT)[5] and we attribute the spectrum to radical **9**. Clear-cut spectroscopic evidence for the ring closed radical **11** was not forthcoming; partly because of sample boiling and weak spectra at higher temperatures.

Photolysis of a solution of amide **7** in DTBP with unfiltered light from a 400 W medium pressure Hg lamp at 50 °C for 8 h afforded γ-lactam **12** as the main product (53%) together with smaller amounts of formamide **10** (37%) from direct reduction. Similar results were obtained simply by heating **7** with dibenzoyl peroxide (1.5 equiv.) in benzene for 24 h. Acyl radicals often cyclise in the *endo* mode[6] and, in the case of **9**, this would have produced 1-benzylpiperidin-2-one containing a 6-membered ring. However, spectral evidence was unequivocal in support of structure **12** and none of the piperidine derivative was perceptible under our conditions.[7] Most significantly, none of the aromatic amide of type **4** was detectable, even by GC-MS, and hence the adverse dissociation of delocalised radical **8** to Me˙ was negligible. This implied that amides of type **1** had high potential as clean aminoacyl radical sources, with promise of considerable generality for syntheses of a variety of lactams.

Carbapenems and nocardicins are important monocyclic antibiotic classes containing smaller, β-lactam rings that might, therefore, be accessible starting from appropriate amidocyclohexadienes. Radical cyclisations to afford 4-membered rings *via* 4-*exo*-*trig* ring closures are not generally favoured, but instances leading to β-lactams have been reported.[8–11] Suitably unsaturated aminoacyl radicals were generated from amides **13** and **17a**,**b**. EPR spectroscopic observations with amide **13** followed the same pattern as with amide **7** *i.e.* on photolysis with DTBP the spectrum showed the cyclohexadienyl radical at lower temperatures and aminoacyl radical **14** at higher temperatures (> *ca.* 40 °C). In preparative scale experiments at 60 °C, carbapenem derivative **15** was isolated as the major product (34%) along with formamide **16** (31%). Analogous aminoacyl radicals containing propargyl and cyanomethyl chains were generated from amides **17a** and **17b**. However, the formamides **18a**,**b** were the major products isolated. Neither of these radicals underwent efficient 4-*exo*-ring closure, pre-

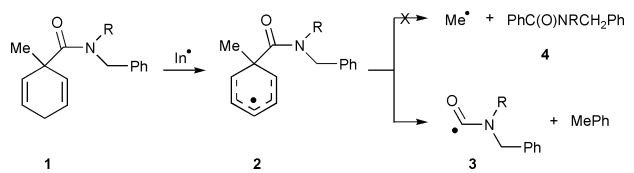

Scheme 1

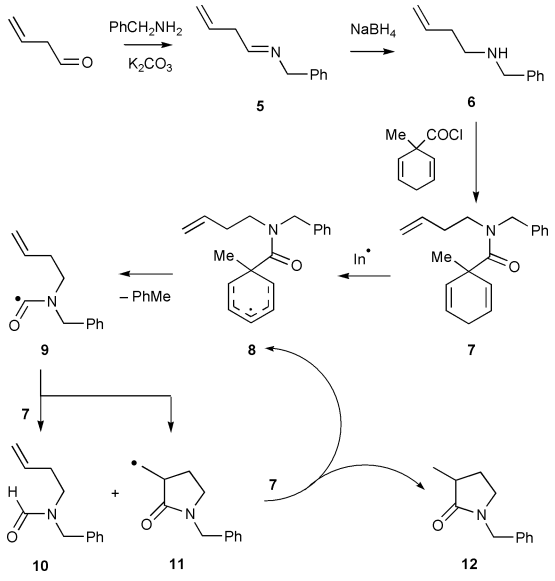

Scheme 2

DOI: 10.1039/b007454n

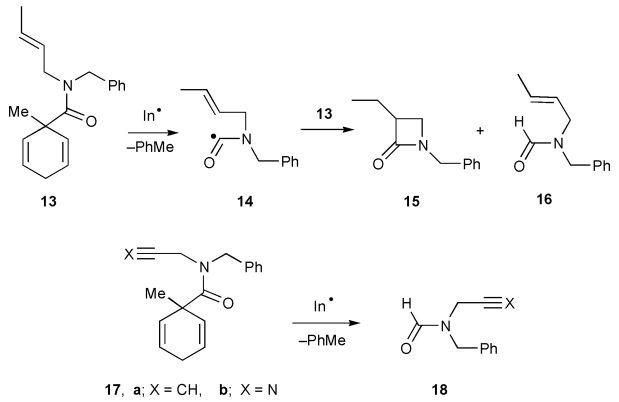

Scheme 3

sumably because of the extra strain involved in forming 4-membered rings containing exocyclic double bonds.

In summary, therefore, radical induced homolyses of cyclohexadienyl amides of type **2** took place cleanly to yield aminoacyl radicals, with no competition from the alternative dissociation to methyl radicals. Model β- and γ-lactams were obtained from ring closures of alkenylaminoacyl radicals. Consequently, these amides, which are easily prepared from unsaturated amines and 1-methylcyclohexa-2,5-diene-1-carboxylic acid, furnish mild, tin-free routes to small, and probably medium ring lactams, eminently suitable for conversion to useful biologically active compounds.

We thank the EPSRC (grant GR/L49185) for financial support.

Notes and references

1 P. A. Baguley and J. C. Walton, *Angew. Chem., Int. Ed.*, 1998, **37**, 3072.
2 G. Binmore, J. C. Walton and L. Cardellini, *J. Chem. Soc., Chem. Commun.*, 1995, 27.
3 G. Binmore, L. Cardellini and J. C. Walton, *J. Chem. Soc., Perkin Trans. 2*, 1997, 757.
4 L. Lunazzi, G. Placucci and L. Grossi, *J. Chem. Soc., Perkin Trans. 2*, 1982, 875; R. H. Schuler, G. P. Laroff and R.W. Fessenden, *J. Chem. Phys.*, 1973, **77**, 456.
5 R. Sutcliffe and K. U. Ingold, *J. Am. Chem. Soc.*, 1981, **103**, 7868; H. Hefter and H. Fischer, *Ber. Bunsen-Ges. Phys. Chem.*, 1970, **74**, 493.
6 C. Chatgilialoglu, D. Crich, M. Komatsu and I. Ryu, *Chem. Rev.*, 1999, **99**, 1991.
7 For example: carbamoylcyclohexadiene **7** (0.5 g, 1.8 mmol) in DTBP (1.3 cm^3) was photolysed in a quartz tube at 60 °C for 6 h with light from a 400 W medium pressure Hg lamp. Remaining DTBP was evaporated and the residue chromatographed to give γ-lactam **12** (0.18 g, 53%); δ_H 1.25 (3H, d, J = 7 Hz), 1.55–1.65 (2H, m), 2.52 (1H, sextet, J = 7 Hz), 3.20 (2H, m), 4.48 (2H, AB), 7.2–7.4 (5H, m); δ_C 16.4 (CH_3), 27.1 (CH_2), 36.8 (CH), 44.6 (CH_2), 46.8 (CH_2), 127.5 (CH), 128.1 (CH), 128.6 (CH), 136.7 (C), 177.4 (C=O). Found: M^+, 189.1158. $C_{12}H_{15}NO$ requires M, 189.1154. Formamide derivative **10** (0.12 g, 37%) was also isolated.
8 G. B. Gill, G. Pattenden and S. J. Reynolds, *Tetrahedron Lett.*, 1989, **30**, 3229; G. B. Gill, G. Pattenden and S. J. Reynolds, *J. Chem. Soc., Perkin Trans. 1*, 1994, 369.
9 H. Ishibashi, C. Kameoka, H. Iriyama, K. Kodama, T. Sato and M. Ikeda, *J. Org. Chem.*, 1995, **60**, 1276; H. Ishibashi, C. Kameoka, K. Kodama, T. Sato and M. Ikeda, *Tetrahedron*, 1996, **52**, 489.
10 A. J. Clark and J. L. Peacock, *Tetrahedron Lett.*, 1998, **39**, 1265.
11 L. Boiteau, J. Boivin, B. Quiclet-Sire and S. Z. Zard, *Tetrahedron*, 1998, **54**, 2087.

Selectivity of cyano-Gilman cuprates: synthesis of 10-membered ring cyclophanes

S. M. Humayun Kabir*† and Masahiko Iyoda

Department of Chemistry, Graduate School of Science, Tokyo Metropolitan University, Hachioji, Tokyo 192-0397, Japan

Received (in Cambridge, UK) 6th October 2000, Accepted 17th October 2000
First published as an Advance Article on the web 10th November 2000

The oxidation of cyano-Gilman cuprates, derived from dibromodithienyl sulfide, dibromodithienyldimethylsilane and dibromodithienylmethane, with molecular oxygen furnishes 10-membered ring cyclophanes selectively and an X-ray analysis of cyclophane 9 reveals that it possesses an *anti* conformation.

Oxidative coupling of Gilman cuprates, prepared from 2 equivalents of an organolithium reagent with 1 equivalent of CuI, was reported to produce bialkyls.[1] Lipshutz *et al*. reported for the first time, the chemistry of lower- and higher-order cyanocuprates and discussed their reactivities in Michael additions and substitution reactions.[2–6] Later, the same group reported the oxidative dimerizations of higher-order cyanocuprates to produce unsymmetrical biaryls.[7] Rajca *et al*. utilized lower-order cyanocuprates for the synthesis of polycyclic aromatics.[8] We recently described the selectivity of lower-order cyanocuprates to produce five-membered rings through intramolecular cyclizations.[9] Here, we report the selectivity of higher-order cyanocuprates or cyano-Gilman cuprates[6] for the formation of 10-membered rings *via* intermolecular cyclization reactions.

The reaction of 3,3′-dibromo-2,2′-dithienylmethane **1**[10,11] with Bu^{n}Li (2 equiv.), followed by treatment with CuCN (2.5 equiv.) produced lower-order cyanocuprates **2**. The oxidation of lower-order cyanocuprates with molecular oxygen produced five-membered ring compound **3**,[9–11] as shown in Scheme 1. Similar reactions were also accessible for compound **6** and its isomer.[9,12] Interestingly, the successive addition of butyllithium and copper(I) cyanide to compounds **1**, **10** and **11**,[9–13] followed by oxidation with molecular oxygen gave 10-membered ring cyclophanes, selectively. Thus the reaction of 3,3′-dibromo-2,2′-dithienylmethane **1** with Bu^{n}Li (2 equiv.) at −78 °C in THF gave a lithio derivative through halogen–lithium exchange, which was treated with CuCN (1 equiv.) to produce cyano-Gilman cuprates **8**. The oxidation of cyano-Gilman cuprates with molecular oxygen afforded 10-membered ring cyclophane **9** in 45% yield. The course of the reaction can be concisely represented as shown in Scheme 2.

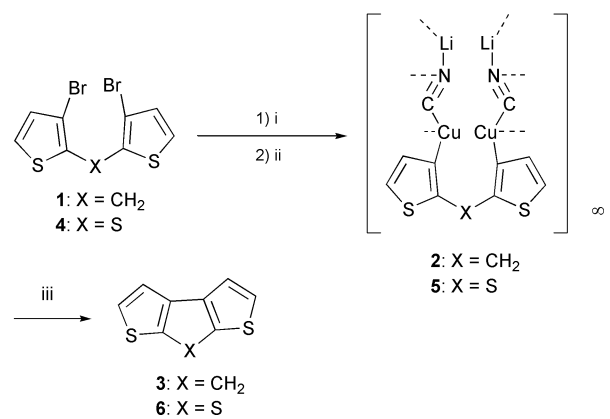

Scheme 1 *Reagents and conditions*: i, Bu^{n}Li (2 equiv.), THF, −78 °C; ii, CuCN (2.5 equiv.), −78 °C to room temp.; iii, O_2, −78 °C to room temp.

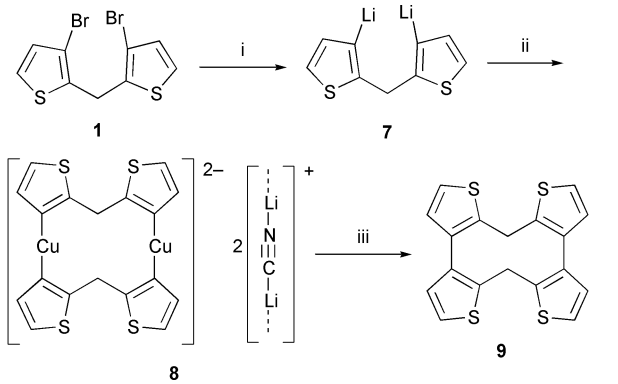

Scheme 2 *Reagents and conditions*: i, Bu^{n}Li (2 equiv.), THF, −78 °C; ii, CuCN (1.0 equiv.), −78 °C to room temp.; iii, O_2, −78 °C to room temp.

Similarly, reactions with 4,4′-dibromo-3,3′-dithienyl sulfide **10** and 4,4′-dibromo-3,3′-dithienyldimethylsilane **11** offered the opportunity to obtain cyclophanes **12** and **13**, as shown in Scheme 3. Analogous reactions afforded cyclophanes **12** and **13** in 40 and 42% yields, respectively.

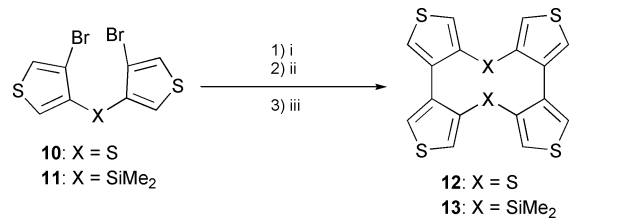

Scheme 3 *Reagents and conditions*: i, Bu^{n}Li (2 equiv.), THF, −78 °C; ii, CuCN (1.0 equiv.), −78 °C to room temp.; iii, O_2, −78 °C to room temp.

The ^{1}H NMR spectrum of **9** shows two doublets for the methylene protons at δ 4.47 and 4.02, which is clearly understood from its X-ray structure (Fig. 1).‡ Owing to the rigidity of the central 10-membered ring, the methylene protons show a coupled AB pattern and thereby appear as doublets.§ The steric repulsion between methylene protons in **9** leads to an *anti* conformation and the dihedral angle between two planes, one defined by the C2–C3 and C2–C6 bonds, and the other defined by the C2–C6 and C6–C7 bonds, is *ca.* 45°. A molecular model of **9** also suggests an *anti* conformation, which forces the bithiophene moieties into a twisted form. This is also the case for **13** with rather bulky $SiMe_2$ bridging moieties. Unlike **9** and **13**, **12** shows a *syn* conformation, owing to the absence of additional atoms on the sulfide bridges. Interestingly, AM 1

† Present Address: Department of Chemistry, Shahjalal University of Science and Technology, Sylhet 3114, Bangladesh. E-mail: hkabir-che@sust.edu

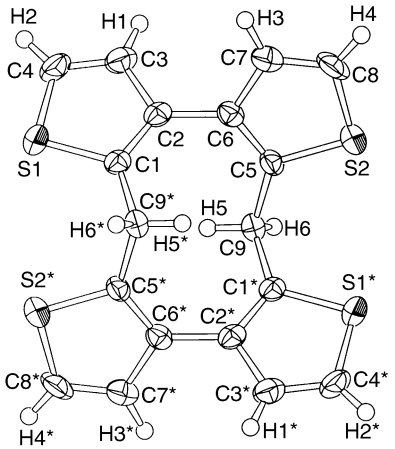

Fig. 1 X-Ray structure of **9**.

calculations on **12** and **13** are consistent with the molecular models.

The absence of π-conjugations in **9** is clearly observed from its UV spectrum. The absorption maximum exhibits a hypsochromic shift in comparison with 3,3′-dithienyl sulfide [**9**: λ_{max} = 245.5 nm (log ε = 4.24); 3,3′-dithienyl sulfide: λ_{max} = 272 nm].[14] A similar hypsochromic shift of the absorption maximum is also observed for **13** [λ_{max} = 243.5 nm (log ε = 4.05)]. Interestingly, the cyclophane **12** exhibits a bathochromic shift [λ_{max} = 289.5 nm (log ε = 4.51)], which indicates extended conjugation and also suggests a *syn* conformation.

Finally, cyclic voltammetry of **12** shows one reversible wave corresponding to radical cation or diradical dication and the half-wave potential ($E_{1/2}$) is 0.1 V (*vs.* Fc/Fc$^+$ in 0.1 M $NBu^n_4ClO_4$– PhCN).

In conclusion, the oxidation of cyano-Gilman cuprates with molecular oxygen produced 10-membered ring cyclophanes selectively and interesting properties of these cyclophanes have been established.

This work was supported by the Japanese Ministry of Education, Science, Sports and Culture (Monbusho) under a fellowship to S. M. H. K. We thank Dr M. Yoshida for helpful discussions.

Notes and references

‡ *Crystal data* for **9**: $C_{18}H_{12}S_4$, M = 356.53, monoclinic, space group $P2_1/a$ (no. 14), a = 8.731(4), b = 18.134(5), c = 9.953(6) Å, β = 90.57(4)°, V = 1575(1) Å^3, Z = 4, T = 296 K, μ(Mo-Kα) = 5.94 cm^{-1}, 3809 reflections measured, 3609 unique, R_{int} = 0.038, final R_1 = 0.046, wR_2 = 0.046 for 3809 [$I > 3.00\sigma(I)$] observed reflections. CCDC 182/1829.
§ *Selected data*: for **9**: colourless crystals, mp 259–259.6 °C; δ_H(500 MHz, $CDCl_3$) 7.30 (d, 4H, *J* 5.2 Hz), 6.89 (d, 4H, *J* 5.2 Hz), 4.47 (d, 2H, *J* 15.9 Hz), 4.02 (d, 2H, *J* 15.9 Hz); δ_C(125 MHz, $CDCl_3$) 138.8, 133.4, 129.0, 124.0, 28.0; *m/z* 356 (M^+); UV (ethanol) λ_{max} (log ε) 245.5 (4.24); Anal. Calc. for $C_{18}H_{12}S_4$: C, 60.63; H, 3.39. Found: C, 60.24; H, 3.49%. For **12**: colourless crystals, mp 196–196.5 °C; δ_H(400 MHz, $CDCl_3$) 7.36 (d, 4H, *J* 5.1 Hz), 7.29 (d, 4H, *J* 5.1 Hz); δ_C(125 MHz, $CDCl_3$) 141.6, 130.9, 125.8, 120.8; *m/z* 392 (M^+); UV (ethanol) λ_{max} (log ε) 289.5 (4.51); Anal. Calc. for $C_{16}H_8S_6$: C, 48.98; H, 2.04. Found: C, 49.18; H, 2.19%. For **13**: colourless crystals, mp 204.5–205 °C; δ_H(500 MHz, $CDCl_3$) 7.00 (d, 4H, *J* 2.7 Hz), 6.99 (d, 4H, *J* 2.7 Hz), 0.36 (s, 12H); δ_C(125 MHz, $CDCl_3$) 142.5, 140.0, 131.8, 123.6, −2.12; *m/z* 444 (M^+); UV (ethanol) λ_{max} (log ε) 243.5 (4.05); Anal. Calc. for $C_{20}H_{20}S_4Si_2$: C, 54.05; H, 4.51. Found: C, 54.30; H, 4.71%.

1 G. M. Whitesides, J. SanFilippo, Jr., C. P. Casey and E. J. Panek, *J. Am. Chem. Soc.*, 1967, **89**, 5302.
2 B. H. Lipshutz, J. Kozlowski and R. S. Wilhelm, *J. Am. Chem. Soc.*, 1982, **104**, 2305.
3 B. H. Lipshutz, R. S. Wilhelm and J. Kozlowski, *Tetrahedron Lett.*, 1982, **23**, 3755.
4 B. H. Lipshutz, R. S. Wilhelm and D. M. Floyed, *J. Am. Chem. Soc.*, 1981, **103**, 7672.
5 G. H.-Vittini, S. Hikichi and F. Sato, *Angew. Chem., Int. Ed.*, 1998, **37**, 2099.
6 N. Krause, *Angew. Chem., Int. Ed.*, 1999, **38**, 79.
7 B. H. Lipshutz, K. Siegmann, E. Garcia and F. Kayser, *J. Am. Chem. Soc.*, 1993, **115**, 9276.
8 A. Rajca, A. Safronov, S. Rajca, C. R. Ross, II and J. J. Stezowski, *J. Am. Chem. Soc.*, 1996, **118**, 7272.
9 S. M. H. Kabir, M. Miura, S. Sasaki, G. Harada, Y. Kuwatani, M. Yoshida and M. Iyoda, *Heterocycles*, 2000, **52**, 761.
10 H. Wynberg and A. Kraak, *J. Org. Chem.*, 1964, **29**, 2455.
11 A. Kraak, A. K. Wiersema, P. Jordens and H. Wynberg, *Tetrahedron*, 1968, **24**, 3381.
12 F. de Jong and M. J. Janssen, *J. Org. Chem.*, 1971, **36**, 1645.
13 M. Iyoda, M. Miura, S. Sasaki, S. M. H. Kabir, Y. Kuwatani and M. Yoshida, *Tetrahedron Lett.*, 1997, **38**, 4581.
14 E. Jones and I. M. Moodie, *Tetrahedron*, 1965, **21**, 2413.

Anionic metal dicyanamide networks with paramagnetic counter-cations

Stuart R. Batten, Paul Jensen, Boujemaa Moubaraki and Keith S. Murray*

School of Chemistry, PO Box 23, Monash University 3800, Australia. E-mail: Keith.S.Murray@sci.monash.edu.au

Received (in Cambridge, UK) 31st August 2000, Accepted 18th October 2000
First published as an Advance Article on the web 10th November 2000

The $M(bipy)_3^{2+}$ cations in the isomorphous structures of $[M(bipy)_3][M'(dca)_3]_2$, [dca = dicyanamide, $N(CN)_2^-$; M = Fe, M′ = Mn 1, Fe 2 or M = Ni, M′ = Mn 3] are contained within hexagonal windows of anionic 2D (6,3) $M(dca)_3^-$ sheets; weak antiferromagnetic coupling is observed between metal centres within the anionic networks of all three compounds.

Our recent work, and that of others, on the topology and magnetism of binary transition metal(II) dicyanamides $M(dca)_2$ [dca = $N(CN)_2^-$] and on neutral adducts of type $M(dca)_2L_x$, where x = 3 for L = H_2O, x = 2 for L = pyridine, MeOH, EtOH, DMF and x = 1 for L = pyrazine, 4,4′-bipyridine, H_2O and 2-aminopyridine, has revealed a fascinating array of structures and magnetic phenomena.[1,2] To date all compounds reported have been homometallic. However, we have recently extended our dicyanamide work to include the anionic coordination polymers $M(dca)_3^-$ and $M(dca)_4^{2-}$ first reported by Köhler *et al.* but without any crystallographic or magnetic characterisation.[3] We have found that the network topology of the anion is dependent on the counter-cation used—the networks are in fact cation templated.[4] We realised that these systems also offered the possibility of making heterometallic systems through the use of paramagnetic metal-containing counter-cations. Thus we report here the structural and magnetic properties of new anionic metal dicyanamide systems containing $M(bipy)_3^{2+}$ (bipy = 2,2′-bipyridine) counter-cations. Future work will involve use of spin-crossover Fe(II) and Co(II) cationic chelates to search for cooperative effects when such centres are dispersed in a 2D host lattice (*vide infra*).

Reaction of sodium dicyanamide, $M(bipy)_3^{2+}$ and the appropriate metal nitrate or perchlorate gave dark red crystals of $[Fe(bipy)_3][M(dca)_3]_2$, M = Mn **1**, Fe **2** and orange/pink crystals of $[Ni(bipy)_3][Mn(dca)_3]_2$ **3**.† The structures were determined by single crystal X-ray crystallography and found to be isomorphous.[5] Bulk sample purities were confirmed by powder X-ray diffraction. The structures consist of infinite hexagonal (6,3) anionic sheets of $M(dca)_3^-$ and $M(bipy)_3^{2+}$

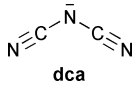

dca

counter-cations (Fig. 1). Each octahedral metal atom in a sheet is bridged by three pairs of dca ligands, coordinating through only the terminal nitrile nitrogen atoms, to three other metal atoms. There are two crystallographically unique metal atoms in the sheets, and within each sheet they are arranged in an alternating fashion [M–N 2.203(3)–2.238(2) Å (**1**), 2.130(2)–2.185(2) Å (**2**) and 2.200(2)–2.242(2) Å (**3**)]. These sheets lie in the *yz* plane, and stack in the *x* direction. The $M(bipy)_3^{2+}$ counter-cations lie inside the hexagonal windows of the sheets (Fig. 2).

There are a number of close contacts between the cations and the anionic networks. The most significant of these are H···C contacts of 2.695 Å (C–H···C = 116.7°), 2.745 Å (148.0°), 2.775 Å (123.6°) for **1**; 2.690 Å (116.6°), 2.674 Å (148.2°), 2.798 Å (121.6°) for **2**; and 2.700 Å (114.0°), 2.714 Å (148.9°), 2.770 Å (126.4°) for **3** and H···N contacts of 2.675 Å (C–H···N = 140.5°), 2.682 Å (121.1°) for **1**; 2.602 Å (140.1°), 2.683 Å (117.0°) for **2**; and 2.663 Å (139.3°), 2.673 Å (119.9°) for **3**.

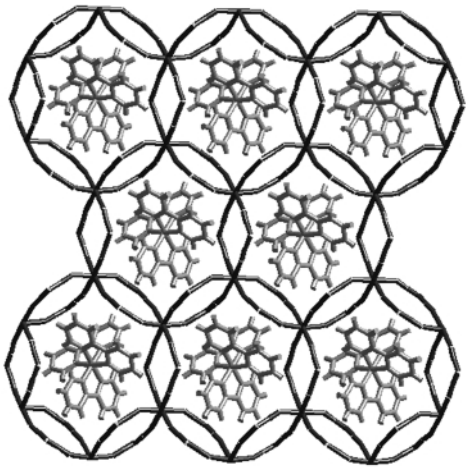

Fig. 1 The sheet structure of **1**–**3**.

There are also edge-to-face [centroid–centroid = 5.07 Å (**1**), 5.02 Å (**2**) and 5.04 Å (**3**)] and vertex-to-face [centroid–centroid = 4.96 Å (**1**), 4.92 Å (**2**) and 4.91 Å (**3**)] inter-cation interactions between the pyridyl rings of cations in adjoining sheets.

It is of interest to compare these structures to a number of closely related oxalate networks reported. Numerous hexagonal 2D (6,3) sheet structures have been reported for metal oxalate $[M_2(ox)_3]^{n-}$ networks with a variety of counter-cations,[6] including paramagnetic ones such as $[(Cp^*)_2M]^+$.[7] In contrast to the structures reported here, however, the counter-cations lie *between* the sheets rather than *within* the planes of the sheets. This is due to the smaller size of the hexagonal windows in the oxalate sheets compared to the dca sheets. Interestingly, when oxalate networks are crystallised with $M(bipy)_3^{n+}$ counter-cations, chiral 3D (10,3)-a networks are formed.[6b,c] Each crystal contains cations of only one handedness, and all $M(ox)_3^{n-}$ centres are also of a single hand. In contrast, the structures described here contain cations of both handedness, with each anionic sheet containing counter-cations of only one hand but successive anionic sheets containing counter-cations of alternating hands. As for the oxalate analogues, each (6,3) $M(dca)_3^-$ sheet contains $M(dca)_6^{4-}$ centres of alternating hands. The structure is nonetheless non-centrosymmetric (space group *Fdd*2) as layers of opposite cation chirality are related by glide planes rather than inversion centres. The alternating layers stack

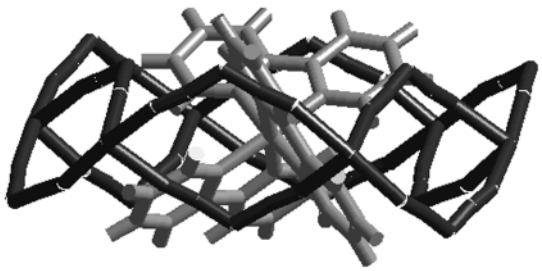

Fig. 2 Location of a $M(bipy)_3^{2+}$ cation inside a hexagonal window of a $M(dca)_3^-$ sheet.

DOI: 10.1039/b007080g

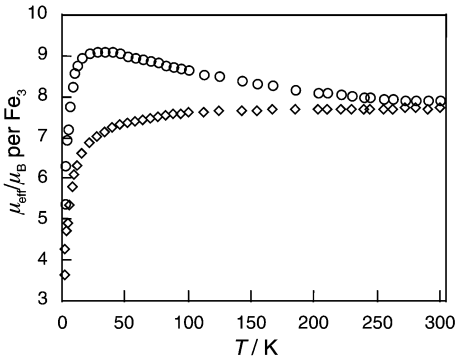

Fig. 3 Plots of μ_{eff} (per Fe_3) *vs.* temperature for $[Fe(bipy)_3][Fe(dca)_3]_2$ **2** measured in a field of 1 T as a neat powder (○) and dispersed in vaseline (◇).

such that successive layers are offset from each other, and hexagonal channels are not formed.

Since it contains a diamagnetic cation, $Fe(bipy)_3^{2+}$, the μ_{eff} value at room temperature of 8.04 μ_B for **1** is that due to $Mn(dca)_3^-$ alone. The variation in temperature mirrors that found for salts such as $PPh_4[Mn(dca)_3]$, which contain a 2D sheet structure, different to that of **1**. μ_{eff} values in **1** remain constant down to 50 K then decrease rapidly below this due to weak antiferromagnetic coupling. In an applied field of 1 T, **2** shows a μ_{eff} value at 300 K of 7.7 μ_B, per Fe_3, which, when the sample is dispersed in a vaseline mull to prevent crystallite torquing, remains constant down to 50 K and then decreases rapidly to 3.6 μ_B at 2 K because of weak antiferromagnetic coupling combined with zero field splitting effects (Fig. 3). Since the $Fe(bipy)_3^{2+}$ group is d^6 low spin the expected μ_{eff} value for uncoupled ($S = 0, S = 2, S = 2$) centres, with $g = 2.0$, is 48 = 6.93 μ_B, excluding orbital contribution/spin–orbit coupling effects on the high spin $Fe^{II}(dca)_3^-$ centre and second order Zeeman effects (TIP) on the $Fe(bipy)_3^{2+}$. An interesting feature, and one possibly overlooked in high-spin Fe(II) systems, including crossover studies, is the field induced torquing which occurs when a neat solid sample was used (Fig. 3). It can be seen that, as the temperature is raised from 2 K, in $H = 1$ T, a ferromagnetic like plot is obtained with a broad maximum in μ_{eff}, the room temperature value being similar to that in the mull sample. This effect arises from anisotropy in the susceptibility of high spin Fe(II), as was also found in Mn(III).[8] It is possible, therefore, to draw wrong conclusions, particularly in extended systems of the present type and caution is warranted.

Compound **3** also displays Curie-like susceptibilities with a value of μ_{eff} (per mol) of 8.7 μ_B at 300 K, which decreases gradually to reach 8.2 μ_B at 50 K then rapidly to 4.9 μ_B at 2 K. The data are again compatible with essentially isolated cationic and extended anionic sublattices, the latter showing weak antiferromagnetism [μ(uncoupled) = 8.83 μ_B for $S = 1 + S = 5/2 + S = 5/2$]. Despite this lack of cation (paramagnet)–anion interaction, the prospect of obtaining unusual magnetic effects when spin-crossover cations are incorporated remains positive since it is well known that weak intermolecular perturbations (*e.g.* solvate, H-bonding, π–π stacking) can sensitively influence the crossover and cooperative behavior in crystals.[9]

Notes and references

† **1**: an ethanol–water solution (5 ml) of Na(dca) (270 mg, 3.0 mmol) and $Mn(ClO_4)_2 \cdot 4H_2O$ (360 mg, 1.1 mmol) was added to an ethanol–water solution (10 ml) of $[Fe(bipy)_3](ClO_4)_2$ (360 mg, 0.50 mmol). Dark red crystals of **1** were obtained after 24 h (400 mg, 0.39 mmol, 77%). Found: C, 48.73; H, 2.31; N, 32.65. Calc. for $C_{42}H_{24}FeMn_2N_{24}$: C, 48.95; H, 2.33; N, 32.63%. Selected IR (2100–2300) (cm^{-1}, Nujol): 2291m, 2232m, 2169s.

2: an ethanol–water solution (10 ml) of Na(dca) (103 mg, 1.16 mmol) and $Fe(BF_4)_2 \cdot 6H_2O$ (129 mg, 0.382 mmol) was added to an ethanol–water solution (25 ml) of $[Fe(bipy)_3](ClO_4)_2$ (135 mg, 0.187 mmol). Dark red crystals of **2** formed after 2 days (25 mg, 0.024 mmol, 13%). Found: C, 49.11; H, 2.32; N, 32.49. Calc. for $C_{42}H_{24}Fe_3N_{24}$: C, 48.86; H, 2.34; N, 32.56%. Selected IR (2100–2300) (cm^{-1}, Nujol): 2288m, 2235m, 2172s.

3: an ethanol–water solution (10 ml) of $Ni(bipy)_3(NO_3)_2$ (162 mg, 0.249 mmol) and Na(dca) (140 mg, 1.57 mmol) was allowed to diffuse slowly into an ethanol–water solution (10 ml) of $Mn(NO_3)_2 \cdot 4H_2O$ (125 mg, 0.498 mmol). After 2 days large orange/pink crystals of **3** were collected (126 mg, 0.122 mmol, 49%). Found: C, 48.98; H, 2.26; N, 32.13. Calc. for $C_{42}H_{24}NiMn_2N_{24}$: C, 48.88; H, 2.32; N, 32.54%. Selected IR (2100–2300) (cm^{-1}, Nujol): 2290m, 2231m, 2165s.

1 S. R. Batten, P. Jensen, B. Moubaraki, K. S. Murray and R. Robson, *Chem. Commun.*, 1998, 439; P. Jensen, S. R. Batten, G. D. Fallon, D. C. R. Hockless, B. Moubaraki, K. S. Murray and R. Robson, *J. Solid State Chem.*, 1999, **145**, 387; P. Jensen, S. R. Batten, G. D. Fallon, B. Moubaraki, K. S. Murray and D. J. Price, *Chem Commun.*, 1999, 177; S. R. Batten, P. Jensen, C. J. Kepert, M. Kurmoo, B. Moubaraki, K. S. Murray and D. J. Price, *J. Chem. Soc., Dalton Trans.*, 1999, 2987; P. Jensen, S. R. Batten, B. Moubaraki and K. S. Murray, *Chem. Commun.*, 2000, 793; P. Jensen, D. J. Price, S. R. Batten, B. Moubaraki and K. S. Murray, *Chem. Eur. J.*, 2000, **6**, 3186; S. R. Batten, A. R. Harris, P. Jensen, K. S. Murray and A. Ziebell, *J. Chem. Soc., Dalton Trans.*, 2000, in press.

2 M. Kurmoo and C. J. Kepert, *New J. Chem.*, 1998, **22**, 1515; J. L. Manson, C. R. Kmety, Q. Huang, J. W. Lynn, G. M. Bendele, S. Pagola, P. W. Stephens, L. M. Liable-Sands, A. L. Rheingold, A. J. Epstein and J. S. Miller, *Chem. Mater.*, 1998, **10**, 2552; J. L. Manson, C. R. Kmety, A. J. Epstein and J. S. Miller, *Inorg. Chem.*, 1999, **38**, 2552; I. Dasna, S. Golhen, L. Ouahab, O. Pena, J. Guillevic and M. Fettouhi, *J. Chem. Soc., Dalton Trans.*, 2000, 129; A. Escuer, F. A. Mautner, N. Sanz and R. Vicente, *Inorg. Chem.*, 2000, **39**, 1668; G. A. van Albada, M. E. Quiroz-Castro, I. Mutikainen, U. Turpeinen and J. Reedijk, *Inorg. Chim. Acta*, 2000, **298**, 221; J. L. Manson, C. D. Incarvito, A. L. Rheingold and J. S. Miller, *J. Chem. Soc., Dalton Trans.*, 1998, 3705; J. L. Manson, A. M. Arif and J. S. Miller, *J. Mater. Chem.*, 1999, **9**, 979; J. L. Manson, A. M. Arif, C. D. Incarvito, L. M. Liable-Sands, A. L. Rheingold and J. S. Miller, *J. Solid State Chem.*, 1999, **145**, 369.

3 H. Köhler and B. Seifert, *Z. Anorg. Allg. Chem.*, 1966, **344**, 63; H. Köhler, H. Hartung and A. M. Golub., *Z. Anorg. Allg. Chem.*, 1974, **403**, 41.

4 K. S. Murray, S. R. Batten, P. Jensen, B. Moubaraki, E. H.-K. Tan and P. van der Werff, *Polyhedron*, in press; P. van der Werff, S. R. Batten, P. Jensen, B. Moubaraki and K. S. Murray, submitted.

5 *Crystal data*: for $C_{42}H_{24}FeMn_2N_{24}$ **1**: $M = 1030.58$, orthorhombic, space group *Fdd*2 (no. 43), $a = 28.7821(7)$, $b = 12.5280(3)$, $c = 23.7374(4)$ Å, $U = 8559.3(3)$ Å^3, $T = 123$ K, $Z = 8$, $D_c = 1.600$ g cm^{-3}, $F(000) = 4160$, μ(Mo-Kα) = 0.981 mm^{-1}, dark red crystal, 28565 reflections measured, 5287 unique ($R_{int} = 0.0635$), 313 parameters, $R_1 = 0.0424$ for 4323 reflections with $I > 2\sigma(I)$, $wR_2 = 0.0699$ (all data). For $C_{42}H_{24}Fe_3N_{24}$ **2**: $M = 1032.40$, orthorhombic, space group *Fdd*2 (no. 43), $a = 28.8799(6)$, $b = 12.4011(3)$, $c = 23.5140(3)$ Å, $U = 8421.4(3)$ Å^3, $T = 123$ K, $Z = 8$, $D_c = 1.629$ g cm^{-3}, $F(000) = 4176$, μ(Mo-Kα) = 1.087 mm^{-1}, dark red crystal, 28083 reflections measured, 4983 unique ($R_{int} = 0.0398$), 313 parameters, $R_1 = 0.0290$ for 4487 reflections with $I > 2\sigma(I)$, $wR_2 = 0.0608$ (all data). For $C_{42}H_{24}Mn_2N_{24}Ni$ **3**: $M = 1033.44$, orthorhombic, space group *Fdd*2 (no. 43), $a = 28.8625(5)$, $b = 12.5231(2)$, $c = 23.9239(3)$ Å, $U = 8647.2(2)$ Å^3, $T = 123$ K, $Z = 8$, $D_c = 1.588$ g cm^{-3}, $F(000) = 4176$, μ(Mo-Kα) = 1.071 mm^{-1}, orange/pink crystal, 28783 reflections measured, 5323 unique ($R_{int} = 0.0334$), 313 parameters, $R_1 = 0.0259$ for 4791 reflections with $I > 2\sigma(I)$, $wR_2 = 0.0564$ (all data). For all structures hydrogens were included at calculated positions (C–H = 0.95 Å) but not refined; H···C/N distances in the text are calculated using these C–H distances. CCDC 182/1821. See http://www.rsc.org/suppdata/cc/b0/b007080g/ for crystallographic files in .cif format.

6 (*a*) P. Day, *J. Chem. Soc., Dalton Trans.*, 1997, 701; (*b*) S. Decurtins, H. Schmalle and R. Pellaux, *New J. Chem.*, 1998, **22**, 117; (*c*) S. Decurtins, R. Pellaux, G. Antorrena and F. Palacio, *Coord. Chem. Rev.*, 1999, **190**–**194**, 841.

7 E. Coronado, J.-R. Galan-Mascaros, C.-J. Gomez-Garcia, J. Ensling and P. Gutlich, *Chem. Eur. J.*, 2000, **6**, 552.

8 B. J. Kennedy and K. S. Murray, *Inorg. Chem.*, 1985, **24**, 1552.

9 See for instance L. Capes, J.-F. Létard and O. Kahn, *Chem. Eur. J.*, 2000, **6**, 2246, and references therein.

ChemComm

Colloidal suspensions of template-removed zeolite nanocrystals†

Huanting Wang, Zhengbao Wang and Yushan Yan*

Department of Chemical and Environmental Engineering, University of California, Riverside, CA 92521, USA. E-mail: yushan.yan@ucr.edu

Received (in Irvine, CA, USA) 1st August 2000, Accepted 13th October 2000
First published as an Advance Article on the web 10th November 2000

Colloidal suspensions of template-removed zeolite nanocrystals were prepared by using an organic polymer network as a temporary barrier during calcination to prevent zeolite nanocrystal aggregation.

There is considerable interest in the synthesis of colloidal zeolite nanocrystals because they can serve as model systems for the fundamental study of zeolite crystal growth.[1–5] Colloidal suspensions of zeolite nanocrystals have also been used to deposit seed layers for preparation of zeolite membranes.[6,7] Very recently, construction of hierarchically porous crystalline structures through templated self-assembly of colloidal zeolite nanocrystals has also been reported.[8,9] Colloidal suspensions of zeolite nanocrystals are usually synthesized *via* hydrothermal procedures using clear aqueous solutions.[1–9] In most of these syntheses, organic templates (or structure-directing agents) are used, and the colloidal crystals so obtained contain organic template in their void spaces. We are interested in using colloidal suspensions of organic-functionalized zeolite nanocrystals as building blocks to construct hierarchical porous inorganic–organic hybrid materials that have potential applications in separation, catalysis, and microelectronics.[10–13] For this purpose, suspensions of template-free nanocrystals are required. Thus far, the most commonly used method for template removal is through high temperature calcination in air or oxygen. This method, however, has proved unsuitable for colloidal nanocrystals because it leads to significant irreversible aggregation.[8,9]

Here we report a novel approach to prepare colloidal suspensions of template-free zeolite nanocrystals by using an organic polymer network as a temporary barrier to isolate as-synthesized nanocrystals during template removal. Scheme 1 shows a flowchart of the preparation process. This approach appears general for all zeolites, however, only the preparation of a colloidal suspensions of template-free silicalite nanocrystals is reported here as an example. To the best of our knowledge, this is the first report on colloidal suspensions of calcined zeolite nanocrystals.

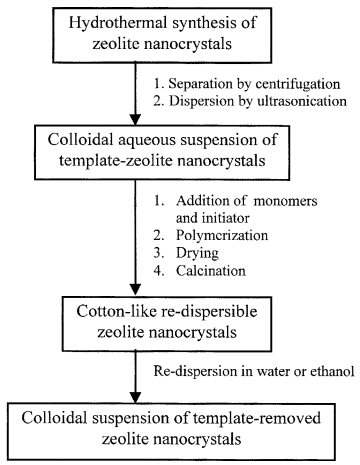

Scheme 1 Preparation protocol for colloidal suspensions of template removed zeolite nanocrystals.

† Electronic supplementary information (ESI) available: Suppl. Figs. 1–3: TGA curves, XRD patterns and IR spectra. See http://www.rsc.org/suppdata/cc/b0/b006518h/

An aqueous colloidal suspension of template-containing silicalite nanocrystals was synthesized as follows.[8] A clear synthesis solution was prepared by dropwise addition of tetrapropylammonium hydroxide solution (TPAOH, Aldrich) into tetraethyl orthosilicate (TEOS, Aldrich) with strong agitation followed by 1–3 days of aging at 30 °C under stirring. The final solution molar composition was 1 TPAOH : 2.8 SiO_2 : 11.2 EtOH : 40 H_2O. Crystallization was carried out at 80 °C for 3 days with constant stirring at 250 rpm. A stable aqueous suspension of silicalite nanocrystals was obtained by repeated cycles of centrifugation at 15 000 rpm, decanting, and ultrasonic redispersion in pure water until pH < 8. Other dispersants such as ethanol could also be used if desired.

The water soluble organic monomers acrylamide CH_2=CHCONH$_2$ (AM, Aldrich), and *N*,*N*′-methylenebisacrylamide, $(CH_2$=CHCONH$_2)_2CH_2$ (MBAM, Aldrich), and the initiator $(NH_4)_2S_2O_8$ (Aldrich) were used to prepare the polymer network. Typically, 1.0 g AM, 0.1 mg MBAM and 25 mg $(NH_4)_2S_2O_8$ were added under stirring into 10 g of a silicalite colloidal suspension with 5 wt% solid loading. After the monomers were dissolved, the mixture was ultrasonicated for 15 min to ensure complete dispersion of the silicalite nanocrystals. The aqueous solution containing the monomers has a fairly low viscosity and could readily be polymerized and crosslinked *via* a free-radical mechanism into an elastic hydrogel once the temperature was increased to 50 °C or a catalyst [*N*,*N*,*N*′,*N*′-tetramethylethylenediamine (TEMED)] was added at room temperature.[14] Polyacrylamide hydrogels have been commonly used as binders in ceramic forming processes[14] and are expected to be compatible with silicalite nanocrystals whose surface silanol groups interact favorably with –NH_2 groups. The solid polymer–silicalite composite was dried at 80–100 °C overnight before it was carbonized under nitrogen at 550 °C for 2 h (heating rate 2 °C min^{-1}) and then calcined at 550 °C for 3 h under air (Scheme 1).

TGA was used to monitor the thermal decomposition of dried polymer–silicalite composite under N_2 and air (ESI†). Under N_2 a weight loss of *ca.* 18% was recorded between room temperature and 280 °C, due to desorption of water and TPAOH. A weight loss of *ca.* 42% occurred between 280 and 600 °C as a result of decomposition of occluded TPA and carbonization of the polymer network. Based on a theoretical value of 11.7% weight loss for TPA decomposition (four TPA^+ cations per silicalite unit cell),[9] the weight loss during carbonization was estimated to be 28 wt%. The residual silicalite was 16 wt% after heating under air at 550 °C which removes carbon completely, and thus the carbon is calculated to be 24 wt%. TG analysis of a sample without incorporation of the polymer network shows that template TPAOH can be removed completely through this procedure.

Fig. 1 shows SEM images of silicalite nanocrystals after direct drying and calcination in the absence of a polymer network barrier. Clearly, direct drying of an as-synthesized silicalite suspension by evaporation leads to densely packed crystals [Fig. 1(a)], which upon calcination aggregate irreversi-

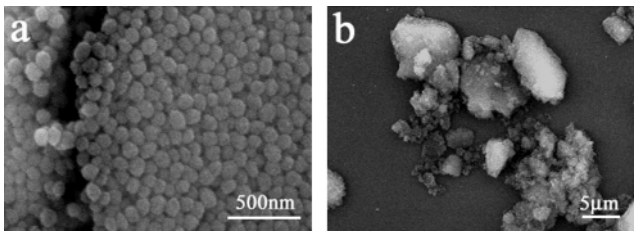

Fig. 1 SEM images of silicalite nanocrystals prepared without polymer network barrier: (a) after drying, (b) after calcination.

bly into large solid particles and grinding using a mortar and pestle for 2 h did not appear to improve its re-dispersibility. These particles cannot be re-dispersed into a suspension, and precipitated quickly after mild shaking [Fig. 1(b)].

The aggregation of zeolite nanocrystals is a result of condensation reactions between surface silanol groups of zeolite nanocrystals.[8,9] For condensation reactions to occur, close packing of the nanocrystals is required [Fig. 1(a)].[8,9] The function of the polymer network used here is to keep the nanocrystals separated during carbonization and calcination. Fig. 2 shows SEM images of the composite after drying, carbonization and calcination. After drying, the silicalite nanocrystals are uniformly distributed and well separated in the polymer network [Fig. 2(a)]. Carbonization at 550 °C generated large voids in the composite owing to production of gaseous products [Fig. 2(b)].[15] SEM examination of the carbon skeleton shows that zeolite nanocrystals are uniformly distributed and well separated within the carbon matrix [Fig. 2(c)]. Final calcination removes the carbon barrier and leads to a loose cotton-like white powder [Fig. 2(d)]. We have carried out extensive SEM studies on suspensions with various solid loading and aging times (*e.g.*, 3–4 months) by dip-coating the nanocrystals onto silicon wafers. The substrate withdrawal rate was 1 cm s^{-1} and clean-room-grade wafers were cut into 2 × 2 cm square pieces and used without further cleaning. Our SEM results suggest that the calcined nanocrystal powders can be easily dispersed in water and many other dispersants such as ethanol to form stable suspensions. Uniform films can be formed using suspensions of template-removed silicalite nanocrystals with an appropriate solid loading, and this indicates that the processed nanocrystals have good film-forming properties. Fig. 2(e) shows an example of such a film (*ca.* 0.3 μm thick).

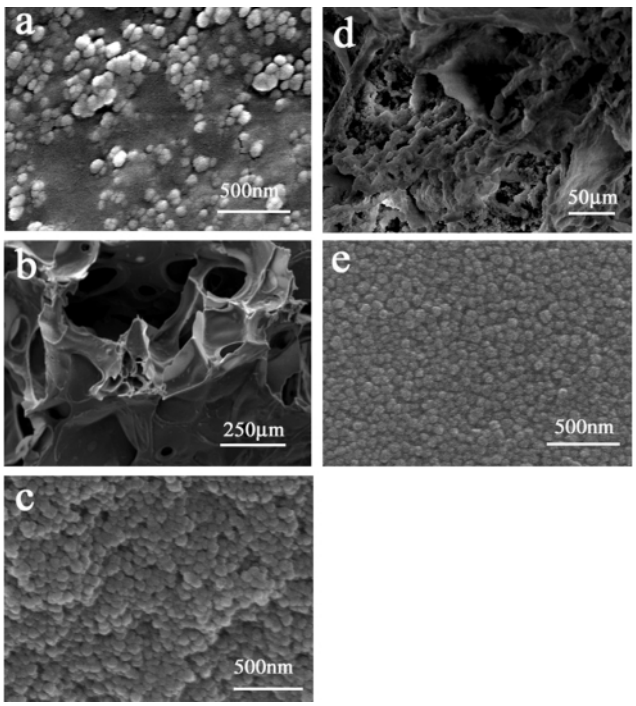

Fig. 2 SEM images of silicalite nanocrystals prepared with a polymer network barrier: (a) after drying, (b) after carbonization (low magnification), (c) after carbonization (high magnification) showing the carbon skeleton, (d) after calcination, (e) silicalite film dip-coated from a colloidal suspension of template-removed nanocrystals.

The powder X-ray diffraction (PXRD) pattern of a re-dispersible white powder sample matches that of a typical 100% crystalline nanoslicalite sample (ESI†).[8,9] FTIR spectra show the nanopowder has an MFI type structure (band at 550 cm^{-1}, with *ca.* 97% crystallinity) and a high concentration of terminal Si–OH groups (band at 972 cm^{-1}) (ESI†).[8,9] N_2 adsorption measurements show that the BET surface area and pore volume for the cotton-like sample are 355 m^2 g^{-1} and 0.18 cm^3 g^{-1}, respectively. These data show that the polymerization, carbonization and calcination processing has no influence on crystallinity and porosity of the nanocrystals.

The weight ratio of polymer to nanocrystals appears important in determining the re-dispersibiltiy of the nanocrystals. We have examined several polymer/zeolite weight ratios and a ratio around 2.0 sufficiently separates nanocrystals. It is recognized that the nanocrystals do move closer and may even contact one another during the final burn-off of carbon. SEM images clearly show that the contact areas among nanocrystals are rather small within the cotton-like nanopowder. It is also possible that during the early stage of calcination some reactive silanol groups on isolated (by carbon) nanocrystals condensed among themselves, and this in turn should reduce the amount of surface silanol groups and the probability of aggregation.

In conclusion, we have demonstrated that colloidal suspensions of template-free zeolite nanocrystals can be prepared by using an organic polymer network as a temporary barrier to avoid nanocrystal aggregation during calcination. Work is under way on organic functionalization of zeolite nanocrystals and construction of hierarchical inorganic–organic hybrid materials using zeolite nanocrystals as building blocks. It is noted here that this approach is not zeolite specific, and thus could become a general strategy for retrieving various nanoparticles from synthetic solutions without aggregation.

This work is partly supported by CE-CERT of UC-Riverside, UC-SMART, UC-TSR&TP, UC-EI, and a UC Regents Faculty Fellowship to Y. Y. We thank Dr. Re Lai and Mr. Piboon Pantu of Caltech for N_2 adsorption measurements.

Notes and references

1 S. Mintova, N. H. Olson, V. Valtechev and T. Bein, *Science*, 1999, **283**, 958.
2 B. J. Schoeman, J. Sterte and J. E. Otterstedt, *Zeolites*, 1994, **14**, 110.
3 G. S. Zhu, S. L. Qiu, J. H. Yu, Y. Sakamoto, F. S. Xiao, R. R. Xu and O. Terasaki, *Chem. Mater.*, 1998, **10**, 1483.
4 M. A. Camblor, A. Mifsud and J. Perez-Pariente, *Zeolites*, 1991, **11**, 792.
5 N. B. Castagnola and P. K. Dutta, *J. Phys. Chem. B*, 1998, **102**, 1696.
6 L. C. Boudreau, J. A. Kuck and M. Tsapatsis, *J. Membr. Sci.*, 1999, **152**, 41.
7 M. C. Lovallo and M. Tsapatsis, *AIChE J.*, 1996, **42**, 3020.
8 L. M. Huang, Z. B. Wang, J. Y. Sun, L. Miao, Q. Z. Li, Y. Yan and D. Y. Zhao, *J. Am. Chem. Soc.*, 2000, **122**, 3530.
9 B. J. Zhao, S. A. Davis, N. H. Mendelson and S. Mann, *Chem. Commun.*, 2000, 781.
10 M. J. MacLachlan, I. Manners and G. A. Ozin, *Adv. Mater.*, 2000, **12**, 675.
11 M. H. Lim, C. F. Blanford and A. Stein, *Chem. Mater.*, 1998, **10**, 467.
12 C. J. Jones, K. Tsuji and M. E. Davis, *Nature*, 1998, **393**, 52.
13 T. Asefa, M. J. MacLachlan, N. Coombs and G. A. Ozin, *Nature*, 1999, **402**, 867.
14 H. T. Wang, X. Q. Liu and G. Y. Meng, *Mater. Res. Bull.*, 1997, **32**, 1705.
15 Y. Yan, M. E. Davis and G. R. Gavalas, *J. Membr. Sci.*, 1997, **126**, 53.

ChemComm

Novel nanoscale gas containers: encapsulation of N_2 in CN_x nanotubes

M. Terrones,*[ab] R. Kamalakaran,[a] T. Seeger[a] and M. Rühle[a]

[a] *Max-Planck-Institut für Metallforschung, Seestr. 92, D-70174 Stuttgart, Germany. E-mail: terrones@hrem.mpi-stuttgart.mpg.de; mterrone@fenix.ifisicacu.unam.mx*

[b] *Instituto de Física, Laboratorio Juriquilla, UNAM, A.P. 1-1010, 76000, Querétaro, México*

Received (in Cambridge, UK) 12th October 2000, Accepted 20th October 2000
First published as an Advance Article on the web

Gaseous N_2 has been efficiently introduced in the hollow cavities of aligned CN_x nanotubes (15–80 nm od) by pyrolysing a jet (spray) solution of $Fe(C_5H_5)_2$ and $PhCH_2NH_2$ in an Ar atmosphere at 850 °C; the aligned material consist of large arrays (2.5 cm²) of CN_x ($x < 0.05$) 'bamboo-like' nanotubes (< 100 μm in length); high resolution electron energy loss spectroscopy (HREELS) line-scans and elemental mapping studies reveal that N gas was encapsulated within the hollow compartments of the CN_x nanotubes; these results demonstrate for the first time, that CN_x nanotubes can be used to fabricate gas storage components.

Carbon nanotubes[1] can behave as efficient gas and metal containers. In particular, it has been demonstrated that metals, metal carbides, oxides, chlorides, *etc*.[2–4] can be introduced into the carbon nanotube cores by methods involving: (a) chemical treatments[5] (by boiling suspensions of nanotubes in aqueous nitric acid for several hours), (b) arc discharge[6] (by arcing graphite electrodes packed with a metal); (c) solid state reactions[7] (by heating nanotubes with halides under vacuum) and (d) electrochemical techniques[8] (by passing a current through graphite electrodes in molten ionic salts at *ca.* 600–700 °C). Unfortunately, these are not able to encapsulate gaseous substances.

Recent studies have revealed that H_2 and Ar can be stored in single[9,10] and multiwalled carbon nanotubes,[11] respectively. However, these processes involve at least two steps including the material production and the gas introduction. In the case of multiwalled nanotubes (MWNTs), Ar has been introduced using high Ar pressures for 48 h at 650 °C. Here we report an alternative route to introduce N_2 inside multiwalled CN_x ($x <$ 0.05) 'bamboo-like' nanotubes using a single step reaction process [spray pyrolysis of $Fe(C_5H_5)_2$ (ferrocene) and $PhCH_2NH_2$ (benzylamine) solutions]. The products were studied using scanning electron microscopy (SEM), high resolution transmission electron microscopy (HRTEM) and HREELS.

The pyrolysis apparatus[12] consists of a 300 mm long furnace fitted with a quartz tube (id 10 mm, 800 mm long). One end of the tube is attached to a Pyrex cone (id 0.35 mm), which is connected to a container used for storing and releasing ferrocene/benzylamine solutions. A nozzle (consisting of a capillary) is contained in the Pyrex cone with an exit diameter of 0.5 mm. The reaction tube was preheated to 850 °C; subsequently the solution (0.2 g. ferrocene in 2 ml benzylamine) was released and sprayed by flowing Ar (Messer Griessheim 99.999%) around the cone/nozzle area into the hot zone. The spraying time lasted between 5 and 10 min, usually using 1 ml of the solution. The furnace was maintained at this temperature for an additional 15 min in order to anneal the products.

SEM studies were carried out using a JEOL-JSM 6300F operated at 2–5 kV and a Zeiss DSM 982 Gemini operated at 1–2 kV. HRTEM observations were made using a JEOL-JEM4000 EX operating at 400 kV. Energy-dispersive X-ray (EDX) spectroscopy data were obtained using a Noran Ins. detector fitted within the JSM 6300F microscope. HREELS studies were performed in a dedicated STEM VG-HB 501UX equipped with a Gatan Digi-PEELS 766 detector.

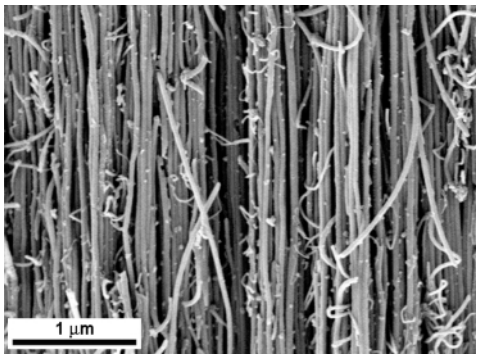

Fig. 1 SEM image of a typical film of aligned CN_x nanotubes of uniform diameter (*ca*. 40 nm od).

The pyrolysed material, scratched from the internal tube surface (hot zone), consists of large black and shiny films of area 2.5 cm² and 100–200 μm thick. SEM studies reveal that the films are composed of aligned tubular structures (100 μm long, 15–80 nm od). Fig. 1 shows a typical region of aligned nanotubes observed within the films.

TEM and HRTEM studies indicate that the material mainly consists of nanotubes exhibiting compartmentalized morpholo-

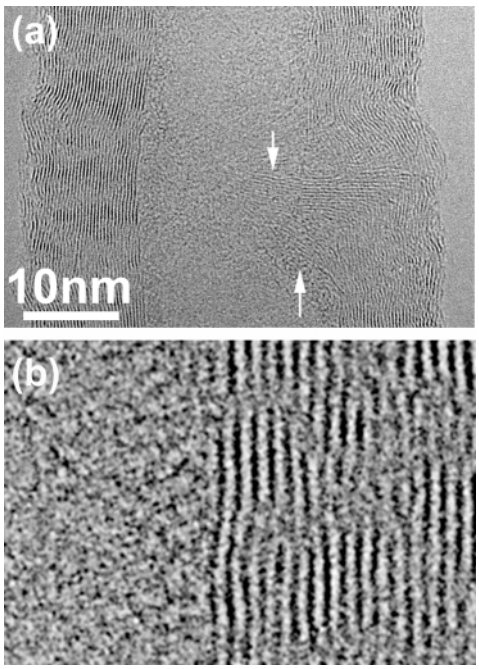

Fig. 2 HRTEM images of a CN_x nanotube: (a) tube segment showing 'graphitic' walls parallel to the tube axis as well as an inner core. It is important to note that the inner core contrast (amorphous-like) suggests the presence of a foreign non-crystalline material. In addition, some inter-linked planes appear to cross the core of the tube, creating compartments (arrows); (b) higher magnification of a CN_x nanotube exhibiting the degree of crystallinity of walls as well as the amorphous-like core (interlayer spacing 0.34 nm).

DOI: 10.1039/b008253h

gies resembling 'bamboo-like' structures, similar to those observed in CN_x nanofibres.[13,14] Fe particles (identified by EDX and electron diffraction) were also observed at the tips of the nanotubes. This confirms that catalytic nanotube growth took place. It is noteworthy that the presence of other carbonaceous material within the samples was notably absent. HRTEM images showed that the tubes were hollow with wide inner cores (>10–20 nm), but compartmentalized forming pockets caused by inter-linkage of graphitic planes across the inner core of the tubes [Fig. 2(a)]. Close inspection of the tubular structures confirmed that the walls consisted of parallel graphite-like sheets [<30 walls; Fig. 2(b)]. We also note that the hollow core of the tubes exhibited an amorphous-like appearance [Fig. 2(a)], suggesting that a foreign material was encapsulated.

EEL spectra of the nanofibres revealed the presence of ionisation edges at *ca.* 284.5 and 400 eV corresponding to the C and N K-excitations. The near edge fine structure of the carbon K-edge confirms that the material is 'graphitic'. Interestingly, a first EELS measurement on a typical CN_x tube revealed a high intensity peak at (401 ± 0.5) eV, clearly indicating the presence of molecular N_2[15] [Fig. 3(a)]. Following this measurement a 'hole' was formed due to the heavy electron irradiation. A subsequent spectrum recorded in the same area revealed a completely different N-K edge exhibiting a π*-peak at (399 ± 0.5) eV and a broad σ*-peak [Fig. 3(a)], which is commensurate with the incorporation of N within the sp^2-carbon network (usually observed in CN_x nanofibres[13,14]). The latter observations suggest that N gas was trapped within the hollow nanotube core, and after our first measurement the effect of focusing the electron beam on the tube caused the tube to open, thus releasing the encapsulated N_2 gas. Once a 'hole' was created, N_2 gas was not detected in neighboring areas.

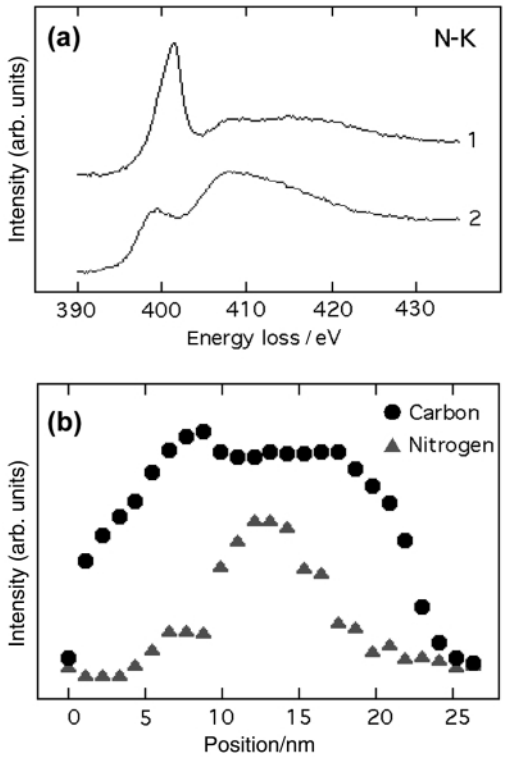

Fig. 3 (a) EEL spectra of the N-K edge representative of a CN_x nanotube. The first measurement (spectrum 1) reveals the presence of molecular nitrogen (peak at 401 ± 0.5 eV). In a second measurement (spectrum 2) recorded at the same position, the sharp peak disappears and a maximum appeared at 399 ± 0.5 eV, corresponding to N incorporated within a C-network. During measurements, we noted that a 'hole' (caused by electron irradiation) was only created when molecular N was trapped inside the tube; (b) concentration profiles of C and N across the diameter of a 25 nm CN_x nanotube derived from EELS line-scans. These indicate the presence of C on the periphery and N mainly within the inner core of the structures. The central 'dip' in the carbon profile is commensurate with an internal core, filled with N.

In order to confirm the presence of N in the nanotube core, HREELS line scans were performed across several tubes. A typical line-scan across the tube axis [Fig. 3(b)] reveals that the C and N concentration profiles 'anticorrelate' across the tubes. A similar behaviour has been observed in Ar filled nanotubes.[11] The line-scans confirm that nitrogen was indeed encapsulated within the hollow cores and not only concentrated within the walls as observed in previous studies.[13,14] Approximately 10–35% of the tubes investigated appeared to be filled with nitrogen gas. In addition, elemental mapping using EELS (not shown here) revealed that N was localised in pockets (consistent with the compartmentalized carbon morphologies) within the nanotube cores. From representative EEL spectra, it was estimated that the N content within the empty CN_x nanotubes (without N_2 gas trapped) was *ca.* $\leqslant$5%. It is noteworthy that the N encapsulation was stable over several weeks and that the gas-filled tubes were not affected after long dispersion periods in acetone.

Our results demonstrate a single-step pyrolytic route to fill CN_x nanotubes with N gas. We have also shown that CN_x nanotubes and nanofibres can be considered as efficient gas containers owing to the presence of pockets (bamboo-like structures), which ensure the encapsulation of gases. The CN_x structures could also serve as containers in order to study liquefaction of N_2 at low temperatures. To the best of our knowledge, this is the first time that N has been incorporated in nanotubes. These observations pave the way to the fabrication of novel gas storage components using spray pyrolysis.

We thank the Alexander von Humboldt Stiftung (M. T.), CONACYT-México grant J31192U (M. T.), the Max-Planck-Gesellschaft (R. K.) and the DFG grant Ru342/11-2 (M. R., T. S.) for financial support. We are also grateful to P. Kopold, H. Labitzke, G. Preininger and S. Kühnemann for electron microscopy support and technical assistance. We also thank N. Grobert, M. Mayne, Ph. Kohler-Redlich and H. Terrones for useful discussions.

Notes and references

1 S. Iijima, *Nature*, 1991, **354**, 56.
2 P. M. Ajayan and S. Iijima, *Nature*, 1993, **361**, 333.
3 N. Grobert, M. Terrones, A. J. Osborne, H. Terrones, W. K. Hsu, S. Trasobares, Y. Q. Zhu, J. P. Hare, H. W. Kroto and D. R. M. Walton, *Appl. Phys. A*, 1998, **67**, 595.
4 M. Terrones, N. Grobert, W. K. Hsu, Y. Q. Zhu, W. B. Hu, H. Terrones, J. P. Hare, H. W. Kroto and D. R. M. Walton, *Mater. Res. Soc. Bull.*, 1999, **24**, 43.
5 S. C. Tsang, Y. K. Chen, P. J. F. Harris and M. L. H. Green, *Nature*, 1994, **372**, 159.
6 C. Guerret-Piécourt, Y. Le Bouar, A. Loisseau and H. Pascard, *Nature*, 1994, **372**, 761.
7 J. Sloan, D. M. Wright, H. G. Woo, S. Brown, A. P. E. York, K. S. Coleman, J. L. Hutchison and M. L. H. Green, *Chem. Commun.*, 1999, 699.
8 W. K. Hsu, H. Terrones, M. Terrones, N. Grobert, A. I. Kirkland, J. P. Hare, K. Prassides, P. D. Townsend, H. W. Kroto and D. R. M. Walton, *Chem. Phys. Lett.*, 1998, **284**, 177.
9 A. C. Dillon, K. M. Jones, T. A. Bekkedahl, C. H. Kiang, D. S. Bethune and M. J. Heben, *Nature*, 1997, **386**, 377.
10 C. Liu, Y. Y. Fan, M. Liu, H. T. Cong, H. M. Cheng and M. S. Dresselhaus, *Science*, 1999, **286**, 1127.
11 G. E. Gadd., M. Blackford, S. Moricca, N. Webb, P. J. Evans, A. M. Smith, G. Jacobsen, S. Leung, A. Day and Q. Hua, *Science*, 1997, **277**, 933.
12 R. Kamalakaran, M. Terrones, T. Seeger, Ph. Kohler-Redlich, M. Rühle, Y. A. Kim, T. Hayashi and M. Endo, *Appl. Phys. Lett.*, 2000, **77**, in press.
13 M. Terrones, Ph. Redlich, N. Grobert, S. Trasobares, W. K. Hsu, H. Terrones, Y. Q. Zhu, J. P. Hare, A. K. Cheetham, M. Rühle, H. W. Kroto and D. R. M. Walton, *Adv. Mater.*, 1999, **11**, 655.
14 M. Terrones, H. Terrones, N. Grobert, W. K. Hsu, Y. Q. Zhu, H. W. Kroto, D. R. M. Walton, Ph. Kohler-Redlich, M. Rühle, J. P. Zhang and A. K. Cheetham, *Appl. Phys. Lett.*, 1999, **75**, 3932.
15 J. Bruley and L. M. Brown, *Philos. Mag. A*, 1989, **59**, 247.

Multiple ligand transfer to planar-chiral cyclopentadienylruthenium complexes inducing metal-centered chirality

Taku Katayama, Yuji Matsushima, Kiyotaka Onitsuka and Shigetoshi Takahashi*

The Institute of Scientific and Industrial Research, Osaka University, 8-1 Mihogaoka, Ibaraki, Osaka 567-0047, Japan. E-mail: takahashi@sanken.osaka-u.ac.jp

Received (in Cambridge, UK) 7th August 2000, Accepted 11th October 2000
First published as an Advance Article on the web 10th November 2000

Multiple ligand transfer reaction between planar-chiral cyclopentadienylruthenium complexes [Cp′Ru(AN)$_3$][PF$_6$] [(Cp′ = 1-(CO$_2$Et)-2-Me-4-RC$_5$H$_2$, R = Me, Ph, Bu^t, AN = acetonitrile] and iron complexes CpFe(CO)(L)X (L = PMe$_3$, PPh$_3$; X = I, Br) results in formation of metal-centered chiral ruthenium complexes Cp′Ru(CO)(L)X with a diastereoselectivity (de) up to 68%.

Half-sandwich transition metal complexes CpML$_3$ with a three-legged piano stool structure are fascinating molecules owing to their potential as catalytic or stoichiometric mediators in precise organic syntheses and some of their chiral versions have recently been applied in asymmetric organic synthesis.[1] Although most chiral organometallic complexes have chiral organic groups on the ligands, chiral half-sandwich complexes can be formed in the absence of chiral ligands. While coordination of three different ligands to a metal generates a stereogenic center at the metal atom,[2] unsymmetrically substituted cyclopentadienyl ligands provide planar chirality.[3] Studies on such chiral complexes give us fundamental and important information that serves for the development of novel asymmetric reactions.

We have been studying planar-chiral Ru complexes with trisubstituted cyclopentadienyl ligands.[4,5] Recently we also reported a novel multiple ligand transfer reaction between [CpRu(L)(AN)$_2$][PF$_6$] [L = AN, CO, P(OMe)$_3$; AN = acetonitrile] and CpFe(CO)(L′)X [L′ = CO, PMe$_3$, PMe$_2$Ph, PMePh$_2$, PPh$_3$, P(OPh)$_3$; X = I, Br, Cl].[6] Now, we have examined multiple ligand transfer reactions using planar-chiral cyclopentadienylruthenium complexes and found the induction of Ru-centered chirality by planar chirality on ligand transfer from Fe complexes.

Table 1 lists the results obtained from the reactions of the trisubstituted cyclopentadienyl ruthenium tris(acetonitrile) complex [Cp′Ru(AN)$_3$][PF$_6$] **1**[4] with Fe complex **2** of the type CpFe(CO)$_2$X. Thus, treatment of Ru complex **1a** [Cp′ = η^5-1-(CO$_2$Et)-2,4-Me$_2$C$_5$H$_2$] with an equimolar amount of CpFe(CO)$_2$I **2a** in refluxing CH$_2$Cl$_2$ for 3 h produced a triple ligand transfer product, Cp′Ru(CO)$_2$I **3a**, in 76% yield (Scheme 1). Similar reactions of **1a** with CpFe(CO)$_2$Br **2b** and CpFe(CO)$_2$Cl **2c** gave Cp′Ru(CO)$_2$Br **3b** and Cp′Ru(CO)$_2$Cl **3c**, respectively. Ru complexes **1b** [Cp′ = η^5-1-(CO$_2$Et)-2-Me-4-PhC$_5$H$_2$) and **1c** [Cp′ = η^5-1-(CO$_2$Et)-2-Me-4-Bu^{t}C$_5$H$_2$] also produced the corresponding dicarbonylruthenium complexes **3d**–**h**. The resulting Ru complex **3** was fully characterized by spectral analyses and X-ray crystallography.† The geometry around the metal atom is similar to those of analogous iron complexes (*R*)- and (*S*)-Cp′Fe(CO)$_2$I [Cp′ = η^5-1-(CO$_2$Men)-2-Me-4-PhC$_5$H$_2$; Men = (*l*)- or (*d*)-menthyl].[7]

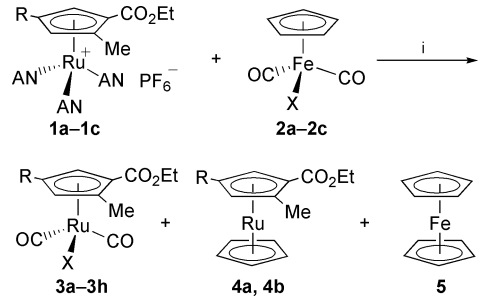

Scheme 1 *Reagents and conditions*: i, CH$_2$Cl$_2$, reflux, 3 h.

When enantiomerically pure planar-chiral complexes (*R*)- and (*S*)-[Cp′Ru(AN)$_3$][PF$_6$] **1d** [Cp′ = η^5-1-(CO$_2$Adm)-2,4-Me$_2$C$_5$H$_2$; Adm = 2-adamantyl] were used as starting materials in the reaction with **2a**, the corresponding Ru complexes (*R*)- and (*S*)-Cp′Ru(CO)$_2$I **3i** were isolated, respectively, in an enantiomerically pure form [(*R*)-**3i**: [α]$_D$ = +143° (*c* 0.100, CH$_2$Cl$_2$); (*R*)-**3i**: [α]$_D$ = −142° (*c* 0.105, CH$_2$Cl$_2$)]. ^{1}H NMR experiments using a chiral shift reagent Eu(hfc)$_3$ unequivocally indicate that no racemization of the planar-chiral cyclopentadienyl ligand occurred in the multiple ligand transfer reactions.

Then, we investigated the influence of planar chirality of the cyclopentadienyl group on the stereochemistry at the Ru center of the triple ligand transfer product Cp′Ru(CO)(L)X **7** from the reaction with CpFe(CO)(L)X **6** (L = PMe$_3$, PPh$_3$; X = I, Br) (Scheme 2). As illustrated in Scheme 3, complex **7** contains two diastereomerically related pairs, each of which consists of enantiomers. Thus, the diastereoselectivity of metal-centered chirality affected by the planar chirality of cyclopentadienyl group was appraised by the diastereomer ratio of **7** (Table 2). Although other Ru complexes **3** and/or **4** were also produced as

Table 1 Triple ligand transfer reactions between [Cp′Ru(AN)$_3$][PF$_6$] **1** and CpFe(CO)$_2$X **2**

	Substrate		Isolated yields of products (%)			
Run	Ru complex	Fe complex	Cp′Ru(CO)$_2$X **3**[a]	Cp′CpRu **4**[a]	Cp$_2$Fe **5**[b]	Recovery of **2**
1	**1a** (R = Me)	**2a** (X = I)	76 (**3a**)			21
2	**1a**	**2b** (X = Br)	91 (**3b**)			9
3	**1a**	**2c** (X = Cl)	47 (**3c**)	9 (**4a**)	43	
4	**1b** (R = Ph)	**2a**	71 (**3d**)		13	26
5	**1b**	**2b**	70 (**3e**)		26	
6	**1b**	**2c**	43 (**3f**)	7 (**4b**)	33	
7	**1c** (R = Bu^t)	**2a**	72 (**3g**)		6	24
8	**1c**	**2b**	79 (**3h**)			

[a] Yields are based on the starting Ru complex **1**. [b] Yields are based on the starting Fe complex **2**.

DOI: 10.1039/b006458k

Table 2 Triple ligand transfer reactions between [Cp′Ru(AN)$_3$][PF$_6$] **1** and CpFe(CO)(L)X **6**

Run	Substrate		Isolated yields of products (%)				
	Ru complex	Fe complex	Cp′Ru(CO)$_2$X **7**[a]	Cp′RuCO)$_2$X **3**[a]	Cp′CpRu **4**[a]	Cp$_2$Fe **5**[b]	Recovery of **6**
1	**1a**	**6a** (L = PMe$_3$, X = I)	49 (68)[c] (**7a**)	12 (**3a**)	6 (**4a**)	12	17
2	**1a**	**6b** (L = PPh$_3$, X = I)		35 (**3b**)	2 (**4b**)		24
3	**1a**	**6c** (L = PPh$_3$, X = Br)	12 (28)[c] (**7b**)	31 (**3c**)	12 (**4c**)	1	
4	**1b**	**6a**	36 (22)[c] (**7c**)	17 (**3d**)	2 (**4a**)	20	23
5	**1c**	**6a**	48 (40)[c] (**7d**)	18 (**3g**)		10	9

[a] Yields are based on the starting Ru complex **1**. [b] Yields are based on the starting Fe complex **6**. [c] Parentheses indicate % de of **7** determined by ^{1}H and ^{31}P NMR spectroscopy.

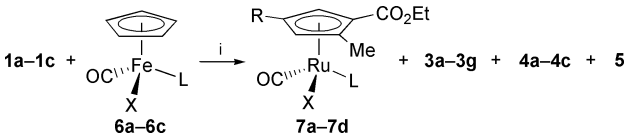

Scheme 2 *Reagents and conditions*: i, CH_2Cl_2, reflux, 3 h.

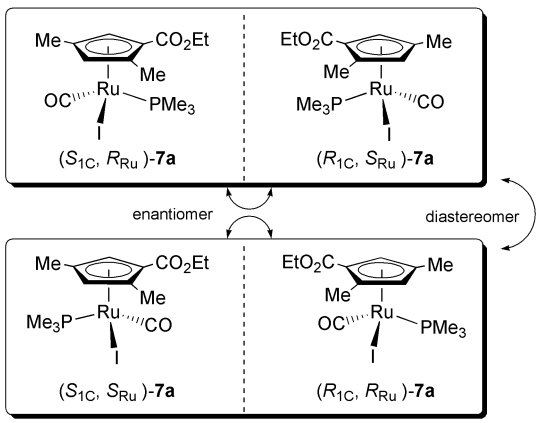

Scheme 3 Stereoisomers of **7a**.

well as **7** in the reaction of **1** and **6**, they were easily separated by column chromatography on silica gel. Yields of products depended both on the substituents on the cyclopentadienyl group as well as the phosphine initially coordinated to Fe. Reactions with **6a** with PMe$_3$ gave desired complex **7** in moderate yields (runs 1, 4 and 5), while yields of **7** were low in the reactions with **6b** and **6c** having PPh$_3$ (runs 2 and 3). To our surprise, the best result (68% de) in the diastereoselectivity of **7** was oberved in the reaction of **1a** having a small substituent (Me) on the cyclopentadienyl group with **6a** having a small phosphine ligand (PMe$_3$) (run 1). Reactions of **1b** and **1c** having a larger substituent (Ph or Bu^t) on the cyclopentadienyl group gave complexes **7c** and **7d** in 22 and 40% de, respectively (runs 4 and 5). Although asymmetric induction at a Ru center by a chiral organic group on the cyclopentadienyl ring has been attempted in the ligand exchange reaction of (η^5-C$_5$H$_4$R*)Ru(CO)$_2$X (R* = neomenthyl) with phosphine and phosphite, the diastereoselectivities of products (η^5-C$_5$H$_4$R*)Ru(CO)(PR$_3$)X were fairly low (up to 19% de).[8]

Fortunately single crystals of the major diastereomer selectively grew on recrystallization of a diastereomeric mixture of **7a** from Et$_2$O–hexane. As seen in Fig. 1 the molecular structure of the major diastereomer of **7a** was established by X-ray analysis to possess the configuration (R_{C1},S_{Ru})/(S_{C1},R_{Ru}).† Previously we also found the induction of metal-centered chirality by CO insertion into the Fe–C bond of planar-chiral Fe complexes giving Cp′Fe(CO)(PPh$_3$)(COMe) **8**.[9] Facile isomerization of complex **8** around the metal center under the employed reaction conditions suggested that the selectivity of the resulting complex is controlled by thermodynamic factors. In contrast, no isomerization at a Ru center was observed for a CH_2Cl_2 solution of the major diastereomer of **7a**, isolated by recrystallization (*vide supra*), under reflux for 3 h. The reactions presented here provide the first induction of metal-centered

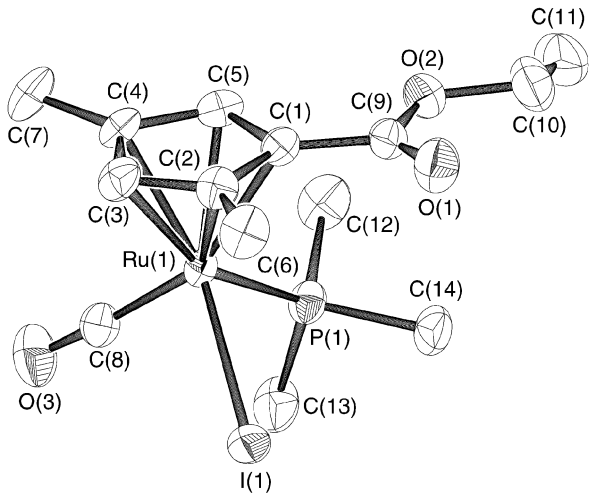

Fig. 1 ORTEP diagram of (R_{C1},S_{Ru})/(S_{C1},R_{Ru})-**7a** (major diastereomer). Hydrogen atoms are omitted for clarity.

chirality in ligand transfer reactions. Further investigation focusing on the mechanism of asymmetric induction is now in progress.

This work was partly supported by Grant-in-Aid for Scientific Research from the Ministry of Education, Science, Sports and Culture. We are grateful to The Material Analysis Center, ISIR, Osaka University, for technical support of spectral measurements and X-ray analysis.

Notes and references

† *Crystal data*: for **3d**: C$_{17}$H$_{15}$IO$_4$Ru, M = 511.28, monoclinic, $P\bar{1}$, a = 9.631(3), b = 11.246(3), c = 8.313(2) Å, α = 98.76(2), β = 100.410(8), γ = 93.71(3)°, V = 868.7(4) Å^3, Z = 2, D_c = 1.954 g cm^{-3}, μ(Mo–Kα) = 26.96 cm^{-1}, 6 < 2θ < 55°, T = −50 °C, R (R_w) = 0.029 (0.069) for 181 parameters *vs*. 3889 reflections with $I > 3.0\sigma(I)$ out of 4122 unique reflections (R_{int} = 0.023), GOF = 1.35. For (R_{C1},S_{Ru})/(S_{C1},R_{Ru})-**7a**: C$_{14}$H$_{22}$IO$_3$PRu, M = 497.27, monoclinic, $P2_1/n$, a = 10.067(2), b = 9.951(2), c = 18.322(1) Å, β = 100.410(8)°, V = 1805.2(4) Å^3, Z = 4, D_c = 1.830 g cm^{-3}, μ(Mo–Kα) = 26.71 cm^{-1}, 6 < 2θ < 55°, T = −75 °C, R (R_w) = 0.037 (0.055) for 208 parameters *vs*. 3645 reflections with $I > 3.0\sigma(I)$ out of 3990 unique reflections (R_{int} = 0.016), GOF = 1.35.

CCDC 182/1818. See http://www.rsc.org/suppdata/cc/b0/b006458k/ for crystallographic files in .cif format.

1 *Catalytic Asymmetric Synthesis*, ed. I. Ojima, VCH, New York, 1993; R. Noyori, *Asymmetric Catalysis in Organic Synthesis*, Wiley, New York, 1994.
2 R. L. Halterman, *Chem. Rev.*, 1992, **92**, 965.
3 H. Brunner, *Angew. Chem., Int. Ed.*, 1999, **38**, 1195.
4 N. Komatsuzaki, M. Uno, H. Kikuchi and S. Takahashi, *Chem. Lett.*, 1996, 677.
5 N. Dodo, Y. Matsushima, M. Uno, K. Onitsuka and S. Takahashi, *J. Chem. Soc., Dalton Trans.*, 2000, 35.
6 T. Katayama, K. Onitsuka and S. Takahashi, *J. Organomet. Chem.*, 2000, **610**, 31.
7 T. Katayama, Y. Morimoto, M. Yuge, M. Uno and S. Takahashi, *Organometallics*, 1999, **18**, 3087.
8 E. Cesarotti, A. Chiesa, G. F. Ciani, A. Sironi, R. Vefghi and C. White, *J. Chem. Soc., Dalton Trans.*, 1984, 653.
9 Y. Morimoto, K. Ando, M. Uno and S. Takahashi, *Chem. Commun.*, 1997, 1785.

An unusually rapid Claisen rearrangement involving ring expansion

Gianluca Dimartino and Jonathan M. Percy*

School of Chemistry, University of Birmingham, Edgbaston, Birmingham, UK B15 2TT.
E-mail: jmpercy@chemistry.bham.ac.uk

Received (in Cambridge, UK) 18th September 2000, Accepted 23rd October 2000
First published as an Advance Article on the web 10th November 2000

A Claisen rearrangement of a partially-fluorinated system involving ring expansion occurred at an unusually low temperature, 100 °C lower than a comparable system from the literature.

Paquette and co-workers showed how the Claisen rearrangement could be used to transform readily available vinylic lactones into medium-ring carbocycles during a series of landmark natural product syntheses.[1] The Tebbe reaction[2] fulfils a critical role in providing the vinyl ether component of the allyl vinyl rearrangement precursor; Scheme 1 summarises the sequence.

The rearrangement step requires the use of high temperatures and some special experimental precautions;[3] after the Tebbe reaction, the allyl vinyl ether is sealed in base washed tubes to minimise decomposition through enol ether protiolysis and Paquette notes that following minimal enol ether purification, traces of the Tebbe reagent by-products may be present in the rearrangement medium. Given that aluminium reagents are indeed known to cause dramatic accelerations of [3,3]-Claisen rearrangements,[4] some assistance to the rearrangement would not be surprising, though the nature of the active Lewis acid is not clear nor is the effect large given the reaction conditions (23 h at 175 °C in Scheme 1). Double bond migration can also compete with rearrangement forming non-productive allyl vinyl ethers.

We were interested to see if halogenation of the allylic fragment would accelerate the ring expansion and lower the reaction temperature. The literature suggests that γ,γ-difluorination accelerates [3,3]-Claisen rearrangements in some cases;[5] though the idea has not been tested fully and definitive theoretical work does not exist, a general concensus exists that the rehybridisation of an sp^2 CF_2 centre to sp^3 is favoured as geminal CF_2-substitution destabilises the alkene. Unambiguous accelerative effects exerted in γ,γ-difluorinated systems have also been reported in other rearrangement systems including [2,3]-Wittigs,[6] heteroatomic [2,3]-rearrangements[7] and oxy-Cope[8] reactions.

Stork enamine chemistry allowed the syntheses of ketoesters **2a** and **2b** and the addition of 1-chloro-2,2-difluoroethenyllithium[9] generated from 1-chloro-2,2,2-trifluoroethane afforded good yields of alcohol products **3a** as a mixture of diastereoisomers (Scheme 2); we assume that the major product has a *trans*-relationship between the sidechains.[3]

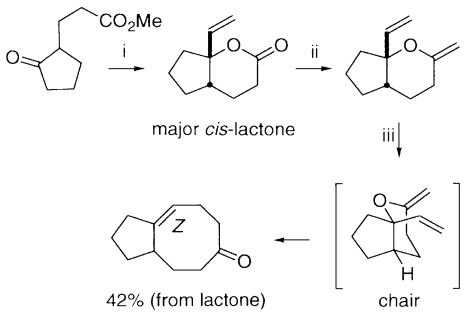

Scheme 1 *Reagents and conditions*: i, vinylmagnesium bromide; ii, $Cp_2TiCl(CH_2)AlMe_3$ (Tebbe reagent); iii, 175 °C, 23 h.

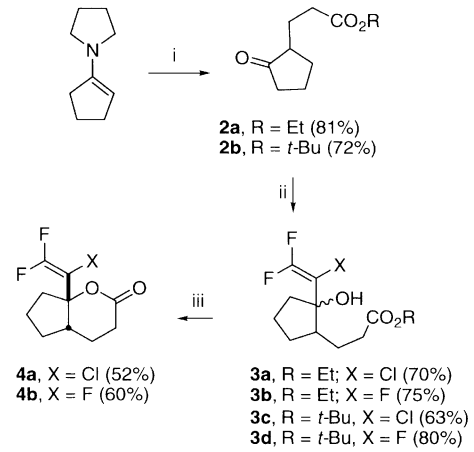

Scheme 2 *Reagents and conditions*: i, ethyl acrylate or *tert*-butyl acrylate, dioxane, rt, 18 h; ii, 1-chloro-2,2-difluoroethenyllithium or 1,2,2-trifluoroethenyllithium, THF, −78 °C to rt; iii, CF_3CO_2H, THF, rt.

No lactone products were detected; what we expected was the collapse of the initial alkoxide onto the ester in at least one of the diastereoisomers. After isolating the hydroxyester, we tried to lactonise it under acidic and basic conditions but failed. Instead of hydrolysing the acid, we synthesised *tert*-butyl ester **3c** as a mixture of diastereoisomers; a single lactone, to which we assigned structure **4a**, was isolated in moderate yield after treatment of these hydroxyesters with trifluoroacetic acid in dichloromethane. Presumably, alkyl–O cleavage and carboxy protonation allows closure to the lactone; it seems less likely that the acid intercepts an allylic cation generated by protonation of, and departure of water from, the hydroxyacid. A similar successful sequence started from 1,2,2,2-tetrafluoroethane (HFC-134a) and afforded lactone **4b**.[10]

With the lactone in hand, we attempted the Tebbe reaction† (Scheme 3) and succeeded in transforming lactone **4a** completely to a new product as evinced by ^{19}F NMR, to which we assign structure **5**.

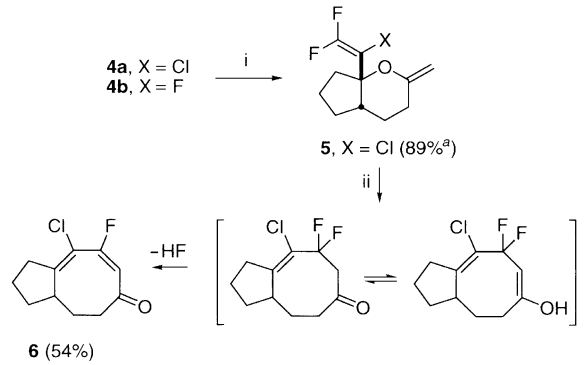

Scheme 3 *Reagents and conditions*: i, $Cp_2TiCl(CH_2)AlMe_3$, PhMe–THF, 0 to 60 °C; ii, xylene, sealed base-washed tube, 85 °C, 4 h. [a] Estimated yield based on clean ^{19}F NMR and full conversion of **4a**.

DOI: 10.1039/b007549n

In contrast, the fluorinated congener **4b** decomposed completely under Tebbe conditions. All attempts to purify and rigorously characterise **5** resulted in decomposition so we simply heated **5** at 85 °C; complete consumption took place within 4 h and a new UV active product **6** was formed.‡ The rearrangement conditions contrast sharply with those in Scheme 1. We contend that this represents an unusually facile [3,3]-Claisen ring expansion; as the Claisen rearrangement is not usually reversible, it is hard to see how dehydrofluorination *after* the rearrangement could accelerate the rearrangement itself. Enol formation from the initial ketonic product followed by elimination of HF does result in the formation of a conjugated system so dienone formation is not surprising.

We are currently in pursuit of **7** in which the fluorine atoms

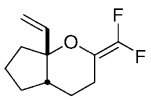

7

are in the vinyl component of the Claisen precursor, so that we can compare the positional effects of fluorine atom substitution and retain both fluorine atoms in a structurally novel product.

In summary, we have shown that the rearrangement precursor can be assembled rapidly, that the fluoroallyl fragment survives Tebbe reaction conditions and that fluorine atoms at C-γ in the allyl fragment appear to lower considerably the barrier to ring expansion Claisen rearrangement.

The authors wish to thank the Engineering and Physical Sciences Research Council of Great Britain for a Project Studentship (to G. D.) under the ROPA Scheme and ICI Klea for a generous donation of HFC-134a.

Notes and references

† Tebbe procedure and ^{19}F NMR data for **5**: Tebbe reagent (2.2 ml of a 0.5 M solution in toluene, 1.1 mmol) was added to a stirred solution of lactone **4a** (0.236 g, 1.0 mmol) in dry THF (10 ml) at 0 °C. Fifteen min after the addition the mixture was allowed to warm to rt and stirred for a further 20 min. The mixture was then heated to 60 °C for 30 min, then cooled to 0 °C before being quenched with 15% NaOH solution (5 ml). After gas evolution had ceased, ether (10 ml) was added and the mixture was dried, filtered and evaporated. The residue was eluted through a short column of alumina with petroleum ether to provide **5** (0.20 g, 89% estimated) as the only fluorine-containing product: δ_F(282 MHz, $CDCl_3$) −81.8 (d, $^2J_{F\text{-}F}$ 38.7, 1F), −84.9 (d, $^2J_{F\text{-}F}$ 38.7, 1F). As **5** was expected to be unstable, it was taken on directly without further purification.

‡ Thermal rearrangement and selected data for **6**: **5** (0.234 g, 1.0 mmol) was dissolved in xylene (5 ml) in an Ace tube that had been washed with NaOH (5 M aqueous solution). The tube was then sealed and heated to 85 °C in an oil bath. The reaction was followed by ^{19}F NMR of aliquots until the starting material was consumed completely (4 h). Concentration and purification *via* silica gel column chromatography (10% ether in light petroleum) gave **6** (0.116 g, 54%) as a yellow oil; R_f (10% ether in light petroleum) 0.2 (95% by GC); δ_H(300 MHz, $CDCl_3$) 5.87 (d, $^3J_{H\text{-}F}$ 20.2, 1H), 3.03–2.88 (m, 1H), 2.87–2.53 (m, 2H), 2.42–2.30 (m, 1H), 2.20–2.02 (m, 1H), 1.98–1.05 (m, 6H); δ_F(282 MHz, $CDCl_3$) −83.9 (d, $^2J_{F\text{-}H}$ 20.0); ν_{max} (film)/cm^{-1} 1662, 1627; [HRMS (CI, M[NH_4^+]) Found: 232.0912. Calc. For $C_{11}H_{16}ClFNO$: 232.0905]; *m/z* (CI) 232 (M+NH_4^+), 215 (M+H^+); λ_{max} (CH_2Cl_2) 284 nm (ε 3600 dm^3 mol^{-1} cm^{-1}).[11]

1 For a recent example, see L. A. Paquette, J. Ezquerra and W. He, *J. Org. Chem.*, 1995, **60**, 1435.
2 F. N. Tebbe, G. W. Parshall and G. S. Reddy, *J. Am. Chem. Soc.*, 1978, **100**, 3611.
3 W. A. Kinney, M. J. Coghlan and L. A. Paquette, *J. Am. Chem. Soc.*, 1985, **107**, 7352.
4 H. Yamamoto, in *Organometallics in Synthesis: A Manual*, ed. M. Schlosser, Wiley, Chichester, 1994, 509. For a recent boron Lewis acid catalysed example involving a fluorinated allyl vinyl ether, see H. Ito, A. Sato, T. Kobayashi and T. Taguchi, *Chem. Commun.*, 1998, 2441.
5 S. T. Purrington and S. C. Weeks, *J. Fluorine Chem.*, 1992, **56**, 165; J. M. Percy, *Top. Curr. Chem.*, 1997, **193**, 131; J. M. Percy and M. E. Prime, *J. Fluorine Chem.*, 1999, **100**, 147. For a discussion relating specifically to Claisen rearrangements, see M. J. Broadhurst, S. J. Brown, J. M. Percy and M. E. Prime, *J. Chem. Soc., Perkin Trans. 1*, 2000, 3217.
6 S. T. Patel, J. M. Percy and R. D. Wilkes, *J. Org. Chem.*, 1996, **61**, 166.
7 K. Blades, S. T. Patel, J. M. Percy and R. D. Wilkes, *Tetrahedron Lett.*, 1996, **37**, 6403.
8 G. Dimartino, T. Gelbrich, M. B. Hursthouse, M. E. Light, J. M. Percy and N. S. Spencer, *Chem. Commun.*, 1999, 2535.
9 J. M. Bainbridge, S. J. Brown, P. N. Ewing, R. R. Gibson and J. M. Percy, *J. Chem. Soc., Perkin Trans. 1*, 1998, 2541. The same method was used to prepare the trifluorovinyl congeners from HFC-134a. See also P. L. Coe, J. Burdon and I. B. Haslock, *J. Fluorine Chem.*, 2000, **102**, 43.
10 In this case alone, the two diastereoisomers of **3d** could be separated. Only one of them lactonised (TFA in CH_2Cl_2) while the other decomposed completely.
11 The only similar compound we were able to find with reported UV data was 1-ethoxycarbonyl-5-oxo-1,3-cyclooctadiene [λ_{max} (95% EtOH) 282 nm (ε 9700 dm^3 mol^{-1} cm^{-1}]: see W. C. Agosta and W. W. Lowrance, *J. Org. Chem.*, 1970, **35**, 3851.

ChemComm

Di-π-methane photorearrangement of *trans*-1,3-diphenylpropene upon excitation to higher singlet states in polar solvents

M. Consuelo Jiménez, Miguel A. Miranda* and Rosa Tormos

Departamento de Química, Instituto de Tecnología Química UPV-CSIC, Camino de Vera s/n, Apdo. 22012, 46071 Valencia, Spain. E-mail: mmiranda@qim.upv.es

Received (in Liverpool, UK) 27th July 2000, Accepted 16th October 2000
First published as an Advance Article on the web 10th November 2000

A dramatic enhancement of the di-π-methane rearrangement is observed upon excitation of *trans*-1,3-diphenylpropene (1) to its higher singlet states in acetonitrile, which leads to *trans*-1,2-diphenylcyclopropane (3) as a major photoproduct.

The photochemistry of *trans*-1,3-diphenylpropene (**1**) has attracted considerable attention in the past.[1–10] In addition to the *cis* isomer **2**, small amounts (*ca*. 5%) of *trans*- and *cis*-1,2-diphenylcyclopropane (**3** and **4**) were also detected after 17 h irradiation in benzene or cyclohexane with 254 nm UV-light (Scheme 1).[1] Under these conditions, the quantum yield of cyclopropane formation was found to be *ca.* 5×10^{-3}, and the reaction rate constant was *ca*. 8×10^{-5} s^{-1}.[10] This cyclization, which in the original paper[1] appeared 'to be without analogy', is considered 'one of the earliest examples of the di-π-methane rearrangement',[7] a reaction named according to Zimmerman and extensively investigated during the last decades.[11–13]

In spite of the considerable efforts devoted to the study of both the synthetic and mechanistic aspects of the di-π-methane rearrangement, there are two issues that have not been studied in a sufficiently systematic way and therefore require further investigation: the wavelength effects and the influence of polar solvents. We have undertaken a study of these two aspects in the case of *trans*-1,3-diphenylpropene (**1**) and found dramatic variations of the reaction efficiency. According to the obtained results, the di-π-methane rearrangement of **1** is markedly enhanced upon excitation to higher singlet states in polar solvents. This provides new mechanistic insights into the reaction and can be used as a tool to increase its preparative value.

Compound **1** was prepared following a known procedure.[14] Solutions of **1** (5 mM) in the indicated solvents were irradiated inside a Luzchem multilamp photoreactor, using the light from four 8W-lamps with emission maxima at 254 or 300 nm (Gaussian distribution), through quartz or Pyrex, respectively. The course of the reaction was followed by GC and ^{1}H-NMR; the degrees of conversion, the product distributions and the mass balances were determined using adequate standards. The results are shown in Fig. 1.

As expected,[1] very minor amounts of *trans*-1,2-diphenylcyclopropane (**3**) were formed in cyclohexane as solvent, whichever the irradiation wavelength employed. Prolonged irradiation at 254 nm resulted in partial isomerization of **3** to the *cis*-cyclopropane **4** (data not shown); in any case the combined yield of cyclopropanes never exceeded 10%. By contrast, upon irradiation of **1** in acetonitrile solution at 254 nm the di-π-methane rearrangement was dramatically enhanced, and **3** became the major product (after 100 min, the chemical yield was almost 50%). This effect was not observed when irradiation of **1** was performed at longer wavelengths. The same trend was found in solvents of intermediate polarity, where **3** was also obtained in significant yields (*e.g.* 30% in THF after 100 min irradiation at 254 nm).

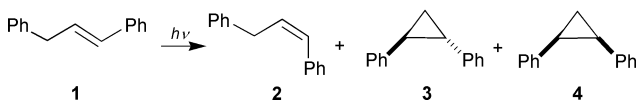

Scheme 1

In order to obtain more reliable quantitative data, the di-π-methane rearrangement quantum yields were determined using the *trans–cis* isomerization of β-methylstyrene (ϕ = 0.2)[15] as actinometer. Table 1 shows that, while in a hydrocarbon solvent $\phi_{di\text{-}\pi}$ was lower than 10^{-2} (in agreement with the literature data of 5.10^{-3}), in acetonitrile it was at least one order of magnitude higher.

As the di-π-methane rearrangement of **1** and related systems is thought to occur from excited singlet states, it appeared of interest to characterise such excited states by carrying out a steady-state and time-resolved fluorescence study in the two solvents. The obtained results are shown in Table 1.

The emission spectrum consisted of a band with maximum at 308 nm. It was found to be independent of the excitation wavelength. The main maximum of the excitation spectra was located at 254 nm; smaller bands appeared at 285 and 294 nm (see Fig. 2). Thus, **1** emits from its lowest lying singlet state, even upon excitation to the higher singlet states.

The fluorescence quantum yields and the singlet lifetimes were smaller in acetonitrile than in hexane (Table 1). No significant effect of the excitation wavelength on these parameters was observed.

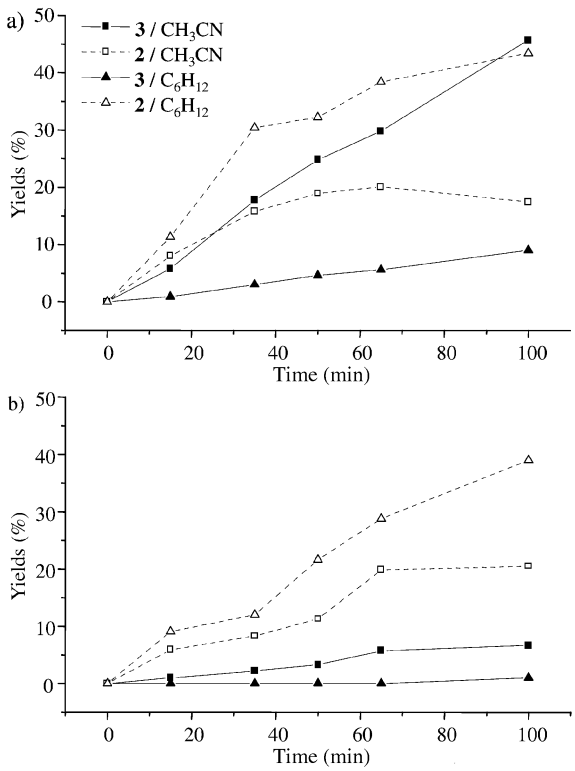

Fig. 1 Preparative yields of formation of **2** and **3**, upon irradiation of **1** in acetonitrile and cyclohexane for different times, a) at 254 nm and b) at 300 nm.

DOI: 10.1039/b006267g

Table 1 Photophysical and photochemical data of **1** at room temperature[a]

Solvent	ϕ_F	$10^{-7}k_F/s^{-1}$	τ_F/ns	$\phi_{di\text{-}\pi}$	$10^{-6}\ k_{di\text{-}\pi}/s^{-1}$	ϕ_{cis}
Hexane	0.27 (0.36)	5.5	6.1 (6.1)	< 0.01	< 1	0.12 (0.12)
Acetonitrile	0.13 (0.15)	10	2.5 (2.6)	0.11 (0.04)	44	0.10 (0.11)

[a] In general, the data have been obtained upon excitation at 254 nm. The fluorescence quantum yield and lifetimes using 285 nm as the excitation wavelength are given in brackets.

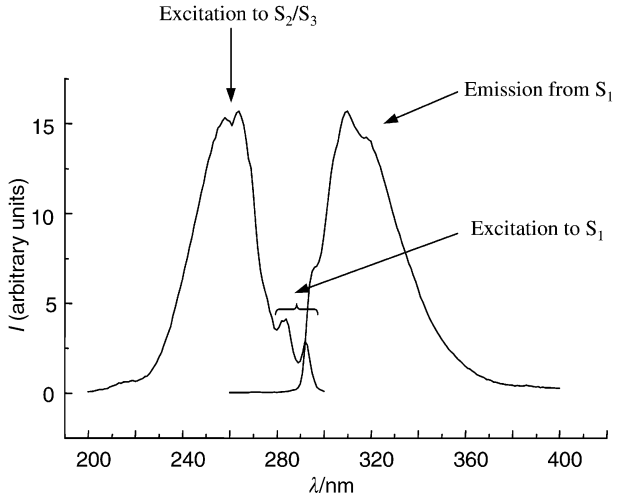

Fig. 2 Excitation and fluorescence emission spectra of **1** in hexane at room temperature.

All the accumulated experimental data on the photochemistry of **1** indicate that, although the nature of the emitting singlet state depends neither on the polarity of the solvent nor on the excitation wavelength, the di-π-methane rearrangement to **3** is strongly influenced by these factors. The sharp enhancement of this reaction upon excitation to higher singlet states in polar solvents is an unexpected behaviour, which is difficult to explain based on the currently accepted models.[11–13] In principle, **1** might photoionize from a higher singlet state in polar solvents, giving rise to the radical cation; this could be the actual rearranging species. An alternative possibility would be to start from the treatment of styrene photoreactivity based on conical intersections.[16] The order of vertically excited singlet states of styrene is believed to be $S_1 < S_2 + S_3$, where S_2 and S_3 (which possesses ionic character) overlap strongly. A conical intersection between S_3/S_2 and S_1 could provide a route to the di-π-methane product **3**. This would explain the need for excitation at shorter wavelength (to populate S_3) and the marked effect of solvents able to modify the energy surfaces of polar excited states.

We are indebted to Professor F. D. Lewis for his helpful comments. Financial support by the DGICYT (PB 97-0339) is gratefully acknowledged. M. C. J. thanks the European Commission for a Grant (MCFI-1999-00101).

Notes and references

1 G. W. Griffin, J. Covell, R. C. Petterson, R. M. Dodson and G. Klose, *J. Am. Chem. Soc.*, 1965, **87**, 1410.
2 S. S. Hixson, *Tetrahedron Lett.*, 1971, 4211.
3 E. W. Valyocsik and P. Sigal, *J. Org. Chem.*, 1971, **36**, 66.
4 E. W. Valyocsik and P. Sigal, *J. Phys. Chem.*, 1971, **75**, 2079.
5 S. S. Hixson, *J. Am. Chem. Soc.*, 1972, **94**, 2505.
6 S. S. Hixson, *J. Am. Chem. Soc.*, 1972, **94**, 2507.
7 S. S. Hixson, *Tetrahedron Lett.*, 1972, 1155.
8 J. M. Figuera and M. T. Serrano, *J. Chem. Soc., Faraday Trans. 1*, 1976, **72**, 1534.
9 J. M. Figuera and M. T. Serrano, *J. Chem. Soc., Faraday Trans. 1*, 1976, **72**, 2265.
10 S. S. Hixson, *J. Am. Chem. Soc.*, 1976, **98**, 1271.
11 S. S. Hixson, P. S. Mariano and H. E. Zimmerman, *Chem. Rev.*, 1973, **73**, 531.
12 H. E. Zimmerman and D. Armesto, *Chem. Rev.*, 1996, **96**, 3065.
13 H. E. Zimmerman, *The Di-π-Methane Rearrangement*, in *CRC Handbook of Organic Photochemistry and Photobiology*, ed. W. M. Horspool and P.-S. Song, CRC Press, Boca Raton, 1995, p. 184.
14 E. K. Raunio and W. A. Bonner, *J. Org. Chem.*, 1966, **31**, 396.
15 F. D. Lewis, D. M. Bassani, R. A. Caldwell and D. J. Unett, *J. Am. Chem. Soc.*, 1994, **116**, 10 477.
16 M. J. Bearpark, M. Olivucci, S. Wilsey, F. Bernardi and M. A. Robb, *J. Am. Chem. Soc.*, 1995, **117**, 6944.

ChemComm

Sol–gel transcription of novel sugar-based superstructures composed of sugar-integrated gelators into silica: creation of a lotus-shaped silica structure†

Jong Hwa Jung, Masato Amaike and Seiji Shinkai*

Chemotransfiguration Project, Japan Science and Technology Corporation (JST), 2432 Aikawa, Kurume, Fukuoka 839-0861, Japan. E-mail: seijitcm@mbox.nc.kyushu-u.ac.jp

Received (in Cambridge, UK) 6th September 2000, Accepted 23rd October 2000
First published as an Advance Article on the web 10th November 2000

Novel silica materials bearing single or multiple (lotus-shaped) hollow fiber structures with 5–10 nm inner diameters and a spherical structure were created using sugar-integrated organogelators (1–4) as templates by sol–gel polymerization of TEOS.

The sol–gel synthesis of well-ordered inorganic materials offers a new and wide-ranging approach to useful materials with controlled architecture and porosity across a range of length scales.[1,2] The direct synthesis of discrete inorganic architectures necessitates the use of dispersed organic supramolecular structures with commensurate dimensionality; for example, hollow fibers of silica have been prepared by self-assembled phospholipid fibers,[3] viroid cylinders,[4] organic crystals[2] or cholesterol-based organogel fibers as templates.[5–9] In particular, cholesterol-based organogel templates have created various hollow silica fibers with linear,[5] helical[6] and multi-layered structures[7] by sol–gel polymerization. Such results indicate that the cholesterol-based organogel fibers act as efficient tubular templates in the polymerization process.[5–9] It is already known that either cationic charge or efficient hydrogen-bonding interaction is necessary for the sol–gel transcription in order to adsorb 'anionic' silica particles onto the organic molecular assemblies.[5–9] Meanwhile, the sugar-based gelators provide various, morphologically novel superstructures such as linear,[10] helical,[10–12] bundled,[12] multi-layered cigar-like[12] and vesicular[13] structures according to their self-assembling manner in the gel phase. Despite their structural variety, however, the transcription of sugar-based organogel structures into the silica gel is unprecedented, because i) introduction of a moderate amount of cationic charge into the organogelator is very difficult and ii) the gelation ability is markedly reduced in the protic sol–gel medium necessary for sol–gel polymerization. To overcome this dilemma, we designed sugar-based organogelators **1**, **3** and **4** in which the amino group not only stabilizes the organogels due to the intensified inter-gelator hydrogen bonds[10] but also binds TEOS through hydrogen-bonding interactions.[7,8] If this idea were to work as expected, one could transcribe the novel sugar-based organogel superstructures into the silica through sol–gel polymerization. We have found that the novel morphologies of the sugar-based gelators are successfully transcribed into the silica prepared under the specific sol–gel polymerization conditions.

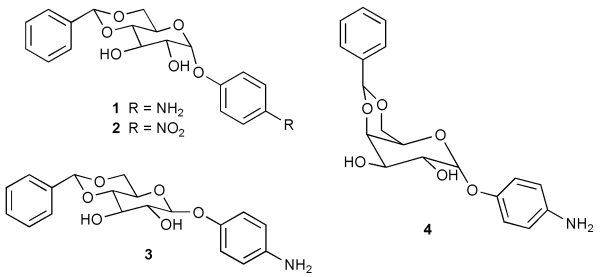

Compounds **1**–**4** were synthesized according to the method reported previously.[10] These compounds could gelate organic solvents such as carbon disulfide, carbon tetrachloride, toluene, ethanol, butan-1-ol, hexan-1-ol or ethylacetate,[14] indicating that they act as versatile gelators of organic solvents. In order to obtain visual insights into the aggregation mode, we observed the xerogel structures of their ethanol (or water) organogels by TEM and SEM. Fig. 1 shows typical pictures obtained from the xerogels **1**, **3** and **4**. The organogel **1** forms a 3-D network with small 5–20 nm frizzled fibrils. On the other hand, the organogel **3** shows a straighter and larger fiber structure with 50–150 nm diameter. One can observe many stripes in a gigantic organogel fiber that was stained prior to organogel fiber growth (Fig. 1c). The size of these stripes is comparable with that of the α-glucose-type organogel fiber. When stained with OsO_4 solution after organogel fiber growth, these stripes could not be observed (Fig. 1b). More interestingly, the α-galactose-type organogel **4** showed the fiber structure in ethanol (the picture is not shown here) and the spherical structure with 200–350 nm outer diameter in water (Fig. 1d).

To transcribe the superstructures formed in the organogels into the silica structure, we carried out sol–gel polymerization of TEOS using **1**–**4** in the ethanol gel phase according to the method described previously.[7,8]† We observed the SEM pictures of the silica obtained from **1** and **2** (Fig. 2a). The silica obtained from **1** shows the tubular structure with outer diameter of 20–30 nm and length of 350–700 nm whereas the silica obtained from **2** showed the conventional granular structure (not shown). It is hardly conceivable that the amino group is protonated in the presence of benzylamine. These results indicate, therefore, that the tubular structure of the silica was successfully transcribed by the hydrogen-bonding interaction

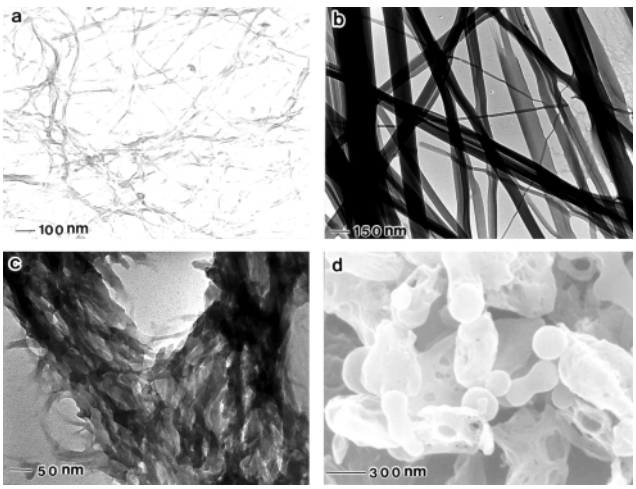

Fig. 1 TEM pictures of xerogels (a) **1** + EtOH, (b and c) **3** + EtOH and (d) SEM picture of xerogel **4** + water. In (c), the organogel was stained with OsO_4 prior to fiber grown up.†

† Electronic supplementary information (ESI) available: the preparation methods of TEM samples for organogels and sol-gel polymerization conditions. See http://www.rsc.org/suppdata/cc/b0/b007218o/

DOI: 10.1039/b007218o

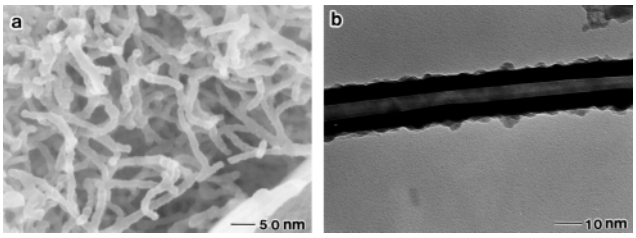

Fig. 2 SEM (a) and TEM (b) pictures of the silica obtained from ethanol organogel **1** after calcination.

between the amino group of **1** and TEOS (or oligomeric silica particles).

To further corroborate that the organogel fibers really acted as template for the growth of the tubular silica, we took the TEM pictures after removal of **1** by calcination. Very interestingly, we found the silica obtained from **1** to have an inner tube structure with 5–10 nm diameter (Fig. 2b). The inner diameter is comparable with that of the outer diameter of the fibrous organogel structure. The results again support the view that oligomeric silica particles are adsorbed onto the neutral organogel fiber through hydrogen-bonding.

In contrast, β-glucose-type organogel **3** resulted in tubular silica with a larger outer diameter of 150–200 nm (Fig. 3a). Why is the diameter of the silica obtained from organogel **3** larger than that obtained from organogel **1**? To solve this problem, we carefully took a number of TEM pictures to confirm the template effect. Very surprisingly, the TEM pictures of the silica obtained from **3** consistently reveal that the silica has an inner diameter of 50–100 nm and an outer diameter of 150–200 nm (Fig. 3b). Furthermore, the silica in the inner tube is composed of micro-tubes of 5–10 nm diameter, in total giving rise to a lotus-like structure. The inner diameter of 5–10 nm is comparable with that of the organogel fiber obtained from **1**. We now consider, therefore, that the silica was transcribed from the hierarchical bundle structure of **3**, because β-glucose-type organogel **3** features stronger intermolecular hydrogen-bonding interaction than that of α-glucose-type organogel **1**, keeping the aggregate structure more stably.[10] This novel structure in silica has been created by transcription of bundled organogel fibers.

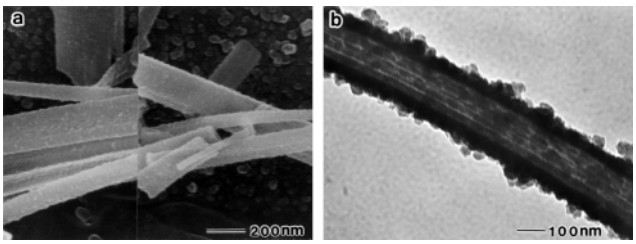

Fig. 3 SEM (a) and TEM (b) pictures of the silica obtained from ethanol organogel **3** after calcination.

Fig. 4 shows SEM pictures of the silica structure obtained from aqueous gel **4** by sol–gel polymerization. The silica obtained from ethanol organogel shows a fiber structure with *ca.* 1400 nm diameter, whereas the silica obtained from aqueous gel shows a hollow spherical structure with 500–1000 nm inner diameter and a 200–300 nm thick wall, which probably consists of multi-layers. These results indicate that the sugar-integrated gel systems can create various silica structures in the gel phase.

As a summary of the foregoing observations, we now propose the mechanism for the formation of the novel lotus-type silica structure from organogel **3** and that of the single hollow fiber silica structure from organogel **1** (Fig. 5). Oligomeric silica species are adsorbed onto the surface of the bundled fibrous structure of **3** and the polymerization further proceeds along these bundled fibrils. This propagation mode eventually yields the lotus-type silica after combustion of gelators by calcination (Fig. 5c; lower). In contrast, **1** provides the minute fibrous structure. Then, the tubular silica grows up by sol–gel

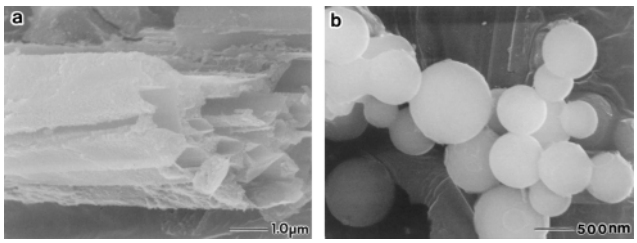

Fig. 4 SEM pictures of the silica obtained from (a) ethanol organogel **4** and (b) aqueous gel **4** after calcination.

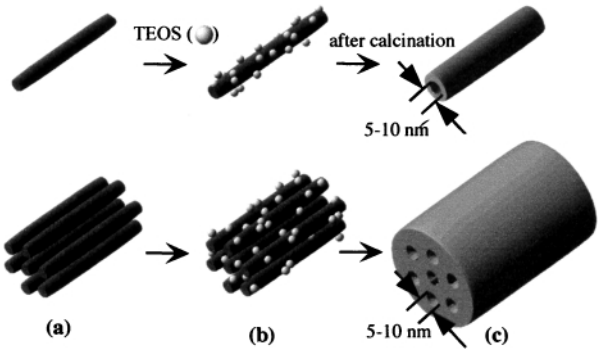

Fig. 5 Schematic representation for the creation of the lotus-like silica structure from the organogel state of **3** (lower) and single hollow fiber silica from **1** (upper) by sol–gel polymerization: (a) gelators; (b) sol–gel polymerization of TEOS and adsorption onto the gelators and (c) lotus-like silica structure (lower) and single hollow fiber structure (upper) of the silica formed after calcination (SEM and TEM pictures in Figs. 2 and 3 were taken at this stage).

polymerization along this surface (Fig. 5b). As supported by the correlation between the xerogel structures (Fig. 1) and the resultant silica gel structures (Figs. 2 and 3), the sugar-based organogel structures are directly and scrupulously transcribed into the silica structures utilizing hydrogen-bonding interactions.

In conclusion, the present paper has demonstrated a new methodology to prepare lotus-like and spherical structures of silica using sugar-integrated organic gelators. These novel silica structures are created by hydrogen-bonding interactions with the fine structure of the gelators. We believe that this concept will be more generally applicable to further new silica preparations using various organogel superstructures as templates.

Notes and references

1 S. Mann, *Biomimetic Materials Chemistry*, ed S. Mann, VCH, New York, 1996.
2 H. Nakamura and Y. Matsui, *J. Am. Chem. Soc.*, 1995, **117**, 2651.
3 S. L. Burkett and S. Mann, *Chem. Commun.*, 1996, 321.
4 W. Shenton, T. Douglas, M. Young, G. Stubbs and S. Mann, *Adv. Mater.*, 1999, **11**, 253.
5 Y. Ono, K. Nakashima, M. Sano, Y. Kanekiyo, K. Inoue, J. Hojo and S. Shinkai, *Chem. Commun.*, 1998, 1477.
6 Y. Ono, K. Nakashima, M. Sano, J. Hojo and S. Shinkai, *Chem. Lett.*, 1999, 1119.
7 J. H. Jung, Y. Ono and S. Shinkai, *Langmuir*, 2000, **16**, 1643; J. H. Jung, Y. Ono and S. Shinkai, *Angew. Chem., Int. Ed. Engl.*, 2000, **39**, 1862.
8 J. H. Jung, Y. Ono and S. Shinkai, *J. Chem. Soc., Perkin Trans. 2*, 1999, 1289.
9 J. H. Jung, Y. Ono, K. Sakurai, M. Sanno and S. Shinkai, *J. Am. Chem. Soc.*, 2000, **122**, 8648.
10 N. Amanokura, Y. Kanekiyo, S. Shinkai and D. N. Reinhoudt, *J. Chem. Soc., Perkin Trans. 2*, 1999, 1995.
11 K. Yoza, Y. Ono, K. Yoshihara, T. Akao, H. Shinmori, M. Takeuchi, S. Shinkai and D. Reinhoudt, *Chem. Commun.*, 1998, 907.
12 R. J. H. Hafkamp, M. C. Feiters and R. J. M. Nolte, *J. Org. Chem.*, 1999, **64**, 412.
13 U. Beginn, S. Keinath and M. Möller, *Macromol. Chem. Phys.*, 1998, **199**, 2379.
14 In addition, organogelator **4** can gelate even water.

Vitamin D_1

Edwin S. Tan,† Fook S. Tham,‡ and William H. Okamura*

Department of Chemistry, University of California, Riverside, CA 92521 USA. E-mail: william.okamura@ucr.edu

Received (in Corvallis, OR, USA) 1st September 2000, Accepted 13th October 2000
First published as an Advance Article on the web 10th November 2000

The X-ray crystallographic structure of vitamin D_1 reveals a sandwich-like 1 : 1 heterodimeric complex of lumisterol$_2$ and vitamin D_2 with the latter in its α-chair conformer.

Vitamin D_1, the very first anti-rachitic factor, which played a historical role in the development of the vitamin D field, was discovered by Windaus[1] with contributions from Askew and co-workers[2] and Reerink and Van Wijk[3] in 1931. This sharp melting, biologically active substance, produced photochemically from ergosterol (provitamin D_2, **3a**), was soon thereafter discovered to be a 1 : 1 crystalline heterodimer of lumisterol$_2$ (**4a**) and vitamin D_2 (**1a**).[1] This was all at a time when the involvement of previtamin D_2 (**2**), pyrocalciferol (**5**) and isopyrocalciferol (**6**) in the now well accepted scheme (Fig. 1) was not yet recognized.[4] Early unsuccessful attempts to obtain the X-ray structure of crystalline, monoclinic D_2 were reported by Bernal in 1932[5] and by Bernal and Crowfoot in 1935,[6] but interestingly, the successful completion of the structure was not completed until 1994![7] The X-ray structure of the monoclinic isomorph revealed that the D_2 was essentially the same as that in the very interesting finding in 1976[8] by Hull *et al.* that the crystalline orthorhombic form of pure **1a** (a feature also characteristic of **1b**, vitamin D_3[9]) exists as a pseudo-homodimer. What is novel about **1a** (and also **1b**) is that it crystallizes as a 1 : 1 complex of α- and β-A-ring chairs (Fig. 2), the former with an equatorial disposition of the C-3 hydroxy and the latter with an axial orientation of the same hydroxy. Not surprising is that in solution vitamin D_2 exists as a dynamically equilibrating mixture of the same α- and β-chairs and that this ratio is solvent dependent.[10]

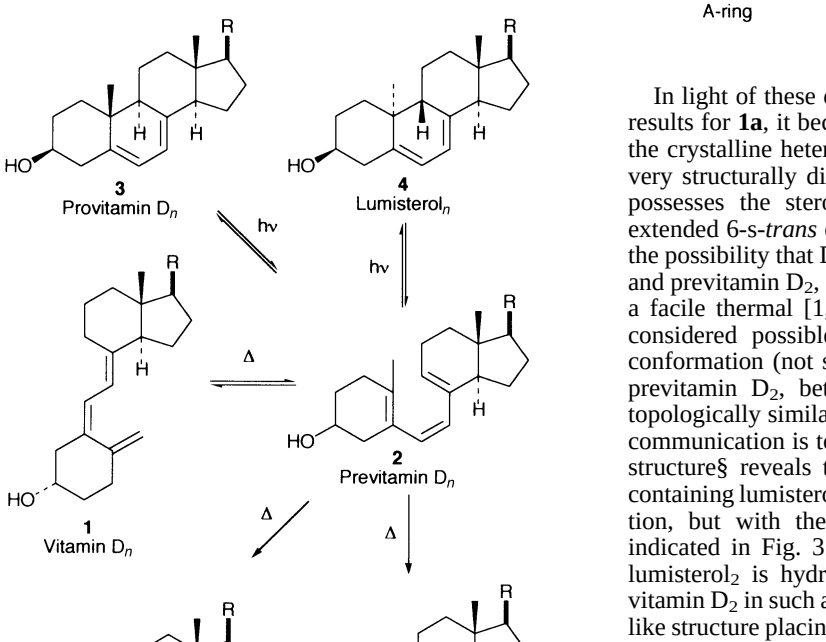

Fig. 1

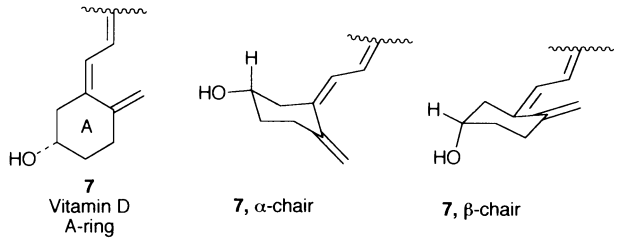

Fig. 2

In light of these divergent solid state and solution structural results for **1a**, it became of interest to consider the structure of the crystalline heterodimeric D_1, a complex of two seemingly very structurally dissimilar molecules **4a** and **1a**. The former possesses the steroid skeleton, but the latter exists in an extended 6-s-*trans* conformation. It was intriguing to entertain the possibility that D_1 might in fact be a complex of lumisterol$_2$ and previtamin D_2, a substance related to vitamin D_2 by way of a facile thermal [1,7]-sigmatropic shift. Alternatively, it was considered possible that the D_2 might exist in its 6-s-*cis* conformation (not shown), thus rendering it, like the putative previtamin D_2, better able to co-crystallize with the more topologically similar lumisterol$_2$ molecule. The purpose of this communication is to report that in fact the single crystal X-ray structure§ reveals that vitamin D_1 is simply a 1 : 1 complex containing lumisterol$_2$ and vitamin D_2 in its 6-s-*trans* conformation, but with the A-ring in the α-chair conformation as indicated in Fig. 3. It is interesting that the axial 3β-OH of lumisterol$_2$ is hydrogen bonded to the equatorial 3β-OH of vitamin D_2 in such a manner as to form a face to face sandwich-like structure placing the two C_{18} angular methyl group carbons in close proximity with one another.

Samples of vitamin D_1 were prepared by collecting crystals (mp, 119–121 °C; literature[2] mp 124–125 °C) from a slowly evaporating solution containing a 1 : 1 mixture of lumisterol$_2$ and vitamin D_2 (acetone). Similar attempts to obtain crystalline

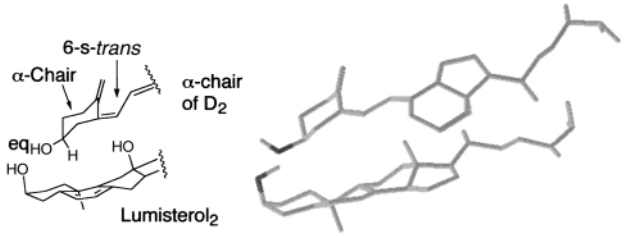

Fig. 3

DOI: 10.1039/b007191i

material from a 1 : 1 mixture of previtamin D_2 (**2a**) and vitamin D_2, lumisterol$_3$ (**4b**) and vitamin D_3 (**1b**), or previtamin D_3 (**2b**) and vitamin D_3 failed. Lumisterol$_2$ and previtamin D_2 were prepared by photochemical irradiation of **3a** (Hanovia 450 W medium pressure mercury lamp, pyrex vessel, EtOH) followed by HPLC purification (20% EtOAc–hexanes, silica column). Previtamin D_2 could also prepared by thermal equilibration with vitamin D_2 followed by HPLC separation.[11] Lumisterol$_3$ and previtamin D_3 were prepared in a similar way from 7-dehydrocholesterol or from vitamin D_3 as appropriate. The X-ray structures of pure lumisterol$_2$ and lumisterol$_3$ have been previously reported[12] as have vitamin D_2 and D_3.[7–9] Thus, the vitamin D_1 result reported herein represents a unique combination of these earlier crystallographic results.

This study was generously supported by grants from the NIH, NSF, and the Committee on Research of the University of California, Riverside. We also acknowledge generous supplies of starting materials from Solvay Pharmaceuticals (Weesp, the Netherlands).

Notes and references

† Undergraduate Honors Thesis Program Participant, University of California, Riverside.

‡ Analytical Chemistry Instrumentation Facility located in the Department of Chemistry, College of Natural and Agricultural Sciences, University of California, Riverside.

§ *Crystal data*: $C_{56}H_{88}O_2$, M = 793.26, monoclinic, a = 20.1072(13), b = 7.2481(5), c = 35.858(3) Å, β = 94.091(2)°, V = 5212.6(6), T = 213(2) K, space group $C2$, Z = 4, μ(Mo-Kα) = 0.059 mm^{-1}, 16502 reflections measured, 9692 unique (R_{int} = 0.0262) which were in all calculations. The final R indices [$I > 2\sigma(I)$] were $R1$ = 0.0497, $wR2$ = 0.1147; R indices (all data) were $R1$ = 0.0725, $wR2$ = 0.1249. There was one lumisterol$_2$ and one vitamin D_2 molecule present in the asymmetry unit. The side chain attached to $C_{23'}$ of vitamin D_2 and C_{23} of lumisterol$_2$ were refined as individual disordered-side chains (the site occupancy ratio for disordered-side chains was 56 : 44% and 52 : 48% for vitamin D_2 and lumisterol$_2$, respectively). The DELU, SIMU, and DFIX restrains (SHELXTL software) were used to model the disorder, where the C–C and C=C–C single bond distances were restrained to 1.53 and 1.51 Å, respectively. Full details have been deposited at the Cambridge Crystallographic Data Centre, Cambridge, UK CB2 1EZ (CCDC 182/1825).

1 A. Windaus, A. Luttringhaus and M. Deppe, *Liebigs Ann. Chem.*, 1931, **489**, 252. See also: A. Windaus, *Proc. R. Soc. London, Ser. B*, 1931, **108**, 568; A. Windaus, O. Linsert, A. Luttringhaus and G. Weidlich, *Liebigs Ann. Chem.*, 1932, **492**, 226.
2 F. A. Askew, H. M. Bruce, R. K. Callow, J. St. L. Philpot and T. A. Webster, *Nature*, 1931, **128**, 758. See also: T. C. Angus, F. A. Askew, R. B. Bourdillon, H. M. Bruce, R. K. Callow, C. F. Fischmann, J. St. L. Philpot and T. A. Webster, *Proc. R. Soc. London, Ser. B*, 1931, **108**, 340; F. A. Askew, R. B. Bourdillon, H. M. Bruce, R. K. Callow, J. St. L. Philpot and T. A. Webster, *Proc. Royal Soc. B*, 1932, **109**, 488.
3 E. H. Reerink and A. Van Wijk, *Biochem. J.*, 1931, **25**, 1001.
4 P. Karlson, *Trends Biochem. Sci.*, 1981, 29.
5 J. D. Bernal, *Nature*, 1932, **129**, 277.
6 J. D. Bernal and D. Crowfoot, *Chem. Ind.*, 1935, **54**, 701.
7 I. Leban, R. A. G. De Graaf, R. De Gelder, J. Turkenburg, K. S. Wilson and Z. Dauter, *The Collected Works of Dorothy Crowfoot Hodgkin: Volume-III, General Crystallography and Essays*, eds. G. G. Dodson, J. P. Glusker, S. Ramaseshan and K. Venkateran, Interline Pub., Bangalore, India, 1994, pp. 43–51.
8 S. E. Hull, I. Leban, P. Main, P. S. White and M. M. Woolfson, *Acta Cryst. B*, 1976, **32**, 2374.
9 Trinh-Toan, H. F. DeLuca and L. F. Dahl, *J. Org. Chem.*, 1976, **41**, 3476.
10 R. M. Wing, W. H. Okamura, M. R. Pirio, S. M. Sine and A. W. Norman, *Science*, 1974, **186**, 939; R. M. Wing, W. H. Okamura, A. Rego, M. R. Pirio and A. W. Norman, *J. Am. Chem.Soc.*, 1975, **97**, 4980; G. N. LaMar and D. L. Budd, *J. Am. Chem. Soc.*, 1974, **96**, 7317; B. Helmer, H. K. Schnoes and H. F. DeLuca, *Arch. Biochem. Biophys.*, 1985, **241**, 608; W. H. Okamura and G.-D. Zhu, *Vitamin D*, eds. D. Feldman, F. H. Glorieux and J. W. Pike, Academic Press, San Diego, 1997, pp. 939–971.
11 W. H. Okamura, H. Y. Elnagar, M. Ruther and S. Dobreff, *J. Org. Chem.*, 1993, **58**, 600.
12 D. C. Hodgkin and P. Sayre, *J. Chem. Soc.*, 1952, 4561; A. J. De Kok and C. Romers, *Acta Cryst. B*, 1974, **30**, 1695.

ChemComm

Synthesis of 1,2-*trans C*-glycosyl compounds by reductive samariation of glycosyl iodides

Nicolas Miquel, Gilles Doisneau and Jean-Marie Beau*

Laboratoire de Synthèse de Biomolécules, UMR CNRS 8614, Institut de Chimie Moléculaire, Université Paris-Sud, F-91405 Orsay Cedex, France. E-mail: jmbeau@icmo.u-psud.fr

Received (in Liverpool, UK) 3rd August 2000, Accepted 16th October 2000
First published as an Advance Article on the web

Reductive samariation of per-*O*-trimethylsilyl or benzyl glycopyranosyl iodides in the presence of carbonyl compounds provides the corresponding 1,2-*trans*-*C*-glycosyl compounds in good yields.

Numerous synthetic methods have been developed for the preparation of *C*-glycosyl compounds, analogues of glycosides in which the interglycosidic oxygen atom has been replaced by a carbon atom.[1] Recent work in our laboratory has focused on a direct method for the synthesis of *C*-glycosyl compounds derived from neutral hexoses by the reductive samariation of anomeric 2-pyridyl sulfones in the presence of carbonyl compounds (Barbier procedure).[2] While the procedure is efficient with the manno series,[3] it is unsatisfactory with the gluco- or the galactopyranosyl series[2] because of too high a level of the competing β-elimination (an elimination–C–C bond formation ratio of approximately 1:1). We now report an unexpected solution to this problem starting from glycosyl iodides as efficient *C*-glycosyl donors in reductive samariation experiments. These glycosyl halides, first prepared by the reaction of glycosyl bromides with sodium iodide[4] and rarely used as electrophilic *O*-glycosyl donors,[5] can be prepared from methyl glycosides, glycosyl acetals and glycosyl acetates,[6] hemiacetals[7] or trimethylsilyl glycosides.[8] Either a rapid synthesis of structurally simple *C*-glycosyl compounds from commercial free sugars *via* the per-*O*-trimethylsilyl glycosyl iodides,[8] or a multi-step construction of more complex *C*-glycosyl compounds with the more practical per-*O*-benzyl iodides is possible.

Silylation of D-mannopyranose **1** and treatment of a DCM solution of the per-*O*-silylated derivative with iodotrimethylsilane (TMSI) according to the procedure of Uchiyama and Hindsgaul[8] provided anomeric iodide **2** which, after solvent removal, was successively treated with the carbonyl compound (2 equiv.) and a THF solution of SmI_2 (2.2 equiv.) at rt (Scheme 1 and Table 1). On completion of the reaction, indicated by the disappearance of the blue color of SmI_2 in approximately 1.5 h, the products were desilylated by addition of acidic MeOH and analyzed as their acetylated compounds. For the acetylation

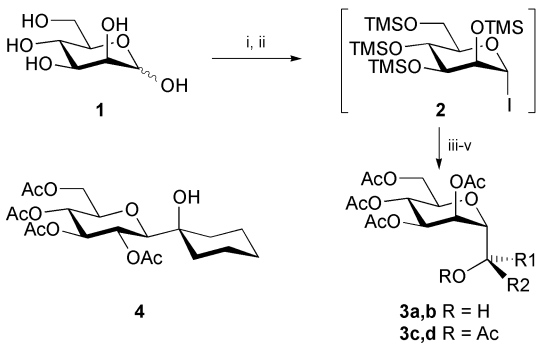

Scheme 1 *Reagents and conditions*: i, TMSCl, Et_3N, DMF, 0 °C; ii, 1.1 equiv. of TMSI, CH_2Cl_2, 25 °C, 0.5 h; iii, 2 equiv. of carbonyl compound, 2.2 equiv. of SmI_2, THF, 25 °C, 1.5 h; iv, MeOH, 1 M HCl, (3:1, v/v), 25°C; v, Ac_2O, 2,6-lutidine, 25 °C.

Table 1 SmI_2-induced coupling of silylated glycopyranosyl iodides with carbonyl compounds[a]

Entry	Substrate	Conditions	*C*-Glycoside (yield)[b]
1	**1**	Cyclohexanone	**3a** (85%)
2	**1**	Pentan-3-one	**3b** (58%)
3	**1**	IsoButyraldehyde	**3c** (71%; 10:1[c])
4	**1**	*n*-Octanal	**3d** (72%; 4:1[c])
5	D-Glucose	Cyclohexanone	**4** (61%)[d]

[a] See Scheme 1 for the reaction conditions. [b] Isolated yields from the free sugar after chromatography on silica gel. [c] Diastereomer ratio at the exocyclic asymmetric center. [d] The only other byproduct is the protonation product, 1,5-anhydro-2,3,4,6-tetra-*O*-acetyl-D-glucohexitol.

step, pyridine which suffered a samarium(III)-induced ring opening was replaced by 2,6-lutidine. This one-pot four-step procedure from the persilylated sugars (steps ii–v, Scheme 1) provided only the α-products **3a**–**d** as determined by ^{1}H-NMR analysis of the crude acetylated reaction mixtures, in yields of 58–85% from the commercial free sugar after silica gel column chromatography. The only identified byproduct was the 1,5-anhydromannohexitol (reprotonation product) in about 10%, presumably arising from traces of HI present in the starting glycosyl iodides. With the two aldehydes tested (entries 3 and 4, Table 1), a mixture of diastereomers were produced with selectivities (10:1 and 4:1, respectively) in line with the results previously obtained with anomeric 2-pyridyl sulfones.[2] D-Glucose provided *C*-glycosyl compound **4** by the same sequence of reactions (entry 5). Noteworthy is the absence of elimination products, particularly striking in the gluco series.

While this procedure is well suited for the rapid conversion of commercial sugars to simple 1,2-*trans*-*C*-glycopyranosyl compounds, more elaborated synthetic schemes would require protecting groups more stable than trimethylsilyl groups. We therefore tested the benzylated mannopyranosyl iodide available by TMSI treatment in DCM at rt of either the glycosyl acetate **5**[5] or the trimethylsilyl glycoside **6** (entries 1 and 2, Table 2). Reductive samariation as reported above in the presence of cyclohexanone provided comparable results. The same one-pot transformation (i, TMSI; ii, SmI_2, cyclohexanone) on the trimethylsilyl glycosides derived from glucose **7**, galactose **8** and fucose **9** also provided an unprecedented level of *C*-glycosylation for these series (72–75% yield), obviously to the detriment of the competing elimination reaction. For these three substrates, it was necessary to conduct the samariation step in the presence of one equiv. of 2,6-lutidine which greatly reduces the amount of the competing protonation leading to the 1,5-anhydro sugars. As usual, the 1,2-*trans* compounds were the only detectable *C*-glycosylation products, as indicated by the values of the H1–H2 coupling constants in the ^{1}H-NMR spectra (9.2 Hz for **11** and 9.3 Hz for **12** and **13** in a chair conformation of the pyranose ring). These results significantly differ from those obtained from anomeric 2-pyridyl sulfones.[2] Substitution of the 2-pyridyl sulfone group by an iodine atom in an otherwise identical structure resulted, under identical conditions, in an improvement of the *C*-glycosylation reaction at a synthetically

DOI: 10.1039/b006455f

Table 2 SmI_2-induced coupling of benzylated glycopyranosyl iodides with cyclohexanone

Entry	Free sugar	Carbonyl compound	*C*-Glycoside (yield)[a]
1	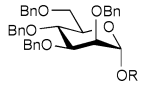 **5** R = Ac	A[b]	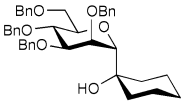 **10** (68%)
2	**6** R = TMS	A[b]	**10** (85%)
3	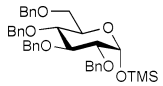 **7**	B[c]	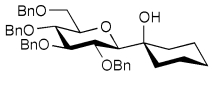 **11** (72%)
4	**7**	C[d]	**11** (80%)
5	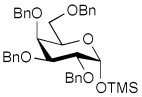 **8** (α:β = 10:1)	B[c]	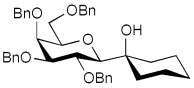 **12** (74%)
6	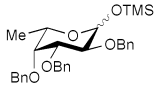 **9** (α:β = 2:1)	B[c]	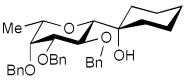 **13** (75%)

[a] Isolated yields from the trimethylsilyl glycoside after chromatography on silica gel. [b] Reaction conditions A: i, 1.1 equiv. of TMSI, CH_2Cl_2, 25°C, 0.5 h; ii, 2 equiv. of cyclohexanone, 2.2 equiv. of SmI_2, THF, 25°C, 0.25 h. [c] Reaction conditions B: see conditions A with 1 equiv. of 2,6-lutidine in step ii. [d] Reaction conditions C: see conditions A with 0.01 equiv. of NiI_2 at −10 °C in step ii.

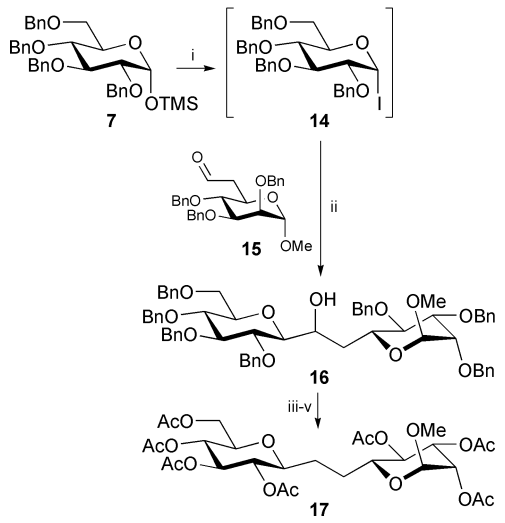

Scheme 2 *Reagents and conditions*: i, 1.1 equiv. of TMSI, CH_2Cl_2, 25 °C, 0.5 h; ii, 1.1 equiv. of **15**, 2.2 equiv. of SmI_2, THF, 25 °C, 0.25 h, 66% from **7**; iii, 1.5 equiv. of NaH, CS_2, CH_3I, 25 °C, 3 h, 96%; iv, 1.5 equiv. of Bu_3SnH, cat. AIBN, toluene, 95 °C, 2.5 h, 89%; v, H_2, Pd/C, MeOH, Ac_2O, py, 94%.

useful level (72 *vs*. 39% yield in the gluco series) with a concomitant decrease in the elimination reaction. We also noticed a further improvement by incorporating catalytic amounts of NiI_2 with SmI_2,[9] and conducting the coupling reaction at −10 °C (80% of **11**, entry 4).

The utility of this new procedure has been demonstrated in a fast synthesis of the carbon-linked mimic of the D-glucopyranosyl(β1→6)-D-mannopyranoside dimer **17** (Scheme 2). Reductive samariation of iodide **14** in the presence of aldehyde **15**[10]† provided the β-*C*-dimer **16** in 66% yield. Only one isomer was detected at the exocyclic asymmetric center. Methyl xanthate formation and radical reduction furnished the methylene-linked dimer which was debenzylated and characterized as its per-*O*-acetyl derivative **17**.‡

In summary, we have shown that the silylated or benzylated glycopyranosyl iodides are useful *C*-glycosyl donors for the synthesis of 1,2-*trans* *C*-glycosyl compounds. Work is in progress to delineate a precise mechanism for the transformation.§

Notes and references

† Aldehyde **15** was prepared from methyl 2,3,4,6 tetra-*O*-benzyl-α-D-mannopyranoside in an overall yield of 54% by the following five-step sequence of reactions: i, Ac_2O, CF_3COOH, (4:1), 25 °C, 1 h; ii, MeONa, MeOH, 25 °C, 12 h; iii, 1.4 equiv. PPh_3, 4 equiv. I_2, imidazole, toluene, 70 °C, 1 h; iv, 1.4 equiv. Bu_4NCN, DMF, 0 to 25 °C, 3 h; v, 3 equiv. DIBAL-H, CH_2Cl_2,, −78 °C, 0.5 h.

‡ *Selected data* for **17**: $[\alpha]_D^{20}$ = + 22 (*c* = 0.2, $CHCl_3$); ^{1}H NMR ($CDCl_3$, 400 MHz, atom numbering of a tridecopyranoside) δ = 5.29 (dd, 1H, *J* 9.8, 3.5, H-3), 5.26 (dd, 1H, *J* 3.5, 1.5, H-2), 5.18, 5.10, 5.04, 4.89 (4 t, 4H, *J* 9.5, H-4,9,10,11), 4.65 (d, 1H, *J* 1.5, H-1), 4.25 (d, 1H, *J* 12, 5.2, H-13), 4.10 (dd, 1H, *J* 12, 2.1, H-13′), 3.70 (ddd, 1H, *J* 10, 9.5, 2, H-12), 3.64 (ddd, 1H, *J* 10, 5, 2, H-5), 3.40 (ddd, 1H, H-8), 3.36 (s, 3H, OMe), 2.16, 2.11, 2.08, 2.06, 2.04, 2.02 and 2.00 (7 s, 21H, OAc), 1.9–1.8 and 1.5–1.4 (2 m, 4H, H-6,6′,7,7′); MS (ES): *m/z* = 671 [*M* + Na]; HR-MS (ES), calcd for $C_{28}H_{40}NaO_{17}$ [*M* + Na]: 671.2163, found: 671.2166.

§ We do not yet have a reasonable explanation for the significant differences between the behavior of anomeric iodides and anomeric 2-pyridyl sulfones. It is possible that there is a change in the electron transfer mechanism (inner *vs*. outer sphere ET) on going from anomeric 2-pyridyl sulfones to anomeric iodides inducing a change in the product distribution (C–C bond formation *vs*. elimination).

1 M. H. D. Postema, *C-Glycoside Synthesis*, CRC Press, Boca Raton, FL, 1995; D. E. Levy and C. Tang, *The Chemistry of C-Glycosides*, Pergamon, Oxford, 1995; G. Casiraghi, F. Zanardi, G. Rassu and P. Spanu, *Chem. Rev.*, 1995, **95**, 1677; J.-M. Beau and T. Gallagher, *Topics Curr. Chem.*, 1997, **187**, 1; Y. Du, R. J. Linhardt and I. R. Vlahov, *Tetrahedron*, 1998, **54**, 9913; T. Skrydstrup, B. Vauzeilles and J.-M. Beau, in *Oligosaccharides in Chemistry and Biology—A Comprehensive Handbook*, Vol. 1, ed. B. Ernst, P. Sinaÿ and G. Hart, Wiley-VCH, Weinheim, 2000, pp. 495–530.

2 D. Mazéas, T. Skrydstrup and J.-M. Beau, *Angew. Chem., Int. Ed. Engl.*, 1995, **34**, 909; T. Skrydstrup, O. Jarreton, D. Mazéas, D. Urban and J.-M. Beau, *Chem. Eur. J.*, 1998, **4**, 655.

3 O. Jarreton, T. Skrydstrup and J.-M. Beau, *Chem. Commun.*, 1996, 1661; O. Jarreton, T. Skrydstrup and J.-M. Beau, *Tetrahedron Lett.*, 1997, **38**, 303; O. Jarreton, T. Skrydstrup and J.-M. Beau, *Chem. Eur. J.*, 1999, **5**, 430; S. L. Krintel, J. Jiménez-Barbero and T. Skrydstrup, *Tetrahedron Lett.*, 1999, **40**, 7565.

4 B. Helferich and R. Gootz, *Chem. Ber.*, 1929, **62**, 2788.

5 M. J. Hadd and J. Gervay, *Carbohydr. Res.*, 1999, **320**, 61 and references cited therein.

6 J. Thiem and B. Meyer, *Chem. Ber.*, 1980, **113**, 3075.

7 B. Ernst and T. Winkler, *Tetrahedron Lett.*, 1989, **30**, 3081; R. Caputo, H. Kunz, D. Mastroianni, G. Palumbo, S. Pedatella and F. Solla, *Eur. J. Org. Chem.*, 1999, 3147.

8 T. Uchiyama and O. Hindsgaul, *Synlett*, 1996, 499; T. Uchiyama and O. Hindsgaul, *J. Carbohydr. Chem.*, 1998, **17**, 1181

9 F. Machrouhi, B. Hamann, J.-L. Namy and H. B. Kagan, *Synlett*, 1996, 633 and references cited therein; P. Girard, J.-L. Namy and H. B. Kagan, *J. Am. Chem. Soc.*, 1980, **102**, 2693.

10 For another synthesis of aldehyde **15** see: H. B. Boren, K. Eklind, P. J. Garegg, B. Lindberg and A. Pilotti, *Acta Chem. Scand.*, 1972, **26**, 4143.

ChemComm

Molecular recognition involving Kemp's triacid: selectivity towards the 8-substituted quinoline system as seen in the cocrystalline adducts with 8-aminoquinoline and 8-hydroxyquinoline

Graham Smith,*[a] Urs D. Wermuth[a] and Jonathan M. White[b]

[a] *Centre for Instrumental and Developmental Chemistry, School of Physical Sciences, Queensland University of Technology, G.P.O. Box 2434, Brisbane QLD. 4001, Australia. E-mail: g.smith@qut.edu.au*
[b] *School of Chemistry, University of Melbourne, Parkville, VIC. 3052 Australia*

Received (in Cambridge, UK) 20th June 2000, Accepted 25th October 2000
First published as an Advance Article on the web

The crystal structure determinations of two molecular adducts of Kemp's triacid (*r*-1,*c*-3,*c*-5-trimethylcyclohexane-1,3,5-tricarboxylic acid = KTA), [$(KTA)_2$(8-aminoquinoline)] (1) and [$(KTA^-)_2$ (8-hydroxyquinoline$^+$)$_2$] (2) have revealed an interactive selectivity towards the 8-substituted quinoline system.

Kemp's triacid (*r*-1,*c*-3,*c*-5-trimethylcyclohexane-1,3,5-tricarboxylic acid) was synthesized in 1981[1] and its unique all-equatorial carboxylic acid configuration demonstrated, and later confirmed in crystal structure analyses.[2,3] Most significantly, the molecules showed no intramolecular hydrogen bonding associations involving the carboxylic acid groups as might have been expected but instead formed an unusual chain structure made up of head-to-tail cyclic hydrogen bonded units, with two at the head and one at the tail. This association is not only unique to Kemp's triacid but the polymeric or 'catemer' mode[4] is itself rare among carboxylic acids where the discrete cyclic hydrogen-bonded dimeric association [graph set $R^2_2(8)$[5]] predominates. The structure also indicates the possible reason for both the high melting point (241–243 °C) and the amomalously small p$K_{a2,3}$ value for the acid (1.5)[1] where the unusually high value for pK_{a3} (for an aliphatic tricarboxylic acid) makes the trianion one of the most basic carboxylate anions known.

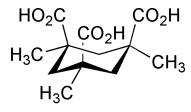

Kemp's triacid (KTA)

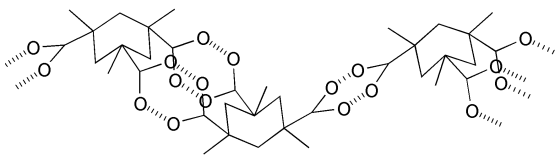
KTA Framework structure

Previous work has indicated that Kemp's triacid and its derivatives, such as the 2 : 1 condensation products with various aromatic diamines (*e.g. m*-xylidenediamine and acridine yellow), possess potential for molecular recognition.[2] These diacid products have discrete encapsulating environments with dimensions which vary with the nature of the parent aromatic diamine used. However, no actual structures of adducts of this type are known. The trianionic form of Kemp's acid has exhibited enhanced affinity compared to the trianions of the *cis-trans*-isomer and other tricarboxylic acids, for the tetraprotonated [21]ane N_7 macromolecule.[6,7] It is proposed that interaction proceeds *via* hydrogen bonding between the favourably oriented carboxylate groups and all or most of the four protonated sites of the macromolecule. These studies in fact involve recognition of Kemp's triacid rather than using it to recognize other simple molecular species. Work in our laboratories has primarily been directed towards both the homogeneous and heterogeneous self-assembly of carboxylic acids as well as co-crystallization of carboxylic acids with Lewis bases, particularly in those cases where proton transfer does not occur.[8] Kemp's triacid was therefore interacted with a series of bifunctional carboxylic acids and Lewis bases with a view to examining the structures of the adducts formed, using single crystal X-ray diffraction. These included compounds having particular associative utility in structure making, including the isomeric monoaminobenzoic acids, 2-aminopyrimidine, 2,6-diaminopyridine, adenine, melamine, xanthine, hypoxanthine, and urea. The very limited success we achieved is reflected in the paucity of structural data on KTA and its compounds in the CSD. However, with 8-aminoquinoline (8-AQ),† large crystals of an adduct were obtained which was confirmed by elemental analysis as having the unexpected stoichiometry [$(KTA)_2$(8-AQ)] (**1**). The crystal structure of **1**‡ indicated that Kemp's triacid has particular affinity for the 8-amino-substituted quinoline system. This structure retains the basic hydrogen-bonded backbone polymer, based upon the KTA repeating unit, as found in the parent acid,[2,3] with the 8-aminoquinoline molecules linking the chains laterally by hydrogen bonds between the 8-amino substituent group [N(2)] and the CO_2H groups in the polymer chains (Fig. 1). Another feature of the structure is the 50% disorder of the 8-AQ molecules across inversion centres in the cell, meaning that half of the molecules lie with the amino group directed towards one carboxylic acid in the first chain [N(2)···O(1), 2.97 Å (x, 1 + y, z)] while the other half are directed towards another acid group in the second chain [N(2)···O(5), 3.14 Å (−1 + x, 1 + y, z)]. The hetero-nitrogen is not involved in intermolecular hydrogen bonding but does form an intramolecular hydrogen bond with the amino group (2.62 Å). Furthermore, this nitrogen is not protonated as might be

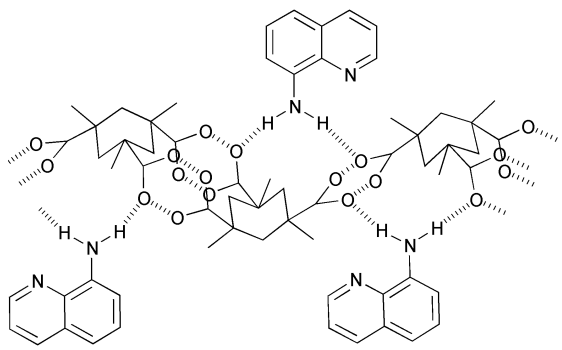

Fig. 1 Molecular associations in the KTA chain polymer structure and the laterally linking 8-aminoquinoline molecules in **1**, shown in the schematic. The 8-AQ molecules are 50% disordered across inversion centres in the unit cell. Hydrogen-bonding distances (Å) in the structure (shown as broken lines) are: intra-chain: O(1)···O(2), 2.68; O(4)···O(6), 2.60; O(3)···O(5), 2.68. Inter-chain: N(2)···O(1), 2.97; N(2)···O(5), 3.14.

DOI: 10.1039/b004945j

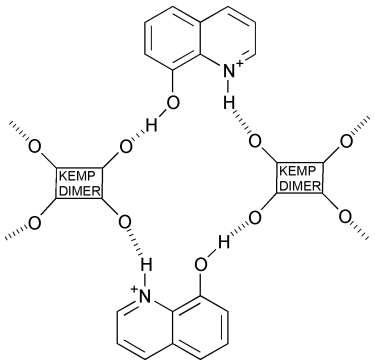

Fig. 2 The centrosymmetric dimeric KTA anion units and the cross-linking 8-hydroxyquinolinium cations in **2**. Schematic shows the hydrogen-bonding associations in the ribbon polymer. Hydrogen-bonding distances (Å) in the structure are: intra-dimer: O(1)···O(6),[a] 2.53; O(3)···O(5), 2.57; inter-dimer: N(1)···O(2), 2.68; O(7)···O(5),[b] 2.66. Unless otherwise indicated, atoms are carbon. [a] $-x$, $1-y$, $1+z$. [b] $-1+x$, y, z.

expected {comparative pK_a values of the acid (pK_{a1} = 3.3) and base [pK_{a2} (hetero-N) = 4.0}.

The apparent size specificity for KTA towards 8-AQ prompted a trial involving another available 8-substituted quinoline, quinolin-8-ol (8-HQ) with Kemp's acid using similar preparative conditions.† This also resulted in the production of good crystals but these had an analysis consistent with a 1:1 complex rather than 2:1 as found in **1**. The crystal structure of [(KTA)(8-HQ)] (**2**)‡ (Fig. 2) unexpectedly showed the presence of a chain polymer based on unusual centrosymmetric hydrogen-bonded KTA dimer repeating units, in contrast to the KTA backbone structure as found in **1** and in the parent acid. These dimer interactions differ from conventional hydrogen-bonded cyclic dimers in that they involve the *cis*-related acid groups [O(1)···O(6), 2.53 Å]. The oxygen of one of these acid groups [O(6)] is devoid of a proton which is located on the hetero-N of the 8-HQ molecule. This protonated group subsequently forms a strong hydrogen bond with the other oxygen of the second CO_2H group [N(1)···O(2), 2.68 Å]. The HO groups of the two bridging 8-HQ molecules provide the links between the dimer units *via* O(5) [O(7)···O(5), 2.66 Å] in a three-centre relationship which involves the third CO_2H group in an intramolecular hydrogen bond [O(3)···O(5), 2.57 Å]. There is a labile partial molecule of 8-HQ in the lattice which appears to be lost during collection of X-ray diffraction data while maintaining crystal stability and further work on this phenomenon is proceeding. The formula for the adduct **2** after removing the effect of the disordered partial molecule of lattice 8-HQ is therefore $[(KTA^-)_2(HQ^+)_2]$.

The presence or absence of proton transfer with examples of this type may be predictable on the basis of pK_a differences between the interacting species. For the pyridine system, this ΔpK_a minimum is found to be 3.5.[10] However, with Kemp's triacid and the 8-substituted quinoline system, the difference would appear to be considerably less than this [for 8-HQ: pK_a = 5.0 (hetero-N); ΔpK_a = 1.7 (proton transfer) while for 8-AQ: pK_a = 4.0; ΔpK_a = 0.7 (no proton transfer)]. The hetero-N in both 8-AQ and 8-HQ is readily protonated by relatively strong nitro-substituted aromatic carboxylic acids [*e.g.* 3,5-dinitrobenzoic acid (pK_a = 2.8), 5-nitrosalicylic acid (pK_a = 2.2) and 3,5-dinitrosalicylic acid (pK_a = 2.1)] giving 1:1 adducts,[10] based on cyclic hydrogen-bonded A–B heterodimers.[11] These form in preference to the B–B homodimer found in the parent structure of 8-HQ[12] and in its adducts with the neutral compounds chloranil[13] and 1,3,5-trinitrobenzene.[14] Adducts **1** and **2** therefore differ significantly in many respects: adduct **1** has 2:1 stoichiometry, involves no proton transfer, is based on a hydrogen bonded polymeric backbone structure and interacts with 8-AQ in a parallel cross-linking mode. Adduct **2** has effectively a 1:1 interactive stoichiometry but involves proton transfer and is based on hydrogen-bonded dimers which interact with two cross-linking 8-HQ molecules in a perpendicular mode. However, these two examples provide chemical evidence of the particular molecular specificity of Kemp's triacid for at least the 8-(interactive group)-substituted quinoline system. This basic proposal is currently being pursued using other similar Lewis bases.

The authors acknowledge financial support from The Centre for Instrumental and Developmental Chemistry of the Queensland University of Technology, The Australian Research Council, and the University of Melbourne.

Notes and references

† *Preparation*. Adducts were prepared by refluxing 0.10 g (0.194 mmol) of KTA with respectively 0.056 g of 8-aminoquinoline or 0.057 g of quinolin-8-ol (0.388 mmol) in 20 cm^3 of 50% aqueous EtOH (compound **1**) or 80% aqueous EtOH (compound **2**) for *ca*. 15 min. The solutions were allowed to evaporate at rt yielding after 1 week, pale brown prisms of **1**, mp 292.5–296.8 °C [Found: C, 60.1; H, 6.9; N, 4.3%. Calc. for $C_{33}H_{44}N_2O_{12}$: C, 60.0; H, 6.7; N, 4.2%], and after 3 weeks, pale yellow prisms of **2**, mp 189.9–192.2 °C [Found: C, 62.5; H, 6.0; N, 3.9%. Calc. for $C_{21}H_{25}NO_7$: C, 62.5; H, 6.3; N, 3.5%]. Variation of the stoichiometric ratio of Kemp's acid to Lewis base gave the same products.

‡ *Crystal analysis* Compound **1**: $C_{33}H_{44}N_2O_{12}$, M = 660.7, triclinic, space group $P\bar{1}$, a = 8.3968(9), b = 8.7615(8), c = 12.3337(9) Å, α = 76.161(6)°, β = 74.331(8)° γ= 70.17(1)°, U = 810.9(1) Å^3, Z = 1, D_c = 1.349 g cm^{-3}, Mo-Kα radiation (λ 0.71073 Å); 3063 reflections measured (2851 unique: R_{int} = 0.0143); R_1 = 0.041 (F) [for 2254 reflections with $I > 2\sigma(I)$], wR_2 = 0.106 (F^2); T = 293(2) K. Compound **2**: $C_{42}H_{50}N_2O_{14}$, M = 806.8, triclinic, space group $P\bar{1}$, a = 8.662(1), b = 10.413(2), c = 14.153(2) Å, α = 99.06(2), β = 103.64(1)°, γ= 102.91(1)°, U = 1179.1(3) Å^3, Z = 1 (dimer repeat), D_c = 1.208 g cm^{-3}; Cu-Kα radiation (μ = 1.5418 Å); 5164 reflections measured (4832 unique: R_{int} = 0.0113); R_1 = 0.053 (F) [4304 reflections with $I > 2\sigma(I)$], wR_2 = 0.159 (F^2); T = 293(2) K. * $R1 = \Sigma[1F_o| - |F_c|]/\Sigma|F_o|$, $wR_2 = \{\Sigma[w(F_o^2 - F_c^2)^2]/\Sigma[w(F_o)^2]\}^{\frac{1}{2}}$. Intensity data were collected on Enraf-Nonius four-circle diffractometers using either Mo-Kα for **1** or Cu-Kα radiation for **2**. Structures were solved and refined using SHELXL97.[15] The 8-AQ molecules in **1** are disordered across inversion centres in the respective cell, indicating that in each the 8-amino groups occupy 50% sites in one orientation and 50% in the inverted orientation. With **2**, as mentioned in the discussion, the disordered partial 8-HQ molecules of crystallization were initially modelled crystallographically with partial occupancy but this did not achieve a completely satisfactory result (*R ca*. 0.08) although the basic hydrogen-bonded polymer framework is quite stable and devoid of any disorder. Subsequently, the use of the programme Squeeze within Platon[16] (which removed the effect of the electron density due to the partial lattice molecule), resolved the problem giving R = 0.054. CCDC 182/1827.

1 D. S. Kemp and K. S. Petrakis, *J. Org. Chem.*, 1981, **46**, 5140.
2 J. Rebek Jr., L. Marshall, R. Wolak, K. Parris, M. Killoran, B. Askew, D. Nameth and N. Islam, *J. Am. Chem. Soc.*, 1985, **107**, 7476.
3 T.-L. Chan, Y.-X. Cui, T. C. W. Mak, R.-J. Wang and H. N. C. Wong, *J. Cryst. Spectrosc.*, 1992, **21**, 297.
4 L. Leiserowitz, *Acta Crystallogr.*, 1976, **B32**, 775.
5 M. C. Etter, *Acc. Chem. Res.*, 1990, **23**, 120; M. C. Etter and J. C. MacDonald, *Acta Crystallogr., Sect. B*, 1990, **46**, 256.
6 A. Bencini, A. Bianchi, M. I. Burguete, E. Garcia-Espana, S. V. Luis and J. Ramirez, *J. Am. Chem. Soc.*, 1992, **114**, 1919.
7 A. Bencini, A. Bianchi, M. I. Burguete, P. Dapporto, A. Domenech, E. Garcia-Espana, S. V. Luis, P. Paoli and J. Ramirez, *J. Chem. Soc., Perkin Trans. 2*, 1994, 569.
8 G. Smith, K. A. Byriel and C. H. L. Kennard, *Aust. J. Chem.*, 1994, **47**, 1413.
9 S. L. Johnson and K. A. Rumon, *J. Phys. Chem.*, 1965, **69**, 74.
10 G. Smith, U. D. Wermuth and J. M. White, unpublished results.
11 G. Smith, D. E. Lynch, K. A. Byriel and C. H. L. Kennard, *J. Chem. Cryst.*, 1997, **27**, 307.
12 W. W. Wendlandt and G. R. Horton, *J. Inorg. Nucl. Chem.*, 1963, **25**, 247; P. Roychowdhury, B. N. Das and B. S. Basak, *Acta Crystallogr., Sect. B*, 1978, **34**, 1047; S. H. Simonsen and D. W. Bechtel, *Am. Cryst. Assoc., Ser. 2*, 1980, **7**, 23; T. Bannerjee and N. N. Saha, *Acta Crystallogr., Sect. C*, 1986, **42**, 1408.
13 C. K. Prout and A. G. Wheeler, *J. Chem. Soc. A*, 1967, 469.
14 E. E. Castellano and C. K. Prout, *J. Chem. Soc. A*, 1970, 550.
15 G. M. Sheldrick: SHELXL 97: Program for Crystal Structure Refinement, University of Göttingen, Germany.
16 A. L. Spek; PLATON: A Multipurpose Crystallographic Tool, Version 111099, Utrecht University, The Netherlands.

ChemComm

Temperature and solvent effects on enzyme stereoselectivity: inversion temperature in kinetic resolutions with lipases

Gianfranco Cainelli,* Valeria De Matteis, Paola Galletti, Daria Giacomini* and Paolo Orioli

Department of Chemistry 'G. Ciamician', University of Bologna Italy. E-mail: cainelli@ciam.unibo.it, giacomin@ciam.unibo.it

Received (in Liverpool, UK) 24th July 2000, Accepted 16th October 2000
First published as an Advance Article on the web

Eyring plots of ln *E vs.* 1/*T* show inversion temperature in kinetic resolution by lipases, demonstrating that clustering effects in the substrate solvation manage the enzymatic selectivity.

Over the past few years, the use of enzymes in organic synthesis has become increasingly important owing to the basic discovery that enzymatic reactions can occur in organic solvents as well as in water.[1] Indeed, enzymatic selectivity is remarkably dependent on the organic solvent[2] and many attempts have been made to explain this influence.[3] However, less attention has been paid to the effect of temperature on selectivity.[4]

We report here the results of our studies on the effect of temperature on the kinetic resolution of racemic β-lactam **1** by

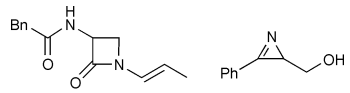

(*R*,*S*)-**1** (*R*,*S*)-**2**

PGA (Penicillin G-Acylase). Furthermore, we also reanalyzed another enzymatic process that has been reported previously, involving the kinetic resolution of azirinol **2** by lipase PS.[5]

Over the past decade, the dependence of stereoselectivity on temperature has been evaluated in several non-enzymatic reactions; *e.g. cis*-dihydroxylation of olefins,[6] reduction of ketones[7] and nucleophilic addition to imines[8] and carbonyl compounds.[9] By plotting the logarithm of selectivity *vs.* the reciprocal of *T*, according to the modified Eyring equation [eqn. (1)], a peculiar behavior is sometimes observed: the existence of two linear regions intersecting at a point defining a temperature denoted the inversion temperature (T_{inv}), whose significance is still a matter of debate.[10]

$$\ln S = -\Delta\Delta H^{\ddagger}/RT + \Delta\Delta S^{\ddagger}/R \qquad (1)$$

This break point leads to two sets of activation parameters: one for $T < T_{inv}$ and the other for $T > T_{inv}$. Our preceding studies demonstrated that the presence of an inversion temperature accounts for a particular effect of the reaction solvent on the stereoselectivity. We have proposed that T_{inv} constitutes a transition temperature between two different solute–solvent clusters, which act as two distinct supramolecules with different thermodynamic properties, reactivity and, therefore, different trends of stereoselectivity with temperature.[11]

We have recently shown[12] that in nucleophilic addition to aldehydes, T_{inv} depends mainly on the aldehyde–solvent couple and its value may be determined by ^{13}C NMR analysis using variable temperature (VT) experiments. NMR techniques provide a powerful method for investigating the local electronic environment of the molecular structure, and nuclear shielding is a sensitive probe of intermolecular interactions and solvent effects.[13] We found that the variation of the C=O chemical shift of the studied aldehydes with temperature presents two linear trends, whose intersection (referred to here as T_{NMR}) lies near the T_{inv} of the same substrate–solvent system, within the experimental error. Therefore, we considered that T_{NMR} and T_{inv} might have a common origin, and could in fact represent two independent experimental observations concerning the same solvation-clustering phenomenon.

We report here the first experimental example of inversion temperature in the field of stereoselective enzymatic reactions[14] and also confirm the presence of interconversion of solute–solvent supramolecules by means of VT ^{13}C NMR analysis.

As part of an ongoing project on the total synthesis of new β-lactam antibiotics,[15] we became interested in the kinetic resolution of racemic 1-*N*-(propen-1-yl)-3-*N*-(phenylacetoxy)-aminoazetidin-2-one **1** by PGA (supported on Eupergit) (Scheme 1). The experiments were carried out by incubating the substrate in phosphate buffer (pH = 7.8) and acetone (2:1 ratio) at different temperatures. Conversion of the reaction was monitored by titration of the phenylacetic acid formed with NaOH solution and the enantiomeric excesses of **3** and unreacted **1** were determined by HPLC analysis on a chiral column.[16] With an increase in temperature, we observed an initial linear lowering of the selectivity ratio *E*[17] until it reached a minimum value of 24 corresponding to $T = 301$ K (Fig. 1). Upon further warming, *E* increased, to reach a maximum value of 130 at $T = 328$ K. Least-squares analysis of these results enabled us to determine that $T_{inv} = 301$ K. Notably, the highest enantioselectivity is reached at the highest temperature.[18] Usually, $E = 100$ is considered the minimum satisfactory value for the industrial application of an enzymatic process. Thus, in our case, a slight variation in temperature made an inadequate enzymatic method very efficient.

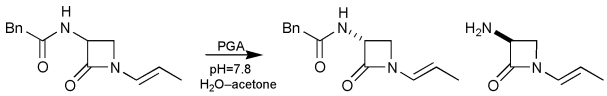

(*R*,*S*)-**1** (*R*)-**1** (*S*)-**3**

Scheme 1

Next, we performed a series of VT ^{13}C NMR analyses of **1** in deuterated water and d_6-acetone (2:1 ratio). The δ value of the phenylacetoxy C=O chemical shift decreases with an increase in temperature between 278 and 323 K, and two linear regions may be clearly recognized by least-squares analysis (Fig. 2). T_{NMR} occurs at $T = 306$ K and corresponds to T_{inv}, within the experimental error. We looked for other studies on temperature dependent selectivity in enzymatic processes in the literature. In 1997 Sakai *et al.*[5] described the kinetic resolution of racemic phenyl-2*H*-azirine-2-methanol **2** in diethyl ether. The selective

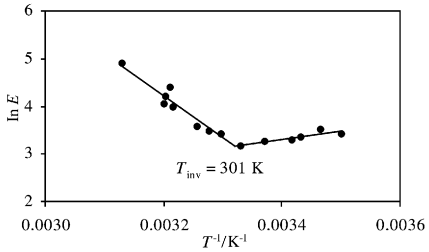

Fig. 1 Eyring plot for the selectivity ratio *E* in the kinetic resolution of **1** by PGA at different temperatures in H_2O–acetone (2:1).

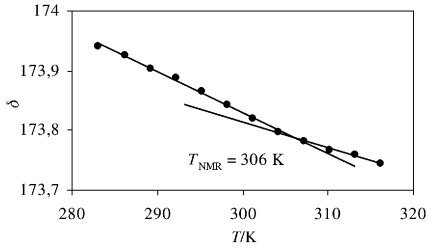

Fig. 2 Plot of the ^{13}C chemical shift of the phenylacetoxy C=O *vs. T* for **1** in D_2O–d_6-acetone (2:1).

acetylation reaction promoted by lipase Amano PS in the presence of vinyl acetate as an acylating agent, proceeded smoothly until 233 K, with progressively higher selectivity (Fig. 3). At T = 233 K, the enantioselection reached a maximum (E = 99) and then decreased. A least-squares analysis of the tabulated data allowed us to determine a T_{inv} at T = 229 K. To test for the presence of a T_{NMR}, we prepared **2** by the reported method[19] and studied the evolution of δ *vs.* T in d_{10}-diethyl ether. The results for the quaternary aromatic carbon[20] are reported in Fig. 4. Again, two linear regions exist and T_{NMR} occurs at T = 222 K, quite near to the corresponding T_{inv}. The different rates of variation of the chemical shift δ *vs.* T indicate an abrupt change in solute–solvent interactions, which reflects a change in substrate solvation.[21] The same solvation change causes the presence of the T_{inv} in an Eyring plot which regards the same substrate in the same solvent of the NMR analysis.

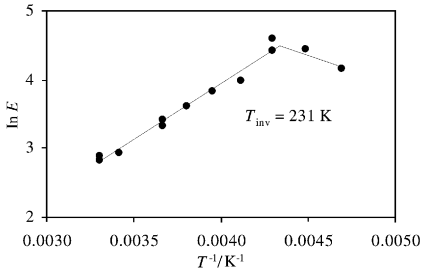

Fig. 3 Eyring plot for the selectivity ratio E in the kinetic resolution of **2** by lipase Amano PS at different temperatures in diethyl ether.

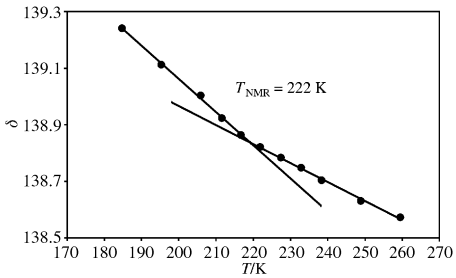

Fig. 4 Plot of the ^{13}C chemical shift of the quaternary aromatic carbon atom *vs. T* for **2** in d_{10}-diethyl ether.

Thus, once again the T_{inv} and the T_{NMR} appear as two independent experimental results due to the same phenomenon. Actually, we think that a reorganization between two differently ordered solvation clusters generates both the T_{inv} and the T_{NMR}. The T_{NMR} reveals the presence of dynamic phenomena on the ground state of solute–solvent clusters which thus appear to be much more structured than generally believed. The T_{inv} reveals the same dynamic phenomena, which now act on diastereomeric transition states leading to a different stereoselectivity below and above the T_{inv}.[22]

From the experimental data reported here, it results that even enzymatic reactions show temperature dependent phenomena of substrate solvation because of the presence of a T_{inv} and a corresponding T_{NMR}, so that even enzymatic reactions experience reorganization of different solute–solvent clusters depending on temperature. Because of the difference in selectivity above and below the T_{inv}, it follows that those solute–solvent clusters contribute to differentiate the Gibbs free energies of the two diastereomeric substrate–enzyme complex transition states. Thus our data provide evidence that solvent molecules are still present in substrate–enzyme transition states.

Our experimental data clearly suggest that enzymatic reactions are only a particular case of a more general phenomenon. Solvation always plays a fundamental role in stereoselectivity and the substrate cannot be considered a mere isolated species in solution, but rather a part of a more complex and well defined solute–solvent cluster.

This work was supported by MURST and by the University of Bologna (funds for selected topics). Penicillin G Acylase was kindly supplied by Recordati (Italy).

Notes and references

1 For a review, see: C. R. Wescott and A. M. Klibanov, *Biochim. Biophys. Acta*, 1994, **12**, 1.
2 A. Zaks and A. M. Klibanov, *J. Am. Chem. Soc.*, 1986, **108**, 2767.
3 T. Ke, C. R. Wescott and A. M. Klibanov, *J. Am. Chem. Soc.*, 1996, **118**, 3366; T. Ke and A. M. Klibanov, *J. Am. Chem. Soc.*, 1998, **120**, 4259.
4 G. Talsky, *Angew. Chem., Int. Ed. Engl.*, 1971, **10**, 548; E. Keinan, E. K. Hafeli, K. K. Seth and R. Lamed, *J. Am. Chem. Soc.*, 1986, **108**, 162; Y.-Y. Huang, T. Hara, S. Sligar, M. J. Coon and T. Kimura, *Biochemistry*, 1986, **25**, 1390; Y.-Y. Chang, R. D. Scott and D. J. Graves, *Biochemistry*, 1986, **25**, 1932; I. H. Segel, *Enzyme Kinetics: behavior and analysis of rapid equilibration and steady-state enzyme systems*, Wiley, New York, 1993; R. S. Phillips, *Trends Biotechnol.*, 1996, **14**, 13.
5 T. Sakai, I. Kawabata, T. Kishimoto, T. Ema and M. Utaka, *J. Org. Chem.*, 1997, **62**, 4906.
6 T. Göbel and K. B. Sharpless, *Angew. Chem., Int. Ed. Engl.*, 1993, **32**, 1329.
7 G. B. Stone, *Tetrahedron: Asymmetry*, 1994, **5**, 465.
8 G. Cainelli, D. Giacomini and M. Walzl, *Angew. Chem., Int. Ed. Engl.*, 1995, **34**, 2150; G. Cainelli, D. Giacomini and P. Galletti, *Eur. J. Org. Chem.*, 1999, 61.
9 G. Cainelli, D. Giacomini, P. Galletti and A. Marini, *Angew. Chem., Int. Ed. Engl.*, 1996, **35**, 2849.
10 H. Buschmann, H.-D. Scharf, N. Hoffmann and P. Esser, *Angew. Chem., Int. Ed. Engl.*, 1991, **30**, 477; K. J. Hale and J. H. Ridd, *J. Chem. Soc., Perkin Trans. 2*, 1995, 1601.
11 G. Cainelli, D. Giacomini and P. Galletti, *Chem. Commun.*, 1999, 567.
12 G. Cainelli, D. Giacomini, P. Galletti and P. Orioli, *Angew. Chem., Int. Ed.*, 2000, **39**, 523.
13 For solvent effects on chemical shift see, for instance: T. Helgaker, M. Jaszunski and K. Ruud, *Chem. Rev.*, 1999, **99**, 293; E. Y. Lau and J. T. Gerig, *J. Am. Chem. Soc.*, 1996, **118**, 1194; E. Y. Lau and J. T. Gerig, *J. Chem. Phys.*, 1995, **103**, 3341 and references therein.
14 Scharf in his review[10] interpreted the T_{inv} on a different basis and suggested its existence in enzymatic reactions without reporting any experimental example.
15 G. Cainelli, D. Giacomini, P. Galletti and M. Da Col, *Tetrahedron: Asymmetry*, 1997, **8**, 3231; G. Cainelli, D. Giacomini and P. Galletti, *Synthesis*, 2000, 289.
16 The chiral column S,S-DACH.DNB Lichosorb was furnished by Professor Gasparrini, University of Rome, Italy.
17 The selectivity ratio E is defined as the ratio of the specificity constants V_{max}/K_M: C.-S. Chen, Y. Fujimoto, G. Girdaukas and C. J. Sih, *J. Am. Chem. Soc.*, 1982, **104**, 7294.
18 This behavior is more common than usually considered. For some examples in diastereoselective reactions, see refs. 8 and 11.
19 G. Hortmann, D. A. Robertson and B. K. Gillard, *J. Org. Chem.*, 1972, **37**, 322.
20 The same conclusion is achieved even in the case of the other carbon atoms.
21 Partial ordering of molecules is possible in solution, and a temperature-dependent change in this order is already manifested in the nonlinearity of some spectroscopic properties. See *e.g.*: J. B. Robert, *Mol. Phys.*, 1997, **90**, 399; M. A. Wendt, J. Meiler, F. Weinhold and T. C. Farrar, *Mol. Phys.*, 1998, **93**, 145.
22 An alternative explanation of T_{inv} could be a change of the enzyme conformation induced by temperature. However, the presence of T_{inv} in many non-enzymatic reactions[6–12] renders our interpretation more plausible (see for instance ref. 3).

Synthesizing silver halide nanoparticles in supercritical carbon dioxide utilizing a water-in-CO_2 microemulsion

Hiroyuki Ohde,[a] Jose M. Rodriguez,[b] Xiang-Rong Ye[a] and Chien M. Wai*[a]

[a] *Department of Chemistry, University of Idaho, Moscow, Idaho 83843, USA. E-mail: cwai@uidaho.edu*
[b] *ECC International, Sandersville, Georgia 31082, USA*

Received (in Irvine, CA, USA) 18th July 2000, Accepted 13th October 2000
First published as an Advance Article on the web

Ionic species can be stabilized in the water core of a water-in-CO_2 microemulsion in supercritical fluid CO_2; by mixing two microemulsions containing Ag^+ and X^- ions separately, silver halide (AgX) nanoparticles were synthesized in supercritical CO_2; the water-in-CO_2 microemulsion may provide a reaction system for a wide range of nanoparticle syntheses involving ionic species in supercritical CO_2.

Reverse micelles and microemulsions formed in liquid and supercritical carbon dioxide (CO_2) allow high polar compounds to be dispersed in this nonpolar fluid.[1] A recent report demonstrated that silver ions in the water core of a water-in-supercritical CO_2 microemulsion could be reduced to nanosized metallic silver particles by a reducing agent dissolved in the fluid phase.[2] The rate of formation of silver nanoparticles in the water-in-supercritical CO_2 microemulsion is fast, suggesting the microemulsion is dynamic in nature.[3] By collision, exchange of contents between two water-in-supercritical CO_2 microemulsions probably would take place effectively. This suggests the possibility of performing nanomaterials synthesis in supercritical CO_2 by mixing water-in-CO_2 microemulsions containing different ions in the water cores. The water-in-CO_2 microemulsion system thus may function like a 'nanoreactor' for a wide range of chemical syntheses involving ionic species as starting materials in supercritical CO_2.

Recently, Ida *et al.* found that the ionic conductivity of silver iodide increased significantly as the particle size decreased to the nanometer-size range.[4] Silver chloride and silver bromide are indirect gap semiconductors and silver iodide is a direct gap semiconductor. Much attention has been paid to the changes in band gap energies for small semiconductor particles as the particle radius decreases.[5] Rosseti *et al.* explained the particle size dependence of the excited state electronic properties of silver iodide and silver bromide as a consequence of electron and hole localization in the small crystallites.[6] Water-in-oil microemulsion technology has been used to synthesize a variety of nanoparticles. Usually, nanometer-sized particles with a high degree of monodispersity can be obtained using this technology.[7] Formation of nanoparticles in supercritical fluids offers significant advantages over conventional liquid-phase systems including rapid separation of solvent and the possibility of depositing the particles *in situ* in porous materials utilizing the unique properties of the supercritical fluid phase.[2]

Sodium bis(2-ethylhexyl) sulfosuccinate (AOT) obtained from Sigma, was purified using a method described by Williams *et al.*[8] The perfluoropolyether–phosphate (PFPE-PO_4) received from Ausimont has a general structure of $CF_3O[OCF(CF_3)CF_2]_n(OCF_2)_mOCF_2CH_2OCH_2CH_2OPO(OH)_2$ with an average molecular weight of 870. The carbon dioxide, SFE grade, was obtained from Oxarc.

Two homemade high-pressure vessels were utilized for the synthesis. One vessel (9.5 ml volume) was equipped with a fiber-optic system (5 mm pathlength) connected to a CCD array UV–VIS spectrometer. The high-pressure fiber-optic spectroscopy cell is described elsewhere.[3] The other vessel was a 15 ml high-pressure view cell with sapphire windows.[2] Each system could be isolated from the other by Valco high-pressure valves.

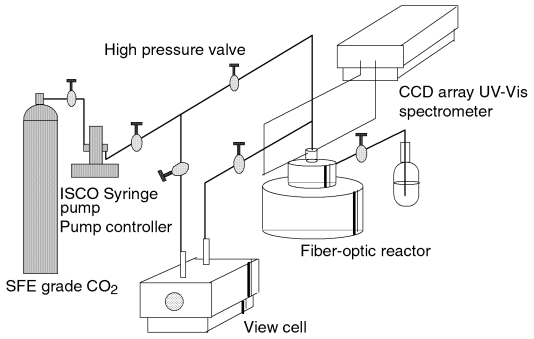

Fig. 1 Schematic diagram of the supercritical CO_2 microemulsion reaction system.

A schematic diagram of the entire supercritical fluid system used for this study is shown in Fig. 1.

The reverse micellar solutions were prepared by using sodium bis(2-ethylhexyl) sulfosuccinate [AOT] (12.8 mM) and the cosurfactant perfluoropolyether phosphate [PFPE-PO_4] (25.3 mM) at the water-to-surfactant ratio, $W = [H_2O]/[AOT] = 12$. The $AgNO_3$ was made to 3.3 mM and NaI, NaBr and NaCl were made to 6.6 mM. The silver nitrate solution was always placed in the 9.5 ml fiber-optic cell and the sodium halide solutions were placed in the 15 ml view-cell. Each solution was stirred for 1 h in the pressurized vessel to ensure the formation of a homogeneous optically transparent microemulsion. For the supercritical fluid carbon dioxide experiments, the vessels were first both pressurized to 80 atm. At the end of 1 h, the 15 ml vessel was pressurized to 200 atm and the microemulsion containing the halide solution was pushed into the fiber-optic cell by opening an interconnecting valve and the spectra were recorded.

Fig. 2 shows the UV–VIS absorption spectra of silver halide nanoparticles observed in the supercritical fluid CO_2 experiments. The spectra for silver iodide show a broad band in the approximate range 410–450 nm. The peak wavelength of the absorption band increased with time after the mixing, varying from *ca.* 422 to 429 nm. About 30 s after the mixing, the peak wavelength reached approximately a constant value at 429 nm and the peak absorption intensity also became constant for the remainder of the experiment. These spectra are consistent with the UV–VIS spectra previously reported by Sato *et al.* for nanosized silver iodide particles formed in an AOT/isooctane reverse micelle system.[9] For silver bromide, we observed shoulder peaks in the range 300–350 nm. Again the observed spectra are consistent with the previously reported observations for silver bromide nanoparticles.[9] The spectra of silver chloride showed an absorption threshold shorter than silver bromide, also in agreement with the literature report.[9]

The size of the silver halide nanoparticles can be estimated by first calculating the band gap energies for the semiconductors. For direct allowed transitions, such as silver iodide, the following equation has been derived by Ravich *et al.*[10]

$$\sigma h\nu = K(h\nu - E_g)^{1/2} \quad (1)$$

DOI: 10.1039/b005924m

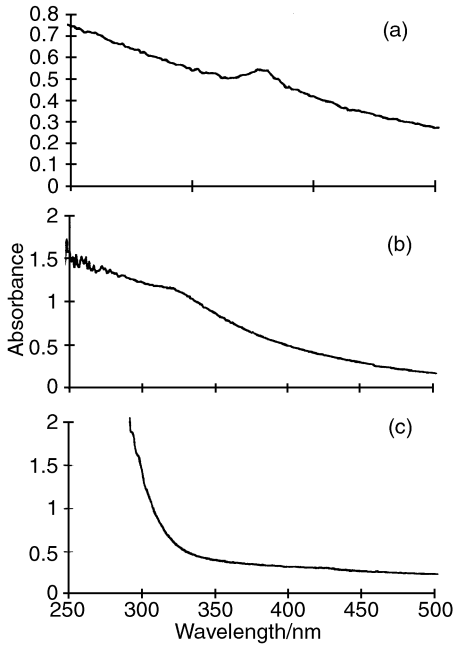

Fig. 2 Absorption spectra of AgX nanoparticles synthesized in the water-in-supercritical CO_2 microemulsion: (a) AgI, (b) AgBr and (c) AgCl.

and for indirect gap semiconductors, like silver bromide and silver chloride,

$$\sigma h\nu = K'(h\nu - E_g')^2 \quad (2)$$

In these equations, σ and $h\nu$ are the absorption coefficient and the photon energy, respectively, K and K' are proportionality constants, and E_g and E_g' are the band gap energy and the indirect energy transition threshold, respectively.

The average diameter of the nanoparticle, d_p, can be estimated from the band gap energy, E_g,[9,11]

$$E_g = E_{g,bulk} + (h^2/2d_p^2)[(1/m_e) + (1m_h)] - [(3.6e^2)/(4\pi\varepsilon d_p)] \quad (3)$$

where m_e and m_h are the effective mass of an electron and a hole in a semiconductor, respectively. In eqn. (3), $E_{g,bulk}$ is the energy of the band gap of the bulk semiconductor, ε is the dielectric constant of the semiconductor and e is the charge of an electron. The following parameters[8] were used for the calculations: for AgI, $E_{g,bulk}$ = 2.83 eV, $\varepsilon/\varepsilon_0$ = 4.91, and m^*/m_0 = 0.2; for AgBr, $E_{g,bulk}$ = 2.5 eV, $\varepsilon/\varepsilon_0$ = 4.62, m_h/m_0 = 0.645, and m_e/m_0 = 0.215. For the other symbols, ε_0 is the dielectric constant of vacuum, m_0 is the rest mass of an electron and m^* is represented by the following equation, $m^* = [(1/m_e) + (1/m_h)]^{-1}$.

The variation of AgI nanoparticle diameters with time during synthesis in supercritical CO_2 can be calculated using eqn. (3) and the UV–VIS spectroscopic data. The results for silver iodide showed a sharp increase in particle size in the first few seconds until a stable size of *ca.* 3.4 nm in supercritical CO_2 was reached. For silver bromide, we obtained a particle size *ca.* 3.0 nm. The size of the silver chloride particles could not be calculated since the effective mass of a hole is not available.

A rapid expansion of supercritical solution (RESS) method[12] was used to collect the synthesized silver halide particles. The size distribution of AgI particles collected on a copper grid by the RESS method is shown in Fig. 3. The particle sizes shown in Fig. 3 (*ca.* 3–15 nm) are larger than the calculated AgI size based on the spectroscopic method. Rapid expansion of the water-in-CO_2 microemulsion apparently can cause agglomeration of the AgI nanoparticles. Other methods of collecting the synthesized nanoparticles in supercritical CO_2 with minimum agglomeration are currently under investigation.

To obtain more information on the mechanism of silver halide nanoparticle formation in supercritical CO_2, the absorbance *vs.* time for the products AgI, AgBr and AgCl were

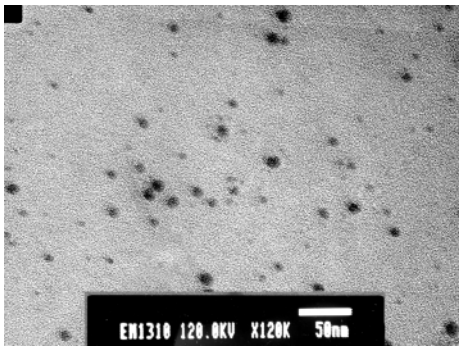

Fig. 3 TEM micrograph of the AgI particles collected on a copper grid using the RESS method.

investigated at 426, 325 and 300 nm, respectively. The time that required for the absorbance–time curve to reach a plateau was used as a measure of the completion of the reaction. The reaction time followed the order AgI (16 s) > AgBr (28 s) > AgCl (40 s). Similar experiments by mixing water/AOT/hexane microemulsions (containing Ag^+ and I^- separately) would require *ca.* 3 min to reach the plateau for the formation of the AgI nanoparticles. The formation of silver halide nanoparticles in the water-in-CO_2 microemulsion system involves several processes including collision, intermicellar exchange and reaction between silver ion and halide ion as shown in the graphical abstract. The intermicellar exchange process involves the distribution of silver nitrate and sodium halide from water droplets to the surfactant phase. This process should depend on the hydrophobicity of sodium halide, *i.e.* NaI > NaBr > NaCl. The observed reaction speed follows the order of hydrophobicity of sodium halide, suggesting that the most hydrophobic species probably reside close to the interface and exchange faster. The reaction between Ag^+ and I^- is expected to be very fast because of the large K_{sp} values for all AgX. The rate-determining step for the formation of silver halide nanoparticles in the water-in-supercritical CO_2 probably is the intermicellar exchange process.

Notes and references

1 J. L. Fulton, D. M. Pfund, J. B. McClain, T. J. Romack, E. E. Maury, J. R. Combes, E. T. Samulski, J. M. DeSimone and M. Capel, *Langmuir*, 1995, **11**, 4241; K. P. Johnston, K. L. Harrison, M. J. Clarke, S. M. Howdle and M. P. Heitz, *Science*, 1996, **271**, 624.
2 M. Ji, X. Chen, C. M. Wai and J. L. Fulton, *J. Am. Chem. Soc.*, 1999, **121**, 2631.
3 F. Hunt, H. Ohde and C. M. Wai, *Rev. Sci. Instrum.*, 1999, **70**, 4661.
4 T. Ida, H. Hamada and K. Kimura, *Surf. Rev. Lett.*, 1996, **3**, 41; T. Ida and K. Kimura, *Solid State Ionics*, 1998, **107**, 313.
5 A. L. Efros, *Sov. Phys. Semicond.*, 1982, **16**, 772; A. I. Ekimov and A. A. Onushchenko, *Sov. Phys. Semicond.*, 1982, **16**, 775; L. Brus, *J. Phys. Chem.*, 1986, **90**, 2555; A. Henglein, *Top. Curr. Chem.*, 1988, **143**, 114.
6 R. Rossetti, R. Hull, J. M. Gibson and L. E. Brus, *J. Chem. Phys.*, 1985, **83**, 1406.
7 J. B. Nagy, D. Barette, A. Fonseca, L. Jeunieau, Ph. Monnoyer, P. Piedigrosso, I. Ravet-Bodart, J. P. Verfaillie and A. Wathelet, in *Nanopartices in Solids and Solutions*, ed. J. H. Fendler and I. Dekany, Dordrecht, 1996, pp. 71–129.
8 E. F. Williams, N. T. Woodberry and J. K. Dixon, *J. Colloid Sci.*, 1957, **12**, 451.
9 C. H. Chew, L. M. Gan and D. O. Shah, *J. Dispersion Sci. Technol.*, 1990, **12**, 593; K. P. Johansson, A. P. Marchetti and G. L. McLendon, *J. Phys. Chem.*, 1992, **96**, 2873; H. Sato, T. Hirai and I. Komasawa, *J. Chem. Eng. Jpn.*, 1996, **29**, 501.
10 I. Y. Ravich, B. A. Efimova and I. A. Smirnov, *Semiconducting Lead Chalcogenides*, Plenum Press, New York, 1970, pp. 52–53.
11 T. Hirai, Y. Tsubaki, H. Sato and I. Komasawa, *J. Chem. Eng. Jpn*, 1995, **28**, 468.
12 R. D. Smith, D. W. Matson, J. L. Fulton and R. C. Peterson, *Ind. Eng. Chem. Res.*, 1987, **26**, 2298.

ChemComm

Ruthenium(II) complex with a notably long excited state lifetime†

Daniel S. Tyson, Jason Bialecki and Felix N. Castellano*

Department of Chemistry and Center for Photochemical Sciences, Bowling Green State University, Bowling Green, Ohio 43403, USA. E-mail: castell@bgnet.bgsu.edu

Received (in Columbia, MO, USA) 25th July 2000, Accepted 10th October 2000
First published as an Advance Article on the web

A new Ru(II) diimine complex, [Ru(5-pyrenyl-1,10-phenanthroline)]$_3$(PF$_6$)$_2$ ([Ru(py-phen)$_3$]$^{2+}$), possesses a room temperature excited state lifetime of 148 ± 8 μs.

Visible-absorbing luminescence probes that display long decay times are becoming increasingly important in biophysics, high-throughput screening, clinical chemistry, and lifetime-based chemical sensing.[1–4] One particular class of luminophores based on transition metal complexes displaying metal-to-ligand charge transfer (MLCT) excited states[5] have shown promise in such luminescence-based technologies.[1–4] In the interest of expanding these initial efforts, new MLCT compounds with prolonged emission decay times deserve special attention.

The photophysical properties of transition metal complexes displaying MLCT excited states are dominated by non-radiative decay processes and can be largely predicted by the energy gap law.[6] Excited state lifetimes in such complexes are modulated through simple modifications of the ligands and/or the central metal atom. Although this approach has proven quite successful, complexes with very long lifetimes consequently possess large energy gaps, generally with MLCT absorption bands in the UV. Alternatively, MLCT complexes containing ligands with large π-systems extend excited state lifetimes by imparting significant electronic delocalization into the charge transfer excited state.[7] Even though such complexes absorb in the visible, useful for analytical luminescence applications, their lifetimes are only slightly larger than that observed in the parent diimine complexes.

The room temperature lifetimes of the charge transfer-based emission in Ru(II) diimine complexes can be dramatically extended (approaching 50 μs) by tethering a pyrene molecule to one of the ligands within the complex.[8–12] The observed MLCT-based emission in such complexes is substantially longer-lived relative to the parent compounds as a result of energy transfer processes between the MLCT fragment and the pyrene unit.[8–12] In previous work, we have suggested that the energy transfer process can be controlled by adding additional pyrene molecules to the ligand periphery, which has the effect of increasing the formation of 'pyrene-like' triplets, further extending the lifetime of the complex. The present work takes advantage of this concept and has successfully generated a new Ru(II) diimine complex, [Ru(py-phen)$_3$](PF$_6$)$_2$ (Fig. 1), where py-phen is 5-pyrenyl-1,10-phenanthroline, with a room temperature lifetime of 148 ± 8 μs.

Full details regarding the synthesis of py-phen and [Ru(py-phen)$_3$](PF$_6$)$_2$ are presented in the ESI†. Briefly, py-phen was prepared from 5-bromo-1,10-phenanthroline and 3-pyreneboronic acid using standard Suzuki coupling conditions. [Ru(py-phen)$_3$](PF$_6$)$_2$ was synthesized by refluxing Ru(DMSO)$_4$Cl$_2$ and py-phen in 95% ethanol, followed by precipitation of the PF$_6$-salt, and final purification accomplished through gel filtration chromatography. The absorption and emission spectra of [Ru(py-phen)$_3$]$^{2+}$ in MeCN are displayed in Fig. 2. The tethered pyrene chromophores are largely responsible for the structured π–π* absorption bands between 300 and 350 nm.

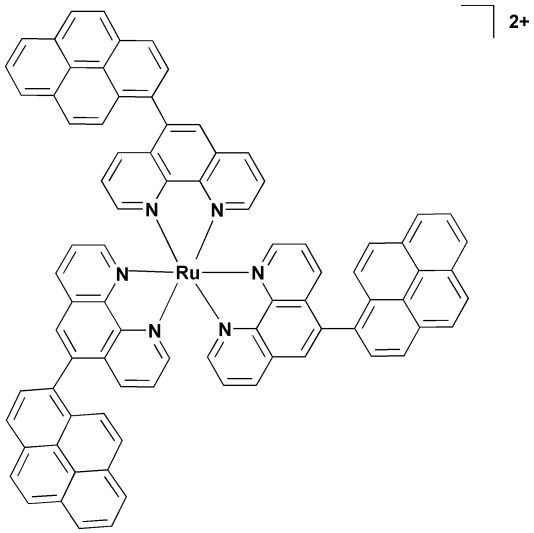

Fig. 1 Molecular structure of [Ru(py-phen)$_3$]$^{2+}$.

The absorption bands in the visible are due to the d$_\pi$(Ru) → π*(py-phen) MLCT transitions in the molecule. Regardless of excitation wavelength (300–532 nm), this complex displays only one visible emission band centered near 600 nm in MeCN at room temperature with a quantum yield of 0.071 ± 0.010. This emission band is characteristic of MLCT-based luminescence typically observed in Ru(II)–diimine complexes.[5] Using single photon counting techniques (342 nm excitation), no singlet emission could be observed from the pyrenyl units when grafted onto the metal complex. The corrected excitation spectrum of [Ru(py-phen)$_3$]$^{2+}$ (600 nm emission) is almost completely superimposible at all wavelengths with its absorption spectrum, suggesting a singlet energy transfer efficiency near unity. Similar behavior has been observed in related Ru(II)–pyrene chromophores.[9,11,12]

The excited state lifetime of [Ru(py-phen)$_3$]$^{2+}$ in thoroughly deaerated MeCN at infinite dilution is 148 ± 8 μs as measured with 458 nm laser pulses from an N$_2$-pumped dye laser (500 ps

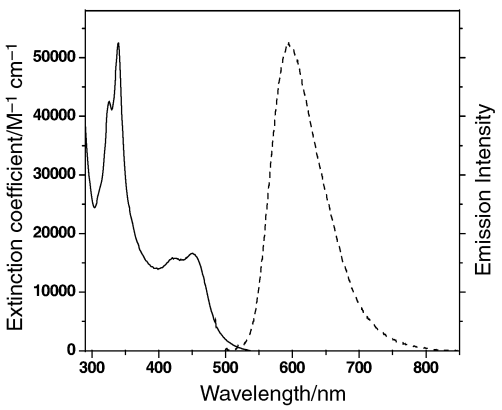

Fig. 2 Absorption (solid line) and emission (dashed line) spectra of [Ru(py-phen)$_3$]$^{2+}$ in MeCN at room temperature. The emission spectrum was recorded with 458 ± 2 nm excitation.

† Electronic supplementary information (ESI) available: experimental details, self quenching plot and excited state absorption difference spectra. See http://www.rsc.org/suppdata/cc/b0/b007336i/

DOI: 10.1039/b007336i

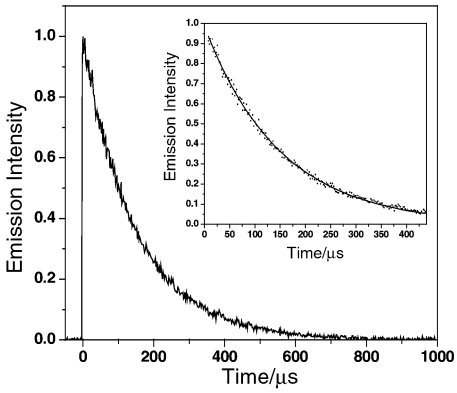

Fig. 3 Time-resolved emission decay of $[Ru(py\text{-}phen)_3]^{2+}$ in deaerated MeCN obtained with 458 ± 2 nm pulsed excitation (500 ps fwhm) detected at 600 nm. The decay represents an average of 128 laser pulses. Inset: data fit to a single exponential decay model.

fwhm), Fig. 3. A fast luminescence decay component (< 16 ns) was also observed, consistent with data obtained on related compounds.[8,10,11] This exceptionally long lifetime agrees well with the decay kinetics observed in the transients from the nanosecond laser flash photolysis experiments. However, the transient absorption profiles observed in $[Ru(py\text{-}phen)_3]^{2+}$ at all times following a 460 or 532 nm laser pulse are similar to that obtained with the uncoordinated py-phen ligand following 355 nm excitation. Therefore, the absorption transients provide evidence for the existence of a 'pyrene-like' triplet state at all delay times while there is no direct observation of a MLCT-based triplet state. The only observed radiative decay pathway for the $[Ru(py\text{-}phen)_3]^{2+}$ complex at room temperature is MLCT-based photoluminescence. In the model complex $[Ru(Ph\text{-}phen)_3]^{2+}$, where Ph-phen is 5-phenyl-1,10-phenanthroline, the lifetime under similar conditions is 1.15 μs.[13] In $[Ru(py\text{-}phen)_3]^{2+}$, the lifetime is extended *ca.* 129-fold relative to $[Ru(Ph\text{-}phen)_3]^{2+}$ as a consequence to the stabilization imparted by the energy transfer processes.

The observed excited state lifetime in $[Ru(py\text{-}phen)_3]^{2+}$ is very sensitive to subtle changes in oxygen concentration. Under our experimental conditions, high purity argon gas was continuously flowed through the cuvette during the measurement cycle, while maintained at a constant temperature of 20 ± 1 °C. Significant changes in lifetime could be correlated to the argon flow rate and temperature.

The long lifetime associated with the $[Ru(py\text{-}phen)_3]^{2+}$ complex permits a dynamic excited state self-quenching reaction at relatively dilute concentrations. Under our experimental conditions we did not observe any deviation in Beer's law behavior in the ground state absorption spectrum nor were we able to identify any new bands in the steady-state emission spectrum at concentrations between 2×10^{-6} and 2×10^{-5} M. Over this concentration range, the rates of emission decay are well modeled by a Stern–Volmer expression, recently used to describe self-quenching processes in Pt(II) diimine compounds.[14] The derived self-quenching rate constant of 1.3×10^8 M^{-1} s^{-1} is valid under optically dilute conditions and is clearly not a result of ground state aggregation.

The uncoordinated py-phen ligand displays structured phosphorescence at 77 K in 4:1 EtOH:MeOH in the presence of ethyl iodide when excited in the UV (342 nm). Visible excitation (458 nm) of $[Ru(py\text{-}phen)_3]^{2+}$ in the same frozen matrix yields a similarly structured emission, reflecting the dominance of pyrene-like triplets in the excited states. The decay kinetics of $[Ru(py\text{-}phen)_3]^{2+}$ at 77 K are complex, containing a long component of 46 ± 2 ms.

Energy transfer processes between the excited MLCT and pyrene states at room temperature facilitates the extension of the excited state lifetime in $[Ru(py\text{-}phen)_3]^{2+}$. The observed 148 μs lifetime is substantially beyond the range of any previously measured lifetime in this class of chromophores. Importantly, this lifetime was obtained without relying on energy gap law predictions. The complex is susceptible to dynamic self-quenching processes under optically dilute conditions. To our knowledge, this is the first example of such behavior in a Ru(II)–diimine complex. The room temperature emission in $[Ru(py\text{-}phen)_3]^{2+}$ is MLCT-based, however at 77 K, the emission emerges as a π–π*-based phosphorescence.

J. B. was supported by the National Science Foundation Research Experience for Undergraduates program.

Notes and references

1 J. R. Lakowicz, *Principles of Fluorescence Spectroscopy*, Kluwer Academic/Plenum Publishers, New York, 1999.
2 E. Terpetschnig, H. Szmacinski, H. Malak and J. R. Lakowicz, *Biophys. J.*, 1995, **68**, 342.
3 X.-Q. Guo, F. N. Castellano, L. Li and J. R. Lakowicz, *Anal. Chem.*, 1998, **70**, 632.
4 *Topics in Fluorescence Spectroscopy Vol. 4: Probe Design and Chemical Sensing*, ed. J. R. Lakowicz, Plenum Press, New York, 1994; J. R. Lakowicz, F. N. Castellano, J. D. Dattelbaum, L. Tolosa, G. Rao and I. Gryczynski, *Anal. Chem.*, 1998, **70**, 5115.
5 A. Juris, V. Balzani, F. Barigelletti, S. Campagna, P. Belser and A. von Zelewsky, *Coord. Chem. Rev.*, 1988, **84**, 85.
6 J. V. Caspar, E. M. Kober, B. P. Sullivan and T. J. Meyer, *J. Am. Chem. Soc.*, 1982, **104**, 630; E. M. Kober, J. L. Marshall, W. J. Dressick, B. P. Sullivan, J. V. Caspar and T. J. Meyer, *Inorg. Chem.*, 1985, **24**, 2755; E. M. Kober, J. V. Caspar, R. S. Lumpkin and T. J. Meyer, *J. Phys. Chem.*, 1986, **90**, 3722.
7 S. Boyde, G. F. Strouse, W. E. Jones and T. J. Meyer, *J. Am. Chem. Soc.*, 1990, **112**, 7395; G. F. Strouse, J. R. Schoonover, R. Duesing, S. Boyde, W. E. Jones and T. J. Meyer, *Inorg. Chem.*, 1995, **34**, 473.
8 W. E. Ford and M. A. J. Rodgers, *J. Phys. Chem.*, 1992, **96**, 2917.
9 G. J. Wilson, W. H. F. Sasse and A. W. H. Mau, *Chem. Phys. Lett.*, 1996, **250**, 583; G. J. Wilson, A. Launikonis, W. H. F. Sasse and A. W. H. Mau, *J. Phys. Chem. A*, 1997, **101**, 4860.
10 J. A. Simon, S. L. Curry, R. H. Schmehl, T. R. Schatz, P. Piotrowiak, X. Jin and R. P. Thummel, *J. Am. Chem. Soc.*, 1997, **119**, 11012.
11 A. Harriman, M. Hissler, A. Khatyr and R. Ziessel, *Chem. Commun.*, 1999, 735; M. Hissler, A. Harriman, A. Khatyr and R. Ziessel, *Chem. J. Eur.*, 1999, **5**, 3366.
12 D. S. Tyson and F. N. Castellano, *J. Phys. Chem. A*, 1999, **103**, 10955.
13 P. C. Alford, M. J. Cook, A. P. Lewis, G. S. G. McAuliffe, V. Skarda, A. J. Thomson, J. L. Glasper and D. J. Robbins, *J. Chem. Soc., Perkin Trans. 2*, 1985, 705.
14 W. B. Connick, D. Geiger and R. Eisenberg, *Inorg. Chem.*, 1999, **38**, 3264.

Synthesis and crystal structure of a C_{60} complex with a bis(ethylenedithio)tetrathiafulvalene radical cation salt: (BEDT-TTF·I_3)C_{60}

D. V. Konarev,[a] A. Yu. Kovalevsky,[b] P. Coppens[b] and R. N. Lyubovskaya*[a]

[a] *Institute of Problems of Chemical Physics RAS, Chernogolovka, 142432 Russia. E-mail: lyurn@icp.ac.ru*
[b] *Crystallography Laboratory, Department of Chemistry, State University of New York at Buffalo, Buffalo, NY 14214, USA*

Received (in Irvine, CA, USA) 5th July 2000, Accepted 13th October 2000
First published as an Advance Article on the web

This communication describes a novel solid, crystals of which are grown by a diffusion technique, consisting of alternating fullerene and radical cation salt layers.

Fullerenes are known to form only neutral molecular complexes with the tetrathiafulvalene derivatives (TTFs†): (BEDT-TTF)$_2C_{60}$;[1] OMTTF•C_{60}·C_6H_6;[2] DBTTF·C_{60}·C_6H_6[3] and some others.[2,3] The lack of charge transfer defines the dielectric properties of these complexes.[2,3] On the other hand, TTF radical cation salts with different inorganic and organic anions demonstrate metallic and superconducting properties.[4] An example is a series of the BEDT-TTF salts with linear and polymeric anions which possess superconducting properties: (BEDT-TTF)$_2$X, X = I_3^-, IBr_2^-, AuI_2^-, ReO_4^-, $Cu(NCS)_2^-$ and (BEDT-TTF)$_4Hg_{2.89}Hal_8$, Hal = Cl, Br.[4] Since the properties of radical cation salts are affected by the polarizability of the molecules, we prepared compounds in which the TTF radical cation salts are surrounded by highly polarizable fullerene molecules (α_M = 85 Å^3 for C_{60}).[5]

In previous work we prepared a number of C_{60} neutral complexes and intercalated them by exposure to iodine vapor. The iodine replaces a solvent molecule and oxidizes a donor to a radical cation to form ($D^{\cdot+}I_n^-$)C_{60}, where $n \leqslant 5$ and D = DBTTF, TPDP or TMDTDM-TTF.[6] The intercalation process results in an increase of the conductivity of the complexes by 1–3 orders of magnitude. However, the diffusion process of intercalation does not allow synthesis of crystals with homogeneously distributed iodine. Therefore, we tried to synthesize such three-component compounds in solution. We reported earlier that cocrystallization of BEDT-TTF·$I_{3.5}$ in a saturated fullerene solution in a chlorobenzene–benzonitrile (1:5) mixture yielded (small) single crystals of (BEDT-TTF·I_3)C_{60}.[7] However, the crystals were not of adequate size to allow crystal structure determination.

Here we report the first crystal structure of (BEDT-TTF·I_3)C_{60} and a new general synthetic procedure for C_{60} complexes comprising radical cation salts of donors. The procedure allows the complexes to be prepared as single crystals suitable for diffraction studies.

(BEDT-TTF·I_3)C_{60} **1** was prepared by slow diffusion of iodine dissolved in acetonitrile which was layered on a solution of C_{60} and BEDT-TTF (1:1) in a 9:1 toluene–1,2-dichlorobenzene mixture. Crystals of **1** were formed as black hexahedrons on the walls of a flask. Simultaneously, planar rhomb-shaped crystals of β-(BEDT-TTF)$_2I_3$ free of C_{60} crystallize as an admixture.

The technique is based on the insolubility of both the fullerene and the donor radical cation salt $D^{\cdot+}I_n^-$ in acetonitrile. In this case the diffusion of the acetonitrile solution of iodine into the toluene–1,2-dichlorobenzene layer results in the formation of the ($D^{\cdot+}I_n^-$)C_{60} compound.

Single crystal X-ray diffraction data of **1**‡ shows that C_{60}, $(BEDT\text{-}TTF)^{\cdot+}$, and I_3^- are fully ordered, with the fullerene, $(BEDT\text{-}TTF)^{\cdot+}$ and I_3^- moieties residing in special positions on two-fold axes. The densely packed C_{60} layers parallel to the *bc* plane alternate with $(BEDT\text{-}TTF)^{\cdot+}$, and I_3^- layers. Fig. 1 shows the view of the crystal structure of **1** along the *b* axis.

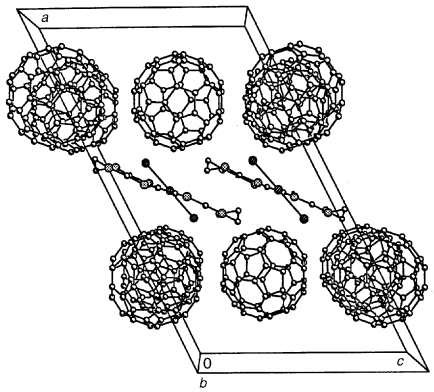

Fig. 1 The projection of the crystal structure of **1** along the *b* axis.

The shortest distance between the centers of the C_{60} molecules in parallel layers is 15.61 Å. Within the layers each C_{60} molecule is surrounded by six adjacent C_{60} molecules with center-to-center distances equal to 9.93–9.97 Å, close to similar distances in neat C_{60} crystals (9.94 Å at 153 K).[8] Adjacent C_{60} molecules within the layers are oriented with the five-membered rings facing each other or with the 6–5 bond of one molecule facing the center of the pentagonal ring of the adjacent molecule, with C···C distances in the range 3.22–3.37 Å.

The ion radical layer (Fig. 2) consists of chains in which the $(BEDT\text{-}TTF)^{\cdot+}$ ion alternates with I_3^-. One of the ethylene hydrogen atoms forms short contacts of 3.10(1) and 3.20(1) Å with two iodine atoms (Fig. 2). Adjacent chains are shifted with respect to each other to form a chequer-like arrangement of $(BEDT\text{-}TTF)^{\cdot+}$ and I_3^- within the layer. Short van der Waals S···I contacts (3.80–3.96 Å) link two $(BEDT\text{-}TTF)^{\cdot+}$ molecules in adjacent chains. The shortest S···S distance between $(BEDT\text{-}TTF)^{\cdot+}$ molecules in neighboring chains is 3.75–3.85 Å, which is larger than the sum of the van der Waals radii of two sulfur atoms (3.6 Å).

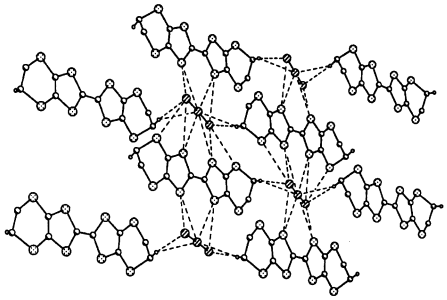

Fig. 2 The projection of the layer comprising $(BEDT\text{-}TTF)^{\cdot+}$ and I_3^- on the *bc* plane. Only H-atoms involved into short van der Waals contacts with I_3^- are shown.

DOI: 10.1039/b005541g

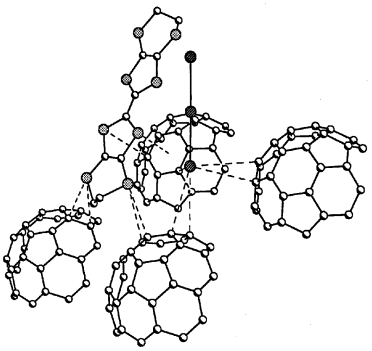

Fig. 3 Short van der Waals contacts between $(BEDT\text{-}TTF)^{\cdot+}$, I_3^- and C_{60}. Only the van der Waals contacts with one layer of C_{60} molecules are shown. Similar contacts are formed in the second adjacent layer.

Short van der Waals contacts exist between the C_{60} and the $(BEDT\text{-}TTF)^{\cdot+}/I_3^-$ layers (Fig. 3). Each $(BEDT\text{-}TTF)^{\cdot+}$ and I_3^- form short contacts with three C_{60} molecules in each of the adjacent layers. The S(BEDT-TTF)···C(C_{60}) distances (3.25–3.40 Å) in **1** are significantly shorter than those in the C_{60} complexes with neutral tetrathiafulvalenes: 3.446–3.556 Å in $(BEDT\text{-}TTF)_2C_{60}$;[1] 3.47–3.72 Å in DBTTF•C_{60}•C_6H_6;[3] 3.412–3.793 Å in $(TMDTDM\text{-}TTF)_2C_{60}(CS_2)_3$.[3] Such shortened contacts of $(BEDT\text{-}TTF)^{\cdot+}$ and C_{60} in **1** are a result of the penetration of the $(BEDT\text{-}TTF)^{\cdot+}$ molecules into the cavities in the fullerene layers (Fig. 3), while in the C_{60} complexes with neutral TTFs, the TTF molecules envelope the spherical surface of C_{60}. The linear I_3^- anions also extend into the cavities in the C_{60} layers to form five shortened van der Waals I···C(C_{60}) contacts [3.77–3.83(3) Å] (Fig. 3).

In contrast to $(BEDT\text{-}TTF)_2C_{60}$, in which the neutral BEDT-TTF molecule has a 'boat' conformation, $(BEDT\text{-}TTF)^{\cdot+}$ has an almost planar shape in **1** (Fig. 4). However, the short contacts with the C_{60} molecules affect the geometry of $(BEDT\text{-}TTF)^{\cdot+}$. In contrast to the η-$BEDT\text{-}TTF\cdot I_3$ salt,[9] $(BEDT\text{-}TTF)^{\cdot+}$ in **1** has a 'chair' conformation with the fold along the S1–S2 and S1a–S2a vectors, and dihedral angles between the planes ≈ 7.4°. The central S_4C_2 fragment of the molecule is not fully planar, but twisted around the double bond. The torsion angle between the plane formed by C1, S1, S2, and C1a, S1a, S2a is 174.1°. The six-membered ring has a sofa conformation, the deviation of the C4 atom from the plane of the other ring atoms being 0.806(4) Å. The central C=C bond length in $(BEDT\text{-}TTF)^{\cdot+}$ is 1.402(8) Å, close to that in η-$BEDT\text{-}TTF\cdot I_3$ [1.40(1) Å][9] and corresponding to a +1 charge on $(BEDT\text{-}TTF)^{\cdot+}$.

The ordering of the C_{60} molecules in **1** allows their bond lengths to be analyzed. The averaged lengths of the 6–6 and 6–5 bonds of C_{60} are 1.395(5) and 1.449(5) Å, respectively, the values being close to those of the 6–6 and 6–5 bonds in neutral $(BEDT\text{-}TTF)_2C_{60}$ [1.389(7) and 1.452(1) Å, respectively].[1] The diameters of the C_{60} molecule in three orthogonal directions running through the centers of the oppositely located 6–6 bonds

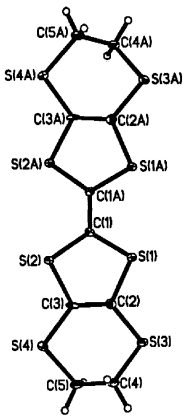

Fig. 4 Geometry of the $(BEDT\text{-}TTF)^{\cdot+}$ radical cation in **1**.

are equal to 6.941, 6.943 and 6.974 Å, thus the deviation from sphericity is only *ca.* 0.03 Å.

Thus, the structure of **1** retains to a great extent the features of the C_{60} structure, with radical cation layers separating the C_{60} layers. The $(BEDT\text{-}TTF)^{\cdot+}$ and I_3^- ions interact mostly electrostatically within the layer, while they form van der Waals contacts with fullerene layers.

1 is a semiconductor with $\sigma = 10^{-4}$ S cm^{-1}. Such behavior is characteristic of simple $BEDT\text{-}TTF\cdot I_3$ salts[9] with an integer charge (+1) on the BEDT-TTF molecule. In the current structure it can be associated also with the nature of the radical cation layer, in which there is no overlap of the π-orbitals of the $(BEDT\text{-}TTF)^{\cdot+}$ radical cations. It is known that BEDT-TTF salts with a formal charge of +0.5 show higher conductivity. However, the compound of composition $((BEDT\text{-}TTF)_2I_3)C_{60}$ cannot be prepared by the diffusion method. Recrystallization of the $(BEDT\text{-}TTF)_2I_3$ salt in fullerene solution yields only the neutral $(BEDT\text{-}TTF)_2C_{60}$ complex and the BEDT-TTF salts free of fullerene.

This work was supported by the Linkage Grant of NATO Science Program, the RFBR grant N00-03-32577, the National Science Foundation (CHE9981864), and the Russian Program 'Fullerenes and Atomic Clusters'.

Notes and references

† Abbreviations used in the text: bis(ethylenedithio)tetrathiafulvalene (BEDT−TTF); octamethyletetrathiafulvalene (OMTTF); dibenzotetrathiafulvalene (DBTTF), tetramethylenedithiodimethyltetrathiafulvalene (TMDTDM−TTF); 2.2′,6,6′-tetraphenyldipyranilydene (TPDP).

‡ *Crystal data* for **1:** $C_{70}H_8S_8I_3$, M = 1485.94; black hexagons, 0.4 × 0.2 × 0.2 mm, monoclinic, *C*2/*c*,*a* = 29.590(2), *b* = 9.9271(7), *c* = 17.2881(12) Å, β = 116.7350(10)°, V = 4535.4(5) Å^3, Z = 4, D_c = 2.176 g cm^{-3}. X-ray data were collected at 90 K using a Bruker SMART1000 CCD diffractometer installed at a rotating anode source (Mo−Kα radiation, λ = 0.71073 Å) and equipped with an Oxford Cryosystems nitrogen gas-flow apparatus. The data were collected by the rotation method with 0.3° frame−width (ω scan) and 20 s exposure time per frame. The data were integrated, scaled, sorted and averaged using the SMART software package of programs.[10] Empirical absorption corrections were applied (μ = 2.49 mm^{-1}) for the data collected using the SADABS program from the SMART software package.

The structure was solved by direct methods using SHELXTL NT version 5.10.[11] Positions of hydrogen atoms were found from the difference electronic density Fourier synthesis and refined using a 'riding model' with variable U_{iso}; 20392 reflections were collected, 4206 unique (R_{int} = 0.0639). Least-squares refinement on F^2 with anisotropic thermal parameters for all non-hydrogen atoms gave R_1 = 0.032 [for 3246 observed reflections with $F > 4\sigma(F)$], wR_2 = 0.085, final GOF = 1.03.

CCDC 182/1823. See http://www.rsc.org/suppdata/cc/b0/b005541g/ for crystallographic files in .cif format.

1 A. Izuoka, T. Tachikawa, T. Sugawara, Y. Suzuki, M. Konno, Y. Saito and H. Shinohara, *J. Chem. Soc., Chem. Commun.*, 1992, 1472.
2 G. Saito, T. Teramoto, A. Otsuka, Y. Sugita, T. Ban, M. Kusunoki and K.-I. Sakaguchi, *Synth. Met.*, 1994, **64**, 359.
3 D. V. Konarev, R. N. Lyubovskaya, N. V. Drichko, E. I. Yudanova, Y. M. Shul'ga, A. L. Litvinov, V. N. Semkin and B. P. Tarasov, *J. Mater. Chem.*, 2000, 803.
4 J. M. Williams, J. R. Ferraro, R. J. Thorn, K. D. Carlson, U. Geiser, H. H. Wang, A. M. Kini and M.-H. Whangbo, *Organic Superconductors (including Fullerenes). Synthesis, Structure, Properties and Theory*, Prentice Hall, Englewood Cliffs, NJ, 1992.
5 M. S. Dresselhaus, G. Dresselhaus, A. M. Rao and P. C. Eklund, *Synth. Met.*, 1996, **78**, 313.
6 R. N. Lyubovskaya, D. V. Konarev, E. I. Yudanova, O. S. Roschupkina, Yu. M. Shul'ga, V. N. Semkin and A. Graja, *Synth. Met.*, 1997, **84**, 741.
7 D. V. Konarev, N. V. Drichko, R. N. Lyubovskaya, E. I. Yudanova, Yu.M. Shul'ga, Ya. V. Zubavichus and V. N. Semkin, *Russ. Chem. Bull.*, 1999, **48**, 1946.
8 H.-B. Burgi, E. Blanc, D. Schwarzenbach, S. Liu, Y.-J. Lu, M. M. Kappes and J. A. Ibers, *Angew. Chem., Int. Ed. Engl.*, 1992, **31**, 640.
9 R. P. Shibaeva, R. M. Lobkovskaya, E. B. Yagubskii and E. E. Laukina, *Sov. Phys. Crystallogr. (Engl. Transl.)*, 1987, **32**, 530.
10 SMART Software Reference Manual, Bruker AXS, Madison, WI, 1998.
11 G. M. Sheldrick, SHELXTL NT Version 5.10, Program for Solution and Refinement of Crystal Structures, University of Göttingen, Germany, 1997.

ChemComm

New unsymmetrical thioether- and thiolate-substituted ferrocene ligands and an unusual bridged-Pd dimer complex

Vernon C. Gibson, Nicholas J. Long,* Andrew J. P. White, Charlotte K. Williams and David J. Williams

Department of Chemistry, Imperial College of Science, Technology and Medicine, South Kensington, London, UK SW7 2AY. E-mail: n.long@ic.ac.uk

Received (in Cambridge, UK) 18th September 2000, Accepted 18th October 2000
First published as an Advance Article on the web

A series of new unsymmetrical 1, 1′-disubstituted ferrocenediyl ligands featuring thioether or thiolate substituents have been conveniently synthesised and, as an example of their coordinating ability, a bridged palladium dimer has been formed and structurally characterised.

Although ferrocene was discovered nearly fifty years ago, the search for new ferrocene derivatives and chemistry continues apace. In particular, versatile, stable and synthetically undemanding ferrocenyl and ferrocenediyl ligands are sought after due to their extensive coordination chemistry and applications within catalysis.[1,2] Ferrocene species with donor heteroatoms (*e.g.* P, N, S, O) substituted onto the cyclopentadienyl rings are well known, especially those featuring homo-substitution (*i.e.* the same donor atom along with the same alkyl or aryl substituents). Much less well-known are unsymmetrical 1,1′-disubstituted ferrocenes featuring hetero-combinations of N, P or S atoms, formed *via* bromo,[3,4] lithio[5,6] or stannyl[7,8] intermediates. These ligands are neutral in character and their preparations are often non-trivial. So far as we are aware, examples of unsymmetrical purely S-substituted neutral and neutral–anionic ferrocenediyl ligands (*i.e.* analogous to the hemilabile P/S$^-$,[9] P/O$^-$,[10,11] and N/O$^-$[12] ('SHOP') based-catalysts) are hitherto unknown. Here, we report the new and convenient syntheses of the first examples of these types of ligands and a preliminary study of their coordination chemistry which has led to the isolation and structural characterisation of a novel palladium dimer complex.

The new ligands **1**–**4** can be synthesised from the well known 1, 2, 3-trithia[3]ferrocenophane[13] (Scheme 1). By utilising an elegant method first described by Herberhold *et al*,[14] the trisulfur bridge can be cleaved by organolithium reagents to form (after air oxidation) bis(1′-organylthiolatoferrocenyl)disulfanes. Herberhold *et al.* have prepared the species RS–Fc–SS–Fc–SR (R = *n*-butyl, phenyl; Fc = 1,1′-ferrocenediyl), but during our research into the formation of redox-active and sterically hindered ligands for homogeneous catalysis, we reacted the ferrocenophane (1 equiv.) with mesityllithium (2 equiv.) and formed RS–Fc–SS–Fc–SR **1** (where R = mesityl). This species may be an interesting, sterically hindered ligand in its own right, but at present, we have concentrated on the formation of the monoferrocenediyl species **2**–**4**.† On reaction of **1** (1 equiv.) with lithium triethylborohydride (2.2 equiv.) in THF and after acid/base work-up, the air-sensitive orange solid **2** was isolated in 88% yield. ^{1}H NMR spectroscopy showed the unsymmetrical substitution of the cyclopentadienyl rings with the presence of signals due to S-mesityl, S–H and *four* pseudo triplets for the C_5H_4 ring protons.

A solution of **1** was also treated with methyllithium (2.2 equiv.) and the reaction mixture stirred for 16 h. Cleavage of the disulfide linkage was effected and the crude orange mixture obtained was washed, extracted and purified *via* column chromatography [neutral grade II alumina, CH_2Cl_2–hexane (1:4)] and **3** was isolated as an air- and moisture-stable orange oil (50%) (*N.B.* 25% of **1** was also isolated). The use at this stage of various organolithium reagents can of course, lead to derivatisation and a possible 'fine-tuning' of the steric and redox properties of the ligands. Finally, a solution of **1** (1 equiv.) in THF was treated with lithium triethylborohydride (2.2 equiv.) and stirred for 1.5 h. On evaporation to dryness, a dark red oily product **4** was formed in quantitative yield but was not isolated due to its unstable nature. As confirmation of its formation and as a preliminary investigation into its coordination chemistry, **4** was treated with *trans*-[Pd(PhCN)$_2$Cl$_2$] (2 equiv.) in toluene and heated to 60 °C for 16 h. Following work-up and crystallisation in CH_2Cl_2–hexane (1:1), the purple–black product **5** was isolated in 81% yield as a crystalline solid. The X-ray analysis of **5**‡ shows that the desired bidentate coordination of the ferrocenediyl species has been achieved. Surprisingly, however, a bridged dimer has been formed where, for each ligand, one of the sulfur atoms is binucleating and carries a formal negative charge whereas the other links to a single palladium ion and is formally neutral (Fig. 1). The complex has non-crystallographic C_2 symmetry about an axis passing through the centre of, and normal to the plane of, the Pd_2S_2 ring, *i.e.* both ferrocenediyl units lie on the same side of the two linked coordination planes. Each ferrocenediyl unit adopts a staggered conformation, their S–C_5H_4 bonds 'subtending' angles of 45 and 46° for Fe(1) and Fe(2), respectively. The two palladium coordination planes are folded by *ca.* 30° out of plane with respect to each other about the S(3)···S(4) vector. The transannular Pd···Pd and S···S distances in the central four-membered ring are 3.394 and 2.998 Å, respectively. The geometry at each palladium centre is distorted square planar with *cis* angles in the ranges 81.1(2)–101.9(2) and 81.0(2)–102.5(2)° at Pd(1) and Pd(2), respectively. The Pd–S distances fall into two distinct groups with those to the negatively charged bridging sulfurs sig-

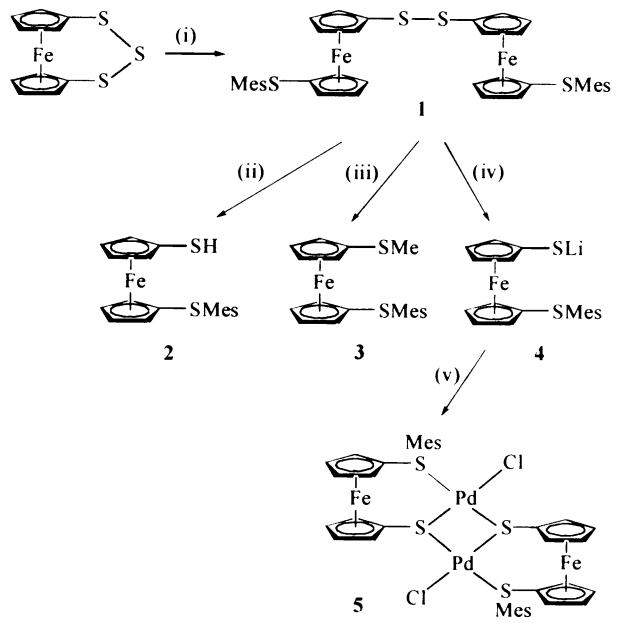

Scheme 1 *Reagents and conditions*: (i) 2 MesLi, THF, 20 h; (ii) 2.2 LiEt$_3$BH, THF, 1.5 h, H$^+$; (iii) 2.2 MeLi, THF, 16 h; (iv) 2.2 LiEt$_3$BH, THF, 1.5 h; (v) *trans*-[Pd(PhCN)$_2$Cl$_2$], toluene, 60 °C, 16 h.

DOI: 10.1039/b007511f

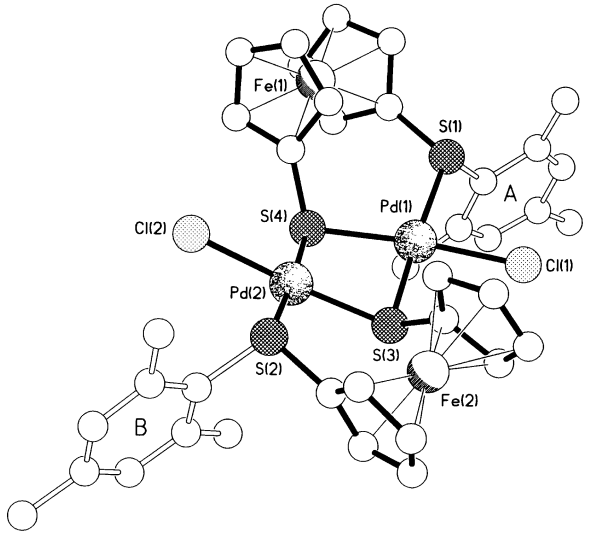

Fig. 1 The molecular structure of **5**. Selected bond lengths (Å) and angles (°); Pd(1)–Cl(1) 2.332(5), Pd(1)–S(1) 2.365(4), Pd(1)–S(3) 2.305(4), Pd(1)–S(4) 2.303(5), Pd(2)–Cl(2) 2.334(5), Pd(2)–S(2) 2.354(4), Pd(2)–S(3) 2.305(5), Pd(2)–S(4) 2.309(4); S(4)–Pd(1)–S(3) 81.1(2), S(4)–Pd(1)–S(1) 101.9(2), S(3)–Pd(1)–S(1) 176.1(2), S(3)–Pd(2)–S(4) 81.0(2), S(3)–Pd(2)–S(2) 102.5(2), S(4)–Pd(2)–S(2) 176.2(2), Pd(2)–S(3)–Pd(1) 94.8(2), Pd(1)–S(4)–Pd(2) 94.7(2).

nificantly shorter than those to the others. Surprisingly, the Pd–S bridge distances are symmetric, *i.e*. there is no *trans* influence of the chloride ligands. The complexes are linked by a combination of C–H···π and π–π interactions to form sheets that extend in the *ab* plane (Fig. 2). The space between adjacent parallel sheets is occupied by disordered dichloromethane molecules. This type of bridged system featuring a thioether/thiolate ligand appears to be unique, the only other similar species being a palladium dimer featuring bridging *di*thiolate ligands.[15]

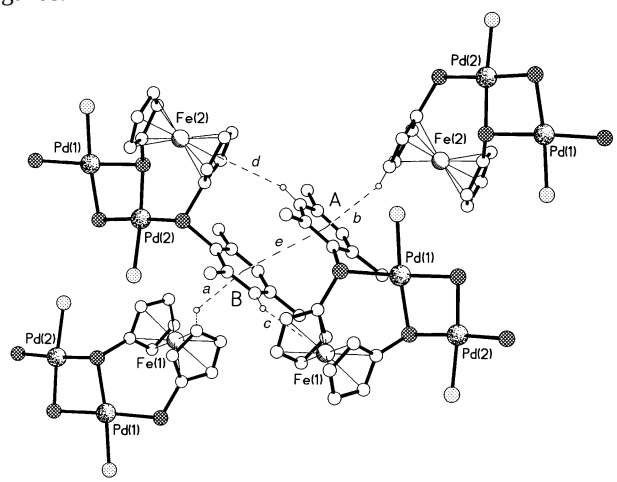

Fig. 2 Part of one of the C–H···π and π–π linked sheets of molecules present in the structure of **5**. The H···π distances (Å) and C–H···π angles (°) are (*a*) 2.76, 136; (*b*) 2.72, 141; (*c*) 2.79, 161; (*d*) 2.87, 159. The centroid···centroid and mean interplanar separations between rings **A** and **B** are (*e*) 3.98, 3.73 Å.

Work is in progress to explore the diverse coordination chemistry expected for these ligands and their role in homogeneous catalysis.

We acknowledge financial support from the EPSRC and Johnson Matthey plc are thanked for the loan of platinum salts.

Notes and references

† *Syntheses*: **2**: compound **1** (0.50 g, 0.65 mmol) was dissolved in dry, deoxygenated THF (30 cm^3) and to this lithium triethylborohydride (1 M solution in THF, 1.40 cm^3, 1.40 mmol) was added and the reaction mixture stirred for 1.5 h. The solvent was removed *in vacuo* and the residue then redissolved in diethyl ether. The dark red solution was poured onto dilute base (1% KOH) (20 cm^3), followed by dropwise addition of conc. HCl. The layers were separated and the aqueous layer extracted with diethyl ether (3 × 20 cm^3). The combined organic layers were dried ($MgSO_4$) and evaporated to dryness to leave an air-sensitive orange solid **2** (0.42 g, 88%); $\delta_H(CDCl_3)$ 2.21 (3H, s, CH_3), 2.47 (6H, s, CH_3), 2.98 (1H, s, SH), 4.10 (2H, t, C_5H_4), 4.21 (4H, t, C_5H_4), 4.33 (2H, t, C_5H_4), 6.86 (2H, s, C_6H_2); *m/z* 367 ($M - H^+$), 334 ($M - SH^+$).

3: a solution of **1** (0.58 g, 0.79 mmol) in THF (40 cm^3) was treated with methyllithium (1.6 M solution in diethyl ether, 1.1 cm^3, 1.74 mmol) and the reaction mixture stirred for 16 h. The solvent was evaporated *in vacuo*, the residue was dissolved in diethyl ether (50 cm^3) and water (10 cm^3) was added. The layers were separated and the aqueous layer extracted with diethyl ether (3 × 20 cm^3). The combined organic layers were dried ($MgSO_4$), then evaporated to dryness. The product was purified by column chromatography [neutral grade II alumina, CH_2Cl_2–hexane (20:80)] and after removal of the solvent, isolated as an orange oil (0.15 g, 50%); $\delta_H(CDCl_3)$ 2.24 (3H, s, CH_3), 2.34 (3H, s, SCH_3), 2.51 (6H, s, CH_3), 4.13 (2H, t, C_5H_4), 4.26 (4H, m, C_5H_4), 4.34 (2H, t, C_5H_4), 6.88 (2H, s, C_6H_2); *m/z* 382 (M^+), 367 ($M - CH_3^+$), 271 ($M - C_5H_4SCH_3^+$).

4 and **5**: a solution of **1** (0.10 g, 0.135 mmol) in THF (30 cm^3) was treated with lithium triethylborohydride (1 M solution in THF, 0.3 cm^3, 0.30 mmol) and the reaction stirred for 1.5 h. The air-sensitive dark red solution of **4** was formed in quantitative yield and due to its instability was reacted *in situ* without work-up. Thus, a toluene (30 cm^3) solution of **4** was treated with bis(benzonitrile)palladium(II) dichloride (0.103 g, 0.27 mmol) also in toluene (30 cm^3). There was an immediate darkening of the solution to deep purple and stirring at 60 °C was continued for 16 h. A black ppt. was filtered off and the filtrate washed with water (2 × 10 cm^3), dried ($MgSO_4$) and evaporated to dryness. The crude residue was washed with hot hexane (2 × 40 cm^3) and recrystallised from CH_2Cl_2–hexane (1:1) to leave a purple crystalline powder **5** (0.11 g, 81%); $\delta_H(CDCl_3)$ 2.16 (6H, s, CH_3), 2.41 (6H, s, CH_3), 3.29 (6H, s, CH_3), 4.07 (2H, m, C_5H_4), 4.28 (2H, m, C_5H_4), 4.44 (2H, m, C_5H_4), 4.57 (2H, m, C_5H_4), 4.60 (2H, m, C_5H_4), 4.66 (2H, m, C_5H_4), 5.07 (2H, m, C_5H_4), 6.80 (2H, m, C_6H_2), 6.93 (2H, s, C_6H_2); *m/z* 982 ($M - Cl^+$), 897 ($M - mes^+$).

‡ *Crystal data* for **5**: $C_{38}H_{38}S_4Cl_2Fe_2Pd_2{\cdot}3.5CH_2Cl_2$, M = 1315.6, monoclinic, space group $P2_1/c$ (no. 14), a = 16.411(4), b = 14.897(3), c = 22.093(4) Å, β = 95.06(1)°, V = 5380(2) Å^3, Z = 4, D_c = 1.624 g cm^{-3}, μ(Mo-Kα) = 18.2 cm^{-1}, $F(000)$ = 2620, T = 293 K; deep red plates, 6985 independent reflections, F^2 refinement to give R_1 = 0.078, wR_2 = 0.161 for 3473 independent observed absorption corrected reflections [$|F_o| > 4\sigma(|F_o|)$, $2\theta \leqslant 45°$], 560 parameters (the high R_1 is a consequence of crystal decomposition and disorder in the CH_2Cl_2 groups). The platinum analogue is isomorphous [a = 16.383(3), b = 14.875(2), c = 22.167(3) Å, β = 94.95(1)°, V = 5382(2) Å^3].[16]

CCDC 182/1826. See http://www.rsc.org/suppdata/cc/b0/b007511f/ for crystallographic files in .cif format.

1 For a detailed literature review, see: *Ferrocenes: Homogeneous Catalysis–Organic Synthesis–Materials Science*, ed. A. Togni and T. Hayashi, VCH, Weinheim, Germany, 1995; *Metallocenes*, ed. A. Togni and R. L. Haltermann, Wiley-VCH, Weinheim, Germany, 1998.
2 For a comprehensive overview of ferrocene and other metallocene chemistry, see: N. J. Long, in *Metallocenes: An Introduction to Sandwich Complexes*, Blackwell Science, Oxford, 1998.
3 T. Y. Dong and C.-K. Chang, *J. Chin. Chem. Soc.*, 1998, **45**, 577.
4 I. R. Butler, U. Griesbach, P. Zanello, M. Fontani, D. Hibbs, M. B. Hursthouse and K. L. M. A. Malik, *J. Organomet. Chem.*, 1998, **565**, 273.
5 I. R. Butler, *J. Organomet. Chem.*, 1997, **552**, 63.
6 N. J. Long, J. Martin, G. Opromolla, A. J. P. White, D. J. Williams and P. Zanello, *J. Chem. Soc., Dalton Trans.*, 1999, 1981.
7 G. A. Balavoine, J.-C. Daran, G. Iftiem, E. Manoury and C. Moveau-Bossuet, *J. Organomet. Chem.*, 1998, **567**, 191.
8 J. A. Adeleke, Y.-W. Chen and L.-K. Liu, *Organometallics*, 1992, **11**, 2443.
9 J. R. Dilworth, J. R. Miller, N. Wheatley, M. J. Baker and J. G. Sunley, *J. Chem. Soc., Chem. Commun.*, 1995, 1579.
10 U. Klabunde and S. D. Ittel, *J. Mol. Catal.*, 1987, **41**, 123.
11 W. Keim, R. Appel, S. Gruppe and F. Knoch, *Angew. Chem., Int. Ed. Engl.*, 1987, **26**, 1012.
12 S. Y. Desjardins, K. J. Cavell, J. L. Hoare, B. W. Skelton, A. N. Sobolev, A. H. White and W. Keim, *J. Organomet. Chem.*, 1997, **544**, 163.
13 J. J. Bishop, A. Davison, M. L. Katcher, D. W. Lichtenberg, R. E. Merrill and J. C. Smart, *J. Organomet. Chem.*, 1971, **27**, 241.
14 M. Herberhold, O. Nuyken and T. Pohlmann, *J. Organomet. Chem.*, 1991, **405**, 217.
15 R. Cao, M. Hong, F. Jiang and H. Liu, *Acta Crystallogr., Sect. C*, 1995, **51**, 1280.
16 V. C. Gibson, N. J. Long, A. J. P. White, C. K. Williams and D. J. Williams, unpublished results.

ChemComm

Hydroxyl radical induced decomposition of *S*-nitrosoglutathione

Veleeparambil M. Manoj and Charuvila T. Aravindakumar*

School of Chemical Sciences, Mahatma Gandhi University, Kottayam 686 560, Kerala, India.
E-mail: mgu@md2.vsnl.net.in

Received (in Cambridge, UK) 13th June 2000, Accepted 16th October 2000
First published as an Advance Article on the web

_S_-Nitrosoglutathione (GSNO) undergoes decomposition induced by hydroxyl radicals (·OH) in aqueous medium at neutral pH forming nitrite (NO_2^-) and glutathione disulfide (GSSG) and therefore it is proposed that ·OH could interfere in the GSNO metabolism.

S-Nitrosothiols (RSNO) are important class of compounds which are now believed to play a major role *in vivo* in connection with the storage and transport of nitric oxide (·NO) within the body.[1,2] The mechanism of the formation of RSNO from the reaction of ·NO with protein thiols in the presence and in the absence of oxygen is reasonably well understood.[3–6] The involvement of RSNOs in the storage and transport of ·NO within the body makes them potential candidates for medical applications. For example *S*-nitrosoglutathione (GSNO) is currently used to inhibit platelet aggregation during some operations.[7,8] Therefore, the kinetics and mechanism of the release of ·NO by RSNO is very important. Excellent reports on the kinetics and mechanism of the degradation of RSNO leading to the release of ·NO by metal ions and some nucleophiles are now available.[9,10] Reaction of *S*-nitrosocysteine (SNCys) with hydrogen peroxide yields peroxynitrite anion.[11] It is also reported that GSNO reacts with superoxide radicals ($O_2^{\cdot -}$) generating glutathione disulfide (GSSG) and equimolar quantities of nitrite and nitrate.[12]

Glutathione (GSH) is the most abundant sulfur-containing intracellular entity (cellular concentration *ca.* 5 mM) and therefore the endothelial nitric oxide has to diffuse through the cells in presence of GSH. This leads to the assumption that *in vivo* conditions, the most likely *S*-nitrosation product could be the GSNO.[13] Hydroxyl radicals (·OH) are the main DNA damaging agent which can be produced *in vivo* during oxidative stress and on exposure to ionizing radiations.[14] Understanding of the reaction between ·OH and GSNO is, therefore, a matter of utmost importance in a biological perspective. The present communication describes a novel reaction pathway for the decomposition of GSNO in presence of ·OH at neutral pH. To our knowledge, this is the first report on the reaction of ·OH with a possible reservoir for ·NO in biological systems.

One of the major difficulties involved in the ·OH reaction with RSNOs is that the components of most of the ·OH generating systems such as H_2O_2 photolysis, Fenton reaction, *etc*., themselves can induce degradation of RSNOs. In this context, radiation chemical method is an ideal choice where ionizing radiations such as γ-rays can radiolyze water and produce both oxidising and reducing radicals. Therefore, in the present work we have used radiation chemical technique to produce ·OH as shown in reactions (1) and (2).

$$H_2O \rightsquigarrow e_{aq}^-, H^{\cdot}, {}^{\cdot}OH, H_2, H_2O_2, H_3O^+ \quad (1)$$

$$N_2O + e_{aq}^- + H_2O \rightarrow {}^{\cdot}OH + OH^- + N_2 \quad (2)$$

The yields of various radicals and molecular products are normally expressed as *G*-values which are defined as the number of molecules formed or destroyed per 100 eV absorption of radiation energy, in SI units, the yields are, $G(^{\cdot}OH) \approx G(e_{aq}^-) \approx G(H_3O^+) = 0.28$, $G(^{\cdot}H) = 0.062$, $G(H_2O_2) = 0.072$ and $G(H_2) = 0.047$ μmol J^{-1}.[15] In the presence of N_2O the $G(^{\cdot}OH) = 0.56$ and $G(OH^-) = 0.28$ μmol J^{-1} as per reaction (2).

GSNO was synthesised from $NaNO_2$ in presence of HCl.[16] N_2O saturated solutions containing GSNO (10^{-3} M) and EDTA (10^{-4} M) at pH 7.3 were irradiated at different doses in a ^{60}Co-γ-source and the decay of GSNO was monitored by both UV–VIS spectrophotometry and HPLC. The unirradiated solution of GSNO was found to be stable for many hours when protected from light. The $G(-GSNO)$ values obtained in both cases were 0.53 and 0.54 μmol J^{-1} respectively. GSSG and nitrite were found to be the major products of radiolysis from the HPLC analysis. The decay of GSNO and the corresponding products build up are shown in Fig. 1. The calculated G(GSSG) and $G(NO_2^-)$ are 0.13 and 0.41 μmol J^{-1}, respectively. The pH of the solutions were determined before and after irradiation and a dose dependent reduction in pH was observed which is tabulated in Table 1. A blank solution without GSNO under similar conditions was also irradiated and obtained no major pH changes.

A good material balance can be observed from the G(GSSG) and $G(NO_2^-)$ values as $G(-GSNO) \approx G(GSSG) + G(NO_2^-)$. A minor contribution of NO_2^- is anticipated from the decay of peroxynitrite which could be formed as a result of the reaction of GSNO with H_2O_2 formed during radiolysis, as reported earlier.[11] However, this contribution is expected to be ⩽ 0.072 μmol J^{-1} [this value corresponds to $G(H_2O_2) = 0.072$ μmol J^{-1}]. Therefore, the major reaction is definitely between ·OH and GSNO. ·OH generally reacts with thiols including GSH by

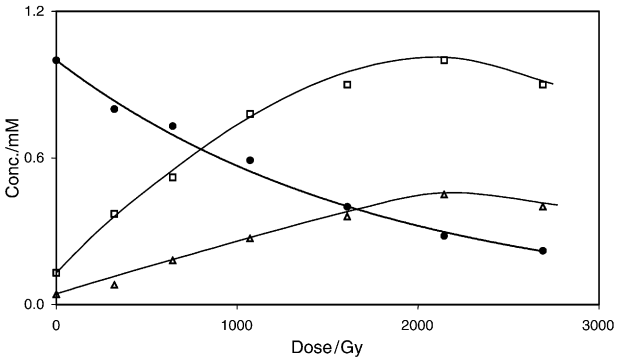

Fig. 1 Dose dependent decay of GSNO (●) at pH 7.3 and the corresponding formation of NO_2^- (□) and GSSG (Δ) determined by using HPLC (Column: 25 cm, Nucleosil, 5C-18; eluent: mixture of sodium phosphate (10^{-3} M) and sodium sulfate (10^{-2} M) in water; flow rate: 1 ml min^{-1}; λ = 210 nm).

Table 1 The observed pH changes in a γ-irradiated N_2O saturated solution containing GSNO (10^{-3} M) and EDTA (10^{-4} M) at different dose values

Dose/Gy	pH
0	7.3
525	5.9
1049	5.1
1574	4.8
2098	4.6
2728	4.1

DOI: 10.1039/b004706f

H-abstraction (from –SH) forming thiyl radicals ($RS^{\cdot}$) as the main intermediate as reported earlier.[17,18] Although the sulfur is bonded to NO in GSNO, the most potential site for $^{\cdot}OH$ attack is expected at the sulfur centre. On the other hand, the H-abstraction reaction which is reported in the case of GSH will not be possible in the present case. Therefore, based on the above observations we propose a reaction mechanism involving the attack of $^{\cdot}OH$ at the electron rich sulfur centre of GSNO [reactions (3)–(6)]. The initial attack of $^{\cdot}OH$ in GSNO (electron transfer) would produce a highly unstable cationic species as shown in reaction (3), which may lead to the breakage of the S–N bond and result in the formation of $GS^{\cdot}$ and NO^{+}. However, such a cationic intermediate ($GS^{+}NO$) is expected to be very short lived and no experimental evidence for its exact identity as well as its transnitrosation reaction [reaction (4)] is available at this moment. The subsequent reactions of NO^{+} with OH^{-} which is formed as shown in reaction (3), can lead to nitrite and H^{+} formation. The combination of two sulfur centered radicals ($RS^{\cdot}$) and the corresponding formation of disulfide (RSSR) is a well known reaction reported in the case of low molecular weight thiols.[19] Therefore, a similar radical–radical reaction of $GS^{\cdot}$ is proposed for the formation of GSSG.

$$GSNO + {}^{\cdot}OH \rightarrow [GS^{+}NO] + OH^{-} \quad (3)$$

$$[GS^{+}NO] \rightarrow GS^{\cdot} + NO^{+} \quad (4)$$

$$OH^{-} + NO^{+} \rightarrow H^{+} + NO_2^{-} \quad (5)$$

$$GS^{\cdot} \rightarrow \tfrac{1}{2}\,GSSG \quad (6)$$

Therefore, the overall reaction mechanism can be written as

$$GSNO + {}^{\cdot}OH \rightarrow \tfrac{1}{2}\,GSSG + NO_2^{-} + H^{+} \quad (7)$$

The dose dependent reduction in the pH values (Table 1) provides clear support to the above mechanism. Further, we exclude the possibility of the formation of nitrate as the reaction is carried out in N_2O saturated solutions where the presence of oxygen is insignificant.

In conclusion, the mechanistic aspects of the reaction of $^{\cdot}OH$ with GSNO, one among the biologically important *S*-nitrosothiols, have been proposed for the first time. The fast decay of GSNO in the presence of $^{\cdot}OH$ and the corresponding formation of nitrite and glutathione disulfide provide evidence for the possible interference of $^{\cdot}OH$ in the GSNO metabolism. One more question to be asked from these findings is, does GSNO have any sacrificial role like glutathione in terms of its protective role against oxidative stress? However, such a role can be established only after a clear understanding of the concentration of GSNO *in vivo* and of the exact rate constant of $^{\cdot}OH$ with GSNO, which are yet to be investigated. Our work is currently being concentrated in these directions.

We thank the Rubber Research Institute of India, Kottayam, for the γ-irradiation experiments. V. M. M. thanks the Nuclear Science Centre, New Delhi, for a fellowship. Part of the financial support for this work is from the Board of Research in Nuclear Sciences (BRNS), Govt. of India.

Notes and references

1 J. S. Stamler, O. Jaraki, J. Osborne, D. I. Simon, J. Keaney, J. Vita, D. Singel, C. R. Valeri and J. Loscalzo, *Proc. Natl. Acad. Sci. USA*, 1992, **89**, 76746.
2 B. Gaston, *Biochim. Biophys. Acta*, 1999, **1411**, 323.
3 V. G. Kharitonov, A. R. Sundquist and V. S. Sharma, *J. Biol. Chem.*, 1995, **270**, 28 158.
4 A. J. Gow, D. G. Buerk and H. Ischiropoulos, *J. Biol. Chem.*, 1997, **272**, 2841.
5 C. T. Aravindakumar, J. Ceulemans and M. De Ley, *Biochem. J.*, 1999, **344**, 253.
6 C. T. Aravindakumar, J. Ceulemans and M. De Ley, *Biophys. Chem.*, 2000, **85**, 1.
7 E. J. Langford, A. S. Brown, R. J. Wainwright, A. J. de Belder, M. R. Thomas, R. E. A. Smith, M. W. Radomski, J. F. Martin and S. Moncada, *Lancet*, 1994, **344**, 1458.
8 A. de Belder, C. Lees, J. Martin, S. Moncada and S. Campbell, *Lancet*, 1995, **345**, 124.
9 H. R. Swift and D. L. H. Williams, *J. Chem. Soc., Perkin Trans. 2*, 1997, 1933.
10 A. P. Munro and D. L. H. Williams, *J. Chem. Soc., Perkin Trans. 2*, 1999, 1989.
11 P. J. Coupe and D. L. H. Williams, *J. Chem. Soc., Perkin Trans. 2*, 1999, 1057.
12 J. David, T. M. Christie, F. L. Stephen, A. W. David and B. G. Matthew, *Biochem. Biophys. Res. Commun.*, 1998, **244**, 525.
13 J. S. Stamler, *Curr. Top. Microbiol. Immunol.*, 1995, **196**, 19.
14 C. von Sonntag, *The Chemical Basis of Radiation Biology*, Taylor & Francis, London, 1987.
15 J. W. Spinks and R. S. Wood, *An Introduction to Radiation Chemistry*, John Wiley & Sons, Inc., New York, 3rd edn., 1990.
16 T. W. Hart, *Tetrahedron Lett.*, 1985, **26**, 2013.
17 W. A. Armstrong and W. G. Humphries, *Can. J. Chem.*, 1967, **45**, 2589.
18 A. B. Ross, W. G. Mallard, W. P. Helman, G.V. Buxton, R. E. Hui and P. Neta, NDRL-NIST Solution Kinetics Database: ver.2.0, National Institute of Standards and Technology, Gaithersburg, MD, 1994.
19 W. A. Pryor, D. F. Church, C. K. Govindan and G. Gank, *J. Org. Chem.*, 1982, **47**, 159.

ChemComm

GUS-1: a mordenite-like molecular sieve with the 12-ring channel of ZSM-12†

Jacques Plévert,*‡[a] Yoshihiro Kubota,*[b] Takahisa Honda,[b] Tatsuya Okubo[a] and Yoshihiro Sugi[b]

[a] *Department of Chemical System Engineering, The University of Tokyo, Tokyo 113-8656, Japan. E-mail: JPlevert@asu.edu*

[b] *Department of Chemistry, Faculty of Engineering, Gifu University, Gifu 501-1193, Japan. E-mail: kubota@apchem.gifu-u.ac.jp*

Received (in Irvine, CA, USA) 26th June 2000, Accepted 12th September 2000
First published as an Advance Article on the web

The framework topology of the novel molecular sieve GUS-1 is reported; the crystalline architecture is characterized by a one-dimensional 12-membered ring channel system that is closely related to the channels of mordenite and ZSM-12.

The search for new microporous solids has shown some successes in recent years as the number of new topologies has doubled within a decade.[1] A key factor is the use of the structure-directing effects of organic species for generating new frameworks. We report here the structure of a novel molecular sieve GUS-1 using 1,1′-butylenedi(4-aza-1-azonia-2,5-dimethylbicyclo[2.2.2]octane) dihydroxide (**1**-hydroxide) as organic structure-directing agent (SDA).

The GUS-1-containing sample was synthesized under hydrothermal conditions. A synthesis mixture of composition $1SiO_2:0.1R^{2+}(OH^-)_2:0.1NaOH:50H_2O$, where the silica source was fumed silica (Cab-O-Sil M-5, Cabot), was heated at 150–175 °C statically under autogeneous pressure for 10–20 d. In order to remove the occluded organics, the sample was calcined at 700 °C for 6 h in air. R^{2+} stands for structure **1** and

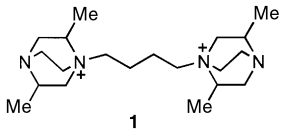

1

its hydroxide form, **1**-hydroxide, was prepared by refluxing 1,4-dibromobutane and excess 2,5-dimethyl-1,4-diazabicyclo[2.2.2]octane in acetone–methanol, followed by ion-exchange.§

The GUS-1 phase tends to come along with ZSM-12, and the synthesis of the new phase in pure form has not been successful so far. Synthesis under all-silica conditions gave a sample with relatively higher GUS-1 content, making structure elucidation of the new phase possible. Further synthetic details are forthcoming.

Structure determination of GUS-1 was carried out from synchrotron powder diffraction data. The powder pattern was collected at the X7A beamline at the National Synchrotron Light Source at Brookhaven Laboratory. The calcined sample was packed in a 1 mm capillary. Acquisition was carried out at room temperature at the wavelength λ = 1.196417 Å.

The reflections of GUS-1 were indexed using the program TREOR.[2] A solution was obtained in the orthorhombic system with lattice constants a = 16.411(2), b = 20.044(2), c = 5.0427(3) Å and figures of merit[3,4] $M(16)$ = 53 and $F(16)$ = 60(0.003,85), after refinement of the unit-cell. Systematic absences indicate C-centering and are consistent with the space groups *Cmmm* and subgroups, and possibly $C222_1$.

A weak, unindexed line is found at position d = 14.4 Å. The interplanar distance is characteristic of the (100) reflection of zeolite SSZ-31.[5] The other peaks of SSZ-31 are not visible in the powder pattern due to the high density of peaks and the structural relations between SSZ-31 and ZSM-12. The SEM pictures show a large number of particles with the typical needle shape of ZSM-12 crystals. Overgrowth of thin needles is observed on the crystallites of ZSM-12, which is assigned to GUS-1. A small number of particles with the fan-like morphology characteristic of SSZ-31 crystallites are also present in the sample.[5]

GUS-1 possesses a small *c*-axis, c = 5.0 Å, reducing the structure determination to a search of the two-dimensional projection of the zeolite into the *ab* plane of the cell. In addition, the N_2 adsorption measurements reveal that the adsorption isotherm of the sample containing the two phases, GUS-1 and ZSM-12, is very similar to the isotherm of pure ZSM-12, suggesting that the unknown phase is a molecular sieve with 12-ring channels too. Models have been built with *Cmmm* symmetry and 12-ring channels running along the *c*-axis. A good candidate was found showing the same projection as mordenite along the pore. The model contains four independent tetrahedral sites of equal multiplicity, in agreement with the ^{29}Si MAS NMR spectrum of the sample where three lines in the ratio 1:2:1 are observed in addition to the seven peaks of ZSM-12.[6]

An optimization of the geometry of the framework has been performed using a distance least squares (DLS)[7] refinement of the atomic positions in space group *Cmmm* and subgroups, assuming a distance $d_{Si–O}$ = 1.61 Å. The model refined in space group *Cmmm* shows a high residual R value, R_{DLS} 0.0150. However, typical R_{DLS} values are obtained for the subgroups *Cmm*2 and *C*222 where R_{DLS} = 0.0024 and 0.0029, respectively. A high R_{DLS} value indicates strong distortions of the framework in the presence of a reflection plane in the *ab* plane. The framework with *Cmmm* symmetry exhibits Si–O–Si bond angles of 180° due to the presence of a bridging oxygen atom on an inversion center. Straight Si–O–Si bond angles are recurrent in the mordenite group, as an oxygen atom is found on an identical symmetry element in mordenite[8] and dachiardite.[9] The 180° bond angle constraint is released by reducing the symmetry of the framework to *Cmm*2 or *C*222.

Further framework searches were performed using the program FOCUS.[10,11] The structure factors of the phase GUS-1 were extracted using the Lebail method[12] in the GSAS software[13] and normalized after estimation of the scale factor by a Wilson plot.

The mordenite-like structure found by model building was generated with the highest frequency. A variety of frameworks with 12-ring channels was also obtained. Most of them are derived from the same mordenite sheet but distorted with the bonds directed up or down at different nodes. All these solutions were discarded based on the poor match of their simulated powder pattern to the experimental data and the high R_{DLS} values.

The Rietveld refinement was performed with the two phases in approximate composition 40% GUS-1 and 60% ZSM-12. The impurity SSZ-31 was ignored during the refinement. The space group *C*222 was selected for the framework of GUS-1 and

† Electronic supplementary information (ESI) available: details of the synthesis of the SDA, crystal data and fractional atomic coordinates for GUS-1. See http://www.rsc.org/suppdata/cc/b0/b005225f/

‡ Current address: Department of Chemistry and Biochemistry, Arizona State University, Tempe, AZ 85287-1604, USA.

the initial atomic coordinates were the positions obtained from the DLS refinement. For ZSM-12 the powder pattern shows the superstructure reflections indicating the doubling of the *c* dimension. The space group is assumed *C*2/*c* and the atomic positions obtained by Fyfe *et al.* were used as starting model.[6] Peak broadening corrections due to particle size effects were applied for both phases. Soft geometric constraints on the Si–O distances were maintained for the two structures until the final stage of the refinement.

Fig. 1 shows a close fit between the calculated and the experimental powder pattern confirming the framework topology of GUS-1. The final residuals are R_{wp} = 7.4%, R_p = 5.5%, and the R_F factors for the individual phases are R_F = 9.8 and R_F = 7.9% for GUS-1 and ZSM-12 respectively.¶

The Si–O distances were maintained for both structures in the range 1.58–1.62 Å. For GUS-1 the averaged Si–O distance $d_{Si–O}$, is 1.60 Å and the Si–O–Si bond angles range from 136 to 169° with an average of 151°.

The Rietveld refinement performed for the space group *Cmm*2 for GUS-1 gave slightly higher *R* factors. The coexistence in the sample of two other phases (including the SSZ-31 impurity) probably introduces a bias in the structure refinement of GUS-1 as the line intensities cannot be properly estimated. It should be noted in particular that the Si–O distances reported by Fyfe *et al.* for the refinement from synchrotron data of all-silica ZSM-12 vary from 1.53–1.70 Å, suggesting that the structure model adopted for ZSM-12 is not completely satisfactory.[6] Therefore, the main result of the Rietveld refinement with the available data is the confirmation of the framework topology of GUS-1.

The structure of GUS-1 is shown in Fig. 2. GUS-1 is a molecular sieve with one-dimensional, 12-ring channels running along the *c*-axis. The projection of the structure in the *ab* plane is similar to the projection of mordenite along the pores [Fig. 2(a)]. GUS-1 shows also common features with ZSM-12. Both structures have the same framework density, *TD* = 19.3 Si atoms per nm^3, have a short axis with a repeat unit of *ca.* 5 Å and possess the same secondary building unit $4^2 5^4 6^2$ [Fig. 2(b)]. But the most striking similarity is the channel structure: both zeolites have an identical channel net composed of six-rings only [Fig. 2(c)]. The channel aperture of GUS-1 is elliptical in shape with deformation from circular shape intermediate between mordenite and ZSM-12. The minor and major free diameters are 5.6 and 7.0 Å, respectively, calculated in the topological symmetry *Cmmm*, with an oxygen radius 1.35 Å.[1]

It is worth mentioning that linear faults along the pore direction have been found in mordenite.[14–16] Different strain-free structures related to mordenite can be obtained by half unit-cell shifts of the four-ring columns along the *c*-axis.[17,18] A simple model describes the faulting as a one-half shift of the *c*-axis,[14,16] which leads to the formation of units $4^2 5^4 6^2$ [Fig. 2(b)]. The framework of mordenite can adopt locally the GUS-1 topology in a highly defective sample by gathering of faults.

In summary, the crystal structure of a new high-silica microporous solid has been elucidated from the synchrotron powder X-ray diffraction data of a mixture of phases. The new framework GUS-1 has symmetrical topology *Cmmm* and shows structural relationships with both mordenite and ZSM-12 frameworks. The formation of ZSM-12 in the presence of GUS-1 may be partly due to the instability of the present SDA.‖ The search for a new SDA that is more stable and suitable for GUS-1 formation is now in progress.

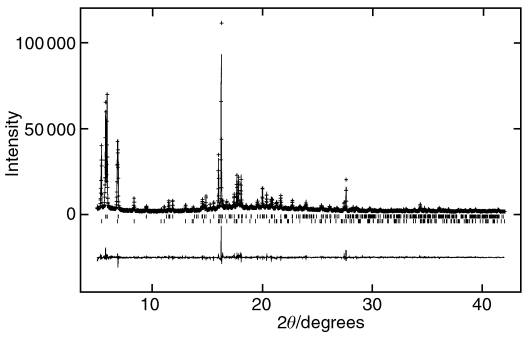

Fig. 1 Observed and calculated synchrotron powder X-ray diffraction pattern of the calcined mixture 40% GUS-1 and 60% ZSM-12 (λ = 1.196417 Å). The upper vertical bars correspond to the peak positions of ZSM-12 and the lower bars represent the peak positions for GUS-1.

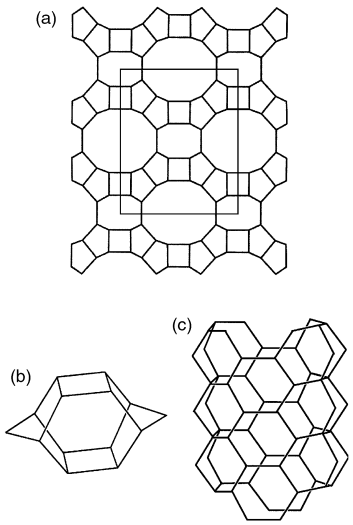

Fig. 2 Structure of GUS-1. (a) projection of the GUS-1 net onto the *ab* plane, (b) the secondary building unit $4^2 5^4 6^2$ and (c) the six-ring net channel.

The authors gratefully acknowledge Dr P. Wagner for collecting the synchrotron data. J. P. thanks Dr T. Tatsumi for providing an opportunity to work at the University of Tokyo and Dr M. O'Keeffe for helpful discussions. Y. K. thanks Dr M. E. Davis for suggestions and Mr M. Ogawa for supplying the precursor of SDA. Y. S. thanks NEDO for financial support.

Notes and references

§ The SDA **1** in both bromide and hydroxide forms gave reasonable ^{1}H and ^{13}C NMR spectra. On a spectroscopic basis, the purity of the SDA was ⩾90% just before use.

¶ CCDC 182/1782. See http://www.rsc.org/suppdata/cc/b0/b005225f/ for crystallographic data in .cif format.

‖ Obvious formation of an allylpiperazine moiety was observed in the ^{13}C CP MAS NMR spectrum of the as-synthesized sample, indicating that some partial decomposition *via* the Hofmann elimination had occurred.

1 W. M. Meier, D. H. Olson and C. Baerlocher, *Atlas of Zeolite Structure Types*, Butterworth-Heinemann, London, 4th rev. edn., 1996.
2 P. E. Werner, L. Eriksson and M. Westdahl, *J. Appl. Crystallogr.*, 1985, **18**, 367.
3 P. M. De Wolff, *J. Appl. Crystallogr.*, 1968, **1**, 108.
4 G. S. Smith and R. L. Snyder, *J. Appl. Crystallogr.*, 1979, **12**, 60.
5 R. F. Lobo, M. Tsapatis, C. C. Freyhardt, I. Chan, C. Y. Chen, S. I. Zones and M. E. Davis, *J. Am. Chem. Soc.*, 1997, **119**, 3732.
6 C. A. Fyfe, H. Gies, G. T. Kokotailo, B. Marler and D. E. Cox, *J. Phys. Chem.*, 1990, **94**, 3718.
7 C. Baerlocher, A. Hepp and W. M. Meier, DLS-76: A Program for Simulation of Crystal Structures by Geometric Refinement, ETH, Zürich, Switzerland, 1977.
8 W. M. Meier, *Z. Kristallogr.*, 1961, **115**, 439.
9 G. Gottardi and W. M. Meier, *Z. Kristallogr.*, 1963, **119**, 53.
10 R. W. Grosse-Kunstleve, PhD thesis, ETH, Zürich, 1996.
11 R. W. Grosse-Kunstleve, L. B. McCusker and Ch. Baerlocher, *J. Appl. Cryst.*, 1997, **30**, 985.
12 A. Lebail, H. Duray and J. L. Fourquet, *Mater. Res. Bull.*, 1988, **23**, 447.
13 A. C. Larson and R. Von Dreele, Generalized Structure Analysis System, Report LAUR 86-748 Los Alamos National Laboratory, NM, USA, 1990.
14 W. J. Mortier, J. J. Pluth and J. V. Smith, *Mater. Res. Bull.*, 1975, **10**, 1319.
15 J. V. Sanders, *Zeolites*, 1985, **5**, 81.
16 P. R. Rudolf and J. M. Garces, *Zeolites*, 1994, **14**, 137.
17 I. S. Kerr, *Nature*, 1963, **197**, 1194.
18 J. D. Sherman and J. M. Bennett, *Molecular Sieves*, A.C.S. Washington, D.C., 1973, p. 52.

ChemComm

Preparation of a high surface area microporous carbon having the structural regularity of Y zeolite

Zhixin Ma, Takashi Kyotani* and Akira Tomita

Institute for Chemical Reaction Science, Tohoku University, 2-1-1 Katahira, Sendai, Japan 980-8577. E-mail: kyotani@icrs.tohoku.ac.jp

Received (in Cambridge, UK) 2nd August 2000, Accepted 24th October 2000
First published as an Advance Article on the web

An ordered microporous carbon that preserves the structural regularity of Y zeolite has been prepared by a template carbonization technique using Y zeolite.

The synthesis of porous carbon materials is of great importance for both practical and fundamental reasons. The recent development of industrial technology requires porous carbons to have a tailored pore structure. The importance of pore structure control has been pointed out for applications such as electrode materials for electric double-layer capacitors and adsorbents for methane storage. To meet the requirements, many novel approaches to control pore structure have been proposed. The detailed features of these techniques have been recently reviewed by Kyotani.[1] One of the most important and elegant techniques is a template carbonization method,[2–7] which utilizes the inorganic templates whose opening or pores are controlled at the nanometer level. We demonstrated that porous carbons with a surface area as high as 2200 $m^2\ g^{-1}$ could be prepared using Y zeolite as a template.[8] There were also a few other reports on such carbon formation in zeolite channels.[9,10] Recently, two Korean research groups have independently obtained mesoporous carbon with ordered structure using mesoporous silica (MCM-48) as a template.[11,12] Their works are the first example of synthesizing an ordered mesoporous carbon. However, none of these porous carbons has a regular microporous structure. Here, by filling as much carbon as possible into the channels of Y zeolite template, we attempted to prepare an ordered microporous carbon that retains the structural regularity of Y zeolite. The obtained microporous carbon has a periodical ordering of 1.4 nm, which is the same as the spacing of (111) plane of Y zeolite.

A two-step method was used in the preparation of carbon material. In the first step, dry Y zeolite powder (Na-form, $SiO_2/Al_2O_3 = 5.6$, Tosoh Inc., HSZ-320NAA) was impregnated with furfuryl alcohol (FA) under reduced pressure at room temperature. The mixture of FA and zeolite powder was stirred for 5 days and then filtered, followed by washing the product with mesitylene. The FA/zeolite composite was placed in a vertical quartz reactor and FA was polymerized in zeolite by heating the composite at 150 °C under N_2 flow. The resultant PFA (polyfurfuryl alcohol)/zeolite composite was heat-treated at 700 °C for 4 h to carbonize the polymer in the zeolite channels. After this first carbon filling, the reactor temperature was raised to 800 °C and then propylene gas (2.0% in N_2) was passed through the reactor for 4 h. This second step resulted in pyrolytic carbon deposition into the remaining opening of the composite. After the propylene CVD, the zeolite framework in the carbon/zeolite composite was dissolved by successive washing with HF and HCl solution. Carbon was obtained as an insoluble fraction. The elemental analysis of the carbon was as follows: C, 94 wt%; H, 2 wt%; O, 4 wt% (difference). The ash content was nearly zero with an experimental error of ±0.1 wt%, indicating almost perfect removal of zeolite template.

The crystallinity and the microscopic features of the carbon were examined using an X-ray diffractometer (XRD, Shimadzu, XD-D1, Cu-Kα radiation) and transmission electron microscopy (TEM, JEOL, JEM-2010). The pore structure was investigated with an automatic volumetric sorption analyzer (Quantachrome, Autosorb-1) using N_2 as the adsorbate at −196 °C. The micropore and mesopore volumes were determined from methods describe elsewhere.[8]

Fig. 1 shows the XRD patterns of the original Y zeolite and the carbon liberated from the carbon/zeolite composite. The former pattern [Fig. 1(a)] is characterized by the appearance of many sharp peaks due to the framework topology of Y zeolite. Among these peaks, the strongest appearing at $2\theta = 6.19°$ can be indexed as the diffraction from the (111) plane. In the XRD pattern of the carbon [Fig. 1(b)], a sharp peak appeared at $2\theta = 6.26°$, together with a very broad and weak peak in the range $2\theta = 23–27°$. This type of broad peak is often observed as the (002) diffraction from carbonaceous materials with poor crystallinity. However, a sharp peak at 2θ *ca.* 6° as observed in Fig. 1(b) has not, to our knowledge, been reported. The presence of the sharp peak indicates that this carbon has a long-range ordering with a periodicity of 1.41 nm, almost the same as the spacing of the (111) plane in Y zeolite (1.43 nm). The presence of such periodical ordering was further confirmed by the lattice fringe image discussed below.

From TEM observation, it was found that each carbon particle consists of a thin and dense envelope with straight lattice fringes present inside each envelope. Fig. 2(a) shows a typical image of lattice fringes, which run along the envelope located on the upper part of this picture. The regular spacing of the observed lattice planes is about 1.3 nm and the diffraction from these planes was clearly observed as a pair of sharp spots in the corresponding electron diffraction pattern [Fig. 2(b)].

Taking the results of our previous work[8] into consideration, we can ascribe the envelopes observed in the particles to the carbon deposited on the external surface of the zeolite particles. When we prepared porous carbon with a shorter CVD period (2 h), many of the resultant carbon particles had no envelope

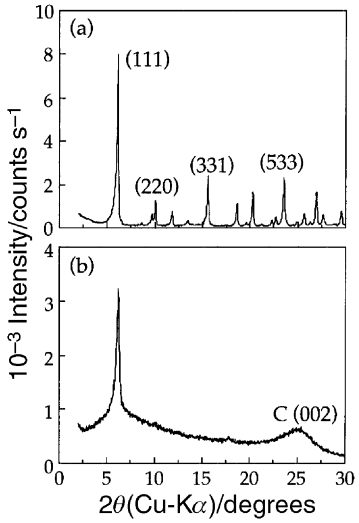

Fig. 1 XRD patterns of Y zeolite (a) and carbon liberated from the carbon/zeolite composite (b).

DOI: 10.1039/b006295m

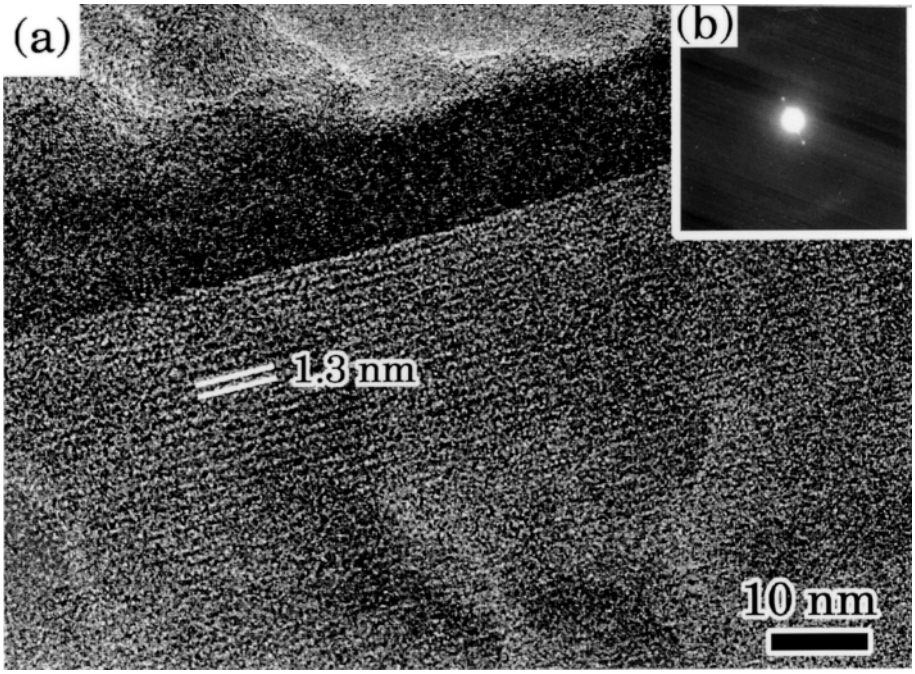

Fig. 2 (a) High-resolution TEM image of part of a carbon particle. (b) Electron diffraction pattern taken from the image of (a).

and the XRD pattern of this carbon did not show such a broad (002) XRD peak as in Fig. 1(b). This finding indicates that the broad XRD peak arises from the envelopes and there is no stacking structure of (002) layers in the ordered carbon.

Fig. 3 shows a N_2 adsorption–desorption isotherm of the carbon. In the relative pressure range of >0.2, the isotherm shows an almost flat sorption characteristic. Furthermore, there is almost no hysteresis loop in the isotherm. These findings clearly indicate the absence of mesoporosity in the carbon. The BET surface area, the micropore and mesopore volumes were calculated from this isotherm to be 1910 $m^2\ g^{-1}$, 1.1 $cm^3\ g^{-1}$ and 0 $cm^3\ g^{-1}$, respectively. In our previous study,[8] we prepared high surface area carbons by a one-step carbon filling method, *via* propylene CVD over Y zeolite. The resultant carbons had both micro- and meso-porosity. The porosity of the carbon obtained here, however, shows highly developed microporous structure without any mesopores.

In conclusion, a microporous carbon with a long-range periodic ordering (d = 1.4 nm) has been synthesized for the first time. Such structural periodicity in the carbon would originate from the structural ordering in Y zeolite. It is well known that Y zeolite consists of a tetrahedral network structure of sodalite units, which results in a supercage, *i.e.* a large cavity with a diameter of 1.3 nm. Each supercage is connected to four other supercages by an opening with a diameter of 0.74 nm. Due to this framework topology, many sharp XRD peaks appeared as in Fig. 1(a). However, the carbon gave only one sharp XRD peak at the angle corresponding to the (111) diffraction [Fig. 2(b)]. No other peak was observed at the angles where sharp peaks from the zeolite appeared. This implies that the carbon retains only the structural ordering of (111) plane stacking of Y zeolite.

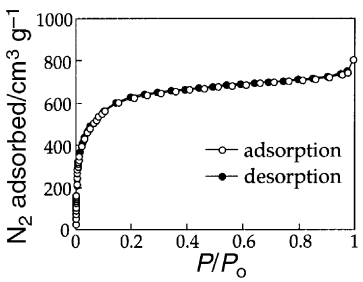

Fig. 3 N_2 adsorption–desorption isotherm at −196 °C for the carbon. The adsorption and desorption curves are plotted using open and filled circles, respectively.

The formation of the ordered microporous carbon suggests that the amount of carbon filled into the zeolite channels by the present method was sufficient to preserve the network structure reflecting the zeolite template. Also, if one can fill zeolite channels with a sufficient amount of carbon for other types of zeolites with three-dimensional structures such as ZSM-5, ZMS-11 and A zeolite, this opens up a possibility for the preparation of a series of microporous carbons having the structural regularity of template zeolites.

We thank the High Voltage Electron Microscope Laboratory of Tohoku University for microscopical analysis. This work was partly supported by the Grant-in-Aid for Scientific Research on the Priority Area 'Fullerene and Nanotubes' by the Ministry of Education, Science, and Culture of Japan.

Notes and references

1 T. Kyotani, *Carbon*, 2000, **38**, 269.
2 T. Kyotani, N. Sonobe and A. Tomita, *Nature*, 1988, **331**, 331.
3 T. Bandosz, K. Putyera, J. Jagiello and J. A. Schwarz, *Carbon*, 1994, **32**, 659.
4 M. T. Gilbert, J. H. Knox and B. Kaur, *Chromatographia*, 1982, **16**, 138.
5 A. A. Zakhidov, R. Baughman, Z. Iqbal, C. Cui, I. Khayrullin, S. O. Dantas, J. Marti and V. G. Ralchenko, *Science*, 1998, **282**, 897.
6 T. Kyotani, L. Tsai and A. Tomita, *Chem. Mater.*, 1995, **7**, 1427.
7 G. Che, B. B. Lakshmi, C. R. Martin, E. R. Fisher and R. S. Ruoff, *Chem. Mater.*, 1998, **10**, 260.
8 T. Kyotani, T. Nagai, S. Inoue and A. Tomita, *Chem. Mater.*, 1997, **9**, 609.
9 S. A. Johnson, E. S. Brigham, P. J. Ollivier and T. E. Mallouk, *Chem. Mater.*, 1997, **9**, 2448.
10 J. Rodriguez-Mirasol, T. Cordero, L. R. Radovic and J. J. Rodriguez, *Chem. Mater.*, 1998, **10**, 550.
11 R. Ryoo, S. H. Joo and S. Jun, *J. Phys. Chem. B*, 1999, **103**, 7743.
12 J. Lee, S. Yoon, T. Hyeon, S. M. Oh and K. B. Kim, *Chem. Commun.*, 1999, 2177.

Synthesis and structures of carbonyl adducts of the boranes $B(BX_2)_3$ (X = F, Cl)

John C. Jeffery, Nicholas C. Norman, Jennifer A. J. Pardoe and Peter L. Timms*

The University of Bristol, School of Chemistry, Bristol, UK BS8 1TS. E-mail: peter.timms@bris.ac.uk

Received (in Cambridge, UK) 14th September 2000, Accepted 18th October 2000
First published as an Advance Article on the web

The borane carbonyl adduct $(Cl_2B)_3BCO$ has been prepared and characterised by spectroscopic methods and X-ray crystallography and is compared with the fluorine analogue $(F_2B)_3BCO$ which has also been structurally characterised by X-ray crystallography.

In recent years the study of carbon monoxide as a ligand has attracted renewed attention largely as a result of the discovery and characterisation of many so-called 'non-classical metal carbonyls' for which metal to CO π-backbonding is thought to be absent or at least much reduced in comparison with more classical species.[1] These compounds merit comparison with the few known boron carbonyl complexes such as the borane carbonyls H_3BCO,[2]† B_4H_8CO,[4] and $(F_2B)_3BCO$ **1** prepared by

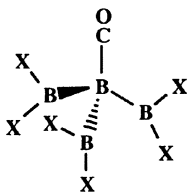

1, X = F; **2**, X = Cl

Timms,[5,6] the related silicon containing species $(Cl_3Si)_2(Cl_2B)BCO$,[7] and the osmium cluster complex $[Os_3(CO)_9(\mu\text{-}H)_3(\mu_3\text{-}BCO)]$ prepared by Shore *et al.*[8] Herein we report the X-ray structure of **1** and the preparation and X-ray structure of the chloro analogue $(Cl_2B)_3BCO$ **2**.

Compound **2** was prepared by two methods. In the first instance, BCl_3 was passed through a column of boron granules contained in a graphite tube inductively heated to *ca.* 2000 °C under high vacuum, using an apparatus slightly modified from that described for the preparation of BF.[5,6] The hot vapour emerging from the graphite tube, believed to be a mixture of BCl and BCl_3 in a mole ratio of about 1 : 3, was then condensed on the liquid nitrogen cooled walls of the surrounding vacuum vessel. When the condensate was allowed to warm to room temperature with continuous pumping through a cold trap, a mixture of BCl_3 and B_2Cl_4 was collected; no B_4Cl_4 was detected in contrast to earlier studies involving BCl.[9] However, when a similar experiment was carried out in which the condensate was allowed to warm to room temperature in the presence of a 3×10^4 Pa pressure of CO, the resulting volatiles comprised not only BCl_3 and B_2Cl_4 but also the white crystalline solid **2**.

Spectroscopic data for **2** were consistent with the formula $(Cl_2B)_3BCO$‡ which was confirmed by X-ray crystallography (*vide infra*). The formation of **2** in the above experiment may involve the intermediacy of $(Cl_2B)_2BCl$, just as the condensation of BF is known to yield $(F_2B)_2BF$ which, in the presence of CO, gives **1** and B_2F_4.[5] Compound **2** was also prepared in a more direct manner and in essentially quantitative yield by treating **1** (prepared as described in ref. 5) with an excess of BCl_3 vapour for a few minutes at room temperature.

The structures of both **1** and **2** were determined by X-ray crystallography.§ Compound **1** crystallises with two molecules in the asymmetric unit one of which is shown in Fig. 1. Compound **2** resides on a crystallographic C_3 axis and part of the crystal structure is shown in Fig. 2. On a molecular level, the structures are very similar and also similar to that reported for the PF_3 analogue of **1**, $(F_2B)_3BPF_3$.[11] The central boron atoms in each structure are all within a degree of being tetrahedral and the B–B bond lengths [1.677(5)–1.690(5) Å for **1** and 1.694(7)

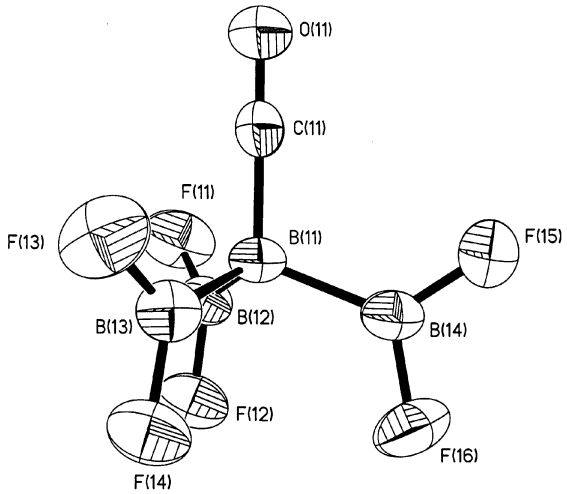

Fig. 1 A view of one of the crystallographically independent molecules of **1**. Ellipsoids are drawn at the 40% level. Bond lengths (Å) and angles (°) for the molecule shown: C(11)–O(11) 1.117(3), C(11)–B(11) 1.522(5), B(11)–B(12) 1.677(5), B(11)–B(13) 1.690(5), B(11)–B(14) 1.681(5), B(12)–F(11) 1.310(4), B(12)–F(12) 1.311(4), B(13)–F(13) 1.317(4), B(13)–F(14) 1.305(4), B(14)–F(15) 1.315(4), B(14)–F(16) 1.302(4); O(11)–C(11)–B(11) 178.8(3), C(11)–B(11)–B(12) 109.6(3), C(11)–B(11)–B(13) 109.3(3), C(11)–B(11)–B(14) 110.5(3), B(12)–B(11)–B(13) 109.5(3), B(12)–B(11)–B(14) 109.9(3), B(13)–B(11)–B(14) 108.0(3), B(11)–B(12)–F(11) 124.9(3), B(11)–B(12)–F(12) 121.1(3), F(11)–B(12)–F(12) 114.0(3), B(11)–B(13)–F(13) 124.3(3), B(11)–B(13)–F(14) 121.8(3), F(13)–B(13)–F(14) 113.9(3), B(11)–B(14)–F(15) 125.0(3), B(11)–B(14)–F(16) 121.5(4), F(15)–B(14)–F(16) 113.5(3).

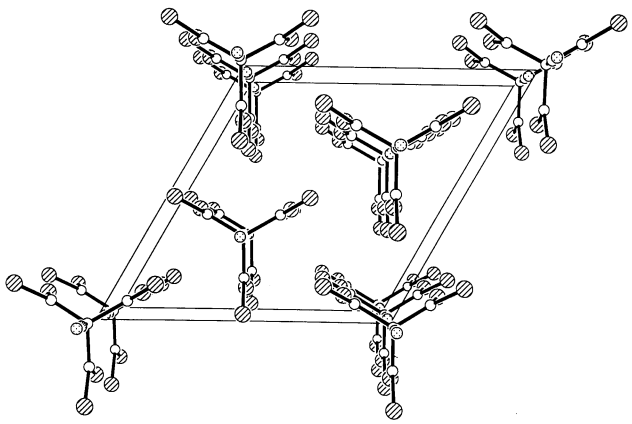

Fig. 2 The crystal structure of **2** viewed down the *c* axis. Bond lengths (Å) and angles (°): C(1)–O(1) 1.091(14), B(1)–C(1) 1.544(15), B(1)–B(2) 1.694(7), B(2)–Cl(1) 1.748(7), B(2)–Cl(2) 1.748(7), O(1)–C(1)–B(1) 180, C(1)–B(1)–B(2) 107.3(4), B(2)–B(1)–B(2a) 111.5(4), B(1)–B(2)–Cl(1) 122.0(5), B(1)–B(2)–Cl(2) 121.9(5), Cl(1)–B(2)–Cl(2) 116.1(4).

DOI: 10.1039/b007484p

Å for **2**] are of the same order as those observed in $(F_2B)_3BPF_3$ [1.677(15) Å][11] and B_2F_4 [1.67(4) Å].[12] The B–F bonds in **1** range from 1.302(4) to 1.317(4) Å [*cf.* 1.30, 1.32(3) and 1.305(15) for BF_3,[13] B_2F_4[12] and $(F_2B)_3BPF_3$[11] respectively] whilst the two B–Cl bond lengths in **2** [1.748(7) Å] are similar to other B–Cl bond distances for trigonal planar boron.[14] Both **1** and **2** have C_{3v} symmetry, crystallographically constrained in the latter case, such that the three BX_2 planes lie parallel to the BCO axis. Despite the similarity in the molecular structures, however, **1** and **2** pack differently in the solid state. Thus, although there are no close intermolecular contacts in either structure, **1** [and $(F_2B)_3BPF_3$] crystallises in a centrosymmetric space group $P2_1/n$ [*Pnma* for $(F_2B)_3BPF_3$] whereas **2** crystallises in the polar space group *R*3*m* with all BCO vectors aligned along the crystallographic *c* axis.

The CO stretching frequencies for **1** (2162 cm^{-1})[5] and **2** (2176 cm^{-1}) are both higher than that of free CO (2143 cm^{-1}) but are close to those observed in many non-classical metal carbonyls[1] and in $(Cl_3Si)_2(Cl_2B)BCO$.[7] Such values are often characteristic of non-classical carbonyls and are associated with increased σ-donation and little if any π-donation into the CO π*-orbitals[1,3] (electrostatic effects are also thought to be important[3]). As expected, both **1** and **2** have C–O bond lengths which appear to be shorter than CO itself [**1**, 1.117(3), 1.116(3) Å; **2**, 1.091(14) Å; CO, 1.1281 Å]. However, given the relatively large esds involved, such comparisons must be made with due caution.

In conclusion, we note that the synthesis of **2** and the structures of **1** and **2** provide a significant contribution to what is known about CO adducts of boron and to the study of non-classical CO complexes in general. Both **1** and **2** are stable to CO loss and future studies, both theoretical and experimental, will address the magnitude of the B–C bond dissociation energy.

We thank the EPSRC for support and for a studentship (J. A. J. P.).

Notes and references

† A recent and comprehensively referenced theoretical analysis of the bonding and stability of the compounds H_3BCO, F_3BCO and $(C_6F_5)_3BCO$ has been carried out by Berke and Erker *et al*.[3] where the analogy between borane carbonyls and non-classical metal carbonyls is also addressed.

‡ *Spectroscopic data* for **2**: ^{11}B NMR (CD_2Cl_2) δ 68.2 [br s, 3B, $(Cl_2B)_3BCO$], −20.7 [br s, 1B, $(Cl_2B)_3BCO$] (referenced to $BF_3{\cdot}Et_2O$). IR (thin film on AgCl window) ν(CO) 2176 cm^{-1}. Mass spectrum (EI), *m/z* 166 (B_3Cl_3CO), 221 (B_4Cl_5), 249 (B_4Cl_5CO) all with correct isotope patterns.

§ A suitable single crystal of **1** was prepared inside a Lindemann tube by condensing its vapour into the tube, sealing it under vacuum and cycling the temperature between 20 and 35 °C. A colourless needle crystal of **2** was grown under vacuum at 4 °C and transferred and sealed under nitrogen in a Lindemann tube prior to mounting on the diffractometer. Both compounds are pyrophoric.

Crystal data: for **1**: CB_4F_6O, M = 185.25, monoclinic, space group $P2_1/n$ (no. 14), a = 10.909(3), b = 11.518(3), c = 11.098(3) Å, β = 90.548(18)°, U = 1394.4(6) $Å^3$, Z = 8, D_c = 1.765 Mg m^{-3}, λ = 0.71073 Å, μ(Mo-Kα) = 0.218 mm^{-1}, F(000) = 704, T = 292(2) K.

For **2**: CB_4Cl_6O, M = 283.95, rhombohedral on hexagonal axes, space group *R*3*m* (no. 160), a = 11.150(5), c = 7.586(4) Å, U = 816.8(7) $Å^3$, Z = 8, D_c = 1.732 Mg m^{-3}, λ = 0.71073 Å, μ(Mo-Kα) = 1.520 mm^{-1}, F(000) = 1700, T = 292(2) K.

Data for both structures were collected on a Siemens SMART diffractometer over the range $2.55 < \theta < 27.51°$ for **1** and $3.42 < \theta < 27.51°$ for **2**. The structures were solved by direct methods using SHELXL97[10] and refined by least squares methods against all 2363 F^2 values with $F^2 > -3\sigma(F^2)$ to $wR2$ = 0.1102 [$R1$ = 0.0419 for 1117 data with $F^2 > 2\sigma(F^2)$] for **1** and all 316 F^2 values with $F^2 > -3\sigma(F^2)$ to $wR2$ = 0.0939 [$R1$ = 0.0391 for 280 data with $F^2 > 2\sigma(F^2)$].

Both crystals suffered significant degradation during the later stages of data collection owing to the propensity of the two compounds to sublime at room temperature and for this reason only the first set of frames in each data set were used in solving the structures. Because of the extreme sensitivity of both compounds they were mounted in Lindemann tubes rather than in frozen oil drops which, owing to the nature of the diffractometer cooling apparatus, precluded data collection at low temperature.

CCDC 182/1824. See http://www.rsc.org/suppdata/cc/b0/b007484p/ for crystallographic files in .cif format.

1 A. J. Lupinetti, G. Frenking and S. H. Strauss, *Angew. Chem., Int. Ed.*, 1998, **37**, 2113; S. H. Strauss, *J. Chem. Soc., Dalton Trans.*, 2000, 1; A. J. Lupinetti, G. Frenking and S. H. Strauss, *Prog. Inorg. Chem.*, 2000, in press.
2 A. B. Burg and H. I. Schlesinger, *J. Am. Chem. Soc.*, 1937, **59**, 780.
3 H. Jacobsen, H. Berke, S. Döring, G. Kehr, G. Erker, R. Fröhlich and O. Meyer, *Organometallics*, 1999, **18**, 1724.
4 A. B. Burg and J. R. Spielman, *J. Am. Chem. Soc.*, 1959, **81**, 3470; J. R. Spielman and A. B. Burg, *Inorg. Chem.*, 1963, **2**, 1139.
5 P. L. Timms, *J. Am. Chem. Soc.*, 1967, **89**, 1629.
6 P. L. Timms, *Acc. Chem. Res.*, 1973, **6**, 118.
7 R. W. Kirk, D. L. Smith, W. Airey and P. L. Timms, *J. Chem. Soc., Dalton Trans.*, 1972, 1392.
8 S. G. Shore, D.-Y. Jan, L.-Y. Hsu and W.-L. Hsu, *J. Am. Chem. Soc.*, 1983, **105**, 5923.
9 P. L. Timms, *Cryochemistry*, ed. M. Moskovits and G. A. Ozin, Wiley-Interscience, New York, 1976, p. 108.
10 G. M. Sheldrick, SHELXL97, Program for Crystal Structure Determination, University of Göttingen, Göttingen, Germany, 1997.
11 B. G. DeBoer, A. Zalkin and D. H. Templeton, *Inorg. Chem.*, 1969, **8**, 836.
12 L. Trefonas and W. N. Lipscomb, *J. Chem. Phys.*, 1958, **28**, 54.
13 *Tables of Interatomic Distances and Configuration in Molecules and Ions*, Special Publication No 11, The Chemical Society, Burlington House, London, 1958, p. M18.
14 F. H. Allen, O. Kennard, D. G. Watson, L. Brammer, A. G. Orpen and R. Taylor, *J. Chem. Soc., Perkin Trans. 2*, 1987, S1.

Toward artificial ion channels: self-assembled nanotubes from calix[4]arene–guanosine conjugates†

Vladimir Sidorov,*[a] Frank W. Kotch,[a] Mahnaz El-Kouedi[b] and Jeffery T. Davis*[a]

[a] *Department of Chemistry and Biochemistry, University of Maryland, College Park, MD 20742, USA. E-mail: jd140@umail.umd.edu*

[b] *Department of Chemistry, Georgetown University, Washington, DC, 20057, USA*

Received (in Columbia, MO, USA) 17th July 2000, Accepted 16th October 2000
First published as an Advance Article on the web

In the presence of Na^+, a 1,3-*alternate*-calix[4]arene bearing four guanosine units forms a self-assembled nanotube.

With the current interest in fabricating nanoscale structures for potential biomedical and materials applications much attention has focused on supramolecular tubes. Nanotubes have been made from cyclic peptides,[1] lipids,[2] oligocyclodextrins,[3] hydrogen-bonded rosettes[4] and coordination complexes.[5,6]

Predicting and controlling structure is essential for optimizing function. Herein, we report our initial efforts on building functional nanotubes, with an eye towards using them as artificial ion channels. Our design hinges on the metal cation-templated self-assembly of guanosine, a nucleobase that readily forms a hydrogen-bonded quartet in the presence of cations (Scheme 1).[7,8] The cyclic G-quartet, stabilized by Na^+ or K^+, can further organize by stacking. Telomeric DNA forms a G-quadruplex with a cation-filled channel;[9] and G-wires, over 1000 nm in length, have been imaged by atomic force microscopy.[10] We have also recently shown by X-ray crystallography that lipophilic G nucleosides self-associate to give extended, tube-like structures upon cation coordination.[11]

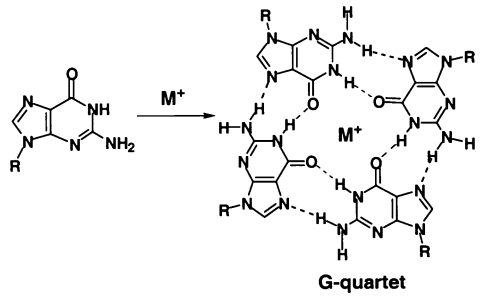

Scheme 1

Our modular approach towards constructing nanotubes involves using sodium cations to trigger the one-dimensional polymerization of G_4-calix **1**, a compound with four G moieties attached to a calix[4]arene-1,3-*alternate* scaffold. The 1,3-*alt* core in monomer **1** orients two orthogonal pairs of self-complementary G nucleosides so that they are well positioned for intermolecular hydrogen bonding with neighboring monomers (Scheme 2). Hosseini and coworkers introduced the calix[4]arene-1,3-*alt* scaffold to organize groups in this alternating 'up-down-up-down' fashion[12] and demonstrated this scaffold's utility by using Ag^+–cyano coordination bonds to form a self-assembled 'metallatubulane.'[6]

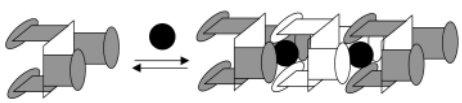

Scheme 2 Representation of nanotube formation by G_4-calixarene **1** upon cation-templated self-assembly. Squares represent the 1,3-*alt*-calix[4]arene core, ovals represent the guanosine moieties, and solid spheres represent the Na^+ cations.

† Electronic supplementary information (ESI) available: experimental and synthetic details. See http://www.rsc.org/suppdata/cc/b0/b007332f/

Compound **1** was readily prepared in six steps from guanosine and the parent *tert*-butylcalix[4]arene.[13] The final step in the synthesis of G_4-calix **1** involved the EDCI-promoted coupling of 5′-amino-2′,3′-isopropylidene G **2**[14] with the calix[4]arene-1,3-*alt* tetraacid **3**[15] (Scheme 3). The G_4-calix **1** was isolated by precipitation from MeOH, purified on microcrystalline cellulose TLC plates, and characterized by FAB-MS and ^1H NMR spectroscopy. The FAB-MS indicated complete substitution of a G residue at each of the calixarene's four sidechains. The symmetrical ^1H NMR spectrum of G_4-calix **1** in DMSO-d_6 confirmed its 1,3-*alt* conformation, and also verified that nucleoside coupling to the calixarene had occurred at the more nucleophilic 5′-amine of G **2**, and not at the less reactive exocyclic N2 amino group.

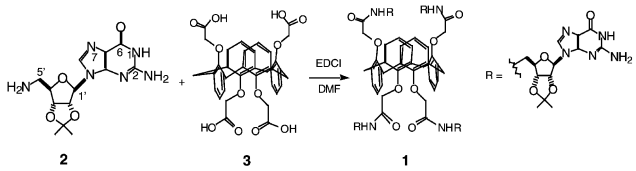

Scheme 3

The G_4-calix **1** was soluble in a MeCN–H_2O (1:1) binary mixture. Addition of $NaBPh_4$ to a solution of G_4-calix **1** in this mixture resulted in the instantaneous and quantitative precipitation of a white solid. The ^1H NMR spectrum of this material in d_6-DMSO confirmed that it was a mixture of G_4-calix **1** and the BPh_4^- anion. Transmission electron microscopy (TEM) images (Fig. 1) show the precipitate to consist of micrometer-long

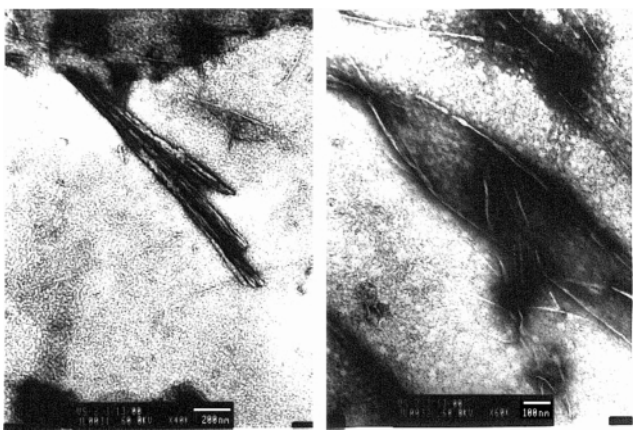

Fig. 1 Representative TEM images of the precipitate formed by G_4-calixarene **1** and $NaBPh_4$ in MeCN–H_2O (1:1) solution. Objects have thicknesses between *ca.* 3 nm (many of the objects in the right image) and *ca.* 50 nm (most objects in the left image), and lengths between 80 nm and 1.5 μm. The thinnest rods, with the approximate thickness of a G-quartet, may correspond to single self-assembled nanotubes. The thicker objects are likely bundles of nanotubes. The unit scale is 200 nm for the left image and 100 nm for the right image.

DOI: 10.1039/b007332f

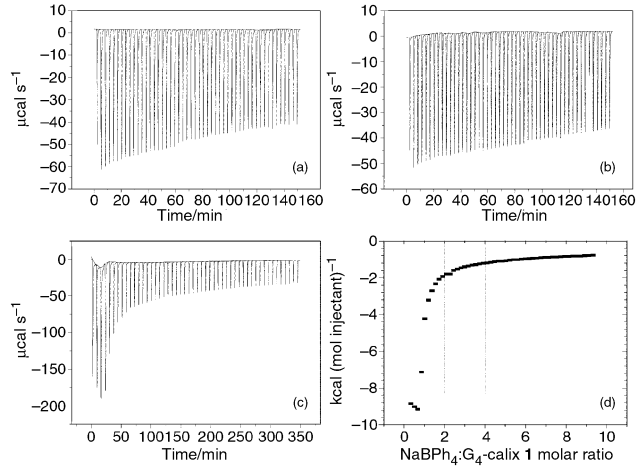

Fig. 2 Isothermal titration calorimetry. (a) Data for titration of $NaBPh_4$ into MeCN–H_2O (1 : 1) solution. (b) Data for titration of $NaBPh_4$ into a MeCN–H_2O (1 : 1) solution containing 2′,3′-isopropylidene guanosine. Note that there is essentially no difference between the results of experiments (a) and (b). (c) Data for titration of $NaBPh_4$ into a MeCN–H_2O (1 : 1) solution containing G_4-calix **1**. Note the difference in the scale of the *y*-axis (heat evolved) for experiment (c), as compared to experiments (a) and (b). (d) Integration curve for raw data from titration (c). The inflection point is consistent with formation of a complex having a 1 : 1 ratio for G_4-calix **1** : $NaBPh_4$. The total enthalpy of the interaction is −9 kcal mol^{-1}.

strands, visible as either single tubes or as bundles of tubes (ranging from *ca.* 3 nm to 50 nm in thickness). The strands are relatively straight, without much bending. The thickness of the individual tubes was near the microscope's limit of resolution, namely *ca.* 3 nm. Since our recent X-ray structure of a lipophilic G-quadruplex showed a tubular structure with a 2.65 nm diameter,[11] the individual rods formed from Na^+ templated aggregation of G_4-calix **1** have dimensions expected for a G-quartet. These electron micrographs of insoluble aggregates, showing such defined structure, are entirely consistent with nanotube formation by G_4-calix **1** upon Na^+ coordination.[16]

The stoichiometry of the insoluble aggregate formed between G_4-calix **1** and $NaBPh_4$ was quantitatively determined using isothermal titration calorimetry (ITC). Titration of a solution of G_4-calix **1** in MeCN–H_2O (1 : 1) with $NaBPh_4$ resulted in the rapid and significant generation of heat, until a 1 : 1 ratio of G_4-calix **1** and $NaBPh_4$ had been reached [Fig. 2(c) and 2(d)]. The total enthalpy of Na^+ binding by G_4-calix **1** was −9 kcal mol^{-1}; and this exothermic reaction coincided with precipitation of the $(\mathbf{1}\cdot Na^+)_n$ aggregate from solution as its BPh_4 salt. The absence of other inflection points in the ITC experiment, besides that for the prominent 1 : 1 G_4-calix **1**–$NaBPh_4$ stoichiometry, suggests that nanotube formation by G_4-calix **1** does not pass through shorter, intermediate structures. In other words, cation-templated nanotube formation of $(\mathbf{1}\cdot Na^+)_n$ is highly cooperative. Control ITC experiments showed that 2′,3′-isopropylidene guanosine, a compound lacking the calixarene framework, does not bind $NaBPh_4$ in this polar MeCN–H_2O (1 : 1) solvent mixture [Fig. 2(a) and (b)]. Thus, the heat evolved upon addition of $NaBPh_4$ to MeCN–H_2O (1 : 1) is the same whether or not 2′,3′-isopropylidene guanosine is present in solution. These ITC experiments clearly illustrate the entropic advantage of attaching the G moieties to the 1,3-*alt*-calixarene scaffold. Moreover, cation-templated aggregation of G_4-calix **1** is kinetically fast, and self-assembly of G_4 tetramers occurs even in this highly competitive hydrogen-bonding solvent mixture.

The assembly process that gives the $(G_4\text{-calix } \mathbf{1}\cdot Na^+)_n$ is completely reversible. Both temperature and pH can be used to control the cation-templated aggregation of G_4-calix **1**. For example, the precipitate formed from G_4-calix **1** and $NaBPh_4$ at 25 °C can be solubilized in MeCN–H_2O (1 : 1) simply by heating. DSC of a suspension of $(\mathbf{1}\cdot Na^+)_n$ in MeCN–H_2O (1 : 1) revealed a sharp transition temperature of 44.5 °C for dissolution. Cooling the sample back to 25 °C resulted, again, in precipitation of $(\mathbf{1}\cdot Na^+)_n(BPh_4^-)_n$. In addition to temperature, pH also had a dramatic effect on the solubility, and presumably the aggregation state, of $(\mathbf{1}\cdot Na^+)_n$. Protonation of the G nucleobase's exocyclic N2 amine and N7 should disrupt the structure of the hydrogen-bonded G-quartet. Indeed, this is consistent with the observation that the insoluble $(\mathbf{1}\cdot Na^+)_n(BPh_4^-)_n$ was completely redissolved in MeCN–H_2O upon changing from pH 7 to 2. This pH-dependent cycle was reversible, as addition of triethylamine base so as to change the solution's pH from 2 to 9 caused reprecipitation of $(\mathbf{1}\cdot Na^+)_n(BPh_4^-)_n$. The thermal lability and acid sensitivity of these hydrogen-bonded nanotubes formed from G_4-calix **1** is consistent with the reversible nature of self-assembly.

Three features of our nanotube design are worth emphasizing: (1) long-range structure can be controlled by cation templation, which triggers formation of an extensive hydrogen-bonded assembly based on the G-quartet; (2) aggregation is enabled by covalent attachment of guanosine units to the *alt*-1,3 calixarene scaffold, and (3) self-association of G_4-calix **1** occurs even in highly polar solvents. Future studies will focus on using temperature, pH, and other variables, to control the polymerization and depolymerization of G_4-calix **1**. The reversible formation of these structures in water at temperatures near 40 °C makes G_4-calix **1** and its analogs interesting as materials for biomedical applications. Finally, we are preparing lipophilic analogs of G_4-calix **1** in an effort to make artificial ion channels that self-assemble within a bilayer membrane.

We thank Professor Robert A. Flowers (Toledo) for the use of his ITC and Professor Larry Sita (Maryland) for use of his DSC. We thank the Department of Energy, BES Separations and Analysis Program for support. The electron microscopy facility is supported by the Lombardi Cancer Center at Georgetown University. J. D. thanks the Dreyfus Foundation for a Teacher-Scholar Award.

Notes and references

1 M. R. Ghadiri, J. R. Granja, R. A. Milligan, D. E. McRee and N. Khazanovich, *Nature*, 1993, **366**, 324.
2 J. M. Schnur, *Science*, 1993, **262**, 1669.
3 A. Harada, J. Li and M. Kamachi, *Nature*, 1993, **364**, 516.
4 N. Kimizuka, T. Kawasaki, K. Hirata and T. Kunitake, *J. Am. Chem. Soc.*, 1995, **117**, 6360.
5 M. Aoyagi, K. Biradha and M. Fujita, *J. Am. Chem. Soc.*, 1999, **121**, 7457.
6 C. Kleina, E. Graf, M. W. Hosseini, A. De Cian and J. Fischer, *Chem. Commun.*, 2000, 239.
7 For a review on metal-templated self-assembly, see: B. Linton and A. D. Hamilton, *Chem. Rev.*, 1997, **97**, 1669.
8 For a review on guanosine self-assembly, see G. Gottarelli, G. P. Spada and A. Garbesi, in *Comprehensive Supramolecular Chemistry*, ed. J.-M. Lehn, Pergamon Press, Oxford, UK, 1996, vol. 9, pp. 483–506.
9 K. Phillips, Z. Dauter, A. I. H. Murchie, D. M. J. Lilley and B. Luisi, *J. Mol. Biol.*, 1997, **273**, 171.
10 T. C. Marsh, J. Vesenka and E. Henderson, *Nucleic Acids Res.*, 1995 **23**, 696.
11 S. L. Forman, J. C. Fettinger, S. Pieraccini, G. Gottarelli and J. T. Davis, *J. Am. Chem. Soc.*, 2000, **122**, 4060.
12 W. Jaunky, M. W. Hosseini, J. M. Planeix, A. De Cian, N. Kyritsakas and J. Fischer, *Chem. Commun.*, 1999, 2313.
13 See ESI† for details of G_4-calix **1** synthesis.
14 M. G. Stout, M. J. Robins, R. K. Olsen and R. K. Robins, *J. Med. Chem.*, 1969, 658.
15 The calix[4]arene-1,3-*alt* tetraacid **3** was prepared by hydrolysis of the known tetraester: K. Iwamoto and S. Shinkai, *J. Org. Chem.*, 1992, **57**, 7066.
16 Control experiments confirmed that the appended guanosine units in G_4-calix **1** are essential for cation-templated aggregation. Thus, addition of $NaBPh_4$ to a solution of a calix[4]arene-1,3-*alt*-tetramethylamide dissolved in MeCN–H_2O (1 : 1) showed no evidence for precipitation. Moreover, ^1H NMR experiments in the same solvent showed no evidence for formation of soluble aggregates from Na^+ and calix[4]arene-1,3-*alt*-tetramethylamide (see ESI† for details regarding these control experiments).

The central 'relay' unit in hydraphile channels as a model for the water-and-ion 'capsule' of channel proteins

Clare L. Murray, Hossein Shabany and George W. Gokel*

Bioorganic Chemistry Program and Dept. of Molecular Biology & Pharmacology, Washington University School of Medicine, 660 South Euclid Ave., Campus Box 8103, St. Louis, MO 63110, USA. E-mail: ggokel@molecool.wustl.edu

Received (in Columbia, MO, USA) 28th June 2000, Accepted 16th October 2000
First published as an Advance Article on the web

The central relay of hydraphile channels is a model for the central ion-capsule of the KcsA K1 K^+-conducting channel of *Streptomyces lividans*; organization of water and concomitant electrostatic stabilization of a transient K^+ appear to be the functions in both cases.

The synthetic ion channels that we call 'hydraphiles' transport Na^+ in phospholipid bilayers.[1] These compounds use crown ethers, typically 4,13-diaza-18-crown-6, as headgroups[2] to maintain their position at the boundary between the bilayer and the aqueous phase on either side of the membrane. Fluorescence studies[3] have shown that the distal macrocycles of **1** are each 14 Å from the bilayer's midplane and in an environment intermediate in polarity between methanol and ethanol. These data are consistent with the macrocycles being proximal to the glyceryl fragment (midpolar regime) of the phospholipid—at opposite ends of the membrane's insulator slab. The headgroups are connected to a 'central relay unit' by means of hydrophobic dodecyl chains that measure *ca.* 14 Å in the extended conformation. The central relay is a polar residue incorported to provide the transient cation a means of sabilization at the bilayer's midplane—the least polar regime in the membrane. In many of the compounds we have studied, this unit is a third crown ether (*e.g.* **1**)

Recently, the solid state structure of a K^+-selective channel from *Streptomyces lividans* (KcsA K1 channel)[4] was reported and has begun to revolutionize our understanding of channel-forming proteins.[5] In this report, the structure of the natural channel is characterized thus: 'From inside the cell…the pore begins as a tunnel 18 Å in length (the internal pore) and then opens into a wide cavity (~ 10 Å across) near the middle of the membrane.' This description applies almost as well to our hydraphile channels. In the same paper, the following question is posed. 'Why is there a 10 Å diameter cavity in the center of the channel with an ion in it?' In a subsequent theoretical report,[6] it was concluded that the central capsule provides a means for electrostatic stabilization of cations in the non-polar midplane of the phospholipid bilayer. We believe that the cavity is equivalent to our 'central relay unit' and we present evidence to that effect in this report.

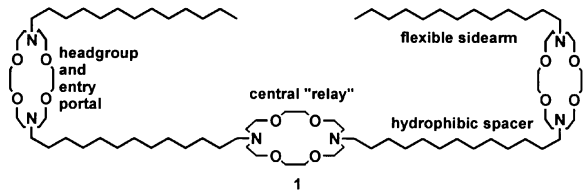

1

Hydraphiles **1**–**8** were prepared by a three-step sequence. First, monobenzyldiaza-18-crown-6 ($PhCH_2 < N18N > H$) was prepared either by benzylation of diaza-18-crown-6 or by partial hydrogenolysis of dibenzyldiaza-18-crown-6.[7] Alkylation of $PhCH_2 < N18N > H$ with an excess of $Br(CH_2)_nBr$ afforded $PhCH_2 < N18N > (CH_2)_nBr$ which was then allowed to react with $H < N18N > H$. Compound **9** was prepared in an analogous fashion except that $H < N18N > H$ was monoalkylated with dansyl chloride rather than benzyl bromide. Based on studies to determine the optimal length,[8] the hydraphiles were designed to be *ca.* 38–42 Å between the proximal nitrogen atoms of the terminal macrocycles. For small central units, proportionally longer hydrophobic chains were incorporated.

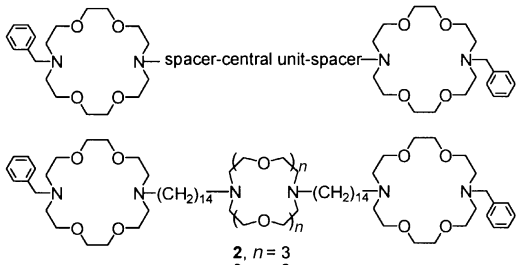

2, $n = 3$
3, $n = 2$
4, $n = 1$

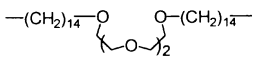

5

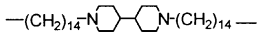

6

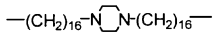

7

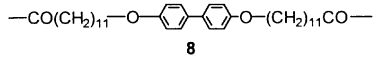

8

Sodium cation flux was measured by using the ^{23}Na NMR-based method of Riddell *et al.*[9] This technique permits quantitative detection of the Na^+ transport rate in vesicles prepared[10] from phosphatidylcholine and phosphatidylglycerol (4:1 w/w, pH = 7.3). The NMR experiment is somewhat complex and we have therefore normalized the data relative to a simultaneously determined standard (**9**).[11] Transport rates for **9** have been determined independently more than 10 times and each of the values shown in Table 1 for **1**–**8** represents at least three independent experiments.

The efficacy of a diaza-15-crown-5 central unit (**3**) is half that of the corresponding 18-membered ring (**1**, **2**). A further reduction in transport efficacy is observed when the central macroring is reduced in size to 12 atoms (**4**): transport efficacy falls again (k_{rel} = 69). Transport is about the same (within *ca.* 10% experimental error) when the 4,4′-bipiperidyl central unit (**6**) replaces diaza-12-crown-4 (**4**). The transport rate falls (to k_{rel} = 50) when the central ring of **4** (2N and 2O donors) is 'lysed' (**5**, 4O donors). All transport efficacy is lost when either pyrazine (**7**) or 4,4′-dioxybiphenyl (**8**) is incorporated as the central unit.

When the hydraphiles were designed, the central unit was intended to be a 'relay' for transient cations. It was presumed that the cations would be partially solvated as is thought to be the case in protein channels. Crown ethers often bind cations that, in turn, are bound to water. In the present case, we postulate that the central unit helps to organize water and that the cation 'passes over' it rather than necessarily being exchanged for water bound in the cavity. 18-Membered crown ethers are well known to bind water. Indeed, we reported the

DOI: 10.1039/b005431n

Table 1 Sodium cation transport by hydraphile ionophores[a]

Compound	Structure	d^a/Å	$k_{rel}{}^b$ (%)
1	$PhCH_2 < N18N > C_{14} < N18N > C_{14} < N18N > CH_2Ph$	43	211
2	$PhCH_2 < N18N > C_{12} < N18N > C_{12} < N18N > CH_2Ph$	38	200
3	$PhCH_2 < N18N > C_{14} < N15N > C_{14} < N18N > CH_2Ph$	42	100
4	$PhCH_2 < N18N > C_{14} < N12N > C_{14} < N18N > CH_2Ph$	41	69
5	$PhCH_2 < N18N > C_{12}O(CH_2CH_2O)_3C_{12} < N18N > CH_2Ph$	42	50
6	$PhCH_2 < N18N > C_{14} < NC_5 > — < C_5N > C_{14} < N18N > CH_2Ph$	42	80
7	$PhCH_2 < N18N > C_{16} < NC_4N > C_{16} < N_{18}N > CH_2Ph$	42	< 2
8	$PhCH_2 < N18N > COC_{11} < OC_6H_4–C_6H_4O > C_{11}CO < N18N > CH_2Ph$	38	< 2
9	$Dn < N18N > C_{12} < N18N > C_{12} < N18N > Dn$	38	100

[a] Distance measured on CPK molecular models between the two proximal nitrogen atoms on the distal macrocycles. [b] Rate relative to dansyl channel, arbitrarily set at 100. Comparative rates are recorded for 10 μM ionophore concentration.

first case of a protonated azacrown complexing a water molecule in 1977.[12] Other examples abound.[13] The solid state structures show a water molecule bridging alternate heteroatoms in the 18-membered ring macrocycles. Such bridging is also possible for the 15- and 12-membered ring compounds but the number of symmetry equivalent bridges is reduced. Thus, on a single surface of 18-crown-6, there are five possible 1,3-heteroatom arrangements that could be bridged by water. In 15-crown-5, there are only three and in 12-crown-4, only two are possible. The Na^+ transport rates observed for **2** (18-crown), **3** (15-crown) and **4** (12-crown) are 211, 100 and 69. This is a ratio (for **2**:**3**:**4**) of 2.1:1:0.7. The ratio of symmetry equivalent water bridges is 1.7:1:0.7. Opened-chained compound **5** can also form water bridges but it is not even as well organized as is **4**. The data presented here for the change from 18- to 15-membered rings and open chains differ some from an earlier,[14] related study.[15] The trend is similar, however.

The 4,4′-bipiperidyl unit of **6** was included because it is a fairly rigid molecule[16] and the N↔N separation is almost identical to the transannular N,N-distance in 4,13-diaza-18-crown-6. When the 4,4′-ring junction is *anti*, the cyclohexane-like units are coplanar. Molecular models show that the overall aspect is concave when the ring junction is *syn*, the nitrogen atoms are focused to a point above the ring junction, and the N↔N separation is barely 6 Å. We speculate that the bipiperidyl unit adds rigidity to the overall structure while providing H-bonding donor or acceptor sites either in the form of neutral nitrogen, protonated nitrogen, or the carbonyl groups. The argument is bolstered by the ESI-MS study that shows **6** to be incapable of binding three cations whereas **1** can easily do so (see following communication).[17]

When a macrocycle comprises the central unit, water may be organized by complexation and appropriately situated either to solvate a transient cation or to exchange with the water present in the partially hydrated cation. Such an arrangement is tantamount to the now well known second-sphere coordination of metal–ammonia complexes.[18] Such a coordinative arrangement is also possible, although probably less effective for the *syn*-oriented bipiperidyl units. In the latter case, however, a partially solvated cation of the form $M(OH_2)_2{}^+$ could bridge the N↔N space as illustrated in Fig. 1. The hydraphiles containing either piperidine in which the nitrogens are clearly very close together (*ca.* 3 Å) or biphenylene, which lacks significant donor groups, fail to transport cations despite the presence of all of the other essential elements.

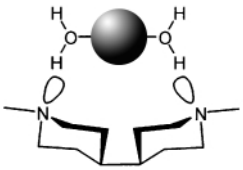

Fig. 1 Presumed coordination of a dihydrated alkali metal cation by 4,4′-dipiperidine.

We believe that simple, structural models such as the hydraphiles offer an effective means to probe complex biological phenomena. Clearly, these central units lack the focused, α-helices that afford electrostatic stabilization in the KcsA K1 channel.[1,4] Still, variations in the structure of the central relay are possible in this model system which permits functional subunits to be transformed—clearly an advantage over single site mutagenesis. Additional structural alterations are in progress and the results will be reported in due course.

We thank the NIH (GM 36262) and NSF (CHE-9805840) for grants that supported this work.

Notes and references

1 G. W. Gokel, *Chem. Commun.*, 2000, 1.
2 (*a*) S. Muñoz, J. Mallén, A. Nakano, Z. Chen, I. Gay, L. Echegoyen and G. W. Gokel, *J. Am. Chem. Soc.*, 1993, **115**, 1705; (*b*) S. L. De Wall, K. Wang, D. L. Berger, S. Watanabe, J. C. Hernandez and G. W. Gokel, *J. Org. Chem.*, 1997, **62**, 6784.
3 E. Abel, G. E. M. Maguire, O. Murillo, I. Suzuki and G. W. Gokel, *J. Am. Chem. Soc.*, 1999, **121**, 9043.
4 D. A. Doyle, J. M. Cabral, R. A. Pfuetzner, A. Kuo, J. M. Gulbis, S. L. Cohen, B. T. Chait and R. MacKinnon, *Science*, 1998, **280**, 69.
5 B. Hille, *Ionic Channels of Excitable Membranes*, Sinauer Press, Sunderland, MA, 2nd edn., 1992.
6 B. Roux and R. MacKinnon, *Science*, 1999, **285**, 100.
7 F. Cuevas and J. de Mendoza, personal communication, 1998.
8 C. L. Murray and G. W. Gokel, *Chem. Commun.*, 1998, 2477.
9 F. G. Riddell and M. K. Hayer, *Biochim. Biophys. Acta*, 1985, **817**, 313.
10 D. Papahadjopoulos and F. Szoka, *Proc. Natl. Acad. Sci. USA*, 1978, **75**, 4194.
11 Gramicidin is so effective at forming channels, it gives positive results even when experimental conditions are less than optimal. Thus, a negative observation for a hydraphile when gramicidin is positive could be misleading. Dansyl channel **9** is effective but frail enough to indicate experimental difficuly.
12 G. W. Gokel and B. J. Garcia, *Tetrahedron Lett.*, 1977, 317.
13 G. R. Newkome, H. C. R. Taylor, F. R. Fronczek, T. J. Delord and D. K. Kohli, *J. Am. Chem. Soc.*, 1981, **103**, 7376; G. S. Heo and R. A. Bartsch, *J. Org. Chem.*, 1982, **47**, 3557; R. Chenevert and A. Rodrique, *J. Chem. Educ.*, 1984, **61**, 465; A. G. Gaikwad, H. Noguchi and M. Yoshio, *Anal. Sci.*, 1987, **3**, 217; J. L. Atwood, S. G. Bott, K. D. Robinson, E. J. Bishop and M. T. May, *J. Crystallogr. Spectrosc. Res.*, 1991, **21**, 459; M. K. Amini and M. Shamsipur, *Iran. J. Chem. Chem. Eng.*, 1992, **11**, 12 (*Chem. Abstr.*, 1993, 119:280027); J. L. Atwood, P. C. Junk, M. T. May and K. D. Robinson, *J. Chem. Crystallogr.*, 1994, **24**, 243.
14 O. Murillo, S. Watanabe, A. Nakano and G. W. Gokel, *J. Am. Chem. Soc.*, 1995, **117**, 7665.
15 In the study reported in ref. 14, sodium transport was about the same for the 18- and 15-membered central ring units of the dodecyl-sidearmed tris(macrocycle) channels. When the central macroring was cleaved, about half of the activity was lost.
16 C. Li, J. C. Medina, E. Abel, G. E. M. Maguire, J. L. Atwood and G. W. Gokel, *J. Am. Chem. Soc.*, 1997, **119**, 1609.
17 H. Shabany, C. L. Murray, C. A. Gloeckner, M. A. Grayson, M. L. Gross and G. W. Gokel, *Chem. Commun.*, 2000, 2375.
18 S. J. Loeb, *Compr. Supramol. Chem.*, 1966, **1**, 733.

ChemComm

Enhancement of cation transport in synthetic hydraphile channels having covalently-linked headgroups

Hossein Shabany and George W. Gokel*

Bioorganic Chemistry Program and Dept. of Molecular Biology & Pharmacology, Washington University School of Medicine, 660 South Euclid Ave., Campus Box 8103, St. Louis, MO 63110, USA. E-mail: ggokel@molecool.wustl.edu

Received (in Columbia, MO, USA) 28th June 2000, Accepted 16th October 2000
First published as an Advance Article on the web

A novel, pentamacrocyclic host molecule has been prepared in which four symmetry-equivalent diazacrown ethers lead to a dramatic enhancement in Na^+ transport, across a phospholipid bilayer, relative to open-chained analogs lacking the fourth crown.

Our strategy[1] to design functional, non-peptide cation-conducting channels[2] has two key elements. First, the system was designed to be flexible so that the structural features could adapt if their exact physical organization had not been correctly evaluated. Second, the planned design was modular so that a compound exhibiting ionophoretic activity in a phospholipid bilayer membrane could be selectively and readily altered. The incorporation of flexibility into the framework could permit minor structural adjustments to compensate for design flaws but could also lead to a non-optimal structural arrangement. This, in turn, could result in poorer function than that of which the system was actually capable.

The first hydraphile structure **1**,[3] a tris(macrocycle), was

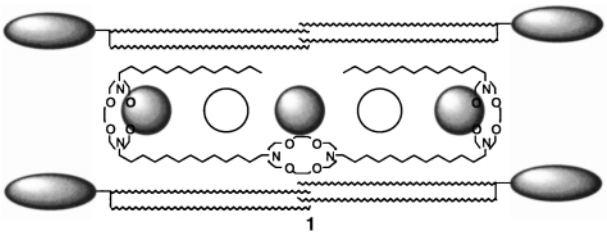

1

covalently-linked to define the overall transmembrane distance but the corresponding opposite side pendant chains were attached only at the distal macrocycles. The conformation shown for structure **1** has been inferred by changing the macroring sizes,[4] by incorporating fluorescent residues,[5] and by other methods.[6] The filled and open circles in the figure are meant to represent Na^+ and H_2O, respectively, but details of the structure within the membrane are not in hand nor are they implied. Note that we use shorthand developed for the purpose[7] to represent **1** as follows: C_{12} < N18N > C_{12} < N18N > C_{12} < N18N > C_{12}.

Studies to determine optimal overall length,[8] coupled with the efforts described above, have led to the conviction that we could connect the two flexible sidechains to form a more rigid and more efficacious structure. Compound **7** (Scheme 1) was a target of this approach. The synthetic plan required a strategy different from that that we had used previously. Compound **1**, which is not cyclic, can be constructed without the requirement for a cyclization reaction.[9] Tetramacrocycle **7**, the key compound in this report, was prepared by a sequence that is detailed in Scheme 1. Monobenzyl-4,13-diaza-18-crown-6[10] ($PhCH_2$ < N18N > H) was alkylated with methyl 12-bromododecanoate. The ester was hydrolyzed, treated with oxalyl chloride to give $PhCH_2$ < N18N > $(CH_2)_{11}COCl$, and then treated with diaza-18-crown-6 to give $PhCH_2$ < N18N > $(CH_2)_{11}CO$ < N18N > - $CO(CH_2)_{11}$ < N18N > CH_2Ph. Debenzylation was accomplished by hydrogenolysis to afford the tris(macrocycle). The diacid, $HO_2C(CH_2)_{11}$ < N18N > $(CH_2)_{11}CO_2H$, a compound that was in hand from previous studies[11] was converted into the corresponding dichloride. The cyclization reaction between H < N18N > $(CH_2)_{11}CO$ < N18N > $CO(CH_2)_{11}$ < N18N > H and $ClCO(CH_2)_{11}$ < N18N > $(CH_2)_{11}COCl$ formed tetramide **6**. Reduction of **6** (BH_3/THF) gave tetraamine **7** as a yellow oil (76% overall from tris(macrocycle). Treatment of Ph_2CH_2 < N18N > H with $ClCOC_{11}O–C_6H_4–C_6H_4–O–C_{11}COCl$ gave $PhCH_2$ < N18N > $CO(CH_2)_{11}O–C_6H_4–C_6H_4–O–(CH_2)_{11}CO$ < N18N > CH_2Ph (65%, yellow oil). Hydrogenolytic debenzylation afforded the biphenyl-bridged bis(macrocycle). The latter underwent cyclization with $ClCO-C_{11}OC_6H_4C_6H_4OC_{11}COCl$ to give tetraamide **2**. Reduction of **2** (BH_3/THF) afforded tetraamine **3** (72%, yellow oil). Compounds **4** (40%), **5** (60%) and **8** (62%) were prepared in a fashion similar to that shown in Scheme 1 and were characterized by standard chemical methods (^1H, ^{13}C NMR and FAB-MS). Dansyl channel **9** has been previously described.[5]

The Na^+ transport efficacies of the compounds prepared as part of this study were assessed in phospholipid bilayers by using the dynamic ^{23}Na NMR method of Riddell *et al.*[12] This method involves the formation of liposomes from phosphatidyl glycerol and phosphatidyl choline in the presence of 100 mM NaCl. The salt is present within the liposomes and in the

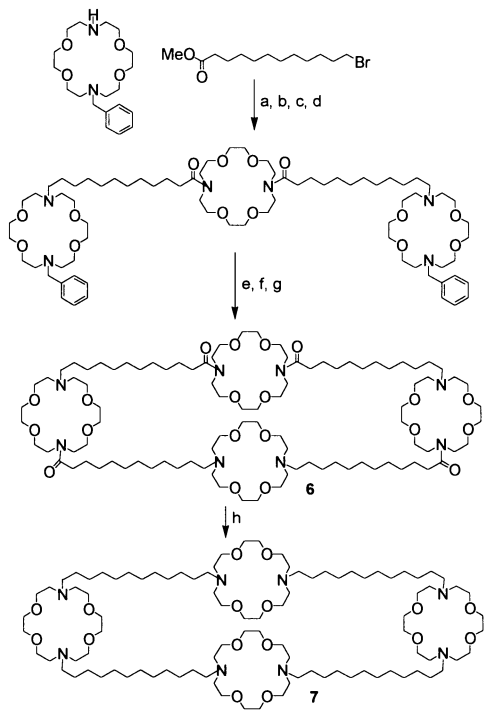

Scheme 1 *Reagents and conditions*: (a) Na_2CO_3, cat. KI, reflux 24 h, 83%; (b) 2 M NaOH, reflux, 18 h, 98%; (c) $(COCl)_2$, cat. DMF, 2 h; (d) diazacrown, Et_3N, cat. DMAP, 48 h, 71%; (e) Pd/C, 24 h, 95%; (f) step (c), $HO_2C(CH_2)_{11}$ < N18N > $(CH_2)_{11}CO_2H$; (g) Et_3N, cat. DMAP, 48 h, 70%; (h) BH_3/THF, −5 °C to rt, 48 h, 65%.

DOI: 10.1039/b005436o

Table 1 Sodium transport by hydraphiles in phospholipid liposomes

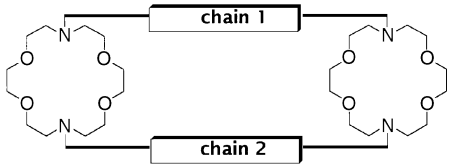

	Chain 1	Chain 2	k_{rel}[a] (%)
1	C_{12}<N18N>C_{12}	$(CH_2)_{11}Me$	105[b]
2	$COC_{11}O$–C_6H_4–C_6H_4–O–$C_{11}CO$	$COC_{11}O$–C_6H_4–C_6H_4–O–$C_{11}CO$	<2
3	$C_{12}O$–C_6H_4–C_6H_4–O–C_{12}	$C_{12}O$–C_6H_4–C_6H_4–O–C_{12}	<2
4	$C_{11}CO$<N18N>COC_{11}	$COC_{11}O$–C_6H_4–C_6H_4–O–$C_{11}CO$	30
5	C_{12}<N18N>C_{12}	$C_{12}O$–C_6H_4–C_6H_4–O–C_{12}	170
6	$C_{11}CO$<N18N>COC_{11}	COC_{11}<N18N>$C_{11}CO$	250
7	C_{12}<N18N>C_{12}	C_{12}<N18N>C_{12}	340
8	C_{12}<N18N>C_{12}	$(CH_2)_{12}S(CH_2)_8S(CH_2)_{12}$	190
9	C_{12}<N18N>C_{12}	Dansyl	100[c]

[a] We estimate the experimental error to be ±10%. [b] The rate relative to gramicidin is 27%. [c] The rate relative to gramicidin is 24%.

surrounding bulk aqueous phase. The ^{23}Na NMR spectrum observed under these conditions is a singlet. Addition of a Dy^{3+} shift reagent to the aqueous phase renders the two Na^+ ions magnetically non-equivalent and two signals are observed. Addition of an ionophore to the bilayer permits exchange of Na^+ ions with a concomitant change in linewidth. The exchange rate constant (k) can be evaluated from the linewidth change according to the relation $k = 1/\tau = \pi[(\Delta\nu - \Delta\nu_0)]$. In this relationship, τ is the half-life and ν represents the linewidth. The experimentally determined values of K are then compared with the value determined for the dansyl channel (Dn<N18N>C_{12}<N18N>C_{12}<N18N>Dn **9**).[13] The compounds that were studied for the present report are recorded in Table 1. Sodium cation transport by ionophores **1**–**9** was investigated at very low concentration (0–20 μM). The rate is reported as the relative rate $k_{rel} = 100\ k_{obs}/k_9$. A value of <2 means that the compound does not transport Na^+ at a rate sufficient to be observed under the experimental conditions. Dansyl channel **9** is used as the standard rather than gramicidin because the latter is 'too robust'. When experiments are not properly executed, gramicidin will still show transport behavior but **9** requires a proper experimental environment and is therefore a better control and standard.

Channel **1** transports Na^+ with a rate 27% that of gramicidin while its rate is 105% relative to **9**, the standard used throughout this study. The most important finding of the study is that when an additional crown ether is present as a central unit to organize water (see preceding communication), joining the flexible sidechains with a fourth crown produces an ionophore significantly (3.5-fold) more active than **1**. The very high efficacy of this structure supports previous conclusions concerning distance and polarity requirements. The family of structures also permits us to probe the effects of certain of the modular subunits.

First, we note that both compounds **2** and **3** are inactive in the ^{23}Na NMR experiment. We attribute this to the lack of a water-organizing central unit (see preceding communication).[14] When the center of the channel possesses one biaryl unit and an amide-substituted diazacrown **4**, activity is restored but it is modest (30% of **9**). Reduction of the amide residues in **4** affords **5** which has substantially increased Na^+ transport activity (150% of **9**). An increase in transport is expected because the amide residues conformationally restrict the macrocycle to which they are attached. The tetraamide precursor to **7**, *i.e.* **6**, is considerably less flexible than **7** but is also 2.5-fold more active than **1**. There may also be a deleterious effect of an arene on cation transport. In the low polarity environment of the phospholipid bilayer, a cation–π interaction between Na^+ and benzene[15] could substantially diminish the transport rate. Thus, the rate for **8**, which lacks an arene, exceeds that of **5** by a small but significant amount.

An important question is whether the increase in Na^+ transport may be attributed to the presence of the crown, to the higher level of organization present where the two flexible sidechains were, or to both. We know from the results reported in the preceding communication that 4,4′-dihydroxybiphenyl is inactive as a 'central ion capsule.' Thus, the fact that ionophoretic activity of **7** is twice that of **5** confirms that both variables are important. When only arenes are present as the central units, no Na^+ transport is measured in the NMR experiment.

The present effort demonstrates that a tetramacrocyclic hydraphile is more efficacious than its flexible counterpart. This confirms that distance relationships, headgroup functions, and ion–capsule interactions occur as previously surmised.

We thank the NIH (GM-36262) and the NSF (CHE-9805840) for grants that supported this work.

Notes and references

1 G. W. Gokel, *Chem. Commun.*, 2000, 1.
2 D. J. Aidley and P. R. Stanfield, *Ion Channels: Molecules in Action*, Cambridge University Press, Cambridge, 1996; G. W. Gokel and O. Murillo, *Acc. Chem. Res.*, 1996, **29**, 425; B. Hille, *Ionic Channels of Excitable Membranes*, Sinauer Press, Sunderland, MA, 2nd edn., 1992.
3 A. Nakano, Q. Xie, J. V. Mallén, L. Echegoyen and G. W. Gokel, *J. Am. Chem. Soc.*, 1990, **112**, 1287.
4 C. L. Murray, E. S. Meadows, O. Murillo and G. W. Gokel, *J. Am. Chem. Soc.*, 1997, **119**, 7887.
5 E. Abel, G. E. M. Maguire, E. S. Meadows, O. Murillo, T. Jin and G. W. Gokel, *J. Am. Chem. Soc.*, 1997, **119**, 9061; E. Abel, G. E. M. Maguire, O. Murillo, I. Suzuki and G. W. Gokel, *J. Am. Chem. Soc.*, 1999, **121**, 9043.
6 O. Murillo, I. Suzuki, E. Abel and G. W. Gokel, *J. Am. Chem. Soc.*, 1996, **118**, 7628.
7 J. C. Hernandez, J. E. Trafton and G. W. Gokel, *Tetrahedron Lett.*, 1991, 6269.
8 C. L. Murray and G. W. Gokel, *Chem. Commun.*, 1998, 2477.
9 O. Murillo, S. Watanabe, A. Nakano and G. W. Gokel, *J. Am. Chem. Soc.*, 1995, **117**, 7665.
10 J. de Mendoza, F. Cuevas, P. Prados, E. S. Meadows and G. W. Gokel, *Angew. Chem., Int. Ed.*, 1998, **37**, 1534.
11 Synthesis of $HO_2C(CH_2)_{11}$<N18N>$(CH_2)_{11}CO_2H$ was achieved from the reaction of H<N18N>H with methyl 12-bromododecanoate, followed by base hydrolysis.
12 F. G. Riddell and M. K. Hayer, *Biochem. Biophys. Acta*, 1985, **817**, 313; F. G. Riddell, S. Arumugam and B. G. Cox, *J. Chem. Soc., Chem. Commun.*, 1987, 1890.
13 E. Abel, G. E. M. Maguire, O. Murillo, I. Suzuki and G. W. Gokel, *J. Am. Chem. Soc.*, 1999, **121**, 9043.
14 C. L. Murray, H. Shabany and G. W. Gokel, *Chem. Commun.*, 2000, 2371.
15 S. L. De Wall, E. S. Meadows, L. J. Barbour and G. W. Gokel, *Proc. Natl. Acad. Sci. USA*, 2000, **97**, 6271.

ChemComm

Evidence for multiple alkali metal cation complexation in membrane-spanning ion transporters

Hossein Shabany,[a] Clare L. Murray,[a] Charles A. Gloeckner,[b] Michael A. Grayson,[b] Michael L. Gross[b] and George W. Gokel*[a]

[a] *Bioorganic Chemistry Program and Dept. of Molecular Biology & Pharmacology, Washington University School of Medicine, 660 South Euclid Ave., Campus Box 8103, St. Louis, MO 63110, USA. E-mail: ggokel@molecool.wustl.edu*

[b] *Department of Chemistry, Washington University, St. Louis, MO 63130, USA*

Received (in Columbia, MO, USA) 28th June 2000, Accepted 16th October 2000
First published as an Advance Article on the web

The polynitrogen-containing cation transporters 1–4 are shown by electrospray mass spectrometry to form multicationic species. In the absence of Na^+, protonated species dominate but increasing the sodium concentration leads to all binding sites being occupied.

The study of cation-conducting channels currently presents an enormous challenge to both chemists and biologists.[1] An important goal for the former is to prepare compounds that are inherently simpler than protein, or even peptide, channels[2] that transport cations at substantial rates across phospholipid bilayer membranes. With functionality achieved, experimental study of the systems should offer insight into the details of such phenomena as ion transport, selectivity, and gating kinetics. A major question concerns the chemical details of cation transport within the pore. A postulate that K^+ transport and selectivity were influenced by cation–π interactions within the pore[3] was disproved by site-directed mutagenesis.[4] The chemical roles of polyarenes in synthetic channels[5] and of the central ion capsule[6] in the KcsA K1 channel of *Streptomyces lividans*[7] beg further exploration of alkali metal cation interactions in low polarity media. In a previous study, electrospray mass spectrometric results demonstrated that all three macrocyclic rings of a hydraphile channel-former could simultaneously bind cations.[8] We now report that the novel tetramacrocyclic[9] and nitrogen-heterocycle-containing[10] channel-formers reported in the preceding two communications can bind a full complement of alkali metal ions by using crown ethers but not piperazine or bipiperidyl donors.

Cation transport through a phospholipid bilayer for the hydraphile family has been demonstrated by using fluorescence (H^+),[11] ^{23}Na NMR (Na^+),[12] and planar bilayer conductance methods (Na^+).[13] The ability of hydraphile channels to span the bilayer[14] has been confirmed and the optimum length for this family of channels has been established.[15] The compounds reported here are elaborations of the previously known systems and all exhibit effective Na^+ transport in a phospholipid bilayer (NMR method). Thus, under comparable conditions, the transport rates in mixed phosphatidyl choline–phosphatidyl glycerol bilayer liposomes, the following Na^+ transport rates were observed at room temperature: **1**, 80%; **2**, 210%; **3**, 50%; and **4**, 340%. In all cases, the values are expressed as a percent of the rate observed for the dansyl-sidearmed channel, **5** (100%).

Compounds **2**[11] and **5**[14] were prepared as previously reported and the synthesis of **4** is described in the preceding communication.[9] Compound **1** was prepared by treatment of $PhCH_2{<}N18N{>}H$ with $Br(CH_2)_{12}Br$ (Na_2CO_3, KI, 2 h) in boiling PrCN to give $PhCH_2{<}N18N{>}(CH_2)_{12}Br$ as a yellow oil (39%). Further reaction of the above with 4,4′-bipiperidine (procedure as above, 16 h) gave **1** as a colorless solid (8%, mp 55–56 °C). The preparation of **3** required a more elaborate approach. Benzyldiaza-18-crown-6 was alkylated with $Br(CH_2)_{11}CO_2Me$ (Na_2CO_3, cat. KI, BuCN, 20 mL, 24 h, 50%)

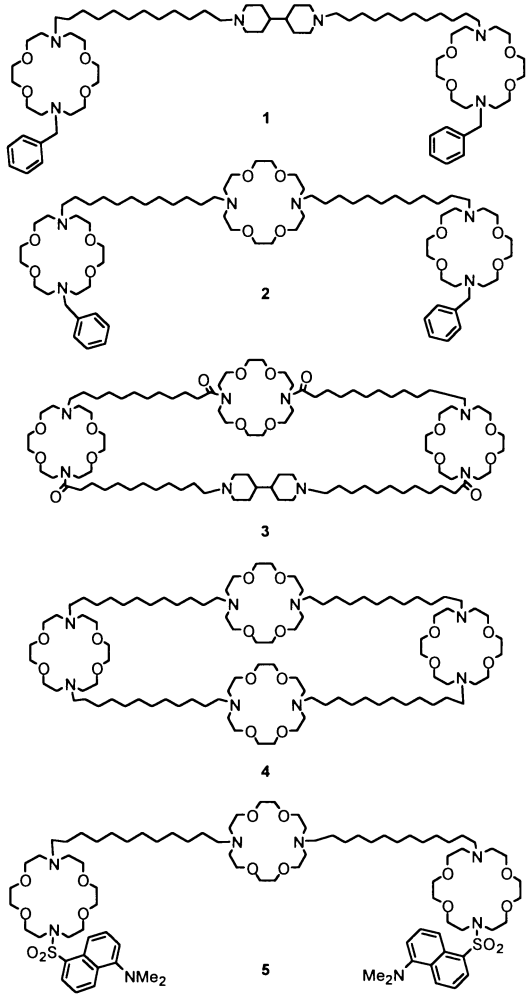

to give $PhCH_2{<}N18N{>}(CH_2)_{11}CO_2Me$. Hydrolysis (2 M NaOH, 93%) followed by treatment with $(COCl)_2$ (2 M solution in CH_2Cl_2, 2 h) gave $PhCH_2{<}N18N{>}(CH_2)_{11}COCl$, which was allowed to react directly in CH_2Cl_2 with $H{<}N18N{>}H$ (Et_3N, 6 equiv., cat. DMAP, to give the tris(crown) diamide as a yellow oil (65%). The tris(crown) diamide was debenzylated (H_2–Pd/C, 60 psi, abs. EtOH) to give $[H{<}N18N{>}(CH_2)_{11}CO]_2{<}N18N{>}$ (yellow oil, 95%). A similar strategy was used to prepare $ClCO(CH_2)_{11}NC_5H_9C_5H_9N(CH_2)_{11}COCl$, beginning with the alkylation of 4,4′-bipiperidine by $Br(CH_2)_{11}CO_2Me/Na_2CO_3$ (cat. KI, BuCN, 20 mL, 24 h) to give $MeO_2C(CH_2)_{11}NC_5H_9C_5H_9N(CH_2)_{11}CO_2Me$ (71%). This, in turn, was hydrolyzed (2 M NaOH, 94%, colorless solid, mp 260 °C, decomposed) and treated with ClCOCOCl (excess, 2 M

DOI: 10.1039/b005442i

Table 1 Electrospray mass spectrometric analysis of compounds **1**–**4**

Ion	*m/z*	Rel. int. (%)
1	1204.98	n/a
[**1**·1Na]$^{+}$	1227.8	30
[**1**·2Na]$^{2+}$	625.5	100
[**1**·3Na]$^{3+}$	424.7	0
[**1**·4Na]$^{4+}$	324.2	0
2	1299.01	n/a
[**2**·1Na]$^{+}$	1322.5	72
[**2**·2Na]$^{2+}$	672.8	100
[**2**·3Na]$^{3+}$	456.2	20
[**2**·4Na]$^{4+}$	347.9	0
3	1675.3	n/a
[**3**·1Na]$^{+}$	1698.7	30
[**3**·2Na]$^{2+}$	861.1	100
[**3**·3Na]$^{3+}$	581.8	45
[**3**·4Na]$^{4+}$	442.1	0
4	1713.5	n/a
[**4**·1Na]$^{+}$	1737.7	38
[**4**·2Na]$^{2+}$	880.2	100
[**4**·3Na]$^{3+}$	594.4	87
[**4**·4Na]$^{4+}$	451.3	47

solution in CH_2Cl_2). The latter was treated with [H < N18N > $(CH_2)_{11}CO]_2$ < N18N > (Et_3N, 6 equiv., cat. DMAP, CH_2Cl_2, 48 h) to afford tetraamide **3** as a yellow oil (30%).

Compounds **1**–**4** present an opportunity to directly assess the interactions of the hydraphile's modular elements and Na^+. Assuming that a crown macroring will bind a single Na^+ ion, we anticipate that we will observe ions corresponding to [**1**·2Na]$^{2+}$, [**2**·3Na]$^{3+}$, [**3**·3Na]$^{3+}$, and [**4**·4Na]$^{4+}$. The projected maximum complexation by **1** or **3** is based on the expectation that 4,4′-bipiperidyl will not complex Na^+. This is particularly important considering the conclusions of the preceding communication that the bipiperidyl unit can organize water but its nitrogen donor groups are too far apart to effectively coordinate with Na^+.[10]

The mass spectrometric analyses were conducted using an electrospray ion source (ESI-MS).[16] The inlet temperature was *ca.* 55 °C. Typically, 1.5 mg of channel was dissolved in 1 mL of $CHCl_3$ and the spray solution was prepared by adding 1 mL of MeOH–$CHCl_3$ 1 : 1 (v/v) and 40 μL of 100 μM NaOH to 60 μL of the sample solution. After mixing, 20 μL of the sample solution was loop injected by continuous infusion [10 μL min^{-1} MeOH–$CHCl_3$ (1 : 1, v/v)]. The instrument continuously scanned (magnetic) at 20 s decade^{-1} of mass over the range from 2000 to 400 Da. The data thus obtained are shown in Table 1.

For each structure, we have calculated the anticipated molecular weights for adducts of **1**–**4** with 1, 2, 3 and 4 Na^+ ions. In each case, the most abundant ion (base peak) observed was the disodium adduct. In all cases, the maximum number of Na^+ ions complexed was equal to the number of macro-rings and no higher order ions were detected. It is also interesting to observe that the ion currents for the complexes containing either three or four Na^+ ions (**2**, **3** or **4**) were significantly larger than observed for either cation complex of **1**.

The most significant finding of the present study is that in all cases, the number of Na^+ ions bound by each host molecule corresponded to the number of macrocycles. In no case did the number of Na^+ ions exceed the number of macro-rings indicating a generalized affinity of the cation for any of these structures. In principle, if 4,4′-bipiperidyl could support cation complexation directly, the complexes [**1**·3Na]$^{3+}$ and [**3**·4Na]$^{4+}$ would have been observed at *m/z* values of 424.7 and 442.1, respectively. Peaks corresponding to such complexes were sought but not observed.

An interesting observation is that the higher organization of **3** relative to **2** appears to result in a more stable tris(Na^+) complex. Thus, the [host·2Na]$^{2+}$: [host·3Na]$^{3+}$ ion abundance ratios for **2** and **3** are 100 : 20 and 100 : 45. The 'central' macrocycle is bis(amidated) in **3** and is expected to be a weaker donor for Na^+. It appears that the diamine opposite can help to stabilize this complex relative to the situation in which the additional structural element is absent.

The critical inference we draw from these data is that direct interaction between the bipiperidyl unit of **1** and a cation is not detectable, even in the low dielectric medium of electrospray mass spectrometry. Extending this to the low polarity, insulating regime of a bilayer, we infer that bipiperidyl cannot directly support cation complexation in that situation either. This does not prove, but strongly supports, the notion that the function of **1** as a channel is due, in part, to the interaction of bipiperidyl with intrapore water or waters of hydration rather than directly with Na^+.[10]

We thank the NIH (GM 36262) and NSF (CHE-9805840) for grants that supported this work. The mass spectrometry research resource is supported by the National Centers for Research Resources of the NIH (Grant P41RR00954).

Notes and references

1 D. J. Aidley and P. R. Stanfield, *Ion Channels: Molecules in Action*, Cambridge University Press, Cambridge, 1996; B. Hille, *Ionic Channels of Excitable Membranes*, Sinauer Press, Sunderland, MA, 2nd edn., 1992.
2 B. Bechinger, *J. Membr. Biol.*, 1997, **156**, 197.
3 R. A. Kumpf and D. A. Dougherty, *Science*, 1993, **261**, 1708.
4 L. Heginbotham, Z. Lu, T. Abramson and R. MacKinnon, *Biophys. J.*, 1994, **66**, 1061.
5 F. Robert, J.-Y. Winum, N. Sakai, D. Gerard and S. Matile, *Org. Lett.*, 2000, **2**, 37.
6 B. Roux and R. MacKinnon, *Science*, 1999, **285**, 100.
7 R. MacKinnon, S. L. Cohen, A. Kuo, A. Lee and B. T. Chait, *Science*, 1998, **280**, 106.
8 O. Murillo, I. Suzuki, E. Abel and G. W. Gokel, *J. Am. Chem. Soc.*, 1996, **118**, 7628.
9 H. Shabany and G. W. Gokel, *Chem. Commun.*, 2000, 2373.
10 C. L. Murray, H. Shabany and G. W. Gokel, *Chem. Commun.*, 2000, 2371.
11 O. Murillo, S. Watanabe, A. Nakano and G. W. Gokel, *J. Am. Chem. Soc.*, 1995, **117**, 7665.
12 O. Murillo, I. Suzuki, E. Abel, C. L. Murray, E. S. Meadows, T. Jin and G. W. Gokel, *J. Am. Chem. Soc.*, 1997, **119**, 5540.
13 E. Abel, E. S. Meadows, I. Suzuki, T. Jin and G. W. Gokel, *Chem. Commun.*, 1997, 1145.
14 E. Abel, G. E. M. Maguire, E. S. Meadows, O. Murillo, T. Jin and G. W. Gokel, *J. Am. Chem. Soc.*, 1997, **119**, 9061; E. Abel, G. E. M. Maguire, O. Murillo, I. Suzuki and G. W. Gokel, *J. Am. Chem. Soc.*, 1999, **121**, 9043.
15 C. L. Murray and G. W. Gokel, *Chem. Commun.*, 1998, 2477.
16 Only sectors one and two, a reversed geometry BE, extended mass range configuration (Vacuum Generators ZAB-T), were used for the mass analysis. The electrospray ion source operated as follows: spray needle voltage, 8940 V; counter electrode, 5255 V; sampling cone, 4200 V; accelerating voltage, 4120 V; source temperature, 75% power (*ca.* 55 °C). Sample preparation was as follows: 1.5 mg of sample was dissolved in 1 mL chloroform.

Pyxophanes: selective gas phase ion complexation by 1,6,13,18-tetraoxa[6.6]paracyclophane-3,15-diyne

Robert Behm,[a] Charles Gloeckner,[b] Michael A. Grayson,[b] Michael L. Gross[b] and George W. Gokel*[a]

[a] *Bioorganic Chemistry Program and Dept. of Molecular Biology & Pharmacology, Washington University School of Medicine, 660 South Euclid Ave., Campus Box 8103, St. Louis, MO 63110, USA. E-mail: ggokel@molecool.wustl.edu*

[b] *Department of Chemistry, Washington University, St. Louis, MO 63130,USA*

Received (in Columbia, MO, USA) 28th June 2000, Accepted 16th October 2000
First published as an Advance Article on the web

Compound 1, synthesized from hydroquinone and 1,4-dichlorobut-2-yne, was characterized by X-ray crystallography and shown by electrospray ionization mass spectrometry to form 1 : 1 complexes with sodium and 2 : 1 complexes with potassium cation.

The interaction of arenes with alkali metal and ammonium ion cations is of considerable theoretical interest but of even greater potential import in biology. Three of the essential amino acids contain aromatic sidechains capable of serving as π-donors. Together, phenylalanine (Phe, F), tryptophan (Trp, W), and tyrosine (Tyr, Y) comprise 8.4% of the amino acids in all known protein sequences. The ability of arenes to complex K^+ was demonstrated experimentally by Kebarle and coworkers in 1981.[1] Additional experiments by the groups of Castleman[2] and Lisy[3] confirmed their observations and extended them to Na^+. Burley and Petsko surveyed data available in the Protein Data Bank and demonstrated the plausibility of ammonium ion–arene interactions in proteins.[4]

Important as this work was, cation–π interactions received little additional attention until it was postulated that the selectivity of protein channels could be understood in terms of K^+–arene interactions.[5] By using site directed mutagenesis, Heginbotham, MacKinnon and coworkers[6] showed that the selectivity filter of the shaker K^+ channel of *Drosophila melanogaster* did not require a cation–π interaction. The crystal structure of the K^+-selective KcsA K1 channel of *Streptomyces lividans* recently reported by MacKinnon and coworkers shows no evidence for K^+–arene interactions.[7] Still, the potential importance of such interactions is great. In recent work of our own, we reported the first crystal structure data confirming K^+–arene, cation–π interactions for the sidechains of phenylalanine,[8] tryptophan,[9] and tyrosine.[10]

We now propose that the ideal 'π-receptor' molecule would possess two arenes held rigidly face-to-face at a distance appropriate to bind an alkali metal cation. For Na^+, this distance should be *ca.* 2 Å, depending on the exact coordination number. To maintain rigidity, electron richness, and symmetry, we chose acetylene units to serve as spacers. Aryl ether links were selected for covalent attachment. Because the oxygen atoms were adjacent to an arene, their π-donicity was expected to be minimal and synthetic access should be facilitated. The target compound **1** was dubbed a 'pyxophane' after the word 'pyx', meaning chest.[11]

Pyxophane **1** was synthesized by alkylation of hydroquinone with 1,4-dichlorobut-2-yne, followed by oligomerization (or dimerization) and cyclization (Scheme 1). Hydroquinone, butyne, potassium carbonate and potassium iodide were heated at reflux for 24 h in acetonitrile. The solvent was removed and the residue was extracted with dichloromethane. The extract was purified by chromatographing over silica using dichloromethane. The purified product was recrystallized from toluene to afford **1** as fine white needles (5% yield, mp 265–266 °C).

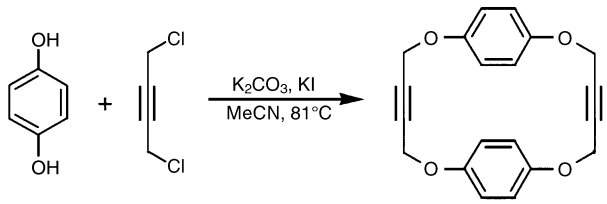

Scheme 1

The solid state structure of **1** (Fig. 1) was obtained by X-ray methods.[12] In the solid state, the molecule lies in a chair conformation with an arene–arene distance of 5.5 Å and an alkyne–alkyne distance of 7.0 Å. By subtracting the arene and alkyne thicknesses (3.4 Å), we deduce a cavity size of 2.1 × 3.6 Å. This distance suggests that a sodium cation, with a diameter of 1.98 Å, should be able to easily fit into the host molecule but a larger cation such as K^+ (2.7 Å diameter) should not.

Cyclophane **1** is related to the cyclophanes synthesized by Jarvi and Whitlock,[13] the primary difference being in the rigid spacer length. In their studies, they used longer diyne spacers which afforded a larger cavity, a necessity for the incorporation of organic guest molecules.

Electrospray ionization mass spectrometry (ESI-MS) is the ideal tool to assess alkali metal cation complexation in the low polarity environments of non-polar solvent and vacuum. Such an environment is clearly relevant to the *ca.* 30 Å non-polar span of a phospholipid bilayer commonly referred to as the insulator regime or the 'hydrocarbon slab'. The study involved three steps. First, an attempt was made to detect intramolecular complexation of Na^+ by **1**. This should lead to an ion of the type $[\mathbf{1}\cdot Na]^+$ having a weight of (320 + 23 =) 343 Da. The corresponding experiments with K^+, Rb^+, and Cs^+ are not expected to produce ions of the type $[\mathbf{1}\cdot M]^+$ because these metal ions are too large to bind intrapyxially. If 2 : 1 complexation is required, the dominant ion will be $[\mathbf{1}_2\cdot M]^+$. The absence of a

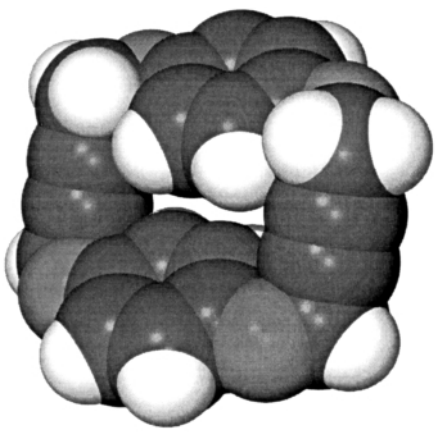

Fig. 1 Solid state structure of pyxophane **1** shown in the CPK metaphor.

DOI: 10.1039/b005443g

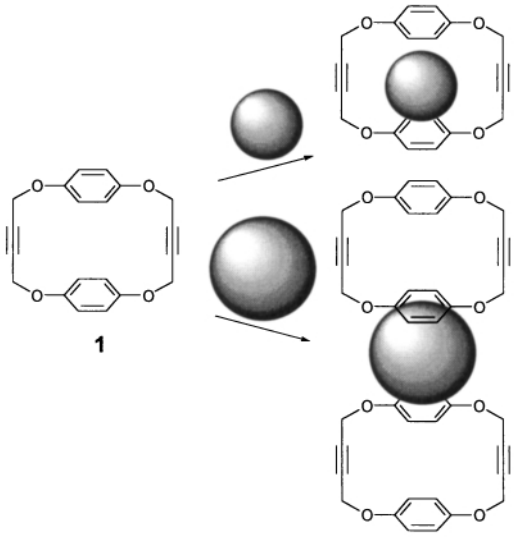

Scheme 2

1·M^+ ion and the presence of one corresponding to $\mathbf{1}_2$·M^+ would be good evidence for 'external' dimer complex formation. Finally, an experiment identical in other respects to those described above but involving Na^+ and 1,4-dimethoxybenzene **2** should not exhibit any significant complexation (neither **2**·M^+ nor $\mathbf{2}_2$·M^+).

The mass spectrometric analyses were conducted using an electrospray ion source (ESI/MS).[14] Pyxophane **1** (typically 1.5 mg) and dry NaCl were dissolved in 1 mL of $CHCl_3$ and the spray solution was prepared by adding 1 mL of MeOH–$CHCl_3$ (1 : 1, v/v) and 40 μL of 100 μM NaOH to 60 μL of the sample solution. After mixing, 20 μL of the sample solution was loop injected by continuous infusion (10 μL min^{-1} MeOH–$CHCl_3$ (1 : 1, v/v)). The instrument continuously scanned (magnetic) at 20 s $decade^{-1}$ of mass over the range from 2000 to 400 Da. The inlet temperature was *ca.* 55 °C. The base peak (100% relative abundance) in the ESI-MS spectrum was observed at *m/z* 343.1 which corresponds to an ion having the composition [**1**·Na]$^+$. A small peak at *m/z* 663.2 (*ca.* 7%) corresponds to [$\mathbf{1}_2$·Na]$^+$.

The binding selectivity was evaluated by comparing the intensity of the electrospray ion signal for the [M·Na]$^+$ complex, with the intensity of the signals for [M·K]$^+$, [M·Cs]$^+$, and [M·Rb]$^+$. These complexes were produced and analyzed separately. By far, the strongest binding was observed for Na^+ as evidenced by an intense *m/z* 343 ion [**1**·Na]$^+$. Although Cs^+ (ionic diameter = 3.32 Å) showed a moderately intense *m/z* 453 ion indicating some affinity for **1**, neither K^+ (2.66 Å) nor Rb^+ (2.94 Å) showed any significant binding. Further, the [M·Na]$^+$ ion was associated with higher mass ions consistent with solvent complexation, offering additional evidence that the Na^+ ion is occupying the central cavity of **1**. As controls, methoxybenzene (anisole) and 1,4-dimethoxybenzene **2** were run under conditions identical to those under which [**1**·Na]$^+$ was found to be the base peak in the spectrum. Sodium complexation was not observed for either compound. The complexation results are suggested by Scheme 2 in which the spheres represent Na^+ (smaller) and K^+ or Rb^+.

The preliminary data presented here support size-selective π-complexation of alkali metal cations. Additional complexation studies in both the gas and solution phases are underway with these and closely related host molecules.

We thank the NIH (GM 36262) and NSF (CHE-9805840) for grants that supported this work. The mass spectrometry research resource is supported by the National Centers for Research Resources of the NIH (Grant P41RR00954).

Notes and references

1 J. Sunner, K. Nishizawa and P. Kebarle, *J. Phys. Chem.*, 1981, **85**, 1814.
2 B. C. Buo, J. W. Purnell and A. W. Castleman Jr., *Chem. Phys. Lett.*, 1990, **168**, 155.
3 O. M. Cabarcos, C. J. Weinheimer and J. M. Lisy, *J. Chem. Phys.*, 1998, **108**, 5151; O. M. Cabarcos, C. J. Weinheimer and J. M. Lisy, *J. Chem. Phys.*, 1999, **110**, 8429.
4 S. K. Burley and G. A. Petsko, *FEBS*, 1986, **203**, 139.
5 R. A. Kumpf and D. A. Dougherty, *Science*, 1993, **261**, 1708.
6 L. Heginbotham, Z. Lu, T. Abramson and R. MacKinnon, *Biophys. J.*, 1994, **66**, 1061.
7 D. A. Doyle, J. M. Cabral, R. A. Pfuetzner, A. Kuo, J. M. Gulbis, S. L. Cohen, B. T. Chait and R. MacKinnon, *Science*, 1998, **280**, 69.
8 S. L. De Wall, E. S. Meadows, L. J. Barbour and G. W. Gokel, *Proc. Natl. Acad. Sci. USA*, 2000, **97**, 627.
9 S. L. De Wall, E. S. Meadows, L. J. Barbour and G. W. Gokel, *J. Am. Chem. Soc.*, 1999, 5613.
10 S. L. De Wall, L. J. Barbour and G. W. Gokel, *J. Am. Chem. Soc.*, 1999, 8405.
11 The second definition given in the shorter *Oxford English Dictionary* is: 'At the Royal Mint, the chest in which specimen gold and silver coins are deposited to be tested annually. Esp. in *trial of the pyx*, the annual test of such specimen coins'.
12 *Crystal data* for **1**: $C_{20}H_{16}O_4$, M = 320.34, space group $P2_1/c$, a = 9.819(2), b = 10.582(3), c = 7.85(2) Å, β = 109.81(2); V = 764.45 Å^3, Z = 2, μ = 5.4 cm^{-1}, λ = 1.5418 Å, 1300 reflections measured, R_w = 0.0533 for 811 reflections with $I > 4\sigma(I)$. CCDC 182/1832. See http://www.rsc.org/suppdata/cc/b0/b005443g/ for crystallographic files in .cif format.
13 E. T. Jarvi and H. W. Whitlock, *J. Am. Chem. Soc.*, 1980, **102**, 657.
14 Only sectors one and two, a reversed geometry BE, extended mass range configuration (Vacuum Generators ZAB-T), were used for the mass analysis. The electrospray ion source operated as follows: spray needle voltage, 8940 V; counter electrode, 5255 V; sampling cone, 4200 V; accelerating voltage, 4120 V; source temperature, 75% power (*ca.* 55 °C). Sample preparation was as follows: 1.5 mg of sample was dissolved in 1 mL $CHCl_3$.

ChemComm

Resin-to-resin Petasis borono-Mannich reaction between dialkylamino resins and supported boronic acids

Kim A. Thompson and Dennis G. Hall*

Department of Chemistry, University of Alberta, Edmonton, Alberta, Canada T6G 2G2. E-mail: dennis.hall@ualberta.ca; Fax: (+1) (780) 492-8231; Phone: (+1) (780) 492-3141

Received (in Corvallis, OR, USA) 28th July 2000, Accepted 18th October 2000
First published as an Advance Article on the web

Iminium intermediates, formed from the condensation of glyoxylic acid and resins functionalized with a secondary amine, are coupled to boronic acids transferred to solution from the corresponding [*N*,*N*-diethanolaminomethyl polystyryl boronates by *in situ* transesterification with the ethanol co-solvent to provide arylglycine derivatives.

In comparison with the traditional approach to solid-phase synthesis where a single resin-bound substrate is employed, the simultaneous use of two or more heterogeneous substrates, reagents or catalysts has seldom found real synthetic utility. Resin-to-resin transfer reactions (RRTR) constitute one type of multiresin system whose particular advantage is to allow the practice of solid-phase synthesis in a convergent fashion.[1] In RRTR, one resin-bound substrate is transferred to solution-phase by action of a phase-transfer agent, or chaperone, and coupled *in situ* to another resin-bound substrate. The concept of RRTR could find applications in combinatorial chemistry where each resin-bound substrate can be a member of a respective library assembled using the practical techniques of solid-phase synthesis. Recently, we have reported a successful RRTR system to effect Suzuki cross-coupling reactions between resin-bound aryl iodides and arylboronic acids supported onto [*N*,*N*-diethanolaminomethyl polystyrene (DEAM-PS).[2] The DEAM-PS resin facilitates the synthesis of functionalized arylboronic acids which can otherwise be difficult to isolate and handle in solution.[3] Their subsequent use in RRTR processes eliminates time-consuming cleavage and transfer operations, thereby considerably simplifying the outlook of library synthesis by manual or automated means. Herein, we describe the preliminary optimization of a resin-to-resin borono-Mannich reaction that produces arylglycine derivatives. Compounds of this nature are of particular interest for their biological activity.[4]

The boronic acid Mannich reaction first reported by Petasis[5] is compatible with a wide range of solvents including hydroxylic ones.[5–8] We envisioned that an alcohol, employed as co-solvent, could act as a neutral phase transfer agent required to cleave the DEAM-PS supported boronic acids under mild conditions appropriate toward a RRTR system. The boronic acid liberated *in situ* as an ester could then add to the imine formed between an amino functionalized resin and an activated aldehyde such as glyoxylic acid (Scheme 1).[6] We have first optimized conditions using DEAM-PS supported *p*-tolylboronic acid (**2**, R = 4-Me-C_6H_4- in Scheme 1), piperazinyltrityl resin, and glyoxylic acid in a semi-automated synthesizer.† The reaction was found to be rather slow and strongly dependent on the nature of the solvent system, THF–EtOH (7:1) and DMF–*n*-BuOH (7:1) being first and second best respectively. The current set of optimal experimental conditions first involve incubating the dialkylamino resin with glyoxylic acid monohydrate (1.1 eq.) for 2 h in dry THF at rt.‡ Then, four eq. of DEAM-PS bound boronic acid are added along with the appropriate volume of 8:3 THF–EtOH. The suspension is shaken at 65 °C for up to 48 h. This way, conversion levels superior to 75% were observed in the case of *p*-tolylboronic acid as seen after cleavage of the final resin mixture **1** and **4** with 5% trifluoroacetic acid/DCM to give the corresponding amino acid product **5a** as a bis(trifluoroacetate) salt (Table 1, entry 1).§ The rest of unreacted starting resin **3** is cleaved into the bis(trifluoroacetate) salt of piperazine (**6**) which can be eventually removed by precipitation. There are no other by-products observed, as the left over DEAM-PS resin (**1**) does not give any artifacts upon treatment with trifluoroacetic acid in the product release step. Interestingly, the transesterification of resin **2** with EtOH, a process required for phase transfer of the DEAM-PS-boronate, appears to be a dynamic equilibrium. The latter is driven forward by the large excess of EtOH, and through consumption of the boronic acid which adds to the putative iminium intermediate to form supported product **4** (Scheme 1). We have devised control experiments aimed at measuring the extent of transesterification of DEAM-PS supported *p*-tolylboronic acid in 7:1 THF–EtOH. Equilibrium is reached within 15 min of exposure of **2** to the 7:1 THF–EtOH solvent. Successive incubations of the resin under constant resin–solvent proportions, followed by rinses with dry THF, revealed that approximately 40% *p*-tolylboronic acid is released from the resin under these conditions.¶ In fact, since there is some left over DEAM-PS-boronate (**2**) at the end because of the transesterification equilibrium, we have found it necessary to include water–THF washes in order to wash off all excess boronic acid from the resin mixture prior to the acidolytic release of product **5**.‖ It is noteworthy to mention that although this RRTR was found to proceed in the absence of ethanol (the water introduced from the aldehyde hydrate may be sufficient to promote phase transfer of the boronic acid) conversion levels were generally higher in THF–EtOH.

Next we have studied substrate generality for this new RRTR system (Scheme 2). As shown in Table 1, conversion values and product yields were generally good except for the RRTR of electron-poor arylboronic acids.§ Thus, conversion values were highest for DEAM-PS supported *p*-methoxybenzeneboronic acid (entries 3, 7, 8), and lowest for *p*-bromophenylboronic acid (entry 4). According to entry 6, DEAM-PS-supported alkenylboronic acids are also appropriate substrates. In this case the use

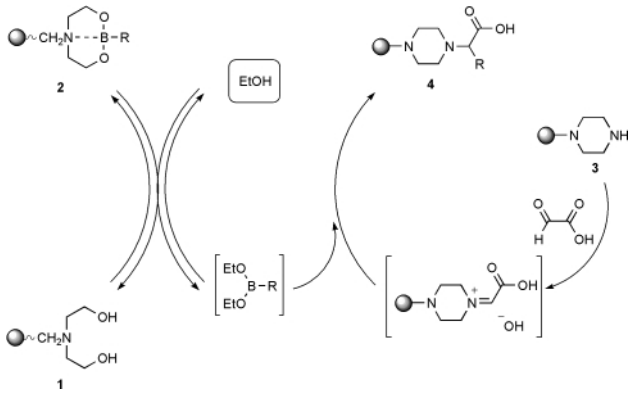

Scheme 1 Borono-Mannich resin-to-resin transfer reaction between boronic acids supported onto [*N*,*N*-diethanolaminomethyl polystyrene (**2**) and the iminium intermediate formed from a dialkylamino resin (**3**) and glyoxylic acid.

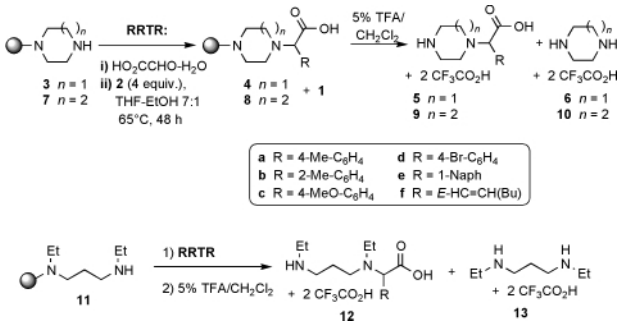

Scheme 2 RRTR of **3**, **7**, **11** with different DEAM-PS-boronates and cleavage of the final resin mixture to provide arylglycine derivatives **5**, **9**, and **12**.

Table 1 Preparation of arylglycine derivatives by borono-Mannich RRTR[a]

Entry	Amino resin	HEAM-PS-boronate **2**	Product	Conversion (%)[b]	Yield[c]
1	**3**	R = 4-Me-C_6H_4	**5a**	79	85
2	**3**	R = 2-Me-C_6H_4	**5b**	81	73
3	**3**	R = 4-MeO-C_6H_4	**5c**	90	> 95
4	**3**	R = 4-Br-C_6H_4	**5d**	21	10
5	**3**	R = 1-Naph	**5e**	85	90
6	**3**	R = *E*-HC=CH(Bu)	**5f**	89	> 95
7	**7**	R = 4-MeO-C_6H_4	**9c**	95	91
8	**11**	R = 4-MeO-C_6H_4	**12c**	76	82

[a] Preparation of resin substrates, RRTR trials, and subsequent cleavage of the resin mixture were carried out as indicated in the Notes and references section.†,‡ [b] Based on the relative amounts of product and respective bis(trifluoroacetate) salt **6**, **10**, or **13** calculated by integration of relevant peaks by ^{1}H NMR after 24–48 h reaction time. [c] Yields of crude product based on ^{1}H NMR analysis with an internal standard.

of a RRTR strategy using DEAM-PS resin is even more advantageous for handling and storage purposes since the otherwise air-sensitive alkenylboronic acids can be stabilized through immobilization as diethanolamine** adducts. An example using an acyclic amine (**11**) was equally successful (entry 8), showing that in principle a variety of secondary amines such as terminal *N*-alkylamino acids could be employed. Although only electron-rich arylboronic acids currently provide satisfactory conversions to crude material of high purity, analytically pure samples of most reported compounds can be obtained following precipitation with MeOH–ether, and filtration of the unreacted dialkylamine as a bis(trifluoroacetate) diammonium salt. We have also confirmed that the examples performed in a RRTR format provide yields comparable to reactions using non-supported boronic acids.

By minimizing cleavage, solvent concentration, and transfer operations this new borono-Mannich RRTR is thus potentially useful in the convergent solid-phase synthesis of libraries of arylglycine derivatives. In principle, this could be achieved by combining libraries of dialkylamino resins with libraries of DEAM-PS-supported arylboronic acids made by solid-phase derivatization of functionalized ones.[2,3] Studies such as this one looking at the structural and electronic preferences of substrates are crucial in order to select the most appropriate types of building blocks.

This work was funded by the Natural Sciences and Engineering Research Council (NSERC) of Canada. NSERC is acknowledged for a Postgraduate Scholarship (to K. T.).

Notes and references

† *Materials and methods*: *N*,*N*-diethanolaminomethyl polystyrene (DEAM-PS) was made according to ref. 3. All boronic acids were purchased from commercial sources (Aldrich, Lancaster, or CombiBlocks) and were loaded onto DEAM-PS as described in ref. 3. The dialkylaminotrityl resins were made by the condensation of excess diamine (20 equiv.) onto commercial chlorotrityl polystyrene (Rapp Polymere) swelled in NMP. Loading measurements were carried out by analysis of nitrogen content. For RRTR's, runs were done in 10 mL Teflon fritted vessels on a Quest 210 instrument with solvent wash unit (Argonaut Technologies). Cleavage was effected on-line and crude products were obtained after evaporation of solvents. Yields and purity were estimated by comparison with an internal NMR standard (EtOAc, 15 s relaxation delay).

‡ *Typical procedure for the borono-Mannich RRTR. Preparation of* **5c**. To piperazinyltrityl resin **3** (32 mg, 0.030 mmol, theor. loading: 0.95 mmol g^{-1}) weighed out in a reaction vessel was added a solution of glyoxylic acid monohydrate (0.032 mmol) in dry THF (2 mL). The suspension was allowed to mix at rt under a nitrogen atmosphere for 2 h. An excess of DEAM-PS boronic ester **2c** (127 mg, 0.120 mmol, theor. loading: 0.95 mmol g^{-1}) was then added followed by 1.5 ml of 8:3 THF–EtOH. The suspension was mixed at 65 °C for 48 h under a nitrogen atmosphere and then cooled to rt. The resin mixture was filtered and rinsed with 8 : 3 THF–EtOH (3×), 2 : 1 THF–H_2O (3×) and CH_2Cl_2 (5×), mixed with 3 ml of 5% TFA/CH_2Cl_2 in the same vessel at rt for 1 h, then filtered and rinsed with CH_2Cl_2 (3×) and MeOH (2×). The combined filtrates were concentrated and dried under high vacuum for 12 h to afford crude **5c** as a clear oil (14 mg, 90% conversion). An analytically pure sample was obtained by dissolving the oil in a small amount of MeOH followed by addition of ether, filtration of the precipitate, and concentration of the resulting solution.

§ *Selected data for all products*: **5a**: ^{1}H NMR (300 MHz, CD_3OD) δ 7.30 (d, J = 8.0 Hz, 2H), 7.20 (d, J = 8 Hz, 2H), 4.17 (s, 1H), 3.23–3.20 (m, 4H), 2.77–2.74 (m, 4H), 2.33 (s, 3H); ^{13}C NMR (75 MHz, CD_3OD) δ 173.5, 140.5, 132.0, 130.7, 130.1, 73.3, 48.1, 44.3, 21.2; ESMS 235.1 (M + H$^+$). **5b**: ^{1}H NMR (300 MHz, CD_3OD) δ 7.40 (d, J = 6.0 Hz, 1H), 7.24–7.18 (m, 3H), 4.50 (s, 1H), 3.20–3.16 (m, 4H), 2.85–2.82 (m, 4H), 2.45 (s, 3H); ^{13}C NMR (75 MHz, CD_3OD) δ 174.2, 138.9, 134.7, 131.8, 129.3, 129.1, 127.1, 69.3, 47.7, 44.9, 19.4; ESMS 235.3 (M + H$^+$). **5c**: ^{1}H NMR (300 MHz, CD_3OD) δ 7.34 (d, J = 8.6 Hz, 2H), 6.93 (d, J = 8.9 Hz, 2H), 4.13 (s, 1H), 3.79 (s, 3H), 3.23–3.19 (m, 4H), 2.75–2.72 (m, 4H); ^{13}C NMR (100 MHz, CD_3OD) δ 174.3, 161.7, 131.2, 127.9, 115.2, 73.1, 55.7, 48.3, 44.7; ESMS 251.1 (M + H$^+$). **5d**: ^{1}H NMR (300 MHz, CD_3OD) δ 7.55 (d, J = 8.5 Hz, 2H), 7.36 (d, J = 8.5 Hz, 2H), 4.22 (s, 1H), 3.25–3.19 (m, 4H), 2.77–2.73 (m, 4H); ESMS 301.1 (M + H$^+$). **5e**: ^{1}H NMR (300 MHz, CD_3OD) δ 8.43 (d, J = 7.9 Hz, 1H) 7.91–7.88 (m, 2H), 7.60–7.45 (m, 4H), 5.06 (s, 1H) 3.16–3.12 (m, 4H), 2.93–2.90 (m, 4H); ^{13}C NMR (75 MHz, CD_3OD) δ 174.3, 135.7, 133.4, 132.4, 130.5, 129.8, 128.4, 127.6, 127.1, 126.2, 125.2, 70.1, 47.9, 45.2; ESMS 271.1 (M + H$^+$). **5f**: ^{1}H NMR (300 MHz, CD_3OD) δ 5.89 (dt, J_1 = 15.0 Hz, J_2 = 7.0 Hz, 1H) 5.48 (dd, J_1 = 15.0 Hz, J_2 = 8.0 Hz, 1H) 3.70 (d, J = 8.0 Hz, 1H) 3.26–3.23 (m, 4H), 2.95–2.87 (m, 2H), 2.84–2.76 (m, 2H), 2.12 (app. q, J = 7.0 Hz, 2H) 1.44–1.29 (m, 4H) 0.92 (t, J = 7.0 Hz, 3H); ^{13}C NMR (100 MHz, CD_3OD) δ 173.9, 140.5, 124.3, 71.8, 48.1, 44.6, 33.2, 32.2, 23.2, 14.2; ESMS 227.2 (M + H$^+$). **9c**: ^{1}H NMR (300 MHz, CD_3OD) δ 7.38 (d, J = 8.7 Hz, 2H), 6.96 (d, J = 8.6 Hz, 2H), 4.65 (s, 1H), 3.80 (s, 3H), 3.34–3.21 (m, 2H) 3.21–3.10 (m, 4H), 3.01–2.97 (m, 2H), 2.07–2.04 (m, 2H); ^{13}C NMR (75 MHz, CD_3OD) δ 174.4, 161.8, 131.5, 128.0, 115.4, 73.1, 55.8, 53.3, 49.2, 46.7, 45.9, 26.1; ESMS 265.1 (*M* + H$^+$). **12c**: ^{1}H NMR (300 MHz, CD_3OD) δ 7.48 (d, J = 8.8 Hz, 2H), 7.03 (d, J = 8.8 Hz, 2H), 4.96 (s, 1H), 3.83 (s, 3H), 3.13–3.01 (m, 8H), 2.18–2.03 (m, 2H), 1.33–1.25 (m, 3H); ESMS 295.4 (M + H$^+$).

¶ The reverse reaction (**1** + *p*-tolylboronic acid) gives a similar outcome under the same conditions, showing that the transesterification process is under equilibrium.

‖ The DEAM-PS boronate linkage is very sensitive to water even in trace amounts. In contrast with alcoholysis, hydrolysis appears to be irreversible and quantitative.

** The IUPAC name for diethanolamine is 2,2′-iminodiethanol, and for DEAM-PS is [*N*,*N*-bis(2-hydroxyethyl)amino]methyl polystyrene.

1 For a recent example, see: Y. Hamuro, M. A. Scialdone and W. F. DeGrado, *J. Am. Chem. Soc.*, 1999, **121**, 1636; and references cited therein.
2 M. Gravel, C. Bérubé and D. G. Hall, *J. Comb. Chem.*, 2000, **2**, 228.
3 D. G. Hall, J. Tailor and M. Gravel, *Angew. Chem., Int. Ed.*, 1999, **38**, 3064.
4 For example, see: J. S. Bedingfield, M. C. Kemp, D. E. Jane, H. W. Tse, P. J. Roberts and J. Watkins, *J. Pharmacol.*, 1995, **116**, 3323.
5 N. A. Petasis and I. Akritopoulou, *Tetrahedron Lett.*, 1993, **34**, 583.
6 N. A. Petasis and I. A. Zavialov, *J. Am. Chem. Soc.*, 1998, **120**, 11 798.
7 T. K. Hansen, N. Schlienger, B. S. Hansen, P. H. Andersen and M. R. Bryce, *Tetrahedron Lett.*, 1999, **40**, 3651.
8 (*a*) S. R. Klopfenstein, J. J. Chen, A. Golebiowski, M. Li, S. X. Peng and X. Shao, *Tetrahedron Lett.*, 2000, **41**, 4835; (*b*) A. Golebiowski, S. R. Klopfenstein, J. J. Chen and X. Shao, *Tetrahedron Lett.*, 2000, **41**, 4841.

ChemComm

Synthesis of substituted α-methylene-γ-butyrolactones from chloroformates *via* palladium catalysed cyclisation–anion capture

Ronald Grigg* and Vladimir Savic

Molecular Innovation, Diversity and Automated Synthesis (MIDAS) Centre, School of Chemistry, Leeds University, Leeds, UK LS2 9JT

Received (in Cambridge, UK) 17th August 2000, Accepted 5th October 2000
First published as an Advance Article on the web

Cyclisation of chloroformates onto proximate alkyne functionality in the presence of a Pd(0) catalyst followed by anion capture affords α-methylene-γ-butyrolactone derivatives in moderate to good yields.

α-Methylene-γ-butyrolactones constitute an important group of natural products possessing a range of biological activities.[1] Their biological profiles are based on the specific reactivity of the α,β-unsaturated functionality acting, in most cases, as a Michael acceptor in reactions with biological nucleophiles.[2] The importance of this class of compounds has led to a number of synthetic procedures for the preparation of α-methylene-γ-butyrolactone derivatives.[2,3] Our approach is based on our palladium catalysed cascade cyclisation–anion capture methodology, (Scheme 1).[4] In the current context cyclisation of appropriate chloroformates onto the alkyne functionality in the presence of a Pd-catalyst would produce a vinylpalladium moiety suitable for further functionalisation by an anion-capture reagent.

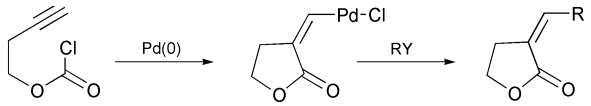

Scheme 1

Compared to the existing Pd-based methodology[5] for the preparation of α-methylene-γ-butyrolactones this approach allows direct access to β-substituted derivatives of this important class of compounds. In a recent communication we report similar methodology for the preparation of oxindole derivatives.[6]

The required chloroformates **(1)** were readily prepared from homopropargylic alcohols **2** by stirring the alcohol with excess of $COCl_2$ in toluene at rt for 16 h, (Scheme 2). These alcohols, if not commercially available, were easily prepared using a standard propargylation procedure of aldehydes in the presence of activated zinc (Scheme 2).

The cyclisation reactions (Scheme 3, Table 1) of chloroformates in the presence of an equimolar amount of $NaBPh_4$ as the anion capture reagent were performed in THF at 65–70 °C (oil bath temperature) in the presence of $Pd(OAc)_2$ (10 mol%)–PPh_3 (20 mol%). In cases of terminally unsubstituted alkyne functionality the expected γ-butyrolactones were isolated in moderate to good yields (Table 1, entries a–e) as the only product. The stereochemistry of all the γ-butyrolactones described in this communication was established from NOE data. The presence of a terminal substituent on the alkyne moiety of the chloroformates (Table 1, entries f and g) resulted in formation of the expected product together with the direct capture product **4**. It is likely that sterically induced slower cyclisation due to the presence of a terminal substituent caused the formation of the direct capture products **4**.

The (*Z*-)-lactone isomer formed in the above reactions can be easily isomerised *via* Michael addition–retro Michael to produce the (*E*)-isomer in almost quantitative yield by heating in the presence of excess of a secondary amine (Scheme 4). The opening of the lactone ring was not observed in this reaction.

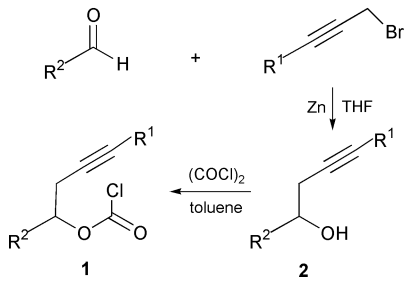

Scheme 2

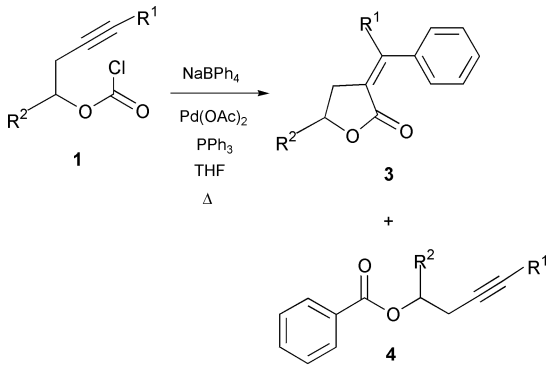

Scheme 3

Table 1

Entry	Chloroformate (**1**)	Lactone (**3**)	Benzoate (**4**)	Yield (%)[a]
a	R^1 + H, R^2 = H	R^1 = H, R^2 = H	—	51
b	R^1 = H, R^2 = CH_3	R^1 = H, R^2 = CH_3	—	51
c	R^1 = H, R^2 = CH_3CH_2	R^1 = H, R^2 = CH_3CH_2	—	55
d	R^1 = H, R^2 = C_6H_{13}	R^1 = H, R^2 = C_6H_{13}	—	73
e	R^1 = H, R^2 = Ph	R^1 = H, R^1 = Ph	—	49
f	R^1 = CH_3, R^2 = H	R^1 = CH_3, R^2 = H	R^1 = CH_3, R^2 = H	64[b]
g	R^1 = CH_3CH_2, R^1 = H	R^1 = CH_3CH_2, R^2 = H	R^1 = CH_3CH_2, R^2 = H	65[c]

[a] Isolated yields. [b] Combined yield, ratio 1:1. [c] Combined yield, ratio 1.3:1.

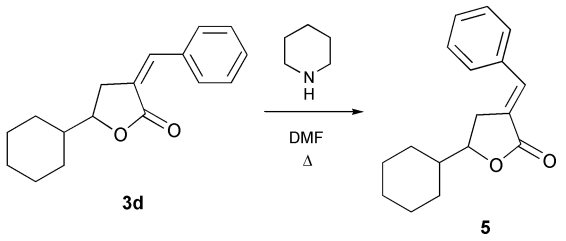

3d 5

Scheme 4

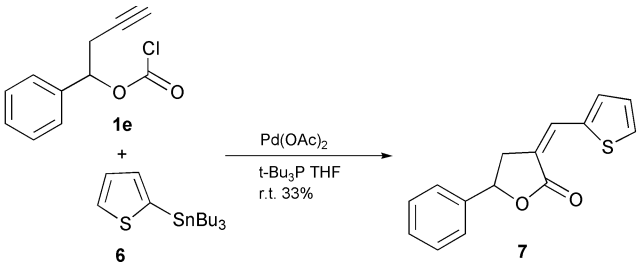

1e + **6** → **7**

Scheme 5

We briefly investigated the application of organostannanes as anion-capture reagents, (Scheme 5). Stirring the chloroformate **1e** and **6** in the presence of $Pd(OAc)_2$ and *t*-Bu_3P at rt afforded the lactone **7** in 33% yield. This reaction remains to be optimised but indicates possible further applications of organostannanes in these processes.

In summary, we have developed a simple procedure for the preparation of (*Z*)-isomers of α-methylene-γ-butyrolactone derivatives from homopropargyl chloroformates. The reaction affords the lactones in good yield but the presence of a terminal substituent on the alkyne induces formation of the direct capture product as well. Isomerisation of the α,β-double bond is possible in the presence of a secondary amine providing access to the (*E*)-stereoisomer. Chloroformates and carbamoyl chlorides constitute new starter species for our wide ranging catalytic cascade cyclisation–anion capture methodology.[4] Further studies involving the application of other anion-capture reagents and the application of this methodology to the synthesis of some naturally occurring lactones are in progress.

We thank Leeds University and the EPSRC for support.

Notes and references

1 E. D. Morgan and I. D. Wilson in *Comprehensive Natural Products Chemistry*, ed. D. Barton, K. Nakanishi and O. Meth-Cohn, Pergamon Press, Oxford, 1999, vol 8, p.308.
2 H. M. R. Hoffmann and J. Rabe, *Angew. Chem., Int. Ed. Engl.*, 1985, **24**, 94.
3 P. A. Grieco, *Synthesis*, 1975, 67; P. K. Choudhury, F. Foubelo and M. Yus, *Tetrahedron*, 1999, **55**, 10 779.
4 R. Grigg and V. Sridharan, *J. Organomet. Chem.*, 1999, **576**, 65.
5 F. Henin and J. P. Pete, *Tetrahedron Lett.*, 1983, 4687; T. F. Murray, E. G. Samsel, V. Varma and J. R. Nortom, *J. Am. Chem. Soc.*, 1981, **103**, 7520.
6 M. R. Fielding, R. Grigg and C. J. Urch, *Chem. Commun.*, 2000, 2239.

ChemComm

Phosphine–phosphite, a new class of auxiliaries in highly active and enantioselective hydrogenation

Oscar Pàmies, Montserrat Diéguez, Gemma Net, Aurora Ruiz* and Carmen Claver

Departament de Química Física i Inorgànica, Universitat Rovira i Virgili, Pl. Imperial Tarraco 1, 43005 Tarragona, Spain. E-mail: aruiz@quimica.urv.es

Received (in Cambridge, UK) 27th September 2000, Accepted 24th October 2000
First published as an Advance Article on the web

Excellent enantioselectivities (ee > 99%) and good activities (TOF > 1200 h^{-1}) are achieved under mild reaction conditions in the Rh-catalyzed hydrogenation of α,β-unsaturated carboxylic acid derivatives with the first family of phosphine–phosphite ligands containing a sugar backbone; these ligands are better than their diphosphine, diphosphite and phosphinite analogues.

The scope of asymmetric hydrogenation of alkenes has been gradually extended both in reactant structure and catalyst efficiency over many years.[1] Chiral bidentate phosphorus ligands have played a dominant role in the success of asymmetric hydrogenation.[1,2] The early excellent enantioselectivities obtained with Binap[3] and Dipamp[4] promoted the synthesis and application of a wide variety of new diphosphanes.[2] Recent reports on the use of chiral diphosphite[5] and diphosphinite[6] ligands in asymmetric hydrogenation have demonstrated their potential utility. Nevertheless, the search for new highly efficient ligand systems derived from readily available simple starting materials is still of great importance. Chiral auxiliaries from the chiral pool have attracted much attention, making tedious optical resolution procedures unnecessary. Carbohydrates are particularly advantageous because they are inexpensive compounds. Nevertheless, despite the accessibility and the excellent enantioselectivities obtained with sugar-derived ligands,[5–7] their full potential in providing chiral ligands has scarcely been exploited.[2a] In a previous paper, different types of phosphorus ligands with a xylofuranoside backbone have been applied to asymmetric hydrogenation with varying degrees of success. Moderate enantioselectivities (up to 35%) with phosphine–phosphinite and diphosphinite ligands have been reported by Brunner and Pieronczyk.[8] More recently, we reported moderate (up to 35%) and good (up to 91%) enantiomeric excesses at room temperature with diphosphites[9] and diphosphines,[10] but in both cases the activities were low.

Continuing our interest in carbohydrates as an available chiral source for preparing ligands and encouraged by the success of diphosphine[2] and diphosphite[5] ligands, we have designed a new family of chiral bidentate phosphine–phosphite ligands **1** with a xylofuranoside backbone which combines the advantages of both ligand types (Scheme 1). A feature of these ligands is that they have two different phosphorus donor sites than can *a priori* match the intermediates better, thus influencing their reactivity and achieving good enantioselectivity.[11] We also report their highly active and enantioselective rhodium catalyzed asymmetric hydrogenation of α,β-unsaturated carboxylic acid derivatives. To the best of our knowledge this is the first example of phosphine–phosphite ligands applied to hydrogenation.[12]

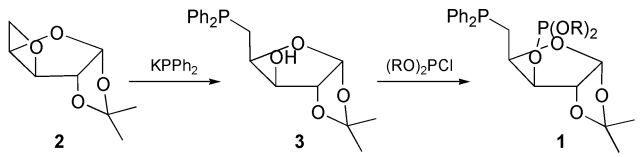

Scheme 1

The new ligands **1a–d** were synthesized very efficiently in two steps from oxetane **2**, as shown in Scheme 1. Compound **2** is easily prepared on a large scale from D-(+)-xylose.[13] The key step is the oxetane ring opening using a slight excess of potassium diphenylphosphide in DMF to afford phosphine **3** in 80% yield after column chromatography.[14] This step is a novel strategy for easily synthesizing related ligands. Reacting **3** with 1 equivalent of the corresponding phosphorochloridite formed *in situ*[15] in the presence of base provided easy access to the desired ligands **1a–d**. These were isolated in good yields as air-stable solids that are fairly robust towards hydrolysis. Selected spectroscopic data are shown in Table 1.

Table 1 ^{31}P NMR spectroscopic data for ligands **1a–d**[a]

Ligand	$(RO)_2PCl$	$\delta(P_1)$[b]	$\delta(P_2)$[c]	$J(P_1–P_2)$/Hz
1a	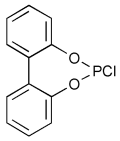	−18.3	148.2	17.0
1b	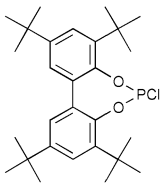	−21.5	144.7	11.9
1c	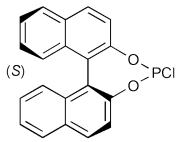	−22.5	150.0	33.1
1d	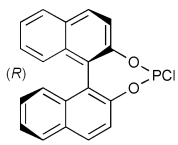	−22.5	148.4	15.5

[a] In $CDCl_3$. [b] P_1 = phosphine. [c] P_2 = phosphite.

In a first set of experiments, we used the rhodium-catalyzed hydrogenation of methyl *N*-acetamidoacrylate **4** to investigate the potential of ligands **1a–d** for asymmetric catalysis (Table 2).[16] The reaction proceeded smoothly at 1 bar of H_2 at room temperature in CH_2Cl_2. Ligand **1a**, with the achiral biphenyl moiety at the phosphite, not only showed high asymmetric induction (88.2%) but also very high catalytic activity (Table 2, entry 1). The presence of bulky *tert*-butyl groups in the *ortho*-positions of the biphenyl moiety (ligand **1b**) have an extremely positive effect on enantioselectivity (ee > 99%, Table 2, entry 2).[17] Interestingly, the sense of the enantioselectivity is reversed; the (*S*) enantiomer was obtained with ligand **1a** and the (*R*)-enantiomer was obtained with ligand **1b**. Ligands **1c** and

DOI: 10.1039/b007850f

Table 2 Asymmetric hydrogenation of methyl *N*-acetamidoacrylate **4** and methyl (*Z*)-*N*-acetamidocinnamate **5** with $[Rh(cod)_2]BF_4$/**1**[a]

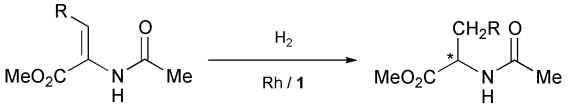

4 R = H
5 R = Ph

Entry	Ligand	Substrate	TOF[b]	% Conv[c] (*t*/min)	% ee[d]
1	**1a**	**4**	>1200	100 (<5)	88.2 (*S*)
2	**1b**	**4**	40	100 (150)	>99 (*R*)
3	**1c**	**4**	330	100 (20)	98.3 (*S*)
4	**1d**	**4**	318	100 (20)	97.6 (*R*)
5	**1a**	**5**	653	100 (10)	84.1 (*S*)
6	**1b**	**5**	31	100 (180)	98.8 (*R*)
7	**1c**	**5**	245	100 (30)	98.0 (*S*)
8	**1d**	**5**	212	100 (30)	94.3 (*R*)
9[e]	**6**	**4**	50	100 (120)	91 (*S*)
10[f]	**7**	**4**	4.2	99 (1440)	35 (*S*)

[a] $[Rh(cod)_2]BF_4$ = 0.01 mmol. **1**/Rh = 1.1. Substrate/Rh = 100. *P* = 1 atm. CH_2Cl_2 = 6 mL. [b] TOF in mol product × mol Rh^{-1} × h^{-1} measured by GC after 5 min. [c] % Conversion measured by GC. [d] % Enantiomeric excess measured by GC using an L-Chirasil-Val column. [e] Data from ref. 10. [f] Data from ref. 9.

1d containing a stereogenic binaphthyl moiety result in a high reaction rate and a high enantioselectivity (Table 2, entries 3 and 4). Ligand **1c**, which has an (*S*)-binaphthyl moiety, produces an ee of 98.3% (*S*), while diastereomer **1d**, which has an (*R*)-binaphthyl moiety, produces an ee of 97.6% (*R*). Therefore, if we compare the results with ligands **1a**–**d**, we can assume that the fast interchanging atropoisomers of ligand **1a** predominantly adopt the same configuration as that of **1c**, while the biphenyl moiety in ligand **1b** predominantly adopts an (*R*) configuration, probably due to the presence of the *tert*-butyl group in the *ortho*-position. We can conclude that the sense of the enantiodiscrimination is predominantly controlled by the configuration of the biphenyl or the binaphthyl at the phosphite moiety.

In general, the hydrogenation of **5** (Table 2, entries 5–8) follows the same trend as for **4**. However, the enantiomeric excesses are somewhat lower and the reaction rate was slightly slower. The configuration of the hydrogenated product is not affected by the presence of the phenyl group in **5**. The catalyst precursor containing ligand **1b** produced the highest enantiomeric excess (98.8%; Table 2, entry 6).

It is remarkable that these phosphine–phosphite ligands showed higher degrees of enantioselectivity and higher reaction rates than their corresponding diphosphine **6**[10] (Table 2, entry 9) and diphosphite **7**[9] (Table 2, entry 10) analogues under the same reaction conditions.

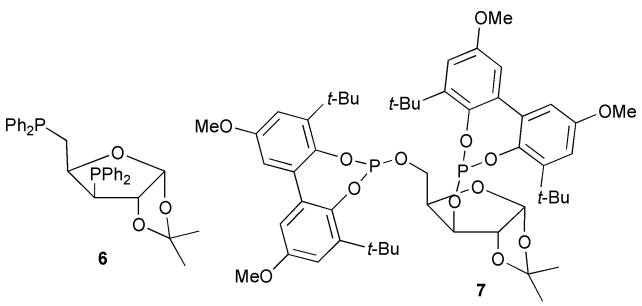

In summary, we have described the first application of phosphine–phosphite ligands in asymmetric hydrogenation. The combination of high enantioselectivities and high performances in simple unoptimized reactions and the low cost of the ligands makes these catalyst systems very attractive for further investigation. Moreover, these ligands were better than their diphosphine and diphosphite counterparts. These results open up a new class of ligands for asymmetric hydrogenation. Research into other substrates and the use of these ligands in other metal-catalyzed reactions is the subject of further investigations.

We thank the Spanish Ministerio de Educación y Cultura and the Generalitat de Catalunya (CIRIT) for their financial support (PB97-0407-CO5-01) and for awarding a research grant (to O. P.).

Notes and references

1 R. Noyori, *Asymmetric Catalysis in Organic Synthesis*, Wiley, New York, 1994; *Catalytic Asymmetric Synthesis*, ed. I. Ojima, Wiley, New York, 2000; *Comprehensive Asymmetric Catalysis*, ed. E. N. Jacobsen, A. Pfaltz and H. Yamamoto, Springer, Berlin, 1999, vol. 1.
2 (*a*) H. Brunner and W. Zettlmeier, *Handbook of Enantioselective Catalysis*, VCH, Weinheim, 1993; (*b*) A. Togni, C. Breutel, A. Schnyder, F. Spindler, H. Landert and A. Tijani, *J. Am. Chem. Soc.*, 1994, **116**, 4062; (*c*) U. Nettekoven, P. C. J. Kamer, P. W. N. M. van Leeuwen, M. Widhalm, A. L. Spek and M. Lutz, *J. Org. Chem.*, 1999, **64**, 3996; (*d*) U. Barens, M. J. Burk, A. Gerlach and W. Hems, *Angew. Chem., Int. Ed.*, 2000, **39**, 1981.
3 R. Noyori and H. Takaya, *Acc. Chem. Res.*, 1990, **23**, 345.
4 W. S. Knowles, M. J. Sabacky and B. D. Vineyard, *J. Chem. Soc., Chem. Commun.*, 1972, 10; B. D. Vineyard, W. S. Knowles, M. J. Sabacky, G. L. Bachman and D. J. Weinkauff, *J. Am. Chem. Soc.*, 1977, **99**, 5946.
5 M. T. Reetz and T. Neugebauer, *Angew. Chem., Int. Ed.*, 1999, **38**, 179.
6 T. V. RajanBabu, T. A. Ayers and A. L. Casalnuovo, *J. Am. Chem. Soc.*, 1994, **116**, 4101; T. A. Ayers and T. V. RajanBabu, in *Process Chemistry in the Pharmaceutical Industry*, ed. K. G. Gadamasetti, Marcel Dekker Inc., New York, 1999.
7 For recent representative examples see: K. Yonehara, T. Hashizyma, K. Mori, K. Ohe and S. Uemura, *Chem. Commun.*, 1999, 415; J.-C. Shi, C.-H. Yueng, D.-X. Wu, Q.-T. Liu and B.-S. Kang, *Organometallics*, 1999, **18**, 3796; M. Diéguez, O. Pàmies, A. Ruiz, S. Castillón and C. Claver, *Chem. Commun.*, 2000, 1607.
8 H. Brunner and W. Pieronczyk, *J. Chem. Res. (S)*, 1980, **3**, 76.
9 O. Pàmies, G. Net, A. Ruiz and C. Claver, *Eur. J. Inorg. Chem.*, 2000, 1287.
10 O. Pàmies, G. Net, A. Ruiz and C. Claver, *Eur. J. Inorg. Chem.*, 2000, 2011.
11 K. Inoguhi, S. Sakuraba and K. Achiwa, *Synlett*, 1992, 169.
12 Few phosphine–phosphite ligands have been described, although some of them have been successfully applied in asymmetric hydroformylation. K. Nozaki, N. Sakai, T. Nanno, T. Higashijima, S. Mano, T. Horiuchi and H. Takaya, *J. Am. Chem. Soc.*, 1997, **119**, 4413; S. Deerenberg, P. C. J. Kamer and P. W. N. M. van Leeuwen, *Organometallics*, 2000, **19**, 2065.
13 Oxetane **2** was prepared by slightly modifying the procedure described: P. Y. Goueth, M. A. Fauvin, M. Mashoudi, A. Ramiz, G. L. Ronco and P. J. Villa, *J. Nat.*, 1994, **6**, 3.
14 Brunner *et al.* previously synthesized this phosphine in low yield (10%) from the related monotosylated compound: H. Brunner and W. Pieronczyk, *J. Chem. Res. (S)*, 1980, 74; H. Brunner and W. Pieronczyk, *J. Chem. Res. (M)*, 1980, 1251.
15 Phosphorochloridites are easily prepared in one step from the corresponding biphenol or binapthol as described: G. J. H. Buisman, P. C. J. Kamer and P. W. N. M. van Leeuwen, *Tetrahedron: Asymmetry*, 1993, **4**, 1625.
16 In a typical run, a Schlenk tube was filled with a dichloromethane solution (6 mL) of substrate (1 mmol), $[Rh(cod)_2]BF_4$ (4.95 mg, 0.01 mmol) and ligand (0.011 mmol). This was then purged three times with H_2 and vacuum. The reaction mixture was then shaken under H_2 (1 atm) at 293 K. To remove the catalyst, the solution was placed on a short silica gel column and eluted with CH_2Cl_2. Conversion and enantiomeric excesses were determined by gas chromatography.
17 Detailed kinetic studies are under way.

Ethylenediamine zinc hydrogen phosphite, $[H_2N(CH_2)_2NH_2]_{0.5}\cdot ZnHPO_3$, containing two independent, interpenetrating, mixed inorganic/organic networks

Jennifer A. Rodgers and William T. A. Harrison*

Department of Chemistry, University of Aberdeen, Aberdeen, UK AB24 3UE. E-mail: w.harrison@abdn.ac.uk

Received (in Cambridge, UK) 7th September 2000, Accepted 31st October 2000
First published as an Advance Article on the web

$[H_2N(CH_2)_2NH_2]_{0.5}\cdot ZnHPO_3$ combines the structural features of templated networks and coordination polymers.

A vast number of inorganic networks templated by organic species have been reported over the last 10 years.[1] The possibilities of incorporating the phosphorus(III) containing, pseudo-pyramidal $[HPO_3]^{2-}$ hydrogen phosphite group into extended structures templated by *inorganic*, alkaline earth cations was explored a few years ago.[2] We have recently described two polymorphs of $ZnHPO_3\cdot N_4C_2H_4$, the first network hydrogen phosphite templated by an organic species (2-cyanoguanidine).[3] Here, we report the synthesis,† crystal structure,‡ and some properties of ethylenediamine (en) zinc hydrogen phosphite, $[H_2N(CH_2)_2NH_2]_{0.5}\cdot ZnHPO_3$, which shows a new type of structure combining the features of templated networks and coordination polymers.

A simulation based on the $[H_2N(CH_2)_2NH_2]_{0.5}\cdot ZnHPO_3$ single crystal structure was in excellent agreement with X-ray powder data, indicating phase purity and high crystallinity. TGA (ramp at 10 °C min^{-1} to 900 °C) for $[H_2N(CH_2)_2NH_2]_{0.5}\cdot ZnHPO_3$ revealed the onset of a 17% weight loss at *ca*. 200 °C, which was complete by *ca*. 700 °C. This is in good agreement (calc. weight loss = 17.1%) with a process involving the loss of all the organic species to result in a residue of nominal stoichiometry '$ZnHPO_3$.' ^{31}P MAS NMR for $[H_2N(CH_2)_2NH_2]_{0.5}\cdot ZnHPO_3$ showed a sharp resonance at δ −1.18 (relative to 85% H_3PO_4). There were strong spinning side bands, consistent with the inherently asymmetric environment of the P atom in the $[H_3PO_3]^{2-}$ grouping. The ^{13}C spectrum consisted of a single line at δ = 42.30 relative to $SiMe_4$.

$[H_2N(CH_2)_2NH_2]_{0.5}\cdot ZnHPO_3$, which is built up from seven framework atoms (Fig. 1), contains ZnO_3N tetrahedra and HPO_3 pseudo-pyramids as the polyhedral building units. The Zn–N bond corresponds to a direct link between zinc and the en template. The Zn species makes three Zn–O–P links to nearby P atoms [d_{av}(Zn–O) = 1.934(1) Å]. P1 makes three bonds to Zn neighbors [d_{av}(P–O) = 1.516(1) Å], with the expected[4] terminal P–H bond as its fourth vertex. The average Zn–O–P bond angle of the three bridging O atoms is 142.08°. The geometrical parameters of the organic component of $[H_2N(CH_2)_2NH_2]_{0.5}\cdot ZnHPO_3$ are typical. Fourier difference maps clearly located two H atoms attached to the N atom, thus the en "template" (if the term is still appropriate for this structure) is neutral, in accordance with the charge balancing requirement. Crystallographic symmetry generates the complete en template, which is therefore bonding to Zn from both its terminal N atoms, as Zn–N–C–C–N–Zn, or Zn–en–Zn (H atoms omitted). This linkage forms the connection between *next*-nearest neighbor sheets (*vide infra*).

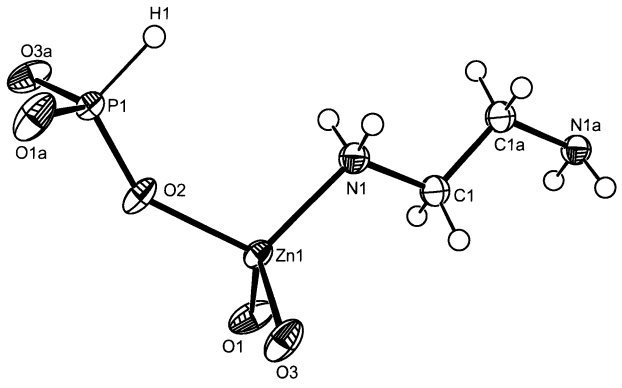

Fig. 1 Detail of the $[H_2N(CH_2)_2NH_2]_{0.5}\cdot ZnHPO_3$ structure (50% thermal ellipsoids) showing the atom labeling scheme. Symmetry generated atoms are indicated by, *e.g.*, O1a.

The connectivity of the strictly alternating ZnO_3N and HPO_3 units in $[H_2N(CH_2)_2NH_2]_{0.5}\cdot ZnHPO_3$ results in infinite layers (Fig. 2) propagating normal to [101]. Polyhedral 4-rings and 8-rings are apparent in these formally neutral sheets, and this topology can be described in terms of a 4.8^2 network (*i.e.*, each nodal Zn or P atom participates in one 4-ring and two 8-rings), which forms a characteristic part of feldspar (*e.g.*, $KAlSi_3O_8$) like phases[5] and various aluminosilicate zeolite structures,[6] although the 8-rings maybe subject to various degrees of distortion. The atom-to-atom dimensions of the $[H_2N(CH_2)_2NH_2]_{0.5}\cdot ZnHPO_3$ 8-ring are approximately 6.51 × 7.14 Å. Each 4-ring has two 'up' (approximately along [101]) and two 'down' vertices, thus both the Zn–N and P–H bonds point into the inter-sheet region.

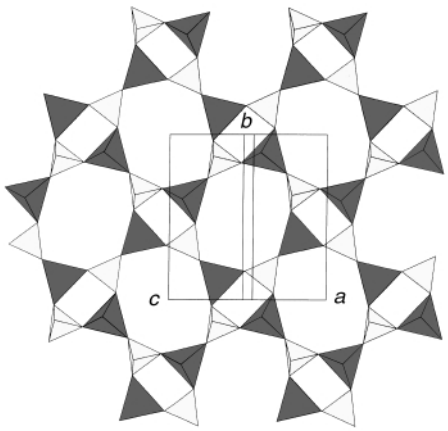

Fig. 2 Polyhedral view approximately down [101] of the 4.8^2 sheet topology of $[H_2N(CH_2)_2NH_2]_{0.5}\cdot ZnHPO_3$ (dark shading for the ZnO_3N groups, light shading for the HPO_3 groups).

An unusual templating effect occurs in $[H_2N(CH_2)_2NH_2]_{0.5}\cdot ZnHPO_3$, with the sheet-to-sheet Zn–en–Zn chain sticking *through* an 8-ring in an intermediate zincophosphite layer (Fig. 3). A somewhat similar effect through-the-ring effect involving a protonated template not bound to the inorganic network (and a totally different overall structure) has been seen in the gallofluorophospahte ULM-18.[7] In $[H_2N(CH_2)_2NH_2]_{0.5}\cdot ZnHPO_3$, every 8-ring is templated in the same way, thus, two completely independent but interpenetrating sets of inorganic sheets (Fig. 4) are 'knitted

DOI: 10.1039/b007268k

together' by a covalent bonding network *via* zinc and the template rather than by H bonds or van der Waals's forces. This configuration has clear parallels with the structures of interpenetrating coordination polymers.[8,9] However, N–H···O hydrogen bonds, as commonly seen in organically-templated zinc phosphates,[10] are also important in $[H_2N(CH_2)_2NH_2]_{0.5}{\cdot}ZnHPO_3$, with N1–H2···O1 [$d$(N1–H2) = 0.85(3) Å, d(H···O) = 2.22(3) Å, d(N···O) = 2.998 (2) Å, θ(N–H···O) = 152(2)°] and N1–H3···O3 bonds [0.90(2), 2.04(2), 2.931(2) Å. 169(3)°] occurring, the latter of these evidently somewhat stronger. Each 8-ring is stabilized by four N–H···O links (two from below, two from above), with all four associated with the same ethylenediamine grouping.

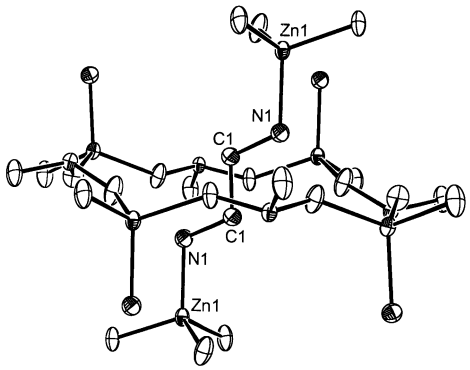

Fig. 3 Side-on view of an 8-ring window in one layer of $[H_2N(CH_2)_2NH_2]_{0.5}{\cdot}ZnHPO_3$ showing the Zn–en–Zn grouping passing through it. For the central 8-ring shown, Zn–en links are terminated at N, and all H atoms are omitted for clarity.

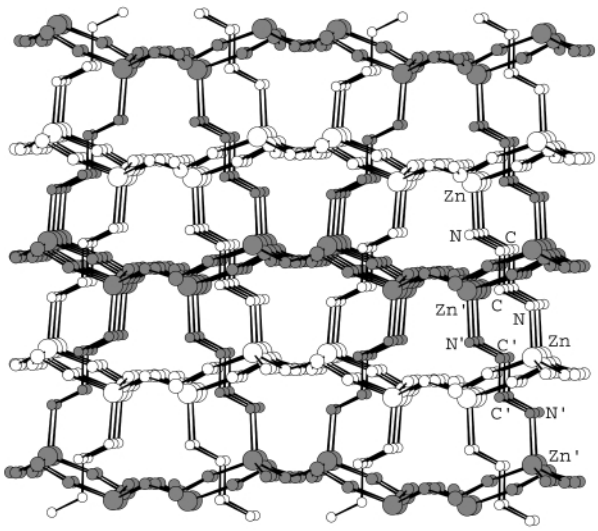

Fig. 4 Side on view approximately down [10$\bar{1}$] of a set of layers in $[H_2N(CH_2)_2NH_2]_{0.5}{\cdot}ZnHPO_3$. The unshaded atoms (unprimed labels) and shaded atoms (primed labels) form separate interpenetrating networks. For clarity, all H atoms are omitted.

We thank David Apperley (University of Durham EPSRC National Solid State NMR Service) for collecting the NMR data.

Notes and references

† *Synthesis*: 0.814 g ZnO, 0.824 g H_3PO_3, 0.602 g ethylenediamine (molar ratio of $Zn:HPO_3^{2-}$:en = 1:1:1) and 18 g of H_2O were added to a PTFE bottle and shaken well. The mixture was transferred to a Teflon-lined, 23 ml hydrothermal bomb, sealed, and heated to 150 °C for two days. The bomb was left to cool for 24 h, and the solid product, consisting of large (up to 2 mm) transparent lumps of the title compound was recovered by vacuum filtration and rinsing with water and methanol.

‡ *Crystal data*: $[H_2N(CH_2)_2NH_2]_{0.5}{\cdot}ZnHPO_3$, M_r = 175.42, monoclinic, space group $P2_1/n$ (no. 14), a = 5.9335(3), b = 10.8863(5), c = 7.7611(4) Å, β = 102.066(1)°, V = 490.25(7) Å^3, Z = 4, μ = 52.2 cm^{-1}, D_c = 2.377 g cm^{-3}, F(000) = 348, $R(F)$ = 0.022, $R_w(F)$ = 0.026. Data collection using a Bruker SMART 1000 CCD diffractometer (graphite-monochromated Mo-Kα radiation, λ = 0.71073 Å, T = 300 K): monoclinic cell parameters from 3479 reflections (6.5 < 2θ < 65.0°), 4999 reflections scanned (2 < 2θ < 65°). After merging (R_{Int} = 0.018), 1649 of the 1752 unique reflections were considered observed [$I > \sigma(I)$]. An absorption correction was applied with SADABS (min., max. equivalent transmission factors = 0.543, 0.928). Hydrogen atoms were located from difference maps and their positions and isotropic thermal factors were refined without constraints.

CCDC 182/1831. See http://www.rsc.org/suppdata/cc/b0/b007268k/ for crystallographic files in .cif format.

1 A. K. Cheetham, G. Férey and T. Loiseau, *Angew. Chem., Int. Ed.*, 1999, **38**, 3268.
2 M. Shieh, K. J. Martin, P. J. Squattrito and A. Clearfield, *Inorg. Chem.*, 1990, **29**, 958.
3 W. T. A. Harrison, M. L. F. Phillips, T. M. Nenoff and J. Stanchfield, *Inorg. Chem.*, 2001, in press.
4 G. Becker, H.-D. Hausen, O. Mundt, W. Schwarz, C. T. Wagner and T. Vogt, *Z. Anorg. Allg. Chem.*, 1990, **591**, 17.
5 F. Liebau, *Structural Chemistry of Silicates*, Springer Verlag, New York, 1985.
6 J. V. Smith and W. J. Dytrych, *Nature* (*London*), 1984, **309**, 607.
7 F. Taulelle, A. Samoson, T. Loiseau and G. Férey, *J. Phys. Chem. B*, 1998, **102**, 8588.
8 T. M. Reineke, M. Eddaoudi, D. Moler, M. OKeeffe and O. M. Yaghi, *J. Am. Chem. Soc.*, 2000, **122**, 4843, and references therein.
9 S. W. Keller, *Angew. Chem., Int. Ed. Engl.*, 1997, **36**, 247.
10 W. Liu, Y. Liu, Z. Shi and W. Pang, *J. Mater. Chem.*, 2000, **10**, 1451 and references therein.

First catalytic dihydroamination of a phosphaalkyne. Crystal and molecular structure of *trans*-[$PdCl_2${$P(Pr^iNH)_2CH_2Bu^t$}$_2$]

F. Geoffrey N. Cloke,* Peter B. Hitchcock, John F. Nixon* and D. James Wilson

School of Chemistry, Physics and Environmental Science, University of Sussex, Brighton, Sussex, UK BN1 9QJ. E-mail: J.Nixon@sussex.ac.uk

Received (in Cambridge, UK) 18th September 2000, Accepted 25th October 2000
First published as an Advance Article on the web

Treatment of a dichloromethane solution of Bu^tCP, containing a catalytic amount of $TiCl_4$, with an excess of the primary amines RNH_2 (R = Pr^i, Bu^t) quantitatively affords the corresponding bis-dialkylaminophosphine $P(Bu^tNH)_2CH_2Bu^t$. $P(Pr^iNH)_2CH_2Bu^t$ is structurally characterised by a single crystal X-ray diffraction study of its bis-*trans*-$PdCl_2$ complex.

The direct addition of nucleophiles HNR_2 to alkenes and alkynes has been shown to be kinetically unfavourable due to high activation barriers caused by unfavourable approach of the substrates.[1] Catalysis is therefore of fundamental importance for the amination of alkynes, by providing alternative lower energy kinetic pathways. A survey of the literature in this area reveals a stronger precedence for catalytic *intra*-molecular hydroamination of alkynes employing complexes of titanium,[2] nickel,[3] palladium,[4] gold[5] and lanthanides.[6] In contrast, catalytic *inter*-molecular hydroamination of alkynes appears much more difficult and these reactions are often hampered by low turnover numbers. The use of Hg^{II} reagents appears to be the most general route for the hydroamination of alkenes and alkynes[7,8] and examples of thallium,[9] lanthanides,[10] uranium and thorium[11] containing catalysts exist.

Recently, Bergman *et al.*[12] have demonstrated the utility of the zirconocene diamide [$Zr(\eta^5$-$C_5H_5)_2(NHC_6H_3$-$Me_2)_2$] **1** for the stoichiometric and catalytic addition of amines to internal alkynes and allenes, yielding enamines and imines respectively. The thermolysis (α-elimination) of **1** yields the transient imide '[$Zr(\eta^5$-$C_5H_5)_2(NC_6H_3$-$Me_2)$]' **2** which catalyses the addition of alkynes (RCCR, R = Me, Ph) to 2,6-dimethylaniline. Although intermediates have not been observed during the catalytic cycle, the proposed intermediate metallacyclobutene complex [$Zr(\eta^5$-$C_5H_5)${$N(C_6H_3$-$Me_2)(Ph)CC(Ph)$}] **3**, formed from a stoichiometric [2 + 2] addition of diphenyl acetylene to the metal nitrogen unsaturated bond of **2**, has been prepared and structurally characterised (see Scheme 1).

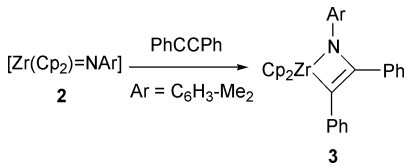

Scheme 1

Although phosphaalkynes, RCP, contain a slightly polarised bond[13] their similarity in reactivity to alkynes is now very well established.[14] However, although nucleophilic, *trans*-metallations and 1,2-additions have been described,[13] there are no examples to date of hydroaminations of this class of unsaturated molecule. Recently we have been interested in the cycloaddition chemistry of the phosphaalkyne Bu^tCP with Ti and Zr imides.[15] The reaction of Bu^tCP with the transient imide '[$Cp_2ZrN(C_6H_3$-$Me_2)$]' **2** affords the azaphosphacyclobutadiene complex [$Cp_2ZrN(C_6H_5$-$Me_2)PC(Bu^t)$] **4** which is isostructural with **3**. The MNPC fragment in **4** is in agreement with the expected bond polarity of the unsaturated reactive sites.

During the course of this work we have discovered that the reaction of catalytic amounts of $TiCl_4$ with the primary amines RNH_2 (R = Bu^t, Pr^i) followed by the addition of $PCBu^t$ yields the dialkyldiaminophosphines $P(NHR)_2CH_2Bu^t$ (R = Pr^i **5**,† Bu^t **6**†) in near quantitative yields (90–95%) (Scheme 2). No reaction occurs in the absence of $TiCl_4$.

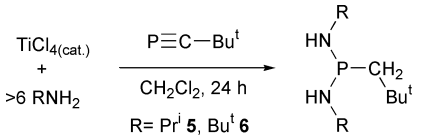

Scheme 2

Compounds **5** and **6** are colourless oils which can be easily purified from the crude reaction mixtures by sublimation *in vacuo* on to a cold finger (liquid nitrogen, 60–70 °C, 10^{-2} mbar, yield 95%). The ^{1}H NMR spectrum of **5** displays the expected five signals. The septet at δ 3.16 and two doublets at δ 1.40, 1.31 are assigned to the methine, methylene and NH protons respectively, the NH resonance being broadened by ^{14}N quadrupolar coupling. The singlet at δ 1.1 is attributed to the *tert*-butyl protons, and the doublet of doublets at δ 1.03 is assigned to the diastereotopic methyl groups of the isopropyl units which are further coupled to the methine protons. The ^{31}P-{^{1}H} NMR spectrum displays a singlet at δ 57.2. In order to unambiguosly assign the connectivity of **5**, the bis-diaminophosphine complex *trans*-[$PdCl_2${$P(Pr^iNH)_2CH_2(Bu^t)$}$_2$] **7**† was prepared from the reaction of [$PdCl_2(NCPh)_2$] **8** and 2 equiv. **5** in acetone. Crystals suitable for X-ray analysis were grown from a concentrated toluene solution cooled to −50 °C and the molecular structure is depicted below together with relevant bond lengths and angles (Fig. 1).‡ The structure is unremarkable, but serves to confirm the dihydroamination of the phosphaalkyne. The bis-aminophosphine units adopt a

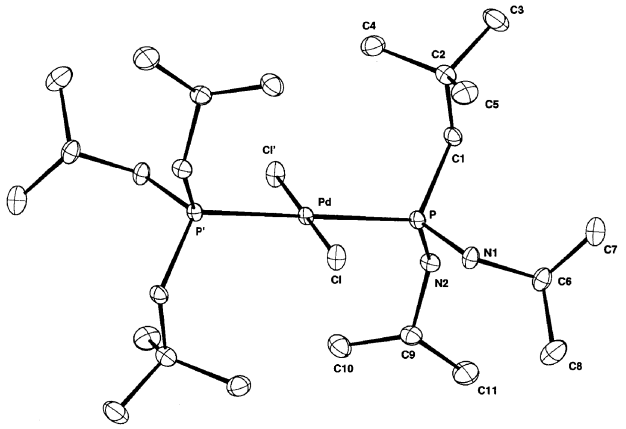

Fig. 1 Molecular structure of [$PdCl_2${$(NHPr^i)_2PCH_2(Bu^t)$}] **7**. Selected distances (Å) and angles (°): Pd–P 2.313(1), P–C(1) 1.829(3), P–N(1) 1.667(2), P–N(2) 1.662(2), Å. P–Pd–Cl′ 87.19(4), N(2)–P–N(1) 103.8(1) P–Pd–Cl 92.81(4) N(1)–P–C(1) 110.0(1), N(2)–P–Pd 116.32(9), N(1)–P–Pd 112.26(8), C(1)–P–Pd 114.49(9)°. Displacement ellipsoids are shown at 50% probability level. Hydrogen atoms are omitted for clarity.

DOI: 10.1039/b007512o

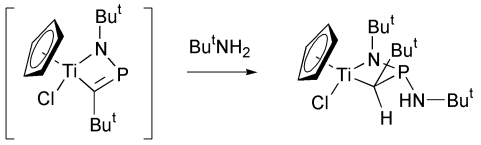

10

Scheme 3

trans-orientation in **7** and the phosphorus atoms display a tetrahedral coordination geometry.

Surprisingly, a survey of the literature shows a relative paucity of structural information on diaminophosphines and only $P(Ar^*NH)_2Ar$ (Ar^* = $C_6H_2Bu^t_3$-2,4,6)[16] and $P(Ar_fNH)_2Ar^*$ (Ar_f = $C_6H_2(CF_3)_3$-2,4,6)[17] have been crystallographically characterised. A few complexes of the group 6 metals have also been reported.[18]

The mechanism of formation of the diaminophosphine has not been fully determined, however Winter *et al.*[19] reported that treatment of $TiCl_4$ with an excess of primary amines affords imido complexes of type $[TiCl_2(NR)(NH_2R)_x)]$ **9** which clearly are likely candidates for the active catalytic species. Furthermore, in unpublished results Regitz and Asmus[20] have recently shown that the reaction of $[Ti(\eta^5\text{-}C_5H_5)Cl_3]$ with Bu^tNH_2 and $PCBu^t$ in toluene yields $[Ti(\eta^5\text{-}C_5H_5)Cl\{PNBu^t(NHBu^t)CHBu^t\}]$ **10**, (probably *via* a [2 + 2] addition of $PCBu^t$ to the intermediate titanium imide $[Ti(C_5H_5)Cl(NBu^t)]$, followed by a 1,2 addition of NH_2Bu^t across the activated P=C bond) (Scheme 3).

The mechanism of formation of the diaminophosphines **5** and **6** by di-hydroamination of $PCBu^t$ probably proceeds *via* the intermediacy of $[TiCl_2(NR)(NH_2R)_x)]$ **9** and $[TiCl_2(NR)P(NHR)CHBu^t]$ which is analogous to **10**, the excess $[NH_3Bu^tCl]$ formed subsequently removing the resulting substrate '{PNR(NHR)CHBu^t}' *via* a double protonation step.

We thank the EPSRC for financial support (D. J. W.) and Professor Manfred Regitz for unpublished results cited in ref. 20.

Notes and references

† *Characterisation data* for: $P(NHPr^i)_2CH_2{}^tBu$ **5**: ^{1}H NMR (d_6-benzene, 295 K) δ 2.36 [sept, 1H, CH, $^3J_{(HH)}$ 6.4 Hz], 1.4 [d, 2H, CH_2, $^2J_{(HP)}$ 2.5 Hz], 1.31 [d, 2H, N*H*C$(CH_3)_3$, $^3J_{(HH)}$ 7.14 Hz], 1.11 [s, $PCH_2C(CH_3)_3$], 1.05, 1.0 [d × 2, 12H, $CH(CH_3)_2$]. ^{31}P-{^{1}H} NMR δ 57.16.

$P(NHBu^t)_2CH_2Bu^t$ **6**: ^{1}H NMR (d_6-benzene, 295 K): δ 1.19 [s, 18H, $CH_2C(CH_3)_3$], 1.09 [s, 9H, $C(CH_3)_3$], 1.27 [d, br, 2H, CH_2]. ^{13}C-{^{1}H} NMR δ 55.9 [d, *C*$(CH_3)_3$, $^2J_{(CP)}$ 6.83 Hz], 50.97 [d, PC, $^1J_{(CP)}$ 14 Hz], 32.69 [d, NHC$(CH_3)_3$, $^3J_{(CP)}$ 8.93 Hz], 31.80 [d, $CH_2C(CH_3)_3$, $^2J_{(CP)}$ 9.03 Hz], 31.1 [d, NHC$(CH_3)_3$, $^2J_{(CP)}$ 12.28 Hz] ^{31}P-{^{1}H}: NMR δ 40.88. EI-MS *m/z* (%): 246 (30) $[M]^+$, 233 (13) $[M - (Me)]^+$, 175 (80) $[M - (NHBu^t) - (Me)]$.

$[PdCl_2\{P(NH_2Pr^i)_2CH_2Bu^t\}_2]$ **7** ^{1}H NMR (d_6-benzene, 295 K): δ 3.5 [s, br, 2H, NH], 2.8 [sept., 2H, C*H*$(CH_3)_2$, $^3J_{(HH)}$ 7.1 Hz], 1.8 [d, 4H, CH_2P, $^2J_{(HP)}$ 3.92 Hz], 1.39 [s, 9H, $C(CH_3)_3$,], 1.05 [d, 12H, $CH(CH_3)_2$, $^3J_{(HH)}$ 4.1 Hz] 1.19 [d, 12H, $CH(CH_3)_2$, $^3J_{(HH)}$ 4.1 Hz]. ^{13}C-{^{1}H} NMR: δ 44.3 [$C(CH_3)_3$], 41.1 [*pseudo*-t, PCH_2, $^1J_{(PC)}$ 22 Hz], 32.6 [br, $C(CH_3)_3$], 31.09 [NCH], 26.1, 25.6 [d, $CH(CH_3)_2$]. ^{31}P-{^{1}H} NMR δ 64.8. EI-MS *m/z* (%): 614 (25) $[M]^+$, 543 (5) $[M - (CC(CH_3)_3]^{+\cdot}$ Analysis calculated for $C_{22}H_{54}Cl_2N_4P_2Pd$: C, 43.04; H, 8.87. Found: C, 43.00; H, 8.90%.

‡ *Crystal data* for $C_{36}H_{66}Cl_2N_4P_2Pd$ **7**: M = 794.2, triclinic, a = 7.869(3), b = 10.919(3), c = 12.754(5) Å, α = 90.44(3), β = 103.26(3), γ = 95.81(3)°, U = 1060.6(6) Å^3, T = 173(2) K, space group $P\bar{1}$ (no. 2), Z = 1, λ(Mo-Kα) = 0.71073 Å, 5107 reflections measured which were used in all calculations. Final R indices for $[I > 2\sigma(I)]$ with 4563 reflections was $R1$ = 0.038. Single crystals of $[PdCl_2\{P(NH_2Pr^i)_2CH_2(Bu^t)\}_2]$ were grown from a saturated toluene solution (−53 °C), mounted in inert oil and transferred to the cold gas stream of the diffractometer. The structure was solved using direct methods and refined by full-matrix least-squares on F^2. CCDC 182/1830. See http://www.rsc.org/suppdata/cc/b0/b007512o/ for crystallographic files in .cif format.

1 R. Tauber, in *Applied Homogeneous Catalysis with Organometallic Compounds*, ed. B. Cornils and W. A. Herrmann, VCH, Weinheim, 1996, vol. 1, p. 507.
2 P. L. McGrane, M. Jensen and T. Livinghouse, *J. Am. Chem. Soc.*, 1992, **114**, 5459.
3 E. M. Campi and W. R. Jackson, *J. Organomet. Chem.*, 1996, **523**, 205.
4 K. Utimoto, *Pure Appl. Chem.*, 1983, **55**, 1845.
5 Y. Fukuda, K. Utimoto and H. Nozaki, *Heterocycles*, 1987, **25**, 297.
6 Y. Li, P. F. Fu and T. J. Marks, *Organometallics*, 1994, **13**, 439.
7 J. Barluenga and F. Azar, *Synthesis*, 1975, 704.
8 F. Esser, *Synthesis*, 1987, **5**, 460; R. C. Larock, *Angew. Chem., Int. Ed. Engl.*, 1978, **17**, 27.
9 J. Barluenga and F. Aznar, *Synthesis*, 1977, 195.
10 Y. Li and T.J. Marks, *J. Am. Chem. Soc.*, 1996, **118**, 707.
11 A. Haskel, T. Straub and M. S. Eisen, *Organometallics*, 1996, **15**, 3773.
12 P. J. Walsh, A. M. Baranger and R. G. Bergman, *J. Am Chem. Soc.*, 1992, **114**, 1708.
13 M. Regitz and P. Binger, in *Multiple bonds and Low Coordination in Phosphorus Chemistry*, ed. M. Regitz and O. J. Scherer, Thieme, Stuttgart, 1990 and references cited therein.
14 K. B. Dillon, F. Mathey and J. F. Nixon, in *Phosphorus the Carbon Copy*, John Wiley and Sons, Chichester, 1998.
15 F. G. N. Cloke, P. B. Hitchcock, J. F. Nixon, D. J. Wilson and P. Mountford, *Chem. Commun.*, 1999, 661.
16 E. G. Bent, R. Schaeffer, R. C. Haltiwanger and A. D. Norman, *Inorg. Chem.*, 1990, **29**, 2608; P. B. Hitchcock, H. A. Jasim, M. F. Lappert and H. D. Williams, *J. Chem. Soc., Chem. Commun.*, 1986, 1634.
17 J. T. Ahlemann, H. W. Roesky, R. Murugavel, E. Parsini, M. Noltemeyer, H. G. Smidt, O. Muller, R. Herbst-Irmer, L. N. Markovskii and Y. G. Shermolovich, *Chem. Ber.*, 1997, **130**, 1113.
18 E. Lindner, H. Rauleder and W. Hiller, *Z. Naturforsch.*, 1983, **38B**, 417.
19 T. S. Lewkebandara, P. H. Sheridan, M. J. Heeg, A. L. Rheingold and C. H. Winter, *Inorg. Chem.*, 1994, **33**, 5879.
20 S. M. F. Asmus, Ph.D. Thesis, University of Kaiserslautern, 1999. M. Regitz, personal communication.

Rapid synthesis of mesoporous SBA-15 molecular sieve by a microwave–hydrothermal process

Bharat L. Newalkar,[a] Sridhar Komarneni*[a] and Hiroaki Katsuki[b]

[a] *Materials Research Laboratory, The Pennsylvania State University, University Park, PA 16802, USA. E-mail: komarneni@psu.edu*

[b] *Saga Ceramics Research Laboratory, Saga 844-0024, Japan*

Received (in Irvine, CA, USA) 30th August 2000, Accepted 31st October 2000
First published as an Advance Article on the web

Ordered, hydrothermally stable mesoporous molecular sieve SBA-15 with hexagonal channel porosity has been synthesized for the first time under microwave–hydrothermal conditions from aged precursor gel within 15 min at 373 K; the crystallized product has been characterized using X-ray diffraction, nitrogen adsorption–desorption and transmission electron microscopy techniques.

Widespread applications of molecular sieves in the fields of separation and catalytic science have emphasised on the search for new structures with new framework compositions.[1] Thus, the last two decades have witnessed a rapid growth of molecular sieve science which has resulted in the discovery of an ordered, mesoporous molecular sieve family (designated as M41S)[2] for the first time. These materials, which can be synthesized with pore sizes from 15 to over 100 Å, are the potential candidates for a wide range of applications such as shape-selective catalysis and sorption of large organic molecules, guest–host chemistry and chromatographic separation. However, poor hydrothermal stability of these materials restricts their application potential. Thus, attempts are being made to improve their hydrothermal stability using various synthesis and post-synthesis routes. These attempts have resulted in the synthesis of the ordered, hydrothermally stable mesoporous molecular sieve SBA-15, which has been synthesized using a triblock organic copolymer as a template under hydrothermal conditions.[3] Here, we report, for the first time, a successful rapid synthesis of SBA-15 molecular sieve under microwave–hydrothermal (M–H) conditions within *ca.* 120 min. The term microwave–hydrothermal process was coined by Komarneni *et al*. in 1992 and this process has been used for the rapid synthesis of numerous ceramic oxides, hydroxylated phases, porous materials and metal powders.[4]

The microwave-assisted synthesis of molecular sieves is a relatively new area of research.[5] This method has been successfully applied for the synthesis of several types of zeolites namely zeolite A, Y, ZSM-5, MCM-41, metal substituted aluminophosphate and gallophosphate.[6–11] Microwave-assisted synthesis of molecular sieves offers many distinct advantages over conventional synthesis. They include rapid heating to crystallization temperature due to volumetric heating resulting in homogeneous nucleation, fast supersaturation by the rapid dissolution of precipitated gels and eventually a shorter crystallization time compared to conventional autoclave heating. Furthermore, it is energy efficient and economical.[4–11]

Microwave–hydrothermal synthesis of SBA-15 molecular sieve was performed using a MARS5 (CEM Corp., Matthews, NC, USA) microwave digestion system. This system operates at a maximum power of 1200 W and the power can be varied from 0 to 100% and is controlled by both pressure and temperature to a maximum of 350 psi and 513 K, respectively. A 2.45 GHz microwave frequency was used which is the same as that in domestic microwave ovens. The syntheses were carried out in double-walled digestion vessels which have an inner liner and cover made up of Teflon PFA and an outer strength vessel shell of Ultem polyetherimide. In a typical synthesis, 4 g of triblock poly(ethylene oxide)–poly(propylene oxide)–poly(ethylene oxide) ($EO_{20}PO_{70}EO_{20;}$ M.W. 5800, Aldrich) was dispersed in 30 g of double distilled water. The resultant solution was mixed with 120 g of 2 M HCl (J. T. Baker) solution under stirring to obtain a homogeneous solution. Finally, 9.50 g tetraethylorthosilicate (TEOS, Aldrich) was added to the homogeneous solution with stirring to form a reactive gel. Thus obtained gel was allowed to crystallize under microwave–hydrothermal conditions at 373 K for the desired time. The crystallized product was filtered off, washed with warm distilled water, dried at 383 K and finally calcined at 813 K in air for 6 h. The calcined product was characterized by X-ray diffraction (X'pert system, Phillips, USA), nitrogen adsorption–desorption isotherm measurements at 77 K (Autosorb, AS-1, Quantachrome, USA) and transmission electron microscopy (JEM-2010, JEOL, Japan). To study the progress of crystallization under microwave–hydrothermal conditions, samples were prepared for 15, 30, 60, 90 and 120 min at 373 K and were characterized using X-ray diffraction and nitrogen adsorption–desorption methods. The standard SBA-15 sample was also prepared by following the reported synthesis preocedure[3b] and was used as a reference to estimate the purity of the samples obtained under microwave–hydrothermal conditions.

The specific surface area, S_{BET}, for crystallized samples was calculated by the standard BET method[12] for nitrogen adsorp-

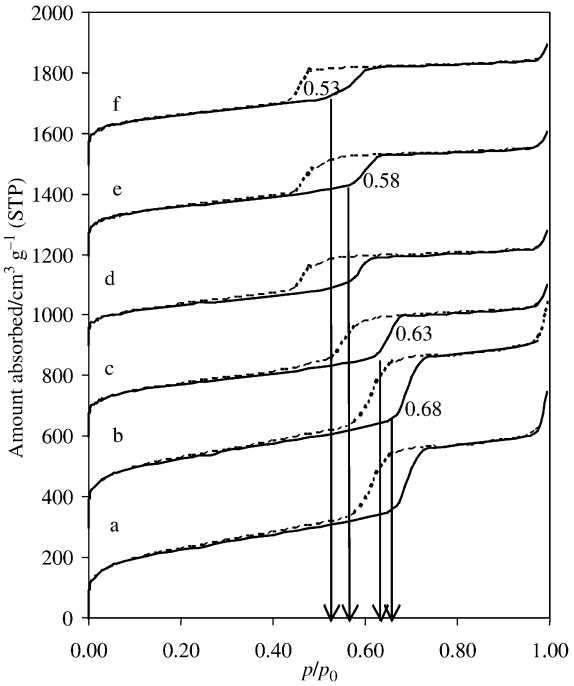

Fig. 1 Nitrogen adsorption (—)/desorption (·····) isotherms for prepared samples: (a) reference, (b) 120 min, (c) 90 min, (d) 60 min, (e) 30 min and (f) 15 min; SBA-15 samples obtained under M–H conditions at 77 K. The adsorption–desorption isotherms for 15, 30, 60, 90 and 120 min samples are shifted by 1500, 1200, 900, 600 and 300 cm^3 (STP) g^{-1}, respectively.

DOI: 10.1039/b007441l

Table 1 Structural parameters for various samples (calcined) obtained at different time intervals

t/min	a_0[a]/Å	S_{BET}/m^2 g^{-1}	S_{ex}/m^2 g^{-1}	$V_{mesopore}$/cm$^-$ g^{-1}	V_{pore} (p/p_0 = 0.95)/cm^3 g^{-1}	p/p_0	W_{KJS}/Å
15	90.4	475.3	3.8	0.46	0.51	≈0.53	52.0
30	93.9	567.8	12.4	0.49	0.52	≈0.58	55.2
60	93.9	583.3	13.5	0.50	0.55	≈0.58	55.8
90	94.8	625.3	16.7	0.62	0.67	≈0.63	62.3
120	105.0	790.9	24.4	0.88	0.96	≈0.68	72.3
Reference[b]	105.0	801.2	24.8	0.90	0.97	≈0.68	72.4

[a] $a_o = 2d_{100}/\sqrt{3}$. [b] Reference sample was prepared by following the reported conventional synthesis route.[3b]

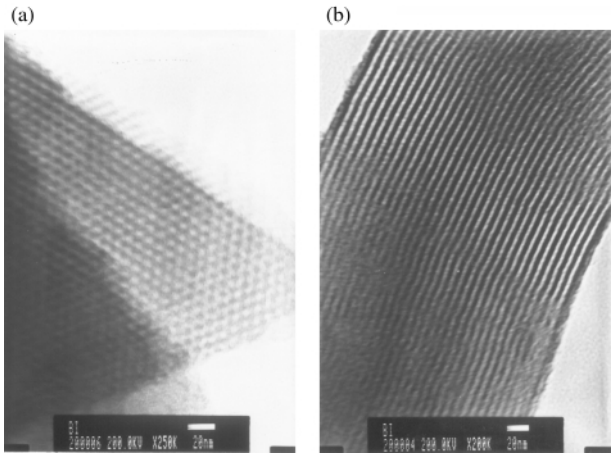

Fig. 2 Transmission electron micrographs with different orientations of a calcined hexagonal SBA-15 sample obtained at 120 min under M–H conditions.

tion data in a relative pressure range from 0.05 to 0.2. The calculation of pore size distribution (PSD) was performed by analyzing the adsorption data of the N_2 adsorption–desorption isotherm using the recently developed KJS (Kurk, Jaroniec, Sayari) approach.[13] The pore diameter corresponding to the maximum of PSD is denoted as W_{KJS}. The total pore volume was estimated from the amount adsorbed at a relative pressure of 0.95. The external surface area S_{ex}, and primary mesopore volume V_p, were estimated using the α_s-plot method, as described elsewhere.[14]

The X-ray diffraction patterns for SBA-15 samples obtained at various time intervals showed a well resolved pattern with a prominent peak at 2θ *ca.* 0.9° and two peaks at 2θ *ca.* 1.6 and 1.7° for all the crystallized samples which match well with the pattern reported for SBA-15.[3b]

Typical nitrogen adsorption–desorption isotherms for various samples are shown in Fig. 1. All the nitrogen adsorption–desorption isotherms are found to be of type IV in nature as per the IUPAC classification. The pore structure parameters for various SBA-15 samples calculated from the X-ray diffraction data and nitrogen adsorption–desorption isotherms are given in Table 1. Interestingly, the relative condensation pressure, which is a function of pore diameter, was found to increase with an increase in crystallization time which in turn reflected an increase in pore dimension and decrease in silica wall thickness for SBA-15 samples. These results are in good agreement with those reported under the conventional hydrothermal route[3b] and may be due to the rapid dehydration of EO blocks of the copolymer[15] at 373 K as a function of time under microwave–hydrothermal conditions. The condensation point for the 120 min sample was found to match with that of the reference sample (Fig. 1). Furthermore, a good agreement of pore structure parameters for the 120 min sample was observed with that of the reference sample. This indicates that the optimum reaction time for this synthesis is *ca.* 120 min at 373 K under microwave–hydrothermal conditions which is extremely short compared to the crystallization time required for conventional synthesis (*i.e.* 1–3 days). This observation is further reinforced by transmission electron microscopy (Fig. 2) which showed the ordered hexagonal pore structure with a one-dimensional channel structure of *ca.* 75 Å size, which is in close agreement with the value obtained from the KJS approach (Table 1), for a 120 min sample crystallized under M–H conditions.

In summary, the present study has established an extremely rapid synthesis method for SBA-15, which should also be applicable to other surfactants.

The support (in part) of this work by the NSF MRSEC program under grant number DMR-0080019 is gratefully acknowledged.

Notes and references

1 R. Szostak, *Molecular Sieves: Principles of Synthesis and Identification*, Van Nostrand Reinhold, New York, 1989.
2 C. T. Kresge, M. E. Leonowicz, W. J. Roth, J. C. Vartuli and J. S. Beck, *Nature*, 1992, **359**, 710.
3 (*a*) D. Zhao, J. Feng, Q. Huo, N. Melosh, G. H. Fredrickson, B. F. Chmelka and G. D. Stucky, *Science*, 1998, **279**, 548; (*b*) D. Zhao, Q. Huo, J. Feng, B. F. Chmelka and G. D. Stucky, *J. Am. Chem. Soc.*, 1998, **120**, 6024.
4 S. Komarneni, R. Roy and Q. H. Li, *Mater. Res. Bull.*, 1992, **27**, 1393; S. Komarneni, Q. H. Li, K. M. Stefansson and R. Roy, *J. Mater. Res.*, 1993, **8**, 3176; S. Komarneni, Q. H. Li and R. Roy, *J. Mater. Chem.*, 1994, **4**, 1903; S. Komarneni, R. Pidugu, Q. H. Li and R. Roy, *J. Mater. Res.*, 1995, **10**, 1687; S. Komarneni, Q. H. Li and R. Roy, *J. Mater. Res.*, 1996, **11**, 1866; S. Komarneni and V. C. Menon, *Mater. Lett.*, 1996, **27**, 313.
5 P. Chu, F. G. Dwyer and J. C. Vartuli, *US Pat.*, 4 778 666, 1988.
6 U. Lohse, R. Bertram, K. Jancke, I. Kurzawski, B. Parlitz, E. Loeffler and E. Schreier, *J. Chem. Soc., Faraday Trans.*, 1995, **91**, 1163.
7 I. Girnus, K. Jancke, R. Vetter, J. Richter-Mendau and J. Caro, *Zeolites*, 1995, **15**, 33.
8 X. Meng, W. Xu, S. Tang and W. Pang, *Chin. Chem. Lett.*, 1992, **3**, 69.
9 A. Arafat, J. C. Jansen, A. R. Ebaid and H. Van Bekkum, *Zeolites*, 1993, **13**, 162.
10 C. G. Wu and T. Bein, *Chem. Commun.*, 1996, 925.
11 M. Park and S. Komarneni, *Microporous Mesoporous Mater.*, 1998, **20**, 39.
12 S. Brunauer, P. H. Emmett and E. Teller, *J. Am. Chem. Soc.*, 1938, **60**, 309.
13 M. Kurk, M. Jaroniec and A. Sayari, *Langmuir*, 1997, **13**, 6267.
14 A. Sayari, P. Liu, M. Kurk and M. Jaroniec, *Langmuir*, 1997, **9**, 2499.
15 M. Kurk, M. Jaroniec, C. H. Ko and R. Ryoo, *Chem. Mater.*, 2000, **12**, 1961.

Crystal engineering a linear polymer of C_{60} fullerene *via* supramolecular pre-organization†

Dayong Sun and Christopher A. Reed*

Department of Chemistry, University of California, Riverside, California 92521-0403, USA.
E-mail: chris.reed@ucr.edu

Received (in Cambridge) 1st September 2000, Accepted 23rd October 2000
First published as an Advance Article on the web

The action of heat and pressure on a co-crystallate of C_{60} and a calixarene, where the fullerenes are pre-organized in separated linear columns, gives a linear [2 + 2] addition polymer of $(C_{60})_n$ without crosslinking.

Co-crystallizations and supramolecular assemblies are giving rise to an explosion of new crystal structures. Aesthetics, apparent ease of synthesis (self assembly), and the challenge of understanding and manipulating the weak forces that dictate crystal structures are driving this very active field.[1]

Fullerenes have three-dimensional arrays of reactive double bonds that present an unusually difficult problem for controlling the topology of multiple addition reactivity. Solid state pre-organization offers a potential solution. Scattered reports support this hypothesis. An unusual addend transfer reaction, not favored in solution, has been observed in the solid state with a Diels–Alder anthracene/C_{60} adduct.[2] A derivatized fullerene has been shown to assemble spontaneously into macroscopic rods and vesicles.[3] Pressure-induced dimerization of C_{60} to produce C_{120} is more efficient in a co-crystallate than in the bulk.[4] Pressure-induced dimerization of bulk C_{70} is interesting because it leads to selection of a single [2 + 2] addition isomer of C_{140}, even though five equi-energy combinations are possible.[5] Bulk C_{60} can be polymerized under pressure to give, depending on conditions, a variety of [2 + 2] addition polymers, some approaching distinct phases.[6]

Fullerenes are particularly prone to co-crystallization with other molecules[7–10] and under fortunate circumstances, the crystallizing components can become organized in useful ways. One such opportunity is provided by the report that C_{60} co-crystallizes with a calixarene in strictly linear, separated columns.[11] As shown in Fig. 1, the C_{60} molecules are in close van der Waals contact within a column (9.92 Å center-to-center distance) but parallel columnar stacks of calixarenes separate the fullerene columns from each other (12.81 Å center-to-center

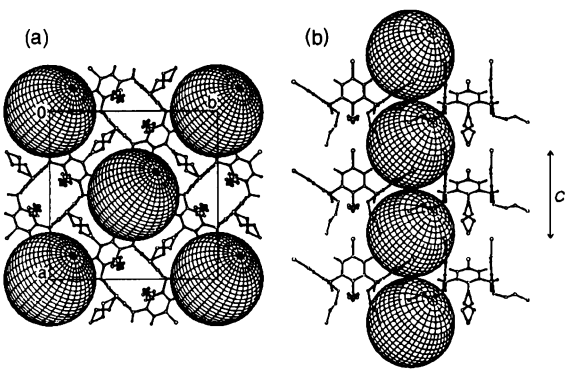

Fig. 1 Two views of the crystal packing of C_{60} and calixarene molecules (a) looking down the columns and (b) side-on. Reproduced with permission from ref. 11.

† Electronic supplementary information (ESI) available: enlarged copies of Figs. 3 and 4 showing peak frequencies. See http://www.rsc.org/suppdata/cc/b0/b007116l/

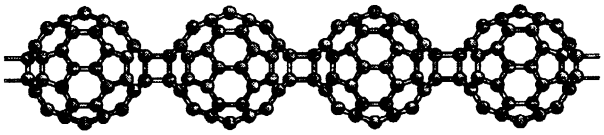

Fig. 2 Schematic depiction of the strictly linear [2 + 2] addition polymer of C_{60}.

distance). We reasoned that the action of heat and pressure should lead to strictly linear nanorods of a [2 + 2] addition polymer $(C_{60})_n$ (Fig. 2) and that the calixarenes would prevent crosslinking. The C_{60} molecules in the co-crystallate are known to be freely rotating at room temperature[12] so the pre-positioned fullerenes can readily adopt the required orientation of bonds[13,14] for mutual [2 + 2] addition.

The co-crystallate of *p*-bromocalix(4)arene propyl ether and C_{60} **1**, was prepared by the published method.[11] The identity of the product was checked by single-crystal X-ray determination. Sample homogeneity was checked by consistency of size, shape and color (dark red) under a microscope. Samples (*ca.* 20 mg) were packed in octahedrally shaped MgO containers, wrapped with Re foil for heating, fitted with a thermocouple, and pressed hydrostatically in a cube anvil. The pressure was increased gradually to the desired value (5 GPa) over a 30 min period followed by 1 h of heating at 200 °C. Samples were allowed to cool prior to the release of pressure since heat without pressure causes depolymerization. The polymerized product **2** had a black obsidian-like appearance. Bulk C_{60} was polymerized in a similar manner at 5 GPa and 200 °C to produce a 'crosslinked' material **3**, and at 1.5 GPa and 400 °C to produce an 'orthorhombic phase' **4**.[6]

Energy dispersive X-ray spectroscopy showed that the atomic composition of co-crystallate **1** and its polymerized product **2** were identical. The IR spectrum of **1** is a simple composite of its constituents: C_{60} and calixarene [Fig. 3(a) and (b)]. After pressure/heat treatment to produce **2**, bands due to the calixarene (1600–800 cm^{-1}) are unchanged, indicating that the calixarene component has not undergone chemical reaction [Fig. 3(c)]. On the other hand, several new bands appear in the 'fingerprint' region for fullerene derivatization (800–500 cm^{-1}) indicative of symmetry-lowering reactivity of C_{60}. Comparison of **2** with pressure/heat-treated pristine C_{60} samples **3** and **4** [Fig. 3(d) and (e)]† reveals a very close similarity to the orthorhombic phase **4** of polymerized C_{60}, but not to the crosslinked phase **3**. The Raman spectra of **2** and **4** are also very similar, in both the high and low energy regions (Fig. 4).† This indicates that the detailed mode of polymerization in **2** and in the orthorhombic phase of C_{60} is the same. Since there is growing consensus that the structure of **4** is a linear [2 + 2] addition polymer,[6] and since it is difficult to understand how **2** could be anything but a linear [2 + 2] addition polymer, the spectral consistency of **2** and **4** supports a correct structural assignment in both (Fig. 2).

Partial polymerization of **1** at 1.5 GPa and 150 °C gives a product from which C_{60}, C_{120}[15] and a presumably linear isomer of C_{180} can be separated by HPLC from the sonicated 1-chloronapthalene extract. The evidence for the linear isomer

DOI: 10.1039/b007116l

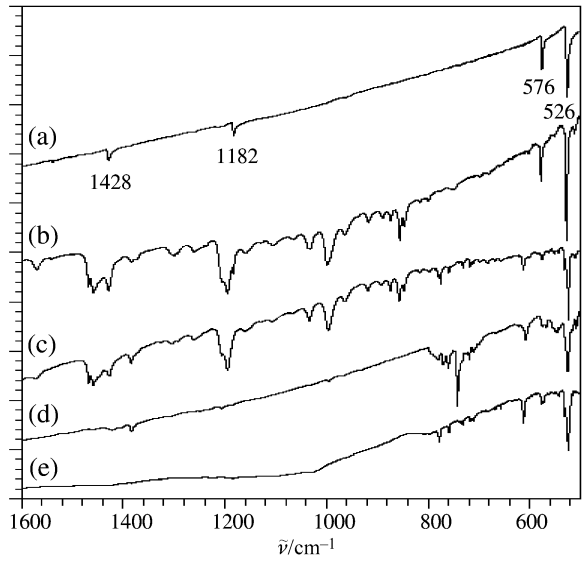

Fig. 3 IR spectra (KBr disk) of (a) C_{60}; (b) co-crystallate of C_{60} and calixarene, **1**; (c) polymerized cocrystallate, **2**; (d) crosslinked $(C_{60})_n$, **3**; and (e) orthorhombic $(C_{60})_n$, **4**. An enlarged copy of this figure which includes peak frequencies is available as ESI.†

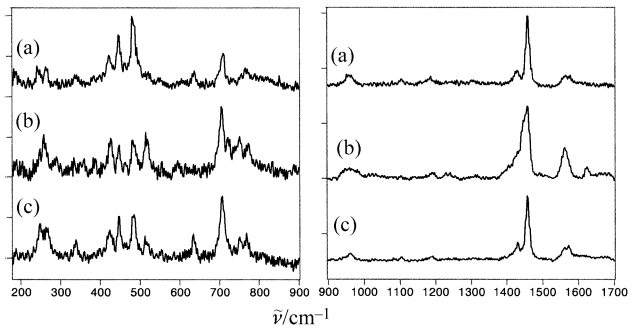

Fig. 4 Raman spectral comparison of [60]-fullerene polymers: (a) polymerized co-crystallate **2**; (b) crosslinked $(C_{60})_n$, **3**; and (c) orthorhombic (linear) $(C_{60})_n$, **4**. Spectra were recorded for samples as 5% KBr pellets with 514 nm Ar laser excitation. An enlarged copy of this figure which includes peak frequencies is available as ESI.†

of C_{180} includes (i) an HPLC retention time [Buckyprep(toluene–1,2-dichlorobenzene (1 : 1)] of 5.3 min compared to C_{60} (4.0 min) and C_{120} (4.6 min), (ii) a *single* HPLC peak rather than *four* that are observed in the low pressure trimerization of bulk C_{60},[16] (iii) an IR spectrum quite different from that of the proposed *triangular* isomer of C_{180},[16] (iv) a fullerene-like UV–VIS spectrum (λ_{max} = 327, 710 nm), and (v) photodegradation to C_{60} and C_{120}. The extremely low solubility and light sensitivity of this material has thwarted attempts to isolate it in significant amounts.

There has been significant effort put into the characterization of photo-[17] and pressure/heat-polymerized[18] C_{60}, partly justified on the basis of potential applications as conductors or nanowires.[6] In order to test the nanowire hypothesis we have subjected the linear polymer to a number of physical and chemical stability tests.

Of potential utility is the observation that it is insoluble in all common solvents and thermally stable at reasonable temperatures. Differential scanning calorimetry at 4 °C min^{-1} heating rate shows an irreversible endothermic process in the range 185–295 °C, consistent with thermal depolymerization at higher temperatures to give C_{60}. This is confirmed by subsequent solubility in organic solvents and UV-VIS identification of C_{60}. HPLC analysis showed traces of C_{120} were also present.

To model charge carrying, the polymer was exposed to reducing agents such as Na/THF or Hg/$R_4N^+Br^-$/THF. In both cases, complete dissolution of the polymer occurred and discrete C_{60}^- ions were detected (λ_{max} = 1075 nm). When smeared onto a platinum electrode and subjected to cyclic voltammetry, cathodic sweep peaks led to the production of C_{60}^- and C_{60}^{2-} in solution. Presumably reduction of the polymer causes monomers to dissociate from the surface like pearls dropping off a necklace. Dimeric C_{120} is known to dissociate immediately upon reduction.[15] In a comparable test for positive hole carrying, the polymer was exposed to oxidizing agents and anodic current. It is stable to aqueous $KMnO_4$ and HNO_3 but a moderate excess of bromine gradually produces $C_{60}Br_8$ (identified by isolation and IR spectroscopy).[19] On a platinum electrode, an irreversible anodic wave was observed at the same potential as C_{60} (*ca.* 1.4 V *vs.* Fc/Fc$^+$) suggesting irreversible decomposition. Although C_{60}^+ is now known as a stable entity,[20] it reacts instantly with errant nucleophiles in the solvent and supporting electrolyte.

In summary, this work shows how crystal engineering can be used fruitfully in fullerene polymer chemistry.[21] With its symmetrical [2 + 2] addition linkages, linear $(C_{60})_n$ is a chemically elegant polymer. One would like it to have a useful application. However, the present work suggests this will not be found as a nanowire. Rather, an analogy can be made to a nano*fuse*. Isolated single chains are unlikely to carry any current at all and bundles of chains are likely to be fragile. We note, however, that the proposed linear-chain isomer of KC_{60} is a metal[22] so stoichiometric intercalation of small cations can stabilize a lattice.

We thank Prof. Harry Green and Dr Larissa Dobrzhinetskaya for assistance with the cube anvil experiments, Prof. David Bocian for assistance in obtaining Raman spectra, Prof. Koichi Komatsu for a preprint of ref. 16 and the US National Institutes of Health NIH (GM 23851) for financial support.

Notes and references

1 G. D. Desiraju, *Angew. Chem., Int. Ed. Engl.*, 1995, **34**, 2311.
2 B. Krautler, T. Müller, J. Maynollo, K. Gruber, C. Kratky, P. Ochsenbein, D. Schwarzenbach and H.-B. Bürgi, *Angew. Chem., Int. Ed. Engl.*, 1996, **35**, 1204.
3 A. M. Cassell, C. L. Asplund and J. M. Tour, *Angew. Chem., Int. Ed.*, 1999, **38**, 2403.
4 Y. Iwasa, K. Tanoue, T. Mitani, A. Izouka, T. Sugawara and T. Yagi, *Chem. Commun.*, 1998, 1411.
5 S. Lebedkin, W. E. Hull, A. Soldatov, B. Renker and M. M. Kappes, *J. Phys. Chem. B*, 2000, **104**, 4101.
6 B. Sundqvist, *Adv. Phys.*, 1999, **48**, 1 and references therein.
7 F. Diederich and M. Gómez-López, *Chem. Soc. Rev.*, 1999, **28**, 263.
8 A. L. Balch and M. M. Olmstead, *Coord. Chem. Rev.*, 1999, **186**, 601.
9 P. D. W. Boyd, M. C. Hodgson, C. E. F. Rickard, A. G. Oliver, L. Chaker, P. J. Brothers, R. D. Bolskar, F. S. Tham and C. A. Reed, *J. Am. Chem. Soc.*, 1999, **121**, 10 487.
10 M. J. Hardie and C. L. Raston, *Chem.Commun.*, 1999, 1153.
11 L. J. Barbour, G. W. Orr and J. L. Atwood, *Chem. Commun.*, 1998, 1901.
12 E. Hughes, J. L. Jordan and T. Gullion, *J. Phys. Chem. B*, 2000, **104**, 691.
13 J. Knol and J. C. Hummelen, *J. Am. Chem. Soc.*, 2000, **122**, 3226.
14 G. M. Schmidt, *J. Pure Appl. Chem.*, 1971, **27**, 647.
15 G.-W. Wang, K. Komatsu, Y. Murata and M. Shiro, *Nature*, 1997, **387**, 583.
16 K. Komatsu, K. Fujiwara and Y. Murata, *Chem. Lett.*, 2000, 1016.
17 A. M. Rao, P. Zhou, K.-A. Wang, G. T. Hager, J. M. Holden, Y. Wang, W.-T. Lee, X.-X. Bi, P. C. Ekland, D. S. Cornett, M. A. Duncan and I. J. Amster, *Science*, 1993, **259**, 955.
18 Y. Iwasa, T. Arima, R. M. Fleming, T. Siegrist, O. Zhou, R. C. Haddon, L. J. Rothberg, K. B. Lyons, H. L. Carter Jr., A. F. Hebard, R. Tycko, G. Dabbagh, J. J. Krajewski, G. A. Thomas and T. Yagi, *Science*, 1994, **264**, 1570.
19 P. R. Birkett, P. B. Hitchcock, H. W. Kroto, R. Taylor and D. R. M. Walton, *Nature*, 1992, **357**, 479.
20 C. A. Reed, K.-C. Kim, R. B. Bolskar and L. J. Mueller, *Science*, 2000, **289**, 101.
21 For a different supramolecular effect in fullerene polymer chemistry, see: S. Samal, B.-J. Choi and K. E. Geckeler, *Chem. Commun.*, 2000, 1373.
22 S. Pekker, A. Jánossy, L. Mihaly, O. Chauvet, M. Carrard and M. Forró, *Science*, 1994, **265**, 1077.

Electrochemical detection of catechol and dopamine as their phenylboronate ester derivatives

Sharon M. Strawbridge, Stephen J. Green* and James H. R. Tucker*

School of Chemistry, University of Exeter, Stocker Road, Exeter, UK EX4 4QD. E-mail: j.h.r.tucker@exeter.ac.uk; stephen.j.green@exeter.ac.uk

Received (in Cambridge, UK) 5th September 2000, Accepted 5th October 2000
First published as an Advance Article on the web

By virtue of its reaction with phenylboronic acid to form a boronate ester, dopamine can be detected electrochemically in aqueous solutions, at physiological pH, in the presence of excess ascorbic acid.

It is well known that, in aqueous media, certain diols and boronic acids react together to form boronate esters, to an extent dependent upon the pH of the solution.[1] Such reactions have previously been used in the detection of sugars both by fluorescence spectroscopy[2] and, as part of recent progress in the electrochemical sensing of organic molecules,[3] by electrochemical measurements.[4] Here, we show that boronate esters, formed by the reaction of the aromatic diol 1,2-dihydroxybenzene (catechol) with phenylboronic acids, are electrochemically oxidised at potentials considerably more positive (by *ca*. 0.5 V) than that necessary to oxidise catechol itself, at a given value of pH. This positive shift indicates that, while formation of the neutral ester is thermodynamically favourable, the oxidised ester tends to revert back to (oxidised) catechol and the phenylboronic acid; cyclic voltammograms of these systems are consistent with such a mechanism. These properties extend to the boronate ester formed by reacting phenylboronic acid (PBA) with the catecholamine neurotransmitter dopamine **1**.

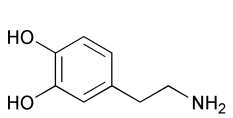

1

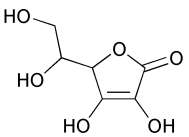

2

This has allowed us to electrochemically detect dopamine in the presence, as would be the case in any human sample, of excess ascorbic acid **2**. Detection is achieved *via* oxidation of the ester, which occurs at a potential positive enough of the values for dopamine and ascorbic acid oxidation to allow resolution by voltammetry (the values for dopamine and ascorbic acid are too close to allow their resolution). Other electrochemical approaches to the problem of dopamine detection, including the use of electrodes modified with ion-exchange membranes,[5] polypyrrole films,[6] templated silicate films,[7] and self-assembled monolayers[8] have met with varying degrees of success but there is presently no direct method, electrochemical or other, of measuring the level of dopamine in human samples; abnormal levels of dopamine have been linked to brain disorders such as Parkinson's disease[9] and schizophrenia.[10]

As aliquots of phenylboronic acid were added to a 1 mM solution of catechol in phosphate buffer at pH = 8, the form of cyclic voltammograms, recorded in this solution using a glassy carbon working electrode, was found to change from the typical form for the quasi-reversible electrode reaction of the catechol itself.[11] With each addition of PBA, a diminution of the catechol oxidation peak was accompanied by the growth of a more positive oxidation peak. Fig. 1 shows voltammograms recorded for catechol alone and for catechol in the presence of 20 equivalents of PBA; the latter clearly shows a new oxidation peak (b) at E_{pa} ('anodic peak potential') = 619 mV *vs*. Ag/AgCl. Since PBA is not electroactive in the potential window

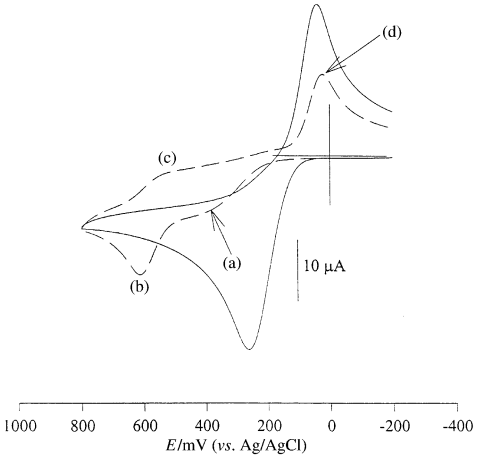

Fig. 1 Cyclic voltammograms, recorded using a glassy carbon working electrode in aqueous buffer at pH = 8 and 298 K, of 1 mM catechol (——) and 1 mM catechol plus 20 molar equiv. of PBA (- - -). Sweep rate 100 mV s^{-1}.

examined, the new oxidation peak is attributed to the oxidation of the boronate ester **3**, the presence of which in equilibrium with PBA and catechol accounts for the positive shift of the remaining catechol oxidation to peak (a). The formation of **3** (Scheme 1) was evidenced by ^{1}H NMR studies conducted over the pH range 6–8 (phosphate buffer, 10% d_4-methanol in H_2O), where the spectra of an equimolar mixture of PBA and catechol (each at 0.05 M) contained signals in the aromatic region consistent with the formation of a 1 : 1 adduct between the two reactants.

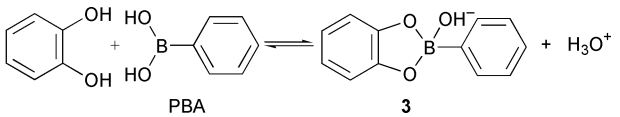

PBA **3**

Scheme 1

The peak (b) associated with the oxidation of **3** appears as for an electrochemically quasi-reversible, two-electron reaction ($E_{pa} - E_{pa/2} \approx 50$ mV; $E_{pa/2}$ is the half-peak potential). The somewhat smaller return peak (c) for reduction of the oxidised ester ($i_{pa}/i_{pc} \approx 0.34$; i_{pa} and i_{pc} are the anodic and cathodic peak currents, respectively), suggests that it is removed by a homogeneous reaction. Given that the second reduction peak (d) is at the potential observed previously for the reduction of oxidised catechol (benzoquinone) and was largely removed by reversal of the voltammogram at 400 mV (*i.e.* just short of oxidising **3**), we conclude that the oxidation of **3** leads to its cleavage to yield benzoquinone and (presumably) PBA.

With a view to obtaining fine control over the oxidation peak potential for the boronate ester, additional voltammetric studies were performed replacing PBA with the *meta*-substituted phenylboronic acids **4** and **5**. Only a slight effect was observed. The oxidation peaks for the esters formed from catechol with **4** and **5** were, respectively, coincident with and only 16 mV

DOI: 10.1039/b007187k

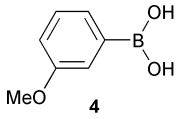

4

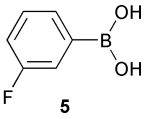

5

positive of that for the oxidation of **3** (results independent of pH over the range 6–8). ^{1}H NMR studies (pH = 7.5, phosphate buffer, 10% d_4-methanol in H_2O, reactants each at 0.05 M) revealed a similar trend in the ratio of boronate ester to boronic acid, following the order **5** > PBA ≈ **4**. The same trend was also observed using ^{11}B NMR (128 MHz, using BF_3:OEt_2 as an external standard), where each spectrum contained a boron signal corresponding to the boronate ester at *ca*. 18 ppm upfield from the signal corresponding to the boronic acid. The trend observed broadly reflects that for esters formed by reacting boronic acid with aliphatic diols,[1c] and is consistent with boronate ester formation being more favourable as the pK_a of the boronic acid decreases.[12] This is expected since electron withdrawing groups on the phenyl ring would tend to stabilise the product.

To demonstrate the possible use of these phenylboronic acid–catechol systems for the detection of biologically important catecholamines, differential pulse voltammetry was performed, using a glassy carbon electrode in pH = 7.5 phosphate buffer solution, to show how the neurotransmitter dopamine **1** could be detected in the presence of excess ascorbic acid **2**. Fig. 2 shows how the oxidation peak for 0.5 mM dopamine [voltammogram (a)] was obscured by that for oxidation of an added 5 mM of ascorbic acid [voltammogram (b)]. Then, after addition of 10 mM of PBA [voltammogram (c)], a new peak emerged at around 600 mV *vs*. Ag/AgCl, which (by analogy to the catechol/PBA case†) is for oxidation of an ester formed between dopamine and PBA, thus allowing the otherwise hidden dopamine to be detected. The figure inset confirms that the new peak recorded in voltammogram (c) does not indicate ester formation between PBA and ascorbic acid. Voltammogram (d) is that for 0.5 mM ascorbic acid in the presence of 10 mM of PBA and shows no peak for oxidation of an ester (the ascorbic acid voltammogram was unchanged by the addition of PBA and we conclude that no significant ester formation occurs). In voltammogram (e), where ascorbic acid was replaced by dopamine, a peak for oxidation of the boronate ester appeared at around 600 mV just as in voltammogram (c) in the main figure.

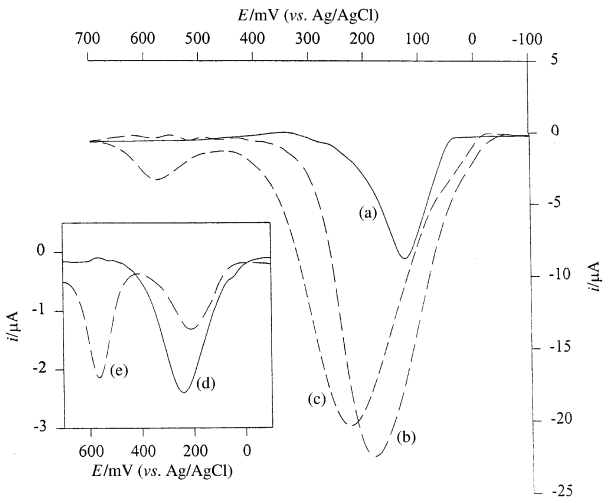

Fig. 2 Differential pulse voltammograms, recorded using a glassy carbon working electrode in aqueous buffer at pH = 7.5 and 298 K, of (a) dopamine **1** (0.5 mM), (b) **1** (0.5 mM) plus ascorbic acid **2** (5 mM), (c) **1** (0.5 mM) plus **2** (5 mM) plus PBA (10 mM), (d) **2** (0.5 mM) plus PBA (10 mM), and (e) **1** (0.5 mM) plus PBA (10 mM). Sweep rate 20 mV s^{-1}; pulse amplitude 50 mV.

Dopamine can thus be detected electrochemically in solutions, at physiological pH, containing an excess of ascorbic acid (we found the limit to be an excess of around 20-fold). We believe that this approach can readily be applied to the development of electrochemical sensors for dopamine and related catecholamines, especially since, once oxidised, the esters formed tend to revert back to the initial reactants, making the sensor re-useable.

We thank the EPSRC for the award of a quota studentship (to S. M. S.).

Notes and references

† The cyclic voltammetry of dopamine/PBA resembles that of catechol/PBA.

1 (*a*) H. Eggert, J. Frederiksen, C. Morin and J. C. Norrild, *J. Org. Chem.*, 1999, **64**, 3846 and references therein; (*b*) M. F. Paugam, L. S. Valencia, B. Boggess and B. D. Smith, *J. Am. Chem. Soc.*, 1994, **116**, 11 203 and references therein; (*c*) R. Pizer and P. J. Ricatto, *Inorg. Chem.*, 1994, **33**, 2402 and references therein.
2 T. D. James, K. R. A. S. Sandanayake, R. Iguchi and S. Shinkai, *J. Am. Chem. Soc.*, 1995, **117**, 8982; C. R. Cooper and T. D. James, *Chem. Commun.*, 1997, 1419.
3 J. D. Carr, L. Lambert, D. E. Hibbs, M. B. Hursthouse, K. M. A. Malik and J. H. R. Tucker, *Chem. Commun.*, 1997, 1649; M. T. Rojas and A. E. Kaifer, *J. Am. Chem. Soc.*, 1995, **117**, 5883; Y. Ge, R. R. Lilienthal and D. K. Smith, *J. Am Chem. Soc.*, 1996, **118**, 3976.
4 A. Ori and S. Shinkai, *J. Chem. Soc., Chem. Commun.*, 1995, 1771; A. N. J. Moore and D. D. M. Wayner, *Can. J. Chem.*, 1999, **77**, 681.
5 J. M. Zen and P. J. Chen, *Anal. Chem.*, 1997, **69**, 5087.
6 Z. Gao and H. Huang, *Chem. Commun.*, 1998, 2107; M. E. G. Breen and J. Cassidy, *J. Chem Soc., Faraday Trans.*, 1991, **87**, 115.
7 R. Makote and M. M. Collinson, *Chem. Commun.*, 1998, 425.
8 M. A. Chen and H. L. Li, *Electroanalysis*, 1998, **10**, 477.
9 C. Martin, *Chem. Br.*, 1998, **34**, 40.
10 M. Pufulete, *Chem. Br.*, 1997, **33**, 31.
11 M. R. Deakin and R. M. Wightman, *J. Electroanal. Chem.*, 1986, **206**, 167.
12 O. Kajimoto, T. Saeki, Y. Nagaoka and T. Fueno, *J. Phys. Chem.*, 1977, **81**, 1712.

ChemComm

Excellent mercury(II) ion selective fluoroionophore based on a 3,6,12,15-tetrathia-9-azaheptadecane derivative bearing a nitrobenzoxadiazolyl moiety

Hidefumi Sakamoto,*[a] Junichi Ishikawa,[b] Shintaro Nakao[b] and Hiroko Wada[b]

[a] *Department of Applied Chemistry, Faculty of Systems Engineering, Wakayama University, 930 Sakaedani, Wakayama 640-8510, Japan. E-mail: skmt@sys.wakayama-u.ac.jp*

[b] *Department of Applied Chemistry, Nagoya Institute of Technology, Gokiso-cho, Showa-ku, Nagoya 466-8555, Japan*

Received (in Cambridge, UK) 18th September 2000, Accepted 23rd October 2000
First published as an Advance Article on the web

Selective and drastic fluorescence enhancement for mercury ion was observed in 1,4-dioxane–water (60/40) using a fluoroionophore bearing a nitrobenzoxadiazolyl group linked to a 3,6,12,15-tetrathia-9-azaheptadecane moiety.

It is very important to develop a easy mercury determination system for monitoring its concentration in polluted areas. Chromo- and/or fluoro-ionophores are very effective for determination for metal ion concentration in terms of handling and equipment. Although several analytical reagents have been made for the determination of Hg^{2+}, most lack selectivity and sensitivity.[1,2] It is well known that Hg^{2+} might quench the fluorescence of fluorescent reagents because of its open-shell, paramagnetic properties.[3,4] A fluoroinophore, constitituted of a thiaaza crown unit and a boron dipyrromethene dye moiety, for Hg^{2+} was reported recently.[5] The emission spectra of the fluoroinophore, however, changed with polarity of the solvent, and so the complexation experiments were mainly carried out in acetonitrile. To the best of our knowledge, we now report the first fluoroionophore which increases the fluorescence intensity according to the concentration of Hg^{2+} selectively in a polar solution containing water.

The novel fluoroionophores **1** and **2**,† prepared by the

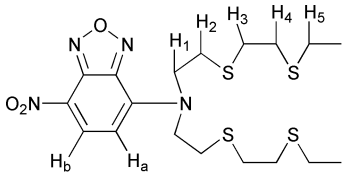

1

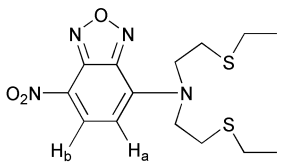

2

reaction of 4-chloro-7-nitrobenzoxadiazole with 3,6,12,15-tetrathia-9-azaheptadecane and 3,9-dithia-6-azaundecane, respectively, are constructed of ionophore and fluorophore moieties. The ionophore moiety contains sulfur atoms which have an affinity for soft metal ions such as Ag^+, Tl^+ and Hg^{2+}, because of its soft donor properties.[6,7] A nitrobenzoxadiazolyl moiety might function both as a fluorophore and as a chromophore.[8] It is expected that the electron density of the fluorophore moiety is reduced by the electron-withdrawing effect of coordinated metal ions and that remarkable changes in the fluorescence intensity and the absorption spectra should be caused when the ionophore moiety is complexed to a metal ion.[9]

On addition of various metal ions, changes in spectral properties of fluoroionophores **1** and **2** were measured by spectrophotometry and spectrofluorometry. 1,4-Dioxane–water (60/40 v/v) solution was used as solvent since the fluoroionophores are insoluble in pure water. The maximum wavelength of absorption (λ_{max}) for **1** is 492 nm, and that (λ_{em}) of the emission spectrum at an excitation wavelength of 492 nm is 536 nm. The spectral properties for **1** are independent of pH between pH 1 (0.1 mol dm^{-3} HNO_3) and neutrality. Fig. 1 shows the absorption and the emission spectra of 1,4-dioxane–water (40/60 v/v) solutions containing 1×10^{-5} mol dm^{-3} **1**, an equimolar quantity of a metal ion, *i.e.*, Mn^{2+}, Co^{2+}, Ni^{2+}, Cu^{2+}, Zn^{2+}, Cd^{2+}, Pb^{2+}, Tl^+, Ag^+ or Hg^{2+}, and 0.1 mol dm^{-3} HNO_3. On addition of Hg^{2+} and Ag^+ to a solution of **1**, blue shifts were observed for the absorption spectra and the absorbances were decreased similarly. On the other hand, the emission spectrum of **1** in the presence of Hg^{2+} ion was enhanced much more than that for Ag^+ ion, while the fluorescence intensity of **1** for Ag^+ was slightly higher than that for free **1**. A hypsochromic shift of *ca.* 18 nm of λ_{max} was observed on addition of Hg^{2+} ion, caused by the interaction between the metal ion and the nitrogen atom, associated with the chromophore moiety on the ionophore unit. Similar hypsochromic shifts have been reported for donor–acceptor type chromoionophores.[10,11] In the presence of other metal ions, *i.e.*, Mn^{2+}, Co^{2+}, Ni^{2+}, Cu^{2+}, Zn^{2+}, Cd^{2+}, Pb^{2+} or Tl^+, no spectral change for **1** was observed. Compound **2** exhibited no spectral change even in the presence of Hg^{2+} and Ag^+ ions under the same conditions as **1**. Such a difference in the spectral changes between **1** and **2** for Hg^{2+} and Ag^+ ions is attributable to a difference of stabilities of their complexes.[12,13]

Fig. 2 shows fluorescence intensity changes for **1** as a function of the concentration of the added metal ions. It is obvious that the fluorescence intensity increases with the concentration of Hg^{2+} and Ag^+. Compound **1** forms a 1:1 complex with Ag^+ quantitatively leading to small change in the

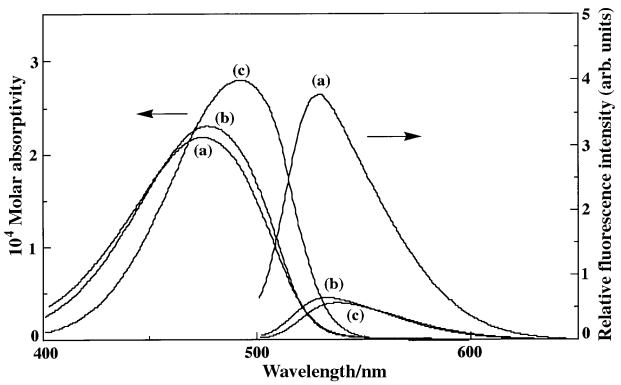

Fig. 1 Absorption and emission spectra of 1,4-dioxane–water (40/60 v/v) solution containing 1.0×10^{-5} mol dm^{-3} **1** 0.1 mol dm^{-3} HNO_3, and 1.0×10^{-5} mol dm^{-3} of metal ion. (a) Hg^{2+} added; (b) Ag^+ added; (c) Mn^{2+}, Co^{2+}, Ni^{2+}, Cu^{2+}, Zn^{2+}, Cd^{2+}, Pb^{2+}, Tl^+ added or absence of metal ion.

DOI: 10.1039/b007577i

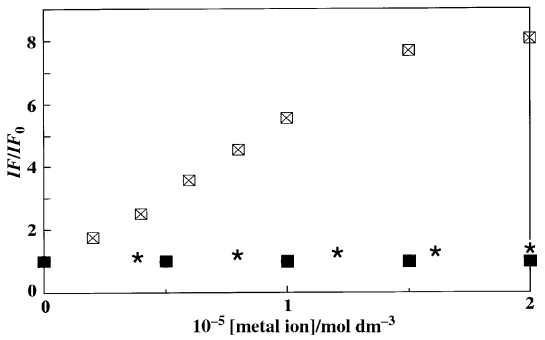

Fig. 2 Relative fluorescence intensity *vs.* metal ion concentration plots for 1×10^{-5} mol dm^{-3} **1** in 0.1 mol dm^{-3} HNO_3; (■) Mn^{2+}, (●) Co^{2+}, (▲) Ni^{2+} (◆) Cu^{2+}, (□) Zn^{2+}, (◇) Cd^{2+}, (○) Pb^{2+}, (⊙) Tl^{+} (all overlapped), Ag^{+} (*), Hg^{2+} (⊠). Values of IF/IF_0 indicate the relative fluorescence intensity for **1** in the presence of metal ion and were calculated using the value corresponding to free **1** as unity.

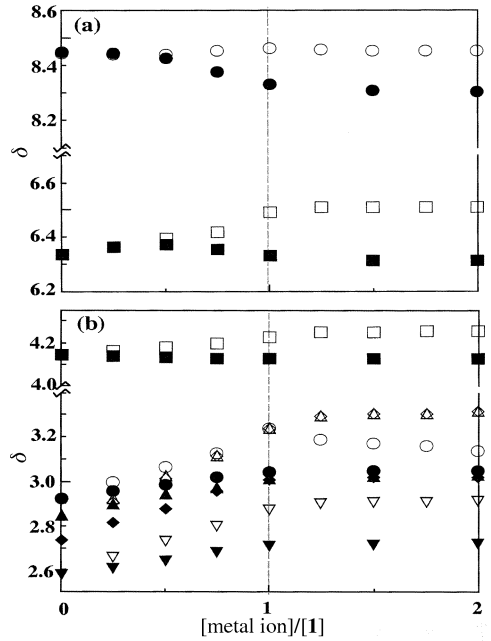

Fig. 3 Metal ion induced changes in chemical shifts for protons of **1** using acetonitrile-d_3 as a solvent. Open and filled symbols are for $(CF_3CO_2)_2Hg$ and CF_3SO_3Ag, respectively. (a) Plots of chemical shifts for protons of fluorophore moiety *vs.* [Metal ion]/[**1**]. (□, ■): H_a, (○, ●): H_b. (b) Plots of chemical shifts for protons of the ionophore moiety *vs.* [Metal ion]/[**1**]. (□, ■) H^1, (○, ●) H^2, (△, ▲) H^3, (◇, ◆) H^4, (▽, ▼) H^5.

fluorescence intensity. On the other hand, the complex of **1** with Hg^{2+} was gradually formed even above an $[Hg^{2+}]/[\mathbf{1}]$ ratio of 1 ($[Hg^{2+}] = 1.0 \times 10^{-5}$ mol dm^{-3}) and drastic enhancement in the fluorescence intensity compared with that for the complex with Ag^{+} was observed. These results demonstrate that the fluorescence intensity of the Hg(II) complex of **1** is much higher than that of the Ag(I) complex, although the former complex is less stable. The spectroscopic properties of the complex should preferentially depend on the strength of the interaction between a metal ion and the nitrogen atom connected to the nitrobenzoxadiazolyl moiety while the stability of the complex is governed by the degree of the affinity of the ionophore moiety to the metal ion.

^{1}H NMR titration of **1** with metal ions was carried out using acetonitrile-d_3 as solvent. Fig. 3 shows Hg^{2+} and Ag^{+} induced changes in the ^{1}H NMR chemical shifts for the protons of **1**. Addition of Hg^{2+} and Ag^{+} caused downfield shifts for the methylene protons of the sulfur containing moiety, indicating the coordination of sulfur atoms to the metal ion in which metal ion is probably wrapped by the tetrathiazaalkane moiety. A drastic downfield shift of H_a was observed on the addition of Hg^{2+}. This phenomenon suggests a decrease in the π-electron density of the nitrobenzoxadiazolyl moiety. The much larger change in the chemical shifts for the protons of the nitrobenzoxadiazolyl moiety upon the addition of Hg^{2+} relative to that of Ag^{+} suggests that the interaction of the nitrogen atom of the tetrathiazaalkane moiety with Hg^{2+} is stronger than with Ag^{+}.

In conclusion, the present study demonstrates that 3,6,12,15-tetrathia-9-azaheptadecane **1** bearing a nitrobenzoxadiazolyl moiety is a viable candidate as a fluoroionophore for a new Hg^{2+} ion sensor. This fluoroionophore **1** can discriminate Hg^{2+} ion well among heavy metal ions by an enhancement of the fluorescence intensity. In this case, the calibration curve for the relative fluorescence intensity *vs.* concentration of added Hg^{2+} shows linearity up to $[Hg^{2+}]$ 1.5×10^{-5} mol dm^{-3} 1,4-dioxane–water (60/40 v/v) (Fig. 2). This fluoroionophore can thus determine trace amounts of Hg^{2+} selectively even in acidic polar media containing water.

Notes and references

† The fluoroionohores **1** and **2** were synthesized as follows: 7-chloro-4-nitrobenzoxadiazole (2.2 mmol), the corresponding thiazaalkane (2 mmol)[13] and potassium carbonate (2 mmol) were dissolved in EtOH (50 mL) and stirred over night. After the reaction was complete, the solvent was evaporated *in vacuo* and 100 mL of water was added to the residue. The aqueous solution was extracted with $CHCl_3$ (3×100 mL) and the extract dried over $MgSO_4$. After removal of the solvent, the product was purified by column chromatography.

Selected data: for **1**: deep red solid, yield 59.9%, mp 55.0–56.0 °C; δ_H($CDCl_3$,TMS): 1.27 (t, 6H, CH_3), 2.48–3.23 (m, 16H, SCH_2), 4.16 (t, 4H, NCH_2), 6.18 (d, 1H, Ar), 8.40 (d, 1H, Ar); EI-MS: *m/z* 471 (M^+); Anal. Calc. for $C_{18}H_{28}N_4O_3S_4$: C, 45.38; H, 5.88; N, 11.74. Found: C, 45.33; H, 5.77; N, 11.62%.

For **2**: deep red solid, yield: 74.0%, mp 74.0–75.0 °C; δ_H($CDCl_3$,TMS): 1.31 (t, 6H, CH_3), 2.56–2.99 (m, 8H, SCH_2), 4.16 (t, 4H, NCH_2), 6.18 (d, 1H, Ar), 8.42 (d, 1H, Ar): EI-MS: *m/z* 356 (M^+); Anal. Calc. for $C_{14}H_{20}N_4O_3S_2$: C, 47.19; H, 5.62; N, 15.73. Found: C, 47.11; H, 5.52; N, 15.45%.

1 E. B. Sandell, *Colorimetric Determination of Trace of Metals*, Interscience publishers, New York, 3rd edn., 1958, p. 621.
2 Z. Marczwnko, *Separation and Spectrophotometric Determination of Elements*, Ellis Horwood Limited, Chichester, 1986, p. 371.
3 D. Y. Sasaki and B. E. Padilla, *Chem. Commun.*, 1998, 1581.
4 G. G. Talanova, N. S. A. Elkarim, V. S. Talanov and B. A. Bartsch, *Anal. Chem.*, 1999, **71**, 3106.
5 K. Rurack, M. Kollmannsberger, U. Resch-Genger and J. Daub, *J. Am. Chem. Soc.*, 2000, **122**, 968.
6 K. Saito, Y. Masuda and E. Sekido, *Anal. Chim. Acta*, 1983, **151**, 447.
7 K. Chayama and E. Sekido, *Anal. Sci.*, 1987, **3**, 535.
8 K. W. Street Jr. and S. A. Krause, *Anal. Lett.*, 1986, **19**, 735.
9 J. Ishikawa, H. Sakamoto and H. Wada, *J. Chem. Soc., Perkin Trans. 2*, 1999, 1273.
10 M. Takagi, in *Cation Binding by Macrocycles*, ed. Y. Inoue and G. W. Gokel, Marcel Dekker, Inc., New York and Basel, 1990, pp. 465–495.
11 H.-G. Hôhr and F. Vôgtle, *Acc. Chem. Res.*, 1985, **18**, 65.
12 H. Sakamoto, J. Ishikawa and M. Otomo, *Bull. Chem. Soc. Jpn.*, 1995, **68**, 2831.
13 J. Ishikawa, H. Sakamoto, T. Mizumo, K. Doi and M. Otomo, *Analyst*, 1998, **123**, 201.

ChemComm

[2]Rotaxane with a cation-binding wheel

Rameshwer Shukla, Martin J. Deetz and Bradley D. Smith*

Department of Chemistry and Biochemistry, University of Notre Dame, Notre Dame, IN 46556-5670, USA. E-mail: smith.115@nd.edu

Received (in Columbia, MO, USA) 7th July 2000, Accepted 4th October 2000
First published as an Advance Article on the web

A [2]rotaxane with a crown ether-containing wheel component is synthesized and shown to bind K^+ which alters the rotaxane's dynamic properties.

There is a growing interest in the chemistry of mechanically interlocked molecules.[1–6] This report concerns rotaxanes, interlocked molecules that are comprised of two molecular components, a wheel and a penetrating axle. Rotaxanes can exhibit a number of dynamic features such as shuttling (the wheel sliding along the axle),[1] pirouetting (the wheel rotating around the axle),[7] and unthreading (loss of the axle from the wheel).[8] There is hope that these dynamic features can be controlled and eventually utilized in molecular machines.[9,10] At present, a major research goal is to develop switching strategies to regulate these dynamic features.

Most of the rotaxanes reported to date have used macrocyclic wheels.[1] We are interested in macrobicyclic wheels with the generalized structure shown in Scheme 1. The structure is composed of a cation-binding macrocycle (*e.g.*, crown ether, porphyrin, *etc.*) and an anion-binding bridge [*e.g.*, diamine, bis(amide), *etc.*]. The anion-binding bridge should allow a range of rotaxanes to be prepared using the versatile anion-templated methodology recently introduced by Vögtle and coworkers.[11,12] The wheel component in these rotaxanes can bind metal cations which in turn should influence the rotaxane's dynamic processes.

In this initial study, we use the bridged crown ether **1** as the rotaxane's wheel component. Recently, we reported a six-step, gram-scale synthesis of **1** and demonstrated that a close structural analogue can simultaneously bind an alkali metal cation and a halide anion.[13] Based on this knowledge, we reasoned that host **1** should be able to bind the potassium salt of 4-tritylphenolate, and that the resulting 'wheeled potassium phenolate' **4** would react with isophthaloyl dichloride to form [2]rotaxane **3**. Indeed, we can consistently produce **3** in 20% isolated yield.† The compound is thermally stable, for example, heating a DMSO solution at 413 K for 3 h produces no evidence of rotaxane unthreading.

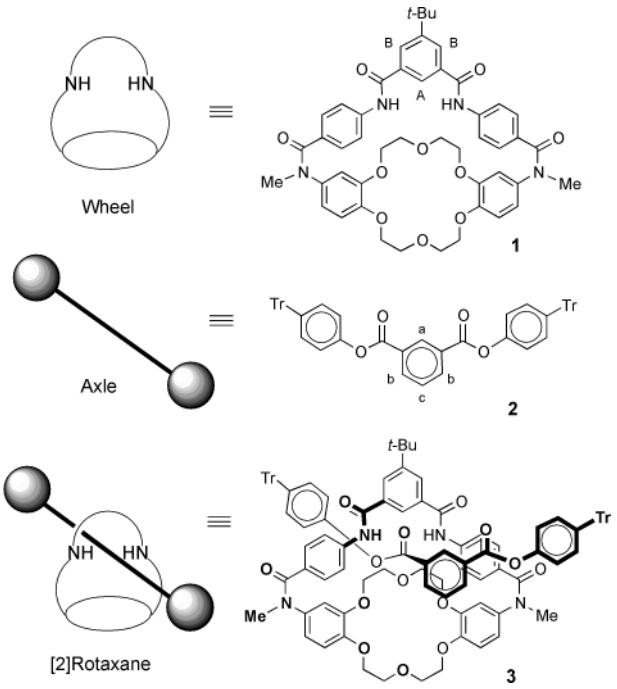

Scheme 1

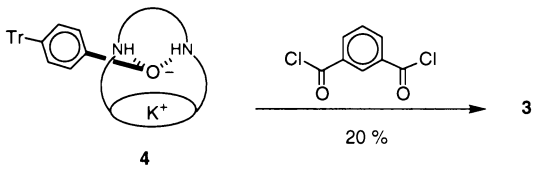

The structure of **3** was proved by NMR and mass spectrometry. A positive ion FAB mass spectrum shows a weak molecular ion signal at *m*/*z* 1646 (M+H), and intense signals at 1668 (M+Na) and 1684 (M+K). A sample treated with KCl shows only the signal at 1684 (M+K). The ^{1}H NMR spectrum is particularly revealing. The signal for the two isophthalate protons, H_b, in axle **2** is a doublet at 8.43 ppm when the axle is free in $CDCl_3$ solution [Fig. 1(a)], but when the axle is part of rotaxane **3** the two protons are no longer chemically equivalent and two doublets at 8.64 and 8.55 ppm are observed (Fig. 1(b)]. The room-temperature ^{1}H NMR spectrum of **3** in $CDCl_3$ was assigned by a combination of COSY and ROESY methods. Formation of the rotaxane shifts the signals for the wheel's internal bridgehead proton H_A and its two NH residues strongly upfield. Conversely, the axle's central phthalate protons, H_b and H_c, are shifted downfield. The ROESY spectrum indicates that the rotaxane adopts a predominant supramolecular co-conformation in $CDCl_3$ with the wheel and axle oriented as shown in structure **3**. For example, the axle proton H_a interacts

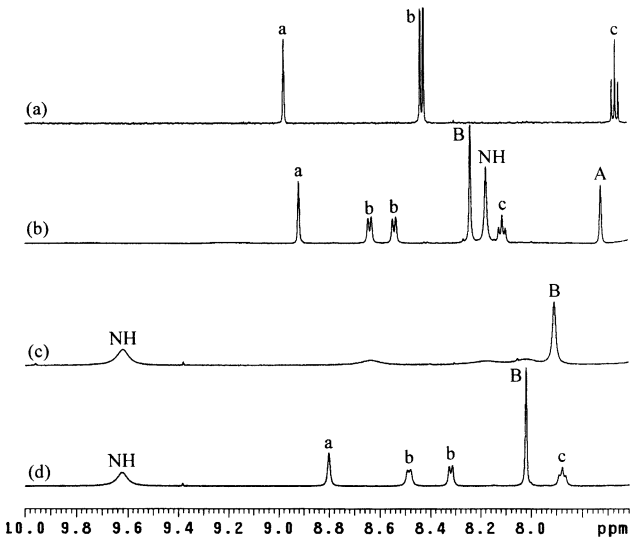

Fig. 1 Partial ^{1}H NMR spectra (600 MHz, 295 K) of (a) axle **2** in $CDCl_3$, (b) rotaxane **3** in $CDCl_3$, (c) rotaxane **3** in DMSO-d_6 and (d) rotaxane **3** and KPF_6 (5 equiv.) in DMSO-d_6.

DOI: 10.1039/b007329f

through-space with the wheel NH residues and proton H_A, there are also cross-peaks between axle protons H_b and H_c and the wheel's benzocrown signals.

The ^{1}H NMR spectrum of **3** in DMSO-d_6 shows broad signals for the axle protons at room temperature [Fig. 1(c)], but they become resolved upon warming. Thus, in DMSO the rotaxane populates multiple axle/wheel orientations.‡ The NMR signals also sharpen upon addition of five mol equivalents of KPF_6 at room temperature [Fig. 1(d)]. There are two possible explanations for this observation: either the added K^+ increases the rate of exchange between different rotaxane co-conformations, or the K^+ freezes out a single co-conformation (Scheme 2).[14] Evidence for the latter explanation is gained from a ROESY spectrum which is consistent with a predominant co-conformation that is different to the one in $CDCl_3$. For example, the axle proton H_a now interacts with the wheel's benzocrown signals whereas the axle proton H_c does not.

Our results suggest that cation-binding macrobicyclic wheels such as **1** can be incorporated into a range of mechanically interlocked structures, and that these compounds are likely to display cation-dependent dynamic behaviour. This is a step towards the eventual development of cation-switchable molecular machines.[9] We gratefully acknowledge financial support from the US National Science Foundation and the University of Notre Dame.

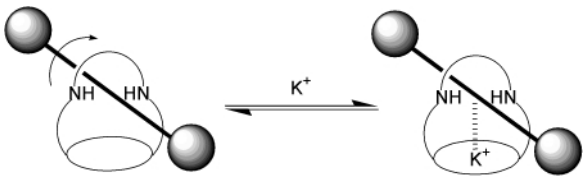

Scheme 2 Binding of K^+ freezes out a single rotaxane co-conformation.

Notes and references

† The anion-templated esterification reactions reported by Vögtle and coworkers require non-polar solvents and a small amount of crown ether to act as a phase-transfer catalyst.[12] In our case, rotaxane formation with salt-binding bicycle **1** is achieved using preformed phenolate salt in a range of organic solvents such as chloroform, THF or even THF–DMF. The reaction fails to yield **3** if the caesium or tetrabutylammonium salt of 4-tritylphenolate is used instead of the potassium salt, which is tentative evidence in favor of **4** as a reactive intermediate.

‡ We have not yet fully characterized the rotaxane's dynamic behaviour. The two most likely motions are pirouetting and shuttling.

1 *Molecular Catenanes, Rotaxanes and Knots*, ed. J. P. Sauvage and C. O. Dietrich-Bucheker, VCH-Wiley, Weinheim, 1999.
2 D. A. Leigh and A. Murphy, *Chem. Ind.*, 1999, 178.
3 F. Vögtle, O. Safarowsky, C. Heim, O. Affeld, O. Braun and A. Mohry, *Pure Appl. Chem.*, 1999, **71**, 247.
4 F. Raymo and J. F. Stoddart, *Chem. Rev.*, 1999, **99**, 1643.
5 W. S. Bryant, I. A. Guzei, A. L. Reingold and H. W. Gibson, *Org. Lett.*, 1999, **1**, 47.
6 K.-S. Jeong, J. S. Choi, S. Y. Chang and H.-Y. Chang, *Angew. Chem., Int. Ed.*, 2000, **39**, 1692.
7 L. Raehm, J.-M. Kern and J.-P. Sauvage, *Chem. Eur. J.*, 1999, **5**, 3310.
8 C. Heim, A. Affeld, M. Nieger and F. Vögtle, *Helv. Chim. Acta*, 1999, **8**, 746.
9 V. Balzani, A. Credi, F. M. Raymo and J. F. Stoddart, *Angew. Chem., Int. Ed.*, 2000, **39**, 3349.
10 J.-P. Sauvage, *Acc. Chem. Res.*, 1998, **31**, 611.
11 C. Seel and F. Vögtle, *Chem. Eur. J.*, 2000, **6**, 21.
12 C. Reuter, W. Wienand, G. M. Hübner, C. Seel and F. Vögtle, *Chem. Eur. J.*, 1999, **5**, 2692.
13 M. J. Deetz, M. Shang and B. D. Smith, *J. Am. Chem. Soc.*, 2000, **122**, 6201.
14 A. Andrievsky, F. Ahuis, J. L. Sessler, F. Vögtle, D. Gudat and M. Moini, *J. Am. Chem. Soc.*, 1998, **120**, 9712.

Typeset and printed by Black Bear Press Limited, Cambridge, England

ChemComm
FEATURE ARTICLE

Controlled polymerizations with constrained geometries

Keisuke Tajima† and Takuzo Aida*

Department of Chemistry and Biotechnology, Graduate School of Engineering, The University of Tokyo, 7-3-1 Hongo, Bunkyo-ku, Tokyo 113-8656, Japan. E-mail: aida@macro.t.u-tokyo.ac.jp

Received (in Cambridge, UK) 20th September 2000, Accepted 20th October 2000
First published as an Advance Article on the web

This short review focuses on recent advances in controlled polymerization and macromolecular architectonics by means of a variety of organized media with constrained geometries.

Introduction

In nature, macromolecules are essential materials for the diversity of life. Plants synthesize cellulose from sugars to support their body, and of course, proteins, polymers of amino acids, exist universally as primary materials for structuring, molecular recognition, electron and energy transfers, catalysis, and so forth. In biological systems, short- and long-range interactions are operative to allow multi-level ordering of macromolecules, which is essential for biological events. Formation of macromolecules in biological systems occurs also in such constrained, organized media, resulting in rigorous control of primary and even higher-ordered structures. On the other hand, chemical synthesis of macromolecules, which is usually conducted in homogeneous, non-constrained media, simply follows statistics of numerous elementary reaction steps, leading to the formation of macromolecules with poorly controlled architectures. In this respect, utilization of constrained media for artificial macromolecular synthesis is an interesting subject, which possibly allows spatial control of the primary structures of polymers and even their two- and three-dimensional multi-level structuring.

This short review focuses on recent advances in controlled polymerization and macromolecular architectonics by means of a variety of organized media with constrained geometries.

Overview

The present article describes some historical background and recent studies on controlled polymerizations in constrained media such as (1) micelles, (2) lipid bilayers, (3) liquid crystals, (4) organic crystals, (5) inclusion complexes, (6) microporous zeolites, and (7) mesoporous materials (Fig. 1), which are arranged in the order of increasing the rigidity of the media (Fig. 2).[1]

For the polymerization with constrained media, there are principally two approaches. One is to conduct polymerization of ordinary monomers in confined spaces of the media, while the other is to polymerize monomers which themselves are organized or co-organized to form constrained media. Studies on the polymerization in inclusion complexes, microporous zeolites, and mesoporous materials include examples only from the former approach. On the other hand, although both approaches are possible in the polymerization with micelles, lipid bilayers, liquid crystals, and organic crystals, this article focuses mostly on recent examples from the latter approach. The review article also focuses on several attempts to stabilize such organized media by polymerization, in order to fabricate well defined two- and three-dimensional macromolecular objects and hybridized materials.

Polymerization in micelles

Amphiphilic molecules having both hydrophobic long alkyl chains and hydrophilic groups are known to form micelles in aqueous media, where the alkyl chains are aggregated to form the core, while the hydrophilic head groups are exposed to water on the exterior surface to minimize the interfacial energy. In general, micelles are spherically shaped with a diameter of 3–4 nm, while under certain conditions rod-like micelles are formed, which have a cylindrical shape with a diameter of the cross section similar to the above. As for the polymerization of surfactant monomers, free radical polymerization has mostly been studied, since it is tolerant to water. In the polymerization in micelles, the chain growth is often affected by the structure and properties of the micelle. Furthermore, micelles are not static but dynamic. Therefore, a rapid exchange of the surfactant monomers between the micellar phase and the aqueous phase takes place during the polymerization (Fig. 3). The average time taken for surfactant molecules to leave a micelle is in the range 10^{-5}–10^{-9} s, which is much shorter than that for the growing radical to propagate (10^{-2}–10^{-6} s).[2–4] Hence, micelles are considered to be more or less soft media for polymerization.

† Former name: Keisuke Kageyama.

Takuzo Aida, born 3rd May 1956 in Japan, received his BSc degree in Physical Chemistry from Yokohama National University in 1979, and his MSc and Ph.D degrees in Macromolecular Chemistry from the University of Tokyo in 1981 and 1984, respectively, on Precision Macromolecular Synthesis with Metalloporphyrins. In 1984, he began an academic career at the University of Tokyo, where he has been Professor of Chemistry since 1996. He received the CSJ Award for Young Chemists in 1988, the SPSJ Award in 1993, and more recently the Wiley Polymer Science Award and IBM Science Award in 1999, and Nagoya Medal Seminar Silver Medal in 2000. His research interests include (1) synthesis of controlled macromolecular and supramolecular architectures, (2) photo- and supra-molecular chemistries of dendritic macromolecules, (3) mesoscopic materials sciences, and (4) bio-related molecular recognition and catalyses. In 1996, he was selected as a researcher of JST PRESTO Project 'Fields and Reactions'. In 2000, he held an appointment as the leader of JST ERATO Project on 'Nanospace'

Keisuke Tajima, born 23rd July 1974 in Japan, received his BSc and MSc degrees in 1996 and 1998, respectively, from the University of Tokyo, where he is currently a Ph.D student, focusing on utilization of mesoporous materials for controlled macromolecular synthesis. In 1999, he was selected for a JSPS Young Scientist Fellowship, and received the Best Presentation Award from CSJ in 1999.

DOI: 10.1039/b007618j

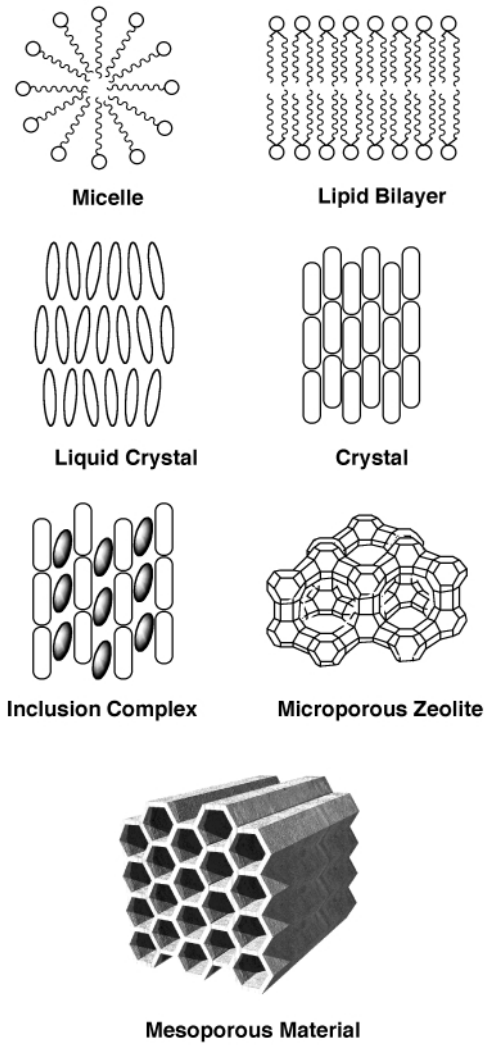

Fig. 1 Schematic representation for constrained media for polymerization.

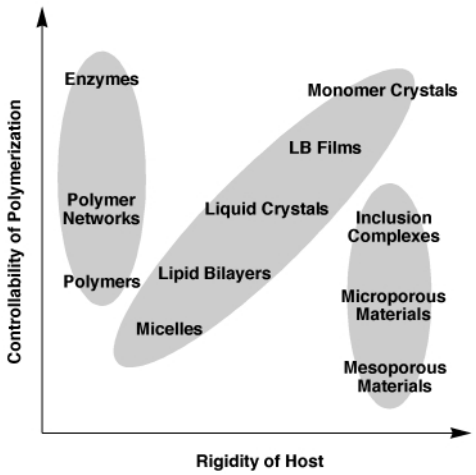

Fig. 2 Rough relationships between host rigidity and controllability of polymerization.

A typical phenomenon in free radical polymerization of surfactant monomers is that the propagation reaction above critical micelle concentration (c.m.c.) can be accelerated by 'condensation effect of monomer'. Examples include polymerization of anionic,[5] cationic,[6] and nonionic[7] surfactant monomers. In some cases, surfactant monomers in micelles spontaneously undergo radical polymerization without externally added initiators.[8,9] For example, the polymerization of sodium dodecyl 2-hydroxy-3-methacryloyloxypropyl phosphate **1** in

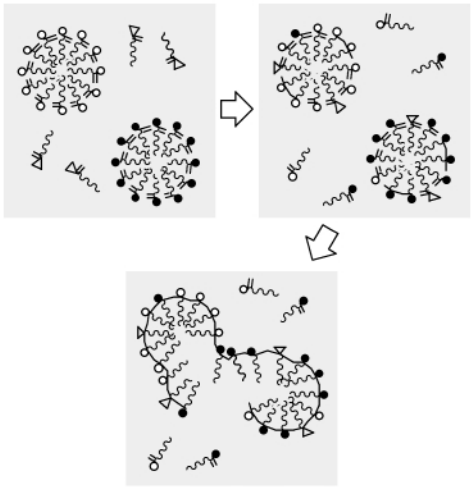

Fig. 3 Dynamical features of polymerization in micelles.

water at a concentration above the c.m.c (*ca.* 10^{-3} mol L^{-1}) takes place even at room temperature (35 °C) without initiator, to attain 100% monomer conversion.[8] In contrast, in methanol where **1** does not aggregate to form micelles, no polymerization

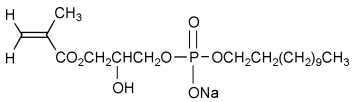

1

occurs unless radical initiators are added. The spontaneous polymerization may also be accounted for by 'condensation effect of monomer'. That is, the methacryloyl group of **1** is condensed at the core of the micelle, where the local monomer concentration must be as high as that in bulk.

Control of molecular weight of polymer by the size of micelle is a challenging subject. However, owing to the dynamic characteristics of micelles, monomer reactivity, rather than micelle size, is the predominant factor for determining the molecular weight. On the other hand, the synthesis of stereoregular polymers in micelles is also an interesting subject, considering possible orientations of polymerizable groups in micelles. However, successful examples are only very limited.[10,11] For example, Dais and coworkers have reported that the polymerization of dodecyl-2-methacryloyloxyethyldimethylammonium bromide **2** initiated by γ-rays at a monomer

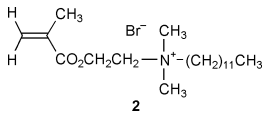

2

concentration above the c.m.c. leads to a polymer consisting exclusively of syndiotactic sequences at 25 °C.[11] In contrast, when a radical initiator such as 2,2′-azobisisobutyronitrile (AIBN) is used in place of γ-rays for initiating the polymerization, the tacticity of the resulting polymer at 50 °C is not directed but almost comparable to that of a polymer formed under homogeneous conditions.[10]

Polymerized micelles with an enhanced physical stability can be formed by free radical polymerization of surfactant monomers but only under very restrictive conditions owing to dynamic characteristics of micelles. For example, a rod-like micelle consisting of cetyltrimethylammonium 4-vinylbenzoate **3** is stabilized by radical polymerization of the vinylic group of the counter anion.[12] The resulting polymer micelle, as observed by small-angle neutron scattering, is likely to retain its original rod-like architecture, which shows an enhanced thermal stability and no longer dissociates upon dilution.

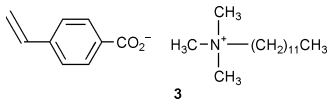

3

Dendrimers can also provide constrained media for polymerization. Percec *et al.* have recently reported an interesting phenomenon in free radical polymerization of self-assembled dendritic monomers. Dendritic monomers **4** and **5** are self-

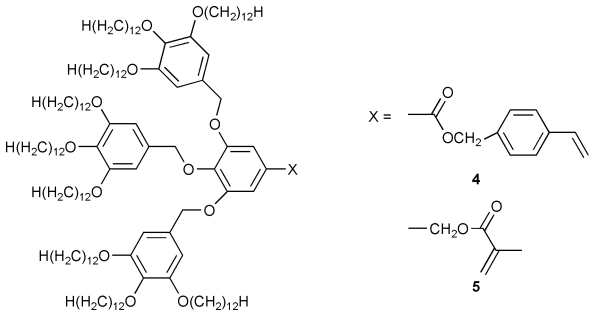

organized at a concentration above 0.20 mol L^{-1} to form spherical micellar aggregates in benzene.[13] In the interior of the aggregate, the polymerizable groups are condensed, so that the polymerization by a free radical initiator is considerably accelerated. As the polymerization proceeds, the interior of the aggregate becomes more constrained and thus protected from invasion of further initiator molecules. Consequently, the polymerization takes place in a 'living' fashion, to give a polymer with a narrow molecular weight distribution (MWD). Of further interest, the shape of the resulting macromolecule depends on the degree of polymerization (D_p) (Fig. 4). When D_p

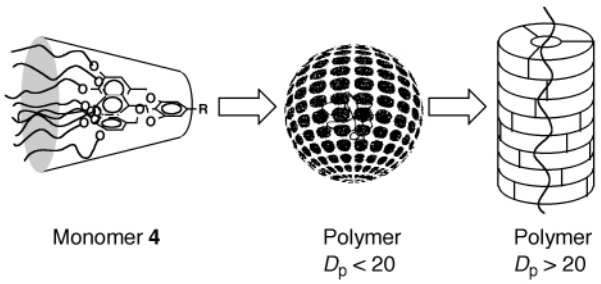

Fig. 4 Illustration for shape transition in free radical polymerization of self-organized dendritic monomers **4** and **5**.

is lower than 20, the polymer remains spherical. On the other hand, when D_p exceeds 20, the polymer becomes cylindrical, as directly observed by atomic force microscopy (AFM). As an extension of the present study, the living ring-opening metathesis polymerization of dendritic monomers having at the focal point a 7-oxanorbornene unit **6** has been reported.[14] Interestingly, the rate constant of propagation is increased discontinuously at a certain monomer conversion where D_p exceeds a critical value for the shape transition from a densely packed, spherical architecture to a more accessible, cylindrical one (Fig. 5).

Polymerization in lipid bilayers

Certain amphiphilic molecules such as lipids are known to form vesicles, *i.e.* liposome-like bilayer assemblies, which have been actively studied as synthetic analogues of biological membranes. In vesicles, the hydrophobic alkyl chains of lipids form two-dimensional (2-D) aggregates, while the hydrophilic head groups form ionic surfaces to contact water. Vesicles are larger

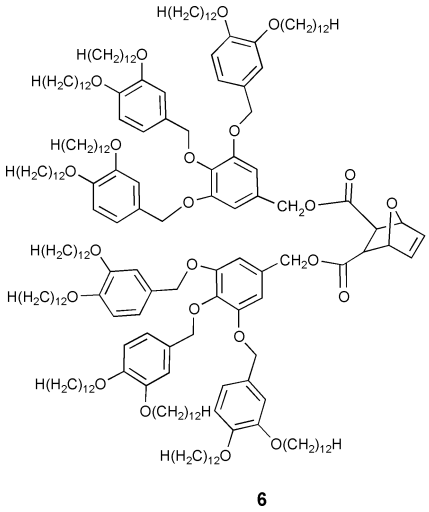

6

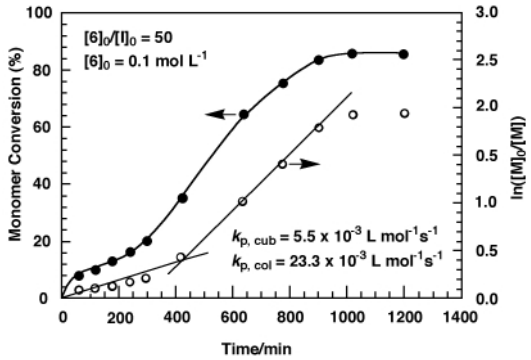

Fig. 5 Self-acceleration characteristics in ring-opening metathesis polymerization of a dendritic monomer **6**; $k_{p,\,cub}$, $k_{p,\,col}$: rate constants of propagation in cubic and columnar phases, respectively.

than micelles and have a much smaller surface curvature. Although a lateral diffusion of lipid molecules within a layer can occur, exchange of the lipid molecules among vesicles is slow. At a given temperature (T_m), vesicles show a main phase transition, which is attributed to a conformational change of the alkyl chains. At temperatures below T_m, the lipid molecules are in a solid-like state with a low mobility, where the alkyl chains adopt a *trans* conformation. On the other hand, at temperatures above T_m, they are in a liquid crystalline state with greater diffusibility, where the alkyl chains adopt a *gauche* conformation.[15] Since the pioneering works by Ringsdorf *et al.* on the formation of polymerized vesicles,[16] extensive studies have been made on free radical and photo-initiated polymerizations of synthetic bilayers.[17] In contrast to micelles, vesicles are stabilized easily through polymerization to give macromolecular containers which can be used for a variety of applications such as drug delivery.

Free radical polymerization of lipid monomers in bilayer membranes shows significantly different kinetics from those in the bulk phase.[18–20] For example, in the polymerization of a vesicle consisting of a phosphatidylcholine derivative having an acryloyl (**7**), methacryloyl (**8**), or sorbyl group (**9**) at the hydrophobic chain end, the degree of polymerization (D_p) is proportional to $[M]^2$ and $[I]^{-1}$ at a high monomer conversion ([M] and [I] are concentrations of monomer and initiator, respectively). In contrast, in bulk under otherwise identical conditions to the above, D_p is proportional to [M] and $[I]^{-0.5}$. These contrasting trends indicate that the polymerization of the lipid monomers in the bilayer state is terminated mostly by recombination of the growing polymer radical with a fragment radical of the initiator, rather than self-recombination of the

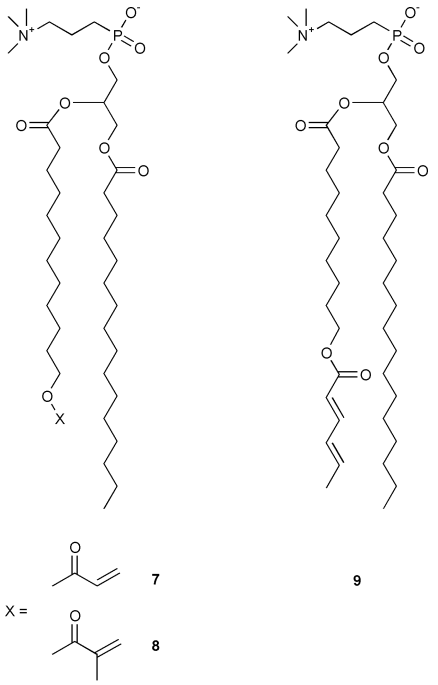

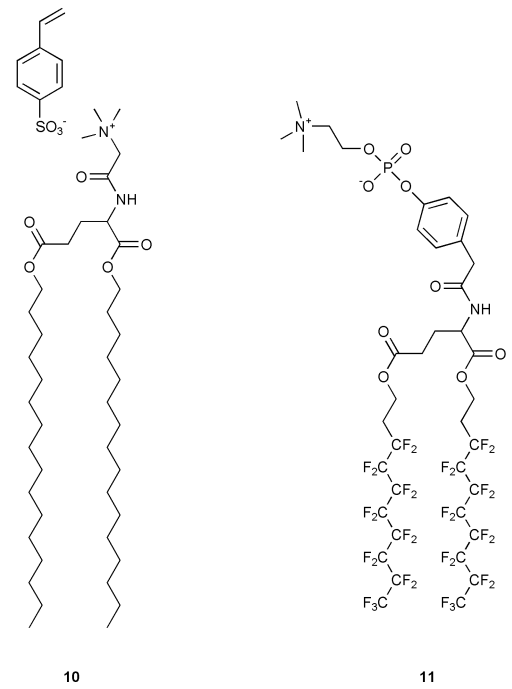

growing polymer radicals.[21] This is likely due to a reduced mobility of long polymer chains in bilayer media.

Phase transitions of bilayer membranes also affect polymerization kinetics. For example, in free radical polymerization of lipid monomer **9**, the activation free energy E_a and frequency factor A, obtained in a temperature range below the phase transition temperature T_m, are 10 kcal mol^{-1} and 10^7, respectively (Fig. 6).[22] On the other hand, at temperatures

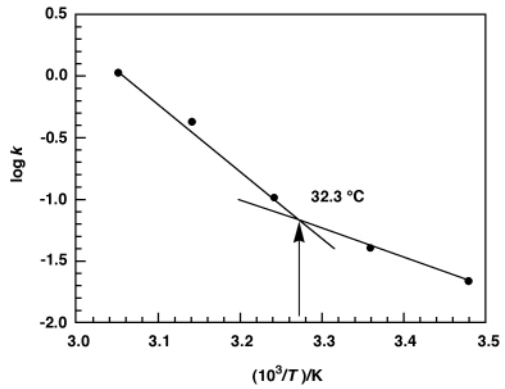

Fig. 6 Effect of phase transition on propagation rate constant in free radical polymerization in a bilayer membrane of a lipid monomer **9**.

higher than T_m, they are 24 kcal mol^{-1} and 10^{16}, respectively. Such discontinuous changes in kinetic parameters upon phase transition indicate a large effect of the lateral diffusibility of **9** on the polymerization kinetics.

Control of molecular weight of the polymer in bilayer membranes is also an interesting subject, and numerous attempts have been made by, *e.g.* changing monomer/initiator mole ratio, phase separation, and addition of chain transfer agents.[19,23] For example, a mixture of a hydrocarbon lipid monomer **10** and a non-polymerizable fluorocarbon lipid **11** forms a phase-separated bilayer membrane (Fig. 7), since fluorocarbons are poorly miscible with hydrocarbons.[23] In this phase-separated system, the molecular weight of the resulting polymer becomes lower as the content of **10** in the membrane (≈ size of the monomer domain) is decreased.

As bilayer membranes are not stiff enough to fix the orientation of polymerizable groups for steric control, only

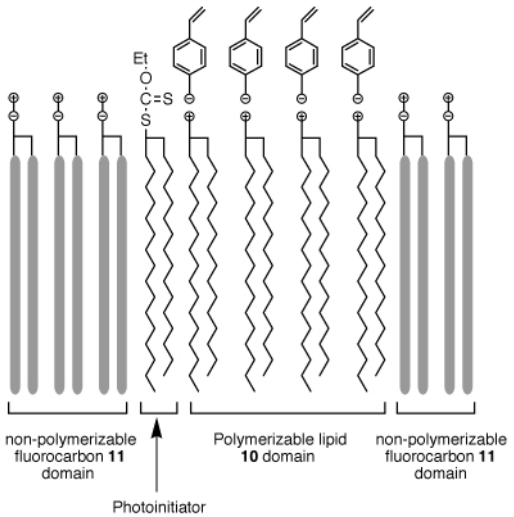

Fig. 7 Illustration for photoinduced polymerization in a phase-separated bilayer membrane of a mixture of a lipid monomer **10** and a non-polymerizable fluorocarbon lipid **11**.

limited examples of stereospecific polymerization in bilayer media have been reported. An old but interesting example is the polymerization of a vesicle consisting of dioctadecyldimethylammonium methacrylate **12**.[24] Upon irradiation of the vesicle, the methacrylate anion on the surface of the vesicle is polymerized to give a highly syndiotactic poly(methacrylate) anion. In contrast, under homogeneous conditions in ethanol, no polymerization occurs under otherwise identical conditions.

Vesicles can be used as templates for the synthesis of topologically unique polymers.[16] Recent examples include selective polymerization of a heterobifunctional lipid monomer **13** containing diene and dienoyl groups at the hydrophobic and hydrophilic termini of its alkyl chain, respectively.[25] O'Brien and coworkers have reported that photoirradiation of vesicles of **13** results in the polymerization of the dienoyl group exclusively, while radical initiation with AIBN gives rise to the selective polymerization of the diene group. Of interest, a simultaneous or a sequential polymerization of both the dienoyl and diene groups of **13** in the vesicular state results in the formation of a novel ladder polymer **14** and not a 2-D cross-

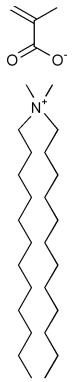

12

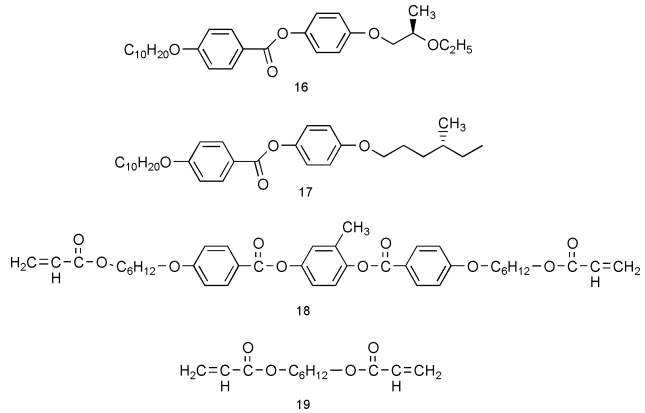

16 17 18 19

linked network **15** (Fig. 8). Addition of a surfactant molecule to polymer **14** in water results in destruction of its vesicular assembly, as observed by light scattering, whereas polymer **15** with a cross-linked architecture is robust under similar conditions. These contrasting trends suggest that polymer **14** is not cross-linked but a ladder.

Polymerization in liquid crystals

Liquid crystals have been utilized for optical materials such as LCDs. Depending on the manner of molecular orientation, several different LC phases such as nematic, smectic, and cholesteric phases are formed. LC media are more constrained than micellar and even bilayer media, and therefore attractive for control of polymerization.

Molecular orientation of monomers considerably affects the polymerization kinetics in LC media. A mixture of **16** and **17** forms a smectic C* (SC*) LC phase at room temperature, which becomes isotropic when heated to 70 °C. Bowman and coworkers have found that free radical polymerization of mesogenic monomer **18** in the SC* LC phase at 25 °C, as observed by differential scanning calorimetry (DSC), proceeds with much higher propagation and termination rates than in the isotropic phase at 70 °C.[26] In contrast, when non-mesogenic monomer **19** is polymerized in the SC* phase (35 °C), the propagation rate is not much different from that under isotropic conditions, but the termination is considerably slower. According to polarized IR spectroscopy, mesogenic and non-mesogenic monomers **18** and **19** are oriented normal and parallel to the smectic layer of the LC phase, respectively. Since addition of **18** to the LC phase does not affect the *d* value, mesogenic **18** most likely exists in the smectic layer (Fig. 9a). In contrast, non-mesogenic monomer **19** is possibly intercalated between the smectic layers, as the *d*-value of the LC phase becomes larger upon addition of **19** (Fig. 9b). This work provides a clear demonstration that the polymerization kinetics depend considerably upon spatial segregation and orientation of monomers in LC media.

In the polymerization in LC media, structural characteristics of the LC phase may give rise to unique organized structures of produced polymers. Recently, Akagi and Shirakawa *et al.* have reported an interesting observation that the polymerization of acetylene in a chiral LC phase leads to helical fibers of polyacetylene.[27] An optically active binaphthol derivative **20** having mesogenic units combined with a 1 : 1 mixture of **21** and **22** forms a chiral nematic LC phase, where the polymerization of acetylene with a homogeneous Ziegler–Natta catalyst ($Ti(OBu^n)_4/Et_3Al$) proceeds to give single-handed helical fibers of polyacetylene, as observed by scanning electron microscopy (SEM). The helical sense of the fibers can be controlled by the absolute configuration of the LC solvent. For example, in the nematic phase of the (*R*)-binaphthol derivative **20**, helical fibers with an anticlockwise sense result (Fig. 10). Circular dichroism spectroscopy of the fibers also shows a clear Cotton effect in the region of a π–π* transition of the conjugated backbone. In this case, the twisted molecular packing of **20** in the chiral nematic

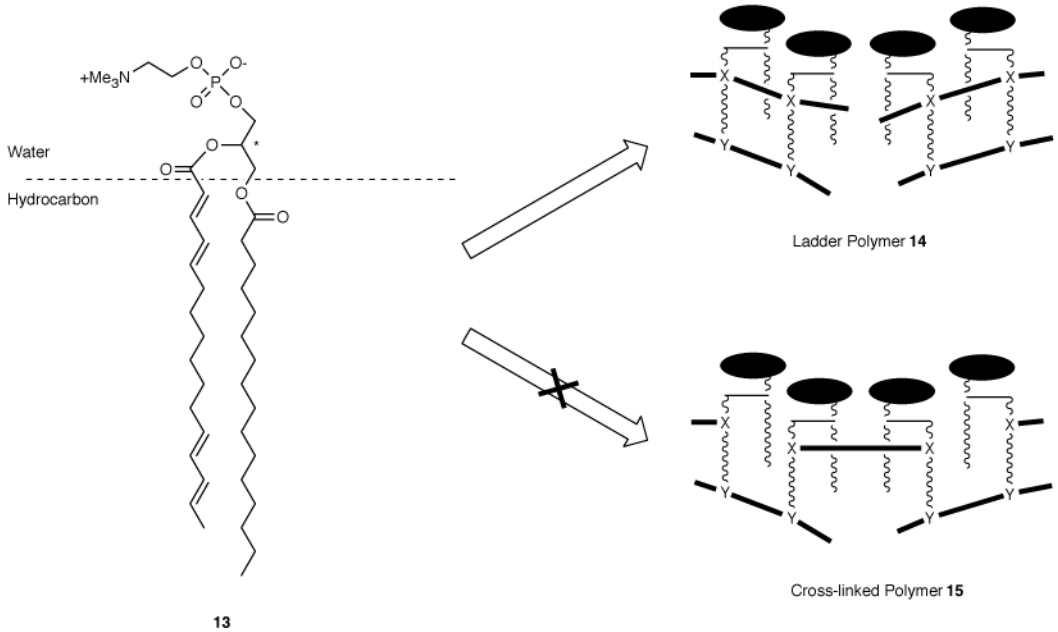

13

Fig. 8 Illustration for different modes of polymerization in a bilayer membrane of a lipid monomer **13**.

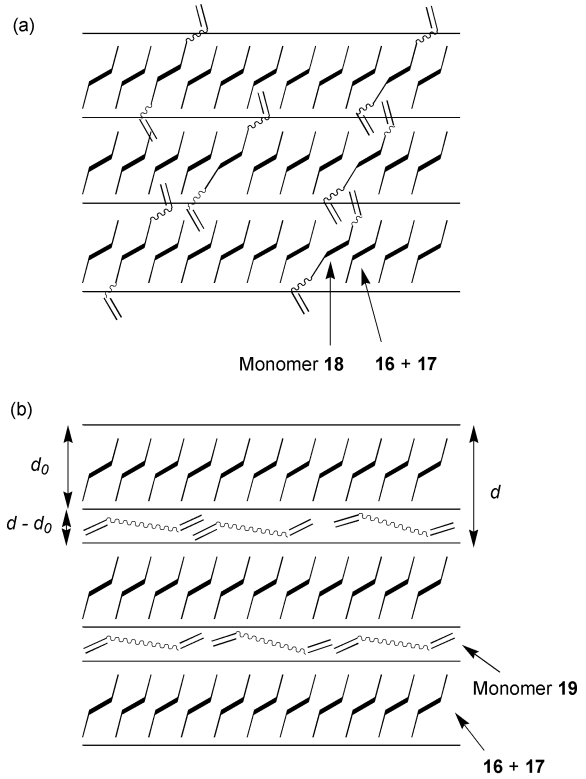

Fig. 9 Proposed models for photoinduced polymerizations of mesogenic and non-mesogenic monomers (**18**, **19**) in a smectic C* liquid crystal.

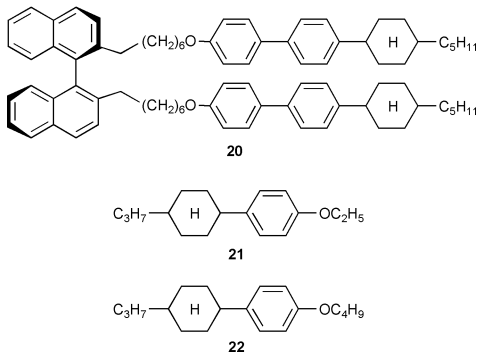

phase is likely to serve as a template for the formation of helical polyacetylene fibers.

Much attention has also been paid to the polymerization of LC monomers for obtaining polymeric materials with predictable structures from their LC phases. Stupp *et al.* have reported the synthesis of a conceptually new two-dimensional (2-D) polymer by the polymerization of a mesogenic monomer in a smectic LC phase (Fig. 11).[28] Monomer **23** has an acrylic group at a terminus, a nitrile group in the middle, and a mesogenic group at the other terminus. **23** is organized to form a smectic LC phase **24** (non-polymerized form of **25**) by a π–π interaction among the mesogenic groups and a homochiral interaction among the chiral nitrile groups. The acrylic and nitrile groups in the LC state are polymerized by heating, to give a cross-linked 2-D network structure **25**, which still shows certain characteristics of the original LC phase. Although the polymer is soluble in chloroform, it most likely retains a sheet-like structure originating from the smectic phase even in solution. Analysis by

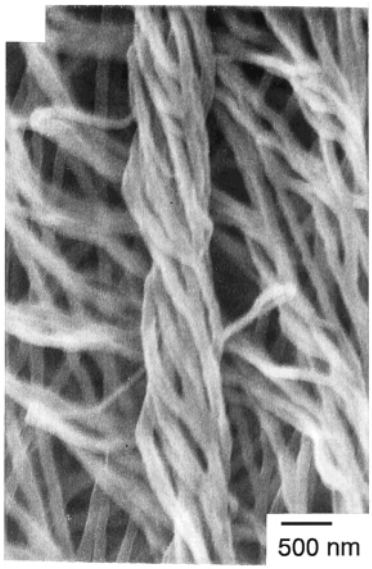

Fig. 10 A SEM micrograph of helical polyacetylene fibers formed with a homogeneous Ziegler–Natta catalyst in a chiral nematic phase of a mesogenic (*R*)-binaphthol derivative **20**. Reprinted in part with permission from: *Science*, 1998, **282**, 1683 (Copyright © 1998, the American Association for the Advancement of Science).

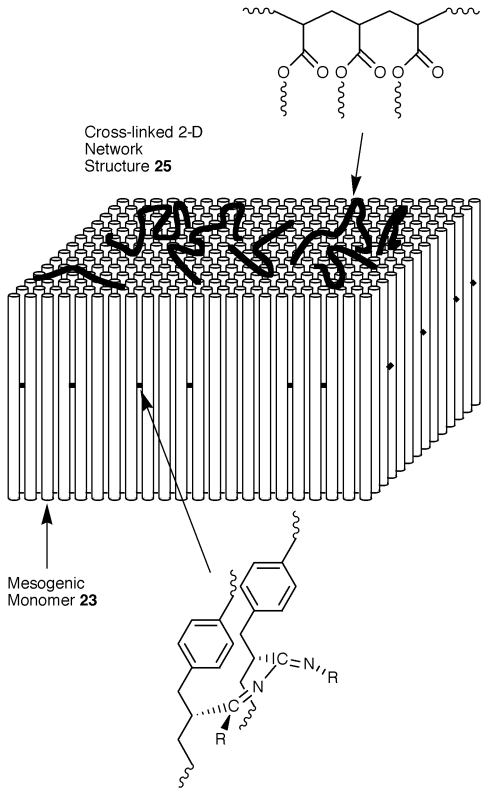

Fig. 11 Illustration for thermal-induced polymerization in a smectic liquid crystalline phase of a mesogenic monomer **23**.

gel permeation chromatography (GPC) indicates that the polymer has an ultrahigh molecular weight (17 000 000) with a broad molecular weight distribution, suggesting that the polymer is a nanometer-sized 2-D object. According to transmission electron microscopy (TEM), this polymer can be spread over a glycerin surface upon casting from its dilute

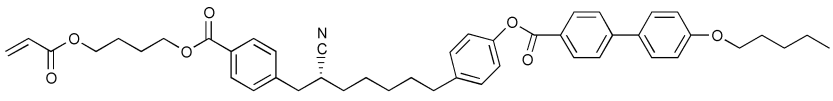

23

chloroform solution, to give a single-layered polymeric film with a thickness of < 100 Å. Along the line of this study, a triblock molecule having a relatively large coiled head group with crosslinkable oligobutadiene units anchored by a rigid mesogenic tail has been synthesized. Owing to the relatively large head group, this rod-coil molecule self-assembles to form a 'mushroom-shaped' cluster of limited size rather than an infinite 2-D sheet as in the case of **23**. Annealing of this molecule in a LC phase at 250 °C resulted in crosslinking of the oligobutadiene domains to form a soluble polymeric nanoscale object with a molecular weight of *ca.* 70 000 (M_w/M_n = 1.11). Although extended annealing promotes the crosslinking and enhances the yield, no substantial increase in molecular weight results. Therefore, the crosslinking occurs within individual clusters to fix the mushroom shape.[29] This is an interesting 2-D approach to the template synthesis of nanoscale polymeric objects.

Not only thermotropic LCs but also lyotropic LCs can be stabilized by polymerization. Gin and co-workers have reported an interesting example of the stabilization of a lyotropic LC phase by polymerization.[30] When a water-soluble polymeric precursor of poly(*p*-phenylenevinylene) (PPV) **26** is mixed with

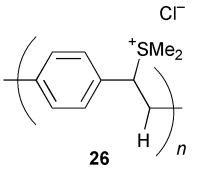

26

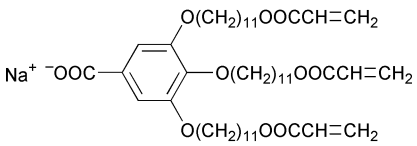

27

amphiphilic acrylate monomer **27** in aqueous media, an inverse hexagonal lyotropic LC phase is formed, in which **26** is likely to be threaded into the hexagonal column and oriented parallel to its *c*-axis (Fig. 12). Subsequently, the acrylate group of **27** is

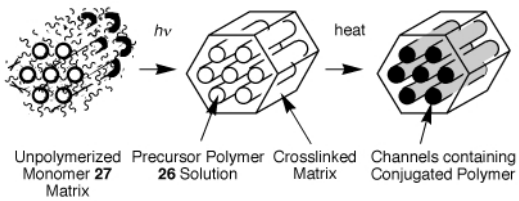

Fig. 12 Illustration for photoinduced polymerization of an amphiphilic acrylate monomer **27** in a lyotropic liquid crystalline phase and subsequent thermal transformation of the precursor polymer **26** into poly(phenylenevinylene).

polymerized by photo-irradiation, and the resulting mixture is heated to promote the removal of dimethyl sulfide and HCl to convert **26** to fluorescing PPV. Interestingly, the fluorescence of PPV from the resulting hybrid material is much stronger than that of bulk PPV, suggesting that the hybridized PPV chains are spatially isolated from one another and protected from self-quenching of the excited state. The present self-assembling/polymerization approach is unique, and can be applied not only to the design of anisotropic optical materials but also to the fabrication of new silica/polymer hybrids[31] and polymer-supported transition metal catalysts.[32]

Polymerization in organic crystals

In the crystalline state, the arrangement and orientation of molecules are strictly determined by crystal packing. Topochemical polymerization, in which the polymerization of a crystallized monomer occurs without changing the symmetry of the crystal lattice, has been well known since the 1960s. Representative examples include topochemical polymerization of diacetylenic monomers in the crystalline state, which occurs upon exposure to UV light or γ-rays.[33] [2 + 2] Photopolymerization of diolefinic monomers in the crystalline state has also been studied extensively.[34] In general, topochemical polymerization is highly sensitive to the crystal structure of monomers. If the crystal packing of monomers is not suited for the active growing end to propagate, no polymerization occurs. For example, for diacetylenic monomers to polymerize topochemically, monomer molecules in the crystalline state are required to adopt a tilted molecular stacking with a distance between the diacetylene centers of *ca.* 4.7–5.2 Å and an angle between the molecular stacking axes of *ca.* 45°. On the other hand, for topochemical polymerization of diolefinic monomers, a center-to-center distance of 3.5–4.2 Å between the polymerizable units is required.

Although crystal engineering of organic molecules has been greatly advanced in recent years, 'crystal design' for topochemical polymerization has not been established yet. A general approach to the 'design' of monomer crystals for topochemical polymerization makes use of some directional forces such as hydrogen-bonding and π–π interactions for suitable alignment of monomer molecules in the crystalline state. For example, Grubbs and coworkers have attempted to prepare polymerizable crystals of diacetylene[35] and diolefin[36] derivatives by using π-stacking interactions. To achieve a suitable orientation of the polymerizable groups, monomers having phenyl and perfluorophenyl groups in proximity to the polymerizable units are co-crystallized. X-Ray crystallography of the co-crystal of **28** and **29** shows a face-to-face stacking of the monomers, where

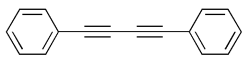

28

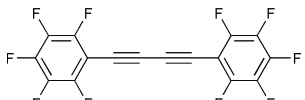

29

the distance between the polymerizable units is short enough for the topochemical polymerization to occur (Fig. 13). In fact, the

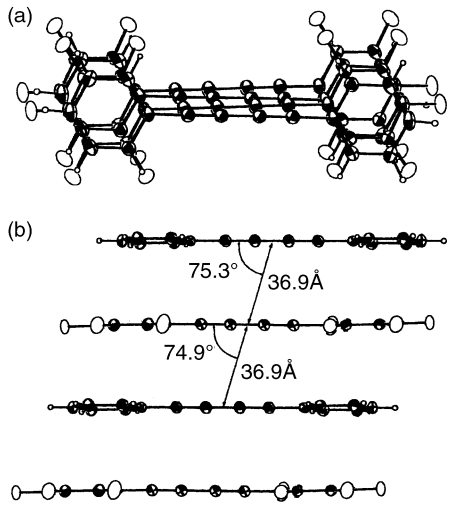

Fig. 13 Crystal packing views of a co-crystal of phenyl- and perfluorophenyl-substituted diacetylenic monomers (**28**, **29**). Reprinted in part with permission from: *Angew. Chem., Int. Ed. Engl.*, 1997, **36**, 248 (© 1997, WILEY-VCH Verlag GmbH).

co-crystals undergo topochemical polymerization upon irradiation with UV light, whereas no polymerization occurs when

unimolecular crystals of **28** and **29** are irradiated under the same conditions.

Stereochemical aspects of topochemical polymerization are also interesting. Single crystals of diethyl (*Z*,*Z*)-hexa-2,4-diene-1,6-dioate **30** have been reported to undergo photoinduced polymerization without change of crystal shape.[37–40] In contrast, methyl, butyl and isopropyl esters of (*Z*,*Z*)-hexa-2,4-diene-1,6-dioic acid in the crystalline state are not polymerized under the same conditions. Interestingly, the topochemical polymerization of **30** is highly stereospecific. When **30** is polymerized by a radical initiator in bulk or solution, a polymer consisting of a mixture of *trans*-1,4- (four possible stereo sequences), *cis*-1,4-, and 1,2-sequences is formed (Fig. 14). On

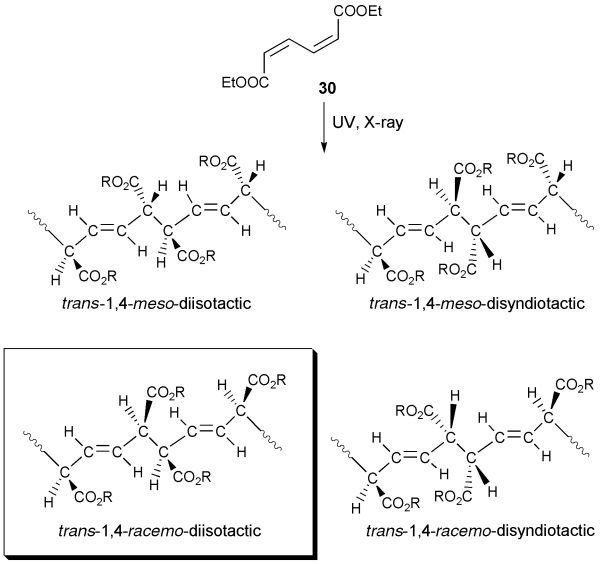

Fig. 14 Schematic representation for stereospecific polymerization in a crystal of diethyl (*Z*,*Z*)-hexa-2,4-dienedioate **30** by UV light.

the other hand, in the crystalline state, an ultrahigh molecular weight polymer consisting exclusively of a *trans*-1,4-*meso*-diisotactic sequence is formed. This perfect steric regulation demonstrates a large effect of crystal packing on the stereochemical course of the polymerization. As observed by X-ray crystallography, the polymer chains are completely oriented along the longer axis of the monomer crystal. Thus, if no structural defect exists in the monomer crystal, the molecular weight of the polymer may be controlled by the length of the longer crystal axis.[41] In relation to this study, Nakanishi and coworkers have reported a novel crystallization method for controlling the size of diacetylene crystals for topochemical polymerization for application to non-linear optics.[42,43]

More recently, topochemical polymerization of long-chain alkylammonium (*Z*,*Z*)-hexa-2,4-diene-1,6-dioates **31** has been

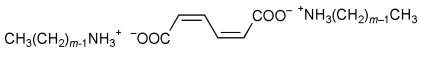

31

reported to produce layered polymer crystals.[44,45] During the polymerization, the alkylammonium group of **31** is intercalated between the crystalline layers of poly(muconic acid) (Fig. 15). The interlayer spacing *d* is increased linearly with the carbon number of the alkylamino group. The intercalated alkylammonium group can be removed from the polymer crystal by stirring in acidified methanol at room temperature, to leave a layered crystal of poly(muconic acid). Interestingly, when crystals thus obtained are exposed to alkylamine, re-intercalation of the amine into the crystalline layers occurs. Thus, this material can be considered as an organic clay, and may be useful for molecular recognition, separation and catalysis.

Although successful examples include only a narrow range of monomers, topochemical polymerization in the crystalline state has a high potential for controlling the locus of polymerization and polymer architectures.

Polymerization in inclusion complexes

It is well known that host molecules such as urea, thiourea, and perhydrotriphenylene are crystallized, in the presence of guest molecules, to form inclusion complexes. In many cases, inclusion complexes consist of one-dimensional columnar channels of crystalline host molecules, which are filled with guest molecules. If the included guest molecules are loosely packed, they can eventually be exchanged with other molecules of similar structures. When the guest molecules have polymer-

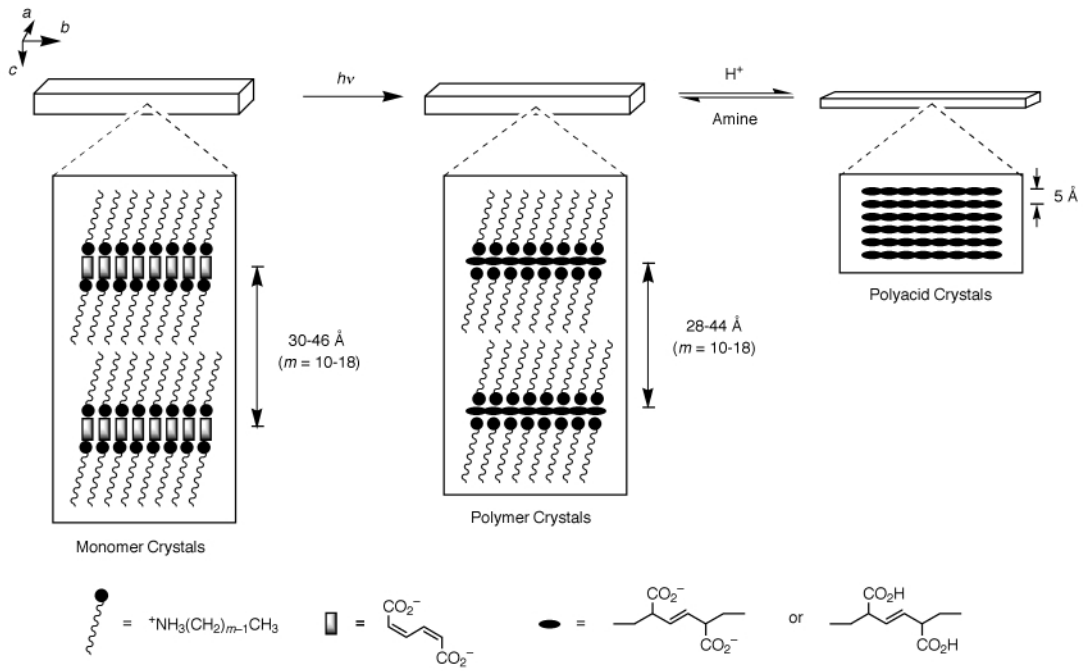

Fig. 15 Proposed models for topochemical polymerization in a crystal of a long-chain alkylammonium (*Z*,*Z*)-hexa-2,4-dienedioate **31** and subsequent transformation into a layered crystal of poly(muconic acid).

izable groups, one can polymerize these monomers in confined spaces of the crystalline channels. This is denoted 'inclusion polymerization'.

Historically, extensive studies on inclusion polymerization have been made in the 1960s–1980s. Farina and coworkers have reported the inclusion polymerization of various diene and triene monomers in the crystalline channels of perhydrotriphenylene **32** with an average diameter of *ca.* 5.5 Å.[46] For

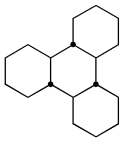

32

example, when an inclusion compound of **32** with *trans*-penta-1,3-diene as the guest is irradiated with γ-rays, a highly isotactic polymer consisting exclusively of 1,4-*trans* sequences is formed, indicating a strong spatial demand of the crystalline channel for the chain growth. Asymmetric synthesis of poly(*trans*-penta-1,3-diene) is also possible by the polymerization of the same monomer in the crystalline channels of optically resolved perhydrotriphenylene. Takemoto and Miyata *et al.* have made systematic studies on inclusion polymerization with crystalline channels of cholic acid derivatives by taking advantage of their high ability to include a variety of monomers (Table 1).[47] As the result, the size of the channel has been found

Table 1 Space size effects on the radical polymerization in inclusion complexes

Cavity size of host	Motion of propagating radicals	Polymerization rate	Selectivity of reaction
Large	Unrestricted	Fast	Low
↕	↕	↕	↕
Small	Restricted	Slow	High

to affect kinetics and specificity of the polymerization. For example, *trans*-2,4-dimethylpenta-1,3-diene can be polymerized in the crystalline channels of apocholic acid **33** at ambient

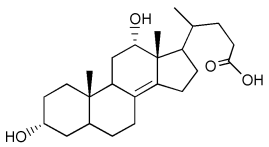

33

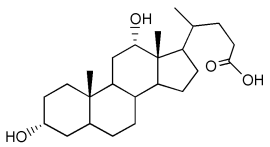

34

temperatures, but no polymerization occurs even at 100 °C in slightly smaller crystalline channels (4 × 6 Å) of deoxycholic acid **34**. According to electron paramagnetic resonance (EPR) spectroscopy, the propagating radicals are included tightly in the channel of **34**, while loosely held by the channel of **33**. Furthermore, when *trans*-penta-1,3-diene is polymerized within the channels of **34**, a polymer with a 99% 1,4-*trans* structure is formed, whereas the selectivity is lower by 10% when the slightly larger channel of **33** is utilized. Cyclophosphazene **35** also forms inclusion compounds with a channel diameter of 5 Å, which have been extensively studied by Allcock *et al.* for the polymerization of various vinyl monomers[48] and dienes.[49] For example, a γ-ray induced polymerization of methacrylonitrile included in the channel of **35** gives a highly isotactic polymer soluble in THF. This is in contrast with a γ-ray induced bulk polymerization of methacrylonitrile, which affords an insoluble, cross-linked polymeric mass.[48]

Recently, α,ω-amino acids and α-cyclodextrin **36** have been found to form inclusion complexes, where the cyclodextrin acts

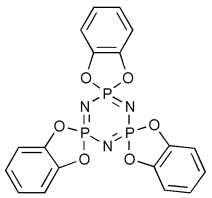

35

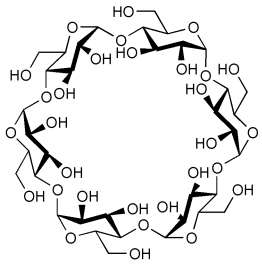

36

as the host for the amino acids to form crystalline channels.[50] Upon heating, polycondensation of the included amino acids takes place to give polyamides in the solid state (Fig. 16).

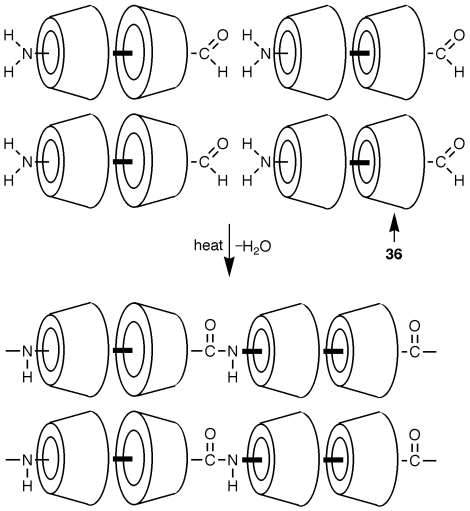

Fig. 16 A proposed scheme for solid state polycondensation of α,ω-amino acid in the presence of α-cyclodextrin **36** to form a polyrotaxane.

Interestingly, the polymerization mixtures are water-soluble, although the polyamides alone are insoluble in water owing to strong intermolecular hydrogen bonding interactions. This observation indicates a high coverage of the polyamide chains by α-cyclodextrin, *i.e.* formation of a polyrotaxane.

Polymerization in microporous zeolites

Microporous zeolites are porous inorganic crystalline materials with a pore diameter of 3–10 Å and possess ion exchangeable sites on the internal surface. Similarly to inclusion complexes, microporous materials can provide confined spaces for controlled polymerization. Historically, radical polymerization of polar vinyl monomers has most extensively been studied with microporous zeolites, by focusing attention on (1) possible elongation effects on the lifetime of growing radicals[51] and (2) possible steric effects on the chain growth step.[52]

Recently, microporous zeolites have been used as catalyst supports for the polymerization of olefins, in which, however, spatial effects of the microporous cavities are not very clear. For example, in the polymerization of ethylene with supported zirconocenes by microporous zeolites, coupled with methylalumoxane (MAO) as cocatalyst, the activity is not related to the internal surface area of the zeolite, but the external surface area and the content of aluminium in the silicate framework appear to be more important.[53]

In view of fabrication of organized hybrid materials, polymerization in microporous zeolites is attractive but somewhat limited, as their pores are too narrow to allow guest molecules to be packed continuously. However, synthesis of nanowires of conducting polymers such as poly(methylacetylenes),[54] polypyrroles[55] and polyanilines[56] has been reported. For example, when a pyrrole vapor is diffused into Cu^{II}-doped

zeolite channels, the polymerization occurs with a color change, to give a polypyrrole/zeolite hybridized material (Fig. 17), which however does not show any significant electronic conductivity.

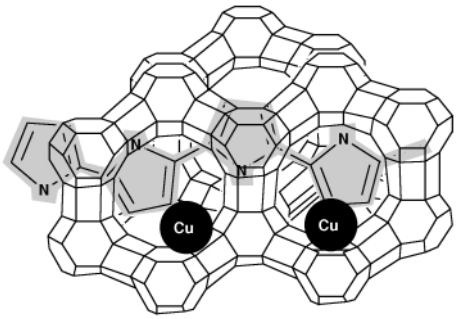

Fig. 17 A proposed model for Cu^{II}-catalyzed oxidative polymerization of pyrrole in zeolite-Y to form a conducting hybrid material.

In relation to microporous zeolites, inorganic materials with layered architectures have been synthesized, which are able to change the interlayer distance upon intercalation of guest molecules. Polymerization with such layered inorganic materials as the reaction media has also been investigated,[57] mainly for the synthesis of functional polymer/inorganic hybridized materials. For example, oxidation polymerization of aniline[58] and pyrrole derivatives[59] within the interlayer spaces gives electroactive composite materials (Fig. 18a). From a more

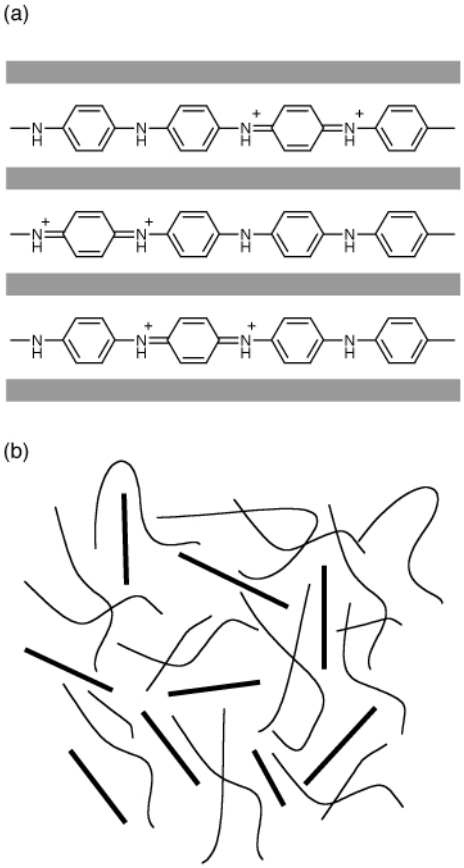

Fig. 18 Proposed structures of (a) an electroactive composite material of polyaniline with a layered inorganic material and (b) a composite material containing uniformly dispersed clay 2-D sheets in a polymer matrix.

practical point of view, certain clays with layered architectures have also been utilized for the ring-opening polymerization of heterocyclic monomers such as lactams,[60] lactones[61] and cyclic carbonates,[62] and coordination polymerization of olefins,[63] where the monomers intercalated between the 2-D inorganic sheets are polymerized to give nanocomposite materials. Because of a uniform dispersion of the clay 2-D sheets at the molecular level in polymer matrices, the hybrid materials exhibit excellent mechanical properties and unique gas barrier characteristics (Fig. 18b).

Polymerization in mesoporous materials

Since the first report on mesoporous silicate MCM-41 in 1992, a variety of mesoporous silicate materials have been developed.[64] These inorganic materials are prepared by using rod-like micelles as templates, and have an ordered hexagonal or cubic array of uniformly sized mesoscopic channels with a pore diameter variable from 15 to 100 Å. Mesoporous materials have an advantage over microporous zeolites for the inclusion of large molecules. A comprehensive review of the inclusion chemistry with mesoporous materials has been reported.[65] Although mesoscopic pores are large enough for the inclusion of ordinary polymers, the included polymer chains may retain their freedom of conformational change. Thus, mesoporous materials are more attractive than microporous materials not only in view of the control of polymerization locus but also for fabrication of polymeric materials.

Recently, several studies on macromolecular synthesis with mesoporous materials have been reported. For example, Aida and coworkers have utilized MCM-41 for the radical polymerization of methyl methacrylate (MMA) with benzoyl peroxide as initiator, and obtained a polymer (PMMA) with a much higher molecular weight than that formed in solution under otherwise identical conditions.[66] Electron paramagnetic resonance study (EPR) has shown the formation of long-lived propagating polymer radicals within the mesoscopic channels, where *ca.* 25% of the initial intensity of the EPR signal remains even after a month (Fig. 19). Furthermore, molecular weight of the

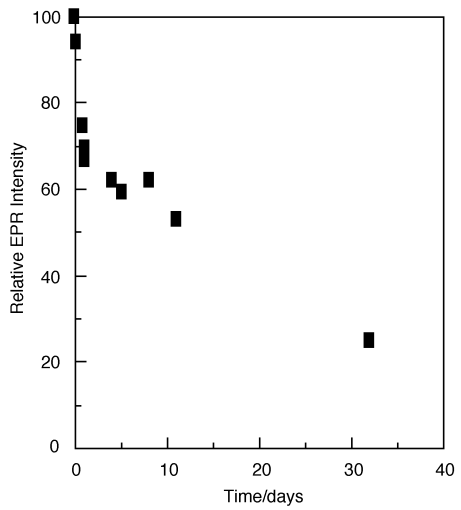

Fig. 19 An electron paramagnetic resonance (EPR) trace of free radical polymerization of methyl methacrylate (MMA) by 2,2′-azobisisobutyronitrile (AIBN) in mesoscopic channels of MCM-41.

polymer can be controlled over a wide range M_n = (1.3–3.0) × 10^5 (M_w/M_n = 2.5) by changing initial molar ratio of MMA to BPO (Fig. 20). On the other hand, the tacticity of the polymer is not particular but almost identical with that of PMMAs obtained by a free radical polymerization in solution.[67] Thus, the mesoscopic pores of MCM-41 are not small enough to affect the stereochemical course of the chain growth. Bein and coworkers have also investigated free radical polymerization of MMA with MCM-41, and reported that PMMA formed within the mesoscopic channels shows no glass transition probably because of a strong interaction between the polymer chain and the internal surface of the mesopore.[68]

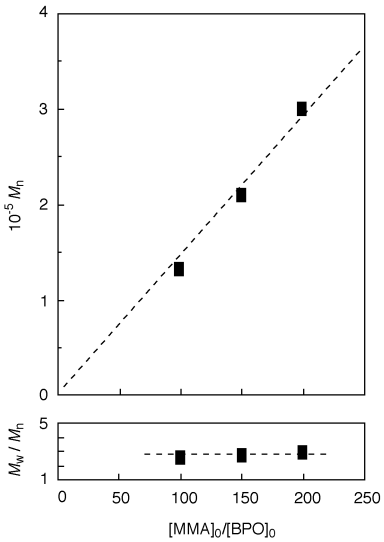

Fig. 20 Molecular weight control in free radical polymerization of methyl methacrylate (MMA) by benzoyl peroxide (BPO) in mesoscopic channels of MCM-41.

Chemical properties of the mesopore surface can be tuned by the introduction of aluminium, titanium, and some other transition metal ions to the silicate framework. For example, a highly Lewis acidic mesoporous silica (Al-MCM-41) can be prepared by doping aluminium in the silicate framework. Aida and coworkers have found that lactones are polymerized in a living manner in the presence of Al-MCM-41 and an alcohol at 50 °C, to give polyesters with narrow molecular weight distribution (MWD).[69] By changing the mole ratio monomer/alcohol, the molecular weight of the polymer can be controlled over a rather wide range. A sequential polymerization of two different lactone monomers with an Al-MCM-41/alcohol system gives the corresponding block copolymer with narrow MWD. Furthermore, Al-MCM-41 is easily separated from the polymerization mixture by filtration, and can be used again for the polymerization. NMR studies have indicated that the alcohol is incorporated into the polymer terminus at the initiation step of the polymerization. In contrast with the case using Al-MCM-41, no polymerization occurs in the presence of a pure silicate MCM-41 or modified MCM-41 with methylated silanol functionalities under otherwise identical conditions to the above. Furthermore, use of a microporous aluminosilicate zeolite-Y (pore diameter = 8 Å), in place of Al-MCM-41, results in no polymerization. These observations suggest that the large pore size as well as the Lewis acidic character of the surface is essential for the polymerization. The postulated mechanism of polymerization is shown in Fig. 21, in which the monomer is activated by a possible cooperation of Lewis acidic aluminium sites and Brønsted acidic silanol functionalities.

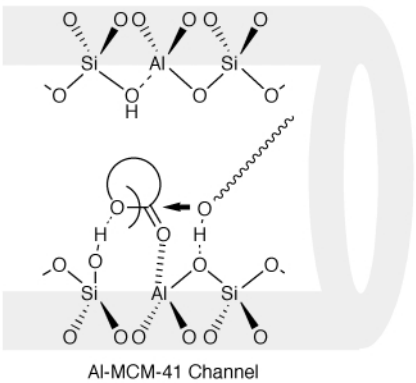

Fig. 21 A proposed mechanism for activation of lactone on the interior wall of Al-MCM-41 for ring-opening polymerization with alcohol.

Mesoporous silicates have been used as inorganic supports for metallocene catalysts for the polymerization of olefins.[70] However, only limited examples have been reported that indicate some spatial effects of mesoscopic pores on the polymerization. For example, co-oligomerization of ethylene and propylene with an MCM-41-supported zirconocene compound, in conjunction with methylalumoxane (MAO) as cocatalyst, has been investigated,[71] where the pore size has been claimed to affect the molecular weight of the resulting co-oligomer. When MCM-41 prepared with a C_{16} surfactant is used as the support, a co-oligomer with M_n of 1280 is formed. On the other hand, when the support is MCM-41 prepared with a shorter-chain C_{14} surfactant, a co-oligomer with M_n of 1730 is formed.

Recently, Aida and Kageyama *et al.* have found that a titanocene complex supported by a particular type of mesoporous silicate denoted mesoporous silica fiber (MSF, pore diameter = 27 Å),[72] in conjunction with MAO, produces crystalline nanofibers of ultrahigh molecular weight (M_n = 6 200 000) linear polyethylene.[73] The polyethylene is obtained as a cocoon-like white mass with a low bulk density. Scanning electron microscopy (SEM) shows that the fibers are 30–50 nm in diameter (Fig. 22), and the crystalline density is close to a

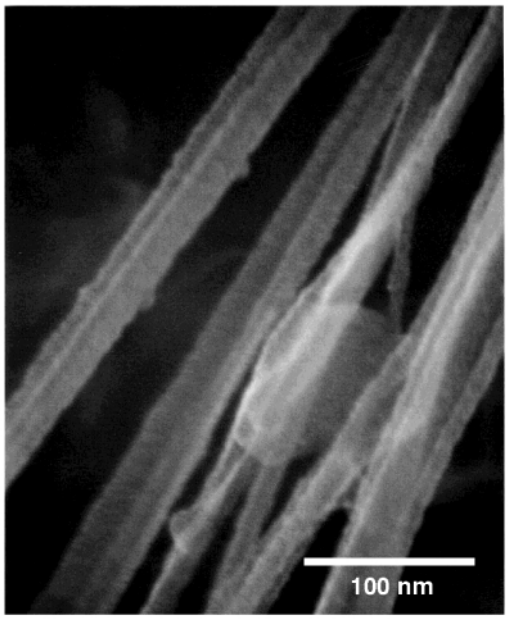

Fig. 22 A SEM micrograph of crystalline polyethylene fibers formed by polymerization with a supported titanocene by mesoporous silica fiber (MSF) in conjunction with methylalumoxane (MAO). Reprinted in part with permission from: *Science*, 1999, **285**, 2113 (Copyright © 1999, the American Association for the Advancement of Science).

theoretical upper limit for polyethylene. Unlike ordinary high-density polyethylenes consisting of folded-chain crystals, the polyethylene fibers thus obtained consist exclusively of extended chain crystals, according to small angle X-ray scattering (SAXS) and differential scanning calorimetry (DSC). For the formation of crystalline nanofibers of polyethylene, the 'extrusion polymerization' mechanism, which mimics biological formation of natural fibers such as crystalline cellulose fibers, has been postulated, where the polymer chains, formed at the activated titanocene sites within the individual mesopores, are extruded into the solvent phase and assembled to form extended-chain crystals (Fig. 23). Thus, the mesoscopic pore in this particular case serves as a template, which can suppress the kinetically favored chain folding process, since the pore diameter (27 Å) is almost one-order of magnitude smaller than the lamellar thickness (270 Å) of the folded-chain crystals of ordinary polyethylenes. Since most studies on precision polymerization have focused on the control of primary structures of polymers, the present finding, which enables control of a

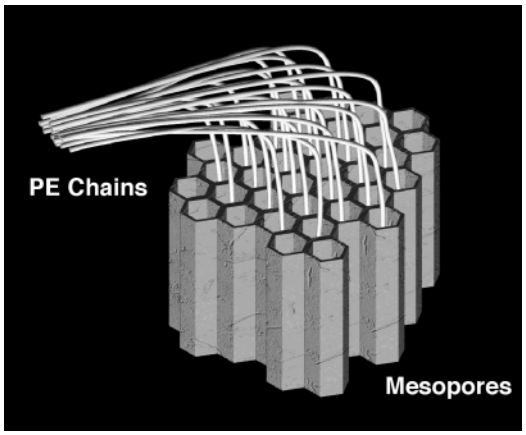

Fig. 23 A proposed mechanism for the formation of fibrous polyethylene with titanocene-mounted mesoporous silica fiber (MSF).

ternary structure, is unique and may have a high potential for the fabrication of novel polymer materials from specialty as well as commodity monomers. Along the line of this study, a novel hybridized thin film of polyethylene and silica (Fig. 24) has

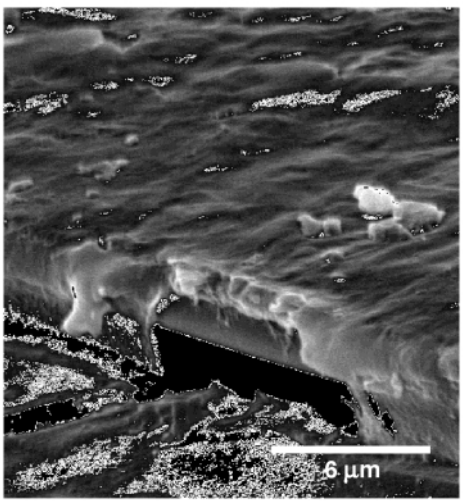

Fig. 24 A SEM micrograph of a polyethylene/silica/mica hybridized thin film formed by polymerization of ethylene on a titanocene-mounted mesoporous silica film in conjunction with methylalumoxane (MAO). Reprinted in part with permission from: *J. Polym. Sci. Part A: Polym. Chem. Ed.*, 2000, in press (© 2000, John Wiley & Sons, Inc.).

been synthesized[74] by the polymerization of ethylene on a mesoporous silica film[75] doped with titanocene.

In relation to the above study, Mallouk and Ozin and coworkers have utilized MCM-41 as a mold for the fabrication of a fibrous poly(phenolformaldehyde) resin.[76] When an acid-catalyzed polyaddition/condensation of phenol and formaldehyde is carried out within the mesoscopic channels of MCM-41, and then the silicate framework is destroyed by HF, mesofibers of poly(phenolformaldehyde) with a diameter of *ca.* 20 Å and an aspect ratio of more than 10^3 is obtained (Fig. 25). In contrast, when the polymerization is conducted in the presence of non-porous silica Cab-O-Sil, only a non-fibrous, agglomerated polymeric mass results.

Since polymer chains included in individual mesoscopic pores are isolated from one another and oriented parallel to the pore axis, fabrication of photo-conducting materials with mesoporous silica has attracted attention. For example, Wu and Bein have reported the synthesis of a graphite-type conducting carbon wire by the polymerization of acrylonitrile within the mesoscopic channels of MCM-41 and its subsequent pyrolysis (Fig. 26).[77] The graphite/MCM-41 adduct, obtained by pyrolysis at 1000 °C, shows a notable microwave conductivity of

Fig. 25 A TEM micrograph of polymer mesofibers formed by polyaddition/condensation of phenol and formaldehyde within the mesoscopic channels of MCM-41. Reprinted in part with permission from: *J. Mater. Chem.*, 1998, **8**, 13 (© 1998, The Royal Society of Chemistry).

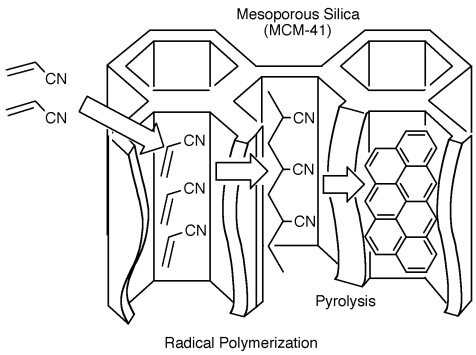

Fig. 26 Illustration for free radical polymerization of acrylonitrile within the mesoscopic channels of MCM-41 and subsequent pyrolysis to form a conducting carbon nanowire.

0.1 S cm^{-1}. A polyaniline wire encapsulated within the mesoscopic silicate channel has also been synthesized, which however shows only a low microwave conductivity (0.0014 S cm^{-1}).[78] Variation of the pore diameter of the mesoscopic channel would make it possible to tune the conducting properties of the hybridized material. Similarly, Ozin and coworkers have reported ring-opening polymerization of [1]silaferrocenophane **37**.[79] Compound **37** is incorporated into the hexagonal channels of MCM-41 by sublimation under vacuum, and then the adduct is heated at 140 °C, whereupon the polymerization occurs to give a poly(ferrocenylsilane)/MCM-41 hybrid (Fig. 27). When the hybrid is pyrolyzed at 900 °C under nitrogen, the included polymer is decomposed to leave iron nanoparticles with an average particle size of 20 ± 5 Å. The magnetic properties of the pyrolyzed product indicate that the iron nanoclusters in the interior are supermagnetic.

Concluding remarks

Template-assisted polymerization, *i.e.* polymerization of pre-organized monomers or in constrained media, has a long history, but is still growing even more rapidly. This is not only from a continuous interest in short- and long-range information transfers in the molecular world but also for a strong demand

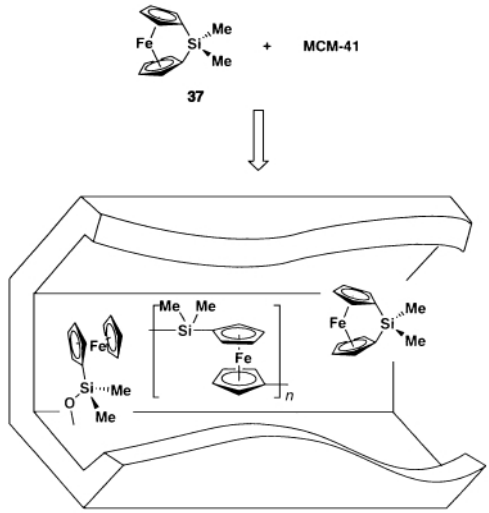

Fig. 27 Illustration for ring-opening polymerization of [1]silaferrocenophane **37** within the mesoscopic channels of MCM-41.

from the next-generation material design for fabrication of well defined nanostructures. Bringing together knowledge about biology and physics as well as organic, inorganic, supramolecular, and macromolecular chemisty into this area will lead to further breakthroughs in science and technology.

References

1 *Polymerization in Organized Media*, ed. C. M. Paleos, Gordon & Breach, New York, 1992.
2 S. Hamid and D. Sherrington, *J. Chem. Soc., Chem. Commun.*, 1986, 936.
3 S. M. Hamid and D. C. Sherrington, *Polymer*, 1987, **28**, 332.
4 D. Cochin, R. Zana and F. Candau, *Macromolecules*, 1993, **26**, 5765.
5 C. E. Larrabee, Jr. and E. D. Sprague, *J. Polym. Sci. Polym. Lett. Ed.*, 1979, **17**, 749; K. W. Yeoh, C. H. Chew, L. M. Gan and L. L. Koh, *Polym. Bull.*, 1989, **22**, 123.
6 K. Nagai, Y. Ohishi, H. Inaba and S. Kudo, *J. Polym. Sci. Part A: Polym. Chem. Ed.*, 1985, **23**, 1221.
7 K. Ito, K. Tanaka, H. Tanaka, G. Imai, S. Kawaguchi and S. Itsuno, *Macromolecules*, 1991, **24**, 2348.
8 Y. Yasuda, K. Rindo and S. Aoki, *Makromol. Chem.*, 1992, **193**, 2875.
9 Y. Yasuda, K. Rindo and S. Aoki, *Polym. J.*, 1993, **25**, 1203; S. Aoki and Y. Morimoto, *Polym. Bull.*, 1996, **37**, 777; S. Aoki, Y. Morimoto and A. Nomura, *Polym. J.*, 1996, **28**, 1014.
10 K. Nagai and Y. Ohishi, *J. Polym. Sci. Part A: Polym. Chem. Ed.*, 1994, **32**, 445.
11 P. Dais, C. M. Paleos, G. Nika and A. Malliaris, *Makromol. Chem.*, 1993, **194**, 445.
12 S. R. Kline, *Langmuir*, 1999, **15**, 2726.
13 V. Percec, C.-H. Ahn and B. Barboiu, *J. Am. Chem. Soc.*, 1997, **119**, 12978; V. Percec, C.-H. Ahn, G. Ungar, D. J. P. Yeardley, M. Möller and S. S. Sheiko, *Nature*, 1998, **391**, 161.
14 V. Percec and M. N. Holerca, *Biomacromolecules*, 2000, **1**, 6.
15 T. Kunitake, in *Comprehensive Supramolecular Chemistry*, ed. J.-P. Sauvage and M. W. Hosseini, Pergamon, Oxford, 1996, vol. 9, p. 351.
16 H. Ringsdorf, B. Schlarb and J. Venzmer, *Angew. Chem., Int. Ed. Engl.*, 1988, **27**, 113.
17 J. H. Fendler, *Science*, 1984, **223**, 888.
18 T. D. Sells and D. F. O'Brien, *Macromolecules*, 1994, **27**, 226.
19 J. Lei and D. F. O'Brien, *Macromolecules*, 1994, **27**, 1381.
20 H. Lamparski and D. F. O'Brien, *Macromolecules*, 1995, **28**, 1786.
21 H. G. Lamparski, E. Oblinger and D. F. O'Brien, *Macromolecues*, 1999, **32**, 5450.
22 J. Lei, T. M. Sisson, H. G. Lamparski and D. F. O'Brien, *Macromolecules*, 1999, **32**, 73.
23 N. Higashi, T. Adachi and M. Niwa, *Macromolecules*, 1990, **23**, 1475.
24 H. Fukuda, T. Diem, J. Stefely, F. J. Kezdy and S. L. Regen, *J. Am. Chem. Soc.*, 1986, **108**, 2321.
25 T. M. Sisson, W. Srisiri and D. F. O'Brien, *J. Am. Chem. Soc.*, 1998, **120**, 2322.
26 C. A. Guymon, E. N. Hoggan, N. A. Clark, T. P. Rieker, D. M. Walba and C. N. Bowman, *Science*, 1997, **275**, 57; C. A. Guymon and C. N. Bowman, *Macromolecules*, 1997, **30**, 1594; C. A. Guymon and C. N. Bowman, *Macromolecules*, 1997, **30**, 5271.
27 K. Akagi, G. Piao, S. Kaneko, K. Sakamaki, H. Shirakawa and M. Kyotani, *Science*, 1998, **282**, 1683.
28 S. I. Stupp, S. Son, H. C. Lin and L. S. Li, *Science*, 1993, **259**, 59; S. I. Stupp, S. Son, L. S. Li, H. C. Lin and M. Keser, *J. Am. Chem. Soc.*, 1995, **117**, 5212.
29 S. I. Stupp, V. Lebonheur, K. Walker, L. S. Li, K. E. Huggins, M. Keser and A. Amstutz, *Science*, 1997, **276**, 384; E. R. Zubarev, M. U. Pralle, L. Li and S. I. Stupp, *Science*, 1999, **283**, 523.
30 R. C. Smith, W. M. Fischer and D. L. Gin, *J. Am. Chem. Soc.*, 1997, **119**, 4092.
31 D. H. Gray, S. Hu, E. Juang and D. L. Gin, *Adv. Mater.*, 1997, **9**, 731; H. Deng, D. L. Gin and R. C. Smith, *J. Am. Chem. Soc.*, 1998, **120**, 3522.
32 S. A. Miller, E. Kim, D. H. Gray and D. L. Gin, *Angew. Chem., Int. Ed.*, 1999, **38**, 3022.
33 H. Bässler, *Adv. Polym. Sci.*, 1984, **63**, 1; H. Sixl, *Adv. Polym. Sci.*, 1984, **63**, 49; V. Enkelman, *Adv. Polym. Sci.*, 1984, **63**, 91.
34 M. Hasegawa, *Adv. Phys. Org. Chem.*, 1995, **30**, 117.
35 G. W. Coates, A. R. Dunn, L. M. Henling, D. A. Dougherty and R. H. Grubbs, *Angew. Chem., Int. Ed. Engl.*, 1997, **36**, 248.
36 G. W. Coates, A. R. Dunn, L. M. Henling, J. W. Ziller, E. B. Lobkovsky and R. H. Grubbs, *J. Am. Chem. Soc.*, 1998, **120**, 3641.
37 A. Matsumoto, T. Matsumura and S. Aoki, *J. Chem. Soc., Chem. Commun.*, 1994, 1389.
38 A. Matsumoto, T. Matsumura and S. Aoki, *Macromolecules*, 1996, **29**, 423.
39 A. Matsumoto, K. Yokoi, S. Aoki, K. Tashiro, T. Kamae and M. Kobayashi, *Macromolecules*, 1998, **31**, 2129.
40 K. Tashiro, T. Kamae, M. Kobayashi, A. Matsumoto, K. Yokoi and S. Aoki, *Macromolecules*, 1999, **32**, 2449; K. Tashiro, A. N. Zadorin, S. Saragai, T. Kamae, A. Matsumoto, K. Yokoi and S. Aoki, *Macromolecules*, 1999, **32**, 7946.
41 A. Matsumoto and K. Yokoi, *J. Polym. Sci., Part A: Polym. Chem. Ed.*, 1998, **36**, 3147.
42 H. Katagi, H. Kasai, S. Okada, H. Oikawa, K. Komatsu, H. Matsuda, Z. Liu and H. Nakanishi, *Jpn. J. Appl. Phys.*, 1996, **35**, L1364.
43 H. Kasai, H. S. Nalwa, H. Oikawa, S. Okada, H. Matsuda, N. Minami, A. Kakuda, K. Ono, A. Mukoh and H. Nakanishi, *Jpn. J. Appl. Phys.*, 1992, **31**, L1132; H. Kasai, H. Kamatani, S. Okada, H. Oikawa, H. Matsuda and H. Nakanishi, *Jpn. J. Appl. Phys.*, 1996, **35**, L221.
44 A. Matsumoto, T. Odani, M. Chikada, K. Sada and M. Miyata, *J. Am. Chem. Soc.*, 1999, **121**, 11122.
45 A. Matsumoto, T. Odani, K. Sada, M. Miyata and K. Tashiro, *Nature*, 2000, **405**, 328.
46 For a review, see M. Farina, in *Encyclopedia of Polymer Science and Engineering*, John Wiley & Sons, New York, 1988, vol. 12, p. 486.
47 For a review, see M. Miyata, in *Comprehensive Supramolecular Chemistry*, ed. D. Reinhoudt, Pergamon, Oxford, 1996, vol. 10, p. 557.
48 H. R. Allcock, E. N. Silverberg and G. K. Dudley, *Macromolecules*, 1994, **27**, 1033.
49 H. R. Allcock, G. K. Dudley and N. Silverberg, *Macromolecules*, 1994, **27**, 1039.
50 M. B. Steinbrunn and G. Wenz, *Angew. Chem., Int. Ed. Engl.*, 1996, **35**, 2139; G. Wenz, M. Boris and K. Landfester, *Tetrahedron*, 1997, **53**, 15575.
51 J. Rychly and M. Lazár, *Eur. Polym. J.*, 1972, 711.
52 J. P. Quaegebeur, T. Seguchi, H. L. Bail and C. Chachaty, *J. Polym. Sci. Part A: Polym. Chem. Ed.*, 1976, **14**, 2703.
53 M. F. V. Marques, C. A. Henriques, J. L. F. Monteiro, S. M. C. Menezes and F. M. B. Coutinho, *Macromol. Chem. Phys.*, 1997, **198**, 3709; M. F. V. Marques, C. A. Henriques, J. L. F. Monteiro, S. M. C. Menezes and F. M. B. Coutinho, *Polym. Bull.*, 1997, **39**, 567; M. Michelotti, A. Altomare, F. Ciardelli and E. Roland, *J. Mol. Catal. A: Chem.*, 1998, **129**, 241.
54 S. D. Cox and G. D. Stucky, *J. Phys. Chem.*, 1991, **95**, 710.
55 T. Bein and P. Enzel, *Angew. Chem., Int. Ed.*, 1989, **28**, 1692; H. Uehara, M. Miyake, M. Matsuda and M. Sato, *J. Mater. Chem.*, 1998, **8**, 2113.
56 P. Enzel and T. Bein, *J. Phys. Chem.*, 1989, **93**, 6270.
57 A. Blumstein, *J. Polym. Sci. Part A*, 1965, **3**, 2653; H. G. Dekking, *J. Appl. Polym. Sci.*, 1967, **11**, 23.
58 M. G. Kanatzidis, C.-G. Wu, H. O. Marcy and C. R. Kannewurf, *J. Am. Chem. Soc.*, 1989, **111**, 4139; C.-G. Wu, D. C. DeGroot, H. O. Marcy,

J. L. Schindler, C. R. Kannewurf, Y.-J. Liu, W. Hirpo and G. Kanatzidis, *Chem. Mater*, 1996, **8**, 1992; T. A. Kerr, H. Wu and L. F. Nazar, *Chem. Mater.*, 1996, **8**, 2005.
59 M. G. Kanatzidis, L. M. Tonge and T. J. Marks, *J. Am. Chem. Soc.*, 1987, **109**, 3797; A. B. Gonçalves, A. S. Mangrich and A. J. G. Zarbin, *Synth. Met.*, 2000, **114**, 119.
60 A. Usuki, M. Kawasumi, Y. Kojima, Y. Fukushima, A. Okada, T. Kurauchi and O. Kamigaito, *J. Mater. Res.*,1993, **8**, 1179; Y. Kojima, A. Usuki, M. Kawasumi, A. Okada, T. Kurauchi and O. Kamigaito, *J. Polym. Sci. Part A: Polym. Chem. Ed.*, 1993, **31**, 1755.
61 P. B. Messersmith and E. P. Giannelis, *J. Polym. Sci. Part A: Polym. Chem. Ed.*, 1995, **33**, 1047.
62 X. Huang, S. Lewis, W. J. Brittain and R. A. Vaia, *Macromolecules*, 2000, **33**, 2000.
63 J. Tudor, L. Willington, D. O'Hare and B. Royan, *Chem. Commun.*, 1996, 2031; J. S. Bergman, H. Chen, E. P. Giannelis, M. G. Thomas and G. W. Coates, *Chem. Commun.*, 1999, 2179.
64 J. S. Beck, J. C. Vartuli, W. J. Roth, M. E. Leonowicz, C. T. Kresge, K. D. Schmitt, C. T. -W. Chu, D. H. Olson, E. W. Sheppard, S. B. McCullen, J. B. Higgins and J. L. Schlenker, *J. Am. Chem. Soc.*, 1992, **114**, 10834; A. Corma, *Chem. Rev.*, 1997, **97**, 2373; J. Y. Ying, C. P. Mehnert and M. S. Wong, *Angew. Chem., Int. Ed.*, 1999, **38**, 56.
65 K. Moller and T. Bein, *Chem. Mater.*, 1998, **10**, 2950.
66 S. M. Ng, S. Ogino and T. Aida, *Macromol. Rapid. Commun.*, 1997, **18**, 991.
67 S. M. Ng, S. Ogino and T. Aida, unpublished data.
68 K. Moller, T. Bein and R. X. Fischer, *Chem. Mater.*, 1998, **10**, 1841.
69 K. Kageyama, S. Ogino, T. Aida and T. Tatsumi, *Macromolecules*, 1988, **31**, 4069; K. Kageyama, T. Tatsumi and T. Aida, *Polym. J.*, 1999, **31**, 1005.
70 Y.-S. Ko, T.-K. Han, J.-W. Park and S.-I. Woo, *Macromol. Rapid Commun.*, 1996, **17**, 749; J. Tudor and D. O'Hare, *Chem. Commun.*, 1997, 603; H. Rahiala, I. Beurroies, T. Eklund, K. Hakala, R. Gougeon, P. Trens and J. B. Rosenholm, *J. Catal.*, 1999, **188**, 14.
71 L. K. van Looveren, D. F. Geysen, K. A. Vercruysse, B. H. Wouters, P. J. Grobet and P. A. Jacobs, *Angew. Chem., Int. Ed.*, 1998, **37**, 517.
72 Q. Huo, D. Zhao, J. Feng, K. Weston, S. K. Buratto, G. D. Stucky, S. Schacht and F. Schüth, *Adv. Mater.*, 1997, **9**, 974.
73 K. Kageyama, J. Tamazawa and T. Aida, *Science*, 1999, **285**, 2113.
74 K. Tajima, G. Ogawa and T. Aida, *J. Polym. Sci. Part. A: Polym. Chem. Ed.*, in press.
75 S. H. Tolbert, T. E. Schäffer, J. Feng, P. K. Hansma and G. D. Stucky, *Chem. Mater.*, 1997, **9**, 1962.
76 S. A. Johnson, D. Khushalani, N. Coombs, T. E. Mallouk and G. A. Ozin, *J. Mater. Chem.*, 1998, **8**, 13.
77 C.-G. Wu and T. Bein, *Science*, 1994, **266**, 1013.
78 C.-G. Wu and T. Bein, *Science*, 1994, **264**, 1757; C.-G. Wu and T. Bein, *Chem. Mater.*, 1994, **6**, 1109.
79 M. J. MacLachlan, P. Aroca, N. Coombs, I. Manners and G. A. Ozin, *Adv. Mater.*, 1998, **10**, 144; M. J. MacLachlan, M. Ginzburg, N. Coombs, Nandyala P. Raju, J. E. Greedan, G. A. Ozin and I. Manners, *J. Am. Chem. Soc.*, 2000, **122**, 3878.

ChemComm

Polycations. Part X. LIPs, a new category of room temperature ionic liquid based on polyammonium salts

Sharon I. Lall, Danny Mancheno, Steve Castro, Valbona Behaj, JaimeLee Iolani Cohen and Robert Engel*

Department of Chemistry and Biochemistry, Queens College of the City University of New York, 65-30 Kissena Boulevard, Flushing, NY 11367, USA. E-mail: robert_engel@qc.edu

Received (in Corvallis, OR, USA) 11th September 2000, Accepted 16th October 2000
First published as an Advance Article on the web 21st November 2000

A series of polyammonium halide salts have been converted to the phosphate ion form. The resultant salts constitute a new category of non-aqueous ionic liquid (NAIL); these new ionic liquids (Liquid Ionic Phosphates) have been characterized by standard methods and have been investigated for their electrical conducting characteristics.

Previously we have reported the preparation of several series of polycationic organic salts.[1] Subsequently, we considered the possibility of converting these new (solid) polyammonium salts into a unique category of ionic liquids through conversion of the gegenion. Numerous reports have been made of the conversion of monoammonium (solid) salts to non-aqueous ionic liquids by such anion conversion. The most extensively investigated series of NAILs include those in which the organic cation is either an *N*-alkylpyridinium or an *N*-alkyl-*N*′-alkylimidazolium species.[2–5] These species have involved *only* organic *mono*cations, with the single exception of a dicationic species involving two imidazolium sites at opposite ends of a long alkyl chain.[6] Of particular interest to us was the use of hexafluorophosphoric acid[7] to generate the corresponding hexafluorophosphate liquid salts from the polycationic species previously synthesized in this laboratory.

Using the established procedure for preparing such salts, with our polycationic organic salts it was observed that only a relatively low yield of such hexafluorophosphate salts could be isolated. Attempts to improve the yield through vacuum evaporation of the aqueous medium resulted in the isolation of a totally new and intriguing category of ionic liquids, liquid ionic phosphates (LIPs). It is with these new materials that the present report is concerned.

Using two separate anion exchange methods we have prepared a series of rt LIPs. The first of these involves vacuum evaporation of the aqueous supernatant solution from the preparation of the hexafluorophosphate species. Moderate yields of clear viscous liquids that exhibit NMR spectra (^{1}H, ^{13}C and ^{31}P) in accord with the assigned structures are isolated (*vide infra*). The second approach involves the more traditional anion exchange using an insoluble resin. Passage of the parent halide salts through a bed of DOWEX™ 21K in the phosphate ion form followed by vacuum evaporation of the eluent also yields the clear, highly viscous liquids providing the same analyses as noted above. A series of LIPs prepared by these methods and so analyzed is illustrated in Fig. 1. LIPs **1**–**8** are derived from the polycationic halide salts prepared in this laboratory. Species **9** has been prepared from the corresponding chloride prepared by a reported procedure,[4] and was included as a general reference to previously available NAILs derived from imidazolium salts.

The ^{1}H and ^{13}C spectra (measured in D_2O) are in total accord with those previously reported[1] in the preparation of the parent halide salts. The ^{31}P NMR spectra (also in D_2O) exhibit sharp singlet signals between δ = 0.91 and 1.20 (relative to 85% phosphoric acid). A representative example of these salts and

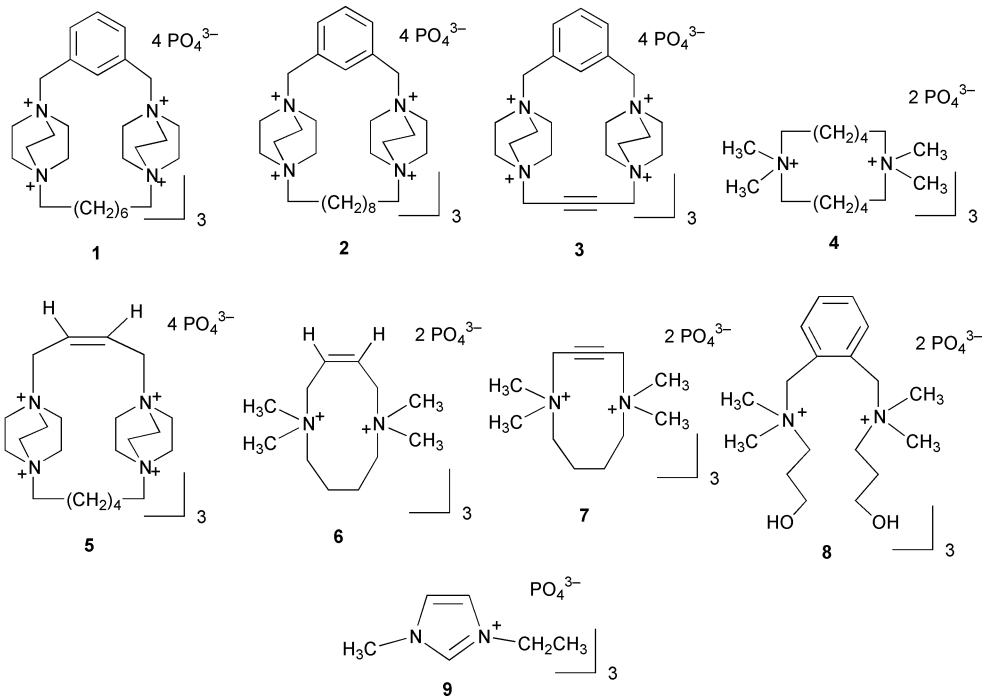

Fig. 1

DOI: 10.1039/b007443h

Table 1 Densities and specific conductivities of LIPs

LIP	Density/ g mL^{-1}	Specific Conductivity, σ/Ω^{-1} cm^{-1} 25 °C	40 °C	60 °C	$\sigma/\sigma_{KCl\ Ref.}$[a]
1	1.78	0.057	0.063	0.061	19
2	1.86	0.063	0.052	0.082	21
3	1.96	0.026	0.027	0.042	9
4	1.82	0.063	0.06	0.071	21
5	1.58	0.064	0.081	0.087	21
6	1.82	0.038	0.052	0.05	13
7	1.58	0.053	0.056	0.071	18
8	1.9	0.042	0.053	0.067	14
9	1.98	0.022	0.03	0.037	7

[a] 0.02 M KCl(aq) reference, specific conductivity = 0.03 Ω^{-1} cm^{-1} at 25 °C.

their spectra is provided by **7**: δ_H: 1.86, br s, 4H; 3.16, s, 12H; 3.49, br s, 4H; 4.35, s, 4H. δ_C: 20.87, 51.98, 56.28, 65.41, 81.35. δ_P: 1.20.

The hexafluorophosphate salts also isolated in these reactions exhibit corresponding ^{1}H and ^{13}C NMR spectra, but the ^{31}P signals appear as symmetrical septets centered at $\delta \sim -144$. Further, the isolated hexafluorophosphate salts appear to be universally contaminated with phosphate. Through quantitative measurement of the ^{1}H NMR spectra for these LIPs their anhydrous nature can be established, although they are fully soluble in water and adsorb water from room air. Specifically, from ^{1}H NMR measurements it is determined that the water content of the new LIPs is below the limit of reliable measurement, that is less than 0.5%. Unlike the hexafluorophosphate salts which are insoluble in water to the point that NMR measurements can not be made, the new LIPs are fully soluble in water. Both types of salts are soluble in DMSO allowing measurement of the ^{1}H and ^{13}C NMR spectra of the crude reaction products.

In addition to the measurement of their densities, specific conductivity measurements were performed on the LIPs **1**–**9**. A YSI Model 31 conductivity bridge was used for these measurements, with a constant temperature bath to maintain temperature of the sample during measurement at several temperatures (25, 40 and 60 °C). A 0.02 M solution of KCl in water was used as reference material (specific conductivity of 0.03 Ω^{-1} cm^{-1} at 25 °C). The results for these determinations are shown in Table 1.

In comparison with previously prepared rt NAILs, the presently described LIPs exhibit particular advantages. These include: (a) ease of preparation, requiring only ordinary ion-exchange in aqueous medium rather than the use of the quite reactive (and under certain circumstances hazardous) hexafluorophosphoric acid, tetrafluoroboric acid or aluminum chloride, which require controlled atmospheric conditions; (b) the resultant salts are unreactive with water; (c) although viscous, the LIPs are liquids at rt, while the hexafluorophosphate salts of monocations melt above rt and the hexafluorophosphate salts of polycations we have synthesized remain solid up to 75 °C; (d) particularly high specific conductivities; and (e) the potential for use as media for electrochemical processes requiring a large electrochemical window.

We are in the process of exploiting this new category of NAILs for utility in a variety of processes, including electrochemical conversions, media for "green" chemical reactions, catalysts for chemical conversions, syntheses of related species exhibiting water-insolubility, and the performance of separations without the use of volatile solvents. Further, determinations of the diffusion coefficients, mobilities of ions within the viscous media, and potential applications for electrochemical storage cells are being made.

The authors wish to acknowledge financial support provided for this project from LSAMP of New York, PFF of NSF/ACS, and ICET, Inc.

Notes and references

1 K. Rengan and R. Engel, *J. Chem. Soc., Chem. Commun.*, 1992, 757; J. Fabian, T. October, A. Cherestes and R. Engel, *Synlett*, 1997, 1007; T. Strekas, R. Engel, K. Locknauth, J. Cohen and J. Fabian, *Arch. Biochem. Biophys.*, 1999, **364**, 129; J. Cohen, L. Traficante, P. Schwatrz and R. Engel, *Tetrahedron Lett.*, 1998, **39**, 8617; J. Cohen, A. Rusinowski, T. Strekas and R. Engel, *Heteroatom Chem.*, 1999, **10**, 559; J. Cohen, V. Shteto and R. Engel, *Synthesis*, 2000, 1263; J. I. Cohen and R. Engel, *Res. Trends*, 2000, **7**,151; J. I. Cohen and R. Engel, *Synth. Commun.*, 2000, **30**, 2161.

2 M. Freemantle, *Chem. Eng. News*, 15 May 2000, 37.

3 H. Carmichael, *Chem. Br.*, January 2000, 36.

4 J. S. Wilkes, J. A. Levisky, R. A. Wilson and C. L. Hussey, *Inorg. Chem.*, 1982, **21**, 1263.

5 A. A. Fannin, D. A. Floreani, L. A. King, J. S. Landers, B. J. Piersma, D. J. Stech, R. L. Vaughn, J. S. Wilkes and J. L. Williams, *J. Phys. Chem.*, 1984, **88**, 2614.

6 W. M. Reichert, A. E. Visser, R. P. Swatloski, R. D. Rogers, Paper #85 presented at the 219th National Meeting of the American Chemical Society, I&EC Division, San Francisco, CA, USA, March 2000.

7 R. A. Carpio, L. A. King, R. E. Lindstrom, J. C. Nardi and C. L. Hussey, *J. Electrochem. Soc.*, 1979, **126**, 1544.

ChemComm

Immobilisation of ketone catalyst: a method to prevent ketone catalyst from decomposing during dioxirane-mediated epoxidation of alkenes

Choong Eui Song,*[a] Jin Seok Lim,[b] Su Chang Kim,[b] Kee-Jung Lee[b] and Dae Yoon Chi[c]

[a] *Life Sciences Division, Korea Institute of Science and Technology, PO Box 131, Cheongryang, Seoul, 130-650, Korea. E-mail: s1673@kist.re.kr*
[b] *Division of Chemical Engineering and Industrial Chemistry, Hanyang University, Seoul, 133-791, Korea*
[c] *Department of Chemistry, Inha University, 253 Yonghyun-Dong, Nam-Ku, Inchon, 402-751, Korea*

Received (in Cambridge, UK) 11th July 2000, Accepted 30th October 2000
First published as an Advance Article on the web 21st November 2000

Covalent attachment of trifluoromethyl ketone catalyst to a solid support such as silica gel increased the stability of catalyst dramatically, so solving an intrinsic problem of dioxirane-mediated epoxidation of alkenes catalysed by ketones.

Dioxiranes have been shown to be powerful and environmentally safe oxidants, which can be generated *in situ* from ketones and Oxone® ($2KHSO_5 \cdot KHSO_4 \cdot K_2SO_4$).[1] In principle, only a catalytic amount of ketone is required and, moreover, with a chiral ketone there exists the opportunity for catalytic asymmetric epoxidation.[2] However, an intrinsic problem of this catalytic epoxidation procedure is that the turnover number (TON) of ketone catalysts is generally very low owing to their instability under the epoxidation conditions. It has been generally known that ketone catalysts can be destroyed *via* Baeyer–Villiger oxidation and/or formation of 1,2,4,5-tetroxane *etc*.[1]

We proposed that the decomposition of ketone catalysts in the dioxirane-mediated epoxidation of alkenes could be prevented by covalent attachment of ketone catalysts to a suitable solid support,[3] since, as shown in Fig. 1, site isolation of catalytic centres can minimise the possibility of 1,2,4,5-tetroxane formation, and, moreover, the migration of a solid-bound alkyl chain in the Baeyer–Villiger oxidation step may need larger movement energy than that of the homogeneous analogue. Of course, this approach can provide an additional advantage of easy recycling of catalyst.

To test our rationale, we prepared a new silica-bound trifluoromethyl ketone **1** and compared its stability in the dioxirane-mediated epoxidation of alkenes with its homogeneous analogue, 1,1,1-trifluorododecan-2-one **2**. Here we report our preliminary results.

The silica-bound trifluoromethyl ketone **1** was simply prepared by the reaction of 1,1,1-trifluorodode-11-cen-2-one **3**[4] with 3-mercaptopropylsilanised silica gel **4**[5] in the presence of α,α′-azoisobutyronitrile (AIBN) as a radical initiator in acetonitrile (Scheme 1).[6] The fluorine and sulfur analyses of **1** (F, 2.61%; S, 2.90%) indicated that 0.45 mmol g^{-1} of trifluoromethyl ketone moiety was incorporated and the coupling yield of **3** with **4** was 50%. Thus, 0.45 mmol g^{-1} of unreacted thiol groups exist in the silica-bound trifluoromethyl ketone **1**. The attachment of trifluoromethyl ketone moieties to silica gel in the silica-bound ketone **1** was also confirmed *via* IR spectroscopy (1766 cm^{-1} for $\nu_{C=O}$).

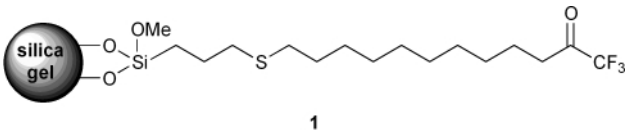

1

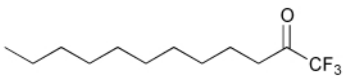

2

In order to compare the catalytic efficiency and stability of silica-bound ketone **1** with its homogeneous analogue **2**, the epoxidation of alkenes were carried out with Oxone® in a MeCN–H_2O solvent system under the modified condition employed by Shi and co-workers.[7] The results are summarised in Table 1.

As shown in Table 1, the silica-bound ketone **1** exhibited comparable catalytic activity with that of its homogeneous analogue **2**. In a ratio of ketone : olefin of 0.5 : 1 at room temperature, epoxidation of alkenes using 2.07 equiv. of Oxone® and 8.7 equiv. of K_2CO_3 was complete within 5 min after addition of Oxone® and K_2CO_3, and afforded the corresponding epoxides in very high yield.[8] Most of the oxidised products were obtained in nearly pure form by simple filtration of the ketone **1**, followed by extraction of organic product and evaporation of the solvent. The observed results suggest that trifluoromethyl ketone moiety on silica gel remains highly exposed to the reactants and thus substrates can access to the catalytic sites easily.

The silica gel supported trifluoromethyl ketone **1** could be easily recovered after reaction by simple filtration and the recovered ketone **1** was reused several times without any significant loss of activity. All epoxidations of *trans*-β-methylstyrene using the recycled ketone **1** afforded *trans*-β-methylstyrene oxide in nearly quantitative yield, even after tenth use.[9] As we proposed, the retainment of the catalytic activity during several cycles can be explained by that the decomposition of the supported ketone catalyst **1** *via* Baeyer–Villiger oxidation and/or 1,2,4,5-tetroxane formation[10] proceeds much more slowly than that of its homogeneous analogue **2**. We could not find any carbonyl peak of the Baeyer–Villiger oxidation product (ester) in the IR spectrum of **1** recovered after

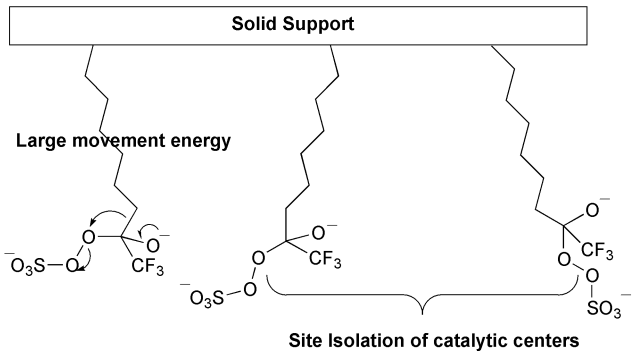

Fig. 1

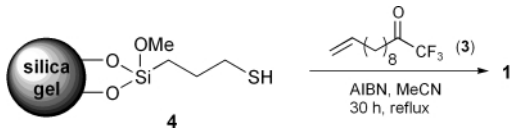

Scheme 1

DOI: 10.1039/b005604i

Table 1 Epoxidations of alkenes with Oxone® catalysed by silica-bound ketone **1** or its homogeneous analogue **2**[a]

Entry	Alkene	Yield (%)[b] Using catalyst **1**	Using catalyst **2**
1	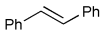	94	93
2		>98	>98
3	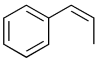	>98	>98
4	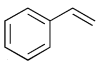	>98	>98
5	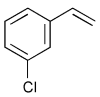	>98	>98
6		>98	>98
7		>98	>98
8	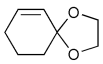	71	67
9		>98[c]	>98[d]

[a] The reaction conditions were not optimised: substrate (1 equiv.), ketone catalyst (0.5 equiv.) Oxone® (2.07 equiv.) and K_2CO_3 (8.7 equiv.) in MeCN–aqueous EDTA (4×10^{-4} M) (1.5/1, v/v) at room temperature. Under such conditions, the blank reaction (the epoxidation of *trans*-β-methylstyrene only with Oxone®) gave the epoxide only up to 16% yield. [b] Yields were determined by GC and ^{1}H NMR analysis of crude products. [c] 93% of α-pinene oxide and *ca*. 5% of α-campholenic aldehyde. [d] 84% of α-pinene oxide and *ca*. 15% of α-campholenic aldehyde.

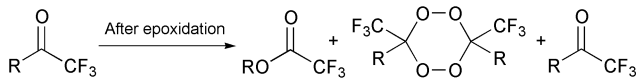

2 (R = $C_{10}H_{21}$) **5** (8%) **6** (77%) **2**

Scheme 2

10 runs. In contrast to the silica-bound catalyst **1**, *ca*. 85% of its homogeneous analogue **2** was decomposed after a first run of the epoxidation of *trans*-β-methylstyrene. The main decomposed products were ester **5** (*ca*. 8%) and 1,2,4,5-tetroxane **6** (*ca*. 77%) (Scheme 2). The structure of **6** was assigned by NMR and HRMS analyses.[11]

In conclusion, we have achieved excellent results for the heterogeneous dioxirane-mediated epoxidation of alkenes using silica gel supported trifluoromethyl ketone **1**. This silica-bound ketone was reused ten times without loss of activity. This retainment of the catalytic activity during several cycles was explained by that the decomposition of the supported ketone catalyst **1** *via* Baeyer–Villiger oxidation and/or 1,2,4,5-tetroxane formation[10] proceeds much more slowly than that of its homogeneous analogue **2**. Thus, this type of immobilisation of ketone catalysts will provide a possibility to increase their stability, which is an intrinsic problem of dioxirane-mediated epoxidation catalysed by ketones. The current study will also provide some insight for the development of new chiral ketone catalysts. In the search for efficient ketone catalysts for asymmetric epoxidation, both turnover number and enantioselectivity are crucial issues to be considered.

This research was supported by a grant from Korea Institute of Science and Technology.

Notes and references

1 R. W. Murray, *Chem. Rev.*, 1989, **89**, 1187; W. Adam, R. Curci and J. O. Edward, *Acc. Chem. Res.*, 1989, **22**, 205; R. Curci, in *Advances in Oxygenated Process*, ed. A. L. Baumstark, JAI, Greenwich CT, 1990, vol. 2, ch. 1, p. 1; W. Adam, L. P. Hadjiarapoglou, R. Curci and R. Mello, in *Organic Peroxides*, ed. W. Ando, John Wiley & Sons, Chichester–New York–Brisbane–Toronto–Singapore, 1992, ch. 4, p. 195; R. Curci, A. Dinoi and M. F. Rubino, *Pure Appl. Chem.*, 1995, **67**, 811; W. Adam and A. K. Smerz, *Bull. Soc. Chim. Belg.*, 1996, **105**, 581; W. Adam, A. K. Smerz and C.-G. Zhao, *J. Prakt. Chem.*, 1997, **339**, 298, and references therein.

2 Review: S. E. Denmark and Z. Wu, *Synlett*, 1999, 847.

3 Recently, simply for the easy separation of catalyst from the reaction mixture, some polymer-bound ketones have been employed: T. R. Boehlow, P. C. Buxton, E. L. Grocock, B. A. Marples and V. L. Waddington, *Tetrahedron Lett.*, 1998, **39**, 1839; A. Shiney, P. K. Rajan and K. Sreekumar, *Polym. Int.*, 1996, **41**, 377.

4 1,1,1-Trifluorododec-11-en-2-one **3** was synthesised by the published procedure: J. Biovin, L. E. Kaim and S. Z. Zard, *Tetrahedron*, 1995, **51**, 2573.

5 3-Mercaptopropylsilanised silica gel **4** (1.14 mmol of S g^{-1}) was prepared by the reaction of Silica gel 60 (70–230 mesh, Merck) and (3-mercaptopropyl)trimethoxysilane according to the published procedure: C. Rosini, C. Bertucci, D. Pini, P. Altemura and P. Salvadori, *Tetrahedron Lett.*, 1985, **26**, 3361; C. Rosini, P. Altemura, D. Pini, C. Bertucci, G. Zullino and P. Salvadori, *J. Chromatogr.*, 1985, **348**, 79; P. Savadori, C. Rosini, D. Pini, C. Bertucci, P. Altemura, G. Uccello-Barretta and A. Raffaelli, *Tetrahedron*, 1987, **43**, 4969.

6 Some of chiral catalysts have been anchored on silica by same methodology: C. E. Song, J. W. Yang and H.-J. Ha, *Tetrahedron: Asymmetry*, 1997, **8**, 841; D. Pini, A. Mandoli, S. Orlandi and P. Salvadori, *Tetrahedron: Asymmetry*, 1999, **10**, 3883.

7 Z.-X. Wang, Y. Tu, M. Frohn and Y. Shi, *J. Org. Chem.*, 1997, **62**, 2328.

8 The epoxidation of *trans*-stilbene in a MeCN–H_2O solvent system under the same reaction conditions[7] reported by Shi (1.38 equiv. of Oxone®, 5.8 equiv. of K_2CO_3 and 0.5 equiv. of ketone) afforded the corresponding epoxide in *ca*. 76% yield. However, the yield was dramatically increased only by increasing the amount used of Oxone® and K_2CO_3. In a 0.5 : 1 ketone : olefin ratio at room temperature, epoxidation of *trans*-stilbene proceeded completely within 5 min after addition of 2.07 equiv. of Oxone® and 8.7 equiv. of K_2CO_3 and afforded the corresponding epoxide in nearly quantitative yield (Table 1).

9 There was some loss of ketone **1** owing to its slight solubility in the reaction medium and thus, in a each run, the amounts of substrate were used based on the amounts of the recovered ketone **1**.

10 However, our site isolation hypothesis is not very convincing yet since the loading of the ketone catalyst on the silica gel is so high that the interaction between immobilised molecules can not be excluded.

11 *Selected physical data* of **6**: ^{13}C NMR (75.5 MHz, $CDCl_3$) δ 123.24 (q, *J* 285.2 Hz), 94.69 (q, *J* 31.5 Hz), 72.09, 36.09, 32.15, 30.43, 29.64, 26.80, 25.57, 22.98, 18.18, 14.43; FAB-HRMS (M^+ + Na). Calc. for $C_{24}H_{42}O_4F_6Na$: *m*/*z* 531.2885. Found: 531.2886.

A third isolated oxidation state for the Mn_{12} family of single-molecule magnets

Monica Soler,[a] Swapan K. Chandra,[a] Daniel Ruiz,[b] Ernest R. Davidson,[a] David N. Hendrickson*[b] and George Christou*[a]

[a] *Department of Chemistry, Indiana University, Bloomington, IN 47405-4001, USA. E-mail: christou@indiana.edu*
[b] *Department of Chemistry-0358, University of California at San Diego, La Jolla, CA 92093-0358, USA. E-mail: dhendrickson@ucsd.edu*

Received (in Irvine, CA, USA) 27th July 2000, Accepted 13th October 2000
First published as an Advance Article on the web 22nd November 2000

Dianionic members of the Mn_{12} family of single-molecule magnets have been prepared by two-electron reduction of the neutral cluster; the $[PPh_4]_2[Mn_{12}O_{12}(O_2CCHCl_2)_{16}(H_2O)_4]$ representative has been shown to possess an $S = 10$ ground state and to exhibit out-of-phase ac susceptibility signals diagnostic of single-molecule magnetism behavior.

An exciting development in nanoscale magnetic materials occurred in 1993 when $[Mn_{12}O_{12}(O_2CMe)_{16}(H_2O)_4]$ **1** was identified as a nanoscale magnet,[1] the first to comprise discrete, (magnetically) non-interacting molecular units rather than a 3D extended lattice (metals, metal oxides, *etc.*). This initiated the field of molecular nanomagnetism and such a molecule has been termed a single-molecule magnet (SMM).[2] Other $[Mn_{12}O_{12}(O_2CR)_{16}(H_2O)_x]$ (R = Et, Ph, *etc.*; x = 3 or 4) derivatives have since been studied,[1,3] and they display similar properties. SMM behaviour is due to a combination of a large ground state spin (S) of S = 10 and negative (easy axis) magnetoanisotropy as gauged by a negative zero-field splitting parameter D. As a result, there is a significant barrier for the relaxation of the cluster's magnetization vector, and these Mn_{12} molecules are thus magnetizable magnets.

More recently, the one-electron reduced complex $[NPr_4][Mn_{12}O_{12}(O_2CEt)_{16}(H_2O)_4]$ and related species with S = 19/2 ground states have also been found to be SMMs.[3] In addition, new examples of SMMs have been found in the family of $[Mn_4O_3X(O_2CMe)_3(dbm)_3]$ (X = Cl^-, Br^-, F^-, N_3^-, $MeCO_2^-$, *etc.*) complexes containing a $[Mn_4(\mu_3\text{-}O)_3(\mu_3\text{-}X)]^{6+}$ core and an S = 9/2 ground state,[2,4] as well as a few other species.[5–7] Here, we report that the two-electron reduced form of the $[Mn_{12}]$ complexes has been successfully isolated and that this retains both a high ground state S value and the SMM properties of the $[Mn_{12}]^{0,-}$ species. This extends the Mn_{12} of SMMs to a third oxidation level and provides an invaluable new datum point for our future understanding of how changing spin state and magnetic anisotropy can affect the properties of these important molecules. We herein report the synthesis and characterization of the new $[Mn_{12}O_{12}(O_2CR)_{16}(H_2O)_4]^{2-}$ species.

$[Mn_{12}O_{12}(O_2CR)_{16}(H_2O)_4]$ complexes with electron-withdrawing groups [R = $CHCl_2$ (**2**), C_6F_5 (**3**), $C_6H_3(NO_2)_2$-2,4 (**4**), *etc.*] to facilitate multi-electron reduction were prepared from **1** using the procedure reported elsewhere.[1,3] The representative CV in MeCN of **2** (Fig. 1) shows three quasi-reversible one-electron reduction processes at 0.91, 0.61 and 0.29 V *vs.* ferrocene, and a fourth irreversible reduction at lower potential. These values are significantly more positive than for the R = Me and Ph derivative (Table 1).[1,3] In addition, the second and third reductions appear more reversible by electrochemical criteria (peak currents and separations) than those for previous $[Mn_{12}]$ derivatives. The dianionic species were therefore targeted and successfully prepared on a large scale using I^- as reducing agent, as employed for one-electron reductions.[3] Thus, addition of 2 equivalents of NPr^n_4I or PPh_4I in MeCN, removal of solvent and recrystallization from MeCN–Et_2O–hexanes or CH_2Cl_2–hexanes gave dark red–brown $[PPh_4]_2[Mn_{12}O_{12}(O_2CCHCl_2)_{16}(H_2O)_4]$ **5**, $[NPr^n_4]_2[Mn_{12}O_{12}(O_2CC_6F_5)_{16}(H_2O)_4]$ **6** and $[NPr^n_4]_2[Mn_{12}O_{12}(O_2CC_6H_3(NO_2)_2\text{-}2,4)_{16}(H_2O)_4]$ **7**,† as well as others [eqn. (1)].

$$[Mn_{12}O_{12}(O_2CR)_{16}(H_2O)_4] + 2NPr^n_4I \rightarrow [NPr^n_4]_2[Mn_{12}O_{12}(O_2CR)_{16}(H_2O)_4] + I_2 \quad (1)$$

The structure‡ of the dianion of **5** (Fig. 2) confirms the same structure as in the neutral and monoanionic species, but now with a $2Mn^{II}$, $6Mn^{III}$, $4Mn^{IV}$ description indicating that the two added electrons are on outer Mn^{II} (formerly Mn^{III}) ions (Mn9 and Mn11 of Fig. 2) rather than Mn^{IV} ions in the cubane, as found in the one-electron reduced complexes,[3] which are Mn^{II}, $7Mn^{III}$, $4Mn^{IV}$. The assignment of $Mn^{II}/Mn^{III}/Mn^{IV}$ is based on relative Mn–O distances, bond valence sum calculations, and Jahn–Teller (JT) axial elongations only on six Mn sites. ^1H NMR studies in solution are consistent with electron-detrapping amongst the outer eight Mn ions on the NMR timescale, as also found for the mono-anionic species.[3]

The ground state of **5** was determined from reduced magnetization ($M/N\mu_B$) *vs.* H/T measurements in the 10–70 kG

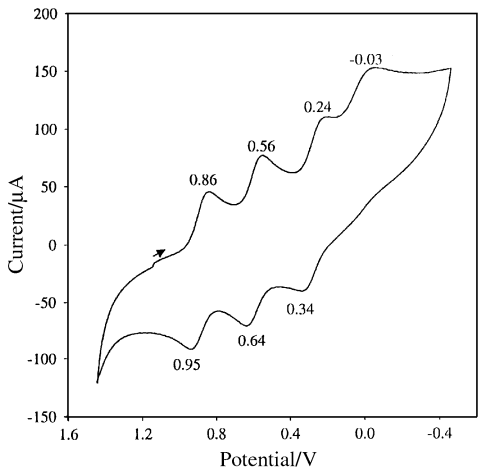

Fig. 1 Cyclic voltammogram at 100 mV s^{-1} for complex **2** in MeCN containing 0.10 M $NBu^n_4PF_6$ as supporting electrolyte. The working and auxiliary electrodes were glassy carbon and Pt wire, respectively. The indicated potentials are *vs.* ferrocene as an internal reference.

Table 1 Electrochemical data for $[Mn_{12}O_{12}(O_2CR)_{16}(H_2O)_4]$ complexes[a]

R	E_1/V[b]	E_2/V[c]
CH_3 (**1**)	0.18	−0.06
CH_2Cl	0.60	0.30
$CHCl_2$ (**2**)	0.91	0.61
C_6H_5[d]	0.12	−0.23
$C_6H_4NO_2$-2	0.47	0.19
$C_6H_4NO_2$-4	0.49	0.23
$C_6H_3(NO_2)_2$-2,4 (**4**)	0.74	0.45
C_6F_5 (**3**)	0.64	0.46

[a] In MeCN, unless otherwise indicated; values are DPV peak potentials *vs.* ferrocene. [b] First reduction. [c] Second reduction. [d] In CH_2Cl_2.

DOI: 10.1039/b006519f

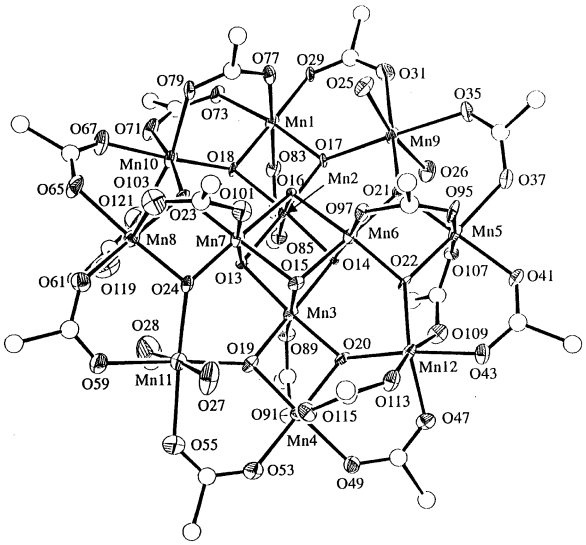

Fig. 2 ORTEP representation of the anion of complex **5** showing 50% probability ellipsoids. For clarity, all H and Cl atoms have been omitted.

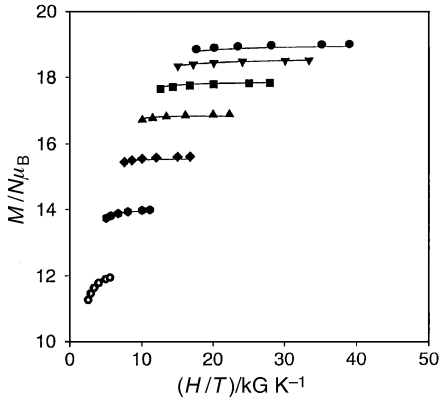

Fig. 3 Plot of (M/N μ_B) *vs.* H/T for complex **5** at 10 (⊕), 20 (●), 30 (◆), 40 (▲), 50 (■), 60 (▼) and 70 (●) kG. The solid lines are fits using the appropriate method;[9] see text for the fit parameters.

and 1.80–4.00 K ranges (Fig. 3). Fitting of the data gave $S = 10$, $D = -0.27$ cm^{-1} (-0.39 K) and $g = 2.00$. The ground state spin is thus similar to the $S = 10$ and 19/2 values for the neutral and monoanionic complexes, respectively. This suggested that the dianionic complexes might also be SMMs, *i.e.* show slow magnetization relaxation (reorientation) rates, and this was confirmed in ac susceptibility studies by an out-of-phase signal (χ_m'') in the 2–3 K range (Fig. 4, bottom). ac Susceptibility studies monitor the response of a material's magnetization (magnetic moment) to an applied, oscillating field, and a non-zero χ_m'' signal shows that the magnetization cannot relax fast enough to keep in-phase with the oscillating field. The positions of the χ_m'' peaks, at which temperature the relaxation rate equals the ac frequency, are in the 2–3 K range, lower than the 4–6 and 6–8 K ranges for the χ_m'' peaks in the monoanionic and neutral complexes, respectively (Fig. 4). This is consistent with the changing S and D values on progressive reduction since the barrier to thermally-activated reversal of the magnetization direction is related to $S^2|D|$ and $(S^2 - \frac{1}{4})|D|$ for integer and half-integer spins, respectively. The $S(D)$ values for the three oxidation levels are: $[Mn_{12}]$, 10 (≈ -0.5 cm^{-1}); $[Mn_{12}]^-$, 19/2 (≈ -0.4 cm^{-1}); $[Mn_{12}]^{2-}$, 10 (≈ -0.3 cm^{-1}).

In conclusion, the $[Mn_{12}]$ family of SMMs now provides three oxidation levels for the study of this important new phenomenon. In particular, the $[Mn_{12}]^{2-}$ *vs.* $[Mn_{12}]$ comparison

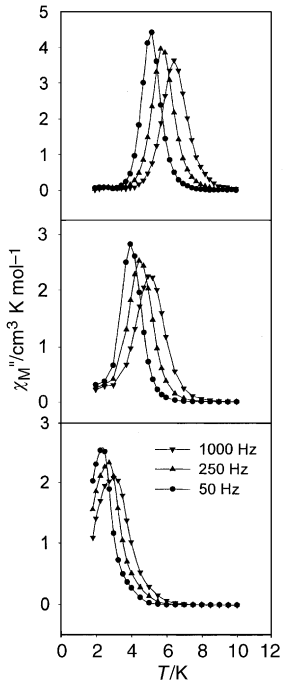

Fig. 4 Plot of the out-of-phase ac susceptibility (χ_m'') for complex **2** (top), $[NPr^n_4][Mn_{12}O_{12}(O_2CCHCl_2)_{16}(H_2O)_4]$ (middle) and complex **5** (bottom) at the indicated oscillation frequencies of the applied field.

provides an invaluable opportunity to study how the magnetic properties and quantum tunneling behaviour of equivalent spin ($S = 10$) systems vary with changing magnetoanisotropy.

This work was supported by the National Science Foundation.

Notes and references

† Complexes **5**–**7** have been fully characterized by NMR, IR, CV and elemental analysis (C, H, N).

‡ *Crystal data*: **5**·4CH_2Cl_2·H_2O: $C_{84}H_{74}Cl_{40}Mn_{12}O_{59}P_2$, $M_r = 4166.79$, triclinic, space group $P\bar{1}$, $a = 15.153(2)$, $b = 21.858(2)$, $c = 22.130(2)$ Å, $\alpha = 109.45(1)$, $\beta = 93.78(1)$, $\gamma = 96.52(1)°$, $U = 6824$ Å^3, $Z = 2$, $T = 115$K, μ(Mo-Kα) = 19.7 mm^{-1}, 146767 reflections measured, 31965 unique ($R_{av} = 0.129$), $R(F) = 0.0638$, $R_w(F) = 0.0551$ using 12440 unique reflections with $I > 2.33\sigma(I)$.

CCDC 182/1822. See http://www.rsc.org/suppdata/cc/b0/b006519f/ for crystallographic files in .cif format.

1 R. Sessoli, H.-L. Tsai, A. R. Schake, S. Wang, J. B. Vincent, K. Folting, D. Gatteschi, G. Christou and D. N. Hendrickson, *J. Am. Chem. Soc.*, 1993, **115**, 1804; R. Sessoli, D. Gatteschi, A. Caneschi and M. Novak, *Nature*, 1993, **365**, 141.

2 S. M. J. Aubin, M. W. Wemple, D. M. Adams, H.-L. Tsai, G. Christou and D. N. Hendrickson, *J. Am. Chem. Soc.*, 1996, **118**, 7746.

3 H. J. Eppley, H.-L. Tsai, N. DeVries, K. Folting, G. Christou and D. N. Hendrickson, *J. Am. Chem. Soc.*, 1995, **117**, 301.

4 S. M. J. Aubin, N. R. Dilley, L. Pardi, J. Krzystek, M. W. Wemple, L.-C. Brunel, M. B. Maple, G. Christou and D. N. Hendrickson, *J. Am. Chem. Soc.*, 1998, **120**, 4991.

5 A.-L. Barra, P. Debrunner, D. Gatteschi, C. E. Schulz and R. Sessoli, *Europhys. Lett.*, 1996, **35**, 133.

6 A.-L. Barra, A. Caneschi, A. Cornia, F. Fabrizi de Biani, D. Gatteschi, C. Sangregorio, R. Sessoli and L. Sorace, *J. Am. Chem. Soc.*, 1999, **121**, 5302.

7 S. L. Castro, Z. Sun, C. M. Grant, J. C. Bollinger, D. N. Hendrickson and G. Christou, *J. Am. Chem. Soc.*, 1998, **120**, 2365.

8 S. M. J. Aubin, Z. Sun, L. Pardi, J. Krzystek, K. Folting, L.-C. Brunel, A. L. Rheingold, G. Christou and D. N. Hendrickson, *Inorg. Chem.*, 1999, **38**, 5329.

9 J. B. Vincent, C. Christmas, H.-R. Chang, Q. Li, P. D. W. Boyd, J. C. Huffman, D. N. Hendrickson and G. Christou, *J. Am. Chem. Soc.*, 1989, **111**, 2086.

Cyclopolymerisation of an oriented 4,6-bis(4-vinylbenzyl)-*myo*-inositol orthoformate

Tae-Hyun Kim,[ab] Peter Dokolas,[b] Neil Feeder,[a] Mark Giles,[b] Andrew B. Holmes*[ab] and Mathias Walther[b]

[a] *University Chemical Laboratory, Department of Chemistry, University of Cambridge, Lensfield Road, Cambridge, UK CB2 1EW. E-mail: abh1@cam.ac.uk*

[b] *Melville Laboratory for Polymer Synthesis, Department of Chemistry, University of Cambridge, Pembroke Street, Cambridge, UK CB2 3RA*

Received (in Cambridge, UK) 30th August 2000, Accepted 19th October 2000
First published as an Advance Article on the web 22nd November 2000

Free radical-promoted cyclopolymerisation of a 4,6-bis(4-vinylbenzyl)-*myo*-inositol orthoformate 4, whose X-ray structure has been determined, was studied and the first formed intermediate was trapped using (tetramethylpiperidine *N*-oxyl) (TEMPO) 7.

Cyclopolymerisation[1,2] is a useful method for controlling the regio- and stereochemistry of monomer additions, leading to polymers with well-defined microstructures.[3] We were interested in the use of a scaffold with oriented hydroxy functionality based on a rigid monomer which would undergo cyclopolymerisation to afford a polymer with an organised backbone and oriented functional groups. We selected the 4,6-bis(4-vinyl)-benzyl)-*myo*-inositol orthoformates **3** and **4** as suitable monomers to deliver these features.

The monomers **3** and **4** were prepared from *myo*-inositol orthoformate **1**[4] either by selective derivatisation[5] at positions 4 and 6 with 4-vinylbenzyl chloride (to give **3**) or selective silylation[6] at the 2-position followed by benzylation at positions 4 and 6 (Scheme 1). The key structural feature offered by these monomers includes the orthoformate group which, after the polymerisation reaction, may be easily deprotected to yield (ideally) an all-axial triol repeat unit.

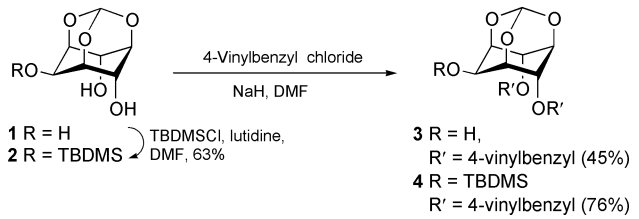

Scheme 1 Preparation of monomers **3** and **4**.

Both monomers gave suitable crystals for X-ray analysis, but disorder in the silyl side chain of **4** yielded data with an unacceptably high *R* factor. The X-ray structure† of monomer **3** revealed two conformations (ratio 3:1) in the unit cell with a characteristic edge-to-face interaction of the aromatic rings.[7] The monomer structures differed only in the relative orientation of the vinyl groups. The important interatomic bond distances of the major conformer of **3** measured from the X-ray data, are presented in Fig. 1.

Heating a toluene solution of the monomer **4** at 65 °C in the presence of 2–3 wt% AIBN afforded an organic soluble polymer of M_n 10 000–20 000 which is formulated as a linear cyclopolymer **5** (Scheme 2).‡ The evidence for the cyclopolymer **5** comes from the X-ray structure of the monomer and the trapping of the first formed cyclic radical intermediate.

Thermal decomposition of the AIBN initiator would give the cyanoisopropyl radical which would add selectively to the less substituted end of the vinyl group.[8] Intramolecular cyclisation by 'head' to 'tail' addition, from C(15) to C(25), is likely to be the more favourable reaction pathway as the distance from C(15) to C(25) shown in Fig. 1, is significantly shorter than the other measured distances. Supporting evidence for this pathway is provided by the trapping experiment discussed below. Similar interatomic bond distances were found in **4**.

Interatomic distances (Å)	
C(15)-C(24)	4.907
C(15)-C(25)	3.935
C(16)-C(24)	5.167
C(16)-C(25)	4.151

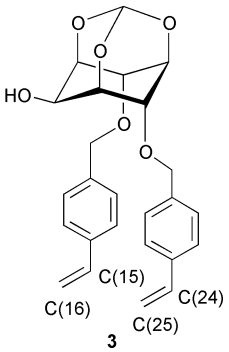

3

Fig. 1 Selected interatomic bond distances in a crystal of the monomer **3**.

The TEMPO radical trapping technique, developed by Rizzardo, Solomon and Moad,[9–11] and also exploited by Busfield and Jenkins,[8] was used to isolate the reactive radical intermediate generated during cyclopolymerisation. The optimum trapping experiment involved heating a 29 mM benzene

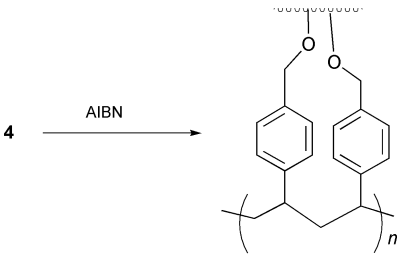

5

Scheme 2 Cyclopolymerisation of the monomer **4**.

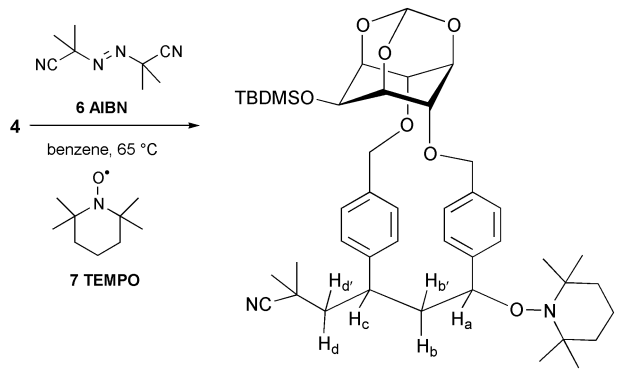

8

Scheme 3 TEMPO trapping of the first formed cyclic intermediate after AIBN-initiated addition to the monomer **4**.

DOI: 10.1039/b007057m

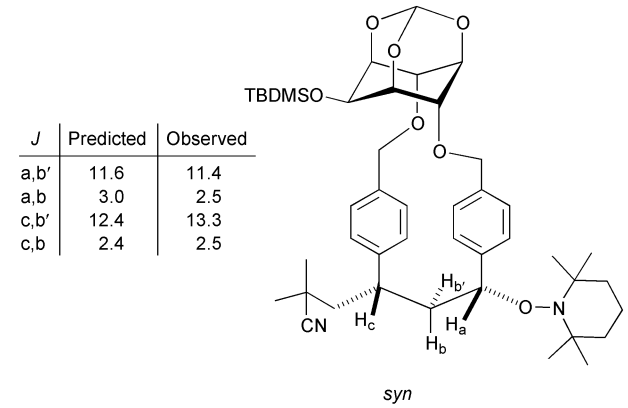

J	Predicted	Observed
a,b′	11.6	11.4
a,b	3.0	2.5
c,b′	12.4	13.3
c,b	2.4	2.5

syn

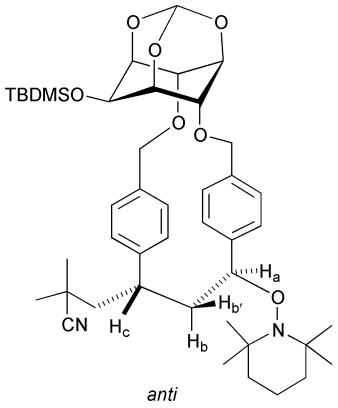

J	Predicted	Observed
a,b′	11.6	11.4
a,b	2.4	2.5
c,b′	4.0	13.3
c,b	3.1	2.5

anti

Fig. 2 Two possible diastereoisomeric structures for the trapped product **8**.

solution of the monomer **4** in the presence of AIBN **6** (28 mM) and TEMPO **7** (10 mM) to give the alkoxyamine **8** in 5% yield (the mass balance was mainly starting material) (Scheme 3). The low yield of product arises from competing reaction of the cyanoisopropyl radical with the aminoxyl agent.[8] To our knowledge this is the first example of trapping of the cyclic intermediate in a styrenic radical cyclopolymerisation, and may offer important opportunities to study the kinetics of the early propagation steps of such processes.

The structure determination of the cyclic product **8** was performed by ^{1}H NMR TOCSY and NOE experiments. Selective 1-D TOCSY experiments assisted in determining the connectivity sequence of atoms. Mutual NOE effects were observed between H_a and H_c in compound **8**, indicating that the methine protons are part of the same cyclic structure. The observed ^{1}H NMR coupling constant (13.3 Hz) between H_c and $H_{b'}$ is more consistent with the *syn* diastereoisomer (predicted 12.4 Hz) than the *anti* (predicted *J* 4.0 Hz) (Fig. 2).§

In conclusion we have confirmed the existence of a cyclopolymerisation by trapping the reactive radical intermediate. Furthermore, interatomic bond distances between the vinyl groups in both **3** and **4**, as established in the solid state, favour the formation of a cyclic structure. Hence, the monomers based on *myo*-inositol orthoformate show interesting opportunities to prepare a rigid scaffold with oriented functionality.

We thank EPSRC for financial support and provision of the Swansea MS service, the Cambridge Overseas Trust, Robinson College, and the CVCP for scholarships (to T.-H. K.) and Dr P. Grice for the ^{1}H TOCSY NMR experiments. We thank Professor I. Jenkins, Dr J. H. G. Steinke and Dr W. McDonald (ICI/DuPont) for their interest in this work.

Notes and references

† *Crystal data* for **3**: Colourless needle-shaped crystals, mp 136 °C, of $C_{25}H_{26}O_6$ were monoclinic, space group $P2_1/c$, with a = 6.072(6), b = 24.506(6), c = 14.217(3) Å, α = 90, β = 99.35(4), γ = 90°, V = 2087(2) Å^3, Z = 4, T = 180 (2) K, μ = 0.96 mm^{-1}, ρ_{calc} = 1.344 Mg m^{-3}, M = 422.46. One of the vinyl groups, C(24) and C(25), appears to be disordered about two orientations. The final $R_w(F^2)$ = 0.1037 with a goodness of fit = 1.014, while the conventional $R(F)$ = 0.0559 for 7948 reflections with $F_o > 4[\sigma(F_o)]$. CCDC 182/1833. See http://www.rsc.org/suppdata/cc/b0/b007057m/ for crystallographic files in .cif format.

‡ Further details of the cyclopolymerisation (see following Communication, DOI: 10.1039/b007058k) will be described in a full paper.

§ Molecular modelling[12] of **8** using the MM2 force field in MacroModel v5.5® indicated that the distance between the methine hydrogens H_a and H_c in either the *syn* or *anti* isomers was 2.43–3.74 Å, within the NOE experimental range. It is impossible to distinguish the two alternative *syn*-diastereoisomers (relative to the 2-TBDMSO substituent).

1 G. B. Butler, *Acc. Chem. Res.*, 1982, **15**, 370.
2 L. J. Mathias, *Trends Polym. Sci.*, 1996, **4**, 330.
3 G. Wulff, S. Glasdow, B. Kühneweg and S. Krieger, *Macromol. Symp.*, 1996, **101**, 355.
4 H. W. Lee and Y. Kishi, *J. Org. Chem.*, 1985, **50**, 4402.
5 D. C. Billington, R. Baker, J. J. Kulagowski, I. M. Mawer, J. P. Vacca, S. J. Desolms and J. R. Huff, *J. Chem. Soc., Perkin Trans. 1*, 1989, 1423.
6 G. Baudin, B. I. Glänzer, K. S. Swaminathan and A. Vasella, *Helv. Chim. Acta*, 1988, **71**, 117.
7 E. G. Cox, D. W. J. Cruickshank and J. A. S. Smith, *Proc. R. Soc. London, Ser. A*, 1958, **247**, 1.
8 W. K. Busfield, I. D. Jenkins and P. Van Le, *Polym. Bull. (Berlin)*, 1997, **38**, 149.
9 E. Rizzardo and D. H. Solomon, *Polym. Bull. (Berlin)*, 1979, **1**, 529.
10 A. L. J. Beckwith, V. W. Bowry and G. Moad, *J. Org. Chem.*, 1988, **53**, 1632.
11 G. Moad, E. Rizzardo and D. H. Solomon, *Macromolecules*, 1982, **15**, 909.
12 F. Mohamadi, N. G. J. Richards, W. C. Guida, R. Liskamp, M. Lipton, C. Caufield, G. Chang, T. Hendrickson and W. C. Still, *J. Comput. Chem.*, 1990, **11**, 440.

Ring closing metathesis of a 4,6-diallyl-*myo*-inositol orthoformate as a model for an inositol cyclopolymer

Tae-Hyun Kim,[a,b] Mark Giles[b] and Andrew B. Holmes*[a,b]

[a] *Department of Chemistry, University Chemical Laboratory, University of Cambridge, Lensfield Road, Cambridge, UK CB2 1EW. E-mail: abh1@cam.ac.uk*

[b] *Melville Laboratory for Polymer Synthesis, Department of Chemistry, University of Cambridge, Pembroke Street, Cambridge, UK CB2 3RA*

Received (in Cambridge, UK) 30th August 2000, Accepted 19th October 2000
First published as an Advance Article on the web 21st November 2000

Ring closing metathesis (RCM) of the diallyl inositol derivative 5 gave the product 6 which after cleavage of the orthoester served as a model for assignment of the preferred conformation of the analogous deprotected inositol cyclopolymer 3.

In the preceding Communication the cyclopolymerisation of the conformationally locked 4,6-bis(4-vinylbenzyl)-*myo*-inositol **1** to the novel cyclopolymer **2** was reported (Scheme 1).[1]

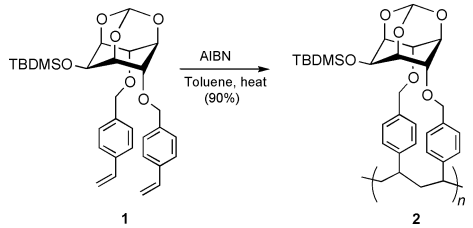

Scheme 1 Polymerisation of the monomer **1** to cyclopolymer **2**.

The rigid inositol unit of the monomer **1** acts as a template to bring both polymerisable styryl groups into close proximity for cyclopolymerisation. The monomer **1** was polymerised at high dilution (0.1 mmol ml^{-1}) in toluene with 2–3 wt% of AIBN as a radical initiator to give a soluble linear cyclic polymer **2** in high yield (80–90%) with molecular weight M_n of 10 000–20 000 as determined by GPC.† It was hoped that removal of the orthoester and silyl groups would release a hydrophilic polymer with oriented fiunctionality. Thus the polymer **2** was heated in a mixture of THF and methanol in the presence of toluene-*p*-sulfonic acid to give the hydroxylated polymer **3** (Scheme 2). The polymer **3** would be expected to exhibit interesting hydrophilic and metal binding properties if all five hydroxy groups remained axial **3ax**.[2,3] However, the alternative conformation **3eq**. would also be feasible. Unfortunately the polymer **3** shows very broad ^{1}H and ^{13}C NMR spectra, making the full conformational interpretation difficult, and hence conformational studies using model small molecules were carried out to gain insight into this feature.

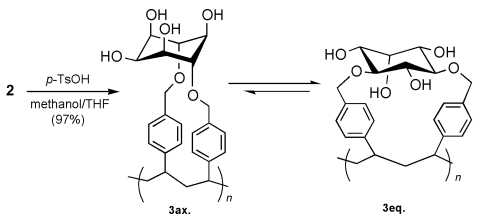

Scheme 2 Deprotection of polymer **2** to give two alternative conformations of **3**.

The model compounds were thought to be accessible by ring closing metathesis (RCM)[4,5] of the monomer **1** using the ruthenium based alkylidene catalyst **4**.[6] However, attempted ring closure of the monomer **1**, under high dilution (11.2 mM),

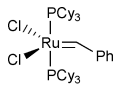

4

failed and gave only oligomeric products. This was ascribed to the rigid steric arrangement of the two styryl groups in a single unit of **1**, making the formation of another ring difficult. RCM of an alternative monomer with flexible alkyl linking groups was therefore carried out. The diallyl inositol **5** was formed in 78% yield by treating **1** with allyl bromide and sodium hydride in DMF. On treatment of the monomer **5** with the ruthenium initiator **4**, the ring closed product **6** and 'dimer' **7** were obtained, together with starting material (35%) and oligomeric products (Scheme 3). The double bond stereochemistry of these symmetrical products has not been assigned, but it is reasonable to assume that compound **6** has the *Z*-double bond configuration.

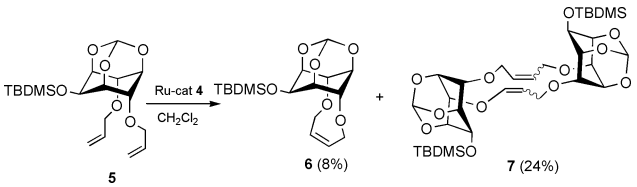

Scheme 3 RCM of the diallyl inositol **5**.

The RCM product **6** was deprotected to give the model compound **8** (Scheme 4).‡

Analysis of the ^{1}H NMR spectrum of the deprotected product **8** indicated that the preferred ring conformation was **8eq**. The protons H_d (δ 3.20, dd, *J* 9 and 3), H_e (δ 3.31, br t, *J* 9, 9) and H_f (δ 2.92, dt, *J* 6 and 9) were all axial and the measured coupling constants were in good agreement with those predicted by computer modelling.[7] A strong ^{1}H NMR NOE effect was also observed between the signals due to H_d and H_f (see Scheme 4) and between H_a (δ 5.75, br s) and H_e.

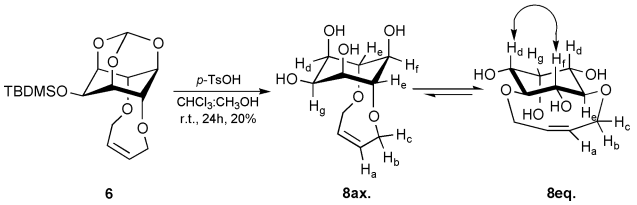

Scheme 4 Deprotection of the ring closed product **6** showing the observed NOE for **8eq**.

Variable temperature (VT) ^{1}H NMR experiments were carried out for both the deprotected RCM product **8** and the analogous 'dimer' in DMSO over the temperature range 300–330 K. However, although the signals due to the OH peaks altered as a result of the breaking of hydrogen bonds, there were

DOI: 10.1039/b007058k

no dramatic changes in the other signals. This demonstrates the rigidity of the structure in inhibiting inositol ring-flipping.

The ^{1}H NMR signals of the inositol ring protons of the 4,6-dibenzyl-*myo*-inositol orthoformate **9**[5] occurred at δ 4.45

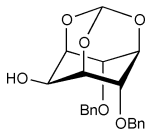

9

(1H, m), 4.30 (2H, m) and 4.23 (3H, m) and resembled closely the analogous signals in the polymer **2** (δ 4.5–4.2, br multiplet), indicating that the ring conformation was maintained, as expected, in the polymer. The ^{1}H NMR chemical shifts (δ 3.60–2.92) of the ring protons of the deprotected metathesis product **8eq.** are shifted upfield compared with those in the model **9**. Similarly the inositol ring protons of the deprotected polymer **3** (δ 3.7–3.0) are shifted upfield from which it is concluded that the inositol ring in **3** has the conformation **3eq.** The ^{13}C NMR spectra peaks of **3** were too broad to be assigned.

In conclusion, we have established the conformation of the novel inositol polymer **3** using the model compound **8** prepared by ring closing metathesis. The ^{1}H NMR analysis strongly suggests that the polymer **3ax**. is converted into **3eq**. when deprotected.

We thank EPSRC for supporting this work and provision of the Swansea MS service, and the Cambridge Overseas Trust, Robinson College, and the CVCP (award of scholarships to T.-H. Kim).

Notes and references

† Full details of the synthesis and properties of polymers based on the monomer **1** will be described in a full paper.

‡ A similar sequence of reactions was carried out using 'dimer' **7**, and the spectroscopic properties of the inositol ring atoms were very similar to those discussed for the small ring analogue **6**.

1 T.-H. Kim, P. Dokolas, N. Feeder, M. Giles, A. B. Holmes and M. Walther, *Chem. Commun.*, 2000; preceding paper DOI: 10.1039/b007057m.
2 S. J. Angyal, *Tetrahedron*, 1974, **30**, 1695.
3 K. Hegetschweiler, M. Ghisletta, T. F. Fässler, R. Nesper, H. W. Schmalle and G. Rihs, *Inorg. Chem.*, 1993, **32**, 2032.
4 R. H. Grubbs and S. Chang, *Tetrahedron*, 1998, **54**, 4413.
5 S. K. Armstrong, *J. Chem. Soc., Perkin Trans. 1*, 1998, 371.
6 G. C. Fu and R. H. Grubbs, *J. Am. Chem. Soc.*, 1992, **114**, 5426.
7 F. Mohamadi, N. G. J. Richards, W. C. Guida, R. Liskamp, M. Lipton, C. Caufield, G. Chang, T. Hendrickson and W. C. Still, *J. Comput. Chem.*, 1990, **11**, 440.
8 H. W. Lee and Y. Kishi, *J. Org. Chem.*, 1985, **50**, 4402.

Pd-catalysed C–C macrocyclisation of a simple tripeptide: efficient total synthesis of K-13

Manuel Pérez-González and Richard F. W. Jackson*

Department of Chemistry, Bedson Building, The University of Newcastle, Newcastle upon Tyne, UK NE1 7RU. E-mail: r.f.w.jackson@ncl.ac.uk

Received (in Liverpool, UK) 29th September 2000, Accepted 31st October 2000
First published as an Advance Article on the web 21st November 2000

The cyclic tripeptide K-13 has been prepared in 11 steps from commercially available starting materials (11% overall yield); the key step is the Pd-catalysed macrocyclisation of the zinc reagent prepared by selective insertion of zinc into the aliphatic C–I bond of the linear tripeptide 3, followed by Pd-catalysed macrocyclisation.

The conformation of peptides is a key parameter in determining their biological activity. Cyclic peptides, in which the degrees of conformational freedom are reduced, are therefore potentially important targets. Some examples of natural products falling into this class include the aminopeptidase inhibitor OF4949-III[1a] and the ACE inhibitor K-13 (**1**).[1b] There is

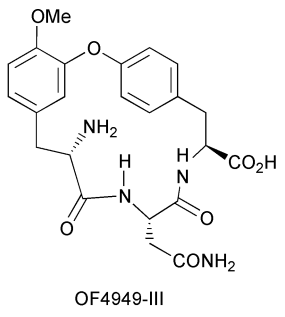

OF4949-III

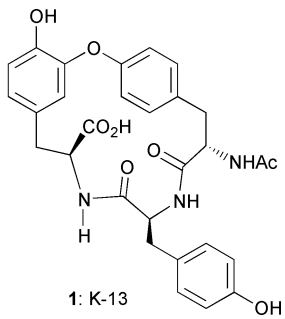

1: K-13

substantial interest in the preparation of these targets,[2] and analogues of these compounds have been proposed as potential therapeutic agents.[3] Previous routes to these and related compounds have relied on macrocyclisation involving classical amide bond formation, or on formation of the biaryl ether. This latter approach has employed oxidative phenol coupling using thallium trinitrate, Ullmann cyclisations and the S_NAr reaction.[4] These approaches have the advantage that the precursors for cyclisation are generally easy to prepare, with minimal reliance on protecting groups.

We have already described the palladium-catalysed reaction between aromatic iodides and the organozinc reagent derived from a protected iodolalanine derivative.[5] The reaction has proved to be versatile and has been extended to dipeptide-derived organozinc reagents.[6] We have therefore explored whether this reaction might be applied to the synthesis of K-13,[7] in which the key macrocyclisation step is a Negishi cross-coupling reaction of the corresponding open chain peptide **3** (Scheme 1).[8] This approach has the benefit of requiring the synthesis of relatively simple macrocyclisation precursors, and the potential for broader application since there is no absolute requirement for a biaryl ether in the target.

It was expected that the crucial C–C bond formation could be achieved after chemoselective Zn insertion into the aliphatic C–I bond, followed by a palladium-catalyzed cross-coupling reaction of the resulting organometallic reagent. The viability of this type of coupling in an intermolecular sense had already been demonstrated.[9] Compound **3** could be obtained by amide bond formation between the peptide **4** and the N-protected biaryl ether amino acid **5**, in which the hydroxy group of the serine residue could then be transformed into an iodide.

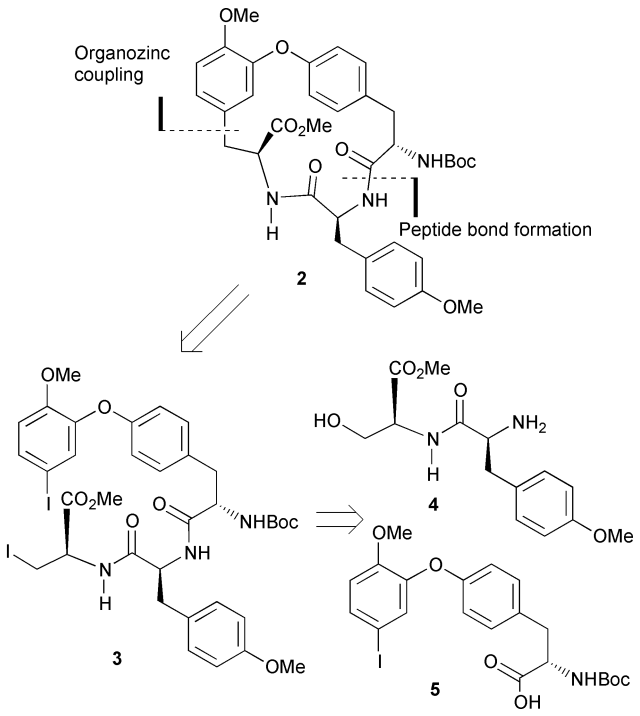

Scheme 1

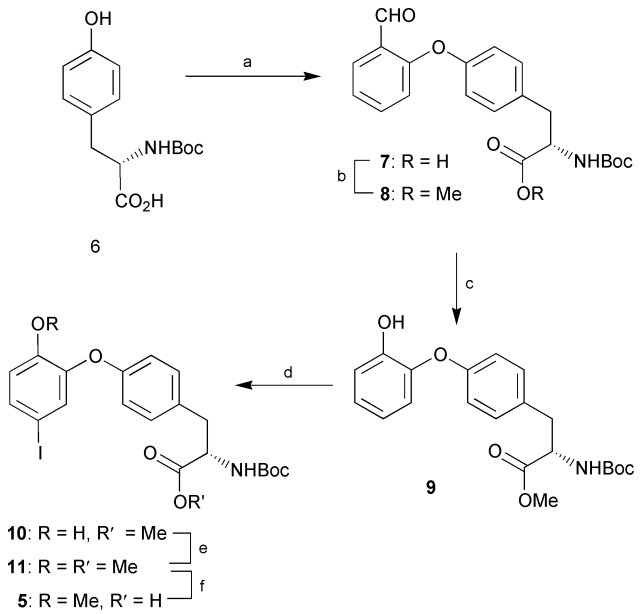

Scheme 2 *Reagents and conditions*: (a) 2-fluorobenzaldehyde, K_2CO_3, DMF, 70 °C, 4 d; (b) MeI, $NaHCO_3$, DMF, rt, 16 h, 85% (two steps); (c) i, MCPBA, $NaHCO_3$, $CHCl_3$, 55 °C, 16 h; ii, K_2CO_3 (cat), MeOH; (d) Chloramine-T, NaI, DMF, rt, 90 min; (e) MeI, K_2CO_3, DMF, rt, 16 h, 71% (three steps); (f) LiOH, THF–H_2O (1 : 4), quantitative.

DOI: 10.1039/b008078k

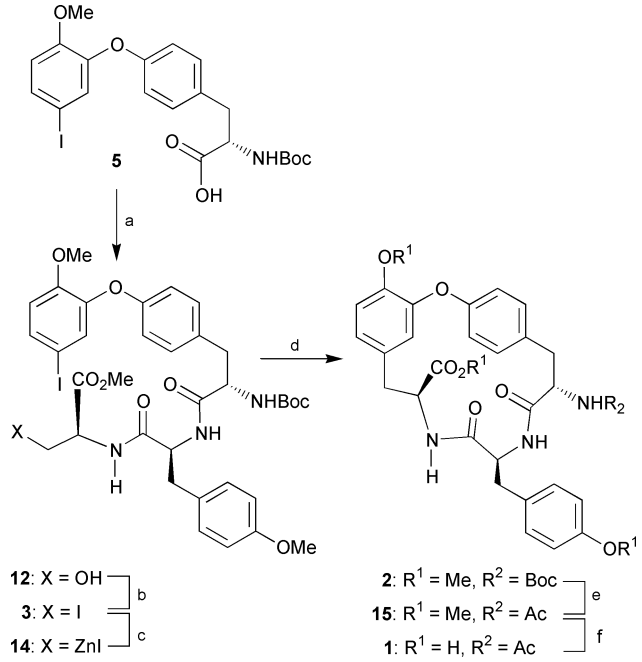

Scheme 3 *Reagents and conditions*: (a) **4**, EDCI, BtOH, iPr_2NEt, DMF, rt, 16 h, 94%; (b) $(PhO)_3PMeI$, DMF, rt, 20 min, 76%; (c) Zn, I_2 (cat), DMF, rt, 30 min; (d) $Pd_2(dba)_3$, (0.03 equiv.), P(*o*-Tol)$_3$, (0.12 equiv.), 3×10^{-3} M THF, 60 °C, 16 h, 35%; (e) i, TFA, thioanisole, CH_2Cl_2; ii, Ac_2O, pyridine 87%; (f) $AlBr_3$, EtSH, CH_2Cl_2, 85%.

The synthesis of fragment **5** started from commercially available *N*-Boc protected tyrosine **6**. Thus, nucleophilic aromatic substitution reaction between *N*-Boc protected tyrosine **6** and 2-fluorobenzaldehyde afforded the diaryl ether **7**, which was directly transformed into the corresponding methyl ester **8** in 85% overall yield (Scheme 2). Perkin reaction on the aromatic aldehyde **8**, using MCPBA in $CHCl_3$, followed by treatment of the formate intermediate with a catalytic amount of K_2CO_3 in MeOH, provided the phenol **9** in quantitative yield, which was used in the next step without further purification. This compound had already been synthesised by Jung using a different route in 30% yield over three steps.[9] At this stage, the enantiomeric purity of compound **9** was checked by removal of the Boc protecting group and Mosher's amide formation using 1-(3-dimethylaminopropyl)-3-ethylcarbodiimide hydrochloride. The enantiomeric purity of **9** was found to be > 95% by ^{1}H-NMR spectroscopy. The use of the free carboxylic acid derivative of tyrosine **6** in the reaction with 2-fluorobenzaldehyde is crucial to ensure high enantiomeric purity; use of the corresponding methyl ester derivative afforded racemic mixtures under a wide variety of conditions. Compound **9** was treated without further purification, following Jung's conditions,[9] with one equivalent of Chloramine-T hydrate (sodium salt of *N*-chlorotoluene-*p*-sulfonamide)–NaI to produce a mixture of 5-iodo **10** and 3,5-diiodo derivatives in a 90 : 10 ratio. This mixture was submitted to methylation (MeI, K_2CO_3, DMF) to give **11** (71% from **8** over three steps).This procedure allowed the synthesis of compound **11** on a multigram scale in 60% overall yield from commercially available *N*-Boc-tyrosine and 2-fluorobenzaldehyde. Finally, acid **5** was obtained in quantitative yield by saponification.

With the key intermediate **5** in hand, the synthesis of the crucial precursor **3** proved straightforward (Scheme 3). Thus, condensation of compound **5** and HCl·**4**[10] gave the dipeptide **12** (94%), which was transformed into the iodide **3** (76%) using $(PhO)_3PMeI$ in DMF.[11] Treatment of iodide **3** with zinc dust in DMF gave a solution of the organometallic intermediate **13**, which was added dropwise to a dilute solution of a catalyst prepared from $Pd_2(dba)_3$ and P(*o*-Tol)$_3$ in THF (maximum conc. of **13**, 3×10^{-3} M at 60 °C, and the solution was then stirred overnight. After extractive work up, cyclic dipeptide **2** was isolated by flash chromatography (35%). Compound **2** was transformed into K-13 following the experimental procedure published by Evans and Ellman[7] in good overall yield (74%). Synthetic K-13 exhibited physical and spectroscopic properties in close agreement with those reported.[12]

We thank the Spanish Ministerio de Educación y Cultura for a fellowship (M. P.-G.), the EU for a Marie Curie fellowship, HPMF-CT-1999-00050 (M. P.-G.), and Professor J. Zhu for providing spectra of synthetic K-13 for comparison.

References

1 (*a*) S. Sano, K. Ikai, K. Katayama, K. Takesako, T. Nakamura, A. Obayashi, Y. Ezure and H. Enomoto, *J. Antibiot.*, 1986, **39**, 1685; (*b*) T. Yasuzawa, K. Shirahata and H. Sano, *J. Antibiot.*, 1987, **40**, 455.
2 For a review, see: A. V. Rama Rao, M. K. Gurjar, K. L. Reddy and A. S. Rao, *Chem. Rev.*, 1995, **95**, 2135.
3 D. W. Hobbs and W. C. Still, *Tetrahedron Lett.*, 1989, **30**, 5405; A. G. Brown, M. J. Crimmin and P. D. Edwards, *J. Chem. Soc., Perkin Trans. 1*, 1992, 13; D. L. Boger and D. Yohannes, *Bioorg. Med. Chem. Lett.*, 1993, **3**, 245; A. D. Abell and M. D. Oldham, *J. Org. Chem.*, 1997, **62**, 1509. For a review, see: D. P. Fairlie, G. Abbenante and S. R. March, *Curr. Med. Chem.*, 1995, **2**, 654.
4 For a review, see: J. Zhu, *Synlett*, 1997, 133.
5 R. F. W. Jackson, R. J. Moore, C. S. Dexter, J. Elliott and C. E. Mowbray, *J. Org. Chem.*, 1998, **63**, 7875. For a review see: S. Gair and R. F. W. Jackson, *Curr. Org. Chem.*, 1998, **2**, 527.
6 M. J. Dunn and R. F. W. Jackson, *Tetrahedron*, 1997, **53**, 13905.
7 D. A. Evans and J. A. Ellman, *J. Am. Chem. Soc.*, 1989, **111**, 1063. For other syntheses of K-13 see: S. Nishiyama, Y. Suzuki and S. Yamamura, *Tetrahedron Lett.*, 1989, **30**, 379; D. L. Boger and D. Yohannes, *J. Org. Chem.*, 1989, **54**, 2498; D. L. Boger and D. Yohannes, *J. Org. Chem.*, 1990, **55**, 6000; A. V. Rama Rao, T. K. Chakraborty, K. Laxma Redy and A. Srinivasa Rao, *Tetrahedron Lett.*, 1992, **33**, 4799; J. W. Janetka and D. H. Rich, *J. Am. Chem. Soc.*, 1997, **119**, 6488; A. Bigot, M. Bois-Choussy and J. Zhu, *Tetrahedron Lett.*, 2000, **41**, 4573.
8 For an early example of a transition metal catalysed macrocyclisation by C–C bond-formation, see: M. F. Semmelhack and L. S. Ryono, *J. Am. Chem. Soc.*, 1975, **97**, 3873. For a review on the intramolecular Stille reaction, see: M. A. J. Duncton and G. Pattenden, *J. Chem. Soc., Perkin Trans. 1*, 1999, 1235.
9 M. E. Jung and L. S. Starkey, *Tetrahedron*, 1997, **53**, 8815.
10 Compound **4** was prepared from the known Boc-Tyr(OMe)-Ser-OMe: S. Lee, H. Aoyagi, Y. Shimohigashi, N. Izumiya, T. Ueno and H. Fukami, *Tetrahedron Lett.*, 1976, **17**, 843.
11 J. P. H. Verheyden and J. G. Moffatt, *J. Org. Chem.*, 1970, **35**, 2319.
12 Synthetic K-13 (**1**): mp (MeOH–diethyl ether) 265–270 °C (decomp.); lit.[1b] mp 260–270 °C (decomp.); $[\alpha]_D = -6.6$ (*c* 1.4, MeOH); lit.[7] $[\alpha]_D = -6.5$ (*c* 0.46, MeOH), natural[1b] $[\alpha]_D = -3.4$ (*c* 0.6, MeOH); ^{1}H-NMR (500 MHz, CD_3OD) δ 7.29 (dd, *J* 8.0, 2.0, 1 H), 7.04 (dd, *J* 8.5, 2.5, 1 H), 6.99–6.93 (m, 3 H), 6.80 (dd, *J* 8.0, 1 H), 6.73 (dd, *J* 8.0, 2.0, 1 H), 6.66 (dd, *J* 8.0, 2.5, 1 H), 6.62–6.57 (BB′, 2 H), 6.38 (d, *J* 2.0, 1 H), 4.48–4.40 (m, 2 H), 4.17 (t, *J* 5.5, 1 H), 3.17 (dd, *J* 15.5, 2.0, 1 H), 3.01 (dd, *J* 12.5, 5.5, 1 H), 2.95 (dd, *J* 13.0, 6.0, 1 H), 2.91 (dd, *J* 15.5, 9.0, 1 H), 2.85 (dd, *J* 13.5, 5.0, 1 H), 2.77 (t, *J* 12.0, H), 2.03 (s, 3 H); ^{13}C-NMR (125.7 MHz, CD_3OD) δ 175.5, 172.9, 172.2, 171.5, 158.2. 157.0, 147.8, 147.5, 132.8, 132.0 (3C), 131.2, 130.7, 128.2, 125.4, 122.1, 120.8, 118.8, 117.5, 115.8 (2C), 57.3, 55.9, 54.3, 39.1, 38.7, 36.6, 22.4.

ChemComm

Direct-space structure solution from laboratory powder diffraction data of an organic cocrystal: 1,2,3-trihydroxybenzene–HMTA (1/1)†

Maryjane Tremayne*[a] and Christopher Glidewell[b]

[a] *School of Chemistry, University of Birmingham, Edgbaston, Birmingham, UK B15 2TT. E-mail: m.tremayne@bham.ac.uk*
[b] *School of Chemistry, University of St Andrews, St Andrews, UK KY16 9ST*

Received (in Cambridge, UK) 5th September 2000, Accepted 23rd October 2000
First published as an Advance Article on the web 22nd November 2000

The crystal structure of an organic cocrystal, 1,2,3-trihydroxybenzene–hexamethylenetetramine (1/1), has been solved from conventional laboratory X-ray powder diffraction data that are significantly affected by preferred orientation, using a direct space structure solution approach based on the Monte Carlo method.

A sound knowledge and understanding of the role that intermolecular forces play in supramolecular assembly is generally obtained from systematic crystallographic studies. Where crystals are available of suitable quality for single-crystal diffraction, these techniques remain the method of choice. However, when no such material is available, this valuable structural information can often be obtained from powder diffraction data.

The use of X-ray powder diffraction for *ab initio* structure determination of purely organic molecular solids is a rapidly expanding field, mainly due to the considerable advances in the development of direct space methods of structure solution.[1–6] Here we report the first application of such a method to the structure determination of an organic cocrystal containing two different molecular building blocks, the 1 : 1 adduct of 1,2,3-trihydroxybenzene [$C_6H_3(OH)_3$; pyrogallol **1**] and hexamethylenetetramine [$(CH_2)_6N_4$; HMTA **2**] from conventional laboratory powder diffraction data. Despite the presence of two different molecular components in the structure and evidence of significant preferred orientation in the data, the Monte Carlo method employed here smoothly generated a starting structure for Rietveld refinement. This structure determination demonstrates both the power of this technique as a tool in the systematic study of intermolecular interactions and as an emerging force in the field of crystal engineering, and the feasibility of using lower resolution powder data collected using laboratory-based powder diffractometers rather than relying on the availability of synchrotron radiation for solving structures with this degree of complexity.

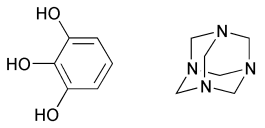

1 **2**

Previous studies have used single-crystal X-ray diffraction to explore the use of bis- and tris-phenols in crystal engineering and the interaction of this type of phenol, acting as a hydrogen bond donor, with HMTA as a hydrogen bond acceptor.[7] However in the case of pyrogallol–HMTA (1/1), investigation of the crystal structure was carried out using powder diffraction data. This type of material is an ideal target for the direct space structure solution technique as it is the organization of these well-defined building blocks within the crystal structure that is of greatest importance.

The direct-space methods approach structure solution by postulation of trial crystal structures constructed from known molecular connectivity, independently of the powder diffraction data. The trial structures are generated by movement of a structural model around the unit cell including variation of molecular conformation when required, and each structure assessed by comparison between the corresponding calculated diffraction pattern and the experimental diffraction data. The structure solution, or global minimum, is then located using a global optimization strategy such as Monte Carlo[2,6] (the method used here), simulated annealing[3,5] or genetic algorithm techniques.[4]

In the application of direct space structure solution methods, the presence of more than one molecule in the asymmetric unit makes the problem more complex in terms of the number of degrees of freedom (*i.e.* the number of structural parameters varied to generate new trial crystal structures), and to an extent, the effect on *R*-factor discrimination. There are few examples of such materials solved from powder diffraction data using the direct space structure solution approach,[8] a situation made more complicated here due to the presence of two entirely different molecules in the cocrystal with the location of each molecule in the unit cell being unique and non-superimposable. The exact hydrogen-bonded relationship between the molecules in this system was not predictable in advance.

The powder diffraction pattern was indexed on a monoclinic unit cell (space group $P2_1/n$) consistent with the presence of one molecule of each component in the asymmetric unit. Hence the structural model used in the Monte Carlo structure solution comprised a complete HMTA molecule and a pyrogallol molecule excluding the hydrogen atoms on the three hydroxyl groups. Both molecules were constructed using standard bond lengths and angles, and treated as rigid units during structure solution, although not in the subsequent refinement. Trial crystal structures were then generated by completely independent translation and rotation of the two molecular components within the unit cell. With more than one independent molecule required to define the structure, the number of degrees of freedom required for random movement is increased (from 6 to 12 in this case) without conformational flexibility being introduced. The calculation was run for 500000 Monte Carlo moves and R_{wp} was found to be typically 52–68% for most random structures whereas the best structure solution corresponded to an R_{wp} value of 18.9%. This solution was used as the starting model for a successful Rietveld refinement (Fig. 1).

Diffraction data had been collected in both disc and capillary geometries and it was clear from the difference in relative intensities of related peaks in these data that there was a significant degree of preferred orientation present. Although these effects were minimized by the use of the capillary data for both solution and refinement, variation of a preferred orientation parameter was still required in refinement.‡ In such cases, this distortion of the data often has a disastrous effect on traditional structure solution, whereas in our experience, direct-

† Electronic supplementary information (ESI) available: atomic coordinates and metrical parameters for 1,2,3-trihydroxybenzene–HMTA (1/1). See http://www.rsc.org/suppdata/cc/b0/b007189g/

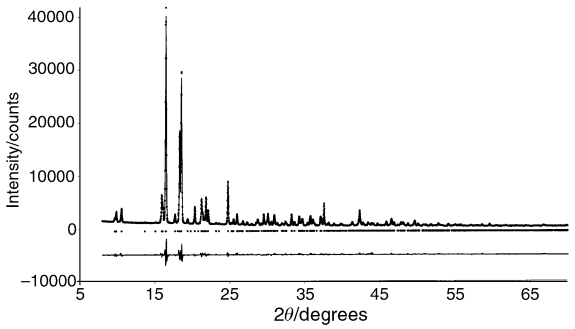

Fig. 1 Final observed (circles), calculated (solid line) and difference (below) X-ray powder diffraction profile for the final Rietveld refinement of pyrogallol–HMTA (1/1). Reflection positions are also marked.

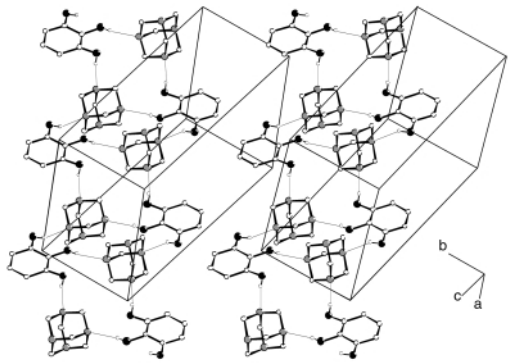

Fig. 2 Stereoview of the crystal structure of pyrogallol–HMTA (1/1) showing the alternating O–H···N rings generating a puckered molecular ribbon. Only hydrogen atoms involved in hydrogen bonding are shown and hydrogen bonds are indicated by thin lines. Intermolecular O···N distances are 2.90(1), 2.79(1) and 2.69(1) Å.

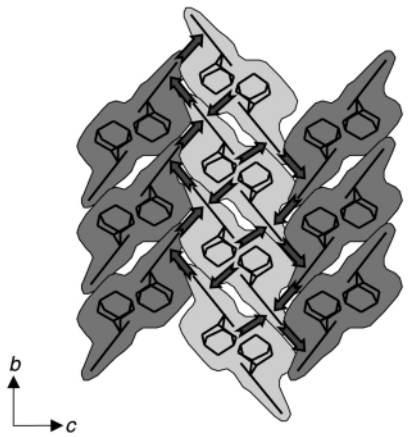

Fig. 3 A schematic diagram of the crystal structure of pyrogallol–HMTA (1/1) with each ribbon shown end-on and represented by a shaded area with the molecular units indicated by black lines. C–H···π(arene) interactions within each stack (light areas) and between neighbouring stacks (dark areas) are indicated by block arrows. C···π(arene) distances, *i.e.*: to the centroid of the ring, are 3.64(1) Å and 3.69(1) Å, respectively.

space methods appear to be more robust, presumably because a substantial amount of structural knowledge is included in the calculation through the use of a structural model.

In the structure, all three hydroxyl groups in the pyrogallol molecule act as hydrogen bond donors, and hence three N atoms in each HMTA molecule act as acceptors. This differs from the majority of systems, in which HMTA acts as a double acceptor of hydrogen bonds:[7] rather less frequently HMTA behaves as an acceptor of just one hydrogen bond, a full complement of four hydrogen bonds, or as in this case, of three hydrogen bonds.[7–9]

O–H···N hydrogen bonds are formed from the hydroxyl groups in the 1 and 3 positions linking alternating pyrogallol and HMTA molecules in a chain running parallel to the [100] direction. Pairs of these chains are linked by further O-H···N hydrogen bonds from the hydroxyl groups in the 2 positions to another N atom in each HMTA unit forming two distinct cyclic $R^4_4(18)$ motifs. The result is a lightly-puckered molecular ribbon running parallel to the [100] direction in which the HMTA cages lie alternately above and below the plane (Fig. 2). These ribbons are then linked into a continuous three-dimensional framework by C–H···π(arene) interactions. There are edge-to-face interactions between pyrogallol units in neighbouring ribbons, occupying one face of each ring: the other face of each ring is involved in a C–H···π(arene) interaction with a C–H bond from an HMTA unit in a neighbouring ribbon. The latter C–H···π(arene) interactions link sets of neighbouring parallel ribbons into columns stacked in the [010] direction, while those between the pyrogallol units link neighbouring stacks together to form a herringbone pattern (Fig. 3). Propagation of these two types of C–H···π(arene) interactions based on aromatic and aliphatic C–H bonds links all the parallel ribbons into a single bundle, so that the overall supramolecular structure is three-dimensional.

In this study we have shown that it is possible to determine the crystal structures of relatively complex materials such as cocrystals with multiple fragments in the structure solution process, from conventional laboratory X-ray powder diffraction data that is significantly affected by the presence of preferred orientation. The successful application of direct space techniques to the structure solution of materials containing a greater number of independent structural fragments or molecules with a considerable degree of conformational flexibility from powder data of this quality is clearly a possibility. Subsequent rationalization of the intermolecular forces in this system show an unpredicted network of both weak and strong hydrogen bonds, demonstrating the invaluable contribution that powder diffraction will have in improving our understanding of non-covalent forces and their role in crystal packing.

This research was supported by the Royal Society through the award of a fellowship to M. T.

Notes and references

‡ *Crystal data* for pyrogallol–HMTA (1/1), $C_{12}H_{18}N_4O_3$: M_r = 266.30, monoclinic, a = 10.7691(2), b = 7.0107(2), c = 16.7519(4) Å, β = 91.402(2)°, V = 1264.38(3) Å^3, space group $P2_1/n$ (no. 14), Z = 4, D_c = 1.39 g cm^{-3}, T = 273 K.

Sample preparation: a microcrystalline sample produced by crystallisation of a methanol solution containing equimolar quantities of **1** and **2**.

Data collection and Rietveld refinement: the powder diffraction data were collected on a Stoe STADI/P diffractometer using Cu-Kα_1 radiation, and a linear PSD. Data were measured over $5 < 2\theta < 75°$ in 0.02° steps for 15 h. In refinement, all atom postions (except the hydroxyl H atoms which were given calculated positions) were refined subject to soft constraints, and isotropic atomic displacement parameters (refined for non-H only) constrained according to atom type. Final refinement gave R_{wp} = 7.40%, R_p = 5.40% for 654 reflections and 117 parameters; preferred orientation fraction = 0.807.

CCDC 182/1828. See http://www.rsc.org/suppdata/cc/b0/b007189g/ for crystallographic files in .cif format.

1 K. D. M. Harris and M. Tremayne, *Chem. Mater.*, 1996, **8**, 2554.
2 K. D. M. Harris, M. Tremayne, P. Lightfoot and P. G. Bruce, *J. Am. Chem. Soc.*, 1994, **116**, 3543.
3 Y. G. Andreev, P. Lightfoot and P. G. Bruce, *J. Appl. Crystallogr.*, 1997, **30**, 294.
4 B. M. Kariuki, K. Psallidas, K. D. M. Harris, R. L. Johnston, R. W. Lancaster, S. E. Staniforth and S. M. Cooper, *Chem. Commun.*, 1999, 1677.
5 W. I. F. David, K. Shankland and N. Shankland, *Chem. Commun.*, 1998, 931.
6 M. Tremayne, E. J. MacLean, C. C. Tang and C. Glidewell, *Acta Crystallogr., Sect. B*, 1999, **55**, 1068.
7 P. I. Coupar, C. Glidewell and G. Ferguson, *Acta Crystallogr., Sect. B*, 1997, **53**, 521.
8 A. M. T. Bell, J. N. B. Smith, J. P. Attfield, J. M. Rawson, K. Shankland and W. I. F. David, *New J. Chem.*, 1999, **23**, 565.
9 E. J. Maclean, C. Glidewell, G. Ferguson, R. M. Gregson and A. J. Lough, *Acta Crystallogr., Sect. C*, 1999, **55**, 1867 and references therein.

1D lanthanide halide crystals inserted into single-walled carbon nanotubes

Cigang Xu,[a] Jeremy Sloan,[ab] Gareth Brown,[ab] Sam Bailey,[a] V. Clifford Williams,[a] Steffi Friedrichs,[a] Karl S. Coleman,[a] Emmanuel Flahaut,[a] John L. Hutchison,[b] Rafal E. Dunin-Borkowski[b] and Malcolm L. H. Green*[a]

[a] *Wolfson Catalysis Centre (Carbon Nanotechnology Group), Inorganic Chemistry Laboratory, University of Oxford, South Parks Road, Oxford, UK OX1 3QR.. E-mail: malcolm.green@chem.ox.ac.uk*
[b] *Department of Materials, University of Oxford, Parks Road, Oxford, UK OX1 3PH*

Received (in Oxford, UK) 21st August 2000, Accepted 24th October 2000
First published as an Advance Article on the web 21st November 2000

1D crystals of lanthanide halides of the form $LnCl_3$ (Ln = La, Nd, Sm, Eu, Gd, Tb or Yb) have been inserted into single-walled carbon nanotubes (SWNTs) using the molten salt capillary filling method; *ca*. 20–40% of all the observed SWNTs were filled with melts in the range 650–910 °C with no observable damage to the carbon tubules; high resolution transmission electron microscopy (HRTEM) studies showed that the nanostructures of the encapsulated crystals varied with tubule diameter.

The unique physical properties of carbon nanotubes[1] have generated considerable interest and the expectation of new types of materials with useful practical applications. Theoretical studies[2–5] suggest that the introduction of foreign materials into their hollow cavities will have interesting effects both on the properties of the filling material and the filled nanotubes. Recently, the filling of SWNTs with Ru, silver metal and other species has been demonstrated.[6–10] Related work has shown that the doping of the interstices of SWNTs with vapour or liquid phase species, including alkali metals, bromine, or charged iodine chains, leads to a 10–100 fold decrease in their measured resistivities and to charge transfer behaviour detectable by Raman spectroscopy.[11,12] Lanthanide (or rare earth) ions have optical and magnetic properties that are particularly interesting when they are situated in a confined geometry. Additionally, as their spectral and dynamic properties alter when the reduced dimensions also affect the chemical and physical properties of the host, these species can act as a local probe for the chemistry and structure of the host material.[13] We present here preliminary results with respect to the incorporation and low-dimensional crystallisation properties of lanthanide halides within SWNTs.

Single-walled carbon nanotubes can be filled both by solution–deposition[6] or by capillarity[7–10] providing, in the latter case, that the filling medium has a surface tension in the range 100–200 mN m^{-1} and a melting temperature ideally below 900 °C.[7,14] The lanthanide halides $LnCl_3$ (Ln = Y, La, Pr, Nd, Gd or Dy) have surface tensions that fall below this threshold in the temperature range 820–950 °C.[15] In this study, we describe the filling properties of three of these halides (Ln = La, Nd and Gd) and four additional halides (Ln = Sm, Eu, Tb and Yb) for which surface tension data were unavailable (Table 1) but for which similar melting behaviour is assumed.

Samples of SWNTs were prepared by a high yield arc synthesis method.[16] The as-prepared SWNTs (*ca.* 30 mg) were intimately mixed with the anhydrous halides (*ca.* 70 mg) by grinding in an agate mortar and pestle under dry-box conditions. The samples were sealed under vacuum in a silica quartz ampoule that was then attached to the tip of a thermocouple and placed in a tube furnace. The temperature was slowly raised (3–5 °C min^{-1}) to a target temperature of *ca.* 10–50 °C above the melting point of the respective lanthanide chloride (Table 1), held at this temperature for 1 h and then furnace cooled to room temp. The specimens were characterised in a JEOL JEM-3000F FEGTEM operated at 300 kV (coefficient of spherical aberration (C_s) = 0.57; point resolution = 0.16 nm). Images were acquired digitally on a Gatan model 794 (1 k × 1 k) CCD camera, and the magnification was calibrated accurately using Si <110> lattice fringes. Energy dispersive X-ray microanalysis (EDX) was performed with a LINK 'ISIS' system using a 0.5 nm diameter electron probe.

All the lanthanide halides in Table 1 filled 20–40% of the observed SWNTs with continuous lanthanide halide single crystals. The HRTEM micrograph in Fig. 1(a) shows an example of $TbCl_3$ filling observed within a SWNT bundle. An enlargement of the tubule on the periphery of the bundle

Table 1 Surface tension data and synthesis conditions for lanthanide halides incorporated into SWNTs

SWNT filling material	Heating ramp rate/ °C min^{-1}	Melting temperature/°C	Target temperature/°C	Surface tension[a]/ mN m^{-1}
$LaCl_3$	3	860	910	109.407
$NdCl_3$	5	784	834	102.093
$SmCl_3$	5	686	706	—
$EuCl_3$	3	850	860	—
$GdCl_3$	3	609	659	91.7798
$TbCl_3$	5	588	638	—
$YbCl_3$	3	854	904	—

[a] Data not available for Ln = Sm, Eu, Tb or Yb.

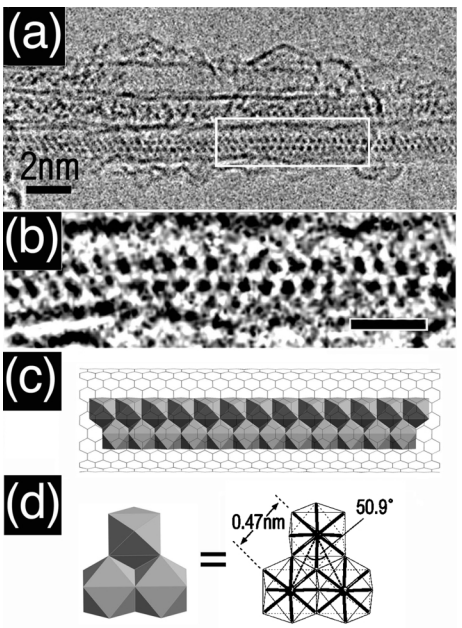

Fig. 1 (a) HRTEM image of $TbCl_3$ filling within a SWNT bundle. (b) Enlargement from boxed region in (a) showing a 'zigzag' arrangement of dark spots attributed to a 1D polyhedral chain of $TbCl_x$ polyhedra (scale bar = 1.6 nm). (c) Structural representation of a 1D polyhedral chain incorporated in a (12,12) SWNT. (d) Detail (left) and schematic depiction (right) of three polyhedra from the encapsulated chain shown in Fig. 1(c). The indicated dimensions in the schematic depiction are estimated from the lattice image [*i.e.* from (a) and (b)].

DOI: 10.1039/b006817i

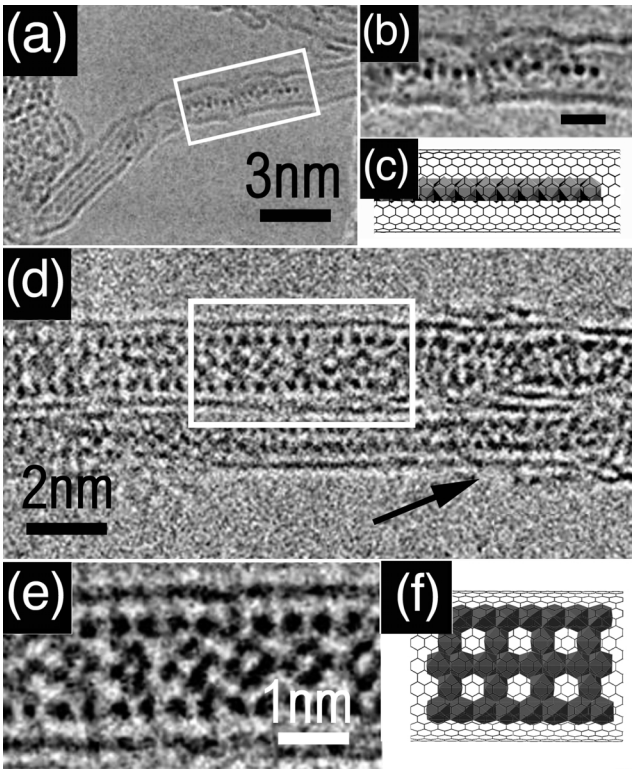

Fig. 2 (a) HRTEM micrograph showing a twisted 1D chain of $GdCl_3$ formed within a (10,10) SWNT. (b) Enlargement of boxed region from (a) showing a linear array of dark spots which terminates towards the right of the micrograph (scale bar = 1 nm). (c) Structural representation showing a 'top-down' view of (b) [*i.e*. similar to Fig. 1(c) but rotated 90°] about the SWNT axis). (d) Bundle consisting of one wide (*ca.* 2.5 nm) and one narrow (arrow = *ca.* 1.6 nm) SWNT both filled with $NdCl_3$. (e) Enlargement of the boxed region in (d) showing the unusual microstructure of the $NdCl_3$ filling. (f) Suggested structural model for (e).

[Fig. 1(b)] reveals that the crystal images as a 'zigzag' array of dark spots which we take to be a chain of $TbCl_x$ polyhedra. Most of the dark contrast in the 1D arrays must originate from the strongly scattering Tb^{3+} centres with the coordinating Cl^- ions being effectively invisible. Groups of three adjacent spots are arranged into nearly equilateral triangles of side *ca*. 0.47 nm. The bulk structure of $TbCl_3$ consists of $TbCl_9$ polyhedra arranged into a 3D hexagonal network (*i.e*. UCl_3-type[17,18]). Within the confines of the 1.6 nm diameter SWNT in Fig. 1(b), it is possible only to accommodate 1D polyhedral chains from the 3D structure, as shown in Fig. 1(c). The individual polyhedra within the chains are likely to be of reduced coordination owing to lattice terminations enforced by capillary confinement and the likeliest candidate structure is therefore a 1D network of edge-sharing $TbCl_6$ octahedra as depicted on the right of Fig. 1(c) (*cf.* $CdCl_2$[18]) and in detail in Fig. 1(d). We have recently reported a related reduction in coordination of 6:6 to 4:4 coordination for bilayer KI crystals incorporated into SWNTs.[19]

Fig. 2(a) shows a 1D chain of $GdCl_3$ incorporated into a 1.4 nm SWNT. The SWNT is bent into an 'elbow' and, on either side of the bend, the crystal images with different contrast suggesting a different orientation formed as a result of a twist induced by the bend. On the right of the bend, the crystal images as an apparently linear array of dark spots, as can be seen in the enlargement in Fig. 2(b). In this case we assume that the crystal has a similar structure to that depicted in Fig. 1(c) but that it is rotated 90° about the SWNT axis [*i.e*. relative to Fig. 1(c)] so that the polyhedral chain is viewed in 'top down' projection as depicted in Fig. 2(c). This crystal can also be seem to terminate within the SWNT capillary.

Fig. 2(d) shows a bundle of two SWNTs, one wide (*ca*. 2.5 nm) and the other narrow (*ca*. 1.6 nm), corresponding approximately to (12,12) and (20,20) SWNTs, respectively, both of which are continuously filled with crystalline $NdCl_3$. This crystal has an unusual microstructure as can be seen by the enlargement in Fig. 2(e). The encapsulated crystal consists of two linear 1D arrays of dark spots separated, in the middle, by a continuous series of groups of four dark spots arranged into diamonds. This microstructure cannot readily be reconciled with the bulk structure of $NdCl_3$,[18] but may instead correspond to the suggested arrangement in Fig. 2(f) in which 'diamond' arrays of $NdCl_x$ polyhedra formed along the centre of the SWNT are bounded by 1D arrays of $NdCl_x$ polyhedra formed along their walls. This arrangement is based using a similar interpretation as for Figs. 1(b) and 2(b), *i.e*. that each dark spot corresponds to a heavy Ln^{3+} centre within one or more $LnCl_x$ polyhedra viewed in projection.

In conclusion, we have demonstrated the first example of lanthanide halide insertion into SWNTs in high yield by a simple and reproducible method, and have also found that the diameter of the host SWNT profoundly influences the obtained structure of the filling material. The nature of these related crystallisation phenomena within SWNTs will be discussed more fully in a forthcoming publication. Experiments are also under way in our laboratory to understand the filling mechanism and to investigate the physical properties of these novel composites.

We acknowledge the Petroleum Research Fund, administered by the American Chemical Society (Grant No. 33765-AC5), the EPSRC (Grant Nos. GR/L59238 and GR/L22324) and Colebrand Ltd. for financial support. C. X. is grateful for a K. C. Wong Scholarship (University of Oxford), a Light Senior Scholarship (St. Catherine's College) and to the Henry Lester Trust. S. F. is indebted to BMBF and Fonds der Chemischen Industrie for additional financial support.

Notes and references

1 S. Iijima, *Nature*, 1991, **354**, 56.
2 K. Laasonen, W. Andreoni and M. Parrinello, *Science*, 1992, **58**, 1916.
3 J. W. Mintmire, B. I. Dunlap and C. T. White, *Phys. Rev. Lett.*, 1992, **68**, 631.
4 R. Saito, M. Fijita, G. Dresselhaus and M. S. Dresselhaus, *Mater. Sci. Eng.*, 1993, **19**, 185.
5 S. C. Tsang, Y. K. Chen, P. J. F. Harris and M. L. H. Green, *Nature*, 1994, **372**, 159.
6 J. Sloan, J. Hammer, M. Zweifka-Sibley and M. L. H. Green, *Chem. Commun.*, 1998, 347.
7 J. Sloan, D. M. Wright, H. G. Woo, S. Bailey, G. Brown, A. P. E. York, K. S. Coleman, J. L. Hutchison and M. L. H. Green, *Chem. Commun.*, 1999, 699.
8 C. H. Kiang, J. S. Choi, T. T. Tran and A. D. Bacher, *J. Phys. Chem. B*, 1999, **103**, 7449.
9 A. Govindaraj, B. C. Satishkumar, M. Nath and C. N. R. Rao, *Chem. Mater.*, 2000, **12**, 202.
10 X. Fan, E. C. Dickey, P. C. Eklund, K. A. Williams, L. Grigorian, R. Buczko, S. T. Pantelides and S. J. Pennycook, *Phys. Rev. Lett.*, 2000, **84**, 4621.
11 R. S. Lee, H. J. Kim, J. E. Fischer, A. Thess and R. E. Smalley, *Nature*, 1997, **388**, 255.
12 L. Grigorian, K. A. Williams, S. Fang, G. U. Sumanasekera, A. L. Loper, E. C. Dickey, S. J. Pennycook and P. C. Eklund, *Phys. Rev. Lett.*, 1998, **80**, 5560.
13 B. M. Tissue, *Chem. Mater.*, 1998, **10**, 2837.
14 T. W. Ebbesen, *J. Phys. Chem. Solids*, 1996, **57**, 951.
15 K. Igarashi, J. Mochinaga and S. Ueda, *Bull. Chem. Soc. Jpn.*, 1978, **51**, 1551.
16 C. Journet, W. K. Maser, P. Bernier, A. Loiseau, M. Lamy, M. L. de la Chapelle, S. Lefrant, P. Derniard and J. E. Fisher, *Nature*, 1997, **388**, 756.
17 H. Gunsilius, H. Borrmann, A. Simon and W. Urland, *Z. Naturforsch., Teil B*, 1988, **43**, 1023.
18 A. F. Wells, in *Structural Inorganic Chemistry*, Oxford University Press, Oxford, 5th edn., 1990, pp. 421–423.
19 J. Sloan, M. C. Novotny, S. R. Bailey, G. Brown, C. Xu, V. C.Williams, S. Friedrichs, E. Flahaut, R. L. Callendar, A. P. E. York, K. S. Coleman, M. L. H. Green, R. E. Dunin-Borkowski and J. L. Hutchison, *Chem. Phys. Lett.*, 2000, **329**, 61.

ChemComm

Polycyclitols. Novel conduritol and carbasugar hybrids as a new class of potent glycosidase inhibitors

Goverdhan Mehta* and Senaiar S. Ramesh

Department of Organic Chemistry, Indian Institute of Science, Bangalore, 560 012, India

Received (in Cambridge, UK) 6th September 2000, Accepted 31st October 2000
First published as an Advance Article on the web 22nd November 2000

We have conceptualized new molecular entities (bicyclitols) in which two conduritol and two carbasugar moieties are embedded in a polyhydroxylated decahydronaphthalene framework and achieved their syntheses in a stereo- and regioselective manner. One of the bicyclitols was found to be a potent and selective α-glucosidase inhibitor.

Conduritols **1** (six diastereomers designated A–F are known)[1] and carbasugars **2** are a class of polyhydroxylated cyclohexanoids that have evoked a great deal of synthetic interest in recent years.[1,2] In view of their promising therapeutic potential in the management of wide ranging disorders like diabetes, viral infections, HIV and cancer among others, many analogues and structural variants of **1** and **2** have been synthesized and their biological activities, particularly glycosidase inhibition has been evaluated.[3] Considering the fundamental importance of competitive and specific glycosidase inhibition in new drug development, we have conceived of a new family of polyhydroxylated polycyclic systems (polycyclitols) represented by **3** as potential glycomimics.[4] Bicyclitol **3** is an interesting entity which can be considered as a hybrid of two conduritols with shared, common ring junction carbon atoms. Alternately, **3** can be regarded as a hybrid of two carbasugars A and B (see, bold portions in **4** and **5**), both of which are ring annulated. Herein,

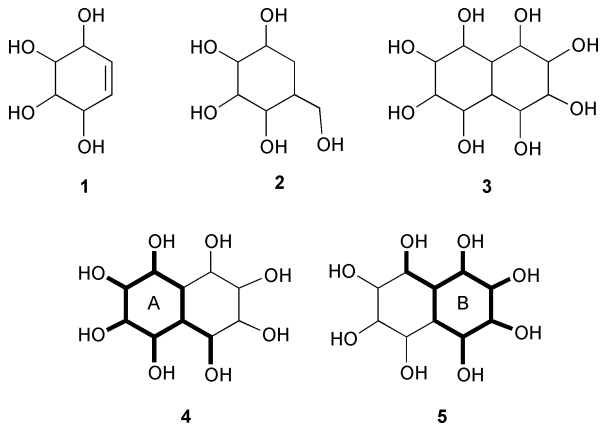

we report the stereo- and regioselective syntheses of two polycyclitols **6** and **7** based on the general structure **3**, and show that one of them **6** is a potent and selective inhibitor of α-glucosidase.

Our synthesis of **6** emanated from the readily available Diels–Alder adduct **8** of 5,5-dimethoxy-1,2,3,4-tetrachlorocyclopentadiene and *p*-benzoquinone, which was elaborated to the tricyclic diene **9** following the tactically modified literature procedure.[5] Exhaustive OsO_4 mediated dihydroxylation of **9** occurred exclusively from the *exo*-face to furnish the all *cis*-tetrol **10**.[6] Selective monoprotection and reductive dechlorination in **10** led to the symmetrical **11**.[6] Careful deketalisation in **11**, while retaining the acetonide protective group led to the desired norbornen-7-one† **12**, Scheme 1. Thermally induced decarbonylation in **12** to the cyclohexadiene derivative **13**[6] was smooth and further catalytic, OsO_4 mediated double dihydroxylation proceeded stereoselectively to furnish **14** as a single diastereomer. Acetonide deprotection in **14** provided the octahydroxydecahydronaphthalene **6**,[6] a hybrid of conduritols D (right ring) and E (left ring), Scheme 1. The absence of symmetry in **6** and **14**, revealed through the presence of 10 and 13 lines, respectively, in the ^{13}C NMR spectra, uniquely settled the stereochemical pattern present in these bicyclitols. Bicyclitol **6** was screened against α- and β-glucosidases (from Bakers' yeast and almonds, respectively) that accept corresponding *p*-nitrophenylglycosides as substrates and it was very satisfying to find impressive inhibition of α-glucosidase with a K_i value[7] of 12 μM (*cf.* K_i = 25.4 μM for deoxynojirimycin, DNJ). Interestingly, **6** exhibited no significant inhibitory activity

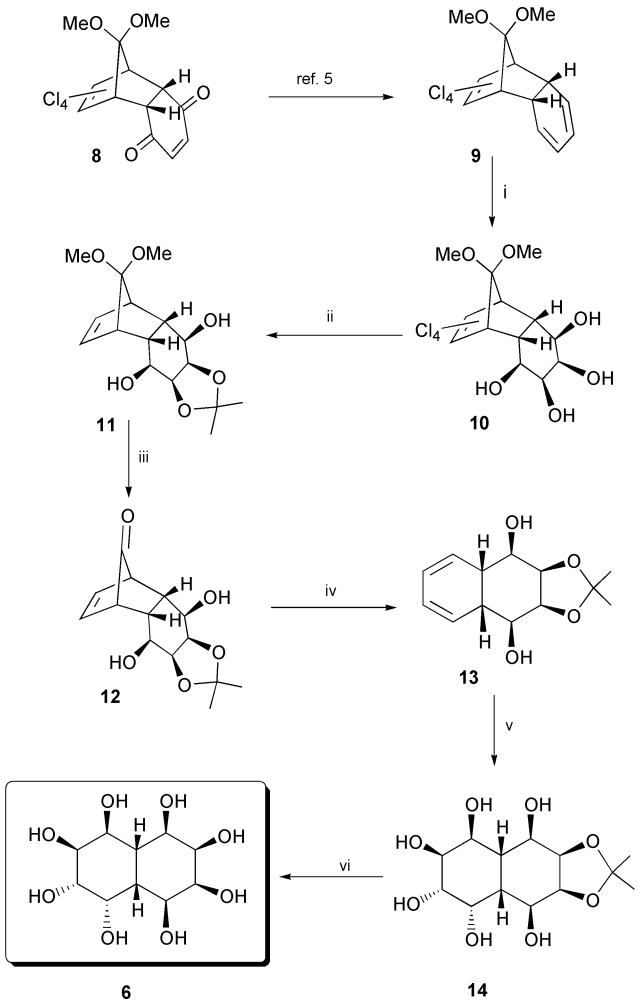

Scheme 1 *Reagents and conditions*: i, OsO_4 (cat.), NMMO, Me_2CO:tBuOH (5:2), 2 d, 66%; ii, (*a*) Amberlyst-15, acetone, mol. sieves 4 A, 75%; (*b*) Na, liq. NH_3, THF, EtOH, 49%; iii, Amberlyst-15, acetone, 98%; iv, $C_6H_5NO_2$, 160 °C, 62%; v, OsO_4 (cat.), NMMO, $Me_2CO:H_2O$:tBuOH (5:5:2), 85%; vi, 30% CF_3COOH, 95%.

DOI: 10.1039/b007224i

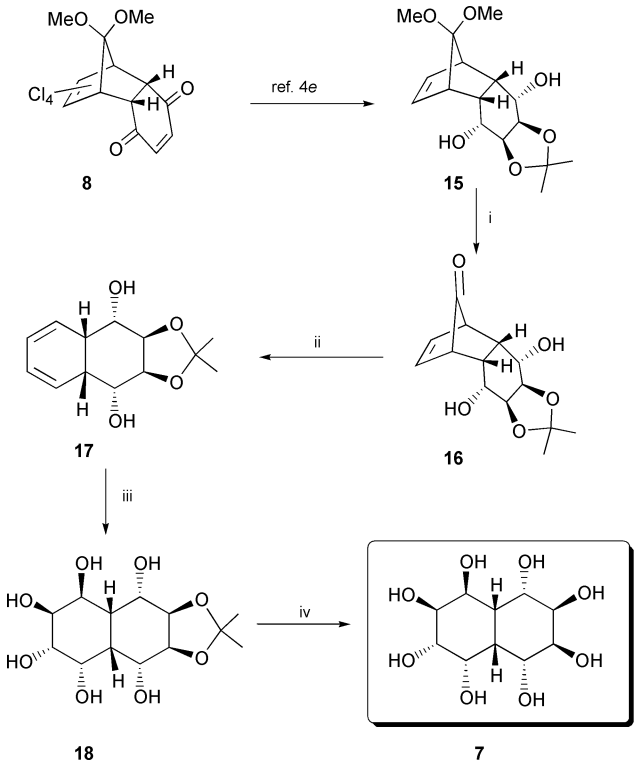

Scheme 2 *Reagents and conditions*: i, Amberlyst-15, acetone, 95%; ii, $C_6H_5NO_2$, 160 °C, 34%; iii, OsO_4 (cat.), NMMO, Me_2CO:H_2O:tBuOH (5:5:2), 73%; iv, 30% CF_3COOH, 90%.

against β-glucosidase at mM concentration, thus highlighting its selectivity towards α-glucosidase.

The promising inhibitory profile of **6**, spurred us to prepare a diastereomer **7** of **6**. Diels–Alder adduct **8** was readily transformed to the *endo*,*endo*-diol-**15**.[6] Deketalisation to **16** and decarbonylation led to the cyclohexadiene derivative **17**,[6] Scheme 2. Catalytic OsO_4 mediated double dihydroxylation was once again highly diastereoselective and the hexahydroxyacetal **18** was obtained. Acetonide deprotection in **18** delivered the projected bicyclitol **7**,[6] a hybrid of conduritols A (right ring) and E (left ring). Once again the lack of symmetry (^{13}C NMR) in **7** and **18**, uniquely delineated the stereochemical pattern generated during the double dihydroxylation of **17**. When **7** was evaluated for its inhibitory activity against α- and β-glucosidases, no significant inhibition was observed for either of the enzymes at mM concentrations, indicating that stereochemical alterations in the hydroxy substituents has a major impact on the enzyme inhibitory activity (*cf.* **6**). This result provides further impetus to prepare many more diastereomers of **6** and **7** for further evaluation and efforts towards that end are underway.

In short, we have devised a new family of glycosidase inhibitors, composed of conduritol and carbasugar hybrid structures and describe the synthesis of an octahydroxydecahydronaphthalene, which exhibits significant and selective α-glucosidase activity.

We thank JNCASR for financial support and the SIF facility at I.I.Sc for the high field NMR spectra. One of us (SSR) thanks CSIR for a research fellowship. We thank Dr Utpal Tatu, Department of Biochemistry for help in enzymatic assays.

Notes and references

† The IUPAC name for norbornen-7-one is bicyclo[2.2.1]hept-2-en-7-one.

1 (*a*) M. Balci, Y. Sutbeyaz and H. Secen, *Tetrahedron*, 1990, **46**, 3715; (*b*) H. A. J. Carless, *Tetrahedron: Asymmetry*, 1992, **3**, 795; (*c*) M. Balci, *Pure Appl. Chem.*, 1997, **69**, 97.

2 (*a*) T. Suami, *Top. Curr. Chem.*, 1990, **154**, 257; (*b*) R. J. Ferrier and S. Middleton, *Chem. Rev.*, 1993, **95**, 2779; (*c*) T. Hudlicky, D. A. Entwistle, K. K. Pitzer and A. J. Thorpe, *Chem. Rev.*, 1996, **96**, 1195; (*d*) C. R. Johnson, *Acc. Chem. Res.*, 1998, **31**, 333; (*e*) Y. Landais, *Chimia*, 1998, **52**, 104.

3 (*a*) B. Ganem, *Acc. Chem. Res.*, 1996, **29**, 340; (*b*) M. Bols, *Acc. Chem. Res.*, 1998, **31**, 1.

4 For a few related examples of syntheses of annulated conduritols, see: (*a*) D. C. Billington, F. Perron-Sierra, I. Picard, S. Beaubras, J. Duhault, J. Espinal and S. Challal, *Bioorg. Med. Chem. Lett.*, 1994, **4**, 2307; (*b*) Y. Kara, M. Balci, S. A. Bourne and W. H. Watson, *Tetrahedron Lett.*, 1994, **35**, 3349; (c) M. Desjardins, M. C. Lallemand, T. Hudlicky and K. A. Abboud, *Synlett.*, 1997, 728; (*d*) G. Mehta and D. S. Reddy, *Tetrahedron Lett.*, 1999, **40**, 9137; (*e*) G. Mehta, D. S. Reddy, S. S. Ramesh and U. Tatu, *Tetrahedron Lett.*, 1999, **40**, 9141.

5 (*a*) M. A. Forman and W. P. Dailey, *J. Org. Chem.*, 1993, **58**, 1501; (*b*) T.-C Chou and J. H. Chiou, *J. Chin. Chem. Soc. (Tapei)*, 1986, **33**, 227.

6 All the new compounds reported here were fully characterised on the basis of their spectral IR, ^1H and ^{13}C NMR, MS) and analytical data. Selected spectral data: **13**: δ_H(300 MHz; $CDCl_3$) 5.87–5.83 (m, 2H), 5.65–5.61 (m, 2H), 4.42–4.40 (m, 2H), 3.74 (br s, 2H), 3.00–2.98 (m, 2H), 2.70–2.67 (m, 2H), 1.55 (s, 3H), 1.40 (s, 3H); δ_C(75 MHz; $CDCl_3$) 125.8(2C), 122.6(2C), 109.3, 74.8(2C), 69.0(2C), 35.4(2C), 26.0, 24.4. **6**: δ_H(300 MHz; D_2O), 4.00–3.60 (m, 2H), 2.22–2.18 (m, 2H); δ_C(100 MHz; D_2O) 77.0, 76.7, 76.0, 74.2, 73.2, 71.2 (2C), 66.4, 43.1, 40.5; MS (70 eV, EI): *m/z* 264 ($M^+ - 2$). **17**: δ_H(300 MHz; $CDCl_3$) 5.97–5.94 (m, 2H), 5.54–5.50 (m, 2H), 4.50–4.49 (m, 2H), 3.86 (br s, 2H), 3.53 (d, 2H, *J* = 6.9 Hz), 3.20 (br s, 2H), 1.46 (s, 3H), 1.37 (s, 3H); δ_C(75 MHz; $CDCl_3$) 125.8(2C), 123.8(2C), 108.6, 74.9(2C), 69.7(2C), 32.4 (2C), 26.6, 24.0. **7**: δ_H(300 MHz; D_2O,) 4.00–3.67 (m, 8H), 2.36–2.28 (m, 2H); δ_C(75 MHz; D_2O) 73.7, 72.8, 71.3, 70.7, 70.4, 69.3, 69.2, 67.4, 40.2, 38.4.

7 Each enzymatic assay contained α- or β-glucosidase (0.1 to 1.0 U ml^{-1}), compounds **6**/**7** in water and the corresponding *p*-nitrophenylglycosides (2–3 mM) at a pH and temperature optimum for the enzyme. K_i (μM) values were determined using Lineweaver–Burk plots of the inhibition data.

ChemComm

A simple regiospecific strategy for labelling hydrogen atoms in α-amino acids

Dierdre A. Pearce,[a] Anders Hammershøi,[b] Jack M. Harrowfield[c] and Alan M. Sargeson*[a]

[a] *Research School of Chemistry, The Australian National University, Canberra, ACT, 0200, Australia. E-mail: sargeson@rsc.anu.edu.au*
[b] *Chemistry Department, University of Copenhagen, Universitetsparken 5, DK-2100, Copenhagen Ø, Denmark*
[c] *Department of Chemistry, University of Western Australia, Nedlands, WA, 6009, Australia*

Received (in Cambridge, UK) 21st September 2000, Accepted 31st October 2000
First published as an Advance Article on the web 22nd November 2000

Simple methods for the regioselective introduction of deuterium labels at the α- and β-carbon atoms of leucine using a Co(III) imino acid complex are described which have a general applicability to the synthesis of a range of labelled amino acids.

Deuterium labelled amino acids are useful probes of protein structure[1] and biosynthetic pathways for interesting, potentially useful, metabolites.[2] As such they are significant synthetic targets and a substantial catalogue of synthetic[3] and biosynthetic[4] strategies for the preparation of labelled α-amino acids now exists in the literature. Many of these strategies involve complex, multi-step syntheses and their application as universal methods for the preparation of families of deuterium labelled amino acids is limited by relatively low yields or relatively high substrate specificity. Given these restrictions, a simple and general synthetic strategy has been developed by which the metal ion activation and protection of sites in α-imino acids coordinated to Co(III) may be harnessed to incorporate, regioselectively, deuterium or tritium labels on the α- and β-carbon atoms of various α-amino acids.

Syntheses of α-amino acid complexes of Co(III) are readily achieved by intramolecular condensation of coordinated amido ion (NH_2^-) with an α-keto acid coordinated *cis* to the amido ion,[5] Scheme 1. These ammine complexes have three useful properties: the complexes are substitutionally inert, the imine is protected from hydrolysis in aqueous solution, and sites, including the imine-N, imine-C and β-carbon atoms are activated for further reaction. For example, the protons on the β-carbon of $[Co(NH_3)_4(2\text{-iminopropanoate})]^{2+}$ readily exchange with deuterium ions in dilute NaOD solution. Then, it is possible to reduce, rapidly, the imino acid ligand to the corresponding amino acid (alanine) with BH_4^- ion in dilute, basic solution without significant reduction of the metal centre.[5] These reactions can be employed to prepare a range of amino acids containing a specific deuterium label at the α-carbon using BD_4^- ion and/or at the β-carbon using basic D_2O and BD_4^- or BH_4^-. To illustrate this strategy, the synthesis and isolation of three deuterium-labelled analogues of leucine are described.

The leucine–iminato complex, **3**†, was prepared by a method analogous to that for the alanine–iminato complex.[5] The 4-methyl-2-oxopentanoate complex, **2**, was treated with aqueous base to induce intramolecular condensation between the coordinated α-keto acid and amido ion, Scheme 1. Treatment of **3** with sodium borodeuteride (at pH 10) for 60 s gave **4**,‡ in which the α-carbon of the coordinated leucine was completely labelled with deuterium. A sample of **3** was dissolved in a carbonate–deuterium carbonate buffer (pD 10) and exchange of the protons on the β-carbon for deuterium was monitored by ^1H NMR spectrometry to completion. The isolated complex, **5**, was then treated with either sodium borohydride or sodium borodeuteride to prepare the corresponding complexes **6** and **7**,‡ in which coordinated leucine was labelled with deuterium at the β-carbon and at the α- and β-carbon atoms, respectively. Direct introduction of the D label from BD_4^- ion at the α-C atom occurs even in H_2O and base catalyzed proton exchange at the β-C atom leads to capture of D^+ from D_2O. Complexes **3**–**7** were purified by cation-exchange chromatography to remove traces of cobalt(II) generated during their preparation.

The deuterium labelled amino acids **8**–**10**§ were isolated following treatment of the corresponding Co(III) complexes (**4**, **6**, **7**) with excess ammonium sulfide and filtration to remove precipitated CoS. They were purified by ion exchange chromatography (dilute aqueous ammonia as eluent)[6] and characterized by ^1H and ^{13}C NMR spectrometry, microanalysis and electrospray mass spectrometry. Examples of ^{13}C NMR spectra of the deuterium labelled leucine are reproduced in Fig. 1. Coupling between the deuterium labels and the α- and β-carbon atoms generates characteristic splitting patterns in the peaks assigned to these atoms.

Analogous chemistry has been used to introduce deuterium labels into other amino acids, including glycine, alanine and valine, details of which will be published elsewhere. A wide range of (α-imino acidato)cobalt(III) complexes is also readily accessible by oxidation of the corresponding (α-amino acidato)cobalt(III) complexes with $SOCl_2$[7] and the chemistry described here whould provide the means to prepare selectively labelled analogues of many amino acids. The methods are

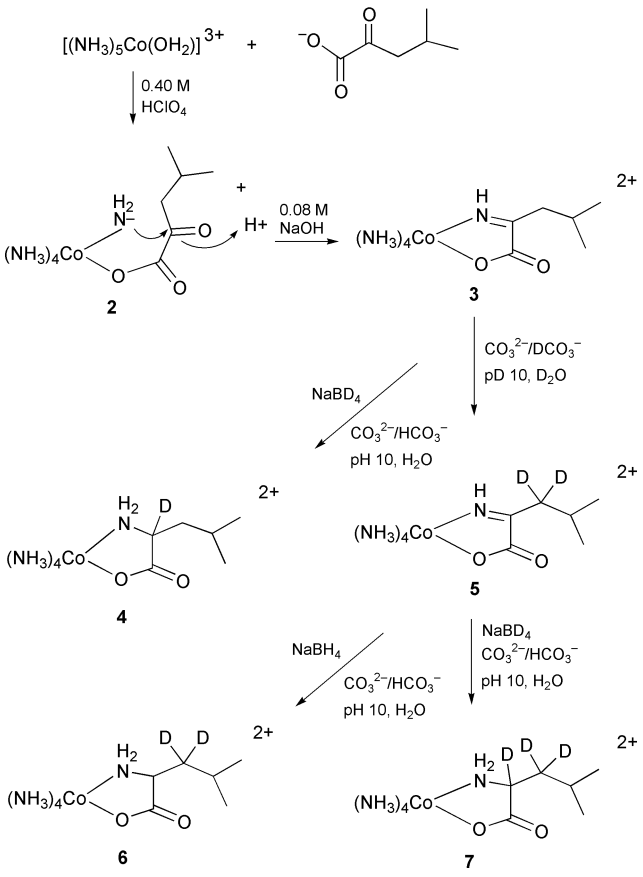

Scheme 1

DOI: 10.1039/b007662g

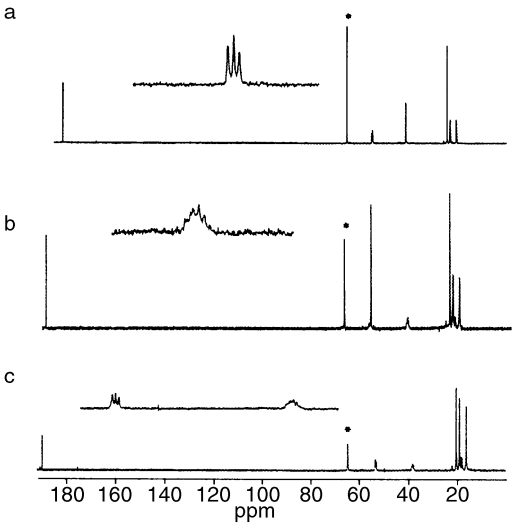

Fig. 1 Comparison of the ^{13}C NMR spectra (D_2O, *1,4-dioxane) of deuteriated-leucines **8**–**10**, a–c respectively from **4**, **6** and **7**. Magnification of spectral peaks due to the α-methine and β-methylene carbon atoms are shown inset, to illustrate splitting of the signals due to the presence of deuterium labels on those atoms.

simple, rt processes and the pure amino acids can be recovered readily.

The stereoselectivity of the chemistry used to prepare the labelled amino acids needs to be addressed. The products isolated from tetraammine complexes are racemic but they can be resolved readily with chiral ion exchange eluents. However, similar chiral cobalt(III) reagents also influence the imino acid[8] reductions stereoselectively and a report on this issue is currently being prepared.

Electrospray mass spectrometric analysis of labelled amino acids by Dr Margaret Shiel and associates of the Department of Chemistry, University of Wollongong, NSW is gratefully acknowledged.

Notes and references

† When necessary, compounds were purified by cation-exchange chromatography (Dowex 50W-X2, 200–400 mesh, BioRad) using HCl solutions as eluents.

For **2**: $[(NH_3)_5Co(OH_2)](ClO_4)_3$[9] (5.00 g, 10 mmol) was added to sodium 4-methyl-2-oxopentanoate (6.1 g, 40 mmol) in $HClO_4$ solution (0.4 M, 4 mmol). The mixture was heated at 45 °C for 3.5 h and the resulting precipitate recrystallized from hot water, producing scarlet crystals of **2** (3.9 g, 76%). δ_H(0.1 M DCl) 4.1 (12 H, br, *cis* 4 × NH_3) 3.5 (3 H, br, *trans* NH_3), 2.73 (2 H, d, β-CH_2), 2.19 (1 H, m, γ-CH), 0.99, 0.98 (6 H, d, 2 × CH_3); δ_C(0.1 M DCl) 188.2 (α-C=O) 174.0 (β-C=O), 44.7 (γ-CH_2), 26.5 (δ-CH), 22.7 (2C, s, 2 × CH_3) (Found: C, 15.3; H, 5.3; N, 15.3; Cl, 14.9; Co, 12.6%. $C_6H_{24}N_5O_{11}Cl_2Co$ requires C, 15.26; H, 5.12; N, 14.83; Cl, 15.02, Co, 12.48%).

For **3**: **2** (3.6 g, 7.6 mmol) was dissolved in NaOH (0.08 M, 7.6 mmol) and stirred at 25 °C (30 s) before addition of acetic acid to pH 4.0. The orange product, **3**, was eluted from ion exchange resin (H^+ form), evaporated to dryness and recrystallized from water by the addition of $HClO_4$ (70%, CAUTION) (2.1 g, 59%). δ_H(0.1 M DCl) 4.1 (3 H, br, NH_3) 3.6 (6 H, br, 2 × NH_3), 3.3 (3 H, br, NH_3), 2.95 (2 H, d, β-CH_2), 2.13 (1 H, m, γ-CH), 0.99, 0.98 (6 H, d, 2 × CH_3); δ_C(0.1 M DCl) 187.6 (O–C=O), 173.0 (α-C=N), 42.3 (β-CH_2), 26.2 (γ-CH), 21.5 (2C, s, 2 × CH_3) (Found: C, 15.6; H, 4.9; N, 15.2; Cl, 14.5; Co, 12.7%. $C_6H_{22}N_5O_{10}Cl_2Co$ requires C, 15.87; H, 4.88; N, 15.42; Cl, 15.61; Co, 12.98%).

‡ For **4**: **3** (0.25 g, 0.8 mmol) was dissolved in a carbonate–bicarbonate buffer solution ($[CO_3^{2-}]$ = $[HCO_3^-]$ = 0.5 M) and $NaBD_4$ (0.08 g, 4 mmol) added. Following vigorous mixing (60 s) the product was rapidly trapped on ion exchange resin (Na^+ form) by suction and washed with water and 0.5 M HCl and the orange product eluted with 2 M HCl. Evaporation gave an orange solid, **4**. The labelled amino acid was removed from this complex without further purification.

Complexes **6** and **7** were prepared by analogous treatment of **5** with $NaBH_4$ and $NaBD_4$, respectively. For **5**: **3** (1.5 mmol, 0.50 g), was dissolved in a carbonate–deuteriobicarbonate buffer ($[CO_3^{2-}]$ = $[DCO_3^-]$ = 0.25 M, pD = 10.0). The resulting deep orange solution was stirred at 25 °C for 10 h and the orange product, **5**, was isolated as above.

§ For **8**–**10**: Complexes **4**, **6** and **7** were individually dissolved in water (10 cm^3) and an 8% solution of $(NH_4)_2S$ added dropwise to reduce and precipitate the cobalt. The resulting CoS suspensions were removed by filtration and the solutions desalted on ion exchange resin (H^+ form); the sorbed material was washed with water before eluting with 0.5 M ammonia solution. Fractions containing the amino acids were evaporated and recrystallized twice from H_2O–propan-2-ol to give white powders (yields from **2** to isolation ~50%). **8**: $\delta_H(D_2O)$ 1.70 (1 H, m, γ-CH), 1.75 (2 H, ABXq, β-CH_2), 0.97, 0.98 (6 H, d, 2 × CH_3); δ_C (D_2O) 187.9 (COOH), 56.8 [1C, t, *J*(CD) 24 Hz, α-CD], 42.4 (β-CH_2), 24.9 (γ-CH), 20.9, 21.0 (2 × CH_3); *m/z* (ES-MS) 133.0 (M^+) (Found: C, 54.4; H, 9.13; N, 10.5%. $C_6H_{12}DNO_2$ requires C, 54.52; H, 9.15; N, 10.6%). **9**: $\delta_H(D_2O)$ 3.73 (1 H, s, α-CH) 1.69 (1 H, m, γ-CH), 0.97, 0.98 (6 H, d, 2 × CH_3); $\delta_C(D_2O)$ 187.8 (COOH) 56.5 (α-CH), 42.3 (1C, m, CD_2), 24.5 (γ-CH), 19.9, 20.9 (2 × CH_3); *m/z* (ES-MS) 134.0 (M^+) (Found: C, 53.2; H, 8.5; N, 10.4%. $C_6H_{11}D_2NO_2$ requires C, 54.1; H, 8.32; N, 10.5%). **10**: δ_H (D_2O) 1.70 (1 H, m, γ-CH), 0.97, 0.98 (6 H, d, 2 × CH_3); $\delta_C(D_2O)$ 187.9 (COOH), 56.6 [1C, t, *J* (CD) 24.45 Hz, α-CD], 42.4 (1C, m, β-CD_2), 24.5 (γ-CH), 19.8, 20.9 (2 × CH_3). *m/z* (ES-MS) 135.0 (M^+) (Found: C, 53.9; H, 7.50; N, 10.3%. $C_6H_{10}D_3NO_2$ requires C, 53.7; H, 7.51; N, 10.4%).

1 A. Ogrel, W. Heerma, K. Versluis, J. Lugtenburg and J. Raap, *Anal. Lett.*, 1997, **30**, 2827; K. H. Gardner and L. E. Kay, *Ann. Rev. Biophys. Biomol. Struct.*, 1998, **27**, 357.
2 G. D. Fate, C. P. Benner, S. H. Grode and T. J. Gilbertson, *J. Am. Chem. Soc.*, 1996, **118**, 11363; A. Ogrel, W. D. Bloemhoff, J. Lugtenburg and J. Raap, *Pep. Sci.*, 1997, **3**, 193.
3 M. Oba, T. Terauchi, J. Hashimoto, T. Tanaka and K. Nishiyama, *Tetrahedron Lett.*, 1997, **38**, 5515; J. C. Shattuck and J. Meniwald, *Tetrahedron Lett.*, 1997, **38**, 8461, and references therein; M. Oba, T. Terauchi, A. Miyakawa, H. Kamo and K. Nishiyama, *Tetrahedron Lett.*, 1998, **39**, 1595; M. Oba, T. Terauchi, A. Miyakawa and K. Nishiyama, *Tetrahedron. Asymmetry*, 1999, **10**, 937.
4 Y. H. Lim, T. Yoshimura, K. Soda and N. Esake, *J. Ferment. Bioeng.*, 1998, **86**, 400; O. U. Mosin, D. A. Skaladner and V. I. Shueb, *Biosci. Biotechnol. Biochem.*, 1998, **62**, 225; J. Raap, S. Nieuenhuis, A. Creemers, S. Hexspoor, U. Kragul and J. Lugtenburg, *Eur. J. Org. Chem.*, 1999, **10**, 2609.
5 J. MacB. Harrowfield and A. M. Sargeson, *J. Am. Chem. Soc.*, 1974, **96**, 2634; J. MacB. Harrowfield and A. M. Sargeson, *J. Am. Chem. Soc.*, 1974, **96**, 3691; J. MacB. Harrowfield and A. M. Sargeson, *J. Am. Chem. Soc.*, 1979, **101**, 1514; P. J. Lawson, M. G. McCarthy and A. M. Sargeson, *J. Am. Chem. Soc.*, 1982, **104**, 6710.
6 R. Barfod, L. Bendahl, A. Hammershøi, D. K. Jensen, A. M. Sargeson and A. C. Willis, *J. Chem. Soc., Dalton Trans.*, 1999, 449.
7 A. Hammershøi, R. M. Hartshorn and A. M. Sargeson, *J. Chem. Soc., Chem. Commun.*, 1988, 1226; A. Hammershøi, R. M. Hartshorn and A. M. Sargeson, *Inorg. Chem.*, 1990, **29**, 4525.
8 K. J. Drok, J. M. Harrowfield, S. J. McNiven, A. M. Sargeson, B. W. Skelton and A. H. White, *Aust. J. Chem.*, 1993, **46**, 1557; L. Bendahl, A. Hammershøi, D. K. Jensen, E. Kaifer, A. M. Sargeson and A. C. Willis, *J. Chem. Soc., Chem. Commun.*, 1996, 1649.
9 D. K. Serbera and H. Taube, *J. Am. Chem. Soc.*, 1961, **83**, 1785.

Asymmetric chemo- and regiospecific addition of organozinc reagents to Baylis–Hillman derived allylic electrophiles

Christoph Börner,[a] Josep Gimeno,[b] Serafino Gladiali,[c] Paul J. Goldsmith,[a] Daniela Ramazzotti[c] and Simon Woodward*[a]

[a] *School of Chemistry, Nottingham University, University Park, Nottingham, UK NG7 2RD. E-mail: simon.woodward@nottingham.ac.uk; Fax: (+44) 115-9513564; Phone: (+44) 115-9513564*
[b] *Departament de Química, Universitat Autònoma de Barcelona, Bellaterra, 08193 Barcelona, Spain*
[c] *Dipartimento di Chimica, Università di Sassari, Via Vienna 2, 07100 Sassari, Italy*

Received (in Liverpool, UK) 21st August 2000, Accepted 23rd October 2000
First published as an Advance Article on the web 22nd November 2000

The copper-catalysed S_N2' addition of ZnR_2 to allylic (*Z*)-ArCH=C(CH_2X)(CO_2Et) (X = Br, Cl, OSO_2Me) fashions only ArCH(R)C(=CH_2)(CO_2Et); use of a chiral ligand gives up to 64% ee for this demanding reaction.

The reactions of organometallic nucleophiles, MR, with allylic halide (or pseudohalide) substrates $R^1CH{=}CR^2CH_2X$ often lead to a mixture of S_N2 (attack α to the leaving group X) and S_N2' (attack γ to X) products.[1] This feature causes problems in metal-catalysed asymmetric γ-additions to unsymmetrical allylic electrophiles where the catalyst must control both the regio- and enantioselectivity. Catalysts showing superlative selectivity for both these aspects are rare.[2–6] Pointers in the stoichiometric literature suggested to us that the regiochemical problem might be overcome with substrates where R^2 is an ester function[7] and if an organozinc reagent[8] is used as the terminal organometallic in the catalytic cycle. In particular, we were keen to apply these ideas to enantioselective copper-catalysed S_N2' additions of MR to allylic halides as very few successes have been reported for this otherwise intrinsically useful transformation.[9,10] Aside from controlling the regiochemistry the ester could play two additional roles. Firstly, a more rigorously bound asymmetric transition state might be attained, *via* carbonyl co-ordination. Secondly, the products from such carbonyl containing substrates are present in many compounds of biological interest.

The allylic bromides **2** (Scheme 1) were selected for initial trials with commercial $ZnEt_2$ to demonstrate the viability of this approach. Compounds **2** are attractive as they are available in just two, chromatography-free, steps *via* known Baylis–Hillman chemistry (Scheme 1).[11] Additionally, bromination of **1** proceeds with very high (*Z*)-selectivity[12] to afford solid products which may be crystallised to high chemical and stereochemical purity. Simple mixture of THF solutions of **2** and $ZnEt_2$ in the presence of $[Cu(MeCN)_4]BF_4$[13] (3 mol%) at −20 °C leads to rapid formation of **4** (R = Et) as apparently the

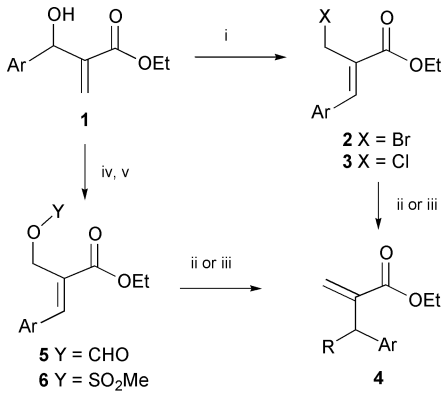

a Ar = Ph; **b** Ar = 4-$C_6H_4NO_2$; **c** Ar = 4-C_6H_4Cl
d Ar = 4-C_6H_4Me; **e** Ar = 1-$C_{10}H_7$

Scheme 1 *Reagents and conditions*: i, conc. HX/H_2SO_4, 16–24 h, rt; ii, ZnR_2, THF, −20 °C, cat. $[Cu(MeCN)_4]BF_4$; iii, $ZnEt_2$, THF, −20 °C, cat. $[Cu(MeCN)_4]BF_4/(S_a)$-**7**; iv, for **5** NEt_3–HCO_2H reflux; v, for **6** treatment of **5** with aq. HCl in MeOH followed by mesylation ($MeSO_2Cl$–NEt_3) of the derived alcohol.

Table 1 Reaction of allylic electrophiles **2**–**6** with organometallics (RM) in the presence of $[Cu(MeCN)_4]BF_4$†

Halide	RM	Cu^I/mol%	Ligand/ mol%	Temp./°C	Time/min	Yield/%[a]	ee/%[b]
2a	$ZnEt_2$	3	None	−20	40	100 (78)	—
2a	$ZnEt_2$	0.5	None	−20	40	100 (73)	—
2b	$ZnEt_2$	3	None	−20	40	100 (63)	—
2c	$ZnEt_2$	3	None	−20	40	100 (80)	—
2d	$ZnEt_2$	3	None	−20	40	86	—
2e	$ZnEt_2$	3	None	−20	40	84	—
2a	$Zn(CH_2TMS)_2$[c]	7	None	0	180	47 (25)	—
2a	$ZnEt_2$	10	**7** 20	−20	20	100 (80)	3 (+)
2a	$ZnEt_2$	10	**7** 20	−40	40	(44)	13 (+)
3a	$ZnEt_2$	10	**7** 20	−20	40	56 (35)	36 (−)
3a	$ZnEt_2$	10	**7** 20	−40	40	(19)	34 (−)
3a	$AlEt_3$	10	**7** 20	0	40	12 (< 5)	8 (−)
3b	$ZnEt_2$	10	**7** 20	−20	40	100 (76)	60 (−)
3b	$ZnEt_2$	10	**7** 20	−40	40	64	64 (−)
3d	$ZnEt_2$	10	**7** 20	−20	40	25 (19)	30 (−)
3e	$ZnEt_2$	10	**7** 20	−20	40	27 (14)	22 (−)
5	$ZnEt_2$	10	**7** 20	−20	20	< 5	—
6	$ZnEt_2$	10	**7** 20	−20	20	100 (90)	2 (+)

[a] Based on NMR conversion, isolated yields in parentheses. [b] Determined by HPLC on a Chiracel OD column, predominant stereoisomer in parentheses. [c] Used in the presence of $MgCl_2$.

DOI: 10.1039/b006943o

sole product (Scheme 1). Extremely high chemo- and regioselectivity, technical simplicity, and high rate ($\sim$50 TON h^{-1}) characterise these reactions (Table 1).† The reactions can be run at even lower copper loadings, for example, **2a** gives a near quantitative yield of **4a** (R = Et) at 0.5 mol% Cu^{I} (>290 TON h^{-1}). In the absence of Cu^{I} polar co-solvents are necessary to provide high chemical yields[7] (in the absence of any copper, yields of <12% were attained in our control reactions). The new catalytic protocol is superior to use of classical Gilman cuprates. For example, reaction of **2a** with $LiCuMe_2$·LiI in THF affords only a 8:1 $S_N2':S_N2$ mixture. Compounds **4** (R = Et) are the intimate precursors of a number of biologically active molecules showing, for example, inhibition of *angiotensin-converting* and *epithelial neutral endopetidase* enzymes[14] or those showing molluscicidal activity against endoparasite carrying *Biomphalaria glabrata*.[15]

Preliminary approaches to rendering these reactions viable as catalytic asymmetric syntheses are also reported in Table 1.† Relatively high copper and ligand loadings were used to maximise the asymmetric induction obtained as this is noted to be a problematic area.[9,10] Ligand **7** was selected as an initial

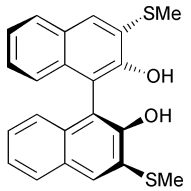

(S_a)-**7**

candidate based on its efficacy in asymmetric conjugate addition.[16] Varying the leaving group indicated chloride to be the best leaving group with respect to enantioselectivity, although the chemical yield suffered somewhat in this case. Very high chemical yields were realised with the mesylate **6**, but the product **4a** is essentially racemic, while the formate **5** does not participate in the reaction. Ligand **7** was confirmed as the optimal structure by screening a small library of compounds against a test reaction of **3a** with $ZnEt_2$; none of the other structures lead to very active catalysts. Similarly, changing to a terminal $AlEt_3$ organometallic source is not tolerated.

In conclusion, a new type of efficient catalytic S_N2' chemistry has been developed. The degree of stereocontrol realised in these reactions appears to be due more to electronic than steric factors, however, more experiments are required before the details of the asymmetric transition state become clear. These studies together with applications of the compounds **4** to the synthesis of biologically active compounds are underway in our laboratories.

We thank the EPSRC for support of this project through grants GR/M75341, GR/M84909, GR/N37339 and for access to their Mass Spectrometry Service (University of Swansea). S. G. and S. W. are grateful to the EU for support through COST (working groups D12/0009/98 and D12/0022/99) and SOCRATES. J. G. acknowledges the support of the Generalitat de Catalunya.

Notes and references

† *Representative procedures and compound data.* An argon-protected solution of $[Cu(MeCN)_4]BF_4$ (6.3 mg, 0.02 mmol, 3 mol%) in THF (0.7 cm^3) at −20 °C was treated sequentially with solid **2b** (211 mg, 0.67 mmol) and $ZnEt_2$ (1.0 cm^3 of 1.0 M hexane solution, 1.0 mmol). After 40 min the pale yellow solution was quenched with aqueous HCl (2 M, 3 cm^3), the product was extracted with diethyl ether, and the organic fraction dried ($MgSO_4$). The solvent was removed and the product assayed directly by ^1H NMR spectroscopy. In all cases the spectra were consistent with a >20:1 $S_N2':S_N2$ selectivity.

For asymmetric runs, ligand **7** (38 mg, 0.10 mmol, 20 mol%) and $[Cu(MeCN)_4]BF_4$ (15.7 mg, 0.05 mmol, 10 mol%) in dry THF (1 ml) were stirred at −20 °C in the presence of $ZnEt_2$ (0.10 mmol). Solutions of the allylic chloride **3b** (140.2 mg, 0.52 mmol) in THF (0.55 cm^3) and $ZnEt_2$ (0.77 ml of a 1.0 M hexane solution, 0.77 mmol) were added by syringe pump over 20 min and the reaction stirred for a further 20 min at −20 °C. The reaction was worked up as above. In cases (Table 1) where the reaction was not complete unreacted allylic chloride was removed by flash chromatography or treatment with DABCO.

(−)-Ethyl 2-methylene-3-(4-nitrophenyl)pentanoate **4b** (R = Et) Yield 76% (60% ee); $[\alpha]_{546}^{21}$ −84 (c = 0.33, in $CHCl_3$); δ_H (400 MHz, $CDCl_3$) 0.88 (3 H, t, J = 7.3, $CHCH_2$*Me*), 1.21 (3 H, t, J = 7.1, OCH_2*Me*), 1.79 (1 H, ddq, J = 13.4, 8.8, 7.3, $CHCH_{2\alpha}$Me), 1.78 (1 H, ddq, J = 13.4, 6.3, 7.3, $CHCH_{2\beta}$Me), 3.84 (1 H, dd, J = 8.8, 6.3, *CH*CH_2), 4.11 (2 H, m, OCH_2Me), 5.76 (1 H, s, $=CH_{2\alpha}$), 6.41 (1 H, s, $=CH_{2\beta}$), 7.39 (2 H, d, J = 8.7, C_6H_4), 8.14 (2 H, d, J = 8.7, C_6H_4); δ_C (67.8 MHz, $CDCl_3$) 12.0 ($CHCH_2$*Me*), 13.8 (OCH_2*Me*), 26.9 ($CHCH_2$), 47.8 (CH), 60.6 (OCH_2), 123.3 (Ar-H), 124.5 ($=CH_2$), 128.8 (Ar-H), 142.4 (Ar-*i*), 146.3 (=*C*CO), 150.7 (Ar-*i*), 166.2 (CO); ν_{max}(thin film)/cm^{-1} 2967m, 2936m, 2876 (3 × C-H), 1714s (C=O), 1520s, 1347s (2 × N=O), 1254m, 1152m, 851m; *m/z* (FAB) 264 ([M + H]$^+$, 13%), 221 (14), 207 (16), 147 (38), 77 (13), 73 (100). [Found (HRMS, FAB): [M + H]$^+$, 264.1244. $C_{14}H_{18}NO_4$ requires *M* + *H*, 264.1236].

1 R. M. Magrid, *Tetrahedron*, 1980, **36**, 1901.
2 T. Hayashi, M. Kawatasura and Y. Kozumi, *Chem. Commun.*, 1997, 561.
3 J. P. Janssen and G. Helmchen, *Tetrahedron Lett.*, 1997, **38**, 8025.
4 R. Pretôt and A. Pfaltz, *Angew. Chem., Int. Ed.*, 1998, **37**, 323.
5 R. Pretôt, G. C. Lloyd-Jones and A. Pfaltz, *Pure Appl. Chem.*, 1998, **70**, 1035.
6 B. M. Trost and I. Hachiya, *J. Am. Chem. Soc.*, 1998, **120**, 1104.
7 L.-H. Xu and E. P. Kündig, *Helv. Chim. Acta*, 1994, **77**, 1480.
8 F. Lambert, B. Kirschleger and J. Villieras, *J. Organomet. Chem.*, 1991, **406**, 71.
9 J. E. Bäckvall, S. E. Karlström, M. van Klaveren, G. van Koten, G. J. Meuzelaar, E. S. M. Persson and A. del Villar, *Tetrahedron*, 2000, **56**, 2895 [18–53% ee values attained].
10 F. Dübner and P. Knochel, *Angew. Chem., Int. Ed. Engl.*, 1999, **38**, 379; P. Knochel and F. Duebner, (Avecia Limited, UK), *PCT Int. Appl.*, 9 March, 2000, [*Chem. Abs.*, 2000, **132**, 222063; 2–87% ee values attained].
11 D. Basavaiah, P. D. Rao and R. S. Hyma, *Tetrahedron*, 1996, **52**, 8001.
12 F. Ameer, S. E. Drewes, N. D. Emslie, P. T. Kaye and R. L. Mann, *J. Chem. Soc., Perkin Trans. 1*, 1983, 2293.
13 G. Kubas, *Inorg. Synth.*, 1990, **28**, 68.
14 C. A. Almansa, A. F. de Arriba, E. Carceller, F. L. Cavalcanti, J. Forn, J. Garcia-Rafanell, L. A. Gomez and R. Rodriguez, *J. Med. Chem.*, 1996, **39**, 2197.
15 G. Ruecker, K. Hostettmann, W. Gajewski, M. Loebbert and P. Boeken, *Arch. Pharm. (Weinheim, Ger.)*, 1993, **326**, 941.
16 S. M. W. Bennett, S. M. Brown, A. Cunningham, M. R. Dennis, J. P. Muxworthy, M. A. Oakley and S. Woodward, *Tetrahedron*, 2000, **56**, 2847.

ChemComm

A novel enantiopure proline-derived triazacyclononane: synthesis, structure and application of its manganese complex

Carsten Bolm,*[a] Nico Meyer,[a] Gerhard Raabe,[a] Thomas Weyhermüller[b] and Eberhard Bothe[b]

[a] *Institut für Organische Chemie der RWTH Aachen, Professor-Pirlet-Straße 1, D-52056 Aachen, Germany. E-mail: Carsten.Bolm@oc.rwth-aachen.de; Fax: (+49) 241 8888 391*

[b] *Max-Planck-Institut für Strahlenchemie, Stiftstr. 34-36, D-45470 Mülheim an der Ruhr, Germany*

Received (in Cambridge, UK) 30th August 2000, Accepted 26th October 2000
First published as an Advance Article on the web 23rd November 2000

The X-ray crystal structure and electrochemical data of a manganese complex $[L_2Mn_2^{III}(\mu\text{-}O)(\mu\text{-}AcO)_2][PF_6]_2$ with L being an enantiopure C_3-symmetric 1,4,7-triazacyclononane derived from L-proline are compared to those of $[Me_3TACN_2Mn_2^{III}(\mu\text{-}O)(\mu\text{-}AcO)_2][PF_6]_2$; catalytic studies reveal the applicability of the complex in enantioselective epoxidations.

The tridentate macrocycle 1,4,7-triazacyclononane (TACN, **1**) and derivatives thereof, in particular 1,4,7-trimethyl-1,4,7-triazacyclononane (Me_3TACN, **2**), have extensively been used as ligands in the coordination chemistry of transition metals (Scheme 1).[1]

Triazacyclononanes imitate the coordination sphere of the three histidines which are often encountered in metalloproteins and therefore such (TACN) metal complexes are of interest as structural and functional enzyme models as well as catalysts. For example, dinuclear TACN–manganese complexes mimic enzymes like manganese superoxide dismutase and manganase catalase,[2] and in 1994 Unilever reported their use in low-temperature bleaching with hydrogen peroxide.[3] Bein and de Vos described stereospecific epoxidations of unfunctionalised olefins,[4] and with manganese complexes bearing chiral TACN derivatives we[5] and others[6] achieved enantioselective epoxidations. Other applications include oxidations of benzylic alcohols[7] and sulfides[8] to benzaldehydes and sulfones, respectively, and the use of perfluorinated TACN–Mn complexes.[9] Moreover, hydroxylation and hydroperoxidation of poorly reactive hydrocarbons was achieved by the activation with such complexes with acetic acid.[10] Here, we present the synthesis of the enantiopure C_3-symmetric trispyrrolidine-1,4,7-triazacyclononane (TP-TACN, **3**) and describe the preparation and characterisation of its dinuclear manganese complex **5** which is capable of catalysing enantioselective epoxidations.

TP-TACN **3** was obtained as an air-sensitive colourless oil by reduction of L-proline-derived cyclotripeptide **4**[11] with a large excess of borane–tetrahydrofuran (Scheme 2).[12] Isolation of the product was achieved by addition of MeOH to destroy the excess of borane followed by refluxing in 4 M HCl–dioxane. Treatment of this acidic mixture with solid NaOH followed by extraction with DCM liberated the triamine. Distillation of the crude product under reduced pressure (120–125 °C; 2.6 10^{-1} mbar) afforded **3** in 83% yield.† The dinuclear manganese(III) complex **6** (74% yield)‡ crystallised from a solvent mixture of MeOH and water containing triamine **3**, manganese(III) acetate, sodium acetate and ammonium hexafluorophosphate providing single crystals suitable for X-ray diffraction analysis.§ The comparison of selected bond distances and angles of **6** with the corresponding values of Wieghardt's Me_3TACN manganese complex **5**[2a] reveals the structural similarity between both compounds. For example, the Mn–Mn distances in **6** [average value 3.155(2) Å] and the one in **5** [3.149(3) Å] overlap within their threefold standard deviation. Similarly, the Mn–O–Mn angle in **6** is 122.2(3)°, while the one reported for **5** is 120.9(1)°.

From temperature-dependent (4–300 K) magnetic susceptibility measurements (SQUID magnetometer) of solid **6** a ferromagnetic coupling (J = +4.6 cm^{-1}; $H = -2JS_1 \times S_2$; $S_1 = S_2 = 2$; $D1 = D2 = 2.3$ cm^{-1}; $g1 = g2 = 1.992$) yielding an $S = 4$ ground state was established in agreement with **5**.

Fig. 1 shows the X-band EPR spectra of the electrochemically generated one electron reduced and oxidised states of the PF_6-salt of **6** in acetonitrile at 30 K. A detailed analysis of the multiline spectra is currently under investigation and will be published elsewhere.

The electrochemical properties of **5** and **6** have been studied by cyclic voltammetry (CV) under identical conditions in acetonitrile solution containing 0.1 M tetra-*n*-butylammonium hexafluorophosphate ($TBAPF_6$) as supporting electrolyte in the potential range +1.6 to −1.0 V. All redox potentials are referenced *vs.* the ferrocenium/ferrocene couple (Fc^+/Fc). Scheme 3 summarises the data.

The CV of **6** exhibits one reversible one-electron reduction at $E_{1/2}$ = −0.62 V corresponding to a $Mn^{III/III}$/ $Mn^{III/II}$ transition and, in addition, two successive quasi reversible [ΔE^p = 109 and 87 mV (scan rate: 50 mVs^{-1})] one-electron oxidations at $E_{1/2}$ = 0.51 and 1.12 V corresponding to $Mn^{III/III}$/$Mn^{III/IV}$ and $Mn^{III/IV}$/$Mn^{IV/IV}$ transitions, respectively. Thus, the redox behaviour of **6** is similar to that of **5**, however, all transitons are shifted towards more negative potentials (by 0.1, 0.08 and 0.09 V, respectively). These results show that TP–TACN and its manganese complex are chiral analogues of Me_3TACN and its corresponding metal complex. Furthermore, the CV data reveal that TP–TACN can better stabilise higher oxidation states than Me_3TACN, which could be particularly useful in oxidation

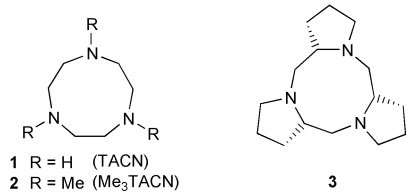

Scheme 1

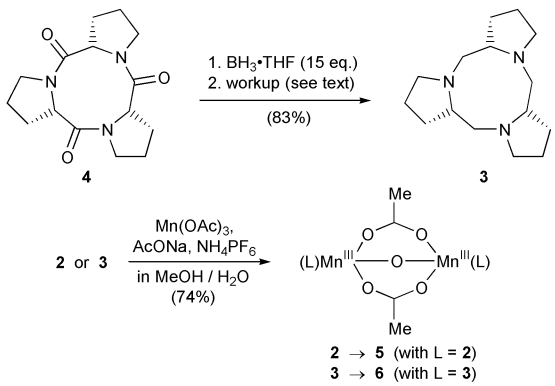

Scheme 2

DOI: 10.1039/b007059i

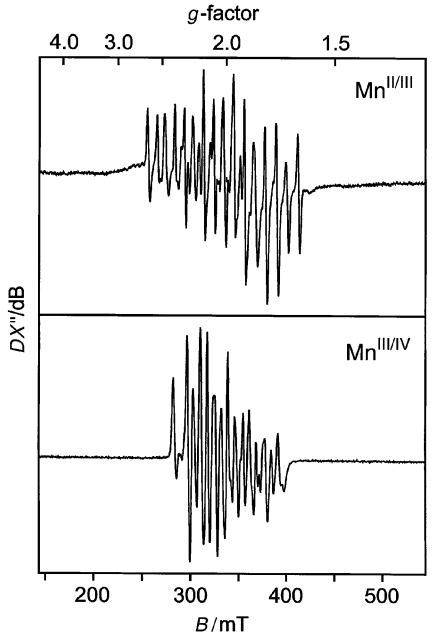

Fig. 1 X-band EPR spectra of the electrochemically generated one electron reduced and oxidised states of the PF_6-salt of **6** in acetonitrile at 30 K.

$[Mn^{IV}Mn^{IV}] \underset{-1e}{\overset{+1e}{\rightleftharpoons}} [Mn^{III}Mn^{IV}] \underset{-1e}{\overset{+1e}{\rightleftharpoons}} [Mn^{III}Mn^{III}] \underset{-1e}{\overset{+1e}{\rightleftharpoons}} [Mn^{III}Mn^{II}]$

for **5**:	**1.21 V**	**0.59 V**	**–0.52 V**
for **6**:	**1.12 V**	**0.51 V**	**–0.62 V**

(for conditions see text)

Scheme 3

catalysis. In order to probe this hypothesis and to investigate the potential of **3** to serve as an asymmetric catalyst we briefly investigated enantioselective epoxidations of styrenes.

Catalytic activity of **5** was observed in the epoxidation of vinylarenes. With H_2O_2 as oxidant and 2 mol% of catalyst in acetone at −25 °C, approximately 28% conversion of styrene was observed after 2 h giving the corresponding epoxide with 24% ee (*S*-enantiomer; all ee-values were determined by GC using a chiral column). Extending the reaction time to 4 h increased the conversion (*ca*. 88%) of the olefin but reduced the enantioselectivity (15% ee). The significantly greater conversion coupled with the lower enantioselectivity after the longer reaction time suggests that the catalytic species is changing during the course of the reaction. Substituted arenes, such as 3-nitrostyrene and 4-chlorostyrene were epoxidised as well giving products with 26 and 21% ee, respectively.

We are grateful to the DFG (SPP Sauerstofftransfer/ Peroxidchemie) and the Fonds der Chemischen Industrie for support of this research. We thank Professor Dr Wieghardt, Dr Bill (MPI für Strahlenchemie, Mülheim) and Professor Dr Kölle (RWTH Aachen) for helpful discussions. We also acknowledge Dr Lehmann (MPI für Kohlenforschung, Mülheim) for the X-ray diffraction data collection.

Notes and references

† NMR data of **3**: ^{1}H NMR (CD_3OD) δ 3.12 (dt, J = 2.0, 6.0 Hz, 1H), 3.04 (m, 1H), 3.05 (t, J = 13.0 Hz, 1H), 2.76 (dd, J = 8.1, 2.7 Hz, 1H), 2.64 (q, J = 9.0 Hz, 1H), 1.95 (m, 1H), 1.70–1.85 (m, 2H), 1.54 (m, 1H); ^{13}C NMR (CD_3OD) δ 23.34, 31.40, 57.95, 59.50, 62.17.

‡ Selected analytical data of **6**: SIMS (NBA): *m/z* 742 (M^+), 363 (LMnOAc), 248 (ligand); $C_{34}H_{60}N_6O_5Mn_2P_2F_{12}$ required C, 39.5; H, 5.9; N, 8.1. Found: C, 39.4; H, 5.8; N, 8.1%. UV-Vis: λ_{max}/nm (ε, L mol^{-1} cm^{-1}) 250 (5500); 314 (8500); 485 (400); 521 (340); $[\alpha]_D$ = +7.1° (*c* 0.05, CH_3CN). The ^{1}H-NMR spectrum of paramagnetic **6** in CD_3CN exhibits broad signals at δ = −157, −108, −76, −50, 34, 55, 62, 102, 108 and 116 ppm and an acetate signal at 80 ppm (assigned by exchange with deutero acetate; see also in ref. 3*c*). Sharper signals were observed in the ranges 0 to 10 and 18 to 28 ppm.

§ *Crystal data* for $C_{34}H_{60}N_6O_5F_{12}P_2Mn_2$ (**6**): The compound crystallises in monoclinic space group $P2_1$ (No. 4) with two symmetrically independent molecules in the asymmetric unit. a = 11.1571(9), b = 16.8538(14), c = 23.1716(18) Å, γ = 98.367(3)°. M_r = 1032.70, Z = 2 × 2, D_c = 1.591 g cm^{-3}, μ = 7.32 cm^{-1}, absorption correction (*Gaussian*): min/max = 0.787/0.915. 47506 reflexions were collected at 100 K on a BRUKER SMART CCD using MoK_α radiation (λ = 0.71073Å). The structure was solved by direct methods (GENSIN/GENTAN) as implemented in the XTAL3.4 program package of crystallographic routines.[13] 7807 observed reflexions ($I > 4\sigma(I)$) in final least-squares full matrix refinement of 1099 parameters on F terminating at $R(R_w)$ = 0.084(0.050, $w = \sigma^{-2}$), a goodness of fit of 1.7924 and a residual electron density of −2.06/1.94 e Å^{-3}. CCDC 182/1847. See http://www.rsc.org/suppdata/cc/b0/b007059i/ for crystallographic files in .cif format.

1 (*a*) P. Chaudhuri and K. Wieghardt, in *Progress in Inorganic Chemistry*, ed. S. J. Lippard, John Wiley and Sons, New York, 1989, vol. 35, p. 329; (*b*) E. Kimura, in *Progress in Inorganic Chemistry*, ed. K. D. Karlin, John Wiley and Sons, New York, 1994, vol. 41, p. 443; (*c*) J. A. Halfen, S. Mahapatra, E. C. Wilkinson, S. Kaderli, V. G. Young, Jr., L. Que, Jr., A. D. Zuberbühler and W. B. Tolman, *Science*, 1996, **271**, 1397; (*d*) C. Stockheim, L. Hoster, T. Weyhermüller, K. Wieghardt and B. Nuber, *J. Chem. Soc., Dalton Trans.*, 1996, 4409; (*e*) K. P. Wainwright, *Coord. Chem. Rev.*, 1997, **166**, 35.

2 (*a*) K. Wieghardt, U. Bossek, D. Ventur and J. Weiss, *J. Chem. Soc., Chem. Commun.*, 1985, 347; (*b*) Review: R. Hage, *Recl. Trav. Chim. Pays-Bas*, 1996, **115**, 385; (*c*) K. Wieghardt, U. Bossek, B. Nuber, J. Weiss, J. Bonvoisin, M. Corbella, S. E. Vitols and J. J. Girerd, *J. Am. Chem. Soc.*, 1988, **110**, 7398; (*d*) U. Bossek, T. Weyhermüller, K. Wieghardt, B. Nuber and J. Weiss, *J. Am. Chem. Soc.*, 1990, **112**, 6387.

3 (*a*) R. Hage, J. E. Iburg, J. Kerschner, J. H. Koek, E. L. M. Lempers, R. J. Martens, U. S. Racherla, S. W. Russell, T. Swarthoff, M. R. P. van Vllet, J. B. Warnaar, L. van der Wolf and B. Krijnen, *Nature*, 1994, **369**, 637; (*b*) J. H. Koek, S. W. Russel, L. van der Wolf, R. Hage, J. B. Warnaar, A. L. Spek, J. Kerschner and L. Del Pizzo, *J. Chem. Soc., Daltan Trans*, 1996, 353; (*c*) R. Hage, E. A. Gunnewegh, J. Niel, F. S. B. Tjan, T. Weyhermüller and K. Wieghardt, *Inorg. Chim. Acta*, 1998, **268**, 43; (*d*) J. H. Koek, E. W. M. J. Kohlen, S. W. Russell, L. van der Wolf, P. F. ter Steeg and J. C. Hellemons, *Inorg. Chim. Acta*, 1999, **295**, 189.

4 (*a*) D. E. De Vos and T. Bein, *J. Organomet. Chem.*, 1996, **520**, 195; (*b*) D. E. De Vos and T. Bein, *Chem. Commun.*, 1996, 917; (*c*) D. E. De Vos, J. L. Meinershagen and T. Bein, *Angew. Chem., Int. Ed.*, 1996, **35**, 2211; (*d*) Y. V. Subba Rao, D. E. De Vos, T. Bein and P. A. Jacobs, *J. Chem. Soc., Chem. Commun.*, 1997, 355; (*e*) D. E. De Vos, B. F. Sels, M. Reynaers, Y. T. Subba Rao and P. A. Jacobs, *Tetrahedron Lett.*, 1998, **39**, 3221; (*f*) D. E. De Vos, S. de Wildeman, B. F. Sels, P. J. Grobet and P. A. Jacobs, *Angew. Chem., Int. Ed.*, 1999, **38**, 980; (*g*) see also: A. Berkessel and C. A. Sklorz, *Tetrahedron Lett.*, 1999, **40**, 7965.

5 C. Bolm, D. Kadereit and M. Valacchi, *Synlett*, 1997, 687.

6 (*a*) M. Beller, A. Tafesh, R. W. Fischer and B. Schabert, DE 195 23 890 C1; 30.06.95; (*b*) M. Beller, A. Tafesh, R. W. Fischer and B. Schabert, DE 195 23 891 C1; 30.06.95.

7 C. Zondervan, R. Hage and B. L. Feringa, *J. Chem. Soc., Chem. Commun.*, 1997, 419.

8 (*a*) D. H. R. Barton, W. Li and J. A. Smith, *Tetrahedron Lett.*, 1998, **39**, 7055; (*b*) R. W. Hay, T. Clifford and N. Govan, *Transition Met. Chem.*, 1998, **23**, 619.

9 (*a*) J. M. Vincent, A. Rabion, V. K. Yachandra and R. H. Fish, *Angew. Chem., Int. Ed.*, 1997, **36**, 2346; (*b*) R. H. Fish, *Chem. Eur. J.*, 1999, **5**, 1677.

10 (*a*) G. B. Shul'pin and J. R. Lindsay Smith, *Russ. Chem. Bull.*, 1998, **47**, 2379; (*b*) G. B. Shul'pin, G. Süss-Fink and J. R. Lindsay Smith, *Tetrahedron*, 1999, **55**, 5345.

11 (*a*) M. Rothe, K. D. Steffen and I. Rothe, *Angew. Chem., Int. Ed. Engl.*, 1965, **4**, 356; (*b*) C. M. Deber, D. A. Torchia and E. R. Blout, *J. Am. Chem. Soc.*, 1971, **93**, 4893; (*c*) H. Kessler and A. Friedrich, *J. Org. Chem.*, 1981, **46**, 3892; (*d*) M. Rothe, M. Fähnle, W. Mästle and K. Feige, in *Peptides, Proceedings of the 9th American Peptide Symposium*, 1985, p. 177; (*e*) M. Rothe and J. Haas, in *Peptides*, 1990, ed. E. Giralt and D. Andreu, ESCOM, Leiden, 1991, p. 212.

12 After concluding our investigations we were informed that **3** has also been synthesized by Reggelin and coworkers. We thank Professor Reggelin (Mainz) for sharing these unpublished results with us.

13 *XTAL3.4 User's Manual*, ed. S. R. Hall, G. S. D. King and J. M. Steward, Universities of Western Australia, Leuven and Maryland, Lamb, Perth, 1995.

ChemComm

One-step synthesis of ordered mesocomposites with non-ionic amphiphilic block copolymers: implications of isoelectric point, hydrolysis rate and fluoride†

Ji Man Kim,[a] Yong-Jin Han,[a] Bradley F. Chmelka[b] and Galen D. Stucky*[a]

[a] *Department of Chemistry and Biochemistry, University of California, Santa Barbara, CA 93106, USA. E-mail: stucky@chem.ucsb.edu*

[b] *Department of Chemical Engineering, University of California, Santa Barbara, CA 93106, USA.*

Received (in Columbia, MO, USA) 7th July 2000, Accepted 18th October 2000
First published as an Advance Article on the web 24th November 2000

Highly ordered hexagonal silica/block copolymer mesostructured composites have been prepared using syntheses with fluoride over a wide range of pH conditions (pH 0–9), by controlling the rates of hydrolysis and condensation of the tetramethoxysilane silica source.

Highly ordered mesoporous silica structures have now been well demonstrated through the use of cationic surfactant (S^+) and anionic silica moieties (I^-) under basic pH conditions[1,2] or by using cationic silica (I^+) assembly through hydrogen bonding mediation with either cationic surfactants (S^+)[2] or hydronium ion solvated neutral block copolymers [$N^0(H_3O^+)$].[3,4] Pinnavaia and coworkers[5,6] have shown that worm-like mesostructures with monodispersed pore sizes can be obtained using non-ionic surfactants (N^0) and partially ionized silica [$N^0(H_3O^+)I^-$] at neutral pH. Prouzet and coworkers[7] have obtained similar results by starting with a clear [$N^0(H_3O^+)X^-I^0$] solution at pH *ca.* 2 and increasing condensation by adding fluoride.

In both the ordered and disordered worm-like structures that have been obtained, a common feature is the independent control of hydrolysis and silica polymerization. For example, highly ordered mesostructures can be created by varying the pH and charge on the silica species at high pH[8] or alternatively near the isoelectric point[9] where the rate of silica polymerization can be readily controlled. Hydrogen-bonding interactions, such as occur among polyethylene oxide–polypropylene oxide–polyethylene oxide (PEO–PPO–PEO) triblock copolymers and silica species in acid media, facilitate simultaneous synthesis and processing of ordered mesostructured materials into thin films,[10] fibers[11] and monoliths.[12] Features of the inorganic species, such as the isoelectric point, associated cations[13,14] and the cosolvent generated on hydrolysis of alkoxide,[15] are important factors in these synthesis approaches.

Fluoride is a well known catalyst for hydrolysis and polymerization of silica species[16] and has been used in the synthesis of mesoporous silica materials under various conditions in order to improve structural order.[5,6,9,17,18] Silva and Pastore[17] first reported the effect of fluoride on synthesis of mesoporous materials with cationic surfactants. Guth and coworkers[18] synthesized mesoporous materials with cationic and non-ionic surfactant species, in the presence of fluoride at a pH between 6.5 and 11. However, use of the non-ionic surfactant species yielded poorly ordered mesostructures compared with those obtained using cationic surfactants. Pinnavaia, Prouzet and their coworkers[6,7] reported the fluoride-mediated synthesis of MSU-*X* materials with worm-like disordered channel structures with poorly defined crystallographic symmetry, using non-ionic surfactant species under neutral conditions. Stucky and coworkers[9] reported synthesis of highly ordered SBA−15 materials using amphiphilic PEO–PPO–PEO triblock copolymer P123 and tetraethoxysilane (TEOS) under acidic conditions (pH ⩽ 3) in the presence of a small amount of fluoride. Here, we report one−step syntheses of well ordered PEO–PPO–PEO/silica mesostructures over a large pH range (0–9), including mild neutral conditions.

The preparation of such materials relies on the control of tetramethoxysilane (TMOS) hydrolysis and silica polymerization in the presence of fluoride and amphiphilic block copolymer, the structure-directing agent. In a typical synthesis batch, 2.0 g of Pluronic P123 ($EO_{20}PO_{70}EO_{20}$, M_{av} = 5800, BASF) was dissolved in 62 g of HCl or NaOH aqueous solution (pH = 0–12) and then 0.3 g of 0.5 M NH_4F solution was added at 313 K with magnetic stirring. To this mixture, 3.2 g of TMOS (98%, Aldrich) was quickly added with vigorous magnetic stirring. The resulting gel mixture was stirred for 1 day at 313 K and aged under static conditions for 1 day at 373 K in an oven. Another set of samples was prepared using P123 and the same procedures, except that NH_4F was not added to the reaction mixtures. The solid products were filtered off and dried at 373 K and subsequently calcined in air at 823 K.

Using these synthesis conditions, clear and homogeneous solutions form first, after which precipitates start to form as the reactions proceed. The times at which precipitates appear are highly dependent on the pH of the reaction mixtures and the presence of fluoride, as shown in Fig. 1. As noted above, the total aqueous solution (TAS) used for the reaction typically consisted of 62 g of HCl or NaOH solution (pH = 0–12). At pH 2 without fluoride, it takes *ca.* 8 h before precipitation begins to occur. This is because pH 2 is near the isoelectric point of silica and the silica polymerization rate is slow under these conditions.[15] Fluoride promotes precipitation, increasing dramatically the rate of silica condensation, for example, more than an order of magnitude at pH 2, due to its catalytic effect on the hydrolysis.[16]

Fig. 2 shows powder X-ray diffraction (XRD) patterns for mesoporous silica produced using structure-directing P123 block copolymer surfactant species and TMOS, with and without fluoride. The patterns in Fig. 2(a) all show an intense

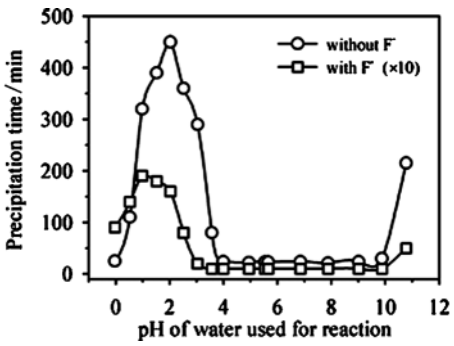

Fig. 1 Silica precipitation time plotted *vs.* pH of the synthesis solutions in the preparation of PEO–PPO–PEO/silica mesophases. The precipitation time is defined to be the cloud point at which the clear reaction mixture forms colloidal silica particles.

† Electronic supplementary information (ESI) available: TEM images and properties for calcined mesoporous silica. See http//www.rsc.org/suppdata/cc/b0/b005608l/

DOI: 10.1039/b005608l

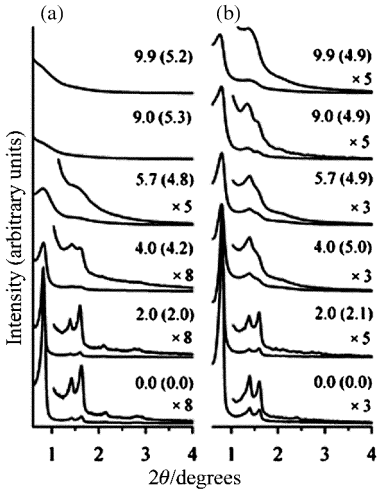

Fig. 2 XRD patterns for calcined mesoporous silica prepared using P123 surfactant species and TMOS: (a) without fluoride and (b) with fluoride. Numbers before parenthesis denote the pH of the precursor HCl or NaOH solution used for the reactions, while the numbers within parenthesis indicate the pH values of the reaction mixture after silica precipitation was complete. The pH of doubly distilled water was 5.7. XRD patterns were collected with a Cu-Kα X-ray source using a Scintag X_2 instrument.

XRD diffraction peak and two or more weaker peaks up to pH 4 (TAS), which are characteristics of a 2-d hexagonally ordered (*P*6*mm*) structure.[1,3,4] This indicates that hexagonal mesoporous silica materials with high mesoscopic ordering are obtained up to pH 4 (TAS) without fluoride. For materials prepared at pH > 4 without F^-, disordered products are obtained. XRD patterns in Fig. 2(b) obtained from the mesoporous silica materials synthesized in the presence of fluoride are very similar to those of the materials obtained without fluoride up to pH 4 (TAS) and indicate the persistence of 2-d hexagonal mesostructural ordering up to pH 9 (TAS). Transmission electron microscopic images for calcined materials confirm that the materials obtained up to pH 9 (TAS) have highly ordered 2-d hexagonal structures.† Lattice parameters, surface areas, pore volumes, and pore sizes are listed in Table 1 (ESI†). It is noteworthy that ordered materials can be obtained from the reaction mixture of P123, doubly distilled water, NH_4F and TMOS without any acid or base catalyst, whereas the absence of fluoride under otherwise identical conditions yields the disordered products [Fig. 2(a)]. A disordered material is obtained at pH 10 (TAS) and there is no precipitation above pH 11 (TAS) with F^-. Morphologies and XRD peak shapes of the hexagonal mesoporous materials are dependent on the reaction pH. Rod-like morphologies, with bundles of silica fibers aligned coaxially with the rods' long axes,[9] are obtained in the SBA-synthesis region below the silica isoelectric point, while above the isoelectric point, where anionic silica species are present, particles with more irregular morphologies are observed.

The results above suggest that suitable oligomeric silica species, formed from fully hydrolyzed monomeric silica species, are needed for interaction with the structure-directing block copolymer to obtain ordered mesostructures. This is due to competition between the condensation of partially hydrolyzed silica species and the hydrolysis of alkoxysilane moieties associated with the silica precursors.[16] Above pH 4 (TAS), silica oligomers may contain the organic moieties from incomplete hydrolysis due to relatively rapid condensation compared to the rate of hydrolysis.[16] The presence of such residual organic moieties leads to weaker interactions between hydrophilic block polymer and silica oligomers, resulting in poorly organized mesocomposites. Indeed, the reaction mixtures above pH 4 without fluoride yield gel-like precipitation and disordered or amorphous silica structures.

On the other hand, addition of fluoride results in the formation of white precipitates and well ordered mesostructures up to pH 9 (TAS). This indicates that hydrolysis of TMOS can be completed before significant condensation of the silica species occurs, which is consistent with the catalytic activity of fluoride for hydrolysis.[16] However, such catalytic activity of fluoride is dependent on the nature of the silica precursors. When TEOS is used as silica source instead of TMOS under the present conditions, ordered mesostructures are obtained up to pH 2.7 with fluoride and disordered mesostructures above pH 2.7[9] because the hydrolysis rate can compete with the rate of condensation. Hydrolysis of TEOS is slower than that of TMOS, because of steric hindrance at ethoxide moieties and reduced solvation of resulting ethanol.[16] The more rapid hydrolysis of TMOS thus makes it a preferable silica precursor to TEOS for producing ordered mesostructures. Nevertheless, such ordered mesostructures can be produced using TEOS or other precursor species, provided the silica sol is pre-hydrolyzed near pH 2[12,19,20] where the hydrolysis rate is fast and the condensation rate is slowest.[15]

In conclusion, highly ordered PEO-PPO-PEO/silica mesostructures can be prepared over a diverse range of pH (0–9) by controlling the relative rates of hydrolysis and condensation of silica species through the use of fluoride and TMOS. Cubic (*Im*3*m*) and 3-d hexagonal ($P6_3/mmc$) block copolymer/silica mesostructures can be synthesized using Pluronic F127 ($EO_{100}PO_{70}EO_{100}$) and Brij 76 [$C_{18}H_{37}(OCH_2CH_2)_{10}OH$] structure-directing surfactant species with TMOS and fluoride near the isoelectric point (pH 2) of silica.

This work was supported by the National Science Foundation under grant DMR 95-20971 and by the Army Research Office under grant DAAH04-96-1-0443. This work made use of MRL Central Facilities supported by the National Science Foundation under Award No. DMR-9123048.

Notes and references

1 C. T. Kresge, M. E. Leonowicz, W. J. Roth, J. C. Vartulli and J. S. Beck, *Nature*, 1992, **359**, 710.
2 Q. Huo, D. I. Margolese, U. Ciesla, P. Feng, T. E. Gier, P. Sieger, R. Leon, P. M. Petroff, F. Schüth and G. D. Stucky, *Nature*, 1994, **368**, 317.
3 G. Attard, J. C. Glyde and C. G. Göltner, *Nature*, 1995, **378**, 366.
4 D. Zhao, J. Feng, Q. Huo, N. Melosh, G. H. Fredrickson, B. F. Chmelka and G. D. Stucky, *Science*, 1998, **279**, 548; D. Zhao, Q. Huo, J. Feng, B. F. Chmelka and G. D. Stucky, *J. Am. Chem. Soc.*, 1998, **120**, 6024.
5 S. A. Bagshaw, E. Prouzet and T. J. Pinnavaia, *Science*, 1995, **269**, 1242.
6 E. Prouzet and T. J. Pinnavaia, *Angew. Chem., Int. Ed. Engl.*, 1997, **36**, 516.
7 C. Boissiere, A. van der Lee, A. El Mansouri, A. Larbot and E. Prouzet, *Chem. Commun.*, 1999, 2047.
8 A. Firouzi, F. Atef, A. G. Oertli, G. D. Stucky and B. F. Chmelka, *J. Am. Chem. Soc.*, 1997, **119**, 3596.
9 P. Schmidt-Winkel, P. Yang, D. I. Margolese, B. F. Chmelka and G. D. Stucky, *Adv. Mater.*, 1999, **11**, 303.
10 D. Zhao, P. Yang, N. Melosh, J. Feng, B. F. Chmelka and G. D. Stucky, *Adv. Mater.*, 1998, **10**, 1380.
11 F. Marlow, M. D. McGehee, D. Zhao, B. F. Chmelka and G. D. Stucky, *Adv. Mater.*, 1999, **11**, 632.
12 P. Feng, X. Bu, G. D. Stucky and D. J. Pine, *J. Am. Chem. Soc.*, 2000, **122**, 994.
13 W. Zhang, B. Glomski, T. R. Pauly and T. J. Pinnavaia, *Chem. Commun.*, 1999, 1803.
14 J. M. Kim and G. D. Stucky, *Chem. Commun.*, 2000, 1159.
15 J. M. Kim, S. K. Kim and R. Ryoo, *Chem. Commun.*, 1998, 259.
16 C. J. Brinker and G. W. Scherer, *Sol–Gel Science*, Academic Press, London, 1990, pp. 97–234.
17 F. H. P. Silva and H. O. Pastore, *Chem. Commun.*, 1996, 833.
18 A. C. Voegtlin, F. Ruch, J. L. Guth, J. Patarin and L. Huve, *Micorporous Mater.*, 1997, **9**, 95.
19 Personal discussion with Prof. Chang-Sik Ha at Pusan National University, Korea.
20 C. Boissière, A. Larbot, A. van der Lee, P. J. Kooyman and E. Prouzet, *Chem. Mater.*, 2000, **12**, 2902.
21 W. W. Lukens, P. Schmidt-Winkel, D. Zhao and G. D. Stucky, *Langmuir*, 1999, **15**, 5403.

The first crystal structure characterization of a semibuckminsterfullerene, and a novel synthetic route

Andrzej Sygula,*[a] Zbigniew Marcinow,[a] Frank R. Fronczek,[b] Ilia Guzei[a] and Peter W. Rabideau*[a]

[a] *Department of Chemistry and Ames Laboratory, Iowa State University, Ames, Iowa 50011, USA. E-mail: asygula@iastate.edu; rabideau@iastate.edu*

[b] *Department of Chemistry, Louisiana State University, Baton Rouge, LA 70103, USA*

Received (in Corvallis, OR) 18th September 2000, Accepted 19th October 2000
First published as an Advance Article on the web 23rd November 2000

Tetrabromosemibuckminsterfullerene 6, obtained by a novel synthetic route, is converted to the tetramethyl derivative 7; X-ray crystal structure determination of the latter reveals a highly nonplanar, bowl-shaped molecule with solvating CCl_4 molecules separating the hydrocarbon moieties.

The considerable attention given to C_{60} and the family of fullerenes has led to renewed interest in curved-surface polynuclear aromatic hydrocarbons known as fullerene fragments or 'buckybowls.'[1] Corannulene (**1**), first synthesized in the 'pre-fullerene' era, is the smallest member of this family.[2] Several other buckybowls are now known,[1] including two semibuckminsterfullerenes $C_{30}H_{12}$ (**2**[3] and **3**[4]) and the largest to date, circumtriindene $C_{36}H_{12}$ (**4**).[5] Most of the buckybowls

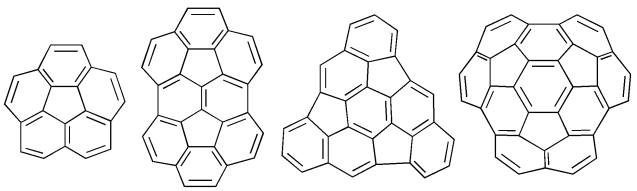

were obtained by flash vacuum pyrolysis (FVP) which involves high temperatures and separation of the precursor molecules in the gas phase; *i.e.* factors believed to be important for the formation of these strained systems.[1] Only recently have more practical, condensed phase alternative synthetic protocols developed.[3b,c,6–8] In this communication we report a novel, convenient route to tetrasubstituted semibuckminsterfullerene **2**, as well as an X-ray crystal structure determination of the tetramethyl derivative. The latter represents the first X-ray crystallographic results for a semibuckminsterfullerene.

Recently we discovered that carbenoid coupling of the dibromomethyl groups of tetrakis(dibromomethyl)fluoranthene leads to the formation of 1,2,5,6-tetrabromocorannulene in high yields.[8] Application of this protocol to dodecabromide **5** is also successful in producing the corresponding tetrabromosemibuckminsterfullerene **6**, although in more modest yield (Scheme 1). Thus, 30 min reflux of **5** in a 3:1 mixture of dioxane and water with sodium hydroxide provides *ca.* 25% yield of **6**.[9] Although the yield of this transformation is similar to that of McMurry coupling,[3b,c] it nonetheless represents a major improvement due to convenience, low cost, and greater reproducibility. The previous method requires long periods of slow addition of the substrate to the reaction mixture (high dilution conditions), as well as strict anhydrous conditions and a deoxygenated environment.[3b,c] None of those requirements are necessary for the present method, since it only involves a short period of reflux in aqueous solvent. Hence this method has much greater potential for the large scale production of **2** and its derivatives.

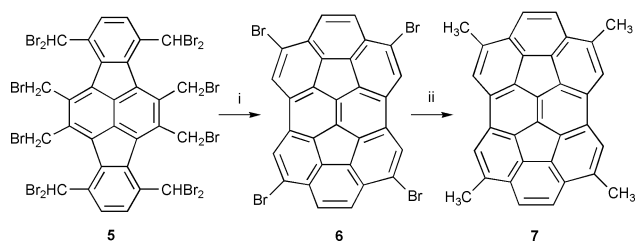

Scheme 1 *Reagents and conditions*: i, NaOH, dioxane–water (3:1), reflux 30 min, 26%; ii, $AlMe_3$, $NiCl_3$(dppp), DME, reflux 12 h, 80%.

Since the carbenoid coupling of **5** leads cleanly to symmetrically substituted **6**, it provides an opportunity for further elaboration of this novel molecule. For example, the four bromine atoms in **6** can easily be replaced by methyl groups leading to **7**.[10] We have been attempting X-ray diffraction studies of semibuckminsterfullerene **2** for some time. Several crystals of **2** were grown from various solvent systems, but they failed to produce useful X-ray diffraction data as a result of poor scattering or multiple twinning. Thus we sought to finally solve this problem with **7** since it produced attractive crystals from a variety of solvents. But again we encountered difficulties—what appeared to be crystals of high quality under the microscope did not produce good diffraction data. Finally we succeeded with a crystal grown by slow evaporation of a carbon tetrachloride solution.[11]

Crystal structure determination shows that **7** crystallizes with two symmetrically independent solvating carbon tetrachloride molecules (Fig. 1). The ideal molecular point symmetry of **7**(C_{2v}) is reduced in the crystal to C_s. The crystallographic mirror plane passes through the carbon atoms and four chlorine atoms of the solvating CCl_4 molecules and bisects the three central carbon–carbon bonds of **7**. The hydrocarbon part exhibits very significant curvature, forming a well developed bowl as predicted for **2** earlier by theory.[3a] The pyramidalization angles defined by the π-orbital axis vector method (POAV)[12] are highest at the central carbon atoms, then

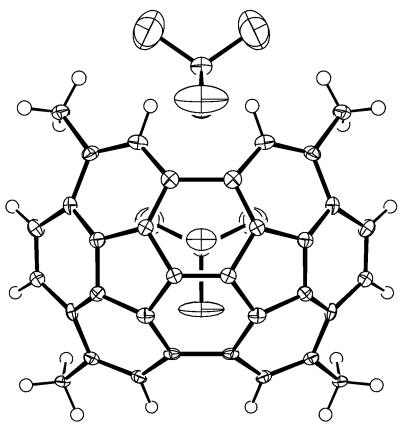

Fig. 1 ORTEP plot of **7***2CCl_4 with 30% thermal elipsoids.

DOI: 10.1039/b007771m

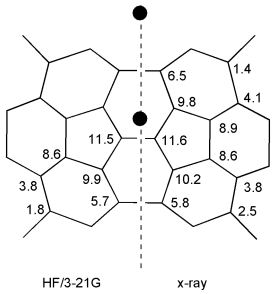

Fig. 2 POAV pyramidalization angles calculated for the crystal structure (right) and for the *ab initio* HF/3-21G optimized geometry (left) of **7**. The dotted line describes the crystallographic mirror plane and the dots represent the solvating CCl_4 molecules.

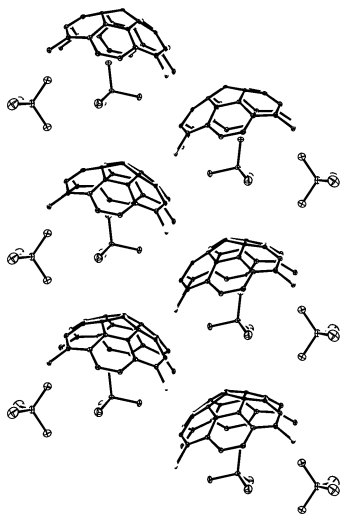

Fig. 3 Crystal packing pattern in **7***2CCl_4. Hydrogen atoms omitted for clarity.

gradually decrease when going toward the rim (Fig. 2). In the region of maximum curvature the pyramidalization of the carbon atoms is quite comparable with that of buckminsterfullerene which has a pyramidalization angle of 11.6°.[12] Comparison of the POAV angles calculated for **7** in the crystal with those based on the *ab initio* optimized geometry of the isolated molecule[13] not only demonstrates the adequacy of the theoretical model, but also suggests that crystal packing forces have very little effect on the curvature of this strained molecule.

Buckybowls have the potential to stack in a concave to convex fashion. Of the very few X-ray crystal structure determinations reported to date, stacking was found in cyclopentacorannulene $C_{22}H_{10}$[14] as well as in $C_{36}H_{10}$,[15] while it is absent in the crystals of corannulene.[16] The present case represents a novel situation, since **7** co-crystallizes with carbon tetrachloride molecules (Fig. 3). One of the solvating CCl_4 molecules separates two molecules of **7** with one of the chlorine atoms in the concave orientation and three chlorine atoms on the convex side. The 'concave' chlorine atom forms twelve nonbonding C···Cl distances in the range of 3.262(7) to 3.501(7) Å, roughly equal or shorter than the sum of the respective van der Waals radii, and in addition, it has six slightly longer C···Cl distances in the range 3.582(7) to 3.747(7) Å. As a consequence of the 'stuffing' of **7** with the solvent molecule, close contacts between the hydrocarbon moieties are minimized. The closest of these, 3.528(9) Å, is between the methyl group carbons, and the nearest intermolecular distance between bowl carbon atoms is 3.654(10) Å. Thus, this solid state arrangement is not, strictly speaking, 'bowl-to-bowl stacking' even though some piling of the solvated molecules is evident.[17]

In conclusion, tetrabromo- and tetramethylsemibuckmisterfullerenes **6** and **7** can be prepared by a convenient, non-pyrolytic route that allows for scale-up. Moreover, the crystal structure of **7** shows that the curvature of this system, at least in the interior region of maximum curvature, is comparable to buckminsterfullerene.

This work was supported by the Ames Laboratory which is operated for the US Department of Energy by Iowa State University under Contract No. W-7405-Eng-82.

Notes and references

1 L. T. Scott, H. E. Bronstein, D. V. Preda, R. B. M. Anselms, M. S. Bratcher and S. Hagen, *Pure Appl. Chem.*, 1999, **71**, 209; G. Mehta and H. S. P. Rao, *Tetrahedron*, 1998, **54**, 13 325; L. T. Scott, *Pure Appl. Chem.*, 1996, **68**, 291; P. W. Rabideau and A. Sygula, *Acc. Chem. Res.*, 1996, **29**, 235.

2 W. E. Barth and R. G. Lawton, *J. Am. Chem. Soc.*, 1966, **88**, 380; W. E. Barth and R. G. Lawton, *J. Am. Chem. Soc.*, 1971, **93**, 1730.

3 (*a*) P. W. Rabideau, A. H. Abdourazak, H. E. Folsom, Z. Marcinow, A. Sygula and R. Sygula, *J. Am. Chem. Soc.*, 1994, **116**, 7891; (*b*) A. Sygula and P. W. Rabideau, *J. Am. Chem. Soc.*, 1998, **120**, 12 666; (*c*) A. Sygula and P. W. Rabideau, *J. Am. Chem. Soc.*, 1999, **121**, 7800.

4 A. H. Abdourazak, Z. Marcinow, A. Sygula, R. Sygula and P. W. Rabideau, *J. Am. Chem. Soc.*, 1995, **117**, 6410.

5 L. T. Scott, M. S. Bratcher and S. Hagen, *J. Am. Chem. Soc.*, 1996, **118**, 8743; R. B. M. Anselms and L. T. Scott, *J. Am. Chem. Soc.*, 2000, **122**, 2719.

6 T. J. Seiders, K. K. Baldridge and J. S. Siegel, *J. Am. Chem. Soc.*, 1996, **118**, 2754; T. J. Seiders, K. K. Baldridge, E. L. Elliott, G. H. Grube and J. S. Siegel, *J. Am. Chem. Soc.*, 1999, **121**, 7439; T. J. Seiders, E. L. Elliott, G. H. Grube and J. S. Siegel, *J. Am. Chem. Soc.*, 1999, **121**, 7804.

7 H. A. Reish, M. S. Bratcher and L. T. Scott, *Org. Lett.*, 2000, **2**, 1427.

8 A. Sygula and P. W. Rabideau, *J. Am. Chem. Soc.*, 2000, **122**, 6323.

9 **6**: Orange crystals (from toluene). Darkens gradually above 300 °C, but does not melt up to 350 °C. ^{1}H NMR (300 MHz, $CDCl_3$) δ 8.06 (s, 4H), 7.69 (s, 4H). ^{13}C NMR (75.44 MHz, $CDCl_3$) δ 128.94, 127.97. Quaternary carbons not detected due to the very limited solubility of **6** in common deuterated solvents. HRMS: calcd for $C_{30}H_8Br_4$ 683.7359; found 683.7350.

10 **7**: Yellow solid (sublimation). Gradually darkens above 350 °C. ^{1}H NMR (300 MHz, $CDCl_3$) δ 7.63 (4H, broad d, J = 0.9 Hz), 7.55 (4H, s), 2.64 (12H, d, J = 0.9 Hz). ^{13}C NMR (75.44 MHz, $CDCl_3$) δ 141.12, 137.05, 136.71, 136.36, 128.14, 124.67, 124.61, 124.57. HRMS: calcd for $C_{34}H_{20}$ 428.1575; found 428.1573.

11 *Crystal data*: $C_{36}H_{20}Cl_8$, FW = 736.12; orthorhombic, *Cmc2*$_1$; a = 16.2594(8), b = 20.0097(10), c = 9.2417(5) Å; V = 3006.7(3) Å^3; Z = 4; D_{calc} = 1.626 g cm^{-3}; F(000) = 1488; T = 173 K; R = 0.0761, Rw = 0.218 for 1841 observed data. Intensity data were collected on a Bruker CCD-1000 diffractometer equipped with Mo-Kα radiation (λ = 0.71073 Å). Hydrogen atoms were placed in calculated positions. CCDC 182/1834. See http://www.rsc.org/suppdata/cc/b0/b007771m/ for crystallographic data in .cif format.

12 R. C. Haddon and L. T. Scott, *Pure. Appl. Chem.*, 1986, **58**, 137; R. C. Haddon, *Acc. Chem. Res.*, 1988, **21**, 243; R. C. Haddon, *Science*, 1993, **261**, 1545.

13 Gaussian 94, Revision E.2, M. J. Frisch, G. W. Trucks, H. B. Schlegel, P. M. W. Gill, B. G. Johnson, M. A. Robb, J. R. Cheeseman, T. Keith, G. A. Petersson, J. A. Montgomery, K. Raghavachari,, M. A. Al-Laham, V. G. Zakrzewski, J. V. Ortiz, J. B. Foresman, J. Cioslowski, B. B. Stefanov, A. Nanayakkara, M. Challacombe, C. Y. Peng, P. Y. Ayala, W. Chen, M. W. Wong, J. L. Andres, E. S. Replogle, R. Gomperts, R. L. Martin, D. J. Fox, J. S. Binkley, D. J. Defrees, J. Baker, J. P. Stewart, M. Head-Gordon, C. Gonzalez, and J. A. Pople, Gaussian, Inc., Pittsburgh PA, 1995. POAV pyramidalization angles calculated for the Becke3/LYP//3-21G optimized geometry of **7** are very similar to the HF geometry with the largest difference being only 0.4 deg.

14 A. Sygula, H. E. Folsom, R. Sygula, A. H. Abdourazak, Z. Marcinow, F. R. Fronczek and P. W. Rabideau, *J. Chem. Soc., Chem. Commun.*, 1994, 2571.

15 D. M. Forkey, S. Attar, B. C. Noll, R. Koerner, M. M. Olmstead and A. L. Balch, *J. Am. Chem. Soc.*, 1997, **119**, 5766.

16 J. C. Hanson and C. E. Nordman, *Acta Cryst.*, 1976, **B32**, 1147.

17 This situation resembles to some extent the solid state arrangements of an interesting class of cup-shaped tribenzoquinacenes, in which either a hydrogen atom or an alkyl group at the vertex of the three fused five-membered rings prevents close packing of the aromatic rings: see D. Kuck, T. Lindenthal and A. Schuster, *Chem. Ber.*, 1992, **125**, 1449 and references therein.

Aluminium-containing mesoporous silica films as nano-vessels for organic photochemical reactions

Makoto Ogawa,*[ab] Kazuyuki Kuroda[cd] and Jun-ichi Mori[c]

[a] *Department of Earth Sciences, Waseda University, Nishiwaseda 1-6-1, Shinjuku-ku, Tokyo 169-8050, Japan. E-mail: makoto@mn.waseda.ac.jp*
[b] *PRESTO, Japan Science and Technology Corporation, Japan*
[c] *Department of Applied Chemistry, Waseda University, Ohkubo 3-4-1, Shinjuku-ku, Tokyo 169-8555, Japan*
[d] *Kagami Memorial Laboratory for Materials Science and Technology, Waseda University, Nishiwaseda 2-8-26, Shinjuku-ku, Tokyo 169-0051, Japan*

Received (in Cambridge, UK) 25th September 2000, Accepted 31st October 2000
First published as an Advance Article on the web 24th November 2000

The adsorption of a cationic azobenzene derivative into both siliceous and aluminium containing mesoporous silica films has been investigated; photoisomerization was found to occur in the temperature range 80–300 K and the mesoporous aluminium containing silica films were proved to be useful reaction media to immobilize organic photochromic species.

Mesoporous materials prepared by supramolecular templating approaches can accommodate guest species in their pores to form host–guest complexes and the resulting nanocomposites may exhibit useful functions in the areas of catalysis, adsorption and sensing.[1] Here we report the synthesis of the aluminium containing mesoporous silica films for the first time and applied these as nano-reactors for organic photochemical reactions. Photochemistry in constrained media is a growing new field which yields a wide variety of useful applications including sensitive optical media, reaction pathways for controlled photochemical reactions, and molecular devices for optics.[3] For such applications, mesoporous silica films possess attractive features such as large surface areas and porosity, controllable pore sizes, reactive pore surfaces, and stability over a wide temperature range.

In the present study, the introduction of a cationic azobenzene into the mesoporous silica films was conducted using *p*-(ω-dimethylhydroxyethylammonioethoxy)azobenzene bromide (AZ) as the guest species. Photochemical reactions of azobenzenes are sensitive to the microenvironment and so can be employed as photoreactive probes to estimate microenvironments (free volume and rigidity), to which conventional characterization techniques do not have an access.[4] Moreover, geometrical changes of azobenzenes have been utilized as a trigger to design photoresponsive supramolecular systems.[5,6] Accordingly, the photochemistry of azobenzenes in mesopores is worth investigating from the viewpoints of probing mesopores as well as constructing photofunctional materials.

Aluminium-containing mesoporous silica films were synthesized by the rapid solvent evaporation method which we have developed.[7] This method is promising for the preparation of silica-surfactant mesostructured materials in a controlled morphology,[8,9] since the reaction is very simple and the resulting films are highly transparent and homogeneous. Aluminium tris(*sec*-butoxide) (ATSB) was used as the aluminium source and co-solidification with silica was conducted by the reported synthesis method for aluminosilica xerogels[10] with slight modification. A typical synthetic procedure for the transparent thin films of aluminium-containing silica-surfactant mesostructured materials is as follows: silicon tetraethoxide (TEOS), ethanol, water and HCl (molar ratio of 1:4:1.2:0.006) were mixed at 60 °C for 10 min with magnetic stirring. ASTB was then added and the mixture allowed to react for a further 10 min at 60 °C. Then, an aqueous solution of octadecyltrimethylammonium chloride was added and the mixture allowed to react for a further 2 h at room temperature. The resulting solution was spin coated on a substrate and calcined in air at 300 °C for 18 h to prepare mesoporous silica films; ASTB/TEOS ratios were set at 0.05, 0.031, 0.025, 0.022 and 0.014.

SEM images of the film surfaces (data not shown) indicate that the films are continuous and crack free when the ASTB/TEOS ratios were 0.031, 0.025, 0.022 and 0.014. When the ASTB/TEOS ratio was increased to 0.05, a homogeneous solution cannot be obtained under the experimental conditions and the resulting film is slightly turbid. The X-ray diffraction patterns of the calcined films with different Al contents are shown in Fig. 1(a)–(c). Although the diffraction peaks broadened with an increase in the loaded Al amount, a single diffraction peak indicative of the surfactant templated mesostructures was observed for all the samples. Nitrogen adsorption isotherms of the calcined films on a glass substrate are of type IV indicating that the films are mesoporous. The average pore sizes as derived from the isotherms by the Horvath–Kawazoe method[11] were 3.2, 2.9 and 2.8 nm for the films with Al/Si = 0, 0.014 and 0.031, respectively.

For the introduction of AZ, the mesoporous silica films were immersed in an ethanol solution of AZ. The amount of AZ adsorbed onto the Al free film was very low even for extended reaction times or if a concentrated AZ solution was used. On the other hand, AZ was adsorbed effectively into the Al containing mesoporous silica films. It is thought that the partial substitution of Si by Al leads to successful introduction of AZ into the mesopores through electrostatic interactions between the dye and the negative charge at the substituted Al site. The UV–VIS absorption spectrum (Fig. 2) of the film (Al/Si = 0.0031) after the reaction with AZ showed an absorption band centered at 338

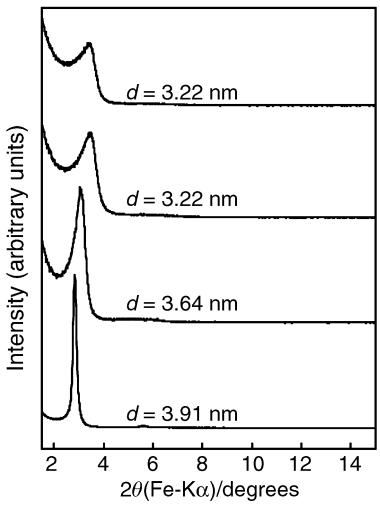

Fig. 1 X-Ray diffraction patterns of mesoporous silica films with Al/Si = 0 (a), 0.0014 (b) and 0.0031 (c); trace (d) is (c) after adsorption of AZ.

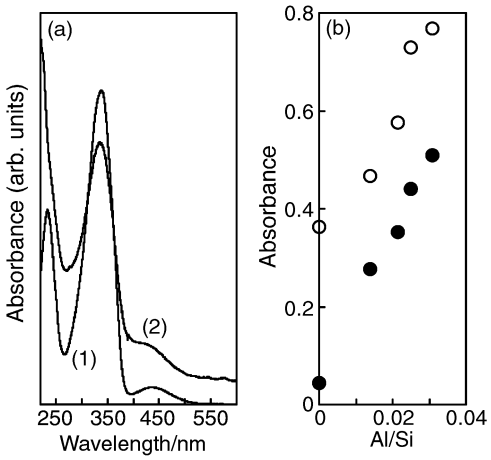

Fig. 2 (a) Absorption spectra of (1) 0.03 mmol L^{-1} AZ ethanol solution and (2) the AZ adsorbed mesoporous silica film (Al/Si = 0.0031). (b) The variation of the absorbance due to *trans*-AZ at 340 nm as a function of the Al/Si ratio. Open and filled circles represent samples before and after washing with ethanol.

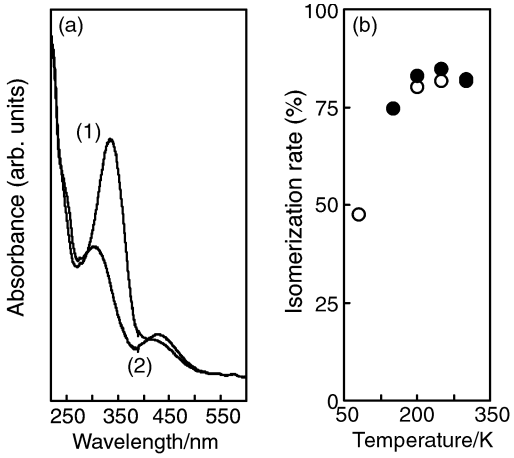

Fig. 3 (a) The change in the absorption spectrum of the AZ adsorbed mesoporous silica film (Al/Si = 0.0031) before (1) and after (2) UV irradiation. (b) The temperature dependence of the fraction of the photochemically formed *cis*-isomer at the photostationary states for the AZ adsorbed mesoporous silica film (Al/Si = 0.0031). Open and filled circles represent the values obtained on cooling and heating, respectively.

nm, which is ascribable to the π–π* transition of *trans*-AZ. With an increase in the Al content, the absorbance due to *trans*-AZ increased as shown in the inset of Fig. 2. The absorbance of the films after washing with ethanol is also shown in Fig. 2(b). The absorbance due to *trans*-AZ was decreased by washing, indicating that weakly bound AZ was removed from the films. As seen in Fig. 2(b), the decrease in the absorbance is almost same irrespective of the amount of loaded Al, suggesting that there are two different adsorption sites for AZ; strongly acidic sites at the substituted Al and weakly acidic sites probably at the silanol groups. Intermolecular interactions between adsorbed AZ may also be a factor leading to differences in behavior of the adsorbed species.

The absorption maximum observed for the film (Al/Si = 0.0031) essentially matched that of a dilute (3×10^{-5} M) ethanol solution of the dye. Considering the fact that the absorption spectra of aggregated AZ molecules such as found in crystals or AZ adsorbed on a layered silicate[12] are quite different from that of the present system, it is clear that the AZ cations are adsorbed and dispersed as monomers on the surface of the mesoporous silica irrespective of the amount of loading. Assuming that the molar absorption coefficient of AZ adsorbed in the mesoporous silica is the same as that of AZ in a dilute ethanol solution and that the film thickness is 0.5 μm, the concentrations of the AZ in the films are determined to be 0.42, 0.37, 0.29 and 0.23 mol L^{-1} for the films with Al/Si ratios of 0.031, 0.025, 0.022 and 0.014, respectively. Such high concentrations of AZ cannot be achieved in any solvents due to solubility limitations. The AZ cations are thought to be distributed in the one-dimensional channels with a mean separation between adjacent AZ molecules of 1.7 nm at the maximum loading level (Al/Si = 0.031).

When the as-coated films were calcined at higher temperature (*i.e.* 450 °C), the capacity for the adsorption of AZ was dramatically decreased. This observation can be rationalized by the condensation of hydroxy groups on the mesopore surfaces as well as diffusion of the loaded Al into the silica walls from the pore surface. Since the films are thin (0.5 μm), oxidative decomposition of the template is facile when compared with surfactant occluded in the bulk samples. Thus, the mesoporous silica films with cation exchangeable sites on the pore surfaces are readily available by surfactant removal at relatively low temperature (300 °C).

The adsorbed AZ in the mesopores exhibits photochemical isomerization upon UV and visible light irradiation.[13] The reactions were monitored by the change in the absorbance of the *trans*-isomer of the AZ at 340 nm and a typical change in the absorption spectrum is shown in Fig. 3(a). The ratio of the *cis*-isomer formed by the UV irradiation at the photostationary state at room temperature was roughly estimated to be no less than *ca.* 90% from the absorbance change. It is known that the photoisomerization is affected by the free volume and the rigidity of the surroundings.[14–16] The van der Waals volume of azobenzene is 144 $Å^3$ and photoisomerization requires an extra 127 $Å^3$.[15] The pore size of the mesoporous silica films used in the present study is large enough for AZ to isomerize. The photochemical isomerization was measured in the temperature range 80–400 K and the temperature dependence of the yield of the photochemical reactions is shown in Fig. 3(b). Photochemical isomerization occurs even at 80 K, showing that the mesoporous silica films can be utilized as a nano-reaction vessel in a wide temperature range for organic photochemical reactions.

Notes and references

1 K. Moller and T. Bein, *Chem. Mater.*, 1998, **10**, 2950.
2 M. Ogawa, *J. Am. Chem. Soc.*, 1994, **116**, 7941.
3 *Photochemistry in Organized & Constrained Media*, ed. V. Ramamurthy, VCH Publishers, Inc., New York, 1991.
4 *Photochromism-Molecules and Systems*, ed. H. Dürr and H. Bouas-Laurent, Elsevier, Amsterdam, 1990.
5 I. Willner, *Acc. Chem. Res.*, 1997, **30**, 347.
6 J. Anzai and T. Osa, *Tetrahedron*, 1994, **50**, 4039.
7 M. Ogawa, *Chem. Commun.*, 1996, 1149.
8 M. Ogawa and T. Kikuchi, *Adv. Mater.*, 1998, **10**, 1077.
9 P. J. Bruinshman, J. A. Kim, Y. Liu and S. Baskaran, *Chem. Mater.*, 1997, **9**, 2507.
10 G. A. Pozamsky and A.V. McCormick, *J. Non-Cryst. Solids*, 1995, **190**, 212.
11 G. Horváth and K. J. Kawazoe, *J. Chem. Eng. Jpn.*, 1983, **16**, 470.
12 Spectral shifts due to aggregation of AZ were observed when the dye was adsorbed into the interlayer space of a layered silicate, montmorillonite, by cation exchange (manuscript in preparation).
13 The photochemical reactions were carried out using a 500 W super high pressure Hg lamp (USHIO USH-500D). A band pass filter, (Toshiba UV-D35) with transmittance centered at 350 nm, was used to cut-off high energy UV light. For the *cis*-to-*trans* reverse reactions, a sharp cut-off filter [HOYA L42 (cut-off wavelength = 420 nm] was used to remove UV light.
14 M. Ueda, H.-B. Kim and K. Ichimura, *Chem. Mater.*, 1994, **6**, 1771.
15 J. G. Victor and J. M. Torkelson, *Macromolecules*, 1987, **20**, 2241.
16 I. Mita, K. Horie and K. Hirao, *Macromolecules*, 1989, **22**, 558.

A host–guest epoxidation catalyst with enhanced activity and stability

Johannes A. A. W. Elemans, Edward J. A. Bijsterveld, Alan E. Rowan* and Roeland J. M. Nolte

Department of Organic Chemistry, NSR Center, University of Nijmegen, Toernooiveld, 6525 ED, Nijmegen, The Netherlands. E-mail: rowan@sci.kun.nl

Received (in Cambridge, UK) 23rd October 2000, Accepted 31st October 2000
First published as an Advance Article on the web 24th November 2000

A porphyrin-capped molecular clip epoxidises olefins, depending on the axial ligand used, with enhanced activity or stability

The mono-oxygenase cytochrome P450 selectively binds substrates in the direct proximity of an Fe(III) protoporphyrin IX, which catalyses the activation of molecular oxygen and the subsequent incorporation of one of the oxygen atoms into the bound substrate and reduction of the other one to water.[1] Much research has been devoted to the elucidation of the complex working mechanisms of the enzyme, and several simplified synthetic models have been constructed which make use of molecular oxygen or a single oxygen donor (*e.g.* sodium hypochlorite) as the oxidant. Many of these model systems utilize Mn(III) porphyrins functionalised with straps or caps to establish an environment in which the oxygen transfer from the metal to the substrate is under steric control.[2] Regio- and stereoselective oxidation has been achieved,[3] in which for example *cis*-stilbene has been oxidised with a major preference for the production of the *cis*-epoxide.[4] Other approaches involve the coupling of a metalloporphyrin to known cavity molecules, such as cyclodextrins[5] and cyclophanes,[6] which can bind substrates and oxidise them with enhanced rates or selectivities. Here we describe initial catalytic studies using the new cavity-containing manganese porphyrin **Mn1** as a catalyst. The molecule consists of a molecular clip[7] equipped with a porphyrin roof situated symmetrically above the receptor, thus creating a rigid and relatively closed cavity with a diameter of approximately 9 Å.[8] Whilst the free base host **$H_2$1** has been applied in the construction of rotaxanes, it was also our intention to utilize its Mn(III) derivative as an olefin epoxidation catalyst. In this paper, the catalytic properties of **Mn1** in the

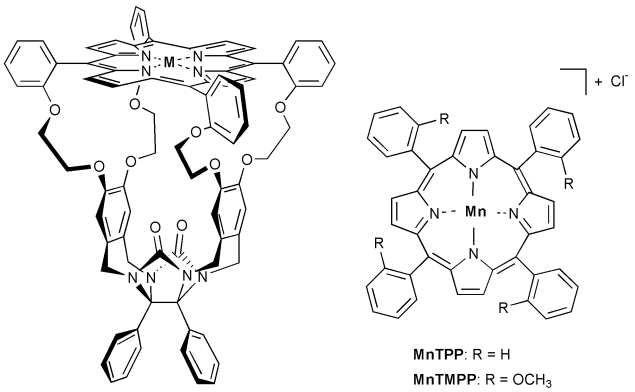

epoxidation of α-pinene and *cis*- and *trans*-stilbene, applying the biphasic dichloromethane–aqueous NaOCl system previously used by us[9] and by other groups,[10] are compared to those of the reference porphyrins **MnTPP** and **MnTMPP**. Particular emphasis is directed toward the relative activity and stability of these catalysts. It will be shown that by a strong host–guest binding of the axial ligand in the cavity of **Mn1** the rate of epoxidation is enhanced, while by shielding the outside of the cavity of **Mn1** the catalyst's stability is increased. Although the Fe(III) porphyrin in cytochrome P450 features axial coordination by a cysteine thiolate, most of its synthetic mimics utilize more stable pyridine, imidazole or phenolate derivatives to enhance the activity and stereoselectivity of the catalytic center. In previous studies in which **MnTPP** was used as the catalyst, it was found that the strength of axial ligand binding was related to the enhancement of the activity of the catalyst, since the electron donating properties of the ligand facilitate the formation of the proposed Mn(V)–oxo species.[9] For optimal results 500 equivalents of pyridine (Py) were, however, required in the reaction, because of its relatively weak binding to the porphyrin metal ($K_a \approx 1000\ M^{-1}$). Since NMR studies had revealed that in host **Zn1** Py is bound within the cavity with a very high association constant ($K_a = 1.1 \times 10^5\ M^{-1}$) due to stabilising cavity effects,[8] it was calculated that under the applied epoxidation reaction conditions† **Mn1** would require only *one* equiv. of Py to achieve a >99% binding to the porphyrin metal (Fig. 1, approach A). Indeed, the effect of this supramolecular activation of **Mn1** by Py, compared to **MnTPP** under the same reaction conditions (*one* equiv. of Py), resulted in a 5–10 fold initial rate enhancement in the epoxidation of olefins (Table 1, Fig. 2). As a result of this, it requires more than 10 h for the reaction to be completed in the case when **MnTPP** is used as the catalyst, while when using **Mn1** it is complete within 2 h. The rate enhancement exhibited by the **Mn1**–Py system is not caused by electronic or steric effects of the alkoxy groups, as control experiments using **MnTMPP** showed that this catalyst exhibited even lower epoxidation rates than **MnTPP** (Table 1). The rate enhancing effect is further illustrated when one equiv. of the even stronger binding axial ligand imidazole (K_a with **Zn1** $= 3.2 \times 10^5\ M^{-1}$) is used as the axial ligand in **Mn1**: α-pinene is epoxidised by **Mn1** within approximately 1 h with an initial rate $k_0 = 17 \times 10^5$/mol dm^{-3} s^{-1}. In addition to rate enhancement, Py-activated epoxidation of *cis*-stilbene by **Mn1** preferentially produced *cis*-stilbene oxide over the *trans*-isomer (Table 1), which is a commonly observed phenomenon for Py–Mn(III) porphyrin catalyst systems.[9,10]

A drawback of the **MnTPP** and **MnTMPP** catalysts is their instability. During the course of the epoxidation reaction the brown organic layer gradually decolourises, especially when the

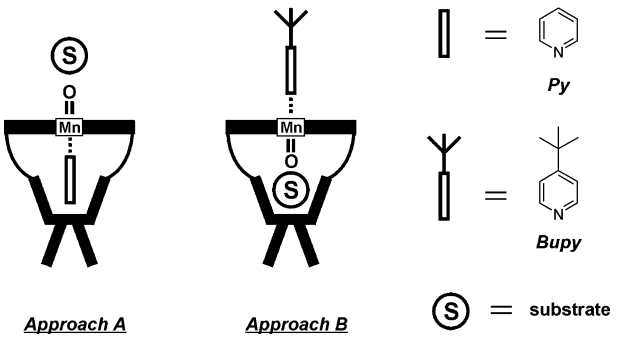

Fig. 1 Two approaches in which **Mn1** is used as an epoxidation catalyst in combination with Py or Bupy as the axial ligand.

DOI: 10.1039/b008567g

Table 1 Epoxidation of olefins by **Mn1** and the reference catalysts **MnTPP** and **MnTMPP**

		Mn1[a]			**MnTPP**[a]			**MnTMPP**[a]		
Substrate	Axial ligand	Yield[b]	Rate[c]	*c*:*t*[d]	Yield[b]	Rate[c]	*c*:*t*[d]	Yield[b]	Rate[c]	*c*:*t*[d]
α-pinene	Py[e]	81	12.0	—	10	1.2	—	—[f]	—[f]	—[f]
cis-stilbene	Py[e]	57	19.9[g]	96:4	39	3.7[g]	65:35	33	2.9	63:37
trans-stilbene	Py[e]	72	18.9	[h]	9	3.8	[h]	8	< 1.0	[h]
α-pinene	Bupy[i]	82	10.9	—	80	12.9	—	—[f]	—[f]	—[f]
cis-stilbene	Bupy[i]	57	15.5[g]	90:10	70	57.0[g]	90:10	52	39.3	92:8
trans-stilbene	Bupy[i]	72	24.1	[h]	63	21.2	[h]	65	20.0	[h]

[a] Standard reaction conditions.† [b] Yield (%) after 3 h. [c] Initial rate × 10^5 mol dm^{-3} s^{-1}. [d] Ratio *cis*–*trans* epoxide product after 3 h. [e] 1 equiv. per Mn(III)-catalyst. [f] Not determined. [g] Rate of formation of the *cis*-epoxide. [h] No *cis*-epoxide was detected. [i] 500 equiv. per Mn-catalyst.

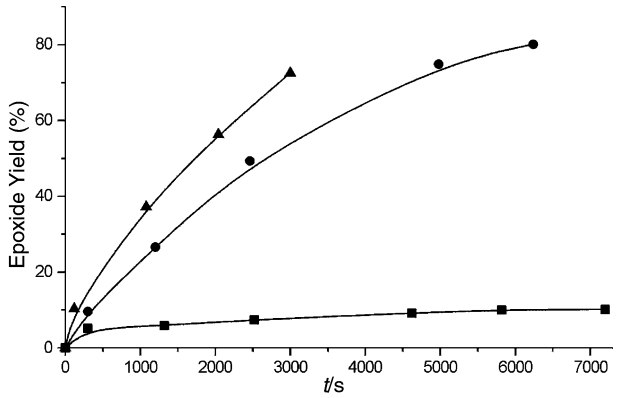

Fig. 2 Epoxidation of α-pinene using 1 equivalent of an axial ligand. **MnTPP**–Py (■), **Mn1**–Py (●), **Mn1**–Im (▲).

amount of unreacted olefin decreases. This phenomenon has been attributed to the formation of μ-oxo-bridged Mn(IV) porphyrin dimeric structures, which are unreactive in further catalysis and rapidly decompose.[9] This rapid decomposition was also found to occur in the case of the **Mn1**–Py system used in approach A. To prevent this, the bulky axial ligand 4-*tert*-butylpyridine (Bupy) was used to coordinate to **Mn1** on the outside of the cavity (Fig. 1, approach B). It was expected that coordination of this ligand, which does not fit within the cavity,‡ would efficiently prevent μ-oxo dimer formation since the other face of the porphyrin is protected by the receptor cavity. When the epoxidation reactions using **Mn1** were carried out in the presence of 500 equiv. of Bupy, catalyst destruction was indeed prevented, as was concluded from the fact that the organic layer retained its brown colour, and, more importantly, that newly added amounts of substrate were epoxidised. The epoxidation experiment was repeated sequentially several times. The observed initial rate was found in all cases to be almost identical, indicating that no decomposition of the catalyst occurred. This gave turnover numbers of > 1000 per catalyst.§ When **MnTPP** or **MnTMPP** were used as the catalyst in combination with Bupy, this stabilization did not occur and the catalysts decomposed.

Assuming complete shielding of the outside of **Mn1** by Bupy implies that the oxygen transfer to the substrate has to occur within the cavity. From molecular modelling studies it became clear that the substrates cannot react *via* the side of the cavity, *i.e.* they need to enter the cavity completely to reach the manganese–oxo species. The epoxidation results of *cis*- and *trans*-stilbene using the **Mn1**–Bupy system are summarised in Table 1 and compared to those when **MnTPP** or **MnTMPP** are used as the catalyst. Whilst for the epoxidation of *trans*-stilbene not much difference is observed between the catalysts with regard to initial rate and epoxide yield, the epoxidation rate of *cis*-stilbene clearly decreases going from **MnTPP** to **MnTMPP** to **Mn1**. This decrease in rate coincides with a simultaneous increase in steric hindrance by the substituents of the *meso*-phenyl rings. Apparently, these groups have more steric influence on a *cis*-stilbene substrate than on a *trans*-stilbene substrate. Remarkably, the rate of epoxidation of *cis*-stilbene catalysed by the **Mn1**–Bupy system (epoxidation within the cavity) is similar to that catalysed by the **Mn1**–Py system (epoxidation outside the cavity) (Table 1). This implies that additional factors play a role in the epoxidation reaction. Further studies are currently under investigation.

In summary, we have shown that by means of a unique supramolecular activation of **Mn1** only one equiv. of the axial ligands pyridine or imidazole are required to activate the catalyst for the epoxidation of olefins. Coordination of a bulky axial ligand on the outside of the cavity of **Mn1** strongly enhances the stability of the catalyst, which in this approach is protected from further oxidative decomposition. Current research is focused on the functionalisation of Mn(III) porphyrins with molecular clip receptors on both faces, so that both approaches of supramolecular activation and catalyst protection are combined.

Notes and references

† *Reaction conditions*: to a CH_2Cl_2 solution (0.65 ml) of the substrate (0.626 M), the manganese catalyst (2.5 mM), the phase transfer catalyst tetrabutylammonium chloride (5 mM), the axial ligand pyridine (2.5 mM) or 4-*tert*-butyl pyridine (1.25 M), and an internal standard (1,3,5-tri-*tert*-butylbenzene (0.17 M) in a Schlenk tube was added an aqueous NaOCl solution (2 ml, 0.6 M). The mixture was stirred at a constant rate under nitrogen for 3 h, and during the course of the reaction samples were taken from the organic layer which were analysed by GLC and ^{1}H NMR.

‡ This was concluded from ^{1}H NMR experiments on mixtures of **Zn1** and Bupy in $CDCl_3$, which indicated no binding within the cavity of the host even when 500 equiv. of the axial ligand were added.

§ More than 4 portions of substrate could be oxidised without any decomposition of the catalyst. Due to phase separation between the solvent and the epoxidation products it then became more difficult to measure a reliable rate of conversion when the number of portions were increased beyond 4.

1 J. T. Groves and Y. Z. Han, *Cytochrome P450: Structure, Mechanism and Biochemistry*, ed. P. R. Oritz de Montellano, Plenum Press, New York, 1995, 2nd edn., pp. 3–48.
2 For reviews see: B. Meunier, *Chem Rev.*, 1992, **92**, 1411; J. P. Collman and L. Fu, *Acc. Chem. Res.*, 1999, **32**, 455.
3 For a review see: J. P. Collman, X. Zhang, V. J. Lee, E. S. Uffelman and J. I. Brauman, *Science*, 1993, **261**, 1404.
4 B. Meunier, M. E. de Carvalho, O. Bortolini and M. Momenteau, *Inorg. Chem.*, 1988, **27**, 161.
5 R. Breslow, Y. Huang and X. Zhang, *J. Am. Chem. Soc.*, 1997, **119**, 4535.
6 D. R. Benson, R. Valentekovich, S.-W. Tam and F. Diederich, *Helv. Chim. Acta*, 1993, **76**, 2034.
7 For a review see: A. E. Rowan, J. A. A. W. Elemans and R. J. M. Nolte, *Acc. Chem. Res.*, 1999, **32**, 995.
8 A. E. Rowan, P. P. M. Aarts and K. W. M. Koutstaal, *Chem. Commun.*, 1998, 611; J. A. A. W. Elemans, M. B. Claase, P. P. M. Aarts, A. E. Rowan, A. P. H. J. Schenning and R. J. M. Nolte, *J. Org. Chem.*, 1999, **64**, 7009.
9 A. W. van der Made, R. J. M. Nolte and W. Drenth, *Recl. Trav. Chim. Pays-Bas.*, 1990, **109**, 537.
10 B. Meunier, E. Guilmet, M.-E. de Carvalho and R. Poilblanc, *J. Am. Chem. Soc.*, 1984, **106**, 6668.

ChemComm

Template synthesis of polymer-insulated colloidal gold nanowires with reactive ends†

Jong-Sung Yu,*[a] Jeong Yeon Kim,[a] Seungho Lee,[a] Jeremiah K. N. Mbindyo,[b] Benjamin R. Martin[b] and Thomas E. Mallouk*[b]

[a] *Department of Chemistry, Hannam University, Taejon, 306-791, Korea*
[b] *Department of Chemistry, Pennsylvania State University, 16802, USA. E-mail: jsyu@mail.hannam.ac.kr*

Received (in Cambridge, UK) 3rd October 2000, Accepted 30th October 2000
First published as an Advance Article on the web 27th November 2000

Alternate adsorption of anionic and cationic polyelectrolytes creates smooth organic films on the walls of template-grown Au nanowires, which can be made chemically reactive on their ends by removal of a sacrificial Ag layer.

Much of the current research on nanophase materials focuses on the synthesis of colloidal particles of controlled size, shape, and surface chemistry. These particles are interesting as building blocks of larger superstructures, which have possible applications in electronics, photonics, catalysis, chemical sensing, and other areas. Monodisperse collections of spherical and polyhedral nanoparticles are known to crystallize into well ordered two- and three-dimensional arrays.[1] On the other hand, it is now becoming clear that less symmetric particles and linkers can give rise to more complex and interesting superstructures, both on the nanoscale[2] and on larger length scales.[3] Recently, we have studied the synthesis and assembly of rod-shaped colloidal particles.[4] This synthesis, which involves the electrochemical replication of porous alumina and polycarbonate membranes, allows one to make cylindrical wires with a controlled sequence of 'stripes' along their length. Different metal stripes selectively adsorb self-assembled monolayers (SAMs) or DNA oligomers, which can be used to direct the assembly of these particles on surfaces. Here, we report the stepwise formation of multilayered organic films on the cylindrical walls of Au nanowires by alternate adsorption of monolayers of poly(styrene sulfonate) (PSS) and poly(allylamine hydrochroride) (PAH). By removing a sacrificial Ag layer from the tips, it is possible to prepare nanowires that are chemically insulated along their length, but reactive at their ends. This reactivity is demonstrated by covalently linking fluorescent dye molecules exclusively to the exposed ends of the nanowires.

The porous templates used for the electrosynthesis of Au nanowires were commercially available Anodisc alumina membranes (200 nm pore size, 8.9×10^8 pores cm^{-2}, 60 μm thickness). Au replicas were made by a modification of the methods of Possin,[5] Martin[6a] and Moskovits.[6b] Ag was thermally evaporated onto the branched side of the alumina membrane to make the membrane electrically conductive (*ca.* 200 nm thick Ag). Ag was then electroplated (using Technic Silver 1025 plating solution) onto the evaporated Ag film to increase its thickness around to *ca.* 2 μm. The narrow branched pores were filled with Ag at a current density of 0.55 mA cm^{-2} of the membrane. Au was then grown electrochemically inside the pores by changing the electroplating solution (to Technic Orotemp 24). After the Au wires were grown to the desired length (2–6 μm), another 500–800 nm of Ag was grown. The metal-filled membrane was then glued to a glass slide and the alumina template was dissolved using NaOH solution. This left the Au nanowire array attached to a silver base, and left each nanowire capped with Ag. Suspensions of free Au nanowires were prepared by first dissolving the alumina membrane in NaOH and then the Ag backing and capping layers in nitric acid.

The surface derivatization of Au nanowires by polyelectrolyte multilayers[7] was performed as shown in Scheme 1. The nanowire array was first reacted with 2-aminoethanethiol hydrochloride to render the Au surface positive. The derivatized surface was then dipped in a solution of poly(sodium 4-styrene sulfonate) (PSS) (average molecular weight ≅ 70,000), which

† Electronic supplementary information (ESI) available: colour versions of Scheme 1 and Figs. 1 and 2. See http://www.rsc.org/suppdata/cc/b0/b007999p/

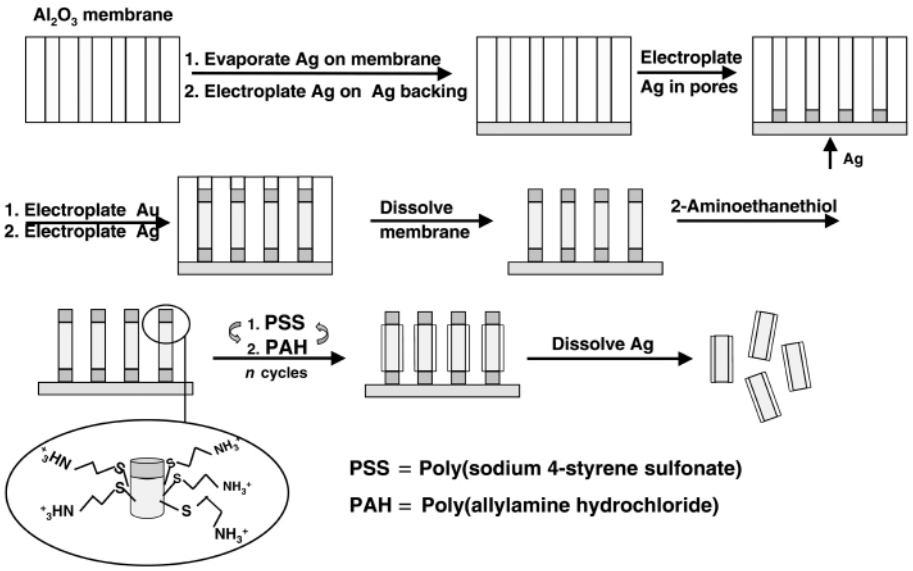

Scheme 1 Strategy for formation of a multilayer polyelectrolyte film on a gold nanowire array.

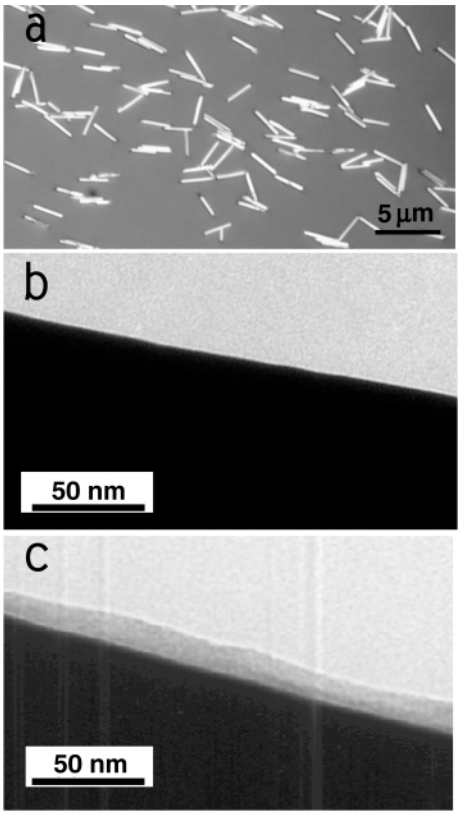

Fig. 1 (a) Optical micrograph at 1000× magnification of 2.4 μm Au nanowires, and TEM images of (b) an untreated Au nanowire and (c) an Au nanowire derivatized with a multilayer film of alternating polyanions and polycations as shown in Scheme 1.

contains negatively charged sulfonate groups in the polymer chain. In this step, anionic PSS adsorbs onto the positively charged surface and inverts the surface charge. The samples were then washed several times with water and reacted with poly(allylamine hydrochroride) (PAH) (average molecular weight ≅ 15,000), which contains positively charged $–NH_3^+$ groups. The polyanion, wash, polycation, wash cycles were repeated 10 times in order to produce multilayer films. Finally, the derivatized Au nanowires were freed from the surface by dissolving their Ag backing and caps in aqueous HNO_3.

Optical and electron microscopy was used to assess the quality of the nanowires and surface films. Fig. 1(a) and (b) show optical and transmission electron micrographs (TEM) of the nanowires. Many identical particles are produced by replication of a single membrane, and the underivatized nanowires have smooth, clean surfaces after the alumina template is dissolved away. Fig. 1(c) shows a TEM image of the surface of a gold nanowire modified by ten alternate adsorptions of PSS and PAH according to Scheme 1. Note the formation of a smooth polymer film with a thickness of *ca.* 13 nm, which is consistent with the 1 nm per bilayer typically found for adsorption of PSS/PAH on planar substrates.[7]

Because the top and bottom of the nanowires are capped with Ag during the polyelectrolyte adsorption steps, removal of Ag creates a clean surface that is chemically distinct from the 'insulated' cylindrical walls. This property was tested by reacting the free nanowires with 2-aminoethanethiol to form a self-assembled monolayer on the exposed surface. The thiol-treated nanowires were then reacted with fluorescein isothiocyanate and imaged using fluorescence microscopy. Studies on fluorescently-tagged monolayers have addressed the issue of fluorescence quenching near a metal surface. Although fluorescence is attenuated by non-radiative energy transfer to the metal, it is still strong enough for detection.[4,8,9] Fig. 2 compares a fluorescence optical micrograph of the derivatized nanowires with brightfield reflectance images from the same regions. Only the tips are fluorescent as a result of the thiourea link between isothiocyanate-functionalized probe molecule and 2-aminoethanethiol bound to the Au surface, confirming that both ends are accessible to the probe molecules. In contrast, the length of the nanowires are non-fluorescent, confirming that they are covered by a multilayer films that is not affected by the thiol–isothiocyanate derivatization steps.

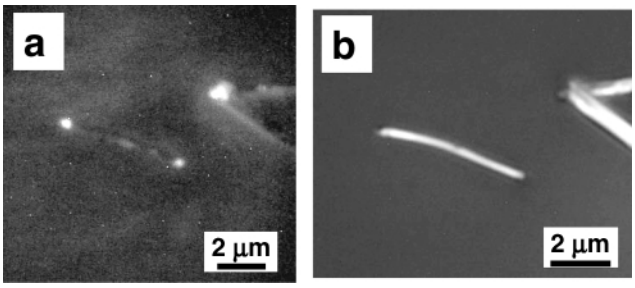

Fig. 2 Optical micrographs of Au rods derivatized with polymer multilayers according to Scheme 1, then etched to remove Ag from the tips and reacted with 2-aminoethanethiol and fluorescein isothiocyanate. (a) Fluorescence micrograph image and (b) a bright-field micrograph image of the derivatized rods on a quartz substrate.

In conclusion, we have successfully derivatized gold nanowires by alternate adsorption of the anionic and cationic polyelectrolytes poly(styrene sulfonate) and poly(allylamine hydrochroride). This process leads to smooth multilayer films around the Au surface, but not on surfaces that are first capped with Ag. It is now possible to selectively derivatize these nanowires, thus opening a door to possible applications in nanoscale electronics and other areas.

This work was supported by Korean Ministry of Science and Technology(I-01-03-A-073), 21C Frontier Project, Korea Research Foundation(KRF-2000-DP0243), DARPA, and the Office of Naval Research.

Notes and references

1 C. B. Murray, D. J. Norris and M. G. Bawendi, *J. Am. Chem. Soc*., 1993, **115**, 8706; S. Sun, C. B. Murray, D. Weller, L. Folks and A. Moser, *Science*, 2000, **287**, 1989; S. A. Harfenist, Z. L. Wang, M. M. Alvarez, I. Vezmar and R. L. Whetten, *J. Phys. Chem.*, 1996, **100**, 13 904; R. P. Andres, J. D. Bielefeld, J. I. Henderson, D. B. Janes, V. R. Kolagunta, C. P. Kubiak, W. J. Mahoney and R. G. Osifchin, *Science*, 1996, **273**, 1690.
2 C. A. Mirkin, R. L. Letsinger, R. C. Mucic and J. J. Sorhoff, *Nature*, 1996, **382**, 607; A. P. Alivisatos, K. P. Johnsson, X. Peng, T. E. Wilson, C. J. Loweth, M. P. Bruchez Jr. and P. G. Schultz, *Nature*, 1996, **382**, 609; J. P. Novak and D. L. Feldheim, *J. Am. Chem. Soc*., 2000, **122**, 3979.
3 N. Bowden, A. Terfort, J. Carbeck and G. M. Whitesides, *Science*, 1997, **267**, 233; I. S. Choi, N. Bowden and G. M. Whitesides, *J. Am. Chem. Soc*., 1999, **121**, 1754.
4 B. R. Martin, D. J. Dermody, B. D. Reiss, M. Fang, L. A. Lyon, M. J. Natan and T. E. Mallouk, *Adv. Mater*., 1999, **11**, 1021.
5 G. E. Possin, *Rev. Sci. Instrum.*, 1970, **41**, 772.
6 (*a*) C. R. Martin, *Chem. Mater*., 1996, **8**, 1739; (*b*) D. Routkevitch, *et al.*, *J. Phys. Chem.*, 1996, **100**, 14037.
7 G. Decher, *Science*, 1997, **277**, 1232.
8 S. H. Chen and C. W. Frank, *Langmuir*, 1991, **7**, 1719.
9 D. S. Karpvoich and G. J. Blanchard, *Langmuir*, 1996, **23**, 5522.

ChemComm

On the effect of catalyst loading in Pd-catalysed allylic alkylation†

Ian J. S. Fairlamb and Guy C. Lloyd-Jones*

School of Chemistry, Cantock's Close, Bristol, UK BS8 1TS. E-mail: guy.lloyd-jones@bris.ac.uk

Received (in Cambridge, UK) 26th September 2000, Accepted 30th October 2000
First published as an Advance Article on the web 24th November 2000

A mononuclear Pd–allyl complex of the Trost modular ligand displays non-C_2-symmetric ligand coordination and is in equilibrium with a hierarchical series of non-chelate oligomers.

We have an ongoing interest in 'memory effects'[1] in Pd-catalysed allylation, particularly in relation to reactions involving the Trost modular ligand **1a**.[2] During such processes, the coordination mode of **1a** to Pd in Pd–allyl intermediates is generally assumed to be exclusively *P*,*P* chelating and C_2-symmetric[3] (*e.g.*, **2**/**3**). However, the crystalline binuclear complex $[Pd_2(\mathbf{1a})(allyl)_2]^{2+}$, an active catalyst for allylation, is readily prepared.[1b] In the solid state and in solution this exists as a single species **4** (X = OTf) in which Pd is *P*,*O*− coordinated. In stark contrast, the mononuclear species '[Pd(**1a**)(allyl)]$^+$' is an amorphous solid which dissolves to give a number of *P*−coordinated species (^{1}H, ^{13}C and ^{31}P NMR).

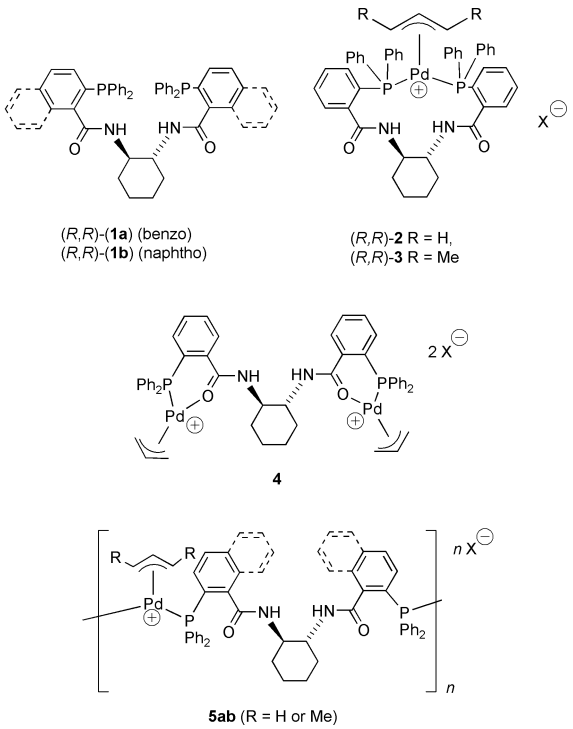

A 23 mM solution of '[Pd(**1a**)(allyl)]$^+$' in CD_2Cl_2 at 25 °C displays two distinct sets of ^{31}P NMR signals of approximately equal abundance [Fig. 1(a)]. The first is a cluster of signals in the range δ 24.5–27. These have no discernible coupling and comprise two outer sets of signals and a broader major central set [Fig. 1(a), open square].

The second set is a pair of AB spin systems in a ratio of 62.5 : 37.5 [Fig. 1(a), open/closed circles] the ratio of which varies with temperature [Fig. 1(b)]‡ but not concentration (1–180 mM). The identical $^2J_{PP}$ coupling (32.9 Hz), similar chemical shifts and low entropic difference (ΔS^0 = 2.4 ± 0.1 J K^{-1} mol^{-1}) suggests these to be diastereoisomers. Note that π-allyl rotamers of **2** can only be non-degenerate through non-C_2-symmetric conformation of coordinated ligand **1a**.[3] Above −15 °C, concentration *independent* line-broadening§ indicates unimolecular diastereoisomer interconversion just below the NMR time-scale [*cf.* Fig. 1(a) and (b)].

When the concentration of '[Pd(**1a**)(allyl)]$^+$' is increased, the proportion of **2** decreases [Fig. 1(c)]. Dilution confirms a reversible equilibrium governed by a term or terms of type $[Pd]^n$, where $n > 1$, and thus a monomer-oligomer equilibrium. As predicted, lower temperatures favour oligomer [see Fg. 1(b)], presumably due to substantial ΔS; however, a reliable van't Hoff relationship (−75 → 25 °C) could not be established owing to precipitation at lower temperatures. ^{31}P NMR analysis of the mol fraction **1a** in monomeric *vs*. oligomeric species at varying concentration (1–180 mM, CD_2Cl_2, 25 °C) yields a curve [Fig. 2(a)]. Using sequential equilibria between hierarchical oligomers [*i.e.* $(X)_n$ + **2** ↔ $(X)_{n+1}$, where '*X*' is an unspecified Pd complex] as a model[4] we could successfully predict equilibrium concentrations (solid line). In DMSO-d_6, near-identical diastereomer ratios (63 : 37) and monomer–oligomer concentration dependences were observed.

The monomer–oligomer equilibria does not cause observable ^{31}P NMR line-broadening in **2**, and thus monomer–oligomer

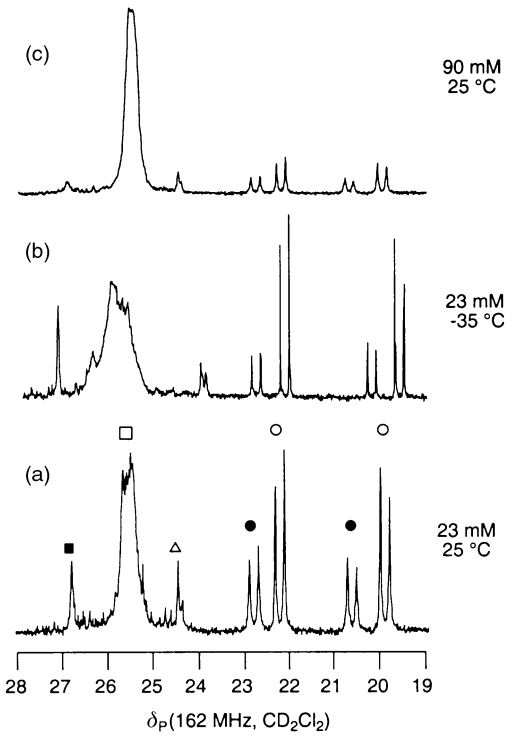

Fig. 1 ^{31}P NMR spectra of [Pd(**1a**)(allyl)][OTf] in CD_2Cl_2 at two temperatures and concentrations. Circles: monomer **2** (R≡H, two diastereomers), open square: oligomer **5a** (R = H), filled square: tentatively assigned as '$[Pd_2(\mathbf{1a})_3(allyl)_2]^{2+}$' (reversibly generated by addition of 0.5 equivalent **1a**), triangle: *P*,*O*-coordinated species analogous to **4** or mono- and *bis*-*P*-allylated **1a** {isochronous with an independently prepared sample of [*P*,*P*′-$allyl_2$-**1a**][$(OTf)_2$]}.

† Electronic supplementary information (ESI) available: explanation of varying ee with catalytic loading. See http://www.rsc.org/suppdata/cc/b0/b007785m/

DOI: 10.1039/b007785m

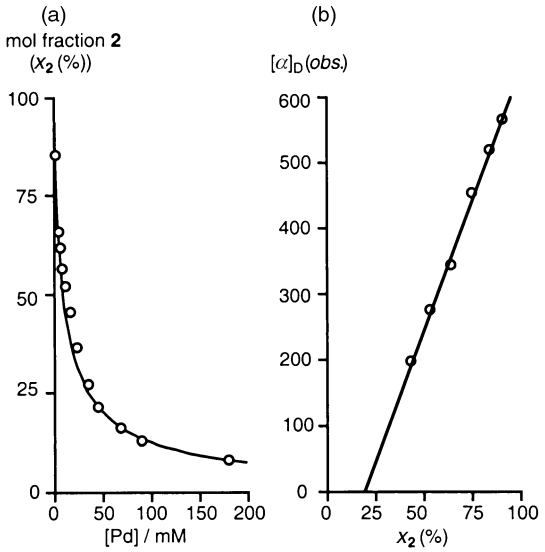

Fig. 2 (a) Concentration of '[Pd(**1a**)(allyl)][OTf]' in CD_2Cl_2 ('[Pd]', *x*-axis) *vs*. mol fraction **2** (x_2, *y*-axis) data: circles (^{31}P NMR) line: best fit. (b) Mol fraction **2** [x_2 (%), *x*-axis] at concentrations of [Pd(**1a**)(allyl)][OTf] in the range 3 → 20 mM *vs*. ($[\alpha]_D$, *y*-axis) circles: data, line: linear regression of $[\alpha]_D$ (obs.) = $[x_2\{\alpha_2\}_D + (100 - x_2)\{\alpha_5\}_D]$.

interconversion is slower than the NMR timescale. However, the specific rotation of [Pd(**1a**)(allyl)][OTf] in CH_2Cl_2 at 22 °C varies dramatically with concentration, *vide infra*, and fast equilibrium ($t_{1/2} \leq 2$ s)[5] at the real time-scale was confirmed by polarimetry after rapid dilution (100 → 10 mM). Analysis of mol fraction monomer (x_2, ^{31}P NMR) and $[\alpha]_D$ over a range of concentrations [Fig. 2(b)] reveals a simple relationship. This demonstrates that the variation of the net specific rotation, $[\alpha]_D$ (obs.), does not arise from large concentration dependent rotations of individual species, but rather from the monomer–oligomer distribution. Linear regression¶ yields an intrinsic specific rotation,[6] $\{\alpha\}_D$ for **2** (R = H) of +644 (±8). The linearity of x_2 *vs*. $[\alpha]_D$ (obs.) also suggests congruence in the $[\alpha]_D$ of the (lower) oligomers and extrapolation to $x_2 = 0$ yields $\{\alpha\}_D = -151$ (±17). This value is significantly different in sign and magnitude from that of **2** and hints that the oligomers are not of the form $(\mathbf{2})_n$. Given the propensity for **1a** to exist in an elongated conformation[1] and the size of the chelate ring in **2** (13-membered) we suggest oligomeric structures of type **5a** (R = H)[7] where the central chirality of the diamide backbone is not within a chelate ring {*cf*. monomer **4** ($[\alpha]_D = 38$, $c = 0.1$, CH_2Cl_2) and ligand **1a** ($[\alpha]_D = 61$, $c = 2.3$, CH_2Cl_2)}.

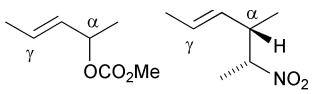

(±)-**6** (2*R*, 3*S*)-**7**

In recent reports on the asymmetric allylation of $EtNO_2$ by (±)-**6** (→**7**) which is suggested to proceed *via* intermediate π-allyl complex **3**, moderate ee values at high catalyst loadings were suggested to be the result of a memory effect arising through slow interconversion of isomers of **3** of differing symmetry. For example with 4 mol% 'Pd(**1a**)', **7** was obtained in 53% ee whilst with 0.5 mol% the ee increased to 97% ee. It was suggested that 'by lowering the catalyst loading which, in effect, reduces the concentration of the π-allylpalladium intermediate, the unimolecular equilibration event now *outcompetes* the bimolecular nucleophilic addition'.[2a] However, if equilibration is unimolecular and capture by nucleophile is bimolecular, as suggested, then the relative rates of these processes is given by $\{k_{eq}[\mathbf{3}]/k_{Nu}[\mathbf{3}][Nu]\}$. Since this reduces to $\{k'[Nu]^{-1}\}$, in which catalyst loading does not feature, this interpretation of memory effect attenuation‖ is unsatisfactory. However, in view of the results described herein, the possibility of analogous equilibrium between **3** and oligomers** such as **5a** (R=Me) must be considered. In contrast to oligomeric intermediates, *P*,*P*-chelation in **3** will allow efficient central chirality transmission through the helical Ar_3P-donor arrays,[8] albeit in a non-C_2-symmetric fashion.[3] Lower catalyst loadings, favouring monomer, would thus lead to higher selectivity. Furthermore, oligomerisation may also account for decreased selectivities at lower temperatures[3b] or the superiority of **1b** over **1a** (see **5b**)[9] in certain processes.

We thank the EPSRC (GR/N05208) and Lancaster Synthesis for generous support.

Notes and references

‡ A van't Hoff analysis of ^{31}P NMR integrals from spectra obtained between +25 and −75 °C yielded: $\ln K_{eq} = (221 \pm 2.9/T) - 0.283 \pm 0.01$; $r^2 = 0.999$.

§ Line width, $\omega_{1/2}$: 6 ± 1.5 Hz (25 °C, 1–180 mM) → 2 ± 0.5 Hz (constant −15 to −75 °C). Strong correlations between A/B′ and A′/B and weak correlations between A/A′ and B/B′ in the 2D ^{31}P{^{1}H} EXSY (500 MHz) spectrum [δ_P, 22.2/19.9 (A,B) and 22.8/20.6 (A′,B′)] suggest that equilibrium proceeds *via* interconversion of ligand conformation rather than ligand dissociation, or π–σ–π allyl fluxionality.

¶ The principle of optical superposition (van't Hoff) is assumed to apply.

‖ The lower selectivity at higher catalyst loading (4 mol%) does not arise exclusively from a regiochemical memory effect (see Fig. 3 in ESI†).

** Ionisation of **6** may generate **3** directly, or indirectly *via* oligomeric Pd(0) species.

1 (*a*) G. C. Lloyd-Jones and S. C. Stephen, *Chem. Eur. J.*, 1998, **4**, 2539 and references therein; (*b*) C. P. Butts, J. Crosby, G. C. Lloyd-Jones and S. C. Stephen, *Chem. Commun.*, 1999, 1707; (*c*) A. J. Blacker, M. L. Clarke, M. S. Loft and J. M. J. Williams, *Org. Lett.*, 1999, **1**, 1969; (*d*) G. C. Lloyd-Jones, S. C. Stephen, M. Murray, C. P. Butts and Š. Vyskočil and P. Kočovský, *Chem. Eur. J.*, 2000, **6**, 4348; (*e*) J. M. Longmire, B. Wang and X. Zhang, *Tetrahedron Lett.*, 2000, **41**, 5435; (*f*) B. Goldfuss and U. Kazmaier, *Tetrahedron*, 2000, **56**, 2493.

2 (*a*) B. M. Trost and J.-P. Surivet, *J. Am. Chem. Soc.*, 2000, **122**, 6291; (*b*) B. M. Trost and J.-P. Surivet, *Angew. Chem., Int. Ed.*, 2000, **39**, 3122.

3 As far as we are aware, there is no published experimental data on the symmetry of *P*,*P*-chelate coordination of **1a** to Pd. However, the working model, based on molecular modelling, always employs fully C_2-symmetric coordination: (*a*) B. M. Trost and F. D. Toste, *J. Am. Chem. Soc.*, 1999, **121**, 4545; however, also see footnote 36 in (*b*) B. M. Trost and X. Ariza, *J. Am. Chem. Soc*, 1999, **121**, 10 727.

4 Quantitative analysis of monomer-oligomer equilibrium will be described elsewhere.

5 Slow equilibration is observed in $PdCl_2$ complexes of simple (achiral) diphosphines with alkyl or polyether backbones: D. C. Smith and G. M. Gray, *J. Chem. Soc., Dalton Trans.*, 2000, 677; however, the ability of **1a** to act as a *P*,*O*-donor to cationic Pd(II) (as in **4**) may catalyse interconversion.

6 There are no observable chromophores in the region of the sodium D-line in the UV spectrum of the mixture of complexes: E. L. Eliel and S. H. Wilen, *Stereochemistry of Organic Compounds*, John Wiley and Sons, New York, 1994.

7 Such oligomers could be linear or cyclic, see *e.g.* B. L. Shaw, *J. Organometal. Chem.*, 1980, **200**, 307.

8 The major contributor to the magnitude and sign of the optical rotation is likely to be the degree of order and sense of the aryl phosphine rotors. The sextuple phenyl array is the mainstay of the 'cartoon' representation of the 'chiral pocket'. Since ligand **1a** is particularly effective with slim cyclic allyl substrates and less so with bulky linear ones (see *e.g.* B. M. Trost, A. C. Krueger, R. C. Bunt and J. Zambrano, *J. Am. Chem. Soc.*, 1996, **118**, 6520) the tightness of the 'chiral pocket' may exacerbate oligomerisation with the latter class.

9 B. M. Trost, R. C. Bunt, R. C. Lemoine and T. L. Calkins, *J. Am. Chem. Soc.*, 2000, **122**, 5968.

An unprecedented mode of association in diselenadiazolyl radicals: crystal structures and magnetic properties of [*p*-$XC_6F_4CNSeSeN]_2$ (X = Cl, Br)†

Neil Feeder,[a] Robert J. Less,[a] Jeremy M. Rawson,*[a] Patricia Oliete[b] and Fernando Palacio[b]

[a] *Department of Chemistry, University of Cambridge, Lensfield Road, Cambridge UK, CB2 1EW. E-mail: jmr31@cam.ac.uk*

[b] *Instituto de Ciencia de Materiales de Aragon, CSIC-Universidad de Zaragoza, E-50009, Zaragoza, Spain*

Received (in Cambridge, UK) 13th June 2000, Accepted 1st November 2000
First published as an Advance Article on the web 27th November 2000

The two title compounds are isostructural with pairs of diselenadiazolyl radicals associating in an unprecedented manner *via* an orthogonal interaction between singly occupied molecular orbitals which renders them essentially diamagnetic in the solid state.

The 1,2,3,5-dithiadiazolyl radical **1** is an extremely persistent stable free radical.[1] Solution EPR studies on several derivatives

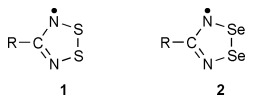

1 **2**

have established[2] that the dimerisation energy is substantial ($\Delta H_{dim} \approx 35$ kJ mol^{-1}). In 1985, Mews and coworkers described[3] the crystal structure of $[CF_3CNSSN]_2$ and predicted that association of dithiadiazolyl radicals could occur through a favourable π-bonding interaction between singly occupied molecular orbitals (SOMOs). The energy differences between *cisoid*, *transoid* and twisted conformations [Fig. 1(i)–(iii)] was estimated[3] at < 10 kJ mol^{-1} and examples of all of these three modes of association have since been established by X-ray crystallography.[1] More recently a fourth, *trans*-cofacial motif has been observed [Fig. 1(iv)].[4]

The isoelectronic diselenadiazolyl radicals **2** have also been prepared[5] and exhibit a greater tendency to dimerise in solution.[6] Theoretical studies have estimated[7] that ΔH_{dim} is higher [*cf.* **1** and **2** (R = H) with $\Delta H_{dim} = 33$ and 46 kJ mol^{-1}, respectively, using the same basis sets]. In the solid state, derivatives of **2** have invariably crystallised in the *cisoid* configuration observed for **1** [Fig. 1(i)]. Here we report the syntheses and characterisation of two diselenadiazolyl radicals **2a** and **2b** (R = *p*-ClC_6F_4 and *p*-BrC_6F_4, respectively), which associate in an unprecedented manner [Fig.1(v)].

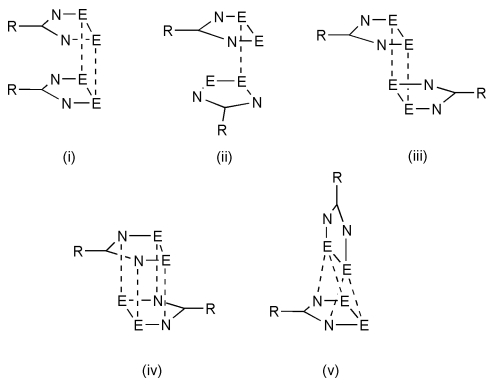

(i) (ii) (iii) (iv) (v)

Fig. 1 Modes of association of dithiadiazolyl (E = S) and diselenadiazolyl (E = Se) radicals: (i) *cis*-cofacial, (ii) twisted, (iii) *trans*-antarafacial, (iv) *trans*-cofacial (v) orthogonal.

† Electronic supplementary information (ESI) available: analytical data for **2a** and **b**. See http//www.rsc.org/suppdata/cc/b0/b004705h/

Radicals **2a** and **2b** were prepared† from *p*-ClC_6F_4CN and *p*-BrC_6F_4CN using standard synthetic procedures,[5] and purified by sublimations under static vacuum (100 °C, 10^{-2} Torr). The crystal structures of **2a** and **2b** are isostructural, although not isomorphous.‡ The structure of **2b** contains two molecules of conventional geometry[8] in the asymmetric unit (Fig. 2). However, their mode of association is exceptional; The two heterocyclic rings in **2b** are inclined at 85° with respect to each other, with each of the selenium atoms of one ring situated approximately equidistant between an N and an Se atom of the second ring. This leads to a set of intermolecular Se···N and Se···Se contacts in the range 3.09–3.21 Å. The Se···Se contact is similar to that observed in conventional *cisoid* diselenadiazolyls. Because of the anisotropy in the van der Waals radius of selenium (*ca*. 2.15 Å perpendicular to the ring plane and *ca*. 1.7 Å in the ring plane),[9] the Se···Se interaction in this orthogonal arrangement (sum of van der Waals radii is 3.85 Å)[9] is likely to be weaker than that observed in the *cisoid* dimers (sum of the van der Waals radii perpendicular to the ring plane is *ca*. 4.3 Å).[9] A packing diagram of **2b** viewed in the *ac* plane (Fig. 3) shows how the dimer pairs pack in an antiparallel fashion along the crystallographic *c*-axis. The inter-dimer separation along the *c*-direction is longer, with the closest inter-dimer Se contacts in the range 3.6–3.7 Å.

Previous magnetic studies on other derivatives of **2** have indicated that the π*–π* interaction between cofacial radicals renders them diamagnetic. In order to establish the strength of the orthogonal interaction between radicals, variable temperature magnetic measurements were carried out on samples of both **2a** and **2b**.

Susceptibility measurements were made on a SQUID magnetometer with an applied field of 1 T in the range 1.8–300 K and isothermal magnetisation curves were recorded at 1.8 and

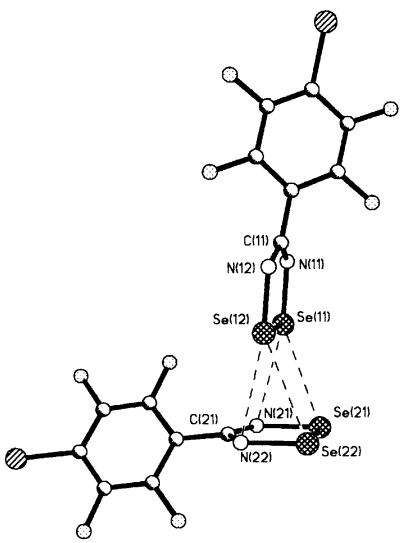

Fig. 2 Asymmetric unit of **2b**, with atom labelling scheme; the structural parameters of **2a** are the same as those for **2b**, within error.

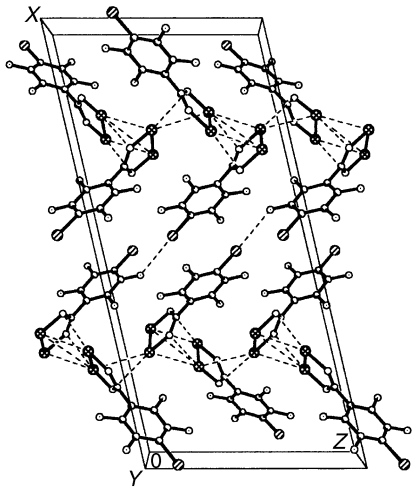

Fig. 3 Crystal structure of **2b** viewed in the *ac* plane. The closest inter-dimer contacts (illustrated) are Se···Se at 3.60 Å and Se···N at 3.46 Å.

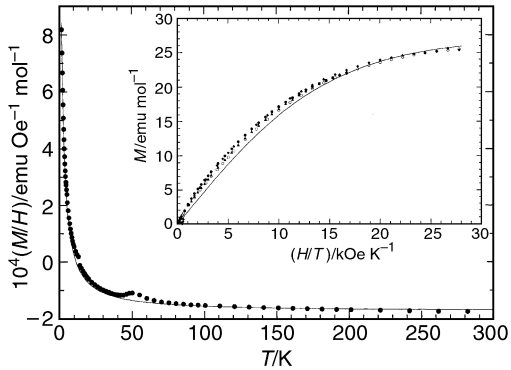

Fig. 4 Magnetic susceptibility as a function of temperature for **2b**. The solid line is the fit to the Curie–Weiss law and a diamagnetic contribution. Inset: Magnetisation behaviour of the unpaired spin moments of **2a** and **2b** as a function of the applied field. The solid line is the Brillouin function corresponding to S = 1/2 and a mol fraction of 0.0049 paramagnetic molecules. The data for **2a** has been scaled to the number of paramagnetic molecules found in **2b**.

3.0 K. A plot of susceptibility *vs.* temperature for both **2a** and **2b** are similar (that for **2b** is shown in Fig. 4) and shows that both **2a** and **2b** are essentially diamagnetic. A rapid increase in susceptibility at low temperatures is due to the presence of a small number of paramagnetic centres in the sample (a small spike can be observed at 50 K due to the antiferromagnetic transition of a minute amount of oxygen in the sample). A good fit to the Curie–Weiss law, including a diamagnetic contribution indicates that, for **2a**, the mol fraction of paramagnetic centres was 0.0045 and for **2b** 0.0054.

After a diamagnetic correction, the behaviour of the magnetisation as a function of the applied field in **2a** and **2b** closely follows a Brillouin function for S = ½ (Fig. 4, inset). A fit to the Brillouin function yielded mol fractions of paramagnetic centres as 0.0031 and 0.0049 for **2a** and **2b** respectively, in good agreement with the susceptibility results.

A preliminary examination of the interaction between SOMOs for this orthogonal mode of association indicates a symmetry-allowed bonding interaction (Fig. 5) which could give rise to a closed-shell singlet and thereby rationalise the observed diamagnetism. However, the poor orbital overlap anticipated from the perpendicular orientation of π* orbitals could also be anticipated to favour an open shell ground state. The magnetic measurements clearly indicate a singlet ground state, although both closed-shell singlet (spin-paired dimer) and open-shell singlet (antiferromagnetically coupled radicals) are possible. In the latter case, the singlet–triplet separation would need to be extremely large to suppress the paramagnetism arising from the triplet state. However, very large exchange

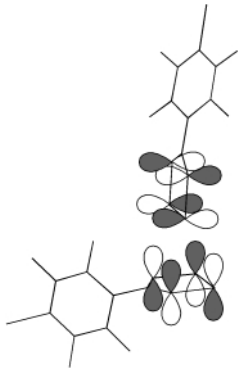

Fig. 5 The π*–π* bonding interaction between orthogonal π-systems on neighbouring diselenadiazolyl radicals.

interactions in group 15/16 radicals are not without precedent; Fujita and Awaga recently reported[10] a dithiazolyl radical with an exchange interaction of −1300 K. Further theoretical and experimental studies are required to confirm the electronic ground state of **2**, *viz-a-viz* an open shell or closed shell singlet. These studies, and additional structural studies on closely related diselenadiazolyl radicals, will be the subject of a future report.

We thank the Royal Society for an equipment grant (J. M. R.) and the EPSRC for a studentship (R. J. L.). This work was also supported by the Materials Program of the Comision Interministerial de Ciencia y Technologia under grant MAT97-951.

Notes and references

‡ *Crystal data* for **2b**: $C_7BrF_4N_2Se_2$, M = 425.92, monoclinic, space group $P2_1/c$, a = 26.275(11), b = 6.131(7), c = 12.513(10) Å, β = 102.85(6)°, Z = 8, T = 180(2) K, μ(Mo-Kα) = 11.620 mm^{-1}. Of a total of 2270 collected reflections, 2197 were unique (R_{int} = 0.0321) and used in all calculations. The final wR_2 = 0.2821 (all data), R_1 [$F > 2\sigma(F)$] = 0.0971. Significant residual electron-density (max: +2.4 e Å^{-3}) was observed in the final difference map close to Se and Br atoms and anisotropic refinement of C and N atoms proved impossible. [The same structural motif was observed for **2a** which crystallises in the orthorhombic space group $Pca2_1$, a = 12.454(3), b = 6.1040(12), c = 25.231(5) Å at T = 150(2) K]. CCDC 182/1838. See http://www.rsc.org/suppdata/b0/b004705h/ for crystallographic files in .cif format.

1 For example see J. M. Rawson, A. J. Banister and I. Lavender, *Adv. Heterocycl. Chem.*, 1995, **62**, 137 and references therein.
2 S. A. Fairhurst, K. M. Johnson, L. H. Sutcliffe, K. F. Preston, A. J. Banister, Z. V. Hauptman and J. Passmore, *J. Chem. Soc., Dalton Trans.*, 1986, 1465.
3 H. U. Höfs, J. W. Bats, R. Gleiter, G. Hartmann, R. Mews, M. Eckert-Maksic, H. Oberhammer and G. M. Sheldrick, *Chem. Ber.*, 1985, **118**, 3781.
4 T. M. Barclay, A. W. Cordes, N. A. George, R. C. Haddon, M. E. Itkis and R. T. Oakley, *Chem. Commun.*, 1999, 2269; N. Bricklebank, S. Hargreaves and S. E. Spey, *Polyhedron*, 2000, **19**, 1163.
5 For example, see: A. W. Cordes, R. C. Haddon, R. G. Hicks, R. T. Oakley and T. T. M. Palstra, *Inorg. Chem.*, 1992, **31**, 1802.
6 J. E. Davies, R. J. Less, I. May and J. M. Rawson, *New. J. Chem.*, 1998, 763.
7 A. W. Cordes, C. D. Bryan, W. M. Davis, R. H. de Laat, S. H. Glarum, J. D. Goddard, R. C. Haddon, R. G. Hicks, D. K. Kennepohl, R. T. Oakley, S. R. Scott and N. P. C. Westwood, *J. Am. Chem. Soc.*, 1993, **115**, 7232.
8 For example of intramolecular dimensions in diselenadiazolyl radicals, see: P. D. B. Belluz, A. W. Cordes, E. M. Kristov, P. V. Kristov, S. W. Liblong and R. T. Oakley, *J. Am. Chem. Soc.*, 1989, **111**, 9276; For examples of twist angles in perfluorophenyl dithiadiazolyl rings see: G. Antorrena, J. E. Davies, M. Hartley, F. Palacio, J. M. Rawson, J. N. B. Smith and A. Steiner, *Chem. Commun.*, 1999, 1393.
9 S. C. Nyburg and C. H. Faerman, *Acta Crystallogr., Sect. B*, 1985, **41**, 274.
10 W. Fujita and K. Awaga, *Science*, 1999, **286**, 261.

An unusual oxidative rearrangement of azabicyclo[2.2.1]heptenes, providing a stereoselective route to 2′- and 3′-hydroxycyclopentylglycines

Patrick D. Bailey,*[a] I. M. McDonald,*[b] Georgina M. Rosair[a] and David Taylor[a]

[a] *Department of Chemistry, Heriot-Watt University, Riccarton, Edinburgh, UK EH14 4AS. E-mail: P.D.Bailey@hw.ac.uk*

[b] *James Black Foundation, 68 Half Moon Lane, Dulwich, London, UK SE24 9JE*

Received (in Liverpool, UK) 11th August 2000, Accepted 30th October 2000
First published as an Advance Article on the web

Treatment of the azabicyclo[2.2.1]heptene derivative 4 with *m*CPBA for 3–5 seconds generates the oxazabicyclo-[3.2.1]octene derivative 7 (X-ray structure) *via* rapid Meisenheimer rearrangement of the *N*-oxide 5, whilst heating 7 in MeCN for 4–6 h leads to further rearrangement to the more thermodynamically stable oxazabicyclo[3.3.0]octene isomer 6; 6 and 7 can be readily reduced to enantio-pure hydroxylated cyclopentylglycine derivatives.

Pharmacologically active peptoids can be generated by attaching the side-chains of a parent peptide to carrier moieties such as sugars, steroids, or porphyrins.[1] We have been exploring the use of azabicyclo[2.2.1]heptanes as rigid templates for such systems which, if they can be derivatised appropriately, offer potential as 3D structures on which to construct peptoid libraries. We were also attracted to such systems because we had developed an extremely short, efficient, and highly stereoselective route to these systems some years ago;[2] the aza-Diels–Alder reaction of the imine **3** with cyclopentadiene gives the azabicyclo[2.2.1]heptene **4** as a single stereoisomer, and we wished to explore the derivatisation of this adduct.[3] This communication, however, reports some unexpected results that have instead provided a short, efficient, stereo- and regio-specific route to hydroxylated cyclopentylglycines.

As outlined in Scheme 1, the adduct **4** could be efficiently prepared using ethyl glyoxylate generated using the procedure developed by Roberts' group.[4] After formation of the imine, the cycloaddition reaction was found to be most reliable when conducted in trifluoroethanol in the presence of TFA (1 equiv.). As reported by ourselves[4] and others,[5] this reaction proceeds both with excellent *exo* diastereo-control (in contrast to the *endo* selectivity observed for acyclic dienes[2]), and with extremely high asymmetric induction resulting from the presence of the α-methylbenzyl auxiliary (72% isolated yield, 95:5 *exo*:*endo*, 90% asymmetric induction). After chromatography, **4** was obtained as a single stereoisomer, from which we hoped an epoxidation/nucleophilic ring-opening sequence would allow derivatisation at site **C**, whilst further pharmacophores could be introduced at sites **A** and **B**. However, treatment with *m*CPBA failed to give the desired epoxide (even under acidic conditions whereby the nitrogen would be expected to be protonated), but instead yielded an isomeric oxygenated product which we initially assigned as the *N*-oxide **5**. Small amounts of a by-product were also generated, which was identified as the oxazabicyclo[3.3.0]octene **6** from NMR data.†

We had expected that an X-ray crystal structure of the '*N*-oxide' would confirm its identity and allow us to assign its stereochemistry at the chiral nitrogen, but this surprisingly revealed that the isomeric oxazabicyclo[3.2.1]octene **7** had been formed instead (Fig. 1‡). Optimisation of the reaction conditions established that the highest yield of **7** was obtained when the cyclo-adduct **4** was reacted at room temperature with *m*CPBA for only *3–5 seconds* and, that clean conversion to **6** could be achieved by refluxing **7** in acetonitrile for 24 h. Presumably **7** is formed *via* a Meisenheimer rearrangement,[6–9] but the rapidity and selectivity of the initial reaction, in which

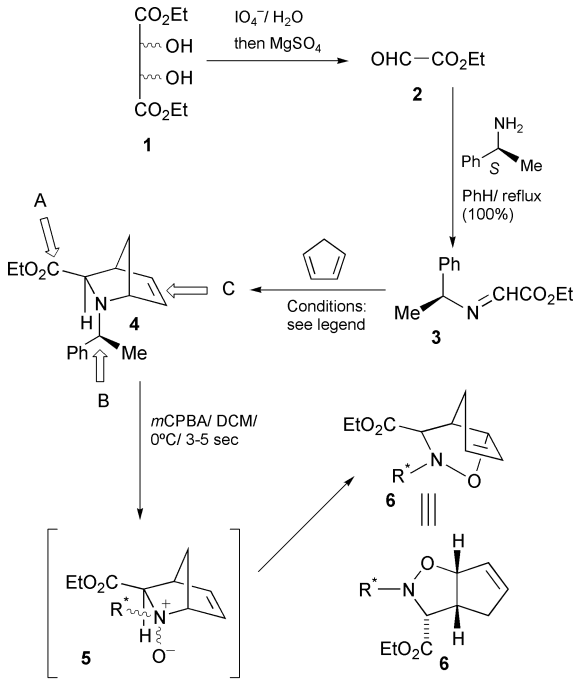

Scheme 1 Formation of the oxazabicyclo[3.3.0]octane system **6**. The aza-Diels–Alder reaction (**3** → **4**) was in TFE, TFA (1 eq.), 0 °C, 3.5 h (72% yield, 95% *exo*, 90% asymmetric induction). See text and Scheme 2 for yields and identification of the products **5** and **6** from *m*CPBA oxidation of **4**. [R* = (*S*)-1-phenylethyl].

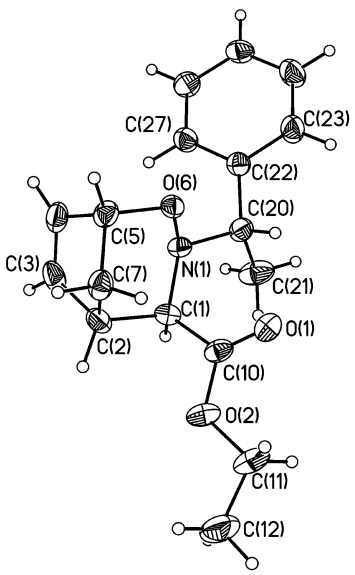

Fig. 1 X-Ray crystal structure of **7** with crystallographic numbering.‡

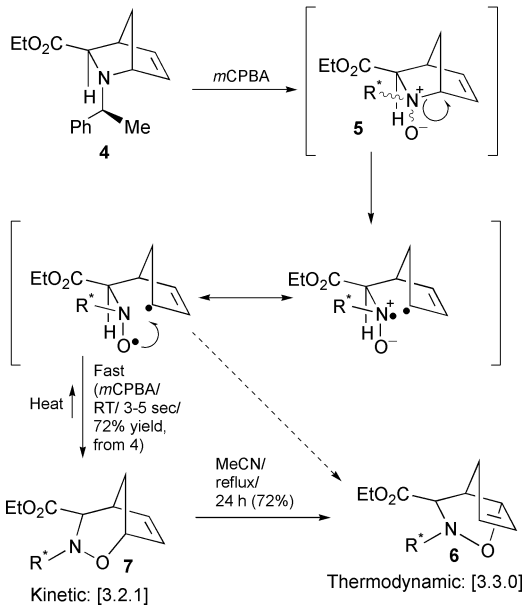

Scheme 2 Possible mechanism for the formation of **6** and **7**; heterolytic bond cleavage of **7** would also be consistent with its thermolysis to **6**. [R* = (*S*)-1-phenylethyl].

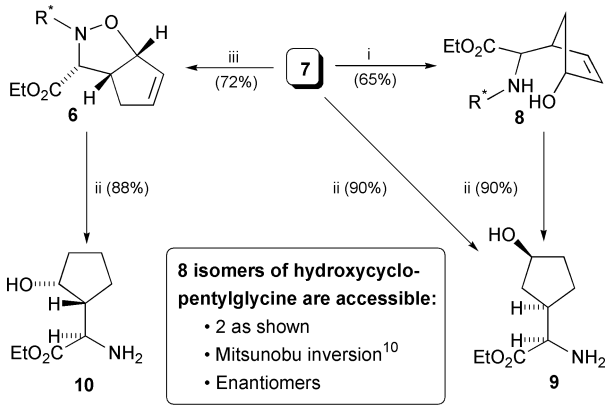

Scheme 3 Conversion of the oxazabicyclooctanes **6** and **7** into hydroxylated cyclopentylglycines such as **9** and **10**. Conditions: (i) Zn–AcOH; (ii) H_2 (50 psi)– $Pd(OH)_2$/C; (iii) MeCN, reflux, 24 h. [R* = (*S*)-1-phenylethyl].

the di-radical must be retained within a solvent cage, is extraordinary. Unprecedented, as far as we are aware, is the establishment of an equilibrium with the Meisenheimer intermediate (or possibly *via* heterolytic bond cleavage of **7**), providing a route by which the thermodynamically more stable adduct **6** can be generated (see Scheme 2).

With an efficient route to two isomeric oxazabicyclooctanes achieved, we wished to explore whether they could be converted into hydroxy-substituted cyclopentylglycines. The key transformations are shown in Scheme 3. In particular, Zn–AcOH treatment of the [3.2.1] isomer **7** allowed selective cleavage of the N–O bond, yielding the 4′-hydroxycyclopent-2′-enyl glycine derivative **8**. Hydrogenation of the double bond (Pearlman's catalyst, 50 psi) resulted in concomitant removal of the α-methylbenzyl auxiliary to afford the 3′-hydroxycyclopentyl glycine **9** as a single (2*R*,1′*R*,3′*S*) stereoisomer; the same hydrogenation conditions also allowed direct conversion of **7** to **9** (90% yield). On the other hand, these hydrogenation conditions enabled us to reduce the [3.3.0] isomer **6** directly to the 2′-hydroxycyclopentyl glycine **10**, also as a single (2*R*,1′*R*,2′*R*) stereoisomer. Closely related analogues of **8** have been used in the synthesis of cyclopentenylglycine,[11] and of carbocyclic analogues of nikkomycin[12] and polyoxin C.[13]

In summary, the asymmetric aza-Diels–Alder adduct **4** reacts with *m*CPBA to generate the Meisenheimer rearranged product **6**, which can be converted into the [3.3.0] system **7** by simple heating. These two isomers can be separately reduced, to provide access to a wide range of cyclopentylglycine derivatives, with complete regio-, diastereo- and enantio-control.

We thank Dr A. S. F. Boyd and Dr R. Fergusson for NMR and mass spectra, the EPSRC for financial support, and we acknowledge the use of the EPSRC's Chemical Database Service at Daresbury.

Notes and references

† Selected data for **6**: $C_{17}H_{21}NO_3$; $\delta_H(CDCl_3)$ 1.1 (3H, t, *J* 7.2), 1.5 (3H, d, *J* 6.6), 2.4 (2H, m), 3.05 (1H, q, *J* 6.6), 3.55 (1H, m), 3.7 (1H, d, *J* 9.1), 3.95 (2H, q, *J* 7.2), 5.3 (1H, dd, *J* 7.4, 0.7), 5.8 (1H, dd, *J* 3.5, 1.7), 5.95 (1H, dd, *J* 1.7, 0.7), 7.2–7.4 (5H, m); $\delta_C(CDCl_3)$ 14.15 (CH_3), 20.47 (CH_3), 34.16 (CH_2), 47.20 (CH), 60.52 (CH_2), 65.68 (CH), 69.85 (CH), 87.35 (CH), 127.66 (CH), 128.25 (2 × CH), 128.30 (2 × CH), 129.49 (CH), 135.17 (CH), 141.91 (C), 169.90 (C).

‡ *Crystal data* for **7**. A single crystal of **7** was grown by slow evaporation of 40–60 pet. ether at rt and coated in Nujol and mounted on a glass fibre covered with vacuum grease for data collection with a Bruker P4 diffractometer[14] at 160 K. Colourless plate, 0.12 × 0.72 × 0.34 mm, $C_{17}H_{21}NO_3$, *M* = 287.35, monoclinic, space group $P2_1$, *a* = 6.0734 (4), *b* = 13.0445 (9), *c* = 10.1045(7) Å , β = 98.280(5)°, *U* = 792.18(13) Å^3, *Z* = 2, μ(Mo–K_α) = 0.082 mm^{-1}. Data measured = 3180, unique data = 1593, *R* = 0.0778 on all data (*wR*2 = 0.0306). Absolute structure parameter = 3.5(19), so the absolute structure could not be confirmed from the X-ray data. Crystallographic computing was performed using the SHELXTL[15] system version 5.1. CCDC 182/1836. See http://www.rsc.org/suppdata/b0/b006683o/ for crystallographic data in .cif format.

1 R. Hirschmann, *Angew. Chem., Int. Ed. Engl.*, 1991, **30**, 1278.
2 P. D. Bailey, R. D. Wilson and G. R. Brown, *J. Chem. Soc., Perkin Trans. 1*, 1991, 1337; P. D. Bailey, G. R. Brown, F. Korber, A. Reid and R. D. Wilson, *Tetrahedron: Asymmetry*, 1991, **2**, 1263.
3 Andersson's group has made extensive use of the azabicyclo-[2.2.1]heptene **4**, as exemplified by P. Pinho and P. G. Andersson, *Chem. Commun.*, 1999, 597, and reference 5 therein; the Malpass group has also developed the chemistry of these azabicyclic systems, as exemplified by J. R. Malpass and C. D. Cox, *Tetrahedron Lett.*, 1999, **40**, 1419.
4 M. B. Hursthouse, K. M. A. Malik, D. E. Hibbs, S. M. Roberts, A. J. H. Seago, V. Sik and R. Storer, *J. Chem. Soc., Perkin Trans 1*, 1995, 2419.
5 L. Stella, H. Abraham, J. Feneu-Dupont, B. Tinant and J. P. Declercq, *Tetrahedron Lett.*, 1990, **31**, 2603; H. Abraham and L. Stella, *Tetrahedron*, 1992, **48**, 9707.
6 For a useful discussion of the Meisenheimer rearrangement, see V. Rautenstrauch, *Helv. Chim. Acta*, 1973, **56**, 2492, and references 8–18 therein.
7 For a study of the 2,3-Meisenheimer rearrangement of allyl *N*-oxides, see Y. Yamamoto, J. Oda and Y. Inouye, *J. Org. Chem.*, 1976, **41**, 303, and references therein; it might be noted that this process is believed to be pericyclic rather than radical, and that **6** is (formally) the product of the 2,3-Meisenheimer rearrangement of **5**.
8 For the synthesis of 7-, 8- and 9-membered 1,2-oxaza ring systems *via* the Meisenheimer rearrangement, see J. B. Bremner, E. J. Browne, P. E. Davies and L. van Thuc, *Aust. J. Chem.*, 1980, **33**, 833; J. B. Bremner E. J. Browne, P. E. Davies, C. L. Raston and A. H. White, *Aust. J. Chem.*, 1980, **33**, 1323; J. B. Bremner E. J. Browne and P. E. Davies, *Aust. J. Chem.*, 1980, **33**, 1335.
9 Spontaneous Meisenheimer rearrangements are rare, but has been observed in the ring expansion of a highly strained azetidine *N*-oxide: T. Kurihara, Y. Sakamoto, K. Tsukamoto, H. Ohishi, S. Harusawa and R. Yoneda, *J. Chem. Soc., Perkin Trans 1*, 1993, 81.
10 O. Mitsunobu, *Synthesis*, 1981, 1.
11 N. Katagiri, M. Okada, Y. Morishita and C. Kaneko, *Chem. Commun.*, 1996, 2137.
12 S. E. Ward, A. B. Holmes and R. McCague, *Chem. Commun.*, 1997, 2085.
13 D. Zhang and M. J. Miller, *J. Org. Chem.*, 1998, **63**, 755; V. K. Aggarwal and N. Monteiro, *J. Chem. Soc., Perkin Trans. 1*, 1997, 2531.
14 XSCANS X-ray Single Crystal Analysis System. Version 2.2. Bruker AXS Inc., Madison, Wisconsin, USA, 1994.
15 G. M. Sheldrick, 1999. SHELXTL Version 5.1, Bruker AXS Inc., Madison, Wisconsin, USA.

Unexpected dimerisation of a 2*H*-azaphosphirene complex

Rainer Streubel,* Hendrik Wilkens, Frank Ruthe and Peter G. Jones

Institut für Anorganische und Analytische Chemie der Technischen Universität Braunschweig, Postfach 3329, D-38023, Braunschweig, Germany. E-mail: r.streubel@tu-bs.de

Received (in Birmingham, UK) 1st September 2000, Accepted 3rd November 2000
First published as an Advance Article on the web

Heating a 2*H*-azaphosphirene complex in the solid state afforded the first head-to-tail dimer, a 2,5-dihydro-2,5-diphosphapyrimidine complex, a η¹-diphosphene complex and another complex having low-coordinated phosphorus centers; whereas the latter was detected only by ^{31}P NMR spectroscopy, the dimer was isolated and structurally characterized.

In comparison to 2*H*-azirenes[1] **I** (Scheme 1), which are versatile building blocks in heterocycle syntheses, the chemistry of heteroatom-substituted ring systems of type **II**–**IV** is much less explored. For example, transiently[2] formed 2*H*-azasilirenes **II** readily dimerise in solution in a head-to-head or head-to-tail manner, the orientation depending mainly on the carbon substituents.[3] Interestingly, even at low temperatures, 1*H*-diazirenes **III**[4] preferentially undergo ring enlargement[4] or rearrangement reactions,[5] but do not form dimers. Although 2*H*-azaphosphirenes **IV** have been claimed as intermediates, no dimerisation was reported; instead, ring cleavage occurred at room temperature to yield a short-lived phosphinidene and a nitrile derivative.[6] 1*H*-diazirene complexes **V** are, to the best of our knowledge, unknown. Recently, we reported syntheses[7] and reactions of 2*H*-azaphosphirene complexes **VI**, which gave access, *e.g.* to differently sized unsaturated phosphorus heterocycles either *via* ring cleavage[8] or *via* selective P–C[9] and P–N bond[10] cleavage ring expansion reactions.

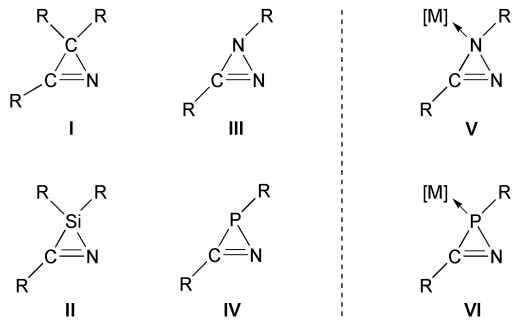

Scheme 1 2*H*-azirenes (**I**), heteroazirenes (**II**–**IV**), 1*H*-diazirene (**V**) and 2*H*-azaphosphirene complexes (**VI**) (**I**–**VI**: R, R′ = alkyl, aryl; [M] = metal complex fragment).

Here we report the first dimerisation of a 2*H*-azaphosphirene complex leading to a head-to-tail dimer, a 2,5-dihydro-2,5-diphosphapyrimidine complex; a η¹-diphosphene complex and another complex having low-coordinated phosphorus centers were detected as by-products.

Heating the neat 2*H*-azaphosphirene tungsten complex **1**[11] for a short period afforded three phosphorus-containing products **2**, **3** and **4** in a ratio of *ca.* 1:3:10 (Scheme 2); heating complex **1** for longer periods, *i.e.* 1 h, did not significantly affect the ratio. Whereas the η¹-diphosphene tungsten complex **2**[12] ([d_8]-toluene): δ 391.3 ppm (^1J(P,P) 513.4 Hz, ^1J(P,W) 230.8 Hz, P=*P*W(CO)$_5$), 443.1 ppm (^1J(P,P) 513.4 Hz) was isolated in 8% yield by column chromatography, the dinuclear complex **3** decomposed during chromatography, but the chemical shifts, phosphorus–phosphorus and phosphorus–tungsten coupling constant magnitudes of **3** (AM-type; δ (P_A) 360.9 ppm, ^3J(P,P) 162.1, ^1J(W,P) 264.3 Hz) (δ (P_M) 160.9 ppm, ^3J(P,P) 162.1, ^1J(W,P) 272.4 Hz) revealed the existence of low-coordinated phosphorus centers,[13] thus allowing a tentative structural assignment with an atom connectivity as shown in Scheme 2 (P_A = P=NR,P_M = P=CR_2). The unusually great ^3J(P,P) value might result from the two-fold η¹-coordination mode of the two phosphorus centers.[14] The main product, the 2,5-dihydro-2,5-diphosphapyrimidine tungsten complex **4**, was confirmed by elemental analyses and NMR spectroscopy.† Further investigations using the analogous 2*H*-azaphosphirene chromium and molybdenum complexes[15] showed that the reaction course strictly depended on the nature of the metal; in contrast to the chromium (and tungsten) complex, heating the 2*H*-azaphosphirene molybdenum complex afforded the corresponding η¹-diphosphene molybdenum complex[12] as main product.

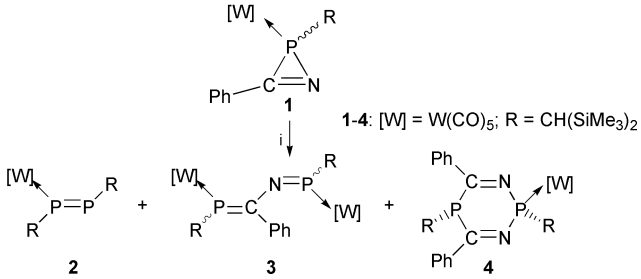

Scheme 2 *Reagents and conditions:* (i) 615 mg of complex **1**, 130 °C, 15 min; column chromatography (Al_2O_3, −50 °C, light petroleum–diethyl ether 90:10); **4**: bright yellow solid, yield: 43%, mp 156 °C (decomp.).

The ^{31}P NMR data of complex **4** are similar to those found for non-coordinated 2,5-dihydro-2,5-diphosphapyrimidine derivatives, which have been recently synthesized for the first time using a completely different approach.[16] The line broadenings in the ^{1}H and ^{13}C{^{1}H} NMR spectra of complex **4** at ambient temperature, which disappear upon cooling to −55 °C are remarkable; *e.g.* in the ^{13}C{^{1}H,^{31}P} NMR spectra two distinct resonances appear for the imino and also for the *ipso* carbon atoms of the phenyl rings. So far, we have no explanation for this phenomenon. Furthermore, the methine carbon atom (δ 9.9 ppm) and also the protons of one trimethylsilyl group (δ −0.73 ppm) of the three-coordinated phosphorus center resonate at remarkably high field, which probably indicates a shielding caused by the ring current of a nearby phenyl group. The molecular structure of complex **4** (Fig. 1), as established for the solid state by X-ray crystallography,‡ shows a slightly distorted boat conformation of the six-membered ring with the P1 and P2 atoms in the bow and stern positions (Fig. 2). The steric situation of the P2-bonded bis(trimethylsilyl)methyl group is noteworthy; as shown by the two different distances P2–C20 1.882(9) Å and P2–C13 1.829(10) Å, this group is asymmetrically flanked by the two phenyl rings, which act like a pincer, but only for one of the two trimethylsilyl groups. If this steric situation is retained in solution, this would convincingly explain the observed shielding of the proton and carbon atoms of the respective methine and trimethylsilyl groups.

Currently we are investigating the reaction of 2*H*-azaphosphirene complexes with various nickel(II) and palladium(0) complexes; such complexes have been shown to catalyze the

DOI: 10.1039/b007107m

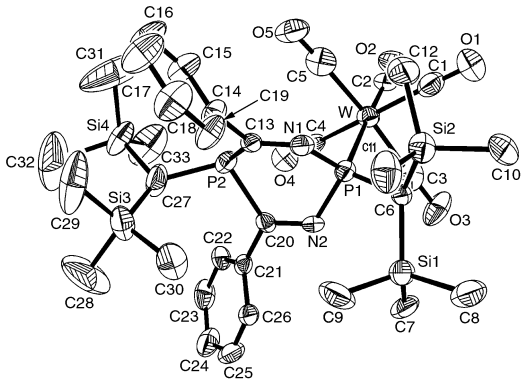

Fig. 1 Molecular structure of **4** in the crystal (ellipsoids represent 50% probability levels, hydrogen atoms are omitted for clarity). Selected bond lengths [Å] and angles [°]: W–C(2) 1.986(10), W–P(1) 2.521(2), P(1)–C(6) 1.796(8), P(1)–N(1) 1.7107(7), P(1)–N(2) 1.698(7), N(1)–C(13) 1.280(9), N(2)–C(20) 1.267(9), P(2)–C(27) 1.852(9), C(13)–C(14) 1.514(11), C(13)–C(14) 1.482(12); C(2)–W–P(1) 176.0(3), W–P(1)–C(6) 115.7(3), N(2)–P(1)–N(1) 103.6(3), N(2)–P(1)–C(6) 107.1(4), N(1)–P(1)–C(6) 102.0(4), C(13)–P(2)–C(20) 95.5(4).

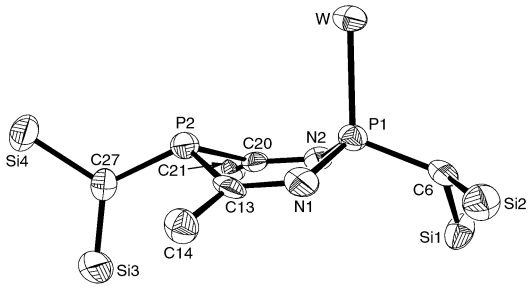

Fig. 2 Side-view showing the boat conformation of **4** (reduced molecular structure).

dimerisation of 1*H*-phosphirenes and 1*H*-phosphirene complexes.[17]

We are grateful to Priv.-Doz. Dr Dietrich Gudat for low-temperature NMR measurements and to the Deutsche Forschungsgemeinschaft and the Fonds der Chemischen Industrie for financial support.

Notes and references

† Satisfactory elemental analysis were obtained for complex **4**. NMR data were recorded in $CDCl_3$ solutions at 50.3 MHz (^{13}C) and 81.0 (^{31}P), using TMS and 85% H_3PO_4 as standard references; *J*/Hz. Selected spectroscopic data for **4**: ^{1}H-NMR (rt): δ −0.15 (v br, 18H, $SiMe_3$), 0.34 (s, 18H, $SiMe_3$), 0.98 (d, ^2J(P,H) 11.8 Hz, 1H, P^{2}C*H*), 1.87 (d, ^2J(P,H) 4.7 Hz, 1H, P^{1}C*H*), 7.43 (s br, 10H, C$H_{aromat.}$). ^{1}H-NMR (−55 °C): δ −0.73 (s, 9H, $SiMe_3$), 0.28 (s, 18H, $SiMe_3$), 0.31 (s, 9H, $SiMe_3$), 0.94 (d, ^2J(P,H) 11.8 Hz, 1H, P^{2}C*H*), 1.80 (d, ^2J(P,H) 4.7 Hz, 1H, P^{1}C*H*), 7.30 (s br, 4H, C$H_{aromat.}$), 7.44 (s br, 6H, C$H_{aromat.}$). ^{13}C{^{1}H}-NMR (rt): δ 2.1 (d br, ^3J(P,C) 3.8 Hz, $SiMe_3$), 3.3 (d, ^3J(P,C) 1.8 Hz, $SiMe_3$), 9.9 (d, ^1J(P,C) 52.6 Hz, *C*H($SiMe_3$)$_2$), 29.2 (dd, ^1J(P,C) 27.0 Hz, ^4J(P,C) 1.5 Hz, *C*H($SiMe_3$)$_2$), 128.2 (s br, *C*H$_{aromat.}$), 128.3 (s br, *C*H$_{aromat.}$), 129.7 (s, *C*H$_{aromat.}$), 130.1 (s br, *C*H$_{aromat.}$), 140.4 (m$_c$, *C*$_{aromat.}$), 184.6 (m, PN*C*), 197.8 (dd, ^2J(P,C) 7.4 Hz, ^4J(P,C) 2.2 Hz, *cis*-*C*O), 199.5 (d, ^2J(P,C) 24.2 Hz, *trans*-*C*O). ^{13}C{^{1}H,^{31}P}-NMR (−55 °C): δ 1.3 (s, $SiMe_3$), 2.4 (s, $SiMe_3$), 3.0 (s, $SiMe_3$), 8.9 (s, *C*H($SiMe_3$)$_2$), 28.4 (s, *C*H($SiMe_3$)$_2$), 128.1 (s, *C*H$_{aromat.}$), 128.7 (s, *C*H$_{aromat.}$), 129.6 (s, *C*H$_{aromat.}$), 130.6 (s, *C*H$_{aromat.}$), 138.9 (s, *C*$_{aromat.}$), 140.3 (s, *C*$_{aromat.}$), 183.6 (s, PN*C*), 185.6 (s, PN*C*), 197.6 (s, *cis*-*C*O), 200.2 (s, *trans*-*C*O). ^{31}P{^{1}H}-NMR: δ −0.6 (m$_c$, P^2), 79.9 (d, ^3J(P,P) 15.2 Hz, ^1J(P,W) 266.1 Hz, P^1).

‡ *Crystal structure determination* for **fidi1**: $C_{33}H_{48}N_2O_5P_2Si_2W$; *M* = 910.90, monoclinic, space group *P*2/*n*, *a* = 18.440(3), *b* = 9.831(3), *c* = 25.145(5) Å, β = 111.491(10)°, *U* = 4241.3(16) Å^3, *Z* = 4, D_c = 1.426 Mg m^{-3}, μ = 2.949 mm^{-1}, *F*(000) = 1840, 7430 independent reflections to $2\theta_{max.}$ 50°, *T* = 173 K, *S* = 0.763, $R(F > 4\sigma(F))$ = 0.0537, $R_w(F^2)$ = 0.0731, 171 restraints and 424 parameters, highest peak 1.162 and deepest hole −0.712 e Å^{-3}. The X-ray dataset was collected with monochromated Mo-Kα radiation (λ = 0.71073 Å) on a Siemens P4 four-circle diffractometer. CCDC 182/1840. See http://www.rsc.org/suppdata/cc/b0/b007107m/ for crystallographic files in .cif format.

1 For reviews on 2*H*-azirenes see: A. Padwa, *Acc. Chem. Res.*, 1976, **9**, 371; V. Nair and K. H. Kim, *Heterocycles*, 1977, **7**, 353; H.-J. Hansen and H. Heimgartner, in *1,3-Dipolar Cycloaddition Chemistry*, ed. A. Padwa, Wiley, New York, 1984, ch. 2, p. 177.

2 A stable 2*H*-azasilirene derivative has been described, but no reactions were mentioned: (*a*) R. Okazaki, H. Suzuki and N. Tokitoh, *XIth International Symposium on Organosilicon Chemistry*, Montpellier, France, 1996, poster abstract PB60; (*b*) R. Okazaki and R. West, in *Multiply Bonded Main Group Metals and Metalloids*, ed. R. West and F. G. A. Stone, Academic Press, London, 1996, p. 232.

3 M. Weidenbruch and A. Schäfer, *J. Organomet. Chem.*, 1986, **314**, 25; M. Weidenbruch and P. Will, *Z. Anorg. Allg. Chem.*, 1996, **622**, 1811.

4 For a review on transiently formed 1*H*-diazirenes, see: X. Creary, *Acc. Chem. Res.*, 1992, **25**, 31.

5 G. Alcaraz, V. Piquet, A. Baceiredo, F. Dahan, W. W. Schoeller and G. Bertrand, *J. Am. Chem. Soc.*, 1996, **118**, 1060.

6 M. Rahmoune, Y. Y. C. Yeung Lam Ko, F. Tonnard and R. Carrie, PSI-BLOCS Conference, Palaiseau, France, 1988, poster abstract.

7 R. Streubel, J. Jeske, P. G. Jones and R. Herbst-Irmer, *Angew. Chem., Int. Ed. Engl.*, 1994, **33**, 80.

8 R. Streubel, A. Ostrowski, H. Wilkens, F. Ruthe, J. Jeske and P. G. Jones, *Angew. Chem., Int. Ed. Engl.*, 1997, **36**, 378.

9 R. Streubel, H. Wilkens, A. Ostrowski, C. Neumann, F. Ruthe and P. G. Jones, *Angew. Chem., Int. Ed. Engl.*, 1997, **36**, 1492.

10 R. Streubel, C. Neumann and P. G. Jones, *J. Chem. Soc., Dalton Trans.*, 2000, 2495.

11 R. Streubel, A. Ostrowski, S. Priemer, U. Rohde, J. Jeske and P. G. Jones, *Eur. J. Inorg. Chem.*, 1998, 257.

12 H. Lang, O. Orama and G. Huttner, *J. Organomet. Chem.*, 1985, **291**, 293.

13 M. Regitz and O. J. Scherer, *Multiple Bonds and Low Coordination in Phosphorus Chemistry*, Thieme, Stuttgart, 1990.

14 On the change of the *J*(P,P) coupling constant value of a 1,3-diphosphabuta-1,3-diene derivative upon metal coordination, see: R. Appel, B. Niemann, W. Schuhn and N. Siabalis, *J. Organomet. Chem.*, 1988, **347**, 299.

15 R. Streubel, F. Ruthe and P. G. Jones, *Eur. J. Inorg. Chem.*, 1998, 571.

16 A. Maraval, B. Donnadieu, A. Igau and J. P. Majoral, *Organometallics*, 1999, **18**, 3138.

17 N. H. Tran Huy, L. Ricard and F. Mathey, *J. Chem. Soc., Chem. Commun.*, 2000, 1137.

Enhanced electron phase-transfer catalysis due to the formation of substrate–catalyst inclusion complexes

Hiromichi Noguchi,*† Haruhiko Tsutsumi and Makoto Komiyama*

Department of Chemistry and Biotechnology, Graduate School of Engineering, The University of Tokyo, Hongo, Bunkyo-ku, Tokyo 113-8656, Japan. E-mail: hnoguchi@cc.eng.toyo.ac.jp

Received (in Cambridge, UK) 12th September 2000, Accepted 4th October 2000
First published as an Advance Article on the web

A redox-active macrocyclic ionene oligomer, cyclobis(paraquat-*p*-phenylene), exhibited an enhanced activity as an electron phase-transfer catalyst for the reduction of quinones compared with acyclic benzyl viologen, due to the inclusion of the substrate into the catalyst cavity.

Compounds having one or more viologen units have attracted much attention because of their versatile applications.[1,2] Of particular interest among recent developments are a series of elaborate works on supramolecular chemistry by Stoddart *et al.*[2] which have led to successful construction of a variety of supramolecular architectures such as pseudorotaxanes, rotaxanes and catenanes mainly using a redox-active macrocyclic ionene oligomer,[3] *i.e.* cyclobis(paraquat-*p*-phenylene)[4] **1**. Theirs as well as work by other research groups[5] unambiguously show that **1** and related compounds form inclusion complexes with a variety of guests. However, little is known to date of their applicability in other fields including catalysis.

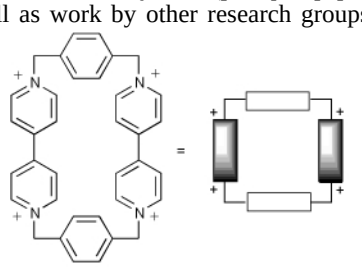

1

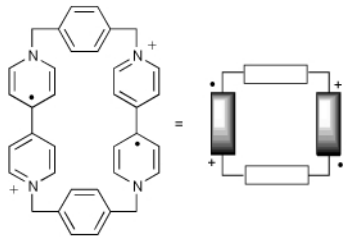

2

On the other hand, electron transfer catalysis by viologen compounds, which function as mediators of electron transfer, has continuously been attracting considerable interest.[1,6] Such compounds have been applied to the reduction of various substrates such as aldehydes and ketones,[6a,b] quinones,[6c] azobenzene,[6d] acrylonitrile,[6e] nitroalkenes,[6f] and nitroarenes,[6g] to the reductive desulfonation of α-nitro sulfones,[6h] and to the dehalogenation of diphenylbromomethane,[6i,j] *gem*- and *vic*-dibromides[6k,l] and α-halogeno ketones[6m] with either zinc or sodium dithionite in either a monophase or a two-phase solvent system. The viologen compounds thus far used include alkyl viologens,[6b,f–h,l,m] ionene polymers[7] having viologen units in the main chains,[6d,i–k] vinyl polymers having viologen units in the pendant groups,[6a,c,e] and so forth. However, no cyclic viologen compounds have ever been examined for catalysis.

The present research combining the above two fields of chemistry was motivated by the premise that, if the substrate is included in the cavity of **2**, a reduced species of **1**, the viologen units might be able to mediate the electron transfer more efficiently than acyclic viologens such as benzyl viologen **3** because of the close vicinity of the substrate to the units, and hence **1** would exhibit a higher activity of electron transfer catalysis than **3**. This communication reports that the experimental results using quinones as substrates validated this conjecture. In addition, to the best of our knowledge, this work presents the first example that the fundamental constituent of a cyclophane, *i.e.* the viologen moiety in the case of **1**, directly plays a pivotal catalytic role for the substrate included in the cavity of the host.

Fig. 1 shows the results of reduction of 1,4-benzoquinone with zinc in the presence of **1** in an alkyl acetate–H_2O (1:1) two-phase system at 25 °C.[8] Conversion of the substrate increased in the order: AcOMe < AcOEt < AcOBu. Thus, in general, the extent of reduction in the two-phase solvent systems became increasingly higher with increase in the hydrophobicity of the organic phase.[9] 1,4-Naphthoquinone could also be reduced similarly to 1,4-dihydroxynaphthalene. It should also be noted that, under the present reaction conditions, the reduction of quinones occurred to a considerable extent even in the absence of catalyst, and that **3** exhibits almost no ability to mediate electron transfer. However, it is obvious that **1** is, as expected, a much better mediator of electrons than **3**.

Fig. 2 depicts the results of the inhibition experiments using compounds having a phenyl or *p*-phenylene group, which can be included in the cavity of **1**, for the reduction of benzoquinone with zinc in different two-phase solvent systems, using either **1** or **3** as a catalyst.[8] The reduction of benzoquinone in AcOBu–H_2O (1:1) with use of **1** was retarded by the addition of 1,4-bis[2(2-hydroxyethoxy)ethoxy]benzene **4**.[10] Similarly, the same reduction in methyl benzoate[11] (BzOMe)–H_2O (1:1) or phenyl acetate[11] (AcOPh)–H_2O (1:1) two-phase systems was also retarded in comparison with the reduction in AcOBu–H_2O (1:1), in spite of the hydrophobic nature of these organic solvents (see above). On the other hand, almost no distinct inhibition effect was observed when **3** was used as a catalyst.

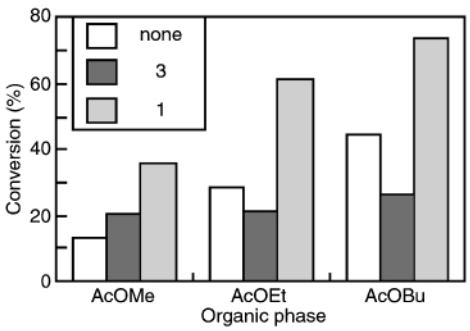

Fig. 1 Reduction of benzoquinone with zinc in alkyl acetate–H_2O (1:1) two-phase systems in the presence of **1** or **3** and in the absence of catalyst. *Conditions*: benzoquinone, 40 mM, 1.0 ml; viologen compound, 20 mM (as viologen unit), 1.0 ml; Zn, 0.20 mmol; 25 °C, 1.0 h.

† Present address: Department of Applied Chemistry, Faculty of Engineering, Toyo University, Kujirai, Kawagoe, Saitama 350-8585, Japan.

DOI: 10.1039/b007404g

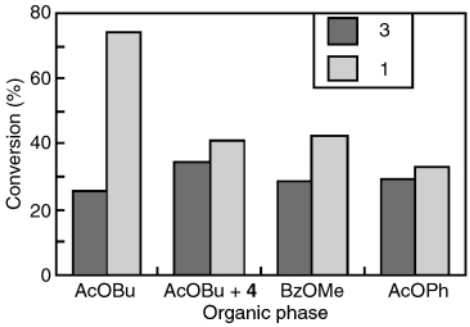

Fig. 2 Reduction of benzoquinone with zinc in the presence of **1** or **3** in different two-phase systems to prove that inclusion of the substrate into the cavity of **1** occurs; AcOBu–H_2O (1:1), AcOBu–H_2O containing 1,4-bis[2(2-hydroxyethoxy)ethoxy]benzene **4**, BzOMe–H_2O (1:1), and AcOPh–H_2O (1:1) (from left to right). *Conditions:* benzoquinone, 40 mM, 1.0 ml; viologen compound, 20 mM (as viologen unit), 1.0 ml; template compound **4**, 0.10 mmol; Zn, 0.20 mmol; 25 °C, 1.0 h.

Thus, it is concluded that inclusion of the substrate in the cavity of **1** does occur, and hence the enhancement of the catalytic activity of **1** compared with that of **3** (*cf.* Figs. 1 and 2) in the two-phase solvent systems can be attributed to the easier electron mediation due to the close proximity of the included substrate to the redox-active viologen units.

Cyclic voltammetry of **1** in acetonitrile exhibits only two reversible reduction processes,[12] suggesting that the two viologen units in **1** are independent of each other in the reduction process. Thus, the species produced by the initial two-electron reduction of **1** with zinc is most likely to be radical cation **2**. From this the fundamental mechanism of the catalysis in a two-phase solvent system can be derived as illustrated in Scheme 1. First, **1** is reduced with zinc in the aqueous phase to **2**, which is then transferred into the organic phase[13] where the substrate (**Q**) is included in the cavity of **2**. The substrate is then reduced to hydroquinone (**QH_2**) with concomitant reoxidation of **2** to **1**. The regenerated **1** is transferred back into the aqueous phase to participate in the next catalytic cycle. The slow reactions in the two-phase solvent systems as compared with that in homogeneous DMSO–H_2O (1:1)[14] could possibly be attributed, at least in part, to the slow extraction rate of **2** from the aqueous phase into the organic phase. The mechanism for the reduction in a homogeneous mixed solvent would be essentially the same as above, apart from the absence of the phase transfer processes. However, since chemical shift values of the protons of **1** were changed on mixing it with quinones in DMSO-d_6–D_2O (4:1), the possibility cannot be ruled out, irrespective of the reaction modes, that the substrate first included in the cavity of **1** is then reduced after reduction of the host in the inclusion complex.

In summary, when a viologen-containing macrocyclic ionene oligomer was used as catalyst, electron transfer catalysis on quinone reduction could be enhanced due to facilitated electron mediation between the substrate and the viologen units in the inclusion complex. Further investigation of catalysis using **1** and related compounds is in progress to reveal the scope and limitations as well as to gain a deeper insight into the reaction mechanism.

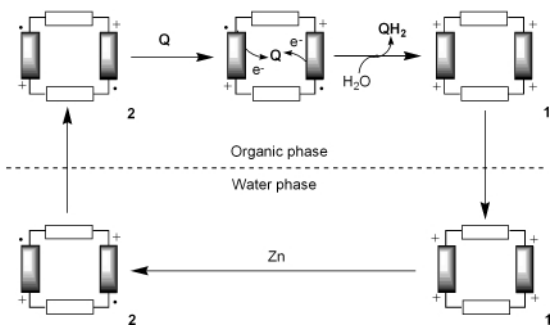

Scheme 1 Fundamental mechanism for the reduction of a quinone compound (**Q**) with zinc in an organic solvent–H_2O (1:1) two-phase system in the presence of **1**.

Part of this work was supported by the Grant-in-Aid for Scientific Research, No. 026550661, from the Ministry of Education, Science and Culture, Japan.

Notes and references

1 X. D. Yu, S. Li and F. Liu, *Polymeric Materials Encyclopedia*, J. C. Salamone (Ed.-in-Chief), CRC Press, Boca Raton, FL, 1996, vol. 11(T–Z), p. 8606, and references therein.

2 For reviews, see for example: D. Philp and J. F. Stoddart, *Synlett*, 1991, 445; D. B. Amabilino and J. F. Stoddart, *Chem. Rev.*, 1995, **95**, 2725; D. Philp and J. F. Stoddart, *Angew. Chem., Int. Ed. Engl.*, 1996, **35**, 1154.

3 H. Noguchi, *Polymeric Materials Encyclopedia*, J. C. Salamone (Ed.-in-Chief), CRC Press, Boca Raton, FL, 1996, vol. 5 (H–L), p. 3381.

4 For synthesis of **1**, see: C. L. Brown, D. Philp and J. F. Stoddart, *Synlett*, 1991, 462; M. Asakawa, W. Dehaen, G. L'abbe, S. Menzer, J. Nouwen, F. M. Raymo, J. F. Stoddart and D. J. Williams, *J. Org. Chem.*, 1996, **61**, 9591.

5 See for example: M. J. Gunter, D. C. R. Hockless, M. R. Johnston, B. W. Skelton and A. H. White, *J. Am. Chem. Soc.*, 1994, **116**, 4810; M. Bauer, W. M. Müller, U. Müller, K. Rissanen and F. Vögtle, *Liebigs Ann.*, 1995, 649; A. C. Benniston, P. R. Mackie and A. Harriman, *Angew. Chem., Int. Ed.*., 1998, **37**, 354; P. E. Mason, W. S. Bryant and H. W. Gibson, *Macromolecules*, 1999, **32**, 1559; S. A. Staley and B. D. Smith, *Tetrahedron Lett.*, 1996, **37**, 283.

6 (*a*) K. Ageishi, T. Endo and M. Okawara, *J. Polym. Sci., Polym. Chem. Ed.*, 1983, **21**, 175; (*b*) T. Endo, Y. Saotome and M. Okawara, *Tetrahedron Lett.*, 1985, **26**, 4525; (*c*) M. Takeishi, Y. Yabe and S. Hayama, *Makromol. Chem., Rapid Commun.*, 1981, **2**, 453; (*d*) F.-T. Liu, N. Song, X.-D. Yu and S.-B. Li, *Macromol. Chem. Phys.*, 1994, **195**, 2169; (*e*) T. Endo, K. Ageishi and M. Okawara, *J. Org. Chem.*, 1986, **51**, 4309; (*f*) H. Tomioka, K. Ueda, H. Ohi and Y. Izawa, *Chem. Lett.*, 1986, 1359; (*g*) K. K. Park, C. H. Oh and W. K. Joung, *Tetrahedron Lett.*, 1993, **34**, 7445; (*h*) K. K. Park, C. W. Lee and S. Y. Choi, *J. Chem. Soc., Perkin Trans. 1*, 1992, 601; (*i*) F. Liu, X. Yu, L. Feng and S. Li, *Eur. Polym. J.*, 1995, **31**, 819; (*j*) F. Liu, X. Yu, S. Li, *J. Polym. Sci., Part A, Polym. Chem.*, 1994, **32**, 1043; (*k*) T. Endo, A. Kameyama, Y. Nambu, Y. Kashi and M. Okawara, *J. Polym. Sci., Part A, Polym. Chem.*, 1990, **28**, 2509; (*l*) R. Maidan, Z. Goren, J. Y. Becker and I. Willner, *J. Am. Chem. Soc.*, 1984, **106**, 6217; (*m*) K. K. Park, C. W. Lee and S.-Y. Oh, *J. Chem. Soc., Perkin Trans. 1*, 1990, 2356.

7 Recent reviews on ionene polymers: W. H. Meyer and L. Dominguez, *Polymer Electrolyte Reviews—2*, ed. J. R. MacCallum and C. A. Vincent, Elsevier Sci. Publ., London, 1989, ch. 6, p. 191; H. Noguchi, *Polymeric Materials Encyclopedia*, J. C. Salamone (Ed.-in-Chief), CRC Press, Boca Raton, FL, 1996, vol. 5 (H–L), p. 3392.

8 A typical reaction procedure was as follows. In an atmosphere of oxygen-free nitrogen 1.0 ml of a 40 mM quinone solution in an organic solvent and 1.0 ml of a 10 mM solution of **1**·4Cl^- in 50 mM phosphate buffer (pH 7.0), were placed in a Schlenk tube, and the mixture was deaerated three times by the freeze–thaw technique. Then, 0.20 mmol of activated zinc powder, was added in an atmosphere of nitrogen. The mixture was vigorously stirred (>1200 rpm) with a Teflon-coated magnetic bar for l h at 25 °C. The product was solely hydroquinone and quantified by HPLC. In all the experiments, the concentration of the viologen unit was the same (20 mM) with chloride as counter ion. To ensure the accuracy of the concentration of **1**·4Cl^-, special care was taken of the water content in its synthesized sample, which was determiend by elemental analysis.

9 It should be noted that this statement is only superficial, because the solubility of the alkyl acetates in water greatly depends on the alkyl groups, indicating that the reaction conditions can be considerably different from one another.

10 This compound has been used as a template in the template-directed synthesis of **1**,[4] and therefore can be included in the cavity of **1**.

11 Note that the phenyl groups of these organic solvents can be included in the cavity of **1**. See for example: T. T. Goodnow, M. V. Reddington, J. F. Stoddart and A. E. Kaifer, *J. Am. Chem. Soc.*, 1991, **113**, 4335.

12 P. R. Ashton, C. L. Brown, E. J. T. Chrystal, T. T. Goodnow, A. E. Kaifer, K. P. Parry, D. Philp, A. M. Z. Slawin, N. Spencer, J. F. Stoddart and D. J. Williams, *J. Chem. Soc., Chem. Commun.*, 1991, 634.

13 Note that **2** is more hydrophobic than **1**, and hence will be transferred into the organic phase more easily than **1**.

14 The reduction of quinones with zinc in a homogeneous mixed solvent such as DMSO–H_2O (1:1) was, on the whole, faster than the same reaction in a two-phase solvent system. However, clear comparison of the catalytic activities of viologen compounds **1** and **3** was hampered by the precipitation of radical cation **2**.

N-Hydroxyphthalimide-catalyzed radical addition of 1,3-dioxolanes and molecular oxygen to alkenes under ambient conditions: a new route to β-oxycarbonyl compounds

Kazutaka Hirano, Takahiro Iwahama, Satoshi Sakaguchi and Yasutaka Ishii*

Department of Applied Chemistry, Faculty of Engineering & High Technology Research Center, Kansai University, Suita, Osaka 564-8680, Japan. E-mail: ishii@ipcku.kansai-u.ac.jp

Received (in Cambridge, UK) 18th October 2000, Accepted 2nd November 2000
First published as an Advance Article on the web

A novel catalytic hydroxyacylation of alkenes using 1,3-dioxolanes and molecular oxygen has been developed, and the reaction of 2-methyl-1,3-dioxolane with methyl acrylate under dioxygen atmosphere in the presence of catalytic amounts of NHPI and $Co(OAc)_2$ produced the corresponding adduct in 81% yield.

Addition of aldehydes to terminal alkenes has received attention as a method for the synthesis of ketones from aldehydes.[1] The frequently used methodologies are the direct hydroacylation of alkenes with aldehydes by transition-metal catalysts[1] and the addition of acyl radicals to alkenes bearing electron-withdrawing substituents such as fumarate by radical initiators.[2] If the concomitant introduction of acyl and hydroxy moieties to alkenes can be carried out by a cascade reaction, this type of reaction is referred to as *hydroxyacylation* and would provide a novel route to β-oxycarbonyl compounds which constitute important structural subunits in key intermediates leading to pharmaceuticals [eqn. (1)].[3] Although there is one report on the hydroxyacylation of alkenes like acrylates with acyl radicals from aldehydes using dioxygen as a hydroxy source assisted by a cobalt(II) Schiff-base complex,[4] the attempt was not fully successful due to the decarbonylation from acyl radicals as well as the reaction of acyl radicals with O_2 leading to carboxylic acids which cause undesired side reactions.

***Hydroxy**acylation*

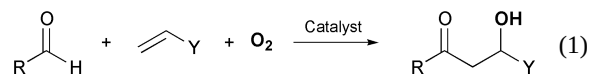

(1)

To overcome these drawbacks arising from acyl radicals, we employed 1,3-dioxolanes, masked aldehydes, as an acyl source in place of an aldehyde.[5] This paper describes the development of a novel catalytic method leading to β-hydroxy carbonyl compounds after deprotection under acidic conditions.

Recently, we have shown that *N*-hydroxyphthalimide (NHPI) combined with a Co(II) species serves as a catalyst for the generation of alkyl radicals from alkanes even under ambient conditions, and that the resulting alkyl radicals are readily captured by O_2 to give oxygenated products.[6] In this catalytic system, phthalimide *N*-oxyl (PINO) is the active species abstracting hydrogen atoms from the alkanes.[6a] This finding prompted us to study the generation of α,α-dioxaalkyl radicals from 1,3-dioxolanes and their addition to alkenes using the NHPI/Co(II)–O_2 catalytic system [eqn. (2)].

At the beginning, a mixture of 2-methyl-1,3-dioxolane (**1a**) (15 mmol) and methyl acrylate (**2a**) (3 mmol) was allowed to react under O_2 (1 atm) in the presence of NHPI (5 mol%) and a small amount of $Co(OAc)_2$ (0.05 mol%) at rt for 3 h (Table 1, Run 1).† The apparent hydroxyacylation based on the concomitant introduction of a dioxaalkyl radical and a hydroxy group to **2a** was achieved to form β-hydroxy ketal (**3a**) in 81% yield. In a previous paper, we showed that a Co(III)–dioxygen complex derived from the Co(II) species and O_2 assists the formation of a PINO radical from the NHPI.[6a] Accordingly, the Co(III) which fails to react with O_2 could not promote the reaction under O_2 at rt (Run 2).[6a,7]

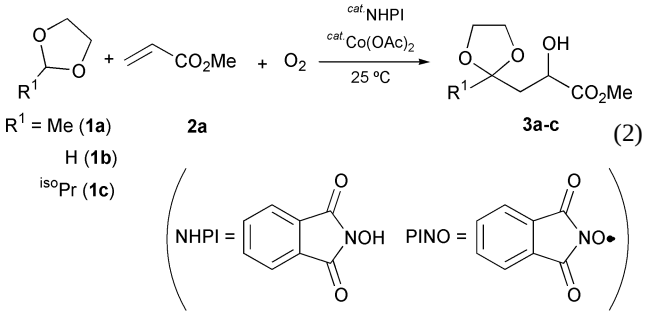

(2)

From 1,3-dioxolane (**1b**), the corresponding adduct **3b** was obtained in high yield (82%) (Run 4). The introduction of the masked formyl group to **2a** is promising, since the direct use of formaldehyde is restricted due to its intractability. These dioxolane moieties could be easily deprotected upon treatment under acidic conditions to form the corresponding carbonyl compounds [eqns. (3) and (4)].

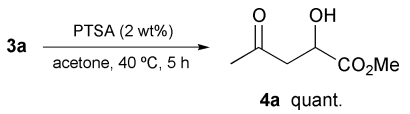

(3)

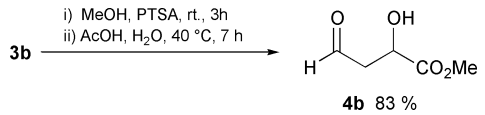

(4)

The reaction of **1a** or **1b** with various alkenes was run under selected reaction conditions (Table 2). Acrylonitrile (**2e**) was found to serve as a good acceptor of **1a** and **1b** in a similar manner as **2a**, giving cyanohydrin derivatives in good yields. However, methyl crotonate (**2c**) bearing a β-methyl group retarded the hydroxyacylation, probably owing to the steric hindrance towards attack by an α,α-dioxaalkyl radical on **2c**.[8] To our surprise, methyl vinyl ketone (**5a**) reacted with **1a** to afford a cleaved product, 3-(1,3-dioxolan-2-yl)butanoic acid (**6**) in 83% yield along with 3-(1,3-dioxolan-2-yl)butylaldehyde (**7**)

Table 1 Reaction of **1a–c** with methyl acrylate (**2a**)[a]

Run	**1a–c**	NHPI/ mol%	Co(II)/ mol%	*t*/h	Yield (%)[b]
1	**1a**	5	0.05	3	81
2[c]	**1a**	5	0.05	3	n.d.
3	**1a**	—	0.05	3	1
4[d]	**1b**	10	0.1	2	82
5	**1c**	5	0.1	14	76

[a] **2a** (3 mmol) was allowed to react with **1a–c** (15 mmol) in the presence of NHPI and $Co(OAc)_2$ under atmospheric oxygen at rt. [b] GC yield. [c] $Co(acac)_3$ was used. [d] **1b** (30 mmol) was used.

DOI: 10.1039/b008418m

Table 2 Reaction of **1a–b** with various alkenes under ambient conditions[a]

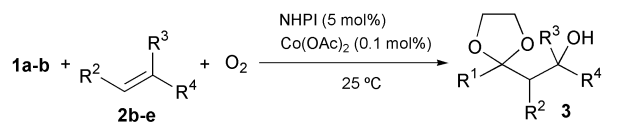

Run	1a–b	2b–e R²	R³	R⁴		t/h	3 (%)[b]
1	**1a**	H	Me	CO_2Me	**2b**	15	84
2[c]	**1a**	Me	H	CO_2Me	**2c**	15	16
3[d]	**1a**	CO_2Et	H	CO_2Et	**2d**	2	77
4	**1a**	H	H	CN	**2e**	16	77[e]
5	**1b**	H	Me	CO_2Me	**2d**	15	60
6	**1b**	H	H	CN	**2e**	16	60[e]

[a] **2b–e** (3 mmol) were allowed to react with **1a–b** (15 mmol) in the presence of NHPI (5 mol%) and $Co(OAc)_2$ (0.1 mol%) under atmospheric oxygen at rt. [b] GC yield. [c] NHPI (10 mol%) was used. [d] $Co(OAc)_2$ (0.05 mol%) was used. [e] Isolated yield.

(4%) [eqn. (5)]. The carboxylic acid **6** is considered to be formed *via* the further oxidation of aldehyde **7**.[9]

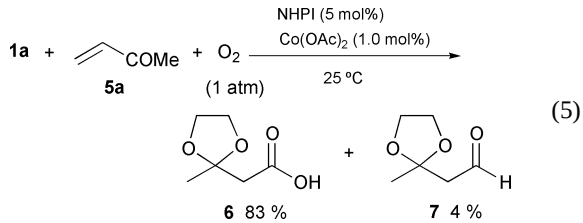

(5)

A plausible reaction path for the apparent hydroxyacylation of **2a** with **1a** under dioxygen is shown in Scheme 1. The reaction may be initiated by the hydrogen atom abstraction from NHPI by the action of the Co(III)–dioxygen complex, giving PINO which then abstracts the dioxolane hydrogen of the **1a** to form an dioxolane radical **I**. The **I** radical having a highly nucleophilic character seems to readily add to **2a**, yielding a radical species **II**. Under the conditions in which O_2 is present in the reaction system, the resulting radical **II** is rapidly trapped by O_2 to give a hydroperoxide **III**. It is well-known that hydroperoxides like **III** are subjected to redox decomposition by Co ions to form an alkoxyl radical **IV** which is eventually

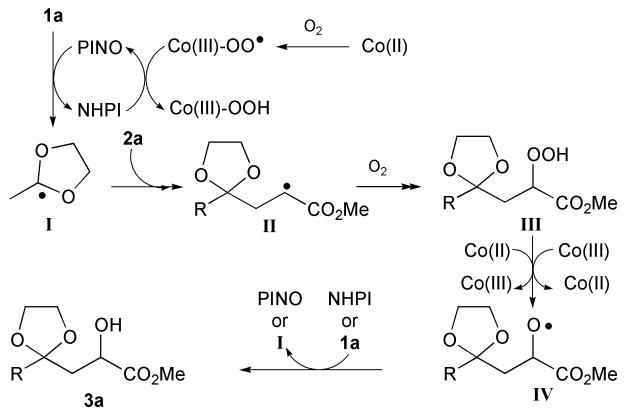

Scheme 1 Proposed reaction path for the radical addition of **1a** to **2a** under dioxygen in the presence of NHPI and $Co(OAc)_2$.

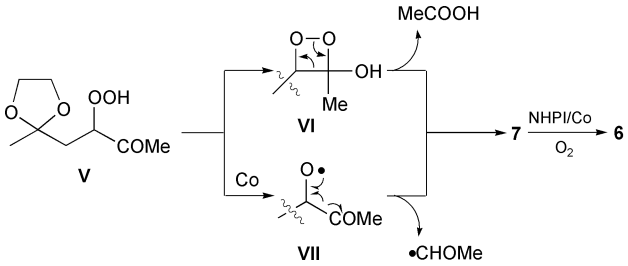

Scheme 2

converted into **3a** through the hydrogen abstraction from either NHPI or **1a**.[10]

Although it seems rather hazardous to make an accurate assessment about the reaction path for the formation of **6** from **1a** and methyl vinyl ketone **5a**, we can make two proposals which seem to agree with the experimental results. It is probable that an α-hydroperoxyketone **V** derived from **1a** and **5a** might decompose into aldehyde **7** *via* formation of a hydroxydioxetane **VI** (Scheme 2). This type of reaction through the hydroxydioxetane is shown in the autoxidation of ketones like diisopropyl ketone.[11] However, an alternative proposal is also possible, *viz.* the hydroperoxide **V** is subject to the redox decomposition to generate an alkoxy radical intermediate **VII** which then is converted into **7** *via* β-scission.

In conclusion, we have developed a novel method for the introduction of both a masked acyl or formyl group and a hydroxy or keto function to a double bond of alkenes. Further work on the extension of this method is actively underway.

This work was partly supported by the Japan Society for the Promotion of Science under the Research for the Future program JSPS.

Notes and references

† *A typical procedure for reaction of 2-methyl-1,3-dioxolane **1a** with methyl acrylate **2a***: To a solution of **1a** (15 mmol), NHPI (0.15 mmol) and $Co(OAc)_2$ (0.0015 mmol) in a two-necked flask, equipped with a balloon filled with O_2 (1 atm), was added **2a** (3 mmol). The mixture was vigorously stirred at rt for 3 h. The recovery of unreacted **1a** under a reduced pressure followed by flash chromatography on silica gel (*n*-hexane–AcOEt = 1 : 2) afforded methyl 2-hydroxy-4-(1,3-dioxolan-2-yl)valerate (**3a**) (462 mg, 81% yield) as a colorless liquid.

1 Recent review: C.-H. Jun, J.-B. Hong and D.-Y. Lee, *Synlett*, 1999, **1**, 1.
2 M. Tracy and Jr. Patrick, *J. Org. Chem.*, 1952, **17**, 1009.
3 M. Braun, *Angew. Chem., Int. Ed. Engl.*, 1987, **26**, 24; C. H. Heathcock, *Comprehensive Carbanion Chemistry*, ed. E. Buncel and T. Durst, Elsevier, Amsterdam, 1984, Chap. 4.
4 T. Punniyamurthy, B. Bhatia and J. Iqbal, *J. Org. Chem.*, 1994, **59**, 850.
5 The use of dioxolanes as masked aldehydes has been extensively studied: H.-S. Dang and B. P. Roberts, *Tetrahedron Lett.*, 1999, **40**, 8929; A. Gross, L. Fensterbank, S. Bogen, R. Thouvenot and M. Malacria, *Tetrahedron*, 1997, **53**, 13797.
6 (*a*) Y. Yoshino, Y. Hayashi, T. Iwahama, S. Sakaguchi and Y. Ishii, *J. Org. Chem.*, 1997, **62**, 6810; (*b*) S. Sakaguchi, T. Takase, T. Iwahama and Y. Ishii, *Chem. Commun.*, 1998, 2037, and references therein.
7 E. C. Niederhoffer, J. H. Timmons and A. E. Martell, *Chem. Rev.*, 1984, **84**, 137.
8 B. Giese, *Angew. Chem., Int. Ed. Engl.*, 1983, **22**, 753.
9 We have reported that aldehydes are readily oxidized to corresponding carboxylic acids with dioxygen by the NHPI–$Co(OAc)_2$ system under ambient conditions: T. Iwahama, Y. Yoshino, T. Keitoku, S. Sakaguchi and Y. Ishii, *J. Org. Chem.*, 2000, in print.
10 R. A. Sheldon and J. K. Kochi, *Metal-Catalyzed Oxidation of Organic Compounds*, Academic Press, New York, 1981.
11 W. Adam, *The Chemistry of Peroxide*, ed. S. Patai, John Wiley & Sons, New York, 1983, p. 830.

ChemComm

A short synthesis of camptothecin *via* a 2-fluoro-1,4-dihydropyridine

M.-Lluïsa Bennasar,* Cecília Juan and Joan Bosch

Laboratory of Organic Chemistry, Faculty of Pharmacy, University of Barcelona, Barcelona 08028, Spain. E-mail: bennasar@farmacia.far.ub.es

Received (in Liverpool, UK) 19th September 2000, Accepted 1st November 2000
First published as an Advance Article on the web

Addition of the enolate derived from isopropyl α-(methylsulfanyl)butyrate to *N*-(quinolylmethyl)-2-fluoropyridinium triflate 7, followed by oxidation–hydrolysis of the resultant 2-fluoro-1,4-dihydropyridine 8b afforded pyridone 9b, from which 20-deoxycamptothecin (11), a known precursor of camptothecin, was synthesized by a radical cyclization–desulfurization, with subsequent elaboration of the lactone E ring by chemoselective reduction.

Camptothecin and 20-deoxycamptothecin[1] are pentacyclic alkaloids with a pyrrolo[3,4-*b*]quinoline nucleus fused to a 2-pyridone ring. First isolated by Wall *et al.* in 1966 from *Camptotheca acuminata*,[2] camptothecin has recently re-emerged as one of the most promising agents for cancer treatment, topoisomerasa I being identified as the intracellular target for the drug.[3] Due to this interesting cytotoxic activity, camptothecin and its structural derivatives have been the objective of many total syntheses using a variety of approaches.[4,5]

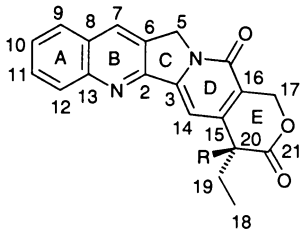

We present here a new, concise synthesis of (±)-20-deoxycamptothecin, a known synthetic precursor of camptothecin. Our approach involves the convergent construction of a suitably substituted and functionalized tetracyclic ABCD derivative **10** and the closure of the lactone E ring at the final synthetic step. For this purpose, we planned to take advantage of the synthetic potential of 1,4-dihydropyridines generated by nucleophilic addition of enolates to *N*-alkyl-3-acylpyridinium salts. In our previous work[6] these dihydropyridines have been further elaborated to complex polycyclic indole alkaloids either after acylation of the unsubstituted enamine moiety or *via* a dihydropyridinium cation generated by protonation or interaction with an electrophile.

For the synthesis of camptothecin we envisaged that, after the regioselective addition of a butyric ester enolate (the C_{18}–C_{21} fragment) to an appropriate *N*-(quinolylmethyl)-2-fluoropyridinium salt, the intermediate 2-fluoro-1,4-dihydropyridine could undergo a different transformation, namely an oxidation with concomitant hydrolysis of the C–F bond, leading to a 4-substituted-2-pyridone. Then, the quinoline and pyridone rings would be connected following the Comins procedure,[5*d–f*] by radical cyclization taking advantage of a bromine atom present at the 2-position of the quinoline nucleus. A methoxycarbonyl substituent at the β-position of the starting pyridinium would not only increase the electrophilicity of the pyridine ring in the nucleophilic attack but would also be subsequently converted to the C-17 oxymethylene group of the alkaloid.

To test the viability of our proposal for the construction of the pyridone moiety we first applied the nucleophilic addition–oxidation sequence to the model *N*-benzyl-2-fluoropyridinium salt **2** (Scheme 1). Knowing the reluctance of 2-halopyridines to undergo alkylation with alkyl halides and tosylates,[7] 2-fluoropyridinium salt **2** was prepared by alkylation of the corresponding 2-fluoropyridine **1**[8] with benzyl triflate. Without isolation, pyridinium triflate **2** was allowed to react with the enolate derived from methyl α-(methylsulfanyl)butyrate, which in related additions had exhibited better C-4 regioselectivity than the corresponding unsubstituted butyrate enolate.[9] Following our synthetic plan, the resulting 1,4-dihydropyridine adduct **3** was converted into the desired pyridone **4**[10] by oxidation with DDQ with hydrolysis of the C–F bond. The overall yield of the three-step sequence from 2-fluoropyridine **1** was 65%.

The application of the above strategy to the synthesis of camptothecin required starting from the pyridinium salt **7**, which incorporates the 2-bromoquinolyl-3-methyl fragment needed for the closure of the five-membered C ring. This salt was obtained by alkylation of 2-fluoropyridine **1** with triflate **6**, prepared from 2-bromo-3-(iodomethyl)quinoline (**5**).[11] Pyridinium triflate **7** was allowed to react as in the above *N*-benzyl series with the enolate derived from methyl α-(methylsulfanyl)butyrate and then with DDQ to provide pyridone **9a** in 50% overall yield from 2-fluoropyridine **1**. This pyridone already incorporates all the carbon atoms of the natural product. As expected, treatment of **9a** with tris(trimethylsilyl)silane–AIBN brought about both a radical arylation[12] and desulfurization to give the key tetracycle **10a** in 65% yield (Scheme 2).

The construction of the lactone E ring of camptothecin required the chemoselective reduction of the conjugate ester rather than the aliphatic one of **10a**. This transformation had already been reported from the diethyl ester analog **10c** by treatment with DIBAL (no details given).[5*k*] However, in our hands, the sequential treatment of **10a** with DIBAL–CH_2Cl_2 at −70 °C or DIBAL–THF at −40 °C and $NaBH_4$ gave the diol **12** as the only isolable product in 80% yield. Neither were we able to induce this transformation from diethyl ester **10c**, prepared in

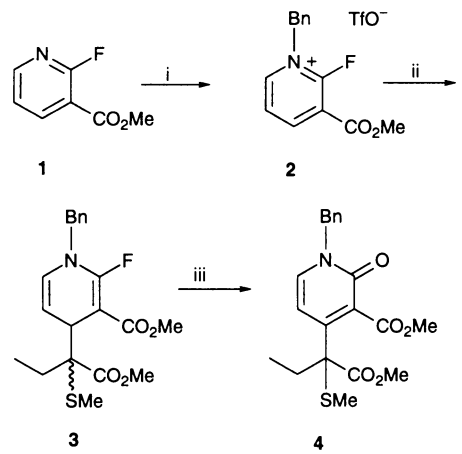

Scheme 1 Model studies. *Reagents and conditions*: i, BnOTf, Et_2O, rt, 10 min; ii, methyl α-(methylsufanyl)butyrate, LDA, THF, −70 °C, then −40 to −10 °C, 1.5 h; iii, DDQ, 3:1 THF–MeOH, rt, 12 h.

DOI: 10.1039/b007814j

90% yield by transesterification of **10a** (EtOH, KF, reflux, 3 days). Diol **12** was also formed as the major product in 75% yield.

The above results prompted us to differentiate the two ester groups as in the pioneering Winterfeldt synthesis of camptothecin from a closely related tetracyclic substrate.[13] Thus, we focused our attention on tetracycle **10b**, which was prepared by reaction of pyridinium triflate **7** with the enolate derived from isopropyl α-(methylsulfanyl)butyrate, followed by DDQ oxidation (50% overall yield from **1**) and subsequent radical cyclization (65% yield). Gratifyingly, treatment of **10b** with DIBAL–hexanes in DME at −70 °C and then with $NaBH_4$ in isopropanol afforded a 1:1 mixture of the target lactone **11** (20-deoxycamptothecin)[5a] and lactol **13** (65% yield), which were easily separated by column chromatography. The conversion of lactol **13** into **11** (65% yield) has recently been reported.[5n] Taking into account that 20-deoxycamptothecin (**11**) has previously been converted by hydroxylation at C-20 either to racemic (Me_2NH, $CuCl_2$, O_2, DMF)[5a] or natural [(+)-(20*S*)]-camptothecin [LHDMS, THF, (+)-(2*R*,8a*S*)-(camphorylsulfonyl)oxaziridine],[5m] the above synthesis constitutes a formal total synthesis of this natural product.

The above results significantly expand the methodology for the synthesis of nitrogen compounds based on the addition of carbon nucleophiles to *N*-alkyl-3-acylpyridinium salts as they open new synthetic possibilities for the subsequent elaboration of the initially formed 1,4-dihydropyridine adducts.

Financial support from the DGICYT, Spain (project PB94-0214) is gratefully acknowledged. Thanks are also due to the

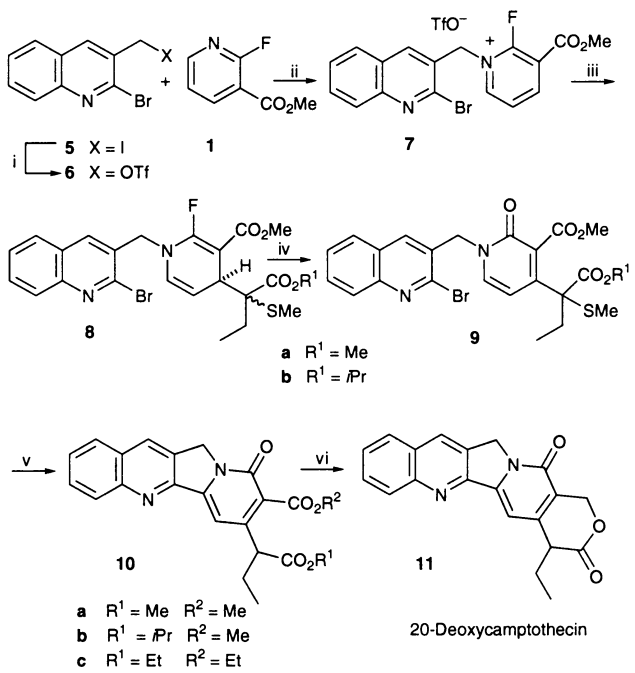

Scheme 2 Synthesis of (±)-20-deoxycamptothecin. *Reagents and conditions*: i, AgOTf, CH_2Cl_2, rt, 45 min; ii, CH_2Cl_2, rt, 1 h; iii, methyl or isopropyl α-(methylsufanyl)butyrate, LDA, THF, −70 °C, then −40 to −10 °C, 1.5 h; iv, DDQ, 3:1 THF–MeOH, rt, 12 h; v, TTMSS (2 equiv.), AIBN, C_6H_6, reflux, 4 h; vi, DIBAL–hexane (3 equiv.), DME, −70 °C, 30 min, then $NaBH_4$, iPrOH, rt, 1 h.

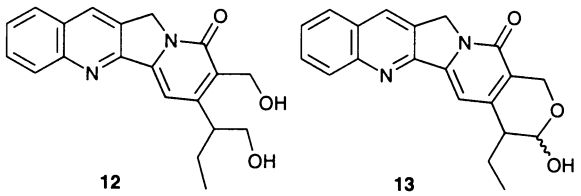

'Comissionat per a Universitats i Recerca' (Generalitat de Catalunya) for Grant 1999SGR00079 and for a fellowship to C. J.

Notes and references

1 C. R. Hutchinson, *Tetrahedron*, 1981, **37**, 1047.

2 M. E. Wall, M. C. Wani, C. E. Cook, K. H. Palmer, A. T. McPhail and G. A. Sim, *J. Am. Chem. Soc.*, 1966, **88**, 3888.

3 Y. Fan, J. N. Weinstein, K. W. Kohn, L. M. Shi and Y. Pommier, *J. Med. Chem.*, 1998, **41**, 2216, and references cited therein.

4 For synthetic references up to 1992, see: J. C. Cai and C. R. Hutchinson, in *Indoles, The Monoterpenoid Indole Alkaloids*, ed. J. E. Saxton, in *The Chemistry of Heterocyclic Compounds*, ed. A. Weissberger and E. C. Taylor, Wiley, New York, 1983, vol. 25, part 4, p. 753; M. E. Wall and M. C. Wani, in *Monoterpenoid Indole Alkaloids*, ed. J. E. Saxton, in *The Chemistry of Heterocyclic Compounds*, ed. E. C. Taylor, Wiley, Chichester, 1994, vol. 25, suppl. to part 4, p. 689.

5 For recent syntheses of camptothecin, see: (*a*) W. Shen, G. A. Coburn, W. G. Bornmann and S. J. Danishefsky, *J. Org. Chem.*, 1993, **58**, 611; (*b*) A. V. Rama Rao, J. S. Yadav and M. Valluri, *Tetrahedron Lett.*, 1994, **35**, 3613; (*c*) F. G. Fang, S. Xie and M. W. Lowery, *J. Org. Chem.*, 1994, **59**, 6142; (*d*) D. L. Comins, H. Hong, J. K. Saha and G. Jianhua, *J. Org. Chem.*, 1994, **59**, 5120; (*e*) D. L. Comins, H. Hoang and G. Jianhua, *Tetrahedron Lett.*, 1994, **35**, 5331; (*f*) D. L. Comins and J. K. Saha, *Tetrahedron Lett.*, 1995, **36**, 7995; (*g*) S. Jew, K. Ok, H. Kim, M. G. Kim, J. M. Kim, J. M. Hah and Y. Cho, *Tetrahedron: Asymmetry*, 1995, **6**, 1245; (*h*) J. M. D. Fortunak, J. Kitteringham, A. R. Mastrocola, M. Mellinger, N. J. Sisti, J. L. Wood and Z.-P. Zhuang, *Tetrahedron Lett.*, 1996, **37**, 5683; (*i*) N. Murata, T. Sugihara, Y. Kondo and T. Sakamoto, *Synlett*, 1997, 298; (*j*) M. A. Ciufolini and F. Roschangar, *Tetrahedron*, 1997, **53**, 11049; (*k*) S. P. Chavan and M. S. Venkatraman, *Tetrahedron Lett.*, 1998, **39**, 6745; (*l*) H. Josien, S.-B. Ko, D. Bom and D. P. Curran, *Chem. Eur. J.*, 1998, **4**, 67; (*m*) K. Tagami, N. Nakazawa, S. Sano and Y. Nagao, *Heterocycles*, 2000, **53**, 771; (*n*) R. T. Brown, L. Jianli and C. A. M. Santos, *Tetrahedron Lett.*, 2000, **41**, 859.

6 For a review, see J. Bosch and M.-L. Bennasar, *Synlett*, 1995, 587. For more recent work, see: M.-L.Bennasar, B. Vidal and J. Bosch, *J. Org. Chem.*, 1997, **62**, 3597; M.-L. Bennasar, J.-M. Jiménez, B. Vidal, B. A. Sufi and J. Bosch, *J. Org. Chem.*, 1999, **64**, 9605.

7 Y. Ban, R. Sakaguchi and M. Nagai, *Chem. Pharm. Bull.*, 1965, **18**, 931; A. P. Dobbs, K. Jones and K. T. Veal, *Tetrahedron Lett.*, 1997, **38**, 5833. See also J. A. Vega, J. J. Vaquero, J. Alvarez-Builla, J. Exquerra and C. Hamdouchi, *Tetrahedron*, 1999, **55**, 2317.

8 Prepared from 2-fluoropyridine and $ClCO_2Me$ according to the procedure reported by T. Güngör, F. Marsais and G. Queguiner, *J. Organomet. Chem.*, 1981, **215**, 139.

9 M.-L. Bennasar, E. Zulaica, C. Juan, L. Llauger and J. Bosch, *Tetrahedron Lett.*, 1999, **40**, 3961.

10 All new compounds were fully characterized by spectroscopic analysis (NMR) and gave satisfactory HRMS and/or combustion data.

11 Prepared by iodine–bromine exchange of 2-bromo-3-(bromomethyl)-quinoline D. L. Comins, M. F. Baevsky and H. Hong, *J. Am. Chem. Soc.*, 1992, **114**, 10971.

12 For the radical arylation of 2-pyridones, see R. Nadin and T. Harrison, *Tetrahedron Lett.*, 1999, **40**, 4073. See also reference 5*e*.

13 E. Winterfeldt, T. Korth, D. Pike and M. Boch, *Angew. Chem., Int. Ed. Engl.*, 1972, **11**, 289; K. Krohn and E. Winterfeldt, *Chem. Ber.*, 1975, **108**, 3030.

Thermally induced gelation of an oil-in-water emulsion stabilised by a graft copolymer

Andrew Y. C. Koh and Brian R. Saunders*

Colloid and Polymer Chemistry Research Group, Department of Chemistry, University of Adelaide, Adelaide, SA, 5005, Australia. E-mail: brian.saunders@adelaide.edu.au

Received (in Cambridge, UK) 16th October 2000, Accepted 7th November 2000
First published as an Advance Article on the web

Oil-in-water (O/W) emulsions exhibiting reversible thermally induced gelation have been prepared using a graft (comb) copolymer containing poly(*N*-isopropylacrylamide) [poly(NIPAM)] as the backbone and poly(ethylene glycol) methacrylate as the side chains.

Emulsions are dispersions of one immiscible liquid in another. They occupy a significant position in colloid science and occur as products (or during processing stages) in a number of areas including the paint, food and agrochemical industries.[1] The majority of emulsions studied or produced commercially are prepared using short-chain surfactants. The properties of these systems are reasonably well understood.[1,2] In recent years copolymers have been employed as macrosurfactants to prepare emulsions.[3,4] One of the advantages of using macrosurfactants for emulsion preparation is the large degree of architectural control that can be exerted in order to explore and optimise copolymer structure—emulsion property relationships. Water-soluble copolymers can be prepared which exhibit solvent–polymer interactions that are thermally responsive. This compositional control thus allows fine control over the lower critical solution temperature of the copolymer.[5] The preparation of emulsions using thermally responsive copolymers is a new area of research and is the subject of this communication.

The objective of the present study was to prepare emulsions with stabilities which are responsive to environmental conditions (*e.g.* temperature). We reasoned that the use of copolymers based on poly(*N*-isopropylacrylamide) [poly(NIPAM)] would provide gross conformational changes at the oil-in-water (O/W) interface at temperatures lower than the cloud point of short-chain ethylene-oxide based surfactants. Perrin *et al.*[3,6] have used hydrophobically modified poly(sodium acrylate) copolymers in order to prepare emulsions the stability of which are sensitive to pH and ionic strength. Mathur *et al.*[7] employed pH sensitive poly(acrylic acid)-g-poly(ethyleneoxide) copolymers in order to break emulsions. Our interest in the use of poly(NIPAM) copolymers to prepare emulsions follows from our earlier work involving swellable poly(NIPAM) microgel particles,[8] linear poly(NIPAM) chains adsorbed at latex particle interfaces[9] and depletion flocculation of emulsions.[10,11] The use of copolymers based on poly(NIPAM) to prepare emulsions was expected to provide large and reversible changes in emulsion properties (*e.g.* viscosity) as the temperature approaches the lower critical solution temperature (LCST). The results presented below show that this is indeed the case.

The copolymer comprised of poly(NIPAM) and poly(ethylene glycol methacrylate) (PEGMa); the latter having a number average molecular weight of 360. AIBN and *tert*-butyl alcohol were used, as the initiator and solvent, respectively, during the free radical copolymerisation stage.[12] Proton NMR data revealed that there was on average one PEGMa group per six NIPAM units in the copolymer. Fig. 1 shows how the turbidity and viscosity vary with temperature for poly(NIPAM–PEGMa) in water. The LCST of the copolymer is taken as *ca.* 34 °C from the turbidity data. This is *ca.* 2 °C higher than that of poly(NIPAM) homopolymer, which is attributed to the hydrophilic nature of the PEGMa in the copolymer.[13] The O/W

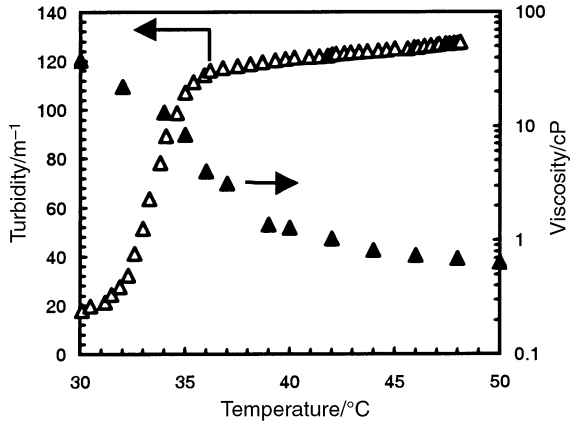

Fig. 1 Variation of the turbidity (Δ) and viscosity (▲) of poly(NIPAM–MPEGMa) solution as a function of temperature. The concentration of copolymer used was 2.5 wt%.

emulsions were prepared by first dissolving the copolymer in water (5 wt%). 1-bromohexadecane was then added to the copolymer solution, before the mixture was sheared using a Silverson SL2T laboratory mixer operating at *ca.* 7500 rpm. A control emulsion was prepared using the short-chain surfactant $Me(CH_2)_8(OCH_2CH_2)_6OH$, ($C_9E_6$) for comparison.

Fig. 2 shows the variation of viscosity with temperature for the emulsions prepared using poly(NIPAM–PEGMa) and C_9E_6. The viscosity data were measured using an Ostwald capillary viscometer. The viscosity for the emulsion prepared using poly(NIPAM–PEGMa) decreases with increasing temperature and reaches a minimum at 44 °C. A dramatic increase in viscosity occurs above 48 °C. The viscosity increased to such an extent that gelation of the emulsion occurred (see Fig. 3). As

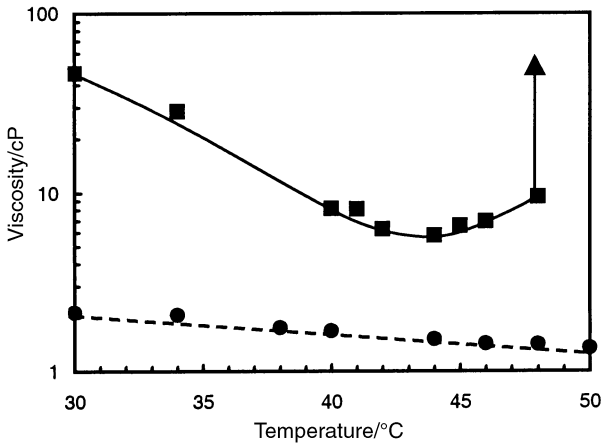

Fig. 2. Effect of temperature on the viscosity of emulsions prepared using poly(NIPAM–MPEGMa) (■) and C_9E_6 (●). The volume average diameters were 9.6 and 4.9 μm, respectively. The volume fraction of the dispersed phase was 0.30. The concentration of copolymer or C_9E_6 present was 2.5 wt% with respect to the total emulsion.

DOI: 10.1039/b008334h

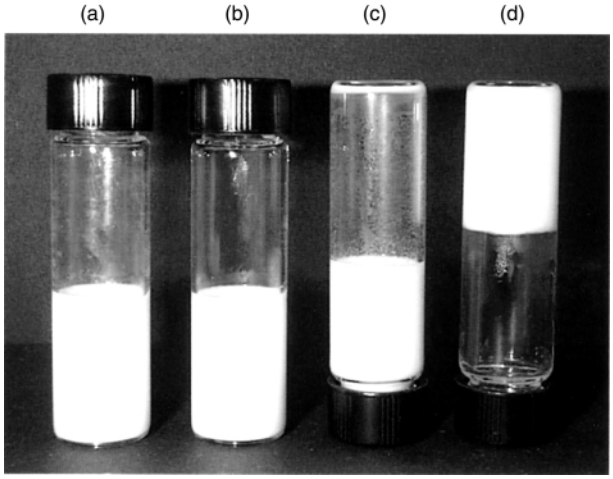

Fig. 3 Emulsions prepared using C_9E_6 (a) at RT and (c) at 50 °C and poly(NIPAM–MPEGMa) (b) at RT and (d) at 50 °C. Note that tubes (c) and (d) have been inverted.

expected, the emulsion prepared using C_9E_6 exhibited a slight decrease in viscosity over the whole experimental temperature range. It should be noted that the rheological behaviour observed for the emulsion prepared using the copolymer is opposite to what is observed for concentrated poly(NIPAM) microgel dispersions, which form gels at room temperature and flow when the temperature exceeds the LCST. It was found that emulsion gelation could be reversed by agitation at 50 °C or cooling to room temperature in the absence of agitation. The emulsions did not break as a result of gelation reversal, although there was evidence of a slight increase in droplet size. Optical microscopy revealed residual flocs were present in the emulsions after one heating/cooling cycle. The emulsion viscosity measured at 30 °C increased by *ca.* 5% as a result of one heating/cooling cycle.

The data shown here demonstrate that it is possible to reversibly gel our O/W emulsion using temperature variation alone. The mechanism by which this occurs is of interest to both the polymer and emulsion science communities. The fact that the gelation temperature is significantly greater than the LCST of the copolymer in solution suggests that the onset of gelation is not solely due to the collapse of the copolymer in the aqueous phase. The viscosity data for the copolymer (Fig. 1) show a decrease in viscosity with increasing temperature and rules out any contribution from temperature-induced continuous phase thickening (*e.g.* associated with the copolymer chains in solution) to emulsion gelation. The zeta potential for the droplets was measured at *ca.* 5 mV, which indicates that electrostatic stabilisation of the emulsions is not significant. The LCST of poly(NIPAM) chains adsorbed at highly charged surfaces is known to increase to values above that for the solution polymer.[14] However, this effect is not likely to occur in the present system due to the low charge of the droplets.

The stability of the emulsions arises primarily from steric stabilisation afforded by the adsorbed copolymer. The mechanism tentatively suggested for emulsion gelation involves thermally induced flocculation due to collapse of the adsorbed poly(NIPAM–PEGMa) layer at temperatures greater than the solution LCST. The depth of the secondary minimum would increase with increasing temperature (decreasing copolymer layer thickness) leading to stronger flocculation at higher temperatures. At 45 °C the minimum is sufficiently greater than *kT* to provide strong gelation *via* adhesive droplets. The collapse of the adsorbed layer presumably results in a rigid interface which opposes coalescence of flocculated droplets. It is likely that interpenetration and entanglement of interfacial copolymer chains contributes to the limits of residual flocculation observed upon cooling. Note that this good degree of reversibility for the copolymer stabilised emulsions is distinctly different to the behaviour of emulsions stabilised by short-chain ethylene oxide surfactants (*e.g.* C_9E_6) when heated to above the phase inversion temperature. For the latter emulsion breaking results from heating to the phase inversion temperature in absence of shear.

The work described above has shown that the use of poly(NIPAM–MPEGMa) graft copolymers allows the reversible gelation of O/W emulsions. This could have significant technological importance in the field of emulsion stability as the thermally induced gelation results in reversible transformation of a liquid emulsion into a highly viscous gel within a short period of time upon application of modest heating. Copolymers based on NIPAM can be prepared that have a range of LCST values. These ratios can be carefully controlled *via* copolymer architecture modification during synthesis. This versatility should allow the gelation temperature to be finely tuned to suit specific applications. The mechanism by which gelation occurs will be further investigated using light scattering, rheological and small-angle neutron scattering measurements and the results of these stuides will be published in due course.

We acknowledge the Department of Chemical Engineering for access to the PCS instrument.

Notes and references

1 B. Binks, in *Modern Aspects of Emulsion Science*, ed. B. P. Binks, RSC, Cambridge, 1998.
2 T. F. Tadros and B. Vincent, in *Encylopedia of Emulsion Technology*, ed. P. Becher, Marcel Dekker, New York, 1983.
3 P. Perrin, *Langmuir*, 2000, **16**, 881.
4 A. E. Cárdenas-Valera and A. I. Bailey, *Colloids Surf. A*, 1995, **97**, 1.
5 M. Hahn, E. Görnitz and H. Dautzenberg, *Macromolecules*, 1998, **31**, 5616.
6 P. Perrin, N. Monfreux, A. L. Dufour and F. Lafuma, *Colloid Polym. Sci.*, 1998, **276**, 945.
7 A. M. Mathur, B. Drescher, A. B. Scranton and J. Klier, *Nature*, 1998, **392**, 367.
8 B. R. Saunders and B. Vincent, *Adv. Colloid Interface Sci.*, 1999, **80**, 1.
9 B. R. Saunders, J. M. Saunders, J. Mrkic and E. H. Dunlop, *Phys. Chem. Chem. Phys.*, 1999, **1**, 1562.
10 A. Koh, G. Gillies, J. Gore and B. R. Saunders, *J. Colloid Interf. Sci.*, 2000, **227**, 390.
11 M. Shields and B. R. Saunders, *Colloids Surf. A*, in press.
12 A. Koh and B. R. Saunders, manuscript in preparation.
13 J. Virtanen and H. Tenhu, *Macromolecules*, 2000, **33**, 5970.
14 P. W. Zhu and D. H. Napper, *J. Colloid Interf. Sci.*, 1994, **164**, 489.

ChemComm

Formation of allylsilanes from $Cl_2[P(C_6H_{11})_3]_2Ru=C(R)H$ and vinylsilanes—β-SiR'_3 elimination from ruthenacyclobutanes as a terminating step in olefin cross-metathesis

Cezary Pietraszuk[a,b] and Helmut Fischer*[a]

[a] *Fachbereich Chemie, Universität Konstanz, Fach M727, D-78457 Konstanz, Germany. E-mail: hfischer@dg6.chemie.uni-konstanz.de*

[b] *Faculty of Chemistry, Adam Mickiewicz University, Grunwaldzka 6, 60-780 Poznan, Poland*

Received (in Cambridge, UK) 23rd October 2000, Accepted 8th November 2000
First published as an Advance Article on the web

Stoichiometric reactions of the Grubbs carbene complex $[Cl_2\{P(C_6H_{11})_3\}_2Ru=C(Ph)H]$ with vinylsilanes, $H_2C=C(SiMe_nR_{3-n})H$ (R = Ph, OEt; *n* = 1, 2, 3), afford metathesis products and allylsilanes formed by β-SiR_3 elimination followed by reductive elimination; the formation of allylsilanes constitutes a terminating step in the Ru-catalysed cross-metathesis of olefins with methylsubstituted vinylsilanes.

Metallacyclobutanes[1] play an important role in a number of stoichiometric and catalytic transformations. Two of the catalytically most important reaction modes of metallacyclobutanes are (a) reductive elimination to give cyclopropanes and a metal–ligand fragment[2] and (b) reductive decoupling to form an olefin–carbene complex (olefin metathesis).[3] In these reactions the metallacyclobutanes are formed as intermediates by addition of the C=C bond of an olefin to the M=C bond of an $L_nM=C(R)R'$ complex. Several types of olefin metathesis are known, such as ring-opening metathesis polymerisation, self- and cross-metathesis of linear olefins, acyclic diene metathesis (ADMET), and ring-closing metathesis (RCM).[3]

We recently reported[4] on the highly selective cross metathesis of styrene $H_2C=C(Ph)H$, with several vinylsilanes $H_2C=C(SiR_3)H$, to give (*E*)-H(Ph)C=C(SiR_3)H and ethylene catalysed by the Grubbs catalyst $[Cl_2\{P(C_6H_{11})_3\}_2Ru=C(Ph)H]$ (**1a**).[5] Very high conversions even at rt were observed when R = OR′ (R′ = Et, $SiMe_3$); however, the conversion significantly decreased with increasing substitution of Me for OR′.[4] To determine the reason for the decreasing selectivity we studied the stoichiometric reaction of **1a** with various vinylsilanes and now report on (a) the first evidence for β-silyl migration in metallacyclobutanes, (b) the very high selectivity of β-SiR_3 *versus* β-H migration and (c) hints for β-migration as the terminating step thus limiting the efficiency of the catalyst.

When an equivalent of trimethylvinylsilane (**2**) was added to a solution of **1a** in C_6D_6 a smooth reaction was observed.† After 6 h at rt 98% of **2** and 99% of **1a** had been consumed. A detailed analysis of the organic reaction products revealed the formation of 15% of **3a**, 57% of **4a**, 6% of **5a**, in addition to small amounts of **6** (5%), **7** (2%), **8** (5%), **9a** (2–5%) (Scheme 1) and unidentified Ru complexes. Cyclopropanes were not detected.

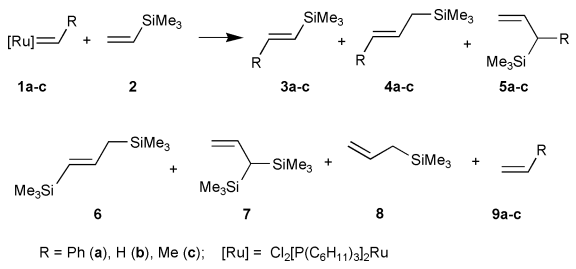

Scheme 1

Only compounds **3a** and **9a** are those expected from olefin metathesis. All other products (**4a**–**8**) are allyl derivatives containing the C_3 fragment of the metallacycle. Obviously, the metallacycle formed by addition of **2** to the Ru=C bond of **1a** breaks down by two different pathways: (a) reductive decoupling to give the metathesis products **3a**, **9a** and a [Ru]=C(R)H species and (b) elimination of an allylsilane derivative and formation of a [Ru] fragment.

Pathway (b) causes a decrease of the catalytically active [Ru]=C(R)H species and presumably is the most important factor in reducing the efficiency of the catalytic system. The conclusion is supported by the following observation: When Me in **2** is replaced stepwise by OEt, both the ratio of the metathesis product (type **3**) to the allyl derivative (type **4**) in the stoichiometric reaction [0.26 ($SiMe_3$), 0.68 ($Si(OEt)Me_2$), 13 ($Si(OEt)_2Me$)] and the cross-metathetical conversion of styrene to vinylsilane mixtures catalysed by **1** drastically increase. Analogously, a strong shift toward the metathesis product is observed when Me is stepwise displaced by Ph.

The reactions of **2** with the methylidene complex **1b** and the ethylidene complex **1c** instead of **1a** proceeded similarly, albeit more slowly. The reaction rate decreased in the series **1a** > **1b** > **1c**. Again mixtures of metathesis products and allyl derivatives were obtained. The reactions of **2** with **1b** and **1c** were accompanied by a substrate-independent decomposition of the Ru complexes[6] which gave rise to a reduction in the conversion of **2** (41% for **1b** and 35% for **1c**, each after 6 h). Within error limits, the product distribution after 6 h was the same as that after 18 h.

The formation of the major allyl derivative (**4a**) in the reaction of **1a** with trimethylvinylsilane (**2**) can be explained in two different ways: (i) by β-$SiMe_3$ elimination to give an allyl(silyl) complex (see Scheme 2: **C**/**D**) followed by reductive elimination or (ii) by β-H elimination to give a hydrido(α-silylallyl) complex (Scheme 2: **E**/**F**) again followed by reductive elimination. The labeling experiment (Scheme 2) allows exclusion of pathway (ii). The ^{2}H-NMR spectrum of the products obtained from the reaction of **1a** with $H_2C=C(D)SiMe_3$ (**2**-d_1) exhibited only signals in the *olefinic* region. From the absence of signals in the *aliphatic* region it follows that **4a′**-d_1 has not been produced. The formation of more than 1% of **4a′**-d_1 (with respect to **4a′**-d_1) would have been detected. Another product of pathway (ii), compound **10**, has not been identified among the reaction products in earlier experiments (see Scheme 1). These results indicate that there is a strong preference for β-SiR_3 elimination over β-H elimination. In fact, products derived from β-H elimination have not been detected in the stoichiometric experiments. Thus the ratio **4a**/**5a** = 57 : 6 presumably reflects the relative stabilities of different allyl(silyl) complex intermediates **C** and **D**.

The bis(silyl)allyl derivatives **6** and **7** are secondary products derived from the reaction of [Ru]=C($SiMe_3$)H with **2**. Their formation establishes that [Ru]=C($SiMe_3$)H species are also formed in the reaction of **1** with **2** as we proposed earlier.[4] Until

DOI: 10.1039/b008536g

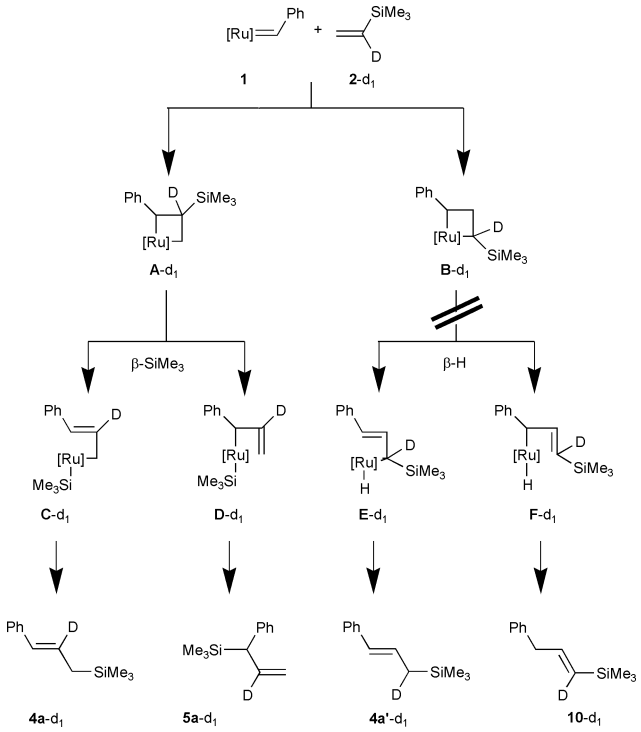

Scheme 2

now, all our attempts to synthesise $[Cl_2\{P(C_6H_{11})_3\}_2Ru{=}C(SiMe_3)H]$ or to spectroscopically detect $Ru{=}C(SiMe_3)H$ species in the cross-metathesis of vinylsilanes with styrene catalysed by **1** have failed.[4]

Our results demonstrate that β-SiR_3 elimination in β-SiR_3-substituted ruthenacyclobutanes followed by reductive elimination strongly competes with olefin metathesis and thus presumably is the most important factor limiting the catalytic efficiency of the system. The migratory aptitude considerably decreases in the series $SiMe_3$ > $Si(OEt)Me_2$ > $Si(OEt)_2Me$ and $SiMe_3$ > $Si(Ph)Me_2$ > $Si(Ph)_2Me$. Although there is a strong preference for SiR_3 migration compared to H migration it seems likely that β-H elimination and subsequent reductive elimination in systems without a SiR_3 substituent could also drain the active species from the catalytic cycle and thus limit the turnover number in cross-metathesis.

C. P. acknowledges a research grant from the Alexander von Humboldt Foundation. We also thank Professor Ulrich Groth for supplying access to GC-MS and Dr A. Geyer for ^{2}H-NMR spectra. Financial support of this work by the Fonds der Chemischen Industrie is gratefully acknowledged.

Notes and references

† Typically, in an NMR tube 1.21×10^{-5} mol of vinylsilane was added by syringe to a solution of $[Cl_2\{P(C_6H_{11})_3\}_2Ru{=}C(Ph)H]$ (0.01 g, 1.21×10^{-5} mol) and anthracene (internal standard) dissolved in 0.65 ml of C_6D_6. The reactions were followed by ^{1}H-NMR spectroscopy for 6 h. Conversions and selectivities were calculated using the internal standard method.[7] Products were identified by GC-MS spectra and by a comparison of their ^{1}H NMR spectra and their retention times (GC) with those of authentic samples.

1 For a representative review on group 8 metallacyclobutanes see W. P. Jennings and L. L. Johnson, *Chem. Rev.*, 1994, **94**, 2241.
2 See *e.g.* M. P. Doyle, *Chem. Rev.*, 1986, **86**, 919; M. Brookhart and W. B. Studabacker, *Chem. Rev.*, 1987, **87**, 411; H.-W. Fruehauf, *Chem. Rev.*, 1997, **97**, 523.
3 For recent reviews see: K. J. Ivin and J. C. Mol, *Olefin Metathesis and Metathesis Polymerization*, Academic Press, San Diego, 1997; *Alkene Metathesis in Organic Synthesis*, ed. A. Fuerstner, Springer, Berlin, 1998; R. H. Grubbs and S. Chang, *Tetrahedron*, 1998, **54**, 4413.
4 C. Pietraszuk, B. Marciniec and H. Fischer, *Organometallics*, 2000, **19**, 913.
5 P. Schwab, M. B. France, J. W. Ziller and R. H. Grubbs, *Angew. Chem.*, 1995, **107**, 2179; *Angew. Chem., Int. Ed. Engl.*, 1995, **34**, 2039; P. Schwab, R. H. Grubbs and J. W. Ziller, *J. Am. Chem. Soc.*, 1996, **118**, 100.
6 M. Ulman and R. H. Grubbs, *J. Org. Chem.*, 1999, **64**, 7202.
7 *Quantitative Analysis using Chromatographic Techniques*, ed. E. Katz, Wiley, Chichester, 1987.

ChemComm

Thiophene S-binding of a conformationally constrained thiophenophane leading to the formation of a copper(I) coordination polymer

Lyall R. Hanton,*[a] Christopher Richardson,[b] Ward T. Robinson[b] and Julia M. Turnbull[a]

[a] *Department of Chemistry, University of Otago, PO Box 56, Dunedin, New Zealand. E-mail: lhanton@alkali.otago.ac.nz*

[b] *Department of Chemistry, University of Canterbury, Private Bag 4800, Christchurch, New Zealand*

Received (in Cambridge, UK) 18th September 2000, Accepted 6th November 2000
First published as an Advance Article on the web

The potentially tetradentate NS_3 thiophenophane binds strongly to Cu(I) through a thiophene S, pyridine N and one thioether S, leaving the remaining thioether S donor in an exodentate arrangement forming an infinite polymeric link between Cu(I) atoms.

The thiophenic sulfur is considered to coordinate poorly to transition metals.[1] Only a few S-bound thiophene coordination complexes exist and for several of these the M–S distances exceed the sum of the covalent radii.[2] However, sterically constrained ligand systems incorporating thiophene have been used to successfully achieve S-binding.[2c,3] If incorporated into a macrocycle the rigid thiophene unit may impose limitations on the possible orientations of donor atoms and hence on the size and shape of the macrocyclic cavity and on the coordination properties.[2d,f,3] For example in macrocyclic thioethers, the thiophene may affect the donor properties of the thioethers by influencing the orientation of the sulfur lone pairs and this property may be used to control the structure of transition metal complexes. When the conformation of the ligand causes some of these lone pairs to be arranged in an exodentate fashion the possibility exists for bridging metal centres or coordination-polymer formation. This property of macrocyclic complexes, that the donor groups within the macrocycle are constrained and so provide a degree of control over the final polymeric structure, has not been widely used in coordination-polymer chemistry. Indeed, the use of macrocyclic complexes as structural elements in coordination polymers is surprisingly rare and typically involves specifically arranged exodentate donor groups[4] on the macrocyclic complexes or separate bridging ligands linking the macrocyclic complexes together.[5]

Herein we report the synthesis of 2,10-dithia[3](2,6)pyridino[3](2,5)thiophenophane (L), a small sterically constrained thiophenophane, and its use in the construction of a Cu(I) coordination polymer in which exodentate thioether donors bridge Cu(I) thiophenophane units containing a bound thiophene sulfur. Thiophenophane L was very difficult to prepare and isolate. Initially, it was prepared by high-dilution base coupling of 2,6-bis(chloromethyl)pyridine[6] and 2,5-bis(methylsulfanyl)thiophene[7] in a 1:1 molar ratio. Purification by column chromatography gave a stable white crystalline solid in 4% yield. 2,5-Bis(methylsulfanyl)thiophene could only be prepared in low yield and was difficult to purify, therefore the alternate precursors 2,6-bis(methylsulfanyl)pyridine[8] and 2,5-bis(bromomethyl)thiophene[9] were used with a slight improvement in yield (10%). CPK models show L is very strained and inflexible. Sulfur inversion is not possible but ring flipping of the pyridine and 'wobbling' of the thioether bridges can occur. These processes are consistent with the presence in the ^{1}H NMR spectrum of signals from two AB methylene proton systems.†

Given the constrained nature of the thiophenophane, it was of interest to determine the conformation in the solid state and to assess the potential for binding to a metal centre.‡ The thiophenophane exists in an *anti*, boat, boat conformation with the thiophene and pyridine rings tilted at 37.5° with respect to each other (Fig. 1). The pyridine N and thiophene S atoms point in opposite directions. Both thioether S atoms adopt a splayed endodentate conformation with respect to the thiophene S and point in the same direction as the thiophene S atom suggesting coordination to a metal ion may be possible. All bond lengths and angles are within the normal range.[10]

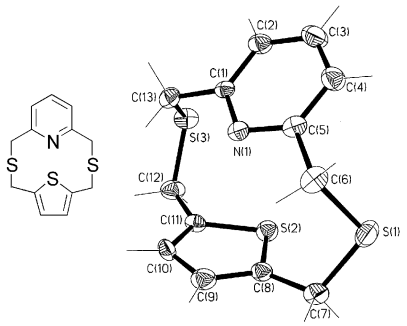

Fig. 1 Thiophenophane L: (left) schematic view; (right) ORTEP view (50% probability ellipsoids). Selected bond lengths (Å) and angles (°): C(6)–S(1) 1.837(3), S(1)–C(7) 1.833(3), C(8)–S(2) 1.735(4), C(8)–C(9) 1.357(5), C(9)–C(10) 1.429(5); C(6)–S(1)–C(7) 103.5(2), C(5)–C(6)–S(1) 113.5(3), C(8)–C(7)–S(1) 115.6(2).

Equimolar reaction of L and $[Cu(MeCN)_4]PF_6$ in MeCN gave an air-stable cream solid in 63% yield, which analysed with a 1:1 ligand to metal ratio and gave ^{1}H and ^{13}C NMR spectra consistent with a symmetrical but dynamic complex.† In order to establish the disposition of the thiophenophane an X-ray structure analysis was undertaken.‡

The crystal structure is severely disordered. The central Cu(I) and thioether S-donors lie on a mirror plane and the mirror operation causes the unsymmetrical L to be disordered equally over two sites (Fig. 2). The disordered thiophene and pyridine rings are intertwined and tilted by 52.9° with respect to each

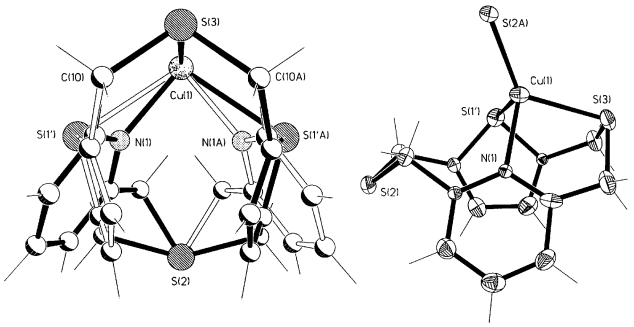

Fig. 2 Cationic $[Cu(L)]^+$ unit with PF_6^- anion omitted: (left) view showing disorder of L about mirror plane; (right) ORTEP view (50% probability ellipsoids). Selected bond lengths (Å) and angles (°): Cu(1)–N(1) 2.017(10), Cu(1)–S(2A) 2.191(3), Cu(1)–S(3) 2.346(3), Cu(1)–S(1′) 2.550(4); S(2A)–Cu(1)–N(1), 131.1(3), N(1)–Cu(1)–S(3) 87.7(3), N(1)–Cu(1)–S(1′) 92.6(3), S(2A)–Cu(1)–S(3) 126.9(1), S(2A)–Cu(1)–S(1′) 115.12(9), S(3)–Cu(1)–S(1′) 93.05(9).

DOI: 10.1039/b007579p

other. The two disordered ligands are required by symmetry to occupy the same thioether and Cu(I) positions but, coincidentally, they also occupy the same C(10) position. The central Cu(I) atom adopts a distorted tetrahedral geometry and is bound to a pyridine N, a thiophene S and an endodentate thioether S from one thiophenophane, and to an exodentate thioether S from the arm of a second symmetry related thiophenophane (Fig. 2). Each $[Cu(L)]^+$ unit is bound to another adjacent $[Cu(L)]^+$ unit *via* one of the exodentate thioether sulfur atoms to form a one-dimensional zigzag chain. This is the first reported thiophenophane polymer and the first polymer containing a bound thiophene sulfur. The ligand adopts a skewed *syn*, chair, boat conformation with the pyridine and thiophene rings lying approximately parallel at 16.8° to each other. From the above-mentioned data, the ligand appeared to be rather inflexible. However, the X-ray structure shows that the ligand is flexible enough to allow flipping of the pyridine ring so that the ligand sits in a *syn* conformation to promote thiophene S-binding to the Cu(I) ion. In each $[Cu(L)]^+$ unit the bound endodentate thioether S points in the same direction as the thiophene S while the other arm adopts an exodentate conformation (Fig. 2). This configuration of the thiophenophane prevents positioning of both thioether S-donors for coordination to the Cu(I) ion and promotes an intramolecular π–π-interaction (3.59 Å) between the thiophene and pyridine rings.

The thiophenophane is responsible for a very irregular coordination geometry about the Cu(I) ion. The Cu–S(exodentate) distance of 2.191(3) Å is short when compared to the normal Cu–S(endodentate) distance. The Cu–S(thiophene) bond length of 2.550(4) Å is around the upper quartile of all reported Cu(I)–S distances (2.18–3.01 Å).[10] The shortest M–S(thiophene) bond is a Ni(II)–S distance of 2.143(6) Å in a Ni(II) thiaporphyrin complex.[3b] The only reported Cu(I)–S(thiophene) distances are 2.960(5)[11] and 3.155(5) Å[2f] which are too long to be considered formal bonds but perhaps indicate weak interactions. The coordinated thiophene sulfur in $\{[Cu(L)]PF_6\}_\infty$ is approximately pyramidal, as indicated by the 103.4° angle between the Cu–S bond and the vector from sulfur to the midpoint of the mean plane of the thiophene ring. This angle is at least 10° smaller than any other reported value[2a,c,10] and is a consequence of the very restricted binding by the rigid ligand. The thiophene ring bond lengths show alternation in both the free and bound thiophenophane consistent with a localised bonding scheme. The one-dimensional polymer lies along the two-fold screw axis parallel to the *a*-axis and has a zigzag motif (Fig. 3).

The symmetrical nature of the complex in CD_3CN, as observed by ^1H and ^{13}C NMR spectroscopy, is inconsistent with the asymmetry found in the crystal structure and suggests dissociation of each polymeric chain in solution. Variable temperature ^1H NMR spectra were measured in CD_3CN down to the solvent limit of 238 K. Results showed the methylene protons nearest the thiophene moiety remained as a singlet resonance with no evidence of broadening or coalescence. However, the signals of the methylene protons adjacent to the pyridine ring collapsed and split into an AB system. These results suggest that in solution the pyridine ring remains bound to copper while the thiophene S is not bound. In addition, the complex must undergo an exchange process involving both of the thioether donor atoms and possibly the solvent. Electrospray mass spectrometry under normal operating conditions showed peaks which could be assigned to a number of species including a parent ion $[Cu(L)]^+$ at *m/z* 342 (100%), $[Cu(L)MeCN]^+$ at *m/z* 383 (78%), $[Cu(L)_2]^+$ at *m/z* 621 (15%) and $\{[Cu_2(L)_2]PF_6\}^+$ at *m/z* 813 (37%). This further indicates that $[Cu(L)]^+$ is dynamic and labile in solution and is probably involved in a series of complex equilibria.

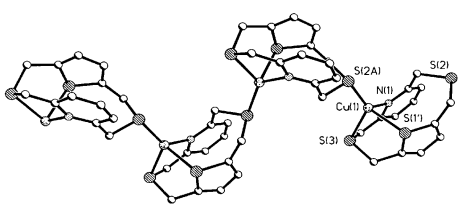

Fig. 3 View of a zigzag polymer chain formed by $[Cu(L)]^+$ units (PF_6^- anions and hydrogen atoms omitted) showing the exodentate thioether coordination linkage.

We have shown that when thiophene was placed in a small sterically constrained macrocycle it not only influenced the conformation of the bound ligand in a metal complex but was also, by its proximity, forced to bind to that metal. In addition, the conformational changes had ramifications for the structure as a whole leading to the formation of a coordination polymer. This work points to the usefulness of macrocyclic complexes as building blocks for coordination polymers.

We thank Associate Professor Bill Henderson (University of Waikato) for electrospray-MS data and the University of Otago for financial support.

Notes and references

† *Selected data* for L: δ_H(300 MHz; $CDCl_3$) 7.44 (t, 1H, ^3J 8 Hz), 7.01 (d, 2H, ^3J 8 Hz), 6.46 (s, 2H), 3.99 (dd, 4H, ^3J 15 Hz), 3.79 (dd, 4H, ^3J 15 Hz). Anal. Calc. for $C_{13}H_{13}NS_3$: C, 55.88; H, 4.70; N, 5.01; S, 34.42. Found: C, 55.84; H, 4.43; N, 4.97; S, 34.20%.

For $\{[Cu(L)]PF_6\}_\infty$: δ_H(300 MHz; CD_3CN) 7.73 (t, 1H, ^3J 8.0 Hz), 7.30 (d, 2H, ^3J 8.0 Hz), 6.23 (s, 2H), 4.14 (d, 4H, ^4J 2.1 Hz), 4.06 (s, 4H). Anal. Calc. for $C_{13}H_{13}NS_3CuPF_6$: C, 32.00; H, 2.69; N, 2.87; S, 19.71. Found: C, 32.27; H, 2.73; N, 3.10; S, 19.04%.

‡ *Crystal data*: L: $C_{13}H_{13}NS_3$, M = 279.42, orthorhombic, space group *Pbca* (no. 61), a = 10.768(5), b = 15.464(5), c = 15.529(5) Å, U = 2586(2) Å^3, T = 163(2) K, Z = 8, μ(Mo-Kα) = 0.549 mm^{-1}, 6628 reflections measured, 1312 independent reflections (R_{int} = 0.041), [959, $I \geqslant 2\sigma(I)$], R_1 = 0.0288, 0.0471 (all data), wR_2 = 0.0649, 0.0680 (all data).

$\{[Cu(L)](PF_6)\}_\infty$: $C_{13}H_{13}CuF_6NPS_3$, M = 487.96, orthorhombic, space group *Pbam* (no. 55), a = 10.727(5), b = 21.194(9), c = 7.553(3) Å, U = 1717(1) Å^3, T = 163(2) K, Z = 4, μ(Mo-Kα) = 1.787 mm^{-1}, 20 131 reflections measured, 1986 independent reflections (R_{int} = 0.027) [1886, $I \geqslant 2\sigma(I)$], R_1 = 0.0876, 0.0900 (all data), wR_2 = 0.1809, 0.1818 (all data). CCDC 182/1842. See http://www.rsc.org/suppdata/cc/b0/b007579p/ for crystallographic files in .cif format.

1 R. J. Angelici, *Coord. Chem. Rev.*, 1990, **105**, 61.

2 (*a*) M. Alvarez, N. Lugan and R. Mathieu, *Inorg. Chem.*, 1993, **32**, 5652; (*b*) C. Amari, S. Ianelli, C. Pelzzi, G. Pelizzi and G. Predieri, *Inorg. Chim. Acta*, 1993, **211**, 89; (*c*) E. C. Constable, R. P. Henney and D. A. Tocher, *J. Chem. Soc., Dalton Trans.*, 1991, 2335; (*d*) S. Liu, C. R. Lucas, M. J. Newlands and J.-P. Charland, *Inorg. Chem.*, 1990, **29**, 4380; (*e*) G. C. van Stein, G. van Koten, F. Blank, L. C. Taylor, K. Vrieze, A. L. Spek, A. J. Duisenberg, A. M. M. Schreurs, B. Kojić-Prodić and C. Brevard, *Inorg. Chim. Acta*, 1985, **98**, 107; (*f*) C. R. Lucas, S. Liu, M. J. Newlands, J.-P. Charland and E. J. Gabe, *Can. J. Chem.*, 1989, **67**, 639.

3 (*a*) L. Latos-Grażyński, J. Lisowski, M. M. Olmstead and A. L. Balch, *J. Am. Chem. Soc.*, 1987, **109**, 4428; (*b*) L. Latos-Grażyński, M. M. Olmstead and A. L. Balch, *Inorg. Chem.*, 1989, **28**, 4065.

4 A. J. Blake, N. R. Champness, S. M. Howdle and P. B. Webb, *Inorg. Chem.*, 2000, **39**, 1035; C. Kaes, M. W. Hosseini, C. E. F. Rickard, B. W. Skelton and A. H. White, *Angew. Chem., Int. Ed.*, 1998, **37**, 920; M. W. Hosseini and A. De Cian, *Chem. Commun.*, 1998, 727; A. J. Blake, G. Reid and M. Schröder, *J. Chem. Soc., Chem. Commun.*, 1992, 1074.

5 H. J. Choi and M. P. Suh, *Inorg. Chem.*, 1999, **38**, 6309; R. J. Pleus, H. Waden, W. Saak, D. Hasse and S. Pohl, *J. Chem. Soc., Dalton Trans.*, 1999, 2601; A. McAuley, S. Subramanian and M. J. Zaworotko, *J. Chem. Soc., Chem. Commun.*, 1992, 1321.

6 G. R. Newkome, G. E. Kiefer, Y.-J. Xia and V. K. Gupta, *Synthesis*, 1984, 676.

7 F. Vögtle and R. Lichtenthaler, *Chem. Ztg.*, 1970, **94**, 727.

8 E. C. Constable, A. C. King and P. R. Raithby, *Polyhedron*, 1998, **17**, 4275.

9 P. R. Ashton, J. A. Reece, J. F. Stoddart, M. S. Tolley, A. J. P. White and D. J. Williams, *Synthesis*, 1995, 1344.

10 F. H. Allen, J. E. Davies, J. J. Galloy, O. Johnson, O. Kennard, C. F. Macrae, E. M. Mitchell, G. F. Mitchell, J. M. Smith and D. G. Watson, *J. Chem. Inf. Comput. Sci.*, 1987, **31**, 187.

11 A. L. Spek, A. J. M. Duisenberg, G. C. van Stein and G. van Koten, *Acta Crystallogr., Sect. C*, 1985, **41**, 374.

ChemComm

Incorporation of nano-sized zeolites in membranes

Ben Moermans, Wouter De Beuckelaer, Ivo F. J. Vankelecom,* Raman Ravishankar, Johan A. Martens and Pierre A. Jacobs

Centre for Surface Chemistry and Catalysis, Department of Interphase Chemistry, Faculty of Agricultural and Applied Biological Sciences, K. U. Leuven, Kard, Mercierlaan 92, B-3001 Leuven, Belgium.
E-mail: ivo.vankelecom@agr.kuleuven.ac.be

Received (in Cambridge, UK) 13th September 2000, Accepted 25th October 2000
First published as an Advance Article on the web

The first incorporation of nano-sized zeolites in membranes is reported and polydimethylsiloxane membranes filled with colloidal silicalite-1 are applied in the pervaporation of ethanol–water mixtures.

The incorporation of zeolites and porous amorphous fillers in dense membranes improves the performance (normalized flux and selectivity) of these membranes in both gas separation and pervaporation for several types of feed mixtures.[1–4] All porous fillers reported up to now have particle sizes in the micron range. As a consequence, the minimal membrane thickness of the composite membranes was inherently higher than that of most unfilled membranes and the absolute fluxes remained low. The recent development of small 'nano-sized' colloidal zeolites leads to the possibility for the preparation of thin, defect-free, filled polymer layers. The synthesis of stable silicalite-1 particles with diameters as small as 70 nm was reported, as well as that of zeolite A (in the range 50–230 nm) and zeolite Y (80–110 nm).[5–7] We report here, the first incorporation of nano-sized zeolite particles in a polymeric membrane, that of silicalite-1 in PDMS (polydimethylsiloxane), and the performance of these membranes in the pervaporation of an aqueous ethanol solution.

Nano-sized silicalite-1 was synthesized following a procedure reported earlier:[8] tetraethylorthosilicate (98%, Acros Chimica), tetrapropylammonium hydroxide (TPAOH, 40% aqueous solution, Alfa) and water were mixed in order to obtain a mixture with a molecular composition of 9 TPAOH : 24.5 SiO_2 : 416 H_2O. The mixture was stirred for 24 h at room temperature and refluxed for 3 days at 100 °C. The silicalite-1 crystals were separated from the mother liquor by repeated centrifugation and washing. After redispersion and freeze-drying, the powder was calcined in air (1 °C min^{-1} heating rate, 2 h at 110 °C and 12 h at 550 °C). The particle size and shape observed by SEM (Fig. 1) and XRD were in good agreement with previous results.[8] The dry zeolite was dispersed in toluene by stirring and ultrasonic treatment. The suspension was then mixed with PDMS (prepolymer and crosslinker in a 10 : 1 ratio, General Electric, RTV 615 A and B) so as to give a 15 vol% solution of membrane constituents (polymer + zeolite) with the desired polymer : zeolite ratio. After a prepolymerisation step at 70 °C for 45 min, the casting solution was poured into a Petri dish and the solvent was evaporated overnight. To obtain complete crosslinking, the membrane was placed in a vacuum oven at 100 °C for 2 h. The maximum silicalite-1 load leading to a macroscopically homogeneous membrane was 30 wt%.

Dispersion of the zeolite in the polymer matrix was investigated by SEM. Fig. 2 shows the cross-section of a PDMS membrane containing 30 wt% nano-sized silicalite-1. Whereas a homogeneous dispersion of large zeolite crystals throughout a polymer matrix has not been reported to be problematic,[1–4] the distribution of the 70 nm crystals in the membrane was not homogeneous. An attempt was made to increase the zeolite loading and the dispersion by improving the contact between the polar zeolite surface and the apolar polymer. The nano-sized silicalite-1 was treated with a silane coupling agent to cover the surface with hydrophobic trimethylsilyl groups. The dry zeolite was dispersed in toluene and *N*-methyl-*N*-(trimethylsilyl)trifluoroacetamide (MSTFA, Acros Chimica, 97%) was added in a five-fold excess, with respect to the amount of silanols present. This number was estimated based on the external surface area of silicalite (45 m^2 g^{-1})[8] and assuming a silanol density of 6 OH nm^{-2}. After ultrasonic treatment, the mixture was stirred at room temperature and refluxed overnight. Removal of unreacted MSTFA was achieved by redispersion in toluene and centrifugation (30 min at 22 100 *g*). The silicalite-1 was finally recovered by evaporating the toluene. Silylation had a positive effect on the maximum amount of zeolite that could be incorporated in the polymer matrix from *ca.* 30 wt% for the non-silylated zeolite up to 40 wt% for the silylated sample. SEM observations of cross-sections of membranes, however, did not reveal an improved dispersion.

The synthesized membranes were evaluated in the pervaporation of a 6 wt% aqueous ethanol solution at three different temperatures. The vacuum at the permeate side was maintained at a pressure below 2 mbar and the permeate was trapped with liquid nitrogen. All reported membranes had thicknesses between 200 and 400 μm. The fluxes were normalized to a thickness of 100 μm assuming an inverse proportionality

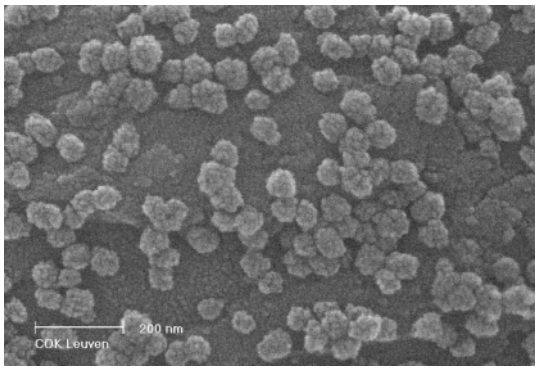

Fig. 1 SEM image of nano-sized silicalite.

Fig. 2 Cross-section of a PDMS membrane filled with 30 wt% nano-sized silicalite.

DOI: 10.1039/b007435g

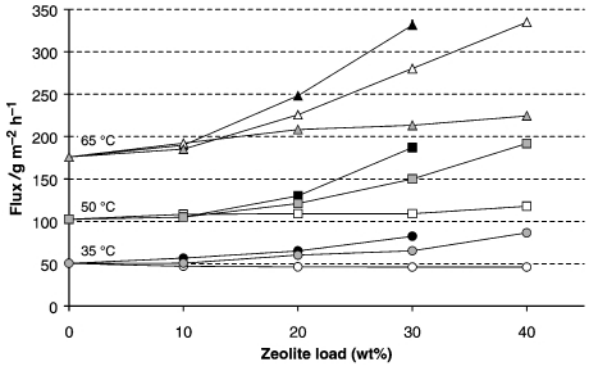

Fig. 3 Total fluxes, normalized to a membrane thickness of 100 μm, at three different temperatures for composite membranes prepared with micron-sized zeolites (open symbols) and nano-sized zeolites: silylated (grey symbols); non-silylated = black symbols).

between the flux and the membrane thickness. Selectivity is expressed as $\alpha = (y_a/y_b)/(x_a/x_b)$ in which y refers to the concentration of the components in the permeate and x to the concentration in the feed. Permeates were analysed by adding methanol as a standard and acetone as a homogenising solvent, followed by analysis with GC. Fig. 3 and Table 1 show the total normalized pervaporation flux and selectivity, respectively. At three different temperatures, a comparison was made between the performance of composite membranes filled with the self-prepared nano-sized silicalite and membranes filled with a commercial micron-sized silicalite (CBV-2802, PQ zeolites, Si : Al ratio = 550 : 1, 0.4–0.8 μm). The nano-sized zeolites show much improved pervaporation results compared with the micron-sized silicate membranes: both flux and selectivity are drastically increased at the highest loadings. Best results were obtained with the PDMS membrane containing 40 wt% of silylated nano-sized silicalite-1.

An explanation for this remarkable effect of nano-sized zeolites in PDMS for the pervaporation of ethanol–water mixtures, is probably related to the mesopores reported to be present in the silicalite-1 samples.[8] These mesopores most probably arise due to voids between the nanocrystals. The extent to which these mesopores and their silylation is responsible for the beneficial effect of the nano-sized zeolites in the pervaporation process, possibly acting as freeways for the preferentially sorbed ethanol, is currently being investigated.

Table 1 Selectivities obtained at different temperatures for composite membranes filled with micron- or nano-sized zeolties

T/°C	Filler load (wt%)	Micron-sized	Nano-sized	Nano-sized (silylated)
35	0	9.0	9.0	9.0
	10	8.8	10.1	9.8
	20	8.6	11.4	12.1
	30	8.9	15.7	13.9
	40	9.2		16.4
50	0	8.6	8.6	8.6
	10	9.2	9.9	9.7
	20	11.3	11.9	10.9
	30	11.5	15.3	12.3
	40	11.8		15.7
65	0	8.7	8.7	8.7
	10	8.9	10.5	9.5
	20	10.6	12.5	10.8
	30	11.7	14.3	11.9
	40	11.9		14.6

B. M. and I. F. J. V. thank the Fund of Scientific Research (F.W.O.) for a grant as an aspirant research fellow and as a post-doctoral researcher, respectively. This research was carried out within the framework of an IUAP-PAI grant.

Notes and references

1 J. te Hennepe, D. Bargeman, M. H. V. Mulder and C. A. Smolders, *J. Membr. Sci.*, 1987, **35**, 39.
2 M.-D. Jia, K.-V. Peinemann and R.-D. Behling, *J. Membr. Sci.*, 1992, **73**, 119.
3 C. Dotremont, S. Goethaert and C. Vandecasteele, *Desalination*, 1993, **91**, 177.
4 I. F. J. Vankelecom, D. Depré, S. De Beuckelaer and J.-B. Uytterhoeven, *J. Phys. Chem.*, 1995, **99**, 13193.
5 A. E. Persson, B. J. Schoeman, J. Sterte and J.-E. Otterstedt, *Zeolites*, 1994, **14**, 557.
6 B. J. Schoeman, J. Sterte and J.-E. Otterstedt, *Zeolites*, 1994, **14**, 110.
7 G. Zhu, S. Qiu, J. Yu, Y. Sakamoto, F. Xiao, R. Xu and O. Terasaki, *Chem. Mater.*, 1998, **10**, 1483.
8 R. Ravishankar, C. Kirschhock, B. J. Schoeman, P. Vanoppen, P. J. Grobet, S. Storck, W. F. Maier, J. A. Martens, F. C. De Schryver and P. A. Jacobs, *J. Phys. Chem.*, 1998, **102**, 2633.

ChemComm

On the electronic character of oxygen-transfer reactions†

Dirk V. Deubel,*[ab] Gernot Frenking,*[a] Hans Martin Senn[c] and Jörg Sundermeyer[a]

[a] *Fachbereich Chemie, Philipps-Universität Marburg, Hans-Meerwein-Str., D-35032 Marburg, Germany*
[b] *Department of Chemistry, University of Calgary, 2500 University Drive N.W., Calgary, Alberta, Canada T2N 1N4*
[c] *Laboratory of Inorganic Chemistry, Swiss Federal Institute of Technology, ETH Zentrum, CH-8092 Zürich, Switzerland*

Received (in Corvallis, OR, USA) 31st July 2000, Accepted 9th October 2000
First published as an Advance Article on the web

Charge Decomposition Analysis (CDA) applied to transition states of ethylene epoxidation is a quantum-chemical probe for the electronic character of oxygen-transfer reactions.

The insight into the electronic character of oxygen-transfer reactions, *i.e.* whether the oxidant attacks the substrate in an electrophilic or nucleophilic way, is used as a tool for an efficient development of catalysts for these reactions.[1] The most popular probe is the chemoselective oxidation of thianthrene 5-oxide introduced by Adam and co-workers.[2] Information about the electronic character of the transition states of olefin epoxidation is also provided by the effect of alkyl[3] and aryl[4] substituents at the C=C double bond on reactivity. A quantum-chemical probe has not been suggested yet, which is somewhat astonishing because the geometry optimization of transition states and the analysis of their electronic structure are key applications of modern computational chemistry. Hence, the principal aim of this work was to find a quantum-chemical probe for the electronic character of oxygen-transfer reactions.

In experimental work and recent theoretical studies by Bach *et al*., Houk *et al*. and others, it was shown that olefin epoxidation with organic peracids[5] and dioxiranes[6] follows a concerted oxygen-transfer mechanism with a *spiro* oxygen atom in the transition state (TS). The topology of the TS is coarctate.[7] Very recently, Rösch *et al.*[8,9] and we[10] supported an analogous mechanism for ethylene epoxidation by Herrmann-type complexes $[ReO(O_2)_2(CH_3)]$[8] and Mimoun-type complexes $[MoO(O_2)_2(OPR_3)]$,[9,10] as postulated by Sharpless *et al.*[11] For this work, we re-optimized TSs for ethylene epoxidation using standard density functional (DFT) methods for oxidations.[12] Calculated TS structures for dimethyldioxirane (DMDO), MCPBA, and $[ReO(O_2)_2(CH_3)]$ as oxidants are shown in the ESI†; selected geometrical parameters are given in Table 1.

† Electronic supplementary information (ESI) available. Geometries optimized at the B3LYP/II level of the transition states for ethylene epoxidation with DMDO, MCPBA, and $[ReO(O_2)_2(CH_3)]$ and predominant orbital interactions of donation *d* and backdonation *b* according to the CDA of the transition states for DMDO and MCPBA. See http://www.rsc.org/suppdata/cc/b0/b006280o/

The most simple tool for electronic-structure analysis is the calculation of atomic partial charges. The sum of NPA charges[13] at ethylene in the TSs are listed in Table 1. The values for all reactants indicate that, at the TSs, electronic charge has migrated from ethylene to the oxidant. In order to gain additional insight into the nature of the electronic interactions in the TSs, we utilized Charge Decomposition Analysis (CDA).[14,15] The Kohn-Sham MOs of a TS are expressed as a linear combination of the MOs of the fragments ethylene ('donor') and oxidant ('acceptor') in the geometry of the TS. We define (i) the interaction among the occupied orbitals of ethylene and the vacant orbitals of the oxidant as donation, *d*, (ii) the interaction among the occupied oxidant orbitals and the vacant ethylene orbitals as back-donation, *b*, (iii) the interaction of the occupied orbitals of both fragments as repulsive polarization, *r*, and (iv) the interaction of the vacant orbitals of both fragments as a rest term, Δ.[14] For the electronic character of oxygen-transfer reactions, the ratio $d:b$ in the TS is important. Oxidants with $d:b > 1$ are electrophilic, those with $d:b < 1$ are nucleophilic. Table 2 shows the CDA results. The most important fragment-orbital interactions in the TS of the ethylene epoxidation with $[ReO(O_2)_2(CH_3)]$ are visualized in Fig. 1. We draw the following conclusions:

(i) Small rest terms ($\Delta \approx 0$, Table 2) indicate that the electronic structure of the epoxidation transition states can be properly described in terms of donor–acceptor interactions between the fragments, ethylene and oxidant. This was to be expected from the Hammond postulate[16] because the strongly exothermic reactions have early TSs.

(ii) For all oxidants, donation, *d*, is an interaction between the ethylene HOMO and the σ* orbital of the O–O bond.[17] Note that the σ* orbital of the O–O bond does not neccessarily correspond to the LUMO of the free oxidant. The interaction between the lone pairs at the transferred oxygen atom and the ethylene LUMO provides the predominant contribution to backdonation, *b*, Fig. 1.

(iii) For all epoxidations investigated here, donation from ethylene to the oxidant is more important than back-donation, indicating an electrophilic attack of the oxidant on the olefin. The reason is that donation occurs earlier on the reaction coordinate. The O–O σ* orbital of the oxidant has a high coefficient from the p orbital pointing directly toward the

Table 1 Analysis of the transition states of ethylene epoxidation. C–O and C–C distances *a* [Å], sum *q* [e] of the NPA charges of the CH_2 moieties of the ethylene fragment, ratio $d:b$ of donation *d* and back-donation *b* in CDA, and activation energies E_a (B3LYP/III+//B3LYP/II)[a] [kcal mol^{-1}]. ZPE-corrected values (B3LYP/II)[a] in parentheses

	a			*q*			
Oxidant	C1–O	C2–O	C1–C2[b]	$C1H_2$	$C2H_2$	$d:b$	E_a
Dimethyldioxirane (DMDO)	1.977	1.977	1.373	0.199	0.199	1.32	17.1 (17.9)
Dioxirane (DO)	2.011	2.011	1.370	0.190	0.190	1.50	12.0 (12.8)
HCO_3H	2.029	2.029	1.369	0.190	0.190	1.55	14.6 (15.2)
m-Chloroperbenzoic acid (MCPBA)	2.037	2.037	1.368	0.185	0.185	1.56	15.4 (16.0)
$[MoO(O_2)_2(OP(CH_3)_3)]$ ($[Mo]O_2$)	2.078	2.186	1.360	0.160	0.129	1.76	16.6 (17.5)
$[ReO(O_2)_2(CH_3)]$ ($[Re]O_2$)	2.051	2.164	1.363	0.191	0.164	2.07	13.7 (14.5)

[a] For computational details, see ESI or: D. V. Deubel and G. Frenking, *J. Am. Chem. Soc.*, 1999, **121**, 2021. [b] Free ethylene: 1.331 Å.

DOI: 10.1039/b006280o

Table 2 CDA results of the transition states. Donation *d* (C_2H_4→oxidant), back-donation *b* (C_2H_4 ← oxidant), repulsive polarization *r* (C_2H_4↔oxidant), and rest term *Δ*

Oxidant	*d*	*b*	*d*:*b*	*r*	*Δ*
DMDO	0.231	0.175	1.32	−0.393	−0.003
DO	0.223	0.149	1.50	−0.353	−0.003
HCO_3H	0.229	0.148	1.55	−0.326	−0.004
MCPBA	0.227	0.146	1.56	−0.319	−0.004
$[Mo]O_2$	0.237	0.135	1.76	−0.312	−0.004
$[Re]O_2$	0.230	0.111	2.07	−0.276	−0.005

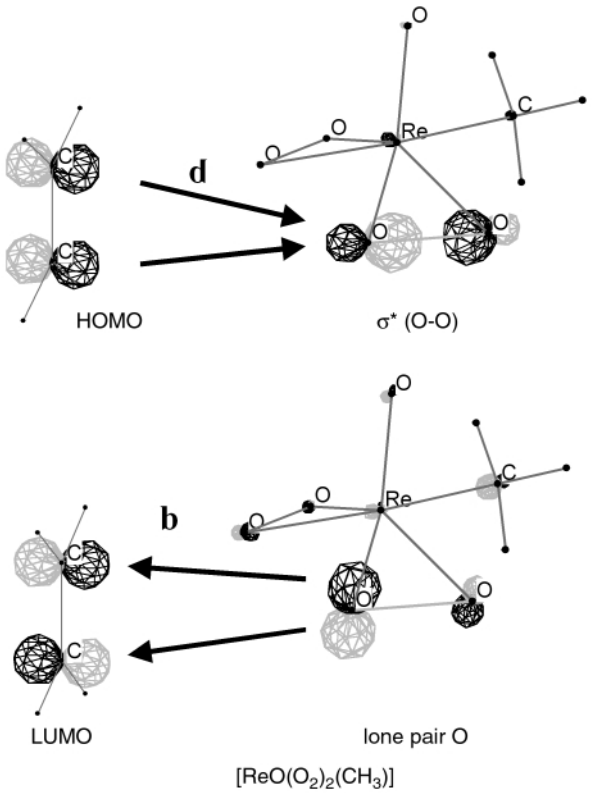

Fig. 1 Predominant orbital interactions of donation *d* and backdonation *b* according to CDA of the transition state for ethylene epoxidation with $[ReO(O_2)_2(CH_3)]$.

ethylene. Thus, at the long C(ethylene)–O distances of about 2.0 Å in the TS, the overlap integral is larger for donation than for back donation. While donation is approximately equal for all investigated epoxidations, the *b* values vary signficantly with the C–O distances (Table 2).

(iv) Due to *d*:*b* > 1, an increase of the olefin HOMO energy originated by alkyl substituents will accelerate epoxidation if steric effects are negligible. This is experimentally[3] and theoretically[5c,5g] confirmed. Negative *ρ* values from Hammett studies indicate a decrease of electron density at the C=C bond in the TS.[4]

(v) The ratio *d*:*b* is a quantum-chemical probe for the electronic character of oxygen-transfer reactions. The larger the value of *d*:*b*, the more electrophilic is the oxidant. Electrophilicity increases in the series DMDO < DO < HCO_3H = MCPBA < $[Mo]O_2$ < $[Re]O_2$. The metal peroxides are the most electrophilic oxidants.

(vi) The attempt to quantitatively correlate our electrophilicity scale with experimental parameters fails due to their dependence on reaction conditions,[2,4] such as temperature and solvent, and because of the lack of accessible data.

(vii) A relation between *electronic character* (*i.e.* *d*:*b*) and *reactivity* (*i.e.* activation energy E_a) is only found within the same class of oxidants, *e.g.* for the two dioxiranes.

D. V. Deubel thanks Professor Dr W. Adam for helpful discussions and the Fonds der Chemischen Industrie for a Kekulé scholarship. This work has also been supported by the Deutsche Forschungsgemeinschaft. Excellent service has been provided by the computer centers HRZ Marburg and HLRS Stuttgart.

Notes and references

1 For a recent example, see: D. V. Deubel, J. Sundermeyer and G. Frenking, submitted.
2 (*a*) W. Adam, D. Golsch and F. C. Görth, *Chem. Eur. J.*, 1996, **2**, 255; (*b*) W. Adam and D. Golsch, *J. Org. Chem.*, 1997, **62**, 115; (*c*) W. Adam, C. M. Mitchell and C. R. Saha-Möller, *J. Mol. Catal. A*, 2000, **154**, 251. Refs, cited therein.
3 (*a*) H. Mimoun, I. Seree de Roch and L. Sajus, *Tetrahedron*, 1970, **26**, 37; (*b*) H. Arakawa, Y. Moro-Oka and A. Ozaki, *Bull. Chem. Soc. Jpn.*, 1974, **47**, 2958; (*c*) A. M. Al-Aljouni and J. H. Espenson, *J. Org. Chem.*, 1996, **61**, 3969.
4 (*a*) R. P. Henzlik and G. O. Shearer, *J. Am. Chem. Soc.*, 1975, **97**, 51; (*b*) A. L. Baumstark and P. C. Vasquez, *J. Org. Chem.*, 1988, **53**, 3437; (*c*) A. M. Al-Aljouni and J. H. Espenson, *J. Am. Chem. Soc.*, 1995, **117**, 9243.
5 (*a*) B. Plesnicar, M. Tasevski and A. Azman, *J. Am. Chem. Soc.*, 1978, **100**, 743; (*b*) R. D. Bach, A. L. Owensby, C. Gonzalez and H. B. Schlegel, *J. Am. Chem. Soc.*, 1991, **113**, 2338; (*c*) S. Yamabe, C. Kondou and T. Minato, *J. Org. Chem.*, 1996, **61**, 616; (*d*) D. A. Singleton, S. R. Merrigan, J. Liu and K. N. Houk, *J. Am. Chem. Soc.*, 1997, **119**, 3385; (*e*) R. D. Bach, C. M. Estévez, J. E. Winter and M. N. Glukhovtsev, *J. Am. Chem. Soc.*, 1998, **120**, 680; (*f*) R. D. Bach, M. N. Glukhovtsev and C. Canepa, *J. Am. Chem. Soc.*, 1998, **120**, 775; (*g*) R. D. Bach, M. N. Glukhovtsev and C. Gonzalez, *J. Am. Chem. Soc.*, 1998, **120**, 9902.
6 (*a*) R. D. Bach, A. L. Owensby, J. L. Andres and H. B. Schlegel, *J. Am. Chem. Soc.*, 1991, **113**, 7031; (*b*) R. D. Bach, J. L. Andres, A. L. Owensby, H. B. Schlegel and J. J. W. McDouall, *J. Am. Chem. Soc.*, 1992, **114**, 7207; (*c*) K. N. Houk, J. Liu, N. C. DeMello and K. R. Condroski, *J. Am. Chem. Soc.*, 1997, **119**, 10 147; (*d*) C. Jenson, J. Liu, K. N. Houk and W. L. Jørgensen, *J. Am. Chem. Soc.*, 1997, **119**, 12 982; (*e*) J. Liu, K. N. Houk, A. Dinoi, C. Fusco and R. Curci, *J. Org. Chem.*, 1998, **63**, 8565; (*f*) A. Armstrong, I. Washington and K. N. Houk, *J. Am. Chem. Soc.*, 2000, **122**, 6297.
7 (*a*) R. Herges, *Angew. Chem.*, 1994, **106**, 261; (*b*) R. Herges, *J. Chem. Inf. Comput. Sci.*, 1994, **34**, 91.
8 P. Gisdakis, S. Antonczak, S. Köstlmeier, W. A. Herrmann and N. Rösch, *Angew. Chem.*, 1998, **110**, 2333; *Angew. Chem., Int. Ed.*, 1998, **37**, 2211.
9 C. Di Valentin, P. Gisdakis, I. V. Yudanov and N. Rösch, *J. Org. Chem.*, 2000, **65**, 2996.
10 D. V. Deubel, J. Sundermeyer and G. Frenking, *J. Am. Chem. Soc.*, 2000, **122**, 10 101.
11 K. B. Sharpless, J. M. Townsend and R. D. Williams, *J. Am. Chem. Soc.*, 1972, **94**, 295.
12 For computational details, see supporting information or: D. V. Deubel and G. Frenking, *J. Am. Chem. Soc.*, 1999, **121**, 2021.
13 A. E. Reed, L. A. Curtiss and F. Weinhold, *Chem. Rev.*, 1988, **88**, 899.
14 S. Dapprich and G. Frenking, *J. Phys. Chem.*, 1995, **99**, 9352.
15 D. V. Deubel, J. Sundermeyer and G. Frenking, *Inorg. Chem.*, 2000, **39**, 2314. Refs. cited therein.
16 G. S. Hammond, *J. Am. Chem. Soc.*, 1955, **77**, 334.
17 R. Curci and J. O. Edwards, in *Catalytic Oxidations with Hydrogen Peroxide as Oxidant*, ed. G. Strukul, Kluwer, Dordrecht, 1992, p. 45.

Solvent-free catalytic enantioselective addition of diethylzinc to aldehydes

Itaru Sato, Takahiro Saito and Kenso Soai*

Department of Applied Chemistry, Faculty of Science, Science University of Tokyo, Kagurazaka, Shinjuku-ku, Tokyo, 162-8601 Japan. E-mail: ksoai@ch.kagu.sut.ac.jp

Received (in Cambridge, UK) 28th September 2000, Accepted 8th November 2000
First published as an Advance Article on the web

Solvent-free enantioselective addition of diethylzinc to aldehydes using β-amino alcohols as chiral catalysts afford chiral *sec*-alcohols with high enantiomeric excesses, and the reaction in solvent-free system is faster than that using organic solvent.

Solvent-free organic synthesis has received much attention.[1,2] From an environmental point of view, potent toxic waste should be minimized and, obviously, bulk wastes in chemical reactions are often organic solvents. Thus, the development of solvent-free organic synthesis is important. Recent advances in this field include, for example, polymerization,[3] radical addition[4] and ionic reactions.[5]

Meanwhile, solvents often play an essential role in catalytic enantioselective synthesis. They not only make the reaction mixtures homogeneous but participate to construct the stereochemically preferable reactive transition state by coordinating with metals. Thus, the use of solvent is generally considered unavoidable in achieving high enantioselectivity in asymmetric reactions.[6] So far, only a few solvent-free enantioselective catalytic reactions are known.[7] We previously reported enantioselective addition of dialkylzincs to aldehydes in the presence of *N*,*N*-dialkylnorephedrines as chiral catalysts using organic solvents such as toluene and hexane.[8]

We here report a solvent-free catalytic enantioselective addition of diethylzinc (Et_2Zn) to aldehydes. In the presence of *N*,*N*-dialkylnorephedrines **2, 4** and **5** as chiral catalysts, aldehydes **1** were reacted with neat Et_2Zn without using any solvent. The reactions were homogeneous and proceeded in highly enantioselective manner to give optically active *sec*-alcohols **3** with high ees (Scheme 1).

The results of the enantioselective addition of Et_2Zn to benzaldehyde **1a** under the solvent-free conditions are summarized in Table 1. In the presence of (1*S*,2*R*)-*N*,*N*-dibutylnorephedrine (DBNE) **2**[8a] (10 mol%) as a chiral catalyst, neat Et_2Zn was added to aldehyde **1a** at 0 °C to give (*S*)-1-phenylpropanol **3a** with 87% ee in an almost quantitative yield (99%) (run 1). When the amount of DBNE **2** was 5 mol%, (*S*)-**3a** was obtained in 97% yield and 87% ee (run 2). The reaction using 3.4 mol% of DBNE **2** and 2.2 mol. equiv. of neat Et_2Zn afforded (*S*)-**3a** with 87% ee in 93% yield (run 3). It should be noted that solvent-free reactions at 0 °C were complete in 2 h (runs 1–3), whereas the same reaction in toluene takes longer time to complete.[8a] *N*,*N*-Dipropylnorephedrine **4**[8a] and 1-phenyl-2-(1-pyrrolidinyl)propan-1-ol **5**[8a,9] were also efficient chiral catalysts which afforded (*S*)-**3a** in 97–99% yields with 85% ee and 86% ee, respectively (runs 4 and 5). An acceleration of the reaction rate under solvent-free conditions is clearly seen in low-temperature reactions. Enantioselective addition of Et_2Zn using (1*S*,2*R*)-DBNE **2** as a chiral catalyst proceeded efficiently at −10 °C within 4 h to give **3a** with 89% ee in 98% yield (run 6). Moreover, the reaction even at −28 °C was complete within 6 h to afford **3a** with 87% ee in 99% yield (run 7). It should be noted that when a solvent (toluene) is used, the reaction hardly proceeds at −28 °C. The high reactivity of Et_2Zn under solvent-free conditions may be attributed to the higher concentration of neat Et_2Zn (*ca.* 9.5–10 M) than that in solvents. Thus, a strong acceleration of the reaction rate was observed in the present solvent-free enantioselective reaction without a decrease in enantioselectivity.[10] The catalytic species is, presumably, zinc monoalkoxide of **2**.[8a,11]

To clarify the generality of substrates, various aldehydes were subjected to the solvent-free enantioselective addition of diethylzinc using (1*S*,2*R*)-**2** (5 mol%) as a chiral catalyst (Table 2). *p*-Tolualdehyde **1b** and 1-naphthaldehyde **1c** were ethylated in a highly enantioselective manner to give the corresponding *sec*-alcohols **3b** and **3c** with *S* configuration in 90% ee and 91% ee, respectively (runs 1 and 2).[12] The reaction with 2-naphthaldehyde **1d** gave (*S*)-**3d** in 98% yield and 86% ee (run 3).

Cyclohexanecarbaldehyde **1g**, an aliphatic aldehyde, was ethylated enantioselectively to afford (*S*)-**3g** with 88% ee in 96% yield (run 6). Enantioselective addition of Et_2Zn to aldehyde **1h**, possessing hydrogen atoms on the α-carbon atom, gave **3h** with 84% ee in 92% yield (run 7).

In conclusion, we have described a highly enantioselective ethylation of aldehydes under solvent-free conditions which is

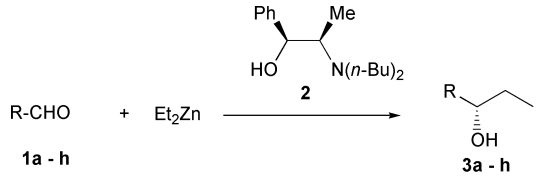

a; R = Ph **e**; R = *p*-ClC_6H_4
b; R = Tolyl **f**; R = *p*-$MeOC_6H_4$
c; R = 1-Naphthyl **g**; R = *c*-C_6H_{11}
d; R = 2-Naphthyl **h**; R = $PhCH_2CH_2$

Scheme 1

Table 1 Solvent-free catalytic enantioselective addition of diethylzinc to benzaldehyde

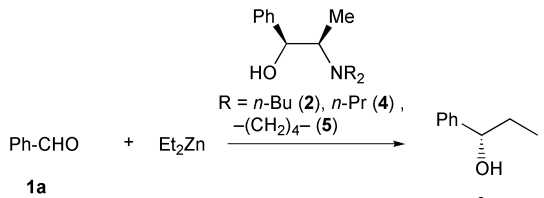

Run[a]	Chiral catalyst (mol%)	*T*/°C	*t*/h	(*S*)-1-phenylpropanol **5a**[b] Yield (%)	Ee (%)
1	(1*S*,2*R*)-**2** (10)	0	2	99	87
2	(1*S*,2*R*)-**2** (5)	0	2	97	87
3[c]	(1*S*,2*R*)-**2** (3.4)	0	2	93	87
4	(1*S*,2*R*)-**3** (5)	0	2	99	85
5	(1*S*,2*R*)-**4** (5)	0	2	97	86
6	(1*S*,2*R*)-**2** (5)	−10	4	98	89
7	(1*S*,2*R*)-**2** (5)	−28	6	99	87

[a] Reactions were carried out using 3–5 mol. equiv. of neat Et_2Zn. [b] Ee was determined by HPLC analysis using a chiral stationary phase (Chiralcel OB-H). [c] Reaction was run using 2.2 mol. equiv. of neat Et_2Zn.

DOI: 10.1039/b007881f

Table 2 Solvent-free enantioselective addition of Et_2Zn to various aldehydes using (1*S*,2*R*)-*N*,*N*-dibutylnorephedrine **2** as a chiral catalyst

		(*S*)-**3**		
Run[a]	Aldehydes		Yield (%)	Ee (%)[b]
1	*p*-Tolualdehyde **1b**	**3b**	99	90
2	1-Naphthaldehyde **1c**	**3c**	80	91
3	2-Naphthaldehyde **1d**	**3d**	98	86[c]
4	*p*-Chlorobenzaldehyde **1e**	**3e**	99	85
5	*p*-Methoxybenzaldehyde **1f**	**3f**	98	89
6	Cyclohexanecarbaldehyde **1g**	**3g**	96	88[d]
7	3-Phenylpropanal **1h**	**3h**	92	84[c]

[a] Reactions were carried out for 2 h at 0 °C using 5 mol% of **2** and 3–5 mol. equiv. of Et_2Zn. [b] Unless otherwise noted, ee was determined by HPLC analysis using a chiral stationary phase (Chiralcel OB-H). [c] Chiralcel OD-H was used as a chiral stationary phase. [d] Ee was determined as *p*-bromobenzoate of **3g** using a chiral stationary phase (Chiralcel OJ-R).

accelerated with respect of the corresponding reaction in organic solvents.

This work was supported by a Grant-in-Aid for Scientific Research from the Ministry of Education, Science, Sports, and Culture of Japan. I. S. thanks a Daicel Award in Synthetic Organic Chemistry.

Notes and references

1 J. O. Metzger, *Angew. Chem., Int. Ed.*, 1998, **37**, 2975.
2 K. Tanaka and F. Toda, *Chem. Rev.*, 2000, **100**, 1025; A. Loupy, A. Petit, J. Hamelin, F. Texier-Boullet, P. Jacquault and D. Mathe, *Synthesis*, 1998, 1213; R. S. Varma, *Green Chem.*, 1999, **1**, 43; S. Deshayes, M. Liagre, A. Loupy, J.-L. Luche and A. Petit, *Tetrahedron*, 1999, **55**, 10 851.
3 J. Hornke, R. Lipphardt and R. Meldt in *Produktionsintegrierter Umweltschutz in der chemischen Industrie*, ed. J. Wiesner, Decheme, Frankfurt/Main, 1990, p. 17; K. Komiya, S. Fukuoka, M. Aminaka, K. Hasegawa, H. Hachiya, H. Okamoto, T. Watanabe, H. Yoneda, J. Fukawa and T. Dozono, in *Green Chemistry, Designing Chemistry for the Environment*, ed. P. T. Anastas and T. C. Williamson, American Chemical Society, Washington, D.C., 1996, p. 20.
4 J. O. Metzger and R. Mahler, *Angew. Chem., Int. Ed. Engl.*, 1995, **34**, 902; J. O. Metzger, R. Mahler and A. Schmidt, *Liebigs Ann.*, 1996, 693.
5 G. Bram and G. Decodts, *Synthesis*, 1985, 543.
6 For example, utilization of acetonitrile is necessary for a highly enantioselective catalytic conjugate addition of Et_2Zn to enones. K. Soai, T. Hatanaka and T. Miyazawa, *J. Chem. Soc., Chem. Commun.*, 1992, 1097.
7 L. E. Martinez, J. L. Leighton, D. H. Carsten and E. N. Jacobsen, *J. Am. Chem. Soc.*, 1995, **117**, 5897; D. Rajagopal, K. Rajagopalan and S. Swaminathan, *Tetrahedron: Asymmetry*, 1996, **7**, 2189.
8 (*a*) K. Soai, S. Yokoyama and T. Hayasaka, *J. Org. Chem.*, 1991, **56**, 4264 (*b*) For a review, K. Soai and S. Niwa, *Chem. Rev.*, 1992, **92**, 833.
9 K. Soai, T. Konishi and T. Shibata, *Heterocycles*, 1999, **51**, 1421; I. Sato, T. Saito, D. Omiya, Y. Takizawa and K. Soai, *Heterocycles*, 1999, **51**, 2753.
10 In addition, enantioselective addition of diisopropylzinc to aldehyde **1a** in the presence of 5 mol% of (1*S*,2*R*)-**2** gave (*S*)-2-methyl-1-phenylpropan-1-ol with 74% ee in 82% yield.
11 It is known that reaction between diethylzinc and *sec*-alcohol easily forms zinc monoalkoxide at 30 °C. Formation of zinc dialkoxide requires heating (80 °C). M. Ishimori and T. Tsuruta, *Mackromol. Chem.*, 1963, **64**, 190.
12 A typical experimental procedure is as follows (Table 2, run 1): To an ice-cooled 2-necked flask containing (1*S*,2*R*)-DBNE **2** (13.7 mg, 0.05 mmol), neat Et_2Zn (370 mg, 3 mmol) was transferred into the flask through a cannula under an argon atmosphere. After the mixture was stirred for 10 min at 0 °C, aldehyde **1b** (120 mg, 1.0 mmol) was added slowly to the mixture, and the mixture was stirred for 2 h. After excess Et_2Zn was removed under a reduced pressure, the reaction was quenched by satd. aq. ammonium chloride. The mixture was extracted with ether and the organic layer was dried over magnesium sulfate. Concentration and purification on silica gel TLC gave (*S*)-**3b** (149 mg, 99%). Ee was determined to be 90% by HPLC analysis using a chiral stationary phase (Chiralcel OB-H).

Are anthocyanidins the immediate products of anthocyanidin synthase?

Jonathan J. Turnbull,[a] Wendy J. Sobey,[a] Robin T. Aplin,[a] Abby Hassan,[a] John L. Firmin,[b] Christopher J. Schofield*[a] and Andy G. Prescott*[b]

[a] *The Dyson Perrins Laboratory and The Oxford Centre for Molecular Sciences, South Parks Road, Oxford, UK OX1 3QY. E-mail: christopher.schofield@chem.ox.ac.uk*

[b] *Department of Applied Genetics, John Innes Centre, Norwich Research Park, Colney, Norwich, UK NR4 7UH. E-mail: andy.prescott@bbsrc.ac.uk*

Received (in Liverpool, UK) 14th September 2000, Accepted 3rd November 2000
First published as an Advance Article on the web

Anthocyanidin synthase catalyses the *in vitro* conversion of its natural substrate, leucocyanidin, to *cis*- and *trans*-dihydroquercetin, quercetin and a small amount of cyanidin; incubation of *trans*-dihydroquercetin gave quercetin.

Flavonoids are an important class of plant metabolites whose roles include attracting pollinators, signalling in plant-microbe interactions, protecting plants against radiation and aiding seed dispersal.[1] There is biomedical interest in flavonoids since they inhibit cell proliferation, are antioxidants and display anti-mutagenic, antinflammatory, antithrombic and antihypertensive effects.[2,3] The anthocyanin sub-family of flavonoids cause pigmentation and are used as food colourants.

The penultimate step in the biosynthesis of the anthocyanin family **1** of flavonoids is catalysed by anthocyanidin synthase (ANS) (Scheme 1).[4] Although there are reports on other enzymes involved in anthocyanin biosynthesis, until recently the only reported work on the ANS concerned the identification of its genetic locus and putative gene sequence.[5] The presence of conserved sequence motifs (*e.g.* HXD and RXS motifs, which are involved in iron and co-substrate binding respectively[6,7]) imply ANS belongs to the family of 2-oxogluatarate (2-OG) dependent dioxygenases.[8] Saito *et al.* reported that ANS from *Perrila fructescens* was indeed a 2-OG dependent oxygenase requiring an unusually high level of ascorbate for activity.[9] It was demonstrated that oxidation of leucocyanidin **2a** (R^1 = OH, R^2 = H) and leucopelargonidin **2b** (R^1 = H, R^2 = H) was coupled with conversion of 2-OG to succinate. However, it was noted that the anticipated anthocyanidin products cyanidin **3a** and pelargonidin **3b**, respectively, were only observed in the crude assay incubations subsequent to acidification. The acidified incubations were analysed by HPLC (monitoring at 520 nm) and peaks corresponding to the appropriate anthocyanidin references identified.[9] Here, we report studies on the selectivity of ANS that lead us to question whether anthocyanidins are the immediate products of the ANS reaction.

The ANS gene from *Arabidopsis thaliana* was over-expressed in *Escherichia coli* BL21 (DE3) using the Novagen pET-24a vector and ANS was purified to *ca.* ~90% purity (by SDS-PAGE analysis) *via* anion-exchange Q-Sepharose and gel filtration chromatography.†

The natural substrates for ANS are relatively difficult to synthesise in enantiomerically pure form and are unstable in solution. Therefore, we investigated the use of a dihydroflavonol, *trans*-dihydroquercetin **4**, as an alternative substrate. Photodiode array (PDA) HPLC analysis identified the product of *trans*-dihydroquercetin incubation as the flavonol quercetin **5**. This result was confirmed by NMR and mass spectrometric analyses. Selected data for the incubation product: (^{1}H NMR 500 MHz; CD_3OD) δ: 4.60 (C-OH, 1H, s br), 6.18 (1H, d, J = 2.0), 6.38 (1H, d, J = 2.0), 6.88 (1H, d, J = 8.5), 7.73 (1H, d, J = 2.0), 7.63 (1H, dd, J = 2.0, J = 8.5); *m/z* (negative ion ESI MS) 301.4 Da.

Using a stopped UV assay the ANS catalysed conversion of *trans*-dihydroquercetin to quercetin was shown to be dependent on both 2-OG and iron(II) and to require a high concentration of ascorbate for significant turnover (40 mM), consistent with the results for ANS from *Perilla fructescens*.[9] Analyses were complicated by precipitation of the flavonoids and their iron

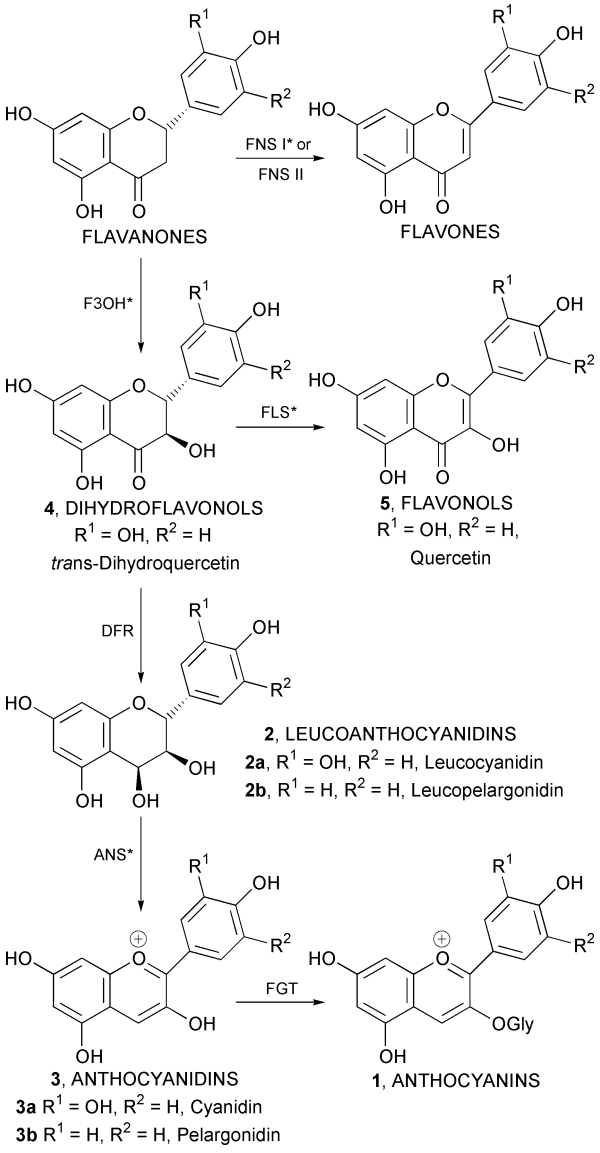

Scheme 1 Later stages of anthocyanin biosynthesis. FNS I , FNS II, flavone synthase I or II; F3OH = flavanone-3β-hydroxylase; FLS = flavonol synthase; DFR = dihydroflavonol-4-reductase; ANS = anthocyanidin synthase; FGT = flavonoid 3-*O*-glucosyltransferase. Asterisked enzymes are 2-OG dependent dioxygenases.[4]

DOI: 10.1039/b007594i

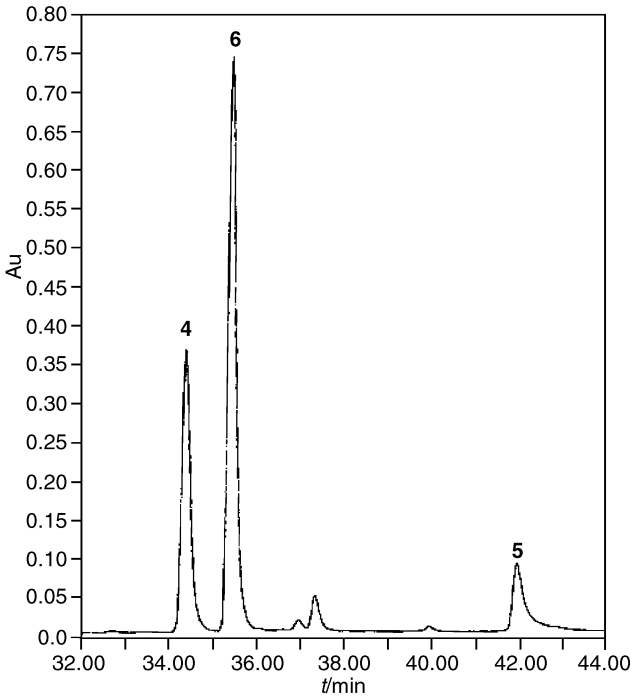

Fig. 1 HPLC trace (λ_{max} 287 nm for **4**, **6**; 372 nm for **5**) of ANS assay with leucocyanidin **2a** after incubation for 20 min. The peaks correspond to *trans*-dihydroquercetin **4**, *cis*-dihydroquercetin **6** and quercetin **5** respectively. Note the **2a** used (Apin) contained contaminating **4** but not **6**.

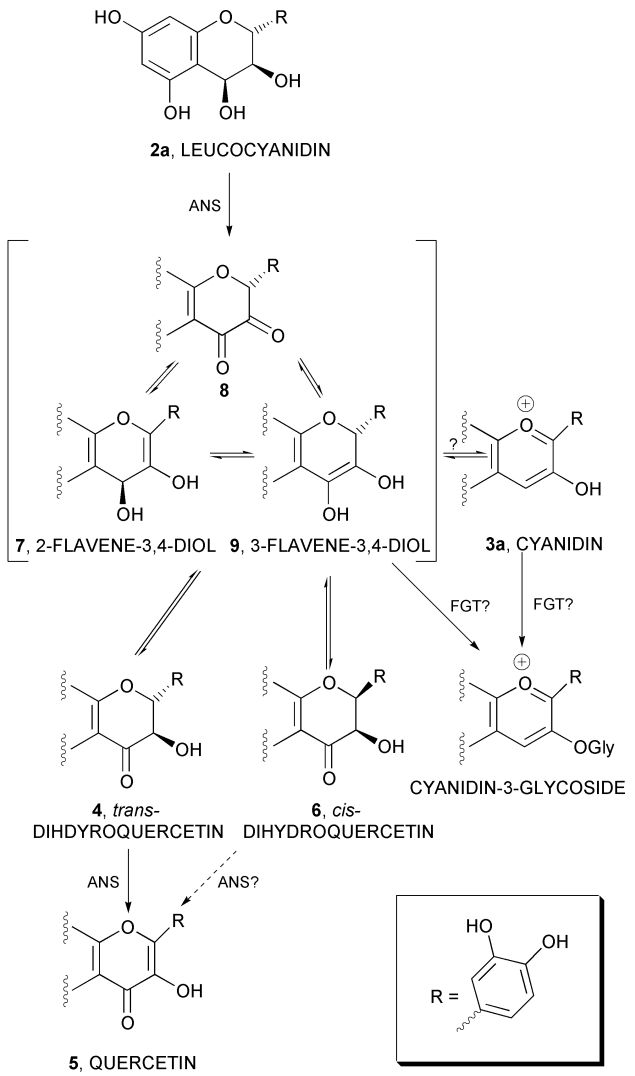

Scheme 2 Proposed intermediates for ANS and FGT turnover of leucocyanidin.[4] The absolute stereochemistry of products **4** and **6** from **2a** has not been determined.

complexes; the maximal catalytical rate was seen at *ca.* pH 6.0. Selwyn analysis[10] indicated that ANS was unstable under the assay conditions at protein concentrations < 70 μg ml^{-1}.

PDA HPLC (monitoring from 200–800 nm) was then used to study ANS catalysed oxidation of a 'natural substrate' leucocyanidin **2a** (Fig. 1). Comparison with known standards identified products as *cis*-**6**‡ and *trans*-**4** dihydroquercetin, quercetin **5** and cyanidin **3a**. The latter was clearly a minor product.

Time course analysis of the leucocyanidin incubation revealed that as the reaction progressed the relative concentration of *trans*-dihydroquercetin decreased as that of quercetin increased. Incubations using mixtures of *cis*-**6** and *trans*-**4** dihydroquercetin demonstrated that *trans*-**4** rather than *cis*-**6** dihydroquercetin was preferentially converted to quercetin **5**.

The observation that both *cis*-**6** and *trans*-**4** dihydroquercetin are produced from leucocyanidin is consistent with the major nascent product of leucocyanidin incubation being a 2-flavene-3,4-diol **7**, as suggested by Heller and Forkmann or ketone **8**, or a 3-flavene-3,4-diol **9** (Scheme 2).[4] Intermediates **7**, **8**, **9** may be non-enzymatically isomerised to give both *cis*-**6** and *trans*-**4** dihydroquercetin. Under the incubation conditions the production of cyanidin is not favoured and it is possible that *in vivo* aromatisation does not occur until the next step,[4] *i.e.* that catalysed by the flavonoid glucosyltransferase (FGT). Alternatively, it is possible that **6** is the (major) product (and substrate for FGT) with the observed **4** arising by isomerisation of **6**.

ANS catalyses conversion of *trans*-dihydroquercetin **4** to quercetin **5**, *i.e.* the same reaction catalysed by flavonol synthase (FLS) (Scheme 1)[4] may reflect incomplete evolution of substrate selectivity or that the pathway has evolved to maintain/develop redundancy in enzymes selectivities. ANS is an interesting enzyme for study due to the ease of tautomerisation/isomerisation of its products, particularly its intermediate products which have not yet been isolated.

We thank Mr A. C. Willis for N-terminal sequencing and the BBSRC, EPSRC and MRC for support of this work.

Notes and references

† The mass and N-terminal protein sequence of the first eleven residues of purified ANS were consistent with the predicted values.[5]

‡ Synthetic **6** reference was obtained by isomerisation of **4** (*trans*:*cis*, 9:1).[11] Leucocyanidin (>95% purity) was from Industrial Research Limited, New Zealand.

1 D. Strack and V. Wray, *Chapter 1, Anthocyanins, in Flavonoids: advances in research since 1986*, ed. J. B. Harborne, Chapman & Hall: London, 1993.
2 Y. T. Huang, J. J. Hwang, P. P. Le, F. C. Ke, J. H. Huang, C. J. Huang, C. Kandaswami, E. Middleton and M. T. Lee, *Brit. J. Pharmacol.*, 1999, **128**, 999.
3 P. C. H. Hollman and M. B. Katan, *Food Chem. Toxicol.*, 1999, **37**, 937.
4 W. Heller and G. Forkmann, *Chapter 11, Biosynthesis in Flavonoids, advances in research since 1986*, ed. J. B. Harborne, Chapman & Hall: London, 1993.
5 M. K. Pelletier, J. R. Murrell and B. W. Shirley, *Plant Physiol.*, 1997, **113**, 1437.
6 P. L. Roach, I. J. Clifton, V. Fulop, K. Harlos, G. J. Barton, J. Hajdu, I. Andersson, C. J. Schofield and J. E. Baldwin, *Nature (London)*, 1995, **375**, 700.
7 C. J. Schofield and Z. H. Zang, *Curr. Opin. Struct. Biol.*, 2000, **9**, 722.
8 A. G. Prescott and M. D. Lloyd, *Nat. Prod. Rep.*, 2000, **17**, 367.
9 K. Saito, M. Kobayashi, Z. Z. Gong, Y. Tanaka and M. Yamazaki, *Plant J.*, 1999, **17**, 181.
10 M. J. Selwyn, *Biochim. Biophys. Acta*, 1965, **105**, 93.
11 E. Kiehlmann and E. P. M. Li, *J. Nat. Prod.*, 1995, **58**, 450.

ChemComm

Molecularly defined palladium(0) monophosphine complexes as catalysts for efficient cross-coupling of aryl chlorides and phenylboronic acid[1]

Mario Gómez Andreu, Alexander Zapf and Matthias Beller*

Institut für Organische Katalyseforschung an der Universität Rostock e.V., Buchbinderstr. 5-6, 18055 Rostock, Germany

Received (in Liverpool, UK) 16th August 2000, Accepted 30th August 2000
First published as an Advance Article on the web

Various 1,6-diene palladium(0) monophosphine complexes have been prepared from tmedaPd(CH_3)$_2$, PR_3, and the corresponding 1,6-diene. These molecularly defined Pd complexes catalyzed the Suzuki coupling of aryl chlorides with phenylboronic acid more efficiently than traditional Pd^{II}–PR_3 pre-catalysts.

The cross-coupling reaction of aryl halides and arylboronic acids (Suzuki reaction) is the most versatile and important method for the synthesis of substituted biaryls.[2] This class of compounds constitute important building blocks for the synthesis of biologically active substances, *e.g.* pharmaceuticals such as the sartan family of drugs for high blood pressure and herbicides.[3] Additionally, biaryls have found application as chiral ligands[4] for catalysis and in materials science, *e.g.* liquid crystals.[5] Suzuki cross-coupling reactions of aryl bromides and iodides have been extensively studied in organic synthesis. Apart from further expanding the scope of this reaction, current interest focuses on the use of economically more attractive aryl chlorides as substrates for this reaction. Notable advances in the cross-coupling reactions of aryl chlorides[6] with arylboronic acids have been described recently by the groups of G. Fu,[7] S. Buchwald,[8] S. A. Guram,[9] S. Nolan,[10] and W. A. Herrmann[11] as well as by our group.[12] In general, important improvements in this area have been made possible by the use of *in situ* 'Pd'–L catalysts consisting of a Pd^{II} source and sterically hindered basic ligands such as dialkylarylphosphines, tri-*tert*-butylphosphine, adamantylphosphines or N-heterocyclic carbenes. It is generally agreed that these *in situ* catalysts are reduced under reaction conditions[13] to afford coordinatively unsaturated complexes such as 16e PdL_3, 14e PdL_2, and 12e PdL, which may constitute the 'real' catalysts. The importance of coordinatively unsaturated Pd^0 species as 'true catalysts' in various cross-coupling reactions has been demonstrated.[14]

In order to avoid side-reactions which may parallel the preformation of the 'real' catalyst and which often lead to loss of catalyst activity, it is desirable to use defined Pd monophosphine complexes as catalysts. To the best of our knowledge there is no report about the use of defined Pd^0 mono- or diphosphine complexes and only one report[11] applying a defined Pd^0 dicarbene species as catalyst in the Suzuki cross-coupling reaction. Recently, we introduced triphenylphosphine palladium(0) diallyl ether as a stable and active catalyst for telomerization of butadiene and methanol.[15] In this paper we describe the use of 1,6-diene stabilized Pd^0–PR_3 complexes as efficient catalysts for the Suzuki cross-coupling of aryl chlorides.

Based on the work of Pörschke[16] *et al.*, who developed a highly effective route for the synthesis of 1,6-diene Pd^0 complexes, we synthesized various monophosphine Pd^0 species as shown in Scheme 1. As phosphine ligands triphenylphosphine, tricyclohexylphosphine, and the so-called 'Buchwald-ligand' *o*-biphenyldicyclohexylphosphine were employed. In order to investigate the influence of the 1,6-diene part on the formation of the L–Pd^0 fragment we decided also to prepare the monotricyclohexylphosphine palladium complex with diallyl ether, diallyl amine and tetramethyldivinyl disiloxane. (Ph_3P)Pd($C_6H_{10}O$) **1**, (Cy_3P)Pd(dvds) **2**, (Cy_3P)Pd($C_6H_{10}NH$) **3**, (Cy_3P)Pd($C_6H_{10}O$) **4**, and (*o*-biphenyl)PCy_2)Pd($C_6H_{10}O$) **5** were obtained by suspending (tmeda)Pd(CH_3)$_2$[17] and PR_3 at −30 °C in the corresponding 1,6-diene. After gently warming the mixtures, elimination of ethane occurred and the desired products were isolated by filtration, washed with cold pentane and dried under vacuum.

A preliminary screening of optimal reaction conditions for the Suzuki coupling of an activated aryl chloride (2-chlorobenzonitrile) with phenylboronic acid in the presence of different palladium catalysts revealed that the coupling proceeds smoothly using THF as the solvent in the presence of a mixture of potassium triphosphate and potassium fluoride as base. In order to compare appropriately the efficiency of the different defined catalysts with each other and with *in situ* catalysts, we performed catalyst tests at low palladium concentration (0.05 mol% Pd). It is important to note that there are relatively few examples of Suzuki cross-couplings of aryl chlorides known that proceed at such low catalyst loading.[8c,18] As shown in Table 1 the cross-coupling reactions of a variety of aryl chlorides with phenylboronic acid proceed in the presence of 1,6-diene stabilized monophosphine in varying yields depending on the catalyst.

Complex **1** ($PPh_3Pd(C_6H_{10}O)$) was shown to be inactive towards all the substrates, although at higher concentrations (0.5 mol% Pd) with the activated 2-chlorobenzonitrile a limited cross-coupling reaction could be observed (32%). 1,6-Diene palladium(0) complexes with the more basic ligand tricyclohexylphosphine **2**–**4** show good conversion with 2-chlorobenzonitrile, chlorobenzene and 4-chlorotoluene (67–96%). Best results were achieved with the 1,6-diene complex containing 'Buchwald's ligand' [**5** (*o*-biphenyl)PCy_2Pd($C_6H_{10}O$)]. With only 0.05 mol% of this catalyst good to excellent yields of biaryls were obtained from activated (2-chlorobenzonitrile: 97%), non-activated (4-chlorotoluene: 82%; chlorobenzene: 87%) and deactivated (4-chloroanisole: 72%) aryl chlorides. The general trend of catalyst activity is in good agreement with previously reported investigations on the corresponding *in situ* systems. However, there are some notable features of the new catalysts: 1. 1,6-Diene palladium(0) monophosphine complexes are significantly more reactive than mixtures of $Pd(OAc)_2$ or $Pd_2(dba)_3$ and phosphines (Table 2). Hence, the obtained

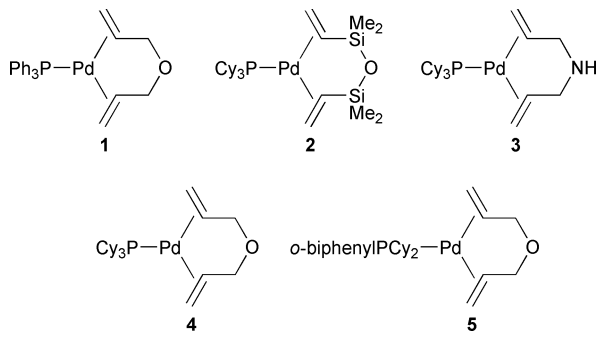

Scheme 1 1,6-Diene complexes of palladium(0).

DOI: 10.1039/b006791l

Table 1 Reactions of aryl chlorides with phenylboronic acid in the presence of various Pd^0 complexes[a]

Entry	Substrate	Product	Catalyst	Yield (%)[b]	TON
1	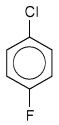	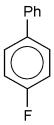	2	15	300
2			3	34	680
3			4	34	680
4			**5**	**67**	**1340**
5	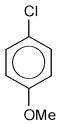	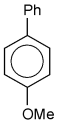	2	28	560
6			3	48	960
7			4	56	1120
8			**5**	**72**	**1440**
9	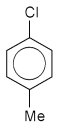	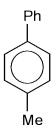	2	23	460
10			3	54	1080
11			4	67	1340
12			**5**	**82**	**1640**
13			2	29	580
14			3	45	900
15			4	79	1580
16			**5**	**87**	**1740**
17			2	96	1920
18			3	95	1900
19			4	96	1920
20			**5**	**97**	**1940**

[a] 3.0 mmol aryl chloride, 4 mmol phenylboronic acid, 3 mmol potassium triphosphate, 3 mmol potassium fluoride, 0.05 mol% catalyst, 8 ml THF, 100 °C, 22 h. [b] Determined by GC with hexadecane as internal standard.

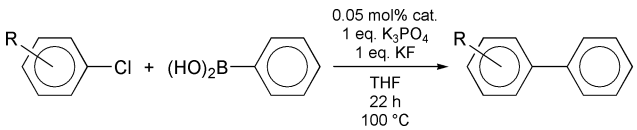

Scheme 2 Suzuki cross-coupling reactions of aryl chlorides with phenylboronic acid.

Table 2 Reactions of aryl chlorides with phenylboronic acid in the presence of various Pd^0 catalysts[a]

Entry	Substrate	Product	Catalyst	Yield (%)[b]	TON
1	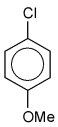	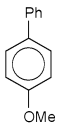	A	5	100
2			B	8	160
3			C	28	560
4			**4**	**56**	**1120**
5			A	8	160
5			B	11	220
7			C	28	560
8			**4**	**79**	**1580**
9			A	91	1820
10			B	91	1820
11			C	95	1900
12			**4**	**96**	**1920**

[a] 3.0 mmol aryl chloride, 4 mmol phenylboronic acid, 3 mmol potassium triphosphate, 3 mmol potassium fluoride, 0.05 mol% catalyst, 8 ml THF, 100 °C, 22 h. [b] Determined by GC with hexadecane as internal standard. A: $Pd_2(dba)_3$–PCy_3 1:1. B: $Pd(OAc)_2$–PCy_3 1:1. C: $Pd(OAc)_2$–PCy_3 1:2.

catalyst turnover numbers are amongst the highest yet reported for the Suzuki reaction of non-activated aryl chlorides. 2. The catalyst properties are mainly determined by the phosphine ligand as shown by an increase of product yields in the series: (*o*-biphenyl)$PCy_2Pd(C_6H_{10}O)$ **5** > $(Cy_3P)Pd(C_6H_{10}O)$ **4** ⩾ $(Ph_3P)Pd(C_6H_{10}O)$ **1**. 3. The effectiveness of the studied complexes **2**–**4** is directly related to their ability to liberate the diene part and to generate the corresponding 12e [L–Pd^0] species. Previously, it has been shown that an increasing acceptor strength of the 1,6-diene moiety results in an increasing stability of the 1,6-diene complex.[16] In agreement with these studies we observe an decrease in reactivity in the order **4** > **3** > **2**.

In summary, we have shown that 1,6-diene palladium(0) monophosphine complexes are extremely efficient catalysts for Suzuki cross-coupling reactions of various aryl chlorides. By variations of both the diene and the phosphine part of the complex the catalytic properties of the complexes can be tuned. It is clearly shown that these defined monophosphine catalysts are superior to generally applied mixtures of Pd-pre-catalysts and phosphines. Thus, this class of catalysts offers promising features for a number of other important palladium-catalyzed coupling reactions.

This work is funded by DMC². We thank Dr O. Briel and Dr Karch (DMC²) for helpful discussions and Dr M. Hateley (IfOK) for help with this manuscript.

Notes and references

1 Part 19 in the series 'Palladium-catalyzed Synthesis of Fine chemicals'; for part 18 see A. Ehrentraut, A. Zapf and M. Beller, *Synlett*, in press.

2 N. Miyaura and A. Suzuki, *Chem. Rev.*, 1995, **95**, 2457; H. Geissler, in *Transition Metals for Organic Synthesis*, Vol. 1, ed. M. Beller and C. Bolm, Wiley-VCH, Weinheim, 1998; A. Suzuki, in *Metal-catalyzed Cross-coupling Reactions*, eds. F. Diederich and P. J. Stang, Wiley-VCH, Weinheim, 1997; A. Suzuki, *J. Organomet. Chem.*, 1999, **576**, 147.

3 H. H. Szmant, *Organic building blocks of the chemical industry*, John Wiley & Sons, New York, 1989.

4 A. S. Parsons, J. M. Garcia and V. Snieckus, *Tetrahedron Lett.*, 1994, **35**, 7537; D. W. Old, J. P. Wolfe and S. L. Buchwald, *J. Am. Chem. Soc.*, 1998, **120**, 9722.

5 E. Poetsch, *Kontakte*, 1988, 15.

6 H. Gröger, *J. Prak. Chem.*, 2000, **342**(4), 334; R. Stürmer, *Angew. Chem.*, 1999, **111**, 3509; *Angew. Chem., Int. Ed.*, 1999, **38**, 3307; T. H. Riermeier, A. Zapf and M. Beller, *Top. Catal.*, 1997, **4**, 301; V. V. Grushin and H. Alper, *Chem. Rev.*, 1994, **94**, 1047.

7 A. F. Littke and G. C. Fu, *Angew. Chem.*, 1998, **110**, 3586; *Angew. Chem., Int. Ed.*, 1998, **38**, 3387; A. F. Littke, C. Dai and G. C. Fu, *J. Am. Chem. Soc.*, 2000, **122**, 4020.

8 (*a*) J. P. Wolfe and S. L. Buchwald, *Angew. Chem.*, 1999, **111**, 2570; *Angew. Chem., Int. Ed.*, 1999, **39**, 2413; (*b*) R. A. Singer and S. L. Buchwald, *Tetrahedron Lett.*, 1999, **40**, 1095; (*c*) J. P. Wolfe, R. A. Singer, B. H. Yang and S. L. Buchwald, *J. Am. Chem. Soc.*, 1999, **121**, 9550.

9 X. Bei, T. Crevier, A. S. Guram, B.Jandeleit, T. S. Powers, H. W. Turner, T. Uno and W. H. Weinberg, *Tetrahedron Lett.*, 1999, **40**, 3855.

10 C. Zhang, J. Huang, M. L. Trudell and S. P. Nolan, *J. Org. Chem.*, 1999, **64**, 3804.

11 V. P. W. Böhm, C. W. K. Gstöttmayr, T. Weskamp and W. A. Herrmann, *J. Organomet. Chem.*, 2000, **595**, 186.

12 M. Beller, H. Fischer, W. A. Herrmann and C. Broßmer, *Angew. Chem.*, 1995, **107**, 1992; A. Zapf and M. Beller, *Chem. Eur. J.*, 2000, **6**, 1830.

13 C. Amatore and A. Jutand, *Acc. Chem. Res.*, 2000, **33**, 314.

14 F. Paul, J. Patt and J. F. Hartwig, *J. Am. Chem. Soc.*, 1994, **116**, 5969; J. F. Hartwig and F. Paul, *J. Am. Chem. Soc.*, 1995, **117**, 5373; P. W. Jolly, *Angew. Chem.*, 1985, **97**, 279; *Angew. Chem., Int. Ed. Engl.*, 1985, **24**, 283.

15 F. Vollmüller, J. Krause, S. Klein, W. Mägerlein and M. Beller, *Eur. J. Inorg. Chem.*, 2000, in press.

16 J. Krause, K.-J. Haack, G. Cestaric, R. Goddard and K.-R. Pörschke, *Chem. Commun.*, 1998, 129; J. Krause, G. Cestaric, K.-J. Haack, K. Seevogel, W. Strom and K.-R. Pörschke, *J. Am. Chem. Soc.*, 1999, **121**, 9807.

17 H. Nakazawa, F. Ozawa and A. Yamamoto, *Organometallics*, 1983, **2**, 241.

18 A. Zapf, A. Ehrentraut and M. Beller, *Angew. Chem.*, in press.

ChemComm

A novel inorganic–organic hybrid membrane for oxygen/nitrogen separation containing a cobalt(II) Schiff base complex as oxygen carrier using poly(*N*-vinylpyrrolidone) as mediator

Koji Kuraoka,*[a] Yoshiki Chujo[b] and Tetsuo Yazawa[a]

[a] *Osaka National Research Institute, AIST, Midorigaoka, Ikeda City, Osaka 563-8577, Japan*
[b] *Kyoto University, Yoshida, Sakyo-ku, Kyoto 606-8501, Japan. E-mail: kuraoka@onri.go.jp*

Received (in Cambridge, UK) 2nd October 2000, Accepted 8th November 2000
First published as an Advance Article on the web

A novel oxygen selective inorganic–organic hybrid membrane containing (*N*,*N*′-disalicylideneethylenediaminato)cobalt(II) (salcomine) as an oxygen carrier was prepared *via* the sol–gel method using poly(*N*-vinylpyrrolidone) (PVP) as the mediation agent.

Oxygen selective membranes are important in various fields such as medicine, oxygen-enriching combustion systems, and fuel cell systems. Much attention for oxygen-enriching organic polymer membranes has been focused on the synthesis of polymers where the solubility of oxygen is greater than that of nitrogen.[1] However, no permselective membrane has been successfully prepared so far using this approach. Recently, the method of oxygen carrier addition to improve the oxygen selectivity of an organic polymer gas separation membrane operating at around room temperature has attracted tremendous attention. Some efforts have been made to facilitate transport using transition-metal complexes such as cobalt porphyrin complexes[2] and cobalt Schiff base complexes.[3] In all earlier investigations it was claimed that high O_2 selectivity could only be achieved at lower operating pressures and temperatures.

A large variety of inorganic–organic hybrids prepared by the sol–gel method has been reported.[4–8] Among these, the most common method utilizes hydrogen bonding interactions between polar functional groups of organic polymers and silanol groups of silica gels. Examples include organic polymers such as poly(2-methyl-2-oxazoline) and poly(*N*-vinylpyrrolidone) incorporated homogeneously into silica gels at the molecular level.[5,6,8]

Here, we report the preparation of a SiO_2–(*N*,*N*′-disalicylideneethylenediaminato)cobalt(II) (salcomine) hybrid membrane using poly (*N*-vinylpyrrolidone) (PVP) as a mediation agent, that is capable of selective separation of oxygen. Salcomine is a well known oxygen carrier complex. Unfortunately, there is no interaction between salcomine and silica, which makes it difficult to integrate it at a molecular level. To solve this problem, we proposed to use PVP as a mediation agent which contains amide carbonyl groups in its structure. Hydrogen bonding interactions between amide carbonyl and silanol groups of silica along with coordinate bonding interactions between nitrogen atoms of amide carbonyl groups and Co(II) in the salcomine can help to disperse organic and inorganic components at a molecular level. Based on this concept, we have prepared novel inorganic–organic hybrid membranes containing oxygen carrier complexes, using the sol–gel technique.

Tetraethoxysilane (TEOS) was used as the silica source and the PVP had a molecular weight of *ca.* 630 000; the concentration of PVP in the TEOS was *ca.* 11 wt%. A selective SiO_2–PVP–salcomine hybrid membrane was prepared using the following molar sol–gel composition: TEOS : EtOH : H_2O : HNO_3 : salcomine = 1 : 20 : 2 : 0.01 : 0.01. In a typical synthesis, the homogeneous sol was prepared by stirring a mixture of TEOS, H_2O, HNO_3 and EtOH for several hours at room temperature. PVP was added to the sol with continuous stirring. Finally, after stirring for 3 h, salcomine was introduced into the sol and resulting sol was vigorously stirred for several hours to obtain a homogeneous sol.

Porous alumina tubes (NGK Insulator, Ltd.; mean pore diameter, 0.1 μm; o.d, 10 mm; i.d, 7 mm; length, *ca.*10 cm) were used as supports. Tubular supports with one end closed were dipped in the sols, withdrawn at a rate of 1 mm s^{-1}, and then dried at room temperature. The dip coating procedure was performed in a class 1000 clean room (295 K and 50% relative humidity) to avoid dust which leads to pinholes on membranes. After the dip-coating was repeated twice, the membranes were heated to 423 K at the rate of 0.5 K min^{-1}, maintained at the same temperature for 2 h, then cooled to room temperature at 0.5 K min^{-1}. These coating and heating procedures were repeated twice in a similar manner. Hybrid membranes without salcomine were also prepared by the same procedure.

The structures of the hybrid membranes were determined using FTIR (FTIR-8700, Shimadzu). FTIR spectra of both SiO_2–PVP–salcomine and SiO_2–PVP hybrids showed a typical band at *ca.* 960 cm^{-1} associated with the stretching mode of Si–OH,[9] along with the characteristic bands related to the Si–O–Si bond (*ca.* 1220, 1080, 800 and 460 cm^{-1}),[9] which confirm the presence of Si–O–Si networks in the hybrids. Other characteristic bands originating from PVP were also observed (Fig. 1). The band at *ca.* 1650 cm^{-1} is due to the stretching band of amide carbonyl groups. Compared to that of PVP, these bands were shifted to lower wavenumbers indicating the existence of hydrogen bonding between amide carbonyl and silanol groups in the hybrids.[5] This provides evidence that in hybrids the inorganic segments (silica) and organic ones (PVP) are very well dispersed at the molecular level in accord with the previous reports.[5,6,8] The spectra of SiO_2–PVP and SiO_2–PVP–salcomine hybrids were quite similar since the amount of salcomine incorporated was very low (1 mol% relative to TEOS). However, PVP aids to dissolve salcomine homogeneously in

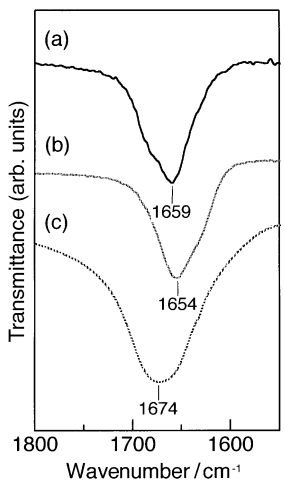

Fig. 1 IR spectra of (a) SiO_2–PVP–salcomine hybrid, (b) SiO_2–PVP hybrid and (c) PVP.

DOI: 10.1039/b007925l

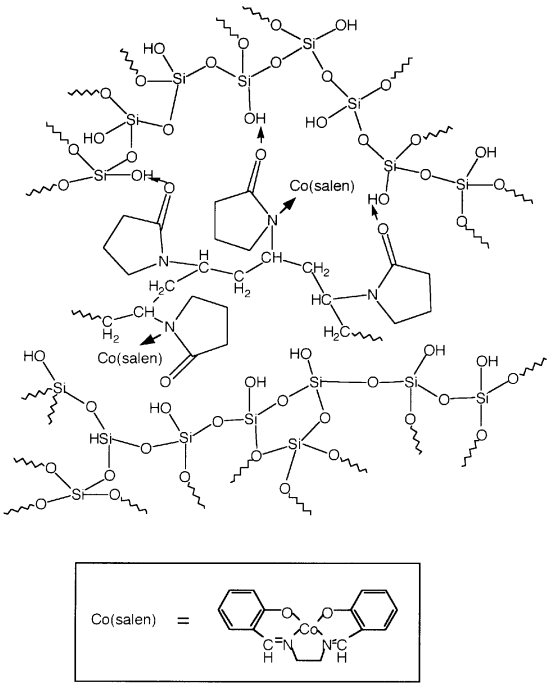

Fig. 2 Schematic representation of the structure of the SiO_2–PVP–salacomine hybrid membrane.

the sol. A possible schematic structure of the membrane is proposed in Fig. 2. As shown, silica and PVP were dispersed at a molecular level due to strong hydrogen bonding between amide carbonyl and silanol groups. Also, PVP and salcomines were well dispersed at a molecular level as nitrogen atoms of amide carbonyl groups were coordinated with Co(II) in the salcomines.[2,3] Therefore, high dispersion of salcomines in the SiO_2–PVP hybrid at the molecular level and a well dispersed inorganic–organic structure of the SiO_2–PVP–salcomine hybrid is evident.

Single gas permeation through these hybrid membranes at different temperatures was measured using O_2 and N_2 using the procedure described elsewhere[10] after drying at 373 K in a vacuum oven for 1 h. Table 1 lists the permeances of O_2 and N_2 through the SiO_2–PVP–salcomine and SiO_2–PVP hybrid membranes and shows the selectivity factor $\alpha = P_{O_2}/P_{N_2}$, where P_{O_2} and P_{N_2} are the permeances of O_2 and N_2, respectively. SiO_2–PVP–salcomine hybrid membrane showed oxygen selectivity even at high temperatures. Although the initial selectivity at 298 K was not that high ($P_{O_2}/P_{N_2} = 1.4$), the selectivity was found to increase with increasing temperature. At 423 K, the O_2/N_2 selectivity factor was 6.1, and the permeance of O_2 was 5.0 $\times$ 10^{-10} (mol m^{-2} s^{-1} Pa^{-1}). This selectivity factor is greater than the theoretical Knudsen value ($P_{O_2}/P_{N_2} = 0.94$) which can be ascribed to the strength of the Co(II)–oxygen complex bonds, which are strong at higher partial pressures of oxygen; therefore, salcomine effectively only releases oxygen at temperatures > 373 K, that is strongly trapped by salcomine at low temperature and thus lowers the mobility of oxygen. The absence of oxygen selectivity for the SiO_2–PVP hybrid membrane (without salcomine) confirms that oxygen selectivity is strongly related to the presence of salcomine.

Table 1 Permeances and selectivity factors of O_2 and N_2 through the SiO_2–PVP–salcomine and SiO_2–PVP hybrid membranes at 298, 373 and 423 K

Membrane	*T*/K	10^{-10} Permeance/ mol m^{-2} s^{-1} Pa^{-1}		Selectivity factor P_{O_2}/P_{N_2}[a]
		O_2	N_2	
SiO_2–PVP–salcomine	298	1.2	0.84	1.4
	373	4.0	0.87	4.6
	423	5.0	0.84	6.1
SiO_2–PVP	298	1.5	1.5	1.0
	373	1.2	1.1	1.0
	423	0.77	0.77	0.99

[a] Theoretical selectivity factor based on Knudsen flow is 0.94.

In conclusion, SiO_2–(*N*,*N*′-disalicylideneethylenediaminato)cobalt(II) (salcomine) hybrid membranes for oxygen separation were prepared by the sol–gel method using poly(*N*-vinylpyrrolidone) (PVP) as a mediation agent. Results indicates that the proposed structure of the membrane consisted of well dispersed inorganic (SiO_2) and organic (PVP, salcomine) segments at a molecular level. This membrane can be classified as a high O_2 selectivity membrane even at high oxygen partial pressure and relatively high temperature.

Notes and references

1 S. A. Stern, *J. Membr. Sci.*, 1994, **94**, 1.
2 H. Nishide, M. Ohyanagi, O. Okada and E. Tsuchida, *Macromolecules*, 1987, **2**, 417.
3 E. Tsuchida, H. Nishide, M. Ohyanagi and H. Kawakami, *Macromolecules*, 1987, **20**, 1907.
4 T. Saegusa and Y. Chujo, *J. Macromol. Sci.*, 1990, **A27** (**13&24**), 1603.
5 Y. Chujo and T. Saegusa, *Adv. Polym. Sci.*, 1992, **100**, 11.
6 M. Toki, T. Y. Chow, T. Ohnaka, H. Samura and T. Saegusa, *Polym. Bull.*, 1992, **29**, 653.
7 J. Wen and G. L. Wilkes, *Chem. Mater.*, 1996, **8**, 1667.
8 R. Tamaki, Y. Chujo, K. Kuraoka and T. Yazawa, *J. Mater. Chem.*, 1999, **9**, 1741.
9 A. Bertoluzza, C. Fagnano, M. A. Morelli, V. Gottardi and M. Guglielmi, *J. Non-Cryst. Solids*, 1982, **48**, 117.
10 T. Yazawa and H. Tanaka, *Ceram. Trans.*, 1993, **31**, 213.

A Zn(II) porphyrin–Ir(III) bis-terpyridine–Au(III) porphyrin triad with a charge-separated state in the microsecond range

Lucia Flamigni,*[a] Isabelle M. Dixon,[b] Jean-Paul Collin*[b] and Jean-Pierre Sauvage*[b]

[a] *Istituto FRAE-CNR, Via P. Gobetti 101, 40129 Bologna, Italy. E-mail: flamigni@frae.bo.cnr.it*
[b] *Laboratoire de Chimie Organo-Minérale, UMR 7513 CNRS, Université Louis Pasteur, Institut Le Bel, 4 rue Blaise Pascal, 67070 Strasbourg, France. E-mail: sauvage@chimie.u-strasbg.fr*

Received (in Cambridge, UK) 25th September 2000, Accepted 7th November 2000
First published as an Advance Article on the web

A photoinduced, multistep electron transfer in a triad containing a zinc porphyrin (electron donor) and a gold(III) porphyrin (electron acceptor) appended to an Ir(III) bis-terpyridine complex produces a charge separated state with a close to unity yield and a lifetime of 450 ns.

Photoinduced charge separation over nanometer distances in artificial arrays is a topic of high relevance both to fundamental[1] and to applied chemical sciences.[2] This function is achieved by molecular triads and higher analogues, able to undergo stepwise electron transfer under the action of light. It is essential that the multicomponent systems be rigid so as to insure good geometrical control and to favor long-lived charge separated (CS) states. In recent years, we have reported rigid triads based on ruthenium(II) bis-terpy complexes (terpy = 2,2′:6′,2″-terpyridine) and differently metallated porphyrins as electron donor and electron acceptor groups.[3,4] In this type of array, energy transfer processes from the porphyrin photosensitizer to the Ru(II) complex could efficiently compete with the desired electron transfer.[4] Ir(III) bis-terpy revealed itself to be particularly well adapted as a component unit, since it displayed a higher ligand centered excited state and remarkable redox properties.[5] Therefore Ru(II) was replaced by Ir(III) as the assembling metal ion in the synthesis of the rigid molecular triads.[6] In the previous Ir(III) bis-terpy based triad the electron donor was a free-base porphyrin (PH_2) and the terminal acceptor was a gold(III) porphyrin (PAu). Clear evidence for the formation of the fully charge-separated state (PH_2^+–Ir–PAu^-) was obtained by transient absorption spectroscopy.[6] However, charge recombination turned out to be fast (*ca.* 3.5 ns at room temperature in nitriles) due to the presence of a low-lying triplet state localized on PH_2. Substitution of the PH_2 unit with zinc porphyrin in this triad is expected to result in an increase in the triplet level; this should leave the CS state as the lowest state with the only possibility to deactivate to the ground state. Since the latter reaction is strongly exergonic (ΔG *ca.* −1.3 eV) we expect it to be placed in the Marcus inverted region[1] in a moderately polar or apolar solvent, and therefore to be slow so allowing for a long-lived CS state.

We now report the detection, upon excitation in the visible region of a toluene solution of **PZn–Ir–PAu** (Fig. 1), of a CS state with a lifetime of 450 ns. The triad **PZn–Ir–PAu**† was prepared by metallation of its free-base analogue[6] with zinc acetate in refluxing MeCN–MeOH (1:1 v/v). The absorption spectrum of this triad in toluene is very little perturbed with respect to the superposition of the spectra of the model components **PAu**, **PZn** (in toluene) and **Ir** (in acetonitrile) indicating little electronic coupling between the components. Similar indications are given by electrochemical determinations in dichloromethane where the oxidation of the PZn unit in the dyad PZn–Ir occurs at the same potential as the model **PZn**, +0.68 V (*vs.* SCE) while the PAu unit, which is reduced at −0.66 V (*vs.* SCE) in PAu–Ir *cf.* −0.70 V (*vs.* SCE) of **PAu**, is somehow affected by the presence of the substituent. Reduction of the Ir complex occurs at −0.71 V in the model dyad PZn–Ir. These data place the energy levels of the CS states PZn^+–Ir^-–PAu and PZn^+–Ir–PAu^- in dichloromethane at *ca.* 1.39 and 1.34 eV, respectively. The excited state properties determined by transient absorption and luminescence experiments‡ at 295 K both for the models and the array are reported in Table 1 with the pertinent energy levels, as derived by the maxima of emissions at 77 K. The emission of zinc porphyrin in the array is quenched with a rate exceeding our resolution time, while the only detectable excited state of the gold porphyrin, the lowest triplet, remains unchanged with respect to the model. The Ir moiety absorbs at higher energies, $\lambda < 400$ nm, therefore this unit is not excited in the present experiment. Upon laser excitation at 532 nm, after the decay of the gold porphyrin triplet (τ = 2.5 ns), a longer lived absorption is left the spectrum of which is displayed in Fig. 2. The decay is monoexponential, identical over the whole spectral region and in air-free solution the lifetime is 450 ns (inset of Fig. 2). Air equilibration of the solution results in a decrease of the exponential lifetime to 310 ns, which allows us to derive a reaction rate with oxygen of *ca.* 5×10^8 M^{-1} s^{-1}. The lifetime was unaffected by changes in the concentration of the array and in the energy of the laser pulse. The spectrum, in full agreement with the bands typical of the zinc porphyrin cation and the reduced gold porphyrin radical, is assigned to the CS state PZn^+–Ir–PAu^-. In oxygen free solutions a very weak absorption ascribable to the triplet localized on the zinc porphyrin, formed with a very low yield and a lifetime of 7 μs, is left after the decay of the CS state. An estimate of the efficiency of the charge separation process with respect to the photons absorbed by the zinc porphyrin moiety only, calculated on the basis of the molar absorption coefficient of 1×10^4 M^{-1} cm^{-1} for the cation of tetraphenyl zinc porphyrin at 680 nm,[7] yields a value very close to unity (1.2 ±

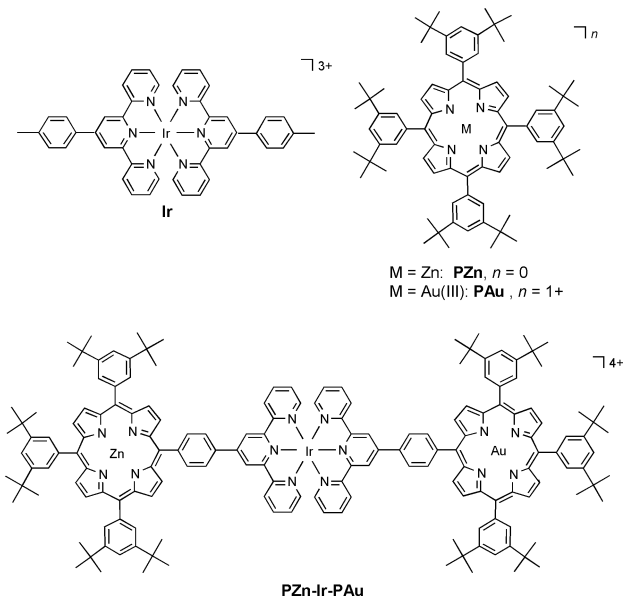

Fig. 1 Chemical formula of the triad and models.

Table 1 Excited state properties from luminescence and transient absorbance[a] data in toluene solutions

		295 K			77 K	
		λ_{max}/nm	τ/ns	Φ_{fluo}	λ_{max}/nm	E/eV
PZn	^{1}PZn	596	2.2	0.08	606	2.05
	^{3}PZn	470[a]	300×10^3[a]		770	1.61
PAu	^{3}PA	630[a]	2.5[a]		712	1.74
PZn–Ir–PAu	^{1}PZn	598	$\leqslant$0.020	0.0006	606	2.05
	^{3}PZn	470[a,b]	7×10^3[a,b]		786	1.58
	^{3}PAu	630[a]	2.5[a]		716	1.73

[a] From transient absorbance. [b] Extremely low yield.

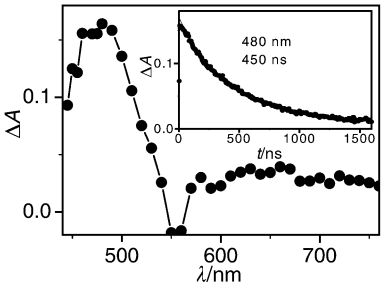

Fig. 2 Transient absorption changes detected in an air free toluene solution of **PZn–Ir–PAu** upon excitation at 532 nm. In the inset the decay at 480 nm and the fitted exponential function corresponding to a lifetime of 450 ns is shown.

0.3). Such high efficiency in the charge separation process requires a very fast primary (from the excited PZn moiety to the Ir complex) and secondary (from the reduced Ir moiety to the gold porphyrin unit) electron transfer, to prevent competition with the back reactions. The detected quenching of the luminescence is faster than 20 ps in agreement with this requirement, so is also the rise of the absorbance assigned to the CS state which cannot be resolved from the excitation profile in an experiment with 20 ps resolution. Any investigation on the model dyad PZn–Ir which could give further information on the elementary steps of the electron transfer sequence is prevented by the insolubility of the dyad in toluene. Fig. 3 shows a schematic energy level diagram for the system along with the processes and the pertinent rates. The energy levels of the CS states are derived from electrochemical data in dichloromethane and this causes some uncertainty in their location in a toluene solution.

We have shown that highly efficient formation of a long lived charge separated state occurs in this triad in toluene solution upon excitation in the visible range.

This work was supported by the French CNRS and the Italian CNR. We thank European Commission COST programme D11/0004/98 and the French Ministry of Education, Research and Technology for a fellowship to I. M. D. We are also grateful to Johnson Matthey for a generous loan of $IrCl_3$.

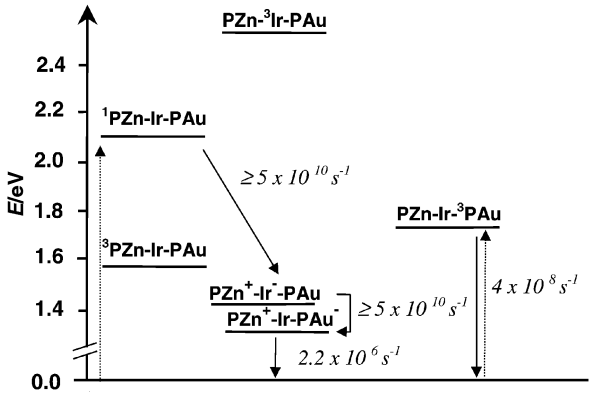

Fig. 3 Schematic energy level diagrams for **PZn–Ir–PAu**. The charge separated state energies are calculated from electrochemical data in dichloromethane.

Notes and references

† ^{1}H NMR (400 MHz, CD_3CN), δ 9.49–9.42 (m, 8H, pyrroles-PAu), 9.37 (s, 4H, $H_{3'}$ + $H_{5'}$), 8.99 (m, 4H, pyrroles-PZn), 8.93 (d, 4H, H_6, ^3J 8.2 Hz), 8.90 (s, 4H, pyrroles-PZn), 8.80–8.70 (m, 8H, H_1 + H_2), 8.36 (dd, 4H, H_4, ^3J 7.8 Hz), 8.18 (d, 4H, H_o-PAu, ^4J 1.7 Hz); 8.16 (d, 2H, $H_{o'}$-PAu, ^4J 1.7 Hz), 8.15 (d, 4H, H_o-PZn, ^4J 2.0 Hz), 8.11 (d, 2H, $H_{o'}$-PZn, ^4J 1.9 Hz), 8.09–8.06 (m, 3H, H_p + $H_{p'}$-PAu), 7.95–7.90 (m, 7H, H_p + $H_{p'}$-PZn + H_3), 7.68–7.62 (m, 4H, H_5), 1.58 (s, 36H, Bu^t-PAu), 1.57 (s, 36H, Bu^t-PZn), 1.56 (s, 18H, Bu$^{t'}$-PAu), 1.55 (s, 18H, Bu$^{t'}$-PZn). MS (FAB^+): *m/z* 3249.3 ([M + H − PF_6]$^+$), 3105.2 ([M − $2PF_6$]$^+$), 2960.2 ([M − $3PF_6$]$^+$), 2813.1 ([M − $4PF_6$]$^+$), 1552.1 ([M − $2PF_6$]$^{2+}$), 1479.1 ([M − $3PF_6$]$^{2+}$), 1408.1 ([M − $4PF_6$]$^{2+}$), 1376.1 ([M − $4PF_6$ − Zn + 3H − terpyPAu]$^+$, *i.e.* [PH_3 − Ph − terpy − Ir]$^+$, 100%).

‡ Time resolved luminescence was determined with an apparatus based on a Nd-YAG laser (35 ps, 1 mJ at 532 nm) and a streak camera (overall resolution: 20 ps). Transient absorbance changes with 20 ps resolution were determined with a pump and probe system based on a Nd-YAG laser (35 ps, 3 mJ at 532 nm) and an OMA detector. For ns to μs time domains a laser flash photolysis based on a Nd-YAG laser (18 ns pulse, 3 mJ at 532 nm), a pulsed xenon lamp and a photomultiplier Hamamatsu R936, was used. For further details on the experimental set-up see refs. 4–6.

1 R. A. Marcus and N. Sutin, *Biochim. Biophys. Acta*, 1985, **811**, 265 and references therein; G. L. Closs and J. R. Miller, *Science*, 1988, **240**, 440.
2 *Energy Resources through Photochemistry and Catalysis*, ed. M. Grätzel, Academic Press, New York, 1983; C. J. Kleverlaan, M. T. Indelli, C. A. Bignozzi, L. Pavanin, F. Scandola, G. Hasselman and G. J. Meyer, *J. Am. Chem. Soc.*, 2000, **122**, 2840 and references therein.
3 A. Harriman, F. Obodel and J.-P. Sauvage, *J. Am. Chem. Soc.*, 1995, **117**, 9461.
4 L. Flamigni, N. Armaroli, F. Barigelletti, V. Balzani, J.-P. Collin, J.-O. Dalbavie, V. Heitz and J.-P. Sauvage, *J. Phys. Chem.*, 1997, **101**, 5936; L. Flamigni, F. Barigelletti, N. Armaroli, J.-P. Collin, J.-P. Sauvage and J. A. G. Williams, *Chem. Eur. J.*, 1998, **4**, 1744.
5 J.-P. Collin, I. M. Dixon, J.-P. Sauvage, J. A. G. Williams, F. Barigelletti and L. Flamigni, *J. Am. Chem. Soc.*, 1999, **121**, 5009.
6 I. M. Dixon, J.-P. Collin, J.-P. Sauvage, F. Barigelletti and L. Flamigni, *Angew. Chem., Int. Ed.*, 2000, **39**, 1292.
7 J. Fajer, D. C. Borg, A. Forman, D. Dolphin and R. H. Felton, *J. Am. Chem. Soc.*, 1970, **92**, 3451.

Synthesis of mesoporous silicon imido nitride with high surface area and narrow pore size distribution

Stefan Kaskel,* David Farrusseng and Klaus Schlichte

Max-Planck-Institut für Kohlenforschung, Kaiser-Wilhelm-Platz 1, D 45470 Mülheim an der Ruhr, Germany. E-mail: kaskel@mpi-muelheim.mpg.de

Received (in Cambridge, UK) 28th September 2000, Accepted 7th November 2000
First published as an Advance Article on the web

Silicon imido nitride with a specific surface area up to 1000 $m^2\ g^{-1}$ is obtained by ammonolysis of silicon tetrachloride in organic solvents and subsequent NH_4Cl removal at elevated temperatures in a stream of anhydrous ammonia. The material has a remarkably narrow pore size distribution and a mean pore size of 5.7 nm. TEM investigations reveal the spherical macromorphology and uniform dendritic mesostructure of the micrometer sized particles. A high number of Si-NH_2 groups on the inner surface of the material is indicated from IR measurements. ^{29}Si MAS NMR indicates the presence of SiN_4^{8-} tetrahedra.

Tailoring inorganic solids is a key feature in the search for purpose-built high-performance materials. High specific surface area and control of pore size and pore morphology are especially needed in heterogeneous catalysis.[1] For oxide materials a wide range of methods has been developed such as flame pyrolysis and sol gel techniques.[2] Due to our recent interest in the development of porous non-oxide ceramics as heterogeneous catalysts we have investigated the synthesis of silicon imido nitride as a high surface area material under various conditions. Even though this material has been widely studied as a precurser to obtain Si_3N_4 for structural applications,[3] sinterability and densification have mainly been stressed, whereas only few attempts have been made to systematically tailor its surface area and pore structure and only recently has its potential in heterogeneous catalysis become apparent.[4–6]

In order to achieve easy access to highly porous materials we have used $SiCl_4$ (Arkos, 99.8%) in various solvents (4% solution) such as pentane, toluene, tetrahydrofuran and polyethyleneglycol dimethyl ether and precipitated the diimide with anhydrous ammonia gas (UHP, Messer).† After filtration, the coprecipitated NH_4Cl was removed by sublimation in a dynamic (40 ml min^{-1}) ammonia atmosphere (1 bar) at elevated temperature [eqn. (1)]

$$SiCl_4 + 6NH_3 \xrightarrow{\text{solvent}} [Si(NH)_2\downarrow + 4NH_4Cl\downarrow] \xrightarrow{NH_3,\ \text{heat}} Si(NH)_2 + 4NH_4Cl\uparrow \quad (1)$$

1 **2**

The composition of the product **2** depends on the heat treatment. According to wet chemical analysis of the powder the N : Si ratio is 1.60 for a sample calcined at 873 K, and 1.50 at 1073 K. The formula $Si_2N_2(NH)$ instead of $Si(NH)_2$ is often assigned to intermediates during the technical process of decomposing $Si(NH)_2/xNH_4Cl$ to prepare Si_3N_4 for structural ceramics. We have therefore adopted the rather unspecific nomenclature 'high surface area silicon imido nitride' (HSA-SIN) for **2**. It is obtained with a BET surface area up to 1000 $m^2\ g^{-1}$ as a white, X-ray amorphous powder if pentane is used as the solvent and the initial precipitation is carried out at room temperature followed by heating the resulting solid to 723 K for 2 h with a rate of 5 K min^{-1}. This is the highest surface area so far reported for $Si(NH)_2$ and comparable to that for MCM-41-like materials.[7] Even though the pores do not form an ordered array according to small-angle X-ray measurements, the adsorption isotherm† (Fig. 1) indicates the presence of mesopores with a narrow pore size distribution, a sharp maximum at 5.1 nm and a mean pore diameter of 5.7 nm. No percolation effect due to ink bottle pores is observed. For applications in heterogeneous catalysis ordering of the pores is not necessary but high surface area, narrow pore size distribution and homogeneity of the inner surface are highly desirable to obtain high performance materials with good selectivity.

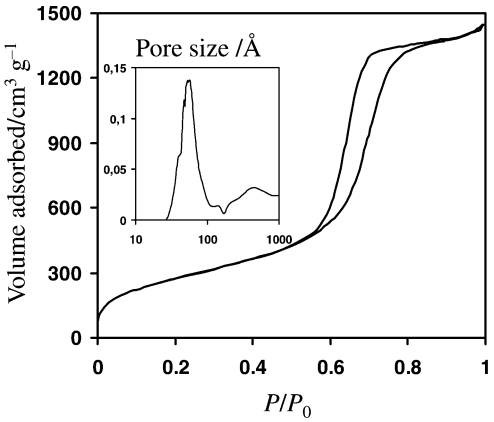

Fig. 1 Nitrogen adsorption isotherm for HSA-SIN synthesized in pentane after calcination in ammonia and its pore size distribution.

TEM investigations (Fig. 2) reveal the spherical morphology of the particles with typical size of 0.1 μm diameter. The radial dendritic channel-like mesostructure is independent of the size of the aggregates. We found that polar solvents such as tetrahydrofuran also give mesoporous silicon imido nitride but with considerably lower surface area (560 $m^2\ g^{-1}$) and two distribution maxima at 7.6 and 40.6 nm. The effect of washing the coprecipitate **1** with liquid ammonia results in an even more drastic reduction of the surface area (*ca.* 300 $m^2\ g^{-1}$) and the

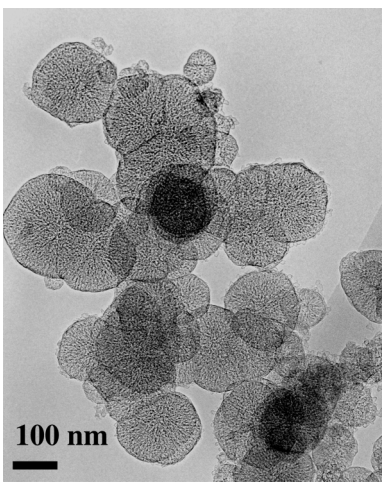

Fig. 2 Transmission electron micrograph of HSA-SIN.

DOI: 10.1039/b007884k

narrow distribution now being completely lost, with a wide range of sizes from micro- to macro-pores being observed. While washing with liquid ammonia is often applied when sinterable $Si(NH)_2$ powder is needed for structural ceramics this method to remove NH_4Cl seems highly inappropriate for specific pore structure design. So far only one group has reported a specific surface area of up to 1000 $m^2\ g^{-1}$ for silicon diimide using the precipitation method and toluene for dilution of $SiCl_4$, but the pore morphology was not discussed.[8] In our experiments, toluene reduces the total yield of the reaction by at least a factor of 10, and is therefore less appropriate.

The particle formation mechanism is still unknown. Some intergrown spheres suggest that the large spheres might have formed by merging of smaller spheres but whether this formation has occurred in solution or during heat treatment is still not clear. However, the strong impact of the solvent on the surface properties as well as the spherical morphology of the aggregates suggests that their formation occurs in solution where surface tension and solubility govern nucleation and growth. In fact we believe that NH_4Cl nanocrystals act as a template for the surrounding $Si(NH)_2$. This view is supported by the fact that polar solvents cause pore collapse due to the higher solubility and recrystallization of the NH_4Cl whereas in pentane the generated ammonium chloride nuclei remain small. This is in accord with the particle size determined from the broadening of the ammonium chloride Bragg reflections in the coprecipitate **1** (*ca*. 8 nm).

IR spectroscopy gives similar results as earlier studies[9] [ν(NH): 3374 cm^{-1}, $\delta(NH_2)$: 1548 cm^{-1}, δ(NH): 1182 cm^{-1}, $\nu_{as}(Si_2N)$: 905 cm^{-1}]. The $\delta(NH_2)$ mode indicates the presence of amino groups located on the inner surface of the material in analogy to silanol groups present on the inner surface of MCM-41. This band is stronger for samples synthesized in pentane *vs*. tetrahydrofuran, corresponding to the higher inner suface area of the former sample; exposure to air as well as lithiation with butyl lithium reduces its relative intensity. No Si–O stretching modes were observed if the material was handled properly with exclusion of moisture or air.

The ^{29}Si MAS NMR spectrum consists of one broad peak centered at −42 ppm, the signal covering the region between −35 and −55 ppm. The broadening originates from the ill defined local structure and is characteristic for amorphous preceramic silicon nitride powders[10] in which different functional groups are present. Thus in HSA-SIN, $Si(NH)_{4/2}$ groups are most abundant but $SiN_{(4-x)/3}(NH)_{x/2}$ (x = 0–3) groups in the bulk and $Si(NH)_{(4-x)/2}(NH_2)_x$ (x = 1,2) groups on the inner surface of the material are also present. A shoulder at −49 ppm indicates a high abundance of $SiN_{4/3}$ groups with a chemical shift comparable to that of β-Si_3N_4[11] at −48.7 ppm. A low level of silicon oxide impurities was also concluded from the absence of any significant peaks close to −100 ppm, though due to the high background noise, such impurities could not be completely excluded. The chlorine contamination was also low (< 2% by EDX).

The high temperature stability and low sintering tendency of the nitride is remarkable and reveals its promising potential as a support in high temperature catalysis: after 2 h of heat treatment at 1273 K in a dynamic ammonia atmosphere (1 bar, 40 ml min^{-1}) the high surface area is only slightly reduced (820 $m^2\ g^{-1}$). The pore size distribution remains narrow with only a slightly reduced mean pore size (4.9 nm).

New compounds will become available as heterogeneous catalysts and supports if morphological syntheses of non-oxide ceramics as high surface area materials are further explored. We have demonstrated that ammonolysis of silicon tetrachloride in solution is an easy route to high surface area silicon imido nitride with uniform pore morphology—a material with potential for base-catalyzed reactions suitable for further functionalization, impregnation and high temperature applications.

We thank F. Schüth for helpful discussions and financial support. A Reimar Lüst Fellowship for Stefan Kaskel was provided by the Max Planck Society. TEM images were recorded by B. Spliethoff while B. Zibrowius measured the ^{29}Si MAS NMR spectra.

Notes and references

† All operations are performed using a vacuum line or an argon-filled glove box and dry solvents. Nitrogen physisorption measurements were performed using an ASAP 2000 (micromeritics) instrument.

1 J. M. Thomas and W. J. Thomas, *Heterogeneous Catalysis*, VCH, Weinheim, 1997.
2 *Advanced Catalysts and Nanostructured Materials*, ed. W. R. Moser, Academic Press, San Diego, 1996.
3 A. W. Weimer, *Carbide, Nitride and Boride Materials Synthesis and Processing*, Chapman & Hall, London, 1997.
4 J. S. Bradley, O. Vollmer, R. Rovai, U. Specht and F. Lefebvre, *Adv. Mater.*, 1998, **10**, 938.
5 J. S. Bradley, O. Vollmer, R. Rovai and F. Lefebvre, *Mater. Res. Soc. Symp. Proc.*, 1999, **549**, 33.
6 D. Hullmann, G. Wendt and U. Ziegenbalg, *Chem.-Ing.-Tech.*, 1999, **71**, 1410.
7 J. S. Beck, J. C. Vartuli, W. J. Roth, M. E. Leonwicz, C. T. Kresge, K. D. Schmitt, C. T.-W. Chu, D. H. Olson, E. W. Sheppard, S. B. McCullen, J. B. Higgins and J. L. Schlenker, *J. Am. Chem. Soc.*, 1992, **114**, 10834.
8 T. Yamada, T. Yamao and K. Shibata, *Ger. Offen.*, DE 19651731 A1, UBE Industries, 1997.
9 R. Rovai, C. W. Lehmann and J. S. Bradley, *Angew. Chem., Int. Ed.*, 1999, **38**, 2036.
10 E. A. Leone, S. Curran and M. E. Kotun, *J. Am. Ceram. Soc.*, 1996, **79**, 513.
11 K. R. Carduner, C. S. Blackwell, W. B. Hammond, F. Reidinger and G. R. Hatfield, *J. Am. Chem. Soc.*, 1990, **112**, 4676.

Electrophilic ring-opening of $[(RP)_nAs]^-$ anions; a simple route to functionalised neutral phosphines of the type $[(Bu^tP)(Bu^tRP)_2]$

David R. Armstrong,[a] Neil Feeder,[b] Alexander D. Hopkins,[b] Martin J. Mays,*[b] David Moncrieff,[c] Jody A. Wood,[b] Anthony D. Woods[b] and Dominic S. Wright*[b]

[a] *Department of Pure and Applied Chemistry, University of Strathclyde, 295 Cathedral Street, Glasgow, UK G1 1XL*
[b] *Chemistry Department, University of Cambridge, Lensfield Road, Cambridge, UK CB2 1EW. E-mail: dsw1000@cus.cam.ac.uk*
[c] *School of Computational Science and Information Technology, Florida State University, Tallahassee, FL 32306, USA*

Received (in Cambridge, UK) 18th September 2000, Accepted 1st November 2000
First published as an Advance Article on the web

Ring opening of the cyclic $[(Bu^tP)_3As]^-$ anion results from reactions with electrophiles (RX = H_2O, MeI, CH_2=$CHCH_2I$, $PhCH_2Br$), providing a simple and general approach to triphosphine ligands of the type $[(Bu^tP)(Bu^tRP)_2]$.

We found recently that heterocyclic anions of the type $[(RP)_nE]^-$ (n = 3 or 4; E = As, Sb; R = Bu^t, 1-adamantyl, cyclohexyl) can be prepared in a single step by the reactions of alkali metal primary phosphides with $E(NMe_2)_3$ (E = As, Sb).[1] Our particular interest in these species stems from their potential to act as sources of group 15 atoms, as suggested by the isolation of Zintl compounds from the same reaction systems at higher temperatures.[1] These heterocyclic anions exhibit unusual reactivity with transition metal metallocenes, the reaction of the Lewis base complex $[\{(Bu^tP)_3As\}Li\cdot 2DABCO\cdot thf]$ **1** [DABCO = $N(CH_2CH_2)_3N$] with $[CpM(CO)_3Cl]$ (M = Mo, W) leading to addition of the $[(Bu^tP)_3As]^-$ anion to the Cp ring rather than displacement of the metal-bonded Cl ligand.[2] Here we show that $[(RP)_nAs]^-$ anions are useful synthons of the corresponding $(RP)_n^{2-}$ dianions, as illustrated by the reactions of $[(Bu^tP)_3As]^-$ with electrophiles which provides direct access to a large range of terminally substituted triphosphine ligands.

The reactions of **1** with a range of electrophiles (1:3 equiv., respectively) occur smoothly at −78 °C in thf–toluene giving insoluble precipitates of HAsO(OH) (in the case of H_2O) or organo-arsenic dihalides $[RAsX_2]$ (with organic halides as electrophiles) which are readily removed by filtration (Scheme 1). Removal of the solvent under vacuum gives 72–98% yields of the terminally substituted triphosphines $[(Bu^tP)(Bu^tRP)_2]$ (R = H **2**, Me **3**, CH_2=$CHCH_2$ **4**, $PhCH_2$ **5**).† The high purity of the materials obtained *directly* by this procedure is confirmed by their room-temperature ^1H and ^{31}P NMR spectra, which show little or no impurities. The ^{31}P NMR spectra of **2**–**5** are consistent with those of previously reported triphosphines,[3] **2** (*meso* and *racemic* isomers), **4** and **5** appearing as characteristic A_2M multiplets and **3** as a more complex eight line A_2B multiplet (*i.e.* $\Delta\delta \approx \Delta J$). A further feature of the ^1H NMR spectra of **3** and **5** is the appearance of the Me and benzyl methylene protons as deceptively simple triplets.[4] Model *ab initio* calculations reveal that the reactions producing **2**–**5** are highly thermodynamically favourable. For example, the gas-phase reaction of 3MeI with $[\{Bu^tP\}_3AsLi]$ is exothermic by 57.4 kcal mol^{-1} (at the B3LYP/6-311G** level).‡ This reaction becomes even more favourable (−66.2 kcal mol^{-1}) once solution effects are included. Calculations of the reactions involving $[\{RP\}_3AsLi]$ (R = H, Me, Bu^t) also reveal that these reactions are enthalpically driven (with negligible entropy changes being associated in solution).

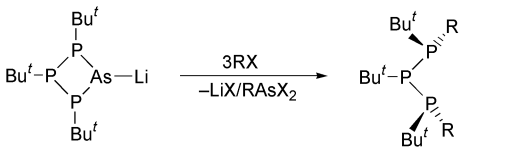

X= OH, R= H **2**; X= Br, I, R = Me **3**, $PhCH_2$ **4**, CH_2=$CHCH_2$ **5**

Scheme 1

A limited number of terminally substituted triphosphines of the type $[(RP)(RR'P)_2]$ have been prepared previously by reactions of $[(RP)_3M_2]$ (M = alkali metal) with electrophiles.[3] These salts can be generated either by cleavage of $(RP)_n$ with an alkali metal (giving the salt as a mixture with other homologues)[5] or by reaction of $[(RP)(RHP)_2]$ (prepared by reduction of terminal halides $[(RP)(RXP)_2]$) with alkali metals.[3a] Importantly, although often efficient these procedures involve several steps starting from the simple dihalides $RPCl_2$, with extensive manipulation and purification at each stage. The electrophilic ring-opening reaction described here provides the potential means by which any primary phosphine (from which **1** and related heterocycles are prepared in a single step in crystalline form) can be converted selectively into a broad range of terminally substituted triphosphines. The closest related approach utilises $[Cp_2Zr(PPh)_3]$ as a source of $[PhP]_3^-$ in the synthesis of the cyclic compounds $[PhP]_4$ and $[(PhP)_3SnBu^t_2]$.[6]

Owing presumably to the involved and specialised synthetic methods previously required in the synthesis of tri- and tetraphosphines, to our knowledge, no studies of their coordination chemistry have been reported. The few structurally characterised examples of coordination compounds of this type are transition metal complexes in which the tri- or tetra-phosphine frameworks have been assembled at the transition metal centre.[7] However, these reactions do not appear to be selective in terms of the chain length of the phosphine incorporated, with the chain length of the phosphines being dependent on the organic substituents[7a,b] as well as the reaction conditions.[8] An illustration that these ligands can indeed be transferred *intact* to a transition metal centre is provided in this study by the synthesis† and structural characterisation§ of $[W(CO_4)\{(Bu^tP)(Bu^tHP)_2\}]$ **6** (Fig. 1). The structural features of **6** are similar to those of $[W(CO)_4\{(Bu^tP)(Me_2P)_2\}]$, the only other complex previously characterised in which a chelating triphosphine ligand is present.[7a] The presence of only one isomer of the triphosphine (the symmetric *meso* form) at the W centres of **6** is of some interest. Previous NMR studies (consistent with those presented in the current work†) have shown that this is the predominant isomer in solutions of free **2**.[3a] The fact that the isomer of **6** incorporating a *racemic* form of the triphosphine is not produced in this reaction may be due to steric factors, leading to the selection of the *meso* form in the complex.

In summary, the new, high yielding method of preparing terminally substituted non-symmetric, triphosphines should allow systematic investigation of the coordination chemistry of

DOI: 10.1039/b007553l

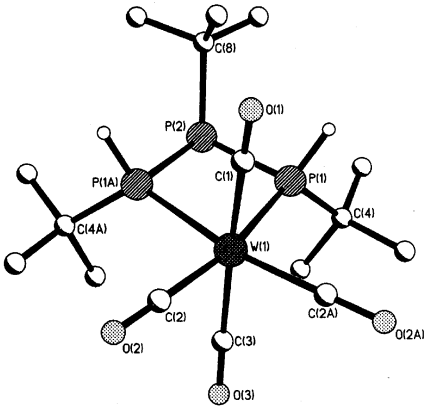

Fig. 1 Structure of **6**; H-atoms (except those attached to the P atoms) have been omitted for clarity. Key bond lengths (Å) and angles (°): W(1)–P(1) 2.512(1), W(1)–C(2) 1.990(5), W(1)–C(3) 2.017(7), P(1)–P(2) 2.215(2); P(1)–W(1)–P(1A) 72.96(5), P(2)–P(1)–W(1) 101.09(5), P(1)–P(2)–P(1A) 84.78(7).

this class of ligands. This should be of particular importance in relation to the widespread application of ligand frameworks such as $(CH_2)_n(PPh_2)_2$ (n = 1 or 2) and the growth of interest in ligand systems with well defined bite, steric and stereochemical characteristics in the field of homogeneous catalysis. Significantly, preliminary studies of the reactions of the heterocyclic anion $[\{CyP\}_4As]^-$ with electrophiles (RX) suggest that analogous tetraphosphines of the type $[(CyP)_2(CyRP)_2]$ are generated.[9]

We gratefully acknowledge the EPSRC (N. F., J. A. W., A. D. W.), Churchill College (Fellowship for A. D. H.), and The Office of Energy Research, Office of Basic Energy Research Sciences, Division of Chemical Sciences, US Department of Energy under grant DE-FG02-97ER-14758 (D. M.).

Notes and references

† *Syntheses* of **2**–**5**: the electrophiles (1.5 mmol) were added dropwise to a solution of **1** (0.64 g, 0.5 mmol) in thf (1 ml)–toluene (20 ml) at −78 °C over a 10 min period. The reactions were allowed to warm to room temperature and stirred for 1 h. For **3**–**5**, white precipitates of the organo-arsenic dihalides in colourless or faint yellow solutions were formed. The precipitates were removed by filtration and the filtrates reduced under vacuum to give crystalline or semi-crystalline solids. For **2**, a yellow solution was produced which was reduced under vacuum to give the triphosphine as a liquid. **2**: 0.13 g (98%); δ_H(+25 °C, d_8-toluene, 400.13 MHz): *meso isomer*, 3.41 (d, P–H, $^1J_{PH}$ 203 Hz), 1.38 (d, Bu^{t}P(2), J 12.9 Hz), 1.30 [d, Bu^{t}P(1,3), J 12.5 Hz]; *racemic isomer*, 3.30 (d, P–H, $^1J_{PH}$ 205 Hz), 1.52 (d, Bu^{t}P(2), J 12.5 Hz), 1.33 [d, Bu^{t}P(1,3), J 12.5 Hz] (ratio of isomer A : B *ca.* 2 : 1); δ_P(+25 °C, d_8-toluene, 161.975 MHz): *meso isomer*, −12.84 [dd, P(1) and P(3)], −46.33 [dd, P(2)] ($^1J_{P(2)P(1,3)}$ 231.5 Hz); *racemic isomer*, −14.0 [dd, P(1) and P(3)], −39.19 [dd, P(2)] ($^1J_{P(2)P(1,3)}$ 207.3 Hz). **3**: yield 0.12 g (82%); δ_H(+25 °C, d_8-toluene, 400.13 MHz) 1.44 (t, 4H, CH_2, av. J 9.7 Hz, Me), 1.25–1.18 (m, 27H, Bu^{t}P); δ_P(+25 °C, d_8-toluene, 161.975 MHz) −40.5 [P(1) and P(3)], −41.8 [P(2)] (8 line multiplet, $^1J_{P(2)P(1,3)}$ 231.0 Hz). **4**: yield 0.14 g (82%); δ_H(+25 °C, d_8-toluene, 400.13 MHz) 5.95 (m, 4H, CH_2=CH–), 4.95 (dd, 2H, CH_2=CHCH_2) 2.75 [q. (overlapped dt), 4H, CH_2=CHCH_2, J 7.6 Hz], 1.24 [d, 9H, Bu^{t}P(2), J 12.5 Hz], 1.22 [d, 18H, Bu^{t}P(1,3), J 12.9 Hz]; δ_P(+25 °C, d_8-toluene, 161.975 MHz) −38.3 [dd, P(1) and P(3)], −47.7 [dd, P(2)] ($^1J_{P(2)P(1,3)}$ 232.6 Hz). **5**: yield 0.16 g (72%); δ_H(+25 °C, d_8-toluene, 400.13 MHz) 7.2–6.9 (m, 10H, Ph), 2.27 (t, 4H, CH_2, av. J 6.7 Hz), 1.25 [d, 9H, Bu^{t}P(2), J 12.9 Hz], 1.11 [d, 18H, Bu^{t}P(1,3), J 13.6 Hz]; δ_P(+25 °C, d_8-toluene, 161.975 MHz) −39.5 [dd, P(1) and P(3)], −46.6 [dd, P(2)] ($^1J_{P(2)P(1,3)}$ 233.4 Hz).

Synthesis of **6**: the complex was prepared by the 1 : 1 reaction of **2** with $[W(CO)_5(thf)]$ in toluene–thf. IR(CH_2Cl_2) ν_{max} = 2015s (*cis* to P), 1913s (sh), 1899vs, 1874s (*trans* to P). δ_H(+25 °C, 400.13 MHz, $CDCl_3$) 4.06 (d, J_{PH} 154 Hz), 1.35 [d, 9H, Bu^{t}P(2), J_{PH} 14 Hz], 1.27 [d, 18H, Bu^{t}P(1,3), J_{PH} 16.5 Hz]. δ_P(+25 °C, $CDCl_3$, 161.975 MHz) 121.1 (t, J 156 Hz), −67.0 [d, 156 Hz (dd, dec. $^1J_{PH}$ 154, $^3J_{PH}$ 16.5 Hz)]. Correct C, H analysis were obtained.

‡ Ab initio *MO calculations*: all calculations were performed using Gaussian 98[11] at the B3LYP/6-311G** level. The solvent effects were incorporated using the PCM[12] model in Gaussian 98. Iodine basis set was obtained from the PNL basis set database.[13] Absolute energies of gas-phase species, solution-phase absolute energies are in parentheses (units E_h): MeI −6959.45606284 (−6959.457283), LiI 6927.13495426 (−6927.158942), $[MeAsI_2]$ 16114.9342294 (−16114.935814), $[\{HP\}_3AsLi]$ −3269.38038964 (−3269.392137), $[\{HP\}_3Me_2]$ −1105.79309134 (−1105.794835), $[\{MeP\}_3AsLi]$ −3387.37832745 (−3387.389669), $[\{MeP\}_3Me_2]$ −1223.78389534 (−1223.786033), $[\{Bu^tP\}_3AsLi]$ −3741.2815255, $[\{Bu^tP\}_3Me_2]$ −15577.67467541. $\Delta H(g)_{reaction}$, for $[\{RP\}_3AsLi]$, $\Delta H(solv)_{reaction}$ and $\Delta G(solv)_{reaction}$ (respectively) are in parentheses (units kcal mol^{-1}): R = H, −71.3 (−79.0, 78.5); R = Me, −66.9 (75.1, 74.6); R = Bu^t, −57.4 (−66.2, 63.5).

§ *Crystal data* for **6**; $C_{16}H_{29}O_4P_3W$, M = 562.15, orthorhombic, space group *Pnma*, Z = 4, a = 17.3386(7), b = 13.7599(5), c = 9.4610(4) Å, V = 2257.2(2) Å^3, μ(Mo-Kα) = 5.345 mm^{-1}, T = 180(2) K. Data were collected using a Nonius Kappa CCD diffractometer. Of a total of 21678 reflections collected, 2087 were independent (R_{int} = 0.082). The structure was solved by direct methods and refined by full-matrix least squares on F^2.[10] Final $R1$ = 0.027 [$I > 2\sigma(I)$] and $wR2$ = 0.066 (all data). CCDC 182/1837. See http://www.rsc.org/suppdata/cc/b0/b007553l/ for crystallographic files in .cif format.

1 M. A. Beswick, N. Choi, C. N. Harmer, A. D. Hopkins, M. McPartlin and D. S. Wright, *Science*, 1998, **281**, 1500; M. A. Beswick, N. Choi, A. D. Hopkins, M. E. G. Mosquera, M. McPartlin, P. R. Raithby, A. Rothenberger, D. Stalke, A. E. H. Wheatley and D. S. Wright, *Chem. Commun.*, 1998, 2485; M. A. Beswick, N. Choi, A. D. Hopkins, M. E. G. Mosquera, M. McPartlin, P. R. Raithby, A. E. H. Wheatley and D. S. Wright, *J. Chem. Soc., Dalton Trans.*, 2000, 479.

2 A. Bashall, A. D. Hopkins, M. McPartlin, J. A. Wood, A. D. Woods and D. S. Wright, *J. Chem. Soc., Dalton Trans.*, 2000, 1825.

3 (*a*) M. Baudler, J. Hellmann and G. Reuschenbach, *Z. Anorg. Allg. Chem.*, 1984, **509**, 38; (*b*) M. Baudler and J. Hellmann, *Z. Anorg. Allg. Chem.*, 1981, **480**, 129.

4 E. D. Becker, *High Resolution NMR: Theory and Chemical Applications*, Academic Press, New York, 1980, pp. 145.

5 For example, K. Issleib and M. Hoffmann, *Chem. Ber.*, 1966, **99**, 1320; K. Isslieb and K. Krech, *Chem. Ber.*, 1966, **99**, 1310; P. R. Hoffmann and K. G. Caulton, *J. Am. Chem. Soc.*, 1978, **111**, 1210.

6 T. L. Breen and D. W. Stephan, *Organometallics*, 1977, **16**, 365.

7 (*a*) W. S. Sheldrick, *Acta Crystallogr., Sect. B*, 1976, **32**, 308; (*b*) W. S. Sheldrick, *Chem. Ber.*, 1975, **108**, 2242; (*c*) W. S. Sheldrick, S. Morton and O. Stelzer, *Z. Anorg. Allg. Chem.*, 1981, **475**, 232; (*d*) A. G. Osborne, H. M. Pain, M. B. Hursthouse and M. A. Mazid, *J. Organomet Chem.*, 1993, **453**, 117; (*e*) O. Stelzer, S. Morton and W. S. Sheldrick, *Acta Crystallogr., Sect. B*, 1981, **37**, 439.

8 R. Bartsch, S. Hietkamp, S. Morton and O. Stelzer, *J. Organomet. Chem.*, 1981, **222**, 263.

9 $[\{CyP\}_4AsLi{\cdot}3Me_2NH]$, generated from the reaction of $As(NMe_2)_3$ with CyPHLi, is a source of $[\{CyP\}_4As]^-$ (the complex was structurally characterised as part of this study). The tetraphosphines are, however, considerably more thermally unstable than the triphosphines at room temperature (see: M. Baudler, G. Reuschenbach and J. Hahn, *Z. Anorg. Allg. Chem.*, 1981, **482**, 27; M. Baudler, G. Reuschenbach and J. Hahn, *Z. Anorg. Allg. Chem.*, 1983, **499**, 89; M. Baudler, G. Reuschenbach, J. Hellmann and J. Hahn, *Z. Anorg. Allg. Chem.*, 1983, **499**, 89). (Full details of the studies involved will be published as a full paper.)

10 SHELXTL PC version 5.03, Siemens Analytical Instruments, Madison, WI, 1994.

11 Gaussin 98: M. J. Frisch, G. W. Trucks, H. B. Schlegel, G. E. Scuseria, M. A. Robb, J. R. Cheeseman, V. G. Zakrzewski, J. A. Montgomery, Jr., R. E. Stratmann, J. C. Burant, S. Dapprich, J. M. Millam, A. D. Daniels, K. N. Kudin, M. C. Strain, O. Farkas, J. Tomasi, V. Barone, M. Cossi, R. Cammi, B. Mennucci, C. Pomelli, C. Adamo, S. Clifford, J. Ochterski, G. A. Petersson, P. Y. Ayala, Q. Cui, K. Morokuma, D. K. Malick, A. D. Rabuck, K. Raghavachari, J. B. Foresman, J. Cioslowski, J. V. Ortiz, A. G. Baboul, B. B. Stefanov, G. Liu, A. Liashenko, P. Piskorz, I. Komaromi, R. Gomperts, R. L. Martin, D. J. Fox, T. Kieth, M. A. Al-Laham, C. Y. Peng, A. Nanayakkara, M. Callacombe, P. M. W. Gill, B. Johnson, W. Chen, M. W. Wong, J. L. Andres, C. Gonzalez, M. Head-Gorden, E. S. Replogle and J. A. Pople, Gaussian, Inc., Pittsburgh PA, 1998.

12 V. Barone, M. Cossi and J. Tomasi, *J. Chem. Phys.*, 1997, **107**, 3210; V. Barone, M. Cossi and J. Tomasi, *J. Comput. Chem.*, 1998, **19**, 404.

13 Basis sets were obtained from the Extendable Computational Chemistry Environment Basis Sets Database, developed by the Molecular Science Computing Facility, Environmental and Molecular Sciences Laboratory, Pacific Northwest Laboratory, P.O. Box 999, Richland 99352, USA. U.S. Department of Energy Contract DE-AC06-76RLO 1830 (http:// www.emsl.pnl.gov:2080/forms/basisform.html).

ChemComm

Supramolecular self-assembly directed by carborane C–H···F interactions

Hans Lee, Carolyn B. Knobler and M. Frederick Hawthorne*

Department of Chemistry and Biochemistry, University of California, Los Angeles, Los Angeles, CA 90095, USA. E-mail; mfh@chem.ucla.edu

Received (in Columbia, MO, USA) 21st August 2000, Accepted 31st October 2000
First published as an Advance Article on the web

The synthesis and crystallization of 9,12-bis-(4-fluorophenyl)-1,2-carborane 1 and 9,12-bis-(3,5-difluorophenyl)-1,2-carborane 2 provide the first examples of a supramolecular assemblage directed by C–$H_{carborane}$···F interactions.

The potential utilization of the isomeric icosahedral carborane ($C_2B_{10}H_{12}$) cages as building blocks for macromolecules and supramolecular assemblies has only recently been explored.[1–3] The versatile chemistry available at the carborane C–H and B–H vertices makes carborane derivatives attractive candidates for crystal engineering.[4] Intermolecular hydrogen bonding is an important factor involved in supramolecular self-assembly motifs. Consequently, the participation of the acidic carborane C–H vertices in hydrogen bonding generates supramolecular structures. The established intermolecular interactions involving carboranes are: classical C–H···O hydrogen bonds,[5] bifurcated C–H···$(O)_2$ hydrogen bonds,[6] non-classical C–H···π hydrogen bonds[7] and B–H···H–N interactions.[1,8] Thus far, known C–H carborane interactions are limited to C–H···Y (Y= O, N, π) systems.[1,9] Fluorocarbon sites (C–F) are poor hydrogen bond components and cannot compete with O and N, although weak C–H···F interactions contribute to crystal-packing organization.[10] We report here the novel *ortho*-carborane derivatives: 9,12-bis-(4-fluorophenyl)-*o*-carborane **1**, and 9,12-bis-(3,5-difluorophenyl)-*o*-carborane **2**. Compounds **1** and **2** provide the first examples of a supramolecular assemblage directed by carborane C–H···F interactions.

Electron-rich boron vertices of *ortho*-carborane were easily functionalized by electrophilic iodination followed by palladium-catalyzed reactions of the regioselectively iodinated carborane with the appropriate fluorophenyl or difluorophenyl Grignard reagent.[11] Colorless crystals of **1** and **2** were grown from a methylene chloride–hexane solution and Et_2O, respectively,† by slow evaporation of the solvent. The structures of compounds **1** and **2** were determined by single-crystal X-ray diffraction analysis.

Crystal structures of both **1** and **2**‡ show intermolecular carborane C–H···F interactions. The unit cell of the solid-state structure of **1** contains four crystallographically unrelated, yet similar carboranes. Carborane C–H···F intermolecular distances lie in the range 2.49–3.05 Å and non-classical C–H···π hydrogen bonds with carborane C–H···aromatic centroid separations of 2.48 and 2.46 Å are observed (see caption to Fig. 1). The observed carborane C–H···F distances are consistent with phenyl C–H···F interactions reported for various fluorobenzene compounds (H···F 2.36–2.86 Å).[10] Also, close phenyl C–H···F distances (H···F 2.25–2.70 Å) are observed. All carborane C–H vertices are in close proximity to either a fluorine atom or π centroid, with the majority participating in C–H···F interactions. The solid-state IR spectrum of **1** exhibits two distinct stretching frequencies for carboranyl C–H at 3088 and 3060 cm^{-1}. These unassigned stretching frequencies represent either a carborane C–H···(F or π) interaction. The C–H stretching frequencies of the *o*-carborane C–H···π bond were reported[7] between 3066 and 3059 cm^{-1} which suggests that the lower energy stretching mode (3060 cm^{-1}) corresponds to those carborane C–H bonds involved in C–H···π interactions.

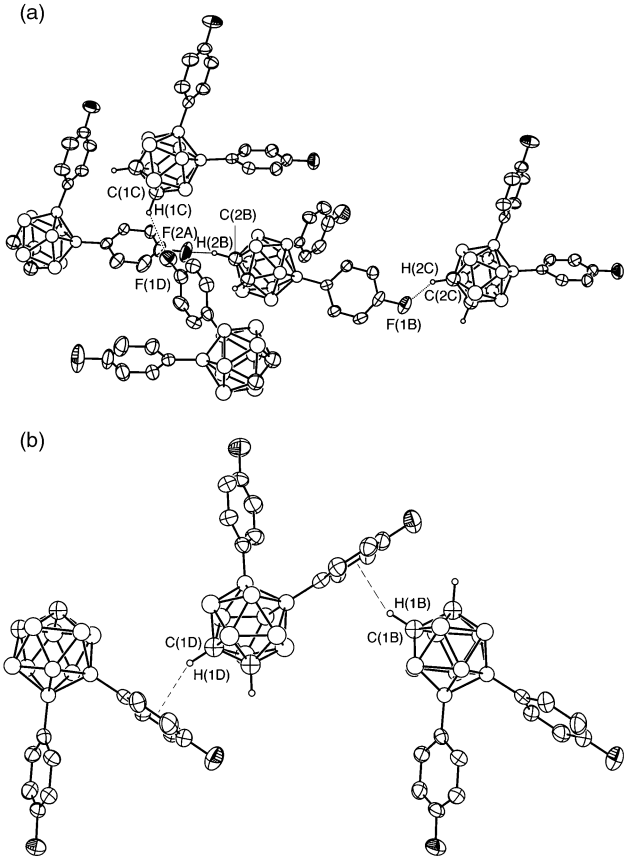

Fig. 1 Crystal packing diagram of **1**. (a) View of carborane C–H···F interactions. Selected distances (Å) and angles (°): C(1C)···F(1D) 3.593(8), H(1C)···F(1D) 2.91, C(2B)···F(2A) 3.416(7), H(2B)···F(2A) 2.49, C(2C)···F(1B) 3.557(8), H(2C)···F(1B) 2.69; C(1C)–H(1C)–F(1D) 120, C(2B)–H(2B)–F(2A) 146, C(2C)–H(2C)–F(1B) 136. (b) View of carborane C–H···π interactions. Selected distances (Å) and angles (°): H(1D)···aromatic centroid(π) 2.48, H(1B)···π 2.46; C(1D)–H(1D)–π 24.3, C(1B)–H(1B)–π 24.7. For clarity, the remaining phenyl and carborane H atoms are not shown.

In the solid state structure, molecules of **2** form a one-dimensional polymeric chain linked by two different carborane interactions having characteristic C–H···F distances. Directionality of both C–H vertices toward the fluorine atoms differ with angles of C(1)–H(1)–F(3P) 160° and C(2)–H(2)–F(11P) 124°. Intermolecular interactions of C(1)–H(1)···F(3P) 2.47 Å and C(2)–H(2)···F(11P) 2.35 Å demonstrate that the hydrogen atom bonded to C(2) interacts more strongly with fluorine than the hydrogen atom bonded to C(1) (Fig. 2). Close phenyl C–H···F interactions are not observed in **2**. The solid-state IR spectrum exhibits two different carborane C–H stretching frequencies of equal intensity (3077 and 3098 cm^{-1}). This observation is consistent with the presence of the two discrete sets of such interactions observed in the X-ray diffraction study. The position of the 3,5-difluorophenyl group in **2** allows the

DOI: 10.1039/b007353i

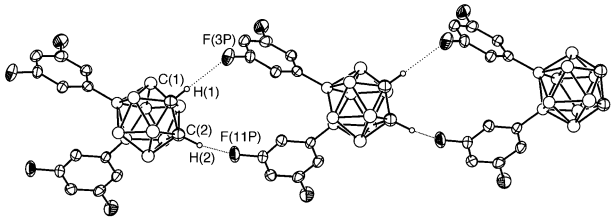

Fig. 2 Crystal packing diagram of **2**. The three molecules are related by translation. Selected distances (Å) and angles (°): C(1)···F(3P) 3.462(5), H(1)···F(3P) 2.47, C(2)···F(11P) 3.107(5), H(2)···F(11P) 2.35; C(1)–H(1)–F(3P) 160, C(2)–H(2)–F(11P) 124. For clarity, the remaining phenyl and carborane H atoms are not shown.

orientation of both carborane C–H vertices to simultaneously be in close proximity to fluorine atoms present on the neighboring molecule. This orientation leads to formation of the observed one-dimensional polymeric structure.

The crystal lattices of **1** and **2** are directed by a network of weak carborane C–H···F and/or C–H···π contacts. Although these C–H···F interactions are weak, their sum in lattice networks provides stabilization. This study demonstrates an additional motif for carboranes in supramolecular self-assembly chemistry.

We are grateful to the National Science Foundation (Grant No. CHE-9730006) for their support of this research.

Notes and references

† *Synthetic procedure* for **1**: to a dry THF (300 ml) solution of 9,12-I_2-1,2-$C_2B_{10}H_{10}$ (4.12 g, 10.4 mmol) was added 52 ml of 4-fluorophenylmagnesium bromide (1 M, in THF) at 0 °C. At 25 °C, *trans*-[$PdCl_2(PPh_3)_2$] (120 mg, 0.17 mmol) was added to the solution. The mixture was heated at the reflux temperature under nitrogen for 2 days, resulting in a black solution. Aqueous 10% HCl was added cautiously to destroy residual Grignard reagent, and all volatiles were removed *in vacuo*. The residue was dissolved in 200 ml of diethyl ether and 10% HCl (aq). The organic phase was separated and the aqueous layer was extracted with diethyl ether (2 × 100 ml). The organic phases were combined, dried over $MgSO_4$, and filtered. The solvent was removed under reduced pressure to yield a red solid. Purification by chromatography on basic aluminum oxide (toluene) gave a white solid. Crystallization from a methylene chloride–hexane solution afforded **1** (2.98 g, 8.95 mmol, 86%).

Selected data for **1**: mp 132–133 °C; ν(KBr)/cm^{-1} 3060, 3088 (carborane C–H); δ_H(400 MHz, $CDCl_3$, *J*/Hz) 1.5–3.4 (BH), 3.68 (br s, 2H), 6.80 (tt, *J* 9.0, 2.3, 4H), 7.13 (br dd, *J* 8, 6, 4H); δ_C(100 MHz, $CDCl_3$, *J*/Hz) 162.8 (d, J_{CF} 245.5, CF), 134.6 (d, J_{CF} 7.3, CH), 114.3 (d, J_{CF} 19.9, CH), 49.4; δ_B(160 MHz, BF_3·Et_2O external standard, *J*/Hz) 8.4 (s, 2B), −8.3 (d, J_{BH} 138, 2B), −13.0 (d, J_{BH} 151, 4B), −15.6 (d, J_{BH} 167, 2B); δ_F(376 MHz, $CDCl_3$, external Freon-113/C_6D_6 solution referenced at −68.0 ppm[12] relative to $CFCl_3$) −116.5; HR-EIMS: *m/z*: found 332.2376; calc. 332.2387.

Synthetic procedure for **2**: the synthesis and separation procedure was similar to that of **1**. Crystallization from Et_2O afforded **2** (79%).

Selected data for **2**: mp 189–190 °C; ν(KBr)/cm^{-1} 3077, 3098 (carborane C–H); δ_H(400 MHz, $CDCl_3$, *J*/Hz) 6.61 (br d, *J* 6.6, 4H), 6.52 (tt, *J* 9.1, 2.4, 2H), 3.74 (2H), 1.5–3.4 (BH); δ_C(100 MHz, $CDCl_3$, *J*/Hz) 50.1, 102.7 (t, J_{CF} 25.2), 115.1 (dd, J_{CF} 17.2), 162.2 (dd, J_{CF} 251.5); δ_F(376 MHz, $CDCl_3$, external Freon-113/C_6D_6 solution referenced at −68.0 ppm[12] relative to $CFCl_3$) −112.4; δ_B(160 MHz, Et_2O, BF_3·Et_2O external standard, *J*/Hz) 7.4 (s, 2B), −8.6 (d, J_{BH} 140, 2B), −13.0 (d, J_{BH} 154, 4B), −15.5 (d, J_{BH} 168, 2B); HR-EIMS: *m/z*: found 368.2196; calc. 368.2191.

‡ Single crystals of 9,12-bis-(4-C_6H_4F)$_2$-1,2-$C_2B_{10}H_{10}$ **1** were crystallized from methylene chloride–hexane, placed on a fiber and mounted on a Syntex P-1 diffractometer.

Crystal data for **1**: $C_{56}B_{40}H_{72}F_8$, M = 1329.54, monoclinic, space group $P2_1/n$, a = 17.504(8), b = 15.015(7), c = 27.57(1) Å, β = 91.16(1)°, V = 7244(6) Å^3, T = 293 K, Z = 4, λ(Cu-Kα) = 1.5418 Å, μ = 0.592 mm^{-1}, 7440 reflections measured, 7440 unique, which were used in all calculations. The final $R1(F^2)$ was 0.0746 [4642 reflections, $I > 2\sigma(I)$].

Single crystals of 9,12-bis-(3,5-$C_6H_3F_2$)$_2$-1,2-$C_2B_{10}H_{10}$ **2** were crystallized from Et_2O, placed on a fiber and mounted on a Syntex P-1 diffractometer.

Crystal data for **2**: $C_{14}B_{10}H_{18}F_2$, M = 332.38, triclinic, space group $P\bar{1}$, a = 6.882(4), b = 9.710(5), c = 13.926(7) Å, α = 84.80(2), β = 81.41(2), γ = 78.50(2)°, V = 900 Å^3, T = 298 K, Z = 2, λ(Cu-Kα) = 1.5418 Å, μ = 0.793 mm^{-1}, 2468 reflections measured. The final $R1(F^2)$ was 0.0616 [1540 reflections, $I > 2\sigma$(I)].

CCDC 182/1844. See http://www.rsc.org/suppdata/cc/b0/b007353i/ for crystallographic files in .cif format.

1 P. C. Andrews, M. J. Hardie and C. L. Raston, *Coord. Chem. Rev.*, 1999, **189**, 169.
2 M. F. Hawthorne and Z. Zheng, *Acc. Chem. Res.*, 1997, **30**, 267.
3 X. Yang, W. Jiang, C. B. Knobler and M. F. Hawthorne, *J. Am. Chem. Soc.*, 1992, **114**, 9719.
4 G. R. Desiraju, *Angew. Chem., Int. Ed. Engl.*, 1995, **34**, 2311.
5 G. Harakas, T. Vu, C. B. Knobler and M. F. Hawthorne, *J. Am. Chem. Soc.*, 1998, **120**, 6405.
6 M. J. Hardie, P. D. Godfrey and C. L. Raston, *Chem. Eur. J.*, 1999, **5**, 1828.
7 M. J. Hardie and C. L. Raston, *Eur. J. Inorg. Chem.*, 1999, 195.
8 P. D. Godfrey, W. J. Grigsby, P. J. Nichols and C. L. Raston, *J. Am. Chem. Soc.*, 1997, **119**, 9283.
9 L. Crâciun and R. Custelcean, *Inorg. Chem.*, 1999, **38**, 4916.
10 V. R. Thalladi, H.-C. Weiss, D. Bläser, R. Boese, A. Nangia and G. R. Desiraju, *J. Am. Chem. Soc.*, 1998, **120**, 8702.
11 J. Li, C. F. Logan and M. Jones, Jr., *Inorg. Chem.*, 1991, **30**, 4866.
12 C. H. Dungan and J. R. van Wazer, *Compilation of Reported ^{19}F NMR Chemical Shifts*, Wiley-Interscience, New York, 1970, appendix 1.

ChemComm

A novel polythiophene with pendant fullerenes: toward donor/acceptor double-cable polymers

Antonio Cravino,[a] Gerald Zerza,[a] Michele Maggini,[b] Stefania Bucella,[b] Mattias Svensson,[c] Mats R. Andersson,[c] Helmut Neugebauer*[a] and N. Serdar Sariciftci[a]

[a] *Linz Institute for Organic Solar Cells (LIOS), Physical Chemistry, Johannes Kepler University Linz, Altenbergerstrasse 69, Linz, A-4040 Austria. E-mail: helmut.neugebauer@jk.uni-linz.ac.at*
[b] *Organic Chemistry Department, University of Padova, Via Marzolo 1, I-35131 Padova, Italy*
[c] *Department of Polymer Technology, Chalmers University of Technology, SE-412 96, Goteborg, Sweden*

Received (in Liverpool, UK) 2nd October 2000, Accepted 1st November 2000
First published as an Advance Article on the web

The synthesis of a novel bithiophene with a pendant fullerene substituent and its electrochemical polymerisation are reported; light induced ESR measurements on the electrodeposited films reveal a photoinduced electron transfer from the donor cable (polythiophene) to the pendant acceptor cable (fullerene moieties).

The ultrafast photoinduced electron transfer from non-degenerate ground state conjugated polymers to fullerenes,[1] in association with the existing technologies for processing polymers, makes these materials potentially suitable for low-cost photovoltaic applications as large-area, flexible solar cells.[2] Within this frame, the most promising devices so far obtained are the so-called bulk heterojunction solar cells.[3–5] The active layer of such devices is a blend of conjugated polymer and fullerene: after photoinduced charge separation, the polymer matrix ensures the transport of positive carriers, while electrons travel through contacting fullerene domains. Because of the limited miscibility of the two components, clusters of fullerenes can form within the active film, so that the transport of electrons is hindered by the 'void' between such separated domains.[4] A convenient solution to overcome phase segregation and reach a homogeneous distribution of the electron transporting sites within the bulk heterojunction should be the preparation of so-called double-cable molecular systems with fullerene substituents grafted to a conjugated polymer chain. Polythiophene/C_{60} mixtures have been already employed for the preparation of prototype bulk heterojunction solar cells,[5] suggesting the investigation of double-cables consisting of a polythiophene backbone with covalently linked fullerene units. Zotti and coworkers and Ferraris *et al.* showed that such fullerene substituted polythiophenes mostly retain the favourable ground state properties of the individual polymer and fullerene moieties.[6] However, the occurrence of photoinduced electron transfer in this type of polymers has, as yet, not been observed.

Here, we report preliminary results on a novel electrosynthesised polythiophene with pendant fullerene substituents, obtained from bithiophene-fulleropyrrolidine dyad **1** (Scheme 1). Compound **1** combines solubility and the superior electropolymerisability of bithiophenes[7] and gives a double-cable polymer that is heavily loaded with fullerene electron conducting moieties.

The synthetic strategy toward bithiophene-fulleropyrrolidine **1** is outlined in Scheme 1. The route to **1** starts with commercially available 4-hydroxybenzaldehyde and 1-iodo-2-[2-(2-iodoethoxy)ethoxy]ethane. Reaction between 4-hydroxybenzaldehyde and the bis-iodo derivative in the presence of K_2CO_3 in acetone at reflux temperature afforded the product of monosubstitution **2** in 20% isolated yield. Palladium-catalysed coupling[8] of 4-bromophenol with 3-thiophene-boronic acid[9] followed by NBS-bromination gave the highly reactive derivative **3** that was coupled directly with 2-thiophene-boronic acid[9] to afford **4**. Reaction of **2** with the potassium salt of bis-thiophene phenol **4** gave functionalised bithiophene **5** in 50% yield. Condensation of **5** with sarcosine in the presence of C_{60}[10] provided **1** in 49% isolated yield. All spectroscopic and analytical data were consistent with the proposed molecular structures.†

The cyclic voltammogram (CV) of **1** shows one anodic peak at *ca.* 1.3 V, which corresponds to the generation of radical cations that *via* subsequent coupling and re-aromatisation steps afford the substituted polythiophene chain[7,11] (Fig. 1). Potential sweeping between 0 and +1.6 V leads to the rapid growth of a new redox wave centered at *ca.* 0.9 V and related to the formed double-cable poly-**1**. Similar results have been obtained in different conditions, *e.g.* by using different electrodes, solvents and substrates. Insoluble and yellow-brownish films, whose UV–VIS absorption spectra show a band ranging from *ca*. 600 nm to the glass cut-off at 300 nm, have been obtained. No photoluminescence could be observed.

The CV of poly-**1** films in monomer-free electrolyte medium (Fig. 2) shows, in positive direction, a stable redox system with

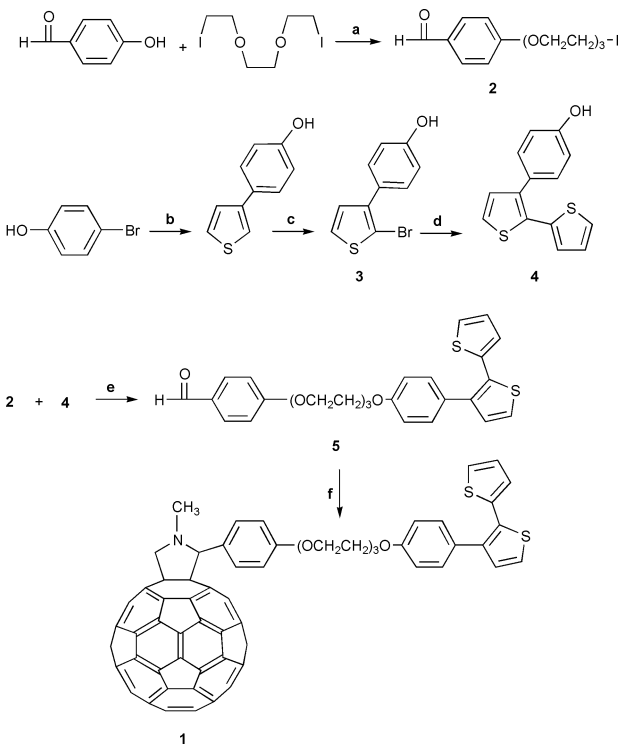

Scheme 1 *Reagents and conditions*: a, K_2CO_3, acetone, reflux, 8 h, 20%; b, 3-thiophene-boronic acid, tetrakis(triphenylphosphine)palladium(0), DME, $NaHCO_3$ (1 M), 12 h, 76%; c, NBS, DMF, 12 h, 87% (crude); d, 2-thiophene-boronic acid, tetrakis(triphenylphosphine)palladium(0), DME, $NaHCO_3$ (1 M), 12 h, 48%; e, K_2CO_3, acetone, reflux, 8 h, 50%; f, *N*-methylglycine, C_{60}, chlorobenzene, reflux, 2 h, 49%.

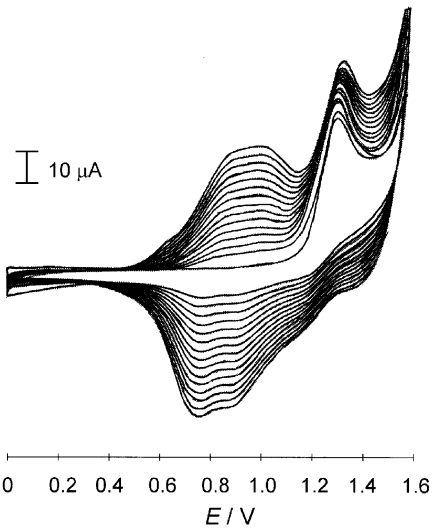

Fig. 1 Anodic CV of **1** (0.1 M Bu_4NPF_6 in CH_2Cl_2). Working electrode: Pt foil; quasi-reference electrode: Ag/AgCl wire. Scan rate: 100 mV s^{-1}.

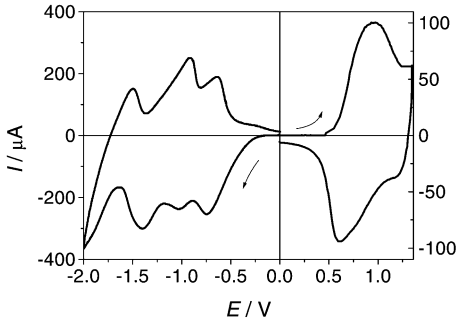

Fig. 2 Anodic (right) and cathodic (left) CV of poly-**1** (0.1 M Bu_4NPF_6 in MeCN). Conditions as in Fig. 1.

anodic and cathodic peak potentials at 0.96 and 0.61 V, respectively, corresponding to the oxidation/re-reduction ('p-doping/dedoping') of the polythiophene chain. Scanning to negative potentials up to −2.0 V shows several waves related to the multiple reduction processes of the fullerene moiety (Fig. 2).[12] The electrochemical behaviour suggests that both the polythiophene chain and the pendant fullerene moieties of the double-cable retain their individual electrochemical properties.

The photogeneration of separated charged states in poly-**1** has been observed by means of light-induced electron spin resonance (LESR) measurements. The LESR spectrum, obtained by subtracting the light-off signal from the light-on signal, is shown in Fig. 3. The spectrum reveals the photoinduced generation of two species with spin = 1/2. The signal at g = 2.0022 corresponds to delocalised radical cations (widely accepted to be polarons) on the conjugated backbone while the signal at g = 2.0004 is typical of low g-factor fullerene radical anions.[13] These results prove the occurrence of a photoinduced electron transfer from the conjugated backbone to the pendant fullerene moieties of poly-**1**, which is an essential prerequisite for photovoltaic applications. In addition, also sub-gap electronic and IR-active vibration (IRAV) bands are observed in the photoinduced UV–VIS and IR spectra of poly-**1**

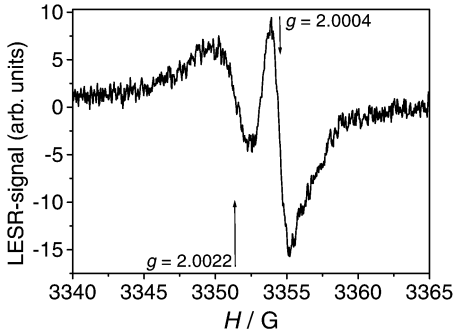

Fig. 3 LESR (light-on minus light-off) spectrum of poly-**1** on ITO coated foil. T = 77 K; excitation at λ = 488 nm (20 mW cm^{-2}).

(not shown here). These spectral features are related to the photoinduced generation of long-living charged states.[14]

In conclusion, we have shown the synthesis of a novel bithiophene-fulleropyrrolidine dyad suitable as a monomer for electrochemical polymerisation. The resulting double-cable polymer retains the peculiar characteristics of polythiophene/fullerene blends, including the ability to generate a charge-separated state after photoinduced electron transfer. Since no phase separation is expected in this type of material, donor–acceptor double-cables represent attractive candidates for photovoltaic applications.

We thank EC, Joule III Programme (Contract No.: JOR3CT980206), for financial support. All partners in this European consortium are gratefully acknowledged.

Notes and references

† *Selected data* for **1**: ^{1}H NMR (400 MHz, $CDCl_3$–CS_2 1:2) δ 7.63 (br s, 2H), 7.16 (m, 3H), 7.09 (dd, 1H), 6.95 (d, 1H), 6.87 (m, 4H), 6.77 (m, 2H), 4.92 (d, 1H), 4.83 (s, 1H), 4.21 (d, 1H), 4.06 (m, 4H), 3.80 (m, 4H), 3.68 (s, 4H), 2.75 (s, 3H); $\lambda_{max}(CH_2Cl_2)$/nm (ε/dm^3 mol^{-1} cm^{-1}) 230 (112530), 256 (125060), 431 (3963); *m/z* (MALDI) 1242 (M^+).

1 N. S. Sariciftci, L. Smilowitz, A. J. Heeger and F. Wudl, *Science*, 1992, **258**, 1474.
2 N. S. Sariciftci, D. Braun, C. Zhang, V. I. Srdanov, A. J. Heeger, G. Stucky and F. Wudl, *Appl. Phys. Lett.*, 1993, **62**, 585.
3 G. Yu, J. Gao, J. C. Hummelen, F. Wudl and A. J. Heeger, *Science*, 1995, **270**, 1789.
4 S. E. Shaheen, C. J. Brabec, F. Padinger, T. Fromherz, J. C. Hummelen and N. S. Sariciftci, *Appl. Phys. Lett.*, in press.
5 D. Gebeyehu, F. Padinger, C. J. Brabec, T. Fromherz, J. C. Hummelen and N. S. Sariciftci, *Int. J. Photoenergy*, 1999, **1**, 95.
6 T. Benincori, E. Brenna, F. Sannicoló, L. Trimarco and G. Zotti, *Angew. Chem., Int. Ed. Engl.*, 1996, **35**, 648; J. P. Ferraris, A. Yassar, D. C. Loveday and M. Hmyene, *Opt. Mater. (Amsterdam)*, 1998, **9**, 34.
7 G. Zotti, *Handbook of Organic Conductive Molecules and Polymers*, ed. H. S. Nalwa, Wiley, Chichester, 1997, vol. 2, ch. 4.
8 S. Gronowitz and D. Peters, *Heterocycles*, 1990, **30**, 645.
9 A. R. Martin and Y. Yang, *Acta Chem. Scand.*, 1993, **47**, 221.
10 M. Prato and M. Maggini, *Acc. Chem. Res.*, 1998, **31**, 519.
11 J. Simonet and J. Rault-Berthelot, *Prog. Solid State Chem.*, 1991, **21**, 1.
12 L. Echegoyen and L. E. Echegoyen, *Acc. Chem. Res.*, 1998, **31**, 593.
13 R. A. J. Janssen, M. P. T. Christiaans, K. Pakbaz, D. Moses, J. C. Hummelen and N. S. Sariciftci, *J. Chem. Phys.*, 1994, **101**, 9519; V. Dyakonov, G. Zoriniants, M. C. Scharber, C. J. Brabec, R. A. J. Janssen, J. C. Hummelen and N. S. Sariciftci, *Phys. Rev. B*, 1999, **59**, 8019.
14 See for example: J. Orenstein, *Handbook of Conducting Polymers*, ed. T. A. Skotheim, Marcel Dekker, New York, 1986, ch. 36; M. Del Zoppo, C. Castiglioni, P. Zuliani and G. Zerbi, *Handbook of Conducting Polymers*, ed. T. A. Skotheim and J. R. Reynolds, Marcel Dekker, New York, 1986, ch. 28.

Synthesis of stable and directly usable hexagonal mesoporous silica by efficient amine extraction in acidified water

K. Cassiers,* P. Van Der Voort and E. F. Vansant

Department of Chemistry–Laboratory of Adsorption and Catalysis, University of Antwerp (U.I.A.), Universiteitsplein 1, B-2610 Wilrijk, Belgium. E-mail: cassiers@uia.ua.ac.be

Received (in Cambridge, UK) 8th September 2000, Accepted 2nd November 2000
First published as an Advance Article on the web

The amine template of hexagonal mesoporous silica (HMS) can be efficiently recovered and re-used by a new extraction procedure in acidified water rendering a directly usable high quality mesoporous support.

Following the earliest reports on M41S materials,[1] Pinnavaia and coworkers[2,3] introduced an alternative route to synthesize mesoporous materials based on a hydrogen bonding interaction between a neutral amine and a non-ionic silica precursor. These materials were denoted hexagonal mesoporous silicas (HMS). An important advantage in the synthesis of these materials is the cost reduction by employing a less expensive and non-toxic surfactant and the mild reaction conditions. HMS materials are claimed to have larger pores, to be more stable and to have thicker pore walls than their MCM-41 counterparts.[4] Owing to the weak hydrogen bonding interactions, more than 90% of the neutral template can be recovered by a simple extraction procedure using ethanol as extracting solvent. A few other attempts to extract the surfactants of mesoporous templated materials have been described in the literature (MCM-41,[5,6] Al-MCM-41,[7] Al-HMS,[8] mesoporous alumino- and galloaluminophosphate[9]). In all cases, a huge amount of organic solvent is required and, mostly, the extraction needs to be followed by a calcination step to remove the remaining surfactant or the surface ethoxy groups produced during extraction.

We report on an optimized HMS synthesis including the complete extraction of the template with acidified water. This procedure yields not only a directly usable high quality support that does not require a further calcination step, but also allows re-use of the recovered template several times. Obviously, a water extraction procedure fits very well in the striving to green or sustainable chemistry.

HMS was prepared at room temperature using dodecylamine (DDA) as structure directing agent and tetraethylorthosilicate (TEOS) as silica source, according to the procedure reported elsewhere.[4] In a typical template removal, 1 g of as-synthesized material was added to 100 ml solvent and refluxed for 1 h. The residual solid was then filtered off and washed with a second 100 ml portion of solvent and dried at room temperature. Several extracted samples were prepared: HMS-E and HMS-W(HCl/DDA), where E and W indicate extraction in ethanol and water, respectively. HCl/DDA indicates the molar ratio of HCl in the solution and DDA in the as-synthesized HMS. Furthermore, portions of the as-synthesized HMS materials that were calcined in air at 550 °C for 16 h were designated as HMS-C.

The amount of template in the extracted samples (see later, Table 1) is calculated from thermogravimetric analysis. The DTG curve for as-synthesized HMS shows weight losses at 225 and 290 °C, attributed to the thermal decomposition of DDA. A notable difference in the shape of the DTG curve can be observed for the ethanol extracted HMS-E (weight loss at 270 and 400 °C). Information on the origin of these weight losses was obtained by refluxing 1 g of calcined HMS in pure ethanol for 1 h, denoted as HMS-RE. This final material shows weight losses at the same temperature as HMS-E, attributed to the esterification of the surface with ethoxy groups. This can also be inferred from IR spectroscopy (Fig. 1) where HMS-E and HMS-RE show the same bands (2905, 2936 and 2982 cm^{-1}) in the C–H vibration region. Although the extraction of surfactant molecules in ethanol is very efficient (no decomposition of DDA in the DTG curve and complete absence of DDA-bands in the IR spectrum), it yields a surface that is completely unreactive toward subsequent activation owing to the presence of chemically bonded ethoxy groups, and a subsequent calcination at 450 °C is required for further possible application of the support.

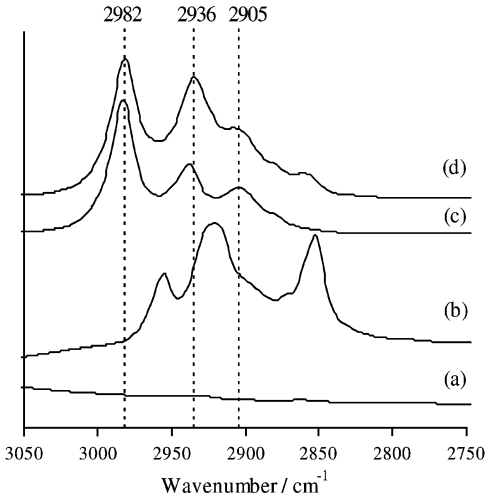

Fig. 1 Diffuse reflectance IR spectra of samples: (a) HMS-W(1), (b) dodecylamine, (c) HMS-RE and (d) HMS-E. The spectra were measured at 200 °C under an oxygen flow.

For the water-extracted HMS-W(0) 69% of the template was present, whereas for the acidified water-extracted HMS-W(1) and HMS-W(2) no weight losses were observed in the DTG curves (Table 1). The absence of template is further evidenced by the IR spectrum of HMS-W(1), where no C–H vibrations are observed. This significant difference in the degree of extraction

Table 1 Amount of template after extraction and physical properties of HMS samples

Sample	Amount of template (%)	BET surface area/ $m^2\ g^{-1}$	$V_{prim.pores}$[a]/ $cm^3\ g^{-1}$	d_{100}[b]/nm	KJS pore diameter/ nm
HMS-C	—	1015	0.71	3.70	3.55
HMS-E	0	932	0.78	3.79	3.70
HMS-W(0)	69	—	—	—	—
HMS-W(1)	0	1051	0.83	3.84	3.70
HMS-W(2)	0	791	0.54	3.63	—[c]
HMS-RC	—	908	0.67	3.78	3.30

[a] Primary pore volume measured after the capillary condensation step ($P/P_0 \approx 0.45$) in the N_2 isotherm. [b] Basal spacing. [c] The pore size distribution was too broad and irregular to determine the peak diameter.

DOI: 10.1039/b007297o

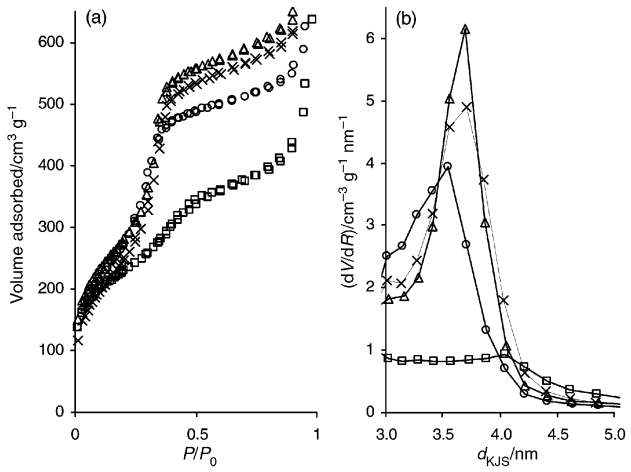

Fig. 2 N_2 sorption isotherms (a) and KJS pore size distributions (b): (□) HMS-W(2), (○) HMS-C, (×) HMS-E and (△) HMS-W(1). The textural mesopore filling of the samples (between P/P_0 = 0.9 and 1) is not shown.

can be attributed to the very low solubility of DDA in pure water, even at elevated temperature. Addition of HCl converts DDA into soluble dodecylammonium chloride (DDAHCl), which facilitates the extraction.

The effect of solvent extraction is shown in Fig. 2(a) and the physical properties of the HMS samples are also listed in Table 1. Compared to the calcined and ethanol-extracted sample, N_2-sorption results show that the template removal in acidified water [HMS-W(1)] also maintained the uniform hexagonal mesoporous structure. To calculate the pore size distribution (PSD), it is generally agreed that the BJH method underestimates the size of pores[10,11] and therefore, the KJS procedure[12] [Fig. 2(b)] is used, which is based on a corrected Kelvin equation for hexagonal materials. It is remarkable that HMS-W(1) has a more narrow PSD, a higher BET-surface area, higher primary pore volume and higher d_{100} value than the calcined and the ethanol-extracted samples. Furthermore, the amount of HCl seems to be a critical parameter in the acidified water extraction procedure. An excess of HCl [HMS-W(2)] results in a poorly ordered structure.

As to its potential use, an important step besides efficient water extraction is the re-usability of the template. To achieve this goal, the recovered DDAHCl was converted to DDA by the addition of NaOH to the extraction solvent. The precipitated DDA was dried and re-used in a fresh synthesis (HMS-RC). As can be seen in Table 1, HMS-RC has very similar characteristics as the calcined HMS-C, indicating that no degradation of the surfactant has occurred.

In summary, the results reported here clearly reveal that the amine template can be recovered easily and efficiently from hexagonal mesoporous silica in acidified water, resulting in a high quality and directly usable molecular sieve. Our synthetic approach therefore provides new opportunities in the synthesis of mesoporous supports while avoiding high-temperature treatment and organic solvents, while the template can also be re-used.

P. V. D. V. acknowledges the FWO-Vlaanderen (Fund for Scientific Research, Flanders, Belgium) for financial support.

Notes and references

1 C. T. Kresge, M. E. Leonowicz, W. J. Roth, J. C. Vartuli and J. S. Beck, *Nature*, 1992, **359**, 710.
2 P. T. Tanev and T. J. Pinnavaia, *Science*, 1995, **267**, 865.
3 P. T. Tanev, M. Chibwe and T. J. Pinnavaia, *Nature*, 1994, **368**, 321.
4 P. T. Tanev and T. J. Pinnavaia, *Chem. Mater.*, 1996, **8**, 2068.
5 X. S. Zhao, G. Q. Lu, A. K. Whittaker, G. J. Millar and H. Y. Zhu, *J. Phys. Chem. B*, 1997, **101**, 6525.
6 A. B. Bourlinos, M. A. Karakassides and D. Petridis, *J. Phys. Chem. B*, 2000, **104**, 4375.
7 S. Hitz and R. Prins, *J. Catal.*, 1997, **168**, 194.
8 R. Mokaya and W. Jones, *J. Mater. Chem.*, 1998, **8**, 2819.
9 B. T. Holland, P. K. Isbeter, C. F. Blanford, E. J. Munson and A. Stein, *J. Am. Chem. Soc.*, 1997, **119**, 6798.
10 A. Galarneau, D. Desplantier, R. Dutartre and F. Di Renzo, *Microporous Mesoporous Mater.*, 1999, **27**, 297.
11 H. Y. Zhu, X. S. Zhao, G. Q. Lu and D. D. Do, *Langmuir*, 1996, **121**, 6513.
12 M. Kruk, M. Jaroniec and A. Sayari, *Langmuir*, 1997, **13**, 6267.

ChemComm

1,3-Diphenyl-2,2,2,4,4,4-hexazido-1,3-diaza-2,4-diphosphetidine: synthesis and structural characterisation of the first nitrogen-penta-coordinated phosphorus with three azide-groups†

Christoph Aubauer, Thomas M. Klapötke,* Heinrich Nöth,‡ Axel Schulz, Max Suter‡ and Jan Weigand

Department of Chemistry, Ludwig-Maximilians-University, Butenandtstr. 5-13 (D), D-81377 Munich, Germany. E-mail: tmk@cup.uni-muenchen.de

Received (in Cambridge, UK) 24th August 2000, Accepted 6th November 2000
First published as an Advance Article on the web

$(C_6H_5)_2N_2P_2(N_3)_6$ 1 has been prepared and characterised by multinuclear NMR, vibrational spectroscopy and single crystal X-ray analysis; the normal modes of 1 have been calculated and the antisymmetric stretching vibration of the azide group has been discussed.

In 1970 Horn reported on the reaction of 1,3-dimethyl-2,2,2,4,4,4-hexachloro-1,3-diaza-2,4-diphosphetidine with NaN_3 in MeCN yielding a highly explosive compound which was only poorly characterised.[1] To our knowledge only a few crystal structures of mono- and di-substituted phosphorus azides[2] and nitrogen-penta-coordinated phosphorus compounds[2c,3] have been published. Here we report on the synthesis and structural characterisation of the first nitrogen-penta-coordinated phosphorus species substituted with three azide groups, which can be considered as a hexazidodiphosphadiazacyclobutane.

1,3-Diphenyl-2,2,2,4,4,4-hexazido-1,3-diaza-2,4-diphosphetidine **1** was obtained in high yield as a colourless solid from the reaction of 1,3-diphenyl-2,2,2,4,4,4-hexachloro-1,3-diaza-2,4-diphosphetidine with trimethylsilyl azide in CH_2Cl_2 solution, [eqn. (1)].

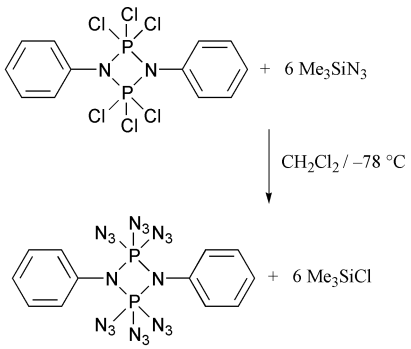

(1)

1

Single crystals suitable for X-ray diffraction determination§ were grown from CH_2Cl_2. A view of the molecular structure of **1** is shown in Fig. 1. Compound **1** crystallises in the triclinic space group $P\bar{1}$ with two formula units in the unit cell. The two crystallographically different molecules display nearly identical bond lengths and angles.

The molecular structure of **1** reveals C_i symmetry in which each phosphorus is coordinated by five nitrogen atoms. The coordination sphere around the phosphorus atom can be regarded as a slightly distorted trigonal bipyramid.

The N_2P_2 ring is planar with a P–N–P angle of 100.6(2)° and a N–P–N angle of 79.4(2)°. The azide groups are slightly bent with N–N–N angles ranging from 171.1(4) to 175.1(4)° which

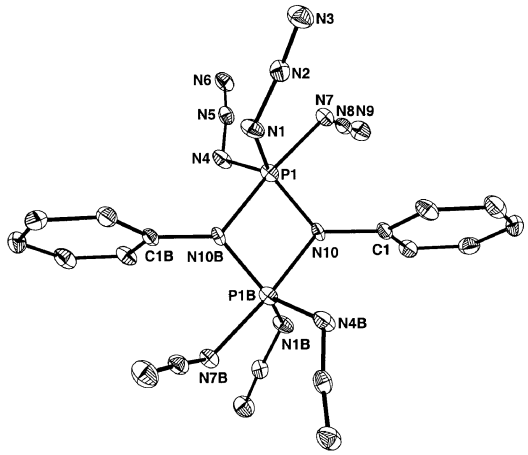

Fig. 1 An ORTEP plot of the molecular structure of compound **1** with thermal ellipsoids at 25% probability level. Hydrogen atoms are omitted for clarity. Selected bond lengths (Å) and angles (°): P(1)–N(1) 1.703(3), P(1)–N(4) 1.713(3), P(1)–N(7) 1.804(3), N(1)–N(2) 1.252(4), N(4)–N(5) 1.253(4), N(7)–N(8) 1.240(4), N(2)–N(3) 1.118(4), N(5)–N(6) 1.118(4), N(8)–N(9) 1.130(4), P(1)–N(10) 1.643(4), N(10)–P(1B) 1.774(3); P(1)–N(10)–P(1B) 100.6(2), N(10)–P(1)–N10(B) 79.4(2).

are in accordance with the structures of other covalent phosphorus azides.[2]

Since the two nitrogen ring atoms occupy different positions in the coordination sphere around the phosphorus atom [N(10) equatorial, N(10B) axial position, with respect to P(1) and *vice versa* for P(1B)] two considerably different $P–N_{ring}$ bond lengths [1.643(4) and 1.774(3) Å] are observed which are similar to the bond lengths found in $Me_2N_2P_2Cl_6$.[4] A similar large difference in the P–N bond length is found for the azide groups [1.703(3), 1.713(3) and 1.804(3) Å] as each phosphorus atom in **1** is surrounded by two equatorial [eq, N(1), N(4)] and one axial [ax, N(7)] azide groups. NBO analysis indicates that this structural feature can be rationalised by a 'weaker' two-electron–three-centre bond unit along the N(10B)–P(1)–N(7) [and N(10)–P(1B)–N(7B)] axis whereas the equatorial positions can be best described by two-electron–two-centre bond units.† This rather special bonding situation can best be understood in the picture of localised bond orbitals (NBOs) by strong non-covalent contributions between the two monomeric units.[5] The one lone pair (p-type atomic orbital) on each $N(Ph)P(N_3)_3$ unit interacts with the antibonding σ $P–N_3$ bond system of the second monomeric unit and *vice versa* (Fig. 2). There are three strong intramolecular donor–acceptor interactions of this type which weaken the $P–N_3$ bonds (especially $P–N_{3,ax}$) and account for the rather long $P–N_3$ bonds. However, since the lone pair (LP) on the ring nitrogen atom lies in-plane with the $P–N_{3,ax}$ bond of the second monomeric unit, the interaction with the unoccupied, antibonding $\sigma^*(P–N_{3,ax})$ is stronger than the interaction with the 'out-of-plane' $\sigma^*(P–N_{3,eq})$ bond orbitals [$LP(N_{ring}) \rightarrow \sigma^*(P–N_{3,ax})$: 85, $LP(N_{ring}) \rightarrow \sigma^*(P–N_{3,eq1})$: 38, $LP(N_{ring}) \rightarrow \sigma^*(P–N_{3,eq2})$: 34 kcal mol^{-1}].† This

† Electronic supplementary information (ESI) available: experimental details for **1**, Fig. SI 1 and computational details. See http://www.rsc.org/suppdata/cc/b0/b006944m/

‡ For queries relating to crystal structure analysis.

DOI: 10.1039/b006944m

Table 1 Selected IR and Raman data for **1**

Calc. IR / Raman[a]	Exp. IR / Raman[b]	Symmetry	Approximate assignment[c]	Displacement vector[d] N(4)	N(1)	N(7)
2164 (0; 472)	2158 (0; 7)	A_g	ν_{as}, i. p., $N_{3,eq}$	↓ N	↓ N	N
				↑ N	↑ N	N
2158 (840; 0)	2154 (s; 0)	A_u	ν_{as}, o. p., $N_{3,eq}$	↓ N	↓ N	N
				↑ N	↑ N	N
2143 (1804; 0)	2142 (s; 0)	A_u	ν_{as}, o. p., $N_{3,eq}$	↑ N	↓ N	N
				↓ N	↑ N	N
2142 (0; 176)	2136 (0; 4)	A_g	ν_{as}, i. p., $N_{3,eq}$	↑ N	↓ N	N
				↓ N	↑ N	N
2105 (0; 250)	2111 (0; 1)	A_g	ν_{as}, i. p., $N_{3,ax}$	N	N	↓ N
				N	N	↑ N
2102 (1918; 0)	2113 (m; 0)	A_u	ν_{as}, o. p., $N_{3,ax}$	N	N	↓ N
				N	N	↑ N

[a] Wavenumbers in cm^{-1}; calculated IR intensities (km mol^{-1}) and Raman activities ($Å^4$ AMU^{-1}) in parenthesis; HF/6-31G(d,p) calculated wavenumbers scaled with f = 0.8317; *cf.* B3LYP/6-31G(d,p) unscaled frequencies (symmetry, IR intensity in km mol^{-1}): 2302 (A_g, 0), 2293 (A_u, 557), 2287 (A_u, 1909); 2287 (A_g, 0); 2270 (A_g, 0) and 2272 (A_u, 943) cm^{-1}. [b] Relative IR and Raman intensities in parenthesis. [c] $N_{eq}(1)$ equivalent to $N_{eq}(1B)$, $N_{eq}(4)$ equivalent to $N_{eq}(4B)$, $N_{ax}(7)$ equivalent to $N_{ax}(7B)$. i. p. = In phase: according to C_i-symmetry all equivalent N_3-groups vibrate in phase; o. p. = out of phase: according to C_i-symmetry the movement of all equivalent N_3-groups is shifted by 180°. [d] These displacement vectors represent approximations. Weak coupling between the axial and the equatorial azide groups is neglected for clarity.

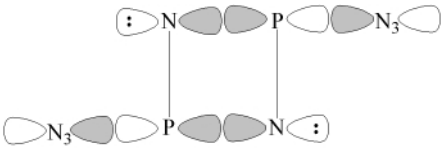

Fig. 2 Intramolecular donor–acceptor interaction in **1**: LP(N_{ring}) → σ*(P–N_3).

strong interaction of the nitrogen lone pair with the σ* P–N_3 bonds can be considered as the main driving force of the cyclisation. Moreover, this donor–acceptor bonding is strengthened by the donor properties of the phenyl ring and accounts for the stability of the dimer. Previous NMR studies on phosphine-imine/diazadiphosphetidine equilibria have shown that the formation of the dimer strongly depends on the donor properties of the nitrogen substituents.[6] Weaker donor substituents (*e.g.* $C_6H_2Cl_3$-2,4,6) result in equilibria between the monomeric and dimeric species.

As a result of this intriguing bond situation, the axial P–N_3 bond displays a higher ionic character which is manifested by a better π delocalisation along the azide unit leading to a longer terminal N(8)–N(9) bond length and a shorter N(7)–N(8) bond length than in the equatorial azide groups with a less polar P–N_3 bond (Fig. 1). In agreement with this, the hybridisation on the nitrogen attached to the P atom increases from $N_{ax}(7)$ ($sp^{1.01}$) < $N_{eq}(1)$ ($sp^{1.23}$) < $N_{eq}(4)$ ($sp^{1.31}$) resulting in a larger N(7)–N(8)–N(9) angle compared to the N(4)–N(5)–N(6) and N(1)–N(2)–N(3) angles.

Since the terminal N(8)–N(9) bond length of the axial azide group is significantly longer, the antisymmetric stretching vibrations of the axial azide group appear at lower wavenumbers than the antisymmetric stretching vibration of the equatorial azide groups (Table 1). The calculated, scaled antisymmetric stretching frequencies are in excellent agreement with the experimentally observed vibrational frequencies and confirm the results of the NBO analysis.† Owing to C_i symmetry of the molecule, there are six normal modes describing the antisymmetric stretching vibration of the N_3 moiety which are either Raman active (3 A_g) or IR active (3 A_u). In agreement with C_i symmetry, the Raman and the IR spectra of solid **1** show each three absorbtions: Raman (2158, 2135, 2111 cm^{-1}); IR (2154, 2142, 2113 cm^{-1}), which are in the typical region for the antisymmetric stretching vibration of azides.[7] The approximate displacement vectors and assignments are given in Table 1.

The difference between the axial and equatorial azide groups was also observed in the ^{14}N NMR spectrum of **1**. The ^{14}N NMR spectrum of a covalently bonded azide group (connectivity X–$N_α$–$N_β$–$N_γ$) usually shows three resonances whereas the signal of the $N_α$ and $N_γ$ are very broad owing to the large quadrupole moment of ^{14}N. The ^{14}N NMR spectrum of **1** reveals three signals for the $N_β$ atoms at −152 (br, sh) and −154 ppm which can be assigned to the two N_{eq} and N_{ax}. The resonances of the $N_γ$ atoms are found in the region of −166 (br, N_{eq}) and −169 (N_{ax}) ppm.[8] A single resonance was observed in the ^{31}P NMR spectrum at −87.6 ppm, in the region typical for penta-coordinated phosphorus.

Financial support of this work by the University of Munich and the Fonds der Chemischen Industrie is gratefully acknowledged. We also wish to thank Prof. K. Karaghiosoff for helpful advice with the NMR spectra. We thank the referees for most valuable comments.

Notes and references

§ *Crystal data*: $C_{12}H_{10}N_{20}P_2$ **1**: M = 496.34, triclinic, space group $P\bar{1}$, a = 7.342(2), b = 8.551(2), c = 17.879(4) Å, α = 88.527(3), β = 85.499(4), γ = 67.684(3)°, V = 1035.1(4) $Å^3$, Z = 2, μ(Mo-Kα) = 0.262 mm^{-1}, λ = 0.71073 Å, T = 193 K, 5983 reflections measured, 3153 unique (R_{int} = 0.0408) which were used in all calculations. Final R indices [$F > 4\sigma(F)$], $R1$ = 0.0488, $wR2$ = 0.1148. The structure was solved using direct methods and refined by full-matrix least squares on F^2 using SHELXL-97. Data for compound **1** were collected on a Siemens CCD Area detector using Mo-Kα radiation. CCDC 182/1843. See http://www.rsc.org/suppdata/cc/b0/b006944m/ for crystallographic files in .cif format.

1 H. G. Horn, *Makromol. Chem.*, 1970, **138**, 163.
2 (*a*) U. Müller, *Chem. Ber.*, 1977, **110**, 788; (*b*) H. W. Roesky, M. Noltemeyer and G. M. Sheldrick, *Z. Naturforsch., Teil B*, 1986, **41**, 803; (*c*) D. Schomburg, U. Wermuth and R. Schmutzler, *Chem. Ber.*, 1987, **120**, 1713; (*d*) A. H. Cowley, F. Gabbai, R. Schluter and D. Atwood, *J. Am. Chem. Soc.*, 1992, **114**, 3142; (*e*) U. Englert, P. Paetzold and E. Eversheim, *Z. Kristallogr.*, 1993, **208**, 307; (*f*) A. H. Cowley, F. P. Gabbai, G. Bertrand, C. J. Carrano and M. R. Bond, *J. Organomet. Chem.*, 1995, **493**, 95; (*g*) M. Larbig, M. Nieger, V. v. d. Gönna, A. V. Ruban and E. Niecke, *Angew. Chem., Int. Ed. Engl.*, 1995, **34**, 460.
3 R. O. Day, A. Schmidpeter and R. R. Holmes, *Inorg. Chem.*, 1983, **22**, 3696; D. Schomburg, U. Wermuth and R. Schmutzler, *Phosphorus Sulfur*, 1986, **26**, 193; P. G. Jones, A. Meyer and R. Schmutzler, *Z. Naturforsch., Teil B*, 1990, **45**, 175.
4 H. Hess and D. Forst, *Z. Anorg. Allg. Chem.*, 1966, **342**, 240; L. G. Hoard and R. A. Jacobson, *J. Chem. Soc.*, 1966, 1203.
5 T. M. Klapötke and A. Schulz, *Quantum Chemical Methods in Main-Group Chemistry* (invited chapter by R. D. Harcourt), Wiley & Sons, Chichester, 1998.
6 H. A. Klein and H. P. Latscha, *Z. Anorg. Allg. Chem.*, 1974, **406**, 214.
7 A. Schulz, I. C. Tornieporth-Oetting and T. M. Klapötke, *Inorg. Chem.*, 1995, **34**, 4343.
8 I. Tornieporth-Oetting and T. M. Klapötke, *Angew. Chem., Int. Ed. Engl.*, 1995, **34**, 511; T. M. Klapötke and P. Geissler, *J. Chem. Soc., Dalton Trans.*, 1995, 3365.

ChemComm

Syntheses and thermal reactivities of symmetrically and asymmetrically substituted acyclic enediynes: steric control of Bergman cyclization temperatures

Diwan S. Rawat and Jeffrey M. Zaleski*

Department of Chemistry and Biochemistry, Indiana University, Bloomington, IN 47405, USA. E-mail: zaleski@indiana.edu

Received (in Corvallis, OR, USA) 6th September 2000, Accepted 6th November 2000
First published as an Advance Article on the web

The steric influences of the functional groups at the termini of acyclic enediynes can dramatically affect the Bergman cyclization temperatures of the resulting compounds.

The potent antitumor activity of the enediyne natural product antibiotics[1] such as calicheamicin,[2] dynemicin,[3] esperamicin,[4] and neocarzinostatin[5] has fostered interest in the development of simple enediynes with low thermal barriers to formation of the lethal 1,4-benzenoid diradical intermediate.[6] To this end, carbocyclic enediyne frameworks,[7] and more recently, novel metalloenediyne structures,[8–13] have shown considerable promise for the development of molecules with tunable thermal reactivities. Key structural considerations within these architectures are the relative disposition of the alkyne termini, as well as the nature of the ring closing motif, both of which provide steric contributions to the thermal barrier to Bergman cyclization.[14,15] In cases of metal assisted enediyne activation, it is now established that the metal center geometry is an important influence on the cyclization thermodynamics.[11–13] However, the structural consequences derived from ligand design also contribute significantly to the initial barrier height prior to metal assisted activation.[12,13] Unfortunately, the steric influences of the metal binding functionalities have not yet been systematically evaluated for simple enediyne ligands.

As a part of our ongoing investigations of novel metalloenediyne structures and reactivities,[11–13,16] we became interested in designing simple nitrogen donor enediyne chelates with variable thermal properties. Within this theme, we report the syntheses and thermal reactivities of two symmetric and two asymmetric enediyne chelates of the form 1,8-bis(R,R′)oct-4-ene-2,6-diyne where R and R′ = dimethylamino, amino, or 3-hydroxypyridine. The asymmetric compounds are synthetically unique, and exhibit cyclization temperatures between the bis(dimethylamino) and the novel diamino compound, the latter of which is substantially more reactive. The thermal reactivities of these enediynes systematically illustrate the importance of intraligand steric hindrance in influencing Bergman cyclization temperatures.

Scheme 1 illustrates the general strategy for our preparation of the symmetric dimethylamino enediyne (1,8-bis(dimethylamino)oct-4-ene-2,6-diyne,[17] **4**),† as well as the dimethylamino (**5**)‡ and 3-hydroxypyridine (**6**) substituted 5-chloropent-4-ene-2-yne synthon. Stephens–Castro coupling of 2.2 equiv. of the 3-dimethylaminoprop-1-yne (**1**) with *cis*-1,2-dichloroethylene (**3**) over a Pd(0) catalyst in the presence of CuI and $BuNH_2$ generates **4** in 79% yield. Comparable reaction conditions using 1 : 1.2 alkyne **1**,**2** : **3** stoichiometries produces the monosubstituted eneyne precursors **5**, **6** in 57–62% yield. Reaction of **5** with 1 equiv. of the *N*-Boc-prop-2-ynyl amine (**10**), or **6** with **1** under analogous conditions yields the asymmetric products **7** and **8**§ (Scheme 2). Subsequent treatment of **7** with acid removes the protecting group and generates the asymmetric primary/tertiary amine species **9**.§ The same *N*-Boc-prop-2-ynyl amine (**10**) is employed for the preparation of the *N*-Boc enediyne precursor **11** and the subsequent diamino product **12** by analogy (Scheme 3).¶

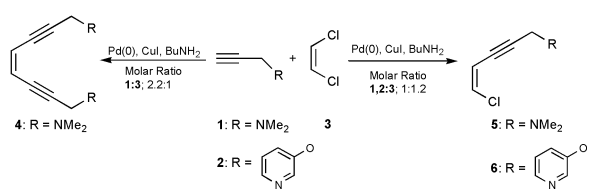

Scheme 1

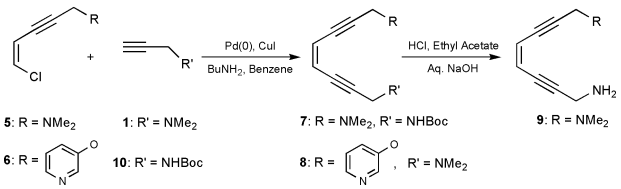

Scheme 2

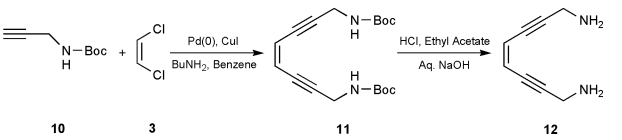

Scheme 3

The Bergman cyclization temperatures of enediyes **4**, **8**, **9**, and **12** (Table 1) were measured on neat materials by DSC and show a remarkable 80 °C variation across the series. The origin of the gradient derives from the steric encumbrance imposed upon the alkyne termini by the nitrogen-containing substitutents at the 1,8 positions of the enediyne framework. Beginning with R = dimethylamino, **4** is a thermally stable compound that exhibits a Bergman cyclization temperature of 186 °C. Substitution of one dimethylamino group with 3-hydroxypyridine (**8**) dramatically reduces the Bergman cyclization temperature to 149 °C. The result derives primarily from two sources. First, the ability of the pyridine ring to rotate out of the enediyne plane about the oxygen bond relieves steric clashes with the opposing substituent.[13] Secondly, the addition of the sp^3 oxygen between the pyridine ring and the alkyne termini

Table 1 Bergman cyclization temperatures of symmetric and asymmetric acyclic enediynes

Compound	Cyclization temperature/°C
4	186
8	149
9	139
12	106
13	136[12]
14	195[13]

DOI: 10.1039/b007360l

effectively distances the pyridine substituent from the alkyne termini by another atom, further reducing the interaction between substituents. This latter effect plays an important role as subsequent substitution to form the 1,8-bis(pyridin-3-yloxy)oct-4-ene-2,6-diyne (**13**) compound[12,16] restores the adjacent proximity of the substituents and results in only a modest decrease of the Bergman cyclization temperature of **13** (136 °C) relative to **8**. In contrast, removal of oxygen and methylene carbon atoms from **13** to form the conjugated 1,6-dipyridin-3-ylhex-3-ene-1,5-diyne (**14**) in which the pyridine rings are adjacent to the alkyne termini restores the high Bergman cyclization temperature (195 °C).[13]

A more pronounced trend is observed between the three compounds in the bis(dimethylamino) to diamino enediyne series (**4**, **9**, **12**). Monosubstitution of amino for dimethylamino (**9**) yields a dramatic 47 °C decrease in the Bergman cyclization temperature (**9** = 139 °C). Further substitution to form the diamino compound **12** produces an additional 33 °C decrease in the Bergman cyclization temperature (**12** = 106 °C, onset: 55 °C) indicating that **12** has one of the most facile thermal reactivities of an acyclic enediyne reported to date. The enhanced thermal reactivity of **12** results from a combination of the reduced steric hindrance of the primary amine functionalities, as well as an additional contribution from intramolecular hydrogen bonding.

To better correlate the thermal reactivity of **12** with that of other enediyne compounds reported in solution, we have measured the pseudo first-order rate constant (20-fold cyclohexadiene) and half-life ($t_{1/2}$) for the reactivity of **12** in DMSO by monitoring the disappearance of the –CH– ^{1}H NMR resonance at 5.7 ppm at 65 °C. A first order plot of ln([**12**]) *vs.* *t* and subsequent linear regression (R = 0.99) yielded k_{obs} = 4.16×10^{-2} h^{-1}, $t_{1/2}$ = 16.6 h. As is often observed in solution cyclization reactions of enediynes, a series of products are produced,[18] which in this case include disubstituted benzenes, and as such no dominant species could be isolated from the reaction. The low onset temperature for reactivity of this acyclic enediyne indicates that **12** may be an extremely important ligand for generating thermally reactive and therapeutically useful metalloenediyne complexes. The series also highlights the importance of ligand design in influencing Bergman cyclization temperatures and points toward the use of sterically innocent ligands in order to achieve lower metalloenediyne cyclization temperatures.

The generous support of the American Cancer Society (RPG-99-156-01-C), the Donors of the Petroleum Research Fund (PRF#33340-G4), administered by the American Chemical Society, and Research Corporation (Research Innovation Award #RI0102 for J. M. Z) are gratefully acknowledged.

Notes and references

† Symmetric enediyne (**4**)[17] was prepared by adding alkyne (2.2 mol) in a mixture of *cis*-1,2-dichloroethylene (1 mol), $Pd(PPh_3)_4$ (0.06 mol), CuI (0.2 mol), *n*-butylamine (5 mol) in benzene at 45 °C and stirring the mixture for 4 h at that temperature. The crude product was purified by flash column chromatography (5% ethyl acetate–dichloromethane). Spectral data for (**4**), yield: 79%; δ_H(400 MHz, $CDCl_3$): 2.19 (s, 12H, CH_3), 3.33 (s, 4H, NCH_2), 5.71 (s, 2H, CH); δ_C($CDCl_3$): 44.16 (NCH_3), 48.84 (NCH_2), 83.02 (Cquart), 93.34 (Cquart), 119.38 (CH); MS: *m/z* 191.2 (M^+ + 1).

‡ Spectral data for (**5**), yield: 62%; δ_H(400 MHz, $CDCl_3$): 2.32 (s, 6H, NCH_3), 3.44 (s, 2H, NCH_2), 5.88 (d, J = 8 Hz, 1H, CH), 6.36 (d, J = 8 Hz, 1H, CH); δ_C($CDCl_3$): 44.39 (NCH_3), 48.93 (NCH_2), 79.50 (Cquart), 93.64 (Cquart), 112.24 (CH), 128.25 (CH); MS: *m/z* 145 (M^+ + 2), 143 (M^+). Spectral data for (**6**), yield: 57%; δ_H(400 MHz, $CDCl_3$): 4.95 (s, 2H, OCH_2), 5.90 (d, J = 8 Hz, 1H, CH), 6.46 (d, J = 8 Hz, 1H, CH), 7.25-7.33 (m, 2H), 8.27 (m, 1H), 8.42 (s, 1H); δ_C($CDCl_3$): 56.95 (OCH_2), 82.0 (Cquart), 91.23 (Cquart), 111.28 (CH), 121.94 (CH), 123.98 (CH), 130.97 (CH), 138.70 (CH), 143.05 (CH), 153.94 (Cquart); MS: *m/z* 195 (M^+ + 2), 193 (M^+), 158, 130.

§ Spectral data for (**7**), yield: 65%; δ_H(400 MHz, $CDCl_3$): 1.45 (s, 9H, CH_3), 2.35 (s, 6H, NCH_3), 3.46 (s, 2H, NCH_2), 4.12 (s, 2H, NCH_2), 5.09 (s, 1H, NH), 5.82 (m, 2H, CH); δ_C($CDCl_3$): 28.66 (CH_3), 31.66 (NCH_2), 44.34 (NCH_3), 49.04 (NCH_2), 80.17 (Cquart), 81.03 (Cquart), 82.96 (Cquart), 93.09 (Cquart), 92.18 (Cquart), 119.18 (CH), 120.29 (CH), 155.59 (CO); MS: *m/z* 262.16 (M^+); Spectral data for (**8**), yield: 62%; δ_H(400 MHz, $CDCl_3$): 2.28 (s, 6H, NCH_3), 3.39 (s, 2H, NCH_2), 4.90 (s, 2H, OCH_2), 5.78 (d, J = 8 Hz, 1H, CH), 5.88 (d, J = 8 Hz, 1H, CH), 7.20–7.27 (m, 1H), 7.28–7.31 (m, 1H), 8.25 (m, 1H), 8.38 (d, J = 4 Hz, 1H); δ_C($CDCl_3$): 44.25 (NCH_3), 48.87 (NCH_2), 57.12 (OCH_2), 82.65 (Cquart), 85.51 (Cquart), 90.19 (Cquart), 93.72 (Cquart), 118.14 (CH), 121.36 (CH), 121.89 (CH), 124.02 (CH), 138.66 (CH), 143.04 (CH), 154.13 (Cquart); MS: *m/z* 239.1 (M^+ − 1), 196.1, 145.1. Spectral data for (**9**), yield: 72%; δ_H(400 MHz, $CDCl_3$): 1.42 (br s, 2H, NH_2), 2.34 (s, 6H, NCH_3), 3.47 (s, 2H, NCH_2), 3.67 (s, 2H, NCH_2), 5.81 (s, 2H, CH); δ_C($CDCl_3$): 32.34 (NCH_2), 44.33 (NCH_3), 49.02 (NCH_2), 80.36 (Cquart), 83.04 (Cquart), 92.65 (Cquart), 119.43 (CH), 119.49 (CH); MS: *m/z* 162.1 (M^+), 132.1.

¶ The syntheses of **11** and **12** are directly analogous to that of **4** and **9**. Spectral data for enediyne (**11**), yield: 68%; δ_H(400 MHz, $CDCl_3$): 1.44 (s, 18H, CH_3), 4.10 (s, 4H, NCH_2), 4.93 (br s, 2H, NH), 5.78 (s, 2H, CH); δ_C($CDCl_3$): 28.67 (CH_3), 31.65 (NCH_2), 80.29 (Cquart), 80.55 (Cquart), 93.70 (Cquart), 119.91 (CH), 155.68 (CO); MS: FAB 335 (M^+ + 1). Deprotection of the Boc group was achieved by stirring (**11**) with 37% HCl in ethyl acetate. Spectral data for (**12**), yield: 70%; δ_H(400 MHz, $CDCl_3$): 1.44 (s, 4H, NH_2), 3.54 (s, 4H, NCH_2), 5.72 (s, 2H, CH); δ_C($CDCl_3$): 32.52 (NCH_2), 79.90 (Cquart), 98.21 (Cquart), 119.15 (CH); MS: *m/z* 134.1 (M^+ + 1).

1 K. C. Nicolaou and W.-M. Dia, *Angew. Chem., Int. Ed. Engl.*, 1991, **30**, 1387.
2 M. D. Lee, T. S. Dunne, C. C. Chang, G. A. Ellestad, M. M. Siegel, G. O. Morton, W. J. McGahren and D. B. Border, *J. Am. Chem. Soc.*, 1987, **109**, 3466.
3 M. Konishi, H. Okhuma, T. Tsuno, G. D. Van Duyne and J. Clardy, *J. Am. Chem. Soc.*, 1990, **112**, 3715.
4 J. Golik, J. Clardy, G. Dubay, G. Groenewold, H. Kawaguchi, M. Konishi, B. Krishnan, H. Ohkuma, K. Saitoh and T. W. Doyle, *J. Am. Chem. Soc.*, 1987, **109**, 3461.
5 K. Edo, M. Mizugaki, Y. Koide, H. Seto, K. Furihata, N. Otake and N. Ishida, *Tetrahedron Lett.*, 1985, **26**, 331.
6 A. L. Smith and K. C. Nicolaou, *J. Med. Chem.*, 1996, **39**, 2103.
7 K. C. Nicolaou, G. Zuccarello, C. Riemer, V. A. Estevez and W.-M. Dia, *J. Am. Chem. Soc.*, 1992, **114**, 7360.
8 B. P. Warner, S. P. Millar, R. D. Broene and S. L. Buchwald, *Science*, 1995, **269**, 814.
9 B. König, W. Pitsh and I. Thondorf, *J. Org. Chem.*, 1996, **61**, 5258.
10 A. Basak, J. C. Shain, U. K. Khamrai, K. R. Rudra and A. Basak, *J. Chem. Soc., Perkin Trans 1*, 2000, 1955.
11 N. L. Coalter, T. E. Concolino, W. E. Streib, C. G. Hughes, A. L. Rheingold and J. M. Zaleski, *J. Am. Chem. Soc.*, 2000, **122**, 3112.
12 P. J. Benites, D. S. Rawat and J. M. Zaleski, *J. Am. Chem. Soc.*, 2000, **122**, 7208.
13 D. S. Rawat, P. J. Benites, C. Incarvito, A. L. Rheingold and J. M. Zaleski, *J. Am. Chem. Soc.*, submitted.
14 P. Magnus, S. Fortt, T. Pitterna and J. P. Snyder, *J. Am. Chem. Soc.*, 1990, **112**, 4986.
15 J. P. Snyder, *J. Am. Chem. Soc.*, 1990, **112**, 5367.
16 D. S. Rawat and J. M. Zaleski, *Synth. Commun.*, submitted.
17 D. Chemin and G. Linstrumelle, *Tetrahedron*, 1994, **50**, 5335.
18 N. Choy and K. C. Russell, *Heterocycles*, 1999, **51**, 13.

ChemComm

$[Pt_2(GaCp^*)_2(\mu_2\text{-}GaCp^*)_3]$: structure and bonding situation of the first homoleptic platinum complex with terminal and bridging Cp*Ga ligands

Dana Weiß,[a] Manuela Winter,[a] Roland A. Fischer,*[a] Chen Yu,[b] Karin Wichmann[b] and Gernot Frenking*[b]

[a] *Lehrstuhl für Anorganische Chemie II, Organometallics & Materials Chemistry, Ruhr-Universität Bochum, Universitätsstraße 150, 44780, Bochum, Germany. E-mail: rfischer@aci.ruhr-uni-bochum.de*

[b] *Fachbereich Chemie, Philipps-Universität Marburg, Hans-Meerwein-Straße, 35032, Marburg, Germany. E-mail: frenking@chemie.uni-marburg.de*

Received (in Cambridge, UK) 9th October 2000, Accepted 30th October 2000
First published as an Advance Article on the web

A new homoleptic diplatinum complex $[Pt_2(GaCp^*)_2(\mu_2\text{-}GaCp^*)_3]$ (Cp* = pentamethylcyclopentadienyl) exhibiting a central unit of two platinum atoms coordinated by five Cp*Ga groups acting as terminal as well as bridging ligands, was synthesized by the reaction of tris(ethylene)platinum(0) with an excess of $(Cp^*Ga)_6$ and was characterized by structural and quantum chemical methods.

In the past decade, the synthesis and structural chemistry of low-valent group 13 compounds and particularly their potential as ligands for the synthesis of novel group 13 element transition metal complexes and clusters, as well as the use of those latter compounds as precursors to new materials, have attracted widespread interest.[1] However, recent studies concerning this subject have almost exclusively focused on the coordination of ER species (E = Al, Ga, In) to metal carbonyl fragments.[2] When in 1998 Uhl *et al*. reported the synthesis of $[Ni\{InC(SiMe_3)_3\}_4]$, the first analogue of a mononuclear, binary carbonyl complex with exclusively terminal ER groups,[3] it was recognised as the starting point of a very fruitful new development in coordination chemistry. However, since then only three (!) other related *homoleptic* complexes have been reported by Uhl *et al*., $[M\{EC(SiMe_3)_3\}_4]$ (M = Ni, E = Ga; M = Pt; E = In),[4] and Jutzi *et al*., $[Ni(GaCp^*)_4]$.[5] We were attracted by the unique properties of ECp* compounds[1e] and have shown recently, that ECp* ligands stabilise reactive 14e L_2Pt centres produced by reductive alkane elimination to yield complexes of the type [(dcpe)Pt(ECp*)$_2$] [E = Al, Ga; dcpe = 1,2-bis(dicyclohexylphosphino)ethane].[6] Herein we describe the first example of the so far unknown series $M_a(ER)_b$ which extends the analogy between CO and ER ligands: $[Pt_2(GaCp^*)_2(\mu_2\text{-}GaCp^*)_3]$ **1**. The ER ligands are often compared to carbon monoxide or phosphine ligands, but regarding **1**, no truly analogous *neutral* homoleptic diplatinum carbonyl or phosphine complexes are known. Compounds of the type $[Pt_2(PPh_3)_2(\mu_2\text{-}dmpm)_3]$ [dmpm = bis(dimethylphosphino)-methane] bridged by a phosphine chelate ligand, may be regarded as closest congeners, at least from a topological point of view.[7]

The synthesis of **1** is outlined in Scheme 1. When tris(ethylene)platinum(0)[8] in pentane solution was treated with a 4.8-fold amount of Cp*Ga[2b] per equivalent of the platinum compound at –100 °C, a reddish brown solution was formed immediately. After warming up to room temperature and evaporation of all volatile components *in vacuo*, a dark red crude crystalline material was collected (quantitative yield based on NMR spectroscopy). After recrystallization from benzene large ruby-red octahedral shaped crystals were gathered in a yield of 70%. Compound **1** was characterised by ^{1}H NMR, ^{13}C NMR and IR spectroscopy, elemental analysis† and single crystal X-ray diffraction.‡ The ^{1}H NMR spectrum in benzene-d_6 exhibits two resonances at δ 2.15 and 2.03, respectively, with a ratio of two to three, that can be assigned to the methyl groups of the terminal and bridging Cp*Ga units, thus showing that there is no exchange between this positions on the NMR time scale. The ^{13}C NMR data show similar features.† Neither ^{71}Ga nor ^{195}Pt NMR resonances have, as yet, been identified, most likely because of extensive quadrupolar line broadening effects caused by the Ga nuclei. A single crystal X-ray diffraction study was performed, the results of which confirm the structural predictions based on analytical and spectroscopic data.

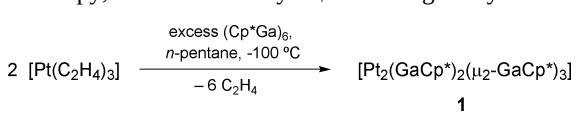

Scheme 1

Compound **1** crystallizes in the monoclinic space group $P2_1/c$ (Z = 4). The molecular structure of **1** (Fig. 1) consists of a central unit of two platinum atoms Pt(1) and Pt(2) with a quite short platinum–platinum bond length of 2.582(1) Å, compared to the common range for Pt^0–Pt^0 bonds of *ca*. 2.65–2.80 Å, *e.g.* in {[Pt(dtbpe)]$_2$} [2.765(1) Å, dtbpe = 1,2-bis(di-*tert*-butylphosphino)ethane] or neutral platinum clusters like $[Pt_3(PCy_3)_3(CO)_3]$ [2.656(2) Å, Cy = cyclohexyl].[9] For the shortest Pt–Pt distances in platinum metal values in the range 2.742–2.848 Å have been reported.[10] The Pt_2 unit of **1** is surrounded by two terminal Cp*Ga ligands [Ga(1) and Ga(2)], and three bridging Cp*Ga ligands [Ga(3)–Ga(5)]. All Cp*

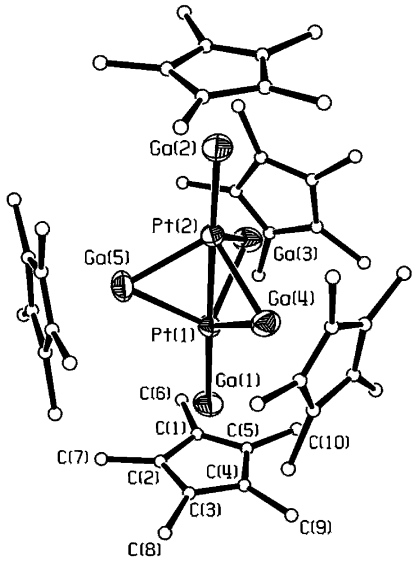

Fig. 1 Molecular structure of **1**. Selected bond lengths (Å) and angles (°): Pt(1)–Pt(2) 2.582(1), Pt(1)–Ga(1) 2.326(2), Pt(2)–Ga(2) 2.331(1), Pt(1)–Ga(3) 2.450(1), Pt(1)–Ga(4) 2.465(1), Pt(1)–Ga(5) 2.464(1), Pt(2)–Ga(3) 2.472(1), Pt(2)–Ga(4) 2.463(1), Pt(2)–Ga(5) 2.470(1), Ga(1)–Ga(3) 4.160, Ga(3)–Ga(4) 3.593, Ga(1)–C(1–5) 2.294(7)–2.310(7), Ga(4)–C(31–35) 2.313(7)–2.338(7), $Cp^*_{centroid}$–Ga(1) 1.968, $Cp^*_{centroid}$–Ga(2) 1.969, $Cp^*_{centroid}$–Ga(3) 2.013, $Cp^*_{centroid}$–Ga(4) 2.001, $Cp^*_{centroid}$–Ga(5) 2.021; Ga(1)–Pt(1)–Pt(2) 178.93(2), Ga(2)–Pt(2)–Pt(1) 178.60(2), Pt(1)–Ga(3)–Pt(2) 63.28(2), Pt(1)–Pt(2)–Ga(3) 57.95(2), Pt(2)–Pt(1)–Ga(3) 58.77(2), Ga(1)–Pt(1)–Ga(3) 121.12(3), Ga(3)–Pt(1)–Ga(4) 93.95(3).

DOI: 10.1039/b008133g

moieties are bound to the Ga centres in a nearly ideal symmetric η^5 mode with average values for the $Cp^*_{centroid}$–Ga distances of 1.969 Å for the terminal Cp*Ga units and 2.013 Å for the bridging ligands, both values being close to the free ligand of 2.081 Å (gas phase, monomer).[1a] Such distances are an indirect measure for the polarity of the Ga–Pt bond, which appears to be low compared to $[(CO)_nM–GaCp^*]$ complexes, especially for the bridging Cp*Ga ligands.[2a,6] The coordination pattern of the five Cp*Ga units at the central Pt(1)–Pt(2) core results in a diplatinum centred trigonal-bipyramidal structure (idealized D_{3h} symmetry) with an essentially linear Cp*Ga–Pt–Pt–GaCp* arrangement. The structure can also be described in terms of two face-sharing $PtGa_4$ tetrahedra. At least formally we can imagine an (unstable ?) intermediate species $[Pt(GaCp^*)_4]$ similar to the corresponding stable $[Ni(GaCp^*)_4]$ adding one reactive [PtGaCp*] fragment to yield **1**. This tendency of the heavier d-metals to form oligonuclear complexes rather than mononuclear species is well known from classical metal carbonyl chemistry. The terminal Pt–Ga distances of 2.326(2) and 2.331(1) Å are the shortest Pt–Ga bonds known and compare with average terminal Pt–Ga bond lengths of 2.369 Å in $[(dcpe)Pt(GaCp^*)_2]$.[6] The bridging Cp*Ga units exhibit an average Pt–Ga bond length of 2.464 Å, with values in the range 2.450(1)–2.472(2) Å. The shortest Pt–Ga distances of the intermetallic alloy systems PtGa and Pt_2Ga_3 amount to 2.60 and 2.45 Å, respectively.[11] A final comparison can be drawn to the complex $[(dcpe)Pt(GaR_2)(R)]$ (R = CH_2Bu^t), which exhibits the only other known Pt–Ga bond in molecular compounds [2.438(1) Å].[12] The Ga–Ga distances of compound **1** are in the range 3.593–3.691 Å for the bridging Cp*Ga units and 4.160–4.197 Å for the distances between terminal and bridging Cp*Ga ligands, which both are regarded as non-bonding. These values can be compared to the situation in $(Cp^*Ga)_6$ with Ga–Ga distances in the range 4.073–4.173 Å as a consequence of very weak bonding interactions in the solid state.[1a]

We examined the bonding situation in **1** with the aid of quantum chemical methods. To this end we first optimized the geometry of the model compound $[Pt_2(GaCp)_2(\mu_2\text{-}GaCp)_3]$ **1M** where the Cp* ligands of **1** are replaced by Cp at the gradient-corrected DFT (BP86) level of theory.[13] The calculated bond lengths of **1M** are $Pt–Ga_{terminal}$ 2.308 Å, $Pt–Ga_{bridge}$ 2.368 Å and Pt–Pt 2.829 Å. The theoretical value for the $Pt–Ga_{bridge}$ bond is significantly shorter than the experimental value of **1**, and the calculated Pt–Pt distance is much too long. Therefore we optimized the geometry of the real compound **1** at the same level of theory.[13] The calculation took three weeks cpu-time on a fast workstation and gave interatomic Pt–Pt distances which are in better agreement with experiment. The theoretical (average) values for **1** are $Pt–Ga_{terminal}$ 2.393 Å, $Pt–Ga_{bridge}$ 2.558 Å and Pt–Pt 2.676 Å. Calculated bond lengths of donor–acceptor bonds are usually longer than experimental values obtained from X-ray structure analysis, since solid state effects tend to shorten the interatomic distances.[15] Analysis of the Pt–Pt bond with the help of the NBO[16a] and AIM[16b] methods suggests weak attractive interactions only. A detailed bonding analysis will be reported in a full paper.

Though to our knowledge no intermetallic Pt_2Ga_5 bulk phase has been reported, the synthesis of heterobimetallic compounds such as **1** might provide prospects for molecular pathways to new intermetallic materials and nanophases as a valid target for further studies, following our work on single molecule sources for OMCVD of alloy thin film materials, which we have been performing for a number of years.[1d]

The support of this work by the Deutsche Forschungsgemeinschaft (Fi 502/6-1), the Degussa-Hüls AG and the W. C. Heraeus GmbH is gratefully acknowledged.

Notes and references

† *Spectroscopic data* for **1**: δ_H(298 K, 250.1 MHz, C_6D_6) 2.03 [s, 45H, CH_3, (μ_2-Cp*Ga)], 2.15 [s, 30H, CH_3, (Cp*Ga, terminal)]; δ_C(298 K, 62.9 MHz, C_6D_6) 10.58 [CH_3, (Cp*Ga, terminal)], 12.35 [CH_3, (μ_2-Cp*Ga)], 112.56 [ring atoms, (μ_2-Cp*Ga)], 114.35 [ring atoms, (Cp*Ga, terminal)]. IR (KBr, cm^{-1}) 2957m (sh), 2903s, 2849s, 1480m, 1445m (sh), 1418s, 1375s, 1260w, 1063w, 1020w, 797m, 585m, 473w. Elemental Anal. Calc. for $C_{50}H_{75}Ga_5Pt_2$, C, 42.44; H, 5.34. Found: C, 42.78; H, 5.49%. Slow decomp. beginning at 50 °C.

‡ *Crystallographic data* for **1** (ruby-red octahedra, 0.35 × 0.30 × 0.28 mm): $C_{50}H_{75}Ga_5Pt_2$, M = 1414.9, monoclinic, a = 14.9284(12), b = 20.1058(15), c = 18.9613(15) Å, β = 100.730(1)°, U = 5591.7(8) Å^3, T = 203 K, space group $P2_1/c$, Z = 4, μ(Mo-Kα, λ = 0.71073 Å) = 7.384 mm^{-1}, 34742 reflections measured, 12822 unique (R_{int} = 0.0639) which were used in all calculations. The final $wR(F^2)$ was 0.0758 (all data); measurements: Bruker-axs-SMART-diffractometer; programs used: SHELXS-86 and SHELXL-97. CCDC 182/1841. See http://www.rsc.org/suppdata/cc/b0/b008133g/ for crystallographic files in .cif format.

1 (*a*) D. Loos, E. Baum, A. Ecker, H. Schnöckel and A. J. Downs, *Angew. Chem.*, 1997, **109**, 894; D. Loos, E. Baum, A. Ecker, H. Schnöckel and A. J. Downs, *Angew. Chem., Int. Ed. Engl.*, 1997, **36**, 860; (*b*) W. Uhl, *Angew. Chem.*, 1993, **105**, 1449; W. Uhl, *Angew. Chem., Int. Ed. Engl.*, 1993, **32**, 1386; (*c*) C. Dohmeier, D. Loos and H. Schnöckel, *Angew. Chem.*, 1996, **108**, 141; C. Dohmeier, D. Loos and H. Schnöckel, *Angew. Chem., Int. Ed. Engl.*, 1996, **35**, 129; (*d*) R. A. Fischer and J. Weiß, *Angew. Chem.*, 1999, **111**, 3002; R. A. Fischer and J. Weiß, *Angew. Chem., Int. Ed.*, 1999, **38**, 2830; (*e*) P. Jutzi and G. Reumann, *J. Chem. Soc., Dalton. Trans.*, 2000, 2237.

2 (*a*) C. Üffing, A. Ecker, R. Köppe and H. Schnöckel, *Organometallics*, 1998, **17**, 2373; (*b*) P. Jutzi, B. Neumann, G. Reumann and H.-G. Stammler, *Organometallics*, 1998, **17**, 1305; (*c*) J. Weiß, D. Stetzkamp, B. Nuber, R. A. Fischer, C. Boehme and G. Frenking, *Angew. Chem.*, 1997, **109**, 95; J. Weiß, D. Stetzkamp, B. Nuber, R. A. Fischer, C. Boehme and G. Frenking, *Angew. Chem., Int. Ed. Engl.*, 1997, **36**, 70; (*d*) G. Linti and W. Köstler, *Chem. Eur. J.*, 1998, **4**, 942; (*e*) C. B. Macdonald and A. H. Cowley, *J. Am. Chem. Soc.*, 1999, **121**, 12 113; (*f*) F. A. Cotton and X. Feng, *Organometallics*, 1998, **17**, 128.

3 W. Uhl, M. Pohlmann and R. Wartchow, *Angew. Chem.*, 1998, **110**, 1007; W. Uhl, M. Pohlmann and R. Wartchow, *Angew. Chem., Int. Ed.*, 1998, **37**, 961.

4 W. Uhl, M. Benter, S. Melle and W. Saak, *Organometallics*, 1999, **18**, 3778; W. Uhl and S. Melle, *Z. Anorg. Allg. Chem.*, 2000, **626**, 1.

5 P. Jutzi, B. Neumann, L. O. Schebaum, A. Stammler and H.-G. Stammler, *Organometallics*, 1999, **18**, 4462.

6 D. Weiß, T. Steinke, M. Winter, R. A. Fischer, N. Fröhlich, J. Uddin and G. Frenking, *Organometallics*, 2000, **22**, 4583.

7 S. S. M. Ling, I. R. Jobe, A. J. McLennan, L. Manojlović-Muir, K. W. Muir and R. J. Puddephatt, *J. Chem. Soc., Chem. Commun.*, 1985, 566.

8 M. Green, J. A. K. Howard, J. L. Spencer and F. G. A. Stone, *J. Chem. Soc., Dalton Trans.*, 1977, 271.

9 T. Yoshida, T. Yamagata, T. H. Tulip, J. A. Ibers and S. Otsuka, *J. Am. Chem. Soc.*, 1978, **100**, 2063; A. Albinati, *Inorg. Chim. Acta*, 1977, **22**, L31.

10 N. Uspenski and S. Konobejewski, *Z. Phys.*, 1923, **16**, 215; A. W. Hull, *Phys. Rev.*, 1921, **17**, 571.

11 E. Hellner and F. Laves, *Z. Naturforsch., Teil A*, 1947, **2**, 17.

12 R. A. Fischer, H. D. Kaesz, S. I. Khan and H.-J. Müller, *Inorg. Chem.*, 1990, **29**, 1601.

13 The calculations were carried out at BP86[14a] with the RI (resolution of identity) approximation[14b] using the following basis sets for the atoms. A quasi-relativistic small-core ECP with a valence double-zeta basis augmented by one set of f-functions was used for Pt.[14c] All-electron DZ+P basis sets have been employed for Ga and the carbon atoms of the Cp ring.[14d] Minimal basis sets have been used for the methyl groups of Cp*.[14e] Auxiliary basis sets for all atoms have been taken from the literature.[14b] The calculations have been carried out with the program package Turbomole.[14f,g] The geometry optimizations were carried out with C_s symmetry constraints.

14 (*a*) A. D. Becke, *Phys. Rev. A*, 1988, **38**, 3098; J. P. Perdew, *Phys. Rev. B*, 1986, **33**, 8822; (*b*) K. Eichkorn, O. Treutler, H. Öhm, M. Häser and R. Ahlrichs, *Chem. Phys. Lett.*, 1995, **240**, 283; (*c*) D. Andrae, U. Häußermann, M. Dolg, H. Stoll and H. Preuß, *Theor. Chim. Acta*, 1990, **77**, 123; (*d*) A. Schäfer, H. Horn and R. Ahlrichs, *J. Chem. Phys.*, 1992, **97**, 2571; (*e*) A. Schäfer, cited in the manual of Turbomole, ref. 14(*f,g*); (*f*) R. Ahlrichs, M. Bär, M. Häser, H. Horn and C. Kölmel, *Chem. Phys. Lett.*, 1989, **162**, 165; (*g*) O. Treutler and R. Ahlrichs, *J. Chem. Phys.*, 1995, **102**, 346.

15 V. Jonas, G. Frenking and M. T. Reetz, *J. Am. Chem. Soc.*, 1994, **116**, 8741.

16 (*a*) A. E. Reed, L. A. Curtiss and F. Weinhold, *Chem. Rev.*, 1988, **88**, 899; (*b*) R. F. W. Bader, *Atoms in Molecules. A Quantum Theory*, Clarendon Press, Oxford, 1990.

Homochiral selection in the montmorillonite-catalyzed and uncatalyzed Prebiotic synthesis of RNA

Prakash C. Joshi,[a] Stefan Pitsch[b] and James P. Ferris[a]

[a] *Department of Chemistry and NY Center for Studies on the Origins of Life, Rensselaer Polytechnic Institute, Troy, NY 12180, USA. E-mail: ferrij@rpi.edu*

[b] *Organic Chemistry Laboratory, Eidgenössischen Technischen Hochschule, Zürich, Switzerland. E-mail: pitsch@org.chem.ethz.ch*

Received (in Corvallis, OR, USA) 11th September 2000, Accepted 9th October 2000
First published as an Advance Article on the web

The reaction of D,L-5′-activated nucleotide of adenosine in the presence and absence of montmorillonite gave 60 : 40 and 96 : 4 ratios, respectively of the D,D- and L,L : D,L- and L,D-dimers.

In the RNA world paradigm for the origin of life, RNA is formed by polymerization of mononucleotides present on the primitive Earth.[1] The RNA provides both the required genetic information and the catalytic activity in the first life. RNA oligomers of A, C, I, G, and U are formed in the reaction of the corresponding activated mononucleotides on montmorillonite clay.[2–4] The information content of the heterogeneous mixture of oligomers formed in the montmorillonite-catalyzed reaction serves as a template for the formation of complementary RNAs.[3] Fifty mers of A form when the phosphoroimidazolide of adenosine (ImpA) is added daily to a decameric primer bound to montmorillonite.[5] RNAs containing about fifty monomer units are long enough to be effective templates and catalysts.[6]

There has been little or no success in the enantioselective formation of biomolecules in prebiotic experiments.[7] While chiral selection was observed in the self-directing oligomerization of activated tetranucleotides of pyranosyl-RNA[8] it has not been observed in the template-directed synthesis of RNA.[9]

It would have been a major impediment to the origins of the RNA world if RNAs composed of equal amounts of D- and L-nucleotides formed. These structures would have had less chance of forming the helices, stem loops, and pseudo knots required for the RNA to fold into the secondary and tertiary structures required for template-directed synthesis and catalysis.[6] In addition, polymers containing both D- and L-nucleotides would have increased the number of isomers formed with the resultant decrease in number of those longer RNAs required to initiate the origin of life.[6]

The potential for oligomer formation from racemic mixtures was explored in the reactions of D,L-ImpA and -ImpU on montmorillonite. The reactions of 15 mM of each of these racemic mixtures on montmorillonite resulted in the formation of oligomers comparable in length[10] to those formed from the corresponding D-enantiomers.[2,4]† This result stands in marked contrast to the RNA template-catalyzed reaction where the formation of oligo(G)s is strongly inhibited by the incorporation of a nucleotide of the opposite absolute configuration into the growing oligomer chain.[9]

The potential for homochiral selection in RNA synthesis was explored in the reaction of D,L-ImpA on montmorillonite to form pApA. Reaction mixtures were digested with alkaline phosphatase to dephosphorylate the pApA products to the corresponding ApAs. The products were separated into four peaks of increasing retention time which contained (1) D,D- and L,L-A$^{2'}$pA, (2) D,L- and L,D-A$^{2'}$pA, (3) D,D and L,L-A$^{3'}$pA and (4) D,L- and L,D-A$^{3'}$pA on two different reverse phase HPLC columns (Table 1).[11] The identity of the reaction products was established by coinjection with authentic samples. The average percentage of the homochiral products D,D- and L,L-ApA to the corresponding D,L- and L,D- diastereomers is 60 : 40 ± 3.8%, respectively.

Control reactions without montmorillonite resulted in the homochiral selection of 94 : 6 ± 3.2% for D,D- and L,L-ApA *vs.* D,L- and L,D-ApA using 0.15 and 0.60 mM D,L-ImpA (Table 2). The yields of dimeric products in the 0.15 and 0.60 mM montmorillonite-catalyzed reactions were 5.9 and 19 times greater, respectively, than those in the uncatalyzed reactions. The difference in the yields reflects the 500 times greater second order rate constant for the catalyzed *vs.* the uncatalyzed reactions of ImpA.[4,12]

The possibility that the homochiral selectivity observed in the montmorillonite-catalyzed reaction was due to an uncatalyzed solution phase process was evaluated. The percentages for the 0.15 and 0.60 mM catalyzed reactions in rows 7 and 9 of Table 1 were recalculated after subtracting the dimer yields in the control reactions. The selectivity would decrease from 65 : 35 to 59 : 41 for the 0.15 mM reaction and from 58 : 42 to 56 : 44 for the 0.6 mM reaction. These data show that the observed homochiral selection is observed in the reaction catalyzed by montmorillonite.

Low concentrations of D,L-ImpA were used to minimize trimer formation so that the product mixture would only be a measure of the chiral selection for dimer synthesis.[11] The amount of trimer formed was estimated from the relative total areas of the dimer and trimer peaks. The trimer fraction was

Table 1 Relative yields and ratios of D,D & L,L and D,L & L,D dimers from the montmorillonite-catalyzed reaction of D,L-ImpA

		μBondapak column				Alltima column			
D,L-ImpA (mM)		0.15	0.15	0.60	0.60	0.15	0.15	0.60	0.60
Reaction Time (h) D,D & L,L (%)		2	18	2	18	2	18	2	18
	A$^{2'}$pA	37	23	33	36	46	27	43	31
	A$^{3'}$pA	21	36	20	30	19	33	15	27
D,L & L,D (%)									
	A$^{2'}$pA	23	20	26	15	19	19	24	19
	A$^{3'}$pA	19	21	21	19	16	21	18	23
D,D & L,L : D,L & L,D[a]		58 : 42	59 : 41	53 : 47	66 : 34	65 : 35	60 : 40	58 : 42	58 : 42

[a] The average of all determinations of D,D & L,L : D,L & L,D is 60 : 40 ± 3.7%.

Table 2 Relative yields and ratios of D,D & L,L and D,L & L,D dimers from the uncatalyzed reaction of D,L-ImpA (%)[a]

D,L-ImpA (mM)		0.15	0.15	0.60	0.60
D,D & L,L (%)					
	$A^{2'}$pA	49	57	60	58
	$A^{3'}$pA	42	39	31	39
D,L & L,D (%)					
	$A^{2'}$pA	2.5	trace	2.5	1
	$A^{3'}$pA	6.5	4	6.5	2
D,D & L,L : D,L & L,D[b]		91:9	96:4	91:9	97:3

[a] Procedures were the same as those given for Table 1. Reactions were carried out for 2 h and the products were analyzed on the Alltima column. [b] The average of all determinations of D,D & L,L : D,L & L,D is 94:6 ± 3.2%.

isolated from the reaction of 15 mM D,L-ImpA on montmorillonite and was dephosphorylated with alkaline phosphatase and coinjected with the products from the 0.15 and 0.6 mM D,L-ImpA reactions. The areas of the peaks with the same retention times as trimers in the 0.15 and 0.6 mM reactions of D,L-ImpA were summed and compared with the corresponding amount of dimers. In the reaction of 0.15 mM ImpA for 2 and 18 h the dimer yield was 12.5 fold higher than that of the total trimer yield. With 0.6 mM ImpA the combined dimer yield was 8.3 and 4.3 times greater than that of the trimer yield for the 2 h and 18 h reactions, respectively. These data show that little dimer is converted to trimer so that the yields in Table 1 mainly reflect the homochiral selectivity for dimer synthesis.

One of the five trimer peaks had the same retention time as the D,L- and L,D-$A^{3'}$pA (peak 4 above) in the dimer fraction. None of the compounds in the trimer fraction, that were not dephosphorylated with alkaline phosphatase, had a retention time that was identical with any of the dimer HPLC peaks. These findings establish that the chiral selectivity is not due to the enhancement of the peaks due to D,D- and L,L-ApA by trimers since the only enhancement is to the D,L- and L,D-$A^{3'}$ pA peak.

The product mixture was further characterized by ribonuclease T_2 digestion where the two HPLC peaks with the longest retention times, peaks 3 and 4 above, were decreased by about 50%. This is consistent with the known cleavage of D,D-$A^{3'}$ pA and, as discovered in this study, the cleavage of D,L-$A^{3'}$ pA with ribonuclease T_2 and the resistance of L,L-$Ap^{3'}A$, L,D-$A^{3'}$ pA, and the 2′, 5′-linked ApAs to cleavage with ribonuclease T_2.

The high homochiral selectivity observed in the uncatalyzed reaction may reflect chiral selection in the stacking of the activated nucleotides[13] coupled with intrastack reactions to form dimers. The lower selectivity in the uncatalyzed reaction may reflect formation of a monolayer of activated purine nucleotides on the montmorillonite platelets.[14]

The observance of both oligomer formation and chiral selection in the montmorillonite-catalyzed reaction of activated D,L-nucleotides on montmorillonite catalysis is consistent with previous findings in montmorillonite-catalyzed reactions. For example, regioselectivity was observed in the phosphodiester bonds formed between purine nucleotides[2] and sequence selectivity was observed in the reaction of mixtures of activated purine and pyrimidine nucleotides.[11] In most of these previous studies selectivity, but not specificity, was observed. This indicates that montmorillonite exhibits partial control on the course of the condensation reactions. This limited control explains why the oligomerization of D,L-mixtures proceeds on montmorillonite. The same limited control resulted here in the preferential formation of homochiral dimers.

It is expected that the bias towards the formation of homochiral oligomers will increase as the chain length increases and the homochiral strands fold into secondary and tertiary structures. This process, together with the potential for the more rapid hydrolysis of those RNAs that contain both enantiomers because they do not form secondary and tertiary structures, could enhance the proportion of homochiral RNAs.[15,16] The scenario of chiral selection and more rapid hydrolysis of heterochiral oligomers could have resulted in an even greater preponderance of homochiral RNA. This may have led to two RNA worlds, one with D- and the other with L-RNA.[17] A chance event may have favored the survival of the D-RNA world which was the precursor to the D-RNA (and D-DNA) present in life on Earth today.

Financial aid from NSF and the NY Center for Studies on the Origins of Life: A NASA Specialized Center of Research and Training.

Notes and references

† The L-enantiomers of adenosine and uridine[18] were phosphorylated at the 5′-position[19] and the phosphate was converted to the L-phosphoroimidazolides of adenosine (ImpA) and uridine (ImpU).[20] Solutions of 0.15 M each of D- and L-ImpA were prepared in 0.2 M NaCl, 0.075 M $MgCl_2$ and 0.1 M HEPES at pH 8. The ImpA concentrations were determined by quantitative HPLC analysis. At the end of the reaction time the mixture was centrifuged and the supernatant was removed. The montmorillonite was washed with two 40 μL portions of ammonium acetate. The combined supernatant and extracts was adjusted to pH 4 with 1 M $HClO_4$ and incubated at 37 °C to cleave the imidazole groups from the activated nucleotides. The pH of 200 μL of the reaction mixture was then adjusted to pH 8 and 0.25 units of alkaline phosphatase (bacterial, Sigma) was added and the mixture was incubated at 37 °C for 1 h. The analysis of the ApA isomers was performed on a Waters μBondapak C-18 column[2] and on an Alltima C-18 column.[11,21] Authentic samples of the 2′,5′- and 3′,5′-isomers of L,L-ApA, D,L-ApA and L,D-ApA were prepared by appropriate reactions of the activated monomers with an excess of the corresponding adenosine derivatives. For example, L,D-ApA was prepared in the reaction of excess L-adenosine with D-ImpA. The D,D- and L,L-enantiomers and the D,L- and L,D-diastereomers had the same retention times on the two different reverse phase HPLC columns used. The D,D-enantiomers were characterized by coinjection with authentic standards.[2] Further characterization was performed on some samples by adjusting the pH of 100 μL of the reaction products to 4, adding 2 units of ribonuclease T_2 (Sigma) and incubating the mixture for 1 h at 37 °C. The ribonuclease T_2 cleaves D,D-$A^{3'}$ pA and D,L-$A^{3'}$ pA. It does not cleave any of the other reaction products. The combined peaks due to D,D-and L,L-$A^{3'}$A and D,L- and L,D-$A^{3'}$pA were diminished by about 50% by treatment with ribonuclease T_2.

1 W. Gilbert, *Nature*, 1986, **319**, 618; F. H. C. Crick, *Mol. Biol.*, 1968, **38**, 367; L. E. Orgel, *J. Mol. Biol.*, 1968, **38**, 381.
2 J. P. Ferris and G. Ertem, *J. Am. Chem. Soc.*, 1993, **115**, 12270.
3 G. Ertem and J. P Ferris, *Nature*, 1996, **379**, 238.
4 K. Kawamura and J. P. Ferris, *Origins Life Evol. Biosphere*, 1999, **29**, 563.
5 J. P. Ferris, A. R. Hill Jr., R. Liu and L. E. Orgel, *Nature*, 1996, **381**, 59.
6 G. F. Joyce and L. E. Orgel, in *The RNA World: The Nature of Modern RNA Suggests a Prebiotic RNA*, Second Edition, ed. R. F. Gesteland, T. R. Cech and J. F. Atkins, Cold Spring Harbor Laboratory Press, Cold Spring Harbor, New York, 1999; J. W. Szostak and A. D. Ellington, in *The RNA World: The Nature of Modern RNA Suggests a Prebiotic RNA*, ed. R. F Gesteland and J. F. Atkins, Cold Spring Harbor Laboratory Press, Cold Spring Harbor, New York, 1993.
7 W. A. Bonner, *Origins Life Evol. Biosphere*, 1999, **21**, 59.
8 M. Bolli, R. Micura and A. Eschenmoser, *Chem. Biol*, 1997, **4**, 309.
9 G. F. Joyce, G. M. Visser, C. A. A. van Boeckel, J. H. van Boom, L. E. Orgel and J. van Westrenen, *Nature*, 1984, **310**, 602.
10 G. Ertem, K. J. Prabahar, P. C. Joshi and J. P. Ferris, in *12th International Conference on the Origins of Life and 9th ISSOL Meeting*, ed. L. Lane, 86, San Diego, CA, 1999.
11 G. Ertem and J. P. Ferris, *Origins Life Evol. Biosphere*, 2000, **30**, 411.
12 K. Kawamura and J. P. Ferris, *J. Am. Chem. Soc.*,1994, **116**, 7564.
13 W. Saenger, *Principles of Nucleic Acid Structure*, Springer-Verlag, New York, 1984, p.132.
14 K.-J. Wang and J. P. Ferris, submitted for publication.
15 N. E. Blair and W. A. Bonner, *Origins Life*, 1981, **11**, 331.
16 D. A. Usher and A. H. McHale, *Proc. Natl. Acad. Sci. USA*, 1976, **73**, 1149.
17 G. Wald, *Ann. N.Y. Acad. Sci.*, 1997, **69**, 352.
18 S. Pitsch, *Helv. Chim. Acta*, 1997, **80**, 2286.
19 T. Ikemoto, A. Haze, H. Hatano, Y. Kitamoto, M. Ishida and K. Nara, *Chem. Pharm. Bull.*, 1995, **43**, 210.
20 G. F. Joyce, T. Inoue and L. E. Orgel, *J. Mol. Biol.*, 1984, **176**, 279.
21 A. Kanavarioti, *Origins Life Evol. Biosphere*, 1997, **24**, 357.

ChemComm

Silica-supported sulfated zirconia: a new effective acid solid for etherification

Shaobin Wang* and James A. Guin

Department of Chemical Engineering, 230 Ross Hall, Auburn University, AL 36849, USA.
E-mail: shaobin@eng.auburn.edu

Received (in Cambridge, UK) 14th September 2000, Accepted 7th November 2000
First published as an Advance Article on the web

Silica-supported sulfated zirconia exhibits a comparable and even higher ether production than a reference acid resin (Amberlyst 15) giving an ether yield of 30% at 50% conversion.

Methyl *tert*-butyl ether (MTBE) has been the major gasoline additive in the past decade. However, its environmental consequences to drinking water have caused intense public attention in recent years.[1] Substantial quantities of unsaturated C_5 and C_6 compounds are present in the light gasoline produced in the fluid catalytic cracking units of refineries. Some of these compounds can be etherified with alcohols and possibly used to meet the demand for oxygenates and as a partial replacement for MTBE. Moreover, these higher ethers have lower vapor pressures and lower water solubilities compared to MTBE. Currently, ion exchange resins are the dominant catalysts for ether production. However, new catalysts could offer improvements over acid resins with respect to thermal stability, poor selectivity under certain conditions, and lack of regeneration ability. Several inorganic acid solids such as zeolites, sulfated zirconia, heteropolyoxoanions (HPA) and supported HPA catalysts have been evaluated for the production of MTBE.[2–5] Essayem *et al.* investigated etherification/esterification over two sulfated zirconia catalysts prepared by different methods and acid resins, but they found that sulfated zirconia showed faster deactivation.[6] No research has been thus far reported for the application of supported sulfated zirconia for etherification, though several researchers have reported the application of such catalysts in isomerization.[7–9] It is believed that unsupported sulfated zirconia suffers from the disadvantages of lower surface area and the very limited accessibility to the acid sites in liquid phase reactions with less polar solvents or in gas phase reactions. Therefore, development of well dispersed sulfated zirconia on supports with high surface areas is important for some acid-catalyzed reactions. This study reports preliminary results on the preparation of some inorganic acid solids, sulfated zirconia, tungstated zirconia, and supported sulfated zirconia, and their performance in the etherification of certain C_6 olefins with alcohols. These particular C_6 olefins, 2,3-dimethylbut-1-ene (23DM1B) or 2,3-dimethylbut-2-ene (23DM2B), were chosen on the basis of their potential for making oxygenated transportation fuel additives.[10]

A sulfated zirconia (SZ) was prepared by acid-treatment of $Zr(OH)_4$, obtained by precipitation of $ZrO(NO_3)_2$ solution with $NH_3{\cdot}H_2O$ at pH = 10, with 0.5 M H_2SO_4 solution, followed by evaporating and drying at 100 °C overnight and calcination at 600 °C for 2 h. A tungstated zirconia with 10 wt% WO_3 was prepared by impregnation of ammonium tungstate hydrate on $Zr(OH)_4$. Two silica-supported sulfated zirconia catalysts, referred to as SZ/SiO_2-S and SZ/SiO_2-N, were prepared by impregnation of 3 g of zirconium sulfate and 2.45 g $ZrO(NO_3)_2$ on 3 g of commercial silica gel support (S_{BET} = 650 $m^2\ g^{-1}$) in 0.5 M sulfuric acid solution, respectively, followed by calcination at 600 °C for 2 h. The third catalyst, SZ/SiO_2-NP, was prepared by precipitation of 2.45 g $ZrO(NO_3)_2$ on SiO_2 using $NH_3{\cdot}H_2O$ at pH = 10 under constant stirring, followed by sulfation in 0.5 M H_2SO_4 solution and calcination at 600 °C for 2 h. A commercial ion exchange resin, Amberlyst 15 (from Aldrich), was used as a reference catalyst. Two other commercial resins, Nafion NR50 and silica-supported Nafion SAC-13 (from Fluka and Aldrich, respectively), were also tested. Additionally, a zeolite sample H-ZSM-5, obtained from United Catalyst, was also tested.

The reactions were carried out at 80 °C for 2 h in a 25 ml stainless steel batch reactor with constant agitation under a pressure of 1.8 MPa of dried helium. The catalyst loading was 0.5 g in all the cases. Before reaction, all catalysts were dried overnight in an oven at 60 °C under vacuum. The reactants, consisting of an appropriate amount of alcohol (0.2 g methanol or 0.27 g ethanol) and 0.5 g 23DM1B with an alcohol : olefin molar ratio of *ca.* 1 : 1, were mixed with heptane (4 g) as a solvent. The products were analyzed in a Varian gas chromatograph equipped with a capillary column and FID.

Table 1 shows the results of 23DM1B etherification with methanol over the various laboratory-prepared and reference catalysts. In the reaction, 23DM2B and the ether are the major products. A small amount of 2,3-dimethylbutan-2-ol was also detected, probably due to the reaction between the olefins and a trace amount of water from the catalysts and reactant mixture. Amberlyst 15 is an active catalyst converting 23DM1B to 23DM2B and ether at an overall rate of 90%; however, this catalyst is non-selective for etherification, having instead a high (undesirable) isomerization selectivity of 80% and 19% ether yield. Nafion NR50 shows low activity and low isomerization selectivity, but an ether yield of about 16%. The silica-supported Nafion SAC-13 is less active than the unsupported Nafion NR50, a behavior which is not the same as in some other reactions, where Nafion SAC-13 exhibited higher activity than Nafion NR50 due to a high surface area and enhanced accessibility of the reactants to the acid sites.[11,12] HZSM-5 shows a similar activity to the Nafion NR50 but the highest isomerization selectivity (94%) among the all catalysts tested in this investigation and thus the lowest ether yield. For the laboratory-prepared solid acid catalysts, sulfated zirconia exhibits higher conversion, ether selectivity and yield than Nafion SAC-13, while tungstated zirconia is the least active catalyst with an isomerization selectivity similar to that of Nafion SAC-13 and SZ. SZ/SiO_2-S exhibits much higher conversion with a lower isomerization selectivity, and an ether yield of 30%, which is substantially higher than that over the reference Amberlyst 15. SZ/SiO_2-N shows 40% conversion and 64% ether selectivity, both higher than Nafion NR50, and an ether yield of 24%, which is also higher than that over

Table 1 Catalytic activity of various acid solids and commercial resins in 23DM1B etherification with methanol

Catalyst	23DM1B conv. (%)	23DM2B sel. (%)	Ether sel. (%)	Ether yield (%)
Amberlyst 15	91.0	78.7	20.6	18.8
Nafion NR50	29.0	44.0	53.9	15.6
Nafion SAC-13	3.2	21.7	58.9	1.9
HZSM-5	23.2	93.5	1.1	0.3
ZrO_2–WO_3	0.9	19.4	64.2	0.6
SZ	4.7	23.2	66.2	3.1
SZ/SiO_2-S	51.8	41.7	57.6	29.8
SZ/SiO_2-N	38.2	34.4	63.8	24.4
SZ/SiO_2-NP	21.2	28.7	67.4	14.3

DOI: 10.1039/b007475f

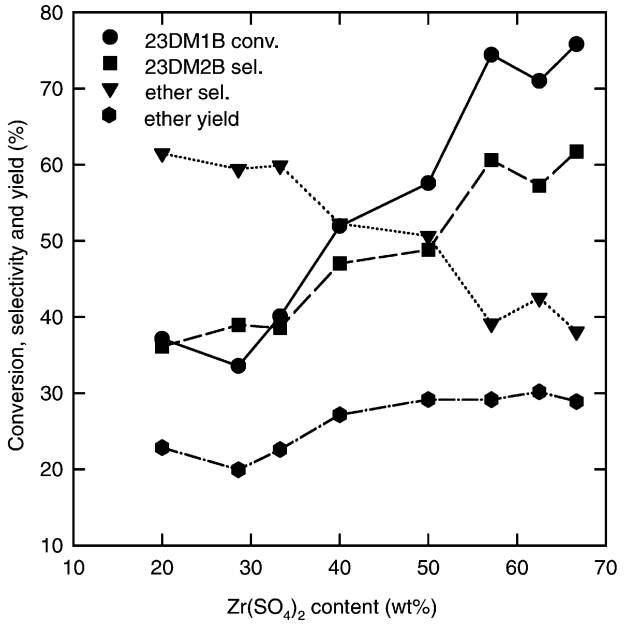

Fig. 1 Effect of $Zr(SO_4)_2$ loading of SZ/SiO_2-S catalysts on catalytic activity.

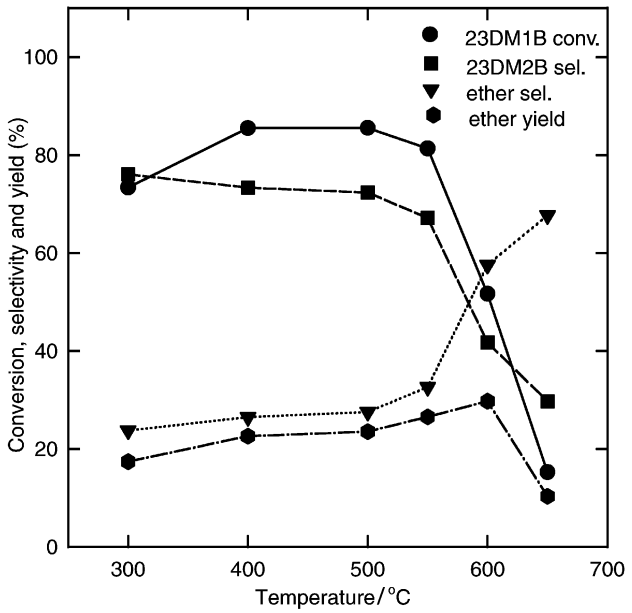

Fig. 2 Effect of calcination temperature on catalytic activity in SZ/SiO_2-S catalysts.

Amberlyst 15. SZ/SiO_2-NP exhibits a lower activity than the other two SiO_2-supported SZ catalysts, but the highest ether selectivity producing an ether yield of 14%, close to those over Amberlyst 15 and Nafion NR50. Therefore, SZ/SiO_2-S is the best catalyst in terms of ether production.

It is well known that etherification or isomerization of olefins generally occurs on acid sites. The acid content is thus an important factor influencing the catalytic activity. The surface areas of catalysts also influence the catalytic activity. Amberlyst 15 has an acid amount of 4.4 $meqH^+\ g^{-1}$ *vs.* 0.89 and 0.12 $meqH^+\ g^{-1}$ for Nafion NR50 and Nafion SAC-13, respectively, making an order: Amberlyst 15 > Nafion NR50 > Nafion SAC-13, which is in agreement with the order of activity. However, in consideration of activity per unit of acidity, the activity of the above catalysts shows a different order; Nafion NR50 > Nafion SAC-13 > Amberlyst 15, which suggests that the catalytic activity also depends on the nature of the acid site. SZ is believed to be a superacid solid, effective for acid-catalyzed reactions such as isomerization. Tungstated zirconia shows little activity probably due to a low acidity. Silica-supported sulfated zirconia could have a better dispersion of active sites for reactions and thus an improved catalytic activity. However, the catalytic behavior of these supported SZ catalysts depends on the preparation technique. Further research on the catalyst characterization is being carried out to elucidate the nature of the active sites responsible for etherification and isomerization.

The effect of varying the composition of $Zr(SO_4)_2$ in SZ/SiO_2-S was further investigated and the results are presented in Fig. 1. It is seen that the loading of $Zr(SO_4)_2$ in SZ/SiO_2-S greatly influences the catalytic activity and selectivity. Both the 23DM1B conversion and 23DM2B selectively generally increase as the $Zr(SO_4)_2$ content increases. The ether yield also increases with increasing $Zr(SO_4)_2$ loading and reaches a stable level of *ca.* 30% for $Zr(SO_4)_2$ exceeding 50 wt%.

Calcination temperature also exerts an influence on the catalytic behavior (Fig. 2). As shown, SZ/SiO_2-S catalysts calcined at 400–550 °C can give much higher conversions, over 80%, comparable to Amberlyst 15. When catalysts are calcined at higher temperatures over 600 °C, the selectivity to ether will be remarkably enhanced, although the overall conversion drops off. In terms of the ether yield, 600 °C is the optimal temperature at which the highest ether yield is achieved.

The catalytic activity of the etherification of 23DM1B with ethanol was also investigated over the resin catalysts and the inorganic acid solids. It was found that Amberlyst 15 is also an effective catalyst for this reaction, exhibiting similar conversion and selectivity to 23DM2B as for the etherification with methanol with an ether yield of 13%. Nafion NR50 and Nafion SAC-13 again are less active than Amberlyst 15, giving ether yields of 9% and 3%, respectively. Sulfated zirconia shows a lower activity than Amberlyst 15 with a conversion of 20% and 58% selectivity to ether but an ether yield of 12%, comparable to that of Amberlyst 15. The SZ/SiO_2-S exhibits 40% conversion and 48% ether selectivity, resulting in an ether yield of 18.4%, higher than that obtained over Amberlyst 15.

In summary, the commercial resin catalyst Amberlyst 15 is an effective but non-selective catalyst in the etherification of C_6 olefins with methanol and ethanol. Silica-supported SZ catalysts exhibit comparable and even higher ether yields than commercial resin catalysts such as Amberlyst 15 and are thus potential alternative catalysts, with the catalytic activity influenced by the zirconium precursor compounds and preparation technique, the ratio of SZ to silica, and calcination temperature.

This research was supported by the U.S. Department of Energy under contract no. DE-FC26-99FT40540 as part of the research program of the Consortium for Fossil Fuel Liquefaction Science.

Notes and references

1 A. Rhodes, *Oil & Gas J.*, 1999, **97**, 39.
2 F. Cillignon, M. Mariani, S. Moreno, M. Remy and G. Poncelet, *J. Catal.*, 1997, **166**, 53.
3 F. Cillignon, R. Loenders, J. A. Martens, P. A. Jacobs and G. Poncelet, *J. Catal.*, 1999, **182**, 302.
4 G. Baronetti, L. Briand, U. Sedran and H. Thomas, *Appl. Catal. A*, 1988, **172**, 265.
5 M. E. Quiroga, N. S. Figoli and U. A. Sedran, *React. Kinet. Catal. Lett.*, 1998, **63**, 75.
6 N. Essayem, V. Martin, A. Riondel, G. Coudurier and J. C. Vedrine, *Spec. Publ. R. Soc. Chem.*, 1998, **216**, 91.
7 J. M. Grau, C. R. Vera and J. M. Parera, *Appl. Catal. A*, 1998, **172**, 311.
8 T. Lei, J. S. Xu, Y. Tang, W. M. Hua and Z. Gao, *Appl. Catal. A*, 2000, **192**, 181.
9 D. J. Zalewsik, S. Alerasool and P. K. Doolin, *Catal. Today*, 1999, **53**, 419.
10 D. E. Hendriksen, *US Pat.*, 5 752 992, Exxon Chemical Patents Inc., May 19, 1998.
11 M. A. Harmer, W. E. Farneth and Q. Sun, *J. Am. Chem. Soc.*, 1996, **118**, 7708.
12 A. Heidekum, M. A. Harmer and W. F. Hoelderich, *J. Catal.*, 1998, **176**, 260.

Remarkable enhancement of the hydrolyses of phosphoesters by dinuclear centers: *Streptomyces* aminopeptidase as a 'natural model system'†

Altan Ercan, Hyun Ik Park and Li-June Ming*

Department of Chemistry and Institute for Biomolecular Science, University of South Florida, Tampa, FL 33620-5250, USA. E-mail: ming@chuma.cas.usf.edu

Received (in Irvine, CA, USA) 2nd June 2000, Accepted 27th October 2000
First published as an Advance Article on the web

The transition-state analogues bis(*p*-nitrophenyl)phosphate and *p*-nitrophenyl phenylphosphonate for peptide hydrolysis are shown to be very effectively hydrolyzed by *Streptomyces* dinuclear aminopeptidase and its Co^{2+}, Ni^{2+}, Mn^{2+} and Cd^{2+} derivatives with high catalytic proficiencies and specific activities comparable to those of some phosphoesterases.

Enzymes are able to specifically recognize a certain type of substrates and stabilize their transition states during reactions to afford enormous rate enhancement.[1,2] Consequently, transition-state analogues can often serve as inhibitors.[2] For peptide, ester, and amide hydrolysis, the transition state is a *gem*-diolate that can be well mimicked by the tetrahedral phospho-center in phosphoesters, phosphonates and phosphoamidates, which are known to inhibit the corresponding enzymes.[3–5] Thus, it would be unusual that peptides and the transition state-like phosphoesters can both be effectively hydrolyzed by the same hydrolytic enzyme because the recognition of the substrates at the ground- and the transition-states and the hydrolytic mechanisms of these two substrate families are quite different.

Proteins from the same origin with structural and sequence similarities may have evolved to exhibit completely different functions that are not related to each other, such as α-lactalbumin and lysozyme,[6] alkaline phosphatase and arylsulfatase,[7] and among the many β-barrel proteins.[8] Some of these enzymes indeed exhibit 'alternative catalysis',[6,9] which demonstrates their evolutionary relatedness and would not by all means be completely unexpected. On the other hand, it would be quite unusual to observe an 'alternative catalysis' of an enzyme that is attributable to an evolutionarily and structurally unrelated enzyme.

Recently, we have observed that the di-Zn aminopeptidase from *Streptomyces griseus* (sAP) exhibits a remarkable hydrolytic activity towards bis(*p*-nitrophenyl)phosphate (BNPP) with a specific activity comparable to several native phosphoesterases.[10] However, it was not clear whether or not this catalysis was unique toward only that particular one phosphoester substrate. Here, we describe an extensive analysis of the hydrolyses of a few different kinds of phosphoesters, including phosphomonoester, phosphodiester, phosphotriester and phosphonate monoester, by metal-substituted derivatives of sAP. The effectiveness toward the hydrolyses of both peptide and phosphoester substrates by sAP offers a rare opportunity to investigate different hydrolytic mechanisms in a single enzymatic system.

The hydrolysis of BNPP by a few homonuclear derivatives of sAP (M_2-sAP; M = Mn^{2+}, Co^{2+}, Ni^{2+}, Zn^{2+} and Cd^{2+})[11,12] has been analyzed with Michaelis–Menten kinetics (Table 1; Fig. S1A in ESI†). The rate constants (k_{cat}/K_m = 0.94–100 M^{-1} s^{-1}) are much higher than the second-order constants of many synthetic chemical models, *e.g.* (1.3–43) × 10^{-5} M^{-1} s^{-1} at 35 °C and pH 7.3–10.5 for several Zn^{2+} complexes[13] (also see footnote 14). The specific activity values (1.6–158 nmol min^{-1} mg^{-1}; Table 1) are in the range for several phosphodiesterases and phosphatases (0.3–2450 and *ca.* 2–40 nmol min^{-1} mg^{-1}, respectively),[15] and comparable to ethyl(*p*-nitrophenyl)phosphate hydrolysis by metal-substituted derivatives of *Pseudomonas* phosphotriesterase (1.7–11.4 nmol min^{-1} mg^{-1} calculated from ref. 16 with k_{cat}/K_m in the range 1.1–7.2 M^{-1} s^{-1}).

In order to demonstrate that BNPP hydrolysis by M_2-sAP is not just an incidental catalysis, the hydrolyses of structurally distinct phosphoesters were investigated. The phosphonate ester *p*-nitrophenylphenylphosphonate (NPPP) contains a P–C bond and resembles the primary hydrolytic products of some chemical warfare agents.[17] Thus, the study of its hydrolysis has practical value. The second order rate constants of NPPP hydrolysis (*ca.* 1–7 M^{-1} s^{-1}; Table 1 and Fig. S1B in ESI†) by M_2-sAP are much greater than those of some metal ions,[18] and are approaching those of a few highly active tetra-valent

† Electronic supplementary information (ESI) available: Michaelis–Menten kinetics plots. See http://www.rsc.org/suppdata/cc/b0/b004544f/

Table 1 The hydrolyses of BNPP and NPPP by several di-metal substituted derivatives of sAP in 0.1 M HEPES buffer at pH 8.0 in the presence of 2 mM Ca^{2+} at 30 °C (BNPP) and 50 °C (NPPP)[a]

	Bis(*p*-nitrophenyl)phosphate (BNPP)[c]					*p*-Nitrophenyl phenylphosphonate (NPPP)[c]				
M,M-sAP[b]	k_{cat}/s^{-1}	K_m/mM	$(k_{cat}/K_m)/M^{-1}$ s^{-1}	CP[d]	SA[e]	k_{cat}/s^{-1}	K_m/mM	$(k_{cat}/K_m)/M^{-1}$ s^{-1}	CP[d]	SA[e]
ZnZn[10]	0.45	4.5	100	4.1×10^{10}	158	0.014	14.9	0.94	1.8×10^{5}	1.7
MnMn	0.21	12.0	18	1.9×10^{10}	31	0.010	4.9	2.0	1.3×10^{5}	3.3
CoCo	0.74	9.5	78	6.7×10^{10}	136	0.022	7.9	2.8	2.9×10^{5}	4.8
NiNi	0.010	10.6	0.94	0.91×10^{9}	1.6	0.0033	3.0	1.1	0.43×10^{5}	1.6
CdCd	0.043	9.7	4.4	3.9×10^{9}	7.8	0.017	2.4	7.1	2.2×10^{5}	9.7

[a] The hydrolyses of the phosphotriesters parathione and tris(*p*-nitrophenyl)phosphate and the phosphomonoester *p*-nitrophenylphosphate by the enzyme are not detectable on the spectrophotometer after several hours at pH 8.0 and 50 °C. [b] Enzyme concentrations were in the range 0.1–0.7 μM. The di-Cu derivative did not show observable activity with a concentration of 2.0 μM under the experimental conditions, which indicates that the activity of CuCu-sAP would be at least *ca.* 10^4 × smaller than the native di-Zn sAP. [c] The substrate concentrations were in the range 1.0–20 mM. The initial rates were obtained from the change of absorbance at 405 nm (ε = 17 500 M^{-1} cm^{-1}), plotted against substrate concentration, and then fitted directly to the hyperbolic Michaelis–Menten equation, rate = $k_{cat}[E_o][S]/(K_m + [S])$ to give the kinetic parameters k_{cat} and K_m. [d] CP: catalytic proficiency.[22] [e] The specific activity (SA) is for the hydrolysis of 1 mM substrate in 1 min by 1 mg enzyme (nmol min^{-1} mg^{-1}) or extrapolated by the use of the Michaelis–Menten equation.

DOI: 10.1039/b004544f

lanthanide micelles (13.1–76.8 M^{-1} s^{-1})[19] which have Lewis acidities several orders of magnitude higher.[20] The specific activities of 1.6–9.7 nmol min^{-1} mg^{-1} against 1 mM NPPP (Table 1) are comparable to those of a few phosphatases and phosphodiesterases at 30 °C (12–355 and *ca*. 1–38 900 nmol min^{-1} mg^{-1}, respectively).[15] Conversely, the hydrolyses of the phosphomonoester *p*-nitrophenylphosphate and the phosphotriesters parathion and tris(*p*-nitrophenyl)phosphate are beyond the spectrophotometric detection limit, indicating the presence of specificity toward different phosphoesters.

Although the *p*-nitrophenol in both BNPP and NPPP is a very good leaving group, the auto-hydrolytic rates of BNPP and NPPP are still *extremely slow* with a rate constant $k_1 = 1.1 \times 10^{-11}$ s^{-1} for BNPP at pH 7.0 and 25 °C[21] and 7.65×10^{-8} s^{-1} for NPPP at pH 8.0 and 50 °C (comparable to 1.7×10^{-7} s^{-1} at 60 °C[18]). Tremendous catalytic proficiencies[22] are obtained for M_2-sAP toward BNPP and NPPP hydrolyses *i.e.* (0.94–67) $\times 10^9$ and (0.43–2.9) $\times 10^5$, respectively (Table 1). Co_2−sAP virtually decreases the half-life of BNPP hydrolysis from *ca*. 2000 years to *ca*. 1 second! These rate enhancements are remarkable when it is taken into account that the phospho-substrates are transition-state analogues of peptides during hydrolysis[1,3–5] In this case their corresponding trigonal bipyramidal transition states requires significantly more stabilization in support of their hydrolysis. For instance, an association constant of 108 M^{-1} (approximated from the average K_m of 9.3 mM for BNPP hydrolysis) would contribute 11.6 kJ mol^{-1} energy in ground-state stabilization at 298 K, which would increase the activation energy by the same amount and would reduce the reaction rate by *ca*. 100×. In the mean time, a 67×10^9 fold rate enhancement requires a decrease of 61.7 kJ mol^{-1} in activation energy at 298 K.

Finally, it is interesting that the Mn^{2+}, Ni^{2+} and Cd^{2+} derivatives of sAP also exhibit potent hydrolytic power [*i.e.* (*ca*. 1–4) $\times 10^9$ and (*ca*. 40–200) $\times 10^3$ fold rate enhancements toward BNPP and NPPP hydrolyses, respectively, Table 1] suggesting that these metal ions should be included in future design of chemical models for more extensive structural and mechanistic studies of metal-centered hydrolysis.[23]

The results have provided some mechanistic insight. The K_m values for BNPP and NPPP are similar, suggesting that they are recognized by sAP in a similar fashion. In both substrates, a hydrophobic *p*-nitrophenyl/phenyl group (as a hydrophobic anchor to bind to the active site) and a $–PO_2^-–$ group (as a *gem*-diolate transition-state analogue) are essential. On the other hand, the non-competitive property of phosphate[24] may be attributable to the lack of a hydrophobic anchor; the competitive inhibitor *p*-nitrophenylphosphate[25] contains both recognition moieties, yet is not hydrolyzed owing to the lack of an additional hydrolyzable group; and the two phosphotriesters are not hydrolyzed owing to the lack of a $–PO_2^-–$ group.

Many synthetic metal complexes have been utilized as models[26] to provide insight into the mechanistic roles of the metal ion(s) and the nucleophilic water in metallohydrolases. The specificity and tremendous effectiveness of enzymes offer a very challenging task for chemical modeling studies to achieve. We describe here that the transition-state analogues BNPP and NPPP are indeed substrates for M_2-sAP, and are hydrolyzed with remarkable rate accelerations. Although the rates of catalysis are not comparable to those of 'perfect enzymes' and much slower than those of the specific substrates of sAP,[11a,b] M_2-sAP can serve as unique '*natural* model systems' (as opposed to '*synthetic* model systems') for further studies of phosphoester hydrolysis. The results from these studies should lead us to a better understanding of dinuclear hydrolysis in chemical and biological systems.

This research was partially supported by the Petroleum Research Funds administrated by the American Chemical Society (ACS-PRF #35313-AC3).

Notes and references

1 L. Pauling, *Am. Sci.*, 1948, **36**, 51.
2 C. Walsh, *Enzymatic Reaction Mechanisms*, Freeman, New York, 1979.
3 K. Nishida, Y. Ohta, M. Ito, Y. Nagamura, S. Kitahara, K. Fujii and I. Ishiguro, *Biochim. Biophys. Acta.*, 1996, **1313**, 47; C. V. Preuss and C. K. Svensson, *Biochem. Pharmacol.*, 1996, **51**, 1661; L. Luan, T. Sugiyama, S. Takai, Y. Usami, T. Adachi, Y. Katagiri and K. Hirano, *Biol. Pharmacol. Bull.*, 1997, **20**, 71.
4 N. Sträter and W. N. Lipscomb, *Biochemistry*, 1995, **34**, 9200; B. Lejczak, P. Kafarski and J. Zygmunt, *Biochemistry*, 1989, **28**, 3549.
5 D. E. Tronrud, H. M. Holden and B. W. Matthews, *Eur. J. Biochem.*, 1986, **157**, 261.
6 E. M. Prager and A. C. Wilson, *J. Mol. Evol.*, 1988, **27**, 326; K. Nitta and S. Sugai, *Eur. J. Biochem.*, 1989, **182**, 111; H. A. McKenzie and F. H. White, Jr., *Adv. Protein Chem.*, 1991, **41**, 173; P. K. Qasba and S. Kumar, *Crit. Rev. Biochem. Mol. Biol.*, 1997, **32**, 255.
7 C. S. Bond, P. R. Clements, S. J. Ashby, C. A. Collyer, S. J. Harrop, J. J. Hopwood and J. M. Guss, *Structure*, 1997, **5**, 277; G. Lukatela, N. Krauss, K. Theis, T. Selmer, V. Gieselmann, K. von Figura and W. Saenger, *Biochemistry*, 1998, **37**, 3654.
8 R. Pickersgill, G. Harris, L. Lo Leggio, O. Mayans and J. Jenkins, *Biochem. Soc. Trans.*, 1998, **26**, 190.
9 P. J. O'Brien and D. Herschlag, *J. Am. Chem. Soc.*, 1998, **120**, 12 369.
10 H. I. Park and L.-J. Ming, *Angew. Chem., Intl. Ed.*, 1999, **38**, 2914.
11 The purification of sAP (*ca*. 30 kDa) and preparation of its apo form followed the literature procedures.[11a,b,12] The kinetic measurements by the metal-substituted derivatives were conducted in the presence of excess amount of the corresponding metal ions to ensure the complete formation of the derivatives. The background hydrolysis of BNPP by the excess metal ion is negligible and that of NPPP is considerably small and has been corrected. (*a*) A. Spungin and S. Blumberg, *Eur J. Biochem.*, 1989, **183**, 471; (*b*) D. Ben-Meir, A. Spungin, R. Ashkenazi and S. Blumberg, *Eur J. Biochem.*, 1993, **212**, 107.
12 L.-Y. Lin, H. I. Park and L.-J. Ming, *J. Biol. Inorg. Chem.*, 1997, **2**, 744.
13 T. Koike and E. Kimura, *J. Am. Chem. Soc.*, 1991, **113**, 8935; E. Kimura, H. Hashimito and T. Koike, *J. Am. Chem. Soc.*, 1996, **118**, 10 963.
14 Second-order rate constants in the range of (0.18–2.8) $\times 10^{-5}$ M^{-1} s^{-1} are calculated from corresponding pseudo-first order rate constants at pH 8.36 and 55 °C[14a] and (5.4–11.5) $\times 10^{-5}$ M^{-1} s^{-1} at pH 10.9–11.5 and 35 °C[14b] for several mono- and di-nuclear Zn^{2+} complexes. (*a*) W. H. Hapman and R. Breslow, *J. Am. Chem. Soc.*, 1995, **117**, 5462; (*b*) A. Bencini, E. Berni, A. Bianchi, V. Fedi, C. Giorgi, P. Paoletti and B. Valtancoli, *Inorg. Chem.*, 1999, **38**, 6323.
15 J. S. Kelly, D. E. Dardinger and L. G. Butler, *Biochemistry*, 1975, **14**, 4983; J. S. Kelly and L. G. Burtler, *Biochem. Biophys. Res. Commun.*, 1975, **66**, 316.
16 H. Shim, S.-B. Hong and F. M. Raushel, *J. Biol. Chem.*, 1998, **273**, 17 445.
17 Y. C. Yang, J. A. Baker and J. R. Ward, *Chem. Rev.*, 1992, **92**, 1729.
18 NPPP hydrolysis by La^{3+} is enhanced only by 100-fold at 60 °C which is much smaller than the catalytic proficiency of sAP (Table 1), whereas Cu^{2+}, Ni^{2+} and Zn^{2+} are ineffective; J. S. Loran, R. A. Naylor and A. Williams, *J. Chem. Soc., Perkin Trans. 2*, 1977, 418.
19 R. Moss and K. G. Ragunathan, *Langmuir*, 1999, **15**, 107.
20 J. Burgess, *Metal Ions in Solution*, Halstead, New York, 1978.
21 B. K. Takasaki and J. Chin, *J. Am. Chem. Soc.*, 1995, **117**, 8582.
22 The catalytic proficiency is expressed as k_{cat}/k_1[22a] instead of $(k_{cat}/K_m)/(k_1/55.5)$,[9] which is not appropriate here since H_2O is not the nucleophile in the hydrolysis. (*a*) A. Radzicka and R. Wolfenden, *Science*, 1995, **26**, 90.
23 Recent references: F. Hampl, F. Liska, F. Mancin, P. Tecilla and U. Tonellato, *Langmuir*, 1999, **15**, 405; J. Suh and W. J. Kwon, *Bioorg. Chem.*, 1998, **26**, 103; C. He, V. Gomez, B. Spingler and S. J. Lippard, *Inorg. Chem.*, 2000, **39**, 4188.
24 M. N. Harris and L.-J. Ming, *FEBS Lett.*, 1999, **455**, 321.
25 H. I. Park, Ph.D. Dissertation 1999, University of South Florida, FL, USA.
26 Some recent reviews: E. Kimura and T. Koike, *Adv. Inorg. Chem.*, 1997, **44**, 229; E. L. Hegg and J. N. Burstyn, *Coord. Chem. Rev.*, 1998, **173**, 133; N. H. Williams, B. Takasaki, M. Wall and J. Chin, *Acc. Chem. Res.*, 1999, **32**, 485; A. Blasko and T. C. Bruice, *Acc. Chem. Res.*, 1999, **32**, 475; H. Vahrenkamp, *Acc. Chem. Res.*, 1999, **32**, 589.

ChemComm

Samarium enolate on crosslinked polystyrene beads: anionic initiator for well defined synthesis of polymethacrylate on a solid support

Masayoshi Tanaka,[a] Atsushi Sudo,[a] Fumio Sanda[a] and Takeshi Endo*[b]

[a] *Chemical Resources Laboratory, Tokyo Institute of Technology, Nagatsuta-cho 4259, Midori-ku, Yokohama 226-8503, Japan*

[b] *Department of Polymer Science and Engineering, Faculty of Engineering, Yamagata University, Jonan, Yonezawa, Yamagata 992-8510, Japan. E-mail: tendo@poly.yz.yamagata-u.ac.jp*

Received (in Cambridge, UK) 7th September 2000, Accepted 6th November 2000
First published as an Advance Article on the web

A resin-supported samarium enolate successfully initiated the living anionic polymerization of methacrylates to afford the corresponding homopolymer as well as block copolymer with well-controlled molecular weights, which could be quantitatively isolated from the resin, so demonstrating the applicability of the present technique for solid supported construction of macromolecular architectures.

Polymer grafting on various organic and inorganic solid supports has been attracting significant attention as an effective technique for modification of functional materials.[1] Living polymerization is one of the most powerful tools for polymer grafting, because its capability in controlling the degree of polymerization together with end-functionalization and block copolymerization allows us to construct macromolecular architectures on solid supports in a well defined manner. Our research interest is in living polymerization of functional monomers on crosslinked polystyrene beads which have been widely applied as solid supports in solid phase organic syntheses which has brought about today's expanding development of combinatorial synthesis of chemical libraries.[2] Our approach would be a promising route to combinatorial synthesis of functional polymeric materials with defined structures. Since bead-supported photo-iniferter radical polymerization has been pioneered by Otsu *et al.*, only a few examples have been reported concerning controlled polymerization on polystyrene beads.[3] Here we describe the first example of living anionic polymerization of methacrylates on polystyrene beads.

Previously we have developed samarium(III) enolate mediated living anionic polymerization of methacrylates (Scheme 1).[4] Based on this technique, we have designed a novel grafting system involving (1) an easy access to immobilized samarium enolate through reduction of the corresponding bromoisobutyrate moiety by divalent samarium iodide (SmI_2), and (2) selective cleavage of the benzyl ester linkage between the formed poly(methacrylate)s and the beads, which enables the isolation of the formed polymer so allowing examination of the polymerization behavior in detail (Scheme 2).

The resin bearing 2-bromoisobutyrate moiety **1** was prepared by the condensation of 2-bromoisobutyric acid with Wang resin (crosslinked polystyrene containing hydroxymethyl groups, 0.68 mmol g^{-1}, 100–200 mesh) using 1-ethyl-3-(3-dimethylaminopropyl)carbodiimide hydrochloride as a dehydrating reagent. The condensation was repeated (usually twice) until

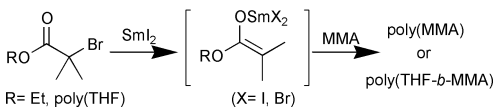

Scheme 1

Table 1 Polymerization of MMA with various feed ratios

Entry	$[MMA]_0/[Sm\text{-enolate}]_0$	M_n[a]	M_w/M_n[a]
1	20	3300	1.24
2	30	4400	1.21
3	50	7700	1.13

[a] Estimated by SEC [eluent: THF, poly(MMA) standards].

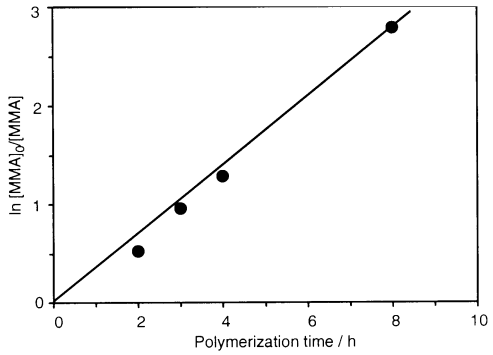

Fig. 1 $\ln[MMA]_0/[MMA]$ *vs.* polymerization time. $[MMA]_0$ = 5 mmol (50 eq. to Sm-enolate).

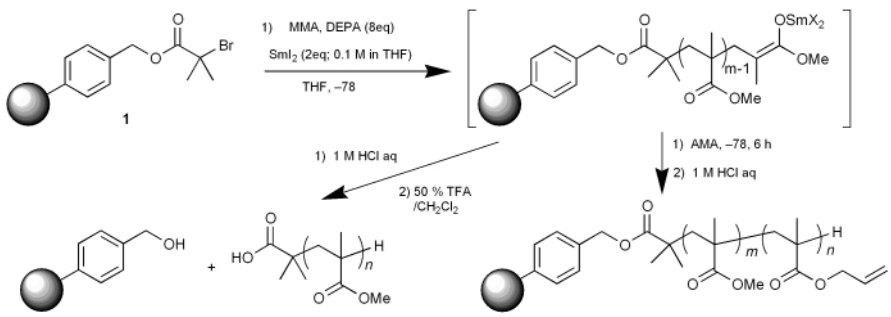

Scheme 2

complete acylation was confirmed by the disappearance of IR absorption of hydroxy groups at 3500 cm^{-1}.

The polymerization of methyl methacrylate (MMA) was performed by the addition of SmI_2 (2.0 eq. to 2-bromoisobutyrate moiety) to **1** in the presence of *N*,*N*-diethylpivaloylamide (DEPA), which is essential to accomplish well controlled polymerization in a homogeneous system, with shaking at −78 °C for 12 h.[5] The dark blue reaction mixture arising from SmI_2 gradually turned into yellow during a few hours, indicating Sm(III) enolate formation. The polymerization was terminated by the addition of 1 M aqueous hydrochloric acid, and the resulting resin was filtered off and washed with appropriate solvents. No polymer was detected in the filtrate by size exclusion chromatography (SEC), while the resin, as expected, gained weight according to the amount of MMA fed. Formation of poly(MMA) on the resin was also confirmed by IR analysis of the resin, which showed strong absorption attributable to ester carbonyl groups at 1740 cm^{-1}. Treatment of the resin with trifluoroacetic acid (TFA, 50% in CH_2Cl_2) resulted in selective cleavage of benzyl ester linkers without cleavage of the methyl ester in the side chain, and consequently poly(MMA) was quantitatively obtained.[6] The presence of carboxylic acid at the chain end of the polymer was confirmed by TLC analysis: the obtained polymer was not eluted by chloroform–THF (9 : 1, v/v) while poly(MMA) having terminal ester groups eluted easily. Isolated poly(MMA) was analyzed by SEC to estimate its number- and weight-average molecular weights (M_n and M_W). Table 1 summarizes the results of the polymerization with various feed ratios. In each case, MMA was completely consumed to give quantitatively poly(MMA) with a narrow M_W/M_n. The M_n of the polymer increased linearly with the feed ratio, demonstrating the ability of the present polymerization system to control the molecular weights of the polymer. We next examined the polymerization process on the solid state. Fixing the feed ratio to 50, separate series of polymerization was carried out with various polymerization times. The monomer conversion was determined based on the weight increase of the resin. Fig. 1 depicts a semi-logarithmic kinetic plot ($\ln[MMA]_0/[MMA]$ *vs.* polymerization time), the linear relationship of which may suggest the living character of the polymerization. The M_n of isolated poly(MMA) increased with monomer conversion (23%: M_n = 1500, 50%: M_n = 4200, > 99 %: M_n = 7700).

Finally, the living character of the present polymerization was confirmed by block copolymerization of MMA with allyl methacrylate (AMA) as shown in Scheme 2. After the polymerization of MMA (20 eq. to the initiator) was complete, AMA (20 eq.) was added and the mixture shaken at −78 °C for 12 h. The resulting resin gained weight according to the total amount of methacrylates fed, and its treatment with TFA resulted in quantitative isolation of the block copolymer. The ^1H NMR spectrum of the block copolymer showed signals assignable to methoxy groups of poly(MMA) and allyl groups of poly(AMA), where the integration ratio was in good agreement with the feed ratio (Fig. 2). SEC analysis showed that the unimodal peak of poly(MMA) shifted toward a higher molecular weight region with a narrow molecular weight distribution being maintained after AMA addition, indicating the successful formation of the block copolymer (Fig. 3).

In summary, we have demonstrated a new solid-supported living anionic polymerization of methacrylates. The initiator samarium enolate was readily and effectively generated by SmI_2-induced reduction of bromoisobutyrate moieties, supported on polystyrene beads. Further applications of the present system to multi-block copolymerization of various functional methacrylates, together with subsequent chemical modifications of the resulting polymer on polymer supports, are now in progress.

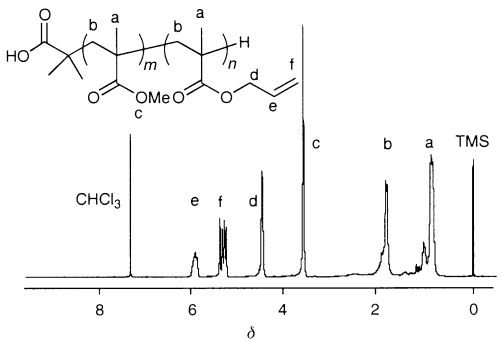

Fig. 2 ^1H NMR spectrum (300 MHz, $CDCl_3$) of poly(MMA-*b*-AMA).

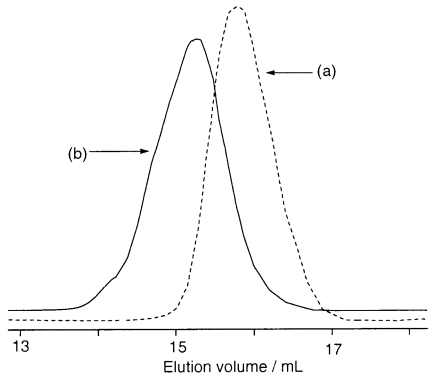

Fig. 3 SEC profiles of polymethacrylates obtained by block copolymerization: (a) poly(MMA) (M_n = 3,300, M_W/M_n = 1.24); (b) poly(MMA-*b*-AMA) (M_n = 6,800, M_W/M_n = 1.21).

Notes and references

1 R. Jordan and A. Ulman, *J. Am. Chem. Soc.*, 1998, **120**, 243; D. M. Haddleton, D. J. Duncalf, D. Kukulj and A. P. Radigue, *Macromolecules*, 1999, **32**, 4769; H. J. Lee, Y. Nakayama and T. Matsuda, *Macromolecules*, 1999, **32**, 6989; B. Zhao and W. J. Brittain, *J. Am. Chem. Soc.*, 1999, **121**, 3557; J. Pyun and K. Matyjaszewski, *Macromolecules*, 2000, **33**, 217; X. Zhang, J. Xia and K. Matyjaszewski, *Macromolecules*, 2000, **33**, 2340; M. Ejaz, K. Ohno, Y. Tsuiji and T. Fukuda, *Macromolecules*, 2000, **33**, 2870; Y. Shen, S. Zhu and W. H. Park, *Macromol. Rapid. Commun.*, 2000, **21**, 956.

2 J. S. Fruchtel and G. Jung, *Angew. Chem., Int. Ed. Engl.*, 1996, **35**, 17; R. C. D. Brown, *J. Chem. Soc., Perkin Trans. 1*, 1998, 3293.

3 T. Otsu, K. Yamashita and K. Tsuda, *Macromolecules*, 1986, **19**, 287; K. Oyanagi, S. Yoshikawa, R. Nishikawa and N. Tsubokawa, *J. Polym. Sci. A: Polym. Chem.*, 1997, **35**, 581; A. G. M. Barrett, S. M. Cramp and R. S. Roberts, *Org. Lett.*, 1999, **1**, 1083; J. C. Hodges, L. S. Harikrishnan and S. Ault-Justus, *J. Comb. Chem.*, 2000, **2**, 80.

4 M. Narita, R. Nomura and T. Endo, *Macromolecules*, 1998, **31**, 2774.

5 *Typical procedure*: to resin **1** (165 mg, bromoisobutyrate unit: 0.1 mmol) swelled in THF (1 mL) were added MMA (500 mg, 5 mmol) and DEPA (126 mg, 0.8 mmol) under N_2. The resulting mixture was cooled to −78 °C, and SmI_2 (0.1 mM solution in THF; 2 mL, 0.2 mmol) was added to the mixture which was shaken at the same temperature for 12 h. Then 1 M HCl (5 mL) was added to quench the reaction. The mixture was filtered and the residual resin washed successively with water, THF and then methanol. It was dried *in vacuo* to obtain the resin bearing poly(MMA) (660 mg; quant.).

6 *Typical procedure*: the resin bearing poly(MMA) (660 mg) was swelled in TFA (50% in CH_2Cl_2, 5 mL) and shaken at room temperature for 6 h. The mixture was filtered and the residual resin was washed with CH_2Cl_2. The filtrate was concentrated by rotary evaporation to give poly(MMA) (500 mg; quant.).

ChemComm

High pressure synthesis of an iodine doped silicon clathrate compound

E. Reny,*[a] S. Yamanaka,[ab] C. Cros[c] and M. Pouchard[c]

[a] *Department of Applied Chemistry, Faculty of Engineering, Hiroshima University, Higashi-Hiroshima 739-8527, Japan. E-mail: reny@ipc.hiroshima-u.ac.jp*
[b] *CREST, Japan Science and Technology Corporation (JST), Japan*
[c] *Institut de Chimie de la Matière Condensée de Bordeaux, Université Bordeaux I, 33608 Pessac, France*

Received (in Cambridge, UK) 20th September 2000, Accepted 9th November 2000
First published as an Advance Article on the web

A silicon clathrate compound doped with an electronegative element, $I_8Si_{46-x}I_x$ (x = 1.5 ± 0.5), has been prepared for the first time using high pressure and high temperature conditions.

In the late 1960s, alkali-metal doped silicon clahrate compounds (M_8Si_{46} and M_xSi_{136}) were prepared by the thermal decomposition of the Zintl phase MSi (M = Na, K, Rb, Cs) under vacuum or inert atmosphere.[1] The two compounds were isostructural with the clathrate hydrates of type I (or gas hydrate) and type II (or liquid hydrate), respectively.[2] The silicon lattice of the M_8Si_{46} structure (type I) is composed of two pentagonal dodecahedra Si_{20} and six tetrakaïdecahedra Si_{24}, offering eight sites per unit cell for guest alkali atoms.[3] Fig. 1 shows the two types of polyhedra connected by a common pentagonal face.

At the period of their discovery, silicon clathrates did not raise any special interest except for their peculiar crystal structures. However, the discovery of carbon clusters, fullerene, and the superconducting properties of the intercalation compounds M_3C_{60} (M = alkali metals) suddenly raised the interest for silicon clathrates: these latter being constructed of an assembly of the smallest possible fullerene type cages.[4] This led to active research of new silicon clathrates and to the discovery of the first superconducting silicon clathrate, $(Na,Ba)_xSi_{46}$ in 1995,[5] which is also the first superconductor composed of an sp^3 Si tetrahedral network. Much attention has also been paid to the thermoelectric properties of some types of clathrate compounds, originating from their special rattling structure.[6]

Very recently, a new synthesis route for silicon clathrates has been developed, *i.e.* high pressure and high temperature (HPHT) synthesis; a silicon clathrate doped with only barium, Ba_8Si_{46}, was obtained for the first time as a bulk phase under a pressure of 3 GPa and at 800 °C.[7] This compound showed a superconductive transition (T_c) at 8.0 K (highest T_c ever found in silicon clathrates). Another type of silicon clathrate, $Ba_{24}Si_{100}$, isostructural with K_6Sn_{25} was also prepared under a pressure of 1.5 GPa at 800 °C.[8] Note that these two new compounds can only be synthesised using high pressure conditions unlike their germanium analogues, Ba_8Ge_{43} and $Ba_{24}Ge_{100}$.[9,10] The iodine doped germanium clathrate $I_8Ge_{46-x}I_x$ with x = 8/3 was synthesised more than ten years ago by thermal decomposition of germanium diiodide by Nesper's group.[11] In this context of the studies of silicon and germanium clathrate compounds, we have focused our research on the synthesis of iodine doped silicon clathrate with the aid of HPHT conditions, the first silicon clathrate structure hosting an electronegative element.

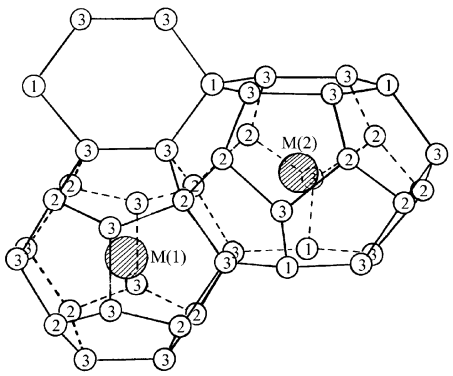

Fig. 1 Schematic illustration of the interconnected polyhedra forming the clathrate type I structure with guest atoms M(1) and M(2). Non-equivalent silicon sites are shown: Si(1), 6c; Si(2), 16i; Si(3), 24k.

Silicon powder (Katayama chemical, 99.999%, 200 mesh) and iodine (Katayama chemical, 99.8%) were mixed in various molar ratios, and finely ground. The mixture was placed in a h-BN cell (8 mm in inner diameter and 6 mm in length) which was in turn placed in a carbon tube heater and in a pyrophyllite cube as a pressure media. A cubic multi-anvil press was used (Riken model CP10). The BN cell was heated electrically by the carbon heater and the temperature was monitored by a thermocouple placed under the cell. A synthesis using a stoichiometric mixture of I/Si = 8/46, and a pressure of 5 GPa at 700 °C for 1 h gave a mixture of many phases: Si and clathrate as major phases and air-sensitive iodides SiI_2 and SiI_4 as minor phases. The iodides could be washed away by ethanol. The change in the conditions (P, T and I/Si ratio) resulted in a drastic change of the relative ratios of the various phases obtained. At a lower temperature of 500 °C under 5 GPa, the major phases were Si, SiI_2 and SiI_4 with a small portion of clathrate. At a lower pressure of < 3 GPa, only SiI_2 and Si were found. The use of higher molar ratios of iodine to silicon (I/Si = 1/2) at 5 GPa and 700 °C, gave no clathrate phase; the major phase was SiI_4. Even under the optimum conditions (P = 5 GPa, T = 700 °C, I/Si = 8/46), the yield of clathrate never exceeded 42 wt%. Surprisingly, however, an addition of only 1% of iodine doped silicon clathrate to the starting mixture (I/Si = 1/5.75) remarkably increased the yield of the clathrate formation up to 90% at P = 5 GPa, T = 700 °C, for 1 h. This suggests that the addition of seed is greatly effective for the growth of the crystals.

The new clathrate compound was found to be stable in acidic solutions like other binary clathrate compounds:[1] it was unreactive in 1 M HCl solution, although it decomposed in a concentrated HF–HNO_3 solution. In hot alkali solution (0.2 M NaOH) silicon dissolves readily but the clathrate phase is much less reactive. This finding provided us with a powerful tool to remove most of the remaining silicon from the final product. The resulting iodine doped clathrate was very fine powder, and the suspension in water had a bright orange colour. The powder sample was separated using a PTFE filter.

The clathrate sample was decomposed by a concentrated HF–HNO_3 solution in a sealed PTFE container at 70 °C. The silicon component was dissolved in the solution, and diluted with a saturated boric acid solution for analysis by inductively coupled plasma atomic emission spectroscopy (ICP, Perkin-Elmer Optima 3000). The iodine component was precipitated in the form of elemental crystals, which could be dissolved by adding potassium iodide. The precipitation of iodine crystals suggested that the iodine was included as electrically neutral atoms in the clathrate. To determine the iodine concentration by ICP, a

DOI: 10.1039/b007632p

separate solution was prepared and the iodine precipitate was dissolved with a sodium thiosulfate solution. The ICP results gave the following formulation: $I_{9.5 \pm 0.5}Si_{44.5 \pm 0.5}$ (*i.e.* an iodine wt% of 48.6 ± 1.4) with a total recovery of 97%. On heating the clathrate sample up to 800 °C for several hours under high vacuum ($< 10^{-4}$ Torr), a wt% loss of 48.1 ± 1.0 was observed. This value was in good agreement with the chemical analysis data.

X-Ray powder diffraction (XRD) data (Fig. 2) were measured using graphite monochromated Cu-Kα radiation and were collected at every 0.02° over the range 2θ = 25–120°. All reflections were indexed on the basis of a cubic unit cell with a = 10.4195(7) Å, which is the largest lattice constant so far observed for binary silicon clathrates. The crystal structure was determined by X-ray Rietveld refinement using Fullprof.[12] The space group ($Pm\bar{3}n$) of type I clathrate was assumed, and the refinements were carried out on the basis of various structural hypotheses. The only reasonable fit was obtained with a structural model, in which iodine atoms occupy all the silicon cages (2a and 6d) and 11% of the Si(2) sites of the network (see Fig. 1). The corresponding stoichiometry ($I_8Si_{44.2}I_{1.8}$) is concordant with the chemical analysis data. The replacement of the Si(1) or Si(3) sites with iodine led to very strong disagreement beween the calculated and the experimental data.

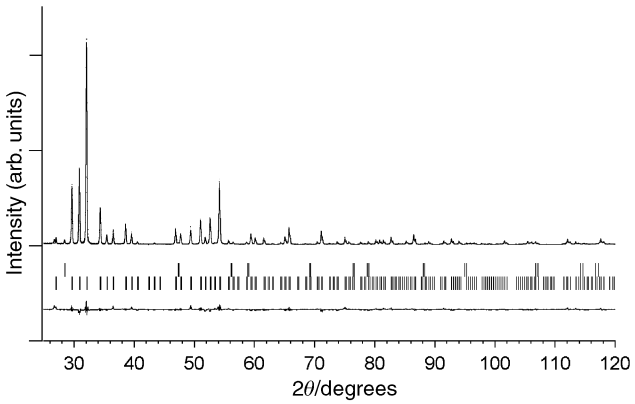

Fig. 2 Plot of the X-ray diffraction data for $I_8Si_{46-x}I_x$ with x = 1.8. Discontinuous and continuous lines represent, respectively, the experimental data points and the calculated spectra. The upper tick marks indicate the calculated reflection positions for some traces of silicon and the lower tick marks the calculated reflection positions for the clathrate phase. The lower continuous line represents the difference.

It was reported that in the germanium doped silicon clathrate ($I_8Ge_{43.3}I_{2.7}$), some iodine was present in the Si(1) sites. Therefore it should be noted that although the compositions of the two iodine doped clathrates are similar, replacement of silicon does not occur in the same sites. The coordinates of Si(2) and Si(3) sites were also refined and led to the following positions respectively: 16i (x, x, x) with x = 0.1831(5) and 24k (0, y, z) with y = 0.3099(8) and z = 0.1161(8). Although the fit is good enough to be sure about the atomic repartitions and positions (S = 2.06, R_{wp} = 0.11, see also Fig. 2), an effort is now being carried out to obtain single crystals for a more precise structural study.

Some preliminary results of the physical properties showed that the new clathrate was an electric insulator as estimated from its orange color, and showed the absence of superconductivity down to 2 K.

This study was supported by the Foreign fellowship division of the Japanese Society for the Promotion of Science (JSPS) and by the Ministry of Education, Science, Sports and Culture of Japan. This study is carried out as a France–Japan joint research project supported by the JSPS and the Centre National de la Recherche Scientifique (CNRS).

Notes and references

1 C. Cros, M. Pouchard and P. Hagenmuller, *C.R. Acad. Sci. Paris*, 1965, **260**, 4764.
2 J. S. Kasper, P. Hagenmuller, M. Pouchard and C. Cros, *Science*, 1965, **3704**, 1713.
3 E. Reny, P. Gravereau, C. Cros and M. Pouchard, *J. Mater. Chem.*, 1998, **8**, 2839.
4 C. Cros, E. Reny and M. Pouchard, *Mol. Cryst. Liq. Cryst.*, 1998, **310**, 199.
5 H. Kawaji, H. Horie, S. Yamanaka and M. Ishikawa, *Phys. Rev. Lett.*, 1995, **74**, 1427.
6 G. S. Nolas, J. L. Cohn, G. A. Slack and S. B. Schujman, *Appl. Phys. Lett.*, 1998, **73**, 178.
7 S. Yamanaka, E. Enishi, H. Fukuoka and M. Yasukawa, *Inorg. Chem.*, 2000, **39**, 56.
8 H. Fukuoka, K. Ueno and S. Yamanaka, *J. Organomet. Chem.*, 2000, **611**, 543
9 H. Fukuoka, K. Iwai and S. Yamanaka, personal communication.
10 H. Fukuoka, K. Iwai, S. Yamanaka, H. Abe, K. Yoza and L. Häming, *J. Solid State Chem.*, 2000, **151**, 117.
11 R. Nesper, J. Curda and H. G. von Schnering, *Angew. Chem., Int. Ed. Engl.*, 1986, **25**, 350.
12 J. Rodriguez-Carjaval, *Collected Abstracts of Powder Diffraction Meeting, Toulouse* (*France)*, 1990, p. 127.

ChemComm

Opal chips: vectorial growth of colloidal crystal patterns inside silicon wafers†

San Ming Yang and Geoffrey A. Ozin*

Materials Chemistry Research Group, Department of Chemistry, 80 St. George Street, Toronto, Ontario, Canada M5S 3H6. E-mail: gozin@alchemy.chem.utoronto.ca

Received (in Cambridge, UK) 23rd October 2000, Accepted 9th November 2000
First published as an Advance Article on the web

A simple, quick, reproducible and inexpensive method is described that combines self-assembly, micro-fluidics and soft lithography, to achieve a novel example of vectorial control of thickness, area, orientation and registry of patterned single crystal silica colloidal crystals in silicon wafers, coined opal chips, for potential applications in photonic chip and lab-on-chip technologies.

Close-packed arrays of mono-disperse silica and latex micro-spheres have numerous uses, such as chromatography and photonics.[1,2] Colloidal crystals are usually prepared from mono-disperse micro-spheres through the use of dip-coating,[3] sedimentation[4] or specially designed micro-cells.[5] These micro-sphere lattices may be prepared in the form of crystals and films. In particular, sphere sizes > 800 nm in silica have proven to be notoriously difficult to make mono-disperse and coerce into well ordered lattices. Colloidal crystals and films display varying degrees of disorder that arise from sphere size polydispersity, site randomness, intrinsic point, line and planar defects, and polycrystalline domains. The defect tolerance of colloidal crystals on properties like completeness of photonic band gaps in photonic crystals and the separation efficiency of chromatographic stationary phases is a subject of intense current interest.

The patterning of mono-disperse micro-spheres on top of various substrates has been explored *via* micro-molding,[6] electrostatic assembly[7] and micro-robotic techniques.[8] These methods of organizing micro-spheres usually require long preparation times and special instrumentation and are unable to simultaneously control order, defects, thickness, area, orientation and registry of patterned colloidal crystals. Moreover, colloidal crystals obtained in these ways have a face centered cubic lattice oriented in the (111) direction. Colloidal crystals displaying a specific (100) orientation have been grown by sedimentation of micro-spheres onto a lithographically patterned substrate, a technique known as colloidal epitaxy.[9] Access to such sophisticated substrates requires use of expensive chrome masks and photolithography, both of which are unfamiliar and unavailable to most research chemists. Further, epitaxial growth of colloidal crystal film is slow and structural order is limited to layers close to the lithographically patterned substrate.

Herein we report a straightforward, fast, reproducible and cost effective way, that combines self-assembly and soft lithography for the fabrication of micron scale patterned single crystal colloidal crystals in silicon wafers and which circumvents many of the aforementioned problems. The attractiveness of this method to opal chips is that it has the capability of controlling defects in colloidal crystals as well as the number, area, orientation and registry of close-packed layer planes of micro-spheres in the colloidal crystals embedded within a single crystal silicon (100) wafer.

Soft lithography encompasses a suite of techniques that have proven to be remarkably useful for the fabrication of micron to sub-micron patterns on a range of planar and curved substrates.[10] The procedures are facile and can be readily handled in an ordinary laboratory environment. In the context of the work described in this study, a line patterned polydimethylsiloxane (PDMS) master is obtained by casting a pre-polymer gel (Sylgard 184, Corning) from the corresponding lithographically defined photo-resist pattern. When access to lithographic instrumentation is not available, PDMS masters may be easily made by non-lithographic methods, such as the use of transmission electron microscopy (TEM) grids or optical gratings as templates for making micro-molds (see below). A procedure for fabricating V-shaped groove patterns inside a Si(100) wafer begins with a PDMS master that is inked with 2 mM hexadecanethiol in ethanol and then printed onto a Au (50 nm) coated Si(100) wafer (5 nm Ti is used as an adhesion layer). The bare gold surface is then etched away by a $Fe(CN)_6^{3-}$/$Fe(CN)_6^{4-}$/$S_2O_3^{2-}$/KOH solution, and the underlying Si(100) substrate is then anisotropically etched by 3 M KOH in Pr^iOH/H_2O at 70 °C to give V-shaped grooves with 70.6° apex angles beneath the surface of the wafer, as seen in the scanning electron microscopy (SEM) image in Fig. 1(a).[11] The etching rate along the Si(100) direction is *ca.* 1 μm min^{-1}.[12]

A flat PDMS block is next put into conformal contact with the patterned wafer and a drop of a 0.1 wt% aqueous dispersion of monodisperse silica micro-spheres (diameter = 840 ± 20 nm, modified Stöber synthesis) was added at the interface between

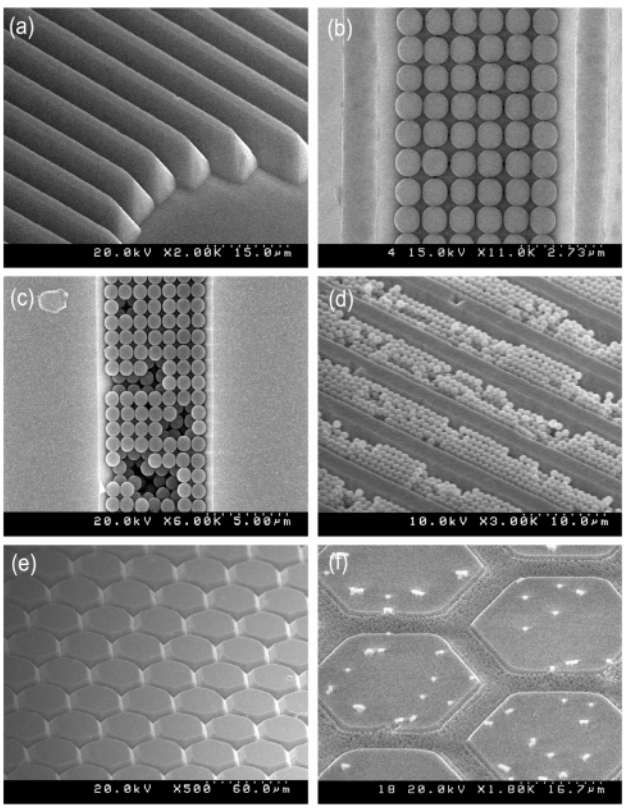

Fig. 1 SEM study illustrating vectorial control of thickness, area, orientation and registry of silica colloidal crystals grown inside silicon wafers – see text.

† Electronic supplementary information (ESI) available: pictorial representation of work described in this communication. See http://www.rsc.org/suppdata/cc/b0/b008534k/

DOI: 10.1039/b008534k

the patterned silicon wafer and the PDMS block. Micro-spheres are driven into the V-shaped grooves by capillary forces and close-pack inside the grooves upon evaporation of the water-dispersing agent. Owing to the 70.6° angular geometry of the V-shaped grooves, micro-spheres nucleate and grow in a vectorial fashion exclusively within the grooves to form a pattern of fcc colloidal crystal parallel lines. It is noteworthy that {100} layer planes are well ordered and organized parallel to the [100] face of the single crystal Si(100) wafer. This can be seen in the SEM images shown in Fig. 1(b)–(d). Over spatial areas sufficiently large for construction of photonic crystal and chromatographic micro-devices, colloidal crystals are seen to be single crystals and can be made essentially free of defects [Figs. 1(b), 2(a)]. When vacancy defects are present in the silica colloidal crystals they can easily be identified and their effect on optical and separation properties evaluated, [Fig. 2(b), (c)].

Interestingly, the first micro-spheres to nucleate in the V-shaped grooves are single-file contiguous arrangements and these linear constructions are found to be located in the apex of the V-shaped groove, [Fig. 3(a)]. These 1-D chains of micro-spheres dominate in the early stages of infiltration and when dilute aqueous dispersions of micro-spheres are used. At later stages the micro-spheres self-assemble adjacent to the 1-D chains and continue to grow up the walls of the V-shaped grooves to eventually fill them with well ordered patterns of colloidal crystals, Fig. 3(b). The edges of the grooves seem to be filled first with well defined lines of micro-spheres. Further, the observed registry of {100} layer planes of micro-spheres between adjacent grooves provides additional evidence for vectorial control of colloidal crystal nucleation and growth. These steps may provide an insight into the control mechanism that enables command of thickness, area, orientation and registry of the patterned colloidal crystal in the silicon wafer.

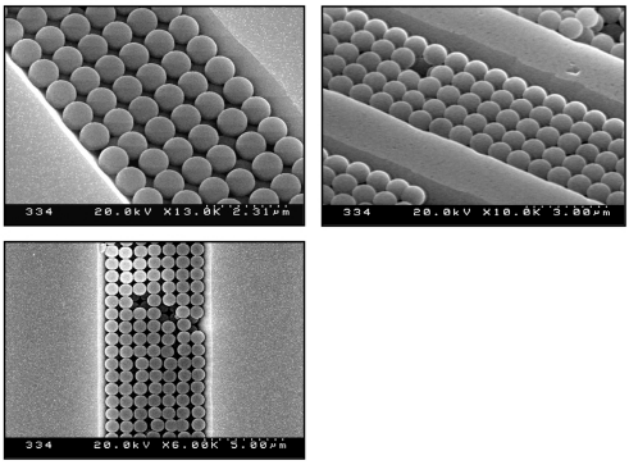

Fig. 2 SEM images depicting (a, top left) *six-layer* (100) single crystal silica colloidal crystal in a V-shaped channel of Si(100) wafer and devoid of vacancy defects. (b, top right) *Five-layer* (100) single crystal silica colloidal crystal in a V-shaped channel of Si(100) wafer depicting a single vacancy defect in top layer of micro-spheres. (c, bottom) *Seven-layer* (100) single crystal silica colloidal crystal in a V-shaped channel of Si(100) wafer depicting three vacancy-type defects in the top layer of micro-spheres.

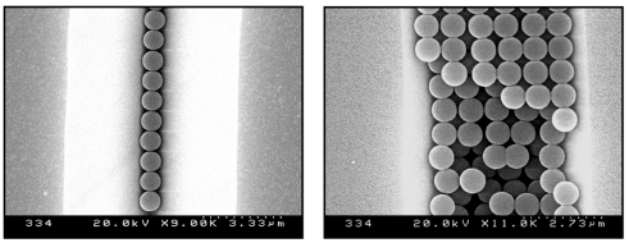

Fig. 3 SEM images depicting (a, left) the formation of a 1-D chain of silica micro-spheres grown in the apex region of a V-shaped groove that had been anisotropically etched within the surface of a single crystal (100) silicon wafer. (b, right) Vectorial growth of *six-layer* (100) oriented silica colloidal crystal within the V-shaped channel exposing the top three micro-sphere layer-planes.

The whole process outlined above is reproducible and can be finished in less than 2 h. The actual capillary infiltration and crystallization of micro-spheres in the patterned silicon wafer can be as short as seconds to minutes. As the depth of the V-shaped grooves in Si(100) is proportional to the etching time, it is easy to control groove depth to accommodate a pre-determined number of layers of silica micro-spheres. This has been achieved for one to ten layers of patterned colloidal crystals. The number of micro-spheres observed in the top (100) layer corresponds to the thickness of the colloidal crystal in the V-shaped grooves. The strategy described in this work alleviates the 'sagging' and 'pairing' problems in PDMS, which has been utilized for patterning latex micro-spheres through micro-molding in capillaries, MIMIC, on top of a silicon substrate.[6,10]

As mentioned above, PDMS masters can be made by non-lithographic approaches involving the use of TEM grids or optical gratings.[13] To exemplify this methodology, we used a hexagonal 600 mesh TEM grid to prepare the PDMS master. The bar width of the grid is *ca*. 7 μm and the pitch width is *ca*. 35 μm. A TEM grid was first laid down to a flat poly-(methylmethacrylate) (PMMA) substrate and a PDMS pre-polymer gel is then cast upon the grid. After curing at 60 °C, the PDMS master is used for the micro-contact printing followed by Au and Si(100) anisotropic etching as described above. The SEM image shown in Fig. 1(e) depicts a representative hexagonal symmetry V-shaped groove network and Fig. 1(f) displays a typical silica micro-sphere array following influx of micro-spheres into the grooves of the hexagonal pattern using the capillary infiltration method described above.

In summary, the process of growing single crystal colloidal crystal patterns of known thickness, area, orientation and registry within a substrate is experimentally straightforward, generally applicable, able to be easily integrated into chip fabrication facilities and amenable to mass production. The creation of colloidal crystal wafers, opal chips, is rapid, reproducible and cheap. They may, for example, be easily adapted for engineering lattice dimensions, refractive index contrast, structural defects, location and integration of photonic crystals coupled to optical fibers on photonic chips.[2] Additionally they may find utility for positioning and connecting lab-on-chip arrays of micro-fluidic and micro-reactor devices that perform chemical and catalytic transformations, as well as ion, molecule and macromolecule separations with simultaneous optical detection.[1] The opal chip described here is a significant advance on anything reported in the open or patent literature.

We are indebted to the Natural Sciences and Engineering Research Council of Canada and the University of Toronto for financial support of this work.

Notes and references

1 R. D. Oleschuk, L. L. Shultz-Lockyear, Y. Ning and D. J. Harrison, *Anal. Chem.*, 2000, **72**, 585.
2 E. Chomski and G. A. Ozin, *Adv. Mater.*, 2000, **12**, 1071.
3 P. Jiang, J. F. Bertone, K. S. Hwang and V. L. Colvin, *Chem. Mater.*, 1999, **11**, 2132.
4 M. Holgado, F. Garcia-Santamaria, A. Blanco, M. Ibisate, A. Cintas, H. Miguez, C. J. Serna, C. Molpeceres, J. Requena, A. Mifsud, F. Meseguer and C. Lopez, *Langmuir*, 1999, **15**, 4701.
5 S. H. Park, D. Qin and Y. Xia, *Adv. Mater.*, 1998, **10**, 1028.
6 E. Kim, Y. Xia and G. M. Whitesides, *Adv. Mater.*, 1996, **8**, 245.
7 J. Aizenberg, P. V. Braun and P. Wiltzius, *Phys. Rev. Lett.*, 2000, **84**, 2997.
8 H. T. Miyazaki, H. Miyazaki, K. Ohtaka and T. Sato, *J. Appl. Phys.*, 2000, **87**, 7152.
9 A. van Blaaderen, R. Ruel and P. Wiltzius, *Nature*, 1997, **385**, 321.
10 Y. Xia and G. M. Whitesides, *Angew. Chem., Int. Ed.*, 1998, **37**, 551.
11 Y. Xia, X.-M. Zhao, E. Kim and G. M. Whitesides, *Chem. Mater.*, 1995, **7**, 2332.
12 I. Zubel, *Sens. Actuators A: Phys.*, 1998, **70**, 260.
13 Y. Xia, J. Tien, D. Qin and G. M. Whitesides, *Langmuir*, 1996, **12**, 4033.

ChemComm

Harnessing thorium(IV) as a catalyst: RNA and phosphate diester cleavage by a thorium(IV) macrocyclic complex†

Congfang Wang, Seema Choudhary, Claire B. Vink, Elizabeth A. Secord and Janet R. Morrow*

Chemistry Department, State University of New York at Buffalo, Amherst, NY 14260-3000, USA

Received (in Cambridge, UK) 20th July 2000, Accepted 8th November 2000
First published as an Advance Article on the web

A robust macrocyclic tetraamide complex of Th(IV) binds phosphate diesters and promotes cleavage of RNA and phosphate diesters at 37 °C in the pH range 5.00–7.90.

Tetravalent cations such as Ce(IV), Th(IV) and Zr(IV) are among the most active catalysts for phosphate diester cleavage.[1–7] There are several reports that these metal ions promote the hydrolysis of phosphate diesters with poor leaving groups including dimethylphosphate and DNA.[1–5] Yet, the basis for this exceptional reactivity is not well understood. Studies reported to date on Ce(IV) or Th(IV) employ free metal ion or weak metal ion complexes and most studies are carried out at acidic pH to prevent precipitation of metal hydroxide complexes.[1–7] The complicated solution speciation of these systems makes mechanistic analysis difficult. Few attempts have been made to prepare well defined, catalytically active complexes of these metal ions.[4,6,7] Here, we report an unusual example of a Th(IV) complex of a neutral macrocycle which is highly resistant to dissociation in aqueous solutions. The complex efficiently promotes RNA cleavage and transesterification of a phosphate diester at neutral pH. Rate constants for RNA cleavage compare favorably to other metal ion macrocyclic complex catalysts including those containing lanthanide ions.[8–13]

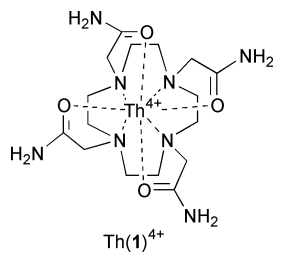

Th(**1**)$^{4+}$

The tetraamide macrocycle **1** binds to 12 members of the lanthanide(III) series with Sm(III) and Eu(III) being the most strongly bound.[12] Given that the ionic radius and coordination geometry of Th(IV) complexes are similar to those of the middle lanthanide(III) ions, **1** was studied as a ligand for Th(IV). Th(**1**)$(NO_3)_4$ was prepared in dry methanol from the free base form of **1** and $Th(NO_3)_4$.‡ NMR studies were carried out to characterize Th(**1**)$^{4+}$ in solution. The six broad ^{1}H NMR resonances observed at room temperature in D_2O sharpened but remained slightly broadened at 4 °C (ESI†).§ The ^{1}H NMR spectrum is analogous to that observed for La(**1**)$^{3+}$ which has **1** coordinated as an octadentate ligand with donor groups coordinated in a square antiprismatic arrangement.¶ The two sets of amide pendent group methylene protons appear as two doublets, the two sets of equatorial ethylene protons give rise to two doublets and the two sets of axial ethylene protons give rise to two triplets. Unfortunately, it was not possible to study the fluxional process further for Th(**1**)$^{4+}$ due to ligand decomposition at high temperatures and the insolubility of the complex in solvents other than water. However, this fluxional process likely involves ring inversion and cooperative pendent group rotation which interconverts the two carbons of the macrocyclic ring, the two sets of lower ring protons, the two sets of upper ring protons and the methylene protons in analogous lanthanide(III) complexes.[13,14] Consistent with such a fluxional process occurring, the ^{13}C NMR spectrum of Th(**1**)$^{4+}$ in D_2O at 22 °C has only three resonances‡ suggesting that, on the ^{13}C NMR timescale, the ethylene carbons are in fast exchange as has been observed for La(**1**)$^{3+}$.[13]

The Th(**1**)$^{4+}$ complex is resistant to dissociation in aqueous solution. Dissociation of Th(**1**)$^{4+}$ was studied in the presence of excess Cu(II) by monitoring formation of the Cu(**1**)$^{2+}$ complex by UV–VIS spectroscopy.[13] No dissociation of the complex (1.00 mM) was observed at pH 6.00 in a buffered solution in the presence of a 10-fold excess of Cu(II) over a period of one week at 37 °C. Remarkably, incubation of the Th(**1**)$^{4+}$ complex in the presence of an equivalent of EDTA at 37 °C and pH 6.00 did not induce dissociation of the complex over a period of a week. This inertness to metal ion release is reminiscent of the Eu(**1**)$^{3+}$ complex which did not release Eu^{3+} over a period of 6 weeks under similar conditions.[13] That this resistance to dissociation is a kinetic effect and not due to an exceptionally high formation constant for Th(**1**)$^{4+}$ relative to Cu(**1**)$^{2+}$ is suggested by competition experiments containing free **1**, $Th(NO_3)_4$ and $Cu(NO_3)_2$. When **1** (1.00 mM) was incubated simultaneously with $Th(NO_3)_4$ (1.00 mM) and $Cu(NO_3)_2$ (10.0 mM) at pH 6.00, 37 °C, all of **1** was complexed as Cu(**1**)$^{2+}$.

The ability to bind phosphate diesters is an integral part of catalysis; lanthanide(III) macrocyclic complexes that do not bind to phosphate diesters are not catalysts for cleavage.[10,13] Binding was studied in solutions containing 5.00 mM diethylphosphate and up to 40 mM Th(**1**)$^{4+}$ at pH 6.90, 21 °C with 0.10 M tetramethylammonium chloride, 5.0 mM triethylphosphate as a reference and 0.100 M Hepes buffer. Two ^{31}P NMR resonances were observed for free (0.81 ppm) and bound phosphate diester (−4.61 ppm), consistent with slow exchange kinetics on the NMR timescale. Fitting of the binding isotherm obtained by plotting the fraction of bound phosphate diester *vs.* concentration of free Th(**1**)$^{4+}$ gave a binding constant of 17 M^{-1}. Th(**1**)$^{4+}$ also bound the RNA analog **2** under similar conditions, but only a few percent was bound at pH 6.90 in the presence of 15 mM Th(**1**)$^{4+}$. In contrast, under similar conditions, diethylphosphate binding to Eu(**1**)$^{3+}$ and La(**1**)$^{3+}$ is too weak to determine binding constants and dissociation of diethylphosphate from La(**1**)$^{3+}$ is rapid on the ^{31}P NMR timescale.[13] The stronger binding and slower exchange rates of Th(**1**)$^{4+}$ are consistent with the higher charge of this actinide complex. These results are consistent with previous studies showing that ligand exchange rates for Th(IV) are slower than those of trivalent cations.[15]

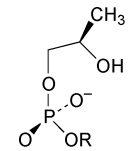

2 R = Ph
3 R= 4-NO_2Ph

Although exchange of bound and free phosphate diester is slow on the NMR timescale, ligand exchange is not likely the

† Electronic supplementary information (ESI) available: ^{1}H NMR spectra for [Th(**1**)]$(NO_3)_4$ in D_2O at 21 and 4 °C. See http://www.rsc.org/suppdata/cc/b0/b005866l

rate determining step in the cleavage studies described below. Binding of Th(**1**)$^{4+}$ (15 mM) to diethyl phosphate (10 mM), pH 6.90, 0.10 M Hepes buffer at 22 °C, is complete within the 90 s it takes to record the ^{31}P NMR spectrum. In comparison, cleavage of RNA analog **3** by 15 mM Th(**1**)$^{4+}$ in 0.10 M Hepes at 22 °C has a half-life of 4.5 min.

Th(**1**)$^{4+}$ promotes transesterification of the phosphate diester **3** to form the cyclic phosphate diester and 4-nitrophenylate as determined by use of ^{31}P NMR and UV–VIS spectroscopy.‖ At pH 7.30, 37 °C with 1.00 mM complex and 0.100 mM **3**, the reaction exhibited good first-order kinetics in **3** for greater than four half-lives. Transesterification of **3** is first-order in Th(**1**)$^{4+}$ complex in the concentration range 0.60–2.00 mM with a second-order rate constant of 0.65 M^{-1} s^{-1}. Addition of 10% EDTA (based on complex concentration) to reaction solutions did not reduce the pseudo-first-order rate constant, suggesting that the reaction is not catalyzed by a small amount of free Th(IV) ion. Transesterification of **3** by Th(**1**)$^{4+}$ is essentially independent of pH in the pH range 5.0–7.9. Phosphate diester cleavage by metal ion complexes is typically pH dependent owing to the formation of metal hydroxide complexes.[6,8–11] That cleavage of **3** by Th(**1**)$^{3+}$ is not pH dependent suggests that the speciation of the Th(IV) complex does not change in this pH range. Pseudo-first-order rate constants for Th(**1**)$^{4+}$ and analogous Ln(III) complexes are listed in Table 1. Th(**1**)$^{4+}$ is 40-times more active than La(**1**)$^{3+}$, the most active lanthanide complex in the series. In addition, Th(**1**)$^{4+}$ promotes cleavage of adenylic acid oligomers more rapidly than does La(**1**)$^{3+}$ under similar conditions.

How does Th(**1**)$^{4+}$ promote RNA cleavage and why is the complex more efficient than analogous Ln(**1**)$^{3+}$ complexes? Given that the ionic radii of Th(IV) and Eu(III) are nearly identical, it is likely that Th(**1**)$^{4+}$ is nine-coordinate with a single site for the binding substrate, analogous to Eu(**1**)$^{3+}$.[13] Thus, Th(**1**)$^{4+}$ activates the phosphate diester to cleavage most probably through interaction at a single coordination site. The greater reactivity of the Th(IV) complex compared to its lanthanide(III) analogs is attributed to the greater Lewis acidity of the Th(IV) center as suggested by its strong interaction with phosphate diesters. In conclusion, we show here that it is feasible to prepare a Th(IV) complex of a neutral macrocycle which is highly resistant to dissociation in neutral aqueous solutions and is active in the cleavage of phosphate diesters and RNA. We demonstrate that the catalytic power of a tetravalent cation can be harnessed in a macrocyclic complex.

Table 1 Pseudo-first-order rate constants for cleavage of RNA and phosphate diester **3** by thorium(IV) and lanthanide(III) complexes of **1** at 37 °C

Complex	Substrate[a,b,c]	$k_{obs}/10^{-4}$ s^{-1}
Th(**1**)$^{4+}$	**3**	7.5[a]
Th(**1**)$^{4+}$	A_{10}	9.2
La(**1**)$^{3+}$	**3**	0.16
La(**1**)$^{3+}$	A_{12}–A_{18}	1.6
Eu(**1**)$^{3+}$	**3**	NR[d]
Eu(**1**)$^{3+}$	A_{12}–A_{18}	NR[d]

[a] For substrate **3** conditions were pH 7.3, 1.00 mM complex, 0.100 mM **3**, 10 mM Hepes buffer, 100 mM $NaNO_3$. [b] For A_{10} conditions were pH 7.4, 0.200 mM complex, 5 mM Hepes buffer, 0.013 mM A_{10} (adenosine concentration). [c] For A_{12}–A_{18} conditions were pH 7.6, 0.200 mM complex, 5 mM Hepes buffer, 0.08 mM A_{12}–A_{18} (adenosine concentration).[13] [d] No cleavage observed under the conditions given above.[13]

We are grateful to the American Chemical Society Petroleum Research Fund (34358-AC) and the National Science Foundation (CHE-9986332) for support of this work.

Notes and references

‡ Equimolar amounts of TCMC and $Th(NO_3)_4$ were heated to reflux in dry methanol for 1.5 h. The methanol was removed and the complex was isolated as a white solid in 43% yield following precipitation twice from a methanol–diethyl ether mixture. Anal. Calc. for $C_{20}H_{42}N_{12}O_{17}Th$ [Th(**1**)-(Et_2O)]$(NO_3)_4$: C, 25.16; H, 4.43; N, 17.60. Found: C, 25.02; H, 4.38; N, 17.27. FAB MS: *m*/*z* 818 [Th(**1**)$(NO_3)_3^+$]. The ^{13}C NMR spectrum of Th(**1**)$^{4+}$ in D_2O showed resonances at 52.5, 57.3, and 177.3 ppm assigned to carbons of the ethylene moiety, methylene and carbonyl carbons, respectively.

§ Only one major diastereomeric form of the complex is observed by ^{1}H or ^{13}C NMR spectroscopy. In contrast, Eu(**1**)$^{3+}$ has two diastereomers present in solution and solid state (see refs. 13 and 14).

¶ In the solid state, [La(**1**)(CF_3SO_3)(EtOH)]$(CF_3SO_3)_2$ is a ten-coordinate complex with an unusual 1,5,4 geometry while [Eu(**1**)(H_2O)]$(CF_3SO_3)_3$ is a nine-coordinate complex with a monocapped distorted square antiprism geometry.[13]

‖ The kinetics of transesterification of **3** were monitored by use of UV–VIS spectroscopy. At pH values > 6.0, the production of 4-nitrophenylate was monitored at 412 nm. At pH values < 6.0, the decrease in the absorbance of **3** at 300 nm was monitored.

1 J. Sumaoka, Y. Azuma and M. Komiyama, *Chem. Eur. J.*, 1998, **4**, 205.
2 R. A. Moss and K. G. Ragunathan, *Chem. Commun.*, 1998, 1871.
3 R. A. Moss and H. Morales-Rojas, *Org. Lett.*, 1999, **11**, 1791.
4 R. Ott and R. Krämer, *Angew. Chem., Int. Ed.*, 1998, **37**, 1957.
5 T. Ihara, H. Shimura, K. Ohmori, H. Tsuji, J. Takeuchi and M. Takagi, *Chem. Lett.*, 1996, 687.
6 R. A. Moss, J. Zhang and K. Bracken, *Chem. Commun*, 1997, 1639.
7 K. Bracken, R. A. Moss and K. G. Ragunathan, *J. Am. Chem. Soc.*, 1997, **119**, 9323.
8 B. N. Trawick, A. T. Daniher and J. K. Bashkin, *Chem. Rev.*, 1998, **98**, 939.
9 R. Haner and J. Hall, *Antisense Nucleic Acid Drug Dev.*, 1997, **7**, 423.
10 J. R. Morrow, in *Metal Ions in Biological Systems*, ed. H. Sigel and A. Sigel, Marcel Dekker, Inc., New York, 1996, vol. 33, pp. 561–592.
11 M. Komiyama, N. Takeda and H. Shigekawa, *Chem. Commun.*, 1999, 1443.
12 D. A. Voss, Jr., Ph.D. Thesis, State University of New York at Buffalo, 2000.
13 (*a*) S. Amin, J. R. Morrow, C. H. Lake and M. R. Churchill, *Angew. Chem., Int. Ed.*, 1994, **33**, 773; (*b*) S. Amin, D. A. Voss, Jr., W. DeW. Horrocks, Jr., C. H. Lake, M. R. Churchill and J. R. Morrow, *Inorg. Chem.*, 1995, **34**, 3294.
14 S. Aime, A. Barge, J. I. Bruce, M. Botta, J. A. K. Howard, J. M. Moloney, D. Parker, A. S. de Souza and M. Woods, *J. Am. Chem. Soc.*, 1999, **121**, 5762.
15 A. Fratiello, R. E. Lee and R. E. Schuster, *Inorg. Chem.*, 1970, **9**, 391.

Typeset and printed by Black Bear Press Limited, Cambridge, England